# Complexing capacity of soil fulvic acid for $Cu^{2+}$, $Cd^{2+}$, $Mn^{2+}$, $Ni^{2+}$, and $Zn^{2+}$ measured by dialysis titration: a model based on soil fulvic acid aggregation

DAVID P. RAINVILLE AND JAMES H. WEBER[1]

*Department of Chemistry, Parsons Hall, University of New Hampshire, Durham, NH 03824, U.S.A.*

Received June 25, 1981

DAVID P. RAINVILLE and JAMES H. WEBER. Can. J. Chem. **60**, 1 (1982).

The dialysis method of metal ion speciation is investigated as a technique to determine complexing capacities of soil fulvic acid (SFA) towards $Cu^{2+}$, $Cd^{2+}$, $Mn^{2+}$, $Ni^{2+}$, and $Zn^{2+}$, between pH 5 and 7. The complexing capacity values for each metal ion usually increase as pH increases. At the same pH the values for $Cd^{2+}$, $Mn^{2+}$, $Ni^{2+}$, and $Zn^{2+}$, are similar, but $Cu^{2+}$ values are significantly higher. The results are interpreted on the basis of a model involving the aggregation of SFA by metal ions, especially $Cu^{2+}$.

DAVID P. RAINVILLE et JAMES H. WEBER. Can. J. Chem. **60**, 1 (1982).

On a étudié la méthode de dialyse des ions métalliques comme technique de détermination des capacités de complexation des acides fulviques du soil (AFS) par rapport aux ions $Cu^{2+}$, $Cd^{2+}$, $Mn^{2+}$, $Ni^{2+}$ et $Zn^{2+}$ à un pH compris entre 5 et 7. La valeur de la capacité de complexation de chaque ion métallique augmente généralement avec le pH. Pour un même pH, les valeurs pour les ions $Cd^{2+}$, $Mn^{2+}$, $Ni^{2+}$ et $Zn^{2+}$ sont semblables, mais elles sont nettement plus élevées dans le cas de l'ion $Cu^{2+}$. On interprète ces résultats en se basant sur un modèle qui implique l'agrégation du AFS par les ions métalliques et plus spécialement par l'ion $Cu^{2+}$.
[Traduit par le journal]

Can. J. Chem. Downloaded from www.nrcresearchpress.com by 210.87.254.42 on 09/06/12
For personal use only.

## Introduction

Increasing public awareness of our environment and the effects of pollutants on it emphasizes a need for additional knowledge about the interaction of metal ions with aquatic humic materials. A variety of methods has been described and utilized to determine the complexing capacity ($C_L$) of both isolated humic matter and humic matter dissolved in natural water systems. These techniques must allow the differentiation of free metal ion species from complexed metal ions without disturbing the equilibrium under study. In a previous paper Truitt and Weber (1) discussed these methods in relation to the determination of complexation capacities of humic materials toward metal ions. Additionally, a recent review (2) has discussed and evaluated critically a variety of metal speciation techniques relevant to the determination of complexing capacities of isolated humic materials and natural water samples.

This paper describes the determination of the complexing capacity of soil fulvic acid (SFA) for $Cu^{2+}$, $Cd^{2+}$, $Mn^{2+}$, $Ni^{2+}$, and $Zn^{2+}$ at various pH values. SFA is a complex mixture of ligands containing phenolic and carboxylic metal binding functional groups. The dialysis titration technique (1) used to determine complexing capacity has a major advantage over other techniques (2). Biological (3), ion selective electrode (4), voltammetric (5), and fluorescence spectrometry (6) techniques all exclude some metal ions of interest. For example, fluorescence quenching studies are most effective for paramagnetic metal ions. In order to study a series of first transition series divalent metal ions and $Cd^{2+}$ we separated free and total metal ions by a dialysis membrane and determined them by atomic absorption spectrometry (AAS). Examination of the complexing capacity results led to a model which involves aggregation of molecules in the SFA mixture induced by metal ions.

## Experimental

*General methods*

Containers used in these experiments were acid washed by soaking in 10% $HNO_3$, and rinsing with distilled, deionized water prior to use.

Solutions were prepared from distilled, deionized water and analytical grade reagents. The soil fulvic acid (SFA) was isolated and characterized by Weber and Wilson (7). The metal ion standard solutions were prepared from Fisher 1000-ppm atomic absorption standard solutions in polypropylene volumetric flasks using disposable polycarbonate tipped pipets.

Dialysis membrane tubing used to prepare dialysis bags (1000 molecular weight cutoff-Spectra/Por 6) and closures were purchased from Spectrum Medical Industries, Los Angeles, CA. They were cleaned prior to use by a procedure already described (1).

Metal ion solutions were acidified by addition of 5 μL of concentrated nitric acid per mL of solution and stored in polypropylene vials prior to atomic absorption spectrometry (AAS) determinations on a Tectron AA5 Spectrometer with less than 3% error. Concentrations of these solutions were determined by a reference to absorbances of standard metal ion solutions. Ultraviolet–visible spectra were recorded on a Cary 14 Spectrophotometer. Solutions were monitored for pH using an Orion Research Model 701A pH potentiometer and a Corning Ag/AgCl glass pH electrode calibrated using buffer solutions.

*Determination of complexing capacity by dialysis*

The complexing capacity of each 10 mg/L SFA aqueous solution was determined by dialysis against an internal 0.001 *M*

[1]To whom all correspondence should be addressed.

0008-4042/82/010001-05$01.00/0

©1982 National Research Council of Canada/Conseil national de recherches du Canada

Can. J. Chem. Downloaded from www.nrcresearchpress.com by 210.87.254.42 on 09/06/12
For personal use only.

$KNO_3$ solution, because 0.001 *M* $KNO_3$ and 10 mg/L SFA solutions have similar ionic strength (8).

To determine the complexing capacity of 10 mg/L SFA solutions toward a metal ion a series of bottled samples (usually 15) was prepared as follows. A strip of dialysis membrane tubing approximately 15 cm in length was tied off at one end with a Teflon string, filled with 10 mL of 0.001 *M* $KNO_3$ solution, and then sealed with a dialysis membrane tubing closure at the other end. The dialysis bag was then placed in a 250 mL polypropylene bottle containing 200 mL of a 10 mg/L SFA solution. All but one sample were then titrated with a volume of a standard metal ion solution so that total metal ion concentrations ranged from 0 to 10 mg/L. After addition of the standard metal ion solutions, the pH of each bottle was adjusted to the proper value by addition of small volumes of 0.1 *M* KOH or 0.1 *M* $HNO_3$. The bottles were then shaken for 48 h with the pH of each bottle being periodically checked for and maintained at the proper value. After the 48 h period, the bottles were sampled. The metal ions in the internal solution within the dialysis bag are considered free since the dialysis bag with its 1000 molecular weight cutoff prevents the migration of most SFA molecules and corresponding complexed metal ions into the dialysis bag (1). The metal ions in the solution external to the dialysis bag are both free and complexed. Since the ratio of the volume of the external solution to the internal solution is 20/1, the external volume approximates the total volume. Thus, metal ion determinations inside the dialysis bag represent free metal ion and those outside the bag are total metal ion. The total metal ion concentration was measured rather than using the calculated values since some metal ions may have been adsorbed onto the containing vessel and dialysis bag.

Figure 1, which for clarity shows only part of the $Cu^{2+}$ pooled data at pH 5 and 6, exemplifies our results. A plot of total metal ion concentration versus free metal ion concentration yields a titration curve which has two linear branches. The lower branch of early data has a slope essentially equal to zero, while the upper branch of data after the titration endpoint is markedly sloped. The complexing capacity ($C_L$) is the *x*-axis intercept of the upper branch as determined by the linear least-squares method.

This procedure was used to determine $C_L$ values of 10 mg/L SFA for $Cu^{2+}$, $Cd^{2+}$, $Mn^{2+}$, $Ni^{2+}$, and $Zn^{2+}$ at pH 5, 6, and 7; and $Cd^{2+}$ at pH 8. In addition $C_L$ values of 0.001 *M* $KNO_3$ for $Cu^{2+}$ were determined at pH 5, 6, and 7 using this procedure (Table 1).

*Determination of the dialysis membrane permeability to $Cu^{2+}$ as a function of time*

The permeability of the 1000 molecular weight cutoff dialysis membrane to $Cu^{2+}$ at pH 5 and 7 in the presence of SFA was determined as a function of time. Typically 2.0 L of either 10 mg/L SFA – 0.001 *M* $KNO_3$ or 10 mg/L SFA – 0.01 *M* $KNO_3$ solutions containing 3.0 mg/L $Cu^{2+}$ (47 μ*M*) were dialyzed against 100 mL of 0.001 *M* or 0.01 *M* $KNO_3$ contained within a dialysis bag 1 m in length. The $Cu^{2+}$ was added on dissolution of SFA or 48 h later. The pH of all internal and external dialysis solutions was adjusted to the desired value by addition of small amounts of 0.1 *M* KOH or 0.1 *M* $HNO_3$. These solutions were stirred by a magnetic stirrer and 5 mL aliquots of internal and external dialysis solutions were withdrawn periodically. The solutions were analyzed for free [$Cu^{2+}$] as a function of time elapsed since addition of $Cu^{2+}$.

*Determination of the dialysis membrane permeability to SFA*

The SFA permeability of the dialysis membrane was determined for the 48 h time period used in the complexing capacity experiment. This was done by dialyzing a 200 mL 10 mg/L SFA solution against a 10 mL 0.001 *M* $KNO_3$ solution at pH 5, 6, and 7. After 48 h 5 mL aliquots of the internal dialysis solutions were withdrawn. The 290 nm absorbance values were obtained and compared to pH 5, 6, and 7 SFA calibration curves (1).

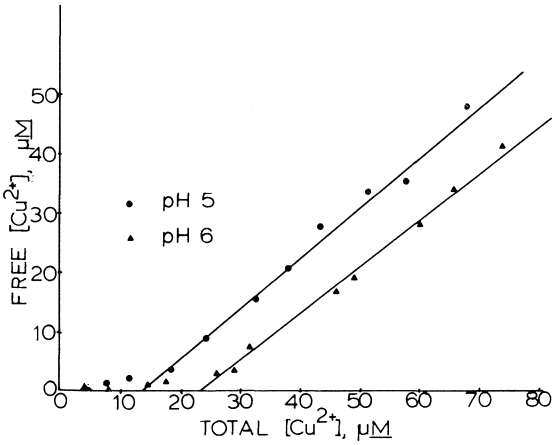


FIG. 1. Sample complexing capacity titration curve, $Cu^{2+}$ at pH 5 and 6.

## Results and Discussion

The complexing capacity ($C_L$) of fulvic acid is defined as its ability to complex free metal ions. In this paper we determined the complexing capacities of well-characterized SFA (7) by dialysis of 10 mg/L SFA – metal ion solutions against 0.001 *M* $KNO_3$. The low [SFA] is similar to that in freshwater samples. We assume that AAS metal ion determinations of internal and external solutions afforded the free metal ion and total metal ion concentrations respectively. The validity of this assumption requires (*1*) that the dialysis membrane effectively excludes complexed metal ions and uncomplexed ligands from the internal solution, and (*2*) that uncomplexed metal ion diffusion through the dialysis membrane is unhindered so that uncomplexed or free metal ion levels are the same in the internal and external solutions. Researchers demonstrated these two points in previous dialysis studies (1, 9–13) and we will prove them valid in the present work.

*Dialysis membrane permeability to SFA*

To test the permeability of the dialysis membrane to SFA we determined the internal/external ratio of SFA absorbance. The ratios determined after 48 h dialysis periods were 14% at pH 5, 4.8% at pH 6, and 3.2% at pH 7. These values are much lower than those of previous 30 day dialysis studies (1). The 48 h dialysis experiments have a major advantage over the 30 day analogs, because metal ions in complexes that permeate the dialysis membrane are considered "free". The net result is that metal complex permeation leads to erroneously low $C_L$ values.

TABLE 1. Complexing capacities ($\mu M$) and slopes for titrations of 10 mg/L soil fulvic acid and 0.001$M$ $KNO_3$ by metal ions[a]

| | pH 5 | | pH 6 | | pH 7 | | pH 8 | |
|---|---|---|---|---|---|---|---|---|
| $M^{2+}$ | $C_L$ | Slope | $C_L$ | Slope | $C_L$ | Slope | $C_L$ | Slope |
| $Cd^{2+}$ | 5.5 | 0.99 | 10.6 | 0.94 | 9.7 | 0.81 | 9.5 | 0.75 |
| $Mn^{2+}$ | 5.2 | 1.02 | 4.8 | 0.94 | 11.6 | 0.94 | | |
| $Ni^{2+}$ | 5.2 | 0.96 | 4.8 | 0.74 | 9.4 | 0.83 | | |
| $Zn^{2+}$ | 0 | 0.95 | 10.2 | 1.08 | 11.8 | 1.09 | | |
| $Cu^{2+}$ | 10.8 | 0.84 | 20.3 | 0.62 | 14.2[d] | 0.24[d] | | |
| $Cu^{2+,b}$ | 0.6 | 0.99 | [c] | 0.92 | [c] | 0.94 | | |

[a] Values obtained by combined linear regression of replicate experiments. At the 90% confidence level the uncertainty is ±8% in slopes and ±15% in $C_L$ values.
[b] Values in 0.001 $M$ $KNO_3$ in absence of soil fulvic acid.
[c] Small, negative value due to experimental error.
[d] This experiment has a large error of ca. 50% in slope and 100% in $C_L$ value.

The error in $C_L$ is not as large as suggested by the absorbance of the internal solution. Templeton and Chasteen (14) found that gel filtration chromatographic separation of our SFA sample produced 91% by weight of larger molecules and 9% of smaller molecules. Furthermore, electron paramagnetic resonance complexation studies revealed that the conditional stability constants of smaller molecules are only 2% that of the larger molecules. In addition Truitt and Weber (1) demonstrated by fluorescence studies that in the absence of metal ions 9% of $Cu^{2+}$ complexing capacity of a 40 mg/L SFA solution permeated the dialysis membrane at pH 5. The 9% value is a high estimate because SFA species increase in size as pH increases (14) and when metal ions are added (1).

*Dialysis membrane permeability to $Cu^{2+}$ in the absence of SFA*

After 48 h the internal and external [$Cu^{2+}$] for 0.001 $M$ $KNO_3$ solutions at pH 5, 6, and 7 are equal. This result means that all $Cu^{2+}$ species, including ones such as $Cu_2(OH)_2^{2+}$ and $Cu(OH)^+$ (15) that might be in the solutions at higher pH, freely permeate the dialysis membrane. The $Cu^{2+}$ species membrane permeability at pH 5 to 7 is important for the future discussion of $Cu^{2+}$ complexation results in that pH range.

*Dialysis membrane permeability to $Cu^{2+}$ as a function of time*

Solutions containing 10 mg/L SFA and 3.0 mg/L $Cu^{2+}$ (47 $\mu M$) were dialyzed against 0.001 $M$ or 0.01 $M$ $KNO_3$ as internal [$Cu^{2+}$] was monitored as a function of time. Some dialysis solutions were prepared and 3 mg/L $Cu^{2+}$ added immediately. Then internal [$Cu^{2+}$] rose rapidly, reaching a maximum after 1.5 h, and then decreased to an equilibrium value within 12 h. In the second experiment, we waited 48 h for equilibrium to occur between the external SFA solution and the internal 0.001 $M$ $KNO_3$ solution before adding $Cu^{2+}$. The [$Cu^{2+}$] rose gradually over 20 h to a maximum level in contrast to the experiment where no equilibrium period was employed. We attribute these observations to minute differences in the ionic environment of the SFA and $KNO_3$ solutions. Additional experiments at pH 5 and 7 in which a 10 mg/L SFA – 0.01 $M$ $KNO_3$ solution containing 3 mg/L $Cu^{2+}$ was dialyzed against a 0.01 $M$ $KNO_3$ solution showed no initial buildup of $Cu^{2+}$ in the internal solution. Despite the fact that [$Cu^{2+}$] reaches a maximum before falling to an equilibrium value in some experiments, this phenomenon does not affect measured $C_L$ values. Anomalous behavior ceases before our 48 h sampling time.

*Complexing capacity results*

Fulvic acid, exemplified in this paper by SFA, is the acid soluble portion of naturally-occurring humic matter. Fulvic acids (FA) are complex mixtures of polyelectrolytes containing carboxyl and phenolic groups. SFA, which is typical of soil- and aquatic-derived fulvic acids, has ca. 50% carbon, ca. 40% oxygen, 8.2 mmol/g carboxyl groups, and 5.2 mmol/g phenolic groups (7). Functional group and elemental analyses are probably the best-known properties of fulvic acids. FA acidic properties, though, have been carefully studied by Gamble and co-workers (16). They found that any equilibrium function measured and defined for a fulvic acid mixture will be a weighted average of values, and will change with changes in FA concentration. This result is not a factor in the present study because of constant 10 mg/L SFA concentration.

There is complication beyond the necessity of using weighted equilibrium functions. Molecules in FA mixtures are thought to undergo conformational and/or aggregation–deaggregation changes as pH, [FA], and solution ionic strength varies. For

Can. J. Chem. Downloaded from www.nrcresearchpress.com by 210.87.254.42 on 09/06/12
For personal use only.

Can. J. Chem. Downloaded from www.nrcresearchpress.com by 210.87.254.42 on 09/06/12
For personal use only.

example, Ghosh and Schnitzer (17) concluded on the bases of viscosity and surface pressure measurements that in 0.001 *M* NaCl FA solutions change from coiled monomers to linear monomers below ca. 4000 mg/L FA. Reuter (18) observed anomalous reduced viscosity changes in FA at concentrations less than 100 mg/L at pH 7. Gel filtration chromatography (GFC) experiments (14) on our SFA sample suggest increased molecular size between pH 3 and 8. Gjessing (19) in GFC experiments noted that humic materials increase in size with increasing pH and lower ionic strength. Other workers (20) noted that pH changes affect various humic acid fractions in different ways.

The above brief description of fulvic acid mixtures suggest difficulties inherent in describing FA complexation of metal ions. It is not surprising that various research groups have different models describing FA – metal ion complexation. Weber and co-workers (21–23), Buffle and co-workers (24), and the Gamble–Langford group (4) have all used different means of calculating conditional stability constants from their data. The latter calculation (4) is the most detailed because it includes the weighted average $Cu^{2+}$ fulvic acid conditional stability constant as well as that for an infinitesimal portion of the binding sites.

Our past $Cu^{2+}$ (21), $Cd^{2+}$ (22), $Pb^{2+}$ (23, 25) ion selective electrode and fluorescence (6) studies exemplify FA metal ion binding results. Observed conditional stability constants depend on variables such as pH and [FA]. Generally conditional stability constants increase as pH increases (21–23). For example, $Cd^{2+}$–SFA conditional stability constants increase from $1.7 \times 10^3$ at pH 4 to $4.3 \times 10^4$ at pH 8 (22). Effects due to changes in [SFA] are less pronounced; an eightfold increase in [SFA] decreases the $Cd^{2+}$ conditional stability constant by ca. 55% (22).

The above discussion of conditional stability constants suggests that interpretation of complexing capacities ($C_L$) will be difficult, but does not explain how to analyze them. The reason is that researchers calculate conditional stability constants from data before the ligand is saturated with metal ion, while they calculate $C_L$ values from data well after the ligand is saturated with metal ion (1, 26). Also any aggregation processes mentioned above may affect availability of metal ion binding sites, i.e. $C_L$ values in this paper are *x*-intercepts of free $M^{2+}$ vs. total $M^{2+}$ curves (Fig. 1).

Most $C_L$ value trends (Table 1) demonstrate that (*1*) $C_L$ values increase as pH increases for each $M^{2+}$; (*2*) at each pH $C_L$ values are similar for $Mn^{2+}$, $Ni^{2+}$, $Zn^{2+}$, and $Cd^{2+}$; and (*3*) the $Cu^{2+}$ $C_L$ value at each pH is appreciably higher than that for the other four $M^{2+}$. Deviations from these three trends, e.g. $C_L$ of $Zn^{2+}$ at pH 5, are beyond our present understanding. It is tempting to rationalize the $C_L$ trends on the basis of the above FA conditional stability constant discussion, because the values typically increase as pH increases (21–23). In addition $Cu^{2+}$ binds more strongly to SFA than $Cd^{2+}$ or $Ni^{2+}$ under the same experimental conditions (6, 21, 22), and probably shows the same trend as with $Mn^{2+}$ and $Zn^{2+}$. Because of the nature of the dialysis experiments and data treatment, the relative $C_L$ values for different $M^{2+}$ cannot be explained on the basis of conditional stability constant results. If, for example, we did experiments similar to those reported here with a model ligand such as $10^{-5}$ *M* salicylic acid, resulting $C_L$ values would not depend on the nature of $M^{2+}$ or pH. $C_L$ represents the *capacity* for metal ion binding, not the equilibrium extent of metal complex formation. The above statement is true for a mixture of salicylic and phthalic acids (a typical fulvic acid model), or a mixture as complex as fulvic acid itself. Thus, different $C_L$ values for any $M^{2+}$ such as $Ni^{2+}$ and $Cu^{2+}$ cannot be due to weaker binding of the former metal ion with SFA. It is also incorrect to attribute enhanced $C_L$ values for any $M^{2+}$ as pH increases to equilibrium considerations. We must look elsewhere for an explanation.

We start with the assumption that in experiments with 10 mg/L SFA solutions at pH 5 and above, there is little inter- or intramolecular SFA binding. First, in the pH range of this study carboxyl groups are predominantly ionized and FA molecules carry a negative charge (16). For this reason SFA molecules would have an extended conformation in which carboxylate ions are widely separated from each other, and intramolecular bonding is minimal. Second, there would also be negligible intermolecular bonding due to the above reason and the small 10 mg/L [SFA]. Addition of metal ions, however, significantly affects the nature of FA molecules.

Several research groups on the basis of stability constant studies have suggested changes in FA aggregation due to complexation by $Cu^{2+}$ (4, 25), $VO^{2+}$ (14), and $Pb^{2+}$ (23, 25). For example, our group (25) showed by light scattering experiments that SFA in a 32 mg/L solution at pH 4.5 in 0.1 *M* $KNO_3$ aggregates when total [$Pb^{2+}$] is 50 $\mu M$, total [$Cu^{2+}$] is 200 $\mu M$ and total [$Cd^{2+}$] is 1000 $\mu M$. SFA and $M^{2+}$ concentrations in this work are somewhat lower, but unpublished results (27) show that scattering does occur in the $M^{2+}$ and SFA concentration ranges of this experiment. A metal ion binding model based on aggregation agrees with the complexation parameters of Table 1.

A first major trend of the data in Table 1 is that $C_L$

Can. J. Chem. Downloaded from www.nrcresearchpress.com by 210.87.254.42 on 09/06/12
For personal use only.

values at constant pH are similar for $Cd^{2+}$, $Mn^{2+}$, $Ni^{2+}$, and $Zn^{2+}$; and significantly higher for $Cu^{2+}$. We contend that the higher $C_L$ values of $Cu^{2+}$ are due to its ability to cause SFA aggregation, because it forms inner sphere complexes. Nuclear magnetic resonance studies (28) have shown that $Mn^{2+}$ forms an outer sphere complex with FA while $Cu^{2+}$ forms an inner sphere one. This result confirms our conclusion that $Cu^{2+}$ forms different kinds of FA complexes than $Mn^{2+}$, and probably weakly-binding $Cd^{2+}$ (22), $Ni^{2+}$, and $Zn^{2+}$ as well. It is a fact that $Cu^{2+}$ is more effective than $Cd^{2+}$ in causing SFA aggregation (25), and we conclude that $Cu^{2+}$–SFA aggregates bind $Cu^{2+}$ more effectively than SFA alone. Another trend in Table 1 for most $M^{2+}$ is that $C_L$ values increase as pH increases. Fluorescence polarization studies (29) demonstrate the absence of conformational change in our SFA sample between pH 4 and 8, and that phenomenon is not an appropriate rationale. Detailed explanation of the two trends based on aggregation is speculative. First, aggregation might convert two or more monodentate ligands into a polydentate one. Second, the aggregates might serve as a site for polymerization or nucleation of hydrolyzed metal ion species. Third, aggregates might induce the formation of mixed M(SFA)(OH) complexes as suggested by Buffle (24).

Finally, the model must be consistent with another trend in Table 1. That is, the experimental slopes of the free $[Cu^{2+}]$ versus total $[Cu^{2+}]$ curves become considerably less than unity as pH increases. This result is unexpected because free and total $[Cu^{2+}]$ well after the $C_L$ endpoint should be equal. The $Cu^{2+}$–SFA aggregates are binding large amounts of $Cu^{2+}$ with no sign of an endpoint. The 70–130 $\mu M$ $Cu^{2+}$ added sometimes approaches the 132 $\mu M$ concentration of carboxylic/phenolic binding sites, and far exceeds the 66 $\mu M$ concentration if all binding sites were bidentate. The non-unity slopes are attributable neither to a precipitate nor to species such as $Cu_2(OH)_2^{2+}$ or $Cu(OH)^+$. Precipitation assures a constant $[Cu^{2+}]$ once a solubility product constant is exceeded (1). The low slopes are not due to $Cu^{2+}$ hydrolysis products that cannot permeate the dialysis membrane, because experiments in the absence of SFA have slopes near unity (Table 1). One explanation is that excess $Cu^{2+}$ binds predominantly to monodentate carboxylic and phenolic sites on the aggregates, via mixed Cu(FA)(OH) complexes as suggested by Buffle (24). The presence of $OH^-$ in the complexes would decrease the excess positive charge due to $Cu^{2+}$ complexed to monodentate anionic sites thus allowing more $Cu^{2+}$ binding. The conditional stability constants based on a 1:1 binding model must be greater than ca. $2 \times 10^4$ for detection of binding past the initial end point.

## Acknowledgements

We thank W. R. Seitz for many helpful discussions and Katherine E. Weber for computer data treatment.

This work was partially supported by Office of Water Resources Technology Grant B004-NH through the University of New Hampshire Water Resources Research Center.

1. R. E. Truitt and J. H. Weber. Anal. Chem. **53**, 337 (1981).
2. T. M. Florence and G. E. Batley. C.R.C. Crit. Rev. Anal. Chem. **9**, 219 (1980).
3. R. Gächter, J. S. Davis, and A. Marès. Environ. Sci. Tech. **12**, 1416 (1978).
4. D. S. Gamble, A. W. Underdown, and C. H. Langford. Anal. Chem. **52**, 1901 (1980).
5. S. A. Wilson, T. C. Huth, R. E. Arndt, and R. K. Skogerboe. Anal. Chem. **52**, 1515 (1980).
6. R. A. Saar and J. H. Weber. Anal. Chem. **52**, 2095 (1980).
7. J. H. Weber and S. A. Wilson. Water Res. **9**, 1079 (1975).
8. R. E. Truitt. Ph.D. Dissertation, University of New Hampshire, Durham, NH. 1980.
9. H. Zunio and J. D. Martin. Soil Sci. **123**, 188 (1977).
10. P. Beneš and E. Steinnes. Water Res. **9**, 741 (1975).
11. P. Beneš, E. T. Gjessing, and E. Steinnes. Water Res. **10**, 711 (1976).
12. B. T. Hart and S. H. R. Davies. Aust. J. Mar. Freshwater Res. **28**, 105 (1977).
13. P. Beneš and E. Steinnes. Water Res. **8**, 947 (1974).
14. G. D. Templeton III and N. D. Chasteen. Geochim. Cosmochim. Acta, **44**, 741 (1980).
15. C. F. Baes Jr. and R. E. Mesmer. The hydrolysis of cations. Wiley-Interscience, New York. 1976. pp. 267–274.
16. R. D. Burch, C. H. Langford, and D. S. Gamble. Can. J. Chem. **56**, 1196 (1978).
17. K. Ghosh and M. Schnitzer. Soil Sci. **129**, 266 (1980).
18. J. H. Reuter. Geol. Soc. Am. Abstr, **9**(7), 1140 (1977).
19. E. T. Gjessing. Schweiz. Z. Hydrol. **33**, 592 (1971).
20. R. L. Wershaw, D. J. Pinckney, and S. E. Booker. J. Res. U.S. Geol. Survey, **5**, 565 (1977).
21. W. T. Bresnahan, C. L. Grant, and J. H. Weber. Anal. Chem. **50**, 1675 (1978).
22. R. A. Saar and J. H. Weber. Can. J. Chem, **57**, 1263 (1979).
23. R. A. Saar and J. H. Weber. Environ. Sci. Tech. **14**, 877 (1980).
24. J. Buffle. Anal. Chim. Acta, **118**, 29 (1980).
25. R. A. Saar and J. H. Weber. Geochim. Cosmochim. Acta, **44**, 1381 (1980).
26. M. S. Shuman and J. L. Cromer. Environ. Sci. Tech. **13**, 543 (1979).
27. D. K. Ryan, C. Thompson, and J. H. Weber. Unpublished results.
28. K. Deczky and C. H. Langford. Can. J. Chem. **56**, 1947 (1978).
29. A. J. Lapen, and W. R. Seitz. Anal. Chim. Acta, In press.

# Comments: Polymérisation du norbornène par des amorceurs au ruthénium. Etude cinétique de la réaction

A. J. Amass

*Department of Chemistry, University of Aston in Birmingham, Gosta Green, Birmingham, B4 7TE, England*

Received May 19, 1981

A. J. Amass. Can. J. Chem. **60**, 6 (1982).

Comments are expressed on the interpretation of experimental data provided by Tanielian *et al.* (Can. J. Chem. **58**, 2813 (1980)).

A. J. Amass. Can. J. Chem. **60**, 6 (1982).

On présent les commentaires sur l'interprétation des donnés expérimentaux publié par Tanielian *et al.* (Can. J. Chem. **58**, 2813 (1980)).

Can. J. Chem. Downloaded from www.nrcresearchpress.com by 210.87.254.40 on 09/06/12
For personal use only.

The paper cited deals with some interesting aspects of the polymerisation of norbornene by the metathesis catalysts $RuCl_3 \cdot 3H_2O$ and $RuCl_2(P\Phi_3)_3$. These comments deal with the analysis of the results and the subsequent interpretation placed upon them by the authors.

Figure 1 shows the behaviour that is typical of metathesis polymerisations and is similar to that shown by the polymerisation of cyclopentene (1). Of great concern to me however is the interpretation that the authors place on Figs. 3 and 4. These figures show the dependence of conversion on time for polymerisations catalysed by $RuCl_2(P\Phi_3)_3$ and $RuCl_3 \cdot 3H_2O$ respectively. In the first case, Fig. 3 is interpreted as showing that the rate of polymerisation is first order in concentration of monomer for monomer concentrations below 0.13 mol $dm^{-3}$ and zero order for concentrations of monomer greater than 0.13 mol $dm^{-3}$. Figure 4 is similarly interpreted as indicating a zero order dependence of rate of polymerisation on monomer concentration. I suggest these interpretations are incorrect.

For a simple first order reaction,

$$-\mathrm{d[M]}/\mathrm{d}t = k[\mathrm{M}]$$

$k$ may be a composite rate constant and in this case includes the concentration of the catalyst. For a reaction of this type, the well known equation:

$$[\mathrm{M}]/[\mathrm{M}]_0 = \exp -kt$$

is obtained. Surely, for a first order reaction, $[\mathrm{M}]/[\mathrm{M}]_0$ is constant and independent of the initial concentration of monomer for a particular reaction time.

Since

$$\%\,\text{conversion} = \frac{[\mathrm{M}]_0 - [\mathrm{M}]}{[\mathrm{M}]_0} \times 100 = \left(1 - \frac{[\mathrm{M}]}{[\mathrm{M}]_0}\right) \times 100$$

it must also follow that a plot of % conversion against time should be close to a straight line at low conversion, the slope of which is independent of the initial concentration of monomer.

Figure 4 therefore leads to the interpretation that the rate of polymerisation of norbornene is first order with respect to the concentration of norbornene when $RuCl_3 \cdot 3H_2O$ is used as catalyst and Fig. 3 shows that at a concentration of norbornene *greater* than 0.13 mol $dm^{-3}$ the rate is first order with respect to monomer concentration when $RuCl_2 \cdot (P\Phi_3)_3$ is used as initiator.

To develop this argument further for a second order reaction,

$$-\mathrm{d[M]}/\mathrm{d}t = k[\mathrm{M}]^2$$

from which

$$\frac{1}{[\mathrm{M}]} - \frac{1}{[\mathrm{M}]_0} = kt$$

may be obtained. Suitable manipulation of this equation leads to

$$1 - \frac{[\mathrm{M}]}{[\mathrm{M}]_0} = \frac{[\mathrm{M}]_0 kt}{1 + [\mathrm{M}]_0 kt}$$

It may be plausible therefore that at low concentrations of monomer, $[\mathrm{M}]_0 kt$ may be much less than 1. If this is the case

$$\left(1 - \frac{[\mathrm{M}]}{[\mathrm{M}]_0}\right) \times 100 \approx 100\,[\mathrm{M}]_0 kt$$

In this case, a plot of % conversion against time would lead to a straight line, the slope of which would depend on the initial concentration of monomer. It would appear therefore that the interpretation to be placed on Fig. 3 is indeed that the measured order of reaction changes as the concentration of monomer is increased but from two to one and not one to zero, as suggested by the authors.

Obviously this now must call for a complete reappraisal of the mechanism that can be formulated for this reaction and the system does not show features typical of the Langmuir–Hinshelwood model.

1. A. J. Amass and J. A. Zurimendi. Eur. Polym. J. **17**, 1 (1981).

0008-4042/82/010006-01$01.00/0

©1982 National Research Council of Canada/Conseil national de recherches du Canada

# Réponses aux commentaires "Polymérisation du norbornène par des amorceurs au ruthénium. Etude cinétique de la réaction"

A. KIENNEMANN

*Laboratoire Chimie Organique Appliquée, 1 rue Blaise Pascal, 67008 Strasbourg, France*

Reçu le 15 juin 1981

A. KIENNEMANN. Can. J. Chem. **60**, 7 (1982).

L'ordre de la réaction de la polymérisation du norbornène catalysée par des amorceurs au ruthénium (entre 0 et 1 ou entre 1 et 2) est discuté. Le rôle du solvant et l'effet du vieillissement du catalyseur permettent de proposer un schéma réactionnel de type dissociatif.

---

A. KIENNEMANN. Can. J. Chem. **60**, 7 (1982).

The reaction order (between 0 and 1 or between 1 and 2) of the polymerization of norbornene catalyzed by ruthenium initiators is discussed. The role of the solvent and the effect of pretreatment of the catalyst allow the proposal of a reaction scheme of the dissociative type.

[Journal Translation]

Le travail de Amass (1) indique clairement la convergence des résultats sur deux points importants: l'ordre 1 de la réaction par rapport au catalyseur et l'ordre variable par rapport au monomère. La divergence provient de la valeur de cet ordre: entre 0 et 1 dans notre étude, entre 1 et 2 d'après son étude cinétique. Les figs 3 et 4 de notre travail (2) montrent l'influence de la concentration en monomère sur la conversion du norbornène par une représentation du % de conversion en fonction du temps. Elles indiquent clairement que le % de conversion est proportionnel au temps et indépendant de la concentration en monomère quelque soit cette concentration pour la fig 4 et pour des valeurs élevées en monomère pour la fig 3. Nous en avons conclu que l'ordre était nul (fig 4) et variable entre 0 et 1 (fig 3).

Cependant, la démonstration de Amass conduit à d'autres conclusions. Il faut donc penser que la cinétique ne permet peut être pas de trancher et regarder d'autres résultats expérimentaux et plus particulièrement le rôle du solvant alcool et du vieillissement du catalyseur.

Dans un travail précédent (3) nous avions montré que la nature du solvant influait sur la vitesse de réaction dans le cas de $RuCl_3 \cdot 3H_2O$ alors qu'elle n'avait pas d'influence avec $RuCl_2(P\phi_3)_3$. Avec $RuCl_3 \cdot 3H_2O$, l'étape lente de la réaction semble donc être la formation d'un complexe ruthénium–alcool qui ne fait pas intervenir le monomère. L'ordre pour $RuCl_3 \cdot 3H_2O$ doit donc être indépendant de la concentration en monomère. Nous avons montré de plus que l'ordre était zéro par rapport à l'alcool dans le domaine étudié ce qui conduit à supposer un mécanisme dissociatif.

L'étude en fonction du vieillissement confirme ces résultats: (*a*) chauffage à 60°C d'une solution alcoolique de $RuCl_3,3H_2O$ ($4 \times 10^{-5}$ mol) pendant 4,24 et 72 h avant d'additionner le monomère (0,04 mol); (*b*) chauffage de $RuCl_3,3H_2O$ ($4 \times 10^{-5}$ mol) en solution alcoolique avec $8 \times 10^{-5}$ mol de norbornène pendant 24 et 72 h avant addition de 0,04 mol de norbornène. Nous constatons: (*1*) une augmentation très nette de la vitesse initiale de polymérisation pour les essais à 24 et 72 h (expérience (*a*)); (*2*) que l'addition préalable de monomère n'a aucune incidence sur le déroulement ultérieur de la réaction ce qui confirme l'aspect dissociatif du processus.

1. A. J. AMASS. Can. J. Chem. **60**, 6 (1982).
2. C. TANIÉLIAN, A. KIENNEMANN, and T. OSPARPUCU. Can. J. Chem. **58**, 2813 (1980).
3. C. TANIÉLIAN, A. KIENNEMANN, and T. OSPARPUCU. Can. J. Chem. **57**, 2022 (1979).

0008-4042/82/010007-01$01.00/0

©1982 National Research Council of Canada/Conseil national de recherches du Canada

Can. J. Chem. Downloaded from www.nrcresearchpress.com by 210.87.254.5 on 09/06/12
For personal use only.

# Détermination du site de chélation dans des systèmes cycliques arylhydrazone–imine à 6 atomes. Échanges intra- et intermoleculaires du proton chélaté

ROGER PICHON, JEAN-YVES LE GALL ET PIERRE COURTOT[1]

*Laboratoire "Photochimie, Electrochimie et Chimie Moléculaires" de l'Université de Bretagne Occidentale, associé au CNRS (LA 322), 6 avenue le Gorgeu, 29283 Brest, France*

Reçu le 28 janvier 1981

ROGER PICHON, JEAN-YVES LE GALL et PIERRE COURTOT. Can. J. Chem. **60**, 8 (1982).

Nous avons déterminé les sites de chélation du proton et les structures des systèmes chélatés cycliques à six atomes que sont les arylhydrazono-2 arylimino-3 propanones-1 et les arylhydrazono-2 bis(arylimino)-1,3 propanes. Deux types d'échange du proton chélaté ont été caractérisés chez ces composés par rmn. Le premier correspond à un échange intramoléculaire entre les deux atomes d'azote des fonctions hydrazone et imine. Nous avons montré que les équilibres de tautomérie interne correspondants dépendent de plusieurs paramètres (solvant, température et substituants des noyaux aromatiques des groupements azo et imino). Le second échange correspond à un échange intermoléculaire, vraisemblablement soluté–soluté, et dépend de la température et de la concentration des solutions.

ROGER PICHON, JEAN-YVES LE GALL, and PIERRE COURTOT. Can. J. Chem. **60**, 8 (1982).

Chelation sites of the proton and structures of chelated six-atom ring systems have been determined for 2-arylhydrazono-3-aryliminopropane-1-ones and 2-arylhydrazono-1,3-bis(arylimino)propanes. Nuclear magnetic resonance spectroscopy allowed determination in these compounds of two types of exchange of the chelated proton. The first type concerns an intramolecular exchange between the two nitrogen atoms of the hydrazono and imino groups. We have shown that the internal tautomeric equilibria are dependent on several factors (solvent, temperature, and substituents fixed on aromatic rings of azo and imino groups). A second type of exchange corresponds to an intermolecular exchange, most probably of the solute–solute type, which depends on the temperature and concentration of the solutions.

La condensation de sels d'aryldiazonium sur les carbanions de composés β-dicarbonylés, β-cétosulfones, β-cétophosphonates conduit à des composés dont la structure hydrazone a été établie et dont les équilibres entre les différents isomères ont été étudiés au cours d'un travail précédent (1, 2). L'absence de tautomérie interne[2] hydrazonocétone–azoénol chez ces composés leur confère des propriétés photochimiques intéressantes résultant de l'isomérisation *syn–anti* de la double liaison C=N (3).

Des propriétés analogues se retrouvent chez les énamines α,α′-dicarbonylées étudiées au laboratoire par Couchouron (10). Ces composés se trouvent en solution sous une seule configuration chélatée énaminocétone **C**, la tautomérie interne énaminocétone–iminohydroxy n'étant pas observée. Afin d'examiner le caractère général des propriétés chimiques et photochimiques des arylhydrazones impliquées dans un cycle de chélation à six atomes et de comparer le pouvoir accepteur du proton chélaté des deux fonctions azo et imine dans un tel environnement, nous nous sommes proposé d'étudier deux séries de composés, les arylhydrazono-2 arylimino-3 propanones **A** et les arylhydrazono-2 bis(arylimino)-1,3 propanes **B**. Une compétition est à prévoir entre les deux atomes d'azote des fonctions azo et imine pour fixer le proton chélaté, ce qui devrait entraîner des propriétés intéressantes.

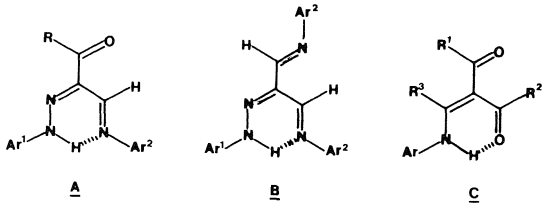

**A** **B** **C**

## Résultats et discussion

### A. *Structure et stéréochimie des arylhydrazono-2 arylimino-3 propanones-1. Echange intramoléculaire du proton chélaté*

Plusieurs séries d'arylhydrazones ont été préparées afin d'étudier l'influence des différents substituants des fonctions azo et imine sur les équilibres thermodynamiques de ces composés en solution. Leur synthèse est réalisée à partir des arylhydrazono-2 propanediones-1,3 diversement substituées en -3 (R = H, $CH_3$, Ar) sur lesquelles on condense un équivalent d'aniline substituée. Ces composés peuvent exister en solution sous plusieurs configurations que nous avons représentées sur le schéma 1 en ne prenant pas en compte les configurations ne possédant pas de chélation: elles ne sont jamais décelées en solution et elles doivent être fortement défavorisées.

[1]Auteur à qui toute correspondance doit être adressée.

[2]Nous désignons comme tautomères internes, deux chélates qui ne diffèrent que par le site du proton chélaté (par exemple **b** et **c**, schéma 1).

0008-4042/82/010008-11$01.00/0

©1982 National Research Council of Canada/Conseil national de recherches du Canada

Can. J. Chem. Downloaded from www.nrcresearchpress.com by 210.87.254.40 on 09/06/12
For personal use only.

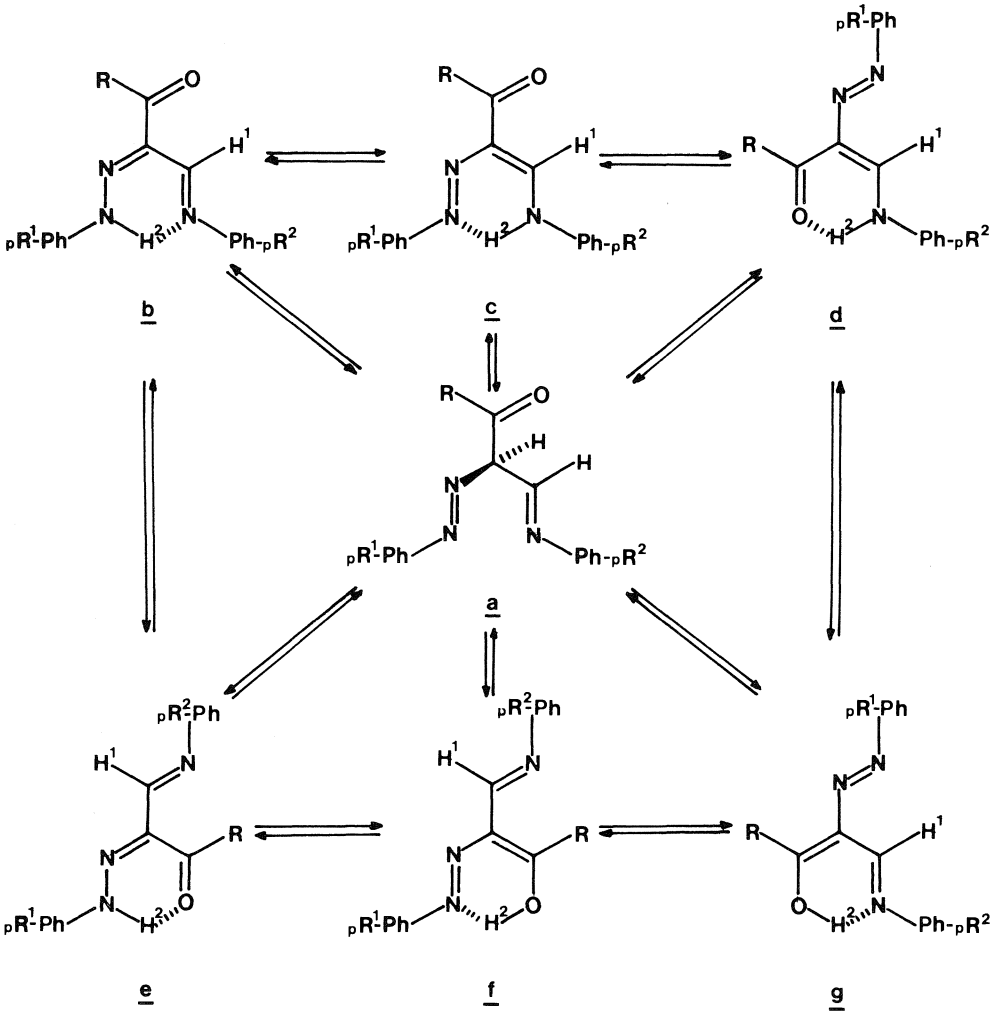


SCHEME 1

Le choix entre les différentes configurations **a**–**g** a pu être effectué à partir des caractéristiques spectroscopiques de ces composés, en particulier à l'aide des arguments rmn dans le cas des arylhydrazono-2 arylimino-3 propanals (R = H), que nous allons exposer en détail avant de généraliser pour les autres séries.

Dans le cas où R = $H^3$, si l'allure des spectres de rmn des composés de cette série (**1** à **10**) reste la même quels que soient les substituants $pR^1Ph$ et $pR^2Ph$ présents (le proton chélaté $H^2$ résonne vers 14,5–15 ppm, les deux protons $H^1$ et $H^3$ entre 8 et 10 ppm et les protons aromatiques entre 6,5 et 8 ppm), la forme du signal correspondant au proton aldimine ou aldéhyde, suivant les configurations envisagées **a**–**g**, diffère selon la nature des substituants. Alors que le premier signal ($H^3$) situé vers 9,5–10 ppm est toujours un singulet, le second ($H^1$) qui résonne à champ plus fort se dédouble plus ou moins nettement suivant les substituants présents sur les noyaux aromatiques des fonctions hydrazone et imine (Fig. 1). Ces deux signaux correspondant chacun à un proton, la présence d'un doublet pour le second signal ne peut résulter que d'un couplage de ce proton avec le proton chélaté, ce qui est vérifié lors d'un découplage de spin en irradiant à la fréquence du proton chélaté. Le signal apparaît alors en singulet, démontrant le couplage de ces protons.

L'allure des spectres nous conduit donc à propo-

Can. J. Chem. Downloaded from www.nrcresearchpress.com by 210.87.254.40 on 09/06/12
For personal use only.

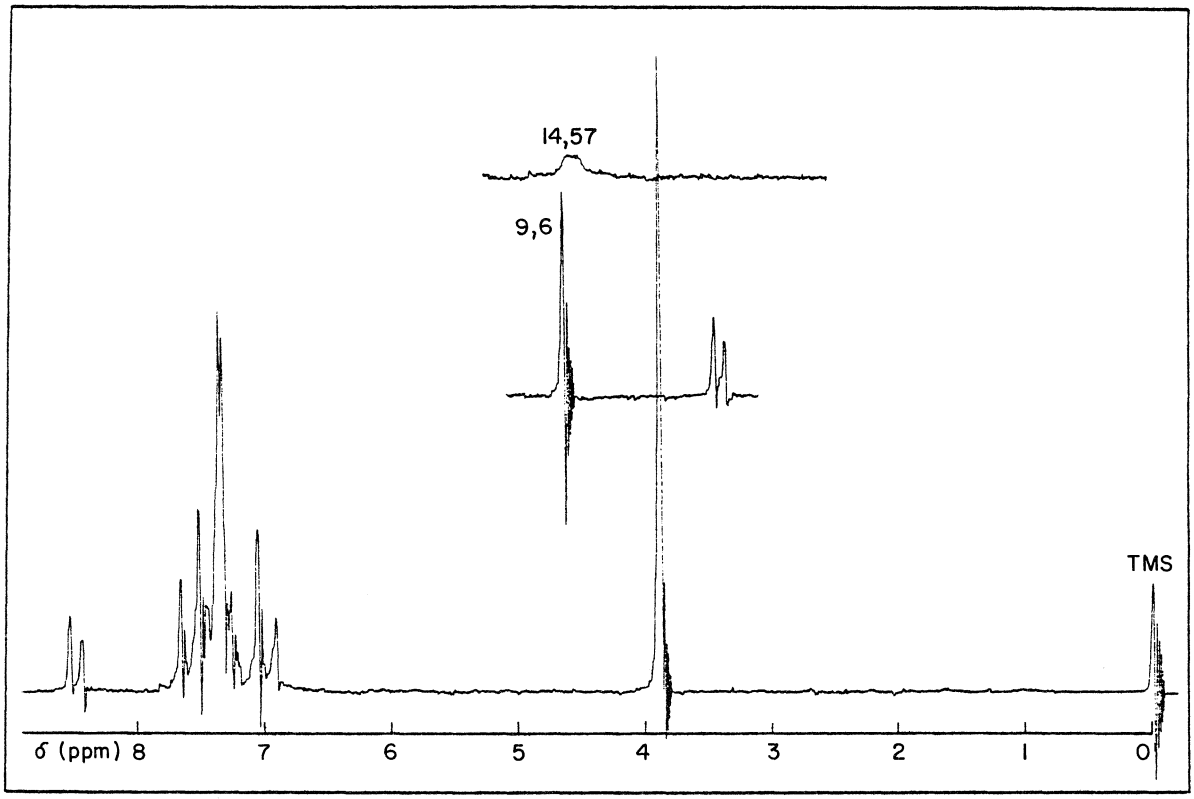


FIG. 1. Spectre rmn du *para*-méthoxyphénylhydrazono-2 phénylimino-3 propanal **4** (R = H, $R^1$ = MeO, $R^2$ = H) en solution dans $CDCl_3$.

ser la présence d'un couple de tautomères "internes" en solution et à exclure – d'une part l'existence de deux isomères, qui auraient entraîné quatre signaux différents pour les protons aldéhydiques et imino libres et chélatés, d'autre part l'existence d'un seul isomère, qui n'expliquerait pas la valeur de la constante de couplage observée sur les spectres rmn. Celle-ci serait nulle dans le cas d'une structure hydrazone ou de 12–13 Hz dans le cas des structures hydroxy ou énamine (4–10).

Si la paire de tautomères internes **d** et **g** peut être exclue, les protons $H^1$ et $H^3$ (R = $H^3$) devant résonner en doublets dédoublés dans ce cas (et le marquage à l'azote-15 le confirme), le choix entre les deux autres paires de tautomères possibles **b** ⇄ **c** et **e** ⇄ **f** peut être réalisé par marquage des atomes d'azote des fonctions imine et azo à l'aide de l'isotope $^{15}N$. Nous avons choisi deux composés caractéristiques pour ce marquage: le phénylhydrazono-2 phénylimino-3 propanal **1** et le *para*-méthoxyphénylhydrazono-2 phénylimino-3 propanal **4**.

La structure arylhydrazone d'un des tautomères est vérifiée dans le cas du composé **1** pour lequel la constante de couplage observée pour le proton aldimino $H^1$ est de l'ordre de 2 Hz dans $CDCl_3$. La fonction hydrazone peut être marquée à l'azote 15 en préparant le sel de phényldiazonium à partir de l'aniline marquée à l'azote 15 (11). L'apparition d'un couplage $^{15}N$—H sur le proton chélaté ($J$ = 77 Hz à 20°C dans $CDCl_3$) confirme la structure hydrazone d'un des tautomères. Le marquage de la fonction imine dans le cas du *para*-méthoxyphénylhydrazono-2 phénylimino-3 propanal **4** conduit également à la mise en évidence d'un couplage $^{15}N$—H ($J$ = 37 Hz dans $CDCl_3$ à 20°C). Ces données permettent d'identifier sans ambiguïté le couple de tautomères internes **b** ⇄ **c** en solution.

Des arguments analogues permettent d'énoncer le caractère général de ce type de tautomérie interne **b** ⇄ **c** chez les autres séries de composés (R = $CH_3$, Ph, *p*MeOPh). Ces configurations sont d'ailleurs confirmées à l'aide des données infrarouge et en ultra-violet.

Tous les composés **1** à **23** possèdent une bande intense correspondant aux fréquences de vibration de valence des carbonyles libres conjugués des fonctions aldéhydes (1680–1690 $cm^{-1}$) ou cétones (1645–1675 $cm^{-1}$) dans un tel environnement (2, 12, 13).

Can. J. Chem. Downloaded from www.nrcresearchpress.com by 210.87.254.40 on 09/06/12
For personal use only.

Can. J. Chem. Downloaded from www.nrcresearchpress.com by 210.87.254.40 on 09/06/12
For personal use only.

TABLEAU 1. Caractéristiques spectrales et physiques des arylhydrazono-2 arylimino-3 propanones (rmn, $CDCl_3$; ir, $CCl_4$)

| R | $R^1$ | $R^2$ | No | δR (ppm) | $\delta H^1$ (ppm) | $\delta H^2$ (ppm) | $J_{H^1-H^2}$ (Hz) | ν(CO) ($cm^{-1}$) ($CCl_4$) | *c* % | *M/e* | *F*(°C) |
|---|---|---|---|---|---|---|---|---|---|---|---|
| H | H | H | **1** | 9,50 | 8,60 | 14,90 | 2 | 1689 | 15 | 251 | 70 |
| | H | $NO_2$ | **2** | 9,56 | 8,65 | 14,85 | 1 | 1680 | 7,5 | 296 | 220 |
| | H | MeO | **3** | 9,55 | 8,69 | 15,08 | 1 | 1686 | 7,5 | 281 | 92 |
| | MeO | H | **4** | 9,6 | 8,33 | 14,57 | 5,25 | 1687 | 40 | 281 | 132 |
| | MeO | MeO | **5** | 9,55 | 8,45 | 14,8 | 3,75 | 1682 | 29 | 311 | 98 |
| | MeO | $NO_2$ | **6** | 9,60 | 8,50 | 14.6 | 3 | 1686 | 23 | 326 | 206 |
| | Me | H | **7** | 9,50 | 8,60 | 15,15 | | 1688 | | — | — |
| | Me | Me | **8** | 9,65 | 8,65 | 14,97 | 2,25 | 1684 | 17 | — | — |
| | $NO_2$ | H | **9** | 9,04 | 8,20 | 14,96 | — | 1687 | — | 296 | 170 |
| | $NO_2$ | MeO | **10** | 9,05 | 8,20 | 15 | — | 1685 | — | 326 | 182 |
| Me | H | H | **11** | 2,55 | 8,78 | 15,2 | 1,5 | 1674 | 11,5 | 265 | 136 |
| | H | MeO | **12** | 2,55 | 8,85 | 15,27 | 1 | 1672 | 5 | 295 | 115 |
| Ph | H | H | **13** | | 8,98 | 15,35 | 1,5 | 1644 | 12 | 327 | 137 |
| | MeO | H | **14** | | 8,82 | 15,2 | 4,5 | 1639 | 35 | — | — |
| | MeO | Cl | **15** | | 8,85 | 15,2 | 3,5 | 1642 | 27 | 391 | 161 |
| | $NO_2$ | $NO_2$ | **16** | | 8,94 | 15,1 | — | 1647 | — | — | — |
| | $NO_2$ | MeO | **17** | | 8,95 | 15,6 | 1 | 1643 | 7,5 | 402 | 190 |
| | Me | H | **18** | | 8,94 | 15,3 | 2 | 1642 | 15 | 341 | 146 |
| MeOPh | H | H | **19** | | 8,97 | 15,5 | 1 | 1639 | 7,5 | — | — |
| | H | MeO | **20** | | 8,88 | 15,68 | 1 | 1636 | 7,5 | 387 | 148 |
| | H | $NO_2$ | **21** | | 9,05 | 15,20 | 1 | 1638 | 7,5 | 402 | 183 |
| | Cl | H | **22** | | 8,80 | 15,20 | 1 | 1638 | 7,5 | 391 | 110 |
| | MeO | H | **23** | | 8,72 | 15 | 4 | 1638 | 31 | 387 | 125 |

Le maximum d'absorption électronique de ces composés en solution dans le cyclohexane se situe entre 405 et 420 nm, les coefficients d'extinction molaire étant de l'ordre $2,5 \times 10^{-4}$ suivant la nature du substituant sur les noyaux aromatiques. Il y a donc un déplacement bathochrome de l'absorption par rapport à la valeur observée chez les arylhydrazones dérivées de composés β-dicarbonylés dont les maximums d'absorption se situent pour la majorité au-dessous de 400 nm (12).

La structure de ces composés étant établie, subsiste le problème du dosage des tautomères en solution. L'échange intramoléculaire du proton entre les deux sites azotés étant plus rapide que la détection rmn, nous sommes dans des conditions analogues à celles décrites en particulier par Garbisch (5, 14). Nous avons donc utilisé les relations établies par cet auteur dans le cas d'un échange intramoléculaire de proton et vérifiées en particulier par Dudek *et al.* (8, 9) et Gindin *et al.* (4) pour le calcul du pourcentage des tautomères en présence. Suivant les composés préparés deux paramètres peuvent être utilisés: d'une part la constante de couplage $J_{HCNH}$ et d'autre part la constante de couplage $J^{15}_{N-H}$ observées sur le spectre des solutions. Ainsi pour le tautomère **b** ($N_b$ et $J_b$) les constantes de couplage $J_{HCNH}$ et $J^{15}_{N-H}$ sont-elles nulles si l'azote de la fonction imine est marqué. Par contre, pour le tautomère **c** ($N_c$ et $J_c$), ces couplages doivent intervenir: les constantes doivent être déterminées par comparaison avec d'autres systèmes chélatés voisins car nous n'obtenons jamais 100% de cette configuration en solution. Ainsi par rapport aux énamines α,α′-dicarbonylées préparées au laboratoire par Couchouron (10) et aux énamines α-carbonylées décrites par Dudek (9) nous avons pris respectivement 13 Hz et 90 Hz pour les constantes $J_{HCNH}$ et $J^{15}_{N-H}$ (azote du groupement imino marqué).

Les pourcentages des tautomères notés dans le tableau 1 sont donc obtenus de deux façons différentes à l'aide de la relation $J_{obs} = N_b J_b + N_c J_c$ soit dans le cas présent: $N_c = \dfrac{J_{HCNH\,observé}}{13}$ ou $\dfrac{J^{15}_{NH\,obs}}{90}$.

Les équilibres de tautomérie interne que nous venons de décrire dépendent de plusieurs paramètres: la substitution des noyaux aromatiques des fonctions hydrazone et imine, la nature du solvant et la température.

1. *Influence de la substitution des noyaux aromatiques des fonctions hydrazone et imine sur la composition des équilibres de tautomérie interne*

La composition des équilibres de tautomérie interne dépend fortement de la nature des substi-

TABLEAU 2. Variation des constantes de couplage $J_{HC-NH}$ suivant la nature du solvant pour quelques arylhydrazono-2 arylimino-3 propanones à 25°C

| | Composé | | | $J_{HC-NH}$ en Hz | | | | |
|---|---|---|---|---|---|---|---|---|
| R | $R^1$ | $R^2$ | No | $CCl_4$ | $CDCl_3$ | $(CD_3)_2CO$ | $CD_3CN$ | DMSO |
| H | H | H | **1** | 1–1,5 | 2 | 2,5 | 3 | — |
| H | MeO | H | **4** | 3 | 5,25 | 6,5 | 7 | 9,3 |
| H | MeO | MeO | **5** | 1,5 | 3,75 | 4,5 | 5,4 | — |
| Ph | MeO | H | **14** | 2,5 | 4,5 | 5 | 5,4 | — |
| *p*MeOPh | MeO | H | **23** | 2 | 4 | 4,5 | 5,25 | — |

tuants sur les noyaux aromatiques. Ainsi la présence en *para* de groupements électrodonneurs tels que Me et MeO sur le noyau aromatique de la fonction phénylhydrazone déplace l'équilibre vers la forme azoénamine **c**, alors que la substitution par un groupement électro-attracteur semble au contraire favoriser la configuration hydrazonoimine **b**.

Inversement la substitution des noyaux aromatiques de la fonction phénylimine par des groupements donneurs d'électrons déplace l'équilibre vers la formation du tautomère de configuration hydrazonoimine **b**.

Ces variations dans les compositions des équilibres sont à rapprocher des observations effectuées par Berrie *et al.* (15) dans le cas de la substitution des arylazonaphtols; les groupements électrodonneurs en *para* sur le noyau aromatique favorisent également le tautomère azohydroxy. Cependant il nous est difficile d'interpréter précisément ce phénomène faute de données quantitatives sur la répartition des charges dans les différents cycles chélatés. La transmission des effets électroniques des groupements arylés peut en effet s'effectuer de deux façons : modification directe de la densité électronique sur l'atome d'azote adjacent ou modification de la répartition électronique sur le cycle chélaté via les groupements azo et imino.

2. *Influence du solvant sur les équilibres*

La composition des équilibres entre les deux tautomères **b** et **c** varie également avec la nature du solvant (Tableau 2). Les pourcentages des tautomères de structure azoénamine étant proportionnels aux constantes de couplage $J_{HCNH}$ observées sur les spectres, nous donnons pour chaque composé les variations des constantes de couplage suivant la nature du solvant. Nous remarquons ainsi que pour tous les composés, la concentration du tautomère **c** de configuration azoénamine croît avec la polarité du solvant. Cependant nous ne pouvons établir une relation quantitative satisfaisante entre les constantes d'équilibre et le pouvoir solvatant ou la polarité du solvant (paramètres $E_T$, $Z$ ou la constante diélectrique ε).

3. *Influence de la température. Mise en évidence de l'échange intermoléculaire du proton chélaté*

Comme pour la majorité des exemples d'équilibres de tautomérie interne décrits dans la littérature, telles les bases de Schiff dérivées d'aldéhydes ou de cétones aromatiques *ortho*-hydroxylées (16), la composition des équilibres décrits dépend de la température. Une élévation de la température entraîne le déplacement de l'équilibre vers la forme hydrozonoimine **b**. En l'absence d'échange intermoléculaire ($10^{-2}$ *M*), nous avons mesuré les variations d'enthalpie pour les réactions d'échange intramoléculaire du proton en traçant les droites de van't Hoff pour différents composés. Ainsi pour le *para*-méthoxyphénylhydrazono-2 phénylimino-3 propanal **4** en solution dans l'acétonitrile, la variation d'enthalpie $\Delta H^0$ est-elle de $-0{,}68$ Kcal $mol^{-1}$ pour l'équilibre hydrazone ⇄ azo et de $-0{,}72$ Kcal $mol^{-1}$ dans l'acétone.

Comme nous venons de le voir, le proton chélaté s'échange de façon intramoléculaire entre les deux sites azotés de la molécule, mais nous avons montré qu'il peut donner également lieu à un échange intermoléculaire. Cette réaction d'échange a été étudiée plus particulièrement pour deux composés **4** (R = H, $R^1$ = OMe, $R^2$ = H), et **5** (R = H, $R^1$ = $R^2$ = OMe) en suivant l'évolution du signal du proton aldimino $H^1$ en fonction de la température et de la concentration de la solution.

Ainsi dans le cas du composé **5**, en solution dans l'acétonitrile à 50°C, le signal du proton aldimino est-il un doublet lorsque la concentration est de $1{,}875 \times 10^{-2}$ *M*. En augmentant la concentration on observe la coalescence de ce signal et son affinement après la coalescence (Fig. 2).

L'effet de la température sur la forme du signal peut être étudié sur les solutions concentrées. On observe ainsi la coalescence du doublet du proton aldimino lors de l'élévation de température, ce signal s'affinant après la coalescence comme le montrent les spectres rmn (Fig. 3).

Les effets de concentration et de température sur les solutions des autres composés dans $CDCl_3$,

Can. J. Chem. Downloaded from www.nrcresearchpress.com by 210.87.254.40 on 09/06/12
For personal use only.

Can. J. Chem. Downloaded from www.nrcresearchpress.com by 210.87.254.40 on 09/06/12
For personal use only.

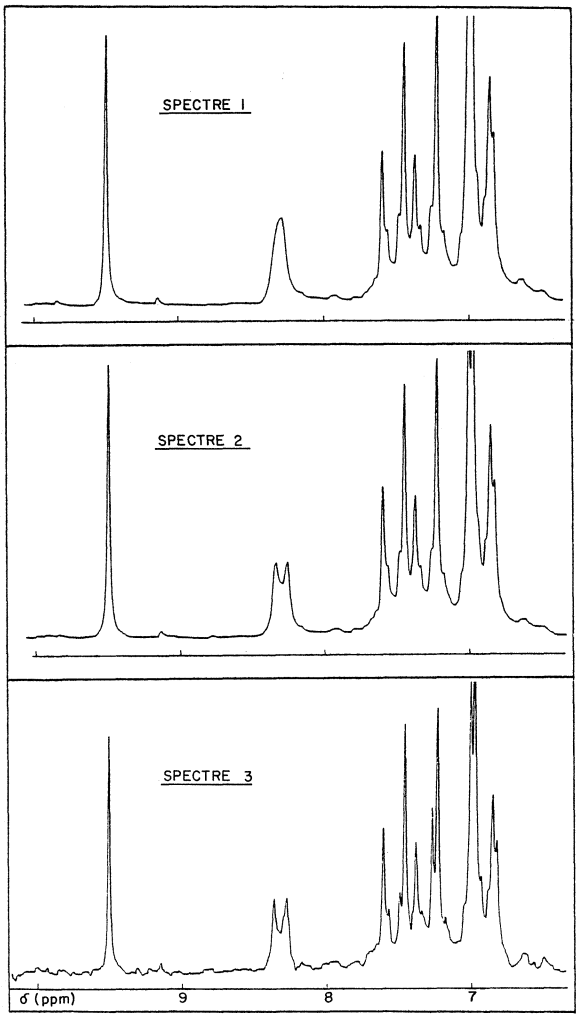


FIG. 2. Spectres rmn du *para*-méthoxyphénylhydrazono-2 *para*-méthoxyphénylimino-3 propanal **5** (R = H, $R^1 = R^2$ = MeO) en solution dans $CD_3CN$ ($t$ = 50°C). Influence de la concentration sur la cinétique d'échange: coalescence du signal du proton aldimino $H^1$ à 8,3 ppm. Spectre 1: concentration $3 \times 10^{-1}$ $M$. Spectre 2: concentration $7{,}5 \times 10^{-2}$ $M$. Spectre 3: concentration $1{,}87 \times 10^{-2}$ $M$.

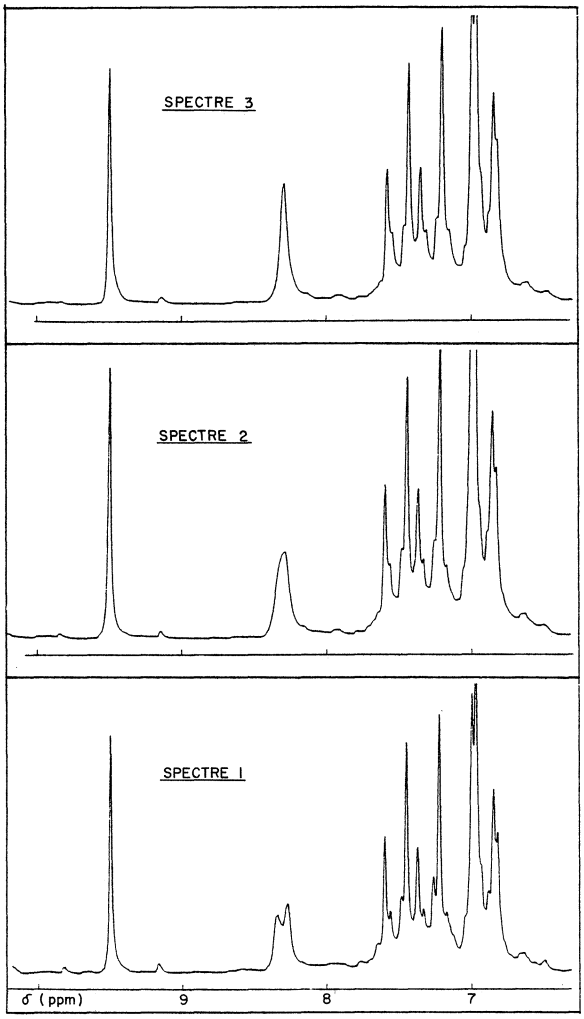


FIG. 3. Spectres rmn du *para*-méthoxyphénylhydrazono-2 *para*-méthoxyphénylimino-3 propanal **5** (R = H, $R^1 = R^2$ = MeO) en solution dans $CD_3CN$ ($C = 3 \times 10^{-1}$ $M$). Influence de la température sur la cinétique d'échange: coalescence du signal du proton aldimino $H^1$ à 8,3 ppm. Spectre 1: 34°C. Spectre 2: 50°C. Spectre 3: 69°C.

$CD_3CN$, $CD_2Cl_2$ et $(CD_3)_2CO$ sont analogues à ceux que nous décrivons. La coalescence des signaux observée sur les spectres rmn caractérise l'échange intermoléculaire du proton $H^2$ dont la fréquence dépasse celle qui permettrait d'observer le couplage des protons $H^1$ et $H^2$.

Dahlqvist et Forsen (17) avaient décrit une situation analogue dans le cas de la formyl-1 phényl-1 acétone. A notre connaissance c'était le seul exemple d'échange intermoléculaire du proton chélaté décrit dans la littérature dans le cas de systèmes à six atomes. La difficulté à observer cet échange provient du fait qu'il faut un environnement favorable (couplage HCNH ou HCOH ou $^{15}N$–H) pour le caractériser facilement par rmn.

B. *Structure et stéréochimie des arylhydrazono-2 bis(arylimino)-1,3 propanes*

Ces composés sont préparés à partir des arylhydrazono-2 propanedials sur lesquels on condense deux équivalents d'aniline.

Afin de faciliter la détermination des structures, les deux équivalents d'aniline condensés possèdent la même substitution.

Deux types de structure peuvent être envisagés pour ces composés: soit une forme hydrazone, soit une forme énamine. Si dans le premier cas le

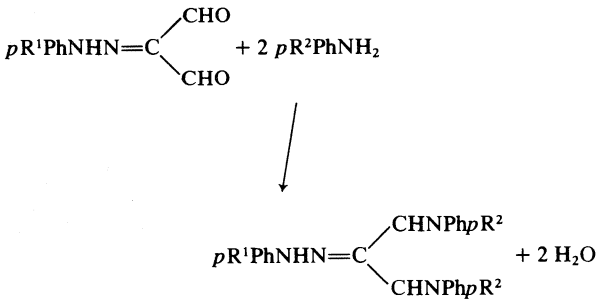

problème du site de chélation ne se pose pas, compte tenu de la symétrie des composés par rapport au motif hydrazone, par contre dans le cas d'une forme énamine nous avons deux sites de chélation possible: la fonction arylazo et la fonction arylimino.

Les éléments les plus intéressants pour la détermination des structures sont fournis par la rmn alors que la spectrophotométrie ultra-violette et l'infra-rouge n'apportent pas d'éléments déterminants pour cette série.

Pour les six composés étudiés (Tableau 3, nos, **24** à **29**), deux isomères peuvent être identifiés facilement en solution par rmn. Le premier, identifié à l'aide du signal du proton chélaté vers 15 ppm et des signaux des protons $H^1$ et $H^2$ respectivement vers 8,2 et 9 ppm (Fig. 4), possède une structure hydrazone **h**. Celle-ci peut être confirmée par marquage de l'atome d'azote porteur du proton de la fonction hydrazone à l'aide de l'isotope $^{15}N$, la présence d'un couplage $^{15}N$–H chez ces composés démontrant la localisation du proton chélaté sur cet atome d'azote.

Le deuxième isomère peut être identifié à l'aide du massif du proton chélaté vers 12,8–13 ppm et du signal correspondant aux deux protons $H^1$ et $H^2$. Le signal unique à 8,7 ppm correspondant à ces deux protons démontre leur équivalence magnétique et seule la structure **k** peut correspondre à de telles caractéristiques. L'évolution de la forme de ce signal en fonction de la concentration et de la température apporte des renseignements complémentaires sur cette structure. A la température ordinaire et pour des concentrations de l'ordre de $3 \times 10^{-2}$ *M*, ces deux protons résonnent en singulet légèrement élargi. Une augmentation de la concentration ou de la température affine ce signal alors

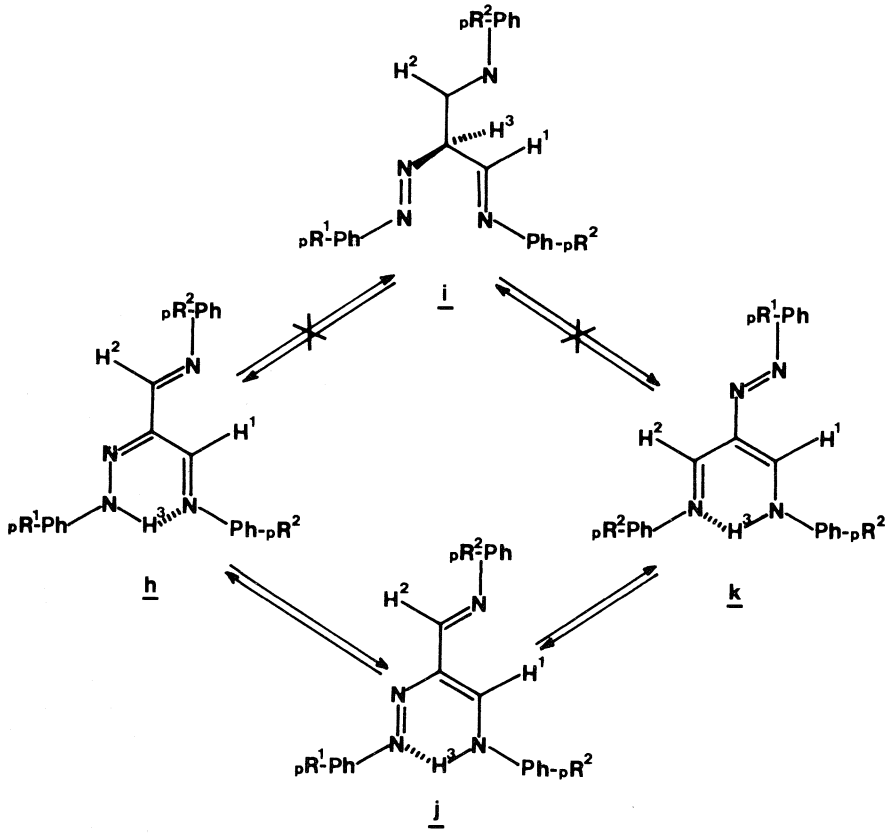

SCHEME 2

Can. J. Chem. Downloaded from www.nrcresearchpress.com by 210.87.254.40 on 09/06/12
For personal use only.

TABLEAU 3. Caractéristiques spectrales et physiques des arylhydrazono-2 bis(arylimino)-1,3 propanes (rmn, $CDCl_3$)

| | | | δH¹ (ppm) | δH² (ppm) | δH¹,H² (ppm) | δH³ (ppm) | | % | | |
|---|---|---|---|---|---|---|---|---|---|---|
| R¹ | R² | No | *h* | *h* | *k* | *h* | *k* | *k* | *M/e* | *F*(°C) |
| H | H | **24** | 9,14 | 8,30 | 8,79 | 15,22 | 13,00 | 18 | 326 | 120 |
| | MeO | **25** | 9,15 | 8,28 | 8,71 | 15,22 | — | 10 | 386 | 97 |
| MeO | H | **26** | 8.98 | 8,22 | 8,68 | 15,08 | 12,8 | 50 | 356 | 99 |
| | MeO | **27** | 9,02 | 8,23 | 8,62 | 15 | 12,75 | 29 | 416 | 100 |
| Me | H | **28** | 9,13 | 8,31 | 8,79 | 15,23 | 12,93 | 25 | 340 | 144 |
| | MeO | **29** | 9,13 | 8,28 | 8,70 | 15,24 | 12,98 | 13 | 400 | 130 |

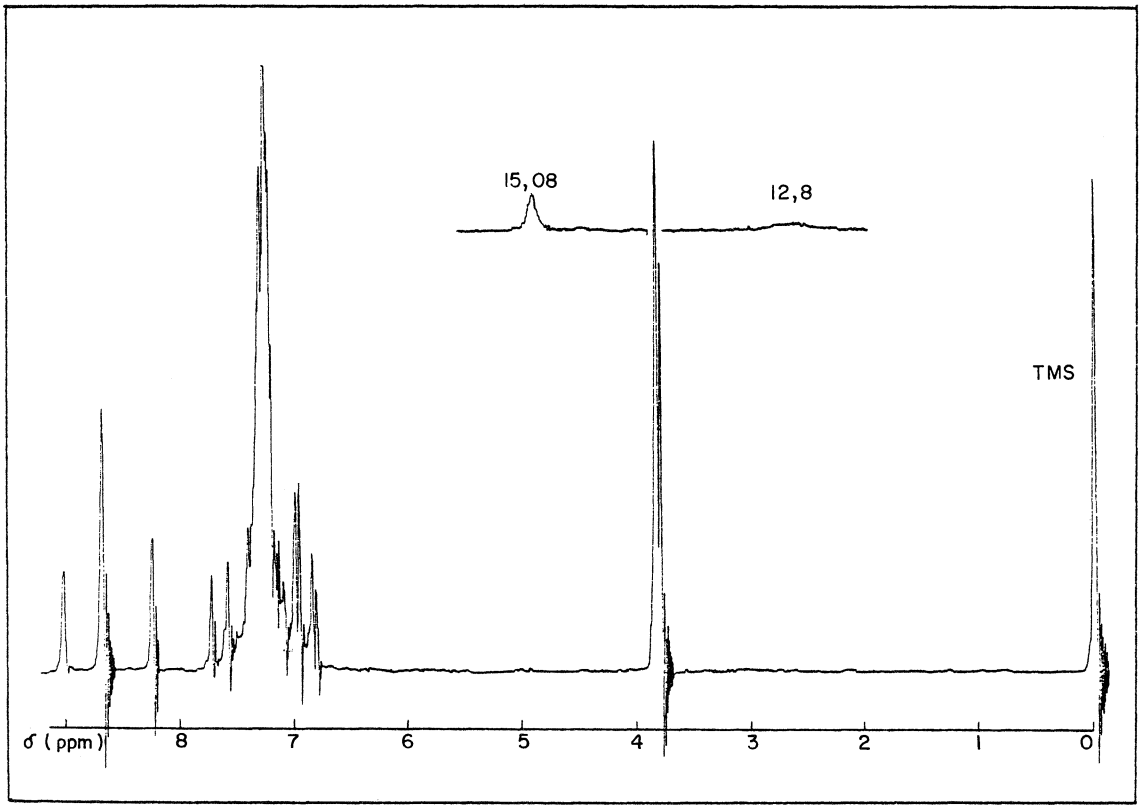


FIG. 4. Spectres rmn du *para*-méthoxyphénylhydrazono-2 bis(phénylimino)-1,3 propane **26** ($R^1$ = MeO, $R^2$ = H) en solution dans $CDCl_3$.

qu'une diminution de la température (−30°C) l'élargit (Fig. 5). Si l'on abaisse encore la température (−76,5°C) on voit le signal à 8,7 ppm se séparer en un singulet à 9,16 (proton $H^2$) et un doublet centré à 8,39 ppm ($H^1$ couplé avec $H^3$ qui sort lui-même en doublet $J$ = 12,2 Hz). Un découplage de spin, à température ordinaire, en irradiant à la fréquence du proton chélaté (12,8–13 ppm) affine le signal des deux protons $H^1$ et $H^2$, démontrant l'existence d'un couplage de ces protons et du proton chélaté.

La disparition du couplage sous l'influence d'une élévation de température ou d'une augmentation de la concentration ne peut s'expliquer que par la présence d'un échange intermoléculaire, vraisemblablement soluté–soluté, du proton chélaté, dont la fréquence devient plus grande que celle du couplage attendu entre les protons $H^1$, $H^2$ et $H^3$, d'où la coalescence du signal correspondant aux deux protons équivalents $H^1$ et $H^2$.

L'existence d'un équilibre entre les deux isomè-

Can. J. Chem. Downloaded from www.nrcresearchpress.com by 210.87.254.40 on 09/06/12
For personal use only.

Can. J. Chem. Downloaded from www.nrcresearchpress.com by 210.87.254.40 on 09/06/12
For personal use only.

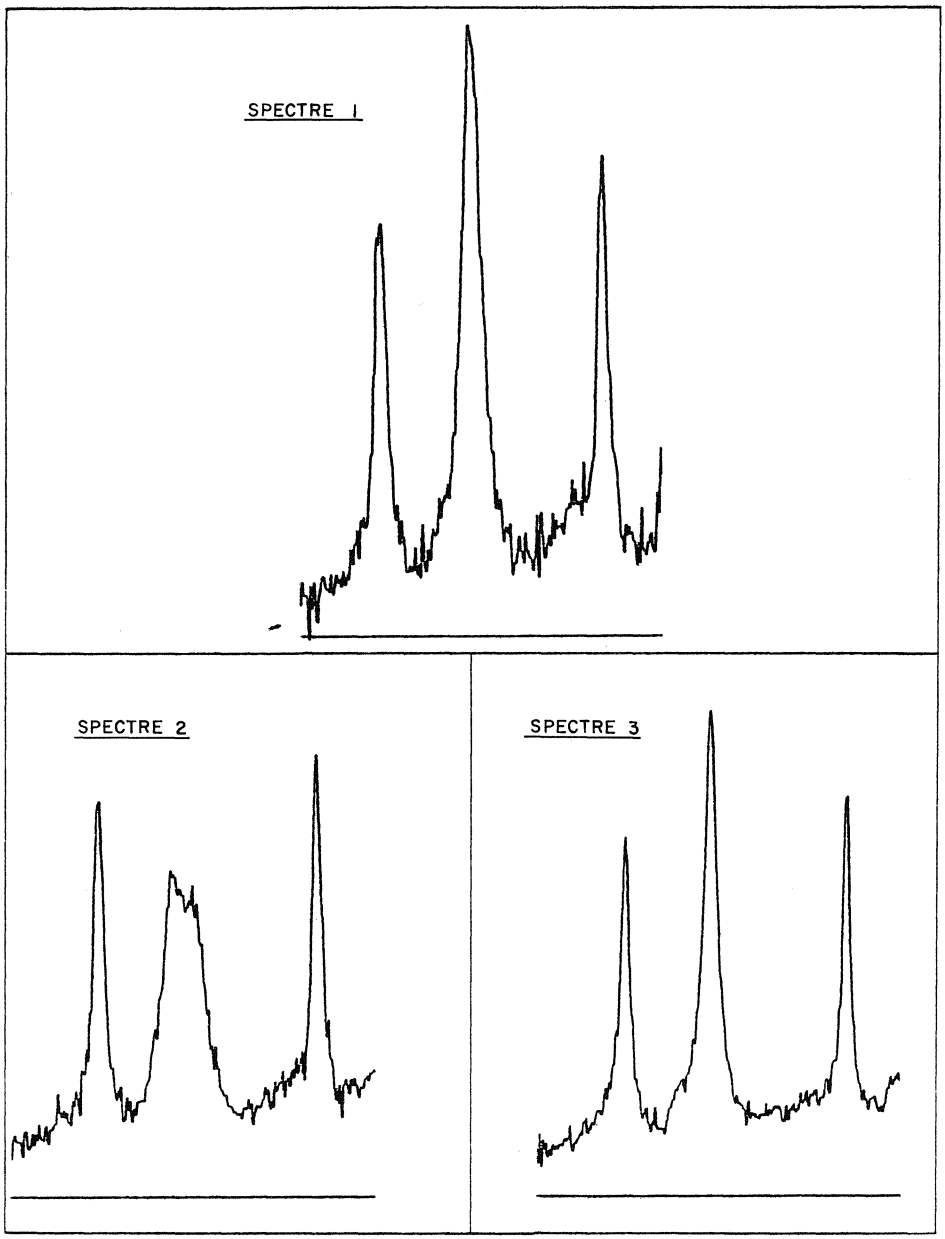


FIG. 5. Evolution des signaux des protons aldimino et énamino en fonction de la température dans le cas du *para*-méthoxyphénylhydrazono-2 bis(phénylimino)-1,3 propane **26** ($R^1$ = MeO, $R^2$ = H). Spectre 1: $t$ = 0°C. Spectre 2: $t$ = −30°C. Spectre 3: découplage de spin à −30°C par irradiation à 12,8 ppm.

res **h** et **k** (auquel s'ajoute l'échange intermoléculaire) implique que l'interconversion de ces deux isomères se fasse obligatoirement via les isomères **i** ou **j**, comme nous le montrerons par la suite.

Les essais de détection de l'isomère **i** en rmn ont été vains quels que soient les composés et les différentes conditions expérimentales utilisées (divers solvants; variations de température).

L'isomère **j** par contre peut être caractérisé lors de l'étude du *para*-méthoxyphénylhydrazono-2 bis(phénylimino)-1,3 propane **26**. Si pour les cinq autres composés préparés les signaux correspondant aux protons $H^1$ et $H^2$ de l'isomère **h** résonnent en singulet fin, dans le cas du composé **26** le signal à champ faible est un singulet élargi. Comme nous l'avons montré dans les séries précédemment décrites (2), ce signal correspond au proton $H^1$ du groupement aldimino impliqué dans la chélation, le

Can. J. Chem. Downloaded from www.nrcresearchpress.com by 210.87.254.40 on 09/06/12
For personal use only.

déblindage de ce proton étant lié à la plus forte polarisation du groupement chélaté par rapport au groupement libre. Le très faible couplage de ce proton $H^1$ ($J < 1$ Hz) avec le proton chélaté (Figs. 4 et 5) peut être mis en évidence par découplage de spin en irradiant à la fréquence du proton chélaté ($\delta$ = 12,8 ppm) ou par addition de $D_2O$ dans la solution. Dans les deux cas, on observe l'affinement du signal causé par la disparition du couplage.

Ces éléments nous incitent à penser que la tautomère **j** existe en solution en très faibles quantités (<8%) dans ce cas particulier. Bien que pour les autres composés la caractérisation de cet isomère ne soit pas réalisable, nous pensons cependant que l'interconversion **h** ⇄ **k** se fait également via le tautomère interne **j** résultant d'une migration [1,5] d'hydrogène à partir de la forme hydrazonoimine et non via l'isomère **i** résultant d'une migration [1,3] d'hydrogène et conduisant à l'isomère **k** par une seconde migration [1,3] d'hydrogène.

1. *Influence de la substitution des noyaux aromatiques sur les équilibres en solution*

Nous nous retrouvons dans une situation identique à celle de la série précédente. La présence de groupements électrodonneurs en *para* sur le noyau aromatique de la fonction hydrazone déplace l'équilibre vers l'isomère de configuration imino-énamine **k**. Inversement la même substitution sur le noyau aromatique de la fonction imine déplace l'équilibre vers l'isomère **h** de configuration hydrazonoimine

2. *Influence du solvant sur les équilibres en solution*

La nature du solvant intervient également sur la composition du mélange des isomères. Tout comme pour les arylhydrazono-2 arylimino-3 propanones-1 précédentes, les solvants polaires favorisent la formation de l'isomère **k** de configuration énamine. Mais pour cette série le déplacement de l'équilibre n'est pas très important puisqu'en passant de $CCl_4$ à $CD_3CN$ l'accroissement du pourcentage de l'isomère **k** de configuration énamine n'est que de 10% dans le meilleur des cas.

3. *Influence de la température sur les équilibres en solution*

L'équilibre entre les deux isomères en solution est légèrement déplacé par variation de température mais ce déplacement est trop faible pour effectuer une étude quantitative satisfaisante, d'autant qu'une variation de température modifie la fréquence de l'échange intermoléculaire du proton chélaté, donc la forme du signal correspondant. Le *para*-méthoxyphénylhydrazono-2 bis(*para*-méthoxyphénylimino)-1,3 propane **27**, qui est le composé le plus sensible à une variation de température, voit ainsi la concentration en isomère **k**, passer de 27% à 32% en élevant la température de −15°C à +50°C dans $CDCl_3$.

La présence en solution des deux structures hydrazone-imine et azo-énamine différencie ces composés des arylhydrazones dérivées de composés β-dicarbonylés, β-cétophosphonates et β-cétosulfones où seule la structure hydrazone était observée (2). On remarque cependant que pour toutes ces séries, la prototropie s'effectue vers l'atome d'azote et non vers l'oxygène d'un groupement carbonylé, quelles que soient les conditions de l'étude: différents solvants et température variable. Les structures du type azohydroxy n'existent pas chez ces composés.

L'orientation de la chélation nous permet de classer les différents groupements en fonction de leur pouvoir accepteur de liaison hydrogène dans un cycle de chélation à six atomes de configuration énamino. Par ordre de pouvoir décroissant on obtient la séquence suivante:

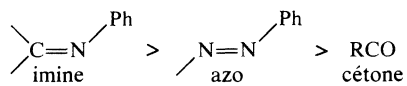


De même, on remarquera l'orientation préférentielle de la chélation du proton de la fonction hydrazone, quels que soient les substituants des noyaux aromatiques, vers le groupement imino et non vers le groupement carbonyle quand ceux-ci sont en compétition.

## Conclusion

L'échange intermoléculaire du proton chélaté est une caractéristique commune aux deux séries de composés étudiés et les distingue des arylhydrazones dérivées de composés β-dicarbonylés pour lesquelles il ne peut être mis en évidence dans les mêmes conditions expérimentales (2). Cet échange intermoléculaire soluté–soluté du proton chélaté, dépendant de la concentration de la solution et de la température, semble donc facilité lorsque les fonctions hydrazone/imine ou imine/énamine sont impliquées dans le cycle de chélation. Cette différence provient vraisemblablement du fait que cet échange est facilité par une plus grande délocalisation sur le cycle de chélation, provenant de l'échange intramoléculaire du proton chélaté entre les deux sites azotés. Par contre, dans le cas des arylhydrazones dérivées de composés β-dicarbonylés nous n'observons pas d'échange intramoléculaire, le proton étant localisé sur l'atome d'azote de la fonction hydrazone. Il semble que l'échange intramoléculaire du proton soit une condition nécessaire mais pas suffisant pour qu'il puisse y avoir échange intermoléculaire à concentration plus élevée.

Can. J. Chem. Downloaded from www.nrcresearchpress.com by 210.87.254.40 on 09/06/12
For personal use only.

## Partie experimentale

Les spectres rmn ont été enregistrés sur appareil JEOL C60HL et JEOL FX60, les spectres infrarouges sur un spectromètre Perkin–Elmer 225 pour les solutions. Les spectres de masse ont été réalisés sur un spectromètre de masse quadripolaire "Riber" de la Société Nermag. Les points de fusion sont mesurés sur banc de Köfler.

*Synthèse des arylhydrazono-2 arylimino-3 propanones-1 et des arylhydrazono-2 bis(arylimino)-1,3 propanes*

Ces deux séries de composés sont préparées à partir des arylhydrazono-2 propanediones-1,3 (2) qui sont condensées avec un ou deux équivalents d'aniline diversement substituée suivant la série envisagée.

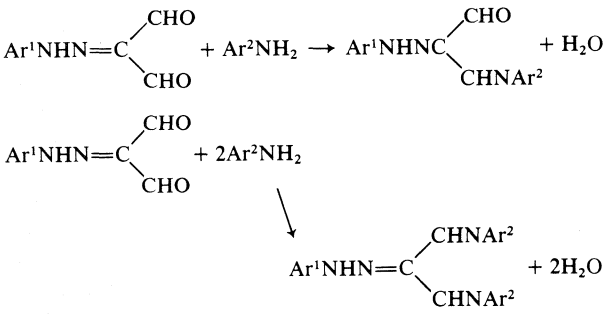

*Mode opératoire général*

Dans un ballon surmonté d'un réfrigérant on place $5 \times 10^{-3}$ mol d'arylhydrazono-2 propanedione-1,3 en solution dans 250 cm³ de chloroforme. On ajoute $5 \times 10^{-3}$ mol ou $10^{-2}$ mol d'aniline diversement substituée suivant la série préparée. La solution est portée à reflux durant six heures au minimum. L'évolution de la réaction peut être suivie directement par rmn. Après évaporation du solvant on obtient des cristaux qui sont recristallisés dans du méthanol. Les caractéristiques principales des composés obtenus sont données dans les tableaux 1 et 3.

*Mesure de la composition des equilibres hydrazonoimine–azoenamine en fonction de la température pour le composé* ***4***

$$\mathbf{4}b \rightleftarrows \mathbf{4}c \quad K = \frac{[\text{azo}]}{[\text{hydrazo}]}$$

(*a*). Dans $CD_3CN$, $10^{-2}$ M

| $t$°(C) | 75 | 51 | 25,8 | 6 | −10 | −17 | −25 |
|---|---|---|---|---|---|---|---|
| ln $K$ | 0,046 | 0,139 | 0,216 | 0,315 | 0,38 | 0,408 | 0,436 |

Equation de la droite, $\ln K = f(1/T)$

$$\ln K = 0{,}338 \left(\frac{10^3}{T}\right) - 0{,}913 \quad (r^2 = 9{,}94 \times 10^{-1})$$

$$\Delta H^0 = -0.68 \pm 0{,}05 \text{ kcal mol}^{-1}$$

(*b*) Dans $(CD_3)_2CO$, $10^{-2}$ M

| $t$°(C) | 40,5 | 29 | 24 | 20 | −3 | −20 | −45 | −56 | −70 | −80 | −97 |
|---|---|---|---|---|---|---|---|---|---|---|---|
| ln $K$ | 0,0123 | 0,043 | 0,074 | 0,102 | 0,222 | 0,345 | 0,47 | 0,496 | 0,68 | 0,74 | 0,89 |

Equation de la droite, $\ln K = f(1/T)$

$$\ln K = 0{,}362 \left(\frac{10^3}{T}\right) - 1{,}136 \quad (r^2 = 9{,}92 \times 10^{-2})$$

$$\Delta H^0 = -0.72 \pm 0{,}05 \text{ kcal mol}^{-1}$$


1. P. Courtot, R. Pichon et J. Le Saint. Tetrahedron Lett. 1177 (1976).
2. R. Pichon, J. Le Saint et P. Courtot. Bull. Soc. Chim. Fr. Partie II, 449 (1980).
3. P. Courtot, R. Pichon et J. Le Saint. Tetrahedron Lett. 1181 (1976).
4. V. A. Gindin, A. Chripun, B. A. Ershov et A. I. Koltsov. Org. Magn. Reson. **4**, 63 (1972).
5. E. W. Garbisch. J. Am. Chem. Soc. **85**, 1696 (1963).
6. A. A. Bothner-By et R. K. Harris. J. Org. Chem. **30**, 254 (1965).
7. S. Forsèn. Acta. Chem. Scand. **18**, 1208 (1964).
8. G. O. Dudek et E. P. Dudek. J. Am. Chem. Soc. **88**, 2407 (1966).
9. G. O. Dudek et V. O. Volpp. J. Am. Chem. Soc. **85**, 2697 (1963).
10. B. Couchouron. Thèse de Doctorat de 3ème cycle, Université de Bretagne Occidentale, Brest. 1977.
11. A. K. Bose et I. Kugagevsky. J. Am. Chem. Soc. **88**, 2325 (1966).
12. R. Pichon. Thèse de Doctorat ès Sciences, Université de Bretagne Occidentale, Brest. 1978.
13. P. Courtot, J. Le Saint et R. Pichon. Bull. Soc. Chim. Fr. 2538 (1975).
14. E. W. Garbisch et J. G. Russel. Tetrahedron Lett. 29 (1967).
15. A. H. Berrie, P. Hampson, S. W. Longworth et A. Mathias. J. Chem. Soc. B, 1308 (1968).
16. S. Forsèn et M. Nilsson. The chemistry of the carbonyl group. Vol. 2. *Edité par* J. Zabicky. Interscience, Londres. 1970. p. 157 et références citées dans cet article.
17. K. I. Dahlqvist et S. Forsèn. Acta. Chem. Scand. **24**, 797 (1970).

# A new cubic-space section model for predicting the specificity of horse liver alcohol dehydrogenase-catalyzed oxidoreductions[1]

J. Bryan Jones and Ignac J. Jakovac

*Department of Chemistry, University of Toronto, Toronto, Ont., Canada M5S 1A1*

Received May 11, 1981

J. Bryan Jones and Ignac J. Jakovac. Can. J. Chem. **60**, 19 (1982).

A new active site model for predicting and interpreting the structural- and stereospecificity of horse liver alcohol dehydrogenase-catalyzed oxidations and reductions has been formulated from the specificity, X-ray, and kinetic data now available. The new model is based on a cubic-space system and is convenient and easy to use. The model is completely reliable and permits HLADH specificity towards all of its currently known substrates to be predicted with confidence. Its application is illustrated by analyses of representative examples of major substrate types.

J. Bryan Jones et Ignac J. Jakovac. Can. J. Chem. **60**, 19 (1982).

A partir des données de spécicité, de diffraction de rayons X et de cinétique disponibles, on a élaboré un nouveau modèle de site actif pour prédire et interpréter la structure et la stéréospécifité des oxydations et des réductions catalysée par la déshydrogénase de l'alcool du foie de cheval (DHAFC). Le nouveau modèle est fondé sur un système d'espace cubique et est d'emploi facile. Le modèle est complètement fiable et permet de prédire en toute confiance la spécifité de la DHAFC envers tous ses substrats connus. On illustre son utilisation par l'analyse d'exemples représentatifs des principaux types de substrats.

[Traduit par le journal]

Can. J. Chem. Downloaded from www.nrcresearchpress.com by 210.87.254.40 on 09/06/12
For personal use only.

The asymmetric synthetic opportunities provided by the chiral catalytic properties of enzymes are becoming increasingly recognized (2*a*,*b*). Alcohol dehydrogenases, which catalyze oxidoreductions of the type depicted in reaction [1],[2] are among the most useful enzymes for organic synthetic purposes, with the commercially available enzyme from horse liver the best documented.

[1] $H^+ + \rangle C{=}O + NADH \rightleftharpoons \rangle CH(OH) + NAD$

HLADH is an extremely versatile alcohol dehydrogenase, capable of effecting highly stereospecific oxidoreductions on a broad structural range of aldehyde, ketone, and alcohol substrates (2–6).

In order for any enzyme to become widely adopted as a practical synthetic catalyst, it is essential that a reliable active site model be available for predicting the structural- and stereospecificity of the enzyme towards both known and potential substrate structures. Predictive systems of varying degrees of sophistication have been developed for a number of enzymes, including proteases (2*a*), mono-oxygenases (7, 8), and some alcohol dehydrogenases (2*a*, 3, 4, 9). For HLADH, the diamond lattice section approach devised by Prelog (3), and subsequently refined (2*a*, 4), has been very successful for interpreting the steric course of catalyses of cyclohexane and decalin substrates. However, for many of the other types of cyclic structures now known to be substrates (2), stereochemical predictions based on diamond lattice analyses have become increasingly subjective and uncertain.[3] It is clear that, after serving as a valuable active site model for nearly twenty years, the diamond lattice section has become totally inadequate for interpreting the stereochemical course of HLADH-catalyzed oxidoreductions of many of the recently identified, and still expanding, range of substrate structures (2, 6*b*).

Recently, the amino acid sequence of the EE-isozyme of HLADH (10) and the X-ray structures of the apoenzyme (11*a*), of the enzyme–NAD complex (11*b*–*d*) and of several ternary complexes (11*e*) have been published. These data, together with the results of new kinetic experiments on

[1]Enzymes in Organic Synthesis, 20. For Part 19 see ref. 1.

[2]Abbreviations used: NAD and NADH, oxidized and reduced forms respectively of the nicotinamide adenine dinucleotide coenzymes; HLADH, horse liver alcohol dehydrogenase; ADP, adenosine diphosphate.

[3]Several factors have contributed to the unsuitability of the diamond lattice section for general current application. The section was drawn up using substrates composed of cyclohexane rings (3, 4), resulting in a lattice framework based on $sp^3$-hybridized carbon bond lengths and angles. This introduces a psychological bias into the analytical process since it almost inevitably leads to attempts to locate substrate atoms at the lattice intersection points, and also to align bonds along the lines of the lattice. The designation of forbidden regions as points at the lattice intersections, rather than as regions of varying degrees of resistance to substrate penetration, is also a major disadvantage. In addition, the use of the "diamond" terminology is itself misleading to many chemists since it conveys, often unconsciously, the impression of a hard, uncompromising and structurally intolerant active site. Furthermore, the use of the diamond bonding framework, with lines drawn throughout the volume, does not permit the empty regions of the active site capable of accommodating substrates, nor the forbidden regions, to be easily visualized.

0008-4042/82/010019-10$01.00/0

©1982 National Research Council of Canada/Conseil national de recherches du Canada

Can. J. Chem. Downloaded from www.nrcresearchpress.com by 210.87.254.40 on 09/06/12
For personal use only.

alkylcyclohexanones (5, 6*c*,*d*), have provided a picture of the hydrophobic, barrel-like, active site pocket and of the relative orientations of the enzyme-bound substrates and coenzyme. The elegant active site representations so obtained are of considerable structural and kinetic significance. However, they do not lend themselves to the type of specificity analyses required by organic chemists utilizing HLADH for asymmetric oxidoreductions on very varied substrate structures. Accordingly, using all of the information now available, we have formulated a new active site section based on a cubic-space system that reliably predicts HLADH specificity throughout the broad structural range of cyclic substrates identified so far.

## Specification of the cubic-space section for the active site region

A model based on cubic space was selected for several reasons. The use of a cubic framework eliminates many of the chemical and conformational bias disadvantages of previous models based on carbon bond lengths and angles or derived directly from X-ray data. Also, the cubic section can be made as specific and flexible as needed by appropriate selection of the unit volume. Furthermore, cubic active site descriptors have already been widely accepted by chemists. They are convenient to use and their practical value in interpreting and predicting stereospecificity has been demonstrated for several enzymes of general organic synthetic interest (7–9), including one very recent specific application to a group of HLADH-substrates of unusual chirality (9*b*).

All of the specificity, kinetic, and X-ray data (2–6, 10, 11) were taken into account, with the following criteria being of primary importance: (*a*) the ADP-ribose portion of the coenzyme is rigidly bound at the active site. It thus firmly anchors the nicotinamide ring, whose freedom of rotation about the glycosyl bond is also restricted, in place. The nicotinamide ring is oriented with its A-face (12) towards the substrate (5, 11*a*,*f*). This fixes the direction of delivery and removal of the hydride equivalent during reduction and oxidation respectively. (*b*) The oxygen atom of the substrate carbonyl or hydroxyl group is liganded to the active site $Zn^{2+}$ atom (11*f*). This requirement, coupled with the fixed hydride delivery and removal site, establishes the location of the C=O and CH(OH) centres undergoing reduction or oxidation. It also severely limits bond rotations adjacent to them. (*c*) From the specificity analyses used initially to create the diamond lattice section (3, 4) and the additional data presently available (2–6), the active site regions that are open to substrate occupation (allowed regions) and those where substrate binding is precluded (forbidden regions) can now be specified with confidence.[4] The forbidden regions identified in this way correlate well with the positions of various amino acid residues in the X-ray structure (5, 11). In addition, the total kinetic data accumulated (2*a*, 3–5) permit estimation of differences in the degrees to which areas adjacent to forbidden regions are resistant to substrate binding.

The cubic-space section selected is depicted in Fig. 1. The 1.3 Å edge basis selected for the lattice provides a suitable compromise between the need to identify different regions as specifically as possible with our desire to minimize their number in order to keep the model convenient to use.

The space in front of the section is occupied by the coenzyme, with C-4 of the nicotinamide ring being positioned to deliver or receive the hydride-equivalent at the position shown. The C—O function, which projects downward along the **U(C1)–U(D1)** boundary, is designated in its alcohol-like configuration since this is considered to resemble most closely the transition state of the reaction (3).

The 1.3 Å per edge scale is well suited to analyzing substrates largely built-up of $sp^3$-hybridized carbon frameworks since these fit easily into the coordinate system. For example, the C-2 – C-6 separation in cyclohexanone is 2.6 Å. The volume defined by **A–R**, **1–9** is 118 $Å^3$. This is somewhat larger than the currently known substrate-accessible volume of the active site and thus allows for any future expansion required.

At present, not all of the cubic space defined in Fig. 1 needs to be used for analyzing the specificity of the enzyme. The regions incorporated into our current working model are shown in Figs. 2 and 3. The forbidden cubes are **A1,2**; **E1–3**; **G4,5**; **L4–6**; **M7–8**; **Q7–9** and the left-hand halves of **B1**, **H4**, and **N7**. Cubes **O9**, **P8**, and **P9** are also limited or forbidden. These latter regions are omitted from the working model because at present they are very seldom involved in analyses of substrate fit. The front of the section, being occupied by the coenzyme, is the remaining forbidden region. The limited cubes are **J4**, **P7**, and the right-hand halves

[4]Most of the systematic mapping-out of the allowed and forbidden regions of the active site was effected by methodically varying the structures of basic six-membered ring substrates and comparing their relative rates of oxidoreductions (3–5, 13). Dutler (5*b*) has provided the most evocative description of the technique. He states that it "can be compared with an imprisoned squid extending its tentacles in all directions around its body and thereby sensing the topography of the cage".

Can. J. Chem. Downloaded from www.nrcresearchpress.com by 210.87.254.40 on 09/06/12
For personal use only.

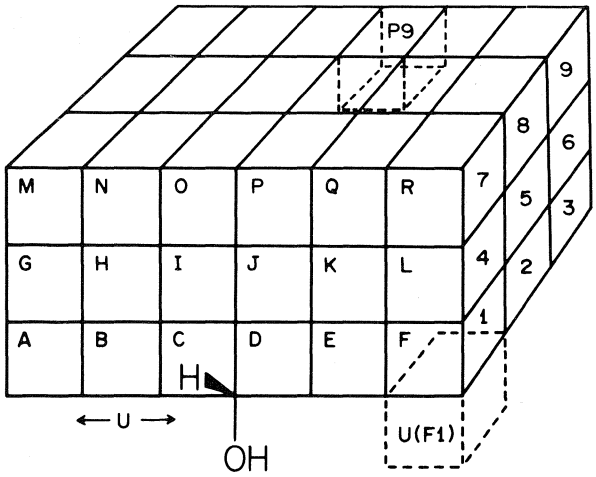


FIG. 1. The cubic-space section encompassing the active site region of HLADH. The cubes each have 1.3 Å edges. The front faces of each cube are labelled alphabetically and the side faces numerically. This permits any individual region to be specified unambiguously, as illustrated for **P9**. Hydride is delivered to or removed from the coenzyme at the front of the lower intersection of **C1** and **D1** as shown. The C—(OH) bond projects downward to coordinate with the active site $Zn^{2+}$ atom. The underneath of the section is designated as **U**. The individual cubes of this bottom region are specified by combining the **U** descriptor with (parenthetically) that of the region immediately above it. Region **U(F1)** is shown.

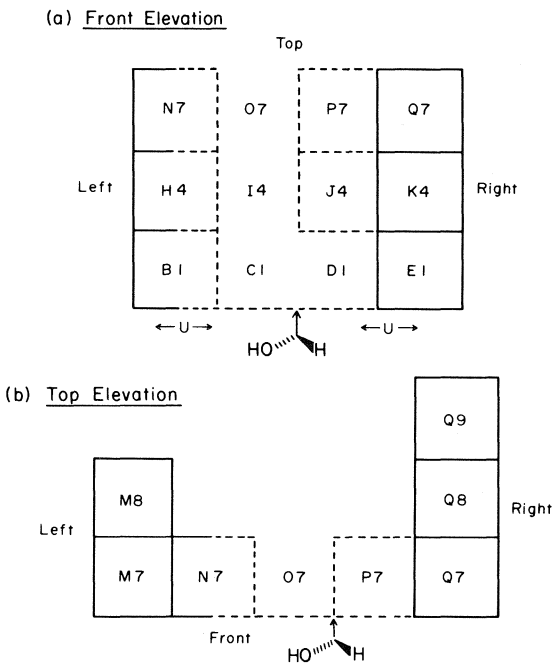


FIG. 2. Specification of the cubic-space model for predicting HLADH stereospecificity. The regions bounded by solid lines (—) are designated as "forbidden". Binding of substrate groups in these regions is precluded because they are already occupied by amino acid side chains of the enzyme. The front of the cubic-space model is occupied by the coenzyme and is also forbidden. The broken-line (---) regions are "limited" in their tolerance of substrate groups due to their being adjacent to amino acid residues or to portions of the coenzyme. While this proximity to forbidden regions does not preclude substrate intrusion into the limited cubes, it does restrict access to these active site areas. Binding in limited areas results in a marked rate decrease. Occupation of limited regions therefore only takes place if binding in the favoured, "allowed", regions is not possible. The allowed regions are represented by the open spaces in the figures. They are areas of the active site that are unoccupied by any enzymic group and can thus readily accommodate substrate groups. In practice, the boundaries between allowed, limited, and forbidden regions are not sharp. Rather, the transition is a graded one where binding of a substrate group becomes increasingly disfavoured the further it penetrates from an allowed space into a limited region and towards a forbidden cube. The projections shown are those of the working model viewed from (*a*) the front and (*b*) the top. Only the outermost cubic faces of each projection are identified alphanumerically. A perspective of the current working model is shown in Fig. 3.

of **B1**, **H4**, and **N7**. The underneath regions reflect the character of the cubes immediately above them. Those below forbidden space, such as **U(E1)**, remain forbidden. Those below limited or allowed cubes will tolerate limited substrate penetration. The cubic portions of the model not specified above are the allowed regions of the active site where substrate binding is freely permitted. This open space corresponds to the "hydrophobic barrel" binding site identified in the X-ray structures (11*f,g*). It curves and opens up towards the rear of the left-hand side of the Fig. 3 model. This active site cleft is depicted from another perspective in Fig. 4.

While our identification of forbidden and limited cubes is largely based on substrate specificity and kinetic data (2–6) it is possible to correlate many of them with the X-ray-derived (5, 11*f, g*) locations of various amino acid residues in the active site region (Fig. 4). Forbidden region **E1** corresponds to the Phe-93 location; **K4**, **Q7** to Ile-116; **E2**, **E3**, **K5** to Phe-110; **O9**, **P9**, and **Q9** to Ile-318. Region **B1** is where Ser-48 is located while Leu-57 occupies the **G4** and **M7**, and half of the **H4** and **N7**, cubes. The **J4** and **P7** cubes are limited regions as a consequence of their proximity to the nicotinamide coenzyme.

It must be stressed that the boundaries between allowed, limited, and forbidden regions are not absolute, with resistance to binding increasing progressively as one proceeds from an allowed region towards a forbidden one. However, as the examples discussed subsequently show, the model permits these distinctions to be made without difficulty.

### General procedure for specificity analyses

Analyses are conveniently performed by constructing the cubic section of Fig. 3, and the

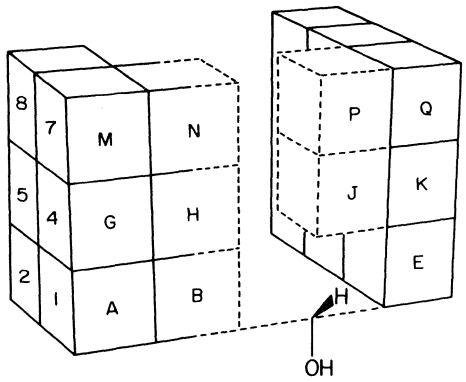


FIG. 3. A perspective of the HLADH cubic-space model used in practice. The model is depicted viewed from a left-front viewpoint. The forbidden regions are shown bounded by solid (—) lines and the limited regions by broken (---) lines. The open spaces are the allowed areas favouring substrate binding. For specificity analyses, the substrate model is built to the same scale. Its C=O or CH(OH) group is first positioned in the required orientation at the oxidation site located at the bottom of the **C1**, **D1** intersection. Its various orientations in the cubic lattice section are then compared in order to identify which, if any, will permit the formation of a productive ES complex. Cubic model and substrate structures constructed from Framework Molecular Models® are convenient.[5]

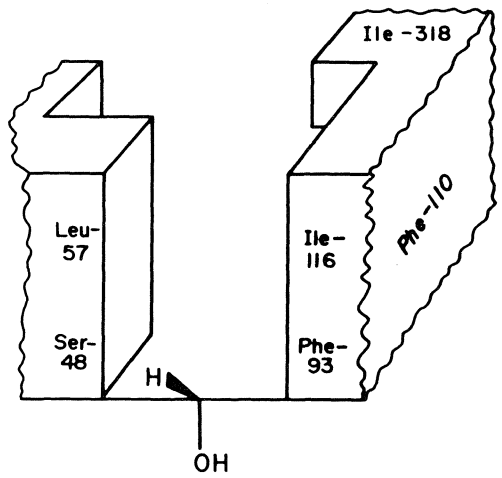


FIG. 4. Schematic representation of the active site binding pocket. The boundaries of the forbidden regions only are shown. The identifications and locations of the amino acid residues responsible for the forbidden regions are based on X-ray data (5*c*, 11).

substrate of interest, from Framework Molecular®, or equivalent, models.[5] The allowed fit, if any, of the substrate at the active site is then established. This is done by identifying, and avoiding if possible, unfavourable interactions that would preclude effective formation of a productive ES complex, in accordance with the following procedure:

(*1*) The carbonyl or hydroxyl group is fixed at the oxidoreduction site such that the C—OH bond being formed or broken is oriented downwards. Hydride delivery or abstraction occurs from the front (the coenzyme binding site) of the cubic section. Because of the rearward-opening nature of the allowed region and the locations of the limited **J4** and **P7** regions (Figs. 2, 3), larger substrates will prefer to bind in a horizontal rather than vertical mode. Thus for cyclohexanol oxidation, the ring adopts a horizontal orientation such that the C—OH bond is axially oriented and the hydride is abstracted from the equatorial direction.

(*2*) For primary alcohol oxidation, the *pro-R* hydrogen atom is removed stereospecifically (14, 15). Conversely, in aldehyde reduction the hydride is delivered to the *Re*-face of the carbonyl group (3).[6]

(*3*) Binding of the substrate must not violate any forbidden regions. A substrate group may occupy a limited region if no allowed cube is accessible, but a slower rate of oxidoreduction must then be anticipated. The rate-reduction effects of occupation of limited areas are cumulative. Location of groups in two or more limited regions becomes virtually equivalent to a forbidden interaction.

(*4*) For potential substrates that are mixtures of stereoisomers, such as racemates or diastereomeric mixtures, each stereoisomer must be analyzed separately.

(*5*) If the substrate is conformationally mobile, the active site interactions of each major conformer of each stereoisomer must be considered independently.

[5]In building the cubic model and substrate structures, we have adopted a 40 mm = 1.54 Å (26 mm = 1 Å) scale. The edge of each cube is 34 mm (1.3 Å). Because the jacks and plastic tubing used to construct the models do take up some space, it is advantageous to extend the edges of cubes **C1**, **D1**, **I1**, and **J1** to 36 mm (1.4 Å) each in order to facilitate positioning of the substrate at the oxidation centre. Octahedral jacks are used for all cubic intersections except for the lower **C1**, **D1** intersection where the CH(OH) function is located. Here a trigonal bipyramidal jack is used to permit the H and OH groups to be oriented in the required directions. Leaving out jacks at structurally non-essential intersections of the framework makes it easier to achieve the positioning of substrate groups in different locations when various substrate orientation possibilities are being compared. We have found it useful to colour-code the cubic model using a traffic light-based convention. The forbidden regions (— in Fig. 3) are bounded in *red* since substrate penetrations are "stopped" by amino acid or coenzyme residues. The limited regions (--- in Fig. 3) are coded *orange* to indicate that one should "proceed with caution" when locating substrate groups in these spaces. The allowed areas are "clear" and *green* tubing is used for their boundaries.

[6]The stereospecificity of hydride delivery always occurs in the same absolute configuration sense. However, for certain ketone substrates, this will not correspond to *Re*-face attack as a consequence of the priority selection rules of the *R*/*S*-system.

Can. J. Chem. Downloaded from www.nrcresearchpress.com by 210.87.254.40 on 09/06/12
For personal use only.

Can. J. Chem. Downloaded from www.nrcresearchpress.com by 210.87.254.40 on 09/06/12
For personal use only.

(*6*) All stereospecificity predictions apply to oxidoreduction products of kinetic control. Reactions carried out for extended periods may give the thermodynamically preferred compounds whose stereochemistries will reflect free energy differences only and will not be influenced by the initially preferred fit of the substrate at the active site (2*a*, 4).

## Applications of the cubic-space section to HLADH-specificity analyses

Representative examples are given for each major substrate type.

### *(A) HLADH-catalyzed Reductions*

#### *(1) Acyclic Aldehydes and Ketones*

The Prelog rule (3) has been totally reliable in predicting the stereochemistry of reductions of aldehydes[7] and our new model offers no advantage over the simple-to-use Prelog rule. Nevertheless it is worth noting that the cubic space model does predict correctly the stereochemistry of aldehyde reduction (Fig. 5).

The stereochemical course of oxidations of acyclic chiral secondary alcohols (16, 17) and the enantiotopically specific *pro-R* hydrogen abstraction in primary alcohol oxidations (14, 15), are also in accord with the Fig. 5 analysis.

#### *(2) Monocyclic ketones*

##### *(a) 2-Alkylcyclohexanones (1)*

The cubic model analysis for such substrates is illustrated schematically in Fig. 6. For the 2*R*-series, reduction is strongly disfavoured because the required binding of both conformations **I** and **II** would place the R-substituent in the forbidden regions of cubes **B1** or **K4**. Formation of an effective ES complex is therefore precluded for the 2*R*-enantiomers. The same situation holds for the thermodynamically preferred conformer **III** in the 2*S*-series, with its equatorial R-group directed towards the forbidden **E1** region. However, conformation **IV** of (2*S*)-**1** can bind effectively to give a productive ES complex since the axial substituent can be accommodated at the boundary of the allowed **I4** and limited **H4** regions. Reduction in this mode would lead to *trans*-(1*S*,2*S*)-**2**-alkylcyclohexanol (**2**) products. The experimental results are in full agreement with this analysis. The predicted *trans*-(1*S*,2*S*)-**2** alcohols of 100% e.e. are formed when R = Me, Et with the 2*R*-ketones recovered unchanged (5*a*, 6*a*, 18).

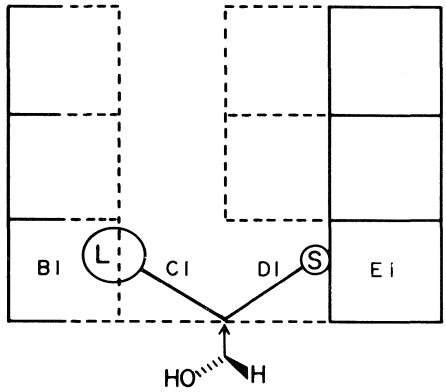


FIG. 5. Analysis of HLADH-catalyzed reductions of acyclic ketones and aldehydes. The favoured orientation is shown in terms of the front elevation of the cubic-space model (Fig. 2*a*), using the Prelog rule convention of (L) and (S) as large and small substituents respectively. The orientation shown permits (S) to occupy the allowed **D1** region while (L) may place itself in the allowed **C1** and limited **B1** sections. The hydride is then delivered to the *Re*-face[6] (for an O > L > S priority sequence (3)) of the carbonyl group to give an alcohol of *S*-configuration (2*a*, *b*, 3). The converse orientation is precluded since it would require (L) to occupy part of **E1**, a strongly forbidden region. Oxidations of chiral acyclic alcohols are analyzed in a microscopic-reverse manner.

Since the productive orientation, conformation **IV** in Fig. 6(*b*), partially occupies the limited region of **H4**, the rate of reduction should be lower than for cyclohexanone itself. This is as found (2*a*, 3–6). Furthermore, as the steric bulk of the R-group is increased, it will intrude further towards the forbidden half of **H4**. This should reflect itself in progressively lower reduction rates, again in accord with the experimental facts. The rate for 2*S*-**1** (R = Et) reduction is less than for 2*S*-**1** (R = Me), while the 2-isopropyl- and 2-*t*-butylcyclohexanones are not substrates at all (5). For the latter two compounds, the substituent at C-2 cannot avoid overlapping a forbidden region, even for conformation **IV**.[8]

[7]HLADH-catalyzed reductions of aldehydes with NAD$^2$H or NAD$^3$H have been widely used for stereospecific preparations of isotopically labelled chiral alcohols for biosynthetic purposes (2*a*,*b*).

[8]Until recently none of the *cis*-isomers of **2**, corresponding to reductions of conformations **I** or **III**, had been detected. However, it has now been demonstrated that when the R-group of **1** is small, such as fluorine (6*a*) or methyl (2*i*), very small amounts (1–4%) of *cis*-2-substituted cyclohexanols of undetermined configurations are produced. These *cis*-isomers must arise from reduction via conformation **I** or **III**. Both orientations are unfavourable (Fig. 6). However, the cubic model predicts that orientation of **I** as in Fig. 6*a* would be the less undesirable since, in contrast to **E1**, the **B1** cube has a limited region that could partially accommodate a small R-group such as fluorine. Thus the minor *cis*-2-fluoro and 2-methylcyclohexanol products should have (1*S*,2*R*) configurations. This point is currently under investigation.

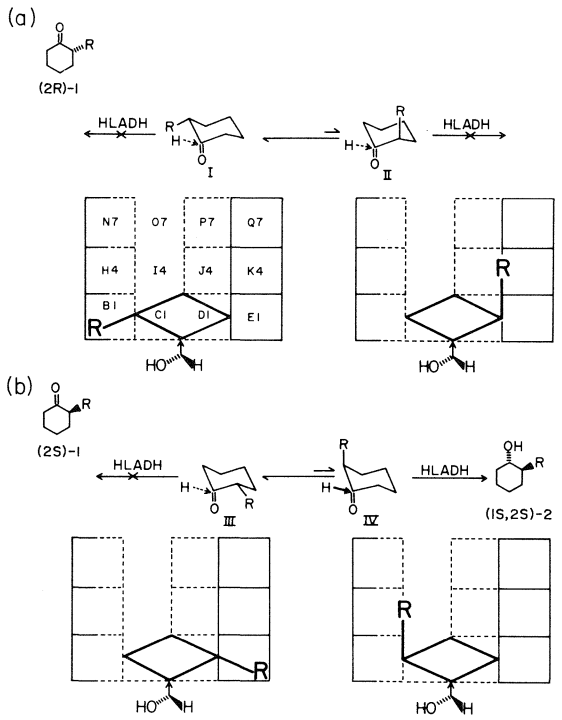


FIG. 6. Interpretation of substrate activity and product stereochemistry for HLADH-catalyzed reductions of 2-alkylcyclohexanones in cubic model terms. Active site binding and orientation of each chair conformation of each enantiomer must be analyzed separately. Part (*a*) covers the 2*R*-series and (*b*) the 2*S*-series. The cyclohexanone rings are shown in the conformations required for correct orientation of the carbonyl group at the hydride delivery site. The direction of hydride delivery from NADH is indicated by the arrows, ---> and → for unreactive and reactive substrate orientations, respectively. The orientations are illustrated with respect to the front elevation of the model (Fig. 2*a*). Only conformation **IV** of the 2*S*-series can bind without violating any forbidden regions.

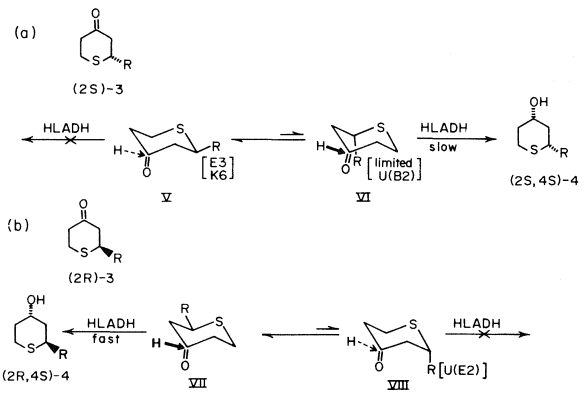


FIG. 7. Interpretations of substrate activity and product stereochemistry for HLADH-catalyzed reductions of 2-alkyltetrahydrothiapyran-4-ones. (*a*) 2*S*[9]-series, (*b*) 2*R*[9]-series. Each conformer is analyzed separately in the manner outlined in the legend for Fig. 6. The orientations of each conformer within the cubic space are depicted from the front elevation perspective (Fig. 2*a*). The regions in which the R-group is required to locate to give a productive ES complex are indicated in square brackets. Reductions via conformations **V** and **VIII** are precluded since R would be placed in forbidden regions **E3,K6** and **U(E2)** respectively. Reduction of **VII** is facile because the **B3,H6** locations accommodating R are allowed. Reduction via **VI** is slower because R must be positioned in **U(B2)**, a cube permitting limited occupation since it lies beneath the allowed area **B2**.

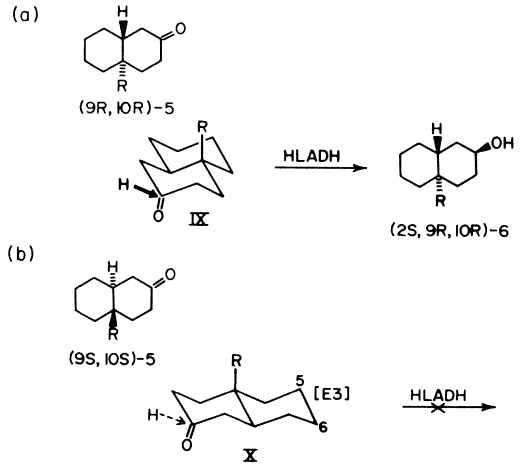


FIG. 8. Representation of *trans*-2-decalone orientations in cubic-space terms. In (*a*), the (9*R*,10*R*)-enantiomers orient as in conformation **IX**, for which all substrate atoms are in allowed regions. Facile reduction to the (2*S*)-alcohol **6** therefore occurs. As shown in (*b*), reduction of the (9*S*,10*S*)-enantiomers is precluded by the fact that binding of conformation **X** cannot avoid locating C-5 and C-6 deep within the forbidden **E3** region.

### *(b) 2-Alkyltetrahydrothiopyran-4-ones (3)*

Heterocyclic substrates can be analyzed in an exactly parallel manner to their carbocyclic analogues. This is illustrated for the sulfur heterocycles (±)-**3**, in Fig. 7. The experimental results with the methyl, ethyl, and isopropyl substituted substrates are as predicted, with the *trans*-alcohols (2*R*,4*S*)-**4** (R = Me, Et) and (2*S*,4*S*)-**4** (R = *i*-Pr)[9] being the major products and *cis*-(2*S*,4*S*)-**4** (R = Me, Et) and (2*R*,4*S*)-**4** (R = *i*-Pr)[9] the minor products (2*c*). With (±)-**3** (R = $C_6H_5$) as substrate, the proportions of *cis*- and *trans*-alcohols are reversed. This is because orientation **VI** has become more preferred than **VII** due to the large phenyl group exceeding the volume of the allowed **B3,H6** region in the direction of the forbidden **G5** cube. All *cis*- and *trans*-alcohol products are of 100% e.e. thus confirming that, as expected, reductions via orientations **V** and **VII** are insignificant.

### *(3) Bicyclic ketones*

### *(a)* trans-*2-Decalones (5)*

Reductions of the *trans*-2-decalones (±)-**5** (R = H, Me) are interpreted in Fig. 8. Formation of the

[9] For **3** or **4** (R = *i*-Pr) the 2*R*- and 2*S*-descriptors are reversed for the Fig. 7 structures.

Can. J. Chem. Downloaded from www.nrcresearchpress.com by 210.87.254.40 on 09/06/12
For personal use only.

Can. J. Chem. Downloaded from www.nrcresearchpress.com by 210.87.254.40 on 09/06/12
For personal use only.

2*S*,9*R*,10*R*-stereoisomers of the 2-decalols **6** (R = H, Me) is heavily favoured, and they can be produced in optically pure form by preparative-scale HLADH-mediated reduction of (±)-**5** (R = H, Me). The unreactive (9*S*,10*S*)-2-decalone enantiomers are also isolable in good yield in optically pure form (3, 4, 19).

*(b)* cis-*2-Decalones (7)*

Analysis of the stereochemistry of reduction of *cis*-2-decalones **7** is less straightforward than for their *trans*-isomers owing to their increased conformational mobility. However, only for one of the two all-chair conformations of the 9*R*,10*S*-enantiomers can orientation avoiding all unfavourable regions be achieved. This is shown in Fig. 9. The experimental facts are as predicted, with 2*S*-2-decalols **8** (R = H, Me) of 100% e.e. being the only reduction products isolated in preparative-scale experiments (4, 19).

*(c) Bicyclo[3,2,1]octan-2-one (9)*

Cubic model analysis of the favoured course of HLADH-catalyzed reduction of the bridged bicyclic ketone (±)-**9** is illustrated in Fig. 10. Only for 1*S*,5*S*-**9** is orientation avoiding all forbidden and limited regions possible. This transcribes into formation of the *exo*-alcohol **10** of 1*S*,2*S*,5*S* absolute configuration (Fig. 10*b*). The formation of the other *exo*-alcohol enantiomer is less favourable because it requires C-7 to be positioned in limited region **J4**. However, occupation of a limited cubic space does not preclude a reaction but merely slows it down significantly (*cf.* Fig. 6). Thus in practice the reduction is found to be stereoselective rather stereospecific, giving the 2*S*-*exo* enantiomer of 83% e.e. (2*d*). The *endo*-alcohol isomers are formed in trace amounts only (2*d*, 6*a*). This is because the active site orientations of **9** that are required to give *endo*-products are even more disfavoured by the intrusion of C-5 and C-8 (for 1*S*-**9**) or C-4 and C-5 (for 1*R*-**9**) into both of the limited **J4** and **P7** cubes. As stated previously, intrusion into two limited regions approximates a forbidden interaction.

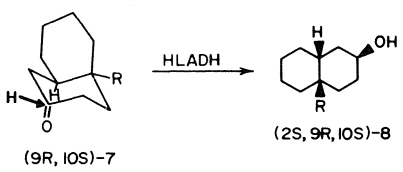


FIG. 9. HLADH-catalyzed reductions of *cis*-2-decalones. Only for the conformation shown of the (9*R*,10*S*)-enantiomers of **7** (R = H,Me) is cubic-space orientation possible that avoids all limited and forbidden regions. Neither of the two all-chair conformations of the (9*S*,10*R*)-enantiomers can be oriented for reduction without C-7 and C-8 violating forbidden positions **E3** and **K5**, or C-6, C-7, and C-8 being placed deep into the limited regions **U(B2)**, **U(B3)**, and **U(C3)**. These enantiomers are thus recovered unchanged.

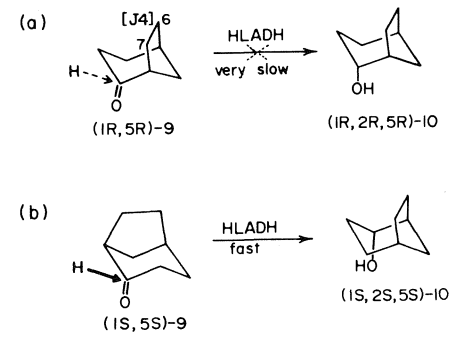


FIG. 10. Interpretation of HLADH-catalyzed reduction of bicyclo-[3,2,1]octan-2-one using the cubic-space system. (*a*) The (1*R*,5*R*)-enantiomer is less readily reduced because its orientation at the oxidation site requires C-7 to locate in limited region **J4**; (*b*) in contrast, the (1*S*,5*S*)-enantiomer can orient with all its atoms in allowed regions. Reduction to 1*S*,2*S*,5*S*-**10** thus occurs readily and is the favoured reaction.

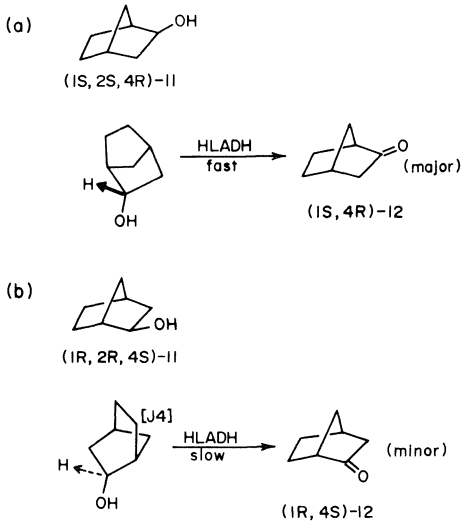


FIG. 11. Analysis of enantioselectivity of HLADH-catalyzed oxidation of (±)-2-norbornanol. (*a*) The (1*S*,2*S*,4*R*)-enantiomer of **11** is readily oxidized since all atoms can be located in allowed positions. (*b*) Oxidation of (1*R*,2*R*,4*S*)-2-norbornanol is slower because C-6 must intrude into limited region **J4**. The net result is a preference for situation (*a*) resulting in the formation of 2-norbornanone (**12**) enriched in the (1*S*,4*R*)-enantiomer as shown.

*(B) HLADH-catalyzed oxidations*

*(1) Mono- and bicyclic secondary alcohols*

Analyses of the stereospecificities of oxidations of such substrates are the microscopic-reverse of the illustrative ketone interpretations described above (Figs. 6–10). The oxidation of (±)-2-norbornanol (**11**) exemplifies this. The stereoselectivity of the catalysis is in accord with the Fig. 11 prediction, with the 2-norboranone (**12**) formed

Can. J. Chem. Downloaded from www.nrcresearchpress.com by 210.87.254.40 on 09/06/12
For personal use only.

being enriched in the (1*S*,4*R*)-enantiomer to the extent of 68% when the reaction is terminated at the 50% oxidation stage (2*d*). The less reactive (1*R*, 2*R*,4*S*)-norbornanol stereoisomer recovered is of 71% e.e.[10]

*(2) Stereospecific and selective oxidations of diols*

In this section, controlled oxidations of substrates possessing one or more primary or secondary alcohol functions are considered. Analyses of primary alcohol oxidations require additional care owing to their increased torsional mobilities.

*(a) Chemo- and enantiospecific oxidation of (±)-*cis*-3(2′-hydroxyethyl)cyclopentanol (13)*

The oxidation of both the primary and secondary alcohol groups must be analyzed separately for each enantiomer. With the primary alcohol functions placed at the oxidation site in the correct orientation for the required *pro-R* hydrogen removal to take place,[11] no orientation can be identified for either enantiomer of **13** for which the C-1 hydroxyl group, or C-1 or C-2, do not violate one or more forbidden regions. Since the forbidden regions are generally hydrophobic, it is particularly unfavourable for a polar group such as the C-1 hydroxyl group even to approach them too closely. Thus oxidation of the primary alcohol function is strongly disfavoured. On the other hand, when the secondary alcohol function of (1*R*,3*S*)-**13** is located at the oxidation site, formation of an unhindered ES complex with all groups in allowed regions is possible (Fig. 12*b*). This cannot be achieved for the (*1S*,3*R*)-enantiomer (Fig. 12*a*). The cubic model analysis is thus in total accord with the experimentally observed results, for which HLADH-catalyzed oxidation of (±)-**13** is found to be totally chemo- and enantiospecific, effecting exclusive oxidation of the secondary alcohol function of the 1*S*,3*R*-enantiomer to give (3*R*)-(2′-hydroxyethyl) cyclopentanone (**14**) of 100% e.e. (2*d*).

Since the determining factor is always the preferred active site fit of a substrate, secondary over primary alcohol oxidation is not always the favoured reaction. For several other substrates possessing both types of hydroxyl functions, exclusive primary alcohol oxidation is observed (2*d*, *e*). In these cases also the enantioselectivities, or lack thereof,[12] and chemospecificities observed are in complete accord with cubic model analyses.

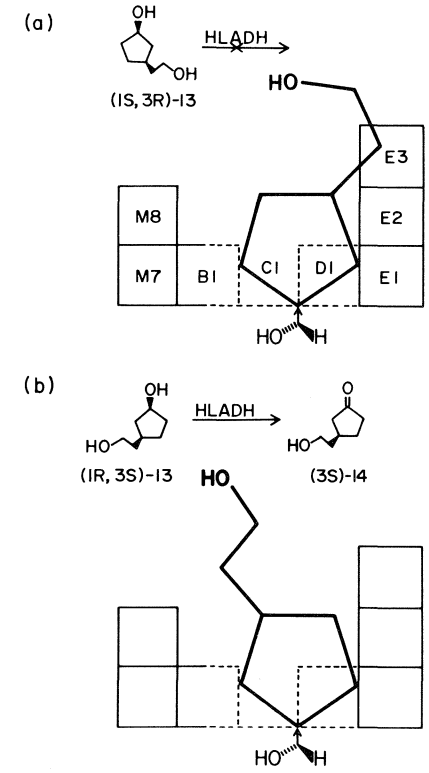


FIG. 12. Interpretation of enantio- and chemospecificity of HLADH-catalyzed oxidation of (±)-*cis*-3-(2′-Hydroxyethyl)-cyclopentanol. Neither $CH_2OH$ group of the enantiomers of **13** can be correctly oriented at the oxidation site for *pro-R* H-removal (11) without C-1, C-2, or the C-1-hydroxyl groups violating one or more of the forbidden positions **U(A3)**, **U(B2)**, **U(C2)**, **U(C3)**, **U(D2)**, **U(D3)**, **U(E3)**, **E2**, **K5**, **M8**, **O9**, or **P9**. Oxidation of the primary alcohol functions is thus precluded. (*a*) Oxidation of the secondary alcohol function of (1*S*,3*R*)-**13** is similarly disfavoured since it would require the C-3—hydroxyethyl function to locate in forbidden region **E3**. This is illustrated using the top elevation perspective of the cubic model (Fig. 2*b*). (*b*) The (1*R*,3*S*)-enantiomer, shown viewed from the same perspective, can be fully accommodated in allowed regions with C-1 at the catalytic site. Oxidation to (3*S*)-**14** is therefore facile.

*(3) Stereospecific oxidations of meso-diols*

All of the cubic-space analyses discussed so far have focussed on identifying differences between binding modes of enantiomeric components of racemic substrates. However, for asymmetric syn-

[10]The enantiomeric excess levels observed in the Figs. 10 and 11 reactions give a semi-quantitative indication of the degree to which requiring a group to be located in a limited rather than allowed region can affect the enantiomeric selectivities of oxidoreductions of such racemates.

[11]The *pro-R* enantiopic specificity of H-abstraction in HLADH-catalyzed oxidations of primary alcohols has been established directly (14, 15). It is also implicit from the stereochemical course of the microscopic-reverse aldehyde-reduction reaction for which delivery of hydride to the *Re*-face of the carbonyl group (*cf.* Figure 5 and discussion thereof) occurs in each of the numerous examples reported (2*a*, *b*, 3).

[12]From the asymmetric synthetic point-of-view the ability to predict when products will be racemic is clearly as important as being able to forecast high enantiomeric discrimination since unproductive enzymic approaches to chiral synthons can then be avoided.

Can. J. Chem. Downloaded from www.nrcresearchpress.com by 210.87.254.40 on 09/06/12
For personal use only.

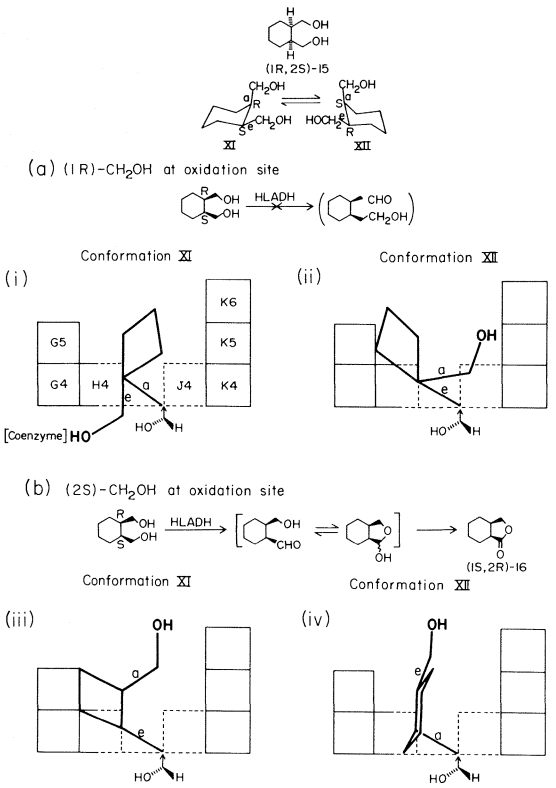


FIG. 13. Analysis of stereospecificity of oxidation of the meso-diol, *cis*-1,2-bis(hydroxymethyl)cyclohexane. The cubic-space orientations of the enantiomeric chair conformers **XI** and **XII** are evaluated separately, with the axial and equatorial $CH_2OH$ groups of each being positioned in turn at the oxidation site, correctly oriented for *pro-R* hydrogen removal. For each analysis, the binding is illustrated from the top elevation perspective (Fig. 2*b*). In (*a*) oxidations of the $CH_2OH$ group attached to the 1*R*-centre are considered. (*i*) Binding for oxidation of the axial-$CH_2OH$ of **XI** to occur cannot take place because the equatorial-$CH_2OH$ attached to the 2*S*-centre would project into the strongly forbidden coenzyme binding zone. Other orientations place parts of the cyclohexane ring in forbidden **U(B2)** and adjacent regions. (*ii*) Oxidations of (1*R*)-$CH_2OH$ group *via* conformation **XII** is also precluded, in this case by the double **H4** and **J4** limited region violations by the cyclohexane C-1—C-6 and (2*S*)-$CH_2OH$ moieties, respectively. (*b*) Oxidation of the (2*S*)-$CH_2OH$ group. (*iii*) Oxidation of the (2*S*)-hydroxymethyl group cannot occur when it is equatorially oriented as in conformation **XI** because the C-3—C-4 region of the cyclohexane ring would violate both limited and forbidden portions of **H4**. (*iv*) Oxidation of the axial (2*S*)-$CH_2OH$ of **XII** is favoured since all of the molecule can occupy allowed regions, except for the minor intrusion of C-3 into the limited region of **B1**. This slows the reaction somewhat but does not prevent it. Oxidation via this ES complex leads initially to the (1*S*,2*R*)-hydroxyaldehyde which undergoes further HLADH-catalyzed oxidation to give the (1*S*,2*R*)-lactone **16** directly (2*f*).

thetic purposes it is much more efficient to perform the desired asymmetric induction on a symmetrical intermediate. Meso-compounds are one such substrate group for which stereospecific enzyme-mediated transformations are possible. HLADH-catalyzed oxidation of *cis*-1,2-di(2′-hydroxymethyl)cyclohexane (**15**) provides a representative example. Interpretation of the reaction in cubic model terms is shown in Fig. 13.

The *cis*-diol **15** is of particular stereochemical interest since its chair conformers are enantiomeric (20, 21). As the Fig. 13 analysis demonstrates, only for oxidation of the axially oriented $CH_2OH$ attached to the 2*S*-centre is formation of a favourable ES complex possible (Fig. 13*b*(*iv*)). The other, unfavourable, binding modes depicted in Fig. 13(*i*), (*ii*), and (*iii*) represent the least disfavoured situations only, with all alternative orientations involving interactions that are equally or more prohibitive. The preparative-scale reaction results confirm this analysis, with HLADH-catalyzed oxidation of the meso-diol **15** occurring with complete stereospecificity to give the (1*S*,2*R*)-lactone **16** of 100% e.e. as the only product (2*f*).

*General applicability of the cubic-space model*

The illustrative examples discussed in this paper represent only a fraction of the known substrates of HLADH. In fact, we have applied the cubic-space analytical method to all of the more than 50 different cyclic and bicyclic compounds presently identified as substrates of HLADH in both published (2–6) and unpublished[13] (22) work. In each case the predictions are in total accord with the experimental observations. The cubic-space model is completely reliable for substrates in which one or more rings are present.[14] It overcomes all of the limitations and uncertainties inherent in the diamond lattice approach[3] and that in recent years have increasingly undermined its credibility. The cubic model is now in routine use in our laboratories and will be extended to new substrate structures as they become known.

**Acknowledgements**

The financial support of the Natural Sciences and Engineering Research Council of Canada (NSERC) and the award of an NSERC Scholarship to I.J.J. are gratefully acknowledged.

1. J. B. JONES and H. M. SCHWARTZ. Can. J. Chem. **59**, 1574 (1981).
2. (*a*) J. B. JONES and J. F. BECK. Tech. Chem. NY **10**, 107

[13]These analyses will be reported shortly.

[14]For bifunctional acyclic substrates such as glycerol (23) and pentane-1,5-diols (2*d*,*g*), cubic section analyses are not yet completely unequivocal owing to the multiplicity of conformational and orientation combinations that must be considered. The cubic model is currently being refined to enable such acyclic substrates to be analyzed with confidence.

(1976); (*b*) J. B. JONES. *In* Enzymic and non-enzymic catalysis. *Edited by* P. Dunnill, A. Wiseman, and N. Blakeborough. Ellis Horwood/J. Wiley, Chichester/New York. 1980. pp. 54–83; (*c*) J. DAVIES and J. B. JONES. J. Am. Chem. Soc. **101**, 5405 (1979); (*d*) A. J. IRWIN and J. B. JONES. J. Am. Chem. Soc. **98**, 8476 (1976); **99**, 556 (1977); **99**, 1625 (1977); (*e*) J. B. JONES and H. B. GOODBRAND. Can. J. Chem. **55**, 2685 (1977); (*f*) H. B. GOODBRAND and J. B. JONES. Chem. Commun. 469 (1977); (*g*) J. B. JONES and K. P. LOK. Can. J. Chem. **57**, 1025 (1979); (*h*) I. J. JAKOVAC, G. NG, K. P. LOK, and J. B. JONES. J. Chem. Soc. Chem. Commun. 515 (1980); (*i*) J. B. JONES and T. TAKEMURA. Unpublished results.

3. V. PRELOG. Pure Appl. Chem. **9**, 119 (1964).
4. J. M. H. GRAVES, A. CLARK, and H. J. RINGOLD. Biochemistry, **4**, 2655 (1965).
5. H. DUTLER. (*a*) Biochem. Soc. Trans. **5**, 617 (1977); (*b*) *In* Pyridine nucleotide-dependent dehydrogenases. *Edited by* H. Sund. Walter de Gruyter, Berlin. 1977. pp. 339–350; (*c*) H. DUTLER and C-I. BRÄNDÉN. Bioorg. Chem. **10**, 1 (1981).
6. (*a*) T. A. VAN OSSELAER, G. L. LEMIERE, E. M. MERCKX, J. A. LEPOIVRE, and F. C. ALDERWEIRELDT. Bull. Soc. Chem. Belg. **87**, 799 (1978); (*b*) J. J. VAN LUPPEN, J. A. LEPOIVRE, T. A. VAN OSSELAER, G. L. LEMIERE, and F. C. ALDERWEIRELDT. Bull. Soc. Chem. Belg. **88**, 829 (1979); (*c*) T. A. VAN OSSELAER, G. L. LEMIERE, J. A. LEPOIVRE, and F. C. ALDERWEIRELDT. Bull. Soc. Chem. Belg. **89**, 133 (1980); (*d*) T. A. VAN OSSELAER, G. L. LEMIERE, J. A. LEPOIVRE, and F. C. ALDERWEIRELDT. Bull. Soc. Chem. Belg. **89**, 389 (1980).
7. C. J. SIH and J. P. ROSAZZA. Tech. Chem. NY. **10**, 69 (1976).
8. R. A. JOHNSON. *In* Oxidation in organic chemistry, Part C. *Edited by* W. S. Trahanovsky. Academic, New York. 1978. pp. 131–210.
9. (*a*) M. NAKAZAKI, H. CHIKAMATSU, K. NAEMURA, and M. ASAO. J. Org. Chem. **45**, 4432 (1980); (*b*) M. NAKAZAKI, H. CHIKAMATSU, K. NAEMURA, Y. SASAKI and T. FUGI. J. Chem. Soc. Chem. Commun. 623 (1980).
10. H. JORNVALL. Eur. J. Biochem. **16**, 25 (1970).
11. (*a*) H. EKLUND, B. NORDSTROM, E. ZEPPERZAUER, G. SODERLUND, I. OHLSSON, T. BOIWE, B. O. SODERBERG, O. TAIPU, C-I. BRÄNDÉN, and A. AKESON. J. Mol. Biol. **102**, 27 (1976); (*b*) C-I. BRÄNDÉN, H. JORNVALL, H. EKLUND, and B. FURUGREN. *In* The enzymes. Vol. 2. 3rd ed. *Edited by* P. D. Boyer. Academic, New York. 1975. pp. 93–190; (*c*) M. ABDALLAH, J-F. BIELLMANN, B. NORDSTROM, and C-I. BRÄNDÉN. Eur. J. Biochem. **50**, 475 (1975); (*d*) J. P. SAMAMA, E. ZEPPERZAUER, J. F. BIELLMANN, and C-I. BRÄNDÉN. Eur. J. Biochem. **81**, 403 (1977); (*e*) B. V. PLAPP, H. EKLUND, and C-I. BRÄNDÉN. J. Mol. Biol. **122**, 23 (1978); (*f*) C-I. BRÄNDÉN. *In* Pyridine nucleotide-dependent dehydrogenases. *Edited by* H. Sund. Walter de Gruyter, Berlin. 1977. p. 325; (*g*) C-I. BRÄNDÉN and H. EKLUND. Molecular interactions and activity in proteins. Ciba Foundation Symposium, Excerpta Medica, Amsterdam. 1978. p. 63.
12. G. POPJAK. *In* The enzymes. Vol. 2. 3rd ed. *Edited by* P. D. Boyer. Academic, New York. 1970. p. 115.
13. R. BENTLEY. Molecular asymmetry in biology. Vol. 2. Academic, New York. 1969. pp. 22–31.
14. C. DONNINGER and G. RYBACK. Biochem. J. **91**, 11P (1964).
15. H. GERLACH and B. ZAGALAK. Chem. Commun. 274 (1973).
16. (*a*) K. DALZIEL. Biochem. J. **84**, 244 (1962); J. Biol. Chem. **238**, 2850 (1963); (*b*) F. M. DICKINSON and K. DALZIEL. Biochem. J. **104**, 165 (1967).
17. (*a*) I. BJORKHEM and M. HAMBERG. J. Biol. Chem. **246**, 7417 (1971); (*b*) I. BJORKHEM, H. JORNVALL, and A. AKESON. Biochem. Biophys. Res. Commun. **57**, 870 (1974).
18. R. E. HELMCHEN-ZEIER. Ph.D. thesis 4991, E.T.H., Zürich. 1973.
19. R. MISLIN. Ph.D. thesis 4169, E.T.H., Zürich. 1968.
20. E. L. ELIEL. Stereochemistry of carbon compounds. McGraw-Hill, New York. 1962. pp. 156–165, 177.
21. S. WOLFE and J. CAMPBELL. Chem. Commun. 874 (1967).
22. J. B. JONES, T. A. HASLEGRAVE, I. J. JAKOVAC, G. Y. NG and D. DODDS. Unpublished results.
23. C. BALLY and F. LEUTHARDT. Helv. Chim. Acta, **53**, 732 (1970); B. HADRON, F. LEUTHARDT, E. MENARD, and D. VISCHER. Helv. Chim. Acta, **46**, 2003 (1963).

Can. J. Chem. Downloaded from www.nrcresearchpress.com by 210.87.254.40 on 09/06/12
For personal use only.

# Stereochemical studies. X. Synthesis of some epimeric δ-lactones

ELLEN COOKE, THEMISTOCLES C. PARADELLIS, AND JOHN T. EDWARD
*Department of Chemistry, McGill University, Montreal, P.Q., Canada H3A 2K6*

Received August 18, 1981

ELLEN COOKE, THEMISTOCLES C. PARADELLIS, and JOHN T. EDWARD. Can. J. Chem. **60**, 29 (1982).
Stereospecific syntheses are reported for the δ-lactones **3**, **5**, **8**, **17**, and **26**.

ELLEN COOKE, THEMISTOCLES C. PARADELLIS et JOHN T. EDWARD. Can. J. Chem. **60**, 29 (1982).
On présente les synthèses stéréospécifiques pour les δ-lactones **3**, **5**, **8**, **17** et **26**.

[Traduit par le journal]

Can. J. Chem. Downloaded from www.nrcresearchpress.com by 210.87.254.6 on 09/06/12
For personal use only.

In connection with studies of the effect of substitution on the tendency of δ-hydroxy-acids to lactonize (1), we required a variety of variously-substituted δ-lactones. In this paper we describe the synthesis of the lactones **3**, **5**, **8**, **17**, and **26**; their equilibrium behaviour is described in a companion paper.

The synthesis of the epimers **3** and **5** is shown in Scheme 1. Hydrogenation of the unsaturated ketone **1** in ethanol over palladium-on-charcoal is known to give a 3:2 mixture of **2** and **4** (2). We have found that hydrogenation in ether at −20°C (cf. ref. 3) gives an approximately 85:15 mixture (as determined by nmr) of **2** and **4**. In alkaline solution such a mixture is isomerized almost completely (~90%) to the *trans* ketone **4**. Baeyer–Villiger oxidation of these ketone mixtures with trifluoroperoxyacetic acid gave products consisting in the one case predominantly of the *cis* (**3**) and in the other case predominantly of the *trans*-disubstituted lactone (**5**).

The lactone **5**, a low-melting solid, could be isolated from the reaction mixture in a pure state, and proved to be stable on standing. However, the *cis* lactone **3**, obtained admixed with some **2**, **4**, and **5** as impurities (as shown by nmr), proved surprisingly unstable. In a few days at room temperature it had decomposed to viscous material (presumably polyester), but also in part to more volatile products (carbon dioxide and diene by a reverse Diels–Alder reaction?). In consequence, our characterization of **3** is very incomplete.

It may be expected that **3** exists about equally in the two conformations **3**ea′ and **3**ae′, having one methyl group axial (a) or pseudo-axial (a′), while **5** should exist almost completely in the single conformation **5**ee′. For this reason, the δ-methyl group (δ 1.21; $J$ = 6 Hz) of **3**, being partially pseudo-axial

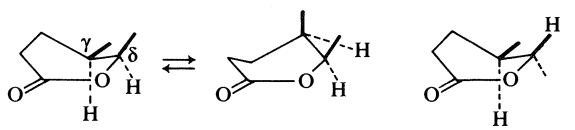

3ea′ 3ae′ 5ee′

and hence more shielded than the (pseudo-equatorial) δ-methyl of **5** (4), absorbs at higher field than the latter (δ 1.26; $J$ = 6 Hz). The reverse holds true for the δ-protons of **3** (δ 4.3) and **5** (δ 3.8). These protons are part of an $A_3BX$ system ($J_{AX}$ = 6 Hz; cf. methyl splitting, above). The splitting pattern indicates that $J_{BX}$ = 3 Hz for **3** and 8 Hz for **5**. This again accords with the conformations shown above, the dihedral angle between $H_\gamma$ and $H_\delta$ in **5** being close to 180°, and in **3** being close to 60°.

The synthesis of **8** is shown in Scheme 2. The

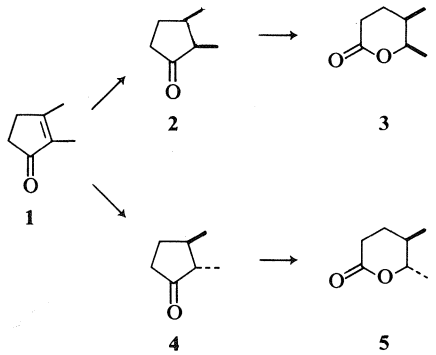

SCHEME 1

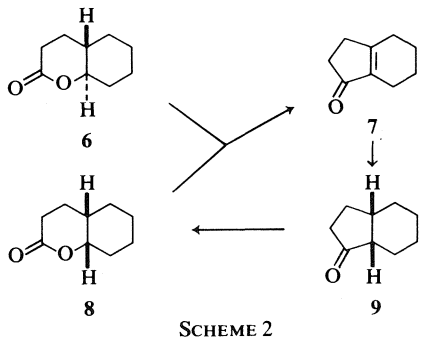

SCHEME 2

0008-4042/82/010029-06$01.00/0
©1982 National Research Council of Canada/Conseil national de recherches du Canada

Can. J. Chem. Downloaded from www.nrcresearchpress.com by 210.87.254.6 on 09/06/12
For personal use only.

lactones **6** and **8** have hitherto been obtained only as inseparable 1:2 or 2:1 mixtures (6). Treatment of these mixtures with hot polyphosphoric acid gave the unsaturated ketone **7**, from which the *cis* ketone **9** was obtained by hydrogenation. Oxidation of **9** with trifluoroperoxyacetic acid yielded the *cis* lactone **8**, free from the *trans* lactone **6**.

The *cis* lactone **12** has been obtained by a similar stereospecific synthesis (5), but the *trans* lactone **10** has been available only in an inseparable mixture with **12** from the catalytic or borohydride reduction of the keto-acid **13** (Scheme 3) (7). Attempts to obtain isomerically-pure **10** were unsuccessful (8, 9), but the proportion of **10**:**12** could be raised to 83:17 by conversion of **13** into the unsaturated lactone **11**, and hydrogenation of the latter (Scheme 3).

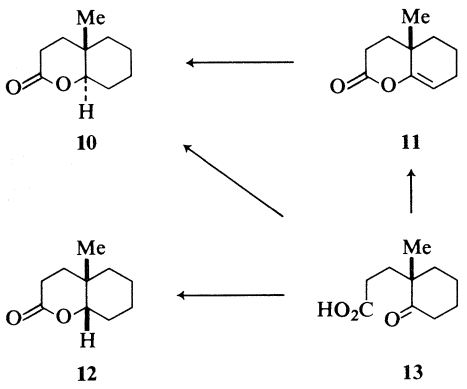


SCHEME 3

The *trans* lactone **16** has been prepared by borohydride reduction of the keto-acid **15**, and the *cis* ("steroid" conformation) lactone **19** by catalytic reduction of **15** in acidic solution (10). The *cis* ("non-steroid" conformation) lactone **17** has now been prepared by the route shown in Scheme 4.

Alkylation of cyclohexanones is known to give initially an axial product (11–13). Consequently, the initial product from the reaction of the enamine of 4-*tert*-butylcyclohexanone with ethyl acrylate, followed by hydrolysis at pH 5–7 (12), must be mostly the axial product **14***c*, contaminated with a small amount of the equatorial ester corresponding to **15***b*. Hydrolysis of the ester group can be expected to be accompanied by epimerization to give mainly the equatorial acid **15** (10). However, this epimerization can be avoided if the carbonyl group is first reduced by hydrogenation over platinum. This gives mainly the β-hydroxy-ester **18**, presumably because approach of the keto group to the catalyst surface takes place more easily when the keto-ester **14** is in the boat conformation **14***b*, so that hydrogen is added to the under-surface of the molecule (see Johnson *et al.* (14) for a closely analogous case). On treatment with acid the hydroxy-ester **18** gave the lactone **17**, accompanied by small amounts of **16** and **19** arising from hydrogenation of the contaminating keto-acid **15**.

The synthesis of **26** (equivalent to **17** with an angular methyl group) is shown in Scheme 5. The stereoelectronic factors which favour the formation of **14** from 4-*tert*-butylcyclohexanone should also favour the formation of the axial product **23** from 4-*tert*-butyl-2-methylcyclohexanone **20**. However, it was found that reaction of the ketone **20** with acrylonitrile went in very low yield. Consequently, the ketone was converted into the trimethylsilyl enol ether **21** (a small amount of the isomeric ether **22** was also formed), and this reacted with methyl lithium to give the lithium enolate. The enolate reacted rapidly with acrylonitrile to give the keto-nitrile **23**, which was hydrolyzed to the keto-acid **24**. Reduction of the latter by either borohydride or catalytic hydrogenation gave only the β-hydroxy-acid **25**, converted by acid to the lactone **26**.

The 9α,10α-configuration of this lactone, advanced above on mechanistic grounds, is supported by its nmr spectrum. The nmr peak for the 9α-proton (δ 3.88) has a band-width $w/2$ at half-height of 18 Hz showing that it is axial (4) and hence 9α.[1] The other possible configuration (9α,10β) with 9α would have the 10-methyl group axial, and hence with an nmr peak at δ ~ 0.97, whereas the peak is at δ 1.12, as expected for an equatorial 10-methyl group (5, 7).

## Experimental

General directions are in ref. 10.

trans-*2,3-Dimethylcyclopentanone (4)*

2,3-Dimethyl-2-cyclopentenone **1** (2) (7.6 g) was hydrogenated over 10% palladium-on-charcoal (8 g) in ethanol (100 mL) until 1460 mL of hydrogen had been absorbed. The catalyst was removed by filtration; vpc (8% QF-1; 6 ft × ¼ in. glass column; 110°C; 100 mL/min $N_2$) of the filtrate showed peaks at 1.4 min (**4**) and 1.8 min (**2**) in the ratio of 1:2. Sodium hydroxide (10 *N*, 2 mL) was added to the filtrate. After 1 h, vpc showed the 1.4 min and 1.8 min peaks in a ratio of 10:1, which did not change further on standing. *trans*-2,3-Dimethylcyclopentanone **4** was isolated in the manner described by Varech *et al.* (2): 6.1 g (79%), bp 30–32°C/5 Torr; $\nu_{max}$ ($CCl_4$): 2955, 2930, 2875, 1740, 1460, 1455, 1408, 1380, 1373, 1355, 1325, 1295, 1270, 1248, 1220, 1215, 1210, 1188, 1158, 1145, 1108, 1080, 1035, 1000, 987, 975, 932, 905, 865, 835 $cm^{-1}$; δ ($CCl_4$): 0.99 (d, 3H, $J$ = 6 Hz), 1.16 (d, 3H, $J$ = 4 Hz), 0.9–2.3 (m, 6H). The semicarbazone had mp 178–179°C (lit. (15) mp 179–180°C), and the 2,4-dinitrophenylhydrazone mp 161.5–164.5°C. *Anal.* calcd. for $C_{13}H_{16}O_4N_4$: C 53.4, H 5.5, N 19.2; found: C 54.4, H 5.8, N 19.6.

[1]The band-width would also be compatible with a 9β,10α-configuration, in which the cyclohexane ring has adopted a boat conformation; however, this lactone would be formed from the hydroxy-acid only under drastic conditions (14), and so it can be excluded.

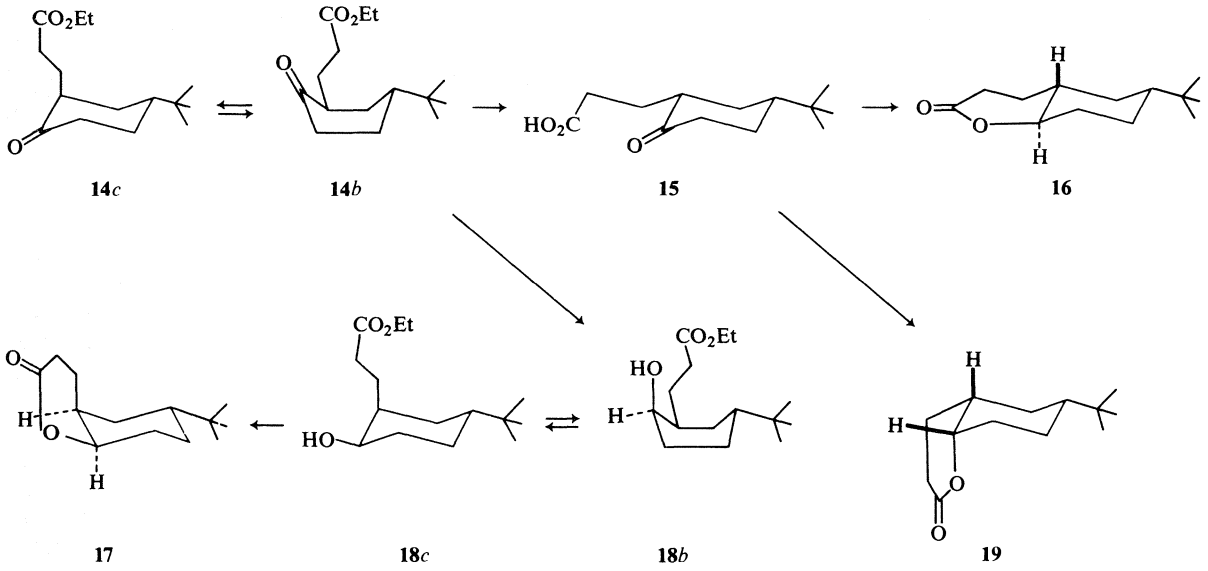


SCHEME 4

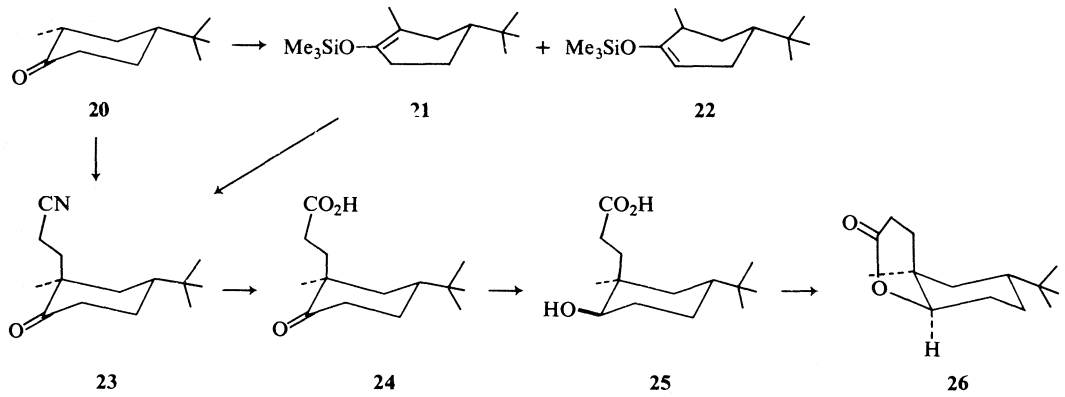


SCHEME 5

trans-γ,δ-*Dimethyl-δ-valerolactone (5)*

A solution of trifluoroperoxyacetic acid was prepared from trifluoroacetic anhydride (39 mL) and 94% hydrogen peroxide (7.8 mL) in methylene chloride (300 mL) (16), and added over 3 h to a stirred solution of *trans*-2,3-dimethylcyclopentanone (6.6 g) in methylene chloride (400 mL) containing suspended disodium hydrogen phosphate (27 g). Stirring was continued for 4 h at room temperature. The solution was filtered, washed with saturated aqueous $NaHCO_3$, saturated aqueous NaCl, and dried ($MgSO_4$). The solvent was then removed by evaporation, and the residue distilled to give a first fraction of starting ketone (0.68 g), bp 30–43°C/5 Torr, followed by the lactone **5** (3.9 g; 51%), bp 100–102°C/5 Torr, purified by a second distillation and then sublimation: mp 26–28°C; $\nu_{max}$ ($CCl_4$): 2980, 2935, 2880, 1740, 1460, 1455, 1419, 1383, 1345, 1326, 1300, 1245, 1220, 1193, 1155, 1110, 1094, 1045, 1031, 982, 968, 910, 850 $cm^{-1}$; nmr δ ($CCl_4$): 0.97 (d, 3H, $J$ = 5 Hz), 1.26 (d, 3H, $J$ = 6 Hz), 1.1–2.5 (m, 5H), 3.87 (m, 1H). *Anal.* calcd. for $C_7H_{12}O_2$: C 65.6, H 9.4; found: C 65.5, H 9.4.

cis-*2,3-Dimethylcyclopentanone (2)*

2,3-Dimethyl-2-cyclopentenone **1** (6.9 g) in diethyl ether (150 mL) was hydrogenated over 10% palladium-on-charcoal (0.08 g) at atmospheric pressure. The temperature was kept between −17°C and −22°C. When hydrogen uptake ceased (4 h), the solution was filtered under $N_2$, and the ether was removed at reduced pressure. Vapor-phase chromatography showed two peaks at 1.4 min (**4**) and 1.8 min (**2**) in the ratio 15:85. To avoid epimerization, the ketone mixture was not distilled: $\nu_{max}$ ($CCl_4$): 2955, 2930, 2875, 1740, 1460, 1450, 1405, 1380, 1370, 1340, 1330, 1295, 1265, 1245, 1215, 1190, 1160, 1155, 1115, 1082, 1045, 1015, 995, 960, 950, 940, 930, 892, 862, 835, $cm^{-1}$; δ ($CCl_4$): 0.92 (d, $J$ = 6.5 Hz), 0.99 and 1.16 (d) (total area: 6H), 1.2–2.6 (m, 6H); δ (benzene-$d_6$): 0.63 (d, $J$ = 6.5 Hz), 0.86 (d, $J$ = 6.5 Hz), 0.92 (d, $J$ = 6 Hz) (total area, 6H), 1.0–2.2 (m, 6H). The 2,4-dinitrophenylhydrazone melted at 161–164°C, and was probably the derivative of **4** because of epimerization under the acidic conditions used to prepare the derivative. *Anal.* calcd. for $C_{13}H_{16}O_4N_4$: C 53.4, H 5.6, N 19.2; found: C 53.9, H 5.7, N 19.2.

Can. J. Chem. Downloaded from www.nrcresearchpress.com by 210.87.254.6 on 09/06/12
For personal use only.

Can. J. Chem. Downloaded from www.nrcresearchpress.com by 210.87.254.6 on 09/06/12
For personal use only.

cis-γ,δ-*Dimethyl-δ-valerolactone (3)*

Baeyer–Villiger oxidation of **2/4** (85:15) (4.6 g) with trifluoroperoxyacetic acid in methylene chloride was carried out under essentially the same conditions as used above for the oxidation of **4**. The residue from evaporation of methylene chloride was distilled to give starting ketone (0.92 g), bp 30–32°C/5 Torr, followed by a colourless liquid which turned brown in the condenser (0.31 g), bp 66–90°C/5 Torr, and finally the lactone **3**, (2.2 g; 42%), bp 99–102°C/5 Torr; $\nu_{max}$ ($CCl_4$): 1740 $cm^{-1}$; vpc of this material showed only one peak at 12.3 min (same retention time as **5**); however, after several days vpc showed several components eluting before the original component at 12.7 min, and additionally it had become viscous.

*4,5,6,7-Tetrahydroindan-1-one (7)*

3-(2-Oxocyclohexyl) propionic acid (8.5 g) was reduced with sodium borohydride following House *et al.* (6), and the resulting crude lactone mixture **6/8** (6.9 g) was added to polyphosphoric acid (105 g) at 120°C according to the method of Dev and co-workers (17). The mixture was stirred for 2 min every 30 min. After 4.5 h the mixture was placed in the refrigerator overnight, then hydrolyzed with 300 mL of ice–water slush. The mixture was extracted with ether, and the ether solution washed with water, aqueous $NaHCO_3$, aqueous NaCl, and dried ($MgSO_4$). The solvent was removed at reduced pressure and the oily residue distilled at 0.1 Torr to give **7**, bp 66–68°C; $\nu_{max}$ (neat): 2945, 2920, 2869, 1690, 1645, 1460, 1440, 1408, 1405, 1390, 1300, 1275, 1250, 1230, 1210, 1180, 1150, 1130, 1120, 1090, 1060, 1010, 990, 950, 870, 855, 840, 800 $cm^{-1}$; δ ($CCl_4$): complex absorption between 1.6 and 2.5; no olefinic proton. The 2,4-dinitrophenylhydrazone melted at 238–239°C (lit. (18) mp 238.5–239.5°C).

cis-*Perhydroindan-1-one (9)*

4,5,6,7-Tetrahydroindan-1-one (4.1 g) was reduced over 10% palladium-on-charcoal (0.42 g) in ethanol (100 mL) at room temperature and atmospheric pressure according to House and Rasmusson (18). After absorption of one equiv. of hydrogen, the solution was filtered and extracted with ether. The ether solution was washed with sodium bicarbonate and dried ($MgSO_4$). Removal of the ether yielded an oil which was distilled at 0.05 Torr to yield **9** (3.3 g, 81%), bp 32–33°C; $\nu_{max}$ ($CCl_4$): 2940, 2880, 2860, 1735, 1470, 1460, 1445, 1440, 1410, 1355, 1345, 1330, 1310, 1305, 1290, 1280, 1250, 1210, 1190, 1155, 1140, 1105, 1055, 1045, 1030, 990, 970, 925, 905, 870, 850 $cm^{-1}$; δ ($CCl_4$): complex absorption between 1.0 and 2.8. The 2,4-dinitrophenylhydrazone melted at 164–166°C (lit. (19) mp 163–165°C, (20) mp 160–162°C).

cis-*1-Oxadecal-2-one (8)*

Oxidation of **9** (2.3 g) with trifluoroperoxyacetic acid was carried out essentially as described above for **4**. The oily residue was distilled at 0.1 Torr to yield starting ketones (0.2 g) bp 40–41°C, and *cis*-lactone **8** (1.48 g; 55%), bp 78–80°C; vpc (8%, QF-1, 6 ft × ¼ in. glass column, 170°C, 120 mL/min $N_2$) showed only one peak for **8** at 4.4 min, and no peak for **6** at 4.8 min; $\nu_{max}$ ($CCl_4$): 2940, 2850, 1735, 1460, 1445, 1435, 1420, 1370, 1350, 1335, 1295, 1240, 1195, 1180, 1162, 1138, 1110, 1068, 1043, 1005, 993, 940 $cm^{-1}$; δ($CCl_4$): 1.1–2.5 (complex absorption, 13H), 4.43 (multiplet, 1H). *Anal.* calcd. for $C_9H_{14}O_2$: C 70.1, H 9.1; found: C 70.2, H 9.2.

*10-Methyl-1-oxa-Δ⁸-octal-2-one (11)*

3-(1′-Methyl-2′-oxocyclohexyl) propionic acid **13** (21) (92 g) was treated with a solution of acetic anhydride (1 *M*) and perchloric acid (0.001 *M*) in ethyl acetate (1000 mL) according to Edwards and Rao (22) to yield the unsaturated lactone **11** as an oil (71 g; 85%), bp 98–100°C/0.7 Torr; $n_D^{20}$ 1.5058; $\nu_{max}$ ($CCl_4$): 1750, 1680 $cm^{-1}$. *Anal.* calcd. for $C_{10}H_{14}O_2$: C 72.3, H 8.5; found: C 72.3, H 8.4.

*Hydrogenation of 10-methyl-1-oxa-Δ⁸-octal-2-one (11)*

The unsaturated lactone **11** (4.9 g) in cyclohexane (50 mL) was hydrogenated over platinized charcoal (1.3 g) at room temperature and pressure. After absorption of 1 equiv. of hydrogen (16 h), the mixture was filtered, washed with aqueous $NaHCO_3$, dried ($MgSO_4$), and concentrated. The residue on distillation gave an oil (3.09 g; 60%), bp 97–100°C/0.2 Torr; $n_D^{20}$ 1.4913; $\nu_{max}$ ($CCl_4$): 1740 $cm^{-1}$, shown by nmr (5) to be a 83:17 mixture of **10/12**.

4-tert-*Butyl-2-(2′-ethoxycarbonylethyl) cyclohexanone (14)*

Freshly distilled ethyl acrylate (22 g) was added to a solution of 4-*tert*-butyl-1-pyrrolidinocyclohexene (12) (33.6 g) in dry dioxane (300 mL). The mixture was refluxed for 8 h under $N_2$, and then hydrolyzed with dilute acetic acid at pH 5–7 and extracted according to Karady *et al.* (12). The keto-ester **14** was obtained as an oil (20 g; 64%), bp 127–131°C/0.3 Torr; $\nu_{max}$ ($CCl_4$): 2960, 2910, 2870, 1740, 1715, 1392, 1375, 1366, 1328, 1300, 1250, 1100, 1040, 985, 965, 950, 927, 855, 780, 685 $cm^{-1}$.

6α-tert-*Butyl-1-oxa-9α,10α-decal-2-one (17)*

The keto-ester **14** (12.4 g) was hydrogenated at room temperature and 40 psi over pre-reduced platinum oxide (1.26 g) in ethanol (150 mL). After hydrogen absorption had ceased, the solution was filtered and the ethanol removed under reduced pressure to yield the crude, hydroxy-ester **18** as an oil ($\nu_{max}$ ($CCl_4$): 3400 (broad, OH), 1740 $cm^{-1}$.

A solution of the crude hydroxy-ester (6.4 g) in 2 *N* hydrochloric acid (50 mL) was refluxed for 10 h. The resulting mixture was extracted with ether, and the ether solution was washed with aqueous $NaHCO_3$, aqueous NaCl, and dried ($Na_2SO_4$). The residue from evaporation of the ether (4.8 g; 91%) on vpc (6 ft × ¼ in. glass column, 8% QF-1, 175°C, 120 mL/min $N_2$) showed components with retention times of 12 min (**19**), 14 min (**16**), and 17 min (**17**) in the ratio 9:30:60. The third component was collected as a pale yellow oil by preparative vpc, and solidified on standing. It sublimed at 40°C/0.1 Torr to yield **17** as a colourless solid, mp 51.7–53°C; $\nu_{max}$: 2930, 2855, 1735, 1468, 1455, 1448, 1420, 1393, 1383, 1363, 1352, 1345, 1325, 1305, 1280, 1265, 1247, 1230, 1219, 1198, 1187, 1165, 1150, 1118, 1092, 1050, 1042, 1038, 1032, 985, 950, 928, 900, 863 $cm^{-1}$; δ ($CCl_4$): 0.84 (s, 9H), 0.90–2.55 (complex multiplet, 12H), 4.32 (1H). *Anal.* calcd. for $C_{13}H_{22}O_2$: C 74.2, H 10.5; found: C 74.1, H 10.3.

*Trimethylsilyl enol ethers of* 4-tert-*butyl-2-methylcyclohexanone (21/22)*

Chlorotrimethylsilane (6 mL) and triethylamine (14 mL) were added to a solution of 4-*tert*-butyl-2-methylcyclohexanone **20** (23) (6.29 g) in 35 mL of dimethylformamide according to the procedure of House *et al.* (24). The mixture was heated for 24 h, then diluted with ether, washed with cold aqueous $NaHCO_3$, cold aqueous NaCl, and dried ($MgSO_4$). The ether was removed by evaporation, and the residue distilled at 0.2 Torr to give three fractions: A (1.42 g), bp 58–64°C; B (2.22 g), bp 64°C; C (3.91 g), bp 65°C (total yield 78%); vpc (8% QF-1, 6 ft × ¼ in. glass column, 110°C, 80 mL/min $N_2$) showed A and B to be made up of approximately 1:2 mixture of **22** (2.6 min) and **21** (3.3 min); and a small amount of **20** (6.8 min); C to be made up of a 1:5.5 mixture of **22** and **21**: δ ($CCl_4$): 0.17 (s, 9H), 0.85 (s, ca. 9H), 1.48 (s, ca. 3H), 1.05–2.2 (complex, ca. 7H).

4α-tert-*Butyl-2β-(2′-cyanoethyl)-2α-methylcyclohexanone (23)*

*(a) By cyanoethylation of* 4α-tert-*butyl-2ξ-methylcyclohexanone*

Freshly distilled acrylonitrile (4.7 g) was added dropwise to 4α-*tert*-butyl-2ξ-methylcyclohexanone **20** (75.6 g) stirred with Triton B (0.9 g) over 15 min. The mixture was stirred at room temperature for 45 min, then acidified with 50% hydrochloric

Can. J. Chem. Downloaded from www.nrcresearchpress.com by 210.87.254.6 on 09/06/12
For personal use only.

acid and diluted with ether. The ether layer was washed with aqueous $NaHCO_3$, aqueous NaCl, dried ($MgSO_4$), and concentrated by evaporation. The residue was distilled, and gave **20** (68.0 g), bp 66–68°C/0.4 Torr, followed by crude ketonitrile as a colourless oil (1.0 g; approximately 5%), bp 132–136°C/0.4 Torr; $\nu_{max}$: 2240, 1710 $cm^{-1}$. Vapor-phase chromatography (175°C, 120 mL/min $N_2$) of the crude material showed three components at 7.4, 10.6, and 12.8 min in the ratio 1:1:8. The components were separated by vpc, but only the third component could be obtained pure. It was crystallized from hexane, and then sublimed at 35°C/0.05 Torr to give the white solid **23**, mp 52–52.5°C; $\nu_{max}$ ($CCl_4$): 2950, 2920, 2855, 2240, 1710, 1478, 1460, 1425, 1393, 1381, 1368, 1335, 1282, 1232, 1160, 1115, 1090, 1020, 1000, 952, 925, 935 $cm^{-1}$; δ ($CCl_4$): 0.92 (s, 9H), 0.99 (s, 3H), 1.2–2.5 (complex, 11H). *Anal.* calcd. for $C_{19}H_{23}NO$: C 76.0, H 10.5, N 6.3; found: C 76.0, H 10.3, N 6.3.

*(b) By cyanoethylation of lithium enolates derived from **21**/**22***

To 4.75 g of the trimethylsilyl enol ether mixture (approximately 88% **21** and 12% **22**) in 25 mL of dry glyme (distilled from lithium aluminum hydride) in a three-necked flask fitted with a septum and flushed with dry nitrogen was added 8.3 mL of 2.4 *N* methyl lithium through the septum, using a dry syringe flushed with dry nitrogen. The mixture was stirred at room temperature for 15 min and then cooled to 0°C; 1.2 mL of freshly-distilled acrylonitrile was added by means of a syringe. After 1 min the mixture was quenched with dilute hydrochloric acid. The mixture was diluted with ether, and the ether layer was washed with aqueous $NaHCO_3$, aqueous NaCl, dried ($MgSO_4$), and concentrated. Fractional distillation of the residue gave an oil, bp 134–138°C/0.05 Torr (2.5 g; 56%); $\nu_{max}$ ($CCl_4$): 2240, 1710 $cm^{-1}$, shown by vpc to have three components in the ratio 1:1:8 with retention times of 7.4, 10.6, and 12.8 min (i.e. ca. 80% **23**).

*3-(5′-*tert*-Butyl-1′-methyl-2′-oxacyclohexyl) propionic acid (**24**)*

The crude ketonitrile (approximately 80% **23**) (2.0 g) from the experiment above was refluxed in 10 mL of 10% aqueous sodium hydroxide for 15 h. The reaction mixture was acidified with 50% hydrochloric acid and extracted with ether. The ether extract was washed with aqueous sodium bicarbonate. The bicarbonate solution was acidified and extracted with ether. This ether extract was washed with aqueous NaCl, dried ($MgSO_4$), and concentrated. The residue solidified on standing and was recrystallized from hexane–ether to yield 1.34 g (62%) of the keto-acid **24**, mp 118–119.5°C; $\nu_{max}$ ($CCl_4$): 3350–2500, 2960, 2940, 2875, 1705, 1480, 1460, 1445, 1425, 1400, 1385, 1370, 1340, 1305, 1295, 1280, 1250, 1230, 1172, 1130, 1090, 1020, 1003, 980, 950, 935, 915, 870 $cm^{-1}$; δ ($CCl_4$): 0.92 (s, 9H), 0.97 (s, 3H), 1.05–2.45 (complex 11H), 11.0 (s, 1H). *Anal.* calcd. for $C_{14}H_{24}O_3$: C 70.0, H 10.0; found: C 70.3, H 9.9.

*3-(5′-*tert*-Butyl-1′-methyl-2′-hydroxycyclohexyl)-propionic acid (**25**)*

Sodium borohydride (60 mg) was added to a solution of the keto-acid **24** (700 mg) in 0.2 *N* aqueous sodium hydroxide (20 mL). The mixture was stirred at room temperature for 10 h, then 50% hydrochloric acid was added to destroy excess borohydride. The mixture was stirred for 45 min and extracted with ether. The ether extract was washed with aqueous sodium bicarbonate, aqueous NaCl, and dried ($MgSO_4$). On evaporation of the ether it yielded 69 mg (11%) of the crude lactone **26** (see below).

The sodium bicarbonate solution was acidified and extracted in the usual way to yield an oily solid which crystallized from cold ether–hexane to give the hydroxy-acid **25** (362 mg), mp 140.5–142°C; $\nu_{max}$ (KBr): 3500–2500 (broad), 1715, 1480, 1460, 1440, 1400, 1390, 1375, 1325, 1320, 1300, 1270, 1215, 1205, 1165, 1145, 1110, 1060, 1035, 1010, 940, 930, 925 $cm^{-1}$. Another 91 mg of **25** was obtained from the mother-liquors by preparative tlc.

*6α-*tert*-Butyl-10α-methyl-1-oxa-9α-decal-2-one (**26**)*

*(a) By lactonization of **25***

The hydroxy-acid **25** (432 mg) was refluxed for 15 min in xylene (200 mL) in the presence of *p*-toluenesulfonic acid (150 mg), following the method of Johnson *et al.* (14). The reaction mixture was diluted with ether, and washed with aqueous $NaHCO_3$, aqueous NaCl, and dried ($MgSO_4$). Concentration of the solution left a heavy yellow oil which solidified on standing. It was recrystallized from hexane and then sublimed at 45°C/0.1 Torr to give the lactone **26** (212 mg; 53%), identical with the product from hydrogenation of the keto-acid **24** (see below).

*(b) By hydrogenation of the keto-acid **24***

The keto-acid **24** (537 mg) was hydrogenated over pre-reduced platinum oxide (60 mg) in 4.5 mL of glacial acetic acid containing 0.5 mL of concentrated hydrochloric acid, at room temperature and 45 psi. When absorption had ceased, the solution was filtered and diluted with ether. The ether extract was washed with aqueous $NaHCO_3$, aqueous NaCl, and dried ($MgSO_4$). Evaporation of the ether under reduced pressure left an oil which solidified on standing. Recrystallization from hexane followed by sublimation at 45°C/0.1 Torr gave the lactone **26** as a colourless solid (395 mg; 76%), mp 65–66°C; $\nu_{max}$ ($CCl_4$): 2955, 2935, 2865, 1740, 1470, 1455, 1435, 1420, 1395, 1385, 1370, 1365, 1340, 1320, 1305, 1260, 1238, 1215, 1187, 1165, 1153, 1130, 1105, 1085, 1058, 1003, 960, 945, 920, 850, 840, 830 $cm^{-1}$; δ ($CCl_4$): 0.95 (s, 9H), 1.12 (s, 3H), 1.15–2.55 (complex, 11H), 3.88 (m, 1H). *Anal.* calcd. for $C_{14}H_{24}O_2$: C 74.9, H 10.8; found: C 74.7, H 10.9.

## Acknowledgments

The financial support of the National Research Council of Canada is gratefully acknowledged, as is financial assistance to T.C.P. from the Institute of State Scholarships, Greece, and Canadian Industries Ltd. J.T.E. is grateful for the hospitality of Prof. R. Schaal, Université Pierre-et-Marie Curie, Paris, in whose laboratory this paper was written.

1. T. C. Paradellis, E. Cooke, and J. T. Edward. Can. J. Chem. In press.
2. D. Varech, C. Ouannes, and J. Jacques. Bull. Soc. Chim. Fr. 1662 (1965).
3. C. A. Brown. J. Am. Chem. Soc. **91**, 5941 (1969).
4. J. T. Edward and J. M. Ferland. Can. J. Chem. **44**, 1311 (1966).
5. J. T. Edward and J. M. Ferland. Can. J. Chem. **44**, 1317 (1966).
6. H. O. House, H. Badad, R. B. Toothill, and A. W. Noltes. J. Org. Chem. **27**, 4141 (1962).
7. H. O. House and M. Schellenbaum. J. Org. Chem. **28**, 34 (1963).
8. T. C. Paradellis. Ph.D. Thesis, McGill University, Montreal, 1969.
9. E. Cooke. Ph.D. Thesis, McGill University, Montreal, 1972.
10. J. T. Edward, E. Cooke, and T. C. Paradellis. Can. J. Chem. **59**, 597 (1981).
11. H. O. House, B. A. Tefertiller, and H. D. Olmstead. J. Org. Chem. **33**, 935 (1968).
12. S. Karady, M. Lenfant, and R. E. Wolff. Bull. Soc. Chim. Fr. 2472 (1965).
13. F. Johnson and A. Whitehead. Tetrahedron Lett. 3825 (1964).
14. W. S. Johnson, V. J. Bauer, J. L. Margrave, M. A.

FRISCH, L. H. DREGER, and W. N. HUBBARD. J. Am. Chem. Soc. **83**, 606 (1961).
15. R. S. GUPTA and P. C. DUTTA. J. Indian Chem. Soc. **25**, 213 (1948).
16. G. R. PETTIT, B. GREEN, T. R. KASTURI, and U. R. GHATAK. Tetrahedron, **18**, 953 (1962).
17. S. B. KULKARNI and S. DEV. Tetrahedron, **24**, 553 (1968); C. RAY and S. DEV. Experientia, **11**, 144 (1955).
18. H. O. HOUSE and G. H. RASMUSSON. J. Org. Chem. **28**, 27 (1963).
19. D. W. MATHIESON. J. Chem. Soc. 3248 (1953).
20. R. GRANGER, F. NAU, and C. FRANCOIS. Bull. Soc. Chim. Fr. 1902 (1962).
21. R. FRANK and R. C. PIERLE. J. Am. Chem. Soc. **73**, 724 (1951).
22. B. E. EDWARDS and P. N. RAO. Angew. Chem. **76**, 795 (1964).
23. N. L. ALLINGER, H. M. BLATTER, L. A. FREIBURG, and F. M. KARKOWSKI. J. Am. Chem. Soc. **88**, 2999 (1966).
24. H. O. HOUSE, L. J. CZUBA, M. GALL, and H. D. OLMSTEAD. J. Org. Chem. **34**, 2324 (1969).

Can. J. Chem. Downloaded from www.nrcresearchpress.com by 210.87.254.6 on 09/06/12
For personal use only.

# The catalytic cracking of arenes on $SiO_2$–$AlPO_4$ catalysts. A study of the mechanism

P. M. DEYÁ, A. COSTA, AND J. V. SINISTERRA
*Organic Chemistry Department, Faculty of Science, University of Palma de Mallorca, Balearic Islands, Spain*
AND
J. M. MARINAS
*Organic Chemistry Department, Faculty of Science, University of Córdoba, Córdoba, Spain*

Received June 4, 1981

P. M. DEYÁ, A. COSTA, J. V. SINISTERRA, and J. M. MARINAS. Can. J. Chem. **60**, 35 (1982).

The catalytic protodealkylation mechanism of arenes (R—Ph), using a $SiO_2$–$AlPO_4$ catalyst has been studied using the microcatalytic pulse technique. Two hydrocarbon series were used: normal series (R = Me, Et, *n*-Pr, and *n*-Bu) and α-methylated series (R = Me, Et, *i*-Pr, and *t*-Bu). In all cases it was shown that the process may be described by means of Bassett–Habgood's kinetics. That is to say, the process is a first order reaction ($r = kP_{HC}$) where the rate-controlling step is the surface reaction.

Real activation energies of the superficial process have been determined, all results showing values of the same order within the experimental error, which indicates that the transition state is the same for all alkylbenzenes because all the kinetics are first order.

Correlations between kinetic constants and electrical (σ*) and steric ($E_s$) parameters have been sought. The best are obtained when values for the α-methylated series are plotted against σ* and those for the normal series against $E_s$.

A possible reaction pathway of the $S_E2$ (Ad–E) type is proposed.

P. M. DEYÁ, A. COSTA, J. V. SINISTERRA et J. M. MARINAS. Can. J. Chem. **60**, 35 (1982).

Faisant appel à la technique d'impulsion microcatalytique on a étudié le mécanisme de la protodésalkylation catalysée des arènes (R—Ph) en utilisant le $SiO_2$–$AlPO_4$ comme catalyseur. On a utilisé deux séries d'hydrocarbures: les séries normales (R = Me, Et, *n*-Pr et *n*-Bu) et les séries α méthylées (R = Me, Et, *i*-Pr et *t*-Bu). On a montré, dans tous les cas, que le processus peut être décrit au moyen des cinétiques de Bassett–Habgood. Ceci signifie que le processus est une réaction d'ordre un ($r = kP_{HC}$) où la réaction de surface est l'étape déterminante.

On a déterminé les énergies réelles d'activation de la réaction de surface. Tous les résultats donnent des valeurs ayant le même ordre de grandeur à l'intérieur des erreurs expérimentales, ce qui signifie que l'état de transition est le même pour tous les alkylbenzènes parce que toutes les cinétiques sont d'ordre un. On a cherché à établir des corrélations entre les constantes cinétiques et les paramètres électrique (σ*) et stérique ($E_s$). On a obtenu les meilleures corrélations en tracant des courbes des valeurs des séries α méthylées en fonction de σ* et celles des séries normales en fonction de $E_s$.

On propose un mécanisme réactionnel possible de type $S_E2$ (Ad–E).

[Traduit par le journal]

## Introduction

The catalytic protodealkylation of arenes using acid catalysts can be referred to a $S_E2$ (Ad–E) type reaction according to most authors (1–3). In spite of this wide consensus of opinion, there is great discrepancy as to what type, or types, of active centers take part in the reaction, some authors proposing Bronsted centers (1) and others those of the Lewis type (2). Yet other investigators propose that both types of centers are involved (3).

Concerning the kinetic scheme of the catalytic cracking of monoalkylbenzenes, most authors accept the kinetics proposed by Prater and Lago (4) with only one center involved. This process can be described as:

$$A + L \underset{k_{-1}}{\overset{k_1}{\rightleftharpoons}} A\cdot L \underset{k_{-2}}{\overset{k_2}{\rightleftharpoons}} L\cdot C + B$$

$$L\cdot C \underset{k_{-3}}{\overset{k_3}{\rightleftharpoons}} L + C$$

Still other authors, such as Garcia de la Banda and co-workers (5), propose the participation of two equal active sites with the adsorption of reagents and products, and other authors, such as Campbell and Wojciechowski (6) propose a more complex mechanism called "Delta".

In the present work, we have approached the study of the catalytic protodealkylation of arenes along the lines of investigation followed for the application of $AlPO_4$ and related systems to different organic reactions (7, 8). Several monoalkylbenzenes corresponding to α-methylated and normal series have been used.

## Experimental

*Catalyst*

The method of synthesis of the catalyst called F-72 (80% $SiO_2$ – 20% $AlPO_4$) used in this work has been published in a previous paper (9). This catalyst has been shown to produce the best results in this cracking process (9).

*Apparatus*

The reactor system was similar to that described by Tobin *et al.* (10). The fixed bed vertical reactor was made of 1/4 in. id and

0008-4042/82/010035-05$01.00/0
©1982 National Research Council of Canada/Conseil national de recherches du Canada

Can. J. Chem. Downloaded from www.nrcresearchpress.com by 210.87.254.105 on 09/06/12
For personal use only.

Can. J. Chem. Downloaded from www.nrcresearchpress.com by 210.87.254.105 on 09/06/12
For personal use only.

40 mm long stainless steel and heated by an electrical microfurnace (180 W at 220 V). The catalyst particles (0.125–0.250 mm) never exceeded 130 mg in order to avoid interparticular diffusion phenomena and were held in place by two plugs of glass wool. The reaction temperature was measured with a NiCr–Ni thermocouple connected to a Getrosist 96 Phillips controller. Pulses of hydrocarbon were introduced in a nitrogen carrier stream (flow rate 15 mL/min) by means of a 10 μL Hamilton CH 701 RN syringe, and the chromatographic separation of reactants and products was then carried out in a Hewlett–Packard 5834A gas chromatograph using a 2 m by 1/4 in. column, packed with polyphenylether on Chromosorb G, AW DM cs 80–100, heated from 130 to 170°C at a rate of 10°C/min. Under these experimental conditions, diffusion phenomena can be considered to be minimal.

*Procedure*

*(a) Operation of the Microreactor Unit*

Catalyst charges of 20–130 mg were used. The catalyst was stabilized by heating to 200°C for 12 h in flowing nitrogen (10 mL/min). Experiments were carried out at temperatures ranging from 300 to 520°C by inserting several pulses of 0.5 μL at each temperature and charge of catalyst.

The temperature used in every case was chosen in order to avoid secondary reaction products that could complicate the study of the mechanism of the process.

*(b) Determination of the Textural and Acidity Properties of the Catalyst*

From the adsorption–desorption nitrogen isotherms at liquid nitrogen temperature, the surface area ($S_{BET}$) and accumulated pore volume ($\Sigma V_p$) were determined by the B.E.T. method (11). The total acidity of the catalyst was measured by titration in a nonaqueous medium, applying the alterations to the original method (12) proposed by Benesi (13) and Balikova (14), using *p*-dimethylaminoazobenzene as Hammett indicator ($pK_a$ = +3.3).

The results obtained were: $S_{BET} = 393.0 \pm 15.7\ m^2/g$; $\Sigma V_p = 0.56 \pm 0.02$ mL/g, and acidity = $0.19 \pm 0.01$ mequiv/g.

## Results and Discussion

*Kinetic Procedure*

The results obtained by the microcatalytic pulse technique perfectly fit the Bassett–Habgood equation [1] (15) as can be seen in Fig. 1.

$$[1] \quad \ln \frac{1}{1-X} = RTkK \frac{W}{F}$$

From this fitting for both α-methylated series and normal series of hydrocarbons (Fig. 1) it can be deduced that, under our experimental conditions, the system can be described in accordance with Bassett and Habgood's postulates as first-order kinetics, $r = kP_{HC}$, the rate-controlling step being the surface reaction (15). From this, the cracking of alkylaromatic hydrocarbons with our catalyst appears to follow a kinetic scheme analogous to that proposed by Prater and Lago (4), verified by other authors for other kinds of cracking catalysts (3, 5, 6, 16, 17).

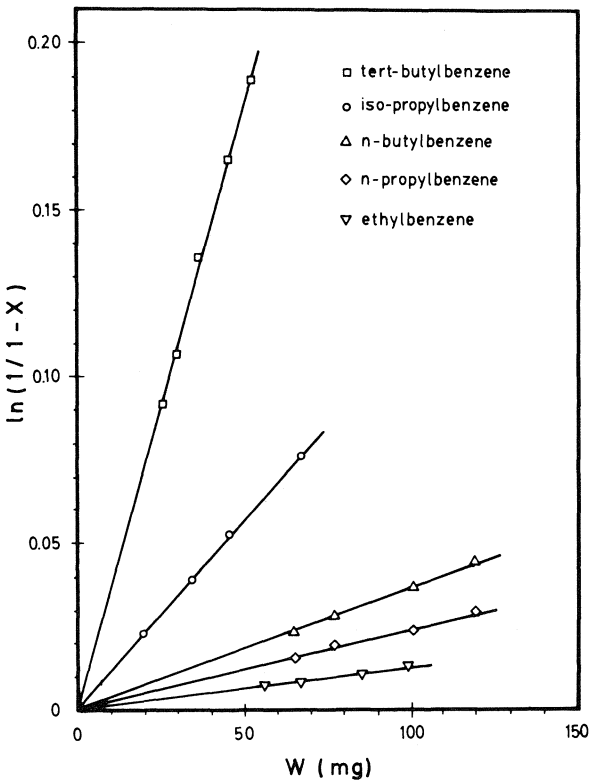


FIG. 1. Plots of ln (1/(1 − *X*)) versus *W* (mg of catalyst).

*Pseudokinetic Constants and Apparent Activation Energies*[1]

Using Bassett and Habgood's kinetic expression [1], it is possible to obtain pseudokinetic constant values (*kK*) at any given temperature by plotting ln (1/(1 − *X*)) versus *W* while the apparent activation energy ($E_{A(ap)}$) is obtained in each case by plotting ln (ln (1/(1 − *X*))) versus 1/*T*. The results obtained are shown in Table 1.

The $E_{A(ap)}$ values are of the same order as some values found in the literature for the cracking of cumene using $SiO_2$–$Al_2O_3$ (5, 18) and zeolites (6, 19).

*Kinetic Constants and Real Activation Energies*

Utilizing adsorption constants (*K*) determined previously (20) by means of a gas-chromatographic technique (21), it is possible to separate the pseudokinetic constant (*kK*) into its component parts: rate constant (*k*) and adsorption constant (*K*). Results are shown in Table 2.

[1]Detailed data are submitted as Supplementary Material. Copies are available at a nominal charge, from the Depository of Unpublished Data, CISTI, National Research Council of Canada, Ottawa, Canada K1A 0S2.

TABLE 1. Pseudokinetic constants and apparent activation energies for certain hydrocarbons

| Hydrocarbon | $T_{cracking}$ (°C) | $kK \times 10^5$ (mol/g atm s) | $(T_1 - T_2)$* (°C) | $E_{A(ap)}$ (kcal/mol) |
|---|---|---|---|---|
| *tert*-Butylbenzene | 300±2 | 1.963±0.137 | 240–340 | 17.7±1.2 |
| Isopropylbenzene | 400±2 | 0.859±0.060 | 350–450 | 21.6±1.4 |
| Ethylbenzene | 520±3 | 0.054±0.004 | 520–580 | 20.0±1.4 |
| *n*-Propylbenzene | 510±3 | 0.097±0.007 | 430–530 | 20.6±1.4 |
| *n*-Butylbenzene | 510±3 | 0.144±0.010 | 430–530 | 20.3±1.4 |

*Range of temperature used in the determination of $E_{A(ap)}$.

TABLE 2. Kinetic constants and real activation energies for certain hydrocarbons

| Hydrocarbon | $K \times 10^5$* (mol/atm g) | $\Delta H_{ads}$* (kcal/mol) | $k$ ($s^{-1}$) | $E_{A(real)}$ (kcal/mol) | ln ($PZ$) | $k_{460}$ ($s^{-1}$) |
|---|---|---|---|---|---|---|
| *tert*-Butylbenzene | 6.356±0.38 | −16.09±0.32 | 0.318±0.029 | 32.7±2.9 | 27.52±0.09 | $1.628 \times 10^2$ |
| Isopropylbenzene | 0.925±0.06 | −14.21±0.28 | 0.929±0.084 | 33.5±3.0 | 24.93±0.09 | 7.192 |
| Ethylbenzene | 0.190±0.01 | −13.20±0.26 | 0.303±0.027 | 31.9±2.9 | 19.05±0.09 | $5.886 \times 10^{-2}$ |
| *n*-Propylbenzene | 0.185±0.01 | −14.70±0.29 | 0.526±0.047 | 33.8±3.0 | 21.12±0.09 | $1.213 \times 10^{-1}$ |
| *n*-Butylbenzene | 0.203±0.01 | −15.75±0.31 | 0.720±0.065 | 34.9±3.0 | 22.08±0.09 | $1.543 \times 10^{-1}$ |

*Reference 20.

The table also shows values for enthalpy of adsorption (20) and activation energies and frequency factors (ln $PZ$) obtained from the study of the variation of ln $k$ with $1/T$. From values obtained in this way, it can be seen that the $E_{A(real)}$ values from the superficial process are practically constant (~33 kcal/mol) within experimental error for all hydrocarbons studied. This, combined with the fact that we are dealing with first order kinetics, seems to indicate that the transition state is of the same type for all the hydrocarbons. The nature of the alkyl chain (R) is not an influencing factor on the transition state type.

This similar transition state can only be explained by supposing that it is analogous to that observed in electrophilic aromatic substitution ($S_E2$) reactions in homogeneous phase where, in the slow step of the reaction, there is a loss of aromaticity leading to the σ complex in which the leaving group, in this case R, has not yet left the ring.

The conceptual distinction between $E_{A(real)}$ and $E_{A(ap)}$ used in this work should be pointed out here to avoid confusion. $E_{A(real)}$ values correspond to the energy difference between the adsorbed state and the transition state, while $E_{A(ap)}$ values refer to the difference in energy between the initial state of the reactants and the transition state. It can be shown in this way that the values obtained by subtracting $E_{A(real)}$ from $E_{A(ap)}$, in every case, coincide with the $\Delta H_{ads}$ values found in a previous study (20) by an experimental technique distinct from that used in the present work, which is in agreement with what we have indicated earlier in this paper.

The $E_{A(real)}$ values found here are of the same order as some values found in the bibliography for the cracking of alkylaromatic hydrocarbons on $SiO_2$–$Al_2O_3$ (4, 22) and zeolites (22, 23).

*Influence of the Nature of R group on the Kinetic Constant*

In an attempt to understand the mechanism of this organic process, the kinetic constants ($k_{460}$, extrapolated by means of ln $k$ vs. $1/T$ plots data at a temperature of 460°C; Table 2) were examined for correlations with electrical (σ* from Taft) and steric ($E_s$ from Taft) parameters taken from the literature (24) in order to observe the behavioural tendency of these plots in the cases where the fit was better.

For the α-methylated series, the best correlations were obtained by plotting the kinetic constant ($k$) against σ* (eq. [2]) and for the normal series, by plotting $k$ values against $E_s$ (eq. [3]):

[2] α-methylated $\log k/k_0 = -17.03\sigma^* + 0.20$ ($r = 0.99$)

[3] normal $\log k/k_0 = -1.22E_s + 0.00$ ($r = 0.99$)

In these equations $k_0$ represents the kinetic constant of ethylbenzene, since no cracking process for toluene was observed.

From the before-mentioned equations it can be deduced that for the α-methylated series the electrical effects (σ*) are primary influences, because plots versus $E_s$ give a correlation coefficient of only 0.91. This is a logical conclusion since the arenes of

Can. J. Chem. Downloaded from www.nrcresearchpress.com by 210.87.254.105 on 09/06/12
For personal use only.

Can. J. Chem. Downloaded from www.nrcresearchpress.com by 210.87.254.105 on 09/06/12
For personal use only.

this series differ only in the nature of the carbon atom directly joined to the aromatic ring (primary, secondary, or tertiary). For the normal series, on the other hand, steric effects ($E_s$) have the greater influence (the correlation coefficient for the plots vs. $\sigma^*$ was only 0.95). This is also logical, considering that the carbon atoms directly joined to the aromatic ring are secondary in all cases, for which reason their inductive effect is comparable and the only difference is in the length of the R chain, which can produce differences in the steric hindrance. Quantitatively, the negative sign of the constant "ρ" (−17.03; eq. [2]) obtained, indicates that a positive charge is produced on the arene when the reaction takes place, which is in accord with what we stated earlier concerning the σ complex type transition state. On the other hand, the negative sign of the constant "δ" (−1.22; eq. [3]) indicates that the steric hindrance makes difficult the surface reaction process.

We can therefore propose the following reaction pathway ($S_E2$ (Ad–E): aromatic electrophilic substitution, addition–elimination) which progresses through a π complex, type I, that involves the aromatic ring and the P—OH active site of the surface of the catalyst, as has been shown in a previous work (20), applying the criteria of the Frontier Orbital Theory (F.O.T.) to deduce the regioselectivity of the process. This intermediate progresses, in the slow step, towards a σ complex (II) in which R has not left the ring. This would explain why the $E_{A(real)}$ values of the superficial process were approximately constant within the limits of experimental error. In subsequent rapid steps, the leaving of the R group would take place with the formation of the olefin.

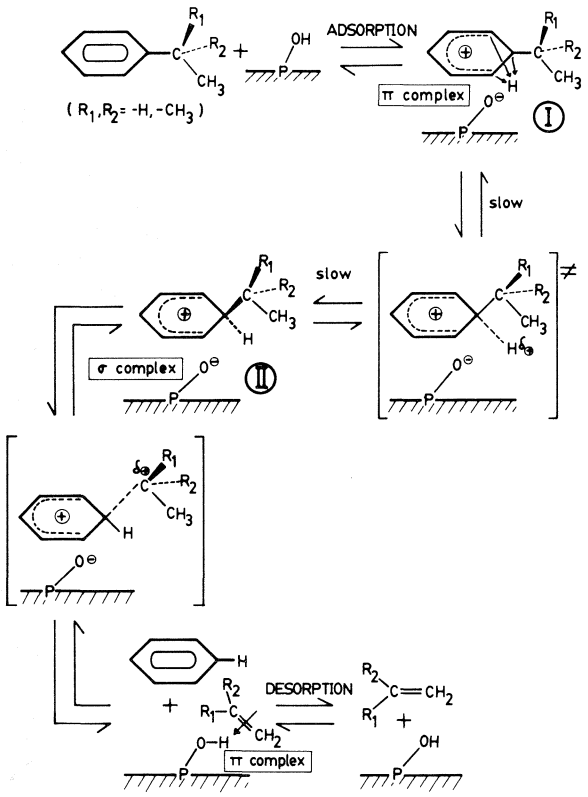


SCHEME 1

1. C. L. THOMAS. Ind. Eng. Chem. **41**, 2564 (1949).
2. A. G. OBLAD, T. H. MILLIKEN, and G. A. MILLS. Adv. Catal. **3**, 238 (1951).
3. P. ANDREU, G. MARTIN, and H. NOLLER. J. Catal. **21**, 255 (1971).
4. C. D. PRATER and R. H. LAGO. Adv. Catal. **8**, 293 (1956).
5. A. C. ARROYO, J. F. GARCIA DE LA BANDA, and E. HERMANA. An. Quim. **8**, 847 (1967).
6. D. R. CAMPBELL and B. W. WOJCIECHOWSKI. J. Catal. **20**, 217 (1971).
7. A. COSTA, P. M. DEYÁ, J. V. SINISTERRA, and J. M. MARINAS. Can. J. Chem. **58**, 1266 (1980).
8. M. A. ARAMENDIA, J. M. MARINAS, J. V. SINISTERRA, C. JIMENEZ, and J. M. CAMPELO. Rev. Inst. Mex. Pet. **12**(3), 61 (1980).
9. C. JIMENEZ, J. M. MARINAS, and J. V. SINISTERRA. An. Quim. **70**, 860 (1974).
10. H. TOBIN, R. J. KOKES, and P. H. EMMETT. J. Am. Chem. Soc. **77**, 5860 (1955).
11. S. BRUNAUER, P. H. EMMETT, and E. TELLER. J. Am. Chem. Soc. **60**, 309 (1930).
12. O. JOHNSON. J. Phys. Chem. **59**, 827 (1955).
13. H. A. BENESI. J. Phys. Chem. **61**, 970 (1957).
14. M. BALIKOVA. React. Kinet. Catal. Lett. **2**, 323 (1975).
15. D. W. BASSETT and H. W. HABGOOD. J. Phys. Chem. **64**, 769 (1960).
16. P. B. VENUTO. Catalysis in organic syntheses. Academic Press, New York. 1977. p. 74.
17. H. F. RASE and R. S. KIRK. Chem. Eng. Prog. **50**, 35 (1954).
18. D. R. CAMPBELL and B. W. WOJCIECHOWSKI. J. Catal. **23**, 307 (1971).
19. D. A. BEST and B. W. WOJCIECHOWSKI. J. Catal. **47**, 343 (1977).
20. P. M. DEYÁ, A. COSTA, J. V. SINISTERRA, and J. M. MARINAS. Proc. VIIth Iber. Symp. Catal. Argentina. 1980. p. 44.
21. D. ATKINSON and G. CURTHOYS. J. Chem. Educ. **55**, 564 (1978).
22. J. T. RICHARDSON. J. Catal. **25**, 182 (1967).
23. B. V. ROMANOVSKII, E. V. BEZRE, and K. V. TOPCHIEVA. Kinet. Katal. **9**, 1111 (1968).
24. T. H. LOWRY and J. T. RICHARDSON. Mechanism and theory in organic chemistry. Harper & Row, New York. 1976.

## Appendix

*Nomenclature*

A = molecule of reactant

B = benzene

C = olefin
$E_{A(ap)}$ = apparent activation energy (kcal/mol)
$E_{A(real)}$ = real activation energy (kcal/mol)
$F$ = flow rate of carrier gas (mL/s)
$k$ = kinetic constant ($s^{-1}$)
$K$ = adsorption constant (mol $atm^{-1}$ $g^{-1}$)
L = active site
$P_{HC}$ = hydrocarbon pressure (atm)
$PZ$ = frequency factor
$r$ = reaction rate
$R$ = gas constant (atm L $K^{-1}$ $mol^{-1}$)
$S_E2(Ad–E)$ = bimolecular electrophilic aromatic substitution, addition–elimination
$T$ = reaction temperature (K)
$W$ = weight of catalyst (g)
$X$ = molar fractionary conversion

Can. J. Chem. Downloaded from www.nrcresearchpress.com by 210.87.254.105 on 09/06/12
For personal use only.

# Solvent extraction separation of Cr(VI)–Mo(VI)–W(VI), Zr(IV)–Hf(IV), and Se(IV)–Te(IV) with sulphoxides

ALAVALAPATI SAMBASIVA REDDY AND BONTHA RAMACHANDRA REDDY
*Department of Chemistry, Sri Venkateswara University, Tirupati – 517 502, India*

Received March 23, 1981

ALAVALAPATI SAMBASIVA REDDY and BONTHA RAMACHANDRA REDDY. Can. J. Chem. **60**, 40 (1982).

Solvent extraction studies have been made on some metals in the same periodic group: Cr(VI)–Mo(VI)–W(VI), Zr(IV)–Hf(IV), and Se(IV)–Te(IV) from hydrochloric acid solutions by dialkyl and aryl sulphoxides. Separation of these metals from one another can be achieved by suitable choice of extraction conditions. The nature of extractable metal species has been elucidated.

ALAVALAPATI SAMBASIVA REDDY et BONTHA RAMACHANDRA REDDY. Can. J. Chem. **60**, 40 (1982).

On a étudié l'extraction à l'aide de sulfoxydes de dialkyles et de diaryles de quelques métaux, en solution dans l'acide chlorhydrique, appartenant à la même période soit Cr(VI), Mo(VI), W(VI); Zr(IV), Hf(IV) et Se(IV), Te(IV). On peut, à l'aide d'un choix judicieux des conditions d'extraction, séparer ces métaux les uns des autres. On a caractérisé la nature des espèces métalliques que l'on peut extraire.

[Traduit par le journal]

Can. J. Chem. Downloaded from www.nrcresearchpress.com by 210.87.254.42 on 09/06/12
For personal use only.

## Introduction

Sulphoxides have gained importance as reagents for the solvent extraction of a number of metals with efficiency and specificity (1–5). It was thought to be of interest therefore, to use dialkyl and aryl sulphoxides for the extraction of some metals in the same periodic group, such as Cr(VI)–Mo(VI)–W(VI), Zr(IV)–Hf(IV), and Se(IV)–Te(IV). Di-*n*-pentyl sulphoxide (DPSO), di-*n*-octyl sulphoxide (DOSO), and diphenyl sulphoxide (DPhSO) have been chosen for this purpose.

## Results and Discussion

*Extraction of Metal Ions*

The distribution ratio, $D$, may be expressed as a function of the metal ion concentration $[M^{m+}]$, $a_{H^+}$, $a_{Cl^-}$, and the ligand concentration [S] (6)

$$\log D = \log K' + (x - 1) \log [M^{m+}] + y \log a_{H^+} + z \log a_{Cl^-} + n \log [S]$$

where

$$K' = \frac{[\text{Complex}]}{[M^{m+}]^x a_{H^+}{}^y a_{Cl^-}{}^z [S]^n}$$

and $x$, $y$, $z$, and $n$ represent the number of metal, hydrogen, and chloride ions and ligand molecules involved in the extracted species. By evaluating $D$ as a function of $[M^{m+}]$, $a_{H^+}$, $a_{Cl^-}$, and [S], the nature of the extracted species has been elucidated.

As shown in Fig. 1, the extraction of W(VI) by 0.03 mol dm$^{-3}$ DPSO in benzene increases with increase in HCl concentration (up to 7 mol dm$^{-3}$) and decreases thereafter. The initial increase in extraction may be attributed to the common ion effect. The slow increase or decrease in extraction at higher acidities is due to compound formation between the extractant and the acid. Because of their basic character, sulphoxides form compounds

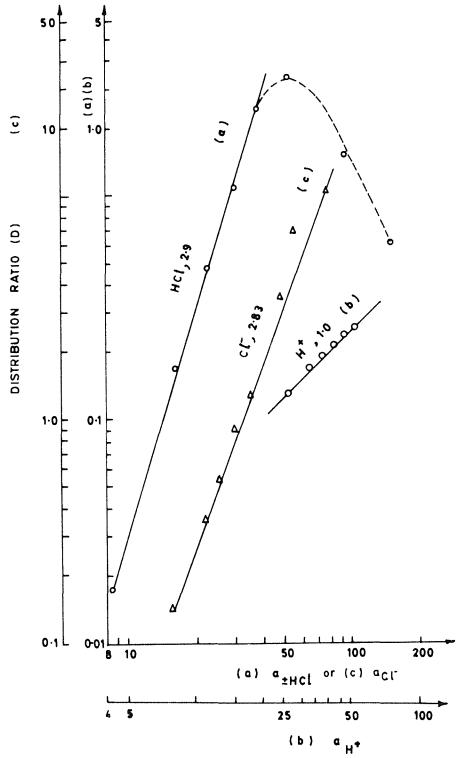


FIG. 1. The distribution of W(VI) between hydrochloric acid solutions (*a*) and DPSO in benzene; and the effect of $H^+$ (*b*) and total $Cl^-$ (*c*) concentrations upon this distribution. Numerical values on the plots are the line gradients.

0008-4042/82/010040-04$01.00/0
©1982 National Research Council of Canada/Conseil national de recherches du Canada

TABLE 1. Extraction of various elements from hydrochloric acid into DPSO

| Element | Elemental concentration (mol dm$^{-3}$) | [HCl] (mol dm$^{-3}$) | [DPSO] (mol dm$^{-3}$) 0.02 | 0.10 | 0.36 | Separation factor |
|---|---|---|---|---|---|---|
| Cr(VI) | $2 \times 10^{-3}$ | 3.5 | 20% | — | — | |
| Mo(VI) | $2 \times 10^{-3}$ | 3.5 | 0% | 58% | — | |
| W(VI) | $1 \times 10^{-3}$ | 3.5 | 0% | 0% | — | |
| Se(IV) | $1 \times 10^{-6}$ | 4.0 | — | — | 1% | |
| Te(IV) | $1 \times 10^{-6}$ | 4.0 | — | — | 93% | |
| Te(IV)/Se(IV) | | 4.0 | | | | $1.4 \times 10^3$ |
| Zr(IV) | $1 \times 10^{-6}$ | 6.0 | — | 50% | — | |
| Hf(IV) | $1 \times 10^{-6}$ | 6.0 | — | 0.4% | — | |
| Zr(IV)/Hf(IV) | | 6.0 | | | | $2.4 \times 10^2$ |

Can. J. Chem. Downloaded from www.nrcresearchpress.com by 210.87.254.42 on 09/06/12
For personal use only.

like HCl·DPSO (7) and HCl·DOSO (7) at high acidities. These adducts may not be able to solvate the metal to the same extent as the free extractants. Partial solubilities of the adducts in the aqueous phase may be an additional factor responsible for the diminution of $D$. At low acidities, the small amount of the acid in the organic phase cannot seriously compete with the metal. The slope of the linear plot of log $D$ versus log $a_{\pm HCl}$ (8) (Fig. 1) is 3, suggesting the extraction of acidic species.

Increase in the $H^+$ concentration at a constant level of $Cl^-$ and that of $Cl^-$ at a given $H^+$ concentration for HCl + LiCl mixtures increases the extraction of the metal. The mean ionic activity coefficients of the mixed electrolyte (HCl + LiCl) system were calculated (9, 10). The log $D$ versus log $a_{H^+}$ (logarithm of the mean ionic activity of HCl at constant $Cl^-$ concentration (5)) plot (Fig. 1) is linear with a slope of unity and the corresponding plot of log $D$ versus log $a_{Cl^-}$ (logarithm of mean ionic activity of HCl at constant $H^+$ concentration (5)) has a slope of 3, confirming the extraction of the monoacidic species, $HWO_2Cl_3$.

At constant HCl concentration (6 mol dm$^{-3}$), the extraction of the metal increases with increase of the ligand concentration (DPSO, DOSO, and DPhSO). The plots of log $D$ versus log [extractant] (Fig. 2) are linear with slopes of 2 for the sulphoxides. Solvation number 2 or 3 is commonly observed with solvating solvents (5, 11, 12). A plot of log equilibrium organic phase metal concentration against log equilibrium aqueous phase metal concentration is linear with a slope of unity indicating the extraction of mononuclear species. Thus the extracted species are disolvates, $HWO_2Cl_3 \cdot 2DPSO$, $HWO_2Cl_3 \cdot 2DOSO$, and $HWO_2Cl_3 \cdot 2DPhSO$.

Analogous experiments to the above using hexavalent Cr, Mo, and W and tetravalent, Zr, Hf, Se, and Te, resulted in identification of the following species: $HCrO_3Cl \cdot 2DPSO$ and $HCrO_3Cl \cdot 2DOSO$, $HMoO_2Cl_3 \cdot 3DPSO$, $HMoO_2Cl_3 \cdot 3DOSO$, and $HMoO_2Cl_3 \cdot 3DPhSO$; $HWO_2Cl_3 \cdot 2DPSO$, $HWO_2Cl_3 \cdot 2DOSO$, and $HWO_2Cl_3 \cdot 2DPhSO$; $ZrCl_4 \cdot 2DPSO$, $ZrCl_4 \cdot 2DOSO$, and $ZrCl_4 \cdot 2DPhSO$; $HfCl_4 \cdot 3DPSO$ and $HfCl_4 \cdot 3DOSO$; $H_2SeOCl_4 \cdot 2DPSO$, $H_2SeOCl_4 \cdot 2DOSO$, and $H_2SeOCl_4 \cdot 2DPhSO$; and $TeOCl_2 \cdot 2DPSO$ and $TeOCl_2 \cdot 2DOSO$.

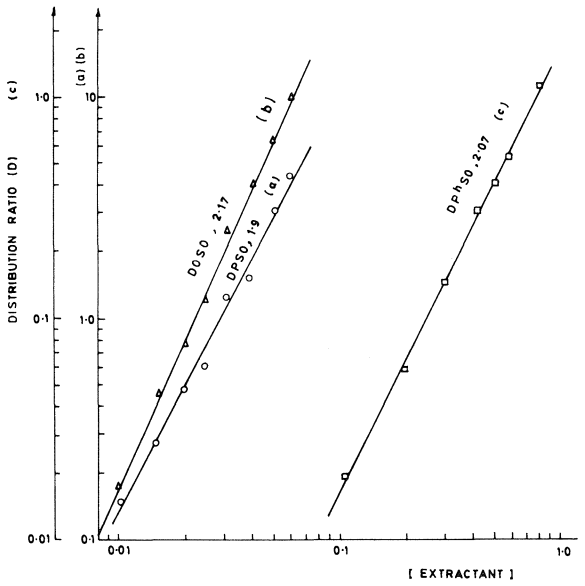


FIG. 2. The distribution of W(VI) as a function of different concentrations of DPSO (*a*), DOSO (*b*), and DPhSO (*c*) at constant hydrochloric acid concentration.

The percentage extraction ($E_{\%}$) and the separation factors ($S$) are given in Table 1.

*Optimum Conditions for Separation of Metals*

The optimum conditions for the separation of the metals from one another are shown in Table 2.

TABLE 2. Optimum conditions for separation of various elements from each other

| Elements to be separated | Aqueous phase | Organic phase | No. of batch extractions | Quantitative extraction |
|---|---|---|---|---|
| Cr(VI), Mo(VI), and W(VI) | 3.5 mol $dm^{-3}$ HCl | 0.02 mol $dm^{-3}$ DPSO in $CCl_4$ | 10 | Cr(VI) |
| | 3.5 mol $dm^{-3}$ HCl | 0.1 mol $dm^{-3}$ DPSO in $CCl_4$ | 6 | Mo(VI) |
| Zr(IV) and Hf(IV) | 6.0 mol $dm^{-3}$ HCl | 0.1 mol $dm^{-3}$ DPSO in $CCl_4$ | 6 | Zr(IV) |
| Se(IV) and Te(IV) | 4.0 mol $dm^{-3}$ HCl | 0.36 mol $dm^{-3}$ DPSO in $C_6H_6$ | 2 | Te(IV) |

TABLE 3. Temperature dependence of distribution ratios ($D$) for various elements for the extraction system hydrochloric acid – DPSO in carbon tetrachloride/benzene

| Element | Aqueous phase | Organic phase | Temperature (K) | | | |
|---|---|---|---|---|---|---|
| | | | 283 | 293 | 303 | 313 |
| Zr(IV) | 6 mol $dm^{-3}$ HCl | 0.1 mol $dm^{-3}$ DPSO | 1.36 | 1.28 | 1.22 | 1.16 |
| Hf(IV) | 7 mol $dm^{-3}$ HCl | 0.1 mol $dm^{-3}$ DPSO | 0.05 | 0.11 | 0.21 | 0.44 |
| Se(IV) | 2 mol $dm^{-3}$ HCl +5 mol $dm^{-3}$ LiCl | 0.2 mol $dm^{-3}$ DPSO | 0.14 | 0.20 | 0.33 | 0.41 |
| Te(IV) | 5 mol $dm^{-3}$ HCl | 0.05 mol $dm^{-3}$ DPSO | 1.34 | 0.73 | 0.43 | 0.30 |

*Temperature Dependence of Extraction*

The dependence of the distribution ratio on temperature for various elements is shown in Table 3. The opposing trend of temperature dependence within a pair of elements further helps to achieve clean separation. Temperature is likely to affect the extraction equilibrium in several ways. Increase in temperature could increase the extraction of the complex due to the increased dehydration of the species, since the complex formation is essentially the replacement of water molecules by the neutral donor groups. On the other hand, increase in temperature could decrease the extraction due to the decreased stability of the complex at higher temperatures (13, 14).

## Experimental

The aqueous phase (3.5 mol $dm^{-3}$ HCl) containing a mixture of Cr(VI), Mo(VI), and W(VI) was equilibrated with an equal volume of the organic phase (0.02 to 1.0 mol $dm^{-3}$ DPSO solution in $CCl_4$) at 303 ± 1 K. Solutions of DOSO (0.01 to 0.06 mol $dm^{-3}$) and DPhSO (0.1 to 0.8 mol $dm^{-3}$) in $C_6H_6$ were also employed. The extraction equilibrium was attained within 5 min in the case of Mo(VI) and W(VI). On the other hand, the extraction of Cr(VI) was found to be a time-dependent process (15). The Cr(VI) content of the equilibrated aqueous phase was estimated spectrophotometrically by the diphenyl carbazide method (16); and the Mo(VI) concentration in the aqueous phase and W(VI) content of the organic phase were determined by the dithiol method (17, 18).

The tracers $^{95}Zr^{4+}$, $^{175+181}Hf^{4+}$, $^{75}Se^{4+}$, and $^{127+129}Te^{4+}$ were supplied by the Isotope Group, Bhabha Atomic Research Centre, India. An aliquot of the tracer stock solution was introduced into a given aqueous phase (pre-equilibrated with an appropriate organic phase) and was equilibrated with an equal volume of 0.1 mol $dm^{-3}$ DPSO solution in $CCl_4$ or in $C_6H_6$ for 30 min. Suitable aliquots of each phase were pipetted out for radioassay of the metals by γ counting using a well-type NaI(Tl) scintillation detector. The distribution ratio, $D$, was taken as the ratio of the activity of the tracer in the organic phase to that present in the aqueous phase.

## Acknowledgements

The authors are grateful to University Grants Commission, New Delhi, for giving a fellowship to one of them (B.R.R.).

1. W. KORPAK. Nukleonika, **7**, 715 (1962); **9**, 1 (1964).
2. D. C. KENNEDY. U.S.A.E.C., IS-T-293, 156 (1969); Nucl. Sci. Abstr. **23**, 43382 (1965).
3. YU. E. NIKITIN, YU. I. MURINOV, and A. M. ROZEN. Russ. Chem. Rev. **45**, 1155 (1976).
4. R. SHANKAR and K. S. VENKATESWARLU. J. Inorg. Nucl. Chem. **32**, 229 (1970); **32**, 2369 (1970).
5. S. R. MOHANTY and A. S. REDDY. J. Inorg. Nucl. Chem. **37**, 1791 (1975); **37**, 1977 (1975).
6. A. S. REDDY and Y. S. SAYI. J. Inorg. Nucl. Chem. **40**, 1125 (1978).
7. W. KORPAK. Nukleonika, **8**, 747 (1963).
8. Y. MARCUS and A. S. KERTES. Ion exchange and solvent extraction of metal complexes. Wiley–Interscience, New York. 1969. p. 922.
9. H. S. HARNED and B. B. OWEN. The physical chemistry of

Can. J. Chem. Downloaded from www.nrcresearchpress.com by 210.87.254.42 on 09/06/12
For personal use only.

electrolytic solution. 3rd ed. Reinhold, New York. 1968. p. 585.
10. R. A. ROBINSON and R. H. STOKES. Electrolyte solution. 2nd ed. Butterworths, London. 1959. p. 450.
11. A. K. DE and M. S. RAHMAN. Talanta, **11**, 601 (1964).
12. G. P. NIKITINA and M. P. PUSHLENKOV. Radiokhimia, **4**, 137 (1962).
13. S. K. PATIL, V. V. RAMAKRISHNA, G. V. N. AVADHANY, and M. V. RAMANIAH. J. Inorg. Nucl. Chem. **35**, 2537 (1973).
14. M. S. SUBRAMANIAN and S. A. PAI. J. Inorg. Nucl. Chem. **32**, 3677 (1970).
15. A. S. REDDY, B. R. REDDY, and Y. S. SAYI. Indian J. Chem. **16**(A), 80 (1978).
16. A. I. VOGEL. A text book of quantitative inorganic analysis. 3rd ed. Longmans, London. 1969. p. 791.
17. L. K. CLERK and J. H. AXLEY. Anal. Chem. **27**, 200 (1955).
18. B. R. REDDY. Ph.D. Thesis, Sri Venkateswara University. 1980.

Can. J. Chem. Downloaded from www.nrcresearchpress.com by 210.87.254.42 on 09/06/12
For personal use only.

# Further justification for the *exo*-anomeric effect. Conformational analysis based on nuclear magnetic resonance spectroscopy of oligosaccharides

HENNING THØGERSEN[1] AND RAYMOND U. LEMIEUX
*Department of Chemistry, University of Alberta, Edmonton, Alta., Canada T6G 2G2*
AND
KLAUS BOCK AND BERND MEYER[2]
*Department of Organic Chemistry, The Technical University of Denmark, DK-2800 Lyngby, Denmark*

Received June 11, 1981

HENNING THØGERSEN, RAYMOND U. LEMIEUX, KLAUS BOCK, and BERND MEYER. Can. J. Chem. **60**, 44 (1982).

Hard-sphere (HS) calculations predict three conformers for the branched B human blood group antigenic determinant (αLFuc(1→2)[αDGal(1→3)]βDGal) and two conformers for the linear tetrasaccharide (αLRha(1→2)αLRha(1→3)αLRha(1→3)-βDGlcNAc), which constitutes a part of the repeating unit of the *Shigella flexneri* O-antigen, which differ in conformational energy by less than 0.7 and 0.2 kcal/mol, respectively. However, a detailed $^1$H nmr study of specific interunit deshielding effects, quantitative treatment of spin-lattice relaxation times, and nuclear Overhauser enhancements requires that only one of the conformers thus predicted be, in fact, conformationally preferred in solution. These conformers are those predicted by hard-sphere *exo*-anomeric (HSEA) calculations.

HENNING THØGERSEN, RAYMOND U. LEMIEUX, KLAUS BOCK et BERND MEYER. Can. J. Chem. **60**, 44 (1982).

Des calculs de sphères dures (SD) prédisent trois conformères pour le déterminant antigénique ramifié du groupe sanguin humain B (αLFuc(1→2)[αDGal(1→3)]βDGal) et deux conformères pour le tétrasaccharide linéaire (αLRha(1→2)αLRha(1→3)αLRha-(1→3)βDGlcNAc) qui constitue une partie du monomère de l'antigène O du *Shigella flenneri* dont la différence d'énergie conformationnelle est respectivement inférieure à 0,7 et 0,2 kcal/mol. Cependant sur la base d'une étude détaillée par le rmn du $^1$H, des effets spécifiques de déblindage entre unités, d'un traitement quantitatif des temps de relaxation spin-réseau et d'un examen des accroissements Overhauser nucléaire, on peut conclure qu'un seul des conformères prévus est de fait présent en solution. Les conformères sont ceux prédits par les calculs *exo*-anomériques de sphères dures (EASD).

[Traduit par le journal]

## Introduction

We have recently published evidence (1) that the addition of the torsion-angle dependent *exo*-anomeric effect to the ground state energy of an oligosaccharide allowed the conformational preferences about the glycosidic linkages to be assessed by hard-sphere molecular modelling in good agreement with physical evidence based on nmr spectroscopy. The evidence was based mainly on specific interunit deshieldings of protons and interunit nuclear Overhauser enhancements (nOe's) (1, 2). Since then, we have gained more ready access to a high frequency (400 MHz) nuclear magnetic resonance spectrometer and we wish to take this occasion to report a much more detailed $^1$H nmr study than was possible at that time of the human blood group B (αLFuc(1→2)[αDGal(1→3)]βDGal) antigenic determinant and the tetrasaccharide (αLRha(1→2)αLRha(1→3)αLRha(1→3)βDGlcNAc) which constitutes a part of the repeating unit of the *Shigella flexneri* O-antigen.

The B determinant and the tetrasaccharide were chosen because these appeared to present very good tests for the worth of this simple empirical method (based on the Kitaigorodsky expression (3, 4) and *ab initio* molecular orbital calculations (5, 6), and which we have termed the HSEA calculations (1)), for the estimation of the preferred conformation for an oligosaccharide. The reason for the choice of the B determinant will become evident from a consideration of the conformational energy – conformation diagrams reproduced in Fig. 1. The objective was to provide firm evidence in support of the *exo*-anomeric effect by showing that the HSEA calculations do provide conformations that are in good accord with the results obtained in a thorough nuclear magnetic resonance study of the nOe, $T_1$, and chemical shift parameters for this molecule. Similarly, the solution conformation of the *Shigella flexneri* tetrasaccharide as determined from the same nmr parameters (7) is only reproduced by hard-sphere calculations with inclusion of the *exo*-anomeric effect. It is expected that, in turn, the information thus gained will be of continuing assistance to interpretation of immunochemical phenomena (8, 9). Results from similar calculations of the Type 1 and Type 2 blood group determinants are therefore included towards the end of this paper.

[1]University of Alberta Postdoctoral Fellow, 1980–1981.
[2]Research Associate, The Technical University of Denmark, 1979–1980.

0008-4042/82/010044-14$01.00/0
©1982 National Research Council of Canada/Conseil national de recherches du Canada

Can. J. Chem. Downloaded from www.nrcresearchpress.com by 210.87.254.5 on 09/06/12
For personal use only.

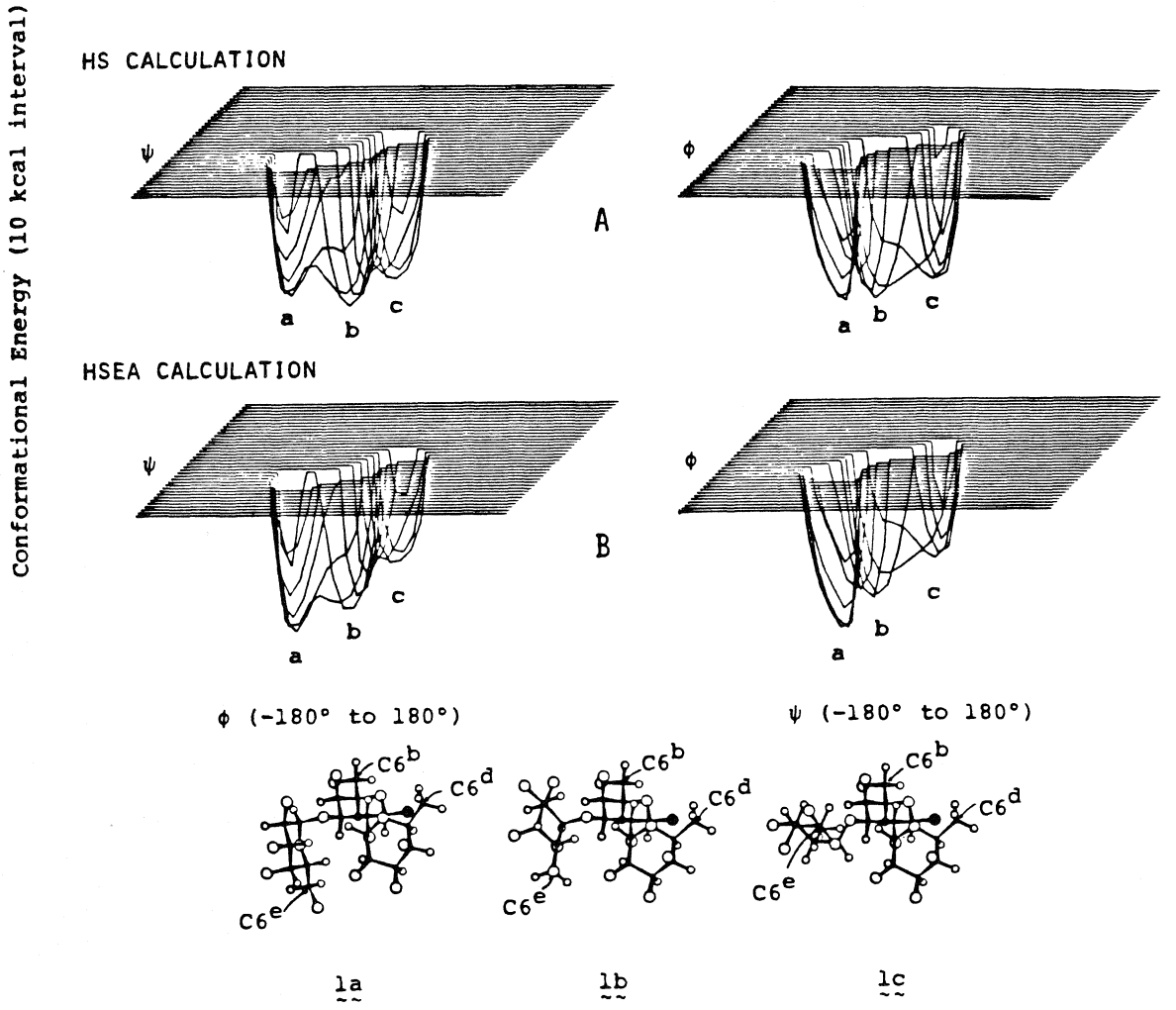


FIG. 1. Three-dimensional diagrams to illustrate the 3 conformational energy wells that are expected to exist for the B human blood group determinant [αLFuc(1→2) (unit d)] [αDGal(1→3) (unit e)]βDGalOR (unit b) with $(\phi,\psi)^d = (55°, 20°)$. Diagrams A were obtained by hard-sphere (HS) calculations. Diagrams B were obtained by hard-sphere *exo*-anomeric (HSEA) calculations. The stick and ball projection formulas are for the lowest energy conformer in each of the wells. The differences in energy for these conformers are given in Table 1.

Figure 1A displays computer-drawn three-dimensional conformational energy plots for the B-trisaccharide that were derived by hard-sphere calculations only and which include all conformers that differ from the minimum energy conformer by 10 kcal/mol or less. On this basis, the trisaccharide would exist in conformations wherein the ϕ and ψ angles (10) have the values listed for the HS calculations in Table 1. Figure 1B provides the same plots but based on the HSEA calculations. The purpose of Fig. 1 is to illustrate clearly that the hard-sphere calculations limit the populations of important conformations to conformers of energy near those of **1***a*, **1***b*, and **1***c*, but that inclusion of a contribution from the *exo*-anomeric effect limits the conformational equilibrium very substantially towards conformers **1***a* of Fig. 1. The purpose of this communication is to provide experimental evidence that, in fact, the B determinant, dissolved in water, resides largely in conformers whose weighted average corresponds well to conformer **1***a* (see Table 1).

The influence of the *exo*-anomeric effect on the conformational equilibrium as judged by the conformational energies of the lowest energy conformer in each of the discernible energy wells can

Can. J. Chem. Downloaded from www.nrcresearchpress.com by 210.87.254.5 on 09/06/12
For personal use only.

TABLE 1. The influence of the *exo*-anomeric effect on the populations of the conformers described in Fig. 1

| Method of calculation | Conformer | Conformational preference* ($\phi, \psi$)[d] | Conformational preference* ($\phi, \psi$)[e] | Conformational energy (kcal/mol) | Mole fraction at 296 K |
|---|---|---|---|---|---|
| HS | **1***a* | 55°, 20° | −65°, −50° | −3.26 | 0.22 |
| | **1***b* | 50°, 15° | −10°, −40° | −3.84 | 0.60 |
| | **1***c* | 50°, 15° | 20°, 15° | −3.14 | 0.18 |
| HSEA | **1***a* | 55°, 20° | −65°, −50° | −3.16 | 0.87 |
| | **1***b* | 55°, 20° | −30°, −45° | −2.02 | 0.13 |
| | **1***c* | 50°, 10° | 15°, 15° | 0.35 | ~0 |

*Except when otherwise noted, the $\phi$ and $\psi$ torsional angles refer to $\phi^H$ and $\psi^H$ angles as defined by Lemieux and Koto (10). Calculated in 5° steps. Superscripts d and e refer to the glycosidic units αLFuc and αDGal, respectively.

be assessed from the data presented in Table 1. It is assumed that the lowest energy conformer in each of the wells will usefully reflect the mole fractions of **1** which are present near the bottom of each of the wells. It is seen that the *exo*-anomeric effect is expected to raise the mole fraction of conformer **1***a* from 0.22 to 0.87 while decreasing that of conformer **1***b* from 0.60 to 0.13 and to eliminate conformer **1***c*. The hope was that the results of the $^1$H nmr experiments would be capable not only of distinguishing between these conformational equilibria but to be in good accord with the conformer predicted and, thereby, reinforce the worth of HSEA calculations in an at least *interim* role for the conformational analysis of glycosidic structures. Of course, the *exo*-anomeric effect is not expected to be constant for all glycosides nor to be independent of the environment. However, we believe that these theoretical considerations should not discourage the use of the thoroughly objectively based and consistent method (HSEA calculations) presented herein since, to date, it has provided conformational preferences that are in good accord with the conformational assignments made using the best physical methods (nmr) presently available for the study of glycosides in aqueous solution. The need for a method that can serve as a routine and apparently reliable method for the assessment of the conformational preferences of glycosides is urgent. The main need is in terms of a start toward an understanding of the role of oligosaccharide structures in biological systems (11). However, it must also be realized that, in the absence of molecular models that define the spatial arrangement of the protons in molecules, even an attempt to assess the significance of nOe, $T_1$ measurements (12), and other nmr parameters is denied. We contend that HSEA calculations can serve well in these regards as an approximation that is amenable to routine laboratory work.

## Results and discussion

Figure 2 displays the 400 MHz spectrum for the B-trisaccharide attached to the linking arm $(CH_2)_8$-$COOCH_3$. The presence of this arm has no bearing on the present investigation. Its presence is only due to the fact that this was the form in which the trisaccharide was available. Its possible influence on $^{13}$C nmr and on some of the $^1$H nmr parameters will be discussed later where it will be seen that its presence does not influence the conclusions reached. Although the signals for the hydrogens at positions $1^b$ and $4^b$ of the βDGal unit,[3] at positions $1^d$ and $5^d$ of the αLFuc unit, and at positions $1^e$ and $5^e$ of the αDGal unit are well separated at 400 MHz, selective saturation for nuclear Overhauser enhancement experiments without some irradiation of neighboring protons was not possible. However, it was possible to adjust to this circumstance and to show by way of nuclear Overhauser interunit enhancements that the compound resides largely in conformer **1***a*. Furthermore, it will be demonstrated that both $T_1$ and specific interunit deshielding effects are in accord with this conclusion.

Prior to a consideration of the $^1$H nmr data, we would like to present an adjustment of the *exo*-anomeric effects for α and β-glycosides which were previously used for the HSEA calculations (1). In our first publication (1), the potential energy surfaces published by Jeffrey, Pople, and co-workers (6) for the internal rotational barriers present in dimethoxymethane, as derived by *ab initio* molecular orbital calculation, were used directly to introduce the influence of the *exo*-anomeric effect. It was considered at the time that the quality of the nmr data did not warrant an effort to further refine the method. Also, the *ab initio* calculations (6)

[3]These units are designated as units b (βDGal), d (αLFuc), and e (αDGal) to conform with designations used in the previous publication (1).

Can. J. Chem. Downloaded from www.nrcresearchpress.com by 210.87.254.5 on 09/06/12
For personal use only.

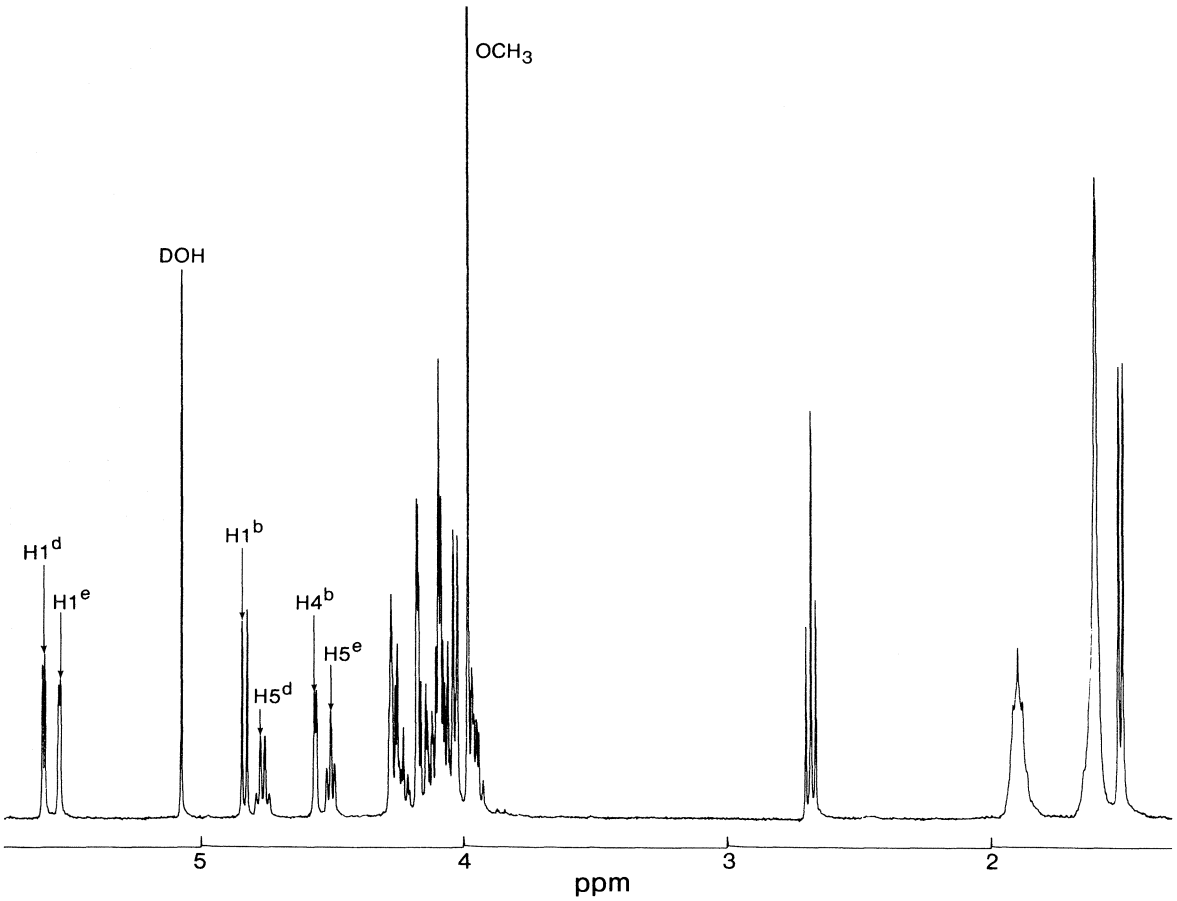


FIG. 2. 400 MHz $^1$H nmr spectrum of αLFuc(unit d) (1→2) [αDGal(unit e) (1→3)]βDGal(unit b)—O$(CH_2)_8COOCH_3$ in $D_2O$ to display the separation of the signals for protons which were saturated in nuclear Overhauser enhancement measurements.

were only carried out in 60° steps and interpolations of these few points were used. Since then, other papers have appeared (13–15) wherein molecular mechanics are used to estimate the conformational preferences for glycosides and which introduce a parameter for the *exo*-anomeric effect. Burkert (16) introduced a torsional potential function of the type:

$$E_{tor} = (V_1/2)(1 - \cos\omega) + (V_2/2)(1 - \cos 2\omega) + (V_3/2)(1 - \cos 3\omega) + \ldots$$

with $V_1 = 0$, $V_2 = -1.80$, and $V_3 = 0.66$ kcal/mol. The negative $V_2$ term was explained as stabilization due to back-donation of the oxygen lone pair orbital into the δ* molecular orbital of the C—O bond and favours the C/O torsion angle of ±90°. Jeffrey and Taylor (17) used a similar expression:

$$E = (V_2/2)(1 - \cos 2\theta)$$

where θ is a lone pair to oxygen torsion angle (e/O in the system —O—C—O—) derived by treating the lone pair of electrons as pseudoatoms with the bond angle e—O—e at an equilibrium value of 140°. Also, Wolfe *et al.* (18) have recently discussed the origin of the anomeric effect as involving lone pair orbital back-bonding interactions. Since for α and β-anomers, the orientations of the lone electron pairs relative to each other are different, it is expected that similar changes in the φ torsion angle will not cause the same changes in energy. Consequently, it is expected that two different curves should be available for assessment of the *exo*-anomeric effect in different anomers. As previously mentioned (19), the *exo*-anomeric effect can be expected to be stronger for β-glycosides.

The atomic parameters for dimethoxymethane which were used in the *ab initio* molecular orbital calculations (6) were also used in hard-sphere

Can. J. Chem. Downloaded from www.nrcresearchpress.com by 210.87.254.5 on 09/06/12
For personal use only.

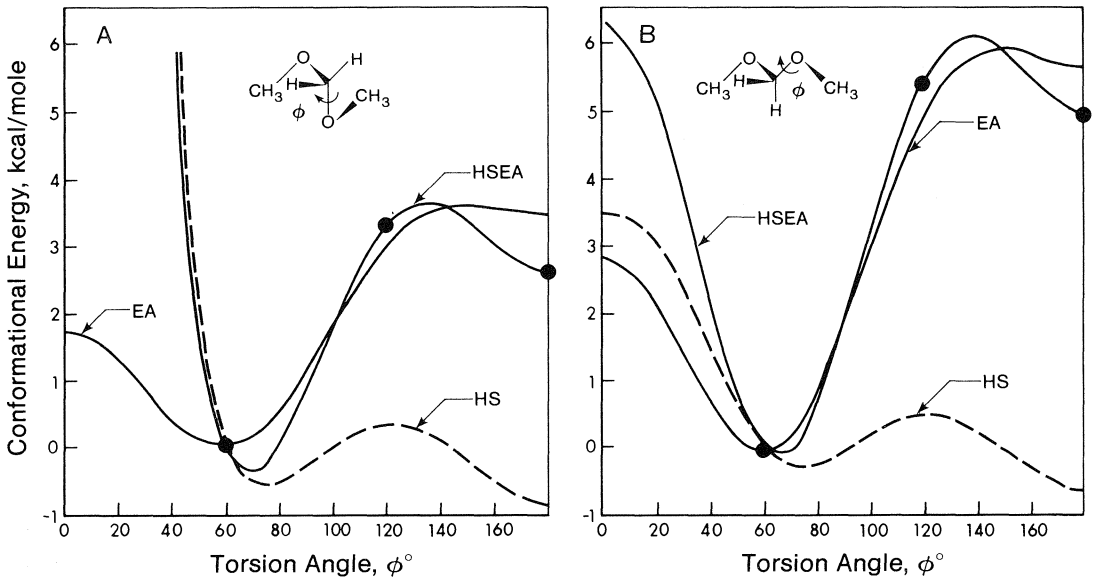


FIG. 3. Potential energy surfaces for dimethoxymethane and involving rotation of one of the $CH_3O—CH_2$ bonds (change in $\phi^o$ torsion angle) while holding the rest of the molecule in the conformations displayed in A and B. A represents changes that occur for rotation about the glycosidic bond of α-glycosides and B similar changes for β-glycosides. The points indicated as black dots are those estimated by *ab initio* molecular orbital calculations (6) except that the energies of the conformers shown in B were lowered so as to bring the energy for $\phi^o = 60°$ to 0 kcal/mol. The curves marked HS were derived by hard-sphere calculation. Those designated EA represent the change in the *exo*-anomeric effect with change in $\phi^o$. The plots termed HSEA are to show that the addition of the HS and EA curves provides curves which in fact pass through the points which were provided (6) by *ab initio* calculations as required by the method used to derive the EA curves.

calculations (20) to estimate the nonbonded interactions for the ranges of conformational change presented in Fig. 3. As seen in Fig. 3A, the conformational changes that correspond to changes in the ϕ torsion angle for α-glycosides contain only three points for the total conformational energy calculated by Jeffrey and co-workers (6). The point at $\phi^o = 0$ is not useful in hard-sphere calculations since it involves very strong van der Waals contacts (17). On the other hand, all four points obtained by the *ab initio* calculations are presented in Fig. 3B which deals with changes in torsion angles encountered in β-glycosides. The goal was to derive an expression using these points and the results of the hard-sphere calculations which would reflect change in the *exo*-anomeric effect with change in the ϕ torsion angle. This was accomplished as is discussed below to provide the curves designated EA in Fig. 3. The EA curves are curves which when added to the HS curves reproduce the points derived by *ab initio* calculation (6).

The four points on the EA curve (0°, 60°, 120°, and 180°) in Fig. 3B were used to set up four expressions of the type mentioned above and used by Burkert (16). The solution of these four simultaneous equations then gave the following expression

$$EA_{\beta\text{-anomers}} = 2.61(1 - \cos\phi^o) - 1.21(1 - \cos 2\phi^o) - 1.18(1 - \cos 3\phi^o) + 2.86\ \text{kcal/mol}$$

The constant (2.86) is the value of *EA* at $\phi^o = 0$.

Since only three points were available for the achievement of the EA curve given in Fig. 3A, the problem was handled in a different way. It was noticed that the ratio of the *EA* value at $\phi^o = 120°$ in Fig. 3A to that in Fig. 3B was 0.60 and that the same ratio existed for these values at $\phi^o = 180°$. It was assumed, therefore, that this relationship would also exist at $\phi^o = 0°$. This assumption then provided the fourth point required to set up the expression,

$$EA_{\alpha\text{-anomers}} = 1.58(1 - \cos\phi^o) - 0.74(1 - \cos 2\phi^o) - 0.70(1 - \cos 3\phi^o) + 1.72\ \text{kcal/mol}$$

As seen in Fig. 3, the assumption provides similar EA curves and implies that the *exo*-anomeric effect is stronger for β-glycosides than for α-glycosides. The use of these expressions provides virtually the same results in HSEA calculations as does the previously described procedure. Furthermore, the

Can. J. Chem. Downloaded from www.nrcresearchpress.com by 210.87.254.5 on 09/06/12
For personal use only.

Can. J. Chem. Downloaded from www.nrcresearchpress.com by 210.87.254.5 on 09/06/12
For personal use only.

computer program has been rewritten in order to facilitate the practical application in routine work.[4] It should be noted that, although $\phi^H$ and $\psi^H$ values are used in the following discussion of the conformational analysis of the oligosaccharides, the computer program calculates $\phi^{O5}$ from the coordinates of the heavy atoms of the glycosidic bond for each $\phi^H$ value in order to evaluate the contribution of the *exo*-anomeric effect from the formulas given above.

It is well recognized (21) that an nOe is dependent not only on the proximity of the proton observed to the proton which is saturated but also on the immediate proton environment of the former. In rigid systems of known geometry and in which the molecules are tumbling isotropically so that the correlation time ($\tau_c$) is the same for every proton vector, and with intramolecular dipole–dipole relaxation predominating, the observed nOe for proton d on the saturation of proton s is well *approximated*, for the purpose of estimating relative nOe's, by the following expression wherein $r_{ds}$ is the distance between proton d and proton s, and $r_{dj}$ is the distance between proton d and each other proton in the molecule.

$$\mathrm{nOe_d(s)} = r_{ds}^{-6} \Big/ \left(2 \sum_{j \neq d} r_{dj}^{-6}\right)$$

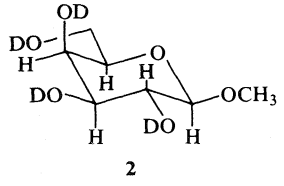


2

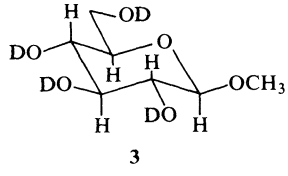


3

The nOe's observed for H2 on saturation of H1 for methyl β-D-galactopyranoside (**2**) and for methyl β-D-glucopyranoside (**3**) (Table 2) provide a good example. Simple examination shows that whereas the distances between H1 and H2 are the same, H2 of **2** is much more isolated from other protons than is H2 of **3**. Consequently, the term $\Sigma_{j \neq d} r_{dj}^{-6}$ will be smaller for **2** and the nOe will be larger as observed. In the case of the glucoside (**3**), the signals for H3 and H5 could not be sufficiently well resolved to allow separate nOe assignments. However, both of these protons are more isolated from H4 than in the galactoside (**2**). Therefore, a greater enhancement of H3 and H5 is expected for **3** than for **2** as was the case. The negative enhancement of H4 for **2** arose because this proton is far from the proton (H1) that was saturated but close to protons (H3 and H5) which were enhanced (21). The positive enhancement of H4 of **3** is due to higher order effects.

[4]Listings of computer programs are available at a nominal charge from the Depository of Unpublished Data, CISTI, National Research Council of Canada, Ottawa, Ontario K1A 0S2, Canada.

TABLE 2. Nuclear Overhauser enhancements by saturating H1 of the methyl β-D-galacto- (**2**) and glucopyranosides (**3**) and spin-lattice relaxation times

| Compound | H2 | H3 | H5 | H4 |
|---|---|---|---|---|
| | nOe (%) | | | |
| **2** | 10 | 9 | 12 | −4 |
| **3** | 5 | —* | 27* | 2 |
| | $T_1$ (s) | | | |
| **2** | 7.1 | 1.7 | 1.1 | 1.8 |
| **3** | 3.4 | 2.0 | 1.5 | 2.0 |
| nOe(**2**)/nOe(**3**)† | 2.0 (2.2) | 0.78 | (0.83)‡ | — |
| $T_1$(**2**)/$T_1$(**3**)† | 2.1 (2.2) | 0.80 | (0.84)‡ | |

*The sum of the nOe's are given due to overlap of signals.
†The ratios in brackets were calculated from appropriate molecular models.
‡The average of the $T_1$ and nOe's for H3 and H5 are used due to overlap of these protons in compound **3**.

The proton spin-lattice relaxation time ($T_1$) is a measure of the relaxation environment of the proton. Thus, the more intimate the proton environment for a given proton, the shorter the relaxation time; following the expression (21),

$$(1/T_1)_i = \text{constant} \cdot \tau_c \cdot \sum_{j \neq i} r_{ij}^{-6}$$

Assuming isotropic motion of the molecule and only intramolecular dipole–dipole relaxation, the ratios between the $T_1$'s for the similar hydrogens in **2** and **3** should be the same (everything else being ideal) as the ratios of the nOe's. This is seen (Table 2) to be the case both for H2 and the sums for H3 and H5.

Table 3 lists coupling constants as evidenced by the spacings of the signals for a number of vicinal protons in the B-trisaccharide. These data confirm that the three hexopyranose units exist in their normal chair conformations.

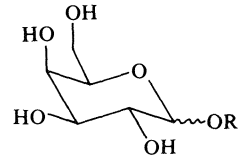


**2(4)***a*

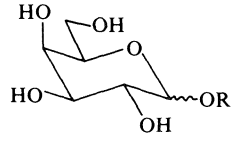


**2(4)***b*

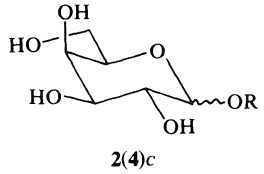


**2(4)***c*

TABLE 3. (*a*). Coupling constants (Hz) for vicinal hydrogen atoms in the B-trisaccharide (**1**)

| Unit | $J_{1,2}$ | $J_{2,3}$ | $J_{3,4}$ | $J_{4,5}$ | $J_{5,6}$ | $J_{5,6}$ |
|---|---|---|---|---|---|---|
| βDGal | 7.8 | 9.8 | 3.2 | ~1 | 7.8* | 4.3* |
| αLFuc | 3.7 | 9.9 | ~3.5 | ~1 | 6.8 | — |
| αDGal | 2.8 | ~10 | — | ~1 | 6.4* | |

*Observed first order coupling constants.

(*b*). Chemical shifts (ppm) of H4 in derivatives of D-galactose

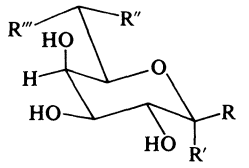


| Compound | R | R′ | R″ | R‴ | Chemical shifts |
|---|---|---|---|---|---|
| **2** | $OCH_3$ | H | H | OH | 4.17 |
| **4** | H | $OCH_3$ | H | OH | 4.21 |
| **5** | H | $OCH_3$ | H | H | 4.04 |
| **6** | $OCH_3$ | H | $CH_3$ | OH | 4.23 |

It was necessary to set a specific conformation for the hydroxymethyl groups in the B-trisaccharide in order to calculate theoretical $T_1$ and nOe values. In the case of the βDGal units, the spacings that reflect $J_{5,6} = 7.8$ Hz and $J_{5,6'} = 4.3$ Hz require that the hydroxymethyl group exist largely in a conformer that has one of the hydrogen atoms at C6 in *anti*-periplanar relationship to H5; i.e., either **2**(**4**)*b* or *c*. This situation was also observed for methyl β-D-galactopyranoside (**2**) (1). The signals for H6 and H6′ could also be sufficiently resolved at 400 MHz to provide this information in the case of methyl α-D-galactopyranoside (**4**). ABX analysis of the H5, H6, and H6′ protons gave $J_{5,6} = 8.2$ Hz and $J_{5,6'} = 4.6$ Hz. Therefore, the orientation of the hydroxymethyl group must be essentially as in **2**(**4**)*b* or **2**(**4**)*c*. The latter orientation could be assigned on the basis of chemical shift data.

The chemical shifts for H4 in the βDGal and αDGal units of the trisaccharide were found (1) to be 4.50 and 4.20 ppm, respectively. The greater deshielding (0.30 ppm) of H4 of the βDGal unit can be assigned to the fact that this unit is substituted by the αDGal unit at the neighboring 3-position (1). As seen in Table 3, the chemical shifts for H4 in methyl β-D- (**2**) and α-D-galactopyranoside (**4**) are nearly the same (4.17 and 4.21 ppm, respectively). This similarity suggests that these hydrogen atoms are in similar environments. If conformer **2**(**4**)*b* existed as the predominant conformer, then the chemical shift could be expected to be near that of methyl 6-deoxy-α-D-galactopyranoside (**5**). However, it is seen to be nearly 0.15 ppm to lower field. This suggests a deshielding of H4 in **2** and **4** by O6 as would be the case for conformer **2**(**4**)*c*. This interpretation is supported by the chemical shift of H4 (4.23 ppm) in methyl 7-deoxy-β-D-*glycero*-D-*galacto*-heptopyranoside (**6**). This compound definitely exists essentially in the conformation shown in Table 3 (22). It is seen that this chemical shift is very nearly the same as that for this atom in **2** and **4**. The previously presented argument (23) based on empirical rules for chemical shifts, in support of a high population of conformer **2**(**4**)*c*, is thus supported and it is on this basis that this orientation was chosen to calculate the $T_1$ and nOe data. The methyl group of the αLFuc unit was considered to be in the staggered conformation.

As was previously discussed in detail (1, 8, 24), the $^1$H nmr spectra of branched oligosaccharides can display large specific interunit chemical shift changes which are attributed to strong nonbonded interaction between the proton and one or more oxygen atoms in another unit. This is seen in Table 4 to be the case for the H5 atoms of both the αLFuc and βDGal units of **1**. We expect that these deshielding interactions occur only when the two atoms are in repulsive van der Waals interaction and, therefore, the internuclear distance should be less than 2.7 Å. On this basis, the internuclear distances listed in Table 5 eliminate conformer **1***c* and would render conformer **1***b* improbable. These conclusions found support in the proton $T_1$ values presented in Table 7. However, it is required to first consider the $^{13}$C spin-lattice relaxation times presented in Table 6.

Assuming isotropic motion and intramolecular dipole–dipole relaxation only, proton $T_1$ values can be related to intramolecular proton–proton distances by the simple expression already presented. Assuming dipole–dipole relaxation only, the anisotropy of molecular tumbling can be judged from a consideration of the $NT_1$ values of the $^{13}$C atoms (Table 6) where $N$ refers to the number of hydrogens directly bound to the carbon atom. It is seen that the $NT_1$ values are in fact almost constant (the values for the C6 atoms are special cases because these are parts of rotating groups). The $NT_1$'s (not listed) for the $(CH_2)_8COOCH_3$ group were larger except for the aglyconic carbon. This indicates, as would be expected, a greater mobility for the side chain. In view of the quality of the data presented in Table 6, it was encouraging to examine the spin-lattice relaxation times and the related nOe phenomena for the protons in **1**. The $T_1$'s that could be accurately measured are listed in Table 7. These values were then used to calculate the $C$ values defined and presented in Table 8 for the B-

Can. J. Chem. Downloaded from www.nrcresearchpress.com by 210.87.254.5 on 09/06/12
For personal use only.

Can. J. Chem. Downloaded from www.nrcresearchpress.com by 210.87.254.5 on 09/06/12
For personal use only.

TABLE 4. Chemical shift differences (ppm) for similar hydrogen atoms in the B-trisaccharide (1) and related methyl glycosides

| | H1 | H2 | H3 | H4 | H5 | H6 | H6′ |
|---|---|---|---|---|---|---|---|
| αLFuc unit of **1** | 5.53 | 3.95 | 4.02 | 3.98 | 4.68 | 1.47 | — |
| αLFuc-$OCH_3$ | 5.00 | 4.03 | 4.06 | 4.04 | 4.28 | 1.47 | — |
| Difference | 0.53 | −0.08 | −0.04 | −0.06 | 0.40 | 0 | — |
| αDGal unit of **1** | 5.48 | 4.09 | 4.09 | 4.20 | 4.47 | 3.96 | 3.96 |
| αDGal-$OCH_3$ | 5.08 | 4.07 | 4.05 | 4.21 | 4.14 | 3.96 | 3.96 |
| Difference | 0.40 | 0.02 | 0.04 | −0.01 | 0.33 | 0 | 0 |

TABLE 5. Internuclear distances*

| | Internuclear distance (Å) | |
|---|---|---|
| Conformer | $H5^d$—$O1^b$ | $H5^e$—$O2^d$ |
| **1***a* | 2.49 | 2.40 |
| **1***b* | 2.53 | 2.83 |
| **1***c* | 2.53 | 4.70 |

*The internuclear distances for the protons involved in strong interunit deshielding interactions (Table 4) and the closest oxygen atom in a different unit for the B-trisaccharide in the three conformations described in Table 1, except for $H5^e$—$O2^d$ of 1*c*. In this case, $H5^e$ was closest to $O4^b$ (4.32 Å).

TABLE 6. Carbon-13 spin-lattice relaxation times for the B-trisaccharide (1) multiplied by the number of directly bound hydrogen atoms ($NT_1$)

| | $NT_1$ (s)* | | | | | |
|---|---|---|---|---|---|---|
| Unit | C1 | C2 | C3 | C4 | C5 | C6 |
| βDGal (b) | 0.20 | — | 0.19 | 0.20 | 0.20 | 0.38 |
| αLFuc (d) | 0.19 | 0.19 | — | — | 0.19 | — |
| αDGal (e) | 0.23 | 0.17 | — | — | 0.17 | 0.38 |

*Measured in $D_2O$ (0.08 *M*) at 22.63 MHz, 302 K, by the inversion recovery method with delay times of 1.5, 0.001, 0.01, 0.02, 0.03, 0.05, 0.1, 0.15, 0.20, 0.25, and 3.0 s. The relaxation delay time was 1.22 s. The $^{13}C$ nmr spectra and signal assignments are reported (1).

TABLE 7. Some proton spin-lattice relaxation times ($T_1$'s) for the B-trisaccharide (1)

| Unit | Relaxation time (s)* | |
|---|---|---|
| βDGal | 0.57 ($H1^b$) | 0.52 ($H4^b$) |
| αLFuc | 0.65 ($H1^d$) | 0.52 ($H5^d$) |
| αDGal | 0.69 ($H1^e$) | 0.56 ($H5^e$) |

*Measured in $D_2O$ (0.02 *M*) at 400 MHz, 296 K, by the inversion recovery method with delay times of 0.001, 0.05, 0.1, 0.15, 0.20, 0.25, 0.3, 0.4, 0.5, 0.7, 1.0, and 6.0 s. The relaxation delay was 9.28 s.

trisaccharide (**1**) in the three conformations described in Table 1. The *C* values for $H1^b$ can be neglected from further consideration since their high value is related to neglecting the $O(CH_2)_8$-$COOCH_3$ aglycon in the calculations.

Since the molecule seems to be tumbling isotropically as indicated by the $^{13}C$-$T_1$'s in Table 6 and should the relative dispositions in space of the various hydrogen atoms in the molecule be well represented by one conformer, then the *C* values are expected to be constant (25). This condition is seen to be the best held for conformer **1***a*. Conformer **1***c* obviously is not in accord with expectations and this conformation can therefore be neglected and will not be considered further. The low *C* values of 65 for $H1^e$ in conformer **1***b* already suggest that this conformer is less important than **1***a* in contrast to the prediction based on hard-sphere calculations only (Table 1). This indication found support in the nOe measurements to be presented in Table 11. However, we must first comment on how these measurements were made.

Table 9 presents the nOe's that would be expected on saturation of one of the six protons listed and assuming that the total of the enhancements would be 100%. It is seen that no significant differences in nOe could be expected from the saturation of either protons $H1^b$ or $H5^d$. The experimental results confirmed these relative values and are not presented in Table 11 since these do not bear on the conformational analysis. Inspection of Table 9 did indicate, however, that certain nOe differences should exist that would allow a decision on conformation preference (**1***a* or **1***b*).[5] These values are underlined in Table 9. It was considered, therefore, that if nOe experiments could be conducted that would provide overall results which were consistent with these expectations, then a decision on the relative importance of conformers **1***a* and **1***b* could be reached.

As was mentioned above, it was not possible under the available experimental conditions to selectively saturate a given proton. The application of the transient nOe experiment described by Heatley *et al.* (27) is not possible to perform with accuracy due to the short relaxation times of this fairly large molecule in aqueous solution. However, it proved possible to adjust to the situation as is indicated in Table 10 which presents some of the results achieved in this regard. The results are also plotted in Fig. 4.

Saturation of $H1^d$ at power level 1 (see Experi-

[5]It is of interest that the results of a two-dimensional nOe experiment (26) qualitatively confirmed the existence of the nOe's predicted in Table 9.

TABLE 8. Comparison of $C$ values for the different conformers using the $T_1$ values presented in Table 7

| | $C$ ($D \cdot 10^3$)* | | | | | |
|---|---|---|---|---|---|---|
| Conformer | H1[b] | H4[b] | H1[d] | H5[d] | H1[e] | H5[e] |
| **1***a* | 134† (13.1) | 84 (23.0) | 96 (16.0) | 82 (23.4) | 79 (18.4) | 75 (23.8) |
| **1***b* | 135† (13.0) | 95 (20.2) | 87 (17.7) | 83 (23.2) | 65 (22.3) | 79 (22.7) |
| **1***c* | 134† (13.1) | 145 (13.3) | 117 (13.2) | 83 (23.2) | 67 (21.5) | 106 (16.8) |

*The values for constant $C$ were calculated from the expression $C = [(T_{1j})D]^{-1}$ where $D = \Sigma_{j \neq i} r_{ij}^{-6}$ (Å$^{-6}$).
† Values too high due to the neglect of the relaxation contributions by the O—$(CH_2)_8$COOMe group.

TABLE 9. Relative nOe's calculated for conformers **1***a* and **1***b* measured under ideal experimental conditions*

| Proton saturated | Unit† | Conformers **1***a* and (**1***b*) position and nOe (% of total) | | | | |
|---|---|---|---|---|---|---|
| | | H1 | H2 | H3 | H4 | H5 |
| | b | ‡ | 22 (21) | 22 (23) | 2 (2) | 49 (50) |
| H1[b] | d | 1 (1) | 0 (0) | 2 (2) | 0 (0) | § |
| | e | 0 (1) | 0 (0) | 0 (0) | 0 (0) | 1 (0) |
| | b | § | 11 (7) | 0 (0) | 0 (0) | 0 (0) |
| H5[d] | d | 3 (2) | 4 (4) | 46 (49) | 35 (36) | ‡ |
| | e | 0 (0) | 0 (0) | 0 (0) | 0 (0) | 0 (0) |
| | b | § | 4 (4) | 21 (27) | ‡ | 19 (24) |
| H4[b] | d | 0 (0) | 0 (0) | 0 (0) | 0 (0) | § |
| | e | 53 (39) | 1 (4) | 0 (1) | 0 (0) | 1 (0) |
| | b | § | 1 (1) | 5 (23) | 35 (25) | 1 (1) |
| H1[e] | d | 1 (0) | 0 (0) | 0 (0) | 0 (0) | § |
| | e | ‡ | 54 (46) | 1 (2) | 0 (0) | 1 (1) |
| | b | § | 30 (34) | 1 (1) | 0 (0) | 0 (0) |
| H1[d] | d | ‡ | 40 (39) | 1 (1) | 0 (0) | § |
| | e | 0 (0) | 1 (0) | 21 (4) | 1 (1) | 4 (19) |
| | b | § | 2 (2) | 25 (1) | 1 (0) | 0 (0) |
| H5[e] | d | 7 (27) | 3 (8) | 1 (0) | 0 (0) | § |
| | e | 2 (2) | 3 (3) | 22 (28) | 33 (29) | ‡ |

*Hypothetical situation wherein the proton is fully saturated without affecting other protons.
† βDGal (b), αLFuc (d), and αDGal (e).
‡ The proton saturated.
§ These values were small and not calculated since these have no significance to the following discussions.

mental) was found (Table 10) by difference spectroscopy (28) both to saturate H1[e] by 20% and to enhance H5[e] by 2.5%. On the other hand, full saturation of H1[e] saturated H1[d] by 15% and produced an enhancement of H5[e] by 0.5%. Thus, at this power level, an indirect enhancement of H5[e] was observed which was 0.5 × 100/2.5 = 25% of that observed when H1[d] was fully saturated. According to Table 9, saturation of H1[e] should not enhance H5[e] appreciably. Therefore, the enhancements obtained for H5[e] in these two experiments arose from saturation of H1[d] only. The data presented in Fig. 4 were obtained in this way using both 200 and 400 MHz data. The conclusion that the effect of partial saturation could be treated in this way was used to calculate the relative nOe's presented in Table 12 using the data presented in Table 9. It is seen that few comparisons could be made without complication. However, the fact that excellent agreement was obtained in the cases which involved a prediction of greater than 10% of the total of the enhancements, which are underlined in Table 12, and all favor **1***a*, is taken as evidence for the actual existence of the conformer as predicted by HSEA calculations.

In conclusion, we wish to comment on the conformational equilibrium for the linear tetrasaccharide **7**. HS calculation indicated that the terminal trisaccharide unit would exist as conformers **7***a* and **7***b* in about equal populations. These conformers are described in Table 13 and by computer-drawn projection formulas in Table 14. In contrast to this prediction, HSEA calculation supports only conformer **7***a*, and this conformer would be some 3.6 kcal/mol more favorable than **7***b*. Compound **7** therefore offered another situation suitable for the examination of the influence of the *exo*-anomeric effect on the conformational equilibria of oligosaccharides.

It is seen from the data presented in Table 14 that

Can. J. Chem. Downloaded from www.nrcresearchpress.com by 210.87.254.5 on 09/06/12
For personal use only.

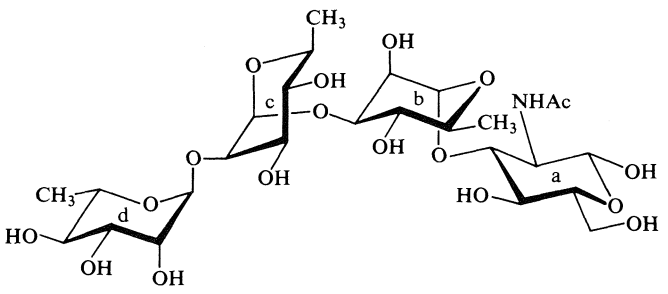

αLRha(1 → 2)αLRha(1 → 3)αLRha(1 → 3)βDGlcNac

the distances between the nuclei of H1$^c$ and H1$^d$ are significantly different and, therefore, an $^1$H nmr study of **7** was expected to allow a further test of HSEA versus HS calculations. In fact, the calculated and found values for the nOe's observed on saturation of H1$^c$ are clearly in favor of conformer **7***a*. Also, it is seen in Table 14 that the observed $T_1$ values are consistent with conformer **7***a* but not with conformer **7***b*. These results therefore provide further strong experimental evidence in support of molecular modelling procedures which include an important contribution to the conformational energy of a glycoside by the *exo*-anomeric effect.

The $^1$H nmr studies of the Type 1 and Type 2 human blood group determinants which are listed in Table 15 also well substantiated the conformational preferences assigned on the basis of HSEA calculation. In the case of the Type 1 structure, the torsion angles listed differ somewhat from those

TABLE 10. Nuclear Overhauser enhancements obtained from partial saturations

| % Saturation* | | % nOe | nOe Ratio (%) |
|---|---|---|---|
| Power level 1 (400 MHz) | | | |
| 100 (H1$^d$) | [20 (H1$^e$)] | 2.5 (H5$^e$) | |
| [100 (H1$^e$)] | 15 (H1$^d$) | 0.5 (H5$^e$) | 20 |
| 100 (H1$^e$) | [15 (H1$^d$)] | 6 (H4$^b$) | |
| [100 (H1$^d$)] | 20 (H1$^e$) | 1 (H4$^b$) | 17 |
| Power level 2 (400 MHz) | | | |
| 100 (H5$^d$) | [33 (H1$^b$)] | 6 (CH$_3^d$) | |
| [100 (H1$^b$)] | 36 (H5$^d$) | 2 (CH$_3^d$) | 33 |
| 100 (H5$^e$) | [41 (H4$^b$)] | 3 (H1$^d$) | |
| [100 (H4$^b$)] | 47 (H5$^e$) | 1.5 (H1$^d$) | 50 |
| Power level 3 (200 MHz) | | | |
| 100 (H5$^e$) | [30 (H4$^b$)] | 3.5 (H1$^d$) | |
| [100 (H4$^b$)] | 64 (H5$^e$) | 2.5 (H1$^d$) | 71 |
| 100 (H5$^d$) | [38 (H1$^b$)] | 11.5 (CH$_3^d$) | |
| [100 (H1$^b$)] | 55 (H5$^d$) | 5.5 (CH$_3^d$) | 48 |
| Power level 4 (200 MHz) | | | |
| 100 (H4$^b$) | [84 (H5$^e$)] | 17 (H1$^e$) | |
| [100 (H5$^e$)] | 60 (H4$^b$) | 10 (H1$^e$) | 59 |
| 100 (H5$^d$) | [54 (H1$^b$)] | 8.5 (CH$_3^d$) | |
| [100 (H1$^b$)] | 77 (H5$^d$) | 6 (CH$_3^d$) | 71 |

*The saturations in square brackets are those not expected (Table 9) to cause the nOe noted.

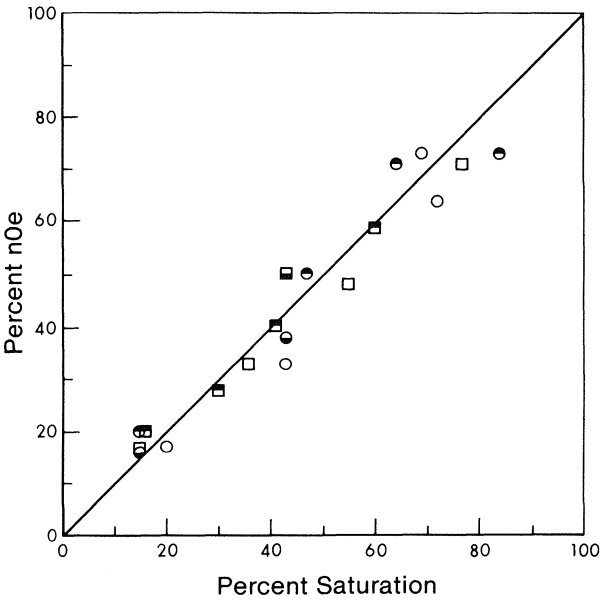


FIG. 4. A plot of the data presented in Table 10 together with the data obtained by the saturation of other signals in the spectrum of the B-trisaccharide (**1**) to show that nuclear Overhauser enhancement is directly proportional to the amount that the signal for the irradiated proton was partly saturated. The symbols indicate which one of the protons was fully saturated; ○ (H4$^b$), ◓ (H1$^d$), ◒ (H2$^d$), □ (CH$_3^d$), ⬒ (H1$^e$), and ⬓ (H5$^e$).

previously reported (1). These differences are not considered significant in the context of what may be expected from HSEA calculations. Nevertheless, these differences arose in part because of the slight modification of the contribution by the *exo*-anomeric effect but also because the improved computer program provided a more extensive iterative procedure than previously used. The $^1$H nmr data will be provided in connection with the syntheses of the structure listed in Table 15.[6]

We have previously (1) commented on the value of nOe experiments for gauging the proximity of

[6]R. U. Lemieux, H. Thøgersen, O. Hindsgaul, and T. Norberg, manuscript in preparation.

Can. J. Chem. Downloaded from www.nrcresearchpress.com by 210.87.254.5 on 09/06/12
For personal use only.

TABLE 11. The nOe's measured for the B-trisaccharide (**1**) at 400 MHz, 296 K (0.02 *M*) in $D_2O$ by difference spectroscopy

| % Saturation | Unit | Observed nOe's (%)* H1 | H2 | H3 | H4 | H5 | H6 |
|---|---|---|---|---|---|---|---|
| | b | — | † | 1.5 | — | 7 | — |
| 100 ($H1^b$), 1 ($H4^b$), | d | — | — | † | 3† | — | 1 |
| 15 ($H5^d$), 1 ($H5^e$) | e | — | — | — | — | — | — |
| | b | — | — | 4† | — | 2 | — |
| 100 ($H4^b$), 15 ($H5^e$) | d | 0.5 | — | — | — | — | — |
| | e | 7.5 | — | — | † | — | — |
| | b | — | † | — | 1 | — | — |
| 100 ($H1^d$), 20 ($H1^e$) | d | — | 9.5 | — | — | — | — |
| | e | — | 10† | † | — | 2.5 | — |
| | b | — | † | — | — | — | — |
| 100 ($H5^d$), 11 ($H1^b$), | d | — | — | † | 14† | — | 6 |
| 1 ($H4^b$), 1 ($H5^e$) | e | — | — | — | — | — | — |
| | b | — | 1 | 1 | 6 | — | — |
| 100 ($H1^e$), 15 ($H1^d$) | d | — | 1.5 | — | — | — | — |
| | e | — | 8† | † | — | 0.5 | — |
| | b | — | — | †† | — | — | — |
| 100 ($H5^e$), 16 ($H4^b$) | d | 2.5 | 0.5 | — | — | — | — |
| | e | 1.5 | † | 5.5† | 7†† | — | 3.5 |

*Measured at 400 MHz, power level 1 (see Table 10).
† or †† Because of signal overlap, this percentage is the sum of the nOe for these protons.

TABLE 12. Relative nOe's calculated for conformers **1***a* and **1***b* taking into account the partial saturation of other protons and comparison of these values with those found (see Table 11)

| Proton fully saturated | Unit | Conformers **1***a* and (**1***b*) nOe (% of total) H1 Calc. | H1 Found | H2 Calc. | H2 Found | H3 Calc. | H3 Found | H4 Calc. | H4 Found | H5 Calc. | H5 Found |
|---|---|---|---|---|---|---|---|---|---|---|---|
| | b | † | § | 4 (4) | § | 22 (24) | $28^+$ | * (*) | — | 17 (21) | 15 |
| $H4^b$ | d | 1 (4) | 3 | 0 (1) | § | 0 (0) | § | 0 (0) | § | † | § |
| | e | 47 (34) | 54 | 1 (4) | § | 3 (5) | § | 4 (4) | + | ‡ (‡) | — |
| | b | † | § | 5 (5) | 5 | 5 (20) | 5 | 31 (22) | 33 | 1 (1) | § |
| $H1^e$ | d | ‡ (‡) | — | 5 (5) | 8 | 0 (0) | § | 0 (0) | § | † | § |
| | e | * (*) | — | 48 (40) | $44^+$ | 4 (2) | + | 0 (0) | § | 1 (3) | 3 |
| | b | † | § | 25 (29) | $41^+$ | 2 (5) | § | 6 (4) | 4 | 0 (0) | § |
| $H1^d$ | d | * (*) | — | 34 (33) | 43 | 1 (1) | § | 0 (0) | § | † | § |
| | e | ‡ (‡) | — | 10 (8) | + | 18 (4) | + | 1 (1) | § | 4 (16) | 10 |
| | b | † | § | 2 (2) | § | 25 (5) | + | ‡ (‡) | — | 3 (3) | § |
| $H5^e$ | d | 6 (23) | 12 | 3 (7) | 2 | 1 (0) | § | 0 (0) | § | † | § |
| | e | 9 (7) | 7 | 3 (3) | ++ | 19 (24) | $27^{++}$ | 29 (25) | $34^+$ | * (*) | — |

*The proton fully saturated.
† These values were small and not calculated since these have no significance for the results discussed.
‡ The proton partly saturated.
§ No measurable nOe.
+ or ++ The sum of the nOe's observed for these protons in the given experiment was used because these signals overlapped. The sum is presented under that signal which was expected to be most strongly enhanced.

anomeric and aglyconic hydrogen atoms. We now wish to note that, as displayed in Fig. 5, a wide range of different sets of $\phi$ and $\psi$ values can set these hydrogen atoms at the same distance. Therefore, it is important in the assessment of the enhancement of the signal for an aglyconic hydrogen from saturation of the anomeric hydrogen that this enhancement be compared to an interunit enhancement observed in the same experiment for another hydrogen whose distance from the anomeric hydrogen also sets a requirement in terms of $\phi$ and $\psi$ torsion angles. In other words, in the absence of the interunit enhancement which was observed for $H5^d$ (Table 14), the only conclusion that could be reached would be that $H1^c$ and $H3^b$ are separated by about the same distance as $H1^c$ is from $H2^c$;

Can. J. Chem. Downloaded from www.nrcresearchpress.com by 210.87.254.5 on 09/06/12
For personal use only.

TABLE 13. The influence of the *exo*-anomeric effect on the populations of conformers of the tetrasaccharide **7**

| Method of calculation | Conformer | Conformation preferred† $(\phi/\psi)^d$ | Conformation preferred† $(\phi/\psi)^c$ | Conformational energy (c—d bond) | Mole fraction 296 K |
|---|---|---|---|---|---|
| HS | 7*a* | 40°/10° | 45°/15° | 0.00 | 0.59 |
| | 7*b* | −30°/−20° | 45°/15° | 0.22 | 0.41 |
| HSEA | 7*a* | 45°/15° | 50°/20° | 0.00 | ~100 |
| | 7*b* | −30°/−20°* | 50°/20° | 3.61 | ~0 |

*Not a minimum.
†Except when otherwise noted, the $\phi$ and $\psi$ torsion angles refer to $\phi^H$ and $\psi^H$ angles as defined by Lemieux and Koto (10). Calculated in 5° steps. Superscripts c and d refer to the glycosidic units αLRha(1→3) and αLRha(1→2), respectively.

TABLE 14. Proton $T_1$ values and nuclear Overhauser enhancements for **7**

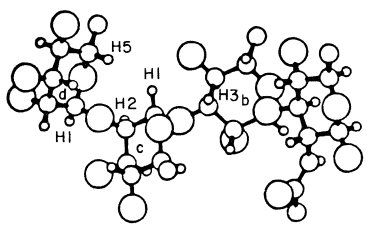


**7a**

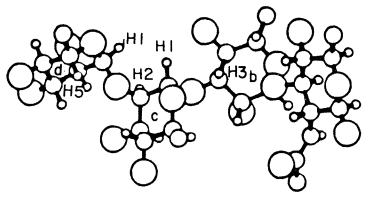


**7b**

(*a*) nOe Data

| Atom | Internuclear distances from H1c (Å) 7*a* | 7*b* | nOe (%), H1c* Calculated 7*a* | 7*b* | Found |
|---|---|---|---|---|---|
| H3b | 2.50 | 2.39 | 13 | 15 | 13 |
| H2c | 2.55 | 2.55 | 12 | 9 | 13 |
| H5d | 2.36 | 4.45 | 12 | 0.3 | 13 |
| H1d | 4.15 | 2.58 | — | — | — |

(*b*) $T_1$ Results

| Atom | $T_1$ values (s) | $\Sigma r^{-6} \times 10^3$ (Å$^{-6}$) 7*a* | 7*b* | *C*-values 7*a* | 7*b* |
|---|---|---|---|---|---|
| H1c | 0.46 | 15.9 | 14.4 | 137 | 151 |
| H1d | 0.78 | 10.8 | 16.0 | 119 | 80 |

*Proton saturated.

i.e., about 2.5 Å. This matter is of special importance to the conformational analysis of disaccharides where on occasions the only interunit nOe which is observed is that for the aglyconic hydrogen.

## Experimental

The solutions of the B-trisaccharide (**1**) (30) used in the $^1H$ nmr studies were prepared by freeze-drying the sample twice from $D_2O$ solutions in a specially prepared (31) 5 mm tube and then adding 100% $D_2O$ to provide a 0.02 *M* solution. This solution was then frozen, pumped, and thawed three times prior to the sealing of the tube under vacuum. The samples of methyl β-D-galacto (**2**) and β-D-glucosides (**3**) were similarly prepared.

*Spectroscopy*

The $^{13}C$ nmr spectra were obtained on a Bruker HFX-10 spectrometer operating at 22.63 MHz. The acquisition time of the free induction decay was 0.82 s in 4K data points (Nicolet 1085). A relaxation delay of 1.22 s was used with 3200 scans for each free induction decay which were then zero filled to 16K prior to Fourier transformation using a line-broadening factor of 3.0 Hz. The sweep width was 2500 Hz.

The $^1H$ nmr spectra were recorded on Bruker WH-200 and WH-400 spectrometers (200 and 400 MHz, respectively) using 16K points (Aspect 2000 computer) for the free induction decay and a 90° pulse width of 10 μs.

Can. J. Chem. Downloaded from www.nrcresearchpress.com by 210.87.254.5 on 09/06/12
For personal use only.

Can. J. Chem. Downloaded from www.nrcresearchpress.com by 210.87.254.5 on 09/06/12
For personal use only.

TABLE 15. Minimum energy conformations of blood-group related oligosaccharides calculated using the HSEA method*

| Compound | Unit† e | d | b | c | a |
|---|---|---|---|---|---|
| Type 1 structures | | | | | |
| Le[a] | | | βDGal(1→3) 55°, 10° | [αLFuc(1→4)] 55°, 25° | βDGlcNAc |
| Le[d] or H (Type 1) | | αLFuc(1→2) 50°, 10° | βDGal(1→3) 60°, 10° | | βDGlcNAc |
| Le[b] | | αLFuc(1→2) 45°, 15° | βDGal(1→3) 55°, 10° | [αLFuc(1→4)] 55°, 25° | βDGlcNAc |
| B‡ | αDGal(1→3) −65°, −50° | [αLFuc(1→2)] 55°, 20° | βDGal | | |
| B‡ | αDGal(1→3) −65°, −50° | [αLFuc(1→2)] 55°, 15° | βDGal(1→3) 60°, 5° | | βDGlcNAc |
| —‡§ | αDGal(1→3) −65°, −55° | [αLFuc(1→2)] 50°, 15° | βDGal(1→3) 55°, 10° | [αLFuc(1→4)] 55°, 25° | βDGlcNAc |
| Type 2 structures | | | | | |
| X | | | βDGal(1→4) 55°, 10° | [αLFuc(1→3)] 55°, 25° | βDGlcNAc |
| H (Type 2) | | αLFuc(1→2) 50°, 15° | βDGal(1→4) 55°, 0° | | βDGlcNAc |
| Y | | αLFuc(1→2) 50°, 10° | βDGal(1→4) 55°, 10° | [αLFuc(1→3)] 50°, 25° | βDGlcNAc |
| B‡ | αDGal(1→3) −65°, −50° | [αLFuc(1→2)] 55°, 15° | βDGal(1→4) 55°, 0° | | βDGlcNAc |
| —‡§ | αDGal(1→3) −65°, −55° | [αLFuc(1→2)] 50°, 15° | βDGal(1→4) 55°, 10° | [αLFuc(1→3)] 50°, 25° | βDGlcNAc |

*Specified as $\phi^H$, $\psi^H$ minimum values, calculated in 5° steps.
†See footnote 3 in text.
‡Similar values are expected for the corresponding A determinants, in which the αDGal(1→3) unit (e) is exchanged with a αDGalNAc unit.
§When this pentasaccharide is linked to a βDGal unit through a (1→3) bond, $(\phi,\psi)_{min}$ values of 60°, −10° are calculated; and when linked to a βDGal unit through a (1→6) bond, $(\phi,\psi^{C5})_{min}$ values of 50°, 130° are calculated. (For discussion of ω angle, see ref. 29.)

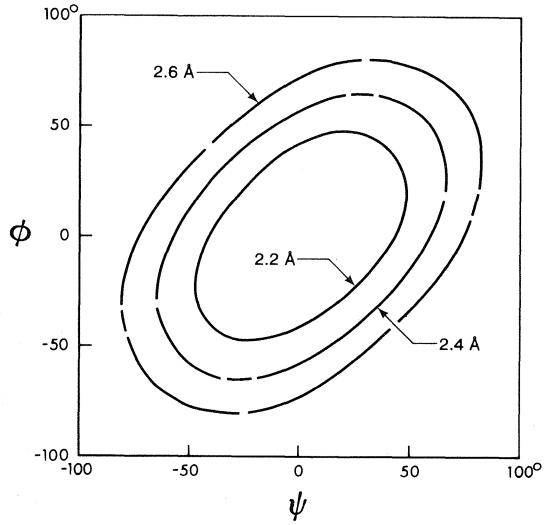


FIG. 5. Plots to illustrate the relationship between the internuclear distance of an anomeric hydrogen atom to its aglyconic hydrogen atom and the φ and ψ torsion angles for the glycosidic bond. The number of discontinuities increases with increasing distance (for a given set of bond angles and bond lengths).

The $T_1$ experiments were done with the inversion recovery method at temperatures and delay times as shown in Tables 6 and 7.

The nOe experiments described in Table 11 were performed in the difference mode (28) with power levels 1, 2, 3, and 4 being 36 db below 0.2 W, 30 db below 0.2 W, 35 db below 0.2 W, and 28 db below 0.2 W, respectively. The enhancements are given in % relative to the proton saturated.

*Hard-sphere calculations*

The procedure was the same as that previously described (1) but using a simplified computer program.[4] The atomic parameters for the αDGal and βDGal units were obtained from the neutron diffraction data obtained on the corresponding methyl D-galactopyranosides recently published by Takagi and Jeffrey (32). X-ray data for the calcium bromide complex of α-L-fucopyranose (33) was used to represent the αLFuc unit except that the coordinates of the hydrogen atoms were synthesized using a C—H bond length of 1.1 Å and a bond vector defined by the appropriate C—C and C—O bond vectors.

The calculations were made with an Amdahl 470V/7 computer. The ball and stick representations used in Fig. 1 were obtained by the Pluto program[7] and the energy profiles by a program which can be used in connection with the HSEA program.[4]

[7]Pluto Plot Program, S. Motherwell, University Chemical Laboratory, Cambridge, England.

## Acknowledgements

The financial support of the Natural Sciences and Engineering Research Council of Canada through a grant (A172) to R. U. Lemieux is gratefully acknowledged. The Danish Natural and Technical Science Research Council and the Otto Mønsted Foundation are thanked for support to K. Bock, B. Meyer, and H. Thøgersen.

We gratefully acknowledge the guidance provided by Mark Botkin of Chembiomed Ltd. in the application of the PLUTO program for drawing molecular models.

1. R. U. Lemieux, K. Bock, L. T. J. Delbaere, S. Koto, and V. S. Rao. Can. J. Chem. **58**, 631 (1980).
2. R. U. Lemieux and K. Bock. J. Antibiot. **32**, S163 (1979).
3. A. I. Kitaigorodsky. Tetrahedron, **14**, 230 (1961).
4. A. I. Kitaigorodsky. Chem. Soc. Rev. **7**, 133 (1978).
5. G. A. Jeffrey, J. A. Pople, and L. Radom. Carbohydr. Res. **25**, 117 (1972).
6. G. A. Jeffrey, J. A. Pople, J. S. Binkley, and S. Vishveshwara. J. Am. Chem. Soc. **100**, 373 (1978).
7. K. Bock, D. Bundle, and S. Josephson. J. Chem. Soc. Perkin Trans. I, Submitted for publication.
8. R. U. Lemieux, J. LePendu, and O. Hindsgaul. J. Antibiot. **32**, S21 (1979).
9. E. A. Kabat, J. Liao, M. H. Burzynska, T. C. Wong, H. Thøgersen, and R. U. Lemieux. Mol. Immunol. **18**, 873 (1981).
10. R. U. Lemieux and S. Koto. Tetrahedron, **30**, 1933 (1974).
11. R. U. Lemieux. Pure Appl. Chem. In press.
12. J. M. Berry, L. D. Hall, D. G. Welder, and K. F. Wong. ACS Symposium Series **87**, 1979. p. 30.
13. I. Tvaroška and T. Kožár. J. Am. Chem. Soc. **102**, 6929 (1980).
14. R. H. Marchessault, T. Bleha, Y. Deslandes, and J.-F. Revol. Can. J. Chem. **58**, 2415 (1980).
15. S. Melberg and K. Rasmussen. Carbohydr. Res. **78**, 215 (1980).
16. U. Burkert. Tetrahedron, **33**, 2237 (1977).
17. G. A. Jeffrey and R. Taylor. J. Comput. Chem. **1**, 99 (1980).
18. S. Wolfe, M.-H. Whangbo, and D. J. Mitchell. Carbohydr. Res. **69**, 1 (1979).
19. R. U. Lemieux, S. Koto, and D. Voisin. ACS Symposium Series **87**, 1979. p. 17.
20. C. M. Venkatachalam and G. N. Ramachandran. Conformation of biopolymers. Vol. 1. *Edited by* G. M. Ramachandran. Academic Press, New York. 1967. p. 83.
21. J. H. Noggle and R. E. Schirmer. The nuclear Overhauser effect. Academic Press, New York. 1971. p. 45.
22. R. U. Lemieux, O. H. Boullanger, D. R. Bundle, D. A. Baker, A. Nagpurkar, and A. Venot. Nouveau J. Chim. **2**, 321 (1978).
23. A. de Bruyn and M. Anteunis. Carbohydr. Res. **47**, 311 (1976).
24. R. U. Lemieux, D. R. Bundle, and D. A. Baker. J. Am. Chem. Soc. **97**, 4076 (1975).
25. R. Rowan III, J. A. McCammon, and B. D. Sykes. J. Am. Chem. Soc. **96**, 4773 (1974).
26. A. Kumar, R. R. Ernst, and K. Wüthrich. Biochem. Biophys. Res. Commun. **95**, 1 (1980).
27. F. Heatley, L. Akhter, and R. T. Brown. J. Chem. Soc. Perkin Trans. I, 919 (1980).
28. R. Richarz and K. Wüthrich. J. Magn. Reson. **30**, 147 (1978).
29. R. U. Lemieux, T. C. Wong, and H. Thøgersen. Can. J. Chem. **60**, 81 (1982).
30. R. U. Lemieux, D. R. Bundle, and D. A. Baker. U.S. Patent No. 4,238,473 (Dec. 9, 1980).
31. Y. Theirault, Y. Morio, and Kotovych. Can. J. Biochem. **57**, 165 (1979).
32. S. Takagi and G. A. Jeffrey. Acta Crystallogr. Sect. B, **35**, 902 (1979).
33. W. J. Cook and C. E. Bugg. Biochem. Biophys. Acta, **389**, 428 (1975).

Can. J. Chem. Downloaded from www.nrcresearchpress.com by 210.87.254.5 on 09/06/12
For personal use only.

# Syntheses of derivatives of lacto-*N*-biose. I. 4,6-Di-*O*-acetyl-3-*O*-(tetra-*O*-acetyl-β-D-galactopyranosyl)-2-deoxy-2-phthalimido-α,β-D-glucopyranosyl chloride

R. U. LEMIEUX, S. Z. ABBAS,[1] AND B. Y. CHUNG[2]

*Department of Chemistry, University of Alberta, Edmonton, Alta., Canada T6G 2G2*

Received March 27, 1981

R. U. LEMIEUX, S. Z. ABBAS, and B. Y. CHUNG. Can. J. Chem. **60**, 58 (1982).

Procedures are reported for the synthesis of 4,6-di-*O*-acetyl-3-*O*-(tetra-*O*-acetyl-β-D-galactopyranosyl)-2-deoxy-2-phthalimido-α,β-D-glucopyranosyl chloride, a reagent useful for the reliable introduction of β-D-Gal*p*-(1→3)-β-D-GlcNAc*p* units (lacto-*N*-biose I units) into oligosaccharide structures. A benzyl glycoside intermediate is hydrogenolyzed to the alcohol which is subsequently converted to the glycosyl chlorides by use of the Vilsmeier reagent in the presence of *sym*-collidine. A comparison is made of the oxazoline method for the preparation of β-glycosides from 2-amino-2-deoxysugars and the phthalimido procedure developed in this laboratory.

R. U. LEMIEUX, S. Z. ABBAS et B. Y. CHUNG. Can. J. Chem. **60**, 58 (1982).

On rapporte des méthodes de synthèse du chlorure de di-*O*-acétyl-4,6-*O*-(tétra-*O*-acétyl-β-D-galactopyrannosyl)-3-déoxy-2-phtalimido-2-α,β-D-glucopyrannosyle, un réactif pratique pour l'introduction d'unités β-D-Galp-(1→3)-β-D-GlcNAc*p* (unités de lacto-*N*-biose I) dans la structure d'oligosaccharides. On hydrogénolyse le glycoside de benzyle intermédiaire en alcool, que l'on transforme ensuite en chlorure de glycosyle en utilisant un réactif de Vilsmeier en présence de *sym*-collidine. On établit une comparaison entre la méthode aux oxazolines pour la préparation des β-glycosides à partir des sucres amino-2-déoxy-2 et la méthode du phtalimide mise au point dans ce laboratoire.

[Traduit par le journal]

Lacto-*N*-biose I (βDGal(1→3)DGlcNAc) was first isolated by partial acid hydrolysis of "lacto-*N*-tetraose" (1) which has this disaccharide β-linked to the 3′-position of lactose. The disaccharide βDGal(1→3)DGlc does not appear to have received a trivial name.

Lacto-*N*-biose I, like *N*-acetyllactosamine, is a building unit of the core chains of human blood group determinants. When present in the terminal tetra- or pentasaccharide of a human ABH antigenic determinant, the resulting structure is said to have the Type 1 chain (2). This is in contrast to the Type 2 chain (2) wherein *N*-acetyllactosamine forms the core structure unit of the ABH determinant. The Lewis family of human blood group determinants are Type 1 structures (3–5). The purpose of this communication is to report the preparation of a reagent **9** which we expect can play an important role in efforts designed to achieve the incorporation of Type 1 (lacto-*N*-biose I) units as β-glycosides.

We consider the use of 2-deoxy-2-phthalimido-glycosyl halides (6) as reagents for the synthesis of a β-linkage between an alcohol and an aminosugar which has the amino group in equatorial orientation to be particularly attractive, both for reasons of reliability and yield. In our experience, the method can be used in the presence of a wide range of both acid- and alkali-labile protecting groups. The yields are generally good to excellent and, to date, the formation of the α-glycoside as a byproduct has not been detected. When the reaction conditions are carefully controlled so as to minimize side reactions (highly pure reagents and solvents, low temperature, and strictly anhydrous conditions), excellent yields are normally achieved using equimolar amounts of the reactants (6).

Since we first announced our interest in the synthesis of the core structural units for the human blood group determinants,[3] a number of contributions to the same end have appeared from other laboratories. These investigations have generally employed the classical oxazoline method (7) for the establishment of a β-linkage between *N*-acetyl-D-glucosamine and another sugar. As a result, there now exists a substantial experimental basis for comparing the oxazoline and phthalimido methods. To do so appears timely since recently condensations using the oxazoline method which led to derivatives of chitobiose were reported (8) and the opinion was stated that the improved oxazoline method which employs 1,2-dichloroethane as solvent (9) provides yields that are as satisfactory as

[1]University of Alberta Postdoctoral Fellow 1975–1977. Present address: Chembiomed Ltd., W5-56 Chemistry Bldg., University of Alberta, Edmonton, Alta., Canada T6G 2G2.

[2]University of Alberta Postdoctoral Fellow 1975–1977. Present address: Dept. of Chemistry, Korea University, Seoul, Korea.

[3]R. U. Lemieux, S. Z. Abbas, and B. Y. Chung. Abstr. Pap. Chem. Soc. Meeting, Norwich, England, April 1977.

0008-4042/82/010058-05$01.00/0

©1982 National Research Council of Canada/Conseil national de recherches du Canada

Can. J. Chem. Downloaded from www.nrcresearchpress.com by 210.87.254.40 on 09/06/12
For personal use only.

Can. J. Chem. Downloaded from www.nrcresearchpress.com by 210.87.254.40 on 09/06/12
For personal use only.

those by the phthalimido route. We do not believe that the facts support this statement and take this occasion to explain why we hold this opinion.

First of all, we consider that it would have been more appropriate for Kiso *et al.* (8) to compare the 30–36% yields obtained in their synthesis of derivatives of chitobiose by the oxazoline method with the 68% yield that was reported for the synthesis of a chitobiose derivative by the phthalimido method (6). It is particularly important in this regard that the latter work employed an alcohol (2,2,2-trichloroethyl 3,6-di-*O*-acetyl-2-deoxy-2-phthalimido-β-D-glucopyranoside) which is of a type notorious for its resistance to glycosylation (10). After finding the oxazoline method unattractive for the synthesis of paragloboside (βDGal(1→4)βDGlcNAc(1→3)βDGal(1→4)βDGlc) analogs,[4] Ponpipom *et al.* turned to the phthalimido method (11). It was reported that the synthesis was then accomplished in high yield and with excellent stereoselectivity.

Similarly, Bundle and Josephson (12) have reported that whereas 2-acetamido-3,4,6-tri-*O*-acetyl-2-deoxy-α-D-glucopyranosyl chloride and the 1,2-oxazoline derivative obtained from it were not effective in the glycosylation of the 2-position of a 3,4-di-*O*-benzyl-α-L-rhamnopyranoside, the phthalimido method provided the desired compound in good yield (70%). These experiences match our own. For example, with a large excess of 2,2,2-trichloroethanol, the oxazoline method after substantial examination provided 2,2,2-trichloroethyl 2-acetamido-3,4,6-tri-*O*-acetyl-2-deoxy-β-D-glucopyranoside in 46% yield along with the α-anomer in 6.1% yield (13). On the other hand, when suitable precautions were taken to exclude water, the phthalimido method provided 2,2,2-trichoroethyl 3,4,6-tri-*O*-acetyl-2-deoxy-2-phthalimido-β-D-glucopyranoside in 89% yield (6) and no α-anomer was detected.

Augé and Veyrières (14) achieved a synthesis of lacto-*N*-triose I (βDGal(1→3)βDGlcNAc(1→3)-DGal) using the oxazoline derived from lacto-*N*-biose I. An 84% yield was reported. However, the yield was based on the alcohol (6-*O*-allyl-1,2,4-tri-*O*-benzyl-α-D-galactose) and a one molar excess of the oxazoline was used in the condensation. Thus, the yield may have been reported as 42%. This is to be contrasted with the condensation of acetylated phthalimido-chloride derived from lactosamine (24) with an equimolar amount of 2,2,2-trichloroethyl 2-*O*-benzoyl-4,6-*O*-benzylidene-α-D-glucopyranoside which proceeded in 80% yield (15).

The condensation of the oxazoline derived from D-glucosamine with 1,2;3,4-di-*O*-isopropylidene-α-D-galactose has provided perhaps the most favorable yield (81%) ever reported (16) using this method. Recently, 6-*O*-(3,4,6-tri-*O*-acetyl-2-deoxy-2-phthalimido-β-D-glucopyranosyl)-1,2;-3,4-di-*O*-isopropylidene-α-D-galactose was synthesized in 86% yield (17). The condensation of **9** with an equimolar amount of 1,2;3,4-di-*O*-isopropylidene-α-D-galactose gave the desired β-glycoside in 75% yield after one recrystallization (15). It is to be noted, however, that the yields were not acceptable when the alcohol was 1,2;5,6-di-*O*-isopropylidene-α-D-galactofuranose (15). In this case, electrophilic attack to open an isopropylidene group appeared to be an important competing reaction.

In contrast to the results obtained by the phthalimido method, virtually all of the yields which have been reported for the establishment of an intersugar glycosidic bond using the oxazoline method are less than 50% when the amount of the oxazoline is used to calculate the yield (18–23). This is of importance since the aminosugar component, especially in the form of higher saccharides, is often the more difficultly available starting material. It is these considerations that prompt us to publish the preparation of the title compound **9**. An accompanying paper (24) describes the preparation of the related structure derived from lactosamine.

The transformations used to achieve **9** are outlined using the formulas **1** to **9** and these are described in detail in the Experimental portion of this paper. The reaction sequence is modelled on the procedure used by Lemieux and Driguez (13) to build the lacto-*N*-biose I portion of the Lewis-a determinant. A point of interest is that the condensation of **4** with acetobromogalactose proceeded in 74% yield under Helferich conditions but using a 133% excess of the bromide. Over one-third of the bromide was converted to tetra-*O*-acetyl-β-D-galactopyranosyl cyanide. This result is to be contrasted with the previously reported (13) condensation of acetobromogalactose with 2,2,2-trichloroethyl 2-acetamido-4,6-*O*-benzylidene-2-deoxy-β-D-glucopyranoside under similar conditions. Using only a 50% excess of the bromide, the β-linked disaccharide was obtained in 91% yield. It is apparent, therefore, that the phthalimido group has an important shielding influence on the reactivity of the 3-hydroxyl of **4** and this property may have an important influence on the success of synthetic strategies which follow similar lines.

[4]M. M. Ponpipom, R. L. Bugianesi, and T. Y. Shen. 2nd Joint Conference CIC/ACS, Montreal, May 30 – June 2, 1977. Abstracts of Papers, CARB 26.

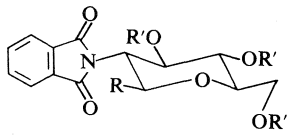

**1** R = Br, R′ = Ac
**2** R = OBn, R′ = Ac
**3** R = OBn, R′ = H

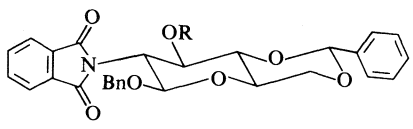

**4** R = H

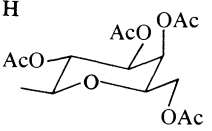

**5** R =

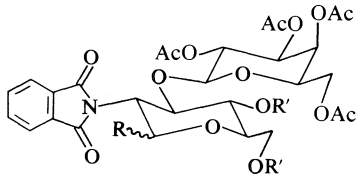

**6** R = OBn(β), R′ = H
**7** R = OBn(β), R′ = Ac
**8** R = OH(α,β), R′ = Ac
**9** R = Cl(α,β), R′ = Ac

The replacement of the anomeric hydroxyls of appropriately blocked structures by chlorine is conveniently accomplished (28)[3] using the Vilsmeier reagent (25–27). We conduct the reaction in the presence of *sym*-collidine to neutralize the liberated hydrogen chloride. Since the Vilsmeier reagent is also available in the bromide form (29, 30), the more reactive glycosyl bromides are also available in this way. We would also like to note that the reaction can be applied to such acid-labile compounds as 2,3,4,6-di-*O*-isopropylidene-D-mannopyranose.[5] In the phthalimido method, under the conditions for glycosylation which utilize an equimolar mixture of silver triflate and *sym*-collidine as promotor (6), the more stable chlorides are adequately reactive. No effort was made to separate the α and β-anomers of the glycosyl halides since the mixture was found to provide as good yields in the glycosylation reactions as did the pure β-form.

## Experimental

All solvent extracts were dried over anhydrous sodium sulfate prior to solvent removal using a rotary evaporator under the vacuum of a water aspirator. The $^1$H nmr spectra were measured at 100 MHz (Varian HA-100). Unless otherwise stated, deuteriochloroform was used as a solvent and internal TMS as a standard. Thin layer chromatograms (tlc) were developed on a Silica Gel G (E. Merck A.B., Darmstadt) and visualized with 5% sulfuric acid in ethanol after heating at 100°C. Column chromatography was performed on silica gel (CAMAG). Nitromethane, benzene, acetonitrile, dichloromethane, and 2,4,6-trimethylpyridine (*sym*-collidine) were dried and freshly distilled prior to use. All solid reactants for glycosylation were dried, prior to use, overnight over phosphorus pentoxide under high vacuum. *N,N*-Dimethylchloroforminium chloride (Vilsmeier reagent) was prepared by the method of Bosshard *et al.* (27).

*Benzyl 3,4,6-tri-*O*-acetyl-2-deoxy-2-phthalimido-β-D-glucopyranoside (2)*

A solution of 3,4,6-tri-*O*-acetyl-2-deoxy-2-phthalimido-β-D-glucopyranosyl bromide (6) (**1**), mp 122–123°C, $[\alpha]_D^{24}$ +57.3° (*c* 1.0, $CHCl_3$), (14.95 g, 30 mmol) in dry nitromethane (20 mL) was added to a cooled (−30°C) solution of benzyl alcohol (3.24 g, 30 mmol), silver trifluoromethanesulfonate (8.0 g, 31 mmol), and 2,4,6-trimethylpyridine (3.75 g, 31 mmol) in dry nitromethane (30 mL) under nitrogen. The mixture was stirred at −30°C for 2 h and then diluted with chloroform (100 mL). The solid was removed by filtration and the filtrate was evaporated *in vacuo*. The foamy residue was dissolved in chloroform (100 mL), and washed sequentially with ice-water, 5% aqueous hydrogen chloride, and with aqueous sodium bicarbonate solution. Solvent removal after drying left a foam which was crystallized from diethyl ether (13.88 g, 88%), mp 106–108°C. Recrystallization from ethanol raised the melting point to 108–109°C, $[\alpha]_D^{22}$ −12.6° (*c* 0.5, $CHCl_3$); $^1$H nmr δ: 7.86–7.60 (m, 4H, phthalimido), 7.07 (s, 5H, $C_6H_5$), 5.78 (dd, 9 and 11 Hz, H-3), 5.37 (d, 8 Hz, H-1), 5.17 (t, 9 Hz, H-4), 4.95–3.75 (m, 6H), 2.12, 2.0, 1.84 (s, 3 OAc). *Anal.* calcd. for $C_{27}H_{27}NO_{10}$: C 61.71, H 5.18, N 2.67; found: C 61.66, H 5.11, N 2.48.

*Benzyl 2-deoxy-2-phthalimido-β-D-glucopyranoside (3)*

A solution of the acetate **2** (12.60 g, 24 mmol) in a mixture of acetone (200 mL), water (100 mL), and concentrated hydrochloric acid (40 mL) was kept at 70°C for 6 h. Evaporation of acetone left a suspension which was collected by filtration, washed with cold water, and dried when a solid was obtained (9.20 g, 97% yield), mp 173–175°C. Recrystallization from ethyl acetate raised the melting point to 176–177°C, $[\alpha]_D^{25}$ −34.2° (*c* 0.76, $Me_2CO$). The $^1$H nmr spectrum was consistent with expectations. *Anal.* calcd. for $C_{21}H_{21}NO_7$: C 63.14, H 5.30, N 3.51; found: C 63.09, H 5.27, N 3.43.

*Benzyl 4,6-*O*-benzylidine-2-deoxy-2-phthalimido-β-D-glucopyranoside (4)*

A solution of glycoside **3** (8.0 g, 20 mmol), α,α-dimethoxytoluene (6.08 g, 40 mmol), and *p*-toluenesulfonic acid (200 mg) in freshly distilled acetonitrile (200 mL) was stirred at room temperature for 16 h. Neutralization with triethylamine (2 mL) and solvent

[5]R. U. Lemieux and S. Z. Abbas, unpublished work.

Can. J. Chem. Downloaded from www.nrcresearchpress.com by 210.87.254.40 on 09/06/12
For personal use only.

Can. J. Chem. Downloaded from www.nrcresearchpress.com by 210.87.254.40 on 09/06/12
For personal use only.

removal left a sticky solid which was triturated several times with Skellysolve "B" and finally collected by filtration. Recrystallization from ethanol yielded colorless needles (8.96 g, 92% yield), mp 183–184°C; $[\alpha]_D^{25}$ −75.4° (*c* 1.2, $CHCl_3$). The $^1H$ nmr spectrum was consistent with expectations. *Anal.* calcd. for $C_{28}H_{25}NO_7$: C 68.98, H 5.17, N 2.88; found: C 68.85, H 5.06, N 2.70.

*Benzyl 3-O-(tetra-O-acetyl-β-D-galactopyranosyl)-4,6-O-benzylidene-2-deoxy-2-phthalimido-β-D-glucopyranoside (5)*

A solution of the alcohol **4** (7.31 g, 15 mmol) in a 1:1 mixture of nitromethane and benzene (600 mL) was distilled until 100 mL of distillate was collected. The temperature was adjusted to 60°C, mercuric cyanide (5.05 g, 20 mmol) and acetobromogalactose (8.22 g, 20 mmol) were added. After the mixture was stirred at 60°C for 24 h, additional amounts of mercuric cyanide (3.74 g) and the bromide (6.17 g, 15 mmol) were added and the mixture was stirred for 28 h at 60°C. The cooled solution was washed with 30% aqueous potassium iodide solution (2 × 250 mL), with aqueous sodium bicarbonate (2 × 250 mL), and with brine (500 mL). Each washing was back-extracted with chloroform (2 × 200 mL). The combined organic layers were evaporated to a foam which was dissolved in 90% aqueous acetic acid (50 mL) and the solution was stirred at room temperature for 30 min in case orthoesters had formed. The solution was diluted with chloroform (200 mL) and washed with ice-water (3 × 200 mL) and sodium bicarbonate solution (2 × 250 mL). Solvent removal left a foam which was passed through a short alumina (Woelm, neutral) column using ethyl acetate – diethyl ether (1:1). Solvent removal yielded a colorless foam (21 g). Addition of diethyl ether caused the crystallization of tetra-*O*-acetyl-β-D-galactopyranosyl cyanide (4.7 g), mp 168–170°C; $[\alpha]_D^{24}$ +36.2° (*c* 2.15, $CHCl_3$) (lit. (31) mp 168–169°C; $[\alpha]_D^{20}$ +37.2° (*c* 7.95, $CHCl_3$)).

Evaporation of the mother liquor left a foam which was applied to a silica gel (180 g) column and eluted with ethyl acetate – hexane–benzene (1:1:1). Solvent removal of the second and main fraction left a colorless foam (12.7 g). This crude product crystallized from diethyl ether but contained traces of tetra-*O*-acetyl-β-D-galactopyranosyl cyanide. Recrystallization from ethanol yielded colorless needles (9.02 g, 73% yield based on compound **4**), mp 170–171°C; $[\alpha]_D^{24}$ −46.3° (*c* 0.66, $CHCl_3$); $^1H$ nmr δ: 7.77 (s, 4H, phthalimido), 7.60–7.32 (m, 5H, phenyl), 7.01 (s, 5H, phenyl), 5.57 (s, 1H, $CHC_6H_5$), 5.14 (d, 9 Hz, H-1), 2.05, 1.90, 1.82, 1.53 (s, 4 OAc). *Anal.* calcd. for $C_{42}H_{43}NO_{16}$: C 61.68, H 5.30, N 1.72; found: C 61.99, H 5.33, N 1.57.

*Benzyl 4,6-di-O-acetyl-3-O-(tetra-O-acetyl-β-D-galactopyranosyl)-2-deoxy-2-phthalimido-β-D-glucopyranoside (7)*

A solution of the benzylidene compound **5** (8.18 g, 10 mmol) in 60% aqueous acetic acid (100 mL) was stirred at 100°C for 30 min and diluted with water (100 mL). Solvent removal left a foam (**6**) which was not characterized but acetylated directly with a 2:1 mixture of pyridine – acetic anhydride (90 mL). Solvent removal left a foam which was dissolved in chloroform (100 mL) and washed with 5% aqueous hydrochloric acid, sodium bicarbonate solution, and then with ice-water. Solvent removal then left a foam which was applied to a silica gel column and eluted with a mixture of ethyl acetate – hexane (1:1). Solvent removal of the second fraction yielded a solid (6.15 g, 75% yield based on compound **5**), mp 89–92°C; $[\alpha]_D^{23}$ −42.3° (*c* 1.3, $CHCl_3$). The $^1H$ nmr spectrum was consistent with expectations. *Anal.* calcd. for $C_{39}H_{43}NO_{18}$: C 57.56, H 5.33, N 1.72; found: C 57.11, H 5.49, N 1.61.

*4,6-Di-O-acetyl-3-O-(tetra-O-acetyl-β-D-galactopyranosyl)-2-deoxy-2-phthalimido-D-glucopyranose (8)*

A mixture of compound **7** (4.88 g, 6 mmol) and 5% palladium on carbon (3.0 g) in a 1:1 mixture of ethanol and ethyl acetate (100 mL) was hydrogenated at 50 psi at room temperature for 16 h. The solid was removed by filtration and the filtrate evaporated. The resulting foam was applied to a silica gel column and eluted with a mixture of ethyl acetate – hexane (2:1). The second and main fraction on evaporation left a solid (4.02 g, 93% yield), mp 123–126°C; $[\alpha]_D^{24}$ +12.2° (*c* 1.0, $CHCl_3$). *Anal.* calcd. for $C_{32}H_{37}NO_{18}\cdot H_2O$: C 51.80, H 5.30, N 1.89; found: C 51.97, H 5.12, N 1.77.

*4,6-Di-O-acetyl-3-O-(tetra-O-acetyl-β-D-galactopyranosyl)-2-deoxy-2-phthalimido-α,β-D-glucopyranosyl chloride (9)*

A solution of compound **8** (3.62 g, 5 mmol), *N,N*-dimethylchloroforminium chloride (Vilsmeier reagent) (2.56 g, 20 mmol), and collidine (2.42 g, 20 mmol) in dry dichloromethane (20 mL) was stirred at 0°C for 3 h. Dilution with dichloromethane (50 mL), washing with cold water, drying over sodium sulfate, and solvent removal gave a foam which crystallized on addition of diethyl ether (3.53 g, 95% yield), mp 104–109°C; $[\alpha]_D^{24}$ +18.7 (*c* 0.7, chloroform). The $^1H$ nmr spectrum of the product showed it to be a 3:7 mixture of α and β-anomers; $^1H$ nmr δ: 8.0–7.74 (m, 4H, phthalimido), 6.11 (d, 0.3H, 4 Hz, H-1), 5.92 (d, 0.7H, 9 Hz, H-1). *Anal.* calcd. for $C_{32}H_{36}NO_{17}Cl$: C 51.79, H 4.89, N 1.88, Cl 4.77; found: C 51.70, H 4.96, N 1.84, Cl 4.90.

## Acknowledgements

The authors are indebted to the National Research Council of Canada for grants (A172) in aid of this research to R.U.L. The nmr and microanalyses were provided by the spectral and analytical service laboratories of this department.

1. R. KUHN, A. GAUHE, and H. H. BAER. Chem. Ber. **87**, 289 (1954).
2. W. M. WATKINS. Adv. Hum. Genet. **10**, 1 (1980).
3. R. U. LEMIEUX, D. A. BAKER, W. M. WEINSTEIN, and C. M. SWITZER. Biochemistry **20**, 199 (1981).
4. W. M. WATKINS and W. T. J. MORGAN. Nature, **180**, 1038 (1957).
5. W. M. WATKINS and W. T. J. MORGAN. Vox Sang. **7**, 129 (1962).
6. R. U. LEMIEUX, T. TAKEDA, and B. Y. CHUNG. Am. Chem. Soc. Symp. Ser. No. 39, 1976, p. 90.
7. F. MICHEEL and H. KÖCHLING. Chem. Ber. **91**, 673 (1958), and earlier work.
8. M. KISO, Y. KANEDA, R. SHIMIZU, and A. HASEGAWA. Carbohydr. Res. **83**, C8 (1980).
9. C. D. WARREN and R. W. JEANLOZ. Carbohydr. Res. **53**, 67 (1977).
10. F. SCHMITT and P. SINAŸ. Carbohydr. Res. **29**, 99 (1973).
11. M. M. PONPIPOM, R. L. BUGIANESI, and T. Y. SHEN. Tetrahedron Lett. **20**, 1717 (1978).
12. D. R. BUNDLE and S. JOSEPHSON. Can. J. Chem. **57**, 662 (1979).
13. R. U. LEMIEUX and H. DRIGUEZ. J. Am. Chem. Soc. **97**, 4063 (1975).
14. C. AUGÉ and A. VEYRIÈRES. J. Chem. Soc. Perkin Trans. I, 1343 (1977).
15. R. U. LEMIEUX, S. Z. ABBAS, and B. Y. CHUNG. Can. J. Chem. **60**, 68 (1982).
16. J.-C. JACQUINET, S. E. ZURABYAN, and A. YA. KHORLIN. Carbohydr. Res. **32**, 137 (1974).
17. B. Y. CHUNG and Y. K. SIM. Taehan Hwahakhoe Chi, **23**, 46 (1979).
18. K. L. MATTA and O. P. BAHL. Carbohydr. Res. **21**, 460 (1972).

19. K. L. MATTA, E. A. JOHNSON, and J. J. BARLOW. Carbohydr. Res. **26**, 215 (1973).
20. S. DAVID and A. VEYRIÈRES. Carbohydr. Res. **40**, 23 (1975).
21. C. AUGÉ, S. DAVID, and A. VEYRIÈRES. Nouv. J. Chim. **3**, 491 (1979).
22. R. KAIFU, T. OSAWA, and R. W. JEANLOZ. Carbohydr. Res. **40**, 111 (1975).
23. R. KAIFU and T. OSAWA. Carbohydr. Res. **52**, 179 (1976).
24. R. U. LEMIEUX, S. Z. ABBAS, M. H. BURZYNSKA, and R. M. RATCLIFFE. Can. J. Chem. **60**, 63 (1982).
25. H. EILINGSFELD, M. SEEFELDER, and H. WEIDINGER. Angew. Chem. **72**, 836 (1960): Chem. Ber. **96**, 2671 (1963).
26. Z. ARNOLD. Collect. Czech. Chem. Commun. **26**, 1723 (1961).
27. H. H. BOSSHARD, R. MORY, M. SCHMID, and HCH. ZOLLINGER. Helv. Chim. Acta, **42**, 1653 (1959).
28. J. R. POUGNY, J. C. JACQUINET, M. NASSR, D. DUCHET, M. L. MILAT, and P. SINAŸ. J. Am. Chem. Soc. **99**, 6762 (1977).
29. Z. ARNOLD and A. HOLY. Collect. Czech. Chem. Commun. **26**, 3059 (1961).
30. D. R. HEPBURN and H. R. HUDSON. J. Chem. Soc. Perkin Trans. I, 754 (1976).
31. N. CONSTANTZAS and J. KOCOUREK. Collect. Czech. Chem. Commun. **24**, 1099 (1959).

Can. J. Chem. Downloaded from www.nrcresearchpress.com by 210.87.254.40 on 09/06/12
For personal use only.

# Syntheses of derivatives of *N*-acetyl-D-lactosamine from D-lactal hexaacetate. Hexa-*O*-acetyl-2-deoxy-2-phthalimido-β-D-lactosyl chloride

R. U. LEMIEUX, S. Z. ABBAS,[1] M. H. BURZYNSKA,[2] AND R. M. RATCLIFFE[3]

*Department of Chemistry, University of Alberta, Edmonton, Alta., Canada T6G 2G2*

Received March 27, 1981

R. U. LEMIEUX, S. Z. ABBAS, H. BURZYNSKA, and R. M. RATCLIFFE. Can. J. Chem. **60**, 63 (1982).

Two reaction routes are presented for the preparation of hexa-*O*-acetyl-2-deoxy-2-phthalimido-β-D-lactosyl chloride (**7**) from lactal hexaacetate (**1**). One route involves, in the first stage, reaction of **1** with nitrosyl chloride and proceeds by way of benzyl 2-amino-2-deoxy-α-D-lactoside (**4**) as an intermediate. The other route, which is considered more efficient, involves reaction of **1** with ceric ammonium nitrate and sodium azide and involves the β-anomer (**12**) of **4** as an intermediate. The preparation of **7** is of interest as a reagent for the preparation of 2-amino-2-deoxy-β-D-lactosides. The procedures offer routes for the preparation of D-lactosamine.

R. U. LEMIEUX, S. Z. ABBAS, M. H. BURZYNSKA et R. M. RATCLIFFE. Can. J. Chem. **60**, 63 (1982).

On présente deux méthodes de préparation du chlorure d'hexa-*O*-acetyl-déoxy-2-phtalimido-2-β-D-lactosyle (**7**) à partir de l'hexaacétate de lactale (**1**). Une méthode fait intervenir, dans la première étape, la réaction du composé **1** avec le chlorure de nitrosyle et passe par un intermédiaire benzylamino-2-déoxy-2-α-D-lactoside (**4**). L'autre méthode, que l'on considère plus efficace, fait intervenir la réaction de **1** avec le nitrate d'ammonium cérique et l'azoture de sodium et implique comme intermédiaire l'anomère β (**12**) du composé **4**. L'intérêt de la préparation du composé **7** réside dans le fait qu'il est un moyen d'accès aux amino-2-déoxy-2-β-D-lactosides. Les méthodes ouvrent la voie à la préparation de la D-lactosamine.

[Traduit par le journal]

*N*-Acetyl-D-lactosamine (D-LacNAc) is of widespread occurrence as a component of the oligosaccharide portions of very many *N*- and *O*-linked glycoproteins and the oligosaccharides of milk (1). It is a building unit for the antigenic determinants of a number of certain Ii human blood group activities (2) as well as of the ABH Type 2 determinants (3).

In 1977[4] we announced our involvement in the chemical synthesis of oligosaccharide structures of possible interest to immunochemical investigations of the Ii determinants. On that occasion, the synthesis, amongst others, of βDLacNAc(1→6) and βDLacNAc(1→3) derivatives of both D-galactose and $\beta DGalO(CH_2)_8COOCH_3$ were reported. These syntheses are now reported in detail in an accompanying paper. The role that these products played in establishing the nature of the combining site of the monoclonal anti-I Ma myeloma protein have been reported in separate communications (5, 6). The synthesis of these β-glycosides of *N*-acetyl-D-lactosamine was accomplished by way of hexa-*O*-acetyl-2-deoxy-2-phthalimido-β-D-lactosyl chloride (**7**) using the silver triflate – collidine complex (7) to promote its condensation with the alcohol. The worth of this approach (the phthalimido-chloride method) for the establishment of β-glycosidic linkage from 2-amino-2-deoxy sugars (wherein the amino group is in equatorial orientation) was considered in an accompanying paper (4). We now wish to report details for the preparation of **7** from D-lactal hexaacetate (**1**) by two different routes. One process is based on the procedure for the preparation of 2-amino-2-deoxy-α-glycopyranoside which was developed in this laboratory (8) and which will be termed the nitroso-chloride route. The other process for the preparation of **7** is based on the azidonitration of glycals (9, 10) to form 2-azido-2-deoxy glycopyranosides and which will be designated as the azidonitrate route.

Ponpipom and co-workers (11, 12) have independently used the nitroso-chloride route for the preparation of the phthalimido-chloride **7**. Although full details have not been reported, these investigators used the same reaction sequences except for the conversion of **6** to **7**. Whereas we used the Vilsmeier reagent for this purpose (4), they chose to acetylate **6** for subsequent conversion to **7** using aluminum chloride. Dimitriev *et al.* (13) had previously prepared *N*-acetyl-D-lactosamine by way of a zinc reduction of the oximino-chloride **2**.

Very recently, Arnarp and Lönngren (14) published the use of the azidonitration route to achieve the bromide form of the chloride **7**. The reagent was used in the course of the preparation of hepta- and

[1]University of Alberta Postdoctoral Fellow 1975–1977. Present address: Chembiomed Ltd., W5-56 Chemistry Bldg., University of Alberta, Edmonton, Alta., Canada T6G 2G2.

[2]University of Alberta Postdoctoral Fellow 1978–1980.

[3]University of Alberta Postdoctoral Fellow (1975–1977) and Research Associate (1977–1979). Present address: Chembiomed Ltd., W5-56 Chemistry Bldg., University of Alberta, Edmonton, Alberta, Canada T6G 2G2.

[4]R. U. Lemieux, S. Z. Abbas, and B. Y. Chung. Abstr. Pap. Chem. Soc. Meeting, Norwich, England, April 8–10, 1977.

0008-4042/82/010063-05$01.00/0

©1982 National Research Council of Canada/Conseil national de recherches du Canada

Can. J. Chem. Downloaded from www.nrcresearchpress.com by 210.87.254.105 on 09/06/12
For personal use only.

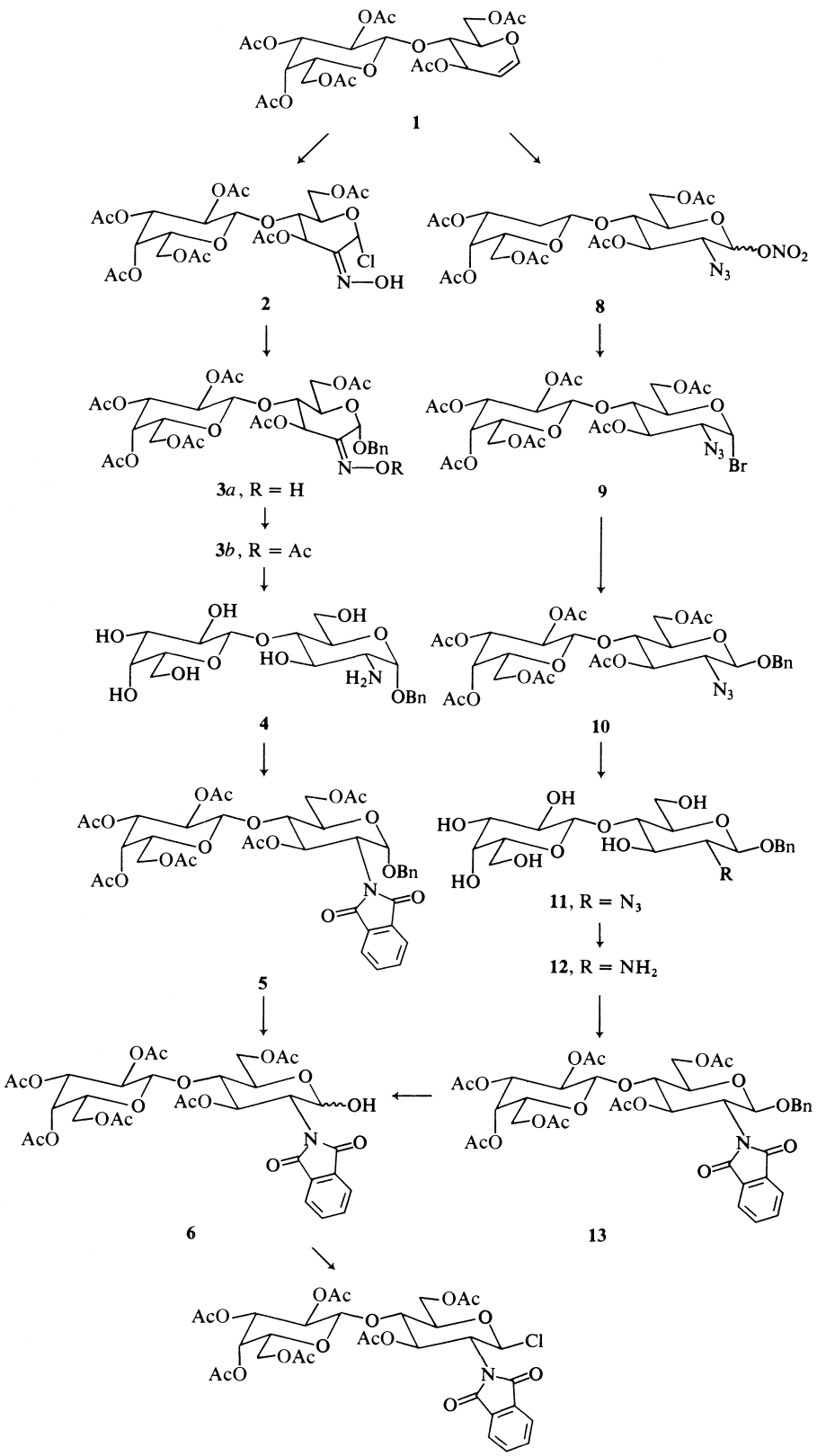


Can. J. Chem. Downloaded from www.nrcresearchpress.com by 210.87.254.105 on 09/06/12
For personal use only.

Can. J. Chem. Downloaded from www.nrcresearchpress.com by 210.87.254.105 on 09/06/12
For personal use only.

pentasaccharides which are building units of "complex type" aspargine-linked glycoproteins.

Although it was not possible to expend much effort toward the optimization of yields, it is noteworthy that the seven-stage process for converting D-lactal hexaacetate (**1**) to **6** by way of the azidonitration route proceeded in 23% overall yield whereas only near half this yield was obtained by way of the six-stage nitroso-chloride route. On the other hand, a number of transformations in the latter process proceeded in yields that likely can be substantially improved. At the time that this process was investigated, the relatively high reactivity of the phthalimido group in α-glycosides toward hydrolysis[5] was not recognized and this property likely had an influence on the low yields obtained in the preparation of compounds **5** (70%) and **6** (60%). Also, the relatively poor yields obtained in the reaction of the nitrosyl chloride adduct **2** with benzyl alcohol and for the diborane reduction of the oximinoacetate **3***b* appear unacceptable in view of our previous experiences (8) with these reactions. Nevertheless, we recommend the process by way of azidonitration as the more convenient and reliable laboratory preparation.

The synthetic sequences are straightforward and warrant little comment beyond the information contained in the experimental portion of this paper. It may be noted that the use (15) of a strongly basic resin for the removal of alkali-labile by-products in the preparation of **4** should prove generally useful for such preparations. The high resistance to hydrogenolysis displayed by the α-benzyl glycoside **5** as compared to its β-anomer **13** was to be expected (16) but was an important disadvantage in the formation of a product **6** which contains groups susceptible to solvolysis. The reduction of the azide **11** to the amine **12** using hydrogen sulfide (17) in the presence of amine proved highly convenient and essentially quantitative. The amine **4** was characterized both as its peracetate and as its *N*-acetyl derivative. The use of the Vilsmeier reagent for the conversion of **6** to **7** has been presented in a separate communication (4). The preparation of the azido-bromide **9** in 42% overall yield by way of the azidonitration of **1** has been reported (10).

## Experimental

The general procedures and analytical methods were the same as previously described (4). The nmr measurements used either TMS (< 1%) as internal standard or 1:1 TMS–$CCl_4$ as external standard.

*Dimeric 3,6-di-*O*-acetyl-(4-*O*-tetra-*O*-acetyl-β-D-galactopyranosyl)-2-deoxy-2-nitroso-α-D-glucopyranosyl chloride (**2**)*

Nitrosyl chloride was added to a solution of D-lactal hexaacetate **1** (18) in dry ethyl acetate (280 mL) (19) to form **2**, mp 122–123°C, $[\alpha]_D^{20}$ +69.2° (*c* 1.0, $CHCl_3$), in 92% yield (lit. (13) mp 120–122°C, $[\alpha]_D^{20}$ +66.7° (*c*, 1.0, $CHCl_3$)).

*Benzyl 3,6-di-*O*-acetyl-4-*O*-(tetra-*O*-acetyl-β-D-galactopyranosyl)-2-deoxy-2-oximino-α-D-*arabino*-hexopyranoside (**3**a)*

A solution of the nitrosyl chloride adduct (**2**) (60.0 g, 0.11 mol) and benzyl alcohol (14.0 g, 0.13 mol) in *N,N*-dimethylformamide (300 mL) was kept at room temperature for 2 days. The solvent was removed, the dark yellow residual oil was dissolved in diethyl ether (500 mL), and this solution was washed with water (3 × 200 mL). Work-up in the usual manner provided a solid foam which was chromatographed on a column of Silica Gel G (E. Merck A.G., Darmstadt) using ethyl acetate – hexane (1:1). The first and main fraction provided a solid (40.0 g, 59% yield), $[\alpha]_D^{24}$ +31.2° (*c* 1.3, $CHCl_3$), whose $^1H$ nmr spectrum was consistent with expectation for the title compound **3***a*. *Anal.* calcd. for $C_{31}H_{39}NO_{17}$: C 53.37, H 5.64, N 2.01; found: C 53.75, H 5.55, N 2.01.

*Benzyl 2-acetoximino-3,6-di-*O*-acetyl-4-*O*-(tetra-*O*-acetyl-β-D-galactopyranosyl)-α-D-*arabino*-hexopyranoside (**3**b)*

Treatment of the oxime **3***a* (27.0 g, 38 mmol) with pyridine – acetic anhydride (2:1) (150 mL) at 5°C for 12 h provided the title compound **3***b* (26.0 g, 90% yield) as a solid, $[\alpha]_D^{24}$ +31.0 (*c* 1, $CHCl_3$) (lit. (13) $[\alpha]_D^{25}$ +12° (*c* 1.45, $CHCl_3$)), with an $^1H$ nmr spectrum consistent with a high degree of purity. *Anal.* calcd. for $C_{33}H_{41}NO_{18}$: C 53.58, H 5.58, N 1.89; found: C 53.19, H 5.51, N 1.72.

*Benzyl 2-amino-2-deoxy-4-*O*-(β-D-galactopyranosyl)-α-D-glucopyranoside (**4**)*

A solution of the oximinoacetate **3***b* (25.0 g, 33.7 mmol) in tetrahydrofuran (200 mL) was added dropwise to a 1 *M* solution of diborane in tetrahydrofuran (800 mL) kept at −70°C in an atmosphere of nitrogen. After completion of the addition, the solution was allowed to warm to room temperature and kept for 24 h and then carefully poured into methanol (600 mL). Evaporation left an oil which was taken up in methanol, rendered acid with acetic acid, and evaporated to a solid residue. This residue was dissolved in methanol and the solution was applied to a column (2.5 × 50 cm) of a basic resin (15) (Dowex I-X8, 200–400 mesh, $OH^-$ form). On elution with methanol and solvent removal, a crystalline solid (8.6 g, mp 138–142°C, 60% yield) was obtained. Recrystallization from ethanol raised the melting point to 164–168°C, $[\alpha]_D^{25}$ +64.6° (*c* 1, $H_2O$). The $^1H$ nmr was consistent with the structural assignment. *Anal.* calcd. for $C_{19}H_{29}NO_{10}\cdot H_2O$: C 49.77, H 7.03, N 3.05; found: C 50.76, H 6.95, N 3.11.

Acetylation of **4** provided benzyl 2-acetamido-3,6-di-*O*-acetyl-4-*O*-(tetra-*O*-acetyl-β-D-galactopyranosyl)-2-deoxy-α-D-glucopyranoside, mp 101–103°C; $[\alpha]_D$N +51° (*c* 0.4, $CHCl_3$) (lit. (12) mp 102–104°C, $[\alpha]_D^{25}$ +56.4 (*c* 1.56, $CHCl_3$)). De-*O*-acetylation readily provided crystalline benzyl 2-acetamido-2-deoxy-4-*O*-(β-D-galactopyranosyl)-α-D-glucopyranoside, mp 226–229°C, $[\alpha]_D^{25}$ +105.5° (*c* 0.85, $H_2O$).

*Benzyl 3,6-di-*O*-acetyl-4-*O*-(tetra-*O*-acetyl-β-D-galactopyranosyl)-2-deoxy-2-phthalimido-α-D-glucopyranoside (**5**)*

Phthalic anhydride (1.2 g, 8 mmol) was added to a solution of the amine **4** (6.0 g, 13.9 mmol) in pyridine (25 mL). The solution was heated to 60–75°C for 20 min. Triethylamine (1.4 g, 13.9 mmol) and more phthalic anhydride (1.2 g, 8 mmol) were added and the heating was continued for 2 h. Methanol (50 mL) was added and the solution was evaporated to a dry residue which was taken up in 30 mL of a mixture of pyridine – acetic anhydride (2:1). After heating at 90°C for 3 h, the crude solid product was isolated in the usual manner and applied to a

[5]R. U. Lemieux and P. Hermentin, in preparation.

Can. J. Chem. Downloaded from www.nrcresearchpress.com by 210.87.254.105 on 09/06/12
For personal use only.

column (2.5 × 50 cm) of Silica Gel G for chromatography using ethyl acetate – hexane (2:1). The first fraction (7.88 g, 70% yield) was recrystallized from ethyl acetate – hexane, mp 177–180°C, $[\alpha]_D^{25}$ +86.1° (*c* 1.1, $CHCl_3$). The $^1H$ nmr was consistent with the structural assignment. The signals for C-1′ and C-1 occurred at 100.97 and 96.35 ppm, respectively. *Anal.* calcd. for $C_{39}H_{43}NO_{18}$: C 57.56, H 5.32, N 1.72; found: C 57.41, H 5.25, N 1.66.

*Benzyl 3,6-di-O-acetyl-4-O-(tetra-O-acetyl-β-D-galacto-pyranosyl)-2-azido-2-deoxy-β-D-glucopyranoside (**10**)*

A solution of the azidobromide **9** (10), (20.5 g, 30 mmol), mp 156–157°C, $[\alpha]_D^{25}$ +87° (*c* 0.93, $CHCl_3$), in nitromethane (50 mL) was added dropwise to a stirred mixture of benzyl alcohol (10.0 g, 92 mmol), silver carbonate (30.0 g, 109 mmol), and Drierite (30.0 g) which was cooled to −22°C and protected from light and moisture. After stirring at this temperature for 18 h, the solids were removed by filtration and washed with dichloromethane. The combined filtrates were taken to dryness and the residue was dissolved in ethyl acetate – hexane (1:1) for passage through a short column of Silica Gel G. Solvent removal left an oily residue from which the title compound **10** crystallized on the addition of diethyl ether. After one recrystallization from diethyl ether (16.4 g, 77% yield), the melting point was 137–138°C, $[\alpha]_D^{25}$ −9.7° (*c* 2.3, $CHCl_3$). The $^1H$- and $^{13}C$ nmr spectra in $CDCl_3$ were entirely consistent with the assigned structure; for example, in confirming the presence of the benzyl group, the six acetyl groups at 1.96, 2.03, 2.05, 2.11, 2 × 2.15 ppm and the two β-anomeric hydrogens at 4.45 (d, 8 Hz, H-1′) and 4.05 ppm (d, 8.5 Hz, H-1). The signals for C-1′ and C-1 were at 100.88 and 100.07 ppm, respectively. Absorption in the infrared (KBr) at 2110 $cm^{-1}$ confirmed the presence of the azido group. *Anal.* calcd. for $C_{31}H_{39}O_{16}N_3$: C 52.47, H 5.54, N 5.92; found: C 52.22, H 5.64, N 5.68.

*Benzyl 2-azido-2-deoxy-4-O-(β-D-galactopyranosyl)-β-D-gluco-pyranoside (**11**)*

The acetate **10** (8.72 g, 12.3 mmol) was dissolved in 150 mL of 0.01 *N* sodium methoxide in methanol. Solvent removal provided crystals which were washed with a little cold methanol (5.01 g, 89% yield), mp 202–204°C, $[\alpha]_D^{25}$ −1.1° (*c* 0.4, $CH_3OH$). *Anal.* calcd. for $C_{19}H_{27}O_{10}N_3$: C 49.89, H 5.95, N 9.19; found: C 49.84, H 5.86, N 8.97.

*Benzyl 2-amino-2-deoxy-4-O-(β-D-galactopyranosyl)-β-D-glucopyranoside (**12**)*

A slow stream of hydrogen sulfide was bubbled through an ice-cold solution of the azide **11** (10.8 g, 23.5 mmol) in pyridine (210 mL) and triethylamine (60 mL) for 2.5 h. The solution was evaporated to dryness and the residue was extracted with a mixture of methanol–water (1:1). The extract was filtered through a bed of diatomaceous earth and evaporated. The residue (10.65 g) appeared to be the desired amine **12** as assessed by $^{13}C$ nmr and tlc. Although it was contaminated with traces of sulfur, it was used directly for the preparation of the phthalimido compound **13**. In order to remove the sulfur and obtain a sample for analysis, the compound was adsorbed on a cation-exchange resin (AG 50W-X2, 200–400 mesh, 40 g) in the $H^+$ form and, after washing, was desorbed with ammonium hydroxide. After solvent removal, the residue was taken up in water, the solution treated with charcoal and evaporated to a syrup which crystallized, mp 108–111°C, $[\alpha]_D^{25}$ −25.3° (*c* 2.4, $H_2O$); $^{13}C$ nmr ($D_2O$, external TMS): 136.68, 128.62, 128.53, 128.31, 102.95 (C-1′), 101.88 (C-1), 78.97 (C-4), 75.17, 74.76, 74.20, 72.53, 71.39, 70.86, 68.42, 60.81 and 60.27 (C-6 and C-6′), 56.02 (C-2). *Anal.* calcd. for $C_{19}H_{29}NO_{10}\cdot 0.5H_2O$: C 51.81, H 6.86, N 3.18; found: C 51.85, H 6.67, N 2.98.

*Benzyl 3,6-di-O-acetyl-4-O-(tetra-O-acetyl-β-D-galactopyrano-syl)-2-deoxy-2-phthalimido-β-D-glucopyranoside (**13**)*

Treatment of the β-amine **12**, under the conditions described above for the conversion of the α-anomer **4** to **5**, provided the title compound **13** in 79% yield after recrystallization from ethyl acetate – hexane, mp 187–188°C, $[\alpha]_D^{25}$ −9.6° (*c* 2.5, $CHCl_3$). The $^1H$- and $^{13}C$ nmr spectra ($CDCl_3$) were consistent with the structural assignment. The signals for the H-1 and H-1′ atoms were at 5.40 and 4.57 ppm each as doublets with spacings of 8.2 Hz. The low-field signal for H-1 is consistent with the deshielding expected by the vicinal phthalimido group. The signals for C-1′ and C-1 occurred at 101.06 and 97.1 ppm, respectively. *Anal.* calcd. for $C_{32}H_{37}NO_{18}$: C 57.57, H 5.33, N 1.73; found: C 57.57, H 5.44, N 1.72.

*3,6-Di-O-acetyl-4-O-(tetra-O-acetyl-β-D-galactopyranosyl)-2-deoxy-2-phthalimido-α,β-D-glucopyranose (**6**)*

(a) *From the α-benzyl glycoside **5***

Hydrogenolysis of compound **5** (6.0 g, 7.3 mmol) dissolved in 5% solution of acetic acid in ethanol (100 mL) and using 5% palladium on charcoal (4.0 g) and 50 psi of hydrogen was incomplete after 24 h. The title compound was obtained in 60% yield by chromatography on Silica Gel G column (3 × 60 cm) and developing the column with ethyl acetate – hexane (2:1). It occurred as the second and main fraction, mp 116–120°C. The identity of the product was evident from a consideration of its $^1H$ nmr which, furthermore, was similar to that for the product obtained below. Moreover, both products could be converted to the phthalimido-chloride (**7**) in 82–85% yields.

(b) *From the β-benzyl glycoside **13***

Hydrogenolysis of compound **13** in ethanol – ethyl acetate (1:1) at 70 psi and room temperature using 10% palladium on charcoal proceeded readily to provide the title product, mp 132–140°C, in quantitative yield.

*3,6-Di-O-acetyl-4-O-(tetra-O-acetyl-β-D-galactopyranosyl)-2-deoxy-2-phthalimido-β-D-glucopyranosyl chloride (**7**)*

The alcohol **6** (2.98 g, 4.13 mmol) was dissolved with *sym*-collidine (0.77 g, 6.4 mmol) in dichloromethane (20 mL). This solution was added dropwise to a suspension of *N*,*N*-dimethylchloroforminium chloride (Vilsmeier reagent) (1.70 g, 12.9 mmol) in dichloromethane (10 mL) kept at 0°C and in an atmosphere of dry nitrogen. The reaction mixture was allowed to warm to room temperature while being stirred for 3 h. Toluene (100 mL) was then added and the solution was washed with cold dilute aqueous hydrochloric acid (30 mL), then with aqueous sodium bicarbonate (30 mL), and finally with water (30 mL). After drying over anhydrous sodium sulfate, the solvent was removed to leave a residue which crystallized readily from dichloromethane – diethyl ether, mp 184–185°C, $[\alpha]_D^{25}$ +34.7° (*c* 1.8, $CHCl_3$) (lit. (12) mp 173–174°C; $[\alpha]_D^{25}$ +29.3° (*c* 1.5, $CHCl_3$)) (2.61 g, 85% yield). The compound was best characterized by its $^{13}C$ nmr spectrum ($CDCl_3$): 170.25, 170.07, 169.96, 169.09, 167.36, 134.54, 131.20, 123.80, 101.07 (C-1′), 85.55 (C-1), 78.60, 77.19, 76.44, 76.30, 75.77, 71.06, 70.96, 70.72, 69.12, 66.65, 62.03, 60.81, 67.91 (C-2), 20.82, 20.58, 20.46. *Anal.* calcd. for $C_{32}H_{36}NO_{17}Cl$: C 51.79, H 4.89, N 1.88, Cl 4.77; found: C 51.63, H 4.85, N 1.87, Cl 4.77.

## Acknowledgements

Financial support of the National Research Council of Canada (Grant A172 to R. U. Lemieux) is gratefully acknowledged. The nmr and microanalyses were provided by the Spectral and Analytical Service Laboratories of this department.

1. A. GOTTSCHALK (*Editor*). Glycoproteins. Elsevier Publishing Company, New York. 1972.
2. E. WOOD and T. FEIZI. FEBS Lett. **104**, 135 (1979).
3. K. O. LLOYD, E. A. KABAT, and E. LICERIO. Biochemistry, **7**, 2976 (1968).
4. R. U. LEMIEUX, S. Z. ABBAS, and B. Y. CHUNG. Can. J. Chem. **60**, 58 (1982).
5. E. A. KABAT, J. LIAO, and R. U. LEMIEUX. Immunochemistry, **15**, 727 (1978).
6. E. A. KABAT, J. LIAO, M. H. BURZYNSKA, T. C. WONG, H. THØGERSEN, and R. U. LEMIEUX. Mol. Immunol. **18**, 873 (1981).
7. R. U. LEMIEUX, T. TAKEDA, and B. Y. CHUNG. Am. Chem. Soc. Symp. Ser. No. 39, 1976. p. 90.
8. R. U. LEMIEUX, K. JAMES, and T. L. NAGABHUSHAN. Can. J. Chem. **51**, 48 (1973).
9. R. U. LEMIEUX and R. M. RATCLIFFE. Can. J. Chem. **57**, 1244 (1979).
10. R. U. LEMIEUX and R. M. RATCLIFFE. U.S. Patent No. 4,195,174. March 25, 1980.
11. M. M. PONPIPOM, R. L. BUGIANESI, and T. Y. SHEN. 2nd Joint Conference CIC/ACS, Montreal, May 30–June 2, 1977. Abstract of Papers, CARB 26.
12. M. M. PONPIPOM, R. L. BUGIANESI, and T. Y. SHEN. Tetrahedron Lett. **20**, 1717 (1978).
13. B. A. DIMITRIEV, YU. A. KNIREL, and N. K. KOCHETKOV. Akad. Nauk SSSR Bull. **22**, 2310 (1973).
14. J. ARNAPP and J. LÖNNGREN, J. Chem. Soc. Chem. Commun. 1000 (1980).
15. P. W. AUSTIN, F. E. HARDY, J. G. BUCHANAN, and J. BADDILEY. J. Chem. Soc. 5350 (1963).
16. C. E. BALLOU, S. ROSEMAN, and K. P. LINK. J. Am. Chem. Soc. **73**, 1140 (1951).
17. T. ADACHI, Y. YAMADA, I. INOUE, and M. SANEYOSHI. Synthesis, 45 (1977).
18. W. N. HAWORTH, E. L. HIRST, M. M. T. PLANT, and R. J. W. REYNOLDS. J. Chem. Soc. 2644 (1930).
19. R. U. LEMIEUX, T. L. NAGABHUSHAN, and I. K. O'NEILL. Can. J. Chem. **46**, 413 (1968).

Can. J. Chem. Downloaded from www.nrcresearchpress.com by 210.87.254.105 on 09/06/12
For personal use only.

# Syntheses of core chain trisaccharides related to human blood group antigenic determinants

R. U. LEMIEUX, S. Z. ABBAS,[1] AND B. Y. CHUNG[2]

*Department of Chemistry, University of Alberta, Edmonton, Alta., Canada T6G 2G2*

Received March 27, 1981

R. U. LEMIEUX, S. Z. ABBAS, and B. Y. CHUNG. Can. J. Chem. **60**, 68 (1982).

Trisaccharides related to the core chain of human blood group determinants were synthesized by way of the phthalimido-chloride method; namely, β-D-Gal*p*-(1→3)-β-D-GlcNAc*p*-(1→6)-D-Gal*p* (**3**), β-D-Gal*p*-(1→3)-β-D-GlcNAc*p*-(1→3)-D-Gal*p* (**5**), β-D-Gal*p*-(1→4)-β-D-GlcNAc*p*-(1→6)-D-Gal*p* (**4**), and β-D-Gal*p*-(1→4)-β-D-GlcNAc*p*-(1→3)-D-Gal*p* (**6**). The syntheses of the 8-methoxycarbonyloctyl β-glycosides of these trisaccharides are also reported.

R. U. LEMIEUX, S. Z. ABBAS et B. Y. CHUNG. Can. J. Chem. **60**, 68 (1982).

Faisant appel à la méthode du chlorure phtalimide, on a synthétisé les trisaccharides correspondant à la chaîne centrale des déterminants du groupe sanguin humain: β-D-Gal*p*-(1→3)-β-D-GlcNAc*p*-(1→6)-D-Galp (**3**), β-D-Gal*p*-(1→3)-β-D-GlcNAc*p*(1→3)-D-Gal*p* (**5**), β-D-Gal*p*-(1→4)-β-D-GlcNAc*p*-(1→6)-D-Gal*p* (**4**) et β-D-Gal*p*-(1→4)-β-D-GlcNAc*p*-(1→3)-D-Gal*p* (**6**). On rapporte également les synthèses des méthoxycarbonyl-8-octyl β-glycosides de ces trisaccharides.

[Traduit par le journal]

The core structure of the oligosaccharide structures which lead to the human ABH and Lewis antigenic determinants as terminal units can occur as linear or branched chains (1). In the case of the blood group specific glycoproteins, the first disaccharide unit (βDGal(1→3)αDGalNAc) is attached to either a serine or threonine residue of the core protein as an *O*-glycoside. The oligosaccharide is then elaborated to produce the structures which are incorporated into the basic chain shown in Fig. 1. This chain is taken from the composite megalosaccharide structure proposed by Lloyd *et al.* (2) to include the known structural features. It is not meant to indicate a specific structure.

In the case of the ABH active glycosphingolipids which have been isolated from human red cells, the basic core structure, as illustrated in Fig. 1 for a very simple structure, begins with a βDGal(1→4)-βDGlc (lactose) unit attached to the ceramide. The oligosaccharide is then mainly elaborated in this case by way of *N*-acetyllactosamine residues. Kościelak[3] has classified these as both oligo- and poly(glycosyl)ceramides.

The Ii antigens (5) consist of a chemically ill-defined group of human antigenic determinants. The I antigens are well expressed on the red cells of the majority of adults and the i antigens are found on red cells from the umbilical cords of newborn infants and the red cells of a rare group of adults which lack the I antigens (6–8). The change from i to I specificity occurs gradually during the first year of life (6) and appears to be related to the branching of the core oligosaccharide structures (9, 10). Recently the i specificity has been associated with at least two *N*-acetyllactosamine units which are linked 1→3′ (11). The I specificities appear numerous since a wide range of anti-I antibodies of different specificities are recognized (12). These antibodies are termed cold agglutinins because these do not agglutinate red cells at body temperature. These can occur in the plasma as autoantibodies and give rise to haemolytic disorders (13). It has become evident (14) that many of these anti-I antibodies are directed against carbohydrate structures and that at least some of these structures constitute the inner portions of the carbohydrate chains in the blood-group specific glycoproteins and glycolipids.

We set out several years ago[4] to synthesize portions of the structures shown in Fig. 1 as possible candidates for Ii activities (14). In this context and judging from the structures in Fig. 1, thirteen trisaccharide structures are indicated. In this regard, it must be noted that, since most of the anti-I cold agglutinins (antibodies) are monoclonal, it cannot be expected that a trisaccharide will have strong I activity unless the combining site is directed to the central sugar unit and only to portions of the two terminal units, as has now been

[1]University of Alberta Postdoctoral Fellow 1975–1977. Present address: Chembiomed Ltd., W5-56 Chemistry Bldg., University of Alberta, Edmonton, Alta., Canada T6G 2G2.

[2]University of Alberta Postdoctoral Fellow 1975–1977. Present address: Dept. of Chemistry, Korea University, Seoul, Korea.

[3]J. Kościelak. Joint Meeting of International Soc. Hematology/International Soc. Blood Transfusion, Montreal, Aug. 16–22, 1980. Abstracts of Papers, No. 298.

[4]R. U. Lemieux, S. Z. Abbas, and B. Y. Chung. Abstr. Pap. Chem. Soc. Meeting, Norwich, England, April 1977.

0008-4042/82/010068-08$01.00/0

©1982 National Research Council of Canada/Conseil national de recherches du Canada

Can. J. Chem. Downloaded from www.nrcresearchpress.com by 210.87.254.42 on 09/06/12
For personal use only.

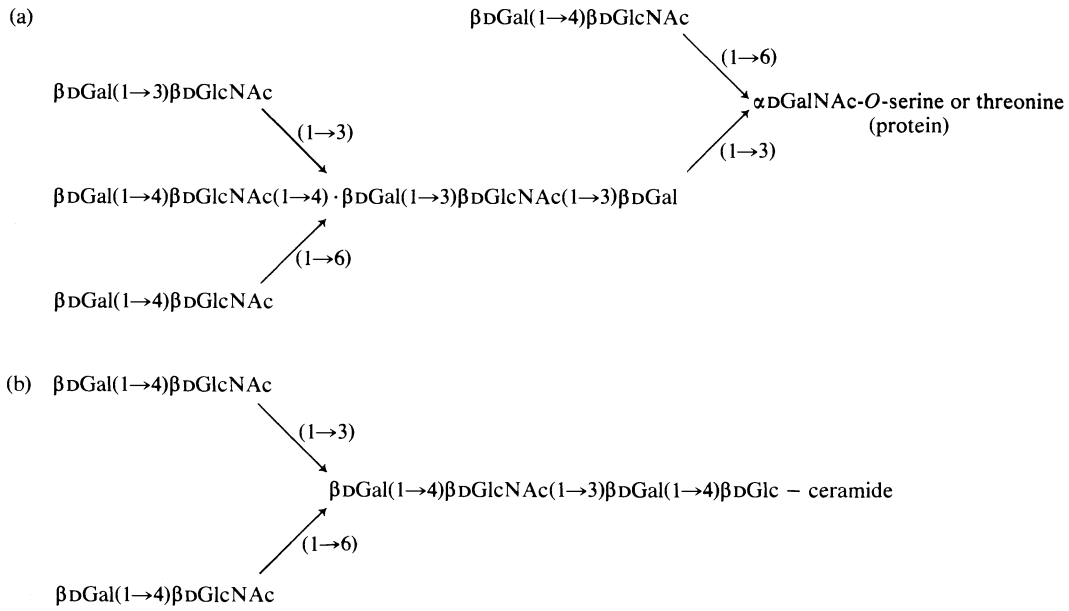


FIG. 1. (a) The composite "megalosaccharide" structure for the branched carbohydrate chains in blood-group specific glycoproteins by Lloyd *et al.* (2). (b) The core structure for the H (Type 2) active glycosphingolipid isolated by Watanabe and co-workers (3) and Kościelak *et al.* (4) have shown that poly(glycosyl)ceramides can have up to 59 glycosyl units and are multibranched.

established for the IMa determinant (15). Consequently, to properly delineate the I activities, it may prove necessary to synthesize tetra-, penta-, and even higher saccharides including branched structures.

We wish to report herein the synthesis of the four core chain trisaccharides both as the reducing trisaccharides (**3** to **6**) and as the glycosides (**9** to **12**). These were synthesized by way of condensation of hexa-*O*-acetyl-2-deoxy-2-phthalimido-α,β-D-lactosyl chloride (16) (**15**) and the corresponding derivative (17) (**14**) of lacto-*N*-biose I with the alcohols **1**, **2**, **7**, **8**, and **13**.

The condensations of the phthalimido-chlorides with the primary hydroxyl of **1** proceeded without complications and in acceptable yield (about 75%). However, the condensations with the secondary hydroxyl group of **2** were not satisfactory. In the case of the Type 1 reagent **14** to form the blocked derivative of **5**, the yield was only 24%. Indeed, attempts to prepare the Type 2 trisaccharide **6** by condensing **2** with the lactosamine derivative **15** also failed. Although the matter was not investigated in detail, we consider that the diisopropylidene compound **2** is unsatisfactory as a starting material because the cationic intermediate, which is liberated on reaction of the silver-triflate – *sym*-collidine complex with the phthalimido-chloride (**14** or **15**), attacks the *O*-isopropylidene groups at an overall faster rate than it attacks the hydroxyl group. Such an occurrence would not be without precedent (18, 19).

In order to achieve a synthesis of **6**, the condensation of hexa-*O*-acetyl-2-deoxy-2-phthalimido-β-D-lactosyl chloride (**15**) with the galactose derivative **13** was examined. In this case, the reaction proceeded smoothly to provide the desired condensation product in 80% yield. The eventual overall yield of **6**, however, proved to be unsatisfactory.

Although the synthesis of oligosaccharides, such as compounds **3** to **6**, which may correspond to antigenic determinants, can play an important role as inhibitors in studies of antibody–antigen interaction, the synthesis of the oligosaccharide attached to an aglycon which can serve as a linking arm for the preparation of artificial antigens and immunoadsorbents (20) should also provide structures which are useful in such inhibition studies. The trisaccharides **3** to **6** were synthesized as β-glycosides (**9** to **12**) of 8-methoxycarbonyloctanol since this aglycon has proven highly attractive as a linking arm (21). These structures were synthesized starting from the alcohols **7** and **8**.

The $^{1}H$- and $^{13}C$-chemical shifts for the glycosides **9** to **12** are presented in Table 1. Inspection of these data will show that the effects of substitutional changes are in accord with previous experi-

Can. J. Chem. Downloaded from www.nrcresearchpress.com by 210.87.254.42 on 09/06/12
For personal use only.

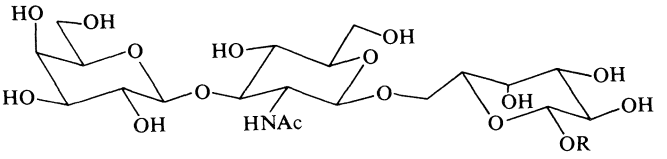

**3** R = H(α, β) **9** R = $(CH_2)_8COOCH_3$

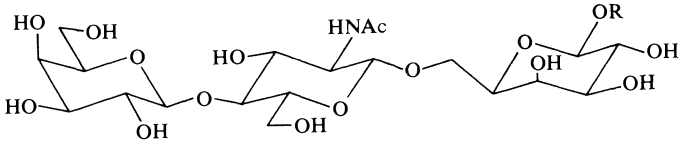

**4** R = H(α, β) **10** R = $(CH_2)_8COOH_3$

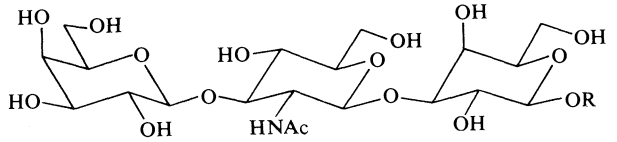

**5** R = H(α, β) **11** R = $(CH_2)_8COOCH_3$

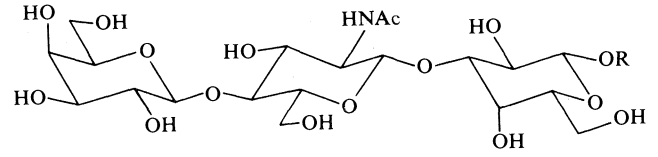

**6** R = H(α, β) **12** R = $(CH_2)_8COOCH_3$

ence in these regards (22) and clearly confirm the structural assignments. The $^{13}C$ chemical shifts are seen to be characteristic of a given disaccharide unit (βDGal(1→3)βDGlcNAc, βDGal(1→4)βDGlcNAc, βDGlcNAc(1→6)βDGal, or βDGlcNAc(1→3)βDGal). The only significant changes which occur are at C1 because of a change in aglycon. These observations support the contention that $^{13}C$ nmr can play an important role in structural investigation of complex oligosaccharides especially since these appear to be less sensitive to changes in environment, such as the specific interunit chemical shifts which may be observed in the case of $^{1}H$-chemical shifts (22).

In the preparations of compounds **9** to **12**, intermediates are encountered wherein it is necessary to remove the phthaloyl group in order to convert the phthalimido group to an acetamido group. Initially, we performed this by alkaline hydrolysis to the amino acid and this stage was followed by peracetylation and then conversion of the carboxyl group of the bridging arm to methyl ester using diazomethane. Since then, a controlled hydrazinolysis of the phthalimido group, to avoid transformation of the methyl ester grouping of the linking arm to acyl hydrazide, was developed by Bundle and Josephson (23), which is the method of choice (24).

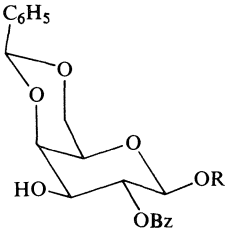

**7** R = $(CH_2)_8COOCH_3$
**13** R = $CH_2CCl_3$

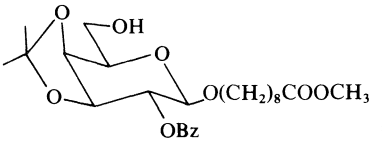

**8**

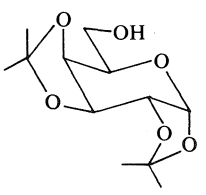

**1**

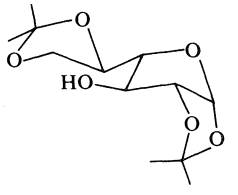

**2**

Compounds **3** to **6** and **9** to **12** have now been examined for I activity by examining their ability to

Can. J. Chem. Downloaded from www.nrcresearchpress.com by 210.87.254.42 on 09/06/12
For personal use only.

Can. J. Chem. Downloaded from www.nrcresearchpress.com by 210.87.254.42 on 09/06/12
For personal use only.

inhibit the precipitation of an I active glycoprotein by a variety of anti-I agglutinins (25, 26). As was to be expected, compounds **4** and **10** were excellent inhibitors and, interestingly, provided, under the test conditions used, identical 50% inhibitions. An accompanying paper (27) follows up on this observation by way of the preparation of the diastereoisomeric 6-*C*-methyl derivatives of **4**. The D-isomer proved to be superior to **4** as an inhibitor whereas the L-isomer was virtually ineffective. In this way, it proved possible to establish the conformation of **4** which is bound by the monoclonal anti-I Ma antibody (15).

## Experimental

The general experimental procedures in terms of preparation of solvents and reagents, evaporations, chromatographic separations, and analytical methods were the same as previously described (17).

*1,2;5,6-Di-*O*-isopropylidene-α-D-galactofuranose (**2**)*

Prepared as previously described (28) (see also Morgenlie (29) and Paulsen and Behre (30)).

*8-Methoxycarbonyloctyl 2-*O*-benzoyl-4,6-*O*-benzylidine-β-D-galactopyranoside (**7**)*[5]

A solution of chloroacetyl chloride (27.3 mL, 0.34 mol) and pyridine (0.34 mol) in dichloroethane (100 mL) was added dropwise over 2 h to a stirred solution of 8-methoxycarbonyloctyl 4,6-*O*-benzylidene-β-D-galactopyranoside (123 g, 0.28 mol) (31) in dichloromethane and kept near −78°C. The temperature was then allowed to rise to −10°C and the solution was poured into vigorously stirred water (5 L). The product was isolated in the usual way and then benzoylated without further purification. The $^{13}C$ nmr spectrum of the syrupy product (220 g) indicated that one component represented about 80% of the mixture. This crude product (215 g) was added to dry methanol (2 L) and the mixture was cooled to −30°C. On adding a saturated (−5°C) solution of ammonia in methanol (180 mL), a clear solution was obtained (32). When none of the starting material remained (tlc using ethyl acetate – *n*-hexane (1:1)), the solution was taken to dryness. Column chromatography (silica gel and graded elution using ethyl acetate and *n*-hexane) of a portion of the solid residue provided a fraction (77% yield) which crystallized from ethanol. Recrystallization from ethanol provided the analytical sample, mp 119–120°C, $[\alpha]_D^{24}$ +7.1° (*c* 1, $CHCl_3$). *Anal.* calcd. for $C_{30}H_{38}O_9$: C 66.41, H 7.06; found: C 66.21, H 7.09.

Both the $^1H$ and $^{13}C$ nmr spectra were in accord with those expected for the title compound. The position of the signal for H2 at 5.33 ppm (dd, 8 and 10 Hz) confirmed the structural assignment. Although *O*-chloroacetyl groups can be removed by treatment with thiourea (32), ammonolysis proved more convenient in this case.

*8-Methoxycarbonyloctyl 2-*O*-benzoyl-3,4-*O*-isopropylidene-β-D-galactopyranoside (**8**)*

A solution of compound **7** (3.5 g, 6.45 mmol) in 80% aqueous acetic acid (60 mL) was kept at 75°C for 1 h. Solvent removal left a residue which was triturated with hexane (200 mL). The residue (2.7 g) was dissolved in dry *N,N*-dimethylformamide

[5]Prepared by Y. Fouron, University of Alberta postdoctoral fellow, 1975–1977.

TABLE 1. The $^1H^a$ and $^{13}C$ nmr[b] chemical shifts for glycosides in $D_2O$ (R = $(CH_2)_8COOCH_3$)

| Compound | βDGal[c] | | | βDGlcNAc | | | | | | βDGal[d]—OR | | | |
|---|---|---|---|---|---|---|---|---|---|---|---|---|---|
| | H1[e] | C1 | C2 | H1[f] | C1 | C2 | C3 | C4 | C5 | C6 | H1[f] | C3 | C4 | C5 | C6 |
| βDGal—OR (22) | — | — | — | — | — | — | — | — | — | — | 4.62 | 72.8 | 68.6 | 75.0 | 60.8 |
| βDGal(1→3)βDGlcNAc—OR (22) | 4.69 | 103.5 | 70.7 | 4.81 | 100.9 | 54.7 | 82.6 | 68.8 | 75.4 | 60.9 | — | — | — | — | — |
| βDGal(1→3)βDGlcNAc(1→6)βDGal—OR (**9**) | 4.73 | 103.6 | 70.7 | 4.88 | 101.2 | 54.6 | 82.6 | 68.9 | 75.4 | 60.9 | 4.66 | 72.8 | 68.8 | 73.4 | 70.7 |
| βDGal(1→3)βDGlcNAc(1→3)βDGal—OR (**11**) | 4.73 | 103.5 | 70.7 | 5.05 | 102.8 | 55.1 | 82.5 | 68.9 | 75.4 | 60.9 | 4.67 | 82.4 | 68.4 | 74.7 | 60.9 |
| βDGal(1→4)βDGlcNAc—OR (22) | 4.74 | 103.0 | 71.0 | 4.79 | 101.0 | 55.2 | 72.6 | 78.9 | 74.8 | 60.3 | — | — | — | — | — |
| βDGal(1→4)βDGlcNAc(1→6)βDGal—OR (**10**) | 4.77 | 102.9 | 71.0 | 4.86 | 101.4 | 55.2 | 72.6 | 78.8 | 75.0 | 60.3 | 4.66 | 72.8 | 68.7 | 73.4 | 70.6 |
| βDGal(1→4)βDGlcNAc(1→3)βDGal—OR (**12**) | 4.77 | 102.9 | 71.0 | 5.02 | 103.0 | 55.7 | 72.6 | 78.7 | 75.0 | 60.3 | 4.66 | 82.4 | 68.3 | 74.7 | 60.8 |

[a] At 400 MHz (305 K) and setting the chemical shift for the methoxyl group of the side chain at 3.98 ppm.
[b] At 22.6 MHz (305 K) and setting the chemical shift for C6 of the terminal βDGal group at 61.0 ppm.
[c] δ (± 0.05 ppm): 72.6 (C3), 68.6 (C4), 75.4 (C5).
[d] δ (± 0.05 ppm): 102.8 (C1), 70.6 (C2).
[e] Doublet, spacing 7.8 Hz.
[f] Doublet, spacing 8.0 Hz.

Can. J. Chem. Downloaded from www.nrcresearchpress.com by 210.87.254.42 on 09/06/12
For personal use only.

(30 mL), and dimethoxypropane (1.17 g, 11.2 mmol) and *p*-toluenesulphonic acid (50 mg) were added. The reaction and isolation of the product were the same as previously described (31) for the preparation of 2,2,2-trichloroethyl 3,4-*O*-isopropylidene-β-D-galactopyranoside. The crude product (2.8 g) was dissolved in dry pyridine (30 mL) and triphenylmethyl chloride (2.28 g) was added. The resulting solution was kept at 65°C for 12 h. The product was isolated in the usual manner and chromatographed on silica gel using a mixture of hexane – ethyl acetate (8:1). The first fraction provided a solid which crystallized from hexane (2.0 g), mp 102–103°C, $[\alpha]_D^{25}$ −5.8° (*c* 1.2, $CHCl_3$). The $^1H$ nmr was consistent with that expected for the 6-*O*-trityl derivative of the title compound **8**. Hydrogenolysis of this product (1.95 g) in ethanol using 5% palladium-on-charcoal at 200 psi of hydrogen pressure gave a solid which was triturated with hexane (100 mL). The residue crystallized from a mixture of hexane–ether (1.18 g, 37% yield from **7**), mp 47–49°C, $[\alpha]_D^{25}$ +17.6° (*c* 0.8, $CHCl_3$). *Anal.* calcd. for $C_{26}H_{38}O_9$: C 63.13, H 7.74; found: C 63.28, H 7.66. The $^{13}C$ nmr spectrum was in complete accord with the structural assignment.

*2,2,2-Trichloroethyl 2-O-benzoyl-4,6-O-benzylidene-β-D-galactopyranoside (**13**)*

2,2,2-Trichloroethyl 3-*O*-benzoyl-4,6-*O*-benzylidene-β-D-galactopyranoside (mp 198–199°C, $[\alpha]s^{24}$ −60.40° (*c* 1, $CHCl_3$)) was readily prepared from 2,2,2-trichloroethyl-β-D-galactopyranoside (33) following the procedure published by Chittenden and Buchanan (34) for the preparation of the analogous benzyl glycoside. In order to have the benzoyl group migrate from the 3- to the 2-position, a solution of the compound (5.0 g, 9.9 mmol) in dimethylsulfoxide (20 mL) was added to 0.05 *N* aqueous sodium hydroxide (20 mL). After 2 min at room temperature, the solution was poured into ice water and immediately extracted with chloroform (250 mL) to afford a product which was subjected to chromatographic separation on a silica gel column using ethyl acetate – chloroform as solvent. The second fraction to appear in the eluate contained a compound (1.7 g, 35% yield) which crystallized readily, mp 206–208°C, $[\alpha]_D^{23}$ −17.5° (*c* 0.9, $CHCl_3$), which was isomeric ($^1H$ nmr) to the starting material, and which necessarily, from a quartet centered at 5.43 ppm with spacings of 8 and 10 Hz, had the benzoyl group at the 2-position. *Anal.* calcd. for $C_{22}H_{21}O_7Cl_3$: C 52.45, H 4.20, Cl 21.11; found: C 52.40, H 4.29, Cl 21.24.

*4,6-Di-O-acetyl-3-O-(tetra-O-acetyl-β-D-galactopyranosyl)-2-deoxy-2-phthalimido-α,β-D-glucopyranosyl chloride (**14**)*

This reagent was prepared as described in a separate communication (17).

*3,6-Di-O-acetyl-4-O-(tetra-O-acetyl-β-D-galactopyranosyl)-2-deoxy-2-phthalimido-α,β-D-glucopyranosyl chloride (**15**)*

This reagent was prepared by way of one of the two procedures described in a separate communication (16). The route involving the azidonitration is recommended.

*General methods*

(a) *Glycosylation reactions*

In general, a solution of the phthalimido-chloride (either **14** or **15**) (3.5 mmol) in nitromethane (10 mL) was added dropwise to a solution of the alcohol (3.5 mmol), silver trifluoromethylsulfonate (3.7 mmol), and *sym*-collidine (3.7 mmol) in nitromethane (20 mL) kept at −15° to −30°C. The resulting mixture was stirred at −15°C for 1 h and then at room temperature for 2 h. Chloroform was then added and the solids removed by filtration prior to washing, first with water, then cold dilute hydrochloric acid, then with dilute aqueous sodium bicarbonate solution, and finally with water. The solid foam which remained after solvent removal was dissolved in ethyl acetate and this solution was applied to a short column of neutral alumina. The product obtained on elution with ethyl acetate was purified as is indicated.

(b) *Hydrolysis of O-isopropylidene groups*

In general, the compound (1 mmol) was dissolved in 95% aqueous trifluoroacetic acid (35) at room temperature. After 15 min the solvents were rapidly removed *in vacuo* near room temperature. The residue was then processed as is indicated.

(c) *Removal of the phthaloyl group and* N*-acetylation*

For the products (about 0.5 mmol) formed on glycosylation of the di-*O*-isopropylidene compounds **1** and **2**, both the acetyl and phthaloyl groups were removed simultaneously by reaction with a large excess of hydrazine hydrate (2 mL) in ethanol (20 mL) at reflux. After solvent removal, the residue was dissolved in 50% aqueous methanol (20 mL), acetic anhydride (5 mL) added, and the solution stirred for 2 h. Solvent removal left a residue which was processed as is indicated.

In the case of the products formed on the glycosylation of the compounds **7** and **8**, the *O*-isopropylidene or the *O*-benzylidene group was first removed by acid hydrolysis. Refluxing 80% acetic acid was used to hydrolyze the benzylidene group. A 10% solution (10 mL) of 99% trifluoracetic acid in dichloromethane was used to remove the *O*-isopropylidene group. The resulting product was taken up in 40% aqueous methanol containing an excess of sodium hydroxide and the solution was heated under reflux for 3 h in order to saponify the methyl ester. The solution was then evaporated to dryness. The residual salt-cake was acetylated overnight with an excess of a mixture (2:1) of pyridine – acetic anhydride. Solvent removal left a residue which was treated with cold 0.1 *N* aqueous hydrochloric acid prior to extraction with dichloromethane. The crude acidic product thus obtained was heated under reflux for 3 h with 40% aqueous methylamine in methanol in order to effect deacetylation and removal of the phthaloyl group. The product was then reacetylated using pyridine – acetic anhydride (2:1) in the usual manner.

The resulting product was then dissolved in dichloromethane for treatment with an excess of diazomethane in ether. The peracetate of the desired compound was then isolated by chromatographic separation on a silica gel column (2.5 × 15 cm) using first ethyl acetate – benzene (1:1) and then this solvent mixture containing 5% methanol. It is to be stressed at this point that this multistep procedure was used only because it was convenient at the time these preparations were made. It is not recommended. The procedure developed by Bundle and Josephson (23) and which was recently used in this laboratory (24) is more convenient and proceeds in better yield.

*6-O-[4,6-Di-O-acetyl-3-O-(tetra-O-acetyl-β-D-galactopyranosyl)-2-deoxy-2-phthalimido-β-D-glucopyranosyl]-1,2;3,4-di-O-isopropylidene-α-D-galactopyranose (**16**)*

The crude product from the reaction of **1** with **14** was applied to a silica-gel column and the chromatogram was developed with ethyl acetate – hexane (1:1). The second fraction contained a colorless solid which was recrystallized from ethanol (76% yield), mp 119–121°C, $[\alpha]_D^{25}$ −39.1° (*c* 0.6, $CHCl_3$). The $^1H$ nmr spectrum required the presence of the phthalimido group, the two isopropylidene groups, and the six acetyl groups. *Anal.* calcd. for $C_{44}H_{55}NO_{23}$: C 54.71, H 5.73, N 1.45; found: C 53.84, H 5.64, N 1.42.

*6-O-[2-Acetamido-2-deoxy-3-O-(β-D-galactopyranosyl)-β-D-glucopyranosyl]-1,2;3,4-di-O-isopropylidene-α-D-galactopyranose (**17**)*

The product from the hydrazinolysis and then *N*-acetylation

Can. J. Chem. Downloaded from www.nrcresearchpress.com by 210.87.254.42 on 09/06/12
For personal use only.

of **16** was passed through a column of Dowex 1-X 8 ($OH^-$ form) using methanol as solvent. Solvent removal left a residue which crystallized from methanol – diethyl ether (74% yield). Recrystallization from methanol–acetone gave an analytically pure compound, mp 225–227°C (dec.), $[\alpha]_D^{24}$ −50.3° (*c* 0.5, $H_2O$). The $^1H$ and $^{13}C$ nmr were consistent with the structural assignment.

*6-O-[2-Acetamido-2-deoxy-3-O-(β-D-galactopyranosyl)-β-D-glucopyranosyl]-D-galactopyranose [βDGal(1→3)βD-GlcNAc(1→6)DGal] (**3**)*

The product from the hydrolysis of **17** using trifluoroacetic acid was recrystallized from methanol (64% yield), mp 175–178°C (dec.), $[\alpha]_D^{23}$ −0.9° (*c* 0.8, $H_2O$) (lit. (36) mp 177–184°C, $[\alpha]_D^{20}$ −9.5° to −1.2° (1 h) (*c* 0.84, water)). *Anal.* calcd. for $C_{20}H_{35}NO_{16}\cdot H_2O$: C 42.62, H 6.61, N 2.38; found: C 42.65, H 6.39, N 2.20.

*6-O-[4,6-Di-O-acetyl-4-O-(tetra-O-acetyl-β-D-galactopyranosyl)-2-deoxy-2-phthalimido-β-D-glucopyranosyl]-1,2;3,4-di-O-isopropylidene-α-D-galactopyranose (**18**)*

The crude product from the reaction of **1** with **15** crystallized on solvent removal (80% yield) and was recrystallized from ethanol, mp 201–202°C, $[\alpha]_D^{29}$ −19.6° (*c* 0.8, $CHCl_3$). The $^1H$ nmr spectrum confirmed the presence of the phthalimido group, the two isopropylidene groups, and the six acetyl groups. *Anal.* calcd. for $C_{44}H_{55}NO_{23}$: C 54.71, H 5.73, N 1.45; found: C 55.04, H 5.68, N 1.50.

*6-O-[2-Acetamido-2-deoxy-4-O-(β-D-galactopyranosyl)-β-D-glucopyranosyl]-1,2-3,4-di-O-isopropylidene-α-D-galactopyranose (**19**)*

The product from the hydrazinolysis and then *N*-acetylation of **18** was treated as described above in the preparation of **17**. The yield was 87%, mp 212–214°C, $[\alpha]_D^{23}$ −47.2° (*c* 0.9, $H_2O$). The $^1H$ and $^{13}C$ nmr spectra were consistent with the structural assignment. *Anal.* calcd. for $C_{26}H_{43}NO_{16}\cdot H_2O$: C 48.51, H 7.04, N 2.17; found: C 48.49, H 6.69, N 2.06.

*6-O-[2-Acetamido-2-deoxy-4-O-(β-D-galactopyranosyl)-β-D-glucopyranosyl]-D-galactopyranose [βDGal(1→4)βD-GlcNAc(1→6)DGal] (**4**)*

The product from the hydrolysis of **19** using trifluoroacetic acid was recrystallized from ethyl acetate – methanol (73% yield), mp 155–159°C (dec.), $[\alpha]_D^{24}$ +9.6 (*c* 0.5, $H_2O$) (lit. (36) $[\alpha]_D^{20}$ +4.0° (*c* 1, $H_2O$)). *Anal.* calcd. for $C_{20}H_{35}NO_{16}\cdot H_2O$: C 42.62, H 6.61, N 2.48; found: C 42.18, H 6.04, N 2.16.

*3-O-[4,6-Di-O-acetyl-3-O-(tetra-O-acetyl-β-D-galactopyranosyl)-2-deoxy-2-phthalimido-β-D-glucopyranosyl]-1,2;5,6-di-O-isopropylidene-α-D-galactofuranose (**20**)*

The crude product from the reaction of **2** with **14** was chromatographed on a silica-gel column using ethyl acetate – hexane (1:1). A fraction (24% yield) crystallized, mp 104–107°C, and was recrystallized from ethanol, mp 106–109°C, $[\alpha]_D^{25}$ −15.5° (*c* 0.5, $CHCl_3$). The $^1H$ nmr spectrum confirmed the presence of the phthalimido group, the two isopropylidene groups, and the six acetyl groups. *Anal.* calcd. for $C_{44}H_{55}NO_{23}\cdot H_2O$: C 53.71, H 5.84, N 1.42; found: C 53.63, H 5.51, N 1.79.

*3-O-[2-Acetamido-2-deoxy-3-O-(β-D-galactopyranosyl)-β-D-glucopyranosyl]-1,2;5,6-di-O-isopropylidene-α-D-galactofuranose (**21**)*

The product from the hydrazinolysis and then *N*-acetylation of **20** was crystallized from methanol – ethyl acetate (50% yield), mp 182–184°C (dec.), $[\alpha]_D^{24}$ −13.4° (*c* 0.4, $H_2O$). The $^1H$ and $^{13}C$ nmr spectra were consistent with the structural assignment.

*3-O-[2-Acetamido-2-deoxy-3-O-(β-D-galactopyranosyl)-β-D-glucopyranosyl]-D-galactopyranose [βDGal(1→3)βD-GlcNAc(1→3)DGal or lacto-N-triose I] (**5**)*

The product from the trifluoroacetic acid hydrolysis of **21** crystallized from methanol (60% yield), mp 139–141°C (dec.), $[\alpha]_D^{23}$ +13.6° (*c* 0.5, $H_2O$). These physical constants are substantially lower than those reported by Kuhn *et al.* (37), mp 183–185°C, $[\alpha]_D^{23}$ +19.3° (*c* 2, $H_2O$), and essentially confirmed by Augé and Veyrières (38). Because of the paucity of material (46 mg), this matter was not investigated further except that sugar analysis required the presence of two galactose units per unit of *N*-acetylglucosamine (performed by Professor E. A. Kabat).

*2,2,2-Trichloroethyl 3-O-[3,6-di-O-acetyl-4-O-(tetra-O-acetyl-β-D-galactopyranosyl)-2-deoxy-2-phthalimido-β-D-glucopyranosyl]-2-O-benzoyl-4,6-O-benzylidene-β-D-galactopyranoside (**22**)*

The product from the reaction of **13** with **15** crystallized in 80% yield (mp 228–231°C) and was recrystallized from ethanol, mp 252–254°C, $[\alpha]_D^{24}$ +8.6° (*c* 0.8, $CHCl_3$). The $^1H$ nmr spectrum confirmed the presence of the three aromatic rings and the six acetyl groups. *Anal.* calcd. for $C_{54}H_{56}NO_{24}Cl_3$: C 53.62, H 4.66, N 1.15, Cl 8.79; found: C 53.26, H 4.58, N 1.04, Cl 8.71.

*2,2,2-Trichloroethyl 2-O-acetyl-3-O-[2-acetamido-3,6-di-O-acetyl-4-O-(tetra-O-acetyl-β-D-galactopyranosyl)-2-deoxy-β-D-glucopyranosyl]-4,6-O-benzylidene-β-D-galactopyranoside (**23**)*

The product of hydrazinolysis of **22** (1.82 g, 1.5 mmol) was acetylated with pyridine – acetic anhydride (2:1). A solution of the peracetate in ethyl acetate was passed through a short column of neutral alumina. Solvent removal left a crystalline solid (mp 144–149°C, 1.35 g, 85% yield) which was recrystallized from ethyl acetate – hexane, mp 150–152°C, $[\alpha]_D^{23}$ −1.9° (*c* 0.8, $CHCl_3$). The $^1H$ nmr spectrum displayed the presence of the benzylidene group and eight acetyl groups. *Anal.* calcd. for $C_{43}H_{54}NO_{23}Cl_3$: C 48.75, H 5.13, N 1.32; found: C 48.60, H 5.19, N 1.23.

*2,2,2-Trichloroethyl 2,4,6-tri-O-acetyl-3-O-[2-acetamido-3,6-di-O-acetyl-4-O-(tetra-O-acetyl-β-D-galactopyranosyl)-2-deoxy-β-D-glucopyranosyl]-β-D-galactopyranoside (**24**)*

Compound **23** (1.00 g, 0.94 mmol) was kept at 100°C in 60% aqueous acetic acid for 40 min. The product was acetylated in pyridine – acetic anhydride (2:1) in the usual manner to provide a solid which crystallized from ethyl acetate – hexane (0.50 g, 50% yield), mp 138–141°C, $[\alpha]_D^{23}$ +2.2° (*c* 1, $CHCl_3$). *Anal.* calcd. for $C_{40}H_{54}NO_{25}Cl_3$: C 45.52, H 5.15, N 1.32, Cl 10.07; found: C 45.19, H 5.09, N 1.24, Cl 10.0.

*2,2,2-Trichloroethyl 3-O-[2-acetamido-2-deoxy-4-O-(β-D-galactopyranosyl)-β-D-glucopyranosyl]-β-D-galactopyranoside (**25**)*

Compound **24** (190 mg, 0.18 mmol) was dissolved in a triethylamine–water–methanol (1:1:8) mixture (12 mL) and the solution left at room temperature for 16 h. The solution was concentrated to dryness and the residue was passed through a short column of Dowex (2-X8, $OH^-$ form) using water. The aqueous fractions were combined and freeze-dried to give a powder (90 mg, 75% yield), $[\alpha]_D^{23}$ −4.88° (*c* 0.84, $H_2O$). The $^1H$ and $^{13}C$ nmr spectra were consistent with the structural assignment. *Anal.* calcd. for $C_{21}H_{36}NO_{16}Cl_3\cdot H_2O$: C 36.93, H 5.60, N 2.05; found: C 36.48, H 5.07, N 1.85.

*3-O-[2-Acetamido-2-deoxy-4-O-(β-D-galactopyranosyl)-β-D-glucopyranosyl]-D-galactopyranose [βDGal(1→4)βD-GlcNAc(1→3)DGal] (**6**)*

Compound **25** (85 mg) in glacial acetic acid (2 mL) was treated

Can. J. Chem. Downloaded from www.nrcresearchpress.com by 210.87.254.42 on 09/06/12
For personal use only.

with a zinc–copper couple (33, 39) (20 mg) at room temperature for 4 h. The product was purified on a silica gel column using chloroform–methanol–water (65:35:8) (40 mg, 57% yield), $[\alpha]_D^{23}$ +17.5° (*c* 0.5, $H_2O$) (lit. (36) $[\alpha]_D^{20}$ +19.5 (*c* 0.62, $H_2O$)). *Anal.* calcd. for $C_{20}H_{35}NO_{16}\cdot H_2O$: C 42.62, H 6.61, N 2.48; found: C 42.27, H 6.29, N 2.20.

*8-Methoxycarbonyloctyl 6-O-[4,6-di-O-acetyl-3-O-(tetra-O-acetyl-β-D-galactopyranosyl)-2-deoxy-2-phthalimido-β-D-glucopyranosyl]-2-O-benzoyl-3,4-O-isopropylidene-β-D-galactopyranoside (**26**)*

The product obtained on the condensation of compounds **8** and **14** was obtained in 71% yield (mp 87–91°C) after passage through a short column of neutral alumina. Since the $^1H$ nmr spectrum was in good accord with expectation, no attempt was made to achieve higher purity. *Anal.* calcd. for $C_{58}H_{73}NO_{26}$: C 58.04, H 6.13, N 1.16; found: C 58.24, H 6.04, N 1.33.

*8-Methoxycarbonyloctyl 2,3,4-tri-O-acetyl-6-O-[2-acetamido-4,6-di-O-acetyl-3-O-(tetra-O-acetyl-β-D-galactopyranosyl)-2-deoxy-β-D-glucopyranosyl]-β-D-galactopyranoside (**27**)*

Compound **26** (1.35 g, 1.1 mmol) was subjected to the multi-step process for the conversion of all the protecting groups to acetyl groups. The major fraction (amorphous, 372 mg, 30% yield) $[\alpha]_D^{23}$ −13.7° (*c* 0.7, $CHCl_3$), appeared chromatographically pure and possessed an $^1H$ nmr spectrum consistent with that expected for the title compound. *Anal.* calcd. for $C_{48}H_{71}NO_{27}$: C 52.69, H 6.54, N 1.28; found: C 53.53, H 6.80, N 1.12.

*8-Methoxycarbonyloctyl 6-O-[2-acetamido-2-deoxy-3-O-(β-D-galactopyranosyl)-β-D-glucopyranosyl]-β-D-galactopyranoside [βDGal(1→3)βDGlcNAc(1→6)βDGalO(CH$_2$)$_8$COOCH$_3$] (**9**)*

Compound **27** (325 mg, 0.29 mmol) was dissolved in 0.01 *N* sodium methoxide in methanol (15 mL) and the solution was kept overnight at room temperature. After deionization with Amberlite 120H$^+$, the solvent was removed and the residue was dissolved in water, the solution clarified and freeze dried to a colorless powder (196 mg, 97% yield), mp 185–188°C, $[\alpha]_D^{23}$ −20.9° (*c* 1, $H_2O$). The $^1H$ and $^{13}C$ nmr (see Table 1) required a high purity and were consistent with the structural assignment. *Anal.* calcd. for $C_{30}H_{53}NO_{18}\cdot H_2O$: C 49.17, H 7.39, N 1.90; found: C 49.20, H 7.30, N 1.87.

*8-Methoxycarbonyloctyl 6-O-[3,6-di-O-acetyl-4-O-(tetra-O-acetyl-β-D-galactopyranosyl)-2-deoxy-2-phthalimido-β-D-glucopyranosyl]-2-O-benzoyl-3,4-O-isopropylidene-β-D-galactopyranoside (**28**)*

The product obtained on the condensation of compounds **8** and **15** was obtained in 64% yield as an amorphous powder, $[\alpha]_D^{23}$ +21.3° (*c* 1.2, $CHCl_3$). The $^1H$ nmr was consistent with the structural assignment. *Anal.* calcd. for $C_{58}H_{73}NO_{26}$: C 58.04, H 6.13, N 1.16; found: C 57.93, H 6.06, N 1.17.

*8-Methoxycarbonyloctyl 2,3,4-tri-O-acetyl-6-O-[2-acetamido-3,6-di-O-acetyl-4-O-(tetra-O-acetyl-β-D-galactopyranosyl)-2-deoxy-β-D-glucopyranosyl]-β-D-galactopyranoside (**29**)*

Compound **28** (1.02 g, 0.84 mmol) was subjected to the multi-step procedure for conversion of all the protecting groups to acetyl groups. The major fraction (318 mg, 44% yield), $[\alpha]_D^{23}$ −18.3° (*c* 0.5, $CHCl_3$), appeared chromatographically pure and possessed an $^1H$ nmr spectrum consistent with that expected for the title compound. *Anal.* calcd. for $C_{48}H_{71}NO_{27}$: C 52.69, H 6.54, N 1.28; found: C 52.42, H 6.47, N 1.20.

*8-Methoxycarbonyloctyl 6-O-[2-acetamido-2-deoxy-4-O-(β-D-galactopyranosyl)-β-D-glucopyranosyl]-β-D-galactopyranoside [βDGal(1→4)βDGlcNAc(1→6)βDGalO(CH$_2$)$_8$COOCH$_3$] (**10**)*

De-*O*-acetylation of **29** (194 mg, 0.17 mmol) as was described for the preparation of **9**, provided a powder (118 mg, 94% yield), mp 202–205°C, $[\alpha]_D^{23}$ −15.7° (*c* 0.8, $H_2O$). The $^1H$ and $^{13}C$ nmr spectra (see Table 1) required high purity and were consistent with structural assignment. *Anal.* calcd. for $C_{30}H_{53}NO_{18}\cdot H_2O$: C 49.17, H 7.39, N 1.90; found: C 48.81, H 7.28, N 1.88.

*8-Methoxycarbonyloctyl 3-O-[4,6-di-O-acetyl-3-O-(tetra-O-acetyl-β-D-galactopyranosyl)-2-deoxy-2-phthalimido-β-D-glucopyranosyl]-2-O-benzoyl-4,6-O-benzylidene-β-D-galactopyranoside (**30**)*

The product obtained on the condensation of compounds **7** and **14** had to be chromatographed on a silica gel column to afford the title compound as an amorphous solid in 34% yield, $[\alpha]_D^{23}$ +1.6° (*c* 0.7, $CHCl_3$). The $^1H$ nmr spectrum was consistent with the structural assignment. *Anal.* calcd. for $C_{62}H_{73}NO_{26}$: C 59.65, H 5.89, N 1.12; found: C 59.38, H 5.85, N 1.12.

*8-Methoxycarbonyloctyl 2,4,6-tri-O-acetyl-3-O-[2-acetamido-4,6-di-O-acetyl-3-O-(tetra-O-acetyl-β-D-galactopyranosyl)-2-deoxy-β-D-glucopyranosyl]-β-D-galactopyranoside (**31**)*

Compound **30** (700 mg, 0.56 mmol) was subjected to the multi-step process for the conversion of all the protecting groups to acetyl groups. The major fraction of the chromatogram provided an amorphous solid (135 mg, 22% yield), $[\alpha]_D^{23}$ +11.1° (*c* 0.9, $CHCl_3$). The $^1H$ nmr spectrum was consistent with the structural assignment and inferred chemical homogeneity. *Anal.* calcd. for $C_{48}H_{71}NO_{27}$: C 52.69, H 6.54, N 1.28; found: C 52.46, H 6.50, N 1.27.

*Methoxycarbonyloctyl 3-O-[2-acetamido-2-deoxy-3-O-(β-D-galactopyranosyl)-β-D-glucopyranosyl]-β-D-galactopyranoside [βDGal(1→3)βDGlcNAc(1→3)βDGalO(CH$_2$)$_8$COOCH$_3$] (**11**)*

De-*O*-acetylation of **31** (125 mg, 0.12 mmol) as was described for the preparation of **9** afforded an amorphous powder (61 mg, 72% yield), $[\alpha]_D^{23}$ −4.7° (*c* 0.9, $H_2O$). The $^1H$ and $^{13}C$ nmr spectra (see Table 1) required high purity and were consistent with the structural assignment.

*8-Methoxycarbonyloctyl 3-O-[3,6-di-O-acetyl-4-O-(tetra-O-acetyl-β-D-galactopyranosyl)-2-deoxy-2-phthalimido-β-D-glucopyranosyl]-2-O-benzoyl-4,6-O-benzylidene-β-D-galactopyranoside (**32**)*

The product obtained on the condensation of compounds **7** and **15** had to be chromatographed on a silica gel column to afford the title compound in 44% yield as a colorless solid, $[\alpha]_D^{23}$ +31.5° (*c* 0.7, $CHCl_3$). The $^1H$ nmr spectrum was consistent with the structural assignment. *Anal.* calcd. for $C_{62}H_{73}NO_{26}$: C 59.65, H 5.89, N 1.12; found: C 59.90, H 6.01, N 1.23.

*8-Methoxycarbonyloctyl 2,4,6-tri-O-acetyl-3-O-[2-acetamido-3,6-di-O-acetyl-4-O-(tetra-O-acetyl-β-D-galactopyranosyl)-2-deoxy-β-D-glucopyranosyl]-β-D-galactopyranoside (**33**)*

Compound **32** (960 mg, 0.77 mmol) was subjected to the multi-step process for the conversion of all the protecting groups to acetyl groups. The major fraction of the chromatogram provided an amorphous solid (256 mg, 30% yield), $[\alpha]_D^{23}$ +4.6° (*c* 0.75, $CHCl_3$). The $^1H$ nmr spectrum was consistent with the structural assignment and inferred chemical homogeneity.

*8-Methoxycarbonyloctyl 3-O-[2-acetamido-2-deoxy-4-O-(β-D-galactopyranosyl)-β-D-glucopyranosyl]-β-D-galactopyranoside [βDGal(1→4)βDGlcNAc(1→3)βDGalO-$(CH_2)_8COOCH_3$] (12)*

De-*O*-acetylation of **33** (220 mg, 0.21 mmol) as was described for the preparation of **9** afforded an amorphous powder (141 mg, 97% yield), $[\alpha]_D^{23}$ −3.8° (*c* 1, $H_2O$). The $^1H$ and $^{13}C$ nmr spectra (see Table 1) required high purity and were consistent with the structural assignment. *Anal.* calcd. for $C_{30}H_{53}NO_{18}\cdot H_2O$: C 49.19, H 7.39, N 1.90; found: C 48.80, H 7.23, N 1.91.

## Acknowledgements

Financial support from the National Research Council (Grant A172 to R. U. Lemieux) is gratefully acknowledged. The nmr and microanalyses were provided by the Spectral and Analytical Service Laboratories of this department.

1. W. M. Watkins. Adv. Hum. Genet. **10**, 1 (1980).
2. K. O. Lloyd, E. A. Kabat, and E. Licerio. Biochemistry, **7**, 2976 (1968).
3. S. Hakomori, K. Watanabe, and R. A. Laine. Pure Appl. Chem. **49**, 1215 (1977).
4. J. Kościelak, H. Miller-Podraza, R. Krauze, and A. Piasek. Eur. J. Biochem. **71**, 9 (1976).
5. R. R. Race and R. Sanger. Blood groups in man. 6th ed. Blackwell Scientific Publications, Oxford. 1975. pp. 447–462.
6. W. L. Marsh. Br. J. Haemat. **7**, 200 (1961).
7. W. L. Marsh and W. L. Jenkins. Nature, **188**, 753 (1960).
8. A. S. Wiener, L. G. Unger, L. Cohen, and J. Feldman. Ann. Intern. Med. **44**, 221 (1956).
9. J. Kościelak. Human blood groups, 5th Intl. Convoc. Immunol. Buffalo, NY. 1976. pp. 143–149 (Karger, Basel. 1977).
10. J. Kościelak, E. Zdebska, Z. Wilczynska, H. Miller-Podraza, and W. Dzierzkowa-Borodej. Eur. J. Biochem. **96**, 331 (1979).
11. H. Niemann, K. Watanabe, S. Hakomori, R. A. Childs, and T. Feizi. Biochem. Biophys. Res. Commun. **81**, 1286 (1978).
12. T. Feizi and E. A. Kabat. J. Exp. Med. **135**, 1247 (1972).
13. D. Roelcke. Clin. Immunol. Immunopathol. **2**, 266 (1974).
14. T. Feizi. Human blood groups, 5th Int. Convoc. Immunol. Buffalo, NY. 1976. pp. 164–171. (Karger, Basel, 1977).
15. E. A. Kabat, J. Liao, M. H. Burzynska, T. C. Wong, H. Thøgersen, and R. U. Lemieux. Mol. Immunol. **18**, 873 (1981).
16. R. U. Lemieux, S. Z. Abbas, H. M. Burzynska, and R. M. Ratcliffe. Can. J. Chem. **60**, 63 (1982).
17. R. U. Lemieux, S. Z. Abbas, and B. Y. Chung. Can. J. Chem. **60**, 58 (1982).
18. K. Matsuda. Chem. Ind. 1627 (1958).
19. J. Baddiley, J. G. Buchanan, and F. E. Hardy. J. Chem. Soc. 2180 (1961).
20. R. U. Lemieux. Chem. Soc. Rev. **7**, 423 (1978).
21. R. U. Lemieux, D. A. Baker, and D. R. Bundle. Can. J. Biochem. **55**, 507 (1977).
22. R. U. Lemieux, K. Bock, L. T. J. Delbaere, S. Koto, and V. S. Rao. Can. J. Chem. **58**, 631 (1980).
23. D. R. Bundle and S. Josephson. Can. J. Chem. **57**, 662 (1979).
24. R. U. Lemieux and M. H. Burzynska. Can. J. Chem. **60**, 76 (1982).
25. E. A. Kabat, J. Liao, and R. U. Lemieux. Immunochemistry, **15**, 727 (1978).
26. T. Feizi, E. Wood, C. Augé, S. David, and A. Veyrières. Immunochemistry, **15**, 733 (1978).
27. R. U. Lemieux, H. Thøgersen, and T. C. Wong. Can. J. Chem. **60**, 81 (1982).
28. R. U. Lemieux and R. V. Stick. Aust. J. Chem. **28**, 1799 (1975).
29. S. Morgenlie. Acta Chem. Scand. **27**, 3609 (1973).
30. H. Paulsen and H. Behre. Carbohydr. Res. **2**, 80 (1966).
31. R. U. Lemieux, D. R. Bundle, and D. A. Baker. U.S. Patent No. 4,238,473 (1980).
32. M. Bertolini and C. P. J. Glaudemans. Carbohydr. Res. **15**, 263 (1970).
33. R. U. Lemieux and H. Driguez. J. Am. Chem. Soc. **97**, 4069 (1975).
34. G. J. F. Chittenden and J. G. Buchanan. Carbohydr. Res. **11**, 379 (1969).
35. J. E. Christensen and L. Goodman. Carbohydr. Res. **7**, 510 (1968).
36. C. Augé, S. David, and A. Veyrières. Nouv. J. Chim. **3**, 491 (1979).
37. R. Kuhn, A. Gauhe, and H. H. Baer. Chem. Ber. **89**, 1027 (1956).
38. C. Augé and A. Veyrières. J. Chem. Soc. Perkin Trans. I, 1343 (1977).
39. R. D. Smith and H. E. Simmons. Org. Synth. **41**, 72 (1961).

Can. J. Chem. Downloaded from www.nrcresearchpress.com by 210.87.254.42 on 09/06/12
For personal use only.

# Synthesis of βDGlcNAc(1→6) and βDGal(1→4)βDGlcNAc(1→6) derivatives of the $T_N$ (αDGalNAc) human blood group determinant

RAYMOND U. LEMIEUX AND MARIA HALINA BURZYNSKA[1]
*Department of Chemistry, University of Alberta, Edmonton, Alta., Canada T6G 2G2*
Received March 27, 1981

RAYMOND U. LEMIEUX and MARIA HALINA BURZYNSKA. Can. J. Chem. **60**, 76 (1982).
In order to investigate the immunological properties of certain I blood group specific glycoproteins, the potential antigenic determinants βDGlcNAc(1→6)αDGalNAc and βDGal(1→4)βDGlcNAc(1→6)αDGalNAc attached as glycosides to 8-methoxycarbonyloctanol were synthesized by way of the phthalimido-chloride method.

RAYMOND U. LEMIEUX et MARIA HALINA BURZYNSKA. Can. J. Chem. **60**, 76 (1982).
Dans le but d'étudier les propriétés immonulogiques de certaines glycoprotéines spécifiques du groupe sanguin I, on a synthétisé, par la méthode du chlorure de phtalimide, les déterminants antigéniques potentiels: βDGlcNAc(1→6)αDGalNAc et βDGal(1→4)-βDGlcNAc(1→6)αDGalNAc attachés en tant que glycosides au méthoxycarbonyl-8-octanol.

[Traduit par le journal]

In 1968, Lloyd *et al.* (1) published a composite structure for the carbohydrate chains of A, B, H, Lewis a, and Lewis b human blood group specific glycoproteins. The structure was presented with the tetrasaccharide,

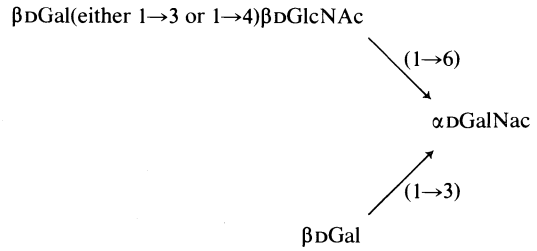


as the structural unit attached to the core protein. This unit was proposed since alkaline borohydride treatment of a Lewis a active human cyst glycoprotein had produced a substance (Lewis $R_L$ 0.41) with composition and chemical properties consistent with the presence of either one of these units. It was to be expected that the oligosaccharide chains in the glycoprotein would be linked through *N*-acetylgalactosamine to serine and threonine units in the polypeptide portion.

It is now well established that the βDGal(1→3)-αDGalNAc disaccharide is the first disaccharide unit in the carbohydrate chains that are attached as *O*-glycosides to the core protein of the blood group active glycoproteins (2). The αDGalNAc residue is characteristic of the $T_N$ determinant (3) and the βDGal(1→3)αDGalNAc structure is characteristic of the T determinant (4). The T determinant is also related to the M and N human blood group determinants (5). It was therefore of interest to examine in more detail the occurrence of the above-mentioned tetrasaccharide units in human blood group specific glycoproteins, by way of chemical synthesis toward structures which would be amenable to the preparation of immunochemical reagents of possible use in these regards (6).

The syntheses of the tetrasaccharide structures have not as yet been accomplished. Nevertheless, we wish to report the syntheses of the structures βDGlcNAc(1→6)αDGalNAc (**8**) and βDGal(1→4)-βDGlcNAc(1→6)αDGalNAc (**13**) attached to the potential linking arm derived from 8-methoxycarbonyloctanol since these substances proved useful to a study of the combining site of the anti-I Ma monoclonal antibody (7, 8). It was found that structure **13** binds this myeloma protein, on a molar basis, equally as well as do βDGal(1→4)βDGlcNAc(1→6)βDGalO$(CH_2)_8COOCH_3$ and βDGal-(1→4)βDGlcNAc(1→6)[βDGal(1→4)βDGlcNAc-(1→3)]βDGalO$(CH_2)_8COOCH_3$. Therefore it is possible that the antigenic determinant, which was involved in the myelomatosis and proliferation of the neoplastic monoclonal anti-I Ma producing cells, was a βDGal(1→4)βDGlcNAc(1→6)αDGal-NAc unit of the glycoprotein and not necessarily a βDGal(1→4)βDGlcNAc(1→6)βDGal unit (8). The synthesis of βDGal(1→3)αDGalNAcO$(CH_2)_8$-$COOCH_3$ (the T determinant) has been reported (9).

The synthesis of **8** from αDGalNAcO$(CH_2)_8$-$COOCH_3$ **1** (9) by way of the intermediates **2–7** warrants a few comments. Treatment of **2** with benzoyl chloride in pyridine was found to lead to *N*-benzoylation as well as the desired *O*-benzoylation (10). The so-called phthalimido-chloride method (11) was used to establish the β(1→6) linkage of **5**

[1]University of Alberta Postdoctoral Fellow (1978–1980).

0008-4042/82/010076-05$01.00/0
©1982 National Research Council of Canada/Conseil national de recherches du Canada

Can. J. Chem. Downloaded from www.nrcresearchpress.com by 210.87.254.40 on 09/06/12
For personal use only.

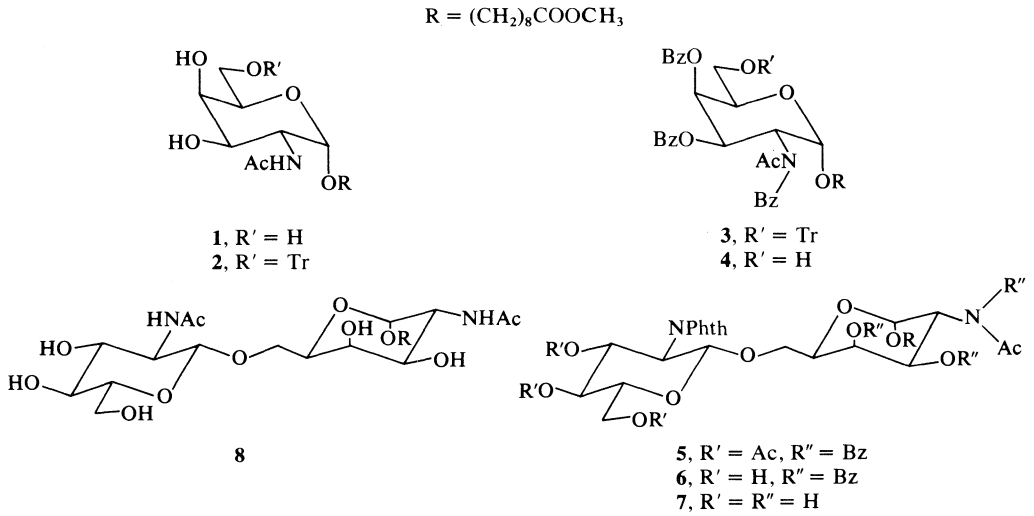


**1**, R′ = H
**2**, R′ = Tr

**3**, R′ = Tr
**4**, R′ = H

**8**

**5**, R′ = Ac, R″ = Bz
**6**, R′ = H, R″ = Bz
**7**, R′ = R″ = H

since this method has proved generally reliable for this purpose (12). Indeed, the yield was 87%. It is of interest that treatment of **5** with sodium methoxide – methanol in the cold allowed the transesterification reaction to be limited to de-*O*-acetylation. The use of magnesium methoxide (13) for this purpose therefore appears advantageous, simply because, as a less active catalyst, it allows more convenient kinetic control. It is remarkable that the treatment of **5** with sodium methoxide under conditions which removed the benzoyl groups preferentially removed the *N*-benzoyl group. Especially in view of the $^{13}C$ nmr data, it seems evident that the compound was an *N*-acetylbenzamido product and not an *O*-benzoyl acetamidate.

In the course of this work, we observed that the phthalimido group remained intact in the course of the deacetylation of **5** and work-up to provide **7**. Meanwhile, Bundle and Josephson (14) reported a similar experience. As was pointed out by Bundle and Josephson (14), this occurrence is a considerable convenience in the context of the need to later remove the phthalimido group without affecting the methoxycarbonyl group of the linking arm. We have now found[2] that the opening of the phthalimido group by the sodium method is strongly influenced by the configurations of the neighboring centers. Our earlier investigations (11) demonstrated the strong nonbonded interaction that exists between an equatorially oriented phthalimido group and an axial neighboring substituent. Thus it was not surprising to find that the reaction of a 2-deoxy-2-phthalimido-α-D-galactopyranosyl unit to form the *o*-methoxycarbonylbenzamido derivative was extremely rapid and quantitative. The product could quite readily be isolated. On the other hand, the reaction of a 2-deoxy-2-phthalimido-β-D-glucopyranosyl unit was relatively much slower, did not proceed quantitatively, and the products could not be isolated. In accordance with these results, the complete removal of the phthalimido group by reaction with hydrazine depends both on the ease of formation of the *o*-hydrazinocarbonylbenzamido intermediate and on how readily this reaction is reversed as compared to the formation of the amine. The method developed by Bundle and Josephson (14) which employs hydrazine at high dilution, followed by *N*-acetylation, was effective for the conversion of **7** to **8** and of **12** to **13** in acceptable yields.

Our initial attempts to prepare the 3,4-*O*-isopropylidene derivative of **1**, namely **9**, met with difficulty and it was for this reason that the preparation of **4** was undertaken. The problem arose because of the ready formation of the 4,6-*O*-isopropylidene derivative. However, it was subsequently found that extended reaction at 5°C gave the desired compound in acceptable (64%) yield. The preparation of **13** by way of the intermediates **10**, **11**, and **12** followed normal procedures for the transformations shown. The conversion of **9** to **10** using hexa-*O*-acetyl-2-deoxy-2-phthalimido-α,β-D-lactosyl chloride (15) and a slight excess of the alcohol **9** proceeded in 75% yield.

## Experimental

The methods used for the isolation of products, solvent purification and removal, spectral analysis, and chromatography were in general the same as those previously reported from this laboratory (12).

[2]R. U. Lemieux and P. Hermentin, in preparation.

Can. J. Chem. Downloaded from www.nrcresearchpress.com by 210.87.254.40 on 09/06/12
For personal use only.

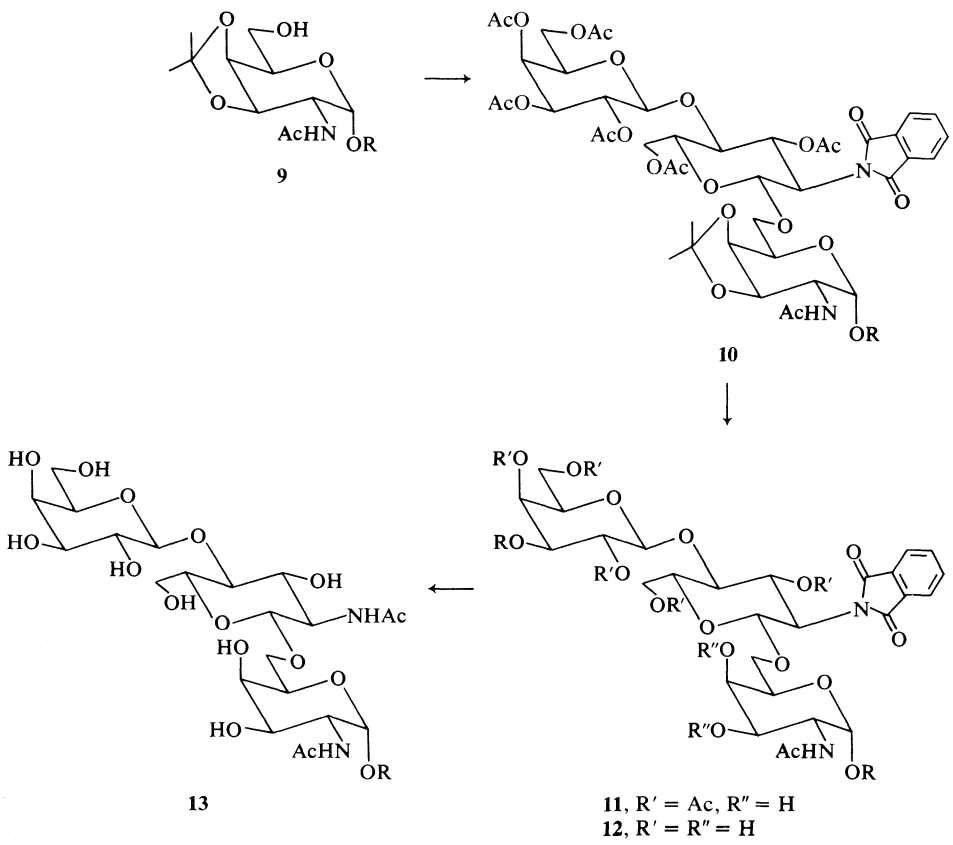


*8-Methoxycarbonyloctyl 2-(*N*-acetylbenzamido)-3,4-di-*O*-benzoyl-2-deoxy-α-*D*-galactopyranoside (4)*

This compound was prepared starting from 8-methoxycarbonyloctyl 2-acetamido-2-deoxy-α-D-galactopyranoside (**1**) which was prepared following the directions reported by Ratcliffe *et al.* (9). In this work, the compound was obtained after recrystallization from methanol as an anhydrous product, mp 134°C, $[\alpha]_D^{25}$ + 143.5° (*c* 1, in chloroform). Both the $^1H$ and $^{13}C$ nmr spectra were in accord with expectations.

A solution of compound **1** (670 mg, 1.71 mmol) and triphenylmethyl chloride (500 mg, 1.79 mmol) in pyridine (12 mL) was kept at 65°C for 24 h. Triphenylmethyl chloride (100 mg, 0.36 mmol) was added and the reaction was continued for a further 24 h. The reaction was monitored by tlc (benzene – ethyl acetate – methanol, 10:5:3). The solution expected to contain the trityl compound **2** was then cooled to room temperature for the addition of benzoyl chloride (1.00 g, 7.1 mmol). The resulting mixture was kept at near 23°C for 24 h prior to the addition of dichloromethane (200 mL). This solution was then processed in the usual manner to provide a yellow oil (1.98 g) which was not further purified. However, in a separate experiment, the main product was isolated by column chromatography and found on examination by $^1H$ nmr to contain three benzoyl groups along with one trityl group and one acetyl group. Therefore the product was assigned structure **3**.

The above-mentioned crude product was dissolved in 1% methanolic hydrogen chloride (30 mL) and the solution was kept at near 23°C for 1 h prior to neutralization with triethylamine. Solvent removal left a residue which was dissolved in dichloromethane (100 mL) for extraction with water. After drying and solvent removal, the residue was applied to a column of silica gel (40 g) for chromatographic separation using ethyl acetate – hexane (6:4). The main fraction contained a product which appeared homogeneous on examination by tlc but which resisted crystallization. The overall yield was 61% (740 mg) of a colorless foam; $[\alpha]_D^{25}$ + 133° (*c* 1.1, in chloroform). The $^{13}C$ nmr ($CDCl_3$) spectrum required a high state of purity and structure **4** was supported by the presence of signals for four carbonyl carbons at 165.2, 166.8, 171.6, and 173.6 ppm in addition to that for the methoxycarbonyl group at 174.3 ppm. The signal at 61.07 ppm was assigned to the $CH_2OH$ group. The $^1H$ nmr confirmed the structural assignment both in terms of the relative intensities of the signals which could be unequivocally assigned and the chemical shifts of the hydrogen atoms of the pyranose ring. The occurrence of the signal for H-2 at exceptionally low field (6.18 ppm, $CDCl_3$) is noteworthy. *Anal.* calcd. for $C_{39}H_{46}O_{11}N$: C 66.45, H 6.58, N 1.99; found: C 66.58, H 6.43, N 1.81.

*8-Methoxycarbonyloctyl 2-(*N*-acetylbenzamido)-3,4-di-*O*-benzoyl-2-deoxy-6-*O*-(3,4,6-tri-*O*-acetyl-2-deoxy-2-phthalimido-β-*D*-glucopyranosyl)-α-*D*-galactopyranoside (5)*

A solution of alcohol **4** (915 mg, 1.30 mmol), silver triflate (481 mg, 1.87 mmol), and *sym*-collidine (226 mg, 1.87 mmol) in nitromethane (6 mL) protected from light and moisture was cooled to −30°C. Tri-*O*-acetyl-2-deoxy-2-phthalimido-β-D-glucopyranosyl chloride (**8**) (850 mg, 1.87 mmol) in nitromethane (3 mL) was added dropwise with stirring so as to maintain the temperature near −30°C. After 1 h, the stirring was continued for 2 h at −5°C. The reaction mixture was then diluted with chloroform (150 mL) and the solids were collected by filtration.

Can. J. Chem. Downloaded from www.nrcresearchpress.com by 210.87.254.40 on 09/06/12
For personal use only.

Can. J. Chem. Downloaded from www.nrcresearchpress.com by 210.87.254.40 on 09/06/12
For personal use only.

The filtrate was washed with ice-cold water (50 mL), cold 3% hydrochloric acid (50 mL), water (50 mL), and dried. Solvent removal left an oily residue (1.85 g) which was purified by chromatography on a silica gel column (60 g) which was developed with a mixture of hexane and ethyl acetate (6:4). On evaporation, the material crystallized and was recrystallized from the same solvents; mp 85–87°C, $[\alpha]_D^{25}$ + 84.7 (*c* 2.12, in chloroform) (1.27 g, 87% yield); $^1$H nmr ($CDCl_3$) δ: 8.1–7.2 (m, 19H, phthalimido and 3 benzoyl groups), 6.06 (dd, 3.5 Hz, 11.5 Hz, 1H, H-2), 5.86 (d, 3.5 Hz, 1H, H-1), 5.74 (dd, 10.5 Hz, 9.5 Hz, 1H, H-3′), 5.56 (dd, 11.5 Hz, 3.5 Hz, 1H, H-3), 5.38 (d, 8.5 Hz, 1H, H-1), 5.14 (t, 9.5 Hz, 1H, H-4′), 4.74 (d, 3.4 Hz, 1H, H-4), 4.35–4.20 (m, 3H, H-2′, H-5, H-6″), 4.08 (dd, 3.2 Hz, 11.0 Hz, 1H, H-6), 3.83 (m, 1H, H-5′), 3.70 (s, 3H, $CH_3O$), 3.61 (dd, 11.0 Hz, 9.0 Hz, 1H, H-6′), 3.30–3.13 (m, 1H, —O—$CH_2$—$(CH_2)_7CO_2CH_3$), 2.58–2.45 (m, 1H, —O$CH_2$—$(CH_2)_7CO_2CH_3$), 2.33 (t, 7 Hz, 2H, $CH_2$—$CO_2CH_3$), 2.08 (s, 3H, $CH_3CONH$), 2.03 (s, 3H, $CH_3CO$), 1.86 (s, 3H, $CH_3CO$), 1.76 (s, 3H, $CH_3CO$), 1.7–1.5 (m, 2H, —$CH_2$—$CH_2CO_2CH_3$), 1.35–0.75 (m, 10H, $CH_2$—$(CH_2)_5CH_2CH_2CO_2CH_3$); $^{13}$C nmr ($CDCl_3$) δ: 174.3 (1C, $CO_2CH_3$), 173.6, 171.6, 170.7 (3C=O), 170.1 (C=O double intensity, 2 C=O phthalimido), 169.4, 167.5, 165.0 (4 C=O), 136.0–123.6 (14C, aromatic carbons), 98.9 (C-1′), 98.3 (C-1). *Anal.* calcd. for $C_{59}H_{64}O_{20}N_2$: C 63.20, H 5.75, N 2.50; found: C 63.08, H 5.79, N 2.39.

*8-Methoxycarbonyloctyl 2-acetamido-2-deoxy-6-O-(2-acetamido-2-deoxy-β-D-glucopyranosyl)-α-D-galactopyranoside (**8**)*

The blocked disaccharide **5** was converted to the desired hapten **8** by way of the intermediate de-*O*-acylated phthalimido compound **7**. It was noted by tlc that treatment of **5** (299 mg, 0.267 mmol) with 0.1 *M* sodium methoxide in methanol (10 mL) at 0°C led after 10 min to essentially one product. Neutralization with Amberlite IR120 ($H^+$) resin and solvent removal provided a product (199 mg) which appeared ($^1$H nmr) to be almost pure **6**. However, when the transesterification was performed at near 23°C for 1.5 h, this product was transformed to compound **7**. The presence of the *N*-acetyl (1.92 ppm) and the methoxycarbonyl (3.68 ppm) groups was clearly evident. The signal for the four hydrogen atoms of the phthalimido group occurred as a broad singlet at 7.83 ppm. The compound was not further purified but used directly for the formation of compound **8** by way of hydrazinolysis followed by *N*-acetylation under conditions similar to those independently developed by Bundle and Josephson (14).

Compound **7** (117.4 mg, 0.172 mmol) was dissolved in methanol (4 mL) containing 97% hydrazine (14.5 mg, 0.44 mmol) and refluxed, monitored by tlc (ethyl acetate – ethanol–water, 8:4:2). After 3 h, an additional amount of hydrazine (7 mg) in methanol (1 mL) was added and the reaction mixture was refluxed for 3 h. Then the solution was cooled to room temperature and acetic anhydride (500 mg) was added. The resulting mixture was left for 30 min and then evaporated to dryness. Ethanol (10%, 4 mL) was added, the solids were gathered by filtration and washed with a small amount of the solvent. The combined filtrates were evaporated and the residue was applied to a Bio-Gel P-2 column and eluted with 10% ethanol. The first fraction to appear in the eluate on evaporation provided an amorphous white powder (70 mg, 79% yield), $[\alpha]_D^{25}$ + 69° (*c* 1.1, water). The nmr spectra required the assigned structure and a high state of purity. Selected parameters are given: $^1$H nmr ($D_2O$) δ: 4.88 (d, 3.8 Hz, H-1), 4.52 (d, 8.5 Hz, 1H, H-1′), 3.68 (s, 3H, $OCH_3$), 2.37 (t, 7.5 Hz, 2H, $CH_2$—$COOCH_3$), 2.03 (s, 3H, $NHCOCH_3$), 2.01 (s, 3H, $NHCOCH_3$); $^{13}$C nmr ($D_2O$) δ: 177.5, 174.3, 174.0 (3 C=O), 101.4 (C-1′), 96.7 (C-1), 75.9 (C-5′), 74.0 (C-3′), 70.1 (C-4′), 69.3 (2C, C-6, C-5), 68.5 (1C, —O—$CH_2$—$(CH_2)_7$—), 67.8, 67.6 (C-4, C-3), 60.9 (C-6′), 55.5 (C-2′), 51.9 ($OCH_3$), 50.0 (C-2). *Anal.* calcd. for $C_{26}H_{46}O_{13}N_2 \cdot H_2O$: C 50.97, H 7.89, N 4.59; found: C 50.88, H 7.42, N 4.54.

*8-Methoxycarbonyloctyl 2-acetamido-2-deoxy-3,4-O-isopropylidene-α-D-galactopyranoside (**9**)*

A solution of compound **1** (9) (1.61 g, 4.12 mmol) in *N,N*-dimethylformamide (50 mL) containing *p*-toluenesulphonic acid (0.1 g, 0.75 mmol) and 2,2′-dimethoxypropane (7 g, 67.30 mmol) was kept at 5°C for 28 h. The reaction mixture was neutralized with triethylamine, evaporated under vacuum, and the residue (2.21 g) was chromatographed on a silica gel column (100 g) eluting with ethyl acetate – hexane (7:3) to provide compound **9** (1.14 g, 64% yield after one recrystallization from the same solvents); mp 64°C, $[\alpha]_D^{25}$ + 109.5° (*c* 2.37, in chloroform); $^1$H nmr ($CDCl_3$) δ: 5.87 (d, 8.5 Hz, 1H, NH), 4.77 (d, 3.5 Hz, 1H, H-1), 4.4–3.2 (m, 8H), 3.65 (s, 3H, $OCH_3$), 2.9–2.7 (m, 1H, O*H*), 2.30 (t, 7 Hz, 2H, $CH_2CO_2CH_3$), 2.02 (s, 3H, NAC), 1.55 (s, 3H, $CH_3$), 1.8–1.2 (m, 15H, $(CH_2)_6CH_2CO_2CH_3$ and $CH_3$); $^{13}$C nmr ($CDCl_3$) δ: 174.36 ($CO_2CH_3$), 170.29 ($NHCOCH_3$), 109.85 (isopropylidene $(CH_3)_2C$), 97.73 (C-1), 74.67, 73.47, 68.22, 67.86 (3 ring carbons and $OCH_2(CH_2)_7CO_2CH_3$), 62.61 (C-6), 51.44 (C-2), 50.81 ($OCH_3$), 34.02, 29.99, 29.33, 29.14, 28.29, 28.05, 26.83, 26.65, 26.03, 24.88, 23.36 ($(CH_2)_7CO_2CH_3$ and 3 $CH_3$). *Anal.* calcd. for $C_{21}H_{37}O_8N$: C 58.45, H 8.64, N 3.25; found: C 58.33, H 8.65, N 3.10.

*8-Methoxycarbonyloctyl 2-acetamido-2-deoxy-6-O-[3,6-di-O-acetyl-4-(2,3,4,6-tetra-O-acetyl-β-D-galactopyranosyl)-2-deoxy-2-phthalimido-β-D-glucopyranosyl]-3,4-O-isopropylidene-α-D-galactopyranoside (**10**)*

A solution of alcohol **9** (575.8 mg, 1.10 mmol), silver triflate (283.3 mg, 1.10 mmol), and *sym*-collidine (133 mg, 1.10 mmol) in nitromethane (protected from light and moisture) (3 mL) was cooled to −30°C. Hexa-*O*-acetyl-2-deoxy-2-phthalimido-D-lactosyl chloride (15) (745.6 mg, 1.00 mmol) in nitromethane (4 mL) was added dropwise. The resulting solution was stirred at −20°C for 2 h and then at room temperature for 4 h. The solution was diluted with chloroform (100 mL) and the solids were filtered and washed with chloroform. The combined filtrates were washed with cold water (30 mL), a cold aqueous hydrochloric acid solution (10%, 30 mL), cold water (30 mL), an aqueous cold sodium bicarbonate solution (30 mL), and water (30 mL), dried, and evaporated under vacuum. The residue was dissolved in a mixture of ethyl acetate – hexane (1:1) and passed through a short alumina column yielding compound **10** (856 mg, 75% yield from **9**); mp 102–105°C, $[\alpha]_D^{25}$ = +57.3° (*c* 1.77, in chloroform); $^1$H nmr ($CDCl_3$) δ: 7.95–7.6 (m, 4H, phthaloyl), 5.76 (dd, 8 Hz, 10 Hz, H-3′), 3.66 (s, 3H, $OCH_3$), 2.33 (t, 7 Hz, 2H, $CH_2CO_2CH_3$), 2.14, 2.12, 2.06, 2.04, 1.94, 1.93, 1.90 (6 *O*-acetyls, 1 *N*-acetyl), 1.47, 1.14 (each s, 3H, —$CH_3$); $^{13}$C nmr ($CDCl_3$) δ: 174.25 ($CO_2CH_3$), 170.41 ($NHCOCH_3$), 170.17, 170.06, 169.87, 169.69, 169.09 ($CH_3CO$), 134.26, 131.76, 128.41, 123.49 (aromatic), 109.80 (isopropylidene $(CH_3)_2C$), 101.4 (C-1″), 98.96 (C-1′), 97.27 (C-1), 79.31, 77.17, 76.99, 75.05, 74.74, 72.85, 71.10, 70.73, 70.37, 69.28, 67.45, 66.70, 66.59, 62.28, 60.81, 55.13 (C-2′), 51.32 ($CH_3O$), 50.51 (C-2), 34.03, 29.14, 27.89, 26.48, 25.99, 24.89, 23.32, 20.87, 20.58 ($(CH_3)_2C$). *Anal.* calcd. for $C_{53}H_{72}O_{25}N_2$: C 55.98, H 6.38, N 2.46; found: C 55.47, H 6.38, N 2.33.

*8-Methoxycarbonyloctyl 2-acetamido-6-O-[2-acetamido-4-O-(β-D-galactopyranosyl)-2-deoxy-β-D-glucopyranosyl]-α-D-galactopyranoside (**13**)*

Compound **10** (177 mg, 0.1556 mmol) was dissolved in a 10% solution of 99% trifluoroacetic acid in dichloromethane (7 mL) and left at room temperature for 1 h. The solution was diluted with dichloromethane (50 mL), washed with ice-cold water

(25 mL), cold aqueous sodium bicarbonate solution (25 mL), and cold water (25 mL), dried, and evaporated to provide a crude compound **11** (136 mg, 70% yield) which was characterized by $^1$H nmr. Without purification, the product was treated with 0.1 *N* sodium methoxide in methanol (5 mL) for 5 min. The solution was then neutralized with Amberlite IR-120 ($H^+$) resin and evaporated to provide compound **12** (103 mg, 94% yield). The material appeared essentially pure; $^1$H nmr ($CDCl_3$) δ: 7.82 (s, 4H, phthalimido), 5.68 (dd, 8 Hz, 10 Hz, H-3′), 3.64 (s, 3H, $OCH_3$), 2.32 (t, 7 Hz, 2H, $CH_2$—$CO_2CH_3$), 1.90 (s, 3H, *N*-acetyl), 1.8–1.2 (m, 12H, $(CH_2)_6CH_2CO_2CH_3$).

Crude compound **12** (94.2 mg) was dissolved in methanol (5 mL) containing 97% hydrazine (14.5 mg) and the solution was brought to reflux. The course of the reaction could be monitored by tlc (ethyl acetate – ethanol–water, 8:4:2). After 2 H, an additional amount of hydrazine was added (10.8 mg in 1.5 mL of methanol) and the reaction mixture was refluxed for a further 2 h. The solution was cooled to room temperature, acetic anhydride (500 mg) was added, and the mixture was left at room temperature for 20 min. Solvent removal left a solid residue which was extracted with 10% ethanol in water. The combined filtrates were evaporated for application to a Biogel P-2 column and elution with 10% ethanol in water. The major fraction was freeze-dried to a powder (75 mg, 89% yield), $[\alpha]_D^{25}$ + 129° (*c* 2.7, in water); $^1$H nmr ($D_2O$, HOD, 400 mHz) δ: 4.96 (d, 3.8 Hz, H-1), 4.75 (d, 8.3 Hz, H-1′), 4.72 (d, 8.3 Hz, H-1″), 4.37 (dd, 10.8 Hz, H-2), 2.63 (t, 7 Hz, 2H, $CH_2CO_2CH_3$), 2.29, 2.26 (2s, 6H, *N*-acetyls); $^{13}$C nmr ($D_2O$, dioxane) δ: 177.2, 174.1, 173.8 ($COOCH_3$, 2 *N*—$COCH_3$), 102.9 (C-1″), 101.3 (C-1′), 96.7 (C-1), 78.83, 75.29 (C-5″), 74.74, 72.58, 72.47 (C-3″), 70.94 (C-2″), 69.26, 68.52 (C-4″), 67.70, 67.56, 66.5, 60.9 (C-6″), 60.2, 54.97 (C-2′), 51.94, 49.99 (C-2, $OCH_3$), 33.63, 28.32, 28.25, 28.19, 25.24, 24.27, 22.22, 21.95.

## Acknowledgements

The financial assistance of the Natural Sciences and Engineering Research Council of Canada (A172) is gratefully acknowledged. The microanalyses and nmr spectra were carried out by the Analytical and Spectral Services Laboratories of this department.

1. K. O. Lloyd, E. A. Kabat, and E. Licerio. Biochemistry, **7**, 2976 (1968).
2. L. Rovis, B. Anderson, E. A. Kabat, F. Gruezo, and J. Liao. Biochemistry, **12**, 5341 (1973).
3. J.-P. Cartron, G. Andrew, J. Cartron, G. W. Bird, C. Salmon, and A. Gerbal. Eur. J. Biochem. **92**, 111 (1978).
4. P. Vaith and G. Uhlenbruck. Z. Immun.-Forsch. **154**, 1 (1978).
5. G. F. Springer, P. R. Desai, M. S. Murthy, H. Tegtmeyer, and E. F. Scanlon. Prog. Allergy, **26**, 42 (Karger, Basel, 1979).
6. R. U. Lemieux, D. A. Baker, W. M. Weinstein, and C. M. Switzer. Biochemistry, **20**, 199 (1981).
7. E. A. Kabat, J. Liao, M. H. Burzynska, T. C. Wong, H. Thøgersen, and R. U. Lemieux. Mol. Immunol. **18**, 873 (1981).
8. E. A. Kabat, J. Liao, and R. U. Lemieux. Immunochemistry, **15**, 727 (1978).
9. R. M. Ratcliffe, D. A. Baker, and R. U. Lemieux. Carbohydr. Res. **93**, 35 (1981).
10. T. D. Inch and H. G. Fletcher, Jr. J. Org. Chem. **31**, 1815 (1966).
11. R. U. Lemieux, T. Takeda, and B. Y. Chung. Am. Chem. Soc. Symp. Ser. **39**, 90 (1976).
12. R. U. Lemieux, S. Z. Abbas, and B. Y. Chung. Can. J. Chem. **60**, 58 (1982).
13. S. Josephson and D. R. Bundle. Can. J. Chem. **57**, 3073 (1979).
14. D. R. Bundle and S. Josephson. Can. J. Chem. **57**, 662 (1979).
15. R. U. Lemieux, S. Z. Abbas, M. H. Burzynska, and R. M. Ratcliffe. Can. J. Chem. **60**, 63 (1982).

Can. J. Chem. Downloaded from www.nrcresearchpress.com by 210.87.254.40 on 09/06/12
For personal use only.

# The synthesis and conformational properties of the diastereoisomeric βDGal(1→4)βDGlcNAc(1→6)6-*C*-$CH_3$-D-Gal trisaccharides

RAYMOND U. LEMIEUX, TING C. WONG,[1] AND HENNING THØGERSEN[2]
*Department of Chemistry, University of Alberta, Edmonton, Alta., Canada T6G 2G2*

Received March 27, 1981

RAYMOND U. LEMIEUX, TING C. WONG, and HENNING THØGERSEN. Can. J. Chem. **60**, 81 (1982).

The trisaccharide βDGal(1→4)βDGlcNAc(1→6)DGal was known to be bound strongly by the so-called anti-I Ma monoclonal antibody. In order to help assess the conformation about the 1→6 glycosidic linkage that is accepted by the antibody combining site, the conformationally well-defined βDGal(1→4)βDGlcNAc(1→6) derivatives of 7-deoxy-L-*glycero*-D-*galacto*-heptopyranose and 7-deoxy-D-*glycero*-D-*galacto*-heptopyranose were synthesized. The conformational preferences for these trisaccharides were established by $^1$H nmr spectroscopy and rationalized by computer-assisted molecular modelling.

RAYMOND U. LEMIEUX, TING C. WONG et HENNING THØGERSEN. Can. J. Chem. **60**, 81 (1982).

On sait que le trisaccharide βDGal(1→4)βDGlcNAc(1→6)DGal est lié fortement à l'anticorps monoclonal anti-I Ma. Dans le but d'aider à déterminer la conformation autour de la liaison glycosidique (1→6) qui est accepté par le site combinant de l'anticorps, on a synthétisé les dérivés conformationnellement bien définis βDGal(1→4)βDGlcNAc(1→6) du déoxy-7-L-*glycéro* D-*galacto*-heptopyrannose et du déoxy-7 D-*glycéro*-D-*galacto*-heptopyrannose. On a établi les préférences conformationnelles de ces trisaccharides par la spectroscopie de rmn du $^1$H et on les a rationalisées par des modèles moléculaires fournis par ordinateur.
[Traduit par le journal]

## Introduction

The myeloma protein which was classified (1) as the monoclonal antibody I Ma (group 1) was found to possess a combining site which binds at the surface of a βDGal(1→4)βDGlcNAc(1→6) structural unit which was common to a number of the oligosacchardies studied.

We have predicted (2) that the conformational preference for the glycosidic linkage at the 4-position of the βDGlcNAc residue should be near $\phi^{C4'/H1''} = 50°$, $\psi^{H4'/C1''} = 10°$. Both for reasons of nonbonded interactions and the *exo*-anomeric effects, it was to be expected that the glycosyl bond of the βDGlcNAc unit to the 6-position of a sugar, which may be either βDGal or αDGalNAc, would possess the $\phi^{C6/H1'}$ torsion angle close to +60°. However, rotation about either the O6—C6 bond (to provide changes in the $\psi^{C5/C1'}$ torsion angle) or the C5—C6 bond (to provide changes in the $\omega^{H5/O6}$ torsion angle) was expected to lead to a number of conformers which differ little in energy (3). Indeed, hard-sphere calculations using the general procedure described by Venkatachalam and Ramachandran (2) while setting $\phi^{C6/H1'} = 60°$ substantiated this expectation.

The procedure was to examine the barriers to rotation about the O6—C6 bond (changes in $\psi^{C5/C1'}$) with the atoms on C5 and C6 in the 3 staggered orientations (namely, $\omega^{H5/O6} = +60°$, 180°, and −60°). In order to simplify the calculation, as in the past (2), the hydroxyl group hydrogen atoms were neglected and the hydroxymethyl groups of the hexose units, when present, were treated as 6-deoxy units. The parameters for the βDGlcNAc unit were derived from the X-ray structures of 4-*N*-(2-acetamido-2-deoxy-β-D-glucopyranosyl)-L-asparagine (4) and lactose (5). The coordinates for the hydrogen atoms attached to carbon were established by fixing the C—H bond length at 1.1 Å and making equal the three bond angles involving this hydrogen atom. The neutron diffraction data (6) for methyl β-D-galactopyranoside were used for the two βDGal units of βDGal(1→4)βDGlcNAc(1→6)βDGal. Since no interaction can be reasonably expected to exist between the two terminal βDGal units, the conformation of the trisaccharide was estimated by examining the structure as two disaccharide units. The calculations showed that the $\psi^{C5/C1'}$ torsion angle could vary within the following ranges without encountering energy barriers greater than ± 0.5 kcal/mol.

Conformers of near equal energy for βDGlcNAc(1→6)βDGal

| $\phi^{C6/H1'}$ | $\omega^{H5/O6}$ | $\psi^{C5/C1'}$ |
|---|---|---|
| 60° | 60° | 120°–290° |
| 60° | 180° | 110°–240° |
| 60° | −60° | 100°–260° |

In view of the very large number of energetically near-equivalent conformers for the βDGlcNAc-(1→6)βDGal disaccharide, no conclusion could be drawn as to which conformer was most likely to be accepted by the I Ma combining site. It was

[1]Ph.D. Student, 1978–present.
[2]University of Alberta Postdoctoral Fellow, 1980–1981.

0008-4042/82/010081-06$01.00/0
©1982 National Research Council of Canada/Conseil national de recherches du Canada

Can. J. Chem. Downloaded from www.nrcresearchpress.com by 210.87.254.42 on 09/06/12
For personal use only.

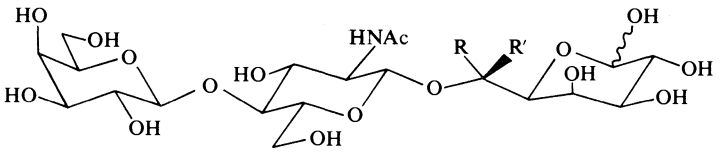

**6** R′ = $CH_3$, R = H
**9** R′ = H, R = $CH_3$

expected, however, that the range of low energy conformers could be narrowed by the substitution of a methyl group for a hydrogen at the C6 atom of the reducing βDGal unit. This would lead to two diastereoisomers depending on which hydrogen atom was substituted; namely, structures **6** and **9**. Since **6** is derived from 7-deoxy-L-*glycero*-D-*galacto*-heptose, it will be referred to as the L-trissaccharide. D-Trisaccharide will be used to refer to the derivative of 7-deoxy-D-*glycero*-D-*galacto*-heptose; namely, **9**. This paper is concerned with the synthesis of the trisaccharides **6** and **9** and a study of their conformational properties. The results obtained in a study of their properties as inhibitors of anti-I Ma is reported in a separate communication (7).

## Discussion

In a study of the binding of antibodies specific for the β-D-galactopyranosyl group, Lemieux *et al.* (8) observed that the addition of methylmagnesium bromide to 1,2;3,4-di-*O*-isopropylidene-α-D-*galacto*-1,6-dialdohexopyranose (9) (**1**) provided the L and D isomers **2** and **3**, respectively, in a ratio of

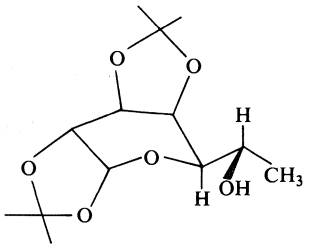

**2**

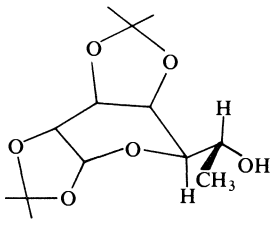

**3**

about 3:1. However, these products were not characterized. Instead, the compounds were converted to their methyl β-glycosides to serve as inhibitors in the immunochemical studies. The configuration of the new asymmetric carbon in the minor component was established to be D by relating its physical properties to the enantiomeric structure which had been previously described by Jackson and Hudson (10). It should be noted at this point that there exists an error in the reporting of these compounds by Lemieux *et al.* (8). The correct names are given in the title of the preparation. The first fraction from the chromatogram should have been reported as the D-isomer and the second fraction as the L-isomer. In the present work, the L-compound **2** was readily isolated by direct crystallization. Compound **3** (the minor D-isomer) was obtained after purification by way of its crystalline benzoate. The spacings for the signals for the hydrogens of the pyranose ring in compounds **2** and **3** were virtually the same as those published by Cone and Hough (11) for 1,2;3,4-di-*O*-isopropylidene-α-D-galactopyranose. The chemical shifts of H1, H2, and H3 were essentially the same. The shift of H4 was 4.26 ppm for both the galactose compound and the L-isomer (**2**), but the signal for H4 of the D-isomer, probably because of electrostatic deshielding by O6, was 0.2 ppm to lower field. In view of the magnitudes of the coupling constants for H5 and H6 (6.8 Hz for **2** and 7.2 Hz for **3** with $CDCl_3$ as solvent), the compounds must exist extensively in the conformer which maintains these two hydrogens in near *anti*-periplanar orientation. It is noted, however, that the pyranose ring in these compounds is strongly distorted away from the $^4C_1$ conformation (11) as is implied in the conformational formulas.

It was planned to confirm the configurations of the products (**2** and **3**), formed in the reaction of the aldehyde (**1**) with methylmagnesium iodide, by nuclear Overhauser enhancement studies (2, 12) since the C6-methyl group could be expected to reside closer to H4 in the L-isomer than in the D-isomer. However, although saturation of the signals assigned to these methyl groups did, in fact, cause a greater enhancement of H4 in the case of the L-isomer, the significance of this result proved to be obscured by the fact that the experiment could not avoid simultaneous saturation of the isopropylidene groups. This interference by the isopropylidene groups was not present in the case of the trisaccharides **6** and **9** and, as will be seen below, the $^1H$ nmr spectra for these compounds further confirmed these configurational assignments.

The chemical syntheses of compounds **6** and **9** were accomplished by condensation of hexa-*O*-acetyl-2-deoxy-2-phthalimidolactosyl chloride (13) with the alcohols **2** and **3** under the conditions

Can. J. Chem. Downloaded from www.nrcresearchpress.com by 210.87.254.42 on 09/06/12
For personal use only.

Can. J. Chem. Downloaded from www.nrcresearchpress.com by 210.87.254.42 on 09/06/12
For personal use only.

reported (14) for the preparation of 6-*O*-[hexa-*O*-acetyl-2-deoxy-2-phthalimido-β-lactopyranosyl]-1,2;3,4-di-*O*-isopropylidene-α-D-galactopyranose. The products (**4** and **7**) were treated first with hydrazine to remove the acyl groups and the resulting amines were then *N*-acetylated to provide **5** and **8**. Removal of the isopropylidene groups by hydrolysis in aqueous trifluoroacetic acid afforded the desired trisaccharides **6** and **9**. The overall yields are poor and not to be taken as representative of the methods used, primarily since the preparations were made only once and no effort was made to optimize the reaction and isolation procedures.

The hard-sphere calculations (5° steps) for the D- and L-trisaccharides (**6** and **9**) employed the same atomic parameters mentioned above in connection with the molecular modelling for the βDGal(1→4)-βDGlcNAc(1→6)βDGal trisaccharide, except that the *C*-methyl group was substituted for the particular H6 atom with a C—C bond length of 1.536 Å. In the case of the D-trisaccharide (**9**), the calculation showed the most favorable conformer to be near that with $\phi^{C6/H1'} = 60°$, $\omega^{H5/O6} = 60°$, and $\psi^{C5/C1'} = 130°$. The minimum energy conformers with $\omega^{H5/O6} = 180°$ and 300° were indicated to be about 1 kcal and 3 kcal/mol, respectively, less favorable. The $\omega^{H5/O6} = 60°$ torsion angle requires that the torsion angle be defined by H5 and that H6 be near 180°. Thus, should this inference as to conformational preference be correct, there should exist a coupling constant between the vicinal *anti*-periplanar H5 and H6 atoms of near 10 Hz. Indeed, a coupling of 8.5 Hz was observed. Examination of a molecular model in this conformation shows the C6-methyl group to be close to H5 and H6 only. In fact, saturation of the methyl group led to nuclear Overhauser enhancement of only these two hydrogens. The signal for H4 at 4.17 and 4.24 ppm (α and β anomers) was not affected. When $\omega^{H5/O6}$ was set at 60° and the $\psi^{C5/C1'}$ torsion angles in the range 120–160° examined by HSEA calculations, the best value for the φ torsion angle was found to be +50° with ψ = 130°. In the context of these calculations, the difference of near 0.1 kcal/mol between this conformation and that with $\phi^{C6/H1'} = 60°$ and $\psi^{C5/C1'} = 130°$ is not significant. A projection formula for the D-trisaccharide (**9**) is presented in Fig. 1.

The hard-sphere calculations for the L-trisaccharide (**6**) indicated the staggered conformation with $\omega^{H5/O6} = 190°$ to be most favorable by nearly 1 kcal and that this conformer involved $\psi^{C5/C1'} = 230°$ (−130°) (for this calculation, $\phi^{C6/H1'}$ had been arbitrarily set at 60°). When this value for ω was

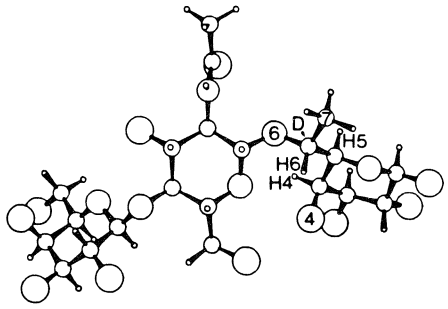


**9**

FIG. 1. Computer drawing of the D-trisaccharide (**9**) in the conformation anticipated by HSEA calculation in order to display the *anti*-periplanar orientation of H5 and H6 and the orientation of the C7-methyl group relative to H4.

used in a second iterative HSEA calculation[3] to estimate the most favorable values for φ and ψ, the values $\phi^{C6/H1'} = 50°$ and $\psi^{C5/C1'} = 230°$ were obtained and the total conformational energy was −0.6 kcal/mol for the compound in the conformation (**6***a*) represented in Fig. 2. On applying the HSEA calculation to the conformer with $\omega^{H5/O6} = 290°$ (−70°), the conformer (**6***b*) with $\phi^{C6/H1'} = 45°$ and $\psi^{C5/C1'} = 250°$ (−110°) was indicated as energetically most favorable with a total conformational energy of 0 kcal/mol.

Thus, it appeared that conformer **6***a* should have a substantially higher abundance than **6***b*. However, the $^1$H nmr properties of the L-isomer clearly demand that the conformational equilibrium favor conformer **6***b*. This followed from the observations that (*a*) the coupling constant for the vicinal H5 and H6 atoms was 8.0 Hz, in keeping with a high population of the conformer **6***b*, which has these atoms in *anti*-periplanar orientation, but not **6***a*, where these atoms are in *syn*-clinal orientations, and (*b*) saturation of the signal for the C-methyl group strongly enhanced the signal for H4 as well as those for H5 and H6 in keeping with conformation **6***b* but not **6***a*.

That the HSEA calculations predicted a greater conformational stability for **6***a* whereas **6***b* is undoubtedly more favorable is not necessarily surprising. The calculations may well have underestimated the *syn*-axial like nonbonded interaction between O4 and O6 in **6***a*. The HSEA calculations assume that the van der Waals radius for an oxygen atom is 1.5 Å. However, evidence has been presented that the effective radius for oxygen can vary

[3]The procedure for hard-sphere, *exo*-anomeric (HSEA) calculations (2) has been improved and ref. 15 should be consulted in this regard.

Can. J. Chem. Downloaded from www.nrcresearchpress.com by 210.87.254.42 on 09/06/12
For personal use only.

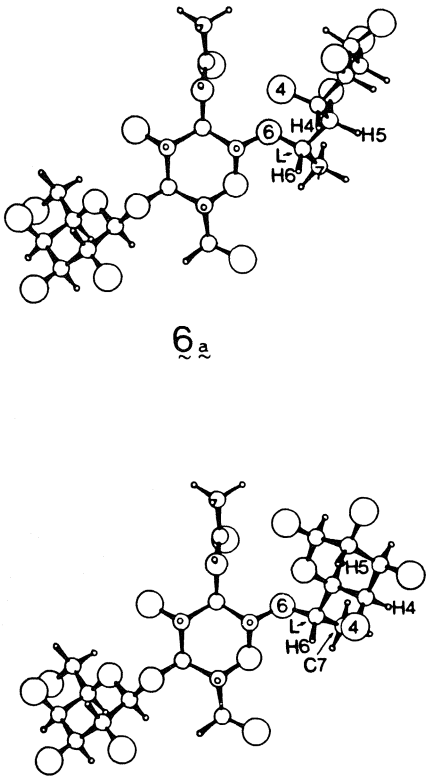


FIG. 2. Computer drawing of the L-trisaccharide (**6**) in the conformation (**6***a*) anticipated to be most favorable by HSEA calculations and in the conformation (**6***b*) best indicated by the $^1$H nmr spectrum. In the case of **6***a*, note the *syn*-axial like arrangement of O4 and O6, the *syn*-clinal orientation of H5 and H6, and that the C7-methyl group is distant from H4. In the case of **6***b*, note that H5 and H6 are in *anti*-periplanar orientation and that the C7-methyl group is in *syn*-axial like orientation with H4.

depending on its substituents (16). Moreover, the calculations do not include either electrostatic terms or a consideration of the effect on the apparent volume of hydroxyl groups when these are hydrogen bonded to the solvent water. We were fortunate in this regard in that **6** proved to be a very poor inhibitor (7) and, therefore, the possible availability of the compound to the antibody combining site in conformation **6***a* did not become an important question.

The study of the interactions of **6** and **9** with the anti-I Ma monoclonal antibody are reported in a separate communication (7) which also reports the results obtained with a number of related compounds. It proved that compound **9** reacts with the antibody even more strongly (about 0.5 kcal/mol) than does the βDGal(1→4)βDGlcNAc(1→6)DGal trisaccharide. This appears to be the first instance in which a complex synthetic structure that is closely related to a natural antigenic determinant binds the antibody more strongly. It is considered that this exceptional event likely occurs, at least in part, because compound **9** is held in the specific conformation that is required for the binding. This matter has a bearing on the notion at times expressed that ground state conformations are not necessarily implicated in antibody–antigen interactions. As expected, the preferred conformation for **9** is amongst the most favorable of the conformations available to the βDGal(1→4)βDGlcNAc-(1→6)DGal trisaccharide.

## Experimental

The purification of the solvents, chromatographic and analytical procedures were the same as previously reported (13).

*1,2;3,4-Di*-O-*isopropylidene*-α-D-galacto-*1,6-dialdo-hexopyranose (1)*

1,2:3,4-Di-*O*-isopropylidene-α-D-galactose was oxidized using the chromium trioxide – pyridine complex in dichloromethane as was described by Arrick *et al.* (9). Examination of the dark green syrupy crude product (95% yield) showed it to be of as good a quality as that obtained by distillation. The $^1$H nmr spectrum was in accord with that published by Horton *et al.* (17).

*1,2;3,4-Di*-O-*isopropylidene-7-deoxy*-β-L-glycero-D-galacto-*heptopyranose(2)*

Methylmagnesium iodide was prepared under standard conditions using magnesium (1.42 g, 58 mmol) and methyl iodide (8.3 g, 58 mmol) in ether (60 mL). A solution of the aldehyde (**1**) (8.0 g, 31 mmol) in diethyl ether (45 mL) was added dropwise with stirring and the mixture was kept at room temperature for 15 h. The reaction mixture was then cooled in ice-water and a 10% solution of ammonium chloride in water (50 mL) was added. Work-up in the usual manner using diethyl ether as extractant, drying over magnesium sulfate, and solvent removal, left a syrup which was decolorized by passing a solution in ethyl acetate through a short column of silica gel. Removal of the solvent left a syrup (7.3 g) which was dissolved in hexane (15 mL). On storage, the solution deposited 3.17 g of crystals which, after three recystallizations from hexane, provided 2.2 g (26%) of **2**, mp 90–91°C; $[\alpha]_D^{23}$ −58.5° (*c* 1.8, chloroform); $^1$H nmr ($CDCl_3$) δ: 5.58 (d, 1H, H-1, $J_{1,2}$ = 4.6 Hz), 4.59 (dd, 1H, H-3, $J_{2,3}$ = 2.1 Hz, $J_{3,4}$ = 8.0 Hz), 4.32 (dd, 1H, H-2), 4.26 (dd, 1H, H-4, $J_{4,5}$ = 2.0 Hz), 3.99 (m, 1H, H-6), 3.48 (dd, 1H, H-5, $J_{5,6}$ = 6.8 Hz), 1.50, 1.44, 1.32 (3s, 12H, O—C(=O)—$C(CH_3)_2$), 1.26 (d, 3H, (C-7)$H_3$, $J_{6,CH_3} \simeq$ 6 Hz). *Anal.* calcd. for $C_{13}H_{22}O_6$: C 56.92, H 8.08; found: C 56.87, H 8.05.

*1,2;3,4-Di*-O-*isopropylidene-7-deoxy*-α-D-glycero-D-galacto-*heptopyranose (3)*

The mother liquor from the first crystallization of the L-isomer (**2**) was taken to a syrup (3.86 g) which was dissolved in dichloromethane (10 mL), pyridine (4 mL), and benzoyl chloride (2 mL). The solution was stirred at room temperature for 3 h and the product was isolated in the usual manner. Solvent removal left a syrup which was taken up in hexane (3 mL) and the solution was kept at −4°C for 2 days. Crystals (0.290 g) were deposited which were debenzoylated in methanol – sodium methoxide without further purification. The product was ap-

Can. J. Chem. Downloaded from www.nrcresearchpress.com by 210.87.254.42 on 09/06/12
For personal use only.

plied to a column of silica gel and eluted with ethyl acetate – hexane (6:4). The main fractions were combined and dissolved in a small amount of hexane and the solution deposited a white solid (0.188 g, 2%) when stored at −4°C overnight. This product, mp 57–58°C, $[\alpha]_D^{23}$ −34.8° (*c* 0.3, chloroform), was not further purified since the $^1$H nmr spectrum revealed it to be a nearly pure substance; $^1$H nmr ($CDCl_3$) δ: 5.55 (d, 1H, H-1, $J_{1,2}$ = 5 Hz), 4.62 (dd, 1H, H-3, $J_{2,3}$ = 2.2 Hz, $J_{3,4}$ = 8.0 Hz), 4.46 (dd, 1H, H-4, $J_{4,5}$ = 2.0 Hz), 4.30 (dd, 1H, H-2), 3.96 (m, 1H, H-6), 3.50 (dd, 1H, H-5, $J_{5,6}$ = 7.2 Hz), 1.51, 1.45, 1.36, 1.32, 1.29 (5 O‖ peaks, 15H, O—C(CH$_3$)$_2$ and (C-7)H$_3$ overlapping). *Anal.* calcd. for $C_{13}H_{22}O_6$: C 56.92, H 8.08; found: C 56.42, H 7.77.

*1,2;3,4-Di-*O*-isopropylidene-6-*O*-[3,6-di-*O*-acetyl-2-deoxy-4-*O*-(tetra-*O*-acetyl-*β*-*D*-galactopyranosyl)-2-phthalimido-*β*-*D*-glucopyranosyl]-7-deoxy-*β*-*L*-glycero-*D*-galacto-heptopyranose (4)*

3,6-Di-*O*-acetyl-4-*O*-(tetra-*O*-acetyl-β-D-galactopyranosyl)-2-deoxy-2-phthalimido-α,β-D-glucopyranosyl chloride (13) (1.3 g, 1.8 mmol) in nitromethane (5 mL) was added to a solution of the alcohol **2** (0.5 g, 1.8 mmol), *sym*-collidine (0.22 g, 1.8 mmol), and silver triflate (0.49 g, 1.9 mmol) in dry nitromethane (15 mL) cooled to −25°C (18). The mixture was stirred at −25°C for 2 h. The reaction mixture was then stirred at room temperature for 8 h. The solids that were deposited after the addition of chloroform (100 mL) were removed by filtration and the filtrate was washed with sodium thiosulfate solution, cold water, dilute aqueous HCl, and saturated sodium bicarbonate solution. Solvent removal, after drying over sodium sulfate, left a foam which was applied to a silica gel column and eluted with ethyl acetate – hexane (1:1). Solvent removal of the second fraction left a white solid (0.63 g, 36%), mp 119–123°C; $[\alpha]_D^{23}$ −21.6° (*c* 1.1, chloroform); $^1$H nmr ($CDCl_3$) δ: 7.80–7.52 (broad m, 4H, phthalimido), 5.70 (dd, 1H, H-3′, $J_{3',4'}$ = 8.0 Hz, $J_{2',3'}$ = 10.5 Hz), 5.39 (d, 1H, H-1′, $J_{1',2'}$ = 8.5 Hz), 5.23 (broad d, 1H, H-4″, $J_{3'',4''}$ = 3.1 Hz), 5.04 (dd, 1H, H-2″, $J_{1'',2''}$ = 7.5 Hz, $J_{2'',3''}$ = 10.5 Hz), 4.87 (dd, 1H, H-3″), 4.73 (d, 1H, H-1, $J_{1,2}$ = 5.0 Hz), 4.44 (d, 1H, H-1″), 3.18 (broad dd, 1H, H-5, $J_{5,6}$ = 8.2 Hz), 2.06, 2.05, 1.99, 1.97, 1.88, 1.80 (6s, 18H, acetyl CH$_3$), 1.32, 1.18, 1.12, O‖ 0.80, 0.75 (5 peaks, 15H, O—C—(CH$_3$)$_2$ and (C-7)H$_3$). *Anal.* calcd. for $C_{45}H_{57}O_{23}N$: C 55.16, H 5.86, N 1.43; found: C 55.02, H 5.83, N 1.31.

*1,2;3,4-Di-*O*-isopropylidene-6-*O*-[2-acetamido-2-deoxy-4-*O*-(β-*D*-galactopyranosyl)-β-*D*-glucopyranosyl]-7-deoxy-β-*L*-glycero-*D*-galacto-heptopyranose (5)*

A solution of compound **4** (0.56 g, 0.57 mmol) and 85% hydrazine hydrate (0.22 g, 4.39 mmol) in ethanol (5 mL) was refluxed for 3 h. Solvent removal left a syrup which was redissolved in water (5 mL). The solution was neutralized with glacial acetic acid and the precipitate formed was removed by filtration. Dialysis of the filtrate through a UMO5 Diaflo membrane (Amicon, Lexington, MA 02173) afforded, after freeze-drying of the dialyzed solution, a solid (0.25 g). This substance was taken up in methanol–water (1:1, 20 mL) containing acetic anhydride (4 mL) and left at room temperature for 2 h. Solvent removal and crystallization from methanol–ether gave a white solid (0.152 g, 42%), mp 165–169°C; $^1$H nmr ($D_2O$, HOD δ = 4.80) δ: 5.62 (d, 1H, H-1, $J_{1,2}$ = 5.0 Hz), 4.44 (2d, 2H, H′ and H″ overlapping, *J* = 7.5 Hz and 8.0 Hz, 2.07 (s, 3H, NHAc O‖ methyl), 1.52, 1.48, 1.38 (3s, 12H, O—C(CH$_3$)$_2$), 1.30 (d, 3H, (C-7)H$_3$), 4.02–3.48 (m, 17H, remaining protons).

*6-*O*-[2-Acetamido-2-deoxy-4-*O*-(β-*D*-galactopyranosyl)-β-*D*-glucopyranosyl]-7-deoxy-*L*-glycero-*D*-galacto-heptopyranose (6)*

A solution of compound **5** (50 mg, 0.078 mmol) in 95% trifluoroacetic acid (2 mL) was stirred for 3 min at room temperature and rapidly evaporated *in vacuo* to a syrup which was applied to a Sephadex LH-20 (Pharmacia Fine Chemicals AB, Uppsala, Sweden) column and eluted with ethanol–water (1:1). Solvent removal and freeze-drying of the main fraction gave a white solid (13.5 mg, 0.024 mmol, 31%); $^1$H nmr ($D_2O$) δ: 5.28 (d, H-1α, $J_{1,2}$ = 2.5 Hz, H-1β not observed, probably obscured by the HOD peak at 4.80), 4.54 (2d, 2H, H-1′ and H-1″ overlapping, *J* = 7.5 Hz and 7.5 Hz), 2.14, 2.13 (2s, NHAc-α and NHAc-β methyl), 1.33 (2d, 3H, (C-7)H$_3$ α and β), 4.08–3.44 (m, 17H, remaining protons).

*1,2;3,4-Di-*O*-isopropylidene-6-*O*-[3,6-di-*O*-acetyl-2-deoxy-4-*O*-(tetra-*O*-acetyl-β-*D*-galactopyranosyl)-2-phthalimido-β-*D*-glucopyranosyl]-7-deoxy-α-*D*-glycero-*D*-galacto-heptopyranose (7)*

3,6-Di-*O*-acetyl-4-*O*-(tetra-*O*-acetyl-β-D-galactopyranosyl)-2-deoxy-2-phthalimido-α,β-D-glucopyranosyl chloride (0.213 g, 0.29 mmol) in dry nitromethane (2 mL) was added to a solution of the alcohol (**3**) (60 mg, 0.22 mmol), *sym*-collidine (33 mg, 0.27 mmol), and silver triflate (60 mg, 0.24 mmol) in dry nitromethane (5 mL) cooled to −25°C. The mixture was stirred at −25°C for 2 h and then warmed to room temperature for 16 h. The reaction mixture was diluted with chloroform (20 mL) and the solids were removed by filtration. The filtrate was washed with cold water, aqueous sodium bicarbonate solution, and dilute aqueous HCl. Solvent removal after drying over sodium sulfate left a foam which was applied to a silica gel column and eluted with ethyl acetate – hexane (1:1). Solvent removal of the second fraction left a white solid (0.14 g, 0.14 mmol, 65%), mp 114–119°C, $[\alpha]_D^{23}$ −20° (*c* 0.5, chloroform); $^1$H nmr ($CDCl_3$) δ: 7.80–7.62 (broad m, 4H, phthalimido), 5.66 (dd, 1H, H-3′, $J_{3',4'}$ = 8.0 Hz, $J_{2',3'}$ = 10.5 Hz), 5.41 (d, 1H, H-1′, $J_{1',2'}$ = 8.5 Hz), 5.34 (d, 1H, H-1, $J_{1,2}$ = 4.5 Hz), 5.25 (broad d, 1H, H-4″, $J_{3'',4''}$ = 3.1 Hz), 5.04 (dd, 1H, H-2″, $J_{1'',2''}$ = 7.5 Hz, $J_{2'',3''}$ = 10.5 Hz), 4.86 (dd, 1H, H-3″), 4.46 (d, 1H, H-1″), 2.07, 1.99, 1.98, 1.89, 1.84 (5s, 15H, acetyl CH$_3$), O‖ 1.32, 1.22, 1.20 (3s, 12H, O—C(CH$_3$)$_2$), 0.88 (d, 3H, (C-7)H$_3$). *Anal.* calcd. for $C_{45}H_{57}O_{23}N$: C 55.16, H 5.86, N 1.43; found: C 54.51, H 5.76, N 1.34.

*1,2;3,4-Di-*O*-isopropylidene-6-*O*-[2-acetamido-2-deoxy-4-*O*-(β-*D*-galactopyranosyl)-α-*D*-glucopyranosyl]-7-deoxy-β-*D*-glycero-*D*-galacto-heptopyranose (8)*

Treatment of compound **7** (0.119 g, 0.12 mmol) with 85% hydrazine hydrate, work-up and *N*-acetylation as described above for the preparation of **5**, resulted in the isolation of a white solid (72 mg) which was applied to a Sephadex LH-20 column and eluted with ethanol–water (1:1). Solvent removal from the main fraction gave a white solid (34 mg, 0.053 mmol, 44%), mp 155–158°C; $^1$H nmr ($D_2O$) δ: 5.66 (d, 1H, H-1, $J_{1,2}$ = 5.0 Hz), 4.50 (2d, 2H, H-1′ and H-1″ overlapping, *J* = 7.5 Hz), 2.10 (s, O‖ 3H, NHAc methyl), 1.65, 1.48, 1.45, 1.43 (4s, 12H, O—C(CH$_3$)$_2$), 1.25 (d, 3H, (C-7)H$_3$), 4.20–3.50 (m, 17H, remaining protons).

*6-*O*-[2-Acetamido-2-deoxy-4-*O*-(β-*D*-galactopyranosyl)-β-*D*-glucopyranosyl]-7-deoxy-*D*-glycero-*D*-galacto-heptopyranose (9)*

A solution of compound **8** (21 mg, 0.033 mmol) in 70% trifluoroacetic acid (2 mL) was stirred at room temperature for 4 min and rapidly evaporated *in vacuo* to about 0.5 mL, and 3

drops of triethylamine was added. Filtration through a column of Sephadex LH-20, as described above for the preparation of **6**, provided a main fraction which was freeze-dried to a white solid (14.5 mg, 79%); $^1$H nmr ($D_2O$) δ: 5.24, 4.66 (2d, 1H, H-1α and H-1β, $J$ = 3.0 Hz and 7.5 Hz), 4.58, 4.49 (2d, 2H, H-1′ and H-1″ which shows up at this field position, $J$ = 7.5 Hz and 7.5 Hz), 2.08 (s, 3H, NHAc methyl), 1.26, 1.24 (2d, 3H, (C-7)$H_3$α and (C-7)$H_3$β), 4.26–3.42 (m, 17H, remaining protons).

## Acknowledgements

The financial support of the Natural Sciences and Engineering Research Council of Canada through a grant (A172) to R. U. Lemieux is gratefully acknowledged. The microanalyses and nmr spectra were carried out by the Analytical and Spectral Services Laboratories of this Department. We gratefully acknowledge the guidance provided by Mark Botkin of Chembiomed Ltd. in the application of the PLUTO program for drawing molecular models and to the Danish Natural Science Research Council for a travel grant to H. Thøgersen.

1. T. Feizi, E. A. Kabat, G. Vicari, B. Anderson, and W. L. Marsh. J. Immunol. **106**, 1578 (1971).
2. R. U. Lemieux, K. Bock, L. T. J. Delbaere, S. Koto, and V. S. Rao. Can. J. Chem. **58**, 631 (1980).
3. I. Tvaroska, S. Pérez, and R. H. Marchessault. Carbohydr. Res. **61**, 97 (1978).
4. L. T. J. Delbaere. Biochem. J. **143**, 197 (1974).
5. D. C. Fries, S. T. Rao, and M. Sundaralingam. Acta Crystallogr. Sect. B, **27**, 994 (1971).
6. S. Takagi and G. A. Jeffrey. Acta Crystallogr. Sect. B, **35**, 902 (1979).
7. E. A. Kabat, J. Liao, M. H. Burzynska, T. C. Wong, H. Thøgersen, and R. U. Lemieux. Mol. Immunol. **18**, 873 (1981).
8. R. U. Lemieux, P. H. Boullanger, D. R. Bundle, D. A. Baker, A. Nagpurkar, and A. Venot. Nouv. J. Chim. **2**, 321 (1978).
9. R. E. Arrick, D. C. Baker, and D. Horton. Carbohydr. Res. **26**, 441 (1973).
10. E. L. Jackson and C. S. Hudson. J. Am. Chem. Soc. **75**, 3000 (1953).
11. C. Cone and L. Hough. Carbohydr. Res. **1**, 1 (1965).
12. R. U. Lemieux and K. Bock. J. Antibiot. **32**, S163 (1979).
13. R. U. Lemieux, S. Z. Abbas, M. H. Burzynska, and R. M. Ratcliffe. Can. J. Chem. **60**, 63 (1982).
14. R. U. Lemieux, S. Z. Abbas, and B. Y. Chung. Can. J. Chem. **60**, 68 (1982).
15. H. Thøgersen, R. U. Lemieux, K. Bock and B. Meyer. Can. J. Chem. **60**, 44 (1982).
16. R. U. Lemieux and A. A. Pavia. Can. J. Chem. **47**, 4441 (1969).
17. D. Horton, M. Nakadate, and J. M. J. Tronchet. Carbohydr. Res. **7**, 56 (1968).
18. R. U. Lemieux, T. Takeda, and B. Y. Chung. Am. Chem. Soc. Symposium Series **39**, 90 (1976).

Can. J. Chem. Downloaded from www.nrcresearchpress.com by 210.87.254.42 on 09/06/12
For personal use only.

Can. J. Chem. Downloaded from www.nrcresearchpress.com by 210.87.254.6 on 09/06/12
For personal use only.



# Hydrogenation of phosphido bridged ruthenium clusters. A view of P—C bond activation and cleavage in the coordinatively unsaturated molecule $Ru_3(CO)_9(\mu_2\text{-}PPh_2)(\mu_2\text{-}H)$: conversion of $\mu_2\text{-}PPh_2$ to $\mu_3\text{-}PPh$

SHANE A. MACLAUGHLIN, ARTHUR J. CARTY,[1] AND NICHOLAS J. TAYLOR

*Guelph–Waterloo Centre, Waterloo Campus, Chemistry Department, University of Waterloo, Waterloo, Ont., Canada N2L 3G1*

Received September 11, 1981

SHANE A. MACLAUGHLIN, ARTHUR J. CARTY, and NICHOLAS J. TAYLOR. Can. J. Chem. **60**, 87 (1982).

Treatment of $Ru_3(CO)_8(\mu_3\text{-}\eta^2\text{-}C{\equiv}CR)(\mu^2\text{-}PPh_2)$ (R = $Bu^t$, $Pr^i$) with dihydrogen liberates olefin ($CH_2{=}CHR$) and generates the coordinatively unsaturated cluster $Ru_3(CO)_9(\mu_2\text{-}PPh_2)(\mu_2\text{-}H)$ which has been shown by X-ray diffraction to have an unprecedented $\mu_2$-phosphido bridge in which a P—phenyl group interacts with an electron deficient ruthenium atom. This molecule provides an insight into P—C bond activation leading to cleavage. Further reaction of $Ru_3(CO)_9(\mu_2\text{-}PPh_2)(\mu_2\text{-}H)$ with $H_2$ leads to the phosphinidene cluster $Ru_3(CO)_9(\mu_3\text{-}PPh)(\mu_2\text{-}H)_2$ via elimination of benzene. Conversion of $Ru_3(CO)_9(\mu_2\text{-}PPh_2)(\mu_2\text{-}H)$ to another phosphinidene cluster $Ru_4(CO)_{13}(\mu_3\text{-}PPh)$ occurs on pyrolysis. Hydrogenation of multi-site bound acetylides with $H_2$ is a potentially useful synthetic route to unsaturated clusters. Hydrogenative conversion of $\mu_2\text{-}PPh_2$ to $\mu_3\text{-}PPh$ groups has significance for the synthesis of phosphinidene capped molecules as well as the chemistry of phosphido bridged clusters.

SHANE A. MACLAUGHLIN, ARTHUR J. CARTY et NICHOLAS J. TAYLOR. Can. J. Chem. **60**, 87 (1982).

Le composé $Ru_3(CO)_8(\mu_3\text{-}\eta^2\text{-}C{\equiv}CR)(\mu^2\text{-}PPh_2)$ (R = *t*-Bu, *i*-Pr) libère par hydrogénation l'oléfine ($CH_2{=}CHR$) et produit le groupe insaturé coordonné $Ru_3(CO)_9(\mu_2\text{-}PPh_2)(\mu_2\text{-}H)$ qui par diffraction de rayons X révèle l'existence d'un pont $\mu_2$-phosphido, jusqu'à présent inconnu, dans lequel le groupe P—phényle interagit avec l'atome de ruthénium déficient en électron. Cette molécule apporte des éclaircissements sur l'activation du groupe P—C conduisant au clivage. Une hydrogénation plus poussée du composé $Ru_3(CO)_9(\mu_2\text{-}PPh_2)(\mu_2\text{-}H)$ conduit au groupe phosphinidène $Ru_3(CO)_9(\mu_3\text{-}PPh_2)(\mu_2\text{-}H_2)$ via l'élimination du benzène. Par pyrolyse, on peut transformer le composé $Ru_3(CO)_9(\mu_2\text{-}PPh_2)(\mu_2\text{-}H)$ en un autre groupe phosphinidène. L'hydrogénation des acétylures est une voie d'accès potentielle très utile aux groupes insaturés. La transformation des groupes $\mu_2\text{-}PPh_2$ en groupe $\mu_3\text{-}PPh$ par hydrogénation a une importance dans la synthèse des molécules portant un groupe phosphinidène ainsi que dans la chimie des groupes ayant un pont phosphido.

[Traduit par le journal]

A major drawback to the use of metal cluster compounds as homogeneous catalysts is their inherent tendency to degrade under conditions appropriate for effective catalysis. Thus many high nuclearity carbonyl clusters undergo fragmentation under pressure of CO or in the presence of Lewis bases (1). A solution to this problem has been sought via the design of molecules with stable but flexible supporting bridges capable of maintaining the integrity of a cluster framework while allowing facile metal–metal bond cleavage and reformation. Considerable attention has recently focussed on the synthesis and catalytic behaviour of phosphido ($PR_2$) (2) and phosphinidene (PR) (3) based carbonyls since these groups have a number of features desirable in edge bridging or face capping ligands (4). Two rather notable examples are the use of the dianion $Fe_2(CO)_6(PPh_2)_2^{2-}$ in the synthesis of aldehydes from alkyl halides (5) and the catalytic hydroformylating ability of the phosphinidene complex $Co_4(CO)_8(\mu_2\text{-}CO)_2(\mu_4\text{-}PPh)_2$ (6). We report herein results pertinent to the chemistry of phosphido and phosphinidene clusters under molecular hydrogen and $H_2$/CO mixtures. In particular we have observed the facile reduction of $\mu_2\text{-}PPh_2$ groups in $Ru_3(CO)_8(\mu_2\text{-}PPh_2)(\mu_3\text{-}\eta^2\text{-}C{\equiv}CR)$ (R = $Bu^t$, $Pr^i$) (7) to a $\mu_3$-PPh unit in $Ru_3(CO)_9(\mu_3\text{-}PPh)(\mu_2\text{-}H)_2$ via an intermediate electron deficient hydride $Ru_3(CO)_9(\mu_2\text{-}PPh_2)(\mu_2\text{-}H)$. This coordinatively unsaturated complex contains a novel $\mu_2$-phosphido group activated by a weak P—Ph interaction with a third ruthenium atom.

The X-ray crystal structure of $Ru_3(CO)_9(PPh_2)(H)$ provides an unprecedented view of how a normally stable ligand entity is activated via coordinative unsaturation in a cluster. In the absence of molecular hydrogen, $Ru_3(CO)_9(PPh_2)(H)$ is converted on pyrolysis to another phosphinidene cluster $Ru_4(CO)_{13}(\mu_3\text{-}PPh)$ having a "butterfly" metal framework. These results are significant not only in demonstrating a new strategy for the synthesis of stable phosphinidene complexes but also in pro-

[1]To whom all correspondence should be addressed.

0008-4042/82/010087-04$01.00/0

©1982 National Research Council of Canada/Conseil national de recherches du Canada

Can. J. Chem. Downloaded from www.nrcresearchpress.com by 210.87.254.6 on 09/06/12
For personal use only.

viding an indication that phosphido bridges may be considerably more reactive than has been previously assumed. Finally, the reduction of multisite bound acetylides by dihydrogen may be a useful method for generating coordinatively unsaturated clusters.

The trinuclear acetylide complexes $Ru_3(CO)_6(\mu_2\text{-}CO)_2(\mu_3\text{-}\eta^2\text{-}C{\equiv}CR)(\mu_2\text{-}PPh_2)$ (**I**, R = $Pr^i$; **II**, R = $Bu^t$) react rapidly with dihydrogen (25°C, 1 atm $H_2$, 2 min) resulting in hydrogenation of the acetylide. The principal organic product from **II** was identified as the olefin $H_2C{=}CHBu^t$ by $^1H$ nmr and by comparison with an authentic sample. Chromatography of the solution on Florisil (heptane eluant) afforded $Ru_3(CO)_9(\mu_2\text{-}PPh_2)(\mu_2\text{-}H)$ (**III**; ~ 40%) and $Ru_3(CO)_9(\mu_3\text{-}PPh)(\mu_2\text{-}H)_2$ (**IV**; ~ 10%). The ν(CO) ir spectra of **III** and **IV** showed only terminal carbonyls (ν(CO)($C_6H_{12}$) **III**, 2083 s, 2055 vs, 2014 s, 1993 m, 1986 m; **IV**, 2104 m, 2073 s, 2048 vs, 2030 m, 2017 s, 1998 m, 1986 m). High field nmr resonances typical of metal hydrides were observed in each case ($^1H$ nmr, $C_6D_6$ **III**, δ −15.8(d) $J_{P-H}$ = 24 Hz; **IV**, δ −18.3(d), $J_{P-H}$ = 15.3 Hz). Orange–red crystals of **III** are monoclinic, space group $P2_1/c$, $a$ = 13.369(2), $b$ = 11.824(1), $c$ = 15.417(2) Å; β = 97.32(1)°; $Z$ = 4, $\rho_c$ = 2.038, $\rho_m$ = 2.03 g cm$^{-3}$; μ(MoKα) = 19.22 cm$^{-1}$, $F$(000) = 1424. Solution and refinement of the structure by Patterson, Fourier and least-squares methods was based on 4703 observed ($I \geq 3\sigma(I)$) (7106 measured) reflections with 3.2° < 2θ < 60°, measured on a Syntex $P2_1$ diffractometer with MoKα radiation. With anisotropic thermal parameters for all non-hydrogen atoms and isotropic coefficients for hydrogen atoms refinement proceeded to $R$ and $R_w$ values of 0.035 and 0.039. The molecular structure is shown in Fig. 1. Within the closed triangle of ruthenium atoms there are two normal Ru—Ru distances (Ru(1)—Ru(2) 2.8350(5); Ru(2)—Ru(3) 2.7996(5) Å); the third, longer Ru—Ru vector (Ru(1)—Ru(3) 2.9049(5) Å) is bridged by a hydride (Ru(1)—H(1)—Ru(3) 109.5°) and by a phosphido group. The stereochemistry of the latter is remarkable, with the phosphorus atom "tipped" towards the centre of the $Ru_3$ triangle as a result of an additional weak P–Ph interaction with Ru(2). The extent of the Ru(2)···P—Ph interaction can be gauged not only by the orientation of the phosphido bridge but also by the contact Ru(2)···P (2.779(1) Å) (cf. Ru(3)—P of 2.336(1) Å) and the distance between Ru(2) and the mid point of the P—C(21) bond (2.489 Å). However, the P—C(21) bond length (1.827(5) Å) does not differ significantly from the P—C(11) (1.832(5) Å) distance and the $^{31}P$ nmr

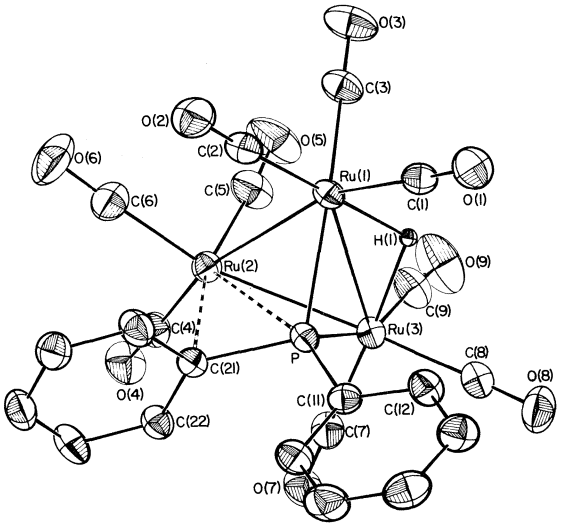


FIG. 1. A perspective view of the molecular structure of $Ru_3(CO)_9(\mu_2\text{-}PPh_2)(\mu_2\text{-}H)$ showing the unusual interaction of a P—phenyl linkage with Ru(2). Important distances and angles not mentioned in the text are: Ru(1)—P 2.331(1), Ru(2)—C(21) 2.518(4) Å; Ru(1)—P—Ru(3) 77.0°, Ru(2)—P—Ru(3) 65.7°.

chemical shift (δ = +134.2 ppm) is not unusual for an Ru(1)—P—Ru(3) angle of 77.0° (2, 7). These results together with the facile formation of 1:1 adducts with Lewis bases (*vide infra*) suggest that the Ru(2)···P—Ph interaction is weak in the solid state and that **III** is indeed coordinatively unsaturated in solution. A formal electron count indicates that **III** is a 46 electron species, two electrons short of a closed shell 48 electron configuration for an $Ru_3$ cluster if the $PPh_2$ group contributes three electrons. In particular, Ru(2), with two electron bonds to three CO groups and two other ruthenium atoms, is electron deficient. The attraction of Ru(2) for one P—Ph group of the phosphido bridge can therefore be seen as a direct consequence of the need for Ru(2) to relieve its unsaturation. To our knowledge such behaviour is unprecedented. In other coordinatively unsaturated clusters such as $H_2Os_3(CO)_{10}$ (8) and $H_2Re_2(CO)_8$ (9) multiple metal–metal bonding provides partial relief of electron deficiency. By analogy with the chemistry of these exceedingly reactive clusters, **III** should be hyperreactive. Reaction of **III** with CO in heptane is rapid, affording high yields of $Ru_3(CO)_{10}(\mu_2\text{-}PPh_2)(\mu_2\text{-}H)$($^1H$ nmr, $C_6D_6$, δ, −16.3(d) $J_{P-H}$ = 30.5 Hz (Ru—H—Ru); 8.1 (m), 7.0 (m) ($C_6H_5$); $^{31}P$ nmr $C_6D_6$ δ($H_3PO_4$) +133.8; ν(CO) $C_6H_{12}$, 2098 w, 2054 s, 2048 m, 2020 s, 2002 w, 1996 m, 1987 w cm$^{-1}$) while phosphines $PR_3$ produce instantly the adducts $Ru_3(CO)_9(\mu_2\text{-}PPh_2)(\mu_2\text{-}H)(PR_3)$.

The structure of **III** (Fig. 1) also provides a

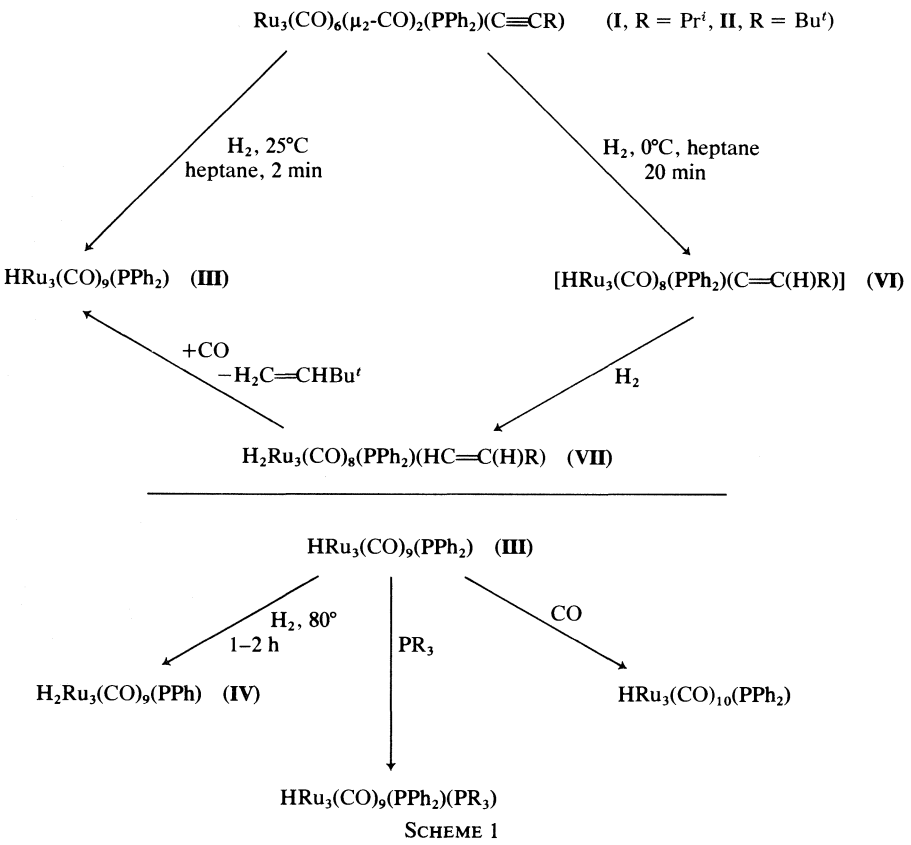


SCHEME 1

unique view of an intermediate stage in P—C bond activation and cleavage leading from a phosphido group to a phosphinidene. The predicted loss of an activated phenyl group from **III** was readily achieved. Passage of dihydrogen through a solution of pure **III** in $C_7H_{16}$ (80°C, 2 h) afforded only $Ru_3(CO)_9(\mu_3\text{-PPh})(\mu_2\text{-H})_2$ **IV** in excellent yield (~ 80%). The structure of **IV** as determined by X-ray analysis[2] consists of a triangle of ruthenium atoms capped by a $\mu_3$-PPh group and edge bridged on two sides by hydride ligands (Scheme 1).

While facile loss of a phenyl group from **III** as $C_6H_6$ occurred under reducing conditions, the presence of an activated $PPh_2$ group and a hydride in **III** suggested the possibility of phosphinidene generation via intramolecular reductive elimination of $C_6H_6$. Pyrolysis of **III** (80°C, 4 h, $C_7H_{16}$) resulted in cluster fragmentation and the synthesis of $Ru_4(CO)_{13}(\mu_3\text{-PPh})$ **V**, (ir, ν(CO) $C_6H_{12}$; 2095 w, 2060 vs, 2048 s, 2041 s, 2020 w, 2010 m, 1988 w, 1969 w, sh) in moderate yields (~ 40%). Crystals of **V** are orthorhombic, space group *Pbca* with $a$ = 15.325(2), $b$ = 17.797(2), $c$ = 18.613(5) Å; $Z$ = 8, $\rho_c$ = 2.293, $\rho_m$ = 2.31 g cm$^{-3}$ and $\mu(MoK_\alpha)$ = 24.05 cm$^{-1}$, $F(000)$ = 3312. The intensities of 3041 observed (4473 measured) reflections ($I \geq 3\sigma(I)$) measured on a $P2_1$ diffractometer in the range 3.2° < 2θ < 50°, were used in structure solution and refinement. $R$ and $R_w$ values are 0.040 and 0.046 respectively. The principal structural features of **V** (Fig. 2) are a metal "butterfly" with a $\mu_3$-PPh group capping an open $Ru_3$ face (Ru(1)—P 2.302(2), Ru(2)—P 2.388(2), Ru(4)—P 2.316(2) Å) and distant from the remaining ruthenium atom (Ru(3)—P 3.199(2) Å). While a few "open" triangular mixed metal phosphinidenes are known (12) **V** is the first example of a homotetranuclear butterfly phosphinidene complex to be characterised.

Preliminary mechanistic studies indicate that conversion of **II** to **III** and **IV** proceeds (scheme) via initial oxidative addition of $H_2$ to the cluster generating a transient hydrido (vinylidene) complex H $Ru_3(CO)_8(PPh_2)(C{=}CHBu^t)$, **VI**, which

[2]This molecule has also been recently prepared and structurally characterised by Mays and co-workers (10) as a product of the reaction of $PH_2Ph$ with $Ru_3(CO)_{12}$. The two structures are essentially identical. The iron analogue $Fe_3(CO)_9(\mu_3\text{-PPh})(\mu_2\text{-H})_2$ was earlier prepared by a similar route (11).

Can. J. Chem. Downloaded from www.nrcresearchpress.com by 210.87.254.6 on 09/06/12
For personal use only.

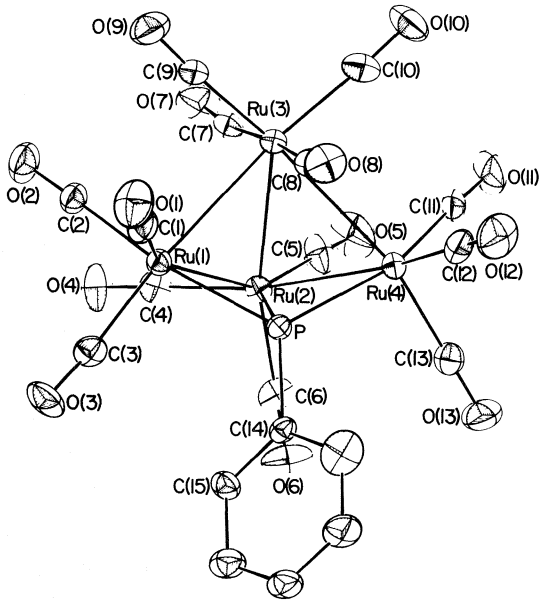


FIG. 2. The molecular structure of $Ru_4(CO)_{13}(\mu_3\text{-PPh})$ showing the atomic numbering. Important bond lengths and angles not included in the text are: Ru(1)—Ru(2) 2.833(1), Ru(1)—Ru(3) 2.861(1), Ru(2)—Ru(3) 2.974(1), Ru(2)—Ru(4) 2.784(1), Ru(3)—Ru(4) 2.924(1) Å; Ru(1)—P—Ru(2) 74.3, Ru(1)—P—Ru(4) 121.1(1), Ru(2)—P—Ru(4) 72.6°.

rapidly adds a second molecule of $H_2$ leading to an unstable dihydrido ($\mu_2$-$\eta^2$-vinyl) complex $H_2Ru_3(CO)_8(PPh_2)(HC{=}C(H)Bu^t)$, **VII**. Under CO **VII** is quantitatively transformed into **III** with loss of *t*-butylethylene. Complex **III** reacts more slowly with CO to yield the coordinatively saturated species $Ru_3(CO)_{10}(H)(PPh_2)$. Carbon monoxide is not, however, required in the direct hydrogenative conversion of **II** to **III**. Complete spectroscopic and structural characterisation of these species will be described elsewhere. It is clear, however, that reduction of $\mu_3$-$\eta^2$-acetylido clusters with $H_2$ under mild conditions is a useful strategy for the synthesis of hydrido-phosphido and hydrido-phosphinidene bridged clusters. Furthermore, our studies indicate that the reactivity of phenyl phosphido bridges under reducing conditions may limit the application of $PPh_2$ bridged clusters in catalysis.[3]


## Acknowledgements

We thank the Natural Sciences and Engineering Research Council of Canada for financial support (A.J.C.) and a scholarship (S.A.M.).



1. P. CHINI, G. LONGONI and V. G. ALBANO. Adv. Organomet. Chem. **14**, 285 (1976).
2. A. J. CARTY. Am. Chem. Soc. Adv. Chem. Ser. In press.
3. (*a*) G. HUTTNER, J. SCHNEIDER, G. MOHR, and J. VON SEYERL. J. Organomet. Chem. **191**, 161 (1980); (*b*) K. NATARAJAN, L. ZSOLNAI, and G. HUTTNER. J. Organomet. Chem. **209**, 85 (1981); (*c*) L. M. FERNANDEZ, B. F. G. JOHNSON, J. LEWIS, and P. R. RAITHBY. J. Chem. Soc. Chem. Commun. 1015 (1978).
4. H. VAHRENKAMP. Angew. Chem. Int. Ed. **17**, 379 (1978).
5. J. P. COLLMAN, R. L. ROTHROCK, R. G. FINKE, and F. ROSE-MUNCH. J. Am. Chem. Soc. **99**, 7381 (1981).
6. C. U. PITTMAN, JR., G. M. WILEMAN, W. D. WILSON, and R. C. RYAN. Angew. Chem. Int. Ed. **19**, 478 (1980).
7. A. J. CARTY, S. A. MACLAUGHLIN, and N. J. TAYLOR. J. Organomet. Chem. **204**, C27 (1981).
8. M. R. CHURCHILL, F. J. HOLLANDER, and J. P. HUTCHINSON. Inorg. Chem. **16**, 2697 (1977).
9. M. J. BENNETT, W. A. G. GRAHAM, J. K. HOYANO, and W. L. HUTCHESON. J. Am. Chem. Soc. **98**, 4687 (1976).
10. F. IWASAKI, M. J. MAYS, P. R. RAITHBY, P. L. TAYLOR, and P. J. WHEATLEY. J. Organomet. Chem. **213**, 185 (1981).
11. G. HUTTNER, J. SCHNEIDER, G. MOHR, and J. VON SEYERL. J. Organomet. Chem. **191**, 161 (1980).
12. G. HUTTNER, J. SCHNEIDER, H. D. MILLER, G. MOHR, J. VON SEYERL, and L. WOHLFAHRT. Angew. Chem. Int. Ed. **18**, 76, (1979).


[3]Complete set of supplementary material is available, at a nominal charge, from the Depository of Unpublished Data, CISTI, National Research Council of Canada, Ottawa, Ont., Canada K1A 0S2.

# Studies toward polyether antibiotics: stereospecific synthesis of polysubstituted tetrahydropyrans


PAK-TSUN HO

*Department of Chemistry, University of Waterloo, Waterloo, Ont., Canada N2L 3G1*



Received July 31, 1981

PAK-TSUN HO. Can. J. Chem. **60**, 90 (1982).



A stereospecific and general method for the preparation of *trans*-tetrahydropyrans **1** and *cis*-tetrahydropyrans **2** from acyclic precursors are described. Compound **12**, a possible intermediate for the synthesis of antibiotic X-14547A, has been synthesized.



0008-4042/82/010090-05$01.00/0



©1982 National Research Council of Canada/Conseil national de recherches du Canada



Can. J. Chem. Downloaded from www.nrcresearchpress.com by 210.87.254.6 on 09/06/12
For personal use only.

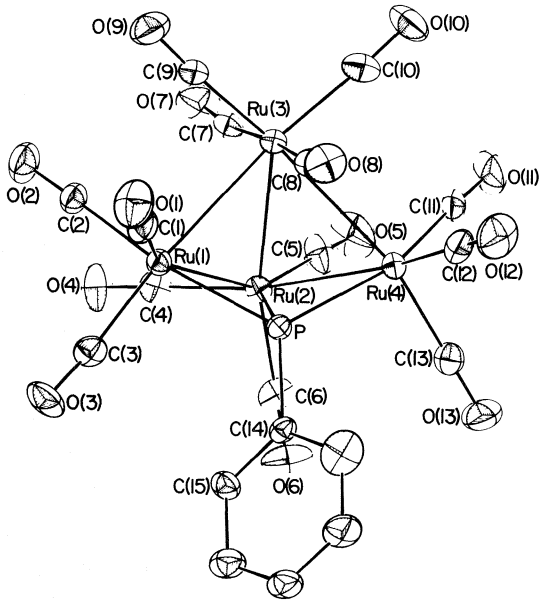


FIG. 2. The molecular structure of $Ru_4(CO)_{13}(\mu_3\text{-PPh})$ showing the atomic numbering. Important bond lengths and angles not included in the text are: Ru(1)—Ru(2) 2.833(1), Ru(1)—Ru(3) 2.861(1), Ru(2)—Ru(3) 2.974(1), Ru(2)—Ru(4) 2.784(1), Ru(3)—Ru(4) 2.924(1) Å; Ru(1)—P—Ru(2) 74.3, Ru(1)—P—Ru(4) 121.1(1), Ru(2)—P—Ru(4) 72.6°.

rapidly adds a second molecule of $H_2$ leading to an unstable dihydrido ($\mu_2$-$\eta^2$-vinyl) complex $H_2Ru_3(CO)_8(PPh_2)(HC{=}C(H)Bu^t)$, **VII**. Under CO **VII** is quantitatively transformed into **III** with loss of *t*-butylethylene. Complex **III** reacts more slowly with CO to yield the coordinatively saturated species $Ru_3(CO)_{10}(H)(PPh_2)$. Carbon monoxide is not, however, required in the direct hydrogenative conversion of **II** to **III**. Complete spectroscopic and structural characterisation of these species will be described elsewhere. It is clear, however, that reduction of $\mu_3$-$\eta^2$-acetylido clusters with $H_2$ under mild conditions is a useful strategy for the synthesis of hydrido-phosphido and hydrido-phosphinidene bridged clusters. Furthermore, our studies indicate that the reactivity of phenyl phosphido bridges under reducing conditions may limit the application of $PPh_2$ bridged clusters in catalysis.[3]


## Acknowledgements

We thank the Natural Sciences and Engineering Research Council of Canada for financial support (A.J.C.) and a scholarship (S.A.M.).



1. P. CHINI, G. LONGONI and V. G. ALBANO. Adv. Organomet. Chem. **14**, 285 (1976).
2. A. J. CARTY. Am. Chem. Soc. Adv. Chem. Ser. In press.
3. (*a*) G. HUTTNER, J. SCHNEIDER, G. MOHR, and J. VON SEYERL. J. Organomet. Chem. **191**, 161 (1980); (*b*) K. NATARAJAN, L. ZSOLNAI, and G. HUTTNER. J. Organomet. Chem. **209**, 85 (1981); (*c*) L. M. FERNANDEZ, B. F. G. JOHNSON, J. LEWIS, and P. R. RAITHBY. J. Chem. Soc. Chem. Commun. 1015 (1978).
4. H. VAHRENKAMP. Angew. Chem. Int. Ed. **17**, 379 (1978).
5. J. P. COLLMAN, R. L. ROTHROCK, R. G. FINKE, and F. ROSE-MUNCH. J. Am. Chem. Soc. **99**, 7381 (1981).
6. C. U. PITTMAN, JR., G. M. WILEMAN, W. D. WILSON, and R. C. RYAN. Angew. Chem. Int. Ed. **19**, 478 (1980).
7. A. J. CARTY, S. A. MACLAUGHLIN, and N. J. TAYLOR. J. Organomet. Chem. **204**, C27 (1981).
8. M. R. CHURCHILL, F. J. HOLLANDER, and J. P. HUTCHINSON. Inorg. Chem. **16**, 2697 (1977).
9. M. J. BENNETT, W. A. G. GRAHAM, J. K. HOYANO, and W. L. HUTCHESON. J. Am. Chem. Soc. **98**, 4687 (1976).
10. F. IWASAKI, M. J. MAYS, P. R. RAITHBY, P. L. TAYLOR, and P. J. WHEATLEY. J. Organomet. Chem. **213**, 185 (1981).
11. G. HUTTNER, J. SCHNEIDER, G. MOHR, and J. VON SEYERL. J. Organomet. Chem. **191**, 161 (1980).
12. G. HUTTNER, J. SCHNEIDER, H. D. MILLER, G. MOHR, J. VON SEYERL, and L. WOHLFAHRT. Angew. Chem. Int. Ed. **18**, 76, (1979).


[3]Complete set of supplementary material is available, at a nominal charge, from the Depository of Unpublished Data, CISTI, National Research Council of Canada, Ottawa, Ont., Canada K1A 0S2.

# Studies toward polyether antibiotics: stereospecific synthesis of polysubstituted tetrahydropyrans


PAK-TSUN HO

*Department of Chemistry, University of Waterloo, Waterloo, Ont., Canada N2L 3G1*



Received July 31, 1981

PAK-TSUN HO. Can. J. Chem. **60**, 90 (1982).



A stereospecific and general method for the preparation of *trans*-tetrahydropyrans **1** and *cis*-tetrahydropyrans **2** from acyclic precursors are described. Compound **12**, a possible intermediate for the synthesis of antibiotic X-14547A, has been synthesized.



0008-4042/82/010090-05$01.00/0



©1982 National Research Council of Canada/Conseil national de recherches du Canada



Can. J. Chem. Downloaded from www.nrcresearchpress.com by 210.87.254.6 on 09/06/12
For personal use only.

PAK-TSUN HO. Can. J. Chem. **60**, 90 (1982).

On décrit une méthode générale de synthèse stéréospécifique des tétrahydropyrannes *trans* (**1**) et des tétrahydropyrannes *cis* (**2**) à partir de précurseurs acyliques. On a synthétisé le composé **12** qui est un intermédiaire éventuel dans la synthèse de l'antibiotique X-14547A.

[Traduit par le journal]

Can. J. Chem. Downloaded from www.nrcresearchpress.com by 210.87.254.6 on 09/06/12
For personal use only.

The polyether antibiotics represent a growing and important class of naturally occurring substances. These compounds have received considerable attention in the synthetic field during recent years, because of their unique ionophoric properties as well as the degree of stereochemical complexity of this class of compounds (1). As a part of our program aimed at the synthesis of a variety of ionophore antibiotics, we have been interested in developing a stereospecific and general method for synthesizing the highly substituted tetrahydropyranyl ring systems **1** and **2** from acyclic intermedi-

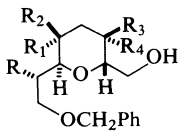

**1**

*a*: R = $R_4$ = Me, $R_1$ = $R_2$ = $R_3$ = H
(ring A of antibiotic X-14547A)
*b*: R = Et, $R_4$ = Me, $R_1$ = $R_2$ = $R_3$ = H
(ring A of salinomycin)
*c*: R = $R_2$ = Me, $R_1$ = $R_3$ = $R_4$ = H
(ring A of nigericin)

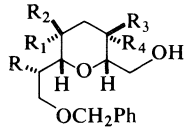

**2**

*a*: R = $R_2$ = Me, $R_1$ = $R_3$ = $R_4$ = H
(ring A of antibiotic X-206)
*b*: R = $R_2$ = $R_3$ = Me, $R_1$ = $R_4$ = H
(ring A of alborixin)

ates. The structural ring systems in the present studies have often been found in the polyether antibiotics. The *trans*-tetrahydropyrans **1** represent ring A of antibiotic X-14547A (for isolation, see ref. 2*a*, for syntheses of the "right wing", see ref. 2*b*–*d*), salinomycin (3), and nigericin (4), while the *cis*-tetrahydropyrans **2** represent ring A of antibiotic X-206 (5) and alborixin (6). Although for future total syntheses of polyether antibiotics, chiral precursors for the construction of tetrahydropyranyl subunits are a crucial point, our exploratory work for the present studies was undertaken with racemic materials.

The starting material **3** for the present investigation was prepared by a modification of literature procedures (7) from commercially available (*Z*)-2-butene 1,4-diol (Scheme 1). The key reaction in the preparation of the enantiomeric pair of the alcohol **3** was the stereospecific *trans* opening of the epoxide with lithium dimethylcuprate. Compound **4**[1] was obtained in quantitative yield by two-step standard procedures from the corresponding primary alcohol **3**. In order to explore the stereospecificity and feasibility of our approach to the tetrahydropyranyl ring systems, two isomeric epoxides **7** and **8** were synthesized from the same enantiomeric pair of alcohol **3** in a straight-forward and unambiguous manner (Scheme 1). The alcohol **3** was converted into the diol **5** in 95% yield by benzylation and mild acidic hydrolysis. For the preparation of the α-epoxide **7**, treatment of the diol **5** with *p*-anisyldiphenylmethyl chloride (1.1 equiv) in pyridine at 0°C overnight and then subsequently with tosyl chloride (1.2 equiv) at room temperature for 1 day gave the crude product, which was treated with 80% aqueous acetic acid at room temperature for 4 h to yield the hydroxyl tosylate **6**. The yield was 84% from the diol **5**. This operation was to invert the configuration at the secondary alcohol when the epoxide was formed in the next step. Exposure of compound **6** to methanolic potassium hydroxide at room temperature for 1 h led to the formation of the desired epoxide **7** in 89% yield. For the preparation of the β-epoxide **8**, the diol **5**, on treatment with tosyl chloride (1 equiv) in pyridine and methylene dichloride at 0°C for 6 h, followed with methanolic potassium hydroxide at room temperature for 1 h furnished the epoxide **8** in 86% yield.

Two alternative elaborations of *trans*-tetrahydropyran **1** by the sequence of reactions shown in Scheme 2 were examined. Thus, treatment of the iodide **4** with *n*-butyllithium (1.1 equiv) in tetrahydrofuran at −70°C for 4 h, followed with cuprous iodide at the same temperature for 1 h resulted in the formation of lithium cuprate derivative, which reacted in the desired manner with the epoxide **8** (the ratio of epoxide-to-iodide was 1 equiv:1.7 equiv) at −70°C for 2 h to give the alcohol **9** in 65–70% yield.[2] Conversion of **9** to the hydroxyl

[1]Satisfactory physical and spectral data have been obtained for all new compounds.

[2]The material obtained from this reaction, as expected, was a pair of diastereoisomers as shown by $^{13}C$ nmr, which could not be separated by HPLC.

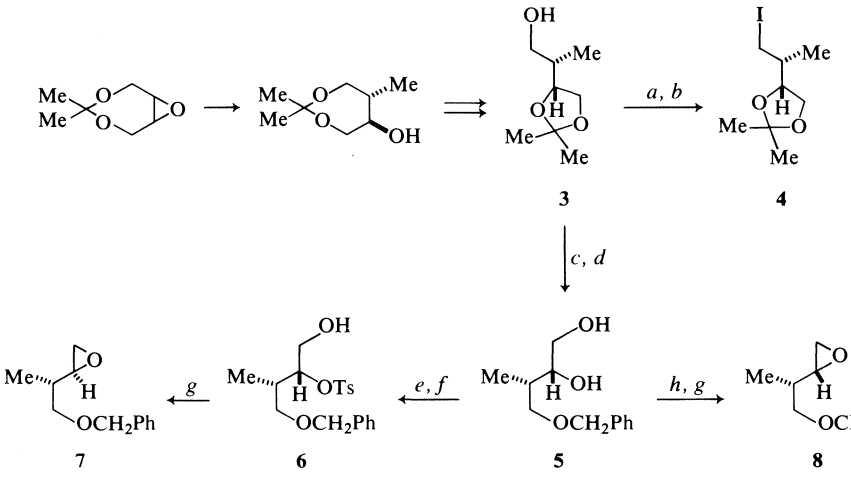

SCHEME 1. Reagents and conditions: *a*, TsCl, pyridine, RT; *b*, NaI, acetone, RT, 2 days; *c*, NaH, $PhCH_2Br$, THF, RT; *d*, 80% aqueous HOAc, RT, 6 h; *e*, *p*-anisyldiphenylmethylchloride (1.1 equiv), pyridine, 0°C, 12 h, then TsCl (1.2 equiv), RT, 1 day; *f*, 80% aqueous HOAc, RT, 4 h; *g*, KOH, MeOH, RT, 1 h; *h*, TsCl (1 equiv), pyridine, $CH_2Cl_2$, 0°C, 10 h.

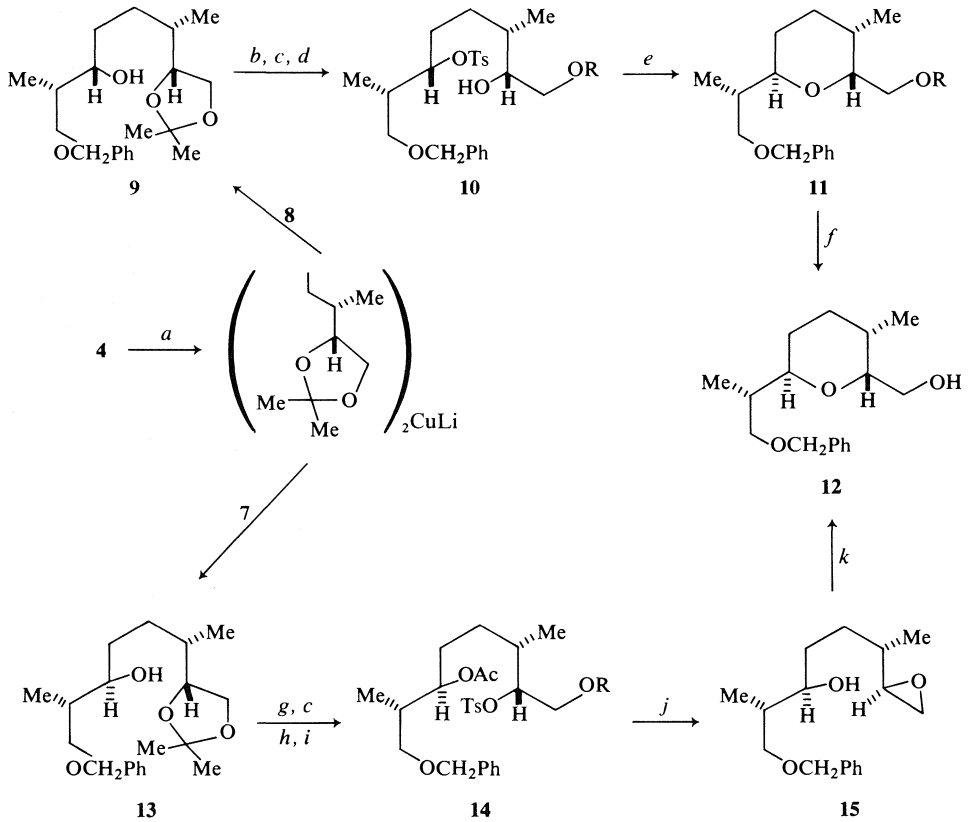

SCHEME 2. R = *p*-anisyldiphenylmethyl. Reagents and conditions: *a*, *n*BuLi (1.1 equiv), THF, −70°C, 4h, then CuI, −70°C, 1h; *b*, TsCl, pyridine, RT; *c*, 80% aqueous HOAc, RT; *d*, *p*-anisyldiphenylmethyl chloride (1.1 equiv), pyridine, RT; *e*, NaH (1.4 equiv), benzene, reflux, 6h; *f*, 80% aqueous HOAc, RT; *g*, $Ac_2O$, pyridine, RT; *h*, *p*-anisyldiphenylmethyl chloride (1.1 equiv), pyridine, RT, 6h, then TsCl (1.2 equiv), RT, 1½ day; *i*, 80% aqueous HOAc, RT, 4h; *j*, KOH, MeOH, RT, 10h; *k*, HOAc, RT, 2 days.

Can. J. Chem. Downloaded from www.nrcresearchpress.com by 210.87.254.6 on 09/06/12
For personal use only.

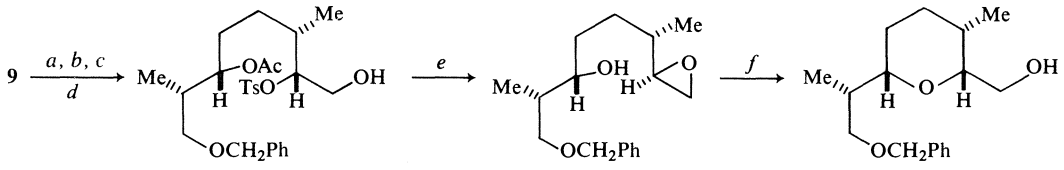

16 17 18

SCHEME 3. Reagents and conditions: *a*, $Ac_2O$, pyridine, RT; *b*, 80% aqueous HOAc, RT; *c*, *p*-anisyldiphenylmethyl chloride (1.1 equiv), pyridine, RT, 6 h, then TsCl (1.2 equiv), RT, 1½ day; *d*, 80% aqueous HOAc, RT, 4 h; *e*, KOH, MeOH, RT, 10 h; *f*, HOAc, RT, 2 days.

tosylate **10** was accomplished in 81% yield by standard procedures, tosylation of the secondary alcohol, generation of the diol by mild acidic hydrolysis, and tritylation of the primary alcohol (Scheme 2). With the complete carbon skeleton and functionality assembled, the *trans*-tetrahydropyranyl ring **11** was smoothly formed in 69% yield by the reaction of compound **10** with sodium hydride (1.4 equiv) in anhydrous benzene under reflux for 6 h.[3] The cyclization reaction from the acyclic intermediate achieved by a $S_N2$ displacement reaction left no doubt about the outcome of the desired stereochemistry of the *trans*-tetrahydropyranyl ring system. Compound **11**, on treatment with 80% aqueous acetic acid at room temperature, afforded quantitatively compound **12**. An alternative route to *trans*-tetrahydropyran **12** was also developed starting with alcohol **13**[2] prepared by the reaction of α-epoxide **7** with the iodide **4** under the same conditions as described above, and proceeding (Scheme 2) via the intermediates **14** and **15**. The overall yield from **7** and **4** to **15** was 53%. When compound **15** was treated with glacial acetic acid at room temperature for 2 days, the cyclization reaction proceeded smoothly to give the identical compound **12** in 92% yield. That two independent routes yielded the identical *trans*-tetrahydropyranyl ring affirm to the complete stereospecificity of the epoxide opening reaction with acetic acid. Clearly, the simplicity and high yield of this approach to compound **12** compared with the first approach make the reaction more attractive to the synthesis of polysubstituted tetrahydropyranyl ring systems.

With the successful development of the *trans*-tetrahydropyran synthesis, we now shifted our direction to the *cis*-ring systems **2**. Scheme 3 summarizes the sequence of reactions for the *cis*-series. Using the same techniques for the preparation of compound **15** from compound **13**, the alcohol **9** was converted into compound **17** in 69% overall yield. Treatment of the hydroxyl epoxide **17** with glacial acetic acid at room temperature for 2 days led to the isolation of the *cis*-tetrahydropyran **18** in 90% yield.[4]

The efficiency and stereospecificity of our method for the construction of various tetrahydropyranyl systems will open a wide synthetic application for many polyether antibiotics. Specifically, compound **12**, which possesses the correct stereochemistry and the required functionality for the synthesis of the recently isolated novel antibiotic X-14547A **19** (2), will be used as a key intermediate for the total synthesis. We are currently synthesizing the optically active compound **12** from tartaric acid and further progress along the line will be reported in due course.

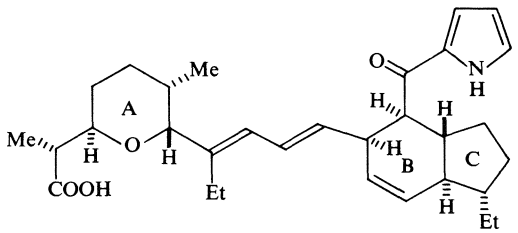

19

### Acknowledgements

The author thanks the Natural Sciences and Engineering Research Council of Canada and

[3]After cyclization, the pair of diastereoisomers **11** and **i**, produced from the reaction of **4** with **8**, could easily be separated by column chromatography on silica gel in 1% methanol in hexane and $CH_2Cl_2$ (**i**, $R_f$ 0.75; **11**, $R_f$ 0.55). The

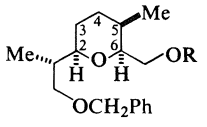

**i**

stereochemistry of **11** and **i** was assigned based on the chemical shift of their $^1H$ and $^{13}C$ nmr. Compound **11** gave $^1H$ nmr signal at 3.95 ppm and $^{13}C$ nmr signal at 72.9 ppm for hydrogen at C-6, while compound **i** had $^1H$ nmr signal at 3.72 ppm and $^{13}C$ nmr signal at 79.3 ppm for axial hydrogen at C-6.

[4]The pair of diastereoisomers was easily separated by column chromatography on silica gel. Compound **18** gave $^{13}C$ nmr signal at 81.3 ppm for C-6; while its isomer showed signal at 74.6 ppm for C-6 in its $^{13}C$ nmr spectrum.

Can. J. Chem. Downloaded from www.nrcresearchpress.com by 210.87.254.6 on 09/06/12
For personal use only.

University of Waterloo Research Grant for financial support of this work.

1. (*a*) J. W. WESTLEY. Adv. Appl. Microbiol. **22**, 177 (1977); (*b*) J. W. WESTLEY. Ann. Rep. Med. Chem. **10**, 246 (1975); (*c*) B. C. PRESSMAN. Ann. Rev. Biochem. **45**, 601 (1976).
2. (*a*) J. W. WESTLEY, R. H. EVANS, L. H. SELLO, N. TROUPE, C. H. LIU, and J. F. BLOUNT. J. Antibiot. **32**, 100 (1979); (*b*) M. P. EDWARDS, S. V. LEY, and S. G. LISTER. Tetrahedron Lett. 361 (1981); (*c*) K. C. NICOLAOU and R. L. MAGOLDA. J. Org. Chem. **46**, 1506 (1981); (*d*) W. R. ROUSH and A. G. MYERS. J. Org. Chem. **46**, 1509 (1981).
3. H. KINASHI, N. OTAKE, and H. YONCHARA. Tetrahedron Lett. 4955 (1973).
4. L. K. STEINRAUF, M. PINKATON, and J. W. CHAMBERLIN. Biochem. Biophys. Res. Commun. **33**, 29 (1968).
5. J. W. WESTLEY and J. F. BOUNT. Chem. Commun. 533 (1975).
6. M. ALLEAUME, B. BUSETTA, G. FARGES, P. GACHON, A. KERGOMASD, and T. STAROW. Chem. Commun. 411 (1975).
7. (*a*) W. J. ELLIOTT and J. FRIED. J. Org. Chem. **41**, 2469 (1976); (*b*) E. J. COREY and M. J. BOCK. Tetrahedron Lett. 2643 (1975).

# Thiol esters in organic synthesis. X.[1] A new approach to 1,5-ketols and 5-hydroxy esters using *S,S'*-diethyl dithiomalonate as an ethanol carbanion equivalent

HSING-JANG LIU AND ISAAC V. OPPONG

*Department of Chemistry, University of Alberta, Edmonton, Alta., Canada T6G 2G2*

Received September 2, 1981

HSING-JANG LIU and ISAAC V. OPPONG. Can. J. Chem. **60**, 94 (1982).

Michael addition of *S,S'*-diethyl dithiomalonate to conjugated enones and α,β-unsaturated esters followed by reduction with Raney nickel gave rise to 1,5-ketols and 5-hydroxy esters respectively in good yields.

HSING-JANG LIU et ISAAC V. OPPONG. Can. J. Chem. **60**, 94 (1982).

L'addition suivant Michael du dithiomalonate de *S,S'*-diéthyle à des énones conjuguées et à des esters α,β-non saturés, suivie par une réduction à l'aide de nickel de Raney conduit, suivant le cas, à la formation de cétols-1,5 et d'hydroxy-5 esters avec de bons rendements.

[Traduit par le journal]

In a recent communication (1*e*), we reported that *S,S'*-diethyl dithiomalonate reacts readily with alkyl halides and other electrophiles and that the dithiomalonate group can be easily reduced by Raney nickel under mild conditions to the ethanol level. One interesting application of *S,S'*-diethyl dithiomalonate as a convenient source of ethanol carbanion equivalent is its use as a Michael donor to facilitate the preparation of 1,5-ketols and 5-hydroxy esters, versatile synthetic intermediates which are particularly useful for the construction of six-membered carbocyclic and heterocyclic systems (2, 3).

In our initial attempts to induce the Michael addition of *S,S'*-diethyl dithiomalonate to α,β-unsaturated carbonyl compounds,[2] the use of the sodium and lithium salts generated *in situ* with strong bases such as NaH, NaSEt, and *t*-BuOLi was found to be ineffective. In each case, the starting material was recovered, presumably due to an unfavorable addition–elimination equilibrium. However, when a tertiary amine was used as a base, the conjugated addition occurred readily. Of several amines examined, 1,4-diazabicyclo[2.2.2]-octane (DABCO) was shown to be most effective, giving consistently high yields of the products under mild conditions. In a typical experiment, a solution of *S,S'*-diethyl dithiomalonate (720 mg, 3.74 mmol), DABCO (420 mg, 3.74 mmol), and 2-cyclohexenone (300 mg, 3.12 mmol) in 1,2-dimethoxyethane (10 mL) was stirred at room temperature under an argon atmosphere for 48 h. The reaction mixture was acidified with 1 *N* aqueous hydrochloric acid and extracted with chloroform. Drying ($MgSO_4$), filtration, and concentration gave the crude product which was purified by column chromatography on silica gel. Elution with a solution

[1]For parts I–IX of this series, see refs. 1*a*–*i* respectively.

[2]The addition of *S,S'*-diethyl dithiomalonate to ethyl acrylate was previously explored by Scheithauer and Mayer (4) using sodium methoxide in methanol to give a mixture of the mono- and bis-adduct in ca. 1:1 ratio.

0008-4042/82/010094-03$01.00/0

©1982 National Research Council of Canada/Conseil national de recherches du Canada

Can. J. Chem. Downloaded from www.nrcresearchpress.com by 210.87.254.6 on 09/06/12
For personal use only.

University of Waterloo Research Grant for financial support of this work.

1. (*a*) J. W. WESTLEY. Adv. Appl. Microbiol. **22**, 177 (1977); (*b*) J. W. WESTLEY. Ann. Rep. Med. Chem. **10**, 246 (1975); (*c*) B. C. PRESSMAN. Ann. Rev. Biochem. **45**, 601 (1976).
2. (*a*) J. W. WESTLEY, R. H. EVANS, L. H. SELLO, N. TROUPE, C. H. LIU, and J. F. BLOUNT. J. Antibiot. **32**, 100 (1979); (*b*) M. P. EDWARDS, S. V. LEY, and S. G. LISTER. Tetrahedron Lett. 361 (1981); (*c*) K. C. NICOLAOU and R. L. MAGOLDA. J. Org. Chem. **46**, 1506 (1981); (*d*) W. R. ROUSH and A. G. MYERS. J. Org. Chem. **46**, 1509 (1981).
3. H. KINASHI, N. OTAKE, and H. YONCHARA. Tetrahedron Lett. 4955 (1973).
4. L. K. STEINRAUF, M. PINKATON, and J. W. CHAMBERLIN. Biochem. Biophys. Res. Commun. **33**, 29 (1968).
5. J. W. WESTLEY and J. F. BOUNT. Chem. Commun. 533 (1975).
6. M. ALLEAUME, B. BUSETTA, G. FARGES, P. GACHON, A. KERGOMASD, and T. STAROW. Chem. Commun. 411 (1975).
7. (*a*) W. J. ELLIOTT and J. FRIED. J. Org. Chem. **41**, 2469 (1976); (*b*) E. J. COREY and M. J. BOCK. Tetrahedron Lett. 2643 (1975).

Can. J. Chem. Downloaded from www.nrcresearchpress.com by 210.87.254.105 on 09/06/12
For personal use only.

# Thiol esters in organic synthesis. X.[1] A new approach to 1,5-ketols and 5-hydroxy esters using *S,S'*-diethyl dithiomalonate as an ethanol carbanion equivalent

HSING-JANG LIU AND ISAAC V. OPPONG

*Department of Chemistry, University of Alberta, Edmonton, Alta., Canada T6G 2G2*

Received September 2, 1981

HSING-JANG LIU and ISAAC V. OPPONG. Can. J. Chem. **60**, 94 (1982).

Michael addition of *S,S'*-diethyl dithiomalonate to conjugated enones and α,β-unsaturated esters followed by reduction with Raney nickel gave rise to 1,5-ketols and 5-hydroxy esters respectively in good yields.

HSING-JANG LIU et ISAAC V. OPPONG. Can. J. Chem. **60**, 94 (1982).

L'addition suivant Michael du dithiomalonate de *S,S'*-diéthyle à des énones conjuguées et à des esters α,β-non saturés, suivie par une réduction à l'aide de nickel de Raney conduit, suivant le cas, à la formation de cétols-1,5 et d'hydroxy-5 esters avec de bons rendements.

[Traduit par le journal]

In a recent communication (1*e*), we reported that *S,S'*-diethyl dithiomalonate reacts readily with alkyl halides and other electrophiles and that the dithiomalonate group can be easily reduced by Raney nickel under mild conditions to the ethanol level. One interesting application of *S,S'*-diethyl dithiomalonate as a convenient source of ethanol carbanion equivalent is its use as a Michael donor to facilitate the preparation of 1,5-ketols and 5-hydroxy esters, versatile synthetic intermediates which are particularly useful for the construction of six-membered carbocyclic and heterocyclic systems (2, 3).

In our initial attempts to induce the Michael addition of *S,S'*-diethyl dithiomalonate to α,β-unsaturated carbonyl compounds,[2] the use of the sodium and lithium salts generated *in situ* with strong bases such as NaH, NaSEt, and *t*-BuOLi was found to be ineffective. In each case, the starting material was recovered, presumably due to an unfavorable addition–elimination equilibrium. However, when a tertiary amine was used as a base, the conjugated addition occurred readily. Of several amines examined, 1,4-diazabicyclo[2.2.2]-octane (DABCO) was shown to be most effective, giving consistently high yields of the products under mild conditions. In a typical experiment, a solution of *S,S'*-diethyl dithiomalonate (720 mg, 3.74 mmol), DABCO (420 mg, 3.74 mmol), and 2-cyclohexenone (300 mg, 3.12 mmol) in 1,2-dimethoxyethane (10 mL) was stirred at room temperature under an argon atmosphere for 48 h. The reaction mixture was acidified with 1 *N* aqueous hydrochloric acid and extracted with chloroform. Drying ($MgSO_4$), filtration, and concentration gave the crude product which was purified by column chromatography on silica gel. Elution with a solution

[1]For parts I–IX of this series, see refs. 1*a–i* respectively.

[2]The addition of *S,S'*-diethyl dithiomalonate to ethyl acrylate was previously explored by Scheithauer and Mayer (4) using sodium methoxide in methanol to give a mixture of the mono- and bis-adduct in ca. 1:1 ratio.

0008-4042/82/010094-03$01.00/0

©1982 National Research Council of Canada/Conseil national de recherches du Canada

Can. J. Chem. Downloaded from www.nrcresearchpress.com by 210.87.254.105 on 09/06/12
For personal use only.

TABLE 1. Michael addition of *S*,*S*′-diethyl dithiomalonate to α,β-unsaturated carbonyl compounds and reduction of adducts with Raney nickel

| Entry | α,β-Unsaturated ketone (ester) | Addition | | | Reduction | | |
|---|---|---|---|---|---|---|---|
| | | Time (h) | Product[a] (% yield) | | Time (h) | Product[a] (% yield) | |
| 1 | | 48 | 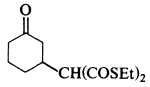 **1** | (93) | 0.5 | 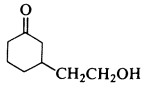 **2** | (80) |
| 2 | $CH_3COCH{=}CH_2$ | 48[b] | $CH_3COCH_2CH_2CH(COSEt)_2$ | (82) | 1 | $CH_3CO(CH_2)_4OH$ | (86) |
| 3 | $CH_3COCH{=}CHCH_3$ | 24 | $CH_3COCH_2\underset{\displaystyle CH_3}{\underset{\vert}{C}}H(COSEt)_2$ | (87) | 1 | $CH_3COCH_2\underset{\displaystyle CH_3}{\underset{\vert}{C}}HCH_2CH_2OH$ | (79) |
| 4 | | 18 | 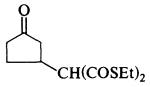 | (95) | 1 | 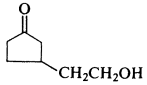 | (70) |
| 5 | 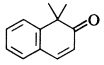 | 24 | 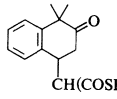 | (87) | 1 | 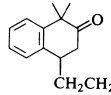 | (86) |
| 6 | 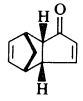 | 10 | 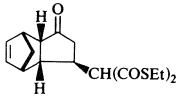 | (100) | 3 | 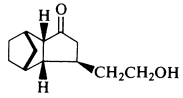 | (93) |
| 7 | 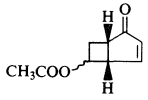 (Two epimers) | 48 | 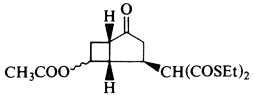 | (77) | 1 | 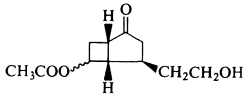 | (95) |
| 8 | $EtOOCCH{=}CH_2$ | 48 | $EtOOCCH_2CH_2CH(COSEt)_2$ | (93) | 4 | $EtOOC(CH_2)_4OH$ | (72) |
| 9 | $(EtOOC)_2C{=}CHCH(CH_3)_2$ | 5 | $(EtOOC)_2\underset{\displaystyle CH(CH_3)_2}{\underset{\vert}{C}}HCH(COSEt)_2$ | (95) | 1 | 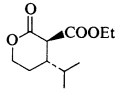 | (70) |
| 10 | 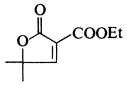 | 1 | 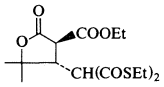 | (100) | 0.5 | 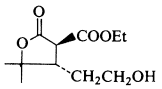 | (75) |

[a]All new compounds were adequately characterized by spectroscopic methods and by exact mass measurement and/or elemental analysis.
[b]This reaction was carried out at −30°C.

Can. J. Chem. Downloaded from www.nrcresearchpress.com by 210.87.254.105 on 09/06/12
For personal use only.

of 30% ether in petroleum ether gave adduct **1** (836 mg; 93% yield): mp 73–74°C (ether – petroleum ether); ir (neat): 1710 (ketone), 1680, and 1658 (thiol esters) $cm^{-1}$; nmr ($CCl_4$) δ: 3.53 (d, 1H, $J = 9$ Hz, —C*H*(COSEt)$_2$), 2.89 (q, 4H, $J = 7$ Hz, —COSC$H_2$—), and 1.26 (t, 6H, $J = 7$ Hz, —C$H_3$); ms $M^+$: 288.0863 (calcd. for $C_{13}H_{20}O_3S_2$: 288.0860). This procedure was found to be general for conjugated enones and α,β-unsaturated esters which are not doubly substituted at the β-carbon. Results obtained for a number of acyclic and cyclic compounds are compiled in Table 1. We have also examined the reactions of *S*,*S*′-diethyl dithiomalonate with mesityl oxide and 3-methyl-2-cyclohexenone, both fully substituted at the β-carbon, but failed to detect any adduct formation.

Upon treatment with Raney nickel, the Michael adducts underwent elimination of one of the thiol ester groups with concomitant reduction of the other to give directly 1,5-ketols or 5-hydroxy esters (Table 1). The best results were obtained using a modified W-2 Ra-Ni prepared by washing sequentially with water, aqueous acetic acid, water, isopropyl alcohol, and benzene instead of the normal water–ethanol combination (5). This acid-washed catalyst suppressed completely the formation of the transesterification products (—COSEt → —COOEt) which were otherwise produced in variable amounts. A general procedure for the reduction is illustrated below with keto dithiomalonate **1**.

At ~5°C, to a suspension of the modified W-2 Ra-Ni (5 mL (settled volume)) in benzene (10 mL), was added a solution of **1** (500 mg, 1.74 mmol) in benzene (10 mL). After stirring at room temperature under an argon atmosphere for 30 min, the mixture was filtered and the residue thoroughly washed with benzene and ethanol. Concentration followed by column chromatography of the crude product on silica gel eluting with ether – petroleum ether (3:1) gave ketol **2** (197 mg; 80% yield).

The foregoing report illustrates a two-step process which allows the overall incorporation of an ethanol unit in a Michael fashion to α,β-unsaturated carbonyl compounds. This procedure for the preparation of 1,5-ketols and 5-hydroxy esters compares favorably with existing methods (2, 3, 6, 7) in terms of simplicity and efficiency.

## Acknowledgments

We are grateful to the Natural Sciences and Engineering Research Council of Canada and the University of Alberta for financial support.

1. (*a*) H. J. Liu, S. P. Lee, and W. H. Chan. Synth. Commun. **9**, 91 (1979); (*b*) H. J. Liu and H. K. Lai. Tetrahedron Lett. 1193 (1979); (*c*) H. J. Liu, S. K. Attah-Poku, and H. K. Lai. Synth. Commun. **9**, 883 (1979); (*d*) H. J. Liu, H. K. Lai, and S. K. Attah-Poku. Tetrahedron Lett. 4121 (1979); (*e*) H. J. Liu and H. K. Lai. Can. J. Chem. **57**, 2522 (1979); (*f*) H. J. Liu and S. I. Sabesan. Can. J. Chem. **58**, 2645 (1980); (*g*) H. J. Liu and H. K. Lai. Synth. Commun. **11**, 65 (1981); (*h*) H. J. Liu, L. K. Ho, and H.K. Lai. Can. J. Chem. **59**, 1685 (1981); (*i*) H. J. Liu, R. R. Bukownik, and P. R. Pednekar. Synth. Commun. In press.
2. H. O. House. Modern synthetic reactions. 2nd ed. W. A. Benjamin Inc., Menlo Park, CA. 1972.
3. J. F. Wolfe and M. A. Ogliaruso. *In* The chemistry of acid derivatives, Supplement B. *Edited by* S. Patai. John Wiley and Sons Ltd., New York, NY. 1979. Chapt. 19.
4. S. Scheithauer and R. Mayer. Chem. Ber. **100**, 1413 (1967).
5. R. Mozingo. Org. Synth. Coll. Vol. **3**, 181 (1955).
6. G. Stork and G. A. Kraus. J. Am. Chem. Soc. **98**, 2351 (1976).
7. M. E. Jung and L. M. Speltz. J. Am. Chem. Soc. **98**, 7882 (1976).

# The crystal structure of 1-phenyl-3,5-dimethyl pyrazolium nitrate

J. ZUKERMAN-SCHPECTOR AND E. E. CASTELLANO

*Instituto de Física e Química de São Carlos, Universidade de São Paulo, Caixa Postal 369, 13560 São Carlos, S.P., Brazil*

AND

A. C. MASSABNI AND A. DERBLI PINTO

*Instituto de Química de Araraquara (UNESP), Caixa Postal 174, 14.800 Araraquara, S.P., Brazil*

Received December 24, 1980[1]

J. ZUKERMAN-SCHPECTOR, E. E. CASTELLANO, A. C. MASSABNI and A. DERBLI PINTO. Can. J. Chem. **60**, 97 (1982).

The crystal structure of the title compound has been determined from diffractometric X-ray data and refined by full-matrix least-squares to a final $R$ factor of 0.055 from 1099 independent reflections above background.

The space group and cell dimensions are : $P2_1/n$, $a$ = 7.916(2), $b$ = 10.934(3), $c$ = 13.638(1) Å, $\beta$ = 97.37(1)°, with $Z$ = 4.

The 1-phenyl-3,5-dimethylpyrazole group was found to be positively charged, forming a strong ionic complex with the nitrate ion.

The dihedral angle between the phenyl and pyrazole rings, corresponding to the minimum intramolecular van der Waals energy, was calculated and compared with those reported in different complexes of known structure, showing that there is a narrow range of rotational freedom about the N(1)—C(6) bond.

J. ZUKERMAN-SCHPECTOR, E. E. CASTELLANO, A. C. MASSABNI et A. DERBLI PINTO. Can. J. Chem. **60**, 97 (1982).

On a déterminé la structure cristalline du composé mentionné dans le titre à partir de données de diffraction de rayons X et on l'a affiné par la méthode des moindres carrés (matrice entière) jusqu'à une valeur conventionnelle de $R$ = 0,055 pour 1099 réflexions indépendantes avec $a$ = 7,916(2), $b$ = 10,934(3), $c$ = 13,638(1) Å, $\beta$ = 97,37(1)°, $Z$ = 4, groupe d'espace $P2_1/n$.

On a trouvé que le groupe phényl-1 diméthyl-3,5 pyrazole est chargé positivement, formant un complexe ionique fort avec l'ion nitrate.

On a calculé l'angle dièdre entre les noyaux phényle et pyrazole correspondant à l'énergie de van der Waals intramoléculaire minimale et on l'a comparé à ceux rapportés pour différents complexes de structure connue; ceci révèle l'existence d'un domaine étroit de rotation libre autour de la liaison N(1)—C(6).

[Traduit par le journal]

## Introduction

1-Phenyl-3,5-dimethylpyrazole (PDMP) has been used as a ligand in some metal complexes of silver(I) (1), copper(II) (2, 3), and cobalt(II) (4). In these complexes the PDMP appears as a neutral group bonded to the metal through the N(2) atom.

At room temperature PDMP is a colourless liquid but addition of nitric acid to the alcoholic solution produces a crystalline precipitate. This fact raised the question of the nature of the PDMP – nitric acid interaction; to investigate this matter, to compare the PDMP molecule with its conformation in the several metal complexes reported, and to see whether the geometry of the pyrazolium moiety was changed or not, a three-dimensional crystal structure analysis was undertaken.

## Experimental

The title compound was prepared as described elsewhere (5) and crystals of adequate size for X-ray analysis were obtained from ethanol by slow evaporation at room temperature.

A prismatic colourless crystal with dimensions 0.7 × 0.25 × 0.3 mm was mounted on an Enraf-Nonius CAD-4 diffractometer. The unit cell dimensions and the orientation matrix for the data collection were obtained by least squares from 25 centered reflections. Systematic absences: $h0l$ for odd $h + l$, and $0k0$ for odd $k$, indicated space group $P2_1/n$.

*Crystal Data*

$C_{11}H_{13}N_2^+ NO_3^-$ fw = 235,24

Monoclinic, space group $P2_1/n$ ($C_{2h}^5$), $a$ = 7.916(2), $b$ = 10.934(3), $c$ = 13.638(1) Å, $\beta$ = 97.37(1)°, $V$ = 1170.6 Å$^3$, $Z$ = 4 formula units per cell, $D_c$ = 1.33 g cm$^{-3}$, $\mu$(CuK$\alpha$) = 8.4 cm$^{-1}$, $\lambda$(CuK$\alpha$) = 1.5418 Å, $t$ = 23°C.

Intensities were measured by the $\theta$–$2\theta$ scan technique at a rate between 1.33 and 20.0 deg min$^{-1}$ determined by a fast prescan of 20.0 deg min$^{-1}$; the $\omega$ scan angle was (0.80 + 0.14 tan $\theta$)° extended at each side by 25% for background determination.

1656 reflections were collected in the range $0 \leq \theta \leq 55°$ using graphite-monochromated CuK$\alpha$ radiation. 1099 reflections having $I \geq 3\sigma(I)$ ($\sigma(I)$ estimated from counting statistics) were retained for structure determination and refinement.

The intensity of one standard reflection was essentially constant over the duration of the experiment. Data were corrected for Lorentz and polarization effects but not for absorption or extinction.

*Structure Solution and Refinement*

The structure was solved by direct methods and refined by full-matrix least-squares using the SHELX-76 system of programs (6). All the non-hydrogen atoms appeared clearly in the first $E$-map. The hydrogen atoms were found from a difference Fourier synthesis calculated when the conventional $R$ was 0.091 and were assigned the isotropic temperature factor of the atom to which they were attached. Further anisotropic refinement for the non-hydrogen atoms was carried out. This resulted in a final $R$ of 0.055 and $R_w$ = 0.061. The function minimized was: $\sum\omega(|F_o| - |F_c|)^2$ with $\omega = 1/[\sigma^2(F_o) + 0.00215\,F_o^2]$, where $\sigma(F_o)$ is the esd for the observed amplitude based on counting statistics. Bonded H-atom scattering factors (7) and complex neutral scattering factors (8, 9) for the remaining atoms were employed. A final difference Fourier map showed no features of

[1]Revision received September 2, 1981.

0008-4042/82/020097-03$01.00/0

©1982 National Research Council of Canada/Conseil national de recherches du Canada

Can. J. Chem. Downloaded from www.nrcresearchpress.com by 210.87.254.105 on 09/06/12
For personal use only.

Can. J. Chem. Downloaded from www.nrcresearchpress.com by 210.87.254.105 on 09/06/12
For personal use only.

TABLE 1. Atomic coordinates and calculated isotropic temperature factors with esd in parentheses*

| Atom | X/A | Y/B | Z/C | $B_{iso}$ (Å$^2$) |
|---|---|---|---|---|
| N(1) | 0.2662(3) | 0.3588(2) | 0.0050(2) | 3.28(8) |
| N(2) | 0.1970(3) | 0.4468(2) | −0.0583(2) | 3.20(8) |
| C(1) | 0.1680(4) | 0.4004(3) | −0.1497(2) | 3.5(1) |
| C(2) | 0.2216(4) | 0.2809(3) | −0.1444(2) | 4.0(1) |
| C(3) | 0.2838(4) | 0.2551(3) | −0.0471(2) | 3.8(1) |
| C(4) | 0.3596(6) | 0.1407(3) | −0.0023(3) | 6.0(1) |
| C(5) | 0.0901(5) | 0.4732(3) | −0.2345(3) | 5.0(1) |
| C(6) | 0.3061(3) | 0.3841(3) | 0.1083(2) | 3.2(1) |
| C(7) | 0.2542(4) | 0.3034(3) | 0.1758(2) | 4.1(1) |
| C(8) | 0.2984(5) | 0.3265(4) | 0.2758(3) | 5.1(1) |
| C(9) | 0.3907(5) | 0.4305(4) | 0.3069(3) | 5.1(1) |
| C(10) | 0.4386(4) | 0.5112(3) | 0.2379(3) | 4.5(1) |
| C(11) | 0.3978(4) | 0.4887(3) | 0.1383(2) | 3.8(1) |
| N(3) | 0.1805(4) | 0.7514(3) | −0.0556(2) | 4.5(1) |
| O(1) | 0.1213(3) | 0.6718(2) | −0.0040(2) | 5.49(9) |
| O(2) | 0.1345(5) | 0.8573(3) | −0.0519(2) | 8.4(1) |
| O(3) | 0.2818(5) | 0.7187(3) | −0.1114(3) | 9.7(2) |

*The standard deviation of $B_{iso}$ was calculated as $\sigma(B_{iso}) = \sum_{ij} T_{ij}\,\sigma(B_{ij})$.

chemical significance. Measured and calculated structure factors, anisotropic thermal parameters for non-hydrogen atoms, and H-atom parameters have been deposited.[2]

Atomic coordinates together with calculated equivalent isotropic temperature factors are given in Table 1. The expression for $B_{iso}$ is of the form:

$$B_{iso} = \sum_{ij} T_{ij}B_{ij},$$

where $T_{ij}$ are the elements of the metric tensor and $B_{ij}$ are the elements of the thermal tensor usually obtained by least-squares refinement (10).

## Discussion

The molecule is depicted in Fig. 1 which also shows intramolecular bond distances and atomic numbering. Thermal ellipsoids are drawn to a 45% probability scale (11). Angles between non-hydrogen bonded atoms are given in Table 2.

The phenyl ring, the pyrazole ring, and the $NO_3^-$ group were found to be planar to within experimental accuracy. Least-squares planes referred to the conventional orthogonalized coordinates, distances of atoms to the planes, and dihedral angles are given in Table 3.

Depending on the different environments the PDMP group is known to have various conformations, as can be seen in Table 4 where the reported dihedral angles between the phenyl and pyrazole rings are given.

The *calculated* dihedral angle corresponding to the conformation of minimum intramolecular van der Waals energy was found using Sakurai and Kobayashi's Molecular Model Building Program (12).

A difference Fourier synthesis unambiguously

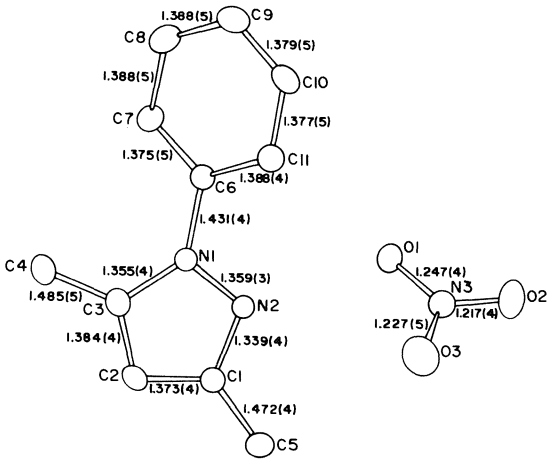


FIG. 1. The title compound, showing the bond distances (Å) with esd in parentheses, and numbering scheme.

TABLE 2. Angles between non-hydrogen bonded atoms with esd in parentheses

| Bonds | Angle |
|---|---|
| C(3)—N(1)—N(2) | 108.6(2) |
| C(6)—N(1)—N(2) | 120.6(2) |
| C(6)—N(1)—C(3) | 130.8(2) |
| C(1)—N(2)—N(1) | 109.3(2) |
| C(2)—C(1)—N(2) | 107.2(3) |
| C(5)—C(1)—N(2) | 122.1(3) |
| C(5)—C(1)—C(2) | 130.7(3) |
| C(3)—C(2)—C(1) | 108.3(3) |
| C(2)—C(3)—N(1) | 106.5(3) |
| C(4)—C(3)—N(1) | 123.5(3) |
| C(4)—C(3)—C(2) | 129.9(3) |
| C(7)—C(6)—N(1) | 119.2(3) |
| C(11)—C(6)—N(1) | 119.4(3) |
| C(11)—C(6)—C(7) | 121.4(3) |
| C(8)—C(7)—C(6) | 118.8(3) |
| C(9)—C(8)—C(7) | 120.4(3) |
| C(10)—C(9)—C(8) | 119.7(3) |
| C(11)—C(10)—C(9) | 120.6(3) |
| C(10)—C(11)—C(6) | 119.1(3) |
| O(2)—N(3)—O(1) | 120.3(3) |
| O(3)—N(3)—O(1) | 118.0(3) |
| O(3)—N(3)—O(2) | 121.7(3) |

showed a hydrogen atom bonded to N(2). The H(N2) ... O(1)—N(3) and the N(2)—H(N2) ... O(1) angles of 112° and 176° together with the N(2) ... O(1) and H(N2) ... O(1) distances of 2.66 and 1.75 Å respectively are strong evidence of hydrogen bonding between O(1) and N(2).

The $NO_3^-$ group shows a very approximate $D_{3h}$ local point symmetry although a slightly longer N(3)—O(1) distance is presumably due to the mentioned hydrogen bond.

We conclude that the PDMP group is positively charged forming a strong ionic complex with the $NO_3^-$ anion.

[2]These tables are available, at a nominal charge, from the Depository of Unpublished Data, CISTI, National Research Council of Canada, Ottawa, Ont., Canada K1A 0S2.

TABLE 3. Least squares planes, deviations of atoms from them,[a] and dihedral angles

| Plane 1[b] | | Plane 2[b] | | Plane 3[b] | |
|---|---|---|---|---|---|
| Atom | Distance (Å) | Atom | Distance (Å) | Atom | Distance (Å) |
| N(1) | −0.004 | C(6) | 0.006 | N | −0.010 |
| N(2) | 0.004 | C(7) | −0.008 | O(1) | 0.003 |
| C(1) | −0.002 | C(8) | 0.003 | O(2) | 0.003 |
| C(2) | 0.000 | C(9) | 0.004 | O(3) | 0.003 |
| C(3) | 0.003 | C(10) | −0.006 | H(N2)* | 0.287 |
| C(4)* | 0.032 | C(11) | 0.001 | | |
| C(5)* | −0.022 | N(1)* | 0.036 | | |
| C(6)* | −0.026 | | | | |

| Plane | Plane | Dihedral angle (deg) |
|---|---|---|
| *1* | *2* | 48.2 |
| *1* | *3* | −56.3 |
| *2* | *3* | −61.4 |

[a] Atoms marked with an asterisk were not included in the calculation of the plane.
[b] Plane *1*: $0.9427X + 0.2892Y - 0.1665Z - 3.1056 = 0$; Plane *2*: $0.8611X - 0.5084Y - 0.0080Z + 0.2296 = 0$; Plane *3*: $-0.6644X - 0.1704Y - 0.7277Z + 1.8576 = 0$.

TABLE 4. Dihedral angle between phenyl and pyrazole rings in different complexes of known structure

| Compound | | Dihedral angle (deg) |
|---|---|---|
| $[Ag(PDMP)_3]NO_3$ | (1) | 57.4 |
| $[CuCl_2(PDMP)_2]$ | (3) | 59.8 |
| $[Co(NCS)_2(PDMP)_2]$ | (4) | 72.9 |
| $(PDMP)^+NO_3^-$ | | 48.2 |
| Calculated | | 60.0 |

It is known that in the pyrazole molecule the C(2)—C(3) distance is systematically shorter than the C(1)—C(2) one (1, 13, 14). In the present case the two nitrogen atoms behave as pyrrolic and unless there is a strong interaction between the $p_\pi$ electrons of the phenyl and pyrazole groups the two C—C internuclear distance should be identical. This is actually observed to within our experimental accuracy. In fact, the dihedral angle of 48.2° does not favor a strong π–π overlap. It may be speculated that the positive charge of the PDMP group gives rise to the two resonance forms:

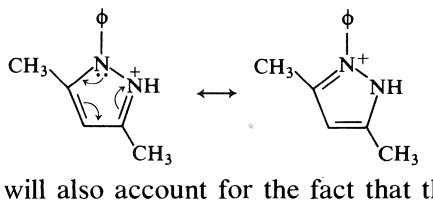

which will also account for the fact that the two C—C bonds in the pyrazolium ion are essentially equal.

## Acknowledgements

We thank one of the referees for many enlightening comments and the Organization of American States for a fellowship (to J. Z-S.).

This work has received the support of BID-FINEP, FAPESP and CNPq, which are hereby gratefully acknowledged.

1. R. H. P. FRANCISCO, Y. P. MASCARENHAS, and J. R. LECHAT. Acta Crystallogr. B**35**, 177 (1979).
2. R. H. P. FRANCISCO, J. R. LECHAT, and Y. P. MASCARENHAS. Acta Crystallogr. B**35**, 1468 (1979).
3. R. H. P. FRANCISCO, J. R. LECHAT, A. C. MASSABNI, C. B. MELIOS, and M. MOLINA. J. Coord. Chem. **10**, 149 (1980).
4. A. M. G. DIAS RODRIGUES, Y. P. MASCARENHAS, and M. M. RODRIGUES. Acta Crystallogr. B**36**, 159 (1980).
5. A. DERBLI PINTO and A. C. MASSABNI. Eclet. Quim. In press.
6. G. M. SHELDRICK. SHELX program for crystal structure determination. University of Cambridge, England. 1975.
7. R. F. STEWART, E. R. DAVIDSON, and W. T. SIMPSON. J. Chem. Phys. **42**, 3175 (1965).
8. D. T. CROMER and D. LIBERMAN. J. Chem. Phys. **53**, 1981 (1970).
9. D. T. CROMER and B. MANN. Acta Crystallogr. A**24**, 321 (1968).
10. W. C. HAMILTON. Acta Crystallogr. **12**, 609 (1959).
11. C. K. JOHNSON. ORTEP, Report No. ORNL-3794, Oak Ridge National Laboratory, Oak Ridge, TN. 1965.
12. T. SAKURAI and K. KOBAYASHI. Rep. Inst. Phys. Chem. Res. **48**, 133 (1972).
13. T. LA COUR and S. E. RASMUSSEN. Acta Chem. Scand. **27**, 1845 (1973).
14. E. N. MASLEN, J. R. CANNON, A. H. WHITE, and A. C. WILLIS. J. Chem. Soc. Perkin II, 1298 (1974).

Can. J. Chem. Downloaded from www.nrcresearchpress.com by 210.87.254.105 on 09/06/12
For personal use only.

# *Ab initio* SCF-MO calculations of features of the lowest triplet state potential surfaces of several tetraatomic carbonyl compounds

A. KAPUR,[1] R. P. STEER, AND P. G. MEZEY

*Department of Chemistry and Chemical Engineering, University of Saskatchewan, Saskatoon, Sask., Canada S7N 0W0*

Received May 28, 1981

A. KAPUR, R. P. STEER, and P. G. MEZEY. Can. J. Chem. **60**, 100 (1982).

Non-empirical SCF-MO calculations have been carried out for a series of tetraatomic carbonyl compounds. Portions of the ground singlet and first triplet state potential energy surfaces, in particular those along the out-of-plane bending coordinates, have been determined. Estimates of the first triplet state out-of-plane vibrational frequencies have been calculated.

A. KAPUR, R. P. STEER et P. G. MEZEY. Can. J. Chem. **60**, 100 (1982).

On a effectué des calculs de MO-SCF non empiriques sur une série de composés carbonylés tétraatomiques. On a déterminé des portions des surfaces d'énergie potentielle de l'état fondamental singulet et du premier état triplet. On a évalué les fréquences de vibration hors du plan du premier état triplet.

[Traduit par le journal]

## Introduction

Tetraatomic carbonyl compounds in their ground and excited electronic states have been the subject of many experimental and theoretical investigations. Foremost among experimental work have been exhaustive studies of the electronic spectroscopy, the photochemistry, and the photophysics of formaldehyde (1–3). Despite these efforts, however, an unequivocal picture of the mechanism(s) of photodissociation of this molecule has yet to emerge, and recent calculations of features of potential energy surfaces relevant to its photofragmentations have proved to be very useful (4). By comparison, little experimental and less theoretical work has been reported on other similar tetraatomic carbonyls, such as the carbonyl halides, a notable exception is an SCF-CI study (5) on the vertical electronic spectrum of $F_2CO$. Tetraatomic carbonyl halides are the subject of the present study.

Recently we reported the results of *ab initio* SCF-MO calculations on the ground and lowest triplet states of several thiocarbonyl compounds (6–8). It was shown that reasonable agreement between computed and experimental ground and lowest triplet equilibrium geometries could be obtained for these molecules even when an economical STO-3G basis set was used. In addition, good estimates of the triplet state inversion frequencies could be obtained by solving the vibrational eigenvalue problem after *ab initio* calculation of the triplet energies at several points along the out-of-plane bending coordinates. A more thorough *ab initio* study of the ground state structures of $H_2CO$, HFCO, HClCO, $F_2CO$, $Cl_2CO$, ClFCO, $H_2CS$, and $F_2CS$ has recently been reported by Oberhammer and Boggs (9). In that work SCF-MO calculations were performed using the Hartree–Fock gradient program of Pulay (10). When 4-21 basis sets were used for second row atoms and 3-3-21 basis sets supplemented with *d* orbitals were used for sulfur and chlorine, good agreement between calculated and experimental geometries was found. With the exception of studies of HFCO and $F_2CO$ (5, 11–12), however, *ab initio* calculations have not been performed on excited states of the tetraatomic carbonyl halides, although several semi-empirical studies have been reported (13–16).

In this paper we present the results of calculations of the lowest triplet state structures and inversion vibrational frequencies of $H_2CO$, HFCO, $F_2CO$, $Cl_2CO$, and ClFCO. Ground state geometries have also been calculated for comparison with previous work.

## Methods of calculation

The *ab initio* calculations were carried out using a modified version of Gaussian-70 (17) adapted for a 36 bit word DEC 2060 computer. The equilibrium geometries of $H_2CO$ and HFCO in their lowest triplet states were obtained by sequential, cyclic optimization of all geometric parameters using both the STO-3G and 4-31G basis sets. In addition, seven other points lying along the out-of-plane bending coordinate on one side of the double minimum potential surface were calculated for these two molecules with both basis sets. For these latter points, all geometric parameters except the out-of-plane angle, $\theta$, were optimized. The equilibrium geometries and energies at various out-of-

[1]Present address: Department of Chemistry, University of New Brunswick, Fredericton, N.B., Canada E3B 6E2.

0008-4042/82/020100-06$01.00/0

©1982 National Research Council of Canada/Conseil national de recherches du Canada

Can. J. Chem. Downloaded from www.nrcresearchpress.com by 210.87.254.40 on 09/06/12
For personal use only.

Can. J. Chem. Downloaded from www.nrcresearchpress.com by 210.87.254.40 on 09/06/12
For personal use only.

plane angles in the lowest triplet states of $F_2CO$, ClFCO, and $Cl_2CO$ were calculated similarly, except that only the more economical STO-3G basis set was employed. For purposes of comparison with previous work, the equilibrium geometries of all five ground state molecules were calculated using the STO-3G basis set and those of $H_2CO$, HFCO, and $F_2CO$ using the 4-31G basis set.

The calculated SCF energies along the out-of-plane bending coordinates of the lowest triplet states of all five molecules were used to find (using a non-linear least-squares fitting program) best values of the parameters, $\lambda$, $A$, and $a^2$, defining the shape of the double minimum potential function (18, 19),

$$[1] \quad V(Q_6) = \frac{1}{2}\lambda Q_6^2 + A \exp(-a^2 Q_6^2)$$

Here $Q_6$ is the mass-weighted out-of-plane bending coordinate whose values must be calculated from the corresponding out-of-plane angles, $\theta$. The eigenvalues and eigenvectors for the inversion vibration were obtained as previously described (6, 7). The vibrational eigenvalues, in multiples of $hc\nu_0$, measured relative to the potential minima, can be obtained in the form (18)

$$[2] \quad \frac{G}{\nu_0} = \frac{E}{hc\nu_0} - \frac{B(\rho + 1)}{(e^\rho - \rho - 1)}$$

where $B = b/\nu_0$ is a dimensionless parameter proportional to the barrier height, $b$; $\rho$ is a shape factor defined by $a^2 = e^\rho\lambda/2A$, and $\nu_0$ is the wavenumber (in $cm^{-1}$) of the harmonic oscillator appropriate to the parabolic part of the potential and is given by $\nu_0 = \lambda^{1/2}/2\pi c$.

Past experience (6, 7) has shown that the eigenvalues are very sensitive to the number of harmonic oscillator basis functions taken and that the number of basis functions required for convergence may be strongly dependent on $\rho$. In the present work, the number of vibrational basis functions has arbitrarily been set to 100. Increasing this number led to no significant numerical change in any of the calculated eigenvalues.

A general method of transforming the out-of-plane angle, $\theta$, to the corresponding mass-weighted coordinate, $Q_6$, involves the use of the appropriate matrix element, $G_{66}$ (ref. 20. For molecules of $C_s$ symmetry the matrix element is $G_{66}$ but is $G_{44}$ for $C_{2v}$ molecules. Here $G_{66}$ is used throughout for convenience). An analytic expression for the $G_{66}$ matrix element of tetraatomic molecules having either $C_{2v}$ or $C_s$ equilibrium symmetry has recently been described (21) and was used in the present work. $Q_6$ and $\theta$ are related via

$$[3] \quad Q_6 = \int_0^\theta G_{66}^{-1/2}\, d\theta$$

and three approximate methods of carrying out this $Q_6$–$\theta$ transformation have been outlined and compared previously (21). The model involves the "best" energy values obtained along the optimized "relaxed" inversion path (corresponding to a non-rigid bender model), combined with the application of a vibrational Hamiltonian preserving some features of a rigid bender. That is, the results refer to a rigid bender model where the energy values along the bending coordinate are replaced by those of the non-rigid molecule. The most general and most accurate of these three methods, involving truncation of the series solution to [3] only after the fourth term, has been used in the present work.

## Results and discussion

The calculated and experimental ground state geometries for the tetraatomic carbonyls considered in this study are given in Table 1. The data of Oberhammer and Boggs (9) are included for comparison. As expected, calculations with the 4-31G basis set reproduce the measured ground state geometries better than those with the STO-3G basis set. It has been noted previously (9, 12) that the use of the latter basis set results in a systematic underestimation of the C=O bond shortening effects of electron-withdrawing substituents. Moreover, the C—Cl bond lengths are systematically overestimated, by as much as 5% in the case of ClFCO. On the other hand, calculations with the 4-31G basis give quite satisfactory agreement with experiment when the differences between the definitions of the calculated and the experimentally measured bond lengths are accounted for (for a discussion of this point see ref. 28).

Despite the fact that either the 4-31G basis set or those used by Oberhammer and Boggs (9) give better ground state geometries, general trends in the predicted geometries are correctly reproduced with the STO-3G basis. Since we were primarily interested in obtaining estimates of the lowest triplet inversion barriers and out-of-plane bending mode frequencies, and since a large number of points along the double minimum paths had to be calculated to do so, only the STO-3G basis set was used for the $F_2CO$, ClFCO, and $Cl_2CO$ triplets.

Table 2 shows the predicted equilibrium geometries and inversion barrier heights for the lowest

TABLE 1. Calculated and experimental ground state geometries of some tetraatomic carbonyls, XYCO[a]

| | r(C=O) | | r(C—X) | | r(C—Y) | | ∠X—C—O | | ∠Y—C—O | | |
|---|---|---|---|---|---|---|---|---|---|---|---|
| X, Y | Calcd[b] | Expt | Calcd | Expt | Calcd | Expt | Calcd | Expt | Calcd | Expt | Ref |
| H, H | 1.227 | | 1.108 | | 1.108 | | 122.6 | | 122.6 | | |
| | 1.206 | 1.2078 | 1.081 | 1.1161 | 1.081 | 1.1161 | 121.8 | 121.8 | 121.8 | 121.8 | 22, 23 |
| | 1.208 | | 1.084 | | 1.084 | | 122.4 | | 122.4 | | |
| H, F | 1.211 | | 1.108 | | 1.352 | | 125.7 | | 122.1 | | |
| | 1.179 | 1.181 | 1.071 | 1.095 | 1.356 | 1.338 | 127.7 | 127.3 | 122.2 | 122.8 | 24 |
| | 1.181 | | 1.072 | | 1.359 | | 127.9 | | 122.9 | | |
| Cl, Cl | 1.195 | | 1.802 | | 1.802 | | 123.9 | | 123.9 | | |
| | — | 1.180 | — | 1.742 | — | 1.742 | — | 124.1 | — | 124.1 | 25 |
| | 1.180 | | 1.754 | | 1.754 | | 124.0 | | 124.0 | | |
| Cl, F | 1.201 | | 1.813 | | 1.342 | | 124.2 | | 125.5 | | |
| | — | 1.173 | — | 1.725 | — | 1.334 | — | 127.5 | — | 123.7 | 26 |
| | 1.175 | | 1.737 | | 1.349 | | 125.3 | | 122.2 | | |
| F, F | 1.209 | | 1.347 | | 1.347 | | 125.1 | | 125.1 | | |
| | 1.170 | 1.170 | 1.329 | 1.317 | 1.329 | 1.317 | 125.8 | 126.2 | 125.8 | 126.2 | 27 |
| | 1.171 | | 1.330 | | 1.330 | | 125.9 | | 125.9 | | |

[a] Bond lengths in Å, bond angles in deg.
[b] For each calculated quantity the value obtained using the STO-3G basis set is given first, followed by that obtained using the 4-31G basis, followed by the value of Oberhammer and Boggs (9).

TABLE 2. Calculated geometries and inversion barrier heights for the lowest triplet states of several tetraatomic carbonyls, XYCO[a]

| X, Y | r(C—O)[b] | r(C—X) | r(C—Y) | ∠ X—C—O | ∠ Y—C—O | θ (deg) | $b$(cm$^{-1}$) | Energy (au) |
|---|---|---|---|---|---|---|---|---|
| H, H | 1.3936 | 1.0888 | 1.0888 | 114.2 | 114.2 | 38.1 | 700 | −112.327673 |
| | 1.3690 | 1.0726 | 1.0726 | 114.4 | 114.4 | 33.0 | 287 | −113.636103 |
| H, F | 1.412 | 1.102 | 1.355 | 112.7 | 112.7 | 44.1 | 2194 | −209.788096 |
| | 1.374 | 1.072 | 1.365 | 113.5 | 112.0 | 44.7 | 2503 | −212.357135 |
| Cl, Cl | 1.400 | 1.793 | 1.793 | 112.1 | 112.1 | 44.4 | 2981 | −1020.331235 |
| Cl, F | 1.414 | 1.815 | 1.343 | 112.5 | 110.7 | 47.6 | 4552 | −663.797903 |
| F, F | 1.425 | 1.356 | 1.356 | 111.5 | 111.5 | 49.1 | 5805 | −307.260175 |

[a] Bond lengths in Å, bond angles in deg.
[b] For each calculated quantity, the value obtained using the STO-3G basis set is given first and is followed by that obtained using the 4-31G basis for $H_2CO$ and HFCO.

triplet states of this series of five tetraatomic carbonyls. Experimental data for θ and $b$ are available only for $H_2CO(^3A'')$, although crude estimates of these quantities may be obtained for triplet HFCO, $F_2CO$, and $Cl_2CO$ from measurements on the corresponding $^1(n,\pi^*)$ states. Thus, there is only limited opportunity to judge the accuracy of the calculated results. Nevertheless, qualitatively the results appear to be reasonable. The C—O bond length generally increases with increasing electronegativity of the substitutent groups ($H_2CO \approx Cl_2CO <$ HFCO ≈ ClFCO < $F_2CO$), and the predicted extent of non-planarity of these triplets is generally in accord with the Walsh postulates (29). As previously noted from CNDO/2 calculations on $n,\pi^*$ states of several carbonyls (13), the change in $p_z$ electron density on the central carbon atom in proceeding from the planar to the equilibrium non-planar conformation, $\Delta\rho(p_z)$, may be correlated with the magnitude of the equilibrium out-of-plane angle and the inversion barrier height. The data for the five molecules chosen for the present study is given in Table 3. In fact, over the range of out-of-plane angles encountered in these five molecules, a linear relationship exists between $\Delta\rho(p_z)$ and $\theta_e$, as shown in Fig. 1. Such a relationship was also observed for a similar series of thiocarbonyl triplets (6, 7) and lends quantitative support to Walsh's Rule.

Figure 2 shows the variation of potential energy along the out-of-plane bending coordinate for all five molecules, calculated with the STO-3G basis set. Only small differences between the parabolic parts of these double minimum curves and those calculated with the 4-31G basis set were noted for HFCO, as illustrated in Fig. 3. The calculated barrier heights were particularly sensitive to choice of basis set for $H_2CO$, however, and, perhaps

Can. J. Chem. Downloaded from www.nrcresearchpress.com by 210.87.254.40 on 09/06/12
For personal use only.

TABLE 3. Carbon $2p$ orbital electron densities for planar and equilibrium non-planar triplet tetraatomic carbonyls

| | $\theta = 0°$ | | | $\theta = \theta_e$ | | | |
|---|---|---|---|---|---|---|---|
| Carbonyl | $2p_x$ | $2p_y$ | $2p_z$ | $2p_x$ | $2p_y$ | $2p_z$ | $\Delta 2p_z$ |
| $H_2CO$ | 0.5086 | 0.6113 | 1.1021 | 0.6272 | 0.6178 | 0.8781 | 0.2240 |
| HFCO | 0.5093 | 0.5343 | 1.1422 | 0.6414 | 0.5458 | 0.8311 | 0.3111 |
| $F_2CO$ | 0.5077 | 0.4804 | 1.1755 | 0.6263 | 0.4884 | 0.7906 | 0.3849 |
| ClFCO | 0.5091 | 0.4791 | 1.1671 | 0.5957 | 0.4891 | 0.8058 | 0.3613 |
| $Cl_2CO$ | 0.5169 | 0.4802 | 1.1557 | 0.5838 | 0.4960 | 0.8397 | 0.3160 |

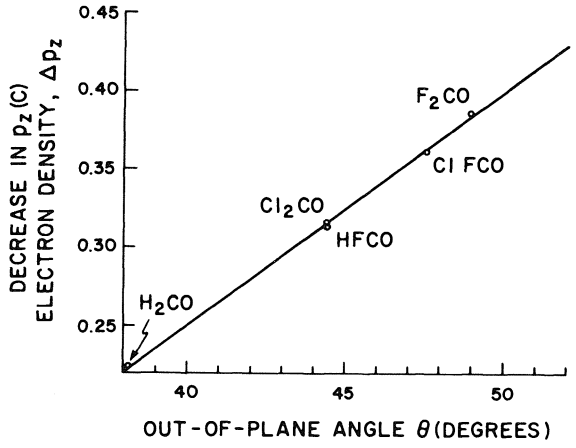


FIG. 1. Correlation between the decrease of electron density on the $p_z$ orbital of carbon atom and the calculated equilibrium out-of-plane angle for a series of tetraatomic carbonyls.

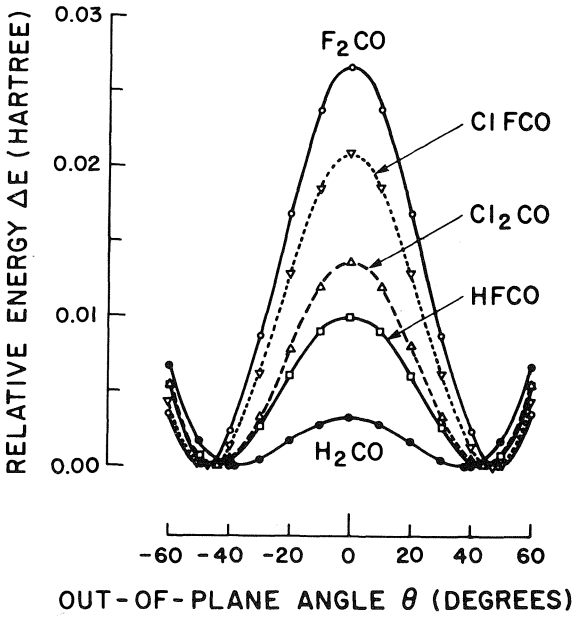


FIG. 2. Calculated out-of-plane bending potentials for the first triplet states of a series of tetraatomic carbonyls (using 3G basis sets).

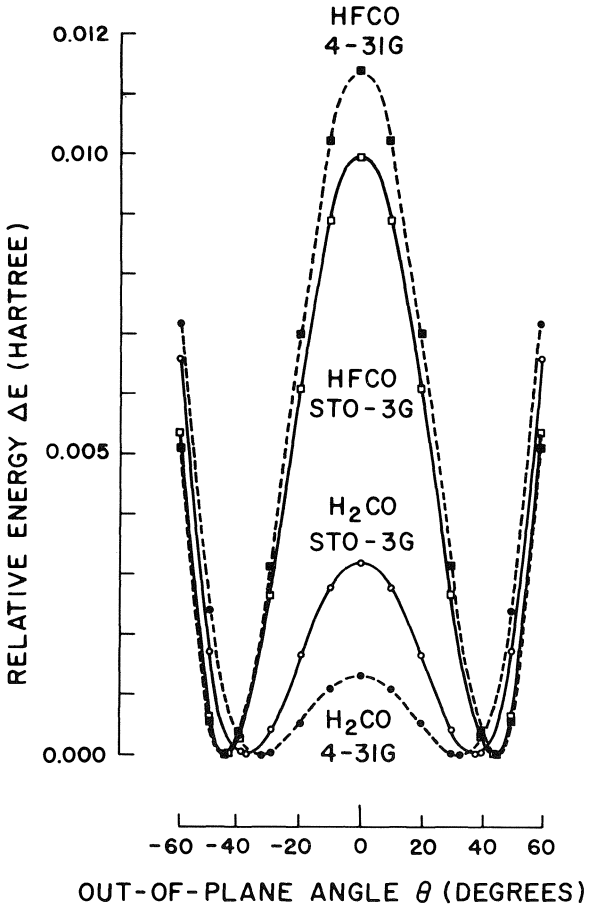


FIG. 3. Comparison of STO-3G and STO-4-31G double minimum out-of-plane bending potentials of triplet states of $H_2CO$ and HFCO.

fortuitously, better agreement with experiment (19) ($\theta = 37.9°$, $b = 775.6$ cm$^{-1}$) was found when the STO-3G basis was employed. Nevertheless, with either basis set the expected trend in variation of barrier height with electron-withdrawing power of the substituent atoms is predicted. If the order of increasing barrier heights is the same for the $^3A''$ states as for the $^1A''$ states, then the predicted trend is confirmed by experimental data. For the $^1A''$

Can. J. Chem. Downloaded from www.nrcresearchpress.com by 210.87.254.40 on 09/06/12
For personal use only.

Can. J. Chem. Downloaded from www.nrcresearchpress.com by 210.87.254.40 on 09/06/12
For personal use only.

states of $H_2CO$, HFCO, $Cl_2CO$, and $F_2CO$ barrier heights of 356.2, 2550, 2170, and >4000 $cm^{-1}$, respectively, have been measured (19, 30–32).

The only direct, quantitative comparison that can be made between experimental and the present calculated lowest triplet state geometries is for formaldehyde. For this molecule agreement between the calculated and the measured equilibrium geometry is relatively poor when either basis set is used, compared with the ground state. Similar difficulties in calculating "good" equilibrium geometries and, in particular, inversion barrier heights for the lowest excited states of formaldehyde have been encountered even when more extensive basis sets and CI methods have been used (11, 33, 34). The fact that there is relatively close agreement between the STO-3G calculated inversion barrier (700 $cm^{-1}$) and the experimental barrier (775.6 $cm^{-1}$) deduced from out-of-plane bending frequencies observed in the $^3A'' \leftarrow {}^1A'$ absorption spectrum of $H_2CO$ (19) must therefore be regarded as fortuitous. Nevertheless, on the basis of comparisons with the triplet thiocarbonyl halides (6, 7, 35), for which more extensive experimental data are available, the worst agreement between experiment and calculation might be expected for the molecules with the lowest barriers; $H_2CZ$ (Z = O, S). Recent results on $H_2CS$ have indicated that in our earlier study, the UHF method produced convergence to a solution dominated by a higher triplet state, possibly due to an erratic convergence of density matrices (36), and the poor agreement with experiment is likely to stem from this, as well as from the approximation used to calculate bond angles, valid only in the case of small amplitudes and small out-of-plane angles (37). We have assumed that the relative potential energies along the out-of-plane bending coordinates, calculated in the present study with a minimal basis set, can be used to give reasonable first estimates of the lowest triplet inversion frequencies in the carbonyl halides. These data are not readily obtainable from spectral measurements.

Table 4 presents the predicted eigenvalues of the out-of-plane bending vibrations of the carbonyl halide triplets, relative to the zero point levels which are assigned energies of zero. Also shown are the values of $\rho$, $b$, and $\nu_0$ which provide the best fit of the potential function, eq. [1], to the potentials calculated with the STO-3G basis set, and values of $G(0^+)$, the estimated zero-point energies. Four and five significant figures are quoted in this table only to provide estimates of the resolving power which might be required to observe inversion splittings in the $^3A'' \leftarrow {}^1A'$ near uv absorption spectra of these compounds.

TABLE 4. Triplet inversion vibrational eigenvalues for several tetraatomic carbonyl halides

| | $G$ ($cm^{-1}$) | | | |
|---|---|---|---|---|
| Level | HFCO | $Cl_2CO$ | ClFCO | $F_2CO$ |
| $0^+$ | 0 | 0 | 0 | 0 |
| $0^-$ | 0.6 | 0.0 | 0.0 | 0.0 |
| $1^+$ | 988 | 607.9 | 755.0 | 919.1 |
| $1^-$ | 1017 | 607.9 | 755.0 | 919.1 |
| $2^+$ | 1689 | 1185.2 | 1483.9 | 1806.6 |
| $2^-$ | 1962 | 1185.3 | 1483.9 | 1806.6 |
| $3^+$ | 2479 | 1724.7 | 2182.3 | 2657.4 |
| $3^-$ | 3005 | 1725.1 | 2182.3 | 2657.4 |
| $\rho$ | 0.334 | 0.211 | 0.507 | 0.287 |
| $B$ | 1.575 | 3.061 | 5.820 | 4.573 |
| $\nu_0$ | 1384 $cm^{-1}$ | 974 $cm^{-1}$ | 773 $cm^{-1}$ | 1251 $cm^{-1}$ |
| $G(0)^+$ | 545.0 $cm^{-1}$ | 312.7 $cm^{-1}$ | 384.7 $cm^{-1}$ | 468.8 $cm^{-1}$ |

**Acknowledgements**

The authors wish to thank the Natural Sciences and Engineering Research Council of Canada for its continuing financial support. The authors are grateful to Drs. J. D. Goddard and D. Cluthier for their thorough checking of our earlier numerical data and for pointing out an error in the assumed geometry of thiocarbonyls used in the calculation of vibrational frequencies.

1. D. C. MOULE and A. D. WALSH. Chem. Rev. **75**, 67 (1975).
2. J. C. WEISSHAAR and C. B. MOORE. J. Chem. Phys. **70**, 5135 (1979) and references therein.
3. K. Y. TANG, P. W. FAIRCHILD, and E. K. C. LEE. J. Phys. Chem. **83**, 569 (1979) and references therein.
4. J. D. GODDARD and H. F. SCHAEFER. J. Chem. Phys. **70**, 5117 (1979) and references therein.
5. K. VASUDEVAN and F. GREIN. Int. J. Quant. Chem. **14**, 717 (1978).
6. A. KAPUR, R. P. STEER, and P. G. MEZEY. J. Chem. Phys. **69**, 968 (1978).
7. A. KAPUR, R. P. STEER, and P. G. MEZEY. J. Chem. Phys. **70**, 745 (1979).
8. A. KAPUR, R. P. STEER, and P. G. MEZEY. J. Chem. Phys. **71**, 5022 (1979).
9. H. OBERHAMMER and J. E. BOGGS. J. Mol. Struct. **55**, 283 (1979).
10. P. PULAY. Theor. Chim. Acta, Berlin, **50**, 299 (1979).
11. R. DITCHFIELD, J. E. DEL BENE, and J. A. POPLE. J. Am. Chem. Soc. **94**, 4806 (1972).
12. J. E. DEL BENE, G. T. WORTH, F. T. MARCHESE, and M. E. CONRAD. Theor. Chim. Acta, Berlin, **36**, 195 (1975).
13. D. A. CONDIRSTON and D. C. MOULE. Theor. Chim. Acta, Berlin, **29**, 133 (1973).
14. E. R. FARNWORTH, G. W. KING, and D. C. MOULE. Chem. Phys. **1**, 82 (1973).
15. Y. YONEZAWA and T. FUENO. Bull. Chem. Soc. Jpn. **48**, 22 (1975).
16. R. ZAHRADNIK and J. LESKA Collect. Czech. Chem. Commun, **42**, 2060 (1977).

17. W. J. HEHRE, W. A. LATHAN, R. DITCHFIELD, J. A. POPLE, and M. D. NEWTON. Quantum Chemistry Program Exchange, Program 236. Indiana University, Bloomington, IN.
18. J. B. COON, N. W. NAUGLE, and R. D. MCKENZIE. J. Mol. Spectrosc. **20**, 107 (1966).
19. V. T. JONES and J. B. COON. J. Mol. Spectrosc. **31**, 137 (1969).
20. E. B. WILSON, JR., J. C. DECIUS, and P. C. CROSS. Molecular vibrations. McGraw-Hill, New York. 1955.
21. A. KAPUR, P. G. MEZEY, and R. P. STEER. Chem. Phys. Lett. **78**, 81 (1981).
22. K. TAKAGI and T. OKA. J. Phys. Soc. Jpn. **18**, 1174 (1963).
23. J. L. DUNCAN. Mol. Phys. **28**, 1177 (1974).
24. R. F. MILLER and R. F. CURL. J. Chem. Phys. **34**, 1847 (1961).
25. K. KUCHITSU. Seventh Austin Symposium on Molecular Structure, Austin, TX. 1978.
26. H. OBERHAMMER. J. Chem. Phys. **73**, 4310 (1980).
27. J. H. CARPENTER. J. Mol. Spectrosc. **50**, 182 (1974).
28. K. KUCHITSU. Molecular structure and vibrations. *Edited by* S. J. Cyvin. Elsevier, Amsterdam. 1972.
29. A. D. WALSH. J. Chem. Soc. 858 (1956).
30. G. FISCHER and Y. SOREK. J. Mol. Spectrosc. **74**, 136 (1979).
31. D. C. MOULE and P. D. FOO. J. Chem. Phys. **55**, 1262 (1971).
32. G. L. WORKMAN and A. B. F. DUNCAN. J. Chem. Phys. **52**, 3204 (1970).
33. S. BELL. Mol. Phys. **37**, 255 (1979).
34. W. MEYER and P. PULAY. Theor. Chim. Acta, Berlin, **32**, 253 (1974).
35. R. P. STEER. Rev. Chem. Intermed. **4**, 1 (1981).
36. P. G. MEZEY, O. P. STRAUSZ, and R. K. GOSAVI. J. Comput. Chem. **1**, 178 (1980).
37. J. D. GODDARD. Private communication.

Can. J. Chem. Downloaded from www.nrcresearchpress.com by 210.87.254.40 on 09/06/12
For personal use only.

# Charge distributions and chemical effects. XXVI. Relationships between nuclear magnetic resonance shifts and atomic charges for $^{17}O$ nuclei in ethers and carbonyl compounds

MARIE-THÉRÈSE BÉRALDIN, EDOUARD VAUTHIER,[1] AND SÁNDOR FLISZÁR

*Department of Chemistry, Université de Montréal, Montreal, P.Q., Canada H3C 3V1*

Received May 21, 1981

MARIE-THÉRÈSE BÉRALDIN, EDOUARD VAUTHIER, and SÁNDOR FLISZÁR. Can. J. Chem. **60**, 106 (1982).

The $^{17}O$ nuclear magnetic resonance shifts of dialkylethers are linearly related to the electron populations on the oxygen atoms, in a range covering L ~ 130 ppm, showing that any increase of electronic charge at the oxygen atom is accompanied by a downfield nmr shift. The opposite trend is observed for the oxygen atoms of ketones and aldehydes.

MARIE-THÉRÈSE BÉRALDIN, EDOUARD VAUTHIER et SÁNDOR FLISZÁR. Can. J. Chem. **60**, 106 (1982).

Les déplacements chimiques des noyaux $^{17}O$ dans les éthers aliphatiques sont linéairement reliés aux populations électroniques des atomes d'oxygène, dans un domaine couvrant L ~ 130 ppm, toute augmentation de population électronique se manifestant par un déplacement vers les champs faibles. L'effet opposé est observé pour l'oxygène des cétones et des aldéhydes.

Can. J. Chem. Downloaded from www.nrcresearchpress.com by 210.87.254.40 on 09/06/12
For personal use only.

## Introduction

Our prime interest in correlations between nuclear magnetic resonance shifts and atomic electron populations originates in the need for practical means enabling the evaluation of atomic charges. The latter play, indeed, an essential role in a number of problems concerning charge-dependent molecular properties, such as thermochemical stabilities (1). Therefore, the theoretical calculation of atomic charges being usually difficult and costly in large systems of chemical interest, while chemical shifts are more readily accessible from experiment, it is felt that some detailed knowledge about charge/shift trends is desirable, despite the fact that the significance or generality of such empirical correlations is not known.

Any attempt at correlating nuclear magnetic resonance shifts with electron populations implies two basic assumptions, namely, (*i*) that one of the major factors governing the shielding of a specific nucleus is its local electron density and (*ii*) that the theoretical method selected for the charge analysis is capable of giving correct results.

Both assumptions are, to a certain extent, empirically justified by simple charge/shift relationships which are verified in a number of occasions (mainly for $^{13}C$ nuclei) in series of closely related compounds. Any additional verification, like the one presented here for $^{17}O$ nuclei in aliphatic ethers, is made with the reservation that results of this sort should not be used to lend unintended support for the unwarranted view that they are necessarily valid in all systems. Of course the validity of any correlation between experimental chemical shifts and calculated atomic charges clearly depends on the validity of the theoretical charge analysis. Interestingly enough, little consideration is usually given to the latter point and a number of different theoretical methods, both semi-empirical and *ab initio*, are used almost indiscriminately for calculating atomic charges for use in charge/shift correlations. A few basic aspects pertaining to this problem are briefly examined as follows.

## Population analysis

Atomic charges are calculated following Mulliken's analysis (2) assuming, however, a more general mode of distributing overlap populations in heteropolar situations. The net (i.e., nuclear minus electronic) charge $q_k$ of atom $k$ is then

$$[2] \quad q_k = q_k^{\text{Mulliken}} + \sum_{l \neq k} p_{kl}$$

where $\sum_{l \neq k} p_{kl}$ is the correction resulting from the departure from the usual halving of the overlap terms (3–5). The overlap populations involving specified $kl$ atom pairs under comparable situations being practically the same in series of closely related compounds, a valid approximation (at least in $\sigma$ systems) is obtained by assuming a constant $p_{kl}$ term for each type of $kl$ bond formed by atom $k$ (4,

[1]Visiting Scientist, on temporary leave from the "Service de Spectroscopie Moléculaire en Milieu Condensé, Laboratoire de Recherches Physiques associé au CNRS, Université Pierre et Marie Curie", Paris. We thank the Authorities of the "France-Québec Exchange Program" who made this cooperation possible.

0008-4042/82/020106-05$01.00/0

©1982 National Research Council of Canada/Conseil national de recherches du Canada

Can. J. Chem. Downloaded from www.nrcresearchpress.com by 210.87.254.40 on 09/06/12
For personal use only.

5).[2] Consequently, anytime $k$ is engaged in the same binding (e.g., in the comparison of the ethane carbon with that of any other $CH_3$ group attached to a $sp^3$ carbon) we apply the same $\sum_{l \neq k} p_{kl}$ correction and find $\Delta q_k = \Delta q_k{}^{\text{Mulliken}}$. This is, namely, the case in the calculation of charge increments in comparisons involving ether oxygens, for which we use $\Delta q_o = \Delta q_o{}^{\text{Mulliken}}$.

Regarding the quality of the wave functions, it has appeared that both semi-empirical and *ab initio* methods yield charge analyses describing a number of relevant trends in quite similar and consistent fashion, despite the fact that numerically the calculated charges differ, sometimes considerably, from method to method. Detailed comparisons of this sort were presented earlier (6, 7), showing that the most consistent results are obtained from STO-3G calculations involving full optimization of all variational parameters. In this way, detailed and subtle structure-related charge effects were recognized in saturated and ethylenic hydrocarbons (5, 8). On the other hand, lack of full geometry and $\zeta$ exponent optimization does not usually prevent the, somewhat less precise, reproduction of the major trends. In short, STO-3G wave functions appear to be quite adequate for deducing consistent atomic charges, permitting valid comparisons, although they are by no means unique in that respect (4–6).

## Results

The STO-3G calculations were carried out following Pople's recipe, with $r_{CH} = 1.09$, $r_{CC} = 1.54$, $r_{CO} = 1.43$ Å and all angles set at 109.47122° (9), using standard $\zeta$ scale factors, i.e., 5.67 (C1s), 1.79 (C2$s$2$p$), 7.66 (O1$s$), 2.24 (O2$s$2$p$), and 1.18 (H), as determined by Hehre and Pople (10). The Mulliken population analyses are indicated in Table 1.

The net $[Z_k - N(k)]$ atomic charges $q_o$ on the oxygen atoms clearly indicate a build-up of electronic charge with increasing electron-releasing ability of the substituents, reflecting the customary inductive effects. A comparison of the ionisation potentials[3] with the oxygen net charges yields a correlation, IP = $0.0274q_o$ + 18.16 eV (with an average error of 0.040 eV and a correlation coefficient of 0.9914), which reflects the expectation that electron withdrawal becomes easier as the oxygen atom becomes electron-richer. This result is worth mentioning because it illustrates a physical aspect linked to the ordering of the oxygen charges given by Mulliken's analysis, in full agreement with all known aspects related to the inductive effects of alkyl groups. In short, it can be assumed with confidence that the oxygen atom in, say, di-*tert*-butylether is electron-richer than that of dimethylether. This confidence is important in the following comparisons involving $^{17}O$ nuclear magnetic resonance shifts (Table 2, Fig. 1).

These results indicate that *in aliphatic ethers, any gain in electronic charge at the oxygen atom is accompanied by a downfield $^{17}O$ nmr shift*. At variance with the commonly held view that any increase in local electron population should bring about a shielding of the nucleus in question and, hence, an upfield shift, this result is the clear echo of a conclusion reached earlier (4, 5, 13), namely, that *in aliphatic and in six-membered (chair and boat) cycloalkanes any gain in electronic charge at an* $sp^3$ *carbon atom is accompanied by a downfield $^{13}C$ nmr shift*. However, contrary to the case of the ether oxygen atoms, whose charge increments $\Delta q_o$ are directly given by differences in Mulliken atomic populations, for carbon atoms use is made of eq. [1]. At this point it is important to stress that this type of analysis for carbon does *not* introduce any artifact which could be held responsible for the conclusion reached above. Indeed, the same conclusion follows from a comparison involving only $CH_3$ carbon atoms and the corresponding Mulliken populations, because the $\sum p_{kl}$ terms of primary carbons cancel in the calculation of the charge increments $\Delta q_c$ relative to ethane.[4]

It is also important to stress that the shift/charge trends exhibited by the ether oxygen and the $sp^3$ carbon atoms are by no means generally valid. Indeed, using exactly the same charge analysis (eq.

[2]For saturated hydrocarbons, it follows, in this approximation, that $q_H = q_H{}^{\text{Mulliken}} - p_{CH}$ and $q_c = q_c{}^{\text{Mulliken}} + N_{CH}p_{CH}$, where $N_{CH}$ is the number of hydrogen atoms bonded to C. This example shows that if $p_{CH}$ is the error introduced with one CH bond by halving all overlap populations, then the total correction required in calculating $q_c$ simply depends on the number of CH bonds formed by that particular carbon atom.

[3]The ionization potentials (11) used in this comparison are 10.00 (dimethylether), 9.53 (diethylether), 9.27 (di-*n*-propylether), and 9.20 eV (diisopropylether).

[4]For example, the $CH_3$ carbon of diisopropylether (δ 23 ppm from TMS) has a Mulliken net charge of ~ −30.9 me, whereas the primary carbon in diethylether has a Mulliken charge of ~ −28.3 me with δ 15.4 ppm from TMS. These charges were obtained from one cycle of optimizations involving the geometries and the scale factors. While these charges are not true optimum values, they clearly reflect a downfield shift with increasing electron population, as described earlier (4, 5, 13) for $sp^3$ carbon atoms. Indeed, the $CH_3$-carbon net charges obtained from fully optimized STO-3G calculations using Mulliken's population analysis are −20.96 me (δ 5.8 ppm from TMS) for ethane, −23.81 (δ 15.6) for propane, −26.39 (δ 24.3) for isobutane, and −28.66 me (δ 31.5) for neopentane (5).

Can. J. Chem. Downloaded from www.nrcresearchpress.com by 210.87.254.40 on 09/06/12
For personal use only.

TABLE 1. Orbital populations of the oxygen atoms in dialkylethers, showing that the changes in net charges occur at the 2*p* level

| Molecule | Orbital population (electron) | | | | |
|---|---|---|---|---|---|
| | 1*s* | 2*s* | $2p_x$ | $2p_y$ | $2p_z$ |
| $CH_3$—O—$CH_3$ | 1.99789 | 1.83322 | 1.95064 | 1.05848 | 1.45684 |
| $CH_3$—O—$C_2H_5$ | 1.99790 | 1.83327 | 1.95069 | 1.06457 | 1.45960 |
| $CH_3$—O—$iC_3H_7$ | 1.99790 | 1.83448 | 1.95088 | 1.06533 | 1.46467 |
| $CH_3$—O—$tC_4H_9$ | 1.99789 | 1.83398 | 1.95065 | 1.06834 | 1.46575 |
| $C_2H_5$—O—$C_2H_5$ | 1.99790 | 1.83322 | 1.95074 | 1.07078 | 1.46213 |
| $C_2H_5$—O—$iC_3H_7$ | 1.99790 | 1.83446 | 1.95087 | 1.07153 | 1.46672 |
| $C_2H_5$—O—$tC_4H_9$ | 1.99790 | 1.83401 | 1.95064 | 1.07465 | 1.46808 |
| $iC_3H_7$—O—$iC_3H_7$ | 1.99790 | 1.83435 | 1.95012 | 1.07520 | 1.47250 |
| $iC_3H_7$—O—$tC_4H_9$ | 1.99790 | 1.83388 | 1.94995 | 1.07828 | 1.47336 |
| $tC_4H_9$—O—$tC_4H_9$ | 1.99789 | 1.83387 | 1.94943 | 1.07564 | 1.47729 |

TABLE 2. $^{17}O$ nmr shifts and net atomic charges of ether oxygen atoms*

| | Molecule | $\delta_0$ | $q_0$ (me) |
|---|---|---|---|
| **1** | $(CH_3)_2O$ | −52.5 | −297.1 |
| **2** | $CH_3$—O—$C_2H_5$ | −22.5 | −306.0 |
| **3** | $CH_3$—O—$iC_3H_7$ | −2.0 | −313.3 |
| **4** | $CH_3$—O—$tC_4H_9$ | 8.5 | −316.6 |
| **5** | $(C_2H_5)_2O$ | 6.5 | −314.9 |
| **6** | $C_2H_5$—O—$tC_4H_9$ | 40.5 | −325.3 |
| **7** | $(iC_3H_7)_2O$ | 52.5 | −330.1 |
| **8** | $iC_3H_7$—O—$tC_4H_9$ | 62.5 | −333.4 |
| **9** | $(tC_4H_9)_2O$ | 76.0 | −334.1 |

*The chemical shifts (ppm from water) are extracted from ref. 12. The numbering corresponds to the points in Fig. 1.

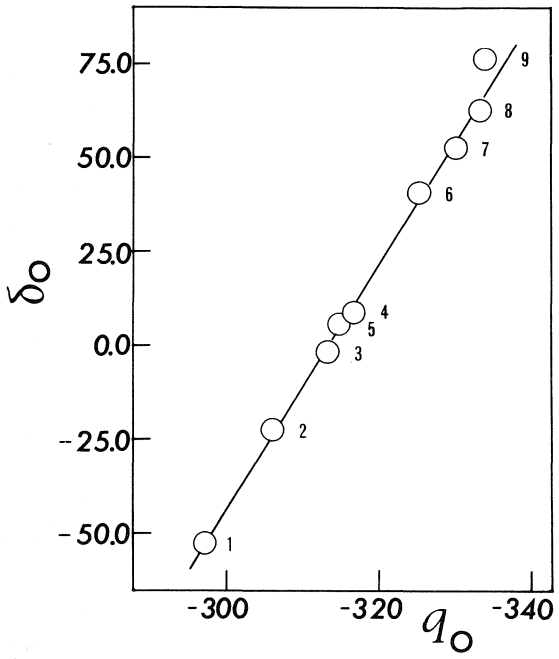


FIG. 1. Comparison of ether $^{17}O$ nmr shifts (ppm) with net atomic charges (me).

[1]) as for the $sp^3$ carbon atoms, it was shown for a series of ethylenic compounds that *any gain in electronic charge at* $sp^2$ *carbon atoms is accompanied by an upfield nmr shift* (8). An examination of results obtained for selected aldehydes and ketones now reveals that *an electron enrichment at carbonyl oxygen atoms is accompanied by an upfield* $^{17}O$ *nmr shift* (Table 3), just as it is the case for $sp^2$ carbon atoms. However, because of the narrow range of $\Delta q_0$ variations, lack of precision (~1–2 me) accompanying standard STO-3G calculations makes it difficult to assess how accurately carbonyl-$^{17}O$ nmr shifts and charges are related to one another. Interestingly, the comparison of the carbonyl-$^{13}C$ nmr shifts with net charges (Fig. 2) indicates the same trend as that observed for $sp^3$ carbon atoms in paraffins, namely, a highfield shift with increasing positive net charge.

While these charge/shift correlations clearly illustrate what is understood by the reservation that results obtained for a given nucleus in a well-defined series of compounds should not be unduly generalized; it also appears that, under proper circumstances, chemical shifts are capable of giving in a simple manner useful information about

TABLE 3. Carbonyl $^{17}O$ and $^{13}C$ nmr shifts and net charges for selected aldehydes and ketones*

| | Molecule | $\delta_0$ | $q_0$ (me) | $\delta_c$ | $q_c$ (me) |
|---|---|---|---|---|---|
| | $CH_3CHO$ | 592.0 | −228.9 | 199.6 | 211.6 |
| | $C_2H_5CHO$ | 579.5 | −229.6 | 202.4 | 204.2 |
| | $iC_3H_7CHO$ | 574.5 | −230.1 | 204.3 | 197.9 |
| **1** | $(CH_3)_2CO$ | 569.0 | −266.7 | 204.9 | 259.7 |
| **2** | $CH_3COC_2H_5$ | 557.5 | −269.5 | 207.0 | 253.6 |
| **3** | $CH_3COiC_3H_7$ | 557.0 | −268.1 | 210.0 | 244.9 |
| **4** | $(C_2H_5)_2CO$ | 547.0 | −272.1 | 209.4 | 247.4 |
| **5** | $C_2H_5COiC_3H_7$ | 543.5 | −270.7 | 212.3 | 238.8 |
| **6** | $(iC_3H_7)_2CO$ | 535±1 | −273.8 | 215.5 | 233.8 |

*The nmr shifts of oxygen (ppm from water) and carbon (ppm from TMS) are extracted from ref. 14. The numbering corresponds to the points in Fig. 2.

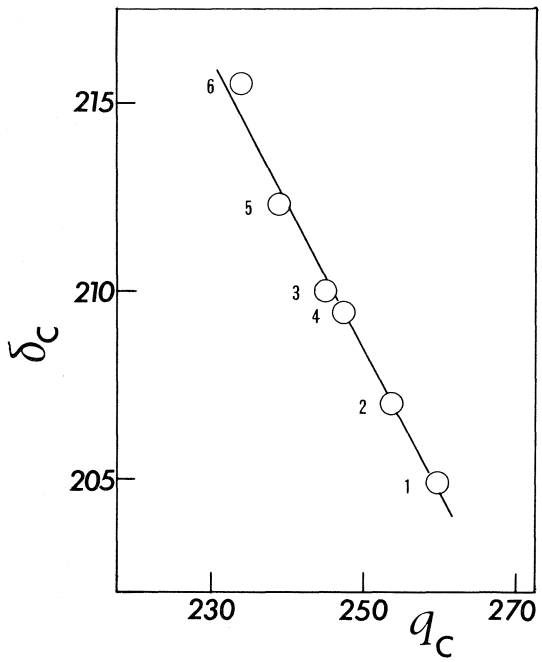


FIG. 2. Comparison of ketone carbonyl – $^{13}C$ nmr shifts (ppm) with net atomic charges (me).

local charges. The use of shift-derived atomic charges of $sp^3$ carbon atoms in the study of charge-dependent thermodynamic properties (1) has met with success, reflected by the accuracy of the calculations in comparisons with experimental results. For future use in the calculation of the enthalpies of formation (and related quantities) of oxygen-containing compounds, we shall now examine more closely the results obtained for the ethers.

In the first place, it is clear that the trends in electron populations at the ROR′ ether oxygen atoms reflect the electron releasing (or withdrawing) abilities of the R,R′ alkyl groups, just as it is the case with the methylene carbons in $RCH_2R'$ hydrocarbons. Since for the ether oxygen and the $sp^3$ carbon atoms it now appears that chemical shifts and atomic charges are linearly related to one another, it follows that the $^{17}O$ nmr shifts of the ROR′ ethers are expected to correlate with the methylene $^{13}C$ shifts of the corresponding $RCH_2R'$ hydrocarbons. This is, indeed, the case, as demonstrated convincingly by Delseth and Kintzinger (12). Moreover, similar correlations (12) between the $^{13}C$ shifts of the carbon atoms in ROR′ ethers and those of the "parent" $RCH_2R'$ hydrocarbons clearly reflect the close correspondence in the structure related effects which govern electron distributions indicating, namely, that the individual C atoms of the alkyl part of the ethers behave quite like hydrocarbon C atoms.

Now, for $sp^3$ carbon atoms, the equation

$$[2] \quad \delta_c = -(237.1/q_c^\circ)\Delta q_c$$

relating their nmr shifts (relative to ethane) to their charge increments (relative to the ethane-C net charge $q_c^\circ$) is accurate in a range of ~40 ppm (at least), with a standard deviation of ~0.3 ppm (4, 5, 13). The charges used in deriving eq. [2] were deduced by means of eq. [1] on the basis of fully optimized STO-3G calculations.[5] In order to deduce an expression for $^{17}O$ nuclei on the same footing as eq. [2], we have carried out an extensive geometry and exponent optimization for the dimethyl-, diethyl-, and diisopropyl-ethers. Although it has appeared that one cycle of optimization is not sufficient for obtaining stable charges for the carbon and hydrogen atoms, which are particularly sensitive to small errors in $\zeta$ exponents, it has also appeared that this type of imperfection in the C and H exponents has little effect on the oxygen charges provided, of course, that the oxygen exponents are properly optimized. Under these conditions, the oxygen STO-3G Mulliken charges of dimethylether (−267 me), diethylether (−295 me), and diisopropylether (−322 me) indicate that the $\delta_o$ vs. $q_o$ slope is ~1/1.8 that of the corresponding $\delta_c$ vs. $q_c$ slope, obtained from the same basis set, *i.e.*

$$\Delta\delta_o/\Delta q_o \simeq (\Delta\delta_c/\Delta q_c)/1.8$$

Consequently, using now the $q_c^\circ = 35.1$ me value determined earlier (1*a*), we obtain from eq. [2] that

$$[3] \quad \Delta q_c = -0.148\delta_c \text{ (me)}$$

$$[4] \quad \Delta q_o = -0.267\delta_o \text{ (me)}$$

These relationships now enable a rapid estimate of atomic charges on the scale which has proven

[5]The validity of eq. [2] does not depend upon the particular choice of the theoretical method selected for calculating charges, since $\Delta q_c/q_c^\circ$ is dimensionless. The $q_c^\circ$ and $\Delta q_c$ values, however, depend on the quality of the wave functions. Fully optimized STO-3G calculations give $q_c^\circ = 69.40$ me (5–7) and larger basis sets lead to a lowering of this value, e.g. 60.0 me (7*s*3*p*/3*s*) and 58 me (6–31G), while the optimum value appears to be 35.1 me (1*a*). Similarly, the $p_{CH}$ value also depends on the quality of the basis set and is, for STO-3G calculations involving full optimization of all variational parameters, $p_{CH} = 30.12$ me (from $^{13}C$ nmr shifts), 30.3 ± 0.3 me (from energies of atomization), and ~ 30.15 invoking the postulate that the carbon net charges in saturated hydrocarbons differ as little as possible from one another (4–6). Finally eq. [2] can be applied directly using SCF-Xα-SW electron populations which are *not* a product of Mulliken's scheme for calculating charges (15).

Can. J. Chem. Downloaded from www.nrcresearchpress.com by 210.87.254.40 on 09/06/12
For personal use only.

Can. J. Chem. Downloaded from www.nrcresearchpress.com by 210.87.254.40 on 09/06/12
For personal use only.

satisfactory for deriving accurately charge-dependent molecular properties involving $sp^3$ carbon atoms. Applications to the study of thermodynamic properties of ethers are presented in a forthcoming paper, along the lines which have led to accurate calculations of saturated hydrocarbons (1*a*).

The physical reasons underlying the observed charge–shift correlations can be roughly described as follows. Extensive gauge invariant calculations of chemical shifts indicate that for atoms other than hydrogen one can safely neglect the three-center integrals (16), meaning that the shielding is mainly governed by "local" charges. It also appears that the variations in local diamagnetic contributions to the total shielding are, indeed, minor and that the major variations are associated with the paramagnetic contributions which reflect most of the "local" charge effect. Specifically, any increase in electron population is accompanied by a more negative paramagnetic contribution, which is a deshielding effect (17). This general behavior is well illustrated by the $sp^3$ carbon atoms (where the variations in charge occur mainly at the 2*s* level) and the ether oxygens (where the main variations occur at the 2*p* level). Present results suggest that the effect of varying the population at the 2*p* level is significantly less pronounced than that of changing the population at the 2*s* level, as regards the accompanying variations in chemical shifts. This observation possibly explains the fact that for vinylic carbon and carbonyl oxygen atoms an increase in total electronic charge is reflected in a highfield shift. In these cases, indeed, $\sigma$ and $\pi$ electron populations vary in an inverse manner (8, 17, 18) so that an increase in $\pi$ population results in a deshielding accompanied by an inverse effect due to the decrease in $\sigma$ population. The effect of the latter being more pronounced results eventually in a highfield shift although the loss in $\sigma$ population is not quite as important as the gain in $\pi$ population, for a total gain in $(\sigma + \pi)$ electron population. A detailed numerical analysis based on theoretical shift calculations is presented elsewhere (17).

## Conclusions

In aliphatic ethers, any gain in electronic charge at the oxygen atom is accompanied by a downfield $^{17}O$ nmr shift, while the opposite trend is observed with carbonyl oxygen atoms. The general behavior of the ether oxygen atoms is thus similar to that of $sp^3$ carbons whereas carbonyl oxygen atoms exhibit the same trends as $sp^2$ carbon atoms. While these results show that any evaluation of charge/shift trends should be confined to series of closely related compounds, it also appears that the ether $^{17}O$ nmr shifts are linearly related to local electron populations. The $\Delta q_o/\Delta\delta_o$ slope is $\sim 1.8$ times that of $\Delta q_c/\Delta\delta_c$ for $sp^3$ carbon atoms. The discussion of these trends in terms of Mulliken population analyses shows that they are not an artifact due to a particular mode of partitioning overlap population terms.

## Acknowledgements

We express our gratitude to le "Centre de Calcul de l'Université de Montréal" for generous computer time made available and to the National Research Council of Canada for financial assistance.

1. (*a*) S. Fliszár. J. Am. Chem. Soc. **102**, 6946 (1980); (*b*) S. Fliszár and J.-L. Cantara. Can. J. Chem. **59**, 1381 (1981); (*c*) H. Henry, G. Kean, and S. Fliszár. J. Am. Chem. Soc. **99**, 5889 (1977); (*d*) H. Henry, S. Fliszár, and A. Julg. Can. J. Chem. **54**, 2085 (1976).
2. R. S. Mulliken. J. Chem. Phys. **23**, 1833 (1955); **23**, 1841 (1955); **23**, 2338 (1955); **23**, 2343 (1955).
3. V. H. Smith. Phys. Scripta, **15**, 147 (1977); A. Julg. Top. Curr. Chem. **58**, 1 (1975).
4. S. Fliszár, A. Goursot, and H. Dugas. J. Am. Chem. Soc. **96**, 4358 (1974).
5. S. Fliszár. Can. J. Chem. **54**, 2839 (1976).
6. S. Fliszár, G. Kean, and R. Macaulay. J. Am. Chem. Soc. **96**, 4353 (1974).
7. G. Kean and S. Fliszár. Can. J. Chem. **52**, 2772 (1974).
8. H. Henry and S. Fliszár. J. Am. Chem. Soc. **100**, 3312 (1978).
9. W. J. Hehre, R. F. Stewart, and J. A. Pople. J. Chem. Phys. **51**, 2657 (1969).
10. W. J. Hehre and J. A. Pople. J. Am. Chem. Soc. **92**, 2191 (1970).
11. K. Watanabe, T. Nakayama, and J. Mottl. J. Quant. Spectrosc. Rad. Transfer, **2**, 369 (1962).
12. C. Delseth and J.-P. Kintzinger. Helv. Chim. Acta, **61**, 1327 (1978).
13. G. Kean, D. Gravel, and S. Fliszár. J. Am. Chem. Soc. **98**, 4749 (1976); R. Roberge and S. Fliszár. Can. J. Chem. **53**, 2400 (1975).
14. C. Delseth and J.-P. Kintzinger. Helv. Chim. Acta, **59**, 466 (1976); Erratum Helv. Chim. Acta, **59**, 1411 (1976).
15. A. E. Foti, V. H. Smith, and S. Fliszár. J. Mol. Struct. **68**, 227 (1980).
16. E. Vauthier, F. Tonnard, and S. Odiot. To be published.
17. E. Vauthier, F. Tonnard, S. Odiot, and S. Fliszár. To be published.
18. W. J. Hehre, R. W. Taft, and R. D. Topsom. Progr. Phys. Org. Chem. **12**, 159 (1976).

# Modified phosphotriester method for chemical synthesis of ribooligonucleotides. Part I. Synthesis of riboundecaadenylate and two fragments constituting the sequence of R-17 translation control signal

WING L. SUNG AND SARAN A. NARANG

*Division of Biological Sciences,[1] National Research Council of Canada, Ottawa, Ont., Canada K1A 0R6*

Received August 4, 1981

WING L. SUNG and SARAN A. NARANG. Can. J. Chem. **60**, 111 (1982).

A modified phosphotriester method has been successfully applied for the chemical synthesis of ribooligonucleotides. The starting material is a fully protected ribomononucleoside containing a 3′-phosphotriester group **5**. The coupling reaction is performed using mesitylenesulfonyl tetrazole and purification of the product achieved using reversed phase column chromatography. The effectiveness of this method has been demonstrated by achieving an efficient and rapid synthesis of r-$A_7$, r-$A_{11}$, r5′-AAACAUGAGGA-3′, and r5′-UUACCCAUGU-3′ (R-17, translation control sequence).

WING L. SUNG et SARAN A. NARANG. Can. J. Chem. **60**, 111 (1982).

On a appliqué avec succès une méthode de phosphotriester modifié à la synthèse chimique des ribooligonucléotides. On utilise comme produit de départ un ribonucléoside entièrement protégé contenant un groupe phosphotriester en position 3′(**5**). On a réalisé le couplage en utilisant le mésitylène sulfonyle tétrazole et on a purifié le produit par chromatographie sur colonne en phase inversée. On démontre l'efficacité de cette méthode en réalisant une synthèse rapide et efficace du r-$A_7$, r-$A_{11}$, r5′-AAACAUGAGGA-3′ et du r5′-UUACCCAUGU-3′ (R-17, unité de contrôle de translation).

[Traduit par le journal]

## Introduction

The availability of ribooligonucleotides of well-defined sequence is of great importance in the biological studies of various RNA-regulatory signals, understanding the splicing mechanism of introns and the synthesis of biologically active RNA molecules such as t-RNA or 5S RNA. The recent discovery that $T_4$-RNA ligase enzyme (1) can join small fragments of RNA end to end without their complementary strand offers an additional impetus for the development of an efficient and rapid method of chemical synthesis. In spite of these incentives, progress in chemical synthesis of ribooligonucleotides has lagged behind deoxy synthesis (2). Although the phosphodiester approach was successfully applied by Khorana and coworkers (3) to synthesize all 64 triplet RNA codons, its application to the synthesis of longer sequences is quite laborious (4). Even use of the phosphotriester approach (5), the phosphite modification (6), or solid phase techniques (7) have only very recently proved capable of synthesizing defined sequences of oligoribonucleotides (8–11) with length of 9–16 units, that are of biological interest.

The main difficulty is the presence of an additional 2′-hydroxyl group, the protection of which presents the most critical problems at all stages of ribooligonucleotide synthesis. At the monomer stage, specificity between the 2′- and 3′-hydroxyls must be achieved; any protecting group must be stable enough to remain intact throughout an extended synthesis yet be complementary in its chemical behaviour, i.e. for selective removal to other protecting groups. Increasingly effective phosphorylation/condensation conditions involving the 3′-hydroxyl must be devised to overcome the additional steric hindrance from the protected 2′-hydroxyl group. Finally deprotection must occur under conditions which prevent any 3′ to 2′ migration of the internucleotidic phosphodiester linkages. The most commonly utilized 2′-hydroxyl protecting groups are substituted tetrahydropyran (9) and *O*-nitrobenzyl (12), but their introduction requires multiple chemical steps, whereas *tert*-butyldimethyl silyl (TBDMS), a bulkier protecting group, has been employed by Ogilvie *et al* (13). The main advantages of this protecting group are its ease of protecting the 2′-hydroxyl function and also stability towards acidic and basic conditions in order to avoid migration and cleavage of 3′ → 5′ phosphodiester linkages.

In this study we present a practical solution to the ribopolynucleotide synthesis by employing the modified phosphotriester approach (14) developed in our laboratory for the deoxy series. The basic feature of our approach is to start the synthesis of an oligonucleotide from the fully protected ribomononucleoside containing the 3′-phosphotriester group **5**. Since each intermediate oligonucleotide synthesized thus contained the fully masked 3′-phosphate group, the necessity for a phosphorylation step at each condensation stage was eliminated.

[1]NRCC No. 19384.

0008-4042/82/020111-10$01.00/0

©1982 National Research Council of Canada/Conseil national de recherches du Canada

Rapid condensations and simple chromatographic purification of intermediates make this approach comparable in speed to polymer support or phosphite techniques with additional advantages of simplicity in handling the large-scale synthesis. In this paper we wish to demonstrate its application in the efficient synthesis of r-$A_7$, r-$A_{11}$, r-AAACAUGAGGA, and r-UUAACCAUGU fragments. The heterosequence fragments constitute a natural sequence of the R-17 translation control signal (15) (Fig. 1). The sequence of each synthetic fragment has been analyzed by the mobility shift method (16) and the radioaudiograms are shown in Fig. 5.

## Discussion

### *Large-scale preparation of fully protected ribomononucleoside 3′-phosphotriester* 5

In our present studies we chose the *tert*-butyldimethyl silyl protecting group (TBDMS) for the 2′-hydroxyl which was easily prepared by treating **1** with *tert*-butyldimethyl silyl chloride and imidazole (13); a mixture of 2′- and 3′-monoprotected isomers was produced. Previously, these isomers were purified by preparative thin layer chromatography (13) which would not be suitable for any large-scale synthesis because of economic and time factors. We have effectively solved this problem using short silica gel column chromatography to collect a pure fraction containing the faster moving 2′-protected isomer. The remaining mixture was eluted from the column and further equilibrated to a mixture of 2′- and 3′-isomers with triethylamine–methanol. On subsequent chromatography, more of the pure 2′-protected isomer was isolated. Repetition of this sequence three times produced pure 2′-protected isomer (25–30 g, 45–64% isolated yield) in less than 7 h. The general method of preparation is outlined in Fig. 2.

The presence of *tert*-butyldimethyl silyl, a bulkier protecting group, at the 2′-position makes the 3′-hydroxyl function less accessible to the phosphorylation reaction due to steric hindrance. Consequently, phosphorylation with *p*-chlorophenyl phosphoryl ditriazolide (17) in dioxane with a stoichiometric amount of triethylamine was found to be slow (overnight) and migration of the 2′-protecting group to the 3′-hydroxyl was also observed under these conditions, possibly due to the presence of residual triethylamine. Obviously, a more powerful phosphorylating reagent was required to phosphorylate the 3′-position quantitatively in a minimum time period to avoid possible migration of the 2′-silyl protecting group. We next attempted phosphorylation with *p*-chlorophenyl phosphoryl ditetrazolide (Fig. 3). As expected, the phosphorylation reaction was over in less than 5 min without any migration and on subsequent addition of β-

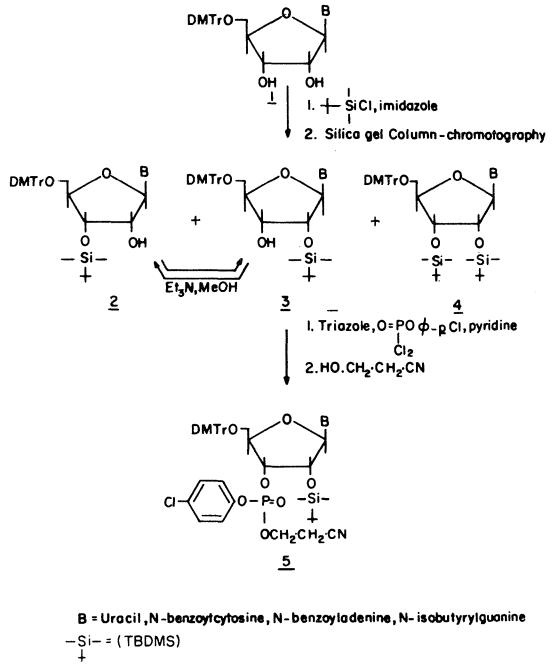


FIG. 2. General method of preparation of fully protected ribomononucleoside containing 3′-phosphotriester group.

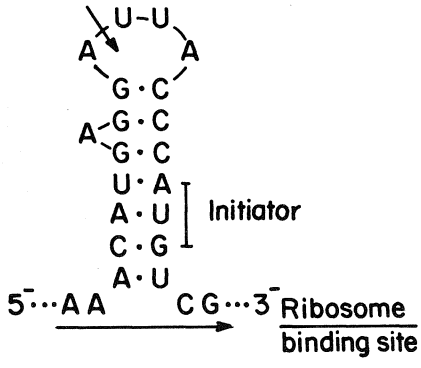


FIG. 1. Sequence of R-17 translational control region.

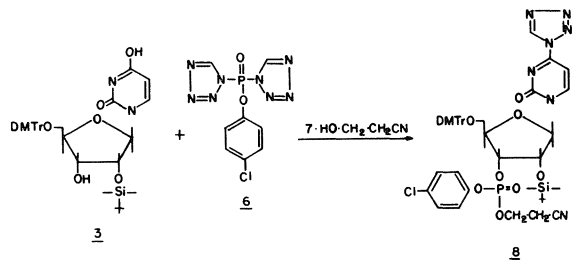


FIG. 3. Modification of uridine moiety.

cyanoethanol, a fully protected ribomononucleotide was prepared and isolated by short silica gel column chromatography in about 70–80% yield. However, in the case of 5′,2′-protected uridine, we observed an unexpected maxima of 324 nm in uv spectra analysis in addition to the regular maximum at 259 nm. Mass spectrometric analysis by the plasma absorption technique (18) also showed an unexpected increase of 52 units in the mass value, which is equivalent to addition of a tetrazole moiety.[2] On complete deblocking the unprotected nucleotidic material had a uv spectra identical to cytidine. Obviously, *p*-chlorophenyl phosphoryl ditetrazolide reagent has introduced a tetrazole moiety at the 4-position of uridine as shown in Fig 3. Subsequently, we discovered that Reese and Ubasawa (19) have also observed a similar modification on prolonged treatment with mesitylenesulfonyl tetrazolide and diphenylphosphate. We overcame this problem by modifying our original phosphorylation procedure by treating 5′-dimethoxytrityl ribomononucleoside 2′-*tert*-butyldimethyl silyl protected compound **3** with *p*-chlorophenyl phosphodichloridate in the presence of excess triazole in pyridine[3] solution *in situ*. Under these conditions, the phosphorylation reaction at the 3′-position was complete in less than 5 min and on subsequent treatment with an excess of β-cyanoethanol the fully protected desired mononucleotide **5** was prepared in 70–80% yield. Under these reaction conditions, no modification and migration were observed. Each of the four fully protected monoribonucleotides in 20–30 g amounts was easily purified on a short reversed phase silanized silica gel column and stored as a dry foamy material at 4°C.

*Modified procedure for amino group protection of cytidine*

Generally, *N*-protection in the case of cytidine, adenosine, and guanosine involves the complete acylation of all the hydroxyl as well as amino functions followed by partial deacylation with sodium hydroxide to generate *N*-protected compound. In the case of cytidine, we have developed a "one-pot" method in which the hydroxyl groups are first silylated on treatment with trimethylsilylchloride followed by the addition of benzoyl chloride *in situ* to benzoylate the amino function. The reaction mixture was decomposed with water–dichloromethane followed by evaporation *in vacuo*. The *O*-silyl groups are hydrolyzed by the benzoic acid produced *in situ* to yield a pure *N*-benzoylated cytidine in quantitative yield. Unfortunately, similar approaches to produce *N*-protected adenosine and guanosine were not successful.

*Di-isopropylamine as a more efficient reagent for the selective removal of the β-cyanoethyl group from* **5**

In our synthetic studies of deoxyribooligonucleotides, it became apparent that a most time-consuming part is the decyanoethylation of the 3′-phosphotriester group **5** on treatment with triethylamine–pyridine (20) (pyrimidine bases required 4 h and purines 2 h). Even in the case of dimer or trimer blocks, the rate of removal of the β-cyanoethyl group was dependent on the nature of the 3′-terminal base. In order to improve on this aspect we examined a variety of bases and found a more suitable base, di-isopropylamine, with $pK_a$ 11.05 compared to triethylamine ($pK_a$ 10.05) which in anhydrous pyridine removes the β-cyanoethyl group in less than 1 h in both the deoxy- and ribo-series. Under this condition, *N*-acyl and *p*-chlorophenyl at the internucleotide phosphate groups were found to be *completely intact* as checked by tlc. The results of these comparative studies are summarized in Table 1.

*Modified phosphotriester approach for oligoribonucleotide synthesis*

The basic strategy of this approach is to start the synthesis from a fully protected ribomononucleoside 3′-phosphotriester **5** as outlined in Fig. 4. The chain was elongated from the 3′- towards the 5′-end by using the 2′,3′-diTBDMS derivative as the 3′-end. Mesitylenesulfonyl tetrazole (21) was used routinely for 15 min as a coupling reagent. One of the major problems in the phosphotriester ap-

TABLE 1. Decyanoethylation of 5′-dimethoxytrityl 2′-*tert*-butyldimethyl silyl *N*-protected ribonucleoside 3′-*p*-chlorophenyl β-cyanoethyl phosphate **5** with di*iso*propylamine

| Mononucleotide[a] | Triethylamine (h) | Di*iso*propylamine (h) |
|---|---|---|
| [(MeO)$_2$]Tr-dbzA∓CE | 3 | 0.6 |
| [(MeO)$_2$]Tr-dIsoG∓CE | 2 | 0.5 |
| [(MeO)$_2$]Tr-dbzC∓CE | 4 | 0.6 |
| [(MeO)$_2$]Tr-dT∓CE | 4 | 0.6 |
| [(MeO)$_2$]Tr-rbzASi∓CE | 4 | 0.8 |
| [(MeO)$_2$]Tr-rIsoGSi∓CE | 4 | 0.6 |
| [(MeO)$_2$]Tr-rbzCSi∓CE | 4 | 0.8 |
| [(MeO)$_2$]Tr-USi∓CE | 4 | 0.8 |

[a]Concentration of mononucleotide (0.1 mmol) in an appropriate amine (0.5 mL) and pyridine (2 mL). The course of reactions was followed by tlc on silanized silica gel using acetone containing 30% water as solvent.

[2]Thanks to C. J. McNeal, Texas A & M University, for performing this experiment.

[3]Gait *et al.* (ref. 2, p. 251) have reported a variation of this reaction condition in which *p*-chlorophenyl phosphorodichloridate was mixed with anhydrous triazole in pyridine solution for 20 min separately and then treated with 5-O′-protected deoxynucleoside.

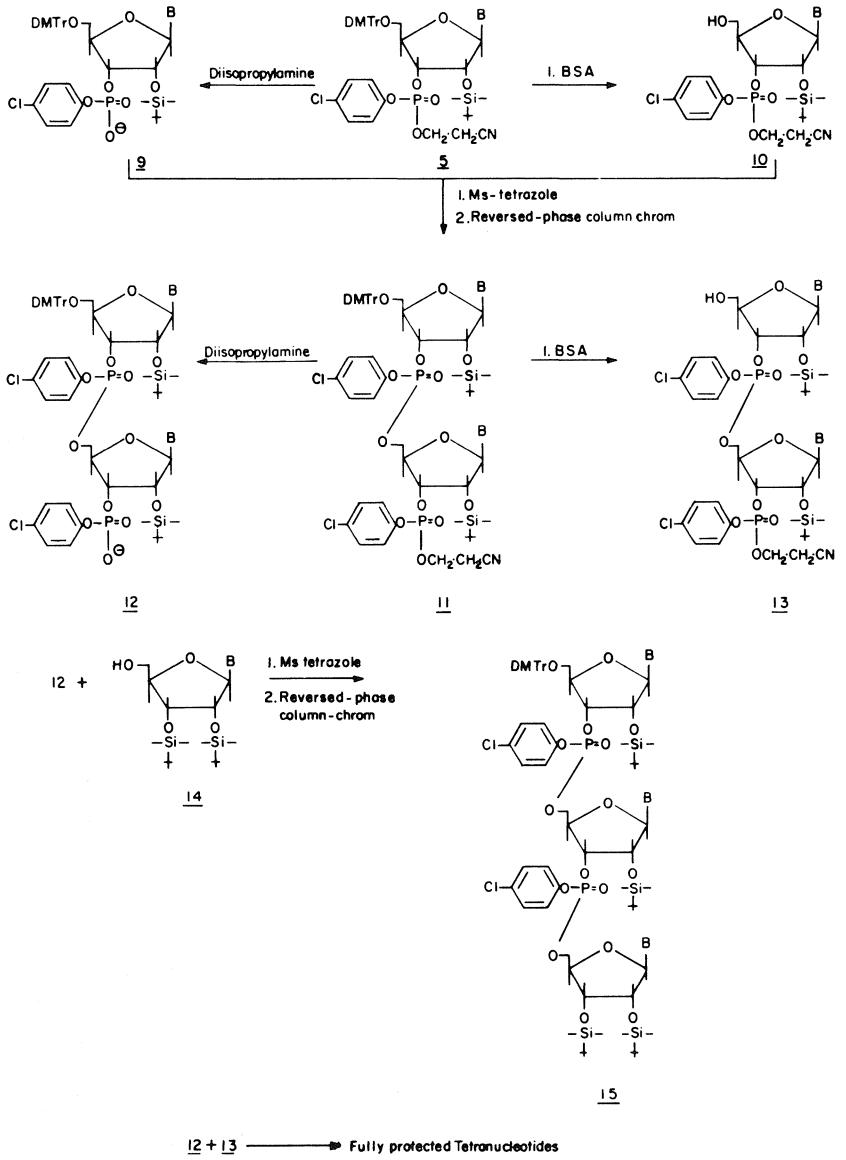


FIG. 4. General method of synthesis by the modified phosphotriester approach.

proach of synthesis is isolation of the pure desired product. In the case of ribooligonucleotide synthesis, the addition of the TBDMS protecting group at each 2′-position causes serious streaking problems in silica gel chromatography. We overcame this problem by developing a short reversed phase column chromatography using an acetone–water solvent system which has the following advantages: (*i*) separation of reaction mixture components is achieved according to the size, i.e. desired product, usually the largest size fragment is the slowest moving component; (*ii*) a 50 mg–10 g amount can be purified easily in less than 1 h time period; and, finally, (*iii*) recovery is quantitative. The reaction conditions and their isolated yields are given in Table 2.

*Final deblocking steps*

The sequential removal of all protecting groups is one of the most difficult as well as critical steps in the successful development of a chemical synthetic approach. Our strategy included initial removal of the 5′-dimethoxytrityl group with 2% benzenesulfonic acid in chloroform–methanol (22), followed by a two-step concentrated ammonia treatment (23) to remove *N*-protecting groups as well as

TABLE 2. Reaction conditions and isolated yield of various ribooligonucleotides synthesized by the modified phosphotriester approach

| 5′-Protected component[a] (mmol) | 3′-Hydroxyl component[b] (mmol) | Condensing[c] reagent (mmol) | Time (min) | Product[d,e] (isolated yield %) |
|---|---|---|---|---|
| | A. r-$A_{11}$ | | | |
| $[(MeO)_2]$rbzA∓bzA-ClPh (0.25) | rbzA-$(OSi)_2$ (0.20) | 0.50 | 15 | $[(MeO)_2]$rbzA∓bzA∓bzA-$(OSi)_2$ (70) |
| $[(MeO)_2]$rbzA(∓bzA)$_2$∓A-ClPh (0.20) | rbzA∓bzA∓bzA-$(OSi)_2$ (0.13) | 0.50 | 15 | $[(MeO)_2]$rbzA(∓bzA)$_5$∓bzA-$(OSi)_2$ (45) |
| $[(MeO)_2]$rbzA(∓bzA)$_2$∓A-ClPh (0.08) | rbzA(∓bzA)$_5$∓A-$(OSi)_2$ (0.04) | 0.20 | 15 | $[(MeO)_2]$rbzA(∓bzA)$_9$∓A-$(OSi)_2$ (35) |
| | B. r-AAACAUGAGGA (11-mer) | | | |
| $[(MeO)_2]$rIsoG∓IsoG-ClPh (0.24) | rbzA-$(OSi)_2$ (0.20) | 0.50 | 15 | $[(MeO)_2]$rIsoG∓IsoG∓bzA-$(OSi)_2$ (55) |
| $[(MeO)_2]$rbzA∓U∓IsoG∓bzA-ClPh (0.15) | rIsoG∓IsoG∓bzA-$(OSi)_2$ (0.10) | 0.30 | 15 | $[(MeO)_2]$rbzA∓U∓IsoG∓bzA∓IsoG∓ IsoG∓bzA-$(OSi)_2$ (45) |
| $[(MeO)_2]$rbzA∓bzA∓bzA∓bzC-ClPh (0.05) | rbzA∓U∓IsoG∓bzA∓IsoG∓ IsoG∓bzA-$(OSi)_2$ (0.03) | 0.15 | 15 | $[(MeO)_2]$rbzA∓bzA∓bzA∓bzC∓bzA∓U∓ IsoG∓bzA∓IsoG∓IsoG∓A-$(OSi)_2$ (30) |
| | C. r-UUACCCAUGU (10-mer) | | | |
| $[(MeO)_2]$rIsoG-ClPh (0.24) | rU-$(OSi)_2$ (0.18) | 0.45 | 15 | $[(MeO)_2]$rIsoG∓U-$(OSi)_2$ (60) |
| $[(MeO)_2]$rbzC∓bzC∓bzA∓U-ClPh (0.13) | rIsoG∓U-$(OSi)_2$ (0.09) | 0.28 | 15 | $[(MeO)_2]$rbzC∓bzC∓bzA∓U∓IsoG∓U-$(OSi)_2$ (50) |
| $[(MeO)_2]$rU∓U∓bzA∓bzC-ClPh (0.06) | rbzC∓bzC∓bzA∓U∓IsoG∓U-$(OSi)_2$ (0.04) | 0.14 | 15 | $[(MeO)_2]$rU∓U∓bzA∓bzC∓bzC∓bzC∓ bzA∓U∓IsoG∓U-$(OSi)_2$ (33) |

[a] Abbreviations are as suggested by IUPAC-IUB (1970) Biochemistry 9, 4022. A phosphodiester linkage is represented by a hyphen and phosphotriester linkage is represented by a (∓) symbol. Each internucleotidic phosphate is protected by a *p*-chlorophenyl (ClPh) group and each 2′-hydroxyl of each nucleoside is protected by a *tert*-butyldimethyl silyl (TBDMS) group.
[b] The 2′- and 3′-*cis*-hydroxyl groups of the 3′-terminal residue are protected by two *tert*-butyldimethyl silyl (TBDMS) groups.
[c] Mesitylenesulfonyl tetrazole (MS-Tet).
[d] Pure fully protected product was isolated by short column RP-2 chromatography.
[e] Using mesitylenesulfonyl tetrazole, in 2 to 3-fold equivalents, the sulfonated side product was obtained in 5–10% yields.

*p*-chlorophenyl from the internucleotidic phosphotriester bonds.[4] Under these conditions, the *tert*-butyldimethyl silyl group is still intact at every 2′-position. After washing with ether the partially deblocked material was then evaporated to dryness *in vacuo* and the dry powdery residue was treated with an excess of tetrabutylammonium fluoride in tetrahydrofuran under anhydrous conditions at room temperature. The time required to deblock all the silyl groups is mainly dependent upon the size of the fragment (dimer, 30 min; undecamer, 4 h). After evaporation, the residual material was applied, and excess salt from the applied band was washed with spray of methanol and water. The isolated yield of the desired pure material after total deblocking was 70–80%. The main side products were degradation products formed during the deblocking procedure.

*Characterization*

*Unprotected ribooligonucleotides containing 3′ → 5′ phosphodiester linkages*

(a) *Confirmation of the presence of 3′ → 5′ phosphodiester linkages*

Of paramount importance in ribo-synthesis is the proof of the preservation of each internucleotidic phosphodiester linkage as a 3′ → 5′ bond after all chemical reactions. The presence of each 3′ → 5′ phosphodiester linkage was established as follows.

Each ribooligonucleotide was labeled at the 3′-end with [$^{32}$P]Cp using $T_4$-RNA ligase (2). The labeled compound was purified on 20% gel electrophoresis which on treatment with spleen phosphodiesterase enzyme completely digested the labeled material to a radioactive monomer thus establishing that each linkage of the phosphodiester band is indeed 3′ → 5′.

(b) *Sequence analysis*

Each of the ribooligomers was labeled with [$\gamma$-$^{32}$P]-ATP with $T_4$-polynucleotide kinase and the labeled compound was sequenced by the mobility shift method (16) after partial digestion with snake venom phosphodiesterase or nuclease $P_1$-enzyme (24), and the results of each sequencing experiment are shown in Fig. 5.

[4]We also carried the deblocking procedure as recommended by de Rooij *et al.* (26) which involved, first, treatment with concentrated ammonia to remove the *p*-chlorophenyl group from the internucleotidic phosphotriester and *N*-acyl groups, followed by acidic treatment to remove the 5′-dimethoxytrityl group. After removing all the TBDMS groups from the 2′-positions, we compared the separation patterns on 20% gel electrophoresis with our original procedure (21) and found that these were almost comparable in terms of yields of the desired product and various side products.

*Conclusion*

In the present studies, we have demonstrated that the rapid and efficient synthesis of ribooligonucleotides can be achieved by a modified phosphotreister approach, comparable to the phosphotriester (5) as well as the phosphite route (6).

## Experimental

*General methods and materials*

Uridine, cytidine, adenosine, and guanosine (Sigma), *tert*-butyldimethyl chlorosilane (TBDMS), diphenyl-*tert*-butyl chlorosilane, triphenyl chlorosilane, tetrabutylammonium fluoride (Aldrich), *p*-chlorophenyl phosphodicloridate (Alfa-Ventron), RP-2 silanized silica gel (Brinkman), $T_4$-RNA ligase (RNAse free) and nuclease-$P_1$ enzyme (P-L Biochemical), and [$^{32}$P]Cp (Amersham) were purchased commercially.

5′-Dimethoxytrityl *N*-benzoyl adenosine, 5′-dimethoxytrityl *N*-isobutyryl guanosine, 5′-dimethoxytrityl uridine, and 5′-dimethoxytrityl *N*-benzoylcytidine were prepared according to the published procedures (3).

*Solvent systems*

The homogeneity of each fully protected compound was established by reversed phase (RP-2) tlc using acetone containing 20–30% water (v/v).

*Modified method of* N-*benzoylcytidine preparation*

Chlorotrimethylsilane (420 g, 3.9 mol) was added, with stirring, to a solution of cytidine (100 g, 0.41 mol) in pyridine (1.7 L) and kept for 1 h at room temperature. This was followed by the addition of benzoyl chloride (72 g, 0.52 mol). After 1 h, the reaction mixture was decomposed by adding a mixture of water and dichloromethane (700 mL each). The organic layer was separated and the removal of solvent from the organic extract *in vacuo* gradually yielded white crystals which were resuspended in dichloromethane (500 mL) overnight. The crystals were filtered, washed with acetone, and on drying *in vacuo* yielded pure *N*-benzoylcytidine (133 g) in 93% yield which was identical to an authentic sample (mp 234–236°C, lit. (25) mp 238–239°C).

*Large-scale silylation of 5′-dimethoxyribonucleoside*

Each of the ribonucleosides was prepared by the modification of the published procedure (13) as described below.

*5′-Dimethoxytrityl 2′-*tert*-butyldimethyl silyl* N-*benzoylcytidine* ***3***

5′-Dimethoxytrityl *N*-benzoylcytidine (50 g, 77 mmol) in pyridine solution (150 mL) was treated with *tert*-butyldimethyl chlorosilane (17 g, 113 mmol) and imidazole (15 g, 220 mmol) at room temperature. After 4 h, the reaction mixture was decomposed with water (200 mL) and dichloromethane (350 mL). The aqueous layer was extracted with dichloromethane (100 mL × 2) which was mixed with the organic layer. Evaporation of solvent *in vacuo* yielded a gum which was dissolved in ether (100 mL) and precipitated by pouring slowly into petroleum ether (40–60°C, 800 mL) with stirring. The precipitate was collected and washed twice with petroleum ether, then was dissolved in 30% petroleum ether – dichloromethane and chromatographed on silica gel (160 g) (short column of 6 cm diameter). Elution of column with (*i*) dichloromethane containing 30% petroleum ether (40–60°C, 400 mL) removed the 2′,3′-disilylated derivative (2.0 g); (*ii*) dichloromethane solvent (500 mL) eluted pure 2′-silylated isomer (30 g); and, finally, (*iii*) dichloromethane containing 8% acetone (2 L) removed the 3′-silylated isomer contaminated with the 2′-isomer (16 g).

The last fraction containing mainly the 3′-*tert*-butyldimethyl

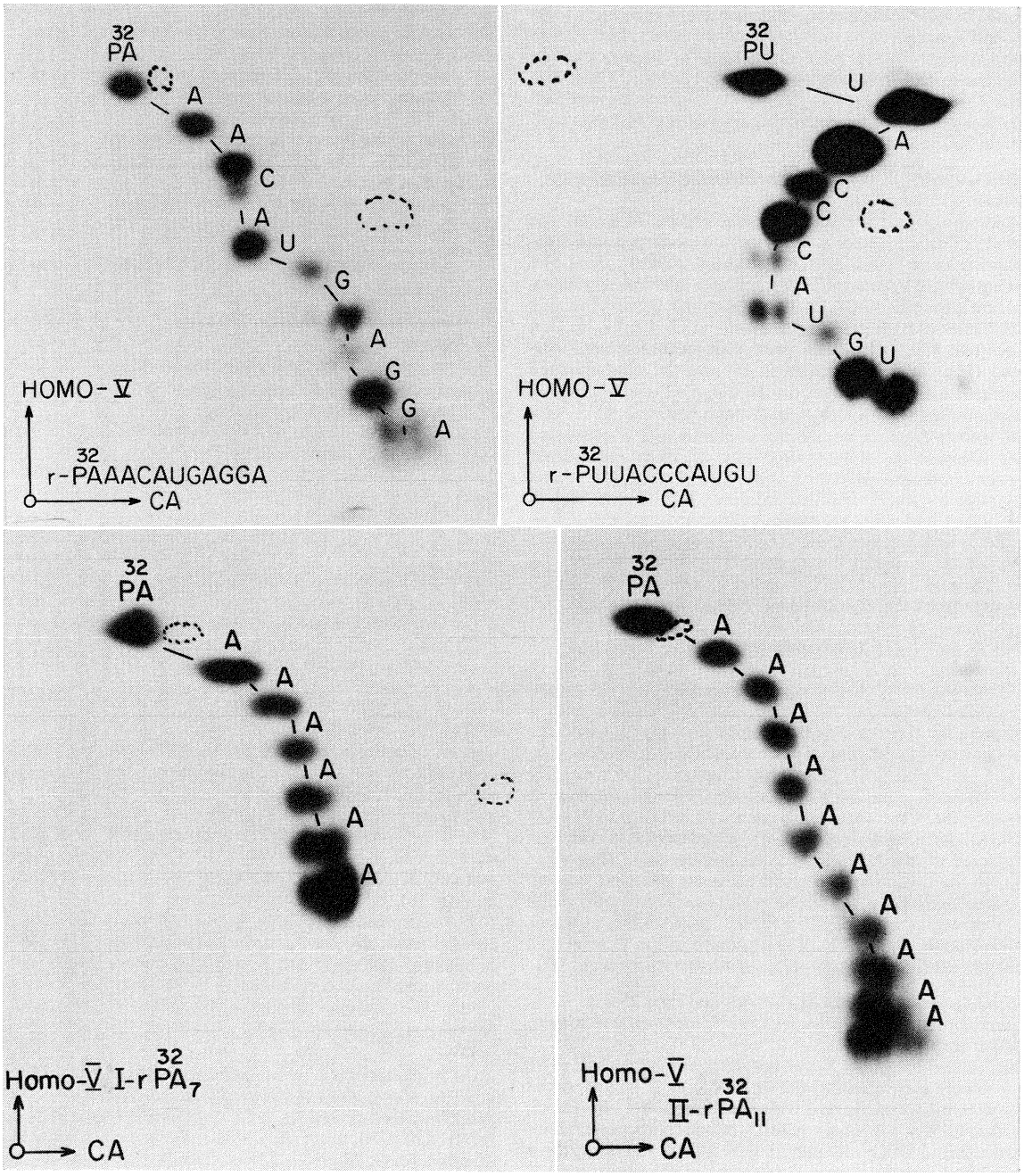


FIG. 5. Two-dimensional chromatographic fingerprints of synthetic ribooligonucleotides after partial digestion with nuclease $P_1$-enzyme. The first dimension is electrophoresis on cellulose acetate strip of pH 3.5 and the second dimension is homochromatography on 20 cm × 20 cm DEAE-cellulose plate in solvent Homo-V.

silylated derivative (16 g) was treated with triethylamine (0.5 mL) in methanol (200 mL) for 40 min at room temperature. On removing the solvent *in vacuo*, a gum was produced which was again chromatographed on a silica gel column as described above to yield a further 9 g of the 2′-protected isomer. The final isolated yields were the 2′-isomer, 39 g (66%); the 3′-isomer, 4.5 g (8%); and the 2′,3′-disilylated product, 2.0 g (4%). The structure of the 2′-protected isomer was confirmed by comparing its nmr spectral data with the literature values (13).

*5′-Dimethoxytrityl 2′-*tert*-butyldimethyl silyl uridine*

5′-Dimethoxytrityluridine (50 g, 93 mmol) in pyridine solution (150 mL) was treated with *tert*-butyldimethyl chlorosilane in the presence of imidazole according to conditions similar to those

described in ref. 13. Purification by silica gel (160 g) chromatography and subsequent isomerization of the 3′-silylated isomer and repeated chromatography (three times) as described above yielded the pure 2′-*tert*-butyldimethyl silyl isomer, 31 g (50%) and the 3′-isomer, 9 g (15%). The structure of the 2′-protected isomer was confirmed by comparing its nmr spectral data with the published values (13).

*5′-Dimethoxytrityl 2′-*tert*-butyldimethyl silyl N-benzoyladenosine*

5′-Dimethoxytrityl *N*-benzoyladenosine (50 g, 74 mmol) was silylated as described above. The reaction mixture was chromatographed on a silica gel (160 g) short column using the following solvent systems: (*i*) ethyl acetate – dichloromethane – petroleum ether (40–60°C) (1:1:3 v/v) (500 mL); (*ii*) ethyl acetate – dichloromethane – petroleum ether (40–60°C) (1:1:2 v/v) (2 L); (*iii*) acetone (800 mL). The pure 2′-protected isomer was isolated (12 g) in fraction number (*ii*) and the contaminated 2′-protected isomer (6 g) with the 3′-protected isomer (18 g) in fraction number (*iii*). Subsequent isomerization of the 3′-protected isomer fraction containing contaminated 2′-protected isomer followed by rechromatography on silica gel column under the conditions described above yielded further amounts of the pure 2′- and 3′-silylated isomers. After two cycles of isomerization and silica gel column chromatographic purification, the overall yield of the 2′-silylated protected isomer was 26 g (45%) and a slightly contaminated 3′-silylated isomer, 9 g (16%). The structure of the 2′-protected isomer was confirmed by comparing its nmr spectral data with the literature (13).

*5′-Dimethoxytrityl 2′-*tert*-butyldimethyl silyl N-isobutyrylguanosine*

5′-Dimethoxytrityl *N*-isobutyrylguanosine (50 g, 76 mmol) was silylated according to the procedure described above. Purification by column chromatography on silica gel with the following solvent systems: (*i*) petroleum ether – dichloromethane (1:1 v/v) (300 mL); (*ii*) dichloromethane (500 mL); (*iii*) dichloromethane containing 4% acetone (2 L); and, finally, (*iv*) acetone, yielded the pure 2′-silylated isomer (10 g) in fraction number (*ii*) and a mixture of the 2′-protected isomer (6 g) and the 3′-protected isomer (23 g) in fraction number (*iii*). After three cycles of isomerization and purification by silica gel column chromatography under the above conditions, the overall yields were 2′-protected isomer, 24.5 g (42%), and a slightly contaminated 3′-isomer, 10 g (17%). The structure of the 2′-protected isomer was confirmed by comparison with literature values (13).

*Attempted phosphorylation of 5′-dimethoxytrityl 2′-*tert*-butyldimethyl silyl uridine with p-chlorophenyl phosphoryl ditetrazolide*

The 5′-dimethoxytrityl 2′-*tert*-butyldimethyl silyl uridine (1.0 g, 1.5 mmol) and tetrazole (0.30 g, 4.8 mmol) in anhydrous pyridine (3 mL) was treated with *p*-chlorophenyl phosphodichloridate (0.59 g, 2.4 mmol). After 20 min at room temperature, β-cyanoethanol (0.8 g, 12 mmol) was added and kept for a further 2 h to complete the reaction. The reaction mixture was decomposed by adding a mixture of water and dichloromethane (30 mL each), then the organic layer was separated and washed with 5% aqueous sodium bicarbonate (30 mL). Evaporation *in vacuo* yielded a gummy residue which was purified on reversed phase (RP-2) (11 g) short column chromatography using the following solvents: (*i*) acetone–water (50:50 v/v) (250 mL) to remove excess β-cyanoethanol and other non-triester components; (*ii*) acetone–water (58:42 v/v) (150 mL) to elute the fully protected product. Extraction of solvent (*ii*) with dichloromethane (50 mL) and subsequent evaporation gave a mixture of two fully protected phosphotriester nucleotide compounds which were further fractionated on preparative silica gel tlc plates developed in dichloromethane–acetone (9:1 v/v) into two bands. Elution of the faster moving band with methanol–dichloromethane (3:7 v/v) and evaporation *in vacuo* yielded 4-tetrazolo-1-(β-D-5′-dimethoxytrityl-2′-*tert*-butyldimethyl silyl ribofuranosyl)-2(1*H*)-pyrimidinone 3′-*p*-chlorophenyl β-cyanoethyl phosphotriester **8** as a foamy material, 0.42 g (35%). The structure was confirmed by its ultraviolet spectra (methanol), $\lambda_{max}$: 324 nm; nmr ($CDCl_3$) δ: 9.44 (1H, s, H(5) of tetrazole), 2.48 (2H, m, $OCH_2CH_2{\cdot}CN$), 0.92 (9H, s, $(CH_3)_3CSi$). The molecular ion ($M^+$) occurs at 957 $m^+/e$ which is an increase of 52 mass units over the corresponding uridine derivative and corresponds to the addition of the tetrazole moiety (18).

On complete deblocking, the resulting product has uv spectra characteristic of cytosine.

*Phosphorylation with p-chlorophenyl phosphodichloridate and triazole*

(i) *Preparation of 5′-dimethoxytrityl 2′-*tert*-butyldimethyl silyl N-benzoyl cytidine-3′-p-chlorophenyl β-cyanoethyl phosphotriester 5*

1,2,4-Triazole (10.0 g, 145 mmol) was added to a pyridine solution (65 mL) containing the 2′-*tert*-butyldimethyl silylated cytidine **3** (33.0 g, 43.3 mmol) at room temperature. *p*-Chlorophenyl phosphodichloridate (17.7 g, 72 mmol) was then added immediately and the reaction mixture stirred for 5 min to complete the phosphorylation reaction as checked by tlc on silica gel and RP-2 plates. β-Cyanoethanol (25 g, 356 mmol) was then added and after a further 3 h at room temperature the reaction mixture was decomposed by adding water (200 mL). The solution was extracted with dichloromethane (500 mL) and the organic layer was washed with 5% aqueous sodium bicarbonate solution (100 mL). Evaporation of solvent *in vacuo* gave a gummy residue which was purified by RP-2, short column chromatography (130 g) using solvents (*i*) acetone–water (50:50 v/v) (1.5 L) to remove excess β-cyanoethanol, followed by (*ii*) acetone containing 45% water (2 L) to elute the fully protected desired product. The desired product was recovered by extracting the solvent (*ii*) with dichloromethane (500 mL), drying, and removing the solvent to produce a foamy material, 31.2 g (71%); uv (MeOH) $\lambda_{max}$: 262, 305 nm; nmr ($CDCl_3$) δ: 2.62 (2H, m, $CH_2{\cdot}CH_2{\cdot}CN$), 0.97 (9H, s, $(CH_3)_3CSi$—). *Anal.* (foamy material) calcd. for $C_{54}H_{26}N_4O_{11}ClPSi$: C 61.99, H 5.60, N 5.56; found: C 61.90, H 5.57, N 5.42.

The corresponding fully protected ribonucleoside 3′-*p*-chlorophenyl, and the β-cyanoethyl phosphotriester of uridine, *N*-benzoyladenosine, and isobutyrylguanosine were also prepared according to the above reaction conditions. The isolated yields were uridine (61%), *N*-benzoyladenosine (75%), and *N*-isobutyrylguanosine (72%). Their analytical data are given below.

(ii) *5′-Dimethoxytrityl 2′-*tert*-butyldimethyl silyl uridine 3′-p-chlorophenyl β-cyanoethyl phosphotriester*

Ultraviolet (MeOH) $\lambda_{max}$: 263 nm; nmr ($CDCl_3$) δ: 2.63 (2H, m, $CH_2CH_2CN$), 0.91 (9H, s, $(CH_3)_3CSi$). *Anal.* (foamy material) calcd. for $C_{45}H_{51}N_3O_{11}ClPSi$: C 60.25, H 5.68, N 4.64; found: C 60.12, H 5.54, N 4.56.

(iii) *5′-Dimethoxytrityl 2′-*tert*-butyldimethyl silyl N-benzoyladenosine 3′-p-chlorophenyl β-cyanoethyl phosphotriester*

Ultraviolet (MeOH) $\lambda_{max}$: 276 nm; nmr ($CDCl_3$) δ: 2.78 (2H, m, $CH_2CH_2CN$), 0.89 (9H, s, $(CH_3)_3CSi$). *Anal.* (foamy material) calcd. for $C_{53}H_{56}N_6O_{10}ClPSi$: C 61.71, H 5.47, N 8.14; found: C 61.50, H 5.57, N, 8.26.

(iv) *5′-Dimethoxytrityl 2′-*tert*-butyldimethyl silyl N-isobutyryl guanosine 3′-p-chlorophenyl β-cyanoethyl phosphotriester*

Ultraviolet (MeOH) $\lambda_{max}$: 274, 281 nm; nmr ($CDCl_3$) δ: 2.75

(2H, m, $CH_2CH_2CN$), 0.93 (9H, s, $(CH_3)_3Si$). *Anal.* (foamy material) calcd. for $C_{50}H_{58}N_6O_{11}ClPSi$: C 59.25, H 5.76, N 8.29; found: C 59.05, H 5.84, N 8.49.

*Selective removal of β-cyanoethyl group from the fully protected ribomononucleotide* **5** *on treatment with diisopropylamine – anhydrous pyridine*

Fully protected ribomononucleotide (2.5 mmol) was dissolved in anhydrous pyridine (5 mL) containing diisopropylamine (1.5 mL) and kept at room temperature. The reaction was over within an hour as monitored on reversed phase tlc and the results are documented in Table 1 for individual nucleotides. After completion of the reaction, the solvent was removed *in vacuo* and the foamy residue was reevaporated in pyridine solvent to dryness.

*General method of large-scale and rapid synthesis of sixteen fully protected ribodinucleotides* **11**

5′-Dimethoxytrityl 2′-*tert*-butyldimethyl silyl *N*-protected ribomononucleoside 3′-*p*-chlorophenylphosphate **9** (4.5 mmol) and 5′-hydroxyl ribomononucleoside, 2′-*tert*-butyldimethyl silyl, 3′-*p*-chlorophenyl, β-cyanoethyl phosphate **10** (4.0 mmol) in anhydrous pyridine (20 mL) were treated with mesitylenesulfonyl tetrazole (9 mmol) at room temperature for 15 min. The reaction mixture was taken up in dichloromethane (100 mL) and 5% aqueous sodium bicarbonate solution (100 mL). The aqueous layer was extracted twice with dichloromethane (50 mL). Evaporation of the organic solvent *in vacuo* yielded a gummy residue which was chromatographed on a reversed phase gel (40 g) packed in a short column (4 cm diameter). The column was eluted with the following solvents: (*i*) acetone containing 40% water (1.0 L) to remove the unreacted 3′-phosphodiester containing material as well as 5′-hydroxyl; (*ii*) acetone containing 25% water (300 mL) eluted the fully protected ribodinucleotide **11**. The desired product was isolated by extracting solvent (*ii*) with an equal volume of dichloromethane. Subsequent evaporation of the dichloromethane solvent *in vacuo* yielded pure fully protected dinucleotide in 50–70% yields. This purification procedure required 90 min.

*General method of ribooligonucleotide synthesis*

The synthesis of fully protected ribooligonucleotide was achieved by condensing 5′-dimethoxytrityl, 2′-*tert*-butyldimethyl silylated, *N*-protected oligonucleotides containing 3′-*p*-chlorophenylphosphate with the 5′-hydroxyl containing component in anhydrous pyridine solution in the presence of mesitylene tetrazole for 15 min at room temperature. After the usual work-up the desired product was isolated by short column chromatography on reversed phase (RP-2) silica gel as described above. The entire operation of coupling, work-up, purification, and isolation was complete within 3 h. The purity of each intermediate was 80–90% as judged by tlc on reversed phase silica gel plates as was the case also after the complete deblocking step, analysis on PEI plate, and sequence determination. The summary of reaction conditions and isolated yields are documented in Table 2.

*Final deblocking and purification step*

A fully protected undecamer containing the base sequence (r-AAACAUGAGGA) (15 mg) was treated with 2% benzenesulfonic acid in methanol–dichloromethane (3:7 v/v) (6 mL) for 1 min at room temperature followed by washing with 5% aqueous sodium bicarbonate solution (6 mL). After separating the aqueous layer, the organic solvent was evaporated *in vacuo* to dryness and then dissolved in concentrated ammonia–pyridine (2:3 v/v) (5 mL). After keeping the reaction mixture at room temperature for 48 h, it was heated to 37°C for 24 h. Subsequent evaporation *in vacuo* gave a gummy residue which was coevaporated in pyridine (1 mL) to a glassy product which was next washed with anhydrous ethyl ether (1 mL) for 15 min. Removal of ethyl ether produced a powder which was then treated with 1.0 *M* tetrabutylammonium fluoride in tetrahydrofuran (1 mL) for 4 h at room temperature. Shorter time periods, e.g. 30 min for the dimer, 2 h for the hexamer, are sufficient for the removal of all the 2′-TBDMS protected groups. The reaction mixture was applied directly on the PEI-tlc plate (~ 300 μL per plate) and the application area washed first by spraying with distilled water and then with methanol to remove excess salts and nonnucleotidic materials. The PEI plate was first developed in water (for a height of 3 cm) followed by 0.6 *M* LiCl–7 *M* urea solvent at 60°C. After 2 h, the plate was removed and then soaked in a methanol tank. The desired major band was eluted with 1 *M* triethylammonium bicarbonate pH 7.5 solution.

*Characterization*

(a) *Confirmation of 3′ → 5′ phosphodiester internucleotidic linkages in snythetic ribooligomers*

The r-AAACAUGAGGA (11-mer) acceptor (1 mmol, 100 μ*M*) and donor [r-5′-$^{32}$P]PCP (0.5 mmol, 50 μ*M*) in reaction buffer (10 μL) containing 50.0 m*M* HEPES, pH 7.5, 20 m*M* $MgCl_2$, 3.3 m*M* (dithiothreitol), 0.1 m*M* ATP, 0.25 μg bovine serum albumin, 10% v/v dimethyl sulfoxide was incubated with RNA ligase (2) (1.5 units) for 30 min at 37°C. The reaction was terminated by heating at 100°C for 2 min. The labeled compound was purified by electrophoresis on a 20% gel slab. The labeled material was then treated with spleen phosphodiesterase in 10 m*M* EDTA and 100 m*M* potassium phosphate (pH 6.5) for 30 min at 37°C. The digested material was analyzed by homochromatography using Homo-V solvent (15). All the radioactivity was found at the solvent front corresponding to mononucleotide.

(b) *Sequence analysis by mobility shift method*

(i) *5′-Labeling of synthetic ribooligonucleotides*

Each synthetic ribooligonucleotide fragment was labeled using [γ-$^{32}$P]-ATP and $T_4$-polynucleotide kinase enzyme. The labeled compound was purified by 20% gel electrophoresis according to the published procedure (22).

(ii) *Partial digest of 5′-$^{32}$P-labeled ribooligonucleotide with nuclease $P_1$ enzyme*

The 5′-labeled ribooligonucleotide in 20 μL containing 50 μg of carrier t-RNA in 50 m*M* ammonium acetate (pH 5.3) was incubated with nuclease $P_1$ enzyme (1 μg) at room temperature. Aliquots (5 μL) were removed at 0, 5, 10, and 20 min and transferred to 5 m*M* EDTA-containing diethyl pyrocarbonate (10 μL/100 mL buffer) (10 μL) and inactivation of the enzyme was accomplished by heating at 100°C for 2 min. An aliquot (1 μL) of each time interval fraction was analyzed in one dimension by homochromatography using solvent V. The appropriate aliquots were mixed, and chromatographed by the two dimensional system. The radioautograms of each oligomer are shown in Fig. 5 which confirms their individual sequences.

## Acknowledgments

We are grateful to Professor Olke Uhlenbeck, University of Illinois, Urbana, for suggesting the R-17 sequence for the chemical synthesis, and to Miss Diana Schmidt for her technical assistance.

1. R. Silber, V. G. Malathi, and J. Hurwitz. Proc. Natl. Acad. Sci. U.S.A. **69**, 3009 (1972); G. C. Walker, O. C. Uhlenbeck, E. Bedows, and R. I. Gumport. Proc. Natl. Acad. Sci. U.S.A. **72**, 122 (1975).
2. Nucleic Acids Res., Symposium Series No. 7, 1980.

3. R. LOHRMANN, D. SÖLL, H. HAYATSU, E. OHTSUKA, and H. G. KHORANA. J. Am. Chem. Soc. **88**, 819 (1966).
4. E. OHTSUKA, M. UBASAWA, and M. IKEHARA. J. Am. Chem. Soc. **93**, 2296 (1971).
5. R. L. LETSINGER and K. K. OGILVIE. J. Am. Chem. Soc. **89**, 4801 (1967).
6. R. L. LETSINGER, J. L. FINNAN, G. A. HEAVER and W. B. LUNSFORD. J. Am. Chem. Soc. **97**, 3278 (1975).
7. K. K. OGILVIE and M. J. NEMER. Tetrahedron Lett. **21**, 4159 (1980); E. OHTSUKA, H. TAKASHIMA, and M. IKEHARA. Tetrahedron Lett. **22**, 765 (1981).
8. T. NEILSON and E. S. WERSTIUK. J. Am. Chem. Soc. **96**, 2295 (1974).
9. S. S. JONES, B. RAYNES, C. B. REESE, A. UBASAWA, and M. UBASAWA. Tetrahedron, **36**, 3075 (1980).
10. K. K. OGILVIE and M. J. NEMER. Can. J. Chem. **58**, 1389 (1980).
11. J. H. VAN BOOM. Heterocycles, **7**, 1197 (1977).
12. E. OHTSUKA, S. TANAKA, and M. IKEHARA. J. Am. Chem. Soc. **100**, 8210 (1978).
13. K. K. OGILVIE, K. K. SCHIFMAN, and C. L. PENNY. Can. J. Chem. **57**, 2230 (1979).
14. K. ITAKURA, C. P. BAHL, N. KATAGIRI, J. MICHNIEWICZ, S. A. NARANG, and R. H. WIGHTMAN. Can. J. Chem. **51**, 3649 (1973); T. C. CATLIN and F. CRAMER. J. Org. Chem. **38**, 245 (1973); S. A. NARANG, R. BROUSSEAU, H. M. HSIUNG, and J. J. MICHNIEWICZ. Methods Enzymol. **65**, 610 (1979).
15. J. GRALLA, J. A. STEITZ, and D. M. CROTHERS. Nature, **248**, 204 (1974).
16. C. D. TU, E. JAY, C. P. BAHL, and R. WU. Anal. Biochem. **74**, 73 (1976).
17. N. KARAGIRI, K. ITAKURA, and S. A. NARANG. J. Am. Chem. Soc. **97**, 7332 (1975).
18. C. MCNEAL, S. A. NARANG, R. D. MACFARLANE, H. M. HSIUNG, and R. BROUSSEAU. Proc. Natl. Acad. Sci. U.S.A. **76**, 735 (1979).
19. C. B. REESE and A. UBASAWA. Nucleic Acids Res., Symp. Series No. 7, 1980. p. 5.
20. A. K. SOOD and S. A. NARANG. Nucleic Acids Res. **4**, 2757 (1977); R. W. ADAMIAK, M. Z. BARCISZEWSKA, E. BIALA, K. GRZESKOWIAK, R. KIERZEK, A. KRASZEWSKI, W. T. MARKIEWICZ, and M. WIEWIOROWSKI. Nucleic Acids Res. **3**, 3397 (1976).
21. J. STAWINSKI, T. HOZUMI, and S. A. NARANG. Can. J. Chem. **54**, 670 (1976).
22. J. STAWINSKI, T. HOZUMI, S. A. NARANG, C. P. BAHL, and R. WU. Nucleic Acids Res. **4**, 353 (1977).
23. H. M. HSIUNG, W. L. SUNG, R. BROUSSEAU, R. WU, and S. A. NARANG. Nucleic Acids Res. **8**, 5753 (1980).
24. M. SILBERKLANG, A. M. GILLUM, and U. L. RAJBHANDARY. Nucleic Acids Res. **4**, 4091 (1977).
25. K. A. WATANABE and J. J. FOX. Angew. Chem. Int. Ed. Engl. **5**, 579 (1966).
26. J. F. M. DE ROOIJ, G. WILLE-HAZELEGER, P. M. J. BURGERS, and J. H. VAN BOOM. Nucleic Acids Res. **6**, 2237 (1979).

# Copper tetrafluoroborate complexes of the potentially binucleating ligand 1,4-di(2′-pyridyl)aminophthalazine. Mononuclear and polynuclear derivatives

JOHN C. DEWAN AND LAURENCE K. THOMPSON[1]

*Department of Chemistry, Memorial University of Newfoundland, St. John's, Nfld., Canada A1B 3X7*

Received July 31, 1981

JOHN C. DEWAN and LAURENCE K. THOMPSON. Can. J. Chem. **60**, 121 (1982).

Three different copper tetrafluoroborate complexes are obtained from the reaction of copper tetrafluoroborate and the title ligand (PAP) in water. Two crystalline modifications of a six-coordinate mononuclear protonated derivative, $[Cu(PAPH)_2(H_2O)_2](BF_4)_4$, a triclinic brown form (**I**) and a monoclinic green form (**II**), and a dark green polynuclear complex containing neutral ligand and formulated as $[Cu_3(PAP)_2(OH)_2](BF_4)(BF_3OH)_3 \cdot 5H_2O$ (**III**), are obtained from the same reaction mixture. The hydrolysis of $BF_4^-$ in water is thought to be responsible for the formation of protonated PAP. In methanol a four-coordinate protonated derivative, $[Cu(PAPH)_2](BF_4)_4$ (**IV**) and a binuclear complex $[Cu_2(PAP)_2(H_2O)_2](BF_4)_4 \cdot 0.5MeOH$ (**V**), containing neutral ligand, are obtained. The molecular structures of both forms of $[Cu(PAPH)_2(H_2O)_2](BF_4)_4$ have been determined by single crystal X-ray diffraction. The brown triclinic form (**I**) belongs to space group $P\bar{1}$ with $a = 9.856(1)$, $b = 12.724(1)$, $c = 9.401(1)$ Å, $\alpha = 101.691(8)$, $\beta = 96.717(9)$, $\gamma = 70.145(8)°$, $V = 1084.4$ Å$^3$, $Z = 1$. The green monoclinic form (**II**) belongs to space group $P2_1/n$ with $a = 12.663(4)$, $b = 9.573(3)$, $c = 18.813(4)$ Å, $\beta = 107.16(2)°$, $V = 2178.9$ Å$^3$, $Z = 2$. Both complexes have tetragonally distorted six-coordinate structures involving axially bound water molecules and two in plane bidentate protonated ligands. The major difference between the structures involves the axial Cu—O(W) bond lengths (triclinic 2.497(9) Å; monoclinic 2.426(9) Å).

JOHN C. DEWAN et LAURENCE K. THOMPSON. Can. J. Chem. **60**, 121 (1982).

On a obtenu trois complexes différents du tétrafluoroborate de cuivre par de la réaction, dans l'eau, entre du tétrafluoroborate de cuivre avec le ligand (PAP) mentionné dans le titre. Le même mélange réactionnel fournit aussi deux modifications cristallines du dérivé protoné mononucléaire hexacoordoné, $[Cu(PAPH)_2(H_2O)_2](BF_4)_4$, une forme brune triclinique (**I**) et une forme verte monoclinique (**II**) ainsi qu'un complexe polynucléaire vert foncé contenant le ligand neutre et considéré comme étant le $[Cu_3(PAP)_2(OH)_2](BF_4)(BF_3OH)_3 \cdot 5H_2O$ (**III**). On croit que l'hydrolyse de $BF_4^-$ dans l'eau est responsable de la formation du PAP protoné. Dans le méthanol, on obtient, un dérivé protoné hexacoordonné, $[Cu(PAPH)_2](BF_4)_4$ (**IV**) et un complexe binucléaire $[Cu_2(PAP)_2(H_2O)_2](BF_4)_4 \cdot 0{,}5$ MeOH (**V**) contenant le ligand neutre. On a déterminé les structures moléculaires des deux formes par diffraction des rayon-X sur un monocristal. La forme triclinique brune appartient au groupe d'espace $P1$ avec $a = 9{,}856(1)$, $b = 12{,}724(1)$, $c = 9{,}401(1)$ Å, $\alpha = 101{,}691(8)$, $\beta = 96{,}717(9)$, $\gamma = 70{,}145(8)$, $V = 1084$ Å$^3$, $Z = 1$. La forme monoclinique verte appartient au groupe d'espace $P2_1/n$ avec $a = 12{,}663(4)$, $b = 9{,}573(3)$, $c = 18{,}813(4)$ Å, $\beta = 107{,}16(2)°$, $V = 2178.9$ Å$^3$, $Z = 2$. Les deux complexes ont des structures hexacoordonnées déformées de façon tétragonale faisant intervenir des molécules d'eau liées en position axiale et deux ligands protonés bidentates dans le plan. La principale différence entre les deux structures se situe au niveau des longueurs de liaison axiale Cu—O(W); elles sont respectivement de 2,497(9) Å dans la forme triclinique, et de 2,426(9) Å dans la forme monoclinique.

[Traduit par le journal]

## Introduction

The binucleating ligand 1,4-di(2′-pyridyl)-aminophthalazine (Fig. 1, ligand abbreviated PAP) has been shown to bind preferentially to two metal centres forming binuclear complexes with copper, cobalt, nickel, and zinc salts (1–3). The metal centres are connected by multiple bridges in all cases; the bridging units include the phthalazine $N_2$ group, hydroxide, halide, and carboxylate. An X-ray study on the complex $[Cu_2(PAP)(OH)Cl_3] \cdot 1.5H_2O$ revealed a triple bridge involving hydroxide, chloride and phthalazine (4) (Fig. 2). Reaction of this complex in acetonitrile/water with 3,5-di-*tert*-butylcatechol produces a binuclear copper(I)/quinone derivative which catalytically oxidizes excess catechol to the corresponding quinone in the presence of excess oxygen (5). Other preliminary X-ray studies on the complexes $[Ni_2(PAPH)_2$-

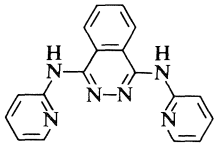

FIG. 1. 1,4-Di-(2′-pyridyl)aminophthalazine, PAP.

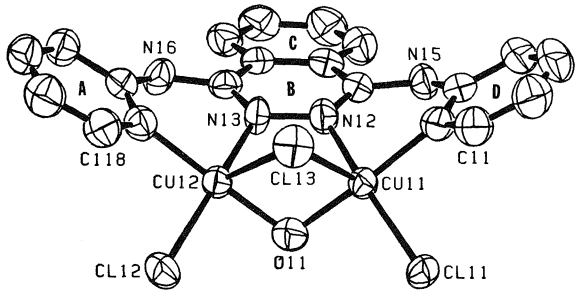


FIG. 2. Geometry of one of the two crystallographically independent molecules in the structure (4) of $[Cu_2(PAP)(OH)Cl_3] \cdot 1.5H_2O$ (**VII**).

[1]To whom all correspondence should be addressed.

0008-4042/82/020121-12$01.00/0

©1982 National Research Council of Canada/Conseil national de recherches du Canada

Can. J. Chem. Downloaded from www.nrcresearchpress.com by 210.87.254.6 on 09/06/12
For personal use only.

Can. J. Chem. Downloaded from www.nrcresearchpress.com by 210.87.254.6 on 09/06/12
For personal use only.

$(PAP)(OH)_2]Br_4 \cdot 6H_2O$ (PAPH = protonated ligand) $[Co_2(PAP)_3(OH)_2]Br_4 \cdot 9H_2O$ and $[Co_2(PAP—H)_2(PAP)(OH_2](ClO_4)_2$ (PAP—H = deprotonated ligand) (6) indicate triple bridges between the cobalt(III) and nickel(II) centres involving a phthalazine $N_2$ bridge and two oxygen bridges. The identity of the oxygen bridges remains in some doubt at present but they have been formulated as hydroxides in keeping with other data. Preliminary structural details of the complex $[Co_2(PAP—H)_2(PAP)(OH)_2](ClO_4)_2$ are given in Fig. 3. The other two complexes have the same basic structure. Full details of the structures of these three complexes will be published elsewhere.

We recently reported the isolation of two mononuclear six-coordinate nickel complexes $[Ni(PAPH)_2(H_2O)_2](BF_4)_4$ and $[Ni(PAPH)_2(H_2O)_2]I_4$ (3) in which the two potentially tetradentate ligands were assumed to be bidentate and that each one was protonated. The formation of such derivatives from aqueous solution was rationalized in terms of the acidity of the solution of the metal salt, at least in the case of the tetrafluoroborate system (3).

$$BF_4^- + H_2O \rightleftharpoons BF_3(OH)^- + HF$$
$$K = 2.0 \times 10^{-3} \quad (7)$$
$$BF_3OH^- + H_2O \rightleftharpoons BF_2(OH)_2^- + HF$$
$$K = 1.8 \times 10^{-4} \quad (8)$$

We report herein that a similar mononuclear protonated system is obtained from the reaction of copper tetrafluoroborate and PAP in a 1:1 ratio in water. Initially a mixture of two different crystalline products is obtained, consisting of light brown blocks (**I**) and light green plates (**II**). Both crystalline products analyse independently as $[Cu(PAPH)_2(H_2O)_2](BF_4)_4$. X-ray analyses of these two compounds reveal the same basic tetragonally distorted six-coordinate structure involving axially coordinated water. The most significant difference between the structures involves the Cu—O(W) bond lengths, which are longer in the brown form.

In addition to the formation of the two mononuclear derivatives a polynuclear derivative is also obtained (**III**) in which the metal-to-ligand ratio appears to be 3:2. $BF_3OH^-$ ions, produced from the hydrolysis of $BF_4^-$, appear as counter ions in this product. If the pH of the copper tetrafluoroborate solution is raised to approximately 5, thus suppressing the hydrolysis of $BF_4^-$, the only product obtained is a polynuclear derivative (**VI**) analogous to **III**, which contains $BF_4^-$ and no $BF_3OH^-$.

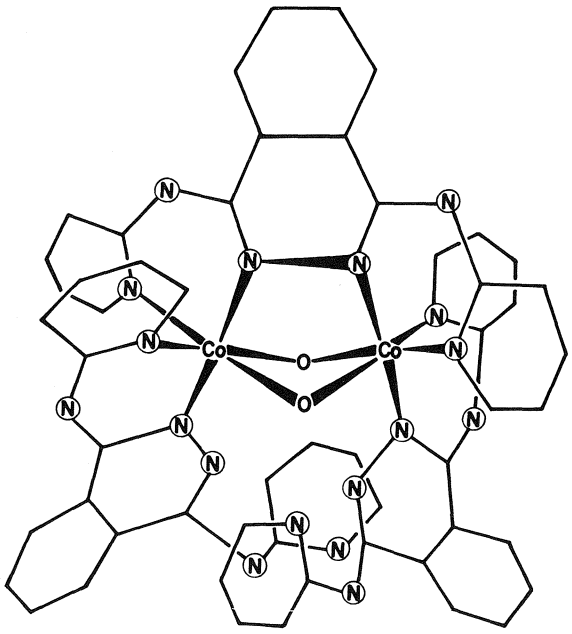


FIG. 3. Preliminary structural details for the $[Co_2(PAP—H)_2(PAP)(OH)_2]^{2+}$ cation (6).

## Experimental

Electronic spectra were recorded on a Cary 17 spectrometer, infrared spectra were obtained with a Perkin-Elmer model 283 spectrometer, and magnetic susceptibilities were obtained at room temperature by the Faraday method with a Cahn model #7600 Faraday Magnetic Susceptibility system, coupled to a Cahn gram electrobalance. Microanalyses were carried out by Canadian Microanalytical Service, Vancouver (C, H, N) and Pascher Microanalytisches Laboratorium, Bonn (F), and metal analyses were determined by Atomic Absorption with a Varian Techtron AA-5, after digestion of the samples in aqua regia.

*1,4-Di(2'-pyridyl)aminophthalazine (PAP)*

The ligand, PAP, was prepared as described previously (1).

*Copper tetrafluoroborate complexes of PAP*

*$[Cu(PAPH)_2(H_2O)_2](BF_4)_4$ (I, II), $[Cu_3(PAP)_2(OH)_2](BF_4)(BF_3OH)_3 \cdot 5H_2O$ (III)*

$Cu(BF_4)_2 \cdot 6H_2O$ (Alfa) (2.2 g; 6.4 mmol) was dissolved in water (150 mL) and the solution filtered. PAP (2.0 g; 5.8 mmol) was added and the mixture refluxed for 1 h. The resulting green solution was filtered hot and left to stand for 1 week. A mixture of brown (**I**) and light green (**II**) crystals was formed. These crystals were used directly for X-ray analysis. The product was filtered, washed with acetone, and air dried. The mother liquor was allowed to stand, open to the atmosphere, for another week. A further crop of brown and light green crystals was obtained, and was treated as before. Further reduction in volume of the mother liquor produced a third crop of mixed crystals. The relative proportions of brown and green crystals appeared to vary in that in the first crop of product the brown crystals predominated whereas, in the last crop there appeared to be more green crystals. (Total yield = 0.6 g.)

The green mother liquor was reduced in volume on a steam bath to 30 mL and ethanol (10 mL) added. On standing, dark green crystals (**III**) formed. The product was filtered, washed with ethanol, and recrystallized from $H_2O$/EtOH (75/25) (yield = 1.3 g).

*Anal.* calcd. for $[Cu(PAPH)_2(H_2O)_2](BF_4)_4$ (**I**, brown): C 40.2, H 3.09, N 15.6, F 28.2, Cu 5.89; found: C 40.0, H 2.99, N 15.5, F 28.6, Cu 6.02.

Can. J. Chem. Downloaded from www.nrcresearchpress.com by 210.87.254.6 on 09/06/12
For personal use only.

*Anal.* calcd. for $[Cu(PAPH)_2(H_2O)_2](BF_4)_4$ (**II**, light green): C 40.2, H 3.09, N 15.6, F 28.2, Cu 5.89; found: C 40.1, H 2.92, N 15.4, F 28.6, Cu 5.91.

*Anal.* calcd. for $[Cu_3(PAP)_2(OH)_2](BF_4)(BF_3OH)_3 \cdot 5H_2O$ (**III**, dark green): C 33.6, H 3.35, N 13.1, F 19.2, Cu 14.8; found: C 33.6, H 3.31, N 13.0, F 19.1, Cu 14.8.

*$[Cu(PAPH)_2](BF_4)_4$ (IV), $[Cu_2(PAP)_2(H_2O)_2](BF_4)_4 \cdot 0.5$-MeOH (V)*

$Cu(BF_4)_2 \cdot 6H_2O$ (1.1 g; 3.2 mmol) was dissolved in methanol (80 mL) and triethylorthoformate (TEOF) (5 mL) added. PAP (1.0 g; 2.9 mmol) was added and the mixture refluxed for $2\frac{1}{2}$ h. A khaki solid (**IV**) was obtained and was filtered, washed with methanol, and dried under vacuum (yield = 0.3 g). The green mother liquor was allowed to stand for 4 days at room temperature. Dark green crystals (**V**) were formed, and were filtered, washed with methanol, and dried under vacuum at room temperature (yield = 0.6 g).

*Anal.* calcd. for $[Cu(PAPH)_2](BF_4)_4$ (**IV**): C 41.5, H 2.88, N 16.1, Cu 6.10; found: C 41.4, H 2.76, N 15.9, Cu 5.90.

*Anal.* calcd. for $[Cu_2(PAP)_2(H_2O)_2](BF_4)_4 \cdot 0.5MeOH$ (**V**): C 37.9, H 2.94, N 14.5, Cu 11.0; found: C 38.3, H 3.08, N 14.5, Cu 10.6.

*$[Cu_3(PAP)_2(OH)_2](BF_4)_4 \cdot 2H_2O$ (VI)*

$Cu(BF_4)_2 \cdot 6H_2O$ (1.0 g; 2.9 mmol) was dissolved in $H_2O$ (30 mL) and the solution filtered. The pH of this solution was about 3.5. Solid sodium fluoride was added to adjust the pH to 4.9. PAP (0.85 g; 2.7 mmol) was added and the mixture refluxed for 1 h. The green solution was filtered to remove a small amount of unreacted ligand and allowed to stand for several days. A dark khaki–green solid was obtained which was recrystallized from water to give dark green crystals. The product was filtered, washed with ethanol and diethyl ether, and dried under vacuum at room temperature.

*Anal.* calcd. for $[Cu_3(PAP)_2(OH)_2](BF_4)_4 \cdot 2H_2O$ (**VI**): C 34.9, H 2.75, N 13.6, Cu 15.4; found: C 34.9, H 2.80, N 13.4, Cu 14.7.

Only crystals of **I** and **II** proved to be suitable for X-ray analysis. Attempts were made to obtain X-ray data on crystals of compound **III** from several different preparations but in all cases the crystals were found not to diffract X-rays.

*X-ray crystallographic analyses*

*$[Cu(PAPH)_2(H_2O)_2](BF_4)_4$ (I) (triclinic modification)*

Crystal data (at 24°C) are:

$C_{36}H_{34}N_{12}B_4CuF_{16}O_2$ fw = 1077.51

Triclinic, $a$ = 9.856(1), $b$ = 12.724(1), $c$ = 9.401(1) Å, $\alpha$ = 101.691(8), $\beta$ = 96.717(9), $\gamma$ = 70.145(8)°, $V$ = 1084.4 Å$^3$, $Z$ = 1, $\rho_c$ = 1.650 g cm$^{-3}$, $F(000)$ = 543, Mo K$\alpha$ radiation ($\lambda_{\bar{\alpha}}$ = 0.71073 Å, $\mu$ = 6.2 cm$^{-1}$) graphite monochromatized. Absent reflections: none. Space group $P\bar{1}$ ($C_i^1$, No. 2) (9) from structure analysis.

The light-brown block shaped crystal used in the diffraction study was bounded by the seven faces: (100) and ($\bar{1}$00), 0.184 mm apart; (010) and (0$\bar{1}$0), 0.096 mm apart; and (001), (0$\bar{1}$1), (02$\bar{3}$) each 0.067 mm from the centre of the crystal. The quality of the data crystal was examined on the diffractometer, by taking open-counter $\omega$ scans of several strong low-angle reflections, and was judged to be acceptable. The average width of the peaks at half-height was 0.16°. Intensity data, in the range $3 \leq 2\theta \leq 55°$, were collected on an Enraf-Nonius CAD-4F $\kappa$-geometry diffractometer employing the $\omega$–$2\theta$ scan technique. Scan rates were automatically selected to make $I/\sigma(I) = 100$, and varied from 1.18 to 20.12° min$^{-1}$ in $\omega$, with a maximum scan time of 53 s being imposed. Prescans were done at 20.12° min$^{-1}$ in $\omega$ and reflections having $I/\sigma(I) < 1.5$ were considered weak and were not remeasured. Scan widths were computed according to $\Delta\omega = (0.70 + 0.35 \tan\theta)°$ and were extended 25% on either side for the measurement of backgrounds. Three standard reflections, (7$\bar{5}$4), (4$\bar{2}$5), and (22$\bar{1}$), measured after each 3600 s of X-ray exposure time (approximately after each 110 reflections) showed only random statistical fluctuations. A total of 6234 reflections ($3 \leq 2\theta \leq 30°$ ($\pm h, \pm k, -l$); $3 \leq 2\theta \leq 55°$ ($\pm h, \pm k, +l$)) were scanned. Data reduction then proceeded as detailed in ref. 10. An absorption correction was not applied. Maximum and minimum transmission factors were 0.95 and 0.92. Averaging of equivalent reflections yielded 4954 data, the 1392 having $F_o > 4\sigma(F_o)$ being used in the structure refinement. The $R$ factor for averaging (10) was 0.012. Unit-cell dimensions were obtained from a least-squares fit to the setting angles of 25 reflections with $2\theta > 30°$.

A systematic search using TRACER-II (11) failed to find any symmetry higher than triclinic and refinement, performed with SHELX-76 (12), has been completed in the centrosymmetric space group $P\bar{1}$. This choice of space group appears to be vindicated based on the successful convergence of the structure refinement. Further weight is added to this assignment of space group by the fact that, in space group $P\bar{1}$, the Cu atoms of the structure are constrained to sites of $\bar{1}$ symmetry. Compound **II** crystallizes in the centrosymmetric space group $P2_1/n$, which is uniquely defined by its systematic absences, and in this case the Cu atoms again occupy sites of $\bar{1}$ symmetry. The structure was solved by conventional heavy atom methods using Patterson and Fourier maps. Full-matrix least-squares refinement of 305 variables converged at $R_1 = 0.083$ and $R_2 = 0.104$ where $R_1 = \sum||F_o| - |F_c||/\sum|F_o|$ and $R_2 = [\sum w(|F_o| - |F_c|)^2/\sum w|F_o|^2]^{1/2}$. The function minimized in the least-squares was $\sum w(|F_o| - |F_c|)^2$ where $w = 2.2787/(\sigma^2(F_o) + 0.000941F_o^2)$. All non-hydrogen atoms were refined anisotropically. Hydrogen atoms could not be located but those attached to carbon were placed in calculated positions and constrained to ride 0.95 Å from their respective carbon atoms (12). A common isotropic temperature factor for these hydrogen atoms converged at $U$ = 0.05(1) Å$^2$. Both tetrafluoroborate anions were refined as rigid groups (B—F, 1.37 Å; F—B—F, 109.5°) pivoting on their respective boron atoms (12).

Towards the final stages of refinement, a check was made on the assignment of N(6) and C(15). With both of these atoms vibrating isotropically and all other non-hydrogen atoms vibrating anisotropically, three cycles of least-squares refinement resulted in $R_1 = 0.083$ and $R_2 = 0.105$. The value of $U$ (Å$^2$) for N(6) was 0.053(3) and for C(15) was 0.057(4). From the same initial parameters, but with N(6) assigned a carbon atom scattering factor and C(15) a nitrogen atom scattering factor, three cycles of refinement were again performed. The residual indices were now $R_1 = 0.088$ and $R_2 = 0.110$. The isotropic temperature factor, $U$ (Å$^2$), for N(6) was 0.026(3) and for C(15) was 0.095(5). The original assignment for these two atoms was therefore considered to be correct.

Neutral atom scattering factors and anomalous dispersion corrections, for the non-hydrogen atoms, were taken from ref. 13. Scattering factors for the hydrogen atoms were those of Stewart *et al.* (14). The three largest peaks on a final difference-Fourier map were 1.10, 0.82, and 0.70 e Å$^{-3}$ located in the vicinity of the tetrafluoroborate groups. All remaining peaks were < 0.45 e Å$^{-3}$. In the final cycle of refinement no parameter shifted by more than 0.001 of its estimated standard deviation. The average $w\Delta^2$ for groups of data sectioned according to parity group, $|F_o|$, $(\sin\theta)/\lambda$, $|h|$, $|k|$, or $|l|$, showed reasonable consistency and the weighting scheme was considered to be satisfactory.

*$[Cu(PAPH)_2(H_2O)_2](BF_4)_4$ (II) (monoclinic modification)*

*Crystal data (at 24°C) are*

$C_{36}H_{34}N_{12}B_4CuF_{16}O_2$ fw = 1077.51

Monoclinic, $a$ = 12.663(4), $b$ = 9.573(3), $c$ = 18.813(4) Å, $\beta$ =

Can. J. Chem. Downloaded from www.nrcresearchpress.com by 210.87.254.6 on 09/06/12
For personal use only.

107.16(2)°, $V = 2178.9$ Å$^3$, $Z = 2$, $\rho_c = 1.642$ g cm$^{-3}$, $F(000) = 1086$, Mo Kα radiation ($\lambda_{\bar{\alpha}} = 0.71073$ Å, $\mu = 6.2$ cm$^{-1}$) graphite monochromatized. Absent reflections: $h0l, h + l \neq 2n$; $0k0, k \neq 2n$. Space group $P2_1/n$, a non-standard setting of space group $P2_1/c$ ($C_{2h}^5$, No. 14) (15) in which the general equivalent positions are $(x, y, z)$; $(\bar{x}, \bar{y}, \bar{z})$; $(\frac{1}{2} + x, \frac{1}{2} - y, \frac{1}{2} + z)$; $(\frac{1}{2} - x, \frac{1}{2} + y, \frac{1}{2} - z)$.

Except as indicated below, the details of the structure analysis for **II** are the same as those for **I**.

The light-green plate-like crystal used in the diffraction study was bounded by eight faces: (011) and (0$\bar{1}\bar{1}$), 0.234 mm apart; (01$\bar{1}$) and (0$\bar{1}$1), 0.384 mm apart; (101) and ($\bar{1}$0$\bar{1}$), 0.366 mm apart; and (10$\bar{1}$) and ($\bar{1}$01), 0.066 mm apart. Three standard reflections, ($\bar{3}$,3,$\bar{1}$0), ($\bar{3}$33), and (225) were measured after approximately every 130 data. A total of 6169 reflections ($3 \leq 2\theta \leq 30°$ ($-h, -k, \pm l$); $3 \leq 2\theta \leq 55°$ ($+h, +k, \pm l$)) were scanned. Maximum and minimum transmission factors were 0.96 and 0.84. Averaging of equivalent reflections yielded 5003 data, the 1493 having $F_o > 4\sigma(F_o)$ being used in the structure refinement. The $R$ factor for averaging (10) was 0.012. Refinement converged at $R_1 = 0.083$ and $R_2 = 0.111$ and the final weighting scheme was $w = 2.7841/(\sigma^2(F_o) + 0.000815F_o^2)$. A common isotropic temperature factor, for the hydrogen atoms attached to carbon, converged at $U = 0.04(1)$ Å$^2$. The largest peaks on a final difference-Fourier map were all < 0.73 e Å$^{-3}$ and were in the vicinity of the tetrafluoroborate groups. The check on the assignment of N(6) and C(15) performed as for **I** yielded $R_1 = 0.084$ and $R_2 = 0.111$ after three cycles of least-squares refinement. The isotropic temperature factor, $U$ (Å$^2$), was 0.053(3) for N(6) and 0.057(4) for C(15). With the scattering factors for these two atoms interchanged, three cycles of refinement from the same initial parameters resulted in $R_1 = 0.087$ and $R_2 = 0.117$. The isotropic $U$ (Å$^2$) for N(6) was now 0.026(3) and for C(15) was 0.091(5). Again, the original assignment for these two atoms was considered to be correct.

Final atomic positional parameters together with their estimated standard deviations, for **I** and **II**, are given in Table 1. Bond lengths and angles, within the cations of both structures, appear in Table 2 while interionic contacts appear in Table 3. Tables S1 and S2 list final observed and calculated structure factors for **I** and **II**, respectively. Tables S3 and S4 list final anisotropic thermal parameters while Table S5 gives a listing of least-squares planes for both structures.[2] The geometry of the cations is depicted in Figs. 5 and S1 for **I** and **II**, respectively. The atom labelling scheme for the cations of **I** and **II** is the same and is shown in Fig. 5.

## Discussion

Our previous studies with binuclear copper and cobalt complexes of PAP (1, 2) had shown that a preferred structural arrangement involved two metal centres bound simultaneously to the same ligand (Fig. 2). In all cases multiple bridging was indicated between the metal centres. Moderate to strong antiferromagnetic exchange was observed for several binuclear copper complexes ($-J = 50$–$170$ cm$^{-1}$) (1) while weaker exchange was observed for the binuclear cobalt systems ($-J < 6$ cm$^{-1}$) (2). Similar 1:2 (ligand:metal) nickel complexes were obtained but here the predominant binuclear species involved 1:1 metal:ligand ratios (3). Weak antiferromagnetic exchange ($-J < 7.3$ cm$^{-1}$) was again observed in these systems.

Since all of the binuclear copper complexes for which antiferromagnetic exchange was observed had multiple bridges between the metal centres ($N_2$ phthalazine bridge plus at least one other bridging group), attempts were made to synthesize systems in which just phthalazine bridges were involved, in order to assess the exchange pathways independently and perhaps decide which bridging groups contributed most to magnetic exchange. Consequently, 1:1 reactions between PAP and metal salts were investigated. In the case of copper tetrafluoroborate, reaction with a 1:1 stoichiometry in water resulted in the formation of three different products. Initially a mixture of brown triclinic (**I**) and green monoclinic (**II**) crystals was obtained, comprising about one third of the total product yield (see Experimental). The mixture contained approximately equal proportions of both products. On reduction of the volume of the mother liquor a dark green crystalline product (**III**) was obtained.

The brown and green crystals were separated by hand and analyzed independently. Both forms were assigned the formula $[Cu(PAPH)_2(H_2O)_2](BF_4)_4$, a system of necessity involving protonated ligand. An elemental analysis of a random sample of the mixture of **I** and **II** was found to be the same, thus supporting the individual analyses. The dark-green product (**III**) has a different elemental analysis in keeping with a product having a 2:3 (ligand:metal) ratio and is assigned a formula $[Cu_3(PAP)_2(OH)_2](BF_4)(BF_3OH)_3 \cdot 5H_2O$. A mixture of products was also obtained from the 1:1 reaction of copper tetrafluoroborate and PAP in methanol/TEOF. Initially a khaki coloured powder (**IV**) was obtained followed by dark-green crystals (**V**) on concentration of the mother liquor. The khaki product **IV** appears to be a mononuclear protonated derivative similar to **I** and **II** and is assigned the formula $[Cu(PAPH)_2](BF_4)_4$. The dark-green product **V** is a binuclear complex, $[Cu_2(PAP)_2(H_2O)_2](BF_4)_4 \cdot 0.5MeOH$.

Electronic spectra (Table 4) for compounds **I** and **II** in the solid state have major absorptions at 18 500 and 17 500 cm$^{-1}$ respectively, consistent with tetragonally distorted six-coordinate structures in which the degree of distortion may be different. Compound **IV** exhibits a weak shoulder at 16 600 cm$^{-1}$. Intense charge transfer absorption at higher energies made it impossible to pick out any further bands assignable to $d$–$d$ transitions. It seems reasonable to assume that compound **IV** is a square

[2]Tables S1-S5 and Figure S1 are available, at a nominal charge, from the Depository of Unpublished Data, CISTI, National Research Council of Canada, Ottawa, Ont., Canada K1A 0S2.

TABLE 1. Final fractional coordinates for the atoms of $[Cu(PAPH)_2(H_2O)_2](BF_4)_4$[a,b]

| Atom | x | y | z | Atom | x | y | z |
|---|---|---|---|---|---|---|---|
| Cu | 0.00 | 0.00 | 0.00 | B(1) | 0.7517(7) | 0.3620(5) | 0.7994(7) |
| | 0.00 | 0.00 | 0.00 | | 0.2838(7) | 0.2240(9) | 0.9041(5) |
| O(W) | -0.2405(10) | 0.1522(8) | 0.0117(11) | F(11) | 0.7006(7) | 0.3939(5) | 0.9364(7) |
| | -0.0264(9) | -0.0477(12) | 0.1203(5) | | 0.3860(7) | 0.1816(9) | 0.9470(5) |
| N(1) | -0.0169(12) | -0.0413(8) | -0.2162(11) | F(12) | 0.8677(7) | 0.3977(5) | 0.7973(7) |
| | 0.0141(9) | -0.2080(11) | -0.0176(7) | | 0.2301(7) | 0.1139(9) | 0.8623(5) |
| N(2) | 0.1960(12) | -0.0027(9) | -0.2415(12) | F(13) | 0.7933(7) | 0.2462(5) | 0.7616(7) |
| | -0.1395(8) | -0.1954(11) | -0.1295(6) | | 0.2236(7) | 0.2707(9) | 0.9490(5) |
| N(3) | 0.0784(11) | 0.1156(9) | -0.0367(12) | F(14) | 0.6451(7) | 0.4101(5) | 0.7024(7) |
| | -0.1622(8) | -0.0295(11) | -0.0450(6) | | 0.2953(7) | 0.3298(9) | 0.8579(5) |
| N(4) | 0.0377(11) | 0.2185(9) | 0.0576(11) | B(2) | -0.5320(8) | 0.1882(9) | 0.2770(10) |
| | -0.2301(8) | 0.0499(10) | -0.0154(6) | | 0.6234(5) | 0.3811(7) | 0.8020(3) |
| N(5) | 0.0534(12) | 0.3968(9) | 0.1484(12) | F(21) | -0.4671(8) | 0.1271(9) | 0.3850(10) |
| | -0.3968(8) | 0.1509(11) | -0.0200(6) | | 0.6675(5) | 0.2567(7) | 0.7885(3) |
| N(6) | -0.1491(13) | 0.3641(10) | 0.2276(12) | F(22) | -0.6743(8) | 0.2446(9) | 0.3046(10) |
| | -0.2639(10) | 0.1872(12) | 0.0946(7) | | 0.6160(5) | 0.3816(7) | 0.8731(3) |
| C(1) | -0.1261(16) | -0.0802(12) | -0.2859(17) | F(23) | -0.5227(8) | 0.1161(9) | 0.1460(10) |
| | 0.0958(10) | -0.2853(16) | 0.0250(8) | | 0.6899(5) | 0.4887(7) | 0.7934(3) |
| C(2) | -0.1196(20) | -0.1373(13) | -0.4244(18) | F(24) | -0.4640(8) | 0.2650(9) | 0.2720(10) |
| | 0.1305(11) | -0.4063(17) | 0.0040(8) | | 0.5201(5) | 0.3973(7) | 0.7527(3) |
| C(3) | 0.0044(20) | -0.1630(12) | -0.4987(17) | H(1) | -0.2096(16) | -0.0664(12) | -0.2345(17) |
| | 0.0774(13) | -0.4524(17) | -0.0667(12) | | 0.1321(10) | -0.2523(16) | 0.0738(8) |
| C(4) | 0.1118(18) | -0.1207(11) | -0.4359(16) | H(2) | -0.1992(20) | -0.1594(13) | -0.4703(18) |
| | -0.0098(11) | -0.3821(15) | -0.1120(8) | | 0.1891(11) | -0.4579(17) | 0.0365(8) |
| C(5) | 0.0939(16) | -0.0547(11) | -0.2968(16) | H(3) | 0.0146(20) | -0.2096(12) | -0.5922(17) |
| | -0.0420(10) | -0.2575(15) | -0.0839(8) | | 0.1023(13) | -0.5354(17) | -0.0844(12) |
| C(6) | 0.1727(14) | 0.0951(12) | -0.1378(15) | H(4) | 0.1966(18) | -0.1358(11) | -0.4858(16) |
| | -0.2048(10) | -0.1055(14) | -0.1037(7) | | -0.0475(11) | -0.4153(15) | -0.1604(8) |
| C(7) | 0.2523(14) | 0.1723(12) | -0.1389(14) | H(8) | 0.3792(14) | 0.0840(12) | -0.3110(14) |
| | -0.3199(10) | -0.0952(14) | -0.1448(7) | | -0.3264(11) | -0.2404(15) | -0.2293(8) |
| C(8) | 0.3588(14) | 0.1500(12) | -0.2378(14) | H(9) | 0.5102(14) | 0.2089(13) | -0.2889(16) |
| | -0.3695(11) | -0.1765(15) | -0.2109(8) | | -0.5082(12) | -0.2171(16) | -0.2873(8) |
| C(9) | 0.4335(14) | 0.2257(13) | -0.2267(16) | H(10) | 0.4475(16) | 0.3808(13) | -0.1205(17) |
| | -0.4756(12) | -0.1600(16) | -0.2452(8) | | -0.6163(11) | -0.0552(16) | -0.2531(8) |
| C(10) | 0.3981(16) | 0.3278(13) | -0.1244(17) | H(11) | 0.2687(16) | 0.4164(12) | 0.0406(17) |
| | -0.5414(11) | -0.0666(16) | -0.2243(8) | | -0.5453(10) | 0.0731(15) | -0.1463(8) |
| C(11) | 0.2909(16) | 0.3492(12) | -0.0306(17) | H(15) | -0.0356(17) | 0.5770(13) | 0.3365(16) |
| | -0.4991(10) | 0.0097(15) | -0.1622(8) | | -0.4982(12) | 0.3334(16) | 0.0341(9) |
| C(12) | 0.2144(14) | 0.2739(12) | -0.0385(16) | H(16) | -0.2229(18) | 0.6318(12) | 0.4920(17) |
| | -0.3863(9) | -0.0037(15) | -0.1203(6) | | -0.4451(15) | 0.4448(16) | 0.1477(11) |
| C(13) | 0.1008(14) | 0.2943(11) | 0.0564(14) | H(17) | -0.3751(18) | 0.5199(15) | 0.4706(19) |
| | -0.3315(10) | 0.0663(14) | -0.0505(7) | | -0.2732(15) | 0.3810(17) | 0.2333(9) |
| C(14) | -0.0601(18) | 0.4273(12) | 0.2373(15) | H(18) | -0.3224(16) | 0.3537(13) | 0.3036(18) |
| | -0.3614(10) | 0.2147(14) | 0.0489(8) | | -0.1619(12) | 0.2267(18) | 0.1967(9) |
| C(15) | -0.0926(17) | 0.5294(13) | 0.3328(16) | | | | |
| | -0.4287(12) | 0.3119(16) | 0.0686(9) | | | | |
| C(16) | -0.2057(18) | 0.5636(12) | 0.4228(17) | | | | |
| | -0.3987(15) | 0.3772(16) | 0.1352(11) | | | | |
| C(17) | -0.2947(18) | 0.4975(15) | 0.4116(19) | | | | |
| | -0.2966(15) | 0.3411(17) | 0.1849(9) | | | | |
| C(18) | -0.2622(16) | 0.3995(13) | 0.3128(18) | | | | |
| | -0.2321(12) | 0.2493(18) | 0.1633(9) | | | | |

[a] Values for the monoclinic modification (II) appear below those for the triclinic modification (I). Atoms are labelled as indicated in Fig. 5. Estimated standard deviations, in parentheses, occur in the last significant figure(s) for each parameter.
[b] Hydrogen atoms are labelled according to the carbon atom to which they are attached.

planar derivative. Compounds **III** and **V** exhibit three major *d–d* absorptions in the range 10 000 – 16 500 $cm^{-1}$ indicative of square pyramidal copper(II) (1). Lower energy absorptions are observed for **V**, suggesting a difference in the metal coordination sphere in these two systems. Compound **VI** has a spectrum identical to that of compound **III**. The lowest energy charge transfer absorptions, which are assigned to a $\pi-\pi^*$ transition, for all the compounds, occur at 27 400 $cm^{-1}$ or above, indicat-

Can. J. Chem. Downloaded from www.nrcresearchpress.com by 210.87.254.6 on 09/06/12
For personal use only.

Can. J. Chem. Downloaded from www.nrcresearchpress.com by 210.87.254.6 on 09/06/12
For personal use only.

TABLE 2. Intramolecular bond distances (Å) and angles (deg) for $[Cu(PAPH)_2(H_2O)_2](BF_4)_4$[a]

| Bond | Distance | Bond | Distance |
|---|---|---|---|
| Cu—O(W) | 2.497(9) | C(4)—C(5) | 1.398(17) |
| | 2.426(9) | | 1.413(17) |
| Cu—N(1) | 1.995(10) | C(6)—C(7) | 1.452(16) |
| | 2.035(11) | | 1.439(15) |
| Cu—N(3) | 1.980(9) | C(7)—C(8) | 1.402(16) |
| | 1.997(10) | | 1.444(18) |
| N(1)—C(1) | 1.378(15) | C(7)—C(12) | 1.400(16) |
| | 1.331(14) | | 1.384(16) |
| N(1)—C(5) | 1.346(16) | C(8)—C(9) | 1.380(17) |
| | 1.328(15) | | 1.318(17) |
| N(2)—C(5) | 1.382(16) | C(9)—C(10) | 1.413(17) |
| | 1.411(14) | | 1.356(18) |
| N(2)—C(6) | 1.385(15) | C(10)—C(11) | 1.376(18) |
| | 1.377(15) | | 1.348(17) |
| N(3)—N(4) | 1.385(13) | C(11)—C(12) | 1.393(17) |
| | 1.381(13) | | 1.419(15) |
| N(3)—C(6) | 1.333(15) | C(12)—C(13) | 1.435(17) |
| | 1.300(14) | | 1.455(16) |
| N(4)—C(13) | 1.315(14) | C(14)—C(15) | 1.381(17) |
| | 1.269(13) | | 1.384(18) |
| N(5)—C(13) | 1.375(15) | C(15)—C(16) | 1.374(18) |
| | 1.396(15) | | 1.350(19) |
| N(5)—C(14) | 1.376(16) | C(16)—C(17) | 1.389(19) |
| | 1.383(15) | | 1.397(20) |
| N(6)—C(14) | 1.362(16) | C(17)—C(18) | 1.359(18) |
| | 1.306(15) | | 1.343(19) |
| N(6)—C(18) | 1.345(16) | N(1)...N(3) | 2.693(16) |
| | 1.371(17) | | 2.737(15) |
| C(1)—C(2) | 1.353(18) | N(1)...N(3*) | 2.924(18) |
| | 1.339(18) | | 2.961(14) |
| C(2)—C(3) | 1.387(19) | N(4)...N(6) | 2.559(14) |
| | 1.374(20) | | 2.591(18) |
| C(3)—C(4) | 1.368(19) | | |
| | 1.357(18) | | |

| Bonds | Angle | Bonds | Angle |
|---|---|---|---|
| O(W)—Cu—O(W*) | 180.0 | N(2)—C(5)—C(4) | 117.7(14) |
| | 180.0 | | 115.2(12) |
| O(W)—Cu—N(1) | 93.3(4) | N(2)—C(6)—N(3) | 118.9(12) |
| | 90.6(4) | | 120.6(11) |
| O(W)—Cu—N(1*) | 86.7(4) | N(2)—C(6)—C(7) | 120.0(13) |
| | 89.4(4) | | 118.1(12) |
| O(W)—Cu—N(3) | 86.5(4) | N(3)—C(6)—C(7) | 121.1(13) |
| | 87.7(4) | | 121.2(12) |
| O(W)—Cu—N(3*) | 93.5(4) | C(6)—C(7)—C(8) | 122.7(13) |
| | 92.3(4) | | 122.7(13) |
| N(1)—Cu—N(1*) | 180.0 | C(6)—C(7)—C(12) | 116.7(12) |
| | 180.0 | | 118.9(12) |
| N(1)—Cu—N(3) | 85.3(4) | C(8)—C(7)—C(12) | 120.5(12) |
| | 85.5(4) | | 118.4(12) |
| N(1)—Cu—N(3*) | 94.7(5) | C(7)—C(8)—C(9) | 118.7(13) |
| | 94.5(4) | | 118.6(13) |

TABLE 2. (*Concluded*)

| Bonds | Angle | Bonds | Angle |
|---|---|---|---|
| N(3)—Cu—N(3*) | 180.0 | C(8)—C(9)—C(10) | 121.2(13) |
| | 180.0 | | 124.2(14) |
| Cu—N(1)—C(1) | 121.8(10) | C(9)—C(10)—C(11) | 119.0(13) |
| | 122.4(10) | | 119.2(13) |
| Cu—N(1)—C(5) | 120.4(9) | C(10)—C(11)—C(12) | 121.0(14) |
| | 116.9(9) | | 120.6(13) |
| C(1)—N(1)—C(5) | 116.4(12) | C(7)—C(12)—C(11) | 119.3(13) |
| | 118.2(12) | | 118.9(12) |
| C(5)—N(2)—C(6) | 125.5(11) | C(7)—C(12)—C(13) | 118.2(12) |
| | 123.8(11) | | 114.7(10) |
| Cu—N(3)—N(4) | 115.6(8) | C(11)—C(12)—C(13) | 122.4(14) |
| | 115.9(8) | | 126.4(12) |
| Cu—N(3)—C(6) | 123.3(9) | N(4)—C(13)—N(5) | 118.0(12) |
| | 123.7(8) | | 119.3(11) |
| N(4)—N(3)—C(6) | 121.0(10) | N(4)—C(13)—C(12) | 122.3(13) |
| | 120.0(10) | | 123.6(12) |
| N(3)—N(4)—C(13) | 120.1(11) | N(5)—C(13)—C(12) | 119.7(12) |
| | 120.8(11) | | 117.1(11) |
| C(13)—N(5)—C(14) | 124.2(11) | N(5)—C(14)—N(6) | 122.3(13) |
| | 125.0(10) | | 120.7(12) |
| C(14)—N(6)—C(18) | 120.2(13) | N(5)—C(14)—C(15) | 119.5(14) |
| | 119.4(13) | | 119.5(12) |
| N(1)—C(1)—C(2) | 122.9(14) | N(6)—C(14)—C(15) | 118.0(15) |
| | 124.5(14) | | 119.8(13) |
| C(1)—C(2)—C(3) | 119.3(14) | C(14)—C(15)—C(16) | 121.5(15) |
| | 117.1(14) | | 122.2(15) |
| C(2)—C(3)—C(4) | 119.3(15) | C(15)—C(16)—C(17) | 119.4(14) |
| | 121.5(15) | | 117.3(15) |
| C(3)—C(4)—C(5) | 118.6(15) | C(16)—C(17)—C(18) | 117.4(15) |
| | 117.1(14) | | 119.0(15) |
| N(1)—C(5)—N(2) | 119.7(12) | N(6)—C(18)—C(17) | 123.4(14) |
| | 123.4(12) | | 122.3(15) |
| N(1)—C(5)—C(4) | 122.6(13) | | |
| | 121.3(12) | | |

[a] See footnote *a* in Table 1. Values reported have not been corrected for thermal motion. Atoms labelled with an asterisk are related to those unlabelled by a centre of symmetry located at the Cu atoms.

ing the absence of an anionic ligand in these systems (1).

Infrared and magnetic data are recorded in Table 5. With the exception of the compound $[Cu(PAPH)_2](BF_4)_4$ (**IV**) all other derivatives exhibit infrared bands that can be assigned to coordinated and/or lattice bound water. In the case of compounds **I** and **II** two OH stretching absorptions can be clearly discerned consistent with the symmetric and antisymmetric OH stretch due to a coordinated water molecule. Single NH stretching absorptions occur in the range 3350–3390 $cm^{-1}$ for all the compounds studied, suggesting the presence of one type of NH group. These absorptions occur at somewhat higher energies than those observed for 2:1 binuclear copper complexes of PAP (1) and indicate that the two hydrogen atoms on the ligand associated with nitrogen are bound to the exocyclic nitrogen atoms. The ligand is therefore expected to exist in all the tetrafluoroborate complexes in the tautomeric form shown in Fig. 1. No other bands in this spectral region could be assigned to the protonated nitrogen site present in compounds **I**, **II**, and **IV**. The NH stretching frequency for such a group, $\overset{+}{N}H$, would be expected to occur at lower energies. Typical pyridinium salts do not have absorptions above 3000 $cm^{-1}$ which can be associated with NH stretch (16). Although compounds **I** and **II** had almost identical infrared absorptions in the OH stretching, NH stretching, and CN stretching regions, some minor differences were observed in other regions of the spectrum. However, the

Can. J. Chem. Downloaded from www.nrcresearchpress.com by 210.87.254.6 on 09/06/12
For personal use only.

Can. J. Chem. Downloaded from www.nrcresearchpress.com by 210.87.254.6 on 09/06/12
For personal use only.

TABLE 3. Intermolecular non-hydrogen atom contacts less than 3.3 Å for $[Cu(PAPH)_2(H_2O)_2](BF_4)_4$

(*a*) Triclinic form (**I**)

| Atoms | Distance | Atoms | Distance |
|---|---|---|---|
| N(5)–F(12[a]) | 2.91(2) | C(11)–F(11[a]) | 3.24(2) |
| N(5)–F(22[b]) | 3.13(1) | C(12)–F(23[b]) | 3.25(2) |
| N(6)–F(11[c]) | 2.99(1) | C(13)–F(22[b]) | 3.03(2) |
| C(1)–F(22[d]) | 3.29(2) | C(15)–F(12[a]) | 3.13(2) |
| C(2)–F(22[d]) | 3.21(2) | C(16)–F(22[f]) | 3.18(2) |
| C(3)–F(13[e]) | 3.14(2) | O(W)–F(11[c]) | 3.14(1) |
| C(4)–F(13[e]) | 3.24(2) | O(W)–F(13[c]) | 2.94(1) |

[a] Atom is at $(1-x, 1-y, 1-z)$.
[b] Atom is at $(1+x, y, z)$.
[c] Atom is at $(-1+x, y, -1+z)$.
[d] Atom is at $(-1-x, -y, -z)$.
[e] Atom is at $(1-x, -y, -z)$.
[f] Atom is at $(-1-x, 1-y, 1-z)$.

(*b*) Monoclinic form (**II**)

| Atoms | Distance | Atoms | Distance |
|---|---|---|---|
| N(2)–F(21[a]) | 2.94(1) | C(12)–F(21[c]) | 3.21(2) |
| N(2)–F(24[a]) | 3.24(1) | C(13)–F(11[b]) | 3.27(2) |
| N(3)–F(13[b]) | 3.17(2) | C(14)–F(11[c]) | 3.22(1) |
| N(4)–F(12[b]) | 3.28(1) | C(15)–F(11[c]) | 3.02(2) |
| N(5)–F(11[c]) | 2.65(1) | C(16)–F(14[f]) | 3.08(2) |
| N(5)–F(22[c]) | 3.02(1) | C(17)–F(14[f]) | 3.25(2) |
| N(6)–F(12[b]) | 2.99(2) | C(17)–F(12[g]) | 3.28(2) |
| C(3)–F(13[d]) | 3.20(2) | O(W)–F(12[b]) | 2.77(2) |
| C(8)–F(23[e]) | 3.29(2) | O(W)–F(13[b]) | 3.25(1) |
| C(11)–F(11[c]) | 3.29(2) | O(W)–F(24[g]) | 2.79(1) |

[a] Atom is at $(\frac{1}{2}-x, -\frac{1}{2}+y, \frac{1}{2}-z)$.
[b] Atom is at $(-x, -y, 1-z)$.
[c] Atom is at $(-1+x, y, -1+z)$.
[d] Atom is at $(x, -1+y, -1+z)$.
[e] Atom is at $(-1+x, -1+y, -1+z)$.
[f] Atom is at $(-x, 1-y, 1-z)$.
[g] Atom is at $(-\frac{1}{2}+x, \frac{1}{2}-y, -\frac{1}{2}+z)$.

complexity of the spectra in these regions prevented the rationalization of these differences in terms of a specific assignment.

One major difference between the infrared spectra of the protonated and neutral ligand complexes occurred in the aromatic CN stretching region (> 1600 $cm^{-1}$) (Table 5). Two bands associated with CN stretch are observed for PAP and compounds **III**, **V**, and **VI** which contain neutral ligand. Three major absorptions are found in this region for **I**, **II**, and **IV**, which contain protonated ligand (an additional shoulder is observed in **I** and **IV**). $[PAPH_2]Cl_2 \cdot 2H_2O$, obtained by reacting PAP with two equivalents of aqueous HCl, exhibits five bands in this region, four of which correspond with those observed for **I** and **IV**. The additional bands observed in the CN stretching region for the protonated complexes, combined with the appearance of bands associated with non-protonated exocyclic NH suggest that the possible sites of protonation are the uncoordinated phthalazine and pyridine nitrogen sites. $pK_b$ values for pyridine and for some 2-substituted pyridines fall in the range 7.2 to 8.8 at room temperature in aqueous solution (17) whereas for phthalazine a value of 10.53 is reported at 20°C (18). The pyridine nitrogen is a more basic site and although infrared data do not indicate which site is protonated the pyridine site seems most likely.

The rationale for the formation of protonated and neutral ligand complexes of PAP with copper tetrafluoroborate in water rests on the hydrolysis equilibrium involving the tetrafluoroborate ion itself. To substantiate the involvement of the tetrafluoroborate hydrolysis in the chemistry of this system would necessitate locating, for example, $BF_3OH^-$ in one of the products. It is evident from the fluorine analyses of compounds **I** and **II** that no hydroxyfluoroborate anion exists in these systems but the fluorine analysis on **III** does indicate the presence of a hydroxyfluoroborate species. However, it was not possible to identify this species by spectroscopic or crystallographic methods, although analytical and other data do suggest $BF_3OH^-$.

Magnetic moments are recorded in Table 5. Normal moments are observed for compounds **I**, **II**, and **IV**, typical of mononuclear copper(II) species. For the other complexes, which involve polynuclear structures, reduced room temperature moments are observed, indicative of systems involving antiferromagnetic exchange between the metal centres. Variable temperature magnetic studies on these systems will be reported elsewhere.

TABLE 4. Electronic spectra ($cm^{-1}$)[a]

| Compound | Colour | | *d–d* | CT |
|---|---|---|---|---|
| **I**, $[Cu(PAPH)_2(H_2O)_2](BF_4)_4$ | Brown | *a*, | [15400]18500 | [28600] |
| | | *b*, | [11000][14300]15500 | |
| **II**, $[Cu(PAPH)_2(H_2O)_2](BF_4)_4$ | Light green | *a*, | 17500 | [27400][28600] |
| **III**, $[Cu_3(PAP)_2(OH)_2](BF_4)(BF_3OH)_3 \cdot 5H_2O$ | Dark green | *a*, | [10900][14700]16400 | 28600 |
| | | *b*, | [11200][14300]15600 | |
| **IV**, $[Cu(PAPH)_2](BF_4)_4$ | Khaki | *a*, | [16600] | 29400 |
| **V**, $[Cu_2(PAP)_2(H_2O)_2](BF_4)_4 \cdot 0.5MeOH$ | Dark green | *a*, | 10400, 13600, 15400 | 28600 |
| **VI**, $[Cu_3(PAP)_2(OH)_2](BF_4)_4 \cdot 2H_2O$ | Dark green | *a*, | [10900][14800]16400 | 28400 |

[a] *a*, Mull transmittance; *b*, solution in water.

TABLE 5. Infrared spectra and magnetism

| Compound | νNH ($cm^{-1}$) | νOH ($cm^{-1}$) | νCN ($cm^{-1}$) | $\mu_{Cu}$(BM) (room temp.) |
|---|---|---|---|---|
| **I**, $[Cu(PAPH)_2(H_2O)_2](BF_4)_4$ | 3360 | 3540, 3615 | 1620, 1632, 1655, 1660(sh) | 1.9 |
| **II**, $[Cu(PAPH)_2(H_2O)_2](BF_4)_4$ | 3370 | 3520, 3590 | 1621, 1634, 1658 | 2.0 |
| **III**, $[Cu_3(PAP)_2(OH)_2](BF_4)(BF_3OH)_3 \cdot 5H_2O$ | 3390 | 3520 | 1615, 1635 | 1.3 |
| **IV**, $[Cu(PAPH)_2](BF_4)_4$ | 3350 | — | 1621, 1634, 1656, 1661(sh) | 1.9 |
| **V**, $[Cu_2(PAP)_2(H_2O)_2](BF_4)_4 \cdot 0.5MeOH$ | 3360 | 3540(sh), 3620 | 1617, 1635 | 1.6 |
| **VI**, $[Cu_3(PAP)_2(OH)_2](BF_4)_2 \cdot 2H_2O$ | 3380 | 3580 | 1612, 1638 | 1.3 |
| **VII**, $[Cu_2(PAP)(OH)Cl_3] \cdot 1.5H_2O$ (ref. 1) | | | 1613, 1635 | |
| $[PAPH_2]Cl_2 \cdot 2H_2O$ | | | 1613(sh), 1620, 1635, 1650, 1660 | |
| PAP | | | 1603, 1628 | |
| $[Cu_2(PAP)(CH_3CH_2COO)_3]$ (ref. 1) | | | 1612, 1635 | |

Spectroscopic and other data indicate compounds **I** and **II** to be mononuclear derivatives involving two bidentate protonated ligands and tetragonal copper with two axially coordinated water molecules (a structural description of these two compounds is to follow). Compound **III** has been formulated as a trinuclear derivative involving tetradentate ligands and possibly hydroxy bridges, with spin-exchanged metal centres. The choice of this unit is largely arbitrary and the cationic component of this system may involve a cluster of copper atoms bridged by both hydroxy and phthalazine groups. The structural identity of this compound awaits a successful X-ray analysis. Compound **VI** is assumed to have the same basic structure as **III**, while for compound **V**, in which the metal-to-ligand ratio is 1:1, a binuclear structure involving two metal centres sandwiched between two adjacent tetradentate ligands is proposed (Fig. 4). Since the ligand is neutral in this system and since no infrared absorption can be associated with a hydroxy bridge the fifth coordination site at each metal is assumed to be occupied by a water molecule. This system appears to be different from other binuclear complexes of PAP involving the metals copper, cobalt, and nickel, in which single atom bridges (e.g. halogen, hydroxide) have been found in addition to the phthalazine bridge (1–4, 6).

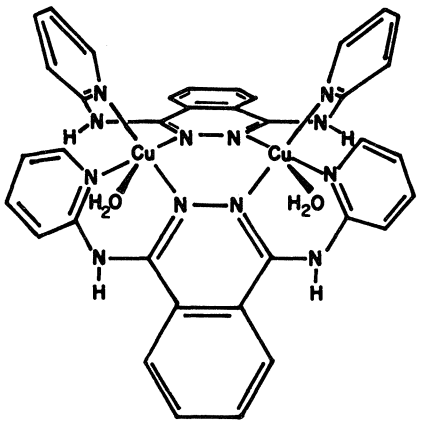


FIG. 4. Proposed structure for the $[Cu_2(PAP)_2(H_2O)_2]^{4+}$ cation in **V**.

*Description of the structures of compounds I and II*

The compound $[Cu(PAPH)_2(H_2O)_2](BF_4)_4$ crystallizes from aqueous solution yielding a brown triclinic form (**I**) and a green monoclinic form (**II**). Both structures of **I** and **II** contain $[Cu(PAPH)_2(H_2O)_2]^{4+}$ cations (Fig. 5) and $BF_4^-$ anions in a ratio of 1:4. The copper atoms of the cations in both structures occupy sites of $\bar{1}$ symmetry and are at the centre of a tetragonally distorted octahedron formed by two *trans* water molecules (Cu—O(W) = 2.497(9) Å in **I** and 2.426(9) Å in **II**) and four nitrogen atoms from two chelating bidentate protonated PAP ligands (Cu—N(pyridine) = 1.995(10) Å in **I** and 2.035(11) Å in **II**; Cu—N(phthalazine) = 1.980(9) Å in **I** and 1.997(10) Å in **II**). The Cu—N distances can be compared to similar distances in the complex $[Cu_2(PAP)(OH)Cl_3] \cdot 1.5H_2O$, **VII**, wherein PAP behaves as a bisbidentate ligand. Figure 2 shows one of the two crystallographically independent molecules of this complex, as determined in a recent X-ray study (4). The Cu—N(pyridine) distances in **I** and **II** are similar, and are comparable to the average of these distances (1.984 Å) in **VII** and to the Cu—N(pyridine) distances of 2.015(7) and 1.989(7) Å in the structure of $[Cu_2(bpim)(NO_3)_2(ClO_4)(H_2O)] \cdot H_2O$ (19). The Cu—N(phthalazine) distances in **I** and **II** are not significantly different, nor are either of them significantly different from the 2.017 Å average for this distance in **VII**. The Cu—N distances of ca. 2 Å, observed in **I** and **II**, are typical of similar distances found in a variety of copper(II) complexes (20–24). The distances and angles within the PAP ligands of both complexes are comparable, and are similar to those observed in both molecules of **VII**.

The distances and angles of **I** and **II** are generally quite comparable. One significant difference be-

Can. J. Chem. Downloaded from www.nrcresearchpress.com by 210.87.254.6 on 09/06/12
For personal use only.

Can. J. Chem. Downloaded from www.nrcresearchpress.com by 210.87.254.6 on 09/06/12
For personal use only.

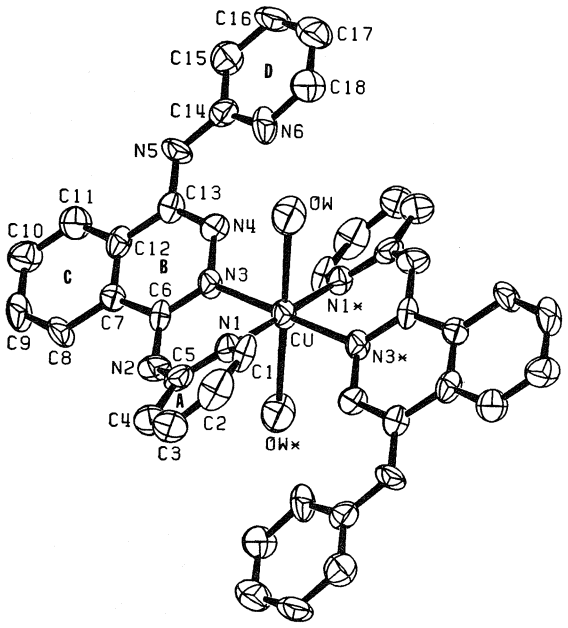


FIG. 5. Geometry and atom labelling scheme for the $[Cu(PAPH)_2(H_2O)_2]^{4+}$ cation in **I**. The geometry and atom labelling for the cation in **II** is similar. Thermal ellipsoids are depicted at the 50% probability level. Hydrogen atoms are not shown. Atoms labelled with an asterisk are related to those unlabelled by a centre of symmetry located at the Cu atom.

tween the structures, however, is the Cu—O(W) bond length which is 2.497(9) Å in **I** and 2.426(9) Å in **II**. This distance presumably reflects the fact that O(W) in **II** is involved in two H-bonding interactions of 2.77(2) and 2.79(1) Å (Table 3) to two different $BF_4^-$ groups while the closest approach to O(W) in **I** is 2.94(1) Å. Lists of interionic contacts less than 3.3 Å appear in Table 3 which summarizes the differences in packing between **I** and **II**. Packing is presumably the main difference between **I** and **II** since the geometry of the cations is quite similar in both structures. All the contacts listed in Table 3 are to fluorine atoms and close contacts to any other atoms of the structure are therefore all greater than 3.3 Å. Reference 25 lists 2.7 Å as the observed O ... F distance in O—H ... F hydrogen bonds and 2.8 Å for the N ... F distance of N—H ... F hydrogen bonds. Accordingly, the only true H-bond appears to occur in **II** between N(5)—F(11$^c$) at 2.65(1) Å but perhaps the short contacts to O(W) should be considered significant as well.

During the solution of the structures of **I** and **II**, it became apparent that there was one more tetrafluoroborate anion per ligand in the lattice of each structure than would be expected for a neutral PAP complex. It became necessary, therefore, to introduce a further positive charge into each lattice and the only plausible way of doing this was to assume that PAP had become protonated during the synthesis of the complex. Direct crystallographic evidence for this proton, however, has not been forthcoming. The possible sites for the protonation of PAP would be N(2), N(4), N(5), and N(6). Of these possibilities, N(4) and N(6) appear to be the most likely candidates (see earlier discussion). The angles at N(2) and N(5) are similar in both **I** and **II**, which suggests that neither is protonated. The location of N(6) in **I** and **II** was determined by utilizing the differences between the scattering factors for carbon and nitrogen. The position of N(6), as determined by experiment, is shown in Fig. 5. The other possibility was the interchange of N(6) with C(15). This was not found to be the case, however. The position of N(6) suggests that there may be some form of hydrogen bonding between N(4) and N(6), either of the form N(4)—H ... N(6) or N(4) ... H—N(6). The N(4) ... N(6) distances of 2.559(14) Å in **I** and 2.591(18) Å in **II** are well below the 3.1 Å indicated in ref. 25 as being the value observed for other N—H ... N hydrogen bonded systems. The small dihedral angles between plane BC and plane D of 8° in **I** and 13° in **II**, also suggest that such a hydrogen bond may exist. Normally, the PAP ligand would be expected to act as a bis-bidentate ligand interacting with two metal ions as observed in **VII** (Fig. 2). The fact that in **I** and **II**, each PAP binds to only one metal ion is also consistent with one potential chelating site being occupied by a proton, as suggested by the hydrogen bonding argument. The location of a proton on N(4) or N(6) cannot be obtained directly from the crystal structures of **I** or **II**, however. The C(14)—N(6)—C(18) angles of 120.2(13)° in **I** and 119.4(13)° in **II** fall between 125 ± 3°, for protonated nitrogen atoms, and 116 ± 3°, for unprotonated nitrogen atoms, as suggested by the empirical rule of Singh (26, 27) for six-membered nitrogen heterocycles. One possible explanation for this observation of a value lying between 125° and 116° is that the site of protonation is disordered between N(4) and N(6). That is, the situation would be N(4)—H ... N(6) approximately 50% of the time and N(4) ... H—N(6) for the remainder. This would lead to an averaging of the actual values. The angles at N(3) and N(4) are all similar to one another in **I** and **II** and reveal no information as to N(4) protonation.

The chemistry of the system described herein suggests the presence of $BF_3(OH)^-$ as well as $BF_4^-$ in aqueous solution. The possibility that $BF_3(OH)^-$ appears in the structures of **I** and **II**, or is indeed the reason for the differences between **I** and **II**, has been recognized. Tetrafluoroborate anions often

Can. J. Chem. Downloaded from www.nrcresearchpress.com by 210.87.254.6 on 09/06/12
For personal use only.

behave badly in the least-squares refinement, however,and the likelihood of being able to differentiate between an oxygen atom and a fluorine atom, in the same manner as was done for carbon and nitrogen (see Experimental), is quite low. Consequently, no attempt was made to explore this possibility in the present work, the tetrafluoroborate anions being refined as rigid groups. The charge balance of structures **I** or **II** would, of course, not be upset by the replacement of $BF_4^-$ by $BF_3(OH)^-$. However, the fluorine analyses on **I** and **II** indicate the absence of $BF_3(OH)^-$ in these systems. Clark and Lynton (28) determined the crystal structure of $NaBF_3OH$ and found that the hydroxyl group could not be distinguished from the isoelectronic fluorine atoms. The $BF_3OH^-$ ion has a distorted tetrahedral geometry.

The dihedral angles between plane A and plane BC (Fig. 5) in **I** and **II** are 34° and 28°, respectively. In **VII**, this angle is similar and averages 29° for the four angles involved. In **I** and **II**, the Cu atom lies 0.64 Å and 0.70 Å out of plane A. This deviation is smaller for **VII** and ranges from 0.08–0.40 Å. The dihedral angle between plane BC and plane D is small in both **I** and **II** (8° and 13°) suggesting that these two rings are more closely planar than planes A and BC which are involved in coordination to copper. Accordingly, the plane A – plane D dihedral angles in **I** and **II** (30° and 19°) are less than the average (58°) for the similar angles in **VII**.

In compound **VII**, there is a dihedral angle of 9° and 11° between planes B and C (Fig. 2) in molecules 1 and 2, respectively. In **I** and **II** the corresponding dihedral angles are only 3.5°, suggesting the phthalazine ring is almost planar in these compounds. The largest deviation of any atom from the mean plane through ring A is 0.05 Å for **I** and 0.03 Å for **II**. For ring D the largest deviations are 0.02 Å for **I** and **II**. In **VII**, the largest deviation from rings A or D is 0.03 Å. The largest deviation from plane BC is 0.08 Å in **I** and 0.07 Å in **II** and this corresponds to N(3) in both structures. The Cu atom is 0.50 Å out of this plane in **I** and 0.56 Å in **II**. For **VII**, the largest deviation from plane BC is 0.15 Å and the Cu atoms range from 0.88 to 1.03 Å out of this plane.

The phenomenon of crystals of the same compound, and having the same composition, crystallizing from the same solution in different crystalline modifications is not unknown. For example, the compound

$$[(OC)_4Mn(\mu\text{-}C_4H_5O)Pt(PMe_3)_2]$$

crystallizes from 1:1 light petroleum/ether in a red monoclinic form, space group $P2_1/n$, and a yellow triclinic form, space group $P\bar{1}$ (29). The two forms of $PdI_2(PMe_2Ph)_2$ crystallize from methanol as red needles, space group $P2_12_12_1$, and yellow plates, space group $P2_1/c$ (30). $[PtCl(NH_3)_2(C_5H_7N_3O)](NO_3)$ crystallizes from water as needles, space group $P2_1/c$, or cubic parallelepipeds, space group $C2/c$ (31). The phenomenon has also been observed before in copper coordination chemistry. Bis(1,3-diaminobutane)copper(II) perchlorate crystallizes from ethanol, methanol, or water as blue–violet prisms and plates or red violet needles (32, 33). Both forms are monoclinic, space group $P2_1/c$. Bis(*N*-*tert*-butylpyrrole-2-carbaldimino)copper(II) crystallizes from *n*-heptane as light-green needles, space group $P\bar{1}$, and dark green tetragonal-pyramids, space group $P4_12_12$ (34). With certain compounds it is possible to transform one crystalline form into another by the application of heat (30, 35–37).

**Acknowledgements**

We thank Professor S. J. Lippard of Columbia University for the use of his X-ray diffraction facilities, Professor E. C. Lingafelter for a preprint of ref. 4, and the Natural Sciences and Engineering Research Council of Canada for financial support.

1. L. K. Thompson, V. T. Chacko, J. A. Elvidge, A. B. P. Lever, and R. V. Parish. Can. J. Chem. **47**, 4141 (1969).
2. A. B. P. Lever, L. K. Thompson, and W. M. Reiff. Inorg. Chem. **11**, 104 (1972).
3. J. A. Doull and L. K. Thompson. Can. J. Chem. **58**, 221 (1980).
4. G. Marongiu and E. C. Lingafelter. Acta Crystallogr. In press.
5. A. B. P. Lever, B. S. Ramaswamy, and S. R. Pickens. Inorg. Chim. Acta, **46**, L59 (1980).
6. L. K. Thompson, P. H. Bird, F. Bottomley, P. S. White, and W. Wickramasinghe. To be published.
7. C. A. Wamser. J. Am. Chem. Soc. **70**, 1209 (1948).
8. R. E. Mesmer, K. M. Palen, and C. F. Baes, Jr. Inorg. Chem. **12**, 89 (1973).
9. International tables for X-ray crystallography. Vol. I. 2nd ed. Kynoch Press, Birmingham, England. 1965. p. 75.
10. L. D. Silverman, J. C. Dewan, C. M. Giandomenico, and S. J. Lippard. Inorg. Chem. **19**, 3379 (1980).
11. S. L. Lawton. J. Appl. Crystallogr. **6**, 309 (1973).
12. G. M. Sheldrick. *In* Computing in crystallography. *Edited by* H. Schenk, R. Olthof-Hazekamp, H. van Koningsveld, and G. C. Bassi. Delft University Press, Delft. 1978. p. 34.
13. International tables for X-ray crystallography. Vol. IV. Kynoch Press, Birmingham, England. 1974. pp. 99, 149.
14. R. F. Stewart, E. R. Davidson, and W. T. Simpson. J. Chem. Phys. **42**, 3175 (1965).
15. International tables for X-ray crystallography. Vol. I. 2nd ed. Kynoch Press, Birmingham, England. 1965. p. 99.
16. C. J. Pouchert. The Aldrich Library of infrared spectra. Aldrich Chemical Company, Milwaukee, WI. 1970.
17. R. C. Weast (*Editor*). Handbook of chemistry and physics. 50th ed. The Chemical Rubber Company. 1969.

18. C. FURLANI, S. BERTOLA, and G. MORPURGO. Ann. Chim. Rome, **50**, 858 (1960).
19. J. C. DEWAN and S. J. LIPPARD. Inorg. Chem. **19**, 2079 (1980).
20. R. R. GAGNÉ, R. S. GALL, G. C. LISENSKY, R. E. MARSH, and C. M. SPELTZ. Inorg. Chem. **18**, 771 (1979).
21. G. KOLKS, S. J. LIPPARD, and J. V. WASZCZAK. J. Am. Chem. Soc. **102**, 4832 (1980).
22. C-L. O'YOUNG, J. C. DEWAN, H. R. LILIENTHAL, and S. J. LIPPARD. J. Am. Chem. Soc. **100**, 7291 (1978).
23. E. I. LERNER and S. J. LIPPARD. Inorg. Chem. **16**, 1546 (1977).
24. B. G. SEGAL and S. J. LIPPARD. Inorg. Chem. **13**, 822 (1974).
25. W. C. HAMILTON and J. A. IBERS. Hydrogen bonding in solids. New York, Benjamin. 1968. p. 16.
26. C. SINGH. Acta Crystallogr. **19**, 861 (1965).
27. H. I. HEITNER and S. J. LIPPARD. Inorg. Chem. **13**, 815 (1974).
28. M. J. R. CLARK and H. LYNTON. Can. J. Chem. **48**, 405 (1970).
29. M. BERRY, J. A. K. HOWARD, and F. G. A. STONE. J. Chem. Soc. Dalton, 1601 (1980).
30. N. A. BAILEY and R. MASON. J. Chem. Soc. A, 2594 (1968).
31. B. LIPPERT, C. J. L. LOCK, and R. A. SPERANZINI. Inorg. Chem. **20**, 335 (1981).
32. A. PAJUNEN. Suom. Kemistil. B**41**, 145 (1968).
33. A. PAJUNEN, K. SMOLANDER, and I. BELINSKY. Suom. Kemistil. B**45**, 317 (1972).
34. C. H. WEI. Inorg. Chem. **11**, 2315 (1972).
35. I. GRENTHE, P. PAOLETTI, M. SANDSTRÖM, and S. GLIKBERG. Inorg. Chem. **18**, 2687 (1979).
36. C. BELLITTO, G. DESSY, V. FARES, and A. FLAMINI. Chem. Commun. 409 (1981).
37. S. A. ROBERTS, D. R. BLOOMQUIST, R. D. WILLETT, and H. W. DODGEN. J. Am. Chem. Soc. **103**, 2603 (1981).

Can. J. Chem. Downloaded from www.nrcresearchpress.com by 210.87.254.6 on 09/06/12
For personal use only.

# Pyrones. VIII.[1] Biosynthetic investigations of the fungal metabolite phacidin

TERRY DONALD CYR[2] AND GERALD ARTHUR POULTON[3]

*Department of Chemistry, University of Victoria, Victoria, B.C., Canada V8W 2Y2*

Received July 15, 1981

TERRY DONALD CYR and GERALD ARTHUR POULTON. Can. J. Chem. **60**, 133 (1982).

Biosynthetic feeding experiments with singly and doubly $^{13}$C-labelled acetate show that phacidin (4-methoxy-6-nonanoyl-2*H*-pyran-2-one-3-carboxaldehyde) is formed from a heptaketide precursor. A similar feeding with sodium $^{13}$C-formate has shown that the methoxyl and aldehyde carbons are derived from the one-carbon pool.

TERRY DONALD CYR et GERALD ARTHUR POULTON. Can. J. Chem. **60**, 133 (1982).

Des expériences d'alimentation biosynthétique avec un acétate marqué avec un ou deux $^{13}$C révèlent que la phacidine (méthoxy-4 nonanoyl-6 2*H*-pyranone-2 carbonaldéhyde-3) se forme à partir d'un précurseur heptacétide. Une alimentation analogue avec le formate $^{13}$C de sodium montre que les carbones du méthoxy et de l'aldehyde proviennent de sources contenant un seul carbone.
[Traduit par le journal]

Can. J. Chem. Downloaded from www.nrcresearchpress.com by 210.87.254.40 on 09/06/12
For personal use only.

## Introduction

Phacidin, 4-methoxy-6-nonanoyl-2*H*-pyran-2-one-3-carboxaldehyde **1**, is an antibiotic (1, 2)

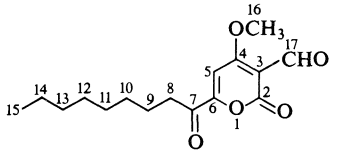

**1**

metabolite isolated (2) from cultures of the fungus *Potebniamyces balsamicola* Smerlis var. *boycei* Funk, whose synthesis we have recently reported (3). During our investigations, we were desirous of obtaining further supportive evidence of the structure of phacidin and information relating to its possible mode of formation by the fungus, and thus undertook to perform some simple biosynthetic experiments. The biogenetic origin of the carbon skeleton of a natural product can now be determined routinely in favourable cases by the use of $^{13}$C-enriched precursors (4). Since phacidin possessed many of the characteristics of an acetogenin (polyoxygenated ring, linear carbon skeleton, long saturated side-chain, etc.), we commenced our investigations with the feeding of singly- and doubly-labelled sodium acetate.

## Results and discussion

In order to test the predictions concerning the biosynthesis of a metabolite, the position of the labelled atom(s) in the product must be determined. The use of carbon-13 magnetic resonance, combined with the use of carbon-13 enriched precursors, has greatly simplified biosynthetic studies of secondary metabolites since chemical degradation of the product becomes unnecessary. Accurate assignment of the $^{13}$Cmr spectrum is, however, a necessity, since any misassignment may lead to false assumptions and/or conclusions about the biosynthesis.

### *(A) Assignment of $^{13}$Cmr spectrum of phacidin*

Many 4-oxy-2-pyrones are known, and the difficulties encountered in accurately assigning resonances due to C-2, C-4, and C-6 have been discussed (5). Indeed, one of the original $^{13}$C-labelled biosynthetic investigations of an α-pyrone (radicinin, **2** (6)) had to be repeated and the resonances reassigned (7). Similar studies such as the assignment (8) and reassignment (9) of the $^{13}$Cmr spectrum of Aurovertin B **3** have further emphasized the need for caution when analyzing the spectra of 2-pyrones. Considerable care was therefore taken in the assignment of the $^{13}$Cmr spectra of phacidin and its derivatives.[4]

An examination of the chemical shift values of a variety of 4-oxypyrones (see Table 1) indicates that the assignment of C-4 is straightforward, since it is consistently the most downfield signal as compared to the other ring carbons. This same trend also holds for most hydroxycoumarins (e.g. compound **12**). It has also been shown that for 2-pyrones the magnitude of the two-bond spin–spin coupling constant between C-2 and a proton at C-3 (H-3) is less than that of C-6 to H-5 or to protons on a side-chain at C-6 (12), resulting in C-6 normally

[1]For Part VII, see ref. 16.

[2]Present address: Hydrocarbon Research Centre, Department of Chemistry, University of Alberta, Edmonton, Alberta.

[3]To whom all correspondence should be addressed.

[4]Copies of $^{13}$Cmr spectra of phacidin (natural abundance, sodium 1-$^{13}$C and 1,2-$^{13}C_2$-acetate derived, and sodium 1-$^{13}$C-formate derived) and of the $^{1}$Hmr spectrum of phacidin ($^{13}$C-formate derived) have been placed with the Depository of Unpublished Data, CISTI, National Research Council of Canada, Ottawa, Ont., Canada K1A 0S2.

0008-4042/82/020133-05$01.00/0

©1982 National Research Council of Canada/Conseil national de recherches du Canada

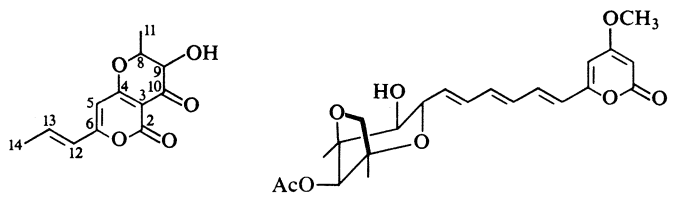

2



3

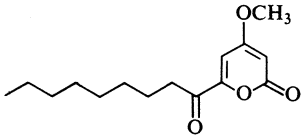

4

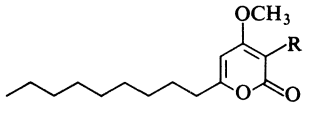

5, R = CHO
6, R = H

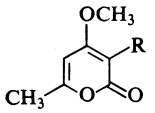

7, R = H
11, R = Br

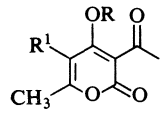

8, R = R¹ = H
9, R = CH₃, R¹ = H
10, R = CH₃, R¹ = Br

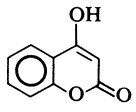

12

appearing as a multiplet, while C-2 remains as a singlet or doublet.

The signals in the $^{13}$Cmr spectrum due to the ring carbons of phacidin were thus assigned as follows:

(*i*) δ 172.9 (m), C-4, being the most deshielded ring carbon.

(*ii*) δ 160.2 (d, $^{3}J_{C-H}$ = 2.5 Hz), C-2. The chemical shift range of C-2's of similar compounds was approximately δ 160–165 ppm, and the analogous compound **5** showed a similar three-bond coupling constant of 3.3 Hz.

(*iii*) δ 158.5 (d, $^{2}J_{C-H}$ = 1.4 Hz), C-6. The chemical shifts for C-6 of a variety of analogous compounds had a relatively wide range of δ 154–175. The two extremes of this range can be represented by compounds **5** (174.4) and **4** (155.2), consistent with the donor/acceptor nature of the carbonyl substituents and its transmission via the conjugated system (13). The carbon α to the carbonyl experiences an increase in electron density (shielding), while those β or δ to it show a decrease (deshielding). In phacidin, the C-6 carbon is influenced by both the aldehyde substituent at C-3 (deshielding on C-6) and the directly attached nonanoyl group (shielding at C-6); the latter is expected to dominate, and phacidin therefore shows the C-6 resonance at δ 158.5, shielded with respect to its analogue **6** which is lacking an aldehyde substituent at C-3 (i.e. no C-17), and which has the resonance at δ 165.8 ppm.

TABLE 1. $^{13}$Cmr spectra of 4-oxy-2-pyrones

| Compound | C-2 | C-3 | C-4 | C-5 | C-6 | Reference |
|---|---|---|---|---|---|---|
| **1** | 160.2 | 105.9 | 172.9 | 97.0 | 158.5 | 3 |
| **2** | 156 | 97.8 | 174.7 | 98.2 | 162.5 | 7 |
| **3** | 163.4 | 88.6 | 170.4 | 107.4 | 154.1 | 9 |
| **4** | 162.5 | 93.7 | 170.2 | 103.8 | 155.2 | 3 |
| **5** | 162.2 | 102.1 | 174.6 | 94.3 | 174.4 | 3 |
| **6** | 165.0 | 87.5 | 171.3 | 99.6 | 165.8 | 3 |
| **7** | 164.6 | 87.3 | 171.4 | 100.3 | 162.1 | 10 |
| **8** | 161.2 | 99.9 | 181.1 | 101.4 | 169.2 | 10 |
| **9** | 161.8 | 105.1 | 170.4 | 95.2 | 166.9 | 10 |
| **10** | 159.5 | 100.0 | 178.2 | 98.3 | 166.9 | 10 |
| **11** | 160.8 | 88.4 | 166.9 | 95.2 | 162.9 | 10 |
| **12** | 161.8 | 91.0 | 165.5 | 115.7 | 153.4 | 11 |

(*iv*) δ 105.9 (dd, $^{2}J_{C-H}$ = 24.5 Hz, $^{3}J_{C-H}$ = 4.2 Hz), C-3. In the series of analogous compounds, C-3 resonated at δ 88–105 ppm. The derivative **5** likewise showed C-3 at δ 102.1 (dd, $^{2}J_{C-H}$ = 23.9 Hz, $^{3}J_{C-H}$ = 4.2 Hz), consistent with this assignment.

(*v*) δ 97.0 (d, $^{1}J_{C-H}$ = 175.3 Hz), C-5. The assignment of C-5 was trivial, since it was the only carbon directly bonded to proton. Normal chemical shift ranges and coupling constants are δ 95–108 and $^{1}J_{C-H}$ = 170–176 Hz.

In addition, it was a trivial matter to assign the nonanoyl ketone C-7 (δ 193.5, m), the 3-carboxaldehyde C-17 (δ 186.3, d, $^{1}J_{C-H}$ = 186.2 Hz), the methoxyl C-16 (δ 58.4, q, $^{1}J_{C-H}$ = 148.4 Hz), and the methylene α to the ketone, C-8 (δ 38.3, t, $^{1}J_{C-H}$ = 123.6 Hz). The remaining carbons of the nonanoyl side chain were assigned by comparison with the assignments of 2-octanone and 1-decanol (14) in Table 2.

Can. J. Chem. Downloaded from www.nrcresearchpress.com by 210.87.254.40 on 09/06/12
For personal use only.

Can. J. Chem. Downloaded from www.nrcresearchpress.com by 210.87.254.40 on 09/06/12
For personal use only.

TABLE 2

(*a*) Assignment of 2-octanone

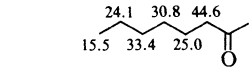


(*b*) Assignment of 1-decanol

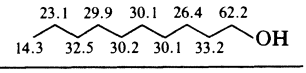


(*c*) Assignment of nonanoyl ketone*

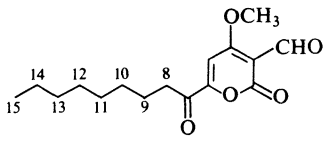


| Carbon | δ (ppm) | $^1J_{C-H}$ (Hz) | Multiplicity |
|---|---|---|---|
| 15 | 14.1 | 124.6 | q |
| 14 | 22.7 | 127.5 | t |
| 13 | 31.8 | 125.5 | t |
| 12 | 29.3 | 125.1 | t |
| 11 | 29.1 | 125.1 | t |
| 10 | 29.0 | 125.1 | t |
| 9 | 23.1 | 127.5 | t |
| 8 | 38.3 | 123.6 | t |

*We were unable to distinguish C-10, C-11, and C-12 since their chemical shift values were only very slightly different from each other.

*(B) Sodium acetate-1-$^{13}C$ labelling experiment*

Labelled sodium acetate was fed to growing cultures of *P. balsamicola* and the distribution of the $^{13}C$ label in the resulting phacidin determined according to the method of McInnes *et al.* (15), by comparing the $^{13}C$mr spectra of natural abundance and enriched compounds recorded under identical instrument parameters. In order to make the comparisons more valid, the carbons to be compared should have similar substituents. Since it was known, *vide infra*, part D, that the aldehyde and methoxyl carbons were not acetate-derived, they were used as reference signals to which the unsaturated (C-2 to C-7) and saturated (C-8 to C-15) were compared.

The results (Table 3) indicate that C-2, C-4, C-6, C-8, and C-14 have been enriched by the feeding of sodium acetate-1-$^{13}C$ to *P. balsamicola*; it is obvious also that C-10 and C-12 are similarly labelled.

*(C) Sodium acetate-1,2-$^{13}C_2$ labelling experiment*

*P. balsamicola* was fed sodium acetate-1,2-$^{13}C_2$ in the same manner and for the same duration as described in the above labelling experiment. The $^{13}C$mr spectrum of labelled phacidin clearly showed the presence of coupled $^{13}C$–$^{13}C$ units (see Table 4) demonstrating the utilization of intact acetate units in the biosynthesis. In addition, the labelling pattern corroborated the chemical shift assignments discussed above.

Intact incorporation of acetate units into the phacidin skeleton was demonstrated for C-2—C-3, C-4—C-5, C-6—C-7, C-8—C-9, C-12—C-13, C-14—C-15, and was assumed for C-10—C-11, thereby indicating its probable biogenesis from an hepta-acetate precursor as indicated below.

*(D) Sodium formate-1-$^{13}C$ labelling experiment*

*P. balsamicola* cultures were fed labelled sodium formate as described below, with the incorporation of $^{13}C$ in the methoxy (C-16) and aldehyde (C-17) groups clearly being indicated by spectral examination. The extent of incorporation was so large in these two positions that it was readily detectable in

TABLE 3. Calculation of incorporation of sodium acetate-1-$^{13}C$ into phacidin

| Carbon | $R = I_N^*/I_S$ | $R^1 = I_L/I_S$ | $r = R^1/R$ | $\%^{13}C = rf$† | Error‡ |
|---|---|---|---|---|---|
| 2 | 0.388 | 0.534 | 1.38 | 2.47 | 0.23 |
| 3 | 0.351 | 0.176 | .501 | | |
| 4 | 0.360 | 0.608 | 1.69 | 3.03 | 0.19 |
| 5 | 1.10 | 0.929 | 0.876 | | |
| 6 | 0.238 | 0.273 | 1.15 | 2.06 | 0.28 |
| 7 | 0.435 | 0.208 | 0.478 | | |
| 8 | 1.06 | 2.54 | 2.40 | 2.17 | 0.031 |
| 9 | 0.923 | 1.17 | 1.27 | | |
| 10, 11, 12 | 1.48 | 4.88 | 3.30 | 2.99 | 0.022 |
| 13 | 0.752 | 0.918 | 1.22 | | |
| 14 | 0.775 | 2.64 | 3.41 | 3.09 | 0.022 |
| 15 | 0.521 | 0.617 | 1.18 | | |

*$I_N$ = peak height in spectrum of unlabelled compound; $I_L$ = peak height in spectrum of labelled compound; $I_S$ = peak height of standard carbon; C-16 used as standard for aliphatic (C-8 to C-15) carbons, C-17 for unsaturated (C-2 to C-7) ones.

†$f$ = factor required to scale average $r$ for unlabelled carbons to natural abundance.

‡Error = standard deviation ($r$) × average enrichment ($r$) ÷ $r$.

Can. J. Chem. Downloaded from www.nrcresearchpress.com by 210.87.254.40 on 09/06/12
For personal use only.

TABLE 4. The $^{13}C-^{13}C$ spin–spin coupling constants of phacidin and radicinin (7)

| Phacidin (1)* | | | Radicinin (2) | |
|---|---|---|---|---|
| Carbon | δ | $^1J_{C-C}$ | Carbon | $^1J_{C-C}$ |
| 2 | 160.2 | 78.7 | 2 | 80 |
| 3 | 105.9 | 78.2 | 3 | 80 |
| 4 | 172.9 | 58.9 | 4 | 62 |
| 5 | 97.0 | 58.8 | 5 | 62 |
| 6 | 158.5 | 59.4 | 6 | 64 |
| 7 | 193.5 | 59.4 | | |
| 8 | 38.3 | 34.8 | 8 | 40 |
| 9 | 23.1 | 34.8 | 9 | 42 |
| 10 | 29.2 | † | 10 | 43 |
| 11 | 29.3 | † | 11 | † |
| 12 | 29.1 | 34.7 | 12 | 64 |
| 13 | 31.8 | 34.7 | 13 | 42 |
| 14 | 22.7 | 34.6 | 14 | † |
| 15 | 14.1 | 34.7 | | |

*Kindly recorded by Dr. A. G. McInnes and co-workers at the Atlantic Regional Laboratory, National Research Council of Canada, Halifax.
†Values not obtained due to overlapping of signals.

the 90 MHz $^1$Hmr spectrum: the methoxy protons appeared as a singlet at 4.14 ppm ($^{12}C$—H) and a doublet centred at 4.15 ppm ($^{13}C$—H, $^1J$ = 148 Hz), the ratio of intensities indicating 29% $^{13}C$ incorporation, while the aldehyde proton appeared as a singlet (10.85 ppm, $^{12}C$—H) overlapped by a doublet centred at 10.84 ($^{13}C$—H, $^1J$ = 188 Hz), the ratio of intensities indicating 36% $^{13}C$ incorporation. This was substantiated further by the 62.8 MHz $^{13}$Cmr spectrum[5] which showed dramatically increased intensities of the 186 (aldehyde) and 58 ppm (methoxyl) carbons as compared to the remaining signals. The methoxy and aldehyde carbons thus do not originate from an acetate-derived precursor, but from the C-1 metabolic pool.

*(E) Possible biogenesis*

The above feeding experiments indicate that phacidin can be formed from seven acetate units with two one-carbon insertions. This may occur via an elaboration of an enzyme-bound caprate (e.g. **13**) produced by normal fatty acid routes to a fourteen-carbon unit (**14**) which may then undergo *O*-cyclization to give a pyrone derivative. The sequence of the other necessary stages, that is, one-carbon introduction and oxidation at C-7, cannot, of course, be determined without much more extensive investigation (see Fig. 1).

## Experimental

Carbon magnetic resonance spectra were obtained on Nicolet TT-14 (15.1 MHz, Victoria), Bruker WP250 (62.8 MHz, Bruker Canada Ltd., Mississauga) and Varian XL100/15 (25.2 MHz, Atlantic Regional Laboratory, Halifax) instruments in $CDCl_3$, and are referenced to internal TMS.

[5]Kindly run by Dr. C. Roger, Bruker Spectrospin Canada, Mississauga, Ont., Canada L5L 1J9.

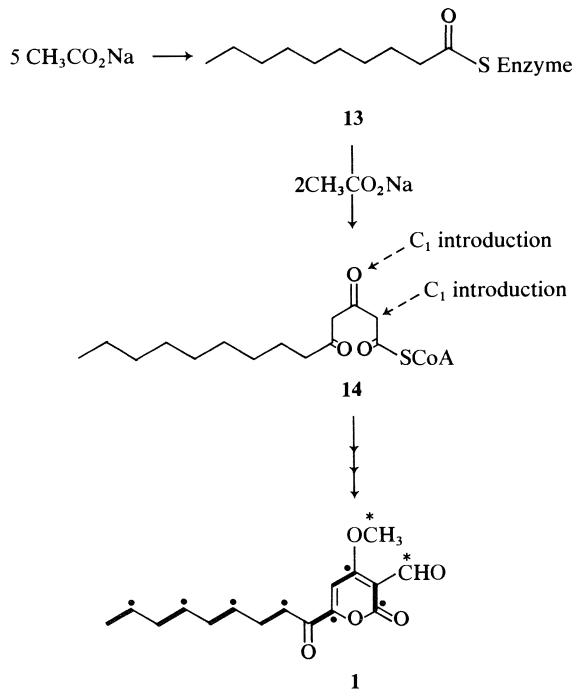


FIG. 1. Feeding of $CH_3{}^{13}\dot{C}O_2Na$, $^{13}CH_3$—$^{13}CO_2Na$, and H—$^{13}CO_2Na$ to *P. balsamicola*; possible biosynthetic route.

*Sodium acetate-1-$^{13}C$ feeding*

Cultures of *P. balsamicola* were grown at the Pacific Forest Research Centre by A. Funk. They were allowed to grow for two weeks, unshaken, at 15°C in 75 mL of 5% malt extract in water. Sodium acetate-1-$^{13}C$ (100 mg, 90% enriched, Stohler Isotope Chemicals) in water (5 mL) was added and the cultures allowed to grow for a further six weeks. Labelled phacidin was then isolated by benzene extraction, and purified by recrystallization from cyclohexane.

*Sodium acetate-1,2-$^{13}C_2$ feeding*

Cultures were grown in a manner similar to that detailed above, and sodium acetate-1,2-$^{13}C_2$ (100 mg, 90% $^{13}C$-enriched, Stohler Isotope Chemicals) added in a similar fashion. Phacidin was isolated by benzene extraction and purified by recrystallization.

*Sodium formate-1-$^{13}C$ feeding*

Cultures were grown in a manner similar to that detailed above. After 10 weeks, labelled sodium formate (90% enriched, Stohler Isotope Chemicals) was added (304 mg in four portions) over a period of two weeks. Blank feedings using unlabelled sodium formate were also carried out. After two further weeks, phacidin was isolated by hot 1,2-dichloroethane extraction and purified by recrystallization.

1. A. S. SEKHON and A. FUNK. J. Antimicrob. Chemother. **3**, 95 (1977).
2. A. FUNK and E. E. MCMULLAN. Can. J. Microbiol. **20**, 422 (1970).
3. G. A. POULTON and T. D. CYR. Can. J. Chem. **58**, 2158 (1980).

4. G. C. LEVY. Topics in carbon-13 N.M.R. spectroscopy. Vol. 1. John Wiley and Sons, Inc., 1974. pp. 238–244.
5. W. V. TURNER and W. H. PIRKLE. J. Org. Chem. **39**, 1935 (1974).
6. M. TANABE, H. SETO, and L. JOHNSON. J. Am. Chem. Soc. **92**, 2157 (1970).
7. H. SETO and S. URANO. Agr. Biol. Chem. **39**, 915 (1975).
8. K. TORI, T. HIRATA, O. KOSHITANI, and T. SUGA. Tetrahedron Lett. 1311 (1976).
9. P. S. STEYN, R. VLEGGAAR, and P. L. WESSELS. J. Chem. Soc. Chem. Commun. 1041 (1979).
10. T. D. CYR. Ph.D. Thesis, University of Victoria, Victoria, B.C. 1980. Diss. Abstr. **41**B, 3447 (1981).
11. K. K. CHAN, D. D. GIANNINI, A. H. CAIN, J. D. ROBERTS, W. PORTER, and W. F. TRAGER. Tetrahedron, **31**, 2719 (1975).
12. A. A. CHALMERS and K. G. PACHLER. Can. J. Chem. **53**, 1980 (1975).
13. D. SEEBACH. Angew. Chem. Int. Ed. Eng. **18**, 239 (1979).
14. J. B. STOTHERS. Carbon-13 N.M.R. spectroscopy. Academic Press, New York, NY. 1972. pp. 140, 146.
15. P. L. CANHAM, L. C. VINING, A. G. MCINNES, J. A. WALTER, and J. L. C. WRIGHT. Can. J. Chem. **55**, 2450 (1977).
16. G. A. POULTON and T. D. CYR. Syn. Commun. **10**, 581 (1980).

Can. J. Chem. Downloaded from www.nrcresearchpress.com by 210.87.254.40 on 09/06/12
For personal use only.

# Thermochromism of 1,2,5-triphenylphosphole and the formation of 1,1,2,2-tetrachloro-1,2-diphenylethane from α,α,α-trichlorotoluene

MARTIN B. HOCKING AND TREVOR A. SMYTH

*Department of Chemistry, University of Victoria, Victoria, B.C., Canada V8W 2Y2*

Received March 17, 1981[1]

MARTIN B. HOCKING and TREVOR A. SMYTH. Can. J. Chem. **60**, 138 (1982).

On boiling a yellow solution of 1,2,5-triphenylphosphole in carbon tetrachloride the colour changes to red, reverting to yellow on cooling. This reversible colour change has been conducted in the presence of various additives in an attempt to determine the cause of the colour change. Boiling 1,2,5-triphenylphosphole in α,α,α-trichlorotoluene similarly showed a colour change and gave a coupling product of the solvent, 1,1,2,2-tetrachloro-1-2-diphenylethane. From this evidence and related synthetic, nmr, and esr experiments it is proposed that the colour change of the former system arises from the incipient formation of a phosphole–trichloromethide salt with carbon tetrachloride. With trichlorotoluene the phosphole undergoes more substantive formation of dichlorophenylmethide and possibly chloride salts which undergo further reaction to the observed coupling product.

MARTIN B. HOCKING et TREVOR A. SMYTH. Can. J. Chem. **60**, 138 (1982).

Une solution de triphényl-1,2,5-phosphole dans le tétrachlorure de carbone portée à ébullition devient rouge, et la couleur passe du rouge au jaune lors du refroidissement. On a réalisé ce changement réversible de couleur en présence de plusieurs additifs dans le but d'en déterminer la cause. Le triphényl-1,2,5-phosphole dans le trichloro-α,α,α-toluène porté à ébullition présente les mêmes caractéristiques et donne un produit de couplage avec le solvant; le tétrachloro-1,1,2,2 diphényl-1,2-éthane. A partir de ces observations et à partir des expériences de synthèse, de rmn et de rpe, on propose que le changement de couleur du premier système provient de la formation d'un sel phosphole-trichlorométhylure par réaction avec le tétrachlorure de carbone. Dans le cas du trichlorotoluène, le phosphole conduit à la formation plus appréciable de dichlorophénylméthylure et éventuellement de chlorures qui, par des réactions subséquentes, conduisent au produit de couplage observé.

[Traduit par le journal]

Can. J. Chem. Downloaded from www.nrcresearchpress.com by 210.87.254.42 on 09/06/12
For personal use only.

## Introduction

Thermochromism, or a reversible colour change obtained on heating (or cooling) a substance from room temperature, has been relatively recently reviewed (1–3). More recently than these summaries and related to this study, the thermochromism demonstrated by solutions of highly arylated pyrryls (4), imidazolyl (5), or benzoquinolinium (6) heterocycles is generally ascribed to a resonance stabilized radical species analogous to that put forward for triphenylchloromethane (7). For solutions of certain spiropyrans (8), equilibrium formation of ring opened zwitterionic products has been implicated in the thermochromic effect, whereas for some anils (9) and benzophenone anthraldazine (10) "aza olefins" *E,Z* isomeric transformations are thought to be the cause. There remain, however, several examples of thermochromic compounds such as tetranisylethylene (11) and an indanedionyl dimer (12) for which no mechanistic proposal for the colour change has yet been made.

Solutions of 1,2,5-triphenylphosphole in carbon tetrachloride under ordinary conditions are yellow with a strong blue fluorescence twice the intensity of fluorescein (13). When the solution is boiled under reflux in a nitrogen atmosphere, however, it slowly changes to a bright red which rapidly reverts to the original yellow colour on cooling (14). This process, which can be repeated many times with the same sample, has now been examined in some detail to determine whether this effect is truly a thermochromic one, or an incipient but reversible reaction to a red product. An additional objective was to obtain some evidence of the probable species involved in either eventuality.

## Experimental

Unless otherwise stated, all solvents used were dried, using fresh 1.5 mm pellets of molecular sieve 4A (Union Carbide), except for α,α,α-trichlorotoluene which was dried by an azeotropic forerun and the remainder distilled.

### *1,2,5-Triphenylphosphole thermochromism in carbon tetrachloride*

A solution of yellow crystals of the phosphole (0.98 g) in carbon tetrachloride was boiled under reflux in a nitrogen atmosphere for 3.25 h during which time the solution gradually became an intense bright red. Within one minute of removing the heating mantle the solution became yellow again. Resuming heating for a further 3 h returned the red colour. The solution was cooled, washed with two small portions of water, dried, and concentrated to recover 0.91 g (93%) of the starting phosphole.

Conducting the experiment as above, but open to the air, more slowly gave the same colour change which reverted to the original yellow colour on cooling, or on the addition of a drop of water or chloroform. Also, in ordinary moist reagent grade carbon tetrachloride, either open to the air or under nitrogen, no colour change was observed.

Boiling a solution of 1,2,5-triphenylphosphole-1-*oxide* in dry

[1]Revision received October 1, 1981.

0008-4042/82/020138-06$01.00/0

©1982 National Research Council of Canada/Conseil national de recherches du Canada

TABLE 1. Ratios of 1,1,2,2-tetrachloro-1,2-diphenylethane (tetrachlorotolan) produced per mole of 1,2,5-triphenylphosphole present

| Experiment number | Time boiled[a] under reflux (h) | Tetrachlorotolan | | Mole ratio, tetrachlorotolan to phosphole | |
|---|---|---|---|---|---|
| | | Crude (g) | Pure (g) | Crude | Pure |
| 1 | 4, 200°C | 0.64 | — | 2.1 | — |
| 2 | 4[b] | 1.03 | 0.63 | 3.3 | 2.1 |
| 3 | 18[c] | 6.16 | 4.35 | 1.9 | 1.4 |
| 4 | 18[d] | 9.69 | 5.29 | 3.0 | 1.7 |
| 5 | 2.5[c] | 3.51 | — | 1.1 | — |
| 6 | 3.5 | 1.45 | — | 0.45[e] | — |

[a] Except where otherwise stated.
[b] Plus at room temperature for six months.
[c] In the presence of one equivalent of acetic acid. See Experimental.
[d] In the presence of one equivalent of butyric acid. See Experimental.
[e] Triphenylphosphine catalyst, rather than 1,2,5-triphenylphosphole.

carbon tetrachloride in the same fashion gave no colour change, and quantitative recovery of the oxide, unchanged.

*Trapping experiments for phosphole/carbon tetrachloride thermochromic species*

Prolonged interaction of benzaldehyde with a solution of the phosphole in carbon tetrachloride under nitrogen failed to demonstrate any change, either at room temperature or when boiled under reflux, by glc, and by quantitative recovery of the reactants.

Addition of a drop of dry butyric acid to a refluxing red solution obtained again as initially described caused immediate reversion to the initial yellow colour. Addition of a total of 0.30 g butyric acid and boiling for a further 24 h under $N_2$ gave no return of red colouration, near quantitative phosphole recovery, and ir bands at 1180 weak (P=O), 1715 strong (acid C=O), and 1823 weak (anhydride or acid Cl C=O) $cm^{-1}$ in the residual mother liquor. Boiling for periods as long as 16 days failed to cause any significant further change.

Repetition of the butyric acid experiment except using vacuum dried stearic, benzoic, and trichloroacetic acids, gave the same initial colour reversion, near quantitative phosphole recovery, and weak or nonexistent ir bands in the region of 1820 $cm^{-1}$ for the mother liquor after periods of boiling under reflux of 7 to 16 days.

*Phosphole coupling of α,α,α-trichlorotoluene*

A solution of 1,2,5-triphenylphosphole (0.30 g) in freshly distilled α,α,α-trichlorotoluene (40 mL) was heated at 200°C for 4 h with protection from atmospheric moisture, and then allowed to stand at room temperature for 14 h. Excess solvent was removed under reduced pressure on a rotary evaporator and the brown residue (1.03 g) sublimed (90–160°C/0.4 Torr) to yield 0.64 g of impure 1,1,2,2-tetrachloro-1,2-diphenylethane (tetrachlorotolan). Resublimation (80°C/0.4 Torr) and recrystallization of a portion of the impure material from acetone provided an analytical sample, mp 160–162°C (lit. (15) mp 162–162.5°C). *Anal.* calcd. for $C_{14}H_{10}Cl_4$: C 52.54, H 3.15; found: C 52.09, H 2.92.

The residue from the initial sublimation was an intractable brown solid that showed no ir band correspondence to the phosphole-1-oxide in the 625 to 900 $cm^{-1}$ region both from spectra obtained on mulls or from solvent-evaporated thin films. The results of other similar coupling experiments using 1,2,5-triphenylphosphole are presented in Table 1.

When triphenylphosphine (2.62 g) was boiled for 4 h in α,α,α-trichlorotoluene, 1.45 g of tetrachlorotolan was isolated by a similar sublimation technique from a tarry residue of triphenylphosphine oxide. When tri-*n*-butylphosphine and α,α,α-trichlorotoluene were boiled together under similar conditions, a residue of 8.17 g of tarry material was obtained on evaporation of the excess trichlorotoluene. Infrared spectra of fractions partially resolved by glc, fractional sublimation experiments, and $^1H$ nmr demonstrated the presence of tetrachlorotolan and traces of tri-*n*-butylphosphine oxide (16) in this residue.

A blank experiment in which 25 mL of α,α,α-trichlorotoluene was boiled under reflux on its own for 4 h left no residue on rotary evaporation under reduced pressure.

*Phosphole plus α,α,α-trichlorotoluene trapping experiments*

A solution of 1,2,5-triphenylphosphole (3.12 g) in α,α,α-trichlorotoluene was boiled under reflux for 1 h, at which time acetic acid (0.57 mL) was added. Refluxing was continued for an additional 16 h. Direct ir examination of the cooled solution, and ir and $^1H$ nmr examination of the first four fractions (1 mL total) of distillate obtained from this solution showed no trace of acetyl chloride. Rotary evaporation of the solvent from the distilland gave 6.2 g of brownish-orange semi-crystalline material from which 4.35 g of pure tetrachlorotolan, mp 158–161.5°C, was isolated. Repetition of the experiment on the same scale again gave no acetyl chloride but yielded 3.45 g of tetrachlorotolan.

Carrying out an experiment similar to the above but using butyric acid (0.86 mL) in place of acetic acid gave no acid chloride but yielded pure tetrachlorotolan (5.29 g). Benzoic acid (≈20 mg; mp 118–121°C), confirmed by ir and $^1H$ nmr, was also recovered.

α,α,α-Trichlorotoluene (15 mL) was boiled under reflux with water (4 mL) for 50 h. After cooling to room temperature, exhaustive extraction with saturated aqueous sodium bicarbonate and filtration of the cold, acidified extracts yielded 7.53 g (56% based on water) of benzoic acid.

*Electron spin resonance experiment*

A 1% solution of 1,2,5-triphenylphosphole in α,α,α-trichlorotoluene placed in a Bruker ER 200 tt esr spectrometer, was carefully scanned over 1000 G range about the free spin *g*-value, followed by a repetition over a 200 G range. No paramagnetic species were detected either at 293 K, or when repeated at 20° intervals up to 413 K or 423 K, at which temperature the solution was virtually black in colour.

*Phosphorus-31 and proton magnetic resonance experiments*

Approximately 1% solutions of twice-recrystallized 1,2,5-triphenylphosphole and its oxide were made up in carbon

Can. J. Chem. Downloaded from www.nrcresearchpress.com by 210.87.254.42 on 09/06/12
For personal use only.

Can. J. Chem. Downloaded from www.nrcresearchpress.com by 210.87.254.42 on 09/06/12
For personal use only.

TABLE 2. $^{31}P$ Magnetic resonance experiments[a]

| Sample | $^{31}P$ Shift,[a] ppm; (% of total signal integral) |
|---|---|
| In carbon tetrachloride, at 30°C: | |
| 1,2,5-triphenylphosphole | +5.1 (>92), +39.6(7) |
| 1,2,5-triphenylphosphole, after heating 2 h at 100°C | +50(60), +39.9(25), +59.0(15) |
| 1,2,5-triphenylphosphole-1-oxide | +39.5(35), +58(20), +59(22), +61(23) |
| In carbon tetrachloride, at 80°C after heating at 80°C, 3 h: | |
| 1,2,5-triphenylphosphole | +6.4(71), +39.7(12), +58.2(17) |
| In α,α,α-trichlorotoluene, at 30°C: | |
| 1,2,5-triphenylphosphole | +4.2(82), +41.0(18) |
| In α,α,α-trichlorotoluene, at 150°C: | |
| 1,2,5-triphenylphosphole | +8.0(15), +15.5(25), +25.0(2), +40.7(59) |

[a] Measured from trimethylphosphite (TMP) reference. Shifts reported here are from 85% phosphoric acid (calculated on the basis that the $^{31}P$ signal for 85% phosphoric acid is 139.6 ppm upfield of TMP).

TABLE 3. Ultraviolet spectra of 1,2,5-triphenylphosphole, triphenylphosphine, and related compounds[a]

| Compound | λ max, nm (log ε) | Reference |
|---|---|---|
| 1,2,5-triphenylphosphole | 222(4.38), 369(4.25) | 13 |
| 1,2,5-triphenylphosphole, P-oxide | 221(4.32), 243(4.22), 394(4.16) | 13 |
| 1,2,5-triphenylphosphole, methiodide | 222(4.56), 405(4.10) | 13 |
| Triphenylphosphine | 260(4.00) | 18, 19 |
| $Ph_3\overset{+}{P}-CH_3I^-$ | 227(4.08), 262(3.35), 268(3.49), 275(3.42) | 20, 21 |
| $Ph_4\overset{+}{P}Br^-$[b] | 233(4.36), 263(3.55), 269(3.68), 276(3.60) | 21 (p. D11/T4) |
| $Ph_3\overset{+}{P}-CHPh_2Br^-$ | 262(3.35), 269(3.38), 277(3.27) | 21 |
| Tri-*o*-tolylphosphine | 276(4.08) | 21 (p. D11/1) |
| $(o\text{-}CH_3Ph)_3\overset{+}{P}-CH_3I^-$ | 274(3.65), 282(3.60) | 21 (p. D11/4) |

[a] Spectra all taken in ethanol, or aqueous ethanol. Duplicate references given reflect very similar spectral data.
[b] Spectra of the chloride and iodide are very similar (20; plus ref. 20, page D11/5).

tetrachloride and α,α,α-trichlorotoluene, and placed in 10 mm diameter nmr tubes each with an axially-positioned, evacuated sealed capillary containing 99.8% deuterium oxide to provide an external lock signal. The tubes to be heated containing carbon tetrachloride solutions were chilled to −30°C and sealed under aspirator vacuum. Trimethyl phosphite, in a separate tube, was used for reference. The results of proton-decoupled $^{31}P$ spectra obtained on a Bruker Cryospec WM 250, Aspect 2000 instrument are summarized in Table 2. Proton spectra were also recorded.

## Results and discussion

Temperature quenching of fluorescence, which has frequently been the cause of thermochromism (1), is apparently not the source of the observed colour change on heating 1,2,5-triphenylphosphole in carbon tetrachloride, both because blue fluorescence is still observed with the boiling solution, and because removing a blue component from yellow does not give a red colour.

Since no colour change was observed on prolonged boiling of a solution of 1,2,5-triphenylphosphole in benzene or xylene, evidently the chloride was a necessary feature of the solvent carbon tetrachloride to obtain the red solution. Tertiary phosphorus was also a requirement from the no-effect observation on the boiling of a solution of 1,2,5-triphenylphosphole-1-oxide in carbon tetrachloride.

It was thought that the red colour might be the result of the bathochromic shift induced by the extension to the cross conjugated system resulting from the direct reversible formation of the dichloromethylene phosphorus compound **2**, by analogy with the triphenylphosphine system (17). Extended boiling of the red phosphole – carbon tetrachloride system in the presence of benzaldehyde, a Wittig-type substrate added to trap any potential phosphorane, only returned unchanged starting materials.

It is evident from Table 3 that phosphonium salts analogous to those postulated here uniformly show a bathochromic wavelength shift coincident with

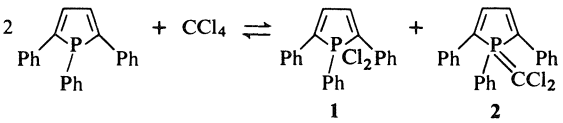


**1** **2**

hypochromic shift in intensity, as compared to the parent phosphine, the same as qualitatively observed here. Accordingly, from precedents set by the preparation of acid chlorides from analogous salts of other tertiary phosphines (22), tests were conducted with a series of carboxylic acids to interact with either of the two salt types, **3** or **4**,

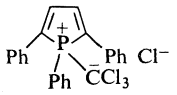

**3**

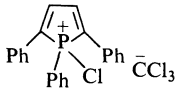

**4**

potentially present in this system. Acetic and stearic acids failed to demonstrate any significant acid chloride formation even though they caused colour reversion. Butyric acid, which was about 8% converted to acid chloride in 28 h, could not, however, be induced to react further even by extending the boiling period to 7 days. Therefore, if phosphonium salt formation was the cause of the red colour, the equilibrium must be well to the left and the colour due to very low salt concentrations, to observe such low acid to acid chloride conversions for acids which have readily afforded acid chloride with other phosphines.

Boiling 1,2,5-triphenylphosphole in α,α,α-trichlorotoluene gave a change to an orange colour in 20 min, and ultimately to a reddish-brown solution, but this solution did not revert to yellow on cooling. After as little as 4 h boiling, no trace of either phosphole or phosphole oxide was detectable in the residue obtained on evaporation of the solvent. However, significant quantities of 1,1,2,2-tetrachloro-1,2-diphenylethane (tetrachlorotolan), a coupling product, was isolated from all reactions conducted in this medium (Table 1). Crude yields ranged from 1.1 to 3.3 moles of tetrachlorotolan per mole of phosphole initially used, which decreased to the 1.4 to 2 mole range for the purified product. A control reaction in the absence of phosphole returned unchanged (although slightly coloured) α,α,α-trichlorotoluene.

The apparent novelty of this phosphine-induced coupling reaction, together with an interest in obtaining further information of potential value towards determining the pathway of this process prompted the testing of similar α,α,α-trichlorotoluene reactions with triphenylphosphine and tri-*n*-butylphosphine. With 10 mmoles of triphenylphosphine, 7.4 mmoles of pure tetrachlorotolan was obtained together with quantitative recovery of impure triphenylphosphine oxide. Tri-*n*-butylphosphine in boiling trichlorotoluene produced a difficultly resolvable mixture which was shown to contain tetrachlorotolan, traces of tri-*n*-butylphosphine oxide, and tar.

It was hypothesized at this stage that phosphonium salt formation from trichlorotoluene occurred with an associated dichlorophenylmethyl counterion **5**, which might be involved in the α,α,α-trichlorotoluene coupling reaction to tetrachlorotolan. Again, however, tests with added acetic and butyric acids in this system failed to demonstrate the formation of acid chloride and yet showed very similar tetrachlorotolan yields to tests carried out in their absence.

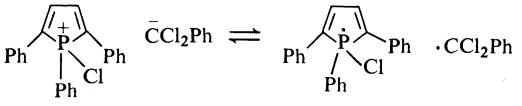

**5** **6**

While tertiary phosphines in the presence of methanol or ethanol have been used to reduce α,α,α-trichlorotoluene to benzal chloride, albeit sluggishly with triphenylphosphine (23), and to obtain tetraphenylethylene from dichlorodiphenylmethane (24), formation of tetrachlorotolan in this way has not been previously demonstrated. Tetrachlorotolan, however, has been obtained from trichlorotoluene using red phosphorus in the presence of hydroiodic acid (25), elemental sulfur (15), di-tertiarybutyl peroxide (26), and finely powdered tin (27), all reducing systems for the generation of radicals. Considering these examples, in the light of our own experiments, it was possible that the coloured species formed with 1,2,5-triphenylphosphole in boiling α,α,α-trichlorotoluene was the radical species **6** thermally produced in equilibrium with the phosphonium salt **5**, neither of which arise to any significant extent at ambient temperatures. But esr scanning of a 1000 G range about the free spin *g*-value failed to demonstrate the presence of any phosphoranyl radicals, which normally have $^{31}P$ coupling constants in the 800 G range (28). Thus, if any radical species was present, the concentration must have been below about $10^{-8}$ *M*, or represent less than one in $10^6$ of the phosphole molecules present, probably not a significant contribution to the colour-forming process in trichlorotoluene.

Phosphorus magnetic resonance experiments provided physical supporting evidence of the chemical evidence of phosphonium salt intermediacy in these colour-forming processes. Phosphorus shifts for 1,2,5-triphenylphosphole and its oxide were determined to be +5.1 (lit. (29) −3 ppm ($CHCl_3$), lit. (30) +3 ppm) and +39.9 ppm respectively, in carbon tetrachloride, +4.2 and +39.5 ppm in carbon

Can. J. Chem. Downloaded from www.nrcresearchpress.com by 210.87.254.42 on 09/06/12
For personal use only.

Can. J. Chem. Downloaded from www.nrcresearchpress.com by 210.87.254.42 on 09/06/12
For personal use only.

tetrachloride, and +4.2 and +39.5 ppm in α,α,α-trichlorotoluene, all at 30°C. Even room temperature measurements of the phosphole solutions, however, by the very gradual appearance of peaks at the appropriate shifts, demonstrated the formation of phosphole oxide. This appearance of phosphole oxide may have occurred via a slow progression of the process of interest, or from direct oxidation, or from a combination of both processes.

Immediately on observation of solutions of phosphole in hot trichlorotoluene, phosphole oxide was the dominant phosphorus species present, although measurable amounts of unchanged phosphole and two other phosphorus-containing species of distinctly different intermediate $^{31}P$ shifts were also present (Table 2). In hot carbon tetrachloride neither of the unknown species observed in trichlorotoluene were present, but a third phosphorus-containing component ($\delta$ = +58.2 ppm), 19 ppm downfield of the phosphole oxide, was present to a significant extent. Probably one or more of the transitory unidentified $^{31}P$ shifts at elevated temperatures in both solvents are caused by the colour-forming substances, and the rapid appearance of phosphole oxide is a strong indication that this is a product of the colour-forming process. The proton nmr spectra run in parallel with the above experiments failed to give any helpful information beyond complex, aromatic-type multiplets.

Thus, the phosphorus nmr exposes the complexity of the colour-forming reaction of the phosphole system in both carbon tetrachloride and α,α,α-trichlorotoluene solvents, the only common feature being the formation of phosphole oxide. Since the normal ranges of $^{31}P$ shifts for phosphine oxides, +20 to +50, and phosphonium salts, +20 to +45 (ref. 30, p. 199), overlap significantly, it can only be speculated that the additional intervening shifts observed in trichlorotoluene are from various possible phosphonium salts or oxidized phosphorus components other than phosphole oxide. With shifts of +52.8, and +74.6 ppm reported for the phosphonium salts **7** and **8** respectively (30), even

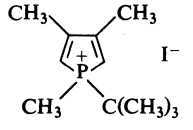


**7**

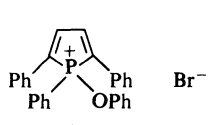


**8**

the observed +58.2 ppm shift observed for the hot carbon tetrachloride solution may well also arise from a phosphonium salt. Certainly all of the unexplained signals from hot solutions are downfield of the +20 to −62 ppm range to be expected from tertiary phosphines (ref. 30, p. 199), which can reasonably therefore be eliminated.

On the basis of the synthetic and spectroscopic evidence obtained, the single likely species responsible for the colour in the phosphole – carbon tetrachloride system is probably a phosphonium trichloromethide salt, with a significant tendency to return to phosphole and carbon tetrachloride on cooling. The combination of higher temperatures and more reactive halide in the phosphole–trichlorotoluene system involves at least two (from $^{31}P$ magnetic resonance) salt-like species which are likely to be the phosphonium dichlorophenylmethide salts, **5**, and phosphonium chloride, **9**, either of

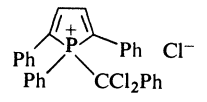


**9**

which can reasonably participate in the coupling reaction observed at these temperatures.

**Acknowledgements**

The authors are grateful to the National Research Council and the University of Victoria for financial support. They thank P. Barker for conducting the esr experiments.

1. J. H. Day. Chem. Rev. **63**, 65 (1963).
2. M. Kobayashi. Kagaku Kyoto, **19**, 18 (1964).
3. J. Vitry. Chim. Ind., Genie Chim. **102**, 1333 (1969).
4. K. Maeda, A. Chinone, and T. Hayashi. Bull. Chem. Soc. Jpn. **43**, 1431 (1970).
5. K. Maeda and T. Hayashi. Bull. Chem. Soc. Jpn. **43**, 429 (1970); S. Gunzenhauser, B. Hellrung, and H. Balli. Helv. Chim. Acta, **62**, 171 (1979).
6. N. S. Kozlov, O. D. Zhikareva, I. P. Mikhailova, and D. I. Burakova. Dokl. Akad. Nauk BSSR, **22**, 434 (1978); Chem. Abstr. **89**, 112286s (1978).
7. R. Simone and M. Toschi. Z. Naturforsch. Teil B, **25**, 461 (1970).
8. F. M. Menger and M. Perinis. Tetrahedron Lett. **47**, 4653 (1978); A. Bertoluzza, C. Concilio, and P. Finelli. J. Appl. Chem. Biotechnol. **27**, 225 (1977); G. G. Gachechiladze, S. A. Akhobadze, N. O. Sepashvili, E. V. Skhirtladze, D. P. Maisuradze, and K. G. Dzhaparidze. Izv. Akad. Nauk Gruz. SSR, Ser. Khim **4**, 230 (1978); Chem. Abstr. **90**, 213159d (1979).
9. E. Hadjoudis, F. Milia, J. Seliger, and R. Blink. Phys. Status Solidi A, **46**, 239 (1978); E. Hadjoudis, F. Milia, J. Seliger, and R. Blink. Chem. Phys. Lett. **56**, 382 (1978); Y. Tipuhi, O. Kalisky, and I. Agranat. J. Org. Chem. **44**, 1949 (1979).
10. R. Paetzold, K. Appenroth, and M. Reichenbaecher. Z. Chem. **16**, 446 (1976).
11. N. Latif, I. Zeid, and N. Mishriky. Chem. Ind. London, 754 (1969).
12. I. V. Kudyakov, A. I. Yasmenko, A. P. Khardin, A. I. Prokof'ev, and V. A. Kuzmin. Izv. Akad. Nauk SSR Ser. Khim. 1499 (1978).
13. I. G. M. Campbell, R. C. Cookson, M. B. Hocking, and A. N. Hughes. J. Chem. Soc. 2184 (1965).
14. M. B. Hocking. Synthesis and chemistry of phospholes. Thesis, University of Southampton, 1963. p. 139.

15. E. J. GEERING. U.S. Pat. No. 3,278,552 (October 11, 1966); Chem. Abstr. **66**, 10920d (1967).
16. W. C. DAVIES and W. J. JONES. J. Chem. Soc. 33 (1929).
17. R. RABINOWITZ and R. MARCUS. J. Am. Chem. Soc. **84**, 1312 (1962); F. RAMIREZ, N. B. DESAI, and N. MCKELVIE. J. Am. Chem. Soc. **84**, 1745 (1962).
18. H. H. JAFFE. J. Chem. Phys. **22**, 1430 (1954).
19. J. C. SHELDON and S. Y. TYREE. J. Am. Chem. Soc. **80**, 2117 (1958).
20. F. G. MANN, I. T. MILLAR, and B. B. SMITH. J. Chem. Soc. 1130 (1953).
21. UV Atlas of Organic Compounds. Vol. I. Butterworths, London, 1966. p. D11/T2.
22. J. B. LEE. J. Am. Chem. Soc. **88**, 3440 (1966); I. M. DOWNIE, J. B. LEE, and M. F. S. MATOUGH. Chem. Commun. 1350 (1968); J. HOOZ and S. S. H. GILANI. Can J. Chem. **46**, 86 (1968); B. CASTRO, Y. CHAPLEUR, B. CROSS, and C. SELVE. Tetrahedron Lett. 500 (1972).
23. I. M. DOWNIE and J. B. LEE. Tetrahedron Lett. 4951 (1968).
24. K. L. FREEMAN and M. J. GALLAGHER. Aust. J. Chem. **21**, 145 (1968).
25. W. M. LE SUER and C. W. STUEBE. U.S. Pat. No. 3,004,076 (July 1, 1960); Chem. Abstr. **56**, 5884 (1962).
26. H. H. HUANG and P. K. K. LIM. J. Chem. Soc. C, 2432 (1967).
27. H. GROHN and R. PAUDERT. Wiss. Z. Tech. Hochsch. Chem. Leuna – Merseberg, **3**, 203 (1960); Chem. Abstr. **56**, 4644 (1962).
28. B. P. ROBERTS. *In* Advances in free-radical chemistry. Vol. 6. *Edited by* G. H. Williams. Heyden, Philadelphia. 1980. p. 240.
29. N. E. WAITE and J. C. TEBBY. J. Chem. Soc. C, 386 (1970).
30. L. D. QUIN. The heterocyclic chemistry of phosphorus: systems based on the phosphorus–carbon bond. Wiley–Interscience, Toronto. 1981. p. 244.

Can. J. Chem. Downloaded from www.nrcresearchpress.com by 210.87.254.42 on 09/06/12
For personal use only.

# Sulfur-free penicillin derivatives. VII. Multiple functionalization of 2-azetidinyl-3-methyl-2-butenoates

SAUL WOLFE AND CHIA-CHENG SHAW

*Department of Chemistry, Queen's University, Kingston, Ont., Canada K7L 3N6*

Received August 10, 1981

SAUL WOLFE and CHIA-CHENG SHAW. Can. J. Chem. **60**, 144 (1982).

The title compounds, substituted with chlorine in the 4′-position and with phthalimido, 2,2,2-trichloroethoxycarbonylamino, or phenoxycarbonylamino in the 3′-position of the azetidinone ring, have been converted to bis-allylic formates via bromination of both methyl groups with excess *N*-bromosuccinimide, and displacement of both bromines by formate ions in methylene chloride solvent. The diformates react smoothly with a deficit of a boron halide to form *E*/*Z* mixtures of halogeno-formates, in which the *E*-isomer predominates. Depending on the 3′-azetidinyl substituent, these halogeno-formates undergo a second displacement with acetate either with retention of olefinic geometry or inversion of olefinic geometry. The mechanisms of these reactions are discussed, along with further transformations leading to hydroxylactones, halogenolactones, halogenohydrins, and other compounds. Examination of the proton magnetic resonance spectra of twenty-one compounds reveals that methylene protons *cis* to the β-lactam nitrogen atom of a methyl 2-azetidinyl-2-butenoate are found at higher field than methylene protons *cis* to the methoxycarbonyl group. This observation appears to provide a more reliable criterion for the assignment of configuration to geometrical isomers than one based on the magnitude of the chemical shift nonequivalence of the *E* and *Z* methylene protons.

SAUL WOLFE et CHIA-CHENG SHAW. Can. J. Chem. **60**, 144 (1982).

Le composé mentionné dans le titre portant une chlore en position 4′ et un groupe phtalimido, trichloro-2,2,2 éthoxycarbonylamino ou phénoxycarbonylamino en position 3′ du cycle azétidinone, soumis à une bromation des groupes méthyles au moyen d'un excès de *N*-bromosuccinimide suivie par déplacement des bromes par des ions formiates dans le chlorure de méthylène, conduit aux formiates bis-allyliques. Les diformiates réagissent avec un défaut d'halogènure de bore en donnant les mélanges *E*/*Z* d'halogénoformiates dans lesquels l'isomère *E* est majoritaire. Dépendant du substituant en position 3′ du cycle azétidinyle, ces halogénoformiates, en présence d'un acétate, subissent une deuxième réaction de déplacement avec rétention ou inversion de la géométrie de l'oléfine. On discute des mécanismes de ces réactions ainsi que des transformation plus poussées qui conduisent à des hydroxylactones, des halogénolactones, des halohydrines et à d'autres composés. Les spectres de rmn du $^1$H de vingt et un composés révèlent que les protons méthyléniques en position 6 par rapport à l'atome d'azote du β-lactame du azétidinyl-2 butène-2 oate de méthyle, sont déplacés vers les champs forts par rapport aux protons méthyléniques en position *cis* du groupe méthoxycarbonyle. Ces observations semblent fournir des critères plus surs, que ceux fondés sur l'ordre de grandeur de la non équivalence des déplacements chimiques des protons méthyliques des isomères *E* et *Z*, pour déterminer la configuration des isomères géométriques.

[Traduit par le journal]

The first synthesis of a 1-oxacephem (**1**; $R^2 = CH_3$) from a penicillin precursor (**2**) was achieved by the sequence shown retrosynthetically in Scheme 1 (1). This approach became feasible following the development of routes from penicillins to the chloroazetidinones **3** (2, 3), and the observation that displacement of chlorine from such compounds proceeds without rupture of the β-lactam ring (2, 4, 5).

Numerous syntheses of 1-oxacephems from β-lactam natural products have since appeared in the literature (6), and two rather different strategies have evolved. One, as in Scheme 1, retains the isoprenoid moiety attached to the azetidinyl nitrogen of **3** and cognate 3-methyl-2-butenoates or 3-methyl-3-butenoates. An advantage of this approach is that these compounds possess the complete carbon skeleton of the target molecule so that,

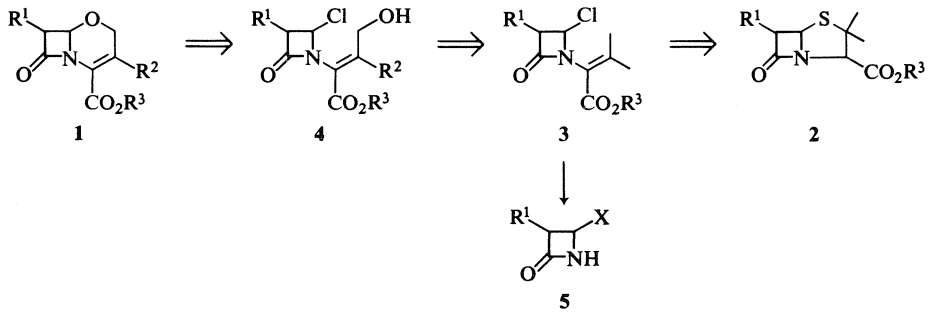

SCHEME 1

0008-4042/82/020144-10$01.00/0

©1982 National Research Council of Canada/Conseil national de recherches du Canada

Can. J. Chem. Downloaded from www.nrcresearchpress.com by 210.87.254.5 on 09/06/12
For personal use only.

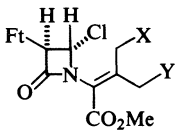


(Ft = phthalimido)

6

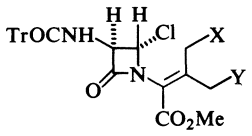


(TrOC = $Cl_3CCH_2OCO$)

7

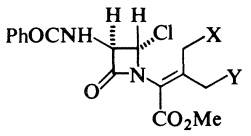


(PhOC = PhOCO)

8

*a* X = Y = OCHO
*b* X = Y = Br
*c* X = Br; Y = H
*d* X = H; Y = Br
*e* X = H; Y = OCHO
*f* X = OCHO; Y = H
*g* X = Y = Cl
*h* X = OCHO; Y = Br
*i* X = Br; Y = OCHO
*j* X = OH; Y = Br
*k* X = OTHP; Y = Br
*l* X = O-*tert*-butyldimethylsilyl; Y = Br
*m* X = OCHO; Y = Cl
*n* X = Cl; Y = OCHO
*o* X = OH; Y = Cl
*p* X = OAc; Y = OCHO
*q* X = OCHO; Y = OAc
*r* X = OH; Y = OAc

in principle, the oxacephem ring system can be reached by an oxidation and a ring closure. An alternative strategy employs methodology first devised by Woodward *et al.* (7). This approach begins with the removal of the butenoate moiety (**3** → **5**) (8); a new ring is then reconstructed by a multistep process (7). The particular advantage of this strategy is that it has allowed the ready laboratory synthesis and biological evaluation of a wide range of bicyclic systems (see, for example, ref. 9). A disadvantage is that the existing multistep sequences cannot be implemented economically on an industrial scale (10).

This paper is concerned with the elaboration of routes to compounds of type **4**, in which $R^2 \neq CH_3$, by functionalization of a 2-azetidinylbutenoate. Important intermediates in these sequences are the diformates **6***a*–**8***a*. A compound of this type (**9**) has been obtained by Campbell *et al.* (11) from the reaction of **10** with formate ions under phase transfer conditions. However, removal of the formate groups with bicarbonate led to loss of the β-lactam ring and concomitant rearrangement to a 1,5-oxazocine. In the present work the diformates **6***a*–**8***a* have been prepared, by a different procedure, from the dibromo precursors **6***b*–**8***b* and have been found to be convertible to the desired compounds **4** ($R^2 \neq CH_3$) under appropriate reaction conditions.

In an earlier investigation of the displacement of bromine from **6***c* and **6***d* (12), it was observed that a 1:1 mixture of these monobromides is converted in over 90% isolated yield to a 2:1 mixture of *E* (**6***e*) and *Z* (**6***f*) formates, using tetramethylguanidinium formate in chloroform solvent at room temperature. Under the same conditions, **6***a* was not obtained from the dibromide **6***b*. It has now been found that simply changing the solvent from chloroform to methylene chloride allows the isolation of **6***a* in 21–28% yield, using tetramethylguanidinium formate at −10°C, and in 42–47% yield using tetra-*n*-butylammonium formate at room temperature. Similar conditions were employed to prepare **7***a* and **8***a*.

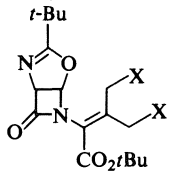


**9** X = OCHO
**10** X = Br

The recovery of a 2:1 mixture of **6***e* and **6***f* from the 1:1 mixture of **6***c* and **6***d* suggested (12) that both geometrical isomers react via the same intermediate, **11** (⇄ **12**), addition of formate to **11** leading to the *Z* isomer, and addition to **12** leading to the *E* isomer. There is precedent for such an elimination–addition pathway in the mechanism proposed for the process **13** → **14** (13). However, it should be noted that the latter reaction proceeds only in hydroxylic solvents, and does not occur with oxygen nucleophiles, in contrast to the observations of ref. 12.

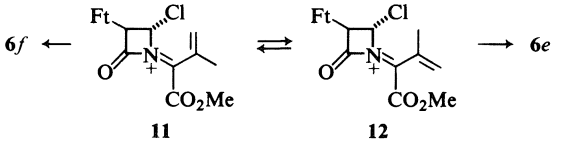


**11** **12**

It is known that the pyramidality of the β-lactam nitrogen atom decreases in the order penicillin > cephalosporin > monocyclic azetidinones. This trend is seen in the solid state (14), and is reflected (15, 16) in the different β-lactam carbonyl stretching frequencies of these compounds (**15**: 1790 $cm^{-1}$; **16**: 1785 $cm^{-1}$; unfused β-lactams: < 1760 $cm^{-1}$).

Can. J. Chem. Downloaded from www.nrcresearchpress.com by 210.87.254.5 on 09/06/12
For personal use only.

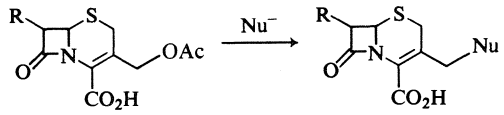

13 14

The azetidinones of type **3** exhibit carbonyl absorption in the range 1773–1779 $cm^{-1}$ (17), suggesting a more nearly planar geometry at the β-lactam nitrogen than in a $\Delta^3$-cephem. Such a geometrical change can lead to an increase in the HOMO–LUMO interaction (18) between the nitrogen lone pair and the allylic halide systems of **6***c* and **6***d*, and thereby facilitate ionization to **11** (**12**).

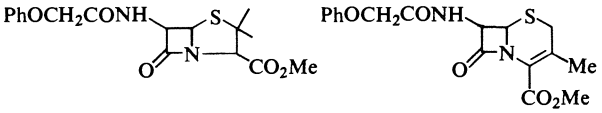

15 16

It was thought that the conversion of a dibromide to a diformate might proceed analogously, via **17** (**18**) (X = Br), leading to a mixture of the bromo-formates **19** and **20** at an intermediate stage, but such compounds could not be isolated from any of the reactions of **6***b*–**8***b*. These multiply-functionalized butenoates were, however, accessible from the reactions of the diformates with boron halides.

Exploratory experiments with the phthalimido compound **6***a* revealed that one mol-equiv. of boron tribromide regenerated the dibromide **6***b* in quantitative yield; use of boron trichloride led to the dichloride **6***g*. With 0.6 mol-equiv. of boron tribromide, **6***a* was converted in 75% yield to a 2:1 mixture of the bromo-formates **6***h* and **6***i*, from which the major isomer **6***h*, mp 135.0–137.0°C, could be isolated in pure form. The assignment of the *E* configuration to this compound is based on the finding that deformylation under acidic conditions (HCl–MeOH–$CH_2Cl_2$) leads to the bromohydrin **6***j*, convertible to the tetrahydropyranyl ether **6***k* and the *tert*-butyldimethylsilyl ether **6***l*. Under the same deformylation conditions the minor isomer **6***i* was converted to the bromolactone **21** (R = Ft; X = Br), and the diformate **6***a* afforded the hydroxylactone **21** (R = Ft; X = OH). The hydroxylactone was convertible to the bromolactone upon further treatment with boron tribromide. The tetrahydropyranyl and *tert*-butyldimethylsilyl derivatives were also prepared.

With 0.6 mol-equiv. of boron trichloride, **6***a* gave, in 68% yield, a 3:1 mixture of the isomeric chloro-formates **6***m* and **6***n*, the assignment of configuration again being based on the deformylation of **6***m* to the chlorohydrin **6***o*, and of **6***n* to the chlorolactone **21** (R = Ft; X = Cl).

The sequences just described proved to be compatible with the TrOC (**7***a*) and PhOC (**8***a*) side chains. Deformylation of **7***a* and **8***a* led to **21** (R = TrOCNH; X = OH) (quantitative) and **21** (R = PhOCNH; X = OH) (91%), respectively. Boron tribromide afforded a separable 4:1 mixture of **7***h* and **7***i* (61%) from **7***a*, and a 4:1 mixture of **8***h* and **8***i* (61%) from **8***a*.

Thus, in the replacement of formate by halogen, as in the earlier replacement of halogen by formate (12), the *E*-geometrical isomer (**6***h*, **6***m*, **7***h*, **8***h*) is formed preferentially. However, despite their stereochemical similarities, the two reactions appear to proceed via different mechanisms. Indeed, that as many as three different mechanistic pathways may

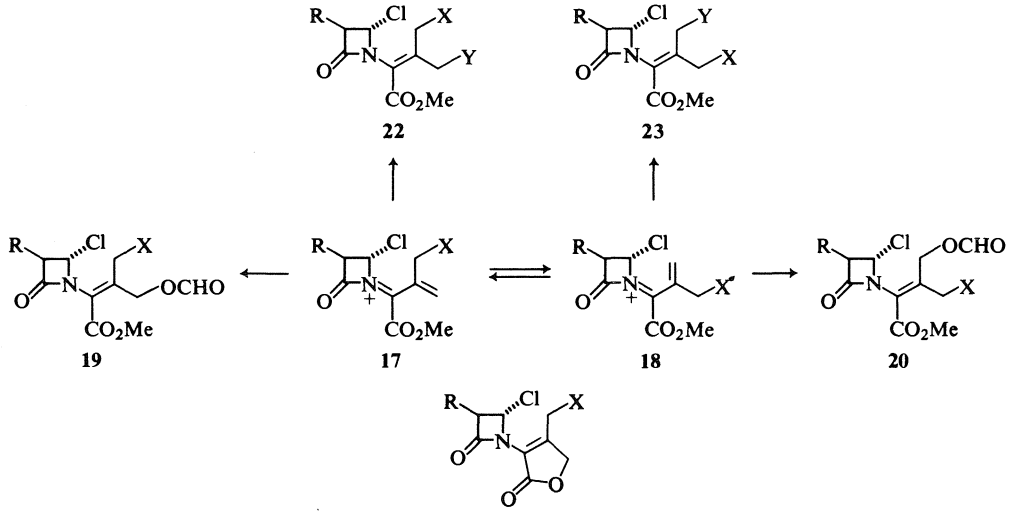

22 23 19 17 18 20 21

Can. J. Chem. Downloaded from www.nrcresearchpress.com by 210.87.254.5 on 09/06/12
For personal use only.

Can. J. Chem. Downloaded from www.nrcresearchpress.com by 210.87.254.5 on 09/06/12
For personal use only.

exist for the displacement of one allylic substituent by another in such compounds became apparent when the bromo-formates **6***h*, **7***h*, and **7***i* were allowed to react with tetraethylammonium acetate, to form acetoxyformates.

In the phthalimido series, this reaction proceeded *with inversion of olefinic geometry* to yield **6***p* (60%), with no trace of the geometrical isomer **6***q*. On the other hand, both TrOC compounds underwent displacement by acetate *with retention of olefinic geometry*. Thus, **7***h* afforded **7***q*, and **7***i* afforded **7***p*. In each case, the configurations of the acetoxyformates were established by deformylation experiments: **6***p* and **7***p* were converted to the acetoxylactones **21** (R = Ft, TrOC; X = OAc), but **7***q* gave the acetoxyhydrin **7***r*. The bromo-formate **7***h* was also converted to the mercaptomethyltetrazole derivative **24**, with mercaptomethyltetrazole in dimethylformamide solvent. Deformylation afforded the alcohol **25**, which appears to be a useful intermediate for further work.

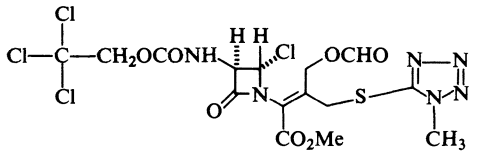

**24**

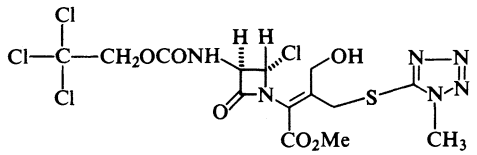

**25**

If the reaction of a diformate with boron tribromide and the reaction of a bromo-formate with a nucleophile both proceed via the elimination–addition pathway postulated earlier, then the same cationic species (**17** ⇄ **18**) (X = OCHO) must intervene in both cases. Since both reactions are conducted in methylene chloride solvent and at similar temperatures (−15° to 0°C), the partitioning of the intermediate (**17** → **22**; **18** → **23**) should not depend greatly on the nature of the entering nucleophile Y.

This behaviour is not observed in the phthalimido series, since **6***a* is converted preferentially to the *E*-bromoformate **6***h*, but **6***h* is, in turn, converted to the *Z*-acetoxyformate **6***p*. The expected behaviour is also not observed in the TrOC series, since the geometrical isomers **7***h* and **7***i* give different products upon reaction with acetate, and **7***h* is converted exclusively to **24** upon treatment with mercaptomethyltetrazole.

The most reasonable interpretation of these observations is that the displacement of bromine in the TrOC series proceeds via an $S_N2$ process and, in the phthalimido series, via the cationic intermediates **17** and **18** (X = OCHO).[1] The replacement of formate by halogen, using a boron halide, then requires a third mechanism; it is suggested that this is the $S_Ni$ process depicted in **26** and **27**.

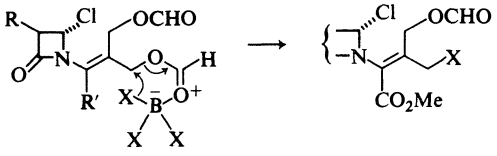

**26** (R′ = $CO_2Me$)

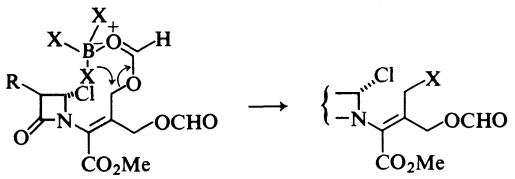

**27**

Inspection of molecular models reveals a possible conformational origin for the mechanistic difference between the phthalimido and TrOC compounds. The azetidinyl nitrogen lone pair will participate optimally in the ionization of the allylic bromine when this lone pair is oriented perpendicular to the 2-butenoate moiety (cf. **28**). Such a conformation can be achieved without difficulty in the phthalimido series. However, in the TrOC series, a hydrogen bond can exist between the TrOC N—H and the carbonyl oxygen of the ester group (cf. **29**). The resulting 90° rotation of the butenoate moiety will greatly diminish orbital interaction between the nitrogen lone pair and the allylic system.

In a recent publication dealing with compounds of type **30**, the Farmitalia group have observed (19) that, for certain combinations of E and Z, the

[1]A multistep process, involving Michael addition of acetate to the conjugated ester to form **i**, followed by displacement of bromine and elimination of acetate, might also be proposed. This seems unlikely for three reasons: (*i*) we have been unable to observe conjugate addition to compounds of type **3** under a variety of conditions; (*ii*) the β-elimination of acetate is expected (1) to lead to a mixture of geometrical isomers; (*iii*) the reaction mixture contains no source of protons to complete the conjugate addition.

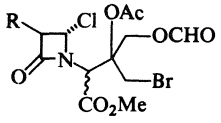

**i**

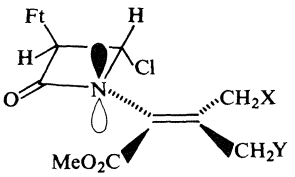

28

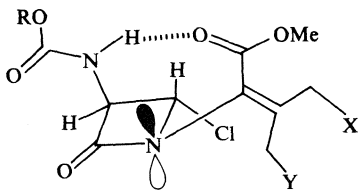

29

methylene protons of the $CH_2E$ moiety exhibit a larger chemical shift nonequivalence than those of the $CH_2Z$ moiety, and suggest that this observation may be useful for the assignment of configurations to such double bond isomers. Using stereochemical assignments apparently based on the generalizations of Martin and Martin (20, 21) for the proton chemical shifts of the methyl groups of compounds of type $CH_3$—CZ=CY—COX, a 0.28–0.36 ppm chemical shift difference was observed for E = Br, SPh and Z = H; and a 0.0–0.09 ppm chemical shift difference was observed for Z = Br, SPh and E = H. No chemical shift nonequivalence was observed when one of E or Z was OMe, O-*t*-Bu or OAc. For example, the bromoacetates **30** (E = Br, Z = OAc) and **30** (E = OAc, Z = Br) each showed singlets for both methylene groups. Although these latter compounds are described separately, it is not clear from the published data how the configurations were assigned.

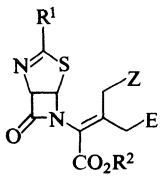

30

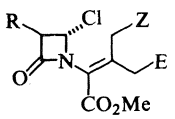

31

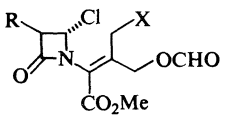

32

The present work has led to a large number of compounds of type **31** of known stereochemistry about the double bond. It has, therefore, been possible to examine in some detail the generality of the earlier proposal concerning the use of chemical shift nonequivalence for configurational assignments. Table 1 summarizes the data for twenty-one compounds. In all cases where $Z \neq E$, $\delta^Z_{av}$ is found at higher field than $\delta^E_{av}$. This observation has been used to assign the $\delta^E_{av}$ and $\delta^Z_{av}$ resonances to compounds in which Z = E, and also to the various acetoxyformates.

Only three compounds (*6a*, *7p*, and *7r*) show no chemical shift nonequivalence in either of the methylene groups. Where nonequivalence is observed, thirteen compounds exhibit greater nonequivalence in $CH_2E$, in agreement with the Farmitalia observations. Five compounds, corresponding to structure **32** (X = Br, Cl, OAc), show the opposite behavior.

Since the reasons for the observed chemical shift nonequivalence of the diastereotopic methylene protons of these complex compounds are not known, the present results suggest that the magnitude of such nonequivalence is not a reliable criterion for the assignment of configuration. It may be more useful to base assignments on the finding that $\delta^Z_{av}$ is at higher field than $\delta^E_{av}$. This result is consistent with the data of Table 2 of ref. 20, if it is supposed that the methoxycarbonyl group of **31** has a greater effect on $\delta_{av}$ than the β-lactam nitrogen.

TABLE 1. Chemical shift data for the $CH_2Z$ and $CH_2E$ protons of compounds **31**[a,b]

| Compound | Z | $\delta^{Z\,c}_{av}$ | Δδ | E | $\delta^{E\,c}_{av}$ | Δδ |
|---|---|---|---|---|---|---|
| *6a* | OCHO | 5.23 | 0 | OCHO | 5.57 | 0 |
| *6b* | Br | 4.52 | 0.19 | Br | 4.79 | 0.31 |
| *6g* | Cl | 4.55 | 0.15 | Cl | 4.80 | 0.18 |
| *6h* | OCHO | 5.17 | 0 | Br | 4.73 | 0.27 |
| *6i* | Br | 4.56 | 0.17 | OCHO | 5.53 | 0 |
| *6j* | OH | 4.43 | 0 | Br | 4.64 | 0.17 |
| *6m* | OCHO | 5.07 | 0 | Cl | 4.72 | 0.12 |
| *6n* | Cl | 4.45 | 0.17 | OCHO | 5.37 | 0 |
| *6o* | OH | 4.41 | 0 | Cl | 4.69 | 0.14 |
| *6p* | OAc | 5.01 | 0.23 | OCHO | 5.13 | 0 |
| *7a* | OCHO | 4.97 | 0 | OCHO | 5.24 | 0.14 |
| *7b* | Br | 4.33 | 0 | Br | 4.62 | 0.17 |
| *7h* | OCHO | 5.02 | 0 | Br | 4.54 | 0.14 |
| *7i* | Br | 4.27 | 0.16 | OCHO | 5.32 | 0 |
| *7p* | OAc | 4.87 | 0 | OCHO | 5.23 | 0 |
| *7q* | OCHO | 4.93 | 0 | OAc | 5.15 | 0.13 |
| *7r* | OH | 4.83 | 0 | OAc | 5.15 | 0 |
| *8a* | OCHO | 4.97 | 0 | OCHO | 5.23 | >0[d] |
| *8b* | Br | 4.30 | 0 | Br | 4.63 | 0.19 |
| *8h* | OCHO | 4.92 | 0 | Br | 4.49 | 0.17 |
| *8i* | Br | 4.19 | 0.17 | OCHO | 5.23 | 0 |

[a]All spectra were recorded on a Varian EM360 spectrometer in $CDCl_3$ solvent.
[b]Chemical shifts are given in ppm relative to internal TMS.
[c]Refers to the position of the singlet, where a singlet was observed, or to the centre of the AB quartet.
[d]A broad singlet was observed in this case.

Can. J. Chem. Downloaded from www.nrcresearchpress.com by 210.87.254.5 on 09/06/12
For personal use only.

Can. J. Chem. Downloaded from www.nrcresearchpress.com by 210.87.254.5 on 09/06/12
For personal use only.

## Experimental

General experimental procedures have been described previously (17). The $^1$Hmr spectra were recorded on a Varian EM360 spectrometer; infrared (ir) spectra were taken on a Perkin Elmer 180 instrument. Analyses are by Galbraith Laboratories, Knoxville, TN.

*Preparation of* **6**a

To a solution of **6***b* (2.35 g, 4.52 mmol) in methylene chloride (5 mL) was added, during 30 min, a solution of tetra-*n*-butylammonium formate (3.73 g, 13.56 mmol) in methylene chloride (20 mL). The reaction mixture was stirred for 48 h under nitrogen at room temperature and was then diluted with 10% acetone–hexane (10 mL) and chromatographed on silica gel. Graded elution with acetone–hexane afforded 919 mg (45%) of the diformate **6***a* as a pale yellow foam; ir ($CHCl_3$): 1795, 1775, 1735 cm$^{-1}$; $^1$Hmr ($CDCl_3$) δ: 3.87 (3H, s), 5.00 (2H, s), 5.23 (2H, s), 5.57 (1H, d, 2 Hz), 6.23 (1H, d, 2 Hz), 7.73 (4H, d), 7.97 (2H, s). *Anal.* calcd. for $C_{19}H_{15}N_2O_9Cl$: C 50.62, H 3.35, N 6.22; found: C 50.37, H 3.46, N 6.18.

*Hydrolysis of* **6**a *to the hydroxylactone* ***21*** *(R = Ft; X = OH)*

The diformate **6***a* (102 mg, 0.226 mmol) was dissolved in methylene chloride (4 mL), and *N* methanolic hydrogen chloride (0.2 mL) was added. The reaction mixture was stirred at 25°C for 2 h, and the solvent was then removed. The residue (89 mg) was a pale yellow foam, which appeared homogeneous on tlc. It was purified by plc (silica gel, acetone–hexane, 2:3) to give 79 mg (96%) of **21** (R = Ft; X = OH); ir ($CHCl_3$): 1790, 1770, 1725 cm$^{-1}$; $^1$Hmr ($CDCl_3$) δ: 3.00 (1H, br s, exch $D_2O$), 4.54, 4.81 (2H, ABq, $J$ = 16 Hz), 4.95 (2H, s), 5.53 (1H, d, 2 Hz), 6.57 (1H, d, 2 Hz), 7.68 (4H, br s).

*Conversion of* **6**a *to* **6**b *with excess boron tribromide*

To an ice-cold solution of the diformate **6***a* (52 mg, 0.115 mmol) in methylene chloride (3 mL) was added an ice-cold solution of boron tribromide (30 mg, 0.116 mmol) in methylene chloride (0.25 mL). The solution was stirred at 0°C for 1.5 h and then poured onto ice-cold brine (20 mL) and the layers separated. The aqueous layer was extracted with chloroform (3 × 40 mL) and the combined organic layers were washed with brine (2 × 5 mL), dried ($MgSO_4$), and evaporated to give 59 mg (100%) of **6***b* as a colourless foam. The $^1$Hmr spectrum of the product was identical with that of authentic material.

*Reaction of* **6**a *with 0.5 mol-equiv. of boron tribromide*

To an ice-cold solution of the diformate (304 mg, 0.675 mmol) in methylene chloride (5 mL) was added dropwise, with stirring, a solution of boron tribromide (86 mg, 0.34 mmol) in methylene chloride (0.8 mL). Stirring was continued for 1.5 h at 0°C, and the solution was then poured onto ice-cold 5% sodium bicarbonate. The layers were separated and the aqueous layer was extracted with methylene chloride (3 × 60 mL). The combined organic layers were washed with brine (3 × 10 mL), dried ($Na_2SO_4$), and evaporated to a colourless foam (322 mg). This was purified by plc (silica gel, acetone–hexane, 1:4) to give three products. The leading band was **6***b* (25 mg). The middle band was a 79:21 mixture of **6***h* and **6***i* (245 mg, 75%). Separation and characterization of these two compounds is described in the following experiment.

*Preparation of* **6**a *and* **6**i

To an ice-cold solution of **6***a* (937 mg, 2.08 mmol) in methylene chloride (10 mL) was added, dropwise under a nitrogen atmosphere, a solution of boron tribromide (321 mg, 1.28 mmol, 0.61 mol-equiv.) in methylene chloride (6 mL). The mixture was stirred for 1.5 h at 0°C and then poured into a large excess of saturated ice-cold sodium bicarbonate. Isolation as described above afforded a crude product which was chromatographed on silica gel. Elution with 1% acetone in hexane afforded successively the dibromide **6***b* (trace), **6***h* (343 mg, 34%), **6***i* (176 mg, 17%), unreacted **6***a* (trace), and an unidentified compound. Compound **6***h*: mp 135.0–137.0°C; ir ($CHCl_3$): 1800, 1780, 1730 cm$^{-1}$; $^1$Hmr ($CDCl_3$) δ: 4.00 (3H, s), 4.59, 4.86 (2H, ABq, 10 Hz), 5.17 (2H, s), 5.67 (1H, d, 2 Hz), 6.35 (1H, d, 2 Hz), 7.90 (4H, br s), 8.17 (1H, s). *Anal.* calcd. for $C_{18}H_{14}N_2O_7BrCl$: C 44.51, H 2.91, N 5.77, Br 16.45, Cl 7.30; found: C 44.37, H 3.02, N 5.74, Br 16.47, Cl, 7.47. Compound **6***i*: foam; $^1$Hmr ($CDCl_3$) δ, 4.05 (3H, s), 4.47, 4.64 (2H, ABq, 10 Hz), 5.53 (2H, s), 5.76 (1H, d, 2 Hz), 6.47 (1H, d, 2 Hz), 8.03 (4H, br s), 8.27 (1H, s).

*Conversion of* **6**a *to* **6**g, **6**m, *and* **6**n *with boron trichloride*

To an ice-cold solution of **6***a* (131 mg, 0.29 mmol) in methylene chloride (4 mL) was added 0.2 mL of a *M* solution of boron trichloride in methylene chloride (0.70 mol-equiv.). The resulting solution was stirred for 2 h at 0°C and then poured into ice-cold 5% sodium bicarbonate. The aqueous layer was extracted with methylene chloride (3 × 50 mL), and the combined organic extracts were washed with brine (2 × 20 mL), dried ($Na_2SO_4$), and evaporated to 133 mg of a foam. This was purified by plc (silica gel, 30% acetone in hexane) to give three products: the dichloride **6***g* (8 mg, 6%); $^1$Hmr ($CDCl_3$) δ: 3.93 (3H, s), 4.47, 4.62 (2H, ABq, 12 Hz), 4.71, 4.89 (2H, ABq, 12 Hz), 5.65 (1H, d, 2 Hz), 6.25 (1H, d, 2 Hz), 7.83 (4H, d); and a 3:1 mixture of **6***m* and **6***n* (84 mg, 68%). Compound **6***m*: $^1$Hmr ($CDCl_3$) δ: 3.93 (3H, s), 4.66, 4.78 (2H, ABq, 12 Hz), 5.07 (2H, br s), 5.61 (1H, d, 2 Hz), 6.27 (1H, d, 2 Hz), 7.80 (4H, d), 8.10 (1H, s). Compound **6***n*: $^1$Hmr ($CDCl_3$) δ: 3.91 (3H, s), 4.36, 4.53 (2H, ABq, 11 Hz), 5.37 (2H, s), 5.61 (1H, d, 2 Hz), 6.27 (1H, d, 2 Hz), 7.80 (4H, d), 8.10 (1H, s).

*Hydrolysis of* **6**h *to the bromohydrin* **6**j

The bromo-formate **6***h* (87 mg, 0.18 mmol) in methylene chloride (4 mL) was cooled to 0°C, and 0.2 mL of 3.2 *M* methanolic hydrogen chloride was added. The resulting solution was stored at 0°C for 1.5 h and then poured onto ice-cold 2.5% potassium bicarbonate (20 mL). The aqueous phase was extracted with methylene chloride (3 × 50 mL), and the combined organic layers were then washed with brine (2 × 20 mL), water (2 × 20 mL), dried ($Na_2SO_4$), and evaporated. The crude product, 73 mg of a nearly colourless foam, was purified by plc on silica gel buffered at pH 7.65 with boric acid – borax. Five developments with 20% acetone in hexane yielded 45 mg of **6***j*; $^1$Hmr ($CDCl_3$) δ: 2.87 (1H, br s, exch $D_2O$), 3.92 (3H, s), 4.43 (2H, s), 4.55, 4.72 (2H, ABq, 10 Hz), 5.60 (1H, d, 1.8 Hz), 6.27 (1H, d, 1.8 Hz), 7.83 (4H, d).

*Hydrolysis of* **6**m *to the chlorohydrin* **6**o

The chloro-formate **6***m* (53 mg, 0.12 mmol) in methylene chloride (3 mL) was cooled to 0°C and 0.15 mL of *N* methanolic hydrogen chloride was added. The resulting solution was stored for 2 h at 0°C, and then worked up as described above for **6***j* to give the chlorohydrin **6***o*, 49 mg; $^1$Hmr ($CDCl_3$) δ: 2.87 (1H, br s, exch $D_2O$), 3.90 (3H, s), 4.41 (2H, s), 4.62, 4.76 (2H, ABq, 12 Hz), 5.60 (1H, d, 1.8 Hz), 6.23 (1H, d, 1.8 Hz), 7.77 (4H, s).

*Hydrolysis of* **6**i *to the bromolactone* ***21*** *(R = Ft; X = Br)*

The bromo-formate **6***i* (59 mg, 0.122 mmol) in methylene chloride (3 mL) was cooled to 0°C and 0.15 mL of 3.2 *M* methanolic hydrogen chloride was added. The resulting solution was stored at 0°C for 1.5 h, and the product was then isolated as described above, 35 mg; $^1$Hmr ($CDCl_3$) δ: 4.41, 4.72 (2H, ABq, 12 Hz), 5.00 (2H, s), 5.67 (1H, d, 2 Hz), 6.70 (1H, d, 2 Hz), 7.87 (4H, d).

Can. J. Chem. Downloaded from www.nrcresearchpress.com by 210.87.254.5 on 09/06/12
For personal use only.

*Conversion of* ***21*** *(R = Ft; X = OH) to* ***21*** *(R = Ft; X = Br)*

The hydroxylactone, prepared by deformylation of **6***a* (92 mg, 0.2 mmol), was dissolved in methylene chloride (3.5 mL) and, at 0°C, boron tribromide (0.1 mL) was added. The resulting solution was stirred at 0°C for 48 h and the product was then isolated in the usual manner to yield 80 mg (94% from **6***a*) of the bromolactone, identical to the material described above.

*Tetrahydropyranylation of* ***21*** *(R = Ft; X = OH)*

The hydroxylactone (86 mg) (prepared from 104 mg, 0.23 mmol of **6***a*) was dissolved in dry tetrahydrofuran (5 mL). To this solution were added freshly purified dihydropyran (0.5 mL) and boron trifluoride etherate (0.2 mL). The resulting solution was stirred for 2 h at room temperature and was then poured into ice-cold 5% sodium bicarbonate (20 mL). The mixture was extracted with chloroform (3 × 40 mL), and the combined organic extracts were washed with brine (2 × 20 mL), dried ($Na_2SO_4$), and evaporated to give the crude product as an oil. This was purified by plc (silica gel, acetone–hexane, 2:3) to yield the tetrahydropyranyl ether **21** (R = Ft; X = OTHP), 97 mg (94% from **6***a*); $^1$Hmr ($CDCl_3$) δ: 1.65 (6H, m), 3.67 (2H, m), 4.59, 4.79 (2H, br ABq, 12 Hz), 4.83 (1H, br, s), 5.00 (2H, br s), 5.60 (1H, d, 2 Hz), 6.67 (1H, d, 2 Hz), 7.80 (4H, d).

*Silylation of* ***21*** *(R = Ft; X = OH)*

The hydroxylactone (72 mg), prepared from **6***a* (86 mg, 0.19 mmol), was dissolved in dimethylformamide (2.5 mL), and the solution was treated successively with imidazole (30 mg, 0.44 mmol) and *tert*-butyldimethylchlorosilane (30 mg, 0.2 mmol). The reaction mixture was stirred for 1 h at room temperature, and the solvent was then removed under reduced pressure at 40–45°C. The residue was purified by plc (silica gel, 20% acetone in hexane) to yield 60 mg (65% from **6***a*) of the *tert*-butyldimethylsilyl ether; $^1$Hmr ($CDCl_3$) δ: 0.13 (6H, s), 0.92 (9H, s), 4.74, 4.98 (2H, ABq, 17 Hz), 4.93 (2H, s), 5.55 (1H, d, 2 Hz), 6.60 (1H, d, 2 Hz), 7.73 (4H, d).

*Tetrahydropyranylation of the bromohydrin* **6**j

The bromohydrin **6***j* (56 mg, 0.12 mmol) was dissolved in methylene chloride (5 mL) and to this solution were added dihydropyran (0.5 mL) and anhydrous *p*-toluenesulfonic acid (2 mg). The mixture was stirred at room temperature for 50 min and was then poured onto ice-cold 5% sodium bicarbonate (30 mL). Extraction with chloroform (3 × 40 mL), followed by washing of the chloroform extracts with brine (2 × 20 mL), drying ($Na_2SO_4$), and evaporation yielded 79 mg of an oil. This was purified by plc (silica gel, 30% acetone in hexane, two developments) to give the tetrahydropyranyl ether **6***k* (36 mg, 55%); $^1$Hmr ($CDCl_3$) δ: 1.68 (6H, m), 3.73 (2H, m), 3.90 (3H, s), 4.40, 4.64 (2H, ABq, 14 Hz), 4.52 (1H, s), 4.72 (2H, s), 5.57 (1H, d, 2 Hz), 6.25 (1H, d, 2 Hz), 7.97 (4H, d).

*Conversion of the bromo-formate* **6**h *to the acetoxyformate* **6***p*

A solution of the bromo-formate **6***h* (137 mg, 0.28 mmol) in methylene chloride (4.5 mL) was cooled to −15°C and, under nitrogen, tetraethylammonium acetate (65 mg, 0.34 mmol) was added. The reaction mixture was stirred at −15°C for 18 h and then at 0°C for 24 h. It was then poured into ice-cold brine (20 mL), the layers were separated, and the aqueous layer was extracted with methylene chloride (3 × 60 mL). The combined organic extracts were washed with brine (2 × 20 mL), dried ($Na_2SO_4$), and evaporated to 114 mg of a pale yellow foam. This was purified by plc (silica gel, acetone–hexane, 3:7) to give 79 mg (60%) of the acetoxyformate **6***p*; $^1$Hmr ($CDCl_3$) δ: 2.07 (3H, s), 3.87 (3H, s), 4.89, 5.12 (2H, ABq, 12 Hz), 5.13 (2H, s), 5.53 (1H, d, 2 Hz), 6.20 (1H, d, 2 Hz), 7.72 (4H, d), 7.97 (1H, s).

The acetoxyformate (79 mg, 0.172 mmol) was dissolved in methylene chloride (3 mL) and, at 0°C under nitrogen, *N* methanolic hydrogen chloride (0.17 mL) was added. The solution was stored at 0°C for 3 h and the solvent was then removed under reduced pressure. The residue was purified by plc (silica gel, acetone–hexane, 2:3, two developments) to give the acetoxylactone **21** (R = Ft; X = OAc), 59 mg (90%); $^1$Hmr ($CDCl_3$) δ: 2.10 (3H, s), 4.87 (2H, s), 5.20 (2H, s), 5.55 (1H, d, 2 Hz), 6.58 (1H, d, 2 Hz), 7.70 (4H, br s).

*Preparation of* ***3*** *($R^1$ = TrOC; $R^3$ = $CH_3$)*

A solution of methyl 6-trichloroethoxycarbonylaminopenicillanate (68.4 g, 0.168 mol) in methylene chloride (600 mL) was cooled to −78°C, and a precooled (−78°C) solution of chlorine (23.9 g, 0.336 mol) in methylene chloride (47 mL) was added dropwise, with stirring. Stirring was continued for 1 h at −78°C, and the reaction mixture was then brought to room temperature. Evaporation of the solvent under reduced pressure afforded a pale yellow foam, which crystallized upon trituration with ice-cold ether. The chloroazetidinone was collected, and washed with ice-cold ether: 48.7 g (70%), mp 139–140°C; $^1$Hmr ($CDCl_3$) δ: 2.03 (3H, s), 2.30 (3H, s), 3.80 (3H, s), 4.77 (2H, s), 4.93 (1H, dd, 2, 8 Hz), 5.83 (1H, br s), 6.47 (1H, br d, 8 Hz).

*Preparation of* **7**b

To a suspension of **3** ($R^1$ = TrOC; $R^3$ = $CH_3$) (49 g, 0.12 mol), in carbon tetrachloride (450 mL), were added *N*-bromosuccinimide (47 g, 0.264 mol) and benzoyl peroxide (0.5 g). The mixture was brought to rapid reflux, under nitrogen, and was then irradiated for 3 h over a Sylvania No. 2 Superflood lamp, cooled to room temperature, and filtered to remove succinimide. The filtrate was washed successively with ice-cold 5% sodium bisulfite (2 × 50 mL) and ice-cold brine (2 × 50 mL), and dried ($MgSO_4$). Evaporation afforded 72.2 g of **7***b* (100%) as a pale yellow foam which could be used directly in further reactions; $^1$Hmr ($CDCl_3$) δ: 3.90 (3H, s), 4.33 (2H, s), 4.53, 4.70 (2H, ABq, 10 Hz), 4.77 (2H, s), 4.90 (1H, dd, 2, 8 Hz), 6.00 (1H, d, 2 Hz), 6.53 (1H, d, 8 Hz).

*Preparation of* **7**a

A solution of **7***b* (2.107 g, 3.72 mmol) in chloroform (20 mL) was cooled to 0°C and, under nitrogen, treated dropwise during 5 min with a solution of tetramethylguanidinium formate (2.576 g, 16 mmol) in chloroform (8 mL). Stirring was continued for 30 min at 0°C and then overnight at room temperature. The reaction mixture was poured onto ice-cold brine (50 mL), and the layers were separated. The aqueous layer was extracted with methylene chloride (3 × 40 mL). The combined organic layers were washed with brine (3 × 20 mL), dried ($Na_2SO_4$), and evaporated to give the crude product as a light brown foam. Purification on silica gel (10% acetone in hexane) afforded 483 mg (26%) of **7***a* as a pale yellow foam; $^1$Hmr ($CDCl_3$) δ: 3.90 (3H, s), 4.77 (2H, s), 4.90 (1H, dd, 2, 8 Hz), 4.97 (2H, s), 5.17, 5.31 (2H, ABq, 12 Hz), 6.00 (1H, d, 2 Hz), 6.37 (1H, d, 8 Hz), 8.10 (2H, s). *Anal.* calcd. for $C_{14}H_{14}N_2O_9Cl_4$: C 33.89, H 2.84, N 5.65; found: C 33.53, H 2.82, N 5.86.

*Hydrolysis of* **7**a

The diformate (250 mg, 0.5 mmol) was dissolved in methylene chloride (6 mL), the solution was cooled to 0°C, and methanolic hydrogen chloride (1 mL of a 2 *M* solution, 2 mmol) was added. The reaction mixture was stirred for 1 h at 0°C by which time the starting material had disappeared. The solvent was removed under reduced pressure, and the product was taken up in methylene chloride (20 mL) and washed with cold brine (1 × 20 mL), dried ($Na_2SO_4$), and evaporated to give **21** (R = TrOC; X = OH) as a white foam which appeared homogeneous by tlc, 202 mg (100%); $^1$Hmr ($CD_3COCD_3$) δ: 4.17 (1H, br s, exch $D_2O$), 4.71, 4.86 (2H, ABq, 18 Hz), 4.90 (2H, s), 5.10 (2H, s), 5.10 (1H, dd, 2, 8 Hz), 6.47 (1H, d, 2 Hz), 7.90 (1H, d, 8 Hz).

Can. J. Chem. Downloaded from www.nrcresearchpress.com by 210.87.254.5 on 09/06/12
For personal use only.

*Conversion of* 7a *to* 7h *and* 7i

An ice-cold solution of **7*a*** (3.394 g, 6.84 mmol) in methylene chloride (40 mL) was treated dropwise, under nitrogen, with a solution of boron tribromide (1.025 g, 4.09 mmol) in methylene chloride (10 mL). The addition required 15 min, and stirring was continued at 0°C for an additional 30 min. The solution was then poured onto ice-cold 2.5% potassium bicarbonate and, after shaking, the layers were separated. The aqueous layer was extracted with methylene chloride (3 × 50 mL) and the combined organic extracts were washed with brine (2 × 10 mL) and dried ($Na_2SO_4$). Evaporation left a pale yellow foam, 3.515 g, which was subjected to silica gel chromatography. Elution with 15% acetone–hexane yielded three fractions. The first was the dibromide **7*b*** (418 mg, 11%); the second was a mixture of **7*h*** and **7*i*** (2.217 g, 61%), and the third fraction was unreacted **7*a*** (315 mg, 9%).

*Separation of* 7h *and* 7i

The above mixture of geometrical isomers (2.2 g) was rechromatographed on silica gel using 20% ethyl acetate in hexane as eluent. This afforded pure **7*h*** (1.6 g) and **7*i*** (0.4 g). For compound **7*h***, $^1$Hmr ($CDCl_3$) δ: 3.88 (3H, s), 4.47, 4.61 (2H, ABq, 11 Hz), 4.75 (2H, s), 4.88 (1H, dd, 2, 7 Hz), 5.02 (2H, s), 5.95 (1H, d, 2 Hz), 6.34 (1H, d, 7 Hz), 8.05 (1H, s). *Anal.* calcd. for $C_{13}H_{13}N_2O_7BrCl_4$: C 29.40, H 2.46, N 5.28; found: C 29.65, H 2.54, N 4.80. For compound **7*i***, $^1$Hmr ($CDCl_3$) δ: 3.88 (3H, s), 4.19, 4.35 (2H, ABq, 10 Hz), 4.73 (2H, s), 4.98 (1H, dd, 2, 6 Hz), 5.32 (2H, s), 5.98 (1H, d, 2 Hz), 6.05 (1H, d, 6 Hz), 8.05 (1H, s).

*Conversion of* 7h *to the acetoxyformate* 7q

A solution of tetramethylguanidinium acetate (300 mg, 1.73 mmol) in chloroform (5 mL) was cooled to 0°C and, with stirring, treated all at once with a solution of the bromo-formate **7*h*** (265 mg, 0.5 mmol) in chloroform (3 mL). Stirring was continued for 1 h at 0°C and then at room temperature for 5 h. The mixture was then poured onto ice-cold brine (50 mL), the layers were separated, and the aqueous layer washed with methylene chloride (3 × 40 mL). The combined organic extracts were washed with brine, dried ($Na_2SO_4$), and evaporated to a light brown foam (239 mg). Purification by plc (silica gel, ethyl acetate – hexane, 3:7) afforded recovered **7*h*** (40 mg) and the acetoxyformate **7*q*** (57 mg, 25%) as a colourless foam; $^1$Hmr ($CDCl_3$) δ: 2.08 (3H, s), 3.88 (3H, s), 4.75 (2H, s), 4.88 (1H, dd, 2, 7 Hz), 4.93 (2H, s), 5.04, 5.17 (2H, ABq, 14 Hz), 5.97 (1H, d, 2 Hz), 6.27 (1H, d, 7 Hz), 8.08 (1H, s).

*Hydrolysis of* 7q *to the acetoxyhydrin* 7r

A solution of the acetoxyformate **7*q*** (57 mg, 0.11 mmol) in methylene chloride (3 mL) was cooled to 0°C and treated with 2 *M* methanolic hydrogen chloride (0.1 mL). The resulting solution was stirred for 1 h at 0°C and was then evaporated to dryness to give a product which retained the methyl ester and acetate groups, but had lost the formate group; $^1$Hmr ($CDCl_3$) δ: 2.10 (3H, s), 3.63 (1H, br s, exch $D_2O$), 3.83 (3H, s), 4.70 (2H, s), 4.83 (2H, s), 5.15 (2H, s), 5.16 (1H, dd, 2, 6 Hz), 6.38 (1H, d, 2 Hz), 6.38 (1H, d, 6 Hz).

*Conversion of* 7i *to the acetoxyformate* 7p

The bromo-formate **7*i*** (217 mg, 0.41 mmol) was dissolved in chloroform (3 mL) and the solution was added to an ice-cold solution of tetrabutylammonium acetate (223 mg, 0.74 mmol) in chloroform (3 mL). The resulting solution was stirred at 0°C for 3 h under nitrogen, and then at room temperature for 22 h. It was then poured onto ice-cold brine (30 mL), the layers were separated, and the aqueous layer was washed with methylene chloride (3 × 40 mL). The combined organic extracts were washed with brine (2 × 20 mL), dried ($Na_2SO_4$), and evaporated. The resulting material was purified by plc (silica gel, ethyl acetate – hexane, 3:7, three developments) to give 100 mg (48%) of the acetoxyformate **7*p***; $^1$Hmr ($CDCl_3$) δ: 2.10 (3H, s), 3.90 (3H, s), 4.80 (2H, s), 4.87 (2H, s), 4.97 (1H, dd, 2, 6 Hz), 5.23 (2H, s), 5.97 (1H, d, 2 Hz), 6.52 (1H, d, 6 Hz), 8.03 (1H, s).

*Hydrolysis of* 7p *to the lactone* ***21*** *(R = TrOC; X = OAc)*

The acetoxyformate **7*p*** (100 mg, 0.20 mmol) was dissolved in methylene chloride (4 mL), the solution was cooled to 0°C, and methanolic hydrogen chloride (1 mL of a 0.8 *M* solution) was added. The resulting solution was stirred for 1.5 h, an additional 0.5 mL of *M* methanolic hydrogen chloride was added, and stirring was continued for 0.5 h. The reaction mixture was poured into cold 2.5% potassium bicarbonate (30 mL) and the layers were separated. The aqueous layer was extracted with methylene chloride (3 × 40 mL) and the combined organic extracts were washed with brine (2 × 20 mL), dried ($Na_2SO_4$), and evaporated to give the acetoxylactone as a colourless foam (74 mg, 83%), homogeneous by tlc; $^1$Hmr ($CDCl_3$) δ: 2.13 (3H, s), 4.77 (2H, s), 4.90 (2H, s), 4.95 (1H, dd, 2, 6 Hz), 5.17 (2H, s), 6.38 (1H, d, 2 Hz), 6.57 (1H, d, 6 Hz).

*Preparation of* ***24***

The bromoformate **7*h*** (133 mg, 0.25 mmol) was dissolved in dimethylformamide (6 mL), mercaptomethyltetrazole (35 mg, 0.30 mmol) was added, and the solution was stirred overnight at room temperature. The reaction mixture was then poured into ice-cold water (50 mL) and extracted with ethyl acetate (2 × 30 mL). This extract was washed successively with water (4 × 10 mL), saturated sodium bicarbonate (1 × 10 mL), and brine (1 × 10 mL), dried and evaporated to yield **24** as a colourless foam, homogeneous on tlc (125 mg, 91% yield); $^1$Hmr ($CDCl_3$) δ: 3.88 (3H, s), 3.95 (3H, s), 4.39, 4.71 (2H, ABq, 14 Hz), 4.75 (2H, s), 4.93 (1H, dd, 2, 8 Hz), 4.98 (2H, br s), 5.95 (1H, d, 2 Hz), 6.67 (1H, d, 8 Hz), 8.03 (1H, s).

*Preparation of* ***25***

Deformylation of **24** in the usual manner afforded **25**; $^1$Hmr ($CDCl_3$) δ: 3.45 (1H, br s, exch $D_2O$), 3.88 (3H, s), 3.98 (3H, s), 4.45 (2H, s), 4.62 (2H, s), 4.77 (2H, s), 4.90 (1H, dd, 2, 8 Hz), 6.02 (1H, d, 2 Hz), 6.95 (1H, d, 8 Hz).

*Preparation of* ***8***a

A slurry of 6-aminopenicillanic acid (21.6 g, 0.1 mol) in water (250 mL) was cooled to 0–5°C, and 2 *N* potassium hydroxide was added dropwise until a clear solution was obtained, and the pH was 7.5. This solution was diluted with tetrahydrofuran (200 mL). Then a solution of phenyl chloroformate (23.5 g, 19.1 mL, 0.15 mol) in dry tetrahydrofuran (40 mL) was added dropwise, with stirring at 5–10°C and simultaneous addition of 2 *N* potassium hydroxide to maintain the pH in the range 7–8. The turbid reaction mixture was extracted with ethyl acetate (2 × 300 mL), and this extract was discarded. The aqueous layer was layered with ethyl acetate (300 mL), the system cooled to 5–10°C and, with stirring, the pH was adjusted to 1 with concentrated hydrochloric acid. The layers were separated, the aqueous layer extracted with ethyl acetate (3 × 150 mL), and the combined organic extracts were washed with saturated brine, dried ($MgSO_4$), and evaporated to yield phenoxycarbonylaminopenicillanic acid (31 g, 92%), as a crisp white foam; $^1$Hmr ($CDCl_3$) δ: 1.60 (3H, s), 1.70 (3H, s), 4.47 (1H, s), 5.40–5.87 (2H, m), 6.00 (1H, br d, 10 Hz), 7.23 (5H, m). Methyl ester: $^1$Hmr ($CDCl_3$) δ: 1.53 (3H, s), 1.67 (3H, s), 3.77 (3H, s), 4.45 (1H, s), 5.38–5.70 (2H, m), 6.12 (1H, br d, 10 Hz), 7.20 (5H, m).

To the methyl ester (7.973 g, 22.78 mmol) in methylene chloride (40 mL) at −78°C was added, in one portion, a precooled solution of chlorine (3.234 g, 45.56 mmol) in methylene chloride (20 mL). The reaction mixture was stirred at −78°C for 1 h, warmed to room temperature, and evaporated. Chroma-

tography of the resulting foam (silica gel, 10–30% ethyl acetate – hexane) gave pure **3** ($R^1$ = PhOC; $R^3$ = $CH_3$) (5.867 g, 73%) as a colourless foam; $^1$Hmr ($CDCl_3$) δ: 2.00 (3H, s), 2.27 (3H, s), 3.73 (3H, s), 4.93 (1H, dd, 1.5, 8 Hz), 5.83 (1H, d, 1.5 Hz), 6.30 (1H, d, 8 Hz), 7.20 (5H, m). *Anal.* calcd. for $C_{16}H_{17}N_2O_5Cl$: C 54.47, H 4.86, N 7.94; found: C 54.18, H 4.95, N 7.62.

To a solution of **3** ($R^1$ = PhOC; $R^3$ = $CH_3$) (2.466 g, 7 mmol), in carbon tetrachloride (25 mL), were added *N*-bromosuccinimide (2.550 g, 14.2 mmol) and benzoyl peroxide (50 mg). Bromination was performed for 15 min, and the product isolated in the usual manner as a light brown foam (3.534 g). Chromatography on silica gel (ethyl acetate – hexane, 3:7) afforded pure **8***b* (2.446 g, 68%) as a colourless foam; $^1$Hmr ($CDCl_3$) δ: 3.85 (3H, s), 4.30 (2H, s), 4.53, 4.72 (2H, ABq, 10.5 Hz), 4.87 (1H, dd, 1.5, 8 Hz), 6.03 (1H, d, 1.5 Hz), 6.10 (1H, d, 8 Hz), 7.22 (5H, m). The dibromide (3.060 g, 6 mmol) was dissolved in chloroform (25 mL), the solution was cooled to 0°C and, under nitrogen, a solution of tetramethylguanidinium formate (4.0 g, 24.84 mmol) in chloroform (15 mL) was added dropwise during 5 min. The resulting solution was stirred at 0°C for 30 min and then at room temperature for 15 h. It was then poured onto a mixture of ice and water and the layers were separated. The aqueous layer was washed with methylene chloride (3 × 40 mL) and the combined organic layers were washed with saturated brine (2 × 10 mL), dried ($Na_2SO_4$), and evaporated to a pale brown foam (2.30 g). The diformate **8***a* was isolated by chromatography on silica gel (10–20% acetone–hexane); 689 mg (26%); $^1$Hmr ($CDCl_3$) δ: 3.87 (3H, s), 4.88 (1H, dd, 1.8, 8 Hz), 4.97 (2H, s) 5.23 (2H, br s), 6.05 (1H, d, 1.8 Hz), 6.23 (1H, d, 8 Hz), 7.27 (5H, m), 8.10 (2H, s).

*Hydrolysis of* **8**a

A solution of **8***a* (214 mg, 0.49 mmol) in methylene chloride (5 mL) was cooled to −10°C, and methanolic hydrogen chloride (2 mL, 29 mg/mL, 1.59 mmol) was added. The solution was allowed to stand overnight, by which time the starting material had disappeared and a single product had formed (tlc, silica gel, acetone–hexane, 3:1). The solvent was removed under reduced pressure and the residual light yellow foam was chromatographed on silica gel (30% acetone in hexane) to yield **21** (R = PhOC; X = OH), 157 mg (91%) as a colourless foam; $^1$Hmr ($CDCl_3$) δ: 3.50 (1H, br s, exch $D_2O$), 4.38, 4.68 (2H, ABq, 16 Hz), 4.85 (2H, br s), 4.95 (1H, dd, 1.8, 8 Hz), 6.32 (1H, d, 1.8 Hz), 6.48 (1H, d, 8 Hz), 7.17 (5H, m).

*Conversion of* **8**a *to* **8**h *and* **8**i

The diformate (184 mg, 0.42 mmol) was dissolved in methylene chloride (4 mL), and the solution was cooled to 0°C, under nitrogen. Then a solution of boron tribromide (61 mg, 0.24 mmol, 0.57 mol-equiv.) in methylene chloride (0.5 mL) was added dropwise during 5 min. The reaction mixture was stirred for 1 h at 0°C and was then poured onto ice-cold 2.5% potassium bicarbonate (20 mL). The layers were separated, and the aqueous layer was extracted with methylene chloride (3 × 40 mL). The combined organic extracts were washed with saturated brine (2 × 20 mL), dried ($Na_2SO_4$), and evaporated to give the crude product (188 mg) as a yellow foam. This was purified by plc (silica gel, 40% acetone–hexane) to give three bands. The leading band (10 mg) was identified as the dibromide **8***b*, and the trailing band (30 mg) was unreacted diformate. The middle band, 102 mg (61%, based on recovered starting material), was the mixture of **8***h* and **8***i*, in the ratio 4:1. For **8***h*, $^1$Hmr ($CDCl_3$) δ: 3.77 (3H, s), 4.40, 4.57 (2H, ABq, 10 Hz), 4.78 (1H, dd, 2, 8 Hz), 4.92 (2H, s), 5.92 (1H, d, 2 Hz), 6.23 (1H, d, 8 Hz), 7.10 (5H, m), 7.90 (1H, s). For **8***i*, $^1$Hmr ($CDCl_3$) δ: 3.67 (3H, s), 4.10, 4.27 (2H, ABq, 10 Hz), 4.78 (1H, dd, 2, 8 Hz), 5.23 (2H, s), 5.92 (1H, d, 2 Hz), 6.23 (1H, d, 8 Hz), 7.10 (5H, m), 7.90 (1H, s).

## Acknowledgements

This research was supported by the Natural Sciences and Engineering Research Council of Canada. Portions of the experimental work were performed in the laboratories of Raylo Chemicals Limited, Edmonton, under an NSERC IRAP grant. The authors thank Dr. R. G. Micetich for his interest and encouragement, and Mr. Peter Wolfert for technical assistance.

1. S. Wolfe, J. B. Ducep, K. C. Tin, and S. L. Lee. Can. J. Chem. **52**, 3996 (1974).
2. S. Kukolja. J. Am. Chem. Soc. **93**, 6267 (1971).
3. S. Wolfe, W. S. Lee, G. Kannengiesser, and J. B. Ducep. Can. J. Chem. **50**, 2894 (1972).
4. S. Wolfe, J. B. Ducep, G. Kannengiesser, and W. S. Lee. Can. J. Chem. **50**, 2902 (1972).
5. S. Wolfe and M. P. Goeldner. Tetrahedron Lett. 5131 (1973).
6. M. Narisada, H. Onoue, and W. Nagata. Heterocycles, **7**, 839 (1977); E. G. Brain, C. L. Branch, A. J. Eglington, J. H. C. Nayler, N. F. Osborne, M. J. Pearson, J. C. Smale, R. Southgate, and P. Tolliday. *In* Recent advances in the chemistry of β-lactam antibiotics. *Edited by* J. Elks. The Chemical Society, London. 1977. p. 204; C. U. Kim and D. N. McGregor. Tetrahedron Lett. 409 (1978); C. L. Branch and M. J. Pearson. J. Chem. Soc. Perkin Trans. I, 2268 (1979); J. E. Baldwin, D. P. Hesson, and M. Jung. Tetrahedron, **36**, 1627 (1980); R. D. G. Cooper. *In* Topics in antibiotic chemistry. Vol. 3. *Edited by* P. G. Sammes. Ellis Horwood Limited, Chichester. 1979.
7. K. Heusler. *In* Cephalosporins and penicillins. Chemistry and biology. *Edited by* E. H. Flynn. Academic Press, New York. 1972. p. 274; R. B. Woodward, K. Heusler, I. Ernest, K. Burri, R. J. Friary, F. Haviv, W. Oppolzer, R. Paioni, K. Syhora, R. Wenger, and J. K. Whitesell. Nouv. J. Chim. **1**, 85 (1977).
8. R. D. G. Cooper and D. O. Spry. *In* Cephalosporins and penicillins. Chemistry and biology. *Edited by* E. H. Flynn. Academic Press, New York. 1972. Chapt. 5; E. G. Brain, A. J. Eglington, J. H. C. Nayler, M. J. Pearson, and R. Southgate. J. Chem. Soc. Perkin Trans. I, 447 (1976); A. C. Kaura, C. D. Maycock, and R. J. Stoodley. J. Chem. Soc. Chem. Commun. 34 (1980).
9. E. T. Gunda and J. Cs. Jászberényi. *In* Progress in medicinal chemistry. *Edited by* G. P. Ellis and G. B. West. Elsevier/North Holland Biomedical Press. Vol. 12. 1975. Chapt. 8; Vol. 14. 1977. Chapt. 4; Topics in antibiotic chemistry. Vol. 4. *Edited by* P. G. Sammes. Ellis Horwood Limited, Chichester. 1980. Chapts. 2 and 3.
10. W. Nagata. Phil. Trans. R. Soc. Lond. Ser. B, **289**, 225 (1980).
11. M. M. Campbell, D. I. Rawson, and A. F. Cameron. Tetrahedron Lett. 1257 (1979).
12. S. Wolfe, W. S. Lee, J. B. Ducep, and G. Kannengiesser. Can. J. Chem. **50**, 2898 (1972).
13. A. B. Taylor. J. Chem. Soc. 7020 (1965); L. D. Hatfield, J. W. Fisher, J. M. Dunigan, R. W. Burchfield, J. M. Greene, J. A. Webber, R. T. Vasileff, and M. D. Kinnick, Phil. Trans. R. Soc. Lond. Ser. B, **289**, 173 (1980).
14. R. B. Woodward. Phil. Trans. R. Soc. Lond. Ser. B, **289**, 239 (1980).

Can. J. Chem. Downloaded from www.nrcresearchpress.com by 210.87.254.5 on 09/06/12
For personal use only.

15. R. B. MORIN, B. G. JACKSON, R. A. MUELLER, E. R. LAVAGNINO, W. B. SCANLON, and S. L. ANDREWS. J. Am. Chem. Soc. **91**, 1401 (1969).
16. L. J. BELLAMY. *In* The infra-red spectra of complex molecules. Methuen and Co. Ltd., London. 1962. p. 205.
17. S. WOLFE, S. L. LEE, J. B. DUCEP, G. KANNENGIESSER, and W. S. LEE. Can. J. Chem. **53**, 497 (1975).
18. I. FLEMING. *In* Frontier orbitals and organic chemical reactions. John Wiley, Toronto. 1976.
19. A. VIGEVANI, M. FOGLIO, G. FRANCESCHI, P. MASI, A. SUARATO, E. GANDINI, and G. PALAMIDESSI. J. Chem. Soc. Perkin Trans. I, 504 (1979).
20. G. J. MARTIN and M. L. MARTIN. *In* Progress in nuclear magnetic resonance spectroscopy. Vol. 8. *Edited by* J. W. Emsley, J. Feeney and L. H. Sutcliffe. Pergamon Press, Oxford. 1972. Part 3.
21. G. FRANCESCHI, M. FOGLIO, P. MASI, A. SUARATO, G. PALAMIDESSI, L. BERNARDI, F. ARCAMONE, and G. CAINELLI. J. Am. Chem. Soc. **99**, 248 (1977).

Can. J. Chem. Downloaded from www.nrcresearchpress.com by 210.87.254.5 on 09/06/12
For personal use only.

# Acid-catalyzed rearrangement of cyclobutanols.[1] Syntheses of chrysenes, cyclopentenophenanthrenes, and diarylmethanes

EDWARD LEE-RUFF, ALAN C. HOPKINSON, HIRA KAZARIANS-MOGHADDAM, BRIJ GUPTA, AND MORRIS KATZ

*Department of Chemistry, York University, Downsview, Ont., Canada M3J 1P3*

Received August 18, 1981

EDWARD LEE-RUFF, ALAN C. HOPKINSON, HIRA KAZARIANS-MOGHADDAM, BRIJ GUPTA, and MORRIS KATZ. Can. J. Chem. **60**, 154 (1982).

Acid-catalyzed reactions of 8-aryl or 8,8-diarylbicyclo[4.2.0]oct-2-en-7-ols lead to tetrahydrophenanthrene derivatives. For example 8-(1-naphthyl)-bicyclo[4.2.0]oct-2-en-7-ols give substituted chrysenes in methanesulphonic acid. In the case of the homologous 7-aryl or 7,7-diarylbicyclo[3.2.0]hept-2-en-6-ols a novel transformation to diarlymethanes is observed. A mechanism is proposed which accounts for the product distribution observed in these rearrangements.

EDWARD LEE-RUFF, ALAN C. HOPKINSON, HIRA KAZARIANS-MOGHADDAM, BRIJ GUPTA et MORRIS KATZ. Can. J. Chem. **60**, 154 (1982).

Les réactions des aryl-8 ou des diaryl-8,8 bicyclo[4.2.0] octène-2 ols-7, catalysées par les acides, conduisent à des dérivés tétrahydrophenanthrènes. Par exemple, les (naphtyl-1)-8 bicyclo[4.2.0] octène-2 ols-7 dans l'acide méthanesulphonique donnent des chrysènes substitués. Dans le cas des homologues aryl-7 ou diaryl-7,7 bicyclo[3.2.0] heptene-2 ols-6, on observe une nouvelle transformation en diarylméthanes. On propose un mécanisme qui tient compte de la distribution des produits observés au cours de ces transpositions.

[Traduit par le journal]

Can. J. Chem. Downloaded from www.nrcresearchpress.com by 210.87.254.42 on 09/06/12
For personal use only.

Cyclobutanones are versatile intermediates in the preparation of polycyclic compounds including steroids and aromatic derivatives (1–3). The key step in these transformations involves the ring opening of a protonated α-arylcyclobutanone and the annelation of the resultant ion to the aromatic nucleus. Thus derivatives such as **1** undergo isomerization to β-tetralones **2** under a variety of acidic

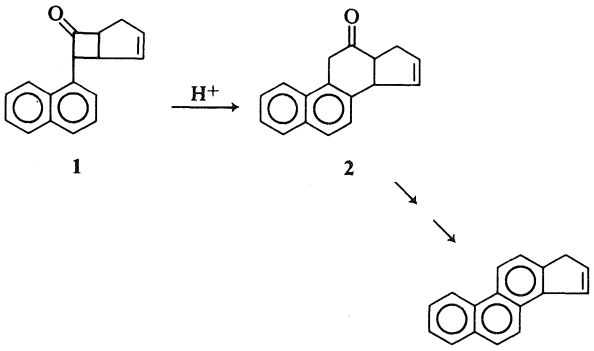


conditions. Further elaboration of these ketones permits the preparation of polycyclic aromatic hydrocarbons. It is proposed that a nonclassical 1-hydroxycyclobutyl cation is involved as an intermediate (4). However, ketones such as **2** cannot be functionalized at the carbonyl position with nucleophilic alkylating agents due to the acidic nature of the benzilic protons. On the other hand, the starting cyclobutanones can be readily alkylated at the carbonyl carbon to produce substituted cyclobutanols. Since cyclobutanols and their esters can be solvolyzed to yield similar cyclobutyl cations (5), we investigated the possibility that such ions can also undergo analogous ring annelations allowing the preparation of substituted perhydroaromatic derivatives, a number of which are of interest for the preparation of oxidized metabolites of polycyclic aromatic hydrocarbons involved in chemical carcinogenesis (6). This study reports on some of the acid-rearrangements of β-aryl cyclobutanols to substituted polycyclic aromatic hydrocarbons as well as a novel conversion of 7-arylbicyclohept-2-en-6-ols to diarylmethanes.

## Results

Cyclobutanols **3–13** were prepared from the corresponding cyclobutanones by reduction with $LiAlH_4$ or methylation with $LiCH_3$. The stereochemistry of the aryl group in **7–12** is assigned the *endo* configuration based on the benzilic-bridgehead hydrogen coupling constants of about 7–8 Hz in the $^1$Hmr spectra. The assignment is consistent with that for the aryl group configuration in the starting cyclobutanones (7). The hydroxyl group in alcohols **5–12** has been assigned the *endo* configuration, again based on the α-hydrogen bridgehead hydrogen coupling constant ($J$ = 7 Hz) as well as the slow exchange of OH hydrogen, indicating possible hydrogen bonding to the aryl group in the monosubstituted aryl alcohols **7**, **9**, and **11** (8). The assignment of the OH configuration is in accord

[1]Part VIII in a series on the acid-catalyzed rearrangement of cyclobutanones.

0008-4042/82/020154-06$01.00/0

©1982 National Research Council of Canada/Conseil national de recherches du Canada

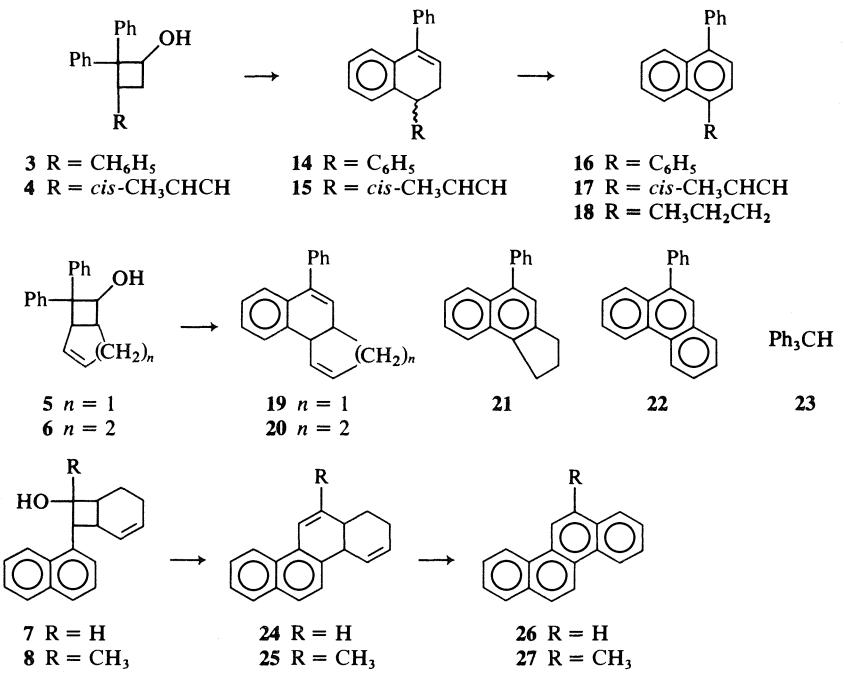


with nucleophilic attack occurring from the less hindered *exo* face in the bicyclic cyclobutanones.

The acid-catalyzed rearrangements were carried out using methanesulphonic acid at 0°C to 25°C or phosphorus pentoxide in benzene heated to reflux. The monocyclic alcohols **3** and **4** gave the 1,4-disubstituted 1,2-dihydronaphthalenes **14** and **15**. The structures of the hydrocarbons were confirmed by comparison with authentic samples (4) as well as the conversion by dehydrogenation with 2,3-dichloro-5,6-dicyano-1,4-benzoquinone (DDQ) to the 1,4-disubstituted naphthalenes **16** and **17**. The naphthalene **17** was hydrogenated to 1-phenyl-4-*n*-propylnaphthalene (**18**). The bicyclo[4.2.0]oct-2-en-7-ols **6–8** undergo dehydration and rearrangement to the tetrahydrophenanthrene **20** and tetrahydrochrysenes **24** and **25**, respectively. The structures of these derivatives were assigned based on their spectral data as well as their conversions to the known 9-phenylphenanthrene **22** (9), chrysene **26**, and 6-methylchrysene **27** (10) by dehydrogenation with DDQ. In the case of the bicyclo[3.2.0]-hept-2-en-6-ols **5**, **9–12**, in addition to formation of the ring fused derivatives **19**, **21**, **30**, and **33**, diarylmethanes **23**, **28**, **29**, **31**, and **32** respectively are produced as major products. The identity of the diarylmethanes **23** and **31** was confirmed by comparison with authentic samples. Hydrocarbons **28** and **32** were assigned structures based on comparison of spectral data with those reported in the

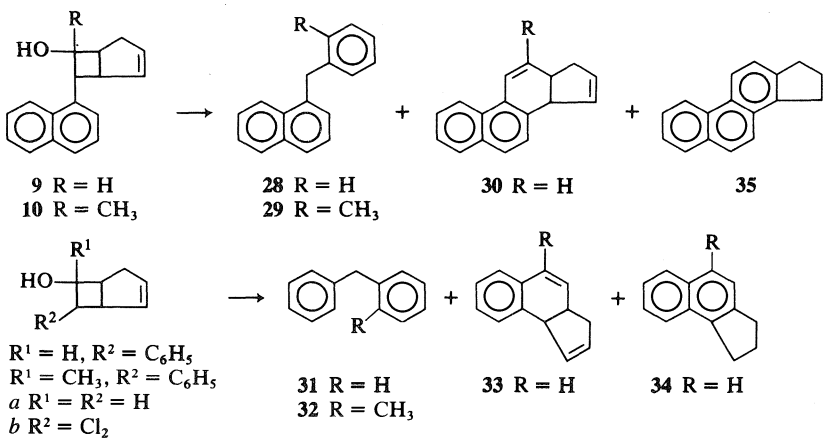


Can. J. Chem. Downloaded from www.nrcresearchpress.com by 210.87.254.42 on 09/06/12
For personal use only.

Can. J. Chem. Downloaded from www.nrcresearchpress.com by 210.87.254.42 on 09/06/12
For personal use only.

literature for these compounds (10, 11). The structure of diarylmethane **29** was based on the similarity of its spectral properties with those of **32**. Structures of the cyclopentane fused derivatives **19**, **30**, and **33** were assigned on the basis of their spectral data and conversion by strong acid to the benzoindans **21**, **34**, and **35**. The latter two compounds exhibited identical properties to those reported in the literature (12, 13). The benzoindan **34** and naphthoindan **35** were synthesized independently by dehydration of the cyclohexanols **38** and **39** with $P_2O_5$ under reflux in benzene. Alcohols **38** and **39** are derived from ketones **36** and **37** respec-

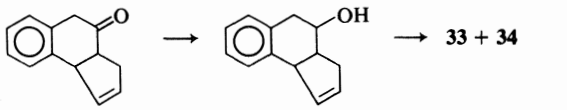


**36** **38**

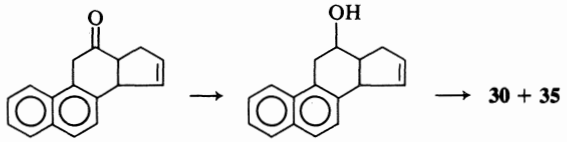


**37** **39**

tively using $LiAlH_4$ (2). Yields of the rearranged hydrocarbons are given in Table 1.

## Discussion

The following scheme (Scheme 1) can be proposed to rationalize the formation of ring annelated products. Cyclobutyl cations are known to interconvert with cyclopropylcarbinyl and allylcarbinyl cations (5). Nuclear magnetic resonance data (14) of certain cyclobutyl cations indicate that these are delocalized species in which structures such as **40**, **41**, and **42** represent resonance contributors. The formation of ring annelated products such as **24** under acid dehydration conditions suggests that such ions undergo intramolecular electrophilic ar-

TABLE 1. Product yields from cyclobutanol rearrangements

| Alcohol | Conditions | Product yields (%)[a] |
|---|---|---|
| **3** | $CH_3SO_3H$/0°C | **14** (95) |
| **4** | $CH_3SO_3H$/0°C | **15** (95) |
| **5** | $CH_3SO_3H$/0°C | **19** (30) **21** (10) **23** (30) |
| **6** | $CH_3SO_3H$/0°C | **20** (70) |
| **7** | $CH_3SO_3H$/r.t. | **24** (70) |
| **8** | $CH_3SO_3H$/r.t. | **25** (75) |
| **9** | $P_2O_5/C_6H_6$ | **28** (60) **30** (20) **35** (5) |
| **10** | $CH_3SO_3H$/r.t. | **29** (65) |
| **11** | $P_2O_5/C_6H_6$ | **31** (55) **33** (30) **34** (5) |
| **12** | $CH_3SO_3H$/r.t. | **32** (70) |

[a]Isolated yields.

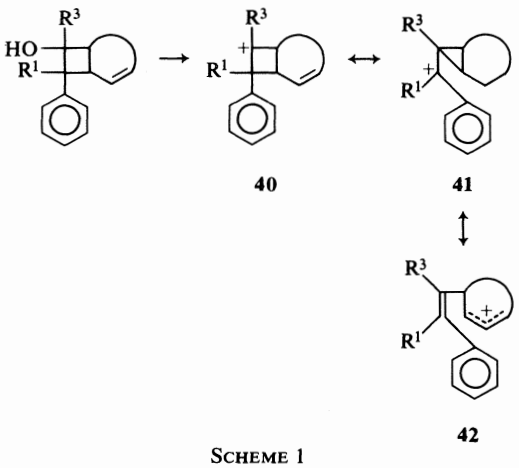


**40** **41** **42**

SCHEME 1

omatic substitution. The formation of diarylmethanes from bicyclohept-2-en-6-ols may involve a competitive *endo* bond cleavage (Scheme 2) of the cyclobutyl cation leading to a norcarenyl ion **43**. In the absence of positive charge stabilizing groups for $R^1$ and $R^3$ such ions are known to rearrange predominantly to products derived from cycloheptadienyl ion **44** (15). However, when $R^1$ and/or $R^2$ are positive charge stabilizing groups (e.g., aryl), *exo* cyclopropane bond scission may be expected, resulting in the formation of 2,5-cyclohexadienylmethyl cation **45**. Subsequent 1,2-hydride shift and proton loss lead to formation of the observed diarylmethanes. Both the unsubstituted bicyclohept-2-en-6-ol (**13***a*) and the β,β-dichloro derivative **13***b* were found to be inert under the same conditions in which β-aryl derivatives undergo rearrangements. Only *endo* to *exo* isomerization of the starting alcohol was observed. However, **13***a* has been reported to be transformed to 1,3,5-cycloheptatriene upon heating at 500°C in the presence of Lewis acids (16). That mono-aryl alcohols **9–12** give predominantly diarylmethanes suggests that *endo* cyclobutyl bond cleavage is preferred in this instance and that ions such as **46** derived from *exo* cleavage are probably more strained than the

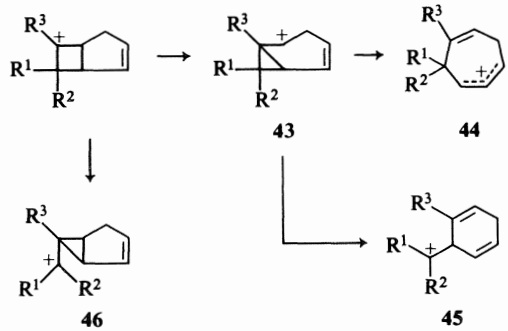


**43** **44**

**46** **45**

SCHEME 2

corresponding homologues derived from bicyclooct-2-en-7-ols. In the case of β,β-diphenyl alcohol **5**, the presence of an additional phenyl group stabilizes ion **46**, making the latter pathway for rearrangement more competitive as seen from the increasing yields of ring fused products **19** and **21**.

## Summary

The present study suggests that the acid assisted dehydration of β-aryl bicyclic cyclobutanols can provide a viable route towards the synthesis of specifically substituted perhydroaromatic compounds. With the convenient availability of the starting cyclobutanones (4) this method provides a simple access to these compounds. A competing reaction in the case of β-arylbicyclohept-2-en-7-ols leads to formation of *ortho*-alkylphenylarylmethanes. Such rearrangements involve a novel pathway for the decomposition of norcar-4-en-2-yl ($C_7H_9^+$) ions. The specific structures of the intermediate ions are being investigated by low temperature nmr spectroscopy.

## Experimental

Melting points were determined on a Reichert melting point apparatus and were uncorrected. The ir spectra were recorded on a Unicam SP 1000 instrument. The nmr spectra were recorded on a Varian EM-360 spectrometer using $CDCl_3$ solutions and TMS as internal standard. Mass spectra were recorded on a V.G. Micromass 16F spectrometer. Vapour phase chromatography (vpc) was performed on a Varian Aerograph 90P instrument using a 6 ft 10% Carbowax column operating at 210°C. Microanalyses were performed by Guelph Chemical Laboratories Ltd. The starting cyclobutanones were prepared according to literature methods: 2,2,3-triphenylcyclobutanone (17), 3-(*cis*-propenyl)-2,2-diphenylcyclobutanone (18), 8,8-diphenylbicyclo[4.2.0]oct-2-en-7-one (18), 7,7-diphenylbicyclo-[3.2.0]hept-2-en-6-one (18), 8-(1-naphthyl)-bicyclo[4.2.0]oct-2-en-7-one (19), 7-(1-naphthyl)-bicyclo[3.2.0]hept-2-en-6-one (19), bicyclo[3.2.0]hept-2-en-6-one (20), 7,7-dichlorobicyclo-[3.2.0]hept-2-en-6-one (20). 7-Phenylbicyclo[3.2.0]hept-2-en-6-one was prepared by a similar synthesis as described for 7-(1-naphthyl)-bicyclo[3.2.0]hept-2-en-6-one using phenylacetyl chloride as the ketene precursor.

*Preparation of cyclobutanols* ***3–13***

The following general procedure was used for the preparation of the starting cyclobutanols. Lithium aluminum hydride (500 mg, 13 mmol) was suspended in anhydrous ether. A solution of the cyclobutanone (2–3 mmol) in anhydrous ether was added to the suspension and the solution stirred at room temperature for 1 h. The following was added to quench the excess $LiAlH_4$, 0.5 mL water, 0.5 mL 15% aqueous sodium hydroxide, and 1.5 mL water. The precipitate was filtered off and the filtrate washed neutral with water. The ether was dried over anhydrous $MgSO_4$ and evaporated. In most instances a single compound was obtained (tlc silica gel, benzene).

*Alcohol* ***3****:* nmr and ir identical with reported values (17).

*Alcohol* ***4****:* ir $\bar{\nu}$ ($cm^{-1}$): 3600, 3400, 1600, 1495, 1445, 1145, 735, 705; nmr δ(ppm): 1.7 (d, $J$ = 5 Hz, 3H), 2.2–2.95 (m, 3H), 3.2–3.7 (d of t, 1H), 4.65 (t, $J$ = 9 Hz, 1H), 5.45 (d of d, 2H, $J$ = 5 Hz), 7.1–7.5 (m, 10H); ms: 220 ($M$ − 44).

*Alcohol* ***5****:* mp 108–109°C; ir $\bar{\nu}$ ($cm^{-1}$): 3600, 3400, 1600, 1495, 1445, 1400, 1130, 1100, 730, 700; nmr δ (ppm): 1.8 (d, $J$ = 12 Hz, 1H), 2.6 (m, 2H), 3.4 (m, 1H), 4.2 (m, 1H), 4.8 (m, 1H), 6.1 (m, 2H), 7.2–7.7 (m, 10H). *Anal.* calcd. for $C_{19}H_{18}O$: C 87.02, H 6.87; found: C 86.85, H: 6.72%.

*Alcohol* ***6****:* ir $\bar{\nu}$ ($cm^{-1}$): 3600, 3400, 1600, 1080, 690; nmr δ (ppm): 1.65 (t, 2H), 2.0 (m, 2H), 2.35 (d, $J$ = 10 Hz, OH, 1H), 2.85 (q, $J$ = 8 Hz, 1H), 3.35 (m, 1H), 5.0 (d of d, $J$ = 8 Hz, 10 Hz, 1H), 6.1 (m, 2H), 7.1–7.8 (m, 10 H); ms: 276 ($M^+$), 258 ($M^+$ − $H_2O$), 196 ($M^+$ − $C_6H_8$).

*Alcohol* ***7***: ir $\bar{\nu}$ ($cm^{-1}$): 3600, 3400, 1600, 790, 765; nmr δ (ppm): 1.9 (d, $J$ = 10 Hz, OH, 1H), 1.8–2.3 (m, 4H), 2.9 (m, 1H), 3.20–3.64 (m, 1H), 4.4 (t, $J$ = 6 Hz, 1H), 5.0 (m, 1H), 5.75 (m, 2H), 7.1–8.2 (m, 7H); ms: 170 ($M^+$ − $C_6H_8$).

*Alcohol* ***8***: ir $\bar{\nu}$ ($cm^{-1}$): 3600, 3400, 1080, 770; nmr δ (ppm): 1.55 (s, 3H), 1.8–2.3 (m, 4H), 2.4–2.8 (m, 1H), 3.2–3.7 (m, 1H), 4.2 (d, $J$ = 8 Hz, 1H), 5.7 (q, $J$ = 12 Hz, 2H), 7.3–8.2 (m, 7H); ms: 184 ($M^+$ − $C_6H_8$).

*Alcohol* ***9***: ir $\bar{\nu}$ ($cm^{-1}$): 3600, 3400, 1590, 1500, 1400, 1090, 780, 760, 650; nmr δ (ppm): 1.8 (br d, $J$ = 10 Hz, 1H), 2.5 (m, 2H), 3.1 (m, 1H), 3.75 (m, 1H), 4.35 (t, $J$ = 8 Hz), 4.7 (d of t, $J$ = 3 Hz, $J$ = 8 Hz, 1H), 5.75 (s, 2H), 7.2–8.0 (m, 7H); ms: 236 ($M^+$), 170 ($M^+$ − $C_5H_6$).

*Alcohol* ***10***: mp 95–96°C; ir $\bar{\nu}$ ($cm^{-1}$): 3550, 1080, 780, 760; nmr δ (ppm): 1.45 (s, 3H), 2.0 (s, 1H), 2.6 (m, 2H), 3.0 (m, 1H), 4.0 (m, 1H), 4.35 (d, $J$ = 9 Hz, 1H), 5.7 (m, 2H), 7.1–8.1 (m, 7H); ms: 250 ($M^+$), 184 ($M^+$ − $C_5H_6$), 232 ($M^+$ − $H_2O$). *Anal.* calcd. for $C_{18}H_{18}O$: C 86.40, H 7.20; found: C 86.15, H 7.08%.

*Alcohol* ***11***: ir $\bar{\nu}$ ($cm^{-1}$): 3600, 3400, 1090, 650; nmr δ (ppm): 1.7 (d, $J$ = 9 Hz, 1H), 2.6 (m, 2H), 3.2 (m, 1H), 3.7 (m, 1H), 4.05 (t, $J$ = 7 Hz, 1H), 4.6 (m, 1H), 5.9 (s, 2H), 7.35 (s, 5H); ms: 186 ($M^+$), 120 ($M^+$ − $C_5H_6$).

*Alcohol* ***12***: ir $\bar{\nu}$ ($cm^{-1}$): 3600, 3400, 1070, 1058, 670; nmr δ (ppm): 1.4 (s, 3H), 1.75 (s, 1H), 2.55 (m, 2H), 2.9 (m, 1H), 3.6 (m, 1H), 3.8 (d, $J$ = 8 Hz, 1H), 5.9 (s, 2H), 7.35 (s, 5H); ms: 200 ($M^+$), 182 ($M^+$ − 18), 134 ($M^+$ − $C_5H_6$).

*Alcohol* ***13***a: exhibited identical spectral properties with literature data (21). An 80:20 mixture of *endo–exo* alcohol was obtained.

*Alcohol* ***13***b: ir $\bar{\nu}$ ($cm^{-1}$): 3400, 1120, 725; nmr δ (ppm): 2.6 (m, 2H), 2.95 (s, 1H), 3.5 (d of q, $J$ = 3 Hz, 7 Hz, 1H), 3.9 (m, 1H), 4.6 (d of d, 1H), 5.9 (m, 2H).

*Acid rearrangements of alcohols* ***3–13***

The following general procedures were used for the acid reactions.

*Methanesulphonic acid method*

To a cooled solution (ice–water bath) of methanesulphonic acid (10–20 mL) was added dropwise a solution of 1–2 g of alcohol in 10–15 mL of ether. A deep colour developed immediately. The solution was warmed to room temperature and stirred for 1 h. This was then poured over ice and extracted with 100 mL of ether. The aqueous layer was reextracted with an additional 50 mL of ether. The combined ether extracts were washed with saturated bicarbonate (3 × 25 mL) and water, dried over $MgSO_4$, and evaporated. The residue was applied on silica gel coated preparative tlc plates, an alumina column (hexane–benzene), or on a vpc column.

*Phosphorous pentoxide method*

A benzene solution (50 mL) of the alcohol (1–2 g) containing 1 equiv. of $P_2O_5$ was heated under reflux for 1–2 h. The solution was concentrated and applied on an alumina column.

*Rearrangement products*

*Hydrocarbons* ***14*** *and* ***15***

These had identical spectral properties with those of authentic samples (4).

Can. J. Chem. Downloaded from www.nrcresearchpress.com by 210.87.254.42 on 09/06/12
For personal use only.

Can. J. Chem. Downloaded from www.nrcresearchpress.com by 210.87.254.42 on 09/06/12
For personal use only.

*Hydrocarbons **16** and **17***

These were prepared from **14** and **15** using a previously reported procedure (4).

*1-Phenyl-4-*n*-propylnaphthalene (**18**)*

A solution containing 100 mg of naphthalene **17** in 50 mL of ethyl acetate and 50 mg of 5% Pd on carbon was hydrogenated in a closed system for 12 h. The catalyst was filtered off and the solvent evaporated to give an oily material; ir $\bar{\nu}$ ($cm^{-1}$): 3070, 770, 700; uv(EtOH): 295, 225 nm (similar to 1-phenylnaphthalene); nmr $\delta$ (ppm): 0.9 (t, $J$ = 6 Hz, 3H), 1.3 (m, 2H), 3.1 (t, $J$ = 7 Hz, 2H), 7.1–8.6 (m, 11 H); ms: 246 ($M^+$).

*Hydrocarbon **20***: showed identical spectral properties with that of previously prepared material (4).

*Conversion of hydrocarbon **20** to 9-phenylphenanthrene **22***

See DDQ method below. 9-Phenylphenanthrene was obtained in 70% yield. Showed identical properties with authentic sample (4).

*Hydrocarbon **24***: ir $\bar{\nu}$ ($cm^{-1}$): 3050, 680; nmr $\delta$ (ppm): 1.5–2.1 (m, 4H), 3.0 (m, 1H), 3.9 (t, $J$ = 6 Hz, 1H), 5.8–6.2 (m, 4H), 7.3–8.0 (m, 6H); ms: 232 ($M^+$).

*Conversion of hydrocarbon **24** to chrysene*

A solution containing 200 mg of **24** in 20 mL of benzene and 500 mL of DDQ was heated under reflux for two hours. The solution was concentrated to 5 mL and applied to an alumina column using benzene as the eluant. A crystalline material (180 mg) was obtained, mp 252–254°C, which was identical in all respects to chrysene.

*Hydrocarbon **25***: ir $\bar{\nu}$ ($cm^{-1}$): 3060, 700; nmr $\delta$ (ppm): 1.6–2.2 (m, 4H), 2.4 (s, 3H), 2.9 (m, 1H), 4.0 (d, $J$ = 6 Hz, 1H), 5.8 (s, 1H), 5.7–6.1 (m, 2H), 7.3–8.1 (m, 6H); ms: 246 ($M^+$).

*6-Methylchrysene (**27**)*

The same procedure was used for conversion of **25** to **27** as described above for the conversion of **24** to chrysene with DDQ. Yield 75%, mp 160–161°C (lit. (22) mp 161°C); uv (EtOH) nm: 324, 310, 298, 284, 268, 260, 244, 224; nmr $\delta$ (ppm): 2.8 (s, 3H), 7.5–8.2 (m, 7H), 8.5–8.9 (m, 4H); ms: 242 ($M^+$, base peak).

*Hydrocarbon **19***: ir $\bar{\nu}$ ($cm^{-1}$): 3050, 3010, 1600, 1500, 1450, 760, 740, 680; nmr $\delta$ (ppm): 2.1–2.7 (m, 3H), 4.1 (d of d, $J$ = 2 Hz, 8 Hz, 1H), 5.5–6.05 (m, 3H), 7.45 (s, 5H), 7.0–7.5 (m, 4H).

*Hydrocarbon **21***: ir $\bar{\nu}$ ($cm^{-1}$): 3050, 1590, 1490, 1440, 740, 685; nmr $\delta$ (ppm): 2.3 (p, $J$ = 7 Hz, 2H), 3.3 (q, $J$ = 7 Hz, 4H), 7.45 (s, 5H), 7.0–7.9 (m, 5H).

*Diarylmethane **28***: mp 54°C (lit. (10) mp 55–57°C); nmr was identical with literature reported data.

*Diarylmethane **29***: ir $\bar{\nu}$ ($cm^{-1}$): 3020, 1590, 1455, 1390, 775, 765, 725; nmr $\delta$ (ppm): 2.3 (s, 3H), 4.4 (s, 2H), 6.9–8.1 (m, 11 H); ms: 232 ($M^+$).

*Diarylmethane **32***: exhibited identical spectral values as reported in the literature (11).

*Hydrocarbon **30***: ir $\bar{\nu}$ ($cm^{-1}$): 3010, 770, 750; nmr $\delta$ (ppm): 2.1–3.4 (m, 3H), 4.0 (m, 1H), 5.7 (m, 3H), 7.0–8.0 (m, 7H); ms: 218 ($M^+$).

*Hydrocarbon **35***: exhibited identical ir and uv spectra as described in the literature (12); mp 131–133°C (lit. (12) mp 133–134°C); nmr $\delta$ (ppm): 2.3 (p, $J$ = 7 Hz, 2H), 3.25 (q, $J$ = 7 Hz, 4H), 7.4–8.0 (m, 6H), 8.6 (m, 2H); ms: 218 ($M^+$).

*Hydrocarbon **33***: ir $\bar{\nu}$ ($cm^{-1}$): 3030, 3000, 1490, 1445, 760, 750; nmr $\delta$ (ppm): 2.1–3.6 (m, 3H), 4.1 (br d, $J$ = 8 Hz, 1H), 5.8 (m, 3H), 6.4 (d of d, $J$ = 2 Hz, 8 Hz, 1H), 7.1 (m, 4H).

*Hydrocarbon **34***: showed identical spectral properties as described in the literature (13).

*Synthesis of naphthoindan **35** from ketone **37***

Ketone **37** was reduced with $LiAlH_4$ as described previously (19) to alcohol **39**. A solution of 300 mg of alcohol **39** in 20 mL benzene and 300 mg of $P_2O_5$ was heated under reflux for two hours. The solution was concentrated and applied on an alumina column. Hexane–benzene eluted 250 mg of an oily mixture containing mostly **35**. A small amount of **30** was present as evident by tlc. Ether–ethanol solution allowed crystallization of naphthoindan **35**, mp 131–132°C. Spectral data were identical in all respects with a sample prepared above.

*Synthesis of benzoindan **34** from ketone **36***

*Preparation of 7-phenylbicyclohept-2-en-6-one*

A solution of 10 g of phenylacetylchloride in 150 mL of benzene was heated to reflux in a three-neck flask containing an addition funnel and condenser in an atmosphere of nitrogen. Cyclopentadiene was rapidly added followed by dropwise addition of 7 g of triethylamine. After addition the solution was heated for a further 15 min. After cooling the resultant precipitate was filtered off and washed with ether. The ether–benzene solution was washed with 2 × 30 mL of 5% HCl, followed by 2 × 30 mL of 10% $Na_2CO_3$, water, dried over anhydrous magnesium sulphate, and evaporated to give 7.2 g of an oil which was applied to a silica gel column (hexane). Hexane eluted 1.2 g of 1,3-cyclopentadiene dimer. Benzene eluted 5.3 g of 7-phenylbicyclohept-2-en-6-one; ir $\bar{\nu}$ ($cm^{-1}$): 3020, 3000, 1780, 1490, 685; nmr $\delta$ (ppm): 2.7 (m, 2H), 3.9 (br t, 2H), 4.8 (d, $J$ = 6 Hz, 1H), 5.7 (m, 2H), 7.2 (s, 5H). *Anal.* calcd. for $C_{13}H_{12}O$: C 84.78, H 6.52; found: C 84.51, H 6.63%.

*Ketone **36***

To a cooled (ice–water bath) solution of 10 mL of methanesulphonic acid was added dropwise the above cyclobutanone (2 g). The solution turned deep red in colour. The reaction mixture was poured over ice and extracted with 50 mL of ether. The ether extract was washed with saturated aqueous $NaHCO_3$ and water, and dried over $MgSO_4$, filtered, and evaporated yielding 1.7 g of an oil. A small amount (200 mg) was purified using preparative tlc (silica gel plates 1000 Å, benzene); ir $\bar{\nu}$ ($cm^{-1}$): 3020, 3000, 1705, 720, 680; nmr $\delta$ (ppm): 2.7 (m, 2H), 3.0 (d of t, $J$ = 4 Hz, 8 Hz, 1H), 3.6 (s, 2H), 4.3 (br d, $J$ = 8 Hz, 1H), 5.8 (s, 2H), 7.2 (q, 4H). *Anal.* calcd. for $C_{13}H_{12}O$: C 84.78, H 6.52; found: C 84.43, H 6.32%.

*Synthesis of benzoindan **34** from ketone **36***

To a suspension of 500 mg of $LiAlH_4$ in 20 mL of anhydrous ether was added dropwise a solution of 1 g of ketone **36** in 10 mL of ether. The reaction mixture was stirred for 1 h. Water (0.5 mL) was carefully added followed by 0.5 mL of 15% NaOH and then by 1.5 mL of water. The resultant precipitate was filtered off and the organic filtrate washed neutral with water, dried over $MgSO_4$, and evaporated to give 0.95 g of an oil; ir $\bar{\nu}$ ($cm^{-1}$): 3600, 3400. The carbonyl peak at 1705 of ketone **36** was absent. The crude alcohol was used for the next step. A solution of 30 mL benzene, 0.8 g of crude alcohol, and 0.8 g of $P_2O_5$ was heated under reflux for 2 h. Water (1 mL) was added to the cooled solution. The benzene layer was washed with saturated $NaHCO_3$, water, dried over $MgSO_4$, and evaporated to give an oily mixture consisting of 60% **34** and 40% **33** (by vpc). The mixture was separated by preparative vpc. Both hydrocarbons **34** and **33** exhibited spectral data identical with those prepared above.

*Preparation of naphthoindan **35** from ketone **37***

The preparation of ketone **37** and alcohol **39** has been described previously (19). The dehydration of alcohol **39** was carried out under identical conditions as described above for alcohol **38**. The mixture contained 80% naphthoindan **35** which was separated by preparative tlc (10% benzene – hexane). The product obtained had properties identical to those of a sample reported above.

## Acknowledgement

We thank the Natural Sciences and Engineering

Research Council of Canada for financial support of this work.

1. J. R. MATZ and T. COHEN. Tetrahedron Lett. 2459 (1981).
2. P. DUPERROUZEL and E. LEE-RUFF. Can. J. Chem. **58**, 51 (1980).
3. L. H. DAO, A. C. HOPKINSON, and E. LEE-RUFF. Tetrahedron Lett. 1413 (1978).
4. V. P. ABEGG, A. C. HOPKINSON, and E. LEE-RUFF. Can. J. Chem. **56**, 99 (1978).
5. H. C. BROWN. The nonclassical ion problem. Plenum Press, New York. 1977. Chapt. 5.
6. K. B. SUKUMARAN and R. G. HARVEY. J. Org. Chem. **45**, 4407 (1980).
7. W. T. BRADY and R. ROE, JR. J. Am. Chem. Soc. **93**, 1662 (1971).
8. W. B. DIXON. J. Chem. Phys. **74**, 1396 (1970).
9. C. F. KOELSCH. J. Am. Chem. Soc. **56**, 480 (1934).
10. T. TEITEI, D. WELLS, and W. H. F. SASSE. Aust. J. Chem. **28**, 571 (1975).
11. K. MAEKAWA, K. NARASAKA, and T. MUKAIYAMA. Bull. Chem. Soc. Jpn. **46**, 3478 (1973).
12. A. RAHMAN and N. M. RODRIGUEZ. Chem. Ber. **104**, 2651 (1971).
13. J. SEPIOL, B. KAWALEK, and J. MIREK. Synthesis, 701 (1977).
14. J. S. STARAL, I. YAVARI, G. K. S. PRAKASH, D. J. DONOVAN, and G. A. OLAH. J. Am. Chem. Soc. **100**, 8016 (1978).
15. P. G. GASSMAN and X. CREARY. J. Am. Chem. Soc. **95**, 6852 (1973).
16. I. FUGITA, R. YAMAMOTO, and K. KOBATA. Jap. Patent No. 7859 (1966); Chem. Abstr. **65**, P12124b (1966).
17. R. HUISGEN and L. A. FEILER. Chem. Ber. **102**, 3391 (1969).
18. R. HUISGEN and P. OTTO. Chem. Ber. **102**, 3475 (1969).
19. E. LEE-RUFF, A. C. HOPKINSON, and L. H. DAO. Can. J. Chem. **59**, 1675 (1981).
20. P. A. GRIECO. J. Org. Chem. **37**, 2363 (1972).
21. M. NEE, W. F. GORHAM and J. D. ROBERTS. J. Org. Chem. **46**, 1021 (1981).
22. M. S. NEWMAN. J. Am. Chem. Soc. **60**, 2947 (1938).

Can. J. Chem. Downloaded from www.nrcresearchpress.com by 210.87.254.42 on 09/06/12
For personal use only.

# Microbial hydroxylation of steroids. 8. Incubation of Cn halo- and other substituted steroids with Cn hydroxylating fungi

HERBERT L. HOLLAND AND EVERTON M. THOMAS

*Department of Chemistry, Brock University, St. Catharines, Ont., Canada, L2S 3A1*

Received June 1, 1981

HERBERT L. HOLLAND and EVERTON M. THOMAS. Can. J. Chem. **60**, 160 (1982).

A series of C-21 substituted progesterone derivatives (R = F, Cl, Br, $CH_3$) has been prepared, and incubated the C-21 hydroxylating fungus *A. niger*. No biotransformation was observed where R = Cl, Br, or $CH_3$, but a minor amount of hydroxylation occurred at an unidentified site where R = F. Two C-11β substituted progesterone derivatives (R = F, OH) were converted to the corresponding C-11 ketone by the C-11α hydroxylator *R. stolonifer*, but a C-11β hydroxylator (*C. lunata*) was unable to perform a similar transformation with a C-11α hydroxy substrate. *C. lunata* hydroxylated a C-11β fluoro substrate at C-14α and C-21 in low yield. C-7α and -7β-hydroxy androst-4-ene-3,17-diones were prepared and incubated with C-7β hydroxylating (*R. stolonifer*) and C-7α hydroxylating (*M. griseocyanus*) fungi respectively. No ketone formation was observed. Similarly, the C-6β hydroxylator *R. arrhizus* was unable to transform a C-6α-hydroxy substrate or C-6α- or C-6β-hydroxy-*B*-norsteroids. No oxidation at halogen was observed for any of the substrates used. $^{13}C-^{19}F$ coupling constants for 11β-fluoroprogesterone suggest the presence of through space interactions between fluorine and both C-18 and C-19.

---

HERBERT L. HOLLAND et EVERTON M. THOMAS. Can. J. Chem. **60**, 160 (1982).

On a préparé une série de dérivés de la progestérone substitués en position C-21 (R = F, Cl, Br, $CH_3$) et on les a incubé avec le champignon hydroxylant en C-21 *A. niger*. On n'a pas observé de biotransformation lorsque R = Cl, Br ou $CH_3$ mais une faible quantité de produit d'hydroxylation apparaît en un site inconnu lorsque R = F. On a transformé deux dérivés des progestérones substituées en C-11β (R = F, OH) en cétone C-11 correspondante à l'aide du *R. stolonifer*, un agent hydroxylant en C-11α. Toutefois le *C. lunata*, un agent hydroxylant en C-11β, ne permet pas d'effectuer une telle transformation avec des substrats hydroxylés en C-11α. Le *C. lunata* hydroxyle un substrat fluoré en C-11β au niveau de C-14α et de C-21 avec un faible rendement. On a préparé les hydroxy-7α (et 7β) androstene-4 diones-3,17 et on les a incubé avec des champignons hydroxylant respectivement en C-7β (*R. stolonifer*) et en C-7α (*M. griséocyanus*). On n'a pas observé la formation de cétone. De la même façon, le champignor *R. arrhizus*, hydroxylant en C-6β, est incapable de transformer des substrats hydroxy-6α ou des hydroxy-6α ou -6β *B*-norstéroides. On n'a pas observé d'oxydation au niveau de l'halogène dans aucun des substrats utilisés. Les constantes de couplage du $^{13}C$ et du $^{19}F$ de la fluoro-11β progestérone suggèrent la présence d'interactions spatiales entre le fluor et les deux carbones en positions 18 et 19.

[Traduit par le journal]

## Introduction

The widespread use of organohalides in both industry and medicine has led to concern about their toxic and/or carcinogenic effects (1). This in turn stimulated research into their metabolic fate, which has indicated that, in many cases, bioactivation of organohalides by a cytochrome P-450 dependant mixed-function oxygenase enzyme is a key step in their degradation, leading in some instances to the formation of toxicologically significant metabolites (2–4). Possible oxidative routes which have been considered (5) for this degradation include hydroxylation at saturated carbon, oxidation of the halogen to a hypervalent state, and epoxidation of C=C bonds. In this study, we have utilized halosteroids, and fungi known to hydroxylate steroids at specific sites, in order to investigate the first of these proposed modes of degradation.

Previous work with fluorosteroids and a series of fungi by the Oxford group (6) has demonstrated that the presence of a fluoro substituent at Cn of an androstane generally results in hydroxylation remote from that site when $C_n$ is a favoured position for hydroxylation, but has little effect in cases where the favoured hydroxylation site is remote from $C_n$. Similarly, the metabolism of a fluorogibberellin derivative by *Gibberella fugikuroi* occurred largely independently of the presence of fluorine (7), although the same group (8) found that *Aspergillus avenaceous* could not produce an ω-fluoro analog of avenaciolide when given the corresponding fluorinated precursors.

## Results and discussion

The substrates were prepared as described in the Experimental. The use of tetraethyl tin (9) to produce 21-methylprogesterone (**1***e*) from the acid chloride of **8** is preferable to the existing methods (10, 11) using diethyl cadmium. The halosteroids were prepared by unexceptional procedures. The synthesis of 11β-fluoroprogesterone (**3***a*) proceeded via the 9α-bromo compound **9** (12); we were unable to reproduce reports of the direct production of **3***a* by reaction of 11α-hydroxyprogesterone (**2***a*) with diethyl-(2-chloro-1,1,2-trifluoroethyl) amine (13, 14). In our hands the only product of this reaction was the corresponding $\Delta^{9(11)}$ olefin.

0008-4042/82/020160-05$01.00/0

©1982 National Research Council of Canada/Conseil national de recherches du Canada

Can. J. Chem. Downloaded from www.nrcresearchpress.com by 210.87.254.5 on 09/06/12
For personal use only.

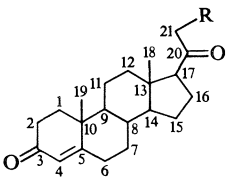

**1**

*a* R = H
*b* R = F
*c* R = Cl
*d* R = Br
*e* R = $CH_3$
*f* R = OH
*g* R = OMs

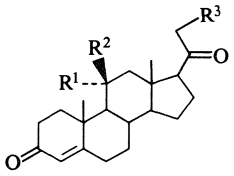

**2**

*a* $R^1$ = OH, $R^2$ = $R^3$ = H
*b* $R^1$ = $R^3$ = H, $R^2$ = OH
*c* $R^1$ + $R^2$ = O, $R^3$ = H

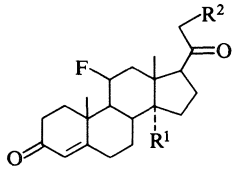

**3**

*a* $R^1$ = $R^2$ = H
*b* $R^1$ = OH, $R^2$ = H
*c* $R^1$ = $R^2$ = OH

The $^{13}C$ nmr spectra of **3***a* and **9**, together with those of other steroids used in this study whose $^{13}C$ nmr spectra are hitherto unreported, are assigned in Table 2. Assignments were straightforward, those of **3***a* and **9** being simplified by the presence of $^{13}C$–$^{19}F$ coupling. The presence of significant coupling to both C-18 and C-19 in these compounds is noteworthy. Long range coupling from a C-6β fluorine to C-19 has been observed (15) and attributed to a through space interaction; a similar phenomenon is presumably operative in the present case.

The results of the incubations performed are summarized in Table 1. The 21-halosteroids **1***b*–**1***d* were incubated with *Aspergillus niger* ATCC 9142, a fungus known to hydroxylate **1***a* at C-21 in good yield (16). The 21-methyl derivative **1***e* was also studied for comparative purposes. In no case was any significant biotransformation observed; with **1***b* as substrate a minor product was obtained, mass spectrometry of which indicated a molecular weight of 348, but a quantity sufficient for structure determination could not be obtained. It is therefore apparent that the presence of halogen or methyl at the favoured site of hydroxylation of this fungus blocks hydroxylation at that site, but does not significantly direct it elsewhere. Control experiments in which **1***a* is efficiently hydroxylated at C-21 in the presence of **1***c* indicate that the failure of *A. niger* to hydroxylate **1***b*–**1***d* was unlikely to have been due to deactivation of the enzyme by the action of these α-haloketones as alkylating agents.[1]

TABLE 1. Incubations with fungi

| Substrate | Fungus | Time (h) | Isolated products (%) |
|---|---|---|---|
| **1***b* | *A. niger* | 120 | **1***b* (44) unknown (0.1) |
| **1***c* | *A. niger* | 96 | **1***c* (60) |
| **1***d* | *A. niger* | 96 | **1***d* (62) |
| **1***e* | *A. niger* | 96 | **1***e* (80) |
| **2***b* | *R. stolonifer* | 35 | **2***c* (85) |
| **3***a* | *R. stolonifer* | 36 | **3***a* (54), **2***c* (33) |
| **2***a* | *C. lunata* | 26 | **2***a* (95) |
| **3***a* | *C. lunata* | 60 | **3***a* (29), **3***b* (17), **3***c* (7) |
| **4***b* | *R. arrhizus* | 24 | **4***b* (72) |
| **5***a* | *M. griseocyanus* | 72 | **5***a* (46), **6** (2) |
| **5***b* | *R. stolonifer* | 24 | **5***b* (66) |
| **7***b* | *R. arrhizus* | 24 | **7***b* (58) |
| **7***c* | *R. arrhizus* | 24 | **7***c* (68) |

The influence of substitution at C-11β and C-11α on hydroxylation at C-11α (by *Rhizopus stolonifer*) (17) and C-11β (by *Curvularia lunata*) (18) was also examined. With *R. stolonifer*, both the C-11β alcohol **2***b* and the C-11β fluorosteroid **3***a* gave rise to the C-11 ketone **2***c*. This can be rationalized by the assumption that *R. stolonifer* hydroxylates **2***b* and **3***a* at the normal C-11α position, the products

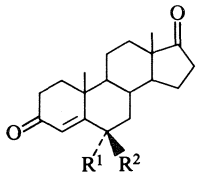

**4**

*a* $R^1$ = $R^2$ = H
*b* $R^1$ = OH, $R^2$ = H
*c* $R^1$ = H, $R^2$ = OH
*d* $R^1$ + $R^2$ = O

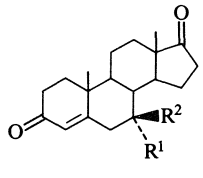

**5**

*a* $R^1$ = H, $R^2$ = OH
*b* $R^1$ = OH, $R^2$ = H
*c* $R^1$ + $R^2$ = O

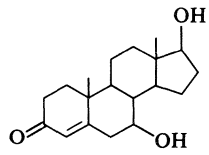

**6**

being formed by subsequent loss of water or HF. The possibility that the alcohol **2***b* is converted to **2***c* by the action of an alcohol dehydrogenase seems unlikely in view of a lack of precedent for such conversions by *R. stolonifer* (19).

The C-11β hydroxylator *C. lunata*, although possessing a low substrate specificity with respect to substitution at sites remote from C-11 (20), is not tolerant of substitution of C-11α (hydroxyl) or

[1]We are indebted to a referee for bringing this possibility to our attention.

Can. J. Chem. Downloaded from www.nrcresearchpress.com by 210.87.254.5 on 09/06/12
For personal use only.

Can. J. Chem. Downloaded from www.nrcresearchpress.com by 210.87.254.5 on 09/06/12
For personal use only.

TABLE 2. $^{13}C$ nmr chemical shifts

| | δ ppm* ($J_{C-F}$ Hz) | | | | | |
|---|---|---|---|---|---|---|
| Carbon | **8** | **1***e* | **3***a* | **9** | **5***b* | **5***a* |
| 1 | 35.8 | 35.7 | 35.3 | 29.9 | 35.4 | 35.6 |
| 2 | 34.0 | 34.0 | 33.7 | 33.8 | 33.9 | 33.9 |
| 3 | 200.0 | 199.5 | 198.9 | 197.8 | 199.3 | 199.4 |
| 4 | 124.0 | 124.0 | 123.2 | 125.0 | 127.0 | 125.0 |
| 5 | 171.3 | 171.1 | 170.5 | 166.8 | 168.0 | 167.4 |
| 6 | 32.9 | 32.8 | 32.1 | 31.6 | 39.4 | 42.5 |
| 7 | 32.0 | 31.9 | 31.7 | 27.7 | 67.0 | 74.3 |
| 8 | 35.8 | 35.7 | 32.1 | 35.5 | 41.1 | 42.8 |
| 9 | 53.7 | 53.7 | 56.4(20) | 88.4(20) | 45.3 | 50.8* |
| 10 | 38.6 | 38.7 | 39.0(0) | 45.7(0) | 38.6 | 38.2 |
| 11 | 21.0 | 21.1 | 89.7(176) | 92.5(183.5) | 20.2 | 20.4 |
| 12 | 38.0 | 38.8 | 44.9(20) | 40.0(20) | 31.0 | 31.3 |
| 13 | 44.1 | 44.1 | 42.7(2) | 42.5(0) | 47.3 | 48.1 |
| 14 | 55.1* | 56.1 | 56.6 | 50.7 | 45.6 | 50.6* |
| 15 | 24.5 | 24.5 | 24.2 | 23.6 | 21.3 | 25.0 |
| 16 | 23.4 | 23.1 | 22.6 | 22.6 | 35.8 | 36.0 |
| 17 | 55.5* | 62.6 | 63.6 | 63.2 | 220.8 | 221.0 |
| 18 | 13.3 | 13.5 | 15.0(6.6) | 15.2(6.6) | 13.5 | 14.0 |
| 19 | 17.4 | 17.4 | 20.4(9.2) | 22.4(13.8) | 17.0 | 17.4 |
| 20 | 179.8 | 211.9 | 208.4 | 208.3 | | |
| 21 | | 37.3 | 31.2 | 31.2 | | |
| 22 | | 7.7 | | | | |

*Chemical shifts marked with asterisks may be interchanged.

C-11β (fluoro). Incubation of 11α-hydroxyprogesterone (**2***a*) with *C. lunata* results in an almost quantitative recovery of starting material, whereas the C-11β fluorosteroid **3***a* was hydroxylated only at C-14α (a normal site of hydroxylation for this fungus (18)) and C-21. Since C-21 hydroxylation by this fungus has not previously been reported, it appears that the fluorine atom at C-11β has directed hydroxylation to this site, a finding consistent with that of previous workers (6).

In view of the apparent insensitivity of the C-11α hydroxylase of *R. stolonifer* to substitution at C-11β, we also examined the same fungus for its ability to metabolize androst-4-ene-3,17-dione-7α-ol (**5***b*); this fungus converts **4***a* to the C-7β hydroxylated product **5***a* in good yield (21). However, incubation of **5***b* with *R. stolonifer* resulted in the recovery of starting material only. The complementary incubation of the C-7β alcohol **5***a* with a C-7α hydroxylator (*Mucor griseocyanus*) (22) gave only a low yield of **6**, the product of reduction at C-17 (cf. 23).

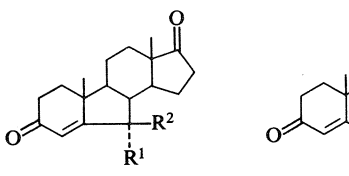


**7**

*a* $R^1 = R^2 = H$
*b* $R^1 = OH, R^2 = H$
*c* $R^1 = H, R^2 = OH$
*d* $R^1 + R^2 = O$

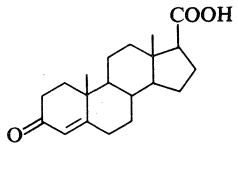


**8**

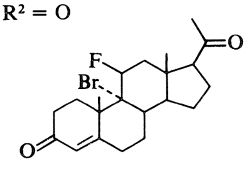


**9**

The C-6α alcohol **4***b* was incubated with the C-6β hydroxylator *Rhizopus arrhizus* (23), and the C-6α and C-6β *B*-nor alcohols, **7***b* and **7***c* were also incubated with the same fungus. *R. arrhizus* is capable of hydroxylation at both C-6α and C-6β of *B*-norandrostanes (24). None of the incubations with *R. arrhizus* produced detectable amounts of the ketosteroids **4***d* or **7***d*. Thus, of the fungi investigated, *R. stolonifer* is unique in its ability to perform hydroxylation at a carbon containing a substituent other than hydrogen. The difficulty of access of C-11 substituted progesterone derivatives has so far precluded a more detailed study of this reaction, but work in this direction is proceeding.

## Experimental

*Apparatus, materials, and methods*

Melting points were determined on a Kofler heating stage and are uncorrected. Infrared spectra were recorded with a Perkin-Elmer 237B, $^1H$ nmr spectra with a Bruker WP-60 or Varian A-60, and $^{13}C$ nmr with a Bruker WP-60 spectrometer using $CDCl_3$ as solvent and TMS as internal standard. Mass spectra were obtained with an AEI MS30 spectrometer. Column

Can. J. Chem. Downloaded from www.nrcresearchpress.com by 210.87.254.5 on 09/06/12
For personal use only.

chromatography was performed on silica gel (60–200 mesh), thin layer chromatography on Merck silica gel 60 F-254 (0.2 mm), and preparative layer chromatography on Merck silica gel F-254 (2.0 mm).

*Preparation of substrates*

With the exception of those listed below, the substrates used in this study were commercial samples.

*21-Methanesulphonyloxypregn-4-ene-3,20-dione (1g) (25)*

Pregn-4-ene-3,20-dione-21-ol (**1***f*) (5 g) was dissolved in dry pyridine (12 mL) and the solution cooled to −10°C. Methanesulphonyl chloride (1.73 g) was added to the solution, and the mixture stirred at −10° to −5°C for 1.25 h. The reaction was terminated by the addition of ether and water, and the white precipitate filtered and crystallized from methanol, giving 4.2 g (67%) of title compound of mp 157–160°C (lit. (26) mp 156–157°C).

*21-Fluoropregn-4-ene-3,20-dione (1b) (27)*

Potassium fluoride (4 g) and 18-crown-6 ether (1,4,7,10,13,16-hexaoxacyclooctadecane, 6 g) were suspended in freshly distilled DMF (25 mL), and **1***g* (3.5 g) added to the mixture, which was then refluxed at water aspirator pressure for 21 h. Water and ether were then added and the precipitated product filtered. Chromatography by gradient elution (benzene/ether) afforded **1***b* (1 g, 35%) mp 138–140°C (lit. (28) mp 141.5–142.2°C); $^1$H nmr included signals at δ 0.72 (3H, s, C-18H), 1.20 (3H, s, C-19H), 4.79 (2H, d, C-21H), and 5.82 (1H, s, C-4H) ppm; $^{13}$C nmr (29); *m/e* (%): 332 (100), 317 (24), 299 (26), 290 (100).

*21-Chloropregn-4-ene-3,20-dione (1c)*

The alcohol **1***f* (5 g) was dissolved in dry pyridine (10 mL) and the solution cooled to 0°C. Methanesulphonyl chloride (2.16 g) was then added, and the solution stirred and allowed to reach room temperature over a 2 h period, by which time the product **1***c* had precipitated. Water was then added and the product collected by filtration and crystallized from methanol to yield 3.8 g (73%), mp 203–205°C (lit. (30) mp 206–208°C); $^1$H nmr included signals at δ 0.71 (3H, s, C-18H), 1.20 (3H, s, C-19H), 4.12 (2H, s, C-21H), and 5.75 (1H, s, C-4H) ppm; $^{13}$C nmr (29); *m/e* (%): 350 (8), 348 (25), 333 (8), 314 (16), 312 (21), 299 (100).

*21-Bromopregn-4-ene-3,20,dione (1d) (25)*

The mesylate **1***g* (2.5 g) was dissolved in acetone (15 mL), and lithium bromide (3.5 g) added to the solution. The mixture was stirred and refluxed for 2 h, and then cooled. The precipitate was collected and dissolved in chloroform, and the resulting solution washed (water), dried (sodium sulphate), and evaporated. The residue was crystallized from acetone affording 1.8 g (76%) **1***d*, mp 159–162°C (lit. (31) mp 190–191°C); $^1$H nmr signals at δ 0.72 (3H, s, C-18H), 1.20 (3H, s, C-19H), 3.96 (2H, s, C-21H), and 5.79 (1H, s, C-4H) ppm; $^{13}$C nmr (29); *m/e* (%): 394 (16), 392 (17), 352 (28), 350 (27), 313 (53), 299 (100).

*Androst-4-ene-3-one, 17β-carboxylic acid (8) (32)*

The alcohol **1***f* (2 g) was dissolved in a mixture of acetone (25 mL) and sulphuric acid (96%, 1 drop). A solution of paraperiodic acid ($H_5IO_6$) in water (6 mL) was then added and the resulting mixture refluxed for 12 h. The acetone was then removed under reduced pressure, and chloroform (50 mL) added to the residue. The resulting solution was then extracted with aqueous sodium hydroxide (4%, 3 times). Fresh chloroform was added to the aqueous extract, which was then acidified with dilute HCl and extracted with chloroform. The extract was dried and evaporated to give 1.4 g (73%) of the title compound, mp 246–250°C (lit. (33) mp 246–250°C); $^1$H nmr included signals at δ 0.75 (3H, s, C-18H), 1.20 (3H, s, C-19), and 5.65 (1H, s, C-4H) ppm; $^{13}$C nmr, Table 2; *m/e* (%): 316 (57), 308 (18), 298 (13), 283 (14), 274 (100).

*21-Methylpregn-4-ene-3,20-dione (9, 10)*

The acid **8** (0.6 g) was suspended in dry benzene (30 mL). The mixture was flushed with dry nitrogen for 10 min, then cooled to 5°C and oxalyl chloride (2 mL) added. The mixture was then stirred and allowed to reach room temperature. After 45 min, dissolution was complete. The solvent was then removed under vacuum and the residual acid chloride dried *in vacuo* for a further 6 h. Dry hexamethylphosphoric triamide (10 mL) was added to the residue and after dissolution was complete, tetraethyl tin (0.56 g) and benzylchlorobis(triphenylphosphine) palladium II (10 mg) were added. The mixture was kept in a water bath at 80°C for 45 min, then cooled and diluted with water. The products were extracted into ether and the extract washed (2% sodium hydroxide), dried, and evaporated. The residue was separated by plc (30% ethyl acetate, 70% benzene solvent), and the resulting product crystallized from aqueous methanol, giving 0.21 g (42%), mp 139–141°C (lit. (11) mp 151–152°C); $^1$H nmr included signals at δ 0.66, (3H, s, C-18H), 1.04 (3H, t, C-22H), 1.19 (3H, s, C-19H), and 5.74 (1H, s, C-19H) ppm; $^{13}$C nmr, Table 2; *m/e* (%): 328 (64), 313 (24), 299 (59), 283 (73), 271 (100).

*9α-Bromo-11β-fluoropregn-4-ene-3,20-dione (9) (12)*

Hydrogen fluoride/pyridine reagent (70%, Aldrich Chemical Co., 50 mL) was added to dry THF (40 mL), and the mixture cooled to −50°C. *N*-Bromosuccinimide (3.5 g) was then added, followed by a solution of pregna-4,9(11)-diene-3,20-dione (5.5 g) in dry THF (10 mL). The resulting mixture was stirred at −50°C for 1 h and then allowed to remain at room temperature for 1 h. Cold saturated sodium carbonate solution was then added cautiously until the solution was basic. The product was then extracted into methylene chloride and the extract dried and evaporated. The residue was crystallized from methanol to give the title compound (6.1 g, 84%), mp 143–145°C (lit. (34) mp 145–150°C); $^1$H nmr included signals at δ 0.81 (3H, d, C-18H), 1.39 (3H, d, C-19H), 2.14 (3H, s, C-21H), 5.15 (1H, m, C-11αH), and 5.69 (1H, s, C-4H); $^{13}$C nmr, Table 2; *m/e* (%): 412 (7), 410 (8), 331 (19), 312 (100), 269 (24).

*11β-Fluoropregn-4-ene-3,20-dione (3a) (35)*

A solution of **9** (2.8 g), tri-*n*-butyltin hydride (10 mL), and azoisobutyronitrile (10 mg) in dry THF (25 mL) was allowed to stand at room temperature for 5 h, after which time several drops of water were added, and the solvent then removed under reduced pressure. The residue was crystallized from an 85% ethanol/water mixture to give 1.95 g (86%) **3***a*, mp 169–172°C (lit. (14) mp 156–158°C); $^1$H nmr included signals at δ 0.81 (3H, d, C-18H), 1.36 (3H, d, C-19H), 2.14 (3H, s, C-21H), 5.13 (1H, m, C-11αH), and 5.71 (1H, s, C-4H) ppm; $^{13}$C nmr, Table 2; *m/e* (%): 332 (54), 317 (10), 312 (100), 304 (16), 297 (46).

*Androst-4-ene-3,17-dione-7α-ol (5b)*

This was prepared from androsta-4,6,diene-3,17-dione by the procedure of Hossain *et al.* (36). Following correspondence with Professor D. N. Kirk, the $^1$H nmr spectrum of the intermediate 6,7α-epoxyandrost-4-ene-3,17-dione has been reassigned as follows: δ 0.95 (3H, s, C-18H), 1.13 (3H, s, C-19H), 3.51 (2H, br s, C-6β,7β H's), and 6.14 (1H, s, C-4H). The title compound had mp 227–230°C (lit. (36) mp 240–245°C); $^1$H nmr included signals at δ 0.92 (3H, s, C-18H), 1.22 (3H, s, C-19H), 4.10 (1H, br s, C-7βH), and 5.79 (1H, s, C-4H); $^{13}$C nmr, Table 2; *m/e* (%): 302 (15), 284 (100), 269 (29).

*Androst-4-ene-3,17-dione-7β-ol (5a)*

The alcohol **5***a* was obtained from androst-4-ene-3,17-dione (**4***a*) by fermentation with *Rhizopus stolonifer* ATCC 6227 b (see below). From 4.2 g of **4***a*, the following were obtained by column chromatography subsequent to a four day incubation with *R. stolonifer* in replacement culture. Recovered starting material (0.92 g), androst-4-ene-3,17-dione-6β-ol (**4***c*, 1.51 g), androst-4-ene-3,17-dione-11α-ol (0.21 g), and androst-4-ene-3,17-dione-7β-ol (**5***a*, 0.32 g), mp 218–220°C (lit. (21) mp 218.5–221°C); $^1$H

nmr included signals at δ 0.94 (3H, s, C-18H), 1.24 (3H, s, C-19H), 3.52 (1H, m, C-7αH), and 5.78 (1H, s, C-4) ppm; $^{13}C$ nmr, Table 2; *m/e* (%): 302 (100), 287 (16), 284 (42), 269 (31).

B-*Norandrost-4-ene-3,17-dione, 6α and 6β-ol (7b, 7c)*

These compounds were obtained by incubation of *B*-norandrost-4-ene-3,17-dione (*7a*) with *Rhizopus arrhizus* ATCC 11145 as described (24). Physical and spectral data were as previously reported (24).

*Incubations with fungi*

The fungi were grown and incubations performed according to the published procedures listed below. Details of time, products, and yields are summarized in Table 1. Data for hitherto unreported compounds are listed below.

*Aspergillus niger* ATCC 9142 (16), *Rhizopus stolonifer* ATCC 6227b (37), *Curvularia lunata* NRRL 2380 (38), *Rhizopus arrhizus* ATCC 11145 (37), and *Mucor griseocyanus* ATCC 1207 (22).

*11β-Fluoropregn-4-ene-3,20-dione-14α-ol (3b)*

Melting point 193–195°C; $R_f$: 0.77 (benzene/ethyl acetate/acetone 3:3.5:3.5), 0.81 (benzene/acetone 3:7), 0.51 (hexane/acetone 2:8); $^1H$ nmr included signals at δ 0.89 (3H, d, C-18H), 1.37 (3H, d, C-19H), 5.11 (1H, m, C-11αH), and 5.69 (1H, s, C-4H) ppm. $M^+$ calcd. for $C_{21}H_{29}O_3F$: 348.210; found: 348.210; *m/e* (%): 348 (6), 330 (36), 310 (36), 287 (43), 123 (100).

*11β-Fluoropregn-4-ene-3,20-dione-14α, 21-diol (3c)*

Melting point 175–178°C; $R_f$: 0.70 (benzene/acetone 3:7), 0.59 (benzene/ethyl acetate/acetone 3:3.5:3.5), 0.29 (hexane/acetone 2:8); $^1H$ nmr included signals at δ 0.92 (3H, d, C-18H), 1.37 (3H, d, C-19H), 4.20 (2H, d, C-21H), 5.08 (1H, m, C-11αH), and 5.70 (1H, s, C-4H) ppm. $M^+$ calcd. for $C_{21}H_{29}O_4F$: 364.205; found: 364.206; *m/e* (%): 364 (1), 346 (2), 333 (27), 315 (100), 295 (9).

## Acknowledgements

Financial support was provided by the Natural Sciences and Engineering Research Council of Canada. We are grateful to Mr. T. Jones for his assistance in recording nmr and mass spectra, and to Professor D. N. Kirk for helpful correspondence.

1. C. Heidelberger. Ann. Rev. Biochem. **44**, 29 (1975).
2. J. L. Stevens and M. W. Anders. Biochem. Pharmacol. **28**, 3189 (1979).
3. V. Ullrich. Top. Curr. Chem. **83**, 67 (1979).
4. F. P. Guengerich, W. M. Crawford, J. Y. Domoradski, T. L. Macdonald, and P. G. Watanabe. Toxicol. Appl. Pharmacol. **55**, 303 (1980).
5. T. L. Macdonald, N. Narasimhan, and L. T. Burka. J. Am. Chem. Soc. **102**, 7760 (1980).
6. T. G. C. Bird, P. M. Fredericks, Sir Ewart R. H. Jones, and G. D. Meakins. J. Chem. Soc. Perkin Trans. I, 750 (1980).
7. B. E. Cross and A. Erasmuson. J. Chem. Soc. Chem. Commun. 1013 (1978).
8. B. E. Cross and P. Hendley. Tetrahedron, **34**, 1281 (1978).
9. D. Milstein and J. K. Stille. J. Org. Chem. **44**, 1613 (1979).
10. F. Rebev, A. Lardon, and T. Reichstein. Helv. Chim. Acta, **37**, 45 (1954).
11. A. Wettstein. Helv. Chim. Acta, **23**, 1371 (1940).
12. A. Bowers, L. C. Ibanez, E. Denot, and R. Becerra. J. Am. Chem. Soc. **82**, 4001 (1960).
13. Syntex Corp. Dutch Patent No. 6,610,921 (Feb. 6, 1967); Chem. Abstr. **68**, 69213t (1968).
14. D. E. Ayer. Tetrahedron Lett. 1065 (1962).
15. H. L. Holland. Tetrahedron Lett. 881 (1978).
16. H. L. Holland and B. J. Auret. Can. J. Chem. **53**, 845 (1975).
17. D. H. Peterson, H. C. Murray, S. H. Eppstein, L. M. Reineke, A. Weintraub, P. D. Meister, and H. M. Leigh. J. Am. Chem. Soc. **74**, 5933 (1952).
18. E. L. Dulaney and W. J. McAleer. U.S. Patent No. 2,888,469 (May 26, 1959); Chem. Abstr. **53**, 22092a (1959).
19. W. C. Charney and H. L. Herzog. Microbial transformations of steroids. A handbook. Academic Press, New York, NY. 1967.
20. K. Kieslich, H. Wieglepp, K. Petzoldt, and F. Hill. Tetrahedron, **27**, 445 (1971).
21. R. C. Tweit, A. H. Goldkamp, and R. M. Dodson. J. Org. Chem. **26**, 2856 (1961).
22. K. Singh, S. N. Sehgal, and C. Vezina. Can. J. Microbiol. **13**, 1271 (1967).
23. H. L. Holland and P. R. P. Diakow. Can. J. Chem. **56**, 694 (1978).
24. H. L. Holland. Can. J. Chem. **59**, 1651 (1981).
25. N. L. Wendler, R. R. Graber, and G. G. Hozen. Tetrahedron, **3**, 144 (1958).
26. E. V. Jensen. U.S. Patent No. 2,953,581 (Sept. 20, 1960); Chem. Abstr. **55**, 5597f (1961).
27. J. E. Herz, J. Fried, P. Grabowich, and E. P. Sabo. J. Am. Chem. Soc. **78**, 4812 (1956).
28. P. Tannhauser, R. T. Pratt, and E. V. Jensen. J. Am. Chem. Soc. **78**, 2658 (1956).
29. H. L. Holland and E. M. Thomas. Can. J. Chem. **57**, 3069 (1979).
30. T. Reichstein and H. G. Fuchs. Helv. Chim. Acta, **23**, 684 (1940).
31. H. Reich and T. Reichstein. Helv. Chim. Acta, **22**, 1124 (1939).
32. L. F. Fieser and S. Rajagopalan. J. Am. Chem. Soc. **71**, 3938 (1949).
33. V. W. Gash. U.S. Patent No. 2,769,822 (Nov. 6, 1956). Chem. Abstr. **51**, 8817d (1957).
34. H. Reimann, E. D. Oliveto, R. Neri, M. Eisler, and P. Perlman. J. Am. Chem. Soc. **82**, 2308 (1960).
35. H. Hofmeister, H. Laurent, R. Weichert, K. Annen, and H. Steinbeck. Ger. Patent No. 2,410,443 (Sept. 11, 1965); Chem. Abstr. **84**, 59868b (1976).
36. A. M. M. Hossain, D. N. Kirk, and G. Mitra. Steroids, **27**, 603 (1976).
37. H. L. Holland and B. J. Auret. Can. J. Chem. **53**, 2041 (1975).
38. Y. Y. Lin, M. Shibahara, and L. L. Smith. J. Org. Chem. **34**, 3530 (1969).

Can. J. Chem. Downloaded from www.nrcresearchpress.com by 210.87.254.5 on 09/06/12
For personal use only.

# Thermal explosions with variable thermal conductivity

AVYGDOR MOISE AND HUW O. PRITCHARD

*Centre for Research in Experimental Space Science, York University, Downsview, Ont., Canada M3J 1P3*

Received June 1, 1981

AVYGDOR MOISE and HUW O. PRITCHARD. Can. J. Chem. **60**, 165 (1982).

Numerical solutions are presented for the case of a thermal explosion in a sphere, in which the thermal conductivity varies linearly with temperature. The behaviour of the critical temperature profiles and of the other critical parameters for variations in the thermal conductivity are demonstrated.

AVYGDOR MOISE and HUW O. PRITCHARD. Can. J. Chem. **60**, 165 (1982).

On présente des solutions numériques dans le cas d'une explosion thermique dans une sphère dont la conductivité thermique varie linéairement avec la température. On démontre le comportement des profils de température critique et d'autres paramètres critiques des variations de la conductivité thermique.

[Traduit par le journal]

Can. J. Chem. Downloaded from www.nrcresearchpress.com by 210.87.254.5 on 09/06/12
For personal use only.

## Introduction

The Frank–Kamenetskii approach to the problem of a thermal explosion has been the subject of much analytic effort in recent years (1, 2), but despite all the progress that has been made, the original simplifying assumptions of the model are unrealistic. We wish to examine in this paper the consequences of the neglect of the variation of thermal conductivity with temperature.

There have been, within the past two or three years, two studies (3, 4) of the case for which the variation of the thermal conductivity ($\kappa$) with temperature ($T$) is considered to be exponential, i.e.

$$[1] \quad \kappa(T) = \kappa(T_0) \exp [a(T - T_0)]$$

where $T_0$ is the wall temperature, and $a$ is a constant. Walker and Jackson (3) provided numerical solutions for all three class A geometries (1), whereas Wake (4) has shown that it is possible to derive isolated analytic solutions for a sphere when $b = a\boldsymbol{R}T_0^2/E = 0.2$ or 1.0, $E$ being the activation energy and $\boldsymbol{R}$ the gas constant.

We use, instead, the form

$$[2] \quad \kappa(T) = \kappa(T_0)[1 + \alpha(T - T_0)]$$

which is certainly more realistic, at least for gases.

## The basic equation

We will not re-derive the basic equation to be solved, but beginning with eq. [2] from Wake's paper (4), and by confining our attention to a first order (unimolecular) reaction taking place in a sphere, the usual manipulations lead us to

$$[1] \quad \frac{\partial^2\theta}{\partial\xi^2} + \frac{2}{\xi}\frac{\partial\theta}{\partial\xi} + \frac{\gamma}{(1+\gamma\theta)}\left(\frac{\partial\theta}{\partial\xi}\right)^2 + \frac{\delta e^{\theta}}{(1+\gamma\theta)} = 0$$

In this equation $\xi = r/R$, where $r$ is the distance from the centre and $R$ is the radius of the vessel, $\theta$, the dimensionless temperature excess (1) and $\delta$, the dimensionless heat production rate (1, 5) have their usual meanings, i.e.

$$\theta = E(T - T_0)/\boldsymbol{R}T_0^2$$

$$\delta = \frac{-\Delta H k_{\text{uni}}(T_0)}{\kappa(T_0)} \cdot \frac{P_0}{\boldsymbol{R}T_0} \cdot \frac{E}{\boldsymbol{R}T_0^2} \cdot R^2$$

and $\gamma = \kappa_0^{-1}\partial\kappa/\partial\theta$ where we now write $\kappa = \kappa(T)$ and $\kappa_0 = \kappa(T_0)$.

## Numerical solution

We have solved this equation by standard numerical methods (6, 7) for various values of $\gamma = \kappa_0^{-1}\,\partial\kappa/\partial\theta$ between zero and unity. We limited our examination to this range of $\gamma$ values because our principal interest is in gaseous explosions where $\gamma$ is rather small; we are, however, indebted to a referee for drawing to our attention a forthcoming paper by Lacey and Wake showing that a solution to [3] exists for all $\gamma$. The integration was started by the Runge–Kutta method (ref. 6, eq. 25.5.20) until sufficient points had been established to proceed with predictor–corrector method (ref. 6, eq. 25.5.21); an acceptable solution was required to fulfil the condition that at both extremities, the product $\xi\theta$ was zero to within $10^{-6}$. For each value of $\gamma$, a systematic search was made through trial values of $\delta$ until no solution could be found: the critical conditions, i.e. $\delta_c$, $\theta_c$ and $\partial\theta_c/\partial\xi|_{\xi=1}$, located in this manner are listed in Table 1.

Before discussing the significance of these solutions, we need to assure ourselves that they are accurate. For the case of $\gamma = 0$ (the standard Frank–Kamenetskii calculation) we agree with

0008-4042/82/020165-03$01.00/0

©1982 National Research Council of Canada/Conseil national de recherches du Canada

Can. J. Chem. Downloaded from www.nrcresearchpress.com by 210.87.254.5 on 09/06/12
For personal use only.

TABLE 1. Dimensionless critical parameters for an exothermic reaction taking place in a sphere, as a function of the rate of change of thermal conductivity with temperature, i.e. $\gamma = \kappa_0^{-1}\,\partial\kappa/\partial\theta$

| $\gamma$ | $\delta_c$ | $\theta_c$ | $-\partial\theta_c/\partial\xi\|_{\xi=1}$ |
|---|---|---|---|
| 0 | 3.322 | 1.607 | 2.000 |
| 0.1 | 3.514 | 1.659 | 2.207 |
| 0.2 | 3.712 | 1.712 | 2.433 |
| 0.3 | 3.917 | 1.760 | 2.674 |
| 0.4 | 4.127 | 1.805 | 2.927 |
| 0.5 | 4.342 | 1.848 | 3.197 |
| 0.7 | 4.784 | 1.925 | 3.771 |
| 1.0 | 5.467 | 2.018 | 4.726 |

the published values (8) of $\delta_c = 3.32199$ and $\theta_c = 1.607$, and also with our own most recent values (9) of $\delta_c = 3.322640$, $\theta_c = 1.60570$ derived from a 20th order power series expansion; the slope of the dimensionless temperature excess at the wall should be exactly $-2$, and our value differs from this by 1 in the 5th figure. Another simple test we can perform is to apply the present numerical procedures to Wake's exactly soluble case (4) i.e. his $b = 0.2$ for exponential thermal conductivity variation, eq. [1]: for this case we obtain $\delta_c = 3.750$ (exact value = 15/4), $\theta_c = 1.733$ (exact value = $5 \ln \sqrt{2} = 1.73287$), and $\delta\theta_c/\partial\xi|_{\xi=1} = -2.500$ (exact value = $-5/2$); our procedure diverges, as it should, for Wake's case $b = 1$. Finally, for values of $b < 1$, we have compared our results with those of Walker and Jackson (3) for the exponential case, and we agree with their results to within the accuracy with which we can read them from their graphical presentation.

Since our work was completed, a new paper by Walker (10) has become available giving numerical solutions for the linear case, eq. [2]. Again, within the accuracy with which we can read his Fig. 4, we agree with Walker's data for the variation of $\delta_c$ with $\gamma$. However, we do not find agreement with his Fig. 1 for the variation of $\theta_c$ with $\gamma$: it appears that these temperature profiles have been misplotted — for example, the slope at the boundary for the $\gamma = 0$ case is $-2.1$ instead of $-2.0$ as is required for the standard solution.

## Discussion

The results found in Table 1 show that the neglect of the variation of thermal conductivity with temperature does not have a profound effect on the behaviour of gaseous explosions, since practical values of $\gamma$ for gases tend to be rather small: for example, for the case of methyl isocyanide for which the thermal conductivity has been measured close to the explosive temperature range (5), $\gamma \approx 0.0604$, whence $\delta_c \approx 3.437$, $\theta_c \approx 1.637$, and $\partial\theta_c/\partial\xi|_{\xi=1} \approx -2.122$. The neglect of this variation, however, may be more significant for other practical cases such as those considered by Walker and by Wake, and their co-workers (3, 4, 10).

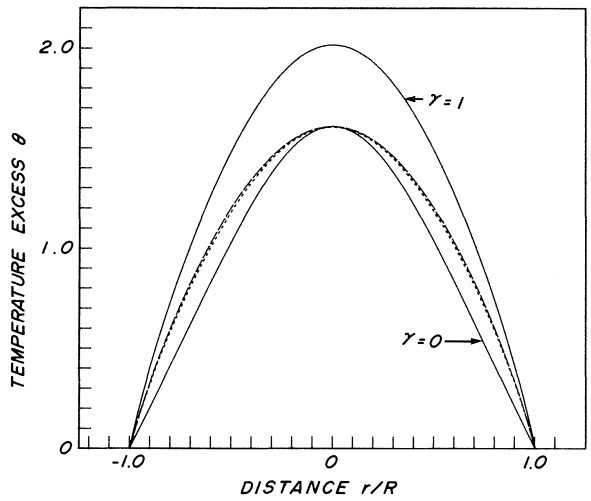


FIG. 1. Dimensionless temperature excess for an exothermic reaction in a sphere. Solid lines: critical temperature profiles for $\gamma = 1$ (top) and $\gamma = 0$ (bottom); broken lines: see Discussion.

Plots of $\delta_c$, $\theta_c$, and of $\partial\theta_c/\partial\xi|_{\xi=1}$ are almost linear over the range $0 \leq \gamma \leq 1$, making interpolation for other interesting cases quite simple. Likewise, the critical temperature profiles are of a similar form to the usual one for $\gamma = 0$, but are raised monotonically everywhere except at the wall. They are, however, of a slightly different shape, as one might expect, and this is demonstrated in Fig. 1. The two solid lines represent the calculated critical temperature profiles for $\gamma = 0$ and $\gamma = 1$: the dashed line is the case of $\gamma = 1$, $\delta = 5.31$ such that $\theta_0 = 1.605$, approximately the same as the value of $\theta_c$ for $\gamma = 0$. It can be seen that the effect of increasing thermal conduction with increasing temperature is to make the temperature profile a little flatter in the middle of the vessel, and rather steeper at the walls. The dotted curve is the critical curve for $\gamma = 1$ scaled down in the ratio of $\theta_c(\gamma = 0)/\theta_c(\gamma = 1)$: it is almost imperceptibly different in shape from that calculated for $\gamma = 1$, $\delta = 5.31$, and gives hope that it may be possible to produce simple empirical expressions for the temperature profiles as a function of $\delta, \gamma$.

1. P. GRAY and M. E. SHERRINGTON. Specialist Periodical Reports. Gas Kinet. Energy Transfer, **2**, 331 (1977).

2. S. R. VATSYA. J. Math. Phys. In press.
3. I. K. WALKER and F. H. JACKSON. New Zealand J. Sci. **21**, 519 (1978).
4. G. C. WAKE. Combust. Flame, **39**, 215 (1980).
5. J. L. COLLISTER and H. O. PRITCHARD. Can. J. Chem. **55**, 3815 (1977).
6. M. ABRAMOWITZ and I. A. STEGUN (*Editors*). Handbook of mathematical functions. U.S. National Bureau of Standards, Applied Mathematics, Series 55, Washington, D.C. 1964. p. 897.
7. B. CARNAHAN, H. A. LUTHER, and J. O. WILKES. Applied numerical methods. Wiley, New York. 1969. pp. 386, 405, 406.
8. T. BODDINGTON and P. GRAY. Proc. R. Soc. London, A**320**, 71 (1970).
9. A. MOISE. Unpublished results.
10. I. K. WALKER. New Zealand J. Sci. **23**, 289 (1980).

Can. J. Chem. Downloaded from www.nrcresearchpress.com by 210.87.254.5 on 09/06/12
For personal use only.

# Program PKAS: a novel algorithm for the computation of successive protonation constants

RAMUNAS J. MOTEKAITIS AND ARTHUR E. MARTELL[1]

*Department of Chemistry, Texas A&M University, College Station, TX 77843, U.S.A.*

Received May 5, 1981

RAMUNAS J. MOTEKAITIS and ARTHUR E. MARTELL. Can. J. Chem. **60**, 168 (1982).

A new algorithm for the simultaneous determination of any number of protonation constants from potentiometric equilibrium data is described. This algorithm is characterized by a unique approach to the internal refinement of the constants and by the analytical nature of the numerical analysis whereby minimization is sought and achieved on the residuals between calculated and observed pH. The FORTRAN IV computer program PKAS utilizing this generalized algorithm has been written and developed and tested on 30 multidentate ligands. The details of the algorithm and the program are described and samples of its recorded usage are provided, indicating its versatility in application.

RAMUNAS J. MOTEKAITIS et ARTHUR E. MARTELL. Can. J. Chem. **60**, 168 (1982).

On décrit un nouvel algorithme qui permet de déterminer simultanément les constantes de protonation successive à partir de données d'équilibre potentiométrique. Cet algorithme se caractérise par son approche spéciale des constantes d'affinage interne et de la nature analytique des analyses numériques grâce auxquelles on a trouvé et minimisé les différences entre les pH calculé et observé. On a mis au point et vérifé, sur trente ligands multidentates, le programme PKAS en langage Fortran IV qui utilise cet algorithme généralisé. On décrit en détail l'algorithme et le programme et on fournit en même temps des exemples de calcul qui indiquent la versatilité de son application.

[Traduit par le journal]

Can. J. Chem. Downloaded from www.nrcresearchpress.com by 210.87.254.40 on 09/06/12
For personal use only.

## Introduction

The efficient determination of the complete set of successive protonation constants of a multidentate ligand or a polyfunctional base is required for the characterization of the acid–base properties of the compound under investigation. The existing algorithms for solving mono and oligoprotic equilibria include such simple expediencies as direct algebraic calculation (1), graphical solution of intercept equations (1, 2), and the half $\bar{n}$ method (3). Such procedures are applicable for either non-overlapping or pairwise overlapping successive reaction steps. Other methodologies (3–5) for protonation constant evaluation include the refinement of initial estimates through inclusion of neighboring overlapping reactions, successive approximations, and computerization of standard graphical methods. Currently, the most common determination of successive overlapping protonation constants employs the rather widely accepted computer programs which had originally been designed for the refinement of metal–ligand formation constants. The more widely known versions include LEAST (6), LETAGROP (7), SCOGS (8), MINIQUAD (9), LETAGROP VRID (10), EQUIL (11), COMICS (12), and GAUSS (13, 14). The use (15) of these generalized programs indicates that the determination of protonation constants represents a subset of a more general problem which involves the interaction of a polyprotic ligand with metal ions. But the subset itself is important enough to merit consideration in its own right for three reasons: (*1*) for polyprotic systems the determination of protonation constants almost always involves simultaneous determination of more equilibrium constants than are needed to describe the metal–ligand systems subsequently investigated after these protonation constants are known (e.g., EDTA possesses four protonation constants, while its complexes are described by one or two formation constants (16)); (*2*) the accuracy with which these protonation constants are known directly affects any subsequent calculations which utilize these constants as parameters (e.g., formation constants, species distribution, etc.); (*3*) the equations are well-ordered and are particularly well-suited for an exact (analytical) mathematical treatment of a generalized refinement process.

Realizing the special nature of this subset (i.e., ligand–proton potentiometry vs. ligand–proton–metal potentiometry) several programs have already appeared which deal with protonation equilibrium specifically. Program TITRA (17) employed an algorithm whereby a ligand of the type $H_NL$ is replaced by $N$ monoprotonated ligands. Program ACBA (18) treats single and mixed acid systems. MUPROT (19) incorporates a technique which refines all parameters describing the titration curve, including a carbon dioxide correction. Most of the above programs utilize the minimization of $U = \sum(v_{obs} - v_{calc})^2$ or similar titer parameter, where $v$ is the volume of titrant added at each point and ($v_{obs}$

[1]To whom all correspondence should be addressed.

0008-4042/82/020168-06$01.00/0

©1982 National Research Council of Canada/Conseil national de recherches du Canada

Can. J. Chem. Downloaded from www.nrcresearchpress.com by 210.87.254.40 on 09/06/12
For personal use only.

$- v_{calc}$) is the difference between the calculated and observed values (15, 20). The other frequently employed minimization parameter is the residual in one or all of the mass balance terms. An exception is a program devised by Siders and Romary (21), in which the areas between experimental and calculated titration curves are minimized. However, in this case refinement is accomplished by incremental variation of each constant and is limited to four constants. Specialized methodology has also been employed for spectral determination of protonation constants (22–25).

This algorithm for the determination of protonation constants differs from those used previously in two important ways: (*1*) the parameter computed at each titration volume is the pH and the parameter minimized is the mean sum of the squares of deviations between the calculated and observed pH values; (*2*) the final refinement of the protonation constants is based on a weighted algebraic mean of the deviations of each interval in which that protonation equilibrium is considered to dominate the reaction. In contrast, all of the previously employed programs compute and minimize either the deviation in "titer" (i.e., volume of base which must be added to achieve the observed pH) or the sums of the squared residuals of one or more of the mass balance equations, while refinement of the calculated parameters itself is based on procedures such as standard numerical analysis techniques for optimization of coefficients, gradient techniques, and Gaussian strategy. These refinement techniques serve to increase program running time as the square of parameters being fitted and can be avoided with our new algorithm.

In these laboratories, the FORTRAN program PKAS, which is based on this new algorithm, has been thoroughly tested since it was formulated more than ten years ago (26). It has evolved from its initial form on the IBM 360/5, CDC 1604A, and its latest version has been adapted as an interactive program for the Micromation CP/M microcomputer system. The algorithm is effective, fast, and very reliable. Program execution times on large computers are extremely rapid when compared to microcomputers, but for dedicated microcomputers, execution times on the order of several minutes are normal.

## The algorithm

### *Mathematical basis*

In the most general case, without making prior assumptions, there are two mass balance equations which must be satisfied at every volume addition point in a potentiometric equilibrium curve:

$$[1] \quad T_L = [L]A_1$$

$$[2] \quad T_H - B = [L]A_2$$

where

$$[3] \quad A_1 = 1 + K_1[H^+] + K_1K_2[H^+]^2 + \ldots\ldots + K_1 \ldots K_N[H^+]^N$$

$$[4] \quad A_2 = K_1[H^+] + 2K_1K_2[H^+]^2 + \ldots\ldots + NK_1 \ldots K_N[H^+]^N$$

and $T_L$ is the analytical concentration of the ligand; $T_H$ is the analytical concentration of ionizable hydrogen; $B = [H^+] - [OH^-] + [\text{titrant added}] + (\text{other corrections})$; and L is the symbol for the most deprotonated form of the ligand $H_NL$.

$$[5] \quad K_i = \frac{[H_iL]}{[H^+][H_{i-1}L]}$$

Dividing eq. [2] by eq. [1] eliminates [L] and gives eq. [6]

$$[6] \quad \frac{T_H - B}{T_L} = \frac{A_2}{A_1}$$

Given a set of protonation constants, $K_i$'s, this simple equation of order $N + 1$ in $[H^+]$ is most efficiently solved for $[H^+]$ at any degree of neutralization by the Newton–Raphson method (27) with the use of the following technique. Define a function $F$ from [6], such that $F = 0$ when the correction solution to [6] in $[H^+]$ is determined.

$$[7] \quad F = \frac{T_H - B}{T_L} - \frac{A_2}{A_1}$$

The iterative methodology involves the determination of the derivative $\partial F/\partial[H^+]$ at an initially estimated value of $[H^+]$. Explicitly stated:

$$[8] \quad F' = \frac{\partial F}{\partial[H^+]} = -\frac{1}{T_L}\frac{\partial B}{\partial[H^+]} - \frac{1}{A_1}\frac{\partial A_2}{\partial[H^+]} + \frac{A_2}{A_1^2}\frac{\partial A_1}{\partial[H^+]}$$

where

$$\frac{\partial B}{\partial[H^+]} = 1 + \frac{K_W}{[H^+]^2}$$

and $\partial A_1/\partial[H^+]$ and $\partial A_2/\partial[H^+]$ may be obtained directly from eqs. [3] and [4] by differentiation. The equation for the $j$th iteration is

$$[9] \quad [H^+]_j = [H^+]_{j-i} - \frac{F}{F'}$$

Can. J. Chem. Downloaded from www.nrcresearchpress.com by 210.87.254.40 on 09/06/12
For personal use only.

When $[H^+]$ is found, the refinement is terminated, and the next experimental point is considered. In general it takes about 2–5 iterations per point for part per million convergence.

*Strategy*

The following strategy is employed in the refinement of $N$ protonation constants for the potentiometric equilibrium curve of a given ligand.

(*1*) Identify $N$ segments $S_i$ of the experimental curve according to "$a$" value, where $a$ = moles of base added to the experimental solution per mol of ligand present. Thus $0 < a \leq 1$ would constitute $S_1$; $1 < a \leq 2$ constitutes $S_2$; etc.

(*2*) Formulate initial tentative values of each $\log K_i$ corresponding to the midpoint pH value in each $S_i$. Since protonation constants are considered (not $pK_a$'s), $\log K_1 = \text{pH}(S_N)$, $\log K_2 = \text{pH}(S_N - 1)$, ..., and $\log K_N = \text{pH}(S_1)$, where $\text{pH}(S_i)$ represents the pH at the midpoint of each segment $S_i$. These values of $K_i$ are the internally determined first approximations of the protonation constants to be refined.

(*3*) Calculate a potentiometric equilibrium curve using the mathematical algorithm given above (eq. [9]).

(*4*) Determine the statistics: (*a*) calculate the standard deviation in pH residuals for the *entire curve* (SD). This is a measure of closeness of fit and is a criterion for deciding when to stop adjusting protonation constants; (*b*) calculate the (weighted) average deviation of pH residuals for *each segment* $A_i$. Since this is an average deviation, $A_i$ is a signed quantity.

(*5*) Adjust each protonation constant according to the average deviation. $\log K_1 = \log K_1 + A_N$; $\log K_2 = \log K_2 + A_{N-1}$; ...; $\log K_N = \log K_N + A_1$.

(*6*) Repeat steps *3–5* until SD for the entire curve cannot be minimized by further refinement. Experience shows that when successive SD's vary by less than one part per thousand refinement is complete.

## Discussion

The new algorithm described above is completely reliable and does not collapse under any circumstances. Furthermore, it is very easy to implement and is versatile in that it can be easily utilized for other purposes such as metal–chelate protonation or deprotonation reactions to form species such as $MLH_i$, and $ML(OH)_i$. Since this algorithm was first employed in these laboratories (26), a number of practical considerations have emerged which should be taken into account to achieve the most precise calculations.

An option should be included in order to discard points near the inflections of the potentiometric curves from consideration. On the other hand, when the compounds are pure substrates it has been repeatedly verified that the number of discarded points near integral "$a$" of neutralization values (moles of base or acid added per mole of ligand) can be kept to a minimum.

The weighting scheme during the calculation of average residual $A_i$ should favor the points near the middle of each segment of the potentiometric curves more heavily than those nearer the integral values of $a$. However, a uniform procedure of discarding values within 0.2 "$a$" values around each integral $a$ value (i.e., consider only $0.2 < a < 0.8$, $1.2 < a < 1.8$, $2.2 < a < 2.8$, etc.) without weighting also gives very rapid convergence accompanied by only a trivial increase in refinement error.

Experience has also revealed one pitfall which results mostly from employing computer programs in "black-box" style. When one considers very low protonation constants, or very high protonation constants, situations arise when the pH data may be mostly out of range of the values of the protonation constants being calculated. Thus in the former case, the ionization may be complete or virtually complete. Refinement by the above algorithm would give rise to constant ($\log K_N$ and/or $\log K_{N-1}$) which may be as much as 0.5 log value too high or two low, as the result of very slight inaccuracies in pH measurement. For alkaline solutions, $\log K_1$ could be much larger than the high pH data and the computed values would be off considerably from the correct value depending on the value of $pK_W$, which determines the concentration of free hydroxide ion. Other errors would result from the pH measurement itself and the possible presence of carbonate. In this version of PKAS, the program prints a message warning the user that the data used as the basis for the calculation may be in question for the extreme (high or low) protonation constants.

An important feature of the algorithm is that the values of pH calculated are exact for the experimental concentration of alkali hydroxide added. The fact that pH values are calculated, but not the added reagent concentration (or volume of base), results in definite advantages, because the pH in potentiometry is the measured probe for the equilibrium under investigation, and it is more natural to fit this variable with the best calculated set of protonation constants. When exact, theoretically calculated potentiometric data are submitted to the algorithm in the program PKAS, and the values of

Can. J. Chem. Downloaded from www.nrcresearchpress.com by 210.87.254.40 on 09/06/12
For personal use only.

log $K_i$'s are reproduced exactly to $\sigma \sim 0.0003$ log units. Most of this residual error arises because the exact input is rounded to 0.001 log units, which is the pH reading limit of research pH meters. When the same input data were randomized to $\pm 0.07$ pH unit, then the protonation constants which resulted were good to $\pm 0.01$ log unit.

The program PKAS, which is the only one that currently employs this algorithm, is adapted for interactive execution. For convenience it requires a simple data file (disk in our case, card if desired) in which the first line is an identifying title card using 80 alphameric characters, while the remaining lines are pairs of volume base and pH. All of the remaining parameters are input as answers to questions as they appear on the CRT screen. These are in order:

1. Millimoles?
2. Molarity base?
3. Initial volume (mL)?
4. Number of dissociable protons on neutral ligand?
5. Number of additional protonations to be considered?
6. Fraction of "*a*" value to be excluded from computation on each end of segment?
7. Type "0" to skip remaining options. Type "1" to consider remaining options.

At this point the program goes into execution when "0" is entered and results are printed out when the calculation is finished. Otherwise, when "1" is entered, more input parameters can be entered, as follows:

8. Normality of excess acid added?
9. Volume of excess acid added?
10. Salt, such as disodium EDTA (2.0)?
11. pH correction?
12. p$K_W$?
13. Percent $CO_2$ in base?
14. First $CO_3^{2-}$ protonation constant?
15. Second $CO_3^{2-}$ protonation constant?

When the computation is complete, an option is presented to change any of the initial parameters and to rerun the program to see whether the fit can be improved or to obtain clues as to why the fit was not satisfactory. The most useful parameters to adjust are the millimoles of ligand and added excess acid. It has been observed in previous experiences that virtually all ligands possess molecular weights in general varying from ~1% to 5% higher than those computed from their molecular formulas. The source of this discrepancy is usually either interstitial (trapped) moisture or some neutral impurity such as NaCl or non-volatile solvent. Nevertheless, adjusting the calculated millimoles by the necessary amount makes possible the calculation of the exact molecular weight, which is required for exact matching of metal/ligand stoichiometry in subsequent stability constant work.

In a similar fashion, hydrochlorides or hydrobromides of bases are frequently found to contain small deficiencies or excesses of acid. This is usually the result of an interstitially trapped quantity of HX or may be caused by the cocrystallization of other sparingly soluble forms of polyhydrohalides containing one more or less hydrohalide molecule. For example, a compound bis-tren hexahydroperchlorate (28) was found to possess a formulation of $BT \cdot 6.028HClO_4$. In this case 82 titration points were considered, to give a $\sigma$ fit = 0.0008 in pH.

Finally, since the availability of self-contained microcomputers has proliferated to the point where almost all research laboratories have access to one, it was considered important to indicate how the common overflow problem was solved for the present systems. A real number $e$ accommodated in the Micromation CP/M system is limited to $10^{-38} \leq e \leq 10^{+38}$ in size. During routine scientific calculation in general, and evaluation of equilibrium expressions in particular, standard programming often gives rise to overflow. For example, at pH 10, $[H^+] = 10^{-10}$ and the last term of equations such as [3] or [4] would produce an underflow since $[H^+]^4$ in this case is $10^{-40}$ which is smaller than $10^{-38}$. A similar situation would occur in larger computer systems where often the limits are $10^{-76}$ to $10^{+76}$. Here the overflow would occur for $[H^+]^8$ at pH 10. One alternative which is practiced in the programming field is to go to logarithmic routines or other devices to maintain records of magnitudes. In order to circumvent this often fatal limitation a simple expedient was developed for this system whereby the evaluation of $A_1$ and $A_2$ in eqs. [3] and [4] and similar expressions were evaluated as if they were written:

$$[10] \quad A_1 = 1 + (K_1[H^+]) + (K_1[H^+])(K_2[H^+]) + (K_1[H^+])(K_2[H^+])(K_3[H^+]) + \ldots$$

$$[11] \quad A_2 = (K_1[H^+]) + 2(K_1[H^+])(K_2[H^+]) + 3(K_1[H^+])(K_2[H^+])(K_3[H^+]) + \ldots..$$

The products of the terms within the parentheses can very seldom exceed the CP/M number size limitation.

*Applications to multidentate ligands*

Table 1 presents a partial list of multidentate ligands of varying basicity for which the reported protonation constants were calculated with pro-

Can. J. Chem. Downloaded from www.nrcresearchpress.com by 210.87.254.40 on 09/06/12
For personal use only.

TABLE 1. Multidentate ligands for which protonation constants were determined with FORTRAN program PKAS

| Ligand | Type | log $K_1^H$ | log $K_2^H$ | log $K_3^H$ | log $K_4^H$ | log $K_5^H$ | log $K_6^H$ | log $K_7^H$ | log $K_8^H$ | Ref. |
|---|---|---|---|---|---|---|---|---|---|---|
| | L | 9.68 | 9.09 | 6.58 | 3.28 | | | | | 29 |
| 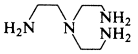 | L | 10.17 | 9.47 | 8.43 | | | | | | 28 |
| | L | 9.85 | 9.27 | 8.19 | 5.08 | 3.43 | | | | 30 |
| 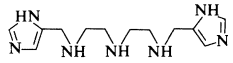 | L | 9.22 | 8.18 | 4.91 | 3.90 | 2.92 | | | | 31 |
| 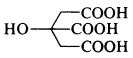 | $H_3L$ | 5.74 | 4.36 | 2.91 | | | | | | 32 |
| 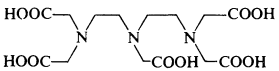 | $H_5L$ | 10.56 | 8.64 | 4.29 | 2.74 | 2.11 | | | | 32 |
| 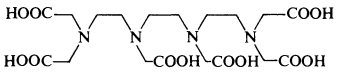 | $H_6L$ | 10.63 | 9.58 | 6.17 | 4.07 | 2.78 | 2.20 | | | 32 |
| 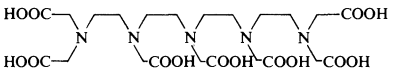 | $H_7L^a$ | 10.76 | 9.87 | 8.13 | 4.75 | 3.78 | 2.69 | 2.00 | | 33 |
| 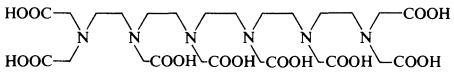 | $H_8L^b$ | 10.85 | 9.96 | 8.85 | 6.20 | 4.48 | 3.57 | 2.52 | 2.02 | 33 |
| 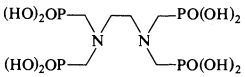 | $H_8L$ | 12.01 | 9.02 | 7.42 | 5.88 | 4.77 | 2.82 | 1.24 | ppt. | 34 |
| 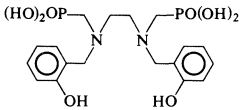 | $H_6L$ | 13.57[c] | 11.48[c] | 9.67 | 7.24 | 5.31 | 3.61 | | | 35 |
| 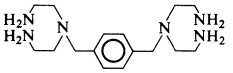 | L | 10.06 | 9.71 | 9.11 | 8.57 | 1.85 | 1.2 | | | 36 |
| 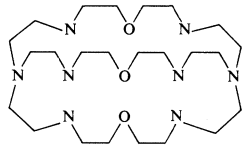 | L | 9.89 | 9.17 | 8.26 | 7.89 | 7.27 | 6.60 | | | 28 |

[a]Two additional protonations 1.70, 1.40.
[b]Two additional protonations 1.70, 1.40.
[c]Determined spectrophotometrically.

Can. J. Chem. Downloaded from www.nrcresearchpress.com by 210.87.254.40 on 09/06/12
For personal use only.

gram PKAS. The results obtained indicate that with this algorithm there is no practical limit to either the number of equilibrium constants or the degree of overlapping (closeness of p$K$'s) that may be handled. In using this method the equilibrium constants of ligands with more than six protonation constants were calculated as easily and smoothly as those of ligands containing only two or three p$K$'s. In the worst cases listed in Table 1 it was found that $\sigma = 0.017$ (log units for the entire pH fit), while in the more favorable cases $\sigma \cong 0.005$ log units. The last entry in Table 1 ("bis-tren") was calculated with the $\sigma = 0.00083$ log units. The deviations in $\sigma$ values apparently were due to the presence of small amounts of impurities in certain ligands. Indeed, the degree to which the data could be refined may be considered a measure of the analytical purity of the ligand.

Most of the ligands in Table 1 also form a series of protonated metal chelates of the type MHL, $MH_2L$, $MH_3L$, etc., as well as a number of hydrolyzed metal chelates such as MOHL and $M(OH)_2L$ with certain metal ions. In most cases cited in the table the protonation constants for the formation of these species have also been calculated with program PKAS.[2]

## Acknowledgement

This research was supported by Grant No. A-259 from The Robert A. Welch Foundation.

1. H. Rossotti. The study of ionic equilibrium. Longman, London. 1978.
2. H. Rossotti. Chemical applications of potentiometry. D. Van Nostrand, London. 1969.
3. F. J. C. Rossotti and H. Rossotti. The determination of stability constants. McGraw Hill Book Co., New York. 1961.
4. F. J. C. Rossotti, H. S. Rossotti, and R. J. Whewell. J. Inorg. Nucl. Chem. **33**, 2051 (1971).
5. C. W. Childs, P. S. Hallman, and D. D. Perrin. Talanta, **16**, 1119 (1969).
6. A. Sabatini and A. Vacca. J. Chem. Soc. Dalton, 1693 (1972).
7. L. G. Sillen. Acta Chem. Scand. **16**, 159 (1962).

[2]Complete program is available, at a nominal charge, from the Depository of Unpublished Data, CISTI, National Research Council of Canada, Ottawa, Ont., Canada K1A 0S2.

8. I. G. Sayce. Talanta, **14**, 1397 (1967).
9. A. Sabatini, A. Vacca, and P. Gans. Talanta, **21**, 53 (1974).
10. N. Ingri and L. G. Sillen. Arkiv. Kemi, **23**, 97 (1965).
11. I. Ting-Po and G. H. Nancollas. Anal. Chem. **44**, 1940 (1972).
12. D. D. Perrin and I. G. Sayce. Talanta, **14**, 833 (1967).
13. D. D. Perrin and I. G. Sayce. J. Chem. Soc. A, 83 (1967).
14. R. S. Tobias and A. A. Hugus. J. Phys. Chem. **65**, 2165 (1961).
15. D. J. Legget. Talanta, **24**, 535 (1977).
16. A. E. Martell and R. M. Smith. Critical stability constants. Vol. 1. Plenum Publishing Corp., New York. 1974.
17. A. Johansson and S. Johansson. Analyst, **104**, 601 (1979).
18. G. Arena, E. Rizzarelli, S. Ssmmartano, and C. Rigano. Talanta, **26**, 1 (1979).
19. M. Wozniak and G. Nowogrocky. Talanta, **25**, 633 (1978).
20. W. A. E. McBryde. Talanta, **21**, 979 (1974).
21. P. D. Siders and J. K. Romary. J. Inorg. Nucl. Chem. **41**, 547 (1979).
22. K. Nagano and D. E. Metzler. J. Am. Chem. Soc. **89**, 2891 (1967); J. A. Thomson and G. F. Atkinson. Talanta, **18**, 817 (1971).
23. D. J. Leggett and W. A. McBryde. Talanta, **22**, 781 (1975).
24. G. Hanisch, T. Kaden, and A. D. Zuberbuhler. Talanta, **26**, 563 (1979).
25. M. Meloun and J. Cermak. Talanta, **26**, 569 (1979).
26. R. J. Motekaitis, I. Murase, and A. E. Martell. J. Inorg. Nucl. Chem. **33**, 3353 (1971).
27. D. D. McCracken. A guide to Fortran VI programming. John Wiley, New York. 1965.
28. R. J. Motekaitis, E. Watanabe, J. M. Lehn, and A. E. Martell. To be published.
29. R. Nakon and A. E. Martell. J. Am. Chem. Soc. **94**, 3026 (1972).
30. R. Nakon and A. E. Martell. J. Inorg. Nucl. Chem. **34**, 1365 (1972); W. R. Harris, I. Murase, J. H. Timmons, and A. E. Martell. Inorg. Chem. **17**, 889 (1978).
31. J. H. Timmons, W. R. Harris, I. Murase, and A. E. Martell. Inorg. Chem. **17**, 2192 (1978).
32. W. R. Harris and A. E. Martell. Inorg. Chem. **15**, 713 (1976).
33. P. Letkeman and A. E. Martell. Inorg. Chem. **18**, 1284 (1979).
34. R. J. Motekaitis, I. Murase, and A. E. Martell. Inorg. Nucl. Chem. Lett. **7**, 1103 (1971); R. J. Motekaitis, I. Murase, and A. E. Martell. Inorg. Chem. **15**, 3403 (1976).
35. D. T. MacMillan, I. Murase, and A. E. Martell. Inorg. Chem. **14**, 468 (1975).
36. C. Y. Ng, A. E. Martell, and R. J. Motekaitis. J. Coord. Chem. **9**, 255 (1979).

# The infrared, Raman, and resonance Raman spectra and normal coordinate analysis of methyl and ethyl dithioacetate[1]

J. J. C. TEIXEIRA-DIAS AND V. M. JARDIM-BARRETO
*University Chemical Laboratory, Coimbra, Portugal*
AND
Y. OZAKI, A. C. STORER, AND P. R. CAREY[2]
*Division of Biological Sciences, National Research Council of Canada, Ottawa, Ont., Canada K1A 0R6*

Received May 21, 1981

J. J. C. TEIXEIRA-DIAS, V. M. JARDIM-BARRETO, Y. OZAKI, A. C. STORER, and P. R. CAREY. Can. J. Chem. **60**, 174 (1982).

Infrared, Raman, and resonance Raman data are reported for ethyl and methyl dithioacetate together with data for their isotopically substituted analogs: $CD_3C(=S)SCH_3$, $CH_3C(=S)SCD_3$, $^{13}CH_3C(=S)SCH_3$, $CH_3{}^{13}C(=S)SCH_3$, $CD_3C(=S)SCH_2CH_3$, $CH_3C(=S)SCD_2CH_3$, and $CH_3{}^{13}C(=S)SCH_2CH_3$. Based on these data and a normal coordinate analysis of methyl dithioacetate, assignments are proposed for the majority of bands appearing in the vibrational spectra. Using excitation wavelengths in the 324–356 nm region strong intensity enhancement is observed for Raman bands near 1195, 1100, 730, and 580 $cm^{-1}$ which are assigned to stretching motions of the CCSSC skeleton. Raman excitation profiles are reported for the 1197 and 581 $cm^{-1}$ bands of ethyl dithioacetate and the electronic absorbance peak near 305 nm is identified as the source of resonance Raman intensity enhancement.

J. J. C. TEIXEIRA-DIAS, V. M. JARDIM-BARRETO, Y. OZAKI, A. C. STORER et P. R. CAREY. Can. J. Chem. **60**, 174 (1982).

On rapporte les des spectres infrarouge, Raman et de résonance Raman des dithioacétates d'éthyle et de méthyle ainsi que les données relatives à leurs analogues substitués par des isotopes: $CD_3C(=S)SCH_3$, $CH_3C(=S)SCD_3$, $^{13}CH_3C(=S)SCH_3$, $CH_3{}^{13}C(=S)SCH_3$, $CD_3C(=S)SCH_2CH_3$, $CH_3C(=S)SCD_2CH_3$, et $CH_3{}^{13}C(=S)SCH_3CH_3$. En fonction de ces données et d'une analyse des coordonnées normales du dithioacétate de méthyle, on propose une identification de la plupart des bandes qui apparaissent dans le spectre de vibration. En utilisant les longueurs d'onde d'excitation dans la région de 324–356 nm, on a observé une forte augmentation de l'intensité des bandes Raman près de 1195, 1100, 730 et 580 $cm^{-1}$ que l'on attribue à des mouvements d'élongation du squelette CCSSC. On rapporte les profils d'excitation Raman pour les bandes à 1197 et 581 $cm^{-1}$ du dithioacétate d'éthyle et on a identifé le pic d'absorption électronique près de 305 nm comme étant la cause de l'augmentation de l'intensité de la résonance Raman.

[Traduit par le journal]

## Introduction

The work presented in this series of papers (this paper and refs. 1 and 2) was motivated by our study of enzyme–substrate complexes using resonance Raman (RR) spectroscopy. In a recent report (3) it was shown that dithioesters (—C(=S)—S—) constitute an ideal RR probe for monitoring those bonds which are undergoing catalytic transformation within an enzyme's active site. The dithioester group forms a transient covalent linkage between enzyme and substrate at the instant of catalysis (4). Since the dithioester moiety has an intense $\pi \rightarrow \pi^*$ absorption band near 310 nm, excitation by 324 nm $Kr^+$ laser irradiation produces a RR spectrum of the —C(=S)—S— group while the normal Raman spectra of the enzyme (which is relatively enormous and has a MW of ~24 000 daltons) and aqueous solvent are too weak to be detected. The utility of the approach depends on our ability to interpret the RR spectrum of the dithioester function. The knowledge of the vibrational (5–10) and chemical (11) properties of dithioesters is minimal and thus we have instigated a series of spectroscopic and chemical studies which will act as a basis for understanding the spectra and properties of the enzyme–substrate intermediates.

This, the first paper in the present series, sets out to determine and assign the vibrational spectra of two of the simplest dithioesters, namely, methyl and ethyl dithioacetate. For these molecules isotopic substitutions and Raman, RR, and infrared data are used to help establish a complete description of the vibrational properties. Additionally, extensive normal coordinate analyses were undertaken for methyl dithioacetate to arrive at a quantitative understanding of the normal mode structure for the heavy atom skeleton. Detailed assignments and RR studies have not been reported hitherto. In the following paper (1) the vibrational spectra of dithioesters that are slightly more complex than methyl and ethyl dithioacetate are discussed with special attention being paid to the consequences of rotational isomerism about

C–C(=S) and —S–C

bonds. The third paper in the series (2) deals with more complex dithioesters which act, in some

[1]NRCC No. 19738.
[2]To whom all correspondence should be addressed.

0008-4042/82/020174-16$01.00/0
©1982 National Research Council of Canada/Conseil national de recherches du Canada

Can. J. Chem. Downloaded from www.nrcresearchpress.com by 210.87.254.105 on 09/06/12
For personal use only.

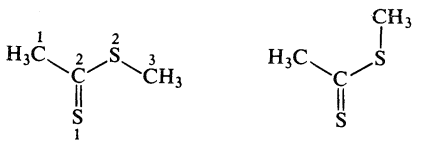


FIG. 1. The s-*cis* and s-*trans* conformers of methyl dithioacetate.

respects, as models for the catalytic region in enzyme substrate complexes.

The conformations and concomitant normal mode structures of dialkyl carboxylic acid esters have been studied in detail and some of the conclusions have been reviewed by Jones and Owen (12). In contrast, the corresponding dithioesters have been little investigated. There is, however, enough evidence in the literature to establish with reasonable certainty the preferred conformer for dithioesters. Infrared and microwave investigations (13) of methyl thiol formate ($HC(=O)SCH_3$) and infrared and Raman studies of $CH_3(=S)SCH_3$ (5) indicated that only the s-*cis* conformer (Fig. 1), with the heavy atoms in a single plane, was present in these compounds. Further support for the *cis* conformer in RC(=O)SR′, RC(=S)OR′, and RC(=S)SR′ came from dipole moment measurements (14–17). Taking this evidence into account we have assumed, unless otherwise stated, that dithioesters are in the s-*cis* conformation.

## Experimental

*Methods*

Raman measurements with visible excitation were recorded using a Jarrell-Ash 25-400 laser Raman spectrophotometer equipped with a RCA 31034A-02 photomultiplier tube and photon-counting detection. The excitation sources were Spectra-Physics model 164 $Ar^+$ and $Kr^+$ lasers. The apparatus used to obtain the Raman spectra with ultraviolet excitation consisted of a Coherent Radiation 3000 K or 2000 K $Kr^+$ laser and a Spex 0.5-m double spectrometer with direct current detection. Peak frequencies were calibrated using emission lines from Ar, Xe, Kr, and Ne lamps and are believed to be accurate to $\pm 2$ $cm^{-1}$ for well-resolved bands.

The resonance Raman spectra were recorded using a flow cell technique (18) to avoid photodecomposition or photoisomerization. A rotating cell was employed for measuring most of the Raman spectra excited by visible irradiation. The spectra showed excellent reproducibility and neither photodecomposition nor photoisomerization were observed. Band intensities were measured by band heights, and intensities reported for the excitation profiles are the average of at least two experiments. Two concentrations of ethyl dithioacetate in $CCl_4$ were prepared for the measurements of the excitation profiles. For the excitation in the range of 356.4–647.1 nm a solution containing 0.96% (v/v) ethyl dithioacetate and 5.8% (v/v) cyclohexane was used. For excitation wavelengths in the range 324.0–356.4 nm a solution containing 0.0033% (v/v) ethyl dithioacetate and 2.4% (v/v) cyclohexane was used. The cyclohexane band at 1033 $cm^{-1}$ was taken as an internal reference. Since the internal standard peak was close to the measured bands and the solutions were of low optical density neither a $\nu^4$ correction nor a self-absorption correction was necessary.

Absorption spectra were recorded using Cary 118 and 219 spectrophotometers. The infrared spectra were recorded by means of a Perkin Elmer 180 spectrophotometer. The methods used in the normal coordinate analysis of methyl dithioacetate are described below under "normal coordinate calculations for methyl dithioacetate".

*Materials*

The dithioesters were synthesised by the procedure outlined for ethyl dithioacetate by Marvel *et al.* (6). For the synthesis of methyl dithioacetate the gaseous methane thiol was liquified by passage down a column jacketed with a dry ice – acetone mixture. The addition of dry HCl to the acetonitrile – methane thiol solution was performed at −10°C. The $^{13}C$-substituted dithioesters were synthesised from acetonitrile labelled in the appropriate position. The deuterated dithioesters were synthesised from either deuterated acetonitrile, or, deuterated ethane or methane thiol prepared from the respective deuterated alkyl iodides (19) (alkyl iodides were used in place of the dialkyl sulphates in the published procedure). Purity of the samples was checked by nmr and elemental analysis of the dithioesters agreed to within 1% of the expected values.

## Results and discussion

*The absorption spectra*

The absorption spectra of methyl and ethyl dithioacetate are similar and both have intense features near 210 and 305 nm and a weak band near 450 nm. The exact positions of the $\lambda_{max}$'s and the extinction coefficients for ethyl dithioacetate in acetonitrile are 209 nm ($\log_{10} \varepsilon = 3.85$), 305.5 nm ($\log_{10} \varepsilon = 4.07$), and 452 nm ($\log_{10} \varepsilon = 1.28$) and for methyl dithioacetate the $\lambda_{max}$'s are at 208, 302, and 446 nm (the extinction coefficients for methyl dithioacetate were not measured but are very similar to those of the ethyl analog). The features near 305 and 450 nm in dithioester absorption spectra have been assigned to $\pi \rightarrow \pi^*$ and $n \rightarrow \pi^*$ transitions respectively (20, 21) and it is likely that the band near 210 nm is due to a higher energy $\pi \rightarrow \pi^*$ transition. The $\pi \rightarrow \pi^*$ transition near 305 nm assumes a special importance since, in the present work, we show that this is the electronic absorbance responsible for RR enhancement. Hence, the 305 nm transition provides the basis of the specific intensity enhancement we observe in dithioester-macromolecules.

*Vibrational spectra of methyl dithioacetate*

Raman and infrared spectra of methyl dithioacetate and its isotopically substituted derivatives in the liquid phase are shown in Figs. 2 and 3 and the observed frequencies are listed in Table 1. Below 1200 $cm^{-1}$ the Raman spectrum of methyl dithioacetate is characterized by three intense bands at 1194, 864, and 580 $cm^{-1}$ while the infrared

Can. J. Chem. Downloaded from www.nrcresearchpress.com by 210.87.254.105 on 09/06/12
For personal use only.

Can. J. Chem. Downloaded from www.nrcresearchpress.com by 210.87.254.105 on 09/06/12
For personal use only.

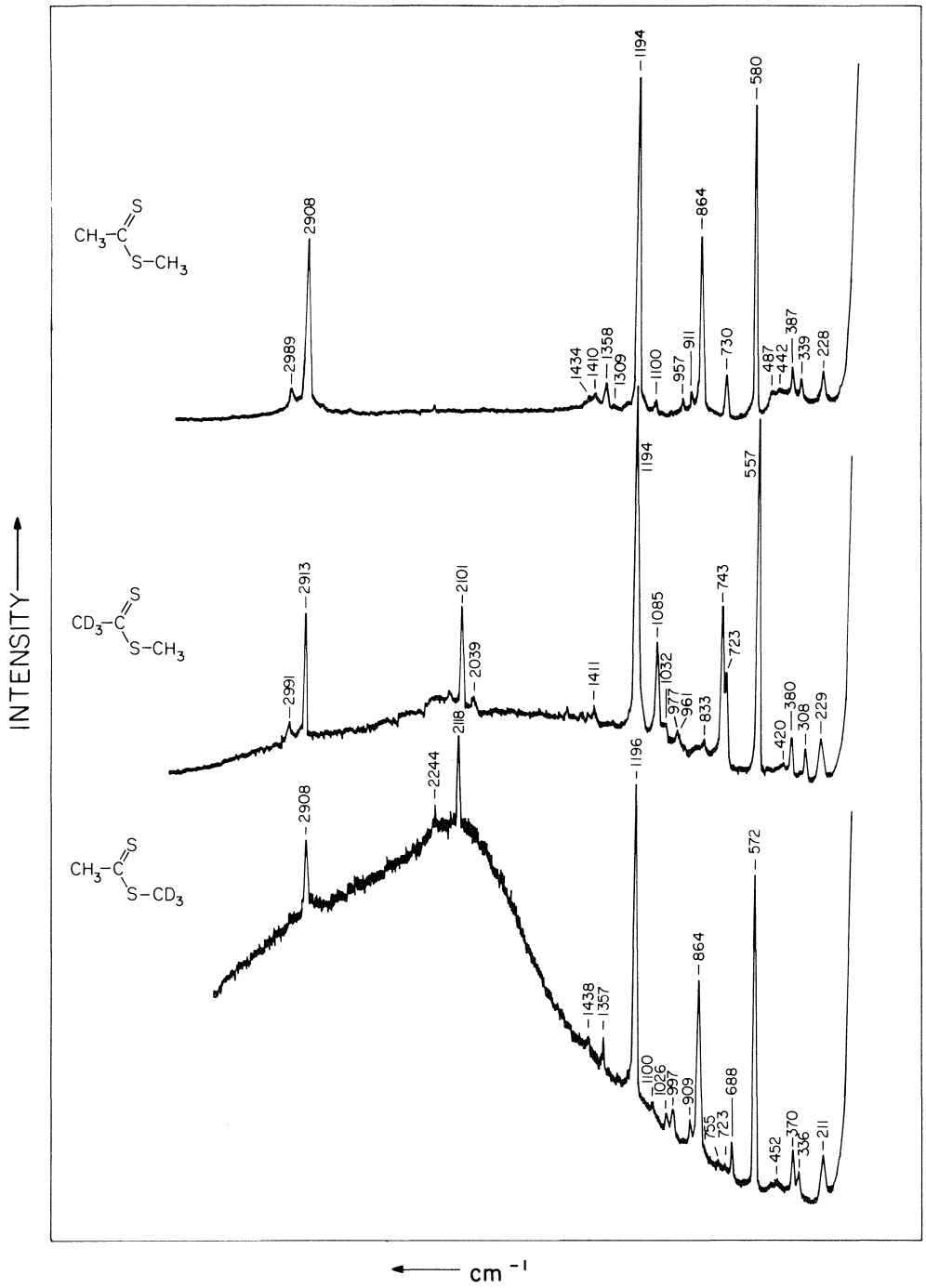


FIG. 2. The 514.5 nm excited Raman spectra of methyl dithioacetate and its isotopically substituted derivatives in the liquid state. Instrumental conditions: laser power, 50 mW; spectral slit width, 8 $cm^{-1}$; scan speed, 0.5 $cm^{-1}$ $s^{-1}$.

spectrum has four intense bands at 1195, 1100, 865, and 580 $cm^{-1}$. Almost all the Raman and infrared bands show individual shifts when various isotopic replacements are made. Upon deuterium substitution of the $CH_3$—C group, the Raman bands at 1434, 1358, and 1100 $cm^{-1}$ shift to the 1090–970 $cm^{-1}$ region while the bands at 911, 864, 730, 580, 387, and 339 $cm^{-1}$ are replaced by features at 833, 743, 723, 557, 380, and 308 $cm^{-1}$. The correspondence between the 730 and 723 $cm^{-1}$ bands in Fig. 2

Can. J. Chem. Downloaded from www.nrcresearchpress.com by 210.87.254.105 on 09/06/12
For personal use only.

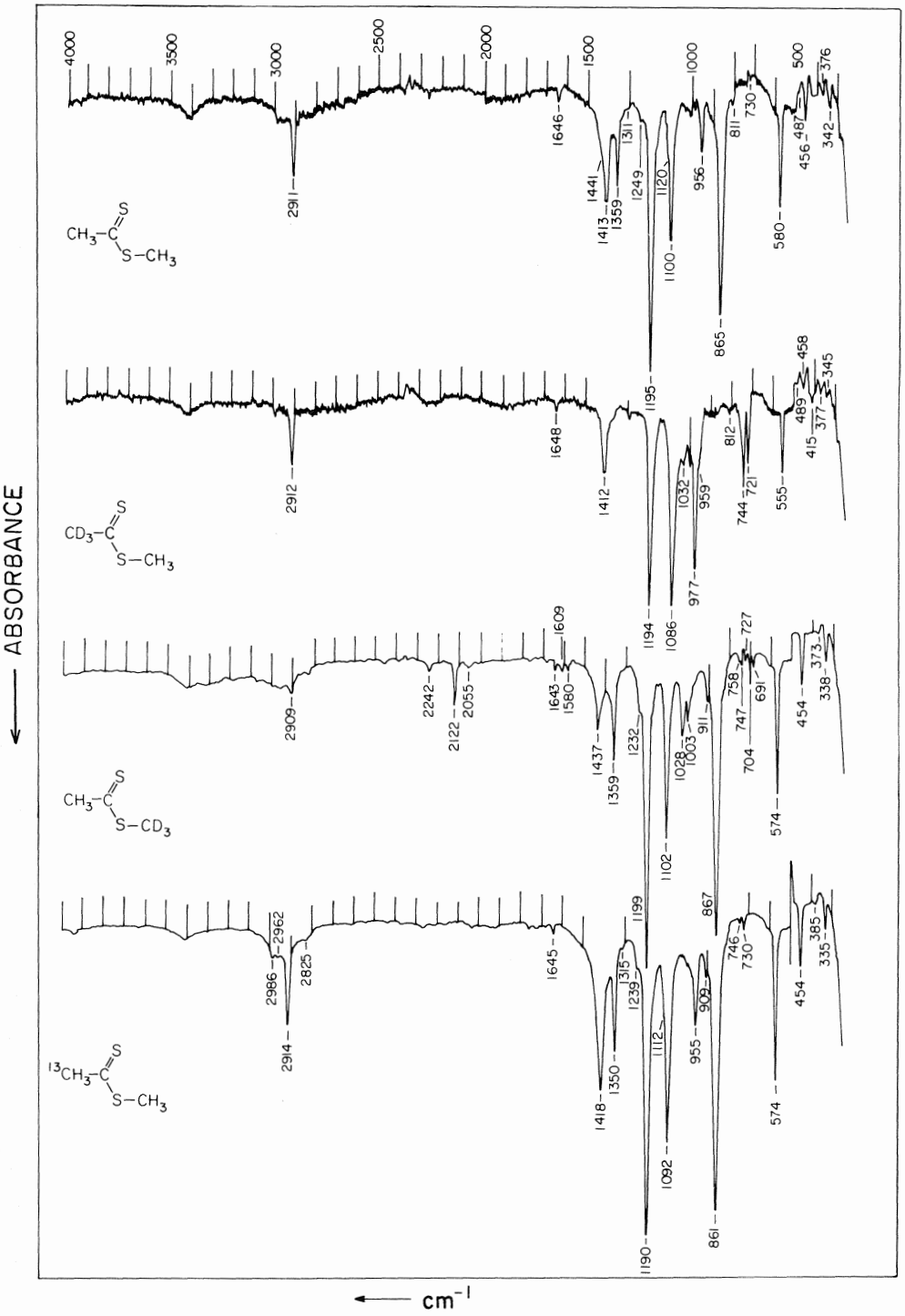


FIG. 3. The infrared spectra of methyl dithioacetate and its isotopically substituted derivatives in the liquid state.

(top and center) was confirmed by the measurement of polarized Raman spectra since only the 730 and 723 $cm^{-1}$ bands are depolarized in the 900–500 $cm^{-1}$ region. The new bands in Fig. 2 (center) at 2101 and 2039 $cm^{-1}$ result from shifts of the bands near 3000 $cm^{-1}$ in Fig. 2 (top). The infrared bands at 1441, 1359, 1100, 865, 730, and 580 $cm^{-1}$ exhibit a shift upon deuterium substitution of the $CH_3$—C

TABLE 1. Observed and calculated frequencies ($cm^{-1}$) for isotopically substituted $CH_3CSSCH_3$*

| $CD_3CSSCH_3$ | | $CH_3CSSCD_3$ | | $^{13}CH_3CSSCH_3$ | | $CH_3CSSCH_3$ | | |
|---|---|---|---|---|---|---|---|---|
| $\nu_{obs}$ | $\nu_{calc}$ | $\nu_{obs}$ | $\nu_{calc}$ | $\nu_{obs}$ | $\nu_{calc}$ | $\nu_{obs}$ | $\nu_{calc}$ | Potential energy distribution for $CH_3CSSCH_3$ |
| 2991 | 2992 | — | 2975 | 2986 | 2992 | 2989 | 2992 | $S_{20}(99)$ |
| — | 2990 | — | 2973 | — | 2990 | — | 2990 | $S_{21}(99)$ |
| 2913 | 2917 | 2908 | 2911 | 2962 | 2962 | — | 2975 | $S_{11}(99)$ |
| — | 2221 | 2244 | 2232 | — | 2961 | — | 2973 | $S_{12}(99)$ |
| — | 2217 | — | 2229 | 2914 | 2916 | 2908 | 2916 | $S_{19}(100)$ |
| 2101 | 2096 | 2118 | 2098 | — | 2908 | — | 2911 | $S_{10}(99)$ |
| — | 1447 | 1437 | 1433 | — | 1447 | — | 1447 | $S_{23}(69)$, $S_{25}(21)$ |
| 1412 | 1417 | — | 1400 | — | 1430 | 1434 | 1433 | $S_{14}(71)$, $S_{16}(20)$ |
| — | 1309 | 1359 | 1359 | 1418 | 1417 | 1413 | 1417 | $S_{23}(22)$, $S_{25}(71)$ |
| 1194 | 1193 | 1196 | 1196 | — | 1398 | — | 1400 | $S_{14}(21)$, $S_{16}(74)$ |
| 1086 | 1089 | 1102 | 1098 | 1350 | 1350 | 1359 | 1359 | $S_{13}(104)$ |
| — | 1037 | — | 1044 | — | 1309 | 1309 | 1309 | $S_{22}(105)$ |
| — | 1031 | 1028 | 1019 | 1190 | 1190 | 1194 | 1194 | $S_1(33)$, $S_2(44)$, $S_5(10)$ |
| 1000 | 1010 | — | 1002 | 1092 | 1095 | 1100 | 1098 | $S_1(24)$, $S_2(10)$, $S_3(55)$, $S_6(11)$ |
| 977 | 974 | 911 | 916 | — | 975 | — | 976 | $S_{24}(81)$ |
| 959 | 957 | 864 | 866 | 955 | 958 | 956 | 958 | $S_{26}(83)$ |
| 744 | 739 | 755 | 752 | 909 | 909 | 911 | 915 | $S_{17}(87)$ |
| 723 | 726 | 723 | 725 | 861 | 857 | 864 | 863 | $S_{15}(74)$, $S_3(10)$ |
| — | 677 | 688 | 686 | 730 | 729 | 730 | 730 | $S_4(87)$ |
| 555 | 555 | 574 | 572 | 574 | 574 | 580 | 582 | $S_1(25)$, $S_2(28)$, $S_3(26)$ |
| 415 | 412 | 454 | 456 | 454 | 458 | 456 | 459 | $S_8(30)$, $S_9(52)$ |
| 380 | 377 | 370 | 371 | 385 | 385 | 387 | 388 | $S_1(14)$, $S_2(13)$, $S_4(15)$, $S_5(22)$, $S_7(44)$ |
| 308 | 304 | 336 | 337 | 335 | 336 | 339 | 340 | $S_6(94)$ |
| 229 | 227 | 211 | 214 | 227 | 230 | 228 | 231 | $S_8(25)$, $S_{18}(12)$, $S_{27}(57)$ |
| 200 | 199 | — | 188 | — | 208 | — | 208 | $S_{18}(67)$, $S_{27}(22)$ |
| — | 170 | — | 181 | (200) | 200 | (200) | 200 | $S_3(15)$, $S_5(57)$, $S_7(35)$ |
| — | 137 | — | 131 | (170) | 157 | (170) | 157 | $S_8(38)$, $S_9(43)$, $S_{27}(12)$ |

*PED contributions less than 10% are ignored. Guessed experimental frequencies are in parentheses.

group. Taking the Raman and infrared data together it is suggested that the features at 911, 864, 730, 580, 387, and 339 in the Raman spectra of the $CH_3$—C compound correspond to the features at 833, 743, 723, 557, 380, and 308 $cm^{-1}$ respectively in the spectrum of the $CD_3$—C analog.

Upon deuterium substitution of the S—$CH_3$ group the Raman bands at 730, 580, 387, and 228 $cm^{-1}$ shift to 688, 572, 370, and 211 $cm^{-1}$, respectively. The shift from 730 to 688 $cm^{-1}$ was again confirmed by the measurement of polarized Raman spectra. The bands at 1410 and 957 $cm^{-1}$ also exhibit a shift. The bands at 2244 and 2118 $cm^{-1}$ result from the shifts of the bands which appear near 3000 $cm^{-1}$ in the spectra of the parent compound. Shifts of the infrared bands at 2911, 1413, 956, 730, and 580 $cm^{-1}$ are also observed for the S—$CD_3$ analog.

Only small amounts of the $^{13}C$-substituted compounds were synthesised. Consequently, we were able to obtain just the infrared and RR spectra of $^{13}CH_3C(=S)SCH_3$ and a poor quality RR spectrum of $CH_3{}^{13}C(=S)SCH_3$. The $^{13}C$ substitution in $^{13}CH_3C(=S)SCH_3$ brought about modest shifts in the infrared spectrum with the bands at 1441, 1359, 1195, 1100, 865, and 580 moving to 1418, 1350, 1190, 1092, 861, and 574 $cm^{-1}$ respectively.

The 324 nm excited RR spectra of 0.01% (v/v) acetonitrile solutions of methyl dithioacetate and its isotopically-substituted derivatives are shown in Fig. 4. Only five RR bands are observed in the 1300–500 $cm^{-1}$ region with two bands being prominent near 1200 and 585 $cm^{-1}$. In the RR spectrum the relative intensity of the 1106 $cm^{-1}$ band increases whereas that of the 872 $cm^{-1}$ band decreases compared to the normal Raman spectrum. In fact, the 1106 $cm^{-1}$ feature undergoes the highest degree of intensity enhancement — a factor of about 9000 fold upon going from 514.5 to 324 nm excitation (c.f. Fig. 8). Some of the bands observed in the Raman spectrum were obscured by the bands of acetonitrile or became too weak to detect under resonance conditions. The bands near 2900 $cm^{-1}$, for example, could not be observed in a 0.01% (v/v) deuterated acetonitrile ($CD_3CN$) solution under the RR condition. Upon deuterium substitution of the $CH_3$—C group, the RR features at 1106, 872, 732, and 585 $cm^{-1}$ shift in frequency as in the case of the normal Raman spectrum of the neat compound. Upon deuterium substitution of the S—$CH_3$ group the 732 $cm^{-1}$ band undergoes a large shift to 694 $cm^{-1}$ while the 585 $cm^{-1}$ band shows a smaller shift to 577 $cm^{-1}$. For $^{13}CH_3C(=S)SCH_3$ the bands at 1200, 1106, 872, and 585 $cm^{-1}$ exhibit small shifts

Can. J. Chem. Downloaded from www.nrcresearchpress.com by 210.87.254.105 on 09/06/12
For personal use only.

Can. J. Chem. Downloaded from www.nrcresearchpress.com by 210.87.254.105 on 09/06/12
For personal use only.

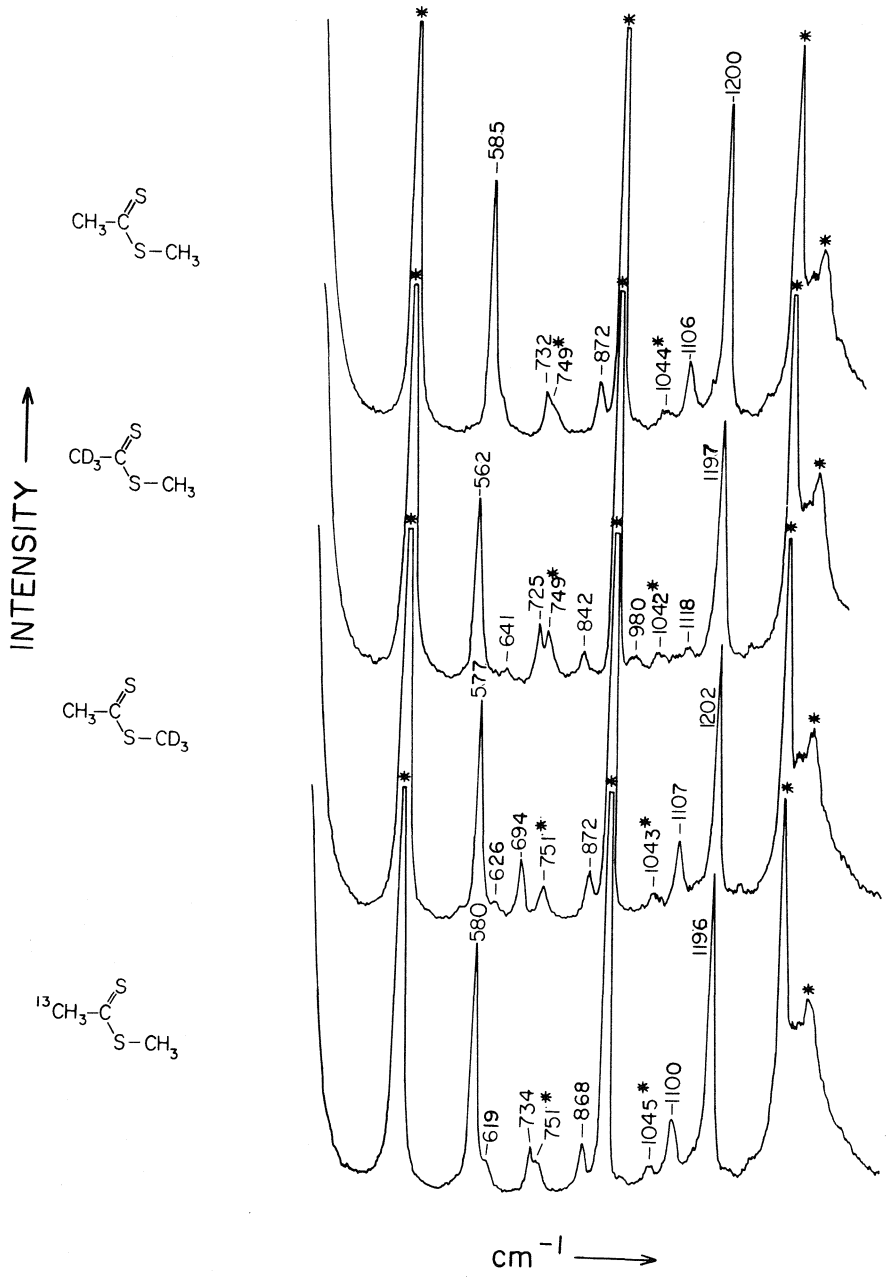


FIG. 4. The 324.0 nm excited RR spectra of methyl dithioacetate and its isotopically substituted derivatives in 0.01% (v/v) $CH_3CN$ solution. Features marked with an asterisk are due to $CH_3CN$. The RR spectrum of $CH_3$—$^{13}C$(=S)—S—$CH_3$ (not shown) has a steep base line due to strong luminescence; however, RR bands were observed at 1175, 1086, and 584 $cm^{-1}$. Instrumental conditions: laser power, 10 mW; spectral slit width, 8 $cm^{-1}$; scan speed, 0.75 $cm^{-1}$ $s^{-1}$.

compared to the parent compound (Fig. 4). However, for $CH_3{}^{13}C(=S)SCH_3$ the intense band found in the parent molecule at 1200 $cm^{-1}$ undergoes a striking shift to 1175 $cm^{-1}$ (data not shown). The band at 1106 $cm^{-1}$ also shifts to 1086 $cm^{-1}$ in the $^{13}C$=S molecule. In contrast, the band at 585 $cm^{-1}$ shifts little upon the $^{13}C$ substitution of the thiocarbonyl group. The measured value for $CH_3{}^{13}C(=S)SCH_3$ is 584 $cm^{-1}$ which, within experimental error, is identical to the value for the $^{12}C$ analog.

Raman spectra were also measured in 1.0% (v/v) acetonitrile solution using 514.5 nm excitation. The relative intensities and frequencies of the Raman bands in 1.0% (v/v) acetonitrile solution are very close to those of the Raman bands in the neat liquid. For example, the most intense band is seen at 1194

Can. J. Chem. Downloaded from www.nrcresearchpress.com by 210.87.254.105 on 09/06/12
For personal use only.

$cm^{-1}$ in the Raman spectrum of liquid and at 1197 $cm^{-1}$ in the Raman spectrum of 1.0% (v/v) acetonitrile solution. Therefore, it is possible to compare directly the 514.5 nm excited Raman spectra of the neat liquids with the 324.0 nm excited RR spectra of 0.01% (v/v) acetonitrile solutions.

*Normal coordinate calculations for methyl dithioacetate*

The normal coordinate analyses were performed using computer programs written by Fuhrer *et al.* (22) and adapted by two of us (J.J.C.T-D and V.M.J-B) to a Univac Sigma 5 computer. The programs were in three parts: CART which converts molecular structural parameters to cartesian coordinates, GMAT which sets up the kinetic energy matrix, and FPERT which calculates and refines the force constants using the least-squares method and the frequency data from several isotopic species.

The geometrical parameters assumed for methyl dithioacetate are listed in Table 2 and were based on previously published data for thioacetic acid (23) and dithioformic acid (24). The numbering of the C and S atoms is shown in Fig. 1. The carbon–sulfur skeleton was assumed to take up the planar S-*cis* conformation shown in Fig. 1, the methyl groups were assigned tetrahedral angles and the CH bond length fixed at the value given by Curl (25).

Table 3 shows the definition of internal coordinates for methyl dithioacetate. Apart from the usual changes in bond lengths and bond angles we have included three torsion coordinates around the C—C, C—S, and S—C bonds and an out-of-plane wagging coordinate for C=S (26).

Before starting the calculation of force constants it is necessary to eliminate any redundant coordinates. In the case of methyl dithioacetate, the internal coordinates we have defined exceed the number of vibrational degrees of freedom ($3N - 6 = 27$) by three. One can separate the redundant coordinates by taking linear combinations of the bending coordinates so that three of them correspond to the sums of the bond angle changes around the atom centres where three or more bonds are coincident (these sums are identically zero). Table 4 shows the new set of internal coordinates grouped in a vector array $S$.

Another remark about the definition of our $S$ coordinates is necessary as we did not use the molecular symmetry group ($C_s$) and preferred instead the highest local symmetry coordinates consistent with the methyl groups ($C_{3v}$ symmetry). While the particular choice of any linear and orthogonal transformation among the basis coordinates is irrelevent as regards to the calculated eigenvalues and to the information contained in the final PED matrix, our choice seems to be justified as we are mainly fitting vibrational frequencies taken from condensed phase spectra and both methyl groups should be considered, for that purpose, to display axial symmetry around the C—C and S—C bonds. Moreover, the primary objective of this work is to analyse the motions of the carbon–sulfur skeleton rather than to accurately reproduce the observed vibrational frequencies of the entire molecule.

The force field adopted in these calculations is the simplified general valence force field (SGVFF). This form of the general valence force field contains a reduced number of interaction constants compatible with a good fit of the fundamental vibrational frequencies. In addition to all the off-diagonal elements relative to the in-plane coordinates of the carbon–sulfur skeleton, we have included the off-diagonal interactions $F_{S_1S_3}$ and $F_{S_4S_{22}}$. This corresponds to having ignored the off-diagonal interactions which are not consistent with

TABLE 2. Geometrical parameters for dithioacetate*

| Bond | Length (Å) |
|---|---|
| $C_1—C_2$ | 1.54 |
| $C_2—S_1$ | 1.63 |
| $C_2—S_2$ | 1.74 |
| $S_2—C_3$ | 1.81 |
| C—H | 1.09 |

| Bonds | Angle (deg.) |
|---|---|
| $C_1C_2S_1$ | 117 |
| $C_1C_2S_2$ | 118 |
| $S_1C_2S_2$ | 125 |
| $C_2S_2C_3$ | 108 |
| $HCH = HC_1C_2 = HC_3S_2$ | 109.4712 |

*Nomenclature as in Fig. 1.

TABLE 3. Definition of internal coordinates*

| | |
|---|---|
| Skeleton: | $CH_3$—C: |
| $r_1 = \Delta(C_1—C_2)$ | $s_i = \Delta(C_1—H_i)$ |
| $r_2 = \Delta(C_2—S_1)$ | $\alpha_i = \Delta(\angle H_jC_1H_k)\ j, k \neq i$ |
| $r_3 = \Delta(C_2—S_2)$ | $\beta_i = \Delta(\angle H_iC_1C_2)$ |
| $r_4 = \Delta(S_2—C_3)$ | $\tau(C_1C_2)$ = torsion around $C_1C_2$ |
| $\varepsilon = \Delta(\angle C_1C_2S_1)$ | $CH_3$—S: |
| $\gamma = \Delta(\angle S_1C_2S_2)$ | $s_i' = \Delta(C_3—H_i)$ |
| $\delta = \Delta(\angle C_1C_2S_2)$ | $\alpha_i' = \Delta(\angle H_jC_3H_k)\ j, k \neq i$ |
| $\omega = \Delta(\angle C_2S_2C_3)$ | $\beta_i' = \Delta(\angle H_iC_3S_2)$ |
| $\tau(C_2S_2)$ = torsion around $C_2S_2$ | $\tau(S_2C_3)$ = torsion around $S_2C_3$ |
| $\zeta$ = out-of-plane of $S_1$ | |

*Atoms numbered as in Fig. 1.

TABLE 4. Definition of a new set of internal coordinates and their approximate description*

| Skeleton | | $CH_3$—C | | $CH_3$—S | |
|---|---|---|---|---|---|
| $S_1 = r_1$ | s | $S_{10} = (1/\sqrt{3})(s_1 + s_2 + s_3)$ | ss | $S_{19} = (1/\sqrt{3})(s_1' + s_2' + s_3')$ | ss |
| $S_2 = r_2$ | s | $S_{11} = (1/\sqrt{6})(2s_1 - s_2 - s_3)$ | as | $S_{20} = (1/\sqrt{6})(2s_1' - s_2' - s_3')$ | as |
| $S_3 = r_3$ | s | $S_{12} = (1/\sqrt{2})(s_2 - s_3)$ | as | $S_{21} = (1/\sqrt{2})(s_2' - s_3')$ | as |
| $S_4 = r_4$ | s | $S_{13} = (1/\sqrt{6})(\alpha_1 + \alpha_2 + \alpha_3 - \beta_1 - \beta_2 - \beta_3)$ | sb | $S_{22} = (1/\sqrt{6})(\alpha_1' + \alpha_2' + \alpha_3' - \beta_1' - \beta_2' - \beta_3')$ | sb |
| $S_5 = (1/\sqrt{6})(2\gamma - \varepsilon - \delta)$ | b | $S_{14} = (1/\sqrt{6})(2\alpha_1 - \alpha_2 - \alpha_3)$ | ab | $S_{23} = (1/\sqrt{6})(2\alpha_1' - \alpha_2' - \alpha_3')$ | ab |
| $S_6 = (1/\sqrt{2})(\delta - \varepsilon)$ | b | $S_{15} = (1/\sqrt{6})(2\beta_1 - \beta_2 - \beta_3)$ | r | $S_{24} = (1/\sqrt{6})(2\beta_1' - \beta_2' - \beta_3')$ | r |
| $S_7 = \omega$ | b | $S_{16} = (1/\sqrt{2})(\alpha_2 - \alpha_3)$ | ab | $S_{25} = (1/2)(\alpha_2' - \alpha_3')$ | ab |
| $S_8 = \tau(C_2S_2)$ | t | $S_{17} = (1/\sqrt{2})(\beta_2 - \beta_3)$ | r | $S_{26} = (1/\sqrt{2})(\beta_2' - \beta_3')$ | r |
| $S_9 = \zeta$ | w | $S_{18} = \tau(C_1C_2)$ | t | $S_{27} = \tau(S_2C_3)$ | t |

*s = stretch; b = bend; t = torsion; w = wag; r = rock; whenever two letters are used the first stands for "symmetric" (s) or "antisymmetric" (a). For the purpose of this calculation, the skeletal and methyl coordinates are herein grouped under different headings.

the hypothesis of axial symmetry for the methyl groups. The simplicity of our force field as regards to the alkyl groups and, in particular, to the interaction elements coupling the dithioester and alkyl groups should not significantly affect the conclusions drawn for the dithioester group vibrations.

The experimental frequency data from four isotopic species, $CH_3CSSCH_3$, $CD_3CSSCH_3$, $CH_3CSSCD_3$, and $^{13}CH_3CSSCH_3$, were simultaneously entered and processed in the least-squares fitting procedure. The calculated valence force constants are reported in Table 5 and the observed and calculated frequencies and their potential energy distribution are shown in Table 1. The conclusions from the PED are also summarised in the assignments given in Table 6 for the region between 500 and 1200 $cm^{-1}$. The calculated valence force constants were subsequently used to evaluate the vibrational frequencies in $CH_3{}^{13}CSSCH_3$. The observed isotopic shifts for the RR spectral data (caption to Fig. 4) were very well reproduced, thus confirming the plausibility of the calculated force field.

TABLE 5. Calculated valence force constants for methyl dithioacetate*

| Diagonal force constants | | Off-diagonal force constants | |
|---|---|---|---|
| *Skeleton* | | *Skeleton–skeleton interactions* | |
| (1, 1) | 3.500 | (1, 2) | 0.309 |
| (2, 2) | 4.934 | (1, 3) | 0.479 |
| (3, 3) | 4.437 | (1, 4) | −0.291 |
| (4, 4) | 3.038 | (1, 5) | 0.021 |
| (5, 5) | 1.099 | (1, 6) | −0.149 |
| (6, 6) | 0.935 | (1, 7) | −0.153 |
| (7, 7) | 1.863 | (2, 3) | −0.301 |
| (8, 8) | 0.562 | (2, 4) | 0.214 |
| (9, 9) | 0.280 | (2, 5) | −0.316 |
| *$CH_3$—C* | | (2, 6) | −0.641 |
| (10, 10) | 4.884 | (2, 7) | −0.088 |
| (11, 11) = (12, 12) | 4.702 | (3, 4) | 0.158 |
| (13, 13) | 0.560 | (3, 5) | −0.302 |
| (14, 14) = (16, 16) | 0.498 | (3, 6) | 0.506 |
| (15, 15) = (17, 17) | 0.503 | (3, 7) | −0.053 |
| (18, 18) | 0.089 | (4, 5) | −0.011 |
| *$CH_3$—S* | | (4, 6) | 0.218 |
| (19, 19) | 4.903 | (4, 7) | −0.214 |
| (20, 20) = (21, 21) | 4.758 | (5, 6) | −0.004 |
| (22, 22) | 0.528 | (5, 7) | 0.015 |
| (23, 23) = (25, 25) | 0.503 | (6, 7) | −0.160 |
| (24, 24) = (26, 26) | 0.626 | *Skeleton–methyl interactions* | |
| (27, 27) | 0.089 | (1, 13) | −0.295 |
| | | (4, 22) | −0.317 |

*Stretching force constants: mdyn $Å^{-1}$; bending force constants: mdyn Å $rad^{-2}$; stretching–bending interaction: mdyn $rad^{-1}$.

*The vibrational assignments of the Raman and infrared bands of methyl dithioacetate*

The Raman band at 2989 $cm^{-1}$ probably contains a contribution from the antisymmetric C—H stretching modes of the S—$CH_3$ and $CH_3$—C groups (27). On the basis of calculations (Table 1) and the different electronegativities of the C and S atoms it is likely that the S—$CH_3$ makes a contribution at slightly higher frequencies within the band profile in this region. The symmetric C—H stretching modes of both methyl groups contribute to the intense 2908 $cm^{-1}$ Raman feature since the infrared absorbance giving rise to this band diminishes upon the deuterium substitution of the $CH_3$—C or the S—$CH_3$ group. Moreover, this conclusion is consistent with the findings in Table 1. The Raman bands at 1434 $cm^{-1}$ and 1358 $cm^{-1}$ (the infrared bands at 1441 and 1359 $cm^{-1}$) undergo a large shift in the Raman (infrared) spectrum of $CD_3$—C(=S)—S—$CH_3$ and therefore these bands may be assigned to the antisymmetric and symmetric deformation modes of the $CH_3$—C methyl group, respectively. The Raman band at 1410 $cm^{-1}$ (the infrared band at 1413 $cm^{-1}$) can be assigned to the antisymmetric deformation mode of the S—$CH_3$ methyl group since the band shifts in the Raman (infrared) spectrum of $CH_3$—C(=S)—S—$CD_3$. The weak band at 1309 $cm^{-1}$ is possibly due to the methyl symmetric deformation mode of the S—$CH_3$ group (28). Support for the $CH_3$ deformation assignments is again found in Table 1.

Can. J. Chem. Downloaded from www.nrcresearchpress.com by 210.87.254.105 on 09/06/12
For personal use only.

Can. J. Chem. Downloaded from www.nrcresearchpress.com by 210.87.254.105 on 09/06/12
For personal use only.

The band at 1194 $cm^{-1}$ is very intense in the Raman and infrared spectra and strongly enhanced in the RR spectrum. Although this band does not shift or shifts little upon the deuterium substitution of the $CH_3$—C or S—$CH_3$ groups or in the $^{13}CH_3C(=S)SCH_3$ analog, the same band does shift by 25 $cm^{-1}$ upon the $^{13}C$ substitution of the thiocarbonyl group. The intensity of the band and the results of the isotopic shifts strongly suggest that the band has a high degree of C=S stretching character. These results and conclusions are in general agreement with the normal coordinate calculations although the latter stress that the C—C stretching motion probably makes a substantial contribution to the 1194 $cm^{-1}$ mode. The band at 1100 $cm^{-1}$ is shifted in the spectra of $CD_3$—C(=S)—S—$CH_3$, $^{13}CH_3$—C(=S)—S—$CH_3$, and $CH_3$—$^{13}$C(=S)—S—$CH_3$, and it does, moreover, undergo a very high degree of intensity enhancement upon going from 514.5 to 324 nm excitation. The results of the calculations indicate that the 1100 $cm^{-1}$ mode has a high degree of C—S and some C—C stretching character (Tables 1, 6). The isotope shifts concerning this mode are faithfully reproduced in the calculations. In addition, the normal coordinate analysis explains the high degree of intensity enhancement observed under resonance conditions since the C—S bond is intimately involved in the chromophore.

The bands at 957 and 911 $cm^{-1}$ shift upon the deuterium substitution of the S—$CH_3$ or the $CH_3$—C group, respectively. This finding and the results from the calculations (Table 1) lead us to assign these bands to methyl rocking modes of the S—$CH_3$ and the $CH_3$—C groups respectively. The band at 864 $cm^{-1}$ is intense in the Raman and infrared spectra, although the relative intensity of this feature becomes weaker in the RR spectrum. Moreover, the 864 $cm^{-1}$ band exhibits a large shift to 743 $cm^{-1}$ upon the deuterium substitution of $CH_3$—C group but only a small shift in the infrared spectrum of the $^{13}CH_3$—C(=S)$SCH_3$ analog (Fig. 3). These observations suggest that the 864 $cm^{-1}$ band, too, may have a substantial degree of $CH_3$ rocking character and is due to the $CH_3$—C group. This assignment is strengthened by the results of the normal coordinate analysis (Table 1) and the fact that the 864 $cm^{-1}$ feature is absent in the spectra of $C_2H_5C(=S)SCH_3$ (1). Methyl rocking modes are prone to coupling with other vibrations in the molecule (29) and such a coupling is indicated for the 864 $cm^{-1}$ feature in the vibrational calculations. The result of the calculations show that the rocking modes at 975, 958, and 915 $cm^{-1}$ (Table 1) are essentially pure modes. However, the 864 $cm^{-1}$ band contains PED contributions of 10% from $\nu_{C-S}$ and 8% from $\nu_{C=S}$. Such coupling may be responsible for the high degree of resonance enhancement seen for this essentially hydrogenic mode. In this regard it is interesting to note that Mathies and co-workers (30) have been able to show that substantial resonance enhancement may be observed for hydrogen out-of-plane bends of certain strained conformers of the retinal molecule.

The band at 730 $cm^{-1}$ undergoes a large shift to 688 $cm^{-1}$ upon deuterium substitution of the S—$CH_3$ group. This finding, taken with the PED distribution of 87% $\nu_{S-C}$ (Tables 1 and 6) prompts us to assign the 730 $cm^{-1}$ mode to a vibration involving a very high degree S—C stretching mode of the S—$CH_3$ group. Such an assignment is in good accord with Miyazawa's finding (31) that for thioethers of the form $RCH_2SCH_3$ the S—$CH_3$ stretching vibration is observed around 725 $cm^{-1}$, and the frequency is fairly independent of the changes in molecular conformation. The band at 580 $cm^{-1}$ is intense in Raman and infrared spectra, and the fact that it is enhanced strongly in the RR spectrum indicates that this band is intimately associated with the motion of atoms in the —C(=S)—S— chromophore. The band exhibits a large shift to 557 $cm^{-1}$ upon the deuterium substitution of the $CH_3$—C group and a small shift upon the deuterium substitution of the S—$CH_3$ group or in $^{13}CH_3(=S)SCH_3$. The results suggest that the 580 $cm^{-1}$ feature contains major contributions from C—S and C—C stretching motions. These expectations are borne out by the calculations which further indicate a sizable contribution from the C=S stretch. Since the 730 $cm^{-1}$ band is weak in both Raman and infrared spectra and the 580 $cm^{-1}$ band is intense in both Raman and infrared spectra, it is not appropriate to ascribe the 730 and 580 $cm^{-1}$ bands to antisymmetric and symmetric C—S—C stretching modes, respectively, and this conclusion is substantiated by the normal coordinate analysis. The situation again parallels Nogami, Sugeta, and Miyazawa's work on thioethers (31) in which these authors found that the best description of the C—S stretches in the $RCH_2$—S—$CH_3$ group is localised $CH_2$—S and S—$CH_3$ stretches. The Raman bands at 387, 339, and 228 $cm^{-1}$ may be due to the skeletal deformation modes. Since the 228 $cm^{-1}$ bands does not show a shift upon the deuterium substitution of the $CH_3$—C group but shifts to 211 $cm^{-1}$ upon the deuterium substitution of S—$CH_3$ group, the band is probably due to a torsional or bending motion in the C—S—$CH_3$ moiety. The vibrational assign-

TABLE 6. Vibrational assignments of methyl dithioacetate*

| Frequency ($cm^{-1}$) | | |
|---|---|---|
| Raman | Infrared | Assignment |
| 2989 (dp) | | Antisymmetric C—H stretching ($CH_3$—C, S—$CH_3$) |
| 2908 (p) | 2911 | Symmetric C—H stretching ($CH_3$—C, S—$CH_3$) |
| 1434 (p) | 1441 | Antisymmetric $CH_3$ deformation ($CH_3$—C) |
| 1410 (dp) | 1413 | Antisymmetric $CH_3$ deformation (S—$CH_3$) |
| 1358 (p) | 1359 | Symmetric $CH_3$ deformation ($CH_3$—C) |
| 1309 | 1311 | Symmetric $CH_3$ deformation (S—$CH_3$) |
| 1194 (p) | 1195 | C=S + C—C stretching (44 + 33) |
| 1100 (p) | 1100 | C—S + C—C stretching (55 + 24) |
| 957 (p) | 956 | $CH_3$ rocking (S—$CH_3$) (83) |
| 911 (p) | | $CH_3$ rocking ($CH_3$—C) (87) |
| 864 (p) | 865 | $CH_3$ rocking ($CH_3$—C) (74) |
| 730 (dp) | 730 | S—C stretching (—S—$CH_3$) (87) |
| 580 (p) | 580 | C—S stretching + C—C stretching + C=S stretching (26 + 25 + 28) |
| 487 (p) | 487 | |
| 422 (p) | 456 | |
| 387 (dp) | 376 | |
| 339 (dp) | 342 | |
| 228 (p) | | |

*The respective PEDs for the modes between 500 and 1200 $cm^{-1}$ (of interest in the RR spectrum) are given in parentheses.

ments for methyl dithioacetate are summarised in Table 6.

A comparison between the diagonal stretching force constants for the CCSSC and CCOOC skeletons of methyl dithioacetate and methyl acetate reveals several interesting facets. In the case of methyl acetate the force constants for $\nu_{C=O}$ and $\nu_{C-O}$ are quite different, 10.8 and 6.1 mdyn $Å^{-1}$ respectively (J.J.C.T.-D, unpublished work), while for methyl dithioacetate the force constants for $\nu_{C=S}$ and $\nu_{C-S}$ are remarkably similar at 4.9 and 4.4 mdyn $Å^{-1}$, respectively. If we relate the ratio of the force constants to the relative degree of double bond character we can say that there is a considerably greater difference in bond order between the formal C=O and C—O bonds than between the formal C=S and C—S bonds. An additional point concerns the force constants for C—C in the dithio and dioxygen analogs. For the latter, the force constant of 4.0 mdyn $Å^{-1}$ is close to that for alkanes (32) while the force constant for C—C in methyl dithioacetate is 3.5 mdyn $Å^{-1}$. The overall similarity of the force constants within the dithioester fragment provide an ample mechanism for the observed vibrational coupling.

A comparison of the PED results and the degrees of RR enhancement shows that modes with a high degree of C=S, C—S, and S—C character are particularly intensity enhanced. Modes associated with $\nu_{C-S}$ and $\nu_{S-C}$ are at least as active as those associated with $\nu_{C=S}$ and this provides evidence for the electronic transition being delocalised over the

—C—S—C moiety rather than being confined to mainly the C=S group.

*Vibrational spectra of ethyl dithioacetate and their assignments*

The Raman, infrared, and RR spectra of ethyl dithioacetate and its isotopically substituted derivatives are shown in Figs. 5, 6, and 7, respectively. There is a striking resemblance between the spectra of methyl dithioacetate and the spectra of ethyl dithioacetate. In the RR spectrum of ethyl dithioacetate, for example, the pattern of bands between 1250 and 500 $cm^{-1}$ closely resembles the pattern of bands in the same region of the RR spectrum of methyl dithioacetate. In fact, in the RR spectrum only the band at 732 $cm^{-1}$ which was assigned to the S—$CH_3$ stretching mode showed a substantial shift upon going from methyl to ethyl ester.

Although the complete assignments of the bands in the C—H stretching vibrational region are not trivial, some comments can be made. The Raman band at 2910 $cm^{-1}$ shifts to 2100 $cm^{-1}$ upon the deuterium substitution of the $CH_3$—C moiety, thus the band can be assigned to the symmetric C—H stretching mode of the $CH_3$—C group. In the infrared spectrum, the shoulder at 2920 $cm^{-1}$ shifts upon the deuterium substitution of the S—$CH_2$

Can. J. Chem. Downloaded from www.nrcresearchpress.com by 210.87.254.105 on 09/06/12
For personal use only.

Can. J. Chem. Downloaded from www.nrcresearchpress.com by 210.87.254.105 on 09/06/12
For personal use only.

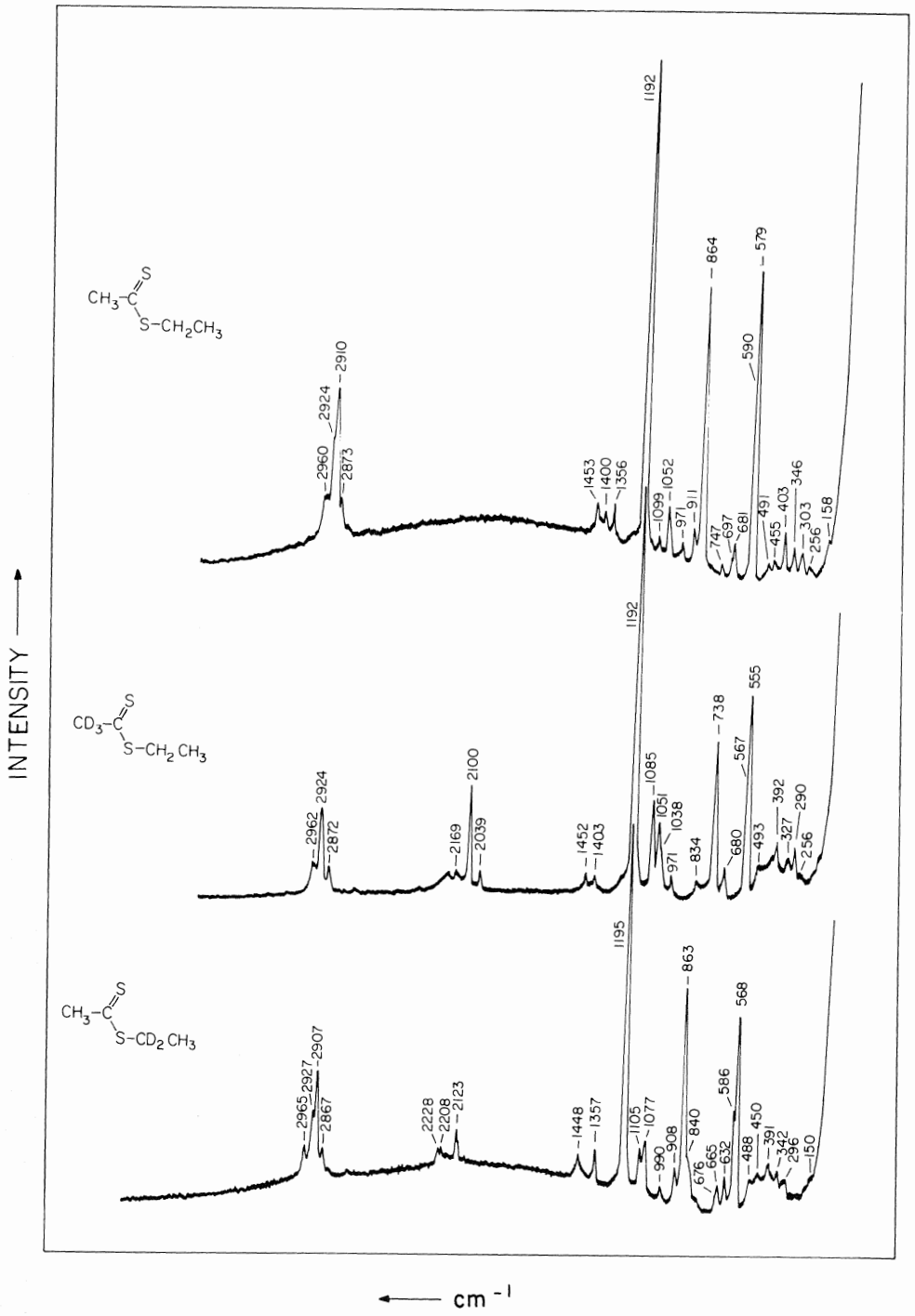


FIG. 5. The 514.5 nm excited Raman spectra of ethyl dithioacetate and its isotopically substituted derivatives in the liquid state. Instrumental conditions are same as those in Fig. 2.

group, thus this band may be due to the antisymmetric C—H stretching mode of the S—$CH_2$ moiety. However, the mode does not make a major contribution to Raman intensity in this spectral region. The infrared bands at 2969, 2929, and 2873 $cm^{-1}$ were observed in the spectra of $CH_3$—C(=S)—S—$CH_2CH_3$, $CD_3$—C(=S)—S—$CH_2$-$CH_3$, and $CH_3$—C(=S)—S—$CD_2CH_3$, therefore

Can. J. Chem. Downloaded from www.nrcresearchpress.com by 210.87.254.105 on 09/06/12
For personal use only.

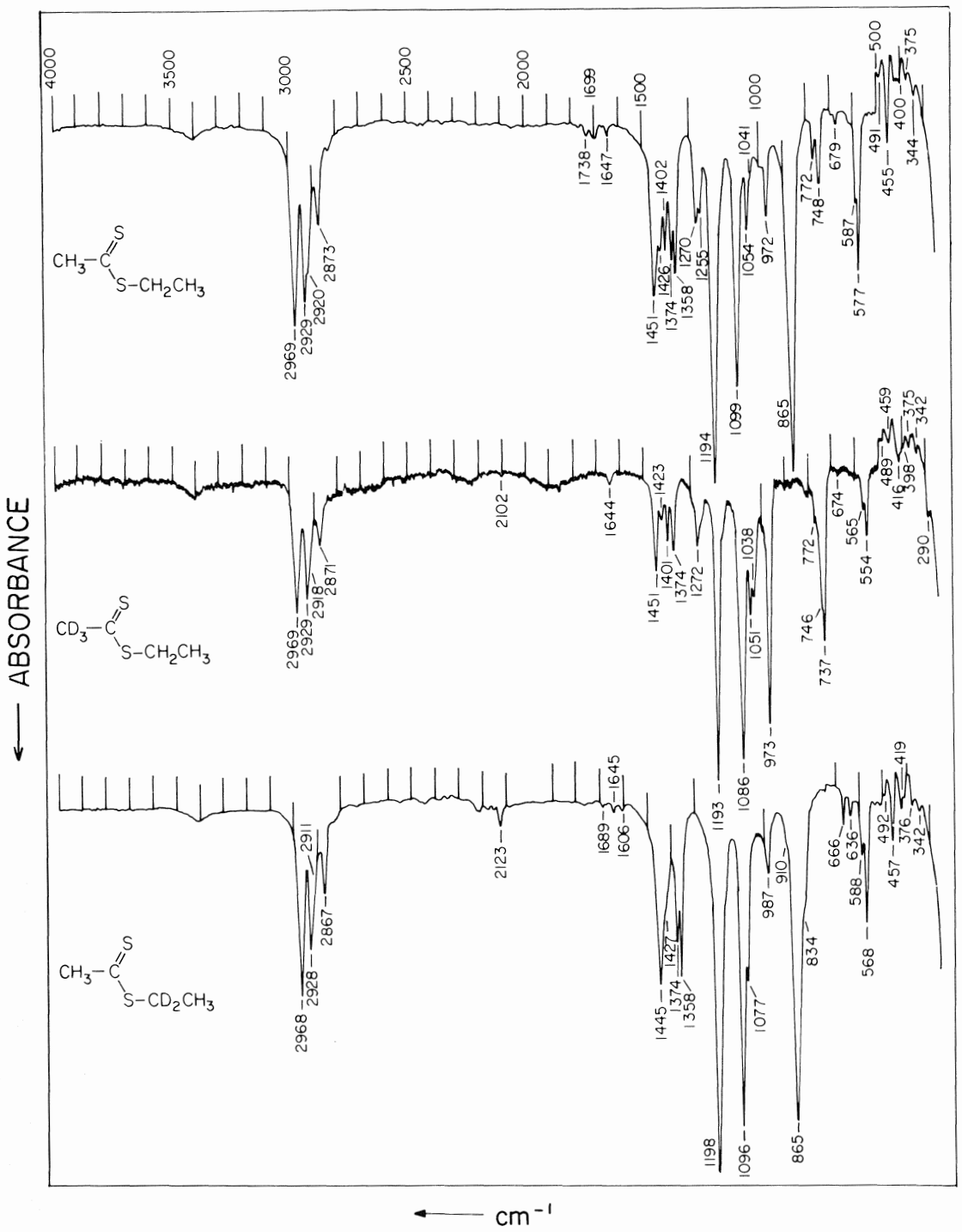


FIG. 6. The infrared spectra of ethyl dithioacetate and its isotopically substituted derivatives in the liquid state.

these bands probably include a contribution from the —$CH_3$ group. In their infrared study of ethyl acetate Nolin and Jones (33) ascribed ethyl acetate bands at 2877 $cm^{-1}$ and 2939 $cm^{-1}$ as due to the symmetrical C—H stretch and a combination band of the —$OCH_2CH_3$ methyl group with the possibility that these assignments may be reversed.

The band at 1453 $cm^{-1}$ can be assigned to the antisymmetric methyl deformation mode of the $CH_2$—$CH_3$ group since the band does not shift upon

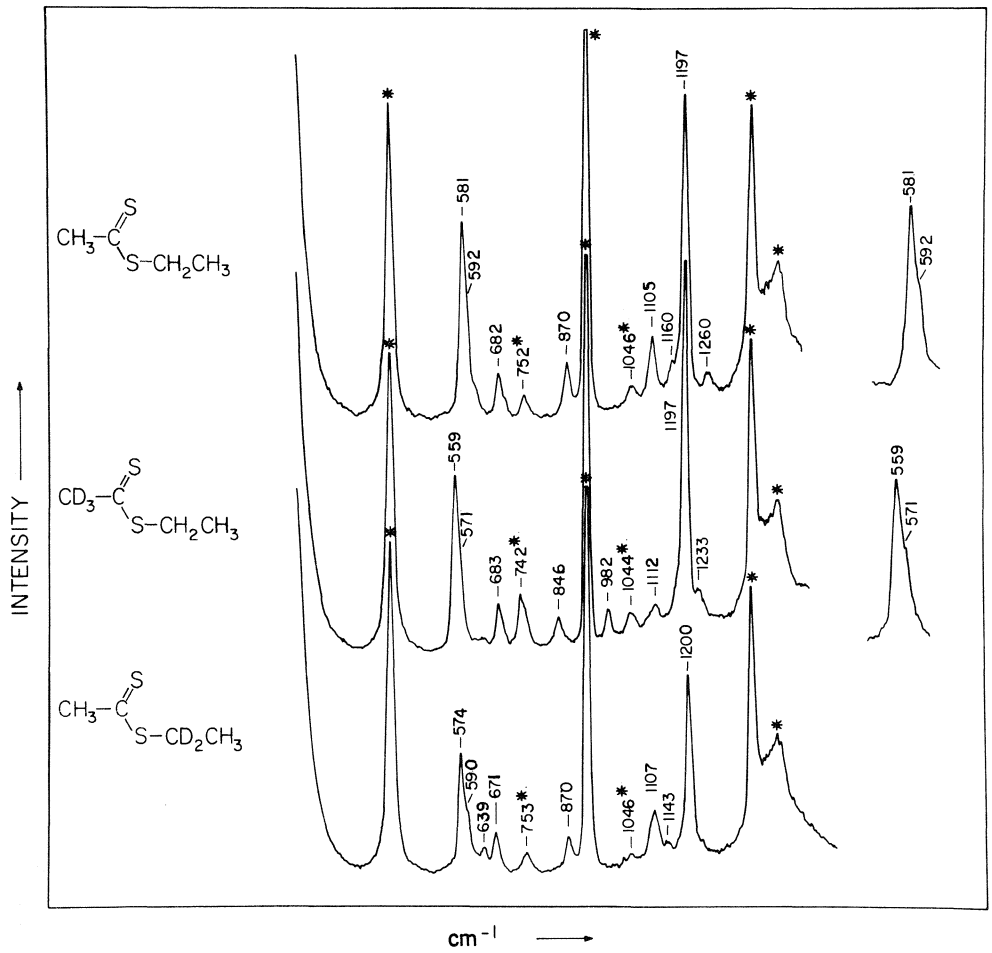


FIG. 7. The 324.0 nm excited RR spectra of ethyl dithioacetate and its isotopically substituted derivatives in 0.01% (v/v) $CH_3CN$ solution. Features marked with an asterisk are due to $CH_3CN$. The RR spectrum of $CH_3$—$^{13}C$(=S)—S—$C_2H_5$ (not shown) had a steep base line due to strong fluorescence; however, RR features were observed at 1172 and 580 $cm^{-1}$ together with a weaker band at 1092 $cm^{-1}$. Instrumental conditions are same as those in Fig. 4.

the deuterium substitution of $CH_3$—C or S—$CH_2$, whereas the infrared band at 1426 $cm^{-1}$ (seen as a shoulder on the Raman band at 1453 $cm^{-1}$) probably includes a contribution from the antisymmetric methyl deformation mode of the $CH_3$—C group, since the intensity of this band became weaker in the infrared spectrum of $CD_3$—C(=S)—S—$CH_2$-$CH_3$. Both these conclusions are in good accord with Nolin and Jones's assignments for ethyl acetate (33). The band at 1400 $cm^{-1}$ shifts upon the deuterium substitution of the methylene group, thus this band is assigned to the $CH_2$ scissoring (deformation) mode. The infrared band at 1374 $cm^{-1}$ does not shift upon the deuterium substitution of the $CH_3$—C group or the S—$CH_2$ group; however, the Raman and infrared band at 1356 $cm^{-1}$ does shift upon the deuterium substitution of the $CH_3$—C group. Thus, the 1374 and 1356 $cm^{-1}$ bands can be assigned to the symmetric methyl deformation mode of the $CH_2CH_3$ and $CH_3$—C groups, respectively. The latter assignment is in accord with the $CH_3$—C symmetric methyl deformation assignment made for methyl dithioacetate above. The infrared bands at 1270 and 1255 $cm^{-1}$ shift in the spectrum of $CH_3$—C(=S)—S—$CD_2$-$CH_3$. Moreover, methyl dithioacetate does not have a band near 1270 $cm^{-1}$, therefore it is possible to assign the feature near 1260 $cm^{-1}$ to the $CH_2$ wagging mode. The assignments concerning the $CH_2$ deformation and wagging modes are in reasonable harmony with those found in the literature (34).

The band at 1192 $cm^{-1}$ is intense in the Raman, infrared, and RR spectra. The band shifts little upon the deuterium substitution of $CH_3$—C group or S—$CH_2$ group, but as in the case of the 1194

Can. J. Chem. Downloaded from www.nrcresearchpress.com by 210.87.254.105 on 09/06/12
For personal use only.

TABLE 7. Vibrational assignments of ethyl dithioacetate

| Frequency ($cm^{-1}$) | | |
|---|---|---|
| Raman | Infrared | Assignment |
| 2960 (dp) | 2969 | |
| 2924 (p) | 2929 | |
| | 2920 | Antisymmetric C—H stretching (S—$CH_2$—) |
| 2910 (p) | | Symmetric C—H stretching ($CH_3$—C) |
| 2873 (p) | 2873 | |
| 1453 (dp) | 1451 | Antisymmetric $CH_3$ deformation ($CH_2$—$CH_3$) |
| | 1426 | Antisymmetric $CH_3$ deformation ($CH_3$—C) |
| 1400 (p) | 1402 | $CH_2$ scissoring |
| | 1374 | Symmetric $CH_3$ deformation ($CH_2$—$CH_3$) |
| 1356 (p) | 1358 | Symmetric $CH_3$ deformation ($CH_3$—C) |
| | 1270, 1255 | $CH_2$ wagging |
| 1192 (p) | 1194 | C=S + C—C stretching |
| 1099 (p) | 1099 | C—S + C—C ($CH_3$—C) stretching |
| 1052 (p) | 1054 | C—C stretching ($CH_2$—$CH_3$) |
| | 1041 | |
| 971 (p) | 972 | $CH_3$ rocking ($CH_2$—$CH_3$) |
| 911 (p) | | $CH_3$ rocking ($CH_3$—C) |
| 864 (p) | 865 | $CH_3$ rocking ($CH_3$—C) |
| | 772 | |
| 747 (p) | 748 | $CH_2$ rocking |
| 697, 681 (dp) | 679 | S—C stretching (—S—$CH_2$—) |
| 590, 579 (p) | 587, 577 | C—S stretching + C—C stretching + C=S stretching |

$cm^{-1}$ band of methyl dithioacetate shows a large shift upon the $^{13}C$ substitution of the thiocarbonyl group. Therefore the 1192 $cm^{-1}$ band probably has a substantial degree of C=S stretching character. This assignment and assignment for the band at 1194 $cm^{-1}$ of methyl dithioacetate are in good agreement with the conclusions reached by several authors using mainly infrared spectroscopy (5–9).

The Raman and infrared bands at 1099, 971, 911, and 864 $cm^{-1}$ of ethyl dithioacetate correspond to those at 1100, 957, 911, and 864 $cm^{-1}$ of methyl dithioacetate, respectively, because the corresponding bands show similar frequencies, intensities, and isotopic shifts. The ethyl dithioacetate band at 1099 $cm^{-1}$, assigned to a mixed vibration involving a C—S stretching and a C—C stretching motion of the $CH_3$—C group, gains intensity under the RR condition and shifts in the spectrum of $CD_3$—C(=S)—S—$CH_2CH_3$ whereas the band at 864 $cm^{-1}$ assigned to the $CH_3$ rocking mode of the $CH_3$—C group loses intensity under the RR condition and shifts to 738 $cm^{-1}$ in the spectrum of $CD_3$—C(=S)—$CH_2CH_3$. This behaviour closely follows that noted for the methyl ester (Figs. 2, 4, 5, and 7). The ethyl ester has an additional band at 1052 $cm^{-1}$ which can be assigned to the C—C stretching mode of the ethyl group. It is marked that in the Raman spectrum, the 1052 $cm^{-1}$ band due to the C—C stretching mode of the ethyl group is much stronger than the 1099 $cm^{-1}$ band due to the C—C stretching mode of the $CH_3$—C group; however, in the RR spectrum the former is very weak or absent and the latter becomes more intense. The 747 $cm^{-1}$ band which shifts to 632 $cm^{-1}$ upon deuterium substitution of the $CH_2$ group may be due to a $CH_2$ rocking mode.

The band at 681 $cm^{-1}$ shifts to lower wavenumbers by 14 $cm^{-1}$ upon the deuterium substitution of S—$CH_2$ and the band is weak in the Raman and infrared spectra but gains intensity in the RR spectra (Figs. 5, 6, and 7). Therefore the band can be assigned to a vibration involving the S—C stretching mode. In contrast to the 681 $cm^{-1}$ band, the intense band at 579 $cm^{-1}$ undergoes a large shift by about 23 $cm^{-1}$ upon the deuterium substitution of $CH_3$—C group and shifts by only 9 $cm^{-1}$ upon the deuterium substitution of S—$CH_2$ group. Thus, by analogy with methyl dithioacetate this band can be assigned to a mode having contributions from C—C, C—S, and C=S stretching coordinates. Accordingly, for both methyl and ethyl dithioacetates the C—C + C—S + C=S stretching mode is intense and is observed near 580 $cm^{-1}$ in the Raman, infrared, and RR spectra; on the other hand, the S—C stretching mode is weak or very weak in the Raman and infrared spectra and is located at 730 $cm^{-1}$ for the methyl ester and at 680 $cm^{-1}$ for the ethyl ester. The shoulders at 697 and

Can. J. Chem. Downloaded from www.nrcresearchpress.com by 210.87.254.105 on 09/06/12
For personal use only.

Can. J. Chem. Downloaded from www.nrcresearchpress.com by 210.87.254.105 on 09/06/12
For personal use only.

590 $cm^{-1}$ of ethyl dithioacetate indicate the coexistence of the rotational isomers as discussed in the following paper (1).

The vibrational assignments for ethyl dithioacetate are summarized in Table 7.

*Excitation profiles*

The dependence of Raman intensity on excitation wavelengths (the excitation profile) can provide information on vibronic structure which lies unresolved in an absorption spectrum, information on the mechanism of Raman intensity enhancement, and provide confirmatory information on assignments of the Raman bands. In the present case excitation wavelengths in the range 647.1 to 324 nm were available and thus it was not possible to scan through the entire dithioester absorbance band centered near 307 nm. The resulting excitation profiles for the 581 and 1197 $cm^{-1}$ bands of ethyl dithioacetate are shown in Fig. 8. Compared to their intensities with 647.1 nm excitation, both bands increase in intensity by a factor of 1500–2000 upon going to 324 nm as an excitation wavelength. Although no significance is attached to the individual "dips" in the excitation profiles in the 450–500 nm region, the data taken together do suggest that a small amount of intensity enhancement is achieved by coupling to the $n \rightarrow \pi^*$ transition near 460 nm. In this region the 1197 $cm^{-1}$ feature shows markedly greater intensity enhancement compared to the 581 $cm^{-1}$ band. Importantly, the excitation profile data establish that the $\pi \rightarrow \pi^*$ transition near 307 nm is the major source of Raman intensity enhancement and, in fact, in the pre-resonance region (412 to 324 nm) there is good agreement between the experimental profile and a theoretical curve generated from an Albrecht and Hutley A type mechanism (35).

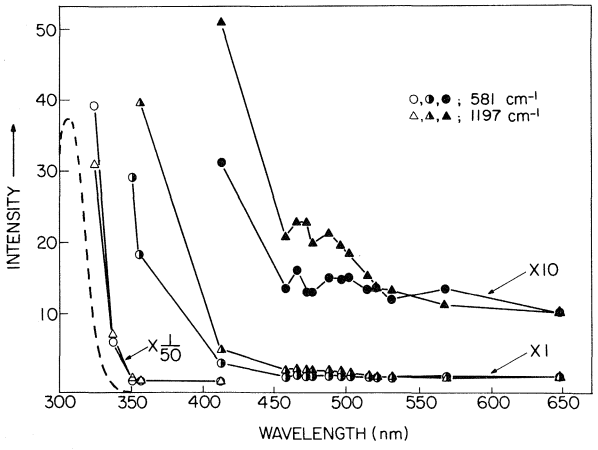


FIG. 8. The observed excitation profiles for the bands at 581 and 1197 $cm^{-1}$ of ethyl dithioacetate. (○, ◑, ● 581 $cm^{-1}$, △, ▲, ▲; 1197 $cm^{-1}$). The absorption spectrum, with an arbitrary absorbance scale, is shown as (---). The $n \rightarrow \pi^*$ transition is too weak to be observed on the same absorbance scale as the main $\pi \rightarrow \pi^*$ transition. The solution used to obtain the excitation profile in the 324 to 350.6 nm range had an O.D. of about 3 at 307 nm.

## Conclusion

By using extensive isotopic substitutions and a detailed normal coordinate treatment we have been able to form a semi-quantitative picture of the assignments of the vibrational bands due to the skeletal modes of methyl dithioacetate. Most of the conclusions can be carried over to ethyl dithioacetate. The present work also establishes that the 305 nm absorption band is the source of RR enhancement for vibrational modes of the dithioester group and indicates that the chromophore responsible for the 305 nm transition involves the entire

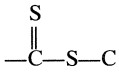

group. Within this group the force constants for the C=S and C—S stretching motions are very similar.

## Acknowledgements

The collaboration between the Canadian and Portuguese laboratories involved in this work was made possible by a NATO grant to J.J.C.T.-D. and P.R.C. J.J.C.T.-D. gratefully acknowledges the cooperation of the computing center in Coimbra.

1. Y. OZAKI, A. C. STORER, and P. R. CAREY. Can. J. Chem. **60**, 190 (1982).
2. A. C. STORER, Y. OZAKI, and P. R. CAREY. Can. J. Chem. **60**, 199 (1982).
3. A. C. STORER, W. F. MURPHY, and P. R. CAREY. J. Biol. Chem. **254**, 3163 (1979).
4. G. LOWE and A. WILLIAMS. Biochem. J. **96**, 189 (1965).
5. K. HERZOG, E. STEGER, P. ROSMUS, S. SHEITHAUER, and R. MAYER. J. Mol. Struct. **3**, 339 (1969).
6. C. S. MARVEL, P. DE RADZITZKY, and J. J. BRADER. J. Am. Chem. Soc. **77**, 5997 (1955).
7. B. BAK, L. HANSEN-NYAARD, and C. PEDERSEN. Acta Chem. Scand. **12**, 1451 (1958).
8. L. J. BELLAMY and P. E. ROGASCH. J. Chem. Soc. 2218 (1960).
9. R. MAYER, E. SCHINKE, P. ROSMUS, and S. SCHEITHAUER. J. Prakt. Chem. **312**, 767 (1970).
10. A. L. VERMA. Y. OZAKI, A. C. STORER, and P. R. CAREY. J. Raman Spectrosc. In press.
11. S. SCHEITHAUER and R. MAYER. Topics in sulfur chemistry. Vol. 4. *Edited by* A. Senning. G. Thieme, Stuttgart. 1979.
12. G. I. L. JONES and N. L. OWEN. J. Mol. Struct. **18**, 1 (1973).
13. G. I. L. JONES, D. G. LISTER, N. L. OWEN, M. C. L. GERRY, and P. PALMIERI. J. Mol. Spectrosc. **60**, 348 (1976).
14. O. EXNER, V. JEHLICKA, and J. FIRL. Collect. Czech. Chem. Commun, **36**, 2948 (1971).

15. H. LUMBROSO and P. J. W. SCHUIJL. C.R. Acad. Sci. C **264**, 925 (1967).
16. O. EXNER, V. JEHLICKA, and A. OHNO. Collect. Czech. Chem. Commun. **36**, 2157 (1971).
17. H. LUMBROSO and P. REYNAUD. C.R. Acad, Sci. C **262**, 1739 (1966).
18. B. A. E. MACCLEMENT, R. G. CARRIERE, D. J. PHELPS, and P. R. CAREY. Biochemistry, **20**, 3438 (1981).
19. F. ARNDT, E. MILDE, and G. ECKERT. Ber. **54B**, 2236 (1921).
20. C. N. R. RAO, A. BALASUBRAMANIAN, and J. RAMACHANDRAN. J. Sci. Industr. Res. **20B**, (1961).
21. M. J. JANSSEN. Recueil, **79**, 382 (1961).
22. H. FUHRER, V. B. KARTHA, K. G. KIDD, P. J. KRUEGER, and H. H. MANTSCH. National Research Council of Canada, Bulletin No. 15. 1976.
23. H. S. RANDHAWA and C. N. R. RAO. J. Mol. Struct. **21**, 123 (1974).
24. (*a*) W. GORDY. J. Chem. Phys. **14**, 560 (1946); (*b*) B. BAK, O. NIELSEN, and H. SVANHOLT. J. Mol. Spectrosc. **75**, 134 (1979).
25. R. F. CURL. J. Chem. Phys. **30**, 529 (1959).
26. J. C. DECIUS. J. Chem. Phys. **17**, 1315 (1949).
27. A. POZEFSKY and N. D. COGGESHALL. Anal. Chem. **23**, 1611 (1951).
28. L. J. BELLAMY. The infrared spectra of complex molecules. Vol. 1. 3rd ed. Chapman and Hall, London. 1975. p. 27.
29. D. HADZI. *In* Infrared spectroscopy and molecular structure. *Edited by* M. Davies. Elsevier, Amsterdam. 1963. Chapt. 7.
30. R. MATHIES, G. EYRING, B. CURRY, A. BROEK, I. PALINGS, R. FRANSEN, and J. LUGTENBURG. Proc. Seventh Int. Conf. Raman Spectrosc. *Edited by* W. F. Murphy. North Holland. 1980. p. 546.
31. N. NOGAMI, H. SUGETA, and T. MIYAZAWA. Bull. Chem. Soc. Jpn. **48**, 2417 (1975).
32. R. G. SNYDER and J. H. SCHACHTSCHNEIDER. Spectrochim. Acta, **21**, 169 (1965).
33. B. NOLIN and R. N. JONES. Can. J. Chem. **34**, 1392 (1956).
34. N. B. COLTHUP, L. H. DALY, and S. E. WIBERLEY. Introduction to infrared and Raman spectroscopy. Academic Press, New York. 1975. p. 228.
35. A. C. ALBRECHT and M. C. HUTLEY. J. Chem. Phys. **55**, 4438 (1971).

Can. J. Chem. Downloaded from www.nrcresearchpress.com by 210.87.254.105 on 09/06/12
For personal use only.

# The Raman and resonance Raman spectra of some substituted dialkyl dithioesters and their rotational isomers[1]

Y. OZAKI, A. C. STORER, AND P. R. CAREY[2]

*Division of Biological Sciences, National Research Council of Canada, Ottawa, Ont., Canada K1A 0R6*

Received May 21, 1981

Y. OZAKI, A. C. STORER, and P. R. CAREY. Can. J. Chem. **60**, 190 (1982).

The Raman spectra of ethyl dithioacetate, methyl dithiopropionate, and ethyl thionoacetate are presented for the liquid phase at 25°C and for the solid phase at approximately −130°C. Certain spectral features disappear upon going from the liquid to the solid phase allowing the assignment of these bands to rotational isomers which are present in the liquid state only. The consequences of placing a *tert*-butyl group proximal to the CSS moiety in dithioesters are explored by considering the absorption, Raman, and resonance Raman spectra of ethyl dithiotrimethylacetate and *tert*-butyl dithioacetate. The resonance Raman spectra of the ionized and unionized forms of dithioacetic acid are also presented. The vibrational spectra of ethyl thiolacetate, and ethyl and methyl thionoacetate are compared to the spectra of the corresponding dithioesters.

Y. OZAKI, A. C. STORER et P. R. CAREY. Can. J. Chem. **60**, 190 (1982).

On présente les spectres Raman du dithioacétate d'éthyle, du dithiopropionate de méthyle et du thionoacétate d'éthyle en phase liquide à 25°C et en phase solide à environ −130°C. Certaines caractéristiques spectrales disparaissent quand on passe de la phase liquide à la phase solide; on peut donc attribuer ces bandes aux isomères de rotation qui sont présents uniquement dans la phase liquide. On a étudié l'influence d'un groupe *tert*-butyle placé au voisinage de la portion CSS des dithioesters en se basant sur l'absorption, les spectres Raman et de résonance Raman du dithiotriméthylacétate d'éthyle et du dithioacétate de *tert*-butyle. On présente également les spectres Raman des formes ionisées et non ionisées de l'acide dithioacétique. On compare les spectres de vibration du thioacétate d'éthyle et des thionoacétates d'éthyle et de méthyle aux spectres des dithioesters correspondants.

[Traduit par le journal]

## Introduction

In the preceding paper (1) we presented data on the infrared, Raman, and resonance Raman (RR) spectra of methyl and ethyl dithioacetates and their isotopically substituted analogs. In the present work we have sought to identify the effects on the vibrational spectra of rotational isomerism about the bonds adjacent to the dithioester moiety. These data are crucial to our understanding of the spectra of more complex dithioesters (2) and, eventually, to our interpretation of the RR spectra of certain enzyme–substrate complexes containing the dithioester group (3). Specifically, we present herein the liquid and solid phase spectra of

$CH_3(C{=}S){-}S{-}CH_2{-}CH_3$,
$CH_3{-}CH_2{-}C(=S){-}S{-}CH_3$,
and $CH_3{-}C(=S){-}O{-}CH_2{-}CH_3$

which provide information on the consequences of rotational isomerism about the bonds indicated.

It is also important for us to delineate the consequences of steric hindrance about the dithioester moiety and to this end we present Raman and RR spectra of $(CH_3)_3CC(=S)SC_2H_5$ and $CH_3C(=S)SC(CH_3)_3$. Finally, our study of enzyme–substrate reactions requires characterization of the Raman and RR spectra of thiono- and thiolesters and of dithioacids; and hence, data for these compounds are presented herein and compared with the data for the corresponding dithioesters.

## Experimental

### *Materials*

Methyl dithiopropionate, *tert*-butyl dithioacetate and ethyl dithiotrimethylacetate were synthesized from their respective nitriles and mercaptans as outlined for ethyl and methyl dithioacetates in the foregoing publication (1). Methyl and ethyl thionoacetates were obtained by a procedure similar to that used for the dithioesters, the only difference being the substitution of alcohols for mercaptans. Dithioacetic acid was prepared from methyl magnesium iodide and carbon disulphide by the method of Houben and Pohl (4). Ethyl thiolacetate was prepared by the action of acetyl chloride on ethyl mercaptan. The purity of all samples was checked by nmr, and elemental analysis gave results within 2% of the calculated values.

### *Methods*

The Raman, RR, infrared, and absorption spectra were recorded using the equipment listed in the preceding paper (1). The low temperature Raman spectra were recorded using a modified Miller–Harney cell (5).

## Results and discussion

### *Absorption spectra*

The absorption maxima of the thiol-, thiono-, and dithioesters studied in the present work are listed in Table 1, where two important generalizations emerge. Firstly, by comparing the thiono- and dithioesters it is seen that the substitution of S for O brings about a very large red shift in the lowest energy $\pi \rightarrow \pi^*$ transition, from about 238 to 305 nm. This provides further support for the conclusion reached in the foregoing paper (1) that

[1]NRCC No. 19739.

[2]To whom all correspondence should be addressed.

0008-4042/82/020190-09$01.00/0

©1982 National Research Council of Canada/Conseil national de recherches du Canada

Can. J. Chem. Downloaded from www.nrcresearchpress.com by 210.87.254.5 on 09/06/12
For personal use only.

TABLE 1. The absorption maxima of various sulfur substituted esters in $CH_3CN$

| Compound | $\lambda_{max}$[b] $\pi \rightarrow \pi^*$ | $n \rightarrow \pi^*$ |
|---|---|---|
| $CH_3C(=O)SC_2H_5$ | 229 | |
| $CH_3C(=S)OCH_3$ | 238[c] | 303[e] |
| $CH_3C(=S)OC_2H_5$ | 239[c] | 368[e] |
| $CH_3C(=S)SC_2H_5$ | 209, 305.5[d] | 452 |
| $C_2H_5C(=S)SCH_3$ | 210.5, 302.5[d] | 452[e] |
| $(CH_3)_3CC(=S)SC_2H_5$ | 213, 308[d] | 463[e] |
| $CH_3C(=S)SC(CH_3)_3$ | 210, 306[d] | 473[e] |
| $CH_3C(=S)SH$ | 203, 296, 338 (wk, sh) | 415 |
| $CH_3CS_2^-$[a] | 212, 244 (sh), 332 | 391.5, 430 (sh) |

[a] In $H_2O$ pH 6.8.
[b] wk = weak, sh = shoulder.
[c] $\log_{10} \varepsilon \approx 3.9$.
[d] $\log_{10} \varepsilon \approx 4.1$.
[e] $\log_{10} \varepsilon \approx 1.25$.

the thiol sulfur in dithioesters makes an important contribution to the intense absorption band near 305 nm. Secondly, in dithioesters, the position of the lowest energy $\pi \rightarrow \pi^*$ transition is relatively insensitive to the nature of the alkyl groups. A further point is that this transition is also insensitive to change in solvent, e.g., the ethyl dithioacetate $\lambda_{max}$ is at 307 nm in $CCl_4$ and at 306 nm in $CH_3CN$.

*The vibrational spectra of ethyl thiolacetate, and ethyl and methyl thionoacetate*

The Raman spectra of the title compounds, taken as neat liquids, are shown in Fig. 1. Infrared spectra were also recorded and although the infrared data are not presented, they are mentioned wherever appropriate in the text. Table 2 lists the assignments for vibrational frequencies of ethyl dithioacetate and the corresponding thiol- and thionoacetates. The analyses for ethyl and methyl dithioacetates in the preceding paper (1) were of value in making assignments for the present compounds. Thus, the assignments of the $CH_3$ antisymmetric and symmetric deformation modes of the $CH_3$—C and —$CH_2$—$CH_3$ methyl groups, and the —$CH_2$ wagging and scissoring modes are consonant with those made for the dithioesters (1). Similarly, the assignments in Table 2 of the $CH_3$ rocking modes in the 975–850 $cm^{-1}$ region and the assignments of the C—C stretching modes between 1100 and 1050 $cm^{-1}$ parallel those for the dithioesters.

For ethyl thiolacetate the bands at 681 and 626 $cm^{-1}$ are assigned, respectively, to the S—C and C—S modes of the —C(=O)—S—$C_2H_5$ group. The band at 626 $cm^{-1}$ is very intense in the Raman spectrum and fairly intense in the infrared spectrum, while the 681 $cm^{-1}$ feature is of medium intensity in the Raman spectrum and weak in the infrared. Again, this is analogous to the situation found in the dithioesters (1) and it is unlikely that the S—C and C—S vibrations are strongly coupled. Thus the designation of the bands to the vibrations of individual bonds is preferred over an assignment to C—S—C symmetric and antisymmetric modes. A similar situation is found in dialkyl thioethers where Nogami and co-workers (6, 7) concluded that stretching vibrations within the C—S—C groups usually were not strongly coupled. This situation contrasts that found for the thionoesters in which the stretching modes of the C—O—C group do appear to be strongly coupled. Methyl thionoacetate has a feature at 701 $cm^{-1}$ which is very intense in the Raman spectrum but absent, or very weak, in the infrared spectrum. However, the mode at 1268 $cm^{-1}$ is weak in the Raman spectrum but very intense in the infrared. These observations suggest that the 701 and 1268 $cm^{-1}$ bands are most suitably described as the symmetric and antisymmetric C—O—C stretching modes, respectively. A similar situation is obtained for ethyl thionoacetate except for the appearance of two symmetric stretch bands at 692 and 724 $cm^{-1}$ due to the presence of two rotational isomers (below).

The band near 1222 $cm^{-1}$ in the Raman spectra of methyl and ethyl thionoacetate is assigned to a mode possessing a high degree of C=S stretching character. This assignment is supported by the infrared studies of several authors (8–10) and by the Raman excitation profile. The Raman spectra of ethyl thionoacetate in 1% (v/v) $CH_3CN$ were measured with 324, 337.5, 350.6, and 356.4 nm excitation. Excitation in the near-uv resulted in the intensity enhancement of the 543, 692, 724, 1103, 1222, and 1262 $cm^{-1}$ features seen in the 514.5 nm excited spectrum shown in Fig. 1. Going from 356.4 to 324 nm excitation resulted in the following enhancements with the intensity at 356.4 nm standardized to 1.0: 543 (1.2), 1103 (1.25), 692 (1.5), 724 (1.6), 1262 (1.9), and 1222 (2.6). The pronounced enhancement of the 1222 $cm^{-1}$ band with decreasing excitation wavelength supports the assignment of this band to $\nu_{C=S}$. An even more pronounced effect is seen upon going from 514.5 to 324 nm excitation: the intensity of the 1222 $cm^{-1}$ peak with 324 nm excitation is approximately twice as great as that of the 543 $cm^{-1}$ peak, whereas with 514.5 nm excitation the same intensity ratio is about 0.3 (Fig. 1). It is also apparent that the features at 1262 and 724, 692 $cm^{-1}$ which we have associated with the C—O—C antisymmetric and symmetric stretches show a high degree of intensity enhancement with uv excitation. It is likely, therefore, that vibrational coupling is prevalent and that the C=S and C—O—C bonds undergo geometric changes upon

Can. J. Chem. Downloaded from www.nrcresearchpress.com by 210.87.254.5 on 09/06/12
For personal use only.

Downloaded from www.nrcresearchpress.com by 210.87.254.5 on 09/06/12
For personal use only.

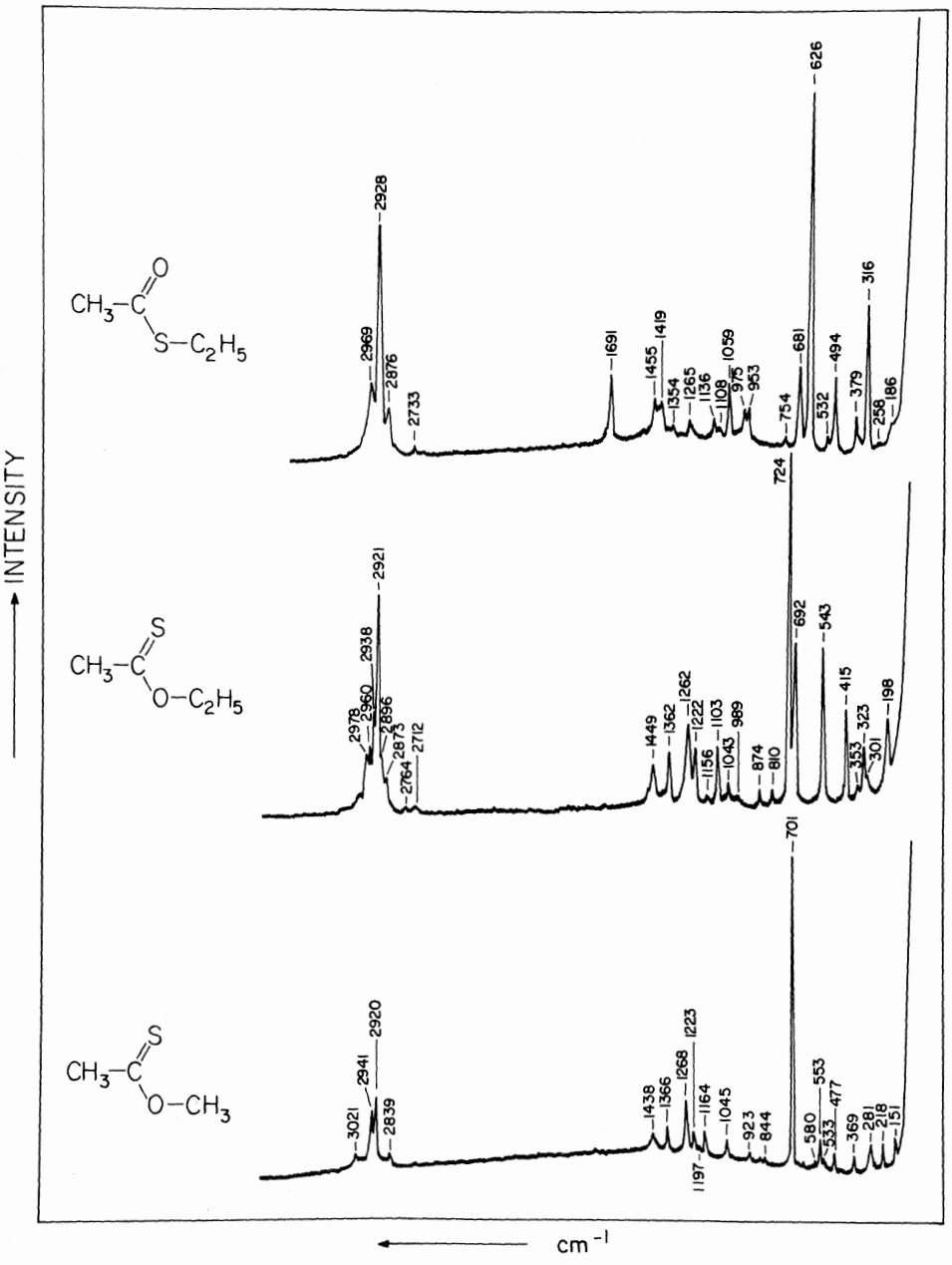


FIG. 1. The 514.5 nm excited Raman spectra of ethyl thiolacetate and methyl and ethyl thionoacetates as neat liquids. Laser power 50 mW; spectral slit width 8 $cm^{-1}$.

going from the ground to the excited electronic state.

*Comparisons between the vibrational spectra of simple dithio-, thiono- and thiolesters*

A mode having a high degree of $\nu_{C=S}$ character appears near 1195 $cm^{-1}$ in dithioesters, whereas it appears near 1222 $cm^{-1}$ in thionoesters. In both cases marked preresonance enhancement is observed. However, for dithioesters $\nu_{C=S}$ is very intense in the normal Raman spectrum and infrared whereas for thionoesters $\nu_{C=S}$ is weak in the Raman effect and intense in the infrared.

Both ethyl dithioacetate and ethyl thiolacetate have a feature near 680 $cm^{-1}$ assigned to a S—C stretching mode, whereas their C—S stretching modes are located near 580 and 626 $cm^{-1}$, respectively. Shoulders on the 580 and 680 $cm^{-1}$ features

TABLE 2. The frequencies of Raman bands and their assignments of ethyl dithioacetate, ethyl thiolacetate, and ethyl thionoacetate

| Frequency | | | |
|---|---|---|---|
| $CH_3CS_2C_2H_5$ | $CH_3C(=O)SC_2H_5$ | $CH_3C(=S)OC_2H_5$ | Tentative assignments |
| | 1691 | | C=O stretching |
| | 1455 (b) | 1449 (b) | $CH_3$ antisymmetric deformation ($CH_2$—$CH_3$, $CH_3$—C) |
| 1453 | | | $CH_3$ antisymmetric deformation ($CH_2$—$CH_3$) |
| 1426[a] | | | $CH_3$ antisymmetric deformation ($CH_3$—C) |
| 1400 | 1419 | | $CH_2$ scissoring |
| 1374[a] | | | $CH_3$ symmetric deformation ($CH_2$—$CH_3$) |
| 1356 | 1354 | 1362 | $CH_3$ symmetric deformation ($CH_3$—C) |
| 1270[a] | 1265 | | $CH_2$ wagging |
| | | 1262 | C—O—C antisymmetric stretching |
| 1192 | | 1222 | C=S stretching |
| | 1136 | 1156 | |
| 1100 | 1108 | | C—C ($CH_3$—C) + C—S stretching |
| 1052 | 1059 | 1103 | C—C stretching ($CH_2$—$CH_3$) |
| | | 1043 | C—C stretching ($CH_3$—C)? |
| 971 | 975 | 989 | |
| 911 | 953 | 874 | $CH_3$ rocking ($CH_2$—$CH_3$, $CH_3$—C) |
| 864 | | 810 | |
| 747 | 754 | | $CH_2$ rocking[b] |
| | | 724 | C—O—C symmetric stretching |
| | | 692 | |
| 697 | 681 | | S—C stretching (—S—$CH_2$) |
| 681 | | | |
| 589 | 626 | | C—S + C=S + C—C stretching (C—C(=S)—S) |
| 579 | | | |

[a] Infrared bands. (b); broad.
[b] Reference 7.

of ethyl dithioacetate provide evidence for the presence of two rotational isomers (below) but no such evidence was found for ethyl thiolacetate. For ethyl dithioacetate and ethyl thiolacetate it is probable that the S—C stretch is coupled to the C—C stretching mode of the $SCH_2$—$CH_3$ group. This C—C mode occurs near 1055 $cm^{-1}$ for ethyl dithioacetate and ethyl thiolacetate and at 1103 $cm^{-1}$ in the spectrum of ethyl thionoacetate.

*Consequences of placing bulky groups in dithioesters*

Ethyl dithiotrimethylacetate and *tert*-butyl dithioacetate were examined as examples of compounds possessing sterically large groups on the thioacetyl and thiol functions, respectively. The major interest lies in the effect of the bulky groups on the appearance of the regions between 1200 and 1050 $cm^{-1}$ and between 750 and 500 $cm^{-1}$ wherein the most intense RR features of the dithioester group occur. The Raman spectra of ethyl dithiotrimethylacetate, and *tert*-butyl dithioacetate are shown in Fig. 2 and the RR spectra of these compounds are shown in Fig. 3.

For ethyl dithiotrimethylacetate, an intense band is observed at 1103 $cm^{-1}$ in the Raman and infrared spectra and the band is strongly enhanced in the RR spectrum. No other band is observed in the 1205–1060 $cm^{-1}$ region except for a weak infrared shoulder at 1191 $cm^{-1}$. Hence, the band at 1103 $cm^{-1}$ probably has C=S stretching character. Consistent with this conclusion Mayer *et al.* (11) pointed out mainly from the results of infrared spectra that aliphatic alkyl dithiocarboxylates of type *A* have a C=S stretching mode near 1100 $cm^{-1}$.

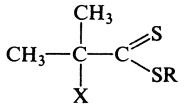


Type *A*, R = $CH_3$, $C_2H_5$; X = $CH_3$, Cl, OH

The low frequency shifts of the C=S stretching mode in the type *A* dithioesters may result from steric hindrance changing the geometry of the dithioester group from that found in unhindered compounds. Since in *tert*-butyl groups C—C stretching vibrations coupled with $CH_3$ rocking modes are usually observed between 1250–1130 $cm^{-1}$ and 950–810 $cm^{-1}$ (12), the Raman band at 1227 $cm^{-1}$ is ascribed to a vibration mode of the *tert*-butyl group. This assignment is supported by the fact that no band is located near 1230 $cm^{-1}$ in the Raman spectrum of methyl or ethyl dithioacetate (1). The dithiotrimethylacetate Raman band at 1049 $cm^{-1}$ is very weak or absent in the RR spectrum as in the

Can. J. Chem. Downloaded from www.nrcresearchpress.com by 210.87.254.5 on 09/06/12
For personal use only.

Can. J. Chem. Downloaded from www.nrcresearchpress.com by 210.87.254.5 on 09/06/12
For personal use only.

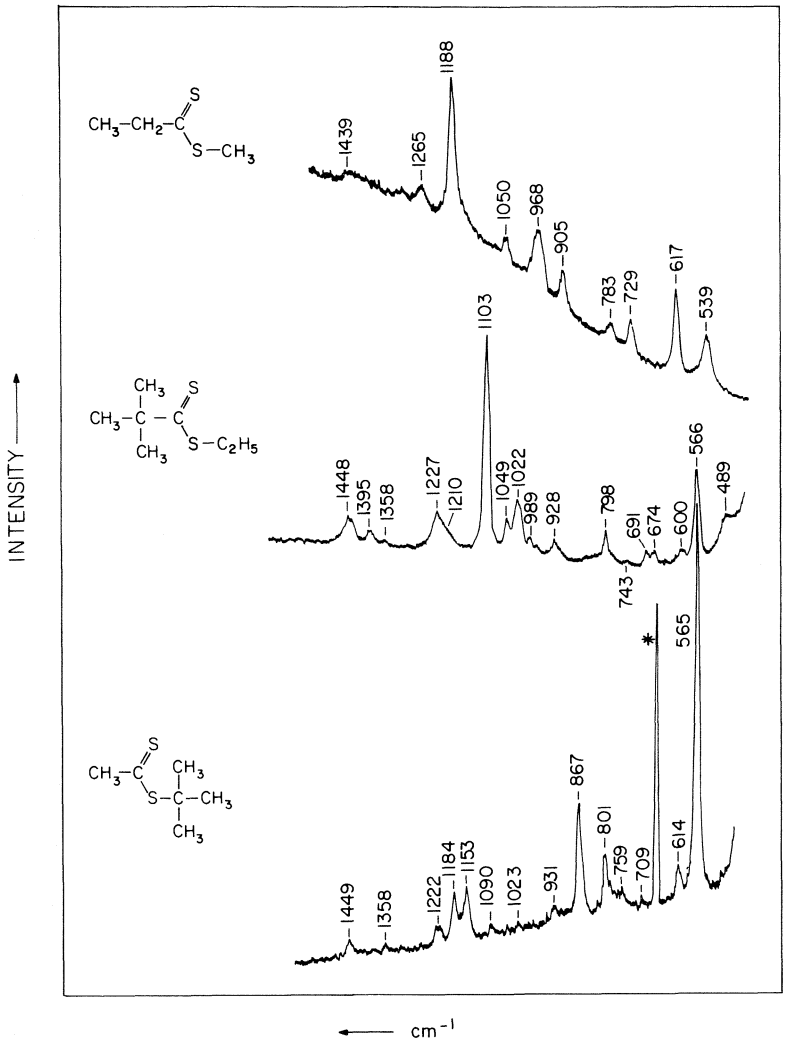


FIG. 2. The 514.5 nm excited Raman spectra of methyl dithiopropionate and ethyl dithiotrimethylacetate and the 647.1 nm excited spectrum of *tert*-butyl dithioacetate as neat liquids. Laser power 50 mW (514.5 nm), 100 mW (647.1 nm); 8 $cm^{-1}$ spectral slit. The asterisk marks a laser plasma line.

case of the 1052 $cm^{-1}$ band of ethyl dithioacetate; thus, the band at 1049 $cm^{-1}$ is ascribed to the C—C stretching mode of the $—CH_2—CH_3$ group. In contrast to the band at 1049 $cm^{-1}$, the band at 1027 $cm^{-1}$ is fairly intense in the RR spectrum; therefore, this band may be ascribed to a mode involving the C—C and C—S stretching motions of the C—C(=S)—S group. From a comparison of the spectrum of ethyl dithiotrimethylacetate with the spectrum of ethyl dithioacetate, the bands at 674 and 566 $cm^{-1}$ are assigned to the S—C and (C—S + C=S + $(CH_3)_3C$—C) stretching modes, respectively. The 681–697 $cm^{-1}$ profile in the Raman spectrum of ethyl dithioacetate has a depolarization ratio of 0.75 (1) whereas the 674–691 $cm^{-1}$ profile (Fig. 2) of dithiotrimethylacetate has a depolarization ratio of 0.60 ± 0.05.

The overall appearance of the RR spectrum of *tert*-butyl dithioacetate (Fig. 3) in the 1200–800 $cm^{-1}$ region is similar to the RR spectra of methyl and ethyl dithioacetate. The Raman band at 1184 $cm^{-1}$ is strongly intensity enhanced and is assigned to a mode possessing a high degree of C=S stretching character. The origin of the shoulder at 1159 $cm^{-1}$ in the RR spectrum of *tert*-butyl dithioacetate is not understood. The shoulder is reduced in intensity compared to the 1184 $cm^{-1}$ as excitation wavelength is reduced, and one possible source for the shoulder is the presence of more than one rotational isomer about the S—$C(CH_3)_3$ bond. Space filling

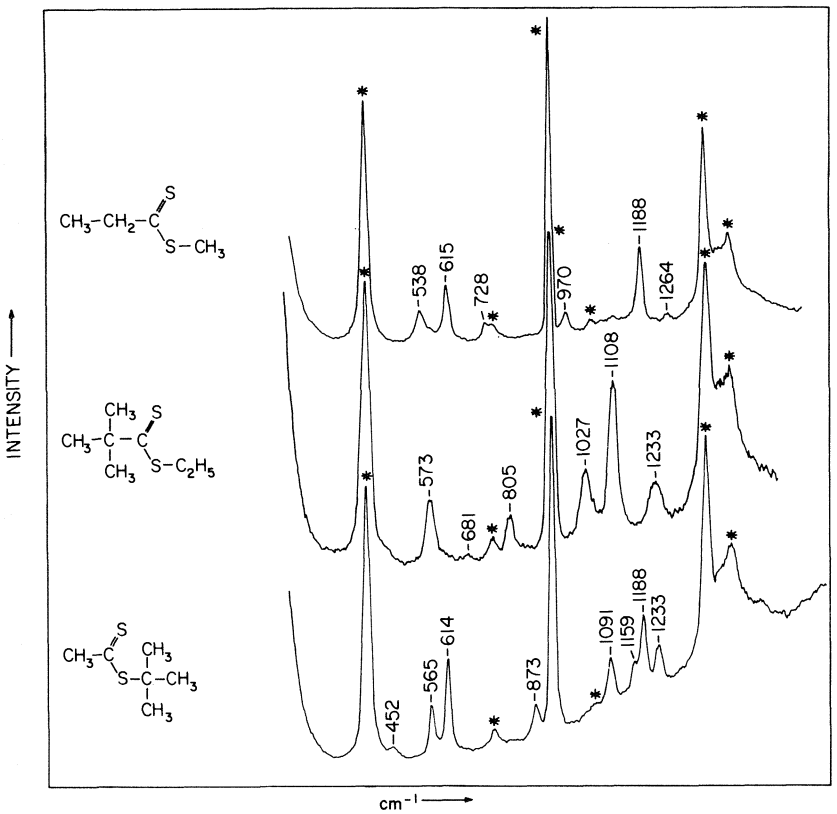


FIG. 3. The 324 nm excited RR spectra of methyl dithiopropionate, ethyl dithiotrimethylacetate and *tert*-butyl dithioacetate in 0.01% (v/v) $CH_3CN$ solutions. Laser power 10 mW; 8 $cm^{-1}$ spectral slit. $CH_3CN$ features are marked by an asterisk.

models show that in any isomer there is steric contact between the C=S sulfur and the *tert*-butyl methyl groups. The band at 1090 $cm^{-1}$ is intense in the infrared spectrum, weak in the Raman effect but becomes relatively more intense with 324 nm excitation (Figs. 2 and 3). This parallels the behaviour of the 1100 $cm^{-1}$ band of ethyl and methyl dithioacetate and, hence, the 1090 $cm^{-1}$ band is assigned to C—S + C—C stretching motions of the $CH_3$—C—S moiety. A possible origin of the 1222 $cm^{-1}$ Raman feature is a motion within the *tert*-butyl group corresponding to a C—C stretch coupled to $CH_3$ rocking modes. Interestingly, there is a band of moderate intensity at 867 $cm^{-1}$ in the Raman, RR, and infrared spectra of *tert*-butyl dithioacetate which probably corresponds to the 864 $cm^{-1}$ band of methyl and ethyl dithioacetate. Thus, the 867 $cm^{-1}$ band is assigned to a $CH_3$ rocking motion of the $CH_3$—C(=S) group. As might be expected, the 500–800 $cm^{-1}$ or "C—S stretching" spectral regions of *tert*-butyl and ethyl dithioacetates are markedly different. For the *tert*-butyl compound both bands at 614 and 565 $cm^{-1}$ can be ascribed to C—S or S—C stretching modes although we do not make specific assignments. The 614 $cm^{-1}$ band undergoes strong resonance enhancement (Fig. 3) and for this reason may be more associated with the C—S bond since the latter is more intimately involved with the chromophore.

Finally, we consider dithioacetic acid. The RR spectrum of dithioacetic acid in the $CH_3CSSH$ form (Fig. 4) strongly resembles the RR spectrum of methyl dithioacetate. The features at 1212 and 596 $cm^{-1}$ are analogous to methyl dithioacetate bands near 1194 and 580 $cm^{-1}$ (1), and the corresponding C—S + C—C (1073 $cm^{-1}$) and methyl rocking motions (845 $cm^{-1}$) are prominent too. The assignment of the 1212 $cm^{-1}$ band to essentially $\nu_{C=S}$ agrees with an earlier assignment made on the basis of Raman and infrared data (13). In the RR spectrum of the $CH_3CSS^-$ form (Fig. 4) the bands at 607 and 1103 $cm^{-1}$ are assigned to the $-CS_2^-$ symmetric and antisymmetric stretches, respectively.

*Rotational isomers of dithio- and thionoesters*

We have previously reported a Raman study on the rotational isomers of ethyl thionoacetate and

Can. J. Chem. Downloaded from www.nrcresearchpress.com by 210.87.254.5 on 09/06/12
For personal use only.

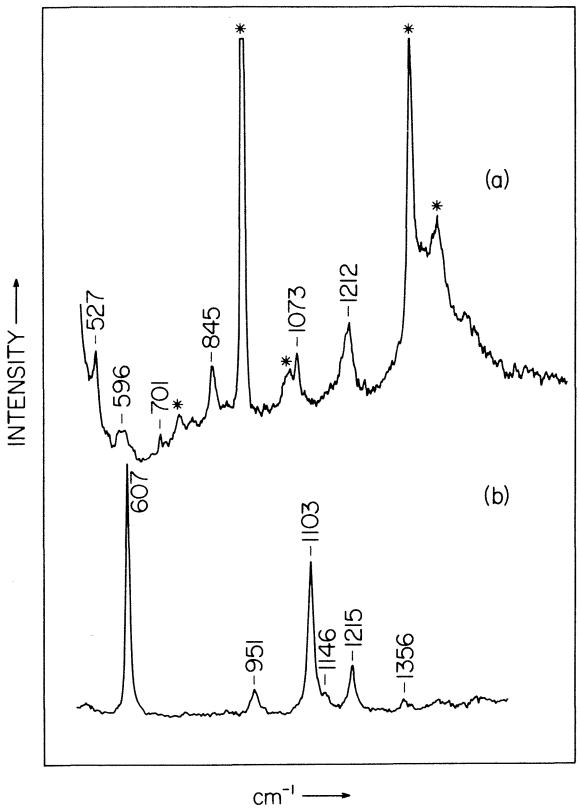


FIG. 4. The 351.6 nm excited RR spectra of dithioacetic acid in 0.01% (v/v) $CH_3CN$ solution, $CH_3CS_2H$ (*a*) and in water at pH 12.3, $CH_3CS_2^-$ (*b*). Laser power 40 mW; 8 $cm^{-1}$ spectral slit. $CH_3CN$ features are marked with an asterisk.

ethyl dithioacetate (14). However, only partial spectral data was given in ref. 14 and we now present complete Raman spectra in the 20–1500 $cm^{-1}$ range. Ethyl thiono- and dithioacetate provide information on the consequences of rotational isomerism about the O—$CH_2$ and the S—$CH_2$ bonds, respectively. In order to explore the consequences of rotational isomerism in the C—C(=S) linkage we also present data on methyl dithiopropionate, $C_2H_5C(=S)SCH_3$.

The Raman spectra of ethyl dithioacetate, methyl dithiopropionate, and ethyl thionoacetate at 25°C and approximately −130°C are shown in Fig. 5. At ~ −130°C the compounds are in the solid phase and the vibrational features which disappear upon solidification have been marked with asterisks. The disappearance of a band is ascribed to the disappearance of a rotational isomer (14); there are two isomers in solution, only one of which remains in the solid phase. For ethyl dithioacetate and ethyl thionoacetate it is thought that the low energy form (which is the one remaining upon solidification) is the *S-cis* with all the heavy atoms in a single plane (14), as shown in Fig. 6.

In the high energy form the —$CH_2CH_3$ methyl moiety rotates by 120° about the X—$CH_2$ bond. The enthalpy differences for the two forms are 598 ± 48 and 1072 ± 65 cal/mol for the ethyl dithio- and thionoacetates, respectively (14). Previously, for ethyl dithioacetate we only discussed the 579 and 589 $cm^{-1}$ bands but now the effect of solidification on the entire spectrum can be seen by referring to Fig. 5. At −132°C the only changes in the 1500–500 $cm^{-1}$ region of the Raman spectrum of ethyl dithioacetate are the disappearance of the 697 and 589 $cm^{-1}$ bands. Thus, we assign the 697 and 589 $cm^{-1}$ features to the S—C and (C—S + C=S + C—C) motions respectively, of the non-polar isomer. The 681 and 579 $cm^{-1}$ bands are the corresponding modes of the planar isomer. Similarly, for ethyl thionoacetate the "disappearing" 692 $cm^{-1}$ feature is ascribed to the C—O—C symmetric stretch of the non-planar rotamer and the 724 $cm^{-1}$ band to the planar rotamer. The situation near 1260 $cm^{-1}$ where the antisymmetric C—O—C stretch occurs is less clear due to the overlap of other spectral features. Importantly, for ethyl dithioacetate we find no evidence for rotational isomerism affecting the C=S stretching region between 1200 and 1050 $cm^{-1}$.

The spectral properties of methyl dithiopropionate have not been discussed hitherto. The Raman and RR spectra are given in Figs. 2 and 3, respectively. By analogy to the compounds discussed above and in ref. 1, the strongly enhanced features at 1188 and 615 $cm^{-1}$ may be assigned to motions involving stretching of the C=S and (C—S + C=S + C—C) bonds, respectively. Interestingly, there is no evidence for a band near 1100 $cm^{-1}$ which would be analogous to the (C—S + C—C) mode found in ethyl and methyl dithioacetate (1). The change in vibrational coupling brought about by the $CH_3CH_2C(=S)$'s methyl group and the effect of rotational isomerism about the $CH_2$—C bond on the normal modes is under active study. The 729 $cm^{-1}$ band is assigned to a mode containing a high degree of S—$CH_3$ stretching character, again by analogy with the foregoing molecules. In the Raman spectrum of the solid state (Fig. 5) the 539 $cm^{-1}$ feature disappears. This band is strongly enhanced in the RR spectrum (Fig. 3) and is therefore assigned to a C—S stretch, with additional unknown contributions from C=S and C—C stretches, for a rotational isomer different from that which gives rise to the 617 $cm^{-1}$ band. Some support for the idea that the C—S stretch is very

Can. J. Chem. Downloaded from www.nrcresearchpress.com by 210.87.254.5 on 09/06/12
For personal use only.

Can. J. Chem. Downloaded from www.nrcresearchpress.com by 210.87.254.5 on 09/06/12
For personal use only.

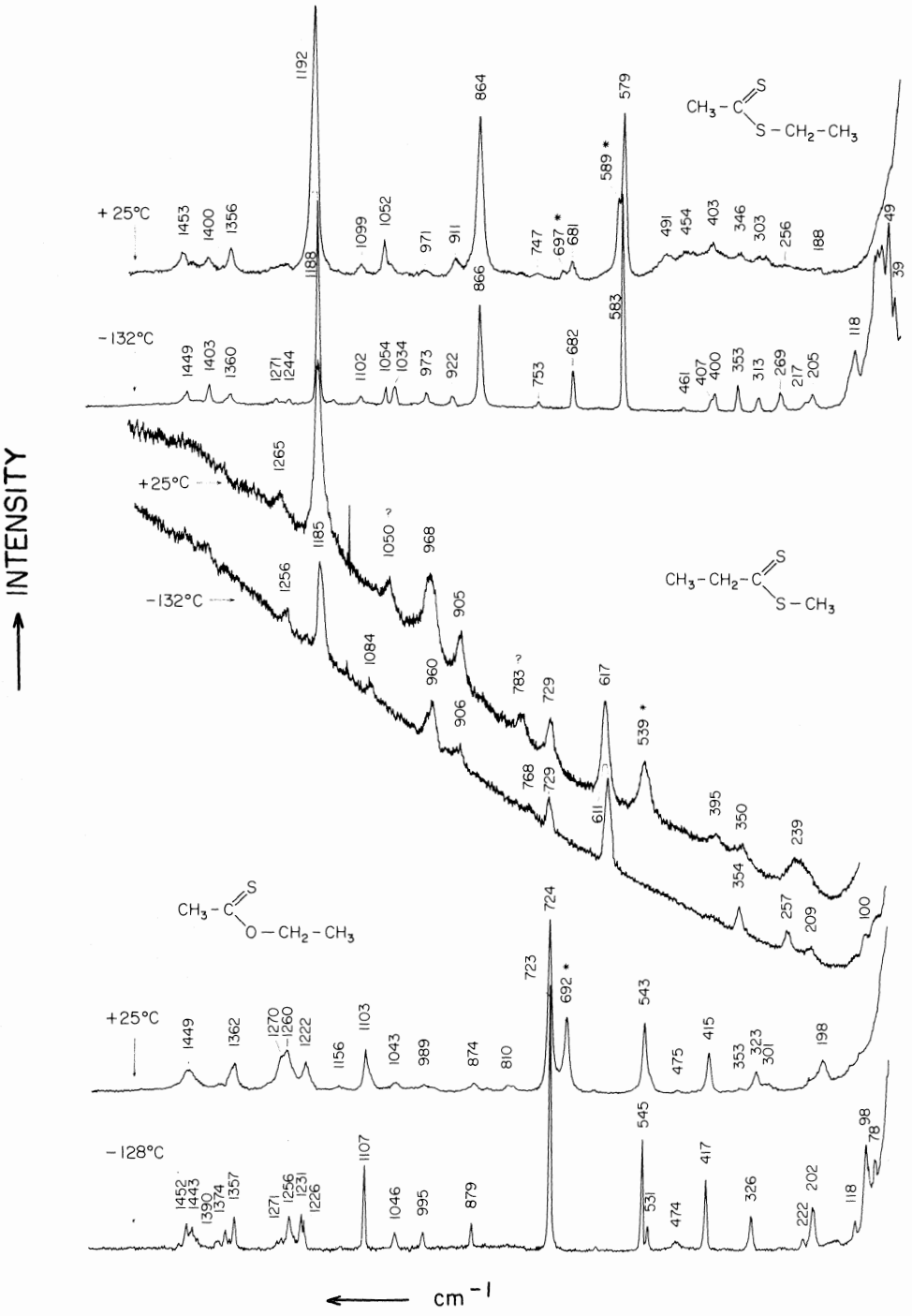


FIG. 5. The 514.5 nm excited Raman spectra of ethyl dithioacetate, methyl dithiopropionate and ethyl thionoacetate at 25°C and ≈ −130°C. Laser power 50–100 mW; 8 $cm^{-1}$ spectral slit. Bands marked with an asterisk are those which disappear in the low temperature, solid phase spectra.

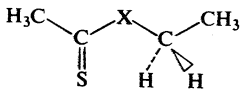


FIG. 6. The preferred conformer for ethyl dithioacetate (X = S) and ethyl thionoacetate (X = O).

sensitive to rotational isomerism comes from Nogami, Sugeta, and Miyazawa's work on dialkyl thioethers (6). These authors have documented the effect of rotational isomerism in, for example, $(CH_3)_2CHCH_2$—S—$CH_3$ on the C—S and S—C stretching modes. They found that the isomer with the H and S *trans* in a projection along the CH—$CH_2$ bond has $\nu_{C-S}$ some 70 $cm^{-1}$ lower compared to the rotamer in which the $CH_3$ and S groups are *trans* across the CH—$CH_2$ bond. In Fig. 5 it also appears that the bands in the room temperature spectrum at 1050 and 783 $cm^{-1}$ have either disappeared in the solid phase spectrum or have shifted to 1084 and 768 $cm^{-1}$, respectively. If the 783 $cm^{-1}$ band has disappeared it is possible that this feature is due to the S—$CH_3$ stretching feature of the same isomer as that giving rise to the 539 $cm^{-1}$ band. Attempts were made to measure the intensity ratio of the 617 and 539 $cm^{-1}$ bands as a function of temperature and thereby calculate the enthalpy difference between the rotamers. The ratio showed only a small change with temperature, for example $I_{617}/I_{539} \approx 1.78$ at −12°C and $\approx 1.84$ at −93°C and there were large experimental errors in the measurement of the ratio. Consequently a reliable value for $\Delta H$ could not be obtained. Similarly we were not able to identify the nature of the rotamers in solution or the preferred form in the solid state. Although measurements were hampered by the sloping baseline (Fig. 5), there appeared to be no depolarized bands in the 1300–400 $cm^{-1}$ spectral range. The band at 729 $cm^{-1}$ has the highest depolarization ratio $\approx 0.60 \pm 0.05$. Thus, we are unable to prove that either of the rotational isomers in solution is planar.

Importantly, the results for $CH_3CH_2CS_2CH_3$ show that rotational isomerism about the $CH_2$—C bond can markedly perturb bands in the 800–500 $cm^{-1}$ region but, as Fig. 5 illustrates, appear to have little or no effect on the "C=S stretching region" between 1200 and 1050 $cm^{-1}$.

1. J. J. C. TEIXEIRA-DIAS, V. M. JARDIM-BARRETO, Y. OZAKI, A. C. STORER, and P. R. CAREY. Can J. Chem. **60**, 174 (1982).
2. A. C. STORER, Y. OZAKI, and P. R. CAREY. Can. J. Chem. **60**, 199 (1982).
3. A. C. STORER, W. F. MURPHY, and P. R. CAREY. J. Biol. Chem. **254**, 3163 (1979).
4. J. HOUBEN and H. POHL. Ber. **40**, 1303 (1907).
5. F. A. MILLER and B. M. HARNEY. Appl. Spectrosc. **24**, 291 (1970).
6. N. NOGAMI, H. SUGETA, and T. MIYAZAWA. Bull. Chem. Soc. Jpn. **48**, 2417 (1975).
7. N. NOGAMI, H. SUGETA, and T. MIYAZAWA. Bull. Chem. Soc. Jpn. **48**, 3573 (1975).
8. R. A. NYQUIST and W. J. POTTS. Spectrochim. Acta, **7**, 514 (1959).
9. A. W. BAKER and G. H. HARRIS. J. Am. Chem. Soc. **82**, 1923 (1960).
10. M. RENSON and J. BIDAINE. Bull. Soc. Chim. Belg. **70**, 519 (1961).
11. R. MAYER, E. SCHINKE, P. ROSMUS, and S. SCHEITHAUER. J. Prakt. Chem. **312**, 767 (1970).
12. N. B. COLTHUP, L. H. DALY, and S. E. WIBERLEY. Introduction to infrared and Raman spectroscopy. Academic Press, New York. 1975. p. 227.
13. R. MECKE and H. SPIESECKE. Chem. Ber. **89**, 1110 (1956).
14. A. L. VERMA, Y. OZAKI, A. C. STORER, and P. R. CAREY. J. Raman Spectrosc. In press.

Can. J. Chem. Downloaded from www.nrcresearchpress.com by 210.87.254.5 on 09/06/12
For personal use only.

# Resonance Raman spectroscopic evidence for an intramolecular interaction involving the amide and dithioester groups of *N*-acyl glycine ethyl dithioesters[1]

A. C. STORER, Y. OZAKI, AND P. R. CAREY

*Division of Biological Sciences, National Research Council of Canada, Ottawa, Ont., Canada K1A 0R6*

Received May 21, 1981

A. C. STORER, Y. OZAKI, and P. R. CAREY. Can. J. Chem. **60**, 199 (1982).

The synthesis and resonance Raman spectra of several new *N*-acyl glycine ethyl dithioesters RC(=O)NH—$CH_2$—C(=S)SR are reported. The resonance Raman spectra of these compounds contain at least two peaks in the "C=S stretching region" between 1050 and 1200 $cm^{-1}$. The solvent, concentration, temperature, and excitation wavelength dependencies of these features have been investigated. The results obtained are consistent with two conformations of the dithioesters co-existing in solution with the conformational differences being controlled by rotational isomerism about one or both of the NH—$CH_2$ and $CH_2$—CS bonds. Strong support for the existence of more than one conformer in solution comes from the Raman spectrum of a single crystal of *N*-acetyl glycine ethyl dithioester. In the spectrum of the single crystal several Raman bands are absent compared to the spectrum of the dithioester in solution indicating that only one of the conformers found in the solution phase is retained in the crystal. In one of the conformers found in solution there is evidence for an intramolecular interaction between the amide group and the dithioester group. The exact nature of the intramolecular interaction is uncertain, although simple H-bonding and enethiol tautomerism have been eliminated as possibilities. Possible contributors to the interaction are dipole–dipole forces and amide π-electrons interacting through space with sulfur $d_\pi$ orbitals. Both of these putative interactions would be modulated by rotational isomerism. Based on deuterium substitution experiments a resonance Raman band is identified in the 1050–1200 $cm^{-1}$ region which contains a contribution from the motion of the amide proton. The unexpected intensity enhancement of an amide mode is attributed to the amide–dithioester intramolecular interaction. The conformer exhibiting the intramolecular interaction is thought to closely resemble the conformation of the substrate in the active site of certain dithioester enzyme–substrate complexes.

A. C. STORER, Y. OZAKI et P. R. CAREY. Can. J. Chem. **60**, 199 (1982).

On rapporte la synthèse et les spectres Raman de plusieurs nouveaux dithiosters du *N*-acyl-glycine d'éthyle, RC(=O)NH—$CH_2$—C(=S)SR. Les spectres Raman de ces composés contiennent au moins deux pics dans la région d'élongation de la liaison C=S entre 1050 et 1200 $cm^{-1}$. On a étudié l'effet du solvant, de la concentration, de la température et de la longueur d'onde d'excitation sur ces caractéristiques. Les résultats obtenus sont en accord avec la présence de deux conformations des dithioesters qui co-existent en solution et dont les différences conformationnelles sont controllées par l'isomérie rotationnelle autour d'une ou des deux liaisons NH—$CH_2$, $CH_2$—CS. Le spectre Raman d'un monocristal de dithioester de *N*-acyl glycine d'éthyle fournit la meilleure preuve de l'existence de plus d'un conformère en solution. Plusieurs bandes Raman sont absentes dans le spectre du monocristal si on le compare avec le spectre du dithioester en solution, indicant ainsi que seulement un des conformères trouvés dans la solution est retenu dans le cristal. Dans l'un des conformères trouvés en solution, on rencontre des caractéristiques d'une interaction intramoléculaire entre le groupe amide et le groupe dithioester. La nature exacte de l'interaction intramoléculaire n'est pas certaine bien qu'on ait éliminé la liaison hydrogène simple et la tautomérie ènethiol comme d'éventuels responsables. L'interaction des forces dipôle–dipôle et les électrons π de l'amide interagissant à travers l'espace avec les orbitales du π du soufre sont éventuellement responsables de cette interaction. Ces deux interactions putatives peuvent être ajustées par l'isomérie rotationnelle. A partir d'expériences de substitution par du deutérium, on a identifié une bande de résonance Raman dans la région de 1050–1200 $cm^{-1}$ qui contient une contribution du mouvement du proton de l'amide. On attribue l'augmentation inattendue de l'intensité d'un mode amide à l'interaction intramoléculaire du dithioester–amide. On pense que le conformère présentant une intramoléculaire ressemble de près à la conformation du substrat dans le site actif de certains complexes enzyme dithioester substrat.

[Traduit par le journal]

## Introduction

This paper is the third of a series aimed at elucidating the vibrational spectroscopic properties of dithioesters with particular emphasis on the resonance Raman (RR) spectra of these compounds. The first paper (1) sought to define the normal modes of the simplest dithioesters, methyl and ethyl dithioacetate, while the second paper (2) dealt with the effects on the vibrational spectra of rotational isomerism about bonds in, for example, $CH_3CH_2$→C(=S)$SCH_3$ and $CH_3C$(=S)S→$CH_2$-$CH_3$. Both papers (1, 2) precede and accompany the present paper. The overall aim of this work is to aid the understanding of the RR spectra of transient dithioesters (3, 4) which are formed during enzyme substrate interactions (5, 6). The structure of the dithioester intermediates can be written as RC(=O)$NHCH_2$C(=S)S—enzyme where the thiol sulfur is from a cysteine in the enzyme's active site. We now report the synthesis and spectroscopic study of a series of six compounds of the type RC(=O)$NHCH_2$C(=S)$SC_2H_5$ which act, in some respects, as models for the enzyme–substrate intermediates. The dithioesters listed in

[1]NRCC No. 19740.

0008-4042/82/020199-11$01.00/0

©1982 National Research Council of Canada/Conseil national de recherches du Canada

Can. J. Chem. Downloaded from www.nrcresearchpress.com by 210.87.254.105 on 09/06/12
For personal use only.

Can. J. Chem. Downloaded from www.nrcresearchpress.com by 210.87.254.105 on 09/06/12
For personal use only.

Table 1 can be considered to be derivatives of *N*-acyl glycine. They were prepared as described under the Methods section and, to our knowledge, only compound **1** has been reported before (7).

A major finding of the present study is that the *N*-acyl glycine ethyl dithioesters exist in more than one conformation in solution. One of these conformers, in which there appears to be strong interaction between the amide and dithioester groups, is common to all the compounds studied. This conformer assumes special importance because, based on the spectral criteria, it resembles the conformation of the corresponding substrate in the active site of enzymes such as papain.

## Methods

Absorption spectra were obtained using a Cary 219 spectrophotometer. The apparatus used to obtain the resonance Raman spectra consisted of either a 3000K or a 2000K Coherent Radiation krypton ion laser with a Spex 0.5 m double spectrometer and direct current detection. The near-uv laser lines were separated using two Pellin–Broca prisms and plasma lines were removed from the selected laser line using a tunable grating filter F100 (PTR Optics Corp., Waltham, MA.). Raman spectra obtained with visible excitation were recorded using a Spectra-Physics model 164 Ar ion laser with a Jarell-Ash 25-400 spectrometer.

The sampling systems consisted of a flow cell for the resonance Raman spectra and a rotating cell for the Raman spectra. The variable temperature study was conducted using a small jacketed rotating cell. Under these conditions there was no evidence for photoisomerisation or photodegradation.

Peak frequencies were calibrated using emission lines from Ar and Ne lamps and are accurate to $\pm 2$ cm$^{-1}$. Peak heights were taken as reliable measures of band intensities for the variable temperature study.

*Synthesis*

The *N*-acyl glycine dithioesters and analogues listed in Table 1 were prepared by first treating their respective nitriles with dry HCl gas and an excess of ethanethiol using methylene chloride as solvent (the Pinner reaction) (7–10):

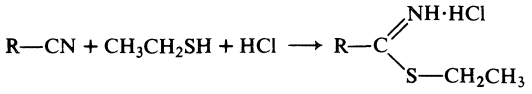

The thioimido ester hydrochlorides produced were treated with $H_2S$ dissolved in pyridine to give the corresponding dithioesters (7–9):

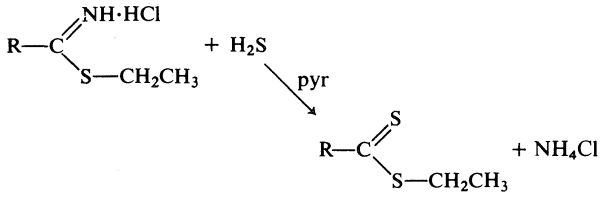

*Nitriles*

The nitriles for the synthesis of dithioesters **1**, **4**, **5**, and **6** (Table 1) were synthesised from aminoacetonitrile bisulphate and the corresponding acid chloride (**1**, **4**, and **5**) or acid chloroformate (**6**). The aminoacetonitrile bisulphate (0.1 equiv.) was dissolved in 50 mL of ice-cold water containing 0.2 equiv. NaOH. The chloride (or chlorformate) (0.1 equiv.) was added dropwise over a period of 30 min while a slightly alkaline pH was maintained by the addition of 5 *M* NaOH. The modified nitriles separated out as white solids which were collected by filtration, washed with cold water, and dried. They required no further purification. The nitriles used in the synthesis of dithioesters **2** and **3** were produced by the methods of Dinizo *et al.* (11) and Johnson and Gatewood (12), respectively.

*Thioimido esters*

The nitriles were converted to their thioimido ester hydrochloride salts by treatment for 30–60 min with dry HCl gas and excess ethanethiol in ice-cold methylene chloride. The thioimido ester salts produced were precipitated by the addition of anhydrous ether, collected by filtration, and washed with more ether. The thioimido ester salt produced for the synthesis of dithioester **3** is extremely hygroscopic and required careful handling. All the thioimido esters were stored in desiccators and used in the next synthetic step as soon as possible.

*Dithioesters*

The thioimido esters were added to pyridine saturated with $H_2S$ at 0°C and $H_2S$ was passed through the solution for 20 min after which the solution was allowed to stand 5 min. The deep yellow solution produced was then poured into sufficient ice-cold 4 *N* HCl to neutralise the pyridine and produce a slightly acidic pH. For some dithioesters crystals of the dithioester formed either immediately or on addition of ice-cold water. The crystals were collected by filtration and washed with water, then recrystallised from an acetone– water mixture. Dithioesters **2** and **4** formed orange or red oils when poured into the HCl solution. These dithioesters were extracted into ether, the ethereal solutions washed with water and dried over anhydrous $Na_2SO_4$. The ether was then removed by rotary evaporation. Dithioester **3** is soluble in water and so the HCl solution was extracted several times with ether and the combined ethereal extracts treated as above. The dithioesters were purified by passage down silica gel columns using 90% ether, 10% acetonitrile as solvent.

The results of elemental analysis of the dithioesters all agreed with the theoretical values to within 2%. The purity of all samples was checked by nmr. The yields obtained varied from about 10% for ester **3** to about 25% for ester **5**.

## Results and discussion

Aliphatic dithioesters normally possess an intense $\pi \rightarrow \pi^*$ absorption band in the range 305–310 nm (13). The $\lambda_{max}$'s and extinction coefficients of this transition, for most of the dithioesters discussed in this paper, were determined in a variety of solvents and are given in Table 2. Results obtained for ethyl dithioacetate are included in the table for comparison.

*(a) Evidence for two forms of dithioester in solution*

The RR spectra of solutions of compounds **1–6** (Table 1) are given in Figs. 1–6. Spectra, taken in several solvent systems, were obtained using 324 nm laser light excitation. The RR spectra of the compounds are more complex than those of ethyl and methyl dithioacetates discussed in the preceding paper (1). For these two simple esters in the region between 1050 and 1200 cm$^{-1}$ a single feature occurs near 1195 cm$^{-1}$. This band is assigned to a

TABLE 1. Dithioesters synthesised

| | |
|---|---|
| **1**, Ethyl dithiohippurate | 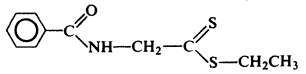 |
| **2**, Benzoyl hydroxyacetyl ethyl dithioester | 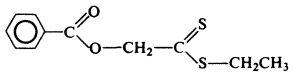 |
| **3**, *N*-acetyl glycine ethyl dithioester | 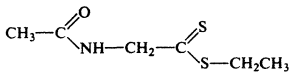 |
| **4**, *N*-phenylacetyl glycine ethyl dithioester | 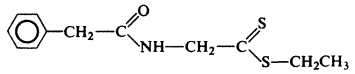 |
| **5**, *N*-β-phenylpropionyl glycine ethyl dithioester | 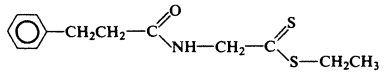 |
| **6**, *N*-carbobenzoxy glycine ethyl dithioester | 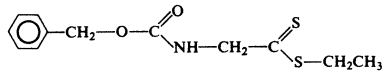 |

TABLE 2. $\lambda_{max}$ and log ε values for various dithioesters

| Dithioester | Solvent | $\lambda_{max}$ (nm) | Extinction coefficient (log ε) |
|---|---|---|---|
| Ethyl dithioacetate[b] | $CH_3CN/H_2O$[a] | 307.5 | 4.10 |
| | $CH_3CN$ | 306 | 4.07 |
| | $CCl_4$ | 307 | 4.13 |
| **1**[b] | $CH_3CN/H_2O$[a] | 309.5 | 4.0 |
| | $CH_3CN$ | 308 | 4.0 |
| | $CCl_4$ | 309 | 4.04 |
| **2** | $CH_3CN/H_2O$[a] | 310.5 | 3.97 |
| **3** | $CH_3CN/H_2O$[a] | 309 | 4.04 |
| **5** | $CH_3CN/H_2O$[a] | 310 | 4.06 |
| | $CH_3CN$ | 308 | 4.03 |
| **6** | $CH_3CN/H_2O$[a] | 309.5 | 4.03 |

[a]20% acetonitrile + 80% water.
[b]Published values for $\lambda_{max}$ and log ε for ethyl dithioacetate are 306 nm and 4.10 in ethanol (13), and for dithioester **1** are 309 nm and 4.03 in methanol (7).

mode possessing significant C=S and some C—C stretching character. Each of the spectra of compounds **1–6** (Table 1) is more complex in that it has more than one feature in the 1050 to 1200 $cm^{-1}$ region. The dithioester solution spectra (Figs. 1–6) all contain one feature between 1160 and 1185 $cm^{-1}$ (which we shall designate band I) and a second feature between 1115 and 1155 $cm^{-1}$ (band II), additionally compounds **3**, **4**, and **5** have a third feature between 1080 and 1100 $cm^{-1}$ (band III). The relative intensities of these three bands exhibit a strong solvent dependency (Figs. 1–6). For all the compounds tested, except dithioester **2**, band I is the most intense in $CCl_4$ solution whereas band II is the most intense in $CH_3CN$ solution. In the spectra of compound **2** in both $CCl_4$ and $CH_3CN$ solution band II is the most intense, however, band I becomes more intense, relative to band II, on changing from $CCl_4$ to $CH_3CN$ solution. This intensity change of band I for dithioester **2** is opposite in sign to that of all the other dithioesters tested. Band III, when it appears, exhibits the same solvent dependency as band II.

The relative intensities of bands I, II, and III were found to be independent of concentration. Spectra were obtained for acetonitrile solutions of dithioester **3** over a concentration range of (0.33–3.65) × $10^{-4}$ *M* and for dithioester **6** over a concentration range of (0.37–3.73) × $10^{-4}$ *M* and for both compounds the relative intensities of bands I and II (both dithioesters) and band III (dithioester **3**) remained constant. The relative intensities of the three bands do, however, exhibit a temperature dependency. Figure 7 shows the changes, in the intensities of bands I and II and where present band III, in the spectra of dithioesters **2**, **3**, and **4** as a function of temperature. In all cases, as the temperature is lowered, band I decreases in intensity relative to bands II and III. These results along with the solvent dependent changes and lack of any concentration dependency in the RR spectra point to the possibility that two forms of the dithioesters exist through some form of intramolecular rearrangement. Band I would be associated with the higher energy form, which we designate form A, and bands II and III with the lower energy form B. With the assumption that the ratio of the intensities of bands I and II is equal to the ratio of the concentrations of the two conformers, a plot of the logarithm of the intensity ratio against the reciprocal of the absolute temperature yields a $\Delta H$ value for the two forms. The $\Delta H$'s obtained for dithioesters **1**, **2**, **3**, and **4** were 1.0, 0.64, 0.89, and 0.88 kcal/mol, respectively.

Can. J. Chem. Downloaded from www.nrcresearchpress.com by 210.87.254.105 on 09/06/12
For personal use only.

Can. J. Chem. Downloaded from www.nrcresearchpress.com by 210.87.254.105 on 09/06/12
For personal use only.

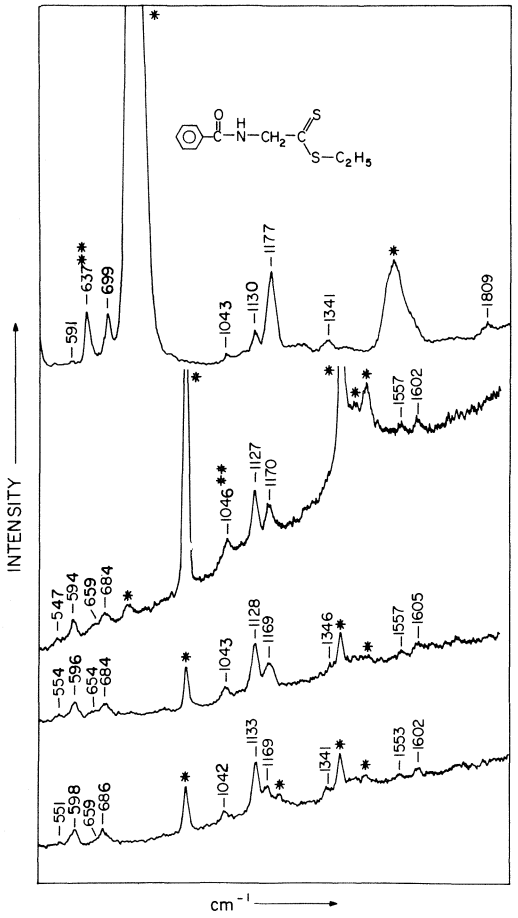


FIG. 1. Resonance Raman spectra of $4 \times 10^{-4}$ *M* solutions of ethyl dithiohippurate (**1**). The solvents used were from top to bottom: carbon tetrachloride, acetonitrile, 20% acetonitrile + 80% $H_2O$, and 20% acetonitrile + 80% $D_2O$. 10 mW of 324 nm laser excitation were used with a spectral slit width of 10 $cm^{-1}$ and a scan speed of 0.75 $cm^{-1}$/s. * denotes peaks due to solvent and ** peaks due to a combination of solute and solvent. The peaks at 637 $cm^{-1}$ in carbon tetrachloride and at 1046 $cm^{-1}$ in acetonitrile contain very weak contributions from the solvent.

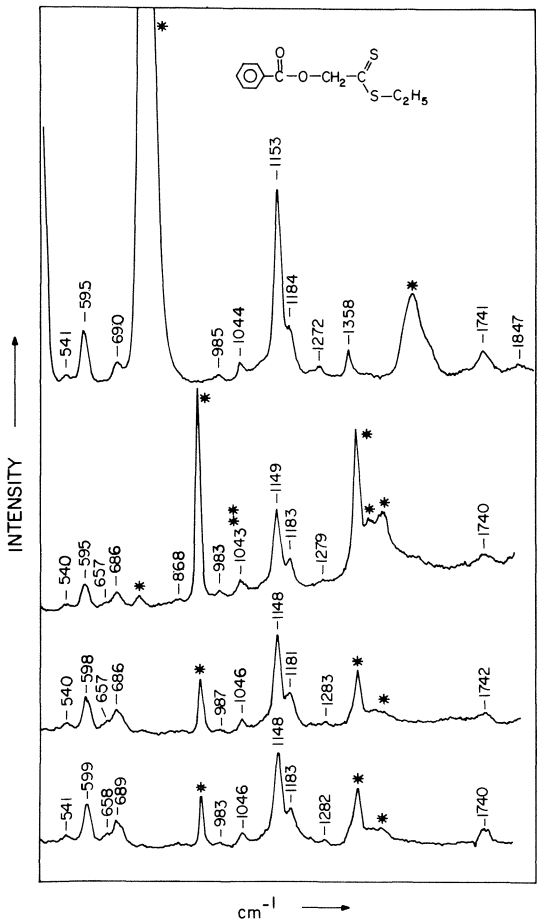


FIG. 2. Resonance Raman spectra of $4 \times 10^{-4}$ *M* solutions of benzoyl hydroxyacetyl ethyl dithioester (**2**). The solvents and other conditions were as given in Fig. 1.

A comparison of the RR spectra obtained for dithioester **3** using three near-uv laser lines (Fig. 8) shows that the intensity ratio of bands II (1145 $cm^{-1}$) and III (1096 $cm^{-1}$) is constant as a function of excitation wavelength whereas the intensity of band I (1165 $cm^{-1}$) changes with respect to bands II and III. There are several possible explanations for these data but they are consistent with the existence of two forms of the dithioester, each form having a slightly different electronic spectrum and a characteristic RR spectrum.

A Raman spectrum obtained from a single crystal of dithioester **3** contains only bands II and III at 1141 $cm^{-1}$ and 1088 $cm^{-1}$, respectively (Fig. 9). Band I is completely absent from this spectrum. Thus, dithioester **3** crystallises entirely in form B. A Raman spectrum of a concentrated acetonitrile solution of dithioester **3** contains all three bands, i.e. bands I, II, and III at 1170, 1143, and 1094 $cm^{-1}$, respectively (Fig. 9). This finding is in agreement with that of the RR study on more dilute solutions of the dithioester (Fig. 3).

The RR spectra of the dithioester solutions (Figs. 1–6) also contain many other features. In the 500–700 $cm^{-1}$ region they all contain a peak between 590 and 600 $cm^{-1}$. This peak appears to be associated with form B in that it exhibits the same solvent dependency as band II, i.e. for dithioesters **1**, and **3–6** it is more intense in acetonitrile solution than in carbon tetrachloride solution. This 590–600 $cm^{-1}$ peak has little or no $D_2O$ dependency. All the RR spectra also contain features near 690, 1045, and 1340 $cm^{-1}$. Other minor features at approximately 550 and 660 $cm^{-1}$ appear in some spectra.

Can. J. Chem. Downloaded from www.nrcresearchpress.com by 210.87.254.105 on 09/06/12
For personal use only.

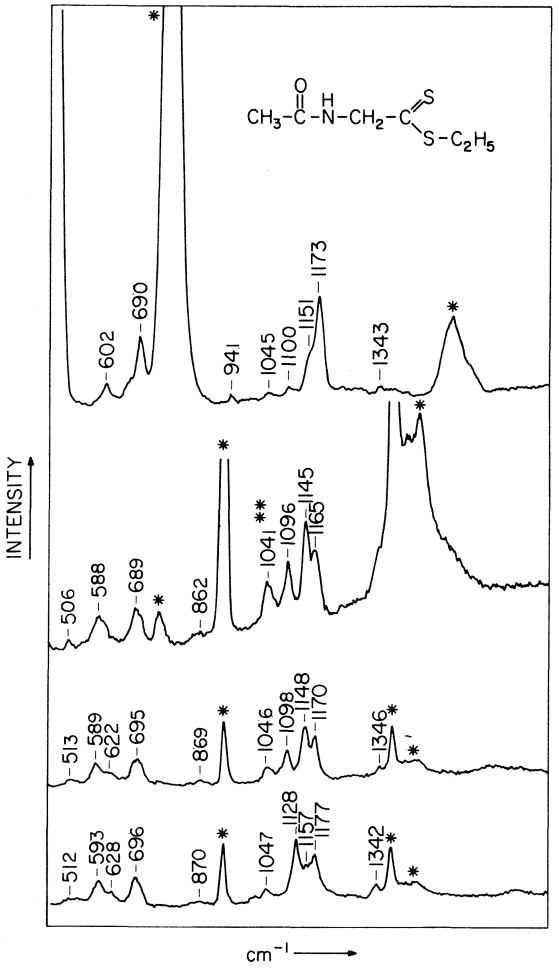


FIG. 3. Resonance Raman spectra of $4 \times 10^{-4}$ *M* solutions of *N*-acetyl glycine ethyl dithioester (**3**). The solvents and other conditions were as given in Fig. 1.

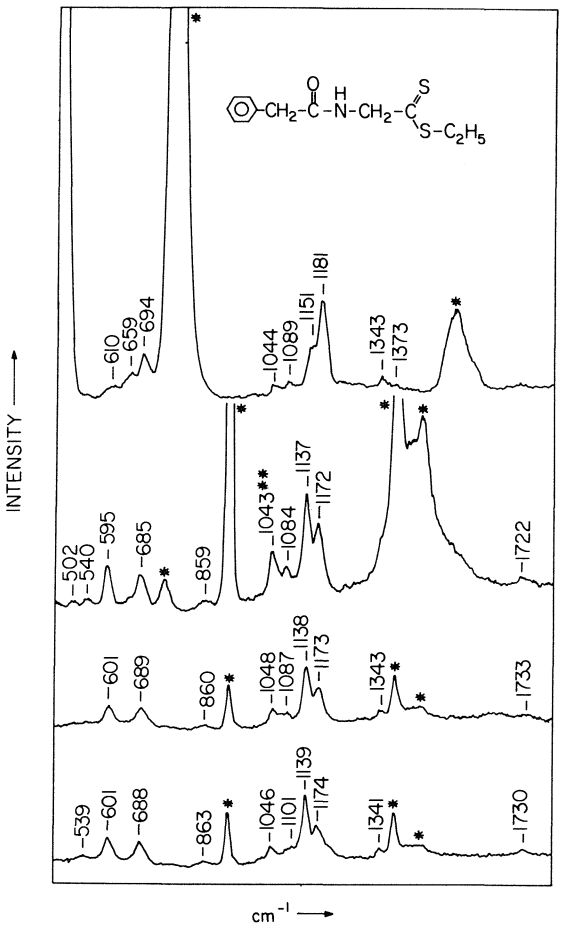


FIG. 4. Resonance Raman spectra of $4 \times 10^{-4}$ *M* solutions of *N*-phenylacetyl glycine ethyl dithioester (**4**). The solvents and other conditions were as given in Fig. 1.

*(b) The RR bands between 1050 and 1200 cm$^{-1}$*

For every *N*-acyl glycine ethyl dithioester, bands I and II appear in the region of the RR spectra associated with C=S stretching motions, and, moreover, derive from different forms of each compound. These facts suggest that bands I and II, respectively, are the corresponding normal modes of forms A and B of the dithioester and that both bands contain some C=S stretching character.

Some insight into the expected positions of C=S stretching bands may be gained by considering the infrared work of Bak *et al.* (14) on dithioesters of type R—CS—$SCH_2COOH$. The analysis of Bak *et al.* allows us to estimate the through bond inductive effect of R on the frequency of $\nu_{C=S}$. Assuming that the effect of the carboxymethyl group is constant throughout a series obtained by varying R then any correlation between R and $\nu_{C=S}$ should, after applying a constant correction for the different effects of $—CH_2COOH$ and $—CH_2CH_3$ on $\nu_{C=S}$, also be applicable to the dithioesters studied here. A plot of the p*K*'s of the series of 21 acids of the type R—COOH against the $\nu_{C=S}$ of the corresponding esters produces a straight line defined by the equation:

$$[1] \quad \nu_{C=S} = 16.8\ pK + 1143$$

The values in this equation were obtained by a regression analysis which gave a correlation coefficient of 0.79 (significant at $P = 0.05$). Using a value of 1197 cm$^{-1}$ for the $\nu_{C=S}$ of ethyl dithioacetate (**1**) and a p*K* of 4.75 for acetic acid the equation for a series of ethyl dithioesters becomes:

$$[2] \quad \nu_{C=S} = 16.8\ pK + 1116$$

A value of 1180 cm$^{-1}$ for the $\nu_{C=S}$ of ethyl dithiohippurate, **1**, can then be calculated using a

Can. J. Chem. Downloaded from www.nrcresearchpress.com by 210.87.254.105 on 09/06/12
For personal use only.

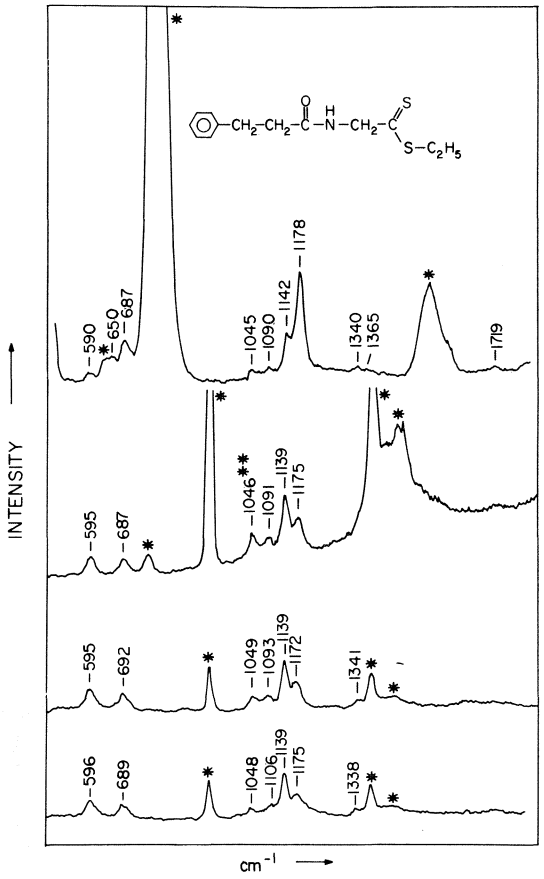


FIG. 5. Resonance Raman spectra of $4 \times 10^{-4}$ *M* solutions of *N*-β-phenylpropionyl glycine ethyl dithioester (**5**). The solvents and other conditions were as given in Fig. 1.

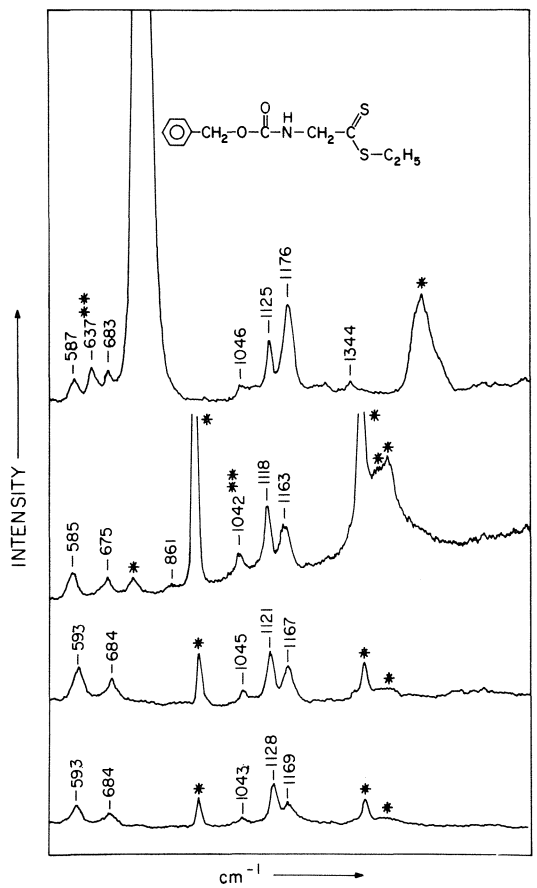


FIG. 6. Resonance Raman spectra of $4 \times 10^{-4}$ *M* solutions of *N*-carbobenzoxy glycine ethyl dithioester (**6**). The solvents and other conditions were as given in Fig. 1.

p*K* of 3.8 for hippuric acid. A similar value (i.e. approx. 1180 $cm^{-1}$) can be calculated for the other *N*-acyl glycine dithioesters studied. The position of band I of the dithioesters falls in the range 1165 $cm^{-1}$ to 1185 $cm^{-1}$, thus this band is very close to the predicted value for $\nu_{C=S}$. Therefore, it seems probable that band I of form A of the dithioesters represents a relatively unperturbed C=S stretching vibration, since it is found in the position to be expected for the C=S stretching vibration after taking into consideration only the through bond effects of the substitution of an *N*-acyl amine onto the acetyl portion of ethyl dithioacetate. By the same token the position of band II is anomalous in that it comes at a lower frequency than that predicted by eq. [2] above. It should be emphasised however that several assumptions, which have not been fully tested, have gone into deriving eq. [2]. For this reason the conclusion we have reached on the expected position for $\nu_{C=S}$ is tentative.

All the dithioesters tested, with the exception of **2**, show some band position shifts on going from solution in 80% $H_2O$, 20% $CH_3CN$, to 80% $D_2O$, 20% $CH_3CN$ (Figs. 1–6). For those compounds that do not possess a band III in their RR spectra, i.e. **1** and **6**, band II shifts to higher wavenumbers in the presence of $D_2O$, whereas band I remains fixed (Figs. 1 and 6). For compounds that do possess a band III, i.e. **4** and **5**, it is this band that shifts to higher wavenumbers, whilst bands I and II remain stationary (Figs. 4 and 5). The behaviour of the *N*-acetyl dithioester **3** is anomalous, since both bands II and III appear to shift and the shifts are also associated with intensity changes, i.e. in $D_2O/CH_3CN$ solution band III is more intense than band II, whereas in $H_2O/CH_3CN$ band II is the more intense, Fig. 3.

On examining the $H_2O/CH_3CN$ and $D_2O/CH_3CN$ dithioester solutions by nmr spectroscopy it was found that in the presence of $D_2O$ the amide proton of the *N*-acyl dithioesters is exchanged for a deuteron. On the time scale of the RR experiments no further proton–deuteron exchanges were ob-

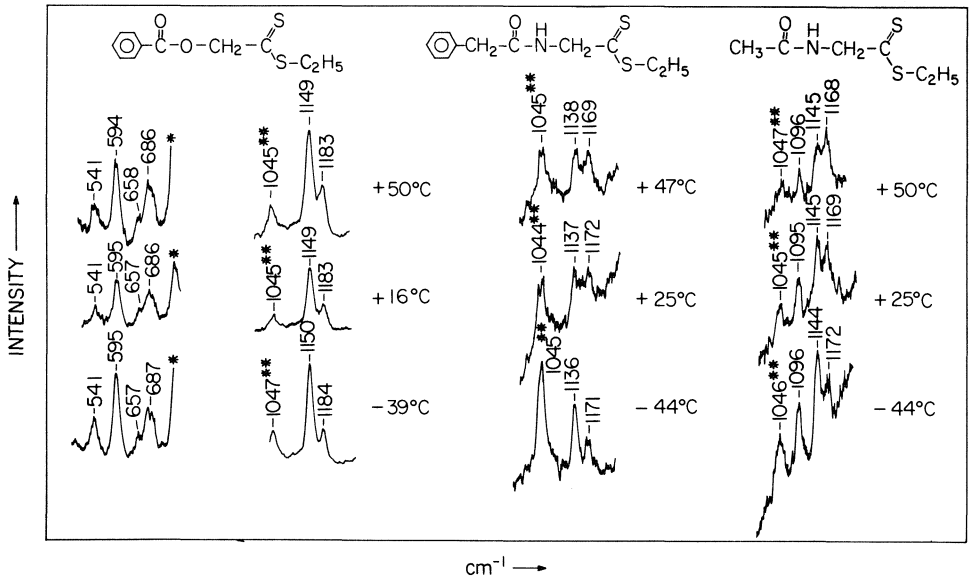


FIG. 7. Sections of the resonance Raman spectra of acetonitrile solutions of dithioesters **2** ($4.2 \times 10^{-3}$ *M*), **3** ($6 \times 10^{-3}$ *M*), and **4** ($3.1 \times 10^{-3}$ *M*) scanned at three different temperatures. 25 mW of 350.7 nm laser excitation were used with a spectral slit width of 10 $cm^{-1}$ and a scan speed of 0.75 $cm^{-1}/s$. The temperature was measured using a copper–constantan thermocouple.

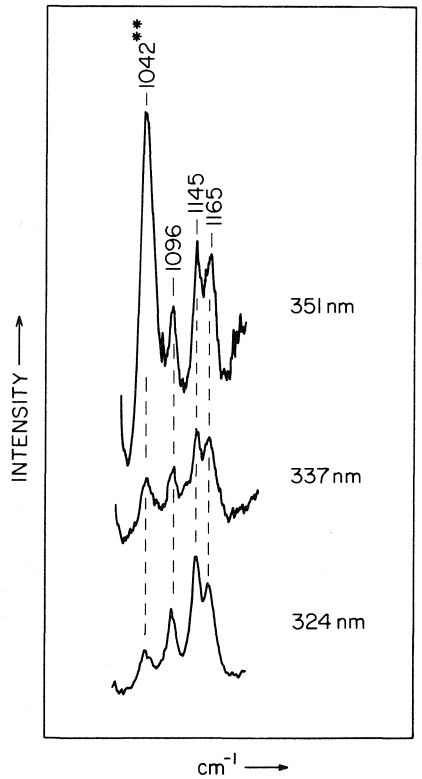


FIG. 8. The variation in the relative intensities of bands I, II, and III in the resonance Raman spectra of dithioester **3** as a function of the excitation wavelength. The concentration of the dithioester was $9.6 \times 10^{-4}$ *M* in a 1:1 acetonitrile–water mixture. The power used was 400, 40, and 15 mW for the 350.7, 337.5, and 324 nm excitation lines, respectively. A spectral slit width of 10 $cm^{-1}$ was used with a scan speed of 0.75 $cm^{-1}/s$.

served. Thus, the exchange of —NH for —ND must be related to the band position shifts in the resonance Raman spectra. Further evidence that the shifts are due to the exchange of the amide proton for a deuteron is the fact that no shift is observed for compound **2** which does not have an amide proton. The position of band I, for all the dithioesters, is not influenced by the presence of $D_2O$, thus the normal mode of form A which gives rise to band I is unaffected by —NH, —ND exchange. Form B gives rise to bands II and III in the RR spectra, and one or both of these bands is affected by deuteration of the amide groups. Band II for compounds **1** and **6** probably contains some C=S stretching character and must contain, in some way, a contribution from the motion of the amide proton. For compounds **4** and **5** band II likely contains C=S stretching character but there is no evidence for a contribution from a NH motion. However, band III in compounds **4** and **5** is sensitive to the motion of the amide proton. The situation for compound **3** is more complex and both bands II and III involve amide proton motions with possible C=S stretching contributions to one or both features.

### *(c) Nature of the two forms found in solution*

Form B, which, according to the temperature dependences of bands I, II, and III, Fig. 7, is of lower energy than form A, must differ from form A by one or more of the following possibilities: (*i*) tautomerism, (*ii*) rotational isomerism, or (*iii*) intramolecular interaction. Intermolecular interac-

Can. J. Chem. Downloaded from www.nrcresearchpress.com by 210.87.254.105 on 09/06/12
For personal use only.

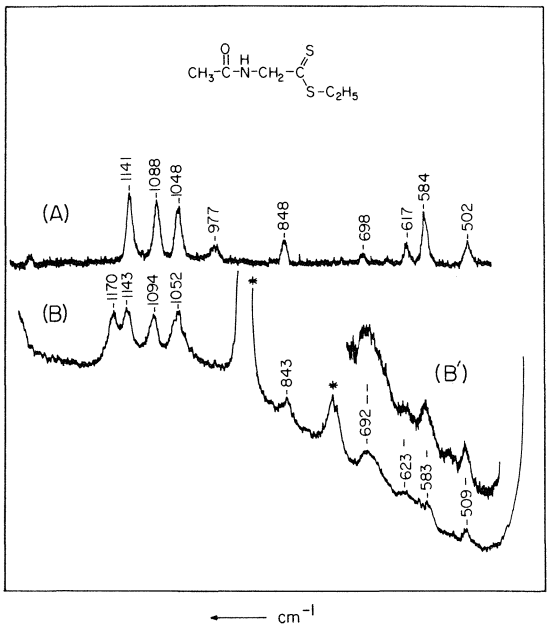


FIG. 9. Raman spectra of *N*-acetyl glycine ethyl dithioester (**3**) *A*, crystals, and *B*, a concentrated solution, 0.11 *M*, in a 1:1 acetonitrile–water mixture. *B'* is a portion of spectrum *B* recorded at higher sensitivity. The power used was 5 and 360 mW of 5145 nm laser light for spectra *A* and *B*, respectively. The spectral slit width was 10 $cm^{-1}$ with a scan speed of 0.25 $cm^{-1}$/s.

tions are ruled out by the lack of a concentration dependence in the RR spectra.

*(i) Tautomerism*

The enethiolization of thioketones is well known (15, 16). In contrast to such simple thiones dithioesters are generally stable in the thione form (17, 18). The exceptions are special dithioesters (19), for example of the type (20):

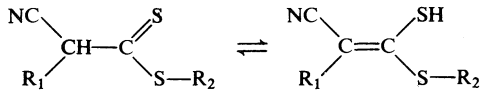


Thione Enethiol

There are three pieces of evidence against enethiolization occurring with the *N*-acyl dithioesters discussed here. Firstly, no band assignable to a C=C stretching vibration can be seen in the spectra of the dithioesters (especially in the Raman spectra of the crystals of dithioester **3** which are entirely in form B, the presumed enethiol). Secondly, if an equilibrium existed between the two tautomers this would provide a mechanism for the exchange of the glycine —$CH_2$—protons, no such exchange is observed in $D_2O$ (except at high pH). Thirdly, the dithioester chromophore would be destroyed by the formation of the enethiol and thus on going from carbon tetrachloride solution (which favours form A) to acetonitrile solution (which favours form B) a large reduction in the measured extinction coefficients should be observed. A small reduction in the extinction coefficients is seen but it is of the same magnitude as that observed for ethyl dithioacetate (Table 2) on changing solvents. Ethyl dithioacetate is known not to undergo enethiolization (17, 18).

*(ii) Rotational isomerism*

We have previously studied rotational isomers of the two dithioesters:

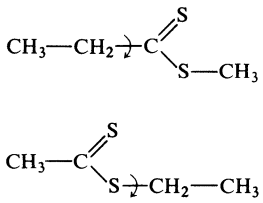


(2, 21) and determined the effect on the RR spectrum of rotations about the C—C and S—C bonds indicated. By altering the vibrational coupling in the molecules, rotational isomerism does bring about changes in the 500–700 $cm^{-1}$ spectral region. However, for ethyl dithioacetate and methyl dithiopropionate rotational isomerism appears to leave the peak near 1195 $cm^{-1}$ unchanged. Thus, it is unlikely that a simple rotation is the sole cause of the changes in the 1050–1200 $cm^{-1}$ region of the RR spectrum of form B of the present compounds. It does not rule out the possibility that the changes are caused by a rotation coupled with some form of intramolecular interaction.

*(iii) Intramolecular interaction — the difference between forms A and B*

Having argued against tautomerism and the effects of rotational isomerism and having dismissed intermolecular interactions as possible causes of the "$\nu_{C=S}$" RR peaks of form B we turn now to consider an intramolecular interaction as the source of form B's "perturbed" RR peaks. There are two examples in the literature of intramolecular interactions which have to be taken into account for the systems discussed here. However, we shall argue that neither of these two cases provides an explanation of the observed RR spectrum of form B.

The first example concerns an intramolecular interaction in *N*-acetyl glycine methylester (22). An intramolecular H-bond was proposed to explain the splitting of the N—H stretching vibration peak in the ir spectra taken in carbon tetrachloride solution, i.e.

Can. J. Chem. Downloaded from www.nrcresearchpress.com by 210.87.254.105 on 09/06/12
For personal use only.

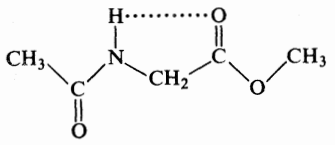

*a*

This interaction is designated $C_5$, since it involves a five-membered ring. Due to the strain in the ring the H-bond must be weak as is reflected by the small change in $\nu_{N-H}$ brought about by the interaction i.e. 24 $cm^{-1}$ (strong hydrogen bonds can change $\nu_{N-H}$ by up to 200 $cm^{-1}$). The lack of any detectable perturbation of the ester $\nu_{C=O}$ frequency (22) also supports the supposition that the $C_5$ interaction must be weak. A dipole–dipole interaction of the amide and ester groups would however help to strengthen the $C_5$ interaction (23). The $C_5$ interaction is thought to be important in the determination of protein structure since it is also present in the amides of *N*-acyl amino acids as well as the esters (22–25).

The second example concerns an intramolecular interaction between a sulfur atom and an amide group in *S*-ethylcysteine methylamide (compound *b*). The ir spectrum of this compound has a strong absorption band at 3402 $cm^{-1}$ which can be assigned to the $N_1—H_1$ stretching vibration (25). However, this frequency is too low to be ascribed to an ordinary $C_5$ interaction between the $N_1—H_1$ and $C_2=O_2$ groups. It was concluded, therefore, that the amide proton is involved in a hydrogen bond with the sulfur atom. The structural similarity between the compound and the dithioesters discussed here is shown below:

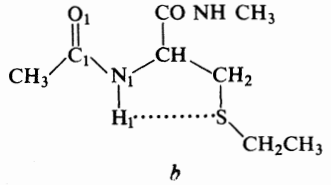

*b*

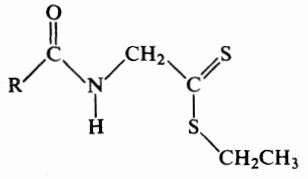

*c*

It is reported that the strength of the N—H....S interaction in *S*-ethylcysteine methylamide is such that all the molecules present in solution are in the intramolecular interacting form (25). This interaction is unusual since it was shown that the optimal ring size for the interaction is five; the equivalent methionine derivative, with its potential to form a six-membered ring, did not possess an interaction of this type. This is unexpected since a less strained H-bond could be formed in a six-membered ring. Also such a supposedly strong H-bonded N—H in *S*-ethylcysteine methylamide would be expected to have a $\nu_{N-H}$ at lower wavenumber than that observed. This suggests that the interaction in this compound is not just a simple H-bond.

In both of the literature examples just cited the formation of the hydrogen bond was proposed as the source of the free energy driving the formation of the intramolecular form. However, for the present *N*-acyl glycine ethyl dithioesters we have good evidence that a hydrogen bond is not energetically important in the intramolecular form. Firstly, compound **2** which does not have an —NH group does have a form B. Secondly, the solvent dependency of the A and B forms argues against the presence of a strong intramolecular H-bond in B. In consequence of the hydrogen-bond accepting nature of its nitrogen atom acetonitrile is a much stronger H-bond acceptor than carbon tetrachloride. Thus, it would be expected that if form B had a strong intramolecular H-bond this form would predominate in $CCl_4$. The opposite is found to be the case; for compounds **1** and **3–6** there is a higher population of form B relative to form A in $CH_3CN$ compared to $CCl_4$.

Although it seems unlikely that either structure *a* or *b*, with their crucial hydrogen bonds, is equivalent to form B, the —NH moiety is implicated in form B by the RR results. The sensitivity of the RR spectrum of form B to —NH, —ND exchange was unexpected since the —NH moiety is two bonds removed from the dithioester chromophore. The amide group itself has a $\pi-\pi^*$ transition at approximately 180 nm ($\varepsilon_{max} \simeq 10^{-4}$) and a $\pi \rightarrow \pi^*$ transition at approximately 220 nm ($\varepsilon_{max} < 100$). However, these electronic absorption bands are too far removed from the Raman excitation wavelength to obtain preresonance enhancement of normal modes of the unperturbed amide chromophore. It is likely, therefore, that the participation of the —NH motion in the RR spectrum takes place by some form of coupling between the amide and dithioester chromophores. This coupling could include both vibrational and electronic interactions and may take place through the —NH—$CH_2$—C(=S) bonds or "through space", i.e. via nonbonded contacts if the chromophores in form B are placed in close juxtaposition. The nature of the coupling is such that it occurs only in form B. Moreover, since it changes the positions of Raman peak positions (for form B compared to form A) it

Can. J. Chem. Downloaded from www.nrcresearchpress.com by 210.87.254.105 on 09/06/12
For personal use only.

Can. J. Chem. Downloaded from www.nrcresearchpress.com by 210.87.254.105 on 09/06/12
For personal use only.

must perturb the electron distribution in the electronic ground state. (Raman and RR peak positions reflect only electronic ground state properties). However, the coupling has only a modest effect on the electronic spectrum of the dithioester chromophore. Compared to the absorption spectrum of ethyl dithioacetate the spectra of the dithioesters in Table 1 show a red shift in $\lambda_{max}$ by 2–3 nm (Table 2) and an increase in peak width at half height of approximately 7% in $CH_3CN/H_2O$ (8:2) solution and 3% in carbon tetrachloride solution.

The nature of the coupling between the amide and dithioesters in form B is not completely understood although literature evidence (26–31) suggests that a substantial part of the coupling may occur through space. The occurrence of the coupling in form B alone suggests that the amide and dithioester chromophores are in closer contact in form B compared to form A. The preferred means of switching from form A to B would be by rotations about either or both of the NH—$CH_2$, $CH_2$—C(=S) bonds. Hence, although rotational isomerism by itself does not change the positions of peaks for form B (by altering the vibrational coupling), it is proposed that it brings the amide and dithioester groups into contact. The chromophore–chromophore interaction (which may include electronic and vibrational components) is then thought to change the position of form B's RR features with respect to those of form A. The interaction between the amide and dithioester groups can also include dipole interactions such as the field effects discussed by Bellamy and Williams (32). Field effects have been used to explain the two carbonyl bands in the ir spectra of α-halogen substituted thiolesters (33). The two bands are due to two conformers, one involving a dipole interaction between the halogen and the carbonyl oxygen (giving rise to the high wavenumber band) and the other involving a dipole interaction between the halogen and the thiol sulfur. The transition between the two forms involves a 180° rotation about a single C—C bond. Another component of the amide–dithioester interaction may be overlap between the sulfur *d*-orbitals and the π-electrons of the amide group. An interaction of this type has been suggested to occur between the π electron cloud and the empty $d_\pi$ orbitals of β,γ-unsaturated thiol esters (34).

Although we strongly favor a model in which forms A and B are different rotamers and that a strong intramolecular interaction in form B is absent in A, it is clear that the details of this interaction are speculative. However, X-ray crystallographic studies are under way and by this means we hope to provide detailed information on the geometries of forms A and B.

The dithioesters discussed in this paper are very useful models for the dithioacyl enzymes produced by the action of cysteine proteases on thiono ester substrates (3–6). The similarities between the dithioacyl enzyme resonance Raman spectra and the spectra of the B form of the dithioesters is very striking (3, 4). Thus, the knowledge obtained about the interactions that define the B form of the dithioesters is important to an understanding of the interactions controlling the catalytic properties of dithioacyl enzymes. This point will be discussed at length in a subsequent publication dealing with the resonance Raman spectra of the dithioacyl enzymes.

1. J. J. C. Teixeira-Dias, V. M. Jardim-Barreto, Y. Ozaki, A. C. Storer, and P. R. Carey. Can. J. Chem. **60**, 174 (1982).
2. Y. Ozaki, A. C. Storer, and P. R. Carey. Can. J. Chem. **60**, 190 (1982).
3. A. C. Storer, W. F. Murphy, and P. R. Carey. J. Biol. Chem. **254**, 3163 (1979).
4. A. C. Storer, Y. Ozaki, and P. R. Carey. Proceedings – VIIth Conference on Raman Spectroscopy. *Edited by* W. F. Murphy North Holland, New York. 1980. p. 624.
5. G. Lowe and A. Williams. Biochem. J. **96**, 189 (1965).
6. K. Brocklehurst, E. M. Crook, and C. W. Wharton. Chem. Commun. 1185 (1967).
7. H. Hartmann, W. Stapf, and J. Heidberg. Liebigs Ann. Chem. **729**, 237 (1969).
8. C. S. Marvel, P. De Radzitzky, and J. J. Brader. J. Am. Chem. Soc. **77**, 5997 (1955).
9. J. Poupaert, A. Bruylants, and P. Crooy. Synthesis, 622 (1972).
10. J. Poupaert and A. Bruylants. Bull. Soc. Chim. Belg. **84**, 61 (1975).
11. S. E. Dinizo, R. W. Freerksen, W. E. Pabst, and D. S. Watt. J. Org. Chem. **41**, 2846 (1976).
12. T. B. Johnson and E. Gatewood. J. Am. Chem. Soc. **51**, 1815 (1929).
13. M. J. Janssen. Recueil, **79**, 464 (1960).
14. B. Bak, L. Hansen-Nygaard, and C. Pedersen. Acta Chem. Scand. **12**, 1451 (1958).
15. R. Mayer. In Sulphur in organic and inorganic chemistry. Vol. 3. *Edited by* A. Senning Marcel Dekker, Inc. New York. 1972. Chapt. 27.
16. F. Duus. Tetrahedron, **28**, 5923 (1972).
17. R. Mayer, S. Scheithauer, S. Bleisch, D. Kunz, G. Bähr, and R. Radeglia. J. Prakt. Chem. **311**, 472 (1969).
18. D. Kunz, S. Scheithauer, S. Bleisch, and R. Mayer. J. Prakt. Chem. **312**, 426 (1970).
19. S. Scheithauer and R. Mayer. Topics in sulfur chemistry. Vol. 4. *Edited by* A. Scanning. 1979. Section 3.9.
20. R. Gompper and W. Töpfl. Chem. Ber. **95**, 2861 (1962).
21. A. L. Verma, Y. Ozaki, A. C. Storer, and P. R. Carey. J. Raman Spectrosc. **11**, 390 (1981).
22. G. Boussard, M. T. Cung. M. Marraud, and J. Néel. Chim. Phys. **71**, 1159 (1974).
23. H. Weiler-Feichenfeld, A. Singerman, and E. D. Bergmann. The Jerusalem Symposia on Quantum Chemistry and Biochemistry, **5**, 87 (1972).

24. J. NÉEL. Pure Appl. Chem. **31**, 201 (1972).
25. M. T. CUNG, M. MARRAUD, and J. NÉEL. The Jerusalem Symposia on Quantum Chemistry and Biochemistry, **5**, 69 (1972).
26. H. H. JAFFÉ and M. ORCHIN. Theory and applications of ultraviolet spectroscopy. John Wiley, New York. 1962. Section 15.6.
27. N. J. LEONARD, M. OKI, and S. CHIAVARELLI. J. Am. Chem. Soc. **77**, 6234 (1955).
28. M. R. BELL and S. ARCHER. J. Am. Chem. Soc. **82**, 151 (1960).
29. N. J. LEONARD, T. L. BROWN, and T. W. MILLIGAN. J. Am. Chem. Soc. **81**, 504 (1959).
30. C. G. OVERBERGER and A. LUSI. J. Am. Chem. Soc. **81**, 506 (1959).
31. N. J. LEONARD, T. W. MILLIGAN, and T. L. BROWN. J. Am. Chem. Soc. **82**, 4075 (1960).
32. L. J. BELLAMY and R. L. WILLIAMS. J. Chem. Soc. 4294 (1957).
33. R. A. NYQUIST and W. J. POTTS. Spectrochim. Acta **7**, 514 (1959).
34. A. C. STORER, D. J. PHELPS, and P. R. CAREY. Biochemistry. **20**, 3454 (1981).

Can. J. Chem. Downloaded from www.nrcresearchpress.com by 210.87.254.105 on 09/06/12
For personal use only.

# Synthesis of β-chloro, β-bromo, and β-iodo α,β-unsaturated ketones

EDWARD PIERS, JOHN R. GRIERSON, CHEUK KUN LAU, AND ISAO NAGAKURA

*Department of Chemistry, University of British Columbia, 2036 Main Mall, University Campus, Vancouver, B.C., Canada V6T 1Y6*

Received August 11, 1981

EDWARD PIERS, JOHN R. GRIERSON, CHEUK KUN LAU, and ISAO NAGAKURA. Can. J. Chem. **60**, 210 (1982).

A new, efficient method for the preparation of β-chloro, β-bromo, and β-iodo α,β-unsaturated ketones is described. The method involves the reaction of β-diketones or α-hydroxymethylenecycloalkanones with triphenylphosphine dihalides in the presence of triethylamine. With the dichloride and dibromide reagents, the reactions are conveniently carried out in benzene at room temperature, while with triphenylphosphine diiodide the reactions are best performed in refluxing acetonitrile (β-diketones) or in acetonitrile–hexamethylphosphoramide (α-hydroxymethylenecycloalkanones). The reaction of triphenylphosphine diiodide – triethylamine with a series of 4-alkyl-1,3-cyclohexanediones provides mainly or exclusively (depending on the size of the alkyl group) 6-alkyl-3-iodo-2-cyclohexen-1-ones, while reaction of this reagent with 2-hydroxymethylenecyclohexanone and 2-hydroxymethylenecyclopentanone affords stereoselectively and regioselectively (*E*)-2-iodomethylenecyclohexanone and (*E*)-2-iodomethylenecyclopentanone, respectively.

EDWARD PIERS, JOHN R. GRIERSON, CHEUK KUN LAU et ISAO NAGAKURA. Can. J. Chem. **60**, 210 (1982).

On décrit une nouvelle méthode efficace de préparation des β-chloro, β-bromo et β-iodo cétones α,β-insaturées. La méthode fait intervenir la réaction des β-dicétones ou des α-hydroxyméthylènecycloalcanones avec les dihalogénures de triphénylphosphine en présence de triéthylamine. Les réactions ont lieu dans le benzène à la température ambiante si on utilise les dichlorures ou les dibromures comme réactifs, tandis qu'avec le diiodure de triphénylphosphine, on obtient de meilleures réactions dans l'acétonitrile au reflux (β-dicétones) ou dans un mélange d'acétonitrile–hexaméthylphosphoramide (α-hydroxyméthylènecycloalcanones). La réaction du diiodure de triphénylphosphine dans la triéthylamine avec une série d'alkyl-4 cyclohexanediones-1,3 conduit principalement ou exclusivement (dépendant de la taille du groupe alkyle) aux alkyl-6 iodo-3-cyclohexèn-2 ones-1, tandis que ce même réactif avec l'hydroxyméthylène-2 cyclohexanone et l'hydroxyméthylène-2 cyclopentanone conduit de façon stéréosélective et régiosélective aux iodométhylène-2 cyclohexanone-(*E*) et iodométhylène-2 cyclopentanone-(*E*) respectivement.

[Traduit par le journal]

## Introduction

β-Chloro α,β-unsaturated ketones have been known for a long time (1) and, over the years, have served as important and versatile intermediates in organic synthesis.[1] On the other hand, the corresponding bromo compounds, although known, do not appear to have been used a great deal by synthetic organic chemists.[2] Furthermore, prior to the initiation of our work in this area[3] reports in the chemical literature concerning the preparation and use of β-iodo α,β-unsaturated ketones were very rare.[4]

The synthesis of β-chloro α,β-unsaturated ketones from β-diketones has been carried out by treatment of the latter substances with a diversity of reagents: phosphorus trichloride (29–36), phosphorus oxychloride (29, 37), phosgene (38), acetyl chloride (39), oxalyl chloride (40, 9), and triphenylphosphine – carbon tetrachloride (41). Of these, the latter two reagents appear to be the best in terms of convenience and efficiency. Conversion of β-diketones into β-bromo enones has traditionally been accomplished by treatment of the former substrates with phosphorus tribromide (29, 36, 42), although the yield of this process does not appear to be very high. More recently, this type of conversion has been accomplished employing triphenylphosphine – carbon tetrabromide (41). To our knowledge, the direct conversion of β-diketones into β-iodo α,β-unsaturated ketones had not been accomplished prior to our work (19). We report herein the details of our study concerning the transformation of β-diketones and β-hydroxymethylenecycloalkanones into the corresponding β-chloro, β-bromo, and/or β-iodo α,β-unsaturated ketones. Subsequent publications will deal with the use of these versatile substances in organic synthesis.[5]

## Results and discussion

### (a) *Conversion of symmetrical β-diketones into β-halo α,β-unsaturated ketones*

When 1,3-cyclohexanedione (**1**) and triethylam-

[1]For some recent examples, see refs. 2–17, inclusive. This list of citations is not meant to be exhaustive, but is provided to give the reader some appreciation for the synthetic utility of β-chloro enones.

[2]For examples, see refs. 11, 13, and 18.

[3]For a preliminary communication regarding part of the work reported herein, see ref. 19.

[4]See, for example, refs. 20 and 21. For some reports concerning the use of β-iodo enones which appeared subsequent to our preliminary communication (19), see refs. 10 and 22–28, inclusive.

[5]For some preliminary reports, see refs. 43–49, inclusive.

0008-4042/82/020210-14$01.00/0

©1982 National Research Council of Canada/Conseil national de recherches du Canada

Can. J. Chem. Downloaded from www.nrcresearchpress.com by 210.87.254.105 on 09/06/12
For personal use only.

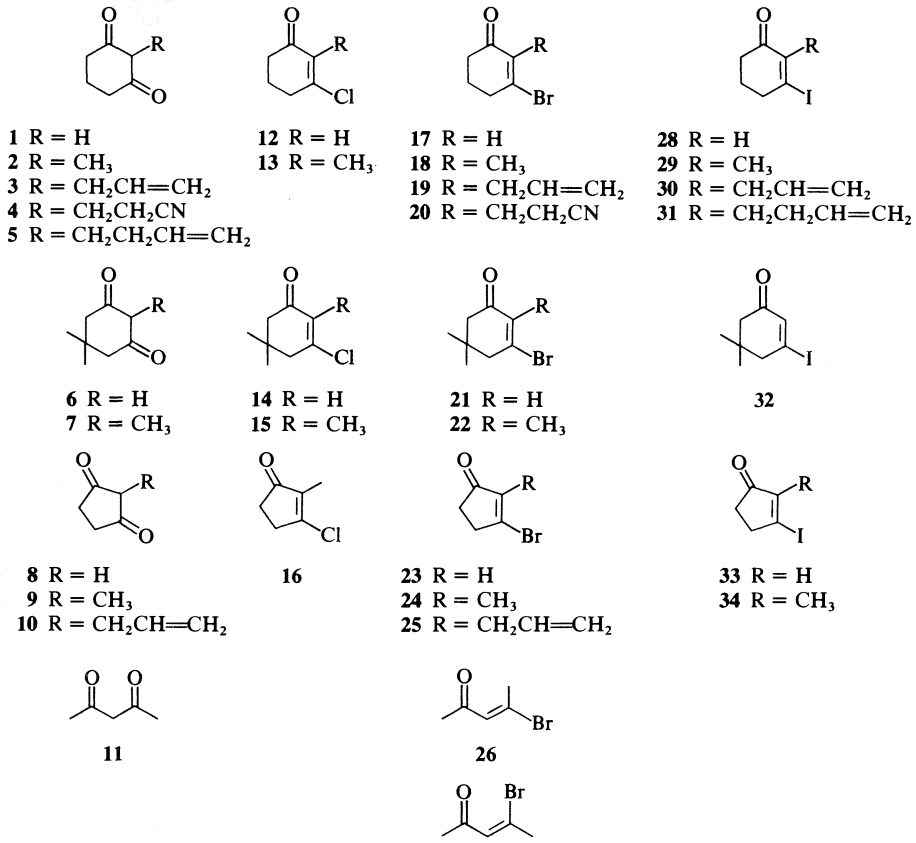


CHART 1

ine were added to a suspension of freshly prepared triphenylphosphine dichloride in benzene and the resulting mixture was stirred at room temperature for 1 h, 3-chloro-2-cyclohexen-1-one (**12**) was produced in 91% yield (see Chart 1). In similar fashion, reaction of **1** with triphenylphosphine dibromide in the presence of triethylamine provided (97%) 3-bromo-2-cyclohexen-1-one (**17**). It seems highly likely that these conversions proceed by way of the phosphonium salt **35**,[6] formed by reaction of the diketone with triphenylphosphine dihalide (see Scheme 1). Conjugate addition of halide ion to **35**, followed by elimination of triphenylphosphine oxide from the resulting intermediate **36** would afford the observed products **12** and **17**.

Reaction of triphenylphosphine dichloride and/or the corresponding dibromide reagent with the symmetrical β-diketones **2–4** and **6–11**, inclusive, gave results comparable to those obtained with 1,3-cyclohexanedione (**1**), and these are summarized in Table 1. Although these results are quite straightforward and require little additional comment, the following points should be noted. It was found to be important to prepare the triphenylphosphine dihalides from freshly recrystallized triphenylphosphine

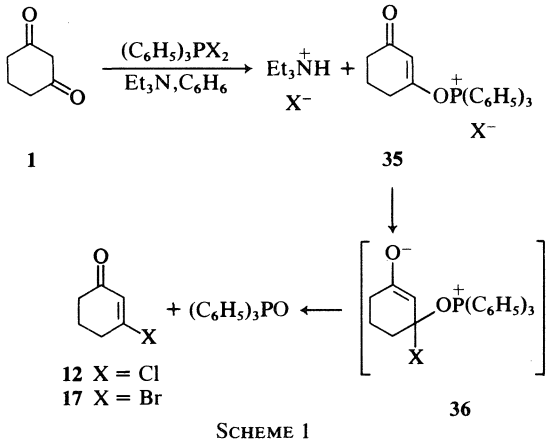


SCHEME 1

[6]This type of intermediate has been proposed previously in connection with the reaction of 2-bromodimedone with triphenylphosphine (51).

Can. J. Chem. Downloaded from www.nrcresearchpress.com by 210.87.254.105 on 09/06/12
For personal use only.

Can. J. Chem. Downloaded from www.nrcresearchpress.com by 210.87.254.105 on 09/06/12
For personal use only.

and to carefully dry and distil the benzene and triethylamine used in the reactions. If these precautions were not taken, the product yields decreased significantly. However, when the reactions were carried out under the conditions prescribed in the Experimental, the yields were uniformly excellent. From the results summarized in Table 1, it is clear that this method for the conversion of β-diketones into β-chloro α,β-unsaturated ketones compares very favorably with the most recently reported methods (9, 41). Furthermore, for the preparation of β-bromo enones, our method appears to be superior to that involving the reaction of β-diketones with phosphorus tribromide (29, 36, 42) and affords yields marginally higher than those obtained from the triphenylphosphine – carbon tetrabromide method (41).

The reactions summarized in Entries 1–14 of Table 1 involved cyclic β-diketones as the starting materials and, therefore, there were no ambiguities with respect to the stereochemistry of the products. However, in the one acyclic case which was investigated, it was found that the reaction of 2,4-pentanedione (**11**) with triphenylphosphine dibromide in 5:1 acetonitrile–benzene was not totally stereoselective, since a mixture of the two geometrically isomeric β-bromo enones **26** and **27** (ratio ~87:13, respectively) was produced (88% yield). A pure sample of each of the two isomers could be obtained by preparative gas–liquid chromatography (glc) and the stereochemistry of these substances was shown to be as indicated on the basis of the $^1$H nmr spectra. Thus the major isomer, which exhibited the signal due to the vinyl methyl group at lower field (δ 2.75), was assigned structure **26**, while structure **27** could be assigned to the minor product, which showed the corresponding resonance at higher field (δ 2.45). Similarly, the olefinic protons of the two isomers exhibited the expected relative chemical shifts (**26**: δ 6.73, proton *cis* to bromine; **27**: δ 6.55, proton *trans* to bromine). It is interesting to note that the reaction of 2,4-pentanedione (**11**) with oxalyl chloride affords (50% yield) a 1:1 mixture of (*E*)- and (*Z*)-4-chloro-3-penten-2-one (40, 9), while treatment of **11** with triphenylphosphine – carbon tetrachloride has been reported (41) to yield (81%) only the (*E*) isomer.

TABLE 1. Conversion of symmetrical β-diketones into β-chloro and β-bromo α,β-unsaturated ketones[a]

| Entry | β-Diketone | Reagent[b] | Reaction time (h) | Product (yield, %)[c] |
|---|---|---|---|---|
| 1 | **1** | A | 1 | **12** (91) |
| 2 | **1** | B | 3 | **17** (97) |
| 3 | **2** | A | 4 | **13** (97) |
| 4 | **2** | B | 4 | **18** (96) |
| 5 | **3** | B | 3 | **19** (96) |
| 6 | **4** | B | 17 | **20** (82) |
| 7 | **6** | A | 1 | **14** (94) |
| 8 | **6** | B | 3 | **21** (93) |
| 9 | **7** | A | 7 | **15** (90) |
| 10 | **7** | B | 4 | **22** (91) |
| 11 | **8** | B | 4 | **23** (80) |
| 12 | **9** | A | 4 | **16** (92) |
| 13 | **9** | B | 4 | **24** (93) |
| 14 | **10** | B | 4 | **25** (86) |
| 15 | **11** | B | 19[d] | **26** + **27**[e] (88) |

[a] All reactions were carried out at room temperature. The reaction solvent was benzene except when otherwise noted.
[b] Reagent A: triphenylphosphine dichloride. Reagent B: triphenylphosphine dibromide.
[c] Yield of distilled product(s).
[d] The solvent in this case was 5:1 acetonitrile–benzene.
[e] The ratio of **26**/**27** was approximately 87:13, respectively. Also present in the product was a minor (~5%), unidentified compound.

The infrared and $^1$H nmr spectral data derived from the β-chloro (**12–16**) and β-bromo (**17–27**) α,β-unsaturated ketones, along with appropriate references or elemental analysis data, are summarized in Table 2.

Reaction of 1,3-cyclohexanedione (**1**) with triphenylphosphine diiodide in benzene via a procedure similar to that used in the case of the dichloride or dibromide reagents (*vide supra*) failed to produce 3-iodo-2-cyclohexen-1-one (**28**) (see Chart 1). When the progress of the reaction was monitored by thin-layer chromatography (tlc) it was found that although the starting material **1** disappeared slowly, only a trace of compound **28** had formed even after a period of 20 h. Apparently, under these conditions, the dione **1** reacted with the diiodide reagent to produce the phosphonium salt **35** (X = I, see Scheme 1), but the latter species did not undergo the conjugate addition–elimination sequence (**35** (X = I) → **36** (X = I) → **28**). Some support for this conclusion was forthcoming when it was found that evaporation of the solvent, followed by heating of the residual material to 145–165°C under reduced pressure with direct distillation of product, gave the iodo enone **28** in 46% yield. In similar fashion, this procedure (Procedure A) could be used to convert other β-diketones into the corresponding β-iodo enones (see Table 3, Entries 1, 4, 9, 12). However, it is clear from the data given in Table 3 that this mode of operation did not provide high yields of the desired products.

In efforts to improve this situation, the use of a more polar reaction medium was investigated. Indeed, it was found that reaction of various β-diketones with triphenylphosphine diiodide – triethylamine in dry acetonitrile at room temperature (Procedure B) produced *directly* improved yields of the corresponding β-iodo enones (Table 3, Entries 2, 5, 7, 10). However, even when this polar solvent was used, the reactions at room temperature were slow and, typically, reaction times of ~4 days were required for complete conversion of the

TABLE 2. Spectral data for β-chloro and β-bromo α,β-unsaturated ketones

| Compound[a] | Infrared ($cm^{-1}$)[b] | $^1H$ Nuclear magnetic resonance (δ) | Reference or analysis |
|---|---|---|---|
| **12** | 1680, 1608 | 1.80–2.90 (complex m, 6H), 6.22 (t, 1H, $J$ = 1.5 Hz) | [c] |
| **13** | 1675, 1626 | 1.86–2.94 (complex m, 6H), 1.90 (t, 3H, $J$ = 2 Hz) | [d] |
| **14** | 1678, 1610 | 1.10 (s, 6H), 2.26 (s, 2H), 2.55 (d, 2H, $J$ = 2 Hz), 6.22 (t, 1H, $J$ = 2 Hz) | [e] |
| **15** | 1675, 1630 | 1.08 (s, 6H), 1.93 (t, 3H, $J$ = 2 Hz), 2.32 (s, 2H), 2.62 (q, 2H, $J$ = 2 Hz) | [f] |
| **16** | 1712, 1640 | 1.78 (t, 3H, $J$ = 2 Hz), 2.40–2.67 (m, 2H), 2.67–2.98 (m, 2H) | [g] |
| **17** | 1682, 1605 | 1.80–2.60 (m, 4H), 2.70–3.00 (m, 2H), 6.50 (t, 1H, $J$ = 2 Hz) | [h] |
| **18** | 1676, 1620 | 1.86–2.26 (m, 2H), 1.94 (t, 3H, $J$ = 2 Hz), 2.30–2.63 (m, 2H), 2.73–3.10 (m, 2H) | *Anal.* calcd. for $C_7H_9BrO$: C 44.41, H 4.79; found: C 44.33, H 4.90 |
| **19** | 3115, 1675 1637, 1613 | 1.80–2.26 (m, 2H), 2.33–2.63 (m, 2H), 2.77–3.06 (m, 2H), 3.10–3.37 (m, 2H), 4.83–5.30 (m, 2H), 5.46–6.14 (m, 1H) | *Anal.* calcd. for $C_9H_{11}BrO$: C 50.20, H 5.15; found: C 50.33, H 5.19 |
| **20** | 2260, 1675 1615 | 1.93–2.43 (m, 2H), 2.47–3.27 (m, 8H) | *Anal.* calcd. for $C_9H_{10}BrNO$: C 47.39, H 4.42, N 6.14; found: C 47.70, H 4.44, N 6.10 |
| **21** | 1680, 1608 | 1.10 (s, 6H), 2.28 (s, 2H), 2.72 (d, 2H, $J$ = 1.5 Hz), 6.49 (t, 1H, $J$ = 1.5 Hz) | [i] |
| **22** | 1675, 1625 | 1.08 (s, 6H), 1.96 (t, 3H, $J$ = 2 Hz), 2.32 (s, 2H), 2.80 (q, 2H, $J$ = 2 Hz) | *Anal.* calcd. for $C_9H_{13}BrO$: C 49.78, H 6.03; found: C 49.65, H 5.98 |
| **23** | 1705, 1580 | 2.43–2.70 (m, 2H), 2.97–3.18 (m, 2H), 6.44 (t, 1H, $J$ = 1.5 Hz) | *Anal.* calcd. for $C_5H_5BrO$: C 37.30, H 3.13; found: C 37.15, H 3.29 |
| **24** | 1705, 1636 | 1.77 (t, 3H, $J$ = 2 Hz), 2.42–2.66 (m, 2H), 2.76–3.14 (m, 2H) | *Anal.* calcd. for $C_6H_7BrO$: C 41.18, H 4.03; found: C 41.38, H 4.15 |
| **25** | 1704, 1626 | 2.47–2.64 (m, 2H), 2.84–3.14 (m, 4H), 4.93–5.22 (m, 2H), 5.58–6.04 (m, 1H) | *Anal.* calcd. for $C_8H_9BrO$: C 47.79, H 4.51; found: C 47.66, H 4.56 |
| **26** | 1693, 1603 | 2.20 (s, 3H), 2.75 (d, 3H, $J$ = 2 Hz), 6.73 (broad s, 1H) | *Anal.* calcd. for $C_5H_7BrO$: C 36.83, H 4.25; found: C 36.80, H 4.22 |
| **27** | 1695, 1610 | 2.33 (s, 3H), 2.45 (d, 3H, $J$ = 1.5 Hz), 6.55 (broad s, 1H) | *Anal.* calcd. for $C_5H_7BrO$: C 36.83, H 4.26; found: C 36.61, H 4.15 |

[a] All compounds (except **18**, which exhibited mp 21.5–23.5°C) were liquids at room temperature, and were purified by bulb-to-bulb distillation under reduced pressure (water aspirator or vacuum pump).
[b] All infrared spectra were taken on liquid films.
[c] References 9, 30, 32, 50.
[d] References 9, 35.
[e] References 9, 29, 31.
[f] References 9, 33.
[g] Reference 9.
[h] References 30, 50.
[i] Reference 51.

Can. J. Chem. Downloaded from www.nrcresearchpress.com by 210.87.254.105 on 09/06/12
For personal use only.

Can. J. Chem. Downloaded from www.nrcresearchpress.com by 210.87.254.105 on 09/06/12
For personal use only.

TABLE 3. Reaction of symmetrical β-diketones with triphenylphosphine diiodide. Preparation of β-iodo α,β-unsaturated ketones

| Entry | β-Diketone | Procedure[a] | Reaction time (h) | Product (yield %)[b] |
|---|---|---|---|---|
| 1 | **1** | A | 20 | **28** (46) |
| 2 | **1** | B | 96 | **28** (72) |
| 3 | **1** | C | 9 | **28** (87) |
| 4 | **2** | A | 24 | **29** (60) |
| 5 | **2** | B | 96 | **29** (73) |
| 6 | **2** | C | 9 | **29** (73) |
| 7 | **3** | B | 96 | **30** (80) |
| 8 | **5** | C | 9 | **31** (86) |
| 9 | **6** | A | 24 | **32** (62) |
| 10 | **6** | B | 96 | **32** (83) |
| 11 | **8** | C | 3 | **33** (85) |
| 12 | **9** | A | 24 | **34** (71) |
| 13 | **9** | C | 3 | **34** (92) |

[a] For details regarding the procedures A, B, and C, see text and the Experimental.
[b] Yield of distilled product.

starting materials into the desired products. Eventually, it was found that the product yields could be improved still further and that the reaction times could be reduced to a matter of hours by carrying out the reactions at elevated temperatures (refluxing acetonitrile, Procedure C). Under these conditions, it was possible to obtain consistently good to excellent yields of the β-iodo enones (Table 3, Entries 3, 6, 8, 11, 13) and this procedure, with few exceptions (*vide infra*), is the preferred one.

The infrared and $^1$H nmr spectral data derived from the β-iodo α,β-unsaturated ketones, along with elemental analysis data, are summarized in Table 4.

### *(b) Conversion of unsymmetrical 1,3-cyclohexanediones into β-iodo α,β-unsaturated ketones*

The reaction of triphenylphosphine diiodide with the unsymmetrically substituted 1,3-cyclohexanediones **37–44** (see Chart 2) was also investigated. This study was carried out in order to determine the regioselectivity of the transformations and to produce substances, more highly substituted than compounds **28–31**, which might be of use as intermediates in organic synthesis.

The substrates **37–44** necessary for this investigation were prepared in a straightforward manner (see Scheme 2). The kinetically formed (lithium diisopropylamide (LDA), tetrahydrofuran (THF), −78°C) enolate anions of the isobutyl enol ethers **63** and **64** were alkylated (52) with methyl iodide, allyl bromide and isopropyl iodide. Although alkylation (tetrahydrofuran solution) of the enolate anions with the former two alkylating agents proceeded in excellent yields (**65**: 95%, **66**: 93%, **69**: 94%, **70**: 95%), similar reactions involving isopropyl iodide gave, not unexpectedly (52), poor yields of the desired products **68** (16%) and **72** (13%), even when hexamethylphosphoramide (HMPA) was used as a cosolvent. Nevertheless, quantities of **68** and **72** sufficient to carry out the present study could be obtained quite readily by this rather simple procedure.

Hydrogenation of the allyl derivatives **66** and **70** in the presence of the homogeneous catalyst tris-(triphenylphosphine)chlororhodium (53) afforded excellent yields of the corresponding *n*-propyl compounds **67** and **71**, respectively.

Careful hydrolysis (54) of the enol ethers **65–72** with 1 *N* hydrochloric acid in acetone provided very good yields of the required 1,3-cyclohexanediones **37–44**, respectively. It is pertinent to point out that this hydrolysis should be done in the absence of oxygen and that the products should be purified carefully and stored under a dry, inert atmosphere. It is well known (55) that 1,3-diones of this type are quite prone to autoxidation, particularly when they are moist.

Treatment of 4-methyl-1,3-cyclohexanedione (**37**) with triphenylphosphine diiodide in refluxing acetonitrile in the presence of triethylamine provided, in 92% yield, a product which on the basis of glc and tlc appeared to consist of two components in a ratio of about 70:30. Separation of these components was achieved by preparative tlc. The major

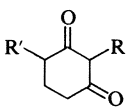

**37** R = H, R′ = $CH_3$
**38** R = H, R′ = $CH_2CH{=}CH_2$
**39** R = H, R′ = $CH_2CH_2CH_3$
**40** R = H, R′ = $CH(CH_3)_2$
**41** R = R′ = $CH_3$
**42** R = $CH_3$, R′ = $CH_2CH{=}CH_2$
**43** R = $CH_3$, R′ = $CH_2CH_2CH_3$
**44** R = $CH_3$, R′ = $CH(CH_3)_2$

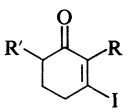

**45** R = H, R′ = $CH_3$
**46** R = H, R′ = $CH_2CH{=}CH_2$
**47** R = H, R′ = $CH_2CH_2CH_3$
**48** R = H, R′ = $CH(CH_3)_2$
**49** R = R′ = $CH_3$
**50** R = $CH_3$, R′ = $CH_2CH{=}CH_2$
**51** R = $CH_3$, R′ = $CH_2CH_2CH_3$
**52** R = $CH_3$, R′ = $CH(CH_3)_2$

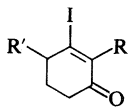

**53** R = H, R′ = $CH_3$
**54** R = H, R′ = $CH_2CH{=}CH_2$
**55** R = H, R′ = $CH_2CH_2CH_3$
**56** R = H, R′ = $CH(CH_3)_2$
**57** R = R′ = $CH_3$
**58** R = $CH_3$, R′ = $CH_2CH{=}CH_2$
**59** R = $CH_3$, R′ = $CH_2CH_2CH_3$
**60** R = $CH_3$, R′ = $CH(CH_3)_2$

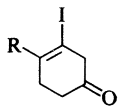

**61** R = $CH_3$
**62** R = $CH_2CH{=}CH_2$

CHART 2

TABLE 4. Infrared, $^1$H nmr, and elemental analysis data for β-iodo α,β-unsaturated ketones derived from symmetrical β-diketones

| Compound | Infrared ($cm^{-1}$)[a] | $^1$H Nuclear magnetic resonance (δ) | Analysis or exact mass determination |
|---|---|---|---|
| **28**[b] | 1675, 1595 | 1.73–2.60 (m, 4H), 2.77–3.10 (m, 2H), 6.80 (t, 1H, $J$ = 2 Hz) | *Anal.* calcd. for $C_6H_7IO$: C 32.45, H 3.17; found: C 32.66, H 3.25 |
| **29**[c] | 1670, 1605 | 1.67–2.20 (m, 2H), 2.03 (t, 3H, $J$ = 2 Hz), 2.30–2.64 (m, 2H), 2.80–3.20 (m, 2H) | *Anal.* calcd. for $C_7H_9IO$: C 36.04, H 3.87; found: C 36.23, H 4.00 |
| **30** | 3115, 1680, 1635, 1600 | 1.83–2.23 (m, 2H), 2.34–2.66 (m, 2H), 2.94–3.40 (m, 4H), 4.90–5.34 (m, 2H), 5.46–6.15 (m, 1H) | *Anal.* calcd. for $C_9H_{11}IO$: C 41.24, H 4.23; found: C 41.54, H 4.23 |
| **31** | 1680, 1601 | 1.66–2.75 (m, 8H), 2.83–3.17 (t, 2H, $J$ = 6 Hz), 4.63–5.20 (m, 2H), 5.46–6.17 (m, 1H) | *Exact Mass* calcd. for $C_{10}H_{13}OI$: 276.0015; found: 276.0019 |
| **32** | 1684, 1596 | 1.08 (s, 6H), 2.27 (s, 2H), 2.80 (d, 2H, $J$ = 2 Hz), 6.81 (t, 1H, $J$ = 2 Hz) | *Anal.* calcd. for $C_8H_{11}IO$: C 38.42, H 4.43; found: C 38.74, H 4.46 |
| **33**[d] | 1710, 1570 | 2.34–2.56 (m, 2H), 2.90–3.16 (m, 2H), 6.64 (t, 1H, $J$ = 2 Hz) | *Anal.* calcd. for $C_5H_5IO$: C 28.88, H 2.42; found: C 28.98, H 2.40 |
| **34**[e] | 1701, 1620 | 1.83 (t, 3H, $J$ = 2 Hz), 2.40–2.68 (m, 2H), 2.80–3.16 (m, 2H) | *Anal.* calcd. for $C_6H_7IO$: C 32.42, H 3.15; found: C 32.36, H 3.30 |

[a] Infrared spectra of compounds which were liquids at room temperature were taken on liquid films, while those of crystalline compounds were recorded on chloroform solutions.
[b] Melting point ~15–16°C.
[c] Melting point 57–59°C.
[d] Melting point 67–68°C.
[e] Melting point 52–53°C.

product provided spectral data consistent with that expected for 3-iodo-6-methyl-2-cyclohexen-1-one (**45**), while the minor component was shown on the basis of the infrared and $^1$H nmr spectra to consist of a mixture of the isomeric iodo ketones **53** and **61** (ratio ≈8:3, respectively). Apparently, under the reaction conditions, the α,β-unsaturated ketone **53** was partially isomerized to the corresponding β,γ-unsaturated isomer **61**. Since we were unable to effect separation of compounds **53** and **61**, these substances were not individually characterized.

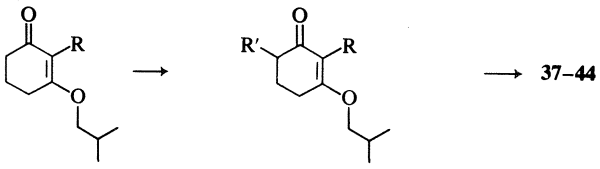


**63** R = H
**64** R = $CH_3$

**65** R = H, R′ = $CH_3$
**66** R = H, R′ = $CH_2CH{=}CH_2$
**67** R = H, R′ = $CH_2CH_2CH_3$
**68** R = H, R′ = $CH(CH_3)_2$
**69** R = R′ = $CH_3$
**70** R = $CH_3$, R′ = $CH_2CH{=}CH_2$
**71** R = $CH_3$, R′ = $CH_2CH_2CH_3$
**72** R = $CH_3$, R′ = $CH(CH_3)_2$

SCHEME 2

Reaction of triphenylphosphine diiodide with the unsymmetrical 1,3-cyclohexanediones **38–44** (see Chart 2) under conditions identical with those used for the dione **37** produced results which are summarized in Table 5. It can be seen that all of the transformations were quite efficient and, in terms of the regioselectivity of the reactions, the trends are not unexpected. For example, if one considers the series of 4-alkyl-1,3-cyclohexanediones **37–40**, it can be seen that as the alkyl group adjacent to the C-3 carbonyl function becomes larger, the regioselectivity of the reaction increases. That is, in the case of 4-methyl-1,3-cyclohexanedione (**37**), the iodine atom becomes attached to carbon atoms 1 and 3 in a ratio of ≈70:30 (Table 5, Entry 1) while in the case of the corresponding isopropyl substrate **40**, the reaction is nearly totally regioselective (Table 5, Entry 4). When the C-4 substituent is intermediate in size (allyl, *n*-propyl), the regioselectivity is between these two extremes (Table 5, Entries 2 and 3). A very similar trend is observed with the 4-alkyl-2-methyl-1,3-cyclohexanediones **41–44** (Table 5, Entries 5–8).

Can. J. Chem. Downloaded from www.nrcresearchpress.com by 210.87.254.105 on 09/06/12
For personal use only.

Can. J. Chem. Downloaded from www.nrcresearchpress.com by 210.87.254.105 on 09/06/12
For personal use only.

TABLE 5. Reaction of unsymmetrical 1,3-cyclohexanediones with triphenylphosphine diiodide[a]

| Entry | β-Diketone | Products (yield, %)[b] | Ratio[c] |
|---|---|---|---|
| 1 | **37** | **45**, **53**, **61** (92) | 70:22:8[d] |
| 2 | **38** | **46**, **54**, **62** (76) | 83:14:3[d] |
| 3 | **39** | **47**, **55** (88) | 89:11 |
| 4 | **40** | **48**, **56** (85) | >99:<1 |
| 5 | **41** | **49**, **57** (91) | 83:17 |
| 6 | **42** | **50**, **58** (71) | 88:12 |
| 7 | **43** | **51**, **59** (78) | 87:13 |
| 8 | **44** | **52**, **60** (90) | >98:<2 |

[a] All reactions were carried out in refluxing acetonitrile.
[b] Yield of distilled products.
[c] Ratios were determined by a combination of glc and $^1$H nmr spectroscopy.
[d] Although it was possible to separate (preparative tlc) compounds **45** and **46** from the mixtures of **53** + **61** and **54** + **62**, respectively, we were not able to effect separation of the latter two pairs of products. The ratios **53**/**61** and **54**/**62** were determined by $^1$H nmr spectroscopy and, in each case, the two compounds were characterized as a mixture (see Table 6).

The observed regioselectivity in these reactions is presumably due to steric factors. Thus, reaction of triphenylphosphine diiodide with the enolate anion **74** of the generalized 1,3-dione **73** would be expected to take place preferentially at the less hindered oxygen atom to provide mainly the phosphonium salt **75**, with species **76** being the minor intermediate (see Scheme 3). On this basis, the ratio of the final products **79** and **80** would be a reflection of the relative proportions of the intermediate phosphonium salts **75** and **76**. As R′ becomes larger, the ratio **75**:**76** should increase, thus accounting for the observed trends.

An alternative rationale is also possible. On the basis of our earlier observations, it appears that the conversion of the phosphonium salts **75** and **76** into the iodo enones **79** and **80** is the rate-determining step in the overall transformation **73** → **79** + **80**. Therefore, if under the reaction conditions the reaction **74** → **75** + **76** were to be readily reversible and a relatively fast equilibrium between **75** and **76** (via **74**) would thus be established, the ratio **79**/**80** would depend upon the relative rates of conversion of **75** and **76** (via **77** and **78**) into the final products. Clearly, attack of iodide ion on the less hindered β carbon of the enone system of **75** would be a more facile process than the corresponding reaction with intermediate **76**. Furthermore, as R′ became larger, this rate difference would be enhanced. In any case, whatever the actual course of events, the observed regioselectivities, especially in those cases where one of the carbonyl groups is quite hindered, should prove to be useful from a synthetic point of view.

The infrared and $^1$H nmr spectral data for the iodo enones listed in Table 5 are summarized in Table 6. The structural assignments for each of the isomeric pairs of compounds were based mainly on the $^1$H nmr spectra and, therefore, it is appropriate to discuss briefly how these conclusions were drawn. Firstly, we have observed that in the $^1$H nmr spectra of all of the substituted 3-iodo-2-cyclohexen-1-ones which we have prepared, the proton or protons at C-4 resonate at lower field (in the region δ 2.75–3.15) than the other ring protons and, in nearly all of the cases, this signal can be identified quite readily. Thus, for example, in the $^1$H nmr spectrum of the β-iodo enone **47**, the C-4 methylene protons give rise to a *two-proton* multiplet at δ 2.78–2.98, while the C-4 proton of the isomeric compound **55** produces a *one-proton*

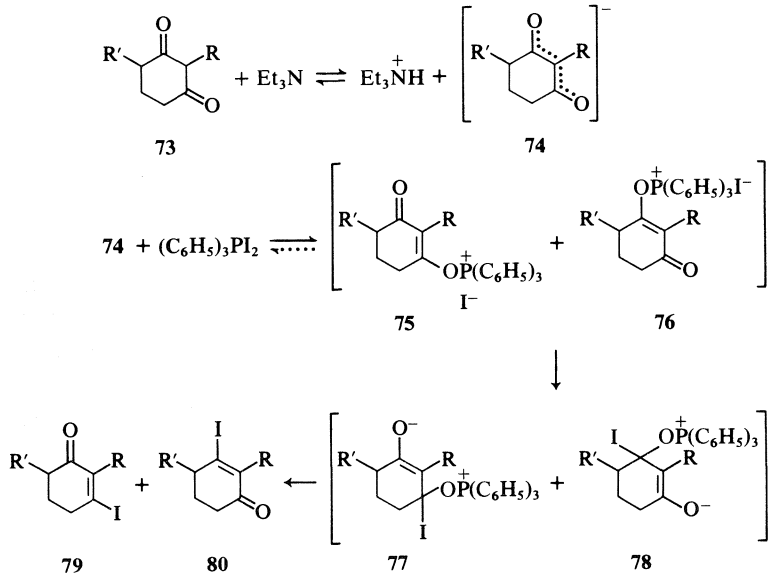


SCHEME 3

TABLE 6. Infrared, $^1$H nmr, and high resolution mass spectrometric data for β-iodo α,β-unsaturated ketones derived from unsymmetrical 1,3-cyclohexanediones

| Compound(s)[a] | Infrared ($cm^{-1}$)[b] | $^1$H Nuclear magnetic resonance (δ) | Exact mass determination[c] |
|---|---|---|---|
| **45** | 1680, 1600 | 1.12 (d, 3H, $J$ = 6.5 Hz), 1.60–2.14 (m, 3H), 2.16–2.54 (m, 1H), 2.76–3.04 (m, 2H), 6.70 (t, 1H, $J$ = 2 Hz) | *Exact Mass* calcd. for $C_7H_9OI$: 235.9698; found: 235.9721 |
| **53** + **61**[d] | 1730, 1680 1595 | 1.30 (d, $J$ = 7.0 Hz, secondary methyl of **53**), 1.70–2.50 (diffuse m), 2.54 (broad s, vinyl methyl of **61**), 2.64–3.00 (m), 3.38 (unresolved m, $w_{1/2} \approx 6$ Hz, C-2 methylene of **61**), 6.72 (d, $J$ = 2 Hz, vinyl proton of **53**) | *Exact Mass* calcd. for $C_7H_9OI$: 235.9698; found: 235.9711 |
| **46** | 1670, 1600 | 1.62–2.72 (diffuse m, 5H), 2.78–3.00 (m, 2H), 4.88–5.16 (m, 2H), 5.48–5.94 (m, 1H), 6.70 (t, 1H, $J$ = 2 Hz) | *Exact Mass* calcd. for $C_9H_{11}OI$: 261.9855; found: 261.9869 |
| **54** + **62**[d] | 1720, 1670 1595 | 1.72–2.94 (diffuse m), 3.09 (broad d, $CH_2CH{=}CH_2$ of **62**), 3.46 (broad s, C-2 methylene of **62**), 5.02–5.32 (m), 5.58–6.04 (m), 6.84 (d, $J$ = 1 Hz, ring vinyl proton of **54**) | *Exact Mass* calcd. for $C_9H_{11}OI$: 261.9855; found: 261.9842 |
| **47** | 1670, 1595 | 0.90 (t, 3H, $J$ = 6 Hz), 1.16–1.58 (m, 4H), 1.60–2.40 (m, 3H), 2.78–2.98 (m, 2H), 6.68 (t, 1H, $J$ = 2 Hz) | *Exact Mass* calcd. for $C_9H_{13}OI$: 264.0011; found: 264.0022 |
| **55** | 1670, 1590 | 1.00 (t, 3H, $J$ = 6 Hz), 1.20–2.55 (diffuse m, 7H), 2.60–2.88 (m, 1H) 6.79 (d, 1H, $J$ = 1.5 Hz) | *Exact Mass* calcd. for $C_9H_{13}OI$: 264.0011; found: 264.0013 |
| **48** | 1670, 1595 | 0.84, 0.91 (d, d, 6H, $J$ = 7 Hz), 1.70–2.48 (m, 4H), 2.76–2.98 (m, 2H), 6.67 (t, 1H, $J$ = 2 Hz) | *Exact Mass* calcd. for $C_9H_{13}OI$: 264.0011; found: 264.0005 |
| **49** | 1670, 1610 | 1.11 (d, 3H, $J$ = 6 Hz), 1.60–2.10 (m, 2H), 1.99 (t, 3H, $J$ = 2 Hz), 2.22–2.56 (m, 1H), 2.90–3.14 (m, 2H) | *Exact Mass* calcd. for $C_8H_{11}OI$: 249.9855; found: 249.9856 |
| **57** | 1680, 1600 | 1.36 (d, 3H, $J$ = 7 Hz), 1.62–2.76 (diffuse m, 4H), 2.03 (d, 3H, $J$ = 1.5 Hz), 2.80–3.12 (m, 1H) | *Exact Mass* calcd. for $C_8H_{11}OI$: 249.9855; found: 249.9858 |
| **50** | 1670, 1600 | 1.52–2.72 (diffuse m, 5H), 2.01 (t, 3H, $J$ = 2 Hz), 2.88–3.12 (m, 2H), 4.86–5.14 (m, 2H), 5.49–5.92 (m, 1H) | *Exact Mass* calcd. for $C_{10}H_{13}OI$: 276.0011; found: 276.0013 |
| **58** | 1670, 1600 | 1.74–3.02 (diffuse m, 7H), 2.01 (d, 3H, $J$ = 1.5 Hz), 4.96–5.22 (m, 2H), 5.52–5.96 (m, 1H) | *Exact Mass* calcd. for $C_{10}H_{13}OI$: 276.0011; found: 276.0024 |
| **51** | 1670, 1600 | 0.91 (t, 3H, $J$ = 6 Hz), 1.14–2.14 (diffuse m, 7H), 2.00 (t, 3H, $J$ = 2 Hz), 2.16–2.46 (m, 1H), 2.88–3.12 (m, 2H) | *Exact Mass* calcd. for $C_{10}H_{15}OI$: 278.0167; found: 278.0167 |
| **59** | 1670, 1600 | 0.98 (t, 3H, $J$ = 6.5 Hz), 1.20–2.60 (diffuse m, 8H), 2.03 (d, 3H, $J$ = 1.5 Hz), 2.70–2.98 (m, 1H) | *Exact Mass* calcd. for $C_{10}H_{15}OI$: 278.0167; found: 278.0168 |
| **52** | 1675, 1610 | 0.84, 0.91 (d, d, 6H, $J$ = 6.5 Hz), 1.62–2.48 (m, 4H), 1.99 (t, 3H, $J$ = 2 Hz), 2.84–3.10 (m, 2H) | *Exact Mass* calcd. for $C_{10}H_{15}OI$: 278.0167; found: 278.0163 |

[a] All compounds were liquids at room temperature and all exhibited one peak on glc analysis and one spot by tlc analysis.
[b] All infrared spectra were taken on liquid films.
[c] Satisfactory C, H elemental analyses were obtained on the following representative, randomly chosen compounds: **46**, **49**, **50**, **55**, **57**, **58**.
[d] We were unable to effect separation of **53** and **61** or of **54** and **62**. On the basis of careful integration of the areas under the $^1$H nmr signals due to the C-2 vinyl protons of **53** (δ 6.72) and **54** (δ 6.84) vs. the C-2 methylene protons of **61** (δ 3.38) and **62** (δ 3.46), the ratios of the two pairs of compounds were estimated to be as follows: **53/61** ≈ 8:3; **54/62** ≈ 4:1.

Can. J. Chem. Downloaded from www.nrcresearchpress.com by 210.87.254.105 on 09/06/12
For personal use only.

multiplet at δ 2.60–2.88. Similar comparisons can be made for the other pairs of isomeric β-iodo enones. Secondly, the C-2 olefinic protons of the β-iodo enones **45–48** and **53–55** exhibit allylic coupling to the C-4 protons, while homoallylic coupling can be observed between the C-2 vinyl methyl protons and the C-4 protons of the iodo enones **49–52** and **57–59**. Thus, for example, in the $^1$H nmr spectra of the isomeric compounds **47** and **55**, the C-2 olefinic protons give rise to a *triplet* (δ 6.68, $J \approx 2$ Hz) and a *doublet* (δ 6.79, $J \approx 1.5$ Hz), clearly showing that C-4 of these two substances contains two protons and one proton, respectively. Similarly, the C-2 vinyl methyl groups of the isomeric β-iodo enones **51** and **59** produce a *triplet* (δ 2.00, $J \approx 2$ Hz) and a *doublet* (δ 2.03, $J \approx 1.5$ Hz), respectively. Analogous observations could be made for the other iodo enones.

### (c) *Conversion of 2-hydroxymethylenecycloalkanones into 2-iodomethylenecycloalkanones*

Attempts to convert 2-hydroxymethylenecyclohexanone (**81**) into 2-iodomethylenecyclohexanone by reaction of the former substance with triphenylphosphine diiodide – triethylamine under conditions previously used for 1,3-diones proved to be unsuccessful. For example, the reaction in acetonitrile at room temperature was prohibitively slow, while in refluxing acetonitrile a good deal of intractable material was formed and the yield of identifiable product was very low. Eventually it was found that the desired conversion could be carried out successfully and reproducibly by carrying out the reaction at room temperature in a mixture of acetonitrile and HMPA. Under these conditions, **81** was transformed into (*E*)-2-iodomethylenecyclohexanone (**82**) in 94% yield (see Chart 3). In similar fashion, (*E*)-2-iodomethylenecyclopentanone (**84**) could be derived in 73% yield from the corresponding hydroxymethylene compound **83**. In each case, the conversion was highly regioselective and stereoselective, since we were unable to detect the presence of isomeric products.

The assignments made regarding the stereochemistry of compounds **82** and **84** require brief comment. It seems clear that these assignments could have been made very readily if the geometric isomers of **82** and **84** had also been formed in the reactions. That is to say, the $^1$H nmr signals of the olefinic protons of the geometric isomers of **82** and **84** would have been expected to appear at higher field than the corresponding signals of **82** and **84** themselves. For example, the protons adjacent to the chlorine atoms of the β-chloro enones **85** and **86**

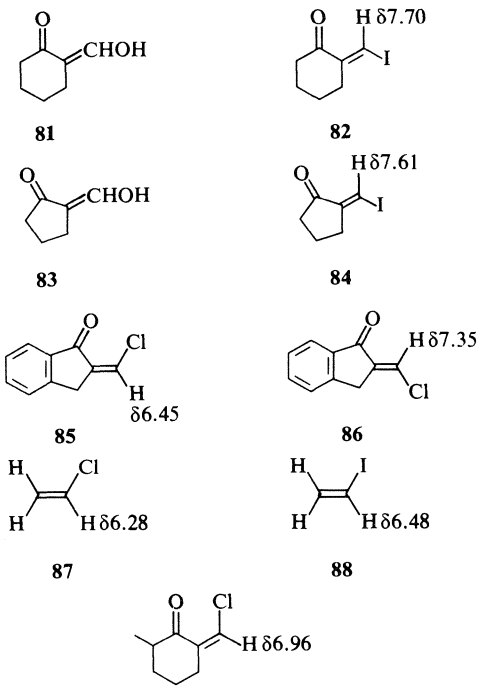


CHART 3

resonate at δ 6.45 and 7.35, respectively (9). However, since the reactions leading to the iodomethylene compounds **82** and **84** were totally stereoselective, only one of the two possible isomers was available in each case, and, therefore, direct comparisons were not possible.

The stereochemical assignments are based on the following arguments. The C-1 protons of vinyl chloride (**87**) and vinyl iodide (**88**) resonate at δ 6.28 and 6.48 respectively (Chart 3). Thus, changing the halogen from Cl to I results in a downfield shift of 0.2 ppm. On this basis, it can be argued that the olefinic protons of the *iodo* compounds corresponding to **85** and **86** (I in place of Cl in each case) should give rise to signals at about δ 6.65 and 7.55, respectively. The latter value is quite close to that of the chemical shift observed for the olefinic proton of the iodomethylenecyclopentanone derived from the reaction discussed above. Therefore, it seems reasonable to conclude that this product has the same relative stereochemistry (i.e. **84**) as that of compound **86**.

A similar argument can be used in the case of the iodomethylenecyclohexanone **82**. Clark and Heathcock (9) have reported that the $^1$H nmr spectrum of (*Z*)-2-chloromethylene-6-methylcyclohexanone (**89**) exhibits the olefinic proton at δ 6.96. The difference (0.74 ppm) between this chemical shift and that of the olefinic proton of **82** (δ 7.70) would

Can. J. Chem. Downloaded from www.nrcresearchpress.com by 210.87.254.105 on 09/06/12
For personal use only.

Can. J. Chem. Downloaded from www.nrcresearchpress.com by 210.87.254.105 on 09/06/12
For personal use only.

appear to be too large for the compounds to possess the same relative stereochemistry. In any case, the olefinic protons of compounds **82** and **84** show very similar chemical shifts and it is therefore highly likely that they have the same configuration.

Finally, a few comments should be made regarding the stability of 2-halomethylenecycloalkanones. It has been stated that 2-chloromethylenecyclohexanone (configuration not specified) "decomposes rapidly at room temperature and even at −20°C under nitrogen is converted into a purple oil in a matter of hours" (56).[7] Indeed, we have found that attempted preparation of 2-chloromethylenecyclohexanone by reaction of **81** with triphenylphosphine dichloride – triethylamine provides a poor yield of a very unstable product. A similar observation was made in the reaction of **81** with triphenylphosphine dibromide – triethylamine. On the other hand, the iodomethylenecycloalkanones **82** and **84**, although certainly less stable than the endocyclic β-iodo enones, can be prepared readily and can be stored in a freezer under an atmosphere of argon for a few months without substantial decomposition. If they are exposed to the air at ambient temperatures, however, they darken in color and decompose extensively in a day or two. Nevertheless, as synthetically employable intermediates, compounds **82** and **84** are certainly to be preferred to the corresponding chloro or bromo derivatives.

### *(d) Ultraviolet spectra of β-iodo α,β-unsaturated ketones*

The well-established Woodward–Fieser rules (57–59) have been employed very successfully in correlating electronic transitions with structural patterns in conjugated chromophores. For example, on the basis of the substitution pattern on the enone system of α,β-unsaturated ketones, it is possible to predict quite accurately the position of the longest wavelength $\pi \rightarrow \pi^*$ absorption band of these compounds (57–59). Since cyclic β-iodo α,β-unsaturated compounds were essentially unknown prior to execution of the work reported herein, nothing was known concerning the effect of a β-iodo substituent on the position of the $\pi \rightarrow \pi^*$ absorption maxima of enones. Therefore, the ultraviolet spectra of methanol solutions of the β-iodo enones prepared in this study were measured, with the hope of establishing the extent of the bathochromic shift caused by a β-iodo group. The results are summarized in Table 7.

The most interesting observation that one can make regarding the data given in Table 7 is that, whether or not there is an alkyl substituent at C-2, the $\pi \rightarrow \pi^*$ absorption maxima of all of the 3-iodo-2-cyclohexen-1-ones which were measured appear in nearly the same position. Thus, the average of the $\lambda_{max}$ values of the 3-iodo-2-cyclohexen-1-ones is 258 nm, with a range of 256–261 nm. The analogous values for 3-iodo-2-alkyl-2-cyclohexen-1-ones are 259 nm and 257–260 nm. Furthermore, if one compares these ultraviolet absorption maxima with those of the "parent" enones (2-cyclohexen-1-one, $\lambda_{max}$ 226 nm; 2-methyl-2-cyclohexen-1-one, $\lambda_{max}$ 234 nm), then the "increments" for a 3-iodo group should be ~32 nm for those cyclohexenones having a proton at C-2 and ~25 nm for the corresponding substances possessing a C-2 alkyl substituent.

The positions of the ultraviolet $\pi \rightarrow \pi^*$ absorption maxima of 3-iodo-2-cyclopenten-1-one (**33**) ($\lambda_{max}$ 249 nm) and the 2-methyl analog **34** ($\lambda_{max}$ 248 nm) are also very similar. Not unexpectedly (2-cyclopenten-1-one, $\lambda_{max}$ 218 nm; 2-methyl-2-cyclopenten-1-one, $\lambda_{max}$ 226 nm), these values are about 10 nm lower than those of the cyclohexenone compounds.

TABLE 7. Longest wavelength $\pi \rightarrow \pi^*$ ultraviolet absorption bands of β-iodo α,β-unsaturated ketones (methanol solution)

| Compound | $\lambda_{max}$, nm (ε) |
|---|---|
| 3-Iodo-2-cyclohexen-1-ones | |
| **28** | 257 (8 430) |
| **32** | 256 (8 380) |
| **45** | 257 (8 700) |
| **46** | 260 (8 860) |
| **47** | 259 (8 680) |
| **48** | 257 (8 150) |
| **55** | 261 (8 330) |
| 3-Iodo-2-alkyl-2-cyclohexen-1-ones | |
| **29** | 258 (9 500) |
| **30** | 259 (9 440) |
| **31** | 260 (9 200) |
| **49** | 256 (8 720) |
| **50** | 258 (8 700) |
| **51** | 257 (9 840) |
| **52** | 262 (7 140) |
| **57** | 260 (9 140) |
| **58** | 260 (8 300) |
| **59** | 259 (8 760) |
| 3-Iodo-2-cyclopenten-1-ones | |
| **33** | 249 (11 350) |
| **34** | 248 (11 520) |

[7]This substance has, however, been employed subsequently as a synthetic intermediate (15). Furthermore, Clark and Heathcock (9) have reported the preparation and characterization of (*Z*)-2-chloromethylene-6-methylcyclohexanone (**89**), although no mention is made regarding the stability (or instability) of this material.

Can. J. Chem. Downloaded from www.nrcresearchpress.com by 210.87.254.105 on 09/06/12
For personal use only.

## Experimental

*General*

Melting points, which were taken on a Fisher–Johns melting point apparatus, and distillation temperatures are uncorrected. Ultraviolet (uv) spectra were recorded on methanol solutions using a Cary 15 spectrophotometer. Infrared (ir) spectra were obtained on liquid films or chloroform solutions, employing Perkin Elmer models 710 or 710B spectrophotometers. Proton magnetic resonance ($^1$H nmr) spectra (deuterochloroform solution) were measured using Varian Associates spectrometers, models T-60 and/or HA-100 or XL-100. Signal positions are given in δ units, with tetramethylsilane as the internal standard. High resolution mass spectrometric measurements were recorded on a Kratos MS-50 mass spectrometer. Gas–liquid chromatography (glc) was carried out with a Hewlett–Packard model 5832 A gas chromatograph (analytical) or with a Varian Aerograph model 90-P instrument (preparative). Microanalyses were performed by Mr. P. Borda, Microanalytical Laboratory, University of British Columbia, Vancouver, B.C.

Triphenylphosphine was recrystallized from ethyl acetate – methanol or from benzene. The solvents and reagents employed were freshly distilled from the following materials: benzene – potassium metal; acetonitrile – phosphorus pentoxide; triethylamine and tetrahydrofuran (THF) – lithium aluminum hydride; hexamethylphosphoramide (HMPA) and diisopropylamine – calcium hydride.

*General procedure for the conversion of β-diketones into β-chloro α,β-unsaturated ketones (Table 1, Entries 1, 3, 7, 9, 12)*

To an ice-cold, stirred solution of recrystallized triphenylphosphine (576 mg, 2.2 mmol) in 20 mL of dry benzene was added 3.7 mL of a 0.6 *M* solution of chlorine in carbon tetrachloride. After the addition was complete, tlc analysis of the mixture indicated that triphenylphosphine was absent. To the resulting suspension was added successively triethylamine (220 mg, 2.2 mmol) and the appropriate β-diketone (2.0 mmol). Stirring was continued at room temperature for the required length of time. The suspension was filtered through a short column of silica gel and the column was eluted with ether. Removal of the solvent from the combined eluate, followed by bulb-to-bulb distillation of the residual oil under reduced pressure (water aspirator, ~10–11 Torr) provided the β-chloro enone as a colorless oil. The yields of the β-chloro enones which were prepared by this procedure are summarized in Table 1, while the spectral data are given in Table 2.

*General procedure for the conversion of β-diketones into β-bromo α,β-unsaturated ketones (Table 1, Entries 2, 4–6, 8, 10, 11, 13, 14)*

To an ice-cold, stirred solution of recrystallized triphenylphosphine (576 mg, 2.2 mmol) in 20 mL of dry benzene was added dropwise 2.2 mL of a 1 *M* solution of bromine in benzene. To the resulting suspension was added successively triethylamine (220 mg, 2.2 mmol) and the appropriate β-diketone (2.0 mmol). Stirring was continued at room temperature for the indicated length of time. The reaction mixture was filtered through a short column of silica gel and the column was eluted with ether. Removal of the solvent from the combined eluate, followed by bulb-to-bulb distillation of the residual oil under reduced pressure (water aspirator, ~10–11 Torr or, in the case of product **20**, vacuum pump, 0.45 Torr) provided the β-bromo enone as a colorless oil. The yields of the β-bromo enones which were prepared by this procedure are summarized in Table 1, while the appropriate spectral data are given in Table 2.

*Conversion of 2,4-pentanedione (**11**) into a mixture of (E)- and (Z)-4-bromo-3-penten-2-one (**26**, **27**) (Table 1, Entry 15)*

To a stirred solution of recrystallized triphenylphosphine (5.76 g, 22 mmol) in dry acetonitrile (100 mL) was added successively a solution of bromine (3.52 g, 22 mmol) in 20 mL of dry benzene, triethylamine (2.2 g, 22 mmol), and 2,4-pentanedione (2.0 g, 20 mmol). The resulting mixture was stirred at room temperature for 19 h. The bulk of the solvent was removed by careful distillation (water aspirator). The residual brown material was diluted with ether (50 mL) and the resulting mixture was filtered through a short column of silica gel (~40 g). The column was washed with ether. Removal of the solvent from the combined eluate, followed by distillation (air-bath temperature 50–70°C/~25 Torr) of the residual oil (which contained some solid triphenylphosphine oxide) gave 3.02 g of a clear liquid. Gas–liquid chromatographic analysis of this material indicated that it consisted of a mixture of **26** and **27** (ratio ~87:13, respectively) along with an unidentified minor compound (~5%). A pure sample of each of the geometric isomers **26** and **27** was obtained by preparative glc, and the spectral data are summarized in Table 2.

*General procedures for the conversion of symmetrical β-diketones into β-iodo α,β-unsaturated ketones*

*(a) Benzene as solvent (Procedure A, Table 3, Entries 1, 4, 9, 12)*

To a stirred solution of recrystallized triphenylphosphine (576 mg, 2.2 mmol) in 20 mL of dry benzene was added 559 mg (2.2 mmol) of iodine and the mixture was stirred at room temperature for 16 h. To the resulting yellow-brown suspension was added successively dry triethylamine (220 mg, 2.2 mmol) and the appropriate β-diketone (2.0 mmol). The mixture was stirred at room temperature for the indicated period of time, during which a brown oil separated from the benzene solution. Examination of the latter by tlc indicated that it contained, at most, only a trace of the desired product. The entire reaction mixture was concentrated under reduced pressure and the residual material was heated at 145–180°C under reduced pressure (water aspirator, ~10–12 Torr) with direct distillation of the product. The distillate thus obtained was redistilled (bulb-to-bulb) under reduced pressure (water aspirator, 10–12 Torr or vacuum pump, 0.2–1 Torr) to provide the β-iodo enone. The yields of the latter substances which were prepared by this procedure are given in Table 3. Physical and spectral data are summarized in Table 4, while ultraviolet absorption maxima are given in Table 7.

*(b) Acetonitrile as solvent (Procedures B and C, Table 3, Entries 2, 3, 5–8, 10, 11, 13)*

To a stirred solution of recrystallized triphenylphosphine (576 mg, 2.2 mmol) in 20 mL of dry acetonitrile was added 559 mg (2.2 mmol) of iodine and the mixture was stirred at room temperature for 2 h. To the resulting orange-yellow suspension was added successively triethylamine (220 mg, 2.2 mmol) and the appropriate β-diketone (2.0 mmol). The mixture was either stirred at room temperature for 4 days (Procedure B, Table 3, Entries 2, 5, 7, 10) or was heated at reflux temperature for the indicated length of time (Procedure C, Table 3, Entries 3, 6, 8, 11, 13). The reaction mixture was concentrated under reduced pressure and the residual material was filtered through a short column of silica gel (~5 g). The column was eluted with 100 mL of ether. Removal of the solvent from the combined eluate, followed by bulb-to-bulb distillation of the residual oil under reduced pressure (water aspirator, ~10–12 Torr or vacuum pump, 0.2–1 Torr) gave the β-iodo enone. The yields of the

Can. J. Chem. Downloaded from www.nrcresearchpress.com by 210.87.254.105 on 09/06/12
For personal use only.

latter substances which were prepared by these procedures are given in Table 3, and the physical and spectral properties of the products are summarized in Table 4. Ultraviolet absorption maxima are provided in Table 7.

*General procedure for the alkylation of 3-isobutoxy-2-cyclohexen-1-one (**63**) and 3-isobutoxy-2-methyl-2-cyclohexen-1-one (**64**) with methyl iodide and allyl bromide*

To a cold (−78°C) stirred solution of LDA (22 mmol) in dry THF (80 mL) under an atmosphere of dry nitrogen was added 20 mmol of the ketone **63** or **64**. The solution was stirred for 1 h. The alkylating agent (methyl iodide or allyl bromide, 26 mmol) was added, the solution was allowed to warm slowly to room temperature, and stirring was continued for 4 h. Brine (50 mL) was added and the resulting mixture was extracted thoroughly with petroleum ether (bp 30–60°C). The combined extracts were washed with brine and dried over anhydrous magnesium sulfate. Removal of the solvent, followed by bulb-to-bulb distillation of the residual oil under reduced pressure, afforded the desired product.

The following compounds were obtained by means of this procedure.

*3-Isobutoxy-6-methyl-2-cyclohexen-1-one* (**65**): 95% yield; distillation temperature 80–90°C (air bath)/0.07 Torr; ir (film): 1690, 1610 $cm^{-1}$; uv (methanol) $\lambda_{max}$: 247 nm (ε 17 800); $^1H$ nmr δ: 0.98 (d, 6H, $J$ = 6 Hz), 1.16 (d, 3H, $J$ = 7 Hz), 1.54–2.58 (diffuse m, 6H), 3.59 (d, 2H, $J$ = 6 Hz), 5.33 (s, 1H). *Anal.* calcd. for $C_{11}H_{18}O_2$: C 72.49, H 9.95; found: C 72.70, H 9.97.

*6-Allyl-3-isobutoxy-2-cyclohexen-1-one* (**66**): 93% yield; distillation temperature 95–100°C (air bath)/0.4 Torr; mp 37–38°C (lit. mp (52) 37–38°C); ir ($CHCl_3$): 1660, 1605 $cm^{-1}$; uv (methanol) $\lambda_{max}$: 247 nm (ε 19 600); $^1H$ nmr δ: 0.98 (d, 6H, $J$ = 6.5 Hz), 1.46–2.78 (diffuse m, 8H), 3.60 (d, 2H, $J$ = 6 Hz), 4.98–5.20 (m, 2H), 5.34 (s, 1H), 5.61–6.05 (m, 1H). *Anal.* calcd. for $C_{13}H_{20}O_2$: C 74.96, H 9.68; found: C 75.05, H 9.54.

*3-Isobutoxy-2,6-dimethyl-2-cyclohexen-1-one* (**69**): 94% yield; distillation temperature 100–110°C (air bath)/0.2 Torr; ir (film): 1650, 1630 $cm^{-1}$; uv (methanol) $\lambda_{max}$: 265 nm (ε 18 800); $^1H$ nmr δ: 0.96 (d, 6H, $J$ = 7 Hz), 1.11 (d, 3H, $J$ = 6.5 Hz), 1.48–2.38 (diffuse m, 5H), 1.68 (t, 3H, $J$ = 2 Hz), 2.40–2.64 (m, 1H), 3.71 (d, 2H, $J$ = 7 Hz). *Exact Mass* calcd. for $C_{12}H_{20}O_2$: 196.1463; found: 196.1470.

*6-Allyl-3-isobutoxy-2-methyl-2-cyclohexen-1-one* (**70**): 95% yield; bp 110°C/0.35 Torr; ir (film): 1640, 1620 $cm^{-1}$; uv (methanol) $\lambda_{max}$: 265 nm (ε 18 600); $^1H$ nmr δ: 1.00 (d, 6H, $J$ = 6.5 Hz), 1.52–2.40 (diffuse m, 6H), 1.72 (t, 3H, $J$ = 1.5 Hz), 3.77 (d, 2H, $J$ = 6.5 Hz), 4.92–5.18 (m, 2H), 5.60–6.04 (m, 1H). *Exact Mass* calcd. for $C_{14}H_{22}O_2$: 222.1620; found: 222.1606.

*Hydrogenation of compounds **66** and **70**. Preparation of 3-isobutoxy-6-*n*-propyl-2-cyclohexen-1-one (**67**) and 3-isobutoxy-2-methyl-6-*n*-propyl-2-cyclohexen-1-one (**71**)*

To a solution of the ketone **66** or **70** (15 mmol) in 150 mL of dry benzene was added approximately 10% by weight of tris(triphenylphosphine)chlororhodium. The resultant solution was stirred vigorously and subjected to an atmosphere of hydrogen at room temperature for 18 h. The solvent was removed under reduced pressure and the residual material was treated with 150 mL of petroleum ether (bp 30–60°C). The mixture was filtered through Celite. Removal of the solvent from the filtrate, followed by distillation of the residual oil under reduced pressure gave the desired products.

*3-Isobutoxy-6-n-propyl-2-cyclohexen-1-one* (**67**): 95% yield; distillation temperature 95–105°C (air bath)/0.1 Torr; mp 25–28°C; ir ($CHCl_3$): 1630, 1600 $cm^{-1}$; uv (methanol) $\lambda_{max}$: 247 nm (ε 19 400); $^1H$ nmr δ: 0.82–1.06 (superimposed d, $J$ = 6.5 Hz, and poorly resolved t, 9H), 1.20–2.30 (diffuse m, 8H), 2.44 (t, 2H, $J$ = 7 Hz), 3.59 (d, 2H, $J$ = 6.5 Hz), 5.30 (s, 1H). *Anal.* calcd. for $C_{13}H_{22}O_2$: C 74.24, H 10.54; found: C 74.47, H 10.40.

*3-Isobutoxy-2-methyl-6-n-propyl-2-cyclohexen-1-one* (**71**): 94% yield; distillation temperature 100–110°C (air bath)/0.2 Torr; ir (film): 1645, 1625 $cm^{-1}$; uv (methanol) $\lambda_{max}$: 265 nm (ε 17 500); $^1H$ nmr δ: 0.91 (t, 3H, $J$ = 7 Hz), 0.98 (d, 6H, $J$ = 6 Hz), 1.14–2.24 (diffuse m, 8H), 1.68 (t, 3H, $J$ = 1.5 Hz), 2.40–2.66 (m, 2H), 3.72 (d, 2H, $J$ = 7 Hz). *Exact Mass* calcd. for $C_{14}H_{24}O_2$: 224.1776; found: 224.1786.

*Preparation of 3-isobutoxy-6-isopropyl-2-cyclohexen-1-one (**68**) and 3-isobutoxy-6-isopropyl-2-methyl-2-cyclohexen-1-one (**72**)*

To a cold (−78°C) stirred solution of LDA (55 mmol) in 60 mL of a 5:1 mixture of dry THF and dry HMPA was added 50 mmol of the ketone **63** or **64**, and the solution was stirred for 1 h. A solution of isopropyl iodide (9.35 g, 55 mmol) in 10 mL of dry THF was added, the resultant mixture was allowed to warm to room temperature, and stirring was continued for 16 h. Water (50 mL) was added and the resultant mixture was extracted thoroughly with petroleum ether (bp 30–60°C). The combined extracts were washed with brine and dried over anhydrous magnesium sulfate. Removal of the solvent produced an oil which was subjected to column chromatography on silica gel (300 g). The eluant was a 7:3 mixture of *n*-hexane – ether. In addition to minor, unidentified products and a major amount of starting material, the following desired products were obtained.

*3-Isobutoxy-6-isopropyl-2-cyclohexen-1-one* (**68**): 16% yield; distillation temperature 70–90°C (air bath)/0.2 Torr; mp 22.5–24°C; ir (film): 1650, 1605 $cm^{-1}$; uv (methanol) $\lambda_{max}$: 247 nm (ε 12 800); $^1H$ nmr δ: 0.83 (d, 3H, $J$ = 6.5 Hz), 0.94 (d, 9H, $J$ = 6.5 Hz), 1.60–2.16 (m, 4H), 2.25–2.56 (m, 3H), 3.53 (d, 2H, $J$ = 6.5 Hz), 5.26 (s, 1H). *Exact Mass* calcd. for $C_{13}H_{22}O_2$: 210.1620; found: 210.1618.

*3-Isobutoxy-3-isopropyl-2-methyl-2-cyclohexen-1-one* (**72**): 13% yield; distillation temperature 85–95°C (air bath)/0.1 Torr; ir (film): 1640, 1620 $cm^{-1}$; uv (methanol) $\lambda_{max}$: 266 (ε 18 300); $^1H$ nmr δ: 0.84 (d, 3H, $J$ = 5 Hz), 0.97 (d, 9H, $J$ = 6 Hz), 1.58 (t, 3H, $J$ = 1.5 Hz), 1.60–2.78 (diffuse m, 7H), 3.77 (d, 2H, $J$ = 6 Hz). *Exact Mass* calcd. for $C_{14}H_{24}O_2$: 224.1770; found: 224.1780.

*General procedure for the hydrolysis of compounds **65–72**. Preparation of the unsymmetrical 1,3-cyclohexanediones **37–44***

To a solution of the β-isobutoxy α,β-unsaturated ketone (**65–72**) (30 mmol) in acetone (80 mL, spectro-grade, previously purged with a stream of nitrogen for 15 min) was added with vigorous stirring 30 mL of 1 *N* hydrochloric acid (previously purged with nitrogen for 15 min). The resultant solution was stirred under an atmosphere of nitrogen for 6 h. Most of the acetone was removed under reduced pressure, the residual material was diluted with 20 mL of brine, and the resultant mixture was extracted thoroughly with dichloromethane. The combined extracts were dried over anhydrous magnesium sulfate. Removal of the solvent, followed by purification of the residual material by distillation under reduced pressure and/or by recrystallization, gave the following desired products.

*4-Methyl-1,3-cyclohexanedione* (**37**): 96% yield; distillation temperature 85–100°C (air bath)/0.03 Torr; recrystallization from ether – petroleum ether (bp 30–60°C), mp 53–57°C; ir ($CHCl_3$): 3400–2400 (broad), 1700, 1610–1580 (broad) $cm^{-1}$; $^1H$ nmr δ: 1.16 (d, 3H, $J$ = 6 Hz), 1.38–2.80 (diffuse m, 5H), 3.38 (s, ~1H, C-2 methylene of keto tautomer), 5.42 (s, ~0.5H, C-2 vinyl proton of enol tautomer). *Anal.* calcd. for $C_7H_{10}O_2$: C 66.75, H 7.99; found: C 66.79, H 7.99.

Can. J. Chem. Downloaded from www.nrcresearchpress.com by 210.87.254.105 on 09/06/12
For personal use only.

*4-Allyl-1,3-cyclohexanedione* (**38**): 90% yield; distillation temperature 90–100°C (air bath)/0.08 Torr; mp 34–36°C; ir ($CHCl_3$): 3600–2400 (broad), 1720, 1710, 1640–1590 (broad) $cm^{-1}$; $^1H$ nmr δ: 1.40–2.80 (diffuse m, 7H), 3.38 (s, ~1H, C-2 methylene of keto tautomer), 4.90–5.20 (m, 2H), 5.42 (s, ~0.5H, C-2 vinyl proton of enol tautomer), 5.52–6.00 (m, 1H). *Exact Mass* calcd. for $C_9H_{12}O_2$: 152.0838; found: 152.0845.

*4-n-Propyl-1,3-cyclohexanedione* (**39**): 60% yield; distillation temperature 110–125°C (air bath)/0.9 Torr; mp 69–71°C; ir ($CHCl_3$): 3500–2400 (broad), 1730, 1710, 1600 (broad) $cm^{-1}$; $^1H$ nmr δ: 0.91 (t, 3H, $J$ = 7 Hz), 1.16–2.72 (diffuse m, 9H), 3.40 (s, ~0.7H, C-2 methylene of keto tautomer), 5.40 (s, ~0.7H, C-2 vinyl proton of enol tautomer). *Exact Mass* calcd. for $C_9H_{14}O_2$: 154.0994; found: 154.1005.

*4-Isopropyl-1,3-cyclohexanedione* (**40**): 95% yield; distillation temperature 110–130°C (air bath)/0.07 Torr; mp 106–107°C; ir ($CHCl_3$): 1730, 1710, 1615 $cm^{-1}$; $^1H$ nmr δ: 0.80–1.14 (series of overlapping d, 6H), 1.58–2.86 (diffuse m, 6H), 3.36 (s, ~1.4H, C-2 methylene of keto tautomer), 5.42 (s, ~0.3H, C-2 vinyl proton of enol tautomer). *Exact Mass* calcd. for $C_9H_{14}O_2$: 154.0994; found: 154.0992.

*2,4-Dimethyl-1,3-cyclohexanedione* (**41**): 97% yield; distillation temperature 80–95°C (air bath)/ 0.3 Torr; mp 108–110°C; ir ($CHCl_3$): 3650–2450 (broad), 1745, 1705, 1630 $cm^{-1}$; $^1H$ nmr δ: 1.10–1.34 (series of d), 1.34–2.94 (diffuse m), 1.72 (s, vinyl methyl of enol tautomer), 3.38–3.68 (m, C-2 protons of diastereomeric keto tautomers). On the basis of the relative integrated areas of the latter two signals, the keto–enol ratio was ~1:1. *Exact Mass* calcd. for $C_8H_{12}O_2$: 140.0838; found: 140.0841.

*4-Allyl-2-methyl-1,3-cyclohexanedione* (**42**): 88% yield; distillation temperature 110–120°C (air bath)/ 0.3 Torr; mp 51–53°C; ir ($CHCl_3$): 3575, 3500–2600 (broad), 1735. 1705, 1615 (broad) $cm^{-1}$; $^1H$ nmr δ: 1.19, 1.21 (d, d, $J$ = 6.5 Hz), 1.32–2.86 (diffuse m), 1.71 (s, vinyl methyl of enol tautomer), 3.50 (q, $J$ = 6.5 Hz, C-2 proton of keto tautomers), 4.90–5.20 (m, 2H), 5.52–6.00 (m, 1H). On the basis of the relative integrated areas of the signals at δ 1.71 and 3.50; the keto–enol ratio was ~1:1. *Exact Mass* calcd. for $C_{10}H_{14}O_2$: 165.9994; found: 166.1007.

*2-Methyl-4-n-propyl-1,3-cyclohexanedione* (**43**): 95% yield; distillation temperature 100–110°C (air bath)/0.03 Torr; mp 67–69°C, ir ($CHCl_3$): 3650–2500 (broad), 1740, 1705, 1635 $cm^{-1}$; $^1H$ nmr δ: 0.82–1.04 (m, 3H), 1.18, 1.20 (d, d, $J$ = 6.5 Hz), 1.24–2.76 (diffuse m), 1.72 (s, vinyl methyl of enol tautomer), 3.36–3.68 (m, C-2 protons of diastereomeric keto tautomers). The relative integrated areas of the latter two signals was ~4:1. *Exact Mass* calcd. for $C_{10}H_{16}O_2$: 168.1150; found: 168.1146.

*4-Isopropyl-2-methyl-1,3-cyclohexanedione* (**44**): 96% yield; sublimes at 95–100°C (air bath)/0.01 Torr; mp 104–105°C; ir ($CHCl_3$): 3560, 3500–3000 (broad), 1735, 1700, 1625 (broad) $cm^{-1}$; $^1H$ nmr δ: 0.80–1.26 (series of d), 1.26–2.90 (diffuse m), 1.70 (s, vinyl methyl of enol tautomer), 3.32–3.62 (m, C-2 protons of diastereomeric keto tautomers). The relative integrated areas of the latter two signals was ~2.5:1. *Exact Mass* calcd. for $C_{10}H_{16}O_2$: 168.1150; found: 168.1151.

*General procedure for the conversion of unsymmetrical 1,3-cyclohexanediones into β-iodo α,β-unsaturated ketones (Table 5)*

To a stirred suspension of iodine (660 mg, 2.6 mmol) in 15 mL of dry acetonitrile under an atmosphere of nitrogen was added 681 mg (2.6 mmol) of recrystallized triphenylphosphine and the mixture was stirred for 30 min. To the resultant yellow suspension was added successively dry triethylamine (263 mg, 2.6 mmol) and 2.4 mmol of the appropriate 1,3-cyclohexanedione (**37**–**44**). The dark solution was stirred at room temperature for 1 h and then was heated at reflux temperature for 12 h. The solvent was removed under reduced pressure and the residue was extracted (decantation) with 6 × 25 mL of ether. Removal of the ether from the combined extracts produced a mixture of a solid and an orange oil. This material was washed with 3 × 15 mL of 7:1 *n*-pentane–ether and the combined washings were applied to a dry column consisting of a mixture of 20 g of Florisil (100–120 mesh) and 10 g of alumina (neutral, activity I). The column was eluted with 7:1 *n*-pentene–ether and the fractions containing the desired products were combined. Removal of the solvent from the combined eluate, followed by bulb-to-bulb distillation of the residual oil, provided the desired product(s). In each case, the distilled material was subjected to analysis by glc (6 ft × 0.125 in. column containing 5% OV-17 on 100–120 mesh HP Chromosorb W) and, where possible (see footnote *d*, Tables 5 and 6), the products were separated by preparative tlc on silica gel (plates developed with 7:3 *n*-pentane–ether). The results are recorded in Table 5, and appropriate characterization data and ultraviolet absorption maxima for the various products are summarized in Table 6 and Table 7, respectively.

*Preparation of (E)-2-iodomethylenecyclopentanone (84) and (E)-2-iodomethylenecyclohexanone (82)*

To a stirred solution of recrystallized triphenylphosphine (2.88 g, 11 mmol) in a mixture of dry acetonitrile (50 mL) and dry HMPA (8 mL) was added 2.79 g (11 mmol) of iodine, and the mixture was stirred at room temperature for 20 min. To the resulting yellow suspension was added successively dry triethylamine (1.1 g, 11 mmol) and the α-hydroxymethylenecycloalkanone (**83**, **81**), and stirring was continued for 72 h when the starting material was **83** and for 15 h when the starting material was **81**. Most of the solvent was removed under reduced pressure. The residual material was extracted by stirring and decantation with 5 × 50 mL of pentane. The combined extracts were washed with 3 × 30 mL of water and dried over anhydrous magnesium sulfate. Removal of the solvent, followed by bulb-to-bulb distillation of the residual oil, provided the following products.

*(E)-2-Iodomethylenecyclopentanone* (**84**): 73% yield; recrystallized from ether, mp 31.5°C; ir ($CHCl_3$): 1720, 1608 $cm^{-1}$; uv (methanol) $\lambda_{max}$: 276 nm (ε 9 200), shoulder at 263 nm; $^1H$ nmr δ: 1.8–3.0 (diffuse m, 6H), 7.61 (t, 1H, $J$ = 2 Hz). *Exact Mass* calcd. for $C_6H_7IO$: 221.9543; found: 221.9544.

*(E)-2-Iodomethylenecyclohexanone* (**82**): 94% yield; distillation temperature 60–70°C (air bath)/ 0.4 Torr; crystallizes in refrigerator, mp ~15°C; ir (film): 1695, 1570 $cm^{-1}$; uv (methanol) $\lambda_{max}$: 265 nm (ε 7 200); $^1H$ nmr δ: 1.60–2.04 (m, 4H), 2.30–2.66 (m, 4H), 7.70 (t, 1H, $J$ = 2 Hz). *Anal.* calcd. for $C_7H_9IO$: C 35.62, H 3.84; found: C 35.65, H 3.76.

## Acknowledgements

Financial support for this work from the Natural Sciences and Engineering Research Council of Canada (N.S.E.R.C.C.) and a N.S.E.R.C.C. scholarship (to C.K.L.) are gratefully acknowledged.

1. A. E. Pohland and W. R. Benson. Chem. Rev. **66**, 161 (1966).
2. E. E. van Tamelen, M. P. Seiler, and W. Wierenga. J. Am. Chem. Soc. **94**, 8229 (1972).
3. J. L. Herrmann, J. E. Richman, and R. H. Schlessinger. Tetrahedron Lett. 2599 (1973).
4. Y. Tamura, T. Miyamoto, T. Nishimura, J. Eiho, and Y. Kita. J. Chem. Soc. Perkin Trans. I, 102 (1974).
5. J. P. Marino and T. Kaneko. J. Org. Chem. **39**, 3175 (1974).
6. Y. Tamura, Y. Sumida, S. Haruki, and M. Ikeda. J. Chem. Soc. Perkin Trans. I, 575 (1975).
7. E. Vedejs and J. P. Bershas. Tetrahedron Lett. 1359 (1975).

Can. J. Chem. Downloaded from www.nrcresearchpress.com by 210.87.254.105 on 09/06/12
For personal use only.

8. J. DROUIN, F. LEYENDECKER, and J. M. CONIA. Tetrahedron Lett. 4053 (1975).
9. R. D. CLARK and C. H. HEATHCOCK. J. Org. Chem. **41**, 636 (1975).
10. D. A. ARCHER and B. W. SINGER. J. Chem. Soc. Perkin Trans. I, 2484 (1976).
11. J. L. COKE, H. J. WILLIAMS, and S. NATARAJAN. J. Org. Chem. **42**, 2380 (1977).
12. R. J. K. TAYLOR and I. T. HARRISON. Tetrahedron Lett. 4793 (1976).
13. P. A. WENDER and S. L. ECK. Tetrahedron Lett. 1245 (1977).
14. R. J. CHORVAT, J. R. PALMER, and R. PAPPO. J. Org. Chem. **43**, 966 (1978).
15. C. R. ENGEL and G. DIONNE. Can. J. Chem. **56**, 424 (1978).
16. J. E. MCMURRY, W. A. ANDRUS, and J. H. MUSSER. Synth. Commun. **8**, 53 (1978).
17. M. GILL and R. W. RICKARDS. Tetrahedron Lett. 1539 (1979).
18. N. OKUKADO, D. E. VAN HORN, W. L. KLIMA, and E. NEGISHI. Tetrahedron Lett. 1027 (1978).
19. E. PIERS and I. NAGAKURA. Synth. Commun. **5**, 193 (1975).
20. E. J. COREY and D. J. BEAMES. J. Am. Chem. Soc. **94**, 7210 (1972).
21. A. F. KLUGE, K. G. UNTCH, and J. H. FRIED. J. Am. Chem. Soc. **94**, 7827 (1972).
22. K. MORI, S. TAMADA, M. UCHIDA, N. MIZUMACHI, Y. TACHIBANA, and M. MATSUI. Tetrahedron, **34**, 1901 (1978).
23. R. T. BUCKLER and D. L. GARLING. Tetrahedron Lett. 2257 (1978).
24. M. L. HAMMOND, A. MOURINO, and W. H. OKAMURA. J. Am. Chem. Soc. **100**, 4907 (1978).
25. J. P. PILLOT, J. DUNOGUES, and R. CALAS. Synth. Commun. **9**, 395 (1979).
26. R. NOYORI, I. TOMINO, and M. NISHIZAWA. J. Am. Chem. Soc. **101**, 5843 (1979).
27. P. CONDRAN, JR., M. L. HAMMOND, A. MOURINO, and W. H. OKAMURA. J. Am. Chem. Soc. **102**, 6259 (1980).
28. A. MOURINO, S. LEWICKA-PIEKUT, A. W. NORMAN, and W. H. OKAMURA. J. Org. Chem. **45**, 4015 (1980).
29. A. W. CROSSLEY and H. R. LE SUEUR. J. Chem. Soc. **83**, 110 (1903).
30. A. W. CROSSLEY and P. HAAS. J. Chem. Soc. **83**, 494 (1903).
31. R. L. FRANK and H. K. HALL, JR. J. Am. Chem. Soc. **72**, 1645 (1950).
32. L. BATEMAN and F. W. SHIPLEY. J. Chem. Soc. 1996 (1955).
33. T. G. HALSALL and D. B. THOMAS. J. Chem. Soc. 2431 (1956).
34. F. SONDHEIMER and S. WOLFE. Can. J. Chem. **37**, 1870 (1959).
35. S. I. ZAV'YALOV and G. V. KONDRAT'EVA. J. Gen. Chem. U.S.S.R. **31**, 3719 (1961).
36. D. PITEA and G. FAVINI. J. Chem. Soc. Perkin Trans. II, 142 (1972).
37. W. PFLEIDERER and K. SCHÜNDEHÜTTE. Justus Liebigs Ann. Chem. **612**, 158 (1958).
38. M. M. SHEMYAKIN, YU. A. ARBUZOV, M. N. KOLOSOV, G. A. SHATENSHTEIN, V. V. ONOPRIENKO, and YU. V. KONNOVA. J. Gen. Chem. U.S.S.R. **30**, 563 (1960).
39. W. HÜCKEL and K. THIELE. Chem. Ber. **94**, 96 (1961).
40. R. D. CLARK and C. H. HEATHCOCK. Synthesis, 47 (1974).
41. L. GRUBER, J. TOMOSKOZI, and L. RADICS. Synthesis, 708 (1975).
42. W. R. BENSON and A. E. POHLAND. J. Org. Chem. **30**, 1129 (1965).
43. E. PIERS and I. NAGAKURA. J. Org. Chem. **40**, 2694 (1975).
44. E. PIERS, C. K. LAU, and I. NAGAKURA. Tetrahedron Lett. 3233 (1976).
45. E. PIERS and I. NAGAKURA. Tetrahedron Lett. 3237 (1976).
46. E. PIERS, I. NAGAKURA, and J. E. SHAW. J. Org. Chem. **43**, 3431 (1978).
47. E. PIERS, I. NAGAKURA, and H. E. MORTON. J. Org. Chem. **43**, 3631 (1978).
48. E. PIERS and H. E. MORTON. J. Chem. Soc. Chem. Commun. 1033 (1978).
49. E. PIERS and E. H. RUEDIGER. J. Chem. Soc. Chem. Commun. 166 (1979).
50. G. HÖFLE. Tetrahedron, **32**, 1431 (1976).
51. I. J. BOROWITZ, K. C. KIRBY, JR., and R. VIRKHAUS. J. Org. Chem. **31**, 4031 (1966).
52. G. STORK and R. L. DANHEISER. J. Org. Chem. **38**, 1775 (1973).
53. F. H. JARDINE and G. WILKINSON. J. Chem. Soc. C, 270 (1967).
54. E. PIERS and J. R. GRIERSON. J. Org. Chem. **42**, 3755 (1977).
55. H. STETTER. Newer methods of preparative organic chemistry. Vol. 2. *Edited by* W. Foerst. Academic Press, New York, NY. 1963. p. 51.
56. J. WOLINSKY, D. CHAN, and R. NOVAK. Chem. Ind. 720 (1965).
57. R. B. WOODWARD. J. Am. Chem. Soc. **63**, 1123 (1941); **64**, 76 (1942).
58. L. F. FIESER and M. FIESER. Steroids. Reinhold Publishing Corp., New York, NY. 1959. pp. 15–21.
59. A. I. SCOTT. Interpretation of the ultraviolet spectra of natural products. The MacMillan Company, New York, NY. 1964. pp. 55–73.

# Metal complexes as antioxidants. 9. Application of the spin scavenging technique to the reaction of transition metal dialkyldithiophosphates and dialkyldithiocarbamates with tertiary alkyl hydroperoxides[1,2]

J. A. HOWARD AND T. YAMADA[3]

*Division of Chemistry, National Research Council of Canada, Ottawa, Ont., Canada K1A 0R9*

Received June 4, 1981

J. A. HOWARD and T. YAMADA. Can. J. Chem. **60**, 224 (1982).

The spin scavenging technique has been applied to the initial homolytic reaction between tertiary alkyl hydroperoxides and zinc and nickel complexes of dialkyldithiophosphoric acids and dialkyldithiocarbamic acids using low concentrations of Galvinoxyl and 2,2,6,6-tetramethyl-4-oxo-1-piperidinyloxyl as radical scavengers. This method has demonstrated that these transition metal complexes react with hydroperoxides at 303 K to generate free-radicals. Quantitative kinetic data have been obtained from zero-order scavenger decays and the efficiency with which the transition metal complexes generate free-radicals increases in the order $Zn[R_2NCS_2]_2 < Zn[(RO)_2PS_2]_2 < Ni[(RO)_2PS_2]_2 < Ni[R_2NCS_2]_2$. Deviations from zero-order scavenger decay have been observed, particularly at high complex concentrations, and have been attributed to reaction of the complex with transient radicals to give products which do not react rapidly with the scavenger.

J. A. HOWARD et T. YAMADA. Can. J. Chem. **60**, 224 (1982).

Utilisant de faibles concentrations de galvinoxyle et de trétraméthyl-2,2,6,6-oxo-4 pipéridinyloxy-1 comme pièges à radicaux, on a appliqué la technique de piégeage de spin à la réaction homolytique initiale entre les hydropéroxydes d'alkyles tertiaires et les acides dialkyldithiocarbamiques. Cette méthode a démontré que ces complexes de métaux de transition réagissent avec les hydroperoxydes à 303K en produisant des radicaux libres. On a obtenu des données cinétiques quantitatives à partir de la désintégration d'ordre zéro des capteurs; l'efficacité avec laquelle les complexes de métaux de transition engendrent les radicaux libres augmente dans l'ordre suivant, $Zn[R_2NCS]_2 < Zn[(RO)_2PS_2] < Ni[(RO)_2PS_2]_2 < Ni[R_2NCS_2]_2$. Toutes les désintégrations du capteur ne sont pas rigoureusement d'ordre zéro, particulièrement aux fortes concentrations du complexe. On a attribué ces déviations à la réaction du complexe avec les radicaux intermédiaires pour donner des produits qui ne réagissent pas rapidement avec le capteur.

[Traduit par le journal]

## Introduction

It has been established that reaction of transition metal complexes, $ML_x$ where M is zinc, nickel, or copper, and L is either dialkyldithiophosphate or dialkyldithiocarbamate, with alkyl hydroperoxides produces free-radicals which can be detected directly by electron spin resonance spectroscopy and indirectly by monitoring the disappearance of a free-radical scavenger such as an aromatic amine or stable free-radical (2, 3). Moreover, these radicals may initiate hydrocarbon autoxidation, induce hydroperoxide decomposition, and give rise to the chemiluminescence usually associated with autoxidation (2).

In addition to qualitatively demonstrating the production of free-radicals, the spin scavenging technique can be used to provide quantitative estimates of rates of free-radical initiation. This method does, however, appear to suffer from several distinct disadvantages which severely limit its usefulness in metal complex – hydroperoxide systems. The present paper discusses the application of this technique to a study of the initial reaction between tertiary alkyl hydroperoxides and several transition metal complexes of dialkyldithiophosphoric and dialkyldithiocarbamic acids.

## Experimental

*Materials*

2,2,6,6-Tetramethyl-4-oxo-1-piperidinyloxyl (Aldrich) was recrystallized from methanol. Galvinoxyl (Aldrich) was used as received. Zinc diisopropyldithiophosphate, nickel diisopropyldithiophosphate, zinc diethyldithiocarbamate, nickel diethyldithiocarbamate, and nickel di-*n*-butyldithiocarbamate had been prepared previously in our laboratory (4–6). *tert*-Butyl hydroperoxide, cumene hydroperoxide, diisopropyldithiophosphoryl disulphide, dimethyldithiuram disulphide, diethyldithiophosphoric acid, *tert*-butyl hyponitrite, and chlorobenzene were prepared and purified by the methods described previously in this series (4–6).

*Procedure*

In most cases runs were performed by adding 50 μL of a standard hydroperoxide solution to 250 μL of a standard solution of the metal complex and stable free-radical in chlorobenzene contained in a 4 mm od suprasil tube directly in the cavity of a Varian E-4 EPR spectrometer. Rapid mixing was achieved by passing a fine steam of argon through the reaction mixture. Before addition of the hydroperoxide the field sweep of the spectrometer was set at the magnetic field corresponding to the maximum peak height of one of the lines of the first derivative signal from the stable free-radical and was switched off. The change in the signal intensity as a function of time was

[1]NRCC No. 19743.

[2]The previous part in this series (1) should have been part 8 and not part 7.

[3]NRCC Research Associate 1979–1981.

0008-4042/82/020224-05$01.00/0

©1982 National Research Council of Canada/Conseil national de recherches du Canada

Can. J. Chem. Downloaded from www.nrcresearchpress.com by 210.87.254.42 on 09/06/12
For personal use only.

Can. J. Chem. Downloaded from www.nrcresearchpress.com by 210.87.254.42 on 09/06/12
For personal use only.

monitored immediately after addition of the hydroperoxide. All decays were recorded on the X-Y recorder provided with the spectrometer. Reaction temperatures were regulated by a Varian variable temperature accessory.

## Results

*Preliminary experiments*

Preliminary experiments demonstrated that 2,2,-6,6-tetramethyl-4-oxo-1-piperidinyloxyl (**1**) does not react with $Zn[(i\text{-}PrO)_2PS_2]_2$, $Ni[(i\text{-}PrO)_2PS_2]_2$, $Zn[Et_2NCS_2]_2$, $Ni[Et_2NCS_2]_2$, *t*-BuOOH, or $[(i\text{-}PrO)_2PS_2]_2$. It does, however, react slowly with $(EtO)_2PS_2H$ by a second-order reaction with a rate constant $\sim 3\ M^{-1}\ s^{-1}$ at 303 K.

Galvinoxyl **2**, on the other hand, reacts slowly with $Zn[(i\text{-}PrO)_2PS_2]_2$, $Zn[Et_2NCS_2]_2$, $Ni[(i\text{-}PrO)_2PS_2]_2$, and $Ni[Et_2NCS_2]_2$. Rates of reaction were, however, slow and no attempt was made to study the kinetics of these reactions. Galvinoxyl also reacts with cumene hydroperoxide and the overall rate was first-order with respect to each reactant. A value of $0.011 \pm 0.002\ M^{-1}\ s^{-1}$ was found for the second-rate constant. Spin scavenging experiments using **2** were, therefore, conducted with reactant concentrations low enough that rates of reaction of **2** with the metal complex and hydroperoxide were negligible compared to rates of destruction of **2** by the radicals produced by reaction of the metal complex with the hydroperoxide. Galvinoxyl also reacts slowly with $[(i\text{-}PrO)_2PS_2]_2$ and $(EtO)_2PS_2H$.

In experiments designed to examine the efficiency with which stable radicals scavenge the transient radicals produced by reaction of $ML_x$ with ROOH, the disappearance of **2** was monitored in the presence of *t*-$BuON_2OBu$-*t*, a thermal source of *tert*-butoxyl and a mixture of *t*-$BuON_2OBu$-*t* and *t*-BuOOH, a thermal source of *tert*-butylperoxyl.

In these experiments, it was demonstrated that **2** was completely destroyed by excess *t*-$BuON_2OBu$-*t* at 303 K and that rates of radical disappearance obeyed the rate expression

$$\frac{-d[\mathbf{2}]}{dt} = 2ek_d[t\text{-}BuON_2OBu\text{-}t]$$

where $e$, the efficiency of production of *t*-BuO$^\cdot$, = 0.9, and $k_d$, the rate constant for unimolecular decomposition of *t*-$BuON_2OBu$-*t*, $= 2.9 \times 10^{-6}\ s^{-1}$ (7). They also showed that rates of disappearance of **2** were not influenced by the presence of *t*-BuOOH (0.001 *M*).

Rates of disappearance of **2** in the presence of *t*-$BuON_2OBu$-*t* were, however, reduced by $Zn[(i\text{-}PrO)_2PS_2]_2$ and at high concentrations of this complex ($> 0.001\ M$) rates were first-order with respect to the concentration of **2**. This implies that there was a competition between **2** and $Zn[(i\text{-}PrO)_2PS_2]_2$ for *t*-BuO$^\cdot$ produced by decomposition of *t*-$BuON_2OBu$-*t* and that the products of the reaction of $Zn[(i\text{-}PrO)_2PS_2]_2$ with *t*-BuO$^\cdot$ did not react rapidly with **2**. This system can probably be described by the elementary reactions [1] to [3].

[1] $t\text{-}BuON_2OBu\text{-}t \xrightarrow{k_1} 2t\text{-}BuO^\cdot + N_2$

[2] $t\text{-}BuO^\cdot + \mathbf{2} \xrightarrow{k_2}$ non-radical products

[3] $t\text{-}BuO^\cdot + Zn[(i\text{-}PrO)_2PS_2]_2 \xrightarrow{k_3}$ unreactive products

Application of the usual steady-state assumptions indicates that the rate of disappearance of **2** should be given by [4].

$$[4] \qquad \frac{-d[\mathbf{2}]}{dt} = \frac{2ek_1k_2[\mathbf{2}][t\text{-}BuON_2OBu\text{-}t]}{k_2[\mathbf{2}] + k_3[Zn[(i\text{-}PrO)_2PS_2]_2]}$$

First-order radical decays in the presence of $Zn[(i\text{-}PrO)_2PS_2]_2$ imply that $k_3[Zn[(i\text{-}PrO)_2PS_2]_2] > k_2$ [**2**] and that the pseudo-first-order rate constant is equal to $2ek_1k_2[t\text{-}BuON_2OBu\text{-}t]/k_3[Zn[(i\text{-}PrO)_2PS_2]_2]$. This rate constant was measured at concentrations of $Zn[(i\text{-}PrO)_2PS_2]_2$ from $10^{-3}$ to $10^{-2}\ M$ and little to no dependence on $[Zn[(i\text{-}PrO)_2PS_2]_2]$ was observed.

The reaction of **2** with *t*-BuO$^\cdot$ was also retarded by $Ni[(i\text{-}PrO)_2PS_2]_2$ and at an initial complex concentration of $2 \times 10^{-3}\ M$ the rate was first-order with respect to the scavenger concentration while little or no decay of the scavenger occurred if the complex concentration was increased above $5 \times 10^{-3}\ M$.

If we assume that *t*-BuO$^\cdot$ reacts with $Zn[(i\text{-}PrO)_2PS_2]_2$ and $Ni[(i\text{-}PrO)_2PS_2]_2$ to give $(i\text{-}PrO)_2PS_2^\cdot$, e.g.,

[5] $t\text{-}BuO^\cdot + Zn[(i\text{-}PrO)_2PS_2]_2 \rightarrow t\text{-}BuOZn[(i\text{-}PrO)_2PS_2] + (i\text{-}PrO)_2PS_2^\cdot$

the results of the above experiments suggest that $(iPrO)_2PS_2^\cdot$ does not react rapidly with **2**.

We have tested this hypothesis by following the disappearance of **2** in the presence of *t*-$BuON_2OBu$-*t* and $(EtO)_2PS_2H$; a system which should give $(EtO)_2PS_2^\cdot$ by reaction [6].

[6] $t\text{-}BuO^\cdot + (EtO)_2PS_2H \rightarrow t\text{-}BuOH + (EtO)_2PS_2^\cdot$

As expected $(-d[\mathbf{2}]/dt)_0$ was slower in the presence of $(EtO)_2PS_2H$ and rates deviated from a zero-order dependence on [**2**] as it fell below one half of its initial concentration. Confirmation of this

TABLE 1. Kinetic data for the disappearance of Galvinoxyl in the presence of $Zn[(i\text{-}PrO)_2PS_2]_2$ and ROOH in PhCl at 303 K

| $10^4[Zn[(i\text{-}PrO)_2PS_2]_2]_0/M$ | $[ROOH]_0/M$ | $10^7(-d[2]/dt)$ $/M\ s^{-1}$ | $nk_7/M^{-1}\ s^{-1}$ |
|---|---|---|---|
| 1 | 0.1[b] | 0.6 | 0.006 |
| 1 | 0.02[b] | 0.1 | 0.005 |
| 1 | 0.049[b] | 0.24 | 0.005 |
| 5.4 | 0.1[a] | 1.0 | 0.002 |
| 0.5 | 0.1[a] | 0.27 | 0.0056 |
| 1 | 0.2[b] | 0.7 | 0.0035 |

[a] *t*-BuOOH.
[b] $PhCMe_2OOH$.

TABLE 2. Kinetic data for the disappearance of Galvinoxyl in the presence of $Ni[(i\text{-}PrO)_2PS_2]_2$ and $PhCMe_2OOH$ in PhCl at 303 K

| $10^4[Ni[(i\text{-}PrO)_2PS_2]_2]_0$ $/M$ | $[ROOH]_0/M$ | $10^7(-d[2]/dt)^a$ $/M\ s^{-1}$ | $nk_8/M^{-1}\ s^{-1}$ |
|---|---|---|---|
| 0.48 | 0.097 | 0.43 | 0.009 |
| 0.24 | 0.097 | 0.22 | $0.009_5$ |
| 0.96 | 0.097 | 0.84 | 0.009 |
| 0.48 | 0.194 | 0.86 | $0.009_3$ |
| 0.48 | 0.048 | 0.24 | 0.010 |
| 19.0 | 0.0019 | 0.39 | 0.011 |

[a] Corrected for rate of reaction of **2** with ROOH.

hypothesis at high concentrations ($> 10^{-4}$ *M*) of $(EtO)_2PS_2H$ could not be obtained because of the direct reaction between **2** and $(EtO)_2PS_2H$.

Rates of destruction of **2** by thermally generated *t*-BuO$^\cdot$ were also reduced by $Zn[n\text{-}Bu_2NCS_2]_2$ and $Ni[Et_2NCS_2]_2$. Thus at a complex concentration of $10^{-4}$ *M* the rate was still zero-order with respect to [**2**] but slower than it was in the absence of the complex, while at higher complex concentrations the usual deviations from zero-order kinetics were observed. Interestingly, dimethyldithiuram disulphide ($10^{-3}$ *M*) did not influence the kinetics for the decay of **2** although the rate was reduced by a factor of about 2. At higher concentrations of this disulphide ($\sim 10^{-2}$ *M*) the kinetics did deviate from zero-order.

*$Zn[(i\text{-}PrO)_2PS_2]_2$*

**1** and **2** began to decay immediately when a solution of *t*-BuOOH or $PhCMe_2OOH$ in chlorobenzene was added to a solution of $Zn[(i\text{-}PrO)_2PS_2]_2$ in chlorobenzene containing a low concentration of scavenger at 303 K, indicating that an initial reaction between the metal complex and hydroperoxide was forming transient free radicals.

[7] $Zn[(i\text{-}PrO)_2PS_2]_2 + ROOH \rightarrow$ free-radicals

The shape of the concentration–time profile for the scavenger did, however, depend very markedly on the initial complex concentration and zero-order decays were only obtained at low complex and low scavenger concentrations and high hydroperoxide concentrations. Under other conditions, the scavenger tended to disappear according to first-order kinetics and at high complex concentrations rates of scavenger disappearance were slower than the rates at low complex concentrations and were almost independent of the complex concentration. Clearly $Zn[(i\text{-}PrO)_2PS_2]_2$ was interfering with the radical scavenging process as it did when the transient radicals were generated by thermolysis of *t*-$BuON_2OBu$-*t*.

Kinetic data obtained under zero-order or close to zero-order conditions are given in Table 1 and initial rates of decay of **2** were approximately first-order with respect to the metal complex and hydroperoxide concentrations, i.e.,

$$\left(\frac{-d[2]}{dt}\right)_0 = nk_7[Zn[(i\text{-}PrO)_2PS_2]_2][ROOH]$$

where $n$ is the number of radicals produced by reaction [7]. The value of the second-order rate constant $nk_7$ was found to be $(5.5 \pm 1) \times 10^{-3}\ M^{-1}\ s^{-1}$.

Initial rates of disappearance of **1** in the presence of $Zn[(i\text{-}PrO)_2PS_2]_2$ and *t*-ROOH, at low initial complex concentrations, gave values of $nk_7$ in good agreement with values obtained from decay of **2**. Deviations from zero-order kinetics were, however, more pronounced with **1** than they were with **2**.

Ivanov and Kateva (8) have studied the initial homolytic reaction between $Zn[(i\text{-}PrO)_2PS_2]_2$ and

Can. J. Chem. Downloaded from www.nrcresearchpress.com by 210.87.254.42 on 09/06/12
For personal use only.

Can. J. Chem. Downloaded from www.nrcresearchpress.com by 210.87.254.42 on 09/06/12
For personal use only.

ROOH using 2,2,6,6-tetramethyl-1-piperidinyloxyl as the radical scavenger. They reported a rate constant of $3.7 \times 10^{-3}$ $M^{-1}$ $s^{-1}$ at 328 K for α-tetralin hydroperoxide (0.3 *M*) and $Zn[(i\text{-}PrO)_2PS_2]_2$ (0.05 *M*) and a value of $7.94 \times 10^{-3}$ using the same concentrations of *t*-BuOOH and metal complex. The agreement between these rate constants and our data is remarkably good considering that Ivanov and Kateva only worked at one rather high concentration of metal complex and one hydroperoxide concentration.

*$Ni[(i\text{-}PrO)_2PS_2]_2$*

Galvinoxyl disappeared completely with zero-order kinetics in the presence of $PhCMe_2OOH$ ($2 \times 10^{-3} - 0.2$ *M*) and $Ni[(i\text{-}PrO)_2PS_2]_2$ ($10^{-5} - 2 \times 10^{-3}$ *M*) at 303 K. Initial rates of radical disappearance are given in Table 2 and obey the rate expression

$$\frac{-d[2]}{dt} = nk_8[Ni[(i\text{-}PrO)_2PS_2]_2][ROOH]$$

where $k_8$ is the rate constant for production of radicals by reaction [8].

[8] $PhCMe_2OOH + Ni[(i\text{-}PrO)_2PS_2]_2 \rightarrow$ free radicals

The value of $nk_8$ at 303 K is $0.01 \pm 0.001$ $M^{-1}$ $s^{-1}$ and values of this rate constant from 293 to 343 K obey the Arrhenius equation

$$\log (nk_8/M^{-1}\ s^{-1}) = (8 \pm 1) - 10.5 \pm 0.5/\theta$$

where $\theta = 2.303RT$ kcal $mol^{-1}$.

The value of $nk_8$ at 303 K obtained by the radical scavenging technique is 2.5–3.8 times larger than rate constants obtained from rates of initiation of styrene autoxidation and rates of nickel complex disappearance (6).

**1** is completely destroyed by mixtures of $Ni[(i\text{-}PrO)_2PS_2]_2$ ($4 \times 10^{-4} - 4 \times 10^{-3}$ *M*) and *t*-BuOOH 0.06–0.6 *M*) in PhCl. In this case, however, radical decays obeyed the rate law

$$\frac{-d[1]}{dt} \propto [t\text{-BuOOH}]^{0.7 \pm 0.2} \times [Ni[(iPrO)_2PS_2]_2]^{0.9 \pm 0.1}[1]^{0.8 \pm 0.5}$$

indicating that the rates were almost first-order with respect to [1]. This suggests that $Ni[(i\text{-}PrO)_2PS_2]_2$ was competing successfully with **1** for the radicals produced by reaction [8].

*$Zn[Et_2NCS_2]_2$*

**2** ($4.8 \times 10^{-6}$ *M*) disappeared completely with zero-order kinetics when $PhCMe_2OOH$ (0.194 *M*) was added to $Zn[Et_2NCS_2]_2$ ($4.8 \times 10^{-5}$ *M*). Deviations from zero-order kinetics were, however, observed at lower hydroperoxide concentrations. Kinetic data for this system are given in Table 3 and it would appear that the rate of reaction is approximately first-order with respect to each reactant and $nk_9 = (1.8 \pm 0.4) \times 10^{-3}$ $M^{-1}$ $s^{-1}$. $Zn[Et_2NCS_2]_2$ is, therefore, only about 32% as efficient as $Zn[(i\text{-}PrO)_2PS_2]_2$ in producing free-radicals by reaction with a tertiary alkyl hydroperoxide.

TABLE 3. Kinetic data for the disappearance of Galvinoxyl in the presence of $Zn[Et_2NCS_2]_2$ and $PhCMe_2OOH$ in PhCl at 303 K

| $10^4[Zn[Et_2NCS_2]_2]_0$ /*M* | $[ROOH]_0$ /*M* | $10^7(-d[2]/dt)_0$ /*M* $s^{-1}$ | $nk_9$ /$M^{-1}$ $s^{-1}$ |
|---|---|---|---|
| 0.24 | 0.097 | 0.046 | 0.002 |
| 0.48 | 0.097 | 0.09 | 0.002 |
| 0.48 | 0.194 | 0.14 | 0.0015 |
| 0.48 | 0.048 | 0.05 | 0.0022 |
| 0.97 | 0.097 | 0.10 | 0.0011 |

[9] $PhCMe_2OOH + Zn[Et_2NCS_2]_2 \rightarrow$ free-radicals

**1** was completely destroyed by a mixture of $Zn[Et_2NCS_2]_2$ and *t*-BuOOH with the rate of radical disappearance depending on the initial concentration of **1** (Table 4).

*$Ni[R_2NCS_2]_2$*

Galvinoxyl ($4.8 \times 10^{-6}$ *M*) disappeared with zero-order kinetics in the presence of $Ni[Et_2NCS_2]_2$ ($2.4 \times 10^{-7} - 10^{-6}$ *M*) and $PhCMe_2OOH$ (0.005 – 0.01 *M*). Rate constants for reaction [10] are summarized in Table 5 and the average value is $1 \pm 0.5$ $M^{-1}$ $s^{-1}$ which is 6–7 times larger than values obtained from rates of initiation of styrene autoxidation and rates of nickel complex disappearance (6)

[10] $PhCMe_2OOH + Ni[Et_2NCS_2]_2 \rightarrow$ free-radicals

Decay of **1** ($2 \times 10^{-4}$ to $2 \times 10^{-5}$ *M*) in the presence of $Ni[n\text{-}Bu_2NCS_2]_2$ (0.001 to 0.0001 *M*) and *t*-BuOOH (0.02 *M*) followed first-order kinetics with respect to the radical concentration indicating that the rate expression [4] was obeyed and that $Ni[n\text{-}Bu_2NCS_2]_2$ was successfully competing with **1** for the free radicals.

## Discussion

It is clear from the present work that although the reaction of transition metal dialkyldithiophosphates and dialkyldithiocarbamates with tertiary alkyl hydroperoxides in the presence of a stable radical gives qualitative information regarding the production of transient free-radicals a great deal of care has to be exercised before rates of free-radical initiation from the metal complex – ROOH system can be obtained. This is because rates of disappearance of low scavenger concentrations are not

TABLE 4. Kinetic data for the disappearance of 2,2,6,6-tetramethyl-4-oxo-1-piperidinyl-oxyl in the presence of $Zn[Et_2NCS_2]_2$ and $PhCMe_2OOH$ in PhCl at 303 K

| $10^3[Zn[Et_2NCS_2]_2]_0$ /M | $[ROOH]_0$ /M | $10^5[1]_0$ /M | $10^8(-d[1]_0/dt)$ /M $s^{-1}$ | $10^5\ nk_9$ /$M^{-1}$ $s^{-1}$ |
|---|---|---|---|---|
| 2 | 1.25 | 5 | 7.0 | 2.8 |
| 4 | 0.156 | 5 | 1.7 | 2.7 |
| 4 | 1.25 | 5 | 10.2 | 2.0 |
| 4 | 1.25 | 10 | 13.4 | 2.7 |
| 4 | 1.25 | 0.5 | 1.65 | 0.33 |

TABLE 5. Kinetic data for the disappearance of Galvinoxyl in the presence of $Ni[Et_2NCS_2]_2$ and $PhCMe_2OOH$ in PhCl at 303 K

| $10^7[Ni[Et_2NCS_2]_2]_0$ /M | $[ROOH]_0$ /M | $10^9(-d[2]/dt)$ /M $s^{-1}$ | $nk_{15}$/$M^{-1}$ $s^{-1}$ |
|---|---|---|---|
| 4.8 | 0.0097 | 7.9 | 1.7 |
| 4.8 | 0.0048 | 1.8 | 0.8 |
| 9.7 | 0.0097 | 5.4 | 0.6 |
| 2.4 | 0.0097 | 2.2 | 0.95 |
| 4.8 | 0.0097 | 7.9 | 1.7 |

TABLE 6. Rate constants for the radical producing reaction between metal complexes and tertiary alkyl hydroperoxides at 303 K

| Metal complex | $nk/M^{-1}$ $s^{-1}$ |
|---|---|
| $Zn[Et_2NCS_2]_2$ | $(1.8\pm0.4) \times 10^{-3}$ |
| $Zn[(i\text{-}PrO)_2PS_2]_2$ | $(5.5\pm1) \times 10^{-3}$ |
| $Ni[(i\text{-}PrO)_2PS_2]_2$ | $(1\pm0.1) \times 10^{-2}$ |
| $Ni[Et_2NCS_2]_2$ | $1.1\pm0.5$ |

always zero-order in the presence of the metal complex and hydroperoxide. Thus the metal complex appears to be able to compete with the scavenger for transient free-radicals to give species which do not react rapidly with the scavenger. We have tested several types of stable radical as scavenger (phenoxyl, nitroxyl, and iminoxyl) and find that the phenoxyl is the only one which can be used to give reliable rates of free-radical production for the $ML_x$–ROOH system.

Rate constants obtained by this technique are summarized in Table 6 and indicate that the ability of the complexes to generate free-radicals increases in the order $Zn[R_2NCS_2]_2 < Zn[(RO)_2PS_2]_2 < Ni[(RO)_2PS_2]_2 < Ni[R_2NCS_2]_2$. Furthermore, where a comparison can be made these rate constants are somewhat larger than the values obtained from rates of initiated autoxidations and rates of metal complex disappearances. We do, however, feel that under conditions of zero-order scavenger decay and over a reasonable range of reactant concentrations that the spin scavenging technique gives the more reliable rate constants.

Although the initiation reactions [7] to [10] have been depicted as simple bimolecular reactions between the hydroperoxide and $ML_x$, the reaction mechanism must be more complicated than this and possibly involves the reversible formation of a co-ordination complex between the reactants followed by first-order decomposition to give radicals (2)

$$ROOH + ML_x \rightleftarrows ROOH \ldots ML_x$$

$$ROOH \ldots ML_x \rightarrow \text{radicals} + ML_x$$

Co-ordination to $ML_x$ could weaken the O—O bond of the hydroperoxide by increasing the electron density at this function. It should, however, be noted that in the case of $Cu[Et_2NCS_2]_2$ no esr evidence could be found for the formation of a co-ordination complex with ROOH (9).

A few preliminary experiments with $Cu[Et_2NCS_2]_2$ and $Cu[(i\text{-}PrO)_2PS_2]_2$ indicated that the homolytic reaction of these complexes with ROOH was either too fast to study by the spin scavenging technique or scavenger decays were too complicated to analyse.

1. J. A. HOWARD and S-B. TONG. Can. J. Chem. **58**, 1962 (1980).
2. J. A. HOWARD. Frontiers Free Rad. Chem. 237 (1980).
3. Y. OHKATSU, K. KIKKAWA, and T. OSA. Sekiyu Gakkai Shi, **23**, 16 (1980).
4. J. A. HOWARD, Y. OHKATSU, J. H. B. CHENIER, and K. U. INGOLD. Can. J. Chem. **51**, 1543 (1973).
5. J. A. HOWARD and J. H. B. CHENIER. Can. J. Chem. **54**, 382 (1976).
6. J. A. HOWARD and J. H. B. CHENIER. Can. J. Chem. **54**, 390 (1976).
7. H. KIEFER and T. G. TRAYLOR. Tetrahedron Lett. 6163 (1966).
8. S. K. IVANOV and Y. D. KATEVA. Dobl. Bolg. Akad. Nauk, **25**, 645 (1972).
9. J. H. B. CHENIER, J. A. HOWARD, and J. C. TAIT. Can. J. Chem. **55**, 1644 (1977).

Can. J. Chem. Downloaded from www.nrcresearchpress.com by 210.87.254.42 on 09/06/12
For personal use only.

Can. J. Chem. Downloaded from www.nrcresearchpress.com by 210.87.254.105 on 09/06/12
For personal use only.



# Lignin and related compounds. 1X. The isolation of a dimer with a benzylisochroman structure from the hydrogenolysis products of aspen lignin

KENICHI SUDO[1] AND JAMES M. PEPPER

*Department of Chemistry and Chemical Engineering, University of Saskatchewan, Saskatoon, Sask., Canada S7N 0W0*

Received September 25, 1981

KENICHI SUDO and JAMES M. PEPPER. Can. J. Chem. **60**, 229 (1982).

A dimer with a benzylisochroman structure, **1**, has been isolated from the products of the catalytic (Rh—C) hydrogenolysis of aspen lignin.

KENICHI SUDO et JAMES M. PEPPER. Can. J. Chem. **60**, 229 (1982).

Des produits résultant de l'hydrogénolyse de la lignin de peuplier catalysée par le (RH—C), on a isolé un dimêr ayant la structure du benzylisochromane (**1**).

[Traduit par le journal]

In a previous paper (1) of this series, several monomeric and dimeric lignin-derived compounds were isolated and identified from the products resulting from the hydrogenolysis of aspen wood (*Populus tremuloides*, Michx) using a rhodium-on-charcoal catalyst. The 51.6 g of chloroform-soluble lignin products (from 400 g wood) were separated into several fractions (A → P) by silica gel chromatography. Fractions C, D and L were discussed earlier. Here we discuss the characterization of a new lignin dimer isolated from Fraction E (3.2 g). Successive column chromatographic separations using silica gel (cyclohexane–acetone (6:1) as eluant), cellulose (xylene–dimethylformamide (15:1) as eluant), silica gel (petroleum ether – diethyl ether (2:1) as eluant), silica gel (cyclohexane – ethyl acetate – absolute ethanol (20:1:1) as eluant), and finally cellulose (xylene–dimethylformamide (25:1) as eluant) resulted in the isolation of pure compound **1** (34.2 mg). Each separation was monitored by thin layer chromatography, developed with toluene – formic acid – ethyl formate (5:1:4), followed by spraying with 50% sulfuric acid and heating to 105°C.

The benzylisochroman-type structure for **1** was determined as follows. The high resolution mass spectrum of the acetate of **1** indicated a molecular formula of $C_{26}H_{32}O_9$ (*m/z* 488.2036). The low resolution spectrum of **1** revealed the molecular ion and base ion peaks at *m/z* 404 and 375 ($M^+$—·$CH_2$-$CH_3$) respectively. Other prominent peaks occurred at *m/z* 237 and 167 ($C_\alpha$—$C_\beta$ cleavage) and at *m/z* 209 ($C_{\alpha'}$—$C_{\beta'}$ cleavage of fragment 237 with hydrogen rearrangement).

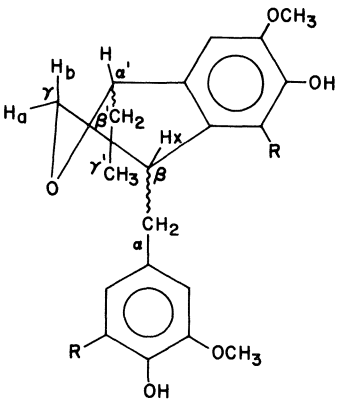


**1** R = $OCH_3$
**2** R = H

The $^1$HMR spectrum of **1** (as diacetate) revealed absorptions which were assigned as follows: δ0.98 (t, 3H, $H_{\gamma'}$, $J$ = 7.0 Hz); δ1.87–2.12 (m, 2H, $H_{\beta'}$); δ2.33 (s, 6H, aryl—OAc); δ2.90–3.06 (m, 2H, $H_\alpha$); δ3.57–3.68 (1H, $H_\beta$ overlapped with singlet peak of δ3.63 of aryl methoxy); δ3.63 (s, 3H, aryl—$OCH_3$); δ3.70–3.98 (m, 2H, $H_\gamma$); δ3.76 (s, 9H, aryl—$OCH_3$); δ4.82 (t, 1H, $H_\alpha$, $J$ = 4.64 Hz); δ6.09 (s, 1H, aryl—H); δ6.36 (s, 2H, aryl—H). Irradiation at the centre of the multiplet at δ1.87–2.12 reduced the triplets at δ0.98 and δ4.82 to singlets. Irradiation at the centre of the triplet at δ0.98 reduced the multiplet at δ1.87–2.12 to a doublet ($J$ = 4.64 Hz). The multiplet at δ3.70–3.98 ($H_\gamma$) would appear to be two quartets with centres at δ3.78 and 3.92 resulting from coupling of $H_a$ and $H_b$ of $C_\gamma$ with $H_x$ of $C_\beta$ ($J$ = 3.0 Hz) and of $H_a$ and $H_b$ with each other

[1]Present address: Forestry and Forest Products Research Institute, P.O. Box 16, Tsukuba Norin Kenkyu, Danchi-Nai, Ibaraki, Japan 305.

0008-4042/82/020229-02$01.00/0

©1982 National Research Council of Canada/Conseil national de recherches du Canada

($J$ = 11 Hz). These assignments are similar to those reported for compound **2** which Yasuda and Sakakibara (2) isolated from the products of the catalytic (copper chromite) hydrogenolysis of compression wood of Karamatsu (*Larix leptolepis* Gord.).

The present work provides evidence for the presence in normal wood lignin of the benzylisochroman structure with $C_\alpha$ and $C_\beta$ linkages. Under the reported conditions of hydrogenolysis, it is difficult to envisage its formation from other accepted structural units of lignin. Indeed, the presence in the lignin macromolecule of structural units such as **1** may be the origin of the trimethoxy-*o*-phthalic acid that has been reported by Freudenberg and Chen (3) as a product obtained by the permanganate oxidation of methylated hardwood lignin.

**Acknowledgements**

The authors wish to acknowledge the financial assistance provided by the Natural Sciences and Engineering Research Council of Canada and the University of Saskatchewan.

1. K. SUDO, D. J. MULLORD, and J. M. PEPPER. Can. J. Chem. **59**, 1028 (1981).
2. S. YASUDA and A. SAKAKIBARA. Mokuzai Gakkaishi, **22**, 606 (1976).
3. K. FREUDENBERG and C. L. CHEN. Ber. **93**, 253 (1960).

Can. J. Chem. Downloaded from www.nrcresearchpress.com by 210.87.254.105 on 09/06/12
For personal use only.

# A $^{13}C$ nuclear magnetic resonance study of the reversible substituent migration in several 2-acyl and 2-silyl derivatives of tropolone. Troponoid-IV[1]

D. MÉNARD AND M. ST-JACQUES

*Département de Chimie, Université de Montréal, C.P. 6210, Succ. A, Montréal (Qué.), Canada H3C 3V1*

AND

J. F. BAGLI

*Department of Chemistry, Ayerst Research Laboratory, Montreal, P.Q., Canada H3C 3J1*

Received June 24, 1981

D. MÉNARD, M. ST-JACQUES, and J. F. BAGLI. Can. J. Chem. **60**, 231 (1982).

The energy barrier for the reversible substituent migration was determined for a number of 2-acyl and 2-silyl derivatives of tropolone. The energy barrier is found to be dependent on the nature of the migrating group. Asymmetric monosubstitution on the ring shifts the equilibrium in favor of one dynamic isomer. In the two cases studied (3-bromotropolone and 3-bromotropolone acetate) it is found that the equilibrium is shifted towards the isomer bearing the bromine atom at the 7-position.

D. MÉNARD, M. ST-JACQUES et J. F. BAGLI. Can. J. Chem. **60**, 231 (1982).

Nous avons mesuré la barrière énergétique pour le processus de migration réversible du substituent en position 2 de quelques dérivés acylés et silylés de la tropolone. La nature du groupe migrateur modifie l'énergie d'activation autant dans le cas des dérivés acylés que dans le cas des dérivés silylés. La présence d'une substitution asymétrique sur le cycle déplace l'équilibre vers un seul isomère dynamique. Dans les deux cas étudiés (bromo-3-tropolone et acétate de bromo-3-tropolone) nous avons montré que l'équilibre favorise l'isomère portant l'atome de brome à la position 7.

Can. J. Chem. Downloaded from www.nrcresearchpress.com by 210.87.254.5 on 09/06/12
For personal use only.

Parallel to other studies on the pharmaceutical activity of tropone and tropolone derivatives (1), we have recently reported on the additivity of substituent effects on $^{13}C$ nmr chemical shifts for a number of 2-methoxytropone derivatives **1** and have shown that $^{13}C$ nmr is quite useful to distinguish between various isomers in the 2-methoxytropone family (2). A more challenging task involves the identification of the dynamic isomer favored by nonsymmetric tropolones and tropolone derivatives for which the 2-substituent is capable of rapid migration at room temperature of the type illustrated by **2***a* ⇌ **2***b*.

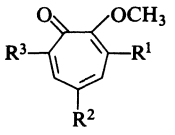

**1**

$R^1, R^2, R^3$ = H, Br, $CH_3$, $OCH_3$, $CH_2CO_2CH_3$

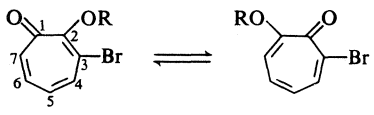

R = H : **2***a* **2***b*
R = Ac: **3***a* **3***b*

It is well known that tropolone acetate undergoes rapid intramolecular acetyl migration at room temperature (**4***a* ⇌ **4***b*) for which $\Delta G^{\ddagger}$ is 10.8 kcal/mol (3*a*). The nonaveraging spectrum can be recorded below −60°C for which the correct line assignment was published in a previous paper in this series (3*b*). A similar exchange process has been observed in substituted tropolone acetates such as 3,7-dibenzyltropolone acetate for which $\Delta G^{\ddagger}$ was found to be 8 kcal/mol (4).

While investigating rearrangements of trialkylsilyl groups bonded to electronegative elements, Reich and Murcia (5) noted that the room temperature $^{13}C$ nmr spectrum of 2-(2-butyldimethylsiloxy)tropone contains only 4 lines, indicating a fast exchange of the trialkylsilyl group between the two oxygen atoms on the tropolone ring (**5***a* ⇌ **5***b*). In addition, they reported line broadening at about −70°C, but the slow exchange spectrum was not observed. Nevertheless, the authors estimated that $\Delta G^{\ddagger}$ for the silyl group migration is about 8.2 kcal/mol. A similar observation was reported by Hobson and co-workers (6) who prepared the trimethylsilyl ethers of tropolone (**6**) and 3-bromotropolone (**7**) and studied their $^1H$ nmr spectra down to −95°C. No significant change was observed for solutions of both trimethylsilyl ethers in toluene-$d_8$, thus indicating a significantly lower energy barrier for the exchange process.

Very few studies concerned with the identifica-

[1]Troponoid III is ref. 1.

0008-4042/82/030231-08$01.00/0

©1982 National Research Council of Canada/Conseil national de recherches du Canada

tion of the major isomer adopted by unsymmetrically substituted tropolones have been reported in the literature. In 1968, Sugiyama (7) used $^1H$ coupling constants and chemical shifts arguments to suggest that the 3-Br form (**2***a*) is favored relative to **2***b*.

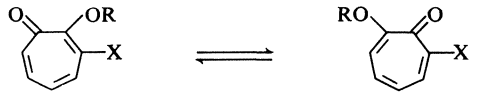

R = Ac; X = H : **4***a* **4***b*

R = $-Si(CH_3)_2CH(CH_3)_2$; X = H : **5***a* **5***b*

R = TMS; X = H : **6***a* **6***b*

R = TMS; X = Br: **7***a* **7***b*

R = TBDMS; X = H : **8***a* **8***b*

R = COPh; X = H : **9***a* **9***b*

In the present work, we report the $\Delta G^{\ddagger}$ value for **6** as well as for other rapidly equilibrating 2-substituted tropolone derivatives. A quantitative description of the dynamic features of these compounds will be presented and extended to nonsymmetric derivatives such as **2** and **3**. Our results show clearly that the published conclusion (7) for **2** is wrong.

## Results and discussion

The partial 22.63 MHz $^{13}C$ nmr spectra of 2-trimethylsiloxytropone (**6**) at several temperatures are shown in Fig. 1. The room temperature spectrum is almost identical to that of the 2-(2-butyldimethylsilyl) derivative investigated by Reich and Murcia (5). At −109°C, the signals of C-3,7 and C-5 overlap but significant broadening is not yet observed. Maximum broadening takes place at −139°C, the coalescence temperature, below which a slow exchange spectrum can be recorded. At −155°C, the low field region of the spectrum of **6** contains 7 lines, one for each carbon of the tropolone ring. The splitting pattern of the C-3,7 signal is represented in Fig. 1. A $\Delta G^{\ddagger}$ of 5.7 kcal/mol was calculated at the coalescence temperature. This value is much lower than the 10.8 kcal/mol determined for the acetate derivative and it suggests that migration of a silyl group is easier than migration of an acyl group. The chemical shifts and $\Delta G^{\ddagger}$ values for all compounds investigated are summarized in Table 1.

In order to test the sensitivity of this barrier to the size of the migrating silyl group we have prepared 2-*tert*-butyldimethylsiloxytropone **8** and have studied its $^{13}C$ nmr (20 MHz) spectrum as a function of temperature. Again the room temperature spectrum contains 4 lines and is similar to the

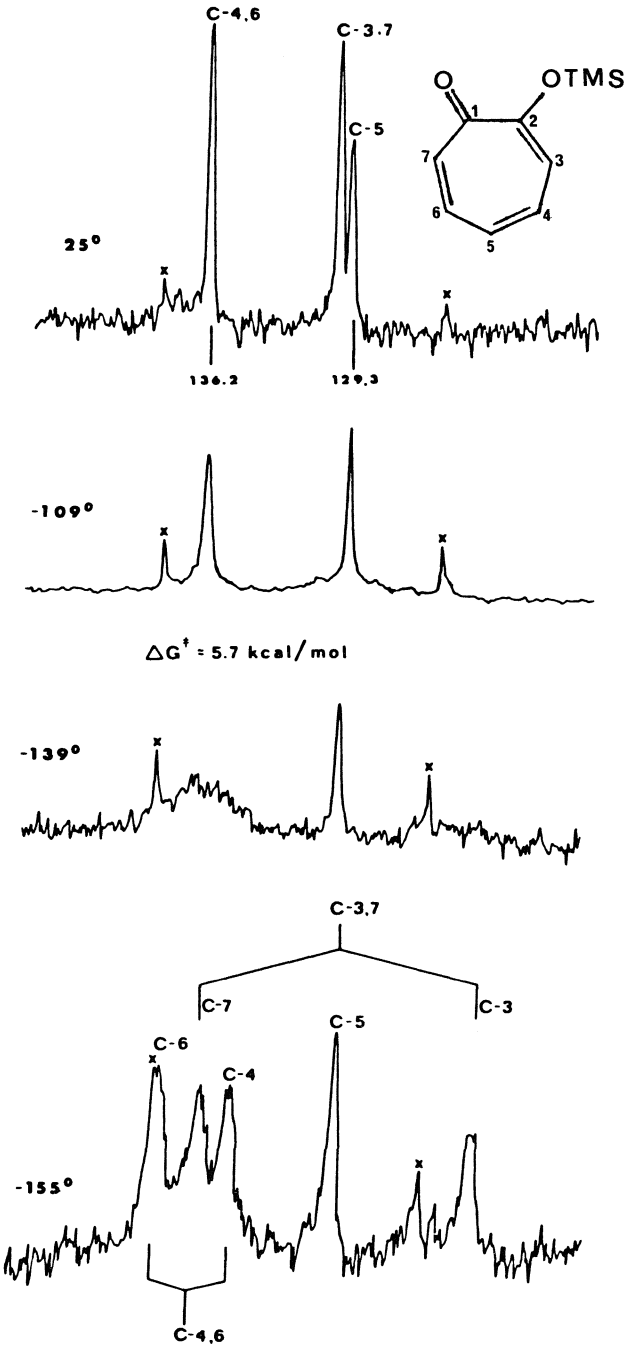


FIG. 1. The partial 22.63 MHz $^{13}C$ nmr spectra of **6** in $CHFCl_2$ at several temperatures (x denotes tropolone impurity). Flip angle = 30°; SW = 6024 Hz; data size = 8K.

spectra of **5** and **6**. As the temperature is lowered to −80°C, broadening occurs; maximum broadening is observed at −104°C, the coalescence temperature for carbons 3 and 7, and finally a well-resolved slow exchange spectrum is recorded at −130°C. A

Can. J. Chem. Downloaded from www.nrcresearchpress.com by 210.87.254.5 on 09/06/12
For personal use only.

TABLE 1. Carbon-13 chemical shifts for ring carbons and dynamic parameters for compounds **2**, **3**, **6**, **8–10**

| Compound | Solvent | $T$ (°C) | C-1 | C-2 | C-3 | C-4 | C-5 | C-6 | C-7 | Δν (Hz) | $T_c$ (°C) | $\Delta G^{\ddagger}$ (kcal/mol) |
|---|---|---|---|---|---|---|---|---|---|---|---|---|
| **6** | $CHFCl_2$ | 25 | — | — | 129.9 | 136.2 | 129.3 | 136.2 | 129.9 | 312.3 | −139 | 5.7 |
| | | −155 | 181.5 | 163.6 | 122.6 | 135.0 | 129.9 | 138.5 | 136.4 | (C-3, 7) | | |
| **8** | $CHFCl_2$ | 25 | — | — | 130.9 | 136.8 | 130.1 | 136.8 | 130.9 | 255.6 | −104 | 7.3 |
| | | −130 | 181.9 | 165.2 | 124.5 | 135.6 | 130.3 | 139.0 | 136.7 | (C-3, 7) | | |
| **9** | $CHFCl_2$ | 25 | — | — | 134.2 | 134.5 | 134.5 | 134.5 | 134.2 | 110.8 | −23 | 11.5 |
| | | −80 | 180.2 | 158.9 | 129.4 | 132.7 | 135 | 138.2 | 140.9 | (C-4, 6) | | |
| **10** | $CHFCl_2$ | 25 | — | — | 136.7 | 138.9 | 129.0 | 138.9 | 136.7 | 42.65 | −43 | 10.9 |
| | | −100 | 171.8 | 153.1 | 132.8 | 138.7 | 130.2 | 140.8 | 142.8 | (C-4, 6) | | |
| **3** | $CHFCl_2$ | 25 | — | — | 129.7 | 132.8 | 131.7 | 140.6 | 141.6 | | | |
| | | −97 | 174.0 | 155.5 | 129.6 | 133.5 | 132.9 | 141.9 | 142.9 | — | — | — |
| **2** | $CDCl_3$ | 25 | 170.8 | 166.0 | 120.1 | 137.1 | 126.0 | 142.3 | 129.3 | — | — | — |
| Tropolone | $CDCl_3$[a] | 25 | 172.6 | 172.6 | 123.5 | 137.6 | 128.1 | 137.6 | 123.5 | — | — | — |
| | Solid[b] | 25 | 177.5 | 165.4 | 113.0 | 133.7 | 128.1 | 141.7 | 133.7 | | | |

[a] Values taken from ref. 10*b*.
[b] Values taken from ref. 10*a*.

$\Delta G^{\ddagger}$ value of 7.3 kcal/mol can be calculated for **8**, indicating that increasing the size of the migrating silyl group raises the energy barrier of the process.

Studies on the lability of *O*-silyl derivatives of *cis* enols of 1,3-diketones (8) have shown that the energy barrier of the migration process is lowered as the polarity of the migrating group increases, presumably because an increase in the electron withdrawing ability of the substituent results in a greater positive charge on silicon and facilitates the use of a d-orbital in achieving the transition state. These results are consistent with a mechanism involving the formation of a five-coordinated silicon intermediate of the type proposed by Reich and Murcia (5). It appears, however, that polarity effects alone cannot account for the 1.6 kcal/mol difference in $\Delta G^{\ddagger}$ observed between **6** and **8** and that steric effects must also contribute to the energy required for the activation process.

Figure 2 illustrates the 100 MHz $^{13}C$ nmr spectrum of tropolone benzoate (**9**) recorded at 20° and −80°C. The room temperature spectrum contains only five signals while there are nine nonequivalent sites on the molecule: four belong to the tropolone ring and five to the benzoate group. Distinguishing between these two types of signals is straightforward since the latter remain unaffected by the temperature change. The slow exchange spectrum of **9** recorded at −80°C contains all 12 expected lines. The assignment of the tropolone carbons in Fig. 2 (and Table 1) respects the order of chemical shifts found for tropolone acetate and 2-methoxytropone (2). The phenyl carbons are assigned directly by comparison with the chemical shifts observed for methyl benzoate. Only the C-5 and C-12 lines cannot be assigned unambiguously because of their proximity.

From the coalescence temperature of −23°C observed for C-4,6 at 20 MHz for this compound, a $\Delta G^{\ddagger}$ of 11.5 kcal/mol is calculated. This value is 0.7 kcal/mol higher than what has been observed for tropolone acetate **4**, indicating that migration of an acetyl group is easier than migration of a benzyl group. A similar behaviour has been observed for *O*-acyl derivatives of the *cis* enols of 1,3-diketones in which replacement of acyl by benzyl raises the energy barrier from 15.4 kcal/mol to 16.3 kcal/mol (9).

The potential influence of ring substituents on the energy barrier of acetyl migration suggested from the published $^1H$ dnmr results for 3,7-dibenzyltropolone acetate (4) was investigated further through analysis of the variable temperature spectra of 3,7-dibromotropolone acetate (**10**).

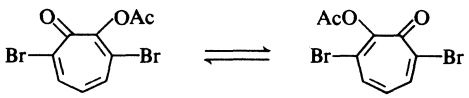


**10***a* **10***b*

Under ordinary recording conditions, the room temperature 20 MHz $^{13}C$ nmr spectrum of **10** shows only three signals instead of five for the unsaturated carbons. Assignments are straightforward from intensity and chemical shifts considerations: there is an intense line at 138.9 ppm which is due to the equivalent C-4 and C-6 carbons and a less intense line at 129.0 ppm which is due to C-5. The weak line observed at 136.7 ppm is due to the nonprotonated C-3,7 carbons. At −100°C, the low field region of

Can. J. Chem. Downloaded from www.nrcresearchpress.com by 210.87.254.5 on 09/06/12
For personal use only.

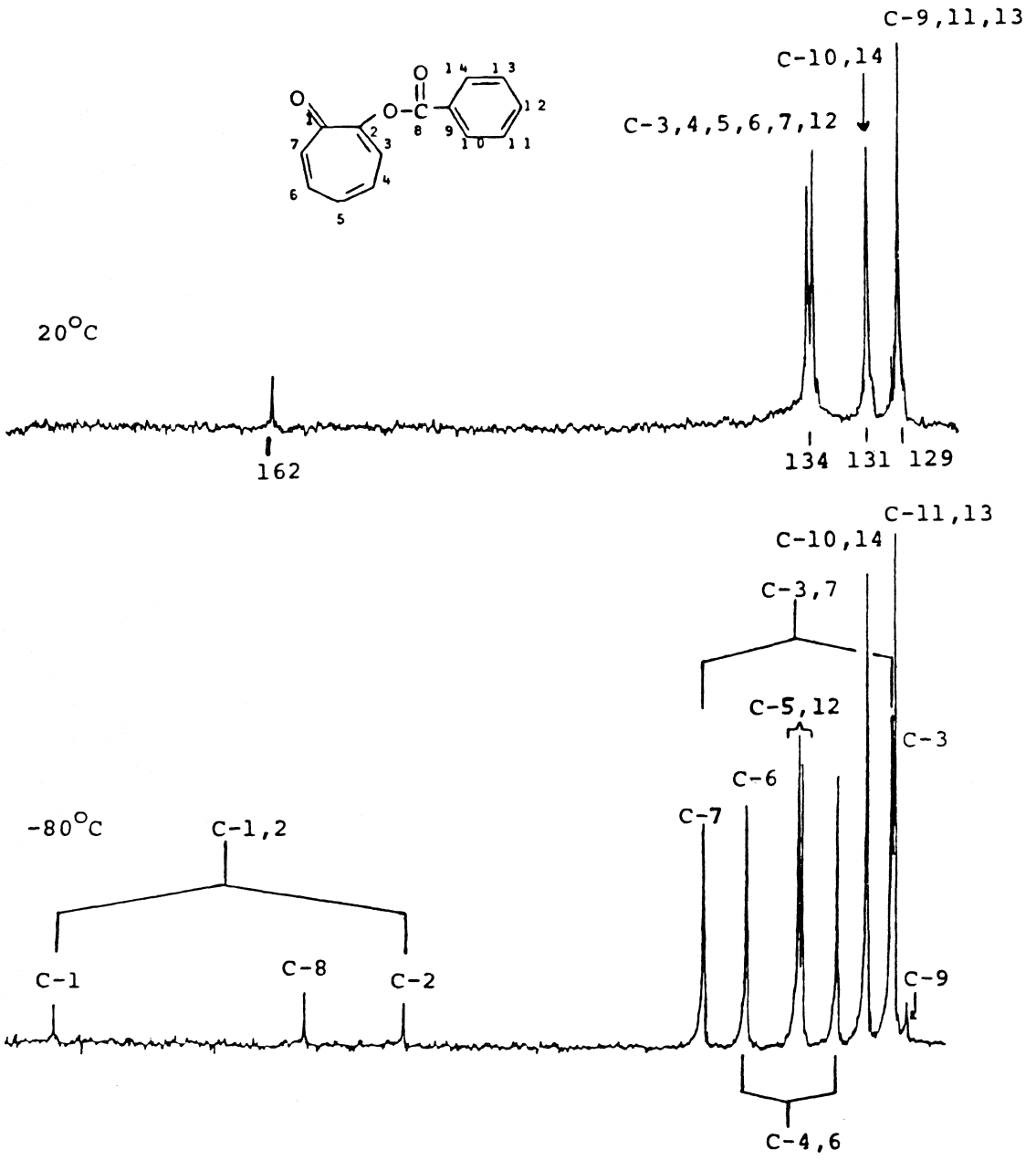


FIG. 2. The 100 MHz $^{13}C$ nmr spectra of **9** in $CHFCl_2$ at 20°C and −80°C. Flip angle = 25°; SW = 8064 Hz; data size = 8K.

the spectrum of **10** contains all expected 8 lines: the C-4,6 line has split into a doublet with components at 140.8 and 138.7 ppm while the C-3,7 line has also split into a doublet with components at 142.8 and 137.8 ppm. The C-1,2 line and the C-8 carbonyl line which were not observed at room temperature are now visible in the slow exchange spectrum: C-1 and C-2 appear at 171.8 and 153.1 ppm respectively.

A $\Delta G^{\ddagger}$ of 10.9 kcal/mol for the acetyl migration process is calculated at the coalescence temperature of −43°C observed for the C-4,6 signal. This value is very similar to that observed for tropolone acetate, indicating little influence of the two adjacent bromine substituents on the energy barrier of the migration process.

At this point it should be mentioned that the energy barrier for tautomerization in tropolone itself is too low for it to be amenable to an

Can. J. Chem. Downloaded from www.nrcresearchpress.com by 210.87.254.5 on 09/06/12
For personal use only.

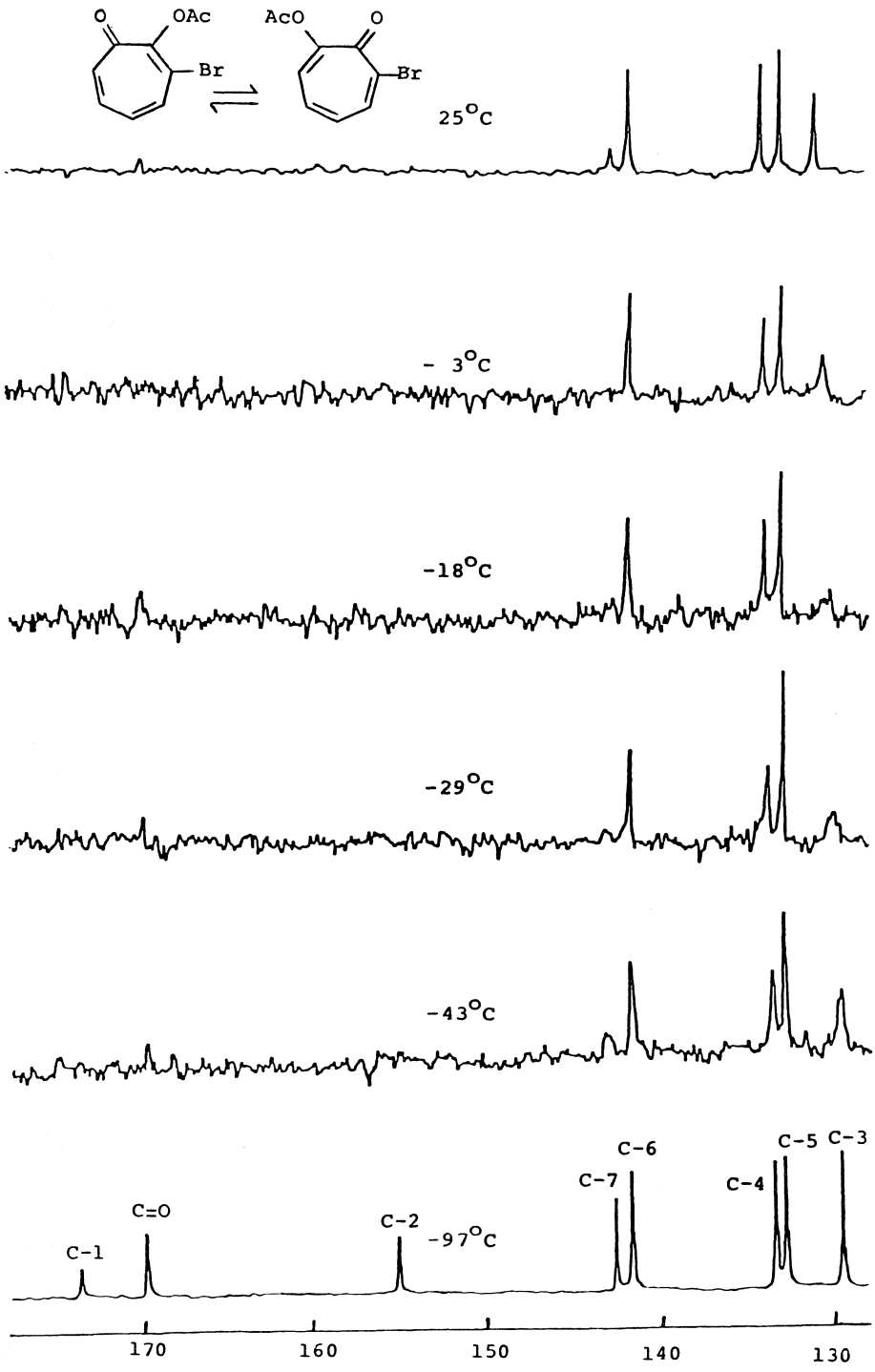


FIG. 3. The 20.15 MHz $^{13}C$ nmr spectra of **3** in $CHFCl_2$ at several temperatures. Flip angle = 35°; SW = 6024 Hz; data size = 8K.

investigation in solution by dynamic nmr techniques and our efforts to determine $\Delta G^{\ddagger}$ for tautomerization by nmr have failed. On the other hand, the 25 MHz $^{13}C$ nmr spectrum of tropolone in the solid state has recently been recorded by Fyfe (10*a*); it contains 7 lines, indicating that proton exchange is slow in the solid state. The chemical shifts of all 7 nonequivalent carbons in tropolone

Can. J. Chem. Downloaded from www.nrcresearchpress.com by 210.87.254.5 on 09/06/12
For personal use only.

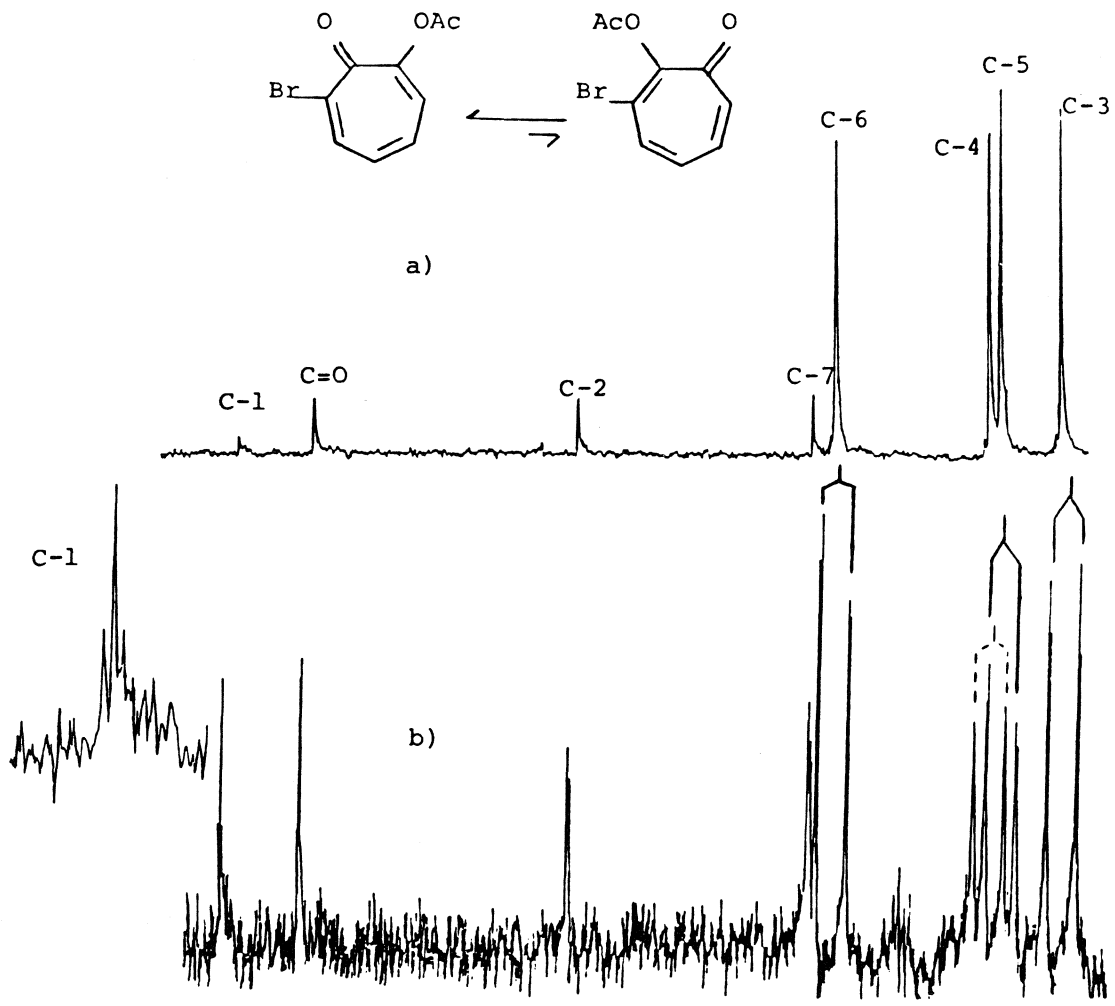


FIG. 4. The 100 MHz $^{13}C$ nmr spectra of **3** in $CHFCl_2$ at −80°C; (a) broad band decoupling; (b) gated decoupling. Flip angle = 25°; SW = 10 000 Hz; data size = 8K.

obtained from that spectrum are given in Table 1. When averaged, these chemical shifts closely match those observed in $CDCl_3$ solution (10*b*).

We now turn our attention to unsymmetrical, singly substituted derivatives at C-3 or C-7, such as **2** and **3**.

Figure 3 illustrates the variable temperature 20 MHz $^{13}C$ nmr spectra of **3** in $CHF_2Cl$ solution. It is immediately apparent that no major changes are observed in the spectrum as the temperature is lowered. At −97°C, the acetyl migration process should be slow and indeed the line broadening observed at intermediate temperatures for the smaller 142.9 and 129.6 ppm lines clearly indicates that the process has been slowed down (11). This absence of new signals suggests that the molecule exists predominantly in only one form. The total absence of weak signals at low temperature and the line broadening phenomenon at intermediate temperatures show that if a minor isomer existed it would account for less than 2% in the **3***a* ⇌ **3***b* equilibrium (11). There thus remains the task of identifying the nature of this predominant isomer, namely that which bears the bromine atom at the 3-position (**3***a*) or at the 7-position (**3***b*).

Our earlier work (2) suggested that substituent effects on $^{13}C$ chemical shifts might allow the determination of the structure of the favored isomer of **3**. Unfortunately the required substituent parameters are not available for the 2-acetoxy derivative but only for the 2-methoxy derivative. Predicted chemical shifts for **3***a* and **3***b* lead to the suggestion that **3***b* is more compatible with the observed spectrum of **3**. On the other hand, no obvious convergence is observed when this method is applied to **2**.

Can. J. Chem. Downloaded from www.nrcresearchpress.com by 210.87.254.5 on 09/06/12
For personal use only.

Can. J. Chem. Downloaded from www.nrcresearchpress.com by 210.87.254.5 on 09/06/12
For personal use only.

Because carbon–proton coupling constants through three bonds ($^3J_{CH}$) offered an alternate probe for locating the position of the bromine atom, proton coupled $^{13}C$ nmr spectra were recorded and analysed. It is well known (12) that in aromatic systems the magnitude of $^1J_{CH}$ coupling constants is close to 160 MHz while $^2J_{CH}$ are smaller (<3 Hz) and frequently nonresolved. Values for $^3J_{CH}$, on the other hand, usually range from 7 to 11 Hz and lead to clearly recognizable patterns in fully coupled $^{13}C$ nmr spectra (12); they therefore constitute a convenient method for determining the number of protons β to a given carbon.

The 20 MHz $^{13}C$ nmr coupled spectrum of 3,7-dibromopolone (**11**) shows that the averaged C-1,2 signal appears as a doublet ($^3J_{CH}$ = 8.8 Hz) because these equivalent carbons are coupled to only one β proton which constitutes a mean of H-6 and H-4. Similarly, the averaged C-1,2 signal in the coupled spectrum of 5-bromotropolone (**12**) appears as a triplet ($^3J_{CH}$ = 9.8 Hz) since both carbons are at all times coupled to two β protons. These results suggest that in the case of the nonsymmetric compounds **2** and **3**, if the 3-Br form was predominant, the C-1 signal should appear as a doublet (coupling with H-6) and the C-2 signal as a triplet (coupling with H-7 and H-4), while the reverse should be observed if the 7-Br form was predominant.

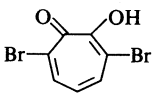


**11**

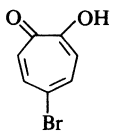


**12**

The 100 MHz coupled $^{13}C$ nmr spectrum of **3** at −80°C (Fig. 4) clearly shows that the C-1 signal appears as a triplet ($^3J_{CH}$ = 9.8 Hz) thereby proving unambiguously that ***3b*** is the major isomer adopted by this molecule. In this case, the C-2 signal revealed additional coupling to $^3J_{CH}$ and is therefore of little use. Similarly, the room temperature 100 MHz coupled $^{13}C$ nmr spectrum of **2** shows that the C-1 signal is a triplet ($^3J_{CH}$ = 8.3 Hz) and the C-2 signal is a doublet ($^3J_{CH}$ = 11.1 Hz), thus confirming that the 7-Br form is also favored by this molecule. This conclusion disproves the earlier claim (7), based on the interpretation of $^1H$ nmr parameters, that ***2a*** should be the more favored form.

## Experimental

Melting points are uncorrected and were determined using a Büchi melting point apparatus. The vpc analyses and separations were carried out on a Varian-Aerograph model 920 instrument using helium as carrier gas.

The variable temperature $^{13}C$ nmr spectra were recorded in the FT mode with Bruker WP-80, WH-90, or WH-400 instruments operating respectively at 20.15, 22.63, and 100.0 MHz and equipped with a Bruker variable temperature accessory. Unless otherwise mentioned, all $^{13}C$ spectra were recorded with proton noise decoupling for solutions in dichlorofluoromethane (100–150 mg in 2.2 mL of solution) containing TMS and about 19% of $CD_2Cl_2$ (for locking purposes) in standard 10 mm tubes which had been degassed and sealed. In the case of 20.15 MHz and 22.63 MHz spectra, temperatures were measured accurately with a calibrated copper–constantan thermocouple placed inside a solvent-containing dummy nmr tube. A precision of ±1°C is expected. $CDCl_3$ solutions containing TMS were used for samples studied only at room temperature. Coupled spectra were recorded using the gated decoupling technique with the decoupler on for 15 s and then switched off 0.005 s before the pulse.

The rate constants were estimated at the coalescence temperature using the equation $k = \pi\Delta\nu/\sqrt{2}$. The free energy values ($\Delta G^{\neq}$) were calculated from standard equations (13) using a transmission coefficient of one-half.

*Synthesis of compounds*

*Monobromotropolone acetate (**3**)*

To a solution of monobromotropolone (**2**) (14) (9.64 g, 48 mmol) in chloroform (12 mL) and pyridine (4.8 mL) was added a solution of acetyl chloride (4.08 mL) in chloroform (8 mL) with cooling. The mixture was stirred for 3 h at room temperature, diluted with chloroform, washed with water, and dried. The solvent was removed to yield the crude acetate. The product was purified by column chromatography to yield the pure product (5.2 g, 44.5%), mp = 72–74°C; *m/e*: 244/242 ($M^+$), 202/200 ($M - COCH_2)^+$, 174/172 [$M - (COCH_3 + CO)$]$^+$.

*2-Trimethylsiloxytropone (**6**)*

Tropolone (0.50 g, 4.1 mmol), pyridine (3 mL), hexamethyldisiloxane (2.7 mL), and chlorotrimethylsilane (1.54 mL, 12.3 mmol) were allowed to react at room temperature for 15 min. The mixture was decanted and 100 μL samples of the resulting clear solution were analysed and separated by gas chromatography. A yellow oil (250 mg) still containing tropolone impurities was obtained after separation on a SE-30 5% column (5 ft × ¼ in.). The $^1H$ nmr spectrum was similar to that already published (6) and the $^{13}C$ nmr data in Table 1 and Fig. 1 confirm the structure; *m/e*: 194 ($M^+$), 179 ($M - CH_3)^+$.

*2-tert-Butyl dimethylsiloxytropone (**8**)*

Tropolone (0.5 g, 4.1 mmol), *tert*-butyldimethylsilyl chloride (1.88 g, 12.5 mmol), and pyridine (1 mL) in hexane (13 mL) were stirred for 3 h and then refluxed for 15 h. The solution was filtered and the residue washed with hexane. Evaporation of the filtrate under reduced pressure gave 0.53 g (55%) of a pale beige solid, mp = 45°C. The structure of this compound was characterized by $^{13}C$ nmr (Table 1); *m/e*: 221 ($M - CH_3)^+$, 179 [$M - (CH_3)_3C$]$^+$.

*Tropolone benzoate (**9**)*

This compound was prepared according to the method reported by Doering and Knox (15). Yield 42.2%, mp = 130°C (lit. (15) yield 31%; mp 130°C).

*3,7-Dibromotropolone (**11**)*

A solution of tropolone (20 g, 160 mmol) in methanol (200 mL) was cooled between −10° and −15°C. Bromine (58 g, 360 mmol) was then added over a period of 30 min while keeping the temperature at −15°C. After the addition, the bath was removed and the reaction mixture was allowed to reach room temperature. Excess bromine was blown out with a stream of nitrogen. The crude product which precipitated was filtered to give a mixture (32.6 g) of 3,7-dibromo and 3,5,7-tribromotropolone.

Recrystallization from methanol gave the pure product (15.6 g, 30.3%), mp = 153–155°C (lit. (16) mp 159–160°C); *m/e*: 278/280/282 ($M^+$, 100%), 250/252/254 [$(M - CO)^+$, 75%], 199/201 [$(M - Br)^+$, 5%]. *Anal.* calcd. for $C_7H_4O_2Br_2$: C 30.04, H 1.44; found: C 30.23, H 1.5. A second crop (16.9 g), also free of tribromo impurity, was obtained on concentration of the solution. Total yield: 43.7%.

*3,7-Dibromotropolone acetate (**10**)*

To a solution of 3,7-dibromotropolone (1.68, 60 mmol) in chloroform (1.5 mL) and dry pyridine (0.6 mL) was added dropwise a solution of acetyl chloride (0.54 mL, 6.6 mmol) in chloroform (1 mL). The mixture was stirred at room temperature for 4 h. The reaction mixture was diluted with chloroform, washed with water, dried, and the solvent was removed to yield the crude product (1.71 g). This was purified by filtering through silica gel to yield the pure product (0.64 g, 33%), mp = 110–112°C; *m/e*: 320/322/324 $(M)^+$, 277/279/271 $(M - COCH_3)^+$, 249/251/253 $[M - (COCH_3 + CO)]^+$.

*5-Bromotropolone (**12**)*

To a suspension of 5-aminotropolone (17) (5 g, 36.5 mmol) in water (34 mL) was added hydrobromic acid 48% (222 mL, 1168 mmol). The mixture was cooled to −10°C and stirred for 15 min. Sodium nitrite (2.5 g) in water (17.2 mL) was added to the mixture over 5 min. The temperature was maintained at −10°C for 1.5 h. The mixture was then allowed to warm up to room temperature over one hour, heated to 45°C for one hour, and then cooled to room temperature. The mixture was then poured on crushed ice (400 g), filtered, and the solid washed with water. The crude solid (3.5 g) was dissolved in chloroform and filtered. The filtrate was treated with charcoal, dried over magnesium sulfate, and filtered. The solvent was removed and the residue (12.7 g) crystallized from chloroform–hexane to yield 1.8 g (24.5%) of pure product, mp = 189–190°C (lit. (18) mp 188°C); *m/e*: 200/202 ($M^+$, 60%), 172/174 [$(M - CO)^+$, 100%], 93 $[(M - (CO + Br)]^+$, 10%].

## Acknowledgements

We wish to acknowledge the technical (nmr) contribution of Mr. Robert Mayer and Dr. Helmut Beierbeck of the "Laboratoire Régional de RMN à haut champ" in Montreal. We thank the Natural Sciences and Engineering Research Council of Canada and the Ministère de l'Education du Québec for their financial assistance.

1. J. F. Bagli, T. Bogri, B. Palameta, R. Martel, W. Robinson, T. Pugsley, and W. Lippmann. J. Med. Chem. **22**, 1186 (1979).
2. J. F. Bagli, T. Bogri, B. Palameta, and M. St-Jacques. Can J. Chem. **57**, 1949 (1979).
3. (*a*) S. Masamune, A. V. Kemp-Jones, J. Green, D. L. Rabenstein, M. Yasunami, K. Takase, and T. Nozoe. J. Chem. Soc. Chem. Commun. 283 (1973); (*b*) J. F. Bagli and M. St-Jacques. Can J. Chem. **56**, 578 (1978).
4. V. I. Minkin, L. P. Olekhnovich, Y. A. Zhdanov, Z. N. Budarina, and V. P. Metlushenko. Tetrahedron Lett. 563 (1974).
5. H. J. Reich and D. A. Murcia. J. Am. Chem. Soc. **95**, 3418 (1973).
6. R. M. Harrison, J. D. Hobson, and A. W. Midgley. J. Chem. Soc. Perkin Trans. I, 2403 (1976).
7. H. Sugiyama. Sci. Rep. Tohoku Univ. **20**, 34 (1968).
8. (*a*) J. J. Howe and T. J. Pinnavaia. J. Am. Chem. Soc. **91**, 5378 (1969); (*b*) T. J. Pinnavaia, W. T. Collins, and J. J. Howe. J. Am. Chem. Soc. **92**, 4544 (1970).
9. V. I. Minkin, L. P. Olekhnovich, Y. A. Zhdanov, V. V. Kiselev, M. A. Voronov, and Z. N. Budarina. J. Org. Chem. USSR, **9**, 1319 (1973).
10. (*a*) C. Fyfe. Personal communication of data presented at the 21st Experimental NMR Conference, Tallahassee, Florida, March 16–20, 1980; (*b*) L. Weiler. Can J. Chem. **50**, 1975 (1972).
11. (*a*) F. A. L. Anet and V. J. Basus. J. Am. Chem. Soc. **95**, 4424 (1973); (*b*) N. Okazawa and T. S. Sorensen. Can J. Chem. **56**, 2737 (1978).
12. F. W. Wherli and T. Wirthlin. Interpretation of carbon-13 nmr spectra. Heyden, New York, NY. 1976.
13. F. A. L. Anet, P. J. Degen, and J. Krane. J. Am. Chem. Soc. **98**, 2059 (1976).
14. T. Toda, H. Kubota, and T. Nozoe. Nippon Kagaku Zasshi, **88**, 1234 (1967); Chem. Abstr. **68**, 101342x (1968).
15. W. von E. Doering and L. H. Knox. J. Am. Chem. Soc. **73**, 828 (1951).
16. T. Nozoe, Y. Kitahara, and K. Yamane. Proc. Jpn. Acad. **27**, 18 (1951).
17. T. Nozoe and S. Seto. Proc. Jpn. Acad. **27**, 188 (1951); Chem. Abstr. **46**, 4522 (1952).
18. J. W. Cook, A. R. M. Gibb, and R. A. Raphael. J. Chem. Soc. 2244 (1951).

Can. J. Chem. Downloaded from www.nrcresearchpress.com by 210.87.254.5 on 09/06/12
For personal use only.

# Relation entre structure et réactivité dans les réactions d'addition nucléophile sur les dérivés carbonylés: influence de la tension angulaire sur la réactivité de cyclanones et cyclanols angulairement contraints

BERNARD BOYER, GÉRARD LAMATY[1] ET CLAUDE MOREAU

*Laboratoire de Chimie Organique Physique, Université des Sciences et Techniques du Languedoc, 34060 Montpellier Cedex, France*

ET

PATRICK GENESTE

*Laboratoire de Chimie Organique Physique Appliquée, Ecole Nationale Supérieure de Chimie de Montpellier, 34080 Montpellier Cedex, France*

Reçu le 5 mai 1981

BERNARD BOYER, GÉRARD LAMATY, CLAUDE MOREAU et PATRICK GENESTE. Can. J. Chem. **60**, 239 (1982).

Les constantes de vitesse d'addition du borohydrure de sodium sur les cyclanones angulairement contraintes, tricyclo[3.3.1.$1^{3,7}$]-décanone-2 (**1**), bicyclo[3.3.1]nonanone-9 (**2**), bicyclo[3.2.1]octanone-8 (**3**) et bicyclo[2.2.1]heptanone-7 (**4**), ont été mesurées dans un mélange eau–dioxanne 50:50 en volumes à 25.0°C. Elles mettent en évidence les énergies dues à la variation de tension angulaire lorsque l'on passe de l'état initial à l'état de transition. Les énergies d'activation mesurées, représentant presque la totalité de l'énergie associée à cette variation de tension angulaire, sont significatives d'un état de transition tardif.

La comparaison des constantes de vitesse de réduction de ces cétones où le carbone siège de la réaction passe d'un état d'hybridation $sp^2$ à un état d'hybridation $sp^3$ avec les vitesses d'oxydation chromique des alcools correspondants qui impliquent le changement d'hybridation opposé montre que l'importance de la variation angulaire peut également servir de critère pour déterminer la position de l'état de transition le long du chemin réactionnel.

BERNARD BOYER, GÉRARD LAMATY, CLAUDE MOREAU, and PATRICK GENESTE. Can. J. Chem. **60**, 239 (1982).

The rate constants for addition of sodium borohydride on the angularly constrained cyclic ketones, tricyclo[3.3.1.1.$^{3,7}$]-2-decanone (**1**), bicyclo[3.3.1]-9-nonanone (**2**), bicyclo[3.2.1.])-8-octanone (**3**), and bicyclo[2.2.1.]-7-heptanone (**4**), have been determined in water/dioxane (50:50 v/v) at 25°C. These values demonstrate the energy differences caused by the changes in torsion angles on passing from the initial state to the transition state. The activation energies determined, representing almost all of the energy associated with the angular torsion, are indicative of a late transition state.

Comparison of rate constants for the reduction of these ketones where the reaction site carbon changes from $sp^2$ to $sp^3$ hybridization with the rates for chromic acid oxidation of the corresponding alcohols (opposite change of hybridization) demonstrates that the effects of the angular variations can also act as criteria for the determination of the position of transition states along the reaction pathway.

[Journal translation]

## Introduction

Dans un précédent article (1), nous avons montré que les constantes de vitesse d'addition du borohydrure de sodium sur des cyclanones stériquement encombrées et les constantes de vitesse d'oxydation chromique des cyclanols correspondants mettaient en évidence les énergies dues aux interactions diaxiales-1,3 lorsque l'on passe de l'état initial à l'état de transition. Cette mise en évidence avait été rendue possible en utilisant plus rationnellement les données conformationnelles, c'est à dire en choisissant des modèles de façon à ne faire varier qu'un seul facteur de réactivité.

Nous souhaitons présenter ici le travail que nous avons effectué afin de mettre en évidence, cette fois, les énergies dues à la variation de tension angulaire lorsque l'on passe d'un état d'hybridation $sp^2$ à un état d'hybridation $sp^3$ et inversement. Les modèles dont le squelette est une cyclohexanone chaise ou une cyclopentanone enveloppe ont été choisis de façon à maintenir constants les autres facteurs de réactivité tels que les interactions diaxiales-1,3, l'hyperconjugaison ou les barrières de torsion.

Notre étude a porté sur la réduction des cyclanones angulairement contraintes **1** à **4** et sur la comparaison avec l'oxydation chromique des cyclanols correspondants **5** à **8**, résultats obtenus dans notre laboratoire (2) ou cités par d'autres auteurs (3).

## Résultats expérimentaux

Les constantes de vitesse d'addition du borohydrure de sodium ont été déterminées à 25.0°C dans un mélange eau–dioxanne 50:50 en volumes, la phase aqueuse contenant 0.05 mol/L de soude; dans ces conditions, les solutions de $BH_4Na$ sont stables (1).

Les constantes de vitesse partielles correspondant à une attaque "équatoriale", $k_\alpha$, ont été cal-

[1]Auteur à qui toute correspondance doit être adressée.

0008-4042/82/030239-04$01.00/0

©1982 National Research Council of Canada/Conseil national de recherches du Canada

Can. J. Chem. Downloaded from www.nrcresearchpress.com by 210.87.254.5 on 09/06/12
For personal use only.

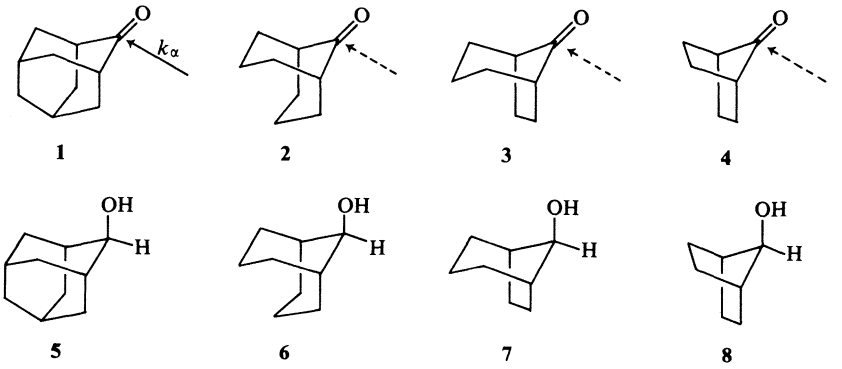


culées à partir des constantes de vitesse totales, $k$, et des résultats stéréochimiques obtenus dans la réduction des cétones **1** à **4** ($k_\alpha = k \times \%$ alcool "axial") malgré les réserves suscitées par ce genre de calculs (4). Les résultats expérimentaux sont rassemblés dans le tableau 1.

TABLEAU 1. Constantes de vitesse de réduction des cétones **1** à **4** par $BH_4Na$ dans le mélange eau–dioxanne 50:50 en volumes à 25.0°C

| Cétones | $k \times 10^2$ ($M^{-1}$ s$^{-1}$) | % Attaque "équatoriale" | $k_\alpha \times 10^2$ ($M^{-1}$ s$^{-1}$) | $\delta\Delta G_{red}^{\neq a}$ (kcal/mol) |
|---|---|---|---|---|
| **1** | 8.566 | 50 | 4.28 | 0.00 |
| **2** | 7.566 | 50 | 3.78 | +0.07 |
| **3** | 478.3 | 100 (5) | 478.3 | −2.78 |
| **4** | 6466.6[b] | 50 | 3233.3 | −3.90 |

[a] $\delta\Delta G_{red}^{\neq} = -RT \ln k_\alpha(n)/k_\alpha(1)$; $n$ = **1**, **2**, **3**, **4**.
[b] Valeur extrapolée par l'intermédiaire de l'énergie d'activation à partir d'une mesure effectuée à 7.8°C (6).

## Interprétation des résultats et discussion

Nous admettons en première approximation que les cycles portant la fonction cétone ont la même conformation, chaise dans le cas d'une cyclohexanone, enveloppe dans le cas d'une cyclopentanone; dans ces conditions, nous pouvons supposer que, pour tous les produits étudiés, l'approche du nucléophile par la face α sera pratiquement la même et que les interactions synpériplanaires-1,3 qui se développent dans l'état de transition seront également les mêmes.[2]

Dans l'introduction de notre article, nous avons mentionné que le but de notre travail était de faire ressortir le facteur tension angulaire lorsque l'on passe d'un état initial $sp^2$ à un état de transition $sp^3$ et réciproquement; il est a priori possible d'évaluer l'énergie associée à la variation de tension angulaire entre un état d'hybridation trigonal et un état d'hybridation tétragonal à l'aide des équations énergétiques établies par Allinger *et al.* (7); les calculs ont été effectués antérieurement pour les produits que nous avons étudiés et sont rassemblés dans le tableau 2.

Le tableau 2 fait apparaitre que l'énergie associée à la variation de tension angulaire entre un état d'hybridation $sp^2$ et un état d'hybridation $sp^3$ est d'autant plus importante que le système est contraint; en d'autres termes, plus le système sera contraint, plus il tendra à se libérer de cette contrainte. Si donc la réactivité de nos produits est influencée d'une manière prépondérante par la tension angulaire, nous devrions observer une correlation entre les valeurs $\delta\Delta E$ calculées et les valeurs $\delta\Delta G_{red}^{\neq}$ expérimentales; en portant $\delta\Delta G_{red}^{\neq}$ en fonction de $\delta\Delta E$ (Fig. 1) on observe effectivement une telle correlation. Et une fois de plus, ces résultats constituent un argument en faveur d'un état de transition tétragonal dans l'addition nucléophile du borohydrure de sodium sur les dérivés carbonylés puisqu'expérimentalement on retrouve environ 80% de l'énergie calculée.

## Comparaison avec l'oxydation chromique des alcools

La comparaison de la réactivité des cyclanones vis-à-vis de $BH_4^-$, où le carbone siège de la réaction passe d'une hybridation $sp^2$ à une hybridation $sp^3$, avec l'oxydation chromique des alcools secondaires correspondants (2) qui implique le changement d'hybridation opposé, met en évidence un comportement symétrique (1, 13).

Il était donc intéressant de comparer les réactivités dans le cas de nos composés et à côté de nos résultats obtenus dans la réduction des cétones nous avons fait figurer dans le tableau 3 les résultats relatifs à l'oxydation chromique des alcools correspondants, résultats obtenus dans notre laboratoire (2) ou cités par d'autres auteurs (3).

Le tableau 3 montre qu'à une augmentation de la

[2] En toute rigueur, les liaisons impliquées dans ce type d'interactions sont axiales dans le cas d'un système cyclohexanique chaise et bissectionnelles dans le cas d'un système cyclopentanique enveloppe.

Can. J. Chem. Downloaded from www.nrcresearchpress.com by 210.87.254.5 on 09/06/12
For personal use only.

Can. J. Chem. Downloaded from www.nrcresearchpress.com by 210.87.254.5 on 09/06/12
For personal use only.

TABLEAU 2. Calcul de la variation de tension angulaire entre un état d'hybridation $sp^2$ et un état d'hybridation $sp^3$

| Produits | | θ (X = O) | θ (X = $H_2$) | $\Delta E(n)^a$ kcal/mol | $\delta\Delta E^b$ kcal/mol |
|---|---|---|---|---|---|
| 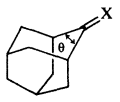 | **1** | 113° (8) | 109° (7) | 0.31 | 0.00 |
| 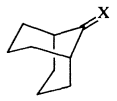 | **2** | 112° (5, 9) | 111° (10, 11) | 0.26 | −0.05 |
| | **3** | 98° (5) | 101° (12) | 3.82 | 3.51 |
| 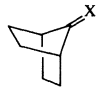 | **4** | 86° (2) | 94° (2) | 5.37 | 5.06 |

[a] $\Delta E(n) = \Delta E$ (X = O) − $\Delta E$ (X = $H_2$); $n$ = **1**, **2**, **3**, **4**.
[b] $\delta\Delta E = \Delta E(n) - \Delta E(1)$.

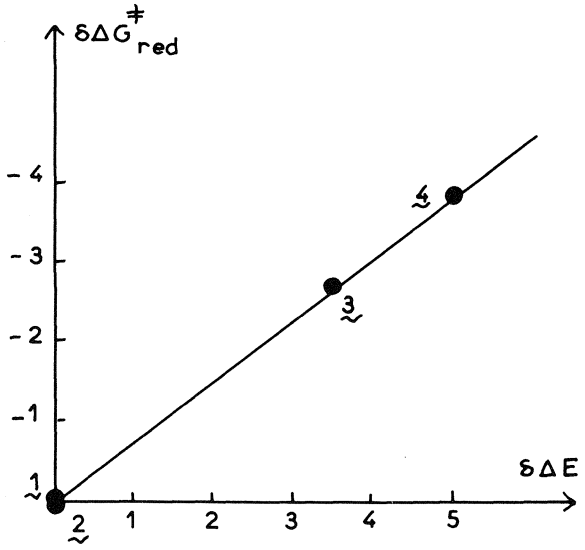


FIG. 1. Variation de $\delta\Delta G_{red}^{\neq}$ en fonction de $\delta\Delta E$ (kcal/mol).

TABLEAU 3. Constantes de vitesse relatives de réduction des cétones **1** à **4** et d'oxydation des alcools correspondants **5** à **8**

| Cétones | $k_\alpha$ rel. | $\delta\Delta G_{red}^{\neq}$ (kcal/mol) | $\delta\Delta G_{ox}^{\neq}$ (kcal/mol) | $k_{ox}$ rel. | Alcools |
|---|---|---|---|---|---|
| **1** | 1 | 0.00 | 0.00 | 1 (2) | **5** |
| **2** | 0.088 | +0.07 | −0.04 | 1.07 (2) | **6** |
| **3** | 112 | −2.78 | +1.43 | 0.088 (3) | **7** |
| **4** | 755 | −3.90 | +1.68 | 0.058 (3) | **8** |

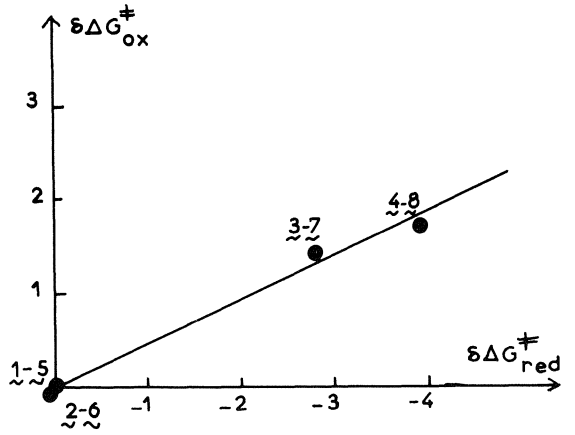


FIG. 2. Variation de $\delta\Delta G_{ox}^{\neq}$ en fonction de $\delta\Delta G_{red}^{\neq}$ (kcal/mol).

vitesse de réduction correspond une diminution de la vitesse d'oxydation. Si la tension angulaire est responsable de l'accélération observée dans la réduction des cétones **1** à **4**, elle doit être également responsable du ralentissement observé dans l'oxydation des alcools **5** à **8**; c'est effectivement ce que l'on constate en portant sur un diagramme $\delta\Delta G_{ox}^{\neq}$ en fonction de $\delta\Delta G_{red}^{\neq}$ (Fig. 2).

## Conclusion

Comme nous l'avons déja fait pour un autre facteur de réactivité, l'utilisation de systèmes rigides judicieusement choisis permet, dans le travail

que nous avons présenté, de mettre en évidence par des méthodes cinétiques l'énergie engendrée par la variation de tension angulaire aussi bien dans la réduction des dérivés carbonylés par $BH_4Na$ ($sp^2 \dashrightarrow sp^{3\ddagger}$) que dans l'oxydation chromique des alcools correspondants ($sp^3 \dashrightarrow sp^{2\ddagger}$).

## Partie expérimentale

La synthèse des cétones est décrite dans la littérature: **1** (14), **2** et **3** (5) et **4** (15).

Pour les alcools **5** et **6**, nous avons utilisé les données de laboratoire (2); pour les alcools **7** et **8**, nous avons utilisé les données de la littérature (3).

Les méthodes cinétiques ont été publiées antérieurement (2, 16).


1. B. Boyer, G. Lamaty, C. Moreau et P. Geneste. Can. J. Chem. **57**, 2848 (1979) et références citées.
2. R. Durand, P. Geneste, G. Lamaty et J. P. Roque. Recl. Trav. Chim. Pays-Bas, **94**, 131 (1975).
3. P. Muller et J. C. Perlberger. J. Am. Chem. Soc. **98**, 8407 (1976).
4. D. C. Wigfield et D. J. Phelps. J. Org. Chem. **41**, 2396 (1976).
5. C. S. Foote et R. B. Woodward. Tetrahedron, **20**, 687 (1964).
6. G. Lamaty, A. Malaval, J. P. Roque et P. Geneste. Bull. Soc. Chim. Fr. 4567 (1972).
7. N. L. Allinger, J. A. Hirsch, M. A. Miller, I. J. Tyminski et F. A. Van Catledge. J. Am. Chem. Soc. **90**, 1199 (1968).
8. P. Von R. Schleyer et R. D. Nicholas. J. Am. Chem. Soc. **83**, 182 (1961).
9. N. C. Webb et M. R. Becker. J. Chem. Soc. B, 1317 (1967).
10. W. A. C. Brown, J. Martin et G. A. Sim. J. Chem. Soc. 1844 (1965).
11. E. L. Osina, V. S. Mastryukov, L. V. Vilkov et N. A. Belikova. J. Chem. Soc. Chem. Commun. 12 (1976).
12. C. L. Stevens, T. A. Treat, P. M. Pillai, W. Schomsees et M. D. Glick. J. Am. Chem. Soc. **95**, 1978 (1973).
13. P. Geneste, M. Bonnet et M. Rodriguez. J. Catal. **57**, 147 (1979).
14. H. W. Geluk et J. L. M. A. Schlatmann. Tetrahedron, **24**, 5361 (1968).
15. P. Gassman et P. G. Pape. J. Org. Chem. **29**, 160 (1964).
16. B. Boyer, G. Lamaty, J. P. Roque et P. Geneste. Recl. Trav. Chim. Pays-Bas, **93**, 260 (1974).


Can. J. Chem. Downloaded from www.nrcresearchpress.com by 210.87.254.5 on 09/06/12
For personal use only.

# The preparation of some thiochroman-3-ones and derivatives

PETER D. CLARK AND DAVID M. MCKINNON[1]

*Department of Chemistry, University of Manitoba, Winnipeg, Man., Canada R3T 2N2*

Received May 22, 1981

PETER D. CLARK and DAVID M. MCKINNON. Can. J. Chem. **60**, 243 (1982).

The use of 2,3-dihydrobenzo[*b*]thiophene-2,3-dione as a source of 2-mercaptophenylacetic acid permits a convenient preparation of 2-carboxymethylthiophenylacetic acid or derivatives. These undergo a Dieckmann cyclization to 3-acetoxybenzothiopyrans, which may be hydrolysed to thiochroman-3-ones. The further reactions of some of these are described.

PETER D. CLARK et DAVID M. MCKINNON. Can. J. Chem. **60**, 243 (1982).

A partir de la dihydro-2,3-benzo[b]thiophènedione-2,3 on peut préparer l'acide *o*-mercaptophénylacétique permettant une synthèse convenable des acides *o*-carboxyméthylthiophénylacétiques ou de leurs dérivés. On obtient par la réaction de cyclisation de type Dieckmann des acétoxy-3-benzothiopyrrannes qui par hydrolyse conduisent aux thiochromannones-3. On décrit les réactions supplémentaires des quelques'uns de ces composés.

In contrast to thiochroman-4-ones and their derivatives (1) few derivatives of thiochroman-3-ones (1) are reported. The parent compound **1***a* may be made by a Dieckmann or modified Dieckmann cyclization of the diacid **2***a* or of derivatives (2, 3), or by photochemical rearrangement of the isomeric isothiochroman-4-one (2). This latter method was also applied to compounds bearing substituents in the aromatic ring, i.e. the 5-methyl and the 6-methoxy derivatives. In connection with another investigation we wished to prepare some examples of **1** bearing substituents in the heterocyclic ring as synthetic precursors of other heterocyclic systems. This work is reported below.

The diacids **2** may be approached in two ways, by an Arndt–Eistert homologation of ethyl 2-(carboxyphenylthioacetate) (**3**) (3), or by carboxyalkylation of 2-mercaptophenylacetic acid derivatives **4** (3). Our initial experiments using the former method to prepare a phenyl-substituted system were unsuccessful, and it appears that this method has limited value. Our experiments were therefore directed to the latter approach, i.e. from 2-mercaptophenylacetic acid (4). While this key acid may be made starting from 2-nitrophenylacetic acid (4), this approach limits the scope of the method. In fact a method starting from benzenethiol, via 2,3-dihydrobenzo[*b*]thiophene-2,3-dione (**5**) (5, 6), with certain modifications gives a very convenient preparation of the acid, as the dione **5** may be readily purified by extraction with base. This method is also capable of application to the preparation of other thiochroman-3-ones with substituents on the aromatic ring.

2-Mercaptophenylacetic acid (**4**) reacted with bromoacetic acid in base to provide the known

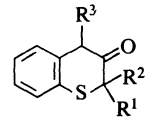

**1**

*a* $R^1 = R^2 = R^3 = H$
*b* $R^1 = CH_3$, $R^2 = R^3 = H$
*c* $R^1 = R^2 = CH_3$, $R^3 = H$
*d* $R^1 = Ph$, $R^2 = R^3 = H$
*e* $R^1 = COPh$, $R^2 = R^3 = H$
*f* $R^1 = R^2 = H$, $R^3 = CH_3$
*g* $R^1 = R^2 = H$, $R^3 = COPh$

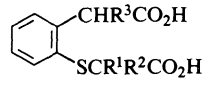

**2**

*a* $R^1 = R^2 = R^3 = H$
*b* $R^1 = CH_3$, $R^2 = R^3 = H$
*c* $R^1 = R^2 = CH_3$, $R^3 = H$
*d* $R^1 = Ph$, $R^2 = R^3 = H$

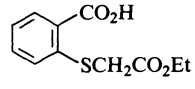

**3**

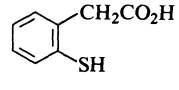

**4**

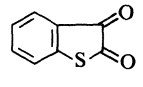

**5**

diacid **2***a*, previously prepared by hydrolysis of its diester (2). For cyclization to **1***a*, Mispelter *et al.* reported the use of acetic anhydride/sodium acetate, followed by aqueous sodium hydroxide, without reporting experimental conditions. In our hands, the treatment of the diacid afforded an oil, which had the properties of an enol-acetate of **1***a*. This compound was assigned the conjugated structure **6***a*, rather than the isomeric **7***a* on the following grounds.

The compound exhibited a 2H singlet at 3.59δ and a 1H singlet at 6.34δ, assigned respectively to the methylene and vinyl protons in **6***a*. Irradiation of the latter resonance produced a larger enhancement of the peak area of the aromatic protons than did the former, by a nuclear Overhauser effect,

[1]Author to whom correspondence should be addressed.

0008-4042/82/030243-06$01.00/0

©1982 National Research Council of Canada/Conseil national de recherches du Canada

Can. J. Chem. Downloaded from www.nrcresearchpress.com by 210.87.254.42 on 09/06/12
For personal use only.

Can. J. Chem. Downloaded from www.nrcresearchpress.com by 210.87.254.42 on 09/06/12
For personal use only.

consistent with the structure **6***a*. In addition this structure is confirmed by comparison of its nmr spectrum with that of the 2-methyl derivatives **6***b*,*c* described below. For instance, the enol-acetate **6***c*, prepared by an unambiguous synthesis, exhibits no absorption in the region 3.59δ.

The hydrolysis of **6***a* to thiochroman-3-one (**1***a*) gave some problems, but eventually it was found that dilute hydrochloric acid in acetic acid gave satisfactory results.

Likewise, treatment of **4** with ethyl-2-bromopropionate afforded the mono-ester **8***b*. This was not purified but was hydrolyzed directly to **2***b* which underwent cyclization by the above conditions to give an enol-acetate. In view of its similar spectral properties to **6***a* it is assigned the structure **6***b*, and mild acid hydrolysis gave 2-methylthiochroman-3-one (**1***b*). Also, reaction of **4** with 2-bromo-2-methylpropanoic acid afforded the acid **2***c* which cyclized to form the enol-acetate **6***c*. Hydrolysis of this afforded the ketone **1***c*.

The synthesis was then extended to produce the 2-phenyl compound **1***d*. Reaction of **4** with ethyl 2-bromophenylacetate gave the monoester **8***d* which on hydrolysis gave the diacid **2***d*. Cyclization of this afforded a mixture, which after chromatography and crystallization was separated into two components, a crystalline solid and an oil. Both of these had absorptions in the nmr corresponding to acetate methyl groups. The solid component also exhibited two singlets at 4.90 and 6.75δ, consistent with the 2- and 4-protons respectively in the enol acetate **6***d*. The other component could not be separated completely from **6***d*, but its nmr spectrum indicated a peak at 3.69δ which is consistent with the methylene protons in the isomeric enol acetate **7***b*. In contrast to the above cyclizations, i.e. to **6***a*,*b*,*c*, both enol-acetates in this case are conjugated and would be expected to be more comparable in stability.

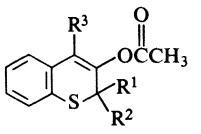

**6**

*a* $R^1 = R^2 = R^3 = H$
*b* $R^1 = CH_3$, $R^2 = R^3 = H$
*c* $R^1 = R^2 = CH_3$, $R^3 = H$
*d* $R^1 = Ph$, $R^2 = R^3 = H$

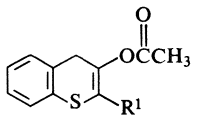

**7**

*a* R = H
*b* R = Ph

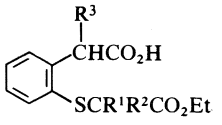

**8**

*b* $R^1 = CH_3$, $R^2 = R^3 = H$
*d* $R^1 = Ph$, $R^2 = R^3 = H$

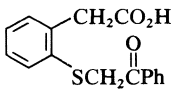

**9**

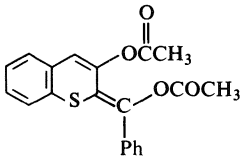

**10***a*

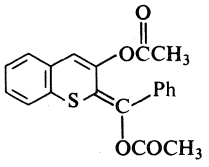

**10***b*

While the enol-acetate **6***d* hydrolysed cleanly to the ketone **1***d*, the isomer **7***d* gave **1***d* along with highly colored material. Consideration of hydrolysis mechanisms indicates that while for **6***d* the production of **1***d* is the most reasonable reaction, for **7***d* a competing reaction involving initial protonation at C-3 could lead to decomposition products.

When 2-phenacylthiophenylacetic acid (**9**), prepared by treatment of **4** with phenacyl bromide, was heated with the acetic anhydride/sodium acetate mixture, a dark green solution was obtained. This appeared to possess two main components, one of which was obtained as pale yellow crystals, whose analysis and properties were consistent with the *bis* enol-acetate **10***a* of the diketone **1***e*. The nmr of this exhibited two $CH_3$ singlets in the region 1.20 and 2.13δ. While the latter is in the usual range for an acetate methyl group, the former is not. However, it may be that one acetate is shielded by the extra aromatic ring. The other component of the mixture was a dark yellow oil but repeated chromatography failed to separate this from impurities. Tentatively it is assigned the structure of a geometrical isomer of **10***a*, i.e. **10***b*. A strongly colored blue component of the mixture was present in only trace amounts.

Attempted hydrolysis of the *bis* enol-acetate **10***a* gave only polymeric and highly colored material. This is not unexpected in view of its 1,3-diene structure.

The ketone **1***a* reacted smoothly with pyrrolidine to form a crystalline enamine, to which was assigned the structure **11**. The nmr spectrum was consistent with this structure rather than the isomeric nonconjugated structure. Reaction with methyl iodide followed by hydrolysis afforded a methyl derivative of **1***a* in good yield. This was not identical to the methyl derivative **1***b* prepared above, confirming its identity as 4-methylbenzothiopyran-3-one (**1***f*). Treatment of **11** with benzoyl chloride afforded, after hydrolysis, 4-benzoylthiochroman-3-one (**1***g*). Since this exhibited a two proton singlet at 3.36δ, and an acidic proton at 16.3δ, it appears to exist as an enolic tautomer, possibly structure **12**.

Can. J. Chem. Downloaded from www.nrcresearchpress.com by 210.87.254.42 on 09/06/12
For personal use only.

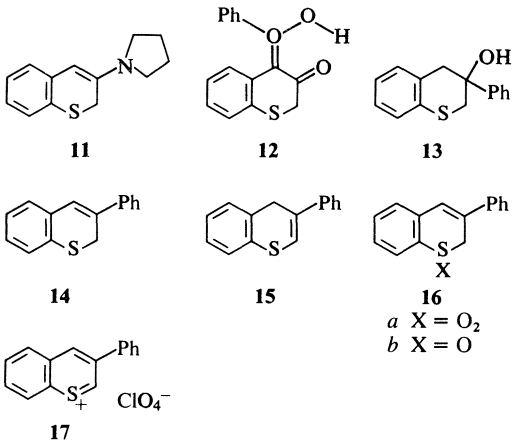


In **1***a* the 4-protons appear to be the more acidic compared to the 2-protons since on treatment with deuterium oxide in the presence of sodium carbonate only the 4-protons were exchanged as determined by nmr. Subsequent treatment with aqueous sodium carbonate regenerated the original spectrum.

When **1***a* was treated with phenylmagnesium bromide it was converted to the alcohol **13**, which dehydrated to 3-phenyl-2-*H*-1-benzothiopyran (**14**) on treatment with acid. This structure is favored over the isomeric structure **15** in view of the similarity of its nmr spectrum to 6-chloro-3-phenyl-2*H*-1-benzothiopyran (7). The compound **14** has been made (8) but no data are reported. Also, treatment with two equivalents of *m*-chloroperoxybenzoic acid afforded a sulfone **16***a*. The differences in chemical shifts of the methylene group in **14** and **16***a* are consistent with those reported for methylene protons adjacent to a sulfide and to a sulfonyl group (9). Oxidation with one equivalent afforded a sulfoxide **19***b*. When this was treated with acetic acid and perchloric acid it produced the known (10) 3-phenylbenzothiopyrylium perchlorate (**17**), although in low yield. The first two stages in a Pummerer type rearrangement of **16** would produce **17**.

While most of the aromatic protons in **12** absorbed in the region δ 7.1–7.6, an absorption at δ 6.73 was also evident, which we attribute to shielding of the 5- and/or 6-protons of the thiopyran ring by the phenyl substituent. The structure **12** has some similar steric features to 4-phenylphenanthrene because of the strong hydrogen bonding of the hydroxyl and carbonyl functions and in 4-phenylphenanthrene and derivatives similar chemical shifts have been observed (11).

The conversion of **1***a* to the condensed indole **18***a*, via a Fischer-type indolization of its phenylhydrazone is reported (2). Likewise **1***d* was converted to its phenylhydrazone which cyclized to the indole **18***b*. The related isomeric dihydrothiopyrano-[4,3-*b*]indoles **20** may be converted into the more conjugated derivatives **21** by dehydrogenation (12, 13) and this was also found for the phenyl-substituted compound **20***a*, prepared by cyclization of 2-phenylthiochromone phenylhydrazone, which formed **21***a* on treatment with chloranil. Under these conditions **18***b* could not be further dehydrogenated. Like **18***a*, **18***b* underwent atmospheric oxidation, but no definite products could be determined.

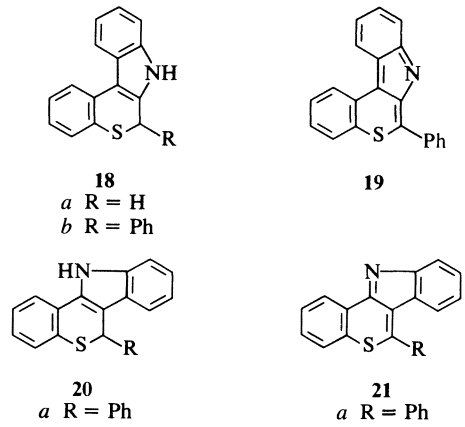


## Experimental

Unless otherwise stated, $^1$H nmr spectra were obtained in deuteriochloroform solution using tetramethylsilane as an internal standard, on a Varian model E.M. 360 spectrometer. Unless otherwise given, nmr spectra are summarized in Table 1. Mass spectra were obtained on a Finnegan model 1015 spectrometer, and ir spectra on a Perkin Elmer model 337 spectrophotometer. Thick layer chromatography (tlc) was performed on "Camag" Silica gel type D.S.F.S. supplied by Terochem Laboratories, and column chromatography (cc) on 60–200 mesh silica gel supplied by Davison Chemical. Solutions were dried over anhydrous magnesium sulfate.

*2-Mercaptophenylacetic acid (4)*

The starting 2,3-dihydrobenzo[*b*]thiophene-2,3-dione was prepared by the method of Papa *et al.* (5), with the following modifications. The crude product obtained by cyclization of 2-oxo(2-mercaptophenyl)acetyl chloride was dissolved in 20% aqueous sodium hydroxide solution. Impurities (mainly phenyl thioloxalate) were removed by extraction with dichloromethane. Acidification of the cooled solution with concentrated hydrochloric acid gave 2,3-dihydrobenzo[*b*]thiophene-2,3-dione as orange prisms, mp 119–121°C (lit. (5) mp 120–121°C). No further purification was necessary. Conversion of this to **4** was effected by the method of Glauert *et al.* (6). The material was used within one day to minimize spontaneous cyclization to 2,3-dihydrobenzo[*b*]thiophene-2-one.

*2-Carboxymethylthiophenylacetic acids (2)*

2-Mercaptophenylacetic acid (**4**) was treated with an equiva-

TABLE 1. Proton chemical shifts (δ) in thiochroman-3-ones (**1**), 2-*H*-1-benzothiopyrans, and 4-*H*-1-benzothiopyrans

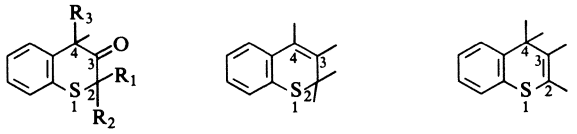

**1** **6, 10, 11, 12, 14, 16** **7**

| Compound | C-2 | C-4 | Aromatic | |
|---|---|---|---|---|
| **1***a* | 3.33s | 3.75s* | 7.03–7.07m | |
| **1***b* | 3.43q | 3.75s | 7.10–7.55m | 1.45 (d, the 2-methyl protons) |
| **1***c* | — | 3.70s | 7.06–7.45m | 1.35 (s, the methyl protons) |
| **1***d* | 4.53 | 3.90 | 7.15–7.33 | — |
| **1***f* | 3.37s | 3.79q | 7.10–7.47m | 1.55 (d, the methyl protons) |
| **6***a* | 3.59s | 6.34s | 7.00–7.61m | 2.21 (s, acetate methyl) |
| **6***b* | 3.60q | 6.32s | 6.95–7.50m | 1.40 (d, the 2-methyl group); 2.20 (s, the acetate methyls) |
| **6***c* | — | 6.17s | 6.91–7.43m | 1.45 (s, the 2-methyl group) 2.18 (s, the acetate methyl) |
| **6***d* | 4.90s | 6.75s | 7.19–7.41m | 2.04 (s, the acetate methyl) |
| **7***b* | — | 3.69s | 7.05–7.50m | 1.95s (the acetate methyl) |
| **10***a* | — | 6.25s | 7.09–7.30m | 1.25s, 2.17s (the acetate methyl) |
| **10***b* | — | 6.32 | 7.05–7.42m | 2.15s, 2.21s (the acetate methyl) |
| **11** | 3.52s | 5.30s | 6.32–7.31m | 1.66–2.0m (β-pyrrolidine protons) 3.05–3.40 (s, the enolic proton) |
| **12** | 3.52s | — | 6.60–7.61m | 16.40 (s, the enolic proton) |
| **14** | 3.73s | 6.72s | 7.05–7.49m | |
| **16***a* | 4.27s | 6.97s | 7.33–7.60m | |
| **18***b* | 5.43 | — | 7.10–8.25 | (m, all other protons) |

*On treatment with $D_2O$, $Na_2CO_3$ these protons rapidly exchanged.

TABLE 2. Preparation of 2-carboxymethylthiophenylacetic acids (**2**)

| Compound | Yield % | Melting point °C | Formula | Analysis Calcd. % C | Calcd. % H | Calcd. % S | Found % C | Found % H | Found % S |
|---|---|---|---|---|---|---|---|---|---|
| 2a | 73 | 185–186* | $C_{10}H_{10}O_4S$ | — | — | — | — | — | — |
| 2b | 64 | 154–155 | $C_{11}H_{12}O_4S$ | 55.00 | 5.00 | 13.35 | 54.80 | 5.05 | 13.10 |
| 2c | 51 | 141–142 | $C_{12}H_{14}O_4S$ | 56.69 | 5.51 | 12.60 | 56.83 | 5.42 | 12.58 |
| 2d | 85 | 197–198 | $C_{16}H_{14}O_4S$ | 63.58 | 4.64 | 10.59 | 63.37 | 4.81 | 10.37 |

*Literature (2) mp 186°C.

lent quantity of the appropriate α-haloacid or ester[2] in ethanol containing two equivalents of sodium ethoxide. The solutions were heated under reflux for 1 h under nitrogen, then the solvent was evaporated and the residues were dissolved in aqueous 2 *M* sodium hydroxide solution. This was heated at 100°C (steam bath) for 1 h. After cooling, the mixtures were acidified, and the products collected and recrystallized from a hexane – ethyl acetate 1:1 mixture. Results are summarized in Table 2.

*2-Phenacylthiophenylacetic acid (9)*

2-Mercaptophenylacetic acid (1.68 g, 0.01 mol) was added to a solution of ethanol (50 mL) containing sodium (0.23 g, 0.01 mol). To the solution was added phenacyl bromide (1.99 g, 0.01 mol) and the mixture was let stand 3 h at room temperature. The ethanol was evaporated *in vacuo* and the residue treated with dilute hydrochloric acid. The liberated oily acid was extracted with chloroform which on evaporation gave an oil which was chromatographed (cc) on silica gel using a benzene–chloroform–methanol 9:6:1 mixture as an eluent. After a yellow forerun a band was obtained which on evaporation yielded the desired ketoacid **9** as a pale yellow oil which crystallized on standing under carbon disulfide and was recrystallized from toluene as pale yellow prisms, mp 116°C (73%). The nmr spectrum in $CD_3OD$, δ: 3.81, 4.15 (two $CH_2$ singlets, the methylene protons), 7.10–7.95 (9H bands, the aromatic protons). The mass spectrum, $M^+$, found: 286, M calcd.: 286. *Anal.* calcd. for $C_{16}H_{14}O_3S$: C 67.13, H 4.89, S 11.19%; found: C 67.36, H 5.03, S 10.93%. Further elution of the column gave small quantities of another yellow oil. This was not examined further.

*3-Acetoxy-2H-1-benzothiopyran (6a)*

A mixture of **2***a* (4.52 g, 0.02 mol) and anhydrous sodium acetate (4.5 g) in acetic anhydride (50 mL) was heated under reflux under nitrogen for 15 min. The solvent was removed *in vacuo*, the residue treated with sodium carbonate solution and extracted with ether. The dried ether extract on evaporation gave a yellow oil which was distilled *in vacuo*, bp 118–120°C at

[2]The use of haloacids or haloesters gave comparable results. Use was determined simply by their availability.

Can. J. Chem. Downloaded from www.nrcresearchpress.com by 210.87.254.42 on 09/06/12
For personal use only.

TABLE 3. Preparation of thiochroman-3-ones (**1**) by hydrolysis of enol acetates **6** or **7**

| Compound | Starting material | Yield % | Boiling (melting) point °C | Formula | Analysis Calcd. % C | Calcd. % H | Calcd. % S | Found % C | Found % H | Found % S |
|---|---|---|---|---|---|---|---|---|---|---|
| **1***a** * | **6***a* | 82 | 115–120 0.9 Torr | $C_9H_8OS$ | — | — | — | — | — | — |
| **1***b*‡ | **6***b* | 85 | 110 0.5 Torr | $C_{10}H_{10}OS$ | 67.40 | 5.00 | 17.95 | 67.50 | 5.45 | 17.60 |
| **1***c*§ | **6***c* | 94 | 104–106 0.4 Torr | $C_{11}H_{12}OS$ | 68.75 | 6.25 | 16.67 | 68.83 | 5.98 | 16.63 |
| **1***d*† | **6***d* | 91 | 117–119 | $C_{15}H_{12}OS$ | 75.00 | 5.00 | 13.33 | 75.00 | 5.03 | 13.66 |
| **1***d* | **7***b* | 51 | 117–119 | $C_{15}H_{12}OS$ | 75.00 | 5.00 | 13.33 | 75.00 | 5.03 | 13.66 |

*The ir spectrum 1723 $cm^{-1}$ (C=O str.).
†The ir spectrum 1711 $cm^{-1}$ (C=O str.), no OH absorption.
‡The ir spectrum 1720 $cm^{-1}$ (C=O str.).
§The ir spectrum 1721 $cm^{-1}$ (C=O str.).

0.9 Torr (82%). The ir spectrum (film): 1765 $cm^{-1}$ (C=O str.). The mass spectrum, $M^+$, found: 206, M calcd.: 206. *Anal.* calcd. for $C_{11}H_{10}SO_2$: C 61.11, H 4.63, S 14.81%; found: C 61.18, H 4.52, S 15.05%.

*3-Acetoxy-2-methyl-2*H*-1-benzothiopyran (**6**b)*

The cyclization of **2***b* was performed as above. The compound **6***b* was obtained as a pale yellow oil, bp 120°C at 0.2 Torr (85%). The ir spectrum (film): 1775 $cm^{-1}$ (C=O str.). The mass spectrum, $M^+$, found: 220, M calcd.: 220. This material was not analysed.

*3-Acetoxy-2,2-dimethyl-2*H*-1-benzothiopyran (**6**c)*

The cyclization of **2***c* was performed as above. Examination by tlc showed a mixture of two main products, identified as the enol acetate **6***c* and the ketone **1***c*. This material was not analysed. The yield, estimated as ketone, was 76%.

*3-Acetoxy-2-phenyl-2*H*-1-benzothiopyran (**6**d)*

The cyclization was performed as above except with a reaction time of 1 h. Work-up afforded a yellow oil which was examined by column chromatography using a hexane–ether 7:3 mixture as an eluent. The first major fraction eluted gave on evaporation an oil which slowly partly crystallized and was recrystallized from methanol as pale yelow needles, mp 108–109°C (40%). The ir spectrum (liquid paraffin mull): 1773 $cm^{-1}$ (C=O str.). The mass spectrum, $M^+$, found: 266, M calcd.: 266. *Anal.* calcd. for $C_{17}H_{14}SO$: C 76.69, H 5.26, S 12.03%; found: C 76.81, H 5.34, S 11.99%.

Evaporation of the methanol mother liquors afforded a viscous oil which appears to be a mixture of **6***d* and what is tentatively assigned the 3-acetoxy-2-phenyl-4*H*-1-benzothiopyran structure (**7***b*); yield 28%. This material was not analysed.

Further elution from the chromatogram yielded traces of a highly fluorescent yellow material.

*Cyclization of 2-phenacylthiophenylacetic acid (**9**)*

The acid (0.268, 1 mmol) in acetic anhydride (10 mL) and anhydrous sodium acetate (0.3 g) was refluxed 20 min. The mixture rapidly became dark green. The solution was treated cautiously with water (10 mL) and cooled. An ether extract was washed with water, then with dilute sodium carbonate solution, dried, and evaporated to give a dark green oil. This was examined by thin layer chromatography using a benzene–chloroform–methanol 8:2:1 mixture as an eluent. Two main yellow bands were obtained with an intense blue band between. Repeated chromatography afforded the first band reasonably pure and this crystallized from methanol as pale yellow needles mp 157–159°C. This is assigned the structure **10***a* (31%). The ir spectrum: 1765 $cm^{-1}$ (C=O str.). The mass spectrum, $M^+$, found: 352, M calcd.: 352. *Anal.* calcd. for $C_{20}H_{16}SO_4$: C 68.12, H 4.56, S 9.09%; found: C 68.35, H 4.31, S 8.93%.

The second yellow band could not be purified properly and was obtained as viscous yellow oil, tentatively identified as **10***b*. The blue material was present only in trace amounts.

*Hydrolyses of 3-acetoxybenzothiopyrans to thiachroman-3-ones **1**a–d*

The enol acetates (1 g) in 60% aqueous acetic acid (20 mL) containing hydrochloric acid (0.1 mL) were refluxed for 6 h under nitrogen. The mixture was diluted with water (40 mL) and ether extracted. The extracts were washed with water, saturated sodium carbonate, dried, and evaporated to give the ketones which were either purified by distillation *in vacuo* or recrystallization.

The results are summarized in Table 3.

*Preparation of 3-pyrrolidino-2-*H*-1-benzothiopyran (**11**)*

A mixture of thiochroman-3-one (1 g), pyrrolidine (2 mL), and *p*-toluenesulfonic acid (5 mg) was heated in benzene (40 mL) under nitrogen for 4 h. Water was removed by continuous azeotropic distillation. The solvent was removed and the product crystallized from hexane as pale yellow plates (91%), mp 95–96°C. The mass spectrum, $M^+$, found: 217, M calcd.: 217. *Anal.* calcd. for $C_{13}H_{15}NS$: C 71.90, H 6.90, N 6.45, S 14.75%; found: C 71.60, H 6.81, N 6.40, S 14.55%.

*4-Methylthiochroman-3-one (**1**f)*

The enamine **11** (2.17 g, 0.01 mol) was dissolved in iodomethane (10 mL) and the solution kept at 20°C for 16 h. The solvent was removed, 5% dilute aqueous acetic acid (20 mL) added, and the mixture warmed at 100°C for 1/2 h. After cooling, the mixture was extracted with dichloromethane (3 × 30 mL). The washed and dried extracts on evaporation gave an oil which was purified by distillation *in vacuo*, bp 105–106°C at 0.4 Torr (63%). The ir spectrum (film): 1720 $cm^{-1}$ (C=O str.). The mass spectrum, $M^+$, found: 178, M calcd.: 178. *Anal.* calcd. for $C_{10}H_{10}OS$: C 67.41, H 5.62, S 17.95%; found: C 67.45, H 5.40, S 17.80%.

*4-Benzoylthiochroman-3-one (**1**g)(**12**)*

The enamine **11** (0.434 g, 2 mmol) and benzoyl chloride (0.280 g, 2 mmol) in methylene chloride (20 mL) were refluxed 4 h. The solvent was removed and the crystalline material refluxed 1/2 h with 5% dilute hydrochloric acid (10 mL). The mixture was extracted with hexane and the solution was shaken with saturated aqueous cupric acetate solution. The copper complex was collected, and decomposed in dilute sulfuric acid. Final

Can. J. Chem. Downloaded from www.nrcresearchpress.com by 210.87.254.42 on 09/06/12
For personal use only.

Can. J. Chem. Downloaded from www.nrcresearchpress.com by 210.87.254.42 on 09/06/12
For personal use only.

purification was effected by chromatography in benzene. Pale yellow needles, mp 118–120°C, were obtained on evaporation (63%). The ir spectrum: 1597 $cm^{-1}$ (C=O str., strongly hydrogen bonded), 2650–3300 (OH str., hydrogen bonded). The mass spectrum, $M^+$, found: 268, M calcd.: 268. *Anal.* calcd. for $C_{16}H_{12}O_2S$: C 71.64, H 4.48, S 11.96%; found: C 71.39, H 4.61, S 12.07%.

*Preparation of 3-phenylthiochroman-3-ol (**13**)*

Into a solution of thiochroman-3-one (**1***a*) (1.64 g, 10 mmol) in anhydrous ether (10 mL) was dropped the equivalent quantity of phenyl magnesium bromide in ether (20 mL). An immediate reaction was evident. After 10 min the solution was worked up by dilution with dilute hydrochloric acid and extraction with ether. The dried extracts on evaporation gave a yellow oil which was purified by chromatography using a benzene–methanol 20:1 mixture as an eluent. A virtually colorless oil was obtained (91%). The nmr spectrum δ: 2.60–3.50 (5H bands, the two diastereotopic methylene and the hydroxy protons), 6.86–7.52 (9H bands, the aromatic protons). The mass spectrum, $M^+$, found: 242, M calcd.: 242. *Anal.* calcd. for $C_{15}H_{14}OS$: C 74.38, H 5.78, S 13.22%; found: C 74.41, H 5.69, S 12.93%.

*Preparation of 2-phenyl-2*H*-1-benzothiopyran (**14**)*

A solution of **13** (0.242 g, 1 mmol) in toluene (10 mL) with *p*-toluenesulfonic acid (10 mg) was refluxed 1 h. Evaporation gave a pale brown oil which was purified by chromatography on silica gel with benzene as an eluent and distillation *in vacuo* (81%). The mass spectrum, $M^+$, found: 224, M calcd.: 224. *Anal.* calcd. for $C_{15}H_{12}S$: C 80.35, H 5.36, S 14.29%; found: C 80.62, H 5.42, S 13.95%.

*3-Phenyl-2*H*-1-benzothiopyran-*S,S*-dioxide (**16**a)*

This was made from **14** by oxidation with two equivalents of *m*-chloroperoxybenzoic acid in acetone. After 5 min the acetone solution was diluted with water and extracted with chloroform. The extract was washed with dilute sodium hydroxide solution, dried, and evaporated to give a colorless oil which was purified by chromatography (tlc) using benzene as an eluent (86%). The mass spectrum, $M^+$, found: 256, M calcd.: 256.

*3-Phenylthiopyrylium perchlorate (**17**)*

The thiopyran **14** was treated with one equivalent of *m*-chloroperoxybenzoic acid in acetone and worked up as above. The pale oil resulting was dissolved in acetic acid, warmed briefly, and to it added perchloric acid. The yellow solution on dilution with ether gave **20** as pale yellow prisms, mp 151°C (lit. (12) mp 151°C) (20%).

*2-Phenyl-2*H*-1-benzothiopyrano[3,4-*b*]indole (**18**b)*

2-Phenylthiochroman-3-one (240 mg, 1 mmol) was treated with a slight excess of phenylhydrazine hydrochloride and sodium acetate in ethanol. After refluxing 15 min the cooled mixture was poured into water. The yellow precipitate was collected and washed with water. A small sample crystallized from ethanol afforded yellow microcrystals, mp 124–127°C. This material was dissolved in acetic acid (10 mL), saturated with hydrogen chloride, and refluxed 45 min. The mixture was poured into water and extracted with ethyl acetate (3 × 30 mL). The washed and dried extracts on evaporation gave a dark red oil which was chromatographed (cc) using a hexane–ether 1:1 mixture as an eluent. The product was obtained as pale yellow microcrystals, mp 146–147°C from hexane (56%). These turned red on standing in air. The mass spectrum, $M^+$, found: 313, M calcd.: 313. *Anal.* calcd. for $C_{21}H_{15}NS$: C 80.51, H 4.79, N 4.47, S 10.22%; found: C 80.32, H 4.03, N 4.51, S 10.25%.

*2-Phenyldihydrobenzothiopyrano[4,3-*b*]indole (**20**)*

This was prepared as **2** above, starting from 2-phenylthiochroman-4-one (14). Yellow needles, mp 182–184°C, were obtained on recrystallization from methanol (81%). The mass spectrum, $M^+$, found: 313, 312; M calcd.: 313. *Anal.* calcd. for $C_{21}H_{15}NS$: C 80.51, H 4.79, N 4.47, S 10.22%; found: C 80.63, H 5.01, N 4.48, S 10.39%.

*2-Phenylbenzothiopyrano[4,3-*b*]indole (**21**)*

A mixture of the dehydro compound **23**, (0.313 g, 1 mmol) and chloranil (0.3 g) in ethyl acetate (20 mL) was heated under reflux 1 h. The solvent was removed *in vacuo* and the residue chromatographed (tlc) on silica gel using an ethyl acetate – hexane 2:1 mixture as an eluent. The product was obtained as orange needles, mp 210–212°C from ethyl acetate (92%). The mass spectrum, $M^+$, found: 311, M calcd.: 311. *Anal.* calcd. for $C_{21}H_{13}NS$: C 81.03, H 4.18, N 4.50, S 10.29%; found: C 81.11, H 4.21, N 4.36, S 10.03%.

## Acknowledgements

Grateful thanks are due to the Natural Sciences and Engineering Research Council of Canada for financial support of this work. We also wish to thank Mr. W. Buchannon and Mr. K. Marat for preparation of mass spectra and $^{13}C$ nmr spectra respectively.

1. S. W. Schneller. Adv. Heterocycl. Chem. **18**, 59 (1975).
2. J. Mispelter, A. Croisy, P. Jacquignon, A. Ricci, C. Rossi, and F. Schiafella. Tetrahedron, **33**, 2383 (1977).
3. W. C. Lumma and G. A. Berchtold. J. Org. Chem. **34**, 1566 (1969).
4. (*a*) C. Marschalk. J. Prakt. Chem. **88**, 237 (1913); (*b*) Z. Pascal and D. S. Tarbell. J. Am. Chem. Soc. **79**, 6015 (1957).
5. D. Papa, E. Schwenk, and H. F. Ginsberg. J. Org. Chem. **14**, 723 (1949).
6. R. H. Glauert and F. G. Mann. J. Chem. Soc. 2127 (1952).
7. G. F. Katekar and R. M. Thomson. Aust. J. Chem. **25**, 647 (1972).
8. A. G. Hortmann, R. B. Harris, and J. A. Miles. J. Am. Chem. Soc. **96**, 6119 (1974).
9. E. Block. *In* Reactions of organosulfur compounds. Academic Press, New York. 1978. Table B-4. p. 297.
10. I. Degani, R. Fochi, and G. Spunta. Ann. Chim. Rome, **61**, 793 (1971).
11. A. H. A. Tinnemans and W. H. Laarhóvern. J. Chem. Soc. Perkin Trans. II, 1115 (1976).
12. T. E. Young and P. H. Scott. J. Org. Chem. **30**, 3613 (1965).
13. N. P. Buu-Hoi, A. Martani, A. Croisy, P. Jacquignon, and F. Perin. J. Chem. Soc. C, 1787 (1966).
14. F. Arndt. Ber. **56**, 1269 (1923).

# Influence complexe d'additifs hydrogénés sur le craquage de substances organiques et analogie hydraulique pour la propagation des chaînes. I. Cas d'une pyrolyse à une seule stoechiométrie

GÉRARD SCACCHI, FRANÇOIS BARONNET ET MICHEL NICLAUSE

*I.N.P.L. et Université de Nancy I, Département de Chimie Physique des Réactions (E.R.A. no 136 C.N.R.S.), 1, rue Grandville, 54042 Nancy Cedex, France*

Reçu le 13 mai 1981

GÉRARD SCACCHI, FRANÇOIS BARONNET et MICHEL NICLAUSE. Can. J. Chem. **60**, 249 (1982).

Dans ce premier mémoire (I), on considère la pyrolyse homogène (à très faible avancement) d'une substance organique μH impliquant *une seule* stoechiométrie principale (μH = m + βH) et relevant d'un mécanisme où les chaînes sont propagées par des radicaux libres (β· et μ·) selon les processus:

$$[2] \quad \mu\cdot \xrightarrow{k_2} m + \beta\cdot$$
$$[3] \quad \beta\cdot + \mu H \xrightarrow{k_3} \beta H + \mu\cdot$$

Le mécanisme "μH, YH" de Niclause et coll. interprète de nombreux effets d'accélération ou d'inhibition, par des additifs hydrogénés YH, de la pyrolyse de telles substances organiques μH.

Pour représenter la *propagation* des chaînes dans ces réactions, on propose une *analogie hydraulique* originale. Elle permet tout d'abord de mieux saisir la notion d'étape limitant la vitesse de propagation dans la décomposition de μH *pur*, à savoir le processus bimoléculaire [3] dans le cas limite [A]: $k_3\,(\mu H)_0 \ll k_2$ ou le processus unimoléculaire [2] dans le cas limite [B]: $k_2 \ll k_3\,(\mu H)_0$.

Cette analogie hydraulique permet aussi de mieux comprendre pourquoi une pyrolyse relevant du cas limite [A] (*néopentane* par ex.) peut être *accélérée* par *certains* additifs hydrogénés (HCl, HBr, $H_2S$), tandis qu'une décomposition thermique relevant du cas limite [B] (*éthane* par ex.) *ne* peut être accélérée, selon ce mécanisme, par *aucun* additif hydrogéné.

Dans un second mémoire (II), on étendra les considérations précédentes au cas d'une substance organique μH se décomposant selon *plusieurs* stoechiométries primaires principales.

---

GÉRARD SCACCHI, FRANÇOIS BARONNET, and MICHEL NICLAUSE. Can. J. Chem. **60**, 249 (1982).

This first article (I) considers the homogeneous pyrolysis at very low conversion of an organic substance, μH, involving a *single* principal stoichiometry (μH = m + βH) and proceeding by a mechanism in which the chains are propagated by free radicals (β· and μ·) according to the steps:

$$[2] \quad \mu\cdot \xrightarrow{k_2} m + \beta\cdot$$
$$[3] \quad \beta\cdot + \mu H \xrightarrow{k_3} \beta H + \mu\cdot$$

The mechanism "μH, YH" of Niclause and co-workers interprets numerous effects of acceleration, or of inhibition, by hydrogenated additives YH, in the pyrolysis of such organic substances μH.

A novel *hydraulic analogy* is proposed to describe the *propagation* of chains in these reactions. This analogy immediately permits a better comprehension of the concept of a step which limits the rate of propagation in the decomposition of *pure* μH, namely the bimolecular process [3] in the limiting case [A] where $k_3[\mu H]_0 \ll k_2$, or the unimolecular process [2] in the limiting case [B] where $k_2 \ll k_3\,[\mu H]_0$. The analogy also leads to a better understanding of why a pyrolysis which follows the limiting case [A] (e.g. neopentane) may be *accelerated* by *certain* hydrogenated additives (HCl, HBr, $H_2S$), while a thermal decomposition following the limiting case [B] (e.g. *ethane*) *cannot* be accelerated by *any* hydrogenated additive according to this mechanism.

In a second article (II), the preceding considerations will be extended to the case of an organic substance μH whose decomposition involves *several* principal primary stoichiometries.

[Journal translation]

## Introduction

Niclause *et al.* (1) ont proposé et étudié théoriquement un mécanisme "μH, YH", qui conduit à attribuer à divers additifs hydrogénés YH, à la fois (dans le cas général) une influence *accélératrice* et une influence *inhibitrice* sur la pyrolyse radicalaire en chaînes d'une substance organique μH impliquant *une seule* stoechiométrie primaire principale: $\mu H = m + \beta H$. Le résultat *global* de ces deux effets cinétiques *opposés* dépend de divers paramètres qui ont été précisés.

De nombreux faits expérimentaux prévus par ce mécanisme ont été vérifiés expérimentalement: (*a*) la pyrolyse du *néopentane* est *accélérée* par $H_2S$ (2), HBr (3) et HCl (3, 4); (*b*) au contraire, $H_2S$ (5, 6) et HBr (3) *inhibent* la décomposition thermique de l'*éthane* et HCl (3) n'a pratiquement pas d'influence cinétique sur cette réaction; et (*c*) le pro-

0008-4042/82/030249-08$01.00/0

©1982 National Research Council of Canada/Conseil national de recherches du Canada

Can. J. Chem. Downloaded from www.nrcresearchpress.com by 210.87.254.40 on 09/06/12
For personal use only.

pène, l'isobutène et les butènes-2 *inhibent* la pyrolyse du *néopentane* (7–9), celle de l'*acétaldéhyde* (10) et celle de l'*éthane* (11, 12).

Ces effets accélérateurs ou inhibiteurs ont pu être interprétés quantitativement par des lois cinétiques calculées à partir du mécanisme "μH, YH".

Mais, pour faciliter l'interprétation synthétique de ces effets et mieux comprendre qualitativement leur signification physique en termes de processus élémentaires, nous proposons et nous utilisons, dans ce qui suit, une *analogie hydraulique* pour représenter la *propagation* des chaînes dans la pyrolyse de μH, pur ou en présence d'un corps hydrogéné YH.

## 1. Pyrolyse d'une substance organique (μH) pure

### *1.1. Mécanisme "βμ"*

Considérons une réaction homogène de pyrolyse radicalaire en chaînes d'une substance organique pure, donnant naissance à deux produits primaires principaux, telle que la décomposition thermique du néopentane ou celle de l'éthane:

$$\text{néo-}C_5H_{12} = \text{i-}C_4H_8 + CH_4$$
$$C_2H_6 = C_2H_4 + H_2$$

*A très faible avancement*, le mécanisme d'une telle réaction peut souvent être schématisé de la manière suivante, en adoptant le symbolisme "βμ" usuel en cinétique chimique (13):

[1] amorçage: $\mu H \xrightarrow{k_1}$ 2 radicaux libres

suivi, éventuellement, de processus de transfert

[2] propagation: $\mu\cdot \xrightarrow{k_2} m + \beta\cdot$

[3] propagation: $\beta\cdot + \mu H \xrightarrow{k_3} \beta H + \mu\cdot$

[ββ] terminaison: $\beta\cdot + \beta\cdot \xrightarrow{k_{\beta\beta}}$ produits

[βμ] terminaison: ou $\beta\cdot + \mu\cdot \xrightarrow{k_{\beta\mu}}$ produits

[μμ] terminaison: ou $\mu\cdot + \mu\cdot \xrightarrow{k_{\mu\mu}}$ produits

μH représente la substance organique soumise à pyrolyse, μ· désigne le radical libre porteur de chaînes qui se décompose de façon *mono*moléculaire (ou unimoléculaire) par rupture d'une liaison C—C ou C—H (processus de propagation [2]) et β· désigne le radical (ou atome) libre porteur de chaînes qui réagit *bi*moléculairement avec une molécule μH en lui arrachant un atome H et en régénérant le radical libre μ· (processus de propagation [3]); enfin, m et βH représentent les produits primaires principaux de la réaction, dont l'équation stoechiométrique s'écrit schématiquement:

$$\mu H = m + \beta H$$

Si l'on suppose que la réaction est en chaînes longues, les vitesses initiales de consommation de μH et de formation de m et βH sont pratiquement égales (soit $V_0$ cette vitesse initiale commune) et l'on a: $k_2\,(\mu\cdot) \simeq k_3\,(\beta\cdot)\,(\mu H)_0$; d'où:

$$\frac{(\mu\cdot)}{(\beta\cdot)} \simeq \frac{k_3(\mu H)_0}{k_2}$$

$$= \frac{\text{réactivité de } \beta\cdot \text{ dans le processus [3]}}{\text{réactivité du } \mu\cdot \text{ dans le processus [2]}}$$

Alors, les valeurs relatives de $k_3\,(\mu H)_0$ et de $k_2$ gouvernent les concentrations relatives des porteurs de chaînes μ· et β· et, par suite, les importances relatives des trois processus possibles [ββ], [βμ] et [μμ] de terminaison des chaînes, du moins si les constantes de vitesse $k_{\beta\beta}$, $k_{\beta\mu}$ et $k_{\mu\mu}$ de ces trois processus sont du même ordre de grandeur, ce que nous supposerons ici.

Deux cas limites sont possibles selon les valeurs relatives de $k_3\,(\mu H)_0$ et de $k_2$.

*Cas limite [A]:* $k_3\,(\mu H)_0 \ll k_2$

Le processus radicalaire [3] est plus difficile que le processus radicalaire [2] et, par suite, règle la vitesse de propagation des chaînes; ón a: $[\mu\cdot] \ll [\beta\cdot]$ et le processus prépondérant de terminaison est du type [ββ].

La pyrolyse, vers 500°C, du *néopentane* (2,2-diméthylpropane) en isobutène et méthane (14–17) relève de ce premier cas limite, avec μH ≡ néo-$C_5H_{12}$, m ≡ i-$C_4H_8$ et βH ≡ $CH_4$; néo-$C_5H_{11}\cdot$ joue le rôle de radical μ· et $CH_3\cdot$ celui de radical β·; le processus [2] consiste en la décomposition unimoléculaire du radical libre néo-$C_5H_{11}\cdot$ par rupture d'une liaison C—C et est plus facile que le processus [3].

Can. J. Chem. Downloaded from www.nrcresearchpress.com by 210.87.254.40 on 09/06/12
For personal use only.

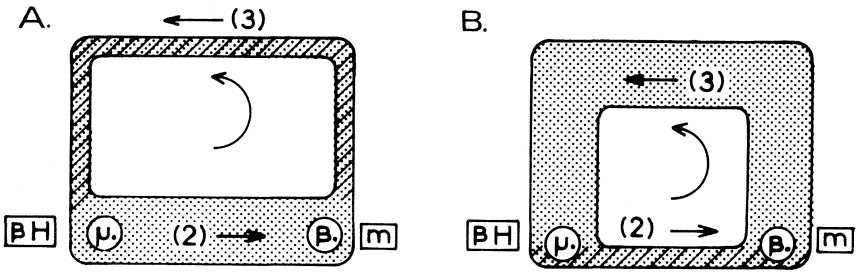


FIG. 1. Analogie hydraulique pour la propagation des chaînes dans la pyrolyse d'une substance organique μH pure.

La pyrolyse de l'*acétaldéhyde* relève également de ce premier cas limite (18).

*Cas limite [B]:* $k_2 \ll k_3 (\mu H)_0$

Le processus radicalaire [2] est plus difficile que le processus radicalaire [3] et, par suite, règle la vitesse de propagation des chaînes; on a: (β·) ≪ (μ·) et le processus prépondérant de terminaison est du type [μμ].

La pyrolyse homogène, vers 540°C, de l'*éthane* en éthylène et hydrogène (19–23) relève de ce second cas limite, avec μH ≡ $C_2H_6$, m ≡ $C_2H_4$ et βH ≡ $H_2$; $C_2H_5$· joue le rôle de radical μ· et H· celui de radical β·; le processus [2] correspond à la décomposition unimoléculaire du radical libre $C_2H_5$· par rupture d'une liaison C—H et est plus difficile que le processus [3].

### *1.2. Analogie hydraulique pour la propagation des chaînes*

Une analogie hydraulique permet de bien distinguer les deux cas limites précédents. On admet que chaque processus de *propagation* des chaînes est représenté par une *conduite*, dont le diamètre est d'autant *plus petit* que le processus est *plus difficile*. Ainsi, le diamètre de la conduite (2) sera d'autant plus petit que la constante de vitesse $k_2$ du processus unimoléculaire [2] sera plus faible; de la même façon, le diamètre de la conduite (3) sera d'autant plus petit que le produit $k_3$ $(\mu H)_0$ de la constante de vitesse $k_3$ du processus bimoléculaire [3] par la concentration initiale du réactif sera plus faible. On fait circuler un "*fluide*" dans les conduites (par exemple au moyen d'une pompe); la *vitesse* d'un processus correspond au "*débit*" du "fluide" dans la conduite correspondante et les concentrations radicalaires peuvent être assimilées à des "pressions".

Dans le *cas limite [A]*: $k_3$ $(\mu H)_0 \ll k_2$ (illustré par l'exemple du *néopentane*), c'est le processus [3] (plus difficile que le processus [2]) qui limite la vitesse de propagation. Le processus [3] sera donc représenté par une conduite (3) de plus petit diamètre que la conduite (2) correspondant au processus [2] (fig. 1A). Les deux conduites formant une boucle, le débit est le même dans (2) et (3): c'est l'équivalent de $v_2 = v_3$. Mais on voit bien que le débit global est, en fait, limité par le petit diamètre de la conduite (3), qui, dans la boucle, a une perte de charge très supérieure à celle de (2) et constitue, par suite, un "goulot d'étranglement" (la conduite (2) pourrait admettre un débit plus grand si la conduite (3) le lui fournissait); de même, la vitesse de propagation est limitée par la difficulté du processus [3] à transformer des radicaux β· en radicaux μ·, c'est-à-dire à fournir des μ· au processus [2] (qui, lui, les transforme facilement en β·). Pour assurer l'égalité des "débits" (c'est-à-dire des vitesses), la "pression" (c'est-à-dire la concentration) des espèces β· doit être très supérieure à celle des espèces μ·, en accord avec l'inégalité définissant le cas limite [A].

Au contraire, dans le *cas limite [B]*: $k_2 \ll k_3$ $(\mu H)_0$ (illustré par l'exemple de l'*éthane*), c'est le processus [2] qui est l'étape limitant la vitesse de propagation. Dans l'analogie hydraulique, le débit est encore le même dans les conduites (2) et (3), ce qui est l'équivalent de $v_2 = v_3$. Mais, cette fois, la perte de charge de la conduite (2) est très supérieure à celle de la conduite (3) et c'est donc maintenant la conduite (2) qui, dans la boucle, constitue le "goulot d'étranglement" (fig. 1B). La "pression" (concentration) des espèces μ· doit alors être très supérieure à celle des espèces β·, en accord avec l'inégalité définissant le cas limite [B].

## 2. Pyrolyse d'une substance organique (μH) en présence d'un corps hydrogéné (YH)

### *2.1. Mécanisme "μH, YH"*

Pour décrire, à très faible avancement, la pyrolyse d'une substance organique μH en présence d'un corps hydrogéné YH comportant aussi un atome (au moins) d'hydrogène "mobile", Niclause *et al.* (1) ont proposé et analysé un mécanisme symbolique "μH, YH":[1]

[1]Ce mécanisme suppose que l'additif YH n'augmente pas la vitesse d'amorçage des chaînes et que le radical (ou atome) libre Y· est thermiquement stable (ce qui est automatiquement le cas lorsque Y· est un atome libre).

Can. J. Chem. Downloaded from www.nrcresearchpress.com by 210.87.254.40 on 09/06/12
For personal use only.

[1] amorçage: $\mu H \xrightarrow{k_1}$ 2 radicaux libres

suivi, éventuellement, de processus de transfert

[2] propagation I $\mu\cdot \xrightarrow{k_2} m + \beta\cdot$

[3] $\beta\cdot + \mu H \xrightarrow{k_3} \beta H + \mu\cdot$

[2] $\mu\cdot \xrightarrow{k_2} m + \beta\cdot$

[4] propagation II $\beta\cdot + YH \xrightarrow{k_4} \beta H + Y\cdot$

[5], [−5] $Y\cdot + \mu H \underset{k_{-5}}{\overset{k_5}{\rightleftharpoons}} YH + \mu\cdot$

terminaison: processus [ββ], [βμ], [μμ], [βY], [μY] et [YY] de combinaison ou de dismutation des radicaux libres β·, μ· et Y·.

Ce mécanisme suppose essentiellement que les radicaux libres β· et μ· (qui sont porteurs de chaînes dans la décomposition de μH pur) peuvent réagir aussi avec l'additif YH en donnant naissance au nouveau radical (ou atome) libre Y· (processus [4] et [−5], Y· pouvant, à son tour, réagir avec μH (processus [5]) en régénérant YH.

En l'absence de YH, les radicaux libres β· et μ· ne peuvent propager que la décomposition en chaînes de μH selon I. Le mécanisme proposé suppose qu'*en présence de l'additif* YH, il se *propage* également *un autre type* II de décomposition en chaînes de μH, faisant participer le nouveau radical (ou atome) libre Y·, mais conduisant à la *même* stoechiométrie que I: μH = m + βH.

Enfin, ce mécanisme implique que YH tend à faire apparaître de *nouveaux* processus de *terminaison* des chaînes.

On note que, dans ce schéma réactionnel, il n'y a pas de consommation de YH dans la propagation des chaînes; une légère consommation de YH peut seulement provenir de certains processus nouveaux de terminaison.

### 2.2. *Analogie hydraulique pour la propagation des chaînes*

En présence de YH, la chaîne cinétique de la réaction globale de décomposition de μH est complexe: elle comporte un certain nombre de "maillons" représentatifs de chacun des deux types I et II de propagation. Le mode II fait intervenir les nouveaux processus [4] et ([5], [−5]) et a le processus [2] *en commun* avec le mode I de propagation. Pour traduire ceci en analogie hydraulique, il suffit d'ajouter, *en parallèle* avec la conduite (3), une nouvelle conduite constituée des éléments (4) et ((5), (−5)). Les deux schémas hydrauliques de la figure 1 se transforment alors en les schémas présentés sur la figure 2.[2] La différence essentielle entre les deux cas limites [A] et [B], en présence de l'additif YH, apparaît sur ces schémas.

Dans le *cas limite [A]*: $k_3 (\mu H)_0 \ll k_2$(*néopentane* par ex.), le nouvel assemblage de tuyaux (4) et ((5), (−5)), ajouté *en parallèle* avec la conduite (3), augmente le débit global du fluide, puisque, dans ce premier cas limite, c'était la conduite (3) qui limitait le débit global. En d'autres termes, l'additif YH a, *au niveau des propagations*, un effet *accélérateur* sur la pyrolyse de μH; il *catalyse*, par transfert d'hydrogène, la propagation de la décomposition en chaînes de μH.

Au contraire, dans le *cas limite [B]*: $k_2 \ll k_3 (\mu H)_0$ (*éthane* par ex.), le nouvel assemblage ajouté ne change pas le débit global du fluide, puisque celui-ci doit emprunter, dans les deux circuits I et II, la conduite commune (2) de faible diamètre, qui était et qui demeure le "goulot d'étranglement" dans ce second cas limite. C'est dire que, cette fois, l'additif YH *ne* peut *pas* avoir d'effet accélérateur, au niveau des propagations, sur la pyrolyse de μH (1).

### 2.3. *Influence cinétique globale de YH sur la pyrolyse de μH*

L'analogie hydraulique vient de nous montrer que, d'après le mécanisme "μH, YH", l'additif YH a, *au niveau des propagations*, un effet *accélérateur* sur la pyrolyse de μH *dans le cas limite [A]* et non dans le cas limite [B].

Mais, *dans les deux cas*, l'additif YH a aussi un

[2]Sur la figure 2, les sections des éléments (4), (5) et (−5) ont été représentées arbitrairement, cet ensemble pouvant avoir un diamètre de passage résultant très différent du diamètre de la conduite (3).

Can. J. Chem. Downloaded from www.nrcresearchpress.com by 210.87.254.40 on 09/06/12
For personal use only.

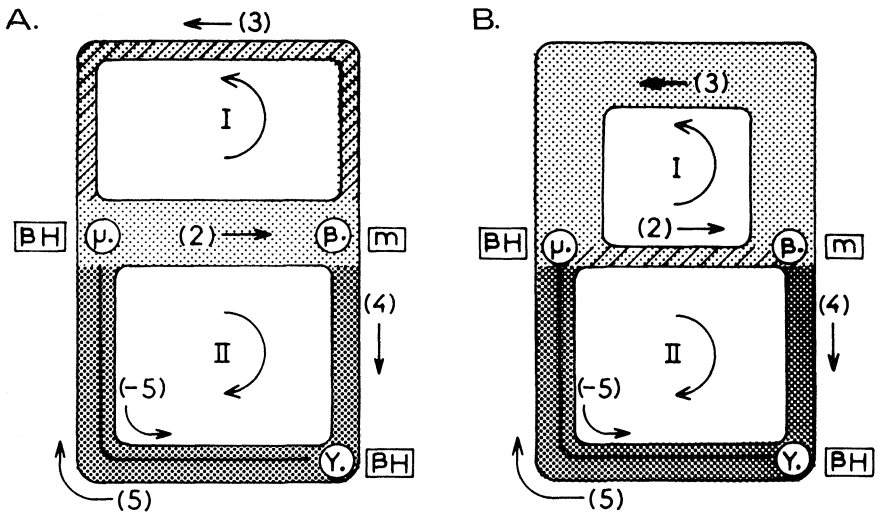


FIG. 2. Analogie hydraulique pour la propagation des chaînes dans la pyrolyse d'une substance organique μH en présence d'un corps hydrogéné YH.

effet *inhibiteur*, du fait que YH fait apparaître de nouveaux processus de *terminaison* des chaînes.

Ces prévisions qualitatives sont confirmées par le calcul, à partir du mécanisme "μH, YH", du rapport $(V_0)_{YH}/V_0$ des vitesses initiales de pyrolyse de μH en présence ou en l'absence de YH (à même concentration initiale de μH et à même température) (1, 24).

Considérons, à nouveau, les deux cas limites [A] et [B].

*Cas limite [A]:* $k_3\,(\mu H)_0 \ll k_2$ (*néopentane* par ex.)

Comme nous venons de le voir, l'additif YH exerce *simultanément deux influences cinétiques opposées* sur la pyrolyse de μH. Le résultat *global* de ces deux effets est une *accélération*, par YH, de la pyrolyse de $\mu$H si l'expression de $(V_0{}^A)_{YH}/V_0{}^A$ est supérieure à 1, une *inhibition* dans le cas contraire.

(*a*) A partir du mécanisme "μH, YH", on peut montrer (1) que si l'on a:

$$k_5 > k_3 \quad [a],$$

c'est-à-dire si le radical (ou atome) libre Y· est *plus réactif* que le radical (ou atome) libre β· vis-à-vis de $\mu$H, l'additif YH doit exercer, *globalement*, une influence *accélératrice* sur la pyrolyse de μH (l'effet accélérateur au niveau des propagations l'emporte sur l'effet inhibiteur dû aux terminaisons nouvelles).

(*b*) Si l'on a, au contraire:

$$k_5 < k_3 \quad [b],$$

c'est-à-dire si Y· est *moins réactif* que β· pour arracher un atome H de μH, l'additif YH doit, *globalement*, *inhiber* la pyrolyse de μH.

On prévoit donc qu'une décomposition relevant du *premier* cas limite [A], telle que la pyrolyse du *néopentane*, doit pouvoir être *accélérée* par certains additifs hydrogénés YH et, au contraire, *inhibée* par d'autres.

(*a*) L'expérience montre effectivement (fig. 3) que la pyrolyse du *néopentane* est *accélérée* par *HCl*, par *HBr* et par $H_2S$ (2–4). Ces effets accélérateurs indiquent donc que les radicaux (ou atomes) libres Cl·, Br· et HS· (Y·) sont *plus* réactifs que le radical libre $CH_3$· (β·) pour arracher un atome H à une molécule de néopentane ($k_5 > k_3$), en accord avec d'autres travaux indépendants.

Dans le cas de *HCl* par exemple, le rapport des vitesses initiales de pyrolyse du néopentane en présence ou en l'absence de HCl peut se mettre sous la forme (3):[3]

$$\frac{(V_0{}^A)_{HCl}}{V_0{}^A} \simeq \frac{1+ax}{1+bx} > 1,$$

avec

$$x = \frac{[HCl]_0}{[\text{néo-}C_5H_{12}]_0} \quad \text{et} \quad a = \frac{k_4{}^{HCl}}{k_3} > b$$

Le terme $1 + ax$ du numérateur traduit l'effet accélérateur de HCl par suite de l'apparition du nouveau type II de propagation; il est *supérieur* au terme $1 + bx$ du dénominateur, qui traduit l'effet inhibiteur de HCl dû aux nouveaux processus de terminaison.

[3] *b* est un paramètre dépendant de constantes de vitesse de processus élémentaires et de la concentration initiale de néopentane (cf. ref. 3).

Can. J. Chem. Downloaded from www.nrcresearchpress.com by 210.87.254.40 on 09/06/12
For personal use only.

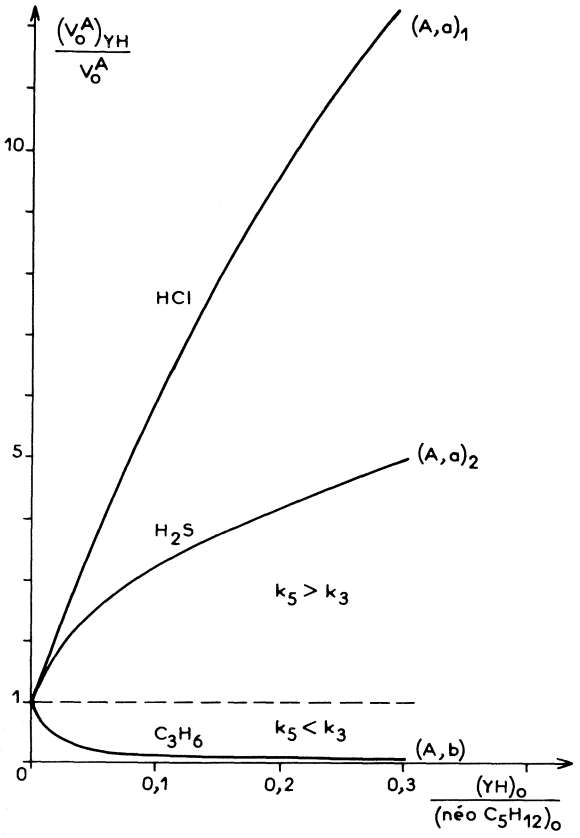


FIG. 3. Cas limite [A]: $k_3$ $(\mu H)_0 \ll k_2$. Accélération ($k_5 > k_3$) ou inhibition ($k_5 < k_3$) par YH de la pyrolyse du néopentane (μH).

| Courbe | YH | $T$ (°C) | $P_0$ (néo-$C_5H_{12}$) (Torr) | Réf. |
|---|---|---|---|---|
| (A, a)$_1$ | HCl | 480 | 100 | 3 |
| (A, a)$_2$ | $H_2S$ | 512 | 50 | 2 |
| (A, b) | $C_3H_6$ | 495 | 100 | 7 |

Rappelons que, dans la pyrolyse du néopentane pur, le processus prépondérant de terminaison des chaînes est:

[ββ] $2CH_3\cdot \rightarrow C_2H_6$

Dans la pyrolyse du néopentane *accélérée* par HCl, il apparaît les nouveaux processus de terminaison (3):

[βμ] $CH_3\cdot$ + néo-$C_5H_{11}\cdot \rightarrow CH_3—CH_2—C(CH_3)_3$

[μμ] 2 néo-$C_5H_{11}\cdot \rightarrow (CH_3)_3C—CH_2—CH_2—C(CH_3)_3$

(*b*) Par ailleurs, il a été observé (fig. 3) que la pyrolyse du *néopentane* est, au contraire, *inhibée* par le *propène* (7), par les *butènes-2* (9) et par l'*isobutène* (8). Ces effets inhibiteurs sont dus au fait que le radical libre $CH_3\cdot$ réagit avec un alcène YH (processus [4]) en donnant un radical libre allylique (Y·), qui est stabilisé par résonance et, par suite, *moins* réactif que le radical libre $CH_3\cdot$ (β·) vis-à-vis du néopentane ($k_5 < k_3$).

Le rapport des vitesses initiales de pyrolyse du néopentane en présence ou en l'absence d'alcène peut s'écrire (7, 8):[4]

$$\frac{(V_0^A)_{YH}}{V_0^A} \simeq \frac{1 + a'x}{1 + b'x} < 1,$$

avec

$$x = \frac{(YH)_0}{(néo\text{-}C_5H_{12})_0} \quad \text{et} \quad a' = \frac{k_4^{YH}}{k_3} < b'$$

Ici, le terme $1 + a'x$ du numérateur est *inférieur* au terme $1 + b'x$ du dénominateur.

(Note: Dans la pyrolyse du néopentane *inhibée* par un alcène (YH), la terminaison des chaînes implique les processus [ββ], [βY] et [YY] (7, 8).)

On peut expliquer, de façon analogue, l'allure fortement auto-inhibée (par l'isobutène formé) de la pyrolyse du néopentane (8), ainsi que l'influence inhibitrice du propène, des butènes-2 et de l'isobutène sur la décomposition thermique de l'acétaldéhyde (10).

*Cas limite [B]:* $k_2 \ll k_3$ $(\mu H)_0$ (*éthane* par ex.)

Nous avons vu que, dans ce second cas limite, l'apparition du nouveau type II de propagation ne conduit pas à un effet accélérateur de YH sur la pyrolyse de μH. L'additif YH a une influence *purement inhibitrice* (due à l'apparition de nouveaux processus de terminaison).

On prévoit donc qu'on *ne* peut *pas* accélérer, par ce mécanisme, une décomposition relevant du *second* cas limite [B], telle que la pyrolyse de l'*éthane*.

L'expérience montre effectivement (fig. 4) que *HCl*, *HBr* et $H_2S$ (qui accélèrent la décomposition du néopentane) *n'*accélèrent *pas* la pyrolyse de l'*éthane*: cette réaction est *inhibée* par *HBr* (3) et par $H_2S$ (5, 6).

Dans le cas de *HBr* par exemple, le rapport des vitesses initiales peut se mettre sous la forme (3):[4]

$$\frac{(V_0^B)_{HBr}}{V_0^B} \simeq \frac{1}{(1 + b''x)^{1/2}} < 1, \text{ avec } x = \frac{(HBr)_0}{(C_2H_6)_0}$$

La valeur 1 du numérateur indique l'absence d'effet accélérateur au niveau des propagations dans le cas limite [B]; le terme $(1 + b''x)^{1/2}$ du dénominateur traduit l'effet inhibiteur au stade de la terminaison des chaînes.

Rappelons que, dans la pyrolyse de l'éthane pur,

[4] $b'$ et $b''$ sont des paramètres dépendant de constantes de vitesse de processus élémentaires et de la concentration initiale de néopentane (cf. refs. 7 et 8 pour $b'$, ref. 3 pour $b''$).

Can. J. Chem. Downloaded from www.nrcresearchpress.com by 210.87.254.40 on 09/06/12
For personal use only.

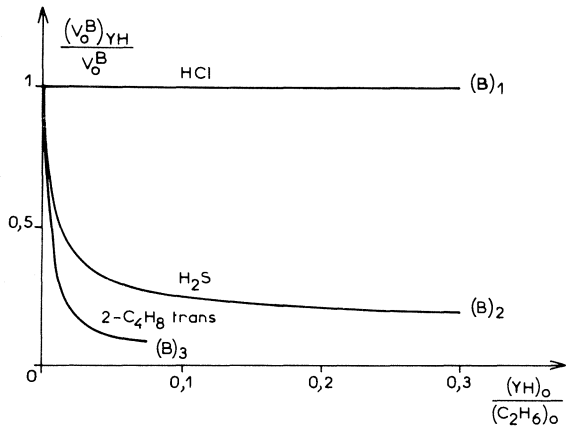


FIG. 4. Cas limite [B]: $k_2 \ll k_3$ $(\mu H)_0$. Inhibition par YH de la pyrolyse de l'éthane (μH).

| Courbe | YH | $T$ (°C) | $P_0$ ($C_2H_6$) (Torr) | Réf. |
|---|---|---|---|---|
| $(B)_1$ | HCl | 540 | 50 | 3 |
| $(B)_2$ | $H_2S$ | 540 | 50 | 5 |
| $(B)_3$ | 2-$C_4H_8$ *trans* | 520 | 100 | 12 |

le processus prépondérant de terminaison est:

$$[\mu\mu] \quad 2C_2H_5\cdot \longrightarrow \begin{matrix} C_2H_4 + C_2H_6 \\ n\text{-}C_4H_{10} \end{matrix}$$

Dans la pyrolyse de l'éthane *inhibée* par HBr, il apparaît essentiellement le nouveau processus de terminaison (3):

$$[\mu Y] \quad C_2H_5\cdot + Br\cdot \rightarrow C_2H_4 + HBr \text{ (ou } C_2H_5Br)$$

Quant à *HCl*, son influence *inhibitrice* sur la pyrolyse de l'*éthane* est *négligeable* (3) devant celle de HBr ou de $H_2S$ (fig. 4), parce que, dans le cas de HCl, le paramètre $b''$ est beaucoup plus petit.

L'expérience montre aussi (fig. 4) que la pyrolyse de l'*éthane* (comme celle du néopentane cette fois) est *inhibée* par divers *alcènes*, tels que le propène (11), les butènes-2 (12) et l'isobutène (11), par suite de l'apparition de nouveaux processus de terminaison importants.

(Note: Dans la pyrolyse de l'éthane *inhibée* par un alcène (YH), la terminaison des chaînes implique les processus $[\mu\mu]$, $[\mu Y]$ et [YY] (11).)

### 2.4. *Remarque*

L'étude théorique de l'influence cinétique globale de YH serait très complexe dans le cas général. Elle est plus simple dans les deux cas limites [A] et [B] examinés ci-dessus.

Mais, pour des raisons de continuité, on s'attend à ce que, dans le *cas intermédiaire* où $k_2$ ne serait ni très grand, ni très petit devant $k_3$ $(\mu H)_0$, l'additif YH exerce, sur la pyrolyse de μH: un effet cinétique intermédiaire au niveau des propagations, c'est-à-dire une influence *accélératrice moins marquée* que dans le cas limite [A]; et un effet *inhibiteur*, dû à l'apparition de nouveaux processus de terminaison des chaînes.

Le calcul confirme cette prévision (1).

## 3. Conclusion

Pour la pyrolyse (à très faible avancement) d'une substance organique μH impliquant *une seule* stoechiométrie principale et un mécanisme radicalaire en chaînes de type "βμ", l'*analogie hydraulique* utilisée ici pour représenter la *propagation* des chaînes nous a permis de mieux saisir la notion d'étape *limitant* la *vitesse* de *propagation*, à savoir: le processus bimoléculaire [3] dans le cas limite [A] (*néopentane* par ex.) ou, au contraire, le processus unimoléculaire [2] dans le cas limite [B] (*éthane* par ex.), bien que, dans chaque cas, les processus de propagation [2] et [3] aient la même vitesse.

L'analogie hydraulique nous a montré par ailleurs que, d'après le mécanisme "μH, YH", un additif hydrogéné YH peut avoir, *au niveau des propagations*, un effet *accélérateur* sur la pyrolyse de μH *dans le cas limite [A]* et non dans le cas limite [B]. Mais, *dans les deux cas*, l'additif YH a aussi un effet *inhibiteur*, du fait que YH fait apparaître de nouveaux processus de *terminaison* des chaînes. On comprend ainsi pourquoi une pyrolyse relevant du *cas limite [A]* (*néopentane* par ex.) peut être *accélérée* par certains additifs hydrogénés (HCl, HBr, $H_2S$) et, au contraire, *inhibée* par divers alcènes et pourquoi on *ne* peut *pas* accélérer, par ce mécanisme, une décomposition thermique relevant du *cas limite [B]* (par exemple, la pyrolyse de l'*éthane* est *inhibée* par HBr, par $H_2S$ et par des alcènes et HCl n'a pratiquement pas d'influence).

Dans un second mémoire, nous étendrons les mécanismes "βμ" et "μH, YH" et l'analogie hydraulique pour la propagation des chaînes au cas d'une substance organique μH se décomposant selon *plusieurs* stoechiométries primaires principales. Ceci nous permettra d'interpréter l'influence d'additifs hydrogénés YH sur la cinétique de la réaction et sur sa sélectivité (c'est-à-dire sur les importances relatives des stoechiométries de décomposition).

1. M. NICLAUSE, R. MARTIN, F. BARONNET et G. SCACCHI. Rev. Inst. Fr. Pétrole, **21**, 1724 (1966).
2. G. SCACCHI, F. BARONNET, R. MARTIN et M. NICLAUSE. J. Chim. Phys. **65**, 1671 (1968).
3. J. MULLER, F. BARONNET, G. SCACCHI, M. DZIERZYNSKI et M. NICLAUSE. Int. J. Chem. Kinet. **9**, 425 (1977).
4. S. W. BENSON et K. H. ANDERSON. J. Chem. Phys. **39**, 1677 (1963).

Can. J. Chem. Downloaded from www.nrcresearchpress.com by 210.87.254.40 on 09/06/12
For personal use only.

5. G. SCACCHI, M. DZIERZYNSKI, R. MARTIN et M. NICLAUSE. Communication au Symposium International "Gas Kinetics", Szeged, Hongrie. 8–11 juillet 1969, Preprints p. 236; Int. J. Chem. Kinet. **2**, 115 (1970).
6. P. R. MCLEAN et D. J. MCKENNEY. Can. J. Chem. **48**, 1782 (1970).
7. F. BARONNET, R. MARTIN et M. NICLAUSE. J. Chim. Phys. **69**, 236 (1972).
8. F. BARONNET, G. M. CÔME et M. NICLAUSE. J. Chim. Phys. **71**, 1214 (1974).
9. F. BARONNET. Thèse de Doctorat ès Sciences Physiques, Nancy, France. 1970.
10. C. RICHARD, R. MARTIN et M. NICLAUSE. J. Chim. Phys. **70**, 1151 (1973); React. Kinet. Catal. Lett. **1**, 37 (1974).
11. F. BILLAUD, F. BARONNET et M. NICLAUSE. J. Chim. Phys. **77**, 175 (1980); F. BILLAUD. Thèse de Doctorat ès Sciences, Nancy, France. 1980.
12. J. F. DECARREAU, B. DESCHAMPS, G. SCACCHI et M. NICLAUSE. J. Chim. Phys. **71**, 1554 (1974).
13. P. GOLDFINGER, M. LETORT et M. NICLAUSE. Volume commémoratif Victor Henri: Contribution à l'étude de la structure moléculaire, Desoer, Liège, Belgique. (1947–1948). p. 283.
14. J. ENGEL, A. COMBE, M. LETORT et M. NICLAUSE. C.R. Acad. Sci. **244**, 453 (1957).
15. F. BARONNET, M. DZIERZYNSKI, R. MARTIN et M. NICLAUSE. C.R. Acad. Sci. Ser. C, **267**, 937 (1968).
16. M. P. HALSTEAD, R. S. KONAR, D. A. LEATHARD, R. M. MARSHALL et J. H. PURNELL. Proc. R. Soc. London, Ser. A, **310**, 525 (1969).
17. F. BARONNET, M. DZIERZYNSKI, G. M. CÔME, R. MARTIN et M. NICLAUSE. Int. J. Chem. Kinet. **3**, 197 (1971).
18. G. M. CÔME, M. DZIERZYNSKI, R. MARTIN et M. NICLAUSE. Rev. Inst. Fr. Pétrole, **23**, 1365 (1968).
19. J. H. PURNELL et C. P. QUINN. Proc. R. Soc. London, Ser. A, **270**, 267 (1962).
20. C. P. QUINN. Proc. R. Soc. London, Ser. A, **275**, 190 (1963).
21. M. C. LIN et M. H. BACK. Can. J. Chem. **44**, 505 (1966); **44**, 2357 (1966); **44**, 2369 (1966).
22. A. B. TRENWITH. Trans. Faraday Soc. **62**, 1538 (1966); **63**, 2452 (1967).
23. G. SCACCHI, R. MARTIN et M. NICLAUSE. Bull. Soc. Chim. Fr. 731 (1971).
24. M. NICLAUSE et R. MARTIN. Ind. Chim. Belge, No spécial, 36ème Congrès International de Chimie Industrielle, Gr. VIII, t. II, 621 (1967).

Can. J. Chem. Downloaded from www.nrcresearchpress.com by 210.87.254.40 on 09/06/12
For personal use only.

# Influence complexe d'additifs hydrogénés sur le craquage de substances organiques et analogie hydraulique pour la propagation des chaînes. II. Cas d'une pyrolyse à plusieurs stoechiométries

GÉRARD SCACCHI, CLOTILDE JUSTE-DARRAS, FRANÇOIS BARONNET ET MICHEL NICLAUSE

*I.N.P.L. et Université de Nancy I, Département de Chimie Physique des Réactions (E.R.A. no 136 C.N.R.S.), 1, rue Grandville, 54042 Nancy Cedex, France*

Reçu le 13 mai 1981

GÉRARD SCACCHI, CLOTILDE JUSTE-DARRAS, FRANÇOIS BARONNET et MICHEL NICLAUSE. Can. J. Chem. **60**, 257 (1982).

Dans un premier mémoire (I), on a considéré le cas simple d'une substance organique μH se décomposant (à très faible avancement) selon *une seule* steochiométrie principale: μH = m + βH. Pour représenter la *propagation* des chaînes dans la pyrolyse de μH, pur ou en présence d'un corps hydrogéné YH, on a introduit une *analogie hydraulique*. En se basant sur le mécanisme "μH, YH" de Niclause et coll., cette analogie a permis, en particulier, de mieux comprendre pourquoi *certains* additifs hydrogénés *accélèrent* certaines décompositions thermiques (e.g. néo-$C_5H_{12}$ = i-$C_4H_8$ + $CH_4$), tandis qu'*aucun* additif hydrogéné n'accélère d'autres pyrolyses (e.g. $C_2H_6 = C_2H_4 + H_2$).

Dans ce second mémoire (II), on étend les considérations précédentes au cas plus complexe d'une substance organique μH se décomposant selon *deux* stoechiométries primaires principales:

[A] $\mu H = m_A + CH_4$

[B] $\mu H = m_B + H_2$

On montre que le mécanisme "μH, YH" généralisé et *l'analogie hydraulique* pour la propagation des chaînes permettent d'interpréter l'influence d'additifs hydrogénés (HCl, HBr, $H_2S$, $H_2$, $C_3H_6$) sur les *vitesses* initiales des réactions [A] et [B] de la pyrolyse du *propane* ou de *l'isobutane* et sur la *sélectivité* de cette décomposition (importance de [A] par rapport à [B]).

Enfin, on examine sommairement le cas, plus complexe encore, d'une substance organique μH se décomposant selon *plus de deux* stoechiométries primaires principales.

---

GÉRARD SCACCHI, CLOTILDE JUSTE-DARRAS, FRANÇOIS BARONNET, and MICHEL NICLAUSE. Can. J. Chem. **60**, 257 (1982).

A first article (I) considered the simple case of an organic substance μH whose decomposition at low conversion follows a *single* principal stoichiometry: μH = m + βH. An *hydraulic analogy* was introduced in order to describe the *propagation* of chains in the pyrolysis of μH, either pure or in the presence of a hydrogenated substance YH. Applying the mechanism "μH, YH" of Niclause and co-workers, this analogy leads, in particular, to a better understanding of why *certain* hydrogenated additives *accelerate* certain thermal decompositions (e.g. neo-$C_5H_{12}$ = i-$C_4H_8$ + $CH_4$), whereas *no* hydrogenated additive accelerates other pyrolyses (e.g. $C_2H_6 = C_2H_4 + H_2$).

This second article (II) extends the preceding considerations to the more complex case of an organic substance μH which decomposes according to *two* principal primary stoichiometries:

[A] $\mu H = m_A + CH_4$

[B] $\mu H = m_B + H_2$

It is shown that the generalized mechanism "μH, YH" and the *hydraulic analogy* for the propagation of chains permit an interpretation of the influence of hydrogenated additives (HCl, HBr, $H_2S$, $H_2$, $C_3H_6$) on the initial *rates* of the reactions [A] and [B] in the pyrolysis of *propane* or of *isobutane* and on the *selectivity* of this decomposition (the importance of [A] relative to that of [B]).

Finally the still more complex case, in which an organic substance μH decomposes according to *more than two* principal primary stoichiometries, is briefly examined.

[Journal translation]

## Introduction

Dans un premier mémoire (1), nous avons considéré le cas simple de la décomposition thermique (à très faible avancement) d'une substance organique μH impliquant *une seule* stoechiométrie principale (μH = m + βH) et relevant d'un mécanisme radicalaire en chaînes "βμ" (2), telle que la pyrolyse du néopentane (néo-$C_5H_{12}$ = i-$C_4H_8$ + $CH_4$) ou celle de l'éthane ($C_2H_6 = C_2H_4 + H_2$).

Le mécanisme "μH, YH" (3) a permis d'interpréter de nombreux effets d'accélération ou d'inhibition, par des additifs hydrogénés YH, de la décomposition thermique de telles substances organiques μH. Pour représenter la *propagation* des chaînes dans le craquage de μH, pur ou en présence d'un corps hydrogéné YH, nous avons utilisé une *analogie hydraulique*. Grâce à celle-ci, on comprend mieux pourquoi certaines pyrolyses (*néopentane* par ex.) sont *accélérées* par certains additifs hydrogénés (HCl, HBr, $H_2S$) et, au contraire, *inhibées* par divers alcènes et pourquoi *aucun* additif hydrogéné n'accélère d'autres décom-

0008-4042/82/030257-17$01.00/0

©1982 National Research Council of Canada/Conseil national de recherches du Canada

Can. J. Chem. Downloaded from www.nrcresearchpress.com by 210.87.254.5 on 09/06/12
For personal use only.

positions thermiques (par ex., la pyrolyse de l'*éthane* est *inhibée* par HBr, par $H_2S$ et par des alcènes et HCl n'a pratiquement pas d'influence).

Dans ce second mémoire, nous allons examiner (Sect. 1 et 2) le cas, plus complexe, d'une substance organique μH se décomposant selon *deux* stoechiométries primaires principales:

[A] $\mu H = m_A + CH_4$

[B] $\mu H = m_B + H_2$

Il en est ainsi pour le *propane* et l'*isobutane*:

$C_3H_8 = C_2H_4 + CH_4$ [A] $i\text{-}C_4H_{10} = C_3H_6 + CH_4$

$C_3H_8 = C_3H_6 + H_2$ [B] $i\text{-}C_4H_{10} = i\text{-}C_4H_8 + H_2$

(Note: Remarquons que, dans chacun de ces deux exemples, la réaction [A] est du type "néopentane", la réaction [B] du type "éthane". En effet, [A] correspond à une perte de méthane, [B] à une déshydrogénation et nous verrons que la propagation des chaînes fait intervenir un processus unimoléculaire de décomposition d'un radical libre de type μ·: par rupture, relativement facile, d'une liaison C—C pour la réaction [A], comme dans le cas du néopentane; par rupture, relativement difficile, d'une liaison C—H pour la réaction [B], comme dans le cas de l'éthane.)

Niclause et coll. (4, 5) ont montré, dans le cas du *propane*, que $H_2S$, HBr et HCl *accélèrent* la réaction [A] (comme la pyrolyse du néopentane); au contraire, $H_2S$ et HBr *inhibent* la réaction [B], qui *n*'est pratiquement *pas* influencée par HCl (comme la décomposition de l'éthane). Les trois additifs précités *orientent* donc la pyrolyse du propane vers la production d'éthylène (et de méthane) au détriment de la formation de propène (et d'hydrogène). Ils *orientent* aussi la pyrolyse de l'*isobutane* vers $C_3H_6 + CH_4$ plutôt que vers $i\text{-}C_4H_8 + H_2$ (5, 6). Il est ainsi possible d'augmenter fortement la *sélectivité* (importance de [A] par rapport à [B]) de ces décompositions. Par ailleurs, l'expérience montre que des alcènes, tels que le propène, l'isobutène et les butènes-2 (qui inhibent la pyrolyse du néopentane et celle de l'éthane), *inhibent*, à la fois, les *deux* réactions [A] et [B] de décomposition du *propane* et de l'*isobutane* (4, 7–13); la sélectivité est alors peu modifiée.

Dans ce qui suit, nous nous proposons d'étendre au cas d'une substance organique μH se décomposant selon *deux* stoechiométries primaires principales [A] et [B], les mécanismes "βμ" et "μH, YH" et l'*analogie hydraulique* (pour la *propagation* des chaînes) utilisés dans le premier mémoire (1) pour une décomposition à une seule stoechiométrie. Ces considérations nous permettront d'interpréter l'influence de divers additifs hydrogénés sur les *vitesses* initiales des réactions [A] et [B] de la pyrolyse du *propane* ou de l'*isobutane* et sur la *sélectivité* de cette décomposition.

Enfin, nous examinerons sommairement (Sect. 3) le cas, plus complexe encore, d'une substance organique μH se décomposant selon *plus de deux* stoechiométries primaires principales, en tenant compte de travaux relatifs à l'influence de $H_2S$ sur la pyrolyse du *n*-butane (14, 15) ou de divers autres hydrocarbures (15, 16).

## 1. Pyrolyse distoechiométrique d'une substance organique (μH) pure

### *1.1. Mécanisme "βμ" généralisé*

Considérons la réaction de pyrolyse d'une substance organique μH se décomposant selon *deux* équations stoechiométriques primaires principales, l'une de *perte de méthane* (comme dans le cas de la pyrolyse du néopentane), l'autre de *déshydrogénation* (comme dans le cas de la pyrolyse de l'éthane):

[A] $\mu H = m_A + CH_4$

[B] $\mu H = m_B + H_2$

La généralisation du mécanisme "βμ" au cas d'une pyrolyse à deux stoechiométries permet d'écrire le mécanisme symbolique suivant (à très faible avancement):

[1] amorçage: $\mu H \xrightarrow{k_1}$ 2 radicaux libres

suivi, éventuellement, de processus de transfert

[2A] propagation Ⓐ $\mu_A\cdot \xrightarrow{k_{2A}} m_A + CH_3\cdot$

[3'A] $CH_3\cdot + \mu H \xrightarrow{k_{3'A}} CH_4 + \mu_A\cdot$

Can. J. Chem. Downloaded from www.nrcresearchpress.com by 210.87.254.5 on 09/06/12
For personal use only.

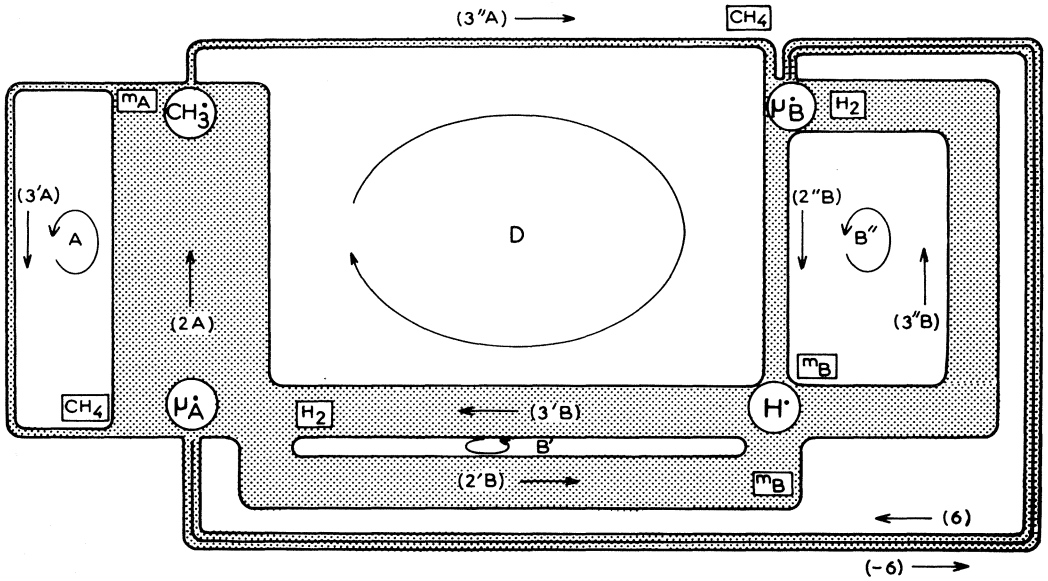


FIG. 1. Analogie hydraulique pour la *propagation* des chaînes dans la pyrolyse d'une substance organique μH pure.

[2′B] [3′B] propagation (B′)

$$\mu_A\cdot \xrightarrow{k_{2'B}} m_B + H\cdot$$
$$H\cdot + \mu H \xrightarrow{k_{3'B}} H_2 + \mu_A\cdot$$

[2″B] [3″B] propagation (B″)

$$\mu_B\cdot \xrightarrow{k_{2''B}} m_B + H\cdot$$
$$H\cdot + \mu H \xrightarrow{k_{3''B}} H_2 + \mu_B\cdot$$

[3″A] processus de croisement de chaînes: $CH_3\cdot + \mu H \xrightarrow{k_{3''A}} CH_4 + \mu_B\cdot$

[6] et [−6] processus d'isomérisation: $\mu_B\cdot + \mu H \underset{k_{-6}}{\overset{k_6}{\rightleftharpoons}} \mu H + \mu_A\cdot$

terminaison: combinaison (et dismutation éventuelle) 2 à 2 des porteurs de chaînes les plus abondants

Il existe deux types de radicaux β·: $CH_3\cdot$ et H· et deux formes isomères du radical μ·: la forme $\mu_A\cdot$, radical primaire qui peut se décomposer unimoléculairement par rupture d'une liaison carbone–carbone (processus [2A]) ou d'une liaison carbone–hydrogène (processus [2′B]); dans le cas du propane, $\mu_A\cdot \equiv$ p-$C_3H_7\cdot$ et dans celui de l'isobutane, $\mu_A\cdot \equiv$ p-$C_4H_9\cdot$ (p veut dire primaire); et la forme $\mu_B\cdot$, radical secondaire ou tertiaire qui ne peut se décomposer que par rupture d'une liaison carbone–hydrogène (processus [2′B]); dans le cas du propane, $\mu_B\cdot \equiv$ s-$C_3H_7\cdot$; dans celui de l'isobutane, $\mu_B\cdot \equiv$ t-$C_4H_9\cdot$. La propagation (A) rend compte de la stoechiométrie [A]; les propagations (B″) et (B′) rendent toutes deux compte de la stoechiométrie [B].

Le calcul des rapports des concentrations radicalaires, dans le cas de la pyrolyse du propane (4, 17) montre clairement que les radicaux libres les plus abondants dans le milieu, à très faible avancement, sont les radicaux $CH_3\cdot$ et $\mu_B\cdot$ (s-$C_3H_7\cdot$); la terminaison des chaînes implique donc essentiellement ces deux types de radicaux. De la même façon, dans la pyrolyse de l'isobutane, les radicaux libres prépondérants sont $CH_3\cdot$ et $\mu_B\cdot$ (t-$C_4H_9\cdot$).

*1.2. Analogie hydraulique pour la propagation des chaînes*

La figure 1 représente l'analogie hydraulique des divers processus de propagation, croisement de chaînes et isomérisation.

On retrouve les 3 boucles: (A) (correspondant à la stoechiométrie [A]) (B′) et (B″) (correspondant à la

Can. J. Chem. Downloaded from www.nrcresearchpress.com by 210.87.254.5 on 09/06/12
For personal use only.

Can. J. Chem. Downloaded from www.nrcresearchpress.com by 210.87.254.5 on 09/06/12
For personal use only.

stoechiométrie [B]). Une quatrième boucle (D) composée des processus [2A], [3″A], [2″B], [3′B] correspond à la somme des stoechiométries [A] + [B].

La stoechiométrie [A] relève du *cas limite* [A]: $(k_{3'A} + k_{3''A})\ (\mu H)_0 \ll k_{2A}$, car le processus unimoléculaire [2A] correspond à la rupture, relativement facile, d'une liaison carbone–carbone. Il est ainsi plus facile que les deux processus bimoléculaires parallèles (et de constantes de vitesse voisines) [3′A] et [3″A]. Le calcul des concentrations radicalaires dans la pyrolyse du propane (4, 17) montre que l'on a bien: $(CH_3\cdot) \gg (\mu_A\cdot)$. C'est une chaîne de ''type néopentane''.

La chaîne représentée par la boucle (B″) relève du *cas limite* [B]: $k_{2''B} < (k_{3'B} + k_{3''B})\ (\mu H)_0$, car le processus unimoléculaire [2″B] correspond à la rupture, relativement difficile, d'une liaison carbone–hydrogène (hydrogène primaire). Il est ainsi plus difficile que les deux processus bimoléculaires parallèles (et de constantes de vitesse voisines) [3′B] et [3″B]. Le calcul (4, 17) montre que l'on a bien: $(\mu_B\cdot) > (H\cdot)$. C'est une chaîne de ''type éthane''.

Dans la chaîne représentée par la boucle (B′) le processus unimoléculaire [2′B] correspond aussi à la rupture d'une liaison carbone–hydrogène, mais cette fois d'un hydrogène secondaire (dans le cas du propane) ou tertiaire (dans le cas de l'isobutane). Le processus [2′B] est donc moins difficile que le processus [2″B] et la chaîne (B′) est plutôt du type ''intermédiaire'' entre les *cas limites* [A] et [B].

(*Remarque*. Rappelons que dans l'analogie hydraulique le diamètre des conduites est fonction de la constante de vitesse (pour les processus unimoléculaires) ou de la constante de vitesse multipliée par la concentration du réactif (pour les processus bimoléculaires). Le débit de fluide (c'est-à-dire la vitesse du processus élémentaire) dépend non seulement de la taille de la conduite mais de la ''pression'' en amont, c'est-à-dire de la concentration du radical impliqué. Ceci explique pourquoi, malgré le diamètre notable de [2′B], le débit dans cette conduite est nettement inférieur à celui dans [2″B], de diamètre pourtant plus faible.)

*1.3. Echanges entre radicaux libres* $\mu_A\cdot$ *et* $\mu_B\cdot$ *et importances relatives des deux stoechiométries [A] et [B]*

Le schéma hydraulique permet de bien visualiser *les échanges entre* $\mu_A\cdot$ *et* $\mu_B\cdot$. Ce phénomène est très important et il servira plus loin de clé à l'interprétation des variations des importances relatives des stoechiométries en présence d'additif YH.

On voit que le passage $\mu_A\cdot \rightarrow \mu_B\cdot$ peut se faire par les conduites: (2A) (suivie de (3″A)), (2′B) (suivie de (3″B)), (−6); le passage $\mu_B\cdot \rightarrow \mu_A\cdot$ peut se faire par les conduites: (2″B) (suivie de (3′B)), (6). Ce sont bien ces *5 termes* que l'on retrouve dans le rapport $R = (\mu_B\cdot)/(\mu_A\cdot)$, calculé par ailleurs (17) dans le cas de la pyrolyse de μH pur:[1]

$$[I] \quad R = \frac{(1+\gamma)k_{-6}(\mu H)_0 + \gamma(k_{2A} + k_{2'B})}{(1+\gamma)k_6(\mu H)_0 + k_{2''B}}$$

L'équilibre dynamique entre $\mu_A\cdot$ et $\mu_B\cdot$ et donc *les importances relatives des stoechiométries [A] et [B]* ne dépendent *que de ces 5 conduites* (dans le cas de la pyrolyse de μH pur). Seule *l'intervention de nouvelles conduites* entre $\mu_A\cdot$ et $\mu_B\cdot$, due à la présence d'un additif YH, pourra, comme nous le verrons, déplacer l'équilibre entre $\mu_A\cdot$ et $\mu_B\cdot$ et *changer la sélectivité de la décomposition de* μH.

Ce schéma hydraulique permet également de comprendre les variations des importances relatives des deux stoechiométries en fonction des conditions expérimentales (température et pression initiale d'hydrocarbure).

Supposons d'abord, pour simplifier, que le processus [2′B] soit absent, ainsi que les processus d'isomérisation [6] et [−6].

Les conduites (3′A) et (3″A) étant de diamètres voisins, il est facile de voir que la stoechiométrie [A] provient: pour moitié environ de la boucle (A); pour moitié environ de la boucle complexe (D) composée de (2A) (3″A) (2″B) (3′B) de stoechiométrie: $2\,\mu H = m_A + CH_4 + m_B + H_2$. De la même façon, les conduites (3′B) et (3″B) ont des diamètres voisins et la stoechiométrie [B] provient: pour moitié environ de la boucle (B″); pour moitié environ de la boucle complexe (D) composée de (2A) (3″A) (2″B) (3′B). Ainsi les deux stoechiométries [A] et [B] sont sensiblement d'*égale importance* dans ce cas simple.

---

[1]On a supposé que l'on a: $\gamma = k_{3''A}/k_{3'A} \simeq k_{3''B}/k_{3'B}$. Ce rapport γ est très voisin de 1 et c'est la raison pour laquelle nous avons attribué aux conduites (3′A) et (3″A) d'une part et (3′B) et (3″B) d'autre part des diamètres très voisins. Les calculs ont été faits, en supposant, d'autre part, que les chaînes étaient longues.

*A suffisamment haute température*, l'intervention des processus d'isomérisation [6] et [−6] ne modifie pas sensiblement le résultat précédent, car les conduites (6) et (−6) sont de faible diamètre par rapport aux autres conduites d'échange entre $\mu_A$ et $\mu_B$.[2]

En revanche, l'intervention de la conduite (2′B), de taille intermédiaire entre (2A) et (2″B), transforme des $\mu_A\cdot$ en H· et tend donc à diminuer l'importance de la stoechiométrie [A] par rapport à [B].

C'est bien ce qui est observé, dans le cas du propane, pour $T \geq 600$°C. Par exemple, à 600°C: [A]/[B] ≃ 0,8 (17).

*A plus basse température* (vers 500°C), l'isomérisation [6], [−6] intervient et tend à transformer $\mu_B\cdot$ en $\mu_A\cdot$.[3] Les processus [6] et [−6] étant bimoléculaires, cet effet est d'autant plus marqué que la pression initiale d'hydrocarbure $P_0$ est plus grande. Au contraire, [2′B] tend à convertir $\mu_A\cdot$ en H· (donc en $\mu_B\cdot$).

Les importances relatives de ces deux effets opposés permettent d'interpréter les faits expérimentaux suivants: (*i*) à basse pression initiale d'hydrocarbure (par exemple: $P_0 < 300$ Torr environ pour le propane) on a: [A]/[B] < 1, aussi bien dans le cas du propane (4) que dans celui de l'isobutane (6, 11). L'influence de [2′B] l'emporte alors sur celle de l'isomérisation [6], [−6]; (*ii*) à plus haute pression initiale d'hydrocarbure (par exemple: $P_0 > 300$ Torr pour le propane) on a: [A]/[B] > 1 (4). L'influence de $P_0$ sur [6] et [−6] fait que l'effet de l'isomérisation l'emporte alors sur celui de [2′B].

## 2. Pyrolyse distoechiométrique d'une substance organique (μH) en présence d'un corps hydrogéné (YH)

### *2.1. Mécanisme "μH, YH" généralisé*

Par analogie avec le mécanisme "μH, YH" vu précédemment (cf. Premier Mémoire (1)), on peut écrire, a priori, un mécanisme "μH, YH" généralisé correspondant à l'action d'un additif YH sur la pyrolyse d'une substance se décomposant selon deux équations stoechiométriques primaires principales:

[1] amorçage: $\mu H \xrightarrow{k_1}$ radicaux libres

suivi, éventuellement, de processus de transfert

[2A], [3′A] propagation $\textcircled{A}_I$

$$\left\{\begin{array}{rl} \mu_A\cdot & \xrightarrow{k_{2A}} m_A + CH_3\cdot \\ CH_3\cdot + \mu H & \xrightarrow{k_{3'A}} CH_4 + \mu_A\cdot \end{array}\right.$$

[2A], [4A], [5A], [−5A] propagation $\textcircled{A}_{II}$

$$\left\{\begin{array}{rl} \mu_A\cdot & \xrightarrow{k_{2A}} m_A + CH_3\cdot \\ CH_3\cdot + YH & \xrightarrow{k_{4A}} CH_4 + Y\cdot \\ Y\cdot + \mu H & \underset{k_{-5A}}{\overset{k_{5A}}{\rightleftharpoons}} YH + \mu_A\cdot \end{array}\right.$$

[2′B], [3′B] propagation $\textcircled{B'}_I$

$$\left\{\begin{array}{rl} \mu_A\cdot & \xrightarrow{k_{2'B}} m_B + H\cdot \\ H\cdot + \mu H & \xrightarrow{k_{3'B}} H_2 + \mu_A\cdot \end{array}\right.$$

[2′B], [4B], [5A], [−5A] propagation $\textcircled{B'}_{II}$

$$\left\{\begin{array}{rl} \mu_A\cdot & \xrightarrow{k_{2'B}} m_B + H\cdot \\ H\cdot + YH & \xrightarrow{k_{4B}} H_2 + Y\cdot \\ Y\cdot + \mu H & \underset{k_{-5A}}{\overset{k_{5A}}{\rightleftharpoons}} YH + \mu_A\cdot \end{array}\right.$$

[2″B], [3″B] propagation $\textcircled{B''}_I$

$$\left\{\begin{array}{rl} \mu_B\cdot & \xrightarrow{k_{2''B}} m_B + H\cdot \\ H\cdot + \mu H & \xrightarrow{k_{3''B}} H_2 + \mu_B\cdot \end{array}\right.$$

[2]Les énergies d'activation des processus *bimoléculaires* [6] et [−6] sont nettement inférieures à celles des processus *unimoléculaires* [2A], [2″B] et [2′B]. Le calcul montre qu'à suffisamment haute température [6] et [−6] sont négligeables devant [2A], [2″B] et [2′B]. En revanche lorsque la température baisse, on doit tenir compte de [6] et [−6].

[3]Bien que $k_{-6}$ soit légèrement supérieur à $k_6$ (4, 10, 18), l'inégalité $(\mu_B\cdot) \gg (\mu_A\cdot)$ conduit à un flux de passage $\mu_B\cdot \rightarrow \mu_A\cdot$ plus important que le flux $\mu_A\cdot \rightarrow \mu_B\cdot$.

Can. J. Chem. Downloaded from www.nrcresearchpress.com by 210.87.254.5 on 09/06/12
For personal use only.

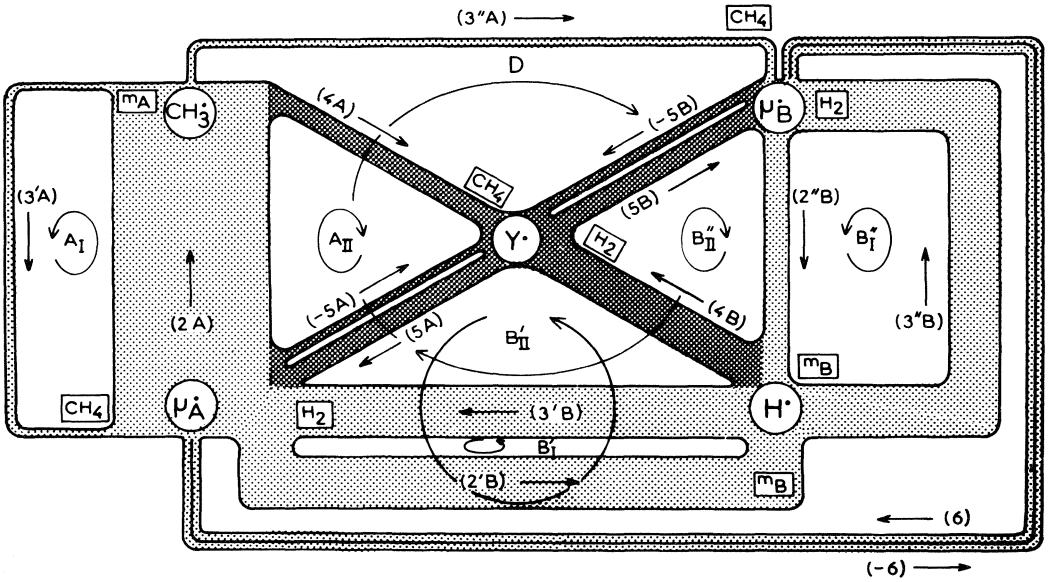


FIG. 2. Analogie hydraulique pour la propagation des chaînes dans la pyrolyse d'une substance organique μH en présence d'un additif YH.

[2″B], [4B], [5B], [−5B] — propagation $(B'')_{II}$:

$$\mu_B\cdot \xrightarrow{k_{2''B}} m_B + H\cdot$$

$$H\cdot + YH \xrightarrow{k_{4B}} H_2 + Y\cdot$$

$$Y\cdot + \mu H \underset{k_{-5B}}{\overset{k_{5B}}{\rightleftharpoons}} YH + \mu_B\cdot$$

[3″A] — processus de croisement des chaînes:

$$CH_3\cdot + \mu H \xrightarrow{k_{3''A}} CH_4 + \mu_B\cdot$$

[6], [−6] — isomérisation:

$$\mu_B\cdot + \mu H \underset{k_{-6}}{\overset{k_6}{\rightleftharpoons}} \mu H + \mu_A\cdot$$

terminaison: combinaison (et dismutation éventuelle) 2 à 2 des porteurs de chaînes les plus abondants, c'est-à-dire $CH_3\cdot$, $\mu_B\cdot$ et éventuellement, Y·, selon la nature de YH.

### 2.2. *Analogie hydraulique pour la propagation des chaînes et influence de YH sur la sélectivité de la pyrolyse de μH*

On complète le schéma de la figure 1 avec les nouvelles conduites pour obtenir le schéma global de la figure 2 représentant les processus de propagation, de croisement de chaînes et d'isomérisation.

Pour la clarté de l'exposé, nous allons d'abord supposer que la présence de YH n'*introduit pas de terminaisons nouvelles*; ceci signifie que nous allons traiter uniquement de l'*effet de YH sur les propagations*, croisement de chaînes et isomérisation, *sans nous préoccuper de l'effet global* qui, comme on l'a vu (cf. Premier Mémoire (1)), fait, en plus, intervenir les terminaisons nouvelles éventuelles.

Nous évoquerons l'influence *globale* de YH sur la pyrolyse de μH au paragraphe 2.3.

Par analogie avec les raisonnements utilisés dans le cas de l'étude des réseaux électriques complexes, nous partirons de circuits hydrauliques simples "extraits" du schéma de la figure 2 et nous les compléterons progressivement jusqu'à l'obtention du schéma complet.

#### 2.2.1. *Influence de YH sur la stoechiométrie [A]*

On a vu précédemment que la décomposition de μH pur selon la stoechiométrie [A] se fait par la boucle $(A)_I$ et la boucle complexe (D) composée de [2A] [3″A] [2″B] [3′B]. Dans ces deux boucles, les "goulots d'étranglement" sont, respectivement, les conduites (3′A) et (3″A).

Can. J. Chem. Downloaded from www.nrcresearchpress.com by 210.87.254.5 on 09/06/12
For personal use only.

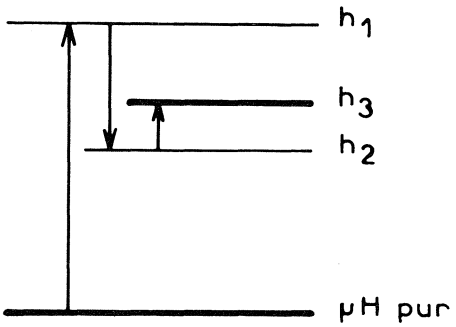


FIG. 3. Concentration de $\mu_A\cdot$ dans les différentes hypothèses.

Considérons successivement les hypothèses suivantes:

*Hypothèse* $h_1$: on suppose que le schéma de la figure 2 *se réduit* aux boucles Ⓐ$_I$, Ⓓ et Ⓐ$_{II}$ "isolées" du reste du système.

La présence de YH permet un nouveau passage de $CH_3\cdot$ vers $\mu_A\cdot$ par (4A) et (5A) (−5A), augmente le débit dans (2A) et donc accélère la stoechiométrie [A], comme dans le cas du néopentane en présence de YH. La concentration de $\mu_A\cdot$ croît (Fig. 3). Cette accélération est d'autant plus forte que la nouvelle conduite (4A) est de diamètre important par rapport aux anciennes conduites (3′A) et (3″A).

*Hypothèse* $h_2$: on suppose maintenant, en plus, que les échanges entre $\mu_A\cdot$ et $\mu_B\cdot$ sont les mêmes qu'en l'absence de YH, c'est-à-dire se font *exclusivement* par les conduites (2A) (2′B) (−6) et (2″B) (6) (cf. Sect. 1.3), aucun échange entre $\mu_A\cdot$ et $\mu_B\cdot$ n'ayant lieu par l'intermédiaire du radical Y·.

L'augmentation de $(\mu_A\cdot)$ due à la présence de YH est limitée par les échanges $\mu_A\cdot \leftrightarrow \mu_B\cdot$ puisque le rapport des concentrations $(\mu_B\cdot)/(\mu_A\cdot)$ est le même qu'en l'absence de YH. Il y a donc passage $\mu_A\cdot \rightarrow \mu_B\cdot$ et ceci bien que $(\mu_B\cdot) \gg (\mu_A\cdot)$ dans la pyrolyse de μH pur. On a indiqué la chute de la concentration $(\mu_A\cdot)$ dans l'hypothèse $h_2$, sur la figure 3.

*Hypothèse* $h_3$: cette fois, on tient compte, des nouvelles conduites d'échange: $\mu_A\cdot \rightarrow \mu_B\cdot$ par (−5A) suivi de (5B); $\mu_B\cdot \rightarrow \mu_A\cdot$ par (−5B) suivi de (5A).

Notons que ce sont bien les deux processus [−5A] et [−5B] qui apparaissent, en plus des anciens termes, dans l'expression théorique du rapport: $R_{YH} = (\mu_B\cdot)/(\mu_A\cdot)$ en présence de YH (6, 17):[4]

$$[II] \quad R_{YH} = \frac{(\mu_B\cdot)}{(\mu_A\cdot)} = \frac{\gamma k_{-5A}(YH)_0 + (1+\gamma)k_{-6}(\mu H)_0 + \gamma(k_{2A} + k_{2'B})}{k_{-5B}(YH)_0 + (1+\gamma)k_6(\mu H)_0 + k_{2''B}}$$

Ces nouvelles conduites (de tailles voisines) augmentent les échanges entre $\mu_A\cdot$ et $\mu_B\cdot$. La concentration $(\mu_B\cdot)$ étant bien supérieure à $(\mu_A\cdot)$ le débit de passage $\mu_B\cdot \rightarrow \mu_A\cdot$ est plus grand que celui de $\mu_A\cdot \rightarrow \mu_B\cdot$. La concentration relative de $\mu_B\cdot$ par rapport à $\mu_A\cdot$ diminue, ce qui tend à augmenter la concentration $(\mu_A\cdot)$ par rapport à sa valeur dans l'hypothèse $h_2$ (cf. Fig. 3).

La vitesse $V_0^A$ de décomposition de μH selon la stoechiométrie [A] s'écrit:

$$V_0^A = V_0^{CH_4} = V_0^{m_A} = k_{2A}(\mu_A\cdot)$$

La figure 3 représente donc également les variations de $V_0^A$ dans les différentes hypothèses.

Ce raisonnement qualitatif concernant l'influence de YH sur la stoechiométrie [A] est compatible avec les calculs théoriques effectués à partir du mécanisme "μH, YH" généralisé. En supposant toujours que la présence de YH ne fait pas apparaître de terminaisons nouvelles,[5] on peut calculer (17) le rapport $\Phi_{YH}^A$ des vitesses initiales de décomposition de μH selon la stoechiométrie [A], en présence de YH, $(V_0^A)_{YH}$ et en l'absence de YH, $V_0^A$:

[4]Dans l'expression de $R_{YH}$, le coefficient γ préalablement défini est aussi supposé égal à: $k_{5B}/k_{5A}$ de sorte que: $\gamma \simeq k_{5B}/k_{5A} \simeq k_{3''A}/k_{3'A} \simeq k_{3''B}/k_{3'B}$.

[5]On a supposé que la terminaison des chaînes, en l'absence de YH, impliquait les radicaux $CH_3\cdot$ et $\mu_B\cdot$: processus [ββ], [$\beta\mu_B$], [$\mu_B\mu_B$].

Can. J. Chem. Downloaded from www.nrcresearchpress.com by 210.87.254.5 on 09/06/12
For personal use only.

$$[III] \quad \Phi_{YH}{}^{A} = \frac{(V_0{}^{A})_{YH}}{V_0{}^{A}} = \frac{r + \left(\frac{k_{\mu_B\mu_B}}{k_{\beta\beta}}\right)^{1/2} R}{r_{YH} + \left(\frac{k_{\mu_B\mu_B}}{k_{\beta\beta}}\right)^{1/2} R_{YH}}$$

où $r_{YH} = (CH_3\cdot)/(\mu_A\cdot)$ et $R_{YH} = (\mu_B\cdot)/(\mu_A\cdot)$. $R$ et $r$ étant relatifs à la pyrolyse de μH *pur*.

*Hypothèse* $h_1$: il n'y a pas d'échange entre $\mu_A\cdot$ et $\mu_B\cdot$ autre que la boucle (D) et on suppose que la terminaison des chaînes ne fait intervenir *que* le radical $\beta\cdot \equiv CH_3\cdot$, comme dans la pyrolyse du néopentane. Le rapport $\Phi_{YH}{}^{A}$ s'écrit alors:[6]

$$[IV] \quad \Phi_{YH}{}^{A} = \frac{(V_0{}^{A})_{YH}}{V_0{}^{A}} = \frac{r}{r_{YH}} = 1 + \frac{k_{4A}}{(k_{3'A} + k_{3''A})} \frac{(YH)_0}{(\mu H)_0}$$

On retrouve, au niveau des propagations, *le terme accélérateur* qui apparaît dans la pyrolyse du néopentane en présence de YH (cf. Premier Mémoire (1) Sect. 2.3.)

*Hypothèse* $h_2$: si les échanges entre $\mu_A\cdot$ et $\mu_B\cdot$ sont les mêmes en présence de YH qu'en l'absence: $R_{YH} \equiv R$ et le rapport $\Phi_{YH}{}^{A}$ s'écrit (en faisant intervenir cette fois le radical $\mu_B\cdot$ dans les terminaisons):

$$[V] \quad \Phi_{YH}{}^{A} = \frac{(V_0{}^{A})_{YH}}{V_0{}^{A}} = \frac{r + \left(\frac{k_{\mu_B\mu_B}}{k_{\beta\beta}}\right)^{1/2} R}{r_{YH} + \left(\frac{k_{\mu_B\mu_B}}{k_{\beta\beta}}\right)^{1/2} R} < \frac{r}{r_{YH}}$$

Le terme accélérateur $r/r_{YH}$ de l'hypothèse $h_1$ est en fait diminué à cause de l'échange $\mu_A\cdot \leftrightarrow \mu_B\cdot$.

*Hypothèse* $h_3$: les échanges font intervenir de nouveaux termes au numérateur et au dénominateur de $R_{YH}$; ces nouveaux termes sont voisins et comme $R \gg 1$ on obtient $R_{YH} < R$. Le dénominateur est ainsi plus petit que dans l'hypothèse $h_2$, ce qui tend à augmenter un peu la valeur du rapport des vitesses initiales par rapport à l'hypothèse $h_2$. Le rapport $\Phi_{YH}{}^{A}$ prend alors la forme (III).

L'analogie hydraulique permet ainsi de bien mettre en évidence l'origine "physique" des différents termes apparaissant dans la formule (III).

*2.2.2. Influence de YH sur la stoechiométrie [B]*

La stoechiométrie [B] provient, en l'absence de YH, des chaînes $(B'')_I$ et $(B')_I$.

(*a*) *Considérons d'abord la boucle* $(B'')_I$. Dans cette boucle, le "goulot d'étranglement" est constitué par la conduite (2″B), comme pour la pyrolyse de l'éthane.

Considérons successivement les hypothèses suivantes:

*Hypothèse* $h_1'$: on suppose que la boucle $(B'')_I$ est *isolée*. L'adjonction de nouvelles conduites: (4B) (5B) (−5B) n'augmente pas le débit dans (2″B): YH est sans effet sur la formation de $m_B$ et $H_2$ et la concentration de $\mu_B\cdot$ reste la même qu'en l'absence de YH (cf. Fig. 4).

*Hypothèse* $h_2'$: en réalité il y a des échanges entre $\mu_A\cdot$ et $\mu_B\cdot$. Supposons qu'ils soient les mêmes qu'en l'absence de YH: échanges par (2A), (2′B), (−6) dans un sens et (2″B), (6) dans l'autre sens. Le rapport des concentrations $(\mu_B\cdot)/(\mu_A\cdot)$ reste le même qu'en l'absence de YH et comme $(\mu_A\cdot)$ augmente, $(\mu_B\cdot)$ augmente aussi, dans les mêmes proportions (cf. Fig. 4).

*Hypothèse* $h_3'$: les échanges entre $\mu_A\cdot$ et $\mu_B\cdot$ se font non seulement par les anciennes conduites, mais aussi par les nouvelles: de $\mu_A\cdot$ vers $\mu_B\cdot$ par (−5A) (5B), et de $\mu_B\cdot$ vers $\mu_A\cdot$ par (−5B) (5A).

Comme on l'a vu dans l'étude de la stoechiométrie [A], ces nouvelles conduites, de tailles voisines, tendent à faire diminuer la concentration $(\mu_B\cdot)$ et à augmenter $(\mu_A\cdot)$ et ceci d'autant plus que leurs diamètres sont gros par rapport à ceux des anciennes conduites d'échange, en l'absence de YH.

La concentration $(\mu_B\cdot)$ chute par rapport à sa valeur dans l'hypothèse $h_2'$: si les nouvelles conduites sont de très faible diamètre, $(\mu_B\cdot)$ chute très peu et la chaîne (B″) *est pratiquement autant accélérée que la*

[6]On a:

$$r_{YH} = \frac{k_{2A}}{k_{4A}(YH)_0 + (k_{3'A} + k_{3''A})(\mu H)_0} \quad \text{et} \quad r = \frac{k_{2A}}{(k_{3'A} + k_{3''A})(\mu H)_0}$$

Can. J. Chem. Downloaded from www.nrcresearchpress.com by 210.87.254.5 on 09/06/12
For personal use only.

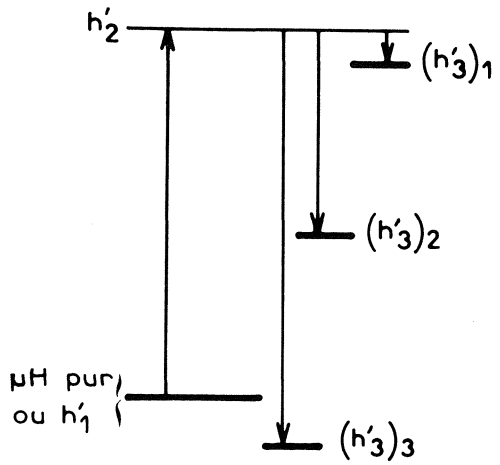


FIG. 4. Concentration de $\mu_B$· dans les différentes hypothèses.

*chaîne* (A) (Cas $(h_3')_1$); si les nouvelles conduites ont des diamètres notables, la diminution de ($\mu_B$·) est importante et la chaîne (B″) *est beaucoup moins accélérée que la chaîne* (A) (Cas $(h_3')_2$); et enfin, si les nouvelles conduites ont des diamètres importants, la diminution de ($\mu_B$·) par rapport à sa valeur $h_2'$ est telle que sa valeur en présence de YH est inférieure à sa valeur dans le cas de μH pur: *la chaîne* (B″) *est alors inhibée, alors que la chaîne* (A) *est accélérée* (Cas $(h_3')_3$).

(*b*) *Considérons maintenant la boucle* $(B')_I$. On a vu qu'elle pouvait être du type "intermédiaire" entre les *cas limites* [A] et [B] de la théorie "μH, YH". L'influence de YH sur cette chaîne est, en fait, très facile à décrire, puisque la vitesse de cette chaîne est: $V_0^{B'} = k_{2'B}(\mu_A\cdot)$. En présence de YH, on a vu que ($\mu_A$·) augmente, donc la *chaîne* (B′) *est accélérée dans les mêmes proportions que la chaîne* (A).

Ainsi, globalement, la stoechiométrie [B] provient de deux chaînes: l'une, (B′) est accélérée par YH dans les mêmes proportions que la stoechiométrie [A]; l'autre, (B″) peut être, soit accélérée comme [A], soit moins accélérée que [A], soit même inhibée.

On retrouve les résultats qualitatifs précédents en considérant la forme du rapport $(V_0^B)_{YH}/V_0^B$ des vitesses initiales de décomposition de μH selon la stoechiométrie [B], en présence et en l'absence de YH.

Avec les mêmes hypothèses concernant les terminaisons (en [ββ], [$\beta\mu_B$] et [$\mu_B\mu_B$]) on peut calculer (17):

$$[VI]\quad \Phi_{YH}{}^{B} = \frac{(V_0^B)_{YH}}{V_0^B} = \frac{r + \left(\frac{k_{\mu_B\mu_B}}{k_{\beta\beta}}\right)^{1/2} R}{r_{YH} + \left(\frac{k_{\mu_B\mu_B}}{k_{\beta\beta}}\right)^{1/2} R_{YH}} \times \frac{k_{2''B}R_{YH} + k_{2'B}}{k_{2''B}R + k_{2'B}}$$

*terme accélérateur* — *terme inhibiteur* car $R_{YH} < R$

Le terme *accélérateur* est le même que celui de la stoechiométrie [A]: on retrouve l'hypothèse $h_2'$ précédente.

Le terme *inhibiteur* contient les termes $k_{2''B}R_{YH}$ au numérateur et $k_{2''B}R$ au dénominateur; le rapport de ces deux termes est inférieur à 1, puisque $R_{YH} < R$. On retrouve l'hypothèse $h_3'$ précédente correspondant à l'effet de YH sur la chaîne (B″). Selon l'importance de l'écart entre $R_{YH}$ et $R$, le résultat *global* sera soit une accélération de [B] identique à celle de [A] (hypothèse $(h_3')_1$: $R_{YH} \simeq R$), soit une accélération moins forte que celle de [A] (hypothèse $(h_3')_2$: $R_{YH} < R$), soit enfin, une inhibition de [B] (hypothèse $(h_3')_3$: $R_{YH} \ll R$). Le terme inhibiteur comprend également au numérateur et au dénominateur le terme $k_{2'B}$. Ce terme rend compte de l'existence de la chaîne (B′) qui, comme on l'a vu, est accélérée dans les mêmes proportions que la stoechiométrie [A]. Ces termes $k_{2'B}$ tendent à rapprocher de 1 la valeur du terme inhibiteur et donc à compenser un peu l'effet inhibiteur de YH sur la chaîne (B″).

Can. J. Chem. Downloaded from www.nrcresearchpress.com by 210.87.254.5 on 09/06/12
For personal use only.

*2.2.3. Influence de YH sur la sélectivité de la décomposition de* μ*H* (proportions relatives des stoechiométries [A] et [B])

L'analyse de l'influence de YH sur les stoechiométries [A] et [B] a montré que *toute variation de la sélectivité de décomposition de* μ*H*, c'est-à-dire des proportions relatives des stoechiométries [A] et [B], ne peut provenir que de *l'effet de YH sur la boucle* (B″) et que cet effet dépend de la taille des nouvelles conduites apparaissant en présence de YH et permettant de nouveaux échanges $\mu_A\cdot \leftrightarrow \mu_B\cdot$: (*a*) si ces nouvelles conduites sont de très faible diamètre, c'est-à-dire si les processus

[−5A] $\mu_A\cdot + YH \rightarrow \mu H + Y\cdot$

et

[−5B] $\mu_B\cdot + YH \rightarrow \mu H + Y\cdot$

sont difficiles, il n'y a pas de variation de la sélectivité, i.e. *(B) sera accélérée comme (A)*; (*b*) si ces nouvelles conduites ont des diamètres notables, la stoechiométrie [B] sera: soit *accélérée*, mais plus faiblement que [A] (processus [−5A] et [−5B] assez faciles); soit *inhibée* (processus [−5A] et [−5B] très faciles).

On retrouve, par le calcul, les conclusions précédentes. Le calcul théorique montre en effet que les sélectivités $S$ et $S_{YH}$ de la décomposition de μH, respectivement en l'absence et en présence de YH s'écrivent:

$$[\text{VII}] \quad S = \frac{V_0^A}{V_0^B} = \frac{k_{2A}}{k_{2''B}R + k_{2'B}} \quad \text{et} \quad S_{YH} = \frac{(V_0^A)_{YH}}{(V_0^B)_{YH}} = \frac{k_{2A}}{k_{2''B}R_{YH} + k_{2'B}}$$

Le rapport des sélectivités en présence et en l'absence de YH s'écrit donc:

$$[\text{VIII}] \quad \frac{S_{YH}}{S} = \frac{1 + \dfrac{k_{2''B}}{k_{2'B}} R}{1 + \dfrac{k_{2''B}}{k_{2'B}} R_{YH}}$$

qui est, évidemment, le rapport inverse du terme inhibiteur vu dans l'étude de la stoechiométrie [B] (cf. relation (VI)).

*La présence de YH tend donc à augmenter, à très faible avancement, la sélectivité en [A] par rapport à [B]*, l'effet étant d'autant plus marqué que $R_{YH}$ est petit par rapport à $R$, c'est-à-dire que les nouveaux processus [−5A] et [−5B] sont *faciles* par rapport aux "anciens" processus d'échange: [2A], [2′B], [−6] d'une part et [2″B], [6] d'autre part.

Pour un corps μH donné, le changement de sélectivité dû à la présence de YH dépend donc des trois facteurs suivants: (*i*) pour une même teneur et une même température, il dépend de *la nature de l'additif YH*, c'est-à-dire des constantes de vitesses des deux processus [−5A] et [−5B]; (*ii*) pour un additif YH donné, il est d'autant plus fort: que la *température est plus basse*: les énergies d'activation des processus bimoléculaires [−5A] et [−5B] étant plus faibles que celles des processus unimoléculaires [2A], [2″B] et [2′B], les nouvelles conduites d'échange (−5A) et (−5B) ne seront comparables aux anciennes ((2A), (2″B), (2′B)) que si la température n'est pas trop élevée; et (*iii*) que la *concentration de YH ajouté est plus* forte: les diamètres des conduites (−5A) et (−5B) dépendent, en effet, des produits $k_{-5A}(YH)_0$ et $k_{-5B}(YH)_0$.

*2.2.4. Changements de sélectivité observés lors de la pyrolyse du propane et de l'isobutane en présence d'additifs YH*

L'influence de YH sur la *sélectivité* des pyrolyses d'alcanes μH se décomposant selon deux équations stoechiométriques primaires principales a été étudiée expérimentalement sur les exemples suivants: pyrolyse du *propane*, étude de l'influence de $H_2$, $C_3H_6$, HCl, HBr et $H_2S$; pyrolyse de l'*isobutane*, étude de l'influence de HCl, HBr, $H_2S$ et $C_3H_6$.

*Remarque préliminaire concernant l'influence de* $H_2$

Bien que $H_2$ soit un produit primaire principal dans la pyrolyse du propane ou de l'isobutane *purs*, on peut montrer (17) que la théorie "μH, YH" généralisée exposée précédemment lui est applicable. Dans ce cas particulier, le schéma hydraulique de la figure 2 se simplifie (le radical Y· étant identique à H·), mais le

Can. J. Chem. Downloaded from www.nrcresearchpress.com by 210.87.254.5 on 09/06/12
For personal use only.

raisonnement général est directement transposable. On considérera donc $H_2$ comme un additif YH ordinaire.

Dans ce qui suit, nous ne nous intéresserons qu'*au changement de sélectivité* dû à la présence de YH, en faisant provisoirement abstraction de l'influence cinétique globale de cet additif, qui ne peut s'interpréter qu'en prenant en considération les terminaisons nouvelles éventuelles et qui sera traitée au paragraphe 2.3.

L'expérience confirme les prévisions du mécanisme et de l'analogie hydraulique. Comparons les sélectivités $S_{YH}$ et $S$, en reprenant, successivement, l'influence des trois facteurs précités.

*(a) Influence de la nature de l'additif YH*

Considérons l'action de $H_2$,[7] de $C_3H_6$, de HCl, de HBr et de $H_2S$ (4, 5) sur la pyrolyse du *propane* ($P_0$ = 100 Torr), à faible teneur ($x = (YH)_0/(C_3H_8)_0$ = quelques %) et dans le même domaine de température (490–550°C).

Avec $H_2$: $S_{YH} \simeq S$ ($T$ = 550°C, $x$ = 5%)
Avec $C_3H_6$: $S_{YH} \simeq 1{,}2 \times S$ ($T$ = 490°C, $x$ = 2,7%)
Avec $H_2S$: $S_{YH} \simeq 3{,}3 \times S$ ($T$ = 490°C, $x$ = 5%)
Avec HCl: $S_{YH} \simeq 4{,}1 \times S$ ($T$ = 490°C, $x$ = 5%)
Avec HBr: $S_{YH} \simeq 5{,}3 \times S$ ($T$ = 490°C, $x$ = 5%)

Ces résultats sont compatibles avec les importances relatives des nouvelles conduites par rapport aux anciennes; on a, en effet[8] (19–22):

$$(k_{-5A})_{C_3H_6} \simeq (k_{-3'B})_{H_2}{}^{9} < (k_{-5A})_{HCl} \simeq (k_{-5A})_{H_2S} < (k_{-5A})_{HBr}$$

et

$$(k_{-5B})_{C_3H_6} \simeq (k_{-3''B})_{H_2}{}^{9} < (k_{-5B})_{HCl} \simeq (k_{-5B})_{H_2S} < (k_{-5B})_{HBr}$$

L'influence relative de HCl, HBr, $H_2S$ (5, 6) et $C_3H_6$ (11, 13) sur la sélectivité de la pyrolyse de l'*isobutane* est analogue à celle observée dans le cas du propane.

*(b) Influence de la teneur en additif*

Lorsque $H_2$ est ajouté en petite quantité au propane (quelques %), vers 550°C, *on n'observé pas de changement de sélectivité*.[7]

En revanche, lorsque la teneur en $H_2$ est grande (par exemple $x = (H_2)_0/(C_3H_8)_0 = 21$), on constate, toujours vers 550°C, *un net changement de sélectivité*: $S_{YH}/S = 2{,}7$. Dans ces conditions les nouvelles conduites (−3′B) et (−3″B) ont des diamètres comparables à ceux des anciennes conduites qui assuraient les échanges $\mu_A\cdot \leftrightarrow \mu_B\cdot$ dans la pyrolyse du propane pur.

*(c) Influence de la température*

Vers 550°C l'addition de 21 fois plus de $H_2$ que de propane conduit, comme on vient de le voir à une *nette augmentation* de la sélectivité.

Vers 600°C, pour une teneur voisine en $H_2$: $x = 23$, on observe seulement une *très légère croissance de la sélectivité* par rapport à sa valeur dans la pyrolyse du propane pur (17).

Au-dessus de 650°C, l'expérience montre (17) que, pour cette même teneur, *aucun changement de sélectivité* ne se produit. Les travaux de Kunugi *et al.* (23) entre 700 et 800°C, pour $x$ = 7,5 sont compatibles avec ces observations.

*2.2.5. Remarque*

Considérons les variations de $R_{YH}$ (relation II) et de $S_{YH}/S$ (relation VIII) en fonction de la teneur en

[7]C. Richard. Résultats non encore publiés.

[8]On a supposé que le rapport des constantes de vitesse $k$ et $k'$ correspondant à:

$$R\cdot + YH \xrightarrow{k} RH + Y\cdot$$

$$R\cdot + Y'H \xrightarrow{k'} RH + Y'\cdot$$

était le même quel que soit le radical alcoyle R· attaquant YH ou Y′H. Les tables fournissent les constantes de vitesse correspondant à l'attaque du radical $CH_3\cdot$ sur différents additifs YH. Nous avons supposé que les rapports des différents $k$ sont conservés si $CH_3\cdot$ est remplacé par p-$C_3H_7\cdot$ ou s-$C_3H_7\cdot$.

[9]Dans le cas particulier où YH est $H_2$, les processus [−5A] et [−5B] deviennent, respectivement, les processus inverses [−3′B] et [−3″B] de deux processus existant dans la pyrolyse de μH pur.

Can. J. Chem. Downloaded from www.nrcresearchpress.com by 210.87.254.5 on 09/06/12
For personal use only.

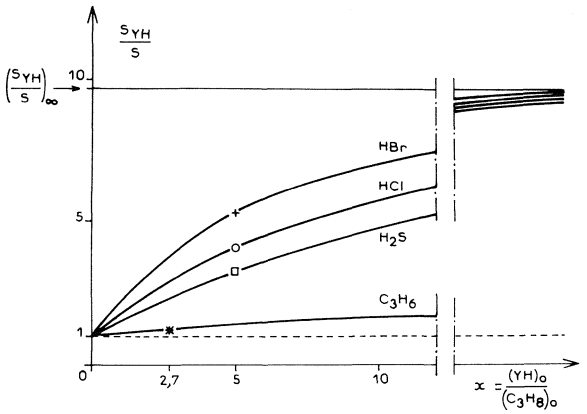


FIG. 5. Pyrolyse du propane en présence d'additifs YH. Variations, qualitatives, du rapport $S_{YH}/S$ des sélectivités en présence et en l'absence de YH en fonction de la teneur $x$ en YH. Réacteur fermé – $T$ = 490°C.

additif: $x = (YH)_0/(\mu H)_0$. Quand $x = 0$, $R_{YH} = R$ et $S_{YH}/S = 1$; quand $x \to \infty$, $R_{YH}$ se simplifie et devient: $R_\infty = \gamma(k_{-5A}/k_{-5B})$.

Compte-tenu de $\gamma = k_{5B}/k_{5A}$, $R_\infty$ s'écrit: $R_\infty = K_{5B}/K_{5A}$, où $K_{5B}$ et $K_{5A}$ sont les constantes d'équilibre des processus [5B] [−5B] et [5A] [−5A].

Ceci signifie que s'établit alors un double équilibre:

$$\mu_A\cdot + YH \underset{5A}{\overset{-5A}{\rightleftharpoons}} Y\cdot + \mu H \underset{-5B}{\overset{5B}{\rightleftharpoons}} \mu_B\cdot + YH$$

et que les radicaux $\mu_A\cdot$ et $\mu_B\cdot$ sont à l'équilibre thermodynamique: $\mu_A\cdot \overset{K}{\rightleftharpoons} \mu_B\cdot$

$$R_\infty = K = (\mu_B\cdot)/(\mu_A\cdot)$$

Les données de la littérature (24) permettent de prévoir, par exemple dans le cas du propane, que:

$$K = \frac{(\mu_B\cdot)}{(\mu_A\cdot)} \simeq 3{,}8 \text{ à } 490°C \quad \text{et} \quad 2{,}6 \text{ à } 650°C$$

Notons que ces valeurs sont compatibles avec le fait que nous avons considéré précédemment que les conduites (−5A) et (−5B) avaient des diamètres voisins (Sect. 2.2.).

Pour un corps μH donné, la valeur de $R_\infty$ est ainsi *indépendante de la nature de YH* et ne dépend que de la *température*. Il en est de même du rapport $(S_{YH}/S)_\infty$ à teneur "infinie" en YH.

La figure 5 représente ainsi, qualitativement, les courbes de variation de $S_{YH}/S$ en fonction de $x$, dans le cas du *propane*, à 490°C, pour 4 additifs: $C_3H_6$, $H_2S$, HCl et HBr. La valeur de l'asymptote $(S_{YH}/S)_\infty$ commune à ces 4 courbes est environ 9,7 à cette température;[10] seule la forme des courbes dépend de la nature de l'additif. Les 4 points expérimentaux permettent de positionner qualitativement les courbes les unes par rapport aux autres.

A 650°C l'asymptote ne correspond plus qu'à $(S_{YH}/S)_\infty = 5{,}6$. Pour un additif et une teneur $x$ donnés, le changement de sélectivité est donc d'autant plus marqué que la température est plus basse.

Ainsi le mécanisme "μH, YH" généralisé et l'analogie hydraulique pour la propagation des chaînes permettent de regrouper et d'interpréter des résultats expérimentaux variés sur les phénomènes de changement de sélectivité par action d'un additif hydrogéné.

*2.3. Influence cinétique globale de YH sur les réactions [A] et [B] de pyrolyse de μH*

Comme on l'a vu sur l'exemple de la pyrolyse du néopentane (Premier Mémoire (1)), l'effet cinétique global dépend: de l'effet cinétique au niveau des propagations (interprété par l'analogie hydraulique); de la présence de *terminaisons nouvelles éventuelles*. Selon l'importance de ces dernières, l'effet cinétique global peut être très variable.

Nous ne traiterons de l'influence de YH que sur la stoechiométrie [A], le comportement de la

[10]Les constantes de vitesses de la littérature utilisées figurent dans la référence 17.

Can. J. Chem. Downloaded from www.nrcresearchpress.com by 210.87.254.5 on 09/06/12
For personal use only.

stoechiométrie [B] se déduisant de celui de [A] par les considérations de *sélectivité* développées précédemment.

Nous avons vu que l'*effet accélérateur au niveau des propagations* dépend de la taille de la nouvelle conduite (4A) par rapport aux conduites (3′A) et (3″A). Pour une même teneur en YH, cet effet dépend donc de la constante de vitesse du processus (4A).

Les données de la littérature (19–22) conduisent, dans le cas de la pyrolyse du *propane*, aux inégalités suivantes:

$$(k_{4A})_{HBr} > (k_{4A})_{HCl} \simeq (k_{4A})_{H_2S} > (k_{4A})_{H_2} \simeq (k_{4A})_{C_3H_6}$$

En ne prenant en compte *que le facteur accélérateur dû au processus [4A]*, on devrait observer les phénomènes suivants.

L'effet accélérateur global $\Phi_{HBr}{}^{A}$, à très faible avancement, de HBr sur la stoechiométrie [A] devrait être supérieur à ceux observés avec HCl ($\Phi_{HCl}{}^{A}$) ou $H_2S$ ($\Phi_{H_2S}{}^{A}$). Or l'expérience (4, 5) montre que, vers 500°C et pour $x = 5\%$: $\Phi_{HBr}{}^{A} \simeq 3{,}7$ (cf. Fig. 6a, courbe 1), $\Phi_{H_2S}{}^{A} \simeq 1{,}8$ (cf. Fig. 6a, courbe 2), $\Phi_{HCl}{}^{A} \simeq 4{,}9$ (cf. Fig. 6a, courbe 3). L'inversion, dans le cas de HBr et HCl, est due aux terminaisons nouvelles, plus importantes avec HBr qu'avec HCl.

HCl devrait plus accélérer la stoechiométrie [A] que $H_2$. C'est effectivement ce que l'on observe vers 500–550°C (4, 5, voir aussi la note en bas de page no 1): $\Phi_{HCl}{}^{A} \simeq 4{,}9$ alors que $\Phi_{H_2}{}^{A} \simeq 1$, pour une même teneur $x = 5\%$ (cf. Fig. 6a: courbes 3 et 4). Il faut ajouter de grosses quantités de $H_2$ pour obtenir un effet accélérateur notable sur la stoechiométrie [A]: $\Phi_{H_2}{}^{A} \simeq 4{,}5$ pour $x = 21$, vers 550°C[7] (cf. Fig. 7: courbe 1).

$H_2$ et $C_3H_6$ devraient avoir le même effet cinétique global sur la stoechiométrie [A]. En réalité $H_2$ n'a pas d'effet (à faible teneur),[7] alors que $C_3H_6$ *inhibe* fortement la stoechiométrie [A]: $\Phi_{C_3H_6}{}^{A} = 0{,}35$ pour $x = 2{,}7\%$ (4) (cf. Fig. 6a: courbes 4 et 5). Les terminaisons nouvelles importantes dues à la présence du radical allyle $C_3H_5\cdot$ peu réactif, sont responsables de cette action inhibitrice.[11]

En combinant maintenant l'effet cinétique de YH sur la stoechiométrie [A] et l'effet de changement de sélectivité, on peut imaginer les 5 cas possibles suivants:

*1er cas*: [A] est accélérée
[B] est accélérée de façon identique

C'est le cas de l'influence de $H_2$ sur $C_3H_8$ à haute température (≥650°C) (17): cf. courbes 3 et 4 de la figure 7.

*2ème cas*: [A] est accélérée
[B] est accélérée plus faiblement ou reste inchangée

C'est le cas: de l'influence de $H_2$ sur $C_3H_8$ à plus basse température (<600°C)[7]: cf.: courbes 1 et 2 de la figure 7; de l'influence de HCl sur $C_3H_8$ vers 500°C (4, 5): cf. courbes 3 des figures 6a et 6b; de l'influence de HCl sur i-$C_4H_{10}$ vers 500°C (5, 6).

*3ème cas*: [A] est accélérée
[B] est inhibée

C'est le cas: de l'influence de HBr ou $H_2S$ sur $C_3H_8$ (4, 5): cf. courbes 1 et 2 des figures 6a et 6b; de l'influence de HBr ou $H_2S$ sur i-$C_4H_{10}$ (5, 6).

*4ème cas*: [A] est inhibée
[B] est inhibée de façon identique

Nous n'avons pas actuellement d'exemple illustrant ce cas.

*5ème cas*: [A] est inhibée
[B] l'est également, mais plus fortement

C'est le cas de l'influence de $C_3H_6$ sur $C_3H_8$ (4). Les courbes 5 des figures 6a et 6b montrent que le changement de sélectivité n'est pas très important. Ce cas correspond également à l'influence de $C_3H_6$ sur i-$C_4H_{10}$ (11, 13).

[11]Rappelons que les radicaux allyle, formés à partir du propène, produit primaire principal dans la pyrolyse du propane *pur*, sont les principaux responsables de l'*auto-inhibition* de cette réaction (7, 9).

Can. J. Chem. Downloaded from www.nrcresearchpress.com by 210.87.254.5 on 09/06/12
For personal use only.

Can. J. Chem. Downloaded from www.nrcresearchpress.com by 210.87.254.5 on 09/06/12
For personal use only.

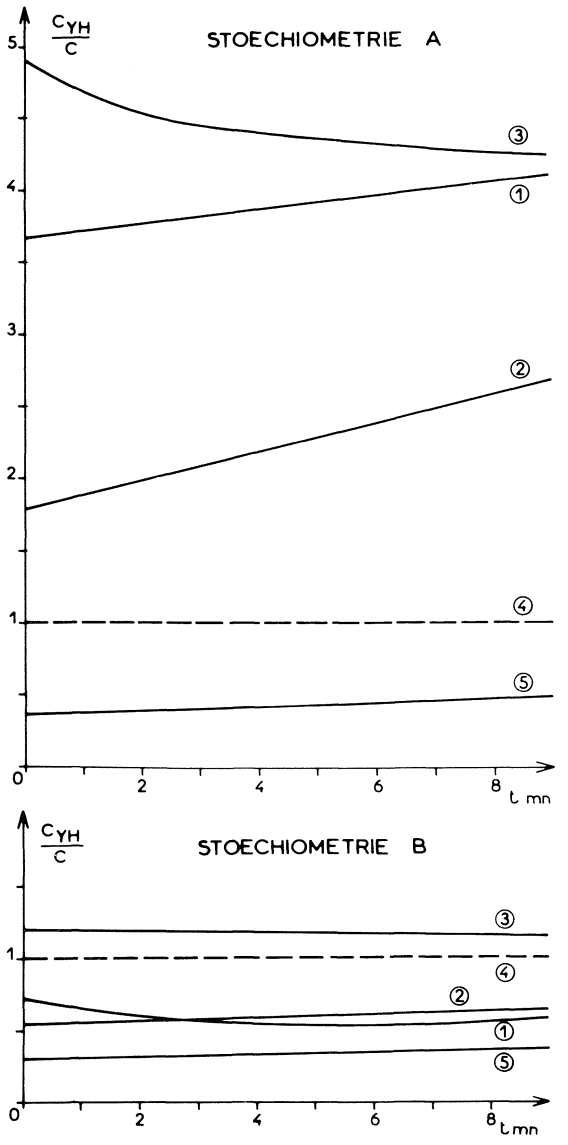


FIG. 6. Pyrolyse du propane en présence d'additifs YH. Réacteur fermé. Variations du rapport $C_{YH}/C$ de la concentration d'un produit primaire en présence de YH sur celle en l'absence de YH, en fonction du temps de séjour; (a): produit principal représentatif de la stoechiométrie [B]: $C_3H_6$ pour les courbes 1, 2, 3 et 4; $H_2$ pour la courbe 5.

| Courbe | YH | $x = (YH)_0/(C_3H_8)_0$ (en %) | $T$ (°C) |
|---|---|---|---|
| 1 | HBr | 5 | 490 |
| 2 | $H_2S$ | 5 | 490 |
| 3 | HCl | 5 | 490 |
| 4 | $H_2$ | 5 | 550 |
| 5 | $C_3H_6$ | 2,7 | 490 |

*2.4. Remarque*

Nous avons noté (cf. Introduction) que, pour le propane ou l'isobutane, la réaction [A] est du type "néopentane" et la réaction [B] du type "éthane". En raison de ces ressemblances, on pourrait être tenté de considérer comme évident le fait qu'en présence d'un corps hydrogéné YH donné, la réaction [A] se comporte cinétiquement comme la pyrolyse du néopentane et la réaction [B] comme la décomposition

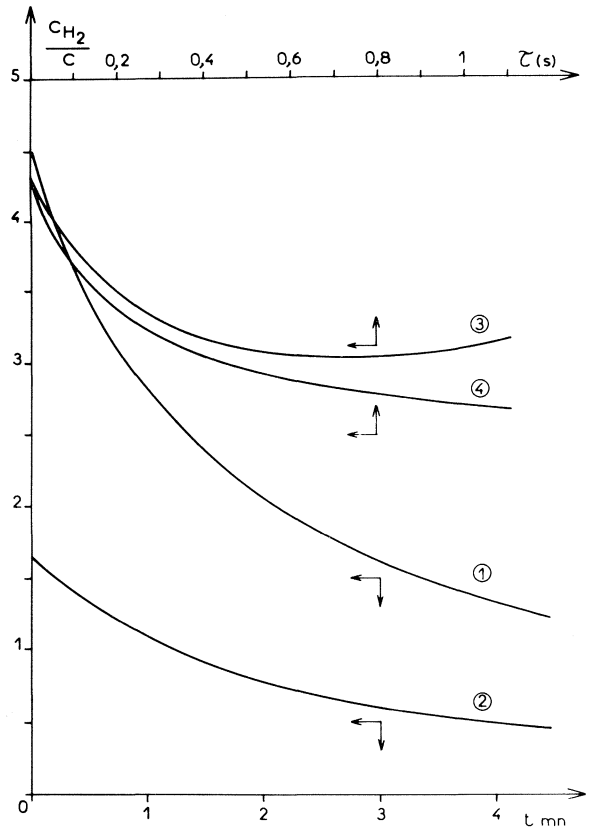


FIG. 7. Pyrolyse du propane en présence d'hydrogène. Variations du rapport $C_{H_2}/C$ de la concentration d'un produit primaire principal en présence d'hydrogène sur celle en l'absenced'hydrogène, en fonction: soit du temps de séjour $t$ (réacteur fermé, $T$ = 550°C, $x = (H_2)_0/(C_3H_8)_0 = 21$)[7], courbe 1: $C_2H_4$ (stoechiométrie [A]), courbe 2: $C_3H_6$ (stoechiométrie [B]); soit du temps de passage τ (réacteur ouvert parfaitement agité en régime permanent, $T$ = 650°C, $x = (H_2)_0/(C_3H_8)_0 = 23$ (17)), courbe 3: $C_2H_4$ (stoechiométrie [A]), courbe 4: $C_3H_6$ (stoechiométrie [B]).

de l'éthane. Mais ce raisonnement serait trop simpliste car, comme nous l'avons vu, des processus complexes de croisement de chaînes interviennent.

L'influence de $H_2$, à forte teneur, sur la pyrolyse du propane représente un contre-exemple typique du raisonnement simpliste (cf. Fig. 7). La stoechiométrie [B] est *accélérée*, aussi bien à 550°C ($\Phi_{H_2}^{B}$ = 1,65, pour $x$ = 21) qu'à 650°C ($\Phi_{H_2}^{B}$ = 4,3, pour $x$ = 23) alors que $H_2$ ne peut accélérer la pyrolyse de l'éthane (25).

### 3. Cas d'une pyrolyse à plus de deux stoechiométries

Dans le premier mémoire (1), nous avons examiné le cas simple d'une substance organique se décomposant selon *une seule* stoechiométrie primaire principale. Aux paragraphes 1 et 2 de ce second mémoire, nous avons considéré le cas, déjà plus complexe, d'une pyrolyse à *deux* stoechiométries. Examinons maintenant le cas, plus complexe encore, d'une substance organique se décomposant selon *plus de deux* stoechiométries.

La pyrolyse du n-*butane* constitue un exemple de ce type, puisqu'elle implique *trois* stoechiométries primaires principales (26, 27):

[$A_1$] $n$-$C_4H_{10} = C_3H_6 + CH_4$

[$A_2$] $n$-$C_4H_{10} = C_2H_4 + C_2H_6$

[B] $n$-$C_4H_{10} = 2C_2H_4 + H_2$

Cette réaction a été interprétée par un mécanisme de type "βμ" généralisé.

Can. J. Chem. Downloaded from www.nrcresearchpress.com by 210.87.254.5 on 09/06/12
For personal use only.

Il a été montré (5, 14) que, vers 500°C, $H_2S$ *inhibe* la réaction [B] et, au contraire, *accélère* les réactions [$A_1$] et [$A_2$], qui tendent ainsi à devenir prépondérantes quand la concentration de $H_2S$ augmente. Ces modifications *cinétiques* et ces changements de *sélectivité* provoqués par $H_2S$ dans la décomposition thermique du *n*-butane ont été confirmés vers 600–650°C (15).

Par ailleurs, Rebick (15) a observé récemment des effets semblables de $H_2S$ sur la pyrolyse d'autres hydrocarbures (*n*-hexadécane, dodécène-1, *n*-butylbenzène, tétraline).

Tous ces effets de $H_2S$ sur des décompositions thermiques ont été expliqués essentiellement sur la base d'une extension du mécanisme "μH, YH" au cas d'une pyrolyse à plusieurs stoechiométries.

Notons enfin qu'au moins un procédé industriel utilise l'influence de $H_2S$ sur le craquage d'hydrocarbures (16).

## 4. Conclusion

Pour la pyrolyse (à très faible avancement) d'une substance organique μH (propane ou isobutane par ex.) impliquant *deux* stoechiométries principales:

[A] $\mu H = m_A + CH_4$

[B] $\mu H = m_B + H_2$

et un mécanisme radicalaire en chaînes de type "βμ" généralisé, l'*analogie hydraulique* utilisée ici pour représenter la *propagation* des chaînes nous a permis d'expliquer l'influence de la température et de la pression initiale sur la *sélectivité* de la décomposition de μH pur (importance de [A] par rapport à [B]).

Le mécanisme "μH, YH" généralisé et l'analogie hydraulique nous ont montré par ailleurs qu'un additif hydrogéné YH doit tendre à *augmenter* la *sélectivité* de la pyrolyse de μH et nous avons pu prévoir l'effet global de YH sur les *vitesses* initiales des réactions [A] et [B] de décomposition de μH. Nous avons montré que ces prévisions théoriques sont bien vérifiées expérimentalement. On rend ainsi compte de nombreuses observations faites lors de l'étude de l'influence d'additifs hydrogénés variés (HCl, HBr, $H_2S$, $H_2$, $C_3H_6$) sur la *cinétique* et la *sélectivité* de la pyrolyse du *propane* ou de l'*isobutane*.

Le mécanisme "μH, YH" généralisé permet également d'interpréter des *effets semblables* de $H_2S$ dans le cas de substances organiques se décomposant selon *plus de deux* stoechiométries primaires principales (*n*-butane, *n*-hexadécane, dodécène-1, *n*-butylbenzène, tétraline).

Rappelons aussi (cf. mémoire I) que le mécanisme "μH, YH" a déjà permis de rendre compte de phénomènes d'*accélération* ou d'*inhibition*, par des corps hydrogénés, de la pyrolyse de substances impliquant *une seule* stoechiométrie primaire principale.

En conclusion, ce mécanisme fournit une représentation synthétique et cohérente d'effets variés de divers additifs hydrogénés sur la *cinétique* et la *sélectivité* du craquage de nombreuses substances organiques; l'*analogie hydraulique* utilisée ici pour représenter la *propagation* des chaînes dans ces réactions aide à mieux saisir la signification microscopique des phénomènes observés.


1. G. Scacchi, F. Baronnet et M. Niclause. Can. J. Chem. **60**, 249 (1982).
2. P. Goldfinger, M. Letort et M. Niclause. Volume commémoratif Victor Henri: Contribution à l'étude de la structure moléculaire. Desoer. Liège. 1947–1948. p. 283.
3. M. Niclause, R. Martin, F. Baronnet et G. Scacchi. Rev. Inst. Fr. Pétrole, **21**, 1724 (1966).
4. J. Y. Jezequel. Thèse de Doctorat ès Sciences physiques, Nancy, 1977.
5. M. Niclause, F. Baronnet, G. Scacchi, J. Muller et J. Y. Jezequel. Communication au 1st Chemical Congress of the North American Continent, Mexico City (Mexique), 30 nov.–5 déc. 1975; A.C.S. Symposium Series no 32, ACS, Washington, 17 à 37 (1976).
6. J. Muller. Thèse de Doctorat ès Sciences physiques, Nancy, 1973.
7. J. Y. Jezequel, F. Baronnet et M. Niclause. J. Chim. phys, **75**, 773 (1978).
8. J. Y. Jezequel, F. Baronnet et M. Niclause. J. Chim. phys, **75**, 991 (1978).
9. J. Y. Jezequel, F. Baronnet et M. Niclause. J. Chim. phys, **71**, 1549 (1974).
10. D. A. Leathard et J. H. Purnell. Proc. R. Soc. London, Ser. A, **305**, 517 (1968); D. A. Leathard et J. H. Purnell. Proc. R. Soc. London, Ser. A, **306**, 553 (1968).
11. J. A. Rondeau, F. Baronnet et M. Niclause. C.R. Acad. Sci. Paris, Ser. C, **274**, 668 (1972).
12. R. S. Konar, R. M. Marshall et J. H. Purnell. Int. J. Chem. Kinet. **5**, 1007 (1973).
13. F. Billaud. Thèse de Doctorat ès Sciences physiques, Nancy, 1980.
14. J. F. Large, R. Martin et M. Niclause. C.R. Acad. Sci. Paris, Ser. C, **274**, 332 (1972).
15. C. Rebick. Hydrogen transfer catalysis in hydrocarbon pyrolysis. *In* Frontiers of free radical chemistry. *Edité par* W. A. Pryor. Academic Press, New York. 1980. pp. 117–137.
16. D. A. Hutchings, K. J. Frech et F. H. Hoppstock. Industrial and laboratory pyrolyses. ACS Symposium Series, **32**, Washington, DC. 1976. pp. 178–196; K. J.


Can. J. Chem. Downloaded from www.nrcresearchpress.com by 210.87.254.5 on 09/06/12
For personal use only.

FRECH, F. H. HOPPSTOCK et D. A. HUTCHINGS. ACS Symposium Series, Washington, DC. 1976. pp. 197–217
17. C. JUSTE. Thèse de Docteur-Ingénieur, Nancy, 1980.
18. R. A. BACK. J. Am. Chem. Soc. **86**, 2558 (1964).
19. V. N. KONDRATIEV. Rate constants of gas phase reactions. NBS (1972).
20. J. A. KERR et M. J. PARSONAGE. Evaluated kinetic data on gas phase hydrogen transfer. Reaction of methyl radicals. Butterworths, London and Boston. 1976.
21. A. F. TROTMAN-DICKENSON et G. S. MILNE. Tables of bimolecular gas reactions. NSRDS–NBS. no 9 (1967).
22. D. L. ALLARA et R. SHAW. J. Phys. Chem. **9**, 523 (1980).
23. T. KUNUGI, H. TOMINAGA, S. ABIKO et A. NAMATAME. Int. Chem. Eng. **7**, 550 (1967).
24. S. W. BENSON. Thermochemical kinetics. 2nd ed. John Wiley and Sons, New York. 1976.
25. G. SCACCHI. Thèse de Doctorat ès Sciences physiques, Nancy, 1969.
26. J. F. LARGE. Thèse de Doctorat ès Sciences physiques, Nancy, 1970.
27. J. F. LARGE, R. MARTIN et M. NICLAUSE. Bull. Soc. Chim. Fr. 961 (1972).

Can. J. Chem. Downloaded from www.nrcresearchpress.com by 210.87.254.5 on 09/06/12
For personal use only.

# Modulation spectroscopy. Kinetics for the self-reactions of some α-aminoalkyl radicals in solution[1]

PAUL R. MARRIOTT, ARLINDO L. CASTELHANO, AND DAVID GRILLER
*Division of Chemistry, National Research Council of Canada, Ottawa, Ont., Canada K1A 0R6*

Received August 6, 1981

PAUL R. MARRIOTT, ARLINDO L. CASTELHANO, and DAVID GRILLER. Can. J. Chem. **60**, 274 (1982).

The optical spectra and reaction kinetics of some α-aminoalkyl radicals, $R\dot{C}HN(CH_2R)_2$; R ≡ H, Me, Ph, were measured in solution using the technique of modulation spectroscopy. These radicals undergo diffusion controlled self-reaction with rate constants $\simeq 10^9\ M^{-1}\ s^{-1}$. When R ≡ Ph, the absorption spectrum has a well defined maximum at 346 nm; $\varepsilon = 3390\ M^{-1}\ cm^{-1}$, while the spectra when R ≡ H or Me were less intense ($\varepsilon_{346}$ nm $\simeq 500\ M^{-1}\ cm^{-1}$) and tailed into the visible. These spectra are substantially red-shifted when compared with those of simple alkyl radicals, an effect which is thought to be due to the interaction between the unpaired electron and the lone pair of electrons on nitrogen.

PAUL R. MARRIOTT, ARLINDO L. CASTELHANO et DAVID GRILLER. Can. J. Chem. **60**, 274 (1982).

Faisant appel à la technique de spectroscopie modulée en solution, on a mesuré les spectres optiques et les cinétiques de réaction de quelques radicaux α-aminoalkyles, $R\dot{C}HN(CH_2R)_2$ où R ≡ H, Me, Ph. Ces radicaux subissent une auto-réaction, contrôlée par la diffusion, avec une constante de vitesse de $10^9\ M^{-1}\ s^{-1}$. Le spectre d'absorption, lorsque R = Ph, a un maximum bien défini à 346 nm; $\varepsilon = 3390\ M^{-1}\ cm^{-1}$. Cette absorption est moins intense quand R = H ou Me ($\varepsilon_{346\ nm}$ de $500\ M^{-1}\ cm^{-1}$) et s'étale dans le visible. Ces spectres glissent de façon marquée vers le rouge si on les compare à ceux des radicaux alkyles simples; c'est un effet que l'on attribue à l'interaction entre l'électron non apparié et le doublet libre de l'azote.

[Traduit par le journal]

## Introduction

Modulation spectroscopy has been successfully applied to the study of transient intermediates in the gas phase (see for example refs. 1 and 2). The technique involves photolytic generation of a transient using modulated initiation coupled with phase sensitive detection of that transient. This combination allows spectroscopic detection of short lived intermediates with high signal-to-noise levels and also provides information on the kinetics of their reactions.

The most recent advance in the field of modulation spectroscopy has been made by Huggenberger *et al.* (3) who have constructed a spectrometer for the study of free radicals *in solution*. With this instrument, radicals are generated using sinusoidally modulated light and are detected optically. In this work, we have used such a spectrometer in a kinetic study of the self-reactions of some α-aminoalkyl radicals.

## Experimental

*Materials*

All materials were commercially available. Iso-octane (Spectrograde) and trimethylamine were used as received. Di-*tert*-butyl peroxide was purified by chromatography through alumina which removes traces of the hydroperoxide impurity. Tribenzylamine was purified by recrystallization from ethanol. Triethylamine was purified by the standard procedure (4) and was distilled under nitrogen.

*Apparatus*

The modulation spectrometer used in this work follows closely on the design developed by Huggenberger and Fischer (3*b*). It is shown diagramatically in Fig. 1.

A fluorescence flow cell (Helma 178f-QS) was used as the sample chamber. Radicals were generated by irradiating solutions through the front window of the cell (10 mm × 10 mm) using light from a 1000 W, dc-powered mercury–xenon lamp (Hanovia 997B001; Oriel 6141 lamp housing). The irradiating light was modulated as a sine wave using a mechanical chopper (Brookdeal 9479) which was fitted with sine shaped irises.

A magnified image of the arc was brought to a focus at the sample cell which was positioned in a region of the image of fairly uniform light intensity. The quality of the sinusoidal modulation and the uniformity of light intensity were checked by manoeuvering a photomultiplier tube and housing with a small entrance slit (0.5 × 0.5 mm) throughout the region normally occupied by the sample chamber. The modulated sine wave generated by the irradiating light was compared on an

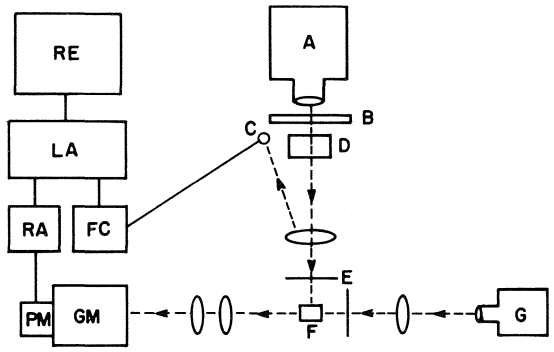


FIG. 1. Block diagram of modulation spectrometer. A, 1000 W mercury xenon lamp. B, light chopper. C, photocell. D, Co/Ni aqueous filter solution. E, cut-off filters. F, sample cell. FC, frequency counter. G, 100 W xenon lamp. GM, grating monochrometer. LA, lock-in amplifier. PM, photomultiplier tube. RA, ratiometer. RE, recorder.

[1]NRCC No. 19749.

0008-4042/82/030274-05$01.00/0
©1982 National Research Council of Canada/Conseil national de recherches du Canada

Can. J. Chem. Downloaded from www.nrcresearchpress.com by 210.87.254.6 on 09/06/12
For personal use only.

Can. J. Chem. Downloaded from www.nrcresearchpress.com by 210.87.254.6 on 09/06/12
For personal use only.

oscilloscope with one of the same amplitude and frequency produced by a sine wave generator and was indistinguishable from it. In addition, the maximum variation of light intensity across the sample cell was ± 8% of the mean.

The irradiating light was always passed through a water filter (10 cm path length) which removed much of the infrared radiation. The light could be further filtered using bandpass or cut-off filters.

Changes of optical density in the sample were followed using a monitoring beam arranged at right angles to the irradiating light path. A 100 W xenon lamp (Bausch and Lomb) provided the monitoring light which was passed through the side windows of the sample cell and then through a grating monochromator (Oriel 7240) fitted with photomultiplier tube (RCA 4840) and housing. In kinetic studies cut-off filters were always placed in the monitoring beam to prevent sample photolysis by the interrogating light.

Output from the photomultiplier tube was "terminated" by a suitable resistance. The signal at this point consisted of a large dc component and a very much smaller oscillating component which was due to the modulated absorption of starting materials, transient, and products. A ratiometer was used to divide ac by dc when recording spectra so as to correct for changes in signal intensity due to wavelength-dependent variations in the output of the monitoring light and in the sensitivity of the monochrometer/photomultiplier tube arrangement. In kinetic runs, which were carried out at fixed wavelength, the ratiometer was not used since its circuitry introduced an additional time constant into the system.

The modulated part of the signal was analysed using a lock-in amplifier (PAR 124A). The reference channel of the amplifier was driven by a photocell positioned so as to detect light from the irradiating beam. Finally, the output of the amplifier was displayed on a strip chart recorder.

*Sample preparation and analysis*

In a typical run an iso-octane solution of amine (5–10% v/v) and di-*tert*-butyl peroxide (5% v/v) was purged for ca. 20 min with a stream of nitrogen. The deoxygenated solution was taken up in a syringe and was then passed through the sample cell as ca. 1 mL/min by the use of a mechanical syringe drive.

Kinetic runs were carried out at fixed wavelength, with a 312 nm cut-off filter and an aqueous cobalt – nickel sulphate filter solution in the photolysis beam. This provides a window for photolysis of the peroxide between 312 and 340 nm. The concentration of reagents was adjusted so that > 90% of the incident light was transmitted in this wavelength range. In addition, the monitoring beam was always filtered with 316 nm or 325 nm cut-off filters. This procedure, combined with uniform irradiation at the front face of the cell, ensures a reasonably homogeneous distribution of transient which is necessary for the accurate analysis of second order kinetics. In addition, the sample flow rate was adjusted so that reagent depletion was < 1% and was further checked spectrophotometrically to ensure that the products did not absorb significantly at the photolysis wavelengths. The photolyzed mixture was analysed by vpc for *tert*-butyl alcohol using benzene as an internal standard (24 ft, 20% Carbowax 20 M).

*Electron paramagnetic resonance experiments*

A limited number of epr experiments were carried out on the amine systems using procedures which have been previously described (5).

## Results and discussion

α-Aminoalkyl radicals are formed extremely efficiently in solution by the reaction of *tert*-butoxyl radicals with amines, eq. [1] and [2]. Rate constants for these reactions are among the largest measured for H abstractions by *tert*-butoxyl with $k_2 \simeq 10^8\ M^{-1}\ s^{-1}$ (5). Only abstractions at molecules such as 1,4-cyclohexadiene, which give rise to highly stabilized radicals, proceed with rate constants of this magnitude (6). Moreover, abstractions at amines show a pronounced stereoelectronic effect. That is, H abstraction is most rapid when the C—H bond being broken is eclipsed with the axis of the lone pair orbital on nitrogen (5).

[1] $t\text{-BuO-OBu-}t \xrightarrow{\hbar\nu} 2t\text{-BuO}\cdot$

[2] $t\text{-BuO}\cdot + (RCH_2)_3N \rightarrow t\text{-BuOH} + \underset{\mathbf{1}}{R\dot{C}HN(CH_2R)_2}$

[3] $\mathbf{1} + \mathbf{1} \rightarrow$ nonradical products

**1***a* R = H; **1***b* R = Me; **1***c* R = Ph

While α-aminoalkyls can be efficiently generated they are nevertheless extremely difficult to detect in solution by using epr spectroscopy (5, 7, 8). Only the spectrum of $Me_2N\dot{C}H_2$ is easily detected and this is probably because the spectral linewidth is small, ca. 0.1 G. In all other cases, spectra are barely detectable, presumably because of the large number of hyperfine interactions and greater linewidths. This means, of course, that α-aminoalkyls cannot be studied generally using the techniques of kinetic epr spectroscopy. To overcome this problem, we have used modulation spectroscopy to characterize the uv–visible spectra of α-aminoalkyl radicals and to determine the kinetics of their self-reactions.

*Spectra*

In modulation spectroscopy the concentration of a transient species is made to oscillate at a predetermined frequency, e.g. by generating the transient using modulated photolysis. The sample is monitored optically and phase sensitive detection is used to find the signals which oscillate at the modulation frequency. These signals can be due to the disappearance of starting material, the formation of a transient intermediate, or the appearance of products. However, these three components can be differentiated by measuring the phase of the signal detected with respect to the phase of the modulated photolyzing light. The phase relationships between the signals have been previously derived (3) and are shown in Fig. 2.

In this work, we have modulated the photolyzing light as a sine wave which considerably simplifies kinetic analysis of the data. Under this condition, the rate of transient generation can be expressed as

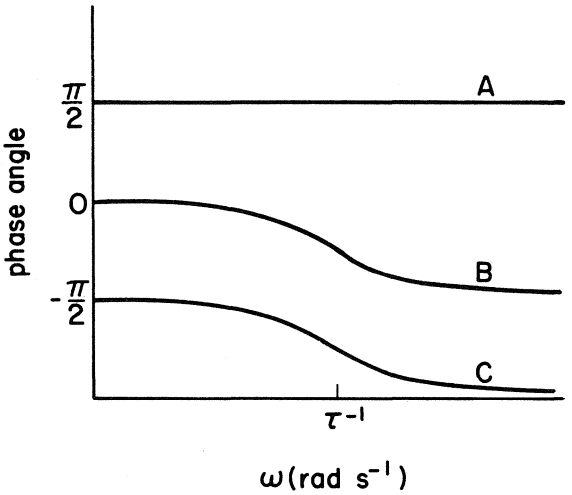


FIG. 2. Frequency dependencies of phases. A, reactant. B, radical. C, product.

a cosine function of the modulation frequency, which leads to simple solutions of the differential equations that describe the reaction kinetics (1, 3, 5, 9). By contrast, square wave or "on–off" modulation (2) requires that the rate of transient generation be expressed as a Fourier series which has obvious disadvantages.

Photolysis of an iso-octane solution of trimethylamine (5% v/v) and di-*tert*-butyl peroxide in the modulation spectrometer gave rise to a spectrum similar to that shown in Fig. 3. In the absence of trimethylamine, only very weak transient absorptions were detected. At the modulation frequencies used in these experiments (10–200 Hz), the phase of the signal lagged behind that of the modulated photolyzing light but did not reach −90° (see Fig. 2). Moreover, the shape of the spectrum was independent of the modulation frequency at which it was recorded. This behaviour implies that the signal is due to a single transient species, which we assign to radical **1***a*.

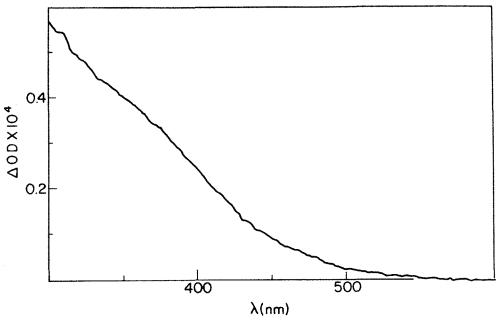


FIG. 3. Optical spectrum of radical **1***b* recorded at a modulation frequency of 43 Hz.

Photolysis of the above solution in the cavity of an epr machine gave rise to an intense spectrum of **1***a* (5), which supports the assignment of the optical spectrum. The signal intensity observed by epr was proportional to the square root of the incident light intensity when the latter was varied by a factor of 100, indicating that the radical decays with second order kinetics. In addition, prolonged photolysis of the sample gave *tert*-butyl alcohol and tetramethylethylenediamine as the major products identified by vpc analysis. Both the epr and modulation results are entirely consistent with the formation and decay of radical **1***a* according to reactions [1]–[3].

A similar optical spectrum was obtained when triethylamine was used in place of trimethylamine in the modulation spectrometer (Fig. 3). However, when tribenzylamine was used, a far more intense spectrum was obtained (Fig. 4) which had a well defined maximum at 346 nm. These spectra showed the properties associated with single transient species and we assign them to radicals **1***b* and **1***c* respectively. Similar spectra have also been obtained in laser flash photolysis experiments[2] and by gas phase modulation spectroscopy.[3]

*Kinetics*

Rate constants, $k_3$, for self-reactions of **1***a–c* were determined at a fixed wavelength. Using the lock-in amplifier, the signals due to the radicals were resolved into components which were out-of-phase and in-phase with the photolyzing light. The ratio of these components is tan $\phi$, where $\phi$ is the *phase angle*, and the vector sum of these components is directly proportional (3) to $\Delta$OD which is the modulated part of the optical density of the transient.

A plot of $-\tan\phi$ versus the modulation frequency, $\omega$, gave the lifetime, $\tau$, of the radicals, eq. [4]. The relationship between $\tau$ and the rate constant for self-reaction of the radicals, $k_3$, is given in eq. [5], where $I_0$ is the maximum rate of radical generation during the modulation cycle. An example of such a plot is given in Fig. 5.

$$[4] \quad -\tan\phi = \omega\tau$$

$$[5] \quad \tau^{-2} = 4k_3I_0$$

An alternative method of analysing the data yields the extinction coefficient for the radical, $\varepsilon$. In this approach, a plot of $(\Delta OD)^{-2}$ versus $\omega^2$ gave a straight line of slope $a$ and intercept $b$ which are related (3) to $\tau$, $\varepsilon$, $I_0$, and $l$, where $l$ is the pathlength of the cell in the monitoring direction, eqs. [6] and

[2]J. C. Scaiano, private communication.
[3]H. Hunziker, private communication.

Can. J. Chem. Downloaded from www.nrcresearchpress.com by 210.87.254.6 on 09/06/12
For personal use only.

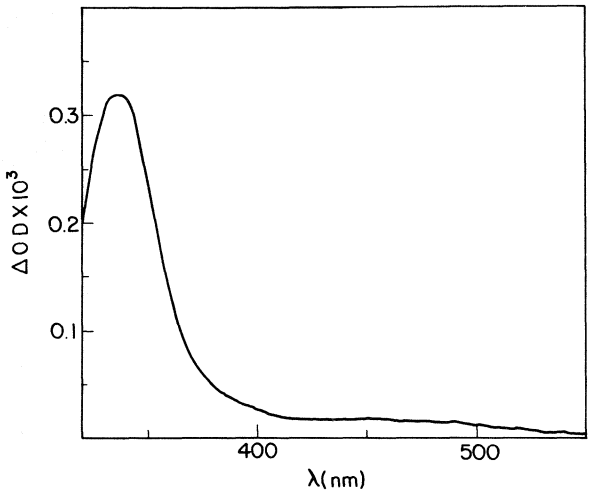


FIG. 4. Optical spectrum of radical 1*c* recorded at a modulation frequency of 43 Hz.

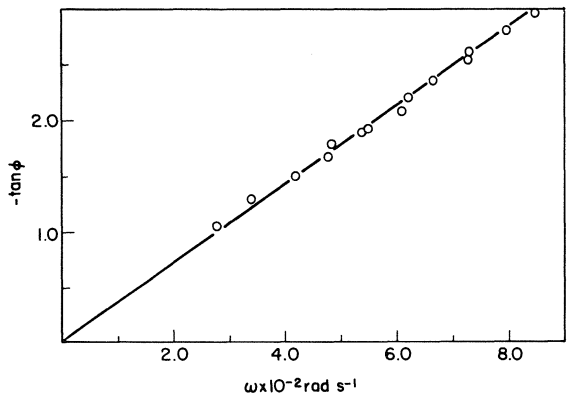


FIG. 5. Frequency dependence of ϕ for radical 1*c* in iso-octane.

[7]; Fig. 6.

[6] $a = 4(\varepsilon l I_0)^{-2}$

[7] $b = 4(\varepsilon l I_0 \tau)^{-2}$

In these experiments the mean rate of radical generation $I_0/2$ was determined by analysing the photolyzed reaction mixtures for *tert*-butanol. Values of τ obtained by the two graphical procedures were identical within experimental error. Moreover, τ was proportional to $I_0^{-\frac{1}{2}}$ when the light intensity was reduced using neutral density filters, which indicates that in all cases the radicals decay by bimolecular reactions. The data are summarized in Table 1. The experimental errors on rate constants and extinction coefficients were ca. ± 30%.

When amines were omitted from the reaction mixture the yield of *tert*-butanol obtained by photolyzing the solution under the conditions of the

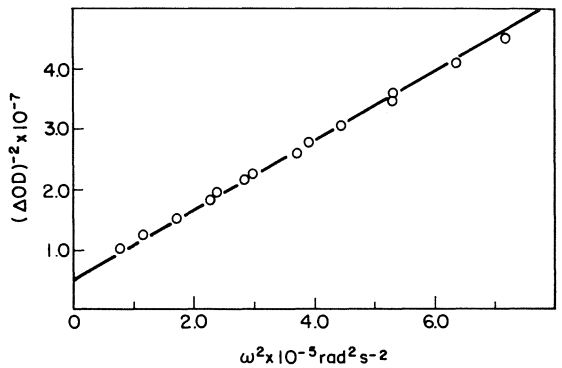


FIG. 6. Frequency dependence of ΔOD for radical 1*c* in iso-octane.

kinetic experiments was the same within experimental error as was obtained in the presence of trimethyl or triethylamine. This indicates that the α-aminoalkyl radicals do not induce decomposition of the peroxide under these experimental conditions. The slight reduction in $I_0/2$ observed when tribenzylamine was used as substrate was presumably due to slight light absorption by the amine in the region where the di-*tert*-butyl peroxide was being photolyzed.

The values of $2k_3$ measured in this work indicate that radicals 1*a–c* undergo diffusion controlled self-reaction. Indeed, $2k_3$ decreases as the size of the radicals increases which is to be expected for a diffusion controlled process. The value of $2k_3$ obtained for 1*a* is in accord with the rate constant for self-reaction of *tert*-butyl (10), i.e. $7.4 \times 10^9$ $M^{-1}$ s$^{-1}$ (294°C; octane solvent) which is a radical of similar size monitored in a solvent of similar viscosity to the iso-octane used in this work. It should be noted that *tert*-butyl has been used as a model for the study of diffusion controlled processes and the kinetics of its self-reaction have been explored in considerable detail (3*b*, 10). Thus, α-aminoalkyl radicals behave kinetically as most other small unhindered alkyls and moreover they do not appear to induce the decomposition of di-*tert*-butyl peroxide at room temperature. We therefore conclude that the failure to detect members of this class of radicals other than 1*a* by epr, in

TABLE 1. Rate constants for the self-reactions of α-aminoalkyl radicals at 298 K

| Radical | $I_0$ ($M^{-1}$ $s^{-1}$) | τ ($s^{-1}$) | ε(340 nm) ($M^{-1}$ cm$^{-1}$) | $2k_3$ ($M^{-1}$ s$^{-1}$) |
|---|---|---|---|---|
| 1*a* | $1.66 \times 10^{-4}$ | $0.94 \times 10^{-3}$ | 493 | $3.4 \times 10^9$ |
| 1*b* | $1.33 \times 10^{-4}$ | $1.41 \times 10^{-3}$ | 445 | $1.9 \times 10^9$ |
| 1*c* | $7.76 \times 10^{-4}$ | $3.57 \times 10^{-3}$ | 3390[a] | $5.1 \times 10^8$ |

[a]Measured at 346 nm.

Can. J. Chem. Downloaded from www.nrcresearchpress.com by 210.87.254.6 on 09/06/12
For personal use only.

solution, must be a consequence of the spectral characteristics of the radicals, e.g. linewidth and number of hyperfine interactions, rather than any intrinsic chemical property.

The uv–visible spectrum of radical **1***c* shows a strong absorption band at 346 nm; $\varepsilon = 3390\ M^{-1}\ cm^{-1}$. This band is typical of benzylic radicals which show strong absorption bands at ~ 316 nm with $\varepsilon_{max} \sim 9000\ M^{-1}\ cm^{-1}$ in hydrocarbon solvents.[4] By contrast, the absorption spectra of **1***a* and **1***b* show no well defined maximum in the accessible wavelength range but "tail" to ca. 500 nm. This "tail" is not generally observed in simple alkyl radicals which tend not to absorb significantly at wavelengths > 280 nm (**3***c*) and must therefore be associated with the interaction of the unpaired electron with the lone pair of electrons on nitrogen.

The electronic interaction in α-aminoalkyl radicals between the unpaired electron and the nitrogen lone pair manifests itself in a number of ways. First, the epr spectra of α-aminoalkyls isolated in matrices (for matrix isolation studies see ref. 8) indicate that there is substantial delocalization of the unpaired electron between the α-carbon and the adjacent nitrogen atom. In addition, the interaction gives rise to a stereoelectronic effect in hydrogen abstractions from amines (5) and to low ionization potentials and high stabilization energies for the radicals themselves (11). The interaction between the unpaired electron and the nitrogen lone pair can be rationalized in terms of the model of the three-electron bond (see, for example, ref. 12). In this picture, two of these three electrons reside on a bonding orbital, while the third lies in the related antibonding orbital. Electronic transitions between these orbitals in α-aminoalkyl radicals presumably give rise to the absorptions observed in the visible region.

[4]For a review of the literature data, see ref. 3*b*.

## Summary

α-Aminoalkyl radicals undergo diffusion controlled self-reaction at 298°C in iso-octane solvent. Their optical absorption spectra are substantially different to those of simple alkyl radicals in that they absorb significantly up to 500 nm. This property is thought to be a consequence of the interaction between the unpaired electron and the lone pair of electrons on the nitrogen atom.

1. H. E. HUNZIKER. IBM J. Res. Dev. **15**, 10 (1971); R. ATKINSON and R. J. CVETANOVIĆ. J. Chem. Phys. **55**, 659 (1971).
2. T. T. PAUKERT and H. S. JOHNSTON. J. Chem. Phys. **56**, 2824 (1972); D. A. PARKES, D. M. PAUL, and C. P. QUINN. J. Chem. Soc. Faraday Trans. I, **72**, 1935 (1976).
3. (*a*) C. HUGGENBERGER, J. LIPSCHER, and H. FISCHER. J. Phys. Chem. **84**, 3467 (1980); (*b*) C. HUGGENBERGER and H. FISCHER. Helv. Chim. Acta, **64**, 338 (1981).
4. L. F. FIESER and M. FIESER. Reagents for organic synthesis. Wiley, New York. 1967.
5. D. GRILLER, J. A. HOWARD, P. R. MARRIOTT, and J. C. SCAIANO. J. Am. Chem. Soc. **103**, 619 (1981).
6. A. EFFIO, D. GRILLER, K. U. INGOLD, J. C. SCAIANO, and S. J. SHENG. J. Am. Chem. Soc. **102**, 6063 (1980).
7. N. H. ANDERSON and R. O. C. NORMAN. J. Chem. Soc. B, 993 (1971).
8. D. E. WOOD and R. V. LLOYD. J. Chem. Phys. **52**, 3840 (1970); **53**, 3932 (1970).
9. H. PAUL. Chem. Phys. **15**, 115 (1976); J. Phys. Chem. **82**, 2754 (1978); Chem. Phys. **40**, 265 (1979); Int. J. Chem. Kinet. **11**, 495 (1979).
10. H. SCUH and H. FISCHER. Int. J. Chem. Kinet. **8**, 341 (1976); Helv. Chim. Acta, **61**, 2463 (1978).
11. D. GRILLER and F. P. LOSSING. J. Am. Chem. Soc. **103**, 1586 (1981).
12. L. PAULING. J. Am. Chem. Soc. **53**, 3225 (1931); R. F. HUDSON. Angew. Chem. Int. Ed. Engl. **12**, 36 (1973); N. C. BAIRD. J. Chem. Educ. **54**, 291 (1977); R. D. HARCOURT. Aust. J. Chem. **31**, 199 (1978); A. R. GREGORY and V. MALATESTA. J. Org. Chem. **45**, 122 (1980); R. D. HARCOURT. J. Am. Chem. Soc. **102**, 5195 (1980).

Can. J. Chem. Downloaded from www.nrcresearchpress.com by 210.87.254.6 on 09/06/12
For personal use only.

# Solubilization sites in micellar sodium octylsulphate solutions by ultrasonic spectroscopy

DAVID J. JOBE, VINCENT C. REINSBOROUGH, AND PETER J. WHITE
*Chemistry Department, Mount Allison University, Sackville, N.B., Canada E0A 3C0*

Received August 11, 1981

DAVID J. JOBE, VINCENT C. REINSBOROUGH, and PETER J. WHITE. Can. J. Chem. **60**, 279 (1982).

Relaxation frequencies $f_c$ and amplitudes $A$ were measured ultrasonically over the 3.5–52.5 MHz range at 25°C for the fast exchange of monomer between micelles and bulk solution in micellar sodium octylsulfate solutions with solubilizates present in small amounts. The additives were cyclohexane, pyridine-2-azo-*p*-dimethylaniline (PADA), benzene, toluene, and *p*-xylene. Only cyclohexane produced no changes in $f_c$ or $A$. The variations in the relaxational parameters suggested that cyclohexane was situated within the micellar core and PADA, primarily in the surface region of the micelle. Benzene and toluene were adsorbed in minute quantities into the micelle surface but, with additive concentrations beyond a few molecules per micelle, were found principally in the micellar core. Toluene, along with *p*-xylene, showed an initial dip in $f_c$ that may indicate that the first few molecules of these additives were incorporated into the palisade layer of the micelle.

DAVID J. JOBE, VINCENT C. REINSBOROUGH et PETER J. WHITE. Can. J. Chem. **60**, 279 (1982).

On a mesuré par ultrason à des fréquences allant de 3,5 à 52,5 MHz et à 25°C les fréquences de relaxation fc et les amplitudes A de l'échange rapide de monomère entre les micelles et la solution dans des solutions micellaires d'octylsulfate de sodium ayant des petites quantités de solubilisants. On a utilisé comme additifs: le cyclohexane, la pyridine-azo-2 diméthylaniline (PADA), le benzène, le toluène et le *p*-xylène. Le cyclohexane est le seul à ne pas influencer les fréquences de relaxation et les amplitudes. Les variations des paramètres de relaxation suggèrent que le cyclohexane est situé dans la masse micellaire alors que la PADA se trouve de façon primaire dans la région de la surface de la micelle. Le benzène et le toluène sont adsorbés en petites quantités dans la surface de la micelle mais, à des concentrations croissantes de l'ordre de quelques molécules par micelle, on les a trouvé principalement dans le noyau micellaire. Le toluène ainsi que le xylène révèlent une diminution initiale de $f_c$ qui indique que les quelques premières molécules de ces additifs sont incorporées dans la couche protectrice de la micelle.

[Traduit par le journal]

## Introduction

The location of solubilizates within micelles in aqueous solution has recently been the object of many spectroscopic studies by various techniques (1–3). The picture that is emerging from these studies is that the surface region of the micelle is much more favoured in this regard than previously thought, especially at low additive concentrations. For example, benzene, which had been reported to be chiefly absorbed into the core of sodium dodecylsulfate micelles (4), was discovered to be primarily in the surface region of the micelles when the mole fraction of benzene was less than 0.01 (1). Since these "mixed micelles" often form microemulsions of industrial, medicinal, and theoretical importance, it is of some value to determine the micellar sites of solubilization for different compounds to throw light on the interactions not only between solubilizate and micelle but also between monomer and micelle. Also, the structure of micelles is still being debated (5, 6) and further probing of these interactions could have bearing on this question.

Ultrasonic spectroscopy has not yet been employed specifically to determine solubilization sites in micelles, but since the fast relaxation observed ultrasonically in micellar solutions has been so well characterized, the technique could well prove to be a useful diagnostic tool in this regard. The process giving rise to this relaxation is the exchange of the monomeric surfactant between the micelle and bulk aqueous solution. Simplistically, one might expect that additives residing in the core of the micelle would have little effect on the dynamics of this exchange while solubilizates adsorbed into the surface region or the palisade layer should appreciably alter the entry or exit rates of the monomer.

To this end, organic compounds of various polarities were introduced in small quantities into micellar sodium octylsulfate (SOS) solutions and the ultrasonic absorptions noted. This particular surfactant, SOS, was chosen because its relaxation frequency fell within the operating frequency range of the equipment (3.5–52.5 MHz). Since some solubilizates, notably alcohols, give rise to a fast relaxation of their own accord involving exchange with the mixed micelles, care must be exercised in their selection to avoid coupling errors. Additives were screened by measuring the ultrasonic absorptions over the frequency range 3.5–52.5 MHz of their solutions in micellar sodium dodecylsulfate, in premicellar concentrations of SOS and in water. Micellar sodium dodecylsulfate solutions show a fast relaxation in the microsecond range which is far removed from the frequency range employed in this work. Thus, if no relaxation process is detectable when additive is present, it can be assumed that the relaxation process observed in additive-

0008-4042/82/030279-06$01.00/0
©1982 National Research Council of Canada/Conseil national de recherches du Canada

Can. J. Chem. Downloaded from www.nrcresearchpress.com by 210.87.254.5 on 09/06/12
For personal use only.

micellar SOS solutions is due only to the monomer–micelle exchange. The other approach that has been already successfully used is to choose a surfactant like sodium dodecylsulphate or tetradecyltrimethylammonium bromide that does not show a relaxation in the ultrasonic range and to work with solubilizates that do (8–10). In this situation, information can be gained about the solubilizate exchange between the bulk solution and micelle.

## Experimental

The pulsed ultrasonic spectrometer has been described in detail elsewhere (11). Sodium octylsulfate (SOS) was obtained from Eastman Kodak while the additives were the highest quality obtainable. No further purifications were carried out. All ultrasonic measurements were conducted at 25.0°C.

Conductivity measurements were performed in benzene–SOS solutions at 25.0°C to determine the critical micelle concentration (cmc). The instrument used was the RC-18A Beckman conductivity bridge with a Jones–Bollinger cell.

## Results

The ultrasonic absorption data ($\alpha/f^2$) over the 3.5–52.5 MHz frequency range for various SOS solutions containing the additives were fitted by computer to the single relaxation equation:

$$[1] \quad \alpha/f^2 = A/[1 + (f/f_c)^2] + B$$

where $A$ and $B$ are relaxational parameters related to the process responsible for the excess absorption and to the background absorption respectively, and $f_c$ is the relaxation frequency. The fit was satisfactory in all instances. The experimental error in $f_c$ is about 5% except in the few cases where $f_c$ fell just outside the experimental range where these essentially extrapolated values admit of greater error, probably about 10%.

For micellar SOS solutions without additives, the $f_c$ values agree with those reported by Gettins *et al.* (12). The cmc values from conductivity measurements for two different additions of benzene, 0.010 and 0.020 *m* θ in SOS solutions, were the same as that for no additive, 0.114 mol dm$^{-3}$, which agrees with previously reported values (12–14).

The $f_c$ values for cyclohexane and pyridine-2-azo-*p*-dimethylaniline (PADA) additions to 0.397 *m* SOS solutions are shown in Figs. 1 and 2. In Fig. 3 is displayed the effect of benzene additions to various SOS solutions with $[C_6H_6]/C_M$ as the concentration co-ordinate where $C_M$ = [SOS] − cmc. $C_M$ is a measure of the micellar concentration and this ratio allows comparison between additive and micellar surfactant on a per mole basis. This same scale was employed to show the $f_c$ and $A$, the relaxation amplitude, dependencies in toluene – micellar SOS solutions (Figs. 4 and 5). Only a few $f_c$ determinations were possible with *p*-xylene in 0.300 *m* SOS solutions because of solubility limitations and these are also included in Fig. 4.

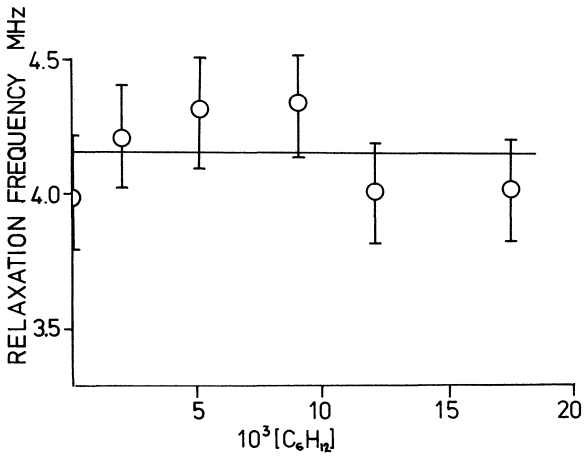


FIG. 1. Effect of cyclohexane additions on the relaxation frequency in 0.397 *m* SOS solutions.

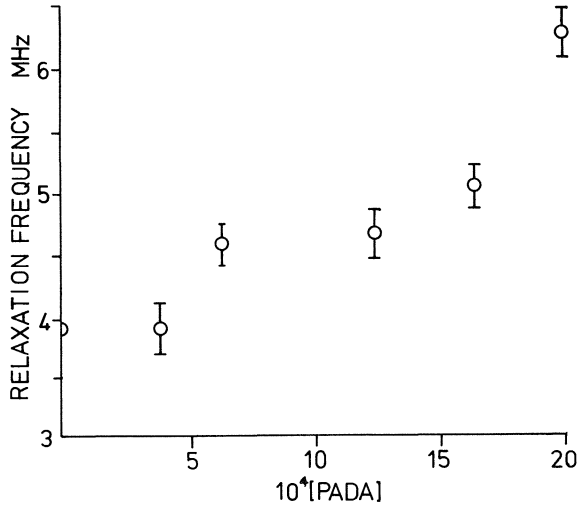


FIG. 2. Effect of PADA additions on the relaxation frequency in 0.397 *m* SOS solutions.

The solubility of benzene in SOS solutions as determined by uv spectroscopy is shown in Fig. 6. These data can be conveniently represented by means of a partitioning constant $K_{benzene}$ defined as $[benzene]_M/[benzene]_B C_M$ where the subscripts M and B refer to the micellar and bulk solution pseudo-phases respectively (15). The value of $K_{benzene}$ in SOS solutions was 30 dm$^3$ mol$^{-1}$.

## Discussion

Aniansson has developed an expression for the relaxation frequency for the fast surfactant exchange in micellar solution for mixed micelles (7), but, for small additions of solubilizate, this expres-

Can. J. Chem. Downloaded from www.nrcresearchpress.com by 210.87.254.5 on 09/06/12
For personal use only.

Can. J. Chem. Downloaded from www.nrcresearchpress.com by 210.87.254.5 on 09/06/12
For personal use only.

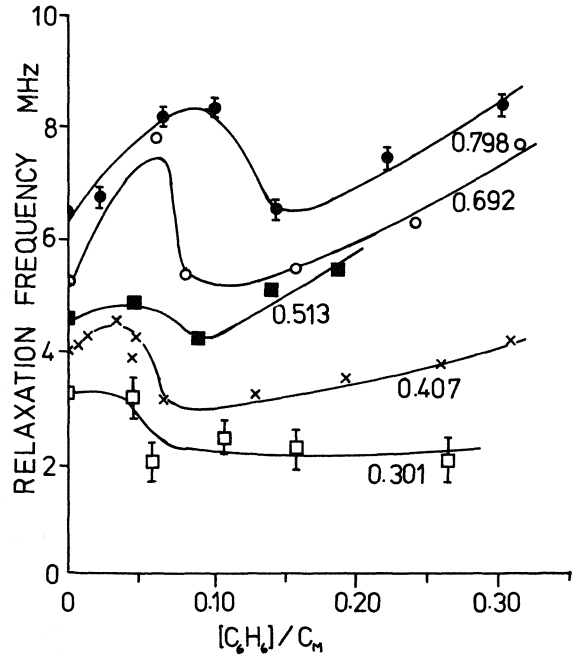


FIG. 3. Effect of benzene additions on the relaxation frequency in various micellar SOS solutions (SOS molalities are displayed).

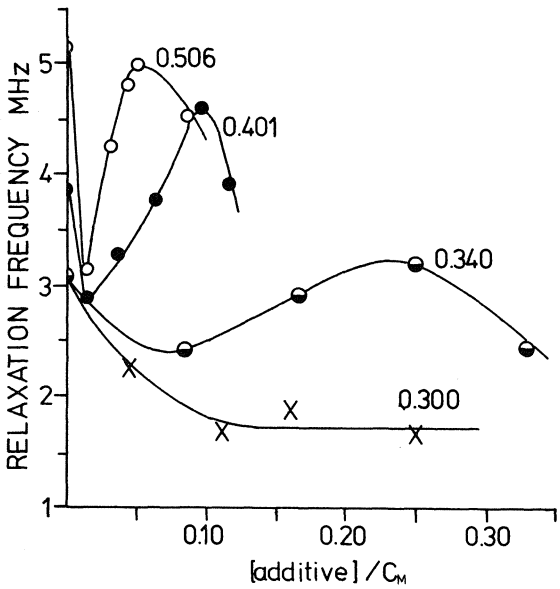


FIG. 4. Effect of toluene and *p*-xylene additions on the relaxation frequency in micellar SOS solutions. The circles represent data for toluene additions to three SOS systems while the *p*-xylene data for 0.300 *m* SOS are shown by crosses (×).

sion can be approximated by the Aniansson equation for one-component micelles (16):

[2] $2\pi f_c = k^-/\sigma^2 + (k^-/n)\,(C_M/\text{cmc})$

where $k^-$ is the rate constant for the exit of the surfactant monomer from the micelle, $\sigma^2$ is the

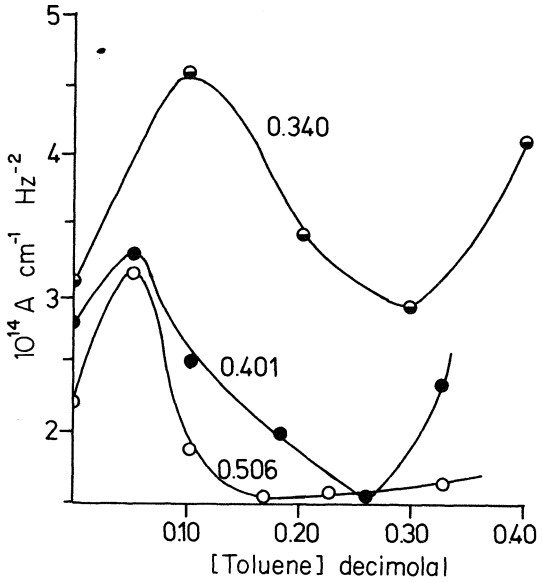


FIG. 5. Relaxation amplitudes (*A*) for toluene additions to various micellar SOS solutions.

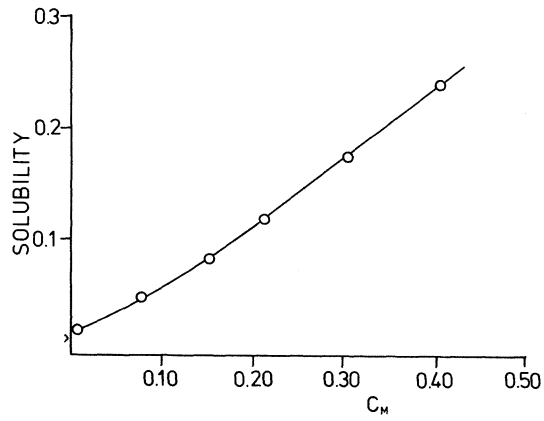


FIG. 6. Solubility of benzene in molality in micellar SOS solutions at 25.0°C. The arrow indicates the pure water solubility of benzene.

variance of the micellar distribution curve, and $n$ is the mean micellar aggregation number.

For the SOS system, $\sigma^2 = 100$ and $n = 25$ (12). Consequently, when $C_M >$ cmc,

[3] $2\pi f_c \simeq (k^-/n)\,(C_M/\text{cmc})$

Thus, for solutions of the same surfactant concentration, $f_c$ is roughly proportional to $k^-$. This assumes that $n$ and $\sigma^2$ are not changed for small additions of additive. The constancy of the cmc within experimental error when benzene was added was some assurance that this was indeed the situation. As far as $k^+$, the entrance rate of the monomers to the micelles, is concerned, this quantity is largely electrostatically controlled and, in

Can. J. Chem. Downloaded from www.nrcresearchpress.com by 210.87.254.5 on 09/06/12
For personal use only.

solutions of high ionic strength such as in micellar SOS solutions, will not be significantly modified by small additions of organic compounds (16). Thus, changes in $f_c$ probably largely reflect changes in $k^-$ and these changes should be roughly directly proportional.

Surfactant concentrations were chosen not only to make eq. [3] more correct but also to avoid the problematical cmc-to-twice-the-cmc range with short-chained surfactants. The decrease in $f_c$ that occurs over this concentration range has never been properly characterized (12, 17).

Less attention has been paid to the relaxation amplitude $A$ which arises from the exchange of the monomers between the micellar and solution environments. Recently, Zana and Yiv (18) have developed an expression for $A$ relating it to $\Delta V_0$, the change in volume associated with the exchange per monomer, and the relaxation frequency:

$$[4] \quad A = \rho u k^- C_M (\Delta V_0)^2/2 \times 10^3 RTn f_c^2$$

where $\rho$ is the solution density and $u$ is the speed of ultrasonic sound through the solution. Teubner (19) has developed a similar expression for the intensity of the ultrasound waves.

From eqs. [3] and [4], then

$$[5] \quad A \simeq \pi \rho u(\text{cmc}) (\Delta V_0)^2/10^3 RTf_c$$

should hold for micellar SOS solutions. The amplitude then should be inversely proportional to $f_c$ where $\rho$, $u$, cmc, and $\Delta V_0$ are relatively constant. In micellar SOS solutions with or without additives, the plot of $A$ against $f_c^{-1}$ was linear (Fig. 7), giving a value of 8 cm$^3$ mol$^{-1}$ for $\Delta V_0$ calculated from the slope. This is remarkably close to 6.3 ± 1.0 cm$^3$ mol$^{-1}$, the $\Delta V_0$ value for the SOS system from density studies (20), given all the assumptions involved. Since the straight line has a non-zero intercept, the analysis may admit of a constant error which cancels when the slope is taken. Apparently, these additives are not affecting significantly the volume change that the SOS monomers undergo on micellization no matter how varied the $f_c$ values are. Thus, it appears consistent to assume that the additives are not affecting the SOS micelles, in any major way, in structure, in aggregation number, and in distribution of micelle sizes, and that the large changes in the relaxation frequency that often occur are a direct reflection of changes in the dissociation rate of the monomer from the micelle.

The $f_c$ values for 0.002–0.02 $m$ cyclohexane additions to 0.397 $m$ SOS solutions did not change within experimental error (Fig. 1). Apparently, the monomers in exchanging between micelle and solution do not "see" the cyclohexane molecules. This argues for a micellar core position for the solubilized cyclohexane which is the conclusion reached with nmr and diffusion studies with this solubilizate in other micellar systems (21–23). Other non-polar solubilizates such as $n$-decane also do not affect the $f_c$ in micellar systems even in greater concentrations (24) (ultrasound often prevents emulsions such as are found in decane (1 $m$) – soap – water systems from separating, allowing sufficient time to measure the ultrasonic absorption).

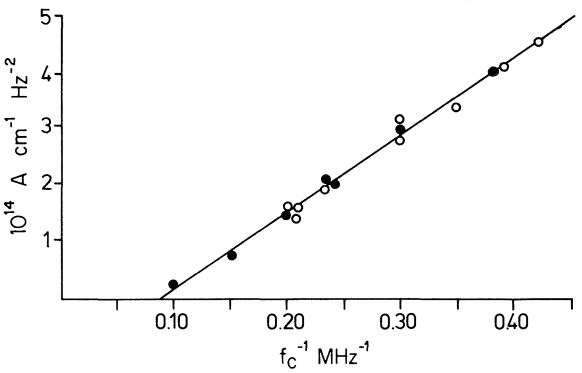


FIG. 7. Dependence of $A$ upon the inverse of the relaxation frequency in micellar SOS solutions without additive (●) and with additive (○).

Through rate enhancement studies by the stopped-flow technique, PADA is known to be preferentially adsorbed by micelles from solution where it is available for metal complexation in the surface region of the micelle (13, 25). Although the micellar-bound PADA molecules could be partitioning rapidly between core and surface in times faster than a millisecond which the stopped-flow technique would not be able to detect, there is good reason to believe from these same studies that the micellar core population of PADA is not significant. Additions of PADA to 0.002 $m$ in a 0.397 $m$ SOS solution cause a significant increase in $f_c$ which indicates, in light of eq. [3], that $k^-$ has undergone an increase of similar magnitude. If PADA were solubilized into the surface region of the micelle, the surface potential would have been lowered, accelerating the rate at which the monomers depart from the micelle. (Another explanation suggested by a referee is that PADA may have ruptured the SOS micelles so that many more but smaller micelles are present. Following his proposal, we measured the conductivity of micellar SOS solutions before and after PADA additions but could find no increase in conductivity beyond experimental error — about 0.2%.) Thus, despite the different time ranges of the techniques, the

Can. J. Chem. Downloaded from www.nrcresearchpress.com by 210.87.254.5 on 09/06/12
For personal use only.

ultrasonic and stopped-flow data agree in assigning PADA to the interfacial region of the micelles.

Concerning the effect of solubilized benzene upon the relaxation frequency in micellar SOS solutions, it is interesting to note that in one of the first ultrasonic investigations in aqueous micellar systems Yasunaga *et al.* (26) had reported that a 1% benzene addition to 0.100 mol $dm^{-3}$ sodium dodecylsulfate solutions markedly shifted the relaxation frequency to a higher value. This solitary measurement with benzene in the literature disguises the complexity in $f_c$ dependence upon additive concentration that is revealed in Fig. 3. Like PADA, benzene in amounts less than $[C_6H_6]/C_M$ values of 0.05–0.10 gives rise to an increase in $f_c$. At this concentration ratio corresponding to 1 to 2 benzene molecules per micelle ($n = 25$), $f_c$ reaches a maximum and then falls off about as rapidly to a value close to the $f_c$ value for the micellar SOS solutions without additive. Further addition of benzene beyond 2–3 molecules per SOS micelle results in a slight, leisurely increase in $f_c$. Benzene in small quantities is much more surface active than one might expect (1) and the initial increase in $f_c$ receives an easy explanation in terms of micellar surface adsorption on benzene. When one to two benzene molecules are adsorbed per micelle, surface adsorption becomes less favourable and may even cease. The $f_c$ data suggest that beyond this concentration inclusion into the micellar core becomes the chief solubilization mechanism for benzene in SOS micelles effectively negating the increase in $k^-$ brought about by the change in surface potential. Had $f_c$ measurements not been conducted in the dilute benzene range, it would have been argued from the near constancy of the $f_c$ values in the more concentrated benzene range that benzene was totally incorporated within the core. That core incorporation does not become the chief solubilization process for benzene until the concentration of benzene exceeds one to two molecules per micelle reconciles the apparently contradictory findings that solubilized benzene in micelles is found chiefly in the surface region (1) and chiefly in the core (4). It is, as Mukerjee and Cardinal (1) expected, just a matter of which site is favoured by the benzene concentration.

Although the error for the $f_c$ determinations for *p*-xylene was greater than that for benzene (Fig. 4), it is clear that *p*-xylene in 0.300 *m* SOS always caused about the same decrease in $f_c$ for $[\text{xylene}]/C_M > 0.1$ (about 2 *p*-xylene molecules per micelle). Solubility restrictions did not permit data to be taken at higher concentrations but a plateau in $f_c$ appears to be developing. This argues for core incorporation for *p*-xylene as in the cyclohexane case. The significant difference from the cyclohexane situation is that a lowering of the $f_c$ was always observed, suggesting that the first few solubilized molecules of *p*-xylene must be interacting with the surfactant monomers in the micelle so as to hinder their escape. This could be accomplished if these additive molecules were vicinal to the monomers as they would be if they were in the palisade layer or in the micellar "fjords" (27). This explanation would rule out any surface adsorption for *p*-xylene in micellar SOS solutions. Fox *et al.* had reported that *p*-xylene in sodium dodecylsulfate solutions had appeared to be solubilized throughout the hydrocarbon core of the micelle (28) with which the ultrasonic evidence does not disagree. In fact, it may be more specific in locating the solubilizate initially close to the micellar surface but then principally within the core with further *p*-xylene additions.

The toluene dependence of the $f_c$, as one might expect from its intermediate position both chemically and in water solubility between benzene and *p*-xylene, was more involved (Fig. 4). All three micellar positions: surface, palisade, and core, appear to be feasible for toluene solubilization depending upon the toluene and micellar concentration. As with *p*-xylene, the first few molecules probably are incorporated into the palisade layer. Then the next few toluene molecules per micelle are adsorbed into the surface region of the micelle as with benzene. Core solubilization, with further addition of toluene, becomes the preferred mechanism. The maxima in $f_c$ for benzene additions all occur at about the same benzene concentration but, with toluene additions, the shift in maxima to lower toluene concentration with increasing SOS concentration likely reflects complications brought about by three competing mechanisms of solubilization.

In summary, the ultrasonic absorption evidence in micellar SOS solutions at this stage suggests that cyclohexane is solubilized within the core of the micelles; PADA, the micellar surface region; benzene, in the surface for concentrations less than a molecule of benzene per micelle then principally in the core for further benzene additions; *p*-xylene, in the palisade layer for concentrations less than one or two molecules of *p*-xylene per micelle, then in the core; toluene, a more complicated pattern with all three sites, palisade, surface, and core, being populated in that order with increasing toluene addition.

The experimental frequency range of the pulse technique limits its applicability to short-chained

surfactants. More "normal" surfactants like sodium dodecylsulfate could accommodate more solubilizate in their micellar solutions but they do not show a relaxation frequency in the MHz range. Other ultasonic techniques such as the resonance or reverberation methods, although slightly less accurate, can be operated in the kHz range and may be useful in this regard. It is clear that the relaxation frequency for surfactant exchange between bulk solution and micelles can be markedly sensitive to solubilizates. From the Aniansson model and from further assumptions regarding constancy of micelle size, distribution, and structure in the presence of minute amounts of solubilizate, we interpret this observed variety of changes in $f_c$ in micellar sodium octylsulfate solutions to indicate the sites of solubilization within the micelles. Although our results appear reasonable and are in agreement with the findings of other structural determination methods where comparison is possible, it remains to be seen whether this is a more general phenomenon with micellar solutions.

**Acknowledgements**

We wish to thank the Natural Sciences and Engineering Research Council of Canada for financial support and Dr. Peeter Kruus of Carleton University for kindly allowing us to use his ultrasonic equipment.

1. P. MUKERJEE and J. R. CARDINAL. J. Phys. Chem. **82**, 1620 (1978).
2. B. LINDMAN and H. WENNERSTROM. Solution chemistry of surfactants — Theoretical and applied aspects. *Edited by* E. J. Fendler and K. L. Mittal. Plenum Press, New York. In press.
3. J. H. FENDLER and E. J. FENDLER. Catalysis in micellar and macromolecular systems. Academic Press, New York. 1975. p. 42.
4. S. J. REHFELD. J. Phys. Chem. **74**, 117 (1970).
5. H. WENNERSTROM and B. LINDMAN. J. Phys. Chem. **83**, 2931 (1979).
6. F. M. MENGER and B. J. BOYER. J. Am. Chem. Soc. **102**, 5936 (1980).
7. E. A. G. ANIANSSON. Techniques and applications of fast reactions in solution. *Edited by* W. J. Gettins and E. Wyn-Jones. D. Reidel Press, Dordrecht, Holland. 1979. p. 249.
8. D. HALL, P. L. JOBLING, J. E. RASSING, and E. WYN-JONES. J. Chem. Soc. Faraday Trans. II, **73**, 1582 (1977).
9. S. YIV and R. ZANA. J. Colloid Interface Sci. **65**, 286 (1978).
10. S. YIV, R. ZANA, W. ULBRICHT, and H. HOFFMANN. J. Colloid Interface Sci. **80**, 224 (1981).
11. R. J. FANNING and P. KRUUS. Can. J. Chem. **48**, 2052 (1970).
12. J. GETTINS, P. L. JOBLING, M. F. WALSH, and E. WYN-JONES. J. Chem. Soc. Faraday Trans. II, **76**, 794 (1980).
13. P. D. I. FLETCHER and V. C. REINSBOROUGH. Can. J. Chem. **59**, 1361 (1981).
14. D. A. W. ADAIR, V. C. REINSBOROUGH, N. PLAVAC, and J. P. VALLEAU. Can. J. Chem. **52**, 429 (1974).
15. V. C. REINSBOROUGH and B. H. ROBINSON. J. Chem. Soc. Faraday Trans. I, **75**, 2395 (1979).
16. E. A. G. ANIANSSON, S. N. WALL, M. ALMGREN, H. HOFFMANN, I. KIELMANN, W. ULBRICHT, R. ZANA, J. LANG, and C. TONDRE. J. Phys. Chem. **80**, 905 (1976).
17. D. A. W. ADAIR, V. C. REINSBOROUGH, H. M. TRENHOLM, and J. P. VALLEAU. Can. J. Chem. **54**, 1162 (1976).
18. R. ZANA and S. YIV. Can. J. Chem. **58**, 1780 (1980).
19. M. TEUBNER. J. Phys. Chem. **83**, 2917 (1979).
20. G. M. MUSBALLY, G. PERRON, and J. E. DESNOYERS. J. Colloid Interface Sci. **48**, 494 (1974).
21. J. C. ERIKSSON and G. GILLBERG. Acta Chem. Scand. **20**, 2019 (1966).
22. G. LINDBLOM, B. LINDMAN, and L. MANDELL. J. Colloid Interface Sci. **42**, 400 (1973).
23. N. KAMENKA, H. FABRE, M. CHORRO and B. LINDMAN. J. Chim. Phys. **74**, 510 (1977).
24. D. A. W. ADAIR, V. C. REINSBOROUGH, and S. J. ZAMORA. Adv. Mol. Relaxation Processes, **11**, 63 (1977).
25. A. D. JAMES and B. H. ROBINSON. J. Chem. Soc. Faraday Trans. I, **74**, 10 (1978).
26. T. YASUNAGA, H. OGURI, and M. MIURA. J. Colloid Interface Sci. **23**, 352 (1967).
27. F. M. MENGER, J. M. JERKUNICA, and J. C. JOHNSTON. J. Am. Chem. Soc. **100**, 4676 (1978).
28. K. K. FOX, I. D. ROBB, and R. SMITH. J. Chem. Soc. Faraday I, **68**, 445 (1972).

Can. J. Chem. Downloaded from www.nrcresearchpress.com by 210.87.254.5 on 09/06/12
For personal use only.

# Synthèse et réactivité de quelques α-amino azocomposés: mécanisme de la cyclisation thermique en triazoles-1,2,4

PIERRE MÉTRA ET JACK HAMELIN[1]

*Groupe de Recherches de Physicochimie Structurale, Equipe de Recherche associée au C.N.R.S., U.E.R.F. "S.P.M.", Université de Rennes, Campus de Beaulieu, 35042 Rennes Cedex, France*

Reçu le 6 mars 1981[2]

PIERRE MÉTRA et JACK HAMELIN. Can. J. Chem. **60**, 285 (1982).

Par addition de l'*O*-mésitylènesulfonylhydroxylamine (MSH) sur des hydrazones d'aldéhydes et de cétones, on observe une amination sur le carbone avec formation d'α-amino azocomposés. La thermolyse de ces composés conduit à des triazoles-1,2,4 dont le mécanisme de formation est discuté.

PIERRE MÉTRA and JACK HAMELIN. Can. J. Chem. **60**, 285 (1982).

The reaction of *O*-mesitylenesulfonylhydroxylamine (MSH) with hydrazones leads to carbon amination with the formation of α-amino azo compounds. Thermolysis of these compounds affords 1,2,4-triazoles. The mechanism of this cyclization is discussed.

## Introduction

Les propriétés nucléophiles et électrophiles de l'*O*-mésitylènesulfonylhydroxylamine (MSH) ont été décrites et discutées dans la littérature (1, 2). En particulier par addition sur des *C*-alkyl *N*-alkyl imines la réaction conduit aux diaziridines correspondantes (1). Dans le but d'accéder aux amino diaziridines qui pouvaient être des amino ylures d'azométhine imine potentiels, nous avons étudié l'addition du MSH sur des hydrazones d'aldéhydes et de cétones **2**.

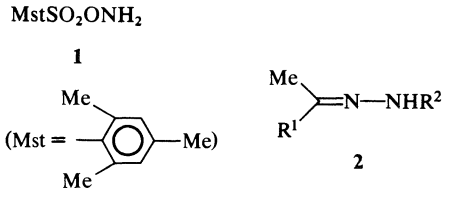


*a* $R^1 = H; R^2 = Ph$
*b* $R^1 = Me; R^2 = Ph$
*c* $R^1 = Me; R^2 = CO_2Me$
*d* $R^1 = R^2 = Me$
*e* $R^1 = H; R^2 = CO_2Me$

## Résultats et discussion

### *1. Addition du MSH sur les hydrazones*

La réaction est effectuée à température ambiante en solution dans l'éther anhydre, sous azote, les réactifs étant en proportions stoechiométriques. Avec les hydrazones **2***a*, **2***b* et **2***c* on obtient après une heure de réaction les sels de formule **3** avec un rendement pratiquement quantitatif.

Les composés **3** (*a*, *b*, *c*) en solution dans $CH_2Cl_2$ sont traités par une quanité stoechiométrique de triéthylamine, et par addition d'éther, on précipite quantitativement le composé **5**. La solution restante est lavée avec une solution aqueuse de chlorure d'ammonium à 10% puis à l'eau. Après évaporation du solvant on obtient les α-amino azocomposés avec des rendements pratiquement quantitatifs (à la précision de la rmn). Les composés **4** purifiés par distillation au four tubulaire sont caractérisés par uv, rmn $^1H$, $^{13}C$, spectrographie de masse et analyse élémentaire.

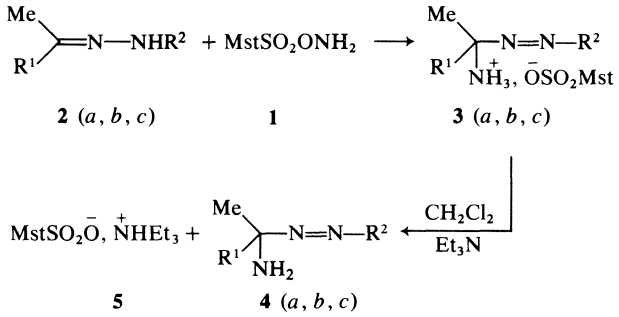


Dans les mêmes conditions de réaction, l'hydrazone **2***d* ne permet pas d'isoler de cristaux primaires analogues à **3** et après traitement à la triéthylamine, on isole avec un bon rendement l'oxime **6** caractèrisée par comparaison avec un échantillon authentique obtenu par réaction du MSH sur l'acétone (1):

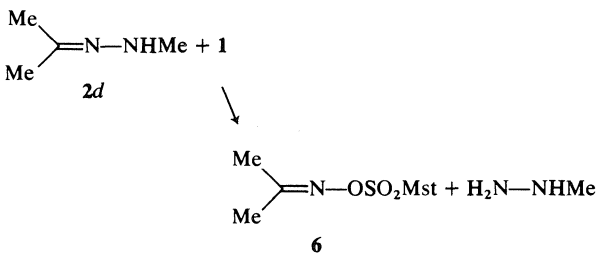


Ces résultats peuvent être interprétés selon le schéma 1:

[1]Auteur auquel doit être adressée la correspondance.
[2]Révision reçue le 6 octobre 1981.

0008-4042/82/030285-06$01.00/0
©1982 National Research Council of Canada/Conseil national de recherches du Canada

Can. J. Chem. Downloaded from www.nrcresearchpress.com by 210.87.254.105 on 09/06/12
For personal use only.

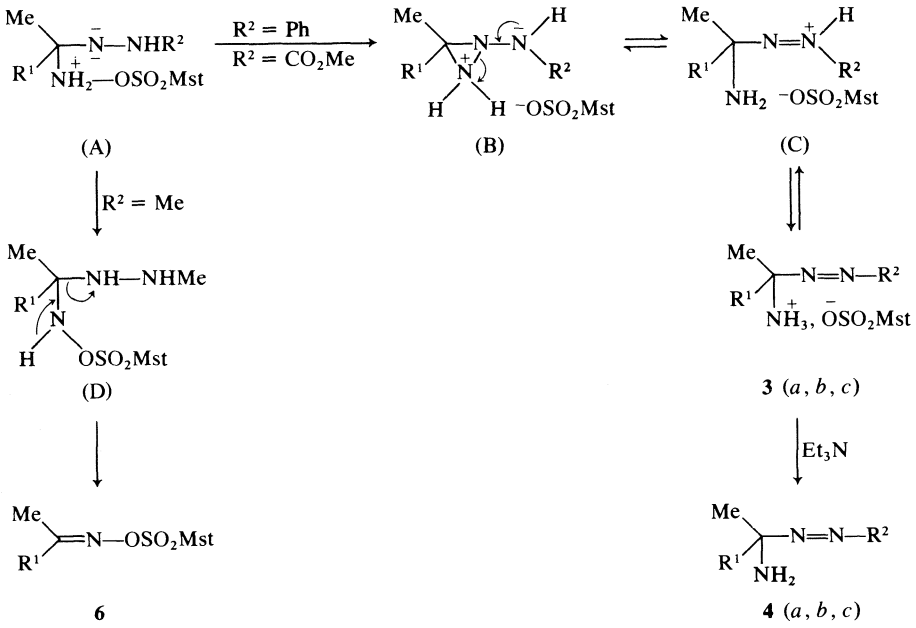

SCHÉMA 1

Il y aurait initialement attaque nucléophile du MSH **1** sur le carbone de l'hydrazone avec formation de la bétaïne (A). Lorsque $R^2$ = Ph ou $CO_2Me$, il y aurait substitution nucléophile intramoléculaire pour former le sel de diaziridinium (B), qui conduirait au sel **3** par l'intermédiaire du sel (C). Par action de la triéthylamine on libère l'azocomposé **4**. Lorsque $R^2$ = Me, l'azote négatif de (A) est plus basique que nucléophile et il y aurait prototropie avec formation de (D) qui conduirait à l'oxime **6** avec élimination de méthylhydrazine.

*2. Réactivité des azocomposés*

Quelques propriétés chimiques ont été étudiées en utilisant plus particulièrement le composé ***4a***.

*(a) Tautomérie azocomposé–hydrazone*

A température ambiante, sous azote, à l'abri de la lumière, ***4a*** se transforme quantitativement, après deux semaines, en aminohydrazone ***7a*** caractérisée par rmn $^1H$ et spectrographie de masse. Le composé ***7a*** peut également être obtenue par traitement de ***4a*** au butyllithium dans le THF (pour donner un anion dont la couleur marron résulte vraissemblablement de la complexation du lithium par l'azote), puis hydrolyse à −15°C. Si l'hydrolyse est effectuée à −90°C on récupère ***4a*** inchangé. Ces résultats sont rassemblés dans le schéma 2.

Par ailleurs, ***7a*** traitée au butyllithium à −90°C conduit à $7a^-$ qui redonne ***7a*** après hydrolyse soit à −90°C soit à −15°C. Le passage irréversible $4a^- \rightarrow 7a^-$ pourrait résulter d'un processus intermoléculaire (schématisé ci-dessous).

L'azocomposé ***4b*** traité par BuLi à −90°C conduit également à un ion marron qui ne peut donner lieu à

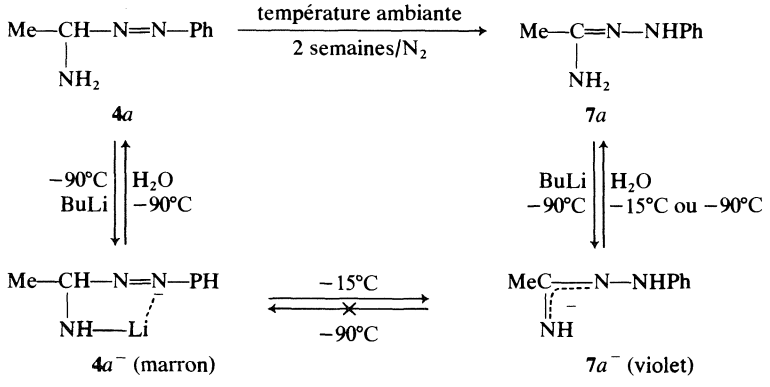

SCHÉMA 2

Can. J. Chem. Downloaded from www.nrcresearchpress.com by 210.87.254.105 on 09/06/12
For personal use only.

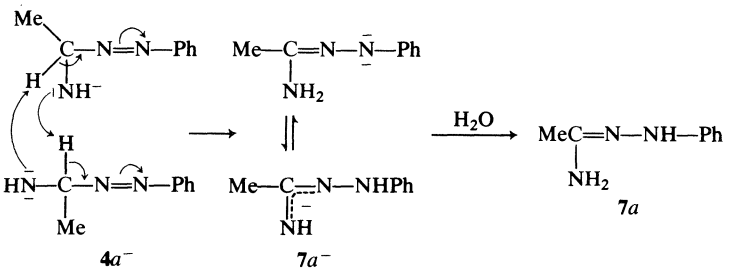

$4a^-$ $7a^-$ $7a$

l'isomérisation précédente et après hydrolyse on récupère **4***b*. Le passage **4***a* → **7***a* à température ambiante pourrait s'effectuer selon un processus analogue. La transformation azocomposé → hydrazone est déjà signalée dans la littérature et s'effectue aussi bien en milieu acide qu'en milieu basique (3), et dans le cas des α-amino azocomposés le groupement amine peut catalyser la transformation. Ce résultat est particulièrement important pour l'interprétation de la formation des triazoles-1,2,4 à partir des α-amino azocomposés ou des aminohydrazones que nous vous étudiés.

*(b) Evolution thermique*

A l'ébullition du benzène durant 24 h, **4***a* se transforme quantitativement en un composé **8***a* auquel la rmn $^1H$ et $^{13}C$ et la spectrographie de masse permettent d'attribuer la structure 1,2,4-triazole.

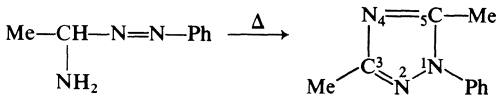

**4***a* **8***a*

Lorsque la thermolyse est réalisée en présence de tertiobutylcatéchol comme inhibiteur de réactions radicalaires, on retrouve après 24 h de reflux dans le benzène, 54% d'azocomposé **4***a* non transformé. Cette observation est en faveur d'un processus radicalaire auquel on pouvait s'attendre pour un azocomposé. De plus **4***a* en solution conduit également à **8***a* à température ambiante et on met en évidence la formation de benzène et un dégagement d'ammoniac.

Les observations précédentes nous conduisent à rationnaliser la formation de **8***a* de la manière suivante (schéma 3):

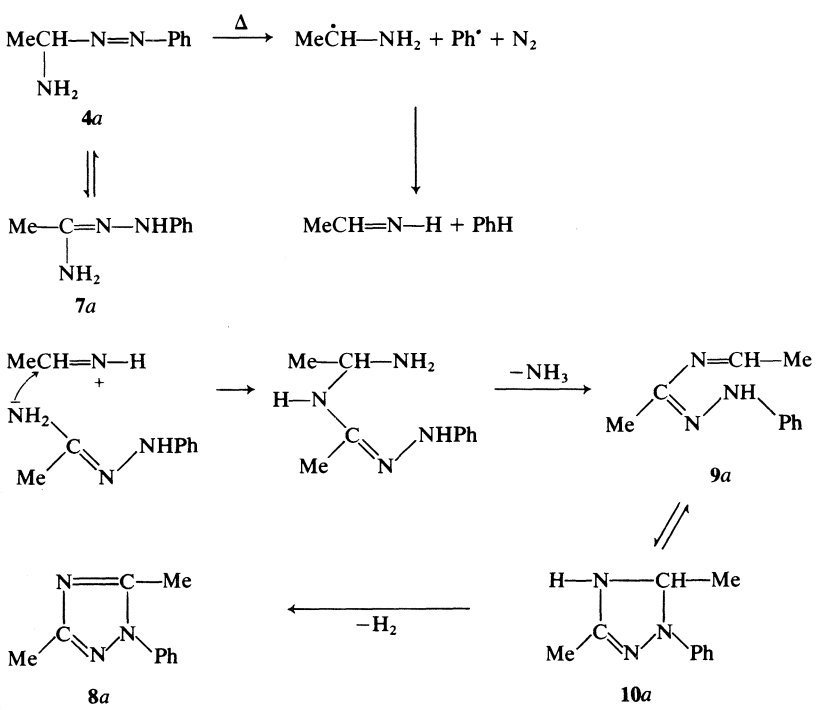

SCHÉMA 3

Can. J. Chem. Downloaded from www.nrcresearchpress.com by 210.87.254.105 on 09/06/12
For personal use only.

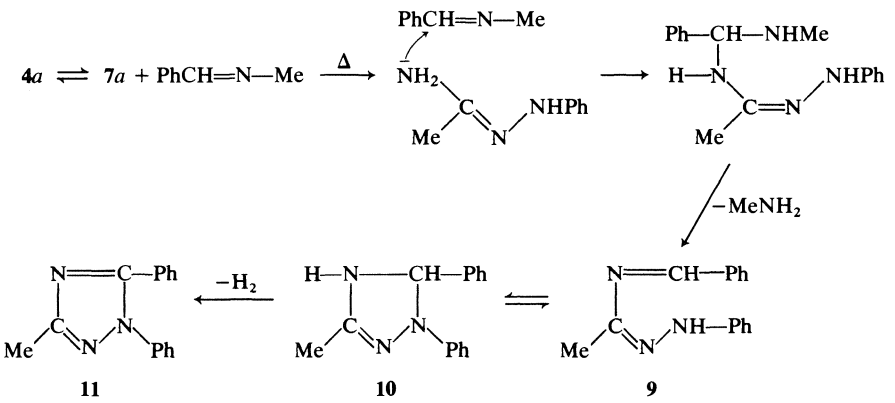

SCHÉMA 4

Il y aurait coupure radicalaire de **4***a* avec formation de deux radicaux MeĊH—$NH_2$ et Ph• et perte d'azote. Par abstraction d'hydrogène il se formerait du benzène et l'imine MeCH=N—H sur laquelle l'aminohydrazone **7***a* en équilibre avec **4***a* s'additionnerait pour former l'iminohydrazone **9***a*[3] avec perte d'ammoniac. Le composé **9***a* se cyclliserait ensuite en triazoline **10***a* dont l'aromatisation conduirait au triazole **8***a*. Il faut signaler que la thermolyse de **7***a* conduit également à **8***a* mais la réaction est plus lente et nécessite 24 h de reflux dans le toluène pour être totale, ceci résulte vraisemblablement du fait que l'équilibre **4***a* ⇌ **7***a* n'est pas en faveur de **4***a*.

Pour vérifier l'hypothèse de l'étape d'addition de l'aminohydrazone sur une imine, nous avons réalisé l'addition de **4***a* sur l'imine PhCH=N—Me. On obtient avec un rendement pratiquement quantitatif, le triazole-1,2,4 de structure **11** caractérisé par rmn $^1$H et comparaison avec un échantillon authentique (dont la synthèse univoque est décrite dans la suite). La réaction s'effectuerait selon le schéma 4, formation d'une iminohydrazone **9** avec perte de méthylamine puis aromatisation en triazole **11** via la triazoline **10**.

La thermolyse de **4***b* a également été étudiée et conduit à une décomposition avec formation de benzène et d'acétone qui ont été caractérisés par rmn et cgl, et dégagement d'azote. Le mécanisme serait initialement le même: rupture radicalaire de l'amino azocomposé avec formation d'imine $Me_2$-C=NH, de benzène et dégagement d'azote. La tautomérie azo ⇌ hydrazone n'étant pas possible dans ce cas, la réaction s'arrête avec hydrolyse de l'imine et formation d'acétone.

[3]Nous remercions l'un des rapporteurs pour son interessante suggestion relative au mécanisme de l'addition de l'aminohydrazone sur l'imine avec formation d'iminohydrazone dont l'existence est d'ailleurs confirmée par addition des aldéhydes sur les amino azocomposés.

Ainsi, l'équilibre azo ⇌ hydrazone que nous avons mis en évidence permet de rationnaliser la formation des triazoles-1,2,4 à partir des α-amino azocomposés ou des aminohydrazones, réaction dont le mécanisme, à notre connaissance, n'était pas signalé dans la littérature (4).

L'amino azocomposé **4***c* présente lors de la thermolyse un comportement particulier. En effet, au reflux du benzène sous azote, **4***c* redonne quantitativement l'hydrazone de départ, avec formellement perte de "NH". Ce résultat est vraisemblablement à l'origine de nos difficultés pour isoler l'amino azocomposé **4***e* dérivé de l'hydrazone MeCH=N—$NHCO_2$Me. En effet, lors de cette réaction on observe bien la formation quantitative du sel de triéthylammonium **5**, mais après évaporation du solvant on récupère l'hydrazone initiale et seulement 10% d'amino azocomposé **4***e*. Cette évolution est actuellement à l'étude au laboratoire.

*(c) Condensation des amino azocomposés* **4** *avec les aldéhydes*

L'amino azocomposé **4***a* donne avec les aldéhydes à température ambiante dans le chloroforme une réaction exothermique ayant pour stade ultime la formation d'un triazole selon le schéma 5.

Dans une première étape, il y a formation de l'azoimine **12** qui s'isomérise en iminohydrazone **9***a* ou **9**, ce qui confirme l'existence de cet intermédiaire postulé dans le mécanisme proposé aux schémas 3 et 4. Les composés **9***a* et **9** se cyclisent ensuite en triazolines **10***a* et **10** respectivement qui s'aromatisent en triazoles **8***a* et **11** selon la nature de R.

Dans le cas de la condensation avec le benzaldéhyde (R = Ph), la réaction à température ambiante est suivie à l'aide de la rmn $^1$H: après 12 h on observe la formation de **12** (64%), **10** (33%) accompagnés de traces de **11**. Après 48 h on obtient **12** (13%), **10** (78%) et **11** (9%), à partir de ce mélange on isole la triazoline **10** (R = Ph). Après 7 jours à

Can. J. Chem. Downloaded from www.nrcresearchpress.com by 210.87.254.105 on 09/06/12
For personal use only.

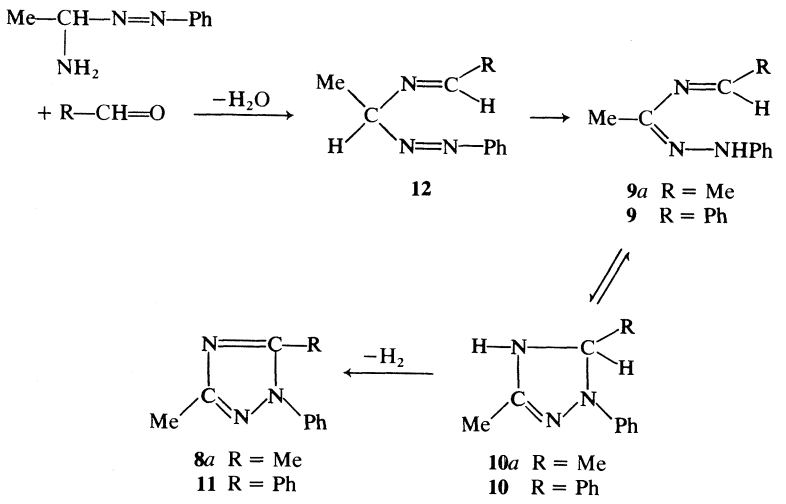

SCHÉMA 5

température ambiante le triazole **11** déjà obtenu par addition de **4***a* sur l'imine PhCH=N—Me est formé avec un rendement quantitatif.

## Partie expérimentale

Les spectres rmn $^1H$ ont été enregistrés sur un apareil JEOL MH 100 à 100 MHz et les spectres $^{13}C$ sur un appareil Brucker WP 80 à 20,115 MHz. Les échantillons sont examinés en solution dans $CDCl_3$ (sauf précision contraire) et les déplacements chimiques δ sont donnés en ppm par rapport au TMS. Les spectres de masse ont été réalisés sur un appareil Varian MAT 311, et les spectres uv sur un spectrophotomètre Beckman DB.

*1. Mésitylène sulfonyl hydroxylamine MSH*

Il est préparé selon la méthode décrite par Tamura *et al.* (1), recristallisé dans le mélange éther–pentane à 0°C ($F$ = 92°C) et conservé à −18°C.

*2. Addition du MSH 1 sur les hydrazones 2*

A une solution de l'hydrazone ($10^{-2}$ mol) dans l'éther anhydre, on ajoute goutte à goutte sous azote $10^{-2}$ mol de MSH dans l'éther à température ambiante. Après une heure sous agitation, le sel **3** généralement formé est essoré et analysé en rmn $^1H$ et $^{13}C$.

Le sel **3** brut est ensuite dissout dans $CH_2Cl_2$ et on ajoute goutte à goutte une quantité stoechiométrique de triéthylamine sous agitation. Après une heure, l'addition d'éther provoque la précipitation de **5** qui est essoré et la solution restante est lavée avec une solution de chlorure d'ammonium à 10%, puis à l'eau. Après évaporation du solvant à température ambiante on obtient l'α-amino azocomposé **4** qui est purifié par distillation au four tubulaire.

*(a) Hydrazone* **2**a

Le composé **3***a* est obtenu avec un rendement de 90% ($F$ = 264°C avec décomposition). Composé **3***a*, rmn $^1H$: 1,53 (d, 3H, *Me*CH); 2,13 et 2,50 (s, 3H, s, 6H, Me en *para* et 2 Me en *ortho* du mésitylène); 5,10 (q, 1H, Me*CH*); 6,65 (s, 2H, H du mésitylène); 8,94 (s large, échangé dans $D_2O$, $NH_3$); rmn $^{13}C$: 17,44; 20,72 et 23,01 (Me du Mésitylène et *Me*CH); 75,99 (Me*C*H, $J$ = 156 Hz) et les C aromatiques.

Le composé **3***a* traité à la triéthylamine donne **4***a* (Rdt = 46% par rapport à **2***a* après distillation au four tubulaire Eb $10^{-2}$ Torr = 70°C). Composé **4***a*, rmn $^1H$: 1,48 (d, 3H, *Me*CH); 2,05 (s, 2H, échange $D_2O$, $NH_2$); 4,58 (q, 1H, Me*CH*); rmn $^{13}C$: 20,63 (*C*$H_3$CH); 80,01 ($CH_3$*C*H, $J$ = 149 Hz) et les carbones aromatiques. Spectrographie de masse: $m/e$ = 149 ($M^+$); $m/e$ = 106 (Ph—N=$NH^+$); $m/e$ = 44 (MeCH=$NH_2^+$); uv (*n*-heptane): $\lambda_{max}$ = 261 nm, $\varepsilon_{max}$ = 7860. *Anal.* calc. pour $C_8H_{11}N_3$: C 64,43; H 7,38; N 28,19%; trouvé: C 64,58; H 7,28; N 28,14%.

*(b) Hydrazone* **2**b

Dans les mêmes conditions on isole **3***b* ($F$ = 135°C avec décomposition). Composé **3***b*, rmn $^1H$: 1,60 (s, 6H, $Me_2$C); 2,14 et 2,52 (s, 3H et s, 6H pour les Me du mésitylène); 6,66 (s, 2H, mésitylène); 8,93 (s, 3H, $NH_3$); rmn $^{13}C$: 20,72; 23,12 et 23,61 (Me en *para*, 2 Me en *ortho* du mésitylène et $Me_2$C); 81,73 ($Me_2$*C*H) et les C aromatiques. Le traitement à $Et_3N$ donne **4***b* avec un rendement de 56% par rapport à **2***b* après distillation au four tubulaire; Eb $10^{-2}$ Torr = 80°C). Composé **4***b*, rmn $^1H$: 1,44 (s, 6H, $Me_2$C); 2,13 (s, large, 2H, $NH_2$); rmn $^{13}C$: 26,75 ($Me_2$C); 80,30 ($Me_2$*C*) et les C aromatiques. Spectrographie de masse: $m/e$ = 163 ($M^+$); $m/e$ = 106 (Ph—N=$NH^+$); $m/e$ = 58 ($Me_2$C=$NH_2^+$); uv (*n*-heptane): $\lambda_{max}$ = 256 nm, $\varepsilon_{max}$ = 4990. *Anal.* calc. pour $C_9H_{13}N_3$: C 66,26; H 7,97; N 25,77%; trouvé: C 66,25; H 8.15; N 25,60%.

*(c) Hydrazone* **2**c

Formation quantitative du sel **3***c*, $F$ = 120°C (avec décomposition). Composé **3***c*, rmn $^1H$: 1,59 (s, 6H, $Me_2$C); 2,22 et 2,53 (s, 3H, s, 6H, Me du mésitylène); 3,93 (s, 3H, $CO_2$*Me*); 6,82 (s, 2H, H du mésitylène) et 9,00 (s, large, 3H, $NH_3$). Composé **4***c* (Rdt = 70% par rapport à **2***c*, non distillé); rmn $^1H$: 1,43 (s, 6H, $Me_2$C); 1,82 (s, large, 2H, $NH_2$); 4,00 (s, 3H, $CO_2$*Me*); uv (10% $CHCl_3$/90% *n*-heptane): $\lambda_{max}$ = 230 nm, $\varepsilon_{max}$ = 2250. Les résultats de l'analyse élémentaire de **3***c* et **4***c* ne sont pas satisfaisants en raison de l'instabilité des produits.

*(d) Hydrazone* **2**d

Dans ce cas on n'observe pas la formation de **3***d* et le traitement à la triéthylamine est effectué sur la solution éthérée. On obtient ainsi l'oxime **6** ($F$ = 96°C) avec un rendement quantitatif.

*(e) Hydrazone* **2**e

La précipitation du sel **3***e* n'est pas observée et après traitement à $Et_3N$ on note la précipitation quantitative de **5** et le spectre de rmn $^1H$ du mélange réactionnel brut révèle l'existence de l'hydrazone **2***e* et de 10% d'un deuxième composé, qui pourrait être **4***e* (q, 5,28 ppm), ce produit n'a pas pu être isolé à l'état pur.

*3. Tautomérie azocomposé–hydrazone*

Comme nous l'avons signalé, **4***a* se transforme quantitative-

Can. J. Chem. Downloaded from www.nrcresearchpress.com by 210.87.254.105 on 09/06/12
For personal use only.

ment en **7***a* en deux semaines sous azote à l'abri de la lumière, sans solvant. Composé **7***a* ($F$ = 100°C, éther/*n*-hexane) est caractèrisé par comparaison avec les données de la littérature relatives au chlorhydrate (5): $F$ = 119–122°C; rmn $^1$H: 1,79 (s, 3H, Me); 5,0 (s, large échange $D_2O$, 3H, NH et $NH_2$). Spectrographie de masse: $C_8H_{11}N_3$: $m/e$ = 149 ($M^+$); $m/e$ = 132 (MeC═N═N—$PH^+$); $m/e$ = 91 (Ph—$N^+$).

*4. Evolution thermique de* **4**a

A l'ébullition du benzène durant 24 h, **4***a* se transforme avec un rendement pratiquement quantitatif en diméthyl-3,5 phényl-1 triazole-1,2,4 de formule **8***a* (Eb 2 × $10^{-2}$ Torr = 110–120°C au four tubulaire) isolé sous forme cristalline après passage au chlorhydrate et relargage; $F$ = 46°C (littérature (6) $F$ = 48°C après sublimation). Composé **8***a*, rmn $^1$H: 2,35 et 2,39 (2s, 3H et 3H, Me en 3 et 5); 7,33 (s, 5H, protons aromatiques); rmn $^{13}$C: 12,96 et 13,59 (Me en 3 et 5); 152,34 et 159,96 (*C*—Me en 3 et 5) et C aromatiques. Spectrographie de masse: $C_{10}H_{11}N_3$: $m/e$ = 173 ($M^+$); $m/e$ = 132 (Ph—N═N═C—$Me^+$); ($M^+$—MeCN); $m/e$ = 91 (PH—$N^+$).

La réaction en présence d'inhibiteur de réaction radicalaire est effectuée en présence de 5% de *para* tertiobutylcatéchol durant 24 h au reflux du benzène.

Par réaction de **4***a* sur une quantité équimoléculaire d'imine PhCH═N—Me durant 48 h au reflux du benzène sous azote on obtient, avec un rendement pratiquement quantitatif (à la précision de la rmn), le triazole **11** cristallisé après passage au chlorhydrate ($F$ = 180°C) et relargage à la soude; $F$ = 92°C. Composé **11**, rmn $^1$H: 2,51 (s, 3H, Me) et 7,36 (s, 10H, ArH). Spectrographie de masse: $C_{15}H_{13}N_3$: $m/e$ = 235 ($M^+$); $m/e$ = 132 ($M^+$—Ph—CN); $m/e$ = 91 (Ph—$N^+$). *Anal.* calc. pour chlorhydrate $C_{15}H_{14}N_3Cl$: C 66,30; H 5,16; N 15,47; Cl 13,07%; trouvé: C 66,23; H 5,19; N 15,47; Cl 13,11%.

*5. Condensation de* **4**a *avec les aldéhydes*

La condensation des aldéhydes est réalisée dans le chloroforme à température ambiante, les réactifs étant en proportions équimoléculaires.

*(a) Acétaldéhyde MeCHO*

On obtient, avec un rendement pratiquement quantitatif, le triazole **8***a* déjà formé par thermolyse de l'amino azocomposé **4***a*.

*(b) Benzaldéhyde PhCHO*

Dans les mêmes conditions, après 12 h à température ambiante, on caractérise par rmn $^1$H l'imine **12**, non isolée; rmn $^1$H: 1,64 (d, 3H, Me); 5,06 (q, 1H, MeC*H*); 8,45 (s, 1H, C*H*). Après 48 h, la triazoline **10** ($F$ = 116°C) est isolée et recristallisée dans le mélange éther/*n*-pentane; rmn $^1$H: 1,93 (s, 3H, Me); 5,95 (s, 1H, C*H*). Ce composé n'a pas pu être analysé en raison de son oxydation rapide en triazole. Après 7 jours à température ambiante, on obtient quantitativement le triazole **11** déjà décrit précédemment.

1. Y. Tamura, J. Minamikawa et M. Ikeda. Synthesis, 1 (1977).
2. J. Streith et C. Fizet. Tetrahedron Lett. 3297, 1977.
3. A. J. Bellamy et R. D. Guthrie. J. Chem. Soc. 3528 (1965), et réf. citées.
4. D. G. Neilson, R. Roger, J. W. M. Heatlie et L. R. Newlands. Chem. Rev. **70**, 151 (1970).
5. D. Jerchel et H. Fischer. Ann. **574**, 85 (1951).
6. A. A. Komzak et J. B. Polya. J. Appl. Chem. 666 (1952).

Can. J. Chem. Downloaded from www.nrcresearchpress.com by 210.87.254.105 on 09/06/12
For personal use only.

# Antitumor activity at the molecular level: binding modes in anthracycline–dinucleotide complexes as determined by optical titration and magnetic circular dichroism[1]

M. J. Bell, G. W. Buchanan,[2] B. R. Hollebone,[2] and E. D. Jones

*Department of Chemistry, Carleton University, Ottawa, Ont., Canada K1S 5B6*

Received January 29, 1981[3]

M. J. Bell, G. W. Buchanan, B. R. Hollebone, and E. D. Jones. Can. J. Chem. **60**, 291 (1982).

The first application of magnetic circular dichroism (mcd) spectroscopy to drug–dinucleotide binding is reported. The mcd spectra have been recorded for complexes of the intercalating anthracyclines carminomycin, marcellomycin, and aclacinomycin with the dinucleotide CpG. Analysis indicates that drugs having OH groups *peri* to each anthraquinone carbonyl (i.e. carminomycin and marcellomycin) bind with only one drug molecule in the central hydrophilic region of the nucleotide. By contrast, aclacinomycin, in which one of the anthraquinone carbonyls lacks a *peri*-OH, is found to cooperatively bind, and has two drug molecules present in the dinucleotide cavity. The cooperativity of binding has been elucidated via an optical titration procedure.

M. J. Bell, G. W. Buchanan, B. R. Hollebone et E. D. Jones. Can. J. Chem. **60**, 291 (1982).

On rapporte la première application de la spectroscopie du dichroisme circulaire magnétique (dcm) à la liaison médicament–dinucléotide. On a enregistré les spectres de dcm des complexes formés par les intercalants anthracycline, carminomycine, marcellomycine et aclacinomycine, avec le dinucléotide CpG. Les analyses révèlent que les médicaments qui ont des groupements OH en *péri* par rapport à chaque carbonyle de l'anthraquinone (comme la carminomycine et la marcellomycine) sont liés à une seule molécule de médicament dans la région hydrophile centrale du nucléotide. On trouve au contraire que l'aclacinomycine, dans laquelle il manque un groupement OH *péri* pour l'un des carbonyles de l'anthraquinone, est liéé coopérativement et que deux molécules de médicament sont présentes dans la cavité du dinucléotide. On a identifié la coopérativité du lien par l'intermédaire d'une méthode de titration optique.

[Traduit par le journal]

## Introduction

A number of anthracyclines are potent antitumor antibiotics, daunomycin and adriamycin being the best known (1). Several other active materials belonging to this general class of compounds have recently been isolated, among which are aclacinomycin, **1**, marcellomycin, **2**, and carminomycin, **3** (2–4) (Fig. 1).

The biological activity of these anthracyclines involves an inhibition of the cellular DNA and RNA dependent replication and transcription processes. This inhibition arises from an intercalative binding mode (5) and it is known that daunomycin and adriamycin intercalate into double-stranded DNA, although these drugs do not show any requirement for a particular base at the intercalation site (1–6).

Among the available physical methods for the study of drug–polynucleotide binding in solution, circular dichroism (cd) spectroscopy has been shown to be particularly sensitive (7). This method does not, however, give any geometrical information regarding the nature of binding. By contrast, magnetic circular dichroism (mcd) spectroscopy has recently been shown (8) to be a powerful method for monitoring subtle geometrical changes in a wide variety of chromophores.

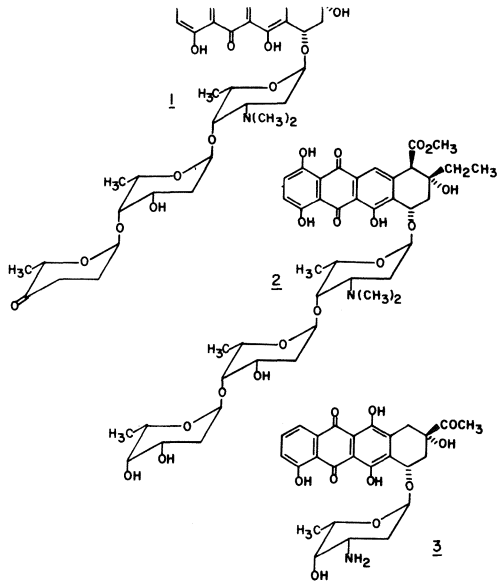

FIG. 1. Structures of aclacinomycin **1**, marcellomycin **2**, and carminomycin **3**.

Presently we have examined the solution interactions between aclacinomycin **1**, marcellomycin **2**, and carminomycin **3**, with the self-complimentary dinucleotide monophosphate CpG (2′-deoxycytidylyl-(3′ → 5′)-2′-deoxyguanosine). In studies of

[1]Presented in part at the 64th annual meeting of the Chemical Institute of Canada, Halifax, N.S., May 31–June 3, 1981.

[2]Authors to whom correspondence may be addressed.

[3]Revision received October 5, 1981.

0008-4042/82/030291-08$01.00/0

©1982 National Research Council of Canada/Conseil national de recherches du Canada

Can. J. Chem. Downloaded from www.nrcresearchpress.com by 210.87.254.6 on 09/06/12
For personal use only.

Can. J. Chem. Downloaded from www.nrcresearchpress.com by 210.87.254.6 on 09/06/12
For personal use only.

DNA binding properties, the use of such self-complimentary systems has been widespread, since it has been found that these dinucleotides associate spontaneously to form a mini-helix in aqueous solution (9).

In addition to the mcd experiments, we have carried out optical titrations and, using the method of Scatchard (10), we have obtained binding isotherms and evidence for cooperativity of binding in one instance.

## Theory

(a) *General considerations of magnetic circular dichroism*

The contribution of an isolated transition to the mcd spectrum of a molecule can be expressed as the sum of three terms, which describe the three possible electronic situations which may be present (11):

$$[\theta]_M = -21.3458\ \{f_1A + f_2[B + C/kT]\}$$

where $[\theta]_M$ is the molar ellipticity per unit magnetic field, $f_1$ is the shape function for a derivative curve, $f_2$ a Gaussian shape function, and $A$, $B$, and $C$ are the Faraday constants for a particular transition.

For an $A$ term to be observed there must be degeneracy in the excited states. A $C$ term arises when the ground state is degenerate, leading to a dependence on temperature.

The mcd spectra of molecules having no 3-fold, or higher, axis of symmetry are composed entirely of $B$ terms (8, 11). These arise from the mixing of the ground state and two or more excited states. The intensities of the $B$ terms are dependent on the energy separation of the excited states and their transition moment directions. The intensities are greatest when the energy separation is small and when the transition moments to the observed and perturbing states are orthogonal.

The mcd spectra of a number of cyclic $\pi$-electron systems have been both calculated and experimentally determined (8). General rules have been derived for substituent effects. This allows the prediction of absolute mcd signs for the most prominent four low energy bands in a large number of compounds based on a simple model of the $\pi$-electron system.

The electronic transitions of aromatic chromophores are classified according to Platt's nomenclature for cata condensed polyacenes (12), based on a simple free electron model. The first excited configuration will give rise to two low energy, weak absorption bands, known as the $L$ states, plus two high energy dipole allowed bands, the $B$ states.

For aromatic ring systems, which contain some bonds parallel or perpendicular to a symmetry axis, the $L_a$, and $B_a$ transition moments will be parallel to these bonds, while the $L_b$ and $B_b$ transition moments will be perpendicular to them.

The mcd spectra of cyclic $(4n + 2)$-electron $(n)$ annulenes can be predicted based on the relative size of two orbital energy differences, ΔHOMO (highest occupied molecular orbital) and ΔLUMO (lowest unoccupied molecular orbital). In general both the HOMO and the LUMO are degenerate; however, perturbations on the parent perimeter will cause orbital splittings.

Of the four possible transitions, from a single electron HOMO → LUMO excitation, two are sense preserving of the magnetic moments and two are sense reversing of the magnetic moments. The sense preserving transitions are the electric dipole allowed $B$ bands, and yield excited configurations with small magnetic moments $\mu^-$. The sense reversing transitions, or $L$ bands, have large magnetic moment contributions $\mu^+$, but are electric dipole forbidden.

In soft chromophores (8), where ΔHOMO is equal to ΔLUMO, all $\mu^+$ contributions vanish and the mcd $B$ terms are controlled by the weaker $\mu^-$ magnetic moments. The most important odd-soft chromophores (8) are the benzenoid hydrocarbons, with the alternate pairing theorum predicting the equality of ΔHOMO and ΔLUMO. Any perturbation affecting this equality of ΔHOMO and ΔLUMO will bring in contributions from the larger $\mu^+$ quantities. This can cause substantial changes in the compound's mcd spectrum.

Substituent effects, both inductive (I) and electrometric (E), are manifested in a change in the quality of ΔHOMO and ΔLUMO. This occurs via a displacement of electrons towards regions of low potential energy, within the constraints of the Pauli exclusion principle.

Substituents presenting a positive charge to the aromatic system (+E, +I), effectively remove electrons from the ring. Conversely, −E or −I substituents will donate charge to the aromatic system.

In a dominant ring position,[4] +E and +I substituents will induce ΔHOMO < ΔLUMO while negative substituents cause ΔHOMO > ΔLUMO. Effects at sub-dominant positions are initially opposite to this, but as the substituent becomes stronger it is able to overcome any inherent molecular orbital ordering and the same changes are observed.

In the perturbed system, the larger $\mu^+$ contribu-

[4]A dominant position has Hückel coefficients $c_{k,1}^2 > c_{k,2}^2$ where $k$ refers to the atom, and 1,2 are orbitals on it (pair belonging to HOMO). In sub-dominant positions $c_{k,1}^2 < c_{k,2}^2$.

Can. J. Chem. Downloaded from www.nrcresearchpress.com by 210.87.254.6 on 09/06/12
For personal use only.

tions may affect the mcd signals. When $\Delta HOMO > \Delta LUMO$ the $\mu^+$ contributions to the mcd bands are $L_b(-)$, $L_a(+)$, $B_b(-)$, $B_a(+)$ in order of increasing energy, if $\Delta HOMO < \Delta LUMO$ then the order is $L_b(+)$, $L_a(-)$, $B_b(+)$, $B_a(-)$.

(b) *Anthracycline transition moments*

An initial step required, before the anthracycline intercalation process can be studied using mcd, is the assignment of the individual transition moments for the components involved.

In determining the transition assignments for the anthracycline drugs, we will begin with a discussion of *p*-benzoquinone and proceed to 9,10-anthraquinone.

In *p*-benzoquinone, two allowed transitions are found at accessible wavelengths, one at 282 nm, the other at 248 nm (13). The effect of OH and $CH_3$ substituents has been determined using a modified Pariser–Parr–Pople method (14).

The introduction of one OH group will red shift the first singlet absorption to 376 nm. A second OH, *ortho* to the first, will cause a further red shift to 600 nm. If the second OH is placed in any other ring position, no further changes occur.

The addition of a $CH_3$ group causes a red shift of both bands, being most pronounced for the lowest energy transition. Each additional $CH_3$ group on the ring further lowers the transition energies.

These substituent effects can be extended to both the calculated (15) and experimental (16–19) transition energies of 9,10-anthraquinone. In 9,10-anthraquinone there is a long axis polarized band at 345 nm which is assigned as the $L_b \leftarrow A$ transition. A weak band, short axis polarized, at 280 nm is the $L_a \leftarrow A$ transition. The two remaining bands at 230 and 250 nm are the $B_a$ and $B_b$ transitions, short and long axis polarized respectively (20).

The introduction of OH groups was found to red shift the low energy transition to 400–500 nm. An additional band appears at $\sim 300$ nm in most derivatives as well. The addition of $CH_3$ groups will cause slight red shifts in each of the bands.

This trend is continued in the experimental spectra of the anthracycline drugs.

(c) *Magnetic circular dichroism spectral assignments*

In considering the mcd assignments of the anthracyclines, we will begin with anthracene as the parent chromophore.

Anthracene is an odd-soft chromophore, the $^1L_b \leftarrow A$ transition having vanishing mcd intensity. Both theoretical and experimental investigations of the mcd spectrum of anthracene have been made (8, 21–26).

In anthracene the bands and their directions are $L_b(+)$, $L_a(-)$, $B_b(-)$, $B_a(+)$ in order of increasing energy (22).

When going to 9,10-anthraquinone, two strong positive electromeric substituents are placed in very dominant ring positions. This will bring in contributions from the larger $\mu^+$ values. The predicted mcd signs, in this case are $L_b(+)$, $L_a(-)$, $B_b(+)$, $B_a(-)$ in order of increasing energy. This sign sequence is observed in the experimental mcd spectra of 9,10-anthraquinone (25, 26). An $n \rightarrow \pi^*$ transition also appears, close in energy to the $L_a$ band. In fact it may split this band in some cases. The $n \rightarrow \pi^*$ band, though forbidden in the absorption spectrum, has a large magnetic moment and may overpower the weaker $L_a$ band, which is magnetically forbidden but optically allowed.

Further substituent effects are observed in going from 9,10-anthraquinone to luteoskyrin and rugulosine (26), as shown in Fig. 2. Here weaker +E and +I substituents in the form of $CH_3$ and OH are added to the anthraquinone chromophore. The effect is opposite to substitution at the 9,10 positions; here $\Delta HOMO > \Delta LUMO$ for substitution in a sub-dominant position, and the $\mu^+$ contributions are $-+-+$ in order of increasing energy. Initially such substitution will affect only the *L* bands, as is seen for luteoskyrin (Fig. 2), the mcd bands being $-++-$ in order of increasing energy.

For the anthracyclines, additional substitution at the sub-dominant positions is sufficient to bring about a sign reversal in the *B* transitions as well, the observed sign sequence being $L_b(-)$, $L_a(+)$, $B_b(-)$, and $B_a(+)$ in order of increasing energy. The $L_a$ transition is hidden under the $n \rightarrow \pi^*$ band of the same sign, as shown by marcellomycin in Fig. 3.

The transition energies (27) and mcd spectra (28) of the individual nucleosides cytidine and guanosine have been determined previously. In both cases there is no absorption of energy at wavelengths longer than 310 nm, so that contributions due to CpG absorption will not be present in the optical titrations or the mcd measurements.

## Results and discussion

(a) *Optical titrations*

The approach taken was essentially identical to that previously used by Muller and Crothers (29) to study the binding of actinomycin to DNA. Binding was followed by measuring the decrease in the extinction coefficient of the drugs when they are mixed with a standard CpG solution. Measurements were taken in the visible region where no interference due to the dinucleotide occurs.

The concentration of the drug–dinucleotide complex, $C_k$ is given by the equation

$$[1] \quad C_k = (\varepsilon_\lambda^k C_T - A/10)/(\varepsilon_\lambda^F - \varepsilon_\lambda^k)$$

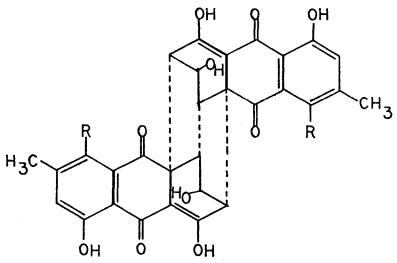


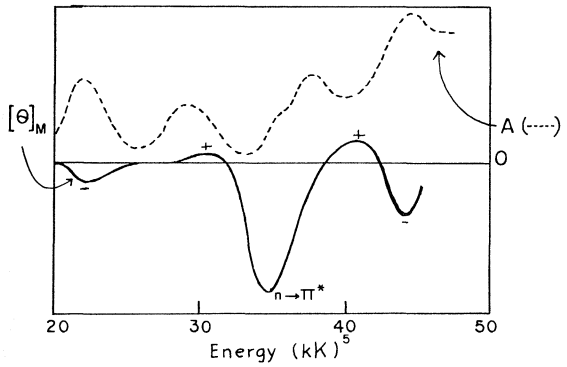


FIG. 2. Absorption (---) and mcd (———) spectra of luteoskyrin.

where $\varepsilon_\lambda^k$ is the extinction coefficient of the complex, $\varepsilon_\lambda^F$ is the extinction coefficient of the free drug, $C_T$ is the total drug concentration, and $A/10$ is the absorbance per cm path length. At very high ratios of dinucleotide to drug, it was assumed that all the drug is bound and thus one can calculate $\varepsilon_\lambda^k$.

It has been shown (30) that by rearrangement of the expression for the equilibrium between a bound and a free species, one can obtain the expression

$$[2] \quad r/m = K_{ap}(B_{ap} - r)$$

which is appropriate to a Scatchard plot (10) of binding isotherms, where $r$ is the ratio of bound drug to total CpG base pair concentration and $m$ is the concentration of the free drug. From a plot of $r/m$ vs. $r$ one can obtain the apparent binding constant, $K_{ap}$ (from the slope) and the number of binding sites per base pair, $B_{ap}$, from the extrapolated intercept at $r/m = 0$.

The results of the Scatchard plots for aclacinomycin **1** and marcellomycin **2** are depicted in Fig. 4. For carminomycin **3**, the plot is nearly identical to that of **2**. Marcellomycin and carminomycin with

[5]kK = kilokaisers, where 1 kK = $10^3$ $cm^{-1}$.

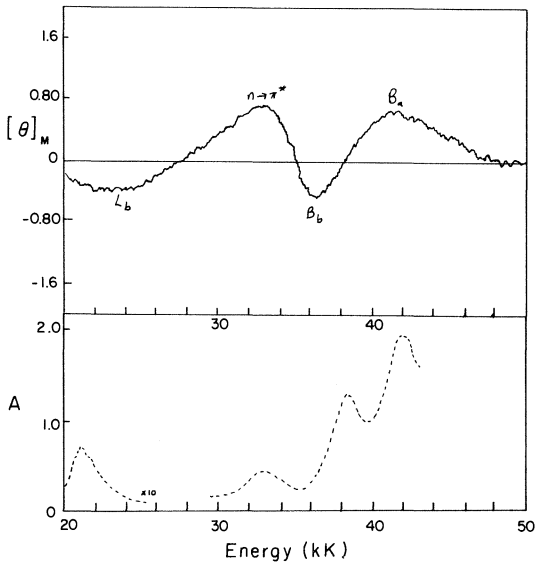


FIG. 3. Absorption (---) and mcd (———) spectra of marcellomycin.

CpG give essentially identical linear binding titrations, falling rapidly with increasing values of bound drug concentration $r$, following the Langmuir isotherm. At low values of $r$, infinity points were obtained for $r/m$, since the concentration of free drug m approaches zero. This indicates complete binding.

For marcellomycin the ratio of bound drug to CpG base pairs, $B_{ap}$, is $0.11 \pm 0.02$ and the apparent binding constant $K_{ap}$ is $4.6 \pm 0.9 \times 10^7$ $M^{-1}$. In the

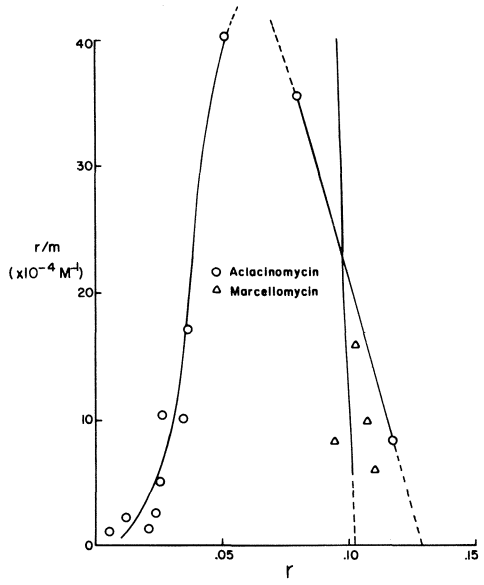


FIG. 4. Scatchard plots.

Can. J. Chem. Downloaded from www.nrcresearchpress.com by 210.87.254.6 on 09/06/12
For personal use only.

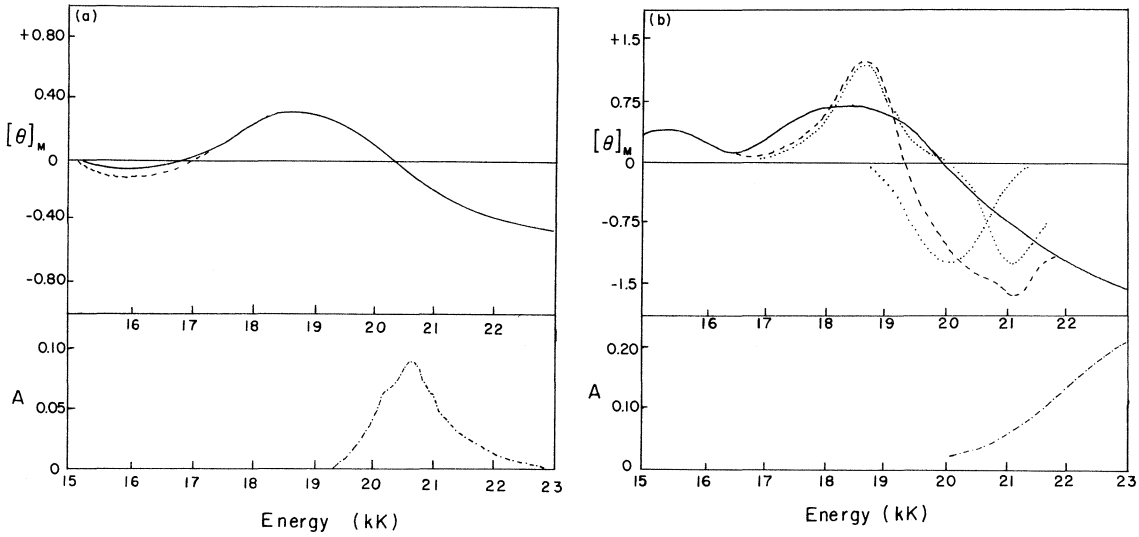


FIG. 5. (a) Absorption (·····) spectrum of marcellomycin; mcd (———) spectrum of marcellomycin; mcd (---) spectrum of marcellomycin–CpG. (b) Absorption (·····) spectrum of aclacinomycin; mcd (———) spectrum of aclacinomycin; mcd(---) spectrum of aclacinomycin–CpG; curve-resolved mcd (····) spectrum of aclacinomycin–CpG.

case of Carminomycin, the corresponding values are $0.08 \pm 0.01$ and $1.2 \pm 0.3 \times 10^7\ M^{-1}$ respectively.

By contrast, the Scatchard plot for aclacinomycin first rises slowly to a maximum value of $r/m$, with complete binding occurring near a value of ca. 0.06 for $B_{ap}$. Subsequently there is a reversion to the Langmuir isotherm above the $r$ value of 0.06. From this portion of the plot, one can calculate $B_{ap}$ to be $0.13 \pm 0.02$ and $K_{ap}$ to be $7.3 \pm 1.0 \times 10^6\ M^{-1}$.

The slope of the plot up to the $r$ value of 0.06 is indicative of cooperative binding (31). The fact that $r/m$ increases as $r$ increases to 0.06 shows that once one drug molecule is initially bound, subsequent binding is facilitated.

(b) *Magnetic circular dichroism spectra*

As stated previously, the dinucleotide CpG has no mcd absorption in the region below 25 000 $cm^{-1}$. Thus any differences between the mcd spectra of the drug itself and the drug–nucleotide complex can be attributed to some specific change in the anthraquinone chromophore due to binding. For marcellomycin, results shown in Fig. 5a indicate little perturbation of the anthraquinone chromophore upon binding. Results for the carminomycin–CpG complex were similar. In each case ratios of dinucleotide to drug of ca. 15:1 were employed to ensure that no free drug was present. Above 25 000 $cm^{-1}$, the mcd spectrum of the excess CpG swamps that of the drug. Thus this region is not included in Fig. 5a or 5b.

In contrast to the slight perturbations in these two cases, the mcd spectrum of the aclacinomycin–CpG complex displays several strong new features. By curve resolution using Gaussian band shapes, three $B$ terms can be identified, with signs, at 18 700(+), 20 100(−), and 21 100(−) wavenumbers (Fig. 5b). The appearance of these bands, in a region of very weak absorption, suggests that a different mode of binding has occurred in this particular complex, which has stimulated forbidden transitions in the drug and the dinucleotide.

In anthraquinones, characterized by $D_{2h}$ symmetry, there is an electric dipole forbidden $\pi \rightarrow \pi^*$ transition to the $^1B_{1g}$ state (25, 26). However, this transition is allowed by an out-of-plane magnetic dipole, and if it could acquire intensity by interaction with a second similar chromophore, a strong mcd signal would be expected. Such an interaction could most easily occur through close contact of the drug chromophore with the aromatic base pairs of the dinucleotide.

(c) *Nature of the drug–dinucleotide interactions*

Clearly two distinct types of interactions are present, based on the optical titration and mcd data. The Scatchard plots for marcellomycin and carminomycin show complete but noncooperative binding when CpG is in excess. The corresponding mcd spectra are not strongly perturbed, indicating that the binding mechanism does not perturb the nature of the anthraquinone chromophore to any large extent.

On the other hand, aclacinomycin is involved in

Can. J. Chem. Downloaded from www.nrcresearchpress.com by 210.87.254.6 on 09/06/12
For personal use only.

Can. J. Chem. Downloaded from www.nrcresearchpress.com by 210.87.254.6 on 09/06/12
For personal use only.

cooperative binding and the mcd spectrum of this drug, complexed with CpG, indicates extensive perturbation of the anthraquinone chromophore.

Previous work indicates that anthracyclines bind via an intercalative mechanism, predominantly in the minor groove of DNA (32). For CpG, this groove corresponds to a slightly displaced set of hydrophilic hydrogen bonds near the centre and hydrophobic base pairs near the edges (Fig. 6). The two drugs carminomycin and marcellomycin possess OH groups in the *peri*-position for each of the anthraquinone carbonyls (Fig. 1). Both molecules could intercalate into the hydrophilic region and be strongly bound without placing the anthraquinone chromophore near any of the bases (Fig. 7). However, aclacinomycin possesses one anthraquinone carbonyl which does not have a *peri*-OH group. Intercalation, placing the hydrophobic side between the base pairs, is therefore favoured.

This sideways shift of **1** relative to **2** and **3** implies that only one half of the CpG slot is occupied by the first molecule of aclacinomycin **1**. The observed cooperative binding strongly suggests that a second molecule of **1** can penetrate the opened slot to lie adjacent to the first (Fig. 8). The initially bound molecule of **1** probably approaches CpG via the minor groove. Intercalation will induce some uncoiling of the helix, thereby permitting the second molecule of **1** to approach via the major groove. For the sugar moieties to have the least steric interference, the two molecules of **1** are probably inverted relative to each other (Fig. 8).

This structural hypothesis is consistent with the observed features in the mcd spectrum. The proposed close association of the anthraquinone moiety between the base pairs provides a strong perturbation of the out-of-plane magnetic dipole transition and a resulting increase in observed intensity. Several new bands have appeared, the first two of which have oppositely signed *B* terms (Fig. 5b). This suggests that similar, out-of-plane, forbidden transitions in the base chromophores have been

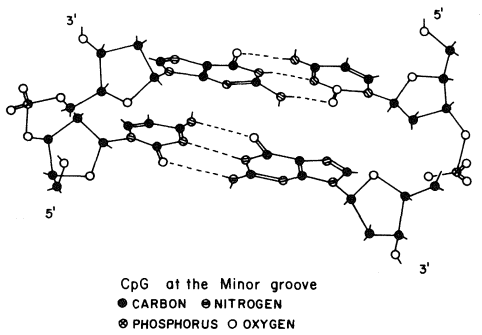


FIG. 6. CpG at the minor groove.

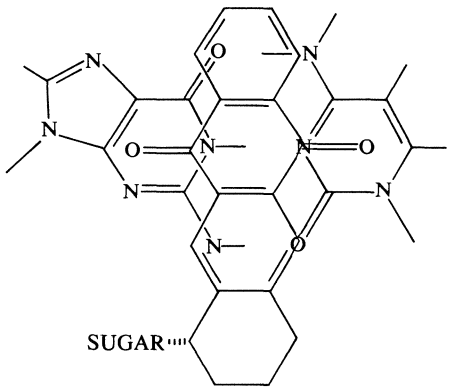


FIG. 7. Proposed interaction between intercalating marcellomycin or carminomycin and CpG base pairs.

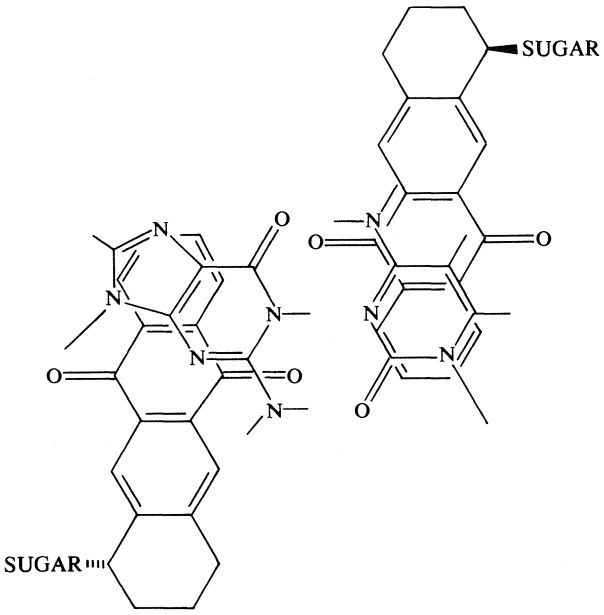


FIG. 8. Proposed interaction between intercalating aclacinomycin and CpG base pairs.

stimulated and that a substantial exiton splitting has occurred. The appearance of oppositely signed *B* terms of similar intensities is often characteristic of systems split by exitons (33).

A more detailed calculation of the orientation of the anthraquinone chromophore relative to the base pairs can be made from the relative intensities of the exiton *B* terms. These *B* terms acquire intensity through the interaction of the forbidden $^1B_{1g}$ state with either the long ($x$-polarized) axis or short ($y$-polarized) axis electric dipole allowed transitions (25, 26). Since the long axis $L_b$ states lie at much closer energy than the short axis *B* states, the $L_b$ states probably dominate the observed *B* term intensities. Thus the relevent exiton dipoles involve the interaction of long axis polarized al-

Can. J. Chem. Downloaded from www.nrcresearchpress.com by 210.87.254.6 on 09/06/12
For personal use only.

lowed transitions in the anthraquinone with the base pair. The exiton is not directly visible in the allowed $L_b$ bands because the band width of 8 000 to 10 000 $cm^{-1}$ is much greater than the exiton splitting of approximately 1 500 $cm^{-1}$.

The equation describing the magnitude of the exiton in the classical transient point dipole model (34) is

$$V_{ab} = \frac{\rho_a \rho_b}{d^3_{ab}} [\sin\theta \sin\phi \cos(\theta-\phi) - 2\cos\theta \cos\phi]$$

where $\rho_a$ and $\rho_b$ are the electric dipole intensities for the transitions in molecules a and b, $d_{ab}$ is the intermolecular distance, and $\theta$ and $\phi$ are the angles formed by the transient dipoles with the line joining their centres.

In the present case, by assuming that the anthraquinone is inserted between the base pairs, the chromophores become stacked in coparallel fashion. The analysis thus reduces to a single orientation angle between the dipoles of the lowest $L_b$ bands in the anthraquinone and the base pair. The near equality of these intensities at 18 700 and 20 100 $cm^{-1}$ indicates that the $L_b$ dipole direction is at an angle near 45° to the $L_b$ dipole in the bases of the dinucleotide. This is quite consistent with structures proposed by Gabbay *et al.* (32).

## Conclusions

It seems clear that the two distinct binding modes are available to intercalating anthracyclines. Those compounds having both anthraquinone carbonyls *peri*-hydroxylated bind one molecule per groove in the central hydrophilic region while those having only one *peri*-hydroxylated anthraquinone carbonyl can bind two per groove and interact directly and strongly with the base pairs. This latter interaction involves a more severe perturbation of both the stereochemistry and electronic structure of the dinucleotide than the first.

This distinction could have important consequences in the understanding of the mode of action of these antitumor agents. Indeed, it has been reported (35) that aclacinomycin possesses a mode of antitumor action which distinguishes it from drugs possessing two *peri*-hydroxylated anthraquinone carbonyls, such as adriamycin, daunomycin, carminomycin, and marcellomycin. Our results indicate that these differing modes of action may reflect the presence or absence of the cooperative binding phenomena described herein.

## Experimental

(a) *Materials*

Aclacinomycin A, carminomycin, and marcellomycin were provided by Bristol Laboratories, Bristol Myers Co., Syracuse, NY. 2′-Deoxycytidylyl-(3′→5′)-2′-deoxyguanosine (CpG) was obtained as the ammonium salt from Sigma Chemical Company. Orthophosphoric acid and sodium phosphate dibasic, both reagent grade, were from Anachemia Chemical Ltd.

All samples were weighed on a Mettler H2O balance. The pH measurements were obtained using a Fisher Accumet 140 meter with a combination electrode. Calibrations were made using standard buffer solutions (pH 4.00 and 8.00), obtained from Anachemia Chemicals Ltd.

(b) *Optical titrations*

Ultraviolet and visible absorption spectra were recorded on a Cary 14 spectrophotometer (Applied Physics Corp., Monrovia, CA). Changeable potentiometers allowed measurements to be taken with 0.5 or 1.0 absorbance units corresponding to a full scale deflection.

Individual absorption spectra were measured in 1 cm quartz cells, whereas binding titrations were performed using quartz cells with a 10 cm path length.

Stock solutions of the three anthracycline drugs were prepared in 5.00 mL of millipore pure water. Binding titrations were performed against an excess of CpG, allowing 24 h for the attainment of equilibrium, during which time samples were stored in the dark. All solutions contained 0.01 *M* $Na_2HPO_4$ with the pH adjusted to 7 using $H_3PO_4$.

The binding interactions were followed at a wavelength corresponding to $\varepsilon_{max}$ for the drugs, 450 nm for aclacinomycin and 550 nm for carminomycin and marcellomycin. Similar (dilute) concentrations of the free drugs were measured under the same conditions.

(c) *Magnetic circular dichroism spectra*

The mcd spectra were obtained on an instrument built in this department. The optics of a Cary 14 spectrophotometer were modified to allow a superconducting magnet (Oxford Instruments) to be placed over the sample compartment.

The field strength was 44.7 kgauss for all experiments. Spectra of 1000 datum points were collected automatically using a scan stepper motor controlled by a Nova 4/c minicomputer (Data General Canada Ltd).

At least 16 values per datum point were collected and averaged, more values (up to 25) were taken as the noise increased. The digitized stored spectrum was then corrected for the baseline. A separate file was created containing the data for the baseline. Both files were rotated about a line connecting two points of zero mcd intensity (lock positions), bringing them to the horizontal. The baseline data were then fitted to the mcd data file and the two subtracted to produce the final spectra. This procedure minimizes the distortion caused by a badly curved baseline.

The instrument was calibrated using 0.01 *M* $CoSO_4$ giving a $[\theta]_M$ value of $-6.1 \times 10^{-3}$ deg $cm^2$ $dmol^{-1}$ $gauss^{-1}$ at 19 800 $cm^{-1}$ (36). A positive mcd signal corresponded to $\varepsilon_L > \varepsilon_R$, where these are the extinction coefficients of left and right circularly polarized light respectively.

Samples were prepared using millipore pure water, and with concentrations previously determined to provide complete binding. Free drug and dinucleotide spectra were obtained under identical conditions. Samples were run in a circular quartz cell with a 1 cm path length.

The natural cd spectra of the drugs and dinucleotide below 30 000 $cm^{-1}$ were obtained on the same instrument. With the magnet turned off, the instrument was calibrated using *d*-camphor sulfonic acid. A [θ] value of 7800 deg $cm^2$ $dmol^{-1}$ was recorded for a $2.0 \times 10^{-3}$*M* solution at 34 500 $cm^{-1}$ (37).

At $\bar{\nu}$ values lower than 30 000 $cm^{-1}$, there was negligible absorption in the cd spectra of CpG and the anthracyclines.

## Acknowledgements

We thank the Natural Sciences and Engineering

Research Council of Canada for financial support. The cooperation of Dr. R. L. Buchanan and Dr. W. T. Bradner of Bristol Laboratories, who furnished the anthracyclines, is gratefully acknowledged.

1. D. W. HENRY. *In* Cancer chemotherapy. *Edited by* A. C. Sartorelli. Am. Chem. Soc. Syn. Ser. **30**, 15 (1976).
2. T. OKI, Y. MATSUZAWA, A. YOSHIMOTO, K. NUMATA, I. KITAMURA, S. HORI, A. TAKAMUTSU, H. UMEZAWA, M. ISHIZUKA, H. NAGANAWA, H. SUDA, M. HAMADA, and T. TAKEUCHI. J. Antibiot. **28**, 830 (1975).
3. D. E. NETTLETON, JR., W. T. BRADNER, J. A. BUSH, A. B. COON, J. E. MOSELEY, R. W. MYLLYMAKI, F. A. O'HERRON, R. H. SCHREIBER, and A. L. VULCANO. J. Antibiot. **30**, 525 (1977).
4. M. G. BRAZNIKOVA, V. B. ZBARSKY, V. I. POMOMARENKO, and N. P. POTAPOVA. J. Antibiot. **27**, 254 (1974).
5. H. KERSTEN and W. SZYBALSKI. Biochemistry, **5**, 236 (1966).
6. J.-B. LE PEQ. Methods Biochem. Anal. **20**, 41 (1971).
7. T. R. KRUGH and M. A. YOUNG. Nature, **269**, 627 (1977).
8. J. MICHL. J. Am. Chem. Soc. **100**, 6801 (1978).
9. P. O. P. TS'O, N. S. KONDO, M. P. SCHWEIZER, and D. P. HOLLIS. Biochemistry, **8**, 997 (1969).
10. G. SCATCHARD. Ann. N.Y. Acad. Sci. **51**, 660 (1949).
11. C. DJERASSI, E. BUNNENBURG, and D. L. ELDER. Pure Appl. Chem. **25**, 57 (1971).
12. J. R. PLATT. J. Chem. Phys. **17**, 484 (1949).
13. M. TITY and M. NEPRAS. Collect. Czech. Chem. Commun. **37**, 2674 (1972).
14. R. P. MITRA and K. L. KAPOOR. Int. J. Quant. Chem. **6**, 387 (1972).
15. A. KUBOYAMA and K. WADA. Bull. Chem. Soc. Jpn. **39**, 1874 (1966).
16. J. W. SIDMAN. J. Am. Chem. Soc. **78**, 4567 (1956).
17. R. A. MORTON and W. T. EARLAM. J. Chem. Soc. 159 (1941).
18. R. SHIMADA and L. GOODMAN. J. Chem. Phys. **43**, 2027 (1965).
19. H. INOUE, T. HOSHI, J. YOSHINO, and Y. IANIZALI. Bull. Chem. Soc. Jpn. **46**, 380 (1973).
20. H. R. DROTT and H. H. DEARMAN. J. Chem. Phys. **47**, 1896 (1967).
21. D. A. SCHOOLEY, E. BUNNENBERG, and C. DJERASSI. Proc. Natl. Acad. Sci. U.S.A. **56**, 1377 (1966).
22. J. P. LARKINDALE and D. J. SIMKIN. J. Chem. Phys. **55**, 5668 (1971).
23. S. F. MASON and R. D. PEACOCK. Chem. Phys. Lett. **21**, 406 (1973).
24. J. G. Foss and M. E. MCCARVILLE. J. Chem. Phys. **44**, 4350 (1966).
25. H. H. DEARMAN. J. Chem. Phys. **58**, 2135 (1973).
26. P. CHUONG, J.-C. BOUCHET, C. SCHNEIDER, and P. FROMAGEOT. J. Chim. Phys. Phys.-Chim. Biol. **71**, 401 (1974).
27. L. B. CLARK and I. TINOCO, JR. J. Am. Chem. Soc. **87**, 11 (1965).
28. D. W. MILES, L. B. TOWNSEND, M. J. ROBINS, R. K. ROBINS, W. H. INSKEEP, and H. EYRING. J. Am. Chem. Soc. **93**, 1600 (1971).
29. W. MULLER and D. M. CROTHERS. J. Mol. Biol. **35**, 251 (1968).
30. R. FOSTER. Molecular complexes. Vol. 2. *Edited by* R. Foster. Crane, Russak and Co. Ltd., New York, NY. 1974.
31. K. G. WAGNER. Eur. J. Biochem. **10**, 261 (1969).
32. E. J. GABBAY, D. GRIER, R. E. FINGERLE, R. REIMER, R. LEVY, S. W. PIERRE, and W. D. WILSON. Biochemistry, **15**, 2062 (1976).
33. M. J. STILLMAN and A. J. THOMSON. J. Chem. Soc. Faraday Trans. II, **70**, 805 (1974).
34. B. R. HOLLEBONE and M. J. STILLMAN. J. Chem. Soc. Faraday Trans. II, **74**, 2107 (1978).
35. S. T. CROOKE, V. H. DURVERNAY, L. GAHVAN, and A. W. PRESTAYKO. Mol. Pharmacol. **14**, 290 (1978).
36. B. HOLMQUIST, T. A. KADIN, and B. L. VALLEE. Biochemistry, **14**, 1454 (1975).
37. G. C. CHEN and J. T. YANG. Anal. Lett. **10**, 1195 (1977).

Can. J. Chem. Downloaded from www.nrcresearchpress.com by 210.87.254.6 on 09/06/12
For personal use only.

# Synthesis of the colitose determinant of *Escherichia coli* O111 and 3,6-di-*O*-(α-D-galactopyranosyl)-α-D-glucopyranoside[1]

TOMMY IVERSEN[2] AND DAVID R. BUNDLE

*Division of Biological Sciences, National Research Council of Canada, Ottawa, Ont., Canada K1A 0R6*

Received September 16, 1981

TOMMY IVERSEN and DAVID R. BUNDLE. Can. J. Chem. **60**, 299 (1982).

The syntheses of two branched trisaccharides, which constitute important elements of enterobacterial lipopolysaccharides are described. The common structural feature of each trisaccharide is α-D-glucopyranoside, upon which branching occurs at the *O*-3 and *O*-6 positions. Selective blocking of this hexoside at *O*-2 and *O*-4 by persistent blocking groups was accomplished by benzylation of 1,6-anhydro-β-D-glucopyranoside (**1**). Acetolysis of the product **2** afforded a mixture of anomeric triacetates **3** from which the corresponding 3,6-di-*O*-acetyl-2,4-*O*-benzyl-α-D-glucopyranosyl chloride (**4**) was prepared. The α and β 8-methoxycarbonyloctyl glycosides **5** and **6** were obtained in the ratio ~2:1, when **4** was reacted with 8-methoxycarbonyloctanol. Transesterification of the α-glycoside **5** gave the aglyconic intermediate **7** from which each trisaccharide could be obtained in a one step reaction. Thus glycosylation of **7** with tetra-*O*-benzyl-α-D-galactopyranosyl chloride (**8**) or 2,4-di-*O*-benzyl-3,6-dideoxy-α-L-*xylo*-hexopyranosyl chloride (**10**) gave the trisaccharides **11** and **13**. In both cases removal of blocking groups was achieved in a single hydrogenolysis step. Trisaccharide **12** represents a trisaccharide sequence present in the core saccharide of Salmonella lipopolysaccharides, while the colitose containing trisaccharide **14** is an essential element of the *E. coli* O111 *O*-antigen.

TOMMY IVERSEN et DAVID R. BUNDLE. Can. J. Chem. **60**, 299 (1982).

On décrit la synthèse de deux trisaccharides ramifiés qui constituent des éléments importants des lipopolysaccharides entérobactériens. La caractéristique structurale commune à chaque trisaccharide est l'α-D-glucopyrannoside, sur lequel s'effectue les ramification en positions *O*-3 et *O*-6. On a pu protéger sélectivement cet hexoside en positions *O*-2 et *O*-4 à l'aide de groupes protecteurs très stables en benzylant l'anhydro-1,6 β-D-glucopyrannose (1). L'acélotyse du composé **2** conduit à un mélange de triacétates **3** anomères à partir duquel on a préparé le chlorure de di-*O*-acétyl-3,6 *O*-benzyl-2,4 α-D-glucopyrannosyle (**4**). On a obtenu les α- et β-glycosides de methoxycarbonyl-8 octyle, **5** et **6**, dans un rapport de 2:1 environ en faisant réagir le composé **4** avec le méthoxycarbonyl-8 octanol. La transestérification de l'α-glycoside conduit à l'intermédiaire aglyconique **7** à partir duquel on peut obtenir chaque trisaccharide en une seule étape. Ainsi la glycosilation du composé **7** par le chlorure de tétra-*O*-benzyl α-D-galactopyrannosyle (**8**) ou par le chlorure de di-*O*-benzyl-2,4 didéoxy-3,6 α-L-xylohexopyrannosyle (**10**) donne les trisaccharides **11** et **13**. Dans les deux cas, l'hydrolyse permet d'effectuer la déprotection en une seule étape. Le trisaccharide **12** représente une suite de trisaccharides présents dans le noyau saccharique des lipopolysaccharides du type Salmonella, tandis que le trisaccharide **14** contenant la colitose est un élément essentiel de l'antigène O de l'*E. Coli* O111.

[Traduit par le journal]

## Introduction

Although antigenic determinants of *Salmonella* O-antigens containing the three 3,6-dideoxyhexoses paratose, abequose, and tyvelose have been synthesized (1–3), none of the colitose (optical antipode of abequose)-containing determinants have yet been prepared. Preliminary data indicate that colitose occurs in a "cross"-like structure as part of the repeating unit of the *E. coli* O111 O-antigen (4). Serological cross-reactions of *E. coli* O111, *Salmonella adelaide* O–35, and *Salmonella greenside* O–50 are related to the presence of colitose in the lipopolysaccharides (LPS) from each of these bacteria (5–7). In order to investigate further the dependence of these serological cross-reactions upon the colitose residues, the branched, colitose-containing trisaccharide, which is part of the *E. coli* O-antigen, was synthesized. The structurally related galactose-containing trisaccharide of *Salmonella* LPS core structures (8) was also synthesized. Since recent work has shown approximately 65% of LPS molecules to be incomplete with respect to addition of the O-chains (9, 10), the accessibility of such incomplete structures to core-specific antibodies is of renewed interest (11).

The synthesis of both trisaccharides was contingent upon an acceptable blocking strategy, which would provide an α-D-glucopyranoside with persistent blocking groups at *O*-2 and *O*-4, leaving *O*-3 and *O*-6 open for glycosylation. Branching at *O*-3 and *O*-6 of galacto- and manno-pyranosides occurs in blood-group substances (12) and glycoproteins (13). Compared with these hexoses, glucose lacks an axial–equatorial vicinal diol system that may be exploited to generate the required substitution pattern of blocking groups (14–16). A solution to this problem is described here, which facilitated the synthesis of two biologically important branched structures.

## Results

The scheme envisaged for the synthesis of branched structures was based upon the requirement

[1]Issued as NRCC No. 19790.

[2]NRCC research associate 1979–1981.

0008-4042/82/030299-05$01.00/0

©1982 National Research Council of Canada/Conseil national de recherches du Canada

Can. J. Chem. Downloaded from www.nrcresearchpress.com by 210.87.254.42 on 09/06/12
For personal use only.

Can. J. Chem. Downloaded from www.nrcresearchpress.com by 210.87.254.42 on 09/06/12
For personal use only.

for a 8-methoxycarbonyloctyl α-D-glycopyranoside bearing persistent blocking groups, preferably benzyl ethers, at *O*-2 and *O*-4. In order to accomplish this, methyl α-D-glucopyranoside and *tert*-butyl β-D-glucopyranoside were reacted with *tert*-butyldiphenylsilyl chloride in DMF (17). Whereas the methyl glycoside gave predominantly the 2,6-disubstituted glucoside, *tert*-butyl β-D-glucopyranoside (18) gave the desired 3,6-disilyl ether. Unfortunately this product proved to be resistant to benzylation conditions, which have been reported to be compatible with the integrity of such silyl ethers (17).

A suitable derivative, 2,4-di-*O*-benzyl-1,6-anhydro-β-D-glucopyranose, has been reported in the literature (19–21). Benzylation of 1,6-anhydro-β-D-glucopyranose (**1**) with benzyl bromide and barium oxide in DMF gave **2** in 95% yield compared with the previously reported yield of 21%. Acetolysis of **2** gave an anomeric mixture of the triacetates **3** in 77% yield. This mixture was converted cleanly and quantitatively to 3,6-di-*O*-acetyl-2,4-di-*O*-benzyl-α-D-glucopyranosyl chloride (**4**), which was used without purification for the glycosylation of 8-methoxycarbonyloctanol. The desired α-glycoside **5** was obtained together with the β-anomer **6** in the ratio ~2:1. Transesterification of **5** gave the selectively blocked α-glucopyranoside **7**, which was used for the one-step syntheses of the branched trisaccharides.

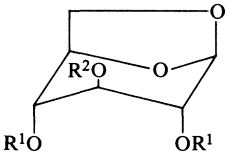

**1** $R^1 = R^2 = H$
**2** $R^1 = Bzl, R^2 = H$

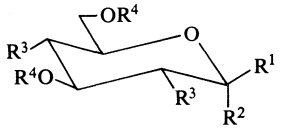

**3** $R^1/R^2 = Ac/H, R^3 = OBzl, R^4 = Ac$
**4** $R^1 = H, R^2 = Cl, R^3 = OBzl, R^4 = Ac$
**5** $R^1 = H, R^2 = O(CH_2)_8CO_2CH_3, R^3 = OBzl, R^4 = Ac$
**6** $R^1 = O(CH_2)_8CO_2CH_3, R^2 = H, R^3 = OBzl, R^4 = Ac$
**7** $R^1 = R^4 = H, R^2 = O(CH_2)_8CO_2CH_3, R^3 = OBzl$

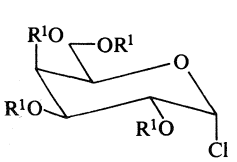

**8** $R^1 = Bzl$

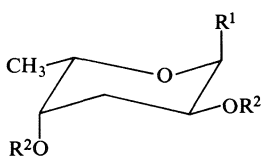

**9** $R^1 = OCH_3, R^2 = Bzl$
**10** $R^1 = Cl, R^2 = Bzl$

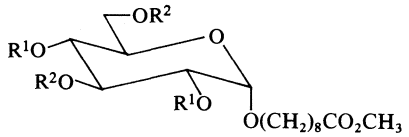

**11** $R^1 = Bzl, R^2 =$

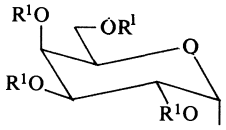

**12** $R^1 = H, R^2 =$



**13** $R^1 = Bzl, R^2 =$

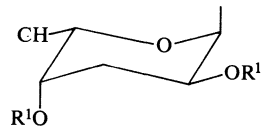

**14** $R^1 = H, R^2 =$



Silver trifluoromethanesulphonate (triflate)-promoted glycosylation of **7** by tetra-*O*-benzyl-α-D-galactopyranosyl chloride (**8**) gave the corresponding trisaccharide **11** in 57% yield. Carbon-13 nmr revealed the presence of three anomeric carbon atoms with chemical shifts characteristic of α-anomers.

Methyl 3,6-dideoxy-α-L-*xylo*-hexopyranoside (22) was benzylated to give the benzylated glycoside **9**. Conversion of this derivative to the glycosyl chloride **10** was accomplished by reaction of the methyl glycoside **9** with dichloromethyl methyl ether in the presence of zinc chloride (23). The chlorosugar **10** was used immediately without purification. Glycosylation of the aglyconic component **7** by **10** under conditions of standard halide-ion catalysis (24) was unsuccessful. Under less conventional conditions the glycosyl chloride **10** reacted with the selectively blocked glucoside **7** in acetonitrile solution to give the required trisaccharide **13** in 53% yield.

The blocked trisaccharides **11** and **13** were hydrogenated to give the deblocked trisaccharides **12** and **14**. Proton and carbon-13 nmr chemical shifts confirm the α-configuration of the glycosidic linkages.

## Discussion

The selective protection of D-glucose residues is made difficult by the equatorial relationship of the secondary hydroxyl groups of the $^4C_1$ (D) conformer. These difficulties may be circumvented for some purposes by the use of 1,6-anhydro-β-D-glucopyranose (**1**) (20). For the purpose of generating 3,6-disubstituted glucopyranose residues, benzylation of **1** to give the 2,4-di-*O*-benzyl-glucopyranose **2** offers the most direct route (19–21), although the published yield is low (19). By comparison, an alternate route to a 2,4-di-*O*-benzyl-D-glucopyranoside was recently reported (24). Modification of the benzylation conditions of **1** gave **2** in

Can. J. Chem. Downloaded from www.nrcresearchpress.com by 210.87.254.42 on 09/06/12
For personal use only.

good yield. Acetolysis followed by conversion to the glycosyl chloride **4** provides a rapid route via glycosylation of 8-methoxycarbonyloctanol to the desired intermediate α-glycosides **5** and **7**. The yields achieved compare favourably with previous work (19).

Methyl 2,4-di-*O*-benzyl-3,6-dideoxy-α-L-*xylo*-hexopyranoside (**9**) was efficiently converted to the corresponding glycosyl chloride **10** by dichloromethyl methyl ether with zinc chloride as the Lewis acid (23). The 3,6-dideoxyglycosyl halides are among the most labile glycosyl halides. These reaction conditions are, therefore, compatible with benzyl ether blocking groups and well suited to the lability of the product.

Throughout this study glycosyl chlorides were employed, a choice based on several considerations. The chlorides are more stable than the glycosyl bromide analogues and the reduced reactivity can be compensated for by judicious choice of promoter, according to the scheme of Paulsen and Kolář (25). Thus tetra-*O*-benzyl-α-D-galactopyranosyl chloride (**8**) readily formed α-glycosidic bonds at *O*-6 and *O*-3 with silver triflate as promoter (26).

When the glycosyl chloride **10** was reacted with 8-methoxycarbonyloctyl 2,4-di-*O*-benzyl-α-D-glucopyranoside (**7**) under conditions of halide ion catalysis, the reaction mixture contained many components from which only decomposition products of **10** and **7** could be isolated. In order to suppress side reactions which could result from the electrophilic nature of reaction intermediates (27), acetonitrile was employed as the solvent for the halide-ion catalysed reaction of **10** with **7**. The solvating action of acetonitrile served to stabilize the glycosyl chloride, the presence of which was evident from tlc examination of the reaction mixture over a five-day period. In this way an efficient yield of the trisaccharide **12** was secured.

The deblocked glycosides showed nmr parameters in agreement with the structures. The $^1$H nmr shift and $^3J$ coupling constant data for the three anomeric protons are consistent only with the presence of α-linkages in both trisaccharides **12** and **14**. The $^{13}$C nmr shifts for the anomeric carbon atoms further corroborate this conclusion.

Binding of antibody, raised against *E. coli* O111 or *Salmonella adelaide* whole cell vaccines, to the respective cell wall lipopolysaccharides was inhibited by methyl 3,6-dideoxy-α-L-*xylo*-hexopyranoside and trisaccharide **14**. In all cases the trisaccharide was at least 50–100 times more effective than the methyl α-glycoside of colitose. These results reflect the crucial spacial disposition of the two colitose residues for antibody binding. Moreover, since trisaccharide **14** inhibits the homologous *S. adelaide* system, both *S. adelaide* and *E. coli* O111 likely possess similar O-antigen structures. This conclusion based on serology is supported by independent structural studies.[3]

## Experimental

The general methods and materials employed in this work are similar to those described in other papers from this laboratory (22, 28). Carbon 13 and $^1$H nmr spectra were recorded at 20 and 79.9 MHz respectively. Proton chemical shifts are expressed relative to 1% tetramethylsilane (TMS) for deuteriochloroform solutions and, in the case of deuterium oxide, relative to sodium 3-trimethyl-silylpropionate-2,2,3,3-$d_4$ (TSP). Carbon-13 shifts are expressed relative to internal and external TMS for deuteriochloroform and deuterium oxide solutions. Medium pressure column chromatography was used for most separations and was conducted according to our published method (29).

*1,6-Anhydro-2,4-di-*O*-benzyl-β-*D*-glucopyranose (**2**)*

A mixture of 1,6-anhydro-β-D-glucopyranose (30) (**1**) (2.0 g, 12 mmol), benzyl bromide (7.5 mL), and barium oxide (7.5 g) in dimethylformamide (50 mL) was stirred at 60°C for 3 h, followed by addition of methanol (25 mL) to destroy excess benzyl bromide. After 30 min the reaction mixture was diluted with chloroform, filtered, and washed with water. Evaporation of the solvents left a syrup that was purified on a silica gel column (Skellysolve B – ethyl acetate 2:1) to give 4.0 g (95%) of **2**: $[\alpha]_D$ −28.8° (*c* 1.0, chloroform), mp 104.5–105°C (recryst. Skellysolve B – ethyl acetate) (lit. (19) $[\alpha]_D$ −28.5°; mp 106.5–107°C); $^1$H nmr ($CDCl_3$) δ: 7.34 (bs, 10H, aromatics), 5.44 (s, 1H, H-1). *Anal.* calcd. for $C_{20}H_{22}O_5$: C 70.16, H 6.48; found: C 70.04, H 6.54.

*1,3,6-Tri-*O*-acetyl-2,4-di-*O*-benzyl-*D*-glucopyranose (**3**)*

Compound **2** (3.0 g, 8.8 mmol) was dissolved in acetic anhydride (50 mL) and 3 drops of concentrated sulfuric acid were added to the stirred reaction mixture. After 30 min the solution was diluted with chloroform, washed with aqueous sodium bicarbonate and water, and evaporated. The resulting syrup was purified on a silica-gel column (Skellysolve B – ethyl acetate 2:1) to give 3.3 g (79%) of **3** as an anomeric mixture; α/β ~3; $[\alpha]_D$ +80.7° (*c* 2.0, chloroform); $^1$H nmr ($CDCl_3$) δ: 7.27 (bs, 10H, aromatics), 6.32 (d, $J_{1,2}$ = 3.6 Hz, H-1α), 5.45 (d, $J_{1,2}$ = 9.7 Hz, H-1β); $^{13}$C nmr ($CDCl_3$) $\delta_c$: 93.8 (C-1β), 89.2 (C-1α).

*3,6-Di-*O*-acetyl-2,4-di-*O*-benzyl-α-*D*-glucopyranosyl chloride (**4**)*

Dichloromethyl methyl ether (7.5 mL) was added to a solution of **3** (2.6 g, 5.3 mmol) and zinc chloride (~100 mg) in dichloromethane (50 mL). The reaction mixture was stirred for 1.5 h, filtered, evaporated, and dried under vacuum to give 2.5 g (~100%) of the syrupy chlorosugar **4**. Carbon-13 nmr and $^1$H nmr indicated the syrup to be at least 95% pure and it was used in the glycosidation step without purification; $^1$H nmr ($CDCl_3$) δ: 6.01 (d, 1-H, $J_{1,2}$ = 3.9 Hz, H-1), 5.59 (t, 1H, $J_{2,3} \approx J_{3,4}$ = 12 Hz, H-3), 2.07 (s, 3H, OAc), 2.00 (s, 3H, OAc); $^{13}$C nmr ($CDCl_3$) $\delta_c$: 92.14 (C-1).

*8-Methoxycarbonyloctyl 3,6-di-*O*-acetyl-2,4-di-*O*-benzyl-α- (**5**) and -β-*D*-glucopyranoside (**6**)*

The chlorosugar **4** (2.5 g, 5.3 mmol) dissolved in dichloromethane (5 mL) was added to a stirred mixture of 8-methoxycarbonyloctanol (31) (1.3 g, 6.9 mmol), mercuric cyanide (2.7 g,

[3]L. Kenne, private communication.

Can. J. Chem. Downloaded from www.nrcresearchpress.com by 210.87.254.42 on 09/06/12
For personal use only.

11 mmol), and mercuric bromide (3.7 g, 10 mmol) in dichloromethane (10 mL) at −70°C. The reaction was allowed to warm to room temperature and stirred overnight. Filtration and evaporation gave a syrupy residue that was purified on a silica-gel column (Skellysolve B – ethyl acetate 3:1) to give 1.6 g (49%) of **5**; $[\alpha]_D$ +68.5° (*c* 1.4, chloroform); $R_f$ = 0.33 (solvent same as above); $^1$H nmr ($CDCl_3$) δ: 7.32 (bs, 10H, aromatics), 5.56 (t, 1H, $J_{2,3} = J_{3,4}$ = 9.4 Hz, H-3), 3.66 (s, 3H, OMe), 2.09 (s, 3H, AcO), 2.00 (s, 3H, AcO), 1.10–1.80 (m, 12H, —$(CH_2)_6$—); $^{13}$C nmr ($CDCl_3$) $\delta_c$: 96.6 (C-1); and 0.9 g (28%) of **6**; $[\alpha]_D$ +33.5° (*c* 1.2, chloroform); $R_f$ = 0.35 (solvent same as above); $^1$H nmr ($CDCl_3$) δ: 9.27 (bs, 10H, aromatics), 3.66 (s, 3H, OMe), 2.04 (s, 3H, AcO), 1.88 (s, 3H, AcO), 1.80–1.10 (m, 12H, —$(CH_2)_6$—); $^{13}$C nmr ($CDCl_3$) $\delta_c$: 103.5 (C-1).

*8-Methoxycarbonyloctyl 2,4-di-*O*-benzyl-α-*D*-glucopyranoside (7)*

Compound **5** (2.3 g, 3.7 mmol) in methanol (50 mL) containing a catalytic amount of sodium methoxide was left overnight. The syrup, obtained after removal of sodium ions with Rexyn 101 ($H^+$) resin, filtration, and evaporation, was purified on a silica-gel column (Skellysolve B – ethyl acetate 2:1) to give 1.6 g (83%) of **7**; $[\alpha]_D$ 79.6° (*c* 1.1, chloroform); $^1$H nmr ($CDCl_3$) δ: 7.34 (bs, 10H, aromatics), 3.65 (s, 3H, OMe), 2.0–1.0 (m, 12H, —$(CH_2)_6$—); $^{13}$C nmr ($CDCl_3$) $\delta_c$: 96.5 (C-1). *Anal.* calcd. for $C_{30}H_{42}O_8$: C 67.90, H 7.98; found: C 67.70, H 7.88.

*8-Methoxycarbonyloctyl 2,4-di-*O*-benzyl-3,6-di-*O*-[tetra-*O*-benzyl-α-*D*-galactopyranosyl]-α-*D*-glucopyranoside (11)*

A solution of tetra-*O*-benzyl-α-D-galactopyranosyl chloride (**8**) (30) (2.0 g, 3.5 mmol) in dichloromethane (10 mL) was added to a stirred mixture of compound **7** (0.40 g, 0.8 mmol), silver triflate (1.5 g, 5.8 mmol), *N*,*N*-tetramethylurea (3 mL), and molecular sieve 4 Å in dichloromethane (15 mL) at −40°C. The reaction mixture was allowed to warm to room temperature and stirred overnight. Filtration followed by evaporation left a syrup that was purified on a silica-gel column (toluene – ethyl acetate 15:1) to give 0.68 g (57%) of **8**; $[\alpha]_D$ +53.1° (*c* 1.4, chloroform); $^{13}$C nmr ($CDCl_3$) $\delta_c$: 98.3, 97.9, 96.5 (C-1″, C-1′, and C-1).

*Methyl 2,4-di-*O*-benzyl-3,6-dideoxy-α-*L*-xylo-hexopyranoside (9)*

A solution of methyl 3,6-dideoxy-α-L-*xylo*-hexopyranoside (22) (5.9 g, 36 mmol) containing sodium hydride (3.5 g, 15 mmol) in dry dimethylformamide (100 mL) was stirred at room temperature for 30 min. Benzyl bromide (20 g) in dimethylformamide (50 mL) was then slowly added to the stirred mixture and the reaction was left for 2 h at room temperature. Excess benzyl bromide was destroyed by the addition of methanol (25 mL). The reaction mixture was diluted with dichloromethane, washed with water, and evaporated to a syrup that was purified on a silica-gel column (Skellysolve B – ethyl acetate 4:1) to give 9.5 g (76%); $[\alpha]_D$ −19.8° (*c* 1.7, chloroform); $^1$H nmr ($CDCl_3$) δ: 3.90 (s, 3H, OMe), 2.20–1.70 (m, 2H, H-4), 1.28 (d, 3H, $J_{5,6}$ = 6 Hz, H-6); $^{13}$C nmr ($CDCl_3$) $\delta_c$: 98.0 (C-1), 27.9 (C-3), 16.6 (C-6). *Anal.* calcd. for $C_{21}H_{26}O_4$: C 73.66, H 7.65; found: C 73.61, H 7.66.

*2,4-Di-*O*-benzyl-3,6-dideoxy-α-*L*-xylo-hexopyranosyl chloride (10)*

Anhydrous zinc chloride (~50 mg) was added to a solution of **9** (0.53 g, 1.5 mmol) in dichloromethyl methyl ether (5 mL). The reaction mixture was stirred at room temperature for 1 h, filtered through glass wool, evaporated, and dried under high vacuum to give 0.53 g (~ 100%) of the syrupy chlorosugar **10**, which was immediately used in the glycosidation step; $^1$H nmr ($CDCl_3$) δ: 6.26 (d, 1H, $J_{1,2} \approx$ 2 Hz, H-1), 2.35–1.95 (m, 2H, H-3), 1.26 (d, 3H, $J_{5,6} \approx$ 6 Hz, H-6); $^{13}$C nmr ($CDCl_3$) $\delta_c$: 95.8 (C-1), 28.1 (C-3), 16.3 (C-6).

*8-Methoxycarbonyloctyl-2,4-di-*O*-benzyl-3,6-di-*O*-[2,4-di-*O*-benzyl-3,6-dideoxy-α-*L*-xylo-hexopyranosyl]-α-*D*-glucopyranoside (13)*

The chlorosugar **10** (0.53 g, 1.5 mmol) from the above preparation, in acetonitrile (5 mL), was added to a stirred mixture of compound **7** (0.35 g, 0.7 mmol), tetraethylammonium chloride (0.66 g, 4 mmol), diisopropylethylamine (0.25 g, 1.9 mmol), and molecular sieve 4 Å in acetonitrile (10 mL) at −40°C. The reaction mixture was allowed to reach room temperature and was stirred for 10 days, after which time the mixture was filtered and evaporated to a syrupy residue that was separated on a silica-gel column (Skellysolve B – ethyl acetate 4:1) to give 0.40 g (53%) of compound **11**; $[\alpha]_D$ −8.5° (*c* 0.7, chloroform); $^{13}$C nmr ($CDCl_3$) $\delta_c$: 96.9, 96.5, 95.9 (C-1″, C-1′, and C-1).

*8-Methoxycarbonyloctyl 3,6-di-*O*-[α-*D*-galactopyranosyl]-α-*D*-glucopyranoside (12)*

The trisaccharide **8** (0.67 g, 0.4 mmol) was dissolved in ethanol – acetic acid (1:1, 80 mL) and hydrogenolyzed for 18 h at 70 psi over 10% palladium on charcoal. Filtration and evaporation of solvents left a syrup that was purified on a silica-gel column (ethyl acetate – methanol–water 7:2:1) to give 0.18 g (63%) of the product **12**. The $^{13}$C nmr of **12** showed the presence of small amounts of disaccharide impurities and an analytically pure sample was obtained by acetylation (acetic anhydride – pyridine) and chromatography on a silica-gel column (Skellysolve B – ethyl acetate 4:1) followed by deacetylation (sodium methoxide – methanol); $[\alpha]_D$ +79.2° (*c* 0.9, in water); $^1$H nmr ($D_2O$, 90°C) δ: 5.96 (s, 1-H, H-1″), 4.97 (dd, 2-H, $J_{1,2} \approx$ 1.4, $J_{1,2}$ = 3.7 Hz, H-1′, H-1), 2.4 (t, —$CH_2CO$—), 2.0–1.1 (m, 12H, —$(CH_2)_6$—); $^{13}$C nmr ($D_2O$) $\delta_c$: 100.5, 99.6, and 99.3 (C-1″, C-1′, and C-1). *Anal.* calcd. for $C_{28}H_{50}O_{18}$: C 49.85, H 7.47; found: C 49.61, H 7.58.

*8-Methoxycarbonyloctyl 3,6-di-*O*-[3,6-dideoxy-α-*L*-xylo-hexopyranosyl]-α-*D*-glucopyranoside (14)*

The trisaccharide (**11**) (180 mg, 0.2 mmol) was dissolved in ethanol (30 mL) and hydrogenolyzed for a week at 70 psi over 10% palladium on charcoal. Filtration and evaporation of the solvent left a syrup that was purified on a silica-gel column (ethyl acetate – methanol–water 85:10:5) to give 80 mg (84%) of the product **13** $[\alpha]_D$ −17.7° (*c* 0.6, $H_2O$); $^1$H nmr ($D_2O$, 90°C) δ: 5.16 (d, 1-H, $J_{1',2'}$ = 3.6 Hz, H-1′), 4.88 (dd, 2H, $J_{1,2}$ = 3.0 Hz, $J_{1,2}$ = 4.2 Hz, H-1, H-1″); $^{13}$C nmr ($D_2O$) $\delta_c$: 100.5, 99.7, 99.5 (C-1″, C-1′, and C-1), 16.7 (C-6″), 16.6 (C-6′). *Anal.* calcd. for $C_{28}H_{50}O_{14}$: C 55.07, H 8.25; found: C 54.91, H 8.42.

## Acknowledgements

We wish to thank Dr. Klaus Bock for valuable discussions and for a generous gift of 1,6-anhydro-β-D-glucopyranose. In addition, the expert assistance of Mr. H. Seguin for microanalyses and the technical assistance of Mr. J. W. L. C. Christ are gratefully acknowledged.

1. G. Ekborg, P. J. Garegg, and B. Gotthammar. Acta Chem. Scand. **29**, 765 (1975).
2. K. Eklind, P. J. Garegg, and B. Gotthammar. Acta Chem. Scand. **30**, 305 (1976).
3. P. J. Garegg and B. Gotthammar. Carbohydr. Res. **58**, 345 (1977).
4. K. Eklind, P. J. Garegg, L. Kenne, A. A. Lindberg, and B. Lindberg. Abstracts of IXth Internat. Symposium on Carbohydrate Chemistry, London. April, 1978. G34.
5. O. Lüderitz, A. M. Staub, S. Stirm, and O. Westphal. Biochem. Z. **330**, 193 (1958).

6. O. WESTPHAL, F. KAUFFMAN, O. LÜDERITZ, and H. STIERLIN. Zentr. Bakteriol. I. Orig. **179**, 336 (1960).
7. O. LÜDERITZ, O. WESTPHAL, A. M. STAUB, and L. LEMINOR. Nature (London), **188**, 556 (1960).
8. O. LÜDERITZ. Angew. Chem. Int. Ed. Engl. **9**, 649 (1970).
9. E. T. PALVA and P. H. MAKELA. Eur. J. Biochem. **107**, 137 (1980).
10. R. C. GOLDMAN and L. LIEVE. Eur. J. Biochem. **107**, 145 (1980).
11. K. K. NIXDORFF, S. SCHLECHT, E. RÜDE, and O. WESTPHAL. Immunology, **29**, 87 (1975).
12. K. O. LLOYD, E. A. KABAT, and E. LICERIO. Biochemistry, **7**, 2976 (1968).
13. R. KORNFELD and S. KORNFELD. Ann. Rev. Biochem. **45**, 217 (1976).
14. T. OGAWA, K. KATANO, and M. MATSUI. Carbohydr. Res. **64**, C3 (1978).
15. J. ARNARP and J. LONNGREN. Acta Chem. Scand. Ser. B, **32**, 696 (1978).
16. C. AUGÉ, S. DAVID, and A. VEYRIERIES. J. Chem. Soc. Chem. Commun. 375 (1976).
17. S. HANESSIAN and P. LAVALLEE. Can. J. Chem. **53**, 2975 (1975).
18. W. A. R. VAN HEESWIJK, H. G. J. VISSER, and J. F. G. VLIEGENTHART. Carbohydr. Res. **58**, 494 (1977).
19. G. ZEMPLÉN, Z. CSUROS, and S. ANGYAL. Chem. Ber. **70**, 1848 (1937).
20. R. EBY and C. SCHUERCH. Carbohydr. Res. **79**, 53 (1980).
21. H. ITO and C. SCHUERCH. J. Am. Chem. Soc. **101**, 5797 (1979).
22. D. R. BUNDLE and S. JOSEPHSON. Can. J. Chem. **56**, 2686 (1978).
23. R. BOGNAR, I. FARKAS-SZABO, I. FARKAS, and H. GROSS. Carbohydr. Res. **5**, 241 (1967).
24. S. KOTO, S. INADA, T. YOSHIDA, M. TOYAMA, and S. ZEN. Can. J. Chem. **59**, 255 (1981).
25. H. PAULSEN and Č. KOLÁŘ. Chem. Ber. **114**, 306 (1981).
26. R. U. LEMIEUX, R. M. RATCLIFFE, B. ARREGUIN, A. ROMO DE VIVAR, and M. J. CASTILLO. Carbohydr. Res. **55**, 113 (1977).
27. R. U. LEMIEUX, S. Z. ABBAS, and B. Y. CHUNG. Can. J. Chem. **60**, 68 (1982).
28. D. R. BUNDLE and S. JOSEPHSON. Carbohydr. Res. **80**, 75 (1980).
29. D. R. BUNDLE, T. IVERSEN, and S. JOSEPHSON. Int. Lab. 21 (1980).
30. R. B. WARD. Methods Carbohydr. Chem. **2**, 394 (1963).
31. R. U. LEMIEUX, D. A. BAKER, and D. R. BUNDLE. J. Am. Chem. Soc. **97**, 4076 (1975).

Can. J. Chem. Downloaded from www.nrcresearchpress.com by 210.87.254.42 on 09/06/12
For personal use only.

# Spectral behaviour and solvent effects of some aminoanthraquinone dyes

SAFAA H. ETAIW, MORSI M. ABOU SEKKINA,[1] GAD B. EL-HEFNAWEY, AND SAMY S. ASSAR
*Department of Chemistry, Faculty of Science, University of Tanta, Tanta, Egypt*
Received October 6, 1980[2]

SAFAA H. ETAIW, MORSI M. ABOU SEKKINA, GAD B. EL-HEFNAWEY, and SAMY S. ASSAR. Can. J. Chem. **60**, 304 (1982).

The electronic absorption spectrum of each of nineteen AAQ dyes has been studied in nine different organic solvents. The acid dissociation constants of dyes containing OH, COOH, or $SO_3H$ groups have also been determined experimentally. The spectra in ethanol display five bands in the uv region and one in the visible region (450–560 nm). This band is assigned to CT transitions of the type $l$–$a_\pi$ which result from the interaction of the lone pair of the nitrogen atom with the phenyl ring of the carbonyl group. The CT nature of the band was supported theoretically and by the effect of solvent on band position.

SAFAA H. ETAIW, MORSI M. ABOU SEKKINA, GAD B. EL-HEFNAWEY et SAMY S. ASSAR. Can. J. Chem. **60**, 304 (1982).

On a étudié le spectre d'absorption électronique de chacun des 19 colorants AAQ dans neuf solvants organiques différents. On a également déterminé expérimentalement les constantes de dissociation acide des colorants contenant les groupes OH, COOH ou $SO_3H$.

Les spectres dans l'éthanol montrent cinq bandes dans la région de l'uv et une dans la région du visible (450–560 nm). On attribue cette bande à une transition TC du type $l$–$a_\pi$ qui résulte de l'interaction entre le doublet libre de l'azote et le cycle phényle du groupe carbonyle. La nature TC de la bande est établie sur des bases théoriques ainsi que par l'influence du solvent sur la position des bandes.

[Traduit par le journal]

Can. J. Chem. Downloaded from www.nrcresearchpress.com by 84.22.46.98 on 09/08/12
For personal use only.

## Introduction

Investigations of the electronic absorption spectra of some anthraquinone derivatives have been reported (1–5). The effect of solvents on the absorption spectra of hydroxy- and aminoanthraquinone dyes have also been studied (6–8). In addition, the electronic absorption spectra of anthraquinone and its amino derivatives have been studied (3, 9, 10) by means of the polarized absorption spectra on stretched PVA sheets and by means of theoretical calculations.

In the course of our research, the major goal was to evaluate a complete band assignment for the electronic absorption spectra of six known aminoanthraquinone dyes and several newly prepared derivatives. In particular, one needs to determine the nature of their lower electronic excited states, e.g. the extent of charge transfer (CT) character, the role of the solvent, and the effect of protonation and substitution on their energy states. The acid properties of the carboxy, sulphonic, and hydroxy groups were also studied.

## Experimental

*Dye preparation and purification*

The first six aminoanthraquinone (AAQ) dyes namely, I-AAQ (**1**); 2-AAQ (**2**); 1,5-di AAQ (**3**); 1,8-di AAQ (**4**); 1-AAQ 2-$SO_3H$ (**5**), and 1-AAQ 4-OH (**6**) were obtained by purifying the Merck chemical grade through crystallization several times from the appropriate solvents. The remainder of the investigated dyes (**7–19**), as listed below, were carefully prepared for the first time and purified by methods similar to those previously recommended (11–13).

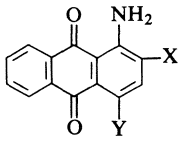

| | X | Y |
|---|---|---|
| **7** | Br | OH |
| **8** | $CH_2OH$ | H |
| **9** | $CH_2OH$ | Cl |
| **10** | $CH_2OSOCl$ | H |
| **11** | $CH_2Cl$ | Cl |
| **12** | $CH_2OCH_3$ | H |
| **13** | $CH_2OC_2H_5$ | H |
| **14** | $CH_2OC_3H_7$ | H |
| **15** | $CH_2OC_8H_{17}$ | H |
| **16** | COOH | H |
| **17** | CHO | H |
| **18** | $CH_3$ | H |
| **19** | $CH_3$ | Cl |

The solids obtained were purified by recrystallization from the appropriate solvents and their purity was checked by mp determination, nmr, and elemental analysis. The electronic absorption spectra were recorded in nine Spec. Pure (SP) organic solvents, namely ethanol, chloroform, carbon tetrachloride, *n*-hexane, cyclohexane, dioxane, dimethylformamide (DMF), 1,2-dichloroethane, and isopropylalcohol, at $4 \times 10^{-5}$ *M* concentration.

The hydrochlorides of the AAQ dyes were obtained by passing dry gaseous hydrogen chloride into solutions of the AAQ in pure dry $CCl_4$. The formation of the salts was accompanied by the deposition of an abundant white precipitate and decolourization of the solution. However, on filtration, the white precipitate rapidly acquired the colour of the initial AAQ, which indicates its decomposition. The chosen concentration of

[1]Author to whom all correspondence should be addressed.
[2]Revision received September 11, 1981.

0008-4042/82/030304-04$01.00/0
©1982 National Research Council of Canada/Conseil national de recherches du Canada

the AAQ dyes in the different organic solvents ($4 \times 10^{-5} M$) was such that, after passing dry hydrogen chloride gas through the solution, the salts were not precipitated but the solution became decolourized. The spectra were recorded several times on a Pye Unicam SP 8000 recording spectrophotometer using 1 cm matched silica cells at 25 ± 0.1°C. The results were found to be reproducible. Universal buffer solutions were prepared (pH = 2–12) and the electronic spectra (400–650 nm) were taken soon after preparation of dye solutions. A radiometer pH-meter type 63 fitted with a combined glass electrode type GK 2301 C was used (accuracy = ±0.01 pH unit).

## Results and discussion

### *1. Electronic absorption spectra in nine different organic solvents*

The uv and visible absorption spectra of AAQ dyes (**1–19**) in ethanol display six absorption bands A, B, C, D, E, and F located near 210, 230, 245, 275, 308, and 450–560 nm respectively. The band A suffers a blue shift as the polarity of the solvent increases and disappears in HCl solution. This band has low absorptivity after background correction and corresponds to that observed at 207 nm in the spectrum of anthraquinone in ethanol (8). Thus, it was assigned to a $n-\pi^*$ transition. However, the spectra of some dyes show that the band A may be obscured by the most intense band B near 230 nm. The bands B, C, D, and E in the 230–275 nm region, corresponding to those observed in the spectra of anthracene (14) and anthraquinone (8, 15), were found to be distinctly shifted to shorter or longer wavelengths on changing the substituents. The relationships between these band shifts and the substituents are in agreement with the observations of Peters and Summer (16). These bands are polarized along Y, X, Y, and X axes respectively, where X and Y axes are perpendicular and parallel to the axis of the carbonyl bond (10) which is the main axis of the molecule. The bands B and C are due to $\pi-\pi^*$ transitions within the benzenoid system and correspond to ($1B_b \leftarrow 1A$) and ($1L_a \leftarrow 1A$) transitions respectively. The bands D and E were absent from the spectrum of anthracene, hence they are assigned to quinonoid transitions ($\pi-\pi^*$). The band D suffers a blue shift on going from aprotic to protic solvents. Also, the band suffers from splitting around 270, 276 nm in the spectra of all dyes except **9**, **11**, **12**, and **19**. Thus, the band D can be assigned to $\pi-\pi^*$ transitions within the carbonyl groups while the splitting of the band is due to the increase of the polar nature of one carbonyl group over the other, i.e. on changing the dye. On the other hand, the band E is slightly affected by the nature and position of the substituent and by the change of the solvent polarity, hence it may be attributed to $\pi-\pi^*$ transitions within the ethylenic system of the quinonoid ring. The broad band F was not observed in the spectra of either anthracene or anthraquinone. It showed a wide variation in both position and intensity under the influence of changing the solvent polarity and the type of substituents. It was previously assigned to $\pi-\pi^*$ transitions (17). Inoue *et al.* (10) assigned this band as due to intramolecular CT from the amino group to the carbonyl group without indicating the type of this CT. El-Ezaby *et al.* (8) observed this band in the spectra of hydroxy-anthraquinone dyes and attributed it to CT (from the effect of solvent on its position). To give a precise assignment of the band F, the energy of this band may be calculated theoretically and experimentally for the dyes **1** and **2** containing one amino group. The energy of the CT could be calculated using the following equation as used by Abou-Eutah and Hamed (18):

$$[1] \quad E_{CT} = I_P - (\text{E.A.} + C)$$

In this case, the coulombic forces ($C$) are estimated, to a good approximation, to be 5.6 eV (18) and the electron affinity (E.A.) of the carbonyl group equals 1.4 eV. This value was determined polarographically for dyes **1** and **2** using eq. [2] (19).

$$[2] \quad \text{E.A.} = -E_{1/2} + 2.49\,\text{eV}$$

Now, if we consider that the CT may originate either from the amino group, the aniline residue, or the benzene ring, ionization potentials of these groups were used to calculate the $E_{CT}$ (20, 21). The corresponding $E_{CT}$ values were 3.15, 0.7, and 2.245 eV, respectively. On the other hand, the experimental values of $E_{CT}$ using cyclohexane were found to be 2.77 and 3.1 eV for dyes **1** and **2**, respectively. These values closely match the value of $E_{CT}$ calculated using the value of $I_P$ of the amino group as donor. The experimental value of $E_{CT}$ for dye **2** was in better agreement with the calculated one than for the case of dye **1**. This could be attributed to the formation of an intramolecular hydrogen bond between the amino and the carbonyl group leading to growth of $s$ orbital character of the amino nitrogen atom which favours approach to the $sp^2$ state for the nitrogen atom. This is reflected in the increase of conjugation between the amino group and the anthraquinone residue. The spectra of AAQ dyes in ethanol are more or less identical with those in 0.1 $N$ HCl and after passing dry HCl gas into an ethanolic solution of the dye. However, when the spectra of these dyes are recorded in $CCl_4$ after passing dry HCl gas, the band F disappears and the solution is decolourized. In this case, the

Can. J. Chem. Downloaded from www.nrcresearchpress.com by 84.22.46.98 on 09/08/12
For personal use only.

corresponding AAQ hydrochlorides are formed. On standing or on addition of a small amount of ethanol or water to the solution of AAQ hydrochloride, the salt solution rapidly acquires the initial colour of the AAQ dye and the band F reappears. The interaction of a proton from HCl with the amino group results in a transition of the nitrogen atom to the pure $sp^2$ state which prohibits the long wavelength CT transition due to the interaction of the lone electron pair of the nitrogen atom with the anthraquinone ring. Since ε is higher than that expected for a $n-\pi^*$ transition, the CT is of the type $l-a_\pi$ (22) resulting from the interaction of the electron pair of the nitrogen with the phenyl ring of the carbonyl group. This opinion is supported by the fact that the amino nitrogen, conjugated with a multiple bond or aromatic rings, deviates from the $sp^2$ state. The bands B, C, D, and E are slightly blue-shifted on going from polar to nonpolar solvents and this is in agreement with the general behaviour of $\pi-\pi^*$ transitions. On the other hand, the band F is highly red-shifted on going from aprotic to protic solvents, supporting its CT character.

It was noted that the spectrum of the dye **5** exhibits the band F at 478 nm in ethanol while it disappears in cyclohexane. In cyclohexane, the lone electron pair of the amino group is self protonated by the acidic hydrogen atom of the sulphonic group and the molecule has zwitterion structure. This is supported by the ir spectrum of this dye which exhibits two bonds at 3040 and 2650 $cm^{-1}$ attributed to $\nu_{NH_3}$ (23).

The addition of a very small amount of ethanol to the solution of dye **5** in cyclohexane rapidly returns the colour of the dye and the solution has the same spectrum as in ethanol, i.e. the CT band reappears. Thus the $l-a_\pi$ nature of the CT, originating from the amino group to the quinone system, is further supported. The zwitterion of dye **5** is formed only in aprotic solvent and has very low stability in protic ones. On this basis one can explain and understand why the amino group of the aminoanthraquinone dyes cannot be protonated in the protic solvents. This observation could be further clarified on the basis that, in protic solvents, the nitrogen atom is close to the $sp^2$ state. The interaction of the lone electron pair of the nitrogen with the anthraquinone ring is so pronounced that it may be regarded as incorporated in the common electronic system of the ring. This may prevent protonation of the amino group in protic solvents and hence prevent zwitterion formation, whereas the reverse case takes place in aprotic solvent.

*2. Acid ionization constants*

The acid ionization constants of dyes **6** and **7** were determined spectrophotometrically in (BR) buffers ranging from pH = 2 up to 12 at 25°C. From results obtained, the spectra are characterized by an isosbestic point around 540 nm indicating the presence of an acid–base equilibrium of the type:

$$AAQ-OH + H_2O \rightleftharpoons AAQ-O^- + H_3O^+$$

The variations of absorbance with pH at four different wavelengths are typical dissociation curves from which the p$K$ values were computed and evaluated by applying four different recommended methods (24, 25). The acid ionization constants of dyes **5** and **16** were determined potentiometrically. The p$K_a$ values can be evaluated from the titration curves using eq. [3]:

$$[3] \quad pH = pK_a + \log \frac{V}{V_0 - V}$$

where $V$ is the volume of alkali used for salt formation at the corresponding pH value and $V_0$ is the volume of alkali used to attain the end point.

A new method was introduced to calculate the ionization constants of the acids. Colleter's method (25) for the determination of the stability constant of complexes is modified to calculate the constant in the forms:

$$[4] \quad K_a = \frac{C_{H_2^+} - MC_{H_3^+}}{M - 1}$$

where

$$M = \frac{V_3 - V_1}{V_2 - V_1} \times \frac{C_{H_1^+} - C_{H_2^+}}{C_{H_1^+} - C_{H_3^+}}$$

The obtained p$K$ values were 3.79, 9.925, 9.104, and 5.74 for dyes **5**, **6**, **7**, and **16** respectively. Using $\Delta G = RT \ln K$ ($T$ = 298 K), values for p$K$ of 5.18, 13.56, 12.44, and 7.84 (kcal $mol^{-1}$) were obtained for dyes **5**, **6**, **7**, and **16** respectively.

1. M. Rolf, D. Harry, and F. Dietrich. Z. Chem. **15**, 400 (1975).
2. G. T. Khachaturova and R. N. Nurmukhametov. Zh. Obshch. Khim. **45**, 2708 (1975).
3. A. Novak, M. Titz, and M. Nepras. Collect. Czech. Chem. Commun. **39**, 1532 (1974).
4. S. N. Singh and R. S. Singh. Indian J. Pure Appl. Phys. **8**, 641 (1970).
5. Z. Yoshida and F. Takabayashi. Tetrahedron, **24**, 933 (1968).
6. S. Roys and M. Eoghan. J. Soc. Dyers Colour. **91**, 399 (1975).
7. R. M. Issa, M. S. El-Ezaby, and A. H. Zewil. Z. Phys. Chem. **244**, 155 (1970).

Can. J. Chem. Downloaded from www.nrcresearchpress.com by 84.22.46.98 on 09/08/12
For personal use only.

8. M. S. EL-EZABY, T. M. SALEM, A. H. ZEWIL, and R. M. ISSA. J. Chem. Soc. B, 1293 (1970).
9. J. C. D. BRAND and T. H. GOODWIN. Trans. Faraday Soc. **53**, 295 (1957).
10. H. INOUE, T. HOSHI, J. YOSHIO, and Y. TANIZAKI. Bull. Chem. Soc. Jpn. **45**, 1018 (1972).
11. A. SCHUHMACHER (BASF-A-O). Ger. Offen. Z. 428 (CI.C.07.C), 18 Dec. (1975). Appl. P.2428337.2-4212, p. 77, June (1974).
12. K. BREDERECK, L. BANHAF, and E. KOCH. Chem. Ber. **105**, 377 (1972).
13. S. A. METWALLY. J. Appl. Chem. Biotechnol. **25**, 161 (1975).
14. C. A. COULSON. Proc. Phys. Soc. **60**, 257 (1948).
15. H. INOUE, T. HOSHI, and Y. TANIZAKI. Nippon Kagaku Zasshi, **92**, 501 (1971).
16. R. H. PETERS and H. H. SUMMER. J. Chem. Soc. 2102 (1953).
17. B. E. ZAITSEV and V. M. ALLENOV. Zh. Fiz. Khim. **45**, 1331 (1971).
18. R. ABOU-EUTAH and M. HAMED. Bull. Chem. Soc. Jpn. **47**, 2578 (1974).
19. S. H. ETAIW, M. ISMAIL, and M. EL-BORAI. Can J. Chem. **58**, 263 (1980).
20. K. WATANABE. J. Chem. Phys. **26**, 542 (1957).
21. K. WATANABE, T. NAKAYAME, and J. MOTTL. Quant. Spectrosc. 361 (1960).
22. G. GEORGE. Fluorescence, theory, instrumentation and practice. Edward Arnold, Ltd., London. 1967.
23. K. NAKANISHI. Infrared spectra and structure of organic compounds. Izd. Mir. Moscow. 1965.
24. R. M. ISSA and J. Y. MAGHRABI. Z. Phys. Chem. **56**, 1120 (1975).
25. J. C. COLLETER. Ann. Chim. **5**, 415 (1960).

Can. J. Chem. Downloaded from www.nrcresearchpress.com by 84.22.46.98 on 09/08/12
For personal use only.

# A synthesis of 11-nor-9-ketohexahydrocannabinol[1]

JOHN W. APSIMON,[2] ANDREW M. HOLMES,[3] AND IAN JOHNSON[4]
*Department of Chemistry, Carleton University, Ottawa, Ont., Canada K1S 5B6*
Received August 4, 1981

JOHN W. APSIMON, A. HOLMES, and IAN JOHNSON. Can. J. Chem. **60**, 308 (1982).

A 12-step synthesis of 11-nor-9-keto-hexahydrocannabionol (**3**) from dimethoxyolivetol (**4**) is described, together with some ancillary synthetic steps. The key step in this route is the reaction of the unsaturated dinitrile **6** with the Danishefsky diene **10**.

JOHN W. APSIMON, A. HOLMES et IAN JOHNSON. Can. J. Chem. **60**, 308 (1982).

On décrit une synthèse en 12 étapes du nor-11 céto-9 hexahydrocannabionol (**3**) à partir du diméthoxyolivétol (**4**); on décrit aussi quelques étapes connexes. La réaction du dinitrile insaturé **6** avec le diène de Danishefsky **10** est l'étape principale de cette synthèse.
[Traduit par le journal]

As part of a wider project aimed at the total synthesis of a variety of metabolites of cannabinoids (1) such as the 11-hydroxylated derivatives of $\Delta^8$ and $\Delta^9$ THC (**1** and **2** respectively), together with the possible requirement for the labelling of such species at nonexchangeable sites (see Scheme 1), we have examined routes proceeding via 11-nor-9-ketohexahydrocannabinol **3** (2).

In this report we describe our studies towards a direct, rational approach to the total synthesis of **3**. Although the final step in the route is of modest yield only, all of the other operations are extremely efficient.

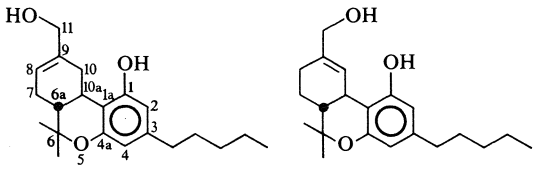

**1**



**2**

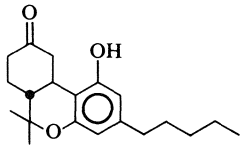

**3**

The basis strategy of our approach is outlined in Scheme 1. The key steps foreseen in such a tactic involve a Diels–Alder reaction between a coumarin and a 2-oxygenated butadiene (3). Precedent for construction of the carbon skeleton of the basic cannabinoid system by a Diels–Alder route is reported (4), but the work described does not involve incorporation of oxygen at the 9-position. In our proposal, this oxygen atom is delivered to the correct site in the form of a trapped enol in the diene synthon. Other efficient routes to the target compound (**3**) must also be noted (3, 5).

The overall pathways studied are outlined in Schemes 2 and 3. That described first, proceeding via cyanocoumarin **7***a* or **7***b*, was not amenable to the elaboration of cannabinoid-like compounds; however, a slight modification of the strategy involved enabled **3** to be prepared.

The first synthetic plan devised for the preparation of **3** is summarized in Scheme 2. The *cis*-ring junction that would be generated in the proposed Diels–Alder reaction of 2-methoxy-1,3-butadiene **8** with the cyanocoumarin **7** presents no problem since decarboxylation (after hydrolysis of the nitrile function), proceeding through an enolate, should cause equilibration to the preferred *trans*-fusion. Both the carbocyclic ring and the requisite oxygen function would be efficiently introduced via the cycloaddition process. Incorporation of the *gem*-dimethyl grouping would involve the action of two equivalents of a methyl Grignard reagent on the lactone, affording a tertiary alcohol. Under acidic conditions, cyclization ensues, yielding the pyran ring. This sequence has been successfully performed with similar substrates, although not with the

[1]Two numbering systems are in use today. One is based on the formal chemical rules for numbering of benzopyran. The second system has a biogenetic basis, regarding cannabinoids as substituted monoterpenes. The former is used exclusively in this work. The naturally occurring enantiomer (6aR, 10aR) is shown for convenience although structures of synthetic materials described herein represent racemates.

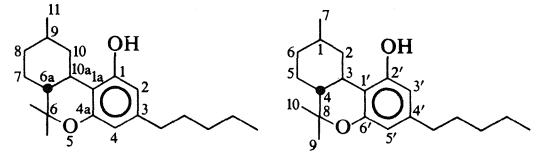

[2]Author to whom inquiries may be addressed.

[3]Portions of this work are taken from the M.Sc. thesis of A.H., Carleton University, 1976.

[4]Portions of this work are taken from the M.Sc. thesis of I.J., Carleton University, 1981.

0008-4042/82/030308-09$01.00/0
©1982 National Research Council of Canada/Conseil national de recherches du Canada

Can. J. Chem. Downloaded from www.nrcresearchpress.com by 210.87.254.40 on 09/06/12
For personal use only.

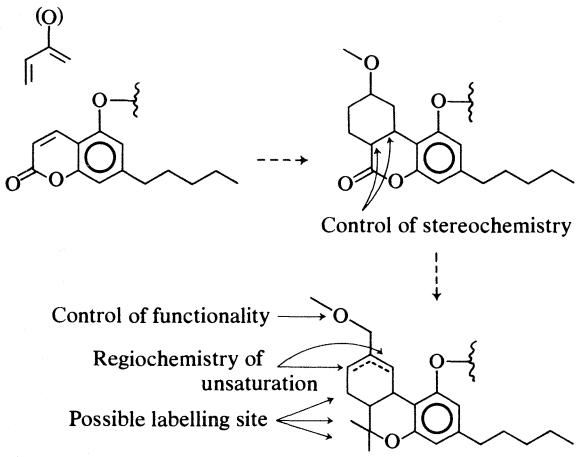


SCHEME 1. Synthetic strategy used in this study.

compounds studied in this work (For a summary of previous synthetic efforts in the cannabinoid field, see ref. 3.).

*Routes towards 11-nor-9-ketohexahydrocannabinol* ***3***

Olivetol dimethyl ether **4** was prepared via the two-step transformation developed by Bailey (6).

Introduction of the aldehyde function to give **5** was achieved through the known procedure (4, 7) involving metallation of **4** and reaction with *N*-methylformanilide. Addition of piperidine to a mixture of **5** and malononitrile initiated an exothermic reaction, producing a homogeneous mass (8) which after purification gave **6**. Cleavage of the methyl ethers of **6** was next undertaken. Refluxing of the dinitrile and aluminum chloride in chlorobenzene for 4 h (9) did not produce the dihydroxy analog of **6**, but instead yielded only the cyanocoumarin **7**. Formation of the lactone presumably occurred as outlined in Scheme 3.

The only difficulty associated with this step occurred in larger-scale preparations, when the solid mass produced during work-up interfered with complete recovery of **7**. The cyanocoumarin **7** was considered a suitable precursor for elaboration to tricyclic material, via a cycloaddition reaction with 2-methoxy-1,3-butadiene (**8**) synthesized using the two-step method of Degraw *et al.* (10).

Heating cyanocoumarin (**7**) in the presence of the substituted butadiene (**8**) failed to produce a Diels–Alder adduct as indicated by the persistence of the nmr resonance (δ 8.56) of the highly deshielded

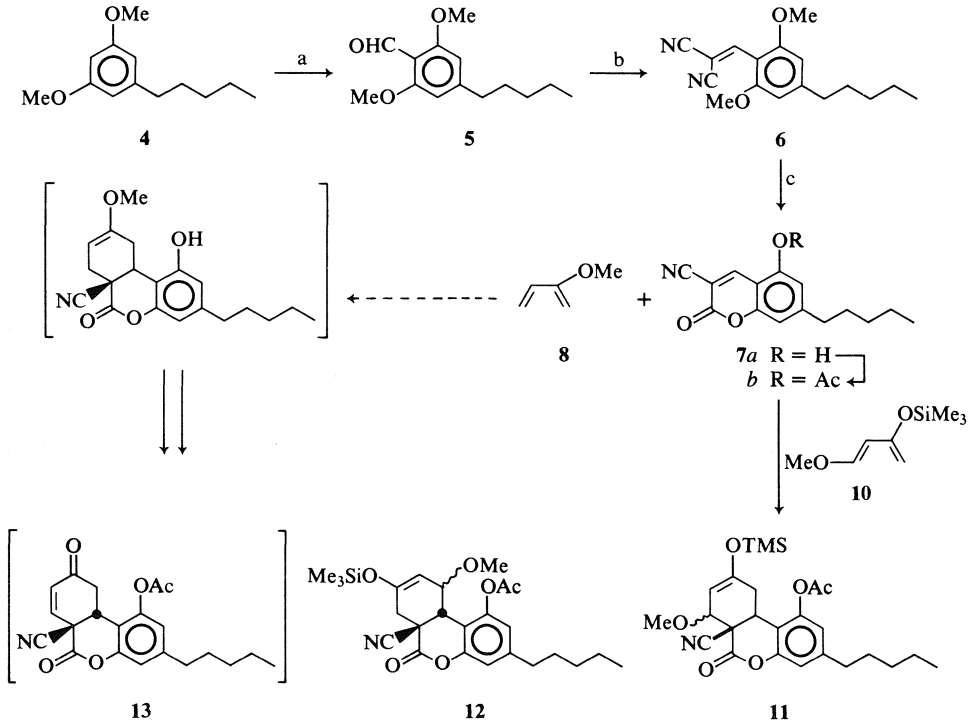


*Reagents*: a, *n*-BuLi, *N*-methylformanilide; b, malononitrile, piperidine; c, $AlCl_3$, chlorobenzene, reflux; d, $Ac_2O$,$H_2SO_4$

SCHEME 2

Can. J. Chem. Downloaded from www.nrcresearchpress.com by 210.87.254.40 on 09/06/12
For personal use only.

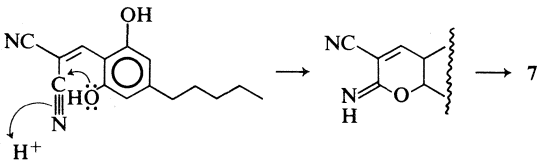

SCHEME 3

proton of the disubstituted styrene. Other features of the nmr spectrum of the product indicated that it possessed one aromatic proton (s, δ 6.76), an ether methyl group (s, δ 3.30), which was not of the enol ether variety, and another methyl group (s, δ 1.68) not coupled to other hydrogens. The ir spectrum showed no hydroxyl absorption, and the mass spectrum indicated a molecular ion of *m/e* 341. In addition, the ultraviolet (uv) absorption of the compound was in agreement with a species possessing extended conjugation to an aromatic system. All of the spectral data are in accord with structure **9**, the formation of which can be accounted for by addition of the phenol to the double bond of the diene, followed by a Claisen rearrangement as indicated in Scheme 4. Analogous processes have been cited (11).

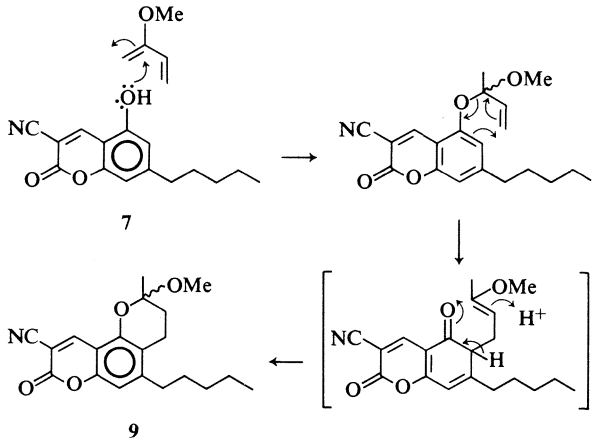

SCHEME 4

The hydroxy function of **7** was next masked as the acetate in order to block the Claisen process, and thereby prevent competition with the Diels–Alder reaction. The acetoxycoumarin **7***b* and the diene **8** resisted all efforts to carry out the cycloaddition reaction. A sealed vessel was used to avoid loss of the relatively volatile diene (bp 74–77°C), and several attempts involved Lewis acid catalysis, known to alter the facility and regioselectivity of Diels–Alder reactions (e.g. ref. 12). The lack of reactivity of this diene–dienophile combination was rather surprising, as both compounds are activated, the former by virtue of an electron-donating function and the coumarin with two electron-withdrawing groups.

At this juncture, the Danishefsky diene (13), 1-methoxy-3-(trimethylsiloxy)-1,3-butadiene (**10**), was examined in view of its ready reaction with a variety of dienophiles, exhibiting a high degree of selectivity in the orientation of addition to unsymmetrical olefins.

Refluxing a benzene solution of the diene **10** and the acetoxycoumarin **7***b* under a nitrogen atmosphere led to complete consumption of starting material as indicated by the disappearance in the nmr spectrum of the crude reaction mixture of the olefinic proton resonance at δ 8.26. Also, the ir spectrum of the product exhibited a carbonyl absorption at 1785 $cm^{-1}$. This Diels–Alder adduct was assigned structure **11**, a conclusion based upon consideration of the "*ortho* and *para* rules".[5] Danishefsky had found that, in all reactions of **10** studied (13), there was a high degree of selectivity in the formation of the isomer in accord with these postulates. Both possible configurations of the methoxyl substituent appear to be generated, a result attributable to competition between the *exo* and *endo* modes of approach of the reactants (14). The nmr spectrum exhibited two singlets (δ 3.57, 3.61), with intensities corresponding to a product ratio of 1.0:1.4. The formation of a diastereomeric mixture in no way affects the outcome of the synthetic route, as the asymmetric centre β to the ketone would be destroyed upon hydrolysis and elimination to give the sought after enone **13**. This conversion was the next goal of the synthesis but, contrary to the previously reported (13, 15) facile hydrolyses to α,β-unsaturated systems, this step presented unforeseen difficulties. The mild conditions (0.005 *N* HCl, THF, 0°C, 10 min) employed by Danishefsky and Kitahara (15) indicated no

[5]These rules are based on the observation that an unsymmetrically substituted diene would orient itself in adding to acrolein or acrylates to produce a predominance of the adduct *a* with a 1-substituted diene, and an excess of *b* with a group at the 3-position of the diene. In the reaction of **7***b* with **10**, both these tendencies favour formation of the positional isomer **11**, rather than **12**.

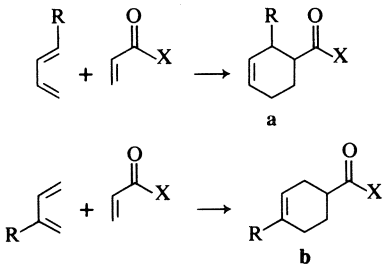

Can. J. Chem. Downloaded from www.nrcresearchpress.com by 210.87.254.40 on 09/06/12
For personal use only.

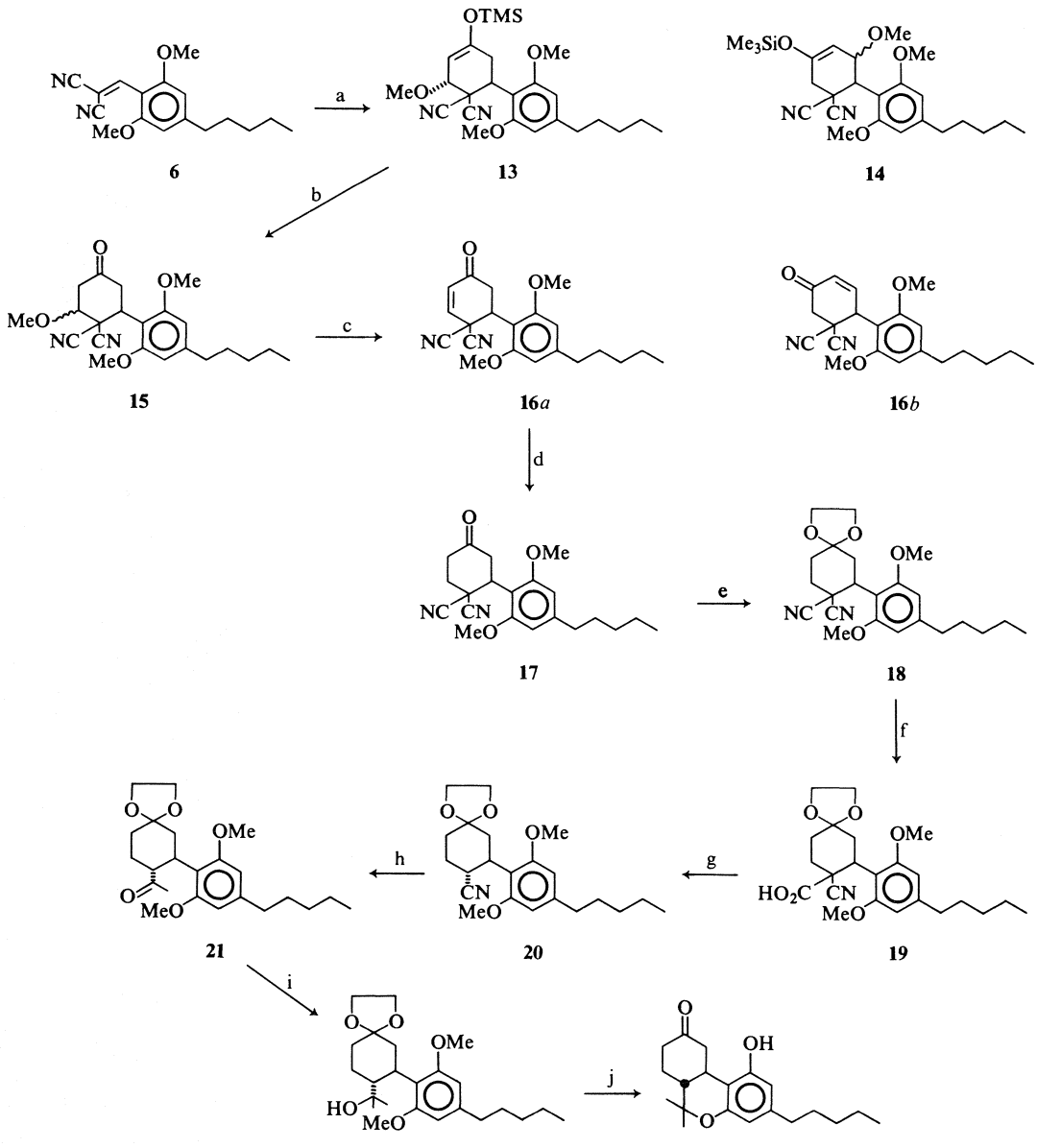


*Reagents*: a, diene **10**; b, HCl, MeOH, $H_2O$; c, *p*-toluene sulfonic acid, benzene; d, $H_2$, Pd/C; e, $HOCH_2CH_2OH$, *p*-TSA; f, 10 *N* NaOH/EtOH; g, NaOH, DMF, 150°C; h, MeMgI, $Et_2O$,6 h; i, MeMgBr; j, $Ph_2PLi$, THF

SCHEME 5

reaction occurring. Attempts at forcing the process with 6 *N* hydrochloric acid in methanol or other reaction conditions produced a complex reaction mixture, with no evidence of the existence of the enone **13**.

In view of these problems, which rendered this synthetic approach unattractive, the scheme was abandoned in favour of the parallel Diels–Alder process between **10** and the unsaturated dinitrile **6** (see Scheme 5).

Reaction of **6** and **10** in dry benzene at reflux caused a high yield conversion to a crystalline bicyclic species that had a proton nmr spectrum consistent with the adduct **13**, but not with the

Can. J. Chem. Downloaded from www.nrcresearchpress.com by 210.87.254.40 on 09/06/12
For personal use only.

Can. J. Chem. Downloaded from www.nrcresearchpress.com by 210.87.254.40 on 09/06/12
For personal use only.

positional isomer **14**. The benzylic methine proton appears as a doublet of doublets ($J$ = 5, 12 Hz), coupled to the hydrogens of the allylic methylene group. In **14** a single splitting would be expected for this proton (coupled only to the allylic methine hydrogen). The large paramagnetic shift of the benzylic proton is likely due to the anisotropy of the neighbouring nitrile functions. The methine proton α to the ether oxygen atom is coupled solely to the olefinic hydrogen, providing further support for the assignment of **13** as the correct representation of the reaction product. The coupling constant of 6 Hz relates to a dihedral angle of 30 to 40° between the methine and olefinic hydrogens, indicating that the former is an equatorial substituent (i.e. the *O*-methyl group is axial). This is the configuration one would expect to arise from *exo* approach of the diene and dienophile (14) (see Scheme 6). Thus, structure **13** was assigned to the Diels–Alder adduct. This adduct was allowed to stand at room temperature for 30 min in a 5:3 mixture of acetone and 6 *N* hydrochloric acid. A β-methoxy ketone (**15**), rather than an enone, was again inferred from the spectral data. The infrared spectrum included a carbonyl absorption at 1735 $cm^{-1}$, and a three-proton singlet at δ 3.53 in the nmr spectrum confirmed that hydrolysis of the enol ether was not accompanied by elimination of methanol. Each methine proton β to the ketone appeared as a doublet of doublets, a result consistent with structure **15**.

Elimination of methanol to give the α,β-unsaturated ketone **16***a* was accomplished in excellent yield by refluxing **15** in benzene in the presence of *p*-toluenesulfonic acid. The $^1H$ nmr pattern of the olefinic protons reinforces the earlier statement that the orientation of the Diels–Alder cycloaddition was that required to generate **13**. The double bond hydrogens give rise to a pair of doublets centred at δ 6.32 and δ 6.90, with a coupling constant of 10 Hz. The alternative enone **16***b* would be expected to exhibit a more complex pattern for the resonance of the olefinic proton β to the ketone, as it would be coupled to the benzylic methine proton in addition to the neighbouring olefinic hydrogen.

A sharp six proton singlet at δ 3.82 in the proton nmr spectrum of **16***a* is a result of the methoxy groups. It is interesting to note that elimination of the aliphatic *O*-methyl substituent causes a collapse to this singlet from the two singlets seen for the enol silyl ether **13**, and the broad multiplet found with the β-methoxy ketone **15**. This variance is attributed to an increase in the ease of rotation about the inter-annular bond. Molecular models of

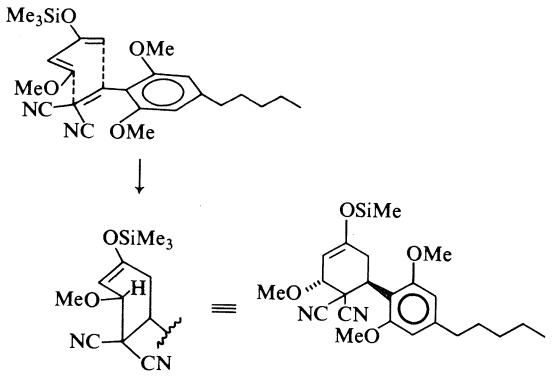


13

SCHEME 6

the compounds involved show that the axial methoxy substituent and the aromatic methoxyls experience severe steric interactions. Hydrogenation of **16***a* in ethanol at atmospheric pressure with palladium on charcoal as a catalyst gave dinitrile ketone **17** in a 99% yield as an unstable solid with a melting point of 54–55°C. The instability of **17** was probably due to aerial oxidation at room temperature leading to aromatization of the C-ring. Ketalization with ethylene glycol gave a colorless solid **18** in a yield of 93% (mp 104–106°C), which proved to be much more stable.

At this point cleavage of the methyl ether groups was, as anticipated, the major obstacle. In the earlier cannabinoid work by Adams *et al.* (4) this problem proved to be insurmountable.

In cannabinoid work, a variety of reagents have been used for this process (3) and recently a large variety of reagents have been reported for effective demethylation of phenol methyl ethers (16). In this study no satisfactory result was obtained on treatment of **17** or **18** with any of these reagents.

A variation in the synthetic route was next studied. Thus, heating **18** in 10 *N* sodium hydroxide and ethanol (1:1) resulted in the hydrolysis of only one nitrile group. The product **19** exhibited a molecular ion in its mass spectrum of *m/e* 417 as well as exhibiting the expected spectral data. This acid (**19**) was decarboxylated by stirring over ground sodium hydroxide in DMF at 150°C to give **20** in an 80% yield from **18**. After 2 h the decarboxylation was complete and analysis of the product **20** by gas chromatography (gc) showed that the two possible epimers about position 6a were present in a ratio of 2:3. After further heating of the reaction for an additional 8 h, the ratio had become 9:1. The thermodynamically more stable *trans*-isomer was assumed to predominate in the final product. The above reaction demonstrated that the nitrile **20** was relatively unreactive, so it appeared that demeth-

Can. J. Chem. Downloaded from www.nrcresearchpress.com by 210.87.254.40 on 09/06/12
For personal use only.

ylation might again be attempted. Demethylation of **20** could lead to the intramolecular hydrolysis of the nitrile and lactonization following a route similar to that observed in the formation of **7***a*.

When **20** was treated with a variety of reagents (16) no useful reaction was observed. Finally treatment of **20** with 30 equivalents of methylmagnesium iodide in ether at gentle reflux for 6 h formed the methyl ketone **21** in a 40% conversion and 60% yield based on recovered starting material.

The methyl ketone **21** was easily methylated with methylmagnesium bromide to give alcohol **22** in a 95% yield. This represents a 28% overall yield of **22** from dimethoxyolivetol (**4**) in eleven steps with an average yield of 89% per step.

Demethylation of alcohol **22** was accomplished following the method of Ireland and Walba (16*f*) with lithium diphenylphosphide. Acidic work-up was used to invoke cyclization and deketalization when a modest yield of ketone **3** was obtained which was identical in all respects with an authentic sample of ketone **3** (prepared following the method of Archer *et al.* (5)). Thus, a total synthetic route to ketone **3** has been completed. Although existing routes would appear better suited to large scale work (3, 5) the present route reveals some useful and interesting chemistry capable of leading to a variety of modified cannabinoids.

## Experimental

Melting points were determined with a Fisher–Johns melting point block and are uncorrected. A Perkin–Elmer 237B Infracord spectrophotometer was used for recording infrared (ir) spectra. Absorptions are noted as strong (s), medium (m), weak (w), or shoulder (sh). Nuclear magnetic resonance (nmr) spectra were taken on a Varian Associates Model T-60A with deuteriochloroform solvent (unless otherwise stated), and tetramethylsilane as internal standard. The following designations are used in characterizating nmr signals: singlet (s), doublet (d), triplet (t), doublet of doublets (dd), multiplet (m), and broadened (br). Gas chromatographs were recorded using a Perkin–Elmer 990 Gas Chromatograph, with a 5.5 ft column of 3% OV-17 at 285°C, with nitrogen as the carrier gas or using a Hewlett Packard 5840B Gas Chromatograph using a 25 M, SP-2100 microcapillary column with nitrogen as the carrier gas. Mass spectra were recorded using an AEI MS12 instrument at Trent University.

Preparative hplc was done using a Waters Prep 500 with two PrepPac silica gel columns. Thin-layer and preparative thin-layer chromatography (tlc and ptlc respectively) were carried out on Merck 60 F-254 precoated silica gel plates of 0.25 mm thickness. Bands were visualized by (*i*) viewing under an ultraviolet (uv) source or (*ii*) spraying with ceric ammonium sulfate and charring the plate. Florosil (activated magnesium silicate, J. T. Baker Chemical Co., 100–200 mesh) was the adsorbent used for column chromatography.

Tetrahydrofuran (THF) was distilled from sodium and stored over 4A molecular sieves (J. T. Baker Chemical Co.) under nitrogen. Azeotropic removal of water followed by distillation afforded dry benzene which was stored over sodium. Anhydrous ether was stored under nitrogen over sodium. Anhydrous dimethylformamide was prepared by drying ACS Spec. grade solvent over molecular sieves (4A).

*((2,6-Dimethoxy-4-pentylphenyl)methylidene)malononitrile (**6**)*

Piperidine (10 mL) was added to a mixture of the 2,6-dimethoxy-4-pentylbenzaldehyde **5** (10.50 g, 44.4 mmol) and malononitrile (3.10 g, 46.9 mmol), causing the mass to become hot and homogeneous. After the red solution had cooled, it was acidified with 6 *N* hydrochloric acid, and extracted with three portions of chloroform. The combined organic solutions were washed with water (×2) and saturated aqueous sodium chloride, before being dried ($MgSO_4$) and concentrated under vacuum. Addition of a little methanol to the resultant oil, accompanied by chilling of the solution, yielded a crop of yellow crystals (2.61 g). Recrystallization from methanol afforded pure **6**, mp 64–65°C; uv: 348 nm (ε 21 500) and 203 nm (28 500); ir (KBr): 2215 (m, conjugated C═N), 1617 (s, C═C), and 825 (m, trisubstituted C═C) $cm^{-1}$; nmr (100 MHz, $CCl_4$) δ: 0.93 (br, t, $J$ = 6 Hz, 3H, terminal $CH_3$), 1.25–1.83 (m, 6H, $3CH_2$'s), 2.61 (br, t, $J$ = 7 Hz, 2H, benzylic $CH_2$), 3.90 (s, 6H, $2ArOCH_3$), 6.15 (s, 2H, aromatic), 7.74 (s, 1H, olefinic CH); *m/e* (relative intensity): 284 (40), 242 (12), 241 (10), 229 (20), 228 (100), 227 (10). *Anal.* calcd. for $C_{17}H_{20}N_2O_2$: C 71.81, H 7.09, N 9.85; found: C 71.86, H 7.05, N 9.92.

Chromatography of the mother liquors on silica gel (elution with benzene) gave a further 8.38 g of product. The total yield of **6** was 87%.

*5-Hydroxy-2-oxo-7-pentyl-2H-1-oxanapthalene-3-carbonitrile (**7***a*)

Employing the demethylation procedure of Bruce and Sutcliffe (9*b*), the dinitrile **6** (1.10 g, 3.87 mmol) was dissolved in chlorobenzene (125 mL), aluminum chloride (3.7 g, 28 mmol) was added to the solution, and the reaction mixture was refluxed under a nitrogen atmosphere for 3.5 h. 2 *N* Hydrochloric acid (100 mL) was added to the cooled flask, and the yellow solid present was removed by filtration. The aqueous layer of the filtrate was separated, and extracted with ether (×4). The pooled ethereal extracts were washed with water and aqueous sodium chloride (saturated), after which this organic solution was added to the chlorobenzene layer, previously washed in the same manner. Drying over $MgSO_4$ and evaporation of solvent afforded **7***a* as a yellow powder (570 mg).

The filter cake separated above was extracted with ether (×4). Work-up (as above) of the combined organic solutions produced a further 381 mg of material, which was combined with the product already isolated. The pooled material (951 mg, 96%) was homogeneous by tlc ($CHCl_3$/EtOAc, 80:20). Ultraviolet: 340 (ε 37 500), 250 (9 000), and 209 nm (28 000); ir (neat): 3345 (m, OH), 2230 (w, conjugated C≡N), 1695 (s, C═O), and 1625 (m, C═C) $cm^{-1}$; ir (KBr): 3270 (sh), 3205 (s, OH), 2255, 2225 (m, conjugated C≡N), 1745, 1705 (s, C═O), and 1635 (s, C═C) $cm^{-1}$; nmr (100 MHz) δ: 0.89 (br t, $J$ = 6 Hz, 3H, terminal $CH_3$), 1.13–1.83 (m, 6H, $3CH_2$'s), 2.65 (br t, $J$ = 7 Hz, 2H, benzylic $CH_2$), 6.69 (m, 2H, aromatic), and 8.61 (s, 1H, olefinic CH); *m/e* (relative intensity): 257 (33), 215 (10), 214 (11), 202 (17), 201 (100), 200 (14). The analytical sample (mp 179–181°C) was prepared by sublimation (170–175°C/0.1 Torr). Compound **7***a* recrystallized with difficulty; benzene was the most effective solvent. *Anal.* calcd. for $C_{15}H_{15}NO_3$: C 70.02, H 5.88, N 5.44; found: C 70.08, H 5.88, N 5.45.

*7,8-Dihydro-6-methoxy-6-methyl-2-oxo-9-pentyl-2H,6H-1,5-dioxaphenanthrene-3-carbonitrile (**9**)*

The cyanocoumarin **7***a* (202 mg, 0.785 mmol), 2-methoxy-1,3-butadiene (**8**, 143 mg, 1.70 mmol), and hydroquinone (53 mg) were combined with xylenes (50 mL) in a sealed pressure vessel, then heated to 165°C (sand bath). After 70 h at this temperature,

Can. J. Chem. Downloaded from www.nrcresearchpress.com by 210.87.254.40 on 09/06/12
For personal use only.

the reaction mixture was cooled and concentrated *in vacuo*. The residue was chromatographed on silica gel. From the early benzene–ether (95:5) fractions was isolated **9** (193 mg, 72%), as white needles. Recrystallization from methanol gave the analytical sample, mp 160–160.5°C; uv: 342 (ε 18 500), 250 (4 000), and 209 nm (35 000); ir (KBr): 2855 (m, $ROCH_3$), 2230 (m, conjugated C≡N), 1745 (s, C=O), and 1625 (s, C=C) $cm^{-1}$; nmr (100 MHz) δ: 0.86 (br t, $J$ = 6 Hz, 3H, terminal $CH_3$), 1.2–1.7 (m, 6H, $3CH_2$'s), 1.68 (s, 3H, $CH_3COR$), 2.65 (br t, $J$ = 7 Hz, 2H, benzylic $CH_2$), 3.30 (s, 3H, $OCH_3$), 6.76 (s, 1H, aromatic), 8.56 (s, 1H, olefinic CH); *m/e* (relative intensity): 341 (100), 310 (57), 309 (37), 204 (42), 270 (23), 269 (92), 252 (31), 240 (24), 214 (35), 213 (24). *Anal.* calcd. for $C_{20}H_{23}NO_4$: C 70.36, H 6.79, N 4.10; found: C 70.43, H 6.69, N 4.04.

*5-(Ethanoyloxy)-2-oxo-7-pentyl-2H-1-oxanaphthalene-3-carbonitrile (7b)*

The cyanocoumarin **7***a* (1.25 g, 4.86 mmol) was covered with distilled acetic anhydride (12.41 g, 122 mmol). Concentrated sulfuric acid (0.5 mL) was added to the mixture, which immediately became hot, forming a tan paste. This material was dissolved in chloroform, and allowed to stand for 0.5 h before water was added. The aqueous layer was separated, and extracted with chloroform (×3). These extracts were combined with the original chloroform phase, which was then washed with water (×2) and saturated aqueous sodium chloride, dried ($MgSO_4$), and concentrated *in vacuo*, yielding **7***b* (1.41 g, 97%). Three recrystallizations from methanol afforded the analytical sample, mp 155–155.5°C; uv: 318 (ε 15 500) and 203 nm (32 500); ir (KBr): 2235 (m, conjugated C≡N), 1777 (s, aryl acetate), 1738 (s, C=O), and 1627 (s, C=C) $cm^{-1}$; nmr (100 MHz) δ: 0.90 (br, t, $J$, 6 Hz, 3H, terminal $CH_3$), 1.17–1.84 (m, 6H, $3CH_2$'s), 2.45 (s, 3H, acetate), 2.73 (t, $J$ = 7 Hz, 2H, benzylic $CH_2$), 7.03 (br s, 2H, aromatic), and 8.26 (s, 1H, olefinic CH); *m/e* (relative intensity): 299 (27), 258 (19), 257 (100), 215 (9), 214 (10), 202 (15), 201 (98), 200 (14). *Anal.* calcd. for $C_{17}H_{17}NO_4$: C 68.22, H 5.72, N 4.68; found: C 68.07, H 5.63, N 4.58.

*Attempted reaction of* **7**b *with 2-methoxy-1,3-butadiene (8)*

*Attempt 1*

2-Methoxy-1,3-butadiene (**8**, 19 mg, 0.23 mmol), **7***b* (68 mg, 0.23 mmol), and hydroquinone (22 mg) were dissolved in 50 mL of xylenes, and heated in a sealed vessel at 160–165°C. After 87 h, the flask was cooled to room temperature and the contents were concentrated at reduced pressure to give a solid, which was recrystallized from methanol. The spectral characteristics of the crystalline substance were identical with those of **7***b*.

*Attempt 2*

A solution of **8** (16.5 mg, 0.20 mmol) and **7***b* (62 mg, 0.21 mmol) in dry benzene (25 mL) was heated (150–152°C) in a sealed vessel for 18 h. Removal of solvent *in vacuo* afforded pure **7***b* with the same physical properties previously reported.

*Attempt 3*

To a solution of **7***b* (28.9 mg, 0.097 mmol) in anhydrous ether (25 mL), stirred under a nitrogen atmosphere, was added boron trifluoride etherate (40 μL, 0.33 mmol), followed after 15 min by the diene **8** (119 mg, 1.41 mmol). After 72 h at ambient temperature, the reaction mixture was poured into water. Extraction with chloroform (×3), washing of the combined extracts with water and aqueous sodium chloride (saturated), drying of the organic solution ($MgSO_4$), and evaporation of solvent gave a white solid that was identical with **7***b* in all respects.

*Attempt 4*

The reaction was repeated as in Attempt 3, except that it was carried out in dry benzene rather than ether. The quantities of the reactants were: **7***b* (21.5 mg, 0.072 mmol), **8** (90 mg, 1.1 mmol), boron trifluoride etherate (30 μL, 0.24 mmol). Again, only the starting coumarin was recovered.

*4-(Ethanoyloxy)-4b,5,8,8a-tetrahydro-8-methoxy-9-oxo-2-pentyl-6-(trimethylsiloxy)-9H-10-oxaphenanthrene-8a-carbonitrile (11)*

The acetoxycoumarin **7***b* (301 mg, 1.01 mmol) and the diene **10** (239 mg, 1.39 mmol) were dissolved in benzene (60 mL), then refluxed under nitrogen for 65 h. The cooled solution was concentrated *in vacuo* to give 458 mg (99%) of an oil, which eventually solidified on standing. Although tlc ($CHCl_3$) showed only one major spot, recrystallization from various solvent systems proved difficult. The product (**11**), mp 119–125°C (dec.), exhibited the following physical properties: ir (neat): 2245 (w, C≡N), 1785 (s, C=O), 1775 (s, aryl acetate), and 1662 (m, enol ether) $cm^{-1}$; nmr (100 MHz) δ: 0.23 (s, 9H, $OSi(CH_3)_3$), 0.94 (br, t, $J$ = 6 Hz, 3H, terminal $CH_3$), 1.21–1.80 (m, 6H, $3CH_2$'s), 2.39 (s, 3H, acetate), 2.64 (br t, $J$ = 7.5 Hz, 2H, benzylic $CH_2$), 2.4–2.9 (obscured m, 2H, allylic $CH_2$), 3.57, 3.61 (two s, ratio 1.0:1.4, 3H total, $OCH_3$), 3.83 (dd, $J$ = 7 Hz, $J'$ = 11 Hz, 1H, benzylic CH), 4.55 (m, 1H, $CHOCH_3$), 5.14 (m, 1H, olefinic CH), and 6.84 (m, 2H, aromatic); *m/e*: 399 ($M^+$ − 72) (relative intensity 22), 358 (24), 357 (100), 325 (10), 301 (29), 299 (15), 258 (12), 257 (40), 201 (35).

*2-(2,2-Dicyano-3-methoxy-5-(trimethylsiloxy)-4-cyclohexenyl)-1,3-dimethoxy-5-pentylbenzene (13)*

A mixture of the dinitrile **6** (515 mg, 1.81 mmol) and the diene **10** (480 mg, 2.79 mmol), in 50 mL of dry benzene, was refluxed under nitrogen for 2 h. Evaporation of the cooled solution left **13** as a solid (817 mg, 99%), which was recrystallized from hexanes. Two further recrystallizations afforded the analytical sample, mp 118.5–119.5°C; ir (KBr): 2240 (w, C≡N), 1655 (s, enol ether), and 1615 (s, C=C) $cm^{-1}$; nmr (100 MHz) δ: 0.25 (s, 9H, $OSi(CH_3)_3$), 0.91 (br t, $J$ = 6 Hz, 3H, terminal $CH_3$), 1.23–1.81 (m, 6H, $3CH_2$'s), 2.23 (dd, $J$ = 5 Hz, $J'$ = 18 Hz, 1H, allylic $CH_2$ proton), 2.58 (t, $J$ = 7.5 Hz, 2H, benzylic $CH_2$), 2.99 (dd, $J$ = 12 Hz, $J'$ = 18 Hz, 1H, allylic $CH_2$ proton), 3.58 (s, 3H, $ROCH_3$), 3.81 (s, 3H, $ArOCH_3$), 3.85 (s, 3H, $ArOCH_3$), 4.30 (d, $J$ = 6 Hz, 1H, $CHOCH_3$), 4.52 (dd, $J$ = 5 Hz, $J'$ = 12 Hz, 1H, benzylic CH), and 6.38 (s, 2H, aromatic); *m/e* (relative intensity): 456 (12), 384 (15), 353 (11), 285 (10), 284 (42), 242 (13), 234 (25), 229 (17), 228 (100), 227 (12). *Anal.* calcd. for $C_{25}H_{36}N_2O_4Si$: C 65.75, H 7.95, N 6.13; found: C 65.74, H 7.91, N 6.09.

*2-(2,2-Dicyano-3-methoxy-5-oxocyclohexyl)-1,3-dimethoxy-5-pentylbenzene (15)*

To an acetone solution (50 mL) of the adduct **13** (724 mg, 1.50 mmol) was added 6*N* hydrochloric acid (30 mL). The solution was allowed to stand at room temperature for 45 min before the organic solvent was removed *in vacuo*. Work-up of the residual liquid yielded the β-methoxy ketone **15** (577 mg, 94%), of sufficient purity (tlc ($CHCl_3$/EtOAc, 80:20)) for use in the next synthetic step. Chromatography on silica gel gave, in the benzene/ether (99:1) fractions, pure **15**, from which the analytical sample was obtained by evaporative distillation at 115–120°C (0.1 Torr); ir (neat): 2240 (w, C≡N) and 1735 (s, C=O) $cm^{-1}$; nmr (100 MHz) δ: 0.91 (br t, $J$ = 6 Hz, 3H, terminal $CH_3$), 1.24–1.81 (m, 6H, $3CH_2$'s), 2.59 (t, $J$ = 7.5 Hz, 2H, benzylic $CH_2$), 2.73–3.14 (m, 4H, $CH_2$'s α to carbonyl), 3.53 (s, 3H, $ROCH_3$), 3.61–3.86 (m, 6H, $2ArOCH_3$'s), 4.03 (dd, $J$ = 5 Hz, $J'$ = 8 Hz, 1H, $CHOCH_3$), 4.68 (dd, $J$ = 5 Hz, $J'$ = 7 Hz, 1H, benzylic CH), and 6.39 (br s, 2H, aromatic); *m/e* (relative intensity): 384 (75), 354 (13), 353 (49), 328 (10), 261 (10), 251 (10), 236 (10), 235 (57), 234 (100), 228 (14), 221 (13). *Anal.* calcd. for $C_{22}H_{28}N_2O_4$: C 68.73, H 7.34, N 7.29; found: C 68.59, H 7.46, N 7.27.

*2-(2,2-Dicyano-5-oxo-3-cyclohexenyl)-1,3-dimethoxy-5-pentylbenzene (16a)*

The ketone **15** (577 mg, 1.50 mmol) was refluxed in benzene (70 mL) under nitrogen, in the presence of a large excess of

Can. J. Chem. Downloaded from www.nrcresearchpress.com by 210.87.254.40 on 09/06/12
For personal use only.

*p*-toluenesulfonic acid (723 mg, 3.80 mmol). After 2.5 h, water was added to the cooled reaction mixture. The benzene layer was separated, washed with water (×3) and aqueous sodium chloride (saturated), dried ($MgSO_4$), and evaporated to a white crystalline solid (481 mg, 91%). In chromatographing the product on silica gel, **16***a* (mp 84–87°C) was eluted with benzene. As recrystallization proved to be troublesome, the analytical sample was prepared by high-vacuum sublimation (134°C/0.1 Torr), ir (KBr): 2250, 2225 (w, C≡N), and 1695 (s, conjugated C=O) $cm^{-1}$; nmr (100 MHz) δ: 0.93 (br t, $J$ = 6 Hz, 3H, terminal $CH_3$), 1.22–1.83 (m, 6H, $3CH_2$'s), 2.61 (br t, $J$ = 7 Hz, 2H, benzylic $CH_2$), 2.78–2.96 (m, 2H, $CH_2$ α to carbonyl), 3.82 (s, 6H, $2ArOCH_3$'s), 4.52–4.75 (m, 1H, benzylic CH), 6.32 (d, $J$ = 10 Hz, 1H, olefinic CH α to carbonyl), 6.41 (s, 2H, aromatic), and 6.90 (d, $J$ = 10 Hz, 1H, olefinic CH β to carbonyl); *m/e* (relative intensity): 352 (26), 310 (5), 284 (8), 235 (22), 234 (100), 228 (17), 178 (28), 177 (8). *Anal.* calcd. for $C_{21}H_{24}N_2O_3$: C 71.57, H 6.86, N 7.95; found: C 71.65, H 6.72, N 7.88.

*2-(2,2-Dicyano-5-oxocyclohexyl)-1,3)-dimethoxy-5-pentylbenzene (17)*

The enone **17** (1.90 g, 5.4 mmol) in ethanol (250 mL) over 10% palladium on charcoal (50 mg) was stirred under hydrogen for 6 h. Filtration through Celite and concentration yielded a yellow oil. Column chromatography on Florisil (benzene) gave **17** as an unstable white solid (1.90 g, 99%), mp 54–55°C; ir ($CHCl_3$): 2240 (w, C≡N), 1710 (s, C=O) $cm^{-1}$; nmr δ: 0.90 (br t, $J$ = 6 Hz, 3H, terminal $CH_3$), 1.2–1.8 (m, 7H, $4CH_2$'s), 2.60 (br t, $J$ = 8 Hz, 2H, benzylic $CH_2$), 2.70–3.25 (m, 4H, $2CH_2$'s, α to carbonyl), 3.80 (s, 6H, $2ArOCH_3$'s), 4.50 (t, $J$ = 6 Hz, 1H, benzylic CH), and 6.40 (s, 2H, aromatic); *m/e* (relative intensity): $M^+$ 354 (81), 324 (100), 298 (29), 262 (41), 234 (95), 221 (47), 178 (62), 91 (35). *Anal.* calcd. for $C_{21}H_{26}N_2O_3$: C 71.16, H 7.39, N 7.90; found: C 71.05, H 7.41, N 7.72.

*2-(2,2)Dicyano-5-ethylenedioxycyclohexyl)-1,3-dimethoxy-5-pentylbenzene (18)*

Ketone **17** (1.90 g, 5.4 mmol), ethylene glycol (1.15 g, 18.5 mmol), and *p*-toluenesulfonic acid (0.2 g) were refluxed in benzene (100 mL) for 4 h with a Dean–Stark trap fitted. The reaction mixture was cooled and the solvent removed *in vacuo*. Chromatography on Florisil (benzene) yielded a yellow oil which was crystallized from hexane to give **18** (1.98 g, 93%) as a colorless solid, mp 104–106°C; ir (KBr): 2250 (w, C≡N) $cm^{-1}$; nmr δ: 0.90 (br t, $J$ = 6 Hz, 3H, terminal $CH_3$), 1.20–2.30 (m, 12H, $6CH_2$'s), 2.50 (br t, $J$ = 6 Hz, 2H, benzylic $CH_2$), 3.80 (s, 6H, $ArOCH_3$), 3.95 (4H, 2 ketal $CH_2$'s), 4.20 (dd, $J$ = 3 Hz, $J'$ = 14 Hz, 1H, benzylic CH), 6.40 (s, 2H, aromatic); *m/e* (relative intensity): 398 (68), 305 (20), 228 (13), 178 (15), 165 (31), 164 (93), 99 (24), 86 (100). *Anal.* calcd. for $C_{23}H_{30}N_2O_4$: C 69.32, H 7.59, N 7.03; found: C 69.11, H 7.52, N 7.01.

*2(2-Cyano-5-ethylenedioxy-2-cyclohexylcarboxylic acid)-1,3-dimethoxy-5-pentylbenzene (19)*

To a solution of ketal (**18**) (1.07 g, 2.7 mmol) in ethanol (200 mL) was added 10 *N* aqueous sodium hydroxide (200 mL). The mixture was refluxed for 20 h. The organic solvent was removed *in vacuo* and the aqueous residue was cooled to below 0°C. The solution was acidified to pH 3 by dropwise addition of *concentrated* hydrochloric acid, maintaining the temperature below 5°C. The aqueous layer was extracted with ether (×3) using ice to maintain the temperature at 0°C. The combined organic layers were dried ($MgSO_4$) and concentrated to give acid **19** as a white foam (1.05 g, 94%). Analysis of the product on tlc (ethyl acetate) showed one trace impurity which later proved to be **20**. The physical properties exhibited were ir (KBr): 3200 (s, acidic OH), 2240 (w, C≡N), 1750, 1720 (acid, C=O) $cm^{-1}$; nmr δ: 0.90 (br t, $J$ = 6 Hz, terminal $CH_3$), 2.60 (br t, $J$ = 6 Hz, 2H, benzylic $CH_2$), 3.80 (s, 6H, a $ArOCH_3$'s), 3.95 (s, 4H, $2CH_2$'s of ketal), 6.40 (s, 2H), aromatic, variable, $D_2O$ exchangeable (s or br s, 1H, acid OH); *m/e* (relative intensity): $M^+$ 417 (13), 373 (23), 315 (32), 234 (14), 183 (55), 139 (58), 86 (100).

*2(2-Cyano-5-ethylenedioxycyclohexyl)-1,3-dimethoxy-5-pentylbenzene (20)*

A stirred solution of acid **19** (555 mg, 1.3 mmol) in 100 mL of dimethylformamide was stirred at reflux over ground sodium hydroxide (2 pellets) under a nitrogen atmosphere for 8 h. The reaction mixture was cooled and poured into water (300 mL). The mixture was cooled to 0°C, acidified with dilute hydrochloric acid, and then extracted with ether (×3, 200 mL). The combined extracts were washed with water (×3), dried ($MgSO_4$), and concentrated *in vacuo*. Filtration through Florisil (20 g; ethyl acetate/benzene, 2:98) afforded mononitrile **20** (435 mg, 88%) as a clear oil; ir (neat): 2225 (m, C≡N) $cm^{-1}$; nmr δ: 0.90 (br t, $J$ = 6 Hz, 3H, terminal $CH_3$), 2.60 (br t, $H$ = 6 Hz, 2H, benzylic $CH_2$), 3.80 (s, 6H, $2ArOCH_3$), 4.00 (s, 4H, $2CH_2$'s of ketal), 6.40 (s, 2H, aromatic); *m/e* (relative intensity): $M^+$ 373 (51), 342 (12), 329 (15), 305 (40), 285 (48), 140 (10), 139 (94), 99 (31), 86 (100). *Anal.* calcd. for $C_{22}H_3NO_4$: C 70.75, H 8.37, N 3.75; found: C 70.51, H 8.17, N 3.54.

*2(2-Ethyloxy-5-ethylenedioxycyclohexyl)-1,3-dimethoxy-5-pentylbenzene (21)*

To oven dried magnesium turnings (0.162 g, 6.7 mmol) covered with anhydrous ether in an oven dried flask, fitted with a condenser, under a dry nitrogen atmosphere, was added methyl iodide (1.04 g, 7.3 mmol) in anhydrous ether (15 mL) via syringe. After 10 h, mononitrile **20** was added to the ice-cooled Grignard reagent. The solution was gently refluxed for 6 H. The reaction was then cooled in an ice bath and saturated aqueous ammonium chloride (10 mL) followed by water (10 mL) were added. After separation the aqueous layer was extracted with ether (×2). The combined ether layers were dried ($MgSO_4$) and concentrated *in vacuo*. Preparative tlc (ethyl acetate/benzene, 10:90) afforded the methyl ketone (28 mg, 40%) as a clear oil, and starting nitrile (18 mg). This represents a yield of 60% based on recovered starting material; ir (neat): 1700 (s, C=O) $cm^{-1}$; nmr δ: 0.90 (br t, $J$ = 6 Hz, 3H, terminal $CH_3$), 1.90 (s, 3H, methyl ketone), 3.85 (s, 6H, $2ArOCH_3$'s), 4.00 (s, 4H, 2 ketal $CH_2$'s), 6.40 (s, 2H, aromatic); *m/e* (relative intensity): $M^+$ 390 (24), 359 (39), 347 (12), 305 (21), 289 (10), 245 (12), 221 (9), 156 (22), 139 (9.4), 124 (12), 99 (31), 86 (100). *Anal.* calcd. for $C_{23}H_{34}O_5$: C 70.74, H 8.78; found: C 70.25, H 9.39.

*2(2(1-Hydroxyisopropyl)-5-ethylenedioxycyclohexyl)-1-3-dimethoxy-5-pentylbenzene (22)*

To a stirred, ice-chilled solution of methyl ketone **21** (51 mg, 0.13 mmol) in anhydrous ether (20 mL), under argon, was added methyl magnesium bromide (0.1 mL, 0.6 mmol) and the solution was refluxed 1 h. The reaction was cooled in an ice bath and saturated aqueous ammonium chloride (10 mL) was added dropwise, followed by water. The mixture was separated and the aqueous layer was extracted with ether (×2). The combined organic layers were dried ($Na_2SO_4$), and concentrated *in vacuo* before ptlc (ethyl acetate/benzene, 10:90) gave 50 mg of alcohol **22** (95%) as a clear oil; ir (neat): 3500 (OH) $cm^{-1}$; nmr δ: 0.90 (br t, $J$ = 6 Hz, 3H, terminal CH), 1.10 (s, 6H, 2CH's α to alcohol), 3.85 (s, 6H, $2ArOCH_3$), 6.40 (br s, 2H, aromatic); *m/e* (relative intensity): $M^+$ 406 (10), 305 (30), 221 (25), 178 (10), 154 (62), 152 (10), 139 (15), 99 (22), 86 (100).

*11-Nor-9-ketohexahydrocannabinol (3)*

To a solution of diphenylphosphine (0.05 mL, 0.29 mmol) in dry THC (2.5 mL) was added 0.25 mL (0.40 mmol) of cold 1.6 *M* *n*-butyllithium – hexane solution via syringe. The reaction was stirred for 15 min before the addition of alcohol **22** (32 mg, 0.08 mmol) in dry THF (2.5 mL) via syringe. The solution was

stirred at room temperature for 2 h before being added to 20 mL of 5% hydrochloric acid and stirred for an additional 2 h. The aqueous mixture was extracted with ether (×3) and the combined extracts were dried ($MgSO_4$) and concentrated *in vacuo*. Separation by ptlc (ethyl acetate/benzene, 10:90) afforded a material **16** (2 mg) identical in all respects to an authentic sample of **1**, prepared by M. Guiver following the method of Archer *et al.* (5).

## Acknowledgements

We thank the Natural Sciences and Engineering Research Council of Canada and Health and Welfare Canada (NMUD Directorate) for financial assistance. A.H. and I.J. thank Carleton University for financial support during graduate studies.

1. R. MECHOULAM. Science, **168**, 1159 (1970); R. MECHOULAM and Y. GAONI. Fortschr. Chem. Org. Naturst. **25**, 175 (1967); C. R. B. JOYCE and S. H. CURRY (*Editors*). The botany and chemistry of cannabis. J. and A. Churchill, London. 1970; W. D. M. PATON and J. CROWN (*Editors*). Cannabis and its derivatives. Oxford University Press, London. 1972; R. K. RAZDAN. Prog. Org. Chem. **8**, 78 (1973); R. MECHOULAM. (*Editor*). Marijuana Chemistry, pharmacology, metabolism, and clinical effects. Academic Press, New York, NY. 1973; R. MECHOULAM, N. K. MCCALLUM, and S. BURSTEIN. Chem. Rev. 75 (1976).
2. M. GUIVER. M.Sc. Thesis, Carleton University, 1980; J. W. APSIMON, L. COLLIER, and M. GUIVER. Can J. Chem. To be submitted.
3. R. K. RAZDAN. *In* The total synthesis of natural products. Vol. 4. *Edited by* J. W. ApSimon. Wiley-Interscience, New York. 1981. p. 185.
4. R. ADAMS and T. E. BOCKSTAHLER. J. Am. Chem. Soc. **74**, 5436 (1952); R. ADAMS and R. CARLIN. J. Am. Chem. Soc. **65**, 360 (1943).
5. R. A. ARCHER, W. BLANCHARD, W. A. DAY, D. W. JOHNSON, E. R. LAVAGNINO, C. W. RYAN, and J. E. BALDWIN. J. Org. Chem. **42**, 2277 (1977).
6. K. BAILEY. Can J. Chem. **52**, 2136 (1974).
7. M. CUSHMAN and N. CASTAGNOLI. J. Org. Chem. **39**, 1546 (1974).
8. L. L. WOODS and J. SAPP. J. Org. Chem. **30**, 312 (1965).
9. (*a*) H. S. MASON. J. Am. Chem. Soc. **69**, 2241 (1947); (*b*) J. M. BRUCE and F. K. SUTCLIFFE. J. Chem. Soc. 4435 (1955).
10. J. I. DEGRAW, L. GOODMAN, and B. R. BAKER. J. Org. Chem. **26**, 1156 (1961).
11. L. J. DOLBY, C. A. ELLIGER, S. ESFANDIARI, and K. S. MARSHALL. J. Org. Chem. **33**, 4508 (1968).
12. Z. STOJANAC, R. A. DICKINSON, N. STOJANAC, R. J. WOZNOW, and Z. VALENTA. Can. J. Chem. **53**, 616 (1975).
13. S. DANISHEFSKY and T. KITAHARA. J. Am. Chem. Soc. **96**, 7807 (1974).
14. A. WASSERMAN. Diels–Alder reactions. Elsevier Publishing Co., Amsterdam. 1965. pp. 29–31.
15. S. DANISHEFSKY and T. KITAHARA. J. Org. Chem. **40**, 583 (1975).
16. (*a*) MeMgI: R. MECHOULAM and Y. GANOI. J. Am. Chem. Soc. **87**, 3237 (1965); (*b*) $AlCl_3$: J. M. BRUCE and F. K. SUTCLIFFE. J. Chem. Soc. 4435 (1955); (*c*) $BBr_3$: F. M. DEAN, J. GOODCHILD, L. E. HOUGHTON, J. A. MARTIN, R. B. MORTON, B. PARTON, A. W. PRICE, and N. SOMVICHIEN. Tetrahedron Lett. 4153 (1966); (*d*) TMSI: M. E. JUNG and M. A. LYSTER. J. Org. Chem. **42**, 3761 (1977); J. MINAMIKAWA and A. BROSSI. Tetrahedron Lett. 3085 (1978); M. E. JUNG and T. A. BLUMENKOPF. Tetrahedron Lett. 3657 (1978); (*e*) $RS^-$: G. I. FEUTRILL and R. N. MIRRINGTON. Tetrahedron Lett. 1327 (1970); P. A. BARLETT and W. S. JOHNSON. Tetrahedron Lett. 4459 (1970); T. R. KELLY, H. M. DALI, and W. G. TSANG. Tetrahedron Lett. 3859 (1977); J. W. WILDES, N. H. MARTIN, C. G. PITT, and M. E. WALL. J. Org. Chem. **36**, 721 (1971); (*f*) $PPh_2Li$: R. E. IRELAND and D. M. WALBA. Org. Synth. **56**, 44 (1976).

Can. J. Chem. Downloaded from www.nrcresearchpress.com by 210.87.254.40 on 09/06/12
For personal use only.

# Condensation of Schiff bases with 2-oxazolin-5-ones: simultaneous introduction of arylidene and amino moieties

ARYA K. MUKERJEE[1] AND PRADEEP KUMAR

*Chemistry Department, Faculty of Science, Banaras Hindu University, Varanasi-221005, India*

Received April 23, 1981

ARYA K. MUKERJEE and PRADEEP KUMAR. Can. J. Chem. **60**, 317 (1982).

Schiff bases condense with 2-oxazolin-5-ones having a C-4 methylene and/or C-2 methyl group, and the reaction in glacial acetic acid, containing freshly fused sodium acetate, produces 4-arylidene- and/or 2-styryl-2-imidazoline-5-ones as a result of simultaneous introduction of arylidene and amino moieties.

ARYA K. MUKERJEE et PRADEEP KUMAR. Can. J. Chem. **60**, 317 (1982).

La condensation des bases de Schiff sur les oxazoline-2 ones-5 ayant un groupe méthylène en position C-4 et éventuellement un groupe méthyle en position C-2, conduit dans l'acide acétique glacial contenant de l'acétate de sodium fraichement fondu, aux arylidène-4 et/ou styryl-2 imidazoline-2 ones-5 provenant de l'introduction simultanée de groupe arylidène et amino.

[Traduit par le journal]

Can. J. Chem. Downloaded from www.nrcresearchpress.com by 210.87.254.105 on 09/06/12
For personal use only.

In connection with our studies on 4-unsubstituted 2-oxazolin-5-ones, we have found that these heterocycles condense with suitable imines in benzene, affording the corresponding 4-alkylidene (arylidene) derivatives (1). In the reaction of 2-methyl-2-oxazolin-5-one with benzylideneaniline under similar conditions, the 2-styryl-2-imidazolin-5-one (**6**, $Ar^1 = Ar^2 = Ph$) was obtained in trace amount, besides the expected 4-benzylidene-2-methyl-2-oxazolin-5-one (**1**). Though several stilbenyl heterocycles have been synthesized by base-catalyzed condensation of anils with nitrogen-containing heteroaromatic systems bearing methyl groups (2, 3), simultaneous introduction of arylidene and amino moieties in suitable heterocycles does not seem to have been attempted. Therefore it was thought worthwhile to explore the possibility of using Schiff bases for the one-pot conversion of suitable O—C=N heterocycles into N—C=N heterocycles having a new exocyclic olefinic centre in conjugation with the imino group of the ring, and with this objective in mind the present investigation was undertaken.

The reaction of 4-benzylidene-2-methyl-2-oxazolin-5-ones (**1**) and Schiff bases was carried out under different conditions. When dry toluene was used as a solvent, the reaction of **1** and benzylideneaniline led to the formation of the anilide (**8**, $Ar^2 = Ph$) and the 2-styryl-2-imidazolin-5-one (**6**, $Ar^1 = Ar^2 = Ph$) in 25% and 2% yields, respectively. Addition of a catalytic amount of an acid, such as glacial acetic acid or *p*-toluenesulphonic acid to the reaction mixture raised the yield of **6** ($Ar^1 = Ar^2 = Ph$) to 10%. When 4-benzylidene-2-methyl-2-oxazolin-5-one (**1**) and Schiff bases were allowed to react in boiling glacial acetic acid in the presence of freshly fused sodium acetate, 1-substituted 4-benzylidene-2-imidazolin-5-ones (**6**) were obtained in moderate to good yields.

One of the possible reaction pathways for the conversion of **1** into **6** involves Michael type addition, followed by extrusion of the amine and subsequent aminolysis of the oxazolinone (path A, Scheme 1). The resultant amides (**5**) on cyclization afford **6**. This was verified by converting **4** into **3** ($Ar^1 = Ph$) by introducing the benzylidene moiety at the C-4 position, followed by aminolysis and subsequent cyclization (Scheme 1).

The alternative route to **6** could be through cleavage of the 1,5-bond of 2-oxazolin-5-one by the imine (path B, Scheme 1), promoted by the acid medium, and formation of **7** and the aldehyde, condensation of which ultimately affords the styryl compound. The mechanism of this route has been elaborated for the synthesis of **12** (Scheme 2). It was found that authentic 4-benzylidene-2-methyl-1-phenyl-2-imidazolin-5-one (**7**, $Ar^2 = Ph$) condenses with aromatic aldehydes in boiling glacial acetic acid to give the corresponding 2-styryl derivatives. With a view to ascertaining the authenticity of the path B, the reaction of **1** with a Schiff base was carried out in the presence of an added aldehyde different to that from which the Schiff base was derived. It was found that the imidazolone (**6**) containing the arylidene group derived from the Schiff base predominates in the reaction mixture, though its yield is considerably reduced. This finding indicates that path A has precedence over path B.

It is noteworthy that when 4-benzylidene-2-phenyl-2-oxazolin-5-one (**10**), which does not have

[1]Author to whom correspondence may be addressed.

0008-4042/82/030317-06$01.00/0

©1982 National Research Council of Canada/Conseil national de recherches du Canada

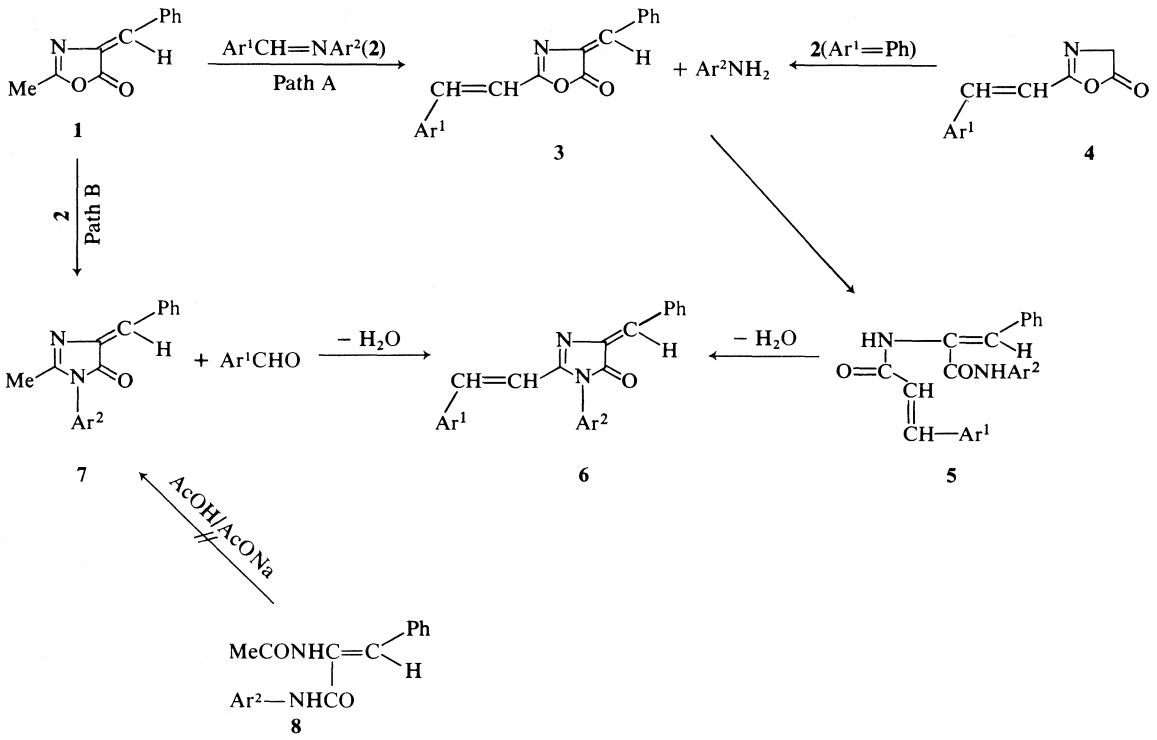


**1** **3** **4** **7** **6** **5** **8**

| 5 and 6 | Ar¹ | Ar² | 5 and 6 | Ar¹ | Ar² |
|---|---|---|---|---|---|
| *a* | Ph | Ph | *e* | 2-HO—$C_6H_4$ | Ph |
| *b* | Ph | 4-Me—$C_6H_4$ | *f* | 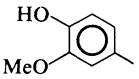 | Ph |
| *c* | Ph | 4-Cl—$C_6H_4$ | *g* | 3-$O_2N$—$C_6H_4$ | Ph |
| *d* | Ph | 4-MeO—$C_6H_4$ | | | |

SCHEME 1

an active methyl group and thereby ruling out Michael type addition, was allowed to react with benzylideneaniline in glacial acetic acid, 4-benzylidene-1,2-diphenyl-2-imidazolin-5-one (**12**) and benzaldehyde were obtained (Scheme 2).

Formation of **12** by cyclodehydration of the anilide (**11**) is known in the literature, but under the reaction conditions of the present study this route is unlikely, because in that case generation of aniline from benzylideneaniline present in the reaction mixture is essential. As already indicated, the reaction is carried out strictly under anhydrous conditions and thus there is no chance of hydrolysis of the imine. Had it been so, 2-methyl-2-oxazolin-5-one (**1**) should also have produced the anilide (**8**, $Ar^2$ = Ph), on reaction with benzylideneaniline in glacial acetic acid, because it is more vulnerable to aminolysis. It should be emphasized that the excellent yield of **6** ($Ar^1$ = $Ar^2$ = Ph) rules out formation of **8** in any appreciable amount. Also, **8** does not undergo cyclodehydration, on boiling in glacial acetic acid in the presence of fused sodium acetate, and the 2-methyl-2-imidazolin-5-one (**7**) does not play the key role in the conversion of **1** into **6**, as already mentioned.

Formation of **12** by the interaction of **10** and **2** is clearly an acid-mediated reaction. For example, when **10** and **2** ($Ar^1$ = $Ar^2$ = Ph) were heated under reflux in dry toluene for about 4 h, 90% of **10** was recovered without any trace of the imidazolone (**12**). Addition of *p*-toluenesulphonic acid in catalytic amount to the reaction mixture in dry toluene led to the formation of **12** in 10% yield, the major portion of **10** remaining unaffected. On using glacial acetic acid as a solvent, the yield of the product was about 50%. The reaction of 2-phenyl-5-oxazolonium perchlorate and benzylideneaniline is known to afford the 4-imidazolone **16** (Z = $CH_2$) and the conversion obviously involves cleavage of the 1,5-bond of **9**, though the mechanism proposed is

Can. J. Chem. Downloaded from www.nrcresearchpress.com by 210.87.254.105 on 09/06/12
For personal use only.

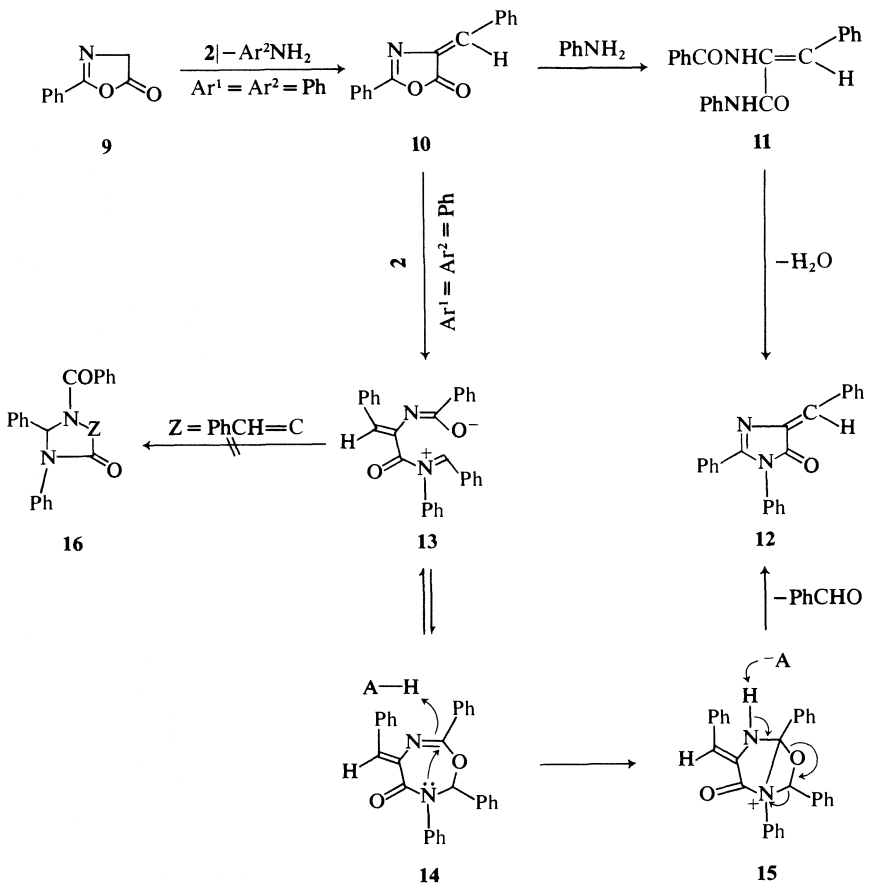

SCHEME 2

rather esoteric (4). It is noteworthy that benzylideneaniline itself does not undergo cleavage in this case. Formation of the 5-imidazolone (**12**), obtained in the present study, and 4-imidazolone (**16**, Z = $CH_2$) and other products reported in the work mentioned (4) can be adequately explained by the intermediates given in Scheme 2. It should be conceded that we could not isolate **14** and there is no precedent of the oxadiazepine in the literature. However, such a system is expected to be vulnerable to acids, and the ring closures outlined (Scheme 2) are in conformity with Baldwin's rules (5).

Simultaneous introduction of the arylidene and amine moieties seems to be advantageous. For example, synthesis of **3** and **4** in which $Ar^1$ carries a free hydroxyl group is difficult. Also, preparation of **3** and **4**, in which $Ar^1$ is a substituted phenyl group, involves several steps because substituted cinnamic acids have to be synthesized for obtaining the corresponding *N*-cinnamoyl glycines required for their synthesis. The alternative route to **3** by condensation of **1** with aromatic aldehydes gives very poor yields (6). Similarly, the condensation of 4-benzylidene-2-methyl-2-imidazolin-5-one (**7**) with aromatic aldehydes is not profitable because yields of the starting material **7** are just moderate (7) and its preparation requires a longer time (about 13 h in boiling xylene). It should be emphasized that the procedure now described overcomes these difficul-

TABLE 1. Preparation of 1-aryl-4-benzylidine-2-styryl-2-imidazolin-5-ones (**6**)

| Compound | Yield (%) method A | B | C | D | Melting point (°C) |
|---|---|---|---|---|---|
| **6***a* | 85.6 | 90 | 68.5 | 71.4 | 240–241 (A)[a] 245 (B)[b] |
| **6***b* | 66.6 | 44.4 | 50 | — | 188 |
| **6***c* | 63 | — | — | — | 222 |
| **6***d* | 68 | — | — | — | 198–199 |
| **6***e* | 30 | 27 | — | — | 245–246 |
| **6***f* | 65.6 | 22 | — | — | 200 |
| **6***g* | 66 | 44 | — | — | 200 (A)[a] 225 (B) |

[a] The product obtained by method A represents the *cisoid*-form which changes to the higher melting *transoid*-isomer on heating for some time in xylene.
[b] The product was obtained earlier by heating 2-cinnamoylamino cinnamanilide in xylene for 13 h (8).

Can. J. Chem. Downloaded from www.nrcresearchpress.com by 210.87.254.105 on 09/06/12
For personal use only.

TABLE 2. Data of combustion analysis of **6**

| Compound | Formula | Analysis (%) | | | | | |
|---|---|---|---|---|---|---|---|
| | | Calculated | | | Found | | |
| | | C | H | N | C | H | N |
| **6***b* | $C_{25}H_{20}N_2O$ | 82.41 | 5.49 | 7.69 | 82.40 | 5.74 | 7.67 |
| **6***c* | $C_{24}H_{17}N_2OCl$ | 74.90 | 4.42 | 7.27 | 75.09 | 4.48 | 7.49 |
| **6***d* | $C_{25}H_{20}N_2O_2$ | 78.94 | 5.26 | 7.36 | 78.94 | 5.49 | 7.23 |
| **6***e* | $C_{24}H_{18}N_2O_2$ | 78.68 | 4.91 | 7.65 | 78.89 | 4.90 | 7.26 |
| **6***f* | $C_{25}H_{20}N_2O_3$ | 75.75 | 5.05 | 7.07 | 75.82 | 4.74 | 7.34 |
| **6***g* | $C_{24}H_{17}N_3O_3$[a] | 72.91 | 4.30 | 10.63 | 73.05 | 4.14 | 10.50 |
| **6***g* | $C_{24}H_{17}N_3O_3$[b] | 72.91 | 4.30 | 10.63 | 72.98 | 3.88 | 10.26 |

[a] The *cisoid*-form.
[b] The *transoid*-form.

ties, affording better overall yields of the products and the time required is short.

It is noteworthy that these compounds can exist as conformers **17** and **18**. For example, condensation of **1** with 3-nitrobenzylideneaniline afforded a compound, mp 200°C. On the other hand condensation of **7** with 3-nitrobenzaldehyde led to the formation of a product, mp 225°C. Both these samples gave correct elemental analysis and they absorb near the same regions in their respective ir spectrum. But in their uv spectra, $\varepsilon_{max}$ values are different though they absorb near the same wavelengths. The sample with higher melting point has higher $\varepsilon_{max}$ values and therefore it was assigned the *transoid*-form which is thermodynamically more stable. As expected, the other conformer having lower melting point and lower $\varepsilon_{max}$ values changed

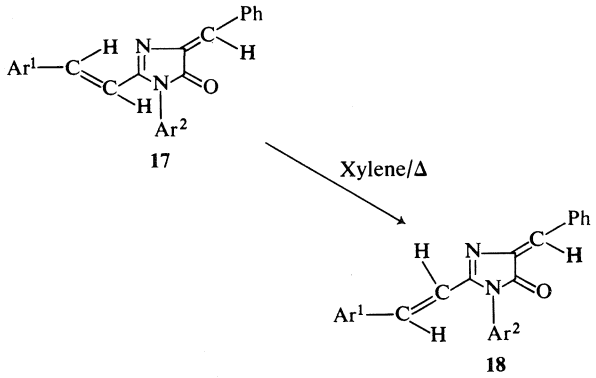


SCHEME 3

to the more stable conformation on heating in xylene for some time (Scheme 3). The compounds reported here were characterized by elemental and spectral analyses, the relevant data being presented in Tables 1 and 2, respectively. Some of the compounds obtained by the present procedure are already known in the literature and they were compared with the authentic samples.

## Experimental

All melting points are uncorrected. The uv, ir, and nmr spectra were recorded on Cary-14, Perkin-Elmer-720, and Varian A-60D spectrometers respectively.

*1-Aryl-4-benzylidene-2-styryl-2-imidazolin-5-ones (**6**); general procedures*

*Method A*

(*Z*)-4-Benzylidene-2-methyl-2-oxazolin-5-one (1, 9, 10) and a suitable Schiff base were taken in equimolar proportions in glacial acetic acid (20 mL/g of the oxazolone) containing freshly fused sodium acetate (0.48 mol) and the mixture was heated under reflux for about 4 h. The solvent was removed under reduced pressure and the pasty mass triturated with ethanol to give a solid which was filtered under suction and recrystallized from glacial acetic acid.

*Method B*

(*Z*)-4-Benzylidene-2-methyl-1-phenyl-2-imidazolin-5-one (**7**, $Ar^2$ = Ph), prepared by a published method (7), and an aromatic aldehyde were taken in equimolar proportions in glacial acetic acid (20 mL/g of the imidazolone) and the mixture was heated under reflux for about 4 h. Finally, it was worked up as in method A.

*Method C*

To a suspension of *N*-cinnamoylamino glycine (**4**, $Ar^1$ = Ph; 1.0 mol) in dry benzene (30 mL/g of the acid) containing triethylamine (1.0 mol), ethyl chloroformate (1.0 mol) was added and the mixture shaken at room temperature till the cinnamoylamino glycine crystals disappeared and triethylamine hydrochloride separated. The hydrochloride was filtered and washed twice with dry benzene. To the combined benzene solution and washings benzylideneaniline (1.0 mol) was added. The mixture was heated under reflux for 10 min and the solvent completely removed under reduced pressure.[2] To this, glacial acetic acid (20 mL/g of the Schiff base) and freshly fused sodium acetate (0.48 mol) were added and the mixture was heated under reflux for about 4 h. Finally, it was worked up as in method A.

*Method D*[3]

A mixture of (*Z*)-4-benzylidene-2-styryl-2-oxazolin-5-one (1, 6, 11) and a suitable primary amine, taken in equimolar proportions in glacial acetic acid containing freshly fused

[2] The (*Z*)-4-benzylidene-2-styryl-2-oxazolin-5-one (**3**) obtained in the reaction was not isolated. For the experimental detail of its separation and characterization see our earlier publication (1).

[3] A similar method was published earlier (12, 13).

Can. J. Chem. Downloaded from www.nrcresearchpress.com by 210.87.254.105 on 09/06/12
For personal use only.

TABLE 3. Spectral data of compounds **6**

| Compound | ir (Nujol) $\nu_{max}$ ($cm^{-1}$) | nmr ($CDCl_3$/TMS) δ (ppm) | uv (95% EtOH) λ ($\varepsilon_{max} \times 10^4$) nm |
|---|---|---|---|
| **6***a* | 1710, 1630, 1620 (mp 240–241°C) | 6.6 (d, 1H, *J* = 16 Hz, PhCH=C*H*), 7.3 (s, 1H, 4C=*CH*), 7.4–7.9 (m, 15H, Ar-*H*), 8.1 (d, 1H, *J* = 16 Hz, PhC*H*=CH)[a] | 235(1.26), 295(2.14), 405(1.7) |
| | 1710, 1630, 1620 (mp 245°C) | 6.7 (d, 1H, *J* = 16 Hz, PhCH=C*H*), 7.36 (s, 1H, 4-C=C*H*), 7.46–7.8 (m, 15H, Ar-*H*), 8.16 (d, 1H, *J* = 16 Hz, PhC*H*=CH)[a] | 235(1.95), 295(2.54), 405(1.70) |
| **6***b* | 1710, 1640, 1630 | 2.5 (s, 3H, $CH_3$), 6.66 (d, 1H, *J* = 16 Hz, PhCH=C*H*), 7.2–7.9 (m, 15H, 4-C=C*H* and Ar-*H*), 8.12 (d, 1H, *J* = 16 Hz, PhC*H*=CH)[a] | 208(2.06), 240(1.7), 295(2.45), 400(1.77) |
| **6***c* | 1710, 1630 | 6.66 (d, 1H, *J* = 16 Hz, PhCH=C*H*), 7.3 (s, 1H, 4-C=C*H*), 7.4–7.7 (m, 14H, Ar-*H*), 8.18 (d, 1H, *J* = 16 Hz, PhC*H*=CH)[a] | 225(2.0), 295(2.72), 405(2.2) |
| **6***d* | 1710, 1630 | 3.9 (s, 3H, $OCH_3$), 6.6 (d, 1H, *J* = 16 Hz, PhCH=C*H*), 7.2 (s, 1H, 4-C=C*H*), 7.3–7.9 (m, 14H, Ar-*H*), 8.1 (d, 1H, *J* = 16 Hz, PhC*H*=CH)[a] | 260(3.07), 283(3.41), 370(0.89) |
| **6***e* | 3400, 1700, 1630 | Insufficiently soluble | 215(4.05), 247(2.54), 297(3.4), 430(2.87) |
| **6***f* | 3230, 1710, 1630 | 3.96 (s, 3H, $OCH_3$), 6.74 (d, 1H, *J* = 16 Hz, 4-HO, 3-MeO—$C_6H_3$—CH=C*H*), 7.4–7.9 (m, 14H, O*H*, and Ar-*H*, one exchangeable), 8.2 (d, 1H, *J* = 16 Hz, 4-HO, 3-MeO—$C_6H_3$—C*H*=CH)[a] | 300(2.0), 435(2.73) |
| **6***g* | 1710, 1630, 1620 (mp 200°C) | 6.74 (d, 1H, *J* = 16 Hz, 3-$O_2N$—$C_6H_4$—CH=C*H*), 7.3 (s, 1H, 4-C=C*H*), 7.4–8.36 (m, 14H, Ar-*H*), 8.14 (d, 1H, *J* = 16 Hz, 3-$O_2N$—$C_6H_4$—C*H*=CH)[a] | 223(1.51), 290(2.37), 320(1.1), 405(1.71) |
| | 1710, 1630, 1620 (mp 225°C) | 6.86 (d, 1H, *J* = 16 Hz, 3-$O_2N$—$C_6H_4$—CH=C*H*), 7.3–8.3 (m, 15H, 4-C=C*H* and Ar-*H*), 8.18 (d, 1H, *J* = 16 Hz, 3-$O_2N$—$C_6H_4$—C*H*=CH)[a] | 245(1.95), 290(2.74), 320(1.29), 405(1.87) |

[a]Not very distinct due to partial overlapping of the peaks of the aromatic protons.

sodium acetate (0.48 mol), was heated under reflux for about 4 h and finally worked up as in method A.

*4-Benzylidene-1,2-diphenyl-2-imidazolin-5-one (**12**)*

The title compound was obtained by starting from hippuric acid and following method C given above; yield, 60%, mp 180°C (lit. (14) mp 180°C);[4] ir (Nujol) $\nu_{max}$: 1710 (CO) and 1640 (C=C) $cm^{-1}$; nmr ($CDCl_3$/TMS) δ: 7.34 (s, 1H, 4-C=C*H*), 7.4–7.7 (m, 15H, Ar-*H*) ppm.

The same product was obtained (in 50% yield) when (*Z*)-4-benzylidene-2-phenyl-2-oxazolin-5-one (**10**) and benzylideneaniline were heated under reflux in glacial acetic acid, containing freshly fused sodium acetate, for about 4 h and worked up as in method A given above.

[4]This method involves cyclization of 2-*N*-benzoylamino cinnamanilide. The yield is just moderate. Recently, **10** and aniline, taken in the molar ratio of 1:1, and anhydrous zinc chloride in catalytic amount were fused and heated for 5 min to give **12** in 70% yield; mp 175°C (15). It was also obtained, in very poor yield, by rearrangement of 3-benzoylamino-1,4-diphenyl-2-azetidinone (16).

## Acknowledgements

We sincerely thank one of the referees for suggesting the experiment to distinguish between path A and path B and for proposing the intermediate **15**. We also thank the Council of Scientific

Can. J. Chem. Downloaded from www.nrcresearchpress.com by 210.87.254.105 on 09/06/12
For personal use only.

and Industrial Research, New Delhi, for the award of a Senior Research Fellowship to one of us (P.K.).

1. P. KUMAR, H. D. MISHRA, and A. K. MUKERJEE. Synthesis, 836 (1980).
2. I. J. FLETCHER and A. E. SIEGRIST. Adv. Heterocycl. Chem. **23**, 171 (1978).
3. J. P. PAUCHARD and A. E. SIEGRIST. Helv. Chim. Acta, **61**, 129 (1978); **61**, 142 (1978).
4. A. M. KNOWLES, A. LAWSON, G. V. BOYD, and R. A. NEWBERRY. Tetrahedron Lett. 485 (1971).
5. J. E. BALDWIN. J. Chem. Soc. Chem. Commun. 734 (1976).
6. K. RÜFENACHT. Helv. Chim. Acta, **37**, 1451 (1954).
7. R. PFLEGER and G. MARKERT. Chem. Ber. **90**, 1494 (1957).
8. A. MUSTAFA, W. ASKER, A. H. HARHASH, T. M. S. ABDIN, and E. M. ZAYED. Justus Liebigs Ann. Chem. **714**, 146 (1968).
9. R. M. HERBST and D. SHEMIN. Org. Synth. Coll. Vol. II. Wiley, New York. 1943. p. 1.
10. R. GLASER and M. TWAIK. Tetrahedron Lett. 1219 (1976).
11. J. M. RIORDAN and C. H. STAMMER. J. Org. Chem. **39**, 654 (1974).
12. A. M. ISLAM, A. M. KHALIL, and I. I. ABD EL-GAWAD. Aust. J. Chem. **26**, 827 (1973).
13. A. M. ISLAM, A. M. KHALIL, and M. S. EL-HOUSENI. Aust. J. Chem. **26**, 1601 (1973).
14. C. GRÄNCHER and G. GULBAS. Helv. Chim. Acta, **10**, 819 (1927).
15. M. Z. A. BADR, H. A. H. EL-SHERIEF, and M. E. TADROS. Indian J. Chem. **18B**, 240 (1979).
16. C. W. BIRD and J. D. TWIBELL. J. Chem. Soc. C, 3155 (1971).

Can. J. Chem. Downloaded from www.nrcresearchpress.com by 210.87.254.105 on 09/06/12
For personal use only.

# Dihydropyridines in synthesis and biosynthesis. III.[1] Coupling of dihydropyridinetricarbonylchromium(0) complexes: bipyridyls[2]

JAMES P. KUTNEY, LUCAS KACZMAREK, DANUTA MOSTOWICZ, AND BRIAN R. WORTH

*Department of Chemistry, University of British Columbia, 2036 Main Mall, Vancouver, B.C., Canada V6T 1Y6*

Received August 24, 1981

JAMES P. KUTNEY, LUCAS KACZMAREK, DANUTA MOSTOWICZ, and BRIAN R. WORTH. Can. J. Chem. **60**, 323 (1982).

Reaction of 1,2- and 1,6-dihydro-3-ethyl-*N*-methyl pyridine tricarbonylchromium(0) complexes with methyllithium at low temperature afforded a high yield of dimeric tricarbonylchromium(0) complexes. Structures of the latter products were established by X-ray crystallographic analysis. Some chemistry of these novel compounds is described.

JAMES P. KUTNEY, LUCAS KACZMAREK, DANUTA MOSTOWICZ et BRIAN R. WORTH. Can. J. Chem. **60**, 323 (1982).

La réaction des complexes de dihydro-1,2 et de dihydro-1,6 éthyl-3 *N*-méthyl pyridine tricarbonylchrome(0) avec le méthyl-lithium à basse température conduit avec un excellent rendement aux complexes dimères de tricarbonylchrome(0). On a établi la structure de ces dernier produits par l'analyse cristallographique aux rayons X. On décrit quelques propriétés chimiques de ces nouveaux composés.

[Traduit par le journal]

Previous work from these laboratories (1–4) described the preparation and characteristics of 1,2- and 1,6-isomers of dihydropyridinetricarbonylchromium(0) complexes. Generally, controlled reduction of pyridinium salts provided labile 1,2-dihydropyridines (e.g. **1**) which were subsequently stabilized as their chromium carbonyl complexes (**2** and **3**, Scheme 1). Facile release of the complexing metal was possible using pyridine or ethylenediamine and subsequent reaction of the enamines gave β-alkylation (5) (**5**). Alternatively, the complexes reacted with lithium salts of substituted acetonitriles to provide an overall nucleophilic substitution reaction (**6–9**, Scheme 1) (6). The stabilization of dihydropyridines as their chromium complexes has also been applied to the synthesis of various alkaloid systems (1, 7).

In order to improve the efficiency of, and/or the position of, nucleophilic substitution we attempted to prepare the cation **10** using, for example, trityl fluoroborate (8, 9). All attempts in this area were unsuccessful presumably due to the considerable electron withdrawing effect of the chromium carbonyl group and the absence of stabilization of positive charge by nitrogen electrons. By the same argument, the corresponding anion **11** seemed a plausible species and attempts were made to abstract a proton from **2** and to subsequently alkylate or acylate the expected intermediate **11**.

Initially the complex **2** was reacted with *tert*-butyllithium (1 mol equiv. at −78°C) and the mixture subsequently treated with an excess of iodomethane. The resulting solution both before and after oxidation with iodine gave mainly decomposition products together with traces of **2** and a product tentatively assigned structure **12**. Anticipated product **13** was not detected. Simply reacting **2** with *tert*-butyllithium at −78°C gave **12** in 7% yield. The major product (> 80%) was "dimeric" material with $M^+$ 382. Analogous reaction, using methyllithium as base, gave a high yield (80–92%) of "dimeric" material together with a trace (ca. 1.5%) of the substitution product **13**. Chromatography on silica gel allowed separation of the "dimeric" fraction into three bright red crystalline components **14** (32–37%), **15** (4–27%), and **16** (25–50%). Structures **14–16** were consistent with spectral data obtained and were confirmed by X-ray crystallographic analysis (2). The diastereomer **17** was not isolated, although in one reaction a low yield of a fourth product was obtained. This material rapidly decomposed in light/air. Under similar (−78°C) conditions, the 1,6-isomer **3** did not react, while at higher temperatures (up to −10°C) an intractable mixture of products was formed.

As with the simple organometallic compounds **2** and **3**, thermal isomerization was possible. In fact heating **14** in refluxing *n*-octane for twelve hours gave a 70% yield of the 1,6-isomer **18** (8% of **14** was recovered) while **16** similarly gave **18** in 41% yield (28% of **14** recovered). Thermal isomerization of either **2** or **3** had given (1) a 1:1 mixture of isomers while, here, the predominance of **18** is likely due to the release of extra steric crowding at the new $sp^3$ carbon atom. This is consistent with the configuration at C2 which is supported by $^1$Hmr data. In **18**, the C2 proton resonated as a double doublet ($J_{2,3} \simeq$ 6 Hz, $J_{2,2'} \simeq$ 8 Hz) at δ 3.18 ppm. Irradiation of the signal for C3-H (δ 3.78) collapsed the C2-H signal to

[1]For Part II, see ref. 1.

[2]For a preliminary report see ref. 2.

0008-4042/82/030323-04$01.00/0

©1982 National Research Council of Canada/Conseil national de recherches du Canada

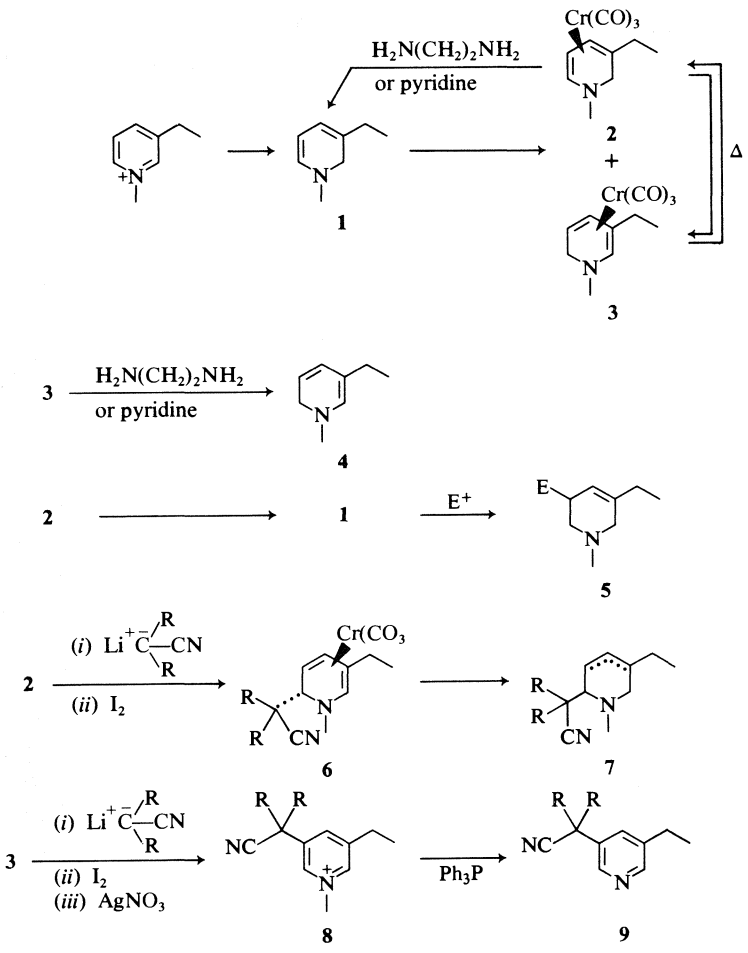


SCHEME 1

a doublet ($J$ = 8 Hz) while irradiation at δ 2.15 (C2′-H) gave a doublet ($J$ = 6 Hz) at δ 3.18. This 6 Hz coupling between C2-H and C3-H is consistent with a pseudo-equatorial orientation for C2-H

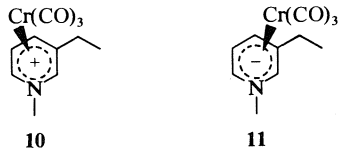


10 11

analogous to that found for **6**. The piperideine substituent is therefore *pseudo*-axial, directed away from the tricarbonylchromium group. This inherent release of steric crowding is consistent with the facile conversion of **14** to **18**. Thermal induced isomerization of **16** was accompanied by double bond migration to the enamine system in **18**.

The dimeric compounds, **14–16**, were converted to a simple bipyridyl (**21**) by two routes. Reaction of a mixture of **14–16** with pyridine at 50°C followed by reduction with sodium borohydride gave a mixture of **19** and **20** which on oxidation with selenium gave the bipyridyl **21** (27%). Direct oxidation of the mixture **14–16** with selenium gave **21** in 15% yield. Attempts to optimize these conversions or to find alternative reagents for the formation of **21** have not been made. The utility of complexes such as **14–16** and **18** was found to be limited by their steric bulk. For example, reactions with nucleophilic species (cf. **2** → **6** or **3** → **8**) were unsuccessful, giving either unreacted complex or, under more forcing conditions, intractable decomposition products.

Finally, the reaction of the 1,2-dihydropyridine complex **2** with alkyllithiums at −78°C gave, rapidly, a high yield of "dimeric" compounds **14–16**, which were subsequently oxidized to the bipyridyl **21**. The mechanism of formation of the "dimers" remains ambiguous.

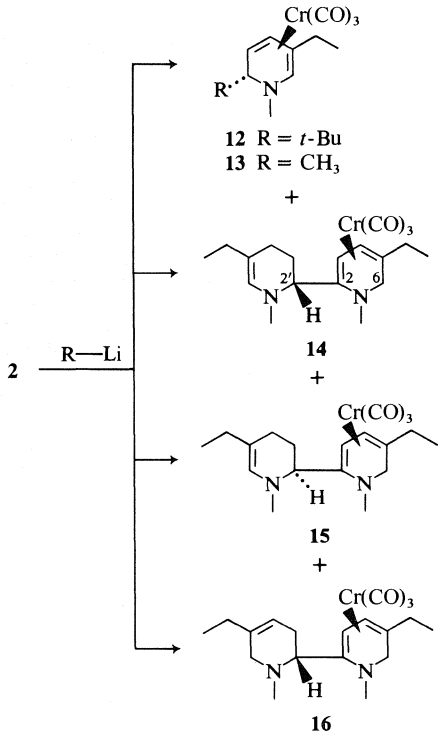


SCHEME 2

## Experimental

Melting points were determined on a Kofler block and are uncorrected. Ultraviolet (uv) spectra were recorded on a Cary 15 spectrophotometer in ethanol solution. The wavelengths of absorption maxima are reported in nanometers (nm). Infrared

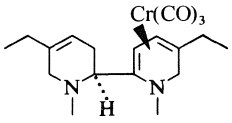


17

(ir) spectra were measured on a Perkin Elmer model 710 or 457 spectrophotometer in chloroform solution. The absorption maxima are reported in wavenumbers ($cm^{-1}$), calibrated with respect to the absorption band of polystyrene at 1601 $cm^{-1}$. Proton magnetic resonance ($^1$Hmr) spectra were measured in deuteriochloroform ($CDCl_3$) solution at ambient temperature on either a Varian HA-100 or XL-100 spectrometer or on a Nicolet

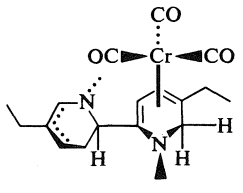


14 or 16

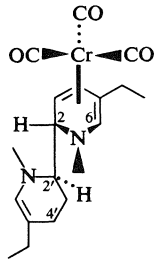


18

270 MHz instrument. Chemical shift values are given in the δ (ppm) scale relative to tetramethylsilane (TMS) used as internal standard. The integrated peak areas, signal multiplicities, and proton assignments are given in parentheses. Low resolution mass spectra (ms) were determined on either an AEI-MS-902 or an Atlas CH-4B spectrometer. High resolution mass spectra were measured on an AEI-MS-902 instrument. Microanalyses were carried out by Mr. P. Borda of the Microanalytical Laboratory, University of British Columbia.

As a matter of routine, all reagents and solvents were recrystallized or distilled before use. Chromium carbonyl complexes were always handled under oxygen free nitrogen or under high vacuum.

*The complex (12)*

A solution of *tert*-butyllithium (0.66 mL of 1.6 *M* solution in *n*-pentane) was added to the complex **2** (0.276 g) in dry THF at −78°C under nitrogen. The solution was cooled to −78°C, treated with iodine (0.254 g), allowed to warm to −10°C over 1 h, concentrated *in vacuo*, and chromatographed on silica gel with petroleum ether (30–60°C)/dichloromethane, *under nitrogen* to give: (*i*) complex **12**; 23.5 mg, 7%; $^1$Hmr ($CDCl_3$) δ: 5.42 (s, 1H, C6-H), 5.20 (1H, d, $J$ = 8 Hz, C4-H), 3.77 (1H, dd, $J$ = 8, 6 Hz, C3-H), 3.26 (1H, d, $J$ = 6 Hz, C2-H), 2.73 (3H, s, $NCH_3$), 1.32 (3H, t, $J$ = 7.5 Hz, $—CH_2CH_3$), 0.70 (9H, s, $—C(CH_3)_3$); ms *m/e*: 315 ($M^+$); (*ii*) a mixture of products with *m/e* 382 ($M^+$), 173 mg (85%).

*The complexes 14–16*

A solution of methyllithium (7.5 mL of 1.43 *M*) was added to the complex **2** (2.16 g) in dry THF (50 mL) at −78°C under nitrogen. After 30 min, degassed methanol (15 mL) was added

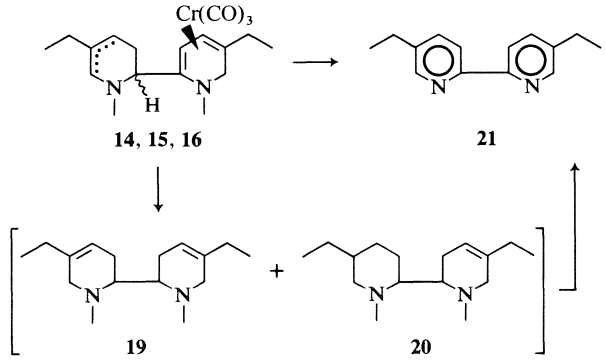


SCHEME 3

and the solution allowed to reach 0°C. The solvents were removed *in vacuo* and the residue chromatographed *under nitrogen* on silica gel with hexane/diethyl ether to give the following.

*Compound 14* (507 mg, 32%); red crystals (dichloromethane/hexane); mp 99–101.5°C; uv $\lambda_{max}$: 402 nm (ε 3821); $\nu_{max}$: 1945, 1863, 1845 $cm^{-1}$; $^1$Hmr ($CDCl_3$) δ: 5.82 (1H, d, $J$ = 5.4 Hz, C3-H), 5.79 (1H, s, C6′-H), 4.94 (1H, d, $J$ = 5.4 Hz, C4-H), 3.92 (1H, s, C2′-H), 3.33 (2H, s, C6-$H_2$), 2.87 (3H, s, $—N'CH_3$), 2.63 (3H, s, $—NCH_3$), 1.02 (3H, t, $J$ = 7.5 Hz, $—CH_2CH_3$), 0.96 (3H, t, $J$ = 7.5 Hz, $—CH_2CH_3$); ($C_6D_6$) δ: 5.50 (1H, d, $J$ = 5.4 Hz, C3-H), 5.44 (1H, s, C6′-H), 4.41 (1H, d, $J$ = 5.4 Hz, C4-H), 3.36 (1H, unresolved triplet, C2′-H), 2.62 (3H, s, $—N'CH_3$), 2.31 (2H, ABq, $\Delta\nu_{AB}$ = 12.1 Hz, $J$ = 10.8 Hz, C6-$H_2$), 1.54 (3H, s, $—NCH_3$), 0.95 (3H, t, $J$ = 7.5 Hz, $—CH_2CH_3$), 0.56 (3H, t, $J$ = 7.5 Hz, $—CH_2CH_3$); ms *m/e*: 382, 354, 326, 298, 296, 245, 122;

*Anal.* calcd. for $C_{19}H_{26}CrN_2O_3$: C 59.94, H 6.80, N 7.33; found: C59.79, H 6.88, N 7.35.

*Compound* ***15*** (427 mg, 27%); red crystals; mp 105–107°C; ms and uv as for **14**; $\nu_{max}$: 1950, 1875, 1850 $cm^{-1}$; $^1$Hmr ($CDCl_3$) δ: 5.79 (1H, d, $J$ = 5.4 Hz, C3-H), 5.76 (1H, s, C6′-H), 4.97 (1H, d, $J$ = 5.4 Hz, C4-H), 3.62 (1H, d, $J$ = 9 Hz, C2′-H), 3.43 (2H, ABq, $\Delta\nu_{AB}$ = 24.7 Hz, $J$ = 10.8 Hz, C6-$H_2$), 2.65 (3H, s, N′-$CH_3$), 2.50 (3H, s, $NCH_3$); ($C_6D_6$) δ: 5.60 (1H, s, C6′-H), 5.32 (1H, d, $J$ = 5.4 Hz, C3-H), 4.50 (1H, d, $J$ = 5.4 Hz, C4-H), 3.42 (1H, dd, $J$ = 10, 2.7 Hz, C2′-H), 2.50 (2H, ABq, $\Delta\nu_{AB}$ = 15.5 Hz, $J$ = 10.8 Hz, C6-$H_2$), 1.97 (3H, s, N′-$CH_3$), 1.78 (3H, s, —$NCH_3$), 0.97 (3H, t, $J$ = 7.5 Hz, —$CH_2CH_3$), 0.72 (3H, t, $J$ = 7.5 Hz, —$CH_2CH_3$); *Anal.* calcd. for $C_{19}H_{26}CrN_2O_3$: C 59.94, H 6.80, N 7.33; found: C 59.34, H 6.88, N 7.30.

*Compound* ***16*** (400 mg, 25%); red crystals; mp 138–142°C; ms and uv as for **6**; $\nu_{max}$: 1945, 1870, 1845 $cm^{-1}$; $^1$Hmr ($CDCl_3$) δ: 5.67 (1H, d, $J$ = 5.4 Hz, C3-H), 5.62 (1H, bs, C4′-H), 4.95 (1H, d, $J$ = 5.4 Hz, C4-H), 3.62 (1H, t, $J$ = 5.4 Hz, C2′-H), 3.36 (2H, ABq, $J$ = 10.8 Hz, C6-$H_2$), 3.19 (2H, ABq, $J$ = 17.5 Hz, C6′-$H_2$), 2.68 (3H, s, —N′$CH_3$), 2.40 (3H, s, —$NCH_3$), 1.03 (3H, t, $J$ = 7.5 Hz, —$CH_2CH_3$), 0.97 (3H, t, $J$ = 7.5 Hz, —$CH_2CH_3$); ($C_6D_6$) δ: 5.39 (1H, bs, C4′-H), 5.35 (1H, d, $J$ = 5.4 Hz, C3-H), 4.60 (1H, d, $J$ = 5.4 Hz, C4-H), 3.48 (1H, t, $J$ = 5.4 Hz, C2′-H), 2.93 (2H, ABq, $J$ = 17.5 Hz, C6′-H), 2.63 (2H, ABq, $J$ = 10.8 Hz, C6-$H_2$), 2.19 (3H, s, —N′$CH_3$), 2.06 (3H, s, —$NCH_3$), 0.94 (3H, t, $J$ = 7.5 Hz, —$CH_2CH_3$), 0.78 (3H, t, $J$ = 7.5 Hz, —$CH_2CH_3$); *Anal.* calcd. for $C_{19}H_{26}CrN_2O_3$: C 59.94, H 6.80, N 7.33; found: C 59.75, H 6.90, N 7.30.

*Isomerization of* ***14*** *to* ***18***

A solution of **14** (476 mg) in degassed *n*-octane (30 mL) was refluxed, under nitrogen, for 12 h. The solution was cooled to room temperature and chromatographed, under nitrogen, on silica gel to give **14** (37 mg, 8%); and **18** (335 mg, 70%), as red crystals (petroleum ether, ether); mp 87–88°C; ir $\nu_{max}$: 1945, 1870, 1845 $cm^{-1}$; uv $\lambda_{max}$: 405 nm (ε 3786); $^1$Hmr ($CDCl_3$) δ: 5.39 (2H, s, C6-H and C6′-H), 5.19 (1H, d, $J$ = 8 Hz, C4-H), 3.78 (1H, dd, $J$ = 8, 6 Hz, C3-H), 3.18 (1H, dd, $J$ = 8, 6 Hz, C2-H), 2.69–2.63 (5H, m, N-$CH_3$, and C5′-$CH_2CH_3$), 2.41 (3H, s, N′-$CH_3$), 2.15 (1H, dd, $J$ = 8, 6 Hz, C2′-H), 1.86 (2H, q, $J$ = 8 Hz, —$CH_2CH_3$), 1.67–1.58 (3H, m, C3′-H and C4′-$H_2$), 1.35 (3H, t, $J$ = 8 Hz, —$CH_2CH_3$), 1.16 (1H, m, C3′-H), 0.91 (3H, t, $J$ = 8 Hz, —$CH_2CH_3$); ms *m/e*: 382 ($M^+$), 354, 326, 298. High resolution molecular weight calcd. for $C_{19}H_{26}N_2O_3Cr$: 382.1349; found: 382.1347. *Anal.* calcd. for $C_{19}H_{26}N_2O_3Cr$: C 59.67, H 6.85, N 7.32; found: C 59.40, H 6.95, N 7.31.

*Isomerization of* ***16*** *to* ***18***

Similarly heating a solution of **16** (413 mg) gave **16** (115 mg, 28%) and **18** (170 mg, 41%) identical with that isolated above.

*Oxidation of* ***14–16*** *to* ***21*** *via* ***19*** *and* ***20***

A mixture of the "dimers" **14–16** (500 mg) in dry pyridine (100 mL) was refluxed under nitrogen for 3 h. The solvent was removed *in vacuo* and the residue treated with sodium borohydride (250 mg) in degassed methanol (15 mL) for 1 h, under nitrogen at room temperature. The mixture was acidified with dilute HCl, stirred for 10 min, and then made alkaline with dilute NaOH and extracted with ether. The ether extract was dried ($Na_2SO_4$) and concentrated *in vacuo* to give **19** and **20** as a clear oil. The mixture was not separated due to the number of possible diastereomeric components, but used directly for the next step.

A mixture of **19** and **20** (325 mg) and selenium (1.0 g) were heated in a sealed tube at 350°C for 15 h. The mixture was dissolved in dilute HCl and filtered. The filtrate was made basic with dilute NaOH and then extracted with ether. The ether layer was dried, concentrated, and chromatographed on silica gel to give **21** (77 mg, 27%) as colourless crystals (hexane), mp 54.5°C; ir $\nu_{max}$ ($CCl_4$): 3120–2890, 1610, 1560, 1470 $cm^{-1}$; uv $\lambda_{max}$ (MeOH): 297 (ε 20 779), 283 (29 221), 275 (27 922), 245 (21 104), 240 (19 156) nm; $^1$Hmr δ: 8.48 (2H, s, C6-H and C6′-H), 8.24 (2H, d, $J$ = 8 Hz, C3-H and C3′-H), 7.61 (2H, dd, $J$ = 8, 2 Hz, C4-H and C4′-H), 2.67 (4H, q, $J$ = 8 Hz, 2 × —$CH_2CH_3$), 1.25 (6H, t, $J$ = 8 Hz, 2 × —$CH_2CH_3$); ms *m/e*: 212 ($M^+$), 197. High resolution molecular weight determination calcd. for $C_{14}H_{16}N_2$: 212.1313; found 212.1317. *Anal.* calcd. for $C_{14}H_{16}N_2$: C 79.20, H 7.60, N 13.20; found: C 79.08, H 7.80, N 13.00.

*Oxidation of* ***14–16*** *to* ***21***

Reaction of a mixture of **14–16** (1.13 g) with selenium (2.5 g) as above gave **21** (95 mg, 15%) identical with a sample prepared earlier.

## Acknowledgement

Financial aid from the Natural Sciences and Engineering Research Council of Canada is gratefully acknowledged.

1. J. P. KUTNEY, R. A. BADGER, W. R. CULLEN, R. GREENHOUSE, M. NODA, V. E. RIDAURA-SANZ, Y. H. SO, A. ZANAROTTI, and B. R. WORTH. Can. J. Chem. **57**, 300 (1979).
2. J. P. KUTNEY, T. C. W. MAK, D. MOSTOWICZ, J. TROTTER, and B. R. WORTH. Heterocycles, **12**, 1517 (1979).
3. C. A. BEAR, W. R. CULLEN, J. P. KUTNEY, V. E. RIDAURA, J. TROTTER, and A. ZANAROTTI. J. Am. Chem. Soc. **95**, 3058 (1973).
4. J. P. KUTNEY. Heterocycles, **7**, 593 (1977).
5. J. P. KUTNEY, R. GREENHOUSE, and V. E. RIDAURA. J. Am. Chem. Soc. **96**, 7364 (1974).
6. J. P. KUTNEY, M. NODA, and B. R. WORTH. Heterocycles, **12**, 1269 (1979).
7. J. P. KUTNEY, M. NODA, N. G. LEWIS, B. MONTEIRO, D. MOSTOWICZ, and B. R. WORTH. Heterocycles, **16**, 1469 (1981).
8. R. P. A. SNEEDEN. Organochromium compounds. Academic Press, New York, NY. 1975. p. 210.
9. K. ÖFELE. Angew. Chem. Int. Ed. Engl. **6**, 988 (1967).

# Stereoselective synthesis of (−)-α-multistriatin from D-glucose

PHAIK-ENG SUM AND LARRY WEILER[1]

*Department of Chemistry, University of British Columbia, Vancouver, B.C., Canada V6T 1Y6*

Received August 17, 1981

PHAIK-ENG SUM and LARRY WEILER. Can. J. Chem. **60**, 327 (1982).

D-Glucose was converted into (−)-α-multistriatin, the aggregation pheromone of the European elm bark beetle, via a highly stereoselective eighteen-step route.

PHAIK-ENG SUM et LARRY WEILER. Can. J. Chem. **60**, 327 (1982).

On a transformé le D-glucose en (−)-α-multistriatine, la phérémone d'agrégation du scolyte de l'orme européen, en utilisant une synthèse hautement stéréosélective en 18 étapes.

[Traduit par le journal]

Can. J. Chem. Downloaded from www.nrcresearchpress.com by 210.87.254.105 on 09/06/12
For personal use only.

The bicyclic ketal, α-multistriatin (**1**), is one of three components of the aggregation pheromone of the European elm bark beetle, *Scolytus multistriatus*, which is the principal vector of Dutch elm disease in North America (1). The severe devastation of the elm populations in eastern North America and the steady march of the disease to the west coast have resulted in extensive studies on the use of pheromones to control this bark beetle and hence the Dutch elm disease. The volatile compounds from virgin female beetles were obtained and fractionated. The active attractant was found to be a combination of three components, α-multistriatin (**1**), 4-methyl-3-heptanol (**2**), and α-cubebene (**3**) (2). Compounds **1** and **2** were produced by the beetles, while compound **3** was produced by the host elm logs. In addition, the β-isomer **4** of multistriatin was also isolated from the beetles, but it was found to be inactive as an attractant (2). The structure of α-multistriatin was determined by extensive use of spectroscopic techniques and spectral analysis of the hydrogenolysis products from **1** (3). The natural α-multistriatin was optically active, $[\alpha]D^{25}$ −47° (hexane) (3) and subsequently the absolute configuration of (−)-α-multistriatin was found to be 1*S*,2*R*,4*S*,5*R* by a chiral synthesis (4).

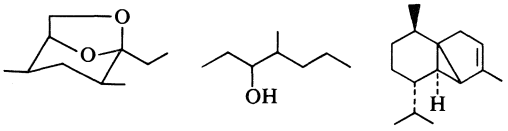


**1** **2** **3**

A nonselective synthesis of multistriatin gave the four isomers α- (**1**), β- (**4**), γ- (**5**), and δ- (**6**) (5). However, only the α-isomer **1** was active as an attractant. Subsequently one of the intermediates in this route was partially resolved and converted into the enantiomers of α-multistriatin (4). This established the absolute configuration of (−)-α-multistriatin as shown in **1**. A second synthesis of (−)-**1** was reported by Mori starting from D-mannitol (6). Cernigliaro and Kocienski have synthesized (−)-**1** from (+)-citronellol (7). Unfortunately the low optical purity of this starting material gave a product with ca. 40% optical purity. Elliott and Fried have also reported a synthesis of (−)-**1** via a resolution of one of the intermediates in their synthesis (8). Bartlett and Myerson have stereoselectively converted the readily available *meso*-2,4-dimethylglutaric anhydride into racemic α-multistriatin (9). Recently Fraser-Reid and co-workers have reported a synthesis of (−)-**1** from D-glucose (10) which has many similarities to the synthesis reported here.[2]

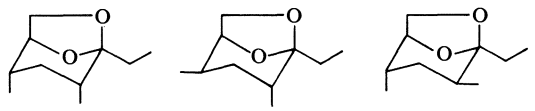


**4** **5** **6**

Earlier, we had developed facile synthetic routes to the 6,8-dioxabicyclo[3.2.1]octane pheromones frontalin (**7**), *exo*-brevicomin (**8**) and *endo*-brevicomin (**9**) (12). However, it was quickly apparent that this synthetic route which involved cyclization of an acyclic epoxy β-keto ester could

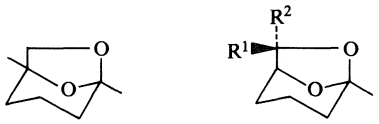


**7**

**8** R¹ = H, R² = Et
**9** R¹ = Et, R² = H

[1]Author to whom correspondence may be addressed.

[2]For a preliminary communication of our work see ref. 11.

0008-4042/82/030327-08$01.00/0

©1982 National Research Council of Canada/Conseil national de recherches du Canada

Can. J. Chem. Downloaded from www.nrcresearchpress.com by 210.87.254.105 on 09/06/12
For personal use only.

not be readily extended to a synthesis of **1**. In addition we recognized that the basic 6,8-dioxabicyclo[3.2.1]octane skeleton of all of these pheromones is present in certain anhydrohexoses (13) and we were intrigued with the potential synthesis of (−)-**1** from a readily available carbohydrate.[3] D-Glucose (**10**) shown in the unstable $^1C_4$ chair has the

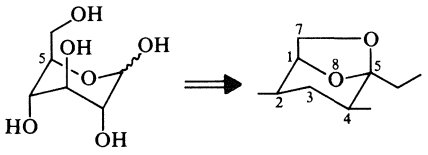


**10** **1**

same absolute stereochemistry at C-5 as C-1 in (−)-α-multistriatin. Our synthetic plan to convert D-glucose into **1** involved: (*a*) deoxygenation of C-3, (*b*) introduction of methyl groups at C-2 and C-4 with "inversion" of configuration, (*c*) introduction of an ethyl group at C-1, and (*d*) formation of the C-1,6 anhydro derivative of glucose.

Methyl α-D-glucopyranoside (**11**) was protected as its benzylidine derivative **12** in 70% yield (15). The benzylidine **12** was converted into the ditosylate which on treatment with base following the procedure of Richtymer (15) gave the epoxide **13** (15) in a yield of ca. 70% for the two steps. However, we have found that we could obtain slightly higher yields (ca. 75%) but after noticeably shorter reaction periods using the dimesylate as an intermediate to epoxide **13**. Reaction of epoxide **13** with lithium dimethylcuprate according to the method of Hicks and Fraser-Reid (16) afforded the 2-deoxy sugar **14** in 75% yield. Deoxygenation of the C-3 hydroxyl group in **14** was accomplished in ca. 85% yield using the method reported by Barton and McCombie (17). The alcohol **14** was first converted into the xanthate ester **15** by treatment with sodium hydride, carbon disulfide, and iodomethane. The xanthate **15** was then heated under reflux with an excess of tri-*n*-butylstannane in toluene to yield the deoxygenated product **16**.

The next objective in our synthetic plan was the introduction of a β-methyl group at C-4 of the glucose derivative. A variety of catalysts was tried to effect the hydrogenolysis of the benzylidene in **16**. However, we were unsuccessful in carrying out a catalytic hydrogenolysis of **16**. We tentatively attribute the failure of this reaction in this case to the presence of trace amounts of tin–sulfur by-products derived from the previous stannane reduction. It was found that, after treatment of **16** with a catalytic amount of *p*-toluenesulfonic acid in methanol and careful work-up, the product **17** could be used directly in the preparation of the trityl ether **18** which was obtained in 77% overall yield for the two steps. The alcohol **18** gave the mesylate **19** in good yield. However, all attempts to displace this mesylate with a one carbon nucleophile failed. We had hoped to carry out a displacement with inversion at C-4 with lithium dimethylcuprate.[4] Presumably the axial methyl at C-2 provided sufficient steric interference to divert any nucleophile from approaching the backside of the mesylate at C-4.

This shielding of the top face of the molecule by the C-2 methyl group was turned to advantage in the following fashion. The alcohol at C-4 of **18** was oxidized (19) to the ketone **20** which on treatment with methylene triphenylphosphorane gave the exocyclic alkene **21** in good yield. In the crucial subsequent step the axial methyl group at C-4 was generated in a stereoselective hydrogenation of **21** using Wilkinson's catalyst (20). The stereoselectivity of this reduction was dependent on solvent and temperature. At 0°C in benzene alkene **21** was cleanly reduced to **22** and we could not detect any of the C-4 epimer by nmr or tlc. However, when ethanol was used as solvent or cosolvent (20) or if the hydrogenation was carried out at higher temperature the stereoselectivity fell. For example, hydrogenation of **21** at room temperature in anhydrous benzene gave **22** and its C-4 epimer in a ratio of 9:1. The effect of solvent (for example, ref. 21) and temperature (for example see ref. 22) on the stereoselectivity of homogeneous hydrogenations has been reported previously.

We had hoped to apply the alkylation of dithioacetal carbanions (23) to add the ethyl group at C-1 of **22** in the third phase of our synthetic plan. Compound **22** was smoothly converted into the diethyl dithioacetal **23** with concomitant cleavage of the trityl group by treatment with concentrated HCl and ethanethiol (24). The resulting diol **23** was then protected as its isopropylidene derivative **24**. Unfortunately all attempts to alkylate **24** were unsuccessful. The difficulty in this reaction was traced to our failure to generate the anion of **24**. We suspected that the methyl group at C-2 is responsible for the inertness of the dithioacetal **24**. Difficulties in alkylating α-substituted dialkyl dithioacetals have been reported (25). In contrast to our failure to alkylate **24**, the carbanion of a diethyl dithioacetal of a C-2 *unsubstituted* carbohydrate derivative has

[3]For two recent reviews on the use of carbohydrates in the synthesis of chiral natural products see ref. 14.

[4]For example (+)-2-butyl tosylate reacts with lithium diphenylcuprate to give (−)-2-phenylbutane with 100% inversion (18).

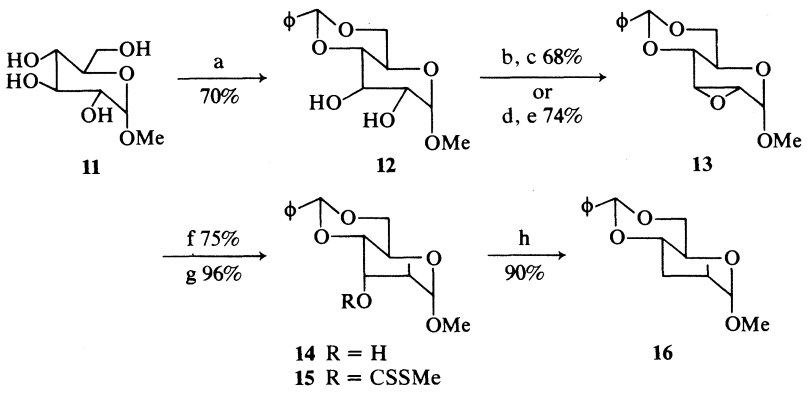

SCHEME 1. (a) $\phi$CHO, $ZnCl_2$; (b) TsCl, py, 7 days; (c) NaOMe, $CH_2Cl_2$, 6 days; (d) MsCl, py, 1 day; (e) NaOMe, $CH_2Cl_2$, $3\frac{1}{2}$ days; (f) $Me_2CuLi$, $Et_2O$; (g) NaH, $CS_2$, MeI, $Et_2O$; (h) $Bu_3SnH$, toluene, $\Delta$.

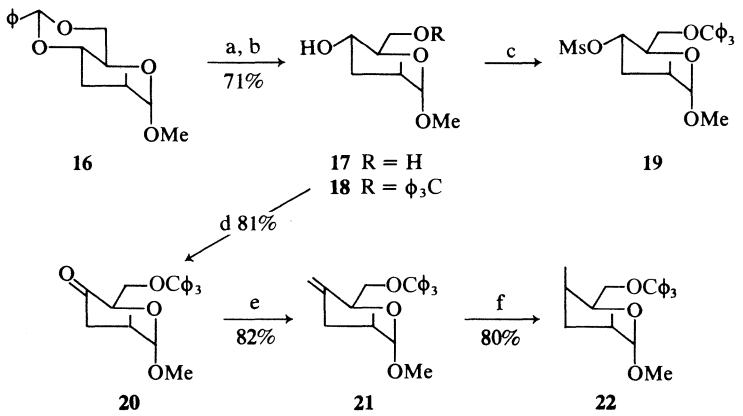

SCHEME 2. (a) TsOH, MeOH; (b) $\phi_3CCl$, py; (c) MsCl, py; (d) $CrO_3 \cdot 2py$, $CH_2Cl_2$; (e) $\phi_3P^{+}\text{-}^{-}CH_2$, $Et_2O$; (f) $H_2$, $(\phi_3P)_3RhCl$, benzene.

been alkylated in good yield (26). Several reports have indicated that the dithiane derivatives of aldehydes are less susceptible to the steric effect of an α-substituent in carbanion alkylation than the corresponding diethyl dithioacetals. For this reason we prepared the protected dithiane as shown in Scheme 3. We found that *n*-butyllithium treatment of **26** followed by a $D_2O$ quench led to partial (ca. 50%) anion formation whereas *tert*-butyllithium gave essentially quantitative formation of the desired carbanion. This carbanion was alkylated with iodoethane in HMPA–hexane to give **27** in 80% yield. A similar alkylation of another dithiane from D-glucose has recently been reported in the synthesis of the pheromone chalcogran (27).

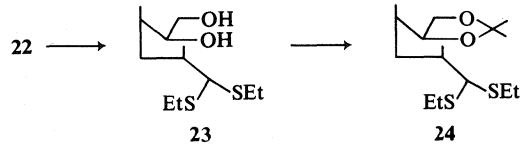

Hydrolysis of the isopropylidene **27** afforded the diol **28** in 90% yield. Several previous syntheses of α-multistriatin involved an acid-catalyzed cyclization of epoxy ketone **29** or diol **30**. These conditions

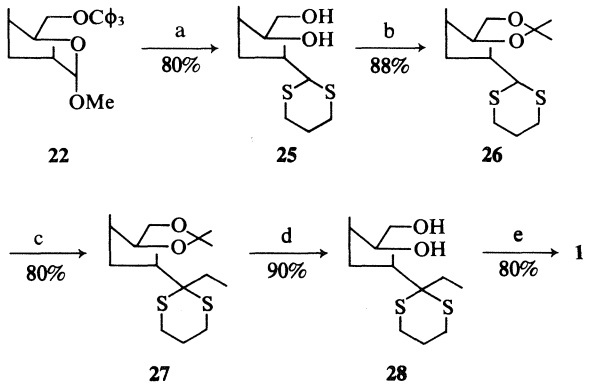

SCHEME 3. (a) $HS(CH_2)_3SH$, $BF_3 \cdot Et_2O$, $CH_2Cl_2$; (b) $Me_2C(OMe)_2$, TsOH; (c) *t*-BuLi, MeI, hexane–HMPA; (d) TsOH, MeOH; (e) $HgCl_2$, HgO, anhydrous MeCN.

Can. J. Chem. Downloaded from www.nrcresearchpress.com by 210.87.254.105 on 09/06/12
For personal use only.

usually resulted in the epimerization of the methyl group at C-4 (adjacent to the carbonyl) and the production of significant amounts of α-multistriatin (5).[5] With this in mind we attempted to cleave the thioketal of **28** with concomitant cyclization, and avoid going through the ketone **30**. Thus the

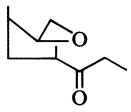

**29**

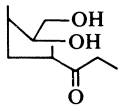

**30**

thioketal **28** in *anhydrous* acetonitrile containing mercuric chloride and mercuric oxide was cleanly converted into **1**. The structure of our synthetic material was fully confirmed by comparison of the spectral data of our synthetic material with that reported for α-multistriatin (3–8). The nmr spectrum (5) is particularly diagnostic in distinguishing the iomers of multistriatin. Our synthetic material had an optical rotation $[\alpha]_D^{25}$ −46.0° (*c* 1.00, hexane) compared with a rotation $[\alpha]_D^{25}$ −47 (*c* 0.19, hexane) for the natural material (1, 4). Finally, vpc analysis of our synthetic (−)-α-multistriatin with a 3% OV 101 column, under a variety of conditions which separated the multistriatin isomers, demonstrated that our product was 99.7% pure and no trace of the other multistriatin isomers could be detected. This confirms the absolute configuration of the natural (−)-α-multistriatin as that shown in **1** (4, 6, 7).

## Experimental

*General*

Melting points (mp) were determined on a Kofler micro heating stage or a Thomas Hoover capillary melting point apparatus and are uncorrected. Gas–liquid chromatography was performed on a Hewlett Packard Model 5831A gas chromatograph, using a 6 ft × 1/8 in. column of 3% OV 101 Chromosorb W(HP) and nitrogen as carrier gas. The 60 MHz nuclear magnetic resonance spectra were recorded on a Varian Associates Model T-60, the 100 MHz spectra were recorded on Varian Associates Model HA-100 or Model XL-100, and the 270 MHz spectra were recorded on a homebuilt high resolution nmr spectrometer consisting of an Oxford Instruments' 63.4 KG magnet. Chemical shifts in ppm are reported using the δ scale with tetramethylsilane (TMS) as internal reference. Infrared spectra were recorded on a Perkin–Elmer model 710B spectrophotometer. Optical rotations $[\alpha]_D$ were measured with a Perkin–Elmer model 241 MC polarimeter. Low resolution mass spectra were determined on a Varian/Mat model CH4B mass spectrometer. High resolution mass measurements were obtained using a Kratos-AEI model MS902 or model MS50 instrument. Microanalyses were performed by Mr. P. Borda, Microanalytical Laboratory, University of British Columbia, Vancouver. All solvents used for nmr, ir, and optical rotations were of Spectral grade.

Analytical thin layer chromatography plates and preparative tlc plates were prepared from silica gel GF-254 from E. Merck Co. Preparative tlc plates were about 1 mm thickness. Column chromatography was carried out with 100–200 mesh ASTM silica gel from Davison Chemical. The petroleum ether used was of boiling range ca. 30–60°C. Dry solvents or reagents, where indicated, were prepared as follows: ethyl ether by refluxing over lithium aluminum hydride followed by distillation; dichloromethane and acetonitrile by distillation from phosphorus pentoxide; hexamethylphosphoramide (HMPA) by distillation from calcium hydride followed by storage over molecular sieve (Type 4A); triethylamine by distillation from and storage over potassium hydroxide pellets; pyridine by distillation from barium oxide followed by storage over potassium hydroxide pellets; benzene, toluene, and *n*-hexane by distillation from calcium hydride; and methanol by refluxing over magnesium methoxide followed by distillation.

Methyllithium (in ethyl ether) and *n*-butyllithium (in hexane) were obtained from Aldrich Chemical Company, Inc. *tert*-Butyllithium (in pentane) was supplied by Alfa Division, Ventron Corporation. The alkyllithium solutions were standardized by titration against 1.0 *M tert*-butyl alcohol in benzene using 1,10-phenanthroline as indicator.

*Methyl 4,6-O-benzylidene-α-D-gluco-pyranoside (12)*

This compound, mp 161–163°C, was prepared from methyl α-*gluco*pyranoside (**11**) in 70% yield following the procedure of Richtymer (15).

*Methyl 4,6-O-benzylidene-2,3-di-O-p-tolylsulfonyl-α-D-gluco-pyranoside*

This compound, mp 148–149°C, was prepared from **12** in 80% yield following the procedure of Richtymer (15).

*Methyl 4,6-O-benzylidene-2,3-di-O-methanesulfonyl-α-D-gluco-pyranoside*

Benzylidene diol **12** (20.0 g, 70.9 mmol) was dissolved in ca. 125 mL of dry pyridine. The solution was cooled in ice and 19.95 g (175 mmol) of methanesulfonyl chloride was added. A white heavy precipitation was observed. The reaction was stirred at room temperature for 24 h. The mixture was then poured onto ice and extracted several times with dichloromethane. The combined extracts were washed several times with dilute hydrochloric acid until no trace of pyridine could be detected. The extracts were then washed once with water and once with aqueous sodium bicarbonate, dried over anhydrous magnesium sulfate, and filtered. The solvent was removed under reduced pressure to ca. 150 mL and ethyl ether was added to induce crystallization. The yield of the recrystallized methyl 4,6-*O*-benzylidene-2,3-di-*O*-methanesulfonyl-α-D-*gluco*-pyranoside was 25.0 g (81%); mp 186–18°C. This compound was characterized by ir ($CHCl_3$): 1100, 1130, 1180, and 1420 $cm^{-1}$; nmr ($CDCl_3$) δ: 2.87 (s, 3H), 3.17 (s, 3H), 3.48 (s, 3H), 3.6–4.8 (m, 5H), 4.8–5.2 (m, 2H), 5.51 (s, 1H), and 7.1–7.6 (m, 5H); mass spectrum: (*a*) high resolution calcd. for $C_{16}H_{22}O_{10}S_2$: 438.0655 amu; found: 438 0655; (*b*) low resolution *m/e* (relative intensity): 47(13), 49(100), 69(4), 79(4), 107(8), 116(6), 121(4), 149(3), 157(4), 185(4), 193(7), 229(3), 289(3), 299(8), 359(3), 437(11), and 438(7).

*Methyl 2,3-anhydro-4,6-O-benzylidene-α-D-allo-pyranoside (13)*

(a) *From the ditosylate of* **12**

Compound **13**, mp 198–200°C, was prepared from the ditosylate of **12**, in 85% following the procedure of Richtymer (15).

[5]Recently Rao and co-workers (28) have suggested that ketal formation of five-membered rings may involve enol ether intermediates which would explain the epimerization of the C-4 methyl in **29** or **30**.

Can. J. Chem. Downloaded from www.nrcresearchpress.com by 210.87.254.105 on 09/06/12
For personal use only.

Can. J. Chem. Downloaded from www.nrcresearchpress.com by 210.87.254.105 on 09/06/12
For personal use only.

(b) *From the dimesylate of* ***12***

A solution of sodium methoxide was prepared using 12.7 g (552 mmol) of sodium and 188 mL of dry methanol. Methyl 4,6-*O*-benzylidene-2,3-di-*O*-methanesulfonyl-α-D-*gluco*-pyranoside from above (48.18 g, 110 mmol) in 780 mL of dichloromethane was added to the sodium methoxide solution at 0°C. The reaction mixture was kept at 0°C for 3 days and stirred at room temperature for 10 h. The reaction mixture was diluted with water and the dichloromethane layer separated. The aqueous layer was extracted several times with dichloromethane. The combined organic extracts were washed with water, dried over anhydrous magnesium sulfate, and solvents were removed under reduced pressure. The product crystallized readily, and was filtered and washed with ether. The crude product was recrystallized from a mixture of dichloromethane and ethyl ether to give 26.40 g (91%) of pure epoxide **13**, mp 198–200°C. The spectral data were identical to the epoxide prepared from the ditosylate.

*Methyl 4,6-*O*-benzylidene-2-deoxy-2-*C*-methyl-α-D-*altro*-pyranoside (**14**)*

This compound, mp 112–113°C, was prepared in 75% from **13** using the procedure of Hicks and Fraser-Reid (16).

*Methyl 4,6-*O*-benzylidene-2-deoxy-2-*C*-methyl-3-*O*-[(thiomethyl)-thiocarbonyl]-α-D-*altro*-pyranoside (**15**)*

Compound **15** was prepared in 96% crude yield from **14** using the procedure of Hicks and Fraser-Reid (16). The crude product was used directly in the next step. A small amount of compound **14** was purified by preparative tlc ($CCl_4$–$Et_2O$, 4:1 v/v) and characterized by the following spectral data. Infrared ($CHCl_3$): 950, 1005, 1040, 1060, 1100, 1140, and 2950 $cm^{-1}$; nmr ($CDCl_3$) δ: 1.18 (d, $J$ = 7 Hz, 3H), 2.55 (s, 3H), 2.4–2.8 (m, 1H), 3.33 (s, 3H), 3.5–4.5 (m, 5H), 5.55 (br s, 1H), 5.75 (m, 1H), and 7.1–7.6 (m, 5H); mass spectrum *m/e* (relative intensity): 41(29), 43(30), 55(21), 57(29), 69(23), 85(44), 91(38), 105(56), 113(44), 121(32), 125(25), 131(29), 149(100), 150(14), 231(20), 262(47), 263(24), and 370(11).

*Methyl 4,6-*O*-benzylidene-2,3-dideoxy-2-*C*-methyl-α-D-*arabino*-hexopyranoside (**16**)*

A solution of 22.2 g (60.0 mmol) of the *S*-methyl dithiocarbonate compound **15** in 260 mL of dry toluene was added over 1.5 h to 34.92 g (120 mmol) of tri-*n*-butylstannane in 240 mL refluxing dry toluene under dry nitrogen. Refluxing was continued overnight, and the solvent was removed under reduced pressure. Purification was achieved by column chromatography using silica gel (100–200 mesh) and a mixture of petroleum ether and ethyl ether (9.5:1, v/v, then 1:1, v/v) to yield 14.30 g (90%) of pure compound **16** as a syrup, $[\alpha]_D^{28}$ +82.7° (*c* 14.2, ethyl ether); ir ($CHCl_3$): 930, 950, 1005, 1050, 1100, 1120, 1140, 1380, and 1460 $cm^{-1}$; nmr ($CDCl_3$) δ: 1.13 (d, $J$ = 7 Hz, 3H), 1.4–2.3 (m, 3H), 3.33 (s, 3H), 3.5–4.3 (m, 4H), 4.33 (s, 1H), 5.50 (s, 1H), and 7.0–7.5 (m, 5H); mass spectrum: (*a*) high resolution calcd. for $C_{15}H_{20}O_4$: 264.1362 amu; found: 264.1374; (*b*) low resolution *m/e* (relative intensity): 55(15), 73(12), 83(19), 105(21), 115(100), 116(11), 149(11), 221(10), and 264(22).

*Methyl 2,3-dideoxy-2-*C*-methyl-α-D-*arabino*-hexopyranoside (**17**)*

To a solution of 12.41 g (47.0 mmol) of compound **16** in ca. 30 mL of methanol was added 0.40 g of *p*-toluenesulfonic acid monohydrate. The reaction mixture was stirred at room temperature and followed by tlc. After the reaction was complete (2.5 h), solid sodium carbonate was added to neutralize the acid. The reaction mixture was filtered, and the methanol was removed under reduced pressure. The residue was dissolved in water and ethyl ether, and extracted several times with water. The combined aqueous extracts were concentrated under reduced pressure and the residue dissolved in dichloromethane, dried over anhydrous magnesium sulfate, and filtered. The dichloromethane was removed under reduced pressure to give a thick oil, 6.81 g (82%) of which was pure enough for the next step. Compound **17** was characterized by the following spectral data. Infrared ($CHCl_3$): 960, 1050, 1100, 1150, 2975, 3500, and 3650 $cm^{-1}$; nmr ($CDCl_3$) δ: 1.03 (d, $J$ = 7 Hz, 3H), 1.5–2.2 (m, 3H), 2.83 (br s, 2H), 3.33 (s, 3H), 3.6–4.2 (m, 4H), and 4.3 (br s, 1H); mass spectrum: (*a*) high resolution calcd. for $C_8H_{16}O_4$: 176.1049 amu, found: 176.1047; (*b*) low resolution *m/e* (relative intensity): 41(24), 43(27), 55(28), 56(29), 57(27), 72(100), 74(55), 83(23), 113(26), 115(27), 145(33), and 176(1).

*Methyl 2,3-dideoxy-2-*C*-methyl-6-*O*-triphenylmethyl-α-D-*arabino*-hexopyranoside (**18**)*

Compound **17** (3.17 g, 18 mmol) was treated with 7.5 g (27 mmol) of trityl chloride in 30 mL of anhydrous pyridine. The reaction mixture was stirred at room temperature for 3 days. It was then poured onto ice cold water, acidified, and extracted several times with dichloromethane. The combined extracts were washed with dilute sodium bicarbonate and brine, dried over anhydrous magnesium sulfate, filtered, and the solvents were removed under reduced pressure. Purification was achieved by column chromatography using silica gel (100–200 mesh) and a mixture of carbon tetrachloride and ethyl ether (4:1, v/v) as eluent to yield 6.465 g (86%) of **18**, mp 147–149°C, $[\alpha]_D^{26}$ +26° (*c* 20.0, chloroform); ir ($CHCl_3$): 1600 and 3570 $cm^{-1}$; nmr ($CDCl_3$) δ: 0.99 (d, $J$ = 7 Hz, 3H), 1.4–2.1 (m, 3H), 2.39 (br s, 1H), 3.31 (s, 3H), 3.0–3.7 (m, 4H), 4.26 (s, 1H), and 6.7–7.4 (m, 15H); mass spectrum *m/e* (relative intensity): 43(4), 55(5), 72(4), 77(6), 83(6), 105(13), 113(13), 127(5), 165(27), 175(21), 183(15), 243(100), 244(27), 258(4), 259(7), 260(5), 309(5), 386(4), and 418(3). *Anal.* calcd. for $C_{17}H_{30}O_4$: C 77.48, H 7.22; found: C 77.61, H 7.21.

*Methyl 2,3-dideoxy-2-*C*-methyl-6-*O*-triphenylmethyl-α-D-*threo*-hexopyranosid-4-ulose (**20**)*

A sample of 6.0 g (60 mmol) of chromium trioxide was added to a magnetically stirred solution of 9.5 g (120 mmol) of anhydrous pyridine in ca. 150 mL anhydrous dichloromethane. The flask was stopped with a drying tube, and the deep burgundy solution stirred for 15 min at room temperature. At the end of this period, a solution of 4.18 g (10 mmol) of alcohol **18** in 5 mL of dry dichloromethane was added in one portion. A tarry, black deposit separated immediately. After stirring for 18 h at room temperature, the solution was decanted and the dichloromethane removed under reduced pressure. The residue was dissolved in ethyl ether and the reaction flask was rinsed several times with ethyl ether. The ether layers were combined and filtered through a bed of Celite. The slight yellow filtrate was washed with dilute hydrochloric acid and aqueous sodium bicarbonate solution, dried over anhydrous magnesium sulfate, filtered, and the solvents were removed under reduced pressure to give 3.99 g (96%) of ketone **20** which was homogeneous from tlc. The crude product was purified by column chromatography using silica gel (100–200 mesh) and a mixture of carbon tetrachloride and ethyl ether (8:1, v/v) as eluent to give 3.35 g (81%) of pure **20**, mp 88–89°C; $[\alpha]_D^{28}$ +98.8° (*c* 20.0, chloroform), which was characterized by ir ($CHCl_3$): 1600, 1730, and 2960 $cm^{-1}$; nmr ($CDCl_3$) δ: 1.14 (d, $J$ = 7 Hz, 3H), 1.9–2.6 (m, 3H), 3.2–3.6 (m, 2H), 3.5 (s, 3H), 3.83 (m, 1H), 4.6 (d, $J$ = 4 Hz, 1H), and 7.0–7.7 (m, 15H); mass spectrum: (*a*) high resolution calcd. for $C_{27}H_{28}O_4$: 416.1988 amu; found: 416.1989; (*b*) low resolution *m/e* (relative intensity): 43(4), 45(6), 55(4), 59(7), 71(6), 72(8), 105(7), 157(6), 165(20), 173(5), 183(5), 243(100), 244(24), 259(6), 339(4), and 416(4).

Can. J. Chem. Downloaded from www.nrcresearchpress.com by 210.87.254.105 on 09/06/12
For personal use only.

*Methyl 2,3,4-trideoxy-2-C-methyl-4-methylene-6-O-triphenylmethyl-α-D-*threo*-hexopyranoside (**21**)*

A 250-mL 3-necked round bottom flask containing ca. 120 mL of anhydrous ethyl ether was fitted with a reflux condenser, an addition funnel, a septum stopper, and a nitrogen outlet. *n*-Butyllithium (8.86 mL of 1.58 *M*, 14 mmol) was added to the flask and 5.00 g (14 mmol) of triphenylmethylphosphonium bromide was added in portions to the *n*-butyllithium solution. The orange reaction mixture was refluxed for 4 h and 5.82 g (14 mmol) of ketone **20** in 30 mL of ethyl ether was added slowly. The orange color discharged and a white precipitate was observed. The reaction mixture was then refluxed for 24 h, cooled, and the precipitate was filtered off. The ether filtrate was washed with water and brine, dried over magnesium sulfate, filtered, and the solvents were evaporated under reduced pressure. Purification of the crude product by column chromatography using silica gel (100–200 mesh) and a mixture of carbon tetrachloride and ethyl ether (10:1, v/v) as eluent gave 4.53 g (78%) of compound **21**, mp 153–154°C, $[\alpha]_D^{22}$ +45.4° (*c* 7.4, chloroform), and 0.5 g of recovered **20**. Thus, the yield was 82% based on recovered starting material **20**. The olefin **21** was characterized by the following spectral data. Infrared ($CHCl_3$): 1600, 1660, 2960, 3040, and 3100 $cm^{-1}$; nmr ($CDCl_3$) δ: 0.93 (d, $J$ = 7 Hz, 3H), 1.6–2.8 (m, 3H), 3.30 (d, $J$ = 6 Hz, 2H), 3.43 (s, 3H), 4.2–4.4 (m, 2H), 4.62 (m, 2H), and 6.8–7.6 (m, 15H); mass spectrum: (*a*) high resolution calcd. for $C_{28}H_{30}O_3$: 414.2195 amu; found: 414.2214; (*b*) low resolution *m/e* (relative intensity); 41(2), 43(2), 77(2), 81(4), 105(5), 109(14), 139(2), 141(50), 142(5), 165(21), 166(4), 183(2), 215(2), 228(3), 241(3), 243(100), 244(21), and 414(1).

*Hydrogenation of compound **21***

A 100-mL round bottom flask containing 50 mL of anhydrous benzene, 0.7 g of tris(triphenylphosphine)rhodium chloride (20), and 3.31 g (8.0 mmol) of alkene **21** was fitted with a magnetic stirrer and connected to an atmospheric pressure hydrogenation apparatus equipped with a graduated burette to measure the uptake of hydrogen. The system was evacuated and filled with hydrogen. After 24 h, about 1 equiv. of hydrogen was absorbed. The solvent was removed under reduced pressure and the product was purified by column chromatography using silica gel (100–200 mesh) and a mixture of ethyl acetate and petroleum ether (10:1, v/v) as eluent. Two components were isolated from this chromatography, and these were, in order of elution: methyl 2,3,4-trideoxy-2,4-di-*C*-methyl-α-D-*arabino*-hexopyranoside (0.29 g, 9%), and methyl 2,3,4-trideoxy-2,4-di-*C*-methyl-α-D-*lyxo*-hexopyranoside (**22**) (2.74 g, 80%).

Methyl 2,3,4-trideoxy-2,4-di-*C*-methyl-α-D-*arabino*-hexopyranoside was characterized by ir ($CHCl_3$): 1600 $cm^{-1}$; nmr ($CDCl_3$) δ: 0.58 (d, $J$ = 6 Hz, 3H), 1.05 (d, $J$ = 7 Hz, 3H), 1.3–2.0 (m, 4H), 2.9–3.6 (m, 3H), 3.38 (s, 3H), 4.4 (br s, 1H), and 6.9–7.6 (m, 15H); mass spectrum: (*a*) high resolution calcd. for $C_{28}H_{32}O_3$: 416.2351 amu; found: 416.2328; (*b*) low resolution *m/e* (relative intensity): 83(10), 85(25), 105(15), 111(17), 141(9), 143(60), 165(40), 173(48), 243(100), 244(31), 258(8), and 416(5).

Methyl 2,3,4-trideoxy-2,4-di-*C*-methyl-α-D-*lyxo*-hexopyranoside (**22**) had mp 153–154°C and $[\alpha]_D^{24}$ +27.0° (*c* 6.6, chloroform) and was characterized by ir ($CHCl_3$): 1600 $cm^{-1}$; nmr ($CDCl_3$) δ: 0.70 (d, $J$ = 7 Hz, 3H), 0.95 (d, $J$ = 7 Hz, 3H), 1.3–2.0 (m, 4H), 3.0–3.3 (m, 2H), 3.45 (s, 3H), 3.8–4.1 (m, 1H), 4.2 (d, $J$ = 5 Hz, 1H), and 6.9–7.6 (m, 15H); $^{13}C$ nmr ($CDCl_3$) δ: 15.93, 18.3, 30.61, 33.75, 34.73, 55.35, 63.10, 71.96, 104.34, 126.98, 127.77, 128.83, and 144.21; mass spectrum: low resolution *m/e* (relative intensity): 55(7), 72(7), 83(8), 85(20), 105(13), 111(16), 115(4), 141(8), 143(65), 144(7), 165(25), 166(6), 173(63), 174(9), 183(7), 229(5), 243(100), 244(36), 258(3), and 416(1). *Anal.* calcd. for $C_{28}H_{32}O_3$: C 80.73, H 7.74; found: C 80.51, H 7.55.

*(2S, 4S, 4'S)-1,1-Diethylthio-2-methyl-4-(2',2'-dimethyl-1',3'-dioxacyclopent-4'-yl)pentane (**24**)*

To a mixture of 0.83 g of **22** and 1.80 mL of concentrated hydrochloric acid at 0°C was added 1.80 mL of ethanethiol. The reaction mixture was stirred for 24 h at 0°C. Ice and water were added to the reaction mixture and the mixture extracted several times with ethyl acetate. The organic extract was washed with brine and saturated aqueous sodium bicarbonate, dried over anhydrous sodium sulfate, filtered, and the solvent was removed under reduced pressure. The crude product was purified by column chromatography (silica gel 100–200 mesh) using a mixture of petroleum ether and ethyl ether (3:1, v/v); after the side-product had completely eluted, the solvent was changed to ethyl ether. The yield of compound **23** from this chromatography was 0.44 g (83%). The nmr ($CDCl_3$) of compound **23** had absorptions at δ: 0.92 (d, $J$ = 7 Hz, 3H), 1.16 (d, $J$ = 7 Hz, 3H), 1.25 (t, $J$ = 7 Hz, 6H), 1.4–2.3 (m, 4H), 2.2–3.0 (m, 4H), 3.26 (br s, 2H), 3.4–3.7 (m, 3H), and 3.75 (d, $J$ = 3 Hz, 1H).

To a solution of diol **23** (0.43 g, 1.60 mmol) in 9 mL of 2,2-dimethoxypropane was added ca. 20 mg of *p*-toluenesulfonic acid. After stirring at room temperature for 2 h, the reaction mixture was diluted with chloroform, washed with 5% aqueous sodium bicarbonate, dried over anhydrous magnesium sulfate, filtered, and solvents were removed under reduced pressure. The crude product was distilled (Kugelrohr, bath temperature 100°C/0.2 Torr) to give 0.40 g (82%) of **24**. A small sample was purified by tlc using a mixture of petroleum ether and ethyl ether (4:1, v/v) to give pure **24** and was characterized by ir ($CHCl_3$): 860, 1060, 1160, 1260, 1280, 1380, and 1460 $cm^{-1}$; 270 MHz nmr ($CDCl_3$) δ: 0.98 (d, $J$ = 6 Hz, 3H), 1.04 (d, $J$ = 6 Hz, 3H), 1.25 (t, $J$ = 7 Hz, 3H), 1.35 (s, 3H), 1.40 (s, 3H), 1.5–1.7 (m, 3H), 2.0–2.2 (m, 1H), 2.5–2.8 (m, 4H), and 3.6–4.2 (m, 4H); mass spectrum: (*a*) high resolution calcd. for $C_{15}H_{30}O_2S_2$: 306.1687 amu; found: 306.1690; (*b*) low resolution *m/e* (relative intensity): 43(38), 55(18), 75(27), 103(19), 107(55), 115(56), 125(29), 135(30), 169(19), 187(100), and 306(30).

*(2'S, 4'R, 5'S)-2-(2',4'-Dimethyl-5',6'-dihydroxyhex-2'-yl)-1,3-dithiane (**25**)*

To a solution of 2.08 g (5.0 mmol) of compound **22** in ca. 40 mL of dry dichloromethane was added 1.63 g (15 mmol) of 1,3-dithiolpropane and 1.4 mL of distilled boron trifluoride etherate at 0°C. The reaction was stirred at 0°C for 18 h. It was then diluted with ethyl acetate, washed with aqueous sodium bicarbonate, dried over anhydrous magnesium sulfate, filtered, and the solvents were removed under reduced pressure. Purification of the crude product was achieved by column chromatography using silica gel (100–200 mesh) and a mixture of petroleum ether and ethyl ether (9:1, v/v) as eluent. After the side product had completely eluted, the eluting solvent was changed to ethyl acetate. The yield of compound **25** from this chromatography was 1.0 g (80%) and this product was characterized by ir ($CHCl_3$): 3500 and 3660 $cm^{-1}$; nmr ($CDCl_3$) δ: 0.98 (d, $J$ = 6 Hz, 3H), 1.1 (d, $J$ = 6 Hz, 3H), 1.5–2.5 (m, 8H), 2.7–3.1 (m, 4H) 3.4–3.7 (m, 3H), and 4.12 (d, $J$ = 4 Hz, 1H); mass spectrum: (*a*) high resolution calcd. for $C_{11}H_{22}O_2S_2$: 250.1061 amu; found: 250.1085; (*b*) low resolution *m/e* (relative intensity): 41(10), 43(7), 55(6), 73(5), 119(100), 120(8), 121(10), 143(5), 219(5), and 250(16).

*(2'S, 4'R, 4"S)-2-[4'-(2",2"-Dimethyl-1", 3"-dioxacyclopent-4"-yl)pent-2'-yl]-1,3-dithiane (**26**)*

To a solution of 1.0 g (4.0 mmol) of diol dithiane **25** in 20 mL of 2,2-dimethoxypropane was added a catalytic amount of *p*-toluenesulfonic acid (0.10 g). The reaction was stirred at room temperature for 1.5 h. It was then diluted with chloroform, washed with aqueous sodium bicarbonate, dried over anhydrous magnesium sulfate, filtered, and the solvents were removed

Can. J. Chem. Downloaded from www.nrcresearchpress.com by 210.87.254.105 on 09/06/12
For personal use only.

under reduced pressure. The crude product was purified by column chromatography using silica gel (100–200 mesh) and a mixture of petroleum ether and ethyl ether (9:1, v/v) as eluent. From this chromatography 1.02 g (88%) of compound **26** was isolated. Kugelrohr distillation (bath temperature 120°C/0.1 Torr) of **26** isolated from this column had $[\alpha]_D^{25}$ −6.2° (*c* 15.0, ethyl ether), and was characterized by ir ($CHCl_3$): 920, 1070, 1380, 1390, and 2975 $cm^{-1}$; 270 MHz nmr ($CDCl_3$) δ: 0.98 (d, $J$ = 7 Hz, 3H), 1.07 (d, $J$ = 7 Hz, 3H), 1.35 (s, 3H), 1.41 (s, 3H), 1.5–1.9 (m, 4H), 1.95–2.2 (m, 2H), 2.75–3.0 (m, 4H), 3.65 (t, $J$ = 7 Hz, 1H), 3.85 (q, $J$ = 7 Hz, 1H), 4.01 (t, $J$ = 7 Hz, 1H), and 4.16 (d, $J$ = 4 Hz, 1H); mass spectrum *m/e* (relative intensity): 41(22), 43(38), 72(21), 119(100), 159(31), 161(18), 232(24), 275(44), and 290(58). *Anal.* calcd. for $C_{14}H_{26}O_2S_2$: C 57.89, H 9.02; found: C 57.70, H 9.00.

*(2'S, 4'R, 4"S)-2-Ethyl-2-[4'-(2",2"-dimethyl-1",3"-dioxacyclopent-4"-yl)pent-2'-yl]-1,3-dithiane (**27**)*

A solution of 0.58 g (2.0 mmol) of compound **26** in ca. 8 mL of dry *n*-hexane was placed in a 25-mL round bottom flask fitted with a magnetic stirrer and nitrogen outlet. The flask was cooled to ca. −20°C (Dry Ice and carbon tetrachloride) and 1.5 mL (2.0 *M* in pentane, 3 mmol) of *tert*-butyllithium was added dropwise. The reaction was stirred at ca. −20°C for 2 h, then kept in the freezer (ca. −10°C) for 16 h. The temperature of the reaction mixture was then raised to 0°C and 0.4 mL (0.78 g, 5 mmol) of iodoethane in 1.74 mL (5 equiv.) of hexamethylphosphoramide was added; a white precipitate formed immediately. The reaction was stirred for 5 h, diluted with ethyl ether, washed with ice cold dilute hydrochloric acid, sodium bicarbonate solution, and brine, dried over anhydrous sodium sulfate, filtered, and the solvents were removed under reduced pressure. The crude product was purified by column chromatography using silica gel (100–200 mesh) and a mixture of petroleum ether and ethyl ether (9:1, v/v) as eluent to yield 0.506 g (80%) of compound **27**. Kugelrohr distillation (bath temperature 128°C/0.1 Torr) of **27** isolated from this column had $[\alpha]_D^{25}$ −28.0° (*c* 5.0, ethyl ether), and was characterized by ir ($CHCl_3$): 860, 1060, 1160, 1380, 1480, and 2970 $cm^{-1}$; 270 MHz nmr ($CDCl_3$) δ: 0.98 (t, $J$ = 7 Hz, 3H), 1.01 (d, $J$ = 7 Hz, 3H), 1.1 (d, $J$ = 7 Hz, 3H), 1.34 (s, 3H), 1.41 (s, 3H), 1.5–2.2 (m, 8H), 2.6–3.0 (m, 2H), 3.7 (t, $J$ = 7 Hz, 3H), and 3.9–4.1 (m, 2H); mass spectrum *m/e* (relative intensity): 41(12), 43(16), 134(15), 147(100), 148(13), 149(15), 303(18), and 320(16). *Anal.* calcd. for $C_{16}H_{30}O_2S_2$: C 60.30, H 9.49; found: C 60.20, H 9.53.

*(2'S, 4'R, 5'S)-2-Ethyl-2-(2',4'-dimethyl-5',6'-dihydroxyhex-2-yl)-1,3-dithiane (**28**)*

To a solution of 0.35 g (1.1 mmol) of compound **27** in ca. 15 mL of methanol was added a catalytic amount of *p*-toluenesulfonic acid monohydrate (0.02 g). The reaction mixture was stirred at room temperature for 24 h. Solid sodium carbonate was added to neutralize the acid. The mixture was filtered and the filtrate concentrated under reduced pressure. The residue was dissolved in ethyl acetate, dried over anhydrous magnesium sulfate, filtered, and the solvents were removed under reduced pressure. Purification was achieved by column chromatography using silica gel (100–200 mesh) and a mixture of petroleum ether and ethyl ether (9:1, v/v) as eluent to yield 0.20 g (90%) of compound **28**, $[\alpha]_D^{24}$ −42.6° (*c* 5.0, ethyl ether). This compound was characterized by the following spectral data. Infrared ($CHCl_3$): 900, 1005, 1050, 1280, 1380, 1460, 2970, 3500, and 3650 $cm^{-1}$; nmr ($CDCl_3$) δ: 0.87 (d, $J$ = 7 Hz, 3H), 1.08 (d, $J$ = 7 Hz, 3H), 1.02 (t, $J$ = 7 Hz, 3H), 1.7–2.3 (m, 8H), 2.38 (br s, 2H), 2.6–3.0 (m, 4H), and 3.4–3.8 (m, 3H); mass spectrum: (*a*) high resolution calcd. for $C_{13}H_{26}O_2S_2$: 278.1374 amu; found: 278.1358; (*b*) low resolution *m/e* (relative intensity): 41(8), 47(11), 83(36), 85(23), 147(100), 148(12), 149(13), and 278(12).

*(−)-α-Multistriatin (**1**)*

To a stirred solution of 0.43 g (1.6 mmol) of mercuric chloride and 0.17 g (0.80 mmol) of mercuric oxide in ca. 5 mL of dry acetonitrile was added a solution of 0.197 g (0.71 mmol) of dithiane **28** in 5 mL of anhydrous acetonitrile under nitrogen. The reaction mixture was refluxed for 4 h with stirring. After cooling, the reaction mixture was filtered and the solid washed with pentane. An equal amount of saturated brine solution was added to the filtrate and this solution was extracted several times with pentane. The organic extracts were washed with aqueous ammonium acetate, dried over anhydrous sodium sulfate, filtered, and the solvents were removed under reduced pressure. Kugelrohr distillation (bath temperature 110°C/20 Torr) of the crude produce gave 0.096 g (80%) of α-multistriatin (**1**), $[\alpha]_D^{24}$ −46.0° (*c* 1.0, hexane) (lit. (3) bp 90°C/20 Torr, bath temperature), and all the spectral data were identical to those reported (3–8). Gas–liquid chromatographic analysis showed a major component (> 98%). This was further identified by comparison with a sample of (±)-α-multistriatin kindly provided by Dr. J. W. Peacock; **1** was characterized by ir ($CHCl_3$): 895, 920, 1035, 1130, 1180, 1255, 1460, 2925, and 2980 $cm^{-1}$; nmr ($CDCl_3$) δ: 0.81 (d, $J$ = 7 Hz, 3H), 0.81 (d, $J$ = 7 Hz, 3H), 0.93 (t, $J$ = 7 Hz, 3H), 1.4–2.2 (m, 6H), 3.68 (m, 1H), 3.89 (m, 1H), and 4.20 (m, 1H); mass spectrum: (*a*) high resolution calcd. for $C_{10}H_{18}O_2$: 170.1307 amu; found: 170.1298, (*b*) low resolution *m/e* (relative intensity): 41(8), 43(6), 54(9), 55(22), 57(100), 71(20), 81(16), 96(25), 99(11), 128(25), and 170(19).

## Acknowledgements

We are grateful to the Natural Sciences and Engineering Research Council of Canada for financial support of this project.

1. G. N. Lanier, R. M. Silverstein, and J. W. Peacock. *In* Perspectives in forest entomology. *Edited by* J. F. Anderson and H. K. Kaya. Academic Press, New York, NY. 1976. Chapt. 12.
2. J. W. Peacock, R. A. Cuthbert, W. E. Gore, G. N. Lanier, G. T. Pearce, and R. M. Silverstein. J. Chem. Ecol. **1**, 149 (1975).
3. G. T. Pearce, W. E. Gore, R. M. Silverstein, J. W. Peacock, R. A. Cuthbert, G. N. Lanier, and J. B. Simone. J. Chem. Ecol. **1**, 115 (1975).
4. G. T. Pearce, W. E. Gore, and R. M. Silverstein. J. Org. Chem. **41**, 2797 (1976).
5. W. E. Gore, G. T. Pearce, and R. M. Silverstein. J. Org. Chem. **40**, 1705 (1975).
6. K. Mori. Tetrahedron, **32**, 1979 (1976).
7. G. J. Cernigliaro and P. J. Kocienski. J. Org. Chem. **42**, 3622 (1977).
8. (*a*) W. J. Elliott and J. Fried. J. Org. Chem. **41**, 2469 (1975); (*b*) **41**, 2475 (1975).
9. P. A. Bartlett and J. Myerson. J. Org. Chem. **44**, 1625 (1979).
10. B. J. Fitzsimmons, D. E. Plaumann, and B. Fraser-Reid. Tetrahedron Lett. 3925 (1979).
11. P. E. Sum and L. Weiler. Can. J. Chem. **56**, 2700 (1978).
12. P. E. Sum and L. Weiler. Can. J. Chem. **57**, 1475 (1979).
13. M. Cerny and J. Stanek, Jr. *In* Advances in carbohydrate chemistry and biochemistry. Vol. 34. *Edited by* R. S. Tipson and D. Horton. Academic Press, New York, NY. 1980. p. 23.
14. (*a*) S. Hanessian. Acc. Chem. Res. **12**, 159 (1979); (*b*) B. Fraser-Reid and R. C. Anderson. *In* Progress in the chemistry of organic natural products. Vol. 39. *Edited by*

W. Herz, H. Grisebach, and G. W. Kirby. Springer-Verlag, New York, NY. 1980.
15. N. K. RICHTYMER. Methods Carbohydr. Chem. **1**, 107 (1962).
16. D. R. HICKS and B. FRASER-REID. Can. J. Chem. **53**, 2017 (1975).
17. D. H. R. BARTON and S. W. MCCOMBIE. J. Chem. Soc. Perkin Trans. I, 1574 (1975).
18. C. R. JOHNSON and G. A. DUTRA. J. Am. Chem. Soc. **95**, 7783 (1973).
19. R. RATCLIFFE and R. RODEHORST. J. Org. Chem. **35**, 4000 (1970).
20. J. A. OSBORN, F. N. JARDINE, J. F. YOUNG, and G. WILKINSON. J. Chem. Soc. A, 1711 (1966).
21. K. E. KOENIG and W. S. KNOWLES. J. Am. Chem. Soc. **100**, 7561 (1978).
22. W. R. CULLEN and Y. SUGI. Tetrahedron Lett. 1635 (1978).
23. E. J. COREY and D. SEEBACH. J. Org. Chem. **40**, 231 (1975).
24. M. L. WOLFROM and K. ANNO. J. Am. Chem. Soc. **74**, 6150 (1952).
25. R. A. MARKOVS. Diss. Abstr. **36**B, 3964 (1975).
26. D. HORTON and R. A. MARKOVS. Carbohydr. Res. **78**, 295 (1980).
27. H. REDLICH and W. FRANCKE. Angew. Chem. Int. Ed. Engl. **19**, 630 (1980).
28. C. P. REDDY, S. M. SINGH and R. B. RAO. Tetrahedron Lett. **22**, 973 (1981).

Can. J. Chem. Downloaded from www.nrcresearchpress.com by 210.87.254.105 on 09/06/12
For personal use only.

# Enzymes in organic synthesis. 22.[1] Effects of organic solvents on horse liver alcohol dehydrogenase-catalyzed reduction

J. Bryan Jones and Harold M. Schwartz

*Department of Chemistry, University of Toronto, Toronto, Ont., Canada M5S 1A1*

Received July 30, 1981

J. Bryan Jones and Harold M. Schwartz. Can. J. Chem. **60**, 335 (1982).

The effects have been evaluated of up to 30% (v/v) of *methanol*, *ethanol*, 2-propanol, tert-*butyl alcohol*, dimethylsulfoxide, sulfolane, *acetonitrile*, dimethylformamide, N-*methyl-2-pyrrolidone*, hexamethylphosphoramide, tetrahydrofuran, *dimethoxymethane*, *diglyme*, and *dioxane* on horse liver alcohol dehydrogenase-catalyzed reduction of the representative ketone cyclohexanone. The most viable solvents are those shown in italics on the above list.

J. Bryan Jones et Harold M. Schwartz. Can. J. Chem. **60**, 335 (1982).

On a étudié l'effet du *méthanol*, de l'*éthanol*, du propanol-2, du tert-*butanol*, du diméthylsulfoxide, du sulfolanne, de l'*acétonitrile*, du diméthylformamide, de la N-*méthyl pyrolidone-2*, de l'hexaméthylphosphoramide, du tétrahydrofuranne, du *diméthoxyméthane*, du *diglyme* et du *dixoanne*, à des compositions allant jusqu'à 30% sur la réduction de la cyclohexanone, comme substrat type, catalysée par la déhydrogénase de l'alcool du foie de cheval. Les solvants les plus efficaces sont en italique.

[Traduit par le journal]

## Introduction

The advantages of using enzymes as chiral catalysts in organic synthesis are becoming increasingly recognized (1*b*, *c*). However, many of the organic substrates of current or potential interest are hydrophobic in nature and are effectively insoluble in the aqueous solutions preferred for enzyme-catalyzed reactions. In such cases, it is usually necessary to add organic cosolvents to the enzyme-containing medium in order to attain at least a minimal solubility of the substrate. The problem can become acute when immobilized enzymes are used in flow systems (2), when complete solubility of the substrate becomes a requirement.

Significant proportions of organic cosolvents, which often exert deleterious effects on enzymic catalyses, may be needed to achieve the desired levels of substrate concentrations. While some organic cosolvent effects have been documented for a few enzymes (1, 3), few data are available on their influence on the oxidoreductase enzymes of greatest current asymmetric synthetic value. In this paper we report on the effect of a broad range of commonly used, water-miscible, protic and aprotic organic solvents on the horse liver alcohol dehydrogenase (HLADH[2])-catalyzed reduction of the representative organic ketone substrate cyclohexanone.

## Results

A range of common protic and aprotic water-miscible solvents of different polarities was evaluated. The solvents selected were: protic – methanol, ethanol, 2-propanol, and *tert*-butyl alcohol; aprotic – DMSO, sulfolane, acetonitrile, DMF, NMP, HMPA, THF, dimethoxyethane, diglyme, and dioxane. The effects of up to 30% of each cosolvent on HLADH-catalyzed reduction were evaluated using cyclohexanone as substrate. The reductions were performed in 0.1 *M* phosphate buffer pH 7.0 at 0.175 m*M* NADH and 0.2, 1, and 5 m*M* cyclohexanone concentrations. The relative activities observed, based on initial reaction velocities, are recorded in Table 1. The activity of the enzyme is seen to be progressively lowered to a greater or lesser extent by each solvent.

While not as complete as from a thorough kinetic study, the Table 1 data did permit satisfactory basic Lineweaver–Burk (3) plots to be derived. With the exception of the data obtained in 2-propanol, ethanol, DMF, HMPA, THF, and dioxane, the double reciprocal plots obtained were linear up to the highest cosolvent concentrations evaluated. The Lineweaver–Burk data indicated that the majority of the solvents were acting as reversible inhibitors of the noncompetitive or mixed type. Further analysis of the Table 1 data by the method of Dixon (3) permitted the $K_I$ values of most cosolvents to be estimated. These are summarized in Table 2.

[1]For Part 21, see ref. 1*a*. Abstracted from the Ph.D. thesis, University of Toronto (1979) of H.M.S.

[2]Abbreviations used: HLADH, horse liver alcohol dehydrogenase; NADH, nicotinamide adenine dinucleotide, reduced form; DMSO, dimethylsulfoxide; DMF, dimethylformamide; NMP, *N*-methyl-2-pyrrolidone; HMPA, hexamethylphosphoramide; THF, tetrahydrofuran.

0008-4042/82/030335-04$01.00/0

©1982 National Research Council of Canada/Conseil national de recherches du Canada

Can. J. Chem. Downloaded from www.nrcresearchpress.com by 210.87.254.42 on 09/06/12
For personal use only.

TABLE 1. Relative rates of HLADH-catalyzed reduction of cyclohexanone in the presence of different organic cosolvents[a]

| Cosolvent (ε) | 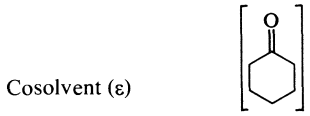 | Relative rate[b] of cosolvent 1% | 5% | 10% | 20% | 30% |
|---|---|---|---|---|---|---|
| Protic | | | | | | |
| Methanol (32.7) | 0.2 | 67 | 34 | <0.1 | | |
| | 1.0 | 59 | 27 | 10 | <0.1 | |
| | 5.0 | 65 | 26 | 18 | 2 | |
| Ethanol (24.6) | 0.2 | 10 | 1[c] | | | |
| | 1.0 | 11 | 1[c] | | | |
| | 5.0 | 9 | 2[c] | | | |
| 2-Propanol (19.9) | 0.2 | 20 | 6 | 3 | 1 | |
| | 1.0 | 20 | 14 | 3 | 1 | |
| | 5.0 | 23 | 7 | 3 | 1 | |
| *tert*-Butyl alcohol (12.5) | 0.2 | 40 | 14 | 9 | 3 | |
| | 1.0 | 44 | 17 | 9 | 4 | |
| | 5.0 | 54 | 21 | 11 | 5 | |
| Aprotic | | | | | | |
| DMSO (46.7) | 1.0 | 3 | 0.4[c] | | | |
| Sulfolane (43.3) | 0.2 | 92 | 52 | 35 | 28 | |
| | 1.0 | 79 | 31 | 15 | 12 | |
| | 5.0 | 69 | 40 | 22 | 12 | |
| Acetonitrile (37.5) | 0.2 | 47 | 18 | 13 | | |
| | 1.0 | 49 | 18 | 8 | | |
| | 5.0 | 65 | 24 | 11 | | |
| DMF (36.7) | 1.0 | 3 | 0.5[c] | | | |
| NMP (32.0) | 0.2 | 53 | 18 | 12 | 7 | |
| | 1.0 | 51 | 21 | 11 | 5 | |
| | 5.0 | 69 | 31 | 18 | 9 | |
| HMPA (30) | 0.2 | 110 | 98 | 75 | 23 | 44 |
| | 1.0 | 104 | 80 | 77 | 55 | 33 |
| | 5.0 | 112 | 92 | 85 | 76 | 37 |
| THF (7.6) | 0.2 | 11 | <0.1 | | | |
| | 1.0 | 11 | 3 | | | |
| | 5.0 | 15 | 3 | | | |
| Dimethoxyethane (7.2) | 0.2 | 50 | 18 | 11 | 6 | |
| | 1.0 | 45 | 20 | 11 | 5 | |
| | 5.0 | 50 | 20 | 11 | 5 | |
| Diglyme | 0.2 | 79 | 47 | 30 | 14 | 12 |
| | 1.0 | 75 | 45 | 33 | 18 | 9 |
| | 5.0 | 83 | 49 | 35 | 20 | 10 |
| Dioxane (2.2) | 0.2 | 50 | <0.1 | | | |
| | 1.0 | 53 | 17 | 9 | | |
| | 5.0 | 55 | 35 | 30 | | |

[a]Determined in 0.1 *M* phosphate buffer pH (app) 7.0, 0.175 m*M* in NADH at 25°C.
[b]Relative to initial velocity of 100 in absence of organic cosolvent.
[c]Intermediate activities were observed at 2 and 3% organic solvent levels.

## Discussion

The solvents were chosen on the basis of their complete water miscibility, their ready availability, and their common use in organic chemistry. Representative solvents of both protic and aprotic character possessing varying protogenic, protophilic, or amphiprotic (4) properties were included. A broad range of polarity was selected using dielectric constant as the guide. No acyclic ketone solvents could be included because they are substrates, albeit often poor ones (1*b*).

Cyclohexanone was picked as the substrate

Can. J. Chem. Downloaded from www.nrcresearchpress.com by 210.87.254.42 on 09/06/12
For personal use only.

Can. J. Chem. Downloaded from www.nrcresearchpress.com by 210.87.254.42 on 09/06/12
For personal use only.

TABLE 2. $K_I$ values estimated for cosolvent inhibition of HLADH[a]

| Cosolvent | $K_I$(m$M$) |
|---|---|
| Methanol | 720 |
| Sulfolane | 600 |
| Acetonitrile | 210 |
| DMF | 15 |
| NMP | 130 |
| THF | 15 |
| Dimethoxyethane | 200 |
| Diglyme | 400 |

[a]Estimated from the Table 2 data using Dixon plots (3).

since its behaviour and properties are representative of those of organic interest (1*b*) and its mechanism of reduction is well documented (5, 6). Many ketone substrates of HLADH possess large Michaelis constants and have limited aqueous solubilities at high substrate concentrations. Consequently, kinetic analyses of ketone substrates are generally performed at concentrations well below $K_m$ levels. Concentrations in the 1 m$M$ range are the most common (1*f*). Thus cyclohexanone levels of 0.2, 1.0, and 5 m$M$, spanning this common concentration region, were evaluated, despite the fact that the $K_m$ of cyclohexanone is 17 m$M$ (5). A saturating concentration (0.175 m$M$) of the NADH coenzyme was used for each assay.

The initial reaction rates were measured for each cosolvent level in phosphate buffer at the pH optimum for reduction of 7.0. Although the pH of phosphate buffers is known to be affected by the addition of organic solvents (7), no corrections were made since, with the exception of HMPA, the apparent pH's of the solutions were not significantly altered by the levels of organic solvents used. For each solvent, the concentration was raised until the observed activity was $\lesssim$ 10% of that in aqueous solution. This level of activity represents the practical lower limit for effective preparative scale applications of HLADH. For the two solvents with the least deactivating effects, HMPA and diglyme, up to 30% (v/v) of organic solvents were required before this lower activity limit was reached (Table 1).

The assays were performed by monitoring the coenzyme absorbance change at 340 nm. With methanol, acetonitrile, HMPA, THF, and dioxane as cosolvents, a change in the 340 nm absorbance was observed on their addition to the assay medium even when cyclohexanone was omitted to preclude the enzyme-induced reaction. These effects are attributed to nucleophilic attack of NADH to form addition products (8) in the case of methanol and HMPA and to oxidation of NADH by the peroxides present in THF and dioxane.[3] The nature of the acetonitrile-induced NADH transformation is not known and was not investigated.[3] The relative rates of reduction cited in Table 1 have been corrected for these solvent effects.

As Table 1 shows, all the cosolvents evaluated are strongly inactivating towards HLDAH at their highest concentrations. However, at the lower organic solvent levels, HLADH retains significant activity in a number of cases. For example, with 5% of sulfolane, HMPA, or dimethoxyethane present, the enzyme retains >40% of its original catalytic power. In fact, when 1% of HMPA is added, the activity of HLADH is actually slightly enhanced, possibly due to induction of a catalytically more effective protein conformation (9).

Identification of a solvent as being protic or aprotic in character is clearly of no benefit with respect to predicting its effect on HLADH catalysis. Furthermore, while the two groups of solvents are arranged in Table 1 in order of decreasing dielectric constant, it is evident from the lack of correlation of inactivation power with polarity that this parameter is of little guidance value either.

Lineweaver–Burk and Dixon plot analyses of the Table 1 data show that the cosolvents are acting as reversible inhibitors, with most (Table 2) being of the noncompetitive (3) type. The linear Dixon plot obtained suggest the addition of only one molecule of cosolvent per subunit in the inactive complex. For the solvents omitted from Table 2, the Lineweaver–Burk or Dixon analyses gave nonlinear plots for the highest organic cosolvent concentration runs. However, the patterns for methanol, HMPA, and dioxane were strongly indicative of mixed (3) inhibition. The strong inactivations by DMSO, known to be a competitive inhibitor, and DMF are due to coordination of their respective functional groups with the catalytically vital active site zinc ion (10). From the $K_I$ values of Table 2, it is seen that none of the cosolvents is a particularly powerful reversible inhibitor, particularly when compared with the better competitive inhibitors such as pyrazoles, some of which have $K_I$'s as low as $10^{-6}$ m$M$ (11).

For the cosolvents acetonitrile, NMP, HMPA,

[3]Although freshly distilled solvents were used, rigorous steps to remove peroxides were not taken. The nonenzymic rate of NADH oxidation was much increased when undistilled THF and dioxane were employed. A referee, to whom we are grateful, has drawn our attention to the fact that Sanyal and Maren (University of Florida) have found that even doubly distilled acetonitrile contains trace quantities of cyanide. Nucleophilic attack of NADH by $CN^-$, in a manner analogous to that of methanol addition (8), may well occur with acetonitrile as solvent.

Can. J. Chem. Downloaded from www.nrcresearchpress.com by 210.87.254.42 on 09/06/12
For personal use only.

and THF, increasing the substrate concentration affords some protection against inactivation. With methanol, ethanol, 2-propanol, dimethoxyethane, and diglyme, no such trend can be seen while in the presence of *tert*-butyl alcohol and sulfolane, the catalytic activity of the enzyme is reduced as the cyclohexane concentration is raised.

For HLADH-catalyzed reductions, the cosolvent with the least deleterious effect is clearly HMPA. Unfortunately, however, the aqueous solubilities of hydrophobic organic substrates are not greatly enhanced by this solvent. DMSO and DMF are not recommended since they eliminate 97% of the enzyme's activity even in 1% (v/v) solutions. The remaining Table 1 solvents should all be preparatively viable, with the best prospects being *tert*-butyl alcohol, acetonitrile, NMP, dimethoxyethane, diglyme, and dioxane.[4] With the ethereal solvents, care must be taken to remove peroxides prior to, and prevent their build-up during, the reaction. The results of the analogous study on solvent effects on HLADH-catalyzed oxidations will be reported shortly.

## Experimental

HLADH, prepared by the method of Roy and Nishikawa (17), was a gift from Hoffmann-La Roche. It is also available from Sigma. Enzyme stock solution was prepared containing 1 mg HLADH/mL of 0.1 *M* Tris buffers pH 7.4. NADH was purchased from Sigma. Cyclohexanone and all solvents were redistilled immediately prior to use, with dimethoxyethane and diglyme being distilled over potassium hydroxide. Dioxane was purified over stannous chloride prior to distillation over lithium aluminum hydride. Acetonitrile was distilled over calcium hydride. Kinetics were performed on a Unicam SP 1800 uv spectrophotometer equipped with a Unican AR 25 linear recorder.

*Relative rate studies*

All kinetic runs were carried out in 3 mL volume uv cuvettes at 25°C in 0.1 *M* potassium phosphate buffer pH 7.0, $1.75 \times 10^{-4}$ *M* in NADH, and with cyclohexanone concentrations of 0.2, 1.0, and $5.0 \times 10^{-3}$ *M*. The volume of buffer was varied so that addition of between 30 μL and 0.9 mL of cosolvent would bring the total volume to 2.95 mL. The solution was then allowed to equilibrate at 25°C in the spectrophotometer and the catalysis initiated by the addition of 50 μL of enzyme stock solution giving a final [HLADH] of $9.92 \times 10^{-8}$ *M*. The initial rates of reduction were determined by monitoring the rate of decrease in optical density at 340 nm. The rates, which are recorded in Table 1, were corrected for the solvent-induced rates when methanol, HMPA, acetonitrile, dioxane, and THF were used as cosolvents. The levels of organic solvents used had no effect on the pH of the buffer solutions except for HMPA. In 30% HMPA, the pH(app) of the solution was 7.6, but the reduction rates were unaltered when pH(app) 7.0 solutions (prepared from aqueous buffer pH 6.45) were used.

[4]The limited preparative-scale data in the literature are in accord with these recommendations. Use of up to 3% methanol or ethanol has been reported (1) as has up to 2.5% of dioxane (12–14). The inhibitory problems reported for dioxane (15) may have been due to the inadvertent presence of peroxides. Dimethoxyethane has been used successfully at 1.66% (v/v) (15); again the inhibitory properties reported in other work (16) could have been due to peroxide contaminants.

## Acknowledgements

We are grateful to the Natural Sciences and Engineering Research Council of Canada for generous financial support, to Hoffmann-La Roche, Nutley, New Jersey for a gift of enzyme and additional financial aid, and to Drs. G. Sanyal and T. H. Maren for providing details of their submitted paper in which the acetonitrile data referred to in footnote 3 are discussed.

1. (*a*) J. B. Jones and D. H. Pliura. Can. J. Chem. **59**, 2921 (1981); (*b*) J. B. Jones and J. F. Beck. Tech. Chem. (N.Y.), **10**, 107 (1976); (*c*) J. B. Jones. *In* Enzymic and nonenzymic catalysis. *Edited by* P. Dunnill, A. Wiseman, and N. Blakeborough. Ellis Horwood (Chichester)/J. Wiley (N.Y.). 1980. pp. 54–83; (*d*) J. B. Jones and M. M. Mehes. Can. J. Chem. **57**, 2245 (1979), and references therein; (*e*) D. H. Pliura and J. B. Jones. Can. J. Chem. **58**, 2633 (1980), and references therein; (*f*) A. J. Irwin, K. P. Lok, K. W-C. Huang, and J. B. Jones. J. Chem. Soc. Perkin Trans. I, 1636 (1978); (*g*) J. Davies and J. B. Jones. J. Am. Chem. Soc. **101**, 5405 (1979).
2. K. Mosbach. Methods Enzymol. **44**, (1976).
3. M. Dixon and E. C. Webb. Enzymes. 2nd ed. Longmans, London. 1964.
4. J. F. Coetzee and C. D. Ritchie. Solute–solvent interactions. Dekker, New York. 1969.
5. K. Dalziel and F. M. Dickinson. Biochem. J. **100**, 491 (1966).
6. J. R. Ainslie, Jr. and W. W. Cleland. J. Biol. Chem. **247**, 946 (1972).
7. (*a*) P. Douzou. Mol. Cell. Biochem. **1**, 15 (1973); (*b*) P. Douzou and C. Balny. Advances in protein chemistry. Vol. 32. *Edited by* C. B. Anfinsen, J. T. Edsall, and F. M. Richards. Academic, New York. 1962. p. 1.
8. U. Eisner and J. Kuthan. Chem. Rev. **72**, 1 (1972).
9. P. M. Hinckle and J. F. Kirsch. Biochemistry, **9**, 4633 (1970).
10. (*a*) R. L. Perlman and J. Wolff. Science, **160**, 317 (1968); (*b*) H. Eklund and C. I. Brändén. J. Biol. Chem. **254**, 3458 (1979); (*c*) B. V. Plapp, H. Eklund, and C. I. Brändén. J. Mol. Biol. **122**, 22 (1978).
11. E. Dahlbom, B. R. Tolf, A. Akeson, C. Lundquist, and H. Theorell. Biochem. Biophys. Res. Commun. **57**, 549 (1974).
12. J. M. H. Graves, A. Clark, and H. J. Ringold. Biochemistry, **4**, 2655 (1965).
13. E. Caspi and C. R. Eck. J. Org. Chem. **42**, 767 (1977).
14. (*a*) A. R. Battersby, D. G. Buckley, J. Staunton, and P. J. Williams. J. Chem. Soc. Perkin Trans. I, 2550 (1979); (*b*) J. Chem. Soc. Perkin Trans. I, 2559 (1979).
15. J. Rétey. Ph.D. thesis 3409, ETH, Zurich (1963).
16. M. A. Abdullah, J. F. Biellmann, and D. Lagrange. Biochemistry, **18**, 836 (1979).
17. S. K. Roy and A. H. Nishikawa. Biotechnol. Bioeng. **21**, 775 (1979).

# Triplet energies of fumaronitrile and maleonitrile[1]

PO CHEONG WONG[2]

*Division of Chemistry, National Research Council of Canada, Ottawa, Ont., Canada K1A 0R6*

Received June 17, 1981

PO CHEONG WONG. Can. J. Chem. **60**, 339 (1982).

The triplet energies of fumaronitrile and maleonitrile measured by laser flash photolysis technique using the Herkstroeter–Hammond method are both 59 ± 2 kcal mol$^{-1}$. Our results show that these olefins are classical triplet energy acceptors for non-electron donating sensitizers. With electron donating sensitizers, quenching through a charge-transfer mechanism also occurs in benzene solution.

PO CHEONG WONG. Can. J. Chem. **60**, 339 (1982).

Les énergies du triplet du fumaronitrile et du maléonitrile, telles que mesurées par la technique de photolyse flash au laser en utilisant la méthode de Hekstroeter-Hammond, sont toutes les deux égales à 59 ± 2 kcal mol$^{-1}$. Nos résultats révèlent que ces oléfines sont des accepteurs classiques d'énergie de triplet pour des sensibilisateurs qui ne sont pas des donneurs d'électrons. Dans le cas des sensibilisateurs donneurs d'électrons, le piégeage par l'intermédiaire d'un mécanisme par transfert de charge se produit également dans une solution de benzène.

[Traduit par le journal]

Can. J. Chem. Downloaded from www.nrcresearchpress.com by 210.87.254.5 on 09/06/12
For personal use only.

## Introduction

In recent years, there has been a substantial increase in the use of fumaronitrile (FN) and maleonitrile (MN) in photochemical reactions. Unfortunately, the mechanisms postulated for these reactions often require the knowledge of the accurate vertical triplet energies ($E_T$) of this olefin pair which are so far unavailable (1).

In our previous study (1*a*), we attempted to measure the triplet energies for FN and MN by the well-known Saltiel method (2). The estimated $E_T$'s were both ca. 50 kcal mol$^{-1}$ since the efficiency of sensitized isomerization dropped significantly when sensitizers of $E_T < 49$ kcal mol$^{-1}$ were used. In the present study, we employed a more accurate method developed by Hammond and Herkstroeter (3) to measure the triplet energies of these olefins. The quenching rates of the triplet sensitizers were measured by using the laser flash photolysis technique. The triplet energies thus measured are both about 9 kcal mol$^{-1}$ higher than our previous estimate.

## Experimental

Fumaronitrile (K & K) was freshly sublimed before use. Maleonitrile was prepared and purified as reported before (1*a*) (vpc pure). All the sensitizers were commercially available and were purified by either recrystallization or distillation. Benzene (Aldrich, Gold Label) was treated with concentrated sulfuric acid, washed, and neutralized before being distilled from calcium hydride. All the sample solutions were deaerated by nitrogen purging.

The laser flash photolysis equipment has been described in detail elsewhere (4). Briefly, pulses (337.1 nm, 8 ns, 1–10 mJ) from the Molectron nitrogen laser were used for sample excitation. The transient absorbances in the sample were monitored by using a detection system with nanosecond response at a preselected wavelength. Signals from the detector system were processed through a R7912 Tektronix transient digitizer and were analyzed by using a dedicated PDP 11 computer.

## Results and discussion

All our experiments involving triplet quenching have been carried out by using laser flash photolysis technique. Quenching of the triplets of a series of sensitizers in benzene by the olefins was observed by monitoring the triplet–triplet absorptions in the presence of various concentrations of the olefin (5). At sufficiently low excitation doses and sensitizer concentrations, all the triplets underwent clean first order decay. The pseudo-first order rate constants of triplet decay ($k_d = \tau_T^{-1}$) are linearly related to the olefin concentrations according to eq. [1].

$$[1] \quad k_d = k_d^0 + k_q[\text{olefin}]$$

Here $k_d^0$ is the rate constant of decay for the triplet in the absence of olefin and $k_q$ is the rate constant of quenching the triplet by the olefin. The reverse triplet energy transfer reaction is probably unimportant here due to the short lifetimes of the olefin triplets.

Figure 1 shows a typical plot according to eq. [1] and the corresponding triplet decay trace (insert). The quenching rate constants ($k_q$) obtained by using this approach are summarized in Table 1. Our $k_q$ values for quenching of high energy triplet sensitizers by fumaronitrile are in good agreement to those reported by Loutfy, Dogra, and Yip using

[1]NRCC No. 18921.

[2]Present address: DuPont Canada, Research Centre, Research Division, P.O. Box 5000, Kingston, Ont., Canada

0008-4042/82/030339-03$01.00/0

©1982 National Research Council of Canada/Conseil national de recherches du Canada

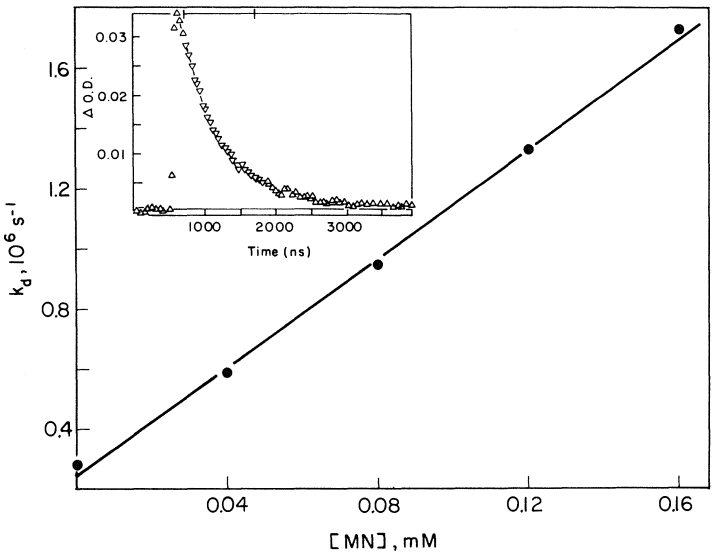


FIG. 1. Determination of $k_q$ for benzophenone in benzene, according to eq. [1]. Insert: trace obtained for maleonitrile, [MN] = 0.16 m$M$ (average of twenty laser shots).

TABLE 1. Quenching rate constants ($k_q$) of sensitizer triplets by fumaronitrile and maleonitrile in benzene

| Sensitizer | Triplet energy (kcal $mol^{-1}$) | $k_q$[a] | |
|---|---|---|---|
| | | Fumaronitrile | Maleonitrile |
| Acetone | 76.0 | $6.50 \times 10^{9}$[b] | — |
| Butyrophenone | 74.5 | $5.80 \times 10^{9}$[b] | — |
| Acetophenone | 74.0 | $4.10 \times 10^{9}$ | $5.46 \times 10^{9}$ |
| *p*-Methoxyacetophenone | 71.8 | $1.44 \times 10^{10}$ | $1.38 \times 10^{10}$ |
| Benzophenone | 69.2 | $7.95 \times 10^{9}$ | $9.10 \times 10^{9}$ |
| Phenanthrene | 62.0 | $7.17 \times 10^{9}$ | $8.38 \times 10^{9}$ |
| 2-Acetonaphthone | 59.0 | $4.55 \times 10^{8}$ | $6.73 \times 10^{8}$ |
| Chrysene | 57.3 | $5.41 \times 10^{8}$ | $6.08 \times 10^{8}$ |
| 1-Nitronaphthalene | 54.9 | $3.51 \times 10^{6}$ | $5.16 \times 10^{6}$ |
| 9-Fluorenone | 53.0 | $8.54 \times 10^{4}$ | $1.36 \times 10^{5}$ |
| Benzil | 50.9 | $3.80 \times 10^{4}$ | $3.25 \times 10^{4}$ |
| Pyrene | 48.2 | [c] | [c] |

[a]In $M^{-1}$ $s^{-1}$, at 25°C, with an error limit of ±10% for $k_q > 10^5$ and ±50% for $k_q < 10^5$.
[b]Taken from ref. 6.
[c]Too slow to be conveniently measured by our instrument.

flash emission technique (6). They claimed that the quenching of acetone, butyrophenone, and benzophenone by FN were purely triplet energy transfer since the quenching rates are faster when using sensitizers of higher $E_T$'s. This is also the general trend observed in Table 1. However, some exceptions are encountered for sensitizers with low oxidation potentials (good electron donors) e.g. *p*-methoxyacetophenone, benzophenone, and chrysene. The quenching rates for these sensitizers are higher than the nonelectron donating sensitizers with the same or even higher $E_T$'s. Such phenomenon has also been observed earlier by other workers (6, 7). The faster quenching rates are probably due to charge-transfer from the excited donors (sensitizers) to the ground state acceptors. Our observation is also in line with the electron-transfer quenching of triplets in aqueous acetonitrile solution (8).

The plot of log $k_q$ versus triplet energies of the sensitizers for both quenching by FN and MN (Fig. 2) are typically saturation curves as observed in the case of *trans*-stilbene (3). From Fig. 2, FN quenches efficiently all triplet sensitizers with $E_T$ greater than 60 kcal $mol^{-1}$. Therefore, the vertical triplet energy for FN is 59 ± 2 kcal $mol^{-1}$. With lower energy sensitizers, the quenching efficiency drops in accord with the Arrhenius equation (3).

Can. J. Chem. Downloaded from www.nrcresearchpress.com by 210.87.254.5 on 09/06/12
For personal use only.

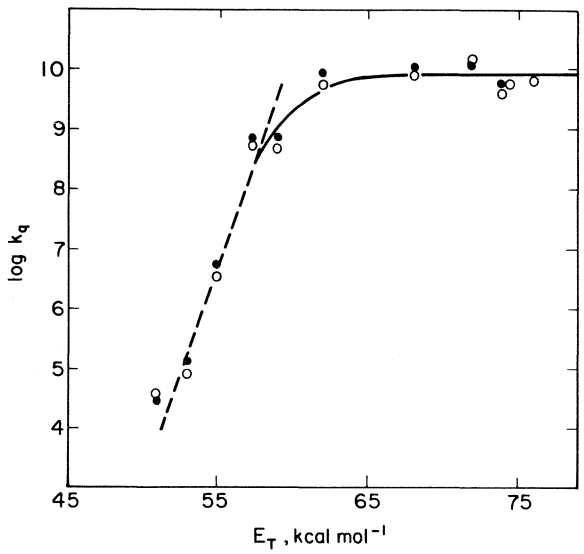


FIG. 2. Dependence of log $k_q$ for fumaronitrile (circles) and maleonitrile (dots) on the triplet energy of the sensitizers. The dotted line represents the slope expected on the basis of the Arrhenius equation.

When plotting the log $k_q$ vs. the sensitizer triplet energy, $E_T$, a slope of $+1/(2.30RT)$ (0.74 at 22°C) is predicted by the Arrhenius equation; a straight line with the slope has been drawn in Fig. 2. Our results in this region are uncomplicated by the charge-transfer mechanism because ketones with low $E_T$ and 1-nitronaphthalene are less likely to donate an electron than the aromatic hydrocarbon sensitizers. Since the slope of the plot in Fig. 2 matches closely the predicted line, this part of our data can be treated the same as the classical triplet quencher like *trans*-stilbene to extract $E_T$.

The behaviour of maleonitrile is very similar to FN as shown in Fig. 2. The triplet energy for MN thus estimated is also $59 \pm 2$ kcal mol$^{-1}$. Therefore, our earlier explanation (1*a*) for the Saltiel plot being a flat line for FN–MN is confirmed. By comparing the quenching rates listed in Table 1, the $k_q$'s for MN are consistently larger than those for FN by a factor of ca. 1.3, except for *p*-methoxyacetophenone. Assuming that the twisted triplet state has equal probability in decaying to FN and MN, the photostationary state concentration ratios can then be deduced from the inverse of the $k_q$ ratios (i.e. FN:MN = 57:43). The agreement between the observed and the photostationary state concentration ratios thus predicted is fairly good (1*a*). The assumption for the 1:1 decay is more or less justified since the heats of formation for FN and MN are almost identical (1*a*, 9).

The higher triplet energies found for FN and MN in the present study are in accord with most of the previous results and interpretations. For example, in the irradiation of *trans*-stilbene and fumaronitrile, there was very little MN formation and no CIDNP signal for MN (1*b*, *d*, *e*).

The triplet energy of *trans*-stilbene is now 9 kcal mol$^{-1}$ below the fumaronitrile triplet. Therefore, when back electron transfer occurs in the radical ion pair, the triplet of *trans*-stilbene will be formed exclusively which will account for the CIDNP signal of *cis*-stilbene upon isomerization.

**Acknowledgements**

This work was supported by the National Research Council of Canada. The author is grateful to Dr. J. C. Scaiano for his valuable advice and generosity in allowing the use of the laser flash photolysis apparatus, and to Dr. D. Griller for his useful comments. Thanks are also due to Mr. S. E. Sugamori and Mr. D. A. Lindsay for their technical assistance.

1. (*a*) P. C. WONG and D. R. ARNOLD. Can. J. Chem. **57**, 1037 (1979); (*b*) P. C. WONG and D. R. ARNOLD. J. Am. Chem. Soc. **101**, 1894 (1979); (*c*) P. C. WONG and D. R. ARNOLD. Can. J. Chem. **58**, 918 (1980); (*d*) F. D. LEWIS and J. T. SIMPSON. J. Phys. Chem. **83**, 2015 (1979); (*e*) H. D. ROTH and M. L. MANION. J. Am. Chem. Soc. **102**, 4303 (1980).
2. G. S. HAMMOND, J. SALTIEL, A. A. LAMOLA, N. J. TURRO, J. S. BRADSHAW, D. O. COWAN, R. C. COUNSELL, V. VOGT, and C. DALTON. J. Am. Chem. Soc. **86**, 3197 (1964).
3. W. G. HERKSTROETER and G. S. HAMMOND. J. Am. Chem. Soc. **88**, 4769 (1966).
4. J. C. SCAIANO. J. Am. Chem. Soc. **102**, 7747 (1980).
5. J. C. SCAIANO and G. G. WUBBELS. J. Am. Chem. Soc. **103**, 640 (1981).
6. R. O. LOUTFY, S. K. DOGRA, and R. W. YIP. Can. J. Chem. **57**, 342 (1979).
7. I. E. KOECHEVAR and P. J. WAGNER. J. Am. Chem. Soc. **94**, 3859 (1972).
8. (*a*) P. K. DAS. Tetrahedron Lett. 1307 (1981); (*b*) R. S. DAVIDSON, R. BONNEAU, P. FORNIER DE VIOLET, and J. JOUSSOT-DUBIEN. Chem. Phys. Lett. **78**, 475 (1981).
9. G. HELLING and D. WOEHRLE. Makromol. Chem. **179**, 101 (1978).

Can. J. Chem. Downloaded from www.nrcresearchpress.com by 210.87.254.5 on 09/06/12
For personal use only.

# Conformational consequences of intramolecular hydrogen bonding by OH to the directional lone-pair of sulfur in derivatives of methyl phenyl sulfide, diphenyl sulfide, and diphenyl disulfide

TED SCHAEFER, SALMAN R. SALMAN[1], TIMOTHY A. WILDMAN, AND PETER D. CLARK[2]

*Department of Chemistry, University of Manitoba, Winnipeg, Man., Canada R3T 2N2*

Received August 7, 1981

TED SCHAEFER, SALMAN R. SALMAN, TIMOTHY A. WILDMAN, and PETER D. CLARK. Can. J. Chem. **60**, 342 (1982).

Complete spectral parameters for the $^1$H nmr spectra of 2-hydroxyphenyl methyl sulfide, **2**, 2-hydroxyphenyl phenyl sulfide, **3**, bis(2-hydroxy-3-*tert*-butyl-5-methylphenyl) sulfide, **4**, and bis(2-hydroxyphenyl) disulfide, **5**, are reported for $CCl_4$ solutions at 305 K. For **2** the parameters are consistent only with a conformation in which the C—S—C plane is roughly perpendicular to the aromatic plane. The conformational determinant is the OH···3*p* hydrogen bond which forces the mainly 3*p* orbital on sulfur into the benzene plane. In **3** a similar arrangement is found about the sulfur atom, with the phenyl group lying in the C—S—C plane and therefore perpendicular to the hydroxyphenyl plane (skew conformation). In **4** two OH···3*p* hydrogen bonds exist, yielding a gable (twist) conformation. Compound **5** exists in the axial conformation with probable $C_2$ symmetry, the CSSC dihedral angle and the CCSS torsion angles all being near 90°. For none of the compounds is there any evidence for OH···π interactions.

TED SCHAEFER, SALMAN R. SALMAN, TIMOTHY A. WILDMAN et PETER D. CLARK. Can. J. Chem. **60**, 342 (1982).

On rapporte les paramètres spectraux complets des spectres de rmn du $^1$H des composés suivants en solution, dans le $CCl_4$, à 305 K: sulfure de l'hydroxy-2 phényle et de méthyle, **2**, sulfure de hydroxy-2 phényle et de phényle, **3**, sulfure du bis(hydroxy-2 *tert*-butyl-3 méthyl-5 phényle), **4** et du disulfure de bis(hydroxy-2 phényle), **5**. Les paramètres du composé **2** sont uniquement en accord avec une conformation dans laquelle le plan C—S—C est approximativement perpendiculaire au plan du noyau aromatique. Le déterminant conformationnel est la liaison hydrogène OH···3*p* qui oblige l'orbitale principale 3*p* du soufre à passer dans le plan du benzène. Dans le cas du composé **3**, on trouve un arrangement semblable autour de l'atome de soufre avec le groupe phényle oriente dans le plan C—S—C et par conséquent perpendiculaire au plan de l'hydroxyphényle (conformation *gauche*). Deux liaisons hydrogènes OH···3*p* existent dans le composé **4**, donnant une conformation gable (twist). Le composé **5** existe dans une conformation axiale avec une symétrie probable $C_2$, l'angle dièdre CSSC et les angles de torsion CCSS étant tous deux pratiquement à 90°. On n'a pas pu établir l'existence d'interactions OH···π dans aucun de ces composés.

[Traduit par le journal]

## Introduction

The existence of intramolecular OH···π hydrogen bonds in 2-phenylphenol and in derivatives of 2-benzylphenol is attested by infrared spectroscopy (1) and by X-ray crystallography (2). Furthermore, infrared, ultraviolet, and nmr data in $CCl_4$ solution are interpreted in terms of predominant intramolecular OH···π bonding in *ortho* hydroxy derivatives of diphenyl sulfide and diphenyl disulfide (3). Apparently, the $^1$H nmr data are not useful in the deduction of the conformations adopted as a consequence of the OH···π bonds (3). A $^{13}$C nmr study concludes that $^{13}$C shifts are insensitive to the intramolecular hydrogen bonding but assumes the OH···π intramolecular interaction as proven (4).

It is interesting, therefore, that a detailed $^1$H nmr investigation of 2-hydroxythiophenol, **1**, in $CCl_4$ shows its conformation as one in which the SH bond prefers to lie perpendicular to the benzene plane (5). In the absence of the hydroxyl group the SH bond prefers the molecular plane by 3.2 kJ/mol (6), the mainly 3*p* orbital conjugating with the π system. Also, the hydroxyl group in phenol shows a preference of 14.6 kJ/mol for the benzene plane (7, 8*a*). The most favorable conformation, **1** (R=H), is therefore a consequence of a stereospecific electrostatic attraction between the directional 3*p* lone pair on the polarizable sulfur atom and the O—H dipole (5).

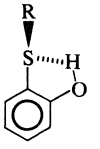


**1** R = H
**2** R = $CH_3$
**3** R = $C_6H_5$

When R=$CH_3$, the preferred conformation may still be determined by the OH···3*p* attraction. Furthermore, the latter may well play an important role in the conformations adopted for R = $C_6H_5$ and perhaps also for R = $SC_6H_5$.

In this paper, chemical shifts and spin–spin coupling constants are used in arguments about the conformations of **2**, **3**, bis(2-hydroxy-3-*tert*-butyl-

[1]Present address, Department of Chemistry, University of Baghdad, Baghdad, Iraq.

[2]Present address, Department of Chemistry, University of Calgary, Calgary, Alta., Canada T2N 1N4.

0008-4042/82/030342-07$01.00/0

©1982 National Research Council of Canada/Conseil national de recherches du Canada

Can. J. Chem. Downloaded from www.nrcresearchpress.com by 210.87.254.40 on 09/06/12
For personal use only.

TABLE 1. The $^1$H nmr spectral parameters for 2-hydroxyphenyl methyl sulfide, **2**, 2-hydroxyphenyl phenyl sulfide, **3**, and bis(2-hydroxyphenyl) disulfide, **5**

| | Value | | | | Value | | |
|---|---|---|---|---|---|---|---|
| Parameter | **2**[a] | **3**[b] | **5**[c] | Parameter | **2** | **3** | **5** |
| νOH | 649.518(2) | 635.674(2)[e] | 613.062 | $^4J_o^{H,OH}$ | −0.114(3) | −0.09(2) | −0.08(2) |
| $\nu CH_3$ | 226.974(2)[d] | — | — | $J_m^{OH,H}$ | 0.449(3) | 0.473(3) | 0.481(5) |
| $\nu_3$ | 689.093(2) | 698.486(2) | 692.452(3) | $J_p^{H,OH}$ | ≤ 0.02 | ≤ 0.02 | ≤ 0.02 |
| $\nu_4$ | 714.983(2) | 727.193(2) | 726.416(3) | $J^{H,CH}$ | ±0.04±0.01 | — | — |
| $\nu_5$ | 676.643(2) | 684.438(2) | 674.701(3) | Root-mean square deviation | 0.009 | 0.007 | 0.011 |
| $\nu_6$ | 738.529(2) | 744.625(2) | 716.157(3) | | | | |
| $^3J_{34}$ | 8.184(2) | 8.215(3) | 8.236(4) | | | | |
| $^3J_{45}$ | 7.373(2) | 7.364(3) | 7.348(5) | Peaks observed | 44[f] | 42 | 39 |
| $^3J_{56}$ | 7.718(3) | 7.743(3) | 7.774(4) | Transitions calculated | 80[g] | 80 | 80 |
| $^4J_{35}$ | 1.340(2) | 1.333(3) | 1.328(4) | | | | |
| $^4J_{46}$ | 1.675(2) | 1.694(3) | 1.694(5) | Transitions assigned | 80 | 77 | 79 |
| $^5J_{36}$ | 0.391(3) | 0.389(3) | 0.384(4) | | | | |

[a] 5 mol% in $CCl_4$.
[b] 1.8 mol% in $CCl_4$.
[c] 3 mol% in $CCl_4$.
[d] In Hz at 100.001$_2$ MHz and 305 K to low field of internal TMS. For the $C_6H_5$ group of **3**, $\nu_o$, $\nu_m$, and $\nu_p$ are 699.602(5), 713.310(4), and 703.901 (7) Hz.
[e] Numbers in parentheses are standard deviations in the last significant figure.
[f] Excluding $CH_3$ peaks.
[g] Above an intensity of 0.05.

5-methyl) sulfide, **4**, and of bis(2-hydroxyphenyl) disulfide, **5**. No evidence for OH···π bonding is found.

## Experimental

*Compounds*

The 2-hydroxyphenyl methyl sulfide, **2**, was prepared from the 2-amino derivative (Parish) via diazotization (8*b*) and **3** was prepared as follows. A mixture of 2-bromophenol (5 g, 0.029 mol), benzenethiol (3.2 g, 0.029 mol), and sodium ethoxide (4.8 g, 0.06 mol) in dry dimethylformamide (100 mL) was heated under reflux for 8 h in a nitrogen atmosphere. The reaction mixture was cooled, poured into 2 *M* HCl solution (200 mL), and the resultant milky solution was extracted with $CH_2Cl_2$ (3 × 50 mL). The combined organic extract (diphenyldisulfide, 3.2 g, 50%, was isolated from these extracts after basic extraction) was washed with water (6 × 100 mL) and then was extracted with 2 *M* NaOH (3 × 30 mL). These basic extracts were acidified with 2 *M* HCl and the mixture was extracted with $CH_2Cl_2$ (3 × 30 mL). Evaporation of the washed ($H_2O$) and dried ($MgSO_4$) organic extracts left an oil which was distilled to give **3** (1.4 g, 20%) as a clear oil, bp 95–103°C at 0.5 Torr. No attempt was made to maximize the yield. $C_{12}H_{10}OS$ requires M 202, found $M^+$202. Compound **4** came from Aldrich and **5** was formed in the presence of air in a $CCl_4$ solution of **1**.

*$^1$H nuclear magnetic resonance measurements*

Samples were prepared as dilute solutions in $CCl_4$ and contained about 4 mol% of tetramethylsilane (TMS). The solutions were degassed by the freeze–pump–thaw method and were then flame-sealed into 5 mm od nmr sample tubes. Care (9) was taken to retard intermolecular hydroxyl proton exchange.

The $^1$H nmr spectra were recorded on an HA100 spectrometer in the frequency sweep mode at a probe temperature of 305 K. Calibrations of peak positions were performed by the reading of sweep and manual oscillator frequencies for markers placed at ca. 5 Hz intervals with a dispersion of 1 Hz/cm and sweep rates of 0.02 and 0.01 Hz/s. Repetition of this procedure and interpolation yielded peak frequencies with a typical rms deviation of ≤ 0.02 Hz.

## Results and discussion

*Spectral analyses*

These used the computer program LAME (10, 11). The derived $^1$H nmr spectral parameters for **2**, **3**, and **5** are presented in Table 1. The $C_6H_5$ spectrum of **3** also yields to analysis; all but a few of its peaks could be unequivocally identified. Figure 1 provides evidence for the high spectral quality obtained in this work.

*The conformation of 2-hydroxyphenyl methyl sulfide, 2*

In **2**, $^5J_m^{H_4,OH}$ is 0.45 ± 0.01 Hz (assuming an accuracy of three times the standard deviation in Table 1), whereas in 2-hydroxythiophenol it is 0.42 ± 0.01 Hz (5). As discussed in detail for the latter compound (5), this stereospecific coupling and the absence of significant coupling to H-5 and H-6 means that at least 95% of **2** exists in a conformation containing an OH···S hydrogen bond (compare **1**); and this interaction involves a negligible out-of-plane twist about the C—O bond.

The conformation about the C—S bond in **2** can be reasonably deduced as follows. Temperature-dependent photoelectron spectra imply that the

Can. J. Chem. Downloaded from www.nrcresearchpress.com by 210.87.254.40 on 09/06/12
For personal use only.

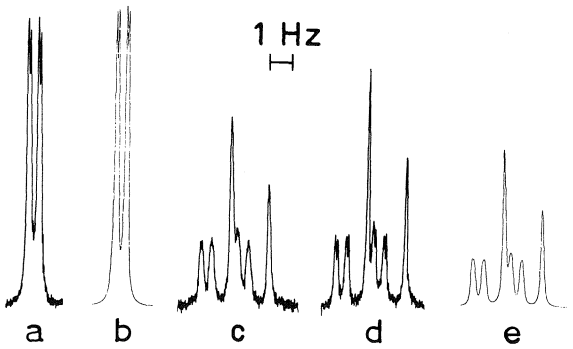


FIG. 1. In (a) is shown the hydroxyl proton spectrum of a 5 mol% solution of **2** in $CCl_4$ at 305 K and 100.001 MHz (centerband). In (b) the calculated spectrum assumes the parameters in Table 1 and a linewidth at half height of 0.10 Hz. *Parts* of the multiplets from H-3 *and* H-5 are displayed in (c), whereas (d) has the same region under conditions of methyl proton decoupling. The small coupling (0.11 Hz) of H-3 to the hydroxyl proton is apparent. In (e) the calculated spectrum assumes that H-3 and H-5 are also coupled to the methyl protons by 0.04 Hz (compare (c)). Altering this coupling by 0.02 Hz produced disagreement. It should be noted that the linewidths of all peaks from H-4 and H-6 were 0.10 ± 0.01 Hz ("spectrometer" or "sample" linewidth) and these protons are coupled to the methyl protons by ≤ 0.02 Hz.

planar ($C_2C_1SC = 0°$) form of thioanisole is favored by 3.5 kJ/mol over the (probably) perpendicular conformer (12). This number is close to the twofold barrier in thiophenol, suggesting $3p\cdots\pi$ conjugation as a major contributor to the stability of the planar forms. MO calculations are also available (13, 14). Therefore it is reasonable that in both **1** and **2** the polar O—H bond seeks the directional lone pair on sulfur, twisting it into the molecular plane and causing the S—H and S—$CH_3$ bonds to move into the perpendicular plane. This conformation of **2** should have three consequences: (*i*) the chemical shift of the methyl protons should show evidence for a perpendicular form, (*ii*) as should the ring proton shifts, and (*iii*) no proximate coupling of $CH_3$ and H-6 protons should exist.

Taking the coupling evidence first, a comparison with *ortho* substituted anisoles, **6** (X = O), is in

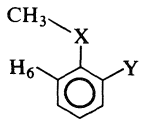


**6**

order. Because of the relatively strong conjugation when X = O, the anisoles usually favor a conformation with a zero angle of twist (15, 16) about the C—O bond (planar). As a consequence (17, 18) a proximate coupling of −0.30 ± 0.02 Hz between the methyl protons and H-6 exists. INDO MO FPT calculations (19) reproduce this phenomenon (20), which has its origin in the close approach of the coupled nuclei and/or the relevant bond orbitals. The coupling is observed also for 2-hydroxyanisole, in which an intramolecular hydrogen bond exists (18).

Now, in *ortho* substituted thioanisoles, such a coupling also occurs (21). Contrary to ref. 21, there is a $^5J_o^{H_6,CH_3}$ of (−) 0.24 Hz in 2-methoxythioanisole and of −0.36 Hz in 2,5-dichlorothioanisole.[3] These numbers and their signs are again consistent with a proximate (through-space) coupling mechanism for a preferred **6** (X = S). However, in **2**, $^5J_o^{H,CH_3}$ is not larger than 0.02 Hz in magnitude (see Fig. 1) indicating that **2**, in which the hydrogen atoms containing the coupled protons are separated by more than their Van der Waals radii, and not **6** (X = S) is the stable conformation.

Furthermore, in **2** the methyl protons resonate at $\delta_{CH_3}$ = 2.27 ppm (Table 1). In 4-hydroxythioanisole, $\delta_{CH_3}$ is 2.41 ppm and is 2.44 ppm in thioanisole (22*a*). The upfield shift in **2** is analogous to that observed for the SH proton in the corresponding hydroxythiophenol (5) and can be attributed to the magnetic anisotropy of the benzene nucleus. Similar calculations to those in refs. 5 and 22*b*, taking reasonable geometries (5, 12) for **2** and **6** (X = S), predict an upfield shift of ca. 0.3 ppm for the methyl protons in **2** relative to **6** (X = S). This is an extreme value because in 4-hydroxythioanisole the relatively low barrier to rotation about the C—S bond implies that the methyl protons sample conformations other than **6**. Therefore an upfield shift of less than 0.3 ppm is anticipated. Accordingly, the observed shift of 0.14 ppm for the methyl protons is consistent with a perpendicular conformation of **2**.

Turning to the ring proton shifts, their equality in **2** and **1** is striking (Table 2). Because the latter exists as the perpendicular **1**, the equalities suggest the same conformation for **2**. A comparison with 2-hydroxyanisole is also useful. In Table 2, two sets of predicted shifts are given, based on the shifts observed for the corresponding phenyl derivatives. One set assumes that the $SCH_3$ and $OCH_3$ substituents do not contribute to the shifts in the two disubstituted compounds. The other set assumes additive contributions from both substituents in a compound. A comparison of the mean deviations between observed and calculated shifts, $\langle\Delta\delta\rangle$, implies that the $SCH_3$ group in **2** is no longer conjugated with the $\pi$ system of the benzene nucleus.

Of course, it is known (25, 26) that a simple

[3]Unpublished work in this laboratory.

Can. J. Chem. Downloaded from www.nrcresearchpress.com by 210.87.254.40 on 09/06/12
For personal use only.

TABLE 2. $^1$H chemical shifts[a] of 1-X-2-Y benzene derivatives in $CCl_4$ solution

| X, Y | $\delta_2$ | $\delta_3$ | $\delta_4$ | $\delta_5$ | $\delta_6$ | $\delta_{CH_3(SH)}$ | $\langle\Delta\delta\rangle$[d] | Ref. |
|---|---|---|---|---|---|---|---|---|
| SH,H | 7.19 | 7.13 | 7.05 | 7.13 | 7.19 | (3.23) | — | 23 |
| $SCH_3$,H | 7.16 | 7.14 | 7.04 | 7.14 | 7.16 | 2.44 | — | 24 |
| SH,OH | — | 6.88 | 7.16 | 6.76 | 7.38 | (2.81) | — | 5 |
| $SCH_3$,OH | — | 6.89 | 7.15 | 6.77 | 7.39 | 2.27 | — | — |
| | — | (6.64)[b] | (6.89) | (6.71) | (7.01) | — | 0.24 | — |
| | — | ((6.73))[c] | ((7.10)) | ((6.82)) | ((7.10)) | — | 0.13 | — |
| OH,H | 6.73 | 7.10 | 6.82 | 7.10 | 6.73 | — | — | 9 |
| $OCH_3$,H | 6.75 | 7.15 | 6.81 | 7.15 | 6.75 | 3.76 | — | 24 |
| $OCH_3$,OH | — | 6.81 | 6.76 | 6.70 | 6.72 | 3.81 | — | 18 |
| | — | (6.63)[b] | (6.67) | (6.72) | (6.60) | — | 0.10 | — |
| | — | ((6.73))[c] | ((7.10)) | ((6.82)) | ((7.10)) | — | 0.23 | — |

[a]In ppm relative to internal TMS; different concentrations will cause variations of ca. 0.02 ppm for various measurements.
[b]On an additive basis, $\delta_{C_6H_6} = 7.25$ in $CCl_4$.
[c]Assuming only OH contributes to the shifts.
[d]The mean deviation between observed and calculated shifts for all four protons.

additivity scheme for the ring proton shifts in *ortho* disubstituted benzenes somewhat lacks predictive power, particularly for protons next to the substituents. Therefore, centering attention on $\delta_4$, i.e., for the proton placed *para* to $SCH_3$ or $OCH_3$, note that a shift to low field occurs in going from methyl phenyl sulfide to **2** whereas a high field shift occurs for the corresponding anisoles (OH causes a high field shift at a *meta* position). Accordingly, conjugation between the 3*p* orbital of the sulfur atom and the $\pi$ system has been decreased in **2**, but not between the corresponding oxygen orbitals and the $\pi$ system in 2-hydroxyanisole. In fact, a detailed comparison of $\delta_4$ in the various compounds suggests almost no conjugative electron donation by $SCH_3$ in **2**.

Note also the marked shift to low field of H-6, the proton *ortho* to the $SCH_3$ group in **2**. The so-called "heavy-atom" perturbation (27, 28) is accentuated in **2**. We attribute this shift to the proximity of the directional, mainly 3*p*, lone-pair in **2**. It should also be noted that H-6 in thiophenol or thioanisole resonates farther to low field than expected for a $\pi$ donor (compare phenol), also a "heavy-atom" effect, observable because the barrier to internal rotation in these two compounds is not large compared to thermal energies.

It seems clear that the ring proton shifts in **2** are compatible with a perpendicular conformation and not with a "planar" conformation as found for 2-hydroxyanisole. Taken together, the present $^1$H nmr data are consistent only with a relatively strong OH···3*p* hydrogen bond in **2**. Because no coupling between the hydroxyl proton and H-6 is observed, the perpendicular conformer **2** must exist to the extent of at least 95% in $CCl_4$ at 305 K. The photoelectron spectrum and a crystal structure of **2** should confirm the $^1$H nmr work. The photoelectron spectrum of thioanisole (29) is describable in terms of a 3*p* model for the delocalization of the sulfur lone pair.

*2-Hydroxyphenyl phenyl sulfide, 3*

The chemical shift of the hydroxyl proton, 6.36 ppm, and its coupling to H-4, 0.47 Hz (Table 1), imply the same conformation at sulfur and oxygen as in **2**, as does the large $\delta$ value for H-6. The four ring protons are all deshielded relative to the corresponding protons in **2**. The largest deshielding occurs for H-4, the proton most distant from the phenyl ring. If the deshielding for **3** relative to **2** arises from the magnetic anisotropy of the phenyl ring, the *only* conformation consistent with the observed $\Delta\delta_3 \sim \Delta\delta_5 < \Delta\delta_4$ is one in which the phenyl group lies roughly perpendicular to the substituted benzene plane, i.e., with a conformation **7**. For this conformation, the anisotropy model

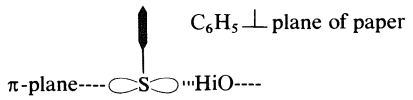


**7**

and reasonable CSC angles and C—S bond lengths (30, 31) predicts $\Delta\delta_4 > \Delta\delta_3 = \Delta\delta_5$, with $\Delta\delta_4 \sim 0.07$ ppm. $\Delta\delta_{OH}$ is calculated as 0.04 ppm. Any other conformation, reached by twisting about the $C_1$—S bond in **7**, involves striking contradictions between model and observation.

In **7** the 3*p* orbital can conjugate most effectively with the second phenyl $\pi$ system and may be favored (by about 3 kJ/mol) for this reason. Because of partial delocalization into the second phenyl, the OH···3*p* bond may also be somewhat weaker than in **2** and could account for the observed shift to high field of 0.14 ppm in **3**. An empirical relationship (32) suggests this weakening as only 0.4 to 0.8 kJ/mol. The partial delocalization

Can. J. Chem. Downloaded from www.nrcresearchpress.com by 210.87.254.40 on 09/06/12
For personal use only.

Can. J. Chem. Downloaded from www.nrcresearchpress.com by 210.87.254.40 on 09/06/12
For personal use only.

might also help to account for the $\Delta\delta_6$ of 0.06 ppm (calculated as 0.10 ppm). Of course, **7** is an idealized structure. The real conformation undergoes torsional motions, among others. Nevertheless, no other conformation is expected to display the low field shifts given in Table 1.

A further test involves $\delta_o$, $\delta_m$, and $\delta_p$ in the $C_6H_5$ group. These are 6.996, 7.133, and 7.039 ppm, respectively, from a full analysis (rms error of 0.014 Hz). Diphenyl sulfide itself may have $C_s$ or $C_2$ symmetry (30) or a twisted (33) conformation. The experimental uncertainties imply marked freedom of motion about the C—S bonds. In $CS_2$ solution, $\delta_o$, $\delta_m$, $\delta_p$ are 7.264, 7.235, 7.170 ppm (33). The striking shift in **3** is $\delta_o$, which now lies at highest field. Indeed, structure **7** places an *ortho* proton into the shielding region of the other benzene ring, so that, on average, the anisotropy model predicts an upfield shift of ca. 0.5 ppm. The observed value relative to diphenyl sulfide is 0.27 ppm. The $C_6H_5$ group is constrained to **7** by only 3 kJ/mol. Therefore it will sample other conformations as well and these have lower anisotropy shifts for the *ortho* protons. Considering the approximate nature of the anisotropy model and the $CS_2$ solvent for diphenyl sulfide, the agreement is satisfactory. Further, $\Delta\delta_m$ is calculated as 0.12 ppm (observed 0.10 ppm) and $\Delta\delta_p$ as 0.05 ppm (observed 0.13 ppm). $\Delta\delta_p$ is independent of the orientation about the $C_1$—S bond. Therefore the additional shift to high field is very likely due to the enhanced $3p,\pi$ conjugation relative to diphenyl sulfide. In fact, in benzenethiol $\delta_p$ is 7.05 ppm (Table 2).

Taken together, the shift and coupling data for **3** firmly imply **7** as the low energy conformation in solution, with the provision that the $C_6H_5$ group is relatively weakly constrained in its motion about the C—S bond. Conformation **7** is usually called a skew conformation (34).

*Bis(2-hydroxy-3-*tert*-butyl-5-methyl) sulfide, 4*

This compound was examined for two reasons. First, its infrared spectrum has been interpreted in terms of two different intramolecular OH···π bonds, together with simultaneous OH···π and OH···O interactions for one hydroxyl group and out-of-plane twisting of both hydroxyl groups (3). Second, these interpretations have been used in $^1H$ and $^{13}C$ nmr studies of related compounds (4).

The most interesting spectral parameters are $\delta_{OH} = 6.42_0$ ppm (3 mol% in $CCl_4$) and $^5J_m^{OH,H_4} = 0.59 \pm 0.04$ Hz (three times the standard deviation). The magnitude of $^5J_m$ is that expected for a trisubstituted phenol (35) and indicates a conformation in which the OH···S bond predominates. No coupling between the hydroxyl and methyl protons was observed. A finite coupling is expected if **4** takes on conformations in which the hydroxyl groups are rotated away from the planes of their respective benzene rings. Again, the hydroxyl proton shift agrees with an OH···S hydrogen bond (compare numbers in Table 1) but not with extensive OH···π interaction. In comparison, the analogous parameters (36) for 2-benzyl-4-chlorophenol imply an intramolecular OH···π interaction of about 1 kJ/mol in free energy, but note that there $\delta_{OH}$ is 4.43 ppm (3 mol% in $CCl_4$ and 305 K).

Characteristic broadening of the H-4 peaks ($6.94_5$ ppm) by small couplings with the *tert*-butyl protons gave an unequivocal assignment of the ring proton shifts with H-6 at $6.90_3$ ppm. In a 2 mol% solution in $CCl_4$ of 2-*tert*-butylphenol, $\delta_3$ is 7.16 ppm and $\delta_5$ is 6.94 ppm. A methyl group causes an upfield shift of 0.18 ppm at an *ortho* position (25). In the absence of sulfur, additivity of shifts predicts $\delta_4$ as 6.98 and $\delta_6$ as 6.76 ppm in **4**. In the gable (butterfly) conformation, in which two OH···3*p* interactions exist (on either end of the 3*p* orbital), the anisotropy of the phenyl groups should cause $\delta_6 = 6.89$ and $\delta_4 = 6.93$ ppm, effectively identical to the observed shifts.[4]

In other words, the present model implies that the low-field shift caused by a coplanar 3*p* orbital at an *ortho* proton, as discussed above for **1** to **3**, is *absent* if the 3*p* orbital is involved in two OH···3*p* hydrogen bonds. This implication is intriguing in terms of chemical shift theory (note that the electronegativity of a $C_6H_5S$ group is thought to be 2.0, i.e., probably the same as that of hydrogen (30)). A first test demands a structure determination of **4** or of 2,2′-dihydroxydiphenyl sulfide.

The detailed $^1H$ nmr data provide no evidence for other than OH···S preferences in **4**.

*Bis(2-hydroxyphenyl) disulfide, 5*

The conformations of diphenyldisulfides have received much experimental (37–39) and theoretical (40–43) attention. Here we take a simple view designed to rationalize the observed chemical shifts in terms of one conformation.

The dihedral angle in $H_2S_2$ is ca. 90° and the HSS angle is also near 90° (44). The filled 3*p* lone pair electrons minimize their mutal repulsion by a twist of 90° to give the observed conformation. If hydrogen atoms are replaced by phenyl groups, the CSSC dihedral angle remains near 90° (38, 45, 46). Furthermore if $3p,\pi$ conjugation is to be maintained, then the CCSS torsion angles are favored at 0°, yielding the observed *equatorial* (47) conformation. In the latter, an *ortho* proton again lies near a

[4]If $\delta_{OH} = 6.03$ ppm from **1** is taken as a reference, the anisotropy model predicts $\delta_{OH}$ as 6.35 ppm (6.42 observed).

Can. J. Chem. Downloaded from www.nrcresearchpress.com by 210.87.254.40 on 09/06/12
For personal use only.

3*p* orbital of the *other* $SC_6H_5$ fragment. The closest H···S distance of about 2.3 Å is much smaller than that of 3.0 Å in **2**. In terms of the discussion in previous sections, this proximity accounts for the large $\delta_o$ of 7.44 ppm in equatorial diphenyl disulfide (the phenyl rings reorient rapidly about the C—S bonds and S—S bonds on this shift scale).

Now, for **5**, $\delta_{OH}$ is 6.13 ppm (similar to the 6.04 ppm in 2-hydroxythiophenol) and $^5J_m^{OH,H_4}$ is 0.48 Hz. Intramolecular hydrogen bonds exist, therefore. The equatorial form of **5** would imply hydrogen bonding to the diffuse 3*s* lone pair on the *ortho* sulfur atom. However, a further twist of 90° about each C—S bond produces the *axial* form in which OH···3*p* bonds can exist. In this form **8**, the hydroxyl groups lie on one side of the molecule, which brings the H-6 protons close to the neighbouring rings but outside each other's contact distance. 3*p*,π conjugation is largely lost and there is a $C_2$ axis perpendicular to the S—S bond.

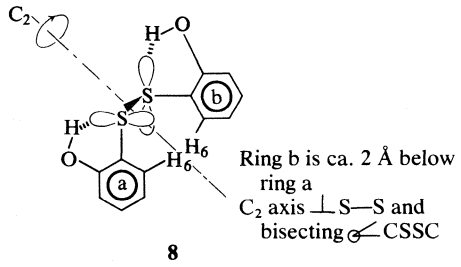


**8**

The anisotropy model for the benzene ring and reasonable geometry about sulfur (37) predicts that for **8**, O—H, H-3, and H-4 should shift (downfield) by 0.09, 0.04, and 0.02 ppm, respectively; whereas H-5 and H-6 should shift (upfield) by −0.03 and −0.36 ppm, respectively. In the above order, the observed shifts relative to **1** are 0.10, 0.04, 0.10, −0.03, and −0.22 ppm. Considering that **8** is not rigid and that the reference compound is not ideal, the agreement is satisfactory. A number of other possible conformers produced much larger discrepancies between observed and calculated shifts. Anisotropy models are semiquantitative at best, of course. The present results provide *no* evidence for OH···π interactions (3). It is of interest that the corresponding diamino compound has this conformation in the crystal, i.e., axial with the amino groups on the same side of the molecule (38, 45). From our viewpoint, this conformation is expected. Again, the corresponding dinitro compound has an equatorial form (48), as anticipated because of the absence of a stereospecific hydrogen bond and probably also because the nitro groups enhance the 3*p*,π conjugation (37, 49).

3,3′-Dihydroxy-2-pyridyl disulfide adopts the equatorial conformation (37) in the crystal. There is one *inter*molecular OH···N hydrogen bond and the other hydroxyl group in the molecule is not involved in hydrogen bonding. Conformation **8** would bring the (negatively charged) nitrogen atoms to within about 3 Å (they replace the C—$H_6$ bonds in **5**). It is quite possible that the N,N electrostatic repulsion, together with the lack of 3*p*,π conjugation, in a conformation **8** is higher in energy than the observed conformation in which 3*p*,π conjugation is retained and one OH···N intermolecular hydrogen bond occurs.

The model used for all the molecules in this paper distinguishes between mainly *s* and mainly *p* type lone-pair orbitals on sulfur. The model rationalizes the approximately perpendicular conformation deduced for **1** (5). The pressure to keep 3*s* orbitals fully occupied (50) supports the simple viewpoint taken in the present discussion. Furthermore, equilibrium bond electron densities can be bent away from the corresponding internuclear axes in a variety of molecules (51). There is also considerable evidence for a nonspherical shape of sulfur in crystals, giving rise to directional preferences in interactions with divalent sulfur (52). In particular, electrophiles approach sulfur in a plane roughly perpendicular to the X—S—Y plane.

The present model is similar to one which would be based on canonical molecular orbitals obtained from, say, single-determinant molecular orbital calculations. An alternative approach would invoke localized molecular orbitals giving equivalent, roughly $sp^3$, lone-pairs on sulfur. This approach could not account in a straightforward way for the observed conformation of **1**, for example, simply because of the equivalency of the lone-pairs (see ref. 53 for a nice discussion of canonical and localized molecular orbitals). An X-ray investigation of **2** would decide the quality of the model used in this paper.

## Acknowledgments

We are grateful to Dr. L. Kruczynski and Dr. R. Laatikainen for their help with the synthesis of 2-hydroxyphenyl methyl sulfide and with the analysis of the phenyl $^1$H nmr spectrum of 2-hydroxyphenyl phenyl sulfide. The Natural Sciences and Engineering Research Council of Canada gave essential financial support. We thank a referee for useful criticism.

1. H. S. Aaron. Top. Stereochem. **11**, 1 (1979).
2. A. D. U. Hardy and D. D. MacNicol. J. Chem. Soc. Perkin Trans. II, 1140 (1976).
3. S. Kovac, E. Solcaniova, and J. Baxa. Tetrahedron, **27**, 2823 (1971).
4. B. Norden, U. Edlund, and C-A. Nilsson. Org. Magn. Reson. **13**, 391 (1980).

5. T. SCHAEFER, T. A. WILDMAN, and S. R. SALMAN. J. Am. Chem. Soc. **102**, 107 (1980).
6. N. W. LARSEN and F. M. NICOLAISEN. J. Mol. Struct. **22**, 29 (1974).
7. E. MATHIER, D. WELTI, A. BAUDER, and Hs. H. GUNTHARD. J. Mol. Spectrosc. **37**, 63 (1971).
8. (*a*) H. D. BIST, J. C. D. BRAND, and D. R. WILLIAMS. J. Mol. Spectrosc. **24**, 402 (1967); (*b*) H. S. HOLT and E. E. REID. J. Am. Chem. Soc. **46**, 2333 (1924).
9. T. SCHAEFER, J. B. ROWBOTHAM, and K. CHUM. Can. J. Chem. **54**, 3666 (1976).
10. S. CASTELLANO and A. A. BOTHNER-BY. J. Chem. Phys. **41**, 3863 (1964).
11. C. W. HAIGH. Ann. Rep. NMR Spectrosc. **4**, 311 (1971).
12. A. SCHWEIG and N. THON. Chem. Phys. Lett. **38**, 482 (1976).
13. T. MATSUSHITA, Y. OSAMURA, N. MISAWA, K. NISHIMOTO, and Y. TSUNO. Bull. Chem. Soc. Jpn. **52**, 2521 (1979).
14. A. ALBERTI, M. GUERRA, G. MARTELLI, F. BERNARDI, A. MANGINI, and G. F. PEDULLI. J. Am. Chem. Soc. **101**, 4627 (1979).
15. D. G. LISTER. J. Mol. Struct. **68**, 33 (1980).
16. G. M. ANDERSON III, P. A. KOLLMAN, L. N. DOMELSMITH, and K. N. HOUK. J. Am. Chem. Soc. **101**, 2344 (1979), and references therein.
17. H. A. GAUR, J. VRIEND, and W. G. B. HUYSMANS. Tetrahedron Lett. 1999 (1966).
18. T. SCHAEFER and T. A. WILDMAN. Can. J. Chem. **57**, 450 (1979).
19. T. SCHAEFER, H. D. GESSER, and J. B. ROWBOTHAM. Can. J. Chem. **54**, 2235 (1976).
20. J. HILTON and L. H. SUTCLIFFE. Prog. NMR Spectrosc. **10**, 27 (1975).
21. L. LUNAZZI and D. MACCIANTELLI. J. Chem. Soc. Chem. Commun. 933 (1971).
22. (*a*) S. H. MARCUS, W. F. REYNOLDS, and S. I. MILLER. J. Org. Chem. **31**, 1872 (1966); (*b*) R. J. ABRAHAM, S. C. M. FELL, and K. M. SMITH. Org. Magn. Reson. **9**, 367 (1977).
23. W. J. E. PARR and T. SCHAEFER. Can. J. Chem. **25**, 171 (1977).
24. G. LLABRÉS, M. BAIWIR, L. CHRISTIAENS, J. DENOEL, L. LAITEM, and J.-L. PIETTE. Can. J. Chem. **56**, 2008 (1978).
25. P. DIEHL. Helv. Chim. Acta, **44**, 829 (1961).
26. J. S. MARTIN and B. P. DAILEY. J. Chem. Phys. **39**, 1722 (1963).
27. T. SCHAEFER, W. F. REYNOLDS, and T. YONEMOTO. Can. J. Chem. **11**, 2969 (1963).
28. I. MORISHIMA, A. MIZUNO, and T. YONEZAWA. Chem. Phys. Lett. **7**, 633 (1970).
29. H. BOCK, G. WAGNER, and J. KRONER. Chem. Ber. **105**, 3850 (1972).
30. B. ROZSONDAI, G. SCHULTZ, and I. HARGITTAI. J. Mol. Struct. **70**, 309 (1981).
31. N. GOODHAND and T. A. HAMOR. J. Fluorine Chem. **14**, 223 (1979).
32. T. SCHAEFER. J. Phys. Chem. **79**, 1888 (1975).
33. G. LLABRÉS, M. BAIWIR, L. CHRISTIAENS, and J.-L. PIETTE. Can. J. Chem. **57**, 2967 (1979).
34. S. P. N. VAN DER HEIJDEN, E. A. H. GRIFFITH, W. D. CHANDLER, and B. A. ROBERTSON. Can. J. Chem. **53**, 2084 (1975).
35. J. B. ROWBOTHAM and T. SCHAEFER. Can. J. Chem. **52**, 3037 (1974).
36. T. SCHAEFER, R. SEBASTIAN, and T. A. WILDMAN. Can. J. Chem. **57**, 3005 (1979).
37. L. S. HIGASHI, M. LUNDEEN, and K. SEFF. J. Am. Chem. Soc. **100**, 8101 (1978), and references therein.
38. J. D. LEE and M. W. R. BRYANT. Acta Crystallogr. Part B, **25**, 2094 (1969); Part B, **26**, 1729 (1970).
39. F. P. COLONNA, G. DISTEFANO, V. GALASSO, K. J. IRGOLIC, G. C. PAPPALARDO, and L. POPE. J. Chem. Soc. Perkin Trans. II, 281 (1981).
40. H. E. VAN WART, L. L. SHIPMAN, and H. A. SCHERAGA. J. Phys. Chem. **79**, 1436 (1975).
41. C. J. SIMMONS, M. LUNDINE, and K. SEFF. Inorg. Chem. **18**, 3444 (1979), and references therein.
42. H. KESSLER and W. RUNDEL. Chem. Ber. **101**, 3350 (1968).
43. J. P. SNYDER and L. CARLSEN. J. Am. Chem. Soc. **99**, 2931 (1977).
44. G. WINNEWISER, M. WINNEWISSER, and W. GORDY. J. Chem. Phys. **49**, 3465 (1968).
45. N. V. RAGHAVAN and K. SEFF. Acta Crystallogr. Part B, **33**, 386 (1977).
46. M. SACERDOTI, G. GILLI, and P. DOMIANO. Acta Crystallogr. Part B, **31**, 327 (1975).
47. E. SHEFTER. J. Chem. Soc. B, 903 (1970).
48. E. SHEFTER and T. I. KALMAN. Chem. Commun. 1027 (1969).
49. T. SCHAEFER and T. A. WILDMAN. Chem. Phys. Lett. **80**, 280 (1981).
50. M. B. HALL. J. Am. Chem. Soc. **100**, 6333 (1978).
51. D. M. CHIPMAN, W. E. PALKE, and B. KIRTMAN. J. Am. Chem. Soc. **102**, 3377 (1980).
52. T. N. GURO ROW and R. PARTHASARATHY. J. Am. Chem. Soc. **103**, 477 (1981).
53. S. WOLFE, M.-H. WHANGBO, and D. J. MITCHELL. Carbohydr. Res. **69**, 1 (1979).


Can. J. Chem. Downloaded from www.nrcresearchpress.com by 210.87.254.40 on 09/06/12
For personal use only.

# Structure in the solid state and conformational analysis in solution of 1,4-diacetyl-1,4-dihydro-2,3-diphenylpyrazine, a potential antiaromatic heterocyclic compound

JOSEPH ARMAND

*Laboratoire de Physicochimie des Solutions, Laboratoire Associé CNRS no 161, Université Pierre et Marie Curie, Bâtiment F, 8, Rue Cuvier, 75230 Paris Cedex 05, France*

CLAUDETTE BOIS AND MICHÈLE PHILOCHE-LEVISALLES

*Laboratoire de Chimie Systématique, Université Pierre et Marie Curie, Bâtiment F, 8, Rue Cuvier, 75230 Paris Cedex 05, France*

AND

MARIE-JOSÉ POUET AND MARIE-PAULE SIMONNIN

*Laboratoire de Spectroscopie, Laboratoire Associé CNRS no 161, E.N.S.C.P. 11 rue Pierre et Marie Curie, 75231 Paris Cedex 05, France*

Received June 9, 1981

JOSEPH ARMAND, CLAUDETTE BOIS, MICHÈLE PHILOCHE-LEVISALLES, MARIE-JOSÉ POUET, and MARIE-PAULE SIMONNIN. Can. J. Chem. **60**, 349 (1982).

It is shown by X-ray crystallography that the 1,4-dihydropyrazine skeleton of 1,4-diacetyl-1,4-dihydro-2,3-diphenylpyrazine **2** has a boat shape. The C(2)–C(3) and C(5)–C(6) double bonds are localized; therefore **2** does not exist as an azahomoaromatic entity with 6 electrons delocalized on the ring and two electrons localized on one nitrogen atom. In the solid state **2** is in a *Z,Z* conformation. The $^1H$ and $^{13}C$ nmr spectra indicate that **2** exists as an equilibrium mixture of *Z,E*, *E,E*, and *Z,Z* conformers in $CD_2Cl_2$ at −80°C. An unambiguous assignment of the different sets of signals has been obtained by nOe experiments performed at −80°C. The conformer distribution is the following: 65% (*Z,E*), 22% (*E,E*), and 13% (*Z,Z*). The relatively low barrier to rotation about the carbonyl nitrogen bonds of the two amide groups ($\Delta G_c^{\neq} \sim 13$ kcal/mol) is in line with a rather large C—N bond length (~1.37$_5$ Å) in the crystal.

---

JOSEPH ARMAND, CLAUDETTE BOIS, MICHÈLE PHILOCHE-LEVISALLES, MARIE-JOSÉ POUET et MARIE-PAULE SIMONNIN. Can. J. Chem. **60**, 349 (1982).

Les données cristallographiques obtenues par diffraction des rayons X montrent que le noyau de la 1,4-diacetyl-1,4-dihydro-2,3-diphenylpyrazine **2** se présente sous la forme d'un bateau sensiblement symétrique. Les doubles liaisons C(2)–C(3) et C(5)–C(6) sont localisées: **2** n'a donc pas une structure de type azahomoaromatique comprenant un ensemble de 6 électrons π délocalisés et une paire d'électrons localisée sur un atome d'azote. A l'état solide **2** adopte une conformation *Z,Z*. Les spectres rmn $^1H$ et $^{13}C$ de **2** indiquent que les trois conformations *Z,E*, *E,E* et *Z,Z* coexistent à −80°C dans $CD_2Cl_2$. Des expériences de nOe effectuées à −80°C ont permis d'attribuer sans ambiguité les différents signaux à chacun de ces conformères. Leurs populations sont respectivement de 65% (*Z,E*), 22% (*E,E*) et 13% (*Z,Z*). La barrière à la rotation autour des liaisons carbone–azote des groupes amides est relativement faible ($\Delta G^{\neq} \sim 13$ kcal/mol), en accord avec la longueur des liaisons C—N (~1.37$_5$ Å) dans le cristal.

## Introduction

The replacement of an ethylene group of cyclooctatetraene by a >N–R group leads to derivatives of 1-*H*-azepine which are potential 8π-electron systems with antiaromatic character (1). But, like cyclooctatetraene (2, 3), these compounds are not planar. X-ray crystallographic study of **1** has shown (4) that the N(1), C(4), and C(5) atoms lie above the best plane through the atoms C(2), C(3), C(6), and C(7) (structure **1***a*). The double bonds are localized at C(2)–C(3), C(4)–C(5), and C(6)–C(7). These results show that 1-*H*-azepines exhibit little propensity to exist as an azahomoaromatic entity (structure **1***b*).

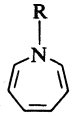

**1**, R = $SO_2C_6H_4pBr$

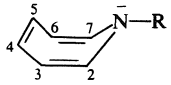

**1***a*

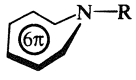

**1***b*

Replacing two opposite ethylene groups in cyclooctatetraene by two N—R groups yields derivatives of 1,4-dihydropyrazine which are also potential 8π-electron systems. 1,4-Dihydropyrazines are very easily oxidized and cannot in general be isolated (5). Only a few stable *N,N'*-substituted derivatives are known: *N,N'*-dialkyl- and *N,N'*-diaryl-1,4-dihydro-2,6-diphenylpyrazines (e.g. **3**) (6) and 1,4-diacetyl-1,4-dihydro-2,3-diphenylpyrazine **2** (7).

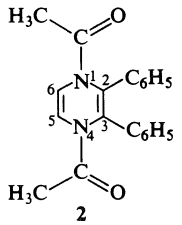

**2**

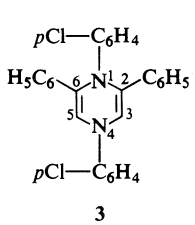

**3**

An X-ray structural analysis of **3** has already been made (8). Its skeleton was found to be an

0008-4042/82/030349-06$01.00/0

©1982 National Research Council of Canada/Conseil national de recherches du Canada

Can. J. Chem. Downloaded from www.nrcresearchpress.com by 210.87.254.5 on 09/06/12
For personal use only.

Can. J. Chem. Downloaded from www.nrcresearchpress.com by 210.87.254.5 on 09/06/12
For personal use only.

unsymmetrical boat and this led Schmidt *et al.* (9) to propose that its structure would be similar to that of **1***b*, namely that the 8π system would be divided into two parts, a delocalized 6π system and a lone pair localized on a nitrogen. This asymmetry could be caused by the two phenyl groups on carbon atoms α to one nitrogen.

We report in the first part of this paper an X-ray structure analysis of **2**. This molecule was selected since, if Schmidt's hypothesis is correct, the skeleton of **2** should be a half-boat because it has a plane of symmetry perpendicular to the N–N axis. On the other hand, it is possible that the presence of the electron-withdrawing substituents on the nitrogen atoms might cause the skeleton to be nearly planar, i.e. antiaromatic in character.

In the second part of this paper we report a conformational study of **2** in solution using $^1H$ and $^{13}C$ nmr. While an extensive study of monoamides (10) and a conformational study of diacetamide (11) have been made, there is to our knowledge no report regarding *N,N'*-diacetyl derivatives of *N*-heterocyclic compounds. Compound **2** appears to be a good model for such studies since there is no apparent steric interaction with the acetyl groups and we have been able to compare the solid state and solution results.

## 1. Structure in the solid state

Tables of atomic positions, bond lengths, bond angles, of some selected dihedral angles, of observed and calculated structure factor amplitudes, and of temperature factors were put on deposit.[1] Figures 1 and 2 give some crystallographic results of **2** and **3**. Figures 3 and 4 are ORTEP diagrams of the crystal structure of **2**.

The carbon atoms of the 1,4-dihydropyrazine ring are nearly coplanar, as indicated by the dihedral angle C(6)C(5)C(3)C(2) (2.6°).

The conformation of the 1,4-dihydropyrazine ring corresponds to a boat form displaying a good mirror symmetry as shown by the values of the α and β angles (Fig. 2) as well as by the similarity of the N(1)C(2) and N(4)C(3), N(1)C(6) and N(4)C(5) distances. In the same way, the values of the C(3)C(2)N(1), C(2)N(1)C(6), and N(1)C(6)C(5) angles are nearly equal to that of the C(2)C(3)N(4), C(3)N(4)C(5), and N(4)C(5)C(6) angles. Points N(1),A, B,N(4) are nearly coplanar, this mediating plane is nearly perpendicular to the C(2)C(3)C(5)C(6) plane (angle equal to 88.5°).

[1]A complete set of tabular data is available, at a nominal charge, from the Depository of Unpublished Data, CISTI, National Research Council of Canada, Ottawa, Ont., Canada K1A 0S2.

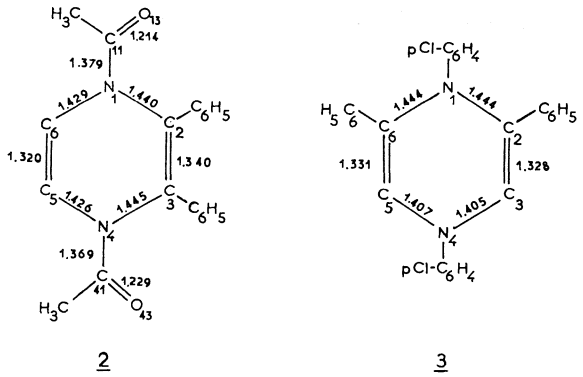


FIG. 1. Bond lengths within **2** and **3**.

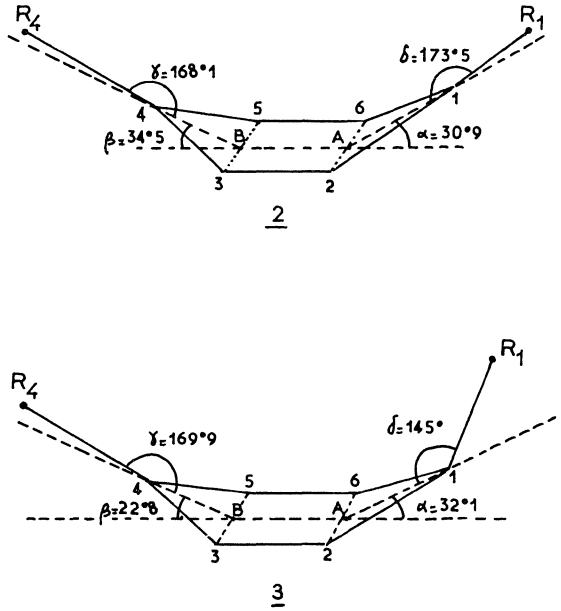


FIG. 2. Angles α, β, γ, and δ within **2** and **3**.

Both phenyl rings make an angle with the mean C(2)C(3)C(5)C(6) plane which precludes any conjugation with the C(2)C(3) double bond. Thus the dihedral angle is 34.2° in the case of $\phi_2$ and 80.3° in the case of $\phi_3$. The angle between $\phi_2$ and $\phi_3$ is 73°.

As could be expected for this diamide, atoms N(1), C(11), C(12), and O(13) on one side and N(4), C(41), C(42), and O(43) on the other side are coplanar. The angles between these planes and the mediating plane of the cycle N(1)ABN(4) are respectively 78.9° and 85.5°. As shown in Fig. 3, both amide groups present a *Z* conformation. These conformations correspond to a minimum of steric hindrance as the methyl groups lie on the less hindered side of the molecule. For each of these

Can. J. Chem. Downloaded from www.nrcresearchpress.com by 210.87.254.5 on 09/06/12
For personal use only.

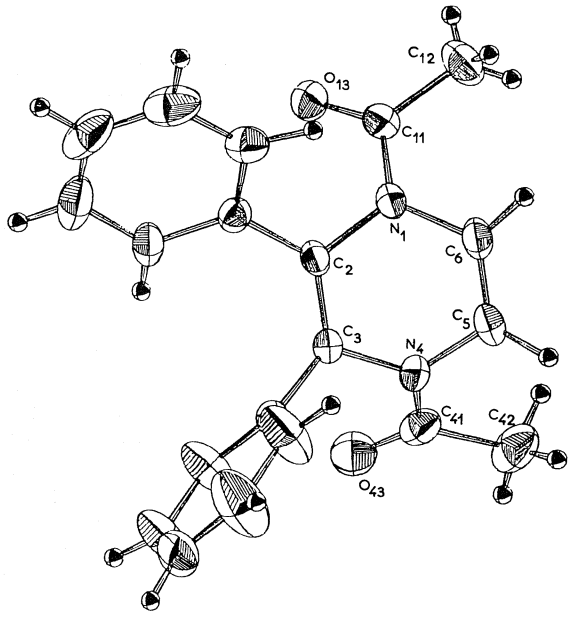


FIG. 3. ORTEP diagram of the crystal structure of **2**.

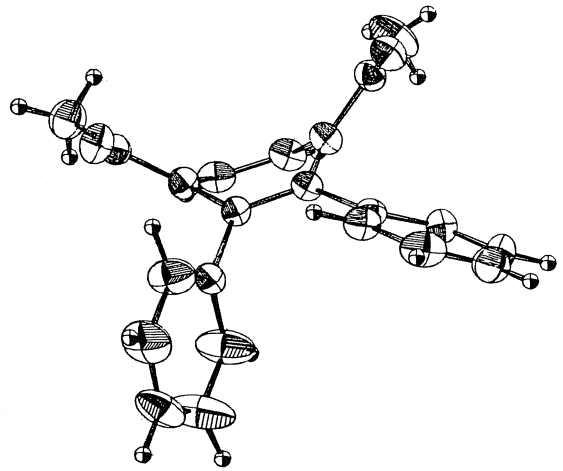

FIG. 4. ORTEP diagram of the crystal structure of **2**.

amide groups the C—O length is slightly shorter than for the open chain alkylamides (~1.24 Å), but the C—N length is somewhat longer (~1.32 Å). The large values of the γ and δ angles (Fig. 2) should be noticed, together with the valency angles around N(1) and N(4) implying a substantial $sp_2$ character for the nitrogen atoms (C(2)N(1)C(11): 121.8°; C(6)N(1)C(11): 122.6°; C(2)N(1)C(6): 115.1°; C(3)N(4)C(41): 121.2°; C(5)N(4)C(41): 123.0°; C(3)-N(4)C(5): 114.3°).

*Discussion*

The main feature of this structure is that the skeleton of this heterocycle is not planar as had been supposed (7). Its nearly symmetrical boat shape rules out the hypothesis of the separation of the eight π electrons into 6 electrons delocalized on the ring and two electrons localized on one of the nitrogen atoms. This hypothesis is also disproved by the values of the C(2)C(3) and C(5)C(6) bond length. In the case of **2** as well as in the case of **3** a mean value of 1.33 Å is obtained; these values correspond to localized ethylenic bonds as the C=C length is 1.34 Å in ethylene and 1.35 Å in cyclooctatetraene (12).

Structures **2** and **3** are thus similar to that of azepine **1** and cyclooctatetraene. They feature localized double bonds and absence of conjugation with the lone pairs of the nitrogen atoms. The difference between the α and β angles in **3** may be assigned to the disymmetry of the molecule (two hydrogens in the 3- and 5-positions, two phenyls in the 2- and 6-positions). The 1,4-dihydropyrazines escape the instability related to antiaromaticity in the same way as cyclooctatetraene and 1-*H*-azepines through the nonplanarity of the heteroaromatic ring.

Another interesting point should be brought forward. The dihedral angle between the mean N(1)C(2)C(3)N(4) and N(1)C(5)C(6)N(4) planes is equal to 38.2° and it has been shown that the 1,5-dihydroalloxazines **4** and **5** present an angular shape (13, 14), the analogous angles being 32° and 35.5° respectively. In the case of **4**, it has been

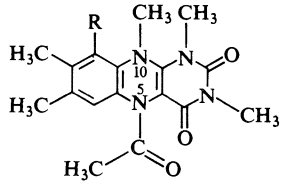


**4** R = H **5** R = Br

shown that the observed interannular angle is at an energy minimum (13). The central ring of **4** and **5** is a 1,4-dihydropyrazine; a good agreement is thus observed between the values of this angle for compounds **2**, **4**, and **5**.

### 2. Conformational study in solution

A variable temperature $^1H$ and $^{13}C$ nmr study of 1,4-diacetyl-1,4-dihydro-2,3-diphenylpyrazine **2** was performed to determine which of the three possible conformers *Z,E*, *E,E*, or *Z,Z* is preferred in solution.

Symmetry arguments allow us to predict that two distinct methyl signals should be observed for the *Z,E* conformer, while only one methyl signal is expected for each of the *E,E* and *Z,Z* conformers. Similarly, the ethylenic protons H(5) and H(6) are

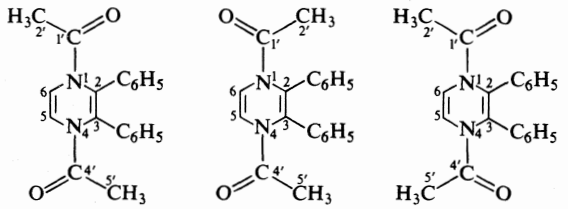

*Z,E* *E,E* *Z,Z*

anisochronous in the *Z,E* conformation and may give rise to an AB system, while they become isochronous in the *E,E* and in the *Z,Z* conformers and their resonance should be a singlet in both cases. Moreover, the aromatic rings bonded to the carbons C(2) and C(3) lie out of the plane of the double bond C(2)–C(3) and it can be anticipated that the $^1$H methyl signal of the *E,E* conformer and one of the methyl signals of the *Z,E* conformer will be shielded by the aromatic ring current.

*$^1$H nuclear magnetic resonance spectra*

At ambient probe temperature (31°C), the 100 MHz $^1$H spectrum of **2** dissolved in $CD_2Cl_2$ showed only one methyl signal (δ 1.80 ppm) and one singlet for the ethylenic protons (δ 6.60 ppm). This spectrum indicates that rotation around the N—CO bond is fast on the nmr time scale at 31°C. Broadening of the signals occurred on decreasing the temperature and a well resolved spectrum was obtained at −80°C. The methyl resonance was split into four lines, two of which had the same intensity, thus showing that the three conformers *Z,E*, *E,E*, and *Z,Z* coexist at −80°C. A five-line pattern was observed at low field instead of the six lines expected for the resonances of the ethylenic H(5)/H(6) protons in the three conformers, i.e. a singlet was superimposed on the low field component of the AB system due to the *Z,E* conformer.

Nuclear Overhauser enhancement (nOe) experiments were performed at −80°C to identify the ethylenic protons which are located spatially close to a methyl group, i.e. in a *Z* conformation. Successive irradiation of the two upfield methyl signals (δ 1.59 and 1.62 ppm) did not produce any detectable enhancement of the ethylenic resonances, while irradiation of the two downfield methyl signals (δ 2.15 and 2.17 ppm) resulted respectively in about 15% and 28% enhancement of the upfield part of the ethylenic resonances. This result indicates that the two methyl groups at low field are *syn* to the upfield ethylenic protons (*Z* conformation) and allows an unambiguous assignment to be made of the low temperature spectrum (Table 1).

The relative populations of the three conformers were obtained by integration of the ethylenic and of the methyl signals at −80°C: *Z,E*: 65%; *E,E*: 22%; *Z,Z*: 13%.

TABLE 1. The $^1$H nmr parameters of the *Z,E*, *E,E*, and *Z,Z* conformers of **2**[a]

| Conformer | $\delta_{H(5)}$ | $\delta_{H(6)}$ | $\delta_{H(2')}$ | $\delta_{H(5')}$ | $^3J_{H(5)H(6)}$ |
|---|---|---|---|---|---|
| *Z,E* | 7.05 | 6.58 | 2.15 | 1.59 | 4.5 |
| *E,E* | 7.07 | | 1.62 | | |
| *Z,Z* | 6.54 | | 2.17 | | |

[a] Temperature −80°C, solvent $CD_2Cl_2$. Chemical shifts in ppm from internal TMS; *J* in Hz. Averaged chemical shifts at ambient probe temperature: H(5)/H(6): 6.80; H(2')/H(5'): 1.80 ppm.

Upon increasing the temperature, a reversible coalescence of the methyl signals and of the ethylenic lines was observed. Three coalescence temperatures were determined for the coalescence of the methyl signals: −38°C for the two lowfield resonances ($\Delta\nu$ = 1.8 Hz), −29°C for the two high-field resonances ($\Delta\nu$ = 3.1 Hz), and −2°C for the two partially coalesced signals ($\Delta\nu$ = 52.5 Hz). A free energy of activation $\Delta G_c^{\ddagger} \sim 13$ kcal/mol was calculated from these three sets of data, using the approximate Gutowsky–Holm formula (15).

*$^{13}$C nuclear magnetic resonance spectra*

At ambient probe temperature, the 25.17 MHz proton noise decoupled $^{13}$C spectrum of **2** was averaged and the assignment of the observed eight lines was straightforward. Below −50°C the rotation around the N—CO bonds becomes slow enough to allow an individual set of signals to be observed for each of the three conformers. Between −50° and −80°C, the resonances of C(2)/C(3) and of carbonyl carbons C(1')/C(4') gave four distinct lines, while only three lines were observed for C(5)/C(6) and for the methyl carbons C(2')/C(5') (Table 2).

Selective proton irradiation and off-resonance decoupling experiments (16) were performed to assign the low temperature $^{13}$C signals. Due to the existence of a two bond $^2J_{CH}$ coupling constant, the carbonyl resonances could be assigned unambiguously.

The four CO resonances observed in the low temperature proton noise decoupled $^{13}$C spectrum indicate that shielding of $^{13}$CO increases in the order: C(1') (*Z,E*) < C(1')/C(4') (*E,E*) < C(4') (*Z,E*) < C(1')/C(4') (*Z,Z*).

The relative populations of the three conformers were calculated from the intensities of the four carbonyl signals and the results are identical to those obtained from low temperature $^1$H spectra.

## Discussion

While assignments deduced from chemical shifts are not reliable, nOe has been shown to be the method of choice in conformational studies of tertiary amides (17). However, it was emphasized that these experiments have to be performed at a sufficiently low temperature ($T \ll T_c$) to avoid

Can. J. Chem. Downloaded from www.nrcresearchpress.com by 210.87.254.5 on 09/06/12
For personal use only.

TABLE 2. $^{13}C$ chemical shifts of the $Z,E$, $E,E$ and $Z,Z$ conformers of **2**[a]

| Conformer | $\delta_{C(1')}$ | $\delta_{C(4')}$ | $\delta_{C(5)}$ | $\delta_{C(6)}$ | $\delta_{C(2')}$ | $\delta_{C(5')}$ |
|---|---|---|---|---|---|---|
| $Z,E$ | $167.3_3$ | $168.8_2$ | $119.5_5$ | $120.0_6$ | $23.3_4$ | $25.0_1$ |
| $E,E$ | $168.4_7$ | | $119.2_4$ | | $25.1_4$ | |
| $Z,Z$ | $167.1_3$ | | $120.0_6$ | | $23.3_4$ | |

[a] Temperature −80°C, solvent $CD_2Cl_2$. Chemical shifts in ppm from internal TMS. Averaged chemical shifts at ambient probe temperature:



$C_i$: 135.4$_5$ $C_o$: 130.9$_9$ $C_p$: 128.4$_3$ $C_m$: 127.9$_3$
C(1')/C(4'): 167.8$_5$ C(5)/C(6): 119.8$_3$ C(2)/C(3): 132.7$_3$ C(2')/C(5'): 23.9$_8$ ppm.

spin-saturation transfer (18, 19). In this study, the nOe experiments were performed at −80°C and the first coalescence process was observed at −38°C, so that the condition $T \ll T_c$ is fulfilled. The absence of nOe effect on irradiating the upfield methyl signals shows that, effectively, no saturation transfer occurs at this temperature so that the assignments deduced from nOe are unequivocal.

Due to the lack of data regarding *N,N'*-diacetyl derivatives of *N*-heterocyclic compounds, $^1H$ and $^{13}C$ chemical shifts can only be compared to those previously reported for *N*-acetyl heterocycles. We selected *N*-acetylpyrrole **6** and *N*-acetyltetrahydroquinoline **7** for model compounds because assignments were deduced from low temperature nOe experiments (18). However, such a comparison has to take into account differences in the geometry of these compounds. *N*-acetylpyrrole is planar (18) and the low barrier to rotation around the amide bond, $\Delta G_{298}^{\neq} = 12.1$ kcal/mol indicates that "the lone pair on the nitrogen is to a great extent localized in the pyrrole ring" (20). On the other hand, it was suggested that the acetyl group of *N*-acetyltetrahydroquinoline lies out of the mean molecular plane corresponding to a low steric interaction between the methyl group and the methylene group α to the nitrogen. This hypothesis is in line with the low barrier determined for this compound, $\Delta G_c^{\neq} = 12.8$ kcal/mol.

(Acetone, −45°C)

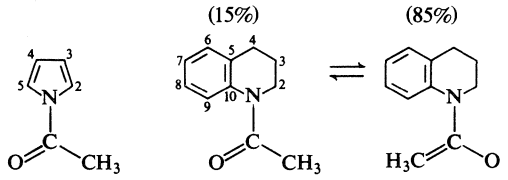


**6** **7a** **7b**

The main factor determining the $^1H$ methyl chemical shifts in the $E,E$ and $Z,Z$ conformers of **2** is the orientation of the $CH_3$ relative to the phenyl substituents, which lie out of the plane of the C(2)–C(3) double bond ($\delta_{CH_3}$ $E,E$: 1.62 ppm; $Z,Z$: 2.17 ppm). A similar result is observed for **7** ($\delta_{CH_3}$ **7***a*: 2.30 ppm, **7***b*: 2.20 ppm) but the difference between these shifts is greater for **2** (0.55 ppm) than for **7** (0.1 ppm). The large difference observed for **2** indicates that the twist angles of the phenyl substituents are significant in solution, suggesting a geometry similar to the one found in the solid state. Such a geometry explains the high shielding observed in the $E,E$ conformer and the $E$ part of the $Z,E$ one.

The ethylenic protons H(5)/H(6) are less shielded when they are *syn* to the carbonyl oxygen ($E$ conformation) than when they are *anti* ($Z$ conformation). Similarly, in *N*-acetylpyrrole **6**, H(5) is deshielded relative to H(2) ($\delta_{H(5)}$: 7.41, $\delta_{H(2)}$: 7.12 ppm).

On going from $^1H$ to $^{13}C$ spectra, a quite different sequence is observed for the methyl groups. While $^1H$ shielding shows an increase in the following order: $Z,Z <$ $Z$ part of $Z,E < E,E <$ $E$ part of $Z,E$, the corresponding $^{13}C$ sequence is: $E,E <$ $E$ part of $Z,E <$ $Z,Z =$ $Z$ part of $Z,E$. Additionally only three signals are observed in the $^{13}C$ spectra instead of four in the $^1H$ spectra. The differences between the above sequences are due to the great sensitivity of proton chemical shifts to anisotropy effects and to the minor importance of these effects on $^{13}C$ shifts.

Four distinct $^{13}C$ resonances are observed for the carbonyl groups and the corresponding carbon is more shielded when the carbonyl oxygen is oriented towards the Ph-substituted C(2)/C(3) $sp^2$ carbons than when the oxygen is oriented towards the nonsubstituted C(5)/C(6) $sp^2$ carbons. Although this behavior seems difficult to explain at first sight, a similar trend is observed in **7**. The carbonyl carbon is more shielded in **7***a* (δ 169.8 ppm) where the oxygen is directed towards the aromatic ring than in **7***b* (δ 169.6 ppm) where the oxygen is oriented towards the unsubstituted $sp^3$ carbon C(2). This suggests that a repulsive interaction could exist between the aromatic ring and the oxygen of the carbonyl group.

The chemical shifts of the $sp^2$ C(5)/C(6) carbons are dependent upon their orientation relative to the

Can. J. Chem. Downloaded from www.nrcresearchpress.com by 210.87.254.5 on 09/06/12
For personal use only.

carbonyl group; this carbon is more shielded when *syn* to the carbonyl oxygen (*E* conformation) than when *anti* to the oxygen (*Z* conformation). Identical results have been reported (18) for **6** (C(2): 120.2 ppm, C(5): 118.5 ppm) and for the $sp^3$ and $sp^2$ carbons of **7** (C(2): **7***b*, 42.8, **7***a*, 46.7 ppm; C(10): **7***a*, 138.8; **7***b*, 140 ppm) and for various acyclic amides (21–23). This effect, which has been attributed to the electric field of the carbonyl (21), seems to be general in the absence of steric compression (18).

It can be noted that $^1H$ and $^{13}C$ chemical shifts of the *Z* or *E* part of **2** are slightly different in the *Z*,*E* conformer and in the *Z*,*Z* or *E*,*E* conformers. Two hypotheses can explain this result; either the chemical shifts are not only dependent on their close but also on their remote surroundings, or geometry of the *Z*,*E* conformer is not exactly identical to the geometry obtained in joining one half of the *Z*,*Z* and one half of the *E*,*E* conformer.

Although the structure of **2** in the solid state indicates that the nitrogen lone pairs are not delocalized towards the 1,4-dihydropyrazine ring, the barrier to rotation about the carbonyl–nitrogen bonds in **2** is rather low ($\Delta G_c^{\ddagger} \sim 13$ kcal/mol) relative to that observed in *N*,*N*-dimethylacetamide ($\Delta G^{\ddagger} \sim 18.1$ kcal/mol) (27). This result is in line with a C—N bond longer in **2** ($\sim 1.37_5$ Å) than in *N*,*N*-dimethylacetamide ($\sim 1.32$ Å).

## Experimental

The 1,4-diacetyl-1,4-dihydro-2,3-diphenylpyrazine has been prepared according to ref. 24. The monocrystal used in the crystallographic study was obtained by slow evaporation of an ethanolic solution.

*Crystallographic study*

Crystal data are used as follows:

$C_{20}H_{18}N_2O_2$ f.w. = 318

Triclinic, $a = 5.684(1)$, $b = 9.299(2)$, $c = 16.516(3)$ Å, $\alpha = 89.62(2)$, $\beta = 90.16(2)$, $\gamma = 107.29(2)°$, $V = 833.49$ Å$^3$, $Z = 2$, $\rho_c = 1.27$ g cm$^{-3}$, $\rho_o = 1.26(2)$ g cm$^{-3}$ (20°C, MoK$_\alpha$ $\lambda = 0.707$ Å, $\mu = 0.86$ cm$^{-1}$). Preliminary X-ray photographs showed triclinic diffraction symmetry; a statistical analysis of the intensity data indicated the centrosymmetric space group $P\bar{1}$. A crystal ($0.7 \times 0.4 \times 0.2$ mm) was mounted with the *a* axis parallel to the $\phi$ axis of a Philips automated diffractometer equipped with a graphite monochromator. The intensities of all reflections having $2\theta$ less than 50° were measured using the variable $\omega$–$2\theta$ scan technique. During the course of the data collection three standard reflections were measured every 54 reflections. A total of 2676 reflections were measured, 2114 of which had $I \geq 4\sigma(I)$. The data were reduced to $|F_o|$ by the routine procedure. Lorentz and polarization but no absorption or extinction corrections were applied. The scattering factors for neutral atoms were taken from ref. 25. The structure was determined by direct methods (MULTAN) (26) and refined by large block least squares $\Sigma\omega(|F_o| - |F_c|)^2 = \min$ with $\omega = 1/6^2$. The refinement with anisotropic thermal parameters on the non-hydrogen atoms converged to $R = 0.126$. At this stage, a difference Fourier map revealing the positions of all the hydrogen atoms was calculated; refinement of their positional parameters was carried out, using the thermal parameters of the corresponding heavy atoms at the end of isotropic refinement. The refinement converged with $R = 0.043$ and $R_w = 0.048$.

*Conformational study in solution*

The $^1H$ and $^{13}C$ spectra were recorded on a Varian XL-100-12-W.G. spectrometer. The $^1H$ and $^{13}C$ chemical shifts were measured relative to TMS as an internal reference. The nOe experiments were performed using carefully degassed solution by three freeze–pump–thaw cycles.


1. R. R. SCHMIDT. Angew. Chem. Int. Ed. Engl. **14**, 581 (1975), and references therein.
2. R. A. RAPHAEL. *In* Nonbenzenoid aromatic compounds. *Edited by* D. Ginsburg. Interscience, New York. 1959. p. 465.
3. G. SCHRODER. Cyclooctatetraen. Verlag Chemie, Weinheim. 1956.
4. I. C. PAUL, S. M. JOHNSON, L. A. PAQUETTE, J. M. BARRETT, and R. J. HALUSKA. J. Am. Chem. Soc. **90**, 5023 (1968).
5. J. ARMAND, K. CHEKIR, and J. PINSON. Can. J. Chem. **23**, 3971 (1974).
6. J. W. LOWN, M. H. AKHTAR, and R. S. MCDANIEL. J. Org. Chem. **39**, 1998 (1974).
7. S. J. CHEN and F. W. FOWLER. J. Org. Chem. **35**, 3987 (1970).
8. J. J. STEZOWSKI. Cryst. Struct. Commun. **4**, 21 (1975).
9. R. R. SCHMIDT, M. DIMMLER, and P. HEMMERICH. Ber. **109**, 2395 (1976).
10. W. E. STEWART and T. H. SIDDALL. Chem. Rev. **70**, 517 (1970).
11. M. RABAN, R. A. KEINTZ, and E. A. NOE. Tetrahedron Lett. 1633 (1979).
12. I. L. KARLE. J. Chem. Phys. **20**, 65 (1952).
13. R. NORRESTAM, P. KIERKEGAARD, B. STENSLAND, and L. TORBJÖRNSSON. J. Chem. Soc. Chem. Commun. 1250 (1969).
14. P. KIERKEGAARD, O. RONNQUIST, and P. E. WERNER. Tetrahedron Lett. 4667 (1969).
15. H. S. GUTOWSKY and C. H. HOLM. J. Chem. Phys. **25**, 1228 (1956).
16. J. BIRDSALL and J. FEENEY. J. Chem. Soc. Chem. Commun. 316 (1972).
17. A. H. LEWIN and M. FRUCHT. Org. Magn. Reson. **7**, 206 (1975).
18. S. COMBRISSON and B. P. ROQUES. Tetrahedron, **32**, 1507 (1976).
19. J. K. SAUNDERS and R. A. BELL. Can. J. Chem. **48**, 512 (1970).
20. K. I. DAHLQVIST and S. FORSEN. J. Phys. Chem. **73**, 4124 (1969).
21. W. MCFARLANE. J. Chem. Soc. Chem. Commun. 418 (1970).
22. G. C. LEVY and G. L. NELSON. J. Am. Chem. Soc. **94**, 4897 (1972).
23. D. E. DORMAN and F. A. BOVEY. J. Org. Chem. **38**, 1719 (1973).
24. P. MARTIGNY, H. LUND, and J. SIMONET. Electrochim. Acta, **21**, 345 (1976).
25. International tables for X-ray crystallography. Vol. IV. The Kynoch Press, Birmingham, England. 1974.
26. G. GERMAIN, P. MAIN, and M. M. WOOLFSON. Acta Crystallogr. Sect. A, **27**, 268 (1971).
27. T. DRAKENBERG, K. I. DAHLQUIST, and S. FORSEN. J. Phys. Chem. **76**, 2178 (1972).


Can. J. Chem. Downloaded from www.nrcresearchpress.com by 210.87.254.5 on 09/06/12
For personal use only.

# Synthesis and incorporation of [3-$^3$H, U-$^{14}$C]-L-valine into penicillin V using *Penicillium chrysogenum*

SAUL WOLFE AND RAYMOND JOHN BOWERS
*Department of Chemistry, Queen's University, Kingston, Ont., Canada K7L 3N6*
AND
DAVID A. LOWE[1] AND ROBERT B. MORIN[1]
*Raylo Chemicals Limited, Edmonton, Alta., Canada T6C 4A9*

Received May 26, 1981

SAUL WOLFE, RAYMOND JOHN BOWERS, DAVID A. LOWE, and ROBERT B. MORIN. Can. J. Chem. **60**, 355 (1982).

The title compound was synthesized by exchange of dimethylpyruvic acid with NaOH–HTO, followed by reductive amination using cyanoborohydride in methanol solvent, resolution of the *N*-chloroacetyl derivative, and admixture with [U-$^{14}$C]-L-valine. Degradation of the compound revealed that 94.5% of the tritium was attached to C3, and 5.5% was located on the methyl groups. Incorporation of this doubly labelled valine into penicillin V, purified as the dibenzylamine salt, proceeded with 100.7% loss of the tritium originally present at C3. Commercial [2,3-$^3$H, U-$^{14}$C]-L-valine, which was found to have 12% of the tritium on the methyl groups, was also incorporated into penicillin V, purified as its methyl ester. Degradation to remove the hydrogen attached to C3 of this ester revealed that no tritium was present at this position. Therefore, in agreement with an earlier result and other related studies, the β-hydrogen of valine is not transferred to C3 of penicillin during the biosynthesis of the latter compound.

SAUL WOLFE, RAYMOND JOHN BOWERS, DAVID A. LOWE et ROBERT B. MORIN. Can. J. Chem. **60**, 355 (1982).

On a synthétisé le composé mentionné dans le titre grâce à un échange de l'acide diméthylpyruvique avec une solution de NaOH–HTO, suivi d'une amination réductrice utilisant le cyanoborohydrure dans le méthanol, d'une résolution du dérivé *N*-chloroacétyle et finalement d'un mélange avec la [U-$^{14}$C]-L-valine. La dégradation du composé a révélé que 94,5% du tritium est attaché au carbone en position 3 et 5,5% se retrouve au niveau des groupes méthyles. L'incorporation de cette valine doublement marquée dans de la pénicilline V, purifié sous forme de sel de dibenzylamine, se fait avec une perte de 100,7% du tritium originalement présent au niveau du carbone en position 3. On a également incorporé la [$^3$H-2,3, U-$^{14}$C] L-valine commerciale qui contient 12% de tritium dans les groupes méthyles à la péniciline V purifiée sous forme d'ester méthylique. La dégradation en vue d'enlever le tritium du carbone en position 3 a révélé qu'il n'y en avait pas dans cette position. Par conséquent, en accord avec un résultat antérieur et d'autres études apparentées, l'hydrogène en position β de la valine n'est pas transférré sur le carbone en position 3 de la pénicilline pendant la biosynthèse de ce dernier composé.

[Traduit par le journal]

Both eukaryotic (1) and prokaryotic (2) organisms synthesize the penicillin nucleus (**1**, X = OH) from the tripeptide precursor **2**, δ-L-(α-aminoadipyl)-L-cysteinyl-D-valine (ACV). The overall process **2** → **1** includes a two-equivalent oxidation in the cysteinyl moiety, and a two-equivalent oxidation in the valinyl moiety of ACV. Although the stereochemical consequences of these processes at the β carbon atoms of cysteine and valine are known (3), their relative timing and detailed chemical mechanisms are not, despite much effort and ingenious speculation.

It has been known for some time that L-valine is a more efficient precursor of the D-valinyl moiety of penicillin than is D-valine (4), and that both enantiomers are incorporated with loss of their α-hydrogen atoms. More recently, it has been found that this loss occurs during the attachment of valine to an aminoadipylcysteine dipeptide, since some (5) or all (6) of the α-valinyl hydrogen of ACV is retained during the oxidative stages of the biosynthesis. This fact suggests (7) that the oft-considered dehydrovalinyl-containing peptide **3** (8) can no longer be regarded as a viable post-ACV intermediate in the overall process.

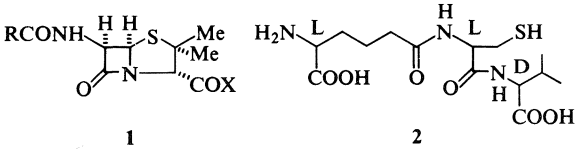

**1**



**2**

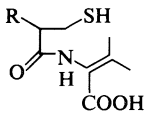

**3**

The present work originated from some mechanistic considerations, based on literature precedents, which suggested that retention of the α-valinyl hydrogen of ACV need not be incompatible with the postulate of **3** as a post-ACV intermediate.

[1]Present address: Bristol Laboratories, Division of Bristol-Myers Company, P.O. Box 657, Syracuse, NY 13201 U.S.A.

0008-4042/82/030355-07$01.00/0
©1982 National Research Council of Canada/Conseil national de recherches du Canada

Can. J. Chem. Downloaded from www.nrcresearchpress.com by 210.87.254.40 on 09/06/12
For personal use only.

Can. J. Chem. Downloaded from www.nrcresearchpress.com by 210.87.254.40 on 09/06/12
For personal use only.

In one version of the Morin–Baldwin hypotheses (9–11), oxidation of ACV at sulfur, followed by intramolecular dehydration, leads to the isothiazolidinone **4**. A β-elimination to the acylimine **5** (12), followed by a second oxidation at sulfur, then affords **6** which, by an ene reaction, is transformed to the mercaptoazetidinone **7**, which cyclizes to penicillin. Although the reported examples of the latter reaction (13, 14) have not been confirmed (15), such cyclizations are known in model systems (16), and the reverse reaction, i.e., **1** (X = Cl, $OCH_3$, OCOR) → **7** (X = Cl, $OCH_3$, OCOR) also exists (17, 18).

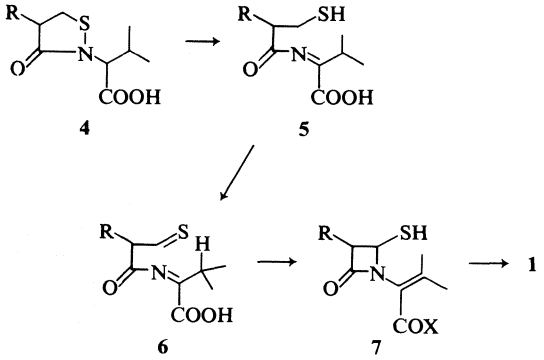

During an investigation of the C6 epimerization of the penicillin derivative **8** (19), it was observed that exposure of this compound to triethylamine in a mixture of *tert*-butanol-*d* and methylene chloride led to **9** *without incorporation of deuterium from the solvent*. Under the same conditions, the anhydropenicillin **10** was epimerized to **11**, again without incorporation of deuterium. To account for these observations, it was proposed that triethylamine promotes a β-elimination to form an ion-pair (e.g., **12**), which is transformed to the mercaptan **13**. This corresponds to an intramolecular 1 → 3 shift of hydrogen from C6 to sulfur. Ring closure by a concerted *cis*-addition of S—H to the β-face of the C5—C6 double bond would then explain the labelling results. The role of ion-pairs in base-catalyzed intramolecular 1,3-proton transfer reactions has since been examined in some detail (20). In addition, there is now good evidence for intramolecular 1,3-hydrogen shifts under enzymatic control, e.g., the C4 to C6 hydrogen transfer during the conversion of cholesterol into cholestenone (21), and the intramolecular hydrogen transfer observed during the enzymatic conversion of 3-carboxymuconolactone into 3-oxoadipic acid (22).

On the basis of these precedents, it was considered that the postulated conversion of **4** to **5** might proceed with transfer of hydrogen from the α-valinyl carbon to sulfur. Prototropic rearrangement

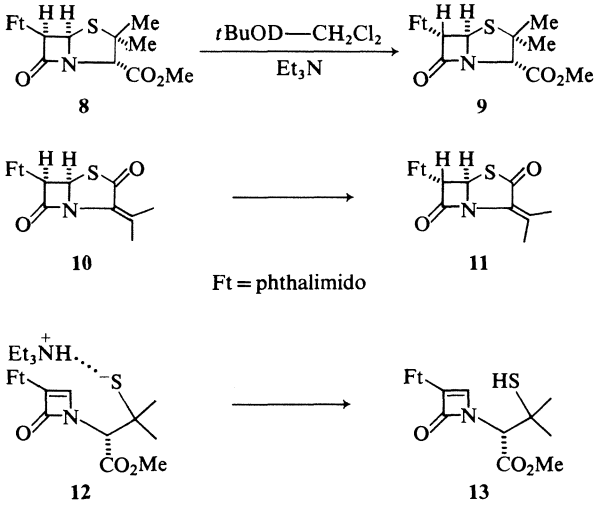

to **14**, followed by *cis*-addition to the carbon–carbon double bond would then lead to the thiazepine **15** (23) with retention of some or all of the α-valinyl hydrogen. This mechanism is consistent with the labelling results, predicts that the β-hydrogen of the valinyl moiety is lost, and provides a new route to the putative (23) intermediate **15**.

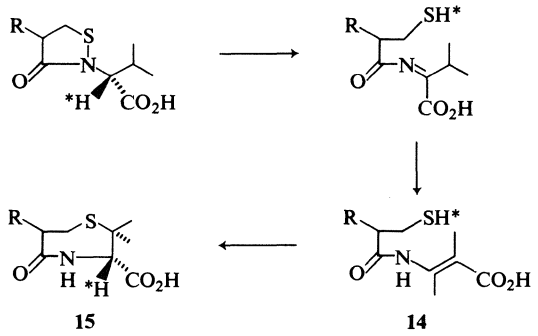

Alternatively, an intramolecular hydrogen transfer during the step **6** → **7**, followed by *cis*-addition of S—H* to the carbon–carbon double bond (*cf.* **16** → **17**) would lead to penicillin, with loss of the α-valinyl hydrogen of ACV, and a transfer of the β-valinyl hydrogen of ACV to the α-valinyl carbon atom of penicillin.

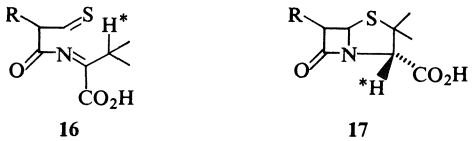

Although this latter pathway is inconsistent with the observations of refs. 5–7, it seemed desirable to reexamine the fate of the β hydrogen atom of valine during the incorporation of this amino acid into penicillin by the eukaryotic *P. chrysogenum*. An experiment of this type has been reported previous-

Can. J. Chem. Downloaded from www.nrcresearchpress.com by 210.87.254.40 on 09/06/12
For personal use only.

ly by Adriaens *et al.* (24). In the latter work, DL-[3-$^3$H]valine was prepared by racemization of L-[2,3-$^3$H]valine, and was found to contain 0.46% tritium on the methyl groups; after admixture with DL-[4,4′-$^{14}$C]valine to a $^3$H/$^{14}$C ratio of 3.0103, the compound was incorporated into penicillin V (**18**), using *P. chrysogenum*. The latter compound exhibited a $^3$H/$^{14}$C ratio of 0.05184 (average of four runs), somewhat higher than the value (0.01385) expected for complete loss of the 3-$^3$H and retention of only the 0.46% tritium on the methyl groups (25). The specific objectives of the present work were, therefore, to develop an alternative synthesis of DL-[3-$^3$H]valine, and a degradation of the labelled penicillin to locate the position(s) of any residual tritium.

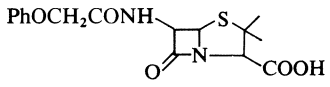


**18**

## Experimental

General experimental procedures have been summarized in ref. 23. Enzymes used in the present work were purchased from Sigma Chemical Company. [2,3-$^3$H]-L-valine was supplied by Schwarzmann, Inc., Division of Medisciences, Spring Valley, NY 10977, U.S.A.

*[3-$^3$H]-Dimethylpyruvic acid*

A solution of dimethylpyruvic acid (1.06 g, 9.1 mmol), sodium hydroxide (600 mg, 15 mmol), and HTO (5.0 mL, specific activity 4 mCi/mmol) was stirred at room temperature for 17 h. The solution was then acidified by addition of concentrated hydrochloric acid (1.6 mL) and was continuously extracted with methylene chloride for 3 h. The organic extract was evaporated and the residual oil dissolved in methanol (40 mL) to exchange the carboxylic acid proton. This solution was evaporated and the residue was again dissolved in methanol (40 mL). After evaporation of the solvent a colourless oil (994 mg) was obtained, with specific activity 25.5 μCi/mmol.

*Reductive amination of dimethylpyruvic acid (26)*

A solution of dimethylpyruvic acid (106 mg, 0.9 mmol) and ammonium acetate (385 mg, 50 mmol) in methanol (20 mL) was treated with sodium cyanoborohydride (126 mg, 2.0 mmol) and stirred at 20°C for 46 h. The reaction was quenched by addition of concentrated hydrochloric acid (5.0 mL), and the solvent was removed under reduced pressure. The white, solid residue was dissolved in water (3.0 mL) and added to an ion exchange column, which had been prepared as follows: Rexyn RG50 (H+) (24 g, 100 mequiv.) was stirred with water (50 mL) and decanted. This process was repeated several times to remove small particles of resin. The slurry was then poured into a glass column and washed with 2 *N* hydrochloric acid (150 mL), followed by water until the eluate was neutral.

The solution of the product (3 mL) was added to the column. The acidic impurities were removed by a distilled water wash (500 mL), after which the product was eluted with 1 *N* ammonium hydroxide (300 mL). Evaporation of the eluate gave a light brown solid (60 mg, 50%), which gave a purple colour with ninhydrin. Analysis by paper chromatography (Whatman 3M; *n*-butanol – acetic acid – water; 27:10:33) showed a single spot, $R_f$ 0.73, identical to that of an authentic sample of valine; ir (Nujol): 3360–1830 (s, br, $NH_3^+$), 2140 (s, $NH_3^+$), 1620 (s, br, $CO_2^-$) cm$^{-1}$; $^3$Hmr ($D_2O/D_2SO_4$) δ: 0.97 (3H, d, $J$ = 7 Hz, $CH_3$), 1.03 (3H, d, $J$ = 7 Hz, $CH_3$), 1.80–2.52 (1H, m, C3 methine), 3.57 (1H, d, $J$ = 5 Hz, C2 methine).

A similar experiment employing ammonium chloride (268 mg, 5.0 mmol) in place of ammonium acetate as the nitrogen source afforded only a 10% yield of valine.

A further experiment with methanol-*d* (99.5 at.%) in place of methanol gave a 50% yield of valine. Analysis of this product by $^1$Hmr indicated that no deuterium had been incorporated into the product. This material was then converted to *N*-acetyl-D,L-valine, mp 149.5–151°C, with *p*-nitrophenyl acetate, and esterified with diazomethane to form *N*-acetyl-D,L-valine methyl ester as a colourless syrup which, on standing, crystallized slowly as large needles, mp 59–60°C; ir (film): 3400 (br, sh, NH), 3290 (s, br, NH), 1735 (s, ester C=O), 1650 (s, amide C=O), 1535 (s, amide II) cm$^{-1}$; $^1$Hmr ($CDCl_3$) δ: 0.93 (3H, d, $J$ = 6.5 Hz, $CH_3$), 0.95 (3H, d, $J$ = 6.5 Hz, $CH_3$), 2.05 (3H, s, $COCH_3$), superimposed on 1.80–2.47 (1H, m, C3 methine), 3.74 (3H, s, $CO_2CH_3$), 4.55 (1H, q, $J$ = 5, 8 Hz, C2 methine), 6.14 (1H, br d, $J$ = 8 Hz, N*H*); ms (70 eV) *m/e* (relative intensity) taking *m/e* 114 ($M^+ - CO_2CH_3$) as the base peak: 116 (3.0), 115 (4.7) 114 (100). A sample prepared from D,L-valine (Aldrich) had: 116 (2.9), 115 (8.8), 114 (100).

*[3-$^3$H]-D,L-Valine*

In the same manner, the reductive amination of [3-$^3$H]-dimethylpyruvic acid (0.99 g, 8.6 mmol) (specific activity 25.5 μCi/mmol) gave [3-$^3$H]-D,L-valine (499 mg, 50%). The product was converted immediately to *N*-chloroacetyl-[3-$^3$H]-D,L-valine (27), mp 126–130°C, specific activity 27.9 μCi/mmol.

*[3-$^3$H, U-$^{14}$C]-L-Valine*

The *N*-chloroacetyl-[3-$^3$H]-D,L-valine (197 mg, 1.013 mmol), specific activity 28 μCi/mmol, was resolved, using hog kidney acylase (28) to give [3-$^3$H]-L-valine (12.19 μCi, 85.5%). A solution of [3-$^3$H, U-$^{14}$C]-L-valine was prepared by mixing a solution of [3-$^3$H]-L-valine (41.72 mg, 9.986 μCi) in water (9.5 mL) with a solution of [U-$^{14}$C]-L-valine (2.28 mg, 3.359 μCi, New England Nuclear) in water (3.0 mL). The solution showed $^3$H/$^{14}$C = 2.91. Aliquots (3.0 mL) of this solution were used for the incorporation experiments.

*Distribution of tritium in [2,3-$^3$H, U-$^{14}$C] or [3-$^3$H, U-$^{14}$C]-L-valine*

Eighty μmoles of doubly labelled L-valine containing approximately 1 μCi $^3$H and 0.3 μCi $^{14}$C were absorbed onto Dowex 50 ($H^+$) at neutral pH, eluted with 2 *M* ammonium hydroxide solution, and the eluate was lyphilized. The eluate was reconstituted at pH 8.0 in 6 mL of a solution containing 500 μmol Tris-HCl and 500 μmol KCl, and shaken with L-amino acid oxidase (10 mg) and catalase (1 mg) at 37°C for 18 h. A further 80 μmol aliquot of unlabelled L-valine was added to the reaction mixture and the incubation was continued for 6 h. The pH of the final solution was adjusted to 5.0 with dilute acetic acid. The solution was then passed through Dowex 50 ($H^+$), and the resin was washed with four volumes of water. The combined eluate and wash were dried by lyophilization, and reconstituted with water. Lyophilization was repeated to ensure the complete removal of tritiated water. The resultant dimethylpyruvic acid was dissolved in water (5 mL) and the pH adjusted to 13 by the addition of 1 *N* ammonium hydroxide (1.5 mL), and the solution was maintained overnight in a sealed tube at 37°C. The alkaline solution was neutralized with dilute hydrochloric acid and dried by lyophilization. The exchange procedure was repeated to ensure the complete removal of tritium from the 3-position.

*Production of penicillin V by* Penicillium chryosogenum *ATC-C26818*

Surface spores were developed on tube slants on an agar

Can. J. Chem. Downloaded from www.nrcresearchpress.com by 210.87.254.40 on 09/06/12
For personal use only.

medium containing 0.75% glycerol, 0.75% molasses, and 0.5% Bactopeptone. Spores from a 10 day culture were suspended in distilled water and inoculated at a density of $10^4$/mL into a seed medium of composition 3% corn steep liquor, 1% distillers' solubles, 2% sucrose, and 0.5% calcium carbonate adjusted to pH 6.5 before sterilization. The seed was cultured in 100 mL volume in a 500 mL Erlenmeyer flask by shaking at 250 rpm at 24°C for 72 h. Production medium consisted of 6% corn steep liquor, 6% lactose, 1.0% $CaCO_3$, 0.3% $MgSO_4 \cdot 7H_2O$, 0.5% $KH_2PO_4$, 0.5% soybean oil, and 0.2% phenoxyacetic acid, adjusted to pH 6.5 before sterilization. Production fermentations were carried out in 100 mL of medium in 500 mL Erlenmeyer flasks shaken at 250 rpm at 24°C for 72 h. A 10% cross volume from the third day of seed was used to inoculate the production medium. Bioassay results using *Bacillus subtilis* indicated that penicillin V was produced at a titre of 1.1 mg/mL filtrate at 72 h.

*Incorporation of doubly labelled* L-*valine into penicillin V*

Doubly labelled L-valine (10 mg) was dissolved in distilled water (15 mL) and sterilized by membrane filtration. Equal aliquots were added to *P. chrysogenum* growing in three flasks of production medium at 52 h and the fermentation was continued for a further 20 h, after which time the contents of the flasks were pooled, unlabelled penicillin V (1.5 g) was added, and the whole broth filtered. The pH of the filtrate was adjusted to 2.5 with dilute sulfuric acid and the mixture was then extracted with an equal volume of ethyl acetate. The organic phase was separated, washed with water, and dried over sodium sulfate. Crude penicillin V was precipitated from the ethyl acetate as the potassium salt by titration to pH 7.5 with 2 *M* potassium 2-ethylhexanoate in *n*-butanol, collected by filtration, and finally washed with ethyl acetate.

*Separation of penicillin V from phenoxyacetic acid via the dibenzylamine salt*

A solution of potassium penicillin V (646 mg, 1.67 mmol) and potassium phenoxyacetate (253 mg, 1.33 mmol), in water (10 mL), was stirred vigorously at room temperature, and a warm solution of dibenzylamine hydrochloride (767 mg, 3.3 mmol), in water (23 mL), was added to give a thick white paste. The mixture was cooled overnight at 5°C and then filtered, washed with ice-cold water (6 mL), and air-dried. Drying under high vacuum gave 894 mg of material. This was suspended in acetonitrile (5.0 mL) and water (8.0 mL), and it dissolved readily upon heating. The hot solution was filtered through a short stemmed, preheated filter funnel, containing a small plug of tissue paper, into a flask containing hot water (8.0 mL). The product crystallized smoothly as the solution cooled. After cooling of the mixture overnight, the product was collected to give a white microcrystalline solid (692 mg) mp 98–100°C; ir (Nujol): 3442, 3355, 3218 (s, NH), 2615, 2445 (s, $NH_2^+$), 1770 (s, β-lactam C=O), 1675 (s, amide C=O), 1628 (s, $CO_2^-$), 1576 (s, amide II and $NH_2^+$) $cm^{-1}$; $^1$Hmr ($CDCl_3$) δ: 1.56 (3H, s $CH_3$), 1.46 (3H, s, $CH_3$), 3.83 (4H, s, $PhCH_2$), 4.49 (2H, s, $PhOCH_2$), 4.23 (1H, s, C3 methine), 5.36 (1H, d, $J$ = 4 Hz, C5 methine), 5.56 (1H, q, $J$ = 4, 8 Hz, collapses to a doublet, $J$ = 4 Hz on exchange of NH with $D_2O$, C6 methine), 5.99–6.39 (3H, exch $D_2O$, N*H* and $NH_2^+$), 7.28 (10H, s, Ph) overlapping with 6.76–7.49 (5H, m, PhO). *Anal.* calcd. for $C_{30}H_{33}N_3O_5S$: C 65.79, H 6.07, N 7.67, S 5.85; found: C 65.78, H 6.04, N 7.51, S 5.70.

*Isolation of [$^3$H, $^{14}$C]-penicillin V dibenzylamine salt from the crude penicillin isolate obtained after incubation of [3-$^3$H, U-$^{14}$C]-*L-*valine*

In a similar manner, the crude penicillin V isolate (824 mg) from the incubation of [3-$^3$H, U-$^{14}$C]-L-valine ($^3$H/$^{14}$C 2.91) with *Penicillium chrysogenum* was dissolved in water (9.0 mL) and treated with a solution of dibenzylamine hydrochloride (700 mg) in hot water (24.0 mL). The precipitated [$^3$H, $^{14}$C]-penicillin V dibenzylamine salt was collected and dried under high vacuum, mp 91–95°C; specific activity: $^3$H, 0.0043; $^{14}$C, 0.031 μCi/mmol. Recrystallization from aqueous acetonitrile gave a fluffy white microcrystalline solid, mp 97–100°C; specific activity: $^3$H, 0.0052; $^{14}$C, 0.0355 μCi/mmol ($^3$H/$^{14}$C 0.146, 5.03% retention of tritium).

A second penicillin V isolate (751 mg) was also treated with dibenzylamine hydrochloride (640 mg) in water. The precipitated salt was recrystallized twice from aqueous acetonitrile to give a fluffy white microcrystalline solid, mp 98.5–100.5°C (mixture mp with an authentic sample, 98–100°C). Specific activity: $^3$H, 0.0045; $^{14}$C, 0.033 μCi/mmol ($^3$H/$^{14}$C 0.136, 4.7% retention of tritium).

*Isolation of [$^3$H, $^{14}$C]-penicillin V methyl ester from the incubation of [2,3-$^3$H, U-$^{14}$C]-*L-*valine with* Penicillium chrysogenum

The crude penicillin V isolate (401.5 mg) was dissolved in water (4.0 mL), and the solution was cooled to 0°C. The pH was adjusted to 2.0 with 6 *N* hydrochloric acid and the product was extracted into ethyl acetate (4 × 10 mL). The combined extracts were dried and evaporated to leave a pale yellow gum (340 mg). The product was dissolved in absolute ether (20 mL and esterified at 0°C with alcohol-free diazomethane. The excess diazomethane was destroyed by the dropwise addition of acetic acid and the solvent was evaporated. The residue was dissolved in methylene chloride (20 mL) and washed with 7% sodium bicarbonate (10 mL). The organic layer was dried and evaporated to leave a golden yellow syrup (363 mg). Chromatography on silica gel (7.0 g) (methylene chloride – ethyl acetate, 19:1) separated methyl phenoxyacetate from the penicillin V methyl ester, which was isolated as two samples; the first, 195.5 mg, was homogenous on tlc, $R_f$ 0.58 (methylene chloride – ethyl acetate, 19:1) and identical by $^1$Hmr with an authentic sample. Specific activity: $^3$H, 0.011; $^{14}$C, 0.023 μCi/mmol; $^3$H/$^{14}$C 0.46.

*Rearrangement of methyl 6-phenoxyacetamido-[$^3$H, $^{14}$C]-penicillanate-1β-oxide (29)*

Methyl 6-phenoxyacetamidopenicillanate-1β-oxide (118 mg, 0.311 mmol, specific activity: $^3$H, 0.011 μCi/mmol; $^3$H/$^{14}$C 0.46) was reacted with trimethyl phosphite (40 mg, 0.32 mmol) in benzene (10 mL). The crude product was purified by column chromatography on 5 g silica gel (methylene chloride – ethyl acetate, 1:1) to give 56 mg of material that was homogenous on tlc ($R_f$ 0.55), and identical by $^1$Hmr with an authentic sample (29). Specific activity: $^3$H, 0.008; $^{14}$C, 0.027 μCi/mmol; $^3$H/$^{14}$C 0.3.

*Isomerization of the β,γ-isomer (29)*

A solution of the β,γ-isomer (173 mg, 0.5 mmol) in methanol (2.5 mL) was stirred with triethylamine (0.07 mL, 51 mg, 1 equiv.) at room temperature for 20 min. The solvent was then evaporated and the residue dissolved in methylene chloride (15 mL) and reevaporated. Repetition of this process with methylene chloride (15 mL) gave a syrup which was dried under high vacuum (174 mg); ir ($CDCl_3$): 1769 (s, β-lactam C=O), 1720 (s, ester C=O) $cm^{-1}$; $^1$Hmr ($CDCl_3$) δ: 1.77 (3H, s, $CH_3$), 2.23 (3H, s, $CH_3$), 3.74 (3H, s, $CO_2CH_3$), 4.95 (2H, s, $PhOCH_2$), 5.83 (1H, d, $J$ = 4 Hz, β-lactam *H*), 6.03 (1H, d, $J$ = 4 Hz, β-lactam *H*), 6.77–7.43 (5H, m, Ar*H*).

*Isomerization in methanol-*d

A similar experiment using methanol-*d* (99.5 at.%) in place of methanol gave the α,β-isomer containing one atom of deuterium by nmr integration; $^1$Hmr ($CDCl_3$) δ: 1.77 (2.8H, s, vinyl $CH_3$), 2.23 (2.2H, s, vinyl $CH_3$).

Can. J. Chem. Downloaded from www.nrcresearchpress.com by 210.87.254.40 on 09/06/12
For personal use only.

*Isomerization of the β,γ-isomer at high dilution*

Triethylamine (0.70 mL) was dissolved in redistilled methanol and the solution was diluted to 50.0 mL in a volumetric flask. An aliquot of this solution (5.0 mL, 0.5 mmol of triethylamine) was added to a solution of the β,γ-isomer (17.3 mg, 0.05 mmol) in redistilled methanol (345 mL). After 5 h the solvent was evaporated and the residue dissolved in methylene chloride (15 mL), filtered, and evaporated to leave a pale yellow oil (17 mg) which was identical ($^1$Hmr) to material prepared previously.

*Isomerization of the [$^3$H, $^{14}$C]-β,γ-isomer*

In the same way, the [$^3$H,$^{14}$C]-β,γ-isomer (27.0 mg, 0.078 mmol), was isomerized using triethylamine (10 equiv.) in redistilled methanol (500 mL). The product (27.0 mg) was purified on silica gel (1.0 g), (methylene chloride – ethyl acetate, 19:1) to give 19.0 mg of the α,β-isomer which was identical ($^1$Hmr, tlc) to material prepared previously; specific activity: $^3$H, 0.007; $^{14}$C, 0.026 μCi/mmol; ($^3$H/$^{14}$C 0.27).

## Results and discussion

Dimethylpyruvic acid **19** was prepared by hydrolysis (30) of 2-phenyl-4-isopropylidene-5-oxazolone **20** (31), and was converted to valine in 50% yield using ammonium acetate as the nitrogen source in the reductive amination. Interestingly, the yield of valine decreased to only 10% when ammonium chloride was employed in place of ammonium acetate.

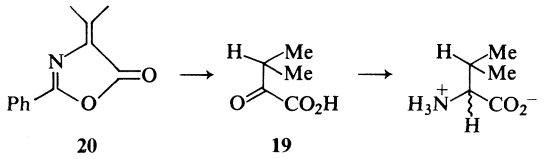


**20** **19**

Exchange of **19** with 1 *M* NaOD–$D_2O$ was complete within 5 min at room temperature. Because of the facility of this exchange, it was necessary to check for loss of isotope to the solvent during the reductive amination step. Therefore, **19** was converted to D,L-valine with cyanoborohydride and ammonium acetate in methanol-*d*. The resulting product showed no incorporation of deuterium by $^1$Hmr and mass spectral examination of the derived *N*-acetyl methyl ester (see Experimental).

Tritiation of **19** was performed in 1 *M* NaOH–HTO and the resulting **19**-*t* was converted to [3-$^3$H]-D,L-valine in 49% yield. The *N*-chloroacetyl derivative of this compound, specific activity 28.0 μCi/mmol, was resolved, using hog kidney acylase, and the product was mixed with [U-$^{14}$C]-L-valine, $^3$H/$^{14}$C = 2.91. The distribution of tritium in this compound was then determined. Incubation with L-amino acid oxidase afforded [3-$^3$H,U-$^{14}$C]-dimethylpyruvic acid, which was exposed to 1 *M* ammonium hydroxide. Reacidification, followed by repetition of the exchange procedure, afforded doubly labelled **19**, $^3$H/$^{14}$C = 0.161. These results indicated that, in the doubly labelled L-valine, 94.5% of the tritium was attached to C3, and 5.5% was located in the methyl groups. The presence of tritium in the methyl groups was unexpected, and is indicative of homoenolization (32) during the exchange of **19** with NaOH in a tritiated medium.

Incorporation of the doubly labelled L-valine into penicillin V was achieved using *P. chrysogenum* in a medium supplemented with phenoxyacetic acid. The crude penicillin was isolated as the potassium salt by filtration of the broth, acidification to pH 2.5, extraction with ethyl acetate, and treatment with potassium 2-ethylhexanoate. Three experiments were performed, with an average incorporation of L-valine of 5.5%, based on recovered $^{14}$C. These crude potassium penicillin V isolates exhibited an average $^3$H/$^{14}$C ratio of 0.407, and suggested retention of 14% of the tritium originally present in the valine, corresponding to ca. 8.5% of the tritium originally located at C3 of the precursor.

Since $^1$Hmr examination of unlabelled crude potassium penicillin V isolates indicated some contamination with potassium phenoxyacetate, separation and purification of the penicillin was necessary. This was accomplished by treatment of the mixture, in water, with a hot aqueous solution of dibenzylamine hydrochloride. The dibenzylamine salt of penicillin V precipitated virtually quantitatively, and could be recrystallized to analytical purity from aqueous acetonitrile. Similar treatment of the labelled material yielded pure dibenzylamine salt of penicillin V having an average $^3$H/$^{14}$C ratio of 0.136, corresponding to 100.7% loss of the tritium originally present at C3 of the valine.

A further set of experiments was performed using commercially available [2,3-$^3$H]-L-valine. Degradation of this material, using L-amino acid oxidase as described above, revealed 12% tritium in the methyl groups. The compound was mixed with [U-$^{14}$C]-L-valine ($^3$H/$^{14}$C = 5.1) and incorporated into Penicillin V as before. Three experiments were performed. In this case, the crude potassium salts were acidified to pH 2, extracted into ethyl acetate, and treated with alcohol-free diazomethane. The pure methyl ester of penicillin V ($^3$H/$^{14}$C = 0.46) was isolated by column chromatography. Although this radioactivity corresponds to ca. 103% loss of tritium from the C3 position of the valine precursor, the methyl ester (**21**) was degraded to the thiazoline **24** via the known sequence **21** → **22** → **23** → **24** (29), to allow the removal of the hydrogen attached to C3.

To validate this degradative sequence, it was necessary to demonstrate that the rearrangement **23** → **24** proceeds in an intermolecular manner, with incorporation of hydrogen from the solvent.

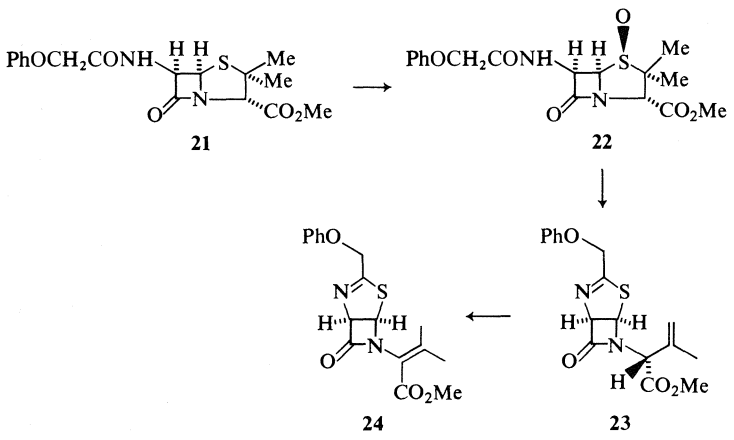


Therefore, **23** was converted to **24**-*d* with triethylamine in methanol-*d*. The product was found, by $^1$Hmr, to contain one deuterium atom, distributed unequally between the two methyl groups, as indicated in **25**. The assignments of the chemical shifts of these methyl groups are based on literature precedents (33). These observations indicate that the conversion of **23** to **24** in methanol solvent is intermolecular, and proceeds via a carbanionic intermediate which protonates most readily in the sickle (**26**) or U (**27**) conformations (34).

In the radioactive series, the conversion of **23** to **24** was performed with triethylamine in a large excess of methanol. The $^3$H/$^{14}$C ratios were found to be: **21**, 0.46; **23**, 0.31; **24**, 0.27. This corresponds to loss of 23% tritium in the sequence **21** → **22** → **23**, slightly higher than the expected 17% and, within the experimental error, no further loss of tritium in the formation of **24**.

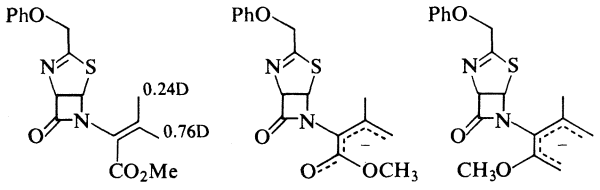


The two sets of experiments confirm the conclusions of Adriaens *et al.* (24), and provide no support for our hypothesis that the β-hydrogen of valine is transferred to C3 of penicillin during the biosynthesis of the latter compound. As has been reported elsewhere (35), the thiazepine **15** (R = δ-L-α-aminoadipyl) (23) is not converted to penicillin by a cell-free preparation of *C. acremonium*.

## Acknowledgement

This research has been supported by grants from the Natural Sciences and Engineering Research Council of Canada. We thank Dr. Derek Hook for helpful discussions and for assistance with some of the experiments.

1. J. O'Sullivan, R. C. Bleaney, J. A. Huddleston, and E. P. Abraham. Biochem. J. **184**, 421 (1979); T. Konomi, S. Herchen, J. E. Baldwin, M. Yoshida, N. A. Hunt, and A. L. Demain. Biochem. J. **184**, 427 (1979); Y. Sawada, J. E. Baldwin, P. D. Singh, N. A. Solomon, and A. L. Demain. Antimicrob. Agents Chemother. **18**, 465 (1980).
2. S. E. Jensen, D. W. S. Westlake, and S. Wolfe. J. Antibiot. In press.
3. D. J. Aberhart. Tetrahedron, **33**, 1545 (1977).
4. B. W. Bycroft, C. M. Wels, K. Corbett, A. P. Maloney, and D. A. Lowe. J. Chem. Soc. Chem. Commun. 923 (1975).
5. P. A. Fawcett, P. B. Loder, M. J. Duncan, T. J. Beesley, and E. P. Abraham. J. Gen. Microbiol. **79**, 293 (1973).
6. B. Meeschaert, P. Adriaens, and H. Eyssen. J. Antibiot. **33**, 722 (1980); J. E. Baldwin, B. L. Johnson, J. J. Usher, E. P. Abraham, J. A. Huddleston, and R. L. White. J. Chem. Soc. Chem. Commun. 1271 (1980).
7. E. P. Abraham. J. Antibiot. Suppl. **30**, 1 (1977).
8. H. R. V. Arnstein and J. C. Crawhall. Biochem. J. **67**, 180 (1957).
9. R. B. Morin, E. M. Gordon, and J. R. Lake. Tetrahedron Lett. 5213 (1973); R. B. Morin, J. R. Lake, and E. M. Gordon. Tetrahedron Lett. 2979 (1974).
10. J. E. Baldwin, S. B. Haber, and J. Kitchin. J. Chem. Soc. Chem. Commun. 790 (1973).
11. J. E. Baldwin, M. Jung, P. Singh, T. Wan, S. Haber, S. Herchen, J. Kitchin, A. L. Demain, N. A. Hunt, M. Kohsaka, T. Konomi, and M. Yoshida. Phil. Trans. R. Soc. London Ser. B, **289**, 169 (1980).
12. B. W. Bycroft. Nature, **224**, 595 (1969).
13. S. Wolfe, R. N. Bassett, S. M. Caldwell, and F. I. Wasson. J. Am. Chem. Soc. **91**, 7205 (1969).
14. R. Thomas. J. Chem. Soc. Chem. Commun. 478 (1972).
15. R. Lattrell. Justus Liebigs Ann. Chem. 1361 (1974); 1937 (1974); M. D. Bachi and O. Goldberg. J. Chem. Soc. Perkin Trans. I, 1184 (1974); M. Narisada and W. Nagata. Heterocycles, **6**, 1646 (1977); J. E. Baldwin. *In* Further perspectives in organic chemistry. Ciba foundation symposium 53. Elsevier. 1978. p. 85.
16. J. Sicher, M. Svoboda, and J. Farkas. Collect. Czech.

Can. J. Chem. Downloaded from www.nrcresearchpress.com by 210.87.254.40 on 09/06/12
For personal use only.

Chem. Commun. **20**, 1439 (1965); R. CHATTERJEE, A. H. COOK, I. M. HEILBRON, and A. L. LEVY. J. Chem. Soc. 1337 (1948).
17. S. WOLFE, J. C. GODFREY, C. T. HOLDREGE, and Y. G. PERRON. Can. J. Chem. **46**, 2549 (1968).
18. E. G. BRAIN, I. MCMILLAN, J. H. C. NAYLER, R. SOUTHGATE, and P. TOLLIDAY. J. Chem. Soc. Perkin Trans. I, 562 (1975).
19. S. WOLFE, W. S. LEE, and R. MISRA. J. Chem. Soc. Chem. Commun. 1067 (1969).
20. A. THIBBLIN, S. BENGTSSON, and P. AHLBERG. J. Chem. Soc. Perkin Trans. II, 1569 (1977).
21. T. NAMBARA, S. IKEGAWA, T. HIRAYAMA, and H. HOSODA. Chem. Pharm. Bull. **26**, 757 (1978).
22. R. A. HILL, G. W. KIRBY, and D. J. ROBINS. J. Chem. Soc. Chem. Commun. 459 (1977).
23. S. WOLFE, R. J. BOWERS, S. K. HASAN, and P. M. KAZMAIER. Can. J. Chem. **59**, 406 (1981).
24. P. ADRIAENS, H. VANDERHAEGHE, B. MEESSCHAERT, and H. EYSSEN. Antimicrob. Agents Chemother. **8**, 15 (1975).
25. D. J. ABERHART, J. Y.-R. CHU, N. NEUSS, C. H. NASH, J. OCCOLOWITZ, L. L. HUCKSTEP, and N. DE LA HIGUERA. J. Chem. Soc. Chem. Commun. 564 (1974); J. E. BALDWIN, M. JUNG, J. J. USHER, E. P. ABRAHAM, J. A. HUDDLESTON, and R. L. WHITE. J. Chem. Soc. Chem. Commun. 246 (1981).
26. R. F. BORCH, M. D. BEERNSTEIN, and H. D. DURST. J. Am. Chem. Soc. **93**, 2897 (1971).
27. H. M. CROOKS. *In* The chemistry of penicillin. *Edited by* H. T. Clarke, J. R. Johnson, and R. Robinson. Princeton University Press, Princeton, NJ. 1949. p. 464.
28. J. P. GREENSTEIN, S. M. BIRNBAUM, and M. C. OTEY. J. Am. Chem. Soc. **75**, 1994 (1953).
29. R. D. G. COOPER and F. L. JOSE. J. Am. Chem. Soc. **92**, 2575 (1970).
30. G. R. RAMAGE and J. L. SIMONSEN. J. Chem. Soc. 532 (1935).
31. J. W. CORNFORTH. *In* The chemistry of penicillin. *Edited by* H. T. Clarke, J. R. Johnson, and R. Robinson. Princeton University Press, Princeton, NJ. 1949. p. 783.
32. A. NICKON, J. L. LAMBERT, J. E. OLIVER, D. F. COVEY, and J. MORGAN. J. Am. Chem. Soc. **98**, 2593 (1976).
33. A. SRINIVASAN, K. D. RICHARDS, and R. K. OLSEN. Tetrahedron Lett. 891 (1976); S. WOLFE and C. C. SHAW. Can. J. Chem. **60**, 144 (1982).
34. R. B. BATES, D. W. GOSSELINK, and J. A. KACZYNSKI. Tetrahedron Lett. 199 (1967).
35. D. J. HOOK and R. P. ELANDER. Symposium on new developments in beta-lactam fermentation. 80th Annual Meeting of the American Society of Microbiology, Miami, FL. 1980; D. J. HOOK, R. P. ELANDER, and R. B. MORIN. *In* Symposium on enzyme biosynthesis of peptides. *Edited by* H. Kleinkauf. In press.

Can. J. Chem. Downloaded from www.nrcresearchpress.com by 210.87.254.40 on 09/06/12
For personal use only.

# The crystal and molecular structure of *syn*-2,11-diselena[3,3]metacyclophane and comparison with the dithia-analogue

GORDON W. BUSHNELL AND REGINALD H. MITCHELL

*Department of Chemistry, University of Victoria, Victoria, B.C., Canada V8W 2Y2*

Received April 30, 1981

GORDON W. BUSHNELL and REGINALD H. MITCHELL. Can. J. Chem. **60**, 362 (1982).

The crystal structure of *syn*-2,11-diselena[3,3]metacyclophane, **1***a*, has been determined by single crystal X-ray diffraction and refined to an *R*-value of 0.039. The crystal structure is monoclinic with $a = 1926(1)$, $b = 801.4(3)$, $c = 924(1)$ pm, $\beta = 98.9(1)°$, and is isomorphous with that of the analogous sulphur compound. The space group is $P2_1/n$ with 4 molecules per cell, $D$(meas) = 1.733 g cm$^{-3}$, $D$(calcd) = 1.726 g cm$^{-3}$. The molecule has the *syn*-conformation with the largest possible Se—Se distance of 721.8 pm. The benzenoid rings form a dihedral angle of 19.1°. The distance between the internal aryl hydrogen atoms on rings **1** and **2** is 285.1 pm. The internal aryl C atoms are 314.6 pm apart. The $^1$Hmr solution spectra of **1***a* are consistent with the solid state structure, and can be explained without involving equilibration with an *anti*-conformer.

GORDON W. BUSHNELL et REGINALD H. MITCHELL. Can. J. Chem. **60**, 362 (1982).

On a déterminé la structure cristalline du *syn*-diséléna-2,11[3,3]métacyclophane (**1***a*) par diffraction de rayons X sur un monocristal et on l'a affinée jusqu'à une valeur de $R = 0{,}039$. Le cristal est monoclinique avec $a = 1926(1)$, $b = 801{,}4(3)$, $c = 924(1)$ pm, $\beta = 98.9(1)°$, et il a la même forme que le composé sulfuré analogue. Le cristal appartient au groupe d'espace $P2_1/n$ avec 4 molécules par maille, $D$(mesuré) = 1,733 g cm$^{-3}$, $D$(calculé) = 1,726 g cm$^{-3}$. La molécule a une conformation syn avec la plus grande distance possible Se—Se égale à 721,8 pm. Les noyaux benzéniques forment un angle dièdre de 19.1°. La distance entre les atomes d'hydrogène aryles internes des cycles 1 et 2 est égale à de 285,1 pm. Les atomes de C aromatiques internes sont à 314,6 pm les uns des autres. Les spectres de rmn du $^1$H en solution du composé **1***a* sont en accord avec la structure à l'état solide et peuvent être expliqués sans faire intervenir l'équilibre avec le conformère *anti*.

[Traduit par le journal]

## Introduction

We have recently reported (1) the preparation and properties of 2,11-diselena[3,3]metacyclophane, **1**.[1] On the basis of its $^1$Hmr spectrum, in which the internal aryl hydrogens ($H_i$) appear at δ6.46, we assigned the solution molecular structure of **1** to be that of the *syn*-conformer **1***a*, or a rapidly equilibrating mixture of *syn*-**1***a* and the *anti*-conformer **1***b*, in which *syn*-conformer predominates. These conclusions were made by comparison to the analogous thiaphane, **2**, which we have previously (2) shown exists as the *syn*-conformer in both the solid state and in solution. However, because the $H_i$ protons of **1***a* (δ6.46) were shielded from those of **2***a* (δ6.82), which *a priori* might not be expected (see below), and because no evidence for *anti*-conformer participation in **2** could be observed, we decided to determine the crystal structure of **1** in order to illuminate these observations, and also to allow the first detailed comparison between the structures of thia- and selenacyclophanes.

This paper reports the results of this study.

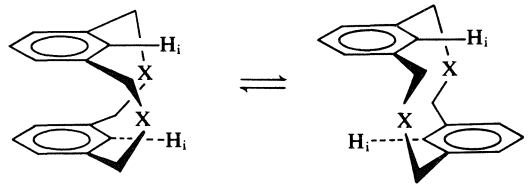


X = Se **1***a* **1***b*
X = S **2***a* **2***b*

[1]For the nomenclature system used in these compounds see ref. 18.

## Experimental

*X-ray measurements*

Preliminary X-ray photographs gave space group $P2_1/n$ with equivalent positions; $x, y, z$; $0.5 + x, 0.5 - y, 0.5 + z$; $-x, -y, -z$; and $0.5 - x, 0.5 + y, 0.5 - z$. Measurements were obtained on a Picker 4-circle diffractometer, using Zr filtered Mo$K_{\bar{\alpha}}$ radiation ($\lambda = 71.069$ pm). The crystal was mounted approximately along the *b*-axis within a glass capillary, and the crystal shape was specified by the following indices and perpendicular distances ±(1,0,−1), 0.132 mm; ±(1,0,0), 0.100 mm; ±(0,1,0), 0.321 mm; ±(1,0,1), 0.130 mm. The crystal data at 26°C were:

$C_{16}H_{16}Se_2$ mw = 366.22

$a = 1926(1)$, $b = 801.4(3)$, $c = 924(1)$ pm, $\beta = 98.9(1)°$, $V$(cell) = 1.409(2) nm$^3$, $D$(meas) = 1.733 Mg m$^{-3}$ (flotation in $CCl_4$/$CHBr_3$ solution). $D$(calcd) = 1.726 Mg m$^{-3}$, $Z = 4$.

Intensity measurements were completed over two octants up to $2\theta = 50°$, (~2480 reflections). A set of three standards 5,0,−5; 0,6,0; and 10,0,0 was used. An instrument instabilty constant of 0.017 (3) was evaluated from the standards. Lorentz and polarisation corrections were applied to the reflections and those for which $I < \sigma(I)$ were eliminated. Absorption corrections were carried out by numerical integration using a 6 × 14 × 6 Gaussian grid ($\mu$ for Mo$K_\alpha$ = 55.65 cm$^{-1}$). After sorting and the merging of a few duplicate measurements there were 2044 independent reflections in the dataset.

0008-4042/82/030362-06$01.00/0

©1982 National Research Council of Canada/Conseil national de recherches du Canada

Can. J. Chem. Downloaded from www.nrcresearchpress.com by 210.87.254.5 on 09/06/12
For personal use only.

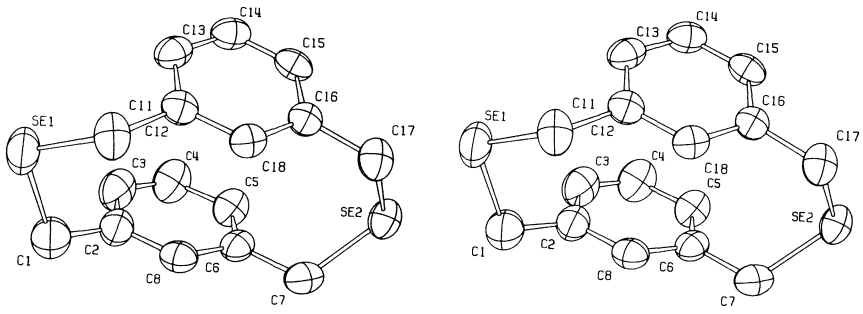


FIG. 1. A stereoview of the molecular structure of *syn*-2,11-diselena[3,3]metacyclophane.

*Structure determination*

A set of programs supplied by Penfold was used, based on ORFLS, FORDAP, ORTEP, and ORFEE (4). From the cell dimensions the crystal structure was seen to be approximately isomorphous with $C_{16}H_{16}S_2$ (2). Atomic scattering curves were taken from International Tables (5), and Se was treated as an anomalous scatterer. The carbon atom co-ordinates were found by means of a difference map. The refinement was by full-matrix least-squares minimisation of $\Sigma w(|F_o| - |F_c|)^2$. The hydrogen atoms were placed at calculated positions using a C—H length of 97 pm, and were given isotropic temperature parameters. The weights derived from counting statistics and experimental considerations did not give constant $w\Delta^2$ when analysed as a function of $|F_o|$, and a weighting scheme was therefore devised: $w = (A + Bx + Cx^2 + Dx^3)^{-1}$ where $x = |F_o|$, $A = 48.7703$, $B = -2.50651$, $C = 0.046833$, $D = -1.63 \times 10^{-4}$. The final agreement factors were $R = 0.039$, $R_w = 0.041$ where $R_w = (\Sigma w\Delta^2/\Sigma w|F_o|^2)^{1/2}$. The final difference map had a maximum of $0.385 \times 10^{-6}$ e pm$^{-3}$, and a minimum of $-0.450 \times 10^{-6}$ e pm$^{-3}$, and $\sigma(\rho) = 0.089 \times 10^{-6}$ e pm$^{-3}$. The fractional atomic co-ordinates for the Se and C atoms are given in Table 1. Supplementary tables have been deposited containing the hydrogen atom and the anisotropic temperature parameters, and the magnitudes of the structure factors.[2]

TABLE 1. Fractional atomic co-ordinates* × $10^4$

| Atom | *x* | *y* | *z* |
|---|---|---|---|
| Se(1) | 103.3(3) | 1968.0(8) | 960.0(7) |
| Se(2) | 3141.9(3) | 2674.7(7) | 6576.2(5) |
| C(1) | 180 (3) | 3904 (8) | 2295 (7) |
| C(2) | 581 (3) | 3540 (6) | 3793 (6) |
| C(3) | 295 (3) | 2622 (8) | 4832 (7) |
| C(4) | 675 (3) | 2266 (8) | 6164 (6) |
| C(5) | 1373 (3) | 2792 (7) | 6504 (6) |
| C(6) | 1678 (2) | 3704 (6) | 5481 (5) |
| C(7) | 2420 (3) | 4300 (6) | 5784 (6) |
| C(8) | 1270 (3) | 4077 (5) | 4142 (5) |
| C(11) | 1095 (3) | 1478 (7) | 921 (6) |
| C(12) | 1489 (2) | 647 (6) | 2282 (5) |
| C(13) | 1208 (2) | −709 (6) | 2940 (6) |
| C(14) | 1586 (3) | −1404 (6) | 4189 (6) |
| C(15) | 2230 (2) | −784 (6) | 4787 (5) |
| C(16) | 2518 (2) | 568 (5) | 4153 (5) |
| C(17) | 3201 (2) | 1327 (7) | 4826 (5) |
| C(18) | 2143 (2) | 1249 (5) | 2892 (5) |

*Estimated standard deviations in parentheses.

## Crystal structure description

A stereoscopic view of a single molecule with atom labels and the thermal ellipsoids containing 50% of the atom probability density is given in Fig. 1. The molecule has an approximate two-fold axis of symmetry passing through the midpoints of C(8)—C(18) and C(4)—C(14). The bond lengths are given in Table 2. There is agreement between columns 1 and 2 within 3 esds, the mean lengths are: Se—C = 196.4 pm, C—C(exocyclic) = 150.3 pm, C—C(aromatic) = 138.5 pm. The bond angles are given in Table 3, in which columns 1 and 2 are related by the approximate two-fold axis of the molecule, and agree satisfactorily. The mean plane results given in Table 4 show that benzene rings are planar and form a dihedral angle of 19.1°. Table 4(*b*) has columns 1 and 2 related by the approximate two-fold molecular axis. The exocyclic C-atoms, C(1) and C(17), lie out of planes *1* and *2* respectively on the inner (Se) sides. A similar displacement for C(7) and C(11) is less definite.

In our previous paper (2) on the isomorphous structure of *syn*-2,11-dithia[3,3]metacyclophane, **2***a*, the emphasis was on the unexpected *syn*-conformation of the compound. Magnetic reso-

TABLE 2. Bond lengths* (pm)

| Bond | Length | Bond | Length |
|---|---|---|---|
| Se(1)—C(1) | 197.3(6) | Se(2)—C(7) | 196.2(5) |
| Se(1)—C(11) | 195.6(5) | Se(2)—C(17) | 196.3(5) |
| C(1) —C(2) | 150.6(8) | C(11)—C(12) | 151.9(7) |
| C(7) —C(6) | 149.1(7) | C(17)—C(16) | 149.5(6) |
| C(2) —C(3) | 138.9(8) | C(12)—C(13) | 139.5(7) |
| C(3) —C(4) | 136.2(8) | C(13)—C(14) | 138.3(7) |
| C(4) —C(5) | 139.6(7) | C(14)—C(15) | 137.0(7) |
| C(5) —C(6) | 139.4(7) | C(15)—C(16) | 138.7(6) |
| C(6) —C(8) | 139.2(7) | C(16)—C(18) | 138.4(6) |
| C(2) —C(8) | 138.4(7) | C(12)—C(18) | 138.4(6) |

*Estimated standard deviations in parentheses.

[2]A complete set of data may be obtained, at a nominal charge, from the Depository of Unpublished Data, CISTI, National Research Council of Canada, Ottawa, Ont., Canada, K1A 0S2.

Can. J. Chem. Downloaded from www.nrcresearchpress.com by 210.87.254.5 on 09/06/12
For personal use only.

Can. J. Chem. Downloaded from www.nrcresearchpress.com by 210.87.254.5 on 09/06/12
For personal use only.

TABLE 3. Bond angles* (deg)

| Atoms | Angle | Atoms | Angle |
|---|---|---|---|
| C(1) —Se(1)—C(11) | 101.0(2) | C(7) —Se(2)—C(17) | 100.7(2) |
| Se(1)—C(1) —C(2) | 113.6(4) | Se(2)—C(17)—C(16) | 114.0(3) |
| Se(2)—C(7) —C(6) | 117.4(3) | Se(1)—C(11)—C(12) | 115.9(4) |
| C(2) —C(8) —C(6) | 121.9(5) | C(12)—C(18)—C(16) | 121.9(4) |
| C(3) —C(4) —C(5) | 120.3(5) | C(13)—C(14)—C(15) | 121.2(4) |
| C(8) —C(2) —C(3) | 118.2(5) | C(18)—C(16)—C(15) | 118.2(4) |
| C(8) —C(6) —C(5) | 118.4(4) | C(18)—C(12)—C(13) | 119.0(4) |
| C(2) —C(3) —C(4) | 121.3(5) | C(16)—C(15)—C(14) | 120.6(4) |
| C(6) —C(5) —C(4) | 119.9(5) | C(12)—C(13)—C(14) | 119.2(4) |
| C(1) —C(2) —C(3) | 122.3(5) | C(17)—C(16)—C(15) | 121.7(4) |
| C(7) —C(6) —C(5) | 122.2(4) | C(11)—C(12)—C(13) | 121.6(4) |
| C(1) —C(2) —C(8) | 119.4(5) | C(17)—C(16)—C(18) | 120.0(4) |
| C(7) —C(6) —C(8) | 119.4(4) | C(11)—C(12)—C(18) | 119.4(4) |

*Estimated standard deviations in parentheses.

nance results were used to extend the scope of the argument in favour of many other related dithia[3,3]metacyclophanes with internal aryl hydrogens, also having the *syn*-conformation. This paper establishes beyond doubt the *syn*-conformation of the diselena[3,3]metacyclophane, **1***a*, and now enables us to discuss in detail the relationship between nmr parameters and structure for the sulphur and selenium analogs.

Table 5 summarises the structural differences between the sulphur and selenium compounds. A difference of 15.3 pm in the bond length C—X (X = S or Se) is accompanied by the selenium atom having a smaller C—X—C bond angle by 3.0°. The strain in the molecules is examined through the X—C—C bond angles and the distortions of the methylene C atoms out of the benzene ring planes on the same side as the S or Se atoms. Averaging over all four X—C—C angles we find that the total distortion is the same in the two compounds. In Table 5 we have averaged pairs of X—C—C bond angles related by the approximate two-fold axis of the molecule. Summing the methylene out-of-plane distortions we come to the conclusion that the sulphur compound is slightly more strained than the selenium one.

Turning our attention now to the distances of the S and Se atoms from the planes of the benzene rings, we find long and short perpendiculars in each compound. These distances are in pairs and related by the approximate two-fold symmetry. A longer perpendicular is associated with a C—C—C—X torsion angle closer to 90°. The strain is then more directly out of the benzene plane, which produces a larger out-of-plane methylene displacement.

The two-fold molecular symmetry approximation is quite good in both compounds, as may be seen by inspecting the groups of four numbers given in the central of part of Table 5. The first and second entries are similar, as are the third and fourth. Both molecules are twisted so that the aromatic rings are not directly one above the other, and the twist is greater for the selenium compound. The various differences in bond lengths and angles combine to give a sizeable increase in the intramolecular X—X distance of 24.4 pm in changing from S to Se. It may be seen from Fig. 1 that this increase in molecular size in the X—X direction is probably responsible for the *a*-axis of the Se compound being 28 pm larger than that of the S compound, a major difference between the unit cell parameters. In the lower section of Table 5 the numbers show that the intramolecular ring-to-ring distances are only slightly larger for the selenium compound, and that the dihedral angle is 1.5° smaller, an almost negligible difference.

We can now amplify our previous statement (2), that in the dithiametacyclophane, **2***a*, the deviations of the benzene ring angles from 120° are collectively greater than the differences between corre-

TABLE 4. The mean planes of the aromatic rings*, plane *1* is through C(2)—C(6) and C(8); plane *2* is through C(12)—C(16) and C(18); the angle between planes *1* and *2* = 19.1°

(*a*) Coefficients of $Ax + By + Cz = D$

| Plane | *A* | *B* | *C* | *D* | $\chi^2$ |
|---|---|---|---|---|---|
| *1* | 0.3722 | −0.8480 | −0.3773 | −349.82 | 7.31 |
| *2* | 0.5366 | −0.6287 | −0.5628 | −12.98 | 7.25 |

(*b*) Perpendicular distances to planes (pm)

| Plane *1* | | Plane *2* | |
|---|---|---|---|
| Atom | Distance | Atom | Distance |
| Se(1) | 185.4(1) | Se(2) | −185.3(1) |
| Se(2) | 131.9(1) | Se(1) | −132.1(1) |
| C(14) | 392.3(5) | C(4) | −395.3(6) |
| C(18) | 303.6(4) | C(8) | −305.6(5) |
| C(1) | 6.3(6) | C(17) | −7.9(5) |
| C(7) | 1.2(5) | C(11) | −2.7(5) |
| C(8) | −0.7(5) | C(18) | 0.8(4) |

*The orthogonal system of axes used has *x* along *a*, *y* in the (*a*, *b*) plane, and *z* along the *c** axis. $\chi^2$ is defined as $\Sigma_i(P_i^2/\sigma^2(P_i))$ where the summation is over all atoms, *i*, in the plane. $P_i$ = the perpendicular distance of atom *i* from the plane.

TABLE 5. A comparison of the structures of *syn*-2,11- dithia- and diselena-[3,3]metacyclophanes*

| Distances and angles (pm and deg) | Dithia | Diselena |
|---|---|---|
| Mean bond length, C—X | 181.1(3) | 196.4(3) |
| Mean bond angle, C—X—C | 103.9(2) | 100.9(2) |
| Mean bond angle, X—C—C | 114.7(3), 116.0(3) | 113.8(3), 116.7(3) |
| Perpendicular distances of methylene C atoms from the ring planes: | | |
| C(1) –plane *1* | 8.9(7) | 6.3(6) |
| C(17)–plane *2* | 10.7(6) | 7.9(5) |
| C(7) –plane *1* | 5.2(6) | 1.2(5) |
| C(11)–plane *2* | 6.9(6) | 2.7(5) |
| X(1) –plane *1* | 171.8(2) | 185.4(1) |
| X(2) –plane *2* | 175.3(2) | 185.3(1) |
| X(2) –plane *1* | 136.0(2) | 131.9(1) |
| X(1) –plane *2* | 136.8(2) | 132.1(1) |
| Torsion angles: | | |
| X(1) C(1) C(2) C(3) | 74.6(7) | 75.2(7) |
| X(2) C(17) C(16) C(15) | 71.2(6) | 74.3(5) |
| X(2) C(7) C(6) C(5) | 51.5(7) | 48.6(6) |
| X(1) C(11) C(12) C(13) | 50.8(7) | 46.5(6) |
| C(11) X(1) C(1) C(2) | 61.1(5) | 59.1(5) |
| C(7) X(2) C(17) C(16) | 61.8(5) | 57.1(4) |
| C(17) X(2) C(7) C(6) | 75.1(5) | 74.0(4) |
| C(1) X(1) C(11) C(12) | 73.6(5) | 74.5(4) |
| Environment of the internal hydrogen atoms: (C–H = 107 pm assumed) | | |
| H(8) –X(1) | 382 | 392 |
| H(18)–X(2) | 388 | 394 |
| H(8) –X(2) | 417 | 434 |
| H(18)–X(1) | 417 | 435 |
| Intramolecular distance, X–X | 697.4(3) | 721.8(1) |
| Distance between benzene ring centres | 350 | 355 |
| Distances C(8)–C(18) and H(8)–H(18) | 305.2(7), 271 | 314.6(6), 284 |
| Dihedral angle between the benzene ring planes | 20.6 | 19.1 |
| H(8) – ring centre 2, in-plane | 287 | 288 |
| ⊥-plane | 260 | 271 |
| H(18) – ring centre 1, in-plane | 299 | 301 |
| ⊥-plane | 259 | 269 |
| H(8) – ring centre 1 | 244 | 244 |
| H(18) – ring centre 2 | 243 | 244 |

*X = S or Se. Estimated standard deviations in parentheses.

sponding angles in the two rings. A comparison of the diselena and dithia compounds reinforces our confidence in the estimated standard deviations derived from the full-matrix least-squares procedure, and shows that the angles are the same in the two compounds as well as between rings *1* and *2*. The angles at the internal carbon atoms such as C(2)—C(8)—C(6) have a mean value of 122.2°. The angles internal to the benzene rings at the bridge junctions have a mean value of 118.4°, and the angles such as C(1)—C(2)—C(3) which are external to both the 6- and 12-membered rings have a mean value of 121.7°.

### Discussion of the nuclear magnetic resonance data relative to the crystal structures of 1 and 2

The pertinent magnetic resonance data are given in Table 6. Whilst there have been a number of studies of $^1H$ and $^{77}Se$ nmr shifts in organoselenium compounds (see for example refs. 8 to 10), apart from correlations to electronegativity, not much has been said about $^1H$ shifts of organosulfur relative to organoselenium compounds. However, as might be expected on the basis of the very similar electronegativities (ref. 11, p. 82) of sulfur and selenium, the $^1H$mr shifts of analogous compounds are very similar. This is also quite clear from Table 6 in which many of the chemical shift differences for the compounds listed there are negligible.

For $H_i$ of **1**, **2** and —$CH_3$ of **5**, **6**, however, the chemical shift difference $\Delta(\delta_S - \delta_{Se})$ is larger and requires some explanation. In the case of **1***a*, **2***a* there are several possible explanations as to why $H_i$ for the selenium analogue **1***a* might be more shielded than $H_i$ of **2***a*. One of the well known (12) consequences of bringing two benzene rings face-

Can. J. Chem. Downloaded from www.nrcresearchpress.com by 210.87.254.5 on 09/06/12
For personal use only.

TABLE 6. Nuclear magnetic resonance data for several thia- and selenacyclophanes and a model

| Compound | Proton type | δ X = S (ref. 6) | δ X = Se (ref. 1) | $\Delta(\delta_S - \delta_{Se})$ |
|---|---|---|---|---|
| 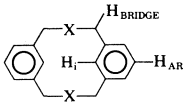 | $H_{AR}$ | 6.91 | 7.04 | −0.13 |
| | $H_i$ | 6.82 | 6.46 | +0.36 |
| | $H_{BRIDGE}$ | 3.71 | 3.78 | −0.07 |
| **1***a*: X = Se **2***a*: X = S | | | | |
| 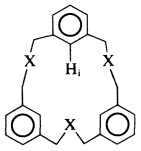 | $H_{AR}$ | 7.26 | 7.20 | +0.06 |
| | $H_i$ | 7.09 | 7.06 | +0.03 |
| | $H_{BRIDGE}$ | 3.52 | 3.60 | −0.08 |
| **3**: X = S **4**: X = Se | | | | |
| 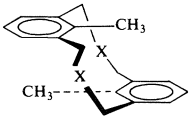 | $H_{AR}$ | 7.4–7.0 | 6.97 | — |
| | $H_{BRIDGE}$ | 3.68 | 3.69 | −0.01 |
| | $H_{CH_3}$ | 1.30 | 1.77 | −0.47 |
| **5**: X = S **6**: X = Se | | | | |
| 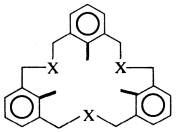 | $H_{AR}$ | 7.11 | 7.00 | +0.11 |
| | $H_{BRIDGE}$ | 3.63 | 3.67 | −0.04 |
| | $H_{CH_3}$ | 1.80 | 2.05 | −0.25 |
| **7**: X = S **8**: X = Se | | | | |
| $(CH_3CH_2)_2X$ | $—CH_2—$ | 2.55 (ref. 7) | 2.53 (ref. 8) | +0.02 |
| | $CH_3—$ | 1.25 | 1.37 | −0.12 |

to-face is that one benzene ring shields the protons of the opposite ring. If the geometry of the molecule is known, the degree of shielding can be calculated using the tables of Johnson and Bovey (ref. 13, ref. 14, p. 595). When this calculation is carried out for H(8) and H(18) (i.e. $H_i$) of **1***a* and **2***a* using the geometry of the crystal (data given in Table 5), the average shielding of $H_i$ for the sulfur analogue (ca. 0.17 ppm) is actually less than for the selenium analogue (ca. 0.19 ppm), but the difference between these two values of only 0.02 ppm is marginal. As well, although the deshielding effect of a benzene ring on its own hydrogens changes rapidly as the distance of a hydrogen varies from the center of the ring, the difference between the calculated distances of H(8) and H(18) from the centers of their own rings in **1***a* and **2***a* is very small and has no significant effect (< 0.01 ppm) on the chemical shift differences of $H_i$.

Thus the observed difference of chemical shift of $H_i$ for **1** and **2** of 0.36 ppm is probably caused by a through space heteroatom anisotropy effect. Whilst the exact calculation of the shielding of a hydrogen close to a heteroatom is rather complex (see, for example, ref. 14, p. 130), certainly it is reasonable that such shielding would be distance dependent. As can be seen from Table 5, the $H_i$–Se distance of **1***a* is notaby greater than the corresponding $H_i$–S distance of **2***a*, and this may explain the observed chemical shift difference, without the necessity of invoking participation of an *anti*-conformer such as **1***b* to account for the shielding of $H_i$ of **1**. This would then be consistent with the results found (2) for **2**.

Can. J. Chem. Downloaded from www.nrcresearchpress.com by 210.87.254.5 on 09/06/12
For personal use only.

Can. J. Chem. Downloaded from www.nrcresearchpress.com by 210.87.254.5 on 09/06/12
For personal use only.

Further support for this suggestion can be found by considering the C(8)–C(18) and H(8)–H(18) distances given in Table 5. In both cases these are greater for the selena compound, which should result in less strain for the latter, and less need to invoke *anti*-conformer involvement. However, as the size of the substituent (Z) on C(8) and C(18) grows then the compression between Z(8) and Z(18) becomes of paramount importance (for a review see ref. 15 and the *anti*-conformer is generally preferred, e.g. in the case of **5**, the *anti:syn* ratio observed experimentally in their preparation is about 7:1 (6). Thus in *syn*-**5** the $CH_3(8)$–$CH_3(18)$ distance measured (16) is 352 pm, considerably less than the normally expected distance of closest approach of about 400 pm (ref. 11, p. 109). In the case of **1***a* and **2***a* however, the H(8)–H(18) distances are greater than the closest approach values of ca. 240 pm, and hence the preference for *syn*-conformation.

The $^{13}$Cmr spectra (1) of **1***a* and **2***a* are very similar to each other with the exception of the methylene bridge carbons (C-1, 7, 11, 17) which for **1***a* appear at δ27.8 whereas for **2***a* are at δ37.7. The shielding in the selenium case is probably due to the neighbour anisotropy shielding term (17) which would be expected to be larger for selenium than sulfur. Presumably this must be counteracted to some extent by any steric effect, since the thia-compound **2***a* is the more strained, and much of this occurs by bending these particular carbon atoms out of the planes of the benzene rings (see Table 5) which would be expected (17) to shield the carbon atoms in their $^{13}$Cmr spectra.

Unfortunately the crystal structures of the *anti*-compounds **5** and **6** are not yet available. Nevertheless, from the data observed in this comparison between **1** and **2** it would seem reasonable to expect that because of the longer C—Se bonds (196.4 pm) relative to C—S (181.1 pm), the internal methyl groups of **6** will not be projected so far into the shielding cavity of the opposite benzene ring, and hence would be expected to be less shielded than those of **5** as observed. We hope to be able to comment further on this in due course.

**Acknowledgements**

We thank the University of Victoria and the Natural Sciences and Engineering Research Council of Canada for operating grants, Mrs. K. Beveridge for technical assistance, and Mr. K. Hartman for the illustrative photography.

1. R. H. MITCHELL. Can. J. Chem. **58**, 1398 (1980).
2. W. ANKER, G. W. BUSHNELL, and R. H. MITCHELL. Can. J. Chem. **57**, 3080 (1979).
3. G. H. STOUT and L. H. JENSEN. X-ray structure determination. Macmillan, New York. 1968. p. 456.
4. B. R. PENFOLD. University of Canterbury, crystallographic programs. Christchurch, New Zealand.
5. D. T. CROMER and J. T. WABER. International tables for X-ray crystallography. Vol. IV. Kynoch Press, Birmingham. 1974. Table 2.2A. p. 72.
6. R. H. MITCHELL and V. BOEKELHEIDE. J. Am. Chem. Soc. **96**, 1547 (1974).
7. C. J. POUCHERT and J. R. CAMBELL. The Aldrich Library of NMR Spectra. Aldrich Chemical Co., Milwaukee, WI. 1974. Vol. I, 158C.
8. M. A. LARDON. J. Am. Chem. Soc. **92**, 5063 (1970).
9. U. SVANHOLM and M. A. LARDON. *In* Organic selenium compounds: their chemistry and biology. *Edited by* D. L. Klayman and W. H. H. Gunther. Wiley-Interscience, New York, NY. 1973. Chapt. XV.
10. W. MCFARLANE and R. J. WOOD. J. Chem. Soc. Dalton, 1397 (1972); A. FREDGA, S. GRONOWITZ, and A. B. HÖRNFELDT. Chem. Script. **8**, 15 (1975).
11. A. J. GORDON and R. A. FORD (*Editors*). The chemist's companion. John Wiley and Sons, New York, NY. 1972.
12. R. H. MITCHELL and F. SONDHEIMER. J. Am. Chem. Soc. **90**, 530 (1968); D. J. CRAM, C. K. DALTON, and G. R. KNOX. J. Am. Chem. Soc. **85**, 1088 (1963); R. H. MARTIN, G. MORREN, and J. J. SCHURTER. Tetrahedron Lett. 3683 (1969).
13. C. E. JOHNSON and F. A. BOVEY. J. Chem. Phys. **29**, 1012 (1958).
14. I. W. EMSLEY, J. FEENY, and L. H. SUTCLIFFE. High resolution nuclear magnetic resonance spectroscopy. Vol. I. Pergamon Press, Oxford. 1965.
15. H. FÖRSTER and F. VÖGTLE. Angew. Chem. Int. Ed. Engl. **16**, 429 (1977).
16. B. R. DAVIS and I. BERNAL. J. Chem. Soc. B, 2307, (1971).
17. F. W. WEHRLI and T. WIRTHLIN. Interpretation of carbon-13 nmr spectra. Heyden, London. 1978. Chapt. 2.
18. F. VÖGTLE AND P. NEUMANN. Tetrahedron, **26**, 5847 (1970).

Can. J. Chem. Downloaded from www.nrcresearchpress.com by 210.87.254.105 on 09/06/12
For personal use only.

COMMUNICATION

# Biogenetic type solid phase phenol coupling synthesis of alkaloids. Prelycorane species

J. W. APSIMON[1] AND D. M. DIXIT

*Department of Chemistry, Carleton University, Ottawa, Ont., Canada K1S 5B6*

Received August 4, 1981

J. W. APSIMON and D. M. DIXIT. Can. J. Chem. **60**, 368 (1982).

The coupling of a norbelladine derivative supported on a modified styrene – 1% divinylbenzene copolymer proceeds in modest yield to provide a coupled product whose structure corresponds to the presently undescribed precursors to the Lycorane alkaloids. The orientation of phenol coupling (*o–o*-) is different to that observed (*o–p*-) on oxidation of the nonsupported substrates.

J. W. APSIMON et D. M. DIXIT. Can. J. Chem. **60**, 368 (1982).

Le couplage d'un dérivé de la norbelladine fixé sur un copolymère modifié de styrène – 1% divinylbenzène se fait avec un rendement modeste et conduit à un produit couplé dont la structure correspond au précurseur d'alcaloïdes du Lycorane qui ne sont pas encore décrits. L'orientation du couplage du phénol (*o–o*) est différente de celle observée (*o–p*) lors de l'oxydation des substrats non fixés sur un support.

[Traduit par le journal]

Oxidative coupling of phenols (1) plays an important role in the biosynthesis of a large variety of natural products. Alkaloids present in the Amaryllidaceae demonstrate beautifully the varied operations of phenol coupling (2). These compounds are present in three skeletal types (**2**, **3**, and **4**) all derived from a single biogenetic precursor, related to 4′-*O*-methylnorbelladine (**1***b*) by the coupling modes a, b, and c, shown.

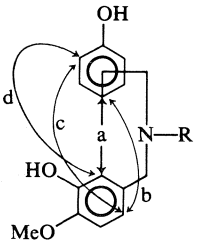


**1***a* R = H
*b* R = Ⓟ

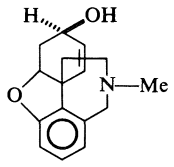


Golanthamine **2** (via a)

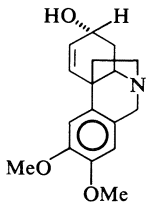


Crinine **3** (via b)

Barton and Cohen (3) outlined a mechanism whereby these three major structural types among these alkaloids were derivable from this parent compound by intramolecular oxidative coupling of two phenolic rings, a hypothesis that has been supported by radioactive tracer evidence (4). In vitro oxidations of norbelladine derivatives have yielded both crinane (**3**) (5) and galanthamine (**2**) (6) type compounds but to date we are unaware of a phenolic coupling route that has led to the lycorane type species (mode c or d), although several

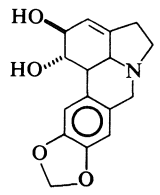


Lycorine **4** (via c)

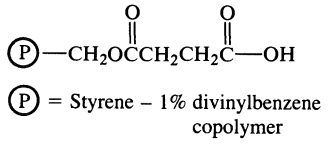


**5**

stepwise syntheses of this type of compound have been recently reported (7). With a couple of exceptions, in vitro biomimetic phenolic coupling reactions have been unsatisfactory because of low yields. Some while ago we became interested in the possibility of solving this problem by examining the oxidation of phenolic precursors supported on a solid phase (8). In this manner we felt that the intermolecular coupling reactions (polymerization) of the phenolic radicals would be reduced and, hopefully, the products of intramolecular reaction would be increased. Although this goal is still not completely realised we have been successful in accomplishing coupling on a polymer support, and our preliminary results are reported here suggesting mode d outlined above.

4′-*O*-methylnorbelladine **1***a* has three sites (2 phenol, 1 amine) available for anchoring onto a polymer support, although bonding at the amino group appears to be preferable since at the same time as leaving two phenolic groups required for the oxidative experiments, the nitrogen atom is also protected from oxidation. Of the many polymers examined as a suitable support (9) for the

[1]Author to whom communications may be addressed.

0008-4042/82/030368-03$01.00/0

©1982 National Research Council of Canada/Conseil national de recherches du Canada

Can. J. Chem. Downloaded from www.nrcresearchpress.com by 210.87.254.105 on 09/06/12
For personal use only.

diphenol, only one was found to be suitable in both specific amine anchoring and deanchoring reactions. This polymer **5** is prepared by the esterification of hydroxymethylated styrene – 1% divinylbenzene polymer with succinic anhydride in DMF and pyridine (ir $\nu_{max}$ (KBr): 1730 (ester), 1710 (acid) $cm^{-1}$ (10)).

Reaction of **1***a* and **5** in the presence of dicyclohexylcarbodiimide provided the supported diphenol **1***c* (ir $\nu_{max}$ (KBr): 1730 (ester), 1645 (amide) $cm^{-1}$) in a concentration of about 0.05 mmol of diphenol per gram of resin. Anchoring appears to have occurred only on nitrogen. Oxidation of **1***c* with a variety of one-electron oxidizing agents, followed by deanchoring of the reaction products from the resin with potassium carbonate in methanol, was disappointing until we chose vanadium oxytrichloride (5, 11) in methylene chloride at −55°C. After deanchoring and tlc purification a product was obtained (approx. 30% yield) to which we assign structure **6***a* (isolated as its methylated derivative **6***b* after treatment of the reaction mixture with diazomethane).[2]

The structure of **6***b* follows from spectroscopic data. The high resolution mass spectrum indicates that coupling has occurred ($M^+$ 399.1697, $C_{22}H_{25}O_6N$ requires $M^+$ 399.1682) and its infrared spectrum shows strong intramolecular hydrogen bonding (3420 $cm^{-1}$) together with ester (1730 $cm^{-1}$) and amide (1645 $cm^{-1}$) absorptions. The uv spectrum ($\lambda_{max}$ EtOH, 225 nm (log ε 3.32), 277.5 (log ε 1.07) suggests a skewed diphenyl. The $^1H$ nmr spectrum (100 MHz FT JEOL) indicates a mixture of conformers at room temperature, but at 120°C in DMSO-$d_6$ simplification is observed (together with thermal decomposition), revealing the two AX aromatic proton systems (centred at 6.95 and 7.28 ppm) together with the single *m*-proton signal (6.98 ppm, $J$ = 1 Hz). The *o*–*m*-cyclophane system and the *o*,*o*′-substituents of **6** presumably lead to this conformational barrier.

It is apparent that **6***a* represents the primary cyclization product leading to the lycorane-type alkaloids (e.g. **4**). Its formation in this case is in distinct contrast to Schwartz's $VOCl_3$ oxidation of the trifluoroacetyl derivative of **1***b* (5) and Tobinaga's electrochemical cyclization of the same compound (12). Both of these reactions yielded *p*–*p*′ coupling products.

Probably the solid matrix used immobilizes the diphenyl system in some way to restrict the previously observed in vitro coupling mode. The vanadium oxytrichloride may also help in the efficient cyclization by the intervention of a cyclic coupling mode as shown in **7**.

The data presented for **6***b*, while indicating that coupling has occurred ($M^+$) and that a diphenyl system is present (nmr, uv, ir), do not distinguish between this structure and the alternate structures **8**, **9**, and **10**. Of these, the proton nmr data eliminated **9** and **10** (2 AX systems in aromatic region) and all are eliminated from consideration by the observation of strong intramolecular hydrogen bonding in the infrared spectrum of **6***b*.

The dibenzo[*c*,*e*]azocine system present in **8** has been reported (13); amongst other spectral data this system displays that are not consistent with the proposed **6***b*, it is to be noted that the $ArCH_2N$ protons are of substantially different chemical shift (~ 2.2 ppm) and show a geminal coupling constant of 14 Hz. No such signals can be detected in the nmr spectrum of **6***b*. Further, work from this laboratory[3] has led to a synthesis of **8***b*, a compound which is far more stable than **6***b* and whose nmr spectrum can be analysed in a first-order manner at room temperature.

A natural product, Nivaldine (14), is also known which possesses the basic structure of **8** (minus the hydroxyl group on the topmost ring). The mass spectral fragmentation of this species is reportedly (15) characteristic for the dibenzazocine ring sys-

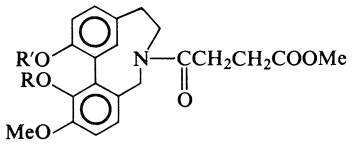


**6***a* R = R′ = H
*b* R or R′ = H,Me

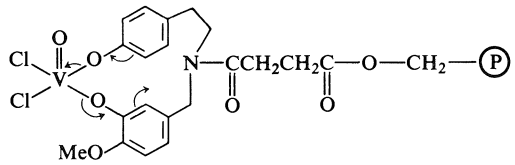


7

[2]Compound **1***b* (200 mg) was anchored to resin **5** (5 g) and suspended in dry methylene chloride (40 mL). The suspension was treated at −55°C under argon with an excess of $VOCl_3$ (2.4 mL) for 48 h. The resin was then filtered, washed successively with $CH_2Cl_2$, $H_2O$, 6 *N* $H_2SO_4$, $H_2O$, and acetone, and dried *in vacuo*. The resin was then transesterified with methanol and $K_2CO_3$ and the product obtained was treated with ethereal-diazomethane. Preparative tlc provided **6***b* (47 mg) which slowly crystallized from ether as conglomerates of fine needles, mp 132–134°C.

[3]J. W. ApSimon and D. M. Dixit. Unpublished data.

tem. The mass spectrum of **6***b* exhibits none of the reported major fragmentation patterns of Nivaldine.

The intriguing possibility of modifying hitherto observed reaction pathways by solid phase conformational restriction, the conversion of **6** to known lycorane alkaloids, and parallel reactions in the benzylisoquinoline field are presently in progress in our laboratories.

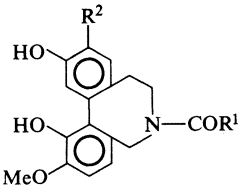


**8***a* $R^1 = COCH_2CH_2COOMe$; $R^2 = H$
**8***b* $R^1 = COCH_2CH_2COOMe$; $R^2 = OMe$

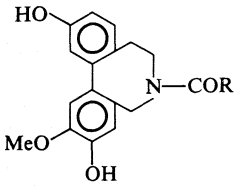


**9**

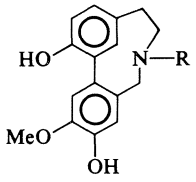


**10**

**Acknowledgements**

We thank the Natural Sciences and Engineering Research Council of Canada and the Hofmann La Roche Foundation for generous financial assistance.

1. A. R. BATTERSBY. Oxidative coupling of phenols. *Edited by* W. I. Taylor and A. R. Battersby. Marcell Dekker, New York. 1967.
2. D. R. DALTON. The alkaloids. Marcel Dekker, New York. 1971. p. 287; R. B. HERBERT. *In* Comprehensive organic chemistry. Vol. 5. *Edited by* D. H. R. Barton and W. D. Ollis. Pergamon Press, Oxford. 1979. p. 1087.
3. D. H. R. BARTON and T. COHEN. Festschr. Arthur Stoll, 117 (1957).
4. B. FRANCK and H. J. HUBS. Angew. Chem. Int. Ed. Engl. **3**, 223 (1968).
5. M. A. SCHWARTZ and R. A. HOLTON. J. Am. Chem. Soc. **92**, 1090 (1970).
6. D. H. R. BARTON and G. W. KIRBY. J. Chem. Soc. 806 (1962).
7. R. V. STEVENS. *In* The total synthesis of natural products. Vol. 3. *Edited by* J. W. ApSimon. Wiley–Interscience, New York. 1977. p. 439.
8. R. B. MERRIFIELD. J. Am. Chem. Soc. **85**, 2149 (1963); J. M. STEWART and J. D. YOUNG. Solid phase peptide synthesis. W. H. Freeman and Co., San Francisco, CA. 1969; C. C. LEZNOFF. Acc. Chem. Res. **11**, 327 (1978).
9. A. M. FELIX and R. B. MERRIFIELD. J. Am. Chem. Soc. **93**, 3272 (1971); D. M. DIXIT. Ph.D. thesis, Carleton University, Ottawa, Canada, 1976.
10. J. W. APSIMON and D. M. DIXIT. Synth. Commun. In press.
11. M. A. SCHWARTZ, R. A. HOLTON, and S. W. SCOTT. J. Am. Chem. Soc. **91**, 2800 (1969).
12. E. KOTANI, N. TAKEUCHI, and S. TOBINAGA. J. Chem. Soc. Chem. Commun. 55 (1973).
13. P. W. JEFFS, J. F. HANSEN, and G. A. BRINE. J. Org. Chem. **40**, 2883 (1975).
14. L. BUBEWA-IWANOWA. Chem. Ber. **95**, 1348 (1962).
15. T. KAMETANI, K. YAMASAKI, S. SHIBUYA, K. FUKUMOTO, K. KIGASAWRA, F. SATOH, M. HIIRAGI, and T. HAYASAKA. J. Chem. Soc. C, 590 (1971).

Can. J. Chem. Downloaded from www.nrcresearchpress.com by 210.87.254.105 on 09/06/12
For personal use only.

# The biosynthesis of cyclopropane fatty acids. II. Mechanistic studies using methionine labelled with one, two, and three deuterium atoms in the methyl group

PETER H. BUIST AND DAVID B. MACLEAN
*Department of Chemistry, McMaster University, Hamilton, Ont., Canada L8S 4M1*

Received May 26, 1981

PETER H. BUIST and DAVID B. MACLEAN. Can. J. Chem. **60**, 371 (1982).

The mechanism of formation of monodeuterated cyclopropane fatty acids on administration of L-methione-methyl-$d_3$ to *L. plantarum* has been investigated. It has been found that the extent of exchange is not affected by the presence of oxygen in the medium, that neither formate-$d_0$ nor formaldehyde-$d_2$ is significantly incorporated into the fatty acid, and that methionine reisolated from the intracellular pool does not contain any exchanged species. These experiments militate against any mechanism involving exchange prior to methyl group transfer. Parallel feeding experiments using methionine labelled in the methyl group with one, two, or three deuterium atoms were carried out and in this way that extent of exchange was quantitated. It was found that at least one-third of the cyclopropane fatty acid from methionine methyl-$d_3$ experiments is derived from an exchanged methyl group. The intramolecular and intermolecular primary deuterium isotope effects for biological cyclopropane ring formation were measured and found to be 3.2 ± 0.5, and 1.01 ± 0.04, respectively. These results are consistent with a mechanism in which a methyl group is transferred in a slow step which is followed by a fast, partially reversible, protonation–deprotonation step.

PETER H. BUIST et DAVID B. MACLEAN. Can. J. Chem. **60**, 371 (1982).

On a étudié le mécanisme de formation du cyclopropane monodeutéré d'acides gras contenant un cyclopropane monodeutéré en administrant de la L-méthionine-méthyl-$d_3$ au *L. plantarum*. On a trouvé que le taux d'échange n'est pas affecté par la présence de l'oxygène dans le milieu et que ni le formiate-$d_0$ ni la formaldéhyde-$d_2$ ne s'incorporent de façon significative dans l'acide gras et que la méthionine réisolée du bain intracellulaire ne contient aucune espèce inchangée. Ces expériences militent contre tout mécanisme impliquant un échange avant le transfert du groupe méthyle. On a réalisé des expériences parallèles d'alimentation utilisant de la méthionine marquée au niveau du groupe méthyle avec un, deux ou trois atomes de deutérium et dans cette voie on a pu mesurer le taux d'échange. A partir des expériences avec la méthionine-méthyl-$d_3$ on a trouvé qu'au moins un tiers du cyclopropane de l'acide gras provient du groupe méthyle échangé. On a mesuré que les effets isotopiques primaires intra et intermoléculaires du deutérium lors de la formation biologique du cyclopropane sont respectivement de 3,2 ± 0,5 et de 1,01 ± 0,4. Ces résultats sont en accord avec un mécanisme dans lequel il y a transfert d'un groupe méthyle dans l'étape lente qui est suivi par une rapide étape de protonation–déprotonation qui est partiellement réversible.

[Traduit par le journal]

The biosynthesis of cyclopropane fatty acids involves the construction of a methylene bridge across the *cis* double bond of an unsaturated precursor. The methylene group is derived from *S*-adenosyl-L-methionine (SAM) which in turn is formed by reaction of L-methionine with adenosine triphosphate (1). Recently, we reported the results of methionine-methyl-$d_3$ feedings, to *Lactobacillus plantarum*, where up to 17% of a monodeuterated cyclopropane fatty acid was formed along with the expected $d_2$ species (2). Clearly, substantial amounts of label had been exchanged out at some stage in the biosynthetic pathway. A similar exchange phenomenon had been observed in biological exomethylene group formation, a process thought to involve the same initial carbocationic intermediate as that postulated for cyclopropane group biosynthesis (Scheme 1) (3). Reversible 1,3 $H^+$ elimination would lead to exchanged product. Lederer has shown quite conclusively that, in methionine-methyl-$d_3$ feedings leading to exomethylene group formation, the methyl group had not undergone exchange prior to the methyl transfer step (3). Here we report experiments designed to investigate whether exchange had occurred in our feeding experiments, by processes unrelated to the cyclopropanation reaction. Furthermore, by carrying out parallel feeding experiments using methionine labelled with one, two, or three deuterons in the methyl group, the extent of exchange could be quantitated. The data from these experiments allowed the calculation of an intramolecular primary deuterium isotope effect for the proton abstraction step in the cyclopropanation reaction. Comparison of this value with the

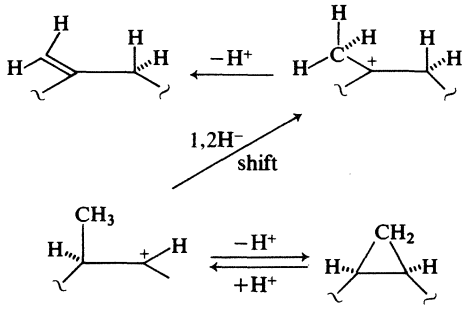


SCHEME 1

0008-4042/82/040371-08$01.00/0
©1982 National Research Council of Canada/Conseil national de recherches du Canada

Can. J. Chem. Downloaded from www.nrcresearchpress.com by 210.87.254.40 on 09/06/12
For personal use only.

TABLE 1. Results of experiments designed to examine the role of one-carbon metabolism in $d_1$-cyclopropane fatty acid formation

| Experiment No. | Compounds added to basal medium 2* (1 L) | Cell yield (mg/100 mL) | Deuterium content of biosynthetic cyclopropane fatty acid | | | |
|---|---|---|---|---|---|---|
| | | | % $d_0$ | % $d_1$ | % $d_2$ | % $d_1$/(% $d_1$ + % $d_2$) |
| 1 (Aerobic) | Methionine-methyl-$d_3$ (0.67 m*M*) | 82 | 16.4 | 11.6 | 72.0 | 13.9 |
| 2 (Anaerobic) | Methionine-methyl-$d_3$ (0.67 m*M*) | 120 | 15.7 | 12.2 | 72.0 | 14.5 |
| 3 (Aerobic) | Methionine (0.67 m*M*) Formaldehyde-$d_2$ (0.63 m*M*) | 55 | 100 | 0 | 0 | 0 |
| 4 (Aerobic) | Methionine-methyl-$d_3$ (0.60 m*M*) Formate (0.40 m*M*) | 135 | 16.8 | 15.3 | 67.9 | 18.4 |
| 5 (Aerobic) | Methionine-methyl-$d_3$ (0.30 m*M*) Formate (0.40 m*M*) | 178 | 16.9 | 12.7 | 70.4 | 15.3 |

*All culture media contained biotin at 10 μg/L.

results of an intermolecular isotope effect experiment yielded further mechanistic information.

One possible mechanism for methyl group exchange would be the degradation of methionine to formaldehyde or formate followed by resynthesis of methionine. Liu and Hofman (4) were able to obtain low levels of incorporation of formate-$^{14}$C into the bridgehead position of cyclopropane fatty acids and low levels of methionine biosynthesis have been detected in *L. casei* (5), a closely related microorganism, also capable of performing the cyclopropanation reaction. A series of experiments, designed to test for methionine degradation and resynthesis, was carried out. Since oxygen might be involved in the oxidative degradation of methionine, two methionine-methyl-$d_3$ feedings, one under anaerobic and one under aerobic conditions, were carried out (Experiments 1 and 2, Table 1). In another experiment, formaldehyde-$d_2$ (Experiment 3) along with L-methionine-methyl-$d_0$ was administered to the organism. Two further experiments were performed in which nonlabelled formate was fed at 0.7 × (Experiment 4) and at 1.3 × (Experiment 5) the concentration of methionine-methyl-$d_3$ to the organism. Finally, intracellular methionine was isolated from the aerobically grown cells (Experiment 1) and the bis-TMS derivative examined by gc-ms (Table 2).

From examination of Tables 1 and 2, it is evident that *de novo* methionine biosynthesis from formaldehyde-$d_2$ is not involved in $d_1$-cyclopropane fatty acid formation.

Removal of oxygen from the culture medium did not reduce $d_1$-cyclopropyl fatty acid formation (Experiments 1, 2). Neither formate or formaldehyde was incorporated into the cyclopropane fatty acid (Experiments 3, 4, 5). Finally, reisolated methionine contained no $d_1$ or $d_2$-species within experimental error (Table 2).

TABLE 2. Intracellular methionine isolation experiment

| Compound analyzed | % $d_0$ | % $d_1$ | % $d_2$ | % $d_3$ |
|---|---|---|---|---|
| Methionine administered | 14.0 | 0 | 1.0 | 85.0 |
| Cyclopropane fatty acid isolated | 16.4 | 11.6 | 72.0 | |
| Methionine isolated | 51* | 1.0 | 0 | 48.0 |

*The large amount of $d_0$-methionine was derived from the methionine tracer used to isolate the intracellular methionine.

It is also possible that SAM-methyl-$d_3$ loses deuterium by a simple exchange process. This seems unlikely for a number of reasons. Firstly, the pH inside fermenting cells of *L. plantarum* has been shown to be approximately 5.4 (6). These slightly acidic conditions would not favor rapid exchange of a methyl sulfoniun salt. Nuclear magnetic resonance experiments have shown that *S*-methyl-methionine does not exchange its methyl protons in neutral medium. Secondly, SAM-methyl-$d_3$ has been isolated from yeast (Fleischmann, Standard Brands, Inc.) and shown to have the same deuterium content, within experimental error, as that of the methionine from which it was biosynthesized (7). Thirdly, natural products, containing methyl groups derived from SAM-methyl-$d_3$ via simple methyl transfer to electron-rich centres, do not contain any significant $d_2$ or $d_1$-species (8–15).

Can. J. Chem. Downloaded from www.nrcresearchpress.com by 210.87.254.40 on 09/06/12
For personal use only.

TABLE 3. Feeding experiments with methionine labelled at the methyl group with one, two, and three deuterium atoms

| Experiment | Compound administered (length of incubation, h) | Compound isolated | pH at end of incubation | Cell yield (mg/100 mL of culture) | % $d_0$ | % $d_1$ | % $d_2$ | % $d_3$ |
|---|---|---|---|---|---|---|---|---|
| A | Methionine-methyl-$d_3$ | | | | 13.8 | 0 | 1.2 | 85.0 |
| | | Cyclopropane | 5.0 | 106 | 16.2 | 10 | 73.8 | |
| | (29) | fatty acid | | | (0.8) | (11.5) | (87.7) | |
| B | Methionine-methyl-$d_2$ | | | | 0.6 | 2.8 | 96.6 | |
| | | Cyclopropane | | | 4.1 | 35.6 | 60.3 | |
| | (29) | fatty acid (I) | 4.8 | 110 | (1.1) | (35.1) | (63.8) | |
| | | Cyclopropane | | | | | | |
| | (48) | fatty acid (II) | 4.5 | 120 | 3.7 | 37.7 | 58.7 | |
| C | Methionine-methyl-$d_1$ | | | | 3.0 | 97.0 | | |
| | | Cyclopropane | | | 17.8 | 82.2 | | |
| | (29) | fatty acid (I) | 5.2 | 111 | (13.5) | (86.5) | | |
| | | Cyclopropane | | | | | | |
| | (48) | fatty acid (II) | 4.6 | 122 | 17.7 | 82.3 | | |

Notes to Table:
1. The results of Experiment II are included to show that even though these cells grew out more slowly than those in Exp. I, the resulting distribution of deuterium in the cyclopropyl product was similar. The results of Exp. I are used for the calculations.
2. Isotopic compositions of the cyclopropane fatty acid were corrected for both the isotopic composition of the labelled methionine (which in all cases did not consist of one isotopic species) and for endogenous $d_0$-methionine and $d_0$-cyclopropane fatty acid in the inoculum. The latter value was estimated to contribute ca. 2% to the $d_0$ content of the cyclopropyl product. The corrected isotopic compositions are given in parentheses to an accuracy of ±2%.

If exchange is actually occurring at the active site of cyclopropane synthetase, it would be of interest to quantitate this process, namely, to determine the percentage of methyl groups that go through the reaction sequence irreversibly. Our approach was to carry out three parallel feeding experiments, using methionine labelled with one, two, or three deuterons in the methyl group, and then determine by mass spectrometry the deuterium distribution in the resulting biosynthetic cyclopropane fatty acid. The results are shown in Table 3.

The extent of exchange at the methyl group in the methionine-methyl-$d_3$ feedings was calculated in the following manner. In the feeding using methionine-methyl-$d_3$ (Table 3, hereafter referred to as Experiment A), a $d_3$-methyl group must have exchanged to give a $d_2$-methyl group which in turn might have exchanged to give a $d_1$ and eventually a $d_0$-methyl group species. In the feeding using methionine-methyl-$d_2$ (Table 3, hereafter referred to as Experiment B), a $d_2$-methyl group might have exchanged to give a $d_1$ and eventually a $d_0$-methyl group species. Assuming, for the moment, that the extent to which a $d_2$-methyl group exchanged was the same in both experiments A and B, then one can calculate the amount of cyclopropyl product derived directly or indirectly from such a species in Experiment A. Thus, associated with the 11.5% of $d_1$-product obtained in Experiment A was a certain amount of $d_2$-product which also arose from a $d_2$-methyl species. This amount can be calculated by taking the ratio of the $d_1$ content obtained in Experiments A and B and multiplying this value by the $d_2$ content obtained in Experiment B. This is $(11.5/35.1 \times 63.8) = 20.9$. Adding this number to the $d_1$ and $d_0$ content obtained in Experiment A gives the total amount of cyclopropane fatty acid derived from an exchanged methyl group species. The extent of this exchange was $(20.9 + 11.5 + 0.8) = 33.2\%$.

However, the extent of exchange of a $d_2$-methyl group in Experiment B may have been greater (never less) than in Experiment A. The ratio of $\%\, d_2/\%\, d_1$ used in the above calculation might, therefore, be too low and thus the above calculated value for the extent of exchange is a minimum value. From the above discussion it is clear that, typically, at least one-third of the cyclopropane fatty acid is derived from an exchanged methyl group species in a methionine-methyl-$d_3$ feeding experiment.

The results of the feeding experiments using methionine-methyl-$d_2$ (Experiment B) and methionine-methyl-$d_1$ (Experiment C) can be used to obtain primary intramolecular isotope effects for the proton abstraction step in the biological cyclopropanation reaction.

Since the extent of exchange at the methyl group in the methionine-methyl-$d_1$ and methionine-methyl-$d_2$ feedings could not be determined, only a minimum intramolecular isotope effect was calculated. This value was calculated to be $k_H/k_D = 2(\%\, d_2/\%\, d_1) = 2(63.8 \pm 2/35.1 \pm 2) = 3.6 \pm 0.2$, for the methionine-methyl-$d_2$ feeding and $k_H/k_D =$

Can. J. Chem. Downloaded from www.nrcresearchpress.com by 210.87.254.40 on 09/06/12
For personal use only.

$\frac{1}{2}(\%\, d_1/\%\, d_0) = \frac{1}{2}(86.5 \pm 2) = 3.2 \pm 0.5$, for the methionine-methyl-$d_1$ feeding.[1] Exchange in the methionine-methyl-$d_1$ feeding would be less than in the methionine-methyl-$d_2$ feeding and thus the calculated $k_H/k_D$ from the former experiment would be more accurate. This value is, therefore, used in the following discussion.

From the experiments of Pohl *et al.* (16), it is possible to extract an approximate intramolecular tritium isotope effect of 5.3 for the biological cyclopropanation reaction.[2] Applying the Swain relationship (17) to the $k_H/k_D$ obtained in the methionine-methyl-$d_1$ experiment gives an intramolecular tritium isotope effect of $(3.2 \pm 0.5)^{1.44} = 5.4 \pm 0.4$, in good agreement with that obtained above.

An enzymic reaction which has been taken as the model for biological cyclopropane ring formation is the 1,3-elimination of a proton to form cycloartenol. The stereochemistry of this reaction has been studied using chiral methyl-labelled oxidosqualene containing 30% tritium enrichment to allow examination of the product by $^3$H nmr (18) (see Scheme 2).

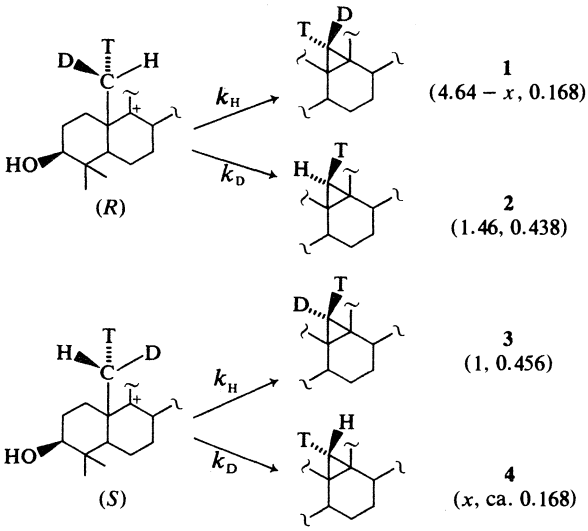


SCHEME 2

From the intensities of the tritium nmr signals corresponding to the two tritiated products,[3] it was possible to calculate an intramolecular deuterium isotope effect of 2.8 which compares reasonably closely to the value of $3.2 \pm 0.5$ obtained from the methionine-methyl-$d_1$ feeding.

The intramolecular isotope effect obtained above are independent of the degree to which proton (deuteron) abstraction is rate limiting. It was of interest to compare these results with a primary intermolecular deuterium isotope effect in order to measure the extent to which the proton removal step is rate limiting.

A 1:1 mixture of nondeuterated L-methionine and L-methionine-methyl-$d_3$ was fed to *L. plantarum*

[1]For the loss of one hydrogen (deuteron) from a methyl-$d_1$ group, the following kinetic scheme obtains:

$$CH_2D\text{—}X \xrightarrow{2k_H} CHD\text{—}Y \qquad CH_2D\text{—}X \xrightarrow{k_D} CH_2\text{—}Y$$

The rate of $d_1$ and $d_0$ cyclopropane formation is given by $d[d_1]/dt = 2k_H[CH_2D\text{—}X]$, $d[d_0]/dt = k_D[CH_2D\text{—}X]$. Taking the ratio of the rates yields the expression for the intramolecular deuterium isotope effect: $d[d_1]/d[d_0] = 2k_H/k_D$. Integration yields: $d_1/d_0 = 2k_H/k_D$. Since $d_1 + d_0 = 1$, $\%d_1/\%d_0 = 2k_H/k_D$. Rearranging, $k_H/k_D = \%\, d_1/2(\%\, d_0)$.

For the conversion of a methyl-$d_2$ group into a methylene group, the following kinetic scheme obtains:

$$CHD_2\text{—}X \xrightarrow{k_H} CD_2\text{—}Y \qquad CHD_2\text{—}X \xrightarrow{2k_D} CHD\text{—}Y$$

The rate of $d_2$ and $d_1$ cyclopropane formation is given by $d[d_2]/dt = k_H[CHD_2\text{—}X]$, $d[d_1]/dt = 2k_D[CHD_2\text{—}X]$. Taking the ratio of the rates, integrating, and rearranging yields the expression for the intramolecular deuterium isotope effect: $d_2/d_1 = k_H/2k_D$. Thus, $k_H/k_D = 2(\%\, d_2)/(\%\, d_1)$.

[2]The above workers fed a mixture of methionine-methyl-$^3$H, and methionine-methyl-$^{14}$C in the ratio of 0.427 to 1. They isolated a biosynthetic cyclopropane which had a $^3$H/$^{14}$C ratio of 0.39 to 1. The following kinetic scheme applies if there is no intermolecular isotope effect where the amount of $^{14}CH_2$—Y formed is equal to the amount of $CH_2$—Y *and* CHT—Y formed:

$$^{14}CH_3\text{—}X \xrightarrow{k_H} {}^{14}CH_2\text{—}Y$$

$$CH_2T\text{—}X \xrightarrow{k_T} CH_2\text{—}Y \qquad CH_2T\text{—}X \xrightarrow{2k_H} CHT\text{—}Y$$

Thus $d[(CHT)]/dt = 2k_H[CH_2T\text{—}X]$ and $d[(CH_2)]/dt = k_T[CH_2T\text{—}X)$. Using similar arithmetic manipulations as in Footnote 1, one arrives at an expression for $k_H/k_T = \%\,(CHT)/2\%(CH_2) = 0.39/(0.427 - 0.39) \times \frac{1}{2} = 0.39/0.037 \times \frac{1}{2} = 5.3$.

[3]The above workers fed chiral-methyl labelled oxidosqualene (80% (*R*)-methyl and 20% (*S*)-methyl) which when cyclized gave the following distribution of products (see Scheme 2; the figures in parentheses represent $^3$H nmr intensities and the chemical shift in ppm).

The value of $x$ could be calculated by assuming identical rates of formation of compounds **2** and **4**. Since the (*R*)-methyl compound was present at four times the concentration of the (*S*)-methyl compound, then $x = 1.46/4 = 0.365$. Thus, the contribution of compound **1** to the intensity of the signal at 0.168 ppm was $4.64 - 0.365 = 4.275$ (this represents an error of 7% from the expected value of 4.0). By taking the ratios $4.275/1.46 = 2.93$ and $1/0.365 = 2.74$, one arrives at an average intramolecular deuterium isotope effect of 2.84.

Can. J. Chem. Downloaded from www.nrcresearchpress.com by 210.87.254.40 on 09/06/12
For personal use only.

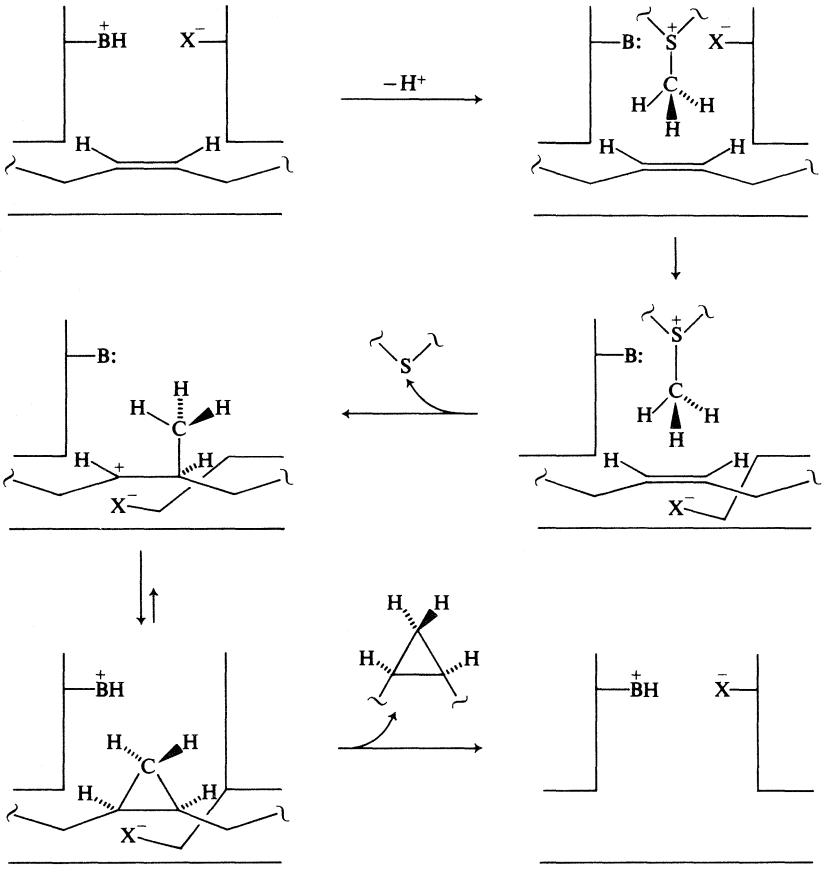

SCHEME 3

and the distribution in the resulting biosynthetic cyclopropane fatty acid measured to be: $d_0$, 51.6%; $d_1$, 5.9%; $d_2$, 42.5%. Analogous feeding experiments using only methionine-methyl-$d_3$ of the same isotopic composition as used in this experiment ($d_0$, 1.9%; $d_1$, 0.9%; $d_2$, 1.4%; $d_3$, 95.8%) gave rise to a biosynthetic cyclopropane fatty acid with the following isotopic composition: $d_0$, 1.5%; $d_1$ 13.8%; $d_2$, 84.7%. Thus in the intermolecular isotope effect study described above the amount of $d_0$ material, "derived from the methionine-methyl-$d_3$", would be ca. 0.8%. Also the mole ratio of methionine-methyl-$d_0$ to methionine-methyl-$d_3$ as calculated by the weights (cf. Experimental) was 1.02. Taking these two corrections into account one arrives at a calculated intermolecular primary deuterium isotope effect, $k_H/k_D$, of $(50.8 \pm 1.4)/(1.02(0.8 + 5.9 + 42.5) \pm 1.7) = (50.8 \pm 1.4)/(50.2 \pm 1.7) = 1.01 \pm 0.04$. The lack of any significant intermolecular isotope effect means that proton–carbon bond cleavage is not a rate-determining step in the cyclopropanation reaction. (This interpretation assumes that biological cyclopropanation does not deplete the cell of SAM, in which case no isotope effect would be observed. The results of Cronan *et al.* suggest that cyclopropanation is not a means of disposing of excess SAM (19).)

It is tempting to account for the negligible intermolecular isotope effect in terms of a carbonium ion mechanism (Scheme 1) where deprotonation of a carbonium ion intermediate would be expected to be a more facile process than methyl transfer to an unactivated double bond. Akhtar and Jones (20) have postulated that biological methylation of isolated double bonds is initiated by an enzymic conformational change which separates the methyl sulfonium cation from its anionic counterion. (Scheme 3).[4] It is possible that a third group (B), such as the ε-amino group from a lysine residue, plays an important role in these reactions.

[4]Bringing the $X^-$ group below the olefinic plane as shown in our scheme could enhance the nucleophilicity of the olefin due to steric compression. (The postulation of an $X^-$ group has recently gained some experimental support from the inhibition studies of P. Benveniste and co-workers using sterols carrying an ammonium group at C-25 (21).)

Can. J. Chem. Downloaded from www.nrcresearchpress.com by 210.87.254.40 on 09/06/12
For personal use only.

Can. J. Chem. Downloaded from www.nrcresearchpress.com by 210.87.254.40 on 09/06/12
For personal use only.

In the absence of SAM, it could serve as the counterion to the $X^-$ group. In its deprotonated form B could abstract a proton from the carbocationic intermediate (formed on transfer of methyl) resulting in a second charge-separated state which could partition via one of two possible pathways: (1) reprotonation of the cyclopropane ring; (2) release of product to form the original ion pair. (The 9β,19 cyclopropane ring cleavage reaction in phytosterol biosynthesis (22) is presumably also initiated by protonation using an unsolvated acid in analogy to the postulated protonation of isolated double bonds in biochemical hydrogenation reactions (20).) The results presented in this paper indicate that approximately one-third of the total cyclopropyl fatty acid is derived from an exchanged methyl group species and thus the ratio of the rate of reprotonation to the rate of product release is at least 1:2. We have also observed that the exchange increases with cell growth or decreasing pH (2). It is not inconceivable that the reprotonation reaction could be favoured at decreased pH. Further work with buffered cell-free systems is needed to clarify this point.

## Experimental

*Apparatus, methods, and materials*

L-Methionine-methyl-$d_3$, methyl iodide-$d_1$, and methyl iodide-$d_2$ were purchased from Merck Sharpe and Dohme, Point Claire, Quebec. L-Methionine-methyl-$^{14}$C was obtained from New England Nuclear. Paraformaldehyde-$d_2$ was a generous gift from Professor D. Moule, Brock University, St. Catharines, Ontario.

Deuterium determinations were performed by mass spectrometry using either a CEC model 21-110-B mass spectrometer at 70 eV, using a direct introduction probe, or a VG micromass 7070 F instrument at 70 eV, coupled to a Varian model 3700 gas chromatograph. The experimental error in the deuterium content measurements was estimated to be ±1% for each isotopic species expressed as a percentage, unless otherwise stated. The mass spectrometry methods were described in detail earlier (2).

The methionine isolation experiment was carried out using a Beckman Model 119 automatic amino acid analyzer, equipped with a single column (32 cm × 0.9 cm id) packed with Durrum DC-6A cation exchange resin.

The microorganism used in this study was *Lactobacillus plantarum* ATC 8014, available from the American Type Culture Collection. The basal medium used for each feeding experiment was that of Henderson and Snell (23). The details of the microbiological aspects of this work have already been described elsewhere (2). The fatty acids were isolated from the microorganism as previously described (2).

*Methionine-methyl-*$d_3$ *feeding under aerobic and anaerobic conditions (Experiments 1 and 2)*

The basal medium (1.65 L), containing biotin (17.0 μg) and methione-methyl-$d_3$ (165.0 mg), was filter sterilized and distributed among 11 × 250 mL Erlenmeyer flasks (150 mL each). A saline cell suspension (1 mL) was used to inoculate each flask. Three flasks were fitted with 2-hole rubber stoppers and sterile argon passed through the medium for 0.5 h. The remaining flasks were fitted with disposable plugs to allow growth under aerobic conditions. The anaerobic and aerobic cultures were grown for 48 h. The anaerobically grown cells were harvested, dried, weighed (542 mg), and extracted to obtain the fatty acids (9.5 mg). The relative proportion of the three major fatty acids was as follows: *cis* vaccenic acid ($C_{18}$), 28%; palmitic acid ($C_{16}$), 38%; lactobacillic acid ($C_{19}$) 34%.

The aerobically grown cells were used to isolate methionine as well as fatty acids and a different procedure was used in the work-up. The cells were harvested, washed with water (2 × 150 mL), and resuspended in water (50 mL) in a round bottomed flask. The mixture was heated to boiling over 0.5 h and kept at 100°C for a further 10 min, with stirring. The mixture was cooled and centrifuged to obtain a pale yellow supernatant. The cells were dried, weighed (994 mg), and extracted to obtain the fatty acids (9.5 mg, $C_{18}$, 29%; $C_{16}$, 35%; $C_{19}$, 36%). The supernatant was reduced in volume to 10 mL and an aliquot (100 μL) subjected to automatic amino acid analysis to determine the methionine present.

*Isolation of methionine*

Automatic amino acid analysis showed that there were ca. 950 μg of methionine present in the 10 mL extract of 994 mg of dry cells. Thus, the intracellular pool of methionine was 0.65 μmol per 100 mg of dry cell weight. To an aliquot of the extract (2.5 mL) was added sulfosalicylic acid to precipitate the protein present in the sample. The sample was concentrated to 500 μL, filtered through a 20 μm Millipore filter, and ca. 0.1 μcurie of methionine-methyl-$^{14}$C was added. The sample was injected onto the automatic amino acid analyzer and the effluent collected at the column exit in 2.5 mL fractions, using a Gilson automatic fraction collector. Each fraction was checked for radioactivity by counting an aliquot (50 μL) which had been dissolved in A.C.S. aqueous counting scintillant. All the radioactivity was contained in 3 fractions, collected at a retention time of ca. 148 min, using a flow rate of 70 mL/h.

The three fractions were individually cleaned up to remove lithium citrate buffer. The procedure used was as follows. Dowex 1 × 8-200 (100–200 mesh) ion exchange resin (6 g) was washed with 2 *M* NaOH (50 mL) by stirring for 15 min, filtered, and washed with water (100 mL). (All water used in this procedure was deionized and passed through a charcoal filter.) The process was repeated with 2.5 *M* HCl and the cycle repeated once more. Two more cycles were carried out with warm 2 *M* NaOH (50°C) and 2 *M* acetic acid. The resin was then suspended in water and a 1.4 cm × 7 cm column made up. The column was washed with 2 *M* NaOH at 45°C (25 mL). (The NaOH solution was made up in $CO_2$-free water and the washing procedure was carried out under a KOH drying tube.) The column was washed with water (20 mL) until the pH of the effluent was ca. 7.0. The 2.5 mL fraction containing methionine and buffer was then placed on the column and the column washed with water (20 mL) until the effluent was neutral. Acetic acid (1 *M*) was added to elute the methionine and one 50 mL fraction collected and evaporated and dissolved in water (2 mL). The column was regenerated by washing with 1 *M* HCl (20 mL) and then water (20 mL).

By tlc (70% ethanol, ninhydrin spray detection), it was estimated that only 1–10 μg of methionine was present in all the fractions combined. This was about 25 times less than anticipated and may have been caused by decomposition of methionine in the extract, which had been kept in the dark for 4 months at 5°C.

The aqueous methionine solution obtained from the Dowex column was evaporated under nitrogen in a 2.0 mL reactivial which had previously been treated with a 5% dimethyldichlorosilane in toluene solution to render the surface hydrophobic. The sample was dried *in vacuo* for several hours. A mixture of

TABLE 4. Analytical data for fatty acids in intramolecular isotope experiments

| Flask | Dry cell wt-(mg) | Cell yield (mg/100 mL) | Total fatty acid (mg) | % $C_{18}$* | % $C_{16}$* | % $C_{19}$* |
|---|---|---|---|---|---|---|
| $A_1$–$A_4$ | 640 | 110 | 14.2 | 27 | 38 | 35 |
| $B_1$–$B_4$ | 646 | 111 | 8.1 | 37 | 36 | 27 |
| $C_1$, $C_2$ | 308 | 106 | 5.8 | 29 | 28 | 43 |
| $A_5$ | 176 | 121 | 2.5 | 20 | 40 | 40 |
| $B_5$ | 177 | 122 | 1.9 | 21 | 41 | 38 |

*$C_{18}$: *cis*-vaccenic acid; $C_{16}$: palmitic acid; $C_{19}$: lactobacillic acid.

acetonitrile/BSTFA (1:3, 100 μL) was added via syringe, the mixture heated at 100°C for 10 min, and the sample analyzed by gc-ms using the following gc conditions: 3% OV-1 on Gas Chrom Q (110/120), 6 ft × 2 mm id, glass, temperature programmed from 50°–250°C at 10°/min. The $M - 117$ ion (loss of carbosiloxy) from the bis-TMS derivative of methionine was monitored at *m/e* 176–179 and the deuterium content calculated from the ion intensities.

*Formaldehyde-*$d_2$ *feeding (Experiment 3)*

Paraformaldehyde-$d_2$ (3.75 mg) was suspended in water (6 mL) and heated under reflux, at which time the white solid had disappeared. To one-half of this solution was added the basal medium (100 mL) which also contained L-methionine (10 mg) and biotin (1 μg). The medium was filter sterilized and placed in a 250 mL Erlenmeyer flask. A saline cell suspension (0.7 mL) was used to inoculate the 2 flasks. After 80 h the cells were harvested, dried, weighed (55 mg), and the fatty acids (1.3 mg) extracted. The relative proportion of the three major fatty acids was as follows: $C_{18}$, 13%; $C_{16}$, 45%; $C_{19}$, 42%.

*Methionine-methyl-*$d_3$*/formate feedings (Experiments 4 and 5)*

The basal medium (290 mL) containing biotin (2.9 μg) was distributed in two flasks (145 mL) each, supplemented with the components listed below and filter sterilized. Flask A contained methionine-methyl-$d_3$ (13.0 mg) and sodium formate (4.0 mg) (Experiment 4), flask B contained methionine-methyl-$d_3$ (6.5 mg) and sodium formate (4.0 mg) (Experiment 5). Each of the above flasks was inoculated with a saline cell suspension (1.0 mL, Klett reading of 400). Growth was monitored by measuring the pH of 5 mL aliquots. After 29 h of growth, the two flasks were harvested, the cells dried and weighed, and the fatty acids extracted.

In Experiment 4, 2.2 mg of total fatty acids were obtained from 175 mg of cells. The relative proportion of the three major fatty acids was as follows: $C_{18}$, 18%; $C_{16}$, 48%; $C_{19}$, 34%.

In Experiment 5, 3.2 mg of total fatty acids were obtained from 232 mg of cells. The relative proportion of the three major fatty acids was as follows: $C_{18}$, 35%; $C_{16}$, 32%; $C_{19}$, 33%.

L-*Methionine-methyl-*$d_2$

*S*-Benzyl-L-homocysteine (Sigma) was converted to the title compound in 80% yield by treatment with methyl iodide-$d_2$ according to the method of Nelville *et al.* (24); $^1$H nmr ($D_2O$): 2.1 (3 H, m, $CH_2CH(NH_2)CO_2H$ + $CHD_2$—S), 2.6 (2 H, m, $CH_2$—S), 3.8 (1 H, t, $NH_2CH$—COOH). Mass spectrum: the bis-TMS derivitive of the title compound was prepared by heating 1 mg of the amino acid with acetonitrile (200 μL) and bis-(trimethylsilyl)-trifluoroacetamide (BSTFA) (200 μL) at 100°C for 5 min; 1 μL of the resulting solution was injected into the gc-ms system. The gc conditions were as follows: 3% OV-1 on Gas Chrom Q (110/120), 6 ft × 2 mm id, glass, temperature programmed from 50°–250°C at 10°/min. The molecular ions at *m/e* 293 ($M^+$, $d_0$), *m/e* 294 ($M^+$, $d_1$), and *m/e* 295 ($M^+$, $d_2$) were scanned and the deuterium distribution was calculated to be: $d_2$, 96.7%; $d_1$ 2.7%; $d_0$ 0.6%.

L-*Methionine-methyl-*$d_1$

The title compound was prepared by a method identical with that described above, except that methyl iodide-$d_1$ was used; $^1$H nmr ($D_2O$): 2.1 (4 H, m, $CH_2CH(NH_2)COOH$, $CH_2D$—S). Mass spectrum: by a similar analysis to that described above, the following deuterium content was calculated: $d_1$, 97%; $d_0$, 3%.

*Intermolecular isotope effect study*

L-Methionine (49.475 mg), L-methionine-methyl-$d_3$ (49.460 mg), and biotin (10 μg) were dissolved in basal medium (1 L). The complete medium, after filter sterilization, was distributed among 14 culture tubes (10 mL each) and among 7 × 250 mL Erlenmeyer flasks (125 mL each). A saline cell suspension (0.05 mL) was used to inoculate each of 14 culture tubes. After 24 h of growth, the resulting cultures (2 × 10 mL each) were used to inoculate each of the 250 mL flasks. The cells were allowed to grow for 24 h, after which they were harvested and the fatty acids extracted. The total fatty acid content was 9.3 mg ($C_{18}$, 9%, $C_{16}$, 34%; $C_{19}$, 57%).

*Intramolecular isotope effect study*

Basal medium (1.75 L) containing biotin(17.5 μg) was supplemented with the components listed below, filter sterilized, and distributed in 145 mL portions among 12 × 250 mL Erlenmeyer flasks ($A_1$–$A_5$, $B_1$–$B_5$, $C_1$, $C_2$). Flasks $A_1$–$A_5$ contained methionine-methyl-$d_2$ (14.5 mg each); flasks $B_1$–$B_5$ contained methionine-methyl-$d_1$ (14.5 mg each); flasks, $C_1$, $C_2$ contained methionine-methyl-$d_3$ (14.5 mg each). Each of the above flasks was inoculated with a saline cell suspension (1.0 mL, Klett reading of 400). Growth was monitored by measuring the pH of 5 mL aliquotes. After 29 h of growth, flasks $A_1$–$A_4$, $B_1$–$B_4$, $C_1$, $C_2$ were harvested, the cells dried and weighed, and the fatty acids extracted. After 48 h of growth, the same procedure was carried out with Flasks $A_5$, $B_5$. The analytical data of the above experiment are listed in Table 4.

## Acknowledgements

We thank the Natural Sciences and Engineering Research Council of Canada for financial support and Dr. J. J. Miller for the use of his laboratory facilities for growing and harvesting the microbial cultures. One of us (P.H.B.) gratefully acknowledges the award of an N.S.E.R.C. postgraduate scholarship.

1. J. W. LAW. Acc. Chem. Res. **4**, 199 (1971).
2. P. H. BUIST and D.B. MACLEAN. Can. J. Chem. **59**, 828 (1981).
3. E. LEDERER. Q. Rev. **23**, 453 (1969).
4. T. Y. LIU and K. HOFMANN. Biochemistry, **1**, 189 (1962).
5. B. SHANE and E. R. R. STOKSTAD. J. Gen. Microbiol. **103**, 261 (1977).

Can. J. Chem. Downloaded from www.nrcresearchpress.com by 210.87.254.40 on 09/06/12
For personal use only.

6. S. MIZUSHIMA, Y. MACHIDA, and K. KITAHARA. J. Bacteriol. **86**, 1295 (1963).
7. M. F. HEGAZI, R. T. BORCHARDT, and R. L. SCHOWEN. J. Am. Chem. Soc. **101**, 4359 (1979).
8. E. B. KELLER, J. R. RACHELE, and V. DU VIGNEAUD. J. Biol. Chem. **177**, 733 (1949).
9. F. SCHLENK. *In* Progress in the chemistry of natural products. Vol. 23. *Edited by* L. Zechmeister. Springer-Verlag, New York 1965. p. 61.
10. F. SCHLENK. *In* Transmethylation and methionine biosynthesis. *Edited by* S. K. Shapiro and F. Schlenk. U. of Chicago Press, Chicago. 1965. Chapt. 4. p. 59.
11. H. PAPE, R. SCHMID, H. GRISEBACH, and H. ACHENBACH. Eur. J. Biochem. **10**, 479 (1969).
12. G. JAUREGUIBERRY, G. FARRUGIA-FOURGEROUSE, H. AUDIER, and E. LEDERER. C. R. Acad. Sci. Ser. B, **259**, 3108 (1964).
13. B. E. TROPP, J. H. LAW, and J. M. HAYES. Biochemistry, **3**, 1837 (1964).
14. D. R. THRELFALL. Biochim. Biophys. Acta, **280**, 472 (1972).
15. M. LENFANT, G. FARRUGIA, and E. LEDERER. C.R. Acad. Sci. Ser. D, **268**, 1986 (1969).
16. S. POHL, J. H. LAW, and R. RYHAGE. Biochem. Biophys. Acta, **70**, 583 (1963).
17. C. G. SWAIN, E. C. STIVERS, J. F. REUWER, JR., and L. J. SCHAAD. J.Am. Chem. Soc. **80**, 5885 (1958).
18. L. J. ALTMANN, C. Y. HAN, A. BERTOLINO, G. HANDY, D. LAUNGANI, W. MULLER, S. SCHWARTZ, D. SHANKER, W. H. DE WOLF, and F. YANG. J. Am. Chem. Soc. **100**, 3235 (1978).
19. J. E. CRONAN, JR., W. D. NUNN, and J. G. BATCHELOR. Biochim Biophys. Acta, **348**, 63 (1974).
20. M. AKHTAR and C. JONES. Tetrahedron, **34**, 813 (1978).
21. A. RAHIER. Thèse de doctorat d'Etat, Strasbourg, 1980.
22. E. CASPI and J. SLIWOWSKI. J. Am. Chem. Soc. **97**, 5032 (1975).
23. L. M. HENDERSON and E. E. SNELL. J. Biol. Chem. **172**, 15 (1948).
24. D. B. MELVILLE, T. R. RACHELL, and E. B. KELLER. J. Biol. Chem. **169**, 419 (1947).

Can. J. Chem. Downloaded from www.nrcresearchpress.com by 210.87.254.40 on 09/06/12
For personal use only.

# Synthesis of chalcone ethynylogues with a pharmaceutical objective

PIERRE BABIN

*Laboratoire de Pharmacie Chimique, Université de Bordeaux II, Place de la Victoire, 33000 Bordeaux, France*

AND

PAULETTE LAPOUYADE AND JACQUES DUNOGUÈS[1]

*Laboratoire de Chimie Organique et Laboratoire de Chimie des Composés Organiques du Silicium et de l'Etain associé au CNRS no 35, 351, Cours de la Libération, 33405 Talence Cédex, France*

Received May 11, 1981

PIERRE BABIN, PAULETTE LAPOUYADE, and JACQUES DUNOGUÈS. Can. J. Chem. **60**, 379 (1982).

A simple route to chalcone ethynylogues, convenient even in the presence of alkoxy or acyloxy substituents, is proposed. This method is based on the use of ethynylsilanes, the involved trimethylsilyl group being recovered during the course of the reaction.

PIERRE BABIN, PAULETTE LAPOUYADE et JACQUES DUNOGUÈS. Can. J. Chem. **60**, 379 (1982).

Une méthode simple de synthèse d'éthynylogues de chalcones, utilisable même avec des substituants alcoxy ou acyloxy, est proposée. Cette méthode met en jeu la voie organosilicique, le groupe triméthylsilyle engagé étant récupérable en fin d'opération.

Several chalcone derivatives have found pharmaceutical uses. Thus, some flavonoids having a chalcone skeleton exhibit anti-aldose reductase properties (1) and a trimethoxy derivative of chalcone (2) is currently used as a qualitative and quantitative choleretic for biliary secretion (commercial name: Vesidryl (3)). Moreover a chalcone vinylogue, the divanillidene cyclohexanone, also is a commercially available choleretic (Vanilone[2]). In the context of our studies concerning the obtention of drug ethynylogues (4, 5) we have focused our interest on the synthesis of chalcone ethynylogues having potential pharmacological properties (products with aryl groups substituted by one or several alkoxy or acyloxy substituents).

In this series only Ph—C≡C—CO—CH=CH—Ph has been described to our knowledge (6–9). It has been made according to three synthetic methods which offer possibilities of comparison.

(*a*) Condensation of Ph—C≡C—Na with cinnamic anhydride, which does not afford chalcone in high yields (~33%) (6) and raises problems with acetoxy substituents (6*b*).

(*b*) Quantitative preparation of Ph—C≡C—Cu used as precursor of chalcone (7) presents danger (9).

(*c*) Chalcone is afforded by the direct condensation of Ph—C≡CH with a stoichiometric amount of cinnamoyl chloride in the presence of triethylamine and $(Ph_3P)_2PdCl_2$ and CuI as the catalyst (9):

$$Ph—C{\equiv}C—H + Ph—CH{=}CH—COCl + Et_3N \xrightarrow[CuI]{(Ph_3P)_2PdCl_2} Ph—C{\equiv}C—CO—CH{=}CH—Ph$$
$$-Et_3N, HCl \qquad 80\%$$

Despite the formation of triethylamine hydrochloride and the use of an expensive catalyst we attempted this process for the synthesis of **13** and **7**, both previously undescribed: we obtained 55% yields in the first case but lower than 20% yield in the presence of the acyloxy substituent after 48 h, while most of the unreacted phenyl acetylene was recovered.

The proposed routes are not generally adaptable to the preparation of alkoxy or acyloxy substituted structures. For all these reasons we decided to investigate the synthesis of chalcone ethynylogues from alkynylsilanes and aryl substituted cinnamoyl chlorides since alkynylsilanes react with electrophiles (10, 11) such as acyl chlorides under Friedel–

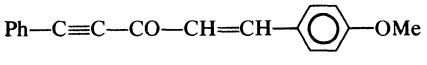

**13**

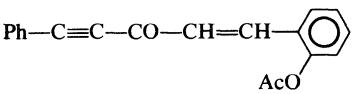

**7**

[1]Author to whom correspondence may be addressed.

[2]See ref. 3, p. 1290.

0008-4042/82/040379-04$01.00/0

©1982 National Research Council of Canada/Conseil national de recherches du Canada

Can. J. Chem. Downloaded from www.nrcresearchpress.com by 210.87.254.105 on 09/06/12
For personal use only.

TABLE 1. Synthesis of chalcone ethynylogues

| Ar | Ar′ | Yields % crude products | Yields % after recrystallization | Number |
|---|---|---|---|---|
| Ph- | Ph- | 55 | 40 | **6** |
| Ph- | | 60 | 40 | **7** |
| | Ph— | 50 | 30 | **8** |
| | | 38 | 38[a] | **9** |
| 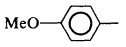 | 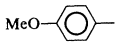 | 40 | 30 | **10** |
| 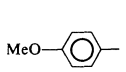 | 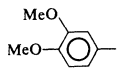 | 60 | 40 | **11** |
| 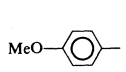 | | 50 | 30 | **12** |

[a]Liquid product.

Crafts conditions, at least in the absence of alkoxy and acyloxy substituents.

Several routes were used for the preparation of ethynylsilanes. Ethynyltrimethylsilane was obtained by silylation of trichloroethylene (12); (*p*-methoxyphenylethynyl)trimethylsilane (15, 16) **5** was synthesized by condensation of ethynyltrimethylsilane on *p*-methoxy iodobenzene (13); (phenylethynyl)-trimethylsilane **1** was prepared from phenylacetylene (14), whereas the other substituted (phenylethynyl)trimethylsilanes (*o*-RO—$C_6H_4$—C≡C—$SiMe_3$, R = H, **2**, $SiMe_3$, **3**, COMe, **4**), also new compounds, were easily obtained from *o*-$Me_3SiO$—$C_6H_4$—C≡CH described in one of our previous publications (4).

Chalcone ethynylogues were formed according to:

$$Ar—C{\equiv}C—SiMe_3 + Ar'—CH{=}CH—COCl \xrightarrow[CH_2Cl_2;\ 0°C]{AlCl_3} Ar—C{\equiv}C—CO—CH{=}CH—Ar' + Me_3SiCl$$

Results are summarized in Table 1. These results require the following comments.

(*i*) All the chalcone ethynylogues have a *trans* structure ($AlCl_3$ isomerizes *cis* to *trans* α,β-ethylenic ketones) (17).

(*ii*) In an attempt to improve the results we replaced $AlCl_3$ by $TiCl_4$, which often limits the formation of degradation products (18). The ethynylogue of the nonsubstituted chalcone was obtained in only 20% yields but the silylated intermediate **14** could be isolated. The stereochemistry of the reaction was not determined.

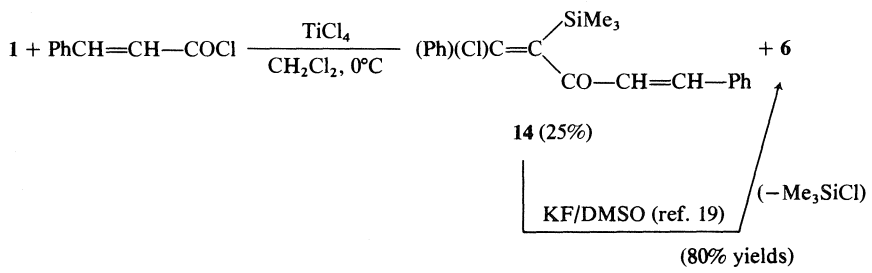


Can. J. Chem. Downloaded from www.nrcresearchpress.com by 210.87.254.105 on 09/06/12
For personal use only.

Can. J. Chem. Downloaded from www.nrcresearchpress.com by 210.87.254.105 on 09/06/12
For personal use only.

The route we propose for the synthesis of chalcone ethynylogues appears to be synthetically convenient even in the presence of acyloxy substituents since the involved trimethylchlorosilane was recovered during the acylation reaction.

## Experimental

All the new compounds exhibit satisfactory C, H analyses. Microanalytical data are available on request.

*Ethynylsilanes*

H—C≡C—$SiMe_3$, **1**, and **5** were prepared according to refs. 12, 14, and 13 respectively. Compounds **2**, **3**, and **4** were synthesized from *o*-$Me_3SiO$—$C_6H_4$—C≡C—H (4) by classical replacement of the acetylenic proton by a $Me_3Si$ group followed by hydrolysis or acetylation. Infrared $cm^{-1}$: 1250, 840, and 755 ($SiMe_3$); 2170 ($\nu_{C\equiv C}$) and 3500 ($\nu_{OH}$) for **2**; 1760 ($\nu_{C=O}$) for **4**.

*(2-Hydroxyphenylethynyl)trimethylsilane* **2**

Boiling point: 80°C/1 Torr; nmr ($CCl_4$, TMS) δ ppm: 0.30 (s, 9H, $SiMe_3$), 6.1 (s, 1H, OH which disappears when added $D_2O$), 7.0–7.8 (m, 4 arom H).

*(2-Trimethylsiloxyphenylethynyl)trimethylsilane* **3**

Boiling point: 80–83°C/1 Torr; nmr δ ppm: 0.24 (s, 9H, $SiMe_3$), 0.30 (s, 9H, $SiMe_3$), 7.3–7.8 (m, 4 arom H).

*(2-Acetoxyphenylethynyl)trimethylsilane* **4**

Boiling point: 105°C/1 Torr; nmr δ ppm: 0.25 (s, 9H, $SiMe_3$), 2.23 (s, 3H, OCOMe), 6.9–7.5 (m, 4 arom H).

*Chalcone etynylogues*

The general procedure given by Birkofer *et al.* (10) was modified as follows: ethynylsilane (15 mmol in 20 mL $Ch_2Cl_2$) was added dropwise at −30°C to the complex formed from acyl chloride (15 mmol) and $AlCl_3$ (15 mmol) in 40 mL $CH_2Cl_2$ under $N_2$ atm. After 1 h at −30°C, the reaction mixture was left 2 h at 0°C, then poured into ice-cold water containing $NH_4Cl$ and $NaHCO_3$. Products were extracted with $CH_2Cl_2$ and the organic layer washed, dried with $Na_2SO_4$, and the solvent and $Me_6Si_2O$ evolved. Then the products were purified on a silica column (Kieselgel 60, 70–230 mesh ASTM) using benzene, benzene–ether, or methylene chloride as the eluent (as specified below).

Compound **6** also was synthesized from PhCH=CH—COCl/$TiCl_4$ according to a similar procedure ($TiCl_4$ replacing $AlCl_3$). Dechlorosilylation of **14** was carried out according to ref. 19 (3 h at 70°C); **7** and **13** also were prepared according to the method of Tohda *et al.* (9) starting from phenylacetylene (15 mmol).

Except for the nonsubstituted chalcone ethynylogue **6** previously described (9), all the other ethynylogues are new compounds.

*5-(2'-Acetoxyphenyl) 1-phenyl pent-1-yn 4-enone* **7**

Melting point (ether/pentane, 1:1 vol) 88°C; eluent: $CH_2Cl_2$; ir $cm^{-1}$: 2225 and 2195 (C≡C), 1775 (C=O ester), 1640 (C=O ketone), 1610 (C=C); nmr δ ppm: 2.23 (s, 3H, OCOMe), 6.56, 6.84, 7.72, 8.00 (AB spectr, $J \simeq 16.5$ Hz, 2H, CH=CH), 6.80–7.75 (m, 9 arom H).

*1-(2'-Acetoxyphenyl) 5-phenyl pent-1-yn 4-enone* **8**

Melting point (pentane) 72°C; **8** was purified by hplc (Jobin–Yvon Chromatospac Prep 100, silica column H 60 10–40 mesh, $CH_2Cl_2$ as the eluent); ir $cm^{-1}$: 2230 (C≡C), 1770 and 1750 (C=O ester), 1640 (C=O ketone), 1600 (C=C); nmr δ ppm: 2.31 (s, 3H, OCOMe), 6.66, 6.94, 7.80, 8.08 (AB spectr, $J \sim 16.5$ Hz, 2H, CH=CH), 7.05–7.80 (m, 9 arom H).

*1,5-Bis(2'-acetoxyphenyl) pent-1-yn 4-enone* **9**

Eluent: $CHS_2Cl_2$; ir $cm^{-1}$: 2220 (C≡C), 1765 (C=O ester), 1635 (C=O ketone), 1605 (C=C); nmr δ ppm: 2.23 (s, 6H, 2 OCOMe), 6.56, 6.83, 7.76, 8.03 (AB spectr, $J \sim 16$ Hz, 2H, CH=CH), 6.80–7.75 (m, 8 arom H).

Compounds **10**, **11**, **12**, and **13** were studied by 90 MHz nmr spectrometry with expansion of the aromatic region to specify some couplings.

*1,5-Bis(4'-methoxyphenyl) pent-1-yn 4-enone* **10**

Melting point ($C_6H_{12}/Et_2O$, 1:1 vol) 106°C; eluent: $C_6H_6/Et_2O$, 19:1 vol; ir $cm^{-1}$: 2220 and 2200 (C≡C), 1685 (C=O ketone), 1610 (C=C); nmr δ ppm: 3.70 (s, 6H, 2MeO), 6.36, 6.63, 7.45, 7.72 (AB spectr, 2H, $J \sim 16.5$ Hz), 6.69, 6.83, 7.36, 7.50 (AA'BB' spectr, $J \sim 9$ Hz, 4 arom H), 6.70, 6.84, 7.37, 7.51 (AA'BB' spectr, $J \sim 9$ Hz, 4 arom H).

*5-(3',4'-Dimethoxyphenyl) 1-(4'-methoxyphenyl) pent-1-yn 4-enone* **11**

Melting point ($C_6H_{12}/Et_2O$, 1:1 vol) 96°C; eluent: $Et_2O/C_6H_6$, 1:1 vol; ir $cm^{-1}$: 2220 and 2195 (C≡C), 1680 (C=O), 1605 (C=C); nmr δ ppm: 3.80 (s, 9H, 3MeO), 6.41, 6.68, 7.50 and 7.77 (AB spectr, $J \sim 16$ Hz, 2H, CH=CH), 6.71, 6.86, 7.40, 7.56 (AA'BB' spectr, $J \sim 9$ Hz, 4H of the disubstituted arom ring), 6.55–7.70 (m, 3 other arom H).

*5-(2'-Acetoxyphenyl) 1-(4'-methoxyphenyl) pent-1-yn 4-enone* **12**

Melting point ($C_6H_{12}/Et_2O$, 1:1 vol) 109°C; eluent: $C_6H_6/Et_2O$, 9:1 vol; ir $cm^{-1}$: 2230 and 2200 (C≡C), 1770 (C=O ester), 1645 (C=O ketone), 1616 (C=C); nmr δ ppm: 2.25 (s, 3H, OCOMe), 3.75 (s, 3H, MeO), 6.46, 6.73, 7.63, 7.90 (AB spectr, $J \sim 16$ Hz, 2H, CH=CH), 6.68, 6.83, 7.36, 7.51 (AA'BB' spectr, $J \sim 9$ Hz, 4H of the disubstituted arom ring), 6.65–7.65 (m, 3 other arom H).

*5-(4'-Methoxyphenyl) 1-phenyl pent-1-yn 4-enone* **13**

Melting point ($Et_2O$/*n*-$C_6H_{14}$, 1:1 vol) 105°C; no elution; ir $cm^{-1}$: 2220 (C≡C), 1640 (C=O), 1610 (C=C); nmr δ ppm: 3.76 (s, 3H, MeO), 6.38, 6.66, 7.48, 7.76 (AB spectr, $J \sim 16.5$ Hz, 2H, CH=CH), 6.70, 6.84, 7.36, 7.50 (AA'BB' spectr, $J \sim 8.5$ Hz, 4H of the disubstituted arom ring), 6.70–7.70 (m, 5 other arom H).

*1,5-Diphenyl 1-chloro 2-trimethylsilyl penta-1,4-dienone* **14**

Melting point ($C_6H_6/C_6H_{12}$, 1:1 vol) 133°C; eluent: $C_6H_6$; ir $cm^{-1}$: 1645 (C=O); nmr δ ppm: 0.15 (s, 9H, $SiMe_3$), 6.72, 6.98 (part A of AB spectr, $J \sim 16$ Hz, 1H of CH=CH), 7.28–7.85 (m, 11 other H); ms: signals at 342 and 340 (mol. peaks), 305 (M − Cl), 131 (PhCH=CH—CO), 103 (PhCH=CH), 73 ($SiMe_3$).

1. Actualités de chimie thérapeutique. 7ème série. 1290 (1980).
2. A. Lespagnol. Chimie des Médicaments. Vol. 2. Entreprise Moderne d'Edition, Paris. 1974. p. 390.
3. Dictionnaire Vidal, O.V.P. (Paris). 56th ed. 1980. p. 1308.
4. P. Babin, P. Bourgeois, and J. Dunoguès. C.R. Acad. Sci. Ser. C, **283**, 149 (1976).
5. P. Babin, J. Dunoguès, and F. Duboudin. J. Heterocycl. Chem. **18**, 519 (1981).
6. (*a*) D. Nightingale and F. T. Wadsworth. J. Am. Chem. Soc. **67**, 416 (1945); (*b*) **69**, 1181 (1947).
7. A. M. Sladkov and I. R. Golding. Khim. Atsetilena, Tr. Vses. Konf., 3rd. *Edited by* A. A. Petrov. Nauka, Moscow, USSR. 1968.
8. L. Rampazzo, A. Inesi, and A. Zeppa. J. Electroanal. Chem. **76**, 175 (1977).
9. Y. Tohda, K. Sonogashira, and N. Hagihara. Synthesis, 777 (1977).
10. L. Birkofer, A. Ritter, and H. Uhlenbrauck. Chem. Ber. **96**, 3280 (1963).
11. (*a*) R. Calas and P. Bourgeois. C.R. Acad. Sci. Ser. C,

**268**, 1525 (1969); (*b*) P. BOURGEOIS and R. CALAS. J. Organometal. Chem. **22**, 89 (1970); (*c*) P. BOURGEOIS, G. MÉRAULT, and R. CALAS. J. Organometal. Chem. **59**, C 4 (1973); (*d*) P. BOURGEOIS, G. MÉRAULT, N. DUFFAUT, and R. CALAS. J. Organometal. Chem. **59**, 145 (1973); (*e*) G. DÉLÉRIS, J. DUNOGUÈS, and R. CALAS. Tetrahedron Lett. 2449 (1976); (*f*) G. DÉLÉRIS, J. DUNOGUÈS, and R. CALAS. J. Organometal. Chem. **116**, C 45 (1976); (*g*) J.-P. PILLOT, J. DUNOGUÈS, and R. CALAS. Synthesis, 469 (1977).

12. Société Rhône–Poulenc. French Patent no. 2079814 (1970).
13. K. SONOGASHIRA, Y. TOHDA, and N. HAGIHARA. Tetrahedron Lett. 4467 (1975).
14. V. CHVALOVSKÝ and J. RATHOUSKÝ. Organosilicon compounds. Academic Press, New York and London. 1965.
15. C. EABORN and D. WALTON. J. Organometal. Chem. **2**, 95 (1964).
16. R. OLIVER and D. R. M. WALTON. Tetrahedron Lett. 5209 (1972).
17. G. COMBAUD and L. GIRAL. Bull. Soc. Chim. Fr. 3258 (1969).
18. T. MUKAIYAMA. Angew. Chem. Int. Ed. Engl. **16**, 817 (1977).
19. R. F. CUNICO and E. M. DEXHEIMER. J. Am. Chem. Soc. **94**, 2868 (1972).

For personal use only.

# Pyrrole chemistry. XXIV. The Vilsmeier formylation and the cyanation of pyrrole acetals. A synthesis of pyrrole-2,3,5-tricarboxaldehyde

CHARLES E. LOADER, GRAHAM H. BARNETT, AND HUGH J. ANDERSON

*Department of Chemistry, Memorial University of Newfoundland, St. John's, Nfld., Canada A1B 3X7*

Received July 15, 1981

CHARLES E. LOADER, GRAHAM H. BARNETT, and HUGH J. ANDERSON. Can. J. Chem. **60**, 383 (1982).

The preparation of the acetals of a number of pyrrole mono- and dicarboxaldehydes is described. It is shown that, provided the reactivity of the unsubstituted ring positions on the pyrrole nucleus is not too low, a carboxyaldehyde or a carbonitrile group may be substituted onto the pyrrole ring using the Vilsmeier reaction or chlorosulfonyl isocyanate respectively. Vilsmeier formylation of the diacetal, 2,4-di(5,5-dimethyl-1,3-dioxan-2-yl)-pyrrole, followed by hydrolysis gave pyrrole-2,3,5-tricarboxaldehyde.

CHARLES E. LOADER, GRAHAM H. BARNETT et HUGH J. ANDERSON. Can. J. Chem. **60**, 383 (1982).

On décrit la préparation des acétals d'un certain nombre de pyrroles mono et de dicarboxaldéhydes. On montre, en admettant que la réactivité des positions non substituées du noyau pyrrole n'est pas trop faible, que l'on peut substituer un groupe carboxaldéhyde ou carbonitrile du cycle pyrrole en utilisant soit la réaction de Vilsmeier ou l'isocyanate de chlorosulfonyle. La formylation de Vilsmeier du diacétal, di (diméthyl-5,5 dioxanne-1,3 yl-2)-2,4 pyrrole, suivie d'une hydrolyse donne le pyrroletricarboxaldéhyde-2,3,5.

[Traduit par le journal]

## Introduction

We recently reported the synthesis of 2-(5,5-dimethyl-1,3-dioxan-2-yl)-pyrrole (**1***a*) (1), and noted that it was formylated by the Vilsmeier reaction in very good yield and without appreciable hydrolysis of the acetal group, to give 5-(5,5-dimethyl-1,3-dioxan-2-yl)-pyrrole-2-carboxaldehyde (**1***b*). We have now synthesized a wide variety of substituted pyrrole acetals to assess the scope of this reaction.

The unsubstituted pyrrole 2- and 3-acetals can be prepared directly from the corresponding aldehydes and 2,2-dimethylpropane-1,3-diol but are obtained in better overall yields using indirect methods. When the 1-position on the pyrrole ring is blocked by a methyl group, excellent yields of both the 1-methyl-2- and 1-methyl-3-pyrrole acetals can be obtained directly from the aldehydes. We were also able to prepare, using similar methods, the diacetals (**1***d*) and (**2***d*) and their 1-methyl analogs. In some cases the most convenient starting material was the dialdehyde, and in others, the monoaldehyde/monoacetal (e.g. **1***d* was prepared from **1***b* rather than from the dialdehyde). Attempts to prepare the diacetal, 2-(5,5-dimethyl-1,3-dioxan-2-yl)-4-(2,5,5-trimethyl-1,3-dioxan-2-yl)-pyrrole, from 4-acetylpyrrole-2-carboxaldehyde gave much lower yields and the product was much less stable than **2***d*. Other acetals prepared directly from the corresponding aldehydes are listed in Table 1.

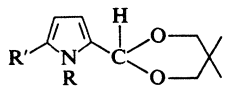

**1**

*a* R = R′ = H
*b* R = H, R′ = CHO
*c* R = $CH_3$, R′ = H

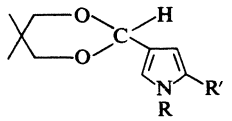

**2**

*d* R = H, R′ = 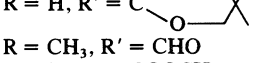
*e* R = $CH_3$, R′ = CHO
*f* R = H, R′ = $COOCH_3$

Like the monoacetals reported earlier (1) the diacetals prepared in this work are fairly stable compounds. They can be stored at room temperature for long periods without visible change provided that they are protected from acid. Decomposition is usually attended by discoloration and the sublimation of the free diol onto the sides of the container.

Pyrrole-2-carboxaldehyde has not been formylated successfully by direct methods. Direct formylation of 1-methypyrrole-2-carboxaldehyde using the Friedel and Crafts reaction has been reported (2) to give mainly the 2,4-dialdehyde. Formylation using the Vilsmeier reaction gives a very poor yield of a mixture of 2,4- and 2,5-dialdehydes.

Vilsmeier formylation of 1-methyl-2-(5,5-dimethyl-1,3-dioxan-2-yl)-pyrrole (**1***c*) using the method that we reported for the corresponding 2-(5,5-dimethyl-1,3-dioxan-2-yl)-pyrrole (**1***a*) (1), gave an excellent yield of 1-methyl-5-(5,5-dimethyl-1,3-dioxan-2-yl)-pyrrole-2-carboxaldehyde (**1***e*) in a much cleaner reaction than that given by the 1-*H* pyrrole 2-acetal. The reaction was very selective and there was no significant amount of 2,4-substitution observed. Hydrolysis of the formylated 1-methyl-2-acetal gives 1-methylpyrrole-2,5-dicarboxaldehyde in almost quantitative yield. Although other syntheses are available (3) this

0008-4042/82/040383-07$01.00/0

©1982 National Research Council of Canada/Conseil national de recherches du Canada

Can. J. Chem. Downloaded from www.nrcresearchpress.com by 210.87.254.6 on 09/06/12
For personal use only.

Can. J. Chem. Downloaded from www.nrcresearchpress.com by 210.87.254.6 on 09/06/12
For personal use only.





TABLE 1. Analytical and physical data for new pyrrole acetals prepared from the corresponding carbonyl compounds[a]

| Starting material | Acetal formed | mp (solvent) or bp (Torr) (°C) | Yield (%) | $^1$H nmr ($CDCl_3$) (δ ppm) | Analysis | *m/e* ($M^+$) |
|---|---|---|---|---|---|---|
| | 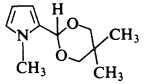 **1c** | 96.5–97.5 (0.5) | 68 | 0.76, 1.26 (each 3H, s, acetal $CH_3$), 3.62 (4H, broad m, acetal $CH_2$), 3.71 (3H, s, N—$CH_3$), 5.36 (1H, s, O—CH—O), 5.96, 6.13, 6.46 (1H, each m, pyrrole H), $J_{3,4}$ = 3.6, $J_{3,5}$ = 1.9, and $J_{4,5}$ = 2.8 Hz | calcd. for $C_{11}H_{17}NO_2$: C 67.66, H 8.78; found: C 67.57, H 8.76 | 195 |
| | 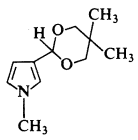 **2c** | 82–83 (0.2) | 89 | 0.75, 1.26 (each 3H, s, acetal $CH_3$), 3.53 (3H, s, N—$CH_3$), 3.62[b] (4H, dd, $J_{AB}$ = 12 Hz, acetal $CH_2$), 5.34 (1H, s, O—CH—O), 6.15, 6.47, 6.67 (each 1H, m, pyrrole H) | calcd. for $C_{11}H_{17}NO_2$: C 67.66, H 8.78; found: C 67.52, H 8.78 | 195 |
| 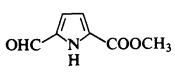 | 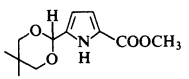 **1f** | 110–111 (ethyl ether/ petroleum) | 85 | 0.76, 1.21 (each 3H, s, acetal $CH_3$), 3.65 (4H, broad s, acetal $CH_2$), 3.79 (3H, s, $CH_3$), 5.41 (1H, s, O—CH—O), 6.20, 6.79, (1H, each m, pyrrole H), 9.3 (1H, broad, N—H) | calcd. for $C_{12}H_{17}NO_4$: C 60.23, H 7.16; found: C 60.38, H 7.23 | 239 |
| 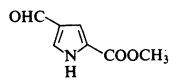 | 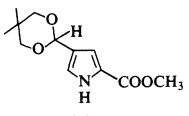 **2f** | 133–134 (ethyl ether/ petroleum) | 80 | 0.75, 1.23 (each 3H, s), 3.63 (4H, broad s), 3.80 (3H, s), 5.37 (1H, s), 6.97 (2H, m), 9.45 (1H, broad s) | calcd. for $C_{12}H_{17}NO_4$: C 60.23, H 7.16; found: C 60.38, H 7.36 | 239 |
| 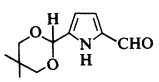 | 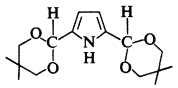 **1d** | 167–168 (ethyl ether/ petroleum) | 60 | 0.75, 1.22 (each 6H, s), 3.66[b] (8H, dd, $J_{AB}$ = 12 Hz), 5.43 (2H, s), 6.13 (2H, d), 8.7 (1H, broad, $J_{1,3}$ = 2.6 Hz) | calcd. for $C_{16}H_{25}NO_4$: C 65.06, H 8.53; found: C 64.92, H 8.58 | 295 |
| 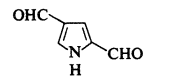 | 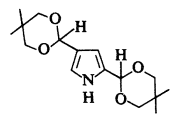 **2d** | 166–167 (petroleum) | 68 | 0.76, 1.25 (each 6H, s), 3.62[b] (8H, dd, $J_{AB}$ = 12 Hz), 5.37, 5.40 (each 1H, s), 6.27, 6.78 (each 1H, m), 8.4 (1H, broad s) | calcd. for $C_{16}H_{25}NO_4$: C 65.06, H 8.53; found: C 65.28, H 8.34 | 295 |

Can. J. Chem. Downloaded from www.nrcresearchpress.com by 210.87.254.6 on 09/06/12
For personal use only.



TABLE 1. (*Continued*)

| Starting material | Acetal formed | mp (solvent) or bp (Torr) (°C) | Yield (%) | $^1$H nmr ($CDCl_3$) (δ ppm) | Analysis | *m/e* ($M^+$) |
|---|---|---|---|---|---|---|
|  |  | 103–104 (petroleum) | 86 | 0.73, 1.22 (each 6H, s), 3.58[a] (8H, dd, $J_{AB}$ = 12 Hz), 3.70 (3H, s), 5.29 (2H, s), 6.20, 6.60 (each 1H, d, $J_{3,5}$ = 1.8 Hz) | calcd. for $C_{17}H_{27}NO_4$: C 65.99, H 8.80; found: C 65.90, H 8.80 | 309 |
|  |  | 146–147 (petroleum) | 13 | 0.60, 0.78, 1.20, 1.27, 1.55 (each 3H, s), 3.27, 3.62 (each 2H, d, $J_{AB}$ = 11 Hz), 3.64 (4H, dd), 5.37 (1H, s), 6.07, 6.57 (each 1H, m), 8.3 (1H, broad N—H) | calcd. for $C_{17}H_{27}NO_4$: C 65.99, H 8.80; found: C 65.98, H 8.81 | 309 |

[a]Prepared by the method described for related acetals in ref. 1.
[b]Centroid of AB quartet.

procedure provides an additional convenient route to this 2,5-dialdehyde.

The acetal grouping on the pyrrole ring appears to behave as a very weakly electron-withdrawing group. Evidence for this is provided by the formation of traces (detected by $^1$H nmr) of the 4-substituted product in the Vilsmeier formylation of the 2-acetal. There is also a greater deshielding effect on the 5-position of the pyrrole ring by the acetal group as shown in both the $^1$H nmr and the $^{13}$C nmr chemical shifts compared to those for 2-methylpyrrole (4*a*, 5*a*). The $^{13}$C nmr spectra of the 5,5-dimethyl-1,3-dioxan-2-yl ring of the 2-acetal and its *N*-methyl derivative were found to be in close agreement with those reported for similar compounds as assigned by Jones *et al.* (5*b*). The observed chemical shifts are shown in Figure 1.

Electrophilic attack on 3-alkyl pyrroles reportedly gives a high proportion of 2,3-disubstituted products relative to the yield of 2,4- and 3,4-disubstituted products (4*b*). We hoped that formylation of the 3-acetals **2***a* and **2***c* would afford primarily the 2-substituted products providing a new route to some 2,3-difunctionalized pyrroles. However, formylation of the 3-(5,5-dimethyl-1,3-doxan-2-yl)-pyrrole (**2***a*) gave a mixture, which was separated by fractional recrystallization. Hydrolysis of the crude mixture of acetals gave a mixture containing 2,3- (54%) and 2,4- (46%) dialdehydes which were separated by chromatography on silica gel. Similarly, Vilsmeier formylation of 1-methyl-3-(5,5-dimethyl-1,3-dioxan-2-yl)-pyrrole (**2***c*) gave 2,3- (~34%) and 2,4- (~62%) substitution with traces of the 3,4- (~4%) disubstituted product.

Other routes available for the synthesis of the 2,3-dialdehyde involve ring synthesis followed by several steps to the desired product (6,7), and poor overall yields. The procedure described here al-




**1***a* **1***c*

FIG. 1. $^{13}$C nmr chemical shifts for **1***a* and **1***c* with shifts for pyrrole and *N*-methylpyrrole in parentheses. Assignments of resonances for C(3) and C(4) of **1***a* and **1***c* may be interchanged.

Can. J. Chem. Downloaded from www.nrcresearchpress.com by 210.87.254.6 on 09/06/12
For personal use only.

lows a stepwise synthesis from pyrrole and is thus of synthetic interest.

The acetals, methyl 5-(5,5-dimethyl-1,3-dioxan-2-yl)-pyrrole-2-carboxylate (**1***f*) and methyl 4-(5,5-dimethyl-1,3-dioxan-2-yl)-pyrrole-2-carboxylate (**2***f*) are readily prepared directly from the corresponding aldehyde-esters and we hoped that formylation of them would lead to interesting trisubstituted pyrroles. In both cases there was evidence (nmr spectrum) that some formylation took place but no product was isolated. Most of the starting material was recovered unchanged, hydrolysed to the aldehyde, or destroyed. The reactivity of the pyrrole ring in both cases is apparently too low to permit reaction with the Vilsmeier reagent under conditions where the acetal can survive.

We found that both pyrrole-2,4-dicarboxaldehyde (**3***a*) and 5-(5,5-dimethyl-1,3-dioxan-2-yl)-pyrrole-2-carboxaldehyde (**1***b*) formed their corresponding diacetals (**2***d* and **1***d* respectively) in good yields. Both of the diacetals were fairly stable crystalline solids so the Vilsmeier reaction was attempted on them. The 2,4-diacetal gave an excellent yield of the formylated product **5***a* (77%). However, the 2,5-diacetal gave only a trace of what appeared to be the desired formylation product. The unreacted 2,5-diacetal could not be recovered because it was partially hydrolysed in the work-up and the main product isolated was 5-(5,5-dimethyl-1,3-dioxan-2-yl)-pyrrole-2-carboxaldehyde (**1***b*). The failure of the 2,5-diacetal (**1***d*) to formylate can be attributed to the relatively low reactivity of the 3- and 4-positions of the pyrrole ring. In contrast, the 2,4-diacetal (**2***d*) has a reactive 5-position still available. This again emphasizes the electron withdrawing and deactivating effect on the pyrrole ring of the acetal group.

The successful formylation of the 2,4-diacetal (**2***d*) gives a route (Scheme 1) to the previously unknown pyrrole-2,3,5-tricarboxaldehyde (**6***a*). The hydrolysis of the formylated acetal (**5***a*) proved to be very difficult. Mild hydrolysis gave a mixture of monoacetals which required long and rather vigorous hydrolysis. Prolonged hydrolysis eventually gave the trialdehyde (**6***a*) in 67% yield. The $^1$H nmr spectrum of the trialdehyde showed resonances for the aldehydic protons at 9.81, 10.22, and 10.25, and for the ring proton at 7.48 ppm. Long range coupling between the ring proton and the aldehydic proton was too small to be resolved by the spectrometer used, indicating that the ring proton was in the 4-position rather than the 2-position. A ring proton in the 2-position would have produced a larger long range coupling to the 5-aldehydic proton (6). Other spectral properties were in accord with the assigned structure.

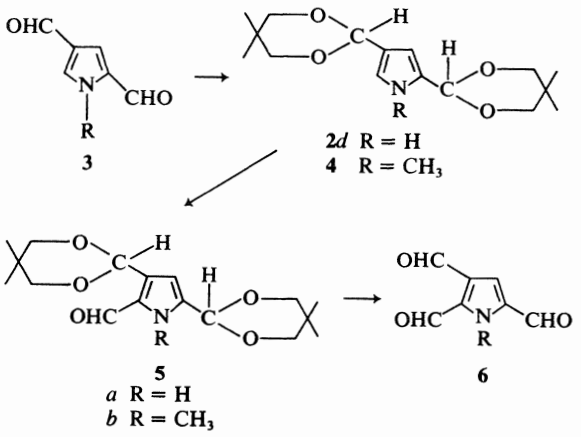


SCHEME 1

A similar series of reactions on 1-methyl-2,4-di(5,5-dimethyl-1,3-dioxan-2-yl)-pyrrole (**4**) gave 1-methyl-2,3,5-tricarboxaldehyde (**6***b*), a known compound. The melting point of our product was much higher and some of the spectral properties differed slightly from those reported by Severin and Krönig (8).[1] Direct comparison of the spectra of authentic material and our product showed them to be the same in all essential details and those differences present could be attributed to concentration effects since the original spectra had been obtained for very dilute solutions. The low melting point previously reported (8) can probably be attributed to the difficulties associated with purifying the small amount of material that was available to the original workers.

The Vilsmeier formylation of the acetals formed from 3-acetylpyrrole and from 4-acetylpyrrole-2-carboxaldehyde was also attempted but led only to extreme decomposition of the acetals. None of the desired products could be isolated from the tarry mass produced in the reaction.

We have lately reported (9) the cyanation of some substituted pyrroles using chlorosulfonyl isocyanate (CSI) in fairly good yield where the pyrrole was not too deactivated by electron-withdrawing substituents. Since the reaction can be carried out under quite mild conditions we attempted this reaction on some of the acetals. The best results were obtained by treating a solution of the acetal in *N*,*N*-dimethylformamide (DMF), with CSI at low temperature (solid $CO_2$/acetone bath) and then allowing the reaction mixture to warm near 0°C, depending on the acetal (cf. the preparation of pyrrole-2-carbonitrile (9)). Cyanation of the

[1]In a private communication Dr. Severin kindly provided additional information including copies of some of the original spectra but he was unable to provide a sample of the authentic compound.

Can. J. Chem. Downloaded from www.nrcresearchpress.com by 210.87.254.6 on 09/06/12
For personal use only.

pyrrole-2-acetal (**1***a*) in this way gave a good yield (~85%) of a mixture of 4- (~10%) and 5- (~75%, ~63% isolated yield) cyanated product. The mixture of cyanoacetals was hydrolysed and separated by fractional crystallization to give 5-cyanopyrrole-2-carboxaldehyde (~75%) and 4-cyanopyrrole-2-carboxaldehyde (~9%). When the 1-methyl homologue (**1***c*) was cyanated in a similar fashion, only the product of 5-cyanation, **7***b*, was isolated (65% yield). Although the cyanation of **1***c* might have been expected to give more 4-substitution than **1***a*, there were no more than trace amounts of the 4-substituted product present in the crude product. This result probably does not indicate abnormal selectivity in the substitution reaction but is more likely a result of the lability of the 2-acetal (**1***a*) towards hydrolysis and other side reactions. Attempts at the cyanation of the 2,5- (**1***d*) and 2,4- (**2***d*) diacetals with CSI gave a very small yield of the 3,5-di(5,5-dimethyl-1,3-dioxan-2-yl)-pyrrole-2-carbonitrile (**7***c*) (Scheme 2) from the 2,4-diacetal but no isolable product from the 2,5-diacetal. When the nitrogen is blocked by a methyl group we again found that the yield in the reaction was greatly improved, so that the 1-methylpyrrole-2,4-di(5,5-dimethyl-1,3-dioxan-2-yl)-pyrrole (**4**) gave a 18% yield of 1-methyl-3,5-di(5,5-dimethyl-1,3-dioxan-2-yl)-pyrrole-2-carbonitrile (**7***d*).

While there is considerable scope for the use of the Vilsmeier reaction for the formylation of pyrrole acetals where the pyrrole ring is reactive towards electrophilic substitution, cyanation using CSI seems to be limited by the lability of the acetal function towards decomposition under the reaction conditions required for substitution.

## Experimental

Melting points are uncorrected. Elemental analyses were by Atlantic Microlabs, GA, U.S.A., or by Memorial University Water Analysis Facility. The ir spectra were recorded on a Perkin–Elmer 237B grating spectrophotometer as Nujol mulls or as liquid films. The $^1$H nmr spectra were determined using a Varian EM 360 instrument and are recorded on the δ scale with tetramethylsilane as internal reference. Mass spectra were recorded on a Hitachi–Perkin–Elmer RMU-6E spectrometer using a direct inlet system. The $^{13}$C nmr spectra were determined at 25.2 MHz in $CDCl_3$ on a Varian Associates XL-100/15 Fourier transform instrument.

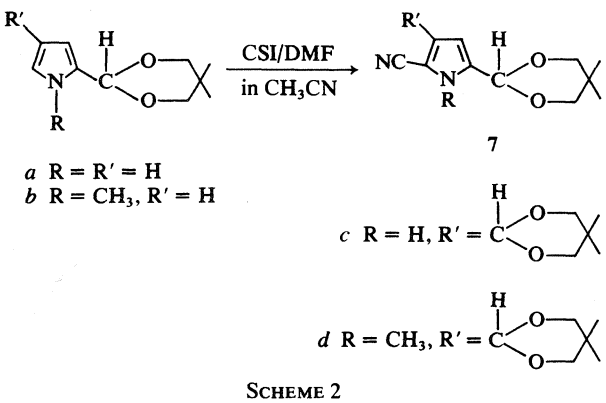


SCHEME 2

*Preparation of acetals*

The acetals were prepared by the method reported earlier for related acetals (1) and are listed in Table 1.

*Vilsmeier formylation of pyrrole monoacetals*

For (1) to (3) below the method given for the formylation of 2-(5,5-dimethyl-1,3-dioxan-2-yl)-pyrrole in ref. 1 was used.

(1) *1-Methyl-2-(5,5-dimethyl-1,3-dioxan-2-yl)-pyrrole-2-carboxaldehyde (1e)*

1-Methyl-2-(5,5-dimethyl-1,3-dioxan-2-yl)-pyrrole gave the product, 1-methyl-5-(5,5-dimethyl-1,3-dioxan-2-yl)-pyrrole-2-carboxaldehyde (**1***e*), (95% yield), as an oil; nmr ($CDCl_3$) δ: 0.77, 1.24 (each 3H, s), 3.67 (4H, dd, $J_{AB}$ = 12 Hz), 3.99 (3H, s), 5.40 (1H, s), 6.29, 6.77 (each 1H, d), 9.47 (1H, s); $J_{3,4}$ = 4.0 Hz.

The product was immediately hydrolysed using the method described for hydrolysis of **1***e* in ref. 1 to give 1-methylpyrrole-2,5-dicarboxaldehyde (94%), mp 96–97°C (lit. (3b) mp 97°C); nmr ($CDCl_3$) δ: 4.25 (3H, s), 6.90 (2H, s), 9.78 (2H, s); *m/e*: 137.

(2) *4- and 3-(5,5-Dimethyl-1,3-dioxan-2-yl)-pyrrole-2-carboxaldehyde*

3-(5,5-Dimethyl-1,3-dioxan-2-yl)-pyrrole gave a mixture (78% yield) which was separated by fractional crystallization from ether/petroleum mixtures to give: (*i*) 4-(5,5-dimethyl-1,3-dioxan-2-yl)-pyrrole-2-carboxaldehyde (**2***b*) (46% of total product), mp 131–132°C; nmr ($CDCl_3$) δ: 0.76, 1.24 (each 3H, s), 3.64 (4H, dd, $J_{AB}$ = 12 Hz), 5.35 (1H, s), 6.97, 7.13 (each 1H, m), 9.41 (1H, s), 9.8 (1H, broad, N—H), *m/e*: 209. *Anal.* calcd. for $C_{11}H_{15}NO_3$: C 63.14, H 7.23, N 6.69; found: C 63.34, H 7.35, N 6.66; and (*ii*) 3-(5,5-dimethyl-1,3-dioxan-2-yl)-pyrrole-2-carboxaldehyde (54%), mp 105–106°C; nmr ($CDCl_3$) δ: 0.77, 1.26 (each 3H, s), 3.68 (4H, dd, $J_{AB}$ = 12 Hz), 5.62 (1H, s), 6.33, 6.93 (each 1H, m), 9.83 (1H, d); $J_{5,CHO}$ = 1.0 and $J_{3,5}$ = 1.5 Hz. *Anal.* calcd. for $C_{11}H_{15}NO_3$: C 63.14, H 7.23, N 6.69; found: C 63.40, H 7.17, N 6.58.

The mixture of acetals was also hydrolysed before purification in the usual way (1) affording a mixture of aldehydes which could be separated by fractional crystallization or by chromatography on silica gel (see ref. 6) to give: pyrrole-2,4-dicarboxaldehyde, mp 151.5–152°C (lit. (6) mp 152°C), the mixture melting point with authentic material was undepressed; and pyrrole-2,3-dicarboxaldehyde, mp 118–120°C (lit. (6) mp 123°C); ir ν: 3260 (N—H), 1660 (C=O) cm$^{-1}$; nmr ($CDCl_3$) δ: 6.72 (1H, d), 7.23 (1H, unresolved dd), 10.06 (1H, d), 10.20 (1H, s); $J_{4,5}$ = 3.0, $J_{2\text{-CHO},5}$ = 0.7 Hz.

(3) *1-Methyl-3-(5,5-dimethyl-1,3-dioxan-2-yl)-pyrrole carboxaldehyde (mixture of isomers)*

1-Methyl-3-(5,5-dimethyl-1,3-dioxan-2-yl)-pyrrole gave a mixture of monoformylated products (~53% yield). The reaction mixture was hydrolysed (1) and then the mixture of aldehydes was chromatographed on a silica gel column. Elution with benzene/ethyl acetate mixtures gave (in order) the following. 1-Methylpyrrole-2,3-dicarboxaldehyde, mp 78°C (lit. (7*a*) mp 77°C); ir ν: 1740 (C=O), 1670 (C=O) cm$^{-1}$; nmr ($CDCl_3$) δ: 3.97 (3H, s), 6.63 (1H, d), 6.80 (1H, unresolved dd), 10.22 (1H, s), 10.38 (1H, d), $J_{4,5}$ = 3.0, $J_{2\text{-CHO},5}$ = 0.7 Hz. 1-Methylpyrrole-2,4-dicarboxaldehyde, mp 96–97°C (lit. (2) mp 95°C); nmr ($CDCl_3$) δ: 3.97 (3H, s), 7.26 (1H, d), 7.40 (1H, unresolved dd), 9.56 (1H, d), 9.67 (1H, s). 1-Methylpyrrole-3,4-dicarboxaldehyde, mp 166–167°C (lit. (7*b*) mp 169°C). ir ν: 1680, 1665 (each C=O) cm$^{-1}$; nmr ($CDCl_3$) δ: 3.73 (3H, s), 7.21 (2H, s), 10.07 (2H, s).

Can. J. Chem. Downloaded from www.nrcresearchpress.com by 210.87.254.6 on 09/06/12
For personal use only.

*3,5-Di(5,5-dimethyl-1,3-dioxan-2-yl)-pyrrole-2-carboxaldehyde (5a)*

*N,N*-Dimethylformamide (20 mL) was cooled in an ice bath and phosphorus oxychloride (3.0 mL) was added to the stirred liquid. The very pale yellow liquid was stirred for 10 min at room temperature and then cooled in an ice bath. Solid 2,4-di(5,5-dimethyl-1,3-dioxan-2-yl)-pyrrole (1.04 g) was added fairly rapidly to the cooled mixture and the red solution formed was stirred in the ice bath for 100 min. The reaction mixture was then poured onto a stirred mixture of 6 mol $L^{-1}$ NaOH/ice/water (~200 mL). The yellow solution was extracted with ether until the aqueous layer was almost colourless. The ether extracts were washed with 10% aqueous $NaHCO_3$ and dried ($K_2CO_3$). Removal of the solvent gave a brown gum which rapidly crystallized (1.14 g after removal of as much DMF as possible under high vacuum). The product was recrystallized from $CH_2Cl_2$/petroleum as light brown crystals (0.877 g, 77%), mp 126–127°C; nmr ($CDCl_3$) δ: 0.76 (6H, s), 1.17, 1.23 (each 3H, s), 3.64 (8H, broad s), 5.37, 5.56 (each 1H, s), 6.31 (1H, d), 9.39 (1H, broad s), 9.79 (1H, s); *m/e*: 323. *Anal.* calcd. for $C_{17}H_{25}NO_5$: C 63.14, H 7.79, N 4.33; found C 63.18, H 7.79, N 4.33.

*1-Methyl-3,5-di(5,5-dimethyl-1,3-dioxan-2-yl)-pyrrole-2-carboxaldehyde (5b)*

Using the same method described above for 3,5-di(5,5-dimethyl-1,3-dioxan-2-yl)-pyrrole-2-carboxaldehyde, 1-methyl-2,4-di(5,5-dimethyl-1,3-dioxan-2-yl)-pyrrole gave the product as colourless crystals (80%), from heptane, mp 168.5°C; nmr ($CDCl_3$) δ: 0.77, 1.24 (each 6H, s), 3.67 (8H, broad s), 3.97, (3H, s), 5.37, 5.59 (each 1H, s), 6.40 (1H, s), 9.90 (1H, s); *m/e*: 337. *Anal.* calcd. for $C_{18}H_{27}NO_5$: C 64.07, H 8.07, N 4.15; found C 64.15, H 8.08, N 4.11.

*Pyrrole-2,3,5-tricarboxaldehyde (6a)*

3,5-Di(5,5-dimethyl-1,3-dioxan-2-yl)-pyrrole-2-carboxaldehyde (200 mg) was added to water (10 mL), ethanol (1 mL), and *p*-toluenesulfonic acid (100 mg), and the mixture was heated first under reflux for 1 h and then open to the atmosphere for 3.3 h with the solvent level maintained by the addition of water. Water (50 mL) was then added and the solution was extracted very thoroughly with chloroform. The extracts were dried ($MgSO_4$) and the solvent was removed to leave a solid residue of the almost pure product (93 mg, 67%), mp 185–187°C; ir ν: 3120 (N—H), 1676, 1660 (each broad C=O) $cm^{-1}$; nmr (acetone-$d_6$) δ: 7.48, 9.81, 10.22, 10.25 (each 1H, s); *m/e*: 151. *Anal.* calcd. for $C_7H_5NO_3$: C 55.64, H 3.34, N 9.27; found: C 55.58, H 3.38, N 9.25.

*1-Methylpyrrole-2,3,5-tricarboxaldehyde (6b)*

Using the method described above for pyrrole-2,3,5-tricarboxaldehyde, 1-methyl-3,5-di(5,5-dimethyl-1,3-dioxan-2-yl)-pyrrole-2-carboxaldehyde gave the product, mp 125.5–126°C; ir ν: 1670 (broad C=O) $cm^{-1}$; nmr ($CDCl_3$) δ: 4.25 (3H, s), 7.28, 9.73, 9.98, 10.35 (each 1H, s); *m/e*: 165. *Anal.* calcd. for $C_8H_7NO_3$: C 58.18, H 4.27, N 8.48; found: C 58.41, H 4.39, N 8.51.

*5-(5,5-Dimethyl-1,3-dioxan-2-yl)-pyrrole-2-carbonitrile (7a)*

2-(5,5-Dimethyl-1,3-dioxan-2-yl)-pyrrole (500 mg) was dissolved in a mixture of $CH_3CN$ (2 mL) and DMF (3 mL) and cooled in a solid $CO_2$/acetone bath. Chlorosulfonyl isocyanate (CSI) (0.43 mL) dissolved in $CH_3CN$ (3 mL) was added to the stirred mixture dropwise over about 5 min. The stirred mixture was held in the cooling bath for about 1 h as it was allowed to warm slowly to −5°C. During this period the solution, yellow at the start of the reaction, became dark red. The reaction mixture was poured into a rapidly stirred mixture of aqueous NaOH (5 mL, 3 mol $L^{-1}$), aqueous $NaHCO_3$ (50 mL, 5% aqueous), and ice (~25 g). The aqueous mixture was extracted with $CH_2Cl_2$, the extracts washed with water, dried ($K_2CO_3$), and the solvent was removed to leave the crude product containing some 4-substituted material (nmr) as a red oil. Molecular distillation of the red oil gave the product as a colourless oil which crystallized very slowly. The product was purified by repeated sublimation (60°C/0.5 Torr) to give colourless crystals, mp 72–73.5°C (360 mg. 63%); ir ν: 3200 (N—H), 2215 (CN) $cm^{-1}$; nmr ($CDCl_3$) δ: 0.77, 1.24 (each 3H, s), 3.64 (4H, dd, $J_{AB}$ = 12 Hz), 5.40 (1H, s), 6.18, 6.72 (each 1H, m), 9.25 (1H, broad); *m/e*: 206. *Anal.* calcd. for $C_{11}H_{14}N_2O_2$: C 64.06, H 6.84, N 13.58; found: C 64.05, H 6.88, N 13.58.

When the reaction mixture was poured into 1.5 mol $L^{-1}$ HCl/ice (200 mL) and then stirred at room temperature for 1 h the acetal group was completely hydrolysed. Extraction with ether gave a solid mixture of 5- and 4-cyanopyrrole-2-carboxaldehyde ($^1H$ nmr). The mixture was easily separated by fractional recrystallization from ethyl acetate/petroleum (bp 60–80°C) to give: 5-cyanopyrrole-2-carboxaldehyde (249 mg, 75%), mp 162–163°C; ir ν: 3170 (N—H), 2233 (CN), 1670 (C=O) $cm^{-1}$; nmr ($CDCl_3$) δ: 6.82, 6.91 (each 1H, d, $J_{3,4}$ = 3.8 Hz), 9.57 (1H, s); *m/e*: 120. *Anal.* calcd. for $C_6H_4N_2O$: C 60.00, H 3.33, N 23.33; found: C 60.19, H 3.18, N 23.37; and the much less soluble 4-cyanopyrrole-2-carboxaldehyde (31 mg, 9%), mp 175.5–177°C (from ethyl acetate/petroleum (bp 80–100°C)) (lit. (9) mp 177°C) was also isolated. The mixture melting point with authentic material was undepressed.

*1-Methyl-5-(5,5-dimethyl-1,3-dioxan-2-yl)-pyrrole-2-carbonitrile (7b)*

1-Methyl-2-(5,5-dimethyl-1,3-dioxan-2-yl)-pyrrole (500 mg) was dissolved in a mixture of $CH_3CN$ (2 mL) and DMF (13 mL) and cooled in a solid $CO_2$/acetone bath. Chlorosulfonyl isocyanate (CSI) (0.4 mL) dissolved in $CH_3CN$ (3.0 mL) was added to the stirred mixture dropwise over about 5 min. The solution became yellow and thickened due to the formation of solid. After 10 min the solid $CO_2$ bath was removed and the mixture was allowed to warm to room temperature (~15 min) and then poured onto ice-cold $NaHCO_3$ (5% aqueous, 100 mL). The aqueous mixture was extracted with chloroform (all of the colour was extracted into the organic layer). The combined chloroform extracts were washed twice with $NaHCO_3$ solution (5% aqueous), dried ($K_2CO_3$), and evaporated. The oily residue was pumped at high vacuum (0.1 Torr) to remove residual DMF and gave the almost pure product (500 mg) as a brownish oil. The oil was subjected to molecular distillation along a glass tube (0.1 Torr, 130°C) and the colourless distillate which slowly crystallized was recrystallized from an ethyl ether/petroleum (bp 60–80°C) mixture (364 mg, 65%), mp 49.5–51°C; ir ν: 2200 (CN) $cm^{-1}$; nmr ($CDCl_3$) δ: 0.80, 1.28 (each 3H, s), 3.67 (4H, dd, $J_{AB}$ = 12 Hz), 3.83 (3H, s), 5.37 (1H, s), 6.19, 6.63 (each 1H, d, $J_{AB}$ = 4.2 Hz); *m/e*: 220. *Anal.* calcd. for $C_{12}H_{16}N_2O_2$: C 65.43, H 7.32; found: C 65.47, H 7.35.

The reaction product was hydrolysed using a dilute HCl/methanol mixture (1) to give 1-methyl-5-cyanopyrrole-2-carboxaldehyde (83% yield), mp 66–67°C; ir ν: 2226 (CN), 1670 (C=O) $cm^{-1}$; nmr ($CDCl_3$) δ: 4.03(3H, s), 6.75, 6.87 (each 1H, d, $J_{AB}$ = 4.3 Hz), 9.62 (1H, s); *m/e*: 134. *Anal.* calcd. for $C_7H_6N_2O$: C 62.68, H 4.52; found C 62.67, H 4.53.

*3,5-Di-(5,5-dimethyl-1,3-dioxan-2-yl)-pyrrole-2-carbonitrile (7c)*

Cyanation of 2,4-di(5,5-dimethyl-1,3-dioxan-2-yl)-pyrrole gave a ~2% yield of the product, which was recrystallized from petroleum (bp 60–80°C), mp 113–115°C; ir ν: 3255 (N—H), 2235 (CN) $cm^{-1}$; nmr ($CDCl_3$) δ: 0.77, 0.77, 1.19, 1.26 (each 3H, s), 3.61 (8H, dd, $J_{AB}$ = 12 Hz), 5.33, 5.39 (each 1H, s), 6.29 (1H, d), 8.87 (1H, broad); *m/e*: 320. *Anal.* calcd. for $C_{17}H_{24}N_2O_4$: C 63.71, H 7.55; found: C 63.67, H 7.56.

*1-Methyl-3,5-di(5,5-dimethyl-1,3-dioxan-2-yl)-pyrrole-2-carbonitrile (7d)*

Cyanation of 1-methyl-2,4-di(5,5-dimethyl-1,3-dioxan-2-yl)-pyrrole as above for **1***a* gave the product in 18% yield after sublimation, mp 162.5–163°C; ir ν: 2202 (CN) $cm^{-1}$; nmr ($CDCl_3$) δ: 0.79, 1.27, (6H, each s), 3.67 (8H, dd), 3.81, (3H, s), 5.34, 5.43 (each 1H, s), 6.36 (1H, s); *m/e*: 334. *Anal.* calcd. for $C_{18}H_{26}N_2O_4$: C 64.65, H 7.84; found: C 64.67, H 7.85.

## Acknowledgements

The authors gratefully acknowledge the financial assistance of the Memorial University of Newfoundland and the Natural Sciences and Engineering Research Council of Canada. They also thank Dr. John A. Walter of the Atlantic Research Laboratory of the National Research Council of Canada for determination of the $^{13}C$ nmr spectra.

1. C. E. Loader and H. J. Anderson. Synthesis, 295 (1978).
2. H. J. Anderson and H. Nagy. Can. J. Chem. **59**, 1961 (1972).
3. (*a*) T. M. Cresp and M. V. Sargent. J. Chem. Soc. Chem. Commun. 807 (1972); (*b*) Th. Severin and I. Ipach. Chem. Ber. **108**, 1768 (1975); (*c*) J. Bergman, L. Renström, and B. Sjöberg. Tetrahedron, **36**, 2505 (1980).
4. A. Gossauer. Die Chemie der Pyrrole. Springer-Verlag, New York Berlin, Heidelberg. 1974. (*a*) p. 87, (*b*) p. 119.
5. (*a*) R. J. Abraham, R. D. Lapper, K. M. Smith, and J. F. Unsworth. J. Chem. Soc. Perkin Trans. II, 104, (1975); (*b*) A. J. Jones, E. L. Eliel, D. M. Grant, M. C. Knoebar, and W.F. Bailey. J. Am. Chem Soc. **93**, 4772 (1971).
6. P. Fournari, M. Farnier, and C. Fournier. Bull. Soc. Chim. Fr. 2831 (1972).
7. (*a*) J. Duflos, D. Letouzé, G. Queguiner, and P. Pastour. J. Heterocycl. Chem. **10**, 1083 (1973); (*b*) J. Duflos, D. Letouzé, G. Queguiner, and P. Pastour. Tetrahedron Lett. 3452 (1973).
8. Th. Severin and U. Krönig. Z. Lebensm.-Unters. Forsch. **152**, 421 (1973).
9. C. E. Loader and H. J. Anderson. Can. J. Chem. **59**, 2673 (1981).

Can. J. Chem. Downloaded from www.nrcresearchpress.com by 210.87.254.6 on 09/06/12
For personal use only.

# A highly stereoselective intramolecular aldol condensation. Part I. Nuclear magnetic resonance spectroscopic investigation of the stereochemistry of the products derived from the reaction of 2,2′-*O*-methylene-bis-D-glycerose with base

WALTER A. SZAREK, B. MARIO PINTO, AND ALAN H. HAINES[1]

*Carbohydrate Research Institute and Department of Chemistry, Queen's University, Kingston, Ont., Canada K7L 3N6*

AND

T. BRUCE GRINDLEY

*Department of Chemistry, Dalhousie University, Halifax, N.S., Canada B3H 4J3*

Received July 16, 1981

WALTER A. SZAREK, B. MARIO PINTO, ALAN H. HAINES, and T. BRUCE GRINDLEY. Can. J. Chem. **60**, 390 (1982).

The intramolecular aldol condensation of 2,2′-*O*-methylene-bis-D-glycerose has been found to yield only two of the four possible diastereomeric products. At higher base concentration or prolonged reaction times, these products undergo a Cannizzaro reaction. The stereochemistry of the products derived from the aldol condensation has been established by means of labelling experiments and by examination of the products by $^1$Hmr and $^{13}$Cmr spectroscopy. The major and minor products of the reaction have been identified as being 2-*C*-hydroxymethyl-2,4-*O*-methylene-D,L-ribose (**7**) and 2-*C*-hydroxymethyl-2,4-*O*-methylene-D,L-xylose (**8**), respectively. The preferential stabilization of these products in the reaction by means of intramolecular hemiacetal formation is proposed as a driving force for the high degree of stereoselectivity; this possibility is supported by the isolation of the bicyclic systems expected from such a reaction. Conditions have been chosen such that **7** is formed exclusively.

WALTER A. SZAREK, B. MARIO PINTO, ALAN H. HAINES et T. BRUCE GRINDLEY. Can. J. Chem. **60**, 390 (1982).

On a trouvé que la condensation aldolique intramoléculaire du *O*-méthylène bis-2,2′ D-glycérose donne seulement deux des quatres diastéroisomères possibles. Ces produits subissent une réaction de Cannizaro si la concentration de la base est plus élevée ou si on prolonge les temps de réaction. On a établi la stéréochimie des produits issus de la condensation aldolique à l'aide d'expériences de marquage et de la spectroscopie de rmn du $^1$H et du $^{13}$C. Les produits majoritaires et secondaires de la réaction sont respectivement le *C*-hydroxyméthyl-2 *O*-méthylène-2,4 D,L ribose (**7**) et le *C*-hydroxyméthyl-2 *O*-méthylène-2,4 D,L xylose (**8**). On croit que le haut degré de stéréosélectivité est dû à la stabilisation préférentielle de ces produits au cours de la réaction par l'intermédiaire de la formation d'un hémiacétal intramoléculaire; on envisage cette possibilité par suite de l'isolement de systèmes bicycliques caractéristiques pour de telles réactions. On a choisi des conditions de façon à obtenir exclusivement le composé **7**.

[Traduit par le journal]

## Introduction

In 1943 Hudson and co-workers (1) reported the formation of a di-*O*-acetoxymethyl-di-*O*-acetyl-*O*-methylene-D-mannitol when tri-*O*-methylene-D-mannitol was subjected to mild acetolysis. In order to characterize this compound it was first deacylated, and the resulting *O*-methylene-D-mannitol was subjected to periodate oxidation. Since one mole of periodate was consumed for every mole of compound, and formaldehyde was not generated, it was concluded that the compound contained a 2,5-*O*-methylene acetal (see **1**). Interestingly, the addition of a slight excess of hot saturated barium hydroxide solution in order to remove iodate and periodate from the reaction mixture resulted in the formation of a new compound, as evidenced by a change in sign of the optical rotation of the solution. Concentration of the solution and reduction of the resulting syrup with Raney nickel and hydrogen afforded a product which partially crystallized. Elemental analyses of the reduced compound and of its acetylated derivative were consistent with those of an *O*-methylene mannitol and its tetraacetate, and a molecular-weight determination indicated that the compound was monomeric. Furthermore, the compounds

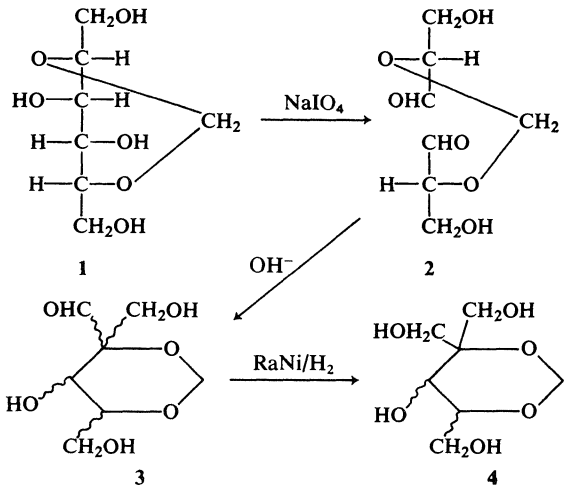


SCHEME 1

[1]On sabbatical leave from the University of East Anglia, Norwich, England NR4 7TJ, May–July 1978.

0008-4042/82/040390-25$01.00/0

©1982 National Research Council of Canada/Conseil national de recherches du Canada

Can. J. Chem. Downloaded from www.nrcresearchpress.com by 210.87.254.40 on 09/06/12
For personal use only.

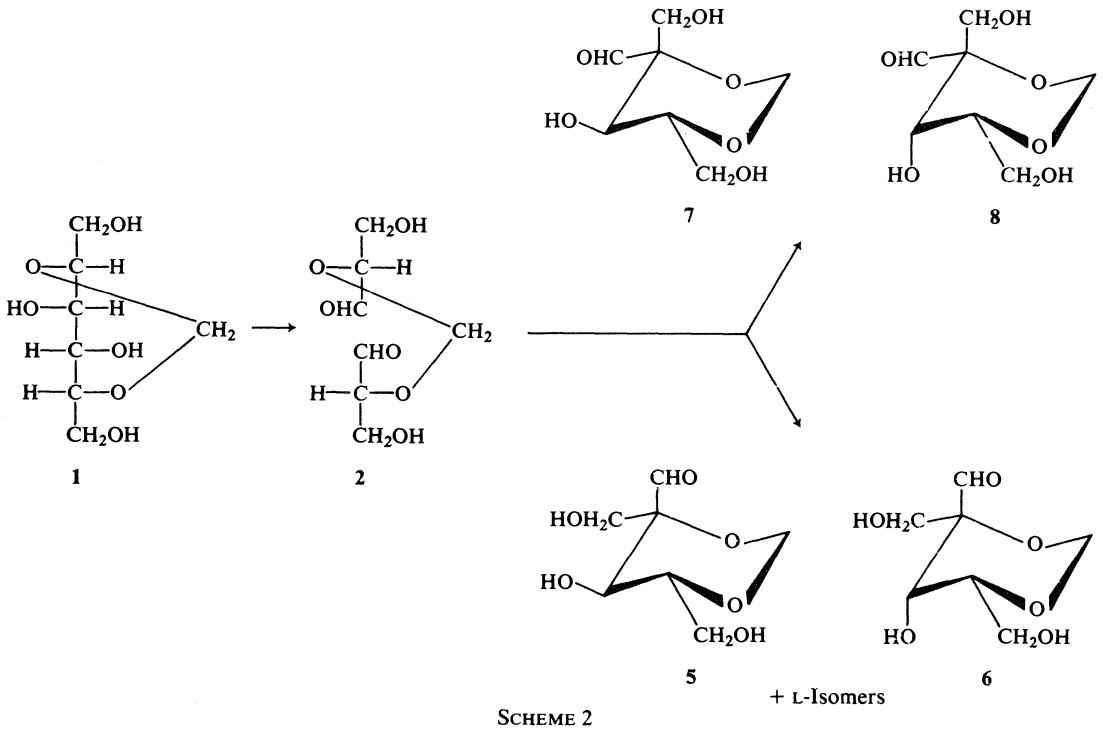


SCHEME 2

were not oxidized by sodium periodate or lead tetraacetate. On the basis of these results, it was concluded that, under the slightly alkaline conditions of the experiment, the primary oxidation product, namely 2,2′-*O*-methylene-bis-D-glycerose (**2**), was converted by an intramolecular aldol condensation into the isomeric cyclic aldehyde, namely 4-formyl-5-hydroxy-4,6-di(hydroxymethyl)-1,3-dioxane (**3**), which was then reduced to form 5-hydroxy-4,4,6-tri(hydroxymethyl)-1,3-dioxane (**4**), as indicated in Scheme 1.

The intramolecular aldol condensation reaction of 2,2′-*O*-methylene-bis-D-glycerose can potentially result in the formation of four enantiomeric pairs of products (**5**, **6**, **7**, and **8** and their enantiomers), as indicated in Scheme 2. Moreover, each of these products can undergo a Cannizzaro reaction to give the corresponding acid and alcohol. It was anticipated that the stereochemistry at C-5 and C-6 of the products would be deducible by examination

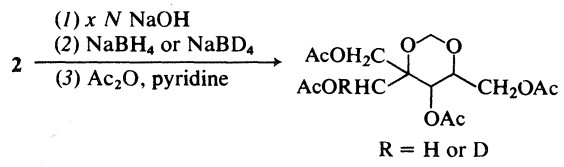


SCHEME 3

of the $^1$Hmr spectra but that the determination of the stereochemistry at the quaternary centre (C-4) would require more sophisticated methods. In order to solve the latter problem, the following strategy was implemented. The products of the reaction were subjected to reduction with sodium borodeuteride followed by acetylation (see Scheme 3). The *gem*-di-(acetoxymethyl) derivatives obtained in this manner were then examined by means of $^{13}$Cmr spectroscopy; the introduction of a deuterium label onto one of the carbon atoms attached to C-4 was expected to result in a change in multiplicity and intensity of the signal attributable to the labelled carbon atom. The unambiguous assignment of the $^{13}$Cmr spectra of the nondeuterated derivatives together with the information obtained from the spectra of the deuterated derivatives would then result in the assignment of stereochemistry at C-4 of the latter compounds and, hence, in the assignment of stereochemistry of the products of the aldol condensation reaction. An alternative route employing the sequence: periodate oxidation, aldol condensation, sodium borohydride reduction, and acetylation, using 2,5-*O*-methylene-D-mannitol-1-*d* (**9**) as starting material, was designed to provide complementary information; in this case, the deuterium label would be present in the diastereotopic counterpart of the

Can. J. Chem. Downloaded from www.nrcresearchpress.com by 210.87.254.40 on 09/06/12
For personal use only.

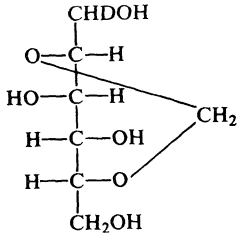

9

acetoxymethyl group at C-4 that was labelled by the first route.

The question of stereochemistry is of some interest, since **7** represents a simple derivative of the naturally occurring branched-chain sugar, hamamelose, and **5**, **6**, and **8** represent isomers of this compound. The intramolecular aldol condensation offers, therefore, an interesting route to this class of compounds.

## Results and discussion

Treatment of 2,2′-*O*-methylene-bis-D-glycerose (**2**) with sodium hydroxide followed by borohydride reduction and subsequent acetylation afforded only two products which were isolated by fractional crystallization. Interestingly, the ratio of the two products was found to be dependent on the conditions of the aldol condensation reaction, namely the base concentration and the reaction time. Thus, for example, when the reaction mixture was 0.3 *N* in sodium hydroxide and the reaction time was 4.5 h, the lower-melting isomer (Isomer 1) and the higher-melting isomer (Isomer 2) were present in a ratio of 63:37. In contrast, treatment of compound **2** with 0.05 *N* sodium hydroxide for 3.5 h afforded Isomer 1 exclusively. The ratio of Isomer 1/Isomer 2 obtained using a base concentration of 0.2 *N* and a reaction time of 24 h was 92:8 and that obtained using a base concentration of 0.1 *N* and a reaction time of 3.5 h was 93:7 (see Table 1). Isomer 1 corresponds to that obtained by Hudson and co-workers (1); these workers utilized a base concentration of 0.1 *N* sodium hydroxide and a reaction time of 3.5 h in order to effect the aldol condensation reaction. Treatment of 2,2′-*O*-methylene-bis-D-glycerose (**2**) under the four conditions described above followed by sodium borodeuteride reduction of the resulting mixtures also furnished some interesting results (see Table 2). Thus, treatment of **2** under the first set of conditions (0.3 *N* NaOH, 4.5 h) followed by borodeuteride reduction and subsequent acetylation afforded Isomer 1 and Isomer 2 as before. Examination of the $^{1}H$-decoupled $^{13}C$mr spectrum of Isomer 1 indicated the presence of a 1:1:1 triplet for one of the signals, attributable to a carbon of an acetoxymethyl group, and the absence of the signal attributable to the corresponding carbon in the nondeuterated derivative (see later). Surprisingly, the $^{13}C$mr spectrum of Isomer 2 showed neither the 1:1:1 triplet for one of the signals nor a reduction in intensity of any of the signals attributable to the carbons of the acetoxymethyl groups relative to those in the spectrum of the nondeuterated derivative. Clearly, deuterium incorporation was unsuccessful in this case. However, when the aldol-condensation reaction was performed at a lower base concentration (0.1 *N* NaOH, 3.5 h), and the products obtained after sequential borodeuteride reduction and acetylation were subjected to analysis by $^{13}C$mr spectroscopy, Isomer 1 was found to have incorporated deuterium as before but Isomer 2 was now found to have partially incorporated deuterium (evidenced by a reduction in intensity of one of the signals, attributable to a carbon of an acetoxymethyl group, relative to that in the nondeuterated derivative). When the aldol-condensation reaction was performed for prolonged reaction times (0.2 *N* NaOH, 24 h), neither of the two isomers obtained after sequential borodeuteride reduction and acetylation showed the incorporation of deuterium. Finally, treatment of **2** at a low base concentration (0.05 *N* NaOH, 3.5 h) afforded Isomer 1 which was shown to have incorporated deuterium.

The production of only two of the four possible diastereomers in the aldol-condensation reaction is noteworthy. Moreover, the observed stereospeci-

TABLE 1. Product distribution obtained from the application of the sequential reactions aldol condensation, borohydride reduction, and acetylation to 2,2′-*O*-methylene-bis-D-glycerose (**2**)

| Conditions of aldol condensation | Composition (%) | |
|---|---|---|
| | Isomer 1 (mp 91–93°C) | Isomer 2 (mp 145.5–146.5°C) |
| 0.3 *N* NaOH, 4.5 h | 63 | 37 |
| 0.2 *N* NaOH, 24 h | 92 | 8 |
| 0.1 *N* NaOH, 3.5 h | 93 | 7 |
| 0.05 *N* NaOH, 3.5 h | 100 | 0 |

TABLE 2. Results of deuterium incorporation experiments from the application of the sequential reactions aldol condensation, borodeuteride reduction, and acetylation to 2,2′-*O*-methylene-bis-D-glycerose (**2**)

| Conditions of aldol condensation | Deuterium incorporation | |
|---|---|---|
| | Isomer 1 | Isomer 2 |
| 0.3 *N* NaOH, 4.5 h | Complete | None |
| 0.2 *N* NaOH, 24 h | None | None |
| 0.1 *N* NaOH, 3.5 h | Complete | Partial |
| 0.05 *N* NaOH, 3.5 h | Complete | — |

Can. J. Chem. Downloaded from www.nrcresearchpress.com by 210.87.254.40 on 09/06/12
For personal use only.

Can. J. Chem. Downloaded from www.nrcresearchpress.com by 210.87.254.40 on 09/06/12
For personal use only.

ficity of the reaction at low base concentration is remarkable in view of the fact that the reaction proceeds through a carbanion. The results of the deuterium incorporation experiments (Table 2) suggest that under certain conditions the formyl group in the products of the aldol-condensation reaction undergoes reduction, presumably by a Cannizzaro reaction, prior to the addition of sodium borodeuteride. Examples of crossed-aldol condensations followed by Cannizzaro reactions to give branched-chain sugars are well documented (2). Apparently, the Cannizzaro reaction occurring in the present study is substrate selective, since, under certain conditions, the aldehyde precursor of Isomer 2 undergoes preferential reduction. For example, at a base concentration of 0.3 *N* or 0.1 *N* and short reaction times, the aldehyde precursor of Isomer 2 undergoes exclusive and partial reduction, respectively, by means of a Cannizzaro reaction, whereas the aldehyde precursor of Isomer 1 is either unaffected by these conditions or serves as the reducing agent and is itself oxidized to the acid. With prolonged reaction times, this selectivity is lost and both compounds undergo reduction by means of a Cannizzaro reaction to furnish, after acetylation, Isomer 1 and Isomer 2. Presumably, the acids that are also formed in these reactions are retained on the basic ion-exchange resin during the processing of the reaction.

The assignment of the relative stereochemistry at C-5 and C-6 of Isomer 1 and Isomer 2 was performed by examination of $^1$Hmr spectra obtained at 220 MHz. The spectra are shown in Figs. 1–8. All spectral assignments were confirmed by means of systematic spin-decoupling experiments. Initially, the spectra were measured in chloroform-*d* solution and later in benzene-$d_6$ solution since it was anticipated that benzene-induced shifts of the proton resonances would result in greater spectral dispersion and thus facilitate assignment of the spectra. The solvent shifts of proton resonances induced by benzene, relative to carbon tetrachloride or chloroform, are well documented, and have been used to advantage in the solution of a variety of structural, stereochemical, and conformational problems (3). These shifts have been attributed (3*a*) to the interaction of the $\pi$-system of the benzene ring with polar sites in solute molecules by way of an induced dipole–dipole mechanism. The nature of the collision complex in various alkyl-substituted 1,3-dioxanes has been considered previously (4, 5). In particular, Carlson *et al.* (5) have postulated a collision complex in which the benzene molecule lies above the solute molecule and in which the plane of the aromatic ring is perpendicular to the molecular dipole moment. However, the presence of additional polar sites in these derivatives (for example, acetates) was found (5) to modify this shielding pattern.

The partial $^1$Hmr spectrum of Isomer 1 (obtained from compound **2** by application of the sequential reactions aldol condensation, borohydride reduction, and acetylation) in chloroform-*d* is shown in Fig. 1. An outstanding feature of this spectrum is the appearance of the H-5 signal as a doublet having a coupling constant of 10.3 Hz; this value for a vicinal coupling constant is only consistent with the existence of an antiperiplanar relationship between H-5 and H-6. Isomer 1, obtained as described above, is, therefore, identified as being 2-*C*-acetoxymethyl-1,3,5-tri-*O*-acetyl-2,4-*O*-methylene-D,L-*erythro*-pentitol (**10**).[2] Another noteworthy feature in the spectrum of **10** is the marked chemical-shift difference between the diastereotopic protons of one of the acetoxymethyl groups. The signal at lower field is attributed to the hydrogen atom of the axial acetoxymethyl group which is directed "inwards" towards the axial hydrogen atoms at C-2 and C-6. The wide separation of the H-4′ and H-4″ signals is indicative of restricted rotation about the $C_4$—$C_{4'}$ bond which results in the preponderance of one rotational conformation. The spectrum of Isomer 1 in benzene-$d_6$ exhibits similar features to those observed in the spectrum measured in chloroform-*d* although greater spectral dispersion obtains (see Fig. 2). It is interesting to note that the H-6 signal is shifted upfield and the H-5 signal is shifted downfield relative to the corresponding signals in the spectrum measured in chloroform-*d* (see Table 3). Since the model proposed by Carlson *et al.* (5) for the benzene – 2-methyl-1,3-dioxane collision complex predicts that both H-5 and H-6 should be shielded in benzene solution relative to chloroform solution, it would appear that the additional sites available for benzene complexation, namely the ester functions, also play an important role in inducing chemical-shift changes. The deshielding of H-5 is most likely caused by the complexation of a benzene molecule with the carbonyl function of the acetoxy group at C-5. In rigid systems, methine protons of secondary acetates are usually deshielded in benzene relative to inert solvents ($\Delta$ = 0.10–0.27 ppm) (3*h*, 3*i*, 3*k*, 6). Similarly, the shielding of H-2, H-2′, H-4′, and H-4″ and the deshielding of H-4‴ and H-4⁗ in benzene relative to chloroform (see Table 3) reflects the

[2]Although the descriptor D,L is used here and elsewhere in this paper, it does not signify in these instances that a racemic mixture of a compound was obtained, but rather that a mixture (not necessarily equimolar) of D- and L-isomers was obtained.

Can. J. Chem. Downloaded from www.nrcresearchpress.com by 210.87.254.40 on 09/06/12
For personal use only.

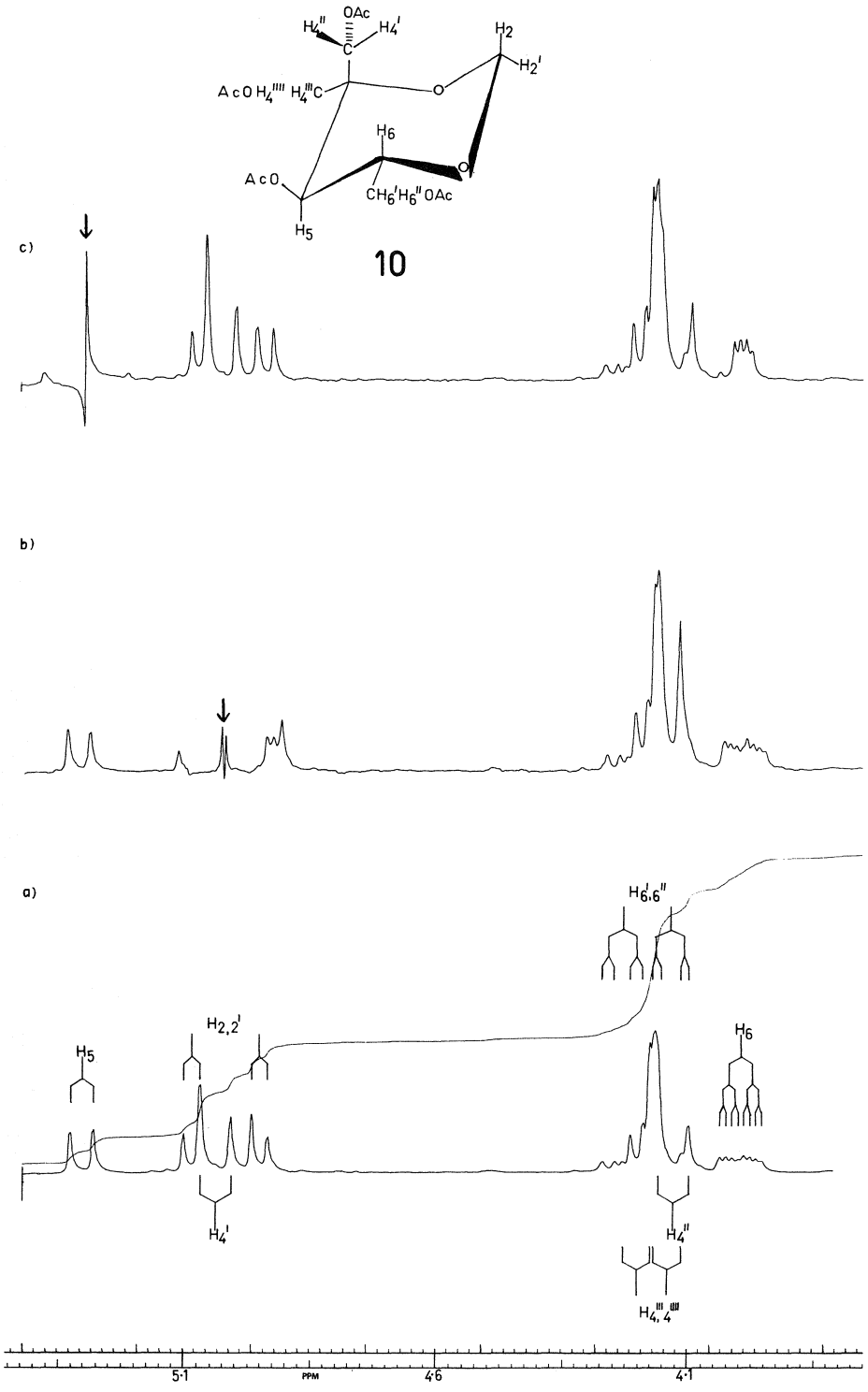


FIG. 1. (a) Partial $^1$Hmr spectrum at 220 MHz of 2-*C*-acetoxymethyl-1,3,5-tri-*O*-acetyl-2,4-*O*-methylene-D,L-*erythro*-pentitol (**10**) in chloroform-*d*; (b) with irradiation at $\nu_{H\text{-}4'}$; (c) with irradiation at $\nu_{H\text{-}5}$.

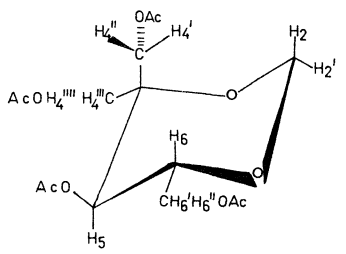


10

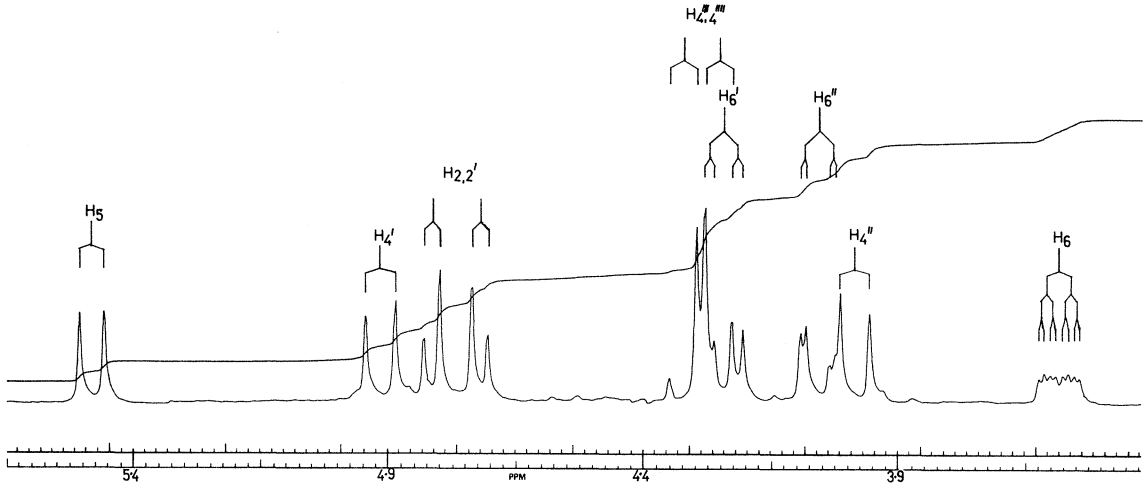


FIG. 2. Partial $^1$Hmr spectrum at 220 MHz of 2-*C*-acetoxymethyl-1,3,5-tri-*O*-acetyl-2,4-*O*-methylene-D,L-*erythro*-pentitol (**10**) in benzene-$d_6$.

TABLE 3. The $^1$Hmr chemical-shift data[a] for nondeuterated derivatives of Isomer 1 and Isomer 2

| | | Chemical shift (δ) | | | | | | | | | | |
|---|---|---|---|---|---|---|---|---|---|---|---|---|
| Compound | Solvent | H-2 | H-2′ | H-4′ | H-4″ | H-4‴ | H-4⁗ | H-5 | H-6 | H-6′ | H-6″ | $CH_3$ |
| Isomer 1 | $CDCl_3$ | 4.92 | 5.05 | 5.01 | 4.10 | 4.17 | 4.11 | 5.27 | 3.96 | 4.20 | 4.10 | 2.09, 2.11 |
| | $C_6D_6$ | 4.71 | 4.81 | 4.91 | 3.98 | 4.31 | 4.24 | 5.47 | 3.58 | 4.23 | 4.05 | 1.60, 1.69 1.74, 1.78 |
| | Δ[b] | −0.21 | −0.24 | −0.10 | −0.12 | 0.14 | 0.13 | 0.20 | −0.38 | 0.03 | −0.05 | — |
| Isomer 2 | $CDCl_3$ | 4.99 | 5.13 | 4.88 | 4.17 | 4.28 | 3.99 | 4.98 | 4.26 | 4.16 | 4.01 | 2.04, 2.09 2.14, 2.16 |
| | $C_6D_6$ | 4.76 | 4.84 | 4.72 | 3.87 | 4.61 | 4.15 | 4.96 | 3.90 | 4.27 | 4.09 | [c] |
| | Δ[b] | −0.23 | −0.29 | −0.16 | −0.30 | 0.33 | 0.16 | −0.02 | −0.36 | 0.11 | 0.08 | |

[a] At 220 MHz; in ppm downfield from internal TMS.
[b] $\Delta = \delta_{C_6D_6} - \delta_{CDCl_3}$, ppm.
[c] Not recorded.

balance of interactions as a result of benzene complexes with the dipole of the 1,3-dioxane ring and with the dipoles of the acetate-carbonyl functions.

The $^1$Hmr spectra of the deuterated derivatives of Isomer 1 (obtained by application of the sequential reactions aldol condensation, borodeuteride reduction, and acetylation to compound **2**) in chloroform-*d* and benzene-$d_6$ are shown in Figs. 3 and 4, respectively. The noteworthy feature of these spectra is the absence of the doublets attributable to H-4‴ and H-4⁗ that are observed in the spectra of the nondeuterated derivative and the presence of two singlets for the H-4‴ signals; the

Can. J. Chem. Downloaded from www.nrcresearchpress.com by 210.87.254.40 on 09/06/12
For personal use only.

Can. J. Chem. Downloaded from www.nrcresearchpress.com by 210.87.254.40 on 09/06/12
For personal use only.

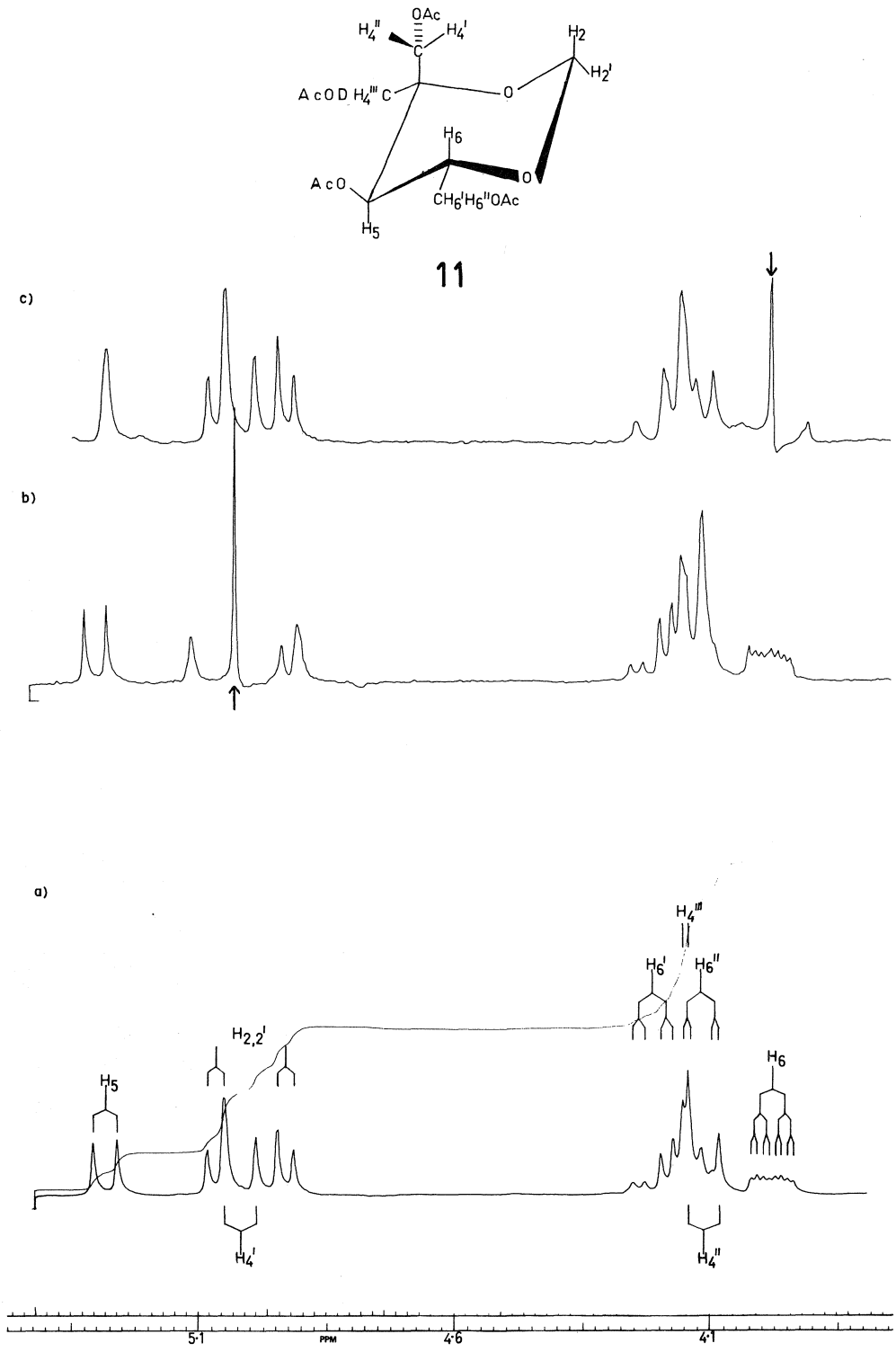


FIG. 3. (a) Partial $^1$Hmr spectrum at 220 MHz of 2-*C*-acetoxymethyl-1,3,5-tri-*O*-acetyl-1-(*R*,*S*)-deuterio-2,4-*O*-methylene-D,L-ribitol (**11**) in chloroform-*d*; (b) with irradiation at $\nu_{H\text{-}4'}$; (c) with irradiation at $\nu_{H\text{-}6}$.

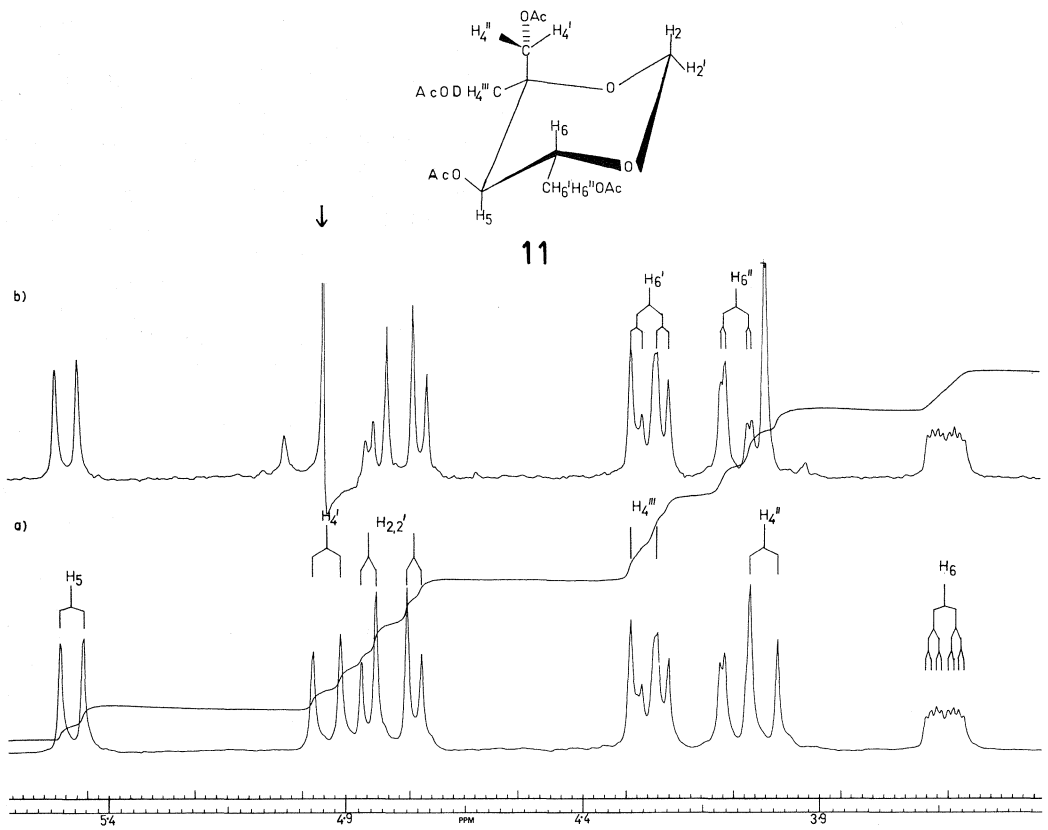


FIG. 4. (a) Partial $^1$Hmr spectrum at 220 MHz of 2-*C*-acetoxymethyl-1,3,5-tri-*O*-acetyl-1-(*R*,*S*)-deuterio-2,4-*O*-methylene-D,L-ribitol (**11**) in benzene-$d_6$; (b) with irradiation at $\nu_{H\text{-}4'}$.

latter two signals are attributed to the methylene proton of the acetoxymethyl group also bearing a deuterium atom in the two diastereomers resulting from generation of a new chiral centre by deuterium substitution. Since the H-4′ and H-4″ signals were tentatively assigned to those belonging to the axial acetoxymethyl group, the acetoxymethyl group bearing a deuterium atom is assigned to the equatorial orientation. The deuterated derivative of Isomer 1 is, therefore, tentatively identified as being 2-*C*-acetoxymethyl-1,3,5-tri-*O*-acetyl-1-(*R*,*S*)-deuterio-2,4-*O*-methylene-D,L-ribitol (**11**). This suggests, therefore, that the aldehyde precursor of **11** contains a formyl group that is equatorially oriented; the major product derived from the aldol-condensation reaction can thus be tentatively identified as being 2-*C*-hydroxymethyl-2,4-*O*-methylene-D,L-ribose (**7**).

The $^1$Hmr spectra of the nondeuterated derivative of Isomer 2 in chloroform-*d* and in benzene-$d_6$ are shown in Figs. 5 and 6, respectively. The signal for H-5 appears as a broadened singlet, signifying a *gauche* relationship of H-5 and H-6 in Isomer 2. The small coupling between these two protons may be attributed to the antiperiplanar arrangement of these protons with vicinal electronegative oxygen atoms (that is, H-5 with O-1; H-6 with O-5) since this is known (7–9) to reduce the magnitude of vicinal coupling constants markedly. The nondeuterated derivative of Isomer 2 is, therefore, identified as being 2-*C*-acetoxymethyl-1,3,5-tri-*O*-acetyl-2,4-*O*-methylene-D,L-*threo*-pentitol (**12**). It is interesting to note that Angyal and James (10) have obtained the L-isomer of **12** in low yield by lead tetraacetate oxidation of 2,4-*O*-methylene-D-glucitol; under the conditions of the processing, namely treatment with barium hydroxide, 2,4-*O*-methylene-L-xylose, the product of oxidation, evidently undergoes a mixed-aldol condensation with formaldehyde, followed by a crossed-Cannizzaro reaction. Another distinctive feature of the spectra of **12** is the appearance of the H-4′ and H-4″ signals as an AK pattern with a substantial chemical-shift difference between signals; this result is interpre-

Can. J. Chem. Downloaded from www.nrcresearchpress.com by 210.87.254.40 on 09/06/12
For personal use only.

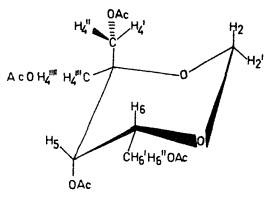

12

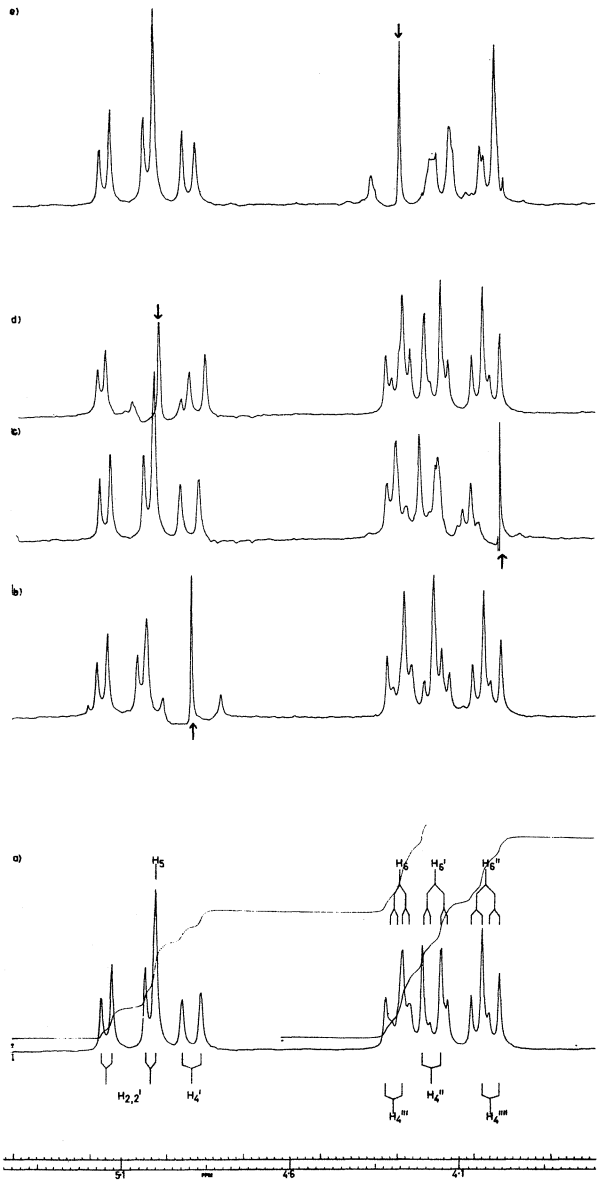

FIG. 5. (a) Partial $^1$Hmr spectrum at 220 MHz of 2-*C*-acetoxymethyl-1,3,5-tri-*O*-acetyl-2,4-*O*-methylene-D,L-*threo*-pentitol (**12**) in chloroform-*d*; (b) with irradiation at $\nu_{H\text{-}4'}$; (c) with irradiation at $\nu_{H\text{-}4'''}$; (d) with irradiation at $\nu_{H\text{-}5}$; (e) with irradiation at $\nu_{H\text{-}4''}$ and $\nu_{H\text{-}6}$.

ted in the same manner as that proposed earlier to account for a similar chemical-shift difference between H-4′ and H-4″ signals in the spectra of Isomer 1. The benzene-induced shifts for the proton resonances of **12** are presented in Table 3. The benzene-induced shift of the H-6 signal is of similar magnitude to that observed in the spectra of Isomer 1. However, the H-5 signal in the spectrum of Isomer 2 in benzene-$d_6$ is only shifted upfield by 0.02 ppm relative to that in the spectrum measured in chloroform-*d*, and is probably indicative of a cancellation of the shielding effect of the benzene molecule associated with the dipole of the 1,3-dioxane ring and the deshielding effect of the benzene molecule associated with the carbonyl function of the acetoxy group at C-5. That H-5 in Isomer 1 should be shielded more than H-5 in Isomer 2 by the benzene – 1,3-dioxane collision complex is evident from the greater benzene-induced shielding of the equatorial proton or equatorial methyl group at C-5, as compared to their axial counterparts, in 2-methyl-1,3-dioxane and 2,5,5-trimethyl-1,3-dioxane, respectively (4). The benzene-induced shifts of the other proton resonances in the spectra of Isomer 2 also probably reflect some balance in the effects of the ring-dipole – benzene complex and the carbonyl-dipole – benzene complexes.

The $^1$Hmr spectra of a mixture of the deuterated and nondeuterated derivatives of Isomer 2 (obtained by application of the sequential reactions aldol condensation, borodeuteride reduction, and acetylation) in chloroform-*d* and benzene-$d_6$ are shown in Figs. 7 and 8, respectively. The spectra are more complicated than those of Isomer 2 owing to the presence of three compounds. Nevertheless, analysis of the spectra indicates that two diastereomers containing a deuterium atom at one of the acetoxymethyl groups are present, in addition to the nondeuterated derivative; the proton resonances corresponding to the remaining proton of each of these acetoxymethyl groups in the two diastereomers appear as singlets, and are labelled as H-4* in the spectra. As was the case with Isomer 1, the acetoxymethyl group that is tentatively assigned to the equatorial orientation bears the deuterium label; this suggests that the formyl group in the aldehyde precursor, obtained from the aldol condensation reaction, is also equatorially oriented. The minor product of the aldol condensation reaction is, therefore, tentatively identified as being 2-*C*-hydroxymethyl-2,4-*O*-methylene-D,L-xylose (**8**).

It thus appears that the two diastereomers obtained in the aldol-condensation differ in configuration only at the newly formed asymmetric centre and that the reaction proceeds with complete

Can. J. Chem. Downloaded from www.nrcresearchpress.com by 210.87.254.40 on 09/06/12
For personal use only.

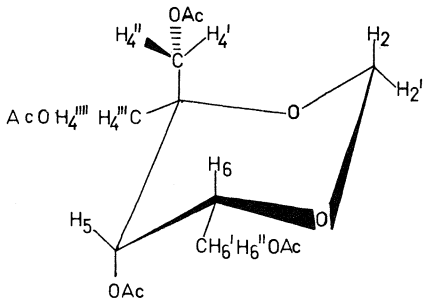


12

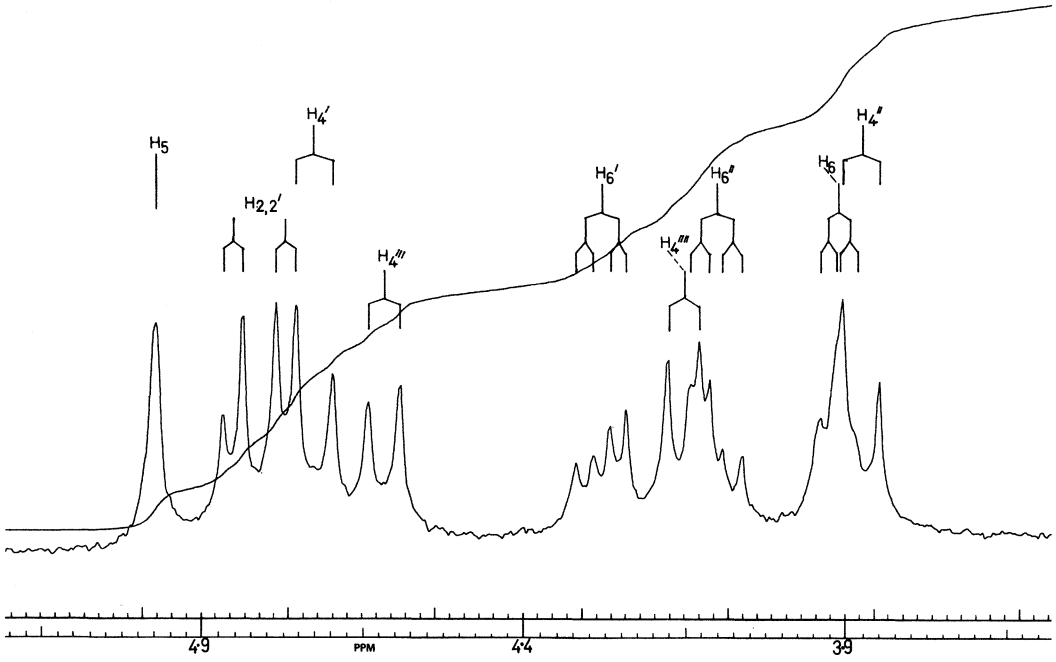


FIG. 6. Partial $^1$Hmr spectrum at 220 MHz of 2-*C*-acetoxymethyl-1,3,5-tri-*O*-acetyl-2,4-*O*-methylene-D,L-*threo*-pentitol (**12**) in benzene-$d_6$.

inversion of configuration at the quaternary centre (see **5** and **6** in Scheme 2). In order to unequivocally establish the stereochemistry at the quaternary centre, however, the products obtained as described in the preceding section were examined by means of $^{13}$Cmr spectroscopy (see Table 4).

Initially, it was necessary to assign unambiguously the $^{13}$Cmr resonances in the $^1$H – noise-decoupled spectra of the nondeuterated derivatives of Isomer 1 and Isomer 2, namely, **10** and **12**. The spectral assignments were made by examination of the coupled spectra, by means of single-frequency off-resonance decoupling (sford) experiments, and by consideration of the effects of substituents on $^{13}$Cmr chemical shifts. The spectra of Isomer 2 will be discussed first. Since the $^{13}$Cmr sford experiments were performed at a spectrum frequency of 20.0 MHz, a description of the $^1$Hmr spectrum at 80 MHz is necessary. The $^1$Hmr spectrum of **12** consisted of two groups of signals; the downfield group consisted of an AB quartet attributable to H-2 and H-2′ (δ 5.02, Δν 0.13 ppm, $J$ = 6.9 Hz), a broadened singlet attributable to H-5 (δ 4.97), and a doublet for one of the six C-methylene protons (δ 4.82, $J$ = 12.3 Hz). The upfield group of signals (δ 3.88–4.33) contained the remainder of the proton resonances (excluding methyl resonances) and could not be assigned. The $^{13}$Cmr signal assignments in the spectrum measured in chloroform-*d* were performed as follows. The signals appearing at 88.0

Can. J. Chem. Downloaded from www.nrcresearchpress.com by 210.87.254.40 on 09/06/12
For personal use only.

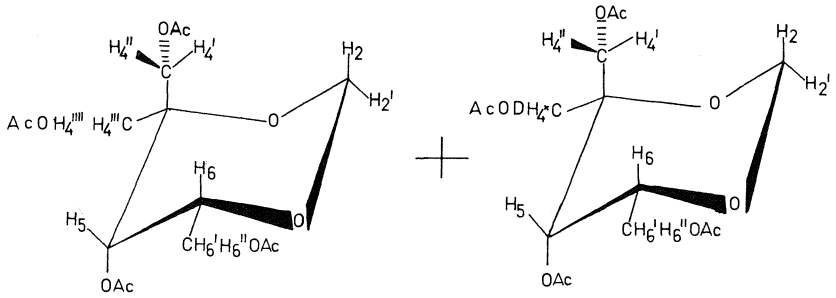

12 13

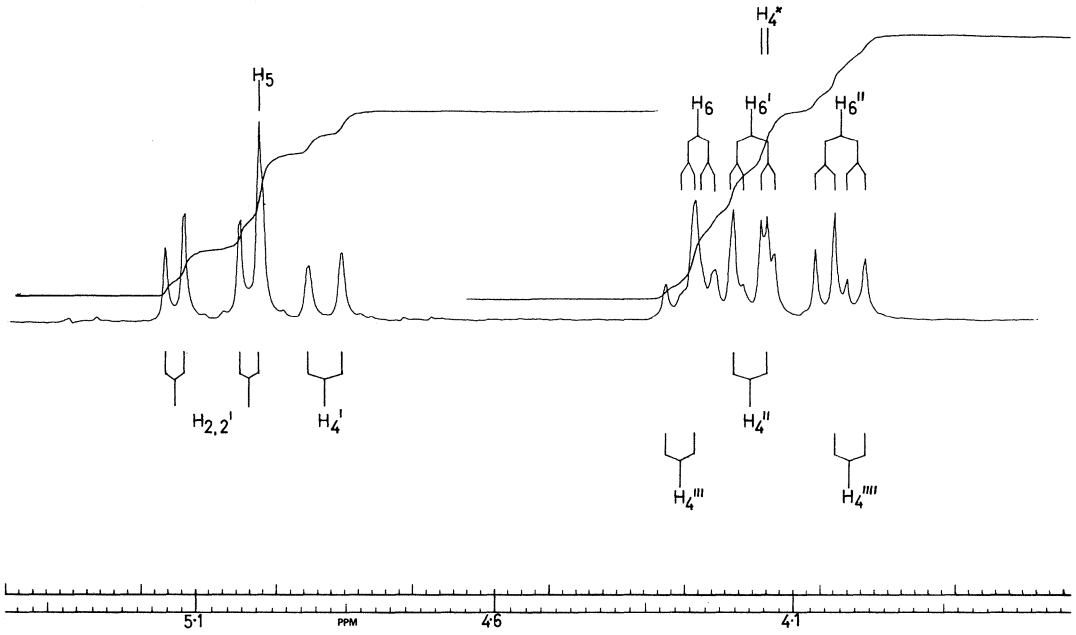


FIG. 7. Partial $^1$Hmr spectrum at 220 MHz of a mixture of 2-*C*-acetoxymethyl-1,3,5-tri-*O*-acetyl-2,4-*O*-methylene-D,L-*threo*-pentitol (**12**) and 2-*C*-acetoxymethyl-1,3,5-tri-*O*-acetyl-1-(*R*,*S*)-deuterio-2,4-*O*-methylene-D,L-xylitol (**13**) in chloroform-*d*.

and 75.6 ppm downfield from tetramethylsilane appeared, in the coupled spectra, as a quartet ($J$ = 162.4 and 170.3 Hz) and a broad singlet, respectively, and were therefore assigned to C-2 and C-4, respectively.[3] The signal at 72.6 ppm appeared as a doublet in the coupled spectrum and collapsed to a singlet upon irradiation at 4.19 ppm in the $^1$Hmr spectrum. Similarly, the signal at 63.7 ppm appeared as a doublet ($J$ = 149.0 Hz) in the coupled spectrum and collapsed to a singlet upon irradiation at 4.94 ppm in the $^1$Hmr spectrum. On the basis of the sford experiments, the signal at 63.7 ppm was assigned to C-5 while that at 72.6 ppm was assigned to C-6. The coupled spectrum of **12** exhibited three triplets at 62.6, 61.8, and 58.4 ppm having coupling constants of 150.0, 151.7, and 147.9 Hz, respectively. The triplet appearing at 62.6 ppm exhibited further splitting into doublets ($J$ = 6.0 Hz) of narrow line width (~2 Hz) while the other two triplets appeared as broad signals (line widths ~9 Hz). Since C-6′ is α to a carbon atom bearing one hydrogen and is also β to a carbon bearing one hydrogen, the signal at 62.6 ppm was assigned to C-6. On the other hand, both C-4′ and C-4″ are β to two carbon atoms, one of which bears two hydrogens and the other one hydrogen, and the signals attributable to C-4′ and C-4″ might not be expected to show individual resolved couplings to these protons. The signals at 62.6 and 61.8 ppm appeared

[3]The numbering of carbon atoms is designated in the formula for **10** in Table 4.

Can. J. Chem. Downloaded from www.nrcresearchpress.com by 210.87.254.40 on 09/06/12
For personal use only.

Can. J. Chem. Downloaded from www.nrcresearchpress.com by 210.87.254.40 on 09/06/12
For personal use only.

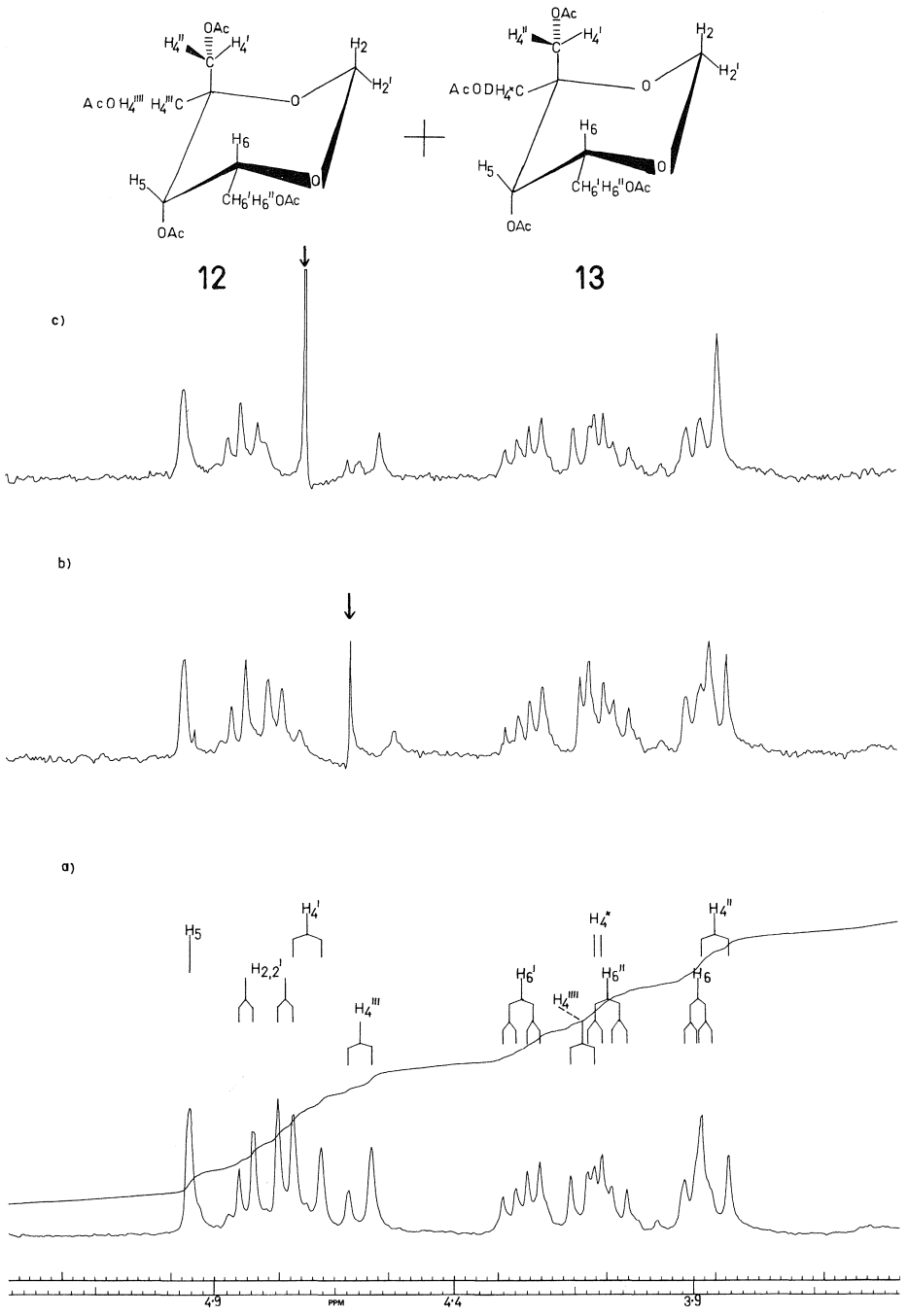


FIG. 8. (a) Partial $^1$Hmr spectrum at 220 MHz of a mixture of 2-*C*-acetoxymethyl-1,3,5-tri-*O*-acetyl-2,4-*O*-methylene-D,L-*threo*-pentitol (**12**) and 2-*C*-acetoxymethyl-1,3,5-tri-*O*-acetyl-1-(*R,S*)-deuterio-2,4-*O*-methylene-D,L-xylitol (**13**) in benzene-$d_6$; (b) with irradiation at $\nu_{H\text{-}4'''}$; (c) with irradiation at $\nu_{H\text{-}4'}$; (d) irradiation at $\nu_{H\text{-}4''}$ and $\nu_{H\text{-}6}$ (not shown) resulted in the collapse of the H-4′ signal to give a singlet and the collapse of the H-6′ and H-6″ signals to give doublets.

TABLE 4. Carbon-13 chemical-shift data[a] for 1,3-dioxane derivatives

| Compound | Carbon 2 | 4 | 4′ | 4″ | 5 | 6 | 6′ |
|---|---|---|---|---|---|---|---|
| 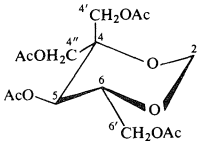 **10** | 87.80 | 75.13 | 58.31 | 65.00 | 64.72 | 72.79 | 62.73 |
| 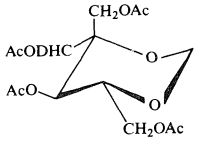 **11** | 87.80 | 75.07 | 58.31 | 64.70[b] | 64.72 | 72.79 | 62.73 |
| | | ($^1J_{^{13}C-^2H}$ = 22.5 Hz) | | | | | |
| 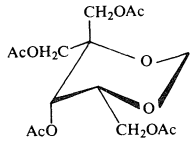 **12** | 88.03 | 75.59 | 58.44 | 61.80 | 63.72 | 72.59 | 62.56 |
| 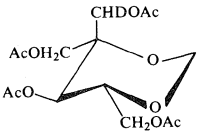 **16** | 87.86 | 75.12 | 58.07[b] | 65.03 | 64.73 | 72.85 | 62.76 |
| | | ($^1J_{^{13}C-^2H}$ = 22.5 Hz) | | | | | |
| 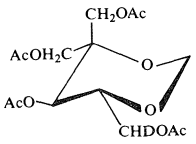 **17** | 87.86 | 75.18 | 58.34 | 65.03 | 64.73 | 72.79 | 62.48[b] |
| | | | | | ($^1J_{^{13}C-^2H}$ = 22.5 Hz) | | |
| 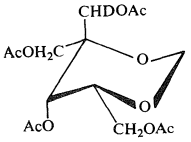 **18** | 88.06 | 75.55 | 58.23[b] | 61.82 | 63.72 | 72.61 | 62.57 |
| | | ($^1J_{^{13}C-^2H}$ = 22.6 Hz) | | | | | |
| 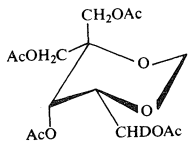 **19** | 88.06 | 75.59 | 58.43 | 61.82 | 63.72 | 72.55 | 62.28[b] |
| | | | | | ($^1J_{^{13}C-^2H}$ = 22.5 Hz) | | |

[a]In ppm downfield from internal tetramethylsilane (TMS); spectra were recorded in chloroform-*d*.
[b]The signal appeared as a 1:1:1 triplet in the $^1$H decoupled spectrum.

as singlets upon irradiation at 4.19 or 4.32 ppm in the $^1$Hmr spectrum. The appearance of the signal at 58.4 ppm varied from a triplet to a quartet to a sextet in the $^{13}$C sford spectrum depending on the frequency of irradiation in the $^1$Hmr spectrum. This behaviour is typical of that of the X portion of an ABX pattern in which A and B exhibit strong chemical-shift nonequivalence, and irradiation is applied at the A or B portion of the spectrum (11). Hagaman (11) has observed such "deviant" $^{13}$C–

Can. J. Chem. Downloaded from www.nrcresearchpress.com by 210.87.254.40 on 09/06/12
For personal use only.

Can. J. Chem. Downloaded from www.nrcresearchpress.com by 210.87.254.40 on 09/06/12
For personal use only.

[$^1$H] multiplets in the sford spectra of C–H systems which show strong geminal-proton nonequivalence. Thus, the signal at 58.4 ppm was assigned to the carbon that is directly coupled to the two methylene protons which exhibit a large chemical-shift difference in the $^1$Hmr spectrum. Nikiforova and co-workers (12) have reported the $^{13}$Cmr spectra of a variety of 2-alkyl-4,4-dimethyl-1,3-dioxanes; in every case, the signal attributable to the axial methyl carbon resonated at higher field (~ 10 ppm) than its equatorial counterpart. Moreover, the carbon atom of an axial hydroxymethyl substituent in the *E*-isomer of 4-*tert*-butyl-1-hydroxymethylcyclohexanol is reportedly shielded (by 6.0 ppm) with respect to its equatorial counterpart in the *Z*-isomer (13), and a similar result has been reported (14) for the $^{13}$Cmr shifts of the axial and equatorial hydroxymethyl carbon atoms in the isomers of 4-*tert*-butyl-1-hydroxymethylcyclohexane. On the basis of these results, one might have expected a substantial chemical-shift difference between the signals for C-4′ and C-4″ in the spectrum of **12**. However, in this case, the anticipated shielding of C-4′ relative to that of C-4″ is offset by the shielding of the C-4″ carbon by virtue of the γ-*gauche* effect of the acetoxy substituent at C-5. Moreover, the shielding of C-4″ by the γ-*gauche* effect is expected to be of greater magnitude than the corresponding shielding of C-4′[4] by virtue of the γ-*anti* effect of the acetoxy substituent at C-5 (15). Since a quantitative estimate of these various effects was not available, it was considered hazardous to assign the signals at 58.4 or 61.8 ppm to the carbons of either the axial or equatorial acetoxymethyl groups at C-4 solely on the basis of anticipated substituent effects on the chemical shifts. However, the assignment of the geminal methylene group showing strong chemical-shift nonequivalence in the $^1$Hmr spectra of **12** to the axially oriented acetoxymethyl group[5] and the demonstration, by means of $^{13}$C sford experiments, that the signal at 58.4 ppm in the $^{13}$Cmr spectrum is indeed attributable to the carbon atom directly coupled to this set of methylene protons, left no doubt that the high-field signal at δ 58.4 was that belonging to the carbon of the axially oriented acetoxymethyl group. The peak at δ 61.8 was then assigned to the carbon of the equatorially oriented acetoxymethyl group.

The $^{13}$Cmr spectral assignments in the spectrum of the nondeuterated derivative of Isomer 1, namely **10**, were made in an analogous manner to that already described for the spectral assignment of **12**. The $^1$Hmr spectrum at 80 MHz of **10** showed the presence of two groups of signals. The group at lower field consisted of an AB quartet (δ 4.97, Δν 0.16 ppm, $J$ = 6.7 Hz) that was assigned to H-2 and H-2′, a doublet at δ 5.26 ($J$ = 10 Hz) that was assigned to H-5, and a doublet at δ 4.98 ($J$ = 12.7 Hz) that was assigned to the methylene proton on the axially oriented acetoxymethyl group. The upfield group of signals (δ 4.0–4.2) appeared as a complex multiplet and contained the remainder of the proton resonances (excluding methyl resonances). The $^{13}$Cmr signal assignments in the spectrum measured in chloroform-*d* were performed as follows. The signals appearing at 87.8 and 75.1 ppm were readily assigned to C-2 and C-4, respectively, on the basis of their appearance in the coupled spectrum. The signal at 72.8 ppm appeared as a doublet in the coupled spectrum and collapsed to a singlet upon irradiation at the high-field group of signals in the $^1$Hmr spectrum. The signal at 64.7 ppm also appeared as a doublet in the coupled spectrum but remained unchanged upon irradiation of the high-field group of signals in the $^1$Hmr spectrum. The signal at 64.7 ppm was assigned to C-5 while that at 72.8 ppm was assigned to C-6. The coupled spectrum of **10** exhibited three triplets at 58.3, 62.7, and 65.0 ppm. The signal at 62.7 ppm was readily assigned to C-6′ on the basis of its appearance in the coupled spectrum, as described for the case of **12**. The assignment of the remaining two signals to the carbons of the axial or equatorial acetoxymethyl groups was also made by analogy with the assignments in the spectrum of **12**. Thus, the upfield signal at 58.3 ppm exhibited the "deviant" $^{13}$C–[$^1$H] multiplets expected of a carbon that was directly bonded to two protons showing strong chemical-shift nonequivalence. This signal was, therefore, assigned to the carbon (C-4′) of the axial acetoxymethyl group at C-4 (see earlier discussion) and the signal appearing at 65.0 ppm was assigned to the carbon (C-4″) of the equatorial acetoxymethyl group. In contrast to the situation with **12**, the C-4′ and C-4″ signals in the spectrum of **10** showed a substantial chemical-shift difference between peaks. This is understandable since the effect of the acetoxy substituent at C-5 on C-4′ and C-4″ should be the shielding of both of these carbons to about the same extent by virtue of the γ-*gauche* effect. The observed chemical-shift difference between the C-4′ and C-4″ signals should then reflect the intrinsic shielding of axial substituents relative to their equatorial counterparts in 1,3-dioxane rings

[4]Since the γ-*anti* effect is transmitted through a quaternary centre, it is also conceivable that the effect of the 5-acetoxy group on C-4′ will be weakly deshielding (16).

[5]It is noteworthy that Angyal and James (10) have made similar assignments in the $^1$Hmr spectra of the L-isomer of **12** and of a closely related compound, namely, 2-*C*-hydroxymethyl-1,3,5-tri-*O*-acetyl-2,4-*O*-benzylidine-L-*threo*-pentitol.

Can. J. Chem. Downloaded from www.nrcresearchpress.com by 210.87.254.40 on 09/06/12
For personal use only.

(12). The $^{13}$Cmr spectral assignments for compounds **10** and **12** are summarized in Table 4.

Having unambiguously assigned the $^{13}$Cmr spectra of the nondeuterated derivatives of Isomer 1 and Isomer 2, it is now possible to settle the question of stereochemistry at the quaternary centre in these compounds by examination of the $^{13}$Cmr spectra of the corresponding deuterated derivatives. The $^{13}$C chemical-shift data for the deuterated derivative of Isomer 1, namely **11**, are presented in Table 4. The distinctive feature of the $^{13}$Cmr spectrum of **11** is the absence of the peak at 65.0 ppm attributed to C-4″, and the presence of a 1:1:1 triplet at 64.7 ppm ($J_{^{13}C-^{2}H}$ = 22.5 Hz), as indicated in Fig. 9. The latter resonance is assigned to the carbon of the equatorial acetoxymethyl group in **11**. Therefore, the product of the aldol-condensation reaction which served as an intermediate to **11** must have had the stereochemistry represented by **7** (see Scheme 2). Another noteworthy feature of the $^{13}$Cmr spectrum of **11** is the displacement of the C-4″ resonance by about 0.3 ppm to higher field and the displacement of the C-4 signal by 0.06 ppm to higher field relative to the corresponding signals in the spectrum of **10**. These shifts are attributed to α- and β-deuterium isotope shifts, respectively.

Examination of the $^{13}$Cmr spectrum of a mixture of the nondeuterated and deuterated derivatives of Isomer 2, namely **12** and **13**, indicated only a reduction in intensity of one of the carbon signals, namely the C-4″ signal (see Fig. 10); this is caused by the partial deuterium incorporation into the sample. Therefore, compound **13** is labelled with deuterium on the carbon of the equatorial acetoxymethyl group. The result suggests that the product of the aldol-condensation reaction which served as an intermediate to **13** must have the stereochemistry represented by **8** (see Scheme 2).

An alternative approach that was intended to provide complementary information about the stereochemistry at the quaternary centre of the aldol-condensation products is discussed below. Thus, D-mannose was converted into D-mannitol-1-*d* (**14**) by simple reduction with sodium borodeuteride and the latter compound was converted by means of the usual reaction sequence into 2,5-*O*-methylene-D-mannitol-1(or 6)-*d* (**9**). Periodate oxidation of **9** to the dialdehyde (**15**), followed by the aldol-condensation reaction and successive borohydride reduction and acetylation, afforded two separable isomers, as before. Owing to the symmetry of the starting material, one would expect that 50% of the molecules of each isomer would contain a deuterium label on C-6′ and that the other 50% of the molecules would be labelled on one of the acetoxymethyl groups attached to C-4 (see Scheme 4). Moreover, the deuterium label in the C-4′ or C-4″ acetoxymethyl group should reside on the opposite carbon to that observed in the previous deuterium-labelling study since the formyl group in the products of the aldol-condensation reaction was subjected to borohydride reduction in this study. One would predict, therefore, that 50% of the molecules should be labelled with deuterium on the *axial* acetoxy group at C-4 in the products of the above reaction sequence.

The $^{13}$Cmr spectral data for the derivatives obtained in this manner are presented in Table 4. The spectrum of Isomer 1 (lower melting point) shows the presence of two species **16** and **17**, as expected, one of which contains deuterium at C-6′ and the other of which contains deuterium at C-4′ (see Fig. 9c). Thus, as predicted, it is the axial acetoxymethyl group at C-4 which contains the deuterium label. Similarly, the spectrum of Isomer 2 shows the presence of two species, **18** and **19**, labelled at C-6′ or C-4′ with deuterium (see Fig. 10c). Once again it is the *axial* acetoxymethyl group at C-4 which bears the deuterium label. The results suggest that the formyl group in both products of the aldol-condensation reaction is equatorially oriented. Another noteworthy feature of the spectra of **16–19** is the manifestation of an α-deuterium isotope shift of about 0.25 ppm and a β-deuterium isotope shift of about 0.05 ppm. Interestingly, the α-deuterium isotope shift of the C-6′ signals in the spectra of **17** and **19** serves to verify the earlier assignments of the signals at 62.7 ppm and 62.6 ppm in the spectra of **10** and **12**, respectively, to the C-6′ carbons.

The remarkable stereoselectivity exhibited by the aldol-condensation reaction, in particular, the total inversion or total retention of configuration at the quaternary centre, strongly suggests the existence of some other controlling influence since a reaction proceeding through a carbanion with 100% inversion or 100% retention, in the absence of such an influence, seems unlikely. Indeed it seems more likely that an enolate anion is formed, and that the products resulting from the reaction are then directed by some other factor. Given that the aldol condensation is an equilibrium reaction, the preferential stabilization of one of the products could be an important factor in directing the equilibrium towards the formation of that product exclusively.

In 1973 Lloyd and Harrison (17) reported the conversion of 2,2′-*O*-methylene-bis-D-glycerose (**2**) into 5-hydroxy-4,4,6-tri(hydroxymethyl)-1,3-dioxane (**4**) by treatment with sodium borohydride.

Can. J. Chem. Downloaded from www.nrcresearchpress.com by 210.87.254.40 on 09/06/12
For personal use only.



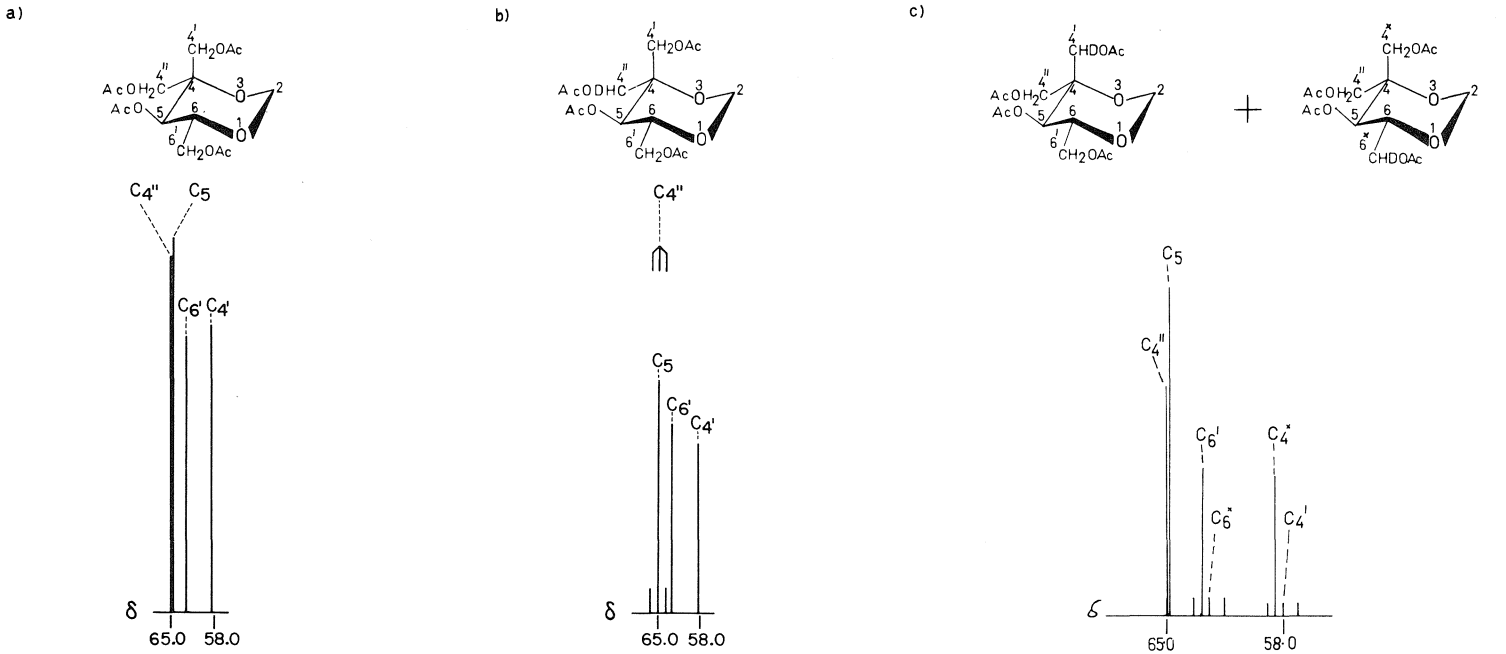


FIG. 9. (a) Partial $^{13}$Cmr spectrum ($^{1}$H-decoupled) of Isomer 1 derived from the products of the intramolecular aldol condensation of 2,2′-*O*-methylene-bis-D-glycerose; (b), (c) the effects of deuterium substitution on the chemical shifts and multiplicities of the signals.

Can. J. Chem. Downloaded from www.nrcresearchpress.com by 210.87.254.40 on 09/06/12
For personal use only.



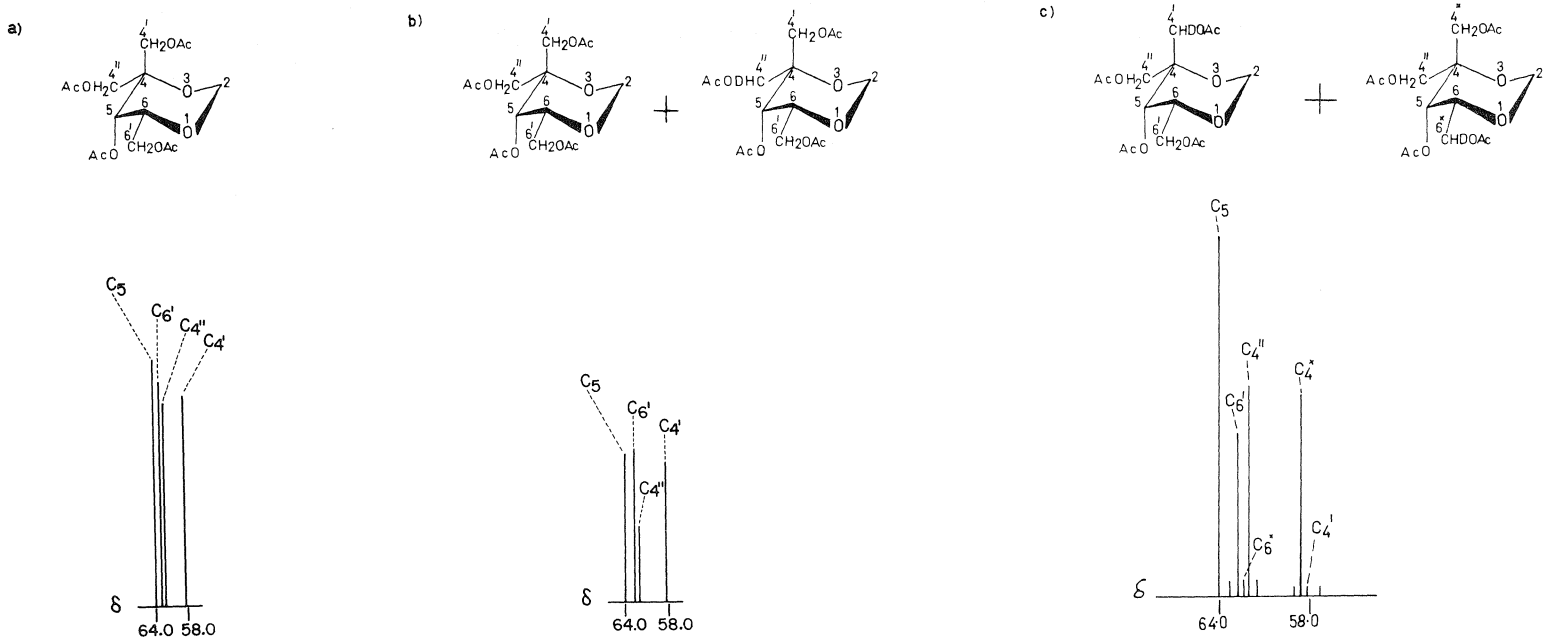


FIG. 10. (a) Partial $^{13}$Cmr spectrum ($^{1}$H-decoupled) of Isomer 2 derived from the products of the intramolecular aldol condensation of 2,2′-*O*-methylene-bis-D-glycerose; (b), (c) the effects of deuterium substitution on the chemical shifts, intensities, and multiplicities of the signals.

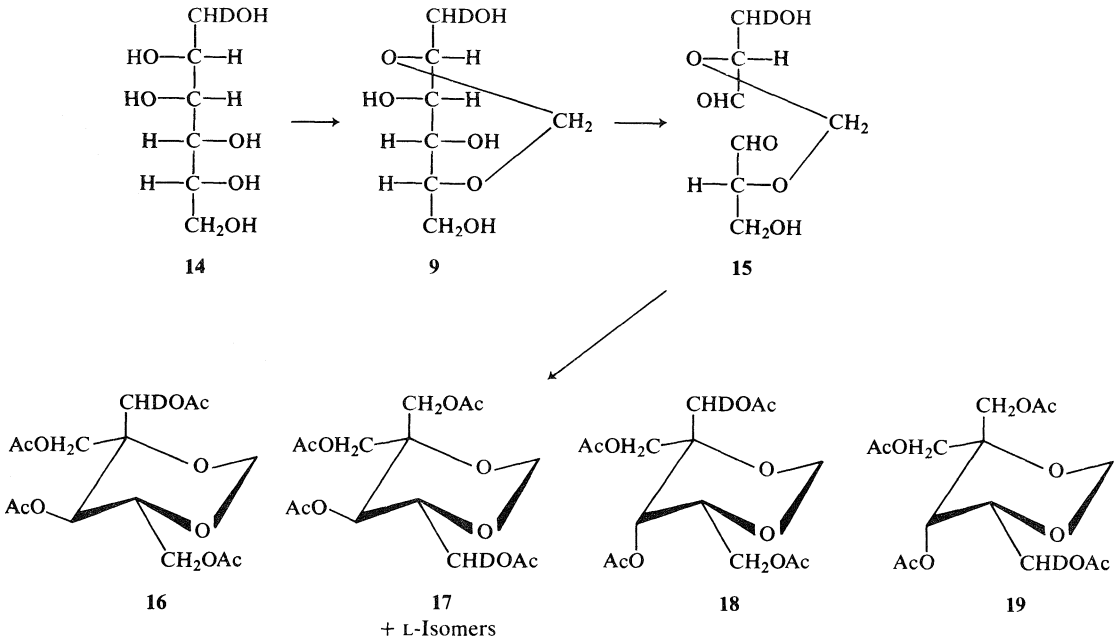


SCHEME 4

Apparently, the intramolecular aldol condensation of **2** proceeds under the conditions of the reaction. Since that time, Jordaan and co-workers (18) have also reported an aldol condensation taking place during sodium borohydride reduction of a furanosidulose. Lloyd and Harrison (17) also observed that sodium borohydride reduction of dialdehyde (**20**) afforded the expected product, namely 2,2′-*O*-methylene-bis(1-deoxy-1-fluoro-L-glycerol) (**21**), and not the reduced aldol product. In order to account for this difference in behaviour, these workers postulated (17) that the base-catalyzed cyclization of the dialdehyde **2** was more facile than that of the difluoride **20** because of greater product stabilization in the former case. Specifically, it was suggested that the product of the aldol condensation derived from **2** might be stabilized by the formation of a cyclic hemiacetal (**22**), provided that its formation was allowed by the relative configuration at C-4 and C-6. The product of the aldol condensation derived from **20** could not, of course, form a cyclic hemiacetal. Harrison also later suggested that the stereochemistry of the products of the aldol-condensation reaction of **2** might be directed by the possibility of later hemiacetal ring closure.[6] The exclusive formation of aldol-condensation products (**7** or **8**) in which the hydroxymethyl group at C-6 and the formyl group at C-4 are *syn* to one another, as demonstrated in the present work, is certainly in accord with Harrison's hypothesis since only these products can undergo internal hemiacetal formation.

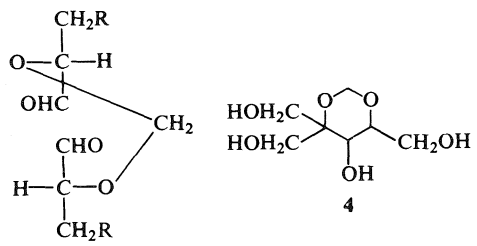


**2** R = OH
**20** R = F

**4**

The possible aldol-condensation products and the hypothetical reaction routes giving rise to these products are shown in Scheme 5. Thus, retention of configuration at the carbon centre bearing the formyl group that is attacked by the enolate ion can give rise to the species labelled as A and B, and inversion of configuration at this centre can give rise to the corresponding enantiomeric species labelled as A′ and B′, respectively. According to Harrison's hypothesis, only A and A′ will be stabilized by intramolecular hemiacetal formation, yielding C and C′, respectively (see Scheme 6); B and B′ should then re-enter the equilibrium to give either A or A′.

The data obtained in the present study suggest that both A and A′ are formed in the aldol-

[6]R. Harrison, private communication.

Can. J. Chem. Downloaded from www.nrcresearchpress.com by 210.87.254.40 on 09/06/12
For personal use only.

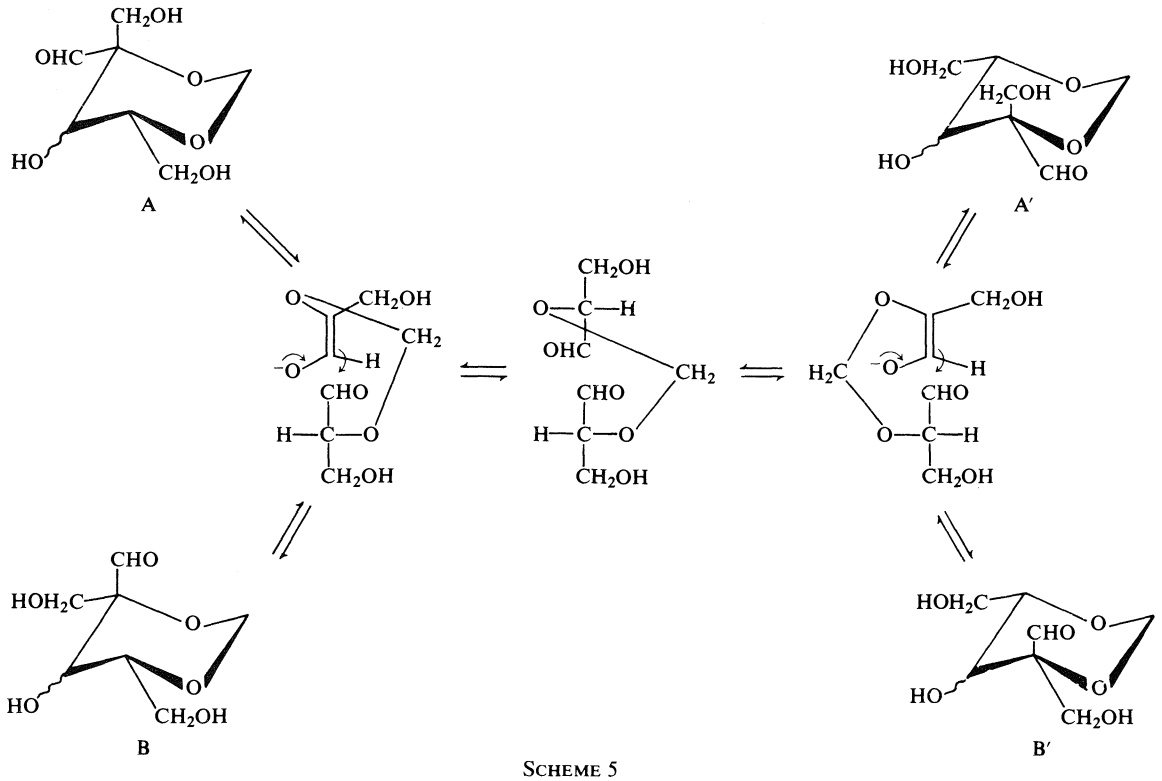


SCHEME 5

condensation reaction, but in a non-equimolar ratio. Thus, for example, variable optical rotations were obtained for the products derived from A or A′, depending on the conditions of the aldol-condensation reactions. Moreover, one of the products of the aldol condensation has been converted into a mixture of 2-*C*-hydroxymethyl-D- and L-ribose (19). Angyal and James (10) have reported an optical rotation of +1.6° for 2-*C*-acetoxymethyl-1,3,5-tri-*O*-acetyl-L-*threo*-pentitol (**23**). In one preparation, the enantiomer of this compound was presumably obtained ($[\alpha]_D = -1.8°$). However, under the particular conditions of the aldol condensation that preceded the formation of this compound, it is likely that this product arose by means

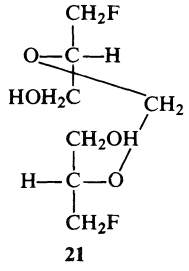


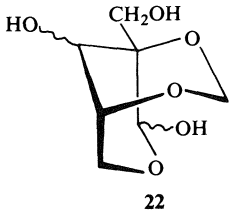


of a Cannizzaro reaction. Therefore, in this case, it would appear that one of the species represented by A in Scheme 5 was reduced before it could re-enter the equilibrium.

The possibility that internal hemiacetal formation provides the driving force for controlling the stereochemistry of the aldol-condensation products is further supported by the fact that the products of the aldol condensation exist to a great extent in aqueous solution as the bicyclic compounds. Thus, examination of the $^1$Hmr spectrum at 220 MHz in deuterium oxide of the aldol-condensation product, obtained under conditions that had previously been shown to yield only one isomer, namely **7**,

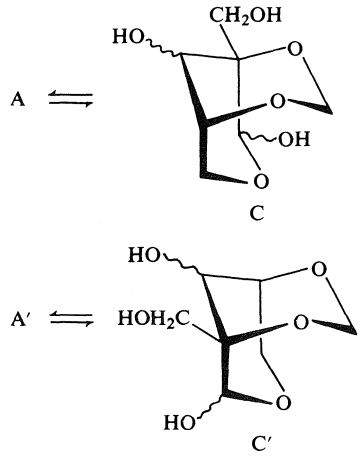


SCHEME 6

Can. J. Chem. Downloaded from www.nrcresearchpress.com by 210.87.254.40 on 09/06/12
For personal use only.

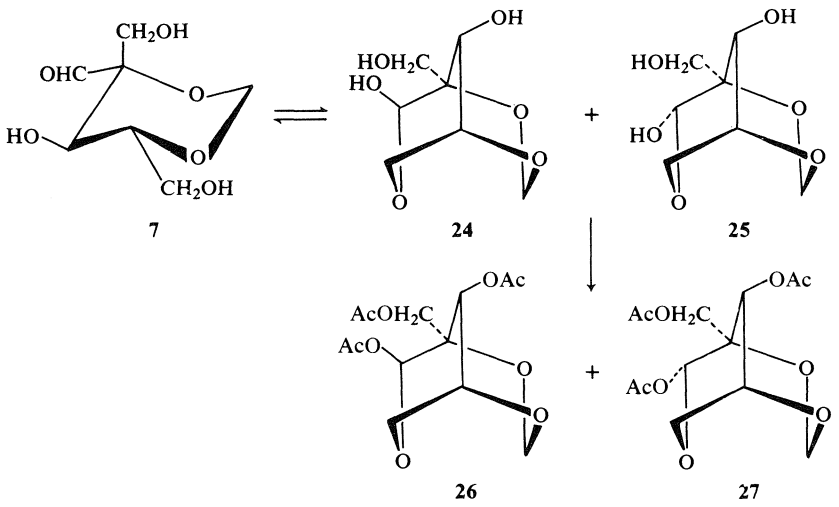

SCHEME 7

indicated the presence of mainly two compounds, one being present in greater proportion. A distinctive feature of the spectrum was the presence of

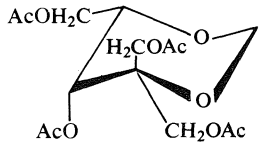

23

two singlets at δ 5.39 (major) and δ 5.19 (minor); these were assigned to the protons at the hemiacetal centres of the bicyclic compounds **24** and **25**, respectively (see Scheme 7), on the basis of the expected shielding of the quasi-axial H-6 proton relative to its quasi-equatorial counterpart. The preponderance of **24** is in agreement with expectations based on the anomeric effect. Interestingly, the signals for the geminal acetal protons displayed substantial chemical-shift nonequivalence. Hence, these signals appeared as AX doublets at δ 5.77 and δ 5.07 ($J$ = 5.2 Hz) for the major isomer and at δ 5.80 and δ 5.01 ($J$ = 5.2 Hz) for the minor isomer. The significance of this result will be discussed later. The H-8 and H-8′ signals for the major isomer appeared as AB doublets at δ 3.84 and 3.71 ($J$ = 12 Hz) and the rest of the $^1$H resonances appeared as complex multiplets at δ 4.33–3.52 and at δ 4.88–5.15. The presence of the bicyclic compounds was corroborated by the appearance of a signal at 96.3 ppm in the $^{13}$Cmr spectrum in deuterium oxide which was assigned to the hemiacetal carbon, C-6. Only the peaks attributable to the major isomer could be assigned unambiguously (see Experimental).

Acetylation of the mixture obtained from the aldol condensation, as described above, afforded, after chromatography, five components. The least polar of these components was identified as being a mixture of the two isomeric bicyclo[3.3.1]nonanes, **26** and **27** derived from **24** and **25** (see Scheme 7). The $^1$Hmr spectrum at 220 MHz of the mixture of **26** and **27** in toluene-$d_8$ is shown in Fig. 11. The distinctive feature of this spectrum is the appearance of the H-6 signals of the major and minor isomers as singlets at δ 6.52 and 6.03, respectively. As before, the major isomer is assigned the structure in which the acetoxy group at C-6 is quasi-axial. The signals for H-3 and H-3′ appear once again as AX doublets for both isomers. The $^{13}$Cmr spectral data for **26** and **27** (see Experimental) are also in accord with the assignment of the stereochemistry at C-6 in the major and minor isomers. Thus, the C-6 signals for both the major and minor isomers appear at 92.94 ppm. However, in the gated-decoupled spectrum, the signal for the major isomer shows a one-bond coupling constant of 177 Hz while that for the minor isomer shows a one-bond coupling constant of about 166 Hz. It is well known that $^1J_{^{13}C_2-H}$ for equatorially oriented protons in 2-substituted tetrahydropyrans is about 10 Hz greater than $^1J_{^{13}C_2-H}$ for axially oriented protons in the analogously substituted isomeric compound (20). Thus, the major isomer **26** is assigned a configuration at C-6 in which the acetoxy group is quasi-axial.

The strong chemical-shift nonequivalence displayed by the geminal methylene protons, H-3 and H-3′, in compounds **24–27** (Δν 0.71–0.97 ppm) may be interpreted in terms of the deshielding of one of the set of protons as a result of the repulsion of electrons in the vicinity of this proton by a proximal

Can. J. Chem. Downloaded from www.nrcresearchpress.com by 210.87.254.40 on 09/06/12
For personal use only.

Can. J. Chem. Downloaded from www.nrcresearchpress.com by 210.87.254.40 on 09/06/12
For personal use only.

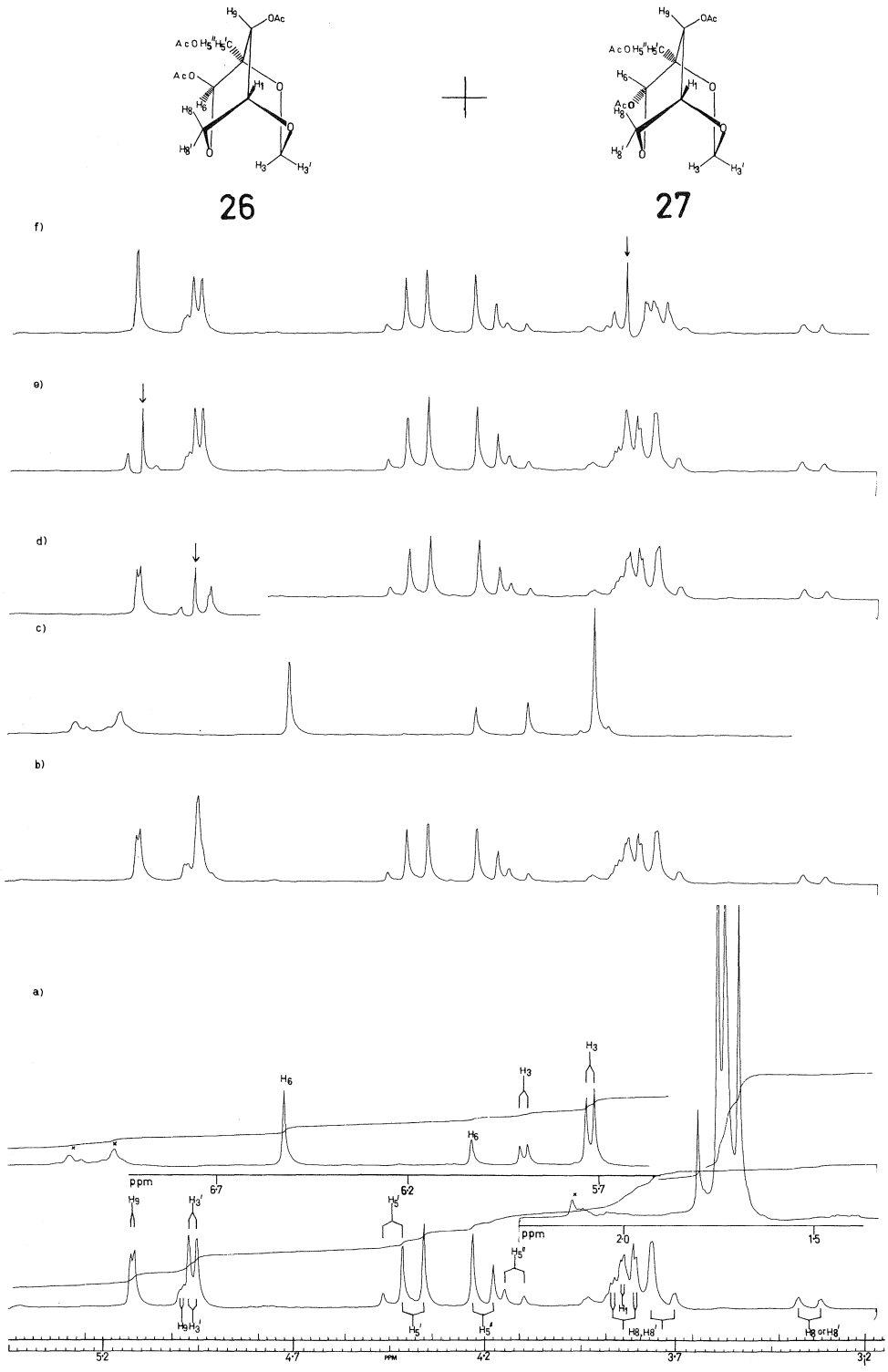


FIG. 11. (a) $^1$Hmr spectrum at 220 MHz of (5*R*, 6*S*, 9*R*)-6,9-diacetoxy-5-acetoxymethyl-2,4,7-trioxabicyclo[3.3.1]nonane (**26**) and (5*R*, 6*R*, 9*R*)-6,9-diacetoxy-5-acetoxymethyl-2,4,7-trioxabicyclo[3.3.1]nonane (**27**); (b) δ 3.2–5.2 with irradiation at $\nu_{H\text{-}3'\ maj.}$; (c) δ 5.2–7.3 with irradiation at $\nu_{H\text{-}3\ maj}$, $\nu_{H\text{-}3\ min}$, and $\nu_{H\text{-}9\ min}$; (d) δ 3.2–5.2 with irradiation at $\nu_{H\text{-}3\ maj}$, $\nu_{H\text{-}3\ min}$, and $\nu_{H\text{-}9\ min}$; (e) δ 3.2–5.2 with irradiation at $\nu_{H\text{-}9\ maj}$; (f) δ 3.2–5.2 with irradiation at $\nu_{H\text{-}1}$.

Can. J. Chem. Downloaded from www.nrcresearchpress.com by 210.87.254.40 on 09/06/12
For personal use only.

substituent atom (21). If it is assumed that these derivatives exist preponderantly in the chair,chair conformation, as shown, then the substituent atom in question may be assigned as O-7. However, if the boat,chair conformation **28** is preferred, then the substituent atom in question is O-9. It is noteworthy that 2,4-dioxabicyclo[3.3.1]nonane has been assigned the boat,chair conformation on the basis of coupling-constant data, nuclear Overhauser effects, and the $T_1$-relaxation times (22). However, it is difficult to rationalize the observed differences in $\Delta\nu_{AX}$ for the major and minor isomers (which differ in configuration only at C-6) if **28** is indeed

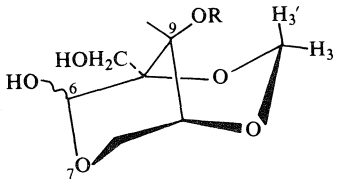


**28** R = H or Ac

the predominant conformation. In particular, $\Delta\nu_{AX}$ in the minor acetylated derivative **27** is 0.2 ppm greater than that in the corresponding major isomer **26**. If the chair,chair conformation is favoured, then this difference might reflect the effect of the anisotropy of the carbonyl group of the equatorially oriented acetoxy group at C-6 in **27** on the chemical shift of H-3. It must be noted that $\Delta\nu_{AX}$ in the minor isomer of the non-acetylated derivative **25** is slightly greater (0.08 ppm) than that in the corresponding major isomer **24**. The choice of the chair conformation for the derivatives obtained in the present work also seems reasonable in view of the fact that the internuclear distance between O-7 and H-3 in the chair,chair conformation is considerably less than the internuclear distance between O-9 and H-3′ in the boat,chair conformation, and should, therefore, result in greater van der Waals shielding in the former case. The magnitude of this effect decreases very rapidly with increasing internuclear distance (21). More definitive conclusions regarding the preponderant conformation of these derivatives must, however, await further studies.

The second component isolated from the acetylation reaction was present in small quantity; it was identified as being 2-*C*-acetoxymethyl-1,3,5-tri-*O*-acetyl-2,4-*O*-methylene-D,L-*threo*-pentitol (**12**), the product of a Cannizzaro reaction. The other three components isolated from this reaction mixture were much more polar in nature and were identified as being the acetylated dimers **29–31** derived from the self-condensation of **7** (see Scheme 8). The condensation of β-hydroxy aldehydes with

Possible structures for **29**, **30**, and **31**.

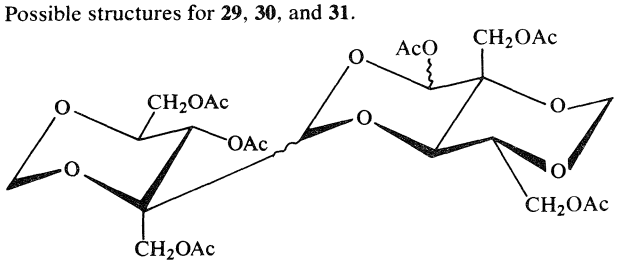


SCHEME 8

themselves and with other aldehydes is well documented (10, 23, 24). Of particular relevance are the dimers derived from 2,4-*O*-ethylidene-D-erythrose (23) and the 2,4-acetals of L-xylose (10) which have analogous structures to those of **29–31**. The proposed structures for **29–31** were supported by the mass-spectral data.

Under the conditions of the aldol-condensation reaction employed in the present work, it is almost certain that the products obtained are under thermodynamic control. Hence, the thermodynamically most stable isomer of the four possible 1,3-dioxanes is that in which the formyl group at C-4, the hydroxymethyl group at C-6, and the hydroxyl group at C-5 are equatorial, as represented by **7** in Scheme 2. It is noteworthy that consideration of the favoured transition state **32** for the aldol-condensation reaction according to Felkin's model (25) or the model proposed by Anh and Eisenstein (26) for 1,2-asymmetric induction on the basis of *ab initio* calculations suggests that the kinetically controlled product should be that in which the hydroxyl group at C-5 adopts the axial orientation (see **8** in Scheme 9). The formation of a substantial

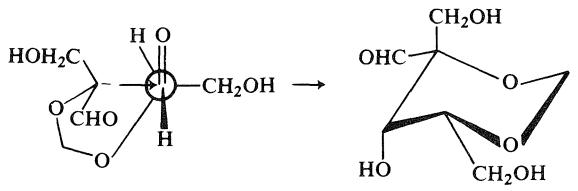


**32** **8**

SCHEME 9

amount of the reduced product derived from **8** (in which the 5-hydroxyl group is axial) at higher base concentration is likely to result from the distortion of the true equilibrium of the aldol condensation by the Cannizzaro reaction of **8**.

## Experimental

Melting points were determined with a Fisher–Johns melting-point apparatus and are uncorrected. Mass spectra were recorded on a CEC21-104 mass spectrometer under electron-impact conditions at 70 eV ionizing voltage. Proton magnetic resonance

Can. J. Chem. Downloaded from www.nrcresearchpress.com by 210.87.254.40 on 09/06/12
For personal use only.

($^1$Hmr) spectra were recorded on a Bruker HX-60, Varian CFT-20, or Varian HR-220 spectrometer. Carbon-13 magnetic resonance ($^{13}$Cmr) spectra were recorded on a Bruker HX-60 spectrometer equipped with a FT60M Fourier transform accessory at 15.09 MHz, a Varian CFT-20 spectrometer at 20.0 MHz, or a JEOL FX-100 spectrometer at 25.05 MHz. Spectra were measured in chloroform-*d* with tetramethylsilane (TMS) as internal standard, unless otherwise stated. Chemical shifts are given in ppm downfield from TMS. Spectra recorded in deuterium oxide solution were measured with respect to internal acetone whose chemical shift was taken as being 2.225 ppm relative to TMS for the $^1$Hmr spectra and 32.78 ppm relative to TMS for the $^{13}$Cmr spectra. Chemical shifts and coupling constants were obtained from first-order analyses of the nmr spectra. Optical rotations were determined on a Perkin–Elmer 141 polarimeter.

Analytical thin-layer chromatography (tlc) was performed on precoated glass plates with Merck silica gel 60F-254 as the adsorbent (layer thickness 0.25 mm). The developed plates were air-dried and exposed to uv light and/or sprayed with a solution of cerium sulfate (1%) and molybdic acid (1.5%) in 10% aqueous sulfuric acid, and heated at 150°C. Column chromatography was performed on Brinkman silica gel (70–325 mesh, E. Merck). The chromatographic solvent systems (v/v) employed in this work are as follows: (A) benzene – ethyl acetate, 1:1; (B) 4:1; (C) toluene – ethyl acetate, 4:1; (D) 1:4; (E) ethyl acetate.

Solvents were evaporated under reduced pressure and below 40°C.

For convenience, the numbering of compounds according to the convention for heterocyclic derivatives has been employed for the presentation of nmr data. However, in order to identify the compounds unequivocally, the names of the compounds are based on accepted carbohydrate nomenclature.

*2,2′-O-Methylene-bis-D-glycerose (**2**)*

To a solution of 2,5-*O*-methylene-D-mannitol (**1**) (10 g), prepared in three steps from D-mannitol by the method of Ness *et al.* (1), in water (50 mL), was added a solution of sodium metaperiodate (12 g) in water (100 mL). After 5 h the solution was carefully neutralized with 0.1 *N* sodium hydroxide, and a solution of barium chloride dihydrate (6.5 g) in water (70 mL) was added. The mixture was refrigerated for 3 h and then filtered to remove the precipitated salts. The filtrate was concentrated to afford a syrup (**2**) (8.6 g), $[\alpha]_D^{24}$ +11.4° (*c* 1.1, water), lit. (1) $[\alpha]_D$ + 10.5°.

In subsequent experiments the filtrate was directly subjected to the conditions of the aldol-condensation reaction, reduction, and acetylation, as follows. The filtrate was diluted with water and the solution was adjusted to the desired pH by dropwise addition of 1 *N* sodium hydroxide. The mixture was let stand at room temperature for the alloted time and was then treated with Amberlite IR-120 (H), followed by Amberlite IR-45 (OH). The neutral solution was treated directly with either sodium borohydride or sodium borodeuteride as required. After 12 h at room temperature the mixture was acidified by addition of Amberlite IR-120 (H) and was subsequently neutralized with Amberlite IR-45 (OH). The solution was concentrated and the residue was acetylated in the usual manner.

A typical procedure is outlined below.

*2-C-Acetoxymethyl-1,3,5-tri-O-acetyl-1-(R,S)-deuterio-2,4-O-methylene-D,L-ribitol (**11**), 2-C-acetoxymethyl-1,3,5-tri-O-acetyl-2,4-O-methylene-D,L-threo-pentitol (**12**), and 2-C-acetoxymethyl-1,3,5-tri-O-acetyl-1-(R,S)-deuterio-2,4-O-methylene-D,L-xylitol (**13**)*

To a solution of 2,5-*O*-methylene-D-mannitol (**1**) (0.5 g) in water (2.5 mL) was added a solution of sodium metaperiodate (0.6 g) in water (5 mL). After 5 h the solution was carefully neutralized with 0.1 *N* sodium hydroxide and a solution of barium chloride dihydrate (0.34 g) in water (3.5 mL) was added. The mixture was refrigerated for 2.5 h and then filtered to remove the precipitated salts. The filtrate was diluted to 40 mL and 1 *N* sodium hydroxide (3.3 mL) was added. The mixture was let stand at room temperature for 3.25 h and was then acidified (pH 4) with Amberlite IR-120 (H), and finally neutralized with Amberlite IR-45 (OH). The resulting solution was made up to a volume of 125 mL, and sodium borodeuteride (0.11 g) was added in small portions. After 12 h at room temperature the mixture was acidified (pH 2) with Amberlite IR-120 (H) and was subsequently neutralized with Amberlite IR-45 (OH). The solution was concentrated to afford a syrup which was repeatedly reconcentrated from methanol to remove boric acid. The resulting syrup was treated with pyridine (10 mL) and acetic anhydride (7.5 mL) and the mixture was shaken to effect complete dissolution. After 12 h the mixture was poured into cold saturated sodium hydrogen carbonate solution (200 mL) and was shaken for 2 h. The mixture was extracted with methylene chloride (4 × 50 mL). The extracts were washed with water (2 × 50 mL) and dried over magnesium sulfate. Evaporation of the solvent afforded a syrup (0.561 g). Thin-layer chromatography (Solvent B) indicated the presence of one component having an $R_f$ value of 0.24. The syrup was dissolved in ethanol and the solution was allowed to stand at room temperature for 12 h. The white needles that deposited were collected and were identified as being a mixture of 2-*C*-acetoxymethyl-1,3,5-tri-*O*-acetyl-2,4-*O*-methylene-D,L-*threo*-pentitol (**12**) and 2-*C*-acetoxymethyl-1,3,5-tri-*O*-acetyl-1-(*R*,*S*)-deuterio-2,4-*O*-methylene-D,L-xylitol (**13**) (0.04 g, 4.3%), mp 145.5–146.5°C, $[\alpha]_D^{33}$ −2.4° (*c* 1.2, $CHCl_3$); $^1$Hmr (220 MHz, $CDCl_3$) δ: 2.04, 2.09, 2.14, 2.16 (12 H, s's, 4 OAc), 3.99 (1H, *J* = 11.2 Hz, H-4‴), 4.01 (1H, d of d, *J* = 11.8, 7.2 Hz, H-6″), 4.13, 4.14 (1H, s's, H-4*'s), 4.16 (1H, d, *J* = 12.2 Hz, H-4″), 4.16 (1H, d of d, *J* = 11.5, 5.1 Hz, H-6′), 4.25 (1H, d of d, *J* = 7.2, 5.2 Hz, H-6), 4.28 (1H, d, *J* = 11.2 Hz, H-4‴), 4.87 (1H, d, *J* = 12.2 Hz, H-4′), 4.98 (1H, br s, H-5), 4.99, 5.12 (two 1H d's, *J* = 6.9 Hz, H-2, H-2′); (220 MHz, $C_6D_6$) δ: 3.85 (1H, d, *J* = 12.6 Hz, H-4″), 3.88 (1H, d of d, *J* = 6.6, 6.0 Hz, H-6), 4.09, 4.10 (1H, s's, H-4*'s), 4.07 (1H, d of d, *J* = 11.0, 6.6 Hz, H-6″), 4.13 (1H, d, *J* = 10.5 Hz, H-4‴), 4.25 (1H, d of d, *J* = 11.0, 6.0 Hz, H-6′), 4.59 (1H, d, *J* = 10.5 Hz, H-4‴), 4.70 (1H, d, *J* = 12.6 Hz, H-4′), 4.74, 4.83 (two 1H d's, *J* = 6.4 Hz, H-2, H-2′), 4.94 (1H, br s, H-5). The filtrate was refrigerated for 12 h upon which orthorhombic crystals deposited. These were collected and were identified as being 2-*C*-acetoxymethyl-1,3,5-tri-*O*-acetyl-1-(*R*,*S*)-deuterio-2,4-*O*-methylene-D,L-ribitol (**11**) (0.164 g, 18%), mp 88–89°C, $[\alpha]_D^{33}$ + 12.2° (*c* 1.4, $CHCl_3$); $^1$Hmr (220 MHz, $CDCl_3$) δ: 2.08 (3H, s, OAc), 2.11 (9H, br s, 3 OAc), 3.96 (1H, d of q, *J* = 2.6, 5.3, 10.4 Hz, H-6), 4.10 (1H, d, *J* = 13.2 Hz, H-4″), 4.10 (1H, d of d, *J* = 12.0, 2.6 Hz, H-6″), 4.13, 4.14 (1H, s's, H-4‴'s), 4.20 (1H, d of d, *J* = 12.0, 5.3 Hz, H-6′), 5.00 (1H, d, *J* = 13.4 Hz, H-4′), 4.91, 5.05 (two 1H d's, *J* = 7.0 Hz, H-2, H-2′), 5.27 (1H, d, *J* = 10.3 Hz, H-5); (220 MHz, $C_6D_6$) δ: 1.64, 1.71, 1.76, 1.79 (12 H, s's, 4 OAc), 3.63 (1H, d of q, *J* = 2.1, 5.0, 10.8 Hz, H-6), 4.01 (1H, d, *J* = 12.5 Hz, H-4″), 4.07 (1H, d of d, *J* = 2.1, 12.7 Hz, H-6″), 4.25 (1H, d of d, *J* = 5.0, 12.7 Hz, H-6′), 4.24, 4.29 (1H, s's, H-4‴'s), 4.75, 4.84 (two 1H d's, *J* = 6.4 Hz, H-2, H-2′), 4.93 (1H, d, *J* = 12.5 Hz, H-4′), 5.47 (1H, d, *J* = 10.8 Hz, H-5). The mother liquor was concentrated to afford a partially crystalline syrup (0.34 g, 36%) which was shown to consist of only compound **11** by $^1$Hmr and $^{13}$Cmr spectroscopy.

*2-C-Acetoxymethyl-1,3,5-tri-O-acetyl-2,4-O-methylene-D,L-erythro-pentitol (**10**) and 2-C-acetoxymethyl-1,3,5-tri-O-acetyl-2,4-O-methylene-D,L-threo-pentitol (**12**)*

When 2,2′-*O*-methylene-bis-D-glycerose (**2**) was subjected to

Can. J. Chem. Downloaded from www.nrcresearchpress.com by 210.87.254.40 on 09/06/12
For personal use only.

the conditions of the aldol condensation, followed by sodium borohydride reduction and then acetylation, as described for the synthesis of compounds **11**, **12**, and **13**, two isomers were obtained by fractional crystallization. Compound **12** was obtained as white needles, mp 147–148°C, lit. (10) mp 147–148°C, $[\alpha]_D^{33}$ −1.8° (*c* 0.8, $CHCl_3$), lit. (10) $[\alpha]_D$ +1.6° (*c* 1, $CHCl_3$) for the L-isomer; $^1$Hmr (220 MHz, $CDCl_3$) δ: 2.04, 2.09, 2.14, 2.16 (12H, s's, 4 OAc), 3.99 (1H, d, *J* = 11.2 Hz, H-4‴), 4.01 (1H, d of d, *J* = 11.5, 7.0 Hz, H-6″), 4.16 (1H, d of d, *J* = 11.5, 4.2 Hz, H-6′), 4.17 (1H, d, *J* = 12.0 Hz, H-4″), 4.26 (1H, d of d, *J* = 7.0, 4.2 Hz, H-6), 4.28 (1H, d, *J* = 11.2 Hz, H-4‴), 4.88 (1H, d, *J* = 12.0 Hz, H-4′), 4.98 (1H, br s, H-5), 4.99, 5.13 (two 1H d's, *J* = 7.0 Hz, H-2, H-2′); (220 MHz, $C_6D_6$) δ: 3.87 (1H, d, *J* = 12.5 Hz, H-4″), 3.90 (1H, d of d, *J* = 6.6, 5.8 Hz, H-6), 4.09 (1H, d of d, *J* = 11.1, 6.6 Hz, H-6″), 4.15 (1H, d, *J* = 11.0 Hz, H-4‴), 4.27 (1H, d of d, *J* = 11.1, 5.8 Hz, H-6′), 4.61 (1H, d, *J* = 11.0 Hz, H-4‴), 4.72 (1H, d, *J* = 12.5 Hz, H-4′), 4.76, 4.84 (two 1H d's, *J* = 6.8 Hz, H-2, H-2′), 4.96 (1H, br s, H-5). *Anal.* calcd. for $C_{15}H_{22}O_{10}$: C 49.72, H 6.12; found: C 49.82, H 6.12.

Compound **10** was obtained as white crystals, mp 91–93°C, lit. (1) mp 93–94°C, $[\alpha]_D^{33}$ +13.9° (*c* 0.44, $CHCl_3$), lit. (1) $[\alpha]_D^{20}$ +12.4° (*c* 1.0, $CHCl_3$); $^1$Hmr (220 MHz, $CDCl_3$) δ: 2.09 (3H, s, OAc), 2.11 (9H, br s, 3 OAc), 3.96 (1H, d of q, *J* = 3.0, 5.4, 10.3 Hz, H-6), 4.10 (1H, d, *J* = 13.5 Hz, H-4″), 4.10 (1H, d of d, *J* = 12.2, 3.0 Hz, H-6″), 4.11 (1H, d, *J* = 12.2 Hz, H-4‴), 4.17 (1H, d, *J* = 12.2 Hz, H-4‴), 4.20 (1H, d of d, *J* = 12.2, 5.4 Hz, H-6′), 5.01 (1H, d, *J* = 13.5 Hz, H-4′), 4.92, 5.05 (two 1H d's, *J* = 7.0 Hz, H-2, H-2′), 5.27 (1H, d, *J* = 10.2 Hz, H-5); (220 MHz, $C_6D_6$) δ: 1.60, 1.69, 1.74, 1.78 (12H, s's, 4 OAc), 3.58 (1H, d of q, *J* = 2.3, 5.0, 10.4 Hz, H-6), 3.98 (1H, d, *J* = 13.0, H-4″), 4.05 (1H, d of d, *J* = 12.3, 2.3 Hz, H-6″), 4.23 (1H, d of d, *J* = 12.3, 5.0 Hz, H-6′), 4.24, 4.31 (two 1H d's, *J* = 11.4 Hz, H-4‴, H-4‴), 4.71, 4.81 (two 1H d's, *J* = 7.2 Hz, H-2, H-2′), 4.91 (1H, d, *J* = 13.0 Hz, H-4′), 5.47 (1H, d, *J* = 10.4 Hz, H-5).

*D-Mannitol-1-*d *(14)*

To a solution of D-mannose (10 g) in water (30 mL) was added dropwise, with stirring, a solution of sodium borodeuteride (1 g) in water (25 mL) over a period of 0.5 h. After 48 h at room temperature, an acidic ion-exchange resin (30 mL of Amberlite IR-120 (H)) was added, and the solution was stirred for 0.5 h, after which the solution had pH 3. The resin was removed by filtration and the filtrate was evaporated to give a residue that was repeatedly reconcentrated from methanol (5 × 30 mL) to remove boric acid as methyl borate. The residue was dissolved in water (15 mL) and to the warmed solution was added methanol (50 mL). A seed crystal of D-mannitol was added and the solution was stored at room temperature. Collection of the crystalline material afforded D-mannitol-1-*d* (**14**) (7.52 g, 74%), mp 166–168°C. This material was, presumably, a mixture of the two diastereomers resulting from the two possible configurations at C-1.

*l-*(R,S)*-Deuterio-2,2′-O-methylene-bis-D-glycerose (15)*

2,5-*O*-Methylene-D-mannitol-1-*d* (**9**), prepared in three steps from D-mannitol-1-*d* (**14**) by the method of Ness *et al.* (1), was treated with sodium metaperiodate, as described for the synthesis of the unlabelled compound **2**, to yield the title compound.

*2-C-Acetoxymethyl-1,3,5-tri-*O*-acetyl-1-*(R,S)*-deuterio-2,4-O-methylene-D,L-arabinitol (16), 2-C-acetoxymethyl-1,3,5-tri-*O*-acetyl-5-*(R,S)*-deuterio-2,4-O-methylene-D,L-*erythro*-pentitol (17), 2-C-acetoxymethyl-1,3,5-tri-O-acetyl-1-*(R,S)*-deuterio-2,4-O-methylene-D,L-lyxitol (18), and 2-C-acetoxymethyl-1,3,5-tri-O-acetyl-5-*(R,S)*-deuterio-2,4-O-methylene-D,L-*threo*-pentitol (19)*

When 1-(*R,S*)-deuterio-2,2′-*O*-methylene-bis-D-glycerose (**15**) was subjected to the conditions of the aldol condensation, followed by sodium borohydride reduction and then acetylation, as described for the synthesis of compounds **11**, **12**, and **13**, two fractions were obtained. The first fraction was shown by $^{13}$Cmr spectroscopy at 25.05 MHz to consist of a mixture of compounds **18** and **19**, mp 144–146°C. Similarly, the second fraction was shown to consist of a mixture of compounds **16** and **17**, mp 90–93°C.

*2-C-Hydroxymethyl-2,4-*O*-methylene-D,L-ribose (7)*

2,2′-*O*-Methylene-bis-D-glycerose (**2**) (12 g) was subjected to the conditions of the aldol condensation that were previously shown to yield compound **7** and at most a trace of compound **8**, namely a 0.05 *N* sodium hydroxide solution for 3.5 h. The mixture was acidified (pH 3) by addition of Amberlite IR-120 (H) and was subsequently neutralized by addition of Amberlite IR-45 (OH). Filtration of the resin and concentration of the solution afforded a hygroscopic foam (12 g). The $^1$Hmr and $^{13}$Cmr spectra of the product in $D_2O$ solution indicated that the major species present were those resulting from intramolecular hemiacetal formation in compound **7**, namely, 6(*S*),9(*R*)-dihydroxy-5(*R*)-hydroxymethyl-2,4,7-trioxabicyclo[3.3.1]nonane (**24**) and 6(*R*),9(*R*)-dihydroxy-5(*R*)-hydroxymethyl-2,4,7-trioxabicyclo[3.3.1]nonane (**25**); the latter compound was present as the minor component. $^1$Hmr (220 MHz, $D_2O$) δ: 3.71, 3.84 (two 1H d's, *J* = 12 Hz, H-5′, H-5″ for **24**), 3.52–4.33 (m's), 4.88–5.15 (m's), 5.01 (1H, d, *J* = 5.2 Hz, H-3 for **25**); 5.07 (1H, d, *J* = 5.2 Hz, H-3 for **24**), 5.19 (1H, s, H-6 for **25**), 5.39 (1H, s, H-6 for **24**), 5.77 (1H, d, *J* = 5.2 Hz, H-3′ for **24**), 5.80 (1H, d, *J* = 5.2 Hz, H-3′ for **25**); $^{13}$Cmr (for **24**, $D_2O$) δ: 64.7 (C-9), 65.4 (C-5′), 67.1 (C-8), 73.5 (C-1), 77.7 (C-5), 90.7 (C-3), 96.3 (C-6).

*5(R)-Acetoxymethyl-6(S),9(R)-diacetoxy-2,4,7-trioxabicyclo-[3.3.1]nonane (26) and 5(R)-acetoxymethyl-6(R),9(R)-diacetoxy-2,4,7-trioxabicyclo[3.3.1]nonane (27)*

A portion of the foam that was obtained in the preceding experiment (0.38 g) was treated with pyridine (20 mL) and acetic anhydride (2.5 mL) for 72 h. The mixture was processed in the usual manner to yield a syrup; tlc (Solvent B) indicated the presence of two components having $R_f$ values of 0.32 and 0.18 as well as a component at the origin. The sample was chromatographed on silica gel using Solvent C as eluant initially and then Solvent E as eluant. The component having an $R_f$ value of 0.32 was obtained as a partially crystalline syrup which was identified as being a mixture of compounds **26** and **27**, present in a ratio of 2.6:1 (0.15 g). $^1$Hmr (220 MHz, toluene-$d_8$) for compound **26**, δ: 1.70, 1.74, 1.75 (three 3H s's, 3 OAc), 3.71 (1H, br d, *J* = 13.2 Hz, H-8), 3.82 (1H, d of d, $J_{8,8'}$ = 13.2 Hz, $J_{1,8'}$ = 2 Hz, H-8′), 3.82 (1H, br d, $J_{1,9}$ = 2 Hz, H-1), 4.18 (1H, d, *J* = 11.8 Hz, H-5″), 4.36 (1H, d, *J* = 11.8 Hz, H-5′), 4.94 (1H, d, *J* = 4.3 Hz, H-3′), 5.10 (1H, d, $J_{9,1}$ = 2 Hz, H-9), 5.72 (1H, d, *J* = 4.3 Hz, H-3), 6.52 (1H, s, H-6); $^1$Hmr (220 MHz, toluene-$d_8$) for compound **27**, δ: 1.74, 1.75, 1.76 (three 3H s's, 3 OAc), 3.33 (1H, d, *J* = 12.5 Hz, H-8), 3.64–3.94 (m's including H-8′ and H-1 signals), 4.10 (1H, d, *J* = 11.2 Hz, H-5″), 4.42 (1H, d, *J* = 11.2 Hz, H-5′), 4.93 (1H, d, *J* = 4.3 Hz, H-3′), 4.96 (1H, d, *J* = 2 Hz, H-9), 5.90 (1H, d, *J* = 4.3 Hz, H-3), 6.03 (1H, s, H-6); $^{13}$Cmr data (toluene-$d_8$) for **26**, δ: 20.24 (Me), 64.35 (C-5′), 65.71 (C-1), 66.81 (C-8), 68.42 (C-9), 72.76 (C-5), 88.86 (C-3), 92.94 ($^1J_{C-H}$ = 177 Hz, C-6), 167.8, 169.6, 169.9 (CO); $^{13}$Cmr (toluene-$d_8$) for **27**, δ: 20.24 (Me), 59.82 (C-5′), 66.29, 67.52, 68.10 (C-5, C-8, C-9), 88.86 (C-3), 92.94 ($^1J_{C-H}$ = 165 Hz, C-6), 168.4, 169.6, 169.9 (CO); mass spectral data: M calcd. for $C_{13}H_{18}O_9$: 318; found: *m/e* 259 ($M^+$ − OAc). *Anal.* calcd. for $C_{13}H_{18}O_9$: C 49.06, H 5.70; found: C 48.97, H 6.18.

The compound having an $R_f$ value of 0.18 was obtained as a solid and was identified as being one of the products derived from the Cannizzaro reaction of compound **8**, namely, 2-*C*-acetoxymethyl-1,3,5-tri-*O*-acetyl-2,4-*O*-methylene-D,L-

*threo*-pentitol (**12**) (0.016 g). The component migrating at the origin in Solvent B was eluted with Solvent E and was shown to consist of three components having $R_f$ values of 0.56, 0.50, and 0.44. The mixture was rechromatographed using Solvent D as eluant to yield each component as a white foam. All three compounds were identified as being the acetylated dimers **29**, **30**, and **31** derived from the self-condensation of **7**; mass spectral data: M calcd. for $C_{26}H_{36}O_{18}$: 636.5; found for **29** ($R_f$ = 0.56, 0.048 g): *m/e* 348, 289 ($M^+ - C_{12}H_{17}O_8$), 275 (348 − $CH_2OAc$), 259 (289 − $CH_2O$), 245 (275 − $CH_2O$), 229 (259 − $CH_2O$), 215 (245 − $CH_2O$), 203 (276 − $CH_2OAc$), 199 (229 −$CH_2O$); found for **30** ($R_f$ 0.50, 0.042 g): *m/e* 577 ($M^+$ − OAc), 563 ($M^+$ − $CH_2OAc$), 461 (563 − $CH_3CO$ − OAc), 445 (563 − 2 OAc); found for **31** ($R_f$ 0.44, 0.029 g): *m/e* 348, 289 ($M^+ - C_{12}H_{17}O_8$), 305 (348 − $CH_3CO$), 275 (348 − $CH_2OAc$), 259 (289 − $CH_2O$), 245 (275 − $CH_2O$). A mixture of compounds **29**, **30**, and **31** was also obtained (0.046 g).

## Acknowledgements

The authors are grateful to the Natural Sciences and Engineering Research Council of Canada for financial assistance in the form of grants (to T.B.G. and W.A.S.) and a scholarship (to B.M.P.). They also wish to thank Dr. A. A. Grey of the Canadian 220 MHz NMR Centre for his assistance and cooperation in the measurement of $^1$Hmr spectra at 220 MHz.

1. A. T. Ness, R. H. Hann, and C. S. Hudson. J. Am. Chem. Soc. **65**, 2215 (1943).
2. R. Schaffer. J. Am. Chem. Soc. **81**, 5452 (1959); D. T. Williams and J. K. N. Jones. Can. J. Chem. **42**, 69 (1964); R. D. Youssefyeh, J. P. H. Verheyden, and J. G. Moffat. J. Org. Chem. **44**, 1301 (1979); G. H. Jones, M. Taniguchi, D. Tegg, and J. G. Moffat. J. Org. Chem. **44**, 1309 (1979).
3. (*a*) J. Ronayne and D. H. Williams. J. Chem. Soc. B, 540 (1967); (*b*) T. Matsuo. J. Phys. Chem. **72**, 1819 (1968); (*c*) T. Ledall. Tetrahedron Lett. 651 (1968); 1683 (1968); (*d*) F. H. Cottee and C. J. Timmons. J. Chem. Soc. B, 326 (1968); (*e*) K. M. Baker and B. R. Davis. J. Chem. Soc. B, 261 (1968); (*f*) D. W. Boykin, Jr., A. B. Turner, and R. E. Lutz. Tetrahedron Lett. 817 (1969); (*g*) J. Seyden-Penne, P. Arnaud, J.-L. Pierre, and M. Plat. Tetrahedron Lett. 3719 (1967); (*h*) M. H. Freemantle and W. G. Overend. Chem. Commun. 503 (1968); (*i*) M. H. Freemantle and W. G. Overend. J. Chem. Soc. B, 547 (1969); 551 (1969); (*j*) D. H. Williams and D. A. Wilson. J. Chem. Soc. B, 144 (1966); (*k*) D. Horton and J. H. Lauterbach. J. Org. Chem. **34**, 86 (1969).
4. J. E. Anderson. Tetrahedron Lett. 4713 (1965); R. C. Cookson, T. A. Crabb, and S. Vary. Tetrahedron, **24**, 4559 (1968).
5. K. D. Carlson, C. R. Smith, Jr., and I. A. Wolff. Carbohydr. Res. **13**, 403 (1970).
6. N. S. Bhacca and D. H. Williams. Tetrahedron Lett. 3127 (1974).
7. T. P. Forrest. Can. J. Chem. **52**, 4095 (1974).
8. T. P. Forrest. Org. Magn. Reson. **6**, 355 (1974).
9. T. P. Forrest. J. Am. Chem. Soc. **97**, 2628 (1975).
10. S. J. Angyal and K. James. Carbohydr. Res. **15**, 91 (1970).
11. E. W. Hagaman. Org. Magn. Reson. **8**, 389 (1976).
12. Y. Y. Samitov, R. S. Musavirov, F. Kh. Karataeva, E. A. Kantor, D. L. Rakhmankulov, and N. A. Nikiforova. J. Org. Chem. U.S.S.R. **14**, 2289 (1978).
13. P. M. Collins and V. R. N. Munasinghe. Carbohydr. Res. **62**, 19 (1978).
14. G. W. Buchanan, J. B. Stothers, and S.-T. Wu. Can. J. Chem. **47**, 3113 (1969).
15. T. P. Forrest and J. G. K. Webb. Org. Magn. Reson. **12**, 371 (1979).
16. W. A. Ayer, L. M. Browne, S. Fung, and J. B. Stothers. Can. J. Chem. **54**, 3272 (1976).
17. W. J. Lloyd and R. Harrison. Carbohydr. Res. **26**, 91 (1973).
18. J. C. Boeyens, A. J. Brink, and A. Jordaan. J. Chem. Res. (S), 187 (1978).
19. B. M. Pinto, W. A. Szarek, and T. B. Grindley. Can. J. Chem. Submitted.
20. A. S. Perlin and B. Casu. Tetrahedron Lett. 2921 (1969); K. Bock, I. Lundt, and C. Pedersen. Tetrahedron Lett. 1037 (1973); K. Bock and C. Pedersen. J. Chem. Soc. Perkin Trans. II, 293 (1974); K. Bock and C. Pedersen. Acta Chem. Scand. B, **29**, 258 (1975); N. J. Cussans and T. N. Huckerby. Tetrahedron, **31**, 2719 (1975); F. R. Taravel and P. J. A. Vottero. Tetrahedron Lett. 2341 (1975).
21. J. B. Lambert. *In* Organic structural analysis, Part 1. *Edited by* A. Streitweiser, Jr. Macmillan Publishing Co. New York, NY. 1976. p. 33.
22. J. A. Peters, W. M. M. J. Bovee, P. E. J. Peters-van Cranenburgh, and H. van Bekkum. Tetrahedron Lett. 2553 (1979).
23. J. R. Hanske and H. Rapoport. J. Org. Chem. **44**, 2472 (1979); R. Anderson, O. Theander, and E. Westerlund. Carbohydr. Res. **61**, 501 (1978); H. Paulsen, W. Bartsch, and J. Thiem. Chem. Ber. **104**, 2545 (1971); K. D. Carlson, C. R. Smith, Jr., and I. A. Wolff. Carbohydr. Res. **13**, 391 (1970).
24. T. D. Inch. Carbohydr. Res. **5**, 53 (1967); R. Schaffer and H. S. Isbell. J. Am. Chem. Soc. **79**, 3864 (1957).
25. M. Chérest, H. Felkin, and N. Prudent. Tetrahedron Lett. 2199 (1968); M. Chérest and H. Felkin. Tetrahedron Lett. 2205 (1968).
26. N. T. Anh and O. Eisenstein. Nouv. J. Chim. **1**, 61 (1977).

Can. J. Chem. Downloaded from www.nrcresearchpress.com by 210.87.254.40 on 09/06/12
For personal use only.

# Quadricyclane–norbornadiene isomerizations on alumina

DOUGLAS N. BUTLER AND INDRANIL GUPTA

*Department of Chemistry, York University, Downsview, Ont., Canada M3J 1P3*

Received August 25, 1981

DOUGLAS N. BUTLER and INDRANIL GUPTA. Can. J. Chem. **60**, 415 (1982).

Standard synthetic steps have been used to convert 7-methylenequadricyclane into the spiro-cyclopropene **1** and the allene **2**. These (and other) quadricyclanes are cleanly isomerized on alumina to the respective bicyclo[2.2.1]hepta-2,5-dienes **3** and **4**.

DOUGLAS N. BUTLER et INDRANIL GUPTA. Can. J. Chem. **60**, 415 (1982).

Faisant appel à des méthodes usuelles de synthèse, on a transformé le méthylène-7 quadricyclane en un spiro cyclopropène **1** et en allène **2**. Ce quadricyclane (ainsi que d'autres), par une isomérisation sur alumine, se transforment respectivement, d'une façon très propre, en bicyclo[2,2,1]heptadiènes-2,5 **3** et **4**.

[Traduit par le journal]

Can. J. Chem. Downloaded from www.nrcresearchpress.com by 210.87.254.6 on 09/06/12
For personal use only.

Interest has recently been shown in the quadricyclane–norbornadiene isomerization using polymer supported catalysts in relation to energy-storage systems (1). Conventionally, noble metal complexes of Ru, Pd, Cu, and Rh have been used (2) and reviewed (3) with respect to the mechanisms of transition metal-catalysed isomerizations of these highly condensed systems. Herein we report the synthesis of novel spiro-annelated norbornadienes via *alumina promoted* cyclo-reversions of quadricyclanes.

The isomeric hydrocarbons **1** to **4** have not been previously reported, though an analysis of through-space and through-bond interactions in these molecules would be of interest in relation to their constitution and properties (4).

The key intermediate **5** (from methylenequadricyclane (5)) was the precursor for all of the isomers **1** to **4**. The synthetic sequences and interconversions are shown in Scheme 1 with the only deviations from standard procedures being the quadricyclane–norbornadiene isomerizations **1** → **3**, **2** → **4**, **5** → **7**, and **9** → **10** which were all brought about by simple passage in pentane through ice-cooled columns of neutral alumina. In each case, the alumina turned orange or pink and in larger samples (~ 3 g) the local heat of reaction disturbed the column packing. In the case of the isomerization of **1** → **3**, these spiro-cyclopropenes slowly reacted on the column to produce uncharacterized products (possibly alcohols by hydration of the strained olefin) and we experienced poor recoveries until we cooled the columns.

It seems indeed surprising to us that this alumina promoted isomerization has not been observed before, but we were not able to find it mentioned in the literature (6). Quadricyclane itself was also shown to be isomerized to norbornadiene but required about three times as much alumina when compared to the more strained cases described above. Also, methylenequadricyclane was cleanly isomerized to 7-methylenenorbornadiene (5). Although it was not tried, we have no reason to doubt that the conversion **6** → **8** could also be effected on alumina in pentane. This cycloreversion phenomenon seems to be associated with the fresh surface of the alumina since once having been used, a column loses its capacity to bring about the isomerization. It should be noted that the thermally sensitive compounds of this study could not be prepared using the conventional noble metal cycloreversion catalysts due to decomposition under the conditions used, and thus this alumina method, being cheap, facile, and applicable to sensitive quadricyclanes, should find ready utilization.

The structures of these new hydrocarbons and their precursors all follow from their mode of synthesis and their consentaneous $^1H$ and $^{13}C$ nuclear magnetic resonance spectra (see Experimental). Isomers **1** to **4** all show very similar mass spectra with a strong P-1 peak at $m/e = 115$ as their most interesting feature.

The stability of the spiro-cyclopropene hydrocarbons **1** and **3** as compared to other 3,3-dialkyl substituted cyclopropenes is noteworthy in relation to the novel type of spiro-conjugation inherent in the constitution of these isomers. Thus, although **1** or **3** polymerized when we attempted to distil them under vacuum (14 Torr), they can be stored at 0°C for weeks without serious loss. This stability contrasts with that of the heretofore unknown norbornane **14** (see Scheme 1 for synthesis) which rapidly polymerized at 0°C on attempted isolation from pentane solution. In turn, this instability should be contrasted with the successful isolation of the spiro-cyclopropene **16** (7) as a stable, crystal-

0008-4042/82/040415-04$01.00/0

©1982 National Research Council of Canada/Conseil national de recherches du Canada

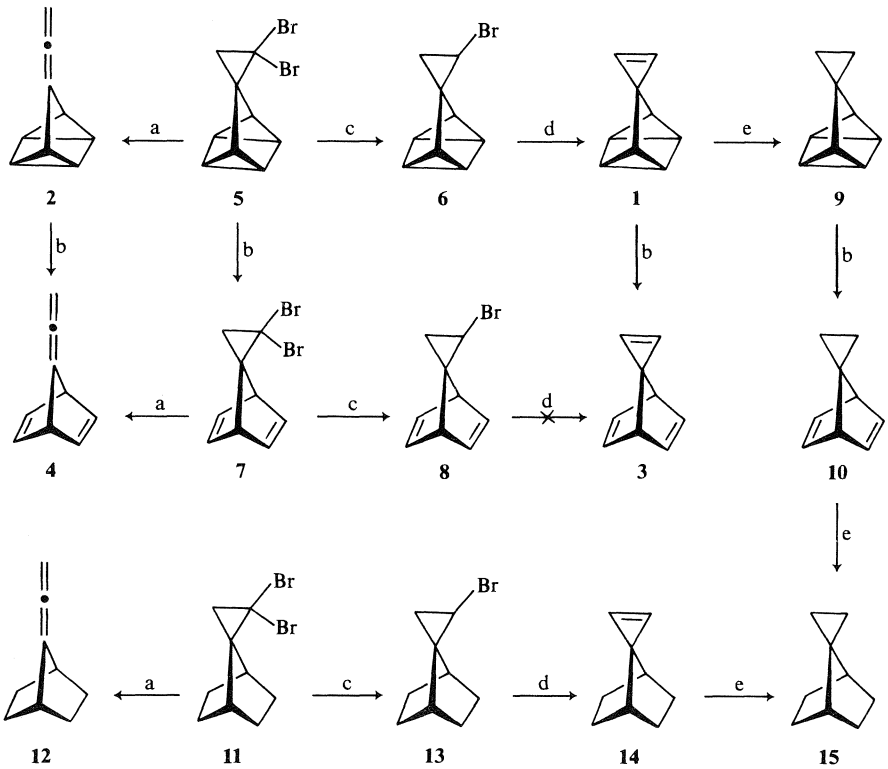


Reagents: a, excess $CH_3Li/(C_2H_5)_20/0°C$; b, $Al_2O_3$/Pentane/0°C; c, $(n\text{-}C_4H_9)_3SnH$/THF//reflux; d, $KOC(CH_3)_3$/DMSO/10°C; e, $H_2$/10% Pd on C/ethyl acetate.

SCHEME 1

line solid. This spiro-conjugation is also evident in the uv spectrum of **3** which shows a pronounced bathochromic shift of the $\lambda_{max}$ (pentane) = 220.5 nm as compared to norbornadiene ($\lambda_{max}$ (pentane) = 205 nm) (8) or the spiro-cyclopropanenorbornadiene **17** (4*a*) ($\lambda_{max}$ (pentane) = 207 nm) (9). A fuller discussion of the orbital interactions involved must await an analysis of the photo-electron spectra currently under way.

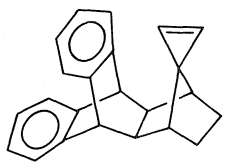

**16**

**17**

## Experimental

The ir spectra were recorded on a Unicam SP1000 spectrophotometer as liquid films or Nujol mulls. The $^1H$ and $^{13}C$ nmr spectra were taken respectively on Varian EM360 or CFT20 instruments in the solvents indicated. The uv spectra were run on a Unicam SP800A spectrophotometer. Mass spectra were taken at 70 eV using a Hitachi–Perkin–Elmer RMU-6E instrument. Vapour phase chromatographic analyses were carried out using a Varian Aerograph instrument, Model 1700, on a 7 ft × 1/4 in. glass column packed with Chromosorb W (60–80 mesh) loaded with a mixture of 6% SE30 and 4% QF1. All melting points are uncorrected.

*Dibromocarbene addition to 3-methylenetetracyclo-[3.2.0.0$^{2,7}$,0$^{4,6}$]heptane. Spiro-tetracyclo[3.2.0.0$^{2,7}$,0$^{4,6}$]-heptane-3:1′-(2′,2′-dibromocyclopropane), 5*

A solution of bromoform (10.04 g, 40 mmol) in hexane (25 mL) was added dropwise over 15 min to a stirred mixture of 3-methylenetetracyclo[3.2.0.0$^{2,7}$,0$^{4,6}$]heptane (2.08 g, 20 mmol) (5) and freshly prepared potassium *tert*-butoxide (11.2 g, 100 mmol) in hexane (50 mL) at 0°C under $N_2$. This mixture was stirred for a further 30 min and then poured into water (200 mL) and the hexane layer separated. The aqueous phase was extracted with hexane (3 × 50 mL) and the combined hexane extracts were washed with ice-water (3 × 50 mL). The organic extract was dried ($Na_2SO_4$) and evaporated to a white solid which was recrystallized from pentane to give the adduct **5** (4.03 g, 72%), mp 54°C; $^1H$ nmr ($CDCl_3$) δ: 1.33 (t, $J$ = 4.5 Hz, 2H), 1.90 (m, 4H), and 2.11 (s, 2H); $^{13}C$ nmr ($CDCl_3$) δ: 16.6 (d), 17.6 (d), 28.6 (t), 31.2 (s + d), and 46.4 (s); mass spectrum *m/e*: 274, 276, 278 ($M^+$). Anal. calcd. for $C_9H_8Br_2$: C 39.17, H 2.92; found: C 38.88, H 2.83.

*Spiro-tetracyclo[3.2.0.0$^{2,7}$,0$^{4,6}$]heptane-3:1′-(2′-bromocyclo-propane), 6*

Tri-*n*-butyl tin hydride (3.5 g) was added to a solution of the dribromide **5** (3.3 g) in dry tetrahydrofuran (20 mL) and the mixture heated to reflux for 3/4 h. The solvent was then removed

Can. J. Chem. Downloaded from www.nrcresearchpress.com by 210.87.254.6 on 09/06/12
For personal use only.

Can. J. Chem. Downloaded from www.nrcresearchpress.com by 210.87.254.6 on 09/06/12
For personal use only.

under vacuum and the residue distilled with the fraction bp 50–52°C /0.1 Torr being collected as the colorless liquid **6** (2.05 g, 84%); $^1$H nmr ($CDCl_3$) δ: 0.9 (m, 1H), 1.1–2.0 (complex multiplets, 7H), and 3.41 (dd, 1H); $^{13}$C nmr ($CDCl_3$) δ: 15.3 (d), 15.6 (d), 15.9 (t), 16.4 (d), 17.8 (d), 22.9 (d), 28.9 (d + d), and 36.7 (s); mass spectrum *m/e*: 196, 198 ($M^+$).

*Spiro-tetracyclo[3.2.0.0$^{2,7}$,0$^{4,6}$]heptane-3:1′-(cyclopropene), **1***

Freshly prepared potassium *tert*-butoxide (2.7 g) was added to a magnetically stirred solution of the monobromide **6** (2.4 g) in dry dimethyl sulfoxide (7 mL) at 10°C. This mixture was stirred at room temperature for 1 h and then worked up by the addition of ice-water (50 mL) followed by extraction with pentane (3 × 50 mL). The combined pentane extracts were washed with water (3 × 50 mL), dried ($Na_2SO_4$), and carefully rotated in an evaporator at water pump pressure using ice-water in the bath until the pentane was removed. The remaining oil (1.1 g, 77%) could not be distilled or vacuum transferred without polymerizing and spectroscopic data were collected directly on this crude reaction product. On standing overnight in the freezer it crystallized, mp approximately 16°C; $^1$H nmr ($CDCl_3$) δ: 0.63 (t, $J$ = 4.3 Hz, 2H), 1.70 (d, $J$ = 2.4 Hz, 4H), and 7.74 (s, 2H); $^{13}$C nmr ($CDCl_3$) δ: 15.1 (d, $J$ = 186 Hz), 26.9 (d, $J$ = 167 Hz), 33.9 (s), and 121.0 (d, $J$ = 221 Hz); mass spectrum *m/e*: 116 ($M^+$).

*Spiro-tetracyclo[3.2.0.0$^{2,7}$,0$^{4,6}$]heptane-3:1′-(cyclopropane), **9***

The hydrocarbon **1** (50 mg) was shaken in pentane (10 mL) in a hydrogen atmosphere with 10% palladium-on-charcoal catalyst (5 mg) until rapid gas uptake stopped. After filtration and careful evaporation the crude product **9** (43 mg) remained as a clear liquid, $^1$H nmr ($CDCl_3$) δ: 0.83 (s and t, $J$ = 4.2 Hz, 6H) and 1.78 (d, $J$ = 4.2 Hz, 4H); $^{13}$C nmr ($CDCl_3$) δ: 5.3 (t, $J$ = 159 Hz), 15.8 (d, $J$ = 183), 28.9 (d, $J$ = 168 Hz), and 29.3 (s); mass spectrum *m/e*: 118 ($M^+$).

*Spiro-bicyclo[2.2.1]hepta-2,5-diene-7:1′(2′,2′-dibromocyclopropane), **7***

A solution of the adduct **5** (700 mg) in hexane (5 mL) was run onto a neutral alumina (Activity Grade 1) (10 g) column (1 cm diameter) packed in hexane and cooled with an ice-jacket. The column was eluted with hexane (100 mL) and the solvent removed from the eluate in a rotary evaporator under vacuum to provide a solid which was recrystallized from pentane to give **7** (554 mg, 79%), mp 42°C; $^1$H nmr ($CDCl_3$) δ: 1.69 (s, 2H), 3.50 (p, $J$ = 2 Hz, 2H), 6.89 (t, $J$ = 2 Hz, 2H), and 7.03 (t, $J$ = 2 Hz, 2H); $^{13}$C nmr ($CDCl_3$) δ: 31.5 (s), 31.9 (t), 54.9 (d), 76.9 (s), 141.5 (d), and 141.7 (d); mass spectrum *m/e*: 274, 276, 278 ($M^+$).

*Spiro-bicyclo[2.2.1]hepta-2,5-diene-7:1′(2′-bromocyclopropane, **8***

Prepared from **7** as described for **6**, monobromide **8** was obtained as a colorless oil (66%), bp 43–47°C/0.1 Torr; $^1$H nmr ($CDCl_3$) δ: 0.8–1.5 (m, 2H), 2.91 (q, 1H), 3.06 (m, 1H), 3.47 (m, 1H), and 6.87 (m, 4H); $^{13}$C nmr ($CDCl_3$) δ: 19.8 (t, $J$ = 161.0 Hz), 23.9 (d, $J$ = 185.6 Hz), 53.8 (d, $J$ = 148.7 Hz), 54.0 (d, $J$ = 148.7 Hz), 71.7 (s), 141.5 (d, $J$ = 176.0 Hz), and 142.6 (d, $J$ = 176.0 Hz); mass spectrum *m/e*: 196. 198 ($M^+$).

*Spiro-bicyclo[2.2.1]hepta-2,5-diene-7,1′-cyclopropene, **3***

Prepared by isomerization of **1** (0.3 g) as described for **7**, hydrocarbon **3** was obtained as an oil which polymerized on attempted distillation (81 mg, 27%); uv (pentane)$\lambda_{max}$: 220.5 nm (ε = 1090); $^1$H nmr ($CDCl_3$) δ: 3.18 (p, $J$ = 2.1 Hz, 2H), 6.80 (t, $J$ = 2.1 Hz, 4H), and 7.41 (s, 2H); $^{13}$C nmr ($CDCl_3$) δ: 58.4 (d, $J$ = 146.4 Hz), 76.0 (s), 126.6 (d, $J$ = 218.4 Hz), and 139.0 (d, $J$ = 168.9 Hz); mass spectrum *m/e*: 116 ($M^+$).

*Spiro-bicyclo[2.2.1]hepta-2,5-diene-7:1′-(cyclopropane), **10***

Prepared from **9** (0.01 g) as described for **1** as an unstable oil (78 mg, 78%) (*4b*); $^1$H nmr ($CDCl_3$) δ: 0.48 (s, 4H), 3.05 (p, $J$ = 2 Hz, 2H), and 6.91 (t, $J$ = 2 Hz, 4H); $^{13}$C nmr ($CDCl_3$) δ: 9.5 (t, $J$ = 159.5 Hz), 55.1 (d, $J$ = 148.4 Hz), 69.7 (s), and 142.5 (d, $J$ = 172.1 Hz); mass spectrum *m/e*: 118 ($M^+$).

*Spiro-bicyclo[2.2.1]heptane-7:1′(2′,2′-dibromocyclopropane), **11***

Prepared from 7-methylenebicyclo[2.2.1]heptane (1.08 g) (5) as for **5** as a white solid (1.98 g, 71%), mp 47°C; $^1$H nmr ($CDCl_3$) δ: 0.75–2.3 with singlets at 1.43, 1.68 and 1.90 (bd); $^{13}$C nmr ($CDCl_3$) δ: 28.3 (t), 28.6 (t), 29.4 (t), 31.0 (s), 43.3 (d), and 48.0 (s); mass spectrum *m/e*: 278, 280, 282 ($M^+$).

*Spiro-bicyclo[2.2.1]heptane-7:1′-(2′-bromocyclopropane), **13***

From the dibromide **11** (0.98 g) as described for **6**, the monobromide **13** was obtained as a liquid (0.525 g, 75%), bp 50–55°C/0.1 Torr; $^1$H nmr ($CDCl_3$) δ: 0.8–2.0 (complex, 12H) and 3.02 (dd, 1H); $^{13}$C nmr ($CDCl_3$) δ: 15.8 (t), 22.9 (d), 28.6 (t), 28.7 (t), 28.8 (t), 29.9 (t), 39.7 (s), 41.2 (d), and 41.3 (d); mass spectrum *m/e*: 200, 202 ($M^+$).

*Spiro-bicyclo[2.2.1]heptane-7:1′-(cyclopropene), **14***

Prepared from mono-bromide **13** (0.56 g) as described for **1**, hydrocarbon **14** was obtained as an unstable oil which rapidly polymerized on warming (180 mg, 54%); $^1$H nmr ($CDCl_3$) δ: 0.75–1.9 (complex, 10H) and 7.43 (s, 2H); $^{13}$C nmr ($CDCl_3$) δ: 28.1, 37.3, 41.1, and 120.8; mass spectrum *m/e*: 120 ($M^+$).

*Spiro-bicyclo[2.2.1]heptane-7:1′-(cyclopropane), **15***

Prepared by hydrogenation of **10** or **14** as described for **9**, liquid (*4b*); $^1$H nmr ($CDCl_3$) δ: 0.40 (s, 4H) and 1.1–1.9 (complex, 10H); $^{13}$C nmr ($CDCl_3$) δ: 4.9 (t, $J$ = 161.0 Hz), 29.4 (t, $J$ = 135.8 Hz), 32.5 (s), and 41.4 (d, $J$ = 138.3 Hz); mass spectrum *m/e*: 122 ($M^+$).

*3-Ethenylidenetetracyclo[3.2.0.0$^{2,7}$,0$^{4,6}$]heptane, **2***

The dibromide **5** (0.46 g) was dissolved in dry ether (15 mL) and the reaction mixture stirred and cooled in an ice-bath under $N_2$ with moisture exclusion. An approximately 1 *N* solution of methyl lithium in ether (6 mL) was added via syringe over 5 min and the mixture kept stirring for 1 h before pouring into water (50 mL) and extraction with pentane (3 × 10 mL). After drying the combined organic extracts and careful evaporation of the solvents, the oily residue (0.16 g, 83%) was shown by gas chromatography to be one major product comprising 90% of the mixture. For characterization, a pure sample was obtained by preparative gas chromatography at 130°C. Compound **2**, colorless liquid, $^1$H nmr ($CDCl_3$) δ: 1.89 (s + m, 6H) and 4.94 (s, 2H); $^{13}$C nmr ($CDCl_3$) δ: 18.4 (d, $J$ = 187.6 Hz), 26.6 (d, $J$ = 168.7 Hz), 77.2 (t, $J$ = 167.2 Hz), 107.0 (s), and 200.5 (s); mass spectrum *m/e*: 116 ($M^+$).

*7-Ethenylidenebicyclo[2.2.1]hepta-2,5-diene, **4***

The dibromide **7** (0.23 g) was reacted with methyl lithium in ether as described for **2**. The hydrocarbon **4** was collected by vacuum transfer at 43–47°C and 0.05 Torr as a colorless oil (0.074 g, 76%); $^1$H nmr ($CDCl_3$) δ: 4.05 (p, $J$ = 2 Hz, 2H), 4.90 (s, 2H), and 6.90 (t, $J$ = 2 Hz, 4H); $^{13}$C nmr ($CDCl_3$) δ: 52.2, 82.4, 142.2 – dilute sample, two lines missing, no coupling constants taken; mass spectrum *m/e*: 116 ($M^+$).

The same allene **4** was also formed by passage of **2** in pentane over alumina as described for **3**.

*7-Ethenylidenebicyclo[2.2.1]heptane, **12***

The dibromide **11** (0.28 g) was reacted with methyl lithium in ether as described for **2**. The hydrocarbon **12** was collected by vacuum transfer at 50°C and 0.05 Torr as a colorless liquid (0.097 g, 81%); $^1$H nmr ($CDCl_3$) δ: 1.1–2.03 ($A_2B_2$ pattern, 8H), 2.66 (m, 2H), and 4.67 (s, 2H); $^{13}$C nmr ($CDCl_3$) δ: 29.7 (t),

40.6 (d), 75.1 (t), 107.4 (s), and 193.6 (s); mass spectrum *m/e*: 120 ($M^+$).


1. (*a*) R. B. KING and E. M. SWEET. J. Org. Chem. **44**, 385 (1979); (*b*) R. J. CARD and D. C. NECKERS. J. Org. Chem. **43**, 2958 (1978).
2. (*a*) K. MARUYAMA, K. TERADA, K. NARUTA, and Y. YAMAMOTO. Chem. Lett. Jpn. 1259 (1980); (*b*) P. A. GRUTSCH and C. KUTAL. J. Am. Chem. Soc. **101**, 4228 (1979); (*c*) H. HOGEVEEN and H. C. VOLGER. J. Am. Chem. Soc. **89**, 2486 (1967); (*d*) L. CASSAR and J. HALPERN. J. Chem. Soc. Chem. Commun. 1082 (1971).
3. (*a*) K. C. BISHOP. Chem. Rev. **76**, 461 (1976); (*b*) R. B. KING (*Editor*). Inorganic compounds with unusual properties. II. Advances in Chemistry Series No. 173. American Chemical Society. 1979.
4. (*a*) F. BROGLI, E. HEILBRONNER, and J. IPAKTSCHI. Helv. Chim. Acta, **55**, 2447 (1972); (*b*) P. BISCHOF, M. BÖHM, R. GLEITER, R. A. SNOW, C. W. DOECKE, and L. A. PAQUETTE. J. Org. Chem. **43**, 2387 (1978).
5. R. W. HOFFMANN, H. KURZ, M. T. REETZ, and R. SCHÜTTLER. Chem. Ber. **108**, 109 (1975).
6. G. H. POSNER. Angew. Chem. Int. Ed. Engl. **17**, 487 (1978).
7. D. N. BUTLER and I. GUPTA. J. Chem. Soc. Chem. Commun. 596 (1980).
8. C. F. WILCOX, S. WINSTEIN, and W. G. MCMILLAN. J. Am. Chem. Soc. **82**, 5450 (1960).
9. C. F. WILCOX and R. R. CRAIG. J. Am. Chem. Soc. **83**, 4258 (1963).


Can. J. Chem. Downloaded from www.nrcresearchpress.com by 210.87.254.6 on 09/06/12
For personal use only.

# The regioselectivity of the formation of dihydro- and tetrahydrocarbazoles by the Fischer indole synthesis

G. W. BRYAN REED, PETER T. W. CHENG, AND STEWART MCLEAN
*Department of Chemistry, University of Toronto, Toronto, Ont., Canada M5S 1A1*

Received August 20, 1981

Can. J. Chem. Downloaded from www.nrcresearchpress.com by 210.87.254.6 on 09/06/12
For personal use only.

G. W. BRYAN REED, PETER T. W. CHENG, and STEWART MCLEAN. Can. J. Chem. **60**, 419 (1982).

The cyclohexanone **3** and the cyclohexenone **13** have been prepared, converted to their phenylhydrazones, and subjected to the Fischer indole synthesis under conditions ranging from 7% to 60% sulfuric acid in methanol. The tetrahydrocarbazoles **4** and **5** were isolated in a 2:1 ratio in the sequence starting from **3** and no significant variation in the ratio was observed through the range of conditions used. In the sequence starting with **13**, the dihydrocarbazoles **14** and **15** were isolated in a 1:1 ratio when 7% or 15% sulfuric acid was used; when more concentrated acid was used, normal Fischer products were not obtained but some transformation products were isolated from the complex mixture of products obtained. The observed regioselectivity of these reactions is not predicted from mechanistic considerations, and no mechanistic explanation for the results is apparent. As part of the proof of structure of **4** and **14**, their *N*-benzyl derivatives were prepared from 1-benzyl-2-vinylindole by Diels–Alder reactions.

G. W. BRYAN REED, PETER T. W. CHENG et STEWART MCLEAN. Can. J. Chem. **60**, 419 (1982).

On a préparé la cyclohexanone **3** et la cyclohexènone **13**, ainsi que leurs phénylhydrazones qui subissent la synthèse de l'indole de Fisher lorsque mises en solution dans de l'acide sulfurique à des concentrations de 7 à 60% dans le méthanol. On a recueilli les tétrahydrocarbazoles **4** et **5** dans un rapport 2:1 en partant du composé **3** et ce rapport reste invariable dans les conditions utilisées. Dans le cas du composé **13**, on pu isoler les tétrahydrocarbazoles **14** et **15** dans un rapport de 1:1 lorsqu'on utilise des solutions d'acide sulfurique à 7 ou 15%. En solutions plus concentrées, on n'obtient pas les produits normaux de Fisher, mais on a isolé quelques produits de transformation à partir d'un mélange complexe de produits obtenus. la régiosélectivité observée pour ces réactions n'est pas prévue à partir des mécanismes connus, et on n'a aucun mécanisme apparent qui permette d'expliquer ces résultats. On établit la structure des composés **4** et **14** en préparant leurs dérivés *N*-benzyle à partir du benzyl-1 vinyl-2 indole par des réactions de Diels–Alder.

[Traduit par le journal]

Tetrahydrocarbazoles carrying reactive substituents at assigned locations could serve as intermediates in syntheses of more complex structures, including a range of indole alkaloids. The classical Fischer indole synthesis (1) offers a convenient route to such tetrahydrocarbazoles, provided that the appropriate cyclohexanone is available as a precursor and that a reasonable degree of regioselectivity can be established when an unsymmetrically substituted cyclohexanone is taken through the Fischer sequence. The regioselectivity observed experimentally and the question of whether it can be controlled by varying the reaction conditions are matters of practical importance in such cases, and are the subject of the present study. It is also of interest to see whether mechanistic considerations can be used to predict and explain the results obtained.

We studied first the simple case using the cyclohexanone **3**, which was conveniently prepared (70% yield) by the Diels–Alder reaction of the trimethylsiloxybutadiene **1** (2) with *N*-methylmaleimide followed by methanolysis of the adduct **2** (see Scheme 1). The phenylhydrazone of **3** was isolated (90% yield) and subjected to the Fischer indole reaction under a range of acidic conditions (see Table 1). The crystalline adducts **4** and **5** were isolated in the yields shown in the table; the overall yields diminished as the concentration of acid used increased, but the **4**/**5** ratio remained close to 2:1 until yields were significantly lowered.

Although the structures assigned to **4** and **5** on the basis of their spectroscopic properties appeared secure, confirmation of the structure of **4** was obtained by the synthesis of a derivative by the unambiguous route outlined in Scheme 2. Indole-2-carboxylic acid (**6**) was converted by diazomethane to its methyl ester, which was *N*-benzylated to provide **7**. The ester was converted by the action of hydrazine in ethanol to the hydrazide, which was tosylated with tosyl chloride, and then subjected to a McFadyen–Stevens reduction. Yields at each step were excellent and the aldehyde **8** was obtained from **6** in 83% overall yield. The vinyl compound **9** was obtained in 85% yield from **8** by a Wittig reaction. A Diels–Alder reaction of **9** with *N*-methylmaleimide then led to the isolation of **10**, the *N*-benzyl derivative of **4**, in 52% yield. Unfortunately, the benzyl group of **10** resisted hydrogenolysis and attempts to *N*-benzylate **4** led to a complex mixture of products none of which was **10**. Nevertheless, comparison of the critical spectroscopic properties of **4** and **10** served to demonstrate that they possessed the same tetracyclic skeleton. Fur-

0008-4042/82/040419-06$01.00/0
©1982 National Research Council of Canada/Conseil national de recherches du Canada

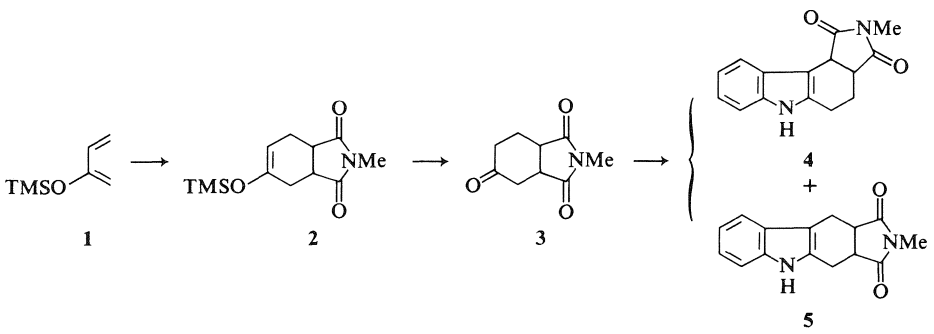


SCHEME 1

thermore, the major product isolated (albeit in only 35% yield) from the treatment of **4** with sodium hydride (1 equiv.) and benzyl chloride in HMPT was a dibenzyl compound. The probable structure of this compound is shown as **11**. Its uv spectrum strongly resembles that of **10** and both compounds show the same carbonyl ir absorptions, but there are key differences in their proton nmr spectra: a one-proton doublet at $\tau$ 5.69 in the spectrum of **10**, assigned to the C-4 proton, is absent in **11**, and a two-proton AB quartet centred at $\tau$ 6.35 appears instead and is assigned to the *C*-benzyl methylene protons; the *N*-benzyl methylene protons have the same chemical shift in both spectra, but those of **10** appear as a singlet, while in the spectrum of **11**, the signal is split. For present purposes, the main importance of this compound obtained from **4** is that it could also be obtained from **10** (in 25% yield) by benzylation, and so demonstrates that **4** and **10** have the same tetracyclic skeleton.

The Diels–Alder reaction of diene **1** with dimethyl acetylenedicarboxylate led to an oily product in 86% yield, the spectroscopic properties of which were consistent with the structure **12** expected for the adduct. Conversion of **12** to a ketone (Scheme 3) even under the mildest conditions (stirring with methanol at room temperature), led to the formation of the conjugated cyclohexenone **13** in excellent yield; this compound showed $\lambda_{max}$ 223 nm ($\varepsilon$ 10 500) in its uv spectrum, a one-proton doublet with $J = 1.5$ Hz at $\tau$ 3.20 in its proton nmr spectrum, and other features in its ir and nmr ($^1$H and $^{13}$C) spectra in accord with the assigned structure. Compound **13** was converted to its crystalline phenylhydrazone which was then subjected to the Fischer indole reaction under the range of acidic conditions used previously. In this series the yields of the Fischer products were lower even from reactions carried out in 7% or 15% sulfuric acid in methanol (see Table 1), and the use of more strongly acidic conditions led to the formation of very complex mixtures of products which afforded none of the normal Fischer products, the dihydrocarbazoles **14** and **15**. The carbazole **16**, presumably an oxidation product of **15**, was isolated from the mixture obtained from reactions in concentrated acids. (It was also detected in some runs even when the reaction was carried out in 15% sulfuric acid.) The corresponding oxidized derivative of **14**, the carbazole **17**, was not identified in the mixture, but a compound that appeared to be **18**, its reduction product, was isolated. (Reference samples of **16** and **17** were prepared by treatment of the corresponding dihydrocarbazole with dichlorodicyanoquinone.) A considerable amount of polymeric material was also evident, and consequently it was deemed unwise to attempt to quantify the regioselectivity of the Fischer reaction under these

TABLE 1. Product distributions in Fischer reactions

| Conditions | Products* from Phenylhydrazone of **3** | | Products* from Phenylhydrazone of **13** | |
|---|---|---|---|---|
| | **4** | **5** | **14** | **15** |
| 7% $H_2SO_4$/MeOH | 45 | 21 | 24 | 23 |
| 15% $H_2SO_4$/MeOH | 45 | 22 | 23 | 22 |
| 30% $H_2SO_4$/MeOH | 45 | 24 | Complex mixture of products | |
| 45% $H_2SO_4$/MeOH | 36 | 18 | | |
| 60% $H_2SO_4$/MeOH | 15 | 6 | | |

*Yields (%) of isolated products are shown.

Can. J. Chem. Downloaded from www.nrcresearchpress.com by 210.87.254.6 on 09/06/12
For personal use only.

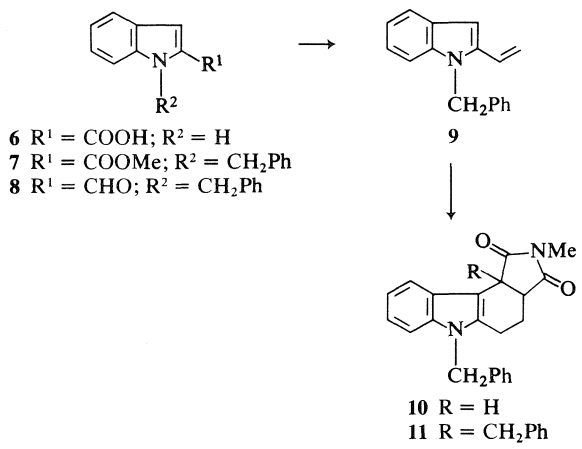


SCHEME 2

circumstances; undoubtedly the reaction of interest is accompanied by undesired competitive and consecutive reactions and even if all of the products from the complex mixture formed could be isolated in the hope of throwing light on any regioselectivity in the Fischer reaction, the procedure under these conditions is of no preparative value. We may note, however, that in the more restricted range of 7% to 15% sulfuric acid, there was no apparent regioselectivity and the **14**/**15** ratio remained 1:1.

As with the previous series, the *N*-benzyl derivative **19** of the diester **14** was prepared by the Diels–Alder reaction of the vinylindole **9** with dimethyl acetylenedicarboxylate. In this case, however, the yield of adduct was only 25%; a complex mixture of by-products was also obtained, some of which appeared to result from oxidation–reduction reactions involving **19** that took place under the Diels–Alder conditions (in the presence of hydroquinone) since the carbazole **20** was isolated from the mixture. Confirmation of the structure assigned to Fischer product **14** was obtained by its *N*-benzylation; in this case monobenzylation could be effected and **19** was isolated in 30% yield. Once again, there was evidence that some of the product had undergone aromatization during the reaction, providing at least a partial explanation for the poor yield.

The mechanism of the Fischer indole synthesis has been the subject of several investigations (1). It is generally agreed that a complex series of events occurs, in which the phenylhydrazone is converted to its enehydrazine tautomer which undergoes a reaction corresponding to a [3,3] sigmatropic rearrangement to form the new C—C bond and cleave the N—N bond; subsequently the indole ring is formed with the elimination of one nitrogen. Normally the reaction is acid-catalyzed, but neither its kinetic dependence on the acid catalyst nor the identity of the rate-determining step has been established unequivocally. In most proposed mechanisms it is a protonated enehydrazine that undergoes rearrangement, and it is the rearrangement step that is probably rate-determining.

The phenylhydrazone of an unsymmetrically substituted cyclohexanone can clearly form two enehydrazine tautomers (e.g. **21** and **22**) and the regioselectivity of the overall Fischer reaction will depend on which of these preferentially undergoes the rearrangement process (Scheme 4). It appeared, *a priori*, that any electronic effects of the substituents ($R^1$, $R^2$) in this case should have a negligible influence on the **21**/**22** ratio; steric effects, if of any significance, would appear to disfavor bond development in the rearrangement of **21**, and consequently favor reaction through **22**. In the case of a cyclohexenone derivative, however, the electronic effects of substituents may be expected to be significant in determining the ratio of enehydrazines (e.g. **23** and **24**) formed; it can also

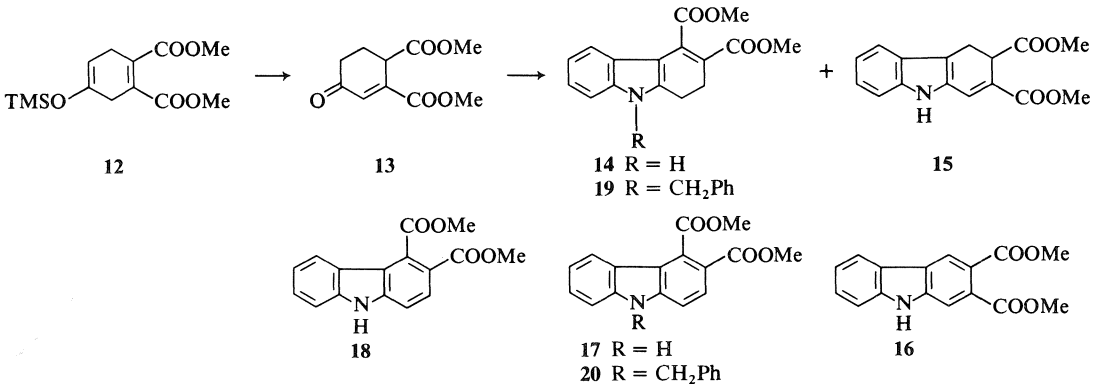


SCHEME 3

Can. J. Chem. Downloaded from www.nrcresearchpress.com by 210.87.254.6 on 09/06/12
For personal use only.

Can. J. Chem. Downloaded from www.nrcresearchpress.com by 210.87.254.6 on 09/06/12
For personal use only.

be seen, however, that the ratio under kinetic control may differ from that under thermodynamic control, and that each isomer may undergo the rearrangement at a different rate. In any event, these factors seem likely to lead to some degree of regioselectivity, and this would probably be sensitive to reaction conditions.

In practice, the distribution of isomers isolated from the Fischer reaction of our cyclohexanone **3** was not approximately 1:1 as predicted, but 2:1 in favor of the route through **21**, and the ratio was not sensitive to the conditions of the reaction. There is a report (3) that only products corresponding to **25** were isolated from the Fischer reaction of a series of compounds corresponding to our **3** but with other substituents on the nitrogen atom; the reaction through **21** again seemed to be favored. However, in another case that appears to be similar, two groups of workers (4) have obtained the opposite regioselectivity; in this case the starting material was cyclohexanone-3-carboxylic acid and only **26** ($R^1$ = COOH; $R^2$ = H) was isolated, indicating that the route through **22** was strongly preferred. It seems clear from these results that the reaction is influenced by effects more subtle than those we have already considered.

In the sequence starting from the cyclohexenone **13**, no regioselectivity was observed when the Fischer reaction was carried out in solutions containing 7% or 15% sulfuric acid, and a 1:1 ratio of isomers was obtained. When more concentrated sulfuric acid was used, no regioselectivity was observable because normal Fischer products were not isolated. Undoubtedly the dihydrocarbazoles are subject to further transformations in the strongly acidic media and they probably undergo some degradation even when the conditions are less acidic. If the two products underwent degradation at different rates, the 1:1 ratio observed for the isolated products could reflect the selective destruction of the major isomer. However, the absence of any significant change in yield or product ratio when the conditions were varied from 7% to 15% sulfuric acid provides some evidence against this possibility, although it does not exclude it. The results in this series must consequently be treated with circumspection but, with the reservations stated, they indicate that reactions through **23** and **24** are equally favored.

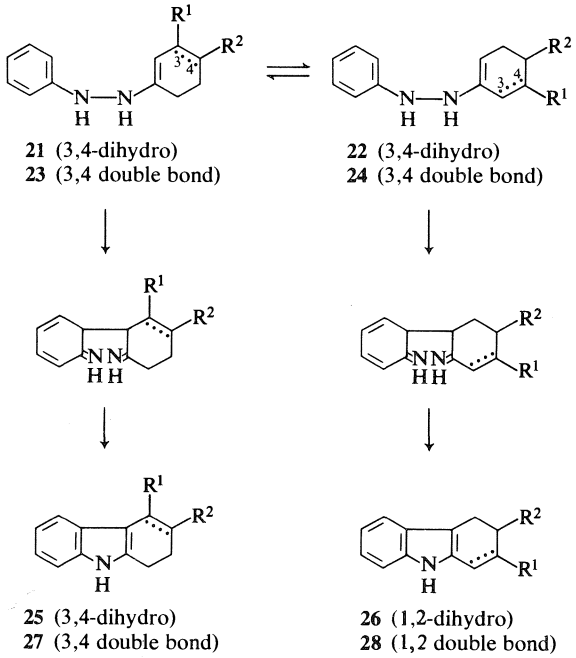


SCHEME 4

In summary then, some regioselectivity (2:1) was observed in the Fischer reaction starting with cyclohexanone **3**, but none was observed in the case of cyclohexenone **13**. These results are not those expected from mechanistic considerations, and we can present no mechanistic explanation for them.

## Experimental

Melting points were determined on a calibrated Thomas–Kofler micro hot stage. A Perkin–Elmer 237B infrared spectrometer was used; the wavelengths (μ) of selected ir absorptions of solutions in chloroform are reported. A Unicam SP 1800 ultraviolet spectrometer was used. The $\lambda_{max}$ values (nm) followed by the extinction coefficients (ε) in parentheses of principal uv absorptions of solutions in methanol are reported. Varian T-60, HA 100, XL 100, and HR 220 nmr spectrometers were used. Unless otherwise indicated, the $^1$Hmr spectra reported were obtained at 100 MHz with solutions in $CDCl_3$; chemical shifts are reported on the τ scale, followed in parentheses by an indication of the multiplicity (initial letter) of the signal, the coupling constant (in Hz units) when available, and the number of protons associated with the signal. Unless otherwise indicated, $^{13}$Cmr spectra were obtained with solutions in $CDCl_3$ and chemical shifts are reported on the $\delta_C$ scale (ppm relative to TMS = 0) followed in parentheses by an indication of the multiplicity of the signal. An AEI MS-902 mass spectrometer was used to make accurate mass measurements.

*The cyclohexanone 3*

A solution of 2-trimethylsiloxy-1,3-butadiene (2) (2.00 g; 0.014 mol) and *N*-methylmaleimide (1.56 g; 14.0 mmol) in 10 mL of dry benzene was heated at 65°C for 24 h. Benzene was removed on a rotary evaporator and adduct **2** (2.99 g) was obtained as an oily residue. The residue was dissolved in 20 mL of methanol and stirred at room temperature for 48 h. Evaporation on a rotary evaporator provided the oily ketone **3** (1.92 g; 11.0 mmol) which was purified by vacuum distillation; ir: 5.66, 5.75, 5.85; $^1$Hmr (220 MHz): 6.62–6.87 (m, 2), 6.98 (s, 3), 7.26 (d, $J$ = 6; 2), 7.56–7.94 (m, 4); $^{13}$Cmr: 207.63 (s), 178.34(s), 177.98(s), 37.96(d), 37.11(d), 36.89(t), 36.14(t), 24.66(q), 21.49(t);

Can. J. Chem. Downloaded from www.nrcresearchpress.com by 210.87.254.6 on 09/06/12
For personal use only.

*Exact Mass* calcd. for $C_9H_{11}NO_3$: 181.0734; found: 181.0740. Phenylhydrazone, mp 190–195°C. 2,4-Dinitrophenylhydrazone, mp 225–227°C. *Anal.* calcd. for $C_{15}H_{15}N_5O_6$: C 49.86, H 4.18, N 19.39; found: C 49.81, H 4.26, N 19.40.

*The cyclohexenone* ***13***

2-Trimethylsiloxy-1,3-butadiene (10.0 g; 0.70 mol) and dimethyl acetylenedicarboxylate (10.0 g; 0.70 mol) were converted by the sequence described above into the cyclohexenone **13** (12.5 g; 0.60 mol), which was purified by vacuum distillation; ir: 5.79, 5.92, 6.13; uv: 223 (10 500); $^1$Hmr: 3.20 (d, $J$ = 1.5; 1), 6.16 (s, 3), 6.2 (m, 1; irradiation collapses τ3.20 doublet), 6.26 (s, 3), 7.6 (m, 4); $^{13}$Cmr: 198.56(s), 171.71(s), 166.29(s), 144.90(s), 133.88(d), 52.86(q), 52.70(q), 40.53(d), 34.91(t), 25.80(t). *Anal.* calcd. for $C_{10}H_{12}O_5$: C 56.60, H 5.70; found: C 56.72, H 5.82. Phenylhydrazone, mp 140–141.5°C. *Anal.* calcd. for $C_{16}H_{18}N_2O_4$: C 63.56, H 6.00, N 9.27; found: C 63.51, H 5.83, N 9.36.

*Fischer indole syntheses*

*Standard procedure*

The phenylhydrazone (1.0 g) was dissolved in 5 g of methanolic sulfuric acid of the required composition (w./w.), and the solution was heated in an oil bath at 80°C for 6 h. The solution was cooled and poured into about 100 mL of water, neutralized with sodium carbonate, and extracted thoroughly with dichloromethane. The combined extracts were washed with water and brine, dried, and evaporated. The residue was chromatographed on silica gel with elution by 1:1 ethyl acetate – hexane, and the separated products were isolated.

*Cyclohexanone* ***3*** *series*

The results obtained by the standard procedure are reported in Table 1. For preparative purposes, the procedure using 15% methanolic sulfuric acid was scaled up. Compound **4** was eluted first, followed by compound **5**, and no other identifiable material was obtained.

Tetrahydrocarbazole **4** was recrystallized from benzene–cyclohexane and obtained as crystals, mp 180–183°C; ir: 2.88, 5.61, 5.88; uv: 223 (30 000), 273 (6040), 278 (6100), 282 (6040), 289 (5150); $^1$Hmr: 2.05 (complex, 2, $D_2O$ reduces to 1), 2.66–2.94 (m, 3), 5.73 (d, $J$ = 8; 1), 6.66 (m, 1), 7.10 (s, 3), 7.26–7.58 (m, 3), 8.05 (m, 1); $^{13}$Cmr: 179.07(s), 177.35(s), 135.56(s), 134.30(s), 126.76(s), 122.03(d), 120.18(d), 119.69(d), 110.59(d), 103.61(s), 40.18(d), 39.58(d), 24.74(q), 21.32(t), 19.79(t). *Anal.* calcd. for $C_{15}H_{14}N_2O_2$: C 70.85, H 5.55, N 11.02; found: C 70.98, H 5.66, N 11.06.

Tetrahydrocarbazole **5** was recrystallized from benzene–methanol and obtained as crystals, mp 219–223°C; ir: 2.89, 5.63, 5.89; uv: 224 (28 000), 274 (6450), 282 (6740), 290 (5500); $^1$Hmr: 1.78 (broad s, 1, $D_2O$ removes), 2.45–3.05 (m, 4), 6.50–6.65 (m, 4), 6.85–7.05 (m, 2), 7.15 (s, 3); $^{13}$Cmr: ($CDCl_3$/DMSO-$d_6$): 181.04(s), 180.80(s), 136.55(s), 133.54(s), 127.51(s), 121.46(d), 119.61(d), 118.16(d), 112.07(d), 107.15(s), 25.81(q), 22.91(t), 21.33(t). *Anal.* calcd. for $C_{15}H_{14}N_2O_2$: C 70.85, H 5.55, N 11.02; found: C 70.75, H 5.71, N 11.13.

*Cyclohexenone* ***13*** *series*

The results obtained by the standard procedure with 7% and 15% methanolic sulfuric acid are reported in Table 1. The reactions in 30%, 45%, and 60% methanolic sulfuric acid produced complex mixtures which were not successfully separated by the standard chromatographic procedure. The material obtained from the 60% sulfuric acid was subsequently subjected to preparative tlc on alumina with elution by 95:5 benzene–methanol; the carbazole **16** (20%) and a trace of material considered to be the tetrahydrocarbazole **18** were isolated in this way. For preparative purposes the procedure using 15% methanolic sulfuric acid was scaled up. Compound **15** was eluted first followed by compound **14**; very small amounts of **16** and **18** were also obtained by a combination of chromatographic and fractional crystallization procedures.

Dihydrocarbazole **14** was recrystallized from benzene and obtained as crystals, mp 223–225°C; ir: 2.88, 5.78, 5.89; uv: 233 (20 750), 272 (8950), 278 (8700), 305 (3550), 369 (12 050); $^1$Hmr (220 MHz): 1.38 (br s, 1), 2.50–2.94 (m, 4), 5.97 (s, 3), 6.21 (s, 3), 7.17 (narrow m, 4; in $C_6D_6$ soln. becomes 7.41 (t, 2), 7.95 (t, 2), $J$ = 8). *Anal.* calcd. for $C_{16}H_{15}NO_4$: C 67.36, H 5.30, N 4.91; found: C 67.49, H 5.31, N 4.81.

Dicarbazole **15** was recrystallized from benzene–cyclohexane and obtained as crystals, mp 192–193°C; ir: 2.79, 5.79, 5.90; uv: 214 (end absorption; 15 350), 258 (10 200), 374 (13 600); $^1$Hmr (220 MHz): 2.33 (br s, 1), 2.44 (s, 1), 2.48–2.95 (complex, 4), 5.97 (dd, $J$ = 9, 2.5; 1), 6.29 (s, 3), 6.36 (s, 3), 6.38 (dd, $J$ = 17, 2.5; 1), 6.88 (dd, $J$ = 17, 9; 1). *Anal.* calcd. for $C_{16}H_{15}NO_4$: C 67.36, H 5.30, N 4.91; found: C 67.03, H 5.51, N 5.17.

Carbazole **16** was recrystallized from benzene and obtained as crystals, mp 136–137°C; ir: 2.89, 5.83; uv: 220 (end absorption; 20 000), 236 (23 600), 245 (25 000), 270 (45 500), 297 (12 800), 305 (11 500), 341 (3750); $^1$Hmr (60 MHz): 0.99 (br s, 1), 1.52–2.96 (complex, 6), 6.06 (s, 3), 6.10 (s, 3). *Anal.* calcd. for $C_{16}H_{13}NO_4$: C 67.84, H 4.63, N 4.95; found: C 67.88, H 4.69, N 5.04. Compound **16** was also prepared by stirring a solution of the dihydrocarbazole **15** (150 mg; 0.53 mmol) and dichlorodicyanoquinone (125 mg; 0.55 mmol) in 10 mL of dioxane at 80°C for 1 h. Filtration and evaporation afforded a residue which was chromatographed on alumina with elution by benzene to provide **16** (110 mg; 0.39 mmol). The same method was used to convert dihydrocarbazole **14** to carbazole **17**, mp 224–225°C; ir: 2.89, 5.80, 5.85; uv: 226 (end absorption; 27 200), 243 (19 200), 264 (25 400), 279 (44 000), 314 (5250), 323 (4800); $^1$Hmr (60 MHz): 2.40–2.80 (complex, 6), 5.83 (s, 3), 6.05 (s, 3). *Anal.* calcd. for $C_{16}H_{13}NO_4$: C 67.84, H 4.63, N 4.95; found: C 67.89, H 4.57, N 4.96.

Compound **18** was recrystallized from benzene in cyclohexane and obtained as crystals, mp 139–142°C; ir: 2.89, 5.79; uv: 225 (13 000), 274 (3050), 278 (3050), 282 (3050), 290 (2400); $^1$Hmr (60 MHz): 2.05 (broad s, 1), 2.44 (m, 1), 2.74–3.06 (complex, 3), 5.70 (d, $J$ = 6; 1), 6.26 (s, 3), 6.33 (s, 3), 6.68 (m, 1), 7.13–8.10 (complex, 4); *Exact Mass* calcd. for $C_{16}H_{17}NO_4$: 287.1157; found: 287.1157.

*Methyl 1-benzylindole-2-carboxylate (****7****)*

A solution of methyl indole-2-carboxylate (12.0 g; 68.6 mmol) in 60 mL of dry hexamethylphosphoric triamide (HMPT) was added over 2 h to a stirred slurry of sodium hydride (83 mmol) in 40 mL of HMPT maintained at 0°C. The reaction mixture was stirred at 0°C for a further hour and then allowed to warm to room temperature. Benzyl chloride (9.1 g; 72 mmol) was added over 0.5 h and the reaction mixture was stirred for a further 2 h. The mixture was poured into 700 mL of water containing 20 mL of concentrated hydrochloric acid and extracted with ether. The ether extract afforded **7** (16.4 g; 61.7 mmol), which was recrystallized from cyclohexane–acetone and obtained as crystals, mp 84–86°C; ir: 5.86; uv: 230 (end absorption, 20 000), 248 (4500), 293 (20 500); $^1$Hmr: 2.31 (dd, $J$ = 6.5, 1.5; 1), 2.61–3.05 (complex, 9), 4.18 (s, 2), 6.17 (s, 3). *Anal.* calcd. for $C_{17}H_{15}NO_2$: C 76.96, H 5.70, N 5.28; found: C 76.94, H 5.79, N 5.22.

*1-Benzylindole-2-carboxaldehyde (****8****)*

A solution of ester **7** (8.2 g; 30.9 mmol) and hydrazine hydrate (15 mL; 0.309 mol) in 25 mL of absolute ethanol was refluxed for 3 h and then allowed to stand. Crystals separated and were collected; the mother liquor afforded a further crop of crystals on evaporation (total yield 95%). Recrystallization from metha-

Can. J. Chem. Downloaded from www.nrcresearchpress.com by 210.87.254.6 on 09/06/12
For personal use only.

nol provided a sample, mp 186–189°C; ir: 2.90, 3.00, 6.00, 6.15; uv: 214 (end absorption; 28 800), 292 (16 100); $^1$Hmr: 2.33 (dd, $J$ = 7, 2; 1), 2.47 (broad m, 1), 2.64–3.10 (complex, 9), 4.22 (s, 2), 6.43 (broad m, 2). *Anal.* calcd. for $C_{16}H_{15}N_3O$: C 72.43, H 5.70, N 15.84; found: C 72.62, H 5.72, N 15.88.

Tosyl chloride (5.7 g; 30.0 mmol) was added to a stirred solution of the hydrazide (7.8 g; 29.4 mmol) in 90 mL of pyridine at 0°C; after 0.5 h at 0°C, the cooling bath was removed, and the stirring was continued for 2 h. The reaction mixture was poured into a mixture of ice and concentrated hydrochloric acid and the product was obtained as a solid which was collected by filtration and washed with dilute hydrochloric acid and water. The partially dry material was dissolved in methylene chloride and dried (magnesium sulfate). The methylene chloride afforded the crystalline tosylhydrazide (97% yield); recrystallization from ethanol provided a sample, mp 231–230°C; ir: 2.99, 5.98, 6.04; uv: 218 (end absorption; 30 200), 294 (17 700); $^1$Hmr: 0.55 (d, $J$ = 4; 1), 1.24 (m, 1), 2.13–3.22 (complex, 14), 4.46 (s, 2), 7.69 (s, 3); *Exact Mass* calcd. for $C_{23}H_{21}N_3SO_3$: 419.1304; found: 419.1304.

The tosylhydrazide (3.0 g; 7.1 mmol) was dissolved in a minimum (about 300 mL) of ethylene glycol at 150°C in a wide-mouthed vessel, and potassium carbonate (2.1 g; 15 mmol) was added in one lot. As soon as the vigorous effervescence ceased (about 1 min), the solution was poured into a large volume of ice. Ether extraction afforded the aldehyde **8** (1.6 g; 6.8 mmol); recrystallization from methanol provided a sample, mp 68–70°C; ir: 3.54, 5.99, 6.04, 6.19; uv: 210 (end absorption; 18 900), 231 (12 100), 307 (18 400); $^1$Hmr: 0.19 (s, 1), 2.33 (dd, $J$ = 8, 1; 1), 2.65–3.00 (complex, 9), 4.27 (s, 2). *Anal.* calcd. for $C_{16}H_{13}NO$: C 81.68, H 5.57, N 5.95; found: C 81.77, H 5.69, N 6.01.

*1-Benzyl-2-vinylindole (9)*

Methyltriphenylphosphonium bromide (3.4 g; 9.5 mmol) and butyllithium (9.5 mmol) in 50 mL of dry ether were stirred at reflux under a nitrogen atmosphere for 1.5 h, and then cooled to 0°C. An ether solution of aldehyde **8** (2.12 g; 9.0 mmol) was added and the mixture was refluxed for 1.5 h. The mixture was cooled and then treated with a solution of sodium sulfate (6.8 g) in 100 mL of water. The organic layer was washed with water, dried, and evaporated. The residue obtained was repeatedly triturated with petroleum ether (30–60°C); the petroleum ether solution was filtered and evaporated to provide the product as a yellow oil (1.78 g; 7.7 mmol): ir: 6.22; uv: 225 (16 000), 242 (10 900), 306 (12 900), 345 (1350); $^1$Hmr: 2.24–3.29 (complex, 10), 3.39 (dd, $J$ = 17.5, 11; 1), 4.31 (dd, $J$ = 17.5, 1.5; 1), 4.80 (s, 2), 4.85 (dd, $J$ = 11, 1.5; 1); *Exact Mass* calcd. for $C_{17}H_{15}N$: 233.1204; found: 233.1204.

*Diels–Alder adduct **10***

A solution of the vinylindole **9** (1.60 g; 6.9 mmol) and *N*-methylmaleimide (0.76 g; 6.9 mmol) in 35 mL of benzene was heated at 70°C for 21 h. Concentration of the solution and addition of cyclohexane caused the product **10** to separate as crystals; several crops were collected (total yield 52%). Recrystallization from benzene–cyclohexane provided a sample, mp 186–188°C; ir: 5.64, 5.86; uv: 224 (21 600), 276 (4100), 283 (4400), 292 (4000); $^1$Hmr: 1.97 (dd, $J$ = 6, 2; 1), 2.60–3.10 (complex, 8), 4.80 (s, 2), 5.69 (d, $J$ = 8; 1), 6.72 (m, 1), 7.10 (s, 3), 7.3–8.0 (complex, 4). *Anal.* calcd. for $C_{22}H_{20}N_2O_2$: C 76.72, H 5.85, N 8.13; found: C 76.77, H 6.04, N 8.06.

*Diels–Alder adduct **19***

A solution of the vinylindole **9** (2.0 g; 8.6 mmol), dimethyl acetylenedicarboxylate (1.2 g; 8.5 mmol), and hydroquinone (50 mg) in 50 mL of benzene was heated at 60°C for 1 h and at 40°C for 20 h. Evaporation of the solvent left a red oily residue; chromatography on an alumina column gave a fraction (1.0 g) that contained adduct **19** and some oxidized material **20**. This mixture of products (about 9:1) was separated by preparative tlc on alumina. Recrystallization of **19** from benzene–cyclohexane gave a sample, mp 151–153°C; ir: 5.75, 5.88; uv: 219 (end absorption; 19 000), 234 (24 900), 274 (11 600), 306 (5600), 369 (16 100); $^1$Hmr: 2.44–3.14 (complex, 9), 4.74 (s, 2), 5.95 (s, 3), 6.22 (s, 3), 7.16 (s, 4; in benzene forms symmetrical complex multiplet centred ~τ 7.5). *Anal.* calcd. for $C_{23}H_{21}NO_4$: C 73.58, H 5.64, N 3.73; found: C 73.74, H 5.76, N 3.76.

The carbazole **20** was also prepared by heating a solution of adduct **19** (250 mg; 0.67 mmol) and dichlorodicyanoquinone (160 mg; 0.70 mmol) in 5 mL of dioxane to 90°C for 25 min. Evaporation, chromatography on alumina, and recrystallization from benzene–cyclohexane provided **20**, mp 164–165°C; ir: 5.80, 5.85; uv: 216 (end absorption; 17 200), 231 (21 600), 247 (17 200), 266 (19 000), 281 (34 000), 316 (3750), 330 (3000), 342 (1500); $^1$Hmr: 1.94–2.10 (complex, 2), 2.57–3.16 (complex, 9), 4.64 (s, 2), 5.85 (s, 3), 6.10 (s, 3). *Anal.* calcd. for $C_{23}H_{19}NO_4$: C 73.98, H 5.13, N 3.75; found: C 74.11, H 4.96, N 3.85.

*Benzylation of **4***

A solution of compound **4** (100 mg; 0.39 mmol) in 5 mL of dry HMPT was added to a stirred slurry of sodium hydride (0.56 mmol) in 3 mL of HMPT maintained at 0°C. After 10 min the mixture was allowed to warm to room temperature, benzyl chloride (55 mg; 0.44 mmol) was added, and stirring was continued for 3 h. The reaction mixture was poured into water and extracted with methylene chloride. The extract afforded the product (**11**) as a white solid (42 mg; 0.10 mmol); recrystallization from benzene provided a sample, mp 264–265°C; ir: 5.63, 5.88; uv: 225 (end absorption; 25 800), 286 (5700), 293 (5750); $^1$Hmr: 1.33 (m, 1), 2.60–3.20 (m, 13), 4.81 (two peaks, 3 Hz separation; 2), 6.19 (d, $J$ = 14; 1), 6.50 (d, $J$ = 14; 1), 6.92 (m, 1), 7.15 (s, 3), 7.48–7.82 (complex, 4).

Compound **11** (31 mg; 0.07 mmol) was also prepared by treating compound **10** (101 mg; 0.29 mmol) with sodium hydride (0.31 mmol) in 5 mL of HMPT and benzyl chloride (45 mg; 0.35 mmol) in the manner just described.

*Benzylation of **14***

Compound **14** (60 mg; 0.20 mmol) was treated with sodium hydride (0.25 mmol) and benzyl chloride (30 mg; 0.26 mmol) in the manner described above, and converted to the compound **19** (20 mg; 0.70 mmol) described previously.

## Acknowledgement

This work was supported by a grant from the Natural Sciences and Engineering Research Council of Canada.

1. (*a*) B. Robinson. Chem. Rev. **63**, 387 (1963); ibid. **69**, 227 (1969); (*b*) F. M. Miller and W. N. Schinske. J. Org. Chem. **43**, 3384 (1978); (*c*) J. McLean, S. McLean, and R. I. Reed. J. Chem. Soc. 2519 (1955).
2. M. E. Jung and C. A. McCombs. Tetrahedron Lett. 2935 (1976); Org. Synth. **58**, 164 (1978).
3. L. G. Rashidyan, S. N. Asratyan, K. S. Karagezyan, A. R. Mkrtchyan, R. O. Sedrakyan, and G. T. Tatevosyan. Arm. Khim. Zh. **21**, 793 (1968); Chem. Abstr. **71**, 21972z (1969).
4. B. Lacoume, G. Milcent, and A. Olivier. Tetrahedron, **28**, 667 (1972); G. R. Allen. J. Heterocycl. Chem. **7**, 239 (1970).

# Biphasic photochemistry: micelle solutions as media for photochemical cycloadditions of enones[1]

NADER BERENJIAN, PAUL DE MAYO, MARY-ELLEN STURGEON, LEIV K. SYDNES, AND ALAN C. WEEDON

*Photochemistry Unit, Department of Chemistry, The University of Western Ontario, London, Ont., Canada N6A 5B7*

Received August 11, 1981

NADER BERENJIAN, PAUL DE MAYO, MARY-ELLEN STURGEON, LEIV K. SYDNES, and ALAN C. WEEDON. Can. J. Chem. **60**, 425 (1982).

The possible application in synthesis of a micellar solution as a medium in the photocycloaddition of enones to alkenes has been examined. It is found that the micelles are useful in increasing the effective concentration of reactants, have some ability in directing reaction regiochemistry, and may reduce hydrogen atom transfer in intermediate biradicals.

NADER BERENJIAN, PAUL DE MAYO, MARY-ELLEN STURGEON, LEIV K. SYDNES et ALAN C. WEEDON. Can. J. Chem. **60**, 425 (1982).

On a étudié la possibilité d'utiliser en synthèse une solution micellaire comme milieu réactionnel lors de l'addition photochimique des énones sur les alcènes. On a trouvé que les micelles servent à augementer la concentration effective des réactifs, qu'elles sont capables de diriger la régiochimie de la réaction et qu'elles peuvent réduire le transfert d'atome d'hydrogène dans les biradicaux intermédiaires.

[Traduit par le journal]

## Introduction

Photochemical cycloaddition between an alkene and an α,β-unsaturated ketone has proved to be a useful tool in synthesis (1–5). The process has been extensively employed for the preparation of cyclobutanes per se (2, 3, 5–8) and the method has also proved to be valuable for the generation of reactive four-membered rings that can undergo subsequent transformations (5, 9). However, the reaction suffers from the disadvantage that a large excess of alkene must be used to avoid enone dimerization and also, since it is bimolecular, reasonably high concentrations of both components are required. The latter can present a technical problem if a small scale reaction is performed,[2] whilst the former represents a source of inefficiency if the alkene used is accessible only with difficulty.

Another problem in the synthetic application of enone photocycloaddition is control of regiochemistry in the reaction between an α,β-unsaturated ketone and a nonsymmetrically substituted olefin. It has been known for some time that the regioselectivity is influenced by the substitution pattern of enone and alkene (8) as well as by the interactions of the overall dipoles of the reacting molecules (7, 10). Since the latter effect is strongly affected by the dielectric constant of the reaction medium, it has been possible, in some cases, to control the regioselectivity to some extent by solvent variation (7, 10). It has recently been demonstrated that photochemical cycloaddition between an enone and an alkene as well as enone photodimerization can occur between species solubilized in aqueous micelle solutions (11, 12). For example, photodimerization of 3-*n*-butylcyclopent-2-en-1-one, **1**, proceeds readily in aqueous potassium dodecanoate micelles (12). Furthermore, the regiochemistry of the addition is reversed as compared with the reaction in homogeneous solution. Thus, in the micellar environment the head-to-head dimer **3** is formed almost exclusively, whilst in benzene the head-to-tail dimer **2** is the major product.

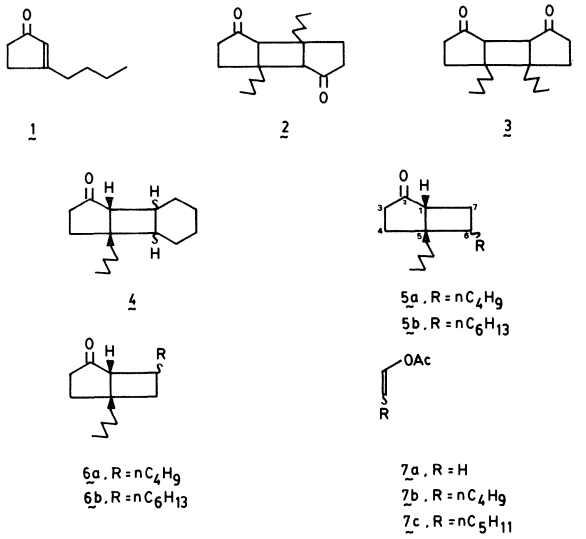


[1]Contribution number 267 from the Photochemistry Unit, Department of Chemistry, The University of Western Ontario.

[2]A 0.1 millimolar scale reaction at 1 molar concentration of reactants requires that 0.1 mL of solution be irradiated.

0008-4042/82/040425-12$01.00/0

©1982 National Research Council of Canada/Conseil national de recherches du Canada

Can. J. Chem. Downloaded from www.nrcresearchpress.com by 210.87.254.5 on 09/06/12
For personal use only.

Can. J. Chem. Downloaded from www.nrcresearchpress.com by 210.87.254.5 on 09/06/12
For personal use only.

TABLE 1. Relative yields[a] of photoadducts **4** and **3** as a function of enone and alkene concentration in potassium dodecanoate micelles.

| Average number of enone molecules per micelles | Average number of alkene molecules per micelle | Alkene | Yield of adduct **4** × 100 / combined yield of **4** + **3** |
|---|---|---|---|
| 0.55 | 0.54 | Cyclohexene | 74 |
| 0.55 | 0.82 | Cyclohexene | 82 |
| 0.55 | 1.09 | Cyclohexene | 88 |
| 0.55 | 2.18 | Cyclohexene | 94 |
| 0.51 | 0.50 | 1,2-Dimethyl cyclohexene | 48 |
| 0.51 | 1.00 | 1,2-Dimethyl cyclohexene | 68 |
| 0.51 | 2.00 | 1,2-Dimethyl cyclohexene | 88 |
| 0.51 | 4.00 | 1,2-Dimethyl cyclohexene | 93 |

[a]All irradiations taken to ca. 30% conversion. Absolute yields of adduct and dimer were determined by glc using *n*-docasane as an internal standard.

We describe here the results of our work[3] concerning the mixed photochemical cycloaddition of α,β-unsaturated ketones with alkenes in aqueous micellar solutions, which show that the micellar environment has potential utility as a medium for overcoming the problems described above.

## Results and discussion

### *Photochemical cycloaddition of 3-*n*-butylcyclopent-2-en-1-one, **1**, to cyclohexene and 1,2-dimethylcyclohexene in micelles; examination of the effect of reactant stoichiometry upon product distribution*

Irradiation of a cyclopentenone in the presence of cyclohexene results in the formation of cyclobutane ring-containing adducts, e.g., **4** (1–3). If the concentration of alkene is low, cyclopentenone dimers (e.g., *syn* and *anti* isomers of **2** and **3**) are also formed; in the absence of alkene, dimers are formed exclusively. It was of interest to us to determine if the reaction could be performed in a micellar environment and to determine the minimum alkene concentration required to prevent appreciable enone dimer formation. Solutions of cyclohexene and 3-*n*-butylcyclopentenone, **1**, in aqueous potassium dodecanoate (0.08 *M*) were irradiated to approximately the same conversion to give the "head-to-head" enone photodimer **3** (12) and the photoadducts **4**. The yields of the products were determined as a function of the mean concentrations of the reactants in the micelles. The study was repeated using 1,2-dimethylcyclohexene and the results are given in Table 1 and expressed graphically in Fig. 1. The mean concentrations of reactants in the micelles were calculated assuming a critical micelle concentration (CMC) for surfactant of 0.024 *M* (13) and an aggregation number of 47 (14). The concentration of micelles is then given by eq. [1]:

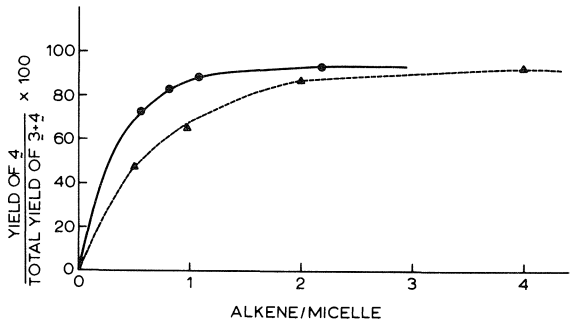


FIG. 1. Relative yield of photoadduct against average number of alkene molecules in each micelle for an average of half an enone/micelle. —●—●—● reaction with cyclohexene; --●-----●--- reaction with dimethylcyclohexene.

$$[1]\quad \text{micelle concentration} = \frac{M - \text{CMC}}{47}$$

Avogadro's number of micelles/L

where *M* is the concentration of potassium dodecanoate. If it is assumed that all alkene and cyclopentenone are dissolved within the micelles and essentially none remains in the aqueous exterior (12), then an average number of molecules of each reactant in each micelle can be calculated. The probability of finding a given number of molecules in each micelle can be determined assuming a Poisson distribution (15). 3-*n*-Butylcyclopentenone

[3]For a preliminary account of part of this work see ref. 12*c*.

Can. J. Chem. Downloaded from www.nrcresearchpress.com by 210.87.254.5 on 09/06/12
For personal use only.

was used in order to ensure that most of the enone would be dissolved in the micelles rather than in the aqueous phase.

The results shown in Table 1 and Fig. 1 indicate that the cycloaddition, to give mixed adducts **4** or dimers, proceeds selectively with respect to mixed adduct formation if the cyclohexene enone ratio is 2:1 or greater, whilst the more hindered 1,2-dimethylcyclohexene requires a ratio of 4:1 for the same selectivity. It was also found that increasing enone and alkene concentration together (i.e., from 1/2 enone/micelle and 1/2 alkene/micelle to 2 enone and 2 alkene/micelle) did not greatly alter the observed photodimer/adduct ratio. These results suggest that micelles are not serving to isolate enone molecules from one another but rather are concentrating the enone and alkene molecules so that their effective concentrations are high even though the bulk concentrations are low. Also, since potassium dodecanoate concentration can be raised as high as 0.5 *M* without drastically altering the aggregation number of the micelle (16), in principle it is possible to handle anywhere from submilligram to gram quantities of reactants.

*Irradiation of 3-*n*-butylcyclopentenone, **1**, in micelles in the presence of nonsymmetrical alkenes; examination of product regiochemistry*

Recently it was demonstrated that the photochemical dimerization of 3-*n*-butylcyclopentenone can be performed in micelles as well as in organic solvents and that the micellar medium greatly affected the regiochemistry of the products. Thus, whereas in nonpolar solvents mainly the head-to-tail dimer **2** was observed and in polar solvents a mixture of head-to-tail and head-to-head dimers **3** and **2** in roughly equal amounts, in micellar potassium dodecanoate the head-to-head dimer **3** was formed almost exclusively (12). The alteration of the reaction regiochemistry is greater than can be reasonably ascribed to change in dielectric constant of the medium (which appears to be the controlling factor in solution (7)) and is possibly owing to some orienting effect of the micelle in which a solubilized molecule containing hydrophilic and hydrophobic components will align itself with the surfactant molecules to maximize hydrophilic and hydrophobic interactions.

Described here are the results of an examination of the stereochemistry of products obtained by mixed photochemical cycloaddition of 3-*n*-butylcyclopentenone and nonsymmetrical olefins in potassium dodecanoate micelles.

*Reactions with simple alkenes*

Photocycloaddition of 3-*n*-butylcyclopentenone in the presence of an excess of 1-hexene and 1-octene in organic solvents proceeded smoothly to afford mixtures of the corresponding adducts **5** and **6**. Regioisomers **5**, resulting from head-to-head[4] attack of the enone to the olefin, could in both cases be unequivocally distinguished from isomers **6**, derived from head-to-tail attack, by comparing the $^{13}C$ nmr spectra of pure samples of the regioisomers obtained by preparative vapour phase chromatography. Thus, in structure **5**, C-5 experiences an α-shielding effect whilst in **6** C-5 experiences a β-deshielding effect from the *n*-butyl substituent at C-7 (17). Similarly C-1 in structure **6** experiences an α-shielding effect and in **5** a β-deshielding effect from the butyl group. Consequently in the head-to-head regioisomer **5** the resonances assigned to C-1 and C-5 should be shifted to lower and higher fields respectively, whilst in the head-to-tail regioisomer **6** the resonances assigned to C-1 and C-5 should be shifted to higher and lower fields respectively. Applying these predictions to the data compiled in Table 2 for the cycloadducts obtained with 1-hexene and 1-octene in organic solvents, it is clear that the major isomer in both cases is formed by head-to-head attack to give **5**. It is also noteworthy that **5** in both cases consists almost exclusively of a single isomer, the stereochemistry of which is unknown, whilst in **6** both possible isomers, epimeric at C-7, are observed.

The photocycloaddition of 3-*n*-butylcyclopentenone to 1-hexene and 1-octene gave the corresponding adducts in near quantitative yield in a variety of solvents, but in both cases the regioisomeric composition of the product mixture was solvent dependent. Thus, with 1-hexene the ratio of **5***a*/**6***a* changed from 51:49 in cyclohexane to 57:43 in diethyl ether. When the reaction was performed in micellar potassium dodecanoate a ratio of 78:22 was obtained. A more pronounced variation was observed with 1-octene; the ratio of **5***b*/**6***b* changed from 53:47 in cyclohexane to 63:38 in acetonitrile (Table 3). When the reaction was performed in micellar potassium dodecanoate a ratio of 88:12 was obtained.

It has been reported (7, 10) that dipole–dipole interactions between reactants in photochemical cycloadditions can control the reaction regiochemistry. These interactions are sensitive to variations in solvent polarity and have been related to the dielectric constant of the medium by the Kirkwood–Onsager equation (18). In Fig. 2, the logarithm of the ratio of cycloadducts, **5***b*/**6***b*, is plotted against

[4]In this context, the more hydrophobic end of the molecule is termed the tail.

TABLE 2. $^{13}C$ nmr chemical shifts of selected carbon atoms in photoadducts **5** and **6** produced from cycloaddition of 1-hexene and 1-octene to 3-*n*-butylcyclopentenone **1** in organic solvents

| Olefin | Isomer | C-1 | C-5 | Assignment |
|---|---|---|---|---|
| 1-Hexene | Major regioisomer: | | | |
| | major stereoisomer | 47.1 | 48.9 | **5***a* |
| | minor stereoisomer[a] | | | |
| | Minor regioisomer: | | | |
| | major stereoisomer | 56.2 | 42.2 | **6***a* |
| | minor stereoisomer | 53.0 | 39.8 | **6***a* |
| 1-Octene | Major regioisomer: | | | |
| | major stereoisomer | 47.1 | 48.9 | **5***b* |
| | minor stereoisomer[a] | | | |
| | Minor regioisomer: | | | |
| | major stereoisomer | 56.2 | 42.2 | **6***b* |
| | minor stereoisomer | 53.1 | 39.8 | **6***b* |

[a]Present in very small amounts only.

TABLE 3. Product composition as a function of medium in the photocycloaddition of 1-hexene to 3-*n*-butylcyclopentenone, **1**

| Solvent | ε[a] | **5***b*:**6***b*[b] |
|---|---|---|
| Cyclohexane | 2.02 | 53:47 |
| Diethylether | 4.34 | 47:43 |
| Ethyl acetate | 6.02 | 59:41 |
| Methanol | 32.63 | 62:38 |
| Acetonitrite | 37.50 | 63:37 |
| 0.08 *M* Aqueous potassium dodecanoate | — | 88:12 |

[a]Dielectric constant at 20°C.
[b]Determined by glc; expressed as a ratio of noncalibrated areas of peaks assigned to each regioisomer.

the Kirkwood–Onsager function; a linear relationship appears to hold for the organic solvents used and the maximum value of the dielectric term (0.5) predicts a value of 64:36 for the maximum ratio of **5***b* to **6***b*. The ratio obtained in micellar potassium dodecanoate (88:12), therefore, suggests factors other than the bulk dielectric constant of the medium are controlling the regiochemistry of the cycloaddition. This was confirmed when the photocycloaddition between 3-*n*-butylcyclopentenone and 1-octene was performed in aqueous potassium dodecanoate below the critical micelle concentration; a ratio of **5***b* to **6***b* of 62:38 was obtained which is similar to that obtained in polar organic solvents even though submicellar aggregates may be present.

These results are consistent with the simplified micelle model shown in Fig. 3 in which the cyclopentenone is oriented in the micelle with the polar carbonyl function in the water–micelle interface and the hydrophobic butyl tail in the micelle interior. Similarly, the hydrophobic alkene is mainly incorporated into the relatively nonpolar micelle

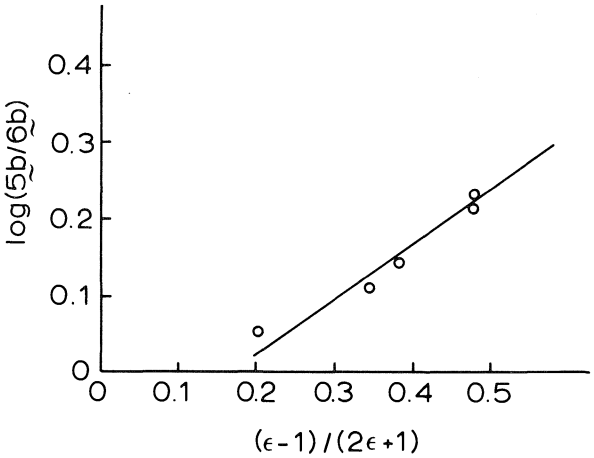


FIG. 2. Variation of the ratio of **5***b* to **6***b* with the solvent dielectric constant (Kirkwood–Onsager plot).

interior; as a result the most likely orientation for reaction between the photoexcited enone and the alkene is that shown in Fig. 3, leading to an increase in the proportion of head-to-head regioisomers **5**.

*Reactions with alkenyl acetates*

If the model suggested above correctly describes the origin of the regioselectivity observed in the irradiation experiments in micelles, then the presence of a polar group on the alkene would be expected to enhance the effect. For example, a 1-acetoxy-1-alkene would orient in a micelle with the polar acetate at the micelle–water interface and the hydrophobic alkyl chain in the nonpolar interior; interaction with a similarly oriented, photoexcited 3-*n*-butylcyclopentenone molecule would afford the head-to-head isomer at the expense of the head-to-head isomer at the expense of the head-to-tail isomer.

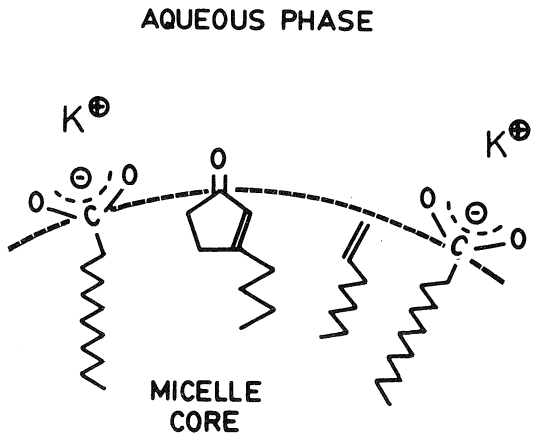


FIG. 3. Representation of proposed model showing orienting effect of micelle upon enone **1** and an alkene.

Can. J. Chem. Downloaded from www.nrcresearchpress.com by 210.87.254.5 on 09/06/12
For personal use only.

Can. J. Chem. Downloaded from www.nrcresearchpress.com by 210.87.254.5 on 09/06/12
For personal use only.

Experimentally, this was found to be the case; irradiation of 3-*n*-butylcyclopentenone in the presence of 1-alkenylacetates, **7**, gave a mixture of regioisomers **8** and **9**, and when the reaction medium was changed from organic solvent to

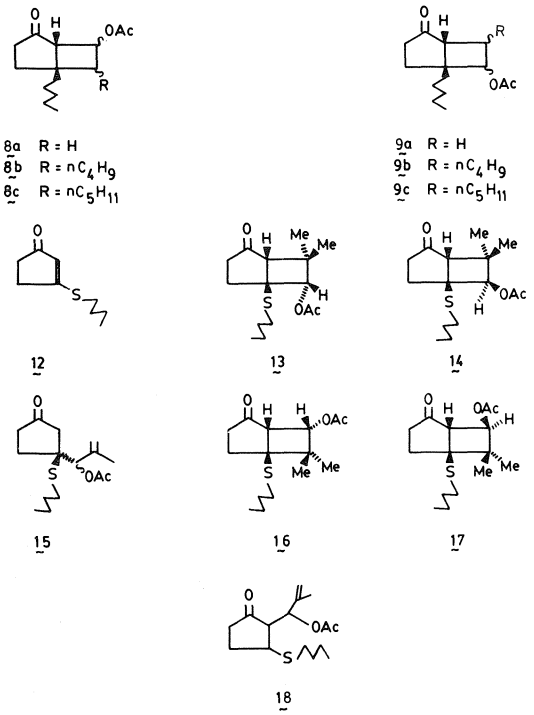


aqueous micellar potassium dodecanoate the proportion of **8** increased relative to **9**. The effect was even discernable in the photoaddition between enone **1** and vinyl acetate which has a very short hydrophobic chain. Thus, the ratio of **8***a* to **9***a* changed from 1:3 in organic solvents to 1:1 in micellar potassium dodecanoate (Table 4).

As was the case with compounds **5** and **6**, the regioisomers derived from reaction of 3-*n*-butylcyclopentenone with vinyl acetate could be conveniently distinguished by their $^{13}C$ nmr spectra, and the results are summarized in Table 5. The assignments were confirmed by hydrolyzing a 1:3 mixture of the acetates **8***a* and **9***a* and oxidizing the alcohols obtained to the corresponding ketones (Scheme 1). Comparison of the $^{13}C$ nmr spectrum of the major component of the mixture of ketones with that of bicyclo[3.2.0]heptan-2,6-dione[5] (Table 6) demonstrates, taking into account $\alpha$, $\beta$, and $\gamma$ shielding and deshielding effects, that the major product is 5-*n*-butylbicyclo[3.2.0]heptan-2,6-dione, **11***a*.

[5]H. J. Leu and J. B. Stothers, private communication.

TABLE 4. Product composition in the photocycloaddition of 3-*n*-butylcyclopentenone, **1**, with vinyl acetate, **7***a*, as a function of medium

| Solvent | **8***a*: **9***a*[a] |
|---|---|
| Cyclohexane | 25:75 |
| Diethyl ether | 26:74 |
| Methanol | 23:77 |
| 0.08 *M* Aqueous potassium dodecanoate | 51:49 |

[a]Determined by glc; expressed as a ratio of noncalibrated areas of peaks assigned to each regioisomer.

TABLE 5. $^{13}C$ nmr chemical shifts of selected carbon atoms of cycloadducts obtained by irradiation of 3-*n*-butylcyclopentenone, **1**, with vinyl acetate **7***a* in diethyl ether

| Isomer | C-1 | C-5 | Assignment |
|---|---|---|---|
| Major regioisomer: | | | |
| major stereoisomer | 43.8 | 52.7 | **9***a* |
| minor stereoisomer | 44.2 | 51.5 | **9***a* |
| Minor regioisomer: | | | |
| major stereoisomer | 54.8 | 41.3 | **8***a* |
| minor stereoisomer | 57.7 | 41.3 | **8***a* |

A more pronounced effect of the micellar environment upon cycloaddition regiochemistry was observed in the reaction of 3-*n*-butylcyclopentenone with 1-hexenyl acetate and 1-heptenyl acetate. Thus, irradiation of 3-*n*-butylcyclopentenone with 1-heptenyl acetate in organic solvents gave four adducts in the ratio 50:20:20:10 as judged by uncalibrated peak areas on glc, whilst in aqueous micellar potassium dodecanoate six adducts were observed in the ratio 10:5:25:35:20:5. Because of the large number of products, and the difficulty of their separation, identification of individual isomers and assignment of relative stereochemistries and regiochemistries was not possible. Instead the adducts were converted to the ketones via hydrolysis and oxidation as depicted in Scheme 1.

Two mixtures of cycloadducts, one obtained by photoaddition of enone to 1-hexenyl acetate in diethyl ether and the other from enone and 1-heptenyl acetate in cyclohexane, were subjected to the hydrolysis/oxidation sequence. The only compounds detected by glc were the stereoisomers **11***b* and **11***c*, and none of the regioisomers **10***b* and **10***c*. Both stereoisomeric mixtures were isolated in good yield (> 80%), and their infrared spectra exhibited the expected strong absorption bands at 1775 $cm^{-1}$ and 1735 $cm^{-1}$ assigned to the cyclobutanone and cyclopentanone carbonyl groups respectively. The

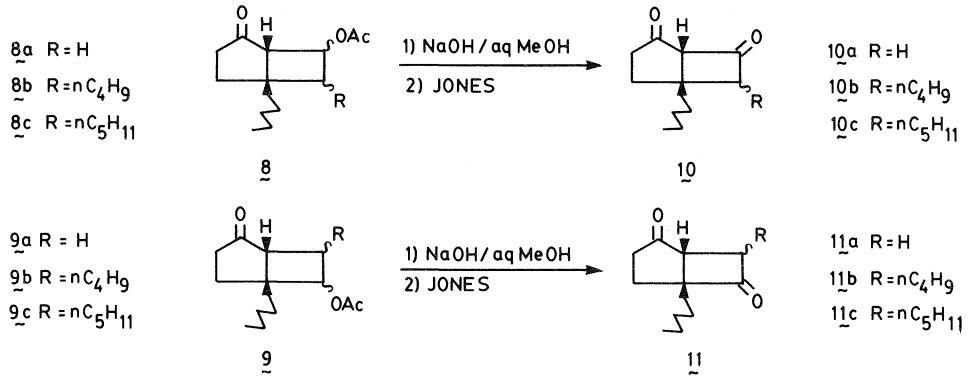


SCHEME 1

$^{13}C$ nmr spectra of the diketones were compared with those of bicyclo[3.2.0]heptan-2,6-dione and 5-*n*-butylbicyclo[3.2.0]heptan-2,6-dione, **11***a*, (Table 6), and allowing for shielding and deshielding effects of alkyl substituents clearly indicate that the products are 2,6-diketones, and not 2,7-diketones (Table 7). The assignment was supported by the failure to observe the formation of ketoacids when the diketones were treated with aqueous potassium hydroxide (8). The cycloaddition between enone **1** and 1-hexenyl and 1-heptenyl acetates in organic solvents appears to be highly regioselective, giving only the head-to-tail adducts.

In the light of this result, a reaction mixture from photocycloaddition between 1-heptenyl acetate and enone **1** in aqueous micellar potassium dodecanoate was treated with base followed by oxidation according to Scheme 1. The base hydrolysis of the acetate adducts proceeded smoothly, but the oxidation of the resulting alcohols, which was followed by glc, proceeded at varying rates for different components of the mixture. Initially, the main product was diketone **11***c*, followed by slower formation of a second product identified as **10***c*. At extended reaction times a secondary process became evident which caused depletion of **10***c* to an unidentified product. Thus, after three hours reaction, uncalibrated glc analysis indicated a mixture of **11***c* (16%), peaks assigned to **10***c* (49%), and unreacted alcohols (35%), whilst after six hours oxidation a mixture of **11***c* (15%), **10***c* (29%), unconverted alcohol (11%), and unidentified secondary product 44% was observed. Work-up gave a mixture of **11***c* and **10***c* in a ratio of approximately 1:2. Attempted separation and purification of **10***c* failed because of decomposition and the structure was deduced from the spectroscopic data of the mixture allowing for the presence of **11***c*. In the infrared spectrum, the expected strong absorptions assigned to the cyclobutanone and cyclopentanone carbonyls were observed at 1775 $cm^{-1}$ and 1745 $cm^{-1}$ respectively. In the $^1H$ nmr spectrum, as well as a complex multiplet in the region 0.50–2.93 ppm, two triplets at 3.20 and 3.23 ppm were observed in a ratio of approximately 1:2. These signals are assigned to the proton at the C-1 position between the carbonyls of the isomeric β-diketones **10***c* epimeric at C-6 and the splitting arises from 1,3 coupling across the cyclobutane ring. The coupling constant of the major triplet was 1.5 Hz, that of the minor 0.5 Hz, suggesting that the predominant stereoisomer of **10***c* has the butyl group and pentyl group *trans* to each other (19). The $^{13}C$ nmr spectrum of regioisomers **10***c* confirmed the structural assignment; the data are given in Table 8 and are substantially different from those for the 2,6-diketones **11***c* given in Tables 6 and 7.

Thus photolysis of 3-*n*-butylcyclopentenone with 1-heptenyl acetate in organic solvents, followed by hydrolysis and oxidation, yields stereoisomeric

TABLE 6. $^{13}C$ nmr chemical shifts of selected carbon atoms of bicyclo[3.2.0]hepta-2,6-dione and 5-*n*-butylbicyclo[3.2.0]-hepta-2,6-dione, **11***a*

| | C-1 | C-5 | C-7 |
|---|---|---|---|
| Bicyclo[3.2.0]hepta-2,6-dione | 36.1 | 61.9 | 52.3 |
| 5-*n*-Butylbicyclo[3.2.0]hepta-2,6-dione | 41.4 | 73.3 | 50.0 |

TABLE 7. $^{13}C$ nmr chemical shifts of selected carbon atoms of cycloadducts **11***b* and **11***c* obtained from photocycloaddition of 3-*n*-butylcyclopentenone, **1**, with 1-heptenyl acetate, **7***c*, and with 1-hexenyl acetate, **7***b*, following hydrolysis and oxidation

| | C-1 | C-5 | C-7 |
|---|---|---|---|
| **11***b* (Major stereoisomer) | 48.7 | 69.7 | 63.5 |
| **11***b* (Minor stereoisomer) | 47.3 | 70.7 | 62.8 |
| **11***c* (Major stereoisomer) | 48.7 | 69.7 | 63.5 |
| **11***c* (Minor stereoisomer) | 47.3 | 70.8 | 62.9 |

Can. J. Chem. Downloaded from www.nrcresearchpress.com by 210.87.254.5 on 09/06/12
For personal use only.

TABLE 8. $^{13}C$ nmr chemical shifts of selected carbon atoms of cycloadducts **10***c* obtained by photocycloaddition of 3-*n*-butylcyclopentenone, **1**, with 1-heptenyl acetate, **7***c*, in aqueous potassium dodecanoate followed by hydrolysis and oxidation

| | C-1 | C-5 | C-6 |
|---|---|---|---|
| Major stereoisomer | 71.4 | 49.7 | 57.9 |
| Minor stereoisomer | 70.2 | 50.0 | 57.8 |

bicyclo[3.2.0]heptan-2,6-diones **11***c* as the only cycloaddition products whereas, if the irradiation is performed in aqueous micellar potassium dodecanoate, a mixture of the 2,6-diones and the regioisomeric bicyclo[3.2.0]heptan-2,7-diones **10***c* are obtained, in which the latter comprises at least 70% of the total. Consequently, whereas head-to-tail addition is the only mode of photochemical cycloaddition in organic solvents, in the micelle the proportion of head-to-head addition rises from zero to a minimum of 70% of the total. This strong directing effect exerted by the micellar environment is greater than in the case of vinyl acetate, possibly because of the relatively long hydrophobic alkyl chain of the heptenyl acetate. This is consistent with the model proposed in Fig. 3.

*Photochemical cycloaddition of 3-(*n*-butylthio)-cyclopent-2-en-1-one,* ***12***

Photochemical additions between alkenes and the enolic derivatives of cyclic β-diketones have been much used in synthesis because of the ability of the intermediate cyclobutanol derivative to open to give a larger ring (4, 9) (Scheme 2). However, inability to control the regiochemistry of this reaction represents a limitation. The directing effect of aqueous potassium dodecanoate micelles described above suggested a method of controlling regiochemistry in this synthetically useful reaction.

Reported here are the results of an investigation of the photochemical cycloaddition reactions of 3-(*n*-butylthio)cyclopent-2-en-1-one **12**. This molecule was chosen in preference to an oxygen analogue because of the relative nonpolarity of the sulphur substituent; it was hoped that the carbonyl function would control the orientation of the molecule in a micellar environment in a similar manner to that observed for 3-*n*-butylcyclopent-2-en-1-one.

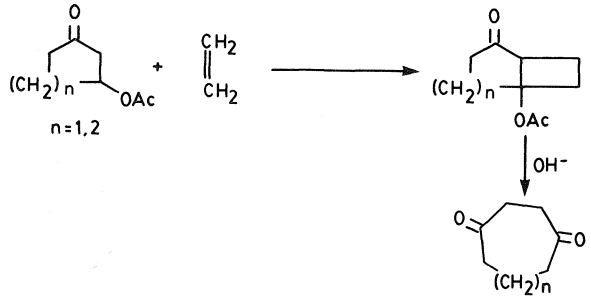


SCHEME 2

The enone **12** was irradiated in the presence of isobutenyl acetate in cyclohexane to 76% conversion to give a mixture of five products as judged by glc. A combination of thin-layer chromatography and preparative glc allowed the isolation of four of these compounds which were assigned the structures **13**, **14**, **15**, and **16**. The fifth component of the mixture was present in too small a quantity to allow isolation.

Repetition of the reaction to 52% conversion in aqueous potassium dodecanoate micelles using concentrations of enone, enol acetate, and surfactant such that on average each micelle contained less than one enone and more than three enol acetate molecules gave five products, four of which were isolated by preparative hplc. The fifth was present in too small a quantity to be isolated. The four products were assigned structures **13**, **14**, **16**, and **17**.

The structures of the products were deduced from their mass spectra and $^1H$ nmr spectra. Compounds **13** and **14** both exhibited weak molecular ions and fragments corresponding to sequential loss of carbon monoxide, an acyl group, and propene, to give base peaks at 161 mass units. The molecular ions of **16** and **17** were not observed, but the fragmentation patterns were consistent with those expected.

Head-to-head adducts **16** and **17** were differentiated from head-to-tail adducts **13** and **14** by comparison of the magnitudes of the coupling constants of the protons geminal to the acetoxy functions. In **16** and **17** these protons experience vicinal coupling with the adjacent methines ($J$ = 9 and 7 Hz respectively) and in **13** and **14** the isolated acetoxyl protons are weakly coupled across the cyclobutane ring ($J$ = 0.9 and 1.1 Hz respectively) (19).

The relative stereochemistries of compounds **13** and **14** were determined by nuclear Overhauser enhancement of the acetoxyl substituted methines following selective irradiation of the adjacent methyls. In structure **13** (Fig. 4) $Me_A$ appears at 0.90 ppm and $Me_B$ appears at lower field (1.40 ppm) owing to a deshielding effect by the carbonyl group. Selective irradiation of $Me_B$ caused a nuclear Overhauser enhancement of $H_A$ which was not observed when $Me_A$ was irradiated. Similarly in **14** (Fig. 4), $Me_A$ appeared at 1.03 ppm and $Me_B$ 1.34 ppm; irradiation of $Me_A$ caused an enhancement of $H_B$,

Can. J. Chem. Downloaded from www.nrcresearchpress.com by 210.87.254.5 on 09/06/12
For personal use only.

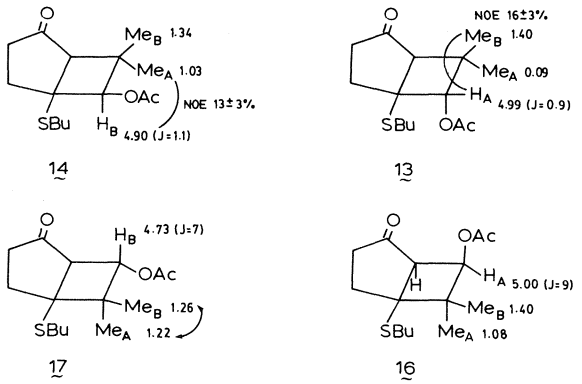


FIG. 4. Structures **13**, **14**, **16**, and **17** with relevant $^1$H nmr data. The assignments for methyls A and B in **17** may be reversed.

which was not observed when Me$_B$ was irradiated. These results are summarized in Table 9.

The assignment of relative stereochemistries to **16** and **17** is based upon a comparison of the chemical shifts of the acetoxyl-substituted methine protons. In compounds **13**, **14**, and **16**, this proton appears at 4.99, 4.90, and 5.00 ppm respectively; in **17** it has been shifted upfield to 4.74 ppm. This is ascribed to the shielding effect of the adjacent carbonyl (Fig. 4).

Compound **15** presumably arises from intramolecular abstraction in the diradical initially formed from the addition of the photoexcited enone **13** to the isobutenyl acetate (3). The mass spectrum of **15** showed a weak molecular ion and a consistent fragmentation pattern in which peaks corresponding to loss of the acetoxy group and the whole acetoxy-containing side chain followed by loss of butene to give the base peak were seen (Scheme 3). The $^1$H nmr spectrum contained a multiplet at 5.07 ppm corresponding to the vinylic methylene and a peak at 5.31 ppm assigned to the acetoxyl-substituted methine. This signal appeared as a broadened singlet, unambiguously distinguishing **15** from the alternative possible structure **18**, where a doublet would be observed.

Compounds **13**, **14**, and **15** are derived from head-to-tail addition of the enol acetate to enone **13**, whilst compounds **16** and **17** derive from head-to-head addition. The relative yields of each product from the reaction performed in cyclohexane, and in aqueous potassium dodecanoate micelles, were determined by glc, and the results are shown in Table 10. It can be seen that whereas in cyclohexane solution the reaction gives predominantly head-to-tail products with considerable amounts of olefinic by-product (compound **15**), in the micellar medium the production of the latter is completely quenched and the proportion of head-to-head adduct is greatly increased.

TABLE 9. Nuclear Overhauser enhancement for cyclobutane ring methines in cycloadducts **13** and **14**

| Proton observed in Fig. 3 | δ (ppm) | Protons irradiated | δ (ppm) | Observed increase in intensity (%) |
|---|---|---|---|---|
| **13** H$_A$ | 4.99 | Me$_A$ | 0.90 | 0 |
| | | Me$_B$ | 1.40 | 16±3 |
| **14** H$_B$ | 4.90 | Me$_A$ | 1.03 | 13±3 |
| | | Me$_B$ | 1.34 | 0 |

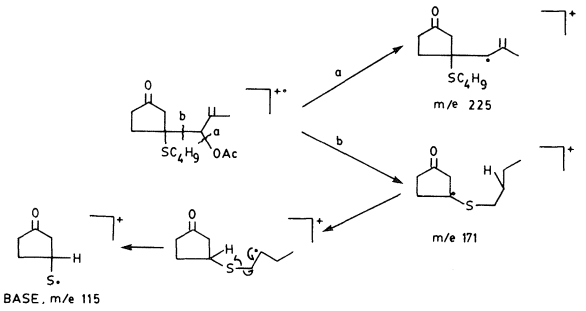


SCHEME 3

## Conclusion

From the foregoing, we conclude that the use of micelles in photocycloaddition has, in special cases, synthetic utility. These are: (a) as a means of increasing effective concentration when small amounts of reactants are available, (b) where head-to-head regioisomers are desired, and (c) when it is desirable to suppress hydrogen transfer in the intermediate biradicals (leading to alkenes).

## Experimental

All proton and carbon nmr spectra were recorded in $CDCl_3$. Carbon spectra were obtained on a Varian XL-100-15 system and assignments were made by comparison of decoupled and off-resonance spectra. All chemical shifts are in δ values relative to tetramethylsilane internal standard. Irradiations were performed using a 450 W Hanovia medium pressure mercury lamp suspended in a water cooled Pyrex jacket, unless otherwise stated. Small scale irradiations in organic solvents were carried out in sealed tubes which had been degassed to a residual pressure of $2 \times 10^{-5}$ Torr by at least three freeze–pump–thaw cycles. Preparative irradiations and micelle solution irradiations were performed under oxygen-free nitrogen using solutions which had been deoxygenated by purging with nitrogen for at least 30 min. Micelle solutions were prepared using triply distilled water and organic substrates were dissolved by immersing solutions in an ultrasonic bath.

*Irradiation of 3-*n*-butylcyclopent-2-en-1-one, 1, with cyclohexene*

3-*n*-Butycyclopentenone, **1**, was prepared by the method of Buchi and Egger (20) and had $\lambda_{max}$ (95% EtOH): 228 nm (ε = 13 500)

Can. J. Chem. Downloaded from www.nrcresearchpress.com by 210.87.254.5 on 09/06/12
For personal use only.

TABLE 10. Product distribution obtained from irradiation of 3-(*n*-butylthio)cyclopentenone, **12**, with isobutenyl acetate in cyclohexane and in aqueous potassium dodecanoate

| Solvent | Product yield[a] 13 + 14 | 15 | 16 | 17 | Ratio of regioisomers[b] (13 + 14 + 15):(16 + 17) |
|---|---|---|---|---|---|
| Cyclohexane[d] | 61 | 27 | 9 | —[c] | 88:9 |
| Potassium dodecanoate micelles[e] | 41 | —[c] | 35 | 14 | 41:49 |

[a]Determined by glc; expressed as a ratio of uncalibrated areas of peaks assigned to each isomer.
[b]For this purpose the olefinic product **15** is designated as a head-to-tail product as it is derived from initial head-to-tail interaction of enone and alkene.
[c]Too small to be measured.
[d]3% unidentified compounds.
[e]9% unidentified compounds.

and 297 nm (ε = 49). Cyclohexene was distilled from calcium hydride under nitrogen.

3-*n*-Butylcyclopentenone (271 mg) was dissolved in cyclohexene (20 mL) and irradiated for 3 h, after which time tlc showed almost complete disappearance of the enone. The glc analysis of the mixture (3% SE 30 at 130°C, and 5% FFAP at 130–170°C) indicated clean formation of two products, in approximately equal amounts. A sample of the reaction mixture was purified by preparative glc (15% FFAP, 180°C). The component with the shorter retention time was a colourless oil and was shown by $^{13}C$ nmr to be a mixture of two isomers of **4**, whilst the component with the longer retention time, which was also a colourless oil, was a single isomer of **4**.

The faster component had the following data: $\nu_{max}$ (film): 2920, 2860, 1730, 1450 $cm^{-1}$; $\lambda_{max}$ (95% EtOH): 289 nm (ε = 35); $^1H$ nmr ($CDCl_3$) (100 MHz): 2.63–2.23 (3H, m), 1.9–1.1 (18H, m), 0.93 (3H, t, 6 Hz), 0.90 (3H, t, 6 Hz); $^{13}C$ nmr ($CDCL_3$): 14.1 (2 methyl groups), 23.3, 23.5, 24.4, 26.1, 26.3, 26.5, 26.7, 27.2, 27.6, 27.8, 28.5, 28.6, 30.5, 31.2, 32.6, 39.3, 40.4, 40.5 (all $CH_2$ groups), 41.7 (methine) 42.5 (methine), 48.3 (methine), 51.2 (quaternary), 51.5 (methine), 53.5 (quaternary), 55.0 (methine), 59.8 (methine), 219.4, 222.5 (carbonyls) ppm; *m/e* (25 eV): 220 ($M^+$, 3%), 191 (3%), 149 (100%); *Mol. Wt.* calcd. for $C_{15}H_{24}O$: 220.1827; found: 220.1825.

The component with the longer retention time had the following data: $\nu_{max}$ (film): 2940, 2870, 1730, 1460 $cm^{-1}$; $\lambda_{max}$ (95% EtOH): 287 nm (ε = 44); $^1H$ nmr ($CDCl_3$) (100 MHz): 2.7–1.9 (6H, m), 1.85–1.05 (15H, m), 0.90 (3H, t, 6 Hz); $^{13}C$ nmr ($CDCl_3$): 14.1 (methyl), 22.0, 22.1, 23.4, 23.5, 26.4, 26.8 (all methylenes), 32.6 (methine), 32.9, 34.9, 39.2 (all methylenes), 40.7 (methine), 46.5 (quaternary), 55.4 (methine), 221 (carbonyl) ppm; *m/e* (25 eV): 220 ($M^+$, 3%), 191 (1%), 149 (100%), *Mol. Wt.* calcd. for $C_{15}H_{24}O$: 220.1827; found: 220.1825.

Repetition of the reaction in potassium dodecanoate solution gave the same cycloadduct products in the same proportions, along with varying quantities of the head-to-head adduct **3** resulting from dimerization of the enone. The ratio of cycloadduct to dimer was determined in a series of reactions where the concentration of cyclohexene was varied. The procedure used was as follows.

A series of stock solutions was prepared. Potassium dodecanoate (9.527 g) was dissolved to 500.0 mL in triply distilled water to give a 0.0800 *M* solution. This solution was deoxygenated by purging with nitrogen gas for one hour to give a stock micelle solution.

3-*n*-Butylcyclopentenone, **1**, (0.0424 g) was dissolved by sonication in 50.0 mL of the potassium dodecanoate solution, to give a solution $6.15 \times 10^{-3}$ *M* in enone.

Cyclohexene (0.0626 g) was dissolved in sonication in 100 mL of the potassium dodecanoate solution, to give a solution $7.63 \times 10^{-3}$ *M* in cyclohexene.

These three solutions were mixed in varying proportions to give solutions $6.15 \times 10^{-4}$ *M* in enone, 0.0800 *M* in potassium dodecanoate, and between $6.11 \times 10^{-4}$ and $2.59 \times 10^{-3}$ *M* in alkene. Total solution volumes were 50.0 mL. All transfers were carried out under nitrogen to minimize dissolution of oxygen in the reaction mixtures. Micelle solutions were irradiated in quartz tubes to allow monitoring of the uv spectrum. Conversion was determined by observing disappearance of the $\pi \rightarrow \pi^*$ band of the enone. Typically, reaction times were in the order of 20 min. Irradiated mixtures were poured into water (500 mL) and extracted with ether (5 × 100 mL). Salt was added carefully in portions to break emulsions; addition of too much salt caused the dodecanoate to come out of solution as a nonfilterable precipate. Combined ether extracts were washed with aqueous $Na_2CO_3$, dried ($MgSO_4$), and concentrated. The concentrate was analysed by glc (3% SE 30, 100–200°C) for cycloadduct **4** and dimer **3** using *n*-docosane as an internal standard. Calibrations of *n*-docosane against **3** and **4** were obtained using purified samples of dimer (12) and the adducts. The results are given in Table 1.

*Irradiation of 3-*n*-butylcyclopent-2-en-1-one, 1, with 1,2-dimethylcyclohexene*

3-*n*-Butylcyclopentenone (166 mg) and 1,2-dimethylcyclohexene (0.554 g) were irradiated together. The progress of the reaction was monitored by recording the $^1H$ nmr spectrum at intervals; disappearance of the olefinic proton of the enone was observed and the reaction was terminated at 70% conversion. Small amounts (< 10%) of olefinic reaction products from intramolecular hydrogen abstraction by the intermediate diradical were observed (3). A glc analysis (3% SE 30) of the reaction mixture showed the presence of a single major peak (> 80% of the total) and four minor peaks travelling closely together. These were assumed to be cycloadduct isomers and small amounts of olefinic by-products. The reaction products we isolated as a mixture by preparative glc (15% SE 30 at 210°C) and used for calibration against *n*-docosane.

Repetition of the reaction in aqueous potassium dodecanoate solution gave a similar result, as indicated by glc analysis of the worked-up reaction mixture. A series of experiments were performed as described above for the reaction of cyclohexene with enone **1** in order to examine the effect of dimethylcyclohexene concentration upon the ratio of cycloadduct to enone dimer. The results are given in Table 1.

*Irradiation of 3-*n*-butylcyclopent-2-en-1-one, 1, with 1-hexene*

A nitrogen purged solution of enone **1** (0.151 g) and 1-hexene (2.77 g) in dry ether (350 mL) was irradiated at room temperature until all enone had been consumed as shown by glc (3% SE 30, 100–175°C). Evaporation gave an isomeric mixture of adducts **5***a* and **6***a* (0.235 g, 97%). Bulb-to-bulb distillation (65°C/0.7 Torr) gave an oil which had $\nu_{max}$ (neat): 1738, 1467, 1457, 1167 $cm^{-1}$; $^1H$ nmr: 0.6–2.8 (complex multiplet) ppm. The glc

Can. J. Chem. Downloaded from www.nrcresearchpress.com by 210.87.254.5 on 09/06/12
For personal use only.

Can. J. Chem. Downloaded from www.nrcresearchpress.com by 210.87.254.5 on 09/06/12
For personal use only.

analysis (5% FFAP, 140°C) of the oil showed the presence of two peaks with areas in the ratio 43:57 (flame ionization detector); separation by preparative glc gave the minor component (shorter retention time) which was identified as the head-to-tail regioisomers **6***a* and had *m/e*: 222 ($M^+$, 3%), 193(3), 165(8), 152(6), 140(3), 139(50), 138(3), 112(100), 111(12), 110(17), 97(66), 96(25), 95(4); *Mol. Wt.* calcd. for $C_{15}H_{26}O$: 222.1984; found: 222.1979; $^{13}C$ nmr, see Table 2. The $^{13}C$ nmr indicated that **6***a* was a mixture of stereoisomers in which one predominated.

The major component was identified as the head-to-head regioisomer **5***a* and had *m/e*: 222 ($M^+$, 2%), 193(2), 165(4), 140(10), 139(100), 138(10), 111(13), 110(18), 97(11), 96(81), 95(22); *Mol. Wt.* calcd. for $C_{15}H_{26}O$: 222.1984; found: 222.1986; $^{13}C$ nmr, see Table 2. The $^{13}C$ nmr indicated that **5***a* was a mixture of stereoisomers present in approximately equal amounts.

*Irradiation of 3-*n*-butylcyclopent-2-en-1-one, **1**, with 1-octene*

A deoxygenated solution of enone **1** (0.168 g) and 1-octene (3.05 g) in dry ether (350 mL) was irradiated for five hours after which time glc indicated all of the enone had been consumed. Evaporation gave a mixture of adducts **5***b* and **6***b* (0.300 g, 99%) which was distilled bulb-to-bulb, 70°C/0.6 Torr) to give an oil which had $\nu_{max}$ (film): 1739, 1470, 1460, 1162 $cm^{-1}$; $^1H$ nmr: 0.6–2.9 (complex multiplet) ppm. The glc analysis (5% FFAP, 150°C) of the mixture indicated two peaks with areas in the ratio 43:57 (flame ionization detector). Separation by preparative glc gave the minor component (shorter retention time) which was identified as regioisomers **6***b*. The $^{13}C$ nmr spectrum (Table 2) indicated that **6***b* was a mixture of isomers present in approximately equal amounts. The major component was identified as regioisomers **6***a* in which one stereoisomer predominated, as indicated by the $^{13}C$ nmr spectrum (Table 2).

*Irradiation of 3-*n*-butylcyclopent-2-en-1-one, **1**, with vinyl acetate, **7**a*

A deoxygenated solution of enone **1** (0.311 g) and freshly distilled vinyl acetate (2.09 g) in dry ether (350 mL) was irradiated until glc (3% SE 30, 100–140°C) indicated no enone remained (4.5 h). Evaporation gave a glassy residue which was triturated with hot pentane (5 × 50 mL) to give a yellow oil (0.51 g). Bulb-to-bulb distillation (92°C/0.3 Torr) yielded a mixture of **8***a* and **9***a* (0.43 g, 85%) as an oil which had $\nu_{max}$ (film): 1739, 1373, 1288, 1070, 1046 $cm^{-1}$; $^1H$ nmr: 0.63–2.93 (19H, m), 4.95 (1H, m) ppm. The glc analysis of the mixture (5% FFAP, 100–180°C, flame ionization detector) showed 3 peaks with areas in the ratio 74:15:11. The $^{13}C$ nmr of the mixture (Table 5) showed the presence of all four possible isomers of **8***a* and **9***a*.

A portion of the mixture of **8***a* and **9***a* (0.20 g) was dissolved in methanol (2.0 mL) and aqueous sodium hydroxide (2.5 *M*, 0.5 mL) was added. The solution was stirred at room temperature for 20 min, hydrochloric acid (0.5 *M*) was added to pH 8, and the products were extracted with ether, dried ($MgSO_4$), and evaporated to give a mixture of alcohols (0.15 g, 90%) which had $\nu_{max}$ (film): 3430, 1730, 1468, 1458, 1240, 1175, 1090 $cm^{-1}$; $^1H$ nmr: 0.57–3.03 (16H, m), 3.17–4.77 (2H, m) ppm. This mixture was dissolved in acetone (2.0 mL) and treated with Jones reagent (0.70 mL) at 3°C. Aqueous work-up gave a yellow oil (0.13 g) which contained (glc analysis; 3% SE 30, 85–150°C) some unreacted alcohols. Chromatography on neutral alumina with ether as eluent followed by bulb-to-bulb distillation (80°C/0.3 Torr) gave 5-*n*-butylbicyclo[3.2.0]heptane-2-6-dione, **11***a*, (0.099 g, 69%) as an oil which had $\nu_{max}$ (film): 1784, 1744, 1468, 1458 $cm^{-1}$; $^1H$ nmr: 0.58–3.80 (complex multiplet) ppm; $^{13}C$ nmr: 13.9 (methyl), 23.0, 27.1, 28.2, 33.2, 37.1 (all methylenes), 41.4 (methine), 50.0 (methylene), 73.3 (quaternary), 211.1 (carbonyl), 216.8 (carbonyl) ppm; *m/e*: 152 $M^+ - 28$, 3%) 151(23), 141(6), 140(3), 139(30), 97(100), 95(27), 81(39), 73(37).

*Irradiation of 3-*n*-butylcyclopent-2-en-1-one, **1**, with 1-hexenyl acetate, **7**b*

1-Hexenyl acetate was synthesized as a mixture of *cis* and *trans* isomers (21), bp 64°C/12 Torr. A deoxygenated solution of enone **1**, (0.443 g) and hexenyl acetate (2.47 g) in dry ether (350 mL) was irradiated until glc (3% SE 30, 100–175°C) indicated that no enone remained (10 h). Bulb-to-bulb distillation (116°C/0.4 Torr) gave a mixture of cycloadducts **8***b* and **9***b* (0.76 g, 85%) which on glc (3% SE 30, 100–175°C) showed four peaks with areas in the ratio 46:18:26:10 (flame ionization detector). The mixture had $\nu_{max}$ (film): 1738, 1467, 1458, 1373, 1236 $cm^{-1}$; $^1H$ nmr: 0.62–2.96 (27H multiplet), 3.10–5.00 (1H, multiplet) ppm. A sample (0.31 g) was dissolved in methanol (3.0 mL) and treated with aqueous NaOH (0.60 mL, 2.5 *M*) at room temperature for 20 min. Dilution with water and extraction into ether gave a mixture of alcohols (0.24 g, 92%), following drying ($MgSO_4$) and evaporation. The alcohol mixture had $\nu_{max}$ (film): 3435, 1735, 1465, 1085 $cm^{-1}$; $^1H$ nmr: 0.50–2.87 (24H, m), 2.93–4.27 (2H, m) ppm. Most of this mixture (0.23 g) was dissolved in acetone (3.0 mL) and treated with Jones reagent (0.75 mL) at 3°C for 1.5 h. The mixture was diluted with water and extracted with ether; the ether extracts were washed (aqueous sodium bicarbonate) and dried ($MgSO_4$). Evaporation gave mainly (glc analysis; 3% SE 30, 100–175°C) 5,7-dibutylbicyclo[3.2.0]heptane-2,6-dione, **11***b*, (0.212 g) as a mixture of isomers. Further purification was unsuccessful. The dione had $\nu_{max}$ (film): 1777, 1738, 1468, 1458 $cm^{-1}$; $^1H$ nmr: 0.50–3.82 (complex multiplet) ppm; $^{13}C$ nmr, see Tables 6 and 7; *m/e*: 222 (0.5%), 221(0.5), 220(1), 205(2), 181(2), 165(4), 140(12), 139(100), 97(5), 96(5), 95(4), 83(12), 73(26).

*Irradiation of 3-*n*-butylcyclopent-2-en-1-one, **1**, with 1-heptenyl acetate, **7**c*

1-Heptenyl acetate was synthesized as a mixture of *cis* and *trans* isomers (21) and had bp 82–88°C/15 Torr. A deoxygenated solution of enone **1** (0.120 g) and heptenyl acetate (1.01 g) was irradiated in dry cyclohexane (65 mL) until all enone was consumed. Distillation (94°C/0.2 Torr) gave a mixture of cycloadducts (0.136 g, 53%). Gas-liquid chromatography (3% SE 30, 100–175°C) indicated four peaks with areas in the ratio 47:22:22:9. The mixture had $\nu_{max}$ (film): 1740, 1471, 1460, 1375, 1236, 1062 $cm^{-1}$; $^1H$ nmr: 0.55–2.92 (29H, m), 4.58–5.25 (1H, m) ppm.

The major part of the cycloadduct mixture (0.124 g) was dissolved in methanol (0.30 mL) and treated with aqueous sodium hydroxide (0.10 mL, 5.0 *M*) at room temperature for 30 min. Neutralization with dilute HCl and extraction with ether gave, after drying ($MgSO_4$), a mixture of alcohols (0.109 g, 99%) which had $\nu_{max}$ (film): 3460, 1730, 1473, 1465, 1100 $cm^{-1}$; $^1H$ nmr: 0.53–3.00 (27H, m), 3.53–4.30 (1H, m) ppm. Most of this mixture (0.100 g) was dissolved in acetone (2.5 mL) and oxidized with Jones Reagent (0.55 mL) at 3°C. Aqueous work-up gave an oil which was a mixture of 5-butyl-7-pentylbicyclo[3.2.0]-heptane-2,6-dione, **11***c*, and the starting alcohols in a ratio of approximately 9:1 as shown by glc (3% SE 30, 100–175°C). Chromatography on neutral alumina followed by bulb-to-bulb distillation (90°C/0.3 Torr) gave **11***c* as an oil (0.088 g, 89%) which had $\nu_{max}$ (film): 1775, 1735, 1469, 1460 $cm^{-1}$; $^1H$ nmr: 0.55–2.94 (25H, m), 2.94–3.78 (1H, m) ppm; $^{13}C$ nmr, see Table 7; *m/e*: 222(1%), 221(5), 220(23), 206(14), 205(95), 177(22), 145(14), 140(8), 139(82), 97(12), 96(43), 95(28), 81(40), 68(36), 58(100).

*Irradiation of 3-*n*-butylcyclopent-2-en-1-one, **1**, with 1-heptenyl acetate in potassium dodecanoate micelles*

A solution (500 mL) of enone **1** and 1-heptenyl acetate in aqueous potassium dodecanoate was made up so as to be $2.5 \times 10^{-3}$ *M* in enone, $1.7 \times 10^{-2}$ *M* in heptenyl acetate, and 0.142 *M*

Can. J. Chem. Downloaded from www.nrcresearchpress.com by 210.87.254.5 on 09/06/12
For personal use only.

in potassium dodecanoate. Under these conditions, each micelle before irradiation contained on average one enone molecule and approximately seven heptenyl acetate molecules. Irradiation followed by aqueous work-up gave a mixture of adducts **8***c* and **9***c* (0.250 g, 68%). The spectroscopic properties of the mixture were identical with those of the product obtained by irradiation in cyclohexane. The mixture of adducts was hydrolysed and oxidized as described in the previous procedure; the extent of the oxidation was monitored by glc (5% FFAP and 3% SE 30, 100–175°C) and the reaction was given an aqueous work-up after six hours to yield an oil (0.149 g). Gas–liquid chromatography (3% SE 30, 90–165°C) showed the presence of 3 products in addition to starting material. Bulb-to-bulb distillation gave a mixture of diones **10***c* and **11***c* (0.072 g) in a ratio of approximately 2:1. Attempted chromatographic separation of these two compounds resulted in decomposition; consequently the isomeric mixture of head-to-head diones **10***c* was characterized spectroscopically allowing for the presence of **11***c* and had $\nu_{max}$ (film): 1775, 1745, 1465 $cm^{-1}$; $^1H$ nmr: 0.50–2.93 (25H, m), 3.20 and 3.23 (total 1 H, two triplets in the ratio of approximately 1:2 with $J$ = 0.5 and 1.5 Hz, respectively) ppm; $^{13}C$ nmr spectrum, see Table 8; *m/e*: 236(2%), 235(1), 234(5), 219(3), 205(9), 179(9), 140(11), 139(100), 97(8), 96(12), 95(12), 81(15), 79(15), 57(42), 54(35).

*Irradiation of 3-(*n*-butylthio)cyclopent-2-en-1-one, **12**, with isobutenyl acetate*

The enone **12** was prepared according to published procedures (22) and was irradiated with the alkenyl acetate in cyclohexane and in aqueous potassium dodecanoate solution.

(a) *In cyclohexane*

A deoxygenated solution of enone **12** (2.00 g) and isobutenyl acetate (10.0 g) in cyclohexane (180 mL) was irradiated in a Rayonet Reactor (300 nm lamps) to 76% conversion. The reaction was followed by monitoring the disappearance of the enone $\pi \rightarrow \pi^*$ absorption at 267 nm. The glc analysis of the reaction mixture (10% SE 30, 170°C) following removal of solvent showed four product peaks in the ratio 61:27:9:3 (flame ionization detector). The major product was found to be a mixture of two compounds (glc 10% FFAP, 200°C). A portion of the mixture (0.10 g) was separated by a combination of tlc, hplc, and glc; the fifth, smallest component of the mixture was present in too small a quantity to allow identification. The isolated compounds were identified as adducts **13**, **14**, **15**, and **16**.

For **13**: $^1H$ nmr: 4.99 (1H, d, $J$ = 1.8 Hz), 2.7–2.0 (7H, m), 2.12 (3H, s), 1.6–1.2 (4H, m), 1.40 (3H, s), 1.1–0.75 (3H, m), 0.90 (3H, s) ppm; *m/e* (25 eV): 284 ($M^+$, 4%), 224(7), 213(67), 171(100), 114(32); *Mol. Wt.* calcd. for $C_{15}H_{24}O_3S$: 284.1448; found: 284.1448.

For **14**: $^1H$ nmr: 4.90 (2H, d, $J$ = 2.4 Hz), 2.7–2.1 (7H, m), 2.16 (3H, s), 0.90 (3H, t, $J$ = 6 Hz) ppm; *m/e* (20 eV): 284 ($M^+$, 2%), 213(24), 171(100), 114(5), 72(7); *Mol. Wt.* calcd. for $C_{15}H_{24}O_3S$: 284.1448; found: 284.1448.

For **15**: $^1H$ nmr: 5.31 (1H, s), 5.07 (2H, m), 2.6–2.3 (6H, m), 2.25–2.0 (2H, m), 2.07 (3H, s), 1.88 (3H, broadened s), 1.63 (4H, m), 0.88 (3H, t, $J$ = 6 Hz) ppm; *m/e*: 284 (2%), 225(23), 171(57), 115(100); *Mol. Wt.* calcd. for $C_{15}H_{24}O_3S$: 284.1448; found: 284.1443.

For **16**: $^1H$ nmr: 4.8 (1H, d, $J$ = 7 Hz), 2.8–2.0 (7H, m), 2.1 (3H, s), 1.7–1.1 (4H, m), 1.28 (3H, s), 1.24 (3H, s), 0.95 (3H, t, $J$ = 6 Hz) ppm; *m/e*: 215(1), 214(3), 213(26), 173(4), 172(8), 171(100), 153(3), 114(5), 72(7).

(b) *In aqueous potassium dodecanoate*

Potassium dodecanoate (75 g) was dissolved to 1200 mL in triply distilled deoxygenated water. Enone **12** (0.761 g) and isobutenyl acetate (3.45 g) were added and the suspension was sonicated to dissolve the reactants. The solution obtained was 0.26 $M$ in dodecanoate, $3.41 \times 10^{-3}$ $M$ in enone, and $3.03 \times 10^{-2}$ $M$ in alkene; the average number of enone and alkene molecules was therefore 0.7 and 6 respectively. The irradiation was performed in a Rayonet reactor using 300 nm lamps and was followed by monitoring the disappearance of the uv absorption of the enone. At 52% conversion the reaction mixture was diluted below the cmc with water and extracted with ether to yield the cycloadducts (0.67 g) which were purified by chromatography on silica. The glc analysis of the adduct mixture (10% SE 30, 170°C) showed four peaks whose areas were in the ratio 41:35:14:9 (flame ionization detector). As in the previous experiment, the major peak was a mixture of compounds **13** and **14**, and the second largest component was compound **16**. The smallest component was not isolated in sufficient quantity to allow identification and the remaining component was identified as **17**.

For **17**: $^1H$ nmr: 5.0 (1H, d, $J$ = 8.8), 2.8–2.2 (7H, m), 2.05 (3H, s), 1.8–1.1 (4H, m), 1.4 (3H, s), 1.08 (3H, s), 0.90 (3H, t, $J$ = 6 Hz) ppm; *m/e*: 213(16), 205(5), 171(100).

1. P. E. Eaton. Acc. Chem. Res. **1**, 50 (1968).
2. P. G. Bauslaugh. Synthesis, 287 (1969).
3. P. de Mayo. Acc. Chem. Res. **4**, 41 (1971).
4. (*a*) K. N. Houk. Acc. Chem. Res. **8**, 361 (1975). (*b*) S. M. Ali, T. V. Lee, and S. M. Roberts. Synthesis, 155 (1977); (*c*) R. W. Guthrie, Z. Valenta, and K. Wiesner. Tetrahedron Lett. 4645 (1966); (*d*) S. W. Baldwin. Org. Photochem. **5**, 123, (1981).
5. W. L. Dilling. Photochem. Photobiol. **25**, 605 (1977), and references therein.
6. (*a*) P. de Mayo, J. P. Pete, and M. Tchir. Can. J. Chem. **46**, 2535 (1968); (*b*) L. Duc, R. A. Mateer, L. Brassier, and G. W. Griffin. Tetrahedron Lett. 6173 (1968); (*c*) T. Matsumoto, H. Shiramhama, A. Ichihara, S. Kagawa, and S. Matsumoto. Tetrahedron Lett. 4103 (1969); (*d*) Y. Tobe, T. Hoshino, Y. Kawakami, Y. Sakai, K. Kimura, and Y. Odaira. J. Org. Chem. **43**, 4334 (1978); (*e*) C. Kaneko, T. Naito, and M. Somei. J. Chem. Soc. Chem. Commun. 804 (1979).
7. B. D. Challand and P. de Mayo. J. Chem. Soc. Chem. Commun. 982 (1968).
8. E. J. Corey, J. D. Bass, R. Lemahieu, and R. B. Mitra. J. Am. Chem. Soc. **86**, 5570 (1964).
9. (*a*) P. de Mayo, and H. Takeshita. Can. J. Chem. **41**, 440 (1963); (*b*) B. D. Challand, H. Hikino, G. Kornis, G. Lange, and P. de Mayo. J. Org. Chem. **34**, 794 (1969), and references therein; (*c*) W. Oppolzer and T. Godel. J. Am. Chem. Soc. **100**, 2583 (1978).
10. (*a*) G. Mark, F. Mark, and O. E. Polansky. Ann. Chem. **719**, 151 (1968); (*b*) P. Margaretha. Chimia, **29**, 203 (1975).
11. (*a*) N. J. Turro, M. Gratzel, and A. M. Braun. Agnew. Chem. Int. Ed. Engl. **19**, 675 (1980); (*b*) R. Fargues, M. T. Maurette, E. Oliveros, M. Riviere, and A. Lattes. Nouveau J. Chim. **3**, 487 (1979); (*c*) Y. Nakamura, T. Kato, and Y. Morita. Tetrahedron Lett. **22**, 1025 (1981).
12. (*a*) K. H. Lee and P. de Mayo. Photochem. Photobiol. **31**, 311 (1980); (*b*) K. H. Lee and P. de Mayo. J. Chem. Soc. Chem. Commun. 493 (1979); (*c*) P. de Mayo and L. K. Sydnes. J. Chem. Soc. Chem. Commun. 994 (1980).
13. T. Yasunaga, H. Oguri, and M. Miura. J. Colloid Interface Sci. **23**, 352 (1967).
14. E. Graber and R. Zana. Kolloid Z.Z. Polym. **238**, 470 (1970); E. Graber, J. Lang, and R. Zana. Kolloid Z.Z. Polym. **238**, 749 (1970).
15. N. J. Turro, M. Gratzel, and A. M. Braun. Angew. Chem. Int. Ed. Engl. **19**, 675 (1980).

16. J. H. FENDLER and E. J. FENDLER. Catalysis in micellar and micromolecular systems. Academic Press, New York. 1975. p. 34.
17. J. B. STOTHERS. Carbon-13 nmr spectroscopy. Academic Press, New York. 1972.
18. (*a*) J. G. KIRKWOOD. J. Chem. Phys. **2**, 351 (1934); **7**, 911 (1937); (*b*) L. ONSAGER. J. Am. Chem. Soc. **58**, 1486 (1936).
19. B. BRAILLON, J. SALAUN, J. GORE, and J. M. CONIA. Bull. Soc. Chim. Fr. 1981 (1964).
20. G. BUCHI and B. EGGER. J. Org. Chem. **36**, 2021 (1971).
21. F. W. SEMMLER. Chem. Ber. **42**, 1161 (1909); D. B. BIGLEY and D. W. PAYLING. J. Chem. Soc. 3974 (1965).
22. J. DROWIN, F. LEYENDECKER, and J. M. CONIA. Tetrahedron, **36**, 1203 (1980).

Downloaded from www.nrcresearchpress.com by 210.87.254.5 on 09/06/12
For personal use only.

# An improved procedure for the preparation of 3-carbomethoxy-4-oxotetrahydrothiopyran, 2- and 4-carbomethoxy-3-oxotetrahydrothiophene

HSING-JANG LIU AND TENG KO NGOOI

*Department of Chemistry, University of Alberta, Edmonton, Alta., Canada T6G 2G2*

Received September 16, 1981

HSING-JANG LIU and TENG KO NGOOI. Can. J. Chem. **60**, 437 (1982).

An improved procedure for the preparation of the title compounds **1–3** has been developed. Direct condensation of methyl 3-mercaptopropionate with methyl acrylate using sodium hydride as a base gave compound **1** in good yield. The reaction of methyl thioglycolate and methyl acrylate at 0°C gave compound **2** as the major product whereas at lower temperature (−40°C) isomer **3** was found as the major product. The condensation reactions of methyl thioglycolate with methyl methacrylate and crotonate were also carried out.

HSING-JANG LIU et TENG KO NGOOI. Can. J. Chem. **60**, 437 (1982).

On a développé une méthode efficace de préparation des composés **1–3** mentionnés dans le titre. La condensation directe du mercapto-3 propionate de méthyle sur l'acrylate de méthyle en présence de l'hydrure de sodium conduit au composé **1** avec un bon rendement. La réaction du thioglycolate de méthyle avec l'acrylate de méthyle à 0°C donne le composé **2** comme produit majoritaire tandis qu'à basse température (−40°C) l'isomère **3** est le produit majoritaire. On a également étudié les réactions de condensations du thioglycolate de méthyle sur le méthacrylate de méthyle et sur le crotonate de méthyle.

[Traduit par le journal]

The title compounds **1–3** are useful synthetic intermediates (1–3) leading to compounds which are of current interest. The conventional methods for their preparation require the formation of the diesters of 3-thioadipic acid and 4-thiopimelic acid followed by a Dieckmann condensation (1, 4–8). Apart from the operational complexity, these procedures often suffer from unsatisfactory yields of the products due to the rather severe conditions required to induce Dieckmann reaction. We wish to report a convenient procedure leading directly to the title compounds with improved yields.

The *S*-anions derived from 3-mercaptopropionate and thioglycolate are expected to undergo conjugate addition to acrylate and the resulting carbanion can conceivably proceed to cyclization under appropriate conditions.[1] This was realized experimentally as follows. Treatment of methyl 3-mercaptopropionate with 1.2 equiv. each of sodium hydride and methyl acrylate in 1,2-dimethoxyethane at 0°C for 4 h gave directly 3-carbomethoxy-4-oxotetrahydrothiopyran (**1**) in 75% yield. In the case of the reaction of methyl thioglycolate and methyl acrylate, the intermediate carbanion resulting from the 1,4-addition can in principle undergo two different modes of cyclization via proton exchange. As a result both compounds **2** and **3** could be produced. Although we were unable to find conditions to facilitate the exclusive formation of either compound, a reasonable selectivity could be achieved by merely adjusting the reaction temperature. At lower temperature (−40°C) the two isomers **2** and **3** were formed in near-quantitative yield and in a ratio of ca. 2:3, whereas at 0°C the former was isolated as the major product in 67% yield along with a lesser quantity (32% yield) of the latter isomer.

The described direct procedure could be further extended to the preparation of derivatives of the title compounds by suitable choice of the two reactants. For example, the reaction of methyl thioglycolate and methyl methacrylate afforded a 94% yield of 3-oxotetrahydrothiophene **4**[2] (12), whereas treatment of methyl thioglycolate with methyl crotonate gave rise to a 1:1 mixture of two isomeric compounds **5** and **6**[3] (13) in 82% yield.

[1]For examples of two related processes, i.e. mercaptide ion induced Wittig reaction and alkoxide induced Dieckmann condensation, see refs. 9 and 10 respectively.

[2]The exclusive formation of this compound is in accordance with the known regioselectivity of Dieckmann condensation (11).

[3]Compounds **5** and **6** were further characterized by acetylation (acetyl chloride in pyridine; 20°C; 5 h) to give the corresponding enol acetates **7** (94% yield; ir (neat): 1775, 1720, and 1660 $cm^{-1}$; nmr ($CCl_4$) δ: 4.34 (q, 1H, $J = 7, J' = 2$ Hz, —CH—), 3.71 (s, 3H, $—COOCH_3$), 3.53–4.01 (complex, 2H, $—CH_2—$), 2.17 (s, 3H, $CH_3COO—$), and 1.51 (d, 3H, $J = 7$ Hz, $—CH_3$); ms $M^+$ 216.0455 (calcd. for $C_9H_{12}O_4S$: 216.0456)) and **8** (92% yield; ir (neat): 1780, 1720, and 1630 $cm^{-1}$; nmr ($CCl_4$) δ: 3.71 (s, 3H, $—COOCH_3$), 3.55 (m, 1H, —CH—), 3.14 (dd, 1H, $J = 17, J' = 9$ Hz, —C*H*H—), 2.51 (dd, 1H, $J = 17, J' = 5$ Hz, —CH*H*—), 2.16 (s, 3H, $CH_3COO—$), and 1.38 (d, 3H, $J = 7$ Hz, $—CH_3$); ms $M^+$ 216.0456 (calcd. for $C_9H_{12}O_4S$: 216.0456)).

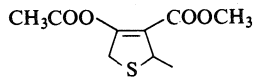


7

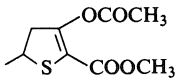


8

0008-4042/82/040437-03$01.00/0

©1982 National Research Council of Canada/Conseil national de recherches du Canada

Can. J. Chem. Downloaded from www.nrcresearchpress.com by 210.87.254.42 on 09/06/12
For personal use only.

Can. J. Chem. Downloaded from www.nrcresearchpress.com by 210.87.254.42 on 09/06/12
For personal use only.

TABLE 1. Mercaptide ion induced Dieckmann condensation

| Reactants | Temperature (time) | Product(s) (yield)[a] | Infrared ($cm^{-1}$)[g] | Nuclear magnetic resonance (δ)[i] | Mass spectra[j] |
|---|---|---|---|---|---|
| $HSCH_2CH_2COOCH_3$<br>$CH_2{=}CHCOOCH_3$ | 0°C (4 h) | 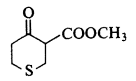 <br>**1** (75%) | 3300, 1740, 1710, 1650, 1605 | 10.85 (s, ~0.8H, -OH), 3.72 (s, 3H, $-CH_3$), 3.54 (dd, ~0.2H, $J = 8$, $J' = 4$ Hz, $-\overset{\vert}{C}H-$), 3.24 (s, ~1.6H, $-\overset{\vert}{C}{=}\overset{\vert}{C}CH_2S-$), 2.52–2.86 (complex, ~4.4H) | 174.0352[k] (174.0351) |
| $HSCH_2COOCH_3$<br>$CH_2{=}CHCOOCH_3$ | −40°C (5 h) | 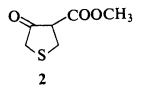 <br>**2** (42%)[b] | 3100, 1755, 1735, 1665, 1620[h] | 10.93 (s, ~0.75H, -OH), 3.63–3.87 (complex, ~6H), 3.11–3.44 (complex, ~1.25H) | 160.0195[k] (160.0194) |
| | | 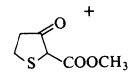 <br>**3** (57%) | 3460, 1750, 1730, 1665, 1610 | 11.0 (s, ~0.1H, -OH), 3.84 (s, ~0.9H, $-\overset{\vert}{C}H-$), 3.77, 3.72 (both s, total 3H, $-CH_3$), 2.11–3.59 (complex, 4H) | 160.0187[k] (160.0191) |
| | 0°C (3 h) | **2** (67%) + **3** (32%) | | | |
| $HSCH_2COOCH_3$<br>$CH_2{=}C(CH_3)COOCH_3$ | 0°C (8.5 h) | 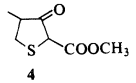 <br>**4** (94%)[c,d] | 3450, 1750, 1730, 1650, 1600 | 10.53 (s, ~0.1H, -OH), 4.01, 3.69 (both s, total ~0.9H, $-\overset{\vert}{C}HS-$), 3.78, 3.72 (both s, total 3H, $-COOCH_3$), 2.44–3.51 (complex, 3H), 1.25, 1.21 (both d, total 3H, $J = 7$ Hz each, $-CH_3$) | 174.0346 (174.0349) |
| $HSCH_2COOCH_3$<br>$CH_3CH{=}CHCOOCH_3$ | 20°C (6 h) | 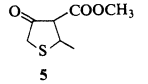 <br>**5** (41%)[c,e] | 3300, 1755, 1730, 1660, 1620 | 11.11 (s, ~0.7H, -OH), 2.99–4.33 (complex, ~3.3H), 3.78, 3.73 (both s, total 3H, $-COOCH_3$), 1.44, 1.41 (both d, total 3H, $J = 7$ Hz each, $-CH_3$) | 174.0353 (174.0352) |
| | | 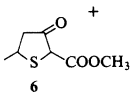 <br>**6** (41%)[c,f] | 3480, 1750, 1730, 1660, 1610 | 4.11, 4.04 (both s, total ~1H, $-SC\overset{\vert}{H}COOCH_3$), 3.76, 3.72 (both s, total 3H, $-COOCH_3$), 2.07–3.93 (complex, 3H), 1.45, 1.39 (both d, total 3H, $J = 7$ Hz each, $-CH_3$) | 174.0352 (174.0351) |

[a]All the products exist partially in the corresponding enol form. In cases of compounds **4–6**, inseparable diastereomers are present.
[b]Melting point 36–37°C.
[c]*Anal.* calcd. for $C_7H_{10}O_3S$: C 48.28, H 5.75, S 18.39.
[d]Found: C 48.19, H 5.61, S 18.15.
[e]Found: C 48.25, H 5.67, S 18.57.
[f]Found: C 48.49, H 5.89, S 18.58.
[g]Except where otherwise stated, the ir spectra were obtained on neat liquid and only diagnostic signals are cited.
[h]Obtained in carbon tetrachloride.
[i]The nmr spectra were obtained on solutions in carbon tetrachloride with tetramethylsilane as internal reference.
[j]Molecular ions are given with calculated values in parentheses.
[k]The spectral data were shown to be identical with those of an authentic sample.

Results of this investigation and the spectral data for products are summarized in Table 1.

## Experimental

*General and material*

Melting points were determined on a Kofler hot stage apparatus and are uncorrected. Infrared spectra were recorded on a Perkin–Elmer model 457 spectrophotometer. Nuclear magnetic resonance spectra were recorded on a 90 MHz Perkin–Elmer 32 spectrometer. Mass spectra were recorded using an A.E.I. Model MS 50 mass spectrometer. Elemental analyses were performed by the microanalytical laboratory of this department. Methyl 3-mercaptopropionate and methyl thioglycolate (Aldrich) were used without purification. 1,2-Dimethoxyethane was freshly distilled over lithium aluminum hydride. Methyl acrylate, methacrylate, and crotonate were distilled prior to use.

*Preparation of 3-carbomethoxy-4-oxotetrahydrothiopyran (**1**), 4-carbomethoxy-3-oxotetrahydrothiophene (**2**), 2-carbomethoxy-3-oxotetrahydrothiophene (**3**), and derivatives **4–6***

The general procedure used for the preparation of these compounds is illustrated below with the reaction of methyl 3-mercaptopropionate and methyl acrylate. Temperature and time of reactions as well as spectral data and yields of products are compiled in Table 1. Separation of the two isomeric pairs, **2** (faster-moving) and **3**, and **5** (faster-moving) and **6**, was effected by flash column chromatography (14) on silica gel, eluting with a solution of 5% ethyl acetate in petroleum ether.

At 0°C, to a solution of methyl 3-mercaptopropionate (490 mg, 4.1 mmol) and methyl acrylate (430 mg, 5 mmol) in 1,2-dimethoxyethane (15 mL), was added sodium hydride (50% dispersion in oil; 240 mg, 5 mmol). The reaction mixture was stirred at 0°C under an atmosphere of nitrogen for 4 h. The mixture was acidified with 1 *N* hydrochloric acid and extracted with methylene chloride. Drying ($MgSO_4$), filtration, and concentration gave the crude product which was purified by column chromatography on silica gel. Elution with ethyl acetate – petroleum ether (1:20) afforded compound **1** (540 mg; 75% yield).

## Acknowledgments

We are grateful to the Natural Sciences and Engineering Research Council of Canada and the University of Alberta for financial support.

1. P. A. Rossy, W. Hoffmann, and N. Müller. J. Org. Chem. **45**, 617 (1980).
2. W. G. Dauben, C. R. Kessel, and K. H. Takemura. J. Am. Chem. Soc. **102**, 6893 (1980).
3. J. B. Jones and H. M. Schwartz. Can. J. Chem. **59**, 1574 (1981).
4. G. M. Bennett and L. V. D. Scorah. J. Chem. Soc. 194 (1927).
5. E. A. Fehnel and M. Carmack. J. Am. Chem. Soc. **70**, 1813 (1948).
6. E. E. Moore and M. B. Moore. J. Am. Chem. Soc. **68**, 910 (1946).
7. R. B. Woodward and R. H. Eastmann. J. Am. Chem. Soc. **68**, 2229 (1946).
8. O. Hromatka, D. Binder, and K. Eichinger. Monatsh. Chem. **104**, 1520 (1973); **105**, 1164 (1974).
9. J. M. McIntosh and R. A. Sieler. Can. J. Chem. **56**, 226 (1978).
10. I. T. Harrison, V. R. Fletcher, and J. H. Fried. Tetrahedron Lett. 2733 (1974); I. Vlattas and L. D. Vecchia. Tetrahedron Lett. 4455 (1974).
11. S. R. Hauser and B. E. Hudson. Org. React. **1**, 274 (1942); J. P. Schaefer and J. J. Bloomfield. Org. React. **15**, 1 (1967).
12. E. Lasson. Svensk Kem. Tidskr. **66**, 114 (1954).
13. H. Fieselman and G. Pfeiffer. Chem. Ber. **87**, 848 (1954).
14. W. C. Still, M. Kahn, and A. Mitra. J. Org. Chem. **43**, 2923 (1978).

Can. J. Chem. Downloaded from www.nrcresearchpress.com by 210.87.254.42 on 09/06/12
For personal use only.

# Nucleophilic attack on 2,1-benzisothiazolium salts

DAVID M. MCKINNON[1], K. ANN DUNCAN, AND LESLEY M. MILLAR

*Department of Chemistry, University of Manitoba, Winnipeg, Man., Canada R3T 2N2*

Received August 10, 1981

DAVID M. MCKINNON, K. ANN DUNCAN, and LESLEY M. MILLAR. Can. J. Chem. **60**, 440 (1982).

2,1-Benzisothiazolium salts react with several stabilized carbanions to give products that are derived by attack at the carbon atom of the heterocyclic ring.

DAVID M. MCKINNON, K. ANN DUNCAN et LESLEY M. MILLAR. Can. J. Chem. **60**, 440 (1982).

Les sels de benzisothiazolium-2,1 réagissent avec plusieurs carbanions stabilisés en donnant des produits qui proviennent de l'attaque au niveau de l'atome de carbone de l'hétérocycle.

[Traduit par le journal]

Can. J. Chem. Downloaded from www.nrcresearchpress.com by 210.87.254.42 on 09/06/12
For personal use only.

Although the site of nucleophilic attack of carbanions on monocyclic isothiazolium salts and the 1,2-benzisothiazolium cation appears to be at ring sulfur rather than at a carbon atom (1–4), little work is reported of the attack of carbanions on 2,1-benzisothiazolium salts. It is known that nucleophilic attack occurs at a ring carbon, i.e. the 3-position by certain oxygen (5), sulfur (6), and nitrogen (7) nucleophiles, and by *N*,*N*-dimethylaniline (on its *para* position) (6). For this investigation we used the salts **1** *a*–*e* which were available from reported syntheses (5–7) or simple modifications. For the reactions of cations of type **1**, a number of reaction possibilities may be envisaged by analogies with other isothiazoles or related heterocyclic species: reaction at ring sulfur with subsequent ring opening (1, 2) as for the isothiazolium (1, 2) and 1,2-benzisothiazolium system (2–4); addition at carbon 3 followed by ring fission or replacement of a reactive substituent with retention of the isothiazole ring (5, 7); dealkylation by nucleophilic displacement at an *N*-alkyl substituent (8), or removal of a C-3 proton giving a carbene (or zwitterion) or further acyclic derivative as for the monocyclic system (9). Other possible reactions of the salts, involving deprotonation of a C-3 alkyl substituent (10), are not possible with the examples we used.

The reaction of the anion of diethyl malonate with **1***a* afforded a mixture of products, from which 2-methylaminobenzaldehyde (**2***a*) and diethyl 1-methyl-2,1-benzisothiazol-3-ylidenemalonate (**3***a*) were isolated. The formation of the latter may be rationalized in terms of nucleophilic attack at carbon to form a saturated derivative **4***a* which is then oxidized by possibly unreacted **1***a* to form **3***a*. The reduction of **1***a* would provide 2-methylaminobenzaldehyde which might be expected to convert to **2***a* under the reaction conditions. It is known (11, 12) that the structurally related 1,2-dithiolium salts react with ketones to produce 3-acylmethylene-1,2-dithioles. On the other hand, if malonate were displaced from **4** by water during the work-up process, ring opening reactions would lead to **2***a*, as described (5). The ester **3***a* was obtained in much better yield by reaction of **1***b* with diethyl malonate. This is again obviously formed by nucleophilic attack at carbon to form **4***b*, which then eliminates methanethiol.

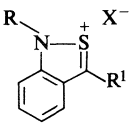

**1**

| | R | R¹ | Y |
|---|---|---|---|
| *a* | Me | H | I |
| *b* | Me | SMe | I |
| *c* | Ph | SMe | I |
| *d* | Ph | Cl | Cl |
| *e* | Me | Ph | $ClO_4$ |
| *f* | Me | $CH(CO_2H)_2$ | $ClO_4$ |
| *g* | Me | $CH_2CO_2H$ | $ClO_4$ |
| *h* | Me | Me | $ClO_4$ |

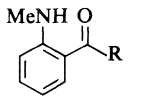

**2**
*a* R = H
*b* R = Ph

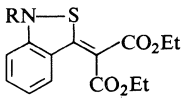

**3**
R = Me
R = Ph

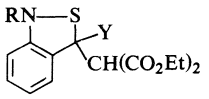

**4**
R = Me; Y = H
R = Me; Y = SMe

When **1***a* was treated with triethylamine or pyridine and the product worked up, the only products obtained were the thione **5** and **2***a*. No products derived from proton abstraction were isolated. The formation of **5** and **2***a* represents a dismutation reaction of a product formed by nucleophilic attack of water on **1***a*, with sulfur being transferred between two molecules. This could have arisen by the mechanism shown (Fig. 1). The addition of extra sulfur to the reaction mixture did not affect the relative yield of the products and therefore this reaction would then appear to pro-

[1]Author to whom correspondence may be addressed.

0008-4042/82/040440-05$01.00/0

©1982 National Research Council of Canada/Conseil national de recherches du Canada

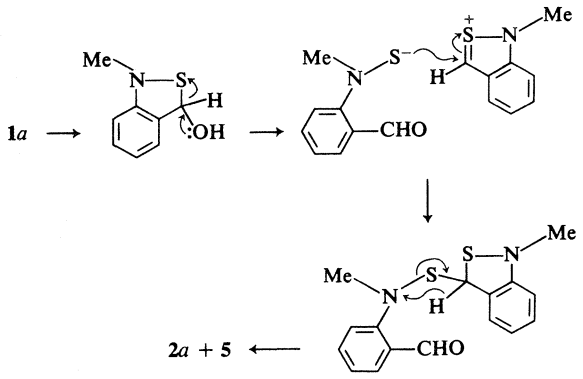

FIG. 1.

ceed via a different mechanism to the base catalysed sulfurizations of 1,2-dithiolium salts to 1,2-dithiole-3-thiones (13) and of isothiazolium salts to isothiazoline 3- and 5-thiones (9). Davis *et al.* (5) obtained **2***a* by treatment of **1***a* with sodium bicarbonate, without reporting the isolation of **5**. In our hands a repeat of this reaction did also yield some thione. The treatment of **1***b* with sodium benzoylacetate in ethanol yielded the ketone **6***a* as a yellow oil. This reaction is analogous to the reactions of sodium benzoylacetate with 3-alkylthio-1,2-dithiolium salts to form 3-phenacylidene-1,2-dithioles (14). The product **6***a* upon thionation with phosphorus pentasulfide yielded the thione **6***b* which is probably best represented by the hypervalent sulfur structure **7**. The product **6***a* was accompanied by small amounts of a red oil, whose properties are consistent with methyl 2-methylaminodithiobenzoate **8***a*, likely formed by reduction of **1***b* with methanethiolate eliminated in the reaction, as for monocyclic isothiazolium salts (1).

Also, treatment of **1***b* with the anion of 2,2-dimethyl-1,3-dioxane-4,6-dione (Meldrum's Acid) afforded the cyclic ester **9***a*. When this was treated with perchloric acid in acetic acid it rapidly converted to the acid derivative **1***f* by ketal hydrolysis and decarboxylation of the malonic acid derivative **1***g*. We were unsuccessful, however, in converting this further to the 1,3-dimethyl-2,1-benzisothiazolium salt **1***h* by further decarboxylation as is described for 1,2-dithioles (15). Similarly **1***d* reacted with Meldrum's acid to form **9***d*.

Reactions of **1***c* or *d* with various anions proceeded similarly with little difference, other than in side products. Thus **1***c* reacted with diethyl malonate or sodium benzoylacetate to yield **3***b* and **6***c* respectively. A side product in these reactions was methyl 2-(*N*-phenylamino)dithiobenzoate (**8***b*) produced by reduction of **1***c* with eliminating methanethiolate. To check this, a sample of **1***c* was treated with methanethiol, giving **8***b* in excellent yield. This product was contaminated, however, with a small amount of 9-methylthioacridine (**10**). This does not appear to arise from **8***b* by base catalysed cyclization since its prolonged treatment with methanethiolate gave no acridine **10**. It therefore may be that it is some initial reduction product of **1***c*, possibly a radical species, that is the direct percursor of **10**. Alternatively it may be formed by initial nucleophilic attack at carbon, with subsequent production of the species **11**, which eventually cyclizes to **10**.[2]

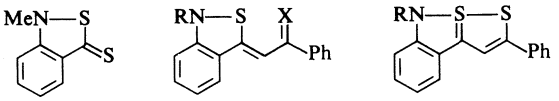

**5** **6** **7**

*a* R = Me; X = O
*b* R = Me; X = S
*c* R = Ph; X = O

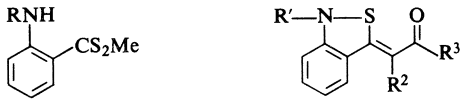

**8** **9**

*a* R = Me
*b* R = Ph

*a* $R^1$ = Me; $R_2$, $R_3$ = $-C(=O)-O-CMe_2-O-$
*b* $R^1$ = Ph; $R_2$ = 2-Py; $R_3$ = OMe
*c* $R^1$ = Ph; $R_2$ = OMe; $R_3$ = 2-Py
*d* $R^1$ = Ph; $R_2$, $R_3$ = $-C(=O)-O-CMe_2-O-$

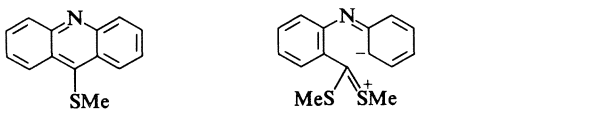

**10** **11**

The treatment of **1***d* with sodium benzoylacetate also afforded **6***c*, and reaction with methyl pyridyl-2-acetate gave a dark yellow oil which could not be separated, but appears to be a mixture of the ester **9***b* and its geometrical isomer **9***c*. With the anion of 2,2-dimethyl-1,3-dioxane-2,6-dione, **9***d* was obtained. Attempted hydrolysis and decarboxylation of this gave only brown polymeric material. Both **9***a* and **9***d* exhibited low field absorptions at ~9.3 δ, no doubt due to the shielding effect of a dioxane-ring carbonyl group on the neighboring aromatic proton. These are in close proximity, due to the steric constraints of the conjugated ring systems.

[2]We are indebted to one of the referees for this suggestion.

Can. J. Chem. Downloaded from www.nrcresearchpress.com by 210.87.254.42 on 09/06/12
For personal use only.

Can. J. Chem. Downloaded from www.nrcresearchpress.com by 210.87.254.42 on 09/06/12
For personal use only.

Treatment of 1-methyl-3-phenyl-2,1-benzisothiazolium perchlorate (**1***e*) with diethyl malonate under a number of conditions gave only 3-phenyl-2,1-benzisothiazole and 2-methylaminobenzophenone (**2***b*). Only a trace of material was isolated whose mass spectrum corresponded to the quinolone **12**, formed by nucleophilic attack on carbon, ring opening, and recyclization. Likewise treatment of **1***e* with sodium benzoylacetate gave 3-phenyl-2,1-benzisothiazole and **2***b*, along with what appear to be traces of the aminoketone **13**, or a tautomer, formed by nucleophilic attack of a phenacyl ion, actual or potential at ring carbon, followed by ring opening, and extrusion of a sulfur atom.

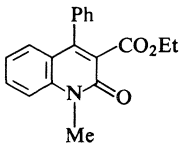


**12**

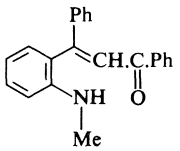


**13**

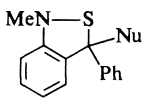


**14**

The low yields of the reaction products with the nucleophiles may be rationalized in terms of initial production of 1:1 addition products which are relatively resistant to ring opening. Nakagawa and co-workers (7) report the isolation of initial products of amines on 2,1-benzisothiazolium salts. Redissociation of adducts of type **14**, with dealkylation, or attack of water on the regenerated cation as alternate reaction pathways could produce the main products isolated. Indeed when **1***e* was treated with sodium bicarbonate, 2-methylaminobenzophenone was isolated. This is comparable to earlier reactions of simpler 2,1-benzisothiazoles (5). Two other unstable products were formed in lesser amounts which may represent side reactions.

Thus all of the products obtained in these reactions, other than dimethylation products, are consistent with nucleophilic attack at ring carbon, in contrast to isothiazolium and 1,2-benzisothiazolium salts which give products by attack of carbanions at sulfur. In terms of "Hard and Soft" acid and base theory, it implies that in the 2,1-system the carbon is "softer," and the sulfur is the "harder" in the latter systems. The low frequencies of the carbonyl stretching frequencies in **6***a* and **6***c*, as well as the two greatly different carbonyl frequencies in **3***a* and **3***c*, are indicative of partial bonding between carbonyl oxygen and sulfur atom. Similar data are available for closely related 1,6,6a$S^{iv}$ trithiapentalenes (16).

## Experimental

The $^1$H nmr spectra were obtained in deuteriochloroform solution, unless otherwise stated, on a Varian model EM 360 spectrometer using tetramethyl silane as an internal standard. Mass spectra were obtained on a Finnegan 1015 spectrometer. Chromatography was performed on Camag silica gel type D.S.F. 5, supplied by Terochem Laboratories, and elution, unless otherwise stated, was by benzene with varying proportions of chloroform. Unless otherwise stated, solutions were dried over anhydrous magnesium sulfate.

*2,1-Benzisothiazolium salts (1*a–e)

These were prepared by literature methods (5–7) or simple modifications of them.

*Reaction of 1-methyl-2,1-benzisothiazolium iodide (1*a) *with sodium bicarbonate*

This was performed as described (5). Examination of the product obtained by tlc afforded 2-methylaminobenzaldehyde (**2***a*) (34%) and 1-methyl-2,1-benzisothiazoline-3-thione (**5***a*) (22%) identical with an authentic sample (6)

*Reaction of 1-methyl-3-phenyl-2,1-benzisothiazolium perchlorate (1e) with sodium bicarbonate*

The perchlorate (326 mg, 1 mmol) was stirred in a warm mixture of ether and saturated sodium bicarbonate. After 30 min the red ether layer was separated, washed with water, dried, and evaporated to give a red oil which on chromatography yielded a broad yellow band. On elution this yielded 2-methylaminobenzophenone (**2***b*) as bright yellow needles from hexane (73%), mp 69°C (lit. (17) mp 69°C).

Two other bands gave small amounts of oily material which appeared to be unstable.

*Reaction of 1-methyl-2,1-benzisothiazolium iodide (1*a) *with triethylamine*

The salt (277 mg, 1 mmol) was added to dry triethylamine and stirred for 30 min. The solution was filtered and partitioned between dilute hydrochloric acid (10%) and ether. The ether layer on evaporation yielded a red oil which on examination by chromatography yielded 2-methylaminobenzaldehyde (36%) and 1-methyl-2,1-benziothiazoline-3-thione (21%), both identical (mixture mp) with authentic specimens (refs. 5 and 6 respectively). Use of pyridine gave similar results.

*Reaction of 1-methyl-2,1-benzisothiazolium iodide (1*a) *with diethyl malonate to form 3*a

The salt (277 mg, 1 mmol) was added to the equivalent quantity of sodium diethyl malonate in ethanol. On stirring, an orange solution resulted which was evaporated and examined by chromatography. Two main bands were evident. A yellow band was found to be 2-methylaminobenzaldehyde (20%), and a slower moving band was isolated as an orange oil which crystallized on standing under ethanol and was recrystallized from hexane as pale orange needles, mp 78–80°C. This is assigned the structure **3***a* (28%). The ir spectrum: 1611, 1702 $cm^{-1}$ (C=O str, the two different carbonyl groups) (in liquid paraffin). The nmr spectrum, δ: 1.20–1.53 (6H, two superimposed methyl triplets), 3.49 (3H, s, the N methyl), 4.12–4.65 (4H, two superimposed methylene quartlets), 6.95–8.02 (4H bands, the aromatic protons). The mass spectrum $M^+$ 307, M calcd. 307.

*Anal.* calcd. for $C_{15}H_{17}NO_4S$: C 58.63, H 5.54, N 4.56, S 10.42; found: C 58.51, H 5.61, N 4.59, S 10.53%.

*Reactions of 3-methylthio- or 3-chloro-2,1-benzisothiazolium salts 1*b, c, d *with diethyl malonate, 2,2-dimethyl-1,3-dioxane-4,6-dione, or benzoylacetic acid*

These were performed under similar conditions. The salts

Can. J. Chem. Downloaded from www.nrcresearchpress.com by 210.87.254.42 on 09/06/12
For personal use only.

were added to slight excesses (1.1 equiv.) of the anions in anhydrous ethanol (prepared by adding the ester or acid to a solution of sodium ethoxide in ethanol). The mixtures were warmed gently until homogeneous, then diluted with water, extracted with chloroform, dried, and examined by chromatography. Products from 2,2-dimethyldioxane-4,6-dione crystallized on dilution of the ethanol with water and were collected. Results of individual experiments are summarized below.

*1-Methyl-3-methylthio-2,1-benzisothiazolium iodide (1b) and sodium benzoyl acetate to form 6a*

Chromatography gave a dark yellow strongly adsorbed material and small amounts of 1-methyl-2,1-benzisothiazoline-3-thione. Separation of the dark yellow material gave an oil which could not be crystallized but had properties consistent with **6a** (76%). It was not analysed.

The ir spectrum: 1000 $cm^{-1}$ (C=O str) (as a liquid film). The nmr spectrum: δ: 3.46 (3 H, s, the *N* methyl protons), 6.85–8.25 (10H bonds, the aromatic and methine protons). The mass spectrum $M^+$ 267, M calcd. 267.

*1-Phenyl-3-methylthio-2,1-benzisothiazolium iodide (1c) and sodium benzoylacetate to form 6c*

Chromatography of the reaction mixture afforded two main products. A dark yellow band on elution and evaporation gave a viscous oil which crystallized on standing under ethanol. Compound **6c** was recrystallized from ethanol as orange prisms, mp 148–50°C (49%). The ir spectrum: 1604 $cm^{-1}$ (C=O str) (in liquid paraffin). The nmr spectrum only exhibited complex bands between δ 7.0 and 8.35. The mass spectrum, $M^+$ 329, M calcd. 329.

*Anal.* calcd. for $C_{21}H_{15}NOS$: C 76.60, H 4.50, N 4.26, S 9.73; found: C 76.73, H 4.31, N 4.28, S 9.80.

A dark orange band on elution and evaporation gave a viscous red oil whose properties were consistent with **8b** (15%). This was identical ($R_f$, nmr) to the product of a preparation described below.

*1-Phenyl-3-chloro-2,1-benzisothiazolium chloride (1d) and sodium benzoylacetate*

This reaction was performed as above. A yellow band obtained on chromatography yielded **6c** as an oil which crystallized under ethanol and was identical to that obtained above (62%).

*Reaction of 1-methyl-3-methylthio-2,1-benzisothiazolium iodide (1b) with 2,2-dimethyl-1,3-dioxane-4,6-dione to form 9a*

The reaction mixture diluted with water gave red needles which recrystallized from ethanol as pale orange needles, mp 165–166°C (43%). The aqueous filtrate on extraction with chloroform yielded more product (19%). The ir spectrum: 1610, 1699 $cm^{-1}$ (C=O str, the two different carbonyl groups) (in liquid paraffin). The nmr spectrum, δ: 1.90 (6H, s, the two C methyl groups), 3.84 (3H, s, the *N*-methyl). The aromatic protons were evident as groups at 7.05–7.83 and 9.15–9.45. The mass spectrum $M^+$ 291, M calcd. 291.

*Anal.* calcd. for $C_{14}H_{13}NO_4S$: C 57.73, H 6.47, N 4.81, S 11.00; found: C 57.62, H 4.48, N 4.90, S 11.13.

*Reaction of 3-chloro-1-phenyl-2,1-benzisothiazolium chloride (1d) with 2,2-dimethyl-1,3-dioxane-4,6-dione to form 9d*

This was performed as above. Dilution with water afforded a dark yellow precipitate which was recrystallized from ethanol as dark yellow prisms, mp 189–190°C (65%). The ir spectrum: 1609, 1699 $cm^{-1}$ (C=O str, the two carbonyl groups) (in liquid paraffin). The nmr spectrum, δ: 1.91 (6H, s, the two methyl groups). The aromatic protons were evident as groups at 7.01–7.86 and 9.13–9.41. The mass spectrum $M^+$ 352, M calcd. 353.

*Anal.* calcd. for $C_{19}H_{15}NO_4S$: C 64.59, H 4.25, N 3.97, S 9.07; found: C 64.81, H 4.26, N 3.83, S 8.94.

*Reaction of 1-methyl-3-methylthio-2,1-benzisothiazolium iodide (1b) with diethyl malonate*

On chromatography a broad yellow band was obtained which on evaporation and standing under ethanol gave **3a** as orange needles from hexane (56%) identical to above.

A faster running orange band gave ~10 mg of a red oil, assigned tentatively to the dithioester **8a**; $M^+$ 197, M calcd. 197.

*Reaction of 3-methylthio-1-phenyl-2,1-benzisothiazolium iodide (1c) with diethyl malonate to form 3b*

Chromatography of the reaction mixture gave a broad strongly absorbed yellow band which on elution gave **3b** as a yellow oil which crystallized from hexane as yellow needles, mp 80°C (42%). The ir spectrum: 1621, 1701 $cm^{-1}$ (C=O str) (in liquid paraffin). The nmr spectrum, δ: 1.31–1.62 (6H, two superimposed methyl triplets), 4.20–4.73 (4H, two superimposed methylene quartets), 6.95–8.11 (9H bands, the aromatic protons). The mass spectrum $M^+$ 369, M calcd. 369.

*Anal.* calcd. for $C_{20}H_{19}NO_4S$: C 65.04, H 5.15, N 3.79, S 8.67; found: C 64.97, H 5.23, N 3.88, S 8.53.

The reaction also yielded **8b** (10%) and small amounts of 1-phenyl-2,1-benzisothiazoline-3-thione as side products.

*Reaction of 3-chloro-1-phenyl-2.1-benzisothiazolium chloride (1d) with methyl 2-pyridylacetate*

The isothiazolium salt (282 mg, 1 mmol) and methyl 2-pyridylacetate (151 mg, 1 mmol) in anhydrous pyridine (10 mL) were refluxed 3 h. The mixture was diluted with water and partitioned between 10% dilute hydrochloric acid and chloroform. The chloroform layer was dried and evaporated to give a dark oil. Chromatography gave a broad yellow band which on elution gave an orange oil. This failed to crystallize and could not be further separated. It was not analysed but its spectral properties are consistent with a mixture of **9b** and **9c**.

The nmr spectrum, δ: 3.78, 4.01 (two singlets of the two isomers). Other protons were evident as bands between 6.95 and 8.85. The mass spectrum $M^+$ 360, M calcd. 360.

*Reaction of 1-methyl-3-phenyl-2,1-benzisothiazolium perchlorate (1e) with diethyl malonate*

The isothiazolium salt (**1e**) (32.6 mg, 1 mmol) and diethyl malonate (~0.2 g) were refluxed together in pyridine for 1.5 h. The pyridine was evaporated under reduced pressure and the product partitioned between dilute hydrochloric acid and chloroform. Examination of the chloroform solution by tlc afforded 3-phenyl-2,1-benzisothiazole (38%) and 2-methylaminobenzophenone (26%), both identical with authentic specimens (refs. 7 and 18, respectively) and only traces of a pale yellow material, mp 135°C, tentatively assigned to **12**.

The mass spectrum $M^+$ 307, M calcd. 307. The use of other reaction conditions gave poorer results.

*Reaction of 1-methyl-3-phenyl-2,1-benzisothiazolium perchlorate (1e) with sodium benzoylacetate*

The perchlorate (326 mg, 1 mmol) was added to a solution of sodium benzoylacetate, prepared from benzoylacetic acid (164 mg, 1 mmol) added to a solution of sodium (23 mg, 1 mmol) in ethanol (10 mL). The mixture was warmed until homogeneous, evaporated under reduced pressure, and examined by chromatography.

The reaction yielded only 3-phenyl-2,1-benzisothiazole, 2-methylaminobenzophenone, and traces of pale orange crystals, mp 68°C, tentatively assigned to **13**.

The mass spectrum $M^+$ 313, M calcd. 313.

*1-Methyl-2,1-benzisothiazole[2,3-b]-5-phenyl-1,2-dithiole (7)*

1-Methyl-3-phenacylidene-2,1-benzisothiazole (**6***a*) (133 mg, 0.5 mmol) in toluene (10 mL) was refluxed with phosphorus pentasulfide (0.5 g) for 30 min. The mixture was cooled and treated with saturated sodium bicarbonate solution and extracted with chloroform. Evaporation yielded a red oil which was separated by chromatography. Elution of the crimson band gave a red oil which crystallized on trituration with ethanol. Dark red prisms, mp 152–153°C, were obtained (61%). The nmr spectrum, δ: 3.60 (3H, s, the *N*-methyl), 6.95–8.29 (9H bands, the aromatic protons), 8.51 (1H, s, the methine proton). The mass spectrum $M^+$ 283, M calcd. 283.

*Anal.* calcd. for $C_{16}H_{13}NS_2$: C 67.84, H 4.59, N 4.95, S 22.61%; found: C 67.91, H 4.66, N 4.61, S 22.89%.

*1-Methyl-3-carboxymethyl-2,1-benzisothiazolium perchlorate (1f)*

The dioxane **9***a* (145 mg, 0.5 mmol) in acetic acid (3 mL) was treated with 70% perchloric acid (0.05 mL) and warmed briefly. The red solution turned pale yellow with gas evolution and separation of a crystalline precipitate. This was recrystallized from acetic acid containing a trace of perchloric acid as buff needles, mp 155°C (dec.).

The ir spectrum: 1710 $cm^{-1}$ (C=O str). It also exhibited a broad absorption between 2800 and 3200 $cm^{-1}$. *Anal.* calcd. for $C_{10}H_{10}ClNO_6S$: C 39.02, H 3.25, Cl 11.54, N 4.55, S 10.41; found: C 39.31, H 3.51, Cl 11.60, N 4.62, S 10.59%.

Further heating of this gave dark yellow polymeric material.

*Methyl 2-phenylaminodithiobenzoate (8b)*

Excess methanethiol was passed into a solution of sodium ethoxide in ethanol (10 mL) (from 13.8 mg sodium). To the solution was added 3-methylthio-1-phenyl-2,1-benzisothiazolium iodide (230 mg, 0.6 mmol), and the mixture warmed until homogeneous. The resulting red solution was treated with charcoal, filtered, and evaporated. The red oil was chromatographed and gave a red and a pale yellow band. The red band on elution gave a red oil which had properties consistent with **8***b* (73%). It was not analysed. The nmr spectrum, δ: 2.80 (3H, s), 6.83–8.40 (9H bands), 9.50–10.03 (1H, broad, the hydrogen bonded NH). The mass spectrum $M^+$ 259, M calcd. 259.

The pale yellow band on elution gave a pale yellow crystalline solid, mp 113°C, identical to a sample of **10** prepared below (5%).

Prolonged treatment of **8***b* with sodium methanethiolate did not produce any of the acridine **10**. Instead a polymeric material was obtained.

*9-Methylthioacridine (10)*

9-Chloracridine (2.13 g, 10 mmol) was treated with excess sodium methanethiolate in methanol (prepared from sodium methoxide and methanethiol) and stirred 4 h. Dilution with water and work-up afforded pale yellow crystals, mp 113–114°C (lit. (17) mp 113–114°C) (81%).

## Acknowledgements

We wish to thank the Natural Sciences and Engineering Research Council of Canada for financial support of this work, and Mr. W. Buchannon for the preparation of mass spectra.

1. D. M. McKinnon and M. E. Hassan. Can. J. Chem. **51**, 3081 (1973).
2. D. M. McKinnon, M. E. Hassan, and M. S. Chauhan. Can. J. Chem. **55**, 1123 (1977).
3. H. Böshagen and W. Geiger. Synthesis, 442 (1979).
4. H. Böshagen and W. Geiger. Justus Liebigs Ann. Chem. **764**, 58 (1972).
5. M. Davis, E. Hornfeld, and K. S. L. Srivastava. J. Chem. Soc. Perkin Trans. I, 1863 (1973).
6. J. Faust and R. Mayer. J. Prakt. Chem. **318**, 161 (1976).
7. O. Aki, Y. Nakagawa, and K. Sirakawa. Chem. Pharm. Bull. **20**, 2372 (1972).
8. J. Faust. Z. Chem. **8**, 170 (1968).
9. G. E. Bachers, D. M. McKinnon, and J. M. Buchshriber. Can. J. Chem. **50**, 2568 (1972).
10. N. F. Haley. J. Org. Chem. **43**, 1233 (1978).
11. E. Klingsberg. J. Org. Chem. **37**, 3226 (1972).
12. D. Festal, J. Tison, Nguyen Kim Son, R. Pinel, and Y. Mollier. Bull. Chem. Soc. Fr. 3339 (1973).
13. E. Klingsberg. J. Org. Chem. **28**: 529 (1963).
14. E. Brown, D. Leaver, and D. M. McKinnon. J. Chem. Soc. C, 1202 (1970).
15. M. Bard and C. Duguay. C. R. Acad Sci. Ser. C. **275**, 905 (1970).
16. N. Losac'h. 1,6,6a$S^{iv}$ Trithiapentalenes and related structures. *In* Advances in heterocyclic chemistry. Vol. 13. New York. 1971. p. 161.
17. H. Staudinger and N. Kon. Justus Liebigs Ann. Chem. **384**, 39 (1911).
18. R. M. Acheson, M. L. Burstall, C. W. Jefford, and B. F. Sanson. J. Chem. Soc. 3742 (1954).

Can. J. Chem. Downloaded from www.nrcresearchpress.com by 210.87.254.42 on 09/06/12
For personal use only.

# Dissociation kinetics of the solvated electron species in methylamine and methylamine–ammonia mixtures

Y. HARIMA, H. KURIHARA, Y. NISHIKI, AND S. AOYAGUI[1]

*Department of Chemical Engineering, Tokyo Institute of Technology, O-okayama, Meguro-ku, Tokyo 152, Japan*

AND

K. TOKUDA AND H. MATSUDA

*Department of Electronic Chemistry, Graduate School at Nagatsuta, Tokyo Institute of Technology, Midori-ku, Yokohama 227, Japan*

Received June 1, 1981

Y. HARIMA, H. KURIHARA, Y. NISHIKI, S. AOYAGUI, K. TOKUDA, and H. MATSUDA. Can. J. Chem. **60**, 445 (1982).

Potential-sweep voltammetric and potential-step chronoamperometric experiments were made at −50°C with solvated electrons in methylamine containing LiCl, KI, or CsI. The dissociation rate constants of the ion pairs, $(M^+ \cdot e_s^-)$, M being alkali metal and $e_s^-$ free solvated electron, were greater than $10^3\ s^{-1}$. The pseudo-first-order rate constant of the dissociation of $K^-$ into the one-electron species, $e_s^-$ and $(K^+ \cdot e_s^-)$ in rapid equilibrium, was determined as $40\ s^{-1}$ by chronoamperometry with 0.5 *M* KI solutions. The formation constants of $K^-$ from the one-electron species determined by chronoamperometry and voltammetry were $4.5 \times 10^4\ M^{-1}$ and $5.6 \times 10^4\ M^{-1}$, respectively. An addition of a small amount of ammonia to methylamine caused a decrease in the formation constant of $K^-$ and an increase in its dissociation rate constant. The appendix deals with a theoretical treatment of chronoamperograms for an electrode process preceded by the dissociation of a dimer. The boundary value problem was solved by the explicit finite difference method and the analytical method which was based on the concept of reaction layer.

Y. HARIMA, H. KURIHARA, Y. NISHIKI, S. AOYAGUI, K. TOKUDA et H. MATSUDA. Can. J. Chem. **60**, 445 (1982).

Opérant à −50°C, on a procédé à des expériences voltammétriques à variation linéaire de potentiel et chronoampèrométriques à saut de potentiel avec des électrons solvatés dans de la méthylamine contenant du LiCL, du KI ou du CsI. Les constantes de vitesse de dissociation des paires d'ions, $(M^+ \cdot e_s^-)$, M étant le métal alcalin et $e_s^-$ l'électron solvaté libre, sont plus grandes que $10^3\ s^{-1}$. On a établi que la constante de vitesse de dissociation de pseudo premier ordre de $K^-$ en espèces mono-électroniques, $e_s^-$ et $(M^+ \cdot e_s^-)$ en équilibre rapide, est égale à $40\ s^{-1}$, en faisant appel à la chronoampèrométrie sur des solutions à 0.5 M de KI. Les constantes de formation de $K^-$, telles que déterminées par chronoampèrométrie et voltammétrie, sont respectivement égales à $4.5 \times 10^4\ M^{-1}$ et $5.6 \times 10^4\ M^{-1}$. L'addition de petites quantités d'ammoniac à la méthylamine a provoqué un accroissement de la vitesse de dissociation de l'espèce bi-électronique et une décroissance de sa constante de formation. L'appendice présente un traitement théorique des chronoampérogrammes pour un processus d'électrode qui est procédé par la dissociation d'un dimère. On a résolu le problème de la valeur aux limites par la méthode de la différence finie explicite et la méthode analytique qui est basée sur le concept de la couche de réaction.

[Traduit par le journal]

## Introduction

Since Hart and Boag (1) in 1963 revealed the presence of solvated electrons in water by generating them with pulse radiolysis and detecting them with spectroscopy, this technique has developed quickly as a powerful tool to investigate solvated electrons in various media, especially those of extremely short lifetimes. Extensive kinetic studies on the formation of chemical species composed of alkali metal cation, $M^+$, and free solvated electron, $e_s^-$, in amines and ethers have been carried out by means of this technique (2–8).

In a previous paper (9) we reported an electrochemical investigation of solvated electrons in methylamine containing an excess alkali metal halide, and concluded that the same solute species as had been proposed in the pulse radiolysis studies on alkali metal – methylamide solutions (2) were present: they were $e_s^-$, the ion pair of $e_s^-$ and $M^+$, $(M^+ \cdot e_s^-)$, and alkali metal anion, $(M^+ \cdot 2e_s^-)$ or $M^-$. In our electrochemical experiments $e_s^-$ and $(M^+ \cdot e_s^-)$ were recognized as species having one excess electron, and $M^-$, two excess electrons. They were termed the one- and the two-electron species, respectively, and the solvated electron species or the solvated electrons, generically. This paper deals with potential-sweep voltammetry and potential-step chronoamperometry of the anodic oxidation of solvated electrons in methylamine and methylamine–ammonia mixtures in order to obtain the rate constants of the dissociation of $(M^+ \cdot e_s^-)$ and $M^-$ as well as the formation constants of $M^-$. A part of the results has been reported in a preliminary note (10).[2]

## Experimental

The test solutions used contained solvated electrons and one of the supporting electrolytes, 0.5 *M* LiCl, 0.5 *M* KI, and 0.1 *M*

[1]Author to whom correspondence should be addressed.

[2]Some of the notations used in refs. 9 and 10 are changed in this paper as follows: $D_{av} \rightarrow D_1$, $D_a \rightarrow D_2$, $K_{ap} \rightarrow K_1$ and $K_a \rightarrow K_2$.

0008-4042/82/040445-11$01.00/0

©1982 National Research Council of Canada/Conseil national de recherches du Canada

Can. J. Chem. Downloaded from www.nrcresearchpress.com by 210.87.254.6 on 09/06/12
For personal use only.

Can. J. Chem. Downloaded from www.nrcresearchpress.com by 210.87.254.6 on 09/06/12
For personal use only.

CsI, in methylamine or methylamine–ammonia mixed solvents. The mixtures were prepared by distillation of a required amount of ammonia into the cell containing a methylamine base solution. The procedures of solvent purification and base solution preparation were described previously (9, 11). Solvated electrons were generated by electrolysis with the cell of Fig. 1 in ref. 11, when their exact concentration must be known, and otherwise with the cell of Fig. 1 in ref. 9. The concentration thus known is the total concentration defined by $c_t = [e_s^-] + [(M^+ \cdot e_s^-)] + 2[M^-]$, where the brackets refer to the concentration in molarity. Tungsten electrodes were used as the working electrode (9–12). Potential-sweep voltammetric and potential-step chronoamperometric experiments were performed in the way described previously (12). In the former experiments the electrode potential was scanned anodically from the equilibrium potential, $E_{eq}$. In the latter ones it was stepped by +50–100 mV from $E_{eq}$ to the limiting current region. The lowest step height was used in the case of low $c_t$ in order to minimize the effect of capacity current. The current–time curves were recorded with a Kawasaki Electronica HR-1200 transient memory and a Riken Denshi F-3DP X-Y recorder. Measurements were made at −50 ± 1°C.

## Results

### *Potential-sweep voltammetry with methylamine solutions*

When $c_t$ and the sweep rate $v$ were below 0.1 m$M$ and 1 V s$^{-1}$, respectively, the potential-sweep voltammograms of 0.5 $M$ LiCl and 0.1 $M$ CsI solutions exhibited features characteristic of the diffusion-controlled electron-transfer process whose number of electron transferred, $n$, is one, as in the case of liquid ammonia solutions (12). In those of 0.5 $M$ KI solutions, however, the difference between $E_{eq}$ and the potential at which the anodic current peak occurs, $E_p$, became greater than 17 mV, a value close to the theoretical value of 16.4 mV which an electrode reaction of $n = 1$ is expected to have at −50°C, when $c_t$ was increased beyond ca. 0.01 m$M$. The $E_p - E_{eq}$ value at a given $c_t$ came to deviate from the theoretical value with increasing $v$. Furthermore, the plot of the peak current $i_p$ vs. $v^{1/2}$ at low $v$ values fitted a straight line through the origin, whereas it bent downwards with increasing $v$. The same behaviour of the $i_p$ vs. $v^{1/2}$ relation has been observed in experiments with an Na–$NaClO_4$ solution of hexamethylphosphoric triamide and attributed to the slow dissociation of some associated species of $e_s^-$ competing with the electron transfer process (13).

Solvated electrons generated by the pre-electrolysis of base solutions decomposed gradually during measurements. They were most unstable in LiCl solutions and most stable in KI solutions. Figure 1 shows a typical $i_p$ change with time in a 0.5 $M$ LiCl solution. No anodic current attributable to the oxidation of any decomposition products of solvated electrons was observed at potentials between 0 and 1.5 V referred to the respective initial $E_{eq}$'s.

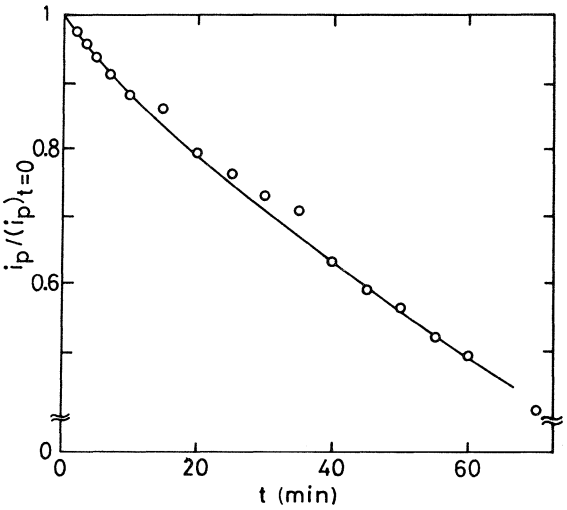


FIG. 1. Decomposition rate of solvated electrons in a 0.5 $M$ LiCl solution of methylamine at −50°C observed by potential-sweep voltammetry. Sweep rate: 50 mV s$^{-1}$.

### *Potential-step chronoamperometry with methylamine solutions*

Figure 2 shows $i_l t^{1/2}$ vs. log $t$ plots, $i_l$ being the limiting current density in potential-step chronoamperometry, obtained with 0.5 $M$ LiCl solutions whose $c_t$ values range from 0.05 to 1 m$M$. In all the curves the $i_l t^{1/2}$ value was independent of time, as in liquid ammonia (11, 12). This fact suggests that the electrode reaction should be a simple diffusion-controlled process. The $i_l t^{1/2}$ values for 0.1 $M$ CsI solutions within the time range of 5 to 600 ms were also almost invariable, when $c_t$ was below ca. 0.1 m$M$. However, an attempt to obtain information on the dissociation kinetics of $Cs^-$ was unsuccessful because of serious ohmic drop error due to high current densities caused by the use of solutions of high $c_t$ where $Cs^-$ is predominant. On the basis of these findings and the reaction schemes proposed previously (9), it is concluded that the lower limit of the rate constant $k_1$ for the dissociation of the ion pairs, $(Li^+ \cdot e_s^-)$ and $(Cs^+ \cdot e_s^-)$, is about $10^3$ s$^{-1}$, which is the reciprocal of the effective rise-time of the potentiostat under the experimental conditions employed.

Figure 3, a reproduction of Fig. 2 in ref. 10, shows $i_l t^{1/2}$ vs. log $t$ plots obtained with 0.5 $M$ KI solutions whose $c_t$ is below 0.1 m$M$. In the lowest curve corresponding to region I in Fig. 1 of ref. 10, the $i_l t^{1/2}$ values are independent of time as in LiCl and CsI solutions. This fact suggests that the $k_1$

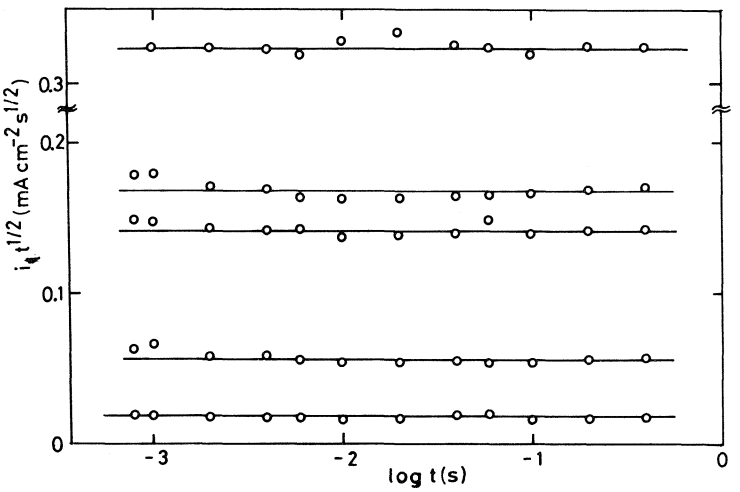


FIG. 2. $i_l t^{1/2}$ vs. log $t$ plots in potential-step chronoamperometry for solvated electrons in 0.5 $M$ LiCl solutions of methylamine at −50°C; $0.05 < c_t(\mathrm{m}M) < 1$.

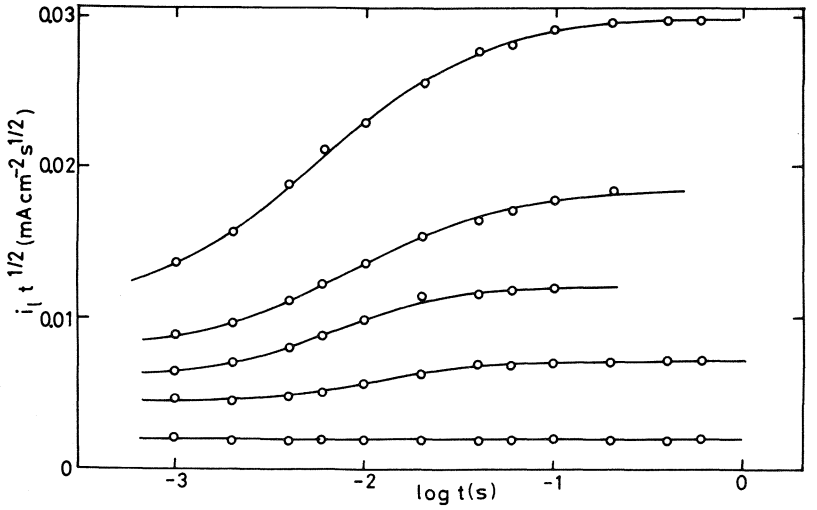


FIG. 3. $i_l t^{1/2}$ vs. log $t$ plots in potential-step chronoamperometry for solvated electrons in 0.5 $M$ KI solutions of methylamine at −50°C; $0.005 < c_t(\mathrm{m}M) < 0.1$.

value for $(K^+ \cdot e_s^-)$ should also be greater than $10^3$ $s^{-1}$. In solutions of higher $c_t$, where $K^-$ coexists with the one-electron species, each $i_l t^{1/2}$ vs. log $t$ curve has two plateaux and a transient region between them. The $i_l t^{1/2}$ values at the left and the right plateaux are denoted by $(i_l t^{1/2})_1$ and $(i_l t^{1/2})_2$, respectively. The transition region comes to be extended on both sides with increasing $c_t$. The current density at the left plateau is considered to be controlled by the diffusion of the one-electron species. The increase in $i_l t^{1/2}$ with time in the transition region may be attributed to the kinetic current (14) due to the formation of the one-electron species from $K^-$:

$$[1] \quad K^+ + K^- \underset{}{\overset{k_2}{\rightleftharpoons}} 2(K^+ \cdot e_s^-), (K^+ \cdot e_s^-) \underset{K^+ + e_s^-,\ e_s^- \rightarrow e_m^-}{\overset{k_1 > 10^3\ s^{-1}}{\rightleftharpoons}}$$

where $k_2$ is the second-order rate constant and $e_m^-$ the electron in electrode metal. In solutions of $c_t > 0.1$ m$M$, the $i_l t^{1/2}$ vs. log $t$ plots were irreproducible. It may be interpreted in terms of potassium metal deposition onto the electrode surface, as was the irreproducibility of the $-E$ vs. log $i$ plots at highly negative potentials (9). Details of the $i_l t^{1/2}$ vs. log $t$ curves for solutions of low $c_t$ are shown in

Can. J. Chem. Downloaded from www.nrcresearchpress.com by 210.87.254.6 on 09/06/12
For personal use only.

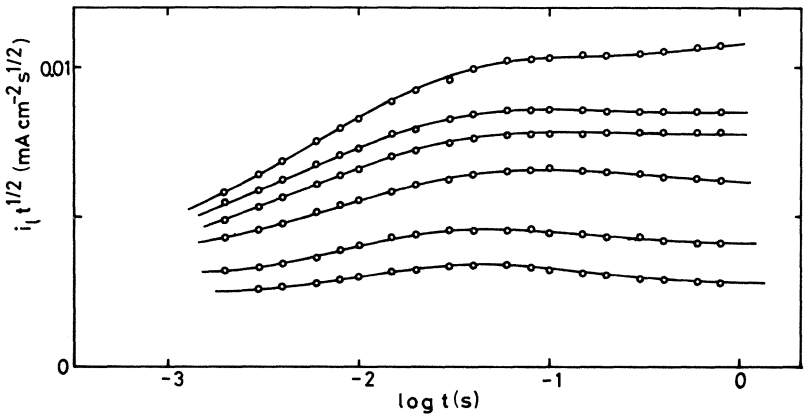


FIG. 4. Detailed plots for $i_l t^{1/2}$ vs. log $t$ in potential-step chronoamperometry for solvated electrons in 0.5 $M$ KI solutions of methylamine at −50°C; $0.005 < c_t(\mathrm{m}M) < 0.03$.

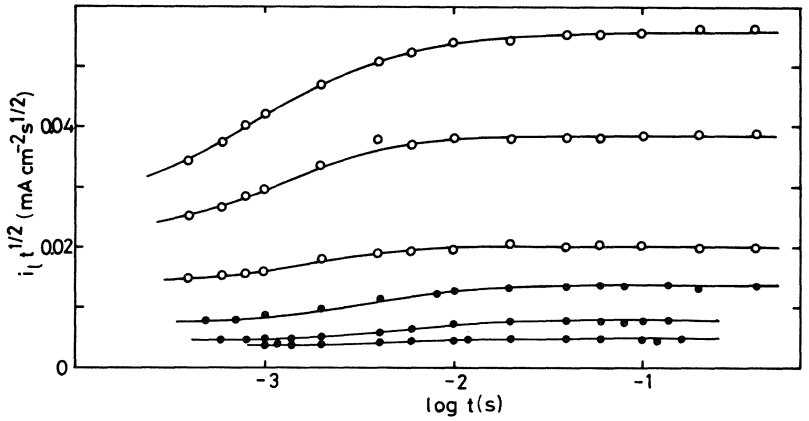


FIG. 5. $i_l t^{1/2}$ vs. log $t$ plots in potential-step chronoamperometry for solvated electrons in 0.5 $M$ KI solutions of (●) methylamine–ammonia (2.5 mol%) ($0.01 < c_t(\mathrm{m}M) < 0.04$) and (○) methylamine–ammonia (5.0 mol%) ($0.04 < c_t(\mathrm{m}M) < 0.15$).

Fig. 4. Each curve exhibited a broad peak at about 50 ms.

*Potential-step chronoamperometry with methylamine–ammonia mixed solutions*

Figure 5 shows $i_l t^{1/2}$ vs. log $t$ plots for solutions containing 0.5 $M$ KI and solvated electrons of various concentrations in methylamine–ammonia mixtures whose ammonia contents are 2.5 and 5.0 mol%. A comparison between Figs. 3 and 5 shows that the transition region of the $i_l t^{1/2}$ vs. log $t$ curve shifts to the left with increasing ammonia content. No such region was observed when ammonia content exceeded 10 mol%. In Fig. 6 are compared the normalized $i_l t^{1/2}$ vs. log $t$ plots for solvated electron solutions providing nearly equal $(i_l t^{1/2})_2$ values in pure methylamine and mixed solvents. The increasing shift of the transition region with increasing ammonia content explains why no transition region was observed when the pure ammonia solvent was used (11, 12).

$D_l$ *values in methylamine solutions of 0.5* M *KI and 0.1* M *CsI*

The results of the previous potential-sweep voltammetric (9) and the present potential-step chronoamperometric experiments suggests that the electrode reaction scheme in the region of $n = 1$ in methylamine should be exactly identical with that in liquid ammonia (12). Consequently, the diffusing species is a composite of $e_s^-$ and $(M^+ \cdot e_s^-)$ in rapid equilibrium. Its diffusion coefficient $D_l$ is given by the following equation (11):

$$[2] \quad D_l = ([e_s^-]D_e + [(M^+ \cdot e_s^-)]D_{ip})/([e_s^-] + [(M^+ \cdot e_s^-)]) = (D_e + K_1 D_{ip})/(1 + K_1)$$

with

Can. J. Chem. Downloaded from www.nrcresearchpress.com by 210.87.254.6 on 09/06/12
For personal use only.

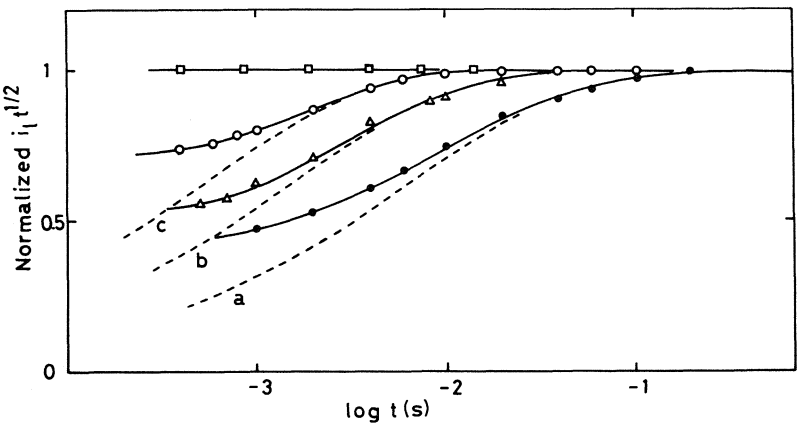


FIG. 6. Normalized plots of $i_l t^{1/2}$ vs. log $t$ for solvated electrons in 0.5 $M$ KI solutions of (●) methylamine, (△) methylamine–ammonia (2.5 mol%), (○) methylamine–ammonia (5.0 mol%), and (□) methylamine–ammonia (> 10 mol%). Broken lines are theoretical curves calculated from eq. [18] with $\alpha$ = (*a*) 15, (b) 67, and (c) 180 $s^{-1}$.

[3] $K_1 = [(M^+ \cdot e_s^-)]/[e_s^-]$

where $D_e$ and $D_{ip}$ are respectively the diffusion coefficients of $e_s^-$ and $(M^+ \cdot e_s^-)$. The $D_1$ values in methylamine were obtained by determining $c_t D_1^{1/2}$ voltammetrically and/or chronoamperometrically and $c_t$, which is practically equal to $[e_s^-] + [(M^+ \cdot e_s^-)]$, coulometrically.

The recovery ratio of solvated electrons in 0.5 $M$ KI solutions was approximately 71%, when determined by coulometric reoxidation which took about 100 min. Since each experimental run, i.e. the electrolytic generation of solvated electrons and the measurement of $c_t D_1^{1/2}$, took no more than 10 min, the decomposition of solvated electrons might affect the $D_1$ value to only a negligible extent. The $D_1$ values obtained by potential-step chronoamperometry and potential-sweep voltammetry were $4.1 \times 10^{-5}$ $cm^2$ $s^{-1}$ and $3.9 \times 10^{-5}$ $cm^2$ $s^{-1}$, respectively. The mean value of $4.0 \times 10^{-5}$ $cm^2$ $s^{-1}$ is used as the $D_1$ value in the 0.5 $M$ KI solution of methylamine at −50°C.

Figure 7 shows $c_t D_1^{1/2}$ vs. $c_t$ plots in 0.1 $M$ CsI solutions at −50°C obtained by potential-sweep voltammetry with sweep rates of 50 and 75 mV $s^{-1}$. All experimental points lie on a straight line. A $D_1$ value of $1.2 \times 10^{-5}$ $cm^2$ $s^{-1}$ could be obtained from its slope, but this might be the lower limit since the decomposition rate of solvated electrons in this solution was faster than in KI solutions.

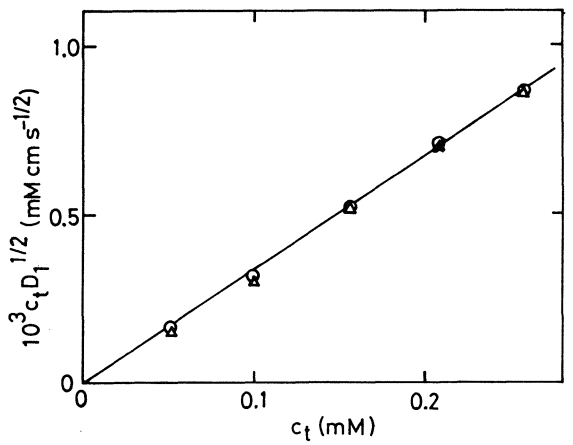


FIG. 7. Plots of $c_t D_1^{1/2}$ vs. $c_t$ for solvated electrons in 0.1 $M$ CsI solutions of methylamine at −50°C. $c_t D_1^{1/2}$ values are obtained by potential-sweep voltammetry with sweep rates of (○) 50 and (△) 75 mV $s^{-1}$. The $c_t$ values are determined coulometrically.

## Discussion

*Formation constant of two-electron species*

The electrode reaction of solvated electron species, $\varepsilon_{sol}$, is written in the form

[4] $n e_m^- \rightleftharpoons \varepsilon_{sol}$

When $n = 1$, $\varepsilon_{sol}$ is the one-electron species, i.e. a mixture of $e_s^-$ and $(M^+ \cdot e_s^-)$ in rapid equilibrium, and when $n = 2$, it is the two-electron species, presumably $M^-$ in the case of methylamine solutions.

The potential-sweep voltammograms in the regions of $n = 1$ and $n = 2$ are expressed respectively by the following equations (12):

[5] $E = -(RT/F) \ln i + (RT/2F) \ln v + A_1$

with

[6] $A_1 = E_1^0 + (RT/F)\{\ln F + \ln (FD_1/RT)^{1/2}\}$

Can. J. Chem. Downloaded from www.nrcresearchpress.com by 210.87.254.6 on 09/06/12
For personal use only.

Can. J. Chem. Downloaded from www.nrcresearchpress.com by 210.87.254.6 on 09/06/12
For personal use only.

and

$$[7] \quad E = -(RT/2F) \ln i + (RT/4F) \ln v + A_2$$

with

$$[8] \quad A_2 = E_2^0 + (RT/2F)\{\ln 2F + \ln(2FD_2/RT)^{1/2}\}$$

where $D_2$ is the diffusion coefficient of $M^-$. $E_1^0$ and $E_2^0$ are respectively the formal standard potentials of the electrode reaction [4] when $n = 1$ and 2 and they are defined respectively at $[e_s^-] + [(M^+ \cdot e_s^-)] = 1\,M$ and $[M^-] = 1\,M$. The difference between them can be given by the following equation, similar to the case where the two-electron species is $(M^+ \cdot e_s^-)_2$ (11):

$$[9] \quad E_1^0 - E_2^0 = -(RT/2F) \ln K_2$$

with

$$[10] \quad K_2 = [M^-]/([e_s^-] + [(M^+ \cdot e_s^-)])^2$$

The quantity $K_2$ is the formation constant of $M^-$ from the one-electron species and can be determined with the experimental values for $A_1, A_2, D_1$, and $D_2$. The $K_2$ value of $K^-$ in a 0.5 $M$ KI solution was $5.6 \times 10^4\ M^{-1}$, when the known values of $A_1 = -2.76$ V (9), $A_2 = -2.73$ V (9), and $D_1 = 4.0 \times 10^{-5}$ cm$^2$ s$^{-1}$ were used together with the $D_2$ value of $1.0 \times 10^{-5}$ cm$^2$ s$^{-1}$. The $D_2$ value was chosen by taking account of the diffusion coefficient of $K^+$ in methylamine, $1.5 \times 10^{-5}$ cm$^2$ s$^{-1}$, estimated from the mobility of $K^+$ in liquid ammonia (15) and the viscosities of liquid ammonia and methylamine (16).

The formation constant of $K^-$ was also obtained by analyzing the chronoamperometric results of Fig. 3. Since $(i_1t^{1/2})_1$ and $(i_1t^{1/2})_2 - (i_1t^{1/2})_1$ are attributed to the diffusion-controlled currents for the one- and the two-electron species, respectively, they can be written as follows:

$$[11] \quad (i_1t^{1/2})_1 = (F/\pi^{1/2})([e_s^-] + [(M^+ \cdot e_s^-)])D_1^{1/2}$$

and

$$[12] \quad (i_1t^{1/2})_2 - (i_1t^{1/2})_1 = (2F/\pi^{1-2})\,[K^-]D_2^{1/2}$$

Combining eqs. [11] and [12], one obtains

$$[13] \quad \{(i_1t^{1/2})_2 - (i_1t^{1/2})_1\}/(i_1t^{1/2})_1 = (2\pi^{1/2}/F)(D_2^{1/2}/D_1)K_2(i_1t^{1/2})_1$$

From the slope of the linear plot of $\{(i_1t^{1/2})_2 - (i_1t^{1/2})_1\}/(i_1t^{1/2})_1$ vs. $(i_1t^{1/2})_1$ in Fig. 8, the formation constant of $K^-$ was evaluated as $4.5 \times 10^4\ M^{-1}$.

The agreement between these $K_2$ values is satisfactory. This fact strongly suggests that the two-electron species in potential-sweep voltammetry should be identical with the slow-dissociating species in potential-step chronoamperometry.

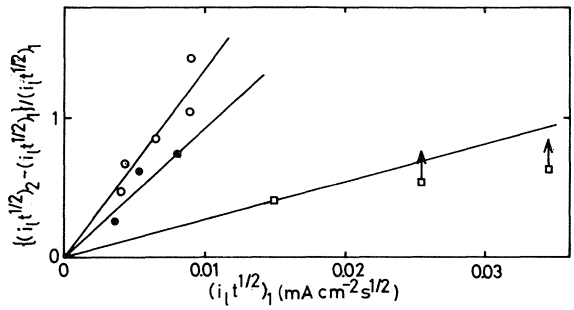


FIG. 8. Plots for obtaining the $K_2$ values in (○) methylamine, (●) methylamine–ammonia (2.5 mol%), and (□) methylamine–ammonia (5.0 mol%). (⇧) indicates a lower limit value.

Figure 9 shows the relative concentrations of the one- and the two-electron species at various $c_t$ values calculated with $K_2 = 5 \times 10^4\ M^{-1}$. The curves for $e_s^-$ and $(K^+ \cdot e_s^-)$ could not be drawn because the $K_1$ value was unavailable. A comparison between this illustration and the similar one obtained with liquid ammonia solutions (11) shows that the two-electron species prevails at much lower $c_t$ values in methylamine than in liquid ammonia.

From the previous potential-sweep voltammogram (9), the approximate value for the formation constant of $Cs^-$ in methylamine was estimated as $5 \times 10^2\ M^{-1}$, by using $A_1 = -2.76$ V, $A_2 = -2.77$ V, $D_1 = 1.2 \times 10^{-5}$ cm$^2$ s$^{-1}$, and $D_2 = 10^{-5}$ cm$^2$ s$^{-1}$. In a similar manner, the upper limit of the formation constant of $Li^-$ was evaluated to be $2 \times 10^1\ M^{-1}$. The order of magnitude of the $K_2$ values of these two-electron species in methylamine is thus as follows:

$$Li^- < Cs^- < K^-$$

It is noted that this is opposite to the solubility order (17) of these alkali metals.

*Dissociation rate constant of potassium anion*

The boundary value problem of the following electrode reaction in potential-step chronoamperometry was solved by the explicit finite difference method and, though applicable only in limited circumstances, the analytical method based on the reaction layer concept of Koutecky (see Appendix):

$$[14] \quad B \overset{k}{\rightleftharpoons} 2A,\ A \pm e_m^- \rightarrow C$$

where $k$ is the first-order rate constant[3] for the dissociation of B defined by $-d[B]/dt = k[B]$.

[3]In a preliminary note (10), the pseudo-first-order rate constant $k_2[K^+]$ for the dissociation of $K^-$ was defined by $-2d[B]/dt = k[B] \equiv (k_2[K^+])\,[B]$. The difference in definition should cause a difference in the $k_2[K^+]$ value by a factor of two.

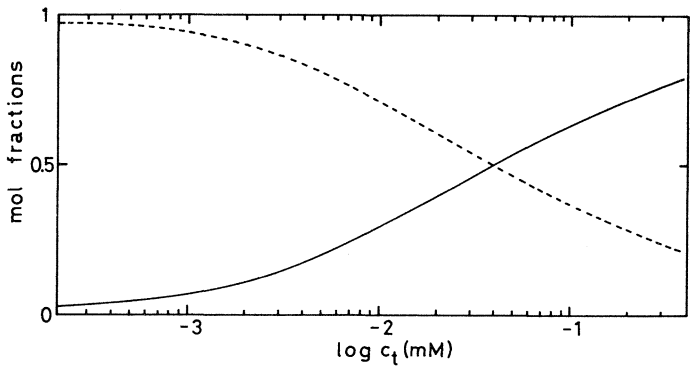


FIG. 9. Mole fractions of (------) the one-electron species and (——) the two-electron species in 0.5 *M* KI solutions of methylamine at −50°C calculated from the $K_2$ value.

The analysis of the electrode reaction of our present concern, reaction [1], can be reduced to that of reaction [14] because of the pseudo-first-order nature of the dissociation reaction of $M^-$ in the presence of a large excess of $M^+$ and the rapidity of the ion-pairing reactions. The chemical species B and A correspond respectively to $K^-$ and the composite one-electron species whose concentration and diffusion coefficient are $[e_s^-] + [(K^+ \cdot e_s^-)]$ and $D_1$, respectively. Then $k$, $K$, and $\alpha$ are given respectively by the following relations:

$$[15] \quad k = k_2[K^+]$$

$$[16] \quad K = K_2$$

and

$$[17] \quad \alpha = (2/3\pi)(D_1/D_2)\{([e_s^-] + [(K^+ \cdot e_s^-)])D_1/2D_2 + [K^-]\}^{-1/2} K_2^{-1/2} \times k_2[K^+]$$

Figure 10 shows the theoretical curves of $\Phi(\alpha t)$ vs. $\alpha t$ obtained by the explicit finite difference method. Each of them has a peak as do the experimental curves for $i_l t^{1/2}$ vs. log $t$ in Fig. 4. In Fig. 11 the two experimental curves at the bottom of Fig. 4 are fitted with the theoretical ones. The best fit was obtained with $k = 37\,s^{-1}$ in both cases, when the following experimental data were used: $D_1 = 4 \times 10^{-5}\,cm^2\,s^{-1}$, $D_2 = 1 \times 10^{-5}\,cm^2\,s^{-1}$, $K_2 = 5 \times 10^4\,M^{-1}$ and $[e_s^-] + [(K^+ \cdot e_s^-)] = 6.7 \times 10^{-3}$ and $8.3 \times 10^{-3}$ m*M* for the lowest and the upper curves, respectively. Those concentrations were determined from the $i_l t^{1/2}$ values at the left plateaux of the corresponding curves in Fig. 4.

Under the specific condition of $[K^-] \gg [e_s^-] + [(K^+ \cdot e_s^-)]$, the analytical method leads to the following expression for $i_l t^{1/2}$:

$$[18] \quad i_l t^{1/2} = (2F/\pi^{1/2})[K^-]D_2^{1/2}\Phi(\alpha t)$$

with

$$[19] \quad \alpha = (2/3\pi)(D_1/D_2)K_2^{-1/2}k_2[K^+][K^-]^{-1/2}$$

The uppermost curve of Fig. 3 was normalized and compared with the theoretical curves calculated from eq. [18] with various $\alpha$ values. The best fit was obtained with $\alpha = 20\,s^{-1}$. The disagreement at low $i_l t^{1/2}$ values, which is typically shown by curve (a) in Fig. 6, may be attributed to the condition $[B_0] \gg [A_0]$. It could not be fulfilled in our experiments because of inevitable metal deposition at $c_t >$ 0.1 m*M*. The same applies to curves (b) and (c). From eq. [19] with this $\alpha$ value the pseudo-first-order rate constant for the dissociation of $K^-$ was evaluated as $40\,s^{-1}$ in a 0.5 *M* KI solution of methylamine at −50°C. The agreement between the two $k_2[K^+]$ values is satisfactory.[4]

By using the $k_2[K^+]$ value of $40\,s^{-1}$, the rate constant for the formation of $K^-$ from the one-electron species, $kK = k_2[K^+]K_2$, was evaluated as $2 \times 10^6\,M^{-1}\,s^{-1}$. It is about three orders of magnitude smaller than the value in ethylamine, obtained with the pulse radiolysis technique, $6.2 \times 10^9\,M^{-1}\,s^{-1}$ (4). This is consistent with the finding that the formation process of $K^-$ in methylamine is too slow to be followed by this technique (2).

*Dissociation rate constants of the two-electron species in methylamine–ammonia mixed solvents*

It is evident from eq. [19] that the increase in the dissociation rate constant of $K^-$, $k_2[K^+]$, is not the only reason for the shift of the transition regions in Fig. 6 towards shorter times, because the quantities, $[K^-]$, $D_1/D_2$, and $K_2$, can also vary with the solvent composition. However, the change in $[K^-]$ cannot be responsible for the shift since the $i_l t^{1/2}$ vs. log $t$ plots in Fig. 6 were compared at nearly equal

[4]This fact suggests that eq. [18] can be used to determine $k_2[K^+]$ even when $[K^-] \simeq [e_s^-] + [(K^+ \cdot e_s^-)]$. The results of chronoamperometry with mixed solvents will be discussed on the basis of eq. [18].

Can. J. Chem. Downloaded from www.nrcresearchpress.com by 210.87.254.6 on 09/06/12
For personal use only.

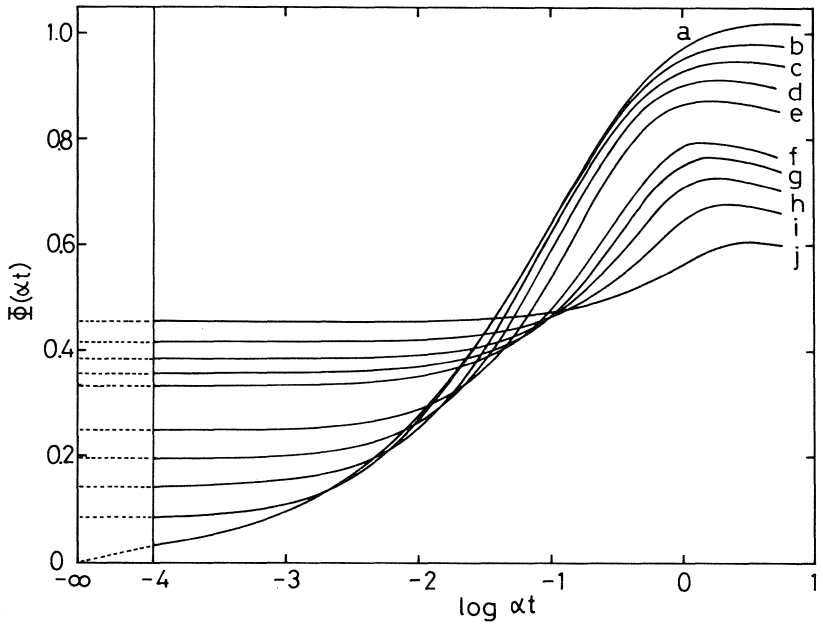


FIG. 10. $\Phi(\alpha t)$ vs. $\alpha t$ curves for $D_B/D_A = 0.25$ obtained by the explicit finite difference method with [B]/[A] = (b) 10, (c) 5, (d) $10^{1/2}$, (e) 2, (f) 1, (g) 0.8, (h) 0.6, (i) 0.4, and (j) 0.2. Curve a is obtained by the analytical method with [B]/[A] = ∞.

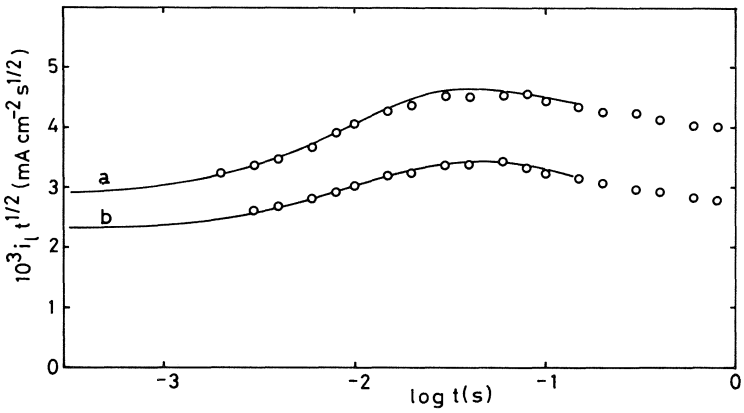


FIG. 11. Simulation analysis for obtaining the $k_2[K^+]$ value. Experimental points are reproductions of the lower two curves in Fig. 4. Solid lines are calculated by using the theoretical curves of Fig. 10 with $k_2[K^+] = 37\ s^{-1}$, $D_1 = 4.0 \times 10^{-5}\ cm^2\ s^{-1}$, $D_2 = 1 \times 10^{-5}\ cm^2\ s^{-1}$, $K_2 = 5 \times 10^4\ M^{-1}$, and $[e_s^-] + [(K^+ \cdot e_s^-)] =$ (a) $8.3 \times 10^{-3}$ m$M$ and (b) $6.7 \times 10^{-3}$ m$M$.

$(i_1 t^{1/2})_2$ values, i.e. $[K^-]$ values. The change in $D_1/D_2$ caused by the solvent composition change may also be unimportant since it ranges between the values of ca. 3 in pure ammonia (11) and 4 in pure methylamine.

The $K_2$ values in mixed solvents were obtained by using the slopes of the $\{(i_1 t^{1/2})_2 - (i_1 t^{1/2})_1\}/(i_1 t^{1/2})_1$ vs. $(i_1 t^{1/2})_1$ plots in Fig. 8 and a constant $D_1/D_2$ value of 4. The values for $\alpha$ and, consequently, $k_2[K^+]$ were obtained from eq. [18] using the uppermost curve for each solvent composition in Fig. 5 in order that the condition $[B_0] \gg [A_0]$ might be satisfied as fully as possible. In Table 1 are listed the values for $\alpha$, $K_2$, and $k_2[K^+]$ in mixed and pure solvents. An increase in ammonia content caused a decrease in $K_2$ as well as an increase in $k_2[K^+]$. According to eq. [19] both changes operate as factors to shift the transition region to shorter times.

The nature of the ion pairs in various solvents has recently been discussed on the basis of the hyperfine structure of the esr spectrum and the third absorption band observed in pulse radiolysis of solvents of relatively low polarity (18). It led to the conclusion that the atomic character of the ion pairs increased with the decreasing dielectric con-

Can. J. Chem. Downloaded from www.nrcresearchpress.com by 210.87.254.6 on 09/06/12
For personal use only.

TABLE 1. Results of potential-step chronoamperometry in methylamine and methylamine–ammonia mixtures

| Solvent | $\alpha(s^{-1})$ | $10^{-4}\ K_2(M^{-1})$ | $k_2[K^+](s^{-1})$ |
|---|---|---|---|
| MA | 20 | 4.5 | 80 |
| MA–$NH_3$ (2.5 mol%) | 67 | 3.1 | 120 |
| MA–$NH_3$ (5.0 mol%) | 170 | 1.0 | 360 |
| $NH_3$ | | 0.069* | $>10^3$* |

*Reference 11.

stant of the solvent. The increase in the atomic character means the decrease in the solvent-separated nature. The values for the dipole moment and the dielectric constant of ammonia, 1.47 D and 22, are greater than those of methylamine, 1.27 D and 15. Consequently, the solvent-separated nature of the two-electron species may become enhanced by the addition of ammonia to methylamine. The increase in dissociation rate constant of the two-electron species caused by the addition of ammonia to methylamine may be interpreted on this basis. The idea of the solvent-separated nature of the two-electron species employed here is consistent with the model proposed for the associated species in alkali metal – ammonia solutions (19).


1. E. J. HART and J. W. BOAG. J. Am. Chem. Soc. **84**, 4090 (1962).
2. J. W. FLETCHER, W. A. SEDDON, J. J. JEVCAK, and F. C. SOPCHYSHYN. Can. J. Chem. **53**, 3571 (1975).
3. J. W. FLETCHER and W. A. SEDDON. J. Phys. Chem. **79**, 3055 (1975).
4. J. W. FLETCHER, W. A. SEDDON, and F. C. SOPCHYSHYN. Can. J. Chem. **51**, 2975 (1973).
5. J. L. DYE, M. G. DEBACKER, J. A. EYRE, and L. M. DORFMAN. J. Phys. Chem. **76**, 839 (1972).
6. W. A. SEDDON, J. W. FLETCHER, and F. C. SOPCHYSHYN. Can. J. Chem. **54**, 2807 (1976).
7. W. A. SEDDON, J. W. FLETCHER, J. J. JEVCAK, and F. C. SOPCHYSHYN. Can. J. Chem. **51**, 3653 (1973).
8. J. L. DYE, M. G. DEBACKER, and L. M. DORFMAN. J. Chem. Phys. **52**, 6251 (1970).
9. Y. HARIMA, H. KURIHARA, and S. AOYAGUI. J. Electroanal. Chem. **124**, 103 (1981).
10. Y. HARIMA, H. KURIHARA, and S. AOYAGUI. Can. J. Chem. **58**, 1151 (1980).
11. Y. HARIMA and S. AOYAGUI. J. Electroanal. Chem. **109**, 167 (1980).
12. Y. HARIMA and S. AOYAGUI. Israel J. Chem. **18**, 81 (1979).
13. Y. KANZAKI and S. AOYAGUI. J. Electroanal. Chem. **36**, 297 (1972); **47**, 109 (1973); E. V. OVSYANNIKOVA, L. I. KRISHTALIK, and N. M. ALPATOVA. Elektrokhim. **12**, 1032 (1976).
14. C. NISHIHARA and H. MATSUDA. J. Electroanal. Chem. **51**, 287 (1974).
15. C. A. KRAUS and W. C. BRAY. J. Am. Chem. Soc. **35**, 1315 (1913).
16. M. YAMAMOTO, Y. NAKAMURA, and M. SHIMOJI. Trans. Faraday Soc. **68**, 135 (1972).
17. Y. NAKAMURA, M. YAMAMOTO, S. SHIMOKAWA, and M. SHIMOJI. Bull. Chem. Soc. Jpn. **44**, 3212 (1971).
18. W. A. SEDDON, J. W. FLETCHER, and R. CATTERALL. Can. J. Chem. **55**, 2017 (1977).
19. M. GOLDEN, W. L. JOLLY, and K. S. PITZER. J. Am. Chem. Soc. **84**, 2264 (1962).
20. S. W. FELDBERG. *In* Electroanalytical chemistry. Vol. 3. *Edited by* A. J. Bard. Marcel Dekker, New York. 1969. p. 199.
21. J. KOUTECKY and V. HANUS. Collect. Czechoslov. Chem. Commun. **20**, 124 (1955).


## Appendix

This appendix describes a theoretical treatment of chronoamperometric curves for an electrode process preceded by the dissociation of a dimer, the general scheme of which is expressed as

[A1] $B \underset{}{\overset{k}{\rightleftharpoons}} 2A,\ A \pm ne_m^- \rightarrow C$

Under the condition of linear diffusion, our boundary value problem is given by

[A2] $\partial[B]/\partial t = D_B\partial^2[B]/\partial x^2 - k([B] - K[A]^2)$

[A3] $\partial[A]/\partial t = D_A\partial^2[A]/\partial x^2 + 2k([B] - K[A]^2)$

with the initial and boundary conditions:

[A2] $$\begin{cases}[A] = [A_0],\ [B] = [B_0] = K[A_0]^2 \text{ for } t = 0,\ x > 0 \text{ and } t > 0,\ x \rightarrow \infty \\ [A] = 0,\ \partial[B]/\partial x = 0,\ D_A\partial[A]/\partial x = i_l/nF \text{ for } t > 0,\ x = 0\end{cases}$$

where $[A_0]$ and $[B_0]$ represent respectively the concentrations of A and B in the bulk of the solution and B is assumed to be electroinactive.

Since it is difficult to solve this nonlinear problem analytically, a digital simulation method outlined by Feldberg (20) was employed. The discretization of time and space into a number of increments of duration $\Delta t$ and JMAX space elements of equal size $\Delta x$, respectively, and transformation of eqs. [A2]–[A4] leads to explicit finite difference equations. Current density is calculated from the concentration of A in the first space element adjacent to the electrode, $C_A$, by using

[A6] $\text{CDNORM} = (\Delta t/\Delta x)(i/nF)/[B_0] = 2DD_AC_A(1)$

Can. J. Chem. Downloaded from www.nrcresearchpress.com by 210.87.254.6 on 09/06/12
For personal use only.

in terms of the dimensionless quantities defined by

$$[A5]\quad \begin{cases} C_A(J) = [A_J]/[B_0],\ C_B(J) = [B_J]/[B_0],\ DD_A = D_A\Delta t/(\Delta x)^2 \\ DD_B = D_B\Delta t/(\Delta x)^2,\ \text{RATE} = k\Delta t,\ \text{EQ} = [B_0]/[A_0] = (k[B_0])^{1/2} \end{cases}$$

where $[A_J]$ and $[B_J]$ denote the concentrations of A and B in the $J$-th space element, respectively. The concentrations in the $J$-th space element are modified according to the following equations,

$$[A7]\quad \begin{cases} C_A'(1) = C_A(1) + DD_A[C_A(2) - C_A(1)] - \text{CDNORM} + 2\ \text{REAC}\ (1) \\ C_B'(1) = C_B(1) + DD_B[C_B(2) - C_B(1)] - \text{REAC}\ (1) \end{cases}$$

$$[A8]\quad \begin{cases} C_A'(J) = C_A(J) + DD_A[C_A(J+1) - 2C_A(J) + C_A(J-1)] + 2\ \text{REAC}\ (J) \\ C_B'(J) = C_B(J) + DD_B[C_B(J+1) - 2C_B(J) + C_B(J-1)] - \text{REAC}\ (J) \\ \qquad\qquad \text{for } 2 < J < \text{JMAX} \end{cases}$$

with

$$[A9]\quad \text{REAC}\ (J) = \text{RATE}\ [C_B(J) - \text{EQ}^2 C_A(J)^2] \text{ for } 1 < J < \text{JMAX}$$

where the primed quantities are evaluated at time $t + \Delta t$ while the unprimed ones are evaluated at $t$ and JMAX is taken as $6(D_A t)^{1/2}/\Delta x$. For each iteration of the time loop, $I = t/\Delta t = 1, 2, 3, \ldots$, values of a dimensionless function, $\Phi$, and a variable, $\xi$, are calculated. They are defined by

$$[A10]\quad \Phi = (\pi t/D_B)^{1/2}(i_l/nF)\{[A_0](D_A/D_B) + 2[B_0]\}^{-1}$$

and

$$[A11]\quad \xi = \alpha t$$

with

$$[A12]\quad \alpha = (2k/3\pi)(D_A/D_B)[K\{[A_0](D_A/2D_B) + [B]\}]^{-1/2}$$

Calculations were made on a computer FACOM M160 for various values of ratios $D_B/D_A$ and $[B_0]/[A_0]$ as parameters. The FORTRAN program is available from the authors (K.T. and H.M.) on request. Figure 10 shows variations of $\Phi$ with $\alpha t$ for a particular case of $D_B/D_A = 0.25$.

When the condition $[B_0] \gg [A_0]$ prevails and a steady-state condition for A is assumed in the reaction layer of thickness $\mu$, i.e.,

$$[A13]\quad \partial[A]/\partial t = 0 \text{ and } [B] = \text{const for } 0 < x < \mu$$

eqs. [A2]–[A4] are converted to an integral equation. Introducing a function

$$[A14]\quad f = [A] + 2(D_B/D_A)[B]$$

and using eq. [A13], we have

$$[A15]\quad \partial f/\partial t = D_B\partial^2 f/\partial x^2$$

and

$$[A16]\quad D_A d^2[A]/dx^2 + 2k([B] - K[A]^2) = 0 \text{ for } 0 < x < \mu$$

Following the procedure used by Koutecky and Hanus (21), we obtain an integral equation with respect to $(i_l/nF)$:

$$[A17]\quad (i_l/nF)^{4/3} = \{(8kD_A)^{2/3}/(9K)^{1/3}\}\{(D_A/2D_B)[A_0] + [B_0] - (1/2(\pi D_B)^{1/2}) \int_0^t (i_l/nF)/(t-u)^{1/2} du\}$$

Introducing the dimensionless variable $\xi$ defined by eq. [A11] and $\Psi$ defined by

Can. J. Chem. Downloaded from www.nrcresearchpress.com by 210.87.254.6 on 09/06/12
For personal use only.

[A18] $\Psi(\xi) = (i_l/nF)(3/8kD_A)^{1/2}K^{1/4}\{[A_0](D_A/2D_B) + B_0]\}^{-3/4}$

into eq. [A17], we have

[A19] $[\Psi(\xi)]^{4/3} = 1 - \int_0^{\xi}(\xi - \eta)^{-1/2}\Psi(\eta)d\eta$

From eqs. [A10], [A11], and [A18], it is easily seen that

[A20] $\Phi(\xi) = \pi\xi^{1/2}\Psi(\xi)$

Equation [A19] was solved by the use of numerical integration. Variation of $\Phi$ with $\alpha t$ its also shown in Fig. 10 (curve a); $\Phi$ has a maximum value of 1.0192 at $\alpha t = 2.34$.

Can. J. Chem. Downloaded from www.nrcresearchpress.com by 210.87.254.6 on 09/06/12
For personal use only.

# La liaison phosphazène dans quelques nouveaux iminophospholanes. Diversité de comportement réactionnel

MARIE ROSE MARRE, MICHEL SANCHEZ, JEAN FRANÇOIS BRAZIER ET ROBERT WOLF

*E.R.A. CNRS 926, Laboratoire des Hétérocycles du Phosphore et de l'Azote, Université Paul Sabatier, 31062 Toulouse Cedex, France*

ET

JACQUES BELLAN

*E.R.A. CNRS 926, Laboratoire des Hétérocycles du Phosphore et de l'Azote et Laboratoire de Chimie Pharmaceutique, Université Paul Sabatier, 31062 Toulouse Cedex, France*

Reçu le 13 mai 1981

MARIE ROSE MARRE, MICHEL SANCHEZ, JEAN FRANÇOIS BRAZIER, ROBERT WOLF et JACQUES BELLAN. Can. J. Chem. **60**, 456 (1982).

Nous avons préparé, suivant la réaction de Staudinger, douze iminophospholanes (**1–12**) à cycle dioxa (**1–4**), oxaza (**5**, **6**) et diaza (**7–12**). Ces derniers composés n'ont jamais conduit au dimère diazadiphosphétidine quelle que soit la nature du substituant sur l'atome d'azote imino. Pour les composés à cycle tétraméthyl dioxaphospholane (**1**, **2**, **4**) le réarrangement thermique

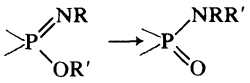

se produit avec l'atome d'oxygène intracyclique. Enfin l'action du méthanol sur ces dérivés, a mis en évidence une différence de comportement: addition conduisant à la pentacoordination pour les composés à cycle pinacolique, associations intermoléculaires de type pont hydrogène pour les dérivés à cycle diazaphospholane.

MARIE ROSE MARRE, MICHEL SANCHEZ, JEAN FRANÇOIS BRAZIER, ROBERT WOLF and JACQUES BELLAN. Can. J. Chem. **60**, 456 (1982).

Using the Staudinger reaction, we have synthesized twelve iminophospholanes (**1–12**) with dioxa (**1–4**), oxaza (**5**, **6**), and diaza (**7–12**) ring systems. We have never observed any phosphazene bond dimerization with diazaphospholane compounds, whatever the nature of the group on the imino atom. For the tetramethyl dioxaphospholane compounds (**1**, **2**, **4**), the thermal rearrangement

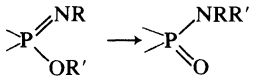

occurs with the intracyclic oxygen atom. Last of all, the reactivity of the phosphazene bond with methanol differs according to the nature of the ring: addition leading to the pentacoordinated species in pinacolic compounds, intermolecular associations (hydrogen bonding) in diazaphospholane derivatives.

## Introduction

Depuis les travaux de Staudinger et Meyer (1) et ceux plus récents de Zhmurova et Kirsanov (2), la chimie des organo-phosphorés tétracoordonnés à liaison phosphazène ( ) s'est largement développée. L'essor des iminophosphanes (3*a*) et surtout des polycyclophosphazènes (3*b*) a marqué la dernière décennie tant par le nombre de réactions originales que par la grande diversité des applications, par exemple dans le domaine des polymères (4) ou des antimitotiques (5).

La liaison phosphazène s'apparente aux liaisons phosphoylure ( ), phosphoryle ( 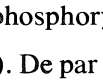 ) ou thiophosphoryle ( ). De par sa réactivité, on lui connait beaucoup d'analogies avec la liaison phosphoylure, en particulier la réaction de type Wittig (6). Les divergences sont toutefois nombreuses. Parmi celles-ci, citons deux exemples.

(*i*) La réaction de dimérisation [1], très courante dans la chimie des iminophosphanes (7), est inconnue dans celle des ylures.

[1] 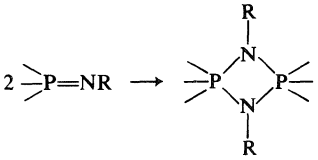

Monomère Dimère

(*ii*) La réaction d'addition de réactifs à hydrogène mobile (XH) qui a été observée dans les phosphoylures (8), reste exceptionnelle dans les iminophosphanes.

0008-4042/82/040456-13$01.00/0

©1982 National Research Council of Canada/Conseil national de recherches du Canada

Can. J. Chem. Downloaded from www.nrcresearchpress.com by 210.87.254.5 on 09/06/12
For personal use only.

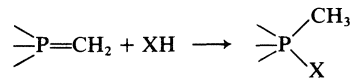

Des travaux récents (9) ont cependant montré que cette réaction d'addition [2] pouvait s'appliquer dans certains cas à la liaison $\rangle P{=}N{-}$:

[2] 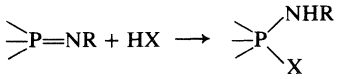

Sur ce thème, nous avons apporté notre contribution (10) en démontrant qu'une addition intramoléculaire dans un intermédiaire iminophosphane conduisait à un amino-phosphorane:

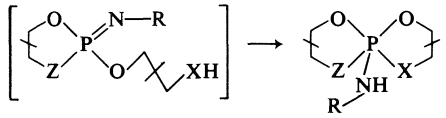

L'objet de cet article est d'exposer et de discuter les particularités de la réaction de synthèse de douze nouveaux iminophospholanes. Sur ces composés, nous avons par ailleurs étudié l'action du méthanol et montré la diversité du comportement de la liaison phosphazène suivant la nature du cycle branché sur l'atome de phosphore.

## Résultats et discussion

I. *Réaction générale de synthèse, choix des substrats phosphorés*

La réaction de Staudinger (1) (schéma [3]), action d'un azoture sur un composé du phosphore tricoordonné, est la voie d'accès aux iminophosphanes utilisée dans la préparation de la totalité de nos composés. Simple dans son principe, cette réaction présente l'avantage de se dérouler dans des conditions douces de température. De plus, l'avancement de la réaction peut être contrôlé par le dégagement d'azote correspondant:

[3] $R_3P + N_3R' \rightarrow [R_3P{=}N_3R'] \xrightarrow{-N_2} R_3P{=}NR'$

Trois azotures (R′ = $-C_6H_5$, $-SO_2-C_6H_4-CH_3$, $-C_2H_5$) ont été opposés à des substrats phosphorés monocycliques. Dans le choix de ces derniers, nous avons été confrontés à une difficulté inhérente à la nature même de la liaison phosphazène, à savoir la dimérisation spontanée du produit attendu en diazadiphosphétidine (réaction [1]).

La frontière dimère ($P^V$) ⇆ monomère ($P^{IV}$) est très sensible à la polarisation de la liaison P=N (*7a*). Celle-ci dépend de la nature des substituants: le seul remplacement d'un substituant sur l'atome de phosphore suffit par exemple à stabiliser l'une ou l'autre des deux formes. C'est ainsi que le cycle orthophénylène dioxaphospholane, par l'effet électroattracteur des atomes d'oxygène, accentue la polarité $P^{\delta+}-N^{\delta-}$ de la liaison phosphazène et entraîne la dimérisation (*7b*):

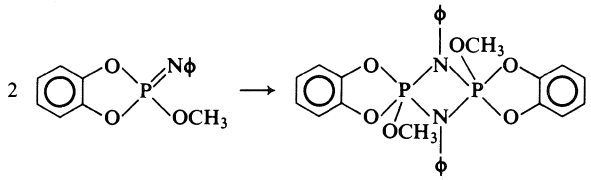

Il en est de même du cycle dioxaphospholane; toutefois, en passant au cycle tétraméthyldioxaphospholane (pinacolique), les substituants méthyle contrebalancent l'effet d'électronégativité des oxygènes et stabilisent la structure monomère.

La présence d'un substituant électronégatif sur l'azote est aussi un facteur favorable à la forme monomère. Les trois exemples suivants résument ce qui précède:

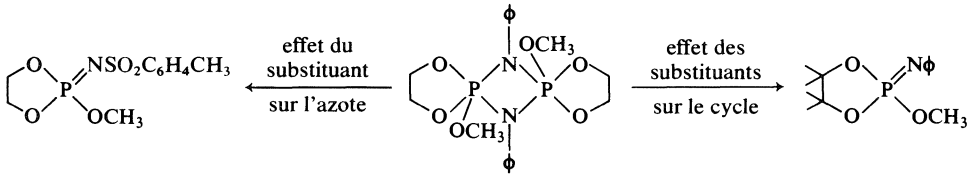


Nous avons également mis récemment (11) en évidence l'équilibre:

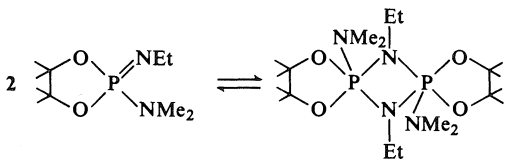

C'est en tenant compte de toutes ces observations que nous avons préparé douze dérivés monocycliques possèdant l'une des trois sortes de cycle: dioxa, oxaza et diaza-phospholanes. Il est remarquable de noter que ces derniers sont les seuls pour lesquels nous n'avons pas observé de forme dimère, quel que soit le substituant sur l'azote imino.

L'ensemble des composés synthétisés et étudiés

Can. J. Chem. Downloaded from www.nrcresearchpress.com by 210.87.254.5 on 09/06/12
For personal use only.

Can. J. Chem. Downloaded from www.nrcresearchpress.com by 210.87.254.5 on 09/06/12
For personal use only.

TABLEAU 1. Conditions de synthèse et caractérisations des iminophospholanes **1** à **12**

| Composé | Synthèse: Solvant Température Temps | Synthèse: δ $^{31}$P du brut | Synthèse: Etat Eb/Torr ou F (°C) | Résonance magnétique nucleaire protonique: Protons du cycle | Résonance magnétique nucleaire protonique: Protons des groupes exocycliques | Analyses ponderales calc. / tr. C—H—N—P— |
|---|---|---|---|---|---|---|
| **1** 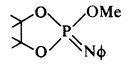 | Benzène 80°C 1 h | 12,6 5,3[a] (benzène) | crist. 53 | $\delta_{CH_3}$ = 0,90, 1,03 | —$OCH_3$ δ = 3,50 $^3J_{H-P}$ = 12,0 | 57,98 7,48 5,20 11,50<br>55,99 7,28 4,72 12,12 |
| **2** 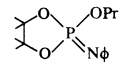 | Toluène 100°C 2 h | 11,7 4,0[a] (toluène) | liq. 58/10$^{-3}$ | $\delta_{CH_3}$ = 0,96, 1,08 | —$OCH_2$— doublet de triplets δ = 4,03 $^3J_{H-P}$ = 9,2 $^3J_{H-H}$ = 6,5 | 60,59 8,13 4,71 10,42<br>59,15 8,13 3,94 10,67 |
| **3** 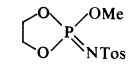 | Toluène 80°C 1 h | 17,5 (toluène) | sol. 120 | $\delta_{CH_2}$ = 4,2 massif | tosyle $\delta_{CH_3}$ = 2,1 —$OCH_3$ δ = 3,5 $^3J_{H-P}$ = 12 | 41,27 4,84 4,81 10,64<br>40,78 4,82 4,58 10,68 |
| **4** 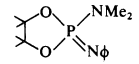 | Benzène 80°C 0,75 h | 13,8 (toluène) | crist. | $\delta_{CH_3}$ = 0,98 1,10 | $N(CH_3)_2$ δ = 2,49 $^3J_{H-P}$ = 10,6 | 59,55 8,21 9,92 10,97<br>55,58 8,16 9,16 10,57 |
| **5** 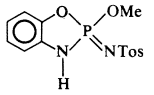 | Toluène 80°C 2 h | 19,3 (DMF) | crist. | $\delta_{N-H}$ = 4,2 singulet large | tosyle $\delta_{CH_3}$ = 2,2 —$OCH_3$ δ = 3,4 $^3J_{H-P}$ = 13 | 49,70 4,47 8,28 9,15<br>48,91 4,60 8,10 9,19 |
| **6** 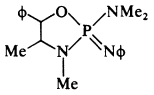 | Acétonitrile 60°C 2 h | 18,7 ($CH_3CN$) | sol. | —C(—$CH_3$ δ = 0,4 $J_{H-H}$ = 6)(—N(—$CH_3$ δ = 2,4 $^3J_{H-P}$ = 10)—C(H)(ϕ) δ = 5,2 $^3J_{H-H}$ = 7, $^3J_{H-P}$ = 2) | —$N(CH_3)_2$ δ = 2,6 $^3J_{H-P}$ = 10,5 | 65,71 7,35 12,77 9,41<br>64,10 7,19 13,21 9,37 |
| **7** 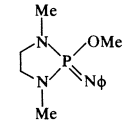 | Toluène 110°C 2 h | 20,1 19,5[a] (toluène) | liq. 75/10$^{-3}$ | N—$CH_3$ δ = 2,3 $^3J_{H-P}$ = 10,1 N—$CH_2$ δ = 2,8 massif | $OCH_3$ δ = 3,5 $^3J_{H-P}$ = 11,2 | 55,28 7,59 17,58 12,95<br>53,71 7,57 16,96 12,95 |
| **8** 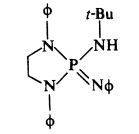 | Acétonitrile 70°C 2 h | 2,8 ($CDCl_3$) | sol. 188 | $\delta_{CH_2}$ = 3,7 (multiplet) | $\delta_{N-H}$ = 3,3 large $\delta_{—C(CH_3)_3}$ = 1 | 71,35 7,23 13,86 7,66<br>69,56 7,11 13,32 7,74 |

Can. J. Chem. Downloaded from www.nrcresearchpress.com by 210.87.254.5 on 09/06/12
For personal use only.



TABLEAU 1. (*Concluded*)

| Composé | Synthèse: Solvant Température Temps | Synthèse: δ $^{31}$P du brut | Synthèse: Etat Eb/Torr ou F (°C) | Résonance magnétique nucleaire protonique: Protons du cycle | Résonance magnétique nucleaire protonique: Protons des groupes exocycliques | Analyses ponderales: calc. / tr. C—H—N—P— |
|---|---|---|---|---|---|---|
| **9** 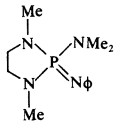 | Toluène<br>80°C<br>2 h | 19,6<br>(toluène) | liq.<br>$40/10^{-3}$ | $\delta_{CH_2}$ = 2,7 (multiplet)<br>N—$CH_3$ δ = 2,6 $^3J_{H-P}$ = 10,2 | —$N(CH_3)_2$ δ = 2,3 $^3J_{H-P}$ = 9,6 | 57,19 8,33 22,23 12,29<br>57,83 8,23 19,22 12,82 |
| **10** 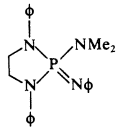 | Toluène<br>70°C<br>3 h | 1,5<br>(toluène) | sol.<br>155 | $\delta_{CH_2}$ = 3,1 doublet | —$N(CH_3)_2$ δ = 2,5 $^3J_{H-P}$ = 10 | 70,27 6,70 14,90 8,23<br>70,58 6,68 14,75 8,11 |
| **11** 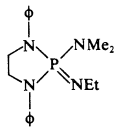 | Toluène<br>50°C<br>1 h | 15,6<br>($CDCl_3$) | sol.<br>120 | $\delta_{CH_2}$ = 3,6 doublet | —$N(CH_3)_2$ δ = 2,6 $^3J_{H-P}$ = 10<br>=N—$CH_2$ δ = 2,9<br>C—$CH_3$ δ = 0,9 $^3J_{H-H}$ = 7 | 65,91 7,68 17,08 9,44<br>64,79 7,69 16,60 9,70 |
| **12** 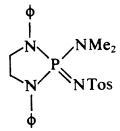 | Toluène<br>Ambiante<br>3 h | 11,9<br>($CDCl_3$) | sol.<br>165 | $\delta_{CH_2}$ = 3,7 massif | —$N(CH_3)_2$ δ = 2,5 $^3J_{H-P}$ = 10<br>tosyle $\delta_{CH_3}$ = 2,2 | 60,84 5,99 12,34 6,82<br>61,11 6,01 12,15 7,20 |

[a]δ$^{31}$P du produit isolé. Solvants rmn $^1$H: $C_6D_6$(**2**, **3**). Toluène-$d_8$ (**1**, **4**, **5**, **6**, **7**, **9**, **10**). $CDCl_3$ (**8**, **11**, **12**).

figurent dans le tableau 1. Nous y avons reporté les principaux paramètres de rmn de $^{31}P$, $^{1}H$, et les conditions de préparation.

II. *Particularités de la réaction de Staudinger rencontrées dans la préparation des iminophospholanes*

1. *Réactivité relative des phosphanes et des azotures*

Dans la préparation des différents iminophospholanes, nous avons constaté que la réactivité du phosphane sur l'azoture est très différenciée quand on passe d'une famille de dérivés à une autre. Ainsi, pour un même azoture ($\phi N_3$ par exemple), les dérivés à cycle diazaphospholane se révèlent plus réactifs que ceux ayant un cycle dioxaphospholane. De plus la présence d'un substituant $NMe_2$ accroît la réactivité du phosphane. Ces observations situent donc les diméthylamino diazaphospholanes comme les phosphanes les plus réactifs que nous ayons utilisés. Les atomes d'azote, par effet donneur d'électrons, augmenteraient la nucléophilie de l'atome de phosphore, ce qui expliquerait ainsi l'ordre décroissant de réactivité rencontré:

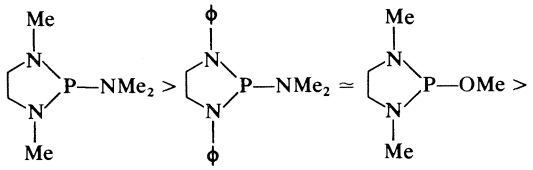

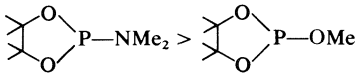

Le deuxième facteur intervenant dans la réaction de Staudinger est lié au caractère électrophile de l'azoture. Celui-ci est d'autant plus grand que les substituants présents sur la fonction azoture sont électroattracteurs. Ainsi la réactivité de ces substrats varie dans l'ordre suivant:

$$Me—C_6H_4—N_3 > C_6H_5—N_3 > C_2H_5—N_3$$

Ces deux facteurs agissent dans le même sens dans la préparation de **12**, synthétisé dans des conditions douces, avec un excellent rendement.

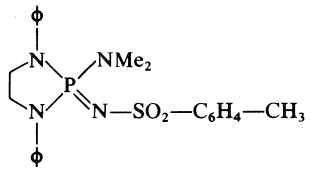

**12**

Dans l'étude de la réactivité des phosphanes vis-à-vis des azotures, nous avons cherché à mettre en évidence l'adduit triazène (phosphane-azoture) intermédiaire de la réaction de Staudinger (12). Ce type de dérivés existe, un petit nombre d'exemples, pour lesquels l'atome de phosphore est entouré de quatre atomes d'azote, ayant été décrits dans la littérature:

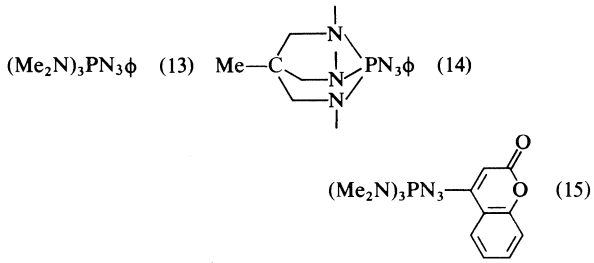

La relation entre basicité du phosphore dans les $P(NR_2)_3$ et stabilité de l'adduit avec $C_6H_5N_3$, établie par Kroshefsky et Verkade (14), nous laissait supposer que le cas le plus favorable pour que cet adduit soit stabilisé pourrait être **9′**.

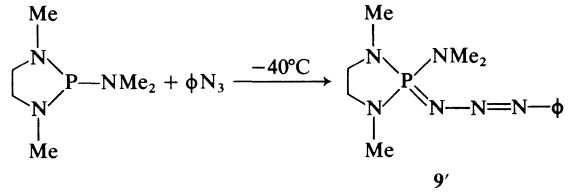

**9′**

En fait, cet adduit est un intermédiaire très labile, qui, dès sa formation, se décompose rapidement pour conduire à l'iminophosphane **9**. Nous avons pu toutefois le caractériser à basse température ($\delta^{31}P = +41$). Il semble que l'adduit triazène, dans les autres composés phosphorés étudiés ici, relèverait plus de l'état de transition que de l'intermédiaire de réaction.

2. *Réarrangement thermique iminophosphane – ester aminophosphorique*

Dans le tableau 1, nous constatons que les $\delta^{31}P$ des mélanges réactionnels bruts des composés **1**, **2**, **7** qui présentent tous le motif:

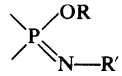

comportent deux valeurs: l'une appartenant à un signal intense (90%) situé à champ fort, est attribuable à l'iminophosphane recherché, l'autre, située à champ plus faible, résulte de la présence d'une entité phosphorylée[1] qui s'est formée en

[1]Selon Kroshefsky et Verkade (14), la variation de $\delta^{31}P$ vers les champs faibles est caractéristique du passage $\geq P=N- \rightarrow \geq P=O$.

Can. J. Chem. Downloaded from www.nrcresearchpress.com by 210.87.254.5 on 09/06/12
For personal use only.

faible proportion (10%) au cours de la synthèse.

Cette forme phosphorylée provient du réarrangement thermique qui assure la migration du groupe R′ de l'alcoxy vers l'atome d'azote imino, formant ainsi une liaison phosphoryle thermodynamiquement plus stable que la liaison phosphazène.

[4] 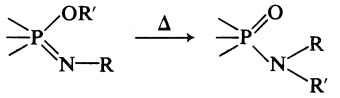

Ce type de réarrangement a été étudié tant en série acyclique (16) que cyclique (17). Dans cette dernière famille, nous avons étudié plus précisément le comportement du composé **1** qui peut s'isomériser thermiquement suivant les deux voies 1a et 1b en fonction des deux ruptures de liaison O—C possibles, cyclique (pour 1a) et exocyclique (pour 1b):

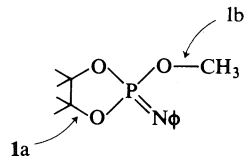

**1**

Une solution de **1** dans le toluène-$d_8$, est chauffée à 100°C pendant 40 h. En rmn de $^{31}P$ nous observons la disparition totale du signal appartenant à **1** ($\delta$ = 4,5) et la croissance de deux signaux d'inégale intensité, l'un à $\delta$ = 12,5 (70%) l'autre à $\delta$ = 14,6 (30%). Ces signaux sont attribuables à deux entités phosphorylées: la première existait déjà et sa concentration a augmenté notablement, la seconde s'est formée au cours du chauffage prolongé. Nous l'avons facilement identifiée comme étant le composé **1***b* synthétisé par la réaction [5]:

[5] 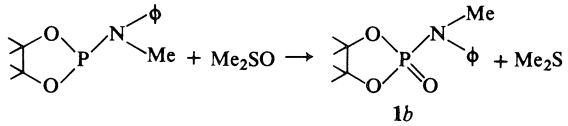

**1***b*

La concordance des paramètres de rmn de $^{31}P$ ($\delta$ = 14,5) et de $^1H$ (doublet P—N—$CH_3$ $\delta$ = 3,0, $J$ = 10 Hz) entre le produit synthétisé et celui qui apparait en solution démontre sa formation à partir de **1** au cours du chauffage.

L'entité à $\delta$ = 12,5 appartient à l'isomère **1***a* qui résulte de l'ouverture du cycle tétraméthyldioxaphospholane. En effet la présence d'un doublet $OCH_3$ ($\delta$ = 3,37, $^3J_{HP}$ = 11,5 Hz) prouve que l'isomérisation thermique n'a pas touché le motif P—$OCH_3$. De plus, les signaux $CH_3$ du cycle pinacolique se sont modifiés très sévèrement: ils se présentent sous la forme de quatre signaux, différents des deux singulets du composé **1**.

Ces arguments nous amènent à proposer pour **1***a* la structure suivante:

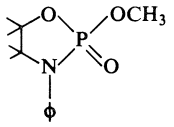

**1***a*

Il est intéressant de noter que, des deux réarrangements thermiques qui conduisent à **1***a* et **1***b*, c'est le premier qui est favorisé. Cela peut résulter de la stabilité relative des deux carbocations qui se forment dans les intermédiaires lors de la rupture de la liaison O—C du cycle (dans **1***a*) ou exocyclique (dans **1***b*). La stabilisation du carbocation tertiaire est la "force motrice" qui conduit préférentiellement à **1***a* par un réarrangement intracyclique.

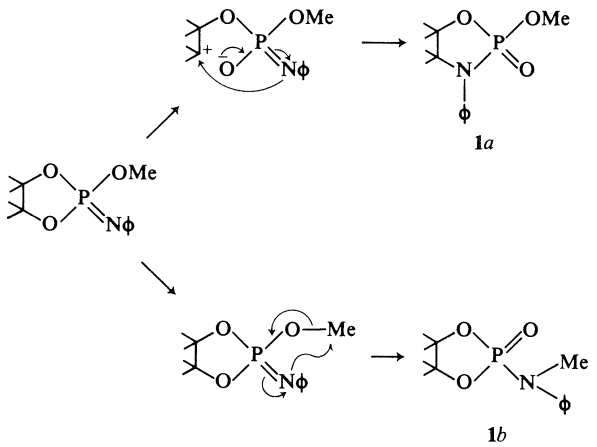

**1***b*

Gilyarov *et al.* (17) a décrit un réarrangement de ce type à des températures plus élevées:

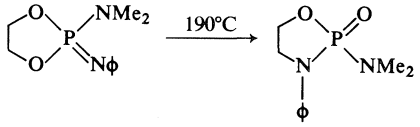

Il est manifeste que, dans notre cas, la substitution du cycle dioxaphospholane par des groupes $CH_3$, abaisse la barrière d'isomérisation thermique de telle sorte que le réarrangement phosphazène → phosphoryle intervient à des températures plus basses.

III. *Addition du méthanol aux iminophospholanes*

Rappelons tout d'abord les travaux antérieurs (9*a*, 10) qui ont montré le caractère quasi général

Can. J. Chem. Downloaded from www.nrcresearchpress.com by 210.87.254.5 on 09/06/12
For personal use only.

Can. J. Chem. Downloaded from www.nrcresearchpress.com by 210.87.254.5 on 09/06/12
For personal use only.

de la réaction d'addition intramoléculaire d'une fonction alcool (ou amine) sur la liaison P=N. Dans le cas où la réaction est menée de manière intermoléculaire elle n'est plus aussi générale; Cadogan *et al.* (*9b*) l'obtiennent encore dans le cas très particulier des α diols qui réagissent sur des iminodioxaphospholanes. Dans notre travail, nous allons mettre en lumière une différence importante de réactivité selon la nature du cycle dans lequel est inséré le phosphore: on peut ainsi classer en deux groupes les comportements rencontrés, suivant qu'on assiste au passage du phosphore à la pentacoordination, ou qu'il y a conservation de la tétracoordination, avec seulement associations moléculaires.

1. *Addition avec passage à la pentacoordination*

Elle a lieu pour les composés (**1**, **2** et **4**) possèdant le cycle tétraméthyl dioxaphospholane. Nous allons présenter en détail l'expérience réalisée avec le composé **1**.

A une solution de **1** dans le toluène-$d_8$, portée à −40°C, nous avons ajouté une quantité équimolaire de $CH_3OH$ à la même température. L'évolution du mélange réactionnel est suivie par rmn de $^{31}P$ de −40°C à +30°C. Le tableau 2 présente les δ des différents signaux observés sur les spectres et leur évolution en fonction de la température. La lecture de ce tableau nous amène à faire les commentaires suivants.

(*i*) Les signaux $\delta_2$ et $\delta_3$ qui apparaissent à champ fort lors de l'addition de $CH_3OH$ sont représentatifs de phosphoranes, l'entité $\delta_2 = -54{,}6$ étant le pentaoxyphosphorane **13** décrit par Bartlett *et al.*

TABLEAU 2. Réaction du méthanol sur l'iminophospholane **1** en solution dans le toluène, dans l'intervalle de température −40°C +30°C, par rmn $^{31}P$

| $n^a$ | T(°C) | $\delta_1$ | $\delta_2$ | $\delta_3$ | Intensités relatives des signaux |
|---|---|---|---|---|---|
| 0 | −40 | 5,9 | | | |
| | +30 | 5,5 | | | |
| 1 | −40 | 9,2 | | −57,5 | |
| | −30 | 8,3 | | −57,3 | |
| | −10 | 6,3 | | −57,3 | |
| | 0 | 6,3 | | −57,2 | $I_3/I_1 = 10$ |
| | +10 | 6,2 | −54,6 | −57,0 | |
| | +30 | 6,0 | −55,0 | −57,0 | $I_2/I_1 = 1$ $I_3$ faible |
| 2 | 0 | 6,4 | −55,4 | −57,3 | $I_2$ faible |
| | +10 | | −55,2 | −57,2 | $I_3/I_2 = 0{,}5$ |
| | +20 | | −55,0 | −57,0[b] | $I_3/I_2 = 0{,}05$ |
| 5 | +20 | | −55,0[c] | | |

[a] $n$ = nombre de moles de $CH_3OH$ par mole de **1**.
[b] Disparition totale deux heures après l'addition.
[c] Apparition d'un signal à δ = −60, dix jours après l'addition.

(18). Ce composé est le produit thermodynamique de la réaction [6]:

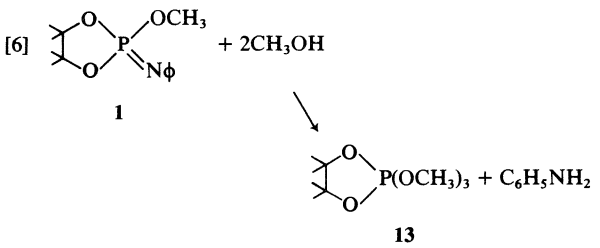


L'aniline formée au cours de la réaction a été caractérisée par chromatographie en phase vapeur. De plus **13** a été préparé suivant la réaction [6].

(*ii*) Le signal à $\delta_3 = -57$ correspond à un intermédiaire **14** résultant de l'addition de $CH_3OH$ sur **1**, stable jusqu'à la température de 0°C. Dans ces conditions la réaction n'est pas totale; en élevant la température, le méthanol en excès dans le milieu réagit sur l'intermédiaire **14** pour conduire au phosphorane **13**. Le dérivé **14** disparait complètement à la température ambiante; seuls le produit de départ et le produit thermodynamique sont, à cette température, présents dans le milieu.

L'addition de deux moles de $CH_3OH$ pour une mole de **1**, confirme les observations précédentes: dès 0°C, le produit final est décelé par rmn de $^{31}P$. Quatre heures après l'addition, à 20°C, la réaction est pratiquement totale. L'addition d'un excès de méthanol fait apparaître, après une dizaine de jours, une entité phosphoranique qui résonne à δ = −60 ppm et qui correspond vraisemblablement à: $P(OMe)_5$ (19).

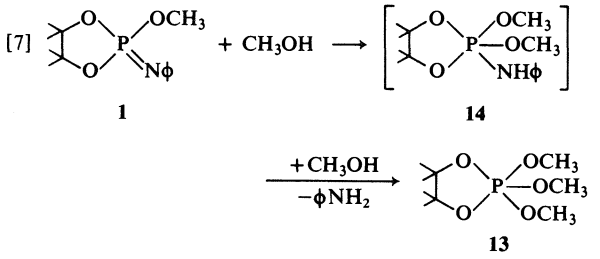


Cette interprétation des spectres de rmn de $^{31}P$ est résumée par le schéma [7] ci-dessus, qui se trouve confirmé par l'étude de la réaction en rmn protonique: l'intermédiaire aminophosphorane **14** est décelé à basse température (−20°C) à partir du doublet (δ = 4,80, $J_{HP}$ = 8,0 Hz) dû au proton P—N*H*-ϕ. Ce doublet, présent jusqu'à la température ambiante, disparait totalement quelques heures après l'addition du méthanol. La rmn protonique montre également la présence d'aniline dans le milieu dès −20°C ($\delta_{H_2N}$ = 4,26) prouvant

ainsi la formation du pentaoxyphosphorane **13** dès cette température.

La même étude par rmn de $^{31}P$ et de $^{1}H$ a été réalisée avec l'iminophosphane **2**: les résultats obtenus dans le cas de **1** sont entièrement confirmés. Ainsi l'intermédiaire aminophosphorane **15** résonne en $^{31}P$ à $\delta = -60{,}1$. Cet intermédiaire a une durée de vie suffisamment longue pour être observé (en rmn de $^{31}P$) à la température ambiante pendant une dizaine d'heures. Le pentaoxyphosphorane **16** donne un signal à $-58{,}3$ qui apparaît dès l'addition du propanol. La figure 1 illustre ces observations: en rmn protonique les trois entités **2**, **15** et **16** peuvent être identifiées au cours du temps par l'évolution des signaux du groupe $CH_2$—O—P.

[8] 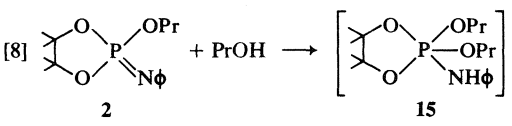


2 15

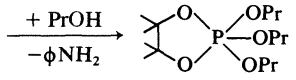


16

Pour le composé **4** à la température ambiante, nous n'avons pas observé de réaction d'addition sur la liaison phosphazène qui aurait conduit à **17**. La première étape de la réaction est en fait l'alcoolyse de la liaison P—$NMe_2$ qui donne le dérivé **1**. Celui-ci évolue comme nous l'avons vu précédemment vers le produit thermodynamique **13**.

[9] 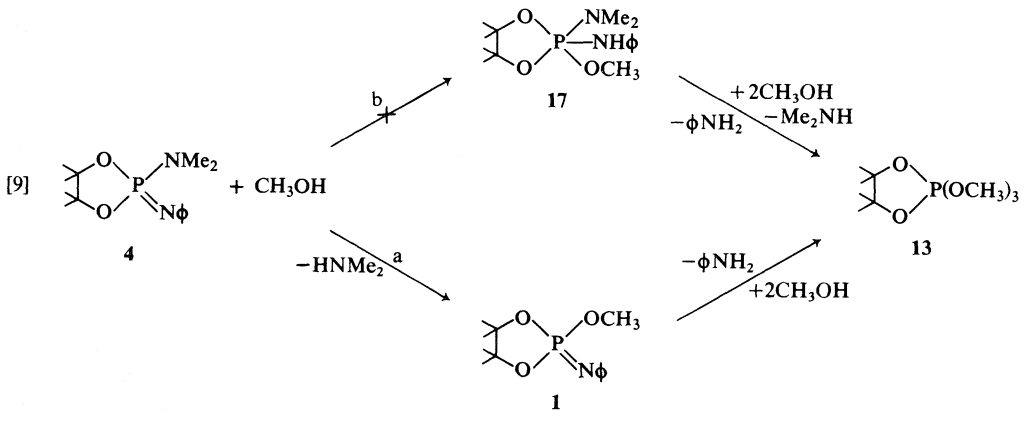


4

Le schéma [9] ci-dessus montre bien que **13** se forme par la voie (a) et non (b). La réaction d'addition est plus lente que la réaction d'alcoolyse de telle sorte qu'en défaut de méthanol, on observe toujours dans le milieu la présence des trois entités **4**, **1** et **13**. L'action de 3 moles de $CH_3OH$ sur une mole de **4** conduit à la seule formation de **13**.

2. *Associations intermoléculaires avec conservation de la tétracoordinance du phosphore*

Nous avons étudié l'action du méthanol sur la série des six diazaiminophosphanes (**7** à **12**) en suivant, par rmn de $^{31}P$, l'évolution d'une solution dans le toluène du dérivé phosphoré, en présence de quantités croissantes de méthanol. L'ensemble des résultats est reporté dans le tableau 3. Nous constatons pour tous ces composés, à l'exception de **12**, qu'il y a un déplacement progressif du signal de résonance du phosphore vers les champs faibles. En aucun cas, nous n'avons observé de signal dans le domaine des phosphoranes ($\delta \sim -60$). Ce comportement particularise les diazaiminophosphanes vis-à-vis des autres composés de ce travail.

Le déplacement chimique de $^{31}P$ varie notablement avec l'addition d'alcool. La variation la plus importante est obtenue avec **11** alors que pour **10**; elle est très faible et nulle pour **12**. La valeur limite de $\delta^{31}P$ intervient pour un excès d'alcool de l'ordre de 3 à 5 fois la quantité du dérivé phosphoré. Après évaporation du méthanol et mise en solution dans le toluène, on retrouve le même déplacement chimique qu'avant l'addition.[2] Ces observations s'interprètent bien comme résultant d'interactions faibles, de type liaison hydrogène, entre les sites basiques de l'iminophosphane considéré et le proton du méthanol. Cette association se retrouve également avec d'autres réactifs à proton acide tels

[2]Dans les composés **9** et **11**, l'addition du méthanol donne, après plusieurs jours, de nouvelles entités du phosphore tétracoordonné (voir partie expérimentale).

Can. J. Chem. Downloaded from www.nrcresearchpress.com by 210.87.254.5 on 09/06/12
For personal use only.

Can. J. Chem. Downloaded from www.nrcresearchpress.com by 210.87.254.5 on 09/06/12
For personal use only.

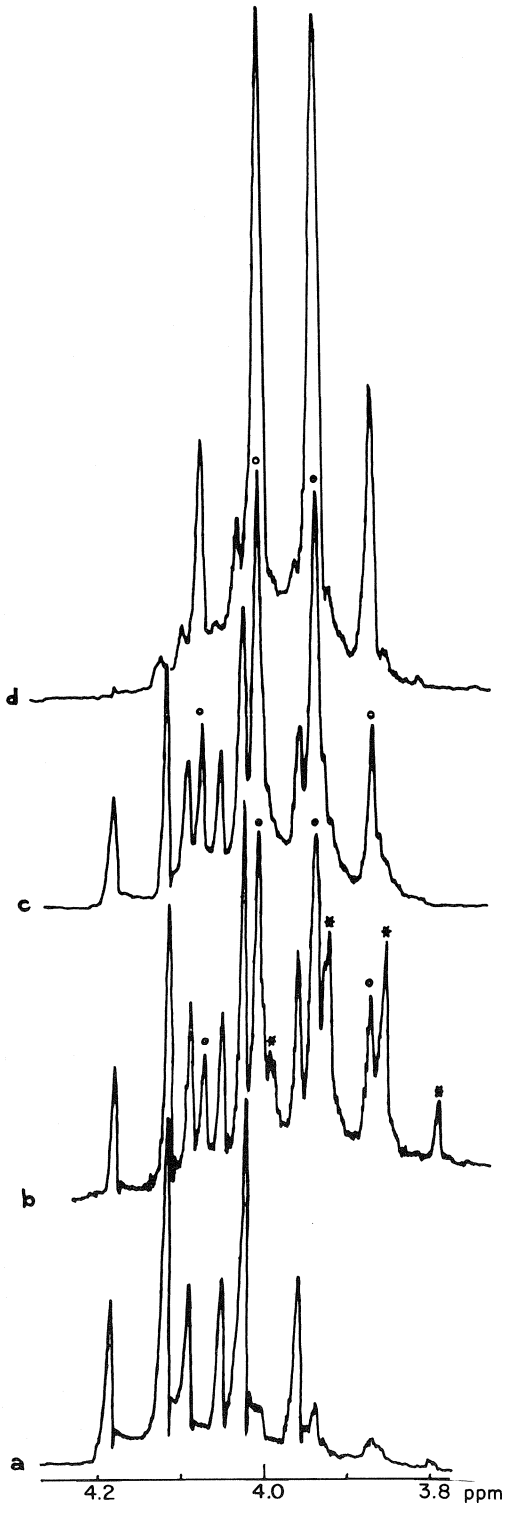


que le phénol,[3] et des solvants ($HCCl_3$) pour lesquels on enregistre également une variation du $\delta^{31}P$ vers les champs faibles.

Ainsi, par le biais de l'addition du méthanol aux diazaiminophosphanes et la variation de $\delta^{31}P$ qui en résulte, on retrouve les propriétés basiques de la liaison phosphazène. Celles-ci ont été très étudiées, par différentes méthodes, dans les aryliminophosphanes diversement substitués ($\phi_3P{=}N{-}C_6H_4X$) (20). Nous mêmes avons montré, par spectroscopie infrarouge dans les dérivés acycliques **18** et **19**, qu'il s'établissait une liaison hydrogène entre le proton du méthanol et l'atome d'azote imino.[4]

$\phi_3P{=}N\phi$ **18** $(CH_3O)_3P{=}N\phi$ **19** $(Me_2N)_3P{=}N\,\phi$ **20**

Les trois dérivés acycliques ci-dessus donnent d'ailleurs le même phénomène de variation de $\delta^{31}P$ en présence de $CH_3OH$. Dans le tableau 3, on notera que **20**, qui a le même environnement atomique que les dérivés cycliques étudiés, subit un $\Delta\delta$ de l'ordre de 10 unités, c'est à dire parmi les plus fortes variations enregistrées.

Les modèles moléculaires étudiés ici présentent trois sites azotés de basicité différente. Mais, de même qu'en série carbonée l'atome d'azote imino est plus basique que celui d'une amine, en série phosphorée, cet atome présente également une forte basicité accentuée par la polarisation de la liaison P=N en $P^{\delta+}{-}N^{\delta-}$ (21). Il est donc raisonnable d'admettre que l'association par liaison hydrogène se produit préférentiellement avec cet atome d'azote, formant un complexe de type 1/1 (22):

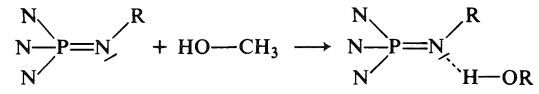


Cette association a pour effet d'accroître la charge effective ($\delta+$) sur P, d'où l'observation du déplacement du signal de résonance de $^{31}P$ vers le domaine des phosphoniums. Le fait d'observer un seul

[3]La variation de $\delta^{31}P$ est d'autant plus forte que le donneur de proton est plus acide. Par exemple, l'addition du phénol sur **11** entraine un $\Delta\delta$ de 17,4 ppm.

[4]R. Mathis, N. Zenati et M. Sanchez, travail en cours.

FIG. 1. Evolution des signaux P—O—$CH_2$— lors de l'addition de propanol sur **2**; (*a*) **2** en solution dans le toluène-$d_8$; (*b*) addition de propanol (0,8 pour 1); (*c*) mêmes conditions que (*b*), trente minutes après: disparition de **15** (*), **2** subsiste; (○): signaux du pentaoxyphosphorane **16**; (*d*) addition de propanol (2 pour 1).

TABLEAU 3. Associations intermoléculaires des iminophospholanes **7** à **12**, en solution dans le toluène, avec le méthanol, par rmn de $^{31}P$

| | Composé | $\delta^{31}P$ $n^a = 0$ | $n = 1$ | $n = 3$ | $n = 5$ | $\Delta\delta$ |
|---|---|---|---|---|---|---|
| **7** | 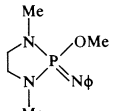 | 19,4 | | 25,6 | 26,3 | 7 |
| **8** | 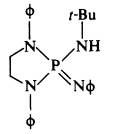 | 2,8 | 6,8 | 6,8 | | 4 |
| **9** | 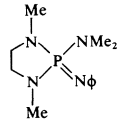 | 18,9 | 19,8 | 22,5 | 23,6 | 4,7 |
| **10** | 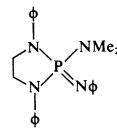 | 1,4 | 2 | | 2,5 | 1,1 |
| **11** | 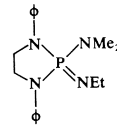 | 10,0<br>15,6[b] | 14,3 | 19,1<br>23,5 | | 9<br>7,9[b] |
| **12** | 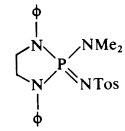 | 11,6 | 11,8 | 11,6 | | 0 |
| | $(Me_2N)_3P{=}N\phi$ | 16,6 | | | 26,6 | 10 |

[a] $n$ = nombre de moles de $CH_3OH$ par mole d'iminophospholane.
[b] Solution dans le chloroforme.

signal en rmn de $^{31}P$ prouve l'existence d'un équilibre dynamique. La possibilité d'associations plus complexes de type 1/2 (réactif phosphoré/solvant) n'est pas à exclure; seule une étude quantitative (détermination des constantes d'équilibre) permettra de préciser le phénomène.

Rappelons que la basicité de la liaison phosphoryle a été également très étudiée (23); en rmn du phosphore la complexation avec R—OH se traduit par une variation notable de $\delta^{31}P$. Cette variation a servi de critère à Mayer et Gutmann (24), dans le cas de $Et_3P{=}O$, pour évaluer les propriétés électrophiles des solvants (D: donicité). D'une manière analogue, en considérant la variation de $\delta^{31}P$ ($\Delta\delta = \delta^{31}P_{CH_3OH} - \delta^{31}P_{Tol}$) comme critère de basicité du motif P=N d'iminophosphanes, nous pouvons établir un ordre relatif de basicité. Dans les composés étudiés, pour les mêmes ligands autour de P, nous observons l'ordre décroissant suivant, qui s'interprète bien avec l'effet inductif du substituant sur l'atome d'azote imino:

$$\text{>P=N—Et} > \text{>P=N—}\phi > \text{>P=N—Tos}$$

| | **11** | **10** | **12** |
|---|---|---|---|
| $\Delta\delta$: | 9 | 1,1 | 0 |

Il est intéressant de noter pour les trois dérivés ci-dessus le même ordre de réactivité vis-à-vis de réactifs électrodéficients tel que l'acétylène dicarboxylate de méthyle (DMA) (15): **11** réagit à la température ambiante plus facilement que **10**, qui nécessite un chauffage prolongé, alors que **12** est sans action sur le DMA.

En conclusion, nous avons synthétisé douze nouveaux iminophosphanes possèdant un cycle à cinq chaînons. Pour la famille de dérivés à cycle

Can. J. Chem. Downloaded from www.nrcresearchpress.com by 210.87.254.5 on 09/06/12
For personal use only.

Can. J. Chem. Downloaded from www.nrcresearchpress.com by 210.87.254.5 on 09/06/12
For personal use only.

diazaphospholane, la présence des substituants azotés est un facteur de stabilisation de la forme monomère iminophosphane quel que soit la nature du groupe présent sur l'azote imino.

L'existence, sur un même modèle, de liaisons P—O (simple) et P=NR est favorable à la réaction de réarrangement iminophosphane → phosphoryle. Dans le cas des composés à cycle tétraméthyldioxaphospholane (**1**, **2**, **4**) un tel réarrangement se produit par voie thermique, à des températures peu élevées, et conduit préférentiellement à l'isomère à cycle oxazaphospholane par introduction de l'azote imino dans le cycle pentagonal. Enfin l'action du méthanol a montré des différences de comportement de la liaison phosphazène. Avec les composés à cycle tétraméthyldioxaphospholane, l'addition du méthanol conduit aux dérivés phosphoraniques. Avec les dérivés à cycle diazaphospholane, des interactions intermoléculaires par liaison hydrogène ont été mises en évidence traduisant ainsi la forte basicité de l'azote imino.

Ceci confirme bien que la nature des substituants présents sur les atomes d'azote et de phosphore influe sur la délocalisation des charges de la liaison P=N, expliquant ainsi les réactions d'addition ou d'association du méthanol.

## Partie expérimentale

Les spectres de rmn du proton ont été enregistrés à 60 et 100 MHz sur des appareils Varian (T-60 et HA-100). En résonance de $^{31}P$ nous avons utilisé un appareil Perkin–Elmer (R-32) fonctionnant à 36,4 MHz en transformée de Fourier. Les déplacements chimiques sont comptés positivement à champ faible à partir de la référence externe ($H_3PO_4$, solution à 85%). Les points de fusion ont été déterminés sur banc Koffler et sont donnés sans correction. Les solvants utilisés dans les réactions chimiques: toluène, chlorure de méthylène, benzène, éther, acétonitrile et diméthylformamide ont été purifiés selon les techniques usuelles.

Nous avons préparé, en suivant les modes opératoires décrits dans la littérature, le phényle azoture (25), l'éthyle azoture (26) et le tosyle azoture (27). Les réactifs phosphorés quant à eux ont été synthétisés soit à partir de réactions mises au point au laboratoire (28) soit à partir de résultats de la littérature (29); c'est ainsi que nous avons réalisé la synthèse de quatre nouveaux diazaphospholanes.

I. *Préparation des réactifs du phosphore tricoordonné*

1. *Chloro-2,*N,N′ *diphényl-1,3 diazaphospholane-1,3,2*

Nous avons mis en oeuvre la réaction ci-dessous en suivant un mode opératoire proposé par Ramirez *et al.* (30).

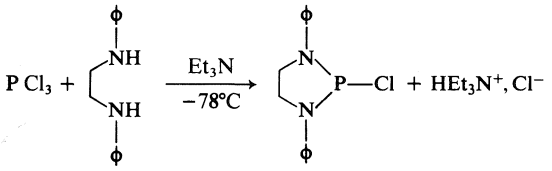


Dans un ballon tricol muni d'un réfrigérant, d'une ampoule isobare, on place sous atmosphère d'argon 13,7 g (0,1 mol) de $PCl_3$ en solution dans 300 cm³ d'éther. La solution refroidie à −78°C est maintenue en agitation permanente. On ajoute goutte à goutte une solution de 21,2 g (0,1 mol) de *N,N′* diphényl éthylènediamine dans 300 cm³ d'éther. A la fin de l'addition, 20,2 g (0,2 mol) de triéthylamine sont ajoutés rapidement; le chlorhydrate précipite et le mélange réactionnel sous agitation est ramené à la température ambiante. Après filtration et évaporation du solvant on obtient un solide blanc qui est lavé à l'éther et séché (Rdt: 90%); F: 140°C; rmn $^{31}P$ ($CHCl_3$): δ = 137,5.

2. *Méthoxy-2,*N,N′ *diphényl-1,3 diazaphospholane-1,3,2*

Ce composé est préparé par alcoolyse du dérivé chloré précédent, en présence de triéthylamine. La réaction se déroule à la température ambiante en 24 h; elle conduit avec un rendement quantitatif au composé attendu; F = 100°C; rmn $^{31}P$ ($CHCl_3$): δ = 103,9; rmn $^1H$ ($CDCl_3$): δ = 3,3 (d, $^3J_{H-P}$ = 8 Hz, 3H, $CH_3O$—), δ = 3,9 (m, 4H, $CH_2$—$CH_2$—).

3. tert-*Butylamino-2,*N,N′ *diphényl-1,3 diazaphospholane-1,3,2*

A une solution de 2,8 g (1 × $10^{-2}$ mol) du dérivé chloré, on ajoute à la température ambiante, un excès (2,2 g soit 3 × $10^{-2}$ mol) de *tert*-butylamine fraichement distillée. Le mélange réactionnel sous atmosphère inerte est maintenu en agitation pendant 12 h. On porte alors le mélange à 0°C puis on ajoute 200 cm³ d'éther pour faire précipiter la totalité du chlorhydrate de *tert*-butylamine. Après filtration et évaporation du solvant, on obtient un solide qui est lavé à l'éther puis séché sous vide (Rdt: 80%); F = 120°C; ir (sol. KBr) $\nu_{N-H}$ = 3350 cm⁻¹; rmn $^{31}P$ ($CHCl_3$): δ = 81; rmn $^1H$ ($CDCl_3$) δ = 1,1 (s, 9H, *t*-butyl), δ = 2,5 (singulet large, H—N), δ = 3,5 (m, 4H, —$CH_2$—$CH_2$—).

4. *Diméthylamino-2,*N,N′ *diphényl-1,3 diaza phospholane-1,3,2*

Ce composé a été préparé suivant la réaction:

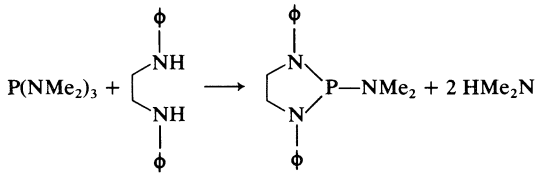


A partir d'un mode opératoire décrit antérieurement (30), on traite 8,15 g (5 × $10^{-2}$ mol) de tris(diméthylamino)phosphane par 10,6 g (5 × $10^{-2}$ mol) de diamine en solution dans 150 cm³ de toluène. Après 10 h de chauffage au reflux du solvant, la réaction est terminée (la quantité théorique de diméthylamine déplacée a été dosée). On obtient avec un bon rendement (85%) le diazaphospholane; F = 145°C; rmn $^{31}P$ (toluène): δ = 97,6; rmn $^1H$ (tol-$d_8$): δ = 2,5 (d, $^3J_{H-P}$ = 10 Hz, 6H, $N(CH_3)_2$), δ = 3,6 (m, 4H, —$CH_2$—$CH_2$—).

II. *Préparation des iminophospholanes*

Nous décrirons deux préparations-types correspondant aux composés **1** et **11** relevant des deux familles dioxa et diaza iminophospholanes.

1. *Tétraméthyl-4,4,5,5,*N *phényl-2, méthoxy-2, dioxaimino-phospholane-1,3,2 (composé 1)*

Dans un ballon tricol muni d'un agitateur magnétique, d'un réfrigérant relié à un volumètre, on place sous atmosphère d'argon 5,8 g (3,5 × $10^{-2}$ mol) de:

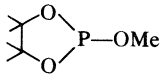


en solution dans 100 cm³ de toluène. On ajoute lentement à l'aide d'une seringue 4,2 g (3,5 × $10^{-2}$ mol) de phényl azoture

Can. J. Chem. Downloaded from www.nrcresearchpress.com by 210.87.254.5 on 09/06/12
For personal use only.

pur. Dès l'addition on observe un dégagement gazeux ($N_2$). On achève la réaction en chauffant le mélange réactionnel 1 h à 80°C. Extraction du solvant et purification par distillation: $Eb_{10^{-3}}$ = 92°C (Rdt = 80%). Le spectre de rmn $^{31}P$ du distillat montre la présence d'une impureté phosphorylée ($\delta$ = 12,5) celle-ci est éliminée en recristallisant le produit dans un mélange de $CH_2Cl_2$ et de pentane ($\delta$ $^{31}P$ = 5,3); F = 52°C.

Suivant le même mode opératoire nous avons préparé les iminophospholanes **2** ($Eb_{10^{-3}}$ = 108–110°C), recristallisé dans un mélange de benzène et d'hexane, **3** recristallisé dans le benzène (F = 120°C), **4** recristallisé dans le toluène et **5** produit peu soluble qui précipite à la fin de la réaction.

2. *Diméthylamino-2,*N,N′ *phénylamino-1,3,*N *éthylimino-2, diazaiminophospholane-1,3,2 (composé 11)*

A l'aide du même appareillage que celui décrit précédemment, on traite 2,85 g ($10^{-2}$ mol) du dérivé phosphoré

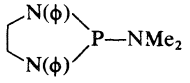

en solution dans 50 cm³ d'acétonitrile (ou de toluène) par 1,4 g d'éthyle azoture en excès ($2 \times 10^{-2}$ mol). Pour que la réaction soit totale (quantité d'azote dégagée 230 cm³), il est nécessaire de chauffer le mélange à 50°C pendant 1 h. Après évaporation du solvant on obtient un solide qui est lavé à l'hexane et séché sous vide (Rdt: 80%); F = 120°C. Les diaza iminophospholanes-1,3,2, **6** à **12** ont été préparés dans des conditions comparables à celles que nous venons de décrire pour **11** (voir tableau 1).

III. *Réaction d'isomérisation de 1 par voie thermique*

Dans une première approche cette réaction a été suivie par rmn du phosphore et du proton. La procédure est la suivante: dans un tube de rmn on place $2 \times 10^{-2}$ mol d'iminophospholane **1** en solution dans 0,5 cm³ de toluène-$d_8$. On enregistre les premiers spectres de référence; le tube est alors porté à une température constante de 100°C, des enregistrements sont effectués à intervalles de temps réguliers. On observe sur les spectres ainsi enregistrés l'apparition progressive de signaux dûs à deux nouvelles entités phosphorées; après 40 h de chauffage la disparition des signaux appartenant à **1** est totale et les deux composés **1***a* (70%) et **1***b* (30%) présentent les paramètres spectroscopiques suivants: **1***a*: rmn $^{31}P$: $\delta$ = 12,5; rmn $^1H$ (tol-$d_8$): $\delta$ = 3,38 (d, $^3J_{H-P}$ = 11,8 Hz, 3H, $CH_3$—O—), $\delta$ = 1,03 (s, 6H, $CH_3$—C—), $\delta$ = 1,08 (s, 6H, $CH_3$C); rmn $^1H$ (tol-$d_8$ + pyr-$d_5$): $\delta$ = 3,50 (d, $^3J_{H-P}$ = 11,6 Hz, 3H, $CH_3$—O—), $\delta$ = 1,08 (s, 6H, $CH_3$—C—), $\delta$ = 1,14 (s, 3H, $CH_3$—C—), $\delta$ = 1,22 (s, 3H, $CH_3$—C—); **1***b*: rmn $^{31}P$: $\delta$ = 14,5; rmn $^1H$ (tol-$d_8$): $\delta$ = 2,90 (d, $^3J_{H-P}$ = 9,5 Hz, 3H, $CH_3$—N), $\delta$ = 1,14 (s, 6H, $CH_3$—C—), $\delta$ = 1,18 (s, 6H, $CH_3$—C—).

Si la solution est laissée dans le tube, à la température ambiante, pendant plusieurs jours, on observe aucune évolution des spectres; par contre un chauffage prolongé (100 h) provoque une décomposition des produits avec apparition de signaux nouveaux d'intensité non négligeable dans les spectres de rmn protonique. Dans une deuxième approche, nous avons tenté d'isoler, sans succès, le composé **1***a* par chromatographie sur plaque de silice. Suivant la même méthode nous avons suivi l'isomérisation thermique de **2** en **2***a* ($\delta$ $^{31}P$ = 11,7). Enfin pour le composé **4** la forme phosphorylée **4***a* n'est pas présente dans le produit brut; par chauffage à 100°C nous avons caractérisé par rmn de $^{31}P$ sa formation ($\delta$ = 18,9).

IV. *Réactions avec le méthanol*

1. *Cas des composés à cycle diazaphospholane (7 à 12)*

Suivant une procédure analogue à celle que nous venons de décrire, nous avons suivi par rmn du phosphore et du proton le comportement d'une solution de $2 \times 10^{-3}$ mol d'iminophospholane dans 0,5 cm³ de tol-$d_8$ lorsqu'on ajoute des quantités croissantes (de 1 à $5 \times 10^{-3}$ mol) de méthanol. Les spectres sont enregistrés avant et après chaque addition; on s'est bien assuré que le signal en rmn de $^{31}P$ ne se déplace pas dans un intervalle de temps de l'ordre de 15 min. Lorsque la variation du déplacement de $^{31}P$ atteint son maximum, on évapore le méthanol puis le produit est remis en solution. On enregistre alors un dernier spectre pour lequel on retouve le même $\delta^{31}P$ qu'avant addition de $CH_3OH$. Ces manipulations ont été réalisées dans un temps de l'ordre de 10 h, à la température ambiante. A l'exception des composés **9** et **11** aucune évolution n'est constatée dans un temps supérieur à 24 h. Pour ces deux composés si le mélange iminophospholane (1 mol) – méthanol (3 mol) est laissé à la température ambiante pendant plusieurs jours on observe l'apparition progressive de signaux nouveaux, autres que celui du composé de départ, dans le domaine des atomes de phosphore tétracoordonné.

Pour **9** les signaux qui apparaissent sur le spectre de rmn de $^{31}P$ se stabilisent en intensité un mois après l'addition de méthanol; ils sont situés aux $\delta$ suivants: $\delta_1$ = 23,5, $\delta_2$ = 18,0, $\delta_3$ = 14,1 $\delta_4$ = 10,0. Après évaporation de $CH_3OH$, quatre entités phosphorées sont caractérisées: $\delta_1$ = 18,9 (composé **9**), $\delta_2$ = $\delta_3$ = 13,9, $\delta_4$ = 9,4. La rmn protonique montre sans ambiguité l'absence totale de signaux de type $OCH_3$ et une grande multiplicité des signaux correspondants à des protons $H_3C$—N; enfin dans deux expériences quantitatives effectuées sur 1 g ($0,4 \times 10^{-2}$ mol) d'iminophospholane pour 0,4 g ($0,4 \times 10^{-2}$ mol) de méthanol, en solution dans le toluène, nous n'avons pas observé de réaction de méthanolyse comparable à [9] et qui interviendrait par coupure de la liaison P—N($CH_3$) exocyclique.

L'étude de **11** confirme les observations faites sur **9**; 24 h après l'addition de 3 moles de méthanol sur une mole d'iminophospholane, le spectre de rmn de $^{31}P$ présente en plus du signal dû à **11** ($\delta$ = 19) un deuxième signal d'égale intensité à $\delta$ = 23,3. La rmn de $^1H$ montre bien que le méthanol n'a pas réagi sur **11**: absence de signaux de type $H_3C$—O, existence de trois doublets $H_3C$—N—P ($^3J_{H-P}$ = 10 Hz) aux $\delta$ suivants: $\delta_1$ = 2,50 (45%), $\delta_2$ = 2,30 (10%), $\delta_3$ = 2,25 (45%) et de trois triplets dus au $H_3C$ du groupe P=N—$CH_2$—$CH_3$ ($^3J_{H-H}$ = 7 Hz) aux $\delta$: $\delta_1$ = 1,40, $\delta_2$ = 1,10 et $\delta_3$ = 0,90.

Ces premiers résultats laisseraient supposer que les nouvelles entités phosphorées qui apparaissent au cours du temps, proviennent d'une ouverture du cycle diazaphospholane (**9** ou **11**) de départ. Les travaux en cours devraient permettre de préciser ces observations.

2. *Cas des composés à cycle dioxaphospholane (1, 2 et 4)*

L'étude de l'évolution au cours du temps et à différentes températures par rmn ($^{31}P$ et $^1H$) a été réalisée sur une solution dans le toluène deutérié (0,5 cm³) de $2 \times 10^{-3}$ mol de l'iminodioxaphospholane **1** en présence de $4 \times 10^{-3}$ mol de méthanol. A −20°C l'intermédiaire anilino phosphorane **14** a été caractérisè en solution: $\delta$ $^{31}P$ = −57,4, rmn $^1H$ $\delta$ = 4,82 (d, 1H, H—N—P, $^2J_{H-P}$ = 8 Hz), $\delta$ = 3,47 (d, 3H, $H_3CO$—P, $^3J_{H-P}$ = 12 Hz). Lorsque la solution est laissée quelques heures à la température ambiante le spectre protonique ne présente plus que les signaux caractéristiques du pentaoxyphosphorane **13** et ceux de l'aniline qui s'est formée dans le milieu.

*Préparation du tris méthoxy-2 tétraméthyl-4,4,5,5, dioxa-1,3 phosphorane-2 (13)*

On traite 4 g ($15 \times 10^{-3}$ mol) de **1** en solution benzènique (30 cm³) par 1 g ($31 \times 10^{-3}$ mol) de méthanol. Le mélange est laissé à la température ambiante pendant 10 h. Extraction du solvant et purification par distillation; $\delta$ $^{31}P$ = −55 (litt. (18) $\delta$ = −54,3); rmn $^1H$ ($CDCl_3$) $\delta$ = 3,54 (d, 9H, $H_3C$—O—P, $^3J_{H-P}$ = 13 Hz), $\delta$ = 1,05 (s, 12H, $H_3C$—C).

L'action du propanol sur l'iminodioxaphospholane **2** a été

également suivie par rmn comme dans le cas de **1**; la figure 1 donne une illustration de l'évolution des signaux correspondant aux protons méthylèniques du groupe P—$OC_3H_7$. L'intermédiaire **15** et le pentaoxyphosphorane **16** ont été aisément caractérisés en solution; **15**: $\delta$ $^{31}P = -60,1$; rmn $^1H$ ($C_6D_6$): $\delta$ = 4,90 (d, 1H, H—N—P, $^2J_{H-P}$ = 9 Hz), $\delta$ = 3,80 (q, 4H, —$CH_2$—O—P, $^3J_{H-H} = {}^3J_{H-P}$ = 6 Hz); **16**: $\delta$ $^{31}P = -58,3$; rmn $^1H$ ($C_6D_6$): $\delta$ = 3,89 (q, 6H, —$CH_2$—O—P, $^3J_{H-H} = {}^3J_{H-P}$ = 6 Hz), $\delta$ = 1,12 (s, 12H, $H_3C$—C).

Enfin l'imino dioxaphospholane **4** a été également soumis à l'action des deux alcools $CH_3OH$ et $n$-$C_3H_7OH$ dans les proportions 1:3. Dans chaque cas on observe la disparition du doublet dû aux protons $(CH_3)_2N$—P ($\delta$ = 2,49, $^3J_{H-P}$ = 10,6 Hz) et l'apparition conjointe d'un singulet dû aux $CH_3$ de la diméthylamine ($\delta$ = 2,14). Lors de l'addition du méthanol le spectre obtenu à la température ambiante est celui du phosphorane **13** alors que dans le cas de l'addition du propanol le spectre obtenu est celui du phosphorane **16** (voir ci-dessus).


1. H. Staudinger et J. Meyer. Helv. Chim. Acta, **2**, 635 (1919).
2. I. N. Zhmurova et A. A. Kirsanov. Zh. Obshch. Khim. **32**, 2576 (1962).
3. (*a*) Yu. G. Gololobov, I. N. Zhmurova et L. F. Kasukhin. Tetrahedron, **37**, 437 (1981); (*b*) H. R. Allcock. Phosphorus–nitrogen compounds. Academic Press, New York 1972; R. Shaw. Phosphorus Sulfur, **4**, 101 (1978).
4. H. R. Allcock. Polymer, **21**, 673 (1980).
5. A. A. Kropatcheva, A. E. Mukhuna, N. M. Kachnikoba et V. A. Parchina. Travaux de la deuxième conférence de Kazan, "Chimie et applications des composés du phosphore". (Dec. 1959). *Edité par* Acad. des Sciences U.R.S.S., Moscou, no 372 (1962); J. F. Labarre, J. P. Faucher, G. Lévy, F. Sourniés, S. Cros et G. François. Eur. J. Cancer, **15**, 637 (1979).
6. A. W. Johnson. Ylid chemistry. Academic Press, New York 1966, chapt. 6; R. Appel et A. Hauss. Chem. Ber. **93**, 405 (1960).
7. (*a*) A. F. Grapov, N. N. Melnikov et L. V. Razvodovskaya. Russ. Chem. Rev. **39**, 20 (1970); (*b*) V. P. Kukhar et V. A. Gilyarov. Pure Appl. Chem. **52**, 891 (1980); V. P. Kukhar, E. V. Grishkun, V. P. Rudavskii and V. A. Gilyarov. Zh. Obshch. Khim. **50**, 1477 (1980).
8. H. Schmidbaur et H. Stuhler. Angew. Chem. Int. Ed. Engl. **11**, 145 (1972).
9. (*a*) H. B. Stegmann, G. Bauer, E. Breitmaier, E. Heimann et K. Scheffler. Phosphorus, **5**, 207 (1975); J. I. G. Cadogan, N. J. Stuart et N. J. Tweddle. J. Chem. Soc. Chem. Commun. 182 (1978); J. I. G. Cadogan, I. Gomey, E. Henry, T. Naishy, B. Nay, N. J. Stuart et N. J. Tweddle. J. Chem. Soc. Chem. Commun. 189 (1979); (*b*) J. I. G. Cadogan, N. J. Stuart et N. J. Tweddle. J. Chem. Soc. Chem. Commun. 191 (1979).
10. M. Sanchez, J. F. Brazier, D. Houalla, A. Munoz et R. Wolf. J. Chem. Soc. Chem. Commun. 730 (1976); M. Sanchez, J. F. Brazier, D. Houalla et R. Wolf. Nouv. J. Chim. **3**, 775 (1979).
11. N. Zenati, M. R. Marre, J. Bellan, J. F. Brazier et M. Sanchez. Colloque national sur la chimie du phosphore, Rennes, France. Mai, 1980.
12. J. E. Leffler et R. D. Temple. J. Am. Chem. Soc. **89**, 5235 (1967); L. F. Kasoukhin et Yu G. Gololobov. Dokl. Akad. Nauk SSSR, **228**, 1380 (1976).
13. H. Goldwhite, P. Gysegem, S. Schow et C. Swyke. J. Chem. Soc. Dalton Trans. 16 (1975).
14. R. D. Kroshefsky et J. G. Verkade. Inorg. Chem. **14**, 3090 (1975).
15. J. Bellan, M. R. Marre, M. Sanchez et R. Wolf. Phosphorus Sulfur. Accepté pour publication.
16. H. Goldwhite, P. Gysegem, S. Schow et C. Swyke. J. Chem. Soc. Dalton Trans. 12 (1975); B. C. Challis, J. A. Challis et J. N. Iley. J. Chem. Soc. Perkin Trans. II, 814 (1978).
17. V. A. Gilyarov, N. A. Tikhonina, V. G. Andrianov, Yu. T. Struchkov et M. I. Kabachnik. Zh. Obshch. Khim. **48**, 732 (1978); V. A. Gilyarov, B. A. Kvasov, T. M. Sheherbina et M. I. Kabachnik. Izv. Akad. Nauk SSSR Ser. Khim. 151 (1978).
18. P. D. Bartlett, A. L. Baumstark, M. E. Landis et C. L. Lerman. J. Am. Chem. Soc. **96**, 5267 (1974).
19. L. L. Chang, D. B. Denney, D. Z. Denney et R. J. Kazior. J. Am. Chem. Soc. **99**, 2293 (1977).
20. V. P. Kukhar, A. A. Petrushenko, I. N. Zhmurova, A. A. Thukar et S. N. Solodushenkov. Zh. Obshch. Khim. **40**, 1696 (1970).
21. T. A. Albright, W. J. Freeman et E. E. Schweizer. J. Org. Chem. **41**, 2716 (1976); I. N. Zhmurova, R. I. Yurchenko, A. A. Thukar, V. G. Yurchenko et O. M. Voitsekhovskaya. Zh. Obshch. Khim. **49**, 2401 (1979).
22. K. A. O. Starzewski et H. Tom Dieck. Inorg. Chem. **18**, 3307 (1979); E. W. Abel et S. A. Mucklejohn. Inorg. Chim. Acta, **37**, 107 (1979).
23. T. Gramstad. Spectrochim. Acta, **20**, 729, (1964); D. Houalla. Thèse de l'Université de Toulouse, no 319, 16 Mars, 1968.
24. U. Mayer. Pure Appl. Chem. **51**, 1697 (1979); V. Gutmann. Pure Appl. Chem. **51**, 2197 (1979).
25. O. Dimroth. Ber. **35**, 1034 (1902).
26. O. E. Oliveri-Mandala et G. Garonna. Gazz. Chim. Ital. **71**, 182 (1941).
27. W. von Doering et C. H. de Puy. J. Am. Chem. Soc. **75**, 5955 (1953).
28. M. Sanchez, R. Wolf, R. Burgada et F. Mathis. Bull. Soc. Chim. Fr. (2), 773 (1968).
29. R. Burgada. Bull. Soc. Chim. Fr. (1), 136 (1973); F. Ramirez, A. V. Pathwardhan, H. J. Kugler et C. P. Smith. J. Am. Chem. Soc. **89**, 6276 (1967).


Can. J. Chem. Downloaded from www.nrcresearchpress.com by 210.87.254.5 on 09/06/12
For personal use only.

# Effective interactions for the configurations $3d^34p + 3d^24s4p + 3d4s^24p$ in the first spectrum of titanium

C. ROTH

*Department of Mathematics, McGill University, Montreal, P.Q., Canada H3A 2K6*

Received July 13, 1981

C. ROTH. Can. J. Chem. **60**, 469 (1982).

Energy levels and Lande $g$-factors for the configurations $3d^34p + 3d^24s4p + 3d4s^24p$ in the first spectra of titanium were calculated and compared with experimental values. The calculations were done in intermediate coupling taking into account explicitly the interactions between configurations, as well as *complete* effective interactions of the core, and effective interactions $d$–$p$.

Due to the insertion of the various effective interactions and a successful starting point based on a general treatment of the odd configurations in the first spectra of the iron group, there was excellent agreement between the experimental and calculated levels.

On fitting 164 levels using 28 free interaction parameters a mean error of only 117 $cm^{-1}$ was obtained, i.e., about 0.3% average difference between the experimental and calculated levels. The experimental and calculated $g$-factors corresponded very closely.

C. ROTH. Can. J. Chem. **60**, 469 (1982).

On a calculé et comparé aux valeurs expérimentales les niveaux d'énergie et les facteurs $g$ de Lande des configurations $3d^34p + 3d^24s4p + 3d4s^24p$ du premier spectre du titane. On a fait les calculs pour un couplage intermédiaire en tenant compte explicitement des interactions entre les configurations ainsi que des interactions effectives complètes du noyau et des interactions effectives $d$–$p$.

L'accord entre les niveaux expérimentaux et calculés est excellent en raison de l'insertion des diverses interactions effectives et un point de départ approprié basé sur le traitement général des configurations impaires des premiers spectres du groupe du fer.

On a obtenu une erreur moyenne de seulement 117 $cm^{-1}$ c'est à dire environ 0,3% pour 164 niveaux en utilisant 28 paramètres d'interaction libre. Les facteurs $g$ calculés et expérimentaux sont très voisins.

[Traduit par le journal]

## Introduction

For the odd configurations in the spectra of the iron group, both strong and weak configuration interactions are significant. The former arise when the perturbing and perturbed configurations are energetically close to each other and there is strong coupling of the configurations by the Coulomb field. These are taken into account by *explicitly* considering the configurations $3d^34p$, $3d^24s4p$, $3d4s^24p$ and the electrostatic interactions between them. Weak interactions occur when the perturbing configurations are well separated from the perturbed configuration, and the coupling of the Coulomb field is weak.

The individual weak interactions may not be significant, but their cumulative influence may be quite large, due to the increasing density of states as the continuum is approached. As it would be completely futile to consider each of these effects individually, the aim should be to modify the energy matrices of the principal configurations so that the major part of *all* the weakly perturbing configurations be included.

By first order perturbation theory, different configurations do not interact. In second order only those configurations which differ in the quantum numbers of at most two electrons interact. Bacher and Goudsmit (1) have shown that the terms of the configuration $l^n$ may be expressed as linear combinations of the terms of $l^2$, so that the perturbation of $l^n$ by all the configurations differing from it by the state of two electrons, and being distant from it, can be accounted for by suitably modifying the terms of $l^2$. Hence these perturbations can be described by two-body effective interactions.

The first correction of this kind for the configurations $d^n$ was the $\alpha L(L+1)$ correction introduced by Trees (2, 3), in the configurations $3d^54s$ of Mn(II) and Fe(III). Trees introduced his correction empirically, but Racah (4) showed that the above effects can be described by a model or effective interaction of the form

$$2\alpha(l_1 \cdot l_2) + \beta q_{12}$$

where $q_{12}$ is the seniority operator (5). For the configuration $d^n$ this becomes

$$\alpha[L(L+1) - 6n] + \beta Q$$

where

$$Q(n,\nu) = (1/4)\,(n-\nu)\,(4l+4-n-\nu)$$
$$= (1/4)\,(n-\nu)\,(12-n-\nu)$$

is the total seniority operator. Here $n$ is the number of $d$ electrons in the configuration $d^np$, $\nu$ is the seniority of the $d^n$ core term, and $l$ is 2 as we are dealing with $d$ electrons. The constant $-6n\alpha$ is usually incorporated into the height of the configuration. Racah (4) showed that the $\alpha L(L+1)$ and

0008-4042/82/040469-11$01.00/0

©1982 National Research Council of Canada/Conseil national de recherches du Canada

Can. J. Chem. Downloaded from www.nrcresearchpress.com by 210.87.254.105 on 09/06/12
For personal use only.

Can. J. Chem. Downloaded from www.nrcresearchpress.com by 210.87.254.105 on 09/06/12
For personal use only.

the $\beta Q$ corrections form a complete set of two-body effective interactions for the $d^n$ configurations. This is due to the fact that together with the Slater integrals $F_0(d^2)$, $F_2(d^2)$, and $F_4(d^2)$, they form a set of five independent parameters that can represent the five terms of $d^2$.

Bacher and Goudsmit (1) also showed that if the far-lying perturbing configuration differs from $l^n$ by the state of only one electron, its effect can be described by expressing the terms of $l^n$ as linear combinations of $l^3$, and modifying the values of these terms. Hence in the linear theory, the Hamiltonian in this case must be augmented by additional three-body interactions.

Rajnak and Wybourne (6) obtained explicit formulas for the effective interactions representing the perturbation of an $l^n$ configuration by far-lying configurations differing from it by one or two electrons or holes.

Rohrlich (7) calculated the energy levels for the configurations $3d^34p$ and $3d^24s4p$ of TiI. He considered the spectrum in the *LS* approximation by taking into account the interaction between the cores $3d^3$ and $3d^24s$, but only as a perturbation to the calculated terms. He obtained an rms error of 1109 $cm^{-1}$.

Roth (8), by taking into account explicitly the three configurations $3d^34p$, $3d^24s4p$, and $3d4s^24p$, the electrostatic interactions between them, and the spin–orbit interactions, but *excluding* the effective interactions (with the exception of the $\alpha$ correction), obtained an rms error of 261 $cm^{-1}$.

At about the same time, Smith and Siddall (9), independently treating the configurations $(3d + 4s)^34p$ in *LS* coupling, obtained an rms error of 355 $cm^{-1}$.

In this project were included the electrostatic and spin–orbit interactions of the individual configurations $3d^34p$, $3d^24s4p$, and $3d4s^24p$; the explicit electrostatic interactions between configurations $3d^34p$–$3d^24s4p$, $3d^24s4p$–$3d4s^24p$, and $3d^3$-$4p$–$3d4s^24p$; and the *complete* two- and three-body effective interactions of the core *d* electrons, as well as two-body mixed effective interactions between the 3*d* and 4*p* electrons.

The value of $\Delta$ is also given by the least-squares routine. The same derivatives can be used for several variations in the least squares, either imposing different conditions on the parameters, inserting the experimental levels with different assignments, or even rejecting some levels from consideration. The parameters of that variation which yielded the best results were used to perform new diagonalizations. This iterative process was continued until mathematical convergence was attained. In the present project four complete iterations were required.

The initial values of the radial parameters were used to multiply the algebraic matrices on tape and the resulting matrices were diagonalized. Besides the eigenvalues, the diagonalization routine also yields the derivatives of the eigenvalues with respect to the parameters, the squares of the eigenvectors (percentage compositions), and the calculated Lande *g*-factors. The appropriate experimental levels were then fitted to the eigenvalues, and using the derivatives obtained in the diagonalization, least-squares optimization calculations were performed. In these calculations, the improved values of the theoretical energy levels, the corrected values of the parameters including their statistical deviations, and the sum of the squares of the differences between the observed and the calculated levels, were obtained. The rms error is then defined as

$$\Delta = \sqrt{\frac{\sum_{i=1}^{n} \Delta_i^2}{n - m}}$$

where the $\Delta_i$'s are the differences between the observed and calculated levels, $n$ is the number of known levels, and $m$ is the number of free parameters. The mean error is quite different from the mean deviation

$$\delta = \sqrt{\frac{\sum_{i=1}^{n} \Delta_i^2}{n}}$$

as the former takes into account the statistical effect of the number of free parameters. Hence in order for a new parameter to have physical significance, it should cause an essential decrease in the rms error, and not simply a decrease in the mean deviation.

## Parameters

The algebraic matrices of $(d + s)^3p$ comprise the electrostatic and spin–orbit interaction matrices of the configurations $d^3p$, $d^2sp$, and $ds^2p$; the electrostatic interactions between configurations $d^3p$–$d^2sp$, $d^2sp$–$ds^2p$, $d^3p$–$ds^2p$; the complete two- and three-body effective interactions of the core *d* electrons, as well as two-body mixed effective interactions between the *d* and *p* electrons. The energy matrix is then a linear combination of these matrices, the coefficients of which are parameters to be discussed below. Unprimed quantities denote the configuration $d^3p$, primes denote $d^2sp$, and double primes denote $ds^2p$.

Can. J. Chem. Downloaded from www.nrcresearchpress.com by 210.87.254.105 on 09/06/12
For personal use only.

$A, A', A''$ = the heights of the configurations:

$$S' = A' - A, \; S'' = A'' - A$$

$B, B'$ = linear combinations of the Slater parameters $F^2(d,d)$ and $F^4(d,d)$:

$$B = \frac{1}{441}[9F^2(dd) - 5F^4(dd)] = F_2(dd) - 5F_4(dd) \quad (10)$$

$C, C'$ = multiples of the Slater parameter $F^4(d,d)$:

$$C = \frac{5}{63}F^4(dd) = 35F_4(dd) \quad (10)$$

$G_{ds}$ = the parameter of the $d$–$s$ interaction in the configuration $d^2sp$:

$$G_{ds} = \frac{1}{5}G^2(ds) \quad (5)$$

$F_2, F_2', F_2''$ = parameters of the direct part of the $d$–$p$ interaction:

$$F^2 = \frac{1}{35}F^2(dp) \quad (10)$$

$G_1, G_1', G_1''$ = parameters of the exchange part of the $d$–$p$ interaction:

$$G_1 = \frac{1}{15}G^1(dp) \quad (10)$$

$G_3, G_3', G_3''$ = parameters of the exchange part of the $d$–$p$ interaction:

$$G_3 = \frac{3}{245}G^3(dp) \quad (10)$$

$G_{ps}$ = the parameter of the $p$–$s$ interaction in the configuration $d^2sp$:

$$G_{ps} = \frac{1}{3}G^1(ps) \quad (11)$$

$H$ = the parameter of the $d^3$–$d^2s$ interaction:

$$H = \frac{R^2(dd,ds)}{35} \quad (5)$$

$H'$ = the parameter of the $d^2s$–$ds^2$ interaction, defined the same as $H$.

$J$ = the parameter of the direct part of the $d^3p$–$d^2sp$ interaction:

$$J = \frac{R^2(dp,sp)}{5} \quad (12)$$

$J'$ = the parameter of the direct part of the $d^2sp$–$ds^2p$ interaction, defined the same as $J$.

$K$ = the parameter of the exchange part of the $d^3p$–$d^2sp$ interaction:

$$K = \frac{R^1(dp,ps)}{3} \quad (12)$$

$K'$ = the parameter of the exchange part of the $d^2sp$–$ds^2p$ interaction, defined the same as $K$.

$G^*$ = the parameter of the $d^3p$–$ds^2p$ interaction:

$$G^* = \frac{R^2(dd,ss)}{5} \quad (5)$$

$\zeta_d, \zeta_d', \zeta_d''$ = parameters of the spin–orbit interactions of the $d$ electrons.

$\zeta_p, \zeta_p', \zeta_p''$ = parameters of the spin–orbit interaction of the $p$ electron.

$\alpha, \alpha'$ = parameters of the $L(L+1)$ correction.

$\beta, \beta'$ = parameters of the $Q$ correction.

$T, T'$ } parameters of the three-body effective
$T_x, T_x'$ } interactions of the core $d$ electrons.

$T$ is the parameter which fully represents the perturbation of $3s^23d^n$ by $3s3d^{n+1}$, while $T_x$ is an additional independent parameter, which is required to make the set of three-body effective interaction parameters complete (13).

$F_1, F_1', F_1''$ = parameters of the direct part of the effective interaction between $d$ and $p$ electrons.

$G_2, G_2', G_2''$ = parameters of the exchange part of the effective interaction between $d$ and $p$ electrons.

The two-body effective Hamiltonian for interactions between $d$ and $p$ electrons is given by (13)

$$H_{\text{eff}}^2 = -\sum_t F_t \sum_{i\neq j}(u_i^{(t)}\cdot v_j^{(t)}) - \sum_t G_t \sum_{i\neq j}(z_i^{(t)}\cdot \tilde{z}_j^{(t)}),$$

where $u^{(t)}$, $v^{(t)}$, $z^{(t)}$, and $\tilde{z}^{(t)}$ are tensor operators of order $t$ whose only non-vanishing reduced matrix elements are

$$(nl||u^{(t)}||nl) = 1$$
$$(n'l'||v^{(t)}||n'l') = 1$$
$$(nl||z^{(t)}||n'l') = 1$$
$$(n'l'||\tilde{z}^{(t)}||nl) = 1$$

The coefficients of $F_t$ in the configuration $d^np$ are found by calculating the matrix elements

$$(d^n(\nu_1 S_1 L_1)pSLJM\,|\sum_{i\neq j}(u_i^{(t)}\cdot v_j^{(t)})\,|d^n(\nu_1' S_1' L_1')pS'L'J'M')$$

Since this involves the reduced matrix element $(p||v^{(t)}||p)$, $t$ may take only the values 0, 1, and 2 because of the triangular relationship $\delta(1,t,1)$ between the two $p$ angular momenta and $t$. For $t$ equal to 0 and 2 the Slater parameters are included

Can. J. Chem. Downloaded from www.nrcresearchpress.com by 210.87.254.105 on 09/06/12
For personal use only.

elsewhere, and thus the only new direct effective parameter is $F_1$.

Similarly for $G_t$, the calculation of the matrix elements

$$(d^n(v_1S_1L_1)pSLJM\,|\sum_{i\neq j}(z_i^{(t)}\cdot\tilde{z}_j^{(t)})\,|d^n(v_1'S_1'L_1')pS'L'J'M')$$

is required.

Due to the reduced matrix element $(d||z^{(t)}||p)$ with the triangular relation $\delta(2,t,1)$, $t$ may take on the values 1, 2, or 3. Since $G_1$ and $G_3$ are already included elsewhere, the only new exchange effective parameter is $G_2$.

The Lande $g$-factors were also computed. Whenever observed $g$-factors exist, they provide useful information to help fit the experimental levels.

The initial values of the parameters $B, B', C, C', G_{ds}, F_2, F_2', F_2'', G_1, G_1', G_1'', G_3, G_3', G_3'', G_{ps}, H, H', J, J', K, K', G^*, \zeta_d, \zeta_d', \zeta_d'', \zeta_p, \zeta_p', \zeta_p'', \alpha$, and $\beta$ were taken as the values obtained for titanium in the general treatment of the configurations $3d^n4p + 3d^{n-1}4s4p + 3d^{n-2}4s^24p$ by the author (13). The initial values of $T$, $T_x$, $F_1$, and $G_2$ were taken as 0.

The initial values of $A$ and $A'$ were obtained by considering the terms $^5F$ and $^5G$ whose electrostatic interaction matrices are of order 2. They are given by (14, 15)

$$^5F\begin{bmatrix} A-15B+3F_2-6G_1-26G_3+12\alpha & -\frac{3\sqrt{5}}{5}(K-J) \\ \frac{-3\sqrt{5}}{5}(K-J) & A'-8B'-2G_{ds}-3F_2'-G_1'-16G_3'-G_{ps}+12\alpha' \end{bmatrix}$$

$$^5G\begin{bmatrix} A-15B-F_2-10G_1-10G_3+12\alpha & \frac{\sqrt{5}}{5}(K-J) \\ \frac{\sqrt{5}}{5}(K-J) & A'-8B'-2G_{ds}+F_2'-9G_1'-4G_3'-G_{ps}+12\alpha \end{bmatrix}$$

Using the initial values in Table 1 below and the experimental centers of gravity of the terms $z^5G$, $z^5F$, $y^5G$, and $y^5F$ which are 16 202 cm$^{-1}$, 17 046 cm$^{-1}$, 26 726 cm$^{-1}$, and 28 767 cm$^{-1}$, respectively (16), we obtain by evaluating the sums and differences of the eigenvalues, the following average values

$$A = 38\,276\ \text{cm}^{-1}$$

$$A' = 32\,264\ \text{cm}^{-1}$$

It was shown (13) that the centers of gravity of the terms $d^2sp$ and $ds^2p$ are given by

$$M'(d^2sp) = A' + \frac{7}{9}(C' - 2B) - 2(G_1' + \frac{7}{2}G_3') - G_{ds} - \frac{1}{2}G_{ps} + \frac{32}{3}\alpha' + \frac{1}{9}\beta' + \frac{980}{9}T' + 2G_2'$$

$$M''(ds^2p) = A'' - (G_1'' + \frac{7}{2}G_3'') - 6\alpha'' + 70T'' + G_2''$$

Then again from ref. 13, using

$$D'' = M'' - M' = 11\,532\ \text{cm}^{-1}$$

we obtain initially

$$A'' = 40\,102\ \text{cm}^{-1}$$

The values of the parameters are listed in Table 1.

In order to obtain well-defined values for the parameters in the least-squares the parameters $F_2, F_2', F_2''; G_1, G_1', G_1''; G_3, G_3', G_3''; \zeta_d, \zeta_d', \zeta_d''; \zeta_p, \zeta_p', \zeta_p''$ were in arithmetic progression. The parameters $H', J', K', G^*$ were fixed at their values in the diagonalization; whereas the parameters $\alpha$, $\beta$, $T$, $T_x, F_1, G_2$ were respectively equal for the different configurations.

The above values of the parameters compare favorably with those obtained by the author using Hartree–Fock calculations (13).

## Discussion

The configurations $(d + s)^3p$ comprise 92 theoretical terms splitting into 212 levels. In AEL (16),

Can. J. Chem. Downloaded from www.nrcresearchpress.com by 210.87.254.105 on 09/06/12
For personal use only.

TABLE 1. Values of the parameters (in $cm^{-1}$)

| Parameter | Initial value | Final value |
|---|---|---|
| $A$ | 38276 | 37995±85 |
| $A'$ | 32264 | 32946±111 |
| $A''$ | 40102 | 40078±198 |
| $B$ | 561 | 547±5 |
| $B'$ | 664 | 653±6 |
| $C$ | 1714 | 1726±26 |
| $C'$ | 2318 | 2326±36 |
| $G_{ds}$ | 1590 | 1562±33 |
| $F_2$ | 176 | 164±5 |
| $F_2'$ | 292 | 319±5 |
| $F_2''$ | 408 | 574 (A.P.) |
| $G_1$ | 290 | 283±5 |
| $G_1'$ | 316 | 326±5 |
| $G_1''$ | 342 | 369 (A.P.) |
| $G_3$ | 13 | 8.1±2.2 |
| $G_3'$ | 21 | 22±2 |
| $G_3''$ | 29 | 36 (A.P.) |
| $G_{ps}$ | 5809 | 5929±61 |
| $H$ | 192 | 183±4 |
| $H'$ | 153 | 153 (FIX) |
| $J$ | 1036 | 1194±40 |
| $J'$ | 1566 | 1566 (FIX) |
| $K$ | 2645 | 2622±26 |
| $K'$ | 3592 | 3592 (FIX) |
| $G^*$ | 1821 | 1821 (FIX) |
| $\zeta_d$ | 74 | 95±22 |
| $\zeta_d'$ | 89 | 104±20 |
| $\zeta_d''$ | 104 | 113 (A.P.) |
| $\zeta_p$ | 101 | 102±49 |
| $\zeta_p'$ | 240 | 178±48 |
| $\zeta_p''$ | 379 | 254 (A.P.) |
| $\alpha = \alpha'$ | 22 | 24±5 |
| $\beta = \beta'$ | −458 | −310±59 |
| $T = T'$ | 0 | −2.1±0.5 |
| $T_x = T_x'$ | 0 | −2.8±0.9 |
| $F_1 = F_1' = F_1''$ | 0 | −9.2±3.2 |
| $G_2 = G_2' = G_2''$ | 0 | 8.9±2.6 |

74 terms splitting into 175 levels are assigned to the configurations $3d^34p + 3d^24s4p$. In addition, 11 odd terms splitting into 28 levels are given without a definite configuration designation. However, in the original work of Russell (17), only the term $w^1G$ was given with no configuration designation. Russell attributed the terms $w^3H$, $p^3D$, $t^3G$, $g^3F$, and $n^3D$, with no configuration designation in AEL, to configurations containing a $5p$ electron. Russell assigned the terms $s^3F$, $q^3D$, and $v^1D$, with no configuration designation in AEL as $3d^3(b^2D)4ps^3F$, $3d^3(b^2D)4pq^3D$, and $3d^3(a^2P)4pv^1D$, respectively. He assigned the term $3d^24s(a^2S)4pt^3P$ of AEL to the configuration $3d4s^24p$.

In the final least-squares, 65 experimental terms splitting into 164 levels were included. The six levels of the terms $s^3G$ and $p^3F$ found by Wilson and Thekaekara (18) and corroborated by Banks *et al.* (19) were included in the calculations. In the least-squares with 28 free parameters the mean error was only 117 $cm^{-1}$.

This value is a great improvement compared to that of 355 $cm^{-1}$ obtained by Smith and Siddall (9). There are several reasons for this very significant decrease. Contrary to Smith and Siddall, who claim that neither effective interactions nor the spin–orbit interactions are important, it turns out that *both* are indeed *very* significant. By including the spin–orbit interactions the mean error was reduced from 342 $cm^{-1}$ to 261 $cm^{-1}$ (8). Smith and Siddall (9), required the parameters $H'$, $J'$, $K'$, and $G^*$ to be respectively equal to $H$, $J$, $K$, and $G_{ds}$, whereas it was shown by the author (13), using Hartree–Fock calculations, that these assumptions are unjustified. Further, by including the various effective interactions, having reliable initial parameters based upon a general treatment (13), and neglecting levels that either belong to or are very strongly perturbed by the configurations $(3d + 4s)^35p$, we are able to obtain the very low final value of 117 $cm^{-1}$ for the rms error.

It should be emphasized that if the configurations with a $5p$ electron are not included in the computations, and if one retains those terms that suffer very large perturbations from these configurations (deviations in excess of 1000 $cm^{-1}$), unwelcome distortions in the parameters may occur. This may explain, for example, why Smith and Siddall's (9) results for $B$ and $B'$ have the very high values of 763 $cm^{-1}$ and 952 $cm^{-1}$, compared with our values of 547 $cm^{-1}$ and 653 $cm^{-1}$, respectively.

Table 2 compares the experimental and calculated levels and $g$-factors.

The column "Theoretical designation" gives the assignments of the calculated levels. For $d^3sp$, as the $p$–$s$ interaction is much stronger than the $d$–$s$ interaction, the coupling scheme is $d^{n-1}(v_1S_1L_1)sp(^{1,3}P)SL$. Whenever terms of the parent $d^m$ have different seniorities these are denoted by the letters $A$ and $B$, the lower calculated term being designated by $A$, and the seniorities summed for each level. Whenever a calculated term has a corresponding experimental term, the letters $z, y, x, \ldots$ are used as in AEL (16). The terms of $d^3p$ are differentiated from those of $ds^2p$ by using an asterisk with the latter terms.

In the column "Experimental designation" the experimental level assignments are given only if different from the calculated designations.

In the column "Percentage" the three highest contributions are specified, provided the lowest is greater than 4%.

The observed and calculated levels, as well as their differences, "O − C", are in $cm^{-1}$.

TABLE 2. Observed and calculated levels of TiI $(3d + 4s)^3 4p$

| Designation | | | | Level | | | $g$ | |
|---|---|---|---|---|---|---|---|---|
| Experimental | Theoretical | Percentage | $J$ | Obsd | Calcd | O − C | Obsd | Calcd |
| $3d^2 4s(a^4F)4pz^5G$ | $^3F(^3P)z^5G$ | 100 | 2 | 15 877.18 | 15 852 | 25 | 0.39 | 0.336 |
| | | 100 | 3 | 15 975.59 | 15 947 | 28 | 0.93 | 0.921 |
| | | 100 | 4 | 16 106.08 | 16 073 | 33 | 1.15 | 1.152 |
| | | 100 | 5 | 16 267.51 | 16 228 | 40 | 1.25 | 1.258 |
| | | 100 | 6 | 16 458.71 | 16 411 | 48 | 1.33 | 1.333 |
| $3d^2 4s(a^4F)4pz^5F$ | $^3F(^3P)z^5F$ | 96 | 1 | 16 817.19 | 16 756 | 61 | 0.00 | 0.001 |
| | | 95 | 2 | 16 875.19 | 16 812 | 63 | | 1.001 |
| | | 97 | 3 | 16 961.42 | 16 896 | 65 | 1.26? | 1.251 |
| | | 98 | 4 | 17 075.31 | 17 007 | 68 | 1.34 | 1.346 |
| | | 99 | 5 | 17 215.44 | 17 143 | 73 | 1.42 | 1.401 |
| $3d^2 4s(a^4F)4pz^5D$ | $^3F(^3P)z^5D$ | 95 | 0 | 18 462.83 | 18 541 | −79 | | — |
| | | 95 | 1 | 18 482.86 | 18 557 | −75 | 1.65? | 1.497 |
| | | 94 | 2 | 18 525.07 | 18 592 | −67 | 1.50 | 1.496 |
| | | 95 | 3 | 18 593.99 | 18 649 | −55 | 1.49 | 1.496 |
| | | 95 | 4 | 18 695.23 | 18 738 | −42 | 1.51 | 1.495 |
| $3d^2 4s(a^2F)4pz^3F$ | $^3F(^3P)z^3F$ | $87 + 10^3P(^3P)^3D$ | 2 | 19 323.00 | 19 323 | 0 | 0.6692 | 0.669 |
| | | $88 + 9^3P(^3P)^3D$ | 3 | 19 421.58 | 19 416 | 5 | 1.0884 | 1.087 |
| | | $88 + 9^3P(^3P)^3D$ | 4 | 19 573.98 | 19 559 | 18 | 1.2542 | 1.252 |
| $3d^2 4s(a^2F)4pz^3D$ | $^3F(^3P)z^3D$ | $85 + 7^3P(^3P)^3D$ | 1 | 19 937.88 | 19 886 | 51 | | 0.502 |
| | | $86 + 8^3P(^3P)^3D$ | 2 | 20 006.05 | 19 959 | 47 | 1.16 | 1.168 |
| | | $85 + 7^3P(^3P)^3D$ | 3 | 20 126.07 | 20 078 | 48 | 1.34 | 1.334 |
| $3d^2 4s(a^2F)4pz^3G$ | $^3F(^3P)z^3G$ | 96 | 3 | 21 469.53 | 21 582 | −113 | 0.75 | 0.758 |
| | | 95 | 4 | 21 588.52 | 21 710 | −122 | 1.05 | 1.052 |
| | | 95 | 5 | 21 739.74 | 21 859 | −119 | 1.21 | 1.206 |
| $3d^2 4s(a^2F)4pz^1D$ | $^3F(^3P)z^1D$ | $88 + 9^3P(^3P)^1D$ | 2 | 22 081.15 | 22 184 | −103 | 1.00 | 1.000 |
| $3d^2 4s(a^2F)4pz^1F$ | $^3F(^3P)z^1F$ | 98 | 3 | 22 404.69 | 22 242 | 163 | 1.00 | 0.996 |
| $3d^2 4s(a^2F)4pz^1G$ | $^3F(^3P)z^1G$ | 96 | 4 | 24 694.81 | 24 740 | −45 | 0.97 | 1.006 |
| $3d^2 4s(b^4P)4pz^3S$ | $^3P(^3P)z^3S$ | $91 + 7(^2P)^3S$ | 1 | 24 921.19 | 24 773 | 148 | 1.99 | 1.982 |
| $3d^2 4s(b^4P)4pz^5S$ | $^3P(^3P)z^5S$ | 95 | 2 | 25 102.88 | 25 013 | 94 | 1.93 | 1.852 |
| $3d^2 4s(a^4F)4py^3F$ | $^3F(^1P)y^3F$ | $48 + 24(^4F)^3F + 23^1D(^3P)^3F$ | 2 | 25 107.45 | 24 997 | 105 | | 0.670 |
| | | $46 + 22(^4F)^3F + 22^1D(^3P)^3F$ | 3 | 25 227.24 | 25 125 | 102 | 1.06 | 1.081 |
| | | $42 + 23(^4F)^3F + 25^1D(^3P)^3F$ | 4 | 25 388.34 | 25 289 | 99 | 1.21 | 1.240 |
| $3d^2 4s(a^4F)4py^3D$ | $(^4F)y^3D$ | $51 + 36^3F(^1P)^3D$ | 1 | 25 317.84 | 25 439 | −121 | 0.50 | 0.542 |
| | | $37 + 32^1D(^3P)^3D + 21^3F(^1P)^3D$ | 2 | 25 438.93 | 25 608 | −169 | 1.17 | 1.283 |
| | | $36 + 34^1D(^3P)^3D + 20^3F(^1P)^3D$ | 3 | 25 643.72 | 25 782 | −139 | 1.33 | 1.362 |
| | $^3P(^3P)^1S$ | $70 + 16(^2P)^1S + 11^1D(^3P)^3P$ | 0 | | 25 358 | | | — |
| $3d^2 4s(b^4P)4pz^3P$ | $^1D(^3P)z^3P$ | $51 + 34^3P(^3P)^5D + 12^3P(^3P)^1S$ | 0 | | 25 714 | | | — |
| | | $63 + 28^3P(^3P)^5D$ | 1 | 25 537.39 | 25 439 | −121 | 1.50 | 1.478 |
| | | $52 + 25^3P(^3P)^5D + 13^3F(^1P)^3D$ | 2 | 25 493.78 | 25 608 | −169 | 1.47 | 1.652 |
| $3d^2 4s(b^4P)4py^5D$ | $^3P(^3P)y^5D$ | $61 + 30^1D(^3P)^3P$ | 0 | 25 605.03 | 25 693 | −88 | | — |
| | | $65 + 23^1D(^3P)^3P$ | 1 | 25 635.74 | 25 708 | −72 | | 1.437 |
| | | $72 \times 18^1D(^3P)^3P$ | 2 | 25 699.95 | 25 716 | −16 | | 1.375 |
| | | $75 + 10(^4F)^3D + 9^3F(^1P)^3D$ | 3 | 25 797.60 | 25 806 | −11 | | 1.452 |
| | | $86 + 7(^4F)^5D$ | 4 | 25 926.80 | 26 025 | −98 | 1.52 | 1.498 |
| | $(^4F)y^5G$ | 96 | 2 | 26 494.37 | 26 584 | −90 | 0.34 | 0.337 |
| | | 96 | 3 | 26 564.43 | 26 658 | −94 | 0.91 | 0.917 |
| | | 98 | 4 | 26 657.41 | 26 755 | −97 | 1.15 | 1.151 |
| | | 100 | 5 | 26 772.98 | 26 875 | −102 | 1.25 | 1.267 |
| | | 100 | 6 | 26 910.69 | 27 019 | −108 | 1.34 | 1.333 |
| $3d^3(b^4F)4px^3F$ | $^1D(^3P)x^3F$ | $57 + 21^3F(^1P)^3F + 12(^4F)^3F$ | 2 | 26 803.46 | 26 814 | −11 | 0.66 | 0.675 |
| | | $60 + 22^3F(^1P)^3F + 9(^4F)^3F$ | 3 | 26 892.95 | 26 911 | −18 | 1.06 | 1.092 |
| | | $59 + 20^3F(^1P)^3F + 10(^4F)^3F$ | 4 | 27 025.67 | 27 055 | −29 | 1.23 | 1.254 |

Can. J. Chem. Downloaded from www.nrcresearchpress.com by 210.87.254.105 on 09/06/12
For personal use only.

TABLE 2. (*continued*)

| Designation | | | | Level | | | $g$ | |
|---|---|---|---|---|---|---|---|---|
| Experimental | Theoretical | Percentage | $J$ | Obsd | Calcd | O − C | Obsd | Calcd |
| $3d^3(b^4F)4px\,^3D$ | $^1D(^3P)x\,^3D$ | $79 + 12^3P(^3P)^3D$ | 1 | 27 355.06 | 27 431 | −76 | 0.51 | 0.531 |
| | | $75 + 11^3P(^3P)^3D + 7^3P(^3P)^5P$ | 2 | 27 418.04 | 27 496 | −78 | 1.17 | 1.237 |
| | | $72 + 13^3P(^3P)^3D + 8^3P(^3P)^5P$ | 3 | 27 480.08 | 27 556 | −76 | 1.36 | 1.402 |
| $3d^3(b^4F)4py\,^3G$ | $^3F(^1P)y\,^3G$ | $50 + 23(^4F)^3G + 10(^2G)^3G$ | 3 | 27 499.03 | 27 488 | 11 | 0.75 | 0.754 |
| | | $49 + 24(^4F)^3G + 11(^2G)^3G$ | 4 | 27 614.69 | 27 600 | 15 | 1.05 | 1.054 |
| | | $49 + 24(^4F)^3G + 9(^2G)^3G$ | 5 | 27 750.16 | 27 735 | 15 | 1.21 | 1.206 |
| $3d^24s(b^4P)4pz\,^5P$ | $^3P(^3P)z\,^5P$ | 95 | 1 | 27 665.57 | 27 690 | −25 | | 2.460 |
| | | 93 | 2 | 27 740.19 | 27 769 | −29 | | 1.743 |
| | | $83 + 12^1D(^1P)^1D$ | 3 | 27 887.74 | 27 926 | −39 | | 1.574 |
| $3d^24s(a^2D)4py\,^1D$ | $^1D(^1P)y\,^1D$ | $39 + 24(^2D)^1D^* + 18(^3P)^1D$ | 2 | 27 906.91 | 27 811 | 96 | 0.98 | 1.003 |
| | $(^4F)y\,^5F$ | 96 | 1 | 28 596.45 | 28 491 | 106 | 0.00 | 0.001 |
| | | 98 | 2 | 28 638.82 | 28 538 | 101 | 1.01 | 1.001 |
| | | 98 | 3 | 28 702.70 | 28 610 | 93 | 1.24 | 1.249 |
| | | 97 | 4 | 28 788.39 | 28 705 | 83 | 1.34 | 1.348 |
| | | 97 | 5 | 28 896.08 | 28 827 | 69 | 1.40 | 1.401 |
| $3d^24s(b^4P)4pw\,^3D$ | $^3F(^1P)w\,^3D$ | $39 + 22(^4F)^3D + 13(^4P)^3D$ | 1 | 29 661.27 | 29 733 | −72 | 0.51 | 0.508 |
| | | $41 + 24(^4F)^3D + 16(^4F)^5D$ | 2 | 29 768.69 | 29 831 | −62 | 1.16 | 1.167 |
| | | $42 + 26(^4F)^3D + 21(^4F)^5D$ | 3 | 29 912.29 | 29 972 | −60 | 1.34 | 1.338 |
| | $(^4F)x\,^5D$ | 94 | 0 | 29 829.16 | 29 837 | −8 | | 0.001 |
| | | $87 + 8^3P(^3P)^5D$ | 1 | 29 855.26 | 29 864 | −9 | 1.46 | 1.498 |
| | | $86 + 9^3P(^3P)^5D$ | 2 | 29 907.29 | 29 917 | −10 | 1.50 | 1.497 |
| | | $75 + 10^3F(^1P)^3D + 7^3P(^3P)^5D$ | 3 | 29 986.24 | 29 991 | −5 | 1.49 | 1.496 |
| | | $88 + 7^3P(^3P)^5D$ | 4 | 30 060.34 | 30 077 | −16 | 1.49 | 1.462 |
| $3d^24s(a^4F)4px\,^3G$ | $^1G(^3P)x\,^3G$ | $76 + 18^3F(^1P)^3G$ | 3 | 29 914.77 | 30 073 | −158 | | 0.753 |
| | | $74 + 17^3F(^1P)^3G + 7(^2H)^3G$ | 4 | 29 971.11 | 30 105 | −134 | | 1.089 |
| | | $75 + 16^3F(^1P)^3G + 7(^2H)^3G$ | 5 | 30 039.25 | 30 156 | −117 | 1.19 | 1.201 |
| $3d^24s(a^2D)4pv\,^3D$ | $^3P(^3P)v\,^3D$ | $79 + 15^1D(^3P)^3D$ | 1 | 31 184.09 | 31 034 | 150 | 0.51 | 0.502 |
| | | $77 + 16^1D(^3P)^3D$ | 2 | 31 190.66 | 31 052 | 139 | 1.17 | 1.169 |
| | | $77 + 14^1D(^3P)^3D$ | 3 | 31 206.01 | 31 077 | 129 | 1.34 | 1.334 |
| $3d^24s(b^2G)4pw\,^3G$ | $(^4F)w\,^3G$ | $72 + 19^3F(^1P)^3G$ | 3 | 31 373.86 | 31 273 | 101 | 0.75 | 0.752 |
| | | $71 + 21^3F(^1P)^3G$ | 4 | 31 489.49 | 31 400 | 89 | 1.05 | 1.052 |
| | | $73 + 20^3F(^1P)^3G$ | 5 | 31 628.70 | 31 547 | 82 | 1.19 | 1.202 |
| $3d^24s(a^2D)4py\,^3P$ | $^3P(^3P)y\,^3P$ | $86 + 7(^2P)^3P$ | 0 | 31 685.90 | 31 681 | 5 | | — |
| | | $87 + 7(^2P)^3P$ | 1 | 31 725.75 | 31 713 | 13 | 1.47 | 1.497 |
| | | $86 + 8(^2P)^3P$ | 2 | 31 805.94 | 31 784 | 22 | | 1.498 |
| $3d^24s(b^2G)4pz\,^3H$ | $^1G(^3P)z\,^3H$ | $84 + 12(^2G)^3H$ | 4 | 31 830.02 | 31 796 | 34 | 0.80 | 0.803 |
| | | $85 + 11(^2G)^3H$ | 5 | 31 914.30 | 31 890 | 24 | 1.04 | 1.036 |
| | | $85 + 12(^2G)^3H$ | 6 | 32 013.56 | 32 001 | 13 | 1.17 | 1.169 |
| $3d^24s(a^2D)4py\,^1F$ | $^1D(^1P)y\,^1F$ | $48 + 34(^2G)^1F + 10^1G(^1P)^1F$ | 3 | 32 857.76 | 32 387 | 271 | 0.99? | 0.998 |
| $3d^24s(b^2P)4px\,^3P$ | $(^4P)x\,^3P$ | $38 + 29^3P(^1P)^3P + 22(^2P)^3P$ | 0 | 33 085.14 | 33 336 | −251 | | — |
| | | $39 + 28^3P(^1P)^3P + 21(^2P)^3P$ | 1 | 33 090.55 | 33 353 | −262 | 1.46 | 1.469 |
| | | $38 + 29^3P(^1P)^3P + 20(^2P)^3P$ | 2 | 33 114.49 | 33 362 | −242 | 1.46 | 1.498 |
| $3d^24s(a^2D)4pw\,^3F$ | $(^4F)w\,^3F$ | $58 + 31^3F(^1P)^3F$ | 2 | 33 655.90 | 33 581 | 75 | 0.66 | 0.669 |
| | | $56 + 29^3F(^1P)^3F$ | 3 | 33 680.16 | 33 638 | 42 | 1.09 | 1.086 |
| | | $59 + 28^3F(^1P)^3F$ | 4 | 33 700.90 | 33 666 | 35 | 1.26 | 1.254 |
| $3d^24s(a^2D)4pz\,^1P$ | $^1D(^1P)z\,^1P$ | $39 + 28^3P(^3P)^1P + 22(^2P)^1P$ | 1 | 33 660.73 | 33 371 | 290 | 0.94 | 1.101 |
| $3d^24s(b^2G)4pv\,^3F$ | $^1G(^3P)v\,^3F$ | $82 + 9(^2D)^3F^*$ | 2 | 33 980.69 | 34 040 | −60 | 0.63 | 0.664 |
| | | $83 + 9(^2D)^3F^*$ | 3 | 34 078.61 | 34 098 | −20 | 1.10 | 1.085 |
| | | $83 + 10(^2D)^3F^*$ | 4 | 34 205.00 | 34 206 | −1 | 1.23 | 1.252 |
| | $^3P(^1P)^3S$ | $64 + 34(^4P)^3S$ | 1 | | 33 984 | | | 1.935 |
| $3d^24s(b^2G)4pz\,^1H$ | $(^2G)z\,^1H$ | $62 + 21(^2H)^1H + 13^1G(^1P)^1H$ | 5 | 34 700.31 | 34 810 | −110 | 1.02 | 1.001 |
| $3d^24s(b^2P)4py\,^1P$ | $^3P(^3P)y\,^1P$ | $59 + 20^1D(^1P)^1P + 13(^2D)^1P^*$ | 1 | 34 947.02 | 34 903 | 44 | | 1.031 |

Can. J. Chem. Downloaded from www.nrcresearchpress.com by 210.87.254.105 on 09/06/12
For personal use only.

TABLE 2. (*continued*)

| Designation | | | | Level | | | $g$ | |
|---|---|---|---|---|---|---|---|---|
| Experimental | Theoretical | Percentage | $J$ | Obsd | Calcd | O − C | Obsd | Calcd |
| $3d^24s(b^2P)4px\,^1D$ | $^3P(^3P)x\,^1D$ | $61 + 14^3F(^3P)^1D + 13^1D(^1P)^1D$ | 2 | 35 035.11 | 35 056 | −21 | | 1.003 |
| | $(^2G)y\,^3H$ | $85 + 12^1G(^3P)^3H$ | 4 | 35 454.10 | 35 253 | 201 | 0.79 | 0.803 |
| | | $84 + 13^1G(^3P)^3H$ | 5 | 35 559.66 | 35 363 | 197 | 1.04 | 1.035 |
| | | $85 + 12^1G(^3P)^3H$ | 6 | 35 685.19 | 35 493 | 192 | 1.17 | 1.168 |
| | $(^4P)w\,^5D$ | 97 | 0 | 35 503.40 | 35 498 | 6 | | — |
| | | 98 | 1 | 35 527.76 | 35 520 | 8 | 1.51 | 1.498 |
| | | 98 | 2 | 35 577.14 | 35 566 | 11 | 1.53 | 1.499 |
| | | 98 | 3 | 35 652.95 | 35 638 | 15 | 1.46 | 1.500 |
| | | 99 | 4 | 35 757.51 | 35 739 | 19 | 1.46 | 1.500 |
| $3d^24s(b^2G)4py\,^1G$ | $^1G(^1P)y\,^1G$ | $49 + 30(^2G)^1G + 17(^2H)^1G$ | 4 | 36 000.25 | 35 732 | 269 | 1.00 | 1.000 |
| | $(^4P)y\,^5P$ | 96 | 1 | 36 298.43 | 36 237 | 62 | 2.47 | 2.486 |
| | | 97 | 2 | 36 340.67 | 36 287 | 54 | 1.81 | 1.827 |
| | | 97 | 3 | 36 414.58 | 36 361 | 53 | 1.66 | 1.665 |
| | $(A^2D)w\,^3P$ | $47 + 31(^4P)^3P + 16(^2P)^3P$ | 0 | 37 090.65 | 37 076 | 14 | | — |
| | | $45 + 32(^4P)^3P + 15(^2P)^3P$ | 1 | 37 173.03 | 37 163 | 10 | 1.53 | 1.508 |
| | | $46 + 35(^4P)^3P + 14(^2P)^3P$ | 2 | 37 325.48 | 37 319 | 6 | 1.48 | 1.503 |
| | $(^4P)y\,^5S$ | 93 | 2 | 37 359.13 | 37 340 | 19 | 1.99 | 1.999 |
| | $(^2G)v\,^3G$ | $78 + 10^1G(^3P)^3G + 7(^4F)^3G$ | 3 | 37 554.99 | 37 658 | −103 | 0.77 | 0.769 |
| | | $80 + 9^1G(^3P)^3G + 7(^4F)^3G$ | 4 | 37 617.93 | 37 748 | −130 | 1.05 | 1.075 |
| | | $81 + 8^1G(^3P)^3G + 8(^4F)^3G$ | 5 | 37 690.37 | 37 750 | −60 | 1.20 | 1.198 |
| $3d^24s(b^2G)4px\,^1F$ | $(^2D)x\,^1F^*$ | $46 + 22^1G(^1P)^1F + 15^1D(^1P)^1F$ | 3 | 37 622.63 | 37 611 | 12 | 0.94 | 0.989 |
| | $(A^2D)u\,^3F$ | $51 + 28(^2G)^3F + 11(^2D)^3F^*$ | 2 | 37 654.77 | 37 752 | −98 | 0.65 | 0.667 |
| | | $47 + 27(^2G)^3F + 12(^2D)^3F^*$ | 3 | 37 743.96 | 37 807 | −63 | 1.08 | 1.078 |
| | | $45 + 28(^2G)^3F + 14(^2D)^3F^*$ | 4 | 37 852.47 | 37 872 | −20 | 1.24 | 1.231 |
| $3d^24s(b^2P)4pu\,^3D$ | $^3P(^1P)u\,^3D$ | $47 + 26(^2P)^3D + 17(^4P)^3D$ | 1 | 37 851.91 | 37 906 | −54 | 0.53 | 0.516 |
| | | $46 + 24(^2P)^3D + 16(^4P)^3D$ | 2 | 37 976.78 | 37 963 | 14 | 1.14 | 1.162 |
| | | $48 + 23(^2P)^3D + 18(^4P)^3D$ | 3 | 38 159.71 | 38 064 | 95 | 1.35 | 1.331 |
| | $(^2D)^1D^*$ | $41 + 28(^2P)^1D + 24(A^2D)^1D$ | 2 | | 37 989 | | | 1.006 |
| | $(^2P)z\,^1S$ | $81 + 16^3P(^3P)^1S$ | 0 | 38 200.94 | 38 331 | −131 | | — |
| | $(^2G)^1G$ | $57 + 27(^2H)^1G + 13^1G(^1P)^1G$ | 4 | | 38 223 | | | 1.001 |
| | $(^2H)z\,^3I$ | 100 | 5 | 38 572.75 | 38 528 | 45 | 0.81 | .834 |
| | | 100 | 6 | 38 669.03 | 38 623 | 46 | 1.02 | 1.024 |
| | | 100 | 7 | 38 779.97 | 38 734 | 46 | 1.15 | 1.143 |
| $3d^3(b^2D)^4pt\,^3D$ | $(^2P)t\,^3D$ | $45 + 24(^2D)^3D^* + 18(^4P)^3D$ | 1 | 38 654.23 | 38 793 | −139 | 0.54 | 0.522 |
| | | $47 + 22(^2D)^3D^* + 17(^4P)^3D$ | 2 | 38 699.95 | 38 831 | −131 | | 1.167 |
| | | $45 + 26(^2D)^3D^* + 18(^4P)^3D$ | 3 | 38 764.96 | 38 918 | −153 | 1.32 | 1.328 |
| | $(A^2D)x\,^1P$ | $74 + 14(^2P)^1P$ | 1 | 39 078.00 | 39 205 | −127 | | 0.981 |
| | $(^2H)x\,^3H$ | 93 | 4 | 39 115.99 | 39 119 | −3 | 0.88 | 0.804 |
| | | $84 + 13^1G(^3P)^3H$ | 5 | 39 152.14 | 39 162 | −10 | 1.02 | 1.035 |
| | | $85 + 10^1G(^3P)^3H$ | 6 | 39 198.39 | 39 210 | −12 | 1.18 | 1.167 |
| | $(^2G)^3F$ | $59 + 27(A^2D)^3F + 10^3F(^1P)^3F$ | 2 | | 39 512 | | | 0.675 |
| | | $58 + 26(A^2D)^3F + 10^3F(^1P)^3F$ | 3 | | 39 578 | | | 1.086 |
| | | $58 + 29(A^2D)^3F + 9^3F(^1P)^3F$ | 4 | | 39 657 | | | 1.250 |
| $3d^3(a^4P)4ps\,^3D$ | $(A^2D)s\,^3D$ | $62 + 17(^2P)^3D + 12^3P(^1P)^3D$ | 1 | 39 662.15 | 39 757 | −95 | 0.52 | 0.506 |
| | | $63 + 16(^2P)^3D + 13^3P(^1P)^3D$ | 2 | 39 686.10 | 39 840 | −154 | | 1.168 |
| | | $62 + 18(^2P)^3D + 11^3P(^1P)^3D$ | 3 | 39 715.51 | 39 873 | −158 | 1.31 | 1.327 |
| | $(A^2D)w\,^1F$ | $84 + 8^1D(^1P)^1F$ | 3 | 40 303.04 | 40 232 | 71 | 1.05 | 1.008 |
| | $(^2H)z\,^1I$ | 100 | 6 | 40 319.80 | 40 359 | −39 | 1.03 | 1.000 |
| $3d^3(a^4P)4Pv\,^3P$ | $(^2P)v\,^3P^*$ | $46 + 27^3P(^1P)^3P + 16(^4P)^3P$ | 0 | 40 369.76 | 40 152 | 217 | | — |
| | | $45 + 28^3P(^1P)^3P + 14(^4P)^3P$ | 1 | 40 384.58 | 40 187 | 198 | | 1.496 |
| | | $46 + 27^3P(^1P)^3P + 13(^4P)^3P$ | 2 | 40 467.04 | 40 245 | 222 | | 1.495 |
| | $(^2P)x\,^3S$ | $62 + 15(^2D)^3P^* + 12^3P(^1P)^3P$ | 1 | 40 844.19 | 40 671 | 173 | | 1.998 |
| | $(^2H)y\,^1H$ | 100 | 5 | 41 039.93 | 41 238 | −198 | 1.03 | 1.000 |

Can. J. Chem. Downloaded from www.nrcresearchpress.com by 210.87.254.105 on 09/06/12
For personal use only.

TABLE 2. (*concluded*)

| Designation | | | | Level | | | $g$ | |
|---|---|---|---|---|---|---|---|---|
| Experimental | Theoretical | Percentage | $J$ | Obsd | Calcd | O − C | Obsd | Calcd |
| $s^3F$ | $(^2D)s^3F^*$ | $61 + 21(A^2D)^3F + 7^1G(^3P)^3F$ | 2 | 41 337.43 | 41 407 | −70 | 0.66 | 0.668 |
| | | $64 + 18(A^2D)^3F + 8^1G(^3P)^3F$ | 3 | 41 457.62 | 41 597 | −139 | 1.09 | 1.146 |
| | | $63 + 15(A^2D)^3F + 10^1G(^3P)^3F$ | 4 | 41 624.13 | 41 775 | −151 | 1.24 | 1.250 |
| $3d^3(a^2P)4pv^3D$ | $(^4P)r^3D$ | $52 + 27(A^2D)^3D$ | 1 | | 41 479 | | | 0.501 |
| | | $51 + 28(A^2D)^3D$ | 2 | | 41 529 | | | 1.113 |
| | | $53 + 29(A^2D)^3D$ | 3 | | 41 597 | | | 1.265 |
| | $(^2G)v^1F$ | $48 + 29^1D(^1P)^1F + 11(^2D)^1F^*$ | 3 | 41 585.24 | 41 708 | −122 | | 1.008 |
| | $(^2P)u^3P$ | $42 + 32(A^2D)^3P + 10^3P(^1P)^3P$ | 0 | 41 959.46 | 41 875 | 85 | | — |
| | | $44 + 31(A^2D)^3P + 9^3P(^1P)^3P$ | 1 | 41 943.95 | 41 857 | 87 | | 1.497 |
| | | $41 + 28(A^2D)^3P + 12^3P(^1P)^3P$ | 2 | 41 928.57 | 41 826 | 103 | | 1.498 |
| | $(^2H)^3G$ | $88 + 7^3F(^1P)^3G$ | 3 | | 42 829 | | | 0.752 |
| | | $89 + 8^3F(^1P)^3G$ | 4 | | 42 841 | | | 1.051 |
| | | $90 + 7^3F(^1P)^3G$ | 5 | | 42 862 | | | 1.498 |
| | $(^2D)^3D^*$ | $42 + 24^3P(^1P)^3D + 14(^2F)^3D$ | 1 | | 43 127 | | | 0.510 |
| | | $40 + 19^3P(^1P)^3D + 18(^2F)^3D$ | 2 | | 43 153 | | | 1.163 |
| | | $49 + 21(^2F)^3D + 16^3P(^1P)^3D$ | 3 | | 43 311 | | | 1.332 |
| | $(^2H)v^1G$ | $51 + 22(^2F)^1G + 19^1G(^1P)^1G$ | 4 | 43 674.31 | 43 767 | −92 | 0.95 | 1.001 |
| | $(A^2D)u^1D$ | $45 + 26^1D(^1P)^1D + 18(^2F)^1D$ | 2 | 43 799.57 | 43 501 | 299 | 0.98 | 1.002 |
| | $(^2P)^1D$ | $41 + 19(^2D)^1D^* + 18(^2D)^3D^*$ | 2 | | 44 623 | | | 1.001 |
| | $(^2P)^1P$ | $43 + 28(^2D)^1P + 15^3P(^3P)^1P$ | 1 | | 45 154 | | | 1.024 |
| | $(^4P)^3S$ | $59 + 28^3P(^1P)^3S$ | 1 | | 46 175 | | | 1.976 |
| | $(^2D)^1P^*$ | $56 + 20^1D(^1P)^1P + 15(^2P)^1P$ | 1 | | 46 189 | | | 1.024 |
| | $^1G(^1P)^1H$ | $73 + 20(^2H)^1H$ | 5 | | 46 386 | | | 1.000 |
| | $(^2F)p^3F$ | 94 | 2 | 47 187.55 | 47 005 | 183 | | 0.668 |
| | | $83 + 11(^2F)^3G$ | 3 | 47 281.90 | 47 099 | 183 | | 1.078 |
| | | $84 + 12(^2F)^3G$ | 4 | 47 463.06 | 47 301 | 162 | | 1.243 |
| | $(^2F)s^3G$ | $86 + 10(^2F)^3F$ | 3 | 46 725.42 | 46 805 | −80 | | 0.756 |
| | | $85 + 11(^2F)^3F$ | 4 | 46 838.09 | 46 936 | −92 | | 1.054 |
| | | 97 | 5 | 46 974.65 | 47 059 | −84 | | 1.203 |
| | $^3P(^1P)^3P$ | $49 + 32(^2D)^3P^*$ | 0 | | 48 747 | | | — |
| | | $46 + 35(^2D)^3P^*$ | 1 | | 48 796 | | | 1.496 |
| | | $52 + 30(^2D)^3P^*$ | 2 | | 48 876 | | | 1.502 |
| | $(^2F)^1F$ | $53 + 24(^2D)^1F^* + 12^1G(^1P)^1F$ | 3 | | 49 223 | | | 1.003 |
| | $^1S(^3P)^3P$ | 91 | 0 | | 49 259 | | | — |
| | | $71 + 23(^2F)^3D$ | 1 | | 49 309 | | | 1.253 |
| | | $72 + 24(^2F)^3D$ | 2 | | 49 428 | | | 1.410 |
| | $(^2F)^1D$ | $66 + 16(A^2D)^1D + 9^1D(^1P)^1D$ | 2 | | 49 520 | | | 1.008 |
| | $(^2F)^1G$ | $62 + 19^1G(^1P)^1G + 18(^2H)^1G$ | 4 | | 49 793 | | | 1.001 |
| | $(^2F)^3D$ | $74 + 19^3P(^1P)^3D$ | 1 | | 50 302 | | | 0.502 |
| | | $61 + 24^1S(^3P)^3P + 9^3P(^1P)^3D$ | 2 | | 50 276 | | | 1.263 |
| | | $78 + 9^3P(^1P)^3D$ | 3 | | 50 236 | | | 1.334 |
| | $^1G(^1P)^1F$ | $51 + 32(^2F)^1F + 12(^2D)^1F^*$ | 3 | | 54 432 | | | 1.000 |
| | $(B^2D)^3D$ | $85 + 7^1S(^3P)^3P$ | 1 | | 56 357 | | | 0.542 |
| | | $84 + 9(B^2D)^3F$ | 2 | | 56 526 | | | 1.112 |
| | | $79 + 15(B^2D)^3F$ | 3 | | 56 528 | | | 1.286 |
| | $(B^2D)^3F$ | $84 + 9(B^2D)^3D$ | 2 | | 56 548 | | | 0.713 |
| | | $80 + 12(B^2D)^3D$ | 3 | | 56 574 | | | 1.103 |
| | | 96 | 4 | | 56 587 | | | 1.250 |
| | $(B^2D)^1P$ | $55 + 37^1S(^1P)^1P$ | 1 | | 56 710 | | | 0.998 |
| | $(B^2D)^1D$ | $89 + 8(^2F)^1D$ | 2 | | 57 419 | | | 1.000 |
| | $(B^2D)^3P$ | 94 | 0 | | 58 324 | | | — |
| | | 93 | 1 | | 58 287 | | | 1.498 |
| | | 94 | 2 | | 58 210 | | | 1.499 |
| | $(B^2D)^1F$ | 97 | 3 | | 58 530 | | | 1.000 |
| | $^1S(^1P)^1P$ | $52 + 42(B^2D)^1P$ | 1 | | 66 315 | | | 1.000 |

Can. J. Chem. Downloaded from www.nrcresearchpress.com by 210.87.254.105 on 09/06/12
For personal use only.

Can. J. Chem. Downloaded from www.nrcresearchpress.com by 210.87.254.105 on 09/06/12
For personal use only.

The columns "Obsd $g$" and "Calcd $g$" give the experimental and calculated $g$-factors respectively.

Below 44000 $cm^{-1}$ there are 76 experimental terms splitting into 185 levels in AEL. The following 13 terms, which split into 27 levels, were rejected in the final least-squares:

| | | | | |
|---|---|---|---|---|
| 1. | $3d^24s(b^2P)4p$ | $y^3S$ | at | 35439.43 $cm^{-1}$ |
| 2. | $3d^3(a^2G)4p$ | $t^3F_{C.G.}$ | at | 38576.37 $cm^{-1}$ |
| 3. | $3d^3(a^2G)4p$ | $x^1G$ | at | 38959.53 $cm^{-1}$ |
| 4. | $3d^3(a^2P)4p$ | $w^1D$ | at | 39265.80 $cm^{-1}$ |
| 5. | $3d^3(a^2P)4p$ | $r^3D_{C.G.}$ | at | 40728.70 $cm^{-1}$ |
| 6. | | $w^1G$ | at | 40883.30 $cm^{-1}$ |
| 7. | $3d^3(a^2H)4p$ | $u^3G_{C.G.}$ | at | 41397.82 $cm^{-1}$ |
| 8. | | $w^3H_{C.G.}$ | at | 41903.49 $cm^{-1}$ |
| 9. | | $q^3D_{C.G.}$ | at | 42243.52 $cm^{-1}$ |
| 10. | | $p^3D_{C.G.}$ | at | 42304.49 $cm^{-1}$ |
| 11. | $3d^24s(a^2S)4p$ | $w^1P$ | at | 42927.55 $cm^{-1}$ |
| 12. | | $r^3F_{C.G.}$ | at | 43624.79 $cm^{-1}$ |
| 13. | | $v^1D$ | at | 43710.28 $cm^{-1}$ |

From Table 2, the calculated value of the term $^3P(^1P)y^3S$ is 33984 $cm^{-1}$. Thus, if the experimental term $y^3S$ were inserted into the least-squares the deviation would be around 1500 $cm^{-1}$. As this deviation is about 13 times the mean error, and furthermore, since the term $y^3S$ has only combinations with the terms $a^3P$ and $b^3P$ (16), it was excluded.

The terms $3d^3(a^2G)4pt^3F$, $3d^3(a^2G)4px^1G$, $3d^3(a^2P)4pw^1D$, and $3d^3(a^2P)4pr^3D$ were excluded as the deviations would be exceedingly large (800–1000 $cm^{-1}$). It is felt that most of this effect is due to the interactions with the configurations $(3d + 4s)^35p$.

Russell does not attribute to $w^1G$ any definite configuration designation, and furthermore, he mentions that "this term depends on only three faint lines and may not even be real". This conclusion is verified by our results, since to all the calculated levels in the vicinity of $w^1G$ there correspond other experimental levels.

From the combinations found by Russell for the levels of $u^3G$, it is apparent that it is a valid term. However, if assigned to the theoretical term $(^2H)^3G$, the deviation would be around $-1500$ $cm^{-1}$. As this deviation is considerably higher than for the other terms, and since the experimental term $u^3G$ is high enough in order to conceivably belong to $(3d + 4s)^35p$, it was excluded.

As the three theoretically predicted terms $^3H$ of $(3d + 4s)^34p$ correspond to $z^3H$, $y^3H$, and $x^3H$, the term $w^3H$ is superfluous. Russell suggested that the term $w^3H$ may be assigned to configurations containing a $5p$ electron. However, in the configurations $(3d + 4s)^34p$, the term $3d^24s(b^2G)4pz^3H_{C.G.}$ at 31930 $cm^{-1}$ is higher by 13330 $cm^{-1}$ than the term $3d^24s(a^4F)4pz^5D_{C.G.}$ at 18600 $cm^{-1}$. Thus $w^3H$ cannot be assigned to $3d^24s(b^2G)5pw^3H$, since the experimental term $3d^24s(a^4F)5pv^5D$ is higher than $w^3H$ (16). Thus the levels of $w^3H$ probably belong to $3d^24s(a^4F)5px^5G$.

If either the term $q^3D_{C.G.}$ at 42243.52 $cm^{-1}$ or the term $p^3D_{C.G.}$ at 42304.49 $cm^{-1}$ were fitted to the only possible calculated term in that vicinity, $3d4s^24p^3D$, the deviations would be around $-1000$ $cm^{-1}$. Hence one of these two terms belongs to the configurations $(3d + 4s)^35p$, and the other is strongly affected by it. Thus both were excluded. Similar conclusions hold for the terms $3d^24s(a^2S)4pw^1P$, $r^3F$, and $v^1D$, as well as for most other terms above 44000 $cm^{-1}$. However, the six levels of $s^3G$ and $p^3F$ in the 47000 $cm^{-1}$ range have very low deviations.

In the configuration $(3d + 4s)^34p$, the lowest six terms are $[d^{2,3}F + (sp)^3P]^{3,5}D, F, G$. It is conceivable that the terms $u^3G$, $w^3H$, $v^5D$, $p^3D$, $r^3F$, and $t^3G$ belong to the lowest terms of $(3d + 4s)^35p$, with the following assignments: $(^3F + {}^3P)$: $z^3D(p^3D)$, $z^3F(r^3F)$, $z^3G(t^3G)$, $z^5D(v^5D)$, $z^5F(u^3G)$, $z^5G(w^3H)$.

In parentheses are the corresponding terms with a $4p$ electron. The term $p^3D$ was chosen over $r^3D$, according to a suggestion already made by Russell (17).

From Table 2 it is evident that the purity of many levels is low. In many cases, the mixing involves eigenfunctions of levels of both configurations $3d^34p$ and $3d^24s4p$, and in some instances even all three configurations.

The lowest calculated levels with no corresponding experimental levels are the levels $^3P(^3P)^1S$ and $^1D(^3P)^3P_0$ at 25356 $cm^{-1}$ and 25593 $cm^{-1}$, respectively.

There was excellent agreement between the experimental and calculated Lande $g$-factors. Hesse (20) has obtained the $g$-factors of the levels of $x^3F$, to four-figure accuracy. These values correspond closely to the calculated values.

All 212 calculated energy levels and $g$-factors are given in Table 2.

**Acknowledgment**

The author would like to thank the Natural Sciences and Engineering Research Council Canada for partial support of this work by Grant No. A3888.

1. R. F. Bacher and S. Goudsmit. Phys. Rev. **46**, 948 (1934).
2. R. E. Trees. Phys. Rev. **83**, 756 (1951).
3. R. E. Trees. Phys. Rev. **84**, 1089 (1951).
4. G. Racah. Phys. Rev. **85**, 381 (1952).
5. G. Racah. Phys. Rev. **63**, 367 (1943).

6. K. RAJNAK and B. G. WYBOURNE. Phys. Rev. **132**, 280 (1963).
7. F. ROHRLICH. Phys. Rev. **74**, 1381 (1948).
8. C. ROTH. J. Res. Natl. Bur. Std. (U.S.); **73*A***, 497 (1969).
9. G. SMITH, and J. SIDDALL. J. Opt. Soc. Am. **59**, 419 (1969).
10. G. RACAH. Phys. Rev. **62**, 438 (1942).
11. E. U. CONDON and G. H. SHORTLEY. The theory of atomic spectra, Cambridge University Press. 1963.
12. N. ROSENZWEIG. Phys. Rev. **88**, 580 (1952).
13. C. ROTH. J. Res. Natl. Bur. Std. (U.S.) Vol. 86, No. 1, 33 (1981).
14. C. ROTH. J. Math. Phys. **9**, 686 (1968).
15. C. ROTH. J. Math. Phys. **10**, 1038 (1969).
16. C. E. MOORE. Atomic Energy Levels, NBS Circ. 467 I (1949), denoted by AEL.
17. H. N. RUSSELL. Astrophys. J. **66**, 347 (1927).
18. C. M. WILSON and M. P. THEKAEKARA. J. Opt. Soc. Am. **51**, 289 (1961).
19. H. W. BANKS, W. R. BOZMAN, and C. M. WILSON. Analysis of the first spectrum of titanium. Georgetown College Observatory Monograph No. 20. 1966.
20. A. HESSE. Z. Naturforsch. A, **27**(2), 188 (1972).

Can. J. Chem. Downloaded from www.nrcresearchpress.com by 210.87.254.105 on 09/06/12
For personal use only.

# The relation of physical properties of alkanes to connectivity indices: a molecular explanation

JOHN T. EDWARD

*Department of Chemistry, McGill University, 801 Sherbrooke St. West, Montreal, P.Q., Canada H3A 2K6*

Received July 30, 1981

JOHN T. EDWARD. Can. J. Chem. **60**, 480 (1982).

Additive schemes for calculating the molar volumes and heats of vaporization of liquid alkanes from increments characteristic of the numbers and different types of carbon atoms (primary, secondary, tertiary, quaternary), of the mole fraction $Z_g$ of *gauche* conformations, and (where necessary) of other steric factors have been developed. It is suggested that schemes for correlating physical properties of alkanes with connectivity indices $^m\chi_t$ are successful because these indices are also correlated with numbers and types of carbon atoms and with $Z_g$.

JOHN T. EDWARD. Can. J. Chem. **60**, 480 (1982).

On a développé des schémas additifs pour calculer les volumes et les chaleurs de vaporisation molaires des alcanes liquides à partir d'incréments caractéristiques de la quantité et des types d'atomes de carbone (primaire, secondaire, tertiaire, quaternaire), de la fraction molaire des conformations gauches, $Z_g$, et (lorsque c'est nécessaire) d'autres facteurs stériques. On pense que les schémas de corrélation des propriétés physiques des alcanes avec les indices de connectivité $^m\chi_t$ sont utiles parce qu'ils permettent aussi d'établir une corrélation avec la quantité et les types d'atomes de carbone et avec $Z_g$.

[Traduit par le journal]

Can. J. Chem. Downloaded from www.nrcresearchpress.com by 210.87.254.40 on 09/06/12
For personal use only.

It has long been recognized that many physical properties of alkanes such as boiling point correlate roughly with the number $n$ of carbon atoms in the molecule. However, the boiling points of isomeric alkanes having the same $n$ differ, and obviously the branching or connectivity of the carbon network must also be taken into account. In fact, it was found by Randić (1) that the boiling point and other physical properties correlate well with a "branching index", which later became the first-order "connectivity index" $^1\chi$ (2). $^1\chi$ is dependent on both $n$ *and* the extent of branching of the molecule.

Better correlations are generally obtained using additional connectivity indices $^m\chi_t$ (3). A full treatment of the calculation and uses of $^m\chi_t$ is given in a book by Kier and Hall (2); here we can give only a brief discussion. To calculate any $^m\chi_t$ we consider the organic molecule (in the present case an alkane) as a graph with the $n$ carbon atoms as vertices and $m(= n - 1)$ bonds as edges (hydrogen atoms are suppressed). The graphs of ethane **1**, propane **2**, butane **3**, and isobutane **4** are shown in Scheme 1, with the valence (≡ number of skeletal bonds) δ of each vertex indicated on the graph. A graph may be made up of subgraphs of various types $t$ (path P, cluster C, path/cluster PC, chain (cycle) CH). Each connectivity index $^m\chi_t$ is evaluated as the sum of terms over all the possible subgraphs of $m$ edges. The subgraphs for $^0\chi$ consist of the vertices only (no edges), and $^0\chi$ is defined by

$$[1] \quad {}^0\chi = \sum_{i=1}^{n} \delta^{-1/2}$$

Values of $^0\chi$ for the alkanes **1**, **2**, **3**, and **4** are shown in Scheme 1. The subgraphs for $^1\chi$ consist of the individual edges, terminating in vertices of valence $\delta_i$ and $\delta_j$, and $^1\chi$ is defined by

$$[2] \quad {}^1\chi = \sum_{i=1}^{m} (\delta_i \delta_j)^{-1/2}$$

Values of $^1\chi$ for **1**, **2**, **3**, and **4** are also shown in Scheme 1.

Higher-order connectivity indices are obtained by summing up contributions from higher-order subgraphs. With $m \geq 3$, a differentiation of subgraphs into types P, C, and CH becomes possible (**3** is made up of paths *abc* and *bcd*, and **4** of *abc*, *abd*, and *dbc* having $m = 2$, whence $^2\chi_P$ may be calculated for these isomers; *abcd* of **4** represents the simplest possible cluster). For our present purposes it suffices that $^m\chi_t$ indices encode information about branching, so that generally isomers of identical $n$ have at least some $^m\chi_t$ different (compare $n$, $^0\chi$, and $^1\chi$, for **3** and **4** in Scheme 1).

Among the physical properties of organic compounds correlated with $^m\chi_t$ by Kier, Hall, and their associates (2) are heats of atomization, molar refractions, molar polarizabilities, diamagnetic susceptibilities, heats of vaporization, boiling points, liquid densities, water solubilities, and partition coefficients; among biological properties are anesthetic potencies, nonspecific narcotic activities, inhibition of various enzymes, vapour toxicities, toxicities against the red spider, and antimicrobial activities. Thus for a set of 46 alkanes for which

0008-4042/82/040480-06$01.00/0

©1982 National Research Council of Canada/Conseil national de recherches du Canada

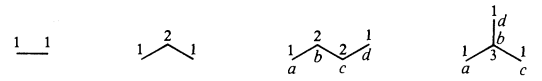

| | 1 | 2 | 3 | 4 |
|---|---|---|---|---|
| $n$ | 2 | 3 | 4 | 4 |
| $^0\chi$ | 2.000 | 2.707 | 3.414 | 3.577 |
| $^1\chi$ | 1.000 | 1.414 | 1.914 | 1.732 |

SCHEME 1

data were considered to be of the highest quality, the liquid density $d$ in g mL$^{-1}$ at 20°C was given by

$$[3]\quad d = 0.7955 - 0.4288/^1\chi + 0.0131^3\chi_P - 0.0079^5\chi_P + 0.0051^4\chi_{PC} + 0.0035^5\chi_{PC}$$

(correlation coefficient $r = 0.9971$, standard deviation $s = 0.0024$) and for a set of 44 alkanes the heat of vaporization $\Delta H_{vap}$ in kcal mol$^{-1}$ was given by

$$[4]\quad \Delta H_{vap} = 0.567 + 1.752^1\chi + 1.301^2\chi - 0.415^4\chi_P - 0.437^5\chi_P - 0.266^6\chi_P - 2.091^3\chi_C + 3.051^4\chi_C$$

($r = 0.9999$, $s = 0.042$).

Regarding the last equation, Kier and Hall write: "We consider this to be a remarkable achievement ... It would be desirable to analyse each coefficient and $^m\chi_t$ variable in terms of intermolecular forces". A start in this direction is made in the present paper, in which it is shown that the densities and heats of vaporization of the alkanes considered by Kier and Hall may be calculated by simple additive schemes *if the molar concentrations of* gauche *conformations* $Z_g$ (4, 5) *are taken into account.*

## An additive scheme for calculating molar volumes of alkanes

We shall calculate, not densities, but what is equivalent, molar volumes $V(\equiv M/d$, $M$ being the molecular weight) of the neat alkanes at 20°C, since a scheme making use of $Z_g$ has proven successful in calculating the partial molal volumes $\bar{V}°$ of alkanes in carbon tetrachloride (4). The corresponding equation for $V$, expanded to take account of several steric factors besides $Z_g$, is

$$[5]\quad V = V_c + \sum_1^m n^k I^k + \sum_1^r m^p S^p$$

where $V_c$ is a constant term (the "co-volume"), $I$ is the volume increment for the groups $CH_3$, $CH_2$, CH, and quaternary[1] C into which the alkane may be dissected, $n$ is the number of such groups, $S$ is a steric term for certain especially crowded groupings, and $m$ is the number of such groupings in the molecule.

The most pervasive steric effect comes from the contraction in volume ($S^1$ in Table 1) associated with the presence of one gauche conformation ($Z_g = 1$) in 1 mol of alkane. Most of the values of $Z_g$ given in Table 2 have been reported already (4–7); others were calculated by standard methods (4, 5). In applying [5], $Z_g$ becomes $m^1$. In calculations of $\bar{V}°$ (4), the other steric terms $S^2$, $S^3$, and $S^4$ (7) were not needed because highly branched hydrocarbons were not examined. Now they become necessary for some of the compounds in Table 2, and are then indicated in the table.

A least-squares fitting of the experimental data in Table 2 to [5] yields a $V_c$ of 17.375 mL mol$^{-1}$ and values of $I$ and $S$ given in Table 1. The steric terms are all associated with a diminution in volume, and all involve arrangements in which the van der Waals surfaces of parts of the molecules would be compressed if the conformations of the carbon network were maintained in ideal diamond-lattice conformations. However, it is probable that little compression of the van der Waals surfaces takes place, and that instead the torsional angles of the carbon network depart from ideal values (8); the reduction in volume most probably comes from a congestion of atoms in certain parts of the molecule, and is discussed further below.

The agreement between most experimental and calculated values of $V$ in Table 2 is highly satisfactory, in view of the simplicity of the model; the particular cases for which agreement is less satisfactory are considered later.

## Molecular basis of effect of structure on V

The volume $V$ occupied by 1 mol of liquid hydrocarbon is made up partly of the van der Waals volumes of the molecules, and partly of empty volumes between them (9). Models of alkane molecules show that hydrogen atoms completely envelope the carbon skeleton (9), and so in any additive scheme it is reasonable to assign a constant volume to the carbon atom (3.40 mL mol$^{-1}$ (4)), and variable volumes to the hydrogen atoms to include the variable empty volumes associated

TABLE 1. Parameters (in mL mol$^{-1}$) for calculation of molar volume $V$ by [5]

| Group | $I$ | Steric effect | $S$ |
|---|---|---|---|
| $-CH_3$ | 24.803 | g ($S^1$) | −2.055 |
| $=CH_2$ | 16.526 | $g^+g^-$ or $g^-g^+$ ($S^2$) | −0.878 |
| $\equiv CH$ | 9.671 | 2,2,3-$Me_3$ ($S^3$) | −1.286 |
| | | 2,2,3,3-$Me_4$ ($S^4$) | −3.565 |

[1]For reasons already discussed (4), $I$ for quaternary carbon is given the value of 3.40 mL mol$^{-1}$.

Can. J. Chem. Downloaded from www.nrcresearchpress.com by 210.87.254.40 on 09/06/12
For personal use only.

TABLE 2. Calculated and experimental molar volumes $V$ (in mL mol$^{-1}$) and heats of vaporization $\Delta H_{vap}$ (in kcal mol$^{-1}$)

| Case number | Compound | $Z_g$ | $V$ | | $\Delta H_{vap}$ | |
|---|---|---|---|---|---|---|
| | | | Calcd | Exptl[a] | Calcd | Exptl[a] |
| 1 | $C_2$ | 0 | — | — | 2.677 | 2.264 |
| 2 | $C_3$ | 0 | — | — | 3.867 | 3.965 |
| 3 | $C_4$ | 0.36 | — | — | 5.069 | 5.191 |
| 4 | 2-Me$C_3$ | 0 | — | — | 4.694 | 4.799 |
| 5 | $C_5$ | 0.66 | 115.20 | 115.21 | 6.270 | 6.395 |
| 6 | 2-Me$C_4$ | 1.13 | 115.66 | 116.43 | 5.924 | 6.030 |
| 7 | 2,2-$Me_2C_3$ | 0 | — | — | 5.355 | 5.345 |
| 8 | $C_6$ | 0.96 | 131.11 | 130.70 | 7.470 | 7.555 |
| 9 | 2-Me$C_5$ | 1.31 | 131.81 | 131.94 | 7.120 | 7.160 |
| 10 | 3-Me$C_5$ | 2.29 | 129.80 | 129.73 | 7.155 | 7.255 |
| 11 | 2,2-$Me_2C_4$ | 2.00 | 132.40 | 132.75 | 6.615 | 6.651 |
| 12 | 2,3-$Me_2C_4$ | 2.64 | 130.50 | 130.25 | 6.805 | 6.985 |
| 13 | $C_7$ | 1.25 | 147.04 | 146.55 | 8.670 | 8.739 |
| 14 | 2-Me$C_6$ | 1.64 | 147.66 | 147.67 | 8.321 | 8.325 |
| 15 | 3-Me$C_6$ | 2.47 | 145.96 | 145.83 | 8.351 | 8.391 |
| 16 | 3-Et$C_5$ | 3.58 | 143.67 | 143.53 | 8.390 | 8.425 |
| 17 | 2,2-$Me_2C_5$ | 2.00 | 148.93 | 148.71 | 7.805 | 7.764 |
| 18 | 2,3-$Me_2C_5$ | 3.55 | 145.16 | 144.16 | 8.027 | 8.191 |
| 19 | 2,4-$Me_2C_5$ | 2.00 | 148.34 | 148.96 | 7.972 | 7.872 |
| 20 | 3,3-$Me_2C_5$ | 4.00 | 144.82 | 144.54 | 7.876 | 7.901 |
| 21 | 2,2,3-$Me_3C_4(S_3)$ | 4.00 | 144.95 | 145.20 | 7.604 | 7.669 |
| 22 | $C_8$ | 1.54 | 162.97 | 162.60 | 9.870 | 9.915 |
| 23 | 2-Me$C_7$ | 1.93 | 163.59 | 163.67 | 9.521 | 9.484 |
| 24 | 3-Me$C_7$ | 2.79 | 161.82 | 161.84 | 9.552 | 9.521 |
| 25 | 4-Me$C_7$ | 2.65 | 162.11 | 162.11 | 9.547 | 9.483 |
| 26 | 3-Et$C_6$ | 3.75 | 159.85 | 160.08 | 9.586 | 9.476 |
| 27 | 2,2-$Me_2C_6$ | 2.38 | 164.67 | 164.29 | 9.008 | 8.915 |
| 28 | 2,3-$Me_2C_6$ | 4.30 | 160.14 | 160.40 | 9.243 | 9.272 |
| 29 | 2,4-$Me_2C_6$ | 3.23 | 162.34 | 163.10 | 9.205 | 9.029 |
| 30 | 2,5-$Me_2C_6$ | 2.34 | 164.17 | 164.71 | 9.173 | 9.051 |
| 31 | 3,3-$Me_2C_6$ | 4.00 | — | — | 9.066 | 8.973 |
| 32 | 3,4-$Me_2C_6$ | 4.69 | 159.34 | 158.82 | 9.257 | 9.316 |
| 33 | 2-Me-3-Et$C_5$ | 5.00 | 158.70 | 158.80 | 9.268 | 9.209 |
| 34 | 3-Me-3-Et$C_5$ | 6.00 | 157.23 | 157.03 | 9.137 | 9.081 |
| 35 | 2,2,3-$Me_3C_5(S_3)$ | 5.00 | 159.42 | 159.53 | 8.829 | 8.826 |
| 36 | 2,2,4-$Me_3C_5(S_2)$ | 3.00 | 163.94 | 165.09 | 8.660 | 8.402 |
| 37 | 2,3,3-$Me_3C_5(S_3)$ | 6.00 | 157.37 | 157.30 | 8.865 | 8.897 |
| 38 | 2,3,4-$Me_3C_5$ | 5.00 | 160.12 | 158.86 | 8.906 | 9.014 |
| 39 | 2,2,3,3-$Me_4C_4(S_4)$ | 6.00 | — | — | 8.510 | 8.410 |
| 40 | $C_9$ | 1.84 | 178.88 | 178.73 | 11.070 | 11.101 |
| 41 | 4-Me$C_8$ | 2.92 | 178.08 | 178.16 | — | — |
| 42 | 2,2-$Me_2C_7$ | 2.66 | 180.62 | 180.52 | — | — |
| 43 | 3,3-Et$C_5$ | 8.00 | 169.65 | 170.20 | — | — |
| 44 | 2,2,3-$Me_3C_6(S_3)$ | 5.34 | 175.25 | 175.89 | 9.940 | 9.871 |
| 45 | 2,2,4-$Me_3C_6(S_2)$ | 4.29 | 177.82 | 179.23 | 9.902 | 9.478 |
| 46 | 2,2,5-$Me_3C_6$ | 2.72 | 181.92 | 181.36 | 9.845 | 9.580 |
| 47 | 2,3,3-$Me_3C_6(S_3)$ | 6.00 | 173.89 | 173.79 | — | — |
| 48 | 2,3,5-$Me_3C_6$ | 4.48 | 177.72 | 177.67 | 10.075 | 9.910 |
| 49 | 2,4,4-$Me_3C_6(S_2)$ | 5.00 | 176.36 | 177.20 | — | — |
| 50 | 2,2,3,3-$Me_4C_5(S_4)$ | 8.00 | 169.51 | 169.51 | 9.771 | 9.871 |
| 51 | 2,2,3,4-$Me_4C_5(S_2 + S_3)$ | 6.00 | 174.44 | 173.57 | 9.684 | 9.478 |
| 52 | 2,2,4,4-$Me_4C_5(2S_2)$ | 4.00 | 179.54 | 178.27 | 9.348 | 9.580 |
| 53 | 2,3,3,4-$Me_4C_5(2S_3)$ | 8.00 | 169.92 | 169.94 | 9.854 | 9.910 |
| 54 | $C_{10}$ | 2.13 | — | — | 12.270 | 12.276 |
| 55 | $C_{12}$ | 2.72 | — | — | 14.670 | 14.650 |
| 56 | $C_{16}$ | 3.89 | — | — | 19.470 | 19.450 |

[a]From ref. 2.

Can. J. Chem. Downloaded from www.nrcresearchpress.com by 210.87.254.40 on 09/06/12
For personal use only.

Can. J. Chem. Downloaded from www.nrcresearchpress.com by 210.87.254.40 on 09/06/12
For personal use only.

with them. On this basis, the increment for the single hydrogen atom depends on the type of carbon to which it is attached, being 7.13 mL mol$^{-1}$ for $CH_3$ (p) hydrogen, 6.56 mL mol$^{-1}$ for $CH_2$ (s) hydrogen, and 6.27 mL mol$^{-1}$ for CH (t) hydrogen.

If we regard the van der Waals volume of the hydrogen atom as being relatively constant, at about 3.43 mL mol$^{-1}$ (9), then the diminishing empty volume associated with hydrogen atoms in the order p > s > t may be explained by the increasing intermolecular attraction in the order p < s < t, so that another molecule X has a greater tendency to remain in the neighbourhood of methine hydrogen, for example (and thereby reduce the empty volume), than in the neighbourhood of methyl hydrogen. This can be understood by a consideration of **5**, **6**, and **7** in Scheme 2. The attraction of X to the portion of the molecular surface covered by methyl hydrogen atoms will be determined by the other atoms shown in **5**; because the energy of attraction falls off as the sixth power of the distance, other atoms of the molecule will be too distant to have any influence. Since carbon is more polarizable than hydrogen, attraction should increase in the order **5** < **6** < **7**, as carbon replaces hydrogen in the sphere in which interatomic attractive forces are appreciable. When considering $\bar{V}^\circ$ of a hydrocarbon in a solvent such as carbon tetrachloride (4), X is $CCl_4$; when considering $V$ of the neat hydrocarbon, X is a portion of a contiguous hydrocarbon molecule.

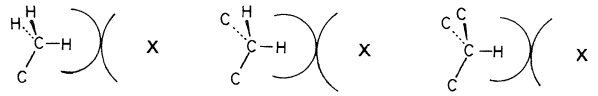

5 6 7

SCHEME 2

### An additive scheme for calculating $\Delta H_{vap}$

Like the molar volume $V$, the enthalpy of vaporization $\Delta H_{vap}$ of alkanes must also depend on the strength of the attractive forces holding the molecules together in the liquid. According to the picture above, this varies over the molecular surface, according to whether the surface is covered by methyl, methylene, or methine hydrogen atoms. It seems likely that the same steric factors $S^1$, $S^2$, $S^3$, and $S^4$ which increase density will also increase molecular attraction, so that the enthalpy of vaporization should be given by the equation

$$[6] \quad \Delta H_{vap} = \sum n^k H^k + \sum m^l S^l$$

where $n$ is the number of hydrogen atoms of a particular type (p, s, or t) and $H$ is the enthalpy increment associated with this type of atom. A least-squares fitting of the experimental data of Table 2 to [6] yields the parameters of Table 3, and using these parameters the calculated values of $\Delta H_{vap}$ in Table 2 are obtained. These agree with the experimental values fairly well (though less well than values calculated from [4]). The steric effects are all positive, as expected, except for $S^2$, which is essentially negligible.

### Failures of the additivity schemes

The degree of success of [5] and [6] is remarkable in view of the naiveté of the model adopted. Thus, if we examine the scale drawing in Fig. 1, we can see that while A and B are not too dissimilar to **5** and **6** (respectively) of Scheme 2, D and E are quite dissimilar, and that more atoms than those shown in **5**, **6**, and **7** are involved in attracting X to the hydrocarbon molecule. This would also be true as the steric effects $S^1$, $S^3$, and $S^4$ crowd atoms of the alkane together, and would explain why these effects are negative for $V$ and positive for $\Delta H_{vap}$. However, with the increased accumulation of branches on the chain, the molecule becomes stiffer, and one can imagine that shape effects, which could only be recognized by a study of individual molecules in their preferred conformations, might become important. Such shape effects could result in some molecules packing together in the liquid more snugly than usual,[2] and so having both $V$ smaller and $\Delta H_{vap}$ greater than expected (i.e. having $\Delta V = V_{exptl} - V_{calcd}$ negative and $\Delta\Delta H_{vap} = \Delta H_{vap(exptl)} - \Delta H_{vap(calcd)}$ positive), and other molecules of awkward shape packing together less well than usual, and having $\Delta V$ positive and $\Delta\Delta H_{vap}$ negative. In Fig. 2 $\Delta\Delta H_{vap}$ is plotted against $\Delta V$ for the fourteen worst cases in Table 2 (Nos. 10, 12, 18, 19, 26, 29, 30, 36, 38, 44, 45, 50, 51, 52), which have $\Delta H_{vap}$ differing by more than 0.1 kcal mol$^{-1}$, or $V$ by more than 0.6 mL mol$^{-1}$ from calculated values. The points do indeed cluster about a line of negative slope, as required by the simple-minded considerations above; the scatter of points is considerable, but is to be expected, since both $\Delta V$ and $\Delta\Delta H_{vap}$ are small differences between large numbers, and the effect of experimental error is magnified.

[2]The evidence in this paper does not support the idea that *n*-alkanes above *n*-octane pack together in the liquid in such a way as to favour the all-extended conformation, with a consequent reduction of $Z_g$ from the value noted in the spherical solvent, carbon tetrachloride.

TABLE 3. Parameters (in kcal mol$^{-1}$) for calculation of heat of vaporization $\Delta H_{vap}$ by [6]

| Type of H atom | $H$ | Steric effect | $S$ |
|---|---|---|---|
| —$CH_3$ (p) | 0.446 | g ($S^1$) | 0.036 |
| =$CH_2$ (s) | 0.595 | $g^+g^-$ or $g^-g^+$ ($S^2$) | −0.008 |
| ≡CH (t) | 0.678 | 2,2,3-$Me_3$ ($S^3$) | 0.090 |
| | | 2,2,3,3-$Me_3$ ($S^4$) | 0.264 |

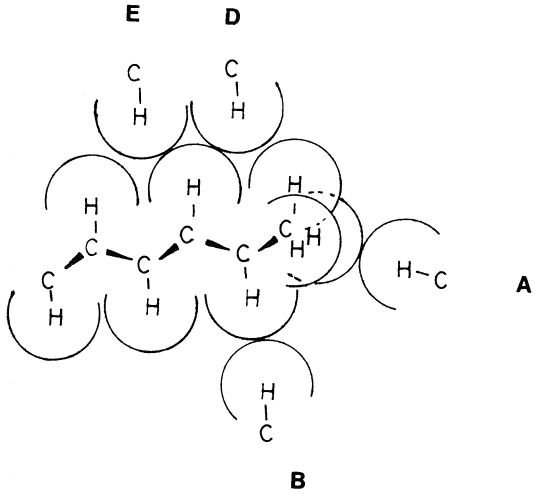


FIG. 1. Scale drawing showing different types of contacts possible between molecules in a liquid alkane.

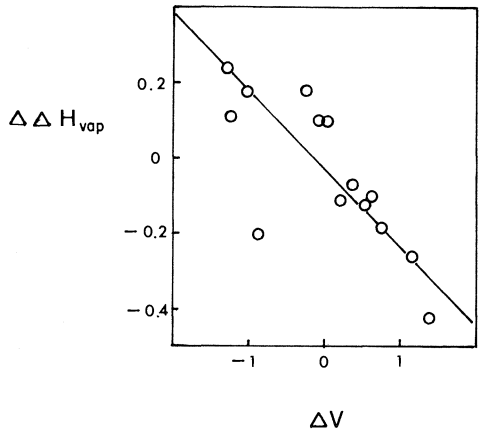


FIG. 2. Relation of $\Delta\Delta H_{vap}$ (in kcal mol$^{-1}$) to $\Delta V$ (in mL mol$^{-1}$).

## Relation of explanations based on molecular additivity to those based on connectivity

We now attempt to relate the empirical equations [3] and [4] based on connectivity to those ([5] and [6]) based on simple additivity schemes.

We may first note that $^0\chi$ is correlated to $n$ with $r = 0.991$; $^1\chi$ to $n$ with $r = 0.978$, and higher order connectivity indices to $n$ with continually decreasing $r$ (ref. 2, p. 250). In fact[3] we can write

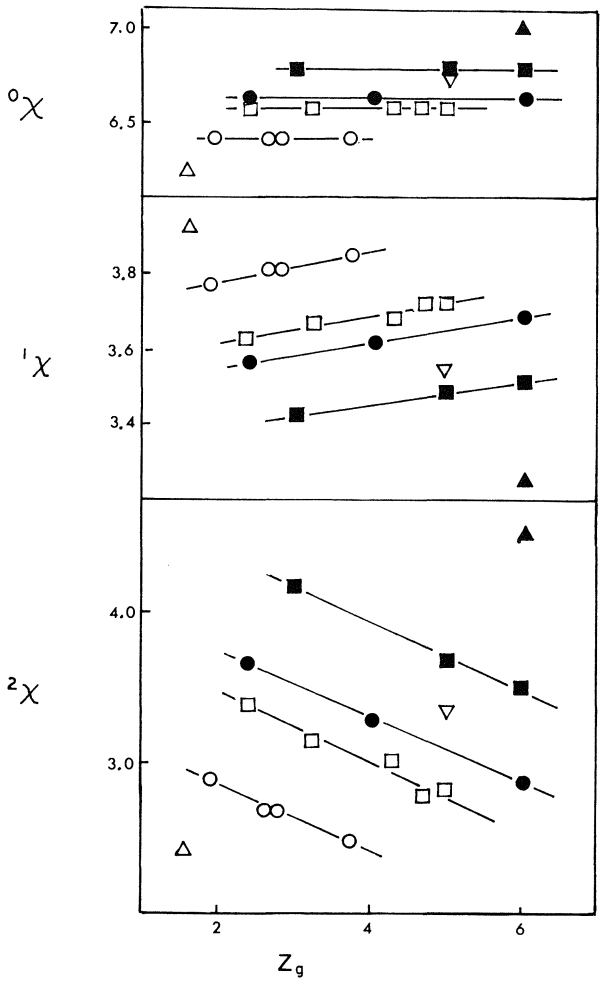


FIG. 3. Variation of $^m\chi$ of isomeric octanes with $Z_g$. Numbers of different types of carbon atoms ($n_p, n_s, n_t, n_q$) are as follows: △: 2,6,0,0 ($C_8$); ○: 3,4,1,0 (2-$MeC_7$, 3-$MeC_7$, 4-$MeC_7$, 3-$EtC_6$); □: 4,2,2,0 (2,3-$Me_2C_6$, 2,4-$Me_2C_6$, 2,5-$Me_2C_6$, 3,4-$Me_2C_6$, 2-Me-3-$EtC_5$); ●: 4,3,0,1 (2,2-$Me_2C_6$, 3,3-$Me_2C_6$, 3-Me-3-$EtC_5$); ▽: 5,0,3,0 (2,3,4-$Me_3C_5$); ■: 5,1,1,1 (2,2,3-$Me_3C_5$, 2,2,4-$Me_3C_5$, 2,3,3-$Me_3C_5$); ▲: 6,0,0,2 (2,2,3,3-$Me_4C_4$).

[7] $$n = n_p + n_s + n_t + n_q$$

[8] $$^0\chi = n_p + \frac{n_s}{\sqrt{2}} + \frac{n_t}{\sqrt{3}} + \frac{n_q}{\sqrt{4}}$$
$$= n_p + 0.707n_s + 0.578n_t + 0.500n_q$$

and for straight chain alkanes (which contain only p and s carbon atoms) having $n \geq 4$

[9] $$^1\chi = 0.457n_p + 0.500n_s$$

[3]Equations [8] and [9] have been obtained by simple inspection of tables of $^m\chi_t$ values (ref. 2, p. 240); doubtless they can be derived by appropriate manipulation of [1] and [2].

Can. J. Chem. Downloaded from www.nrcresearchpress.com by 210.87.254.40 on 09/06/12
For personal use only.

Consequently, the different $\chi$ values give different weights to the contributions of $CH_3$, $CH_2$, CH, or quaternary carbon atoms, a feature also found in the additive schemes of [5] and [6]. Furthermore, when we consider isomers having the same $n_p$, $n_s$, $n_t$, and $n_q$, $^1\chi$ and $^2\chi$ are roughly linear with $Z_g$, as illustrated for the isomeric octanes in Fig. 2 *B* and *C*. Figure 2*A* shows that $^0\chi$ is independent of $Z_g$, and depends only on $n_p$, $n_s$, $n_t$, and $n_q$, as required by [8].

We can accordingly see that the various $^m\chi_t$ terms encode information, in varying proportions, about *both* the nature and number of carbon atoms in the alkanes *and* the degree of folding of the molecule ($Z_g$). This answers in part the problem raised by Kier and Hall (ref. 2, p. 221): "The difficulty encountered in considering molecular connectivity is that there is not yet a developed intuition as to what familiar structural characteristics are described by $^1\chi$, $^2\chi^v$, $^5\chi_p{}^v$, etc." It might prove profitable to examine the other physical properties of alkanes which correlate with various mixtures of $^m\chi_t$ to see whether they too can be accommodated by simple additive schemes making use of $n_p$, $n_s$, $n_t$, $n_q$, and $Z_g$.

**Acknowledgments**

The financial support of the Natural Sciences and Engineering Research Council of Canada is gratefully acknowledged. I am grateful also to Dr. S. C. Wong, who performed the least-squares fitting of [5] and [6] to the experimental data, and to referees for helpful comments.

1. M. RANDIĆ. J. Am. Chem. Soc. **97**, 6609 (1975).
2. L. B. KIER and L. H. HALL. Molecular connectivity in chemistry and drug research. Academic Press, New York. 1976.
3. L. B. KIER, W. J. MURRAY, M. RANDIĆ, and L. B. HALL. J. Pharm. Sci. **65**, 1226 (1976).
4. J. T. EDWARD, P. G. FARRELL, and F. SHAHIDI. J. Phys. Chem. **82**, 2310 (1978).
5. G. MANN. Tetrahedron, **23**, 3375 (1967).
6. J. T. EDWARD. Can J. Chem. **58**, 1897 (1980).
7. J. T. EDWARD. Can J. Chem. **59**, 3192 (1981).
8. V. PRELOG. Progress in stereochemistry. Vol. 3. *Edited by* P. B. D. de la Mare and W. Klyne. Butterworths, London. 1962. p. 205.
9. J. T. EDWARD. J. Chem. Educ. **47**, 261 (1970).

Can. J. Chem. Downloaded from www.nrcresearchpress.com by 210.87.254.40 on 09/06/12
For personal use only.

# Thermochemistry of ion exchange and particle interaction in clay suspensions

LAURIER L. SCHRAMM[1] AND JAN C. T. KWAK
*Department of Chemistry, Dalhousie University, Halifax, N.S., Canada B3H 4J3*

Received January 7, 1981[2]

LAURIER L. SCHRAMM and JAN C. T. KWAK. Can. J. Chem. **60**, 486 (1982).

The measurement of enthalpies of ion exchange for a number of homovalent and heterovalent exchange pairs by titration calorimetry is described. A self-consistent addition to previous measurements on such systems is reported. In addition to the enthalpies of ion exchange the heats of tactoid formation and breakdown were observed. The apparent heat of tactoid formation for the Na–Ca exchange pair is estimated to be −4.9 kJ per equivalent of ion exchange.

LAURIER L. SCHRAMM et JAN C. T. KWAK. Can. J. Chem. **60**, 486 (1982).

On décrit la mesure des enthalpies d'échanges d'ions d'une série de paires d'échanges homovalent et hétérovalent par titrage calorimétrique. On rapporte une addition auto-cohérente qui complète les mesures antérieures relatives à de tels systèmes. En plus des enthalpies d'échanges d'ions, on a observé les chaleurs de formation et de décomposition tactoide. On a évalué à −4,9 kJ par équivalent d'échanges d'ions la chaleur apparente de formation tactoide pour la paire d'échanges Na–Ca.

[Traduit par le journal]

## Introduction

Thermodynamic quantities provide useful information about interactions in clay suspensions. Although the usefulness of calorimetry in clay research has been demonstrated, relatively few studies have been carried out on the thermochemistry of ion exchange reactions in suspension. One reason for the scarcity of data in this connection is the low heat of reaction that characterizes the ion exchange process. As a result, careful calorimetric techniques are required to adequately determine the enthalpies of exchange.

Homshaw and Chaussidon (1) used calorimetry to study the distribution of water in montmorillonite samples of low water concent and to show the strong effect of water on the arrangement of clay plates. A number of studies have been concerned with measuring heats of immersion in water of clays. For example Keren and Shainberg (2, 3) measured heats of immersion of Na- and Ca-montmorillonite and mixed Na/Ca-montmorillonite. Keren and Shainberg found that the interplate adsorption process is different from that which takes place on external surfaces. These authors separated the heat of immersion into contributions from hydration reactions and from ion mixing and tactoid formation. They concluded that a strongly exothermic condensation of plates to form tactoids is the driving force for the demixing of adsorbed ions.

The more common studies involving calorimetry applied to clays have been concerned with observing ion exchange reactions, usually only to provide data for comparison with the results of the temperature dependence of equilibrium constant or selectivity coefficient measurements. Early measurements were made on H-form clays (4, 5). These experiments raise some uncertainty as to the proper interpretation of results when taking into account the possibility of acid attack of the clay lattice and the accompanying changes in surface composition. Another significant problem with such measurements is that the effect of the large heat of formation of water (H-form clay is titrated with base) makes it difficult to determine accurately the relatively small heat effect of the actual ion exchange reaction. Despite these difficulties, Martin and Laudelout (4) obtained heats of exchange by correcting the measured heat for the heats of formation of water, neutralization of $Al(H_2O)_6^{3+}$ (in aged clay), exchange of $Al^{3+}$ by the titrant cations, dilution of the base and gelation (from changes in aggregation). The values thus obtained are in reasonable agreement with values which they obtained directly by adding the appropriate salt to a clay suspension and correcting for a first small amount of reaction. The values obtained also agree with the results they obtained from the method of common final states in which equivalent amounts of reactants were mixed with clay, first with one ion on the clay and then the other, with a correction for the difference in apparent molal enthalpy of the two salts at their final concentration. The enthalpy change obtained in this fashion and from the previous methods is the value corresponding to the simple reaction:

[1] $B^+ + A\text{-clay} \rightarrow B\text{-Clay} + A^+$

[1]Present address: Syncrude Canada Ltd., Research, P.O. Box 5790, Edmonton, Alta., Canada T6C 4G3.

[2]Revision received October 6, 1981.

0008-4042/82/040486-09$01.00/0

©1982 National Research Council of Canada/Conseil national de recherches du Canada

Can. J. Chem. Downloaded from www.nrcresearchpress.com by 210.87.254.5 on 09/06/12
For personal use only.

TABLE 1. Some enthalpies of ion exchange from the literature*

| | $\Delta H°$ (kJ/equiv) | | | | |
|---|---|---|---|---|---|
| | Martin and Laudelout (4) Camp Berteau montmorillonite | | | Gast *et al.* (6) Wyoming bentonite | Gast (7) Chambers montmorillonite |
| A-clay → B-clay | *1* | *2* | *3* | *4* | *5* |
| Li–Na | 0† | (+1.00±0.29)§ | +0.59‡ | −0.63±0.43‡ | −0.46±0.08‡ |
| Li–$NH_4$ | −6.7 | (+4.22±0.33) | −5.19 | — | — |
| Li–K | −6.7 | (+4.39±0.29) | −5.61 | −2.98±0.17 | −4.84±0.17 |
| Li–Rb | −8.8 | — | −9.00 | — | −7.43±0.11 |
| Li–Cs | −19.2 | — | −15.5 | −10.69±0.41 | −10.34±0.28 |
| Na–$NH_4$ | — | −3.84±0.46 | −3.89 | — | — |
| | — | (+3.51±0.17) | | — | — |
| Na–K | — | −4.06±0.38 | −4.52 | −2.65±0.12 | −4.86±0.27 |
| | — | (+3.56±0.25) | | −2.41±0.05 | |
| Na–Rb | — | −10.88±0.29 | — | — | −8.03±0.41 |
| Na–Cs | — | −16.32±0.33 | — | −10.75±0.57 | −11.08±0.69 |
| | — | | — | −10.64±0.48 | |
| $NH_4$–K | — | −1.46±1.09 | +0.84 | — | — |
| | — | (+0.75±0.46) | | — | — |
| $NH_4$–Rb | — | −5.15±0.21 | −4.60 | — | — |
| $NH_4$–Cs | — | −12.55±0.29 | −9.79 | — | — |
| K–Rb | — | −5.86±0.21 | — | — | −5.06±0.18 |
| K–Cs | — | −11.46±0.54 | — | −8.83±0.22 | −8.57±0.31 |
| | — | | — | −7.54±0.54 | |
| Rb–Cs | — | — | — | — | −4.52±0.18 |

| | $\Delta H°$ (kJ/equiv) | | |
|---|---|---|---|
| | | Maes and Cremers (10, 12) | |
| A-clay → B-clay | Laudelout *et al.* (8) Camp Berteau montmorillonite *6* | Otay montmorillonite *7* | Camp Berteau montmorillonite *8* |
| Na–Ba | +2.85‡ | — | — |
| $NH_4$–Mg | +10.67 | — | — |
| $NH_4$–Ca | +10.46 | — | — |
| $NH_4$–Sr | +8.74 | — | — |
| $NH_4$–Ba | +7.74 | — | — |
| Na–Ca | +5.10 | +1.72¶ | +1.41¶ |

*Parentheses indicate that $\Delta H°$ is for the reverse reaction, as actually measured.
†Determined by neutralization.
‡Determined by the common final state method.
§Determined by exchange in dilute suspension.
¶Determined using a separate determination of the equilibrium state.

The results of Martin and Laudelout for each of these methods are included in Table 1 (columns *1–3*), in which the results of a number of calorimetric studies on comparable montmorillonite samples are listed. Given the difficulties in interpretation inherent in the heat of neutralization method (column *1*), many authors use sensitive microcalorimeters to determine directly the small thermal changes in exchange reactions such as

[2] $Na^+ + Li\text{-clay} \rightarrow Na\text{-clay} + Li^+$

Gast *et al.* (6, 7), Laudelout *et al.* (8), and Van Bladel (9) used the method of common final states with a Calvet microcalorimeter to determine $\Delta H°$ for ion exchange reactions. Their results are summarized in Table 1. In a series of papers Maes *et al.* (10–12) reported enthalpies of ion exchange using an LKB batch microcalorimeter and a method in which a salt was added to a clay suspension and the equilibrium state determined separately. Some of their results are also included in Table 1. These authors also followed the changes in enthalpy of ion exchange on montmorillonite of varying degrees of charge density (prepared using the Hofmann–Klemen effect, ref. 13). The variation in $\Delta H°$ observed with changing charge density was explained on the basis that the enthalpy effects are due to differences in partial dehydration of the counterion.

Can. J. Chem. Downloaded from www.nrcresearchpress.com by 210.87.254.5 on 09/06/12
For personal use only.

Can. J. Chem. Downloaded from www.nrcresearchpress.com by 210.87.254.5 on 09/06/12
For personal use only.

While most of the results cited were measured by a batch technique using very small cells, titration calorimetry has also been applied to the study of clay suspensions (5) and, for example, humic acid solutions (14). Ewin, Erno, and Hepler (15) describe the application of titration calorimetry to the study of clay suspensions. The titration mode has advantages in simplicity of operation, low-cost instrumentation, and efficiency since the equivalent of a large number of batch experiments can be obtained in a single run, at least when considerations of reaction kinetics can be managed appropriately. An added advantage of the method is its potential to yield not only the enthalpy of exchange, but also the exchange selectivity coefficient and the cation exchange capacity of the clay. We have used the method of Ewin, Erno, and Hepler to measure the heat effect of ion-exchange reactions in relatively dilute montmorillonite suspensions, employing the titration calorimeter built and described by these authors (15). In order to obtain more detailed data for one particular exchange reaction, that of Na–Ca exchange, a second, commercial titration calorimeter (the LKB 8700-2, LKB Instruments, Malmo, Sweden) more suited to the measurement of heat evolved during discrete additions of titrant was used. A difficulty arising in the use of these titration calorimeters, and especially with the LKB unit, is the lack of efficient stirring of clay suspensions containing added electrolyte. The use of a flow microcalorimeter (Sodev Inc., Sherbrooke, P.Q.), which might in principle overcome this difficulty, was also investigated. The main advantage of the flow microcalorimeter would be its ability under steady state conditions to continuously detect thermal changes, thus yielding results equivalent to a large number of static measurements and using only very small volumes of suspension. Although we could demonstrate the sensitivity of the flow microcalorimeter in detecting heat effects from ion-exchange reactions in dilute clay suspensions, experimental difficulties besetting the method finally forced us to abandon this technique.

## Experimental

*Materials*

A sample of montmorillonite, API No. 27 (Ward's Natural Science Establishment) from Belle Fourche, South Dakota (Kerr *et al.*, ref. 16), was ground to −270 mesh. Samples (30 g) were converted to the sodium form by washing three times in 500 mL each 1 *M* NaCl. A sample of bentonite (Fisher Scientific), used for several measurements, was used as received and converted to the sodium form in the same fashion. Total equilibration time was in excess of 70 h. Preliminary desalting was accomplished by decanting and diluting until 1 L of stable suspension was obtained. This suspension was allowed to stand until the > 2 μm equivalent spherical diameter fraction had settled out. The final suspension was desalted by an ultrafiltration/dialysis procedure described previously by Schramm and Kwak (17). This suspension before final desalting was about 1.2 w% in clay and 0.05 *M* in NaCl. Briefly, the procedure consists of passing the suspension through porous hollow fibers at a slightly elevated pressure so that dissolved salts are efficiently removed via ultrafiltration and dialysis simultaneously. The same apparatus was used to convert the sodium form clay into other ionic forms (17). In this method no clay compaction of any kind takes place and the suspension concentration remains the same throughout the desalting, conversion, and final desalting steps. The final suspensions were freeze dried for storage.

The clay samples prepared by this method, or any method involving washing with water to remove salts, are subject to hydrolysis. As a result, the clays are not homoionic but from approximately 90% to 100% homoionic (18). This is a necessary disadvantage in working with suspensions at low ionic strengths. It was found that the total charge density of the clay is not affected by our procedures (18).

*Apparatus and methods*

The titration calorimeter used to obtain most of the enthalpy of exchange data has been described in detail by Ewin, Erno, and Hepler (15). Briefly, the reaction vessel is a 250 mL polypropylene beaker fitted with a Teflon lid, and suspended in a stainless steel canister which in turn was submerged in a constant temperature bath. In our experiments, the bath was maintained at 25.00°C. A stirrer, thermistor, heater, and titrant delivery tube are passed through the Teflon lid. The temperature outside the beaker was maintained constant to ±0.001°C. In our experiments a syringe pump delivered titrant at a rate of 1.126 ± 0.002 mL/min through 1.5 mm id Teflon tubing, 90 cm of which was coiled inside the constant temperature bath. Stirring was by a glass, multibladed stirrer. The output from the thermistor bridge was amplified and measured on a Keithley 160 B digital multimeter and on a stripchart recorder.

In each determination 2 g of montmorillonite (M27) in the appropriate ionic form was suspended in 200 mL of distilled water and titrated with a solution of 0.1 *M* in the chloride salt of the cation to be exchanged. Enthalpies of dilution were measured in separate experiments and subtracted from the enthalpies of ion exchange.[3] Titrant is added continuously from point *b* to point *c*. As the titration continues the heat effects observed at each point in time depend upon the enthalpy of ion exchange for the surface exchangeable composition present at that time, the selectivity coefficient and the exchange reaction rate. If we assume instantaneous equilibrium and an enthalpy of ion exchange and selectivity coefficient which are independent of the surface exchangeable composition, both the enthalpy of ion exchange and the selectivity coefficient can be obtained from a thermogram. For strongly favoured reactions a linear thermogram results and the enthalpy of ion exchange alone is determined.

Temperature data were taken at intervals along the curve *b*–*c* illustrated in Fig. 1. The raw data were then corrected, point by point, for the heat of dilution of the salt (and any associated instrumental heat effects) and for any change in stirring (background) slopes (shown as regions *a*–*b* and *c*–*d*). In the calculations for each run at least 20 points were taken from the region *b*–*c*. Typically, these titrations correspond to adding about 1 mmol of titrant to 2 mequiv of titrate (clay suspension). The heat gained or lost was calculated using the heat capacity of the suspension as measured before and after each run. For the

[3]Most of the enthalpies of dilution used in this study were measured by Dr. G. J. Ewin at the University of Lethbridge.

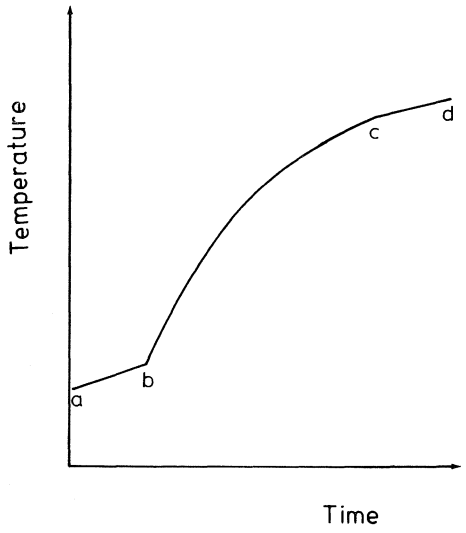


FIG. 1. Illustration of the shape of a typical thermogram as obtained from the continuous calorimeter (arbitrary units).

ion exchange reaction, $\Delta H°$ was assumed to be independent of the surface exchangeable composition. In using a molal selectivity coefficient it is not necessary to choose a special standard state (such as the homoionic solid in contact with an infinitely dilute solution of the corresponding salt). Rather, we take clay plus its counterions as an electrolyte and choose the hypothetical electrolyte solution of unit activity as the standard state. In order to calculate $\Delta H°$ and $K$ values for each thermogram, an initial guess at the value of $K$ is made, the corresponding equilibrium concentrations of competing species calculated, and from the measured heat $\Delta H°$ values for each point on the thermogram are obtained. By refining our choice of $K$ values in an iterative procedure a $K$ value which yields the most nearly constant value for $\Delta H°$ throughout the exchange reaction is obtained. For nearly linear thermograms the exchange reaction can be assumed to proceed to completion and $\Delta H°$ was calculated directly from the number of equivalents of titrant added. The entire group of calculations was carried out using a computer program written by Ewin. A further discussion of the instrumentation and data analysis of this type of calorimetry has been given elsewhere (19).

For additional Na-clay + $CaCl_2$ exchange experiments, use was made of the LKB model 8700-2 precision calorimetry system fitted for titration calorimetry with a Metrohm–Herisau motor buret.[4] This well known instrument has a 100 mL glass reaction cell immersed in a thermostat. In our experiments the temperature was maintained at 25.00°C. The configuration and principle of operation of the instrument are essentially the same as for the calorimeter described above, except that for the LKB the thermistor bridge is balanced manually after each addition of titrant. Stirring in the reaction cell was achieved by means of a small rotating gold clamp normally used to hold glass ampoules (for batch calorimetry). Stirring proved to be the limiting factor for the amounts of clay and salt solution which could be used in this instrument. The stirrer used could not disperse the thixotropic gel formed when sufficient $CaCl_2$ is added to a 2% suspension of Na-montmorillonite.

In each determination 2 g of Na-montmorillonite (M27) suspended in a total volume of 90.0 mL was placed in the cell and titrated stepwise with up to 10.0 mL 0.1 $M$ $CaCl_2$. After each titrant addition, time was allowed to ensure complete equilibration. Heat capacities were measured before and after each titration, but due to experimental difficulties associated with insufficient stirring, only the former was used in the calculations. Each titration took about 7 h to complete. The heat of dilution of $CaCl_2$ and other heat contributions were determined separately.

[4]This calorimeter was also made available to us by Dr. L. G. Hepler of the University of Lethbridge.

## Results and discussion

A summary of the measured enthalpies of ion exchange (reaction [1]) obtained from continuous titrations (Ewin, Erno, Hepler calorimeter) is given in Table 2. We do not report the selectivity coefficients of the exchange reactions because of the fairly large relative uncertainties associated with these quantities in the case of uni-univalent exchanges. However, the uncertainties in the enthalpy of exchange determinations are large enough to cover completely the influence of the relative error in the $K$ values observed. Uncertainties as reported for $\Delta H°$ partly stem from this source of error. That the data are self-consistent can be seen from Fig. 2. Additivities for all the reactions hold within the sum of the uncertainties reported. Referring to Table 1, it is clear that the values obtained for the ion exchange reactions fall within the range of literature values obtained for ion exchange on similar montmorillonite samples. From Tables 1 and 2 it can be seen that the enthalpies of ion exchange are very small, the largest values being observed for the endothermic ion exchanges of monovalent cations by divalent cations. For the heterovalent ion exchange reactions there are several reported values for enthalpies of exchange calculated from the temperature dependence of $\Delta G°$ (e.g. refs. 20, 21) but as might be inferred from Table 1 there are few direct experimental $\Delta H°$ data available. The value obtained here for the K–Ca exchange, +8.4 ± 0.3 kJ/equiv is in good agreement with the value of

TABLE 2. Enthalpies of ion exchange measured by titration calorimetry

| A-clay → B-clay | $\Delta H°$ (kJ/equiv) | Number of titrations |
|---|---|---|
| Li–Na | +0.8±1.7 | 2 |
| Li–K | −8.4±1.3 | 2 |
| Li–Cs | −15.9±1.3 | 3 |
| Na–K | −5.9±0.8 | 5 |
| Na–Cs | −14.3±2.1 | 3 |
| K–Cs | −10.0±1.3 | 3 |
| $NH_4$–Cs | −16.7±2.1 | 2 |
| Na–Ca | +1.65±0.54 | 3 |
| K–Ca* | +8.4±1.3 | 3 |
| Cs–Ca* | +13.4±1.3 | 2 |

*Reverse of reaction actually measured.

Can. J. Chem. Downloaded from www.nrcresearchpress.com by 210.87.254.5 on 09/06/12
For personal use only.

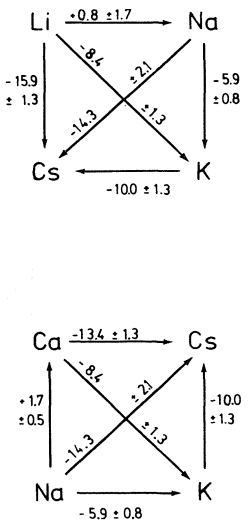


FIG. 2. Additivity diagrams for the measured enthalpies of ion exchange (kJ/equiv) on montmorillonite (M27). The arrows indicate the direction of reaction actually measured.

+8.1 kJ/equiv calculated by Hutcheon (20). The value obtained for the Na–Ca exchange, +1.7 ± 0.5 kJ/equiv is close to those measured by Maes and Cremers (10) for two montmorillonites: +1.72 and +1.4 kJ/equiv. Other values have been calculated or observed for this reaction, however. Tymochowicz (21) calculated 4.8321 kJ/equiv and Laudelout *et al.* (8) measured 5.10 kJ/equiv. This latter value agrees with that which can be inferred from these authors' other values in Table 1, column *1*, i.e. 5.6 kJ/equiv. Ewin *et al.* (15), using the same instrument and methods as in the present work, found a value of +1.7 ± 0.4 kJ/equiv in agreement with the present work and that of Maes and Cremers. Ewin *et al.* (15) observed values of −5.3 ± 0.4 and −18.4 ± 0.8 kJ/equiv for the Na–K and Na–Cs exchanges respectively. These values again are in good agreement with those of the present work, and somewhat more exothermic than the literature values tend to be.

A comparison of all the data presented indicates that while the homovalent exchange reactions are fairly well described, there is some variability in the data reported for heterovalent exchanges. Maes and Cremers (10) note that for heterovalent exchange reactions there seems to be some "partial and apparent irreversibility ... which seems to be restricted to the bivalent-rich end of the composition scale." In view of our earlier observations (22) concerning particle size changes in the same surface exchangeable composition range, it is worth examining in this context the features of some of the actual thermograms obtained.

In a separate paper (22) we describe the variations in the numbers of clay plates per aggregate (tactoid) as a function of surface ionic composition. It is observed that there are fairly narrow regions of surface ionic fraction over which these tactoids form or break down. Figure 3 shows the variation in tactoid size for the Na–Ca exchange pair, as determined from light scattering measurements, in terms of the relative number of plates per tactoid, $N$ ($N$ is relative to the Li-form having $N = 1$). A somewhat similar curve is observed for the Na–Cs exchange reaction (22). If we interpret the sharp rise in $N$ below Na equivalent fractions of 0.2 as a region of tactoid formation, we might expect this tactoid formation to influence the measured exchange enthalpies. The thermograms obtained for the homovalent exchanges are all fairly regularly shaped curves giving no indication of any additional enthalpy changes at any point, even in systems where considerable tactoid size changes are known to occur. As an example, Fig. 4 shows a typical curve, in this case for the Na–Cs exchange reaction. Considering the amount of $Cs^+$ added, the region of tactoid formation which occurs during this particular exchange reaction (22) is contained in this figure but no region of altered slope appears; hence any associated enthalpy effects are apparently too small to affect the curve. One other reaction

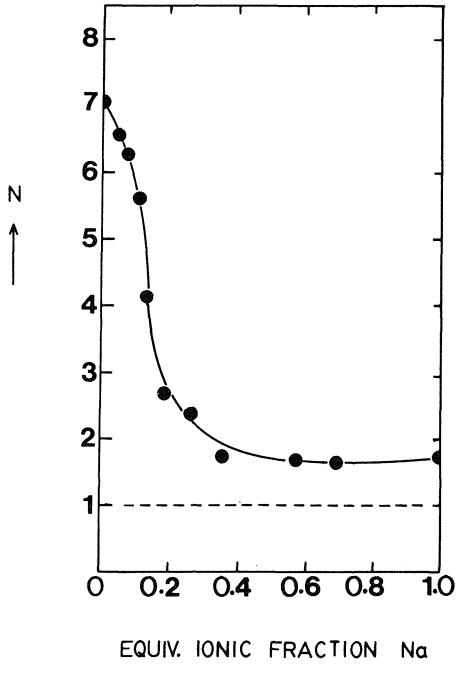


FIG. 3. Graph of relative plate numbers per tactoid versus surface ionic fraction of ions for exchange of Na with Ca on montmorillonite.

Can. J. Chem. Downloaded from www.nrcresearchpress.com by 210.87.254.5 on 09/06/12
For personal use only.

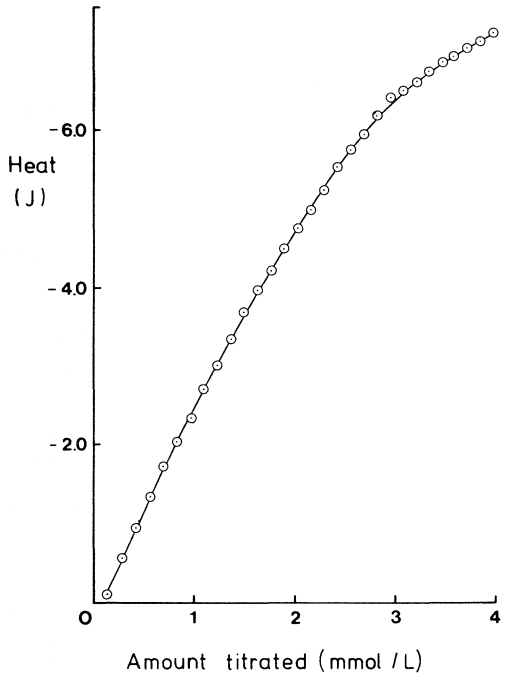


FIG. 4. Thermogram (continuous titration) obtained for the Na–Cs exchange reaction on 1.98 g of Na-montmorillonite (M27). The vertical axis shows the measured heat corrected for the heat of dilution of the titrant CsCl. The horizontal axis gives the amount of CsCl added.

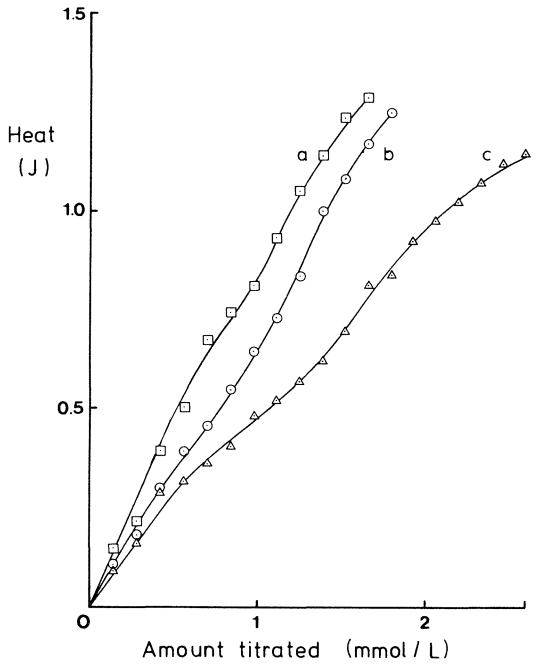


FIG. 5. Thermograms obtained for the Na–Ca exchange on (*a*) 2.12, (*b*) 0.95, and (*c*) 2.11 g of Na-montmorillonite (M27). The vertical axis gives the measured heat corrected for the heat of dilution of the titrant $CaCl_2$. The horizontal axis gives the amount of $CaCl_2$ added.

studied which should include the effect of tactoid formation is the Na–Ca exchange. The thermograms obtained for this case are given in Fig. 5. Since the value of $K$ for the Na–Ca exchange is fairly large, the thermogram curves should be nearly linear and in any case of regularly decreasing slope. It is clear that for each curve there is a region of distinctly altered slope, in each case covering a region corresponding to the same surface composition. It is evident that were these regions of altered slope not present the curves would indeed have the expected shape. For each titration an exothermic change in slope occurred at $\bar{X}_{Ca} = 0.15 \pm 0.03$ (equivalent fraction) and the original slope was regained at $\bar{X}_{Ca} = 0.4 \pm 0.1$. On the other hand, Fig. 3 indicates that under equilibrium conditions tactoids form over the region $\bar{X}_{Ca} = 0.5$–$0.7$. Our present results point to an initial formation of tactoids in regions of high *local* $Ca^{2+}$ concentrations caused by inadequate stirring. These tactoids then may not disperse quickly enough during the rest of the titration. The aggregation indicated by the enthalpy change does continue to the point where it *is* favoured at equilibrium. As has been reported by Shainberg and Kaiserman (23), tactoid formation is very fast, while tactoid breakdown can take place in the order of minutes: enough time to cause the observed effects. The heat effect causing the shift in the curves shown in Fig. 4 can be estimated by extrapolating the "regular" portions of the curve below $\bar{X}_{Ca} = 0.15$ and above $\bar{X}_{Ca} = 0.4$. Using this method we can estimate both (*a*) the overall $\Delta H°$ which would result were the observed irregularity in the thermograms not present, and (*b*) a "$\Delta H$ of tactoid formation". The average $\Delta H°$ of ion exchange would then be about +1.9 kJ/equiv compared to 1.7 kJ/equiv from Table 2. This is in fact within the estimated uncertainty of the earlier value. The "heat of tactoid formation" from curve (*c*) in Fig. 5 is in the order of −0.5 kJ/equiv of ion exchange over the range of ion exchange in which it was observed. If the tactoid formation was due to high local concentrations of titrant, then the units become meaningless and we can conclude only that the reaction to form tactoids is exothermic and of the order of a kJ or so per equivalent of exchange reaction. The exothermic nature of tactoid formation is expected and will be discussed later.

In the exchange of $Ca^{2+}$ by $K^+$ illustrated in Fig. 6, a change in slope over a narrow region of surface coverage is again observed. In this case the change in slope is endothermic and is interpreted to be the result of tactoid breakdown as $K^+$ ions penetrate

Can. J. Chem. Downloaded from www.nrcresearchpress.com by 210.87.254.5 on 09/06/12
For personal use only.

Can. J. Chem. Downloaded from www.nrcresearchpress.com by 210.87.254.5 on 09/06/12
For personal use only.

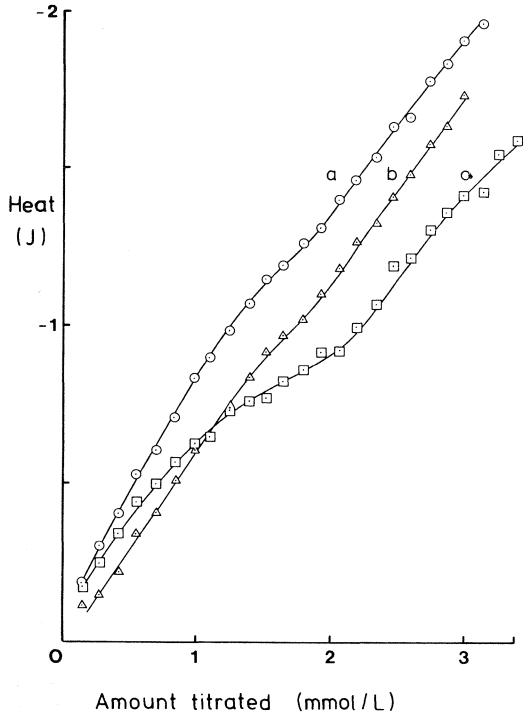


FIG. 6. Thermograms obtained for the Ca–K exchange on (*a*) 1.52, (*b*) 1.99, and (*c*) 2.89 g of Ca-montmorillonite (M27). The vertical axis gives the measured heat corrected for the heat of dilution of the KCl.

the tactoids. Using the value of selectivity coefficient which was fitted to the overall Ca–K thermogram ($K_{Ca/K} = 5 \times 10^{-2}$), and the surface equivalent fraction value required for tactoid breakup predicted from previous work (22), the total KCl concentration for breakup should be 0.001 *M* for curve (*c*) in Fig. 6, as observed. Similarly, significant enthalpy effects due to tactoid breakdown should disappear in the concentration range 0.002–0.003 *M* for curve (*c*), again, as observed.

While the observed enthalpies of tactoid formation and breakdown are not of sufficient magnitude to invalidate the enthalpy data for ion exchange presented here, they may contribute a significant error to measurements made using more sensitive methods or calorimeters (e.g. the Calvet or LKB batch microcalorimeters).

*Stepwise titrations*

Based on the results presented so far, in which apparent heats of tactoid formation and breakdown were observed but could not be quantified, it was of interest to determine whether allowing more time for equilibration would produce the same results, or results in closer agreement with expectations, based on a consideration of tactoid formation. While such measurements could in principle be made with the continuous calorimeter, the LKB calorimeter was considered to be more convenient for this purpose. As an example, Fig. 7 shows a thermogram obtained from a series of steps in the titration of $CaCl_2$ into a Na-montmorillonite (M27) suspension. Resistance values were converted to temperatures directly without correction for heats of leakage, stirring etc., except to the extent that they are the same for the reaction and dilution experiments. Comparison of the values thus obtained with those calculated by the Regnault–Pfaundler method (24) indicated that this was sufficient.

It can be seen from Fig. 7 that at a certain point (ca. $\bar{X}_{Ca} = 0.7$) the endothermic heat of exchange has diminished somewhat, and that by $\bar{X}_{Ca} \approx 0.9$ a definite exothermic apparent heat of exchange is observed. If the enthalpy of exchange as determined from the first addition of titrant is subtracted from each of the apparent enthalpies of exchange at each step in the titration, then (having corrected for the heat of dilution) an approximate heat of tactoid

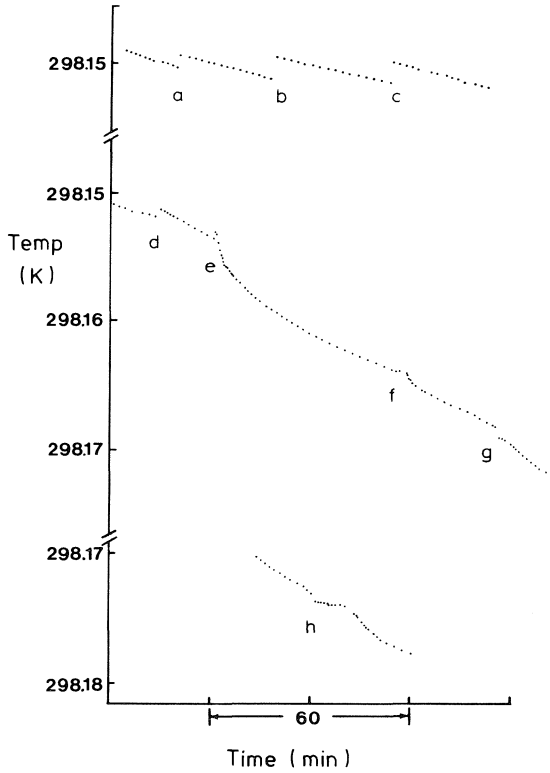


FIG. 7. Thermogram obtained from an LKB calorimeter titration of Na-montmorillonite with $CaCl_2$. In this case temperature is plotted versus time. Additions of titrant are 1 mL at points *a*, *d*–*h* and 2 mL at points *b* and *c*. Note changes in scale, the three segments are all from the same thermogram.

Can. J. Chem. Downloaded from www.nrcresearchpress.com by 210.87.254.5 on 09/06/12
For personal use only.

formation per equivalent of ion exchange is obtained. This quantity, averaged over two separate titrations, is plotted in Fig. 8 as a function of surface ionic fraction sodium, assuming $K$ is large. This curve has the same features as Fig. 3 and shows that under conditions where equilibrium can be attained, the heat effect associated with tactoid formation apparently is indeed observed, and at about the same surface fractions as are other tactoid related properties. The enthalpies for Na–Ca exchange are:

$$\Delta H^\circ_{\text{exchange}} = +1.9 \pm 0.2 \text{ kJ/equiv}$$

$$\Delta H^\circ_{\text{tactoid formation}} = -4.9 \text{ kJ/equiv of ion exchange}$$

The enthalpy of ion exchange is in good agreement with the value obtained using the continuous calorimeter (+1.7 kJ/equiv, see above) and with the results of Ewin *et al.* (15) and Maes and Cremers (10). The apparent heat of tactoid formation is expressed per equivalent of ion exchange reaction for the region of ion exchange in which it is observed. The exothermic character of the reaction is in agreement with the previous results as will be discussed.

*On tactoid formation*

The results presented so far have demonstrated that tactoid formation and breakdown is accompanied by significant heat changes. The reaction to form tactoids is exothermic and for the Na–Ca reaction a value of −4.9 kJ/equiv of ion exchange was determined. So far as the authors are aware the only previous observations of such heat effects have been made by Keren and Shainberg (3) and Goulding and Talibudeen (25). In measuring heats of immersion of montmorillonite, Keren and Shainberg (3) noticed a difference between the heat of immersion for a "chemical" mixture of Na/Ca montmorillonite and for a "physical" mixture. They proposed that the difference gives a heat of mixing of Na and Ca on the montmorillonite surfaces and measured −5.8 kJ/equiv for the formation of the mixed surface composition. Keren and Shainberg apparently observed the same effect as in the present work and the two values agree quite well considering the uncertainty involved in estimating them. In fact, it will not be easy to separate the heat of demixing of the ions on the surfaces from the heat of tactoid formation, since the reactions are intimately connected. However, in physical terms, since the demixing ions are already adsorbed, it seems reasonable to expect that the observed heat is largely due to the tactoid formation itself. Goulding and Talibudeen interpreted the heat effect as arising from a separate homogeneous group of exchange sites within the mineral.

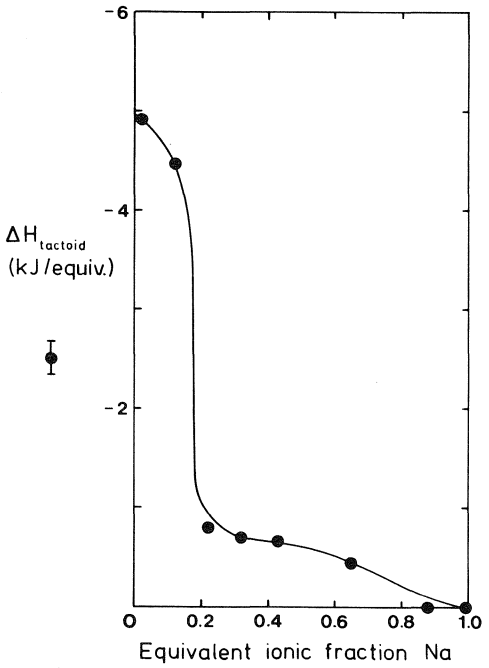


FIG. 8. Plot of observed heat of tactoid formation as a function of surface coverage for the Na–Ca exchange. The units of $\Delta H_{\text{tactoid}}$ are kJ/equiv of ion exchange reaction. An estimate of the experimental reproducibility is given along the axis.

That the reaction should be exothermic follows from the facts that the free energy is lower for plates in tactoids and that the $\Delta S$ term for the reaction will be negative. As concluded by Keren and Shainberg (3) it seems that the heat release is the driving force for the demixing of adsorbed ions.

We conclude that titration calorimetry provides a convenient method for the determination of enthalpies of ion exchange in clay suspensions. Both continuous and stepwise titration calorimeters produce self-consistent results which are in general agreement with literature data. For heterovalent ion exchange reactions the continuous titration method was found to suffer from the effects of inefficient stirring. The results indicate that some kind of batch or stepwise series of measurements in clay suspensions are necessary to establish that equilibrium properties are indeed being measured when expanding clay minerals are studied. Both instruments (methods) were limited in the end by the stirring efficiency. Because of this the final few percent of Na–Ca exchange could not be observed calorimetrically using either technique.

The positive values of $\Delta H^\circ$ obtained for the heterovalent $M^+$–$M^{2+}$ exchanges indicate that these

reactions are entropy driven, in agreement with the conclusions of Ewin *et al.* (15). Considering the enthalpy only, tactoid formation apparently also favours the $M^+$–$M^{2+}$ exchange, since we find tactoid formation to be enthalpy driven (the entropy of tactoid formation is expected to be negative, i.e. opposing tactoid formation). Tactoid formation may lead to complications in clay suspension calorimetry since during the addition of salt solution high local concentrations of exchanging counterions may cause premature tactoid formation, with reestablishment of equilibrium taking as long as several minutes.

In stepwise titration calorimetry we have observed the heat effects of tactoid formation and breakdown in the same regions of surface composition of the exchanging ions as can be predicted from light scattering and viscosity measurements (22). We were able to estimate the enthalpy change accompanying tactoid formation in the Na–Ca exchange on montmorillonite at −4.9 kJ/equiv of ion exchange, in remarkable agreement with the only other known (indirect) determination of this heat effect (3). This means, in the worst possible case, that if for instance in titration calorimetry one were to titrate Ca-montmorillonite with NaCl (notice this is the opposite of the exchange reaction reported in Table 2) only to the point where 20% or so of the Ca ions is replaced, the observed enthalpy of exchange would be positive rather than negative as expected from Table 2, and in the order of +1 kJ/equiv.

**Acknowledgements**

The authors thank Dr. L. Hepler of the University of Lethbridge for his hospitality and valuable assistance and discussions. Travel funds for L.L.S. were available through a grant from the Industrial Colloids Division of Enka b.v., an Akzo group member. The authors are grateful to the Natural Sciences and Engineering Research Council of Canada and to the Killam Trust for Postgraduate Scholarships to the first author. This research is supported by the Natural Sciences and Engineering Research Council of Canada.

1. L. G. Homshaw and J. Chaussidon. Proc. Int. Clay Conf. Oxford. 1979. p. 141.
2. R. Keren and I. Shainberg. Clays Clay Miner. **23**, 193 (1975).
3. R. Keren and I. Shainberg. Clays Clay Miner. **27**, 145 (1979).
4. H. Martin and H. Laudelout. J. Chim. Phys. **60**, 1086 (1963).
5. J. L. Ragland. Soil Sci. Soc. Am. Proc. **26**, 133 (1962).
6. R. G. Gast, R. VanBladel, and K. B. Deshpande. Soil Sci. Soc. Am. Proc. **33**, 661 (1969).
7. R. G. Gast. Soil Sci. Soc. Am. Proc. **36**, 14 (1972).
8. H. Laudelout, R. VanBladel, G. H. Bolt, and A. L. Page. Trans. Faraday Soc. **64**, 1477 (1968).
9. R. VanBladel and R. Menzel. Proc. Int. Clay Conf. Tokyo, 1969. p. 619.
10. A. Maes and A. Cremers. J. Chem. Soc. Faraday Trans. I, **73**, 1807 (1977).
11. A. Maes, P. Peigneur, and A. Cremers. Proc. Int. Clay Conf., Mexico City. 1975. p. 319.
12. A. Maes and A. Cremers. J. Chem. Soc. Faraday Trans. I, **74**, 1234 (1978).
13. V. U. Hofmann and R. Klemen. Z. Anorg. Chem. **262**, 95 (1950).
14. E. M. Perdue. Geochim. Cosmochim. Acta, **42**, 1351 (1978).
15. G. J. Ewin, B. P. Erno, and L. G. Hepler. Can. J. Chem. **59**, 2927 (1981).
16. P. F. Kerr, P. K. Hamilton, and R. J. Pill. Analytical data on reference clay minerals. Am. Petrol. Inst. Project 49, Clay Mineral Standards, Prelim. Rept. 7. 1950.
17. L. L. Schramm and J. C. T. Kwak. Clays Clay Miner. **28**, 67 (1980).
18. L. L. Schramm. Ph.D. Thesis. Dalhousie University, Halifax, N.S. 1980.
19. G. J. Ewin. Ph.D. Thesis. Latrobe University, Victoria, Australia. 1978.
20. A. T. Hutcheon. J. Soil. Sci. **17**, 339 (1966).
21. S. Tymochowicz. Nukleonika, **23**, 931 (1978).
22. L. L. Schramm and J. C. T. Kwak. Clays Clay Miner. In press.
23. I. Shainberg and A. Kaiserman. Soil Sci. Soc. Am. Proc. **33**, 547 (1969).
24. I. Wadso. Science Tools, **13**, 33 (1966).
25. K. W. T. Goulding and O. Talibudeen. J. Colloid Interface Sci. **78**, 15 (1980).

Can. J. Chem. Downloaded from www.nrcresearchpress.com by 210.87.254.5 on 09/06/12
For personal use only.

# The single crystal electronic spectra of *cis*-octahedral nickel(II) diamine complexes at 10 K

A. B. P. LEVER AND I. M. WALKER
*Department of Chemistry, York University, Downsview, Ont., Canada M3J 1P3*
AND
P. J. MCCARTHY
*Department of Chemistry, Canisius College, Buffalo, NY 14208, U.S.A.*

Received August 20, 1981

Can. J. Chem. Downloaded from www.nrcresearchpress.com by 210.87.254.6 on 09/06/12
For personal use only.

A. B. P. LEVER, I. M. WALKER, and P. J. MCCARTHY. Can. J. Chem. **60**, 495 (1982).

The single crystal polarised spectra, at 10 K, of a series of nickel(II) complexes containing the *cis*-chromophore $NiN_4O_2$ are reported. The four N ligands are provided by the diamines *N,N'*-diethylethylenediamine or *meso*-stilbenediamine, and the two O ligands by chelating nitrate or nitrite ion. The spectra are assigned in the point group $C_{2v}$(III). The energies are calculated within the Normalised Spherical Harmonic Hamiltonian and the Orbital Angular Overlap formalisms. The parameters so derived are consistent with previous experience obtained with *trans*-analogs once the small bite of the chelating nitrite ligand is accounted for.

A. B. P. LEVER, I. M. WALKER et P. J. MCCARTHY. Can. J. Chem. **60**, 495 (1982).

Opérant à 10 K, on a mesuré les spectres polarisés de monocristaux d'une série de complexes de nickel(II) contenant le chromophore $NiN_4O_2$ *cis*. Les diamines, *N,N'*-diéthylènediamine ou la meso stilbènediamine, constituent les quatre ligands azotés alors que la chélation des ions nitrate ou nitrite fournissent les deux ligands oxygénés. On attribue les spectres au groupe de symétrie $C_{2v}$(III). On a calculé les énergies à l'intérieur de l'Hamiltonien d'harmonie sphérique normalisée et des formules de recouvrement angulaire d'orbitale. Les paramètres ainsi obtenus sont en accord avec les expériences antérieures obtenues avec les analogues *trans* dès qu'on tient compte de la petite interaction du ligand nitrite chelatant.

[Traduit par le journal]

## Introduction

During the past ten years the electronic spectra of tetragonal complexes of a range of metal ions have been extensively studied (1–8). Complexes with chromium(III), nickel(II), and copper(II) are now particularly well understood (1) while those of cobalt(II) seem to have been studied less often (2, 3, 6). These complexes generally belong to a class of *trans*-octahedral species of general formula $ML_4Z_2$ of $D_{4h}$, or $ML_4ZZ'$ of $C_{4v}$ symmetry. The spectra have generally been treated in terms of the crystal field theory (9), the orbital angular overlap (OAM) model (10, 11), or the normalised spherical harmonic Hamiltonian (NSH) procedure (8, 12).

The earlier literature contains very few examples of systematic studies of complexes of symmetry lower than axial. The reasons for this omission are primarily the difficulty in assigning such spectra unequivocally, and the difficulty in fitting a limited number of observed transitions to the rather lengthy Hamiltonian which appears necessary for such systems.

The best early work on a rhombic six-coordinate complex appears to be the study by Meredith and Palmer (13*a*) on the nickel bis[histidinate], in which cryogenic temperatures, polarised light, and known crystal axes were used to definitively assign all the spin-allowed bands in $C_{2v}$(III) symmetry (12).

With the rising popularity of the Orbital Angular Overlap theory, a growing number of studies of low symmetry complexes are now appearing from the research groups of Gerloch (13*b*), Bertini (13*c*,*d*), and others. An extensive compilation of data and OAM parameters for low symmetry systems has recently appeared (13*e*).

In this article, we discuss single crystal polarised electronic spectra for a series of *cis*-octahedral nickel(II) complexes of general formula $M(diamine)_2(Z)_2$ where diamine is *meso*-stilbenediamine (*ms*-stien), or *sym-N,N'*-diethylethylenediamine (*s*-$Et_2$en) and $(Z_2)$ is bidentate (O,O) chelating nitrate or nitrite ion. Several of these spectra have already appeared in conjunction with our analysis of the vibronic spectrum of the nitrite ion (14). The *d*–*d* spectra of these complexes have unique features, such as their dichroism, which distinguish them from the analogous *trans* complexes. However, the OAM and NSH parameters derived from the *cis* systems parallel in a remarkable way those derivable from the *trans* systems.

## Experimental

The substituted diamines, supplied by Koch-Light (UK), were distilled and stored over KOH pellets. All other materials were of reagent grade. The preparation of the nitrito complexes has already been reported (15).

The preparation of crystals and the methods employed to obtain spectra have also been previously reported (5, 6, 15–18). $Ni(s\text{-}Et_2en)_2(NO_3)_2$ was prepared by the stoichiometric reaction

0008-4042/82/040495-06$01.00/0
©1982 National Research Council of Canada/Conseil national de recherches du Canada

Can. J. Chem. Downloaded from www.nrcresearchpress.com by 210.87.254.6 on 09/06/12
For personal use only.

of *N,N'*-diethylethylenediamine with nickel nitrate in ethanol. Metal analyses, performed by EDTA back-titration (14) were satisfactory for all complexes.

## Results

X-Ray structures exist for [Ni(*s*-$Et_2$en)$_2$($O_2$N)]X, where X is nitrite (**I**) (19) or tetrafluoroborate (**II**) (15), and for [Ni(*ms*-stien)$_2$($O_2$N)]$NO_2$ (**III**) (20). These demonstrate a *cis*-octahedral cation as shown in an idealised fashion in **A**. In general, all the

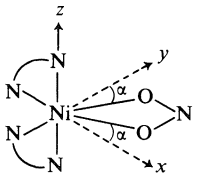


**A**

N—Ni—N angles are within a few degrees of 90°, while the O—Ni—O angle is close to 60°. The deviation of each Ni—O vector from the *x* or *y* axes is measured by the angle α. The point group is $C_{2v}$(III) (12).

The complex Ni(*s*-$Et_2$en)$_2$($NO_3$)$_2$ (**IV**) has electronic spectroscopic features (see Fig. 1) very similar to those of the previously published nitrite complexes (14) suggesting that it also has a *cis* structure. Moreover, the infrared spectrum of this species shows combination bands consistent with the presence of both bidentate bound and ionic nitrate (21). The corresponding nitrite complex (**I**) has two cationic groups in the asymmetric unit (19). The nitrate complex (**IV**) appears to be similar in that the combination infrared spectrum consists of

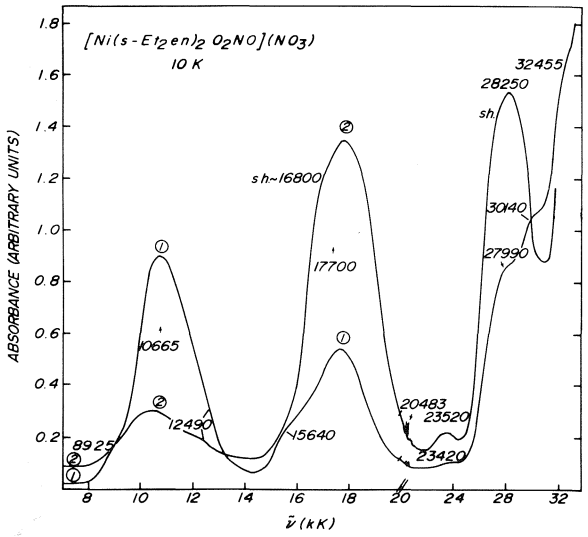


FIG. 1. Polarised crystal spectra of Ni(*s*-$Et_2$en)$_2$($NO_3$)$_2$ at 10 K, in two orthogonal polarisations. Note the change in horizontal scale at 20 kK.

two pairs of weak peaks (at 1719, 1768, and 1730, 1773 $cm^{-1}$) indicative of a pair of slightly different bidentate bound nitrate groups (21), and a sharp spike at 1756.5, with a shoulder at 1754 $cm^{-1}$ suggesting two slightly different ionic nitrate groups. We tentatively suppose therefore that the nitrate complex (**IV**) is isostructural with the cation shown in **A**.

We display single crystal polarised spectra of two of the four nickel(II) complexes at 10 K in Figs. 1, 2. The remaining spectra were reported in our discussion of their vibronic spectra (Figs. 1–5 in ref. 14). The utility of presenting such data obtained along orthogonal extinction axes has been discussed elsewhere (5). In general, with these low symmetry systems, the space groups frequently do not permit unambiguous assignments based solely on dichroism.

We note in Figs. 1–2 (and in ref. 14) that the lower two orbital triplets in cubic symmetry are each split in these derivatives. The very weak feature near 8500 $cm^{-1}$ is regarded to be a genuine crystal field feature and not a vibrational overtone because (*a*), it is absent from the electronic spectrum of Ni(*s*-$Et_2$en)$_2$($NCS)_2$ (5), (*b*), very narrow overtones seen in such species as Ni(*s*-$Et_2$en)$_2$($H_2O)_2^{2+}$ (5) are quite different from the broad bands seen here, and (*c*), calculations suggest that a crystal field band should indeed be observed here.

## Discussion

The principal features of the spectra below 20 kK must arise primarily from spin-allowed *d*–*d* transitions to the components of the $^3T_{1g}(F)$ octahedral parents in $C_{2v}$ symmetry. Except in complex **IV** the components of the $^3T_{1g}(P)$ multiplet are obscured by internal nitrite absorption. Spin singlet transitions may appear as weak features near 12–15 kK. It is evident, however, that the energies of these various spin-allowed components cannot be identified with assurance *a priori*. For this reason we do not believe it profitable to attempt to fit the spectra by allowing all parameters to vary freely, especially as the number of observable parameters does not significantly exceed the number of variables.

Prior experience suggests that OAM parameters can be transferred from one complex to another if the bonding is fairly ionic, rather than significantly covalent, and in the absence of important steric effects (22). This appears to be the situation here. Therefore, the OAM parameters derived from analogous *trans*-nickel(II) complexes (5, 7) should serve in this *cis* case also.

In an initial attempt to fit the spectra we, therefore, adopted the values $\sigma_N$ ca. 4200, $\sigma_O$ ca.

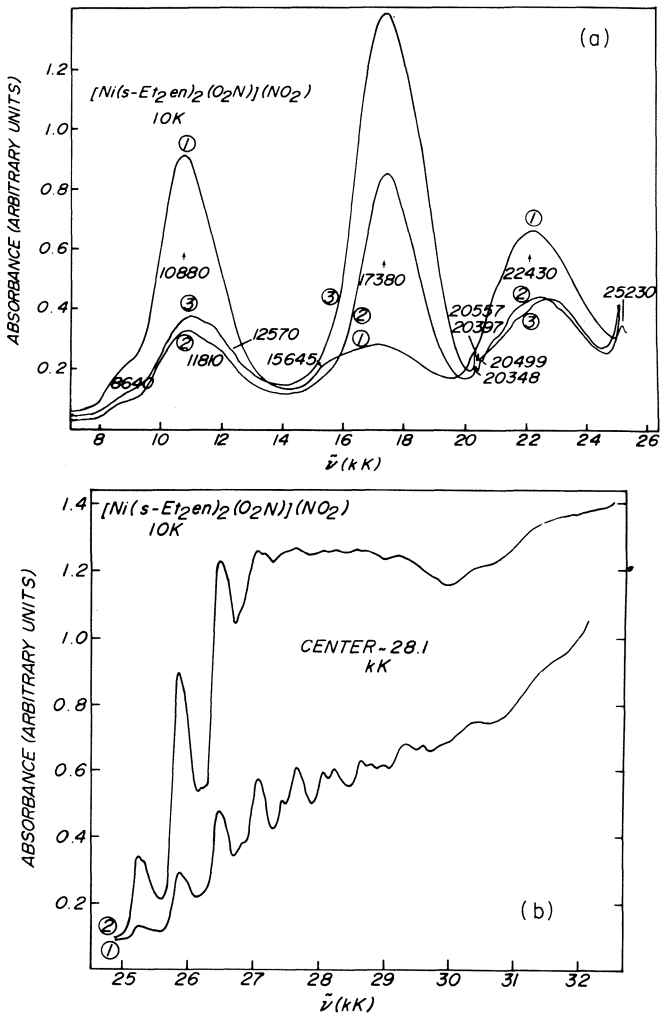


FIG. 2. Polarised crystal spectra of (Ni(*s*-$Et_2en)_2(O_2N)$) $NO_2$ at 10 K. (*a*) Region 7 500–25 000 $cm^{-1}$, three orthogonal polarisations are shown. (*b*) Region 25 000–32 000 $cm^{-1}$, two orthogonal polarisations are shown.

2400, $\pi_O$ ca. $\pm 500$, $\pi_N = 0\,cm^{-1}$, appropriate for *trans*-nickel(II) octahedral complexes and calculated the *d*-orbital energies in these complexes assuming an angle of 59.4° for the nitrite bite ($\alpha$ = 15.3°, see Appendix). Since the nitrito group is not ortho-axial, there is no constraint that in-plane $\pi$ bonding be equal to out-of-plane $\pi$ bonding. In face, we assume, in common with others (23) that in-plane $\pi$ bonding is negligible and write the corresponding OAM parameters equal zero. This is also necessary if the problem is to be tractable considering the small number of observables.

Calculated transition energies fall very close to the observed peaks and shoulders in these various spectra. Iteration around the initial choice of OAM parameters provides a good fit to the spectra as displayed in Table 1. The resulting OAM parameters (Table 2) fall well within the range of parameters expected for a fairly ionic six-coordinate nickel(II) complex with nitrogen and oxygen ligands. In the nitrate complex (**IV**) transitions to the components of the $^3T_{1g}(P)$ state can also be observed and are fitted moderately well.

The NSH approach has been used with other distorted octahedral nickel(II) complexes and for comparison purposes we report the NSH parameters for these complexes. This was achieved by mapping the NSH onto the OAM parameters (see Appendix). The NSH data have the advantage that, given a correct assignment, the parameter values are defined by the spectra and do not require knowledge of the angle $\alpha$ which may vary from one complex to another.

It is important to decide whether this assignment

Can. J. Chem. Downloaded from www.nrcresearchpress.com by 210.87.254.6 on 09/06/12
For personal use only.

TABLE 1. Calculated and observed transition energies and assignments[a]

| Assignments | | Ni(*s*-$Et_2en)_2(O_2N)_2$ (I) | | Ni(*s*-$Et_2en)_2(O_2N)(BF_4)$ (II) | | Ni(*ms*-stien)$_2(O_2N)_2$ (III) | | Ni(*s*-$Et_2en)_2(NO_3)_2$ (IV) | |
|---|---|---|---|---|---|---|---|---|---|
| $D_{4h}$ | $C_{2v}$ | Obsd | Calcd | Obsd | Calcd | Obsd | Calcd | Obsd | Calcd |
| $^3B_{2g}$ | $^3A_1$ | 8640 | 8631 | 8490 | 8400 | 8400 | 8400 | 8925 | 8850 |
| | $^3B_2$ | | 10790 | | 10530 | | 10530 | | 10590 |
| $^3E_g$ | | 10880 | | 10780 | | 10700 | | 10665 | |
| | $^3A_2$ | | 11105 | | 10820 | | 10820 | | 10880 |
| $^1A_{1g}$ | $^1A_1$ | 11810sh | 11770[b] | 11795sh | 11950[b] | 11680sh | 11950[b] | | |
| $^1B_{1g}$ | $^1B_1$ | 12570sh | 12610[b] | 12600sh | 12755[b] | 12640sh | 12755[b] | 12490sh | 12480[b] |
| | $^3B_2$ | | 15505 | | 15255 | | 15255 | | 15600 |
| $^3E_g$ | | 15645 | | 15180sh | | 15440 | | 15640sh | |
| | $^3A_2$ | | 17785 | | 17535 | | 17535 | | 17945 |
| | | 17380 | | 17330 | | 17650 | | 17700 | |
| $^3A_{2g}$ | $^3B_1$ | ~18000sh | 17650 | | 17350 | | 17350 | | 17840 |
| $^1B_{2g}$[c] | $^1A_1$ | | | 20595 | 20785[b] | | | 20483 | |

[a] The calculated spectra should be compared with the data shown in Figs. 1–4. Not all features illustrated in these figures are listed in this table. The calculated energies of the components of the $^3T_{1g}(P)$ term are as follows: I, 26000 ($A_2$), 27970 ($B_1$), 28075 ($B_2$); II, III, 26170 ($A_2$), 28170 ($B_1$), 28220 ($B_2$); IV, 26845 ($A_2$), 28450 ($B_2$), 28620 ($B_1$).
[b] Calculated using $D_{4h}$ matrices.
[c] Tentative assignment.

TABLE 2. NSH and OAM parameters for complexes I, II, III, and IV[a]

| Parameter | Value | | |
|---|---|---|---|
| | I | II, III | IV |
| DQ | 28424 | 27690 | 28423 |
| DS | 2500 | 2500 | 3300 |
| DT | 4246 | 4138 | 3712 |
| DM | −2708 | −2582 | −2136 |
| DN | 4356 | 4209 | 4900 |
| *B* | 850 | 900 | 900 |
| *C* | 3100 | 3000 | 2860 |
| $DQ_{ax}$ | 38472 | 37483 | 37208 |
| $DQ_{eq}$ | 23400 | 22794 | 24031 |
| $\sigma_N$ | 4500 | 4400 | 4700 |
| $\sigma_O$ | 2500 | 2400 | 2400 |
| $\pi_O$ | 500 | 500 | 1000 |

[a] The reader is reminded that the calculation is based on only three OAM parameters. All other radial parameters are calculated therefrom. The numbers so derived are reported here without being rounded off; however, it is recognised that the final digit will not be significant.

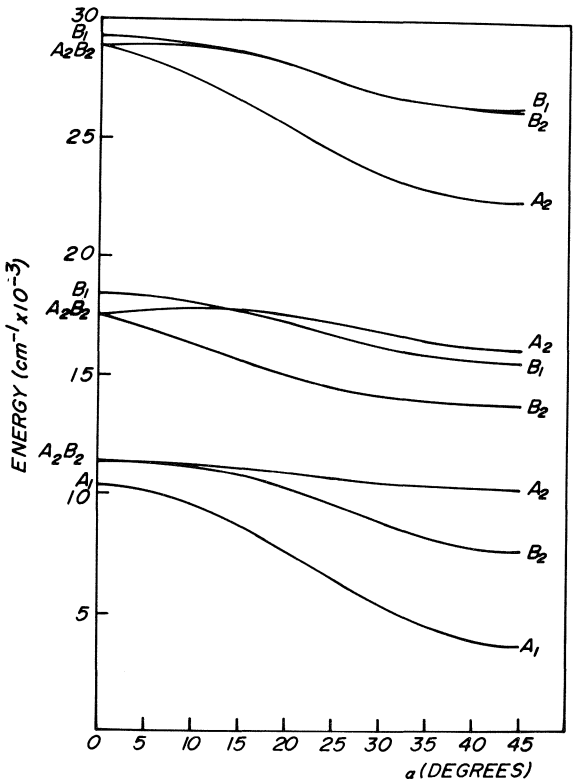


FIG. 3. The dependence of the energy of the states in $C_{2v}$(III) symmetry as a function of the angle α (see (A)). The baseline is the $^3B_1$ ground term energy. This scheme assumes $\sigma_N = 4500$, $\sigma_O = 2400$ and $\pi_O = 500\,cm^{-1}$. An angle of α near 15° is appropriate for the nitrite complexes discussed here.

is internally consistent since others are clearly feasible. Unfortunately the very low symmetry of these complexes precludes the direct use of dichroism to unequivocally assign excited state labels. In Fig. 3 we display the energy sequence for the splitting of the octahedral orbital triplets in these systems as a function of distortion angle α. The spectra show intensities largely independent of temperature, implying that electronic rather than vibronic selection rules are operative (14). All transitions are electronically allowed except for $^3B_2 \leftarrow {}^3A_1$ which is electronically forbidden but vibronically allowed. Our complexes possess α = 15.3° at a region of the diagram (Fig. 3) where there is close accidental degeneracy of two levels, thereby reducing the resolution of the spectra.

Generalising for these nickel(II) complexes, we note the following: (*i*) The weak band near 8.5 kK – 9 kK is assigned to the allowed transition to $^3A_1$ whose energy to first order is 10 Dq. The position of this transition is defined by the $NiN_2O_2$ plane. (*ii*) The $^3E(T_{2g})$ state splits into the $A_2$ and $B_2$ states. Transition to the former is electronically allowed, but is forbidden to the latter. However, the splitting is predicted to be small. Both bands lie inside the

Can. J. Chem. Downloaded from www.nrcresearchpress.com by 210.87.254.6 on 09/06/12
For personal use only.

Can. J. Chem. Downloaded from www.nrcresearchpress.com by 210.87.254.6 on 09/06/12
For personal use only.

envelope observed near 11 kK. (*iii*) Transition to the second $^3B_2$ level is observed weakly near 15–16 kK. Evidently it is allowed vibronically. (*iv*) Additional shoulders in the spectra of some of these complexes near 11.5–13 kK are reasonably assigned as spin singlet transitions (5). (*v*) The dichroism while it does not provide us with unequivocal assignment must nevertheless be itself internally consistent. Thus the transitions to the two $^3A_2$ levels within the *F* term, for example, should show maximum intensity in the same polarisation, not in different polarisations. Using complex **I** as an example, the internal consistency of the dichroism can be demonstrated.

In polarisation 1 (Fig. 2) the intense peak at 10.88 kK must be assigned to the $^3A_2$ component, since the other transition is orbitally forbidden. The strongest feature near 17 kK in this polarisation is also assigned to $^3A_2$. In the other two polarisations the strong peak at 17.38 kK must then be assigned to $^3B_1$. This has no counterpart near 11 kK so absorption here is relatively weak. It is rather strange that, considering polarisation 1, the intensity of the lower energy $^3A_2$ transition should be greater than that of the higher $^3A_2$ transition; this may arise because their octahedral parentage is different. We note that other rather distorted nickel(II) complexes also exhibit this unusual intensity reversal (24). This dichroism is very different from that generally observed with the usual *trans*-nickel (diamine)$_2X_2$ complexes with tetragonal distortion (1*f*, 5, 7). We may conclude that OAM parameters similar to those employed for analogous *trans*-nickel(II) $NiN_4O_2$ species can reproduce the dominant features in the electronic spectra of these *cis*-complexes. The resulting parameters, optimised to fit these spectra, are entirely reasonable.

Even so, we cannot conclude that the assignments demonstrated in Table 1 are unequivocally correct, but do regard that it is consistent with all available information at this time. Such low symmetry complexes have been rarely studied. A larger data base of such systems must be accumulated before further conclusions may be drawn. Clearly there is a great deal of chemical information within the spectra of such complexes and their analysis is certainly worthwhile.

In closing, we note that we have extended these studies to another class of *cis*-nickel(II) complexes, those with the general formula Ni(*s*-$Et_2$en)$_2$(LL) where (LL) is bidentate maleate, succinate, phthalate, malonate. These complexes are freely soluble in such non-polar solvents as dichloromethane providing strong evidence for a mononuclear, and necessarily *cis*-structure. Unfortunately, we have not been able to grow sufficiently large crystals for single crystal study. The solution spectra of these complexes appear close to octahedral (22) which would be anticipated in keeping with the smaller splitting of the octahedral orbital triplets. Certainly they show less structure than the *trans*-$NiN_4O_2$ analogs; thus even solution spectra may serve to distinguish *cis* from *trans* isomers in this series of complexes.

**Acknowledgements**

A.B.P.L. and I.M.W. are indebted to the Natural Sciences and Engineering Research Council for financial support. P.J.Mc. thanks the Research Corporation for funds to purchase the Displex refrigerator.

1. (*a*) M. Gerloch, R. F. McMeeking, and A. M. White. J. Chem. Soc. Dalton, 655 (1976); (*b*) J. Catterick and P. Thornton. J. Chem. Soc. Dalton, 1634 (1976); (*c*) A. Bencini, C. Benelli, and D. Gatteschi. Inorg. Chem. **17**, 3313 (1978); (*d*) M. Gerloch, J. Kohl, J. Lewis, and W. Urland. J. Chem. Soc. A, 3269 (1970); (*e*) J. Glerup, O. Monsted, and C. E. Schäffer. Inorg. Chem. **15**, 1399 (1976); (*f*) I. Bertini, D. Gatteschi, and A. Scozzafava. Inorg. Chem. **15**, 203 (1976); (*g*) D. A. Cruse and M. Gerloch. J. Chem. Soc. Dalton, 152 (1977); 1613 (1977); (*h*) L. Y. Martin, C. R. Sperati, and D. H. Busch. J. Am. Chem. Soc. **99**, 2968 (1977).
2. (*a*) J. Ferguson, T. E. Wood, and H. J. Guggenheim. Inorg. Chem. **14**, 177 (1975); (*b*) J. Ferguson and T. E. Wood. Inorg. Chem. **14**, 184 (1975); **14**, 190 (1975).
3. M. Gerloch, J. Kohl, J. Lewis, and W. J. Urland. J. Chem. Soc. A, 3283 (1970).
4. M. Keeton, B. F. C. Chou, and A. B. P. Lever. Can. J. Chem. **49**, 192 (1971). Erratum, Can. J. Chem. **51**, 3690 (1973).
5. A. B. P. Lever, G. London, and P. J. McCarthy. Can. J. Chem. **55**, 3172 (1977).
6. A. B. P. Lever, I. M. Walker, and P. J. McCarthy. Inorg. Chim. Acta, **39**, 81 (1980).
7. A. B. P. Lever, I. M. Walker, and P. J. McCarthy. Spectrosco. Lett. **12**, 739 (1979).
8. J. C. Donini, B. R. Hollebone, G. London, A. B. P. Lever, and J. C. Hempel. Inorg. Chem. **14**, 455 (1975).
9. A. B. P. Lever. Inorganic electronic spectroscopy. Elsevier, Amsterdam. 1968.
10. C. E. Schaffer. Struct. Bond. **5**, 68 (1968); **14**, 69 (1973).
11. D. W. Smith. Struct. Bond. **35**, 87 (1978).
12. J. C. Donini, B. R. Hollebone, and A. B. P. Lever. Prog. Inorg. Chem. **22**, 225 (1977).
13. (*a*) P. L. Meredith and R. A. Palmer. Inorg. Chem. **10**, 1049 (1971); **10**, 1546 (1971); (*b*) M. Gerloch, L. R. Hanton, and M. R. Manning. Inorg. Chim. Acta, **48**, 205 (1981); (*c*) I. Bertini, P. Dapporto, D. Gatteschi, and A. Scozzafava. Inorg. Chem. **14**, 1639 (1975); (*d*) I. Bertini, D. Gatteschi, and F. Mani. Inorg. Chim. Acta, **7**, 717 (1973); (*e*) M. DiVaira. Inorg. Chim. Acta, **38**, 21 (1980).
14. I. M. Walker, A. B. P. Lever, and P. J. McCarthy. Can. J. Chem. **58**, 823 (1980).
15. R. Birdy, D. M. L. Goodgame, J. C. McConway, and D. Rogers. J. Chem. Soc. Dalton, 1730 (1977).
16. M. N. H. Irving and R. M. Parkins. J. Inorg. Nucl. Chem. **27**, 270 (1965).

17. D. M. L. GOODGAME and M. A. HITCHMAN. Inorg. Chem. **3**, 1389 (1964).
18. D. M. L. GOODGAME and M. A. HITCHMAN. Inorg. Chem. **4**, 721 (1965).
19. M. J. GOLDBERG and R. E. MARSH. Acta Crystallogr. B**35**, 960 (1979).
20. M. A. HITCHMAN. Private communication.
21. A. B. P. LEVER, E. MANTOVANI, and B. S. RAMASWAMY. Can. J. Chem. **49**, 1957 (1971).
22. A. B. P. LEVER. Coord. Chem. Rev. To be published.
23. M. A. HITCHMAN. Coord. Chem. Rev. In press.
24. L. FABBRIZZI, M. MICHELONI, P. PAOLETTI, A. POGGI, and A. B. P. LEVER. J. Chem. Soc. Dalton. 1438 (1981).

Can. J. Chem. Downloaded from www.nrcresearchpress.com by 210.87.254.6 on 09/06/12
For personal use only.

## Appendix

The N.S.H. Hamiltonian (12) appropriate for these $C_{2v}$(III) complexes is given by:

$$\mathcal{H} = \mathrm{DQ}|A_{1g}O(i)|^4_{Oh} + \mathrm{DS}|E_g(\theta)|^2_{Oh} + \mathrm{DT}|E_g(\theta)|^4_{Oh} + \mathrm{DM}|T_{2g}(xy)|^2_{Oh} + \mathrm{DN}|T_{2g}(xy)|^4_{Oh}$$

Since it possesses five variables, and we must add a sixth, the Racah $B$ parameter, it is of limited value with this data set, unless the number of variables can be reduced. By mapping onto the OAM model we note that the DM and DN parameters are not linearly independent, but have a fixed ratio independent of the angle $\alpha$. Moreover within the approximation used here (only three OAM parameters) the values of DM and DN are, in fact, defined by the values of DQ, DS, and DT, and the angle $\alpha$.

(*A*) General OAM matrix elements:

$$\langle z^2|\hat{O}|z^2\rangle = 2.5\sigma_N + 0.5\sigma_O$$
$$\langle 1/\sqrt{2}(xz + yz)|\hat{O}|1/\sqrt{2}(xz + yz)\rangle = 3\pi_N + \pi_O(1 + \sin 2\alpha)$$
$$\langle 1/\sqrt{2}(yz - xz)|\hat{O}|1/\sqrt{2}(yz - xz)\rangle = 3\pi_N + \pi_O(1 - \sin 2\alpha)$$
$$\langle xy|\hat{O}|xy\rangle = 2\pi_N + \sigma_O(1.5 \sin^2 2\alpha) + \pi_O'(2 \cos^2 2\alpha)$$
$$\langle x^2 - y^2|\hat{O}|x^2 - y^2\rangle = 1.5\sigma_N + \sigma_O(1.5 \cos^2 2\alpha) + \pi_O'(2 \sin^2 2\alpha)$$
$$\langle xy|\hat{O}|z^2\rangle = -\sigma_O((\sqrt{3}/\sqrt{2}) \sin 2\alpha)$$

($\pi_O'$, the in-plane $\pi$ bonding, is set equal to zero in our calculations).

(*B*) Mapping:

The zero reference energies of the OAM and NSH models differ from one another and are initially unknown. Mapping is achieved by equating sums and differences from which the zero reference energies cancel.

Since the mapping is independent of the number of electrons, the problem may be kept simple by working with $d^1$. The $d^1$ NSH energies may be used directly from Table VIII of ref. 12. The $d^1$ OAM energies are just those shown in (*A*) above.

Utilising the above procedure we derive, neglecting $\pi_N$ and $\pi_O'$ (in-plane $\pi$ bonding)

$$\mathrm{DQ} = \sqrt{21}\{(6/5)\sigma_N + \sigma_O((3/5) - (3/4) \sin^2 2\alpha)) - (2/5)\pi_O\}$$
$$\mathrm{DS} = \sigma_N - \sigma_O + \pi_O$$
$$\mathrm{DT} = \sqrt{15}\{(3/10)\sigma_N + \sigma_O[(21/20) \sin^2 2\alpha - (3/10)] - (2/5)\pi_O\}$$
$$\mathrm{DM} = \{-\sqrt{6}\sigma_O + \sqrt{3}\pi_O\} \sin 2\alpha$$
$$\mathrm{DN} = \{(9/\sqrt{10})\sigma_O + (6/\sqrt{5})\pi_O\} \sin 2\alpha$$

and the axial and equatorial field parameters:

$$\mathrm{DQ}_{ax} = \sqrt{21}\{(9/5)\sigma_N + \sigma_O[(27/20) \sin^2 2\alpha] - (6/5)\pi_O\}$$
$$\mathrm{DQ}_{eq} = \sqrt{21}\{(9/10)\sigma_N + \sigma_O[(9/10) - (9/5) \sin^2 2\alpha]\}$$

(*C*) The NSH parameters for $d^2$, $d^3$, $d^7$, and $d^8$ ions in $C_{2v}$(III) symmetry are reported in Table XI of ref. 12. Unfortunately there are some errors in the labelling of various rows of this table. To permit accurate use of this table, we correct these errors here. Within the body of the table, the following rows should be replaced as follows:

| | | | |
|---|---|---|---|
| Row 3 | $T_1 1 + (P)$ | $T_1 1 + 0.14548\mathrm{DQ} + 0.17143$ DS $- 0.06148$ DT $+ 0.19795\mathrm{DM} - 0.05324$*DN | |
| Row 4 | $T_1 1 + (P)$ | $T_2 1 -$ $- 0.22131$*DS $- 0.14286$*DT $+ 0.25555\mathrm{DM} + 0.12372$ DN | |
| Row 10 | $T_1 0(P)$ | $A_2 2 -$ $- 0.25555\mathrm{DM} + 0.16496$ DN | |
| Row 12 | $T_1 0$ | $A_2 2 -$ $- 0.12778\mathrm{DM} + 0.08248$ DN | |
| Row 13 | $A_2 2 -$ | $A_2 2 - 0.43644\mathrm{DQ}$ | |

# Apparent carbon–carbon bond cleavage in an epoxide. 2,3,4,5,6-Hexachloro-12-oxopentacyclo[5.4.1.1.$^{8,11}$.0$^{3,10}$.0$^{5,9}$]tridecane; a minor product from the acid treatment of endrin[1,4,5]

JOHN W. APSIMON[2,3] AND KAZU YAMASAKI
*Department of Chemistry, Carleton University, Ottawa, Ont., Canada K1S 5B6*
ALAIN FRUCHIER
*Centre de Chimie Organique, Université des Sciences et Techniques de Languedoc, 34060 Montpellier, France*
ALFRED S. CHAU
*National Water Research Institute, Canada Centre for Inland Waters, Department of Fisheries and Environment, Burlington, Ont., Canada L7R 4A6*
AND
CAROL P. HUBER
*Division of Biological Sciences, National Research Council of Canada, Ottawa, Ont., Canada K1A 0R6*

Received May 11, 1981

JOHN W. APSIMON, KAZU YAMASAKI, ALAIN FRUCHIER, ALFRED S. CHAU, and CAROL P. HUBER. Can. J. Chem. **60**, 501 (1982).

The treatment of *endrin* (**1**) with sulfuric acid produces ketoendrin **2** and from 6 to 8% of another product that we show to be 2,3,4,4,5,6-hexachloro-12-oxapentacyclo[5.4.1.1.$^{8,11}$.0$^{3,10}$.0$^{5,9}$]tridecane **3**, based initially on spectral evidence and confirmed by a single crystal X-ray diffraction study. The formation of **3** involves an apparent and unusual carbon–carbon single bond cleavage in an epoxide accompanied by cycloaddition to a proximate carbon–carbon double bond. This transformation probably proceeds by the route outlined in ref. 1. Some of the observed nmr parameters of **3** are discussed in the light of its structure and a comparison is made with the observed spectra for endrin (**1**).

JOHN W. APSIMON, KAZU YAMASAKI, ALAIN FRUCHIER, ALFRED S. CHAU et CAROL P. HUBER. Can. J. Chem. **60**, 501 (1982).

L'*endrine* (**1**) réagit dans l'acide sulfurique en produisant la cétoendrine (**2**) ainsi que 6 à 8% d'hexachloro-2,3,4,4,5,6 oxa-12 pentacyclo[5.4.1.1.$^{8,11}$.0$^{3,10}$.0$^{5,9}$]-tridécane (**3**) dont la structure avait été proposée initialement sur la base de données spectrales et que nous avons confirmée par diffraction de rayons X sur un monocristal. La formation du composé **3** implique apparemment un clivage inusité d'une liaison simple carbone–carbone d'un epoxyde accompagné d'une cycloaddition avec la double liaison carbone–carbone à proximité. Cette transformation se fait probablement selon la voie suggérée dans la référence 1. On discute, à la lumière de sa structure, de quelques paramètres observés en rmn et on établit des comparaisons avec les spectres observés dans l'endrine (**1**).

[Traduit par le journal]

During a study of the nuclear magnetic resonance spectral properties of the rearrangement products of polychlorocyclodiene insecticides, we have systematically examined the transformation products of endrin **1**. Thus, with sulfuric acid, endrin **1** yields ketoendrin **2** (2) together with a minor product (6–8%) to which we have previously assigned structure **3** (1) based on spectral evidence.[6,7] We now report confirmation of this proposal based on further nmr studies and a single crystal X-ray diffraction study.

[1]For a preliminary communication see ref. 1.
[2]To whom inquiries may be addressed.
[3]Professor Associé, USTL 1976–1977.
[4]NRCC No. 19793.
[5]The numbering system used for **3** in this article varies in order to aid the reader. Thus, the IUPAC derived numbering system is shown in **3***a* while the numbering system used in the nmr spectral discussion in the text is shown in **3***b*. This choice is made since it is essential to our arguments that comparison be made to endrin **1**. This comparison is best appreciated if the two numbering systems correspond. The crystallographic work unfortunately uses another set of numbers to locate the atoms in the two independent molecules found in the unit cell. This system is indicated in Fig. 1.

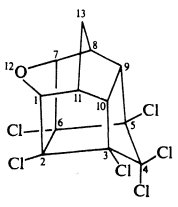

*3a*

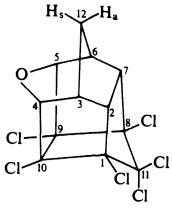

*3b*

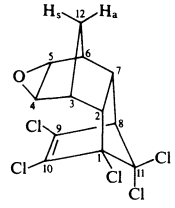

*1*

[6]The assignments for H-12a and H-12s in Table 1 of this reference should be reversed as should the attributions to C-3/C-6 and C-2/C-7 in Table 2. This is amplified in the later discussion.
[7]A referee has correctly pointed out that the formation of **3** does not really involve C—C bond cleavage in an epoxide. Rather, if our proposed mechanism for the formation of **3** from **1** is correct (1), then the C—C bond cleavage occurs after epoxide C—O bond cleavage. The final product appears only as the net effect of C—C bond cleavage.

0008-4042/82/040501-08$01.00/0
©1982 National Research Council of Canada/Conseil national de recherches du Canada

Can. J. Chem. Downloaded from www.nrcresearchpress.com by 210.87.254.40 on 09/06/12
For personal use only.

Can. J. Chem. Downloaded from www.nrcresearchpress.com by 210.87.254.40 on 09/06/12
For personal use only.

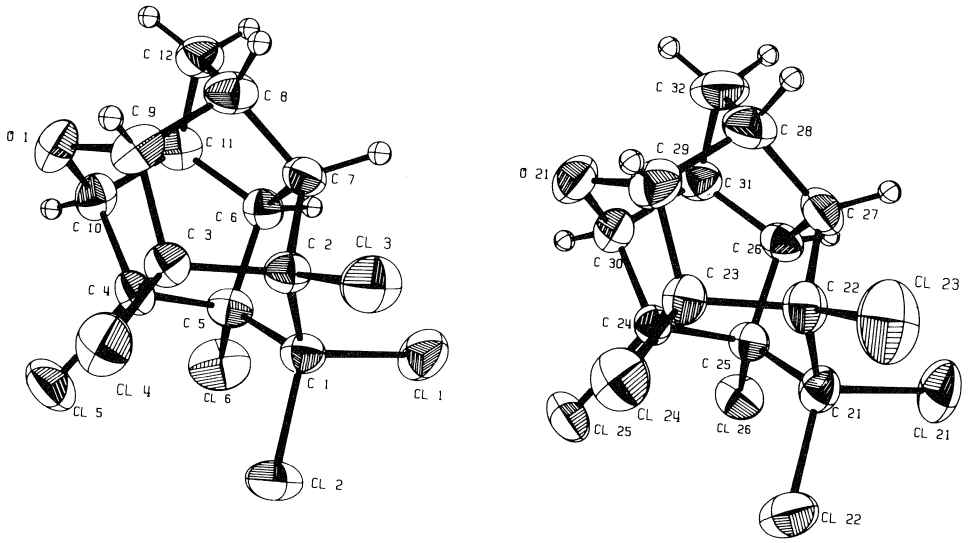


FIG. 1. ORTEP views of the two crystallographically independent molecules of **3**. The thermal ellipsoids enclose 50% probability (5).

*X-ray structural studies*

The results indicated that two independent molecules exist per asymmetric unit in the crystal of **3**. Views of these as established by the X-ray analysis are shown in Fig. 1. Final atomic parameters are listed in Table 1, and bond lengths and bond angles are given in Table 2. The C—H bond distances vary from 0.89 to 1.04 Å with mean 0.96 Å, and the bond angles involving hydrogen atoms vary from 103 to 122°, with mean 112°. The angles involving hydrogens are expected to be larger than 109° in compensation for the small angles formed by the heavier atoms in five-membered rings.

As in other related structures (endrin (3), aldrin (3), and dieldrin (4)), the molecules have essentially mirror symmetry with the mirror planes here defined by C(1), O(1), and C(12) and by C(21), O(21), and C(32). Agreement is reasonably good between chemically related bonds and angles in individual molecules as well as between corresponding values in the two molecules. Allowing for differences in the molecular structures, agreement between bond lengths and angles in the present structure and equivalent values in endrin, aldrin, and dieldrin is satisfactory.

The five-membered rings are all in envelope conformation and the six-membered ring is in the boat form. Because of the formation of bonds between the hexachloro system and what was the epoxide ring in endrin, the present molecule is more nearly spherical and more compact than endrin or dieldrin. The distances Cl(3)···Cl(6), Cl(2)···C(12), and O(1)···Cl(1) in this structure are 5.51, 5.98, and 5.82 Å respectively, while the corresponding Cl···Cl and Cl···epoxide oxygen distances in endrin and dieldrin are 5.47 and 5.52 (Cl···Cl) and 6.78 and 7.36 Å (Cl···O).

A parallel study of the nmr spectra of **3** was undertaken and some data are presented here. Using the computer program LACX (6) we have examined the eight spin system of **3** taking into account the inherent symmetry of the molecules. This calculation involved about 1000 observable transitions and provides the first complete analysis of this type of compound. Figure 2 shows the experimental 250 MHz proton nmr spectrum compared to the calculated spectrum after iteration. The signal for the 12s proton in the experimental

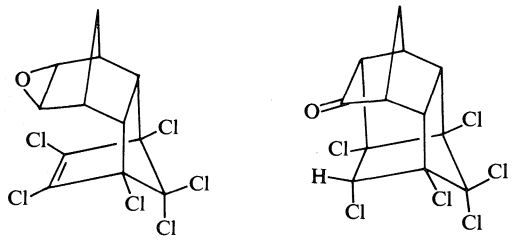


1 2

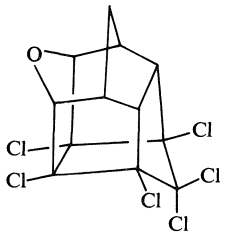


3

Can. J. Chem. Downloaded from www.nrcresearchpress.com by 210.87.254.40 on 09/06/12
For personal use only.

TABLE 1. Final fractional coordinates and their estimated standard deviations (which refer to the least significant digit). The hydrogen coordinates have been multiplied by $10^3$, the $x$ and $y$ coordinates of the other atoms by $10^4$ and $z$ by $10^5$

| | $x$ | $y$ | $z$ |
|---|---|---|---|
| Molecule 1 | | | |
| Cl(1) | 3908(1) | −631(1) | 4804(5) |
| Cl(2) | 3866(1) | −2673(1) | 13461(5) |
| Cl(3) | 5429(1) | 601(1) | 18513(5) |
| Cl(4) | 4029(1) | −650(1) | 24953(4) |
| Cl(5) | 1746(1) | −1789(1) | 16475(6) |
| Cl(6) | 1356(1) | −1441(2) | 3453(5) |
| O(1) | 2091(2) | 2117(4) | 19273(11) |
| C(1) | 3528(3) | −757(4) | 10477(15) |
| C(2) | 4008(3) | 555(4) | 14855(15) |
| C(3) | 3401(3) | 480(4) | 18657(15) |
| C(4) | 2232(3) | −118(5) | 14223(16) |
| C(5) | 2347(3) | −268(4) | 8723(15) |
| C(6) | 2330(3) | 1456(5) | 7091(15) |
| C(7) | 3487(3) | 2045(4) | 11366(17) |
| C(8) | 3267(3) | 3211(5) | 15234(18) |
| C(9) | 3182(3) | 2169(5) | 19932(16) |
| C(10) | 1536(3) | 1366(5) | 13882(17) |
| C(11) | 1557(3) | 2351(5) | 8937(16) |
| C(12) | 2152(3) | 3876(5) | 11384(18) |
| H(6) | 221(3) | 158(5) | 30(2) |
| H(7) | 402(3) | 252(5) | 99(2) |
| H(8) | 380(3) | 394(5) | 168(2) |
| H(9) | 362(3) | 255(5) | 238(2) |
| H(10) | 86(3) | 107(5) | 134(2) |
| H(11) | 93(3) | 245(5) | 59(2) |
| H(12) | 220(3) | 448(5) | 87(2) |
| H(13) | 180(3) | 447(5) | 131(2) |
| Molecule 2 | | | |
| Cl(21) | 8459(1) | 2672(1) | 20461(5) |
| Cl(22) | 8460(1) | 2229(1) | 9532(5) |
| Cl(23) | 6024(1) | 3366(2) | 9033(6) |
| Cl(24) | 6762(1) | 4745(1) | −303(4) |
| Cl(25) | 9223(1) | 5549(1) | 5107(4) |
| Cl(26) | 10380(1) | 4777(1) | 18567(4) |
| O(21) | 7526(2) | 8273(3) | 6260(12) |
| C(21) | 8269(3) | 3623(5) | 14023(15) |
| C(22) | 7193(3) | 4521(5) | 11286(17) |
| C(23) | 7286(3) | 5558(5) | 6616(15) |
| C(24) | 8544(3) | 5972(4) | 9375(15) |
| C(25) | 8979(3) | 5100(5) | 15222(15) |
| C(26) | 8543(3) | 6188(5) | 18423(15) |
| C(27) | 7312(3) | 5790(5) | 15754(17) |
| C(28) | 6751(3) | 7291(6) | 12601(19) |
| C(29) | 6776(3) | 7163(5) | 6680(18) |
| C(30) | 8534(3) | 7753(5) | 10497(17) |
| C(31) | 8586(3) | 7896(5) | 16621(17) |
| C(32) | 7515(4) | 8575(6) | 16049(21) |
| H(26) | 886(4) | 603(6) | 226(2) |
| H(27) | 716(5) | 549(7) | 189(2) |
| H(28) | 600(4) | 725(6) | 125(2) |
| H(29) | 611(3) | 725(5) | 35(2) |
| H(30) | 911(3) | 831(5) | 99(2) |
| H(31) | 925(3) | 841(5) | 193(2) |
| H(32) | 733(5) | 956(7) | 142(2) |
| H(33) | 755(4) | 880(6) | 199(2) |

spectrum is broader compared to the simulated version where we did not introduce any small nonmeasurable long-range couplings. This accounts also for the difference in resolution between the signals for $H_4$ and $H_5$ in the two spectra since irradiation indicates these couplings to be present. Table 3 presents the chemical shifts and coupling constants for **3** and compares these data with those reported for endrin **1** (7).

The availability of the X-ray data for **3** and **1** (3) enables us to make the following comments comparing the nmr spectra of both compounds.

1. The value of $J_{12s,12a}$ is larger in **3** than in endrin (absolute value). In the former, it is close to the cyclohexane value (−12.6 Hz). The X-ray data show clearly that in **3** the $H_{12s}$—C—$H_{12a}$ angle is 108° (i.e. close to the tetrahedral angle), whereas in endrin (**1**) this angle is 123°. The relief of strain on formation of the five-membered tetrahydrofuran ring in **3** is evident here.

2. The value of $J_{3,4}$ is larger in **3** than in endrin (**1**) (8.6 Hz vs. 0.9 Hz). These values are unexceptional when the dihedral angles $H_4$—$C_4$—$C_3$—$H_3$ are examined (8.5° in **3***a* and 51° in endrin). The same Karplus-type agreement can be seen for $J_{2,3}$ (5.1 Hz in **3***a* and 2.5 Hz in endrin) where the dihedral angles are 22.5° and 65° respectively.

3. The modified geometry of **3** resulting from the epoxide C—C bond opening and the consequent relief of strain is further demonstrated by the observed coupling constants for $J_{3,12a}$ and $J_{3,12s}$ as follows. In **3** the $H_{12a}$—$C_{12}$—$C_3$—$H_3$ dihedral angle is 50° with a $J_{3,12}$ being 3.7 Hz and in endrin the corresponding angle is 71° reflected by a coupling constant of 1.3 Hz. The $H_{12s}$—$C_{12}$—$H_3$ dihedral angle in **3***a* is 70° with $J_{3,12s}$ being 1.3 Hz; in endrin this angle becomes 61° and $J_{3,12s}$ is 2.0 Hz.

4. The unambiguous assignment of the $H_{12a}$ and $H_{12s}$ signals can be made by a shift reagent study (8) for endrin (**1**) and **3**. The results obtained are outlined in Table 4. Assuming the oxygen atom is involved as the major complexation site with $Eu(fod)_3$, the assignments are self evident.

5. It is to be noted that the signal for $H_{12a}$ is more sensitive to the transformation of endrin (**1**) to **3** than that for $H_{12s}$, even though this proton is more proximate to the site of chemical change (0.50 ppm and 0.16 ppm downfield shifts respectively). One interpretation of these results is that the major contribution to the shielding of $H_{12}$ is the epoxide-group ring-current which is destroyed on conversion of endrin (**1**) to **3**; whereas for $H_{12s}$ the major shielding contribution arises from the proximate oxygen atom.

It is apparent from the above observations that **3**

Can. J. Chem. Downloaded from www.nrcresearchpress.com by 210.87.254.40 on 09/06/12
For personal use only.

TABLE 2. Bond lengths and bond angles for both molecules of **3** observed in the crystal

| Molecule 1 | | Molecule 2 | |
|---|---|---|---|
| | Bond lengths | | |
| Cl(1)—C(1) | 1.765(4) Å | Cl(21)—C(21) | 1.722(4) Å |
| Cl(2)—C(1) | 1.780(4) | Cl(22)—C(21) | 1.761(4) |
| Cl(3)—C(2) | 1.754(4) | Cl(23)—C(22) | 1.749(5) |
| Cl(4)—C(3) | 1.765(4) | Cl(24)—C(23) | 1.762(4) |
| Cl(5)—C(4) | 1.761(4) | Cl(25)—C(24) | 1.764(4) |
| Cl(6)—C(5) | 1.760(4) | Cl(26)—C(25) | 1.749(4) |
| O(1)—C(9) | 1.427(6) | O(21)—C(29) | 1.433(6) |
| O(1)—C(10) | 1.422(5) | O(21)—C(30) | 1.411(5) |
| C(1)—C(2) | 1.524(5) | C(21)—C(22) | 1.532(6) |
| C(1)—C(5) | 1.534(6) | C(21)—C(25) | 1.537(6) |
| C(2)—C(3) | 1.543(6) | C(22)—C(23) | 1.549(6) |
| C(2)—C(7) | 1.543(5) | C(22)—C(27) | 1.541(6) |
| C(3)—C(4) | 1.588(6) | C(23)—C(24) | 1.590(6) |
| C(3)—C(9) | 1.535(6) | C(23)—C(29) | 1.537(6) |
| C(4)—C(5) | 1.534(6) | C(24)—C(25) | 1.557(5) |
| C(4)—C(10) | 1.556(6) | C(24)—C(30) | 1.546(6) |
| C(5)—C(6) | 1.525(6) | C(25)—C(26) | 1.529(6) |
| C(6)—C(7) | 1.570(6) | C(26)—C(27) | 1.555(7) |
| C(6)—C(11) | 1.539(6) | C(26)—C(31) | 1.536(6) |
| C(7)—C(8) | 1.532(6) | C(27)—C(28) | 1.532(7) |
| C(8)—C(9) | 1.553(6) | C(28)—C(29) | 1.557(6) |
| C(8)—C(12) | 1.524(6) | C(28)—C(32) | 1.510(7) |
| C(10)—C(11) | 1.544(6) | C(30)—C(31) | 1.565(6) |
| C(11)—C(12) | 1.518(6) | C(31)—C(32) | 1.522(8) |
| C(6)—H(6) | 1.01(4) | C(26)—H(26) | 0.98(5) |
| C(7)—H(7) | 1.04(5) | C(27)—H(27) | 0.95(6) |
| C(8)—H(8) | 0.91(4) | C(28)—H(28) | 1.01(6) |
| C(9)—H(9) | 0.98(4) | C(29)—H(29) | 0.93(4) |
| C(10)—H(10) | 0.91(4) | C(30)—H(30) | 0.98(5) |
| C(11)—H(11) | 0.89(5) | C(31)—H(31) | 0.98(5) |
| C(12)—H(12) | 0.90(4) | C(32)—H(32) | 0.94(6) |
| C(12)—H(13) | 0.93(4) | C(32)—H(33) | 1.00(5) |
| | Bond angles | | |
| C(9)—O(1)—C(10) | 102.5(3)° | C(29)—O(21)—C(30) | 102.9(3)° |
| Cl(1)—C(1)—Cl(2) | 107.7(2) | Cl(21)—C(21)—Cl(22) | 108.4(2) |
| Cl(1)—C(1)—C(2) | 113.0(3) | Cl(21)—C(21)—C(22) | 112.6(3) |
| Cl(1)—C(1)—C(5) | 112.9(3) | Cl(21)—C(21)—C(25) | 111.2(3) |
| Cl(2)—C(1)—C(2) | 113.6(3) | Cl(22)—C(21)—C(22) | 114.7(3) |
| Cl(2)—C(1)—C(5) | 114.8(3) | Cl(22)—C(21)—C(25) | 115.0(3) |
| C(2)—C(1)—C(5) | 94.6(3) | C(22)—C(21)—C(25) | 94.7(3) |
| Cl(3)—C(2)—C(1) | 116.0(3) | Cl(23)—C(22)—C(21) | 115.4(3) |
| Cl(3)—C(2)—C(3) | 115.6(3) | Cl(23)—C(22)—C(23) | 115.6(3) |
| Cl(3)—C(2)—C(7) | 114.9(3) | Cl(23)—C(22)—C(27) | 115.3(3) |
| C(1)—C(2)—C(3) | 105.6(3) | C(21)—C(22)—C(23) | 105.0(3) |
| C(1)—C(2)—C(7) | 103.0(3) | C(21)—C(22)—C(27) | 103.6(3) |
| C(3)—C(2)—C(7) | 99.8(3) | C(23)—C(22)—C(27) | 99.9(3) |
| Cl(4)—C(3)—C(2) | 115.8(3) | Cl(24)—C(23)—C(22) | 116.0(3) |
| Cl(4)—C(3)—C(4) | 114.6(3) | Cl(24)—C(23)—C(24) | 115.4(3) |
| Cl(4)—C(3)—C(9) | 111.9(3) | Cl(24)—C(23)—C(29) | 112.0(3) |
| C(2)—C(3)—C(4) | 102.5(3) | C(22)—C(23)—C(24) | 102.3(3) |
| C(2)—C(3)—C(9) | 108.0(3) | C(22)—C(23)—C(29) | 107.8(3) |
| C(4)—C(3)—C(9) | 102.9(3) | C(24)—C(23)—C(29) | 101.9(3) |
| Cl(5)—C(4)—C(3) | 115.9(3) | Cl(25)—C(24)—C(23) | 115.7(3) |
| Cl(5)—C(4)—C(5) | 116.2(3) | Cl(25)—C(24)—C(25) | 115.6(3) |
| Cl(5)—C(4)—C(10) | 112.1(3) | Cl(25)—C(24)—C(30) | 111.6(3) |
| C(3)—C(4)—C(5) | 102.3(3) | C(23)—C(24)—C(25) | 102.4(3) |
| C(3)—C(4)—C(10) | 100.8(3) | C(23)—C(24)—C(30) | 101.9(3) |
| C(5)—C(4)—C(10) | 108.0(3) | C(25)—C(24)—C(30) | 108.3(3) |
| Cl(6)—C(5)—C(1) | 115.7(3) | Cl(26)—C(25)—C(21) | 115.6(3) |
| Cl(6)—C(5)—C(4) | 115.0(3) | Cl(26)—C(25)—C(24) | 115.6(3) |

TABLE 2 (*Concluded*)

| Molecule 1 | | Molecule 2 | |
|---|---|---|---|
| Cl(6)—C(5)—C(6) | 114.6(3) | Cl(26)—C(25)—C(26) | 115.4(3) |
| C(1)—C(5)—C(4) | 105.6(3) | C(21)—C(25)—C(24) | 104.6(3) |
| C(1)—C(5)—C(6) | 103.4(3) | C(21)—C(25)—C(26) | 104.1(3) |
| C(4)—C(5)—C(6) | 100.8(3) | C(24)—C(25)—C(26) | 99.6(3) |
| C(5)—C(6)—C(7) | 102.8(3) | C(25)—C(26)—C(27) | 103.2(3) |
| C(5)—C(6)—C(11) | 108.7(3) | C(25)—C(26)—C(31) | 109.4(3) |
| C(7)—C(6)—C(11) | 103.9(3) | C(27)—C(26)—C(31) | 104.4(3) |
| C(2)—C(7)—C(6) | 102.7(3) | C(22)—C(27)—C(26) | 103.2(3) |
| C(2)—C(7)—C(8) | 108.7(3) | C(22)—C(27)—C(28) | 108.5(4) |
| C(6)—C(7)—C(8) | 104.3(3) | C(26)—C(27)—C(28) | 104.5(4) |
| C(7)—C(8)—C(9) | 104.4(3) | C(27)—C(28)—C(29) | 104.4(4) |
| C(7)—C(8)—C(12) | 103.7(3) | C(27)—C(28)—C(32) | 103.3(4) |
| C(9)—C(8)—C(12) | 109.4(4) | C(29)—C(28)—C(32) | 109.3(4) |
| O(1)—C(9)—C(3) | 103.7(3) | O(21)—C(29)—C(23) | 104.0(3) |
| O(1)—C(9)—C(8) | 110.8(3) | O(21)—C(29)—C(28) | 110.6(4) |
| C(3)—C(9)—C(8) | 106.1(3) | C(23)—C(29)—C(28) | 106.1(4) |
| O(1)—C(10)—C(4) | 104.2(3) | O(21)—C(30)—C(24) | 104.3(3) |
| O(1)—C(10)—C(11) | 112.3(3) | O(21)—C(30)—C(31) | 111.5(3) |
| C(4)—C(10)—C(11) | 105.7(3) | C(24)—C(30)—C(31) | 105.5(3) |
| C(6)—C(11)—C(10) | 104.7(3) | C(26)—C(31)—C(30) | 104.2(3) |
| C(6)—C(11)—C(12) | 103.7(3) | C(26)—C(31)—C(32) | 103.1(4) |
| C(10)—C(11)—C(12) | 108.5(3) | C(30)—C(31)—C(32) | 108.2(4) |
| C(8)—C(12)—C(11) | 99.2(3) | C(28)—C(32)—C(31) | 99.9(4) |
| C(5)—C(6)—H(6) | 112(2) | C(25)—C(26)—H(26) | 115(3) |
| C(7)—C(6)—H(6) | 112(2) | C(27)—C(26)—H(26) | 110(3) |
| C(11)—C(6)—H(6) | 117(2) | C(31)—C(26)—H(26) | 114(3) |
| C(2)—C(7)—H(7) | 108(3) | C(22)—C(27)—H(27) | 117(4) |
| C(6)—C(7)—H(7) | 122(3) | C(26)—C(27)—H(27) | 106(4) |
| C(8)—C(7)—H(7) | 111(3) | C(28)—C(27)—H(27) | 116(4) |
| C(7)—C(8)—H(8) | 113(3) | C(27)—C(28)—H(28) | 105(3) |
| C(9)—C(8)—H(8) | 111(3) | C(29)—C(28)—H(28) | 115(3) |
| C(12)—C(8)—H(8) | 115(3) | C(32)—C(28)—H(28) | 118(3) |
| O(1)—C(9)—H(9) | 106(3) | O(21)—C(29)—H(29) | 110(3) |
| C(3)—C(9)—H(9) | 116(3) | C(23)—C(29)—H(29) | 110(3) |
| C(8)—C(9)—H(9) | 113(3) | C(28)—C(29)—H(29) | 116(3) |
| O(1)—C(10)—H(10) | 110(3) | O(21)—C(30)—H(30) | 108(3) |
| C(4)—C(10)—H(10) | 110(3) | C(24)—C(30)—H(30) | 112(3) |
| C(11)—C(10)—H(10) | 115(3) | C(31)—C(30)—H(30) | 115(3) |
| C(6)—C(11)—H(11) | 108(3) | C(26)—C(31)—H(31) | 111(3) |
| C(10)—C(11)—H(11) | 116(3) | C(30)—C(31)—H(31) | 112(3) |
| C(12)—C(11)—H(11) | 115(3) | C(32)—C(31)—H(31) | 118(3) |
| C(8)—C(12)—H(12) | 109(3) | C(28)—C(32)—H(32) | 112(4) |
| C(8)—C(12)—H(13) | 117(3) | C(28)—C(32)—H(33) | 116(3) |
| C(11)—C(12)—H(12) | 112(3) | C(31)—C(32)—H(32) | 115(4) |
| C(11)—C(12)—H(13) | 112(3) | C(31)—C(32)—H(33) | 111(3) |
| H(12)—C(12)—H(13) | 108(4) | H(32)—C(32)—H(33) | 103(5) |

Can. J. Chem. Downloaded from www.nrcresearchpress.com by 210.87.254.40 on 09/06/12
For personal use only.

suffers much less angular strain than the parent endrin (**1**) and its derivatives.

The formation of **3** is of mechanistic interest but at this stage we can make no further comment to that made in our preliminary communication (1) except to stress that this compound arises only via the acid-catalysed route.

## Experimental

*Reaction of endrin (1) with sulfuric acid*

Endrin (5 g) was dissolved with stirring in concentrated sulfuric acid (65 mL) and allowed to stand for 48 h. The resulting clear solution was poured into ice water (300 mL). The crystalline precipitate obtained was filtered and washed with aqueous sodium bicarbonate (saturated) and water. Preparative thin layer chromatography on silica gel plates eluted with benzene/5% acetone provided, after isolation in the usual manner, ketoendrin **2** (4.1 g) and **3** (0.34 g), mp 286°C. A sample was recrystallized twice from $CCl_4$ for analysis; $M^+$ (mass spectral): 381. *Anal.* calcd. for $C_{12}H_8OCl_6$: C 37.84, H 2.12, O 4.30, Cl 55.9; found: C 37.93, H 2.12, O 4.20, Cl 55.57. See text for nmr spectral data. All chemical operations were standard. Mass spectra were determined on an AE1 MS 10 spectrometer at Trent University, Peterborough, Ontario. The nmr spectra were originally determined on a Varian T-60 and XL-100 spectrometer at Carleton University. The 250 MHz nmr spectra were recorded on a CAMECA spectrometer at the Faculté de Pharmacie de Marseilles.

Crystal data are:

Monoclinic, space group $P2_1/c$, $a$ = 13.680(1), $b$, 8.515(2), $c$ =

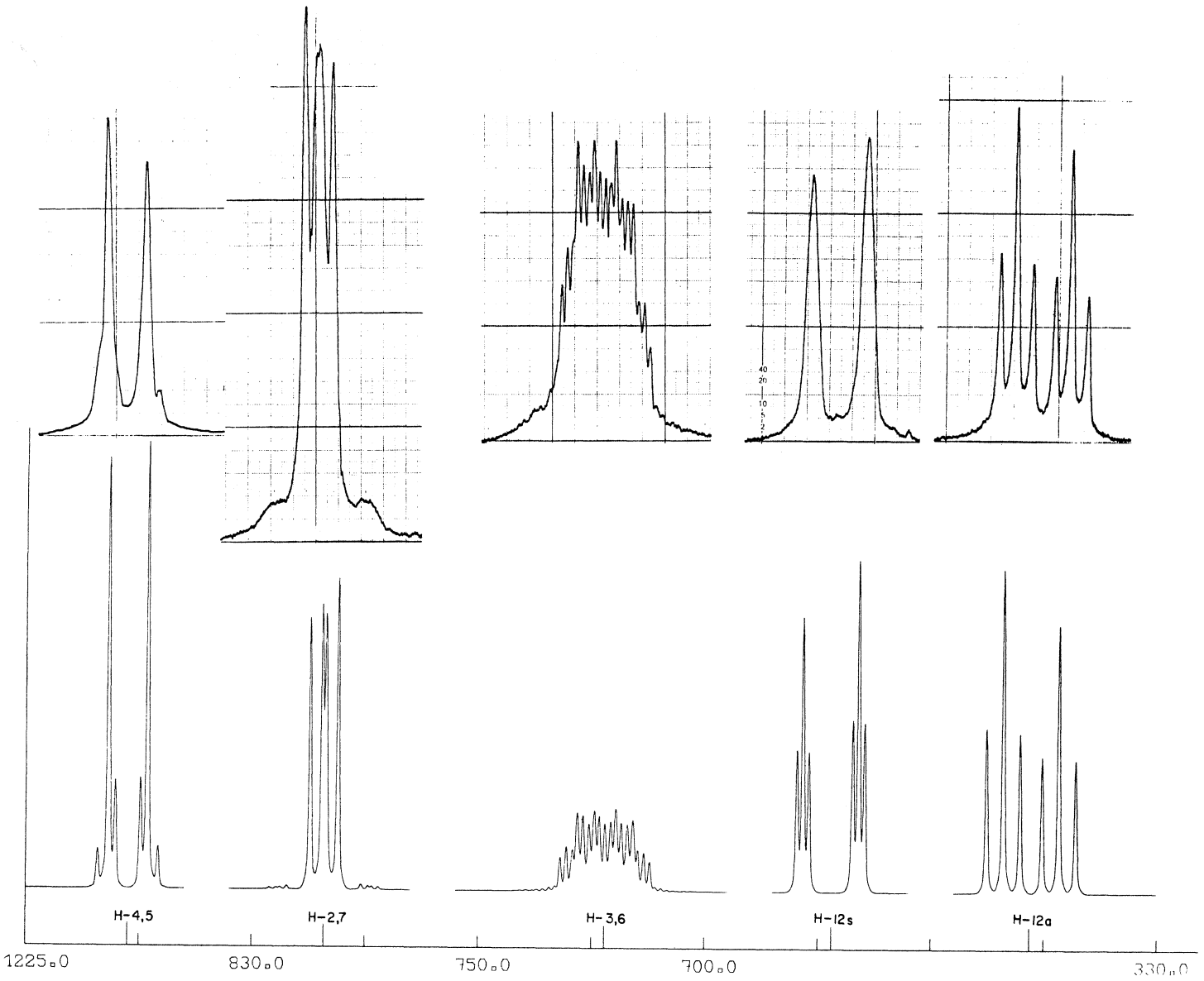


FIG. 2. Experimental 250 MHz $^1$H nmr spectrum of **3** compared with simulated spectrum using LACX. (Note: this spectrum presentation shows only the peaks observed, omitting the baselines in between signals. No effort has been made to equalize the amplitudes of the signals. The multiplicities only are of interest.)

Can. J. Chem. Downloaded from www.nrcresearchpress.com by 210.87.254.40 on 09/06/12
For personal use only.

TABLE 3. Chemical shifts (in ppm/TMS, solvent $CDCl_3$) and coupling constants (in Hz)

| | Minor product (LACX analysis) | Endrin (Keith *et al.* (7)) | Difference (MP − Endrin) |
|---|---|---|---|
| $\nu_2 = \nu_7$ | 3.256 | 3.22 | +0.04 |
| $\nu_3 = \nu_6$ | 2.888 | 2.89 | 0.0 |
| $\nu_4 = \nu_5$ | 4.810 | 3.30 | +1.51 |
| $\nu_{12a}$ | 1.433[a] | 0.93 | +0.50 |
| $\nu_{12s}$ | 1.947[a] | 1.79 | +0.16 |
| $J_{2,3} = J_{6,7}$ | 5.1 | 2.5 | |
| $J_{2,4} = J_{5,7}$ | [b] | 0 | |
| $J_{2,5} = J_{4,7}$ | 0 | 0 | |
| $J_{2,6} = J_{3,7}$ | 1.1 | 1.5 | |
| $J_{2,7}$ | 9.7 | 0[c] | |
| $J_{2,12s} = J_{7,12s}$ | [b] | 0 | |
| $J_{2,12a} = J_{7,12a}$ | 0 | 0 | |
| $J_{3,4} + J_{5,6}$ | 8.6 | 0.9 | |
| $J_{3,5} = J_{4,6}$ | 0 | 0.9 | |
| $J_{3,6}$ | 2.0 | 0[c] | |
| $J_{3,12s} = J_{6,12s}$ | 1.3 | 2.0 | |
| $J_{3,12a} = J_{6,12a}$ | 3.7 | 1.3 | |
| $J_{4,5}$ | 2.0 | 0[c] | |
| $J_{4,12s} = J_{5,12s}$ | [b] | <0.5 | |
| $J_{4,12a} = J_{5,12a}$ | 0 | 0.5 | |
| $J_{12s,12a}$ | −12.3 | −10.3 | |

[a] See footnote 6.
[b] Double irradiation experiments seem to indicate that a small coupling exists which has not been measured.
[c] The authors assumed this value to be zero, presumably due to symmetry.

TABLE 4. Shift reagents comparison studies ($Eu(fod)_3$) on endrin and the title compound, **3**. Chemical shifts are present in ppm from internal TMS at 100 MHz

| | Endrin | | Compound **3** | |
|---|---|---|---|---|
| | Chem. shifts | Rel. bound shifts | Chem. shifts | Rel. bound shifts |
| $H_2$ and $H_7$ | 3.22 | 100 | 3.26 | 100 |
| $H_3$ and $H_6$ | 2.89 | 170 | 2.89 | 128 |
| $H_4$ and $H_5$ | 3.30 | 421 | 4.81 | 397 |
| $H_{12a}$ | 0.93 | 150 | 1.43 | 104 |
| $H_{12s}$ | 1.79 | 379 | 1.95 | 251 |

25.963(2) Å, β = 115.71(3)°, $V$ = 2724.9 Å$^3$, $d_x$ = 1.857 g cm$^{-3}$, $Z$ = 8 (two independent molecules per asymmetric unit) (λ(Cu-Kα$_1$) = 1.54051, λ(CuKα$_2$) = 1.54433 Å), μ(CuKα) = 114.1 cm$^{-1}$.

The material crystallized from $CCl_4$ as clear colourless prisms. Data were collected from a specimen with maximum dimensions 0.30 × 0.15 × 0.40 mm, mounted parallel to the elongation direction (along *b*). Precession photographs showed monoclinic symmetry with systematic absences (0*k*0) with *k* odd, and (*h*0*l*) with *l* odd. Intensity data and cell dimensions were measured on a Picker diffractiometer using Ni-filtered Cu radiation. The θ/2θ scan mode was employed in measuring intensity data; the (2θ) scan speed was 2° min$^{-1}$, scan ranges were 2.0° for 0 < 2θ < 100°, 3.0° for 100 < 2θ ≤ 130°, and a 20 s background count was taken at the end of each scan. Of the 4611 independent reflections accessible in this range in two octants (*hkl* and $\bar{h}kl$) of reciprocal space, 3383 were considered "observed" on the basis of having net counts ≥ 15 and at least 10% of the total background count. Lorentz and polarization corrections were applied, and absorption corrections were made using a Gaussian integration formula; maximum and minimum transmission factors were 0.282 and 0.054 respectively.

The structure was solved by the symbolic addition procedure, and refined by block-diagonal least-squares calculations minimizing $\Sigma w(|F_o| - |F_c|)^2$. The nonhydrogen atoms were refined with anisotropic thermal parameters, and the hydrogen atoms were refined isotropically. The weighting scheme was $w = 1.0$ if $|F_o| < 35.0$, otherwise $w = (35.0/F_o)^2$, and six reflections were assigned zero weight in the later least-squares cycles. (Three (−1 1 3, −1 2 5, and −2 2 8) were affected by extinction and three (−2 0 6, 1 1 0, and 2 4 0) seemed to be Renninger reflections.) Scattering factor values for Cl, O, C, and H were taken from International Tables for X-ray Crystallography, Vol. IV (9). The Cl scattering curve was corrected (9) for the real part ($\Delta f' = 0.348$) of anomalous dispersion. In the last refinement cycle all shifts were less than one-third of their respective estimated standard deviations, and the mean (shift/esd) was 0.05. The final $R$ value for all (3383) observed reflections was 0.039. A difference map calculated from the final structure factors[8] showed 15 significant peaks (none larger than 0.40 e/Å$^3$), all of which occurred near Cl atom sites, most in locations consistent with lone-pair electron density. Computations were performed with the NRCC set of crystallographic computer programs (10).

## Acknowledgements

We thank the National Research Council of Canada and Le Centre National de la Recherche Scientifique de France for support of this work (JWA, KY, and AF) under the auspices of a Canada/France cooperation agreement.

1. J. W. APSIMON, K. YAMASAKI, A. FRUCHIER, and A. S. Y. CHAU. Tetrahedron Lett. 3677 (1977).

[8] The atomic thermal parameters and the structure amplitudes are available, at a nominal charge, from the Depository of Unpublished Data, CISTI, National Research Council of Canada, Ottawa, Ont., Canada K1A 0S2.

Can. J. Chem. Downloaded from www.nrcresearchpress.com by 210.87.254.40 on 09/06/12
For personal use only.

2. S. B. SOLOWAY, A. M. DAMIANA, J. W. SIMS, H. BLUESTONE, and R. E. LIDOU. J. Am. Chem. Soc. **82**, 5377 (1960).
3. T. P. DELACY and C. H. L. KENNARD. J. Chem. Soc. Perkin Trans. II, 2153 (1972).
4. M. E. GRESS and R. A. JACOBSON. Cryst. Struct. Commun. **3**, 485 (1973).
5. C. K. JOHNSON. ORTEP, Report ORNL-3794. 2nd Rev. Oak Ridge National Laboratory, Oak Ridge, TN. 1970.
6. C. W. HAIGH. *In* Annual reports on nmr spectroscopy. Vol. 4. *Edited by* E. F. Mooney. Academic Press, London. 1971. p. 311.
7. L. H. KEITH, A. L. ALFORD, and J. D. MCKINNEY. Anal. Chim. Acta, **60**, 1 (1972).
8. J. W. APSIMON, H. BEIERBECK, and A. FRUCHIER. Org. Magn. Reson. **8**, 483 (1976).
9. International Tables for X-ray Crystallography. Vol. IV. Kynoch Press, Birmingham. 1974. p. 72.
10. F. R. AHMED, S. R. HALL, M. E. PIPPY, and C. HUBER. J. Appl. Crystallogr. **6**, 309 (1973).

Can. J. Chem. Downloaded from www.nrcresearchpress.com by 210.87.254.40 on 09/06/12
For personal use only.

# Approaches to the total synthesis of triterpenes. VIII. The ABC + D/E approach. Synthesis and X-ray structure determination of 1β,4aβ-dimethyl-7-methoxy-1α-(7′,7′-ethyleneketal-6′,6′-dimethyl-3′-ketooctyl)-3,4,4a,9,10,10aα-hexahydro-2(1-*H*)phenanthrone[1,2]

JOHN W. APSIMON[3] AND RICK P. SEQUIN

*Department of Chemistry, Carleton University, Ottawa, Ont., Canada K1S 5B6*

AND

CAROL P. HUBER

*Division of Biological Sciences, National Research Council of Canada, Ottawa, Ont., Canada K1A 0R6*

Received August 4, 1981

JOHN W. APSIMON, RICK P. SEGUIN, and CAROL P. HUBER. Can. J. Chem. **60**, 509 (1982).

The title compound was made following a projected synthetic route to pentacyclic triterpenes. The key step in the route is the alkylative trapping of the enolate derived from the enol trimethylsilyl ether **8**. The stereochemical consequence of this reaction is confirmed by a single crystal X-ray structure determination on **4**, which although of no further utility in the projected synthesis, nevertheless served as a useful template for this determination. In this way, ongoing work in a parallel series of compounds rests on a firm stereochemical footing.

JOHN W. APSIMON, RICK P. SEGUIN et CAROL P. HUBER. Can. J. Chem. **60**, 509 (1982).

On a préparé le composé mentionné dans le titre en suivant une méthode de synthèse prévue pour les triterpènes pentacycliques. L'étape principale est le piègeage par alkylation de l'énolate provenant de l'énol de l'éther triméthylsilylé (**8**). On confirme la conséquence stéréochimique de cette réaction en déterminant la structure par diffraction de rayons X sur un monocristal du composé **4**, pour lequel on ne prévoit pas d'autre utilité au cours de la synthèse mais qui n'en demeure pas moins un modèle très utile pour cette détermination. De ce point de vue, les travaux en cours sur des séries parallèles reposent sur une base stéréochimique solide.

[Traduit par le journal]

## Introduction

During the past several years we have examined several ring construction sequences in our synthetic approaches to pentacyclic triterpenes.[4] In this brief article we describe an approach via the ABC-fragment plus side chain-route as outlined in **1** aimed at providing species such as friedelin **2** and related compounds.

Although this particular work proved fruitless in providing pentacyclic (or tetracyclic) species capable of conversion to triterpenoids, it nevertheless revealed a crucial stereoselective step necessary for the pursual of a parallel series. Thus, our synthetic sub-goal was compound **3** envisioned as arising as shown in Scheme 1 in the retrosynthetic sense.

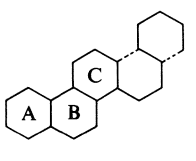


**1**

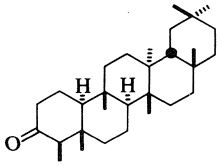


**2**

We describe here the preparation of the title compound **4** and its single crystal X-ray structure determination. In our hands this material could not be further elaborated to compound **7**. In view of this singular failure we have abandoned this route in favour of a closely related study in which the side-chain *gem*-dimethyl groups are absent. These studies will be the subject of a future report from these laboratories when completed.[5]

The condensation of **5** and **6** in this case was envisioned as presenting no real problem in view of established precedent and the improved alkylation characteristics of trimethylsilylvinyl ketones (6). In the event, the trimethylsilyl enol ether **8** was obtained by lithium – liquid ammonia reduction of **5** followed by trapping of the enolate with trimethyl-

[1]Taken in part from the M.Sc. dissertation of R.S. Carleton University, Ottawa, 1980. For part VII see ref. 1.

[2]NRCC No. 19792.

[3]Author to whom inquiries should be addressed.

[4]Our strategies have involved the following ring assembly sequences aimed at the pentacyclic skeleton.

| | |
|---|---|
| BC + E →BCDE | ref. 1 |
| AB + C→ABC + D→ABCD + E | ref. 2 |
| ABC + E | ref. 3 |
| CDE + A | ref. 4 |
| DE + C→CDE + B→BCDE | ref. 5 |

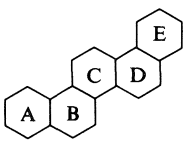


[5]In this series aldol cyclization occurs readily to species such as **7** when the *gem*-dimethyl group is absent.

0008-4042/82/040509-05$01.00/0

©1982 National Research Council of Canada/Conseil national de recherches du Canada

Can. J. Chem. Downloaded from www.nrcresearchpress.com by 210.87.254.105 on 09/06/12
For personal use only.

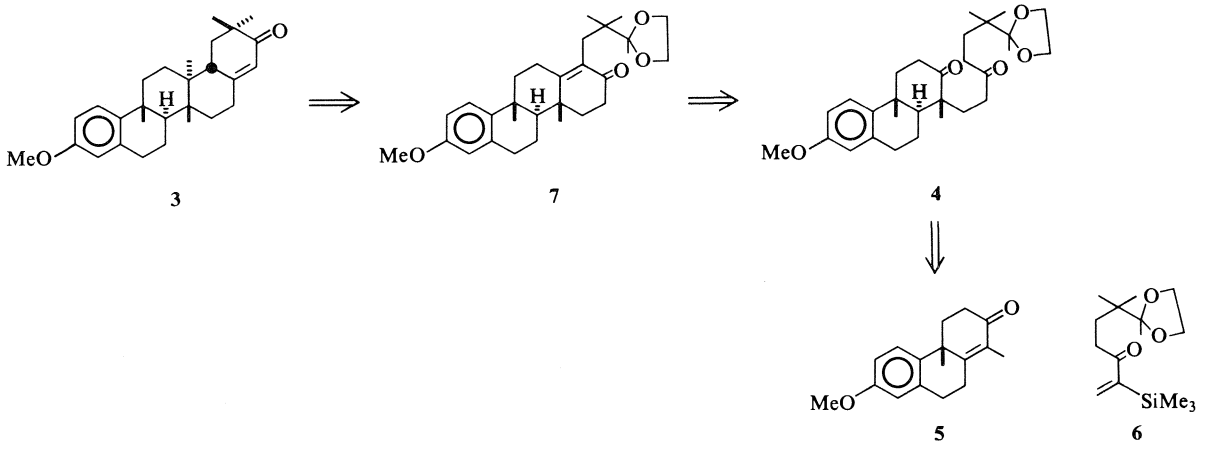


SCHEME 1

silyl chloride. Regeneration of the lithium enolate by reaction of purified **8** with methyllithium, followed by treatment with the trimethylsilylvinyl ketone **6**, provided a modest yield of **4** (42%) after isolation. Experiments aimed at the direct trapping of the enolate of **8** formed in the reductive process led to a low yield of **4** (<20%). By recycling ketone **9**, also isolated in this reaction, the yield can be raised to about 65–70%.

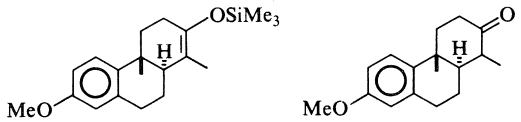


**8** **9**

The structure would appear to be secure on the basis of precedent (2) and benzene-induced solvent shifts observed in the proton nmr spectra of these compounds (3). However, in view of the potential pivotal position of these compounds in the control of other chiral centres in the developing synthetic route and the pleasing fact that **4** was crystalline, we performed a single crystal X-ray study on this material.

The vinyl ketone **6** was prepared as outlined in Scheme 2. This route is straightforward and requires no further comment other than the experimental details described later and to point out that the transformation of the nitrile to the aldehyde as shown worked best using the three-step procedure involving hydrolysis to the carboxylic acid, reduction to the primary alcohol, and oxidation back to the aldehyde (conditions *d* in Scheme 2).

With compound **4** on hand, many attempts were made to effect the aldol-type cyclization to **7** using a large variety of bases and acids. Under no conditions could we detect any cyclization products. Comparison of the structure of our substrates with the multitudinous systems described in the literature (7) suggested that the *gem*-dimethyl group, although seemingly distant from the reaction site, plays a role in the poor reactivity of this compound towards cyclization. Examination of molecular models of the correct enolate derived from **4** reveals that approach of this along a trajectory allowing for ready cyclization (1, 3) is sterically congested in the conceivable conformational modes for the respective transition states.

At this stage we abandoned this work for the more promising bis-normethyl series (**4** less the *gem*-dimethyl groups).[5]

*X-ray crystal structure of* ***4***

Final parameters for the nonhydrogen atoms are listed in Table 1.[6] Figure 1 gives the numbering scheme used in the analysis, and shows that the molecule is in the extended conformation. The final bond lengths not involving H atoms are shown in Fig. 2, and are unexceptional. The C—H bond lengths vary from 0.92 to 1.07 Å, with average 0.98 Å, and their esd's are between 0.019 and 0.041 Å. Endocyclic torsion angles are shown in Fig. 3. Ring A is planar within ±0.003 Å, ring B is in the half-chair conformation, and ring C is in the twist-boat form. The B/C ring junction is *trans*. Repulsion between the 1,3 diaxial methyl groups increases the C(25)—C(9)—C(8), C(9)—C(8)—C(14), and C(8)—C(14)—C(26) bond angles to 113.3, 113.2, and 113.5° respectively and results in an angle of 37.2° between the C(9)—C(25) and C(14)—C(26) vectors. Repulsion between O(2) and C(26) seems to affect the pertinent geometry less;

[6]Tables of final parameters for the hydrogen atoms, of bond angles, and of observed and calculated structure amplitudes are available, at a nominal charge, from the Depository of Unpublished Data, CISTI, National Research Council of Canada, Ottawa, Ont. Canada K1A 0S2.

Can. J. Chem. Downloaded from www.nrcresearchpress.com by 210.87.254.105 on 09/06/12
For personal use only.

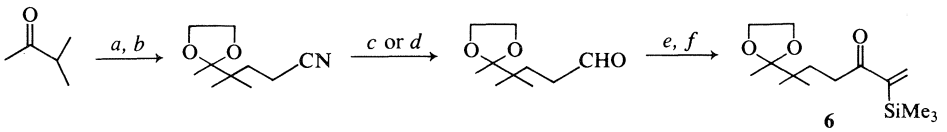


6

SCHEME 2. Reagents: *a*, *t*-BuOK, *t*-BuOH, $\overset{}{=}\!\!\backslash$ CN : *b*, *p*-TsOH, $HOCH_2CH_2OH$, benzene, azeotropic removal $H_2O$: *c*, diBAL—H, $H_3O^+$: *d*, KOH, $HOCH_2CH_2OH$, reflux; $LiAlH_4$, THF; pyridinium chlorochromate (PCC)/, $CH_2Cl_2$: *e*, $CH_2{=}CHBrSiMe_3$, Mg, THF: *f*, PCC, $CH_2Cl_2$, NaOAc.

the O(2)—C(13)—C(14) and C(13)—C(14)—C(26) angles are increased by only about 1° from expected values. The O(2)—C(13)—C(14)—C(26) torsion angle is 30.4°, but a decrease in this would lead towards the less favorable boat conformation.

The dioxolane ring is envelope shaped, with C(21) displaced 0.42 Å from the exact plane formed by O(4), O(5), C(22), C(23).

The molecules are held in the crystal structure by van der Waals forces; there are no hydrogen bonds or other short intermolecular contacts.

*Conclusion*

Although this study did not lead to polycyclic materials capable of conversion to triterpenoids, the work performed, coupled with the X-ray structural analysis, provides concrete proof for the hitherto generally accepted stereochemical consequences of the lithium–ammonia reduction of fused enones and the subsequent trapping of the enolates formed as the trimethylsilyl ether followed by alkylation of the regenerated enolate. This observation places the ongoing stereo- and regio-selective routes in these laboratories on a firm basis.

## Experimental

Melting points were determined on a Fisher hot stage or Buchi model SMP-20 and are uncorrected. The nmr spectra were obtained on a Varian T-60, Varian EM-360, or Varian XL-100 spectrometer with tetramethylsilane (TMS) as internal standard. Chemical shifts are expressed in the δ scale and the following abbreviations apply: s, singlet; d, doublet; t, triplet; q, quartet; m, multiplet. Infrared spectra were determined on a

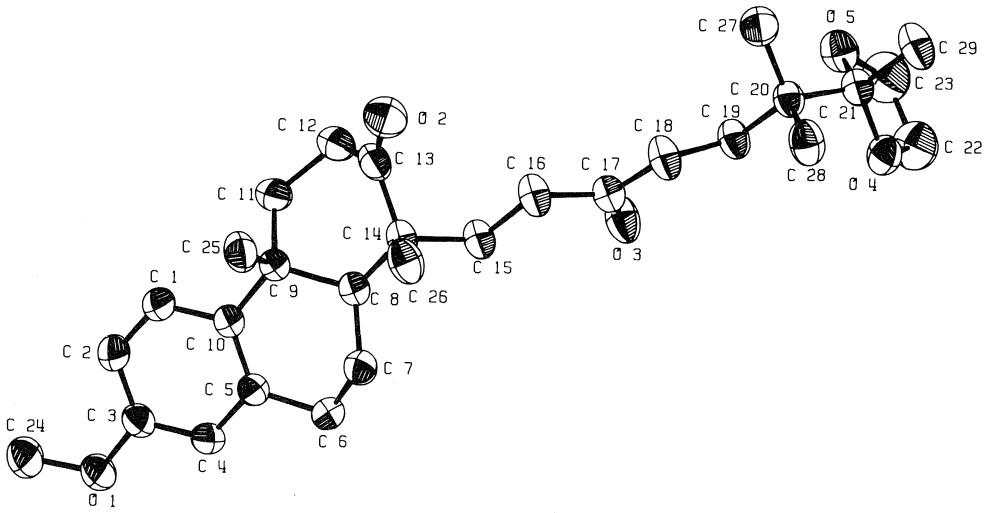


FIG. 1. A view of the title compound (**4**), drawn with the ORTEP program (8), showing the numbering scheme. The thermal ellipsoids enclose 50% probability.

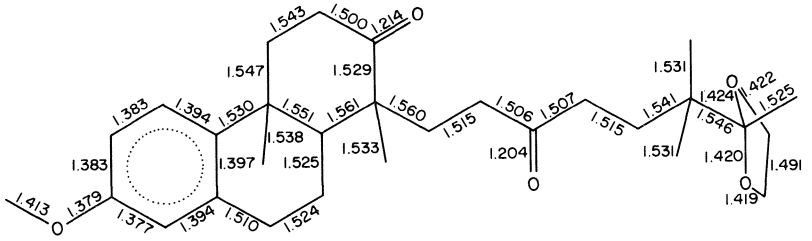


FIG. 2. Bond lengths (Å). The esd's are 0.002–0.004 Å.

Can. J. Chem. Downloaded from www.nrcresearchpress.com by 210.87.254.105 on 09/06/12
For personal use only.

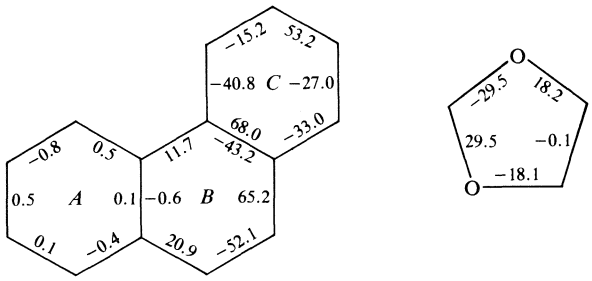


FIG. 3. Endocyclic torsional angles.

Perkin–Elmer 237B grating spectrophotometer. Mass spectra were obtained on an AE-1 MS-12 spectrometer at Trent University, Peterborough, Ont. Combustion analyses were performed by Canadian Microanalytical Laboratories, Guelph, Ontario and Spang Microanalytical Laboratory, Eagle Harbour, MI. Thin layer chromatograms (tlc) were run using precoated plates from E. Merck Reagents (silica gel 5-254, 0.25 or 2.0 mm layer thickness).

The term "work-up" refers to separation of aqueous and organic phases, neutralization of the organic phase by washing with dilute mineral acid or saturated bicarbonate as required, followed by a wash with aqueous brine, drying ($MgSO_4$ or $Na_2SO_4$), and rotary evaporation of the organic solvents.

*1,4aβ-dimethyl-7-methoxy-2-trimethylsilyloxy-3,4,4a,9,10,10aα-hexahydrophenanthrene (8)*

Dry ammonia (150 mL) was stirred for 15 min with 166 mg (23.7 mmol) of lithium metal followed by the addition of a solution of tricyclic enone **5** (2) (2.05 g, 8.0 mmol) in dry THF (150 mL) with 590 mg of *tert*-butanol as proton donor. The reaction mixture was stirred for 10 min and then the excess lithium carefully quenched by addition of small amounts of solid sodium benzoate until the dark blue color disappeared. The ammonia was removed under water aspirator vacuum pressure with the aid of a warm (40°C) water bath. Dry THF (50 mL) was added at such a point as to prevent the enolate/ammonia solution from evaporating to dryness. This was followed by the addition of 3.3 mL of a 1:1 v/v mixture of chlorotrimethylsilane and triethylamine (previously centrifuged to remove solid $Et_3N{\cdot}HCl$). The solution was stirred at room temperature for 2 h, followed by addition of pentane and work-up (sodium bicarbonate and brine wash). The pentane was removed, the residue taken up in benzene and filtered on a Florisil pad using benzene as eluant. Column chromatography using 40% benzene in petroleum ether 30–60°C accomplished separation of the silyl enol ether isomers. The desired $\Delta^1$-isomer (**8**) was isolated as an oil (1.37 g, 52%); nmr δ ($CDCl_3$): 0.2 (s, 9H, Si—*Me*), 1.05 (s, 3H, C-4a Me), 1.66 (broad s, 3H C-1 Me), 3.8 (s, 3H, -OMe), 6.6–7.4 (m, 3H, ArH); ms *m/e* (rel. int.): $M^+$ at 330 (27), 175 (15), 174 (100), 159 (15), 87 (15), 73 (40). *Anal.* calcd. for $C_{20}H_{30}SiO_2$: C 72.68, H 9.15, Si 8.50; found: C 72.88, H 9.21, Si 8.88.

The $\Delta^2$-isomer crystallized on standing (~8%), mp 34°C; nmr ($CDCl_3$) δ: 1.35 (d, 3H, C-1 Me), 4.85 (m, 1H, vinyl H); $M^+$ (mass spectrometer): 330.

*1β,4aβ-Dimethyl-7-methoxy-1α-(7',7'ethylene ketal-6',6'-dimethyl-3'-ketooctyl)-3,4,4a,9,10,10aα-hexahydro-2-(1H)-phenanthrone (4)*

Crystalline silylenol ether **8** (300 mg, 0.91 mmol) was dissolved in dry dimethoxyethane (8 mL) and titrated with methyllithium to a triphenylmethane indicator endpoint. The solution was stirred for 0.5 h and cooled to −78°C. Vinyl ketone **6** (300 mg, 1.09 mmol, 1.2 equiv.) in DME (4 mL) was added, followed by stirring for 10 min at −78°C, then allowing the mixture to warm to room temperature with stirring for 5 h. Addition of ammonium chloride and work-up gave 550 mg of a yellow viscous oil. Preparative tlc (10% ethyl acetate–benzene) gave diketone **4** (230 mg, 42%) which was crystallized from aqueous methanol, mp 156°C; $\bar{\nu}_{max}$: 1695–1705 (broad, C=O) $cm^{-1}$; nmr ($CDCl_3$) δ: 1.0 (s, 6H, 2-Me), 1.2 (s, 3H, Me), 1.35 (s, 6H, 2-Me), 3.8 (s, 3H, O-Me), 4.0 (s, 4H, ketal $CH_2$), 6.6–7.4 (m, 3H, Ar—H); ms *m/e*: 470 $M^+$ (0.05). *Anal.* calcd. for $C_{29}H_{42}O_5$: C 74.01, H 8.99, $M^+$ 470; found: C 73.80, H 9.13, $M^+$ 470.

*5,5-Ethylenedioxy-4,4-dimethylhexanenitrile*

3-Methyl-2-butanone (30 g, 0.34 mol) in dry *tert*-butanol (80 mL) and potassium metal (367 mg, 0.03 equiv.) were stirred for 45 min at room temperature and the acrylonitrile (14.2 g, 0.26 mol) added dropwise over a period of 1 h. Stirring was continued for a further 1 h; *tert*-butanol was removed and 0.7 mL of acetic acid in 100 mL of water was added. Work-up and vacuum distillation gave the keto-nitrile. Ketalization in the usual manner afforded the above nitrile (34.3 g, 68% based on acrylonitrile); $\bar{\nu}_{max}$ (neat): 2250 (CN) $cm^{-1}$; nmr ($CDCl_3$) δ: 1.0 (s, 6H, *gem* × di-Me), 1.25 (s, 3H, C-6 Me), 4.0 (s, 4H, ketal $CH_2$); $M^+$ 183; $C_{10}H_{17}O_2N$ requires $M^+$ 183.

*5,5-Ethylenedioxy-4,4-dimethylhexanal*

The above nitrile (14.5 g, 78 mmol) in 2 L of dry toluene was cooled to −10°C and diisobutylaluminum hydride (633 mL of 25.2% solution in toluene) was added dropwise. The reaction was allowed to warm to room temperature and stirred for 40 h. Saturated ammonium chloride (2 L) was added, followed by cooling to 0°C, and addition of ice-cold sulfuric acid (150 mL in 500 mL $H_2O$). Ether extraction, work-up, and filtration through a Florisil pad furnished pure aldehyde (5.3 g, 37%); $\bar{\nu}_{max}$ 1700 $cm^{-1}$; nmr ($CDCl_3$) δ: 0.98 (s, 6H, 2C-4 Me), 1.25 (s, 3H, C-6 Me), 3.95 (s, 4H, ketal $CH_2$), 9.8 (t (fine splitting), 1H, C*H*O); $M^+$ 186; $C_{10}H_{18}O_3$ requires $M^+$ 186.

Alternatively, the nitrile, (29.6 g, 1.6 mmol) was refluxed overnight with potassium hydroxide (20 g) in ethylene glycol (200 mL). Saturated brine was added and the aqueous layer extracted with ether (isolate nitrile starting material) and then carefully acidified with 50% hydrochloric acid at 0°C to pH 0.5. Rapid extraction with ether and chloroform, washing the extracts with brine and drying, gave the acid (28 g ~ 90%); $\bar{\nu}_{max}$ (neat): 3400–3500 (broad, $CO_2H$), 1710 (C=O) $cm^{-1}$; nmr ($CDCl_3$) δ: 9.95 (s broad, 1H, $CO_2H$). Prolonged treatment, elevated temperatures, or lower pH values led to extensive deketalization. The acid (27 g) in 350 mL of dry ether was then added dropwise to a suspension of lithium aluminum hydride (14.6 g, 0.386 mol) in ether (450 mL) and the mixture stirred for 5 h at room temperature. Addition (sequentially) of water (14.6 mL), 3*N* sodium hydroxide (14.6 mL), and water (43.8 mL) with continued stirring, furnished the ketal alcohol (29.4 g, 88%) which was stirred with pyridinium chlorochromate (46.5 g, 1.5 equiv.) in dichloromethane (300 mL) at room temperature for 15 h. Addition of ether, repeated ether washing of the solids, and filtration through Florisil gave, after removal of solvent, the aldehyde (20 g, 75%) identical in all respects to that prepared above.

*6,6-Dimethyl-7,7-ethylenedioxy-2-trimethylsilyl-3-oct-1-enone (6)*

α-Bromovinyltrimethylsilane (9) (29.4 g, 0.164 mol, 1.25 equiv.) was stirred in THF (40 mL) with dry magnesium turnings for 0.5 h at room temperature and then at reflux for 1 h followed by cooling to 0°C. The above aldehyde (24.4 g, 0.131 mol) in ether (60 mL) was added, the solution was allowed to warm up to room temperature and stirred overnight. Saturated ammonium chloride was added and the reaction worked up and filtered on Florisil. Column chromatography (10% ethyl acetate/benzene)

Can. J. Chem. Downloaded from www.nrcresearchpress.com by 210.87.254.105 on 09/06/12
For personal use only.

gave the allylic alcohol (26.3 g, 70%); nmr ($CDCl_3$) δ: 0.95 (s, 6H, 2C-6 Me), 0.1 (s, 9H, Si-$Me_3$), 1.25 (s, 3H, C-8 Me), 3.95 (s, 4H, ketal $CH_2$), 5.4 (d, 1H, vinyl H), 5.8 (d, $J$ = 3 Hz, vinyl H).

The allylic alcohol (500 mg, 1.75 mmol), pyridinium chlorochromate (0.564 g, 1.5 equiv.), and sodium acetate buffer (143 mg, 1.0 equiv.) were stirred for 3 h at room temperature in dichloromethane (6 mL). Addition of ether and ether washing of the tarry precipitate followed by filtration through a Florisil pad gave ketone **6** (450 mg, 90%); $\bar{\nu}_{max}$: 1665 (C=O) $cm^{-1}$; nmr ($CDCl_3$) δ: 0.1 (s, 9H, $SiMe_3$), 1.25 (s, 3H, C-8 Me), 3.95 (s, 4H, ketal $CH_2$), 6.05 (t, 1H, vinyl H), 6.45 (t, 1H, vinyl H); ms $M^+$ at 284, 139 (10.9), 88 (7.5), 87 (100), 75 (16.5), 73 (28.5). *Anal.* calcd. for $C_{15}H_{28}SiO_3$: C 63.34, H 9.92, Si 9.87; found: C 63.37, H 9.84, Si 9.85.

*X-ray data collection*

The compound was crystallized from methanol/water as clear, colourless parallelopipeds. The specimen used for data collection had approximate dimensions 0.5 × 0.2 × 0.5 mm. Crystal data are as follows.

$C_{29}H_{42}O_5$ f.w. 470.6

Triclinic, $a$ = 12.843(2), $b$ = 17.427(3), $c$ = 7.012(3) Å, α = 119.47(2), β = 106.03(3), γ = 85.37(4)° (based on λ(CuKα$_1$) = 1.54051 and λ(CuKα$_2$) = 1.54433 Å), $V$ = 1310.3(7) Å$^3$. $Z$ = 2, $\rho_c$ = 1.193 g cm$^{-3}$, space group $P\bar{1}$, μ(CuKα) = 6.4 cm$^{-1}$.

Cell dimensions and intensity data were measured at room temperature on a four-circle diffractometer using Ni-filtered Cu radiation. The cell parameters were derived by a least-squares procedure from 2θ values of 12 carefully-centered high-angle reflections. Relative intensities were measured using θ/2θ scans with (2θ) scan ranges of 2–3°. All 4430 independent reflections in a hemisphere of reciprocal space (2θ ≤ 130°) were measured, of which 3824 were considered "observed". The remainder, with net counts less than 10 (deca-) counts or less than 1/10 of the total background count, were classified as "unobservably weak" and omitted from the least-squares refinement. The intensities of two "check" reflections were monitored at frequent intervals during the data collection, and indicated no crystal deterioration. Lorentz and polarization corrections were made, and an extinction correction ($g/u$ = 0.336 × 10$^{-5}$) was applied during the refinement stage.

The structure was solved by the symbolic addition procedure, and refined by block-diagonal least-squares calculations minimizing $\Sigma\, w(|F_o| - |F_c|)^2$. The hydrogen atoms were all located on a difference map and were refined isotropically while nonhydrogen atoms were refined anisotropically. Scattering factor values for C, H, O were taken from International Tables for X-ray Crystallography, Vol. IV (10). The weighting scheme used was $w = 1/[1 + \{(|F_o| - P_2)/P_1\}^2]$ with $P_1$ = 10.0, $P_2$ = 3.0. Ten reflections were given zero weight during the later stages of refinement because of poor structure-factor agreement; the largest discrepancies among these appear to be due to undercorrection for extinction. In the final least-squares cycle, the mean (shift/estimated standard deviation) was 0.06 and the largest shift was 0.3σ. The final $R$ value was 0.051 for all observed reflections. A difference Fourier synthesis calculated from the final structure factors showed no peaks higher than 0.25 e/Å$^3$.

Computer programs of Ahmed *et al.* (11) and Johnson (8) were used in the analysis.


1. J. W. APSIMON, A. M. GREAVES, N.D. THO, and C. P. HUBER. Tetrahedron, **37**, Supp. No. 1, 117 (1981).
2. J. W. APSIMON, P. BAKER, J. BUCCINI, J. W. HOOPER, and S. MACAULEY. Can. J. Chem. **50**, 1944 (1972).
3. J. W. APSIMON, S. BADRIPERSAUD, J. W. HOOPER, R. PIKE, G. I. BIRNBAUM, C. HUBER, and M. L. POST. Can. J. Chem. **56**, 2139 (1978).
4. J. W. APSIMON, D. MOIR, and K. YAMASAKI. Can. J. Chem. **59**, 1010 (1981).
5. J. W. APSIMON, S. BADRIPERSAUD, T. T. T. NGUYEN, and R. PIKE. Can. J. Chem. **56**, 1646 (1978).
6. G. STORK and B. GANEM. J. Am. Chem. Soc. **95**, 6152 (1973); R. K. BOECKMAN. J. Am. Chem. Soc. **96**, 6179 (1974); M. JUNG. Tetrahedron, **32**, 3 (1976).
7. J. W. APSIMON (*Editor*). The total synthesis of natural products. Vols. 1–4. John Wiley and Sons, New York. 1981 and earlier.
8. C. K. JOHNSON. ORTEP, Report ORNL-3794. 2nd rev. Oak Ridge National Laboratory, Oak Ridge, TN. 1970.
9. A. OTTOLENGHI, M. FRIDKIN, and A. ZILKHA. Can. J. Chem. **41**, 2977 (1963).
10. International Tables for X-ray Crystallography. Vol. IV. Kynoch Press, Birmingham. 1974.
11. F. R. AHMED, S. R. HALL, M. E. PIPPY, and C. HUBER. J. Appl. Crystallogr. **6**, 309 (1973).


Can. J. Chem. Downloaded from www.nrcresearchpress.com by 210.87.254.105 on 09/06/12
For personal use only.

# Complexes of substituted benzothiazoles 4. Nickel(II) complexes of the bidentate benzothiazoles 1,2-bis(2-benzothiazolyl)benzene and 1,2-bis(2-benzothiazolyl)ethane

LAURENCE KENNETH THOMPSON,[1] JOHN CHARLES THOMAS RENDELL, AND GEORGE CHARLES WELLON

*Department of Chemistry, Memorial University of Newfoundland, St. John's, Nfld., Canada A1B 3X7*

Received May 29, 1981

LAURENCE KENNETH THOMPSON, JOHN CHARLES THOMAS RENDELL, and GEORGE CHARLES WELLON. Can. J. Chem. **60**, 514 (1982).

The nickel coordination chemistry of two potentially bidentate bis-benzothiazole ligands is compared. 1,2-Bis(2-benzothiazolyl)-benzene (OBT), which has an *o*-phenylene bridge, forms square planar derivatives with $NiX_2$ (X = I, $ClO_4$, $BF_4$), octahedral derivatives with $NiX_2$ (X = NCS, $NO_3$), and five-coordinate derivatives with $NiX_2$ (X = Cl, Br). 1,2-Bis(2-benzothiazolyl)ethane (BBTE), which has an ethylene bridge, forms tetrahedral derivatives with $NiX_2$ (X = Cl, Br, I) and an octahedral complex with $Ni(NO_3)_2$. Although both ligands are capable of tetrahedral coordination about a cobalt centre, the apparent preference of tetrahedral coordination with nickel complexes of BBTE seems unusual. The only difference between the two ligands lies in the bridging group between the benzothiazole rings. Structural assignments are supported by ligand field and infrared spectra, magnetic data, and an X-ray structure of the complex $[Ni(BBTE)Br_2]$, which has been shown to have a distorted tetrahedral stereochemistry.

LAURENCE KENNETH THOMPSON, JOHN CHARLES THOMAS RENDELL et GEORGE CHARLES WELLON. Can. J. Chem. **60**, 514 (1982).

On compare la chimie de coordination du nickel de deux ligands bis-benzothiazoles, potentiellement bidentates. Le bis(benzo-2 thiazolyl)-1,2 benzène (OBT), qui a un pont *o*-phénylène, forme des dérivés plan carrés avec $NiX_2$ (X = I, $ClO_4$, $BF_4$), des dérivés octaédriques avec $NiX_2$ (X = NCS, $NO_3$) et des dérivés pentacoordonnés avec $NiX_2$ (X = Cl, Br). Le bis(benzo-2 thiazolyl)-1,2 éthane (BBTE), qui a un pont éthylène, forme des dérivés tétraédriques avec $NiX_2$ (C = Cl, Br, I) et un complexe octaédrique avec $Ni(NO_3)_2$. En dépit du fait que les deux ligands peuvent avoir une coordination tétraétrique autour du centre cobalt, la préférence apparente pour une coordination tétraédrique avec les complexes de nickel du BBTE semble inhabituelle. La seule différence entre les deux ligands réside dans le groupe qui fait le pont entre les cycles benzothiazoles. Les déterminations de structure s'appuient sur le champ de ligand et les spectres infrarouges, les données magnétiques et la structure, déterminée par diffraction de rayons X, du complexe $[Ni(BBTE)Br_2]$ qui ont révélé la stéréochimie tétraédrique déformée de ce complexe.

[Traduit par le journal]

## Introduction

Histidine imidazole figures prominently at the active sites of numerous metalloprotein and metalloenzyme systems. The type 1 copper centres in such enzymes as plastocyanin (1) and azurin (2) contain imidazole groups, as well as sulphur donor groups. We have investigated a number of polyfunctional pseudoimidazole ligand systems in which the donor groups have included benzimidazoles, benzothiazoles, and imidazolines, all of which are nitrogen donors similar to histidine (3–7). The bisbenzothiazole ligand 1,2-bis(2-benzothiazolyl)-benzene (OBT; Fig. 1) behaves as an $N_2$ donor towards cobalt(II), copper(II), and zinc(II) salts, with the formation of four-coordinate pseudo-tetrahedral and square planar and six-coordinate derivatives (4). An X-ray structural determination revealed that an almost square planar $CuN_2Cl_2$ chromophore exists in the case of the complex $[Cu(OBT)Cl_2]$ (8). Little tendency towards tetrahedral coordination with copper was observed for this system. The bis-imidazoline ligands 1,2-bis(2′-imidazolin-2′-yl) benzene (LP) and 1,2-bis(2′-imidazolin-2′-yl)ethane (LE) form square planar bis-ligand complexes with nickel salts while cobalt complexes are for the most part tetrahedral (3).

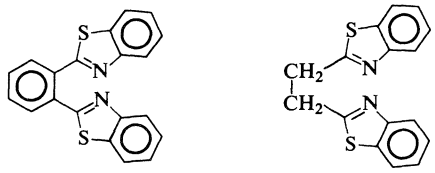

OBT BBTE

FIG. 1. Structure of 1,2-bis(2-benzothiazolyl)benzene, OBT and 1,2-bis(2-benzothiazolylethane, BBTE.

In this study we have investigated the nickel coordination chemistry of the two closely related bis-benzothiazole ligands, OBT and BBTE (Fig. 1; BBTE = 1,2-bis(2-benzothiazolyl)ethane). These ligands are similar to LP and LE except that the imidazoline groups are replaced by benzothiazoles. Reaction of OBT with nickel(II) salts produced several square planar and octahedral derivatives, but in addition, in the case of the chloro- and bromo-complexes spectral and other data suggest the formation of square pyramidal dimers. In

[1]To whom all correspondence should be addressed.

0008-4042/82/040514-07$01.00/0

©1982 National Research Council of Canada/Conseil national de recherches du Canada

Can. J. Chem. Downloaded from www.nrcresearchpress.com by 210.87.254.5 on 09/06/12
For personal use only.

Can. J. Chem. Downloaded from www.nrcresearchpress.com by 210.87.254.5 on 09/06/12
For personal use only.

contrast, BBTE produces four-coordinate 1:1 halide derivatives which appear to be tetrahedral, a structural difference which must in part be a function of the bridging entity between the benzothiazole rings. A six-coordinate nitrate derivative is also formed, which appears to be analogous to the OBT derivative and shows that although in general BBTE seems to prefer a tetrahedral bite it can be accommodated at a nickel centre with an N—Ni—N angle of around 90°.

## Experimental

Electronic spectra were recorded on a Cary 17 spectrometer and infrared spectra were obtained with a Perkin-Elmer model 283 spectrometer. Magnetic susceptibilities were obtained at room temperature by the Faraday method with a Cahn model #7600 Faraday Magnetic Susceptibility system, coupled to a Cahn gram electrobalance. Microanalyses were carried out by Canadian Microanalytical Service, Vancouver. Metal analyses were determined by Atomic Absorption with a Varian techtron AA-5 after digestion of the samples in concentrated $HNO_3$ or aqua-regia.

*Nickel complexes of OBT and BBTE*

OBT and BBTE were synthesized according to the procedure of Rai and Braunwarth (9).

*$[Ni_2(OBT)_2Cl_4]\cdot(CH_3)_2CO$ (I)*

OBT (0.75 g; 2.2 mmol) was dissolved in hot acetone (50 mL) and $NiCl_2\cdot 6H_2O$ (0.52 g; 2.2 mmol) dissolved in hot ethanol. The two solutions were mixed and refluxed for 30 min. After 5 min a pale orange solid formed. The product was filtered, washed with acetone, and dried *in vacuo* at 80°C for 3 h.

*$[Ni_2(OBT)_2Br_4]\cdot EtOH$ (II)*

OBT (0.75 g; 2.2 mmol) was dissolved in ethanol (15 mL) and triethylorthoformate (TEOF) (10 mL) added. $NiBr_2\cdot 3H_2O$ (2.0 g; 7.3 mmol) was dissolved in ethanol (30 mL), the two solutions mixed and heated on a steam bath. As the volume reduced, an orange semicrystalline solid formed. The product was filtered, washed with TEOF, diethylether, and dried *in vacuo* at 80°C for 3 h.

*$[Ni(OBT)I_2]$ (III)*

OBT (0.52 g; 1.5 mmol) was dissolved in hot acetone (35 mL). $NiI_2$ (0.54 g; 1.5 mmol) was dissolved in hot acetone (50 mL) and the solution filtered into the solution of the ligand. The mixture was refluxed until dark green crystals began to form. The product was filtered, washed with acetone, and dried *in vacuo* at 80°C for 3 h.

*$[Ni(OBT)_2(NCS)_2]$ (IV), $[Ni_2(OBT)_2(NCS)_4(H_2O)_2]\cdot(CH_3)_2CO$ (V)*

OBT (0.75 g; 2.2 mmol) was dissolved in hot ethanol (15 mL) and added to a solution of $Ni(NCS)_2$ (0.19 g; 1.1 mmol) in ethanol (50 mL). The mixture was refluxed for 1/2 h and the volume of the solution reduced to approximately 2 mL. Acetone (10 mL) was added and the green solution allowed to stand overnight. A green crystalline product (**IV**) was obtained, which was filtered, washed with ethanol/petroleum ether (30/70), and dried *in vacuo* at 80°C for 3 h. The 1:1 thiocyanate complex **V** was prepared similarly using equimolar quantities of ligand and metal salt.

*$[Ni(OBT)(NO_3)_2]\cdot\frac{1}{2}(CH_3)_2CO$ (VI)*

OBT (0.52 g; 1.5 mmol) was dissolved in ethanol (30 mL). $Ni(NO_3)_2\cdot 6H_2O$ (0.44 g; 1.5 mmol) was dissolved in ethanol (30 mL), and the two solutions mixed and refluxed for 1/2 h. The volume of the resulting green solution was reduced to about 2 mL and acetone added until a light green solid formed. The product was filtered, washed with acetone, diethyl ether, and dried *in vacuo* at 80°C for 3 h.

*$[Ni(OBT)_2](ClO_4)_2\cdot 2H_2O$ (VII), $[Ni(OBT)_2](BF_4)_2\cdot 2H_2O\cdot 2(CH_3)_2CO$ (VIII)*

OBT (0.52 g; 1.5 mmol) was dissolved in hot ethanol (20 mL) and $Ni(ClO_4)_2\cdot 6H_2O$ ( 0.28 g; 0.75 mmol) was dissolved in hot ethanol (30 mL). The solutions were mixed and refluxed for 1/2 h. On reducing the volume of the solution a yellow–orange solid began to form. Acetone was added to aid precipitation and the product filtered, washed with acetone, and dried *in vacuo* at 80°C for 3 h. $[Ni(OBT)_2](BF_4)_2\cdot 2H_2O\cdot 2(CH_3)_2CO$ was prepared similarly using acetone as solvent.

*$[Ni(BBTE)X_2]$ (X = Cl, Br) (IX, X), $[Ni(BBTE)I_2]\cdot EtOH$ (XI), $[Ni(BBTE)(NO_3)_2]\cdot\frac{1}{2}EtOH$ (XII)*

BBTE (0.75 g; 2.5 mmol) was dissolved in hot ethanol (50 mL), $NiCl_2\cdot 6H_2O$ (1.8 g; 7.5 mmol) was dissolved in hot ethanol (50 mL), and the two solutions mixed. TEOF (10 mL) was added and the mixture heated under vacuum until the solution volume was reduced sufficiently to produce purple crystals. The reaction mixture was warmed for an additional 2 h and the product filtered, washed with TEOF, petroleum ether and dried *in vacuo* at 80°C for 3 h. The bromide, iodide, and nitrate complexes were prepared similarly.

Analytical data for all the complexes are given in Table 1. Physical measurements on the nickel complexes of OBT and BBTE were possible only in the solid state because of their general insolubility in common solvents and also their solvolytic instability. Also none of the OBT complexes could be obtained in a crystalline form suitable for X-ray analysis.

## Results and discussion

The chloride and bromide complexes (**I**, **II**) have electronic spectra which are not typical of square planar, octahedral, or tetrahedral nickel(II) derivatives. They are paramagnetic compounds with major absorptions around 12 000 and 21 000 $cm^{-1}$ (Cl) and 11 000 and 20 000 $cm^{-1}$ (Br) (Table 2; Fig. 2). Five-coordinate trigonal bipyramidal nickel(II) derivatives with nitrogen ligands in general have some absorption below 10 000 $cm^{-1}$ with up to five major absorptions in the spectrum. For the trigonal bipyramidal complex $[Ni(Me_6tren)(NCS)]NCS\cdot H_2O$ absorptions are observed at 7 700, 13 200, 16 200, 12 100, 24 600 $cm^{-1}$. A similar spectrum is observed for $[Ni(Me_6tren)Br]Br$ with the band positions shifted to slightly lower energy (10). It seems unlikely therefore that **I**, **II** have trigonal bipyramidal structures. However, a square pyramidal stereochemistry at nickel seems quite plausible. Systems of the type $[Ni(dtp)_2am]$ (dtp = $(C_2H_5O)_2PSS^-$; am = secondary amine, pyridine, quinoline) (11, 12) are reported to have square pyramidal structures and exhibit two major absorptions around 13 000 and 21 000 $cm^{-1}$.

The infrared spectra of compounds **I**, **II** are similar, except in the low energy region (Table 3).

TABLE 1. Analytical and other data

| Compound | Colour | Found (%) C | H | N | M | Calcd. (%) C | H | N | M |
|---|---|---|---|---|---|---|---|---|---|
| **I**, $[Ni_2(OBT)_2Cl_4]\cdot(CH_3)_2CO$ | Orange–brown | 50.9 | 2.97 | 5.49 | 11.4 | 51.3 | 2.98 | 5.56 | 11.7 |
| **II**, $[Ni_2(OBT)_2Br_4]\cdot EtOH$ | Orange–brown | 43.3 | 2.47 | 4.58 | 9.87 | 43.0 | 2.56 | 4.78 | 10.1 |
| **III**, $[Ni(OBT)I_2]$ | Dark green | 36.6 | 1.99 | 4.12 | 9.20 | 36.5 | 1.83 | 4.26 | 9.00 |
| **IV**, $[Ni(OBT)_2(NCS)_2]$ | Pale green | 58.2 | 2.82 | 9.62 | 6.51 | 58.4 | 2.78 | 9.73 | 6.83 |
| **V**, $[Ni_2(OBT)_2(NCS)_4(H_2O)_2]\cdot(CH_3)_2CO$ | Pale green | 49.6 | 2.98 | 9.81 | 9.83 | 49.8 | 3.00 | 9.89 | 10.42 |
| **VI**, $[Ni(OBT)(NO_3)_2]\cdot\frac{1}{2}(CH_3)_2CO$ | Green | 46.6 | 2.96 | 10.3 | 11.2 | 46.4 | 2.70 | 10.1 | 10.6 |
| **VII**, $[Ni(OBT)_2](ClO_4)_2\cdot 2H_2O$ | Orange | 48.5 | 2.88 | 5.36 | 5.83 | 48.9 | 2.85 | 5.70 | 6.01 |
| **VIII**, $[Ni(OBT)_2](BF_4)_2\cdot 2(CH_3)_2CO\cdot 2H_2O$ | Orange | 51.7 | 3.47 | 5.21 | 5.48 | 51.4 | 3.73 | 5.22 | 5.49 |
| **IX**, $[Ni(BBTE)Cl_2]$ | Purple | 45.1 | 2.63 | 6.52 | 13.1 | 45.1 | 2.84 | 6.58 | 13.8 |
| **X**, $[Ni(BBTE)Br_2]$ | Purple | 37.2 | 2.07 | 5.39 | 11.2 | 37.3 | 2.38 | 5.44 | 11.4 |
| **XI**, $[Ni(BBTE)I_2]\cdot EtOH$ | Green | 33.1 | 2.55 | 4.40 | 8.90 | 33.0 | 2.75 | 4.30 | 8.96 |
| **XII**, $[Ni(BBTE)(NO_3)_2]\cdot\frac{1}{2}EtOH$ | Green | 40.5 | 2.29 | 11.4 | 11.3 | 40.6 | 2.98 | 11.2 | 11.7 |

TABLE 2. Electronic spectra (mull transmittance) ($cm^{-1}$)

(*a*) Five-coordinate and square planar

| Compound | Spectra |
|---|---|
| **I**, $[Ni_2(OBT)_2Cl_4]\cdot(CH_3)_2CO$ | [8 400], [11 500], 12 500, 16 100, 21 300 |
| **II**, $[Ni_2(OBT)_2Br_4]\cdot EtOH$ | [8 700], [10 900], 11 700, 15 300, 20 300 [25 000] |
| **III**, $[Ni(OBT)I_2]$ | 10 400, 18 500, 27 800 (CT) |
| **VII**, $[Ni(OBT)_2](ClO_4)_2\cdot 2H_2O$ | — |
| **VIII**, $[Ni(OBT)_2](BF_4)_2\cdot 2(CH_3)_2CO\cdot 2H_2O$ | — |

(*b*) Octahedral

| Compound | $^3T_{2g} \leftarrow {}^3A_{2g}$ $\nu_1$ | $^1E_g \leftarrow {}^3A_{2g}$ | $^3T_{1g} \leftarrow {}^3A_{2g}$ $\nu_2$ | $^3T_{1g}(P) \leftarrow {}^3A_{2g}$ $\nu_3$ | *Dq* | *B* | β |
|---|---|---|---|---|---|---|---|
| **IV**, $[Ni(OBT)_2(NCS)_2]$ | 9 800 | | 16 100 | — | 980 | 933 | 0.90 |
| **V**, $[Ni_2(OBT)_2(NCS)_4(H_2O)_2]\cdot(CH_3)_2CO$ | 9 500 | | 15 400 | — | 950 | 826 | 0.79 |
| **VI**, $[Ni(OBT)(NO_3)_2]\cdot\frac{1}{2}(CH_3)_2CO$ | 9 100 | [12 700] | 15 400 | 25 800 | 910 | 866 | 0.83 |
| **XII**, $[Ni(BBTE)(NO_3)_2]\cdot\frac{1}{2}EtOH$ | 8 800 | 14 000 | 17 500 | 23 800 | 880 | 765 | 0.74 |

(*c*) Tetrahedral

| Compound | $^3A_2 \leftarrow {}^3T_1$ $\nu_2$ | $^1E \leftarrow {}^3T_1$ | $^3T_1(P) \leftarrow {}^3T_1$ $\nu_3$ | *CT* | *Dq* | *B* | β |
|---|---|---|---|---|---|---|---|
| **IX**, $[Ni(BBTE)Cl_2]$ | 9 800 | [12 100] | 17 200[18 700] | | 530 | 947 | 0.91 |
| **X**, $[Ni(BBTE)Br_2]$ | 10 100 | [11 600] | 15 900[18 700] | | 547 | 901 | 0.86 |
| **XI**, $[Ni(BBTE)I_2]\cdot EtOH$ | [10 000]10 600 | | 14 600[16 400] | 17 900 | 553 | 767 | 0.74 |

A single band in the chloro-complex, assigned to terminal Ni—Cl stretch, occurs at 300 $cm^{-1}$, while for the bromo-derivative a similar band occurs at 236 $cm^{-1}$. Other absorptions at 238, 245 $cm^{-1}$ (Cl) and 219 $cm^{-1}$ (Br) are assigned to bridging nickel halogen stretch. The similarity of the electronic spectra of these complexes with known square pyramidal systems and the presence of infrared bands attributable to both terminal and bridging nickel–halogen bonds suggests a square pyramidal dimeric structure for **I** and **II** involving halogen bridges. The presence of single absorptions associated with terminal nickel–halogen stretch also indicates *trans*- rather than *cis*-dimeric structures (Fig. 3). The other isomer involving a *trans*-arrangement of terminal metal halogen bonds in which a non-equatorial arrangement of ligands would exist is considered unlikely on steric grounds.

The iodide complex (**III**) exhibits three major bands in its mull transmittance spectrum. The high energy absorption at 27 800 $cm^{-1}$ is clearly charge transfer in origin while the other bands at 18 500 and 10 400 $cm^{-1}$ can be associated with a square planar iodo-derivative (13, 14). The diamagnetic nature of this system also supports the square planar structure.

The thiocyanate complexes (**IV**, **V**) exhibit typically octahedral mull transmittance spectra (Table 2) although in both bases the $\nu_3$ transition appears

Can. J. Chem. Downloaded from www.nrcresearchpress.com by 210.87.254.5 on 09/06/12
For personal use only.

Can. J. Chem. Downloaded from www.nrcresearchpress.com by 210.87.254.5 on 09/06/12
For personal use only.

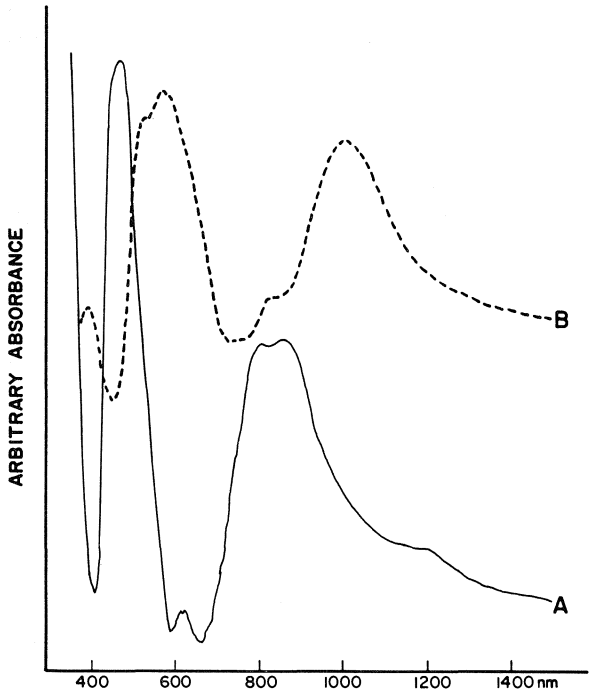


FIG. 2. Electronic spectra (mull transmittance) of $[Ni_2(OBT)_2Cl_4]\cdot(CH_3)_2CO$ (*A*) and $[Ni(BBTE)Cl_2]$ (*B*).

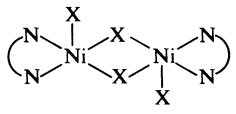

FIG. 3. Proposed structure for $[Ni_2(OBT)_2X_4]$ (X = Cl, Br).

to be hidden among high energy charge transfer absorptions. Although stereochemically compounds **IV** and **V** appear to be similar, in other respects they differ structurally. The 1:2 complex $[Ni(OBT)_2(NCS)_2]$ (**IV**) exhibits CN stretching bands at 2095 and 2106 $cm^{-1}$, associated with two *cis*-isothiocyanate groups. Other bands at 296 and 310 $cm^{-1}$, assigned to Ni—N stretch, are also consistent with such an arrangement. Consequently a *cis*-octahedral structure involving a $NiN_6$ chromophore is indicated for this system. The 1:1 thiocyanate complete (**V**) exhibits a more complex infrared spectrum in the CN stretching region. Three bands are observed at 2100, 2117, and 2140 $cm^{-1}$. The 2140 $cm^{-1}$ band is too high in energy to be associated with a terminally bound isothiocyanate and a thiocyanate bridge is suggested. The two lower energy absorptions appear to be more typical of terminally bound thiocyanate. In light of the stoichiometry of the complex and the fact that it has a pseudo-octahedral stereochemistry a di-μ-thiocyanate bridged dimeric structure appears to be

TABLE 3. Infrared data ($cm^{-1}$)* and magnetic data

| | Compound | μ (BM)† (room temp.) | $\nu_t$ (M—X) | $\nu_b$ (M—X) | νCN (NCS) | Other |
|---|---|---|---|---|---|---|
| **I**, | $[Ni_2(OBT)_2Cl_4]\cdot(CH_3)_2CO$ | 3.49 | 300 | 238, 245 | | 1717 (acetone) |
| **II**, | $[Ni_2(OBT)_2Br_4]\cdot EtOH$ | 3.47 | 236 | 219 | | |
| **III**, | $[Ni(OBT)I_2]$ | Diamagnetic | | | | |
| **IV**, | $[Ni(OBT)_2(NCS)_2]$ | 3.18 | 296, 310 | | 2095, 2106 | |
| **V**, | $[Ni_2(OBT)_2(NCS)_4(H_2O)_2]\cdot(CH_3)_2CO$ | 3.29 | 280, 290 | | 2100, 2117, 2140 | 1705 (acetone) |
| **VI**, | $[Ni(OBT)(NO_3)_2]\cdot\frac{1}{2}(CH_3)_2CO$ | 3.22 | 281, 290 | | | 804, 1275, 1525 ($NO_3$) |
| | | | | | | 1739, 1771, ($\nu_1 + \nu_4$, $NO_3$) |
| | | | | | | 1715 (acetone) |
| **VII**, | $[Ni(OBT)_2](ClO_4)_2\cdot 2H_2O$ | Diamagnetic | | | | 3520, 3610 ($H_2O$) 1085 ($ClO_4^-$) |
| **VIII**, | $[Ni(OBT)_2](BF_4)_2\cdot 2(CH_3)_2CO\cdot 2H_2O$ | Diamagnetic | | | | 3560, 3620 ($H_2O$) 1710 (acetone) |
| | | | | | | 1060 ($BF_4^-$) |
| **IX**, | $[Ni(BBTE)Cl_2]$ | 3.56 | 300, 325 | | | |
| **X**, | $[Ni(BBTE)Br_2]$ | 3.43 | 253, 258 | | | |
| **XI**, | $[Ni(BBTE)I_2]\cdot EtOH$ | 3.62 | 224, 230 | | | |
| **XII**, | $[Ni(BBTE)(NO_3)_2]\cdot\frac{1}{2}EtOH$ | 3.24 | | | | 1720, 1770 ($\nu_1 + \nu_4$, $NO_3$) |

*Infrared spectra obtained as Nujol or hexachlorobutadiene mulls between KBr or CsI plates.
†Magnetic moment measured in the solid state by Faraday method.

Can. J. Chem. Downloaded from www.nrcresearchpress.com by 210.87.254.5 on 09/06/12
For personal use only.

reasonable with a *trans*-arrangement of OBT ligands and two *cis*-terminal thiocyanates. The remaining coordination sites appear to be occupied by water molecules as indicated by infrared absorptions at 3340 and 3390 $cm^{-1}$ (Fig. 4). Molecular models indicate that the isomer involving a *cis* non-equatorial arrangement of OBT ligands is unlikely because of steric crowding.

The nitrate complex $[Ni(OBT)(NO_3)_2]\cdot\frac{1}{2}(CH_3)_2CO$ (**VI**) exhibits mull transmittance bands typical of pseudo-octahedral nickel(II) (Table 2). Nitrate fundamental infrared absorptions (Table 3) suggest the presence of bidentate nitrate (15) and this is confirmed by the appearance of just two bands in the combination ($\nu_1 + \nu_4$) region separated by 32 $cm^{-1}$ (16). A *cis*-octahedral structure is therefore suggested involving one coordinated OBT and two bidentate nitrate groups.

The nickel perchlorate and tetrafluoroborate derivatives of OBT (**VII**, **VIII**) are clearly square planar in structure involving two bidentate ligands acting as $N_2$ donors. No clearly defined *d–d* bands are observed below 25 000 $cm^{-1}$ in their mull transmittance spectra (Table 2) where one might reasonably expect to see such absorptions due to a square planar $NiN_4$ chromophore and it is assumed that they are buried beneath high energy charge transfer bands. The diamagnetism of **VII** and **VIII** (Table 3), coupled with infrared data (Table 3) indicating the ionic role of the perchlorate and tetrafluoroborate groups confirms the square planar nature of these systems.

The nickel coordination chemistry of the ethylene bridged bis-benzothiazole BBTE (Fig. 1) differs markedly from that of OBT. It has not been found possible to synthesize square planar derivatives of BBTE. In fact with nickel perchlorate and tetrafluoroborate no significant complex formation was observed. $NiX_2$ (X = $ClO_4$, $BF_4$) and BBTE were reacted in ethanol/TEOF with warming but on cooling the ligand crystallized out and no complexes were formed. In the cases involving nickel halide complexes forcing conditions were required to effect complex formation. Excess metal salt was employed in each case under anhydrous conditions using TEOF and the mixtures were heated until the product crystallized from the hot solution. The products are solvolytically unstable and if the reaction solutions are cooled before the product is allowed to crystallize only the ligand is obtained.

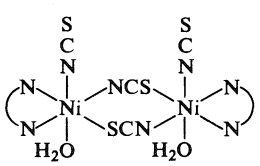


FIG. 4. Proposed structure for $[Ni_2(OBT)_2(NCS)_4(H_2O)_2]\cdot(CH_3)_2CO$.

Highly coloured paramagnetic derivatives are obtained with nickel halides, $NiX_2$ (X = Cl, Br, I) (**IX–XI**). Two major areas of absorption are observed in their mull transmittance spectra (Table 2; Fig. 2) corresponding to the $\nu_2$ and $\nu_3$ transitions associated with tetrahedral nickel (**II**). A high energy absorption at 17 900 $cm^{-1}$ in the case of the iodo-complex is associated with iodine-to-metal charge transfer. In each case two infrared absorptions associated with nickel halogen stretch are observed (Table 3) consistent with a pseudo-tetrahedral stereochemistry. The nitrate complex $[Ni(BBTE)(NO_3)_2]\cdot\frac{1}{2}EtOH$ (**XII**) exhibits electronic spectral bands typical of a pseudo-octahedral nickel(II) system (Table 2) and nitrate combination bands in the infrared (Table 3) separated by 50 $cm^{-1}$ indicate the presence of two bidentate nitrate groups. Structurally therefore the nitrate derivatives of both OBT and BBTE appear to be analogous.

Crystal field splittings for the pseudo-tetrahedral halide complexes are very similar, but it is somewhat surprising that the *Dq* values rise slightly in the series Cl < Br < I. The Racah parameter *B* decreases as expected (Cl > Br > I) reflecting more covalent character in the complexes as the size of the halogen increases. The $\nu_2$ transition increases in energy in the series Cl < Br < I while the $\nu_3$ transition decreases in energy (Cl > Br > I). It was not possible to observe the $\nu_1$ transition in any of these complexes. The slight increase in $\nu_2$ may reflect a distortion towards a square planar stereochemistry as the size of the halogen increases. In the case of the bromo-complex X-ray data indicate a somewhat flattened tetrahedron. This slight increase in $\nu_2$ appears to be responsible for the slight increase in *Dq* in the series Cl < Br < I. In the tetrahedral complexes $Ni(Ph_3PO)_2X_2$ (X = Cl, Br, I) $\nu_2$ decreases slightly in the series Cl > Br > I paralleling the trend in *Dq* (17). The complex $Ni(BBTE)Br_2$ has a crystal field splitting comparable with that of the tetrahedral complex Ni(2,3-dimethylpyridine)$_2Br_2$ (*Dq* = 540 $cm^{-1}$). However, the dimethylpyridine complex has more covalent character ($\beta$ = 0.75) (18).

A comparison of the two ligands, both of which act as $N_2$ donors and form seven-membered chelate rings, reveals a possible reason why square planar $NiN_4$ derivatives are not formed in the case of BBTE. The only difference between the two ligands lies in the bridging unit which is an *o*-disubstituted

Can. J. Chem. Downloaded from www.nrcresearchpress.com by 210.87.254.5 on 09/06/12
For personal use only.

benzene in OBT and an ethylene, $—CH_2CH_2—$, in BBTE. Molecular models indicate that two OBT ligands fit, without serious steric problems, in a *trans*-configuration about a square planar metal centre but that axial coordination would be effectively prevented by the proximity of two α benzene ring protons per ligand to the fifth and sixth coordination sites. (A *cis*-configuration proposed in the case of the complex $[Ni(OBT)_2(NCS)_2]$ also seems reasonable.) The formation of a similar bis-ligand derivative involving BBTE seems less likely in either a *cis*- or a *trans*-configuration because of potential steric interactions between ethylene bridge protons and α benzene ring protons. Although molecular models indicate that a square planar mono-ligand system involving BBTE is reasonable, the fact that tetrahedral derivatives predominate may be a consequence of the larger ethylene bridge, which is more flexible than the *o*-phenylene bridge present in OBT and which can accommodate a larger bite about the metal centre.

An X-ray structural investigation of the complex $[Ni(BBTE)Br_2]$ confirms the pseudo-tetrahedral nature of this molecule (Fig. 5) (19).

Crystal data for $C_{16}H_{12}Br_2N_2S_2Ni$ fw = 514.5 Space group $A2/a$, $a$ = 19.401(1), $b$ = 7.7995(4), $c$ = 13.340(1) Å, β = 122.280(4)°, $V$ = 1706.6 Å$^3$, $Z$ = 4, $D_c$ = 1.996 g cm$^{-3}$, μ = 9.9 mm$^{-1}$, molecular symmetry, 2-fold axis. (CuKα radiation, $\lambda\alpha_1$ = 1.54056 Å)

Selected bond lengths and bond angles are listed in Table 4.

The N—Ni—N angle is very close to the tetrahedral angle but the Br—Ni—Br angle is significantly larger than 109½° and the tetrahedron itself is somewhat compressed. Bond lengths to the nickel centre and in the ligand itself are considered to be normal and the molecule has a two-fold symmetry axis through the nickel centre and a torsional angle of 99.1° in the ethylene bridge.

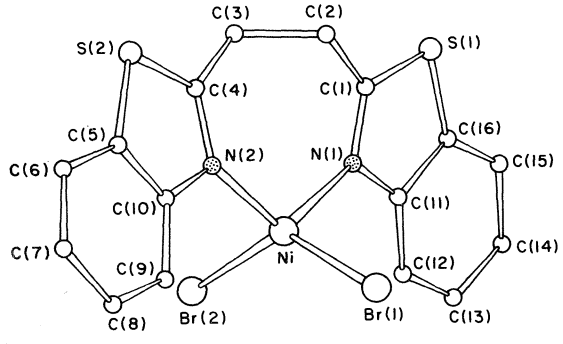


FIG. 5. X-ray structure for $[Ni(BBTE)Br_2]$ ($R$ = 0.027).

TABLE 4. Selected bond lengths and bond angles for $C_{16}H_{12}Br_2N_2S_2Ni$ (esd in parentheses)

| Bond | Length (Å) | Bonds | Angle (deg) |
|---|---|---|---|
| Ni—Br(1) | 2.3631(5) | Br(1)—Ni—Br(2) | 131.79(4) |
| Ni—N(1) | 2.010(3) | Br(1)—Ni—N(1) | 105.40(7) |
| N(1)—C(1) | 1.297(5) | Br(1)—Ni—N(2) | 101.83(8) |
| C(1)—C(2) | 1.484(5) | N(1)—Ni—N(2) | 109.6(1) |
| C(2)—C(3) | 1.541(8) | | |

The tetrahedral structure observed for this system and also for the corresponding chloro- and iodo-complexes seems somewhat unusual on two counts; nickel does not usually have a strong preference for tetrahedral geometries, although in some cases steric factors influence the situation, and also other bidentate pseudo-imidazole ligands have been shown to form only square planar and octahedral complexes with nickel even with a system involving an ethylene bridge. In earlier work we have shown that for the ethylene bridged bis-imidazoline LE (3) square planar bis-ligand complexes are formed with nickel halides, while cobalt derivatives, $Co(LE)X_2$ (X = Cl, Br, I, NCS), are tetrahedral. X-ray data confirm that the cobalt derivative $Co(LE)I_2$ has a tetrahedral structure in which the seven-membered chelate ring has similar dimensions to that in $Ni(BBTE)Br_2$ and the torsional angle in the ethylene bridge is 113.6° (20). BBTE also forms tetrahedral derivatives, $Co(BBTE)X_2$ (X = Cl, Br, I, NCS), with cobalt salts (21).

The formation of 1:1 tetrahedral derivatives of BBTE with the nickel halides appears, in part, to be a function of the ethylene bridge, which is somewhat larger and more flexible than an *o*-phenylene bridge and so would allow the ligand to span two tetrahedral coordination sites more readily than OBT. Also the size of the benzothiazole groups themselves must be taken into account. They are larger than the imidazoline rings found in LE and could be responsible for a steric effect which is helping to stabilize the tetrahedral structure. There appear to be no other steric phenomena in the structure, e.g., hydrogen bonding contacts, which could contribute to the stability of the tetrahedral arrangement. The crystal field strengths of the two ligands must of necessity be very similar and so it is unlikely that electronic effects are responsible for the enhanced stability of the tetrahedral stereochemistry in the cases of the BBTE complexes.

**Acknowledgement**

We thank the Natural Sciences and Engineering Research Council of Canada for financial support.

1. D. M. COLMAN, H. C. FREEMAN, J. M. GUSS, M. MURATA, V. A. NORRIS, J. A. M. RAMSHAW, and M. P. VENKATAPPA. Nature, London, **272**, 319 (1978).
2. E. T. ADMAN, R. E. STENKAMP, L. C. SIEKER, and L. H. JENSEN. J. Mol. Biol. **123**, 35 (1978).
3. A. B. P. LEVER, B. S. RAMASWAMY, S. H. SIMONSEN, and L. K. THOMPSON. Can. J. Chem. **48**, 3076 (1970).
4. J. C. T. RENDELL and L. K. THOMPSON. Can. J. Chem. **57**, 1 (1979).
5. L. K. THOMPSON, R. G. BALL, and J. TROTTER. Can. J. Chem. **58**, 1566 (1980).
6. D. V. BAUTISTA and L. K. THOMPSON. Inorg. Chim. Acta, **42**, 203 (1980).
7. A. W. ADDISON, H. M. J. HENDRIKS, J. REEDIJK, and L. K. THOMPSON. Inorg. Chem. **20**, 103 (1981).
8. R. G. BALL and J. TROTTER. Can. J. Chem. **57**, 1368 (1979).
9. C. RAI and J. B. BRAUNWARTH. J. Org. Chem. **26**, 3634 (1961).
10. I. BERTINI, M. CIAMPOLINI, P. DAPPORTO, and D. GATTESCHI. Inorg. Chem. **11**, 2254 (1972).
11. C. K. JØRGENSEN. Acta Chem. Scand. **17**, 533 (1963).
12. R. L. CARLIN, J. S. DUBNOFF, and W. T. HUNTRESS. Proc. Chem. Soc. 228 (1964).
13. A. B. P. LEVER. J. Inorg. Nucl. Chem. **27**, 149 (1965).
14. M. GOODGAME and D. M. L. GOODGAME. J. Chem. Soc. 207 (1963).
15. N. F. CURTIS and Y. M. CURTIS. Inorg. Chem. **4**, 804 (1965).
16. A. B. P. LEVER, E. MANTOVANI, and B. S. RAMASWAMY. Can. J. Chem. **49**, 1957 (1971).
17. M. GOODGAME, D. M. L. GOODGAME, and F. A. COTTON. J. Am. Chem. Soc. **83**, 4161 (1961).
18. S. BUTTAGNI. L. M. VALLARINO, and J. V. QUAGLIANO. Inorg. Chem. **3**, 480 (1964).
19. A. W. HANSON. Cryst. Struct. Commun. In press.
20. S. H. SIMONSEN. Private communication.
21. L. K. THOMPSON and G. C. WELLON. Unpublished results.

Can. J. Chem. Downloaded from www.nrcresearchpress.com by 210.87.254.5 on 09/06/12
For personal use only.

# 1-Pyrazolyl phosphazenes and their complexes with palladium(II) chloride and platinum(II) chloride

KEITH D. GALLICANO AND NORMAN L. PADDOCK

*Department of Chemistry, The University of British Columbia, 2035 Main Mall, University Campus, Vancouver, B.C., Canada V6T 1Y6*

Received June 25, 1981

KEITH D. GALLICANO and NORMAN L. PADDOCK. Can. J. Chem. **60**, 521 (1982).

The chlorophosphazenes $(NPCl_2)_{3-6}$ and the phenylchlorophosphazenes *gem*-$N_3P_3Ph_4Cl_2$ and *gem*-$N_3P_3Ph_2Cl_4$ react with pyrazole, 3-methylpyrazole, and 3,5-dimethylpyrazole to give $(NPpz_2)_{3-6}$, $[NP(Mepz)_2]_{3-5}$, $[NP(Me_2pz)_2]_{3,4}$, $N_3P_3Ph_4(Mepz)_2$, $N_3P_3Ph_4(Me_2pz)_2$, and $N_3P_3Ph_2(Me_2pz)_4$. Infrared and nmr spectroscopy show the pyrazolyl group to be an electron-withdrawing substituent on the phosphazene ring, resembling a halogen rather than an amino-group. The pyrazolyl group also acts as a donor through its pyridinic nitrogen atom, both intramolecularly and in the formation of the complexes *gem*-$N_3P_3Ph_4(Me_2pz)_2 \cdot PdCl_2$, *gem*-$N_3P_3Ph_2(Me_2pz)_4 \cdot PdCl_2$, $N_3P_3(Me_2pz)_6 \cdot 2PdCl_2$, $N_3P_3(Me_2pz)_6 \cdot 2PtCl_2$, and $N_3P_3(Me_2pz)_6 \cdot 3PdCl_2$. No bonding between the metal and a nitrtogen atom in the ring was detected.

KEITH D. GALLICANO et NORMAN L. PADDOCK. Can. J. Chem. **60**, 521 (1982).

Les chlorophosphazènes $(NPCl_2)_{3-6}$ et les phénylchlorophosphazènes *gem*-$N_3P_3Ph_4Cl_2$ et *gem*-$N_3P_3Ph_2Cl_4$ réagissent avec le pyrazole, le méthyl-3 pyrazole et le diméthyl-3,5 pyrazole pour donner les composés suivants: $(NPpz_2)_{3-6}$, $[NP(Mepz)_2]_{3-5}$, $[NP(Me_2pz)_2]_{3,4}$, $N_3P_3Ph_4(Mepz)_2$, $N_3P_3Ph_4(Me_2pz)$ et $N_3P_3Ph_2(Me_2pz)_4$. La spectroscopie infrarouge et la RMN montrent que le groupe pyrazolyle est un substituant électroattracteur du cycle phosphazène ressemblant plutôt à un halogène qu'à un groupe amino. Le groupe pyrazolyle agit également comme donneur par l'intermédiaire de son atome d'azote à la fois de façon intramoléculaire et lors de la formation des complexes *gem*-$N_3P_3Ph_4(Me_2pz)_2 \cdot PdCl_2$, *gem*-$N_3P_3Ph_2(Me_2pz)_4 \cdot PdCl_2$, $N_3P_3(Me_2pz)_6 \cdot 2PdCl_2$, $N_3Pe(Me_2pz)_6 \cdot 2PtCl_2$ et $N_3P_3(Me_2pz)_6 \cdot 3PdCl_2$. On n'a pas décelé de liaison entre le métal et l'atome d'azote dans le cycle.

[Traduit par le journal]

## Introduction

The phosphazene ring normally acts as an acceptor to substituent groups with unshared electrons. The electron transfer from such ligands as the dimethylamido-group shortens the exocyclic bonds, makes the phosphorus atom to which they are attached less electrophilic, and accentuates the donor properties of the nitrogen atoms in the phosphazene ring. The properties of the pyrazolyl group as a substituent (Fig. 1*a*) are different, in that the formally unshared electrons on nitrogen form part of the aromatic sextet, and their reduced availability for transfer to the phosphazene ring is diminished still further by an adjacent pyridinic nitrogen atom, which is more electronegative than carbon. The same conclusion applies to other heteroaromatic rings, and the validity of the basic concepts is confirmed by a study of the rates of hydrolysis of *N*-acylazoles (1), which increase both with the number of nitrogen atoms in the ring and with their separation, as expected theoretically.

One object of the present work was to compare the general properties of the pyrazolylphosphazenes with those of other phosphazene series, so as to clarify the electronic interactions between azole and phosphazene rings. A second object was to examine their coordination behaviour, to see how far the concentration of charge within the azole ring might shift the donor site from the phosphazene ring to the exocyclic groups. Among heteroaromatic rings, pyrazole is particularly appropriate, because of the stability conferred by chelation in its most usual coordination (Fig. 1*b*). We give below details of the preparation of the series of 1-pyrazolylphosphazenes shown in Fig. 2. The complexes *gem*-$N_3P_3Ph_4(Me_2pz)_2 \cdot PdCl_2$ (**7***a*) and *gem*-$N_3P_3Ph_2(Me_2pz)_4 \cdot PdCl_2$ (**7***b*) were prepared from $PdCl_2$ and **6***b* and **5** respectively, **1***c* gave $N_3P_3(Me_2pz)_6 \cdot 2PtCl_2$ (**8***b*) with $PtCl_2$ and $N_3P_3(Me_2pz)_6 \cdot 2PdCl_2$ (**8***a*) and $N_3P_3(Me_2pz)_6 \cdot 3PdCl_2$ (**9**) with $PdCl_2$. The spectroscopic results confirm the conclusion of a preliminary report (2), and show (*i*) that the pyrazolyl group is an electron-withdrawing substituent, and (*ii*) that coordination occurs exclusively at the pyrazolyl groups, as in Fig. 1*b*.

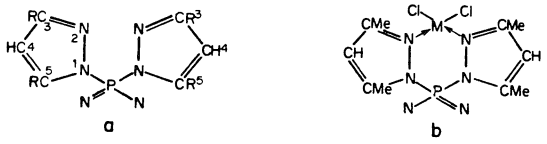


FIG. 1. (*a*) Numbering scheme of pyrazolyl group L. (*b*) Coordination scheme.

## Results and Discussion

All the pyrazolylphosphazenes are crystalline

0008-4042/82/040521-08$01.00/0

©1982 National Research Council of Canada/Conseil national de recherches du Canada

Can. J. Chem. Downloaded from www.nrcresearchpress.com by 210.87.254.42 on 09/06/12
For personal use only.

Can. J. Chem. Downloaded from www.nrcresearchpress.com by 210.87.254.42 on 09/06/12
For personal use only.

TABLE 1. Nuclear magnetic resonance parameters[a] and vibrational frequencies[b] of pyrazolylphosphazenes

| Compound | ν(P=N) (cm$^{-1}$)[j] | Proton shifts, $\delta_H$ (ppm) R(3) | H(4)[c] | R(5) | Coupling constants (Hz) $J_{3,4}$ | $J_{4,5}$ | $\delta_P$ (ppm)[i] |
|---|---|---|---|---|---|---|---|
| pzH[d] | — | 7.61 | 6.31 | 7.61 | 1.9 | 1.9 | — |
| **1***a*[k] | 1238 | 7.82[c] | 6.37 | 8.04 | 1.5 | 1.9 | −111.9 |
| **2***a*[e] | 1428 | 7.75[c] | 6.28 | 8.49 | 1.4 | 2.8 | −137.8 |
| **3***a* | 1425, 1447 | 7.56[c] | 6.18 | 8.22 | 1.5 | 2.7 | −137.1 |
| **4***a*[f] | 1356 | 7.61[c] (7.52)[g] | 6.21 (6.24) | 8.06 (7.52) | 1.5 (2.1) | 2.9 (2.1) | −136.9 |
| MepzH[d] | — | 2.32 | 6.06 | 7.48 | — | 1.7 | — |
| **1***b*[k] | 1234 | 2.22 | 6.10 | 7.90 | — | 2.8 | −112.8 |
| **2***b* | [h] | 2.21 | 6.02 | 8.34 | — | 2.7 | −137.6 |
| **3***b* | [h] | 2.13 | 5.98 | 8.21 | — | 2.6 | −137.2 |
| $Me_2$pzH[d] | — | 2.21 | 5.76 | 2.21 | — | — | — |
| **1***c*[k] | 1228 | 2.09 | 5.81 | 2.19 | — | — | −114.3 |
| **2***c* | [h] | 2.02 | 5.67 | 2.16 | — | — | −131.1 |

[a]Dilute solutions in $CDCl_3$, $\delta_H$, internal TMS, $\delta_P$, negative shifts to high field of external $P_4O_6$.
[b]From mulls in Nujol or hexachlorobutadiene.
[c]$J_{PH} < 1.0$ Hz.
[d]Reference 3.
[e]$J_{3,5} \sim 0.5$ Hz.
[f]$J_{3,5} \sim 0.7$ Hz.
[g]Parenthesised numbers refer to solution in $CCl_4$.
[h]Obscured.
[i]Cf. $\delta_P$ for $(NPF_2)_{3,4}$ = −98.6, −129.5 (4), $(NPCl_2)_{3,4}$ = −92.5, −119.5 (5), $(NPBr_2)_{3,4}$ = −162.0, −184.3 (6), $[NP(NMe_2)_2]_{3,4}$ = −87.7, −102.9 (7), $(NPMe_2)_{3,4}$ = −80.6, −86.2 (8).
[j]Cf. ν(P=N) for $(NPF_2)_{3,4}$ = 1305, 1425/1445 (32), $(NPCl_2)_{3,4}$ = 1218, 1315 (33), $(NPBr_2)_{3,4}$ = 1126/1175, 1272 (6), $[NP(NMe_2)_2]_{3,4}$ = 1195, 1265 (34), $(NPMe_2)_{3,4}$ = 1180, 1220 (9).
[k]Pyrazole ring frequency almost independent of ring size of phosphazene: **1***a*–**4***a*, ~ 1520; **1***b*–**3***b*, ~ 1540; **1***c*, **2***c*, ~ 1570 cm$^{-1}$.

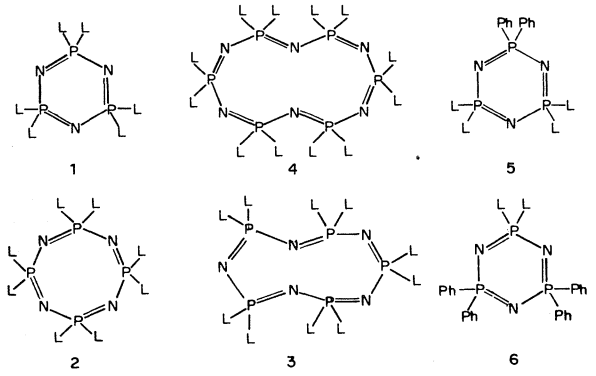


FIG. 2. L is the pyrazolyl group (Fig. 1*a*); **1***a*–**4***a*, $R^3 = R^5 =$ H; **1***b*–**3***b*, **6***a*, $R^3$ = Me, $R^5$ = H, **1***c*, **2***c*, **5**, **6***b*, $R^3 = R^5$ = Me. The following abbreviations are used throughout: pz = 1-pyrazolyl, Mepz = 1-(3-methylpyrazolyl), $Me_2$pz = 1-(3,5-dimethylpyrazolyl).

white solids, that either melt or decompose above 200°C. They are stable to moist air, insoluble in acetonitrile and acetone, increasingly soluble (especially the methyl derivatives) in tetrahydrofuran, diethyl ether, benzene, and chloroform. The pyrazolylphenylphosphazenes are soluble in aromatic solvents.

Spectroscopic information on **1**–**6** is given in Tables 1 and 2. The proton nmr spectra show that the pyrazolyl groups on a particular phosphorus atom are magnetically equivalent. The 3- and 5-positions are differentiated. If $R^3$ and $R^5$ are identical, and contain protons which couple to $H^4$, $R^5$ is identified through the larger coupling constant $J_{4,5}$, arising from the greater double bond character of $C^4$—$C^5$. In the series **1***a*–**4***a*, the order H(5) > H(3) > H(4) for $\delta_H$ was confirmed by comparing the $^{31}$P-decoupled spectra to those of the corresponding methylpyrazolyl compounds (Table 1). The same order is found in $Ppz_3$ and $PhPpz_2$ (11); in $(Me_2N)_2Ppz$ (12) the H(3) resonance is at low field. The methyl signals themselves appear as sharp singlets. The lower-field methyl resonance in **1***c*, **2***c* is arbitrarily assigned to Me(5) by analogy with **1***a*–**4***a*. The peak separation $\Delta = \delta_H R(5) - \delta_H R(3)$ varies with solvent and temperature. Some typical results for **5** are shown in Table 3. Similar phenomena are observed in the spectra of (trimethylsilyl)pyrazoles (13) and in phosphino- and phosphinato-azoles (11). In the former, an intramolecular migration of the $Me_3Si$ group has been suggested to account for the coalescence of the 3- and 5-substituent resonances upon increasing the temperature. The behaviour of the pyrazolylphosphazenes is evidently different, because the coalescence is unsymmetrical, and in $CCl_4$ the bands separate when the temperature is increased. The significantly larger separations found for aromatic

TABLE 2. Nuclear magnetic resonance parameters[a] and vibrational frequencies[b] of phenylpyrazolylphosphazenes

| Compound | ν(P=N) (cm$^{-1}$) | Proton shifts $\delta_H$ (ppm) | | | Phosphorus: $\delta_P$ (ppm) | | J(PP) (Hz) |
|---|---|---|---|---|---|---|---|
| | | R(3) | H(4) | R(5) | $Ppz_2$ | $PPh_2$[e] | |
| **5** | 1219, 1231 | 2.04 | 5.77 | 2.11 | −115.8 | −90.6 | 25 |
| **6***b*[c] | 1214–1224 | 2.12 | 5.81 | 2.18 | −117.5 | −94.1 | 19.9 |
| **6***a*[d] | 1212, 1188 | 2.28 | 6.04 | 7.88 | −118.4 | −93.2 | 19.9 |

[a]Dilute solutions in $CDCl_3$, $\delta_h$, internal TMS, $\delta_P$, negative shifts to high field of external $P_4O_6$.
[b]From mulls in Nujol or hexachlorobutadiene.
[c]$J_{PH(4)}$ = 2.8 Hz.
[d]$J_{PH(4)}$ = 2.7 Hz, $J_{PH(5)}$ = 1.7 Hz, $J_{H(4)H(5)}$ = 2.7 Hz.
[e]Cf. −98.2 ppm in $N_3P_3Ph_6$ (10).

TABLE 3. Peak separation Δ (Hz) of **5** in different solvents[a]

| $CDCl_3$ | | $C_6H_5NO_2$ | | $C_6D_5CD_3$ | | $CS_2$ | | $CCl_4$ | |
|---|---|---|---|---|---|---|---|---|---|
| *T* | Δ | *T* | Δ | *T* | Δ | *T* | Δ | *T* | Δ |
| −30 | 14 | Amb | 19.5 | Amb | 27 | −75 | 3.3 | Amb | 0 |
| Amb | 7.0 | 50 | 20.5 | | | Amb | 0 | 55 | 3.2 |
| 55 | 4.5 | 70 | 21.4 | | | | | 70 | 4.4 |

[a]Amb for ambient.

solvents is probably a result of the interaction of the induced magnetic fields of the solvent and the pyrazole ring.

The $^{31}P$ chemical shifts (Table 1) vary with ring size in qualitatively the same way as in other phosphazene series; shielding is greater in the tetramer than in the trimer, and is greater for compounds with the more electronegative ligands. A similar statement applies to $\nu_{as}$ (P=N). Both criteria suggest that the pyrazolyl group resembles the more electronegative ligands F, Cl, Br, in withdrawing electrons from the phosphazene ring, rather than the methyl- or dimethylamido-groups which release them. Table 2 shows that the introduction of $PPh_2$ groups increases the shielding of neighbouring $Ppz_2$ groups, as expected.

The mass spectra of the trimeric pyrazolyl derivatives are similar to those of the halogen-derivatives, in that the parent ion is dominant; the appearance of metastable peaks shows that $R_2pz$ groups are lost consecutively. The significant difference is that the intensity of the parent peak of the pyrazolyls decreases rapidly with increase in ring size; no parent ion was found in the spectrum of **4***a* (Fig. 3). It is probable that the transannular attack, suggested as an explanation for the formation of $N_3P_3$ fragments from $N_6P_6Cl_{12}$ (14), would be facilitated by the good donor properties of the pyrazolyl groups. A similar interaction could account for the low yield obtained in the preparation of the pyrazolylphosphazenes, as discussed below.

All the pyrazolylphosphazenes, **1–6** were prepared from the chlorophosphazene and an excess of the pyrazole in THF or benzene, triethylamine

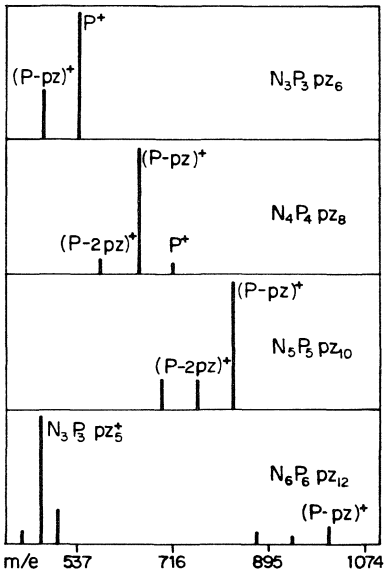


FIG. 3. The mass spectra of **1***a*–**4***a*. The mass numbers of the parent ions are marked; the individual base peaks are given the same intensity. Fragments less abundant than 5% of the base peak are omitted.

being used as an acceptor for hydrogen chloride. Triethylamine hydrochloride was precipitated almost quantitatively, and was variably contaminated by unidentified by-products. The yields of pyrazolylphosphazenes were also variable. They decreased with increase in the size of the phosphazene ring, and with the excess of the pyrazole and triethylamine; broadly speaking, by those changes in reaction conditions which would facilitate parasitic attack of a pyrazolyl group, free or combined, on phosphorus. In agreement, and with the exception of the trimeric derivatives (in which the ring is too small to allow transannular attack), methylation of the pyrazole ring also reduces the yield. Within the same molecule (reaction [1]), nucleophilic attack is made easier by an increase in electron density at the pyridinic nitrogen atom, the greater flexibility of the larger rings, and the partial

Can. J. Chem. Downloaded from www.nrcresearchpress.com by 210.87.254.42 on 09/06/12
For personal use only.

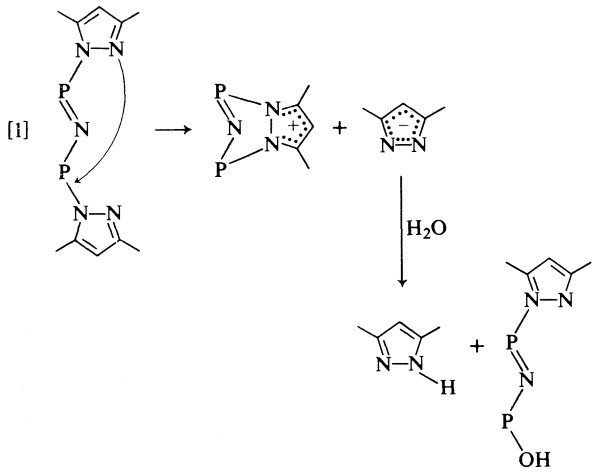


positive charge on phosphorus induced by the substituent. A similar intermolecular reaction is clearly also possible; either would account for the large amounts of $Me_2pzH$ and MepzH recovered (with near-quantitative formation of $Et_3N{\cdot}HCl$) in their reactions with $(NPCl_2)_{5,6}$. In the later stages of this investigation, it was found that benzene was a better solvent than tetrahydrofuran, in that smaller amounts of by-products were formed and yields were improved. Such compounds as $[NP(Me_2pz)]_5$ could probably be obtained by using it.

The reaction appears to resemble that of catechol with the chlorophosphazenes (15), in which, also, the precipitation of $Et_3N{\cdot}HCl$ in high yield is accompanied by ring degradation; in this case no cyclic derivative of larger size than the trimer could be obtained. No such difficulties are found with the reaction of the phenylchlorophosphazenes with the pyrazoles, in which the reactivity of $PCl_2$ groups to nucleophiles is drastically reduced. The reactions of *gem*-$N_3P_3Ph_2Cl_4$ and *gem*-$N_3P_3Ph_4Cl_2$ are slow, those of the latter especially so, but by-products are absent and the yields are excellent.

The chemical properties of the pyrazolylphosphazenes are consistent with the general concepts developed above. As reported earlier (2), and confirmed here for **2***b*, they are cleaved by HCl more easily than are the dimethylamidophosphazenes, but qualitatively appear to be more stable to hydrolysis than is the trimeric imidazolide $N_3P_3Im_6$ (16); similarly, *N*-acetylimidazole is hydrolysed faster than *N*-acetylpyrazole (1). Since, also, pyrazolylphosphines are hydrolysed faster than are pyrrolylphosphines (17), it is likely that the first stage in the reaction is the protonation of the pyridinic nitrogen (16, 17). For the pyrazolylphosphazenes, its completion is aided by both the induced partial positive charge on phosphorus, and the slight extension (relative to dimethylamidophosphazenes) of the exocyclic P—N bond (2).

The donor sites of phosphazenes are almost always the nitrogen atoms in the ring, whether the acceptor group is a proton (18) or a metal ion (19), even when the use of other sites might reduce steric strain (20). Exceptionally, quaternisation of dimethylamidophosphazenes can occur exocyclically (21), and one tungsten carbonyl complex is known in which the metal is bound to ring and exocyclic nitrogen atoms (22). The structures of the five complexes reported here (Fig. 4) have been established spectroscopically, the numerical detail being given in Table 4.

The low electrical conductivities of **7***a*, *b*; **8***a*, *b* in nitromethane reported in the Experimental part show that ionisation plays no important part in determining the stereochemistry. The ν(Pd—Cl) frequencies in **7***a*, **7***b* are assigned to the $A_1$ (sym) and $B_1$ (asym) vibrations of a *cis*-coordinated $PdCl_2$ group of symmetry $C_{2v}$, by comparison with the spectra of *cis*-$PdCl_2(py)_2$ (23), *cis*-$PdCl_2(im)_2$ (24), and *cis*-$PdCl_2(Me_2pzH)_2$ (25), and the broad lines found in the spectra of **8***a*, **8***b*, and **9** are also more in accord with this type of coordination than with a *trans*-configuration, for which a single sharp line would be expected. Coordination at the nitrogen atoms of the phosphazene ring of **7***a* is ruled out by the magnetic equivalence of the two $Me_2pz$ groups. The $^{31}P$ spectrum of **7***a* is of the ABX type, the two $PPh_2$ phosphorus atoms being distinguished. The molecule is therefore stereochemically rigid, in the form shown in Fig. 4; the more downfield $PPh_2$ resonance is assigned to the phosphorus atom $P_A$ closest to the $PdCl_2$ unit. Compound **7***b* introduces a new feature, in that it contains four pyrazolyl groups and coordination might occur at two pyrazolyl groups on the same, or different, phosphorus atoms. The $^1H$ nmr spectrum shows two sets of pyrazolyl groups, consistent with both possibilities. The ABX pattern of the $^{31}P$ spectrum excludes the second possibility, which would require an $A_2X$

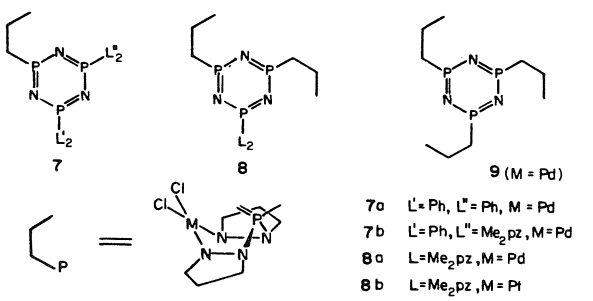


FIG. 4. Schematic stereochemistry of pyrazolylphosphazene complexes.

Can. J. Chem. Downloaded from www.nrcresearchpress.com by 210.87.254.42 on 09/06/12
For personal use only.

TABLE 4. Nuclear magnetic resonance parameters[a] and vibrational frequencies[b] of Pd and Pt complexes of pyrazolylphosphazenes

| Compound | ν(P=N) ($cm^{-1}$) | ν(M—Cl) ($cm^{-1}$) | Proton shifts $\delta_H$ (ppm)[c] H(4) | Me | Phosphorus shifts $\delta_P$ (ppm) $PPh_2$ | $P(Me_2pz)_2$ | $J_{PP}$(Hz)[d] |
|---|---|---|---|---|---|---|---|
| **7***a* | 1230 | 325, 329 | 5.74 (~ 4.0) | 2.04[e] | $1P_A$, −93.0 | $1P_X$, − 122.7 | 0.0 (AB) |
| | 1197 | 341 | | 2.68 | $1P_B$, −95.0 | | 14.2 (AX) |
| | 1180 | | | | | | 27.3 (BX) |
| **7***b* | 1200 | 332 | 5.83 (~ 4.0) | 2.16[f] | $1P_X$, −91.5 | $1P_A$, −113.8 | 49.7 (AB) |
| | 1246 | 347 | | 2.38 | | $1P_B$, −118.1 | 18.1 (AX) |
| | | | 6.02 (~ 4.0) | 2.70 | | | 32.7 (BX) |
| **8***a* | 1212 | 344 br | 5.92 (4.8) | 2.05, 2.32 | | | |
| | 1225 sh | | 5.98 (4.0) | 2.35, 2.61 | | | |
| | | | 6.03 (4.8) | 2.63, 2.72 | | | |
| **8***b* | 1212 | 344 br | 6.02 (5.0) | 2.10, 2.27 | | | |
| | 1225 sh | | 6.12 (5.0) | 2.35, 2.61 | | | |
| | | | | 2.63, 2.70 | | | |
| **9** | 1227 | 344 br | 6.19 br | 2.52, 2.73 | | 3P, −123.8 | |

[a] $CDCl_3$ or $CD_2Cl_2$ (**9**) solutions. Referred to internal TMS or external $P_4O_6$. Negative shifts to high field of reference.
[b] From Nujol mulls; br = broad.
[c] Coupling constants in parentheses.
[d] AX = $P_AP_X$, BX = $P_BP_X$, AB = $P_AP_B$.
[e] Cf. 1.93, 2.69δ in $PdCl_2(Me_2PzH)_2$ (25)
[f] Successive relative intensities 2:1:1.

pattern. The nmr evidence does not distinguish between the two isomers shown (Fig. 5).

Apart from the substitution of platinum for palladium, the empirical formulae of **8***a* and **8***b* are the same, and their $^1H$, $^{31}P$, and infrared spectra suggest that they are isostructural. The $^{31}P$-decoupled $^1H$ nmr spectrum of **8***a* shows six singlets of equal intensity in the methyl region and three singlets of equal intensity in the H(4) region, corresponding to three non-equivalent sets containing two $Me_2pz$ groups each. The $^{31}P$ nmr spectrum of **8***a* is of the ABC type (Fig. 6), which is uniquely consistent with the schematic stereochemistry of Fig. 4. If the boat-shaped complexed pyrazolyl groups were turned towards one another, the two sets of $Me_2pz$ groups would be magnetically equivalent; a doublet and a triplet would be seen in the $^{31}P$ spectrum, and there would be two resonances of intensity ratio 2:1 for H(4), and at most four methyl resonances.

The introduction of a third metal atom simplifies the spectra. The infrared spectrum of **9** is almost identical to that of the ligand, particularly in the region of 1200 $cm^{-1}$, where $\nu_{as}$(P=N) remains

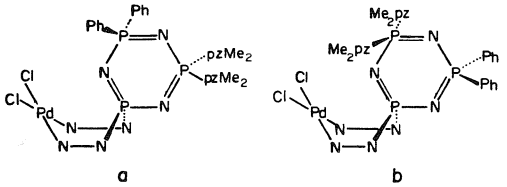


FIG. 5. Alternative structures of **7***b*.

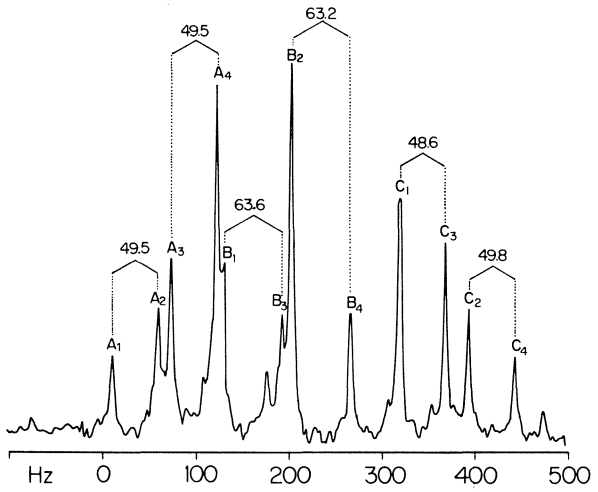


FIG. 6. The $^1H$-decoupled $^{31}P$ nmr spectrum of **8***a* (40.5 MHz, $CDCl_3$). Analysis, by method of ref. 35, in Table 4.

single, suggesting that the complex has a high symmetry. The symmetrical nature of the coordination is confirmed by the pair of singlets in the methyl region of the proton spectrum and by the singlet in the $^{31}P$ spectrum. The H(4) resonance remains as a broad unresolved band, in contrast to the observable couplings of ~ 4.0 Hz apparent in the spectra of the other palladium derivatives. The schematic stereochemistry is therefore that shown in Fig. 4.

We can conclude that in all the complexes, as in other pyrazolyl complexes of the same metals (26), the palladium or platinum has its normal square

Can. J. Chem. Downloaded from www.nrcresearchpress.com by 210.87.254.42 on 09/06/12
For personal use only.

Can. J. Chem. Downloaded from www.nrcresearchpress.com by 210.87.254.42 on 09/06/12
For personal use only.

planar coordination, that coordination occurs through two pyrazolyl groups on the same phosphorus atom, and that, where there is more than one coordination group in the same molecule, the boat-shaped groups are oriented in the same direction; successive addition of metal halides takes place in the sense **7** → **8** → **9** of Fig. 4. The infrared spectra show no evidence of additional coordination of the metal to the nitrogen atoms of the phosphazene ring, which would be expected to lower ν(M—Cl) by 15–20 $cm^{-1}$ (27). Such a lowering is in fact found in the complexes of **5** with $ZnCl_2$ and with $CoCl_2$, to be reported later in detail. The coordination chemistry of the Pd, Pt complexes confirms the spectroscopic results on the ligands, that the pyrazolyl group is an electronegative substituent on the phosphazene ring, which withdraws electron density sufficiently strongly to overcome the normal coordination properties of the phosphazene ring.

## Experimental

The chlorophosphazenes $(NPCl_2)_{3-6}$ (5) and the phenylchlorophosphazenes *gem*-$N_3P_3Ph_4Cl_2$ (28) and *gem*-$N_3P_3Ph_2Cl_4$ (29) were prepared as described in the literature. Pyrazole, 3-methylpyrazole, and 3,5-dimethylpyrazole (Aldrich) were purified by sublimation or distillation. Diethyl ether and tetrahydrofuran were distilled from sodium/benzophenone, benzene and xylene from $LiAlH_4$, and dichloromethane from $P_2O_5$. Methanol was dried over 4A molecular sieves, and acetonitrile and triethylamine over $CaH_2$. Standard methods (30) were used to make *cis*-bis(benzonitrile)dichloroplatinum (II) and *trans*-bis(benzonitrile)dichloropalladium (II). The pyrazolylphosphazenes were dried at 110°C.

Infrared spectra, calibrated against polystyrene, were obtained from Nujol or hexachlorobutadiene mulls on CsI or polyethylene plates, using Perkin-Elmer 457 or 225 spectrophotometers. Mass spectra were recorded at 70 eV on Varian (Atlas) CH 4-B and (for compounds with m.w. > 1000) Kratos AEI MS-902 mass spectrometers. Nuclear magnetic resonance spectra were run on Varian XL-100 ($^1H$, 100 MHz; $^{31}P$, 40.5 MHz), HA-100 ($^1H$, 100 MHz), and Nicolet-Oxford H-270 ($^1H$, 270 MHz) spectrometers. Double resonance techniques were used for $^{31}P$–$^1H$ decoupling (31). Conductance measurements were made with a Wayne Kerr Universal Bridge, Model B221A on solutions in nitromethane, ~ $10^{-3}$ *M*.

*$N_3P_3(pz)_6$ (1a)*

A solution of pyrazole (1.62 g, 23.8 mmol, 25% excess) and triethylamine (2.11 g, 20.9 mmol, 10% excess) in 50 mL THF was added dropwise to a stirred solution of $N_3P_3Cl_6$ (1.10 g, 3.16 mmol) in 60 mL THF. After heating under reflux for 24 h, the white precipitate (3.32 g) was filtered off, and the part soluble in chloroform (2.50 g) was identified as $Et_3N{\cdot}HCl$ (96%). Some of the product (0.15 g) was crystallised from the concentrated and cooled filtrate. The solvent was removed, and the residual white solid was heated at 110°C/0.1 Torr for 2 h, to remove traces of $Et_3N{\cdot}HCl$ and the excess of pyrazole. Crystallisation from acetonitrile yielded a further 0.15 g, of **1***a* (total 18%) as colourless prismatic needles, decomp. 268°C. *Anal.* calcd. for $C_{18}H_{18}N_{15}P_3$: C 40.2, H 3.4, N 39.1; found: C 40.1, H 3.3, N 39.2.

*$N_4P_4(pz)_8$ (2a)*

In a similar but faster reaction, 1.06 g of $N_4P_4Cl_8$ gave $Et_3N{\cdot}HCl$ (2.30 g, 92%), insoluble by-products (1.318 g) and **2***a* (0.30 g, 20%), which was recrystallised from acetonitrile/1,2-dichloroethane; decomp. 361°C. *Anal.* found: C 40.6, H 3.3, N 39.4.

*$N_5P_5(pz)_{10}$ (3a)*

By a similar method, but with a reduced excess of pyrazole (10%) and triethylamine (5%), $N_5P_5Cl_{10}$ (3.89 g, 6.7 mmol) gave a clear colourless oil, which was dissolved in 100 mL 1:1 acetonitrile/toluene and passed through a column of alumina. Slow evaporation of the solvent yielded colourless crystals (2.71 g, 45%) of **3***a*; decomp. 249°C. *Anal.* found: C 40.5, H 3.4, N 38.8.

*$N_6P_6(pz)_{12}$ (4a)*

The reaction product from $N_6P_6Cl_{12}$ (2.13 g, 3.1 mmol) was crystallised from acetonitrile/1,2-dichloroethane as **4***a* (0.692 g, 21%); decomp. 316°C. *Anal.* found: C 40.4, H 3.3, N 38.9.

*$N_3P_3(Mepz)_6$ (1b)*

3-Methylpyrazole (2.40 g, 29.2 mmol, 6% excess) and triethylamine (3.08 g, 30.4 mmol, 10% excess) were heated under reflux with $N_3P_3Cl_6$ (1.60 g, 4.6 mmol in 110 mL THF for 24 h. The $Et_3N{\cdot}HCl$ and by-products were filtered off, and the solvent removed *in vacuo*. The semisolid residue was washed with acetonitrile and crystallised from acetonitrile/1,2-dichloroethane as **1***b* (0.87 g, 30%); mp 213–218.5°C. *Anal.* calcd. for $C_{24}H_{30}N_{15}P_3$: C 46.4, H 4.9, N 33.8; found: C 46.7, H 4.9, N 33.9.

*$N_4P_4(Mepz)_8$ (2b)*

In a similar reaction, the product from $N_4P_4Cl_8$ (1.52 g, 3.3 mmol) was recrystallised from acetonitrile as **2***b* (1.60 g, 59%); mp 253.5–255°C. *Anal.* found: C 46.5, H 4.8, N 33.5. Hydrogen chloride was bubbled into a benzene solution of **2***b* (0.12 g, 0.15 mmol) for 10 min. The clear colourless solution was heated under reflux for 10 min and the solvent removed. The product was a mixture of $N_4P_4Cl_8$ and MepzH·HCl.

*$N_5P_5(Mepz)_{10}$ (3b)*

In a similar preparative experiment with $N_5P_5Cl_{10}$, the colourless oily product was identified by $^1H$ nmr spectroscopy as a mixture of 3-methylpyrazole and **3***b*. The pure compound was not isolated.

*$N_3P_3(Me_2pz)_6$ (1c)*

From $N_3P_3Cl_6$ (1.66 g, 4.8 mmol), 3,5-dimethylpyrazole (3.21 g, 33.3 mmol), and triethylamine (3.18 g, 31.4 mmol) in 115 mL THF, a white solid product (1.92 g) was obtained, which was crystallised from acetonitrile/1,2-dichloroethane as colourless blocks of **1***c*, 58%; mp 253.5–254.5°C. *Anal.* calcd. for $C_{30}H_{42}N_{15}P_3$: C 51.1, H 6.0, N 29.8; found: C 51.1, H 5.9, N 29.7. The product was also obtained in 91% yield by using benzene as a solvent, and a 5% excess of both triethylamine and 3,5-dimethylpyrazole. No by-products were found.

*$N_4P_4(Me_2pz)_8$ (2c)*

From $N_4P_4Cl_8$ (1.86 g, 4.0 mmol), 3,5-dimethylpyrazole (3.50 g, 36.4 mmol, 13% excess) and triethylamine (3.58 g, 35.4 mmol) in 115 mL THF, a colourless product was obtained, which was crystallised from benzene as **2***c*, 0.303 g; 8%, mp 222.5°C (gels). *Anal.* found: C 51.3, H 6.1, N 29.7. The yield was improved (to 17%) and the quantity of by-products diminished, by using the theoretical quantity of the pyrazole.

gem-*$N_3P_3Ph_2(Me_2pz)_4$ (5)*

A solution of 3,5-dimethylpyrazole (0.85 g, 8.9 mmol) and triethylamine (0.99 g, 9.8 mmol) in 50 mL THF was added to a

Can. J. Chem. Downloaded from www.nrcresearchpress.com by 210.87.254.42 on 09/06/12
For personal use only.

stirred solution of *gem*$N_3P_3Ph_2Cl_4$ (0.96 g, 2.2 mmol) in 70 mL THF, and the mixture heated under reflux for 8 days. The white precipitate consisted solely of $Et_3N{\cdot}HCl$. The solvent was evaporated from the filtrate, leaving a clear pale yellow oil which solidified on standing. Residual $Et_3N{\cdot}HCl$ and 3,5-dimethylpyrazole were removed by sublimation *in vacuo*, and the residue crystallised from acetonitrile/1,2-dichloroethane as colourless needles of **5** (1.34 g, 90%); mp 217.5–219°C. *Anal.* calcd. for $C_{32}H_{38}N_{11}P_3$: C 57.4, H 5.7, N 23.0; found: C 57.1; H 5.6, N 22.8.

gem-$N_3P_3Ph_4(Me_2pz)_2$ (**6***b*)

In a similar but slower reaction, *gem*-$N_3P_3Ph_4Cl_2$ (1.50 g, 2.9 mmol), 3,5-dimethylpyrazole and triethylamine (both in 10% excess) in 120 mL xylene were heated under reflux for 8 days, when 81% of the pyrazole had reacted. The product was crystallised from acetonitrile/1,2-dichloroethane as colourless blocks of **6***b* (1.10 g, 73%); mp 211–212.5°C. *Anal.* calcd. for $C_{34}H_{34}N_7P_3$: C 64.5, H 5.4, N 15.5; found: C 64.7, H 5.4, N 15.5.

gem-$N_3P_3Ph_4(Mepz)_2$ (**6***a*)

The product from a similar reaction of *gem*-$N_3P_3Ph_4Cl_2$ in 80 mL xylene was obtained as an adduct with acetonitrile. The acetonitrile was removed by heating the powdered crystals at 100°C/0.1 Torr for 3 h, giving **6***a* (0.77 g, 71%) mp 203–208°C. *Anal.* calcd. for $C_{32}H_{30}N_7P_3$: C 63.5, H 5.0, N 16.2; found: C 63.4, H 5.0, N 16.0.

gem-$N_3P_3Ph_4(Me_2pz)_2{\cdot}PdCl_2$ (**7***a*)

A solution of $PdCl_2(PhCN)_2$ (0.045 g, 0.12 mmol) in 10 mL dichloromethane was filtered into a stirred solution of **6***b* (0.070 g, 0.11 mmol) in 5 mL dichloromethane. The solution gradually became orange, and deposited a yellow precipitate during 24 h at room temperature. The precipitate was crystallised from chloroform as **7***a* (0.081 g, 90%); decomp. 250°C. *Anal.* calcd. for $C_{34}H_{34}Cl_2N_7P_3Pd$: C 50.4, H 4.2, N 12.1; found: C 51.0, H 4.1, N 11.6. $\Lambda_M$(nitromethane) = 1.21 $cm^2$ $ohm^2$ $mol^{-1}$.

gem-$N_3P_3Ph_2(Me_2pz)_4{\cdot}PdCl_2$ (**7***b*)

In a similar experiment, in which benzene was used as a solvent, **5** with an excess of $PdCl_2(PhCN)_2$ yielded an orange solid, which was recrystallised from chloroform as orange needles of **7***b* (34%); decomp. 225°C, *Anal.* calcd. for $C_{32}H_{38}Cl_2N_{11}P_3Pd$: C 45.4, H 4.5, Cl 8.4, N 18.2; found: C 45.2, H 4.4, Cl 8.1, N 17.9. $\Lambda_M$(nitromethane) = 3.41 $cm^2$ $ohm^{-1}$ $mol^{-1}$.

$N_3P_3(Me_2pz)_6{\cdot}2PtCl_2$ (**8***b*)

In a slower reaction, a suspension of **1***c* (0.101 g, 0.14 mmol) in 30 mL benzene was heated under reflux with $PtCl_2(PhCN)_2$ (0.203 g, 0.43 mmol) for 7 days. The yellow precipitate was filtered off, washed with 50 mL benzene, and crystallised from chloroform/benzene as **8***b* (0.076 g, 43%); mp 275–280°C. *Anal.* calcd. for $C_{30}H_{42}Cl_4N_{15}P_3Pt_2$: C 29.1, H 3.4, N 17.0; found: C 29.5, H 3.4, N 15.7. The sample contained traces of benzene which could not be removed by heating it *in vacuo*. $\Lambda_M$(nitromethane) = 1.68 $cm^2$ $ohm^{-1}$ $mol^{-1}$.

$N_3P_3(Me_2pz)_6{\cdot}2PdCl_2$ (**8***a*)

The similar reaction of **1***c* with $PdCl_2(PhCN)_2$ was complete after 4 days. The dull yellow solid was crystallised from chloroform/benzene as orange blocks of **8***a* (80%); decomp. 250°C. *Anal.* calcd. for $C_{30}H_{42}Cl_4N_{15}P_3Pd_2$: C 34.0, H 4.0, Cl 13.4, N 19.8; found: C 34.1, H 4.8, Cl 13.8, N 19.5. Alternatively, the reaction was carried out in dichloromethane (**1***c*:Pd = 1:2) for 16 h. The orange solution was concentrated and added to a large volume of hexane. The yellow solid was filtered off and washed with benzene: yield 99%. $\Lambda_M$(nitromethane) = 2.26 $cm^2$ $ohm^{-1}$ $mol^{-1}$.

$N_3P_3(Me_2pz)_6{\cdot}3PdCl_2$ (**9**)

In the above reactions, no more than two $MCl_2$ groups could be introduced because the complexes were insoluble in benzene. The better solvent dichloromethane allowed further reaction. A solution of $PdCl_2(PhCN)_2$ (0.145 g, 0.38 mmol) in 30 mL dichloromethane was filtered into a solution of **1***c* (0.085 g, 0.12 mmol) in 3 mL dichloromethane. The orange solution was heated under reflux for 24 h, concentrated to 3 mL, and added dropwise to a large volume of hexane. The orange–yellow solid was filtered off and crystallised from dichloromethane as **9** (0.143 g, 96%); decomp. 250°C. *Anal.* calcd. for $C_{30}H_{42}Cl_6N_{15}P_3Pd_3$: C 29.1, H 3.4, N 17.0; found: C 29.9, H 3.8, N 16.6.

## Acknowledgements

We thank the Natural Sciences and Engineering Research Council of Canada for financial support, and the technical staff of the Department of Chemistry for the analyses, the nmr and mass spectra, and the illustrations.

1. H. A. STAAB. Angew. Chem. Int. Ed. Engl. **1**, 351 (1962).
2. K. D. GALLICANO, N. L. PADDOCK, S. J. RETTIG, and J. TROTTER. Inorg. Nucl. Chem. Lett. **15**, 417 (1979).
3. J. ELGUERO, R. JACQUIER, and H. C. N. TIEN DUC. Bull. Soc. Chim. Fr. 3727 (1966).
4. C. W. ALLEN, T. MOELLER, and F. Y. TSANG. Inorg. Chem. **7**, 2183 (1968); V. MARK, C. H. DUNGAN, M. M. CRUTCHFIELD, and J. R. VAN WAZER. Top. Phosphorus Chem. **5**, 227 (1967).
5. L. G. LUND, N. L. PADDOCK, J. E. PROCTOR, and H. T. SEARLE. J. Chem. Soc. 2542 (1960).
6. K. JOHN and T. MOELLER. J. Inorg. Nucl. Chem. **22**, 199 (1961).
7. R. KEAT, R. A. SHAW, and M. WOODS. J. Chem. Soc. Dalton, 1582 (1976).
8. H. T. SEARLE, J. DYSON, T. N. RANGANATHAN, and N. L. PADDOCK. J. Chem. Soc. Dalton, 203 (1975).
9. H. T. SEARLE. Proc. Chem. Soc. 7 (1959).
10. H. P. LATSCHA. Z. Anorg. Chem. **382**, 7 (1968).
11. S. FISCHER, L. K. PETERSON, and J. F. NIXON. Can. J. Chem. **52**, 3981 (1974).
12. J. ELGUERO and R. WOLF. Compt. Rend. Ser. C, **265**, 1507 (1967).
13. D. H. O'BRIEN and C.-P. HRUNG. J. Organomet. Chem. **27**, 185 (1971); V. N. TOROCHESHNIKOV, N. M. SERGEYEV, N. A. VIKTOROV, G. S. GOLDIN, V. G. PODDUBNY, and A. N. KOLTSOVA. J. Organomet. Chem. **70**, 347 (1974).
14. C. E. BRION and N. L. PADDOCK. J. Chem. Soc. A, 388 (1968).
15. H. R. ALLCOCK. J. Am. Chem. Soc. **86**, 2591 (1964).
16. H. R. ALLCOCK and T. J. FULLER. J. Am. Chem. Soc. **103**, 2250 (1981).
17. S. FISCHER, J. HOYANO, and L. K. PETERSON. Can. J. Chem. **54**, 2710 (1976).
18. D. FEAKINS, W. A. LAST, and R. A. SHAW. J. Chem. Soc. 4464 (1964); N. V. MANI and A. J. WAGNER. Acta Crystallogr. B**27**, 51 (1971).
19. H. P. CALHOUN, N. L. PADDOCK, and J. N. WINGFIELD. Can. J. Chem. **53**, 1765 (1975).
20. R. W. ALLEN, J. P. O'BRIEN, and H. R. ALLCOCK. J. Am. Chem. Soc. **99**, 3987 (1977).
21. J. N. RAPKO and G. R. FEISTEL. Inorg. Chem. **9**, 1401 (1970).
22. H. P. CALHOUN, N. L. PADDOCK, and J. TROTTER. J. Chem. Soc. 2708 (1973).

23. J. R. DURIG, R. LAYTON, D. W. SINK, and B. R. MITCHELL. Spectrochim. Acta, **21**, 1367 (1965).
24. J. REEDIJK and J. K. DE RIDDER. Inorg. Nucl. Chem. Lett. **12**, 585 (1976).
25. F. COLETTA, R. ETTORE, and A. GAMBARO. J. Inorg. Nucl. Chem. **37**, 314 (1975).
26. G. MINGHETTI, G. BANDITELLI, and F. BONATI. J. Chem. Soc. Dalton Trans. 1851 (1979); F. BONATI and H. C. CLARK. Can. J. Chem. **56**, 2513 (1978); J. POWELL and A. KUKSIS. Can. J. Chem. **57**, 2527 (1979).
27. T. THEOPHANIDES and P. C. KONG. Can. J. Chem. **48**, 1084 (1970).
28. E. T. MCBEE, K. OKUHARA, and C. J. MORTON. Inorg. Chem. **4**, 1672 (1965).
29. C. D. SCHMULBACH and C. DERDERIAN. J. Inorg. Nucl. Chem. **25**, 1395 (1963).
30. F. R. HARTLEY. Organomet. Chem. Rev. A, **6**, 119 (1970).
31. L. D. HALL and R. BURTON. Can. J. Chem. **48**, 59 (1970).
32. H. J. BECHER and F. SEEL. Z. Anorg. Chem. **305**, 148 (1960).
33. L. W. DAASCH. J. Am. Chem. Soc. **76**, 3403 (1954).
34. R. A. CHITTENDEN and L. C. THOMAS. Spectrochim. Acta, **22**, 1449 (1966).
35. S. CASTELLANO and J. S. WAUGH. J. Chem. Phys. **34**, 295 (1961).

Can. J. Chem. Downloaded from www.nrcresearchpress.com by 210.87.254.42 on 09/06/12
For personal use only.

# Crystalline structure and vibrational spectra of *cis*-dichlorodiammine-*trans*-dihydroxo-platinum(IV), $PtCl_2(NH_3)_2(OH)_2$

R. FAGGIANI, H. E. HOWARD-LOCK, AND C. J. L. LOCK

*Institute for Materials Research, McMaster University, 1280 Main St. W., Hamilton, Ont., Canada L8S 4M1*

AND

B. LIPPERT[1] AND B. ROSENBERG

*Department of Biophysics, Michigan State University, East Lansing, MI 48823, U.S.A.*

Received July 7, 1981

R. FAGGIANI, H. E. HOWARD-LOCK, C. J. L. LOCK, B. LIPPERT, and B. ROSENBERG. Can. J. Chem. **60**, 529 (1982).

The structure of *cis*-dichlorodiammine-*trans*-dihydroxoplatinum(IV), $PtCl_2(OH)_2(NH_3)_2$, has been determined by X-ray diffraction. The tetragonal space group, $P4_2/n$ has cell dimensions $a = 7.328(4)$, $c = 11.362(5)$ Å and has four formula units in the cell. Intensities were measured using MoKα radiation and a Syntex $P2_1$ diffractometer. The crystal structure was determined by standard methods and refined to $R_1 = 0.0460$, $R_2 = 0.0639$ based on 447 independent reflections. The platinum atom has roughly octahedral coordination and Pt—Cl, Pt—N, Pt—O distances (2.306(4), 2.00(1), 2.00(1) Å) are normal. The crystal is held together by hydrogen bonds, and the vibrational spectra have been correlated with observed features of the hydrogen bonding.

R. FAGGIANI, H. E. HOWARD-LOCK, C. J. L. LOCK, B. LIPPERT et B. ROSENBERG. Can. J. Chem. **60**, 529 (1982).

On a déterminé, par diffraction de rayons X, la structure du dichorodiamine-*cis* dihydroxo-*trans* platine(IV), $PtCl_2(OH)_2(NH_3)_2$. Le cristal appartient au groupe d'espace tétragonal $P4_2/n$; les dimensions de la maille sont: $a = 7{,}328(4)$, $c = 11{,}362(5)$ Å et comporte quatre unités par maille. On a mesuré les intensités en utilisant la radiation MoKα et un diffractomètre Syntex $P2_1$. On a résolu la structure du cristal par des méthodes normales et on l'a affiné jusqu'à une valeur conventionnelle de $R_1 = 0{,}0460$ et de $R_2 = 0{,}0639$ à partir de 447 réflexions indépendantes. L'atome de platine a grossièrement une géométrie de coordination octaédrique et les distances Pt—Cl, Pt—N, Pt—O (2,306(4), 2,00(1), 2,00(1) Å) sont normales. Le cristal est maintenu par des liaisons hydrogènes et on a fait correspondre les spectres de vibration aux caractéristiques de la liaison hydrogène.

[Traduit par le journal]

## Introduction

Since the original report on the antitumor activity of two platinum(IV) compounds, *cis*-$Pt(NH_3)_2Cl_4$ and $Pt(en)Cl_4$ (1), relatively little work has been done on the field of cancerostatic Pt(IV) complexes until recently. It had earlier been suggested that Pt(IV) complexes might be superior to Pt(II) compounds because of membrane transport properties (2). It was further assumed that the antitumor activity of Pt(IV) involves reduction inside the cell to the corresponding Pt(II) complexes with loss of the two *trans* ligands. Such an assumption is reasonable and it has been verified that ascorbic acid and cysteine, for example, can reduce Pt(IV) to Pt(II) (3). In a recent systematic study, Tobe *et al.* examined the differences in solubility, toxicity, and antitumor activity between *cis*-$Pta_2Cl_2$ (with a = amine) and *cis*-$Pta_2Cl_2(OH)_2$ (4). As a result no clear-cut structure–activity relation emerged, yet it became obvious that for a = $NH_3$ the compound *cis*-dichlorodiammine-*trans*-dihydroxyplatinum(IV), $PtCl_2(NH_3)_2(OH)_2$, in the test systems used, was clearly superior to *cis*-$Pt(NH_3)_2Cl_2$, the most widely used Pt-compound in cancer treatment of humans presently.

We were interested in this compound both for its antitumor activity and for structural comparison with hydroxo-bridged complexes of Pt(II) we isolated recently (5). Hydroxo-complexes of tetravalent platinum exist in a wide variety both with terminal and bridging hydroxo groups (6), yet only for two such compounds are crystallographic data available at present (7, 8).

## Experimental section

The compound was prepared as described previously (9). Elemental analysis (Glabraith Laboratories): H 2.50, N 8.35, O 9.72, Pt 58.56, Cl 21.29; calcd: H 2.39, N 8.40, O 9.58, Pt 58.4, Cl 21.23.

Solubility in $H_2O$: ~635 mg/100 mL at room temperature. The deuterated compound was prepared by recrystallization from boiling $D_2O$.

Infrared spectra were recorded on Perkin Elmer 577 and 580 grating spectrometers from 4000 to 180 $cm^{-1}$ as KBr and CsI pellets and from 4000 to 300 $cm^{-1}$ as Nujol mulls (KBr plates). The spectra were calibrated against polystyrene. Raman spectra were obtained from polycrystalline samples between 1800 and 150 $cm^{-1}$ on a Coderg PH1 spectrometer with a He–Ne Laser (Spectraphysics) and calibrated against Laser plasma lines.

*Collection of the X-ray diffraction data*

A crystal, homogeneous under the polarizing microscope, was used for crystallographic studies. Precession photographs

[1]Present address: Anorganische Chemische Institut der Technische Universitat Munchen, Lichtenbergstrasse 4, 8046 Garching, W. Germany.

0008-4042/82/040529-06$01.00/0

©1982 National Research Council of Canada/Conseil national de recherches du Canada

Can. J. Chem. Downloaded from www.nrcresearchpress.com by 210.87.254.42 on 09/06/12
For personal use only.

showed the crystal was tetragonal and unit cell parameters were obtained from least squares fit of $\chi$, $\Phi$, and $2\theta$ for 15 reflections in the range $11° < 2\theta < 26°$ recorded on a $P2_1$ diffractometer using graphite-monochromated MoK$\alpha$ radiation ($\lambda$ 0.71069 Å at 20°C). Crystal data and other numbers related to the data collection are given in Table 1. The density was not determined but was shown to be greater than 3.0 since the crystal sank in aqueous thallium formate solution of that density. Intensity data were recorded on a Syntex $P2_1$ diffractometer using a coupled $\theta$(crystal) – $2\theta$(counter) scan. The methods of selection of scan rates and initial data treatment have been described (10, 11). Corrections were made for Lorentz-polarization effects and absorption.

*Solution of the structure*

The coordinates of the platinum atom were found from a three-dimensional Patterson synthesis, and a three-dimensional electron density difference synthesis revealed the remaining non-hydrogen atoms. All atoms were given anisotropic temperature factors and further refinement using full-matrix least-squares minimizing $\Sigma w(|F_o| - |F_c|)^2$ was terminated when the maximum shift/error was 0.01. No attempt was made to locate the hydrogen atoms. Corrections were made for extinction using the method of Larson (12). Throughout the refinement, the scattering curves were taken from ref. 13 and anomalous dispersion corrections from ref. 14 were applied to the curves for platinum and chlorine. The atom parameters are listed in Table 2.[2]

## Results and discussion[3]

The molecule is shown in Fig. 1 and selected interatomic distances are given in Table 3. The bond lengths (Pt—O, 2.00(1), Pt—N; 2.00(1), Pt—Cl, 2.306(4) Å) agree well with those found previously in Pt(IV) compounds (Pt—N range, 1.97(4) to 2.068(17) Å, Pt—Cl range 2.26 Å to 2.309(6) Å, Pt—O, 1.96 Å) (7, 15, 16). Because of the errors it is not possible to differentiate between these values and those observed previously by us for Pt(II) compounds (17), but overall, it appears that the mean distances for the Pt(IV) complexes are about 0.05–0.1 Å shorter than corresponding values in Pt(II) complexes. All angles are close to the 90° or 180° expected for an octahedral complex.

The packing of the molecule within the cell is shown in Fig. 2. The molecules are arranged in layers centred at $z = 0$, $z = 1/4$. The lattice is held together by an extensive hydrogen bonding network, but it is not possible to decide unambiguously which atoms are hydrogen bonded since there are six distances in the range expected for hydrogen bonds (two short N···O, two medium O···Cl, two long, N···Cl) but only four hydrogen atoms (three on $NH_3$, one on OH). A consideration of probable interactions, distances, and angles suggests that the hydrogen bonds are probably disordered with two N—H···O (strong), one N—H···Cl (disordered, weak), and one O—H···Cl (disordered, medium). Within the layers, the sets of molecules related by the $\bar{4}$ axis are held together by the relatively strong $NH_3$···O bonds (N···O, 2.88(2) Å) and the somewhat weaker OH···Cl bonds (O···Cl, 3.39(1) Å). The very weak $NH_3$···Cl bonds (N···Cl, 3.48(1) Å) bind molecules along ***c*** related by the $4_2$ axis. In addition, the molecules in the ***c*** direction are arranged so that dipolar interactions will be maximized.

Infrared and Raman spectra are reported in Table 4, and the modes have been assigned by comparison with *cis*- and *trans*-$Pt(NH_3)_2Cl_4$ (18, 19), *cis*- and *trans*-$[Pt(NH_3)_4Cl_2)]Cl_2$ (18) $Pt(NH_3)_6Cl_4$, *mer*-$[Pt(NH_3)_3Cl_3]Cl{\cdot}H_2O$, $K[Pt(NH_3)Cl_5]{\cdot}H_2O$, $[Pt(NH_3)_5Cl]Cl_3{\cdot}H_2O$ (20, 21), *cis*-$Pt(NH_3)_2Cl_2$ (21, 22), and $K_2[PtCl_4(OH)_2]$ (23) and on the basis of the arguments given below. The isolated $(NH_3)_2PtCl_2$-

TABLE 1. Crystal data

| | |
|---|---|
| Compound | $H_8Cl_2N_2O_2Pt$ |
| Formula weight | 334.07 |
| Crystal size | Rough cube (110) 0.0625 mm, (001) 0.075 from centre |
| Systematic absences | $hk0$, $h + k \neq 2n$, $00l$, $l \neq 2n$ |
| Space group | $P4_2/n$ |
| Unit cell parameters (Å and deg) | $a = 7.328(4)$, $c = 11.362(5)$ |
| Volume (Å$^3$) | 610.1(3) |
| $Z$ | 4 |
| $\rho_{calcd}$ (g cm$^{-3}$) | 3.64 |
| $\rho_{obsd}$ (g cm$^{-3}$) | >3.0 |
| Linear absorption coefficient (cm$^{-1}$) | 249.7 |
| Absorption correction factor, $A$, limits | 8.066 to 36.748 |
| Max $2\theta$, reflections collected | 55° |
| Standard reflections (esd %) | −3 1 −2 (2.0), −1 1 0 (3.6) |
| Temperature (°C) | 22 |
| No. of independent reflections | 447 |
| No. with $I > 3\sigma(I)$ | 302 |
| $3\sigma(I) > I > \sigma(I)$, $F_c > F_o$ | 6 |
| $3\sigma(I) > I > \sigma(I)$, $F_c < F_o$ | 111 |
| $I < \sigma(I)$, rejected | 28 |
| Final $R_1$, $R_2$[a] | 0.0460, 0.0639 |
| Final shift/error, maximum, average | 0.030, 0.008 |
| $g$ (secondary extinction) | $4.21 \times 10^{-7}$ |
| Final difference map | |
| Highest peak (e/Å$^3$), location | 2,0; 0.20, 0.75, 0.50 |
| Lowest valley (e/Å$^3$), location | −3.4; 0.34, 0.66, 0.50 |
| Weight | $w = (\sigma^2 + (0.05F_o)^2)^{-1}$ |

[a] $R_1 = \Sigma||F_o| - |F_c||/\Sigma|F_o|$; $R_2 = \{\Sigma w(|F_o| - |F_c|)^2/\Sigma wF_o^2\}^{1/2}$.

[2]All calculations were carried out on CDC6400 and CYBER 170/730 Computers. Initial data treatment used programs from the X-Ray 76 package (27). The structure was solved using the Fourier program, SYMFOU, and full-matrix least-squares program, CUDLS, written internally by Rutherford and Stephens, respectively. Diagrams were prepared using ORTEP-II (28).

[3]A table of the moduli of $F_o$ and $F_c$ is available on request, at a nominal charge, from the Depository of Unpublished Data, CISTI, National Research Council of Canada, Ottawa, Ont., Canada K1A 0S2.

Can. J. Chem. Downloaded from www.nrcresearchpress.com by 210.87.254.42 on 09/06/12
For personal use only.

TABLE 2. Final positional and thermal parameters[a] (Å²) (×10³)

| Atom | $x$ | $y$ | $z$ | $U_{11}$ | $U_{22}$ | $U_{33}$ | $U_{12}$ | $U_{13}$ | $U_{23}$ |
|---|---|---|---|---|---|---|---|---|---|
| Pt | 750 | 250 | 20.77(5)[b] | 9.2(5) | 7.8(7) | 14.5(6) | 0 | 0 | 0 |
| Cl | 750.1(5) | 26.6(5) | 163.7(3) | 27(2) | 19(2) | 22(1) | 3(2) | 0(2) | −4(2) |
| N | 750(2) | 50(2) | −98.9(7) | 21(7) | 5(6) | 8(4) | 10(6) | 11(5) | 1(4) |
| O | 477(1) | 250(2) | 25.6(6) | 7(6) | 8(5) | 6(5) | 5(6) | −7(6) | 3(5) |

[a] The form of the anisotropic thermal ellipsoid is $\exp[-(\beta_{11}h^2 + \cdots + 2\beta_{12}hk + \cdots)]$ and $U_{ij}$ was obtained from $\beta_{ij} = 2\pi^2 b_i b_j U_{ij}$ where $b_i$ are the reciprocal lattice vectors.
[b] Standard deviations of the least significant figures are given here and in subsequent tables in parentheses.

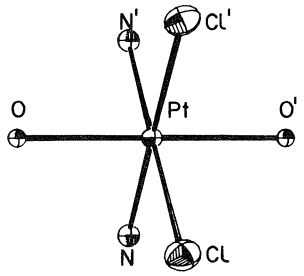


FIG. 1. The molecule *cis*-dichlorodiammine-*trans*-dihydroxoplatinum(IV).

$(OH)_2$ molecule is of point group $C_{2v}$ if $NH_3$ and OH are treated as monoatomic groups, but the site symmetry of $(NH_3)_2PtCl_2(OH)_2$ is reduced to $C_2$ in the crystal. The vibrational modes can be classified, in a first approximation, into those caused by the $NH_3$ and OH ligands and those caused by the $N_2PtCl_2O_2$ skeleton. The latter will be considered first.

The normal modes expected for the $N_2PtCl_2O_2$ system, having $C_2$ site symmetry, are $8A + 7B$, all both infrared- and Raman-active. The stretching modes for this skeleton are distributed as follows: $\nu(Pt—Cl) = A + B$, $\nu(Pt—N) = A + B$, and $\nu(Pt—O) = A + B$. A classification of the skeletal stretching vibrations on a site group approach is reasonable for most of the bands observed, since a multiplicity of bands as expected in a factor group analysis is not observed (c.f. Table 4). Because of the low solubility of the title compound in the solvents used, Raman polarization studies could not be performed and thus no definitive assignment of bands to particular symmetry species was possible. The two Pt—Cl stretching vibrations are observed at 335 and 350 $cm^{-1}$ in the ir spectrum and at 338 and 347 $cm^{-1}$ in the Raman spectrum. They are almost unaffected by deuteration, thus indicating that they are not significantly coupled to Pt—N modes of the same symmetry. The Pt—Cl stretching vibrations absorb in the range observed for other complexes of Pt(IV) with chloro ligands *trans* to $NH_3$ groups (18, 19).

For Pt—N and Pt—O modes of the same symmetry coupling must be taken into consideration, since $NH_3$ and OH have not only almost identical point masses but also identical distances to platinum (2.00 Å) in our compound. Comparison with other complexes of Pt(IV) suggests that Pt—N and Pt—O stretching vibrations can be expected at very similar energies (Pt—N range, 512–603 $cm^{-1}$ (18–22), Pt—O, 540, 548 $cm^{-1}$ (23)). The relatively low energy Pt—O stretching modes in $[(CH_3)_3Pt(OH)]_4$ (340 and 430 $cm^{-1}$ (24)) do not contradict the above assumption because of the relatively weak Pt—O bond (2.22 Å) and its partially ionic character (8*a*). Pt—N, Pt—O stretching modes are observed in the ir spectrum of the title compound at 575, 558, 457, and 420 $cm^{-1}$. The highest frequency band can be observed only under high resolution (1.3 $cm^{-1}$) and is, with lower resolution, buried under the strong 558 $cm^{-1}$ band. In the Raman spectrum, bands are observed 578, 550, 535, 448, and 410 $cm^{-1}$. There is one band more than predicted by $C_2$ site symmetry considerations in both the ir and Raman spectra in the range expected for Pt—N and Pt—O stretching vibrations. Moreover, the demanded "coincidence" between the bands at 457 (ir) and 448 (Raman), 420 (ir) and 410 (Raman),

TABLE 3.[a]

(*a*) Selected interatomic distances (Å)

| Atoms | Distance | Atoms | Distance |
|---|---|---|---|
| Pt—O | 2.00(1) | N···O[a] | 2.88(2) |
| Pt—N | 2.00(1) | N···Cl[d] | 3.48(1) |
| Pt—Cl | 2.306(4) | N···O[b] | 2.88(2) |
| | | O···Cl[a] | 3.39(1) |
| | | N···Cl[c] | 3.48(1) |
| | | O···Cl[e] | 3.39(1) |

(*b*) Selected angles (deg)

| Bonds | Angle | Bonds | Angle |
|---|---|---|---|
| N—Pt—N[f] | 94.3(4) | Pt—NO[a] | 111.3(5) |
| N—Pt—O | 91.1(5) | Pt—NCl[d] | 102.6(5) |
| Cl—Pt—O[f] | 88.9(4) | Pt—ON[a] | 125.8(7) |
| N—Pt—Cl | 87.6(3) | Pt—NO[b] | 111.3(5) |
| N—Pt—O[f] | 91.0(5) | Pt—OCl[a] | 118.2(5) |
| Cl—Pt—O | 88.9(4) | Pt—ON[e] | 126.0(7) |
| N—Pt—Cl[f] | 178.0(3) | Pt—NCl[c] | 102.6(5) |
| Cl—Pt—Cl[f] | 90.4(1) | Pt—OCl[e] | 118.2(5) |
| O—Pt—O[f] | 176.9(3) | | |

[a] Atoms are related to those in Table 2 by *a*, $1-x, -y, -z$; *b*, $\frac{1}{2}+x, y-\frac{1}{2}, -z$; *c*, $1-y, x-\frac{1}{2}, z-\frac{1}{2}$; *d*, $\frac{1}{2}+y, 1-x, z-\frac{1}{2}$; *e*, $x-\frac{1}{2}, \frac{1}{2}+y, -z$; *f*, $1.5-x, \frac{1}{2}-y, z$.

Can. J. Chem. Downloaded from www.nrcresearchpress.com by 210.87.254.42 on 09/06/12
For personal use only.

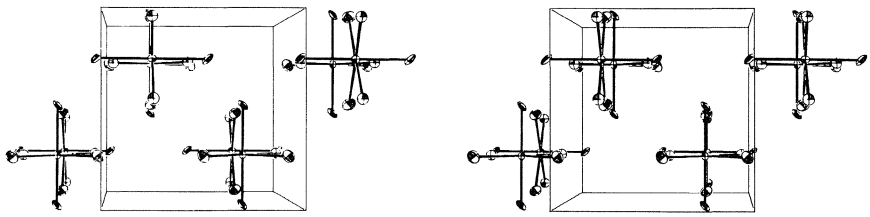

FIG. 2. The packing of the molecule in the unit cell. *a* and *b* are parallel to the bottom and side of the page respectively and the view is down *c*.

Can. J. Chem. Downloaded from www.nrcresearchpress.com by 210.87.254.42 on 09/06/12
For personal use only.

558 (ir) and 550 $cm^{-1}$ (Raman) is poorer than with those of the higher frequency bands (578 (575) and 535 (535 $cm^{-1}$)) and the Pt—Cl modes. The intensity of the ir band at 457 $cm^{-1}$ indicates the latter is a fundamental, and it is not possible to determine the position of the 448 $cm^{-1}$ Raman bands with high accuracy because of its low intensity and the steep slope of the baseline. We assume that the 457 (ir) and the 448 $cm^{-1}$ (Raman) bands are actually coincident, and thus the 420 (ir) and the 410 $cm^{-1}$ (Raman) bands are interpreted as combination bands of skeletal deformation modes (cf. Table 4). An alternative interpretation, namely that factor group coupling causes splitting of one or two (if coupled intramolecularly) skeletal stretching vibrations and results in noncoincidence seems unreasonable because such splittings are usually considerably smaller than those observed (35 $cm^{-1}$ in ir, 38 $cm^{-1}$ in Raman). In the spectra of the deuterated compound the identification of five of the six expected skeletal stretching modes is straightforward since the three high frequency bands and the Pt—Cl modes (in the ir spectrum not resolved) coincide reasonably well. The most prominent change in the ir spectrum of the deuterated compound is the "disappearance", or at least considerable loss of intensity, of the original 457 $cm^{-1}$ band. In the 400–500 $cm^{-1}$ range of the ir-spectra of the deuterated compound, only a weak and broad band around 450 $cm^{-1}$ (KBr, CsI pellet) is observed, and the corresponding band in the Nujol mull (448 $cm^{-1}$) is even weaker. In the same range of the Raman spectrum only one distinct band of low intensity is observed at 434 $cm^{-1}$, though there are several other features at 418, 458, 469, 480, and 490 $cm^{-1}$ whose intensities, however, are too low to interpret them unambiguously as real bands. It is therefore not possible to identify the "missing" sixth band of the skeletal stretching modes with certainty.

Because of vibrational coupling between the Pt—N and Pt—O stretching motions and because hydrogen bonding affects these two motions differently, these vibrations cannot be unambiguously assigned without a detailed force constant analysis. Nevertheless, we suggest a tentative way of estimating which of the two stretching motions (Pt—N or Pt—O) makes the predominant contribution to each band, based on the fact that the Pt—N and Pt—O skeletal stretching vibrations are shifted to a different degree upon deuteration. The very strong Raman band at 578 $cm^{-1}$ is shifted to 567 $cm^{-1}$ in the deuterated species (567/578 = 0.981), the very strong Raman band from 535 $cm^{-1}$ to 502 $cm^{-1}$ (502/535 = 0.938), and the most intense ir band at 558 $cm^{-1}$ is shifted to 538 $cm^{-1}$ giving an isotopic shift of 0.964. Treating $NH_3/ND_3$ and OH/OD, respectively, as point masses vibrating against the heavy Pt-mass, and assuming no coupling, the isotopic/normal frequency ratios should approximate the value $\sqrt{17/20} = 0.922$ for $ND_3/NH_3$ and $\sqrt{17/18} = 0.972$ for OD/OH platinum vibrations. Therefore, we suggest the band at 535 $cm^{-1}$ (Raman), 538 $cm^{-1}$ (ir) is caused mainly by a Pt—N stretching motion and the 578 $cm^{-1}$ band (Raman), 575 $cm^{-1}$ (ir) is caused mainly by a Pt—O motion.

The Raman bands observed below the Pt—Cl stretching modes are listed in Table 4. No attempt was made to classify these skeletal deformation bands.

The ir spectrum above 600 $cm^{-1}$ consists of the absorptions of the individual $NH_3$ and OH group vibrations and combination and overtone vibrations, respectively. The stretching vibrations of the OH groups are well separated from those of the $NH_3$ ligands and appear at 3515 $cm^{-1}$ with multiple slight shoulders between 3495 and 3350 $cm^{-1}$. These shoulders, as well as their shifts in the spectrum of the deuterated compound ($\nu_{OH}/\nu_{OD}$ = 1.352), indicate some hydrogen bonding between hydroxo protons and chloro ligands. The PtO—$H_1$ bending vibration appears at 1039 $cm^{-1}$ in the ir spectrum of the undeuterated compound and at 773 $cm^{-1}$ in the deuterated compound. The position of this vibration falls in the range observed also for δ(PtO—H) modes in *trans*-$K_2[PtCl_4(OH)_2]$ (23) and in a series of hydroxo bridged complexes of Pt(II) (5) as well as other metal complexes containing terminal hydroxo groups (25).

Can. J. Chem. Downloaded from www.nrcresearchpress.com by 210.87.254.42 on 09/06/12
For personal use only.

TABLE 4. Infrared and Raman bands of *cis*-dichlorodiammine, *trans*-dihydroxoplatinum(IV), (*A*), and its deuterated analogue (*B*) in $cm^{-1}$

| Infrared (Nujol, KBr plates)[a] | | Raman (solid)[b] | | |
|---|---|---|---|---|
| *A* | *B* | *A* | *B* | Assignment |
| 3515 s, sh<br>3495···3350 m, sh | 2599 s<br>2570···2500 m, sh | | | νOH (OD) |
| 3260 s<br>3170 m<br>3100···2900 s, b[c] | 2426 s<br>2342 m<br>2322 m, 2180 s,<br>2072 m | | | $\nu NH_3$ ($ND_3$) |
| 2716 w | | | | $2 \times \delta_s(NH_3)$ |
| 2671 vw; 2516 vw;<br>2446 w; 2276 w;<br>2106 vw; 1876 vw;<br>1814 w | | | | |
| | 1840 vw; 1810 vw;<br>1720 w | | | |
| 1606 w<br>1585 m<br>1551 w | 1177 sh<br>1165 m<br>1132 w | 1604 (1)<br><br>1560 (2) | | $\delta_d NH_3$ ($ND_3$) |
| | | 1412 (2)<br>1393 (2)<br>1379 (7) | | |
| 1361 m | 1040 m | | | $\delta_s NH_3$ ($ND_3$) |
| 1171 w | | 1160 (1) | | $2 \times 578\,cm^{-1}$ |
| | | 1103 (2) | | $2 \times 558\,cm^{-1}$ |
| 1039 vs | 773 s, 739 sh | | | δPtO—H (PtO—D) |
| 966 s<br>907 s | 725 w[c]<br>695 m, 687 sh | | | $\rho_r NH_3$ ($ND_3$) |
| 917 sh, sp | | 924 (1) | | $2 \times 457\,cm^{-1}$ |
| 826 vw | | 821 (1) | | |
| | | 658 (1) | | |
| 575 sh<br>558 vs<br>535 m<br>457 s | 570 sh<br>538 vs<br>499 m<br>450 vw, br | 578 (100)<br>550 (17)<br>535 (64)<br>448 (5) | 567 (100)<br>548 (7)<br>502 (72)<br>434 (8) | νPtO, νPtN<br>(2*A* + 2*B*) |
| 420 sh | | 410 (8) | | $238 + 190\,cm^{-1}$ |
| 350 sh<br>335 s | 350 sh<br>332 s | 347 (66)<br>338 (48) | 347 (75)<br>340 (56) | νPtCl (*A* + *B*) |
| 290 sh, s; 276 s;<br>238 s; 190 m[d] | 278 s; 259 s;<br>225 s[d] | 311 (1); 272 (6);<br>248 (11); 230 (1);<br>210 (1); 170 (2) | 332 (10); 293 (1);<br>265 (4); 248 (1);<br>236 (8); 216 (8) | δPtO, δPtN, δPtCl[e]<br>(5*A* + 4*B*) |

[a] Infrared intensities: vs = very strong, s = strong, m = medium, w = weak, vw = very weak, sh = shoulder, br = broad, sp = sharp.
[b] Raman intensities relative to strongest Raman band at 578 (567) $cm^{-1}$ with arbitrary intensity 10.
[c] Only observable in KBr and CsI spectra.
[d] Bands below 300 $cm^{-1}$ only observable in CsI spectra.
[e] Typically δPt—N occurs at ~200 $cm^{-1}$; δPt—Cl at ~170 $cm^{-1}$.

The $NH_3$ stretching vibrations cover a rather large range with distinct bands at 3260 and 3170 $cm^{-1}$ and a broad, unresolved band centered around 3000 $cm^{-1}$. The last is caused by the ammine protons hydrogen bonded to oxygen atoms of neighbouring molecules whereas the two former are probably caused by the NH weakly bonded to Cl. The absorptions of the degenerate deformation modes of the $NH_3$ ligands appear at 1606, 1585, and 1551 $cm^{-1}$, those of the symmetric deformation modes as a single band at 1361 $cm^{-1}$. The somewhat higher positions of these bands in $Pt(NH_3)_2Cl(OH)_2$ compared to *cis*-$Pt(NH_3)_2Cl_4$ (18) are interpreted in terms of strong intermolecular hydrogen bonding between NH and O. The splitting of the degenerate deformation modes in $Pt(NH_3)_2Cl_2(OH)_2$

is preserved in the spectrum of the deuterated compound; this supports our interpretation of differing ammine protons.

There are two bands of approximate equal intensity at 966 and 907 $cm^{-1}$ in the ir spectrum of our compound, which, because they are shifted upon deuteration, are attributed to $NH_3$ vibrations. $NH_3$ rocking frequencies are known to be very sensitive to both the nature and the oxidation state of a metal (26) and thus a shift to higher energy is expected when *cis*-$Pt(NH_3)_2Cl_2^-$ ($\rho_r(NH_3) = 805, 790\ cm^{-1}$) (22) is compared to a closely related Pt(IV) complex. Even higher frequencies for $NH_3$ rocking vibrations are expected and observed for positively charged complexes of Pt(IV) (18, 20–22). The high positions for the $NH_3$ rocking modes in our complex, $Pt(NH_3)_2Cl_2(OH)_2$, undoubtedly are caused by hydrogen bonding. We assign the 966 band to the strongly-hydrogen bonded ammine protons and the other band to the weakly bonded one. The sharp shoulder at 917 $cm^{-1}$ is interpreted as the overtone of the 457 $cm^{-1}$ skeletal vibration. The $NH_3$ rocking frequencies are shifted in the deuterated compound to 725 and 695 $cm^{-1}$. The former band is observed only in spectra obtained from samples in discs KBr and CsI spectra since it falls under the Nujol absorption in this range.

## Acknowledgements

We thank the Natural Sciences and Engineering Research Council of Canada, the McMaster University Science and Engineering Research Board, Johnson, Matthey, Mallory Ltd., Englehard Industries, Matthey Bishop Inc., and the National Cancer Institute of Canada for financial support of this work.

1. B. Rosenberg, L. Van Camp, J. E. Trosko, and V. H. Mansour. Nature, **222**, 385 (1969).
2. A. J. Thomson, R. J. P. Williams, and S. Reslova. Struct. Bonding, **11**, 1 (1972).
3. M. J. Cleare, P. C. Hydes, D. R. Hepburn, and B. W. Malerbi. *In* Cisplatin, current status and new developments. *Edited by* A. W. Prestayko, S. T. Crooke, and S. K. Carter. Academic Press, New York. 1980.
4. (*a*) M. L. Tobe and A. R. Khokhar. J. Clinical Hemat. Oncol. **7**, 114 (1977); (*b*) A. H. W. Nias and I. I. Szumiel. J. Clinical Hemat. Oncol. **7**, 562 (1977).
5. R. Faggiani, B. Lippert, C. J. L. Lock, and B. Rosenberg. Inorg. Chem. **17**, 2971 (1978) and references therein.
6. F. R. Hartley. The chemistry of platinum and palladium. Applied Science Publishers, London. 1973.
7. C. O. Bjorling. Arkiv. Kemi. Min. Geol. **B15**, No. 2 (1941).
8. (*a*) T. G. Spiro, D. H. Templeton, and A. Zalkin. Inorg. Chem. **7**, 2165 (1968); (*b*) H. S. Preston, J. C. Mills, and C. H. L. Kennard. J. Organomet. Chem. **14**, 447 (1968).
9. L. Tschugajeff and W. Chlopin. Z. Anorg. Chem. **151**, 253 (1926).
10. B. Lippert, C. J. L. Lock, B. Rosenberg, and M. Zvagulis. Inorg. Chem. **16**, 1525 (1977).
11. R. P. Highes, N. Krishnamachari, C. J. L. Lock, J. Powell, and G. Turner. Inorg. Chem. **16**, 314 (1977).
12. A. C. Larson. Acta Crystallogr. **23**, 664 (1967).
13. D. T. Cromer and J. T. Waber. *In* International tables for X-ray crystallography. Vol. IV. *Edited by* J. A. Ibers and W. C. Hamilton. Kynoch Press, Birmingham, England. 1974. Table 2.2A, p. 72*ff*.
14. D. T. Cromer. *In* International tables for X-ray crystallography. Vol. IV. *Edited by* J. A. Ibers and W. C. Hamilton. Kynoch Press, Birmingham, England. 1974. Table 2.3.1, pp. 149–150.
15. B. M. Craven and D. Hall. Acta Crystallogr. **14**, 475 (1961).
16. C. F. Liu and J. A. Ibers. Inorg. Chem. **9**, 773 (1970).
17. C. J. L. Lock, R. A. Speranzini, and M. Zvagulis. Acta Crystallogr. B**36**, 1789 (1980) and references therein.
18. D. W. James and M. J. Nolan. J. Raman Spectrosc. **1**, 271 (1973).
19. D. M. Adams and P. J. Chandler. J. Chem. Soc. A, 1009 (1967).
20. M. J. Nolan and D. W. James. J. Raman Spectrosc. **1**, 259 (1973).
21. J. Haraishi, I. Nakagawa, and T. Shimanouchi. Spectrochim. Acta, **24**, 819 (1968).
22. H. Ponlet, P. Delorme, and J. P. Mathieu. Spectrochim. Acta, **20**, 1855 (1964).
23. L. E. Cox and D. G. Peters. Inorg. Chem. **9**, 1927 (1970).
24. P. A. Bulliner and T. G. Spiro. Inorg. Chem. **8**, 1023 (1969).
25. (*a*) D. Scargill. J. Chem. Soc. 4444 (1961); (*b*) R. L. Williams and R. J. Page. J. Chem. Soc. 4143 (1957).
26. G. F. Sratos, D. M. Sweeny, S. I. Mizushima, C. Curran, and J. V. Quagliano. J. Am. Chem. Soc. **79**, 3313 (1957).
27. J. M. Stewart. The X-ray 76 system. Tech. Rep. Tr-446, Computer Science Center, University of Maryland, College Park, MD. 1976.
28. C. K. Johnson. Rep. ORNL-5138 Oak Ridge National Laboratory, TE. 1976.

Can. J. Chem. Downloaded from www.nrcresearchpress.com by 210.87.254.42 on 09/06/12
For personal use only.

# Conjugative interactions in 1-methylpyrrol-2-yl derivatives of the cyclic phosphazenes $(NPF_2)_n$ ($n$ = 3–6): the crystal and molecular structure of 1-methylpyrrol-2-ylheptafluorocyclotetraphosphazene

RAJENDRA D. SHARMA, STEVEN J. RETTIG, NORMAN L. PADDOCK, AND JAMES TROTTER

*Department of Chemistry, University of British Columbia, 2036 Main Mall, Vancouver, B.C., Canada V6T 1Y6*

Received April 27, 1981

RAJENDRA D. SHARMA, STEVEN J. RETTIG, NORMAN L. PADDOCK, and JAMES TROTTER. Can. J. Chem. **60**, 535 (1982).

1-Methylpyrroles, in which the 2-position is occupied by a pentafluorocyclotriphosphazenyl (**1***a*), heptafluorocyclotetraphosphazenyl (**1***b*), nonafluorocyclopentaphosphazenyl (**1***c*), or undecafluorocyclohexaphosphazenyl group (**1***d*), have been prepared from 2-lithio-1-methylpyrrole and the corresponding fluorophosphazene. Crystals of **1***b* are monoclinic, $a$ = 17.300(2), $b$ = 5.0281(3), $c$ = 16.902(2) Å, β = 108.904(4)°, $Z$ = 4, space group $P2_1/n$. The structure was solved by direct methods and was refined by full-matrix least-squares procedures to $R$ = 0.038 and $R_w$ = 0.047 for 1167 observed reflections. The $N_4P_4$ ring is nearly planar. The P—N bond lengths (corrected for libration) range from 1.524(5) to 1.562(5) Å with a mean value of 1.541(17) Å, and the mean ring angles are 122.9(20)° at phosphorus and 146.4(23)° at nitrogen. The geometry of the 1-methylpyrryl group shows no unexpected features, but the P—C bond (1.756(5) Å) is significantly shorter than in typical P-phenyl derivatives, and the P—F bond at the same atom is comparatively long (1.561(4) Å). Conjugative electron release from the pyrryl group, involving $p_\pi$–$d_\pi$ bonding, is indicated both by these geometrical features and by the appearance of intramolecular charge transfer bands in the electronic spectra of **1**(*a*–*d*).

RAJENDRA D. SHARMA, STEVEN J. RETTIG, NORMAN L. PADDOCK et JAMES TROTTER. Can. J. Chem. **60**, 535 (1982).

La réaction du lithio-2 méthyl-1 pyrrole avec un fluorophospazène approprié conduit à des méthyl-1 pyrroles dans lesquels on trouve en position 2 soit un pentafluorocyclotriphosphazényle (**1***a*), soit un heptafluorocyclotétraphosphazényle (**1***b*), soit un nonafluorocyclopentaphosphazényle (**1***c*) ou undécafluorocyclohexaphosphazényle (**1***d*). Les cristaux du composé **1***b* appartiennent au groupe d'espace $P2_1/n$ avec $a$ = 17,300(2), $b$ = 5,0281(3) $c$ = 16,902(2) Å, β = 108,904(4)°, $Z$ = 4. On a résolu la structure par des méthodes directes et on l'a affinée par la méthode des moindres carrés (matrice entière) jusqu'à des valeurs de $R$ = 0,038 et $R_w$ = 0,047 pour 1167 réflexions observées. Le cycle $N_4P_4$ est presque plan. Les longueurs de liaison P—N corrigées pour la libration varient de 1,524(5) à 1,562(5) Å avec une valeur moyenne de 1,541(17) Å alors que les angles moyens de cycle sont de 122,9(20)° au niveau du phosphore et de 146,4(23)° au niveau de l'azote. La géométrie du groupe méthyl-1 pyrrole ne révèle aucune caractéristique imprévue; toutefois la liaison P—C (1,756(5) Å) est d'une façon significative beaucoup courte que dans les dérivés P-phényles typiques alors que la liaison P—F au niveau du même atome est comparativement longue (1,561(4) Å). Les caractéristiques géométriques et l'apparence de bandes de transfers de charge intermoléculaires dans les spectres électroniques de **1**(*a*–*d*) indiquent que la libération conjuguée d'électron à partir du groupe pyrole, fait intervenir une liaison $p_\pi$–$d_\pi$.

[Traduit par le journal]

## Introduction

Although the inductive effect of substituents on a phosphazene ring has been recognized for some time, conjugative interactions are less well established. The Taft $\sigma_{R^0}$ parameters of fluorophosphazenyl groups are similar to those of cyano- or nitro-groups (1), but the electronic spectrum of a phenyl group is little changed by attachment to a phosphazene ring (2), and the results of a photoelectron spectroscopic investigation are in better agreement with the transmission of the electronic effects of a phenyl group through the σ-bond system (3).

The bonding system in phosphazenes is closely analogous to that in phosphoryl compounds, in which, again, the spectroscopic evidence (4) indicates only weak $p_\pi$–$d_\pi$ bonding between phenyl and phosphoryl groups. Electronic delocalization on to phosphorus is limited by the relatively high electronegativity of carbon, and in general the chemical and spectroscopic evidence for conjugation to a phosphoryl group, reviewed elsewhere (5),

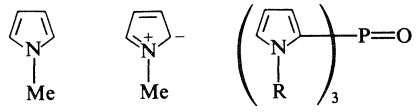


**2***a* **2***b* **3**

is strongest for electron-releasing substituents. The pyrryl group is a good electron donor, because canonical forms of pyrrole like **2***b* make an important contribution to its electronic structure; experimentally, the first ionization energies of pyrrole (8.20 eV) (6) and especially 1-methylpyrrole **2** (7.95 eV) (7) are significantly less than that of benzene (9.25 eV) (8). As a consequence of the conjugative charge transfer to phosphorus, the tri(pyrryl) phosphine oxides **3** show an intense low frequency band in their electronic spectra (9), similar to that found in formyl- and acetyl-pyrroles (10), which is attributed to $p_\pi$–$d_\pi$ bonding (9).

In the expectation that phosphazenyl and phosphoryl groups would behave similarly, we have prepared the 1-methylpyrrol-2-yl fluorophosphazenes $N_nP_nF_{2n-1}\cdot C_4H_3NMe$, ($n$ = 3–6, **1***a*–*d*), and

0008-4042/82/040535-07$01.00/0

©1982 National Research Council of Canada/Conseil national de recherches du Canada

Can. J. Chem. Downloaded from www.nrcresearchpress.com by 210.87.254.105 on 09/06/12
For personal use only.

Can. J. Chem. Downloaded from www.nrcresearchpress.com by 210.87.254.105 on 09/06/12
For personal use only.

have measured their electronic spectra. Since it is conceivable that any conjugation found in this way might be confined to the upper state of the electronic transition, we have also determined the crystal structure of **1***b*, to see whether its geometry might show evidence of conjugation in the ground state.

## Experimental

The fluorocyclophosphazenes $(NPF_2)_n$ ($n$ = 3–6) were prepared by the fluorination of the corresponding chlorides with activated KF. *N,N,N′,N′*-Tetramethylethylenediamine (TMEDA) was stirred over $CaH_2$ for 24 h and distilled at reduced pressure. Diethyl ether was heated with sodium benzophenone under reflux for 12 h, and distilled. 1-Methylpyrrole (Aldrich) was distilled at reduced pressure. All operations were carried out in an atmosphere of dry nitrogen. Ultraviolet spectra were obtained on a Cary 17 spectrophotometer, and nmr spectra were obtained using the following instruments; Varian XL100 ($^1$H, $^{31}$P), Varian CFT20 ($^{13}$C), Bruker WH 400 ($^{13}$C), and Varian EM 360/390 ($^{19}$F).

*Reaction of 2-lithio-1-methylpyrrole with hexafluorocyclotriphosphazene*

An equimolar mixture of *n*-butyllithium (2.2 *M* in hexane, 7.4 mL) and TMEDA (1.89 g, 16.3 mmol) was added dropwise to a solution of 1-methylpyrrole (1.32 g, 16.3 mmol) in 40 mL ether. The resulting solution was added dropwise to a stirred solution of hexafluorocyclotriphosphazene (4.12 g, 16.5 mmol) in 40 mL ether at −20°C. Lithium fluoride was precipitated immediately, and was filtered off (0.425 g, 16.4 mmol) after 2 h at −20°C and 6 h at room temperature. The solvent and the TMEDA were removed at 5 Torr, and the yellow liquid was fractionated at 0.02 Torr to give two components, boiling at 30°C, 50°C. They were purified by gas–liquid chromatography at 180°C: Varian A90P, column 2 ft × 0.25 in, SE30 on 60–80 mesh Chromosorb A treated with HMDS, retention times 3 and 7 min. The major component (50%) was identified as 1-methylpyrrol-2-ylpentafluorocyclotriphosphazene, **1***a*. *Anal.* calcd. for $C_5H_6F_5N_4P_3$: C 19.4, H 1.9, N 18.1; found: C 19.5, H 1.9, N 18.0. The minor component (20%) was bis(1-methylpyrrol-2-yl)tetrafluorocyclotriphosphazene, **4**, a colorless oil which slowly crystallized. *Anal.* calcd. for $C_{10}H_{12}F_4N_5P_3$: C 32.3, H 3.2, N 18.9; found: C 32.6, H 3.3, N 18.7.

The monosubstituted derivatives of $N_4P_4F_8$, $N_5P_5F_{10}$, and $N_6P_6F_{12}$ were prepared similarly. The yield of each was variable in different experiments, but always exceeded 50%. **1***b*, mp 37°C; *Anal.* calcd. for $C_5H_6F_7N_5P_4$: C 15.3, H 1.5, N 17.8; found: C 15.5, H 1.5, N 17.7. **1***c*; *Anal.* calcd. for $C_5H_6F_9N_6P_5$: C 12.6, H 1.3, N 17.6; found: C 12.8, H 1.2, N 17.7. **1***d*; *Anal.* calcd. for $C_5H_6F_{11}N_7P_6$: C 10.7, H 1.1, N 17.5; found C 11.0, H 1.1, N 17.3. Compounds **1***a*,*c*,*d* are liquid at room temperature.

*X-ray crystallographic analysis of* **1***b*

Colorless crystals of **1***b* were obtained from hexane. A crystal ca. 0.19 × 0.28 × 0.48 mm in size was mounted in a general orientation. Unit-cell parameters were refined by least-squares on 2 sin θ/λ values for 25 reflections measured on a diffractometer with Mo Kα Radiation (λ = 0.71073 Å). Crystal data at 22°C are:

$C_5H_6F_7N_5P_4$ fw = 393.0

Monoclinic, $a$ = 17.300(2), $b$ = 5.0281(3), $c$ = 16.902(2) Å, β = 108.904(4)°, $V$ = 1391.0(2) Å$^3$, $Z$ = 4, $\rho_c$ = 1.877 g cm$^{-3}$, $F(000)$ = 776, μ(Mo Kα) = 5.43 cm$^{-1}$. Absent reflections: $h0l$, $h + l \neq 2n$ and $0k0$, $k \neq 2n$ uniquely indicate the space group $P2_1/n$ (non-standard setting of $P2_1/c$, $C_{2h}^5$, No. 14).

Intensities were measured with graphite-monochromated Mo Kα Radiation on an Enraf-Nonius CAD4-F diffractometer. An ω–2θ scan at 1.18–10.06° min$^{-1}$ over a range of (1.00 + 0.35 tan θ) degrees in ω (extended by 25% on both sides for background measurement) was employed. Data were measured to 2θ = 50°. The intensities of three check reflections, measured every 5000 s throughout the data collection, remained constant within 2%.

After data reduction, no absorption correction was made in view of the low value of μ. Of the 2430 independent reflections measured, 1167 (48%) had intensities greater than 3σ($I$) above background where $\sigma^2(I) = S + 2B + (0.04(S - B))^2$ with $S$ = scan count and $B$ = background count.

The structure was solved by direct methods. The positions of the four phosphorus atoms were determined from an $E$-map and those of the remaining non-hydrogen atoms from a subsequent difference map. After full-matrix least-squares refinement of the non-hydrogen atoms with anisotropic thermal parameters to $R$ = 0.047, a difference map gave positions for all six hydrogen atoms which were included in subsequent cycles of refinement with isotropic thermal parameters. The scattering factors of ref. 11 were used for non-hydrogen atoms and those of ref. 12 for hydrogen atoms. Anomalous scattering factors from ref. 13 were used for the P atoms. The weighting scheme $w = 1/\sigma^2(F)$, where $\sigma^2(F)$ is derived from the previously defined $\sigma^2(I)$, gave uniform average values of $w(|F_o| - |F_c|)^2$ over ranges of $|F_o|$ and was employed in the final stages of refinement. Convergence was reached at $R$ = 0.038 and $R_w$ = 0.047 for 1167 reflections with $I \geq 3\sigma(I)$. For all 2430 reflections $R$ = 0.111 and $R_w$ = 0.055. The function minimized was $\sum w(|F_o| - |F_c|)^2$, $R = \sum ||F_o| - |F_c|| / \sum |F_o|$ and $R_w = (\sum w(|F_o| - |F_c|)^2 / \sum w|F_o|^2)^{1/2}$.

On the final cycle of refinement the mean and maximum

TABLE 1. Final positional (fractional; F, N, and C × 10$^4$; P × 10$^5$; H × 10$^3$) and isotropic thermal parameters ($U$ × 10$^3$ Å$^2$) with estimated standard deviations in parentheses

| Atom | $x$ | $y$ | $z$ | $U_{eq.}/U_{iso.}$ |
|---|---|---|---|---|
| P(1) | −6474( 8) | 60335(34) | 21189( 9) | 50 |
| P(2) | 2951( 8) | 36421(38) | 37111( 9) | 54 |
| P(3) | 15032( 9) | 17361(39) | 29930(10) | 62 |
| P(4) | 5372(10) | 38042(41) | 13911(10) | 63 |
| F(1) | −601( 2) | 9086( 7) | 2204( 3) | 90 |
| F(2) | 575( 2) | 5555( 9) | 4440( 2) | 103 |
| F(3) | −63( 2) | 1555( 9) | 4132( 2) | 96 |
| F(4) | 2361( 2) | 2740(12) | 3357( 3) | 122 |
| F(5) | 1696( 3) | −1188(10) | 3082( 3) | 128 |
| F(6) | 949( 2) | 5561(10) | 921( 3) | 108 |
| F(7) | 174( 3) | 1839(11) | 711( 3) | 140 |
| N(1) | −392( 3) | 4924(12) | 3021( 3) | 68 |
| N(2) | 1059( 3) | 2463(14) | 3588( 3) | 96 |
| N(3) | 1207( 3) | 2388(13) | 2081( 3) | 90 |
| N(4) | −129( 3) | 5403(13) | 1550( 3) | 82 |
| N(5) | −2158( 3) | 6324(11) | 876( 3) | 62 |
| C(1) | −1683( 3) | 5374(12) | 1643( 3) | 48 |
| C(2) | −2149( 4) | 3667(16) | 1924( 4) | 63 |
| C(3) | −2923( 4) | 3580(18) | 1332( 5) | 81 |
| C(4) | −2909( 4) | 5233(18) | 714( 5) | 83 |
| C(5) | −1928( 7) | 8326(29) | 385( 6) | 95 |
| H(2) | −201( 3) | 283(11) | 242( 3) | 56(19) |
| H(3) | −339( 4) | 271(13) | 141( 3) | 82(21) |
| H(4) | −333( 3) | 563(12) | 16( 4) | 79(19) |
| H(5a) | −229( 5) | 894(17) | −4( 5) | 114(30) |
| H(5b) | −143( 4) | 881(16) | 47( 4) | 88(28) |
| H(5c) | −190( 6) | 720(20) | 2( 6) | 138(47) |

*Equivalent positions: ±($x$, $y$, $z$; 1/2 − $x$, 1/2 + $y$, 1/2 − $z$) $U_{eq.}$ = (1/3) trace ($U_{diag}$).

TABLE 4. Bond lengths (Å) with estimated standard deviations in parentheses

| Bond | Length | | Bond | Length | |
|---|---|---|---|---|---|
| | Uncorr. | Corr. | | Uncorr. | Corr. |
| P(1)—F(1) | 1.542(4) | 1.561 | P(3)—N(2) | 1.496(5) | 1.522 |
| P(2)—F(2) | 1.513(4) | 1.542 | P(3)—N(3) | 1.495(5) | 1.524 |
| P(2)—F(3) | 1.509(4) | 1.538 | P(4)—N(3) | 1.528(5) | 1.552 |
| P(3)—F(4) | 1.498(4) | 1.533 | P(4)—N(4) | 1.499(5) | 1.524 |
| P(3)—F(5) | 1.505(5) | 1.539 | P(1)—C(1) | 1.741(5) | 1.756 |
| P(4)—F(6) | 1.512(4) | 1.541 | N(5)—C(1) | 1.376(7) | 1.386 |
| P(4)—F(7) | 1.492(5) | 1.524 | N(5)—C(4) | 1.353(8) | 1.363 |
| P(1)—N(1) | 1.547(5) | 1.562 | N(5)—C(5) | 1.441(11) | 1.450 |
| P(1)—N(4) | 1.545(5) | 1.561 | C(1)—C(2) | 1.365(9) | 1.376 |
| P(2)—N(1) | 1.514(5) | 1.537 | C(2)—C(3) | 1.388(8) | 1.396 |
| P(2)—N(2) | 1.523(5) | 1.546 | C(3)—C(4) | 1.342(10) | 1.353 |

TABLE 5. Bond angles (deg) with estimated standard deviations in parentheses, non-hydrogen atoms

| Bonds | Angle (deg) | Bonds | Angle (deg) |
|---|---|---|---|
| F(1)—P(1)—N(1) | 106.1(3) | F(6)—P(4)—N(3) | 107.7(3) |
| F(1)—P(1)—N(4) | 103.8(3) | F(6)—P(4)—N(4) | 107.5(3) |
| F(1)—P(1)—C(1) | 104.3(2) | F(7)—P(4)—N(3) | 107.8(3) |
| N(1)—P(1)—N(4) | 120.0(3) | F(7)—P(4)—N(4) | 109.7(3) |
| N(1)—P(1)—C(1) | 108.1(3) | N(3)—P(4)—N(4) | 123.4(3) |
| N(4)—P(1)—C(1) | 113.0(3) | P(1)—N(1)—P(2) | 144.7(3) |
| F(2)—P(2)—F(3) | 97.5(2) | P(2)—N(2)—P(3) | 147.6(4) |
| F(2)—P(2)—N(1) | 108.7(3) | P(3)—N(3)—P(4) | 144.2(4) |
| F(2)—P(2)—N(2) | 107.2(3) | P(1)—N(4)—P(4) | 148.9(4) |
| F(3)—P(2)—N(1) | 108.7(3) | C(1)—N(5)—C(4) | 107.0(6) |
| F(3)—P(2)—N(2) | 107.5(3) | C(1)—N(5)—C(5) | 126.3(6) |
| N(1)—P(2)—N(2) | 124.1(3) | C(4)—N(5)—C(5) | 126.4(7) |
| F(4)—P(3)—F(5) | 97.5(3) | P(1)—C(1)—N(5) | 125.5(5) |
| F(4)—P(3)—N(2) | 107.3(3) | P(1)—C(1)—C(2) | 126.4(4) |
| F(4)—P(3)—N(3) | 108.2(3) | N(5)—C(1)—C(2) | 107.8(5) |
| F(5)—P(3)—N(2) | 108.4(3) | C(1)—C(2)—C(3) | 108.0(7) |
| F(5)—P(3)—N(3) | 108.0(3) | C(2)—C(3)—C(4) | 106.6(7) |
| N(2)—P(3)—N(3) | 124.1(3) | N(5)—C(4)—C(3) | 110.6(6) |
| F(6)—P(4)—F(7) | 97.7(3) | | |

parameter shifts corresponded to 0.01 and 0.16 σ respectively. The mean error in an observation of unit weight was 1.466. A final difference map showed no unusual features. The final positional and thermal parameters appear in Tables 1 and 2[1] respectively. Measured and calculated structure factors have been placed in the Depository of Unpublished Data.[1]

The ellipsoids of thermal motion for the non-hydrogen atoms are shown in Fig. 1. The thermal motion has been analysed in terms of the rigid-body modes of translation, libration, and screw motion (14). The rms standard error in the temperature factors $\sigma U_{ij}$ (derived from the least-squares analysis) is 0.0036 Å$^2$. The molecule as a whole does not behave as a rigid body, but can be broken down into five smaller rigid groups consisting of the four phosphorus tetrahedra and the pyrrole group plus P(1) (rms $\Delta U_{ij} = 21, 14, 19, 14$, and $44 \times 10^{-4}$ Å$^2$ respectively, details in Table 3).[1] The appropriate bond distances have been corrected for libration (15), using shape parameters $q^2$ of 0.08 for all atoms involved. Corrected bond lengths appear in Table 4 along with the uncorrected values; corrected bond angles do not differ by more than 1σ from the uncorrected values given in Table 5. Intra-annular torsion angles defining the conformation of the phosphazene ring are listed in Table 6.

The corrections to the bond lengths in this case are much larger than those usually obtained from this type of analysis, but in view of the high degree of thermal motion in this low-melting compound the corrections seem realistic. Simple riding-motion analysis yields even larger corrections.

## Results and discussion

The occurrence and extent of conjugation between a phosphorus atom and its substituents is a long-standing and important problem. We are concerned here with compounds in which phosphorus is tetrahedrally 4-coordinated. In so far as the 3*s* and 3*p* orbitals are totally used in σ-bonding, conjugation involves the 3*d*-orbitals of phos-

[1]The structure factor table, Table 2 (anisotropic thermal parameters) and other material mentioned in the text are available, at a nominal charge, from the Depository of Unpublished Data, CISTI, National Research Council of Canada, Ottawa, Canada K1A 0S2.

Can. J. Chem. Downloaded from www.nrcresearchpress.com by 210.87.254.105 on 09/06/12
For personal use only.

TABLE 6. Intra-annular torsion angles (deg)

| Atoms | Value | Atoms | Value |
|---|---|---|---|
| N(4)—P(1)—N(1)—P(2) | 14.4(4) | N(2)—P(3)—N(3)—P(4) | 3.3(4) |
| P(1)—N(1)—P(2)—N(2) | −13.0(4) | P(3)—N(3)—P(4)—N(4) | 4.3(4) |
| N(1)—P(2)—N(2)—P(3) | −6.0(4) | N(3)—P(4)—N(4)—P(1) | −21.7(4) |
| P(2)—N(2)—P(3)—N(3) | 5.7(4) | P(4)—N(4)—P(1)—N(1) | 12.4(4) |

phorus. A considerable amount of structural information has been systematized on the basis of the competitive sharing of a pair of $d_\pi$-orbitals, doubly degenerate in $T_d$ symmetry (16). The better donors take the bigger $\pi$-share, and the exocyclic P—N bonds in, for instance, $(NP(NMe_2)_2)_{3,4}$ (17, 18) are short (mean values 1.652(4), 1.678(9) Å) and the $PNMe_2$ groups are close to planarity, in agreement with a substantial contribution to bonding in the sense of **5**. Since the carbon atoms in pyrrole carry no formally unshared pair of electrons, the 1-methylpyrrol-2-yl group should release electrons to a phosphazene ring, but less strongly than a dimethylamido group.

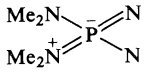

**5**

Pyrrolyl derivatives prepared from $(NPCl_2)_{3,4}$ have been reported previously (19), but few details are available, and the position of substitution in the pyrrole ring is unknown. In the present work, the use of 1-methylpyrrole in conjunction with TMEDA (20) was expected to restrict substitution to the 2-position. The patterns of the $^1H$ and $^{13}C$ shifts of **1***a–d* (Tables 7, 8)[2] are substantially independent of the size of the phosphazene ring, and show that the 2-substitution expected from the preparative method and proved crystallographically for **1***b* is uniform within the series. The shifts of Table 7 were assigned by comparison with those of other 2-substituted pyrroles (21). The resonances of H3 and H5 are shifted downfield from those of 1-methylpyrrole (22), the relationship being approximately that of 2-formylpyrrole to pyrrole (21). In the $^{13}C\{^1H\}$ spectra of **1***a–d*, the $CH_3$ resonance is a singlet, and that of C2 is split into two doublets by phosphorus and fluorine; its assignment is unambiguous. The other assignments are made comparatively (23), C4 at the highest field, and C3 to high field of C5. Comparison of the relative shifts (Table 8) with those of other substituted pyrroles (23) shows that the effect of a 2-(fluorophosphazenyl) group on C3 and C5 is similar to that of a 2-formyl group (relative shifts 13.2, 10.9 ppm respectively). The exceptionally high value of $J_{PC2}$ has no obvious interpretation, but a comparable value (224 Hz) for $J_{PC}$ was found for 3-fluorophenylpentafluorocyclotriphosphazene, and it may be typical of the bond between an aromatic and a phosphazene ring.

The $^{19}F$ spectra consist of doublets for the PFX and $PF_2$ groups, the former being at lower field, as in other mono-substituted fluorophosphazenes (1, 24). As for the analogous fluorophenyl derivatives, two types of $PF_2$ groups are found for **1***c,d*. The $^{31}P$ spectra of **1***a–d*, similar to those of the dimethylamido derivatives, are more complex, and have not been analysed completely. Their main features are given in Table 7. Taken in conjunction with the $^{13}C$ spectra, the $^{19}F$ and $^{31}P$ spectra show that the fluorophosphazenyl group withdraws electrons from C3 and C5, possibly concentrating them more on C2 than on P(1), but a more detailed discrimination of the electronic effects is not possible.

The electronic spectra are more informative. Pyrrole itself has two $\pi-\pi^*$ bands, at 207.5 nm (25) and 183 nm (26). 1-Methylpyrrole has a strong band at 213 nm (9); the vacuum ultraviolet region has apparently not been examined. Both bands of pyrrole are shifted to longer wavelength by electron-withdrawing groups capable of conjugation, such as 2-formyl (279, 246 nm), 1-methyl-2-formyl (280, 246 nm) (10), 2-nitro (335, 231 nm) (21), and 1-methyl-2-cyano (248, 230.5 nm) (27). Inductive shifts are much smaller. The charge transfer nature of the low frequency band has been established by the study of solvent effects (10, 28) and of ν(CO) (29), and confirmed theoretically (10, 28). The higher frequency band is also of the $\pi-\pi^*$ type, but its detailed nature is less certain (10). Two intense bands also appear in the spectrum of the pyrrol-2-yl phosphine oxides (9), similar to those of 2-formylpyrrole, but at higher frequency. The comparability of the pairs of bands in the acylpyrroles and the phosphine oxides in both position and intensity makes it highly likely that the transitions have the same cause, and argues in favour of conjugation in the pyrrylphosphine oxides (10). On this basis, conjugation is stronger in the heteroaryl com-

[2]In Tables 7, 8, and subsequent text, the standard numbering scheme of the pyrrole ring (denoted by unparenthesized numerals, e.g. C3, H3) is used to facilitate comparison with other work.

Can. J. Chem. Downloaded from www.nrcresearchpress.com by 210.87.254.105 on 09/06/12
For personal use only.

TABLE 7. $^{31}P$, $^{19}F$, and $^{1}H$ nmr parameters of 1-methylpyrrol-2-ylfluorocyclophosphazenes[a]

| | $PF_2$ | | | PF(pyrryl) | | | | | | |
|---|---|---|---|---|---|---|---|---|---|---|
| Cpd. | $\delta_P$ | $\delta_F$ | $J_{PF}$[c] | $\delta_P$ | $\delta_F$ | $J_{PF}$[c] | $J_{PP}$[d] | $\delta_H(CH_3)$[b] | δ(H4)[b] | δ(H3, H5)[b] |
| 1*a* | −105.2 | −67.0 | 903 | −88.5 | −47.9 | 937 | 90 | 3.83 | 6.20 | 6.95 |
| 1*b* | −127.9 | −67.2 | 869 | −111.6 | −49.7 | 892 | 80 | 3.84 | 6.18 | 6.92 |
| 1*c* | −134.4 | −64.8 | 835 | −116.0 | −48.6 | 858 | 80 | 3.82 | 6.20 | 6.94 |
| 1*d* | −134.8 | −64.5 | 886 | −114.6 | −49.6 | 903 | 80 | 3.82 | 6.20 | 6.93 |

[a]In $CDCl_3$. Positive shifts (ppm) downfield of TMS (internal), $P_4O_6$ (external) or $CFCl_3$ (external). Coupling constants in Hz.
[b]$^1H$ shifts of **2** (21): $CH_3$, 3.55; Hα, 6.43; Hβ, 6.03 ppm.
[c]From $^{19}F$ spectrum.
[d]Approximate (first-order) values.

TABLE 8. $^{13}C$ nmr parameters of 1-methylpyrrol-2-ylfluorocyclophosphazenes[a]

| Cpd. | $\delta(CH_3)$ | δ(C2) | δ(C3) | δ(C4) | δ(C5) | $J_{PC2}$ | $J_{FC2}$ | $J_{PC3}$ | $J_{PC4}$ | $J_{PC5}$ |
|---|---|---|---|---|---|---|---|---|---|---|
| 1*a* | 36.3 | 118.1 (−3.0)[b] | 123.7 (15.9) | 109.2 (1.4) | 131.6 (10.5) | 249.0 | 38.2[d] | 22.2 | 16.7 | 12.5 |
| 1*b* | 36.3 | 118.3 (−2.8) | 124.5 (16.7) | 109.1 (1.3) | 132.0 (10.9) | 255.2 | 33.3 | 23.6 | 18.0 | 13.9 |
| 1*c* | 36.2 | 118.2 (−2.9) | 124.2 (16.4) | 109.2 (1.4) | 131.9 (10.8) | 252.5 | 33.3 | 23.6 | 18.0 | 12.5 |
| 1*d* | 36.2 | 118.3 (−2.8) | 124.1 (16.3) | 109.2 (1.4) | 131.8 (10.7) | 251.1 | 33.3 | 22.2 | 16.7 | 13.9 |
| 2[c] | 35.8 | 121.1 | 107.8 | 107.8 | 121.1 | — | — | — | — | — |

[a]In $CDCl_3$; positive shifts (ppm) downfield of internal TMS. P = P(1), F = F(1), coupling constants in Hz.
[b]The parenthesized entries are shifts relative to those of **2**.
[c]Reference 23.
[d]Mean value.

pounds than in their phenyl-phosphoryl counterparts, though it is appreciably weaker than to a carbonyl group.

As Table 9 shows, the spectra of 1*a–d* are similar to those of the phosphine oxides **3**, but the shift of the low energy band to longer wavelength (relative to 1-methylpyrrole, **2**) is slightly reduced. A similar statement applies to the intensities. The results again indicate conjugative bonding, comparable to but slightly weaker than that to the phosphoryl group, perhaps reflecting the lower electronegativity of nitrogen compared to oxygen. The spectra show another interesting feature, in the small but significant oscillations in $\lambda_{max}$ of the longer wavelength band. They show the same type of variation with ring size as the ionization energies of the fluorophosphazenes themselves (30).[3] Since the oscillation is small, the conjugative perturbation induced by the pyrryl group may not extend far beyond the phosphorus atom to which it is attached. The position of the shorter wavelength band is independent of ring size, at 220 nm. In nitropyrroles (28) the corresponding band has contributions from the local excitation of both the pyrrole ring and the nitro-group, and in the phosphazenyl derivatives, the shorter wavelength band is perhaps the less likely to be affected by ring size. Further work is required both on the nature of this band and, for the band at longer wavelength, the extent of conjugation within the phosphazene ring, possibly by the *ab initio* methods used to assess the σ- and π-interactions of a pyrryl group with organic substituents (31).

Although these measurements establish a conjugative connection between the pyrryl and phosphazenyl rings, they do not show the relative extent of charge transfer in the ground and excited state of the molecules. The molecular structure of 1*b* (Fig. 1, Tables 4, 5) is more informative. All the intermolecular distances exceed normal van der Waals distances, so that the molecule can be considered in

TABLE 9. Electronic spectra of 1-methylpyrrol-2-ylfluorocyclophosphazenes

| Cpd. | $\lambda_{max}$, nm | $10^{-3} \times \varepsilon_{max}$ | $\lambda_{max}$, nm | $10^{-3} \times \varepsilon_{max}$ |
|---|---|---|---|---|
| 1*a* | 220 | 10.1 | 237 | 10.9 |
| 1*b* | 220 | 10.4 | 240 | 12.4 |
| 1*c* | 220 | 9.9 | 235 | 11.5 |
| 1*d* | 220 | 10.1 | 240 | 11.8 |
| 3[a] | 218 | 8.4 | 243 | 12.9 |
| 2[a] | — | — | 213 | 6.7 |

[a]Reference 9.

[3]The photoelectron spectra of 1*a–d* (38) show that the two highest occupied orbitals of 1-methylpyrrole are stabilized by the fluorophosphazenyl groups by 0.9 and 0.6 eV respectively, but conjugation need not be restricted to the ground state.

Can. J. Chem. Downloaded from www.nrcresearchpress.com by 210.87.254.105 on 09/06/12
For personal use only.

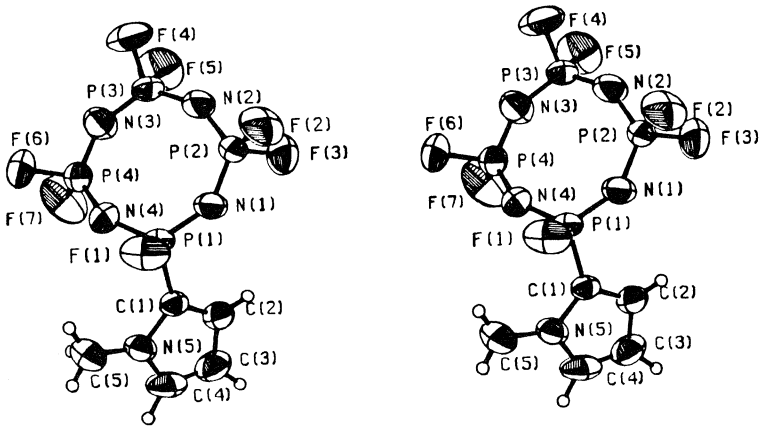


FIG. 1. Stereo view of the 1-methylpyrrol-2-ylheptafluorocyclotetraphosphazene molecule; 50% probability thermal ellipsoids are shown for the non-hydrogen atoms.

isolation. In pyrrole itself, the N—C2, C2—C3, C3—C4, C4—C5, and N—C5 distances are 1.370(1), 1.382(5), 1.417(3), 1.382(5), and 1.370(1) Å respectively (32). The corresponding distances in **1***b* are 1.386(7), 1.376(9), 1.396(8), 1.353(10), and 1.363(8) Å and those in the related molecule (*E*)-2-methyl-3-(pyrrol-2-yl)prop-2-enal (33) (in which exocyclic conjugation also occurs) are 1.37(1), 1.39(1), 1.40(1), 1.35(1), and 1.37(1) Å. Substitution of pyrrole at C2 results in a slight decrease in the mean[4] C—C distance to 1.378(22) from 1.394(27) Å. It is noteworthy that in both the above 2-substituted pyrroles the C4—C5 distance is significantly shortened, rather than lengthened as would be expected to result from contribution by resonance forms such as **2***b*.

In the phosphazene part of the molecule, the changes from the structure of $N_4P_4F_8$ (34) are a little larger but more significant. The $N_4P_4$ ring itself is close to planarity (deviations from the mean plane; mean 0.062, max. 0.122(6) Å), and the sum of the ring angles at phosphorus and nitrogen is 1077.0(10)°, against 1080° required for a planar eight-membered ring. The temperature factors are large, and the ring must be regarded as conformationally flexible. The mean $PF_2$ angles (97.6(1)°) are slightly smaller than in $N_4P_4F_8$ (99.9(5)°), corresponding to the increase of the ring angle at phosphorus from 122.7(10)° to 123.9(4)°; the mean angle at nitrogen is 146.4(24)°, compared with 147.2(14)° in $N_4P_4F_8$. The replacement of fluorine by the less electronegative 1-methylpyrrol-2-yl group has several characteristic geometrical effects, whose general nature in related compounds is discussed elsewhere (35). The *endo*-angle at P(1) is decreased to 120.0(3)° and the *exo*-angle (C—P—F) increased to 104.3(2)°. The ring bonds to P(1) (1.562(1) Å) are lengthened by 0.027(12) Å relative to the other ring bonds (mean P—N excluding P(1) = 1.535(12) Å), and the P(1)—F(1) bond (1.561(4) Å) is lengthened (relative to the mean length in the $PF_2$ groups of 1.536(7) Å) by 0.025(8) Å. In phenylphosphazenes, the length of the P—C bond is close to 1.800 Å; relatively, P—C in **1***b* is shortened by 0.044 Å, to 1.756(5) Å. This reduction is chemically significant, but less than that expected for a formal double bond; in $Ph_3P{=}CH_2$, the length of the ylidic bond is 1.661(2) Å (36). Similar geometrical relationships are found in all-*trans* $N_4P_4(NMe_2)_4F_4$ (37), in which the strong exocyclic conjugation shortens P—N (*exo*) to 1.621(5) Å, the $PNMe_2$ group being nearly planar. The mean *endo*- and *exo*-angles at phosphorus in this compound are 122.3(5)° and 105.3(8)° and the mean (ring) P—N and the P—F bond lengths are 1.557(11) and 1.566 (11) Å respectively (37).

The general conclusion is that conjugative interactions to a phosphorus centre depend upon electron donation to it from the ligand, which increases in the order phenyl < 1-methylpyrryl < dimethylamido. Electron release from the 1-methylpyrryl group to acceptor groups decreases in the order acyl > phosphoryl > fluorophosphazenyl. The crystallographic results on **1***b* show a moderate degree of conjugative stabilization in the ground state, and the electronic spectra show that the acceptor level in the phosphazene has homomorphic character. Conjugation to a phosphoryl centre was earlier supposed (9) to involve 3*d*-orbitals at phosphorus, and the present results are consistent with that view; any appreciable use of a 3*p* orbital

[4]Here and elsewhere in this report mean values refer to weighted means with rms deviations from the mean in parentheses.

Can. J. Chem. Downloaded from www.nrcresearchpress.com by 210.87.254.105 on 09/06/12
For personal use only.

at phosphorus would reduce both *endo*- and *exo*-angles there. The interaction is not restricted to a single *d*-orbital, and $\pi$-interactions are not likely to introduce any large barrier to rotation about P(1)—C(1). In this respect, the conjugation differs from that of an acyl group.


## Acknowledgments

We thank the Natural Sciences and Engineering Research Council Canada for financial support and the University of British Columbia Computing Centre for assistance.



1. T. Chivers and N. L. Paddock. Inorg. Chem. **11**, 848 (1972).
2. A. J. Wagner and T. Moeller. J. Inorg. Nucl. Chem. **33**, 1307 (1971).
3. C. W. Allen and J. C. Green. Inorg. Chem. **19**, 1719 (1980).
4. H. H. Jaffé and M. Orchin. *In* Theory and applications of ultraviolet spectroscopy. John Wiley and Sons, Inc., New York. 1962. pp. 497–501.
5. N. L. Paddock. Q. Rev. Chem. Soc. **18**, 168 (1964).
6. J. H. D. Eland. J. Mass Spectrom. Ion Phys. **2**, 471 (1969).
7. A. D. Baker, D. Betteridge, N. R. Kemp, and R. E. Kirby. Anal. Chem. **42**, 1064 (1970).
8. K. Wanatabe. J. Chem. Phys. **26**, 542 (1957).
9. C. E. Griffin, R. P. Peller, K. R. Marton, and J. A. Peters. J. Org. Chem. **30**, 97 (1965).
10. T. Matsuo and H. Shosenji. Bull. Chem. Soc. Jpn. **45**, 1349 (1972).
11. D. T. Cromer and J. B. Mann. Acta Crystallogr. Sect. A, **24**, 321 (1968).
12. R. F. Stewart, E. R. Davidson, and W. T. Simpson. J. Chem. Phys. **42**, 3175 (1965).
13. D. T. Cromer and D. Liberman. J. Chem. Phys. **53**, 1891 (1970).
14. V. Schomaker and K. N. Trueblood. Acta Crystallogr. Sect. B, **24**, 63 (1968).
15. D. W. J. Cruickshank. Acta Crystallogr. **9**, 747 (1956); **9**, 754 (1956); **14**, 896 (1961).
16. D. W. J. Cruickshank. J. Chem. Soc. 5481 (1961).
17. S. J. Rettig and J. Trotter. Can. J. Chem. **51**, 1295 (1973).
18. G. J. Bullen. J. Chem. Soc. 3193 (1962).
19. E. T. McBee, P. Johncock, S. E. French, and H. P. Braendlin. U.S. Govt. Tech. Ser. Rep., AD 254 985 **36**, No. 1, 14 (1961).
20. D. J. Chadwick and C. Willbe. J. Chem. Soc. Perkin I, 887 (1977).
21. K. J. Morgan and D. P. Morrey. Tetrahedron, **27**, 245 (1971).
22. H. J. Anderson. Can. J. Chem. **43**, 2387 (1965).
23. R. J. Abraham, R. D. Lapper, and K. M. Smith. J. Chem. Soc. Perkin II, 1004 (1974).
24. T. Chivers, R. T. Oakley, and N. L. Paddock. J. Chem. Soc. Sect. A, 2324 (1970).
25. G. Horvath and A. I. Kiss. Spectrochim. Acta, **23A**, 921 (1967).
26. L. W. Pickett, M. E. Corning, G. M. Wieder, D. A. Semenow, and J. M. Buckley. J. Am. Chem. Soc. **75**, 1618 (1953).
27. L. F. Elsom and R. A. Jones. J. Chem. Soc. Sect. B, 79 (1970).
28. Z. Yoshida, T. Kobayashi, and H. Yamada. Bull. Chem. Soc. Jpn. **45**, 313 (1972).
29. M. K. A. Khan and K. J. Morgan. J. Chem. Soc. 2579 (1964).
30. G. R. Branton, C. E. Brion, D. C. Frost, K. A. R. Mitchell, and N. L. Paddock. J. Chem. Soc. 151 (1970).
31. J. Kao, A. L. Hinde, and L. Radom. Nouveau J. Chim. **3**, 473 (1979).
32. L. Nygaard, J. T. Nielsen, J. Kirchheiner, G. Maltesen, J. Rastrup-Andersen, and G. O. Sorensen. J. Mol. Struct. **3**, 491 (1969).
33. Y. Badar, A. K. Choppa, H. W. Dias, M. B. Hursthouse, A. R. Khokhar, M. Ito, T. P. Toube, and B. C. L. Weedon. J. Chem. Soc. Perkin Trans. I, 1372 (1977).
34. H. McD. McGeachin and F. R. Tromans. J. Chem. Soc. 4777 (1961).
35. G. J. Bullen and P. A. Tucker. J. Chem. Soc. Dalton Trans. 1651 (1972).
36. J. C. J. Bart. J. Chem. Soc. Sect. B, 350 (1969).
37. M. J. Begley, D. Millington, and D. B. Sowerby. J. Chem. Soc. Dalton Trans. 1162 (1974).
38. C. Kirby, N. P. C. Westwood, R. D. Sharma, and N. L. Paddock. Unpublished results.


Can. J. Chem. Downloaded from www.nrcresearchpress.com by 210.87.254.105 on 09/06/12
For personal use only.

Can. J. Chem. Downloaded from www.nrcresearchpress.com by 210.87.254.105 on 09/06/12
For personal use only.



# Bimolecular production of proton bound dimers in the gas phase. A low pressure ion cyclotron resonance technique for examination of solvent exchange equilibria and determination of single molecule solvation energetics

J. W. LARSON,[1] R. L. CLAIR, AND T. B. MCMAHON

*Department of Chemistry, University of New Brunswick, Fredericton, N.B., Canada E3B 6E2*

Received October 13, 1981

J. W. LARSON, R. L. CLAIR, and T. B. MCMAHON. Can. J. Chem. **60**, 542 (1982).

A scheme is presented whereby sequences of fast bimolecular gas phase ion molecule reactions in mixtures containing $(CHF_2)_2O$ may be used to generate proton bound dimer species at low pressures in an ion cyclotron resonance spectrometer. Using competitive solvent switching reactions it is demonstrated that solvent exchange equilibria may be readily established and from the thermochemical data derived from such equilibria accurate relative single molecule solvation energetics obtained.

J. W. LARSON, R. L. CLAIR et T. B. MCMAHON. Can. J. Chem. **60**, 542 (1982).

On présente un schéma d'après lequel on peut utiliser les suites de réactions bimoléculaires rapides ion–molécule en phase gazeuse dans des mélanges contenant le $(CHF_2)_2O$ pour produire des espèces dimères liées par le proton à de faibles pressions dans un spectromètre à résonance de l'ion dans un cyclotron. Faisant appel à des réactions compétitives d'échange du solvant, on démontre que les équilibres d'échange du solvant peuvent être facilement établis; à partir des données thermo-chimiques déduites de ces équilibres, on peut obtenir les énergies de solvatation relative d'une molécule unique de façon précise.

[Traduit par le journal]

A detailed knowledge of the nature of ion–solvent interactions is central to the understanding of the behaviour of ions in solution and of the reasons for differences between relative stabilities and reactivities of ions in the gas phase versus solution. Fortunately, several mass spectrometric techniques are available which allow examination of ion–neutral interactions and, as Kebarle has noted recently, relative solvation energetics of solution phase ions can generally be inferred from relative enthalpies of attachment of the first solvent molecules to ions in the gas phase (1). Thus the examination of gas phase ions co-ordinated to one or more solvent molecules becomes an extremely valuable means of understanding solvent effects on stability and reactivity (see, for example, ref. 2). Such examinations are usually not possible in trapped ion ion cyclotron resonance experiments because of the low pressures necessarily involved (3). However, we have recently demonstrated that the dihydrated proton, $H_5O_2^+$, may be rapidly and efficiently generated by a sequence of rapid bimolecular reactions in $H_2O$–$(CHF_2)_2O$ mixtures (4). In the present communication we wish to report experiments in which the chemistry of ternary mixtures containing $(CHF_2)_2O$ may be used to examine solvent exchange equilibria of proton bound dimer ions and thus provide a means whereby ion cyclotron resonance spectroscopy may be used to examine these important phenomena.

As shown previously (4) gas phase ion–molecule reactions in $H_2O$–$(CHF_2)_2O$ mixtures lead rapidly to production of the proton bound dimer of water, $H_5O_2^+$. If a ternary mixture is used containing $H_2O$, $(CHF_2)_2O$, and an n-donor base, B, of greater base strength than water, solvent displacement reactions, [1] and [2], are observed.

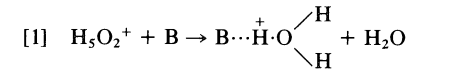

[1] $H_5O_2^+ + B \rightarrow B\cdots\overset{+}{H}\cdot O(H)(H) + H_2O$

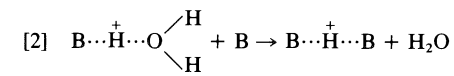

[2] $B\cdots\overset{+}{H}\cdots O(H)(H) + B \rightarrow B\cdots\overset{+}{H}\cdots B + H_2O$

If the species B is of comparable base strength to water, a solvent switching equilibrium may be established and the relative free energies of solvation of $H_3O^+$ and $BH^+$ by single molecules of $H_2O$ and B obtained. For example, in mixtures of $CH_2O$, $H_2O$, and $(CHF_2)_2O$ the equilibria of [3] and [4] are established, as demonstrated by the experimental data shown in Fig. 1. From these data equilibrium constants of $K_3 = 3.9$ and $K_4 = 1.0$ may be obtained

[1]On sabbatical leave from Marshall University, Huntington, WV, U.S.A.

0008-4042/82/040542-03$01.00/0

©1982 National Research Council of Canada/Conseil national de recherches du Canada

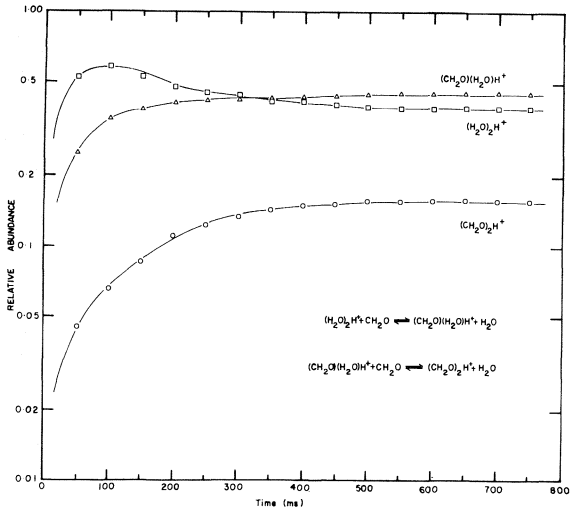


FIG. 1. Variation of relative abundances of proton bound dimers in a 3:3:1 mixture of $(CHF_2)_2O$:$H_2O$:$CH_2O$ at a total pressure of $1.4 \times 10^{-6}$ Torr following a 70 eV, 6 ms ionizing electron beam pulse.

[3] $H_5O_2^+ + CH_2O \rightleftharpoons H_2C{=}O\cdots\overset{+}{H}\cdots OH_2 + H_2O$

[4] $H_2C{=}O\cdots\overset{+}{H}\cdots OH_2 + CH_2O \rightarrow H_2C{=}O\cdots\overset{+}{H}\cdots O{=}CH_2 + H_2O$

which yield free energy changes of $\Delta G_3 = -0.8 \pm 0.1$ kcal mol$^{-1}$ and $\Delta G_4 = 0.0 \pm 0.1$ kcal mol$^{-1}$. Entropy changes for the solvent exchange equilibria may be estimated from changes in rotational entropy due to overall symmetry changes between reactants and products and translational entropy changes. Rotational entropy changes due to changes in moments of inertia have been calculated using the theoretically calculated geometries of $H_5O_2^+$, $CH_2OHOH_2^+$, and $(CH_2O)_2H^+$. The $\Delta S_{rot}$ thus determined have been found to be smaller than entropy changes due to translation and symmetry and have thus been ignored. Vibrational entropies and hence vibrational entropy changes are expected to be minor. Neutron diffraction analysis (5) reveals that solid state $H_5O_2^+$ is a species of $C_{2v}$ symmetry with a linear O···H···O bond in which each oxygen assumes a pyramidal arrangement of hydrogens with the opposing terminal hydrogens in a *trans* configuration. This is in contrast to the more stable species of $D_{2d}$ symmetry found on the basis of *ab initio* calculations (6). More recent calculations using larger basis sets show, however, that the energy difference between the $C_{2v}$ and $D_{2d}$ forms is very small (7) and on the basis of the greater entropy of the $C_{2v}$ form, this species may be the lowest in free energy and hence dominate in the gas phase also. The proton bound dimer of formaldehyde and water has been shown to be of $C_s$ symmetry (8) and further to be the most stable geometrical isomer of molecular formula $CH_5O_2^+$. Thus any rearrangement from the proton bound dimer species to other isomeric forms is unlikely. The proton bound dimer of formaldehyde has been shown by *ab initio* calculation to be of $C_{2v}$ symmetry (9). These symmetries taken with translational entropy changes give rise to estimates of the overall entropy change for these equilibria of $\Delta S_3 = +0.7$ cal mol$^{-1}$ K$^{-1}$ and $\Delta S_4 = -2.3$ cal mol$^{-1}$ K$^{-1}$. These entropy changes combined with the experimentally determined free energy changes yield values for the enthalpy changes of the two reactions of $\Delta H_3 = -0.6 \pm 0.1$ kcal mol$^{-1}$ and $\Delta H_4 = -0.7 \pm 0.1$ kcal mol$^{-1}$. The results obtained for reaction [3] are in good agreement with those of other authors using flowing afterglow (10, 11) and ion cyclotron resonance techniques (12). The only other determination of thermochemical data for reaction [4] is also in good agreement with the present result (10).

In similar fashion to the chemistry of $H_2O$–$(CHF_2)_2O$ mixtures, we have found that mixtures of $(CHF_2)_2O$ with n-donor bases, B, in favourable cases lead to production of proton bound dimer ions, $BHB^+$, via analogous bimolecular sequences. In such cases binary solvent mixtures can also lead to observation of solvent exchange equilibria. For example, in the 11:10:1 mixture of $(CHF_2)_2O$:-$(CH_3)_2CO$:THF shown in Fig. 2 the solvent exchange equilibria, reactions [5] and [6], may be obtained.

[5] $[(CH_3)_2CO]_2H^+ +$ 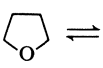 $\rightleftharpoons (CH_3)_2C{=}O\cdots\overset{+}{H}\cdots$ 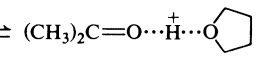 $+ (CH_3)_2CO$

[6] $(CH_3)_2C{=}O\cdots\overset{+}{H}\cdots$ 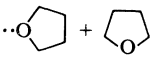 $+$ 

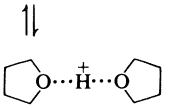 $+ (CH_3)_2CO$

From the steady state ionic abundances at long reaction times equilibrium constants $K_5 = 43.5$ and $K_6 = 5.6$ may be calculated which yield free energy changes of $\Delta G_5 = -2.2 \pm 0.1$ kcal mol$^{-1}$, and $\Delta G_6 = -1.0 \pm 0.1$ kcal mol$^{-1}$. Using symmetry considerations and translational entropy differences the overall entropy change for each reaction may be estimated as $\Delta S_5 = 1.1$ cal mol$^{-1}$ K$^{-1}$ and $\Delta S_6 = -1.7$ cal mol$^{-1}$ K$^{-1}$ to yield overall enthalpy changes of $\Delta H_5 = -1.9 \pm 0.1$ kcal mol$^{-1}$ and $\Delta H_6 = -1.5 \pm 0.1$ kcal mol$^{-1}$. As in the $H_2O$–$CH_2O$ case the higher entropy of the mixed proton bound dimer

Can. J. Chem. Downloaded from www.nrcresearchpress.com by 210.87.254.105 on 09/06/12
For personal use only.

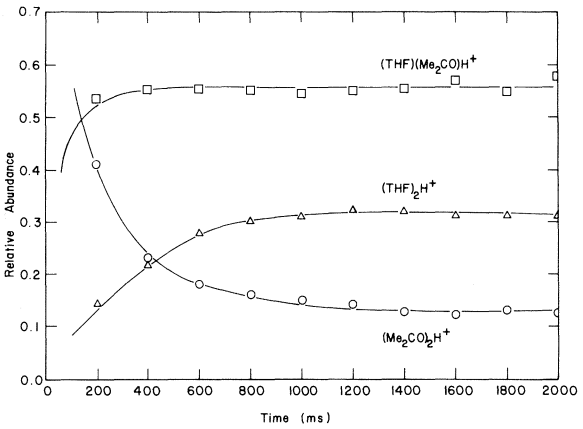


FIG. 2. Variation of relative abundances of proton bound dimers in an 11:10:1 mixture of $(CHF_2)_2O$:$(CH_3)_2CO$:THF at a total pressure of $2 \times 10^{-6}$ Torr following a 70 eV, 6 ms ionizing electron beam pulse.

due to its lower symmetry contributes significantly to the dominant intensity of this ion.

From the enthalpy data for these two cases it may be seen that the more basic molecule is the more strongly co-ordinating solvent for both protonated species involved. Thus $CH_2O$ "solvates" both $CH_2OH^+$ and $H_3O^+$ more strongly than does $H_2O$, and THF "solvates" both protonated THF and protonated acetone more strongly than does acetone. This correlation of solvating ability with gas phase basicity is a generally observed phenomenon (13).

From the above examples it is evident that at low pressures in the ion cyclotron resonance spectrometer using bimolecular reaction sequences associated with the ion chemistry of $(CHF_2)_2O$ a wide range of solvent switching equilibria may be studied. We are currently extending our studies to obtain binding energetics of proton bound dimers for a variety of solvents intermediate in basicity between water and ammonia to obtain a more complete understanding of the effects of basicity and heteroatom identity on these important quantities.

### Acknowledgements

Financial support of the Natural Sciences and Engineering Research Council of Canada is gratefully acknowledged. Professor F. Grein (U.N.B.) is thanked for several useful discussions regarding the structure of $H_5O_2^+$.

1. P. KEBARLE, W. R. DAVIDSON, J. SUNNER, and S. MEZA-HÖJER. Pure Appl. Chem. **51**, 63 (1979).
2. S. D. TANNER, G. I. MACKAY, and D. K. BOHME. Can. J. Chem. **59**, 1615 (1981).
3. T. E. SHARP, J. R. EYLER, and E. LI. Int. J. Mass Spec. Ion Phys. **9**, 421 (1972).
4. R. L. CLAIR and T. B. MCMAHON. Can. J. Chem. **58**, 863 (1980).
5. J. ROZIERE and J. M. WILLIAMS. Inorg. Chem. **15**, 1174 (1976).
6. M. D. NEWTON and S. EHRENSON. J. Am. Chem. Soc. **93**, 4971 (1971).
7. F. GREIN. Private communication.
8. I. H. WILLIAMS, G. M. MAGGIORA, and R. L. SCHOWEN. J. Am. Chem. Soc. **102**, 7831 (1980).
9. A. T. HAGLER, Z. KARPAS, and F. S. KLEIN. J. Am. Chem. Soc. **101**, 2191 (1979).
10. F. C. FEHSENFELD, I. DOTAN, D. L. ALBRITTON, C. J. HOWARD, and E. E. FERGUSON. J. Geophys. Res. **83C**, 1333 (1978).
11. D. K. BOHME, G. I. MACKAY, and S. D. TANNER. J. Am. Chem. Soc. **101**, 3724 (1979).
12. D. W. BERMAN and J. L. BEAUCHAMP. J. Phys. Chem. **84**, 2233 (1980).
13. W. R. DAVIDSON, J. SUNNER, and P. KEBARLE. J. Am. Chem. Soc. **101**, 1675 (1979).

# The isolation and structure of phyllanthostatins 2 and 3[1]

GEORGE R. PETTIT,[2] GORDON M. CRAGG, DEVENS GUST, AND PETER BROWN[3]

*Cancer Research Institute and Department of Chemistry, Arizona State University, Tempe, AZ 85287, U.S.A.*

Received November 9, 1981

GEORGE R. PETTIT, GORDON M. CRAGG, DEVENS GUST, and PETER BROWN. Can. J. Chem. **60**, 544 (1982).

A new antineoplastic glycoside, phyllanthostatin 2, and a related glycoside, phyllanthostatin 3, have been isolated from the Central American tree, *Phyllanthus acuminatus* and their structures assigned as **1***c* and **2** respectively.

[1]Contribution 82 of the series Antineoplastic Agents. For previous contribution (contribution 81) see ref. 1.
[2]Author to whom correspondence should be addressed.
[3]The study reported herein is dedicated to the memory of Professor Peter Brown who passed away March 1981.

0008-4042/82/040544-03$01.00/0
©1982 National Research Council of Canada/Conseil national de recherches du Canada

Can. J. Chem. Downloaded from www.nrcresearchpress.com by 210.87.254.105 on 09/06/12
For personal use only.

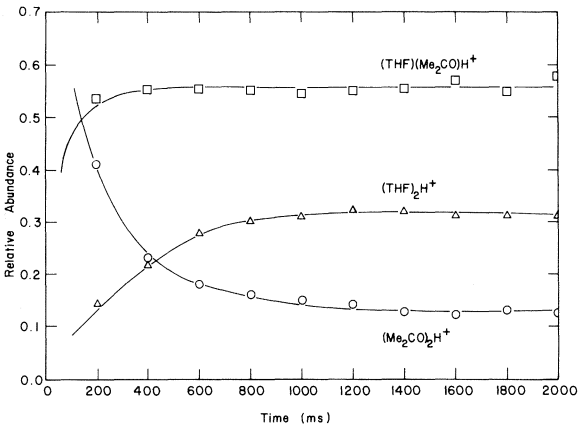


FIG. 2. Variation of relative abundances of proton bound dimers in an 11:10:1 mixture of $(CHF_2)_2O$:$(CH_3)_2CO$:THF at a total pressure of $2 \times 10^{-6}$ Torr following a 70 eV, 6 ms ionizing electron beam pulse.

due to its lower symmetry contributes significantly to the dominant intensity of this ion.

From the enthalpy data for these two cases it may be seen that the more basic molecule is the more strongly co-ordinating solvent for both protonated species involved. Thus $CH_2O$ "solvates" both $CH_2OH^+$ and $H_3O^+$ more strongly than does $H_2O$, and THF "solvates" both protonated THF and protonated acetone more strongly than does acetone. This correlation of solvating ability with gas phase basicity is a generally observed phenomenon (13).

From the above examples it is evident that at low pressures in the ion cyclotron resonance spectrometer using bimolecular reaction sequences associated with the ion chemistry of $(CHF_2)_2O$ a wide range of solvent switching equilibria may be studied. We are currently extending our studies to obtain binding energetics of proton bound dimers for a variety of solvents intermediate in basicity between water and ammonia to obtain a more complete understanding of the effects of basicity and heteroatom identity on these important quantities.

### Acknowledgements

Financial support of the Natural Sciences and Engineering Research Council of Canada is gratefully acknowledged. Professor F. Grein (U.N.B.) is thanked for several useful discussions regarding the structure of $H_5O_2^+$.

1. P. KEBARLE, W. R. DAVIDSON, J. SUNNER, and S. MEZA-HÖJER. Pure Appl. Chem. **51**, 63 (1979).
2. S. D. TANNER, G. I. MACKAY, and D. K. BOHME. Can. J. Chem. **59**, 1615 (1981).
3. T. E. SHARP, J. R. EYLER, and E. LI. Int. J. Mass Spec. Ion Phys. **9**, 421 (1972).
4. R. L. CLAIR and T. B. MCMAHON. Can. J. Chem. **58**, 863 (1980).
5. J. ROZIERE and J. M. WILLIAMS. Inorg. Chem. **15**, 1174 (1976).
6. M. D. NEWTON and S. EHRENSON. J. Am. Chem. Soc. **93**, 4971 (1971).
7. F. GREIN. Private communication.
8. I. H. WILLIAMS, G. M. MAGGIORA, and R. L. SCHOWEN. J. Am. Chem. Soc. **102**, 7831 (1980).
9. A. T. HAGLER, Z. KARPAS, and F. S. KLEIN. J. Am. Chem. Soc. **101**, 2191 (1979).
10. F. C. FEHSENFELD, I. DOTAN, D. L. ALBRITTON, C. J. HOWARD, and E. E. FERGUSON. J. Geophys. Res. **83C**, 1333 (1978).
11. D. K. BOHME, G. I. MACKAY, and S. D. TANNER. J. Am. Chem. Soc. **101**, 3724 (1979).
12. D. W. BERMAN and J. L. BEAUCHAMP. J. Phys. Chem. **84**, 2233 (1980).
13. W. R. DAVIDSON, J. SUNNER, and P. KEBARLE. J. Am. Chem. Soc. **101**, 1675 (1979).

Can. J. Chem. Downloaded from www.nrcresearchpress.com by 210.87.254.5 on 09/06/12
For personal use only.

# The isolation and structure of phyllanthostatins 2 and 3[1]

GEORGE R. PETTIT,[2] GORDON M. CRAGG, DEVENS GUST, AND PETER BROWN[3]

*Cancer Research Institute and Department of Chemistry, Arizona State University, Tempe, AZ 85287, U.S.A.*

Received November 9, 1981

GEORGE R. PETTIT, GORDON M. CRAGG, DEVENS GUST, and PETER BROWN. Can. J. Chem. **60**, 544 (1982).

A new antineoplastic glycoside, phyllanthostatin 2, and a related glycoside, phyllanthostatin 3, have been isolated from the Central American tree, *Phyllanthus acuminatus* and their structures assigned as **1***c* and **2** respectively.

[1]Contribution 82 of the series Antineoplastic Agents. For previous contribution (contribution 81) see ref. 1.
[2]Author to whom correspondence should be addressed.
[3]The study reported herein is dedicated to the memory of Professor Peter Brown who passed away March 1981.

0008-4042/82/040544-03$01.00/0
©1982 National Research Council of Canada/Conseil national de recherches du Canada

GEORGE R. PETTIT, GORDON M. CRAGG, DEVENS GUST et PETER BROWN. Can. J. Chem. **60**, 544 (1982).

A partir d'un arbre de l'Amérique Centrale, le *phyllantus acuminatus*, on a isolé un nouveau glycoside antinéoplastique, la phyllanthostatine (**2**), et un glycoside apparenté, la phyllanthostatine (**3**), et on leur a attribué respectivement les structures **1***c* et **2**.
[Traduit par le journal]

Can. J. Chem. Downloaded from www.nrcresearchpress.com by 210.87.254.5 on 09/06/12
For personal use only.

The *Phyllanthus* genus (Euphorbiaceae) occurs in tropical areas and contains species purported to be useful in treatment of tubercular ulcers, sores, malaria, ring-worm, jaundice, and diarrhoea (*P. niruri*) (2–7), and as a diuretic (*P. discoides* (8–10) and *P. moderospotensis* (11)). Three species, *P. emblica* L., *P. niruri* L., and *P. urinoria* L., have been used in the primitive medical treatment of cancer.

We recently summarized the isolation and complete characterization of the antineoplastic glycosides, phyllanthostatin 1 (**1***a*), and phyllanthoside (**1***b*), from roots of the Central American tree *Phyllanthus acuminatus* Vahl (12). We now report that further detailed studies (guided by the murine P388 lymphocytic leukemia in vitro and in vivo bioassay, PS system) (12) of companion glycosides in *P. acuminatus* have revealed the presence of two new antineoplastic constituents designated phyllanthostatins 2 (**1***c*) and 3 (**2**). Initial biological evaluation of phyllanthostatins 2 and 3 against the PS leukemia has resulted in, respectively, 43% (at 12 mg/kg and $ED_{50}$ 0.12 μg/mL) and 41% (at 80 mg/kg) life extensions.

A recollection (1978) of *P. acuminatus* roots (81.5 kg) from Costa Rica was extracted employing

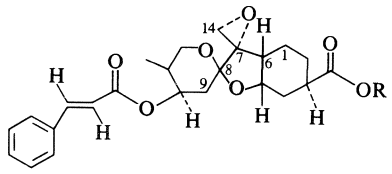

**1***a*, R =

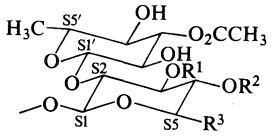

**1***a*, $R^1 = H$; $R^2 = COCH_3$; $R^3 = CH_3$
**1***b*, $R^1 = COCH_3$; $R^2 = H$; $R^3 = CH_3$
**1***c*, $R^1 = COCH_3$; $R^2 = H$; $R^3 = CH_2OH$

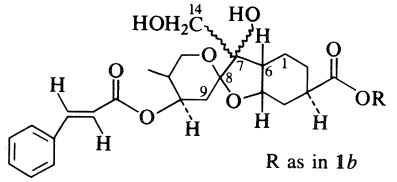

R as in **1***b*

**2**

our new 1:1 methylene chloride – methanol procedure (12). The methylene chloride fraction (475 g) was further separated by a solvent partition sequence (9:1 → 4:1 → 3:2 methanol–water with ligroin → carbon tetrachloride → methylene chloride) (13) and a 38 g aliquot of the chlorinated hydrocarbon fractions (254 g) was subjected to careful separation by column chromatography (Sephadex LH-20 → silica gel) (12). Finally, chromatography on reverse phase (RP-2) silica (70 → 20% aqueous methanol gradient) afforded 0.10 g of phyllanthostatin 2 (**1***c*) as a colorless amorphous solid: mp 134–136°C; $[\alpha]_D^{24}$ +9.33° (*c* 0.75, $CHCl_3$); $\lambda_{max}$ (MeOH) nm (log ε): 216 (4.28), 222 (4.21), and 278 (4.38); ir (KBr) $\nu_{max}$: 3470, 1750, 1730, 1710, 1640, 1452, 1380, 1311, 1257, 1171, 1075, and 770 $cm^{-1}$; FD mass spectrum *m/e*: 821 ($M^+$ +H). Additional silica gel chromatography yielded 0.26 g of phyllanthostatin 3 (**2**) as a colorless amorphous solid: mp 126–130°C; $[\alpha]_D$ +15.7° (*c* 0.76, $CHCl_3$); $\lambda_{max}$ (MeOH) (log ε): 216 (4.25), 222 (4.18), and 278 (4.35) nm; ir (KBr) $\nu_{max}$: 3450, 1755, 1730, 1700, 1640, 1455, 1380, 1311, 1258, 1175, 1070, and 772 $cm^{-1}$; FD mass spectrum *m/e*: 323 ($M^+$ +H).

Comparison of the spectral data[4] recorded for phyllanthostatin 2 (**1***c*) and phyllanthoside (**1***b*, ref. 12) indicated a difference in one of the disaccharide 6-deoxy-D-glucose units. The nmr signal arising from one of the 6-deoxy-D-glucose methyl groups in **1***b* ($^1H$ nmr: d at 1.28 ppm; $^{13}C$ nmr 17.48 ppm) was replaced by a signal due to a $CH_2OH$ group ($^1H$ nmr: dd at 3.83 ppm; $^{13}C$ nmr 61.90 ppm appearing as a triplet in the off-resonance decoupled spectrum) in **1***c*. When $^1H$ nmr decoupling studies revealed that the $CH_2OH$ moiety was located at position S-5, it was apparent that one of the 6-deoxy-D-glucose units of phyllanthoside was replaced by glucose. Therefore structure **1***c* was assigned to phyllanthostatin 2.

Phyllanthostatin 3 (**2**) was found to differe significantly from phyllanthoside (**1***b*, ref. 12) in the

[4]The spectral and elemental microanalytical data were quite consistent with the assigned structures and will be summarized in a future full report. Instrumental analyses were performed using Varian-MAT 731, Bruker WH-90, and Bruker WH-400 instruments. We wish to thank Drs. R. R. Inners, P. D. Ellis, J. A. McCloskey, and J. Witschel, Jr. for expert assistance with these measurements.

aglycone moiety but possesses an identical disaccharide portion. The AB quartet at 2.92 and 2.95 ppm in the $^1$H nmr spectrum of **1***b* due to the epoxide methylene protons was replaced by two doubled doublets at 3.51 and 4.01 ppm in the spectrum of glycoside **2**. Analogous marked differences were apparent in the $^{13}$C nmr spectra. The signals due to C-7 and C-14 (71.00 and 50.01 ppm in **1***b*) of the phyllanthoside epoxide occurred instead at 85.27 and 66.61 ppm respectively in glycoside **2**. Less pronounced changes were observed in the chemical shift values of C-1, C-6, C-8, and C-9. These observations, together with mass spectral and elemental analytical data, established that phyllanthostatin 3 was a vicinal 7,14-diol counterpart of the 7,14-epoxide phyllanthoside. Therefore structure **2** was assigned to phyllanthostatin 3.

Further antineoplastic evaluation of phyllanthostatins 2 and 3 is underway in the U.S. National Cancer Institute's program.

**Acknowledgments**

We are pleased to acknowledge assistance provided by Contract NO1-CM-97297 with the Division of Cancer Treatment, NCI, National Institutes of Health, DHW, Grant Nos. CA16049-06 and 07 awarded by the National Cancer Institute, DHW, Mrs. Mary Dell Pritzlaff, the Olin Foundation, (Spencer T. and Ann W.), the Fannie E. Rippel Foundation, and the National Science Foundation Regional Facility at the University of South Carolina (CH78-18723). Also we are pleased to thank Drs. M. I. Suffness, J. D. Douros, M. E. Wall, C. L. Herald, D. L. Herald, Mr. H. Taylor, Miss M. S. Pettit, and Mr. R. Booze for very helpful assistance.

1. G. R. PETTIT and Y. FUJII. J. Nat. Prod. Submitted.
2. J. S. CHAUHAN, M. SULTAN, and S. K. SRIVASTAVA. Planta Med. **32**, 217 (1977).
3. A. J. LOUSTALOT and C. PAGÁN. El Crisol (Puerto Rico), **3**, 3 (1949).
4. R. M. SERRA. An. Univ. St. Domingo, **8**, 295 (1944).
5. J. S. CHAUHAN, M. SULTAN, and S. K. SRIVASTAVA. J. Indian Chem. Soc. **56**, 326 (1979).
6. T. K. NARA, J. GLEYE, E. L. DE CERVAL, and E. STANISLAS. Plant. Med. Phytothér. **11**, 82 (1977).
7. A. S. R. ANJANEYULU, K. J. RAO, L. R. ROW, and C. SUBRAHMANYAM, Tetrahedron, **29**, 1291 (1973).
8. S. A. OLETTA. Brit. Pat. No. 890614 (1962); Chem. Abstr. **57**, 9963 (1962).
9. Z. HORII, T. IMANISHI, M. YAMAUCHI, M. HANAOKA, J. PARELLO, and S. MUNAVALLI. Tetrahedron Lett. **19**, 1877 (1972).
10. J. PARELLO. Bull. Soc. Chim. Fr. **3**, 1117 (1968).
11. D. S. BHAKUNI. J. Sci. Ind. Res. Sect. B, **18**, 446 (1959); J. L. HARTWELL. Lloydia, **32**, 153 (1969).
12. G. R. PETTIT, G. M. CRAGG, D. GUST, P. BROWN, and J. M. SCHMIDT. Can. J. Chem. In press.
13. G. R. PETTIT, Y. FUJII, J. A. HASLER, J. M. SCHMIDT, and C. MICHEL. J. Nat. Prod. Submitted; G. R. PETTIT and G. M. CRAGG. Biosynthetic products for cancer chemotherapy. Vol. 2. Plenum Publishing Corp., New York. 1978; G. R. PETTIT and R. H. ODE. Biosynthetic products for cancer chemotherapy. Vol. 3. Plenum Publishing Corp., New York. 1979.

Can. J. Chem. Downloaded from www.nrcresearchpress.com by 210.87.254.5 on 09/06/12
For personal use only.

# Nucleic acid related compounds. 37. Convenient and high-yield syntheses of *N*-[(2-hydroxyethoxy)methyl] heterocycles as "acyclic nucleoside" analogues[1]

MORRIS J. ROBINS AND PETER W. HATFIELD[2]

*Department of Chemistry, The University of Alberta, Edmonton, Alta., Canada T6G 2G2*

Received July 13, 1981

MORRIS J. ROBINS and PETER W. HATFIELD. Can. J. Chem. **60**, 547 (1982).

Treatment of 1,3-dioxolane with acetyl bromide gave (2-acetoxyethoxy)methyl bromide (**2***a*) in 88% yield. A number of pyrimidines and three chloropurines were trimethylsilylated and coupled with **2***a*. The respective *N*-1 and *N*-9 alkylated products (obtained in 79–89% yields) were deacetylated to give *N*-[(2-hydroxyethoxy)methyl] heterocycles. The 6-amino or 6-chloro substituent of the 2-amino-6-substituted-purine derivatives was hydrolyzed smoothly with adenosine deaminase to give 9-[(2-hydroxyethoxy)methyl]guanine (acycloguanosine), the potent antiviral agent.

MORRIS J. ROBINS et PETER W. HATFIELD. Can. J. Chem. **60**, 547 (1982).

Le dioxolanne-1,3 réagit avec le bromure d'acétyle en donnant le bromure de (acétoxy-2 éthoxy)méthyle (**2***a*) avec un rendement de 88%. On a couplé ce produit **2***a* avec un certain nombre de pyrimidines et trois chloropurines sur lesquelles on a fixé un groupement triméthylsilyle. Les produits alkyles respectivement *N*-1 et *N*-9 (obtenus avec des rendements allant de 79 à 89%), soumis à une désacétylation conduisent à des hétérocycles substitués par des groupes *N*-[(hydroxy-2 éthoxy)méthyle]. On a hydrolysé, dans des conditions douces en utilisant la désaminase d'adénosine, les substituants amino-6 ou chloro-6 des dérivés de l'amino-2 purine substitué en position 6 pour obtenir la [(hydroxy-2 éthoxy)méthyl]-9 guanine (acylguanosine), un agent antiviral puissant.

[Traduit par le journal]

A surge of interest in the application of nucleosides and acyclic nucleoside analogues as antiviral agents is underway. The well known 5-iodo-2′-deoxyuridine has been in clinical use for over a decade and 5-trifluoromethyl-2′-deoxyuridine has been employed. Approval of 9-(β-D-arabinofuranosyl)adenine (araA) for treatment of human herpes encephalitis has been given. Potent antiviral activity has been reported for 1-(β-D-ribofuranosyl)-1,2,-4-triazole-3-carboxamide (ribavirin), (*E*)-5-(2-bromovinyl)-2′-deoxyuridine, and 1-(2-fluoro-2-deoxy-β-D-arabinofuranosyl)-5-iodocytosine (FIAC) (2). Schaeffer and co-workers had prepared 9-(hydroxyalkyl)adenine derivatives as putative inhibitors of adenosine deaminase and found that 9-[(2-hydroxyethoxy)methyl]adenine was a substrate of the enzyme (3). They later reported the synthesis and potent antiviral activity of the acycloguanosine analogue, 9-[(2-hydroxyethoxy)-methyl]guanine (4). This agent has been carried into clinical trials (5). Other types of "acyclic nucleoside" analogues have been reported by De Clercq and Holý (6), Barrio and co-workers (7), Ogilvie and Gillen (8), McCormick and McElhinney (9), and ourselves (10).

Schaeffer employed alkylation of 6-chloropurine with (2-benzyloxyethoxy)methyl chloride to give the *N*-9 product in 44% yield. Ammonolysis and hydrogenolytic debenzylation gave 9-[(2-hydroxyethoxy)methyl]adenine (3). A similar sequence using 2,6-dichloropurine and (2-benzoyloxyethoxy)methyl chloride (41% yield) gave acycloguanosine (4). Barrio and co-workers studied reactions of chloro- and methylthio-substituted purines with (2-trimethylsilyloxyethoxy)methyl iodide (**7***a*). Alkylations proceeded in 50–80% yields at −63°C with this reagent (**7***a*,*c*). Two very recent abstracts noted work on related pyrimidine acyclonucleosides (11, 12).[3]

We have developed methods for the convenient and high-yield syntheses of *N*-[(2-hydroxyethoxy)-methyl] heterocycles. Acetolysis of 1,3-dioxolane (**1**) (see Scheme 1) gave (2-acetoxyethoxy)methyl acetate (**2***c*) as reported (13). However, treatment of trimethylsilylated pyrimidines with **2***c* in the presence of tin(IV) chloride according to the glycosylation procedure of Vorbrüggen (14) gave ~ 50% yields of *N*-1 products. Similar results have been noted recently (12). We repeated the cleavage

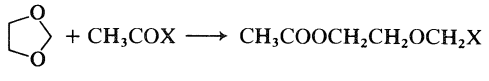


**1**

**2***a* X = Br
*b* X = Cl
*c* X = $OCOCH_3$

SCHEME 1

[1]For the previous paper in this series see ref. 1.

[2]Alberta Heritage Foundation for Medical Research Graduate Studentship Awardee 1980 to present.

[3]Note added in proof: publications by these authors (19, 20) have appeared since submission of the present work.

0008-4042/82/050547-07$01.00/0

©1982 National Research Council of Canada/Conseil national de recherches du Canada

Can. J. Chem. Downloaded from www.nrcresearchpress.com by 210.87.254.6 on 09/06/12
For personal use only.

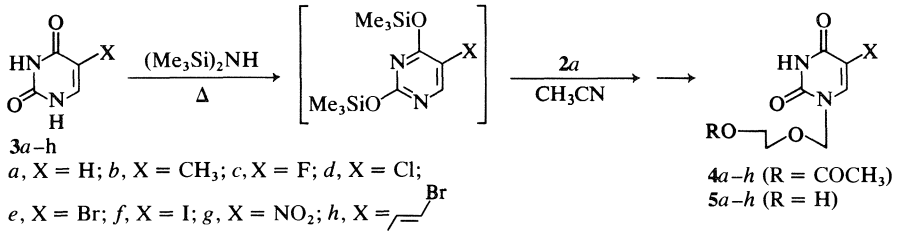


SCHEME 2

of **1** with trimethylsilyl iodide at −78°C (*7a*). However, this preparation was sensitive to moisture and temperature. The failure to isolate an alkylating agent (*7b*) necessitated repetitious *in situ* generation, and attempted use of this preparation with the sodium salt of adenine was not successful. Treatment of **1** with acetyl chloride in the presence of sulfuric acid gave (2-acetoxyethoxy)methyl chloride (**2***b*) contaminated with a tenacious by-product. Coupling yields using this preparation were depressed.

Treatment of **1** with neat acetyl bromide gave pure (2-acetoxyethoxy)methyl bromide (**2***a*) in 88% yield as a readily distilled colorless oil. Storage of **2***a* in a refrigerator for several months with frequent use resulted in no apparent decomposition. Trimethylsilylation of a series of uracils (**3***a–h*) (see Scheme 2), whose nucleosides are of biological interest (2), and *in situ* coupling with **2***a* in dry acetonitrile proceeded without difficulty. The same procedure was applied successfully to cytosine (**6***a*) and 3-deazauracil (4-hydroxy-2-pyridinone) (**7***a*) (see Fig. 1). The *N*-1 derivatives (**4***a–h*, **6***b*, **7***b*) were obtained regiospecifically in yields of 79–88% after recrystallization.

Analogous trimethylsilylation of 6-chloro- (**8***a*), 2,6-dichloro- (**9***a*), and 2-amino-6-chloropurine (**10***a*) and treatment with **2***a* in the presence of mercury(II) cyanide resulted in *N*-9 coupling to give **8***b*, **9***b*, and **10***b* (83–89% conversions). Use of this silylation/mercuric cyanide procedure (15) enhanced yields and effectively eliminated the *N*-7 isomers normally found in alkylations of purine sodium salts (*7c*). However, this method did not give high yields with adenine (**11***a*). Alkylation of the adenine anion with **2***a* in purified DMF gave 75% of 9-[(2-acetoxyethoxy)methyl]adenine (**11***b*). The coupling results and characterization data are summarized in Table 1 and spectral data in Table 2. Deacetylation of these compounds with methanolic ammonia or sodium methoxide occurred readily. Data for the deprotected acyclonucleosides (**5***a–h*, **6***c*, **7***c*, **10***c*, **11***c*) are summarized in Tables 3 and 4.

High-temperature ammonolysis of the 2-chloro group was required previously to prepare acycloguanosine (4, *7c*). Analogous ammonolysis of **9***b* at 150°C gave 2,6-diamino-9-[(2-hydroxyethoxy)-methyl]purine (**12**) (see Scheme 3). Adenosine deaminase was known to effect hydrolytic deamination and dechlorination at C-6 of related purine nucleosides (16) and 6-amino-9-[(2-hydroxyethoxy)methyl]purine (**11***c*) (3). Treatment of **12** with this enzyme effected clean conversion to 9-[(2-hydroxyethoxy)methyl]guanine (**13**). A route to this antiviral drug then was developed that employed convenient ambient temperature and pressure conditions. Mild deprotection of **10***b* followed by enzymatic dechlorination of **10***c* gave

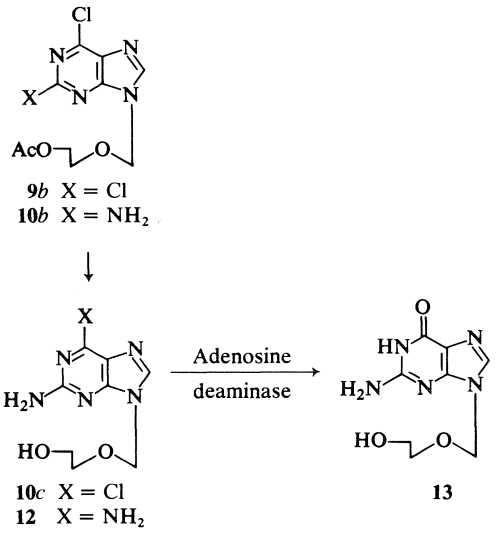


SCHEME 3

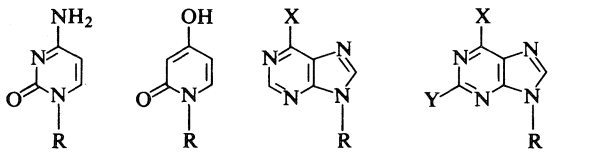


Series: *a*, R = H; *b*, R = $CH_2OCH_2CH_2OCOCH_3$;
*c*, R = $CH_2OCH_2CH_2OH$

FIG. 1

Can. J. Chem. Downloaded from www.nrcresearchpress.com by 210.87.254.6 on 09/06/12
For personal use only.

Can. J. Chem. Downloaded from www.nrcresearchpress.com by 210.87.254.6 on 09/06/12
For personal use only.

acycloguanosine (**13**) in 76% yield overall for the 3-step sequence (**10***a* → **10***b* → **10***c* → **13**).

This study has provided convenient procedures for the high-yield syntheses of *N*-[(2-hydroxyethoxy)methyl] heterocycles. The facile preparation of (2-acetoxyethoxy)methyl bromide from 1,3-dioxolane provided a stable alkylating bromomethyl ether. Coupling of a number of silylated bases with this agent proceeded smoothly. Adenosine deaminase effected hydrolytic deamination or dechlorination at C-6 of the purine acyclonucleosides to give a mild synthetic route to the antiviral guanine compound (17).

## Experimental

*General*

Melting points were determined on a Reichert microstage block and are uncorrected. Ultraviolet (uv) spectra were recorded on a Cary 15 spectrophotometer. The high-field nmr laboratory of this department obtained $^1$H spectra on Varian 100, Bruker WH-200, and WH-400 spectrometers. The $^{13}$C nmr spectra were measured at 22.6 MHz with proton decoupling on a Bruker HFX-90 instrument. Tetramethylsilane was used as internal standard for all nmr data. The mass spectra (ms) laboratory of this department measured EI spectra on an AEI MS-50 instrument with coupled computer analysis at 70 eV using direct probe sample introduction. Compounds that failed to give a molecular ion peak were examined by chemical ionization (ammonia gas) with an AEI MS-12 instrument at 70 eV. Elemental analyses were determined by the microanalytical laboratory of this department.

Evaporations were effected at room temperature with a Buchler rotary evaporator equipped with a Dewar "Dry-Ice" condenser under water tap or mechanical oil pump vacuum. Reagent grade acetonitrile and *N*,*N*-dimethylformamide (DMF) were refluxed with and then distilled from $P_2O_5$ into oven-dried flasks. Adenosine deaminase (adenosine aminohydrolase, E. C. 3.5.4.4) was purchased from Sigma Chemical Co. (crude, Type II). Silica gel for column chromatography was J. T. Baker 5-3405 and thin-layer chromatography was performed on small glass plates coated with E. Merck silica gel PF-254 for tlc using solvent systems (A) 10% MeOH in $CHCl_3$ or (B) EtOAc/*n*-PrOH/$H_2O$ (4:1:2) upper phase.

Solvent systems for recrystallization were: A, chloroform with diffusion of diethyl ether; B, methanol with diffusion of ether; C, 2-propanol with diffusion of ether; D, dichloromethane with diffusion of ether; E, methanol; F, methanol–water; G, 95% ethanol; H, acetone with diffusion of *n*-pentane; I, 2-propanol; J, ethanol–water. "Diffusion crystallization" is described in ref. 18.

*(2-Acetoxyethoxy)methyl bromide (***2***a)*

Freshly distilled acetyl bromide (13.0 g, 106 mmol) was stirred magnetically with cooling in an ice bath while 7.4 g (100 mmol) of 1,3-dioxolane (**1**) was added slowly. A rapid exothermic reaction occurred giving quantitative conversion to **2***a* (as judged by $^1$H nmr). Vacuum distillation of this material gave 17.4 g (88%) of **2***a*, bp 58–60°C/0.1 Torr; $^1$H nmr ($CDCl_3$) δ: 2.10 (s, 3, $COCH_3$), 3.88 ($A_2B_2$m, 2, $AcOCH_2CH_2$), 4.27 ($A_2B_2$m, 2, $AcOCH_2CH_2$), 5.72 (s, 2, $OCH_2Br$); $^{13}$C nmr ($CDCl_3$) δ: 20.80 ($CH_3CO$), 62.14 ($AcOCH_2CH_2$), 69.22 ($AcOCH_2CH_2$), 75.60 ($OCH_2Br$), 170.69 ($CH_3CO$); ms (CI) *m*/*z*: 214, 216 ($M^+$ + 18 [$^{79}$Br, $^{81}$Br]). *Anal.* calcd. for $C_5H_9BrO_3$: C 30.48, H 4.60, Br 40.55; found: C 30.55, H 4.59, Br 40.72.

TABLE 1. Synthetic and characterization data for preparation of acetylated products

| Starting material | | | | Product | | | | | | | | | | | | | |
|---|---|---|---|---|---|---|---|---|---|---|---|---|---|---|---|---|---|
| | | | | | Yield | | Melting | | Calculated | | | | Found | | | Molecular ion | |
| Compound | X | mg | Method[a] | Compound | mg | % | point °C | Solvent[a] | C | H | N | C | H | N | Calculated | Found |
| **3***a* | H | 168 | A | **4***a* | 181 | 79 | 77–78 | A | 47.38 | 5.30 | 12.28 | 47.10 | 5.39 | 12.16 | 228.0742 | 228.0747 |
| *b* | $CH_3$ | 189 | A | *b* | 203 | 84 | 123–125 | A | 49.59 | 5.83 | 11.57 | 49.32 | 5.72 | 11.57 | 242.0903 | 242.0903 |
| *c* | F | 195 | A | *c* | 207 | 84 | 148–149 | A | 43.91 | 4.50 | 11.38 | 43.68 | 4.63 | 11.20 | 246.0652 | 246.0652 |
| *d* | Cl | 220 | A | *d* | 228 | 87 | 119–120 | A | 41.16 | 4.22 | 10.67 | 41.10 | 4.06 | 10.66 | 262.0357[b] | 262.0359[b] |
| *e* | Br | 287 | A | *e* | 264 | 86 | 131–132 | A | 35.20 | 3.61 | 9.12 | 35.04 | 3.66 | 8.99 | | 324[c,d] |
| *f* | I | 357 | A | *f* | 280 | 79 | 121–123 | A | 30.53 | 3.13 | 7.91 | 30.53 | 3.18 | 7.60 | 353.9713 | 353.9727 |
| *g* | $NO_2$ | 236 | A | *g* | 236 | 86 | 134–135 | B | 39.57 | 4.06 | 15.38 | 39.31 | 4.03 | 15.22 | | 291[d] |
| *h* | ≈Br | 326 | A | *h* | 289 | 87 | 109–110 | A | 39.66 | 3.93 | 8.41 | 39.53 | 4.02 | 8.31 | | 350[c,d] |
| **6***a* | | 167 | A | **6***b* | 193 | 85 | 184–186 | B | 47.58 | 5.77 | 18.49 | 47.43 | 5.71 | 18.42 | 227.0907 | 227.0907 |
| **7***a* | | 122 | A | **7***b* | 200 | 88 | 123–124 | C | 52.87 | 5.77 | 6.17 | 52.87 | 5.76 | 6.15 | 227.0794 | 227.0795 |
| **8***a* | | 170 | B | **8***b* | 224 | 83 | 96–97 | D | 44.38 | 4.10 | 20.70 | 44.02 | 4.04 | 20.78 | | 271[b,d] |
| **9***a* | | 208 | B | **9***b* | 270 | 88 | 96–97 | A | 39.37 | 3.30 | 18.36 | 39.18 | 3.44 | 18.22 | 304.0130[b] | 304.0124[b] |
| **10***a* | | 187 | B | **10***b* | 239 | 84 | 132–133 | A | 42.04 | 4.23 | 24.52 | 41.81 | 4.21 | 24.56 | 285.0628[b] | 285.0633[b] |
| **11***a* | | 149 | C | **11***b* | 188 | 75 | 156–158 | A | 47.81 | 5.22 | 27.88 | 47.51 | 5.05 | 28.01 | 251.1019 | 251.1020 |

[a]See the Experimental for coupling methods A–C and recrystallization solvent systems A–D.
[b]For ions containing $^{35}$Cl.
[c]For ions containing $^{79}$Br.
[d]Chemical ionization ($NH_3$) molecular ion plus ammonium ($M^+$ + 18). No $M^+$ was observed at 70 eV EI.

Can. J. Chem. Downloaded from www.nrcresearchpress.com by 210.87.254.6 on 09/06/12
For personal use only.

TABLE 2. Ultraviolet and $^1$H nmr spectral data for acetylated products

| Compound | X | Ultraviolet data: 0.1 *N* HCl max nm (ε) | Ultraviolet data: 0.1 *N* HCl min nm (ε) | Ultraviolet data: 0.1 *N* NaOH max nm (ε) | Ultraviolet data: 0.1 *N* NaOH min nm (ε) | $^1$H nmr data: δ ppm from $Me_4Si$ internal in $Me_2SO$-$d_6$ solution[a]: $CH_3COO$[b] | $AcOCH_2CH_2$[c] | $AcOCH_2CH_2$[c] | $OCH_2$-Base[b] | Base |
|---|---|---|---|---|---|---|---|---|---|---|
| **4***a*[a] | H | 259(9800) | 228(2300) | 259(6800) | 243(5700) | 2.07 | 3.81 | 4.23 | 5.21 | 5.80 (d, $J$ = 8 Hz, H-5), 7.33 (H-6) |
| *b* | $CH_3$ | 264(9600) | 233(2500) | 265(7000) | 246(4800) | 2.01 | 3.70 | 4.11 | 5.08 | 1.78 (s, $CH_3$), 7.56 (s, H-6) |
| *c* | F | 266(8600) | 232(2000) | 265(6200) | 248(5000) | 1.98 | 3.74 | 4.13 | 5.04 | 8.10 (d, $J$ = 6.6 Hz, H-6) |
| *d* | Cl | 274(8700) | 238(1500) | 271(5900) | 249(3600) | 2.01 | 3.73 | 4.11 | 5.11 | 8.20 (s, H-6) |
| *e* | Br | 277(8600) | 241(1100) | 274(5900) | 250(3300) | 2.00 | 3.73 | 4.10 | 5.10 | 8.26 (s, H-6) |
| *f* | I | 285(7000) | 246(2000) | 276(5000) | 252(3300) | 1.99 | 3.70 | 4.09 | 5.08 | 8.25 (s, H-6) |
| *g* | $NO_2$ | 296(9900) 234(8000) | 257(3200) | 323(13 000) | 264(2700) | 1.99 | 3.79 | 4.11 | 5.27 | 9.29 (s, H-6) |
| *h* |  | 289(11 300) 249(16 400) | 270(8900) 214(8300) | 280(9800)[d] 251(16 500) | 230(14 000) | 1.99 | 3.72 | 4.10 | 5.12 | 6.85 (d, $J$ = 13.5 Hz, ), 7.28 (d, 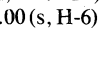 ), 8.00 (s, H-6) |
| **6***b* | | 275(12 000) | 240(1600) | 266(7700) | 249(6200) | 1.98 | 3.66 | 4.06 | 5.06 | 5.68 (d, $J$ = 7.5 Hz, H-5), 7.15 (br, $NH_2$), 7.58 (d, H-6) |
| **7***b* | | 280(4600) | 247(700) | 256(6800) | 232(3700) | 2.00 | 3.66 | 4.08 | 5.21 | 5.59 (d, $J$ = 2.4 Hz, H-3), 5.90 (dd, H-5), 7.54 (d, $J$ = 7.6 Hz, H-6) |
| **8***b* | | 263(9100) 250(6300)[d] | 222(2100) | 263(8800) 250(6300) | 230(3300) | 1.91 | 3.76 | 4.06 | 5.74 | 8.84, 8.86 (s, s, H-2, H-8) |
| **9***b* | | 273(9400) 250(4800)[d] | 228(2400) | 274(8900) 250(4800)[d] | 233(2800) | 2.03 | 3.80 | 4.20 | 5.68 | 8.27 (s, H-8) |
| **10***b*[a] | | 309(7800) 246(6900) | 262(700) 232(5000) | 309(7800) 246(6900) | 262(700) 232(5000) | 2.03 | 3.75 | 4.18 | 5.52 | 5.28 (br, $NH_2$), 7.92 (s, H-8) |
| **11***b* | | 256(16 600) | 225(2400) | 260(16 900) | 227(3300) | 1.92 | 3.72 | 4.06 | 5.56 | 7.23 (br, $NH_2$), 8.16 (s, H-2), 8.26 (s, H-8) |

[a] $^1$H nmr spectra of **4***a* and **10***b* were determined in $CDCl_3$.
[b] Singlet.
[c] $A_2B_2$ multiplet.
[d] Shoulder.

Can. J. Chem. Downloaded from www.nrcresearchpress.com by 210.87.254.6 on 09/06/12
For personal use only.

*Coupling Method A*

*1-[(2-Acetoxyethoxy)methyl]uracil (4a)*

To a suspension of 168 mg (1.5 mmol) of uracil (**3***a*) in 5 mL of hexamethyldisilazane was added a drop of chlorotrimethylsilane and the stirred mixture was heated at reflux with exclusion of moisture until a clear solution was obtained. Excess silylating reagent was removed *in vacuo* with protection against moisture. The residual clear oil was dissolved in 15 mL of dry acetonitrile and cooled to 0°C. A solution of 197 mg (1 mmol) of (2-acetoxyethoxy)methyl bromide (**2***a*) in 5 mL of dry acetonitrile was added slowly with stirring. The solution was allowed to stir for 2 h while warming to room temperature at which time tlc(A) indicated complete reaction. Volatile materials were evaporated *in vacuo*. The resulting yellow oil was chromatographed on a column (3 cm diameter) of 20 g of silica gel using 2% MeOH/$CHCl_3$ for elution. Fractions containing **4***a* were combined and evaporated. The residue was crystallized from $CHCl_3$ with diffusion of $Et_2O$ to give 181 mg (79%) of pure **4***a* with the physical and analytical data recorded in Tables 1 and 2.

This procedure was used to couple 1.5 mmol samples of **3***b–h* and **6***a*, and 1.1 mmol of **7***a* with 1 mmol of **2***a* to give **4***b–h*, **6***b*, and **7***b* as indicated in Tables 1 and 2. In the case of **3***f* → **4***f*, rigorous removal of the coupling by-product $Me_3SiBr$ was necessary in order to avoid deiodination of **4***f* to given contaminating **4***a* during processing and recrystallization.

*Coupling Method B*

*9-[(2-Acetoxyethoxy)methyl]-2-amino-6-chloropurine (10b)*

A stirred mixture of 187 mg (1.1 mmol) of 2-amino-6-chloropurine (**10***a*), 45 mg of $(NH_4)_2SO_4$, and 5 mL of hexamethyldisilazane was heated at reflux for 3 h with exclusion of moisture. Volatile materials were evaporated *in vacuo* with protection against moisture. The residue was stirred with 15 mL of dry benzene and 344 mg of $Hg(CN)_2$ was added. This mixture was stirred at reflux under a dry nitrogen atmosphere for 30 min. A solution of 197 mg (1 mmol) of (2-acetoxyethoxy)methyl bromide (**2***a*) in 5 mL of benzene was added and reflux was continued for 2 h. The mixture was cooled, 150 mL of $CHCl_3$ was added, and the organic phase was washed with 30 mL of saturated $NaHCO_3/H_2O$ followed by 30 mL of 1 *M* $KI/H_2O$. The organic solution was dried over $Na_2SO_4$, filtered, and evaporated to give 239 mg (84%) of an oil that was homogeneous by tlc(A). This product was crystallized from $CHCl_3$ with diffusion of $Et_2O$ to give pure **10***b* with the physical and analytical data given in Tables 1 and 2.

This procedure was used to couple 1.1 mmol samples of **8***a* and **9***a* to give **8***b* and **9***b* as indicated in Tables 1 and 2.

*Coupling Method C*

*9-[(2-Acetoxyethoxy)methyl]adenine (11b)*

To a stirred solution of 149 mg (1.1 mmol) of adenine (**11***a*) in 25 mL of dry (and *amine-free*) DMF was added 29 mg (1.2 mmol) of NaH. After evolution of hydrogen had ceased, the mixture was cooled to −63°C and a solution of 197 mg (1 mmol) of (2-acetoxyethoxy)methyl bromide (**2***a*) in 5 mL of DMF was added slowly. The stirred mixture was allowed to warm slowly to room temperature over a period of 2 h, 0.5 mL of 1 *M* $NaHCO_3/H_2O$ was added, and volatile materials were evaporated *in vacuo*. The residue was chromatographed on a column (30 g) of silica gel using 5% MeOH/$CHCl_3$ for elution. Appropriate fractions were combined and evaporated to give 188 mg (75%) of an oily product. This material was crystallized from $CHCl_3$ with diffusion of $Et_2O$ to give pure **11***b* with physical and analytical data as indicated in Tables 1 and 2.

TABLE 3. Synthetic and characterization data for preparation of deprotected acyclonucleosides

| Starting material | | | | Product | | | | | | | | | | | |
|---|---|---|---|---|---|---|---|---|---|---|---|---|---|---|---|
| | | | | | Yield | | Melting | | Calculated | | | Found | | | Molecular ion |
| Compound | X | mg | Method[a] | Compound | mg | % | point °C | Solvent[a] | C | H | N | C | H | N | Calculated | Found |
| **4***a* | H | 228 | A | **5***a* | 169 | 91 | 147–148 | E | 45.17 | 5.41 | 15.05 | 44.93 | 5.33 | 15.06 | 186.0641 | 186.0640 |
| *b* | $CH_3$ | 4000 | B | *b* | 3077 | 93 | 150.5–152 | E | 48.00 | 6.04 | 13.99 | 48.00 | 5.95 | 13.95 | 200.0797 | 200.0801 |
| *c* | F | 1476 | B | *c* | 1175 | 96 | 154–156 | F | 41.19 | 4.44 | 13.72 | 41.12 | 4.56 | 13.63 | 204.0546 | 204.0541 |
| *d* | Cl | 200 | A | *d* | 164 | 98 | 167–168 | G | 38.11 | 4.11 | 12.70 | 37.88 | 3.96 | 12.42 | 220.0251[b] | 220.0248[b] |
| *e* | Br | 307 | A | *e* | 206 | 78 | 152–153 | G | 31.72 | 3.42 | 10.57 | 31.91 | 3.52 | 10.46 | 263.9746[c] | 263.9746[c] |
| *f* | I | 708 | B | *f* | 576 | 92 | 175–176 | A | 26.94 | 2.91 | 8.98 | 27.02 | 3.00 | 8.84 | 311.9607 | 311.9612 |
| *g* | $NO_2$ | 180 | B | *g* | 140 | 92 | 173–175 | B | 36.38 | 3.92 | 18.18 | 36.24 | 3.88 | 18.21 | 231.0491 | 231.0487 |
| *h* | ≷Br | 500 | A | *h* | 398 | 91 | 130–133 | H | 37.14 | 3.81 | 9.62 | 37.04 | 3.87 | 9.51 | | 308[c,d] |
| **6***b* | | 2905 | B | **6***c*[e] | 2220 | 94 | 170–171 | C | 45.41 | 5.99 | 22.69 | 45.37 | 6.10 | 22.66 | 185.0800 | 185.0803 |
| **7***b* | | 250 | B | **7***c* | 169 | 83 | 137–139 | C | 51.90 | 5.99 | 7.56 | 51.80 | 6.00 | 7.53 | 185.0688 | 185.0689 |
| **10***b* | | 226 | A | **10***c* | 168 | 87 | 204–205 | I | 39.44 | 4.14 | 28.74 | 39.25 | 4.12 | 28.54 | 243.0523[b] | 243.0520[b] |
| **11***b* | | 830 | B | **11***c*[f] | 648 | 94 | 204–206 | E | 45.93 | 5.30 | 33.48 | 45.69 | 5.29 | 33.24 | 209.0913 | 209.0910 |
| **10***c* | | 110 | *g* | **13** | 88 | 87 | 265–266 | J | 42.67 | 4.92 | 31.10 | 42.45 | 4.93 | 30.95 | 225.0862 | 225.0863 |

[a]See the Experimental for deprotection methods A and B and recrystallization solvent systems A–J.
[b]For ions containing $^{35}Cl$.
[c]For ions containing $^{79}Br$.
[d]Chemical ionization ($NH_3$) molecular ion plus ammonium ($M^+ + 18$). No $M^+$ was observed at 70 eV EI.
[e]See ref. 7*c* for prior synthesis and data.
[f]See refs. 3, 7*c* for prior synthesis and data.
[g]See the Experimental.

Can. J. Chem. Downloaded from www.nrcresearchpress.com by 210.87.254.6 on 09/06/12
For personal use only.

TABLE 4. Ultraviolet and $^1$H nmr spectral data for deprotected acyclonucleosides

| | | Ultraviolet data | | | | $^1$H nmr data | | | |
|---|---|---|---|---|---|---|---|---|---|
| | | 0.1 *N* HCl | | 0.1 *N* NaOH | | δ ppm from $Me_4Si$ internal in $Me_2SO$-$d_6$ solution | | | |
| Compound | X | max nm (ε) | min nm (ε) | max nm (ε) | min nm (ε) | $OCH_2CH_2O$[a] | OH[b] | $OCH_2$-Base[a] | Base |
| **5***a*[a] | H | 259(9700) | 229(2500) | 260(6700) | 243(5400) | 3.48 | 4.64 | 5.08 | 5.60 (d, *J* = 8 Hz, H-5), 7.67 (d, H-6) |
| *b* | $CH_3$ | 265(9000) | 234(2200) | 264(6500) | 245(4400) | 3.50 | 4.65 | 5.06 | 1.78 (s, $CH_3$), 7.55 (s, H-6) |
| *c* | F | 266(8200) | 232(1800) | 265(6100) | 248(4700) | 3.48 | 4.61 | 5.05 | 8.10 (d, *J* = 6.6 Hz, H-6) |
| *d* | Cl | 274(8500) | 238(1500) | 272(5800) | 249(3500) | 3.50 | 4.62 | 5.08 | 8.16 (s, H-6) |
| *e* | Br | 276(8600) | 241(1700) | 274(5700) | 251(3300) | 3.51 | 4.65 | 5.10 | 8.25 (s, H-6) |
| *f* | I | 286(7100) | 245(2000) | 277(5000) | 251(3100) | 3.50 | 4.65 | 5.08 | 8.20 (s, H-6) |
| *g* | $NO_2$ | 297(9900)<br>232(7700) | 257(3100)<br>209(4800) | 323(13 300) | 263(2800) | 3.58[c] | 5.70[d] | 5.28 | 9.30 (s, H-6) |
| *h* |  | 290(10 300)<br>249(14 900) | 270(7900)<br>213(6600) | 280(8900)[e]<br>253(15 300) | 230(12 500) | 3.50 | 4.60 | 5.10 | 6.83 (d, *J* = 14 Hz, 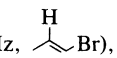 ), 7.28 (d, 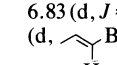 ), 7.97 (s, H-6) |
| **6***c* | | 276(12 000) | 240(1700) | 267(7900) | 250(6400) | 3.46 | 4.60 | 5.06 | 5.72 (d, *J* = 7.5 Hz, H-5), 7.2 (br, $NH_2$), 7.60 (d, H-6) |
| **7***c* | | 280(4600) | 247(800) | 256(6900) | 232(3700) | 3.46 | 4.55 | 5.18 | 5.56 (d, *J* = 2.5 Hz, H-3), 5.87 (dd, H-5), 7.52 (d, *J* = 7.5 Hz, H-6) |
| **10***c* | | 307(7600)<br>246(7200) | 264(1000)<br>232(5300) | 307(7600)<br>246(7200) | 265(1100)<br>232(5400) | 3.50 | 4.66 | 5.47 | 6.99 (br, $NH_2$), 8.28 (s, H-8) |
| **11***c* | | 256(14 200) | 225(2300) | 259(14 500) | 227(3200) | 3.50 | 4.65 | 5.56 | 7.24 (br, $NH_2$), 8.17 (s, H-2), 8.26 (s, H-8) |
| **13** | | 271(8800)[e]<br>252(13 000) | 224(2800) | 260(11 400) | 229(4700) | 3.34[c] | 4.56 | 5.34 | 6.49 (br, $NH_2$), 7.81 (s, H-8) |

[a]Singlet.
[b]Broad singlet.
[c]Multiplet.
[d]Triplet.
[e]Shoulder.

*Deprotection Method A*

*2-Amino-6-chloro-9-[(2-hydroxyethoxy)methyl]purine (**10**c)*

A 226 mg (0.79 mmol) sample of **10***b* was added to 40 mL of MeOH saturated with $NH_3$ at −10°C. The flask was stoppered tightly and the solution was stirred for 5 h at room temperature. Thin-layer chromatography(A) indicated that complete deprotection of **10***b* had occurred. Volatile materials were evaporated and the resulting solid was recrystallized from 2-propanol to give 168 mg (87%) of pure **10***c* with physical and analytical data as indicated in Tables 3 and 4.

*Deprotection Method B*

*5-Fluoro-1-[(2-hydroxyethoxy)methyl]uracil (5*c*)*

To 60 mL of dry MeOH was added 0.23 g (10 mmol) of sodium metal. After hydrogen evolution was complete, 1.476 g (6 mmol) of **4***c* was added and stirring was continued for 2 h at room temperature. Thin-layer chromatography(A) indicated that complete deprotection of **4***c* had occurred. Amberlite IR-120 ($H^+$) resin was added until the solution was neutral to moist pH paper. The mixture was filtered, the resin washed with MeOH, and the combined filtrate evaporated. The colorless residual powder was recrystallized from MeOH–$H_2O$ to give 1.175 g (96%) of pure **5***c* with physical and analytical data as indicated in Tables 3 and 4.

*9-[(2-Hydroxyethoxy)methyl]guanine (acycloguanosine) (**13**) (4, 7c)*

A. *From 2-amino-6-chloro-9-[(2-hydroxyethoxy)methyl]-purine (10c)*

To a solution of 110 mg (0.45 mmol) of **10***c* in 25 mL of aqueous phosphate buffer (0.05 *M*, pH 7.5) was added 30 mg of adenosine deaminase. The reaction mixture was stirred magnetically at room temperature and monitored by tlc(B) until complete hydrolytic dechlorination had occurred. The crude product could be obtained directly by crystallization from the concentrated reaction mixture. However, a convenient purification procedure employed adsorption of the product from the aqueous medium on a carbon column (18), washing the column with water, and elution of **13** with 35% $CH_3CN/H_2O$. Evaporation of the appropriately pooled fractions, recrystallization of the solid from EtOH–$H_2O$, and thorough drying of the product *in vacuo* over $P_2O_5$ gave 88 mg (87%) of pure **13** with physical and analytical data as indicated in Tables 3 and 4.

B. *From 9-[(2-acetoxyethoxy)methyl]-2,6-dichloropurine (9b)*

A solution of 510 mg (1.67 mmol) of **9***b* in 15 mL of liquid ammonia was sealed in a Parr steel bomb and heated at 150°C for 3 days. After cooling, the bomb was vented and tlc(B) indicated complete conversion to the 2,6-diamino product (**12**) (none of the 6-amino-2-chloropurine analogue was detected). The residue was purified on a column of silica gel using 10% MeOH/$CHCl_3$ for elution to give 350 mg (93%) of oily **12**. This material was treated with adenosine deaminase as described above (A. **10***c* → **13**) to give 312 mg (89%) of pure **13**.

C. *Overall from 2-amino-6-chloropurine (**10**a)*

A 187 mg (1.1 mmol) sample of **10***a* was coupled with 197 mg (1 mmol) of **2***a* as described under Coupling Method B. The oily **10***b* obtained was treated by Deprotection Method A to give a crude solid, **10***c*, that was subjected directly to adenosine deaminase as described above (A. **10***c* → **13**). The resulting carbon column-purified product was recrystallized and dried to give 172 mg (76% overall from **2***a*) of pure **13**.

## Acknowledgements

We thank the National Cancer Institute of Canada, the Natural Sciences and Engineering Research Council of Canada (A5890), and The University of Alberta for generous financial support.

1. M. J. Robins, F. Hansske, and S. E. Bernier. Can. J. Chem. **59**, 3360 (1981).
2. (*a*) R. W. Sidwell and J. T. Witkowski. *In* Burger's medicinal chemistry. 4th ed. Part II. *Edited by* M. E. Wolff. John Wiley & Sons, New York. 1979. pp. 543–593; (*b*) E. De Clercq. Arch. Int. Physiol. Biochim. **87**, 353 (1979); (*c*) W. H. Prusoff and P. H. Fisher. *In* Nucleoside analogues: chemistry, biology, and medical applications. *Edited by* R. T. Walker, E. De Clercq, and F. Eckstein. NATO Advanced Study Institute Series. Vol. 26A. Plenum Press, New York. 1979. pp. 281–318; (*d*) J. C. Drach. *In* Annual Reports in Medicinal Chemistry. Vol. 15. *Edited by* H.-J. Hess. Academic Press, New York. 1980. pp. 149–161.
3. H. J. Schaeffer, S. Gurwars, R. Vince, and S. Bittner. J. Med. Chem. **14**, 367 (1971).
4. H. J. Schaeffer, L. Beauchamp, P. de Miranda, G. B. Elion, D. J. Bauer, and P. Collins. Nature, **272**, 583 (1978).
5. J. M. Goldman, P. M. Chipping, G. Agnarsdottir, and D. Brigden. Lancet, **1**, 820 (1979).
6. E. De Clercq and A. Holý. J. Med. Chem. **22**, 510 (1979).
7. (*a*) G. E. Keyser, J. D. Bryant, and J. R. Barrio. Tetrahedron Lett. 3263 (1979); (*b*) J. D. Bryant, G. E. Keyser, and J. R. Barrio. J. Org. Chem. **44**, 3733 (1979); (*c*) J. R. Barrio, J. D. Bryant, and G. E. Keyser. J. Med. Chem. **23**, 572 (1980).
8. K. K. Ogilvie and M. F. Gillen. Tetrahedron Lett. 327 (1980).
9. J. E. McCormick and R. S. McElhinney. J. Chem. Res. (S), 12 (1981).
10. M. J. Robins. *In* Nucleosides, nucleotides, and their biological applications. *Edited by* J.-L. Barascut and J.-L. Imbach. INSERM Colloque 1978. Vol. 81. INSERM, Paris. 1979. pp. 13–35.
11. J. L. Kelley, J. E. Kelsey, W. R. Hall, M. P. Krochmal, and H. J. Schaeffer. Abstracts of Papers, 181st National Meeting of the American Chemical Society, Atlanta, Mar.–Apr. 1981. MEDI 33.
12. A. Rosowsky and S.-H. Kim. Abstracts of Papers, 181st National Meeting of the American Chemical Society, Atlanta, Mar.–Apr. 1981. MEDI 34.
13. M. Senkus. J. Am. Chem. Soc. **68**, 734 (1946).
14. U. Niedballa and H. Vorbrüggen. J. Org. Chem. **39**, 3654 (1974).
15. W. W. Lee, A. P. Martinez, L. Goodman, and D. W. Henry. J. Org. Chem. **37**, 2923 (1972).
16. (*a*) O. P. Chilson and J. R. Fisher. Arch. Biochem. Biophys. **102**, 77 (1963); (*b*) H.-P. Baer, G. I. Drummond, and E. L. Duncan. Mol. Pharmacol. **2**, 67 (1966).
17. (*a*) H. J. Schaeffer. German Patent No. 2,539.963, 1976; Chem. Abstr. **84**, 180300p (1976); (*b*) G. B. Elion, P. A. Furman, J. A. Fyfe, P. de Miranda, L. Beauchamp, and H. J. Schaeffer. Proc. Natl. Acad. Sci. U.S.A. **74**, 5716 (1977); (*c*) J. A. Fyfe, P. M. Keller, P. A. Furman, R. L. Miller, and G. B. Elion. J. Biol. Chem. **253**, 8721 (1978).
18. M. J. Robins, R. Mengel, R. A. Jones, and Y. Fouron. J. Am. Chem. Soc. **98**, 8204 (1976).
19. J. L. Kelley, J. E. Kelsey, W. R. Hall, M. P. Krochmal, and H. J. Schaeffer. J. Med. Chem. **24**, 753 (1981).
20. A. Rosowsky, S.-H. Kim, and M. Wick. J. Med. Chem. **24**, 1177 (1981).

Can. J. Chem. Downloaded from www.nrcresearchpress.com by 210.87.254.6 on 09/06/12
For personal use only.

# Nucleic acid related compounds. 38. Smooth and high-yield iodination and chlorination at C-5 of uracil bases and *p*-toluyl-protected nucleosides[1]

MORRIS J. ROBINS, PHILIP J. BARR,[2] AND JERZY GIZIEWICZ[3]

*Department of Chemistry, The University of Alberta, Edmonton, Alta., Canada T6G 2G2*

Received July 13, 1981

MORRIS J. ROBINS, PHILIP J. BARR, and JERZY GIZIEWICZ. Can. J. Chem. **60**, 554 (1982).

Treatment of uracil bases and protected nucleosides with iodine monochloride (ICl) gave the corresponding 5-iodouracil products in over 95% purified yields. Analogously facile chlorination was effected with iodobenzene dichloride ($PhICl_2$). Protection of the nucleosides as *p*-toluyl esters provided reactants that were soluble in organic solvents and crystallized readily in high yields.

MORRIS J. ROBINS, PHILIP J. BARR et JERZY GIZIEWICZ. Can. J. Chem. **60**, 554 (1982).

Les bases du type uracile et les nucléosides protégés réagissent avec le monochlorure d'iode (ICl) en donnant les produits iodo-5 uraciles correspondants avec un rendement en produits purs supérieur à 95%. D'une façon analogue, on a pu faire facilement une chloration à l'aide du dichlorure d'iodobenzène ($PhICl_2$). La protection des nucléosides par un groupe ester *p*-tolyle fournit des réactifs solubles dans les solvants organiques et qui peuvent être cristallisés facilement avec d'excellents rendements.

[Traduit par le journal]

Can. J. Chem. Downloaded from www.nrcresearchpress.com by 210.87.254.40 on 09/06/12
For personal use only.

A number of 5-substituted uracil derivatives, especially 2′-deoxyuridines, have been investigated extensively in the experimental and clinical treatment of neoplastic and viral diseases (2–4). The 5-fluorouracil and 2′-deoxyuridine compounds are potent inhibitors of cell growth and 5-fluorouracil has been used widely in the clinical treatment of cancer (2). The related 5-iodo-2′-deoxyuridine has been in clinical use as a herpes antiviral drug for over a decade (3). Recently (*E*)-5-(2-bromovinyl)-2′-deoxyuridine has been reported to have extraordinary activity and selectivity against herpes type I viruses (4, 5). There is strong current interest in the study of 5-substituted-2′-deoxyuridine 5′-monophosphates as mechanism based inhibitors of the crucial anabolic enzyme thymidylate synthetase (see ref. 6 and references therein).

We recently have devised an efficient route to uracil nucleosides with a functionalizable carbon chain at C-5 via the palladium–copper catalyzed coupling of terminal alkynes with 5-iodouracil compounds (7). A second reported coupling of terminal alkynes (as their chlorozinc derivatives) with a protected 5-iodo-2′-deoxyuridine gave the 5-(1-alkynyl) derivatives in variable yields (8). Both of these syntheses utilize 5-iodouracil precursors. The availability of the iodo compound in high yield is especially important when beginning with the expensive 2′-deoxyuridine.

Prior reports on the direct iodination of uridine, 2′-deoxyuridine, and their nucleotides have frequently employed the classical iodine/nitric acid/organic solvent mixture of Prusoff *et al.* (9). More recently, iodination of 5-mercuriuridine derivatives in aqueous alcohol has been described (10). However, these procedures can give troublesome by-products with resulting moderate yields of the purified 5-iodo compounds. The use of *N*-iodosuccinimide with pyrimidine nucleosides has been reasonably successful (11) and iodine monochloride has given moderate yields of uracil nucleosides with "unnatural" sugars (12).

We have found that treatment of uracil compounds with iodine monochloride under appropriate conditions gives clean conversion to the 5-iodo derivatives. Yields of the purified products depend primarily on the ease of crystallization. Treatment of 1-methyluracil (**1***b*) (see Scheme 1) with 2 equivalents of ICl in methanol at 50°C gave 5-iodo-1-methyluracil (**2***b*) in 95% yield after purification. Analogous treatment of uridine (**1***c*) and 2′-deoxyuridine (**1***d*) gave the corresponding 5-iodo nucleosides **2***c* and **2***d* in 82% and 76% yields.

Protection of the sugar hydroxyl groups as *p*-toluyl esters gave the organic soluble and readily crystallized derivatives **1***f* and **1***g*. Treatment of 2′,3′,5′-tri-*O*-*p*-toluyluridine (**1***f*), 3′,5′-di-*O*-*p*-toluyl-2′-deoxyuridine (**1***g*), and 1-(2,3,5-tri-*O*-*p*-toluyl-β-D-arabinofuranosyl)uracil (**1***h*) with 1.5 equivalents of ICl in dichloromethane at reflux gave 96%, 98%, and 95% crystallized yields of the 5-iodo products **2***f*, *g*, and *h*. Synthetic and characterization data are given in Table 1.

Chlorination of uracil compounds has been effected previously using elemental chlorine (13) or

[1]For the previous paper in this series see ref. 1.

[2]Isaak Walton Killam memorial postdoctoral fellow of The University of Alberta, 1978–1980.

[3]Postdoctoral fellow on leave from the Warsaw Agricultural University, Warsaw, Poland, 1980–1982.

0008-4042/82/050554-04$01.00/0

©1982 National Research Council of Canada/Conseil national de recherches du Canada

Can. J. Chem. Downloaded from www.nrcresearchpress.com by 210.87.254.40 on 09/06/12
For personal use only.





TABLE 1. Synthetic and characterization data

| Starting material | | | Product | | | | | | | | | | | |
|---|---|---|---|---|---|---|---|---|---|---|---|---|---|---|
| | | | | Yield | | Melting point | | Calculated | | | Found | | |
| Compound | Weight (g) | Method[a] | Compound | (g) | % | °C | Solvent[a] | C | H | N | C | H | N |
| **1***c* | 4.88 | A | **1***f* | 11.2 | 94 | 198–201 | A | 66.22 | 5.05 | 4.68 | 66.38 | 4.89 | 4.64 |
| *d* | 11.4 | A | *g* | 21.8 | 94 | 215–217[b] | A | 64.65 | 5.21 | 6.03 | 64.52 | 5.26 | 5.78 |
| *e* | 10.98 | A | *h* | 25.6 | 95 | 245–246 | A | 66.22 | 5.05 | 4.68 | 66.05 | 5.01 | 4.68 |
| **1***b* | 2.52 | B | **2***b* | 4.77 | 95 | 260–264 | B | 23.83 | 2.00 | 11.12 | 23.93 | 2.03 | 11.29 |
| *c* | 2.44 | B | *c* | 3.04 | 82 | 208–210[c,d] | B | 29.21 | 3.00 | 7.57 | 29.03 | 2.95 | 7.56 |
| *f* | 2.99 | C | *f* | 3.47 | 96 | 230–232 | A | 54.71 | 4.03 | 3.87 | 54.64 | 4.14 | 3.66 |
| *g* | 16.3 | C | *g* | 20.3 | 98 | 195–196[e] | A | 50.87 | 3.93 | 4.75 | 50.88 | 3.98 | 4.67 |
| *h* | 25.1 | C | *h* | 28.74 | 95 | 214–216 | A | 54.71 | 4.03 | 3.87 | 54.80 | 4.06 | 3.71 |
| **1***a* | 0.224 | D[f] | **3***a* | 0.268 | 92 | >325[g] | C | 32.79 | 2.06 | 19.12 | 32.77 | 1.95 | 18.83 |
| *b* | 0.252 | D | *b* | 0.301 | 94 | >270[h] | D | 37.41 | 3.14 | 17.45 | 37.31 | 3.03 | 17.22 |
| *f* | 8.38 | D | *f* | 7.45 | 84 | 224–226 | A | 62.62 | 4.62 | 4.43 | 62.46 | 4.70 | 4.22 |
| *g* | 1.16 | D | *g* | 1.17 | 94 | 214–215[i] | A | 60.19 | 4.65 | 5.62 | 59.99 | 4.71 | 5.30 |

[a]See the Experimental for Methods A–D and crystallization solvents A–D.
[b]Literature (20) mp 216–217°C.
[c]With decomposition.
[d]Literature (9) mp 205–208°C dec.
[e]Literature (21) mp 196–197°C.
[f]Reaction solvent was 50% AcOH/$H_2O$.
[g]Sublimed at >240°C and the resulting condensed prisms melted with decomposition at >325°C; lit. (14) mp 324–325°C dec.
[h]Sublimed without melting; lit. (15) mp 285°C dec.
[i]Literature (22) mp 213.5–214.5°C.

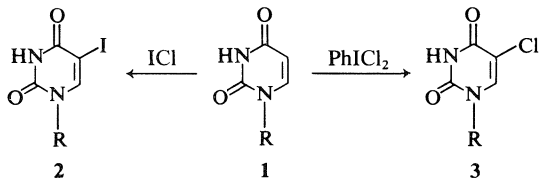


Series: *a*, R = H
*b*, R = $CH_3$
*c–h*, R =

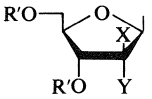

*c*, R′ = X = H, Y = OH
*d*, R′ = X = Y = H
*e*, R′ = Y = H, X = OH
*f*, R′ = $COC_6H_4CH_3$-*p*, X = H, Y = $OCOC_6H_4CH_3$-*p*
*g*, R′ = $COC_6H_4CH_3$-*p*, X = Y = H
*h*, R′ = $COC_6H_4CH_3$-*p*, X = $OCOC_6H_4CH_3$-*p*, Y = H

SCHEME 1

*N*-chlorosuccinimide in acetic acid (14, 15) to provide the 5-chlorouracils in moderate yields. A new procedure that utilizes hydrogen chloride and *m*-chloroperoxybenzoic acid has been described very recently by Ryu and MacCoss (16).

We have found that treatment of uracil compounds with 1.2 equivalents of iodobenzene dichloride in warm acetic acid solutions gives rapid and clean conversion to the 5-chloro products. Treatment of 1-methyluracil (**1***b*) with $PhICl_2$ in acetic acid at 80°C for 15 min gave 94% of purified 5-chloro-1-methyluracil (**3***b*). Analogous treatment of 3′,5′-di-*O*-*p*-toluyl-2′-deoxyuridine (**1***g*) gave 94% of the purified 5-chloro nucleoside (**3***g*). Other examples and data are given in the table.

This investigation has determined convenient access to the readily crystallized *p*-toluyl esters of uridine, 2′-deoxyuridine, and their 5-chloro and 5-iodo analogues. High-yield iodination and chlorination of uracil bases and protected nucleosides have been achieved using iodine monochloride and iodobenzene dichloride, respectively. These procedures complement known methods for efficient access to the corresponding 5-fluoro (17) and 5-bromo (18) series. The precursor 5-iodouracils (**2**) now are readily available for coupling with terminal alkynes (7).

## Experimental

*General*

General procedures and instrumentation used are given in ref. 1. Melting points were determined on a Gallenkamp block apparatus in open capillary tubes and are uncorrected. Iodine monochloride (ICl) was purchased from Aldrich Chemical Co. and used directly without purification. Iodobenzene dichloride (phenyliodine(III) chloride, $PhICl_2$) was prepared as described by Lucas and Kennedy (19). Crystallization solvents used are: A, product dissolved in a minimum volume of hot $CHCl_3$ and ~5 volumes of MeOH added, followed by chilling at −18°C (further crops obtained by concentration and chilling of the mother liquor); B, MeOH (with addition of $Et_2O$ for additional crops); C, MeOH–$H_2O$; D, MeOH.

*Method A*

*3′,5′-Di*-O-p-*toluyl-2′-deoxyuridine* (**1**g)

A magnetically stirred solution of 11.4 g (0.05 mol) of 2′-deoxyuridine (**1***d*) in 250 mL of dry pyridine was cooled to 0°C and 17 g (0.11 mol) of freshly distilled *p*-toluyl chloride was added slowly. The solution was allowed to warm to room temperature, heated at 50°C for 2 h, and evaporated *in vacuo* to give a white solid mass. Chloroform (400 mL) was added and the organic phase was washed with 2 × 300 mL of 1 *M* $H_2SO_4/H_2O$, 2 × 300 mL of $H_2O$, dried over $Na_2SO_4$, filtered, and evaporated to ~150 mL. Methanol (~750 mL) was added and the resulting colorless crystalline mass was filtered. The filtrate was reduced to a small volume and chilled at −18°C to give further crystalline product. The combined crystals were dried to give 21.8 g (94%) of **1***g*, mp 215–217°C; $^1H$ nmr ($Me_2SO$-$d_6$) δ: 2.40 (br, 6, two $CH_3$'s), 4.50 (m, 3, H-4′,5′,5″), 5.58 (m, 2, H-3′ and H-5), 6.28 (t, 1, H-1′), 7.3–7.9 (m, 9, H-6 and aromatic), 11.39 (br, 1, NH).

*Method B*

*5-Iodo-1-methyluracil* (**2**b)

Iodine monochloride (6.5 g, 0.04 mol) was added to a stirred suspension of 2.52 g (0.02 mol) of 1-methyluracil (**1***b*) in 40 mL of MeOH and the resulting solution was heated at 50°C for 1.5 h. Separation of a crystalline mass occurred and tlc indicated complete conversion of **1***b* → **2***b*. The mixture was filtered and the crystals were washed with $Et_2O$. The combined filtrate and washings was chilled at 0°C for several hours and a second crop of crystals was collected to give 4.77 g (95%) of **2***b* after drying. This product had mp 220–224°C; $^1H$ nmr ($Me_2SO$-$d_6$) δ: 3.25 (s, 3, $CH_3$), 8.17 (s, 1, H-6), 11.74 (br, 1, NH).

*Method C*

*5-Iodo-3′,5′-di*-O-p-*toluyl-2′-deoxyuridine* (**2**g)

A stirred solution of 16.3 g (0.035 mol) of **1***g* and 8.53 g (0.0525 mol) of ICl in 300 mL of $CH_2Cl_2$ was heated at reflux for 2 h. Thin-layer chromatography indicated complete conversion of **1***g* → **2***g*. The solution was cooled, diluted with 200 mL of $CH_2Cl_2$, and decolorized (ICl) by careful washing with the *minimum* required volume of 2% $NaHSO_3/H_2O$ solution. The organic phase was washed with $H_2O$, dried over $Na_2SO_4$, filtered, and evaporated. The residue was dissolved in a minimum volume of hot $CHCl_3$, MeOH (~5 volumes) was added, and the mixture was chilled at −18°C to give (in three crops) 20.3 g (98%) of crystalline **2***g*, mp 195–196°C.

*Method D*

*5-Chloro-3′,5′-di*-O-p-*toluyl-2′-deoxyuridine* (**3**g)

Iodobenzene dichloride (825 mg, 3 mmol) was added to a stirred solution of 1.16 g (2.5 mmol) of **1***g* in 15 mL of acetic acid at 80°C. Stirring was continued at 80°C for 15 min and tlc indicated complete conversion of **1***g* → **3***g*. The mixture was evaporated *in vacuo*. Repeated addition and evaporation of MeOH/$H_2O$ and then MeOH gave 1.21 g (97%) of **3***g* as a white powder. This product was dissolved in a minimum volume of hot $CHCl_3$, MeOH (~5 volumes) was added, and the mixture was chilled at −18°C to give (in two crops) 1.17 g (94%) of crystalline **3***g*, mp 214–215°C.

## Acknowledgements

We thank the National Cancer Institute of Canada, the Natural Sciences and Engineering Research

Can. J. Chem. Downloaded from www.nrcresearchpress.com by 210.87.254.40 on 09/06/12
For personal use only.

Council of Canada (A5890), and The University of Alberta for generous financial support.


1. M. J. ROBINS and P. W. HATFIELD. Can. J. Chem. **60**, 547 (1982).
2. C. HEIDELBERGER. Prog. Nucleic Acid Res. Mol. Biol. **4**, 1 (1965).
3. W. H. PRUSOFF and P. H. FISHER. *In* Nucleoside analogues: chemistry, biology, and medical applications. *Edited by* R. T. Walker, E. De Clercq, and F. Eckstein. NATO Advanced Study Institute Series. Vol. 26A. Plenum Press, New York. 1979. pp. 281–318.
4. E. DE CLERCQ. Arch. Int. Physiol. Biochim. **87**, 353 (1979).
5. E. DE CLERCQ, J. DESCAMPS, P. DE SOMER, P. J. BARR, A. S. JONES, and R. T. WALKER. Proc. Natl. Acad. Sci. U.S.A. **76**, 2947 (1979).
6. (*a*) D. V. SANTI. J. Med. Chem. **23**, 103 (1980); (*b*) J. S. PARK, C. T.-C. CHANG, and M. P. MERTES. J. Med. Chem. **22**, 1134 (1978).
7. M. J. ROBINS and P. J. BARR. Tetrahedron Lett. **22**, 421 (1981).
8. P. VINCENT, J.-P. BEAUCOURT, and L. PICHAT. Tetrahedron Lett. **22**, 945 (1981).
9. W. H. PRUSOFF, W. L. HOLMES, and A. D. WELCH. Cancer Res. **13**, 221 (1953).
10. R. M. K. DALE, D. C. WARD, D. C. LIVINGSTON, and E. MARTIN. Nucleic Acids Res. **2**, 915 (1975).
11. (*a*) D. LIPKIN, F. B. HOWARD, D. NOWOTNY, and M. SANO. J. Biol. Chem. **238**, PC 2249 (1963); (*b*) J. H. HUNTER. French Patent No. 1,513,754; Chem. Abstr. **71**, 50465s (1969).
12. (*a*) T. NAITO and N. HIRATA. Japanese Patent No. 68 11,459; Chem. Abstr. **70**, 4543x (1969); (*b*) T. NAITO, M. HIRATA, T. KOBAYASHI, and M. KANEO. Japanese Patent No. 69 17,911; Chem. Abstr. **71**, 113227p (1969).
13. (*a*) T. K. FUKUHARA and D. W. VISSER. J. Biol. Chem. **190**, 95 (1951); (*b*) A. M. MICHELSON. *In* Synthetic procedures in nucleic acid chemistry. Vol. I. *Edited by* W. W. Zorbach and R. S. Tipson. Wiley–Interscience, New York. 1968. pp. 491–492.
14. R. A. WEST and H. W. BARRETT. J. Am. Chem. Soc. **76**, 3146 (1954).
15. B. C. PAL. J. Am. Chem. Soc. **100**, 5170 (1978).
16. E. K. RYU and M. MACCOSS. J. Org. Chem. **46**, 2819 (1981).
17. M. J. ROBINS, M. MACCOSS, S. R. NAIK, and G. RAMANI. J. Am. Chem. Soc. **98**, 7381 (1976).
18. D. W. VISSER. *In* Synthetic procedures in nucleic acid chemistry. Vol. I. *Edited by* W. W. Zorbach and R. S. Tipson. Wiley–Interscience, New York. 1968. pp. 409–411.
19. H. J. LUCAS and E. R. KENNEDY. Organic syntheses. Coll. Vol. III, John Wiley & Sons, Inc., New York. 1955. pp. 482–483.
20. N. PRYSTAŠ, J. FARKAŠ, and F. ŠORM. Collect. Czech. Chem. Commun. **28**, 3140 (1963).
21. M. PRYSTAŠ and F. ŠORM. Collect. Czech. Chem. Commun. **29**, 121 (1964).
22. M. PRYSTAŠ and F. ŠORM. Collect. Czech. Chem. Commun. **29**, 131 (1964).


Can. J. Chem. Downloaded from www.nrcresearchpress.com by 210.87.254.40 on 09/06/12
For personal use only.

# Addition photochimique de nitrènes sur les éthers vinyliques et sucres insaturés

ELZBIETA KOZLOWSKA-GRAMSZ

*Université de Łodz, Laboratoire de Chimie Organique, Narutowicza 901-36-Łodz, Pologne*

ET

GÉRARD DESCOTES

*Université de Lyon I, Laboratoire de Chimie Organique II, E.R.A. 689 C.N.R.S. – E.S.C.I.L., 69622 Villeurbanne, France*

Reçu le 19 mars 1981[1]

ELZBIETA KOZLOWSKA-GRAMSZ et GÉRARD DESCOTES. Can. J. Chem. **60**, 558 (1982).

L'addition photochimique des nitrènes sur les éthers vinyliques cycliques et les sucres insaturés permet d'aboutir en présence d'alcool aux produits d'alcoolyse d'aziridines intermédiairement formées. La réactivité et la stéréosélectivité de cette addition sont discutées. L'application de cette réaction à la synthèse d'aminosucres est décrite.

ELZBIETA KOZLOWSKA-GRAMSZ and GÉRARD DESCOTES. Can. J. Chem. **60**, 558 (1982).

The photochemical addition of nitrenes to cyclic vinylic ethers and unsaturated sugars, in the presence of alcohols, gave the products of alcoholysis of the aziridine intermediates. The reactivity and stereoselectivity of this addition is discussed. The application of this reaction to the synthesis of aminosugars is described.

Les nitrènes constituent des espèces intermédiaires électrophiles très réactives vis-à-vis de sites nucléophiles et en particulier des oléfines (1). L'utilisation des nitrènes pour la synthèse d'aziridines a fait l'objet de très nombreuses recherches et l'étude de la stéréosélectivité de l'addition constitue une des méthodes d'approche du mécanisme réactionnel (2–4). Les éthers vinyliques et plus spécialement le dihydropyranne présentent des insaturations électroniquement riches qui ont été relativement peu étudiées dans leurs réactions avec les nitrènes. Les travaux de Brown et Edwards (5) et de Steiner (6) ont montré que l'obtention d'aziridines était possible avec le dihydropyranne mais l'étude stéréochimique de cette réaction et les applications éventuelles à la synthèse d'aminosucres n'ont pas été abordées. Ce mémoire présente une étude de la réactivité des éthers vinyliques cycliques vis-à-vis des nitrènes, une description de la stéréosélectivité de l'addition des nitrènes sur ces substrats et des applications pour la synthèse d'aminosucres à partir de sucres insaturés.

## *I. Réactivité relative des éthers vinyliques cycliques et sucres insaturés*

Les éthers utilisés de type **1** sont mis en réaction avec l'azidoformiate d'éthyle soumis à une photolyse durant 18 h à 25°C. La comparaison des vitesses de disparition de **1** lors de l'addition compétitive des nitrènes permet par rmn ou cpv de préciser les réactivités relatives (voir Partie expérimentale) qui s'établissent selon la séquence suivante:

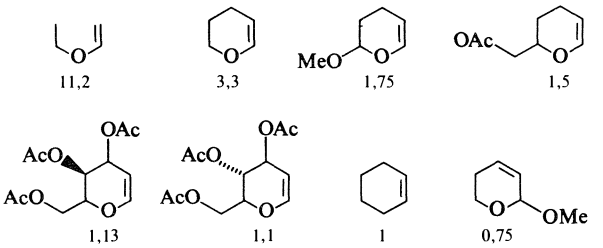


Cette séquence confirme principalement: (*i*) la plus grande réactivité des éthers vinyliques cycliques plus riches en électrons comparée à celle du cyclohexène ou d'un acétal insaturé; (*ii*) l'influence défavorable d'ordre vraisemblablement stérique des substituants en α ou en β des insaturations sur leur réactivité vis-à-vis des nitrènes.

Cependant, les faibles différences observées permettent d'envisager cette réaction pour la synthèse d'aminosucres. L'étude de la stéréosélectivité d'une telle addition a donc été entreprise.

## *II. Stéréosélectivité de l'addition des nitrènes sur 1*

### *1. Identification structurale des produits d'addition*

L'analyse rmn des produits obtenus par addition des nitrènes sur **1** permet de déterminer les configurations relatives des substituants du cycle, en particulier d'après le déplacement chimique et le couplage du proton acétalique (tableau 1).

Avec le dihydropyranne (**1***a*), l'effet anomère oriente la conformation de **5***a cis* avec un groupe alcoxy axial ($\delta_{H\text{-}1} = 4{,}7$ ppm, $J_{H\text{-}1\text{–}H\text{-}2} = 3$ Hz) quel que soit le solvant, alors que **3***a trans* modifie son

[1]Revision reçue le 12 juin 1981.

0008-4042/82/050558-06$01.00/0

©1982 National Research Council of Canada/Conseil national de recherches du Canada

Can. J. Chem. Downloaded from www.nrcresearchpress.com by 210.87.254.105 on 09/06/12
For personal use only.

TABLEAU 1. Données rmn de **2**, **3**, **4**, **5**

| Composé | $\delta_{H-1}$ | $J_{H-1-H-2}(CD_3COCD_3)$ | $\delta_{C-1\text{ et }C-5}$ ($CDCl_3$) | Autres signaux | % |
|---|---|---|---|---|---|
| ***3a*** | | | | | |
| R′ = H | 4,62 | 5 | — | — | 10 |
| R′ = Me | 4,42 | 4 (DMSO: 5) | — | — | 53 |
| R′ = *t*Bu | 4,95 | 3,5 (DMSO: 6) | — | — | 69 |
| ***5a*** | | | | | |
| R′ = H | 5,07 | 3 | — | — | 50 |
| R′ = Me | 4,58 | 3,5 (DMSO: 3,5) | — | — | 10 |
| R′ = *t*Bu | 4,70 | 3 (DMSO: 3) | — | — | 7 |
| ***2b*** | | | | | |
| R′ = Me | 4,60 | 1,5 | 99,7 | — | 41* |
| R′ = *t*Bu | 4,9 | 1,5 | 93,0 | — | 36 |
| ***3b*** | | | | | |
| R′ = Me | 4,25 | 8 | 103,9 | — | 20* |
| R′ = *t*Bu | 4,5 | 8 | 97,6 | — | 20 |
| ***5b*** | | | | | |
| R′ = Me | 4,70 | 4 | 98,2 | — | 6* |
| R′ = *t*Bu | 5,02 | 3 | 91,6 | — | Traces |
| ***2c*** | | | | | |
| R′ = Me | 4,4 | 7,5 | 101,5<br>100,5 | $\delta_{H-5}$ = 4,52 (dd, *J* = 8 et 3 Hz)<br>$\delta_{OMe}$ = 3,4 | 27 |
| R′ = *t*Bu | 4,6 | 8 ($CDCl_3$) | — | $\delta_{H-5}$ = 4,45 (dd, *J* = 7,5 et 3 Hz)<br>$\delta_{OMe}$ = 3,43 | 51 |
| ***3c*** | | | | | |
| R′ = Me | 4,6 | 5 | 97,5<br>100,5 | $\delta_{H-5}$ = 4,73 (t), $\delta_{OMe}$ = 3,38 et 3,35 | 13 |
| R′ = *t*Bu | — | — | — | — | 0 |
| ***4c*** | | | | | |
| R′ = Me | 4,7 | 3 | 98,7<br>97,2 | $\delta_{H-5}$ = 4,73 (t), $\delta_{OMe}$ = 3,38 et 3,35 | 9 |
| R′ = *t*Bu | 5,10 | 3,5 ($CDCl_3$) | — | $\delta_{H-5}$ = 4,8 (dd), $\delta_{OMe}$ = 3,4 ou 3,42 | 18 |
| ***5c*** | | | | | |
| R′ = Me | — | — | — | — | 0 |
| R′ = *t*Bu | 4,97 | 4 ($CDCl_3$) | — | $\delta_{H-5}$ = 4,8 (dd, *J* = 5,5 et 3,5 Hz)<br>$\delta_{OMe}$ = 3,4 ou 3,42 | 11 |
| ***2d*** | 4,65 | 1,5 | 100,1 | $\delta_{OMe}$ = 3,2 | 5 |
| ***3d*** | 4,6 | 8,5 | 101,8 | $\delta_{OMe}$ = 3,45 | 26 |
| ***5d*** | 4,7 | 3,5 | 98,4 | $\delta_{OMe}$ = 3,37 | 11 |
| ***2e*** | 4,98 | 1,5 | 100,5 | $\delta_{OMe}$ = 3,25 | 4 |
| ***3e*** | 4,55 | 8,5 | 102,3 | $\delta_{OMe}$ = 3,45 | 4 |
| ***5e*** | 4,8 | 3 | 98,9 | $\delta_{OMe}$ = 3,38 | 34 |

*Valeurs estimées d'après la cpv analytique et corrigées par rapport aux valeurs erronées données dans la note préliminaire (10).

équilibre conformationnel selon le solvant ($J_{H-1-H-2}$ de 3,5 dans le chloroforme à 6 Hz dans le DMSO-$d_6$). Par contre, les hydroxyuréthannes isomères dont l'un avait été précédemment décrit (5) ont été détectés et identifiés (*cis*/*trans* = 5:1) montrant également l'influence prédominante de l'effet anomère dans l'équilibre de ces isomères.

Pour le composé **1***b*, le blocage de la conformation permet d'identifier les produits d'addition de type *trans* diéquatorial ou diaxial grâce aux couplages respectifs pour $J_{H-1-H-2}$ de 8 Hz et 1,5 Hz. Le dérivé de type *cis* isolé **5***b* (R′ = *t*Bu) présente un groupe alcoxy axial ($\delta_{H-1}$ = 5,02 et $J_{H-1-H-2}$ = 3 Hz).

Des observations de type analogue permettent d'attribuer les configurations et conformations des produits d'addition d'après le tableau 1 avec **1***c*.

Cependant, si les dérivés **2***c* (R′ = Me, *t*Bu) de type "*trans*" sont aisément identifiés d'après $J_{H-1-H-2}$ ~ 8 Hz, d'après la forme du signal de H-5 (dd) et la présence d'un seul signal méthoxy, les autres composés d'addition présentent des problèmes d'analyse conformationnelle résumée dans les équilibres ci-dessous. Les critères rmn $^1H$ utilisés sont les déplacements chimiques et les couplages de H-1, la forme du signal de H-5 et sont complétés par les données rmn $^{13}C$ (Tableau 1). D'après ces

Can. J. Chem. Downloaded from www.nrcresearchpress.com by 210.87.254.105 on 09/06/12
For personal use only.

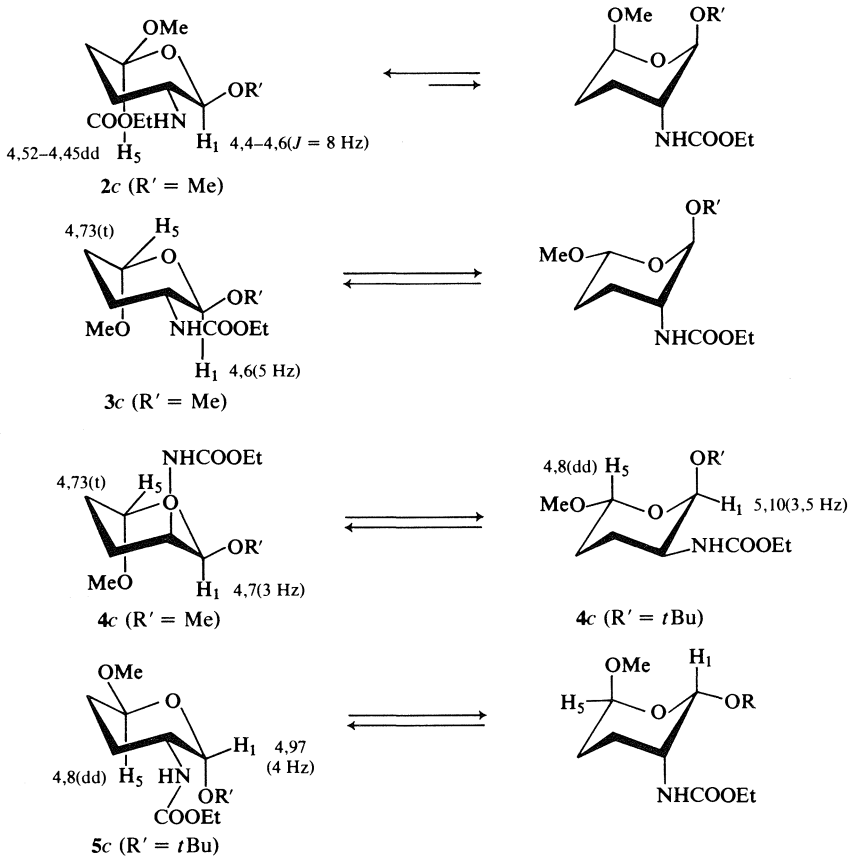


indications, **2***c* est dans une conformation privilégiée de type *C*1.

De même, **3***c* (R' = Me), **4***c* (R' = Me) et **5***c* (R' = *t*Bu) présenteraient un équilibre conformationnel déplacé vers les formes *C*1 alors que **4***c* (R' = *t*Bu) adopterait plutôt une conformation de type 1*C*. Les attributions pour chaque carbone acétalique n'ont pas été effectuées.

Dans le cas des sucres insaturés (**1***d* et **1***e*) quelques précédentes données de rmn $^1$H (7) ont été complétées par notre étude rmn $^{13}$C (tableau 1) pour l'établissement des configurations des produits d'addition obtenus. On n'observe pas de produit d'addition de type **4***d* ou **4***e* (β-*manno* et β-*talo*). Les autres isomères sont identifiés d'après le déplacement chimique et le couplage du proton anomère. En outre, les données cmr indiquent des variations de déplacements chimiques du carbone anomère répétitives puisque: (**3** − **5**) = 3,4 ppm; (**3** − **2**) = 1,6 à 1,7 ppm.

L'ensemble de ces données rmn permettent d'identifier sans ambiguité les isomères **2**, **3** et **5** en série *gluco* et *galacto* (8).

*2. Influence des conditions opératoires*

Divers facteurs expérimentaux ont été étudiés sur l'orientation stéréochimique des additions de nitrènes sur les éthers vinyliques de type **1** qui permettent de préciser: l'orientation initiale de l'attaque du nitrène: A/B, et l'addition *cis* ou *trans* des groupes azotés et oxygénés.

Si les effets de températures (15°C à 45°C) et de concentrations (éther/azidure = 1:1, 1:2) paraissent limités, les différentes données stéréochimiques pour la photolyse "directe" en présence d'alcools (méthode a) montrent que l'attaque du nitrène selon la voie A est privilégiée. Cette influence est limitée si $R_6$ est en position équatoriale (**1***b*) alors que pour $R_6$ préférentiellement axial selon l'effet anomère (**1***c*) (9), la stéréoorientation est beaucoup plus marquée. La gène stérique qui se développe lors de la formation de l'aziridine selon la voie B permet de justifier l'approche préférentielle selon la voie A. Néanmoins, dans le dernier cas, la *trans*-addition de l'alcool est moins importante. Cette observation sera retrouvée dans le cas de certains sucres insaturés (**1***e*) utilisés dans ce même type de réaction. L'amélioration de la stéréo sélectivité (*trans*-addition) est obtenue avec l'emploi d'un alcool encombré (*t*BuOH).

La réaction de **1***a* avec l'azidoformiate de méthyle permet d'aboutir à un intermédiaire de type aziri-

Can. J. Chem. Downloaded from www.nrcresearchpress.com by 210.87.254.105 on 09/06/12
For personal use only.

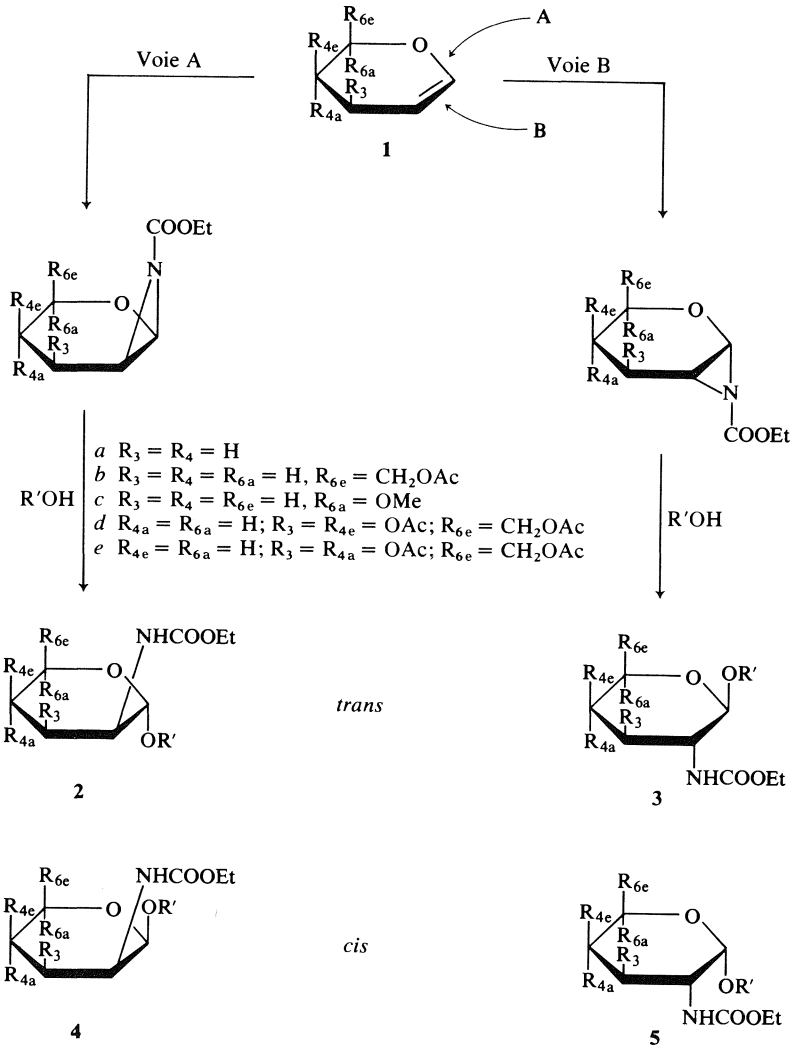


SCHÉMA 1

dine instable isolé par distillation (60°C/5 Torr) ($\delta_{H\text{-}1}$ = 5,95 ppm, $J$ = 6,5 Hz; $\delta_{H\text{-}2}$ = 3,95 ppm) qui donne par addition ultérieure d'alcool les mêmes produits d'alcoolyse que précédemment (tableau 2, méthode b).

La comparaison des résultats de photolyse "directe" avec ceux de réaction "photosensibilisée" (nitrènes à l'état triplet) (1, 4) montre que la présence de photosensibilisateurs diminue nettement les rendements en produits d'addition (avec apparition d'autres produits non isolés). Par contre, la stéréoorientation de l'attaque du nitrène à l'état triplet (rapport A/B) est accrue et le taux d'isomère 2*b* (R' = Me) est augmenté par rapport à la photolyse "directe". On peut expliquer ces différences de résultats par une addition non concertée des nitrènes à l'état triplet sur l'insaturation suivie d'une fixation d'alcool pour conduire aux alcoxyuréthannes de type préférentiellement *cis* en fonction de l'effet anomère. Ainsi, l'ensemble de ces données semble montrer que l'addition des nitrènes sur **1** par la photolyse "directe" dans nos conditions particulières se déroule préférentiellement par l'intermédiaire de nitrène à l'état singulet.

### *III. Application à la synthèse d'aminosucres*

L'obtention d'aminosucres par voie directe à partir des sucres insaturés constitue une intéressante synthèse qui a été récemment utilisée (7) dans des conditions ioniques (addition de *N*-chloroamide catalysée par le chlorure chromeux suivie d'une réaction de type Koenigs–Knorr). Les conditions photochimiques d'addition de nitrènes en présence d'alcools précédemment décrites permettaient d'envisager une synthèse "in one pot" de ces mêmes aminosucres avec une stéréosélectivité satisfaisante.

Can. J. Chem. Downloaded from www.nrcresearchpress.com by 210.87.254.105 on 09/06/12
For personal use only.

Can. J. Chem. Downloaded from www.nrcresearchpress.com by 210.87.254.105 on 09/06/12
For personal use only.

TABLEAU 2. Stéréoselectivité de l'addition des nitrènes sur **1***a*, **1***b*, **1***c*

| Composé | Rdt % total a | Rdt % total b | A/B a | A/B b | *trans*/*cis* a | *trans*/*cis* b |
|---|---|---|---|---|---|---|
| Réactions photosensibilisées* | | | | | | |
| (acétophénone) | | | | | | |
| **1***a* | | | | | | |
| R′ = Me | 30 | Traces | — | — | 54 | — |
| **1***b* | | | | | | |
| R′ = Me | 37 | 23 | 2,8 | 2,8 | 80 | 80 |
| Réactions non photosensibilisées* | | | | | | |
| **1***a* | | | | | | |
| R′ = Me | 63 | 65 | — | — | 83 | 83 |
| R′ = *t*Bu | 76 | — | — | — | 91 | — |
| **1***b* | | | | | | |
| R′ = Me | 67 | 68 | 1,6 | 2 | 90 | 94 |
| R′ = *t*Bu | 56 | — | 1,8 | — | 100 | — |
| **1***c* | | | | | | |
| R′ = *t*Bu | 80 | — | 6 | — | 63 | — |

*Conditions 36 h, 25°C.

TABLEAU 3. Stéréosélectivité de l'addition des nitrènes sur **1***d* et **1***e*

| | Rdt global % | *trans* **2** | *trans* **3** | *cis* **4** | *cis* **5** | B/A | *trans*/*cis* % |
|---|---|---|---|---|---|---|---|
| **1***d* | 42 | 5 | 26 | — | 11 | 7,4 | 75 |
| **1***e* | 42 | 4 | 4 | — | 34 | 9,5 | 18 |

Les essais effectués avec le tri-*O*-acétyl-3,4,6-D-glucal (**1***d*) et le tri-*O*-acétyl-3,4,6-D-galactal (**1***e*) permettent de montrer l'intérêt de cette méthode (tableau 3). En effet, dans les deux cas, l'attaque du nitrène se fait très nettement selon la voie B. Cette approche montre donc l'influence prédominante du groupe $R_3$ = OAc en position quasiéquatoriale comme précédemment observé dans d'autres conditions.[2] Cette stéréoorientation permet ensuite d'obtenir par *trans*-addition de l'alcool, le β-D-aminoglucopyranoside **3***d* majoritaire (plus de 60% du mélange). Par contre, dans le cas du D-galactal **1***e*, si l'approche du nitrène selon la voie B est encore plus marquée, l'addition *cis* du méthanol devient prépondérante puisque l' α-D-aminogalactopyranoside **5***e* devient le composé majoritaire (plus de 80% du mélange). Cette différence de comportement des intermédiaires dérivés de **5***d* et **5***e* doit se justifier par la participation du groupe $R_{4a}$ = OAc qui faciliterait l'ouverture de l'aziridine intermédiaire et favoriserait la formation du dérivé de *cis*-addition répondant à l'effet anomère.

[2]B. Gross, communication personnelle.

*Conclusion*

La photolyse de l'azidoformiate d'éthyle en présence d'alcool sur les éthers vinyliques cycliques et sucres insaturés de type **1** conduit à la formation directe des produits d'alcoolyse d'aziridines intermédiaires. Si l'addition du nitrène est stéréoorientée selon les substituants du cycle, l'ouverture est régiospécifique et stéréosélective avec formation des produits de *trans*-addition prépondérants. Ces additions sont utilisables pour la synthèse d'amino sucres et sont étudiées pour l'obtention d'aminodisaccharides.

## Partie expérimentale

Les points de fusion non corrigés ont été déterminés sur un appareil Buchi. Les spectres rmn ont été tracés à température ambiante avec un appareil Varian A 60 et un Brucker WP 80 CW. Les spectres de masse ont été effectués sur un appareil VG Micromass 70-70 F (70 eV). Les séparations chromatographiques ont été réalisées sur colonne de silice avec un éluant de type pentane – acétate d'éthyle ou selon les indications données ci-dessous.

*Procédé a: Photolyse "directe" en présence d'alcool*

On place dans un photoréacteur en quartz 0,005 mol d'éther vinylique anhydre avec 0,01 mol d'azidure ($ROCON_3$) fraiche-

Can. J. Chem. Downloaded from www.nrcresearchpress.com by 210.87.254.105 on 09/06/12
For personal use only.

ment distillé dans 3 mL d'alcool (méthanol ou tertiobutanol). L'irradiation avec une lampe Hanovia moyenne pression de 450 W est effectuée sous azote durant une période de 24 à 60 h à une température maintenue à 25°C. L'évolution de la réaction est suivie par ir avec la disparition des bandes caractéristiques des groupes azido ($\nu_{max}$ = 2120–2170 $cm^{-1}$). Après évaporation de l'alcool, le mélange est chromatographié sur silicagel. Dans certains cas (**1***e*), le mélange est chromatographié en hplc sur colonne "Lichroprep" Si 60 (5–20 μm) détection réfractométrique; éluant:acétate d'éthyle – hexane 30:70; 2 mL/min). La séparation du produit d'insertion du nitrène sur les alcools (EtOCONHOR′) est facilement obtenue dans les fractions de tête chromatographiques.

*Procédé b: Photolyse suivie d'addition d'alcool*

La photolyse est effectuée sans alcool dans les mêmes conditions que précédemment sans solvant pendant 36 h. L'alcool (méthanol ou tertiobutanol) est ensuite additionné (3 mL) au mélange qui est agité durant une heure. Les produits sont détectés par chromatographie en phase vapeur (à partir de **1***a* et **1***b*) et directement comparés avec ceux précédemment décrits.

*Photolyse photosensibilisée*

On opère de la même façon que précédemment (procédé a ou b) pour les réactions photosensibilisées en rajoutant 0,02 mol d'acétophénone ou d'acétone et en utilisant un filtre Pyrex. La photolyse poursuivie par les méthodes spectrales ou chromatographiques précédentes a été réalisée.

*Photoaddition compétitive*

On irradie un mélange d'oléfines, par exemple de 0,0025 mol de dihydropyranne et de 0,0025 mole de cyclohexène, en présence de 0,005 mol d'azidoformiate d'éthyle durant 18 h à 25°C sans solvant ou en présence de 1,5 $cm^3$ de $CH_2Cl_2$. La concentration restante des deux composés insaturés est mesurée au bout de cette période par rmn ou par chromatographie en phase gazeuse.

*Produits d'addition sur le dihydropyranne* **1**a (**2**a, **5**a)

R′ = H: composés partiellement décrits par la référence 5.

R′ = Me: composés décrits par la référence 7.

R′ = *t*Bu. *Anal.* calc. pour $C_{12}H_{23}O_4N$: C 58,75, H 9,45, N 5,71; trouvé: C 58,45, H 9,61, N 6,14.

*Produits d'addition sur* **1**b (**2**b, **3**b, **5**b)

R′ = Me: *Anal.* calc. pour $C_{12}H_{21}O_6N$: C 52,35, H 7,7, N 5,09; trouvé: C 52,37, H 7,56, N 5,0. Du mélange, le composé **3***b* (R′ = Me) a été obtenu cristallisé; $F$ = 105–106°C; rmn: $\delta_{H\text{-}1}$ = 4,5, $J_{H\text{-}1\text{–}H\text{-}2}$ = 8 Hz; $\delta_{OCH_3}$ = 3,35; $\delta_{OAc}$ = 2,0; $\delta_{NH}$ = 5,95. Spectre de masse: 244 (M + 1), 202 (4%), 186 (6%), 156 (4%), 155 (4%), 115 (100%).

R′ = *t*Bu: *Anal.* calc. pour $C_{15}H_{27}O_6N$: C 56,76, H 8,58, N 4,41; trouvé: C 56,1, H 8,85, N 4,6.

*Produits d'addition sur* **1**c (**2**c, **3**c, **4**c)

R′ = Me: *Anal.* calc. pour $C_{10}H_{19}O_5N$: C 51,49, H 8,21, N 6,01; trouvé: C 51,2, H 8,0, N 6,1. Outre le mélange dont la constitution est précisée dans le tableau 2 on isole un composé (17%) correspondant vraisemblablement au produit d'hydrolyse **3***c* (R′ = H) d'après la rmn: $\delta_{H\text{-}1}$ = 4,72 (d, $J$ = 7 Hz); $\delta_{NH+OH}$ = 6 ppm; $\delta_{OCH_3}$ 3,25; le spectre de masse: 220 (M + 1), 202 (17%), 172 (92%), 140 (65%), 115 (50%), 71 (67%), 68 (100%), et l'ir ($\nu_{OH}$ = 3620 $cm^{-1}$).

R′ = *t*Bu: *Anal.* calc. pour $C_{13}H_{25}O_5N$: C 56,70, H 9,15, N 5,09; trouvé: C 56,6, H 8,8, N 4,8. Du mélange, cristallise le composé **2***c* (R′ = *t*Bu); $F$ = 93–95°C; rmn: $\delta_{H\text{-}2}$ = 4,6, $J_{H\text{-}1\text{–}H\text{-}2}$ = 8 Hz; $\delta_{H\text{-}5}$ = 4,45 (dd, $J$ = 7,5 et 3 Hz); $\delta_{OCH_3}$ = 3,43; $\delta_{tBu}$ = 1,25; $\delta_{NH}$ = 5,0 dans $CDCl_3$.

*Produits d'addition sur le 1,5-anhydro-2-deoxy-*D-arabino-*hex-1 enitol (***1**d) (D-*glucal)* **2**d, **3**d, **5**d

Du mélange obtenu par photolyse directe (procédé a) (*Anal.* calc. pour $C_{16}H_{25}O_{10}N$: C 49,10, H 6,44, N 3,58; trouvé: C 48,5, H 6,4, N 4,0), le dérivé de type β-D-gluco **3***d* a été isolé, $F$ = 133°C, et présente les mêmes caractéristiques physiques et spectrales (tableau 1) que celles précédemment décrites (7). Spectre de masse: 392 (M + 1), 360 (43%), 169 (80%), 144 (56%), 131 (100%).

*Produits d'addition sur le 1,5-anhydro-2-deoxy-*D-lyxo-*hex-1 enitol (***1**e) (D-*galactal)* **2**e, **3**e, **5**e

Après séparation en chromatographie en phase liquide (hexane – acétate d'éthyle, 30:70), du mélange obtenu par photolyse "directe" de **1***e* (*Anal.* calc. pour $C_{16}H_{25}O_{10}N$: C 49,10, H 6,44, N 3,58; trouvé: C 48,8, H 6,5, N 3,9) on peut les caractériser par rmn. **2***e*: voir tableau 1. **3***e*: $\delta_{OAc}$ = 2,0 et 2,15; $\delta_{OCH_3}$ = 3,45; $\delta_{H\text{-}1}$ = 4,55 (d, $J_{H\text{-}1\text{–}H\text{-}2}$ = 8,5 Hz); $\delta_{H_3}$ = 5,1 (dd, $J$ = 6,5 et 3 Hz); $\delta_{H\text{-}4}$ = 5,4 (t, $J$ = 3 Hz); $\delta_{NH}$ = 5,85 dans $CD_3COCD_3$. **5***e*: $\delta_{OAc}$ = 2,0 et 2,15; $\delta_{OCH_3}$ = 3,38; $\delta_{H\text{-}1}$ = 4,8 (d, $J_{H\text{-}1\text{–}H\text{-}2}$ = 3,5 Hz); $\delta_{H\text{-}3}$ = 5,05 (dd, $J$ = 7 Hz et 3 Hz); $\delta_{H\text{-}4}$ = 5,35 (d, $J$ = 3 Hz) dans $CD_3COCD_3$.

1. W. Lwowski. Nitrènes. J. Wiley and Sons, New York. 1970.
2. W. Lwowski et T. W. Mattingly Jr. J. Am. Chem. Soc. **87**, 1947 (1965).
3. J. S. McConaghy et W. Lwowski. J. Am. Chem. Soc. **89**, 2357 (1967); **89**, 4450 (1967).
4. H. Durr et H. Kober. Top. Curr. Chem. **66**, 89 (1976).
5. I. Brown et O. E. Edward. Can. J. Chem. **43**, 1266 (1965).
6. P. S. Steiner. J. Org. Chem. **32**, 2022 (1967).
7. H. Driguez, J. P. Vermes et J. Lessard. Can. J. Chem. **56**, 119 (1978).
8. R. C. Beier, B. P. Mundy et G. A. Strobel. Can. J. Chem. **58**, 2800 (1980).
9. G. Descotes, J. C. Martin et N. Mathicolonis. Bull. Soc. Chim. Fr. 1077 (1972).
10. E. Kozlowska-Gramsz et G. Descotes. Tetrahedron Lett. **22**, 563 (1981).

# La polymérisation anionique en masse de l'α-méthyl styrène. I. Etude de la stabilité des centres actifs

DOMINIQUE ADES ET MICHEL FONTANILLE

*Laboratoire de Recherches sur les Macromolécules de l'Université Paris-Nord (Equipe de Recherche Associée au C.N.R.S.), Avenue J.B. Clément, 93430 Villetaneuse, France*

ET

JACQUES LEONARD

*Groupe de Recherches sur les Macromolécules et Département de Chimie, Université Laval, Québec (Qué.), Canada G1K 7P4*

Reçu le 1 avril 1981

DOMINIQUE ADES, MICHEL FONTANILLE et JACQUES LEONARD. Can. J. Chem. **60**, 564 (1982).

La polymérisation anionique en masse de l'α-méthyl styrène (αMS) a été réalisée en utilisant comme amorceur le *tert*-butyllithium (*t*-BuLi) avec ou sans *N*,*N*,*N'*,*N'*-tétraméthyl éthylène diamine (TMEDA). En absence de TMEDA, les centres actifs formés se dégradent rapidement à 62°C tandis qu'ils sont relativement plus stables à 25°C. En présence de TMEDA, la stabilité des centres actifs est beaucoup plus grande mais elle est fonction de l'ordre dans lequel le *t*-BuLi et la TMEDA sont ajoutés à l'αMS. La stabilité des centres actifs est aussi fonction du rapport $r$ = [TMEDA]/[*t*-BuLi] et les meilleurs résultats sont obtenus pour un rapport égal à un. A température élevée, on observe l'apparition d'espèces qui absorbent à 390 et 424 nm et un élargissement de la répartition des masses molaires. Ces observations sont interprétées comme étant le résultat d'une réaction de transfert au monomère ou au polymère dégradé.

DOMINIQUE ADES, MICHEL FONTANILLE, and JACQUES LEONARD. Can. J. Chem. **60**, 564 (1982).

The anionic bulk polymerization of α-methylstyrene (αMS) has been carried out using *tert*-butyllithium (*t*-BuLi) as initiator with or without *N*,*N*,*N'*,*N'*-tetramethylethylenediamine (TMEDA). In absence of TMEDA, the "living ends" are rapidly deactivated at 62°C whereas they are relatively more stable at 25°C. The "living ends" are much more stable in presence of TMEDA; however, their stability is a function of the order in which *t*-BuLi and TMEDA are added to αMS. The stability of "living ends" is also a function of the ratio $r$ = [TMEDA]/[*t*-BuLi] and best results are obtained with a one to one ratio. At high temperature, the formation of species with absorption bands at 390 and 424 nm and the broadening of the molecular weight distribution are observed. These results are explained in terms of a transfer reaction to the monomer or to the deactivated polymer.

## Introduction

La polymérisation anionique de l'α-méthyl styrène représente l'exemple typique d'une polymérisation réversible et les études cinétiques et thermodynamiques de cette polymérisation en solution ont fait l'objet de nombreux travaux. Cependant, tel n'est pas le cas de la polymérisation anionique en masse même si l'absence d'un composant (le solvant) devrait simplifier l'étude de ce système de polymérisation. Les difficultés inhérentes aux manipulations des systèmes de polymérisation en masse et les anomalies observées au cours de cette polymérisation, comme l'absence de dépropagation et l'accroissement des quantités de polymère obtenu avec augmentation de la température dans un certain domaine de températures, peuvent expliquer le petit nombre d'études sur le sujet (1, 2).

Avant de pouvoir utiliser les données de la polymérisation en masse pour en déterminer les paramètres thermodynamiques, une connaissance approfondie de ce système est nécessaire pour en établir les conditions de réversibilité. Comme première étape de ce travail, nous présentons une étude sur la stabilité des centres actifs qui va de pair avec la réversibilité de la polymérisation. A cette fin, nous avons utilisé comme amorceur le *tert*-butyllithium (*t*-BuLi) seul ou complexé avec la *N*,*N*,*N'*,*N'*-tétraméthyl éthylène diamine (TMEDA). Cet amorceur est facile à mettre en œuvre, est soluble en milieu hydrocarboné et mène à la formation de chaînes monofonctionnelles.

## Partie expérimentale

Afin de réaliser cette étude dans les meilleures conditions de stabilité des centres actifs, nous avons utilisé les techniques expérimentales de travail sous haut vide mises au point par Fontanille et Sigwalt (3).

1. *Purification des réactifs*

α-*Méthyl styrène* (αMS) (Merck)

Distillation sur colonne à bande tournante, sous pression réduite (= 100 Torr), immédiatement suivie d'un séchage sur miroir de potassium. Un début de polymérisation a lieu et le monomère non polymérisé est récupéré sous vide et mis en présence de *n*-BuLi. Dès que l'amorçage est effectif, le monomère est distribué par distillation sur paroi froide, dans des tubes gradués. L'α-méthyl styrène, dont la pureté est testée par cpv, contient moins de 100 ppm d'impuretés non réactives.

t-*BuLi* (Aldrich)

La purification, à partir d'une solution dans l'hexane est réalisée par évaporation du solvant suivie d'une sublimation. Le *t*-BuLi sublimé est redissous dans de l'hexane purifié et

0008-4042/82/050564-08$01.00/0

©1982 National Research Council of Canada/Conseil national de recherches du Canada

Can. J. Chem. Downloaded from www.nrcresearchpress.com by 210.87.254.6 on 09/06/12
For personal use only.

distribué dans des "bulles" fragiles à partir desquelles le solvant est à nouveau évaporé. Le dosage est effectué sur une "bulle" témoin, par addition de diphényl-1,1 éthylène et dosage spectrophotométrique des carbanions diméthyl-3,3', diphényl-1,1' butyl lithium ($\varepsilon = 16\,000$ mol$^{-1}$ L cm$^{-1}$) (4).

*N,N,N',N'-tétraméthyl éthylène diamine* (TMEDA) (Merck)
La purification est effectuée par distillation sous azote dans une colonne à bande tournante suivie d'un séchage sur $CaH_2$ puis sur un miroir de sodium et sur *n*-BuLi. La distillation dans des tubes capillaires étalonnés est effectuée par condensation sur paroi froide.

2. *Techniques d'étude*
La stabilité des centres actifs est déterminée par spectrophotométrie visible–uv (Cary 118 C). Les polymérisations sont effectuées directement dans la cellule de spectrophotométrie. Il convient de signaler que la prise en masse dans la cellule ne conduit à son bris que si une élévation de température supérieure à 10°C est imposée au système. Le polymère "vivant" est désactivé par addition d'une solution de méthanol dans le toluène.

Pour des raisons d'opportunité, les distributions de masses molaires ont été déterminées par gpc dans le trichlorobenzène (TCB) à 140°C en présence de stabilisants. La distribution très étroite des masses molaires de certains échantillons montre que, même à cette température, aucune dégradation des polymères ne se produit. L'absence de dégradation a, en outre, été vérifiée sur un échantillon maintenu à 140°C dans le TCB pendant 24 h.

Les $\overline{M}_n$ ont été mesurées par osmométrie ou par tonométrie suivant la gamme de masses molaires.

## Résultats et discussion

1. *Stabilité des centres actifs lithiés en l'absence de complexant*

La réaction d'addition du *t*-BuLi sur l'α-méthyl styrène en masse à 25°C, peut être suivie par mesure de la densité optique *D* du maximum d'absorption du carbanion à 321,5 nm. Nous donnons ci-dessous (Fig. 1) les courbes permettant de suivre l'évolution des concentrations en centres actifs au cours du temps, pour deux concentrations initiales en *t*-BuLi ($7{,}4 \times 10^{-3}$ *M* et $11{,}4 \times 10^{-3}$ *M*) et à la température de 25°C.

Les courbes montrent que l'amorçage est pratiquement terminé au bout de 20 min mais qu'une légère dégradation a déjà eu lieu. La durée de 1/2 vie est environ de 5 h, ce qui est du même ordre de grandeur que le temps de prise en masse du système.

L'étude prolongée de la stabilité des centres actifs à la température ambiante permet de constater que $D_{321,5}$ tend vers une valeur asymptotique différente de zéro. Nous avions initialement pensé que cela pouvait provenir d'un effet de gel, mais ce phénomène a été observé aussi en présence de TMEDA, dans des conditions où la prise en masse n'a pas lieu.

La décroissance de la concentration en centres actifs est beaucoup plus rapide lorsque la température s'élève, et à 60°C la durée de demi-vie n'est que de quelques minutes et il n'y a pas d'apparition de nouvelles espèces décelables par spectrophotométrie uv–visible.

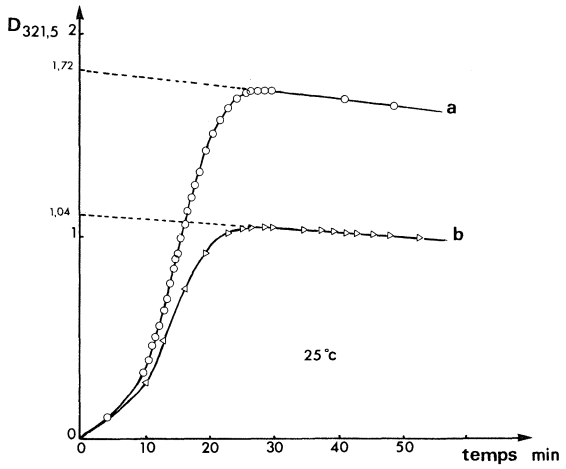


FIG. 1. Evolution de $D_{321,5}$ pour deux concentrations en amorceur à 25°C. (a): [*t*-BuLi] = 0,0114 *M*; (b): [*t*-BuLi] = 0,0074 *M*.

La dégradation peut être décrite par la réaction suivante:

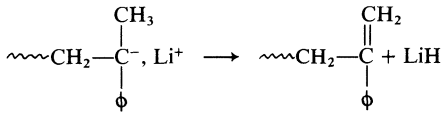


dont l'existence est corroborée par l'apparition d'un léger trouble (LiH) en fin de réaction; l'absorption uv vers 304 et 314 nm du polymère désactivé caractérise la présence des insaturations. Ce résultat ne concorde pas avec le mécanisme proposé par Margerison et Nyss (5), lequel fait intervenir la formation d'une espèce indénique par cyclisation intramoléculaire pour des conditions de polymérisation très différentes.

La valeur asymptotique non nulle de $D_{321,5}$ résulterait de l'addition de l'ion hydrure formé à l'α-méthyl styrène résiduel. L'ensemble des deux réactions peut donc être considéré comme un transfert au monomère et la stabilité observée n'est qu'apparente, la stabilité réelle étant inférieure.

Une étude de la réversibilité de la polymérisation ne peut donc pas être entreprise avec des centres actifs dont la stabilité est si faible.

2. *Stabilité des centres actifs lithiés en présence de TMEDA*

(a) *Rôle de la TMEDA*

Cette diamine tertiaire a souvent été utilisée pour accélérer la polymérisation d'un certain nombre de

Can. J. Chem. Downloaded from www.nrcresearchpress.com by 210.87.254.6 on 09/06/12
For personal use only.

Can. J. Chem. Downloaded from www.nrcresearchpress.com by 210.87.254.6 on 09/06/12
For personal use only.

monomères: éthylène (6), dienes (7), styrène (8), ... en milieu hydrocarboné.

Son rôle peut être schématisé comme suit: dans les hydrocarbures, les composés organolithiés sont fortement agrégés (9) et la complexation de la diamine au cation $Li^+$ favorise leur désagrégation.

Il a été montré par Hélary et Fontanille (8) que l'espèce organométallique ainsi complexée est plus réactive que l'espèce agrégée et moins réactive que l'espèce non agrégée non complexée.

Selon le domaine de concentration en centres actifs, l'addition de la diamine peut donc provoquer soit une accélération (concentration élevée) soit un ralentissement (concentration faible) de la polymérisation.

Pour la polymérisation anionique de l'α-méthyl styrène avec contre ion $Li^+$ et sans agent complexant, l'équilibre entre espèces agrégées et non agrégées doit être influencé par la présence du groupement méthyle et la constante de désagrégation doit être supérieure à celle du polystyryl$^-$,$Li^+$.

L'addition de la TMEDA doit donc se traduire par une stabilité plus grande des centres actifs, à une concentration plus élevée que celle qui a été déterminée pour le polystyryl$^-$,$Li^+$ (8). Cet effet stabilisant vis-à-vis de la réaction de polyaddition doit aussi se manifester vis-à-vis de la désactivation et nous avons recherché les conditions dans lesquelles la réactivité des centres actifs et leur stabilité dans le temps sont compatibles avec la réversibilité et l'étude cinétique de la polymérisation.

(b) *Influence du mode de préparation des centres actifs sur leur stabilité*

Deux méthodes ont été utilisées pour préparer les centres actifs.

*1ère Méthode*: addition du *t*-BuLi à l'αMS en masse puis, lorsque l'amorçage est complet (voir Fig. 1), addition de la TMEDA dans le rapport $r$ = [TMEDA]/[*t*-BuLi].

*2ème Méthode*: addition du *t*-BuLi au mélange (TMEDA + αMS), la quantité de TMEDA étant déterminée par la quantité de *t*-BuLi.

Nous avons établi que, quel que soit le processus choisi, les masses molaires mesurées sont voisines de celles calculées à partir de la concentration en centres actifs. Sur le plan spectrophotométrique, toutes les espèces décelables présentent initialement un maximum d'absorption à 330 nm (espèce A); au cours du temps, apparaît lentement une espèce absorbant à 390 nm (espèce B) avec ou sans formation d'un point isosbestique selon la valeur de $r$ et la méthode retenue (Figs 2a et 2b). La concentration de cette deuxième espèce passe par un maximum, puis décroît très lentement.

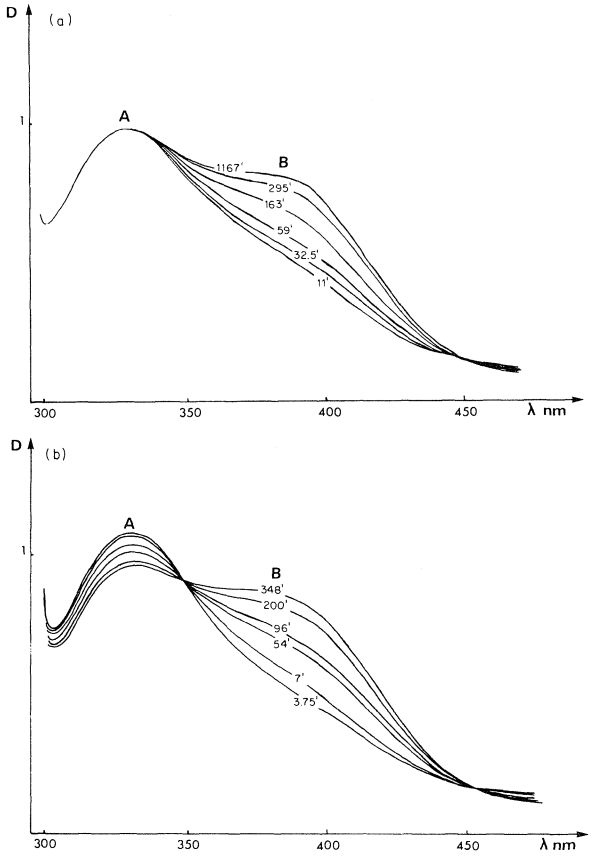


FIG. 2. Evolution spectrale postérieure à l'amorçage à 25°C formation de l'espèce B. (a): (αMS + *t*-BuLi) puis TMEDA. [*t*-BuLi] = 6,95 × $10^{-3}$ *M*; (b): (αMS + TMEDA) puis *t*-BuLi. [*t*-BuLi] = 6,60 × $10^{-3}$ *M*.

L'examen des Figures 2a et 2b montre que, quelle que soit la méthode d'amorçage utilisée, les espèces A se forment rapidement soit à partir du *t*-BuLi, soit à partir du poly(α-méthyl styryl)$^-$,$Li^+$. Par la deuxième méthode, l'espèce B prend naissance à partir de A (point isosbestique).

L'analyse de la distribution des masses molaires par gpc montre que, lorsque la polymérisation est lente, la distribution est élargie et asymétrique (Fig. 3), ce qui était prévisible en raison des évolutions spectrales.

Nous avons retenu la première méthode pour l'amorçage des polymérisations ultérieures. Il convient d'ores et déjà de remarquer que les espèces ainsi formées sont apparemment stables pendant des durées très supérieures à celles de la polymérisation.

(c) *Influence du rapport* r = *[TMEDA]/[t-BuLi] sur la stabilité*

Pour la plupart des expériences réalisées, les concentrations initiales en amorceur sont du même

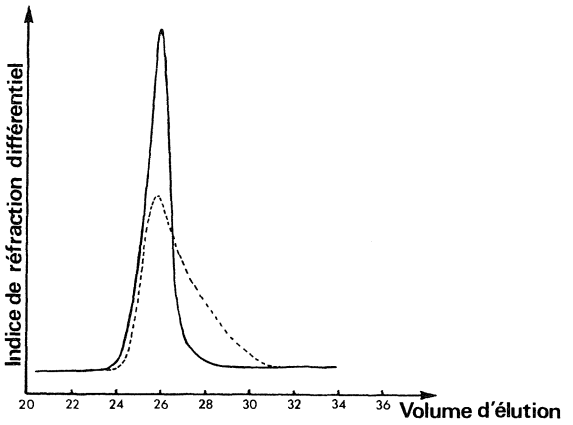


FIG. 3. Les chromatogrammes gpc d'échantillons de poly-(αMS) obtenus à 25°C, pour $r = 2$, par amorçage selon des deux méthodes: ——— *t*-BuLi puis amine; ---------- amine puis *t*-BuLi.

ordre de grandeur ($\simeq 7 \times 10^{-3}$ *M*). Nous avons fait varier le rapport $r$ entre 0,50 et des valeurs très élevées (jusqu'à 208!).

Ainsi que le montre la Fig. 4, la variation de densité optique à 330 nm (maximum d'absorption des espèces de type A) ne dépend que peu de la value de $r$. Néanmoins, il convient de remarquer que la valeur de la densité optique à 330 nm résulte de la simultanéité de plusieurs phénomènes: consommation des espèces A par la réaction de dégradation; contraction de la solution, liée à la polymérisation; reformation éventuelle d'espèces A à partir des formes dégradées susceptibles de réagir avec le monomère résiduel; et absorption non nulle à 330 nm des espèces résultant de la dégradation. Pour cette dernière raison, les valeurs de la Fig. 4 sont celles obtenues après déconvolution des spectres en chacun de leurs constituants.

L'appréciation de la stabilité doit donc tenir compte de ces différents facteurs. Nous constatons en outre que la densité optique à 330 nm atteint

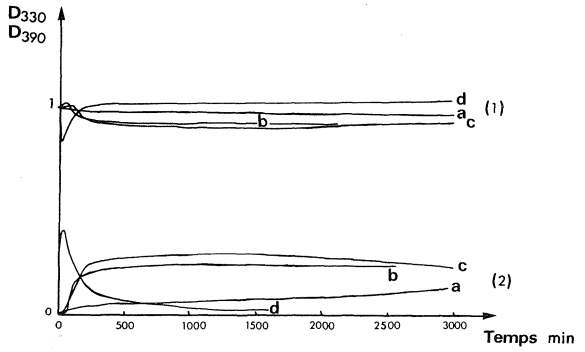


FIG. 4. Influence du rapport $r$ à 25°C sur l'évolution des maximums d'absorption à 330 nm (courbes 1) et à 390 nm (courbes 2). (a): $r = 0,5$; (b): $r = 1$; (c): $r = 2$; (d): $r = 25$.

rapidement une valuer asymptotique dépendant légèrement de $r$ et de la température de l'expérience.

Dans le cas de $r = 1$, on constate que l'abaissement de concentration maximal est de l'ordre de 10% à la température ambiante et seulement de 5% environ au moment de la prise en masse. On peut donc considérer comme négligeable la variation de concentration en centres actifs A pour les 30 premiers % de conversion.

Nous reviendrons ultérieurement sur l'éventuelle reformation de centres actifs à partir des espèces dégradées.

(d) *Influence de la température*

L'influence prépondérante de la température sur la position de l'équilibre polymère ⇄ monomère dans le cas de la polymérisation de l'αMS, nous a conduit à étudier la stabilité des centres actifs aux températures supérieures à la température ambiante.

Nous avons étudié la stabilité des centres actifs à des températures voisines de la température-plafond du système. Dans ces conditions, la polymérisation n'est que partielle et la contraction de volume peut être négligée.

*Pour* r = *1*

*A 75°C* (Fig. 5a), $D_{330}$ décroît de 30% de la valeur initiale, jusqu'à un palier qui est atteint au bout de 2 jours environ. Une observation prolongée du système fait apparaître une décroissance ultérieure de $D_{330}$, avec apparition d'une nouvelle espèce dont le $\lambda_{max} = 424$ nm (espèce C).

*A 62°C* (Fig. 5b), $D_{330}$ décroît de 80% avant d'atteindre le palier mais, si le système est porté à 75°C, il se produit une augmentation de la densité optique du maximum d'absorption principal. Cette augmentation est limitée et suivie d'une nouvelle décroissance simultanée de l'apparition de l'espèce C.

*Pour* r = *0,5* (Fig. 5c)

Le comportement est similaire, les évolutions sont toutefois plus lentes. Après 40 jours on ajoute du monomère. On observe d'abord un effet de dilution puis une évolution lente des espèces.

Pour les deux valeurs de $r$ retenues, une attente suffisamment longue permet de n'observer qu'un seul pic à 424 nm.

(e) *Nature des différentes espèces formées*

La concentration de l'espèce B croît avec $r$ jusqu'à $r = 2$, les vitesses d'apparition et de disparition de ces espèces sont d'autant plus rapides que $r$ est grand (Fig. 4).

Lorsque les polymérisations sont réalisées dans des conditions telles que la prise en masse n'inter-

Can. J. Chem. Downloaded from www.nrcresearchpress.com by 210.87.254.6 on 09/06/12
For personal use only.

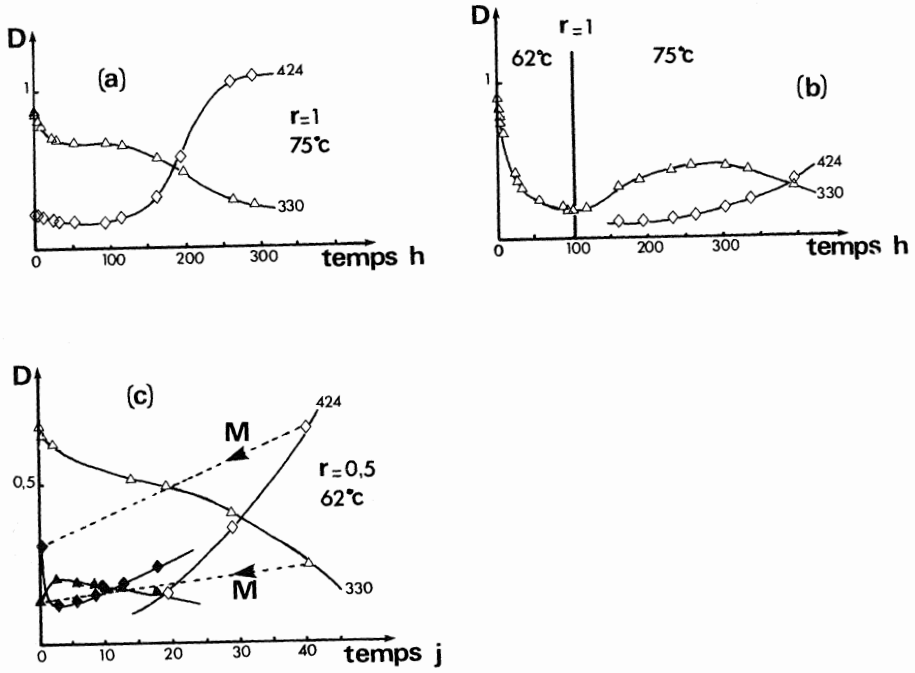


FIG. 5. Evolution de $D_{330}$ et $D_{424}$ pour différentes températures et rapports $r$. (a): $r = 1$ à 75°C; (b): $r = 1$ à 62° et 75°C; (c): Effect de dilution sur l'intensité des maximums: △◇ évolution des spectres au cours de 40 jours; ▲◆ après 40 jours et après addition de monomère. L'effet de dilution est indiqué par le pointillé.

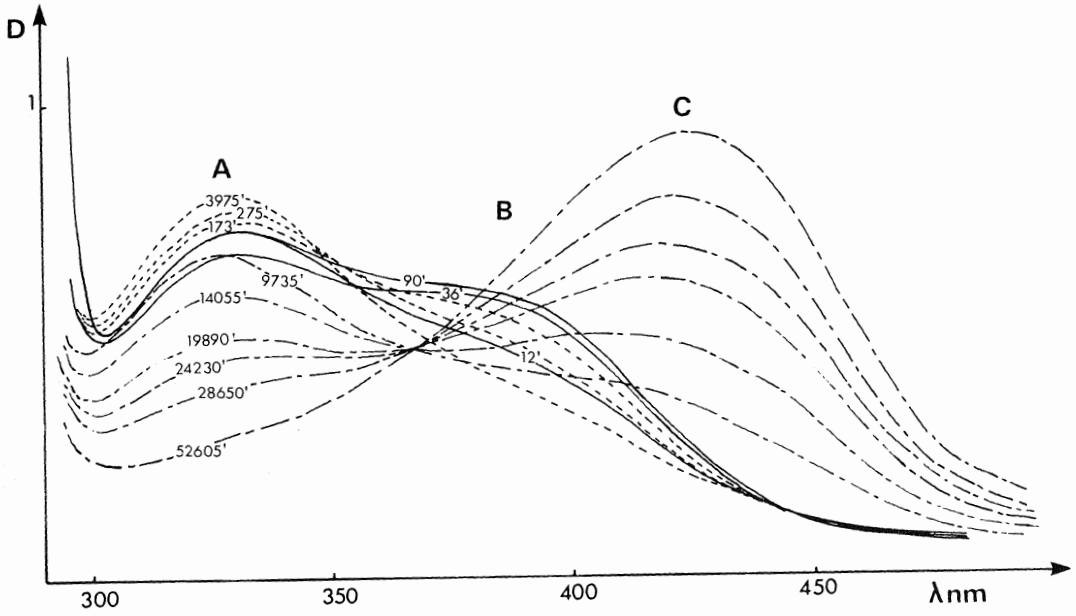


FIG. 6. Evolution spectrale des différentes espèces, obtenue pour $r = 208$ à 25°C; $t = 0$ correspond à l'addition du TMEDA au système amorcé selon la première méthode ($[t\text{-BuLi}]_i = 16 \times 10^{-3}$ équiv./L).

vient pas ou n'intervient que très lentement (haute température ou $r$ élevé), l'espèce C apparaît. La Figure 6 montre une évolution spectrale complète à partir de l'espèce A. Les deux points isosbestiques observés démontrent que B se forme à partir de A ainsi que C et que ce dernier n'est décelable que lorsqu'il n'y a pratiquement plus d'espèces B visibles.

L'hypothèse rendant le mieux compte de ces observations consiste à admettre l'existence de

Can. J. Chem. Downloaded from www.nrcresearchpress.com by 210.87.254.6 on 09/06/12
For personal use only.

deux réactions de dégradation simultanées conduisant respectivement à B et à C.

Par ailleurs, nous avons constaté que l'addition de monomère à un système vieilli dans lequel seule l'espèce C est décelable et dans lequel la concentration de monomère doit être faible, provoque la diminution de la concentration de C et la réapparition soit des espèces A, soit des espèces B selon la valeur de $r$ (Fig. 5c).

L'ensemble de nos observations peut s'expliquer par le schéma suivant:

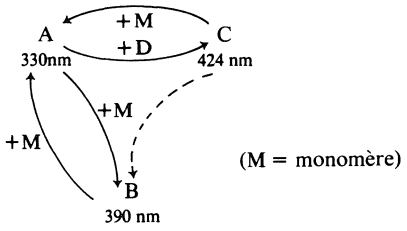


D'après les données de la littérature (10–12), la structure probable de l'espèce C est de type phénylallylique.

L'espèce B absorbant à 390 nm résulterait de l'arranchement d'un proton allylique du monomère par l'espèce A. Cette réaction serait concurrentielle de l'addition.

Les concentrations relatives des espèces B et C dépendraient de leur réactivité respective vis-à-vis du monomère résiduel ainsi que de la concentration de ce dernier.

Le retour aux espèces de type A se produit par addition 1,3 du monomère sur les carbanions phényl allyliques B et C. Une réaction analogue, en présence d'agents complexants, a été précédemment signalée pour différents systèmes (10–12). La nouvelle espèce cylique formée présente une structure électronique très proche de celle de l'espèce A et doit donc absorber sensiblement à la même longueur d'onde. Elle doit aussi pouvoir s'additionner au monomère pour redonner l'espèce A ou

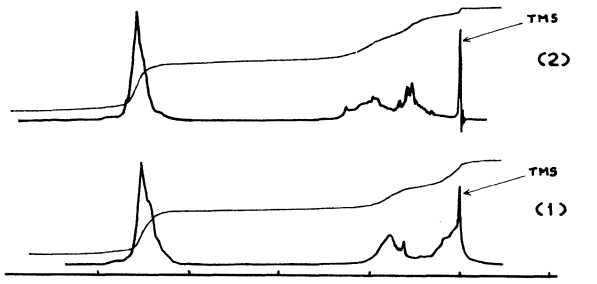


FIG. 7. Les spectres rmn $^1H$ à 60 MHz dans $CDCl_3$. Spectre 1: Polymère issu d'une polymérisation à −10°C. Spectre 2: Oligomères totaux issus d'une réaction conduite à 62°C.

même lui arracher un proton pour redonner l'espèce B. L'ensemble de ce schéma réactionnel est sur plusieurs points semblable à celui proposé par Comyn et Glasse (13).

Ces réactions peuvent être considérées comme des transferts au monomère ou au polymère conduisant à des irrégularités de structure cycliques. Nous avons observé des spectres de rmn $^1H$ très différents pour le poly(αMS) de haute masse molaire d'une part et pour des oligomères résultant d'un transfert important d'autre part (Fig. 7).

(f) *Evaluation du transfert*

Il ne faut pas perdre de vue que, pour réaliser une étude cinétique faisant intervenir un équilibre polymérisation–dépolymérisation, la constante de la concentration en centres actifs est une condition nécessaire mais non suffisante. Selon les schémas réactionnels que nous avons proposés, il se forme des extrémités de chaînes saturées et des cycles situés topochimiquement le long des chaînes qui bloquent la dépolymérisation et perturbent ainsi les équilibres thermodynamiques.

Le taux des irrégularités de structure est proportionnel à l'importance du transfert et les méthodes que nous avons retenues pour son évaluation consistent à comparer les masses molaires expérimentales aux masses théoriques et à mettre en évidence par gpc le défaut d'isomolécularité.

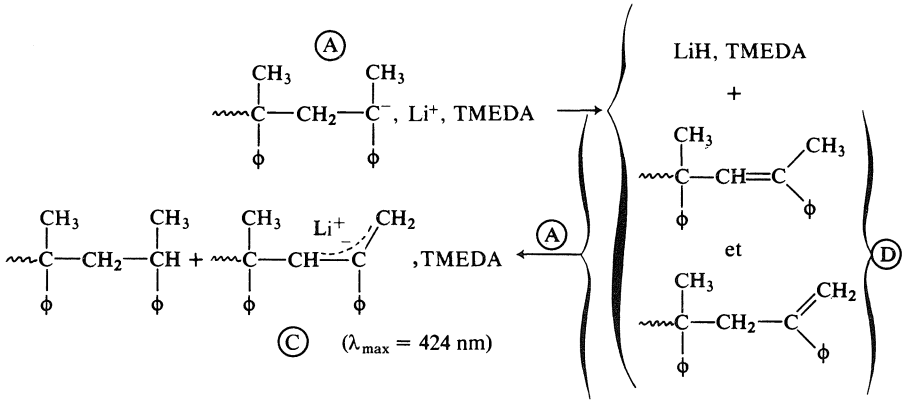


Can. J. Chem. Downloaded from www.nrcresearchpress.com by 210.87.254.6 on 09/06/12
For personal use only.

Can. J. Chem. Downloaded from www.nrcresearchpress.com by 210.87.254.6 on 09/06/12
For personal use only.

TABLEAU 1. Masses molaires et rendements des polymérisations ($[t\text{-BuLi}]_{initial} = 8{,}5 \times 10^{-3}$ équiv./L)

| No. d'l'ampoule | θ (°C) de manipulation | Durée de la polymérisation (jours) | Rdt en polymère (%) | Masse molaire (× $10^{-3}$) | | Ecart (en %) entre les masses théoriques et mesurées |
|---|---|---|---|---|---|---|
| | | | | Théorique | Moyenne | |
| 1 | −31 | 56 | 58,8 | 63 | 44[a] | 30 |
| 2 | −10 | 15 | 67,35 | 72 | 49[a] | 31 |
| 3 | 0 | 15 | 70,2 | 75 | 51[a] | 32,5 |
| 4 | 15 | 15 | 74,7 | 80 | 57[a] | 29 |
| 5 | 25 | 13 | 77,1 | 82 | 59[a] | 28 |
| 6 | 35 | 13 | 78,3 | 84 | 35[a] | 58 |
| 7 | 62 | 9 | 11,7 | 12 | 2,6[b] | 79 |
| 8 | 62 puis −31 | 9 puis 55 | 61,2 | — | — | — |

[a]Nombre obtenu par osmométrie.
[b]Nombre obtenu par tonométrie.

Chaque transfert contribue à l'élargissement de la courbe de répartition des masses molaires. Cette tendance s'accentue lors des transferts au monomère où chaque transfert divise par deux la masse molaire.

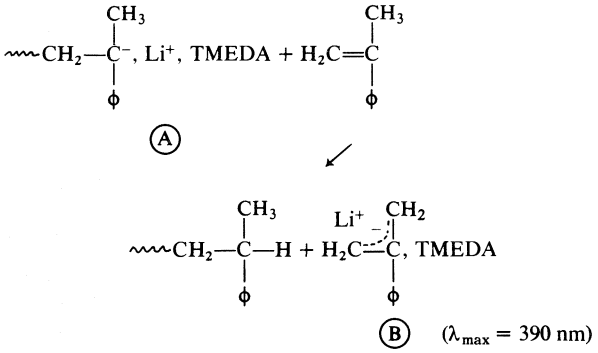


Une solution initiale est distribuée en 8 ampoules d'égale concentration en centres actifs en présence de TMEDA avec $r = 0{,}5$. Chacune d'elles est maintenue à une certaine température pendant une durée déterminée, puis désactivée par le méthanol. Le polymère formé est récupéré par évaporation du monomère résiduel et analysé par gpc. Les résultats correspondants sont exprimés dans le Tableau 1 et par la Fig. 8.

Il apparaît ainsi que la distribution des masses molaires et l'accord avec les masses molaires théoriques varient avec la température de la polymérisation. Pour les expériences réalisées au-dessous de 25°C environ, la répartition des masses molaires est étroite et leur valeur mesurée est en bon accord avec la valeur théorique.

Par contre, dès 35°C, on décèle un élargissement et une dissymétrie de la courbe de répartition qui peut être imputable au transfert.

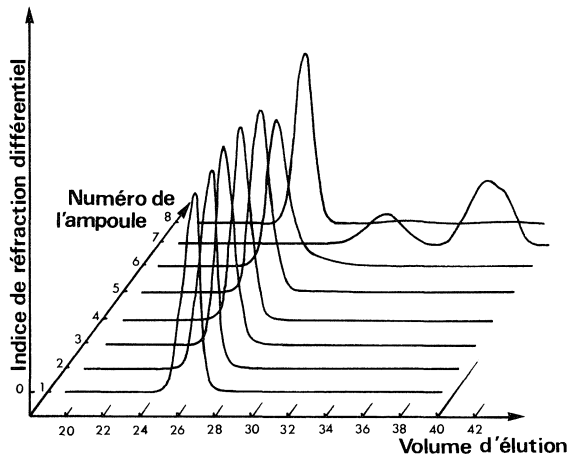


FIG. 8. Chromatogrammes gpc de poly(αMS) préparés à différentes températures (voir Tableau 1).

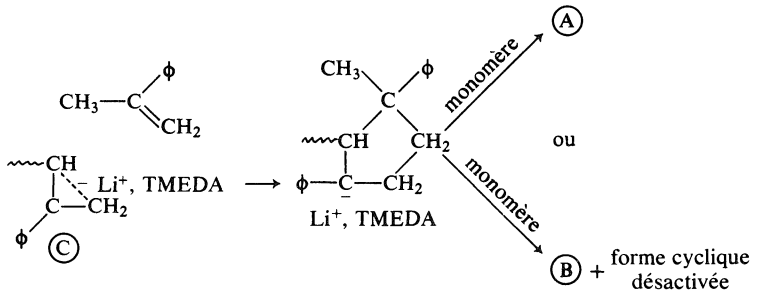

## Conclusion

Nous avions recherché les conditions dans lesquelles une étude cinétique de la polymérisation en masse de l'αMS est possible. Nous avons montré que la présence de TMEDA dans le rapport $r$ = [TMEDA]/[Li] = 1 induit une stabilisation du système qui permet de négliger la dégradation jusqu'à une température voisine de 35°C. Au delà de cette température, le transfert au monomère ou au polymère devient important et l'étude cinétique devra en tenir compte.

## Remerciements

Ce travail a été rendu possible en partie grâce à l'aide de la Sous-Commission à la Recherche Scientifique et Technologique de la Coopération France–Québec. J. Léonard remercie également le Conseil de recherches en sciences naturelles et en génie du Canada pour son soutien financier.

1. D. P. Wyman et I. H. Song. Makromol. Chem. **115**, 64 (1968).
2. I. Mita et H. Okuyama. J. Polym. Sci. Part A-1, **9**, 3437 (1971).
3. M. Fontanille et P. Sigwalt. Bull. Soc. Chim. Fr. 4083 (1967); 4087 (1967); 4095 (1967).
4. R. A. H. Casling, A. G. Evans et N. H. Kees. J. Chem. Soc. 519 (1966).
5. D. Margerison et V. A. Nyss. J. Chem. Soc. C, 3065 (1968).
6. A. W. Langer. Trans. N.Y. Acad. Sci., **27**, 741 (1965).
7. J. N. Hay, J. F. McCabe et J. C. Robb. J. Chem. Soc. Faraday Trans. I, **68**, 1 (1972).
8. G. Hélary et M. Fontanille. Eur. Polym. J. **14**, 345 (1978).
9. D. Margerison et J. P. Newport. Trans. Faraday Soc. **59**, 2058 (1963); G. Witting, F. J. Meyer et G. Lange. Ann. **571**, 167 (1951); M. Weiner, G. Vogel et R. West. Inorg. Chem. **1**, 654 (1962); S. Bywater. Adv. Polym. Sci. **4**, 66 (1965).
10. T. Kauffmann. Angew. Chem. Int. Ed. Engl. **13**, 627 (1974).
11. G. F. Luteri et W. T. Ford. J. Organomet. Chem. **105**, 139 (1976).
12. G. F. Luteri et W. T. Ford. J. Org. Chem. **42**, 820 (1977).
13. J. Comyn et M. D. Glasse. J. Polym. Sci. Part B, **18**, 703 (1980).

Can. J. Chem. Downloaded from www.nrcresearchpress.com by 210.87.254.6 on 09/06/12
For personal use only.

# High yield "one-pot" synthesis of 2-hydroxy-3-methylcyclopent-2-en-1-one and related compounds

GEORGE M. STRUNZ AND G. SANKAR LAL

*Maritimes Forest Research Centre, Canadian Forestry Service, Department of the Environment, P.O. Box 4000, Fredericton, N.B., Canada E3B 5P7*

Received October 1, 1981

GEORGE M. STRUNZ and G. SANKAR LAL. Can. J. Chem. **60**, 572 (1982).

A convenient "one-pot" modification of a conventional synthetic route affords 2-hydroxy-3-methylcyclopent-2-en-1-one and related compounds in high overall yields.

GEORGE M. STRUNZ et G. SANKAR LAL. Can. J. Chem. **60**, 572 (1982).

Une modification très simple d'une synthèse conventionnelle conduit, sans isoler les intermédiaires, au produit hydroxy-2-méthyl-3-cyclopentèn-2-one-1 et d'autres produits apparentés avec des bons rendements.

Can. J. Chem. Downloaded from www.nrcresearchpress.com by 210.87.254.6 on 09/06/12
For personal use only.

An interest in synthetic pyrethroids (1) with alcohol components derived from 2-hydroxy-3-substituted-cyclopent-2-en-1-ones (cf. refs. 2, 3) prompted us to seek a versatile and efficient synthetic route to the latter class of compounds. In large part because of the importance conferred on it by its organoleptic properties, 2-hydroxy-3-methylcyclopent-2-en-1-one (**1**, R = $CH_3$), a flavour constituent of coffee aroma (4) and maple syrup (5), has been a popular synthetic target: more than a score of papers describing syntheses of this and related compounds have been published (6).[1] The majority, according to Cookson and Smith (6*b*) "suffer from low yields, multistep procedures, and/or expensive reagents."

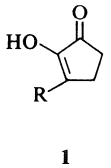


**1**

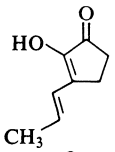


**2**

One of the earlier synthetic approaches, employed by Litchenberger and Litchenberger (7), Hesse and Bücking (8), and Gianturco and Friedel (9), appealed to us by virtue of its simplicity and because it allowed the introduction of a wide variety of substituent groups, R. The synthesis involves alkylation of 3,5-dicarboalkoxycyclopentane-1,2-dione, obtained by condensation of glutaric and oxalic acid esters. Subsequent hydrolysis and decarboxylation afford the 3-alkyl-2-hydroxycyclopent-2-en-1-one.

We have found that by the simple expedient of conducting these reactions sequentially in one flask, without isolation of intermediates, yields are substantially increased. (Additional modifications, such as the use of dimethylformamide as solvent for the alkylation and aqueous phosphoric acid for the hydrolysis–decarboxylation, were also found to be advantageous.) Using this modified procedure, **1** (R = $CH_3$) is obtained in an overall yield of 80% based on dimethyl glutarate. To our knowledge this is the highest yield reported for synthesis of 2-hydroxy-3-methylcyclopent-2-en-1-one from simple readily available noncyclic precursors.

Results for some related compounds prepared by the same procedure are presented in Table 1.

[1]The compound is available from several commercial sources.

## Experimental

The standard procedure is exemplified by the synthesis of **1** (R = $CH_3$).

*2-Hydroxy-3-methylcyclopent-2-en-1-one (1, R = $CH_3$)*

A solution of diethyl oxalate (11.65 g, 0.080 mol) in anhydrous ether (50 mL) was added during 30 min, by dropping funnel, to sodium methoxide (3.60 g, 0.067 mol) in a 100 mL two-neck flask fitted with a reflux condenser. Operations were conducted in an atmosphere of dry nitrogen, and the mixture was stirred and cooled in an ice-bath throughout the addition. When the initially formed lumps had broken down to give a smooth slurry, a solution of dimethyl glutarate (2.13 g, 0.013 mol) in anhydrous ether (10 mL) was added dropwise with stirring and cooling over a period of 30 min. Stirring was continued for 1 h while the mixture was allowed to warm to 22°C. The flask was then fitted for distillation and the apparatus was wrapped with glass wool.

The reaction mixture was gently heated on an oil bath until the ether was removed. The temperature was then gradually raised to 120°C. After 3 h at 120°C, the temperature was raised to 140°C where it was maintained for 14 h.

The residue was allowed to cool, and the apparatus was again fitted with a dropping funnel and reflux condenser. A solution of methyl iodide (3.78 g, 0.027 mol) in dry dimethylformamide (50 mL) was added to the residue, and the mixture was stirred at 22°C under nitrogen for 16 h, then heated under reflux for 2 h. Dimethylformamide and excess methyl iodide were removed by distillation *in vacuo*, and the product was refluxed with 42% aqueous phosphoric acid (50 mL) for 72 h.

The acidic aqueous mixture was extracted with ether (5 × 40 mL) and the extracts, after drying and evaporation of solvent, yielded a crude crystalline product. Elution with hexane–ace-

0008-4042/82/050572-02$01.00/0
©1982 National Research Council of Canada/Conseil national de recherches du Canada

TABLE 1. 3-Substituted-2-hydroxycyclopent-2-en-1-ones[a]

| Alkylating agent | Product | Melting point (°C)[b] | Overall yield,[c] % |
|---|---|---|---|
| Methyl iodide | **1** (R = $CH_3$) | 103–106 | 80 |
| Ethyl iodide | **1** (R = $C_2H_5$) | Oil[d] | 70 |
| Benzyl bromide | **1** (R = $CH_2Ph$) | 97–99 | 70 |
| Allyl bromide | **2** | 156–160 | 44 |

[a]Yields and melting points are reported for material obtained directly from silica gel chromatography without recrystallization.
[b]Literature values for melting points of the methyl, ethyl, and benzyl products respectively: 103–105°C (6*a*), 42–44°C (decomposes on standing) (6*d*), 99°C (6*c*).
[c]Based on dimethyl glutarate.
[d]Pure by tlc and spectra.

tone (9:1) from a silica gel column afforded pure **1** (R = $CH_3$), 1.20 g, mp 103–106°C (lit. (6*a*) mp 103–105°C).

*2-Hydroxy-3-*trans*-allylcyclopent-2-en-1-one (2)*

Prepared as above, using allyl bromide as alkylating agent. (The acid conditions employed for the hydrolysis–decarboxylation cause the double bond of the allyl group to migrate into conjugation.) The spectroscopic characteristics of the product are consistent with structure **2**: ir ($CHCl_3$): (*inter alia*) 3685, 3495, 3320 (br), 2920, 1685, 1635, 1405, 1395, 1105, and 960 $cm^{-1}$; uv $\lambda_{max}$ (EtOH): 296 nm (ε 22 000); $\lambda_{max}$ (EtOH + 1 drop 10% NaOH): 340 nm (ε 8400); nmr (acetone-$d_6$, 60 MHz) δ: 1.97 (3H, d, $J \sim 6$ Hz), 2.53 (4H, narrow m), 5.92–6.87 (2H, AB part of $ABX_3$, $J_{AB} \sim 16$ Hz), 7.16 (br, OH); mass spectrum *m/e*: 138 (base peak) ($M^+$), 123 (87%) $(M - CH_3)^+$.


1. M. ELLIOTT and N. F. JANES. Chem. Soc. Rev. **7**, 473 (1978).
2. R. A. LE MAHIEU, B. TABENKIN, J. BERGER, and R. W. KIERSTEAD. J. Org. Chem. **35**, 1687 (1970); R. A. LE MAHIEU, M. CARSON, and R. W. KIERSTEAD. J. Org. Chem. **33**, 3660 (1968).
3. R. T. DAHILL, JR. J. Org. Chem. **31**, 2694 (1966).
4. M. A. GIANTURCO, A. S. GIAMMARINO, and R. G. PITCHER. Tetrahedron, **19**, 2051 (1963).
5. V. J. FILIPIC, J. C. UNDERWOOD, and C. O. WILLITS. J. Food Sci. **30**, 1008 (1965).
6. (*a*) H. STETTER and W. SCHLENKER. Tetrahedron Lett. 3479 (1980); (*b*) R. C. COOKSON and S. A. SMITH. J. Chem. Soc. Perkin Trans. I, 2447 (1979), and references therein; (*c*) A. BARCO, S. BENETTI, G. P. POLLINI, and R. TADDIA. Synthesis, 104 (1975); (*d*) C. M. LEIR. J. Org. Chem. **35**, 3203 (1970), and references therein; (*e*) K. SATO, S. SUZUKI, and Y. KOJIMA. J. Org. Chem. **32**, 339 (1967), and references therein.
7. J. LITCHENBERGER and R. M. LITCHENBERGER. French Patent No. 839,062. March 23, 1939. (Chem. Abstr. **33**, 82132 (1939)).
8. G. HESSE and E. BÜCKING. Justus Liebigs Ann. Chem. **563**, 37 (1949).
9. M. A. GIANTURCO and P. FRIEDEL. Tetrahedron, **19**, 2039 (1963).


Can. J. Chem. Downloaded from www.nrcresearchpress.com by 210.87.254.6 on 09/06/12
For personal use only.

# On the origin of regioselectivity in the photorearrangement of 4,4-diphenyl-2,5-cyclohexadiene systems. Synthesis and photochemistry of 4,4-diphenyl-γ-thiopyran and -γ-thiopyran-1,1-dioxide[1,2]

DENIS GRAVEL[3] AND CHRISTIAN LEBOEUF[4]

*Département de Chimie, Université de Montréal, C.P. 6210, Succ. A, Montréal (Qué.), Canada H3C 3V1*

Received August 28, 1981

DENIS GRAVEL and CHRISTIAN LEBOEUF. Can. J. Chem. **60**, 574 (1982).

The synthesis from diphenylmethane of 4,4-diphenyl-γ-thiopyran and 4,4-diphenyl-γ-thiopyran-1,1-dioxide is described. Upon direct photolysis at 254 nm the γ-thiopyran derivative undergoes rearrangement to a mixture of 5,6-diphenyl-2-thiabicyclo-[3.1.0]hexene and 2,4-diphenyl-α-thiopyran. The corresponding 1,1-dioxide derivative on the other hand undergoes, upon direct photolysis at 254 nm or sensitized (acetone) photolysis at 350 nm, rearrangement to 6,6-diphenyl-2-thiabicyclo[3.1.0]hexene-2,2-dioxide accompanied by a solvent addition product: 3-methoxy-4,4-diphenyl-2,3-dihydro-γ-thiopyran-1,1-dioxide. The results, along with those observed for 4,4-diphenyl-γ-pyran studied in this series, and other literature results are rationalized in terms of Zimmerman's reacting chromophore simulation using the Möbius–Hückel concept to evaluate competing excited state energies of the isoconjugate chromophores.

DENIS GRAVEL et CHRISTIAN LEBOEUF. Can. J. Chem. **60**, 574 (1982).

La synthèse à partir du diphenylméthane des diphényl-4,4-γ-thiopyranne et diphényl-4,4-γ-thiopyranne-1,1-dioxyde est rapportée. Lors de la photolyse directe à 254 nm le dérivé γ-thiopyranne se réarrange en un mélange de diphényl-5,6-thia-2-bicyclo[3.1.0]hexene et de diphényl-2,4-α-thiopyranne. Le dérivé 1,1-dioxyde correspondant d'autre part subit, lors de la photolyse directe à 254 nm ou sensibilisée (acétone) à 350 nm, un réarrangement en diphényl-6,6-thio-2-bicyclo[3.1.0]hexene-2,2-dioxyde accompagné d'un produit d'addition du solvant, le méthoxy-3-diphényl-4,4-dihydro-2,3-γ-thiopyranne-1,1-dioxyde. Les résultats ainsi que ceux observés pour le diphényl-4,4-γ-pyranne étudié dans cette série ainsi que d'autres résultats puisés de la littérature sont rationalisés en terme de la "simulation du chromophore en réaction" de Zimmerman, utilisant le concept de Möbius–Hückel pour évaluer les énergies en compétition des chromophores isoconjugués excités.

## Introduction

Previously we reported (1) on the photochemistry of 4,4-diphenyl-γ-pyran (**1***a*) which upon irradiation undergoes a di-π-methane rearrangement (2) to yield the corresponding *trans-endo*-5,6-diphenyl-2-oxabicyclo[3.1.0]hexene (**2***a*) as primary photoproduct, along with a series of secondary products which were characterized and interrelated (see Scheme 1).

As stated earlier (1*a*), our aim in undertaking these studies was to investigate some cyclic di-π-methane systems of general structure (**1**) where the two π moieties in the ring are joined by a heteroatom. Such models should provide a further test of the generality of the rearrangement, provide further insight into its mechanism, and also give access to new heterobicyclo[3.1.0] systems **2** and/or **3** and their chemistry. The interesting mechanistic aspect contributed by our original study (1*a*) on compound **1***a* was the observation of an absolute regioselectivity in the reaction, i.e., rearrangement takes place solely with phenyl–vinyl (P–V) bonding (path a) to yield the corresponding phenyl migrated oxabicyclo[3.1.0] product **2***a*; none of the alternative *gem*-diphenyl oxabicyclo[3.1.0] product **3***a* could be found, which shows that vinyl–vinyl (V–V) bonding (path b) does not take place, at least to any significant extent (see Scheme 2) in that system.

These results are to be compared (*vide infra*) with the well documented fundamental systems **1***b* and **1***c* studied by Zimmerman *et al.* (3, 4), which are also totally regioselective in their behavior: **1***b*, where X = C=CH$_2$, yields exclusively via path a the phenyl migrated bicyclo[3.1.0] product **2***b*, of the same *trans-endo* stereochemistry as **2***a* (3), whereas **1***c*, where X = C=O, yields exclusively via path b the *gem*-diphenyl bicyclo[3.1.0] product **3***c* (4); rearrangements following this particular path have been termed Type A rearrangements by Zimmerman (4).

The present study deals with the preparation and photochemistry of two new compounds of general structure **1**, namely: 4,4-diphenyl-γ-thiopyran (**1***d*), where X = S, and 4,4-diphenyl-γ-thiopyran-1,1-dioxyde (**1***e*), where X = SO$_2$. The first compound should yield information regarding the possible influence of the nature of the heteroatom on the

[1]Presented in part at the CIC Annual Conference, Montreal, June 1977.

[2]Taken in part from the thesis submitted by C. Leboeuf in partial fulfillment for the Ph.D. degree, Université de Montréal, Montréal, 1978.

[3]Author to whom correspondence should be addressed.

[4]Predoctoral Fellow, Ministère de l'Education du Québec and National Sciences and Engineering Research Council of Canada: 1973–1977.

0008-4042/82/050574-14$01.00/0

©1982 National Research Council of Canada/Conseil national de recherches du Canada

Can. J. Chem. Downloaded from www.nrcresearchpress.com by 210.87.254.42 on 09/06/12
For personal use only.

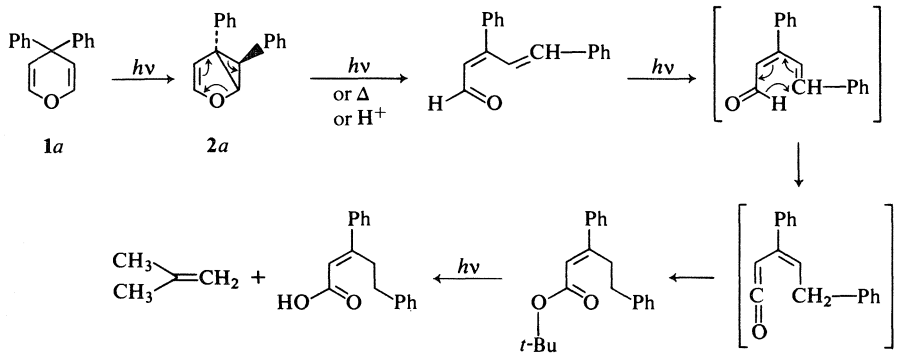

SCHEME 1. Photochemistry of 4,4-diphenyl-γ-pyran (1*a*). Interrelation between photoproducts.

regioselectivity of the rearrangement while the second should provide information regarding the possible influence on the regioselectivity of (*i*) the electronegativity of group X and/or (*ii*) the presence or absence of unshared electrons on group X.

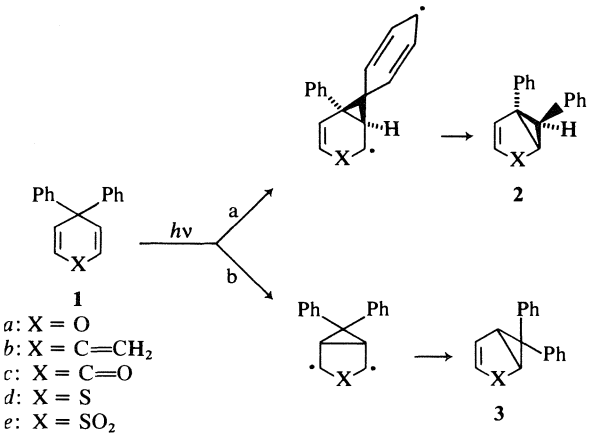

SCHEME 2. Odd-electron representation of *a priori* possible reaction pathways in the 4,4-diphenyl-2,5-cyclohexadiene system.

## Results

### *Synthesis of γ-thiopyrans 1*d *and 1*e

As exemplified (1*a*) by our synthesis of 4,4-diphenyl-γ-pyran (1*a*), our approach to the problem of gaining access to heterocyclic compounds of general structure **1** has been to synthesize the tetramethoxydiacetal derivative of 3,3-diphenylglutaraldehyde (**4**), which is a general synthon for our purpose.

Hence, in the present case, treatment of a dichloromethane solution of diacetal **4** by a gaseous mixture of hydrogen sulfide and hydrogen chloride leads to the 2,6-dihalotetrahydrothiopyran intermediate **5** which is immediately treated with *N*,*N*-dimethylaniline at 160°C to lead directly to the desired 4,4-diphenyl-γ-thiopyran (1*d*) with a 60% yield after purification (see Scheme 3). Compound 1*d* presents in its mass spectrum a molecular ion at *m/e* 250; in the nmr, a multiplet at 7.2 ppm in the form of a broadened singlet, characteristic of the phenyl protons, and an AB quartet centered at 6.0 ppm ($J_{AB}$ = 10.5 Hz) for the vinyl protons; the thioenol ether linkages are characterized in the ir by an absorption at 1600 $cm^{-1}$; finally, compound 1*d* shows in the uv a $\lambda_{max}$ at 240 nm with an ε of 1470 and a second $\lambda_{max}$ at 285 nm with an ε of 1090.

The corresponding sulfone 1*e* was obtained in a 93% yield by oxidation of thiopyran 1*d* with ruthenium tetroxide (5). The mass spectrum of sulfone 1*e* is devoid of a molecular ion peak at *m/e* 282, however, an ion at $M - 64$ corresponds to the loss of $SO_2$ by the molecular ion; furthermore, elemental analysis confirms the molecular formula $C_{17}H_{14}O_2S$ for the sulfone. In the nmr, the phenyl groups are characterized by a narrow multiplet at 7.35 ppm and the vinyl protons appear in the form of an AB quartet centered at 6.70 ppm ($J_{AB}$ = 12 Hz). In the infrared, two intense absorptions at 1295 and 1115 $cm^{-1}$ confirm the presence of the sulfone group.

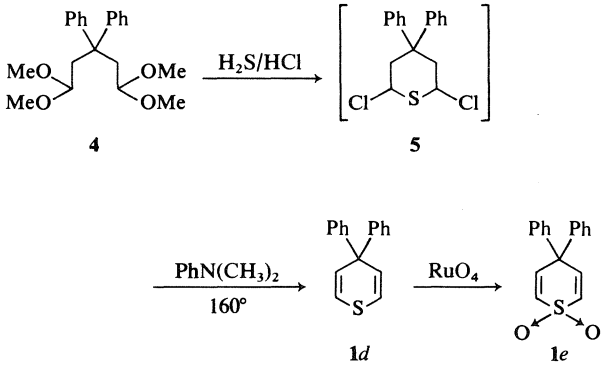

SCHEME 3. Synthesis of 4,4-diphenyl-γ-thiopyran (1*d*) and 4,4-diphenyl-γ-thiopyran-1,1-dioxide (1*e*).

Can. J. Chem. Downloaded from www.nrcresearchpress.com by 210.87.254.42 on 09/06/12
For personal use only.

Can. J. Chem. Downloaded from www.nrcresearchpress.com by 210.87.254.42 on 09/06/12
For personal use only.

*Preparative scale photolysis of thiopyran 1*d *and characterization of photoproducts*

Irradiation for 2 h of a $10^{-3}$ *M* solution of thiopyran **1***d* in anhydrous ether leads to a mixture of photoproducts. Preparative scale thin layer chromatography (tlc) on silica gel allows the recovery of the two main fractions: the first being composed of unreacted starting material **1***d* (7%) and the second, (55%), apparently composed of a mixture of 5,6-diphenyl-2-thiabicyclo[3.1.0]-hexene (**2***d*†)[5] and 2,4-diphenyl-α-thiopyran (**6**) (see eq. [1]). This mixture is unfortunately unstable

[1] 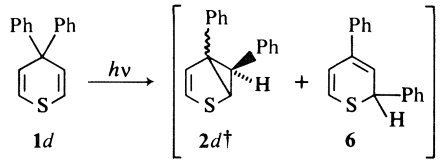


Photolysis of 4,4-diphenyl-γ-thiopyran (**1***d*)

at room temperature and was not amenable, in our hands, to separation into its components.

In the nmr, the mixture of sulfides shows signals characteristic of both structures, i.e. a complex region from 2.1 to 3.7 ppm is typical of cyclopropane protons such as in **2***d*† and also of similar bicyclo[3.1.0] systems (6) such as 5,6-diphenyl-2-oxabicyclo[3.1.0]hexene (**2***a*) (1*a*). An AB system centered at 6.40 ppm ($J$ = 10.5 Hz) could be attributed to the 5,6 vinyl protons of α-thiopyran **6** while a multiplet at 5.80 ppm could very well be a superimposition of the vinyl AB system of the thiabicyclo[3.1.0] derivative **2***d*† and a doublet or multiplet expected for the vinyl proton in the 3-position of α-thiopyran **6**. A doublet at 4.85 ppm $J$ = 8 Hz could be attributed to $H_2$ in the same molecule and finally a broad signal centered at 7.35 ppm is characteristic of the phenyl groups in both compounds.

The formation of such a mixture of photoproducts from γ-thiopyran **1***d* is *a priori* in accord with the expected behavior of these systems (see Scheme 2) as far as the formation of the bicyclo[3.1.0] derivative **2***d*† is concerned. On the other hand, as we have shown in a previous paper (1*a*) and as was observed (6) in a study of the addition of carbenes to furans and thiophenes prior to our work, 2-heterobicyclo[3.1.0]hexenes are labile at room temperature or with acid and are known to rearrange to the corresponding open chain unsaturated aldehyde or thioaldehyde as illustrated in Scheme 1.

[5]The dagger (†) should be taken to indicate unspecified stereochemistry.

In our case, this immediately suggests that the expected primary photoproduct, the thiabicyclo-[3.1.0] derivative **2***d*†, could either thermally or photochemically have evolved to the corresponding thioaldehyde **7** which could have equilibrated [6] with α-thiopyran **6** in competition with decomposition and/or polymerization. With this hypothesis in mind and in the hope of obtaining a more stable and characterizable product we applied a desulfurization procedure reported by Corey and Shulman (7) in their study of the thio-Claisen rearrangement. According to the authors (7), carrying out the rearrangement by heating in the presence of red mercuric oxide allows trapping of the resulting thioaldehyde and conversion to the corresponding aldehyde in high yield. When this procedure was applied to the mixture (**2***d*† + **6**), the known (1*a*) 3,5-diphenylpentadienal (**8**) was obtained in a 63% yield and as a mixture of two stereoisomers[7] (see Scheme 4). Presumably, the thermal processes a, b, and c are initiated at 110–115°C and the intermediate thioaldehyde[7] trapped and converted to aldehyde **8**; a possible electrophilic catalysis by mercury on path a is highly probable since conversion of 2-oxabicyclo[3.1.0]hexenes to the corresponding unsaturated aldehydes is known to be also acid catalyzed (1*a*, 6).

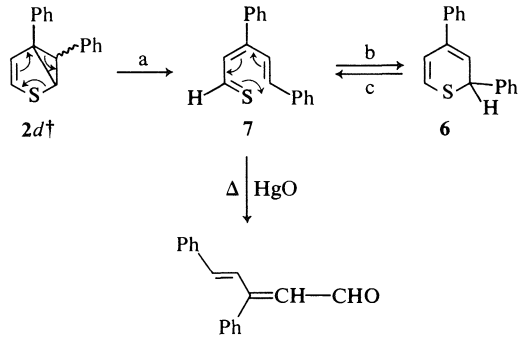


SCHEME 4. Conversion of photoproduct mixture **2***d*† + **6** to fully characterizable 3,5-diphenylpentadienal (**8**).

In the nmr, the 3,5-diphenylpentadienal (**8**) presents a pair of doublets at 10.30 ppm ($J$ = 8 Hz) and 9.50 ppm ($J$ = 8 Hz) having respective relative intensities of 0.8H and 0.2H characteristic of an aldehyde mixture; at 7.72 ppm and 6.80 ppm, a pair of AB doublets ($J$ = 16 Hz) of relative intensities 1H characteristic of the 4,5 vinyl protons in a *trans*

[6]In support of this hypothesis, Jackson (6) has reported that, upon standing at 0–5°C, 3-chloro-2-thiabicyclo[3.1.0]hexene isomerizes to 6-chloro-2*H*-thiopyran.

[7]The ratio of isomers in the resulting mixture is different from that observed in the photolysis of γ-pyran **1***a* (see Scheme 1).

Can. J. Chem. Downloaded from www.nrcresearchpress.com by 210.87.254.42 on 09/06/12
For personal use only.

arrangement; at 7.40 ppm the phenyl groups appear in the form of a complex pattern; further upfield at 6.25 and 6.18 ppm appears another pair of doublets ($J$ = 8 Hz), having a relative total intensity of 1H, characteristic of the vinyl proton on carbon-2. The nmr spectrum is therefore in accord with that expected for a mixture of 2,3-*cis*-4,5-*trans* and 2,3-*trans*-4,5-*trans*-3,5-diphenylpentadienals (**8**). The ultraviolet spectrum is typical of such a conjugated system with a $\lambda_{max}$ at 334 nm ($\varepsilon \simeq$ 18 000) (1).

*Synthesis of authentic 3,5-diphenylpentadienal (8)*

In our previous paper (1*a*), the mixture of 3,5-diphenylpentadienal (**8**) was correlated chemically with authentic methyl 3,5-diphenylpentanoate using tlc and vpc techniques. In the present paper we sought a more direct and absolute proof of structure of the aldehyde mixture and embarked on a synthesis of the desired compound.

The most direct approach to synthesize the unsaturated aldehyde **8** is by formylolefination of chalcone (**9**). All attempts having failed using 2,2-ethylenedioxyethylenetriphenylphosphonium ylid (8), we attempted an alternative method developed by Wittig and Reiff (9) using metallated Schiff bases to effect aldol condensation as a route to α,β-unsaturated carbonyl compounds. This method presumably is superior to phosphorus ylids when ketones are used as starting material and greatly superior when conjugated ketones are used as starting material. Hence, we were most gratified to find that Wittig and Suchanek (10) had already reported the condensation of the lithium anion of ethylidenecyclohexylamine (**10**) with chalcone (**9**) which leads to the desired 3-hydroxy-3,5-diphenylpent-4-enylidenecyclohexylamine (**11**) when the reaction is carried out at −70°C; at room temperature, however, the main product isolated is that of the conjugate addition on the enone **9**. Although Wittig and Suchanek (10) had not reported the hydrolysis–dehydration step to the desired unsaturated aldehyde **8**, we envisaged that treatment by aqueous oxalic acid which has been used with success in many other cases (9) should also be applicable in this case. In the event, our assumption proved correct and the synthesis was carried out successfully (see Scheme 5 and Experimental).

The authentic 3,5-diphenylpentadienal (**8**), obtained in a 35% yield starting from ethylidenecyclohexylamine, presents in its mass spectrum a molecular ion at *m/e* 234 and a $M - 29$ peak typical of aldehydes. The infrared is characterized by an intense conjugated carbonyl absorption at 1660 $cm^{-1}$. In the nmr, there appears the typical pair of

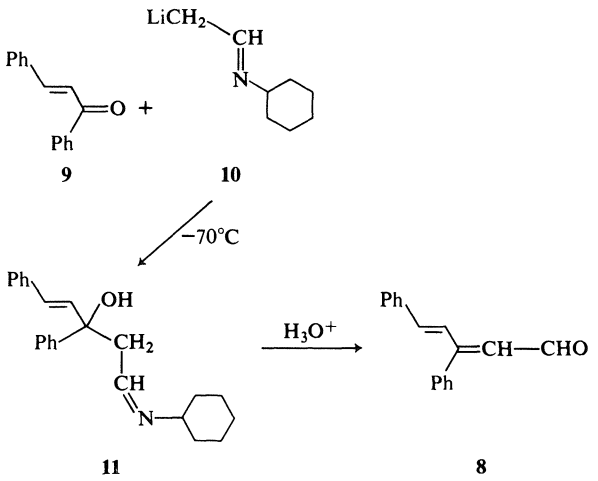


SCHEME 5. Synthesis of authentic 3,5-diphenylpentadienal (**8**).

doublets at 10.18 ppm ($J$ = 8 Hz) and 9.40 ppm ($J$ = 8 Hz) but this time with respective relative intensities of 0.2H and 0.8H, i.e. proportions exactly opposite to those observed in the mercuric oxide experiment described above. Aside from the observed discrepancies in the signal intensities, the general aspect of the spectra regarding chemical shifts was identical.

The present correlation, although chemically sound, was not totally satisfactory to us because the different product ratios in each mixture prevented their full comparison by nmr and ir. We were therefore happy to find that *trans-trans*-3,5-diphenylpentadienoic acid (**12**) and its 2,3-*cis*-4,5-*trans* isomer had been reported in the literature (11) and were separated by crystallization. We thus required a smooth method to efficiently convert the 3,5-diphenylpentadienal mixture of isomers **8** to the corresponding mixture of acids.

*Oxidation of the 3,5-diphenylpentadienal mixture of isomers 8 and correlation with authentic* trans–trans-*3,5-diphenylpentadienoic acid (12)*

For the conversion of the unsaturated aldehyde mixture **8** to the corresponding acids we chose a method described by Corey *et al.* (12) as useful for such conversions and which gives little or no isomerization (see below). The method involves the use of silver oxide as oxidizing agent in presence of cyanide ions. When this procedure was applied to the mixture of unsaturated aldehydes **8** obtained from the mercuric oxide experiment (see Scheme 4), there was obtained a 1:1 mixture of 3,5-diphenylpentadienoic acid (**12**) and unreacted unsaturated aldehydes **8** (see Scheme 6).

Much to our surprise, the acid obtained was

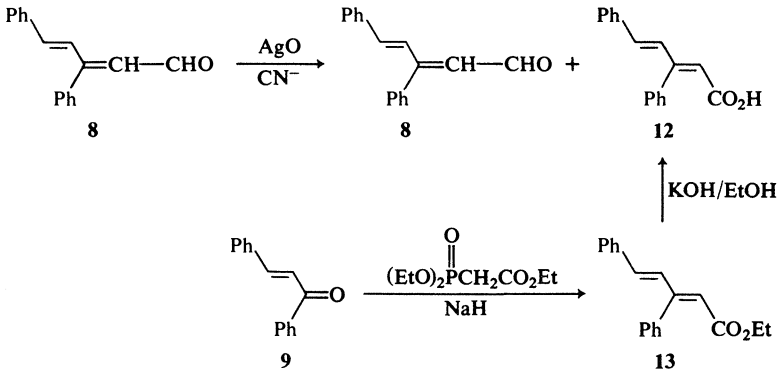


SCHEME 6. Structure correlation of 3,5-diphenylpentadienoic acid (**12**)

unique and had the *trans-trans* stereochemistry while the unreacted unsaturated aldehyde had exactly the opposite isomer ratio to the starting aldehyde mixture, i.e. the aldehydic proton at 10.20 ppm had a relative integration of 0.2H while that at 9.40 ppm had 0.8H. This ratio, however, is exactly that obtained in the unambiguous synthesis of the aldehydes by the Wittig and Suchanek (10) procedure (see Scheme 5); hence, quite by chance, we were in a position to compare the nmr spectra of identical isomer ratios of 3,5-diphenylpentadienal (**8**) originating from the mercuric oxide desulfurization experiment (see Scheme 4) and from the unambiguous synthesis route (see Scheme 5); these proved identical in all respects.

The original desired correlation having thus been obtained (by coincidence) there was no further great need to prepare the *trans-trans* acid **12** but this was done for the sake of completeness using triethylphosphonoacetate and chalcone (**9**) (11) (see Scheme 6). The *trans-trans* ethyl ester **13** obtained by chromatography was saponified to the desired authentic *trans-trans* acid **12** which proved identical in all respects to the *trans-trans* acid **12** obtained by oxidation of the aldehyde mixture **8** using the silver oxide – cyanide method (12) (see Experimental).

With the structure of aldehyde **8** now firmly established, it can safely be concluded that photorearrangement of 4,4-diphenylthiopyran **1***d* involves phenyl migration, most probably by a di-π-methane rearrangement resulting from a phenyl–vinyl (P–V) bonding interaction (see path a, Scheme

*Preparative scale photolysis of 4,4-diphenylthiopyran-1,1-dioxide (1e) and characterization of photoproducts*

In a typical experiment, irradiation for 1 h at 254 nm of 500 mL of a $3.5 \times 10^{-3}$ *M* methanol solution of sulfone **1***e* leads to a mixture of photoproducts. Preparative scale tlc on silica gel allows the recovery of 3 products: (*i*) unreacted starting sulfone **1***e*, 52%; (*ii*) 5-methoxy-4,4-diphenyl-5,6-dihydrothiopyran-1,1-dioxide (**14**) 13%; (*iii*) 6,6-diphenyl-2-thiabicyclo[3.1.0]hexene-2,2-dioxide (**3***e*), 15% (see Scheme 7).

Like the starting sulfone **1***e*, the methanol photoadduct **14** does not show a molecular ion in its mass spectrum but an ion at $M - 64$ is in accord with the loss of $SO_2$. In the ir, intense bands at 1300, 1125, and 1085 $cm^{-1}$ are characteristic of the $SO_2$ group and the C—O bond. The nmr, on the other hand, presents a narrow multiplet at 7.26 ppm for the aromatic protons; the two vinyl protons appear in the form of a singlet at 6.46 ppm while $H_5$ appears as a doublet of doublets ($J_1 \simeq 11.5$ Hz, $J_2 \simeq 2.5$ Hz) at 4.67 ppm. The methoxyl singlet appears at 3.33 ppm, in the midst of a complex signal extending from 3.53 to 2.93 ppm and due to the methylene group α to the sulfone. The structure of the proposed methoxysulfone **14** was corroborated by synthesis, *vide infra*.

The third and most relevant (for this study) product isolated shows in its mass spectrum a molecular ion at *m/e* 282 and an ion at $M - 64$ corresponding to the loss of $SO_2$, typical in this series; a microanalysis corroborated fully the molecular formula of $C_{17}H_{14}O_2S$. The ir spectrum clearly shows the presence of a sulfone group by

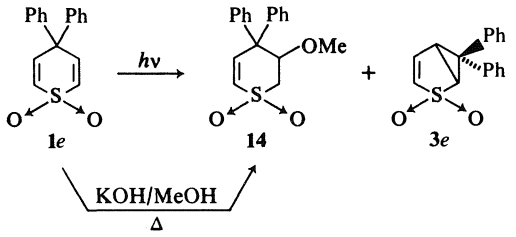


SCHEME 7. Photolysis of 4,4-diphenyl-γ-thiopyran-1,1-dioxide (**1***e*).

Can. J. Chem. Downloaded from www.nrcresearchpress.com by 210.87.254.42 on 09/06/12
For personal use only.

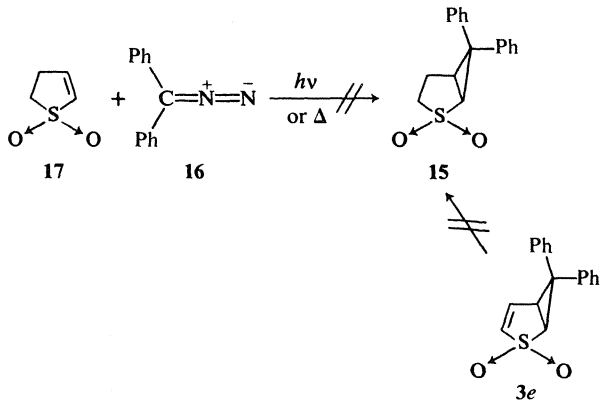


SCHEME 8. Attempted correlation of photoproduct **3e** by way of its dihydroderivative **15**.

characteristic absorptions at 1300 and 1140 $cm^{-1}$. In the nmr, the aromatic protons appear in the form of a narrow multiplet at 7.25 ppm. The vinyl proton $H_4$, β to sulfone, gives rise to a doublet of doublets centered at 6.88 ppm ($J_{3,4} \simeq 6.5$ Hz and $J_{4,5} \simeq 3.0$ Hz), while $H_3$, α to sulfone, gives rise to a doublet of doublets centered at 6.16 ppm ($J_{3,4} \simeq 6.5$ Hz and $J_{1,3} \simeq 1.5$ Hz); the cyclopropyl proton $H_1$ appears also as a doublet of doublets centered at 3.49 ppm ($J_{1,5} \simeq 6.5$ Hz and $J_{1,3} \simeq 1.5$ Hz) and $H_5$ as a doublet of doublets at 3.29 ppm ($J_{1,5} \simeq 6.5$ Hz and $J_{4,5} \simeq 3.0$ Hz).

Due to the all-importance of establishing absolutely and unambiguously the relative position of the phenyl groups on the bicyclic sulfone **3e** because it holds the key to the question of regioselectivity in this system, we attempted, but quite unsuccessfully, to synthesize the 3,4-dihydro derivative **15** of the bicyclic sulfone **3e** (see Scheme 8). We carried out the decomposition of diphenyldiazomethane **16** (13) in the presence of 2,3-dihydrothiophene-1,1-dioxide **17** (14) both photochemically (15) and thermally (16) but unfortunately could not isolate any of the desired bicyclic sulfone **15**.

Confronted with the impossibility of readily preparing authentic bicyclic sulfone **15** for correlation, we had to rely solely on nmr to determine the structural features of bicyclic sulfone **3e**. Although the spectrum described above is perfectly clear and consistent with the structure proposed (**3e**), we nevertheless must dissipate any possibility of error in establishing the structure. In order to do so, we present in Table 1 a series of pertinent nmr values taken from our work (1*a*) and that of Zimmerman *et al.* (3*b*, 17). Inspection shows clearly that all structures originating from phenyl migration present $H_6$ as a doublet as a result of coupling with $H_1$. *No* other coupling with any other proton of the skeleton has ever been observed. Also, $H_4$ in these structures only shows coupling to $H_3$. On the other hand, it is also readily apparent that bicyclic sulfone **3e** has an nmr which is very closely related to structures originating from vinyl migration (i.e. *gem*-diphenyl compounds); indeed, in these structures, $H_4$ or $H_5$ always appears as a doublet of doublets with $J_{4,5} \simeq 2$–3 Hz.

Hence it is now clear that the bicyclic sulfone **3e** bears a *gem*-diphenyl group on carbon-6 and stems from a vinyl–vinyl (V–V) interaction in the mechanism (see path b, Scheme 2).

*Preparation of authentic 5-methoxy-4,4-diphenyl-5,6-dihydrothiopyran-1,1-dioxide (**14**)*

A sample of authentic methoxysulfone **14** was prepared by Michael-type addition (19) of methanol to the cross-conjugated sulfone **1e** (see Scheme 7). The desired compound **14** was obtained in a 30% yield after a methanolic solution of sulfone **1e** was heated to reflux for 98 h in the presence of potassium hydroxide. The authentic methoxysulfone **14** was identical in all respects to that isolated from the photolysis (see Experimental).

*Sensitization experiments*

It has long been established by Zimmerman *et al.* (2) that constrained di-π-methane systems rearranging via a π–π* excited state normally proceed through the triplet state as a more efficient pathway; reaction through the singlet is also observed but is much less efficient.[8]

In the present case and in the case of our earlier work on 4,4-diphenylpyran **1a** (1) it is to be expected, on the basis of the structure–multiplicity relationship cited above, that the systems **1a**, **1d**, and **1e** should rearrange preferably via the triplet state.

Since we have already reported, in collaboration with Durocher and co-workers (1*b*), that pyran **1a** and thiopyran **1d** have lowest triplet states of π–π* configuration and respective energies of 77.8 and 76.4 Kcal/mol, it became apparent that acetone could be a useful sensitizer to carry out these studies. Although the sulfone **1e** does not phosphoresce at 77 K it should be safe to assume that its triplet is of π–π* configuration and energy comparable to that of **1a** and **1d**.

Acetone has a triplet energy of 79–82 Kcal/mol (20, 21) which puts it slightly above the energy of the acceptors. Hence, the conditions chosen for

[8]It will be recalled that unconstrained systems rearrange via the singlet excited state because in these systems the triplets deactivate by the so-called "free rotor effect" which is more efficient than the competing di-π-methane rearrangement.

Can. J. Chem. Downloaded from www.nrcresearchpress.com by 210.87.254.42 on 09/06/12
For personal use only.

TABLE 1. $^1$H nmr parameters of bicyclo[3.1.0]hexene derivatives

| Compound | Proton | Multiplicity | Coupling constants | δ ppm | Reference |
|---|---|---|---|---|---|
| 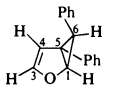 **2*a*** | $H_1$ | d | $J_{1,6}$ = 7 Hz | 4.73 | 1*a* |
| | $H_3$ | d | $J_{3,4}$ = 2.5 Hz | 5.96 | |
| | $H_4$ | d | $J_{3,4}$ = 2.5 Hz | 5.10 | |
| | $H_6$ | d | $J_{1,6}$ = 7 Hz | 2.50 | |
| 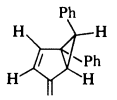 **2*b trans*** | $H_1$ | d | $J_{1,6}$ = 8.5 Hz | 2.70 | 3 |
| | $H_3$ | d | $J_{3,4}$ = 5.5 Hz | 5.59 | |
| | $H_4$ | d | $J_{3,4}$ = 5.5 Hz | 6.00 | |
| | $H_6$ | d | $J_{1,6}$ = 8.5 Hz | 2.99 | |
| 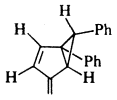 **2*b cis*** | $H_1$ | m | — | 2.90 | 3 |
| | $H_3$ | d | $J$ = 5 Hz | 6.34 | |
| | $H_4$ | d | $J$ = 5 Hz | 5.87 | |
| | $H_6$ | d | $J$ = 4.0 Hz | 2.25 | |
| 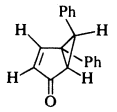 **2*c*** | $H_1$ | dd | $J_{1,6}$ = 9 Hz<br>$J_{1,3}$ = 1.0. Hz | 2.60 | 17 |
| | $H_3$ | dd | $J_{3,4}$ = 5.5 Hz<br>$J_{1,3}$ = 1.0 Hz | 5.57 | |
| | $H_4$ | d | $J_{3,4}$ = 5.5 Hz | 7.40 | |
| | $H_6$ | d | $J_{1,6}$ = 9.0 Hz | 3.56 | |
| 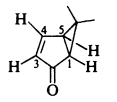 | $H_1$ | d | $J_{1,5}$ = 4 Hz | 1.94 | 3 |
| | $H_3$ | d | $J_{3,4}$ = 6 Hz | 5.89 | |
| | $H_4$ | dd | $J_{3,4}$ = 6 Hz<br>$J_{4,5}$ = 2 Hz | 7.36 | |
| | $H_5$ | dd | $J_{1,5}$ = 4 Hz<br>$J_{4,5}$ = 2 Hz | 2.42 | |
| 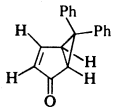 **3*c*[a]** | $H_1$ | d | $J_{1,5}$ = 5 Hz | 2.81 | This work[a] |
| | $H_3$ | d | $J_{3,4}$ ≃ 6.3 Hz | 5.55 | |
| | $H_4$ | dd | $J_{3,4}$ ≃ 6.3 Hz<br>$J_{4,5}$ = 2.5 Hz | 7.41 | |
| | $H_5$ | dd | $J_{5,1}$ = 5 Hz<br>$J_{4,5}$ = 2.5 Hz | 3.24 | |
| 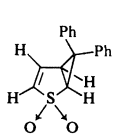 **3*e*** | $H_1$ | dd | $J_{1,5}$ = 6.5 Hz<br>$J_{1,3}$ = 1.5 Hz | 3.49 | This work |
| | $H_3$ | dd | $J_{3,4}$ = 6.5 Hz<br>$J_{1,3}$ = 1.5 Hz | 6.16 | |
| | $H_4$ | dd | $J_{3,4}$ = 6.5 Hz<br>$J_{4,5}$ = 3 Hz | 6.88 | |
| | $H_5$ | dd | $J_{5,1}$ = 6.5 Hz<br>$J_{4,5}$ = 3.0 Hz | 3.29 | |

[a]This compound was reported in the literature (*4b*) but the nmr data did not seem to correspond to those of **3*e***. We therefore repeated the photolysis of 4,4-diphenylcyclohexadienone (**1*c***) (18), isolated the reported bicyclo[3.1.0]hexenone photoproduct **3*c***, mp 138–139°C (lit. (18) 140°C) and herein report its nmr.

sensitization were to use acetone as solvent and 350 nm light in Pyrex vessels. Acetone absorbs only slightly at this wavelength, but pyran **1*a***, thiopyran **1*d***, and sulfone **1*e*** do not.

In a preliminary test, however, we irradiated solutions of pyran **1*a***, thiopyran **1*d***, and sulfone **1*e*** in anhydrous ether using 350 nm lamps (Rayonet) and Pyrex vessels. It was found that **1*a*** and **1*e*** are inert while thiopyran **1*d*** reacts to give the usual products; this is most probably due to the emission of a small amount of 300 nm light by the lamp and, since thiopyran **1*d*** has an $\varepsilon = 800\ M^{-1}\ cm^{-1}$ at 300 nm (*1b*), direct excitation takes place. Attempts to filter out this stray light using a 2 in. × 2 in. 320 nm 0-transmittance filter window even prevented pyran **1*a*** in acetone as sensitizer from reacting; this was most probably due to a lack of radiation energy reaching the sample due to the small size of the

Can. J. Chem. Downloaded from www.nrcresearchpress.com by 210.87.254.42 on 09/06/12
For personal use only.

Can. J. Chem. Downloaded from www.nrcresearchpress.com by 210.87.254.42 on 09/06/12
For personal use only.

window and not to a filter effect. Be that as it may, we abandoned the idea of sensitizing the thiopyran **1***d* reaction because it could not be realized under the best unambiguous conditions.

The preparative scale sensitized photolysis of pyran **1***a* was carried out in 1:1 acetone – *tert*-butanol solution using 350 nm lamps and a Pyrex vessel. The structures of the products isolated corresponded fully to those obtained by direct photolysis (**1***a*) (see Experimental).

As stated above, due to the nonphosphorescence of sulfone **1***e* we assumed a triplet energy of 76–78 Kcal/mol and used acetone as sensitizer. The experiment was carried out using the sensitizer as solvent, 350 nm lamps, and a Pyrex vessel. The bicyclo[3.1.0] product **3***e* isolated from the reaction was identical in all respects to that isolated from the direct irradiation (see Experimental).

These sensitization experiments therefore show that the lowest $\pi$–$\pi^*$ triplet $T_1$ can be the excited state by which rearrangement takes place in pyran **1***a* and sulfone **1***e*. These results are fully in accord with the structure–multiplicity relationship scheme proposed by Zimmerman and co-workers (2). Although we have no direct experimental results to that effect, it would seem reasonable to suggest, on the basis of Zimmerman's scheme (2) and the spectroscopic and photochemical results we have in this homologous series, that thiopyran **1***d* can most probably also undergo the rearrangement via its lowest $\pi$–$\pi^*$ triplet $T_1$. These results and considerations of course do not exclude the singlet $S_1$ as responsible for the rearrangement but according to the scheme (2) it should be less efficient than the triplet.

## Discussion

The results reported above have shown that di-$\pi$-methane systems in the 4,4-diphenyl-2,5-cyclohexadiene series, where the vinyl moieties are bound by a heteroatom, rearrange to yield *phenyl migrated products via phenyl–vinyl (P–V) bonding, when the heteroatom bears unshared electrons*; this is the case for the 4,4-diphenylpyran **1***a* and thiopyran **1***d*. On the other hand, the results also show that *when the heteroatom bears no unshared electrons* as in the case of 4,4-diphenylthiopyran-1,1-dioxide **1***e*, *the rearrangement leads to a vinyl migration product (type A) via vinyl–vinyl (V–V) bonding* (see Table 2).

In an effort to broaden the scope of the discussion we will take into consideration the rearrangement results of other 4,4-diphenyl-2,5-cyclohexadiene systems which have been reported in the literature (see Table 2); these are: the thoroughly studied 1-methylene-4,4-diphenyl-2,5-cyclohexadiene (**1***b*) (3), which has been shown by Zimmerman to give phenyl migration via phenyl–vinyl (P–V) bonding in a di-$\pi$-methane rearrangement; 4,4-diphenylcyclohexadienone **1***c* (4), which has been shown by the same author to give Type A rearrangement via vinyl–vinyl (V–V) bonding; and 1-hydroxy-4,4-diphenyl-2,5-cyclohexadiene (**1***f*) (22), which has been shown indirectly (see note at bottom of Table 2) to give Type A rearrangment via vinyl–vinyl (V–V) bonding. We have also included in the table two recent cases studied by Zimmerman and Diehl (23) to determine the controlling factors governing the differing reactivity between dienone **1***c*, triene **1***b*, and its 4,4-dimethyl analog. These are: 1-dicyanomethylene-4,4-diphenyl-2,5-cyclohexadiene (**1***g*) and 1-diphenylmethylene-4,4-diphenyl-2,5-cyclohexadiene (**1***h*), which in the first case leads to $\alpha,\alpha$-dicyano-3,4-diphenyltoluene (**18**) via phenyl–vinyl (P–V) bonding, while the second leads to 2-diphenylmethylene-6,6-diphenylbicyclo[3.1.0]hex-3-ene (**3***h*) via vinyl–vinyl (V–V) bonding in a Type A rearrangement.

Finally, we have included the interesting case of 4,4-disubstituted 4-sila-2,5-cyclohexadienones (**19**) (24) which yield ring contracted cyclopentenones (**20**) via vinyl–vinyl bonding in a presumed Type A rearrangement, where the zwitterionic intermediate would undergo a nucleophilic attack from the solvent to yield the corresponding cyclopentenone **20** rather than collapse to the usual type A product, the corresponding bicyclo[3.1.0] derivative. This type of interception of the Type A rearrangement by solvent attack on the intermediate zwitterion has already been observed in other cases (25).

In order to shed light on the problem of regioselectivity in the rearrangement of these 4,4-diphenyl-2,5-cyclohexadiene systems we must try to understand the factors which control the preferred mode of $\pi$–$\pi$ interaction and, eventually, bridging as depicted in a simplified fashion in Scheme 2.

In the present case, inspection of Table 2 reveals that compounds **1***a*, **1***b*, **1***d*, and **1***g*, where X = O, C=$CH_2$, S, and C=$(CN)_2$ respectively, give phenyl–vinyl (P–V) bonding while compounds **1***c*, **1***e*, **1***f*, **1***h*, and **19**, where X = C=O, $SO_2$, CH(OH), C=$CPh_2$, and C=O respectively, give vinyl–vinyl (V–V) bonding. For the purpose of our discussion we will try to adapt Zimmerman's "reacting chromophore simulation" concept (26) to the molecules at hand bearing in mind that it was developed and used mainly for benzobarrelene and aliphatic, i.e. non-2,5-cyclohexadienic, di-$\pi$-methane systems. It is important to remember here that excitation energy tends to localize in a mini-

Can. J. Chem. Downloaded from www.nrcresearchpress.com by 210.87.254.42 on 09/06/12
For personal use only.

TABLE 2. Regioselectivity in the photorearrangement of 4,4-diphenyl-2,5-cyclohexadiene systems

| Starting compound | Primary photoproduct | | |
|---|---|---|---|
| | P–V bonding | V–V bonding | |
| 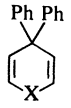 | 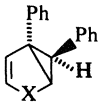 | 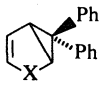 | |
| **1** | **2** | **3** | Reference |
| *a*: X = O | Isolated | — | 1*a* |
| *b*: X = C=CH$_2$ | Isolated | — | 3 |
| *c*: X = C=O | — | Isolated | 4 |
| *d*: X = S | Isolated[a] | — | This work |
| *e*: X = SO$_2$ | — | Isolated | This work |
| *f*: X = CHOH | — | Presumed[b] | 22 |
| *g*: X = C=C(CN)$_2$ | 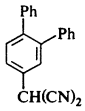 **18** | — | 23 |
| *h*: X = C=C(Ph)$_2$ | — | Isolated | 23 |
| 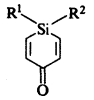 **19** | — | 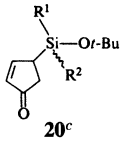 **20**[c] | 24 |
| *a*: R$^1$ = Me, R$^2$ = Ph | | *a*: R$^1$ = Me, R$^2$ = Ph | |
| *b*: R$^1$ = R$^2$ = Ph | | *b*: R$^1$ = R$^2$ = Ph | |

[a]Isolated as a mixture with 2,4-diphenyl-α-thiopyran (**6**)) *vide infra*.
[b]Not isolated but synthesized and shown, under the same photolysis conditions, to yield the same products.
[c]Vinyl–vinyl bonding products; isolated as 1:1 diastereoisomeric mixture in the case of R$^1$ = Me, R$^2$ = Ph (*vide infra*).

mum energy MO and that "electronically excited species react by pathways minimizing energy as the reaction coordinate is traversed" (23). Although both the theoretical (27) and the empirical (28) approaches have been used by the authors we will consider here the latter. To do so, we must estimate the energy of the coupled isoconjugate chromophores as the π moieties begin to interact, i.e. the various vinyl–vinyl (V–V) and phenyl–vinyl (P–V) coupled chromophores. Normally this should be done for the excited singlet chromophores and for the corresponding triplets since some reactions are efficient via the singlet while others are efficient via the triplet. Unfortunately, however, this refinement of the method cannot be applied here because too few of the required energies are available in the literature. Let us nevertheless proceed and identify these coupled chromophores; they are represented in Scheme 9.

It is readily apparent from the scheme that, while phenyl–vinyl (P–V) bonding gives rise to various β-substituted styrenes, vinyl–vinyl (V–V) bonding gives rise to a most interesting series of fundamental five-membered ring chromophores which fall

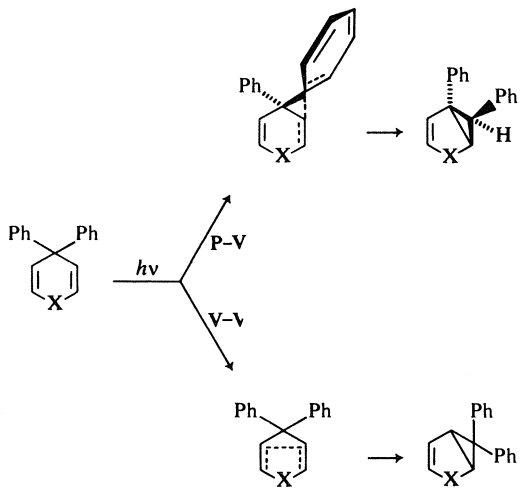


**1*a*: X = O
**1*b*: X = C=CH$_2$
*1*c*: X = C=O
**1*d*: X = S
*1*e*: X = SO$_2$
*1*f*: X = CH(OH)
*1*g*: X = C=C(CN)$_2$
**1*h*: X = C=C(Ph)$_2$
*19*b*: X = C=O (C4 = Si)

SCHEME 9. Standard representation of coupled chromophores for P–V versus V–V bonding.

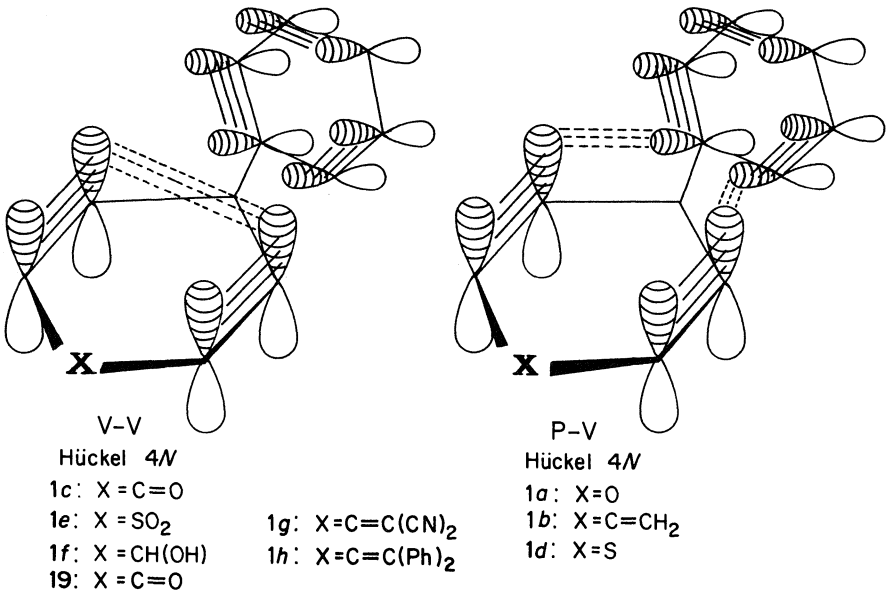


FIG. 1. Possibility of formation of Hückel arrays in V–V versus P–V coupled chromophores.

into two main categories. Firstly there are those which, according to Hückel's $4N$ vs. $4N + 2$ rule (29) or perhaps more appropriately the "Möbius–Hückel concept" developed by Zimmerman[9] (30), should show some aromatic character in the ground state and antiaromatic character in the excited state; they arise from the doubly starred compounds in Scheme 9. Secondly there are those which should show antiaromatic character in the ground state and aromatic character in the excited state; they arise from the singly starred compound in the same scheme. It is also important to note at this point that, apart from two exceptions, **1***g* and **1***h*, the V–V coupled chromophores arising from the doubly starred compounds (i.e. those that should show antiaromatic character, therefore high energy, in the excited state) correspond to an observed P–V regioselectivity and those from the starred compounds (i.e. those that should show aromatic character, therefore low energy, in the excited state) correspond to an observed V–V regioselectivity. In other words, it appears that using the Möbius–Hückel concept of aromaticity and antiaromaticity one may be able, for "*simple*" *cyclically conjugated coupled chromophores*, to evaluate the excited state energy with respect to that of the competing β-substituted styrene-coupled chromophore and thus, on the basis of energy localization, to predict the regioselectivity of the rearrangement.

Furthermore, it becomes readily apparent, upon consideration of molecular models, that phenyl–vinyl (P–V) overlap could also take place in these systems to conceivably generate another set of "*cyclically conjugated coupled chromophores*" whose excited state energies could also be evaluated using the aromaticity concept. Figure 1 illustrates in a generalized fashion the two competing interactions, i.e. V–V versus P–V, where cyclical conjugation takes place through a *p*-type lobe on X when X = O, C=$CR_2$, C=O, or S, and directly through space between lobes 2 and 5 when X = $SO_2$ or CH(OH). Some comments are, however, in order here before we proceed further with the discussion: (1) there should be no problem in applying the Möbius–Hückel concept (30) in the case of **1***a* and **1***d* since Aihara (32) has shown that Hückel's $4N + 2$ rule can still be applied to all heteroannulenes containing single heteroatoms; (2) also, cases **1***e* and **1***f* should be amenable to discussion by the same concept (30) since V–V or P–V coupling generates homoconjugated annulenes to which again Hückel's rule may be applied (32*b*); (3) finally, cases **1***b*, **1***c*, **1***g*, **1***h*, and **19**, upon V–V or P–V coupling, generate cyclic arrays of overlapping orbitals which at first glance should be treatable by the aromaticity rules above; however, Anh has pointed out the pitfalls of indiscriminately applying these rules to systems which are not monocyclic or which are generated by leaving out

[9]Dewar, using his nonbonding MO perturbation method, has arrived at the same conclusion and therefore Anh refers to the "Dewar–Zimmerman rule" (31).

Can. J. Chem. Downloaded from www.nrcresearchpress.com by 210.87.254.42 on 09/06/12
For personal use only.

Can. J. Chem. Downloaded from www.nrcresearchpress.com by 210.87.254.42 on 09/06/12
For personal use only.

of the cyclic array one or more *p*-lobes (31, 33). It is therefore possible that some erroneous conclusions or predictions could be made upon simple application of Hückel's $4N + 2$ rule to these cases. It is nevertheless interesting to note that Aihara's calculations also show that the "rule" can be applied to annulenones and methylene annulenes (32).

Returning to Fig. 1, and inspecting the basis set orbitals for the cyclic Hückel arrays generated upon V–V versus P–V overlap, it can readily be seen that *when X has a* p*-lobe which contains the charge of one or more electrons, the V–V array then behaves as a 6(4*N + 2*) electron system which should be destabilized (antiaromatic) in the excited state, whereas the P–V array behaves as a 12(4*N*) electron system which should be stabilized (aromatic) in the excited state*. Therefore, it can reasonably be predicted that compounds **1***a* (X = O), **1***b* (X = C=$CH_2$), **1***d* (X = S), and **1***h* (X = C=$CPh_2$) should give preferential P–V bonding, which is the case with one exception, **1***h* (X = C=$CPh_2$), most probably attributable to the breakdown of the rule as pointed out by Anh (31, 33) because of the extended conjugation outside of the cyclic array (*vide supra*).

On the other hand, *when X has a* p*-lobe which is practically devoid of electronic charge due to polarization* such as in **1***c* (X = $C^{\delta+}$=$O^{\delta-}$), **1***g* (X = $C^{\delta+}$=$C^{\delta-}(CN)_2$, and **19** (X = $C^{\delta+}$=$O^{\delta-}$), *or when X has no* p*-lobe* as in **1***e* (X = CH(OH)) and **1***f* (X = $SO_2$), *then the V–V arrays possible* in **1***c*, **1***g*, and **19** *as well as the homoconjugated V–V arrays possible* in **1***e* and **1***f* behave as 4(4N) *electron systems which should be stabilized (aromatic) in the excited state, whereas the corresponding P–V arrays behave as 10(4*N + 2*) electron systems which should be destabilized (antiaromatic) in the excited state*. Therefore, it can reasonably be predicted that compounds **1***c*, **1***g*, **1***e*, **1***f*, and **19** should give preferential V–V bonding, which is the case, again with one exception, namely **1***g*, which, as in **1***h*, has conjugation outside of the cyclic arrays considered (*vide supra*).

In conclusion we have expanded in this work the list of 4,4-diphenyl-2,5-cyclohexadiene systems which give either di-π-methane or Type A rearrangement and have proposed a reasonable explanation for the regioselectivity observed in all but two cases, which is based on the Möbius–Hückel concept (30) of evaluating the relative energies of cyclic arrays of overlapping orbitals in competing processes. Although the proposed explanation is qualitative and will require eventual MO calculations, it has the merit of rationalizing for the first time, using a single concept, the problem of regioselectivity in the di-π-methane and dienone (Type A) rearrangements of 4,4-diphenyl-2,5-cyclohexadiene systems.

## Experimental

The silica gel used for all analytical and preparative (20 × 40 cm) tlc is of the G/UV 254 grade from Machery–Nagel. The melting points were taken on a "Büchi" apparatus and are uncorrected. The ir spectra were recorded on a Perkin–Elmer model 710-B apparatus. The routine nmr spectra were recorded either on a Varian A-60 or EM-360 model apparatus, while the high resolution spectra were taken on a JEOL 100 MHz, JNM-4H-100 apparatus. The reported chemical shifts are expressed on the δ scale in ppm and tetramethylsilane was used as internal reference. The letters s, d, t, q, and m are used as abbreviation for singlet, doublet, triplet, quartet, and multiplet. The uv spectra were recorded on a Bausch and Lomb Spectronic 505. The high resolution mass spectra were obtained on an AEI model MS-902 apparatus while the low resolution spectra were obtained on a Hitachi–Perkin–Elmer model RMU-6-D apparatus. All photolyses were carried out using a "Rayonet" photochemical reactor equipped with 16 "monochromatic" lamps emitting either at 254, 300, or 350 nm according to the case.

Finally, the reported microanalyses were done by Midwest Microlab, 6000 East 46th Street, Indianapolis, IN 46226, U.S.A.

*4,4-Diphenyl-γ-thiopyran (***1d***) (ref. 1a)*

A stirred solution of 1,1,5,5-tetramethoxy-3,3-diphenylpentane (**4**) (**1***a*, 34) (51.4 g, 0.15 mol) in 500 mL of dichloromethane is treated at room temperature by a 2:1 gaseous mixture of hydrogen chloride and hydrogen sulfide during a period of 2 h. The excess gas is flushed by a stream of nitrogen during 15 min. The solvent is then immediately evaporated and the crude 2,6-dichloro-4,4-diphenyltetrahydro-2,3,5,6-thiopyran (**5**) heated to reflux during a period of 3 h in 400 mL of *N*,*N*-dimethylaniline.

The reaction mixture is diluted with 300 mL of ether and the solution washed with 10% HCl and then with water. The organic layer is dried over anhydrous magnesium sulfate, filtered, and the solvent evaporated. The crude product obtained is purified by column chromatography over silica gel (8 cm × 80 cm) using hexane as eluent to yield 22.3 g (60%) of 4,4-diphenyl-γ-thiopyran (**1***d*) as a white solid, mp 83°C; ir ($CHCl_3$): 1600 $cm^{-1}$; uv (ethanol 95%): $\lambda_{max}$ = 240 nm (ε ≃ 1470) and $\lambda_{max}$ = 285 nm (ε ≃ 1090); nmr ($CDCl_3$): 7.20 (narrow m, 10H) and 6.00 (pair of d, AB, $J_{AB}$ = 10.5 Hz, $\Delta\nu_{AB}$ = 19 Hz, 4 H). Mass spectrum, calculated mass: 250.0815, measured mass: 250.0795.

*4,4-Diphenyl-γ-thiopyran-1,1-dioxide (***1e***)*

A solution of 4,4-diphenyl-γ-thiopyran (**1***d*) (5 g, 20 mmol) in 100 mL of carbon tetrachloride is added to a suspension of ruthenium dioxide (*n* $H_2O$) (100 mg) in 20 mL of water (5). A solution of 125 mL of 10% sodium periodate in water (58 mmol $NaIO_4$) is then added over a period of 20 min. The resulting suspension is then stirred at room temperature during 3 h. The excess of ruthenium tetroxide (formed *in situ*) is destroyed by addition of a few mL of isopropanol. A portion of 100 mL of chloroform is added to the reaction mixture which is then filtered and the organic phase separated from the aqueous phase. The latter is extracted with 2 portions of 50 mL of chloroform. The organic extracts are combined, dried over anhydrous magnesium sulfate, and the solvent evaporated to yield 5.25 g (93%) of crude product. Purification by crystallization from chloroform–hexane gives a white solid, mp 213.5–

Can. J. Chem. Downloaded from www.nrcresearchpress.com by 210.87.254.42 on 09/06/12
For personal use only.

214°C; ir ($CHCl_3$): 3040, 1645, 1295, and 1115 $cm^{-1}$; uv (ethanol 95%): $\lambda_{max}$ = 235 nm ($\varepsilon \simeq 850$) and $\lambda_{max}$ = 260 ($\varepsilon \simeq 240$); nmr ($CDCl_3$): 7.35 (narrow m, 10H) and 6.70 (pair of d, AB, $J_{AB}$ = 12 Hz, $\Delta\nu_{AB}$ = 5 Hz, 4H). Mass spectrum: base peak at *m/z* 218 (M − $SO_2$). *Anal.* calcd. for $C_{17}H_{14}O_2S$: C 72.31, H 5.00, S 11.36; found: C 72.16, H 4.90, S 11.14.

*Preparative scale photolysis of* **1***d and characterization of photoproducts*

*Photolysis*

Two solutions of 500 mg of thiopyran **1***d* in 500 mL of anhydrous ether ($10^{-3}$ *M*) are irradiated at 254 nm during 2 h and the reaction monitored by tlc. The solvent is evaporated *in vacuo* without heating and the crude mixture separated on 20 preparative tlc plates using ether–hexane (1.5:98.5) as eluent. The products are extracted from the silica gel by successive washings with 75 mL anhydrous ether at room temperature.

The first fraction, 70 mg (7%), is identified as unreacted thiopyran **1***d* by nmr and tlc. The second fraction, 550 mg (55%), is identified as a mixture of 5,6-diphenyl-2-thiabicyclo[3.1.0]-3-hexene (**2***d*) and 2,4-diphenyl-(2*H*)-thiopyran (**6**) by nmr ($CDCl_3$): 7.35 (narrow m), 6.40 (pair of d, AB, $J_{AB}$ = 10.5 Hz, $\Delta\nu_{AB}$ = 11Hz), 5.80 (m), 4.85 (d, *J* = 8 Hz), and 3.70 to 2.10 (m).

*Desulfurization (7) of the photoproduct mixture* **2**d *and* **6**

A solution of the mixture of photoproducts **2***d* and **6** (480 mg, 1.9 mmol) in 200 mL of diglyme is heated to 110–115°C for 30 min in the presence of 1.5 g of commercial red mercuric oxide in the form of a fine powder (Malinckrodt). The reaction mixture is filtered and evaporated to dryness *in vacuo*. The residue is taken up with dichloromethane and separated on 10 preparative tlc plates using ether–hexane (1:4) as eluent. The silica bearing the product of $R_f$ 0.55 is scraped and washed with three portions of 125 mL of anhydrous ether to yield, after evaporation, 285 mg (63%) of a mixture of two 3,5-diphenylpentadienal stereoisomers (**8**); uv (ethanol 95%): $\lambda_{max}$ = 334 nm ($\varepsilon \simeq 18\,000$); nmr ($CDCl_3$): 10.30 (d, *J* = 8 Hz, 0.8H), 9.50 (d, *J* = 8 Hz, 0.2H), 7.72 (d, *J* = 16 Hz, 1H), 7.40 (m, 10H), 6.80 (d, *J* = 16 Hz, 1H), 6.25 (d, *J* = 8 Hz), and 6.18 (d, *J* = 8 Hz).

*Synthesis of authentic 3,5-diphenylpentadienals (8)*

*Condensation of the lithium anion of ethylidenecyclohexylamine (10) with chalcone (9)* (ref. 10)

Condensation of the lithium anion of ethylidenecyclohexylamine (**10**) with chalcone (**9**) is carried out in anhydrous ether at −78°C under argon, following the procedure of Wittig and Suchanek (10). The desired 3-hydroxy-3,5-diphenylpent-4-enylidenecyclohexylamine (**11**) is obtained as an unstable solid (64%, lit. (10) 65%) which is submitted to hydrolysis without further purification (see next procedure); nmr ($CDCl_3$): 7.68 (t, *J* ≃ 3.5 Hz, 1H), 7.33 (m, 10H), 6.46 (pair of d, AB, $J_{AB}$ = 16 Hz, $\Delta\nu_{AB} \simeq$ 10 Hz, 2H), 2.87 (d, broadened, *J* ≃ 3.5 Hz, 3H), and 1.43 (m, broad, 11H).

*Hydrolysis of 3-hydroxy-3,5-diphenylpent-4-enylidenecyclohexylamine (11) to 3,5-diphenylpentadienals (8)*

The β-hydroxy-alkylidenamine **11** from the previous experiment (10.7 g), oxalic acid (54 g, 0.6 mol), and water (250 mL) are heated to 100°C during a period of 2 h. The solution is cooled and extracted three times with 200 mL of ether. The organic layer is washed with aqueous $Na_2CO_3$, with water, dried over anhydrous magnesium sulfate, and evaporated. The crude oily product thus obtained (7.1 g) is purified by column chromatography over silica gel (5 cm × 50 cm), using ether–hexane (1:9) as eluent, to yield the desired authentic 3,5-diphenylpentadienal (**8**) as a mixture of isomers (4.25 g, 35% overall); ir ($CHCl_3$): 3040, 2750, 1660, and 1610 $cm^{-1}$; uv (ethanol 95%): $\lambda_{max}$ = 334 nm ($\varepsilon \simeq 18\,000$); nmr ($CDCl_3$): 10.18 (d, *J* = 8 Hz, 0.2H), 9.40 (d, *J* = 8 Hz, 0.8H), and 7.60 to 6.10 (m, 13H). Mass spectrum: molecular ion at *m/z* 234, loss of -CHO at *m/z* 205, tropylium ion at *m/z* 91, base peak at *m/z* 77 (probably $C_6H_5^{\cdot+}$).

*Chemical correlation of 3,5-diphenylpentadienal (8) with* trans–trans-*3,5-diphenylpentadienoic acid (12)*

*Oxidation of 3,5-diphenylpentadienals (8)*

According to the procedure of Corey *et al.* (12), silver oxide (1.22 g, 9.1 mmol) which has been freshly prepared and dried at 50°C for 30 min under 0.5 Torr, is suspended in 1.5 mL of dry methanol and treated rapidly with a solution of 3,5-diphenylpentadienal (**8**) (220 mg, 0.94 mmol) in 3 mL of methanol. A solution of sodium cyanide (231 mg, 4.7 mmol) in 12 mL methanol is then slowly added. Once the addition is completed, a solution of 0.8 mL of glacial acetic acid in 0.5 mL of methanol is added and the reaction mixture stirred for 3 h at room temperature, after which it is acidified with concentrated HCl, further stirred for a few minutes, filtered, and evaporated to dryness. The residue is taken up in 50 mL of ether and washed once with 30 mL of water. The aqueous layer is then extracted twice with 25 mL of ether; the ethereal layers are combined, dried over magnesium sulfate, and evaporated to yield 210 mg of a mixture of acid and aldehyde in a 1:1 ratio as shown by nmr; nmr ($CDCl_3$): 10.70 (s, broad, 0.5H), 10.25 (d, *J* = 8 Hz, 0.2H), 9.45 (d, *J* = 8 Hz, 0.3H), 8.70 to 6.10 (m, 12.5H), and 5.87 (s, 0.5H).

The mixture is separated by column chromatography on silica gel (2 cm × 25 cm), using chloroform–hexane (1:4) as eluent, to yield: (a) 90 mg of 3,5-diphenylpentadienal (**8**) as a mixture of isomers, *identical by nmr with the mixture of authentic 3,5-diphenylpentadienals (8) prepared above*; (b) 95 mg of crude 3,5-diphenylpentadienoic acid; recrystallization from dichloromethane–hexane yields the pure *trans-trans* acid **12**, mp 145–146°C, *identical with an authentic sample (mp 145–146.5°C) prepared as described below, mixture mp 145–146°C*; nmr ($CDCl_3$), see below.

*Preparation of authentic* trans–trans-*3,5-diphenylpentadienoic acid* **12**

trans–trans-*Ethyl-3,5-diphenylpentadienoate (13)* (ref. 11)

The title compound **13** is obtained, following the procedure of Bergman and Solomonovici (11), by treating chalcone (**9**) (4.16 g, 0.02 mol) with the anion of triethylphosphonoacetate. The crude oily product (5.61 g) obtained could not be separated by vacuum distillation and was therefore chromatographed on silica gel (5 cm × 50 cm) using chloroform–hexane (1:4) as eluent to yield pure *trans-trans*-ethyl-3,5-diphenylpentadienoate (**13**) (1.10 g, 20%, lit. (11) 52%); nmr ($CDCl_3$): 8.58 (d, AB, $J_{AB}$ = 16 Hz, $\Delta\nu_{AB}$ = 117 Hz, 1H), 7.40 (narrow m, 10H), 6.61 (d, AB, $J_{AB}$ = 16 Hz, $\Delta\nu_{AB}$ = 117 Hz, 1H), 5.83 (s, 1H), 4.27 (q, *J* = 7 Hz, 2H), and 1.33 (t, *J* = 7 Hz, 3H).

trans–trans-*3,5-Diphenylpentadienoic acid (12)* (ref. 11)

Saponification of the above ester **13** (160 mg, 0.58 mmol) using KOH in 95% ethanol yields, after work-up and recrystallization from dichloromethane–hexane, pure *trans-trans*-3,5-diphenylpentadienoic acid (133 mg, 93%), mp 145–146.5°C (lit. (11) mp 145°C); ir ($CHCl_3$): 3500–2500, 1680, and 1610 $cm^{-1}$; nmr ($CDCl_3$): 12.18 (s, 1H), 8.50 (d, AB, $J_{AB}$ = 16 Hz, $\Delta\nu_{AB}$ = 111 Hz, 1H), 7.45 (narrow m, 10H), 6.63 (d, AB, $J_{AB}$ = 16 Hz, $\Delta\nu_{AB}$ = 111 Hz, 1H), and 5.86 (s, 1H): Mass spectrum: molecular ion at *m/z* 250, loss of -OH at *m/z* 233, loss of -$CO_2$H at *m/z* 205 (base peak), tropylium at *m/z* 91, $C_6H_5^{\cdot+}$ at *m/z* 77.

*2,3-*cis*-4,5-*trans*-3,5-Diphenylpentadienoic acid*

It is possible to obtain the 2,3-*cis* isomer of the acid **12** simply by recrystallizing the crude saponification product above in a minimum of hot hexane. This procedure was repeated and the pure 2,3-*cis* isomer was obtained, mp 160–162°C; ir ($CHCl_3$):

Can. J. Chem. Downloaded from www.nrcresearchpress.com by 210.87.254.42 on 09/06/12
For personal use only.

3600–2500, 1670, and 1610 $cm^{-1}$; nmr ($CDCl_3$): 11.76 (s, 1H), 7.36 (m, 10H), 7.06 (d, AB, $J_{AB}$ = 16 Hz, $\Delta\nu_{AB}$ = 39 Hz, 1H), 6.36 (d, AB, $J_{AB}$ = 16 Hz, $\Delta\nu_{AB}$ = 39 Hz, 1H), and 6.05 (s, 1H). Mass spectrum: molecular ion at *m/z* 250, loss of -OH at *m/z* 233, loss of $-CO_2H$ at *m/z* 205 (base peak), tropylium at *m/z* 91, $C_2H_5^{\cdot+}$ at *m/z* 77.

*Preparative scale photolysis of* 1e *and characterization of photoproducts*

*Photolysis*

A solution of 500 mg of the thiopyran-1,1-dioxide **1e** in 500 mL of methanol ($3.5 \times 10^{-3}$ *M*) is irradiated during 1 h at 254 nm and the reaction monitored by tlc. The solvent is evaporated *in vacuo* and the crude product mixture separated on 10 preparative tlc plates using dichloromethane–hexane–acetone (15:9:1) as eluent. Three major products are thus obtained: (a) unreacted starting sulfone **1e** (52%); (b) a solvent addition product, 5-methoxy-4,4-diphenyl-5,6-dihydrothiopyran-1,1-dioxide (**14**) (13%), which is obtained as a mixture with starting material and purified by crystallization in dichloromethane–hexane, mp 161–162.5°C; ir ($CHCl_3$): 3040, 2960, 1600, 1300, 1125, and 1085 $cm^{-1}$; nmr ($CDCl_3$): 7.26 (narrow m, 10 H), 6.46 (s, 2H), 4.67 (dd, $J_1 \simeq 11.5$ Hz, $J_2 \simeq 2.5$ Hz, 1H), 3.33 (s), and 3.53–2.93 (s and m, 5H). Mass spectrum: no molecular ion present at *m/z* 314, loss of $CH_3OH$ and $SO_2$ at *m/z* 218, loss of $CH_3OH + SO_2 + C_2H_2$ at *m/z* 192 (base peak).

This material was identical in all respects (nmr, ir, mixture mp) to an authentic sample prepared as described further below. (c) The third fraction isolated was purified by crystallization from dichloromethane–hexane, mp 210°C (dec.), and identified as 6,6-diphenyl-2-thiabicyclo[3.1.0]-3-hexene-2,2-dioxide (**3e**) (15%); nmr ($CDCl_3$); 7.25 (narrow m, 10H), 6.88 (dd, $J_{3,4} \simeq 6.5$ Hz, $J_{4,5} \simeq 3.0$ Hz, 1H), 6.16 (dd, $J_{3,4} \simeq 6.5$ Hz, $J_{1,3} \simeq 1.5$ Hz, 1H), 3.49 (dd, $J_{3,4} \simeq 6.5$ Hz, $J_{1,3} \simeq 1.5$ Hz, 1H), and 3.29 (dd, $J_{1,5} \simeq 6.5$ Hz, $J_{4,5} \simeq 3$Hz, 1H). Mass spectrum: very weak molecular ion peak at *m/z* 282, loss of $SO_2$ at *m/z* 218, loss of $HSO_2$ at *m/z* 217 (base peak). *Anal.* calcd. for $C_{17}H_{14}O_2S$: C 72.31, H 5.00, S 11.36; found: C 72.00, H 5.11, S 11.20.

*Preparation of authentic 5-methoxy-4,4-diphenyl-5,6-dihydrothiopyran-1,1-dioxide (14)*

A solution of 500 mg of 4,4-diphenylthiopyran-1,1-dioxide (**1e**) in 100 mL of anhydrous methanol is heated to reflux for 98 h in presence of five KOH pellets and under a nitrogen atmosphere. The mixture is diluted with 75 mL of chloroform and 75 mL of water; the two phases are separated and the aqueous layer extracted with 150 mL of chlorform. The organic extracts are combined, dried over anhydrous magnesium sulfate, and evaporated to dryness. The desired β-methoxysulfone (**14**) is formed in a 30% yield as shown by nmr. Three successive recrystallizations from dichloromethane–hexane yield pure authentic 5-methoxy-4,4-diphenyl-5,6-dihydrothiopyran-1,1-dioxide (**14**), mp 161–162.5°C, identical in all respects to the solvent addition photolysis product; mixture mp 161°C. The nmr and ir are identical to those of the photolysis product, see above.

*Preparation of authentic 6,6-diphenylbicyclo[3.1.0]-3-hexene-2-one (3c)* (ref. 18)

A solution of 500 mg of 4,4-diphenylcyclohexadienone (**1c**) (4) in 100 mL of anhydrous ether ($2.03 \times 10^{-2}$ *M*) is irradiated during 75 min at 300 nm. The photolysis mixture is separated on 10 preparative tlc plates and eluted with chloroform. This separation yields 270 mg of a mixture of starting dienone (**1c**) (45%) and bicyclic enone **3c** (55%), both having the same $R_f$ under these conditions. Recrystallization from dichloromethane–hexane yields the desired authentic 6,6-diphenylbicyclo[3.1.0]-3-hexene-2-one (**3c**), mp 135–138°C; sublimation at 110°C under 0.15 Torr gives mp 138–139°C (lit. (18) mp 140°C); ir ($CHCl_3$): 3065 and 1690 $cm^{-1}$. The nmr ($CDCl_3$) is less well resolved than that reported and this was the reason for preparing an authentic sample following the published procedure (4); nmr ($CDCl_3$): 7.41 (dd, $J_1 \simeq 2.5$ Hz, $J_2 \simeq 6.3$ Hz, 1H), 7.20 (narrow m, 5H), 7.17 (narrow m, 5H), 5.55 (d, $J \simeq 6.3$ Hz, 1H), 3.24 (dd, $J_1 \simeq 2.5$ Hz, $J_2 \simeq 5$ Hz, 1H), and 2.81 (d, $J \simeq 5$ Hz, 1H). These data are fully in accord with the published structure **3c**.

*Sensitized photolyses in acetone*

*Preliminary qualitative sensitized photolyses of pyran* 1a, *thiopyran* 1d, *and sulfone* 1e

The irradiation in a Pyrex vessel of 10 mg portions of compounds **1a**, **1d**, and **1e**, in 10 mL of anhydrous ether and using 350 nm light, shows that after 5 h of irradiation pyran **1a** and sulfone **1e** do not react and therefore do not absorb light, while thiopyran **1d** reacts and therefore absorbs light under these conditions. In the case of **1a** and **1d** the reaction is monitored by tlc on silica gel using ether–hexane (3:97) as eluent, while in the case of **1e** the eluent was dichloromethane–hexane–acetone (15:9:1).

*Preparative sensitized photolysis of 4,4-diphenylpyran (1a) in acetone*

A solution of 500 mg of title compound **1a** in 400 mL ($5.2 \times 10^{-3}$ *M*) of a 1:1 mixture of acetone and *tert*-butanol is distributed in sixteen 30 mL Pyrex tubes and irradiated during 20 h using 350 nm light. The solvent is evaporated and the residue taken up in 25 mL of anhydrous ether. The later is treated with an ethereal solution of diazomethane, prepared from Diazald (Aldrich), until the evolution of nitrogen has ceased. The excess reagent is destroyed by the addition of 2–3 drops of glacial acetic acid. The resultant ethereal solution is washed with 10% aqueous NaOH, with water, dried over magnesium sulfate, and evaporated to dryness. The residue is separated on 5 preparative tlc plates by eluting twice with ether–hexane (6:94). This procedure allows the recovery of the following two products, which we have reported earlier (1*a*) in the unsensitized photolysis, with the exception that in the present case the mixture of photoacids is obtained as methyl esters. (a) 3,5-Diphenylpentadienal (**8**), mixture of isomers. This material was identical in all respects with the compound which we obtained from the direct photolysis (1*a*) and also with the authentic material (**8**) reported herein (*vide supra*). (b) *trans*-Methyl-3,5-diphenylpent-2-enoate, isolated in the form of a clear oil, identical (tlc, ms, and nmr) with an authentic sample prepared as described below.

*Preparation of authentic* trans*-methyl-3,5-diphenylpent-2-enoate*

A solution of *trans*-ethyl-3,5-diphenylpent-2-enoate (1*a*) (840 mg, 3 mmol) in 10 mL of methanol, previously treated with 25 mg of sodium metal, is heated to reflux over molecular sieves 4A for a period of 24 h. After evaporation of the solvent, the residue is taken up in ether; the latter is washed with water, dried over anhydrous magnesium sulfate, filtered, and evaporated to yield 800 mg (100%) of authentic *trans*-methyl-3,5-diphenylpent-2-enoate in the form of a clear oil; nmr ($CDCl_3$): 7.36 (narrow m, 5H), 7.16 (narrow m, 5H), 6.03 (s, 1H), 3.70 (s, 3H), and 3.53–2.56 (m, AA'MM' portion of a AA'MM'X system, 4H). Mass spectrum: molecular ion at *m/z* 266, loss of $-OCH_3$ at *m/z* 235, loss of $CH_3OH$ at *m/z* 234, loss of $-CO_2CH_3$ at *m/z* 207, tropylium ion at *m/z* 91 (base peak).

*Preparative sensitized photolysis of 4,4-diphenylthiopyran-1,1-dioxide (1e)*

A solution of 500 mg of the title compound **1e** in 400 mL of "Spectrograde" acetone ($3.9 \times 10^{-3}$ *M*) is distributed in sixteen 30 mL Pyrex tubes and irradiated during 20 h using 350 nm light.

The solvent is evaporated and the residue separated on 5 preparative tlc plates eluting with dichloromethane–hexane–acetone (15:9:1) to yield the previously characterized (*vide supra*) 6,6-diphenyl-2-thiabicyclo[3.1.0]-3-hexene-1,1-dioxide (**3***e*) as a solid, mp 210°C (dec.), after recrystallization from dichloromethane–hexane. The nmr, in this case obtained on a Brucker Spectrospin 90 MHz apparatus using a $^1H$ probe and Fourier transform, and the mass spectra were identical in all respects with those of compound **3***e* isolated in the direct photolysis (*vide supra*).

## Acknowledgements

Financial assistance from the Natural Sciences and Engineering Research Council of Canada, le Ministère de l'Education du Québec (FCAC), and Shell Canada Ltd. is gratefully acknowledged.

1. (*a*) D. GRAVEL, C. LEBOEUF, and S. CARON. Can. J. Chem. **55**, 2373 (1977); (*b*) G. LORD, L. FOISY, L. BARIL, D. GRAVEL, and G. DUROCHER. Can. J. Chem. **55**, 4010 (1977).
2. S. S. HIXSON, P. B. MARIANO, and H. E. ZIMMERMAN. Chem. Rev. **73**, 531 (1973).
3. (*a*) H. E. ZIMMERMAN, P. HACKETT, D. F. JUERS, and B. SCHRÖDER. J. Am. Chem. Soc. **89**, 5973 (1967); (*b*) H. E. ZIMMERMAN, P. KACKETT, D. F. JUERS, J. M. MCCALL, and B. SCHRÖDER. J. Am. Chem. Soc. **93**, 3653 (1971).
4. (*a*) H. E. ZIMMERMAN and D. I. SCHUSTER. J. Am. Chem. Soc. **83**, 4486 (1961); (*b*) H. E. ZIMMERMAN and D. I. SCHUSTER. J. Am. Chem. Soc. **84**, 4527 (1962).
5. (*a*) C. DJERASSI and R. R. ENGLE. J. Am. Chem. Soc. **75**, 3838 (1953); (*b*) V. M. PARIKH and J. K. N. JONES. Can. J. Chem. **43**, 3452 (1965).
6. L. L. JACKSON. Ph.D. Thesis, Ohio State University, Columbus, OH (1967), and references cited therein.
7. E. J. COREY and J. I. SHULMAN. J. Am. Chem. Soc. **92**, 5522 (1970).
8. T. M. CRESP, M. V. SARGENT, and P. VOGEL. J. Chem. Soc. Perkin Trans. I, 37 (1974).
9. G. WITTIG and H. REIFF. Angew. Chem. Int. Ed. Engl. **7**, 7 (1968).
10. G. WITTIG and P. SUCHANEK. Tetrahedron, **22**, Supp. 8, I, 347 (1966).
11. E. D. BERGMAN and A. SOLOMONOVICI. Tetrahedron, **27**, 2675 (1971).
12. E. J. COREY, N. W. GILMAN, and B. E. GANEM. J. Am. Chem. Soc. **90**, 5616 (1968).
13. K. NAKAGAWA, H. ONOUE, and K. MIRIAMI. J. Chem. Soc. Chem. Commun. 730 (1966).
14. H. ZIMMERMANOVA and M. PROCKAZKA. Collect. Czech. Chem. Commun. **30**, 286 (1965).
15. J. A. GREEN and L. A. SINGER. Tetrahedron Lett. 5093 (1969).
16. H. NOZAKI, H. TAKAYAMA, S. MORIUTI, and R. NOYORI. Tetrahedron, **24** 3655 (1968).
17. H. E. ZIMMERMAN and R. L. MORSE. J. Am. Chem. Soc. **90**, 954 (1968).
18. H. E. ZIMMERMAN, R. KIESE, J. NASIELSKI, and J. S. SWENTON. J. Am. Chem. Soc. **88**, 4895 (1966).
19. C. C. PRICE and S. OAE. Sulfur bonding. Ronald Press Co., New York, NY. 1962. p. 113.
20. M. O'SULLIVAN and A. C. TESTA. J. Am. Chem. Soc. **92**, 258 (1970).
21. R. F. BORKMAN and D. R. KEARNS. J. Chem. Phys. **44**, 945 (1966).
22. W. G. DAUBEN, W. A. SPITZER, and R. M. BODEN. J. Org. Chem. **36**, 2384 (1971).
23. H. E. ZIMMERMAN and D. R. DIEHL. J. Am. Chem. Soc. **101**, 1841 (1979).
24. T. H. KOCH and J. A. SODERQUIST. J. Am. Chem. Soc. **96**, 5576 (1974).
25. (*a*) H. E. ZIMMERMAN. Adv. Photochem. **1**, 183 (1963); (*b*) K. SCHAFFNER. Adv. Photochem. **4**, 81 (1966); (*c*) P. J. KROPP. *In* Organic photochemistry. Vol. 1. *Edited by* O. L. CHAPMAN. Marcel Dekker, New York, NY. 1967. p. 1.
26. H. E. ZIMMERMAN, D. ARMESTO, M. G. AMEZUA, T. P. GANNETT, and R. P. JOHNSON. J. Am. Chem. Soc. **101**, 6367 (1979), and references cited therein.
27. H. E. ZIMMERMAN, W. T. GRUENBAUM, R. T. KLUN, M. G. STEINMETZ, and T. R. WELTER. J. Chem. Soc. Chem. Commun. 228 (1978).
28. (*a*) H. E. ZIMMERMAN, R. S. GIVENS, and R. M. PAGNI. J. Am. Chem. Soc. **90**, 6069 (1968); (*b*) H. E. ZIMMERMAN and A. C. PRATT. J. Am. Chem. Soc. **92**, 6259 (1970); (*c*) H. E. ZIMMERMAN and A. A. BAUM. J. Am. Chem. Soc. **93**, 3646 (1971).
29. E. HÜCKEL. Z. Phys. **70**, 204 (1931); **76**, 628 (1932); **83**, 632 (1933).
30. H. E. ZIMMERMAN. Acc. Chem. Res. **4**, 272 (1971), and references cited therein.
31. N. T. ANH. Les règles de Woodward–Hoffmann. Ediscience, Paris. 1970. Chapt. IX.
32. (*a*) J. AIHARA. Bull. Chem. Soc. Jpn. **48**, 1501 (1975); (*b*) J. AIHARA. J. Am. Chem. Soc. **98**, 2750 (1976); see also references cited therein for the pioneering work of M. J. S. Dewar and also the related calculations of Hess and Schaad.
33. (*a*) N. T. ANH. Personal communication; (*b*) Lecture given at the 3e Séminaire International sur la Théorie Quantique de la Réactivité Chimique, Paris, October 21, 1977.
34. S. CARON. Mémoire de maîtrise, Université de Montréal, Montréal (Que.), 1973.

Can. J. Chem. Downloaded from www.nrcresearchpress.com by 210.87.254.42 on 09/06/12
For personal use only.

# Optical and Raman spectra of single crystals of perylene-TCNQ charge transfer complexes

A. D. BANDRAUK,[1] K. D. TRUONG,[1] AND C. CARLONE[2]

*Groupe de recherche sur les semiconducteurs et diélectriques, Faculté des Sciences, Université de Sherbrooke, Sherbrooke, P.Q., Canada J1K 2R1*

Received August 12, 1981

A. D. BANDRAUK, K. D. TRUONG, and C. CARLONE. Can. J. Chem. **60**, 588 (1982).

Optical transmission and reflection measurements are reported for the quasi one dimensional solids perylene-TCNQ (P1T1) and (perylene)$_3$-TCNQ (P3T1) in the region from 300 to 1200 nm. Raman spectra of single crystals of both compounds were obtained from 20 to 3000 cm$^{-1}$. With 457.9 nm excitation, combinations and overtones of perylene are observed for the first time. A complete Raman spectrum of perylene and its deuterated homologue including librations is thus obtained via selective resonance enhancement of that molecule.

A. D. BANDRAUK, K. D. TRUONG et C. CARLONE. Can. J. Chem. **60**, 588 (1982).

On rapporte les mesures de transmission optique et de réflexion des solides quasi unidimensionnels pérylène-TCNQ (P1T1) et (perylène)$_3$-TCNQ(P3T1), dans la région allant de 300 à 1200 nm. On a obtenu les spectres Raman d'un monocristal des deux composés de 20 à 3000 cm$^{-1}$. Grâce à une excitation à 457,9 nm, on a pu observé pour la première fois les combinaisons et les harmoniques du pérylène. On a alors obtenu un spectre Raman complet du pérylène et de son homologue deutéré incluant les librations par l'intermédiaire d'une augmentation sélective de la résonance de la molécule.

[Traduit par le journal]

## I. Introduction

Compounds involving the molecule tetracyanoquinodimethane (TCNQ) are of current interest to solid state physicists, chemists, and materials scientists because they exhibit remarkable physical properties (1). In this work we study the optical properties of the compounds formed between TCNQ and perylene. At present, two such compounds are known to exist: perylene-TCNQ and (perylene)$_3$-TCNQ denoted as P1T1 and P3T1 respectively. From X-ray work (2), the former belongs to the class of one dimensional compounds in which the donor (perylene) and acceptor (TCNQ) alternate along one crystal axis in a monoclinic lattice. Some optical properties (3, 4), an infrared spectrum (3) and a partial Raman spectrum (5) of the powders in KBr pellets have been studied. The P3T1 compound has only been recently synthesized (3). Its structure is now known from the X-ray work (6). It seems appropriate to describe its structure as unidimensional chains of units of $P_2T$ intercalated by single perylene molecules in a triclinic lattice, Fig. 1. Some optical, infrared, and partial Raman spectra were reported simultaneously with P1T1 powders (3–5) from KBr measurements.

Both compounds are known to have very low electric conductivities (7, 8) ($< 10^{-9}$ ($\Omega$ cm)$^{-1}$) and are therefore classified as insulators since their ground state is neutral whereas the first electronic excited state is a charge transfer (CT) band (1, 9).

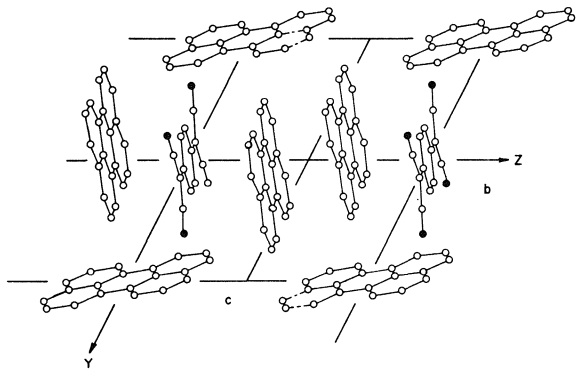


FIG. 1. Disposition of perylene and TCNQ molecules in the *bc* (*zy*) crystal plane of the P3T1 complex.

Since single crystal optical studies were lacking on these two systems, we present here detailed *polarization* transmission and reflection measurements on P1T1 crystals and polarized reflection measurements on P3T1 crystals. This enabled us to establish precisely the polarization of the electronic absorption bands present in these two solid compounds. Finally, the Raman spectra of single crystals of both complexes are also investigated. By working with individual surfaces and at lower temperatures, resolution was significantly increased. We thus report more Raman transitions, including previously undetected overtones and combinations of perylene and deuterated perylene molecules ($P_d$) in P3T1. This second order spectrum is readily excited with a 457.9 nm laser line. It is worth noting that the complexed perylenes do not fluoresce at

[1]Département de chimie.
[2]Département de physique.

0008-4042/82/050588-08$01.00/0
©1982 National Research Council of Canada/Conseil national de recherches du Canada

Can. J. Chem. Downloaded from www.nrcresearchpress.com by 210.87.254.40 on 09/06/12
For personal use only.

Can. J. Chem. Downloaded from www.nrcresearchpress.com by 210.87.254.40 on 09/06/12
For personal use only.

this and other laser frequencies, as opposed to pure solid perylene for which a resonant Raman spectrum is impossible to obtain (10). The present single crystal work allowed the investigation of the Raman spectrum down to $20\,cm^{-1}$, i.e., in the region of molecular librations. This work is partly motivated by the recent discovery that under pressure, neutral organic CT complexes such as those studied here can undergo reversible phase transitions to an ionic ground state (11). The present detailed spectroscopic study of perylene TCNQ complexes should contribute to a better understanding of these and other organic materials.

## II. Experimental

The method of compound preparation and of crystal growth has been given (3, 5).

The P1T1 crystals were needle shaped, between 3 and 10 mm long. For the optical measurements, several crystals were shattered in order to make them thinner. One such fragment, about 50 μ long and about 5 μ thick was used for the transmission and reflection measurements in Figs. 2 and 3.

The P3T1 crystals were much larger, about 2 × 3 × 4 mm. Several of the crystals grew into the shape of the unit cell, i.e. well-defined parallelepipeds. It was impossible to obtain transmission measurements as the crystals were too thick, but we took normal incidence reflection. The neutral perylene band at 450 nm was always found on the two larger surfaces, but never on the smaller one. Similarly, the second order Raman spectrum of the neutral perylene molecule appeared on the same two larger surfaces, but never on the smaller one. The axes were identified this way.

The electronic spectra were taken on Nanometer Spectrometers. In the visible, the Nano Spec/105 had a resolution of 1 nm, and in the infrared the Nano/IONIR had a resolution of 2 nm. The equipment used to obtain the Raman spectrum is standard and has been described previously in our KTCNQ work (12). All spectra were taken at 90° scattering. Excitation was via a Spectra Physics Model 170 Argon in laser. A Jobin-Yvon Ramanor HG2S monochromator equipped with a scrambler was used for spectral analysis.

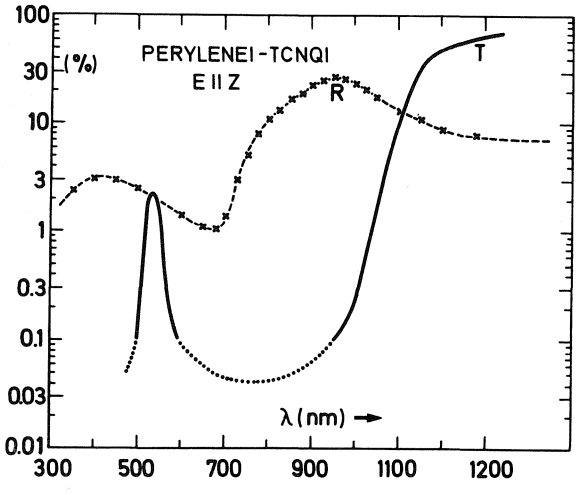


FIG. 2. Polarized transmission (T) and reflection (R) spectra of P1T1 single crystals along the $z$ axis (stacking axis).

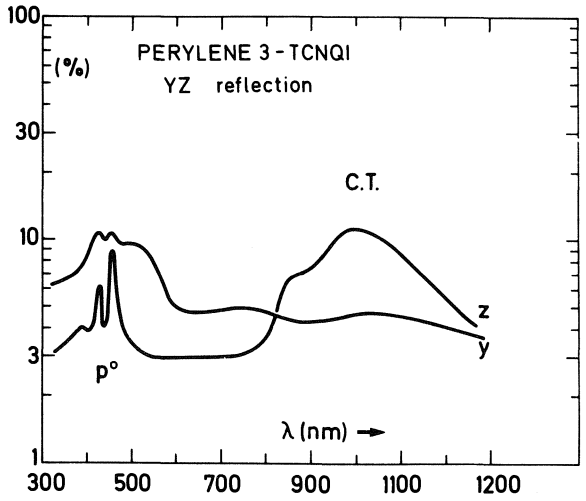


FIG. 3. Polarized reflection spectra of P3T1 single crystals along the $yz$ surface, $z(y)$ is direction of incidence and reflection.

## III. Optical data

In planar molecules, those transitions between states composed of linear combinations of π orbitals perpendicular to the plane of the molecule have their transition moment in the plane of the molecule, and this moment can be resolved into the long axis (LA) or short axis (SA) component. Charge transfer bands, in which the electron hops from the donor planar molecule to the acceptor planar molecule, have their moments perpendicular to the planes. The planes of the molecules are usually not exactly perpendicular to the crystal axis. In P1T1, the angle is 86° (2), so that one can distinguish the nature of the transitions by orienting the exciting field parallel or perpendicular to the axis. Thus, one sees from Fig. 2 where the incoming and outgoing field is parallel to the axis, that there are two parallel electronic bands (with respect to the crystal axis). The reflectivity peaks occur at 410 and 950 nm. The first occurs in the region of the in-plane-polarized electronic absorptions of TCNQ and perylene (13, 14) and probably is a second charge-transfer band. The high reflectivity at 950 nm for the parallel band is established as due to the first CT band in P1T1 since no such absorption occurs in isolated molecules (3). The polarization of this band determines therefore the stacking axis ($z$ axis), perpendicular to the molecular planes.

In the case of P3T1 complex (Fig. 3) we see that the maximum in the CT band is shifted to 1000 nm

Can. J. Chem. Downloaded from www.nrcresearchpress.com by 210.87.254.40 on 09/06/12
For personal use only.

with a weak shoulder at 900 nm. A more complicated structure must be expected since now two perylenes interact with one TCNQ. Again, following the crystal axis designations in Fig. 1, the stacking axis ($z$ axis) for the $P_2T$ units was thus determined for any crystal. The sharp reflection peaks in the 450 nm region are readily attributed to the isolated perylenes, denoted by $P^0$, which are parallel to the $z$ axis and hence perpendicular to the $P_2T$ units (6). Based on these and other surface polarization measurements, we were able to assign appropriate crystal surfaces following the axis notation in Fig. 1. Thus a $yz$ surface contains flat isolated perylenes ($P^0$) and $P_2T$ units perpendicular to it, so that reflection along the $y$ axis (Fig. 3) exhibits the peaks of the free perylenes ($P^0$) excited along their short axis (SA) and a broad spectrum from the $P_2T$ units which are excited along their long axis (LA). In Table 1, we present the various molecular transitions excited depending on the polarization of the exciting and emitted light. These results will be used to analyse the polarized Raman spectra presented below.

## IV. Raman spectra

### *(a) High frequency modes*

We present in Fig. 4 the frequency dependence of the Raman spectrum of intramolecular modes in the region 1000–2200 $cm^{-1}$ for single crystals of P1T1 and $P_d$1T1 where $P_d$ is deuterated perylene. The spectra in both figures correspond to $\rho\rho$ polarization where $\rho$ stands for either $x$ or $y$, (i.e. perpendicular to the stacking axis and therefore essentially in-plane with the molecular axes). Measurements done for $zz$ polarization, (i.e., perpendicular to the molecular axes) gave the same frequency dependence but with much weaker signals as expected. As in the case of our previous powder spectra taken in KBr (5), there is a selective enhancement of the perylene vibrations as one increases the argon laser frequency. Comparing with the KBr results we note that firstly, one obtains better resolution for single crystals. Thus, the 1454 $cm^{-1}$ C=C stretching vibration (15) of TCNQ always appears as a doublet in the single crystals of both compounds. This structure was suppressed in the powder spectra. Furthermore, it was found from the KBr work that the perylene vibrations were much more intense than the TCNQ modes at 457.9 nm excitation. For the isolated crystals this effect is less pronounced, both intensities being comparable at this excitation for the perylene and deuterated perylene complexes. Since this was surface dependent, the KBr results represent an orientational average of the polarization dependent intensities in the single crystal. It is worth noting that the vibrational frequencies are unshifted, in the single crystals and KBr, since the ground state is neutral and very little perturbed by environments.

We made the same measurements on P3T1 and $P_d$3T1 crystals and reached the same conclusion in so far as the first-order spectrum is concerned. Thus in Fig. 5 we represent the frequency dependence of the Raman spectra of the intramolecular modes of P3T1 in single crystals form for $yy$ polarization. From Table 1 and Fig. 1, this polarization corresponds to exciting neutral perylenes $P^0$ along their short axis (SA) and the $P_2T$ units along their long axis (LA). Measurements for $xx$ polarizations showed only TCNQ vibrations, indicating from Table 1 that perylene excitation along their short axis is negligible. Thus the spectra in Fig. 5 correspond essentially to the $P_2T$ units. Since there are twice as many perylenes as compared to P1T1 the resonance effects for perylene are much more important than for the monometric units, Fig. 3. Furthermore, a triplet structure appears well defined for the perylene vibrations at 1299 and 1568 $cm^{-1}$ and a doublet at 1366 $cm^{-1}$. Measurements were done at low temperatures to obtain better resolution for the frequencies reported in Tables 2 and 3. Measurements of scattering with $zz$ polarization corresponding to excitation of $P^0$ (LA) only (Table 1) showed the *same* frequencies and splittings. We thus conclude that the uncomplexed perylene, $P^0$, and the complexed perylene P, are indistinguishable in frequencies as far as Raman spectra are concerned. This is in agreement with the conductivity measurements (8) which indicate a neutral covalent group state for P1T1 and P3T1 compounds. It is worth noting that the deuterated perylene shows an isotopic intensity effect when comparing the equal perylene triplet in Fig. 5*a* to the equivalent unequal triplet in Fig. 5*b* for the deuterated perylene.

Since the P3T1 compound gave a strong resonant Raman spectrum for the perylene as compared to the usual fluorescence of pure perylene in the

TABLE 1. Expected optical transitions from the (perylene)$_3$-TCNQ surfaces*

| Surface | Electric field direction | Transition excited |
|---|---|---|
| $yz$ | $y$ | $P^0$ (SA), T (LA), P (LA) |
| | $z$ | $P^0$ (LA), CT |
| $xz$ | $x$ | T (SA), P (SA) |
| | $z$ | $P^0$ (LA), CT |
| $xy$ | $x$ | T (SA), P (SA) |
| | $y$ | $P^0$ (SA), T (LA), P (LA) |

*$x$, $y$, and $z$ stand for the direction of simultaneous ingoing and outgoing field, SA stands for short axis component, LA for long axis component, $P^0$ corresponds to the free, uncomplexed perylene.

Can. J. Chem. Downloaded from www.nrcresearchpress.com by 210.87.254.40 on 09/06/12
For personal use only.

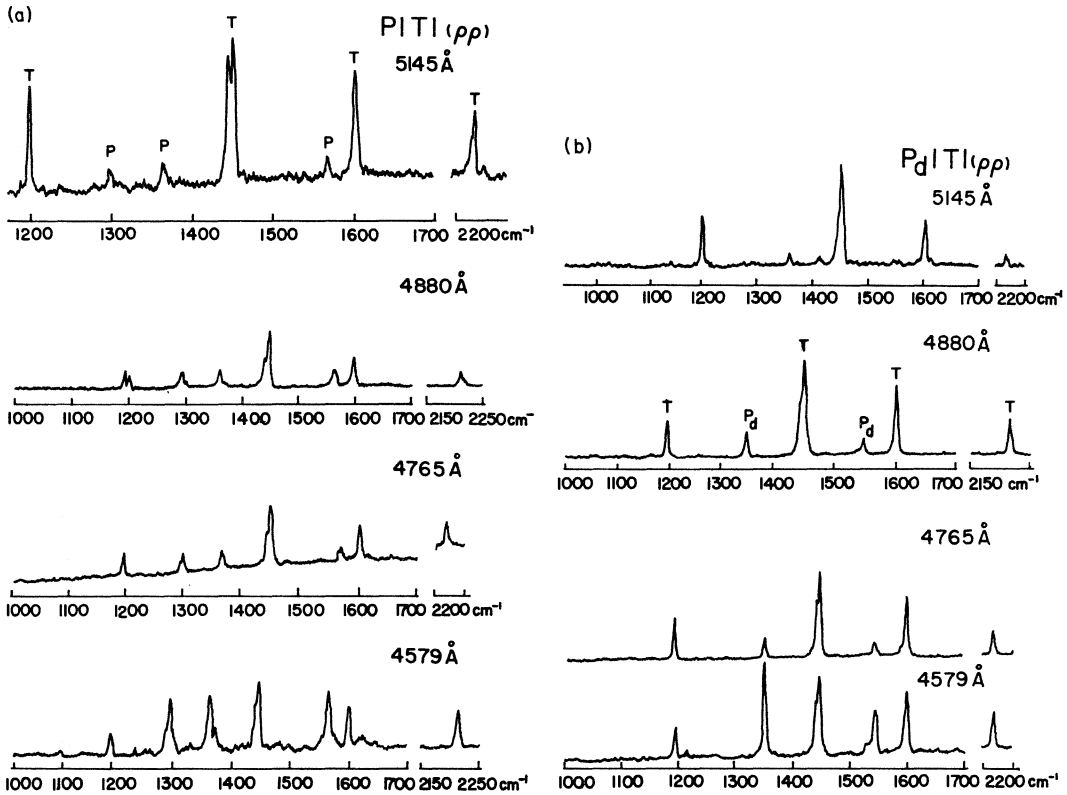


FIG. 4. Raman spectra as a function of laser wavelength for polarization in the plane of the molecules. (*a*) P1T1 crystals; (*b*) $P_d$1T1 ($P_d$ = deuterated perylene) (5 $cm^{-1}$ spectral slit, 3 s time constant, scan 20 $cm^{-1}$/min).

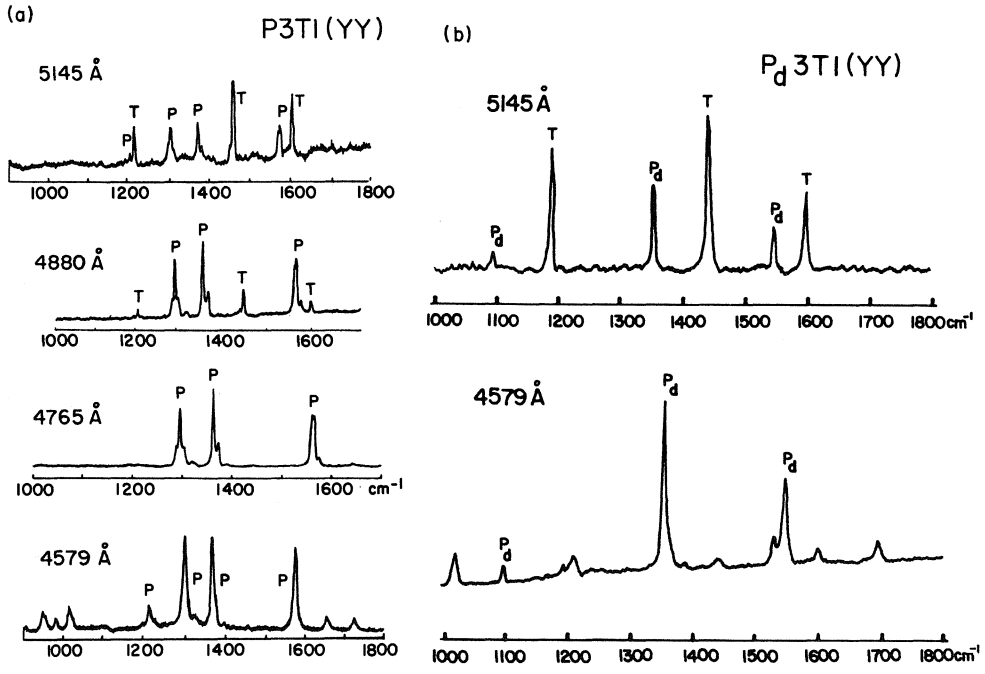


FIG. 5. Raman spectra of (*a*) P3T1 and (*b*) $P_d$3T1 crystals as a function of wavelength for polarization along the *yy* axis, i.e., in the plane of $P_2T$ units (4.5 $cm^{-1}$ spectral slit, 3 s time constant, scan 10 $cm^{-1}$/min).

Can. J. Chem. Downloaded from www.nrcresearchpress.com by 210.87.254.40 on 09/06/12
For personal use only.

TABLE 2. Intramolecular Raman frequencies of P in P3T1 single crystals at 37 K and 457.9 nm excitation (no intensities: < 1%)

| ν ($cm^{-1}$) | Intensity (100% for 1367 $cm^{-1}$) | Assignment |
|---|---|---|
| 336 | | |
| 354 | 47.1 | $A_g$ |
| 426 | 8.6 | $B_{2g}$ (ref. 17) |
| 548 | 32.9 | $A_g$ |
| 708 | 3.3 | (2 × 354) $A_g$ |
| 796 | 6.7 | $A_g$ |
| 898 | | $B_{3g}$ (ref. 17) |
| 950 | 9.5 | $B_{2g}$ (ref. 17) |
| 980 | 8.1 | $A_g$ |
| 1014 | 1.2 | (1367–354) $A_g$ |
| 1097 | | (2 × 548) $A_g$ |
| 1106 | | $A_g$ (ref. 10) |
| 1197 | | |
| 1219 | | (1573–354) $A_g$ |
| 1293 | 25.2 | $A_g$ |
| 1300 | 77.1 | $A_g$ |
| 1308 | 24.8 | $A_g$ |
| 1327 | | |
| 1335 | | |
| 1367 | 100.0 | $A_g$ |
| 1376 | 33.7 | $A_g$ |
| 1396 | | |
| 1568 | 48.1 | $A_g$ |
| 1573 | 66.2 | $A_g$ |
| 1580 | 14.3 | $A_g$ |
| 1602 | | |
| 1654 | 8.1 | (1300 + 354) $A_g$ |
| 1719 | 8.1 | (1367 + 354) $A_g$ |
| 1728 | | (1376 + 354) $A_g$ |
| 1846 | 17.6 | (1300 + 548) $A_g$ |
| 1921 | 44.8 | (1567 + 354) $A_g$ |
| 2112 | 1.6 | (1567 + 548) $A_g$ |
| 2310 | 2.1 | |
| 2593 | 4.2 | (2 × 1296) $A_g$ |
| 2666 | 7.5 | (1300 + 1367) $A_g$ |
| 2731 | 4.3 | (2 × 1367) $A_g$ |
| 2741 | 3.3 | (1367 + 1376) $A_g$ |
| 2866 | 4.9 | (1300 + 1567) $A_g$ |
| 2930 | 7.4 | (1567 + 1367) $A_g$ |
| 2940 | | $A_g$ |
| 2945 | 2.7 | (1567 + 1376) $A_g$ |
| 3140 | 2.4 | (1567 + 1573) $A_g$ |

TABLE 3. Intramolecular Raman frequencies for $P_d$ in $P_d$3T1 single crystals at 37 K and 457.9 nm excitation (no intensities: < 1%)

| ν ($cm^{-1}$) | Intensity | Assignment |
|---|---|---|
| 326 | | |
| 340 | 22.2 | $A_g$ |
| 400 | | $B_{2g}$ |
| 525 | 9.0 | $A_g$ |
| 680 | | (2 × 340) $A_g$ |
| 740 | | (400 + 340) $A_g$ |
| 825 | | $A_g$ |
| 938 | | |
| 1020 | | (1357 − 340) $A_g$ |
| 1096 | 10.7 | |
| 1212 | | (1550 − 340) $A_g$ |
| 1357 | 100.0 | $A_g$ |
| 1386 | | $A_g$ |
| 1532 | 10.7 | $A_g$ |
| 1550 | 22.2 | $A_g$ |
| 1698 | 8.7 | (1357 + 340) $A_g$ |
| 1758 | 1.1 | (1357 + 400) $A_g$ |
| 1872 | 1.3 | (1532 + 340) $A_g$ |
| 1881 | | (1350 + 525) $A_g$ |
| 1890 | 2.4 | (1550 + 340) $A_g$ |
| 1950 | | (1550 + 400) $A_g$ |
| 2032 | | (1357 + (2 × 340)) $A_g$ |
| 2075 | | (1550 + 525) $A_g$ |
| 2095 | | |
| 2192 | | (2 × 1096) |
| *2375* | | (2(1357) − 340) $A_g$ |
| 2452 | 2.4 | (1357 + 1096) $A_g$ |
| *2570* | | (1550 + 1357 − 340) $A_g$ |
| 2716 | 9.6 | (2 × 1357) $A_g$ |
| 2891 | 2.7 | (1532 + 1357) $A_g$ |
| 2908 | 4.9 | (1550 + 1357) $A_g$ |
| 3052 | | (340 + (2 × 1357)) $A_g$ |
| 3082 | | (1550 + 1532) $A_g$ |
| 3100 | | (2 × 1550) $A_g$ |
| 3246 | | (1550 + 1356 + 340) $A_g$ |

457.9 nm excitation region (10), we observed many overtones and combinations of perylene at that excitation frequency. This is the first observation of these frequencies in perylene. We show the complete spectra in Fig. 6, where we show two different temperature measurements to ascertain that the lines in $P_d$3T1 at 1020 and 1212 $cm^{-1}$, Table 3, were actually *difference* vibrations, i.e., $\nu = \nu_1 - \nu_2$ where $\nu_2$ is a low frequency vibration excited thermally with negligible population at low temperatures. This explains the temperature dependence of these two lines and their frequencies. The same phenomenon was observed at 2375 $cm^{-1}$ ((2 × 1537) − 340) and at 2570 $cm^{-1}$ (1550 + 1357 − 340) in Fig. 6*b*. Assignments are made in Tables 2 and 3 from the known frequencies of the now well-established fundamentals of TCNQ (15) and perylene (5, 10). We remark that this overtone spectrum was not obtainable at reasonable laser powers for P1T1 crystals. Furthermore, this second order spectrum was excited *mainly* on the *yz* surface, for which all perylenes have their long axis in the direction of the external field. Finally, no TCNQ second order spectrum was observed at 457.9 nm, indicating once more the high selectivity of this resonance effect.

The sharpening of these broad overtones and combinations as a function of temperature are indicative of a second order spectrum since if the two phonons involved have opposite momentum, each phonon's wave vector spans the entire Bril-

Can. J. Chem. Downloaded from www.nrcresearchpress.com by 210.87.254.40 on 09/06/12
For personal use only.

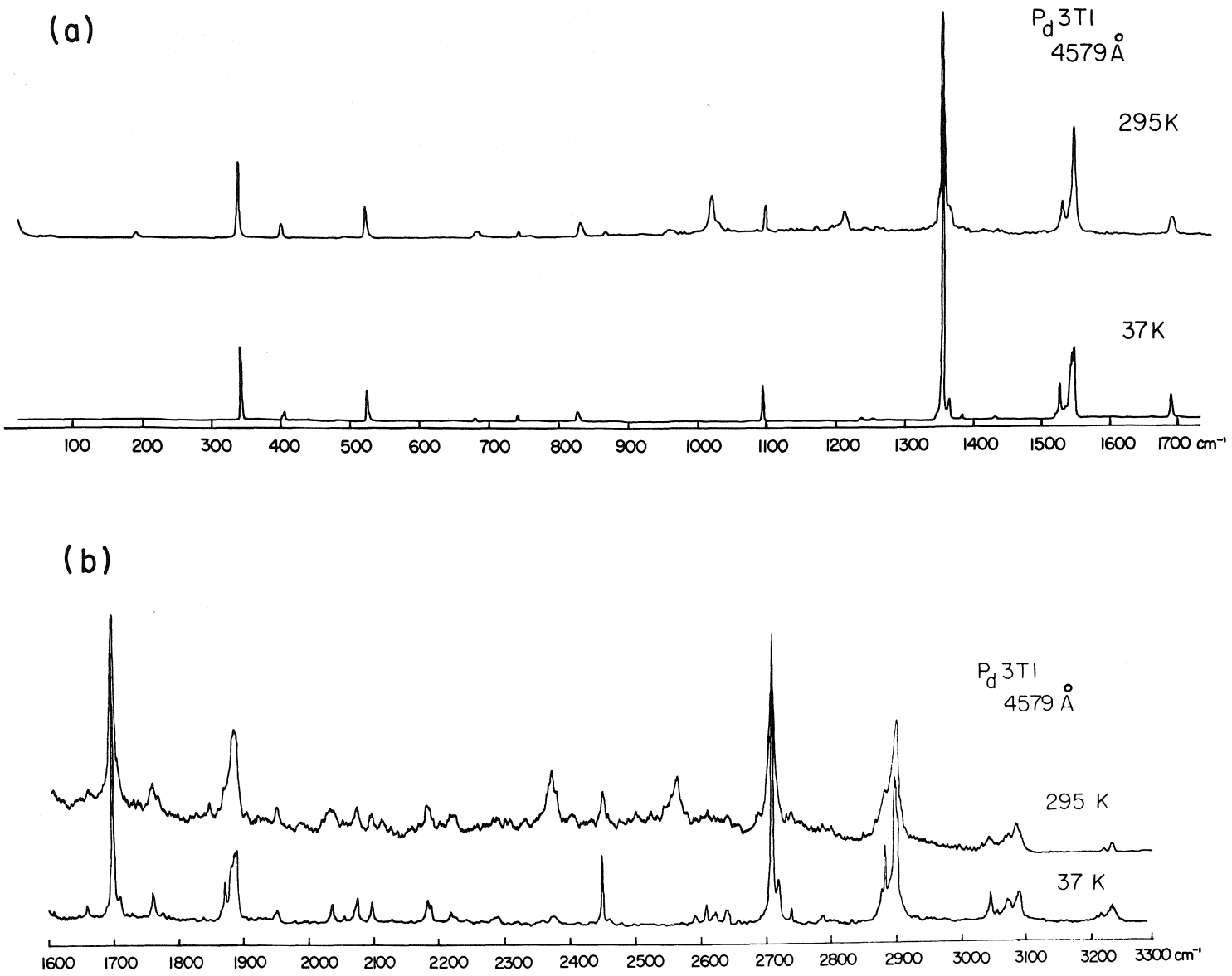


FIG. 6. Temperature dependence of Raman spectra of single crystals of $P_d3T1$; *yz* surface, *z* incident polarization, no analyser (2 $cm^{-1}$ spectral slit, 3 s time constant, scan 10 $cm^{-1}$/min).

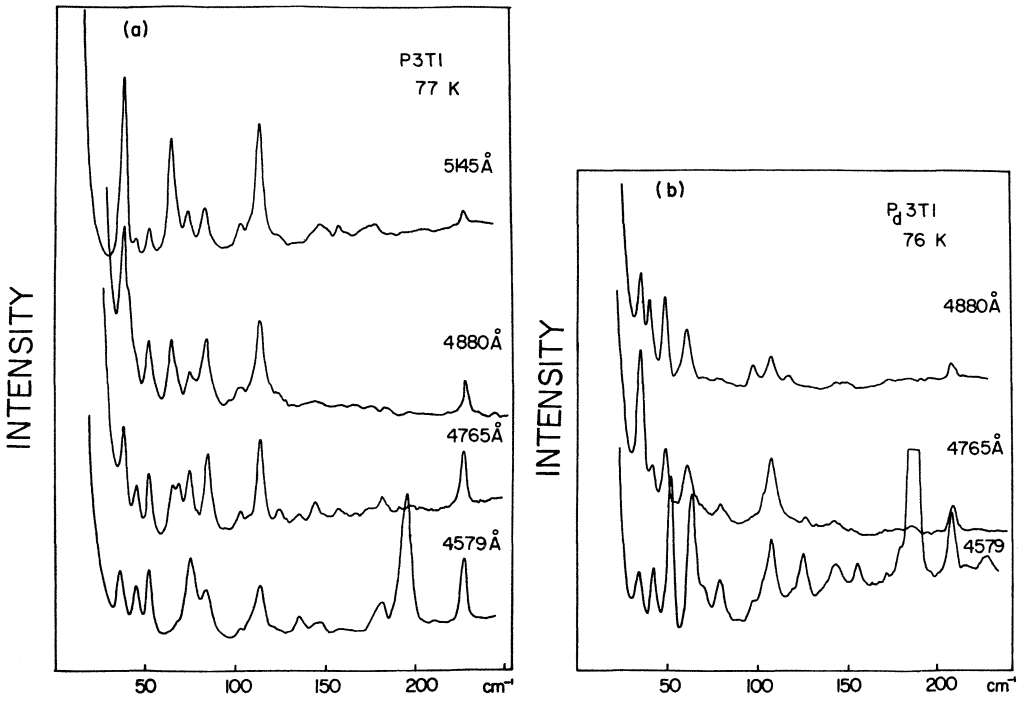


FIG. 7. Frequency dependence of phonons in single crystals of (*a*) P3T1; (*b*) $P_d$3T1; *yz* surface, *z* incident polarization, no analyser (2.5 $cm^{-1}$ spectral slit, 10 s time constant, scan 2 $cm^{-1}$/min).

louin zone (16). Phonon scattering will decrease at lower temperatures, thus inducing sharper lines.

*(b) Low frequency modes*

The selective resonance scattering from the perylene and deuterated perylene molecules at the laser wavelength of 457.9 nm was also used to identify the low frequency modes of these molecules, Figs. 6 and 7. Thus, the sharp lines at 37 and 65 $cm^{-1}$ in both compounds decrease rapidly in intensity with increasing laser frequency and are easily attributed to TCNQ as for solid TCNQ (15). The line at 110 $cm^{-1}$ is weak in both solid perylene (10) and solid TCNQ (15). The most interesting features are the two lines at 195 (189) and 227 (209) $cm^{-1}$ where the frequencies in parentheses correspond to $P_d$. The 195 $cm^{-1}$ was found to be very weak in pure perylene and the other line was not detected (10). Considering the appearance of overtones of the higher frequency modes at 457.9 nm excitation, Fig. 6, we assign these last two lines as overtones and combinations of low frequency modes of perylene, Table 4. The nature of these modes remains to be established. From the crystal structure, Fig. 1, each TCNQ has $C_i$ site symmetry, so that we can expect $3A_g$ librations and no translation in the Raman spectrum for these molecules (15). For the perylene molecules we have two different site symmetries. The free molecules, $P^0$, are at $C_i$ sites and therefore give $3A_g$ librations as TCNQ. The P molecules in the $P_2T$ units are at $C_1$ sites and will give $3A_g$ librations and $3A_g$ translations each. The moments of inertia of the TCNQ molecule are respectively 0.8 ($I_x$), 2.6 ($I_y$), and 3.3 ($I_z$) $\times 10^{-37}$ g $cm^2$ where *z* is perpendicular to the molecular plane. For perylene, these are 1.33 ($I_x$), 3.25 ($I_y$), and 3.99 ($I_z$) $\times 10^{-37}$ g $cm^2$. Thus for isotropic librations, the assignments of three TCNQ librations at 75, 96, and 155 $cm^{-1}$ agrees reasonably with the ratio of the reciprocals of the square roots of the moments, i.e., 1:1.2:2. For perylene, this ratio should be 1:1.1:1.75. The assignments in Table 4 agree qualitatively with this ratio. Due to the similarity in values of the $I_y$ and $I_z$ moments, for T and P, there will be considerable overlap of lines and the assignments cannot be absolute. With this in mind, we present also in Table 4 frequencies of phonons we obtained for pure TCNQ and pyrene-TCNQ crystals. All these low frequency modes belong to TCNQ as no pyrene vibrations were observed at 457.9 nm excitation. Considerable overlap is seen to occur between perylene and TCNQ librations in the 70–85 $cm^{-1}$ region and the 100–110 $cm^{-1}$ regions, so that these modes must be

Can. J. Chem. Downloaded from www.nrcresearchpress.com by 210.87.254.40 on 09/06/12
For personal use only.

TABLE 4. Low frequency modes ($cm^{-1}$) for perylene (P), pyrene ($P_y$) and TCNQ (T)

| 77 K | | 298 K | | |
|---|---|---|---|---|
| P3T1 | $P_d$3T1 | $P_y$T | T | Assignments |
| 38 | 36 | 40 | 40 | Intramolecular $A_g$ (ref. 18) |
| 45 | 42 | | | P libration |
| 50 | 50 | | | P libration |
| 65 | 64 | 65 | 63 | Intramolecular $A_g$* |
| 75 | 73 | 75 | 77 | P and T libration |
| 84 | 81 | | | P libration |
| 103 | 103 | | 104 | T libration |
| 113 | 107 | | | P libration |
| 133 | 126 | | | P combination: $50 + \begin{pmatrix} 84 \\ 81 \end{pmatrix}$ |
| 144 | 144 | 145 | 144 | Intramolecular $A_g$ (refs. 15, 18) |
| 155 | 155 | | 158 | T libration (ref. 15) |
| 180 | 180 | 167 | 169 | Intramolecular $B_{2g}$ (ref. 15) |
| 195† | 189† | | | P difference band $\begin{pmatrix} 548 - 354 \\ 525 - 340 \end{pmatrix}$ |
| 227 | 207 | | | P overtone $\begin{pmatrix} 113 \times 2 \\ 107 \times 2 \end{pmatrix}$ |

*This mode appears at 75 $cm^{-1}$ in gas phase Raman spectra of TCNQ (18).
†This mode is very weak at 37 K and increases with temperature.

strongly coupled. In addition, there may be some mixing with low frequency internal modes as has been suggested recently (18).

## Conclusion

We have presented above optical and Raman spectra of single crystals of P1T1 and P3T1. The optical electronic spectra enabled us to establish the polarization axes in the crystals, so that in the case of P3T1 we were able to infer which perylenes are excited. Raman spectra as a function of excitation frequency show that perylene and its deuterated analogue show selective resonance enhancements at 457.9 nm. In fact, at this wavelength we have obtained for the first time overtone and combination spectra of P and $P_d$ (deuterated). Combinations and overtones were also observed for the librations of perylene in P3T1. Polarization studies of the Raman spectra show that the free perylene and the complexed perylene in P3T1 are indistinguishable in frequencies so that P–T interactions must be very weak. The polarized optical spectra were essential for the differentiation of the excitation of these two different perylenes.

These results should be very useful in studying the pressure dependence of the neutral to ionic phase transition thought to occur in these and similar organic materials. Thus by increasing the pressure along the $P_2T$ stacking axis ($z$ axis, Fig. 1), one should observe a gradual change in the properties of complexed perylenes as opposed to the free molecules. Such measurements are now in progress as well as temperature dependent measurements of the frequencies and widths of the low frequency modes in order to understand the lattice dynamics of these interesting organic materials.

## Acknowledgements

We thank the Natural Sciences and Engineering Research Council of Canada for a special equipment grant to set up the Raman apparatus and also the "Ministère de l'Education-Québec" for operating grants to pursue this work.

1. H. MEIER. Monographs in modern chemistry. Vol. 2. Organic semiconductors. Verlag Chemie, Weinheim. 1974.
2. I. J. TICKLE and C. K. PROUT. J. Chem. Soc. Perkin Trans. II, 720 (1973).
3. K. D. TRUONG and A. D. BANDRAUK. Chem. Phys. Lett. **44**, 232 (1976).
4. M. MICHAUD, C. CARLONE, N. K. HOTA, and J. ZAUHAR. Chem. Phys. **36**, 79 (1979).
5. A. D. BANDRAUK, K. D. TRUONG, H. J. BERNSTEIN, and V. R. SALARES. J. Raman Spectrosc. **8**, 5 (1979).
6. A. W. HANSON. Acta Crystallogr. B**34**, 2339 (1978).
7. P. I. MUNNOCH and J. D. WRIGHT. J. Chem. Soc. Faraday I, 1981 (1976).
8. J. P. FARGES. Private communication.
9. J. B. TORRANCE. Acc. Chem. Res. **12**, 79 (1979).
10. R. M. HOCHSTRASSER and C. A. NYI. J. Chem. Phys. **72**, 2591 (1980).
11. J. B. TORRANCE, J. E. VAZQUEZ, J. J. MAYERLE, and V. Y. LEE. Phys. Rev. Lett. **46**, 253 (1981).
12. K. D. TRUONG and C. CARLONE. Phys. Rev. B**20**, 2238 (1979).
13. R. R. PENNELLY and C. J. ECKHARDT. Chem. Phys. **12**, 89 (1976).
14. K. FUKE, K. KAYA, T. KAJIWARA, and S. NAKAGURA. J. Mol. Spectrosc. **63**, 98 (1976).
15. A. GIRLANDO and C. PECILE. Spectrochim. Acta, **29A**, 1859 (1973).
16. S. P. S. PORTO. Light scattering spectra of solids. *Edited by* G. B. Wright. Springer-Verlag, NY. 1969. p. 1.
17. L. M. BABKOV, M. A. KOVNER, and V. B. PENTS. Opt. Spectrosc. **34**, 354 (1973).
18. C. CARLONE *et al.* J. Chem. Phys. **75**, 3220 (1981).

Can. J. Chem. Downloaded from www.nrcresearchpress.com by 210.87.254.40 on 09/06/12
For personal use only.

# Carbon-13 nuclear magnetic resonance studies of organotellurium compounds. II. Chemical shift trends

RAJ. K. CHADHA AND JACK M. MILLER

*Chemistry Department, Brock University, St. Catharines, Ont., Canada L2S 3A1*

Received July 21, 1981

RAJ. K. CHADHA and JACK M. MILLER. Can. J. Chem. **60**, 596 (1982).

$^{13}C$ nmr chemical shifts are reported for some aromatic and aliphatic tellurium compounds. For a given organic group, the shift of the $C^1$ atom varies in the order $RTeCl_4^- \gtrsim RTeCl_3 > R_2TeCl_2 > R_2Te > R_2Te_2$, as expected from electronegative considerations. The $C^2$ atom experiences an opposite trend while the $C^3$ and $C^4$ atoms of the ring experience smaller changes. The chemical shifts of *para*-substituted aromatic tellurium compounds do not show additivity of contributions from the substituents.

RAJ. K. CHADHA et JACK M. MILLER. Can. J. Chem. **60**, 596 (1982).

On rapporte les déplacements chimiques en rmn du $^{13}C$ de quelques composés aromatiques et aliphatiques du tellure. Pour un groupe organique donné, le déplacement de l'atome $C^1$ varie dans l'ordre $RTeCl_4^- > RTeCl_3 \gtrsim R_2TeCl_2 > R_2Te > R_2Te_2$ que l'on peut prévoir sur la base de considérations d'électronégativité. L'atome $C^2$ subit une tendance inverse alors que les atomes $C^3$ et $C^4$ ne subissent que de faibles changements. Les déplacements chimiques des composés aromatiques du tellure substitués en para ne présentent pas de contributions d'additivité de la part de ces substituants.

[Traduit par le journal]

Can. J. Chem. Downloaded from www.nrcresearchpress.com by 210.87.254.5 on 09/06/12
For personal use only.

## Introduction

$^{13}C$ chemical shift measurements have been found to reflect total carbon atom electron density and, therefore, they have been particularly useful as probes for the study of organometallic compounds. In recent years there have been many publications on $^{13}C$ nmr studies of organometallic compounds (1–4). However, the available data on tellurium compounds are limited compared with those for sulphur and selenium compounds (5–14). We have recently reported our studies on $^{13}C$ nmr spectra of phenyl and *p*-methoxyphenyl tellurium compounds (15). We now report here $^{13}C$ chemical shift data for *p*-phenoxy, *p*-methyl, *p*-chloro, and *p*-bromo phenyl tellurium compounds and some aliphatic tellurium compounds.

## Results and discussion

$^{13}C$ chemical shifts are recorded in Table 1. Assignments of the aromatic signals were based on previous studies (8, 15). The assignments in compounds of the type RR'Te and $RR'TeCl_2$ were made by comparison with assignments in $R_2Te$, $R'_2Te$, and their dichlorides. Where the C signals from R and R' are close together, the assignment should be considered tentative. Assignments of aliphatic signals were made by comparison with assignments in closely related compounds (16).

Examination of Table 1 reveals that the effect of change in tellurium substituent is most strongly observed at $C^1$, to which the tellurium is directly attached, less so at $C^2$ (*ortho*) and $C^4$ (*para*), and least at $C^3$ (*meta*). Plots of the shifts of $C^1$ (tellurium compound) versus $C^1$ (carbon *para* to X in $C_6H_5X$) (Fig. 1) for these compounds show a general linear correlation ($r = 0.99$) with a slope of 1.4. For a given organic substituent, $C^1$ chemical shifts vary according to the number of chlorine atoms attached to tellurium, $RTeCl_4^- \gtrsim RTeCl_3 > R_2Te > R_2Te_2$. On going from tetrachloroaryltellurates to ditellurides, there is a decreasing positive charge on tellurium which corresponds to a decrease in the polarity of the Te—C bond. Magnetic anisotropic effects originating in the tellurium substituents are not expected to vary much in this closely related series; moreover, they are expected to be small (8). Thus the polarity of the C—Te bond appears to have the largest effect on the $C^1$ resonance. $C^1$ chemical shifts of compounds **1**, **2**, **6**, **7**, and **20** are also dependant upon the inductive effect of $—NEt_2$ and $—CH_2COCH_3$.

Figure 1 also shows that there is a linear relationship between $\delta C^2$ (aromatic tellurium compounds) and $\delta C^2(C_6H_5X)$ with a slope of 1.9. For a particular R, $\delta C^2$ changes in the opposite direction, i.e., $RTeCl_4^- \simeq RTeCl_3 < R_2TeCl_2 < R_2Te \simeq R_2Te_2$. A similar curve for $C^4$ signal gives a slope of 1.0.

The substituent shifts ($\Delta\delta^{13}C$ values) are calculated by using $\delta^{13}C$ values for aromatic hydrocarbons obtained on the same instrument under similar experimental conditions and are recorded in parentheses in Table 1. The use of $\Delta\delta^{13}C$ *para* values as a probe for understanding the $\pi$ inductive effects of the substituents in aromatic rings has been very well established (4, 17). The generally upfield shift of $\Delta\delta^{13}C^4$ in the case of diaryl tellurides and ditellurides suggests that $C^4$ in the Te derivative is shielded compared to the aromatic

0008-4042/82/050596-05$01.00/0

©1982 National Research Council of Canada/Conseil national de recherches du Canada

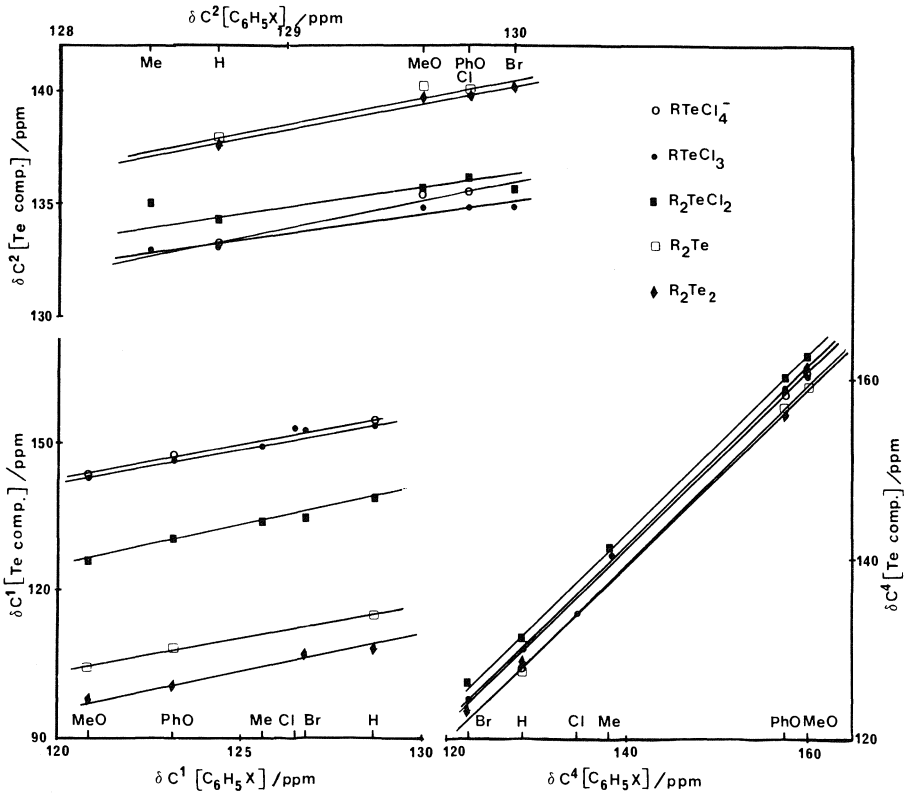


FIG. 1. Plots of $\delta C^n$ ($n$ = 1, 2, 4) for $C_6H_5X$ vs. $\delta C^n$ for organotellurium compounds. Data for X = H and MeO are taken from ref. 18.

hydrocarbon. The downfield shift for $\Delta\delta^{13}C^4$ for organotellurium halides suggests that the tellurium substituents are $\pi$ acceptors in nature.

The deviations of chemical shift values ($\Delta\Delta\delta^{13}C$) from the values calculated according to additivity principles (16) are presented in Table 2. The failure of additivity is clearly evident for $C^1$ and $C^2$, in particular, from this table. Kalabin *et al.* (6) suggested on the basis of the dipole moments and Kerr's constants that the failure of additivity in *p*-substituted aromatic selenium compounds is due to the deviation of the conformation of the molecule from coplanarity, which occurs with a decrease in the strength of the *para*-substituent X. The signs of $\Delta\Delta\delta^{13}C^1$ for different *para*-substituents on the aromatic ring in tellurium compounds (Table 2) are similar to the corresponding substituents in selenium compounds studied by Kalabin *et al.* (6). This similarity between selenium and tellurium compounds suggests that the factor affecting non-additivity in tellurium compounds may also be conformational, though there is not much information available from the dipole moment data (18–21).

For the aliphatic compounds it can be seen that the $C^1$ resonances in the tellurides and ditelluride show an upfield shift whereas in the tellurium halides, it shows a downfield shift, dependant upon the halogens attached to the tellurium atom.

*Coupling constants*

In some of the aliphatic compounds $^{125}$Te satellites are observed. The values lie in the range 127–168 Hz and are of the same order of magnitude as the reported $^1J$ (Te—C) value of 158.5 ± 0.5 Hz in $Me_2Te$ (22) and 118–146 Hz in pentane-2,4-dione tellurium(II) compounds (9). Two bond coupling constants have been observed in some cases and it appears that $^2J$ depends upon steric as well as electronic factors.

## Experimental

$^{13}$C nmr spectra were obtained on a Bruker WP-60FT NMR according to the method described previously (15).

A majority of the compounds studied are described in the literature (23–25). *p*BrPh(Ph)$TeCl_2$ was prepared by refluxing an equimolar mixture of *p*BrPh$TeCl_3$ and $Ph_3SnCl$ in toluene for 2 h. After removing any suspended impurity by filtration, ligroin

Can. J. Chem. Downloaded from www.nrcresearchpress.com by 210.87.254.5 on 09/06/12
For personal use only.

Can. J. Chem. Downloaded from www.nrcresearchpress.com by 210.87.254.5 on 09/06/12
For personal use only.

TABLE 1. Carbon-13 nmr data[a] and substituent shifts[b,c] of organotellurium compounds

| No. | Compound | Solvent | δC¹ | δC² | δC³ | δC⁴ | $^1J$ (C—Te) | $^2J$ (C—Te) | δC$^{others}$ | | | |
|---|---|---|---|---|---|---|---|---|---|---|---|---|
| 1 | $Ph(Et_2N)TeCl_2$ | $CDCl_3$ | 138.1<br>(+ 9.4) | 133.8<br>(+ 5.1) | 129.8<br>(+ 1.1) | 132.3<br>(+ 3.6) | 306.5 | 29.4 | 45.7 | 15.6 | | |
| 2 | $p$MeOPh$(Et_2N)TeCl_2$ | $CDCl_3$ | 127.6<br>(+ 6.8) | 135.8<br>(+ 6.2) | 115.5<br>(+ 1.4) | 162.9<br>(+ 2.9) | 260.0 | 30.3 | 55.7 | 45.7 | 15.6 | |
| 3 | $(p$PhOPh$)_2Te$ | $CDCl_3$ | 107.8<br>(− 16.0) | 140.1<br>(+ 10.3) | 119.9<br>(+ 1.0) | 157.1<br>(− 0.3) | | | 158.0 | 119.5 | 132.6 | 122.1 |
| 4 | $(p$PhOPh$)_2Te_2$ | $CDCl_3$ | 100.3<br>(− 22.9) | 139.8<br>(+ 10.0) | 119.2<br>(+ 0.3) | 156.3<br>(− 1.1) | | 21.1 | 158.0 | 119.2 | 129.7 | 121.2 |
| 5 | $(p$PhOPh$)_2TeCl_2$ | DMSO-$d_6$:<br>$CDCl_3$ (1:4) | 130.1<br>(+ 6.9) | 136.2<br>(+ 6.4) | 119.1<br>(+ 0.2) | 160.1<br>(+ 2.7) | | | 158.2 | 119.4 | 133.4 | 124.8 |
| 6 | $p$PhOPh$(Et_2N)TeCl_2$ | $CDCl_3$ | 129.7<br>(+ 6.5) | 136.0<br>(+ 6.2) | 118.5<br>(− 0.4) | 161.6<br>(+ 4.2) | | | 154.9<br>45.5 | 120.3<br>15.6 | 130.0 | 124.9 |
| 7 | $(p$PhOPh$)(C_4H_8N)TeCl_2$ | DMSO-$d_6$ | 129.0<br>(+ 5.8) | 136.2<br>(+ 6.4) | 117.6<br>(− 1.3) | 160.0<br>(+ 2.6) | | | 155.6<br>45.5 | 120.4<br>24.2 | 131.0 | 125.2 |
| 8 | $(p$PhOPh$)TeCl_3$ | DMSO-$d_6$ | 145.5<br>(+ 22.3) | 134.9<br>(+ 5.1) | 117.0<br>(− 1.9) | 158.6<br>(+ 1.2) | | 22.0 | 155.1 | 119.5 | 130.1 | 124.4 |
| 9 | $[Et_2NH_2]^+[p$PhOPhTe$Cl_4]^-$ | DMSO-$d_6$ | 146.7<br>(+ 23.5) | 135.6<br>(+ 5.8) | 117.0<br>(− 1.9) | 158.3<br>(+ 0.9) | | | 155.4<br>41.3 | 119.6<br>10.9 | 130.2 | 124.5 |
| 10 | $Ph_2(C_4H_4O_2N)TeBr$ | $CDCl_3$ | 137.3<br>(+ 8.6) | 132.0<br>(+ 3.3) | 129.6<br>(+ 0.9) | 131.1<br>(+ 2.4) | | | 178.5 | 29.7 | | |
| 11 | $p$MePh$TeCl_3$ | DMSO-$d_6$<br>$CDCl_3$(1:2) | 148.4<br>(+ 22.8) | 132.9<br>(+ 4.5) | 129.2<br>(0.0) | 141.4<br>(+ 3.6) | 340.0 | 20.2 | 21.2 | | | |
| 12 | $(p$MePh$)_2TeCl_2$ | DMSO-$d_6$<br>$CDCl_3$ (1:3) | 133.0<br>(+ 7.4) | 135.0<br>(+ 6.6) | 129.5<br>(+ 0.3) | 141.5<br>(+ 3.7) | | | | | | |
| 13 | $(p$BrPh$)_2Te_2$ | DMSO-$d_6$:<br>$CDCl_3$ (1:3) | 106.8<br>(− 20.0) | 140.2<br>(+ 10.2) | 132.4<br>(+ 0.9) | 123.0<br>(+ 0.5) | | | | | | |
| 14 | $p$BrPh$TeCl_3$ | DMSO-$d_6$ | 151.7<br>(+ 24.9) | 134.9<br>(+ 4.9) | 131.2<br>(− 0.3) | 124.5<br>(+ 2.0) | | 18.0 | | | | |
| 15 | $p$ClPh$TeCl_3$ | DMSO-$d_6$:<br>$CDCl_3$ (1:1) | 152.3<br>(+ 25.8) | 135.0<br>(+ 5.2) | 128.0<br>(− 0.7) | 134.0<br>(− 0.5) | | | | | | |
| 16 | $p$BrPh<br>Te[d]<br>Ph | $CDCl_3$ | 113.2<br>(− 13.6)<br>114.3<br>(− 14.4) | 139.4<br>(+ 9.4)<br>138.3<br>(+ 9.6) | 132.6<br>(+ 1.1)<br>129.6<br>(+ 0.9) | 122.5<br>(0.0)<br>128.2<br>(− 0.5) | | | | | | |
| 17 | $p$BrPh<br>$TeCl_2$[d]<br>Ph | $CDCl_3$ | 134.2<br>(+ 7.4)<br>135.3<br>(+ 6.6) | 135.3<br>(+ 5.3)<br>133.8<br>(+ 5.1) | 133.2<br>(+ 1.7)<br>130.2<br>(+ 1.5) | 127.1<br>(+ 4.6)<br>132.0<br>(+ 3.3) | | | | | | |

Can. J. Chem. Downloaded from www.nrcresearchpress.com by 210.87.254.5 on 09/06/12
For personal use only.



TABLE 1. (*Concluded*)

| No. | Compound | Solvent | δC[1] | δC[2] | δC[3] | δC[4] | $^1J$ (C—Te) | $^2J$ (C—Te) | δC[others] | | | |
|---|---|---|---|---|---|---|---|---|---|---|---|---|
| **18** | pMeOPh, Te[d], Ph | $CDCl_3$ | 103.3<br>(− 17.5)<br>116.0<br>(− 12.7) | 141.1<br>(+ 11.5)<br>136.4<br>(+ 7.7) | 115.5<br>(+ 1.4)<br>129.3<br>(+ 0.6) | 160.0<br>(0.0)<br>127.2<br>(− 1.5) | | 22.9<br>22.9 | 55.0 | | | |
| **19** | *p*MeOPh, $TeCl_2$[d], Ph | DMSO-$d_6$:<br>$CDCl_3$ (1:1) | 127.0<br>(+ 6.2)<br>138.2<br>(+ 9.5) | 136.1<br>(+ 6.5)<br>134.0<br>(+ 5.3) | 115.0<br>(+ 0.9)<br>129.4<br>(+ 0.7) | 161.2<br>(+ 1.2)<br>131.0<br>(+ 2.3) | | | 55.9 | | | |
| **20** | *p*MeOPh, $TeCl_2$[d], $CH_3COCH_2$ | $CDCl_3$ | 118.3<br>(− 2.5)<br>67.4<br>(+ 38.2) | 135.6<br>(+ 6.0)<br>200.1<br>(− 4.5) | 115.8<br>(+ 1.7)<br>29.8<br>(+ 0.6) | 162.4<br>(+ 2.4) | 301.0<br>165.2 | | 55.6 | | | |
| **21** | Ph, Te[e], Me | $CCl_4$ | 112.5<br>(− 16.6)<br>−16.8<br>(− 14.7) | 136.7<br>(+ 8.0) | 129.0<br>(+ 0.3) | 127.1<br>(− 1.6) | | | | | | |
| **22** | $Me_2Te$ | $CDCl_3$ | −20.2<br>(− 18.1) | | | | 158.8[f] | | | | | |
| **23** | $nBu_2Te$ | $CDCl_3$ | 4.1<br>(− 20.9) | 35.7<br>(+ 15.7) | 29.5<br>(− 0.5) | 13.2<br>(0.0) | | | | | | |
| **24** | $(PhCH_2)_2Te_2$[g] | $CDCl_3$ | 6.6<br>(− 14.8) | | | | | | 141.5 | 128.2 | 127.9 | 126.0 |
| **25** | $Me_2TeI_2$ | DMSO-$d_6$ | 19.1<br>(+ 21.2) | | | | 149.6 | | | | | |
| **26** | $Me_2TeI_4$ | $CDCl_3$ | 20.5<br>(+ 22.6) | | | | | | | | | |
| **27** | $Et_2TeBr_2$ | $CDCl_3$ | 39.1<br>(+ 33.2) | 10.3<br>(+ 4.4) | | | 167.9 | | | | | |
| **28** | $Et_2TeI_2$ | $CDCl_3$ | 34.9<br>(+ 29.0) | 11.3<br>(+ 5.4) | | | 127.6 | | | | | |
| **29** | $Et_2TeI_4$ | $CDCl_3$ | 34.9<br>(+ 29.0) | 11.8<br>(+ 5.9) | | | | | | | | |
| **30** | $Et_3Te^+Br^-$ | $CDCl_3$ | 19.3<br>(+ 13.4) | 11.0<br>(+ 5.1) | | | 145.9 | 18.4 | | | | |

[a]Chemical shift values in ppm, coupling constants in Hz.
[b]In parentheses.
[c]A negative value indicates a upfield shift.
[d]Data from R and R′ given in respective lines.
[e]Taken from ref. 7.
[f]Literature (22) value is 158.5 ± 0.5 Hz.
[g]Taken from ref. 27.

TABLE 2. Deviations of the chemical shift values from the calculated values[a], $\Delta\Delta\delta^{13}C$

| Compound | $\Delta\Delta\delta^{13}C$ | | | |
|---|---|---|---|---|
| | $C^1$ | $C^2$ | $C^3$ | $C^4$ |
| **2** | − 2.6 | + 1.1 | + 0.3 | − 0.7 |
| **3** | − 2.0 | + 1.1 | + 0.3 | + 0.7 |
| **4** | − 2.2 | + 1.1 | − 0.2 | − 0.4 |
| **5** | − 2.4 | + 0.8 | − 0.3 | + 0.5 |
| **6** | − 3.0 | + 1.1 | − 1.5 | + 0.6 |
| **8** | − 1.5 | + 0.8 | − 1.7 | − 0.1 |
| **9** | − 1.2 | + 1.3 | − 1.0 | − 0.2 |
| **11** | − 1.0 | + 0.2 | + 0.2 | + 2.2 |
| **12** | − 1.9 | + 1.0 | − 0.2 | + 1.5 |
| **13** | + 0.7 | + 1.3 | + 0.4 | + 1.2 |
| **14** | + 1.1 | + 0.6 | − 0.1 | + 0.7 |
| **15** | + 2.0 | + 0.9 | − 0.5 | − 1.8 |
| **16** | + 0.4 | + 0.2 | + 0.4 | + 1.0 |
| | − 0.4 | + 0.4 | + 0.2 | + 0.5 |
| **17** | − 1.9 | − 0.3 | + 1.2 | + 2.4 |
| | − 2.7 | − 0.5 | + 1.0 | + 1.1 |
| **18** | − 3.5 | + 2.3 | + 0.7 | + 1.0 |
| | + 1.3 | − 1.5 | − 0.1 | − 0.5 |
| **19** | − 3.1 | + 0.9 | + 0.4 | − 1.0 |
| | + 0.2 | − 0.3 | + 0.2 | + 0.1 |
| **21** | − 2.8 | − 1.2 | − 0.4 | − 0.6 |

[a]Calculated by subtracting $\Delta\delta^{13}C$ values for phenyl compound (15) from $\Delta\delta^{13}C$ values for compounds **2** to **21**.

(30–60°C) was added, and white needles precipitated. The product was filtered, dried, and recrystallised from $CH_2Cl_2$ to give *p*BrPh(Ph)$TeCl_2$, mp 142–143°C (20), yield 85%. *p*MeOPh(Ph)$TeCl_2$ was obtained in a similar manner from *p*MeOPh$TeCl_3$ and $Ph_3SnCl$, mp 113–144°C, lit. 114–115°C (26). These unsymmetric RR′$TeCl_2$ compounds were reduced with $N_2H_4$/EtOH (25) and recrystallised from $CH_3OH$. *p*BrPh(Ph)Te, mp 67–68°C, lit. 68°C (19), *p*MeOPh(Ph)Te, mp 60–61°C, lit. 61°C (26).

Hydrazine reduction of aryl(dialkylamino)tellurium dichlorides gave diaryl ditellurides instead of aryl(dialkylamino) tellurides.

## Acknowledgement

The authors wish to thank the Natural Sciences and Engineering Research Council of Canada for financial support.

1. G. A. GANSOW and W. D. VERNON. Topics in carbon-13 nmr spectroscopy. Vol. 2. Wiley, New York. NY. 1976.
2. B. E. MANN. Adv. Organomet Chem. **12**, 135 (1974).
3. V. S. PETROSYAN. Prog. Nucl. Magn. Reson. Spectrosc. **11**, 115 (1975).
4. G. C. LEVY, R. L. LICHTER, and G. L. NELSON. Carbon-13 nuclear magnetic resonance spectroscopy. 2nd ed. John Wiley and Sons, New York, NY. 1980. p. 182.
5. P. GRANGER, S. CHAPELLE, and C. PAULMIER. Org. Magn. Res. **14**, 240 (1980).
6. G. A. KALABIN, D. F. KUSHNAREV, G. A. CHMUTOVA, and L. V. KASHURNIKOVA. Zh. Org. Khim. **15**, 24 (1979).
7. G. LLABRES, M. BAIWIR, L. CHRISTIAENS, J. DENOEL, L. LAITEM, and J. L. PIETTE. Can. J. Chem. **56**, 2008 (1977).
8. A. FORCHINONI, V. GALASSO, K. J. IRGOLIC, and G. C. PAPPALARDO. J. Organomet. **135**, 327 (1977).
9. J. C. DEWAN, W. B. JENNINGS, J. SILVER, and M. S. TOLLEY. Org. Magn. Res. **11**, 449 (1978).
10. M. L. MARTIN, M. TRIERWEILER, V. GALASSO, F. FRINGUELLI, and A. TATICCHI. J. Magn. Res. **12**, 155 (1981).
11. G. LLABRES, M. BAIWIR, L. CHRISTIAENS, and J. L. PIETTE. Bull. Soc. R. Sci. Liege. **49**, 178 (1980).
12. L. LAITEM, L. CHRISTIAENS, and M. RENSON. Org. Magn. Res. **13**, 319 (1980).
13. G. LLABRES, M. BAIWIR, L. CHRISTIAENS, and J. L. PIETTE. J. Mol. Struct. **70**, 231 (1981).
14. G. V. FAZAKERLEY and M. CELOTTI. J. Magn. Res. **33**, 219 (1979).
15. R. K. CHADHA and J. M. MILLER. J. Chem. Soc. Dalton Trans. In press.
16. J. B. STOTHERS. Carbon-13 nmr spectroscopy. Academic Press, New York, NY. 1972.
17. F. EWING. Org. Magn. Res. **12**, 499 (1979).
18. G. C. PAPPALARDO, S. GRUTTADAURIA, and K. J. IRGOLIC. J. Organomet. Chem. **97**, 173 (1975).
19. I. D. SADEKOV, A. Y. BUSHKOV, and V. I. MINKIN. Zh. Obshch. Khim. **47**, 631 (1977).
20. I. D. SADEKOV, A. Y. BUSHKOV, V. L. PAVLOVA, V. S. YUREVA, and V. I. MINKIN. Zh. Obshch. Khim. **47**, 1305 (1977).
21. R. M. MINAEV, I. D. SADEKOV, and M. I. MINKIN. Zh. Obshch. Khim. **47**, 2011 (1977).
22. H. DREESKAMP and G. PFISTERER. Mol. Phys. **14**, 295 (1968).
23. K. J. IRGOLIC and R. A. ZINGARO. Organometallic reactions. Vol. 2, 117 (1970).
24. J. M. MILLER and R. K. CHADHA. J. Organomet. Chem. **216**, 177 (1981).
25. J. BERGMAN. Tetrahedron, **28**, 3323 (1972).
26. H. RHEINBOLDT and G. VINCENTINI. Chem. Ber. **89**, 624 (1956).
27. H. K. SPENCER and M. P. CAVA. J. Org. Chem. **42**, 2937 (1977).

Can. J. Chem. Downloaded from www.nrcresearchpress.com by 210.87.254.5 on 09/06/12
For personal use only.

# Excited states of acrolein: *ab initio* model studies on α,β-unsaturated carbonyl compounds

KATHERINE VALENTA AND FRIEDRICH GREIN

*Department of Chemistry, University of New Brunswick, Fredericton, N.B., Canada E3B 6E2*

Received August 11, 1981

KATHERINE VALENTA and FRIEDRICH GREIN. Can. J. Chem. **60**, 601 (1982).

As an explanation of the stereochemistry of photoaddition between α,β-unsaturated carbonyl compounds and olefins, Wiesner suggested that the excited state of the α,β-unsaturated carbonyl compound is pyramidal at the β-carbon. It is shown by *ab initio* SCF and CI studies that for acrolein in the $^1n\pi^*$, $^3n\pi^*$, and $^3\pi\pi^*$ excited states the β-carbon remains planar. In addition, vertical excitation energies for the $^1n\pi^*$ and $^1\pi\pi^*$, and adiabatic excitation energies for the $^1n\pi^*$ and $^3n\pi^*$ states of *trans*-acrolein have been calculated.

KATHERINE VALENTA et FRIEDRICH GREIN. Can. J. Chem. **60**, 601 (1982).

Pour expliquer la stéréochimie de l'addition photochimique des composés carbonylés α,β-insaturés sur des oléfines, Wiesner suggère que l'état excité du composé carbonylé α,β-insaturé est pyramidal au niveau du carbone en β. On montre par des calculs *ab initio* SCF et des études CI que dans les états excités $^1n\pi^*$ et $^3\pi\pi^*$ de l'acroléine, le carbone β reste plan. De plus, on a calculé les énergies d'excitation verticale des états $^1n\pi^*$ et $^1\pi\pi^*$ et les énergies d'excitation adiabatique des états $^1n\pi^*$ et $^3n\pi^*$ de l'acroléine *trans*.

[Traduit par le journal]

## 1. Introduction

In the photoaddition of allene and other olefins to α,β-unsaturated carbonyl compounds for the synthesis of polycyclic bridged natural products examples are found where the allene approaches from the more sterically hindered side of the enone. In order to explain this, Wiesner (1) proposed a general rule for predicting the stereochemistry of such photoadducts. He postulated that the excited state of the enone is the controlling factor of the reaction, and that in this excited state the β-carbon inverts to select the more stable configuration. Since then, other studies were found in agreement with this rule (2, 3).

At the basis of Wiesner's empirical rule is a consideration of the change in charge distribution of α,β-unsaturated carbonyl compounds upon excitation. According to Corey (4), the lowest excited singlet state ($^1n\pi^*$) is positively charged at the α-carbon, and negatively at the β-carbon. Placing the negative charge of the β-carbon into an orbital suggests a pyramidal structure of the β-carbon in the excited state (reaction [1]). The orbital accommodating the negative charge is directed upwards or downwards depending on steric effects.

If the geometry of the excited state is not the controlling factor of the reaction, then the configuration controlling species would have to be found in the reaction subsequent to the excitation. Corey *et al.* (4) and de Mayo and co-workers (5) postulated that in this reaction a π-complex is formed between the excited carbonyl compound and the olefin. This complex then becomes a diradical which cyclizes to form the product.

[1] 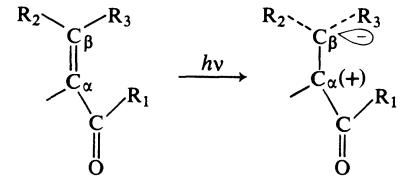


Photoexcitation from the ground state of α,β-unsaturated carbonyl compounds will initially lead to the $^1n\pi^*$ excited state (see ref. 6 for acrolein, ref. 4 for other compounds). Since rapid intersystem crossover may occur to either $^3n\pi^*$ or $^3\pi\pi^*$ (4, 6, 7), the geometries of these two excited states are also of interest.

In this study, theoretical methods are used in order to determine whether or not the above-mentioned excited states of α,β-unsaturated carbonyl compounds are pyramidal at the β-position. We have restricted ourselves to the smallest such compound, acrolein (Fig. 1).

In its ground state acrolein is planar, with the *trans*-isomer more stable than the *cis*-isomer. The singlet $n\pi^*$ transition has been observed at 3860 Å, and is well characterized (8, 9). In both the ground state and the $^1n\pi^*$ state, the out-of-plane vibrational modes $\nu_{15}$ and $\nu_{16}$ have been assigned, the

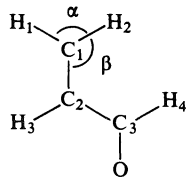


FIG. 1. Schematic diagram of *trans*-acrolein.

0008-4042/82/050601-06$01.00/0

©1982 National Research Council of Canada/Conseil national de recherches du Canada

Can. J. Chem. Downloaded from www.nrcresearchpress.com by 210.87.254.5 on 09/06/12
For personal use only.

Can. J. Chem. Downloaded from www.nrcresearchpress.com by 210.87.254.5 on 09/06/12
For personal use only.

former being the formyl CH wag, the latter being the vinyl $CH_2$ wag. Brand and Williamson (8) found that $\nu_{15}'/\nu_{15}'' = 644/980$, and $\nu_{16}'/\nu_{16}'' = 582/959$. So upon excitation, the vinyl hydrogen wagging mode decreases more than the formyl wagging mode, which is quite unusual. The corresponding potential curve is broadened or may even have a double minimum, in which case the vinyl out-of-plane configuration of the $^1n\pi^*$ state would be more stable.

A weak system at 4060 Å has recently been assigned to correspond to the transition from the ground state of *cis*-acrolein to the singlet $n\pi^*$ state of *cis*-acrolein (10). Similarly, at 4322 Å a transition to $^3n\pi^*$ of *cis*-acrolein has been observed (11). In the $n\pi^*$ excited states, the *cis*-isomer of acrolein appears to be more stable than the *trans*-isomer.

Becker *et al.* (6) suggested that in the lowest $\pi\pi^*$ triplet state twisting about the carbon–carbon double bond may occur, leading to intersystem crossover to the ground state. Their semiempirical PPP-CI calculations indicated that $^3\pi\pi^*$ is most stable at a 90° twist angle. This was subsequently confirmed by minimal basis *ab initio* SCF calculations of Devaquet and co-workers (12, 13). Dykstra (14) considered the possibility that the $^3\pi\pi^*$ state of acrolein is rotated about the CC single bond, with a minimum energy between the *cis* and *trans* form. However, due to the mixing of $\pi\pi^*$ with $n\pi^*$ for nonplanar acrolein, and in the absence of CI calculations, no definite conclusions could be reached.

The out-of-plane motion of the hydrogen atom at the α-carbon was studied by Devaquet (13), and was found to increase the energy. However, it was noted that for cyclic systems (such as cyclohexenone) a smaller ethylenic twist accompanied by an out-of-plane motion of the hydrogen attached to the α-carbon might stabilize the system in $^3\pi\pi^*$.

In summary, there is no conclusive spectroscopic or theoretical evidence for α,β-unsaturated carbonyl compounds to be pyramidal at the β-carbon in any of the excited states. However, only very limited studies have been performed in the past, and more work needs to be done.

In the present work, our ultimate goal is the study of the pyramidal nonplanarity at the β-position of the singlet $n\pi^*$, triplet $n\pi^*$, and triplet $\pi\pi^*$ states of *trans*-acrolein. In addition, we obtained vertical excitation energies for the singlet $n\pi^*$ and $\pi\pi^*$ states, optimized the geometries of the planar $^1n\pi^*$ and $^3n\pi^*$ species of *trans*-acrolein, and obtained the adiabatic excitation energies of these states.

## 2. Results and Discussion

Self-consistent-field (SCF) calculations were performed in the restricted Hartree–Fock formalism, using the (9*s*5*p*/4*s*2*p*) contracted Gaussian basis set according to Dunning (15) for C and O, and the (4*s*/2*s*) basis for H. The configuration-interaction (CI) method of Buenker and Peyerimhoff (16–18) was used. In this method, single and double excitations of a set of reference configurations are generated, and those configurations are selected for the final CI diagonalization which give energy contributions in excess of a properly chosen threshold value $T$. Only CI energy values extrapolated to $T \rightarrow 0$ will be given.

### *A. Vertical excitation energies of singlet states*

CI calculations at the experimental ground state geometry of acrolein ($R_{C_1C_2} = 1.36$ Å, $R_{C_2C_3} = 1.46$ Å, $R_{C_3O} = 1.22$ Å, 120° bond angles (19) were used; a more recent and more accurate ground state geometry (20) is $R_{C_1C_2} = 1.345$ Å, $R_{C_2C_3} = 1.470$ Å, $R_{C_3O} = 1.219$ Å, $R_{C-H} = 1.084$–$1.108$ Å, $H_1C_1H_2 = 118°35'$, $H_1C_1C_2 = 121°27'$, $H_2C_1C_2 = 119°58'$, $C_1C_2H_3 = 122°50'$, $C_1C_2C_3 = 119°50'$, $C_2C_3H_4 = 115°6'$, $C_2C_3O = 123°16'$) were performed for the $^1A'$ ground state, and the $^1A''(n\pi^*)$ and $^1A'(\pi\pi^*)$ excited states. Ground state SCF orbitals were used, with the ground state SCF energy being −190.6949 hartree. The four lowest energy orbitals $1a'$–$4a'$ were "frozen", and the four highest orbitals $37a'$–$40a'$ were excluded from any possible occupancy. The selection threshold was 50 μhartree. Here, and in all following CI calculations, configurations with a coefficient greater than 0.15(absolute) were included as reference (or main) configurations.

The results are given in Table 1. The vertical excitation energy for $^1n\pi^*$ is 4.37 eV, and for $^1\pi\pi^*$ 7.53 eV. The experimental values are 6.5 eV for the vertical excitation energy to $^1\pi\pi^*$ (21, 22). For $^1n\pi^*$, no experimental value could be found. Other theoretical values for $^1n\pi^*$, all obtained by SCF methods, are 4.44 eV (23) and 2.77 eV (14). A recent theoretical CI value for the vertical excitation energy to $^1\pi\pi^*$ is 7.52 eV (24), in close agreement with our results.

Vertical excitation energies to $^3n\pi^*$ and $^3\pi\pi^*$ were calculated by Lucchese *et al.* (25), using double ζ basis sets and CI methods. Their results are 3.38 eV for $^3n\pi^*$ and 3.97 eV for $^3\pi\pi^*$.

### *B. SCF geometry optimizations on planar $^1n\pi^*$ and $^3n\pi^*$ states*

Both the singlet and the triplet $n\pi^*$ states can be dealt with by SCF methods provided the molecule

TABLE 1. Vertical excitation energies of acrolein

| Root | State | # Mains | Gen/select[a] | $E_{CI}$ (hartree) | $\Delta E$(eV)[b] |
|---|---|---|---|---|---|
| 1 | $^1A'$(gs) | 9 | 497768/2346 | −191.0572 | |
| 2 | $^1A'(\pi\pi^*)$ | | | −190.7805 | 7.53 |
| 1 | $^1A''(n\pi^*)$ | 3 | 182105/1425 | −190.8965 | 4.37 |

[a]Number of configurations generated/selected.
[b]Vertical excitation energy from ground state.

TABLE 2. Optimized excited state geometries of *trans*-acrolein[a]

| State | $R_{C_1-C_2}$ | $R_{C_2-C_3}$ | $R_{C_3-O}$ |
|---|---|---|---|
| $^1A''(n\pi^*)$ | 1.45 | 1.34 | 1.39 |
| Ref. 14 | 1.35 | 1.43 | 1.39 |
| Expt.[b] | 1.46 | 1.35 | 1.32 |
| $^3A''(n\pi^*)$ | 1.44 | 1.35 | 1.38 |
| Ref. 14 | 1.34 | 1.44 | 1.37 |

[a]All bond lengths in Å, 120° bond angles.
[b]Reference 9.

is planar. Cyclic geometry optimizations on *trans*-acrolein in the $^1n\pi^*$ and $^3n\pi^*$ states were performed, varying the carbon–carbon and carbon–oxygen distances, but fixing the carbon–hydrogen distances at 1.09 Å, and all bond angles at 120°.

The results are given in Table 2. The minimized SCF energies are −109.6275 hartree for $^1n\pi^*$, and −190.6295 hartree for $^3n\pi^*$. A reversal of the C—C and C—O bond characters with respect to the ground state can be noticed. For both states the terminal C—C bond changes into a single bond, whereas the intermediate C—C bond becomes a double bond. Our results for $^1n\pi^*$ are in good agreement with experimental results (9) (Table 2), except for the C—O distance which is optimized to be much larger than experimental. However, according to Brand and Williamson (8), the experimental C—O distance may be as high as 1.35 Å.

Another experimental confirmation of the single bond – double bond interchange in the excited state is the barrier to internal rotation as reported by Brand and Williamson (8). For the $^1n\pi^*$ excited state, the barrier to rotation about the terminal C—C bond is 2700 $cm^{-1}$, whereas it is 5300 $cm^{-1}$ for the central C—C bond.

Our findings differ significantly from those of Dykstra (14) (also in Table 2), who obtained little change in the carbon–carbon distances upon excitation to the $n\pi^*$ states. His CO distance, however, is similar to ours. Dykstra used the same basis set as used in this work (probably scaled, since his SCF energies are lower), but he used bond angles that were optimized for the ground state ($C_1C_2C_3$ = 123.4°, $C_2C_3O$ = 121.4°, $H_1C_1H_2$ = 116.5°, $C_1C_2H_3$ = 116.3°, $C_2C_3H_4$ = 116.2°, see Fig. 1) instead of our uniform 120° bond angles. Dykstra's geometry parameters gave a higher energy than ours when checking for the discrepancy in results (using our basis set).

### C. *Adiabatic $n\pi^*$ excitation energies of planar trans-acrolein*

CI calculations were performed at the optimized geometries of $^1n\pi^*$ and $^3n\pi^*$, using the respective SCF molecular orbitals (MO). The selection threshold was again 50 μh, and the active orbital space the same as before.

SCF and CI adiabatic excitation energies are given in Table 3. The CI values are in reasonable agreement with experimental values for the transitions to excited states of *trans*-acrolein (since *cis*-acrolein in $^1n\pi^*$ and $^3n\pi^*$ is at lower energy than *trans*-acrolein, the cited excitation energies are not fully adiabatic). Dykstra (14), by SCF methods, obtained 2.01 eV for $^1n\pi^*$ and 1.81 eV for $^3n\pi^*$, whereas Lucchese *et al.* (25) obtained 2.68 eV for the adiabatic transition to $^3n\pi^*$, using Dykstra's optimized geometry that was discussed earlier. The same authors obtained a CI value of 2.86 eV for the adiabatic transition energy to $^3\pi\pi^*$.

### D. *Nonplanar methylene group studies*

In this section, the main problem of this paper will be addressed. Is acrolein (and other α,β-unsaturated carbonyl compounds) in any one of the $n\pi^*$ or $\pi\pi^*$ excited states pyramidal at the β-position? The two methylene hydrogens $H_1$ and $H_2$ will be moved below the plane of the molecule towards a tetrahedral arrangement. Three deformation angles were considered, starting with the planar geometry and going partially to a tetrahedral structure.

Due to a reduction in the symmetry of nonplanar acrolein, from $C_s$ to $C_1$, the SCF method is only capable of handling the lowest singlet state (ground state) and the lowest triplet state, which should be mainly $^3n\pi^*$, but has some admixture of $^3\pi\pi^*$. For simplicity we continue calling this state $^3n\pi^*$.

SCF and CI studies on the out-of-plane motions of the methylene group were conducted in the following way: The $H_1C_1H_2$ angle was reduced gradually from 120° to 115°, in such a way that α

Can. J. Chem. Downloaded from www.nrcresearchpress.com by 210.87.254.5 on 09/06/12
For personal use only.

TABLE 3. Adiabatic excitation energies of *trans*-acrolein

| State | #Mains | Gen/select[a] | $E_{SCF}$ (hartree) | $E_{CI}$ (hartree) | $\Delta E_{SCF}$ (eV) | $\Delta E_{CI}$ (eV) | $\Delta E_{expt}$[b] (eV) |
|---|---|---|---|---|---|---|---|
| $^3A''(n\pi^*)$ | 2 | 419012/1582 | −190.6295 | −190.9500 | 1.78 | 2.92 | 3.01 |
| $^1A''(n\pi^*)$ | 2 | 224537/1593 | −190.6275 | −190.9493 | 1.83 | 2.94 | 3.21 |

[a]Number of configurations generated/selected.
[b]0–0 transition energies, ref. 8 and 9.

TABLE 4. SCF and CI results for $CH_2$ bending of acrolein

| γ degree | $E_{SCF}$ (hartree) $^3n\pi^*$ | Singlet states Gen/Sel | Singlet states $E_{CI}$ (hartree)[a] | Triplet states Gen/Sel | Triplet states $E_{CI}$ (hartree)[a] |
|---|---|---|---|---|---|
| 0 | −109.6294 | 355841/ | −190.9334 | 862201/ | −190.8823 |
| | | 5344 | −190.8767 | 4919 | −190.8612 |
| 10 | −190.6292 | 355841 | −190.9315 | 924186/ | −190.8793 |
| | | 5288 | −190.8754 | 4826 | −190.8589 |
| 25 | −190.6274 | 355841/ | −190.9215 | — | — |
| | | 4352 | −190.8747 | — | — |
| 38.13 | −190.6238 | 355841/ | −190.9080 | 924186/ | −190.8739 |
| | | 2894 | −190.8719 | 4186 | −190.8538 |

[a]The two numbers listed for each γ are the energies corresponding to roots 1 and 2, respectively.

TABLE 5. Energy changes (in kcal/mol) for nonplanar acrolein (relative to planar structure)

| γ (deg) | Ground state $\Delta E_{CI}$ | $^1n\pi^*$ $\Delta E_{CI}$ | $^3n\pi^*$ $\Delta E_{SCF}$ | $^3n\pi^*$ $\Delta E_{CI}$ | $^3\pi\pi^*$ $\Delta E_{CI}$ |
|---|---|---|---|---|---|
| 10 | 1.19 | 0.81 | 0.12 | 1.88 | 1.44 |
| 25 | 7.47 | 1.26 | 1.26 | — | — |
| 38.13 | 15.94 | 3.01 | 3.51 | 5.27 | 4.64 |

was always kept equal to β (Fig. 1). Values for γ (the angle the $CH_2$ group makes with the plane of the rest of the molecule) were 0° (planar), 10°, 25°, and 38.13° ($\alpha = \beta = 115°$; a tetrahedral arrangement corresponds to $\gamma = 54.7°$). Thus, γ fixes the angles of bending unambiguously. For all states considered, the same bond distances, namely the ones optimized for $^1n\pi^*$, and the same bond angles were used. The reason for taking the same bond distances is that the optimized bond distances for $^3n\pi^*$ differ little from those of $^1n\pi^*$ (Table 2), and the $^3\pi\pi^*$ distances optimized by Dykstra (14) are also very similar. For the ground state, these bond distances are of course inadequate; however, the ground state is only a necessary ingredient for the CI calculations, and of no particular interest to the methylene nonplanarity studies. In all cases SCF orbitals for $^3n\pi^*$ were used. In the CI calculations the frozen MOs were as previously described while the highest ten MOs were excluded from possible occupations. Due to inconsistencies in the extrapolated CI energies at a threshold of 50 μhartree, a lower selection threshold of 20 μhartree had to be chosen.

For the singlet states, the lowest root (#1) corresponds to the ground state, and the second root to $^1n\pi^*$. For triplet states, root 1 correlates with $^3n\pi^*$, and root 2 with $^3\pi\pi^*$. Therefore, CI calculations on the $^1A$ and $^3A$ states, with 2 roots each, give results for all states of interest in the study of the methylene nonplanarity of acrolein.

Details of the CI calculations, and SCF and CI energies are given in Table 4. Five or six main configurations were used. The important results are summarized in Table 5. The conclusion is quite clearly that neither the initial state reached in the photoexcitation process, nor any of the triplet states that might be reached through intersystem crossover, have a pyramidal $CH_2$ group in the case of *trans*-acrolein. The CI energy barrier to the maximum deformation calculated is 3.0 kcal/mol for $^1n\pi^*$, 5.3 for $^3n\pi^*$ and 4.6 for $^3\pi\pi^*$.

As expected, the deformation barrier is much larger for the ground state (this should be true even

Can. J. Chem. Downloaded from www.nrcresearchpress.com by 210.87.254.5 on 09/06/12
For personal use only.

with good ground state bond distances). The calculated SCF values for $^3n\pi^*$ are similar to the CI values, but generally smaller.

### 3. Conclusion

According to the results presented for acrolein, none of the excited states of interest are pyramidal at the β-carbon. However, the energy barriers to becoming pyramidal are small, and certainly much smaller than for the ground state.

In the absence of any experimental evidence, and in light of the theoretical work presented here, it is reasonable to assume that α,β-unsaturated carbonyl compounds are planar or twisted at the β-carbon position, but not pyramidal. Therefore, the reason for Wiesner's empirical rule, stated in the Introduction, cannot be found in the geometry of the excited species of the carbonyl compound, and must be determined somehow by the subsequent reaction of the α,β-unsaturated carbonyl compound in the excited state with the olefin.

Considering that Wiesner's rule, relating the stereochemistry of the product to the geometry of the excited state of the carbonyl compound, works in all cases studied so far, one has to conclude that at the initial stages of the reaction with the olefin, the excited carbonyl compound does indeed pyramidalize at the β-position seeking the sterically less-hindered configuration. Due to the low energy barrier for pyramidalization, sufficient energy for this process should be available.

According to previously mentioned experimental evidence, one might assume that the α,β-unsaturated carbonyl compound, after initial photo excitation to $^1n\pi^*$, rapidly crosses over to a lower-lying triplet state, either $^3n\pi^*$ or $^3\pi\pi^*$. Bunce, Ridley, and Zerner (26) presented interesting experimental and theoretical results on *p*-quinones. They proposed that in these systems photo-cycloaddition with an olefin will lead to oxetane formation if the lowest triplet was $n\pi^*$, whereas cyclobutane will be formed if the lowest triplet was $\pi\pi^*$. This also follows from qualitative arguments if one assumes that the $n\pi^*$ excitation is mainly localized at the carbonyl group, whereas $\pi\pi^*$ is localized at the terminal C—C bond. Since in the reactions studied by Wiesner cyclobutane adducts are formed, this would imply that $^3\pi\pi^*$ is lower that $^3n\pi^*$. Although this is not the case for acrolein (but the two energies are close), it might be true for larger such compounds. (For steroidal ketones it was found that $^3\pi\pi^*$ is the lowest triplet state (27).) Bunce *et al.* also pointed out that the ordering of the triplet states is extremely sensitive to substitution.

Besides addressing the problem of a pyramidal β-carbon in excited states of acrolein, CI values were obtained for the singlet $n\pi^*$ and singlet $\pi\pi^*$ vertical excitation energies. Geometry optimizations for $^1n\pi^*$ and $^3n\pi^*$ gave bond distances corresponding to single bond – double bond reversals, similar to values previously obtained for the $^3\pi\pi^*$ state of acrolein. Corresponding calculated adiabatic excitation energies are in good agreement with experimental values.

### Acknowledgments

We are much obliged to Professor K. Wiesner for suggesting this problem, and for many valuable discussions. We also thank Dr. M. Zerner for his interest, and for pointing out useful references. Financial support from the Natural Sciences and Engineering Research Council of Canada and the University of New Brunswick is gratefully acknowledged. One of us (K.V.) would like to acknowledge the support of the Natural Sciences and Engineering Research Council in the form of a postgraduate scholarship, and the University of New Brunswick for support in the form of the Magee Postgraduate Merit award.

We are grateful to one of the referees for helpful comments.

1. K. Wiesner. Tetrahedron, **31**, 1655 (1975).
2. J. F.Blount, G. D. Gray, K. S. Atwal, T. Y. R. Tsai, and K. Wiesner. Tetrahedron Lett. **21**, 4413 (1980).
3. G. Marini-Bettòlo, S. P. Sahoo, G. A. Poulton, T. Y. R. Tsai, and K. Wiesner. Tetrahedron, **36**, 719 (1980).
4. E. J. Corey, J. D. Bass, R. LeMahieu, and R. B. Mitra. J. Am. Chem. Soc. **86**, 5570 (1964).
5. R. O. Loutfy and P. de Mayo. J. Am. Chem. Soc. **99**, 3559 (1977).
6. R. S. Becker, K. Inuzuka, and J. King. J. Chem. Phys. **52**, 5164 (1970).
7. P. de Mayo, A. A. Nicholson, and M. F. Tehir. Can. J. Chem. **48**, 225 (1970).
8. J. C. D. Brand and D. G. Williamson. Discuss. Faraday Soc. **35**, 184 (1963).
9. J. M. Hollas. Spectrochim. Acta, **19**, 1425 (1963).
10. A. C. P. Alves, J. Christoffersen, and J. M. Hollas. Mol. Phys. **20**, 625 (1971).
11. E. J. Blair, W. Goetz, and D. A. Ramsay. Can. J. Phys. **49**, 2710 (1971).
12. A. Devaquet and L. Salem. Can. J. Chem. **49**, 977 (1971).
13. A. Devaquet. J. Am. Chem. Soc. **94**, 5160 (1972).
14. C. E. Dykstra. J. Am. Chem. Soc. **98**, 7182 (1976).
15. T. H. Dunning. J. Chem. Phys. **53**, 2823 (1970).
16. R. J. Buenker and S. D. Peyerimhoff. Theor. Chim. Acta, Berlin, **35**, 33 (1974).
17. R. J. Buenker and S. D. Peyerimhoff. Theor. Chim. Acta, Berlin, **39**, 217 (1975).

Can. J. Chem. Downloaded from www.nrcresearchpress.com by 210.87.254.5 on 09/06/12
For personal use only.

18. R. J. BUENKER, S. D. PEYERIMHOFF, and W. BUTSCHER. Mol. Phys. **35**, 771 (1978).
19. H. MACKLE and L. E. SUTTON. Trans. Faraday Soc. **47**, 691 (1951).
20. E. A. CHERNIAK and C. C. COSTAIN. J. Chem. Phys. **45**, 104 (1966).
21. A. D. WALSH. Trans. Faraday Soc. **41**, 498 (1945).
22. M. B. ROBIN. Higher excited states of polyatomic molecules. Vol. II. Academic Press, New York. 1975.
23. S. IWATA and K. MOROKUMA. J. Am. Chem. Soc. **97**, 966 (1975).
24. E. R. DAVIDSON and L. E. NITZSCHE. J. Am. Chem. Soc. **101**, 6524 (1979).
25. R. R. LUCCHESE, H. F. SCHAEFER III, and C. E. DYKSTRA. Chem. Phys. Lett. **51**, 600 (1977).
26. N. J. BUNCE, J. E. RIDLEY, and M. C. ZERNER. Theor. Chim. Acta, Berlin, **45**, 283 (1977).
27. G. MARSH, D. R. KEARNS, and K. SCHAFFNER. J. Am. Chem. Soc. **93**, 3129 (1971).

Can. J. Chem. Downloaded from www.nrcresearchpress.com by 210.87.254.5 on 09/06/12
For personal use only.

# Sterically hindered aromatic compounds. XI. Spectral and product studies of the decomposition of *N*-nitrosoacetanilides

L. Ross C. Barclay[1] and Julian M. Dust[2]

*Department of Chemistry, Mount Allison University, Sackville, N.B., Canada E0A 3C0*

Received September 28, 1981

L. Ross C. Barclay and Julian M. Dust. Can. J. Chem. **60**, 607 (1982).

Decomposition of *N*-nitroso-2,4,6-tri-*tert*-butylacetanilide (**1**) in benzene forms products 2,4,6-tri-*tert*-butylphenyl acetate (**3**), 3-(3,5-di-*tert*-butylphenyl)-2-acetoxy-2-methylpropane (**4**), and hydrocarbons 3-(3,5-di-*tert*-butylphenyl)- and 1-(3,5-di-*tert*-butylphenyl)-2-methylpropene (**5** and **6**) explained by a reactive aryl cation (**2**), the rearranged products (**4**, **5**, **6**) originating from a 1,5-hydride shift from an *ortho tert*-butyl group in **2**. In contrast, decomposition of **1** in triethylamine forms products 1,3,5-tri-*tert*-butylbenzene (**10**), 2,4,6-tri-*tert*-butylacetanilide (**15**), and 2-(3,5-di-*tert*-butylphenyl)-2-methylpropanal oxime (**13**), expected of a free radical pathway. Electron spin resonance evidence is given for intermediates formed by rearrangement of the 2,4,6-tri-*tert*-butylphenyl radical and spin trapped by the nitroso group of **1**. CIDNP and esr studies on the dediazoniation of *N*-nitrosoacetanilide and aniline in the presence of tertiary amines support the proposed electron transfer mechanism. The results are briefly discussed in terms of the role of steric effects and electron transfer in the dediazoniation of nitrosoacetanilides and diazonium salts.

L. Ross C. Barclay et Julian M. Dust. Can. J. Chem. **60**, 607 (1982).

La décomposition du *N*-nitroso tri-*tert*-butyl-2,4,6 acétanilide (**1**) dans le benzène conduit à la formation de l'acétate de tri-*tert*-butyl-2,4,6 phényle (**3**), de (di-*tert*-butyl-3,5 phényl)-3 acétoxy-2 méthyl-2 propane (**4**) et des (di-*tert*-butyl-3,5 phényl)-3 et (di-*tert*-butyl-3,5 phényl)-1 méthyl-2 propènes (**5** et **6**) dont on explique la formation à l'aide d'un cation aryle réactif (**2**), les produits de transposition (**4**, **5** et **6**) proviennent d'un déplacement-1,5 d'un hydrure provenant d'un groupement *tert*-butyle *ortho* dans **2**. Par opposition, la décomposition de **1** dans la triéthylamine conduit à la formation de tri-*tert*-butyl-1,3,5 benzène (**10**), de tri-*tert*-butyl-2,4,6 acétanilide (**15**) et de l'oxime du (di-*tert*-butyl-3,5 phényl)-2 méthyl-2 propanal (**13**) dont la formation est prévue pour un processus radicalaire. Les données de la rpe suggèrent la présence d'intermédiaires formés par une transposition du radical tri-*tert*-butyl-2,4,6 phényle qui est piégé par le nitroso de **1**. Des études de CIDNP et rpe sur la dédiazotation du *N*-nitrosoacétanilide et de l'aniline en présence d'amines tertiaires est en accord avec le mécanisme de transfert d'électron proposé. On discute brièvement des résultats obtenus en termes du rôle des effets stériques et des transferts d'électrons lors de la dédiazotation des nitrosoacétanilides et des sels de diazonium.

[Traduit par le journal]

## Introduction

The aromatic dediazoniation reaction has been the subject of renewed interest by a number of investigators (1–12). The variety of reactive intermediates involved: diazonium ions (5), aryl cations (6–8), nitrogen – aryl cation molecule – ion pairs (1, 9, 10), aryl radicals (2), and benzynes (3, 4, 11), have attracted considerable interest as have newer methods of deamination of arylamines for synthetic purposes (12).

Earlier (13) we studied the aprotic diazotization of hindered amines, such as 2,4,6-tri-*tert*-butylaniline, with butyl nitrite. The results of spin trapping of the hindered aryl radical and derived radicals from this reaction together with product analysis were rationalized on the basis of a predominantly radical pathway for the dediazoniation. On the other hand, oxygenated compounds accounted for at least 50 per cent of the products; these probably arise by ionic pathways, and the usual question arises as to the relationship between the free radical and cationic pathways. To provide some answers to this question we selected *N*-nitroso-2,4,6-tri-*tert*-butylacetanilide (**1**) for dediazoniation studies. This compound will undergo the reaction without added reagents and is therefore a "cleaner" system for studying the effect of varying conditions such as the presence of an electron transfer medium on the reactive intermediates involved and products formed. Some spectroscopic studies (CIDNP) will also be reported for the comparable decomposition of *N*-nitrosoacetanilide (NNA) in order to further explore the relationships between the various pathways involved in the dediazoniation (i.e. cationic, electron transfer, and free radical).

## Results

### A. *Product analysis*

#### 1. *Decomposition of **1** in benzene*

The nitroso compound (**1**) proved to be slow to decompose in benzene at room temperature or even at 80°C. The major products found are given in Table 1. They can readily be explained by a cationic mechanism involving combination of an aryl cation (**2**) with the acetate anion and rear-

[1]Author to whom correspondence should be addressed.

[2]Present address: Department of Chemistry, Dalhousie University, Halifax, Nova Scotia.

0008-4042/82/050607-09$01.00/0

©1982 National Research Council of Canada/Conseil national de recherches du Canada

Can. J. Chem. Downloaded from www.nrcresearchpress.com by 210.87.254.5 on 09/06/12
For personal use only.

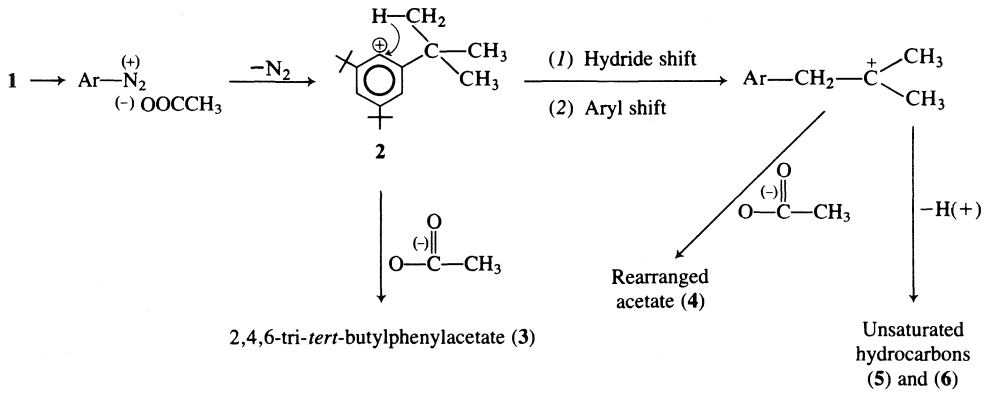


SCHEME 1

TABLE 1. Products from decomposition of *N*-nitroso-2,4,6-tri-*tert*-butylacetanilide in benzene[a]

| Compound | % Yield |
|---|---|
| 2,4,6-Tri-*tert*-butylphenyl acetate **3** | 70.1 |
| 3-(3,5-Di-*tert*-butylphenyl)-2-methylpropene **5**[b] and 1-(3,5-di-*tert*-butylphenyl)-2-methylpropene **6**[b] | 15.9 |
| 3-(3,5-Di-*tert*-butylphenyl-2-acetoxy-2-methylpropane **4**[c] | 7.2 |

[a]Under nitrogen at 80°C for six days. Yields were determined by isolation using preparative tlc.
[b]Hydrocarbon **5** was the major component (as in ref. 13), according to nmr analysis.
[c]The structure is tentatively assigned from spectroscopic properties.

TABLE 2. Products from decomposition of *N*-nitroso-2,4,6-tri-*tert*-butylacetanilide in triethylamine[a]

| Compound | % Yield |
|---|---|
| 2,4,6-Tri-*tert*-butylacetanilide[b] **15** | 40.0 |
| 1,3,5-Tri-*tert*-butylbenzene **10** | 20.0 |
| 2-(3,5-Di-*tert*-butylphenyl)-2-methylpropanal oxime **13** | 18.3 |
| 2,4,6-Tri-*tert*-butylaniline | 2.5 |
| Hydrocarbons **5** and **6** | Trace |
| Unidentified mixture[c] | 11.0 |

[a]Under nitrogen at 80°C for 8 h. Compound **15** was isolated by filtration. The other products were separated and isolated yields determined by preparative tlc.
[b]Precipitated from reaction, filtered, and weighed.
[c]Comparison of the nmr spectrum of this mixture with that of the dimer of **12** (17) indicates that the mixture may consist of a mixture of dimers of nitroso compounds **12** and **17**, 3 peaks upfield at 1.30, 1.35, and 1.49 (*gem*-dimethyl, and *tert*-butyls), 2.55 (benzylic-$CH_2$), near 4.1 and 4.2 (—$CH_2$—NO—NO—), and two sets of multiplets at 7.2 and 7.58 (aromatic).

rangement of this aryl cation via a 1,5 hydride shift with subsequent carbonium ion reactions as outlined in Scheme 1.

It is interesting to contrast our observed rearrangement of **2** with cyclialkylations observed for other *ortho*-alkyl aryl cations (15) including that generated from the diazonium salt of 3-amino-4-*tert*-butyl-5-nitrobenzoic acid (16). Cyclialkylation in **2** would undoubtedly be hindered by an *ortho-tert*-butyl group.

2. *Decomposition of **1** in triethylamine*

The decomposition of **1** proceeded more rapidly in triethylamine than in benzene and the products (Table 2) are remarkably different. These products are explained by an electron transfer mechanism[3] operating between the aryl diazonium ion (or possibly the aryl cation **2**) and triethylamine to yield the 2,4,6-tri-*tert*-butylphenyl radical **7** and derived hydrocarbon radicals **8** and **9**. The products such as 1,3,5-tri-*tert*-butylbenzene (**10**), oxime (**13**), and 2,4,6-tri-*tert*-butylacetanilide (**15**) could then follow by hydrogen atom transfers (**7** to **10**) and radical trapping by the substrate **1** (or derived products, i.e. **17**) according to the proposal given in Scheme 2.[4] This scheme is somewhat speculative in that not all of the products or radical intermediates have been found. Nevertheless it does account for the rather large proportion of 2,4,6-tri-*tert*-butylacetanilide (**15**) found, since there are two routes for its formation: **11** → **14** → **15** and **16** → **14** → **15**.

The oxime **13** (derived from a spontaneous rearrangement of the nitroso compound **12**) was observed earlier (17) from the photorearrangement of 2,4,5-tri-*tert*-butylnitrosobenzene and its formation here is consistent with a radical pathway such as that shown. One would also expect to find some rearranged nitroso compound (**17**, or derived dimers) and this appears to be present in the "unidentified mixture" (Table 2).

[3]A referee has pointed out that there are two possibilities for the electron transfer. It may be either a "free" transfer or by a homolytic dissociation of the diazoaminonium cation formed from diazonium ion + triethylamine as a steady state intermediate.

[4]The intermediates **7**, **8**, and **9** were detected earlier in a kinetic study (14). The bracketed species are postulated ones, while the others (**16** and **17**) are reported herein by esr observations (*vide infra*).

Can. J. Chem. Downloaded from www.nrcresearchpress.com by 210.87.254.5 on 09/06/12
For personal use only.

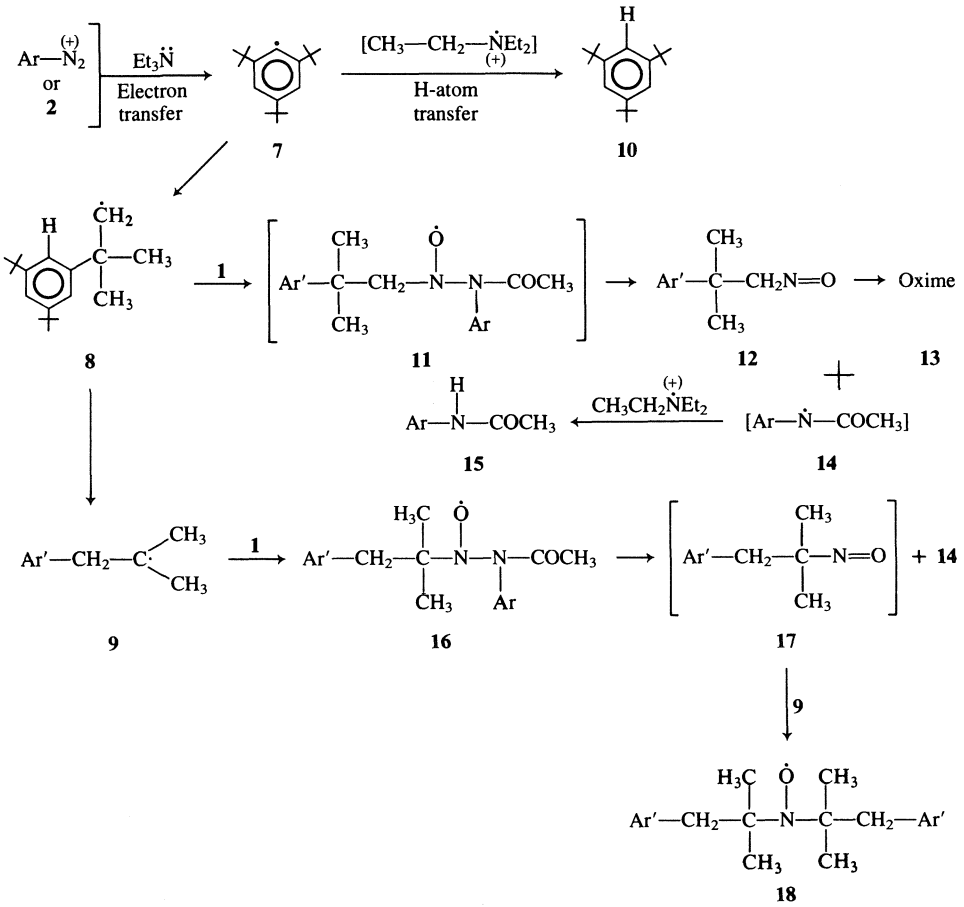

SCHEME 2

B. *Spectroscopic studies*

The pathways shown in Scheme 2 include a number of nitroxide radicals which should be detectable by esr measurements. In addition the proposed electron transfer from triethylamine to the diazonium ion or aryl cation is somewhat unusual. It was desirable to check the validity of this electron transfer and for this purpose we turned to chemically induced dynamic nuclear polarization (CIDNP), since a hydrocarbon (**10** from **2** or benzene from nitrosoacetanilide) formed from a radical pair as proposed is expected to exhibit polarization in the nmr experiment.

1. *Electron spin resonance*

The results from esr observations on the dediazoniations of **1** and nitrosoacetanilide (NNA) are given in Table 3. Earlier (13), we observed the formation of nitroxide radical **16** from **1** in methylene chloride. When this experiment was carried out in the presence of triethylamine (No. 2), the typical triplet of triplets for **16** appeared immediately upon addition of this base and the signals were much more intense and persistent than with **1** alone (No. 1). After longer contact time (3 hours) at room temperature, the spectrum of **16** was replaced by a single triplet assigned to the nitroxide radical (**18**). These results are entirely consistent with the proposal in Scheme 2 for the interconversions **9** → **16** → **17** → **18**. Separate attempts to observe the 2,4,6-tri-*tert*-butylacetanilino radical (**14**) (Scheme 2) by photolysis of the amide with di-*tert*-butylperoxide or oxidation of the amide with lead dioxide were not successful. The proposed **14** may abstract hydrogen readily from solvent or reagents as proposed in Scheme 2.

The effect of triethylamine indicates that it is acting as an electron donor. The earlier (13) observation of the radical (**16**) from **1** alone was probably a result of a minor route of decomposition of an intermediate diazoanhydride Ar—N=N—O—N=N—Ar →Ar· + $N_2$ + ·O—N=N—Ar according to the Rüchardt mechanism (21). An electron donor could cut in on that pathway by forming the

Can. J. Chem. Downloaded from www.nrcresearchpress.com by 210.87.254.5 on 09/06/12
For personal use only.

Can. J. Chem. Downloaded from www.nrcresearchpress.com by 210.87.254.5 on 09/06/12
For personal use only.





TABLE 3. Electron spin resonance observations of dediazoniations[a]

| No. | Substrate[b] | Reagent[c] | Solvent | Temperature °C | Radicals observed | *Hyperfine* splittings (gauss) | *g*-Values | Reference |
|---|---|---|---|---|---|---|---|---|
| 1 | NNTBA (**1**) | — | $CH_2Cl_2$ | 20 | $Ar'—CH_2C(CH_3)_2—\underset{\displaystyle\dot{O}}{\overset{|}{N}}—\underset{\displaystyle Ar}{\overset{|}{N}}—COCH_3$ (**16**) | $a_{N\alpha}$13.8, $a_{N\beta}$3.3 | 2.0062 | 13 |
| 2 | **1** | TEA (excess) | $C_6H_6$ | −40 | **16** Ar | | | |
| | | | | 25 | $Ar'—CH_2C(CH_3)_2—\underset{\displaystyle\dot{O}}{\overset{|}{N}}—C(CH_3)_2CH_2—Ar'$ (**18**) | $a_N$15.3 | 2.0063 | This work |
| 3 | **1** (1) | TPA (3.4) | $CH_2Cl_2$ | 10 | $(C_6H_5)_3\overset{(+)}{N}\cdot$ | $a_N$6.3[g] | — | This work |
| 4 | **1** (1) | TMP (2) | $C_6H_6$ | 25 | $\overset{(+)}{TMP}\cdot$ | F | 2.0031<br>2.0031 | This work<br>18 |
| 5a | NNA (1) | TMP (1) | $C_6H_6$ | 40 | $C_6H_5—\underset{\displaystyle\dot{O}}{\overset{|}{N}}—\underset{\displaystyle COCH_3{}^d}{\overset{|}{N}}—C_6H_5$ | $a_{N\alpha}$9.9, $a_{N\beta}$1.1 | 2.0055 | This work |
| 5b | | | | 10 | $\overset{(+)^e}{TMP}\cdot$ | $a_{N\alpha}$11.7, $a_{N\beta}$1.7 | | 23 |

[a]Studies were carried out by scanning the substrate alone in degassed ($N_2$ purged) solvent and then adding the reagent and recording spectra.
[b,c]NNTBA = *N*-nitroso-2,4,6-tri-*tert*-butylacetanilide, NNA = N-nitrosoacetanilide, TEA = triethylamine, TPA = triphenylamine, TMP = *N*,*NN*′,*N*′-tetramethylparaphenylenediamine. Reactions were generally carried out on one mmol of substrate. The mole ratios of substrates to reagents are shown in parentheses.
[d,e]A combination of signals including *d* + *e* results; *d* is observed by adding NNA to TMP and *e* by adding TMP to NNA.
[f]The spectrum was the same as that for the $\overset{(+)}{TMP}\cdot$ (radical cation) generated independently according to ref. 19 or 20.
[g]The triplet for $(C_6H_5)_3\overset{(+)}{N}\cdot$ exhibited partly resolved fine structure due to coupling with aryl hydrogens. The reported $a_N$ has varied from 8.55 in $CH_2Cl_2$ (24) to 10.16 in liquid $SO_2$ (25).

TABLE 4. CIDNP observations of dediazoniations

| No. | Substrate[a] | Reagent[b] | Solvent | Temperature°C[d] Initial | CIDNP | (time/min) | Polarization observed |
|---|---|---|---|---|---|---|---|
| 1 | NNA | TEA | — | −22 | 0 | — | [e] |
| 2 | NNA | — | $C_6D_6$ | 10 | 30 | (1) | Benzene E |
| | | | | | 50 | (4) | Benzene E, biphenyl E |
| 3 | NNA | Biphenyl[c] | $C_6D_6$ | 10 | 50 | (5) | Benzene E, biphenyl E (Fig. 1) |
| 4 | NNA | TEA | — | −25 | 30 | (8) | Benzene E |
| 5 | NNA | TMP | $C_6D_6$ | 10 | 50 | (4) | Benzene E (Fig. 2) |
| 6 | Aniline | BONO | $C_6D_6$ | 5 | 30 | (4) | Benzene E |
| 7 | Aniline | BONO/TEA | — | 6 | 50 | (6) | Benzene E |
| 8 | Aniline | BONO/TMP | — | 30 | 30 | (2) | Benzene E |

[a,b]NNA = *N*-nitrosoacetanilide, TEA = triethylamine, TMP = *N*,*N*,*N*′,*N*′-tetramethyl-paraphenylenediamine, BONO = butylnitrite.
[c]Biphenyl was added as an internal reference to detect the polarized form.
[d]The temperatures include the initial setting of the nmr probe and the temperature (higher) when CIDNP was observed and the corresponding elapsed time is given in parentheses.
[e]Ordinary benzene was observed, i.e. no CIDNP.

unstable aryl diazenyl radical directly from the diazonium ion

$$Ar{-}\overset{(+)}{N}_2 \xrightarrow[\text{donor}]{\text{electron}} [Ar{-}N{=}N\cdot] \xrightarrow{-N_2} Ar\cdot$$

We did not observe the $Et_3\overset{(+)}{N}\cdot$ radical cation shown in this pathway, presumably because it would rapidly undergo the transformation $Et_3\overset{(+)}{N}\cdot \xrightarrow{\dot{H}\ \text{transfer}}$ $CH_3CH{=}\overset{(+)}{N}Et_2$. However, when aromatic amines such as triphenylamine or tetramethylparaphenylenediamine (22) were used, their radical cations were readily observed in the esr (Nos. 3, 4, 5). These observations were extended to the parent compounds *N*-nitrosoacetanilide which yielded both the known hydrazoxyl radical (23) and the aromatic radical cation ($TMP\overset{(+)}{\cdot}$) (No. 5a, 5b).

2. *Chemically induced dynamic nuclear polarization (CIDNP)*

The CIDNP observations during dediazoniations are outlined in Table 4. Treatment of *N*-nitrosoacetanilide (NNA) with triethylamine in the cold (No. 1) resulted in slow formation of unpolarized benzene. Slow reactions of diazonium ions do not lead to CIDNP effects (26). This may be attributed to the resulting slow formation of radicals (phenyl) which then react comparatively quickly so that they reside in the solvent cage for shorter periods than required for polarization (27, 28). Similarly we found that *N*-nitroso-2,4,6-tri-*tert*-butylacetanilide (**1**) underwent very slow decomposition even at 80°C and did not exhibit CIDNP up to 110°C in perdeuterotoluene, nor at 140°C in cyclohexanone.

Decomposition of NNA at elevated temperatures (30–50°C) resulted in both polarized benzene and polarized biphenyl (Table 4, Nos. 2 and 3) (see Fig. 1). On the other hand, decomposition of NNA in the presence of electron transfer reagents gave only polarized benzene (Nos. 4 and 5) (see Fig. 2). Similarly the dediazoniation of aniline with butyl nitrite in the absence or presence of amines (Nos. 6–8) gave benzene as the only detectable polarized species by our method. Polarized benzene and substituted benzenes have been found in CIDNP studies of various dediazoniations (29–33), including pyrolysis of NNA in acetonitrile at low field (34), whereas spin polarized biphenyl from these systems is unusual and was not reported in CIDNP studies even when biaryls were formed in significant yields (33). Both polarized benzene and biphenyl were reported in $^{13}C$ CIDNP studies of the decomposition of diazoaminobenzene where the enhanced absorption of two carbons of biphenyl was assigned to cage recombination of two phenyl radicals (35). However, spin polarized biphenyl was not found in the $^1H$ CIDNP study of the same system (36).

Our CIDNP emissions for benzene in the *absence* of electron donors (i.e. Nos. 2, 3, and 6) can be accounted for by spin selection using the radical pair model (27, 28), where radical pairs such as $[ArN_2\cdot\ \cdot ON_2Ar]$ and $[Ar\cdot\ \cdot ON_2Ar]$ originate from the diazoanhydride according to the Rüchardt (21) mechanism. When organic bases are present as electron donors (Nos. 1, 4, 5, 7, and 8), the electron pairs involved are probably of the types $[Ar{-}\overset{(+)}{N}_2\cdot\ \cdot N{-}R_3]$ and $[Ar\cdot\ \cdot\overset{(+)}{N}{-}R_3]$. (In the latter pair the different *g* factors as required for the emission polarization are 2.00277 (37) and 2.00306 $TMP\overset{(+)}{\cdot}$.)

The polarized biphenyl, observed in certain experiments in the *absence* of organic bases (Nos. 2 and 3), could arise from attack of phenyl radicals, which escape the cage, on the solvent perdeutero-

Can. J. Chem. Downloaded from www.nrcresearchpress.com by 210.87.254.5 on 09/06/12
For personal use only.

Can. J. Chem. Downloaded from www.nrcresearchpress.com by 210.87.254.5 on 09/06/12
For personal use only.

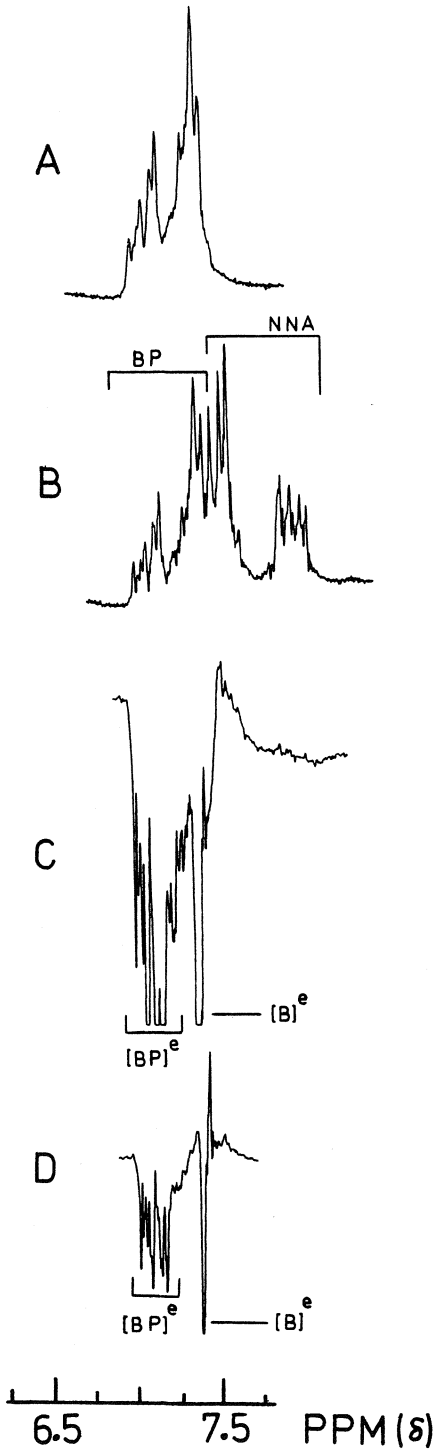


FIG. 1. $^1$H nmr spectra of aromatic protons during the decomposition of *N*-nitrosoacetanilide (NNA) in the presence of biphenyl as internal reference. Spectra were measured in $C_6D_6$ with TMS reference. A. Spectrum of biphenyl. B. Initial spectrum of NNA with biphenyl recorded at 10°C. C. Spectrum recorded at 50°C after 5 min, showing CIDNP emissions for biphenyl, [BP]$^e$, and benzene, [B]$^e$; both off scale. D. Spectrum recorded at reduced amplitude after 6 min at 50°C, showing CIDNP emissions for biphenyl, [BP]$^e$ and benzene [B]$^e$.

benzene. This known (3, 21) scavenging reaction of phenyl radicals could give a polarized product.[5]

## Discussion

These current results permit some conclusions on the role of steric effects and the effect of an electron transfer medium on the pathway of aryl dediazoniations.

1. In the absence of an effective electron transfer agent, the pyrolysis of *N*-nitroso-2,4,6-tri-*tert*-butylacetanilide (**1**) in benzene proceeds mainly by a cationic pathway through the very reactive 2,4,6-tri-*tert*-butylaryl cation (**2**). The major products from this reaction (Table 1) result from a hydride transfer from an *ortho tert*-butyl group via a five-membered transition state followed by subsequent rearrangements (Scheme 1). Similar rearrangements observed earlier (13) during the aprotic diazotization of 2,4,6-tri-*tert*-butylaniline were rationalized on the basis of free radical rearrangements based on esr evidence (e.g. spin trapping of the 2,4,6-tri-*tert*-butylphenyl radical (**7**)). It is more likely that those rearrangements were also cationic in nature, especially those forming oxygen containing products.

2. The *ortho tert*-butyl groups in **1** significantly retard its decomposition (compared to the unsubstituted NNA). This is most probably due to the severe steric restrictions exerted on the four-membered transition state required for the rearrangement of **1** $\rightarrow$ Ar—N=N—O—$\overset{\overset{O}{\|}}{C}$—$CH_3$ (4). On the other hand, the derived hindered diazonium ion Ar—$\overset{(+)}{N}_2$, once formed, is subject to the steric compression of two *ortho tert*-butyl groups and its decomposition may be sterically accelerated. This latter effect was confirmed in a qualitative manner by studying the decomposition of 2,4,6-tri-*tert*-butylphenyl diazonium nitrate. A suspension of this salt in ethyl ether appeared to be stable for several hours below −50°C. A sample of this suspension exhibited an infrared absorption band at 2250 cm$^{-1}$ for Ar—$\overset{(+)}{N}\equiv N$ *when handled rapidly*.

[5]It appears that our nmr method does not distinguish between the proposed product $C_6H_5$–$C_6D_5$, and biphenyl.

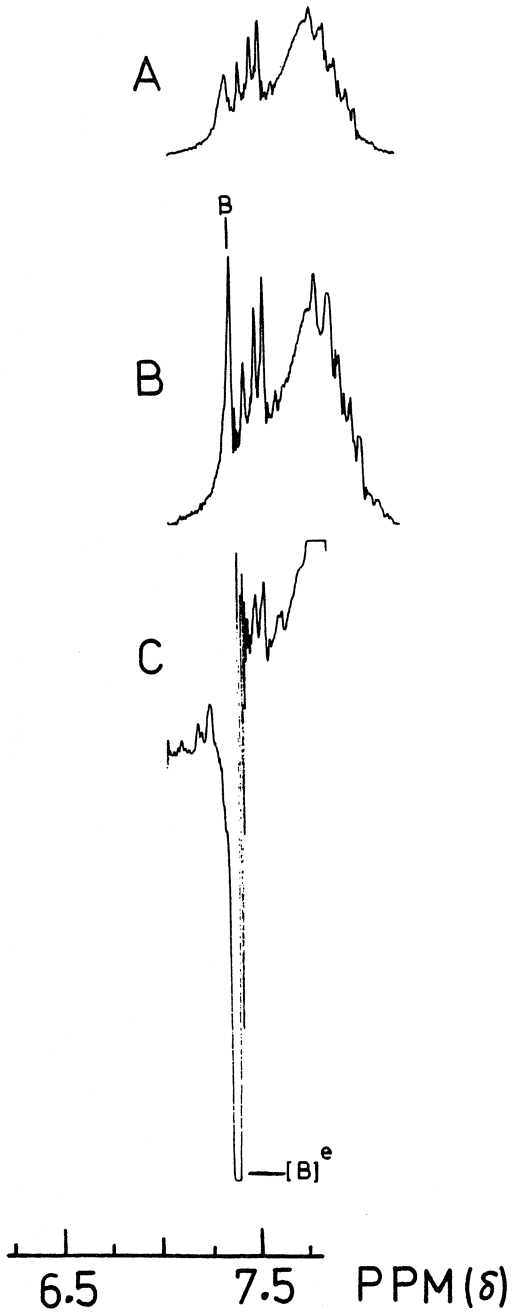


FIG. 2. $^1$H nmr spectra of aromatic protons during the decomposition of *N*-nitrosoacetanilide (NNA) in the presence of *N*,*N*,*N*,*N*-tetramethylparaphenylenediamine. Spectra were measured in $C_6D_6$ with TMS reference. A. Initial spectrum of NNA recorded at 10°C. The upfield portion is only partially resolved. B. Spectrum recorded after 2 min at 10°C, showing a trace of benzene, B, formed. C. Spectrum recorded after 3 min at 50°C, showing the CIDNP emissions for benzene, [B]$^e$, off scale.

Repetitive scans of this band indicated rapid decomposition of the salt at 25°C so that it was completely decomposed in five minutes. This contrasts with the rather *slow* decomposition observed for **1** in boiling benzene. This result is consistent with the proposed rapid ionic decomposition of the hindered Ar—$\overset{(+)}{N}_2$ (Scheme 1) as the main dediazoniation pathway.

3. The presence of tertiary amines as electron transfer agents switches the decomposition of **1** from an ionic to a free radical pathway. The products are accounted for by free radical reactions (Table 2, Scheme 2)[6] which are consistent with intense signals for radicals trapped as nitroxides such as **16** and **18**, as well as the signals for the expected amino cation radicals (e.g. $(C_6H_5)\overset{(+)}{N}\cdot$ and TMP$\overset{(+)}{\cdot}$, Table 3). CIDNP observations (Table 4) on the decomposition of NNA (and aprotic diazotization of aniline) in the presence of tertiary bases are also consistent with a pathway involving rapid electron transfer resulting in a radical pair of the type

$$[Ar—N_2\cdot \quad \cdot\overset{(+)}{N}—R_3]$$

The relatively uncomplicated nmr signal in the aromatic region on decomposition of NNA in triethylamine (a singlet for benzene is observed after the emission period) indicates that this may be a simple and efficient synthetic method for carrying out the well-known hydrodediazoniation reaction. Our failure to observe CIDNP signals for the decomposition of **1** is probably due to the relatively slow decomposition of **1**.

Our results for the hindered system (**1**) provide some insight into the role of steric effects on the dediazoniation reaction. This is a somewhat specialized system and our conclusions cannot readily be generalized. Nevertheless, the fact that radicals are trapped while at the same time products form from ionic pathways, in these and earlier (13) studies, indicates that ionic and radical reactions are independently occurring as shown in simplified form in Scheme 3. More detailed arguments in

[6]An alternative scheme suggested by a referee involves the radical $Et_2N\dot{C}HMe$ in the decomposition in triethylamine. It could form by rapid hydrogen abstraction from $Et_3N$ according to the following chain reaction sequence:

$$Ar\cdot + Et_3N \rightarrow ArH + Et_2N\dot{C}HMe$$
$$Et_2N\dot{C}HMe + Ar\overset{(+)}{N}_2 \rightarrow ArN{=}N\cdot + Et_2\overset{(+)}{N}{=}CHMe$$
$$ArN{=}N\cdot \rightarrow Ar\cdot + N_2$$

Can. J. Chem. Downloaded from www.nrcresearchpress.com by 210.87.254.5 on 09/06/12
For personal use only.

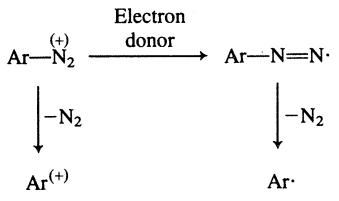


SCHEME 3

favour of a similar scheme have been given by Bunnett and co-workers (38).

## Experimental

*Materials and methods*

*N*-Nitroso-2,4,6-tri-*tert*-butylacetanilide (**1**) was prepared as described (13) and purified by preparative tlc immediately before use. *N*-Nitrosoacetanilide was prepared as described (39) and stored at −20°C over potassium hydroxide pellets. 2,4,6-Tri-*tert*-butylphenyldiazonium nitrate was prepared by the reaction of 2,4,6-tri-*tert*-butylaniline with nitric oxide (40). *N*,*N*,*N*′,*N*′-Tetramethylparaphenylenediamine and triphenylamine were reagent grade. All solvents were reagent grade, distilled before use. Triethylamine was distilled from 1% phenylisothiocyanate before use. Perdeuterobenzene and perdeuterotoluene of minimum isotopic purity 99 at.% deuterium were obtained from Merck, Sharpe and Dohme. The tlc separations were carried out on 20 × 20 cm and 0.5 mm-thick plates of silica gel using benzene eluant. The nmr measurements were made with a Varian EM360-L spectrometer and ir spectra were determined on a Perkin–Elmer 467 spectrometer. Electron spin resonance spectra were recorded on a Varian E-3 spectrometer using an esr reactor tube as previously described (13) and the $g$ values measured relative to that of tetracene in sulfuric acid, $g = 2.002604$ (41). Melting points were determined on a hot stage and are uncorrected.

*Product studies*

In a typical decomposition, a solution of **1** (931 mg, 2.80 mmol) in 50 mL of benzene or triethylamine was heated under a nitrogen atmosphere in an oil bath at 80°C until the carbonyl absorbance of the starting material (ir 1750 $cm^{-1}$) had disappeared. Experiments in triethylamine precipitated the highly insoluble 2,4,6-tri-*tert*-butylacetanilide (mp 270°C, lit. (13) mp 273°C) which was removed by filtration. The solvent was removed under reduced pressure and the residue separated on a number (e.g. 10) of preparative tlc plates. The products were identified, where applicable (e.g. hydrocarbons **5** and **6**, 2,4,6-tri-*tert*-butylacetanilide, 2-(3,5-di-*tert*-butylphenyl)-2-methylpropanal oxime **13**), by comparison of their nmr and ir spectra and melting points with those previously found (13, 17). 2,4,6-Tri-*tert*-butylphenyl acetate (**3**), the major product from **1** in benzene, gave mp 100–102°C (lit. (42) mp 101–102°C), ir band at 1780 $cm^{-1}$ for C=O ester, and nmr bands at δ 1.34 (s, 27H, 3 × $(CH_3)_3C$-), 2.25 (s, 3H, $CH_3COO$-), and 7.25 (s, 2H, aryl H). The minor product from this reaction, rearranged acetate (**4**), was separated from other compounds (e.g. **3**) by repeated preparative tlc. There was not sufficient sample for a complete analysis. Its ir spectrum showed a band at 1760 $cm^{-1}$ for C=O ester, and nmr bands at δ 1.33 (s, 18H, 2 × $(CH_3)_3C$-), 1.54 (s, 6H, $(CH_3)_2C$-), 2.23 (s, 3H, $CH_3COO$-), 2.54 (s, 2H, $CH_2$-), and 7.20 (m, 3H, aryl H).

*Chemically induced dynamic nuclear polarization*

Samples were prepared by rapidly dissolving the *N*-nitrosoacetanilide or aniline (1 mmol) in the cold solvent (0.40 mL of perdeuterobenzene, perdeuterotoluene, or triethylamine containing 50 μL tetramethylsilane) at approximately 0°C. The sample was degassed in the cold in the nmr tube by bubbling with nitrogen. The tube was sealed and the contents frozen in liquid nitrogen. The tube was warmed to −30°C in a methanol–liquid nitrogen bath just before placing in the nmr probe. The temperature of the probe was varied (usually from 10° to 50°C for samples in the deuterated solvents and −25° to 30°C for samples in triethylamine) and rapid repetitive scans were made through the aromatic proton region with the instrument locked on TMS. Benzene was confirmed as a product by peak enhancement on addition of benzene after the CIDNP effect was over. To confirm the presence of polarized biphenyl, a decomposition was carried out with biphenyl present (0.1 mmol to 1 mmol of *N*-nitrosoacetanilide). The ordinary biphenyl absorption was matched (and subsequently lost) by the intense polarized biphenyl emission.

## Acknowledgements

Research grants provided by the Natural Sciences and Engineering Research Council of Canada in support of this research are gratefully acknowledged. We thank Mr. Paul Johns for assistance with the nmr measurements.

1. I. SZELE and H. ZOLLINGER. J. Am. Chem. Soc. **100**, 2811 (1978); Helv. Chim. Acta, **167**, 1721 (1978), and references therein.
2. J. I. G. CADOGAN, J. COOK, R. G. M. LANDELLS, and J. T. SHARP. J. Chem. Soc. Perkin Trans. I, 1835 (1977), and references therein.
3. H. ZOLLINGER. Angew. Chem. **17**, 141 (1978).
4. J. I. G. CADOGAN. Acc. Chem. Res. **4**, 186 (1971).
5. G. A. OLAH and J. L. GRANT. J. Am. Chem. Soc. **97**, 1546 (1975).
6. A. COX, T. J. KEMP, D. R. PAYNE, M. C. R. SYMONS, and P. P. DE MOIRA. J. Am. Chem. Soc. **100**, 4779 (1978).
7. J. D. DILL, P. V. R. SCHLEYER, and J. A. POPLE. J. Am. Chem. Soc. **99**, 1 (1977).
8. C. G. SWAIN *et al.* J. Am. Chem. Soc. **97**, 783 (1975); **97**, 791 (1975); **97**, 796 (1975); **97**, 799 (1975).
9. W. MAURER, I. SZELE, and H. ZOLLINGER. Helv. Chim. Acta, **62**, 1079 (1979).
10. F. TRÖNDLIN, R. MEDINA, and C. RÜCHARDT. Chem. Ber. **112**, 1835 (1979).
11. J. BRENNAN, J. I. G. CADOGAN, and J. T. SHARP. J. Chem. Res. (S), 107 (1977).
12. M. P. DOYLE, J. F. DELLARIA, B. SIEGFRIED, and S. W. BISHOP. J. Org. Chem. **42**, 3494 (1977).
13. L. R. C. BARCLAY, A. G. BRIGGS, W. E. BRIGGS, J. M. DUST, and J. A. GRAY. Can. J. Chem. **57**, 2172 (1979).
14. G. BRUNTON, D. GRILLER, L. R. C. BARCLAY, and K. U. INGOLD. J. Am. Chem. Soc. **98**, 6803 (1976).
15. T. COHEN and J. LIPOWITZ. J. Am. Chem. Soc. **86**, 2515 (1964).
16. M. H. KNIGHT, T. PUTKEY, and H. S. MOSHER. J. Org. Chem. **36**, 1483 (1971).
17. L. R. C. BARCLAY, D. L. CARSON, J. A. GRAY, M. GROSSMAN, P. G. KHAZANIE, J. R. MILTON, and C. E. SCOTT. Can. J. Chem. **56**, 2665 (1978).
18. J. E. WERTZ and J. R. BOLTON. Electron spin resonance. McGraw-Hill, New York. 1972. p. 465.
19. T. R. TUTTLE. J. Chem. Phys. **30**, 331 (1959).
20. L. MICHAELIS and S. GRANICK. J. Am. Chem. Soc. **65**, 1747 (1943).

Can. J. Chem. Downloaded from www.nrcresearchpress.com by 210.87.254.5 on 09/06/12
For personal use only.

21. C. RÜCHARDT and B. FREUDENBERG. Tetrahedron Lett. 3623 (1964); C. RÜCHARDT and C. C. TAN. Chem. Ber. **103**, 1774 (1970).
22. N. N. BUBNOV, B. YA. MEDVEDEV, L. A. POLYAKOVA, K. A. BILEVICH, and O. YU. OKHLOBYSTIN. Org. Magn. Reson. **5**, 437 (1973).
23. G. R. CHALFONT and M. J. PERKINS. J. Am. Chem. Soc. **89**, 3054 (1967).
24. D. L. ALLARA, B. C. GILBERT, and R. O. C. NORMAN. J. Chem. Soc. Chem. Commun. 319 (1965).
25. H. VAN WILLIGAN. J. Am. Chem. Soc. **89**, 2229 (1967).
26. W. T. EVANOCHKO and P. B. SHEVLIN. J. Am. Chem. Soc. **100**, 6428 (1978).
27. H. R. WARD. Acc. Chem. Res. **5**, 18 (1972).
28. R. G. LAWLER. Acc. Chem. Res. **5**, 25 (1972).
29. I. P. GRAGEROV, A. F. LEVIT, L. A. KIPRIANOVA, and A. L. BUCHACHENKO. Org. Magn. Reson. **5**, 455 (1973).
30. A. RIEKER, P. NIEDERER, and D. LEIBFRITZ. Tetrahedron Lett. 4287 (1969).
31. A. RIEKER, P. NIEDERER, and H. STEGMANN. Tetrahedron Lett. 3873 (1971).
32. A. RIEKER. Ind. Chim. Belge, **36**, 1978 (1971).
33. R. M. PATON and R. U. WEBER. J. Chem. Soc. Chem. Commun. 769 (1977).
34. A. V. DUSHKIN, YU. A. GRISHIN, T. V. LECHINA, and R. Z. SAGDEEV. Tetrahedron Lett. 1309 (1977).
35. E. LIPPMAA, T. PEHK, and T. SALUVERE. Ind. Chim. Belge, **36**, 1070 (1971).
36. J. BARGON and H. FISCHER. Z. Naturforsch. **239**, 2109 (1968).
37. H. STERK and G. LECHNER. Org. Magn. Reson. **11**, 453 (1978).
38. J. F. BUNNETT and C. YIJIMA. J. Org. Chem. **42**, 639 (1977); T. J. BROXTON, J. F. BUNNETT, and C. H. PAIK. J. Org. Chem. **42**, 643 (1977).
39. H. FRANCE, I. M. HEILBRON, and D. H. HEY. J. Chem. Soc. 369 (1940).
40. J. RIGAUDY and J. C. VERNIERES. C. R. Acad. Sci. **261**, 5516 (1965).
41. B. G. SEGAL, M. KAPLAN, and G. K. FRAENKEL. J. Chem. Phys. **43**, 4191 (1965).
42. A. RIEKER and P. NIEDERER. Chem. Ber. **102**, 3947 (1969).

Can. J. Chem. Downloaded from www.nrcresearchpress.com by 210.87.254.5 on 09/06/12
For personal use only.

# La dissolution du chlorure cuivreux formé par oxydation électrochimique du cuivre

ROBERT-LOUIS BROSSARD

*Institut de recherche d'Hydro-Québec, C.P. 1000, 1800 Montée Ste-Julie, Varennes (Qué.), Canada J0L 2P0*

Reçu le 27 juillet 1981

ROBERT-LOUIS BROSSARD. Can. J. Chem. **60**, 616 (1982).

La dissolution du chlorure cuivreux, formée par oxydation électrochimique du cuivre immergé en solution aqueuse avec LiCl dissout, a été étudiée. Le pH était compris entre 3 et 5 alors que la concentration en LiCl dissous a été variée de $2{,}36 \times 10^{-2}$ *M* à $16{,}5 \times 10^{-2}$ *M*. Le produit de corrosion accumulé sur l'électrode est constitué de cristaux de nantokite (CuCl) formés par précipitation.

La présence de ce précipité contribue à l'enrichissement local de la solution qui est dans un état voisin de la saturation près de l'électrode. Cet enrichissement se traduit par une tension d'électrode en circuit ouvert bien caractéristique. Elle est approximativement égale à −40 mV (/ECS) sur une électrode en stationnaire. La dissolution complète du CuCl coïncide, pour sa part, à une chute rapide de la tension. Cette chute de tension a permis de définir le temps de transition $\tau$ à partir duquel la vitesse de dissolution du CuCl a été calculée. Par exemple, la vitesse de dissolution est de $0{,}15 \pm 0{,}01$ mC $s^{-1}$ $cm^{-2}$ en courant équivalent pour une électrode stationnaire en présence de $2{,}36 \times 10^{-2}$ *M* de LiCl dissous. Elle est aussi constante jusqu'à la disparition complète du précipité.

Par ailleurs, l'utilisation de l'électrode à disque tournant a mis en évidence que la dissolution est entièrement dominée par la diffusion d'une espèce ionique en phase liquide. Les résultats expérimentaux sont compatibles avec la présence de $CuCl_2^-$ comme espèce diffusante.

---

ROBERT-LOUIS BROSSARD. Can. J. Chem. **60**, 616 (1982).

We have studied the dissolution of copper chloride formed by the electrochemical oxidation of copper immersed in aqueous lithium chloride. The pH was maintained between 3 and 5 while the concentration of LiCl in solution was varied between $2.36 \times 10^{-2}$ *M* to $16.5 \times 10^{-2}$ *M*. The corrosion product accumulating on the electrode consists of crystals of nantokite (CuCl) formed by precipitation.

The presence of this precipitate contributes to the local enrichment of the solution which is close to saturation near the electrode. This enrichment is revealed by an electrode voltage in a well characterized open circuit. This current is about −40 mV (/ECS) on a stationary electrode. The complete dissolution of CuCl coincides with a rapid drop in voltage which allows the transition time $\tau$ to be defined from which the speed of dissolution of CuCl has been calculated. For example, the speed of dissolution is $0.15 \pm 0.01$ mC $s^{-1}$ $cm^{-2}$ in a current equivalent for a stationary electrode in the presence of $2.36 \times 10^{-2}$ *M* of dissolved LiCl. This is also constant until the complete disappearance of the precipitate.

In another study, the use of a rotating disc electrode shows that the dissolution is completely dominated by the diffusion of ionic species in the liquid phase. The experimental results are compatible with the presence of $CuCl_2^-$ as the diffusing species.

[Journal translation]

## 1. Introduction

La corrosion du cuivre en solution aqueuse est intimement liée à la nature des anions présents dans la solution (1) avec lesquels il a tendance à former de nombreux complexes (2–4). En présence d'ions chlorures, notamment, la dissolution anodique du cuivre s'accompagne généralement de la formation de complexes comme le $CuCl_2^-$ et le $CuCl_3^{2-}$, selon la concentration en $Cl^-$ (5–9). Il a aussi été clairement établi que la vitesse de dissolution du cuivre est contrôlée par la diffusion des ions dans la phase liquide (5–12), le cuivre ayant habituellement une valence de +1.

Par ailleurs, le chlorure cuivreux est susceptible de précipiter à la surface de l'électrode (7, 9–11, 13). La seule étude actuellement disponible dans la littérature au sujet de la dissolution du CuCl formé par précipitation électrochimique sur une électrode de cuivre a été réalisée en solution aqueuse contenant 2 *M* de HCl (7). Une méthode optique a permis de suivre, de façon qualitative, le gradient de concentration des différentes espèces ioniques près de la surface d'une électrode en stationnaire. L'étape déterminante de la dissolution du CuCl est attribuée à la diffusion du $CuCl_2^-$ dans la phase liquide. Enfin, il a été observé que la dissolution du CuCl, formé par voie non électrochimique, est contrôlée par la diffusion d'un complexe dans la solution (14). La solution contenait entre 0,11 et 0,89 *M* en NaCl dissous.

Le présent travail, pour sa part, se propose d'approfondir en utilisant une approche originale, l'étude de la dissolution du CuCl fraîchement formé à partir de l'oxydation électrochimique du cuivre en solution aqueuse. Les solutions aqueuses contiennent entre $2{,}36 \times 10^{-2}$ *M* et $16{,}49 \times 10^{-2}$ *M* de LiCl dissous.

## 2. Partie expérimentale

### 2.1 *La cellule et ses accessoires*

Les cellules électrochimiques utilisées étaient d'un type conventionnel avec une électrode de travail en cuivre, une contre-électrode en platine platinée et une électrode de référence au calomel saturé. La solution en contact avec la contre-électrode était séparée de la solution mère par du verre fritté

0008-4042/82/050616-08$01.00/0

©1982 National Research Council of Canada/Conseil national de recherches du Canada

Can. J. Chem. Downloaded from www.nrcresearchpress.com by 210.87.254.42 on 09/06/12
For personal use only.

Can. J. Chem. Downloaded from www.nrcresearchpress.com by 210.87.254.42 on 09/06/12
For personal use only.

alors que l'électrode de référence était immergée dans la partie supérieure du capillaire de Luggin dont l'extrémité venait à près de 1 mm de la surface de l'électrode en cuivre.

L'électrode de cuivre (Ventron Corp., 99,99%) se présentait sous la forme d'un fil de 0,64 cm de diamètre, d'une plaque de 1 cm × 2 cm ou d'un disque de 0,95 cm de diamètre; la surface de l'échantillon était de ~ 0,5 $cm^2$, ~ 4 $cm^2$ et 0,71 $cm^2$ respectivement. Le fil et la plaque étaient en position verticale tandis que le disque était en position horizontale. Les échantillons n'ont subi aucun traitement thermique préalable, tandis qu'une eau triplement distillée a été utilisée dans la préparation des solutions.

2.2 *La préparation des essais*

Un barbotage d'argon de 6 h précédait l'immersion de l'électrode de travail dans la solution. Les solutions étaient légèrement acides, le pH étant compris entre 3 et 5, et contenaient entre 1 et 7 g/L de LiCl. Un tampon à base de phtalate de potassium a été utilisé pour stabiliser le pH.

La méthode utilisée par Shoesmith et Lee (16) a été retenue pour le polissage du cuivre: l'échantillon était poli mécaniquement par abrasion avec du papier au carbure de silicium pour se terminer par un polissage avec une pâte de diament de 1 μ. L'échantillon était alors rincé à l'alcool, à l'acétone puis à l'eau distillée avant sont immersion.

2.3 *Les techniques expérimentales utilisées*

Les courbes cyclovoltammétriques ont été obtenues par les méthodes courantes. Un générateur de Tacussel G-STP2C, couplé à un potentiostat Wenking # 771068FR05, permettait de faire varier de façon continue ou brusque la tension de consigne imposée à l'électrode de cuivre. Un coulomètre Koslow Sci. Co. # 541 servait à mesurer la quantité d'électricité qui traversait l'électrode de travail durant l'oxydation et la réduction.

Par ailleurs, l'oxydation et la réduction en mode potentiostatique, i.e. à tension d'électrode constante, ont été effectuées en l'absence de toute agitation sur une électrode de travail stationnaire. Le cas échéant, l'agitation était imposée par barbotage d'un gaz inerte ou par rotation de l'électrode durant les périodes en circuit ouvert seulement.

Enfin, l'approche expérimentale mise au point pour la mesure de la vitesse de dissolution du chlorure cuivreux est décrite plus loin tandis que toutes les valeurs de la tension d'électrode sont données par rapport à l'électrode au calomel saturé.

## 3. Résultats expérimentaux et discussion

3.1 *Formation de la nantokite*

L'examen de l'enregistrement cyclovoltammétrique, reproduit à la figure 1, est représentatif du comportement de l'électrode de cuivre. L'accroissement de la vitesse de dissolution ($i_a$) est détectable au delà de −50 mV (/ECS). Pour des valeurs de tension croissantes, cet accroissement est continu de sorte que 4,1 mA/$cm^2$ coïncide avec + 100 mV.

Par ailleurs, $i_a$ est légèrement inférieur lors du balayage de retour tandis qu'un courant de réduction ($i_c$) est observé lorsque la tension franchit −15 mV. $i_c$ passe par un maximum de 4 mA/$cm^2$ environ pour devenir négligeable lorsque la tension atteint −180 mV, environ.

Dans ce cas, les quantités d'électricité mises en jeu sont de 48,5 mC/$cm^2$ en anodique ($Q_{oxy}$) contre

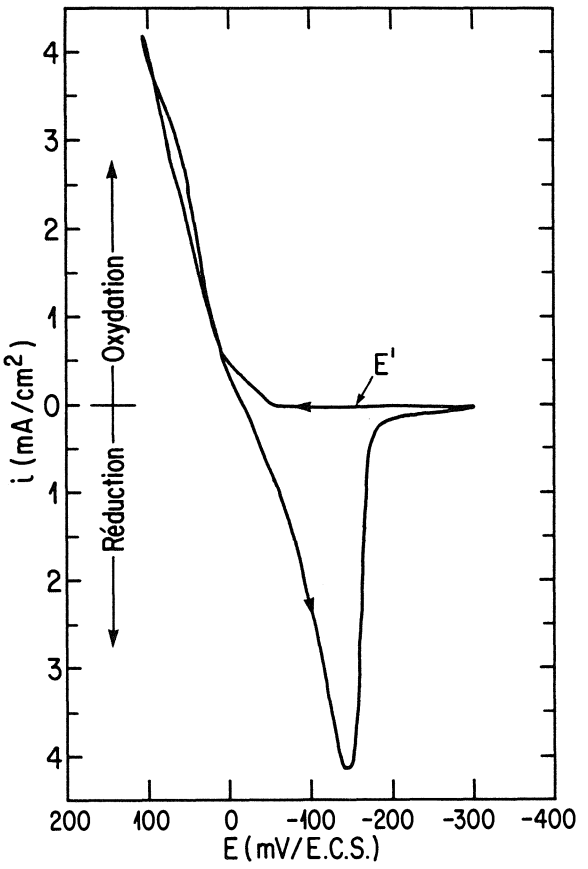


FIG. 1. Courbe de polarisation cyclovoltammétrique sur un fil de cuivre. E': tension du cuivre en circuit ouvert. Balayage à 10 mV/s. LiCl: 1 g/L, pH = 4.

32,5 mC/$cm^2$ en cathodique ($Q_{red}$). Le rapport $Q_{red}/Q_{oxy}$ est alors de 0,67. Ce comportement est généralement associé à la réduction d'un film peu ou pas protecteur formé durant le balayage anodique (15).

Le produit de corrosion qui s'accumule sur l'anode a été examiné par le microscope optique et à balayage ainsi que par diffraction aux rayons-X. Ces examens ont montré des cristaux de nantokite (CuCl) qui s'enchevêtrent pour recouvrir partiellement une surface sous-jacente à l'aspect rugueux (Fig. 2) et qui correspond au cuivre. On remarque, aussi, que les cristaux de nantokite sont souvent de forme tétraédrique. Dans l'exemple reproduit à la fig. 2, la portion de surface couverte par le précipité est de l'ordre de 0,5.

L'ensemble de ces observations suggère que la dissolution du cuivre est relativement uniforme tandis que les cristaux sont le résultat de la précipitation du CuCl suite à l'enrichissement de la solution en $Cu^+$ et en $Cl^-$ près de l'électrode.

Can. J. Chem. Downloaded from www.nrcresearchpress.com by 210.87.254.42 on 09/06/12
For personal use only.

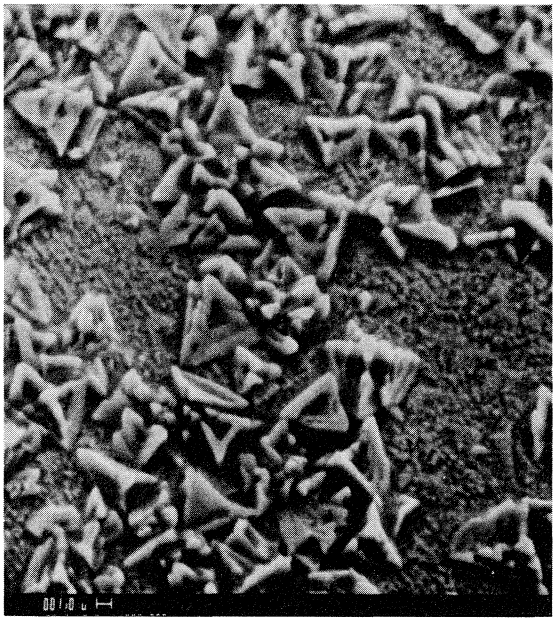

FIG. 2. Aspect de la surface de l'anode de cuivre en présence de nantokite. Tension imposée: +50 mV, durant 8 min.

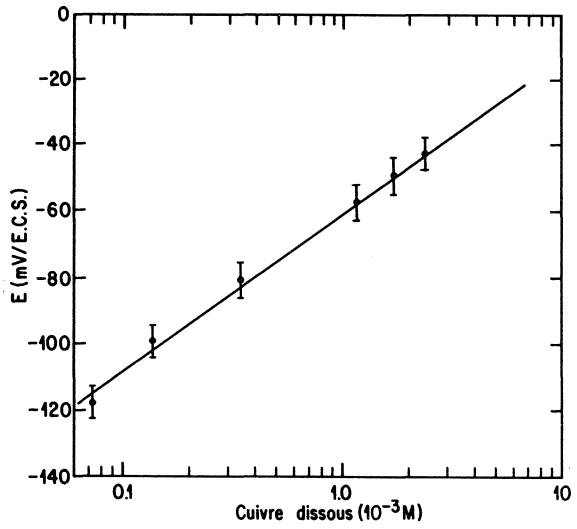


FIG. 3. Tension de l'électrode de cuivre en circuit ouvert ($E_{co}$) en l'absence de précipité en fonction de la concentration en cuivre dissous. LiCl: 1 g/L, pH = 4, solution désaérée.

### 3.2 *Passivation transitoire du cuivre*

La dissolution du CuCl, dès le retour en circuit ouvert, est susceptible de contribuer à l'enrichissement local de la solution. Il est alors prévisible que la tension du cuivre traduise cet enrichissement local.

La tension en circuit ouvert ($E_{co}$) du cuivre, en l'absence de précipité à sa surface, est représentée en fonction de la concentration en cuivre dissous à la fig. 3 tandis que $E_{co}$ du cuivre, en présence de précipité formé à sa surface, est donnée en fonction du temps à la fig. 4. $E_{co}$ du cuivre en présence de précipité présente deux plateaux. Le premier plateau se situe à −40 mV environ; cette valeur est voisine de la tension théorique de −10 mV qui correspond à l'équilibre Cu/CuCl (2). Par ailleurs, la saturation de la solution en $CuCl_2^-$ en présence de 1 g/L de LiCl dissous est de $1{,}34 \times 10^{-3}$ *M* d'après les valeurs thermodynamiques (2). Cette concentration de $1{,}34 \times 10^{-3}$ *M* en cuivre coïncide à $E_{co}$ égal à $-54 \pm 5$ mV (Fig. 3). Il est alors raisonnable d'envisager que la solution est dans un état proche de la saturation près de l'électrode alors recouverte de précipité.

Près du temps de transition τ, une baisse rapide de la tension se manifeste et un deuxième plateau est atteint au-delà de τ (Fig. 4). La tension du deuxième plateau dépend de la concentration en cuivre dissous au coeur de la solution. Quant au temps de transition τ, il est défini en suivant la même procédure que Shoesmith et Lee (16) pour l'étude de films d'oxydes de cuivre métastables.

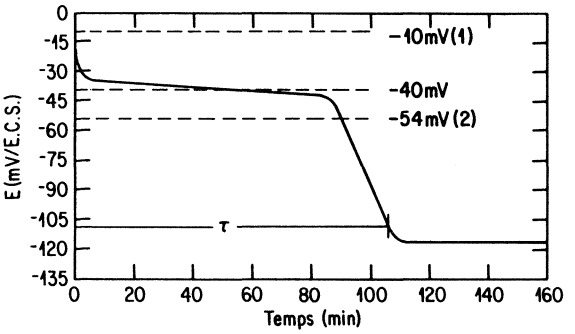


FIG. 4. Tension de l'électrode de cuivre en circuit ouvert après la formation de CuCl. *E*: tension d'électrode en circuit ouvert. LiCl: 1 g/L, pH = 4, solution désaérée. (1) $E_{co}$ théorique de l'équilibre Cu/CuCl; (2) $E_{co}$ pour $1{,}34 \times 10^{-3}$ *M* en cuivre dissous (Fig. 3).

De plus, l'examen de la surface au microscope a mis en évidence la disparition graduelle du produit de corrosion entre $t = 0$ et $t = \tau$ (Fig. 5a, b, c) tandis que le cuivre est complètement à nu à partir de τ (Fig. 5d, e).

La dissolution du précipité doit aussi se traduire par une augmentation de la concentration en cuivre dissous au sein de la solution jusqu'au temps $t = \tau$. Comme le montre l'example reproduit à la figure 6, la concentration en cuivre augmente de façon quasi linéaire avec le temps. L'enrichissement en cuivre ralentit en approchant de τ pour cesser au-delà de τ. Ce comportement incite à croire que la vitesse de dissolution de la nantokite est constante dans le temps jusqu'au voisinage du temps de transition.

Can. J. Chem. Downloaded from www.nrcresearchpress.com by 210.87.254.42 on 09/06/12
For personal use only.

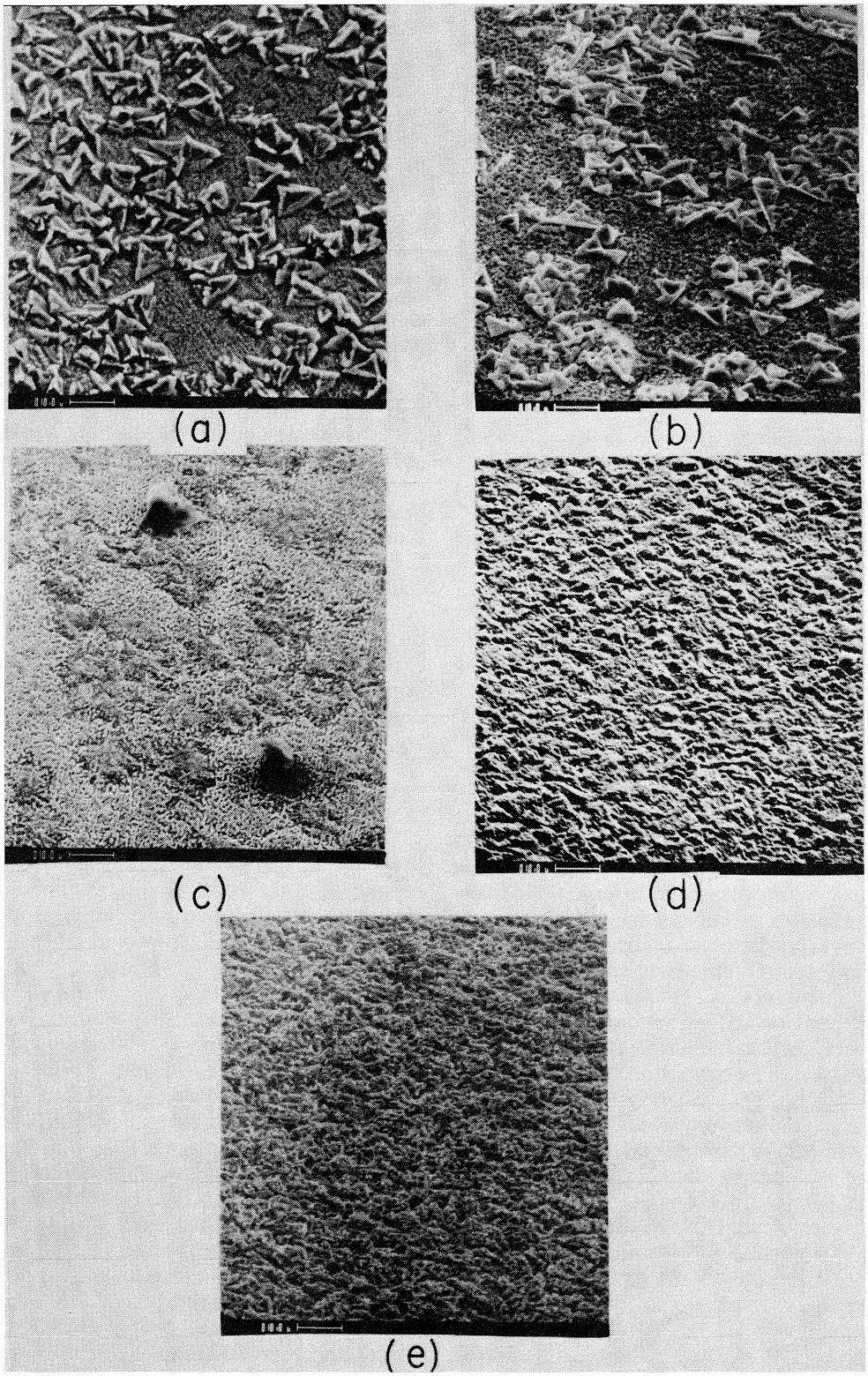


FIG. 5. Apparence de la surface de l'électrode durant la dissolution du CuCl. Condition d'oxydation: + 50 mV durant 8 min. LiCl: 1 g/L, pH = 4. Les durées d'immersion sont: (a) 0,05 $\tau$, (b) 0,40 $\tau$, (c) 0,91 $\tau$, (d) 0,99 $\tau$, (e) 1,17 $\tau$.

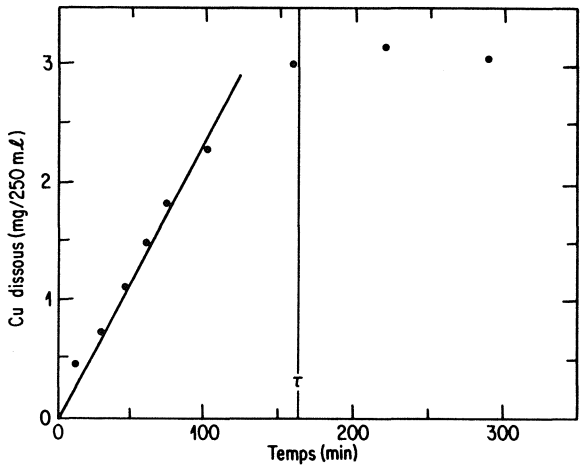


FIG. 6. Enrichissement de la solution en cuivre durant la dissolution de la nantokite. Concentration en cuivre obtenue à l'aide de la spectroscopie par absorption atomique.

### 3.3 *Mesure de la quantité de CuCl présent sur le cuivre*

La surface du cuivre était complètement à nu au départ. L'échantillon subissait, dans un premier temps, une oxydation électrochimique par enclenchement d'une tension anodique. La valeur de + 50 mV a été choisie. Un second enclenchement à −300 mV, destiné à réduire le précipité, suivait immédiatement l'oxydation. Les charges électriques mises en jeu durant l'oxydation ($Q_{oxy}$) et la réduction $(Q_{red})_{t=0}$ étaient mesurées.

Dans ces conditions, la réduction du précipité dépasse rarement 1 min. Le courant devient négligeable au pied de la vague de réduction, ce qui suggère la réduction complète du précipité. L'absence de précipité a été confirmée à partir de l'examen de la surface au microscope et de la mesure de la tension d'électrode en circuit ouvert. Le comportement du CuCl soumis à une réduction rappelle celui du $Cu(OH)_2$ en solution alcaline (16).

Par ailleurs, la charge de réduction $(Q_{red})_{t=0}$ dépend de la charge en oxydation ($Q_{oxy}$) tandis que le rapport $(Q_{red})_{t=0}/Q_{oxy}$ est constant lorsque les conditions d'oxydation demeurent les mêmes et ce, malgré les variations importantes de $Q_{oxy}$ (Fig. 7) qui ont été observées. Dans cet exemple, les charges $Q_{oxy}$ et $(Q_{red})_{t=0}$ ont été mesurées pour plusieurs cycles successifs oxydation–réduction avec +50 mV imposé durant 8 min en oxydation et −300 mV imposé durant 5 min en réduction.

En l'absence d'agitation, le rapport $(Q_{red})_{t=0}/Q_{oxy}$ demeure voisin de 0,5 tandis que $Q_{oxy}$ est compris entre 1100 et 2350 mC/cm². Ce rapport tend a diminuer lorsque l'agitation de la solution devient plus intense. La perte qui correspond à $Q_{oxy} - (Q_{red})_{t=0}$ est attribuée à la non précipitation d'une partie du cuivre qui va en solution, à la dissolution partielle du précipité et, enfin, au fait observable à l'oeil nu que des cristaux de nantokite ne sont pas retenus à la surface de l'électrode. Ainsi, la constance du rapport $(Q_{red})_{t=0}/Q_{oxy}$ permet de déduire la quantité de précipité présent en terme de charge $Q_{red}$ à partir de la valeur de $Q_{oxy}$.

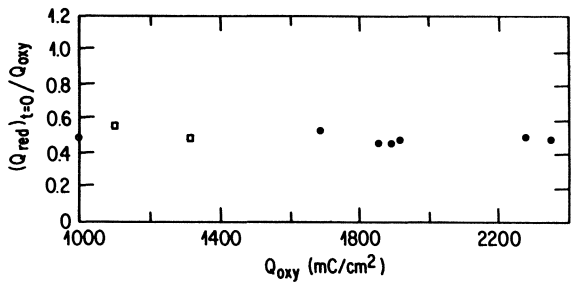


FIG. 7. Rapport $(Q_{red})_{t=0}/Q_{oxy}$ en fonction de $Q_{oxy}$ pour deux échantillons différents. $Q_{oxy}$: quantité d'électricité impliquée durant l'oxydation. $(Q_{red})_{t=0}$: quantité d'électricité obtenue par réduction complète du CuCl immédiatement après oxydation. $E_{oxy}$ = +50 mV durant 8 min; $E_{red}$ = −300 mV durant 5 min.

Le rapport $(Q_{red})_{t=0}/Q_{oxy}$ varie sensiblement d'un échantillon à l'autre même si les conditions expérimentales sont rigoureusement les mêmes. Par conséquent, ce rapport a été déterminé pour chaque immersion et $Q_{red}$ a été calculé à partir de $Q_{oxy}$.

### 3.4 *Vitesse de dissolution de la nantokite sur une électrode stationnaire*

On a vu, d'une part, que la quantité de précipité présent à la surface de l'échantillon est calculable et que, d'autre part, la dissolution du CuCl en circuit ouvert s'achève complètement au temps de transition τ. De plus, l'enrichissement de la solution en cuivre est quasi-linéaire avec le temps jusqu'en τ (Fig. 6); ce qui est compatible avec une vitesse de dissolution ($v$) constante. La vitesse $v$, en courant équivalent, est donc évaluable à partir du rapport $(Q_{red})_{t=0}/\tau$. Les mesures de $v$, à partir de cette approche, ont données 0,14 mC $s^{-1}$ $cm^{-2}$ en courant équivalent pour 1 g/L de LiCl dissous.

Par ailleurs, la constance de $v$ a été vérifiée à partir de la réduction à −300 mV du précipité après des durées variables de séjour en circuit ouvert (Fig. 8.). La différence entre $(Q_{red})_{t=0}$ et $(Q_{red})_{t=t}$ est associée à la perte de nantokite durant le temps $t$ où l'électrode est en circuit ouvert. La pente de la droite obtenue, qui correspond à $v$ en courant équivalent, est ici de 0,16 mC $s^{-1}$ $cm^{-2}$. La perte en nantokite cesse au temps τ où la dissolution du précipité est complète.

Enfin, on a observé que la vitesse de dissolution

Can. J. Chem. Downloaded from www.nrcresearchpress.com by 210.87.254.42 on 09/06/12
For personal use only.

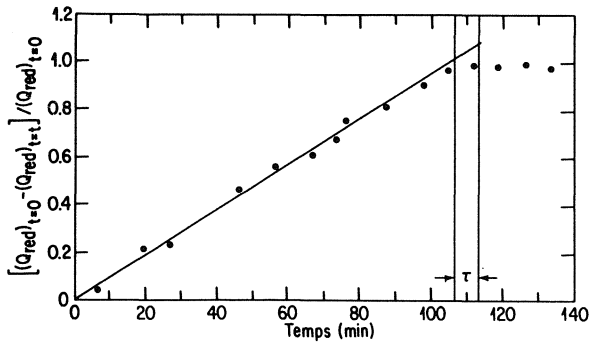


FIG. 8. Quantité de précipité qui passe en solution durant la période en circuit ouvert. $(Q_{red})_{t=0}$: quantité d'électricité disponible par réduction du CuCl immédiatement après formation du précipité. $(Q_{red})_{t=t}$: quantité d'électricité obtenue par réduction du précipité après le temps $t$. $(Q_{red})_{t=0} - (Q_{red})_{t=t}$: quantité de précipité qui va en solution durant le temps $t$.

est intimement liée à l'agitation de la solution réalisée à l'aide d'un barbotage d'un gaz inerte, par exemple, ainsi qu'à la position de l'électrode par rapport à la verticale alors que $v$ est maximum en position verticale et minimum à l'horizontal. L'utilisation d'une électrode à disque tournant en cuivre a permis de fixer les conditions d'agitation et d'établir que la vitesse de dissolution est contrôlée par la diffusion en phase liquide.

### 3.5 *Influence de l'agitation*

Les enregistrements de la tension en circuit ouvert en fonction du temps, reproduits à la figure 9, confirment l'influence déterminante de l'agitation pour des vitesses de rotation comprises entre 4 et 100 t/s. La vitesse de dissolution du CuCl, calculée à partir de la variation de la tension transitoire du cuivre en circuit ouvert, est donnée en fonction de la racine carrée de la vitesse de rotation de l'électrode (Fig. 10) où ω est compris entre 1 et 100 t/s.

L'augmentation linéaire de $v$ avec la racine carrée de ω est caractéristique d'un processus de dissoluton entièrement contrôlé par la diffusion dans la phase liquide (17). En langage mathématique:

[1] $$v = K\omega^{\frac{1}{2}}$$

avec

[2] $$K = 0{,}62\, nFD^{2/3}\nu^{-1/6}(C_s - C_0)$$

où ν correspond à la viscosité de la solution. $C_s$ et $C_0$ représentent la concentration de l'espèce considérée en surface et au sein de la solution, respectivement.

Ainsi, le coefficient de diffusion $D$ est calculable à partir de la relation [2] selon

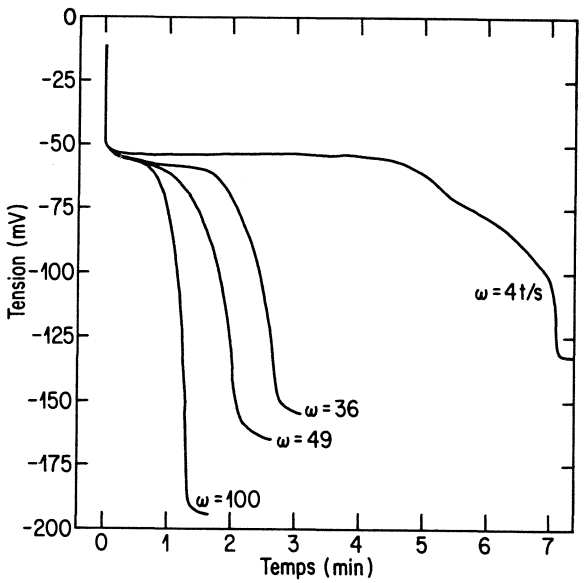


FIG. 9. Influence de la vitesse de rotation de l'électrode sur la tension en circuit ouvert. ω: vitesse de rotation de l'électrode en tours par seconde. pH = 4, LiCl = 5 g/L, $A$ = 0,71 cm².

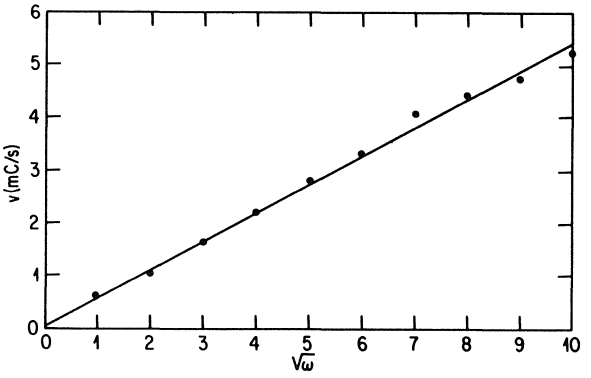


FIG. 10. Vitesse de dissolution en fonction de $\sqrt{\omega}$. $v$: vitesse de dissolution du CuCl en courant équivalent; pH = 4, LiCl = 5 g/L, $A$ = 0,71 cm².

[3] $$D = 2{,}05\, K^{3/2}\nu^{1/4}(nF)^{-3/2}(C_s - C_0)^{-3/2}$$

Par ailleurs, on a vu que la solution au voisinage de l'électrode est saturée en ion cuivreux (Figs. 2, 3, 9) tandis que le cuivre dissous doit exister sous forme de $CuCl_2^-$ dans la gamme de concentration en $Cl^-$ considérée (5, 14). La formation du $CuCl_2^-$ à partir de la nantokite est compatible avec la réaction globale:

[4] $$CuCl + Cl^- \rightleftarrows CuCl_2^-$$

La saturation en $CuCl_2^-(C_s)$, évaluée à partir des valeurs des enthalpies libres de formation standard (2) pour la réaction [4], est donnée en fonction de la concentration en LiCl dissous (Tableau 1). Pour sa

Can. J. Chem. Downloaded from www.nrcresearchpress.com by 210.87.254.42 on 09/06/12
For personal use only.

Can. J. Chem. Downloaded from www.nrcresearchpress.com by 210.87.254.42 on 09/06/12
For personal use only.

TABLEAU 1. Saturation en $CuCl_2^-$ en fonction de la concentration en LiCl dissous

| LiCl dissous (g/L) | $C_s$ ($10^{-3}$ $M$)[a] |
|---|---|
| 1 | 1,34 |
| 2 | 2,68 |
| 3 | 4,02 |
| 5 | 6,7 |
| 7 | 9,38 |

[a]Saturation évaluée à partir des valeurs des enthalpies libres de formation standard (2) pour la réaction [4].

part, ν est égal à $0,96 \times 10^{-2}$ cm²/s (18, 19) contre 1 pour $n$ alors que $C_o$ est estimée négligeable par rapport à $C_s$.

Le rapport $v/\omega^{\frac{1}{2}}$ ou $K$ obtenu avec l'électrode à disque tournant est donné en fonction de la concentration en LiCl dissous à la figure 11. A l'aide de la relation [3], on trouve $D = 0,6 \times 10^{-5}$ cm²/s tandis que $D_{CuCl_2^-}$ généralement admis dans la littérature est compris entre 1 et $0,6 \times 10^{-5}$ cm²/s (20, 21).

De plus, rappelons que

$$[5] \quad C_s = K_e[Cl^-]$$

où $K_e$ est la constante à l'équilibre de la réaction [4] égale à 0,057 [2]. La combinaison des relations [2] et [5] avec $C_o \ll C_s$ conduit à:

$$[6] \quad K = 0,62\, nFD^{2/3}\nu^{-1/6}K_e[Cl^-]$$

Par conséquent, le rapport $v/\omega^{\frac{1}{2}}$ ou $K$ doit être proportionnel à $[Cl^-]$ dans le cas où la réaction [4] est envisagée. Ce qui est tout à fait conforme à nos mesures expérimentales (Fig. 11). Il est aussi prévisible que l'influence du pH entre 3 et 5 soit marginale (Fig. 12). Ainsi l'ensemble des résultats expérimentaux s'expliquent de façon cohérente à partir de la présence du $CuCl_2^-$ comme espèce ionique qui diffuse.

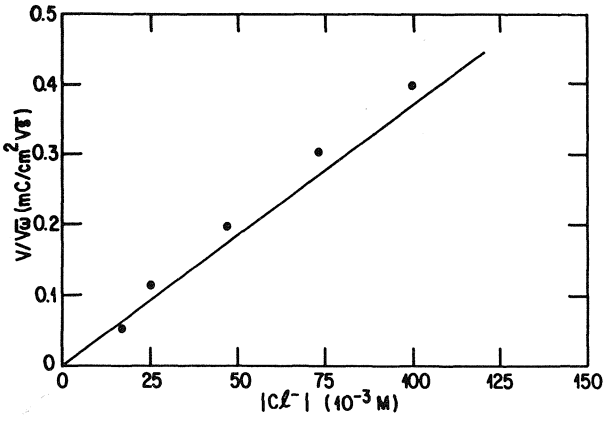


FIG. 11. Rapport $v/\omega^{\frac{1}{2}}$ en fonction de la concentration en LiCl dissous. Ces résultats ont été obtenus à l'aide de l'électrode à disque tournant.

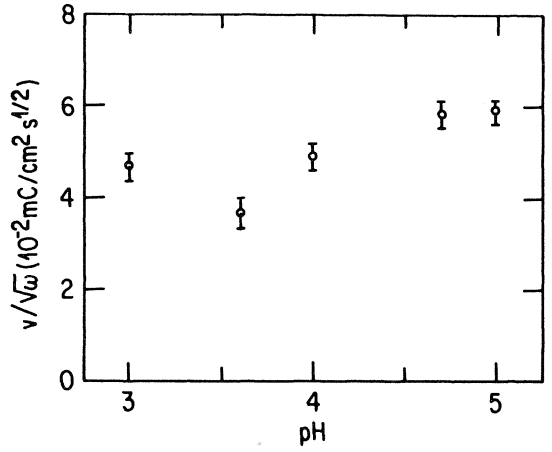


FIG. 12. Influence du pH sur la vitesse de dissolution de la nantokite. LiCl = 1 g/L.

## 4. Conclusion

1. La présence de chlorure cuivreux, formé par précipitation à la surface de l'électrode de cuivre, contribue à l'enrichissement local de la solution qui est alors dans un état voisin de la saturation en cuivre dissous. Cet enrichissement se traduit par une tension d'électrode bien caractéristique qui tombe dès la dissolution complète du précipité.

2. La vitesse de dissolution du précipité est constante jusque dans les instants qui précèdent sa dissolution complète. Elle est indépendante du pH entre 3 et 5 mais est proportionnelle à la concentration en $Cl^-$.

3. La dissolution de la nantokite est entièrement dominée par la diffusion d'une espèce ionique qui se déplace depuis l'électrode jusqu'au coeur de la solution. Les résultats expérimentaux s'expliquent entièrement à partir de la présence du $CuCl_2^-$ comme espèce ionique qui diffuse.

4. La mesure de la vitesse de dissolution du CuCl à partir de la détermination du temps de transition τ est un outil simple et efficace qui donne accès à l'étude de films peu épais fraîchement formés par oxydation électrochimique.

## Remerciements

L'auteur tient à remercier le Dr G. Bélanger (I.R.E.Q.) avec qui il a eu des discussions fort utiles ainsi que G. Larochelle pour l'analyse des solutions.

1. H. LEIDHEISER. The corrosion of copper, tin, and their alloys. J. Wiley & Sons, New York. 1971. Chapt. 4.
2. J. VANMUYLDER, N. DE ZOUBOV et M. POURBAIX. CEBELCOR. Rapp. Tech. No 101. Bruxelles. juillet 1962.

3. V. V. ISAEV, V. I. KUCHERENKO et V. N. FLEROV. Sov. Electrochem. **14**, 637 (1978).
4. Yu. I. NAUMOV, L. I. MOLVINA, G. V. KOROLEV, V. I. KUCHERENKO et V. N. FLEROV. Sov. Electrochem. **15**, 597 (1979).
5. M. BRAUN and K. NOBE. J. Electrochem. Soc. **126**, 1666 (1979).
6. A. L. BACARELLA et J. C. GRIESS. J. Electrochem. Soc. **120**, 459 (1973).
7. R. S. COOPER et J. H. BARTLETT. J. Electrochem. Soc. **105**, 109 (1958).
8. R. K. ASTAKHOVA et B. S. KRASIKOV. Zh. Prikl. Khim. **44**, 363 (1972).
9. C. H. BONFIGLIO, H. C. ALBAYA et O. A. COBO. Corros. Sci. **13**, 717 (1973).
10. L. KISS, J. FARKAS et A. KOROSI. Acta Chim. (Budapest), **67**, 179 (1971).
11. L. KISS, J. FARKAS et A. KOROSI, Magy. Kem. Foly. **77**, 35 (1971).
12. V. K. ALTUKHOV, A. V. VVEDENSKII, I. K. MARSHADOV et T. N. KLEDININA. Sov. Electrochem. **15**, 242 (1979).
13. S. NAGESWAR et T. H. V. SETTY. Proc. Ind. Acad. Sci. Sect. A, **71**, 282 (1972).
14. I. A. SEMENOV, V. F. LAZAREV et A. I. LEVIN. Sov. Electrochem. **11**, 1013 (1975).
15. R. L. BROSSARD et D. L. PIRON. Can. J. Chem. **58**, 30 (1980).
16. D. W. SHOESMITH et W. LEE. Electrochim. Acta, **22**, 1411 (1977).
17. V. G. LEVICH. Physicochemical hydrodynamics. Prentice Hall, Englewood Cliffs, NJ. 1962.
18. R. B. BIRD, W. E. STEWART et E. N. LIGHTFOOT. Transport phenomena. J. Wiley & Sons, New York. 1960. p. 8.
19. R. PARSONS. Handbook of electrochemical constants. Butterworths Scientific Publ., London. 1959. p. 77.
20. A. RIZENKAMPS et E. BELTOVSKA. Electrokhimiya, **11**, 374 (1975).
21. A. MOREAU. Electrochim. Acta, **26**, 497 (1981).

Can. J. Chem. Downloaded from www.nrcresearchpress.com by 210.87.254.42 on 09/06/12
For personal use only.

# The Schmidt reaction of anthraquinones

CECILY A. FLEMMING, SHAM S. GANDHI, MARTIN S. GIBSON,[1] AND EDWARD H. RUEDIGER
*Department of Chemistry, Brock University, St. Catharines, Ont., Canada L2S 3A1*

Received August 26, 1981

CECILY A. FLEMMING, SHAM S. GANDHI, MARTIN S. GIBSON, and EDWARD H. RUEDIGER. Can. J. Chem. **60**, 624 (1982).

Schmidt reaction (sodium azide/sulfuric acid) of 1,5- and of 1,8-dichloroanthraquinones gives, in each case, both of the theoretically possible lactams (2,3,5,6-dibenzoazepin-4,7-diones). Two of the four theoretically possible lactams have been identified from Schmidt reaction of 1- and 2-chloroanthraquinones respectively. Methods used include: (a) preferential hydrolysis of one lactam and identification of the isomeric aminoanthraquinone formed on cyclodehydration of the resulting amino acid; (b) identification of the isomeric aminoanthraquinone(s) formed on direct treatment of a lactam (or mixture of lactams) by sulfuric acid; (c) cleavage by potassium *tert*-butoxide of the amino acid formed by preferential hydrolysis of one lactam and identification of the resulting benzoic acid as its methyl ester.

CECILY A. FLEMMING, SHAM S. GANDHI, MARTIN S. GIBSON et EDWARD H. RUEDIGER. Can. J. Chem. **60**, 624 (1982).

Les dichloro-1,5 et -1,8 anthraquinones soumises à la réaction de Schmidt (azoture de sodium/acide sulfurique) conduisent chacun aux deux lactames qui sont theoriquement possibles (dibenzo-2,3,5,6 azépinediones-4,7). On a identifié deux des quatres lactames pouvant provenir de la reaction de Schmidt sur les chloro-1 et chloro-2 anthraquinones respectivement. Les méthodes utilisées comprennent: (a) l'hydrolyse préférentielle d'un lactame et l'identification de l'aminoanthraquinone isomère formée par la cyclodeshydratation de l'acide amine formé; (b) l'identification des aminoanthraquinones isomères formées par la réaction directe du lactame (ou d'un melange de lactames) avec l'acide sulfurique; (c) l'utilisation du *tert*-butylate de potassium pour cliver l'acide aminé formé par l'hydrolyse préferentielle d'un lactame et l'identification de l'acide benzoique résultant sous forme d'ester méthylique.

[Traduit par le journal]

Substituted 2-aminobenzophenones are of interest as sources of various heterocyclic compounds, including acridones (1, 2). The reports of Caronna and Palazzo that five monosubstituted anthraquinones react with sodium azide in concentrated sulfuric acid (Schmidt reaction) to give in each case a single lactam (2,3,5,6-dibenzoazepin-4,7-dione) are thus of interest since these lactams can be hydrolyzed to the corresponding 2-aminobenzophenone-2′-carboxylic acid (3, 4). Structures were assigned to these lactams and were supported in three cases by hydrolysis and alternate cyclodehydration to the corresponding aminoanthraquinone. In particular, the lactams obtained from 1- and 2-chloroanthraquinones were formulated as **1** and **2** respectively.

Schmidt reaction of a number of alkyl-substituted 1,4-benzo- and naphthoquinones has similarly been reported to give single lactams (5). However, structures were incorrectly assigned and in the course of correction it was noted that lactam mixtures were produced in some reactions (6, 7). It was concluded that these Schmidt reactions proceeded primarily under steric control, with electronic effects exerting a minor influence. Preferential attack occurred at the more hindered, less basic carbonyl group, followed by preferential migration of the larger attached substituent with loss of nitrogen.

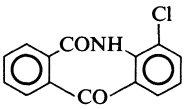


**1**

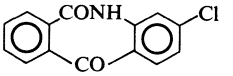


**2**

Our objectives have been to verify, or otherwise, the course of the Schmidt reaction of 1- and 2-chloroanthraquinones, and to extend the study to 1,8- and 1,5-dichloroanthraquinones.

Schmidt reaction of 1-chloroanthraquinone gave a lactam product in high yield. It was, however, immediately apparent from thin-layer chromatography (tlc) and mass spectrometry that this product was a mixture of two or more lactams (four being theoretically possible) with closely related $R_f$ values. It was in fact possible by careful chromatography to separate two lactam fractions which for discussion we designate as lactam **A** (mp 178–180°C) and, in slightly larger quantity, lactam **B** (mp 227–229°C). This separation could, in effect, also be achieved by partial hydrolysis of the crude mixture using 2% ethanolic potassium hydroxide when lactam **A** was preferentially hydrolyzed. The amino acid thus produced (from lactam **A**) was heated with sulfuric acid to effect cyclization to the corresponding anthraquinone (3, 4). This gave a material (ca. 20%) which was separated by chromatography into 1-amino-2-chloroanthraquinone and lactam **A**, alternate products of cyclization of 2-amino-3-chlorobenzophenone-2′-carboxylic acid.

[1]Author to whom correspondence may be addressed.

0008-4042/82/050624-05$01.00/0

©1982 National Research Council of Canada/Conseil national de recherches du Canada

Can. J. Chem. Downloaded from www.nrcresearchpress.com by 210.87.254.40 on 09/06/12
For personal use only.

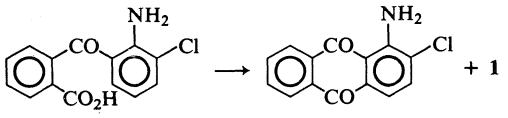

These are evidently derived from **1** as reported previously (4).

Lactam **B** was hydrolyzed using 25% aqueous potassium hydroxide. Cyclization of the resulting amino acid using sulfuric acid gave a material (ca. 30%) which on chromatography gave an aminoanthraquinone fraction and lactam **B**. The former was tentatively identified as (impure) 1,8-aminochloroanthraquinone since a mixture mp with the alternative 1,5-isomer showed depression; tlc and mass spectral characteristics were not sufficiently definitive to corroborate this identification. With this proviso, lactam **B** may be formulated as:

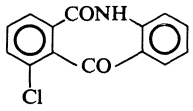

LACTAM B

The case of 2-chloroanthraquinone also presents the possibility of four isomeric lactams being produced, of which **2** is one. Schmidt reaction gave a lactam mixture in good yield. The product showed simply a broad spot on tlc and, while assumed to be a mixture, did not lend itself to chromatographic separation or to attempts at preferential hydrolysis. In an attempt to identify (some of) the lactams present, this mixture was submitted to direct treatment with sulfuric acid (8). This gave a complex mixture (tlc) containing none of the starting lactams. Chromatography gave, in order of elution, compounds **3**, **4**, and **5**, each of which was

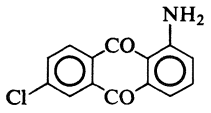

3

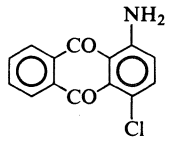

4

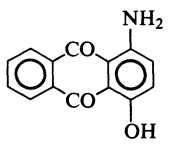

5

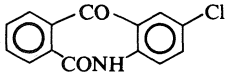

6

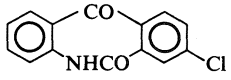

7

identified by comparison with authentic samples; recovery was ca. 50%. Compound **5** is evidently an artifact arising from hydrolytic displacement of chlorine either before or after formation of **4**. These compounds would have lactam **6** as precursor and compound **3** would similarly be derived from lactam **7**. Caronna and Palazzo's lactam **2** or the fourth possible isomer may have been present in the crude lactam mixture, but we obtained no evidence on this point.

The cases of 1,8- and 1,5-dichloroanthraquinones are in principle more tractable in that each of the quinones can yield at most two lactams. Schmidt reaction of 1,8-dichloroanthraquinone gave a mixture of two isomeric lactams (tlc) in good yield. Partial hydrolysis of this mixture with 2% ethanolic potassium hydroxide gave the (unhydrolyzed) lactam of slightly lower $R_f$ value and, after acidification, an amino acid derived from the other lactam. The lactam mixture was treated directly with sulfuric acid (8) and the product was chromatographed giving 1-amino-2,5-dichloroanthraquinone together with the lactam of lower $R_f$ value. A separate experiment confirmed that the lactam of lower $R_f$ value was only slightly affected under these reaction conditions. The quinone was evidently derived from **8** (lactam of higher $R_f$) since **9** (lactam of lower $R_f$) could not give a quinone without substituent displacement. The lactam of lower $R_f$ was hydrolyzed separately using 25% aqueous potassium hydroxide and the resulting amino acid was treated with sulfuric acid. Reversion to the lactam occurred, consistent with its formulation as **9**; interestingly, formation of 3-

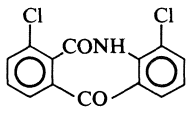

8

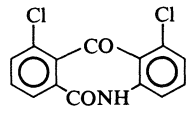

9

chlorophthalic anhydride as a minor product was observed. The amino acid from **8**, similarly treated, gave the aforementioned quinone, together with **8** and 3-chlorophthalic anhydride (tlc, mass spectrum).

Implicit in methods of identifying these difficultly separable isomeric lactams by direct treatment with sulfuric acid or by preferential hydrolysis to an amino acid followed by treatment with sulfuric acid is the assumption that only direct cyclization to a quinone, where possible, occurs; i.e. there is no electrophilic displacement (or migration) of chlorine, nor do quinones arise by dismutation/recombination reactions. There are additional practical

Can. J. Chem. Downloaded from www.nrcresearchpress.com by 210.87.254.40 on 09/06/12
For personal use only.

problems of low yields and the absence of reference quinones for comparison as well as similarities in properties of isomeric quinones. For the Schmidt reaction of 1,5-dichloroanthraquinone, we have therefore developed an alternative approach. This reaction gave a mixture of two isomeric lactams, **10** and **11**, with closely related $R_f$ values. The lactam

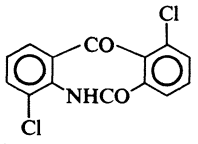


**10**

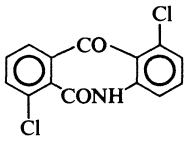


**11**

of higher $R_f$ was preferentially hydrolyzed on treatment of the mixture with 2% ethanolic potassium hydroxide. The amino acid thus obtained is a substituted benzophenone and should thus be amenable to base cleavage to substituted benzoic (or phthalic) acids. Since cleavage of 2-chloro- and 2-carboxybenzophenones has been found to occur mainly on the side of the carbonyl group closer to the substituent (9), examination of cleavage product(s) should permit identification of the amino acid and hence of the precursory lactam. The amino acid in question was successfully cleaved by potassium *tert*-butoxide in 1,2-dimethoxyethane and the acid(s) isolated were converted to the methyl ester(s). Examination of the methyl ester(s) by gas–liquid chromatography (glc), using methyl 2- and 3-chlorobenzoates as standards, revealed the presence of the latter but none of the former ester. This is consistent only with the formulation of the preferentially hydrolyzed lactam as **10** and the other lactam as **11**. This method is reasonably convenient and likely to be useful in cases where the requisite anthraquinones are not available as standards for application of the earlier procedures for assigning lactam structures (3, 4, 8).

The synthetic usefulness of the Schmidt reaction of substituted anthraquinones is thus marred by the production of difficultly separable isomers rather than single lactams as previously reported (3, 4). Isomer production is a feature in common with the Schmidt reaction of some 1,4-benzo- and naphthoquinones (6, 7).

## Experimental

The ir spectra are quoted for KBr discs. The $^1$H nmr spectra were obtained on a Bruker WP-60FT spectrometer (60 MHz; tetramethylsilane as internal standard). Mass spectra were determined with an AEI MS-30 double-beam spectrometer; *m/e* values are reported for the lowest isotopic species (relative intensities in parentheses).

The tlc and plate chromatography were performed on silica gel; glc was carried out on an F and M Laboratory Chromatograph Model 700 using a six-foot column of diethylene glycol succinate on Chromosorb (80–100 mesh); column temperature 150°C, flow rate 40 mL/min.

Purity of all samples was checked before use. Commercial 1-amino-5-chloroanthraquinone was purified by plate chromatography, followed by sublimation, and had mp 221°C (lit. (10) mp 215–217°C); 1-amino-8-chloroanthraquinone was a prepared sample and had mp 225–229°C (lit. (10) mp 225–227°C), but was not quite pure.

*Schmidt reaction of 1-chloroanthraquinone*

To a stirred solution of the quinone (11.0 g) in concentrated $H_2SO_4$ (160 mL) was added $NaN_3$ (9.75 g) in portions so as to maintain a reaction temperature of 40–50°C. Stirring was continued at 40–50°C for 4 h and the mixture was then poured into water to give an off-white solid (10.6 g), mp 185–190°C, consisting apparently of two or more isomeric compounds (tlc, mass spectrum) similar in $R_f$ value.

A sample (1.0 g) of the crude product was chromatographed (silica gel, benzene). Elution gave lactam **A** (i.e. **1**) as a colorless solid (325 mg), mp 178–180°C (after crystallization from aqueous $Me_2SO$); ir: 3185, 1670 and 1655 cm$^{-1}$; $^1$H nmr ($Me_2SO$-$d_6$) δ: 10.09–10.04 (br s, 1H, exchangeable with $D_2O$); mass spectrum *m/e*: 257 ($M^+$, 75), 256 (M − H, 100), 229 (M − CO, 75), 222(M − Cl, 5), 201 (M − 2CO, 17), 166 (M − 2CO − Cl, 25), 139 (166 − HCN, 15). *Anal.* calcd. for $C_{14}H_8ClNO_2$: C 65.26, H 3.13, Cl 13.76, N 5.44; found: C 64.90, H 3.21, Cl 13.46, N 5.57.

Further elution gave lactam **B** as a colorless solid (500 mg), mp 227–229°C (after crystallization from aqueous $Me_2SO$); ir: 3180, 1670, and 1655 cm$^{-1}$; $^1$H nmr ($Me_2SO$-$d_6$) δ: 11.2 (br s, 1H, exchangeable with $D_2O$); mass spectrum *m/e*: 257 ($M^+$, 90), 256 (100), 229 (70), 222 (33), 201 (38), 166 (45), 139 (23). *Anal.* calcd. for $C_{14}H_8ClNO_2$: C 65.26, H 3.13, Cl 13.76, N 5.44; found: C 65.21, H 3.14, Cl 13.84, N 5.54.

*Hydrolysis of the foregoing lactams*

(a) A sample of the crude lactam mixture (5.0 g) from the previous experiment was boiled with 2% ethanolic KOH solution (100 mL) for 15 min. When cool, the solution was filtered and the filtrate was poured into water. The precipitated solid was crystallized from aqueous $Me_2SO$ to give the unhydrolyzed lactam **B** (2.45 g), mp 225–227°C, identical with the reference sample (mixture mp, tlc, ir spectrum).

The ethanolic filtrate from the hydrolysis was carefully acidified (concentrated $H_2SO_4$). Next day, the precipitated solid was collected and crystallized from aqueous ethanol to give 2-amino-3-chlorobenzophenone-2′-carboxylic acid (1.1 g), mp 180–181°C (lit. (11) mp 188°C); ir: 3465, 3345, 1690, and 1650 cm$^{-1}$; mass spectrum *m/e*: 275 ($M^+$). *Anal.* calcd. for $C_{14}H_{10}ClNO_3$: C 60.99, H 3.66, Cl 12.86, N 5.08; found: C 60.94, H 3.67, Cl 12.73, N 5.09.

(b) The lactam **B** (1.3 g, mp 225–227°C) was boiled with 25% aqueous KOH solution (60 mL) for 15 min and the solution was then filtered. When cool, the solution was carefully acidified (concentrated $H_2SO_4$) and left to stand overnight. The precipitated solid was collected, dried, and crystallized from benzene to give 2-amino-6′-chlorobenzophenone-2′-carboxylic acid (450 mg), mp 152–153°C; ir: 3460, 3345, 1720, and 1690 cm$^{-1}$; mass spectrum *m/e*: 275 ($M^+$). *Anal.* calcd. for $C_{14}H_{10}ClNO_3$: C 60.99, H 3.66, Cl 12.86, N 5.08; found: C 60.97, H 3.74, Cl 12.81, N 5.08.

*Treatment of the foregoing amino acids with concentrated sulfuric acid*

(a) A solution of 2-amino-3-chlorobenzophenone-2′-carboxylic acid (400 mg, mp 181–183°C) in concentrated $H_2SO_4$ (2.0 g) was slowly heated to 140–145°C and this reaction temperature was maintained for 6 h. When cool, the mixture was poured into ice-cold water. The precipitated solid (75 mg, mp 175–177°C),

Can. J. Chem. Downloaded from www.nrcresearchpress.com by 210.87.254.40 on 09/06/12
For personal use only.

Can. J. Chem. Downloaded from www.nrcresearchpress.com by 210.87.254.40 on 09/06/12
For personal use only.

which apparently contained two components (tlc), was chromatographed on silica gel using benzene/petroleum ether as eluant. An orange solid (50 mg) was collected which crystallized from benzene/petroleum ether to give orange needles of 1-amino-2-chloroanthraquinone, mp 192–193°C (lit. (4) mp 197–198°C), identical with an authentic sample (mixture mp, tlc, mass spectrum); mass spectrum *m/e*: 257 ($M^+$).

Further elution (benzene) gave lactam **A** (**1**) (15 mg), mp 175–177°C, after crystallization from aqueous $Me_2SO$, identical with the reference sample (mixture mp tlc, ir spectrum).

(b) A solution of 2-amino-6′-chlorobenzophenone-2′-carboxylic acid (250 mg, mp 151–153°C) in concentrated $H_2SO_4$ (3.0 g) was heated slowly to 160–165°C and this temperature was maintained for 7 h. Isolated as in (a) above, the product (70 mg), which apparently contained two components (tlc), was chromatographed on silica gel (benzene/petroleum ether). This gave a brownish red solid (35 mg) which was crystallized twice from benzene to give red needles, mp 212–217°C, slightly contaminated with lactam **B** (mp 227–230°C); a mixture mp with 1,5-aminochloroanthraquinone was 189–210°C.

Further elution (benzene) gave lactam **B** (30 mg), mp 225–227°C after crystallization from aqueous $Me_2SO$, identical with the reference sample (mixture mp, tlc, ir, and mass spectra).

*Schmidt reaction of 2-chloroanthraquinone*

2-Chloroanthraquinone (16.5 g) was treated as for the 1-isomer above to give a crude product (14.8 g) consisting of two or more components with almost identical $R_f$ values. The mass spectrum suggested the presence of isomeric lactams (*m/e* 257; $M^+$). Attempts at chromatographic separation were unsuccessful as were attempts at preferential hydrolysis which gave presumably a mixture of amino acids with similar $R_f$ values.

A sample of the crude lactam mixture (6.0 g) was heated with concentrated $H_2SO_4$ (90 g) at 160–170°C for 6 h. When cool, the mixture was poured into ice-cold water and the purple solid (1.7 g) was filtered off, and dried.

A sample (900 mg) of the purple solid, shown by tlc to be a complex mixture, was chromatographed on silica gel using benzene/petroleum ether (1:3) as eluant. First eluted was 1-amino-6-chloroanthraquinone **3** (40 mg) as a red solid, mp 206–208°C (from nitrobenzene) (lit. (12) mp 210–211°C), identical with an authentic sample (mixture mp, tlc, mass spectrum); mass spectrum *m/e*: 257 ($M^+$). Continued elution with benzene/petroleum ether (1:1) gave 1-amino-4-chloroanthraquinone **4** (70 mg), mp 182–184°C (from toluene) (lit. (13) mp 179–180°C), identical with an authentic sample (mixture mp, tlc, mass spectrum); mass spectrum *m/e*: 257 ($M^+$). Finally, benzene eluted 1-amino-4-hydroxyanthraquinone **5** (315 mg) which crystallized from benzene/petroleum ether as violet needles, mp 210–212°C (lit. (14) mp 215°C), identical with an authentic sample (mixture mp, tlc, mass spectrum); $^1H$ nmr ($CDCl_3$) δ: 13.55 (s, 1H, -OH); mass spectrum *m/e*: 239 ($M^+$).

*Schmidt reaction of 1,8-dichloroanthraquinone*

Treatment of 1,8-dichloroanthraquinone (13.8 g) as above gave an off-white solid (12.9 g), mp 230–233°C, which apparently contained two isomeric lactams, **8** and **9** (tlc).

A sample of the lactam mixture (2.5 g) was heated with concentrated $H_2SO_4$ (35 g) at 140–145°C for 7 h. A portion (1.0 g) of the resulting brown solid, which was apparently a mixture of two components (tlc), was chromatographed on silica using toluene/petroleum ether (1:1) as eluant to give 1-amino-2,5-dichloroanthraquinone as orange-red needles (100 mg), mp 182–183°C (from toluene); mass spectrum *m/e*: 291 ($M^+$, 100), 263 (20), 239 (7), 237 (10), 200 (15), 173 (12), 164 (24), 127 (12), and 88 (12). *Anal.* calcd. for $C_{14}H_7Cl_2NO_2$: C 57.73, H 2.40, Cl 24.05, N 4.81; found: C 57.48, H 2.40, Cl 23.84, N 4.70.

Further elution gave lactam **9** (650 mg), mp 306–308°C, identical (mixture mp, ir spectrum, tlc) with the lactam of corresponding mp described below. A sample of this lactam (200 mg), similarly treated with $H_2SO_4$, was recovered (140 mg) in slightly impure form, a trace of a second compound being indicated by tlc.

*Hydrolysis of the foregoing lactams (8 and 9)*

(a) The crude lactam mixture (5.8 g) was boiled with 2% ethanolic KOH solution (65 mL) for 15 min, and unhydrolyzed material was collected as before. Crystallization from aqueous $Me_2SO$ gave lactam **9** (2.1 g), mp 306–308°C (homogeneous by tlc). An analytical sample had mp 313–315°C (from ethanol); mass spectrum *m/e*: 291 ($M^+$, 100), 290 (53), 263 (93), 256 (81), 235 (24), 228 (14), 200 (41), 173 (16), and 164 (43). *Anal.* calcd. for $C_{14}H_7Cl_2NO_2$: C 57.56, H 2.42, N 4.80; found: C 57.51, H 2.47, N 4.83.

The hydrolysis filtrate was carefully acidified ($H_2SO_4$). Next day, the yellow solid (1.45 g) was collected and crystallized from ethanol to give 2-amino-3,3′-dichlorobenzophenone-2′-carboxylic acid, mp 170–171°C; mass spectrum *m/e*: 309 ($M^+$). *Anal.* calcd. for $C_{14}H_9Cl_2NO_3$: C 54.22, H 2.92, Cl 22.86, N 4.52; found: C 54.37, H 2.94, Cl 23.09, N 4.45.

(b) Lactam **9** (700 mg, mp 306–308°C) was boiled with 25% aqueous KOH solution (30 mL) for 30 min and the solution was then filtered. When cool, the solution was carefully acidified ($H_2SO_4$). The gummy solid was collected, dried, and crystallized from benzene to yield yellow flakes of 2-amino-6,6′-dichlorobenzophenone-2′-carboxylic acid (450 mg), mp 179–180°C; mass spectrum *m/e*: 309 ($M^+$). *Anal.* calcd. for $C_{14}H_9Cl_2NO_3$: C 54.22, H 2.92, Cl 22.86, N 4.52; found: C 54.18, H 2.99, Cl 22.81; N 4.50.

*Treatment of the foregoing amino acids with concentrated sulfuric acid*

(a) The amino acid (70 mg, mp 170–171°C) derived from **8** was heated in concentrated $H_2SO_4$ (1.5 g) at 140–145°C for 6 h. This gave a brown solid (40 mg) consisting (tlc and mass spectra) of 1-amino-2,5-dichloroanthraquinone, 3-chlorophthalic anhydride, and lactam **8**.

(b) The amino acid (100 mg, mp 179–180°C) derived from **9** when similarly treated gave a near colourless solid (30 mg), shown (tlc and mass spectra) to consist of 3-chlorophthalic anhydride and lactam **9**. Chromatographic separation followed by sublimation gave the anhydride (6 mg), mp 126–127°C (lit (15) mp 126°C); ir: 1810 and 1750 (C=O) $cm^{-1}$; mass spectrum *m/e*: 182 ($M^+$).

*Schmidt reaction of 1,5-dichloroanthraquinone*

Treatment of 1,5-dichloroanthraquinone (8.5 g) as above gave a creamy-white powder (8.78 g) which apparently contained two isomeric lactams, **10** and **11** (tlc).

The lactam mixture (8.78 g) was boiled with 2% ethanolic KOH solution (100 mL) as before and unhydrolyzed material was filtered off. The filtrate was carefully acidified ($H_2SO_4$). The resulting gum was extracted with ethanol (35 mL), a small amount of insoluble solid being combined (tlc) with the unhydrolyzed material collected previously. The ethanolic solution was diluted with water and the resulting yellow solid was collected and crystallized from aqueous ethanol to give 2-amino-2′,3-dichlorobenzophenone-6′-carboxylic acid (3.2 g) as yellow spikes, mp 182–184°C; mass spectrum *m/e*: 309 ($M^+$). *Anal.* calcd. for $C_{14}H_9Cl_2NO_3$: C 54.22, H 2.92, Cl 22.86; found: C 54.13, H 2.96, Cl 23.07.

Crystallization of the unhydrolyzed lactam fraction from ethanol gave **11** (4.2 g) as white prisms, mp 321–322°C; mass spectrum *m/e*: 291 ($M^+$, 84), 290 (82), 263 (100), 256 (88), 235 (62), 200 (88), 173 (33), and 164 (85). *Anal.* calcd. for $C_{14}H_7Cl_2NO_2$: C 57.56, H 2.42, Cl 24.27; found: C 57.63, H 2.38, Cl 24.05.

*Cleavage of 2-amino-2',3-dichlorobenzophenone-6'-carboxylic acid*

The amino acid (1.6 g, mp 182–184°C) was added to a mixture made by adding water (0.28 g, 16 mmol) to a rapidly stirred solution of potassium *tert*-butoxide (5.8 g) in 1,2-dimethoxyethane (50 mL) under nitrogen. The mixture was stirred at 20°C for 3 h and then poured into water (250 mL). The solution was washed with ether (washings discarded), acidified (concentrated $H_2SO_4$), and then extracted with ether (3 × 50 mL). The combined ether extracts were washed with saturated aqueous $KHCO_3$ solution (2 × 50 mL). The bicarbonate washings were carefully acidified (concentrated HCl) and extracted with ether (2 × 50 mL). The ether solution was washed with water, dried ($Na_2SO_4$), and the solvent evaporated to give a light yellow residue (1.3 g). This mixture was esterified by refluxing in methanol (25 mL) and concentrated $H_2SO_4$ (2 mL) for 3 h. The mixture was then poured into water and extracted with ether. The ether was washed with saturated aqueous $KHCO_3$ solution (to remove any unreacted acid), then with water, and dried ($Na_2SO_4$).

The ethereal solution was then concentrated and the residue analyzed by glc. This showed the presence of methyl 3-chlorobenzoate (by comparison with an authentic sample).

## Acknowledgements

We are greatly indebted to Dr. G. Hallas (University of Leeds) for a sample of 1-amino-4-hydroxyanthraquinone and to Imperial Chemical Industries Ltd. (Dyestuffs Division) for research samples of several aminochloroanthraquinones. Financial support from the N.S.E.R.C., and from the Government of Ontario for graduate scholarships (to E.H.R.), is gratefully acknowledged.

1. I. H. Bowen, P. Gupta, and J. R. Lewis. Chem. Commun. 1625 (1970); I. H. Bowen, P. Gupta, M. S. Khan, and J. R. Lewis. J. Chem. Soc. Perkin Trans. I, 2524 (1972); J. H. Adams, P. Gupta, M. S. Khan, J. R. Lewis, and R. A. Watt. J. Chem. Soc. Perkin Trans. I, 2089 (1976); J. H. Adams, P. Gupta, M. S. Khan, and J. R. Lewis. J. Chem. Soc. Perkin Trans. I, 2173 (1977).
2. G. J. Chen and M. S. Gibson. J. Chem. Soc. Perkin Trans. I, 1138 (1975).
3. G. Caronna and S. Palazzo. Gazz. Chim. Ital. **83**, 533 (1953).
4. G. Caronna and S. Palazzo. Gazz. Chim. Ital. **84**, 1135 (1954).
5. D. Misiti, H. W. Moore, and K. Folkers. Tetrahedron Lett. 1071 (1965); D. Misiti, H. W. Moore, and K. Folkers. Tetrahedron, **22**, 1201 (1966).
6. R. W. Rickards and R. M. Smith. Tetrahedron Lett. 2361 (1966).
7. G. R. Bedford, G. Jones, and B. R. Webster. Tetrahedron Lett. 2367 (1966); G. Jones. J. Chem. Soc. C, 1808 (1967).
8. Ger. Patent No. 2,230,122; Chem. Abstr. **81**, 78 (1974).
9. D. G. Davies, M. Derenberg, and P. Hodge. J. Chem. Soc. C, 455 (1971); D. G. Davies and P. Hodge. J. Chem. Soc. C, 3158 (1971).
10. R. S. Cahn, W. O. Jones, and J. L. Simonsen. J. Chem. Soc. 444 (1933).
11. Ger. Patent No. 551,256; Chem. Abstr. **26**, 4344 (1932).
12. H. E. Fierz-David, A. Krebser, and W. Anderau. Helv. Chim. Acta, **10**, 197 (1927); Chem. Abstr. **21**, 1811 (1927).
13. Ger. Patent No. 199,758; Chem. Zentr. II, 461 (1908).
14. Y. Bansho and K. Kondo. J. Chem. Soc. Jpn. **57**, 751 (1954); Chem. Abstr. **49**, 9279 (1955).
15. J. C. Smith. J. Chem. Soc. 1643 (1933).

Can. J. Chem. Downloaded from www.nrcresearchpress.com by 210.87.254.40 on 09/06/12
For personal use only.

# Structure of the Cornubert ketone

GEORGE R. PETTIT[1] AND EVAN G. THOMAS

*Cancer Research Institute and Department of Chemistry, Arizona State University, Tempe, AZ 85287, U.S.A.*
*and Department of Chemistry, University of Maine, Orono, ME 04473, U.S.A.*

Received August 11, 1981

GEORGE R. PETTIT and EVAN G. THOMAS. Can. J. Chem. **60**, 629 (1982).

The self-condensation of cyclohexanone in diethyl ether catalyzed by sodium amide has been found to provide a one-step route to pyran **3**. Evidence is presented that the Cornubert ketone formed by this reaction corresponds to ketol **2** which readily rearranges under dehydrating conditions to afford pyran **3**. Structural elucidation of pyran **3** was achieved by a combination of degradative (**3** → **5***b*), synthetic (**8** → **5***b*), and spectral methods. Xanthene **7**, a key dehydrogenation product of ketol **2**, was converted by selective reduction to dihydropyran **5***b*. The five-step synthesis of dihydroxypyran **5***b* from 1-carbomethoxycyclopentanol (**8**) provided unequivocal evidence for the structure assigned pyran **3** and xanthene **7**.

GEORGE R. PETTIT et EVAN G. THOMAS. Can. J. Chem. **60**, 629 (1982).

On a trouvé que l'auto-condensation de la cyclohexanone dans l'éther, catalysée par l'amidure de sodium, fournit une voie d'accès en une étape au pyranne **3**. On prouve que la cétone de Cornubert, formée par cette réaction, correspond au cétol **2** qui se transpose facilement en pyranne **3** dans des conditions de déshydratation. On a caractérisé le pyranne **3** en faisant appel à une combinaison de méthodes de dégradation (**3** → **5***b*), de synthèse (**8** → **5***b*) et spectrales. Par réduction sélective, on a transformé le xanthène **7**, un produit fondamental de déshydrogénation du cetol **2**, en dihydropyranne **5***b*. La synthèse en 5 étapes du dihydropyranne **5***b* à partir du carbométhoxy-1 cyclopentanol (**8**) fournit la preuve sans équivoque de la structure attribuée au pyranne **3** et au xanthène **7**.

[Traduit par le journal]

Over 50 years ago, while investigating the alkylation of cyclohexanone with methyl iodide using sodium hydride or amide, Cornubert (1) found that a simple mixture of the ketone, sodium amide, and diethyl ether yielded a new substance ($C_{18}H_{28}O_2$) melting at 186°C. After 2 h at 150°C in acetic anhydride – sodium acetate solution the new ketone was recovered unchanged. Failure of this attempt at acetylation suggested an ether group and the new ketone was formulated as tetrahydropyran **1**. In our previous study (2) of cyclohexanone intramolecular condensation reactions, mild treatment with sodium methoxide – dimethylformamide was found to yield a ketone ($C_{18}H_{28}O_2$) melting at 186.5–187°C. Chemical and physical evidence culminating in an X-ray crystal structure determination led to the definitive assignment of structure **2** (2).

To ascertain whether the Cornubert ketone (mp 186°C) actually corresponded to ketol **2**, attempts were made to repeat the sodium amide – ether experiment as originally (but briefly) outlined. The only $C_{18}$ product obtained (and in poor yield) using the original (1) fractional distillation (to 145°C at 0.5 Torr) procedure for isolation was pyran **3** (mp 40.5–41.5°C). Previously (2) we obtained the same pyran (**3**) by potassium hydrogen sulfate dehydration (at 190–200°C) of ketol **2**. Presumably Cornubert actually obtained ketol **2** instead of tetrahydroxy pyran **1** and depending on the isolation conditions, especially elevated temperatures, the ketol was easily rearranged (**2** → **4**) and dehydrated (**4** → **3**).[2]

Evidence for this conclusion was obtained by subjecting the reaction mixture prepared from cyclohexanone, sodium methoxide, and dimethylformamide, and known to yield ketol **2**, to an analogous fractional distillation. By this means a good yield of pyran **3** was obtained. Although the distillation procedure for obtaining **3** proved to be capricious and was not reproducible, it did seem likely that pyran **3** would be the principal result of subjecting ketol **2** to pyrolytic dehydration. By means of this evidence and that noted in the sequel, the structure of pyran **3** was unequivocally established.

[2]Cyclization of a 1,5-diketone to a 4*H*-pyran system is analogous to the intramolecular condensation reaction observed when dimedone aldehyde derivatives are heated under acid conditions (**i** → **ii**; see ref. 3*a*–*c*).

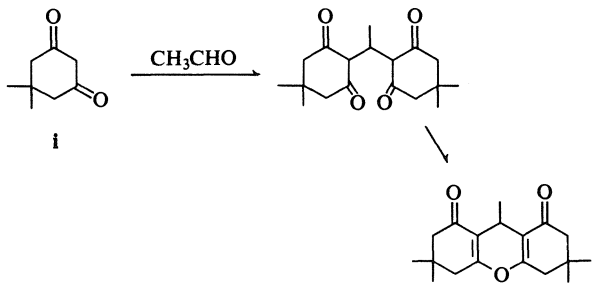


**i** **ii**

[1]Author to whom correspondence should be addressed.

0008-4042/82/050629-05$01.00/0

©1982 National Research Council of Canada/Conseil national de recherches du Canada

Can. J. Chem. Downloaded from www.nrcresearchpress.com by 210.87.254.42 on 09/06/12
For personal use only.

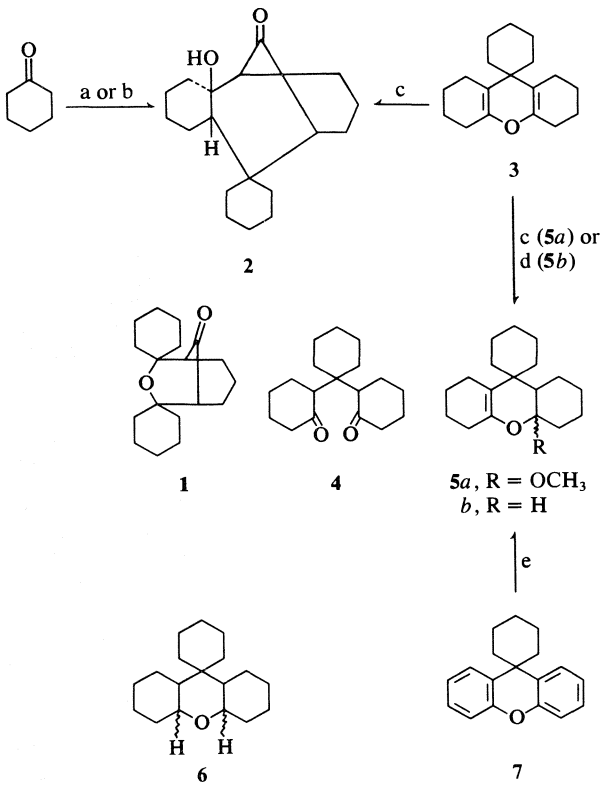


a:$(CH_3)_2NCHO$, $NaOCH_3$, RT, 5 days; b: $NH_3$, $NaNH_2$; c: $CH_3OH$, HCl, Δ, 12 h; d: 5% $Rh/Al_2O_3$, $H_2$; e, 5% $Rh/Al_2O_3$, $H_2$, $CH_3CH_2OH$, 50 psi, RT, 12 h–3 days.

Both the infrared and proton magnetic resonance spectra of pyran **3** were quite compatible with this assignment. Furthermore, partial reconversion to ketol **2** via the hypothetical 1,5-diketone **4** was realized by hydrolysis of pyran **3** in methanol containing concentrated hydrochloric acid. The main product was ketal **5***a*, and its infrared spectrum showed absorption at 1678 $cm^{-1}$ typical of a dihydropyran.

Complete reduction of pyran **3** employing palladium-catalyzed hydrogenation consumed two moles of hydrogen and provided ether **6**. Selective hydrogenation of pyran **3** using 5% rhodium-on-aluminum oxide led to dihydropyran **5***b*. Meanwhile, in a parallel study of the ketol **2** structure problem (2), xanthene **7** was found to be one of the three products formed by dehydrogenation over 10% palladium-on-carbon (at 290°C). Firm evidence for the structure of xanthene **7** was not obtained until the following experiments were completed. Reduction of xanthene **7** with 5% rhodium-on-aluminum oxide and hydrogen gave as main product dihydropyran **5***b* accompanied by a small quantity of ketol **2**. Isolation of the latter substance suggested that pyran **3** is an important intermediate in the course of hydrogenation and an alternative synthesis of dihydropyran **5***b* was considered necessary.

The route selected for a confirming synthesis was initiated by preparation of 1-carbomethoxycyclopentanol (**8**) by a method developed by Burger and Bennet (4). Cyclopentanone cyanohydrin, obtained by treating cyclopentanone bisulphite addition product with potassium cyanide, was hydrolyzed with concentrated hydrochloric acid to 1-hydroxycyclopentanoic acid. After esterification (Fischer) the ester was treated with *o*-methoxyphenylmagnesium bromide in tetrahydrofuran. The new glycol (**9**, 63%) was converted to the spirocyclohexanone **10** by a pinacol rearrangement (81.5% yield) with iodine in acetic acid. Wolff–Kishner reduction of ketone **10** proved to be somewhat more eventful. In addition to the expected methyl ether (**11**, 34% yield) a minor (13%) product was found to be xanthene **7**.[3]

The next step was intended to yield diketone **4** by a Birch reduction sequence. Attempts at reducing anisole **11** by lithium in liquid ammonia containing *tert*-butyl alcohol according to the Dryden (5)[4] variation of the Birch reduction proved unsuccessful. The Birch reduction appeared to proceed well in only one of the aromatic rings and efforts to hydrolyze the resulting enol ethers to an α,β-unsaturated ketone gave a mixture of ketones unsuitable for the synthetic objective. So the attractive alternative of first demethylating and then reducing the resulting bisphenol (**12**) to a cyclohexanol that could be oxidized to diketone **4** was evaluated. Simple cleavage with hydrobromic or hydriodic acids in hot acid led to mixtures. A reasonable conversion to phenol **12** was realized with refluxing 47% hydriodic acid. In model experiments with bis(2-methoxyphenyl)methane a mixture of sodium and pyridine gave the corresponding bisphenol in 80% yield. When this technique (6) was applied to ether **11** only poor yields of phenol **12** were obtained.

In order to reduce the possibility of competing hydrogenolysis during reduction of phenol **12** a rhodium catalyst was chosen for the reduction step (7). Perhaps due to steric difficulties presented by

[3]Except for two preliminary attempts, which were unsuccessful, to prepare xanthene by subjecting both bis(2-hydroxyphenyl)methane and bis(2-methoxyphenyl)methane to reaction with potassium hydroxide in diethylene glycol at 190°C, no further effort was devoted to the scope of this potentially useful route to certain diaryl ethers.

[4]By this procedure any trace amount of iron that would catalyze a competing reaction between lithium and the *tert*-butyl alcohol is removed by distilling the ammonia (see ref. 5)

Can. J. Chem. Downloaded from www.nrcresearchpress.com by 210.87.254.42 on 09/06/12
For personal use only.

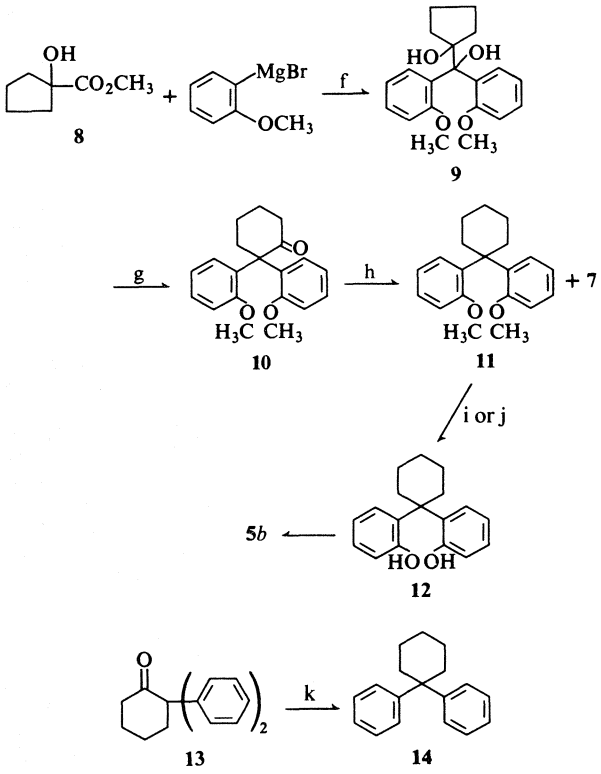

f: THF, $N_2$, 10°C, RT, 12 h; g: $I_2$, $CH_3CO_2H$, Δ, 5 min, RT, 12 h; h: 85% $NH_2NH_2$, $(HOCH_2CH_2OCH_2)_2$, KOH, 195°C; i: 47% HI, Δ, 9 h; j: Na, Py, $N_2$, Δ, 6 h; k: $RuO_2 \cdot x\ H_2O$, $CH_3CH_2OH$, 1500 psi, 60°C, 43 h.

the spirocyclohexane ring, hydrogenation of bisphenol **12** with 5% rhodium-on-aluminum oxide as catalyst proved unsatisfactory (incomplete reduction). Since hydrogenolysis can also be minimized by using ruthenium oxide as catalyst (8), application of this method at 1500 psi afforded in one step dihydropyran ***5b***, albeit in low (15%) yield. The specimens of dihydropyran ***5b*** obtained by ruthenium oxide catalyzed hydrogenation of bisphenol **12** and by rhodium – aluminum oxide catalyzed hydrogenation of pyran **3** and xanthene **7** were found to be identical.

Completion of the above synthetic interconversions and interpretation of the various physical measurement results firmly established pyran **3** as an important product that may result from the intramolecular self-condensation of cyclohexanone and related ketones.

## Experimental

All solvent extracts of aqueous solutions were dried over anhydrous magnesium sulphate. Ether refers to diethyl ether. Solvents employed for chromatography were redistilled and basic alumina refers to either Merck "Suitable for Chromatography" or Alcoa F-20 grades. All melting points are uncorrected. Instruments employed for determining the ultraviolet (95% ethanol solution), infrared (in potassium bromide unless otherwise noted), $^1H$ nmr (deuteriochloroform solution), $^{13}C$ (deuteriochloroform solution with tetramethylsilane as reference), and mass (electron impact) spectra have been outlined in the introduction to the experimental section of ref. 2. We are pleased to thank Drs. C. L. Herald, R. Hill, G. Slomp, R. O. Mumma, and J. Witschel, Jr. for assistance with these measurements. Other general aspects of this experimental section also appear in ref. 2.

*1',2',3',4',5',6',7',8'-Octahydro-spiro[cyclohexane-1,9'-xanthene] (3)*

*Method A*

Without benefit of details the experiment (that gave a substance melting at 186°C) reported by Cornubert (1) entailing the auto-condensation of cyclohexanone in liquid ammonia solution containing sodium amide was repeated. A mixture of cyclohexanone (20 g), 1.38 g of sodium amide (prepared from 0.815 g of sodium and excess liquid ammonia containing ferric nitrate), and anhydrous ether (80 mL) was stirred (under dry nitrogen) at ca. 25°C for three days. The reaction mixture was cautiously decomposed (in a nitrogen atmosphere) with water, extracted with ether, and purified by distillation. The fraction (0.60 g) boiling at 135–142°C and 0.5 Torr was crystallized from ethanol to afford 0.085 g of plates, mp 34–40.5°C. Recrystallization from ethanol brought the melting point to 40.5–41.5°C, undepressed upon admixture with a sample of 1',2',3',4',5',6',7',8'-octahydro-spiro[cyclohexane-1,9'-xanthene] (**3**) prepared by method B and previously (2). Comparison infrared spectra confirmed the mutual identity.

*Method B*

Cyclohexanone (98.0 g, 1.0 mol) was dissolved in 300 mL of anhydrous *N,N*-dimethylformamide. Freshly prepared sodium methoxide (81.0 g, 1.5 mol) was added and the mixture vigorously stirred with cooling (ice-bath). After the temperature was lowered to 10°C it was allowed to rise to ca. 25°C and stirring was continued five days. The sodium methoxide was removed by filtration and the solvent and unreacted cyclohexanone were removed by distillation (atmospheric pressure). Vacuum distillation of the residue gave a fraction (36.9 g) boiling at 148.5–152°C and 1.3 Torr which crystallized from ethanol giving two crops of plates, 22.4 g (mp 40–41.5°C) and 3.1 g (mp 39.5–40.5°C). The first fraction was recrystallized twice from ethanol to afford a pure specimen of pyran **3** (tetranitromethane gave a red-brown color); $\nu_{max}$ ($CCl_4$): 1694, 1660, 1228, and 1180 $cm^{-1}$; $^1H$ nmr δ: 1.52–1.67 (18H, m), 2.16 (8H, m); $^{13}C$ nmr δ: 22.68 (2C), 23.95 (2C), 24.01, 25.64 (2C), 26.22 (2C), 27.46 (2C), 34.44 (2C), 36.00, 114.48 (2C, C=C), 145.18 (2C, =C—O); mass spectrum *m/e*: 258 ($M^+$), 250, 229, 215 (base peak), 207, 202. *Anal.* calcd. for $C_{18}H_{26}O$: C 83.66, H 10.14, O 6.18; found: C 83.64, 83.52; H 9.99, 10.01; O 6.39.

Preparation of pyran **3** by this procedure was not routinely reproducible.

*Acid hydrolysis of 1',2',3',4',5',6',7',8'-octahydro-spiro-[cyclohexane-1,9'-xanthene] (3)*

To a solution of pyran **3** (1.0 g) in 20 mL methanol was added five drops of concentrated hydrochloric acid. After 12 h at reflux the solution was diluted with an equal volume of water, the products were extracted with ether, and the extract was concentrated to about 2 mL. Upon cooling, crystalline plates (0.190 g) separated and melted at 185–186°C. The melting point upon admixture with spiro*[3,4-cyclohexano-4-hydroxybicyclo-[3.3.1]nonan-9-one-2,1'-cyclohexane] (2)* was undepressed. The mother liquor yielded *1',2',3',4',4a',5',6',7',8',9a'-decahydro-spiro[cyclohexane-1,9'-9a'-methoxy xanthene]* (***5a***) as

Can. J. Chem. Downloaded from www.nrcresearchpress.com by 210.87.254.42 on 09/06/12
For personal use only.

Can. J. Chem. Downloaded from www.nrcresearchpress.com by 210.87.254.42 on 09/06/12
For personal use only.

plates (mp 79–79.5°C) following three recrystallizations from methanol; $\nu_{max}$: 1678, 1146, 1130, 1090 $cm^{-1}$. *Anal.* calcd. for $C_{19}H_{30}O_2$: C 78.57, H 10.41, *Mol. Wt.*: 290.43; found: C 78.35, H 10.08; *Mol. Wt.* (Rast): 263.

*1',2',3',4',4a',5',6',7',8',8a',9a',10a'-Dodecahydro-spiro-[cyclohexane-1,9'-xanthene] (**6**)*

A solution of pyran **3** (2.0 g) in 95% ethanol (75 mL) was shaken with platinum oxide (Adams catalyst 0.10 g) in a Towers atmospheric pressure hydrogenation apparatus for 12 h. The hydrogen uptake (corrected for catalyst) was 372 mL (the volume calcd. for two double bonds was 359 mL). The crude sample (1.85 g, mp 63–73°C) of tetrahydropyran **6** was purified by recrystallization from ethanol. Three recrystallizations yielded rhombahedra; mp 99.5–100.5°C; $\nu_{max}$: 1100, 1056, 1005 (C—O) $cm^{-1}$. *Anal.* calcd. for $C_{18}H_{28}O$: C 82.38, H 11.52; found: C 82.38, H 11.64.

*Catalytic hydrogenation of spiro[cyclohexane-1,9'-xanthene] (**7**)*

A 0.74 g sample of xanthene **7** (mp 56–57°C) was dissolved in absolute ethanol, 5% rhodium-on-alumina (0.80 g) was added, and the mixture was hydrogenated (50 psi, room temperature, Parr Shaker) for 3 days. To a solution of the crude hydrogenation product in 95% ethanol (15 mL) was added concentrated hydrochloric acid (0.5 mL). After heating 2 h at reflux the mixture was diluted with an equal volume of water, neutralized by adding 5% aqueous sodium bicarbonate, and extracted with ether. The ether was evaporated and the residual oil was triturated with hexane. The remaining solid (0.04 g) gave a melting point of 187–188°C that was undepressed upon admixture with a sample of spiro*[3,4-cyclohexano-4-hydroxybicyclo-[3.3.1]nonan-9-one-2,1'-cyclohexane]* (**2**). Comparison infrared spectra (KBr) confirmed the identity as ketol **2**.

The hexane-soluble portion of the hydrolyzate (0.39 g) was chromatographed on 15 g of basic alumina (Alcoa). A colorless oil (0.39 g) eluted by hexane was crystallized from methanol yielding prisms (0.150 g) of *1',2',3',4',4a',5',6',7',8',9a'-decahydro-spiro[cyclohexane-1,9'-xanthene]* (**5***b*, mp 79–82°C). Two recrystallizations from ethanol afforded dihydropyran **5***b* as prisms melting at 82–82.5°C (Kofler hot stage); $\nu_{max}$: 1672, 1228, 1194, 1172 $cm^{-1}$. *Anal.* calcd. for $C_{18}H_{28}O$: C 83.02, H 10.84; found: C 83.06, H 10.65, 10.79.

*Hydrogenation of 1',2',3',4',5',6',7',8'-octahydro-spiro-[cyclohexane-1,9'-xanthene] (**3**)*

To a solution of pyran **3** (0.50 g) in absolute ethanol (100 mL) was added 5% rhodium-on-alumina and the mixture was hydrogenated (Parr Shaker, room temperature) at 49 psi for 12 h. The crude oily product crystallized (0.31 g, mp 50–55°C) from ethanol. One recrystallization from ethanol gave prisms, mp 80–81.5°C, and another raised the melting point to 83.5–84°C which was not depressed upon admixture with *1',2',3',4',4a',-5',6',7',8',9a'-decahydro-spiro[cyclohexane-1,9'-xanthene]* (**5***b*) from the hydrogenation of spiro[cyclohexane-1,9'-xanthene] (**7**). Comparison infrared spectra confirmed the mutual identity.

*Di(2-methoxyphenyl)-(1-hydroxycyclopentyl)methanol (**9**)*

The Grignard reagent prepared from magnesium turnings (24.3 g, 0.566 mol), *ortho*-bromoanisole (105.8 g, 0.566 mol, bp 114–115°C and 22 Torr), and tetrahydrofuran under nitrogen, was cooled to 10°C and a solution of 1-carbomethoxycyclopentanol (**8**, 27.1 g, 0.189 mol) (4) in tetrahydrofuran was slowly added (over 15 min) with stirring. The reaction mixture was stirred at room temperature for 12 h and heated at reflux for 6.5 h. The tetrahydrofuran was replaced by benzene and the solution was poured onto ice (500 mL) – concentrated sulfuric acid (50 mL). Following extraction with chloroform the insoluble portion was collected and treated (steam-bath) for 30 min with 6 *N* hydrochloric acid (100 mL). The hydrolyzate was extracted with chloroform and both chloroform extracts were combined, washed with 5% sodium bicarbonate, and solvent was removed. The residual oil was washed with cold (10°C) hexane and the insoluble crude product (42.0 g) was crystallized from ethanol–acetone yielding a crystalline solid (33.9 g, 54.7%), mp 179–180°C. Recrystallization from ethanol gave diol **9**: mp 180.5–181°C (Kofler hot stage); $\lambda_{max}$: 272.4 ($\log \varepsilon = 3.55$), 278.4 ($\log \varepsilon = 3.52$) nm; $\nu_{max}$: 3460 (-OH), 1596, 1580, 1486 (aromatic), 1240 (aryl ether), 1034 ($-OCH_3$), 770 (1,2-disubstituted phenyl) $cm^{-1}$. *Anal.* calcd. for $C_{20}H_{24}O_4$: C 73.14, H 7.37; found: C 73.55, 73.40; H 7.39, 7.69.

*2,2-Bis(2-methoxyphenyl)cyclohexanone (**10**)*

To a solution of diol **9** (36.1 g) in hot glacial acetic acid (250 mL) was added iodine (0.250 g), and the solution was heated at reflux for 5 min, then poured onto ice. The mixture was left at room temperature for 12 h and the crude product was collected by filtration. Recrystallization from acetone afforded 28.0 g (81.8%) of ketone **10** melting at 108–111°C. Another recrystallization from ethanol yielded an analytical specimen as plates; mp 110.5–111.5°C (capillary); $\lambda_{max}$: 278 ($\log \varepsilon = 3.80$), 300 (shoulder, $\log \varepsilon = 2.92$) nm; $\nu_{max}$: 1724 (C=O), 1240 (aryl ether), 1025 ($-OCH_3$), (*o*-substituted phenyl) $cm^{-1}$. *Anal.* calcd. for $C_{20}H_{22}O_3$: C 77.39, H 7.14; found: C 77.07, H 7.10.

*Wolff–Kishner reduction of 2,2-bis(2-methoxyphenyl)-cyclohexanone (**10**)*

A mixture of ketone **10** (18.2 g), sodium hydroxide (7.4 g), 85% hydrazine hydrate (24 mL), and diethylene glycol (144 mL) was heated at reflux for 30 min. The reflux temperature was then raised to 190°C by removing water and excess hydrazine by distillation. Heating was continued at this temperature for 4.5 h. The reaction mixture was poured into water and concentrated hydrochloric acid was added until a red litmus test was obtained. Products were isolated in a chloroform solution, washed with 5% aqueous sodium bicarbonate, and dried. The solvent was removed *in vacuo* leaving a crude oil (19.0 g) which was dissolved in ether and the solution was extracted with 5% aqueous potassium hydroxide. After solvent removal the residual oil (14.5 g) was dissolved in hot ethanol and upon cooling *2,2-bis(2-methoxyphenyl)cyclohexane* (**11**) (4.5 g, mp 92–95°C) crystallized. Another crystallization from ethanol raised the melting point to 96–96.5°C. The mother liquor residual oil (10.0 g) was chromatographed on basic alumina (Alcoa). The fraction (1.82 g, mp 53.5–55°C) eluted by hexane was recrystallized from ethanol giving plates melting at 55–56°C and identical (by comparison infrared spectra and undepressed mixture melting point) with *spiro[cyclohexane-1,9'-xanthene]* (**7**) obtained from the dehydrogenation of ketol **2**.

A fraction (1.34 g, mp 96–97°C) containing cyclohexane **11** was obtained by elution with 1:9 benzene–hexane. Two recrystallizations from ethanol gave an analytical sample: mp 96.5–97.5°C (Kofler hot stage); $\lambda_{max}$: 281 ($\log \varepsilon = 3.56$), 274 ($\log \varepsilon = 3.56$) nm; $\nu_{max}$: 1594, 1580, 1490 (phenyl), 1248 (aryl ether), 1030 ($-OCH_3$), 764, 750 (1,2-disubstituted phenyl) $cm^{-1}$. *Anal.* calcd. for $C_{20}H_{24}O_2$: C 81.04, H 8.16; found: C 81.07, H 8.30.

*Demethylation of bis(2'-methoxyphenyl)cyclohexane (**11**)*

*Method A. With hydriodic acid*

A mixture of *bis(2-methoxyphenyl)cyclohexane* (**11**, 2.0 g), 47% hydriodic acid (20 mL), and glacial acetic acid (40 mL) was heated at reflux for 9 h, cooled to room temperature, and poured onto ice. An ether extract of the product was washed with 10% aqueous sodium hydroxide and concentrated to an oil (0.93 g neutral fraction). The combined sodium hydroxide extract was acidified with concentrated hydrochloric acid and the acid

Can. J. Chem. Downloaded from www.nrcresearchpress.com by 210.87.254.42 on 09/06/12
For personal use only.

fraction was isolated in ether. Sublimation of the acid fraction (0.625 g) led to 0.585 g of bis(2′-hydroxyphenyl)cyclohexane (**12**) which did not depress the melting point of phenol **12** prepared by Method B and both specimens showed identical infrared spectra.

*Method B. With sodium*

A mixture of *bis(2′-methoxyphenyl)cyclohexane* (**11**, 1.50 g), sodium (0.92 g), and dry pyridine (10 mL) was heated (nitrogen atmosphere) at reflux for 6 h. After cooling to room temperature excess sodium was removed by cautiously adding, in succession, pyridine, 1:1 pyridine–water, and water. A neutral fraction (0.90 g, mp 84–88°C), obtained by extracting the mixture with ether, was identified as unreacted starting material. The aqueous phase was adjusted to pH 6 (Hydrion paper) with hydrochloric acid and an acidic fraction (0.178 g) was isolated in ether and recrystallized three times from hexane. The analytical sample of phenol **12** melted at 111–111.5°C (Kofler hot stage); $\lambda_{max}$: 282.5 (log ε = 3.98), 277 (log ε = 3.99) nm; $\nu_{max}$: 3390 (-OH), 1366 (phenol), 768, 755 (1,2-disubstituted phenyl $cm^{-1}$. *Anal.* calcd. for $C_{18}H_{20}O_2$: C 80.56, H 7.51; found: C 80.57, 80.71; H 7.52, 7.53.

*Catalytic hydrogenation of bis(2′-hydroxyphenyl)cyclohexane (**12**)*

A mixture of bisphenol **12** (0.168 g), absolute ethanol (25 mL), and 60.13% ruthenium oxide (0.200 g) (8)[5] was hydrogenated at 1500 psi and 60°C for 43 h (Magnadash autoclave with 250 mL bomb container). The crude product (0.132 g of oil) was chromatographed on basic alumina (5 g). The fraction (0.026 g) eluted by hexane was crystallized from absolute ethanol to provide *1′,2′,3′,4′,4a′,5′,6′,7′,8′,9a′-decahydro-spiro[cyclohexane-1,9′-xanthene]* (**5***b*) as prisms, mp 82–83°C. A mixture melting point with the product (**5***b*) obtained from hydrogenation of spiro[cyclohexane-1,9′-xanthene] (**7**) was undepressed. The infrared spectra (KBr) of both samples were identical.

*2,2-Diphenylcyclohexane (**14**)*

A mixture composed of 2,2-diphenylcyclohexanone (**13**, prepared by the method of Burger and Bennet (4), 3 g, mp 101–102°C), 85% hydrazine hydrate (5 mL), diethylene glycol (25 mL), and potassium hydroxide pellets (3 g) was heated at reflux for 30 min. The reaction temperature was raised to 195°C by removing water and excess hydrazine by distillation and maintained there for 45 min. After cooling to room temperature, the mixture was poured into water (150 mL) and the crude product isolated in ether. The ether solution was concentrated to an oil which was chromatographed on 90 g of basic alumina. Hydrocarbon **14** (1.64 g, mp 45–46.5°C) was eluted by hexane and recrystallized from ethanol giving plates melting at 47–47.5°C (Kofler hot stage); $\lambda_{max}$: 269 (log ε = 2.71), 262 (log ε = 2.86), 255 (log ε = 2.80) nm; $\nu_{max}$ ($CCl_4$): 1600, 1504, 1495 (phenyl), 1452 ($CH_2$), 700 (phenyl) $cm^{-1}$. *Anal.* calcd. for $C_{18}H_{20}$: C 91.47, H 8.53; found: C 91.52, H 8.59.

[5]From Engelhard Minerals and Chemicals, Newark, NJ.

## Acknowledgments

This investigation was supported by Grant No. CA16049-06 awarded by the National Cancer Institute, DHEW, Mary Dell Pritzlaff, the Olin Foundation (Spencer T. and Ann W.), the Fannie E. Rippel Foundation, and a Frederick Gardner Cottrell grant from the Research Corporation. We are pleased to acknowledge this very necessary assistance.

1. R. Cornubert. C. R. Acad. Sci. **184**, 1258 (1927); Chem. Abstr. **21**, 2464 (1927).
2. G. R. Pettit and E. G. Thomas. (*a*) J. Org. Chem. **46**, 4167 (1981); (*b*) Chem. Ind. 1758 (1963).
3. (*a*) B. D. Akehurst and J. R. Bartels-Keith. J. Chem. Soc. 4798 (1957); (*b*) G. Klein and H. Linser. Mikrochem. Pregl. Festschr. **1929**, 204 (1929); Chem. Abstr. **24**, 2441 (1930); (*c*) C. F. H. Allen and H. R. Sallans. Can. J. Res. **9**, 574 (1933); Chem. Abstr. **28**, 2006 (1934).
4. A. Burger and W. B. Bennet. J. Am. Chem. Soc. **72**, 5414 (1950).
5. H. L. Dryden, G. M. Webber, R. R. Burtner, and J. A. Cella. J. Org. Chem. **26**, 3237 (1961).
6. V. Prey. Ber. **76**, 156 (1943).
7. H. A. Smith and B. L. Stump. J. Am. Chem. Soc. **83**, 2739 (1961).
8. W. S. Johnson, E. R. Rogier, and J. Ackerman. J. Am. Chem. Soc. **78**, 6322 (1956).

# Enolates de β-cétoesters: conformations et stabilités des formes dissociées

C. CAMBILLAU[1] ET F. GUIBE[2]

*Groupe de Recherche No 12, C.N.R.S., B.P. 28, 94320 Thiais, France*

Reçu le 24 avril 1981[3]

C. CAMBILLAU et F. GUIBE. Can. J. Chem. **60**, 634 (1982).

La conformation d'énolates de β-cétoesters a été étudiée par $^1$H rmn et par conductimétrie. Nous avons comparé les dissociations des énolates de $K^+$ de β-cétoesters acycliques qui peuvent à priori adopter une quelconque des quatre conformations *ZE*, *ZZ*, *EE* ou *EZ* avec ceux de β-cétoesters hémicycliques (carbéthoxy-2 cyclopentanone, acétyl-2 γ-butyrolactone) qui ne peuvent en adopter qu'un nombre limité. Les résultats montrent que la conformation *EE* est plus stable que les conformations *ZZ* et *EZ*. Ce résultat, qui implique que les énolates acycliques dissociés sont de conformation *EE*, est confirmé par rmn du proton. Ces résultats expérimentaux ont été complétés par des calculs *ab-initio* STO-3G effectués sur l'anion du formylacétate de méthyle et sur celui de la formylacétone, son analogue dicétonique. La méthode de titrage conductimétrique par le cryptand (2,2,2), utilisée pour déterminer les coefficients de dissociation des énolates de $K^+$ dans le DMSO est discutée en détail.

C. CAMBILLAU and F. GUIBE. Can. J. Chem. **60**, 634 (1982).

The problem of the conformation of β-ketoester enolates has been investigated through $^1$H nmr studies and through conductimetric studies. We have compared the dissociative properties of the $K^+$ enolates of acyclic β-ketoesters which can a priori adopt any possible *ZE*, *ZZ*, *EE*, or *EZ* conformations and of hemicyclic β-ketoesters (2-carbethoxycyclopentanone, 2-acetyl γ-butyrolactone) in which geometrical constraints excluded some of them. The results lead to the conclusion that the *EE* conformation is more stable than either the *ZZ* or *EZ* ones. Confirmation of this point, which implies that the acyclic dissociated enolates exist in the *EE* conformation, is afforded by $^1$H nmr spectroscopy. Those experimental results have been complemented with *ab initio* STO-3G calculations performed on the methyl formylacetate anion and on the formylacetone anion (the diketonic analog). The method of conductimetric titration by cryptand (2,2,2) used for the determination of the dissociation coefficient of $K^+$ enolates in DMSO is discussed in some detail.

Outre son intérêt propre, la connaissance de la conformation des énolates de composés β-dicarbonylés est importante à plusieurs titres.

De la conformation adoptée par l'énolate dépend, en effet, la stéréosélectivité (*Z*, *E*) du produit obtenu dans des réactions mettant en jeu les atomes d'oxygène du système mésomère (*O*-alkylation, *O*-acylation) (1). Par ailleurs, les équilibres conformationnels de ces énolates sont très sensibles aux interactions avec l'environnement (cation, solvant, etc...) et de ce fait, ils constituent une sonde commode pour étudier la structure des solutions, en relation ou non avec des problèmes de réactivité (1–5).

Comme pour les énolates de composés β-dicarbonylés en général, quatre conformations (6) sont à priori possible pour les énolates de β-cétoesters: une conformation en *U* (*ZE*), une conformation en *W* (*EZ*) et deux conformations en *S* ("Sickle Shaped"): *S-cis* (*ZZ*) et *S-trans* (*EE*)[4] (Fig. 1).

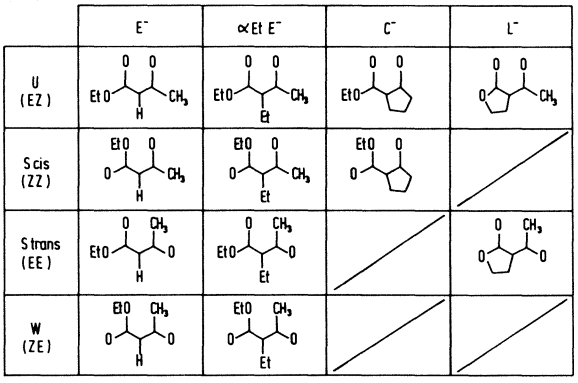


FIG. 1. Conformations que peuvent théoriquement présenter les énolates de l'acétylacétate d'éthyle ($E^-$), de l'α-éthyl-acétylacétate d'éthyle (αEt-$E^-$), de la carbéthoxy-2-cyclopentanone ($C^-$), et de l'acétyl-2-butyrolactone ($L^-$).

La structure en *U* des énolates au contact du cation est en accord avec les résultats des études de rmn du proton ou du $^{13}$C (4, 8, 9). Elle a récemment pu être observée directement par diffraction des rayons X sur des espèces monomères (paires d'ions solvatées extérieurement par des éthers couronnes)[5] (2, 10) ou dimères (ions triples du lithium) (11).

[1]Ce travail fait partie de la thèse d'Etat de C. Cambillau (13).

[2]Auteur à qui la correspondance doit être adressée.

[3]Revision reçu le 9 novembre 1981.

[4]Contrairement à la terminologie *E* et *Z*, la terminologie *U*, *W* et *S* présente l'avantage de rester invariante en passant de la série des β-cétoesters à la série des β-dicétones, et sera donc utilisée de préférence dans la suite de cet article. Les termes *S-cis* et *S-trans* appliqués ici aux énolates de β-cétoesters font référence à la position relative de l'oxygène pseudo-cétonique et du groupement carbalkoxy, en accord avec la terminologie originale de Miller *et al.* (7) concernant les esters ou éthers d'énols de composés β-dicétoniques.

[5]Pour le complexe [$CH_3COCHNaCO_2Et$, 15-couronne-5] (résultat non publié) voir réf. 12.

0008-4042/82/050634-09$01.00/0

©1982 National Research Council of Canada/Conseil national de recherches du Canada

Can. J. Chem. Downloaded from www.nrcresearchpress.com by 210.87.254.5 on 09/06/12
For personal use only.

Can. J. Chem. Downloaded from www.nrcresearchpress.com by 210.87.254.5 on 09/06/12
For personal use only.

Cette structure en *U* est conservée en solution dans le THF pour la paire d'ions (2), et dans $CH_2Cl_2$ ou même le DMSO pour l'anion triple (11). Ces résultats sont facilement expliqués par la stabilité du cycle chélate ($C_3O_2^-$ $M^+$).

Le problème de la conformation des énolates dissociés ou en interaction lâche avec leur cation n'est pas aussi bien documenté. Aucune structure d'énolate alcalin dans une conformation non chélatante n'a été observée aux rayons X. Dans le cas de solutions d'acétylacétonates alcalins ($R^1 = R^2 = CH_3$), Raban *et al.* ont montré sans ambiguité par rmn ($^1H$ ou $^{13}C$) que l'ion dissocié adopte une conformation en *S* (4). Toujours par rmn, Ershov et coll. ont montré que les énolates de β-cétoesters (8) ($R^1$ = H ou $CH_3$, $R^2$ = OR) ou de β-cétoaldéhydes (9) ($R^1$ = H, $R^2 = CH_3$) devaient

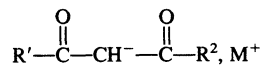

exister sous une forme "transoïde" *W* ou *S*; ces conformations sont toutes deux compatibles avec la géométrie "*trans*" des éthers d'énol (1) obtenus dans les réactions d'alkylation en milieu dissociant.

Nous présentons ici nos résultats concernant la conformation d'énolates de composés β-dicarbonylés. Afin de préciser les stabilités relatives des diverses conformations, nous avons étudié comparativement les énolates de composés linéaires (acétylacétate d'éthyle, E; α-éthyl-acétylacétate d'éthyle, αEt-E) pour lesquels toute conformation est a priori possible, et des énolates de β-cétoesters cycliques (carbéthoxy-2 cyclopentanone, C; acétyl-2 γ-butyrolactone, L) qui ne peuvent en adopter qu'un nombre restreint (voir Fig. 1). Les techniques utilisées sont la rmn et la conductimétrie. Cette étude expérimentale a été complétée par des calculs théoriques (*ab initio* STO-3G) sur des molécules modèles afin de préciser les facteurs de stabilité des différents conformères.

## I. Conductimétrie

*Présentation de la technique utilisée*

Nous avons étudié la dissociation des énolates de potassium de E ($E^-K^+$), αEt-E ($\alpha Et\text{-}E^-K^+$), C ($C^-K^+$) et L ($L^-K^+$) dans le DMSO à 25°C au moyen de la méthode de *titrage conductimétrique* par le cryptand (2,2,2) proposée initialement par Collmann *et al.* (13). Cette méthode consiste à étudier la conductivité de l'électrolyte d'abord sans complexant, puis en présence de quantités croissantes de celui-ci, jusqu'à obtention d'un plateau de conductivité (Fig. 2). Elle permet de travailler facilement dans une gamme de concentrations

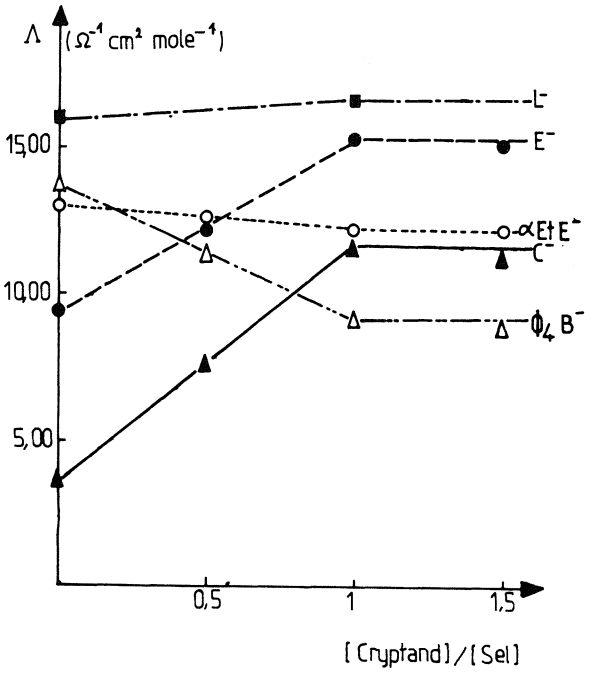


FIG. 2. Courbes de conductivité de quelques énolates de composés β-dicarbonylés et de $Ph_4B^-K^+$ 0,1 *M* dans le DMSO à 25°C, en fonction du nombre d'équivalents de cryptand (2,2,2) ajoutés. (L: acétyl-2-butyrolactone; E: acétylacétate d'éthyle; C: carboéthoxy-2-cyclopentanone; αEt-E: α-ethyl-acétyl-acétate d'éthyle).

inaccessibles à la conductimétrie classique. A partir des valeurs de conductivité équivalente $\Lambda_i$ au point initial (sans complexant) et $\Lambda_{pl}$ (au plateau) il est possible de calculer le coefficient α de l'électrolyte au point initial. Les valeurs $\Lambda_i$ et $\Lambda_{pl}$ obtenues sur un sel totalement dissocié dans le milieu en présence ou non de complexant permet d'effectuer les corrections de mobilités entre le cation et son cryptate. Notons que cette méthode ne s'applique qu'en milieu nettement dissociant (l'électrolyte crypté doit être totalement dissocié) et qu'elle ne permet d'accèder qu'à une valeur approchée de α (l'influence de la force ionique sur la mobilité des ions est négligée). L'ensemble de cette technique est discuté plus en détail dans l'annexe conductimétrique.

*Résultats et discussion* (Fig. 2, Tableau 1)

Pour les quatre énolates de $K^+$ étudiés, comme pour le tétraphénylborate de $K^+$, le plateau de conductivité est atteint dès un équivalent de cryptand ajouté (Fig. 2). Ceci est en accord avec les résultats obtenus par infrarouge (ir) sur des solutions de $E^-K^+$ dans le THF et le DMSO, montrant que, dès un équivalent de cryptand (2,2,2) ajouté,

TABLEAU 1. Résultats conductimétriques concernant quelques énolates de composés β-dicarbonylés et $\phi_4B^-K^+$ en solution 0,1 *M* dans le DMSO à 25°C

| Composé | $\Lambda_{sel}$[a] | $\Lambda_{pl,\,sel\,+\,(2,2,2)}$[a] | $\frac{\Lambda_{pl,sel\,+\,(2,2,2)}}{\Lambda_{pl,\phi_4B^-K^+\,(2,2,2)}}$ | $\alpha \times 100$ | $10^3 \times K_d$ |
|---|---|---|---|---|---|
| $\phi_4B^-K^+$ | 13,70 | 9,15 | 1 | 100 | |
| Carbéthoxy-2-cyclopentanone ($C^-K^+$) | 3,60 | 11,70 | 1,28 | 22,2 | 6,3 |
| αEt AAE (Et-$E^-K^+$) | 13,00 | 12,20 | 1,34 | 77,6 | 269 |
| AAE ($E^-K^+$) | 9,40 | 15,30 | 1,67 | 47,4 | 43 |
| Acétyl-2-butyrolactone ($L^-K^+$) | 16,00 | 16,60 | 1,82 | 75,6 | 234 |

[a]Λ: $\Omega^{-1}$ cm$^2$ mol$^{-1}$.

l'énolate est entièrement dans une conformation non chélatante (2). Les valeurs de conductivité au plateau $\Lambda_{pl}$ des énolates étudiés augmentent dans l'ordre $C^- \simeq$ αEt-$E^- < E^- < L^-$ correspondant aux tailles respectives des anions. Les constantes de dissociation croissent dans l'ordre $C^- < E^-$[6] < αEt-$E^- \sim L^-$. Ces données font apparaître trois faits significatifs et qui seront discutés successivement en se référant aux stabilités intrinsèques des diverses conformations possibles pour les énolates ainsi qu'aux interactions stériques qu'elles impliquent : (*i*) l'énolate acyclique $E^-$ non substitué sur le carbone central est moins dissocié que son homologue éthylé αEt-$E^-$. (*ii*) De tous les énolates étudiés $C^-$ est celui qui présente la plus faible tendance à la dissociation. (*iii*) La tendance à la dissociation des énolates $L^-$ et αEt-$E^-$ est pratiquement la même.

Les constantes de dissociation des énolates $E^-K^+$ et αEt-$E^-K^+$ sont à peu près dans le rapport 0,16 ($\Delta\Delta G \simeq 1{,}1$ kcal). La substitution de l'hydrogène sur le carbone central par le groupement éthyle se traduit donc par une tendance accrue à la dissociation. Des phénomènes analogues ont été récemment mis en évidence par Raban et Haritos (4*b*) dans l'étude par rmn du $^{13}C$ des énolates de lithium β-dicétones. Ils s'expliquent par la déstabilisation du conformère en *U* (donc de la forme associée) due aux interactions stériques 1–2 entre le substituant sur le carbone central et les groupements terminaux (Schéma 1).

Ainsi l'énolate de lithium de l'α-méthylacétyl acétone ($R^1 = R^2 = R^3 = CH_3$) présente une constante $K_d$ dans le méthanol 100 fois supérieure à celle de l'acétylacétonate. On remarque que l'effet de substituant observé dans la série des β-dicétones est donc beaucoup plus marqué que dans la série des β-cétoesters. Ceci pourrait s'expliquer par le fait que les énolates de dicétones α-substituées présentent deux interactions alkyl–alkyl 1–2 *contigues*, ce qui limite les possibilités de déformation de la molécule permettant de les soulager. Dans le cas de β-cétoesters, l'une de ces interactions alkyl–alkyl est remplacée par une interaction alkyl–alkoxy beaucoup moins sérieuse. Un effet de cation peut aussi être envisagé: dans le cas des énolates de lithium, les oxygènes du cycle chélate sont beaucoup plus fortement liés au cation que dans le cas des énolates de potassium ce qui doit impliquer des contraintes géométriques plus rigoureuses.[7]

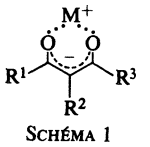

SCHÉMA 1

Dans la série des énolates hémicycliques, la faible dissociation de $C^-$ par rapport à $L^-$ (rapport des constantes de dissociation: 0,027, $\Delta\Delta G \simeq 2{,}15$ kcal) s'explique probablement en partie par le fait que le passage du chelate à la forme *S-cis* dans le cas de $C^-$ ne s'accompagne pas de la suppression d'une interaction alkyl–alkyl 1–3 défavorable comme cela est le cas lors du passage du chélate à la forme *S-trans* de $L^-$. Ceci ne saurait cependent être le seul facteur en cause. La constante de dissociation de $C^-$ est également plus faible, d'un facteur

[6]La valeur de α obtenue ici par conductimétrie concorde avec celle tirée de l'examen de spectres infrarouge (2, 12). Une décomposition graphique des absorptions ($\upsilon_s$CO) de la paire d'ions de contact et de l'ion libre indique la présence d'environ 35–45% de l'ion libre pour une solution 0.1 *M* dans le DMSO. Ainsi qu'il est indiqué dans l'annexe conductimétrique les valeurs de α obtenues par conductimétrie sont probablement légèrement surestimées.

[7]Des données récentes de Olmstead et Bordwell (23) vont à l'appui de cette dernière hypothèse. Le rapport des constantes de dissociation des énolates alcalins de l'acétylacétone et de l'α-méthylacétylacétone mesurées par ces auteurs dans le DMSO est en effet de 0,25 pour $K^+$, 0,08 pour $Na^+$ et 0,04 pour $Li^+$ (note ajoutée à la correction des épreuves).

Can. J. Chem. Downloaded from www.nrcresearchpress.com by 210.87.254.5 on 09/06/12
For personal use only.

Can. J. Chem. Downloaded from www.nrcresearchpress.com by 210.87.254.5 on 09/06/12
For personal use only.

environ 7 ($\Delta\Delta G \simeq 1{,}15$ kcal), que celle de l'énolate $E^-$ qui ne porte pas de substituant sur le carbone central et dont il est prouvé plus loin, notamment par rmn, qu'il adopte la conformation en *S-trans* à l'état dissocié. Ceci montre sans ambiguité que la conformation *S-cis*, dans laquelle l'atome d'oxygène du groupement éthoxy fait face à l'atome d'oxygène du groupement pseudo-cétonique est intrinsèquement défavorable. Ce résultat est corroboré par les calculs *ab initio* présentés plus loin.

Les valeurs très voisines de $K_d$ obtenues avec αEt-$E^-$ et $L^-$ $K^+$ plaident en faveur d'une structure commune *S-trans* pour ces deux énolates, l'énolate cyclique $L^-$ ne pouvant adopter la conformation en *W*. Sur la base de ces seules données conductimétriques, on ne peut exclure totalement la possibilité de coexistence des deux formes *W* et *S-trans* pour l'énolate acyclique; simplement, la forme *W* ne saurait être largement prédominante, auquel cas αEt-$E^-K^+$ serait nettement plus dissocié que $L^-K^+$. La forte dissociation de αEt-$E^-K^+$ comparée à celle de $C^-K^+$ avait déjà été mise en évidence par Rhoads et Holder (14) sur les sels de sodium dans le DMSO, mais elle avait été interprétée en termes de stabilités relatives de conformères *W* pour αEt-$E^-$ et *S-cis* pour $C^-$. La possibilité pour αEt-$E^-$ d'adopter la conformation *S-trans* n'avait pas été prise en considération.

## II. Etude par rmn du proton

L'étude conductimétrique à elle seule ne permet pas de trancher définitivement le problème de la conformation des énolates non cycliques. Nous l'avons donc étayée d'une étude par rmn du proton à basse température dans le méthanol-$d_4$ en comparant les déplacements chimiques de groupements méthyles des énolates $E^-$ et $L^-$. Les déplacements chimiques des protons des groupements éthoxy ne sont pas suffisamment sensibles à la conformation de l'énolate et cette étude n'a pu être étendue avec profit à l'énolate $C^-$.

*Enolate de l'acétyl γ-butyrolactone* ($L^-M^+$)
(Fig. 3, Tableau 2)

Le spectre d'une solution de $L^-K^+$ dans le méthanol à −30°C présente deux signaux pour le $CH_3$: l'un à 1,87 ppm, l'autre à 2,21 ppm. L'addition d'INa à cette solution fait croître le pic à 1,87 ppm. Une dilution de moitié d'une solution de $L^-Li^+$ fait croître celui à 2,21 ppm. Le premier pic correspond donc à un chélate et le second à l'ion relaché.

*Enolates de l'acétylacétate d'éthyle* ($E^-M^+$)
(Fig. 3, Tableau 2)

Le spectre de $E^-K^+$ dans MeOH à −30°C présente pour le $CH_3$ une absorption à 1,78 ppm et une autre à 2,20 ppm. L'addition d'INa à cette solution de $E^-K^+$ fait diminuer le pic à 2,20 ppm alors que l'addition de quantités croissantes de 15-couronne-5 à une solution de ENa le fait augmenter.

Nous concluons que le pic à 2,20 ppm correspond à $E^-$ relaché et celui à 1,78 ppm au chélate. Les déplacements observés sont identiques à ceux de la littérature (9).

La comparaison des intensités relatives des pics observés pour $E^-$ $K^+$ et $L^-$ $K^+$ montre que $L^-$ $K^+$ est beaucoup plus dissocié que $E^-$ $K^+$ ce qui est en accord avec les résultats conductimétriques.

La présence d'un seul pic $CH_3$ pour l'énolate relaché de l'acétylacétate d'éthyle montre que celui-ci existe sous une seule forme *W* ou *S-trans*; en effet à basse température les différents conformères d'énolates de composés β-dicarbonylés ne s'équilibrent pas rapidement à l'échelle de temps de la rmn ainsi qu'en témoigne par exemple la non-équivalence des deux méthyles terminaux du conformère *S-trans* de l'ion acétylacétonate (4*a*). Un seul pic pour $E^-$ relaché (δ = 2,18 ppm) est également observé par Esakov et coll. dans le DMF à −60°C (9).

La quasi identité, à 0,01 ppm près, des déplacements chimiques des groupements $CH_3$ de $E^-$ et $L^-$ observée ici indique par ailleurs que la conformation unique de $E^-$ relaché doit être du type *S-trans*. Raban *et al.* (15) ont montré que le groupement méthyle de l'énolate relaché de l'hexanedione-2,4 à structure en *S* présente des déplacements chimiques différents dans les deux conformères *EZ* et *ZE*. Un Δδ encore plus important (0,38 ppm) est observé pour les deux groupements méthyle non équivalents de l'énolate en *S* de l'acétylacétone (Schéma 2).

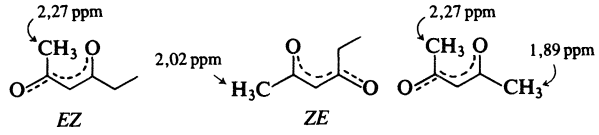


SCHÉMA 2

Dans les deux conformères en *S* de l'anion de l'hexanedione comme dans celui de l'anion de l'acétylacétone, les groupements méthyle sont situés très différemment par rapport au pseudo-carbonyle de l'extrémité opposée de la molécule et les différences de déplacement chimiques observées en rmn sont vraisemblablement le reflet de l'anisotropie magnétique de ce dernier (15). Il est bien établi, dans le cas des composés carbonylés α,β-insaturés et porteurs d'un méthyle en β, que les

Can. J. Chem. Downloaded from www.nrcresearchpress.com by 210.87.254.5 on 09/06/12
For personal use only.

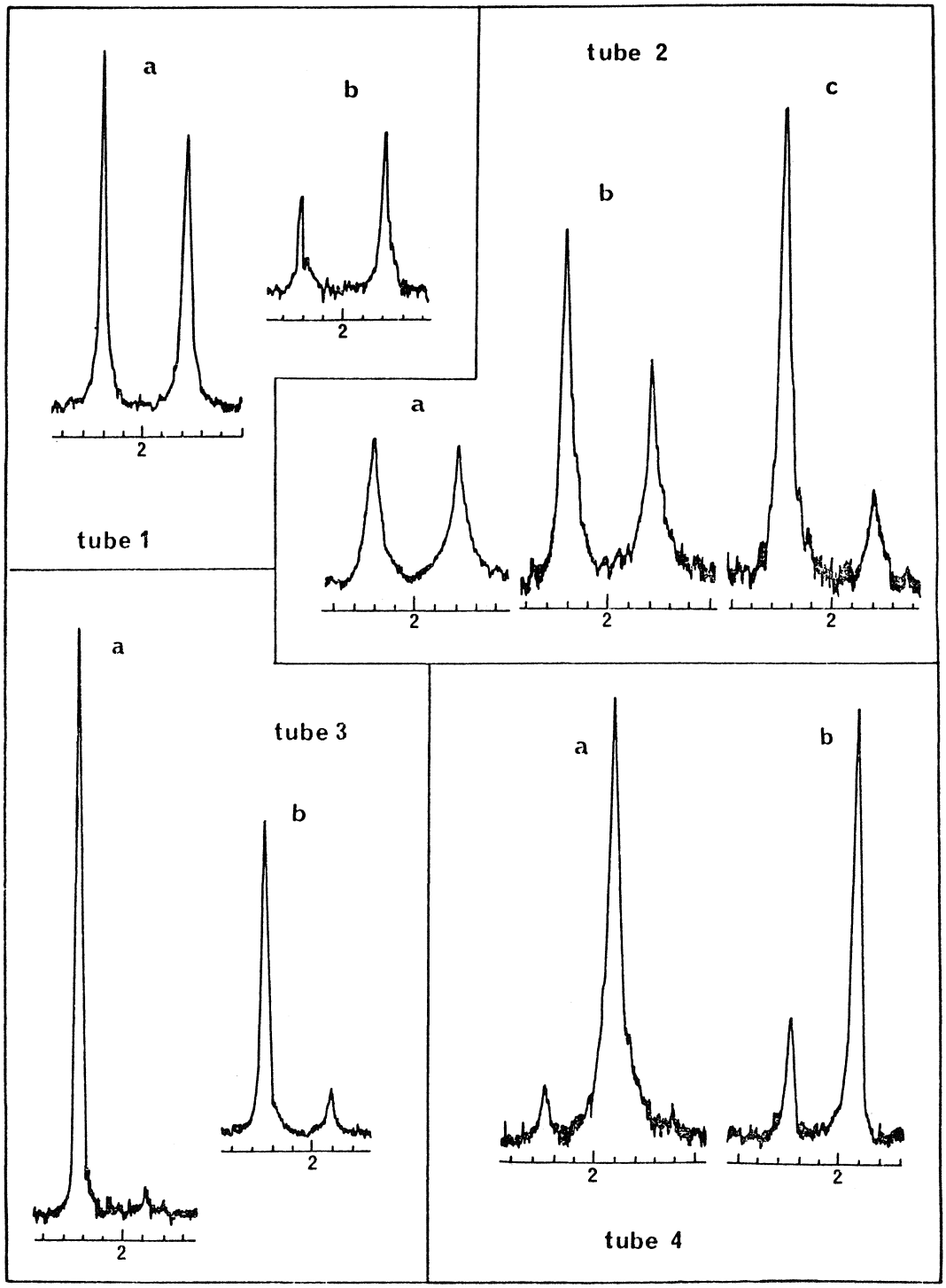


FIG. 3. Spectres de rmn du proton des énolates de l'acétylacétate d'éthyle et de l'acétyl-2-butyrolactone en solution dans le méthanol-$d_4$ à basse température (−40°C). Concentration approximative en énolate: 0,5 *M*. Tube no 1: (a) $E^-K^+$; (b) $E^-K^+$ + INa (2 equiv.). Tube no 2: (a) $E^-Na^+$; (b) et (c): $E^-Na^+$ + 15-couronne-5 (1 et 2 equiv. respectivement). Tube no 3: (a) $L^-K^+$ (b) $L^-K^+$ + INa (1 equiv.). Tube no 4: (a) $L^-Li^+$; (b) $L^-Li^+$ après dilution d'un facteur 2.

TABLEAU 2. Déplacements en ppm par rapport au TMS observés pour les singulets méthyliques d'énolates de l'acétylacétate d'éthyle et de l'acétyl-2-butyrolactone en solution dans le méthanol ($t = -40 \mp 5°C$); (a), (b), (c): voir Fig. 3

| Tube | Sel et additif | | $CH_3$ (chélate): δ ppm | % | $CH_3$ (relâché): δ ppm | % |
|---|---|---|---|---|---|---|
| 1 | $E^-K^+$ | (a) | 1,78 | 43 | 2,22 | 57 |
| | $E^-K^+$ + INa 2 equiv. | (b) | 1,79 | 62 | 2,20 | 38 |
| 2 | $E^-Na^+$ | (a) | 1,79 | 52 | 2,21 | 48 |
| | $E^-Na^+$ + 15C5 | (b) | 1,77 | 38 | 2,20 | 62 |
| | $E^-Na^+$ + 15C5 excès | (c) | 1,75 | 16 | 2,19 | 84 |
| 3 | $L^-K^+$ | (a) | 1,87 | 4 | 2,21 | 96 |
| | $L^-K^+$ + INa | (b) | 1,90 | 12 | 2,22 | 88 |
| 4 | $L^-Li^+$ | (a) | 1,90 | 89 | 2,23 | 11 |
| | $L^-Li^+$ (C/2) | (b) | 1,89 | 78 | 2,22 | 22 |

protons méthyliques résonnent à champ plus fort en série *trans* qu'en série *cis* (16). Il a de plus été montré que l'effet de déblindage observé en série *cis* était associé à une conformation *S-cis* du groupement carbonyle (Schéma 3) (voir ref. 17*a*; pour une analyse semblable concernant les protons oléfiniques en β des cétones α,β-insaturées voir ref. 17*b*).

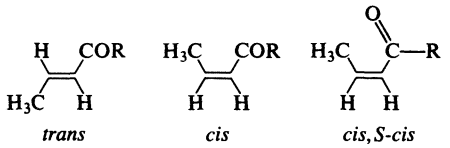


SCHÉMA 3

En accord avec ces données concernant des molécules neutres, on observe dans la série des énolates que le méthyle du conformère *EZ* de l'anion de l'hexanedione-2,4, maintenu dans le voisinage du pseudo-carbonyle, résonne à champ plus faible que le méthyle du conformère *ZE* dirigé vers l'extérieur de la molécule.

Dans le conformère en *W* de $E^-$ le groupement méthyle occupe vis à vis du pseudo-carbonyle de la partie opposée de la molécule une position éloignée, assez similaire à celle du méthyle de la forme *ZE* de l'hexadionate ou du méthyle extérieur de la forme *S-trans* de l'ion acétylacétonate et radicalement différente de celle du méthyle de la forme *S-trans* de $L^-$. Ce dernier occupe par contre une position équivalente à celle du méthyle de la forme *EZ* de l'hexadionate et du méthyle intérieur de la forme *S-trans* de l'acétylacétonate (Schémas 2 et 4). Sur la base de l'identité des déplacements chimiques observés pour $E^-$ et $L^-$, il est donc raisonnable d'exclure la conformation en *W* pour l'énolate $E^-$ et de conclure à l'existence d'une conformation *S-trans* analogue à celle de $L^-$.

Les déplacements chimiques à champ fort, δ < 2 ppm, des groupements méthyles de $E^-$ et $L^-$ sous forme de chélate sont en accord avec les données de la littérature (4, 8, 9, 15). Le Δδ de 0,09 ppm observé sur le chélate de $E^-$ et celui de $L^-$ est significatif et peut s'expliquer par un effet de substituant sur le carbone central du motif conjugué. Une différence de déplacement chimique très voisine (0,07 ppm) est observée par Esakov entre les chélates de l'acétylacétate d'éthyle et de l'α-méthyl-acétylacétate d'éthyle dans le DMF (9). A l'état relaché, l'énolate de l'α-méthyl-acétylacétate présente un δ($CH_3$) identique à celui de $E^-$ (9), ce qui est aussi en faveur d'une conformation *S-trans* pour le dérivé substitué sur le carbone central.

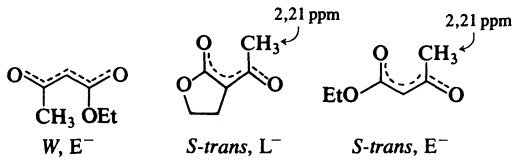


SCHÉMA 4

## III. Calculs théoriques

Les calculs théoriques (*ab initio* STO-3G) ont été réalisés à l'aide du programme Gauss 70. Les carbanions modèles choisis pour cette étude sont ceux du dimalonaldéhyde, de l'acide formylacétique et du formyl acétate de méthyle. Dans tous les cas les atomes appartenant ou directement attachés au système délocalisé $C_3O_2^-$ ont été pris dans le même plan;[8] les longueurs de liaison C—O et C—C du système délocalisé ont été fixées arbitrairement à 1,30 et 1,40 Å respectivement et les angles de liaison autour des atomes de carbone à 120°. Les paramètres géométriques standard ont été utilisés pour les autres parties des molécules (18).

[8]Les structures cristallines des complexes $E^-M^+$ – couronne montrent que le motif $C_3O_2^-$ est plan (2).

Can. J. Chem. Downloaded from www.nrcresearchpress.com by 210.87.254.5 on 09/06/12
For personal use only.

Can. J. Chem. Downloaded from www.nrcresearchpress.com by 210.87.254.5 on 09/06/12
For personal use only.

TABLEAU 3. Energie calculée (*ab initio* STO-3G) pour les carbanions du malonaldehyde, de l'acide formylacétique et du formylacétate de méthyle dans diverses conformations

| Anion | | *E* (en ua) | Energie relative[a] (en kcal) |
|---|---|---|---|
| 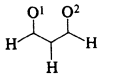 | *ZZ* (*U*) | −261,397 292 | +8,35 |
| 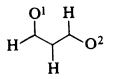 | *ZE* (*S*) | −261,409 667 | +0,58 |
| 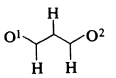 | *EE* (*W*) | −261,410 597 | 0 |
| 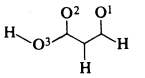 | *EZ* (*U*) | −335,262 107 | +7,25 |
| 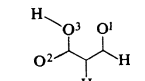 | *ZZ* (*S-cis*) | −335,266 130 | +4,72 |
| 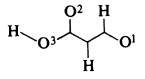 | *EE* (*S-trans*) | −335,275 269 | −1,01 |
| 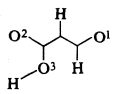 | *ZE* (*W*) | −335,273 653 | 0 |
| 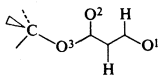 | *EE* (*S-trans*) | −373,853 607 | −1,12 |
| 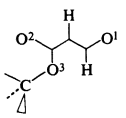 | *ZE* (*W*) | −373,851 820 | 0 |

[a]Le conformère en *W* étant pris comme référence pour chacun des trois énolates.

Le tableau 3 rassemble les valeurs de l'énergie totale obtenues pour les différents conformères étudiés.

Dans tous les cas où il a été calculé (anions du dimalonaldéhyde et de l'acide formylacétique) le conformère en *U* apparaît très destabilisé en absence de cation ainsi que l'on pourrait s'y attendre sur la base de simples considérations électrostatiques (répulsion $O^1$–$O^2$). Le même phénomène s'observe, bien qu'à un degré moindre, pour le conformère *S-cis* de l'anion de l'acide formylacétique (répulsion $O^1$ – oxygène du groupement hydroxy) dont l'énergie calculée est supérieure de 0,00914 ua (5,73 kcal) à celle du conformère *S-trans*.

Concernant les stabilités respectives des formes *S-trans* et *W*, le calcul donne la forme *W* plus stable ($\Delta E$ = 0,58 kcal) dans le cas de l'énolate du malonaldehyde tandis que pour les énolates de l'acide formylacétique et de son ester méthylique utilisés comme modèles d'énolates de β-cétoesters la forme *S-trans* est favorisée ($\Delta E$ = 1,01 et 1,10 kcal respectivement). L'ordre de stabilité des deux formes ainsi trouvé est en accord avec les données expérimentales aussi bien en ce qui concerne l'énolate du malonaldéhyde (19) que celui du formylacétate de méthyle (8). Les différences d'énergie calculées sont cependant faibles et compte tenu du caractère fragmentaire des calculs réalisés ici (absence d'optimisation des paramètres géométriques, utilisation d'une base minimale pour la description des anions) un tel accord est peut être fortuit. Compte tenu de l'étroite parenté de structure des divers énolates étudiés, on peut cependant considérer comme vraisemblablement significative la tendance à la stabilisation, mise en évidence par le calcul, de la forme *S-trans relativement à la forme W* lorsque l'on passe de l'énolate du malonaldéhyde aux énolates de β-cétoesters.[9]

En résumé les résultats de ces calculs montrent que dans la série des énolates de β-cétoesters les facteurs purement électroniques sont nettement défavorables à la conformation *S-cis* et tendraient à favoriser la forme *S-trans* par rapport à la forme *W*. Ceci n'exclut pas la possibilité d'intervention d'autres facteurs, de nature stérique ou liés aux phénomènes de solvatation par exemple. Notamment les interactions stériques entre substituants placés en position 1 et 3 de la molécule, qui jouent

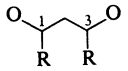

un rôle important dans la série des dicétones (*4b* et références citées) pourraient encore constituer dans le cas des β-cétoesters un facteur non négligeable de déstabilisation du conformère en *W*.

[9]Parmi les facteurs responsables des stabilités respectives des diverses formes, on peut penser que la répulsion électrostatique s'exerçant entre les deux oxygènes chargés négativement du système mésomère joue un rôle important. De ce point de vue, le passage de la forme *S-trans* à la forme en *W* doit s'accompagner d'un gain de stabilité dans la mesure où les deux atomes d'oxygène sont plus éloignés dans la seconde conformation (4,68 Å contre 4,01 Å avec les paramètres géométriques utilisés ici). Dans le cas des énolates de β-cétoesters cependant, la diminution de la répulsion électrostatique entre les deux atomes $O^1$ et $O^2$ du système délocalisé consécutive au passage *S-trans* → *W* est en partie compensée par l'augmentation de la répulsion électrostatique entre l'atome d'oxygène $O^1$ et l'atome d'oxygène $O^3$ du groupement alkoxy; ceci pourrait expliquer la déstabilisation relative du conformère en *W*. A titre d'illustration, si l'on se base sur les charges nettes données par le calcul *ab initio* STO-3G pour les atomes d'oxygène $O^1$, $O^2$ et $O^3$ on trouve, pour le passage *S-trans* → *W*, un gain de stabilité électrostatique d'environ 2 kcal/mol dans le cas de l'anion du formaldéhyde alors qu'il est inférieur à 1 kcal/mol dans le cas de l'anion du formylacétate de méthyle.

Can. J. Chem. Downloaded from www.nrcresearchpress.com by 210.87.254.5 on 09/06/12
For personal use only.

## Partie expérimentale

*Matières premières*

La préparation des énolates alcalins de l'acétylacétate d'éthyle a déjà été décrite (3). La même préparation a été suivie pour les énolates des autres composés β-dicarbonylés.

Le cryptand (2,2,2) (Kryptofix (2,2,2), Merck) a été utilisé tel quel. La 15-couronne-5 (Borregard) a été purifiée sur colonne d'alumine. $\phi_4B^-K^+$ et $I^-Na^+$ ont été sèchés dans un dessicateur sous vide à 80°C pendant une nuit.

Le DMSO a été distillé sous pression réduite avant utilisation, et le méthanol-$d_4$ utilisé tel quel.

*Appareils*

L'étude conductimétrique a été réalisée sur un conductimètre Philips PW 9501/01 équipé d'une cellule de mesure PR 9512/00 possèdant une constante de 0,685 $cm^{-1}$. La fréquence utilisée (2000 Hz) permet des mesures dans la gamme de $\chi$ de $10^{-4}$ à 0,1 $\Omega^{-1}$ $cm^{-1}$.

Les spectres de rmn à basse température ont été réalisés sur un Varian A 60D (60 MHz).

## Remerciements

Nous remercions le Dr J. Corset, Maître de Recherche au C.N.R.S. pour de fructueuses discussions, et Mme M. Ourevitch pour l'enregistrement des spectres rmn.

1. L. M. Jackman et B. C. Lange. Tetrahedron, **33**, 2737 (1977).
2. C. Cambillau, G. Bram, J. Corset, C. Riche et C. Pascard-Billy. Tetrahedron, **34**, 2675 (1978).
3. (*a*) F. Guibe, P. Sarthou et G. Bram. Tetrahedron, **30**, 3139 (1974); (*b*) P. Sarthou, G. Bram et F. Guibe. Can. J. Chem. **58**, 786 (1980).
4. (*a*) M. Raban, E. A. Noe et G. Yamamoto. J. Am. Chem. Soc. **99**, 6527 (1977); (*b*) M. Raban et D. P. Haritos. J. Am. Chem. Soc. **101**, 5178 (1979).
5. A. L. Kurts, A. Macias, I. P. Beletskaya et O. A. Reutov. Tetrahedron Lett. 3037 (1971).
6. H. E. Zaugg et A. D. Schaeffer. J. Am. Chem. Soc. **85**, 1857 (1965).
7. B. Miller, H. Margulies, T. Drabb, Jr. et R. Wayne. Tetrahedron Lett. 3801 (1970); 3805 (1970).
8. S. M. Esakov, Al. An. Petrov et B. A. Ershov. Zh. Org. Khim. (Trad. Anglaise), **11**, 679 (1975).
9. Al. An. Petrov, S. M. Esakov et B. A. Ershov. Zh. Org. Khim. (Trad. Anglaise), **12**, 774 (1976).
10. C. Riche, C. Pascard-Billy, C. Cambillau et G. Bram. J. Chem. Soc. Chem. Commun. 183 (1977).
11. C. Cambillau, G. Bram, J. Corset et C. Riche. Nouv. J. Chim. **3**, 9 (1979); C. Cambillau et M. Ourevitch. J. Chem. Soc. Chem. Commun, 996 (1981).
12. C. Cambillau. Thèse de Doctorat d'Etat, Université de Paris-Sud (Orsay), 29 Juin 1978.
13. J. P. Collman, R. G. Finke, J. N. Cawse et J. I. Brauman. J. Am. Chem. Soc. **99**, 2515 (1977).
14. S. J. Rhoads et R. N. Holder. Tetrahedron, **25**, 5443 (1969).
15. M. Raban, R. Keintz, D. P. Haritos et J. Greenblatt. J. Org. Chem. **45**, 2672 (1980).
16. L. M. Jackman et S. Sternhell. Applications of nuclear magnetic resonance spectroscopy, 2 ième éd. Pergamon Press, 1969. p. 91 et suiv., 223 et suiv.
17. (*a*) L. M. Jackman et R. H. Wiley. J. Chem. Soc. 2886 (1960); (*b*) J. Kossanyi. Bull. Soc. Chim. Fr. 704 (1965).
18. J. A. Pople et M. Gordon. J. Am. Chem. Soc. **89**, 4257 (1967).
19. N. Bacon, N. O. George et B. H. Stringer. Chem. Ind. London, 1377 (1965).
20. R. M. Fuoss. J. Am. Chem. Soc. **57**, 488 (1935).
21. L. Onsager. Z. Phys. **28**, 277 (1927).
22. (*a*) C. M. French et K. H. Glover. Trans. Faraday Soc. **52**, 1418 (1955); **52**, 1427 (1955); (*b*) P. G. Sears, G. R. Lester et L. R. Dawson. J. Phys. Chem. **60**, 1433 (1956).
23. W. N. Olmstead et F. G. Bordwell. J. Org. Chem. **45**, 3299 (1980).

## Annexe conductimétrique

*Dosage conductimétrique à l'aide du cryptand (2,2,2)*

Il est admis en première approximation que la mobilité des ions est indépendante de la concentration en espèces ioniques dans le milieu. Les conductivités équivalentes $\Lambda_i$ du tétraphénylborate de $K^+$ et de l'énolate de $K^+$ étudié en l'absence de cryptand sont alors donnés par les relations

$$[1] \quad \Lambda_{i,EK} = \alpha\lambda_{E^-} + \alpha\lambda_{K^+}$$

$$[2] \quad \Lambda_{i\phi_4BK} = \lambda_{\phi_4B^-} + \lambda_{K^+}$$

$\alpha$ désignant le coefficient de dissociation de l'énolate et les $\lambda$ les conductivités ioniques équivalents des ions.

En présence de cryptand l'énolate est totalement dissocié et les conductivités équivalentes au plateau sont égales à:

$$[3] \quad \Lambda_{pl,EK} = \lambda_{E^-} + \lambda_{K^+ \text{ crypté}}$$

$$[4] \quad \Lambda_{pl,\phi_4BK} = \lambda_{\phi_4B} + \lambda_{K^+ \text{ crypté}}$$

Des équations [1]–[4] on tire la relation [5] utilisée pour la détermination approchée du coefficient de dissociation des énolates:

$$[5] \quad \alpha_{approx.} = \frac{\Lambda_{i,EK}}{\Lambda_{pl,EK} + \Lambda_{i,\phi_4BK} - \Lambda_{pl,\phi_4BK}}$$

L'équation [5] est de la forme:

$$\alpha = \frac{\Lambda_{i,EK}}{\Lambda_{pl,EK} + C}$$

$C = \Lambda_{i,\phi_4BK} - \Lambda_{pl,\phi_4BK}$ étant le terme correctif qui permet de tenir compte de la variation de la mobilité de l'ion $K^+$ consécutive à sa cryptation. Notons qu'elle est différente de l'équation proposée par Collmann *et al.* (13)

$$\alpha = \frac{\Lambda_{i,AM}}{\Lambda_{pl,AM}} \times C'$$

où le terme correctif $C'$ est égal au rapport $\Lambda_{i,\phi_4BM}/\Lambda_{pl,\phi_4BM}$

La conductivité équivalente d'un électrolyte n'est pas en réalité indépendante de sa concentra-

TABLEAU 4. Paramètres conductimétriques calculés pour les différents énolates (estimation) en tenant compte de l'effet de la concentration en espèces ioniques sur la mobilité des ions (cf. Annexe conductimétrique)

| Enolate | $\Lambda^\circ$ | $\alpha \times 100$ | $K_d$ |
|---|---|---|---|
| $E^-K^+$ | 36,93 | 35,1 | $19 \times 10^{-3}$ |
| $\alpha EtE^-K^+$ | 33,25 | 65,3 | $123 \times 10^{-3}$ |
| $C^-K^+$ | 32,62 | 14,3 | $2,1 \times 10^{-3}$ |
| $L^-K^+$ | 38,47 | 65,5 | $124 \times 10^{-3}$ |
| $\phi_4B^-K^+$ | 29,63 | | |
| $E^-K^+$ crypté | 31,53 | | |
| $E^-K^+$ crypté | 27,22 | | |
| $\phi_4B^-K^+$ crypté | 24,23 | | |
| $\alpha EtE^-K^+$ crypté | 27,85 | | |
| $E^-K^+$ crypté | 33,07 | | |

tion $c$ dans le milieu. Dans le cas d'un électrolyte complètement dissocié et pour des valeurs de $c$ suffisamment faibles, la variation de $\Lambda$ en fonction de $c$ est donnée par la relation d'Onsager (20, 21)

$$[6] \quad \Lambda = \Lambda^0 - a\sqrt{c}$$

Pour un électrolyte incomplètement dissocié, cette relation devient:

$$[7] \quad \Lambda = \alpha\,(\Lambda^0 - a\sqrt{\alpha c})$$

Le dosage conductimétrique par le cryptand (2,2,2) peut alors être traité de la façon suivante. Pour l'énolate en l'absence de cryptand nous avons la relation:

$$\Lambda_{i,EK} = \alpha\,(\Lambda^0{}_{EK} - a\sqrt{\alpha c})$$

soit

$$\alpha = \frac{\Lambda_{i,EK}}{\Lambda^0{}_{EK} - a\sqrt{\alpha c}}$$

La conductivité équivalente limite $\Lambda^0{}_{EK}$ de l'énolate de potassium peut être exprimée en fonction des conductivités équivalentes limites de l'énolate crypté et du tetraphényl borate de $K^+$ en présence et en l'absence de cryptand, en effet:

$$\Lambda^0{}_{EK} = \lambda^0{}_{E^-} + \lambda^0{}_{K^+} = \lambda^0{}_{E^-} + \lambda^0{}_{K^+\,\text{crypté}} + \lambda^0{}_{K^+} + \lambda^0{}_{\phi_4B^-} - \lambda^0{}_{\phi_4B^-} - \lambda^0{}_{K^+\,\text{crypté}}$$

et

$$\Lambda^0{}_{EK} = \Lambda^0{}_{EK\text{crypté}} + \Lambda^0{}_{\phi_4BK} - \Lambda^0{}_{\phi_4BK\text{crypté}}$$

et finalement:

$$[8] \quad \alpha = \frac{\Lambda_{i,EK}}{\Lambda^0{}_{EK\text{crypté}} + \Lambda^0{}_{\phi_4BK} - \Lambda^0{}_{\phi_4BK\text{crypté}} - a\sqrt{\alpha c}}$$

A la concentration choisie dans cette étude (0,1 *M*) les déviations par rapport à la loi d'Onsager sont déjà souvent substantielles (22). Il nous a néanmoins paru intéressant de calculer les nouvelles valeurs de $\alpha$ à l'aide de la relation [8] afin *d'estimer* l'importance des approximations faites dans le traitement initial (relation [5]). Les valeurs des conductivités équivalentes limites $\Lambda^0$ des électrolytes complètement dissociés ont été calculées à l'aide de la relation [6], la pente limite de Onsager:

$$a = \frac{8{,}20 \times 10^5\,\Lambda^0}{(DT)^{3/2}} + \frac{82{,}4}{n\,(DT)^{1/2}}$$

étant prise égale à:

$$a = 0{,}5\,\Lambda^0 + 35{,}6$$

dans le DMSO à 25°C ($n = 19{,}6 \times 10^{-3}$ poise et $D = 46{,}6$). $\alpha$ est ensuite calculé à l'aide de la relation [8] et par ajustement successif en prenant pour valeur de départ la valeur $\alpha_{app}$ obtenue à l'aide de [5].

Les valeurs de $\Lambda^0$, $\alpha$ et $K_d$ ainsi obtenues sont résumées dans le tableau 4. Notons que la valeur de $\alpha$ pour l'énolate $E^-M^+$ ($\alpha = 0{,}35$) trouvée ici est cohérente avec le résultat de spectroscopie ir pour une même solution qui donne $\alpha \simeq 0{,}40$ (12).

Les valeurs de $\alpha$ calculées selon [8] sont inférieures aux valeurs de $\alpha$ calculées selon [5]. Comme il était prévisible, l'écart maximum est observé dans le cas de l'énolate $C^-$ le moins dissocié (0,143 contre 0,22 soit un écart relatif de 35%). Les valeurs des constantes $K_d$ de dissociation sont diminuées d'un facteur voisin de 2 pour $E^-$, $\alpha$Et-$E^-$ et $L^-$ et d'un facteur 3 pour l'énolate $C^-$. Les approximations faites dans le traitement initial conduisent donc indiscutablement à surestimer la tendance à la dissociation des électrolytes étudiés. Elles ne remettent néanmoins pas en cause les conclusions tirées dans cette étude puisque celles-ci étaient basées non sur les valeurs absolues des constantes $K_d$ mais sur leur variation d'un énolate à l'autre.

En contre partie de son caractère approximatif, la méthode du titrage conductimétrique par le cryptand a pour avantage sa facilité de mise en œuvre; surtout elle nous a permis de travailler à une concentration élevée (0,1 *M*), où les énolates présentaient encore une forte tendance à l'association. Dans ces conditions, les variations de $K_d$ se sont traduites par des variations relatives de $\alpha$ importantes et ont donc pu être observées sans risque d'erreurs expérimentales.

Can. J. Chem. Downloaded from www.nrcresearchpress.com by 210.87.254.5 on 09/06/12
For personal use only.

# The biosynthesis of retronecine

GUNNAR GRUE-SØRENSEN AND IAN D. SPENSER[1]

*Department of Chemistry, McMaster University, Hamilton, Ont., Canada, L8S 4M1*

Received October 8, 1981

GUNNAR GRUE-SØRENSEN and IAN D. SPENSER. Can. J. Chem. **60**, 643 (1982).

An experiment with putrescine, doubly labelled intramolecularly, with $^{15}N$ and $^{13}C$ at the adjacent C-atom, demonstrates that a $C_4$–N–$C_4$ compound with $C_{2v}$ symmetry serves as a precursor of retronecine, the most common base of the Senecio alkaloids. The $C_4$–N–$C_4$ compound is, in turn, generated from two ornithine-derived precursor units. This was demonstrated by a degradation sequence whereby the distribution of label from [5-$^{14}$C]-, [5-$^{3}$H]-, and [4-$^{3}$H]ornithine within retronecine was fully accounted for.

GUNNAR GRUE-SØRENSEN et IAN D. SPENSER. Can. J. Chem. **60**, 643 (1982).

Une experience, avec de la putrescine doublement marquée avec du $^{13}C$ et du $^{15}N$ sur l'atome de carbone voisin, permet de démontrer que le précurseur de la rétronecine, la base la plus commune des alcoloïdes du Senecio, est un composé $C_4$–N–$C_4$ de symétrie $C_{2v}$. Le composé $C_4$–N–$C_4$ est pour sa part généré à partir de deux unités ayant des dérivés de l'ornithine comme précurseurs. Ceci a été démontré par une séquence de dégradation grâce à laquelle on a pu expliquer complètement la distribution des [5-$^{14}$C]-, [5-$^{3}$H]- et [4-$^{3}$H]ornithines dans la rétronécine.

[Traduit par le journal]

## Introduction

Retronecine (**1**) is the most common of the necine bases of the Senecio alkaloids (1–5). Nonrandom incorporation of carbon-14 from ornithine (6–8) putrescine (6, 8), spermidine (8), and spermine (8) as well as carbon-13 from putrescine (9) into retronecine provides experimental support for the postulate of Sir Robert Robinson (10) that the pyrrolizidine skeleton of the Senecio alkaloids is generated from two $C_4$ units related to ornithine.

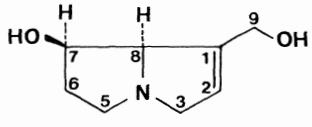


**1**

The manner in which the two ornithine-derived $C_4$ units are incorporated into retronecine is still in question. There is general agreement that one quarter of the activity derived from [2-$^{14}$C]ornithine (6,7) and from [5-$^{14}$C]ornithine (3, 6, 8) resides at C-9 (isolated as formaldehyde (6, 8) or as iodoform (7)). The location of the remaining activity is in dispute, however.

On the one hand, it is reported (8) that retronecine derived from [5-$^{14}$C]ornithine in *Senecio isatideus* contains one quarter of its label at C-5 (isolated together with C-6 and C-7 as β-alanine). If the assumption is made that the activity which is not accounted for by degradation is located at C-3 (25%) and C-8 (25%), this result suggests that two ornithine-derived $C_4$ units enter retronecine, each in symmetrical fashion. Putrescine (**3**), which originates from ornithine (**2**) or from arginine (11), is a nondissymmetric ($C_{2v}$) molecule whose intermediacy would lead to the observed labelling pattern. Label from (1,4-$^{13}C_2$)- and from (2,3-$^{13}C_2$)-putrescine is indeed incorporated into retronecine, leading to equal enrichment, within experimental error, at C-3,-5,-8, and -9, and at C-1,-2,-6, and -7, respectively (9), as expected. This distribution of label has been regarded also as an indication of the intermediacy of a "symmetrical dimeric" intermediate (Scheme 1, Route A) such as **6**. In fact, the same distribution of label would be obtained by a route (Scheme 1, Route B) which excludes a "symmetrical dimeric" intermediate.

On the other hand, it is claimed (7) that retronecine derived from [2-$^{14}$C]ornithine, in the same Senecio species, is not labelled either at C-3 or at C-5, and that the remaining activity (ca. 75%) resides at C-8. This result suggests that two nonidentical ornithine-derived $C_4$ units enter retronecine, each in nonsymmetrical fashion.

The two sets of results are clearly incompatible.

We have re-investigated the biosynthesis of retronecine in *Senecio vulgaris* (common groundsel).

To clarify the question of the distribution of label derived from ornithine, we have devised a degradation sequence which permits assay of label at each of the four crucial positions of retronecine, C-3, C-5, C-8, and C-9 (Scheme 2). By means of this degradation we have determined the mode of incorporation into retronecine of activity from [5-$^{14}$C]ornithine and from [4-$^{3}$H,5-$^{14}$C]- and [5-$^{3}$H,5-$^{14}$C]ornithine, as well as from a $^{3}$H,$^{14}$C-labelled sample of spermidine.

[1]Author to whom correspondence may be addressed.

0008-4042/82/050643-20$01.00/0

©1982 National Research Council of Canada/Conseil national de recherches du Canada

Can. J. Chem. Downloaded from www.nrcresearchpress.com by 210.87.254.42 on 09/06/12
For personal use only.

Can. J. Chem. Downloaded from www.nrcresearchpress.com by 210.87.254.42 on 09/06/12
For personal use only.

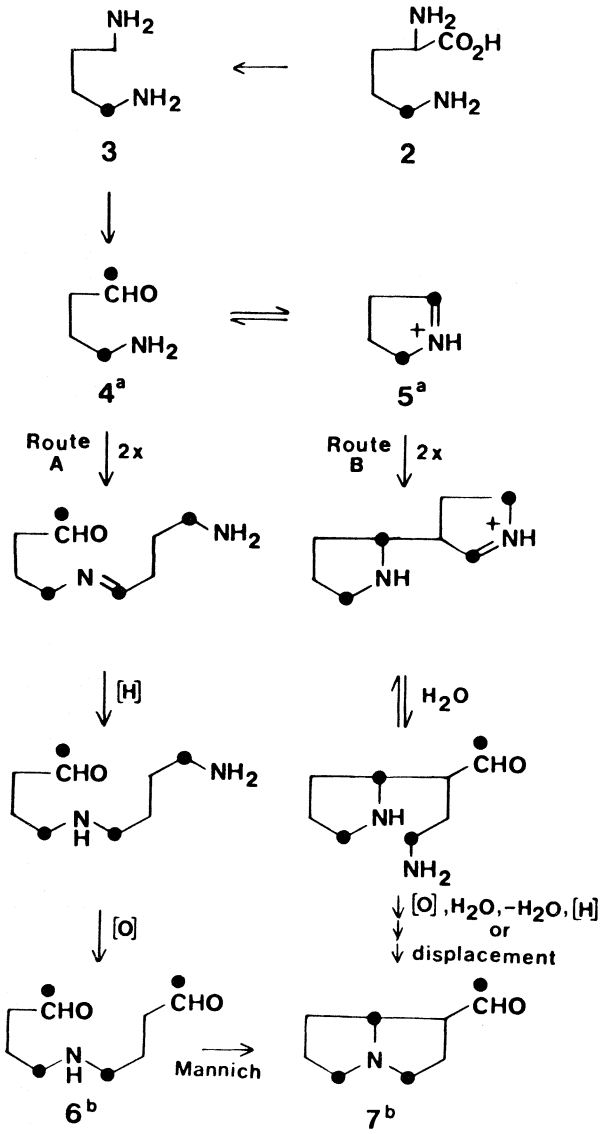


SCHEME 1. Two routes from ornithine into retronecine. Route A, via a symmetrical (i.e., nondissymmetric, $C_{2v}$) intermediate (**6**); Route B, via dissymmetric ($C_1$) intermediates. (a) Formulae **4** and **5** of labelled "monomeric" intermediates represent a 50/50 mixture of two singly labelled species. (b) Formulae of all labelled "dimeric" intermediates and of **7** represent mixtures of four singly labelled and four doubly labelled species, whose relative contribution is determined by the relative quantities of labelled and unlabelled putrescine available to the plant during the period of biosynthesis.

Furthermore, to show whether or not a "symmetrical dimeric" intermediate lies on the pathway to retronecine, we have determined the mode of incorporation of intramolecularly doubly $^{13}C,^{15}N$-labelled putrescine by means of $^{13}C$ nmr.

From our results we conclude that a "symmetrical dimeric" intermediate, $C_4$–N–$C_4$, generated from two L-ornithine-derived[2] "monomer" units, lies on the biosynthetic route. Whether or not these "monomer units" are "symmetrical" (i.e. nondissymmetric) cannot be decided with certainty on the basis of existing evidence.

## Methods and results

The plant species used in this study was *Senecio vulgaris* (common groundsel), a tough and persistent weed which re-appears every spring in the rose beds on the McMaster campus, much to the annoyance of the grounds supervisor, who each year has his staff do their utmost to eradicate it. During the summer months of 1978, 1979, and 1980, when these experiments were carried out, he was persuaded to tolerate the plants in a few unobtrusive locations until they were transferred to the greenhouse for use in our investigation.

In 8 separate tracer experiments specifically labelled samples of ornithine (Experiments 1–4), putrescine (Experiment 5), spermidine (Experiment 6), and 1-pyrroline (Experiments 7 and 8) were administered to *S. vulgaris* by the wick method. In each of the experiments with radioactive tracers (Experiments 1–4, 6, 8) approximately 30 plants were used; in the experiments with stable isotopes (Experiment 5, $^{13}C,^{15}N$; Experiment 7, $^{2}H$) approximately 130 plants were used. In Experiment 5, plants were grown in contact with labelled substrate for two weeks. In all other cases the experiments lasted 3–5 days. Experimental details are summarized in Table 1.

Work-up of the plants yielded a mixture of alkaloids (senecionine, seneciphylline, and retrorsine (13–15)) and a mixture of the corresponding *N*-oxides. Retronecine (**1**) was isolated from the alkaloid mixture after hydrolysis and from the *N*-oxides after reduction and hydrolysis. Labelled samples of retronecine were obtained in the experiments with ornithine (Experiments 1–4), putrescine (Experiment 5), and spermidine (Experiment 6). The experiments with 1-pyrroline did not yield labelled alkaloids (Experiments 7 and 8).

The distribution of label within retronecine derived from radioactive precursors (Experiments 1–4, 6) was determined by the degradation sequence shown in Scheme 2. The distribution of label within retronecine derived from ($^{13}C,^{15}N$)putrescine was determined by $^{13}C$ nmr.

The degradation sequence shown in Scheme 2

[2]That the precursor is L-ornithine follows from the results of an investigation, to be published separately, of the relative efficiencies of incorporation of label from L- and D-ornithine, by a method previously developed (12) for establishing the chirality of precursor product relationships in intact systems.

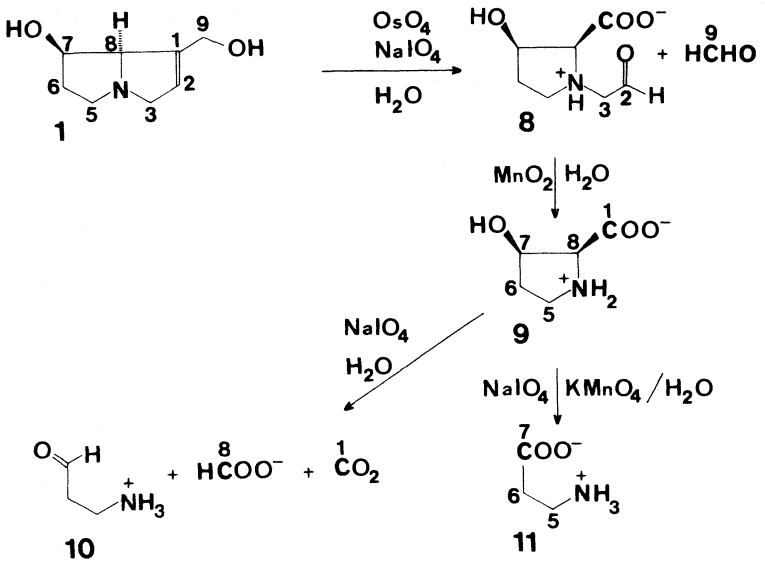

SCHEME 2. Degradation of retronecine.

TABLE 1. Administration of tracers to *Senecio vulgaris*

| Expt. No. | Date | Precursor (source) | Nominal total activity mCi | Nominal specific activity mCi/mmol | $^3H/^{14}C$ ratio of administered sample[a] | No. of plants | Fresh weight: Tops (g) | Fresh weight: Roots (g) | Days |
|---|---|---|---|---|---|---|---|---|---|
| 1 | 1978 | DL-[5-$^{14}$C]ornithine[b] | 0.1 | 7.7 | — | 21 | 192 | 68 | 3 |
| 2 | 1979 | DL-[5-$^{14}$C]ornithine[c] plus DL-[5-$^3$H]ornithine[d,e] | 0.05<br>0.5 | 11.5<br>5 × $10^3$ | 7.0 | 30 | 125 | 75 | 4 |
| 3 | 1979 | DL-[5-$^{14}$C]ornithine[c] plus L-[5-$^3$H]ornithine[f] | 0.1<br>1.0 | 11.5<br>20 × $10^3$ | 5.5 | 33 | 161 | 60 | 5 |
| 4 | 1979 | DL-[5-$^{14}$C]ornithine[c] plus L-[4-$^3$H]ornithine[c] | 0.06<br>0.8 | 11.5<br>13.6 × $10^3$ | 7.0 | 30 | 120 | 75 | 4 |
| 5 | 1980 | (1-$^{13}$C,1-$^{15}$N)putrescine[g] from potassium ($^{13}$C,$^{15}$N)cyanide[h] plus [1-$^{14}$C]putrescine[b] | —<br>0.05 | —<br>90 | — | 133 | 350 | 150 | 13 |
| 6 | 1980 | [1,4-tetramethylene-$^{14}C_2$]-spermidine[b] plus [1,8-$^3H_2$]spermidine[b] | 0.05<br>1.0 | 100<br>35 × $10^3$ | 14.8 | 36 | 110 | 55 | 4 |
| 7 | 1979 | (2-$^2$H)-1-pyrroline[g] from DL-(2-$^2$H)proline[i] | — | — | — | 128 | 600 | 250 | 3 |
| 8 | 1979 | [5-$^3$H,5-$^{14}$C]-1-pyrroline[g] from L-[5-$^3$H]proline[d] and from DL-[5-$^{14}$C]proline[c] | 1.0<br>0.1 | 14 × $10^3$<br>41 | 8.3 | 33 | 180 | 64 | 4 |

[a]The $^3H/^{14}C$ ratio was determined as follows. The solutions containing the two tracers were combined, diluted to 10 mL, and thoroughly mixed. Approximately 100 μL of the diluted solution was withdrawn and added to a solution containing the appropriate nonradioactive compound (200–500 mg) (Experiments 2–4, DL-ornithine monohydrochloride; Experiment 6, spermidine trihydrochloride, Experiment 8, DL-proline), which was then re-isolated and crystallized to constant activity and $^3H/^{14}C$ ratio.
[b]New England Nuclear, Boston, Mass.
[c]CEA, Gif-sur-Yvette, France.
[d]Radiochemical Centre, Amersham, England.
[e]A $^3$H nmr spectrum supplied by the RCC showed that this sample was a mixture of [5-$^3$H]ornithine (86%) and [4-$^3$H]ornithine (14%).
[f]Schwartz/Mann Inc., Orangeburg, New York.
[g]See Experimental.
[h]Prochem, London, England.
[i]Merck, Sharp and Dohme, Point-Claire, Canada.

Can. J. Chem. Downloaded from www.nrcresearchpress.com by 210.87.254.42 on 09/06/12
For personal use only.

Can. J. Chem. Downloaded from www.nrcresearchpress.com by 210.87.254.42 on 09/06/12
For personal use only.

permits individual assay of activity at each of the four predicted sites, C-3, C-5, C-8, and C-9. Oxidation of retronecine with periodate/osmium tetroxide (6) yields formaldehyde (C-9) (isolated as dimethone) and an amino acid, presumably **8**, which was not isolated but was further oxidized with manganese dioxide to yield L-cis-3-hydroxyproline[3] (**9**) (C-1,-5,-6,-7,-8). Periodate oxidation of the latter gave formic acid (C-8) (isolated as *N*-formyl-α-naphthylamine) and 3-aminopropanal (**10**) which was not isolated but oxidized with permanganate to β-alanine (**11**) (C-5,-6,-7) (isolated as *N*-phthaloyl-β-alanine). This degradation permits assay also of tritium at C-9 (formaldehyde), at C-8 (formic acid), and at C-5 + C-6 (β-alanine), and less directly, at C-7 (L-*cis*-3-hydroxyproline minus β-alanine minus formic acid) and at C-2 plus C-3 (retronecine minus L-*cis*-3-hydroxyproline minus formaldehyde).

In some instances the samples of retronecine obtained from alkaloids and alkaloid-*N*-oxides were each degraded separately (Experiments 4 and 6), in other cases only the sample obtained from the alkaloids was degraded (Experiments 2 and 3), and in one case (Experiment 1) the retronecine samples from the two sources were combined before degradation. The samples of retronecine derived from DL-[5-$^{14}$C]ornithine (Experiments 1–4) and from [1,4-tetramethylene-$^{14}C_2$]spermidine (Experiment 6) showed a characteristic labelling pattern (Table 2). In each case, formaldehyde (C-9), formic acid (C-8), and β-alanine (C-5,-6,-7) each accounted for one quarter of the $^{14}$C-activity of the intact retronecine molecule, within experimental error. L-*cis*-3-Hydroxyproline (C-1,-5,-6,-7,-8) accounted for one half of the $^{14}$C-activity. The distribution of label from DL-[5-$^{3}$H]- and from L-[5-$^{3}$H]ornithine (Experiments 2 and 3, respectively) was identical within experimental error (Table 3). Formaldehyde (H atoms at C-9) and formic acid (H atom at C-8) each accounted for approximately one fifth of label, β-alanine (H atoms at C-5 plus C-6) for one third, and L-*cis*-3-hydroxyproline (H atoms at C-5,-6,-7,-8) for one half of the $^{3}$H-activity of intact retronecine.

The distribution of label from L-[4-$^{3}$H]ornithine (Table 3, Experiment 4) was different. Formaldehyde (H-atoms at C-9) and formic acid (H-atom at C-8) were essentially inactive. β-Alanine (H-atoms at C-5 plus C-6) accounted for half the activity of the intact retronecine, L-*cis*-3-hydroxyproline (H-atoms at C-5,-6,-7,-8) for three quarters. The distribution of label within the two samples of retronecine isolated in this experiment, one from the alkaloids (4*A*), the other from the *N*-oxides (4*O*), was identical (Table 3).

The two corresponding retronecine samples, 6*A* and 6*O*, derived from the experiment with spermidine (Experiment 6) did not show identical distributions of tritium activity (Table 3), even though the $^{14}$C distribution was identical in the two samples (Table 2). In the sample obtained from the *N*-oxides, formate (H at C-8) and β-alanine (H at C-5 and C-6) each accounted for one quarter of the $^{3}$H-activity, formaldehyde (H at C-9) for somewhat more than one quarter and L-*cis*-3-hydroxyproline (H at C-5,-6,-7,-8) for one half. A different $^{3}$H-distribution was observed in the case of the other retronecine sample from this experiment (Table 3). As will be shown in the discussion this discrepancy illustrates an experimental pitfall in the use of intermolecularly doubly $^{3}$H,$^{14}$C-labelled samples.

The sample of retronecine, labelled with $^{13}$C and $^{15}$N, which was obtained in Experiment 5 was analyzed by means of $^{13}$C nmr. The precursor, used in this experiment, (1-$^{13}$C,1-$^{15}$N)putrescine dihydrochloride, was synthesized in 3 steps from intramolecularly doubly labelled cyanide (90 at.% $^{13}$C, 99 at.% $^{15}$N,K$^{13}$C$^{15}$N) (Scheme 3). Reaction of 1-bromo-3-phthalimidopropane (**12**) with the cyanide yielded 4-phthalimidobutyronitrile (**13**) which was reduced catalytically (Raney nickel). Acid hydrolysis then gave (1-$^{13}$C,1-$^{15}$N)putrescine dihydrochloride (**15**). This was mixed with [1-$^{14}$C]-putrescine dihydrochloride and administered to 133 plants over a period of 13 days. The alkaloids were isolated (16) and purified by column chromatography. Hydrolysis gave a mixture of retronecine hydrochloride and retronecine *N*-oxide (17, 18) in the ratio 1 to 5, as determined by $^{13}$C nmr (19) (Table 4). Reduction and work-up under exclusion of oxygen gave retronecine hydrochloride which was chemically ($^{13}$C nmr) and radiochemically pure. Four positions within retronecine, C-3,-5,-8, and -9, were equally enriched in $^{13}$C (Fig. 1, Table 4). Furthermore, the $^{13}$C nmr signals due to C-3 and C-5 each showed a doublet (due to $^{13}$C,$^{15}$N coupling) superimposed on a singlet. The ratio, area of doublet/area of singlet, for C-3 was identical with that for C-5 (Fig. 2, Table 5).

Administration to *S. vulgaris* of labelled samples of 1-pyrroline did not yield labelled alkaloids (Experiments 7 and 8). The samples of 1-pyrroline, a compound which is chemically labile (20, 21), were

[3]The stereochemistry of this degradation product provides confirmation of the established configuration at C-7 and C-8 of retronecine.

Can. J. Chem. Downloaded from www.nrcresearchpress.com by 210.87.254.42 on 09/06/12
For personal use only.



TABLE 2. Incorporation of $^{14}C$ into retronecine

| Precursor | Expt. No. | Specific activity[d] (relative specific activity)[e] Retronecine | Retronecine HCl | Formaldehyde dimethone | L-*cis*-3-Hydroxyproline | *N*-Formyl-1-naphthylamine | *N*-Phthaloyl-β-alanine |
|---|---|---|---|---|---|---|---|
| DL-[5-$^{14}C$]ornithine | 1[a] | 12.7 (100±1) | 12.7 (100±1) | 3.1 (24±1) | 6.4 (50±1) | — | 3.2 (25±1) |
| | 2[b] | 4.66 (100±1) | 4.68 (100±1) | 1.21 (26±1) | 2.35 (50±1) | 1.12 (24±1) | 1.20 (26±1) |
| | 3[b] | 5.53 (100±1) | 5.27 (95±1) | 1.35 (24±1) | 2.69 (49±1) | 1.24 (22±1) | 1.34 (24±1) |
| | 4*A*[b] | 1.27 (100±1) | 1.33 (105±1) | 0.32 (25±2) | 0.69 (54±1) | — | 0.33 (26±3) |
| | 4*O*[c] | 2.09 (100±1) | 2.16 (103±1) | 0.53 (25±1) | 1.09 (52±1) | 0.49 (23±1) | 0.56 (27±1) |
| [1,4-Tetramethylene-$^{14}C_2$]spermidine | 6*A*[b] | 8.31 (100±1) | 8.03 (97±1) | 1.95 (23±1) | 4.01 (48±1) | 1.88 (23±1) | 1.97 (24±1) |
| | 6*O*[c] | 5.11 (100±1) | 5.07 (99±1) | 1.23 (24±1) | 2.47 (48±1) | 1.23 (24±1) | 1.23 (24±1) |
| C-atom(s) of retronecine | | All | All | 9 | 1, 5, 6, 7, 8 | 8 | 5, 6, 7 |

[a]Retronecine derived from alkaloids present in the plant as such and as *N*-oxides.
[b]Retronecine derived from alkaloids present in the plant as such.
[c]Retronecine derived from alkaloids present in the plant as *N*-oxides.
[d]Specific activity (dpm per mmol) × $10^{-4}$.
[e]Relative specific activity (per cent) (retronecine = 100%).

TABLE 3. Incorporation of $^{3}H$ into retronecine

| Precursor | Experiment No. | Specific activity[d] (relative specific activity)[e] Retronecine | Retronecine HCl | Formaldehyde dimethone | L-*cis*-3-Hydroxyproline | *N*-Formyl-1-naphthylamine | *N*-Phthaloyl-β-alanine |
|---|---|---|---|---|---|---|---|
| DL-[5-$^{3}H$]ornithine | 2[b] | 24.9 (100±1) | 25.1 (101±1) | 5.5 (22±1) | 13.3 (53±1) | 5.3 (21±1) | 8.7 (35±1) |
| L-[5-$^{3}H$]ornithine | 3[b] | 32.4 (100±1) | 30.9 (95±1) | 6.6 (20±1) | 16.8 (52±1) | 5.0 (15±1) | 10.9 (34±1) |
| L-[4-$^{3}H$]ornithine | 4*A*[b] | 6.37 (100±1) | 6.24 (98±1) | 0.23 (4±1) | 4.54 (71±1) | — | 3.10 (49±2) |
| | 4*O*[c] | 10.2 (100±1) | 10.2 (100±1) | 0.1 (1±1) | 7.5 (74±1) | 0.0 (0±1) | 4.8 (47±1) |
| [1,8-$^{3}H_2$]Spermidine | 6*A*[b] | 31.0 (100±1) | 30.0 (97±1) | 11.5 (37±1) | 13.1 (42±1) | 5.6 (18±1) | 7.0 (23±1) |
| | 6*O*[c] | 23.4 (100±1) | 23.0 (98±1) | 7.2 (31±1) | 11.0 (47±1) | 5.3 (23±1) | 5.5 (24±1) |
| H-atom(s) of retronecine | | All | All | 9α, 9β | 5α, 5β, 6α, 6β, 7, 8 | 8 | 5α, 5β, 6α, 6β |

[b,c,d,e]See corresponding footnotes in Table 2.

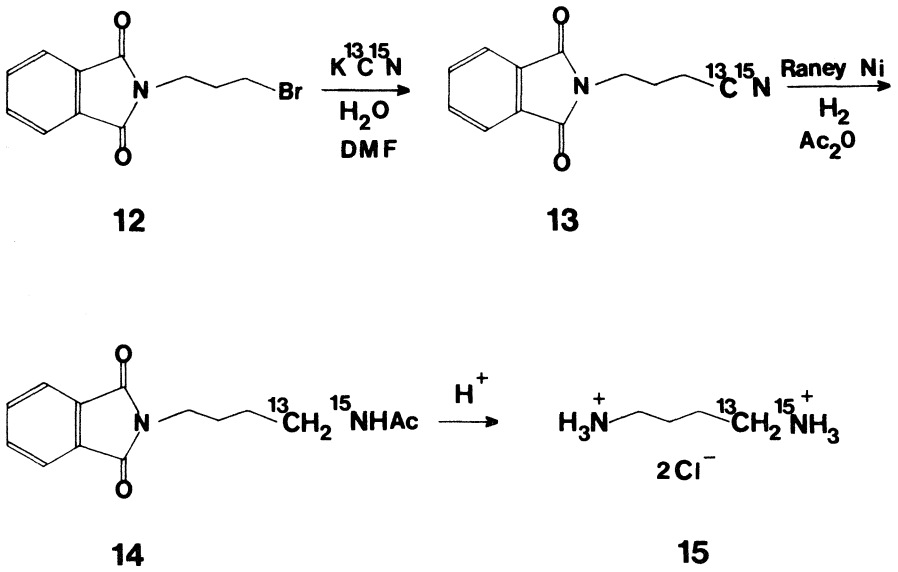


SCHEME 3. Synthesis of (1-$^{13}$C,1-$^{15}$N)putrescine.

TABLE 4. Incorporation of (1-$^{13}$C,1-$^{15}$N)putrescine into retronecine; $^{13}$C nmr analysis (Experiment 5)

| Carbon atom | Retronecine *N*-oxide[a] Chemical shift ppm | Retronecine hydrochloride[a] Chemical shift ppm | Natural abundance $^{13}$C normalized peak area[b] ($A_{NA}$) | Enriched in $^{13}$C normalized peak area[b] ($A_E$) | $1.09\,A_E/A_{NA}$[c] | Percent enrichment above natural abundance[d,e] | Relative percent excess $^{13}$C above natural abundance at individual C atoms |
|---|---|---|---|---|---|---|---|
| 1 | 137.3 | 138.0 | 41 | 42 | 1.12 | 0.13±0.14 | 2±2 |
| 2 | 121.5 | 122.6 | 117 | 95 | 0.89 | −0.12±0.11 | −2±2 |
| 3 | 79.4 | 62.7 | 107 | 202 | 2.06 | 1.17±0.26 | 20±4 |
| 5 | 69.6 | 55.3 | 103 | 223 | 2.36 | 1.50±0.29 | 26±5 |
| 6 | 35.1 | 36.4 | 109 | 92 | 0.92 | −0.09±0.11 | −2±2 |
| 7 | 70.9 | 70.6 | 100 | 100 | 1.09 | 0.10±0.14 | 2±2 |
| 8 | 96.4 | 80.1 | 91 | 205 | 2.46 | 1.61±0.31 | 27±5 |
| 9 | 59.5 | 59.0 | 107 | 240 | 2.44 | 1.58±0.30 | 27±5 |

[a]Samples were contained in 2 mm tubes. Acquisition time, 0.68 s; 1.5 Hz/data point; 0.6 μs pulses.
[b]Peak areas are normalized relative to C-7 (= 100). Estimated standard deviation, ± 8%.
[c]The ratio $A_E/A_{NA}$ is normalized so that the average value for carbon atoms 1, 2, 6, and 7 equals 1.0.
[d]$(1.09\,(A_E/A_{NA})-1) \times 1.1\%$.
[e]The average specific incorporation per carbon atom is [(¼) (1.17 + 1.50 + 1.61 + 1.58)/(90/2) × 100% = 3.3%, where (90/2) at.% $^{13}$C is the average enrichment at each terminal position of putrescine.

prepared by oxidation of DL-proline with periodate (22).

## Discussion

Tracer experiments with $^{14}$C-labelled (6–8) and $^{13}$C-enriched (9) substrates provide evidence which tends to support the prediction of Robinson (10) that the carbon atoms of the $C_4$–N–$C_4$ skeleton of retronecine are derived from two $C_4$ units, both of which ultimately originate from the $C_4$ chain, C-2,-3,-4,-5, of ornithine. The steps of the route from ornithine into the retronecine skeleton are almost totally unexplored, however. Before an attempt can be made to define some of the stages of the pathway, the following questions must be answered.

Does the route from ornithine (**2**) into the $C_4$ chains, i.e., C-9,-1,-2,-3 (chain B) and C-5,-6,-7,-8 (chain A) of retronecine (**1**), pass through a nondissymmetric intermediate (e.g., free putrescine (**3**)), or are the intermediates dissymmetric?

Do the two $C_4$ chains originate from ornithine by a common route, i.e., are they formed from a common intermediate, or is each generated from a different ornithine-derived $C_4$-intermediate?

Does the route include a "dimeric" intermedi-

Can. J. Chem. Downloaded from www.nrcresearchpress.com by 210.87.254.42 on 09/06/12
For personal use only.

Can. J. Chem. Downloaded from www.nrcresearchpress.com by 210.87.254.42 on 09/06/12
For personal use only.

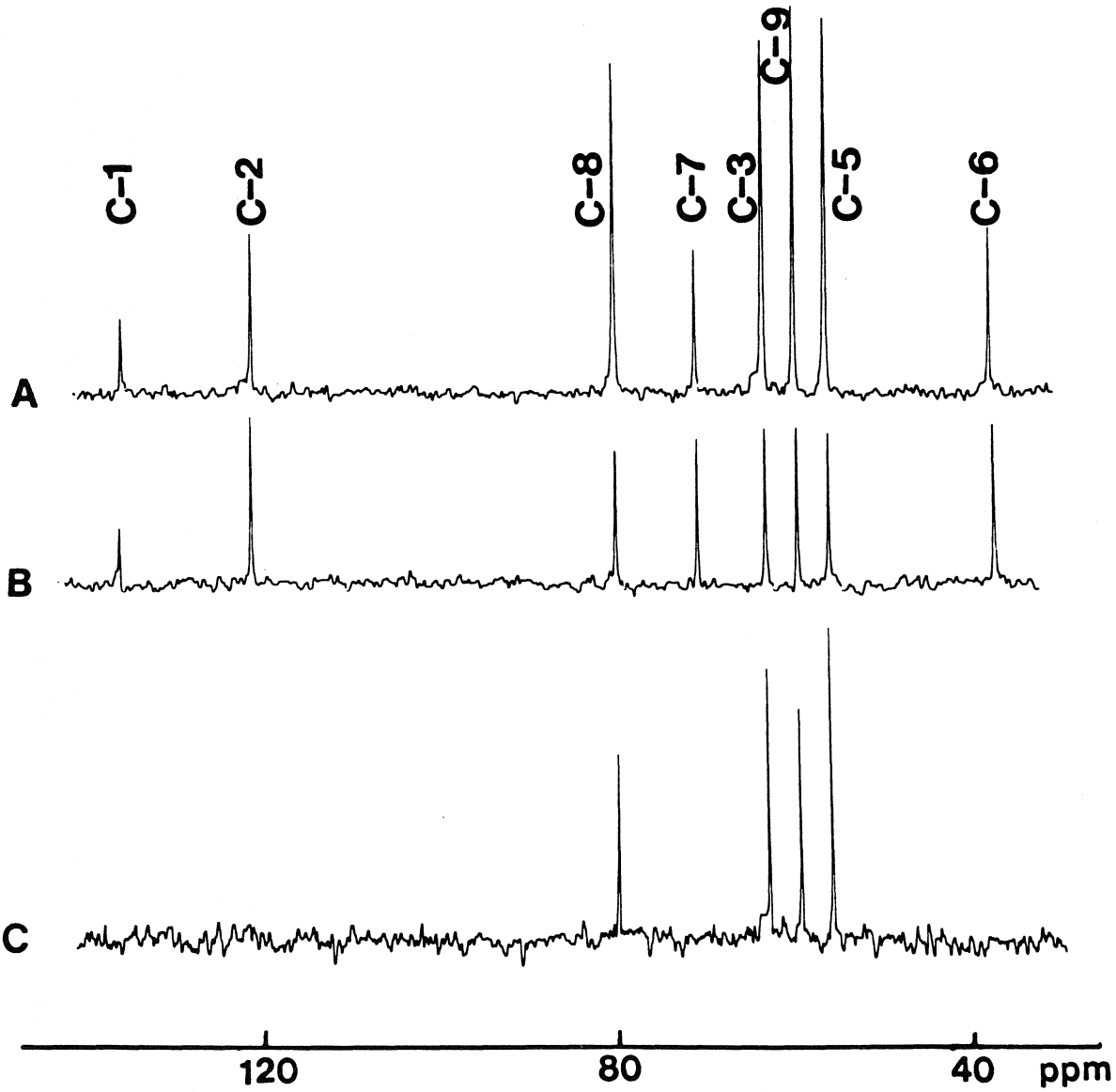


FIG. 1. 20.15 MHz $^{13}C$ nmr spectra of retronecine hydrochloride (13 mg) in $^{2}H_2O$ (50 μL) (See Table 4, Footnote *a*). A: proton noise decoupled (PND) spectrum (85819 scans) of $^{13}C,^{15}N$ enriched sample, derived from (1-$^{13}C$,1-$^{15}N$)putrescine. B: PND spectrum (90482 scans) of natural abundance sample. C: difference spectrum (A minus B).

ate, $C_4$–N–$C_4$, which is nondissymmetric, or are all such intermediates dissymmetric?

Published experimental results (6–9) yield data which are incomplete and mutually contradictory. The present experiments were intended to resolve these questions.

The answers to the questions concerning the nature of the monomer precursor(s) of the $C_4$ units must be looked for in the labelling pattern within retronecine derived from specifically labelled ornithine. Experiments with C-labelled putrescine, a nondissymmetric ($C_{2v}$) molecule, cannot provide an answer, since incorporation of putrescine must, of structural necessity, take place in "symmetrical" fashion, as indeed it does (9). Furthermore, even though label from putrescine is incorporated into retronecine (6, 8, 9), it does not necessarily follow that ornithine, the precursor of putrescine, also enters retronecine in "symmetrical" fashion. It is well documented that putrescine is incorporat-

Can. J. Chem. Downloaded from www.nrcresearchpress.com by 210.87.254.42 on 09/06/12
For personal use only.

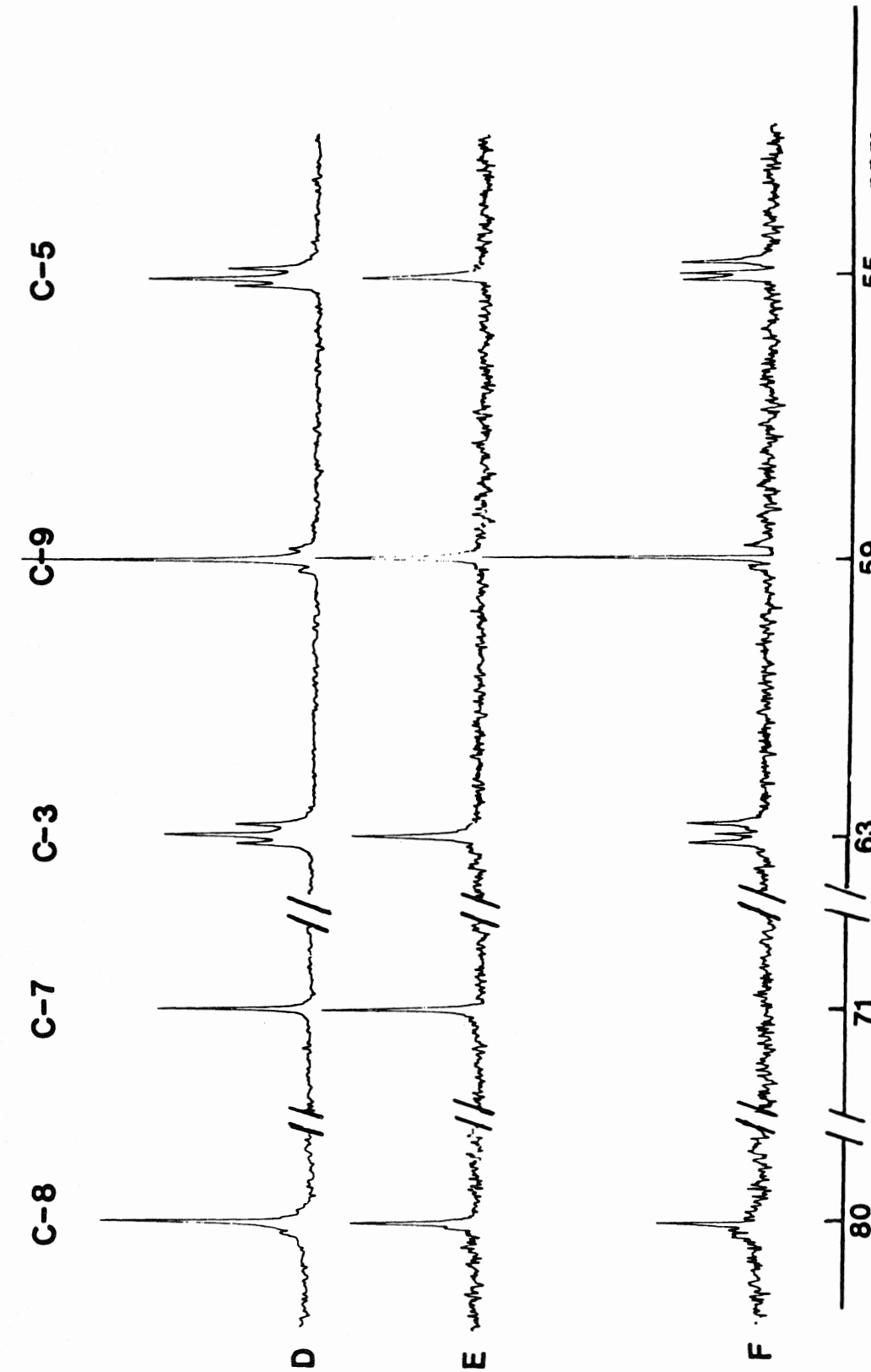


FIG. 2. 20.15 MHz $^{13}C$ nmr spectra of retronecine hydrochloride (13 mg) in $^{2}H_2O$ (50 μL) (See Table 5, Footnote *a*). D: PND spectrum (9720 scans) of $^{13}C$, $^{15}N$ enriched sample, derived from (1-$^{13}C$,1-$^{15}N$)putrescine. E: PND spectrum (9111 scans) of natural abundance sample. F: difference spectrum (D minus E).

TABLE 5. Incorporation of (1-$^{13}$C,1-$^{15}$N)putrescine into retronecine; $^{13}$C nmr analysis (Experiment 5)

| Carbon atom | Type of signal[b] | Retronecine hydrochloride[a] Natural abundance $^{13}$C normalized peak area[c] ($A_{NA}$) | Enriched in $^{13}$C normalized peak area[c] ($A_E$) | $A_E/A_{NA}$ | Percent enrichment above natural abundance[d] | | Relative percent excess $^{13}$C above natural abundance at individual C atoms |
|---|---|---|---|---|---|---|---|
| 3 | s | 106 | 149 | 1.41 | 0.45±0.20 | 1.64±0.25 | 27±4 |
| | d[e] | | 115 | 1.08 | 1.19±0.15 | | |
| 5 | s | 106 | 154 | 1.45 | 0.50±0.20 | 1.72±0.26 | 28±4 |
| | d[f] | | 118 | 1.11 | 1.22±0.16 | | |
| 7 | s | 100 | 100 | 1.00 | 0±0.12 | | 0±2 |
| 8 | s,m | 101(s) | 219(m) | 2.17 | 1.29±0.27 | | 21±4 |
| 9 | s | 108 | 209 | 1.94 | 1.03±0.27 | 1.43±0.27 | 24±4 |
| | d[g] | | 39 | 0.36 | 0.40±0.05 | | |

[a]Samples were contained in 2 mm tubes. Acquisition time, 6.8 s; 0.15 Hz/data point; 2.5 μs pulses.
[b]Abbreviations: s = singlet, d = doublet, m = multiplet.
[c]Peak areas are normalized relative to C-7 (= 100). Estimated standard deviation, ± 8% for singlet signals, ± 10% for composite signals.
[d]$((A_E/A_{NA})-1) \times 1.1\%$ for singlet signals, $(A_E/A_{NA}) \times 1.1\%$ for doublet signals.
[e]$J_{^{13}C\text{-}3,\ ^{15}N}$ 5.1 Hz; isotope shift, −0.02 ppm.
[f]$J_{^{13}C\text{-}5,\ ^{15}N}$ 4.4 Hz; isotope shift, −0.02 ppm.
[g]$J_{^{13}C\text{-}8,\ ^{13}C\text{-}9}$ 5.8 Hz.

ed into hyoscyamine "symmetrically" (23–26), as a matter of structural necessity, but that ornithine enters "nonsymmetrically" (27).[4]

Label from [2-$^{14}$C]ornithine (6, 7) as well as from [5-$^{14}$C]ornithine (6, 8) was found at C-9 of retronecine, obtained from the alkaloids isolated from *Senecio douglasii* and *S. isatideus*. In each case one quarter of the total specific activity of retronecine was found at this site. This was interpreted to show that C-2 and C-5 of ornithine become equivalent before entering chain B of retronecine and to suggest that chain B is derived from a nondissymmetric $C_4$ intermediate, such as putrescine. Yet, a degradation product regarded as representing C-3 of retronecine, the second site within chain B which should have carried label if chain B were derived from a "symmetrical" precursor, was not radioactive when a sample of retronecine derived from [2-$^{14}$C]ornithine was degraded (7). The mode of entry of label into the A chain is similarly in dispute. On the one hand it is reported that retronecine from [5-$^{14}$C]ornithine contains one quarter of its label at C-5 (isolated, together with C-6,-7 as β-alanine) (8), on the other hand a degradation product regarded as representing C-5 of retronecine was nonradioactive, and another, thought to be derived from C-7,-8, accounted for three quarters of the specific activity of retronecine derived from [2-$^{14}$C]ornithine (7). The reported labeling patterns are summarized in Scheme 4 (Figs. A–D).

The results shown in Figs. A and C (Scheme 4) (6) led to the inference that chain B is derived from a "symmetrical" $C_4$-intermediate, and left open the origin of chain A. The results shown in Fig. D (Scheme 4) (8), together with the assumption that the rest of the activity, not accounted for by degradation, is divided equally between C-3 and C-8, suggested that chain A as well as chain B are "symmetrically" derived and that they originated from a common source. The results shown in Fig. B (7) on the other hand, appeared to show that chains A and B were derived independently and nonsymmetrically.

As will be shown in the sequel none of these inferences are valid, for different reasons.

It was apparent that the first step towards the resolution of these experimental contradictions was a reliable degradation permitting independent assay of radioactivity at each of the four crucial positions, C-3,-5,-8, and -9 of retronecine, and not merely at C-5 and -9, as hitherto. Such a degradation (Scheme 2) has now been employed to determine the distribution of label in samples of retronecine obtained from a mixture of the alkaloids retrorsine, senecionine, and seneciphylline, as well as from their *N*-oxides, isolated in four experiments from *S. vulgaris* to which DL-[5-$^{14}$C]-ornithine had been administered (Experiments 1–4, Table 1). The distribution of $^{14}$C within the samples of retronecine (Table 2) is shown in Fig. E, Scheme 4.

In each case formaldehyde (C-9) and formic acid (C-8) each accounts for one quarter of the $^{14}$C activity of the intact retronecine molecule, within

[4]Analogously, incorporation of lysine into piperidine alkaloids such as sedamine (28) and anabasine (29, 30) takes place "nonsymmetrically", while incorporation of cadaverine, the decarboxylation product of lysine, takes place "symmetrically" (31). A possible explanation of this apparent paradox has been advanced (32).

Can. J. Chem. Downloaded from www.nrcresearchpress.com by 210.87.254.42 on 09/06/12
For personal use only.

Can. J. Chem. Downloaded from www.nrcresearchpress.com by 210.87.254.42 on 09/06/12
For personal use only.

experimental error. L-*cis*-3-Hydroxyproline (C-1,-5,-6,-7,-8) accounts for one half of the $^{14}C$ activity, that is, one quarter must be present at one or more of C-1,-5,-6,-7. Since all of this activity is accounted for by β-alanine (C-5,-6,-7), C-1 must be unlabelled. The remaining quarter of the activity of the intact molecule must be present at C-2 and/or C-3 (by difference: retronecine minus formaldehyde (C-9; 25%) minus L-*cis*-3-hydroxyproline (C-1,-5,-6,-7,-8; 50%)). It is a reasonable supposition, based on structural relations, that a quarter of the activity resides at C-5 (and that C-6 and C-7 are unlabelled) and that a quarter of the activity resides at C-3 (and that C-2 is unlabelled). Thus, the four crucial sites, C-9,-3,-5, and -8, account for the activity of the intact molecule and are equally labelled. This result confirms and completes two of the earlier reports (6, 8) and controverts the third one (7).[5]

It would appear at first glance that the observed distribution of label proves that each of the $C_4$ units of retronecine is derived from ornithine via a nondissymmetric intermediate, and that the two $C_4$ units originate from a common source. The distribution is indeed consistent with such a derivation, but there are several other possibilities. The crucial problem which must be solved before the distribution of label can be interpreted is whether among the "dimeric" intermediates, $(C_4)_2N$, there is one that is nondissymmetric or not. Only in the absence of a nondissymmetric dimeric intermediate does the observed distribution prove that the two $C_4$ monomer units are necessarily derived from a common "symmetrical" intermediate, such as free putrescine (Scheme 5A).

If a "symmetrical dimeric" intermediate is implicated in the pathway, then in addition to such a derivation from a common symmetrical intermediate (Scheme 5B) several other routes into the product are possible. These are summarized in Schemes 5C, D, and E. Several other derivations of the two monomer units are excluded by the observed distribution pattern.

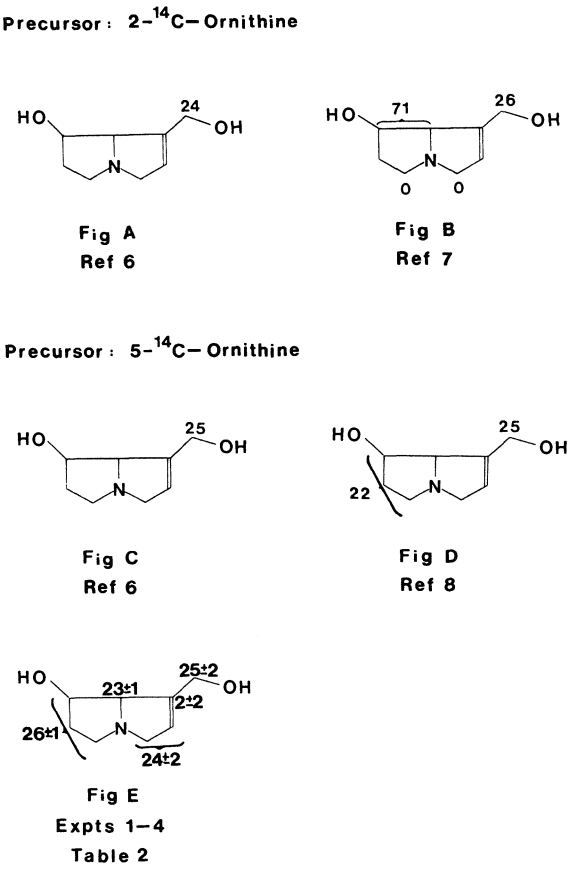


SCHEME 4. Distribution of label from [$^{14}$C]ornithine in retronecine. Figs. A, B, C, D: Reported partial distribution (6, 7, 8). Fig. E. Distribution of label from [5-$^{14}$C]ornithine, now determined.

In order to permit further interpretation of the labelling pattern from [5-$^{14}$C]ornithine it is thus necessary to determine whether or not a nondissymmetric "dimer" of the type $C_4$–N–$C_4$ plays a part in retronecine biosynthesis.

An answer to this question may be obtained, in principle, by a feeding experiment with 1-pyrroline, or with the corresponding open chain compound, 4-aminobutanal, substrates derivable from ornithine. Incorporation of labelled samples of either of these compounds by one or the other of the two routes shown in Scheme 1 would lead to recognizably different labelling patterns (Scheme 6). Feeding experiments with (2-$^2$H)-1-pyrroline (Experiment 7) and [5-$^3$H,5-$^{14}$C]-1-pyrroline (Experiment 8) were unsuccessful, however. Incorporation of tracer into retronecine in either experiment was too low for accurate determination by $^2$H

[5]It is likely that the erroneous results (7) have their basis in the chemistry of the degradation reactions that were employed. Ozonolysis of a Hofmann base leads to formaldehyde not only from the methylene carbon atom of the vinyl group but also from the *N*-methyl groups (33). It must be assumed that the apparent lack of radioactivity in the formaldehyde, derived from C-3 and C-5 by ozonolysis of Hofmann bases, was due to dilution of active formaldehyde derived from these carbons by inactive formaldehyde derived from the *N*-methyl groups, to yield samples whose radioactivity was beyond the limits of detection. Furthermore, evaluation of the contribution to a product of material from more than one site within the molecule (e.g. acetate from C-6,-5 and C-3,-2, as well as from C-9,-1, in the Kuhn–Roth oxidation of the second stage Hofmann base) is too uncertain for determining distribution patterns of radioactivity, as are reactions which yield $CO_2$ from a multiplicity of carbon atoms.

Can. J. Chem. Downloaded from www.nrcresearchpress.com by 210.87.254.42 on 09/06/12
For personal use only.

NON-SYMMETRICAL (I.E. DISSYMMETRIC) DIMER (CF SCHEME 1, ROUTE B)

A TWO IDENTICAL SYMMETRICAL MONOMERS

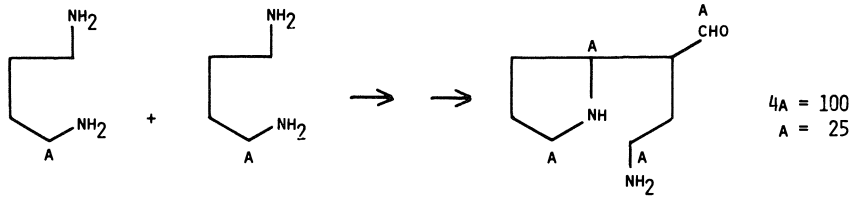


SYMMETRICAL (I.E. NON-DISSYMMETRIC) DIMER (CF SCHEME 1, ROUTE A)

B TWO IDENTICAL SYMMETRICAL MONOMERS

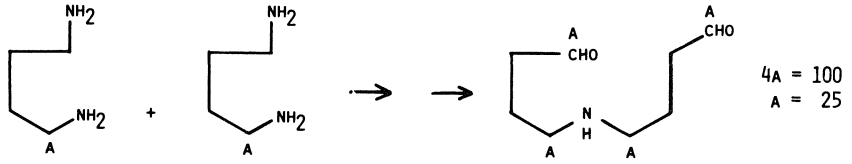


C TWO DIFFERENT MONOMERS, BOTH SYMMETRICAL

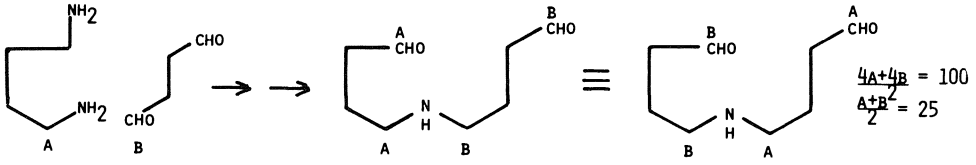


D TWO DIFFERENT MONOMERS, ONE SYMMETRICAL, ONE NOT RELATED TO ORNITHINE

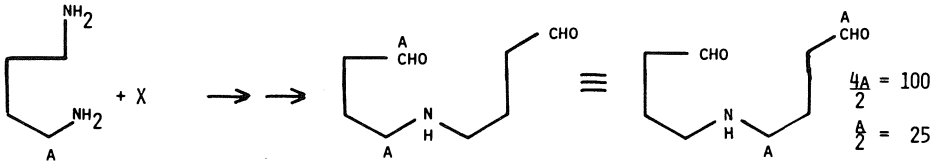


E TWO IDENTICAL NON-SYMMETRICAL MONOMERS

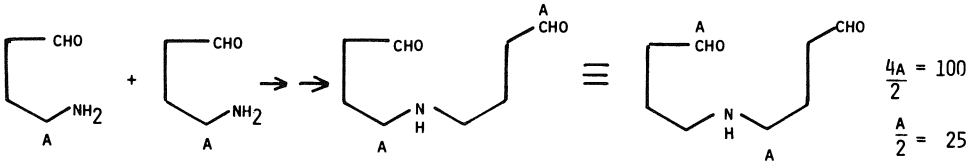


SCHEME 5. Five possible modes of incorporation of [5-$^{14}$C]ornithine-derived $C_4$ units which account for the observed distribution of label in retronecine (i.e. 25% of total specific radioactivity at each of C-3, C-5, C-8, and C-9).

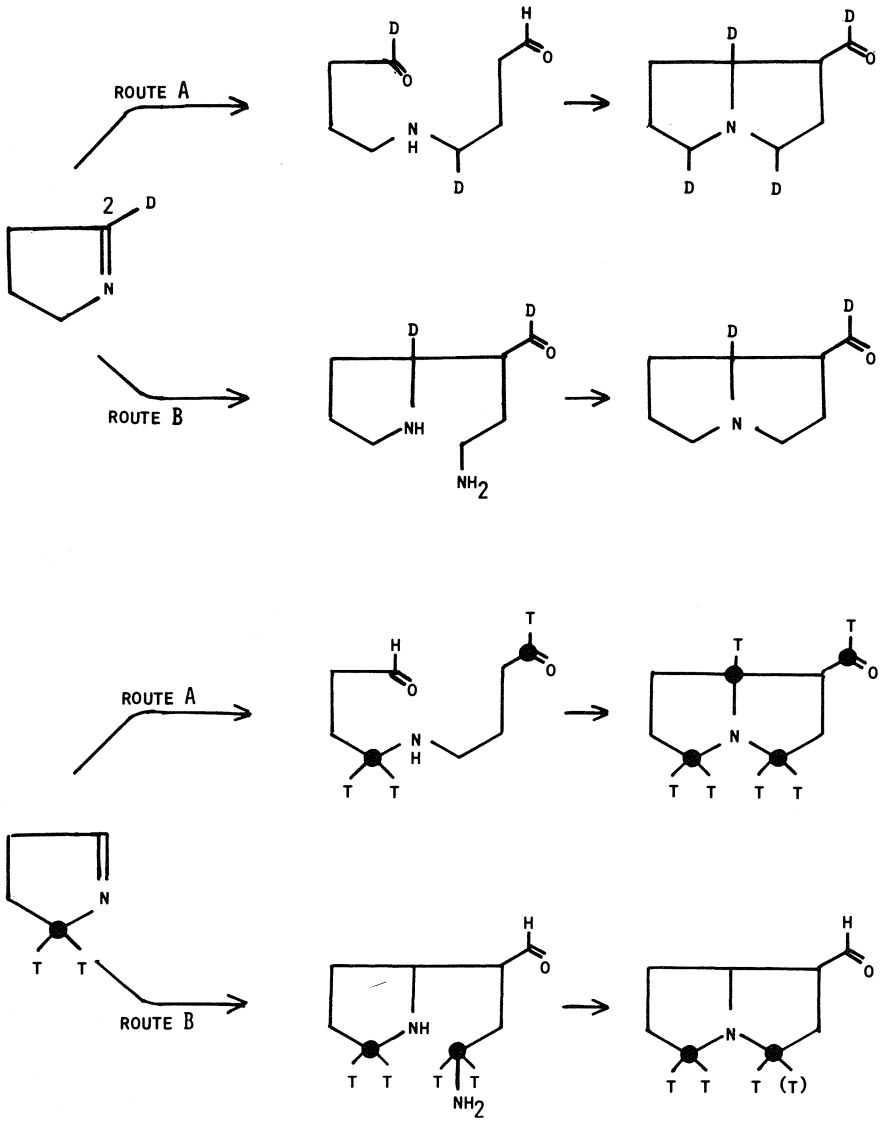


SCHEME 6. Predicted distribution of label from (2-$^2$H)- and from [5-$^3$H]-1-pyrroline within retronecine.

nmr spectroscopy and liquid scintillation counting, respectively. 1-Pyrroline thus may not be an intermediate of biosynthesis. It is more likely, however, that the administered 1-pyrroline did not reach the site of biosynthesis. 1-Pyrroline rapidly polymerizes at basic and neutral pH (20, 21) and the polymer may not be available as a substrate for biosynthesis. In Experiment 8 the crude alkaloid fraction contained an unidentified component, not observed in other experiments, which accounted for ca. 90% of the total radioactivity of the fraction. This may have been a self-condensation product of 1-pyrroline.

Another possible way of establishing whether or not a nondissymmetric "dimeric" intermediate is involved in the pathway to retronecine is by studying the distribution of label from doubly $^3$H,$^{14}$C-labelled ornithines. The incorporation patterns, predicted for retronecine derived from [4-$^3$H,5-$^{14}$C]- and [5-$^3$H,5-$^{14}$C]ornithine, by Routes A and B (Scheme 1), via "nonsymmetrical" and via "symmetrical" monomer units, are summarized in Scheme 7.

The distribution of $^3$H within the samples of retronecine from [4-$^3$H]-ornithine (Experiment 4) and [5-$^3$H]ornithine (Experiments 2, 3), which were administered in admixture with [5-$^{14}$C]ornithine to provide an internal reference standard, was de-

Can. J. Chem. Downloaded from www.nrcresearchpress.com by 210.87.254.42 on 09/06/12
For personal use only.

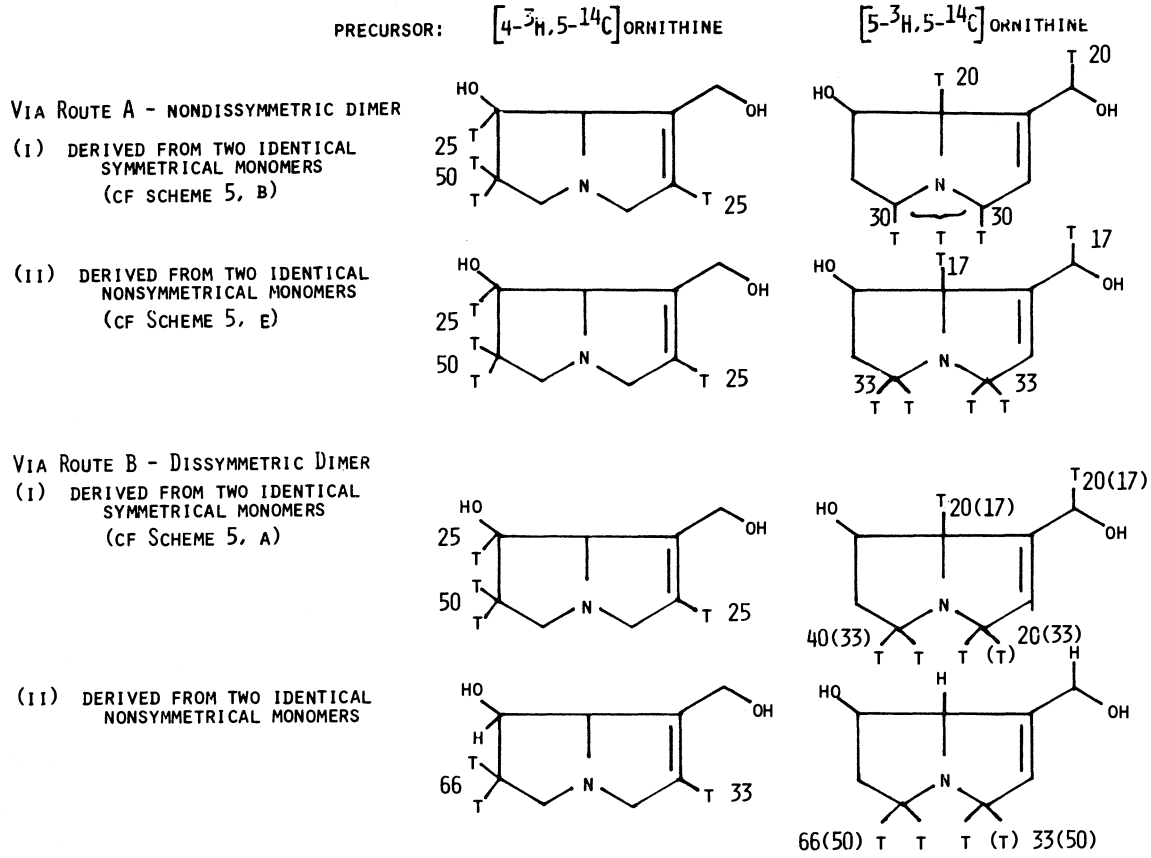


SCHEME 7. Predicted distribution of tritium from [4-$^3$H]- and [5-$^3$H]ornithine within retronecine.

duced from the radioactivity of the products of chemical degradation of these samples (Table 3).

The labeling pattern of $^3$H within the two samples of retronecine derived from L-[4-$^3$H]ornithine was essentially identical and is shown in Fig. F, Scheme 8. No tritium is present at C-9 (formaldehyde) or at C-8 (formic acid). Three quarters of the tritium is accounted for by the hydrogen atoms at C-5,-6,-7, and -8 (L-*cis*-3-hydroxyproline), one half by those at C-5,-6 (β-alanine). Assuming no migration of label from the initial C-4 position of ornithine to C-5 in the course of biosynthesis, tritium is then located at positions C-2 (25%, 1H), C-6 (50%, 2H), and C-7 (25%, 1H) of retronecine. This distribution is consistent with three of the four patterns shown in Scheme 7, and eliminates the fourth. Retention of tritium at C-7 demonstrates that introduction of the hydroxyl group does not involve a keto or enol intermediate.

The distribution of label within the two samples of retronecine from this experiment, derived from the alkaloids, present as such, and from the *N*-oxides (Experiment 4*A* and 4*O*, respectively, Table 3), was identical. If the ease of oxidation of retronecine during the work-up in Experiment 5 (see later) is any guide, the conversion of free alkaloids to *N*-oxides within the plant may well be a nonenzymatic process.

The labeling pattern of $^3$H within the samples of retronecine derived from DL-[5-$^3$H]- and L-[5-$^3$H]ornithine, identical in all but one value[6] (Experiments 2 and 3, Table 3) is shown in Fig. G, Scheme 8. Approximately one fifth of the total label was present at C-9 (formaldehyde) and one fifth at C-8 (formic acid).[6] Half of the tritium is accounted for by the hydrogen atoms at C-5,-6,-7, and -8 (L-*cis*-3-hydroxyproline) and one third by those at C-5,-6 (β-alanine).

The observed distribution of tritium lies within the range of two of the four predicted distribution patterns (Scheme 7, AI, AII, BI). A choice among them on the basis of the experimental data would

[6]The low value for the formic acid in Experiment 3 may have been due to contamination of the product by a nonradioactive contaminant.

Can. J. Chem. Downloaded from www.nrcresearchpress.com by 210.87.254.42 on 09/06/12
For personal use only.

OBSERVED DISTRIBUTION OF TRITIUM IN RETRONECINE

PRECURSOR: [4-$^3$H,5-$^{14}$C] ORNITHINE (EXPERIMENTS 4A, 4O, TABLE 3)

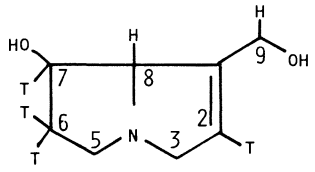

FIG. F

[5-$^3$H,5-$^{14}$C] ORNITHINE (EXPERIMENTS 2,3, TABLE 3)

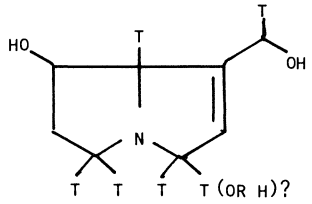

FIG. G

| | | | | |
|---|---|---|---|---|
| FOUND: | C-9 | 4±1, | 1±1 | 22±1, 20±1% |
| | C-8 | 0±1, | | 21±1, 15±1% |
| | C-5,6,7,8 | 71±1, | 74±1 | 53±1, 52±1% |
| | C-5,6 | 49±2, | 47±1 | 35±1, 34±1% |
| | C-2,3 (BY DIFFERENCE) | 25±2, | 25±2 | 25±2, 28±2% |
| | C-7 (BY DIFFERENCE) | 22±2, | 27±2 | -3±2, 3±2% |

SCHEME 8. Observed distribution of tritium from [4-$^3$H]- and [5-$^3$H]ornithine within retronecine.

appear to be unwarranted. It is unfortunate that the sample of DL-[5-$^3$H]ornithine was contaminated with [4-$^3$H]ornithine (See Table 1, footnote *e*). If the observed values are corrected for this contamination, on the basis of the experimental results of the experiment with [4-$^3$H]ornithine (Experiment 4, above), the resulting values correspond closely to three of the predicted distributions (Scheme 7, AI, or AII ≡ BI).

One tritium is present at each of C-9 and C-8 and three or four, respectively, are shared equally among C-3 and C-5. Only one of the hydrogen atoms at the prochiral site, C-9, is labelled. This is predicted by a pathway (Route A, Scheme 1) which involves oxidation of a primary amino function at C-9 to yield an imine which is subsequently hydrolyzed to an aldehyde. The possibility that each of the two sites, C-3 and C-5, accounts for one and a half tritium atoms would support the intermediacy of a nondissymmetric dimer, $C_4$–N–$C_4$, generated from two identical nondissymmetric ornithine-derived monomer units (Scheme 5B). Two other derivations of the nondissymmetric dimer are also consistent with this distribution, however.

The possibility that, on average, 1.5 tritium atoms are located at each of C-3 and C-5 requires comment. Route A (Scheme 1) predicts a reduction step during which a hydrogen atom is introduced at the imino group carbon atom of an intermediate which in subsequent steps is converted into a compound with $C_{2v}$ symmetry. A tritium-labelled compound of this type would be composed of various tritiated species in which, on averaging, 3 labelled hydrogen atoms are shared by the two carbon atoms which are destined to become C-3 and C-5 of retronecine. If this interpretation is correct then the two labelled centres, C-3 and C-5, must be chiral in some of the contributing labelled species and must be of opposite configuration (α and β) at C-3 and C-5. This inference has yet to be tested.

The inference that a nondissymmetric dimer serves as an intermediate rests on values obtained by correcting experimental data. The experimental data themselves did not permit a direct and clearcut differentiation among two sets of predicted values both of which were within experimental range. For this reason the conclusions drawn from the experiments with [5-$^3$H]ornithine must be regarded as tentative. A further experimental approach was sought to solve the problem of the symmetry of the "dimeric" intermediate in a conclusive manner.

In the third attempt to answer the question concerning the intermediacy of a nondissymmetric dimer, we exploited the fact that retronecine contains a single nitrogen atom. If this nitrogen atom, like the carbon atoms, were derived from ornithine, then, assuming a unique route of retronecine biosynthesis, only one of the three C-atoms, C-3, C-5, or, less likely, C-8, can be transferred from a precursor into retronecine without ever having been separated from direct attachment to nitrogen.

Maintenance of a C—N bond in the conversion of a suitably labelled precursor into a product can be recognized by $^{13}$C or $^{15}$N nmr techniques (34–37). If the retronecine obtained in an experi-

Can. J. Chem. Downloaded from www.nrcresearchpress.com by 210.87.254.42 on 09/06/12
For personal use only.

Can. J. Chem. Downloaded from www.nrcresearchpress.com by 210.87.254.42 on 09/06/12
For personal use only.

ment with an appropriately $^{13}C—^{15}N$ labelled precursor contains a single $^{13}C—^{15}N$ bond, transferred intact from a labelled substrate, then all $(C_4)_2N$ intermediates must have been dissymmetric. If two intact $^{13}C—^{15}N$ bonds appear in the product, a nondissymmetric $C_4–N–C_4$ intermediate must have served as a stage of the biosynthetic route.

A substrate, intramolecularly doubly labelled, with $^{15}N$, as well as with $^{13}C$ at the adjacent C atom, would be suitable for such an experiment. A doubly labelled sample of ornithine or of any other compound known to be incorporated into retronecine (e.g. putrescine) could be used for such an experiment.

(1-$^{13}$C,1-$^{15}$N)Putrescine dihydrochloride was synthesized from K$^{13}$C$^{15}$N, with isotopic enrichments of 90 at.% $^{13}C$ and 99 at.% $^{15}N$ (Scheme 3). To obviate the possibility of a multiplicity of couplings in the $^{13}C$ nmr spectrum of the biosynthetic product, the putrescine was labelled only at one of the C—N termini.

A large amount (472 mg) of (1-$^{13}$C,1-$^{15}$N)putrescine dihydrochloride was used in the hope of achieving $^{13}C$ enrichment above natural abundance high enough for quantitative assay. In order to minimize a change in the internal environment of the plants due to this large quantity of extraneous material, the compound was administered in small doses over a prolonged period (13 days). Simultaneous administration of $^{14}C$-labelled putrescine served as an independent check on the incorporation of substrate into retronecine. The plants were growing actively at the end of the 13-day period and had not sustained any evident damage.

An unexpectedly low yield of alkaloid was obtained in the feeding experiment with putrescine (Experiment 5), and a problem, not encountered when larger amounts of alkaloids were handled, was the partial oxidation of the pyrrolizidine moiety to the corresponding *N*-oxide during work-up, when oxygen-free conditions were not employed. As it turned out, the isolation of retronecine-*N*-oxide, the product of this oxidation, was useful in that comparison of the signals in the $^{13}C$ nmr spectra of retronecine hydrochloride and *N*-oxide served as an independent check on the assignment of the signals. There has been some confusion in the assignment of signals in the $^{13}C$ nmr spectra of the pyrrolizidine alkaloids (38, 39). Our own findings (Table 4) are in agreement with those of Barreiro *et al.* (19).

Reduction of the alkaloid *N*-oxides and further work-up under exclusion of oxygen yielded retronecine hydrochloride which was chemically and radiochemically pure. The specific incorporation of substrate per $C_4$ unit of retronecine, as determined by assay of radioactivity, was 3.3%.[7,8]

The $^{13}C$ nmr spectrum of the retronecine sample (Fig. 1 and Table 4) shows that, as expected, four of its eight carbon atoms are enriched in $^{13}C$, to an equal extent. The average specific incorporation per $C_4$-unit, based on $^{13}C$ nmr data (Table 4), is 3.3%, identical with the value obtained from $^{14}C$ assay.

To enhance the resolution of the signals due to the enriched carbon atoms, the number of Hz per data point was decreased tenfold from 1.5 to 0.15, and the acquisition time was correspondingly increased from 0.68 to 6.8 s. The spectrum thus obtained (Fig. 2 and Table 5) comprises the signals due to C-3,-5,-7,-8, and -9, of which only that due to C-7 is a nonenriched singlet. The other four signals show higher multiplicity, reflecting the different labelled species present in the retronecine hydrochloride isolated from the feeding experiment with (1-$^{13}$C,1-$^{15}$N)putrescine.

Most noticeable are the signals due to C-3 and C-5, which each appear as a doublet superimposed on a singlet. The coupling constants are different from one another. This shows that the doublets are due to $^{13}C–^{15}N$ coupling ($^{13}$C-3,$^{15}$N, 5.1 Hz; $^{13}$C-5,-$^{15}$N, 4.4 Hz) and do not arise from $^{13}$C-5,$^{13}$C-3 coupling.

The ratio of the areas of singlet and of doublet, due to enrichment above natural abundance, for each of the two signals, is identical (ca. 28/72). This shows that the $^{13}C—^{15}N$ moiety of putrescine had been transferred intact into positions C-3,N and C-5,N of retronecine to an equal extent, that is, that the retronecine contains equimolar amounts of two species, one of which is labelled at C-3,N, the other at C-5,N. The simplest interpretation of this result is that a nondissymmetric "dimeric" intermediate, $C_4–N–C_4$, such as **6**, lies on the pathway to retronecine. Two other, less likely, possibilities, which exclude a nondissymmetric "dimeric" intermediate, cannot be entirely ruled out, however. One is the intermediacy of a dissymmetric compound, capable of undergoing a degenerate sigmatropic rearrangement (e.g. $NH_2CH_2CH_2CH_2CH_2$-$N{=}CHCH_2CH_2CH_2NH_2$), the other is the occur-

[7] $\dfrac{\text{Molar specific activity of retonecine (dpm/mmol)} \times \frac{1}{2}}{\text{Molar specific activity of putrescine (dpm/mmol)}} \times$

$$100 = \frac{3.4 \times 10^6}{5.2 \times 10^7} \times \frac{10^2}{2} = 3.3.$$

[8] An account of this experiment has appeared in a preliminary communication (40). More recently the results of a similar experiment were reported independently (44).

Can. J. Chem. Downloaded from www.nrcresearchpress.com by 210.87.254.42 on 09/06/12
For personal use only.

rence of two independent pathways fortuitously yielding equal amounts of the two labelled species.

Disregarding these remote possibilities, the nmr evidence thus suggests that a nondissymmetric "dimeric" intermediate is implicated in the biosynthesis of retronecine. As discussed earlier, this leaves open four variants (Scheme 5B, C, D, E) of the mode whereby $C_4$ monomer units combine to yield the $C_4$–N–$C_4$ skeleton.

One of these four possibilities can be eliminated on the basis of a feature of the nmr spectrum which has yet to be discussed, the signal due to C-9. The $^{13}C$ enrichment at this signal is composed of a singlet and a doublet, 72:28 in area. The doublet is due to coupling between C-9 and C-8, and the singlet/doublet ratio is a measure of the contribution to the $^{13}C$-labelled retronecine of molecules enriched in both $C_4$ chains. The fact that such doubly enriched retronecine molecules are found eliminates from further consideration the possibility shown in Scheme 5D, which considers that only one of the two $C_4$ chains is derived from ornithine. No doubly enriched retronecine molecules would occur if this were its mode of origin.

The ratio of the areas singlet/doublet in the signal due to C-9 reflects the dilution of the administered doubly labelled putrescine by natural abundance material produced endogenously by the plant. The observed ratio corresponds to that expected if the administered putrescine were diluted with 63% of its own weight of natural abundance material (40).

The C-9,C-8 coupling is barely observable at C-8, presumably due to superimposed low intensity coupling to $^{15}N$ and C-3. Coupling due to C-8,C-3 or C-5,C-3 (through $^{15}N$) is not observed. Their intensities are presumably low and their contribution to the singlet and doublet integrals of C-3 and C-5 insignificant.

Coupling between C-3 and C-9 does not appear since the labelling pattern in the substrates precludes the possibility of formation of a retronecine molecule, doubly labelled in one $C_4$ chain.

The three remaining possibilities for the origin of the $C_4$–N–$C_4$ unit of retronecine cannot be differentiated on the basis of the experiment with (1-$^{13}C$,1-$^{15}N$)putrescine. In each case the retronecine that would be formed from this precursor would be predicted to yield an nmr spectrum showing C-8,C-9 coupling.

However, an experiment with (5-$^{13}C$,5-$^{15}N$)-ornithine would distinguish between the derivation shown in Scheme 5E (no C-8,C-9 coupling, if retronecine were generated from two identical ornithine-derived dissymmetric $C_4$ units) and those shown in Schemes 5B and C. Such an experiment is in hand.

The final experiment to be mentioned, a study of the incorporation of spermidine into retronecine (Experiment 6), does not contribute to the main thesis of this paper, but provides an illustration of one of the pitfalls which may be encountered in the use of intermolecularly $^3H$,$^{14}C$-doubly labelled substrates in biosynthetic studies. The incorporation of label from [1,4-tetramethylene-$^{14}C$]spermidine into retronecine has been previously reported (8). Presumably it serves as a source of putrescine or of 4-aminobutanal, or both.

A sample of [1-tetramethylene-$^3H$,1,4-tetramethylene-$^{14}C$,8-trimethylene-$^3H$]spermidine was administered, retronecine was obtained from the alkaloids and from the *N*-oxides that were isolated, and the samples were degraded to establish the labelling pattern.

The distribution of $^{14}C$ in the two samples was unexceptional (Experiment 6, Table 2). One quarter of label of each sample was present at each of C-9,-8,-5, and -3. However, the distribution of tritium (Experiment 6, Table 3) differed significantly from that observed in the experiment with [5-$^3H$]ornithine (Experiments 2, 3, Table 3), in that, in both spermidine-derived samples C-3 and C-5 each made the same contribution to the total activity as C-8, whereas in the ornithine-derived samples C-3 and C-5 each accounted for 50% more label than C-8. The observed distribution of label in retronecine derived from the labelled spermidine is readily explicable if the latter were first oxidized to the corresponding aldehyde, OTC—$CH_2$—$CH_2$—$CH_2$—NH—$CH_2$—$CH_2$—$CT_2$—$NH_2$ (11, 41), which then yields as the sole labelled product which enters retronecine, 4-amino-[1-$^3H$]butanal, OTC—$CH_2$—$CH_2$—$CH_2$—$NH_2$. The distribution is also explicable, somewhat less readily, if degradation of the spermidine had yielded both [1-$^3H$]-putrescine, $NH_2$—$CT_2$—$CH_2$—$CH_2$—$CH_2$—$NH_2$, and 4-amino-[4-$^3H$]butanal, $NH_2$—$CT_2$—$CH_2$—$CH_2$—CHO (11). The experiment thus raises questions concerning the mode of degradation of spermidine in *S. vulgaris* rather than answering questions regarding the biosynthesis of retronecine. Further work is required to clarify this problem.

What is of more immediate interest is the difference in the distribution of tritium observed in the two spermidine-derived samples of retronecine, 6*A* and 6*O* (Table 3). These samples differed in the relative contribution which C-9 (formaldehyde) makes to the total activity. In both cases this is higher than the contribution made by tritium at C-8 (formic acid). An explanation for this finding must be sought in an isotope effect or a reverse isotope effect in one of the reactions involved in the

TABLE 6. $^3H/^{14}C$ ratios in retronecine and its degradation products, derived from Expt. 6

| | Sample 6*O* degraded without further chromatography | Sample 6*A* degraded after further chromatography | Difference % |
|---|---|---|---|
| Retronecine | $\frac{23.4}{5.11} = 4.6$ | $\frac{31.0}{8.31} = 3.7$ | −20 |
| Retronecine HCl | $\frac{23.0}{5.07} = 4.5$ | $\frac{30.0}{8.03} = 3.7$ | −18 |
| Formaldehyde dimethone | $\frac{7.2}{1.23} = 5.8$ | $\frac{11.5}{1.95} = 5.9$ | +2 |
| L-*cis*-3-Hydroxyproline | $\frac{11.0}{2.47} = 4.5$ | $\frac{13.1}{4.01} = 3.3$ | −27 |
| *N*-Formyl-1-naphthylamine | $\frac{5.3}{1.23} = 4.3$ | $\frac{5.6}{1.88} = 3.0$ | −30 |
| *N*-Phthaloyl-β-alanine | $\frac{5.5}{1.23} = 4.5$ | $\frac{7.0}{1.97} = 3.6$ | −20 |

formation of retronecine from the "symmetrical dimeric" intermediate, e.g., in the ring closure or in the reduction of the aldehyde function at C-9 to a carbinol.

The differences of distribution within the two samples were due to isotope fractionation in the course of the chromatographic purification of the retronecine samples. The sample isolated from the free alkaloids was chromatographed more extensively than that isolated from the *N*-oxides. When originally isolated, both retronecine samples were radiochemically pure and each showed a $^3H/^{14}C$ ratio 4.6. The retronecine sample derived from the *N*-oxides was degraded without further chromatography. The retronecine sample from the free alkaloids, $^3H/^{14}C$ 4.6, was chromatographed on a silica gel column with chloroform–methanol – concentrated ammonia (74:24:2). The retronecine-containing effluent was collected in several fractions which maintained the specific activity with respect to $^{14}C$ but differed in $^3H/^{14}C$ ratio, which rose from 2.9 to 5.2 and then leapt to 20 in the final retronecine-containing fraction. Retronecine with a $^3H/^{14}C$ ratio of 3.7, isolated from the combined early fractions, was degraded (Tables 2 and 3). Table 6 shows the $^3H/^{14}C$ ratios of the various degradation products derived from the two retronecine samples.

It is evident that the $^3H/^{14}C$ ratio within the samples of formaldehyde (i.e. within C-9 of the two retronecine samples) is the same, i.e., no loss of $^3H$, relative to $^{14}C$, has occurred at this position in the course of chromatography. The other breakdown products, representing samples containing tritium adjacent to the basic nitrogen, have all suffered loss of tritium, relative to $^{14}C$. It would appear that the discrimination of the $^{14}C$-labelled, i.e., the protonated species, versus the tritiated species is a function of small differences in the $pK_a$ due to replacement of $^1H$ by $^3H$ at the carbon atoms adjacent to nitrogen. Such small differences in $pK_a$ are evidently sufficient to cause separation of the two species in the course of chromatography, particularly when the pH of the eluent is numerically close to the $pK_a$ of the dissociating group in question.

Experiments whose interpretation is based on a measurement of $^3H/^{14}C$ ratios must be designed in such a way that such isotope fractionation is avoided.

## Experimental

*Synthesis of (1-$^{13}C$,1-$^{15}N$)putrescine dihydrochloride (**15**)*

1-Bromo-3-phthalimidopropane (**12**) (1.94 g, 7.24 mmol), dissolved in *N*,*N*-dimethylformamide (7.2 mL), was added to a solution of potassium ($^{13}C$,$^{15}N$)cyanide (90.6 at.% $^{13}C$, 99.4 at.% $^{15}N$, Prochem) (0.48 g, 7.16 mmol) in water (2.4 mL). The mixture was heated on a steambath for 90 min. After cooling to 25°C and addition of water (70 mL) the reaction mixture was extracted with ether (2 × 70 mL). The combined ether extracts were re-extracted with water (70 mL) and dried over anhydrous sodium sulfate. Filtration and evaporation of solvent *in vacuo* yielded an oil (1.08 g). Repeated extraction of the combined aqueous phases with ether (2 × 70 mL) and washing of the ether extracts with water (35 mL) gave, upon evaporation of solvent *in vacuo*, an additional 0.18 g. The total yield of crude 4-phthalimidobutyro-(1-$^{13}C$,1-$^{15}N$)nitrile (**13**) was 1.26 g (5.83 mmol, 81%); $^1H$ nmr[9] ($CDCl_3$) δ: 8.95–8.65 (m, 4H), 3.80 (t, $J$ = 6.5 Hz, 2H), 2.60–2.35 (m, 2H), 2.25–1.75 (m, 2H) ppm; $^{13}C$ nmr[10] ($CDCl_3$) δ: 118.8 (d, $J_{^{13}C,^{15}N}$ = 17.6 Hz) ppm; ms *m/e*: 217 (2.3%), 216 (10.5%), 215 (1.3%), 161 (26%), 160 (100%), 105 (15%), 104 (14%), 77 (17%), 76 (22%).

Crude 4-phthalimidobutyro-(1-$^{13}C$,1-$^{15}N$)nitrile (**13**) (1.24 g,

[9]Recorded at 90 MHz on a Varian EM390 spectrometer.

[10] $^{13}C$ nmr spectra were recorded at 20.15 MHz in the Fourier mode on a Bruker WP 80 spectrometer with proton noise decoupling.

Can. J. Chem. Downloaded from www.nrcresearchpress.com by 210.87.254.42 on 09/06/12
For personal use only.

Can. J. Chem. Downloaded from www.nrcresearchpress.com by 210.87.254.42 on 09/06/12
For personal use only.

5.74 mmol) was dissolved in acetic anhydride (7 mL) and added to Raney-Ni (0.5 g, BDH, stabilized, washed with ethanol (2 × 20 mL) and acetic anhydride (10 mL)) in acetic anhydride (5 mL). Hydrogenation was carried out with vigorous stirring at 90°C and 1 atm for 15 h. The reaction was followed by tlc (silica gel, ethyl acetate): 4-phthalimidobutyronitrile (**13**), $R_f$ 0.75, and 4-phthalimido-1-acetamidobutane (**14**), $R_f$ 0.15 (monitored with uv-light). The reaction mixture was centrifuged and the supernate concentrated *in vacuo* to an oil. Hydrochloric acid (25 mL, 6 *M*) was added and the mixture kept in a sealed flask at 92°C for 20 h. Upon cooling to 25°C the mixture was seeded with phthalic acid crystals and kept at 5°C for 1 h. Phthalic acid was removed by centrifugation, washed with hydrochloric acid (2 × 10 mL, 6 *M*), and the supernatant liquids evaporated to dryness *in vacuo*. The residue was dissolved in sodium hydroxide (20 mL, 1 *M*), and the solution was saturated with sodium chloride and extracted with 1-butanol (5 × 20 mL). Hydrochloric acid (2 mL, 6 *M*) was added to the combined extracts and the mixture was evaporated to dryness and dried *in vacuo* over calcium chloride. The crude (1-$^{13}$C,1-$^{15}$N)putrescine dihydrochloride (**15**) (954 mg) was recrystallized from water/ethanol. Yield, 544 mg (3.34 mmol); $^1$H nmr[9] ($D_2O$) δ: 4.0–3.8 (m, 0.9 H), 3.2–3.0 (m, 2.2 H), 2.4–2.2 (m, 0.9 H), 2.0–1.7 (m, 4.0 H) ppm, $J_{^{13}C,H\text{-}1}$ = 143 Hz; $^{13}$C nmr[10] ($D_2O$) δ: 40.3 (d, $J_{C\text{-}1,N}$ = 4.4 Hz), 25.11 (d, $J_{C\text{-}2,C\text{-}1}$ = 37 Hz), 25.15 (s, C-3) ppm.

*Synthesis of (2-$^2$H)-1-pyrroline*

DL-(2-$^2$H)Proline (98 at.%, Merck, Sharp and Dohme) (294 mg, 2.53 mmol) was dissolved in sulfuric acid (20 mL, 0.1 *M*) and sodium metaperiodate (635 mg, 2.97 mmol) in water (10 mL) was added. The mixture was kept in the dark for 16 h. After cooling to 0°C a saturated solution of barium chloride dihydrate (863 mg, 3.53 mmol) in water was added. A saturated solution of sodium bicarbonate was added until the pH was 7.5. The ice-cold reaction mixture was filtered (Celite) and the pH was immediately adjusted to 6.5 with dilute hydrochloric acid. The mixture was immediately used for feeding (experiment 7).

*Synthesis of [5-$^3$H,5-$^{14}$C]-1-pyrroline*

Sodium metaperiodate (13.2 mg, 0.062 mmol) was added to a solution containing L-[5-$^3$H]proline (see Table 1), DL-[5-$^{14}$C]-proline (see Table 1), and L-proline (5.6 mg, 0.049 mmol) in sulfuric acid (0.5 mL, 0.1 *M*). The mixture was left in the dark for 23 h. A solution of barium chloride dihydrate (17.9 mg, 0.073 mmol) in water (0.5 mL) was added and the mixture centrifuged. The precipitate was washed with water (1 × 0.5 mL) and to the combined supernatant liquids was added a solution of sodium bicarbonate (3.5 mg, 0.042 mmol) in water (0.5 mL). Centrifugation and washing of the precipitate with water (1 × 0.5 mL) gave a solution (pH ca. 6) which was immediately used for feeding (experiment 8).

*Administration of tracers to* Senecio vulgaris

The plants used in this study were collected on the McMaster University Campus, keeping as much of the original soil around the roots as possible, and transferred to the greenhouse, where they were allowed to acclimatize for 2–10 days. The plants used in the feeding experiments were 15–30 cm tall. Tracer solution was administered by the wick method.

*Experiment 5*

The mixture of (1-$^{13}$C,1-$^{15}$N)putrescine dihydrochloride (90 at.% $^{13}$C, 99 at.% $^{15}$N, *vide supra*) (472 mg, 2.90 mmol) and [1-$^{14}$C]putrescine (68 μCi, see Table 1)[11] in water (50 mL) was administered to 133 plants over a period of 13 days (July). An equal volume of tracer solution was administered each day.

*Experiments 1–4, 6–8*

Tracer solution was administered in a single dose. The plants were allowed to grow in contact with tracer for various lengths of time before being harvested (see Table 1).

*Extraction of alkaloids*

The procedure described is typical for the experiments with radioactive substrates (Experiments 1–4, 6, 8). In the experiments with stable isotopic tracers (Experiments 5, 7) the amounts used were twice those given below. The plants were harvested and the fresh plant material was immediately ground in a blender with methanol and extracted in a Soxhlet extractor with methanol (approx. 10 h). The extract was concentrated *in vacuo*. Sulfuric acid (50 mL, 1 *M*) was added to the residue and the mixture extracted with ether (3 × 50 mL). The aqueous phase was basified to pH ca. 9 with concentrated ammonium hydroxide and extracted with chloroform (4 × 50 mL). The chloroform extracts were dried over anhydrous sodium sulfate, filtered, and concentrated *in vacuo* to yield a mixture of crude alkaloids. The composition of the mixture was determined by $^1$H nmr (42) and tlc (silica gel, $CHCl_3$/MeOH/concentrated $NH_4OH$; 85:14:1) using Dragendorff's reagent (43*a*) for visualization (retrorsine $R_f$ 0.40; seneciphylline $R_f$ 0.73; senecionine $R_f$ 0.73). These alkaloids accounted for 0–10%, 40–50%, and 50–60%, respectively of the mixture.

The aqueous phase from the chloroform extractions was partly concentrated *in vacuo* to remove excess ammonia. The mixture was acidified to pH ca. 1 with concentrated sulfuric acid and stirred with zinc dust (ca. 2 g) for 30 min. Excess concentrated ammonium hydroxide was added and the mixture extracted with chloroform (4 × 50 mL). The extracts were dried over anhydrous sodium sulfate, filtered, and concentrated *in vacuo* to yield a mixture of crude alkaloids originating from the alkaloid *N*-oxides. The composition of the mixture fell within the limits given above. The aqueous phase from the chloroform extractions was kept for the isolation of ornithine (see Footnote 2).

*Isolation of retronecine*

*Experiment 5*

Each of the two mixtures of the crude alkaloids (*vide supra*) was applied to a column of silica gel 40 (Merck, 70–230 mesh, 25 × 1 cm) and eluted with $CHCl_3$/MeOH/concentrated $NH_4OH$ (90:9:1). The fractions containing the alkaloids were identified by tlc (*vide supra*) and evaporated to dryness *in vacuo*. The yield of crude alkaloids was 47 mg.

Water (1.3 mL) and barium hydroxide octahydrate (186 mg, 0.59 mmol) were added to the crude alkaloids and the mixture heated with stirring on a steambath for 10 min. Sulfuric acid (50% v/v) was added at 20°C to pH ca. 1, the mixture was centrifuged, the precipitate washed with water (3 × 1 mL), and the combined supernate and washings were applied to an ion exchange column (Dowex 2-X8, $OH^-$-form, 5 mL). The eluate was acidified with dilute hydrochloric acid and the solution was evaporated to dryness *in vacuo*. The residue was a mixture (17 mg) of retronecine hydrochloride and retronecine *N*-oxide (1:5, as determined by $^{13}$C nmr, see Table 4).

This mixture was dissolved in hydrochloric acid (1 mL, 1 *M*) and stirred with an excess of Zn dust for 1 h. The mixture was centrifuged, the precipitate washed with water (2 × 1 mL), and the combined supernatant solutions applied to an ion exchange column (Dowex 50W-X4, $H^+$-form, 3 mL). The column was washed with degassed water until the eluate was neutral, then with oxygen-free ammonium hydroxide (3 *M*). The basic eluate (ca. 10 mL) was collected under nitrogen and evaporated to dryness *in vacuo*. The residue was immediately acidified with hydrochloric acid (2 mL, 0.1 *M*) and evaporated to dryness *in*

[11] The radioactivity of the putrescine dihydrochloride which was administered to the plants was determined after recrystallization to constant activity. Specific activity 5.2 × $10^7$ dpm/mmol; total activity administered: 5.2 × $10^7$ dpm/mmol × 2.9 mmol = 1.5 × $10^8$ dpm = 68 μCi.

Can. J. Chem. Downloaded from www.nrcresearchpress.com by 210.87.254.42 on 09/06/12
For personal use only.

*vacuo* to yield retronecine hydrochloride (13 mg, 0.068 mmol). The $^{13}C$ nmr spectrum (see Table 4) showed no signals other than those of retronecine hydrochloride. The specific radioactivity of this material ($3.4 (\pm 0.1) \times 10^6$ dpm per mmol) did not change with repeated recrystallizations from ethanol/acetone, indicating that the sample was radiochemically pure.

*Experiment 7*

The two crude alkaloid fractions (*vide supra*) were separately applied to a Merck silica gel prepacked column (size B) and eluted with $CHCl_3$/MeOH/concentrated $NH_4OH$ (90:9:1) with continuous monitoring of the effluent at 254 nm. The fraction from 35–55 min (flow rate 2.7 mL/min) containing senecionine and seneciphylline (1:1) was collected and evaporated to dryness *in vacuo*. Yield 168 mg (from "free" alkaloids) and 87 mg (from alkaloid *N*-oxides). The two samples were combined and recrystallized from methanol to yield a mixture (177 mg) of senecionine (0.25 mmol) and seneciphylline (0.28 mmol). A 13.8 MHz $^2H$ nmr spectrum ($CHCl_3$, 42 000 scans, pulse width 35 μs, acquisition time 2.0 s) of a saturated solution (ca. 75 mg/mL) showed a line due to the natural abundance of $^2H$ in the chloroform used as solvent. Work-up was discontinued.

*Experiments 1–4, 6, 8*

The two crude alkaloid fractions (*vide supra*) were worked up separately. A typical experiment will be described. To a crude alkaloid fraction was added crude retrorsine (200 mg, 0.57 mmol), water (4 mL), and barium hydroxide octahydrate (650 mg, 2.06 mmol) and the mixture was heated on a steambath with stirring for 10 min. Sulfuric acid (50%, v/v) was added till the pH was ca. 1, and barium sulfate was removed by centrifugation. The supernate was extracted with ether continuously for 24 h. The aqueous phase was applied to an ion exchange column (Dowex 2-X8, $OH^-$-form, 10 mL) and eluted with water. The basic eluate was collected and evaporated to dryness *in vacuo*. The residue was chromatographed on a Silica Gel column (Baker, 60–200 mesh, 50 × 0.7 cm) with $CHCl_3$/MeOH/concentrated $NH_4OH$ (74:24:2) with continuous monitoring of the effluent at 254 nm.[12] The fraction containing retronecine was collected and evaporated to dryness *in vacuo* to yield crude retronecine (103 mg, 0.66 mmol). Addition of excess dilute hydrochloric acid, evaporation to dryness *in vacuo*, and repeated recrystallization from ethanol/acetone yielded retronecine hydrochloride (50 mg, 0.26 mmol). Nonradioactive retronecine hydrochloride (52 mg, 0.27 mmol) was added, the mixture applied to an ion exchange column (Dowex 2-X8, $OH^-$-form, 10 mL), and eluted with water. The basic eluate was evaporated to dryness *in vacuo*. Recrystallization from acetone yielded retronecine (63 mg, 0.41 mmol), mp 119–120°C (lit. (6) mp 119–120°C).

Retronecine (60 mg, 0.39 mmol) was dissolved in excess dilute hydrochloric acid, the solution was evaporated to dryness *in vacuo*, and the residue recrystallized from ethanol/acetone to yield retronecine hydrochloride (68 mg, 0.35 mmol), mp 163–164°C (lit. (16) mp 164°C).

*Degradation of retronecine hydrochloride (Experiments 1–4, 6)*

*Carbon-9 as formaldehyde*

A solution of retronecine hydrochloride (63 mg, 0.33 mmol), osmium tetroxide (4 mg, 0.01 mmol), and sodium metaperiodate (223 mg, 1.04 mmol) in water (2.5 mL) was allowed to stand 2 h at 25°C. Part of this solution (0.15 mL) was added to a solution of 5,5-dimethylcyclohexane-1,3-dione (28 mg, 0.20 mmol) and sodium bicarbonate (8 mg, 0.10 mmol) in water (7 mL). After 2 h at 25°C the precipitate was isolated, washed with water (2 × 2 mL), and recrystallized from ethanol/water to yield formaldehyde dimethone: 4 mg (0.014 mmol, 71%), mp 190–191°C (lit. 43*b*) mp 189°C).

*Carbon-1 and carbons 5–8 as* L-cis-*3-hydroxyproline*

The remaining part of the oxidation mixture (2.35 mL, *vide supra*) was applied to an ion exchange column (Dowex 50W (50-4X200), $H^+$-form, 3 mL). The column was washed with water until the eluate was neutral, and was then eluted with aqueous pyridine (1 *M*). The basic eluate (ca. 15 mL) was concentrated *in vacuo* to 1.0 mL. After addition of manganese dioxide (300 mg, 3.45 mmol) the mixture was stirred with a magnetic bar in a stoppered flask 24 h (or more, if necessary) at 25°C. The course of the reaction was followed by tlc (silica gel, 1-BuOH/AcOH/$H_2O$; 2:1:1), *N*-(2′-oxoethyl)-L-*cis*-3-hydroxyproline, $R_f$ 0.5 (visualized with iodine vapor) and L-*cis*-3-hydroxyproline, $R_f$ 0.3 (visualized with iodine vapor (weak reaction) and ninhydrin (yellow)). The reaction mixture was centrifuged and the supernate applied to an ion exchange column (Dowex 50W (50-4X200), $H^+$-form, 3 mL). The column was washed with water and then eluted with aqueous pyridine (1 *M*). The basic eluate (ca. 15 mL) was evaporated to dryness *in vacuo*, to yield crude L-*cis*-3-hydroxyproline (26 mg, 0.20 mmol, 64%). Recrystallization from water/ethanol yielded 14 mg (0.114 mmol, 34%).

$[\alpha]_D^{25}$ −96° ± 1° (*c* 1.0, $H_2O$) (lit. (45) $[\alpha]_D^{25}$ −102.7° ± 1.5° (*c* 1.0, $H_2O$)); $^1H$ nmr ($D_2O$): δ and *J* values identical with those given for DL-*cis*-3-hydroxyproline (46).

*Carbon-8 as formic acid*

L-*cis*-3-Hydroxyproline (8 mg, 0.061 mmol) and sodium metaperiodate (31 mg, 0.145 mmol) were dissolved in water (0.7 mL). The solution was kept 2 h at 25°C, sulfuric acid (1.1 mL, 0.1 *M*) was then added, and the reaction mixture was solidified by immersing the reaction flask into liquid nitrogen. The frozen mixture, now kept at room temperature, was then submitted to sublimation (0.1 Torr) and the sublimate collected in a flask cooled in liquid nitrogen. The sublimate was allowed to warm to room temperature and the resulting solution was basified to pH 8 with dilute sodium hydroxide (0.1 *M*) and concentrated *in vacuo* to 1.0 mL. 1-Naphthylamine hydrochloride (14 mg, 0.078 mmol) and *N*-ethyl-*N*′-3′-(dimethylamino)propylcarbodiimide hydrochloride (40 mg, 0.21 mmol) was added and the mixture was stirred 15 min. Hydrochloric acid (1 mL, 1 *M*) was added and the mixture was extracted with ether (3 × 1 mL). The ether extracts were evaporated to dryness and the product, *N*-formyl-1-naphthylamine, recrystallized from benzene/hexane: 8 mg (0.047 mmol, 77%), mp 139°C (lit. (47) mp 141–142°C).

*Carbons 5–7 as* β-*alanine*

L-*cis*-3-Hydroxyproline (16 mg, 0.122 mmol) and sodium metaperiodate (107 mg, 0.50 mmol) were dissolved in water (0.75 mL) and allowed to stand at 25°C for 1 h. Potassium permanganate (1.0 mg, 0.006 mmol) was added and the temperature kept at 75°C for 20 min. The reaction mixture was cooled to 25°C, the pH was adjusted to ca. 8 with sodium bicarbonate, and *N*-carbethoxyphthalimide (36 mg, 0.16 mmol) was then added. The mixture was stirred for 10–15 min and then extracted with chloroform (2 × 2 mL). The aqueous phase was acidified with hydrochloric acid (0.5 mL, 1 *M*) and extracted with chloroform (2 × 2 mL). The chloroform extract was evaporated to dryness *in vacuo* and the residue recrystallized from water. Yield of *N*-phthaloyl-β-alanine: 4 mg (0.018 mmol, 15%), mp 151–152°C (lit. (48) mp 152°C).

*Determination of radioactivity*

Radioactivity was assayed by liquid scintillation counting (Beckman LS 9000 Liquid Scintillation System). All samples counted were recrystallized to constant specific radioactivity,

[12]It is of the utmost importance to collect the *whole* fraction containing retronecine to avoid partial separation of $^3H$-containing from $^{14}C$-containing retronecine molecules. Differences in distribution of label within the two samples of retronecine in experiment 6*A* and 6*O* were due to isotope fractionation in the course of chromatographic purification (see Discussion).

dissolved in Aquasol (New England Nuclear), and counted in triplicate, if possible, under comparable conditions of quenching. Confidence limits shown in the tables are standard deviation from the mean.

## Acknowledgments

We thank Dr. D. H. G. Crout, University of Exeter, for a generous sample of retrorsine. This investigation was supported by a grant from the Natural Sciences and Engineering Research Council of Canada. One of us (I.D.S.) thanks the Scientific Affairs Division of the North Atlantic Treaty Organization for the award of a Senior Fellowship.

1. N. J. Leonard. *In* The alkaloids. Vol. 6. *Edited by* R. H. F. Manske. Academic Press, New York. 1960. p. 35.
2. H.-G. Boit. Ergebnisse der Alkaloid-Chemie bis 1960. Akademie-Verlag, Berlin. 1961. p. 88.
3. F. L. Warren. Fortschr. Chem. Org. Naturst. **24**, 329 (1966).
4. F. L. Warren. *In* The alkaloids. Vol. 12. *Edited by* R. H. F. Manske. Academic Press, New York. 1970. p. 245.
5. H. C. S. Wood and R. Wrigglesworth. *In* Rodd's chemistry of carbon compounds. 2nd ed. Vol. 4. Part B. *Edited by* S. Coffey. Elsevier Scientific Publishing Company, Amsterdam. 1977. p. 7.
6. W. Bottomley and T. A. Geissman. Phytochemistry, **3**, 357 (1964).
7. C. A. Hughes, R. Letcher, and F. L. Warren. J. Chem. Soc. 4974 (1964).
8. D. J. Robins and J. R. Sweeney. J. Chem. Soc. Chem. Commun. 120 (1979).
9. H. A. Khan and D. J. Robins. J. Chem. Soc. Chem. Commun. 146 (1981).
10. R. Robinson. The structural relations of natural products. Clarendon Press, Oxford. 1955. p. 72.
11. T. A. Smith. Ann. N. Y. Acad. Sci. **171**, 988 (1970).
12. E. Leistner, R. N. Gupta, and I. D. Spenser. J. Am. Chem. Soc. **95**, 4040 (1973).
13. T. Shun, J. Koluch, and F. Šantavý. Collect. Czech. Chem. Commun. **25**, 934 (1960).
14. S. Ferry and J. L. Brazier. Ann. Pharm. Fr. **34**, 133 (1976).
15. C. W. Qualls, Jr. and H. J. Segall. J. Chromatogr. **150**, 202 (1978).
16. D. H. G. Crout, N. M. Davies, E. H. Smith, and D. Whitehouse. J. Chem. Soc. Perkin Trans. I, 671 (1972).
17. E. C. Leisegang and F. L. Warren. J. Chem. Soc. 486 (1949).
18. C. C. J. Culvenor and L. W. Smith. Austr. J. Chem. **10**, 464 (1957).
19. E. J. Barreiro, A. De L. Pereira, L. Nelson, L. F. Gomes, and A. J. R. Da Silva. J. Chem. Res. Synop. 330 (1980).
20. C. Schöpf. Angew. Chem. **59**, 174 (1947).
21. W. B. Jakoby and J. Fredericks. J. Biol. Chem. **234**, 2145 (1959).
22. P. D. Bragg and L. Hough. J. Chem. Soc. 4050 (1958).
23. J. Kaczkowski and L. Marion. Can. J. Chem. **41**, 2651 (1963).
24. E. Leete and M. C. L. Louden. Chem. Ind. London, 1725 (1963).
25. H. W. Liebisch, H. R. Schütte, and K. Mothes. Justus Liebig's Ann. Chem. **668**, 139 (1963).
26. H. W. Liebisch, H. Ramin, I. Schöffinius, and H. R. Schütte. Z. Naturforsch. Teil B, **20**, 1183 (1965).
27. E. Leete. J. Am. Chem. Soc. **84**, 55 (1962).
28. R. N. Gupta and I. D. Spenser. Can. J. Chem. **45**, 1275 (1967).
29. E. Leete. J. Am. Chem. Soc. **78**, 3520 (1956).
30. E. Leete, E. G. Gros, and T. J. Gilbertson. J. Am. Chem. Soc. **86**, 3907 (1964).
31. E. Leete. J. Am. Chem. Soc. **80**, 4393 (1958).
32. E. Leistner and I. D. Spenser. J. Am. Chem. Soc. **95**, 4715 (1973).
33. R. N. Gupta and I. D. Spenser. Can. J. Chem. **49**, 384 (1971).
34. A. Haber, R. D. Johnson, and K. L. Rinehart, Jr. J. Am. Chem. Soc. **99**, 3541 (1977).
35. G. Burton, H. Nordlöv, S. Hosozawa, H. Matsumoto, P. M. Jordan, P. E. Fagerness, L. M. Pryde, and A. I. Scott. J. Am. Chem. Soc. **101**, 3114 (1979).
36. S. J. Gould, C. C. Chang, D. S. Darling, J. D. Roberts, and M. Squillacote. J. Am. Chem. Soc. **102**, 1707 (1980).
37. E. Leete and J. A. McDonell. J. Am. Chem. Soc. **103**, 658 (1981).
38. N. V. Mody, R. S. Sawhney, and S. W. Pelletier. J. Nat. Prod. **42**, 417 (1979).
39. S. E. Drewes, I. Antonowitz, P. T. Kaye, and P. C. Coleman. J. Chem. Soc. Perkin Trans. I, 287 (1981).
40. G. Grue-Sørensen and I. D. Spenser. J. Am. Chem. Soc. **103**, 3208 (1981).
41. K. Hasse and K. Schührer. Biochem. Z. **336**, 20 (1962).
42. R. J. Molyneux, A. E. Johnson, J. N. Roitman, and M. E. Benson. J. Agric. Food Chem. **27**, 494 (1979).
43. R. M. C. Dawson, D. C. Elliott, W. H. Elliott, and K. M. Jones (*Editors*). Data for biochemical research. 2nd ed. Oxford University Press, Oxford. 1969. (*a*) p. 519; (*b*) p. 79.
44. H. A. Khan and D. J. Robins. J. Chem. Soc. Chem. Commun. 554 (1981).
45. J. S. Wolff, III, J. D. Ogle, and M. A. Logan. J. Biol. Chem. **241**, 1300 (1966).
46. R. Tschesche, E. U. Kaussmann, and H.-W. Fehlhaber. Chem. Ber. **105**, 3094 (1972).
47. I. Ojima, S. Inaba, and Y. Nagai. Tetrahedron Lett. 4363 (1973).
48. G. H. L. Nefkens, G. I. Tesser, and R. J. F. Nivard. Recl. Trav. Chim. Pays-Bas, **79**, 688 (1960).

Can. J. Chem. Downloaded from www.nrcresearchpress.com by 210.87.254.42 on 09/06/12
For personal use only.

# Regiospecific addition of benzeneselenenyl halide to 1,1-disubstituted olefins[1]

PAK-TSUN HO[2] AND RALPH J. KOLT

*Division of Chemistry, National Research Council of Canada, Ottawa, Ont., Canada K1A 0R6*

Received August 24, 1981

PAK-TSUN HO and RALPH J. KOLT. Can. J. Chem. **60**, 663 (1982).

The reaction of benzeneselenenyl halide with a variety of 1,1-disubstituted olefins under controlled conditions yields regiospecifically the anti-Markovnikov adducts which have been converted into the synthetically useful vinyl halides and allyl halides.

PAK-TSUN HO et RALPH J. KOLT. Can. J. Chem. **60**, 663 (1982).

L'halogènure de benzenesélényle réagit avec différentes oléfines disubstituées en position 1,1 dans des conditions controlées pour conduire de manière régiospécifique à des adduits du type anti-Markonikov. On transforme ces derniers en halogènure vinyliques et allyliques qui sont très utiles en synthèse.

[Traduit par le journal]

Can. J. Chem. Downloaded from www.nrcresearchpress.com by 210.87.254.5 on 09/06/12
For personal use only.

Organolselenium compounds have become increasingly important reagents for organic synthesis, because selenides can be converted into olefins in high yield under relatively mild conditions. The reaction of areneselenenyl halides with carbon–carbon double bonds which provide an easy route to selenides has received considerable attention (1). This reaction is observed to be a clean anti-stereospecific addition, but is characterized by low regiospecificity (1*a*, 2). Most studies of the addition have mainly been concerned with simple olefinic hydrocarbons. It has been observed that the reaction of some 1,1-disubstituted alkenes with benzeneselenenyl halide yielded the Markovnikov adducts (3, 4). Recently, it has also been shown that addition of benzeneselenenyl halide to simple monosubstituted terminal olefins produced the unstable anti-Markovnikov adducts with high regioselectivity (5). It seems that the nature of the products obtained from the reaction of olefins with benzeneselenenyl halide is sensitive to the substituted pattern of alkenes. We are interested in the reaction between benzeneselenenyl halide and alkenes that arose from the need of substituted allylic halide for our synthetic effort. We report herein our findings with experimental detail along the lines.

Addition of benzeneselenenyl halide to 1,1-disubstituted alkenes under controlled conditions gives the anti-Markovnikov adducts and is highly regiospecific. When a solution of benzeneselenenyl chloride (1 equiv) in dichloromethane was added dropwise to a stirring solution of methylenecyclohexane **1** in dichloromethane at −70°C under argon, a single adduct was obtained quantitatively. The $^1$H nmr spectrum of the product showed a singlet at 3.76 ppm for two protons deshielded by a chlorine atom and indicated that only the anti-Markovnikov adduct was formed within the experimental limit of our $^1$H nmr analysis. The adduct could survive at −16°C and isomerized slowly at room temperature to its isomer. A new signal at 3.43 ppm (singlet, 2 H, —$CH_2$SePh) appeared in its $^1$H nmr spectrum, which suggested the anti-Markovnikov product had rearranged to the Markovnikov regioisomer. The reaction of methylenecyclopentane **2**, methylenecyclobutane **3**, 2-methyl-3-propenyl benzoate **4**, 3-chloro-2-methyl propene **5**, and the optically active olefinic lactone **6** with benzeneselenenyl chloride under the same conditions all yielded the anti-Markovnikov adducts (Table 1). This observation is similar to the results reported by Raucher (5).

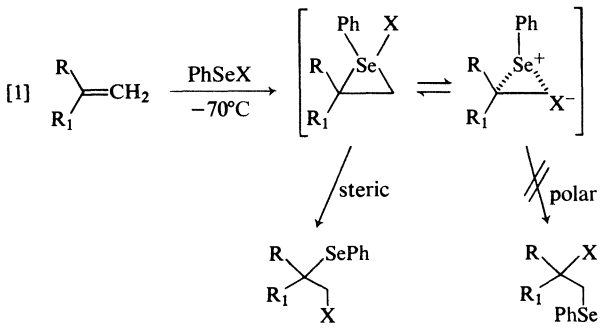


It is of note that under the reaction conditions as described above, the effect of solvent for the reaction is not observed. Thus, the addition of benzeneselenenyl chloride to a solution of olefins in polar solvent such as acetonitrile at −45°C yielded the same anti-Markovnikov adduct as dichloromethane was used as solvent for the reaction. Further, it is worth noting that the introduction of

[1]NRCC No. 19828.

[2]Author to whom correspondence should be addressed; present address: Department of Chemistry, University of Waterloo, Waterloo, Ont., Canada N2L 3G1.

0008-4042/82/050663-04$01.00/0

©1982 National Research Council of Canada/Conseil national de recherches du Canada

TABLE 1. Reaction of PhSeCl with olefins

| Entry | Olefin | Adduct[a] | Elimination product[b] | | Isolated overall yield |
|---|---|---|---|---|---|
| 1 | 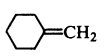 | 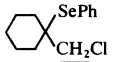 | 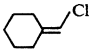 | 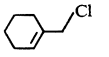 | 74% |
| | **1** | **7** 3.76(S) | **13** (96%) | **14** (4%) | |
| 2 | 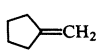 | 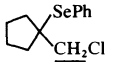 | | 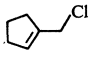 | 50% |
| | **2** | **8** 3.82(S) | | **15** | |
| 3 | 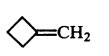 | 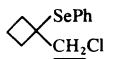 | 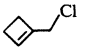 | 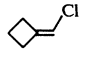 | 51% |
| | **3** | **9** 3.79(S) | **16** (55%) | **17** (45%) | |
| 4 | 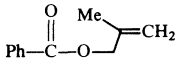 | 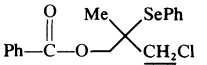 | 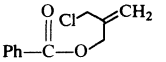 | 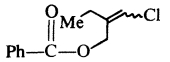 | 80% |
| | **4** | **10** 3.88(q) | **18** (87%) | **19** (13%) | |
| 5 | 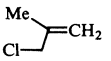 | 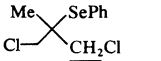 | 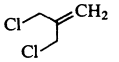 | 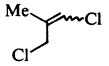 | 56% |
| | **5** | **11** 3.92(q) 3.78(q) | **20** (76%) | **21** (24%) | |
| 6 | 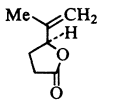 | 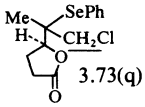 | 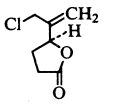 | 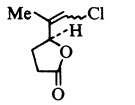 | 84% |
| | **6** | **12** 3.73(q) | **22** (65%) | **23** (35%) | |

[a]For $^1$H nmr analysis, all reactions were carried out in an nmr tube using deuterated solvents.
[b]Pure products were obtained either by tlc or by glc.

functional groups to the 1,1-disubstituted olefins results in a remarkable increase of the stability of the anti-Markovnikov adduct. A crystalline adduct **12** could be prepared from the olefinic lactone **6** at room temperature and was stored at 0°C for several days without significant isomerization.

The result clearly indicates that temperature is the key factor in determining the product with anti-Markovnikov orientation. The addition of benzeneselenenyl halide to olefin presumably involves the formation of a bridged selenurane intermediate (reaction [1]). Which of the two carbon atoms in the intermediate will be attacked by the nucleophilic halide will probably depend on the polar and steric factors. The quantitative formation of anti-Markovnikov product under the reaction conditions strongly suggests that at low temperature the steric factor is preferred and leads to regiospecific formation of the product. Moreover, the use of a polar solvent such as acetonitrile for the reaction does not affect the product composition further supports our view that the reaction carried out at low temperature is not determined by polar factors.

For further characterization, the anti-Markovnikov adduct was converted into the allyl chlorides and vinyl chlorides by simple oxidative elimination process. Typically, the adduct obtained by the reaction of olefines with benzeneselenenyl chloride at −70°C was not isolated and subsequent oxidation elimination with *m*-chloroperbenzoic acid in the presence of pyridine was carried out in the same pot at −70°C. The products were isolated by distillation. The results are summarized in Table 1.

The regiospecificity of the reaction of olefins with benzeneselenenyl chloride described above will provide a simple method for the preparation of substituted allyl chlorides from 1,1-disubstituted alkenes, although the selectivity in the elimination of PhSeOH is rather low. However, it is expected

Can. J. Chem. Downloaded from www.nrcresearchpress.com by 210.87.254.5 on 09/06/12
For personal use only.

that this weakness could be improved by using benzeneselenenyl bromide instead of chloride for the reaction. The reaction of benzeneselenenyl bromide with the optically active olefinic lactone **6** under the same conditions gave 80% yield of the allyl bromide **24** contaminated about 15% of the vinyl bromide.

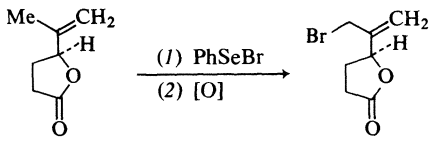


**6** **24**

## Experimental

Melting points were determined on a Reichert hot stage apparatus and are uncorrected. Optical rotations were measured with a Perkin-Elmer Model 141 automatic polarimeter at room temperature. Infrared spectra were of chloroform solution and $^1$H nmr spectra were of deuteriodichloromethane with TMS as an internal reference. A Varian Autoprep Model A-700 gas chromatograph was used in the glc experiment. Thin-layer and preparative-layer chromatography was done using silica gel containing a fluorescent indicator ($G_{254}$).

*General procedure for reaction of benzeneselenenyl chloride with olefins*

*(a) Preparation of the adduct*

A solution of benzeneselenenyl chloride (3.1 mmol) in dichloromethane (6 mL) was added dropwise to a stirring solution of olefins (3 mmol) in dichloromethane (10 mL) at −70°C under argon. Stirring was continued until the orange colour disappeared (10 min).

*(b) Oxidative elimination*

The above adduct obtained at −70°C was not isolated, but was subsequently oxidized with *m*-chloroperbenzoic acid (1.1 equiv) in the presence of pyridine (2 equiv) in the same pot at −70°C. The reaction mixture was stirred at −70°C for 2 h and kept at room temperature overnight. The mixture was diluted with dichloromethane. The solution was washed with 5% sodium metabisulfite, 2% hydrochloric acid, 10% sodium carbonate, and water. Evaporation of the solvent gave the crude product which was purified either by bulb-to-bulb distillation or by chromatography on silica gel.

*Reaction of methylenecyclohexane **1** with PhSeCl*

(*a*) $^1$H nmr of the adduct **7** ($CD_2Cl_2$): δ 1.65 (m, 10 H), 3.76 (s, 2H, —$CH_2Cl$), and 7.32 ppm (m, 5 H aromatic). The adduct **7**, which was left at room temperature overnight, isomerized completely to its Markovnikov isomer. $^1$H nmr ($CD_2Cl_2$): δ 1.73 (m, 10 H), 3.38 (s, 2 H, —$CH_2SePh$), 7.42 ppm (m, 5 H, aromatic).

(*b*) The elimination product from **7** was obtained by distillation (bp 40–45°C at 80 Torr) in 74% yield as a mixture, which was separated by glc to give 96% of compound **13** and 4% of compound **14**. $^1$H nmr of compound **13** ($CDCl_3$): δ 2.21 (m, 4 H, allylic protons), and 5.74 ppm (broad s, 1 H, olefinic proton). *Anal.* calcd. for $C_7H_{14}Cl$: C 64.37, H 8.49, Cl 27.14; found: C 64.47, H 8.57, Cl 27.13. $^1$H nmr of compound **14** ($CDCl_3$): δ 3.95 (s, 2 H, —$CH_2Cl$), and 5.84 ppm (broad s, 1 H, olefinic proton). *Anal.* calcd. for $C_7H_{14}Cl$: C 64.37, H 8.49, Cl 27.14; found: C 64.42, H 8.57, Cl 27.19.

*Reaction of methylenecyclopentane **2** with PhSeCl*

(*a*) $^1$H nmr of the adduct **8** ($CD_2Cl_2$): δ 1.68 (m, 8 H), 3.82 (s, 2 H, —$CH_2Cl$), and 7.38 ppm (m, 5 H, aromatic).

(*b*) The elimination product **15** was obtained in 50% yield. Compound **15** was identical with the sample prepared from known procedure (6). $^1$H nmr ($CDCl_3$): δ 2.62–1.67 (m, 6 H), 4.17 (s, 2 H, —$CH_2Cl$), and 5.76 ppm (broad s, 1 H, olefinic proton).

*Reaction of methylenecyclobutane **3** with PhSeCl*

(*a*) $^1$H nmr of the adduct **9** ($CD_2Cl_2$): δ 2.41 (m, 6 H), 3.79 (s, 2 H, —$CH_2Cl$), and 7.31 ppm (m, 5 H, aromatic).

(*b*) The elimination product from **9** was obtained by distillation (bp 70°C at 120 Torr) in 57% yield based on the 80% commercial material as a mixture, which was separated by glc on a 20% Carbowax column at 100°C to give 65% of compound **16** and 35% of compound **17**. Their $^1$H nmr spectra were identical with the authentic samples respectively (7). $^1$H nmr of compound **16** ($CDCl_3$): δ 2.45 (m, 4H), 4.03 (s, 2 H, —$CH_2Cl$), and 5.95 ppm (broad s, 1 H, olefinic proton). $^1$H nmr of compound **17** ($CDCl_3$): δ 2.03 (q, 2 H), 2.64 (m, 4 H, allylic protons), and 5.69 ppm (5, 1 H, olefinic proton).

*Reaction of 2-methyl-3-propenyl benzoate **4** with PhSeCl*

(*a*) $^1$H nmr of the adduct **10** ($CD_2Cl_2$): δ 1.42 (s, 3 H, $CH_3$), 3.88 (q, 2 H, —$CH_2Cl$), and 4.46 ppm (s, 2 H, Ph—C(=O)—O—$CH_2$).

(*b*) The elimination product from **10** was obtained by distillation (bp 46–50°C at 5 × $10^{-2}$ Torr) in 80% yield as a mixture, which was separated by chromatography on silica gel to give 87% of compound **18** and 13% of compound **19**. For compound **18**: ir ($CHCl_3$): 1720 $cm^{-1}$ (benzoate); $^1$H nmr ($CDCl_3$): δ 4.15 (s, 2 H, —$CH_2Cl$), 4.93 (s, 2 H, Ph—C(=O)—O—$CH_2$—), and 5.38 ppm (m, 2 H, >C=$CH_2$); *Anal.* calcd. for $C_{11}H_{11}O_2Cl$: C 62.72, H 5.22, Cl 16.82; found: C 62.83, H 5.11, Cl 16.77.

*Reaction of 3-chloro-2-methyl propene **5** with PhSeCl*

(*a*) $^1$H nmr of the adduct **11** ($CD_2Cl_2$): δ 1.41 (s, 3 H, —$CH_3$), 3.78 (q, 2 H, —$CH_2Cl$), 3.92 (q, 2 H, —$CH_2Cl$), and 7.32 ppm (m, 5 H, aromatic).

(*b*) The elimination product from **11** was obtained by distillation (bp 45–50°C at 75 Torr) in 56% yield as a mixture, which was separated by glc on a 20% OS-136 column at 110°C to yield 76% of compound **20** and 24% of compound **21**. Their spectra were identical with the literature reported respectively (8). $^1$H nmr of **20** ($CDCl_3$): δ 4.19 (s, 4 H, —$CH_2Cl$), and 5.32 ppm (s, 2 H, >C=$CH_2$). $^1$H nmr of **21** ($CDCl_3$): δ 1.89 (s, 3 H, methyl), 4.21 (s, 2 H, —$CH_2Cl$), and 5.98 ppm (broad s, 1 H, olefinic proton).

*Preparation of the olefinic lactone **6***

(*a*) A solution of the lactonic acid chloride (24.9 g, 0.163 mol) in tetrahydrofuran (75 mL), prepared from L-glutamic acid (9), was added over 20 min to a solution (−10°C) of dimethyl cadmium, prepared from the reaction of methylmagnesium bromide (0.216 mol) with anhydrous cadmium chloride (20.8 g, 0.113 mol) in tetrahydrofuran (250 mL) under argon. The reaction mixture was stirred at −10°C for an additional 8 h, at which time 4 *N* aqueous sulfuric acid (50 mL) was added slowly and the mixture was stirred for 30 min. It was extracted with dichloromethane (3 × 200 mL). The extracts were washed with 5% sodium carbonate and water, and dried over anhydrous magnesium sulfate. Removal of the solvent gave the methyl ketone lactone

Can. J. Chem. Downloaded from www.nrcresearchpress.com by 210.87.254.5 on 09/06/12
For personal use only.

(14.5 g, 70% yield), which was pure enough for further reaction $[\alpha]_D$ −11.9° (c 1.0, $CHCl_3$); ir ($CHCl_3$): 1725 (ketone) and 1785 cm$^{-1}$ (lactone); $^1$H nmr ($CDCl_3$): δ 2.25 (s, 3 H, —C(=O)—$CH_3$), and 4.90 ppm (m, 1 H, —C(=O)—O—CH(—O—C(=O)—)—).

(*b*) A solution of the methyl ketone lactone (2.56 g, 20 mmol) in tetrahydrofuran (10 mL) was added over 15 min to a Wittig reagent, prepared by the reaction of methyltriphenylphosphorium bromide (7.6 g, 21 mmol) in tetrahydrofuran (30 mL) with *n*-butyl lithium (20 mmol) at −78°C under argon. The reaction mixture was stirred at room temperature for 2 days, after which time the mixture was diluted with ether (200 mL), and the solid was filtered. Evaporation of the solvent gave a residue which was chromatographed on silica gel (100 g) to yield the pure olefinic lactone **6** (1.3 g) in 51% yield. $[\alpha]_D$ +6.3° (c 1.3, chloroform); ir ($CHCl_3$) 1775 cm$^{-1}$ (lactone); $^1$H nmr ($CDCl_3$): δ 1.75 (s, 3 H, $CH_3$), and 4.97 ppm (m, 3 H, $>C{=}CH_2$ and —CH(—O—C(=O)—)—). *Anal.* calcd. for $C_7H_{10}O_2$: C 66.64, H 7.99; found: C 66.56, H 8.01.

*Reaction of olefinic lactone **6** with PhSeCl*

(*a*) The crystalline adduct **12** was a mixture of two diastereoisomers (7:3 based on $^1$H nmr analysis), which was stable at 0°C for several days. $^1$H nmr ($CDCl_3$): δ 1.18 (s, 3 H, $CH_3$), 3.73 (q, 2 H, —$CH_2$Cl), 4.76 ppm (m, 1 H, —CH(—O—C(=O)—)—).

(*b*) The elimination product was a mixture which was separated by preparative tlc on silica gel to give 65% of the allyl chloride **22** and 35% of the vinyl chloride **23**. For compound **22**: $[\alpha]_D$ +9.7° (c 1.8, chloroform); ir ($CHCl_3$): 1778 cm$^{-1}$ (lactone); $^1$H nmr ($CDCl_3$): δ 4.10 (s, 2 H, —$CH_2$Cl), 5.07 (broad t, 1 H, —CH(—O—C(=O)—)—), 5.36 ppm (broad d, 2 H, $>C{=}CH_2$). *Anal.* calcd. for $C_7H_9ClO_2$: C 52.35, H 5.65, Cl 22.08; found: C 52.29, H 5.79, Cl 22.23.

*Reaction of olefinic lactone **6** with PhSeBr*

The product, prepared under the same conditions as described in the general procedure, was obtained in 80% yield as a mixture, which could be purified by chromatography on silica gel using benzene and ethyl acetate (10:1) as the solvent. $^1$H nmr of the allyl bromide **24** ($CDCl_3$): δ 4.01 (s, 2 H, —$CH_2$Br), and 5.39 ppm (broad d, 2H, $>C{=}CH_2$); ir ($CHCl_3$): 1778 cm$^{-1}$ (lactone); $[\alpha]_D$ +8.6° (c 1.7, methanol).

## Acknowledgements

We thank Mr. H. Seguin for the microanalyses and Mr. F. Cooper for recording the $^1$H nmr spectra at low temperature.

1. (*a*) K. B. Sharpless and R. T. Lauer. J. Org. Chem. **39** 429 (1974); (*b*) D. G. Garratt and A. Kabo. Can. J. Chem. **58**, 1030 (1980) and references cited therein.
2. (*a*) J. Reich. J. Org. Chem. **39**, 428 (1974); (*b*) D. L. J. Clive. Chem. Commun. 100 (1974); (*c*) N. Miyoshi, S. Furui, S. Murai, and N. Sonoda. Chem. Commun. 293 (1975).
3. D. G. Garratt. Ph.D. Dissertation, University of Toronto. 1975.
4. E. G. Kataev, T. G. Manafov, E. A. Berdnikov, and O. A. Komarovskaya. Zh. Org. Khim. (Engl), **9**, 1983 (1973).
5. (*a*) S. Raucher. J. Org. Chem. **42**, 2950 (1977); (*b*) S. Raucher. Tetrahedron Lett. 3909 (1977); (*c*) D. Liotta and G. Zima. Tetrahedron Lett. 4977 (1978).
6. J. A. Landerebe and D. E. Applequist. J. Am. Chem. Soc. **86**, 1536 (1964).
7. S. A. Sherrod and R. G. Bergman. J. Am. Chem. Soc. **93**, 1925 (1971).
8. P. S. Skell and R. G. Doerr, J. Am. Chem. Soc. **89**, 4688 (1967).
9. S. Iwaki, S. Marumo, Y. Saito, M. Yamada, and K. Katagiri. J. Am. Chem. Soc. **96**, 7842 (1974).

Can. J. Chem. Downloaded from www.nrcresearchpress.com by 210.87.254.5 on 09/06/12
For personal use only.

# Lanthanide complexes of potentially heptadentate Schiff base ligands

ELMER C. ALYEA, ABDUL MALEK,[1] AND ANGELOS E. VOUGIOUKAS

*Guelph-Waterloo Centre for Graduate Work in Chemistry, Guelph Campus, University of Guelph, Guelph, Ont., Canada N1G 2W1*

Received July 6, 1981

ELMER C. ALYEA, ABDUL MALEK, and ANGELOS E. VOUGIOUKAS. Can. J. Chem. **60**, 667 (1982).

The potentially heptadentate trianionic Schiff base ligands derived from tris(2-aminoethyl)amine and 3 mol of (substituted) salicylaldehyde react with lanthanide metal nitrates to form neutral 1:1 compounds of formula Ln(X-Saltren). Physicochemical measurements are described for the following complexes: Ln = La, Pr, Nd, Eu, Gd, Dy, Ho, Yb, X= 3,5-$Cl_2$; Ln = La, X = 5-Cl and 5-$NO_2$; and the analogous complexes, M = Sc, Y, Co, X = 3,5-$Cl_2$. Discussion of the spectroscopic data focuses on far infrared ν(Ln—O) and ν(Ln—N) bands, $^1$H nmr pseudocontact shifts and hypersensitive *f–f* transitions.

ELMER C. ALYEA, ABDUL MALEK, and ANGELOS E. VOUGIOUKAS. Can. J. Chem. **60**, 667 (1982).

Les ligands du type base de Schiff potentiellement heptadentates et trianioniques provenant de la réaction de la tris(amino-2 éthyl) amine avec trois moles de salicylaldehyde (substitué) réagissent avec les nitrates des métaux de la série des lanthanides en formant des composés neutres 1:1 de formule Ln(X-Saltren). On a effectué les mesures physicochimiques sur les complexes suivants: Ln = La, Pr, Nd, Eu, Gd, Dy, Ho, Yb, X = $Cl_2$-3,5; Ln = La, X = Cl-5 et $NO_2$-5 ainsi que sur des complexes analogues, M = Sc, Y, Co, X = $Cl_2$-3,5. La discussion des données spectroscopiques porte sur les bandes ν(Ln—O) et ν(Ln—N) dans l'infrarouge lointain, sur la rmn du $^1$H des réactifs de pseudo déplacement et sur les transitions hypersensibles *f—f*.

[Traduit par le journal]

## Introduction

Studies of metal complexes involving ligands having seven potential donor atoms are relatively rare (1). The number of Schiff base complexes of the lanthanide elements is similarly limited to a few reports (2). In the present work, we accordingly explore the ligating properties of potentially heptadentate Schiff base ligands (**I**) with several trivalent lanthanide metals.

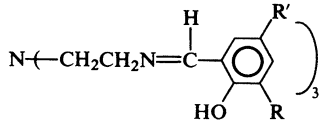

R = H, R′ = H $H_3$Saltren (**I***a*)
R = H, R′ = $NO_2$ $H_3$5-$NO_2$Saltren (**I***b*)
R = H, R′ = Cl $H_3$5-ClSaltren (**I***c*)
R = Cl, R′ = Cl $H_3$3,5-$Cl_2$Saltren (**I***d*)

Earlier work in our laboratory (3) described the synthesis of these trianionic ligands derived from tris(2-aminoethyl)amine(tren) and 3 mol of (substituted) salicylaldehydes and the characterization of M(3,5-$Cl_2$Saltren) (M = Cr, Fe, La), where $H_3$3,5-$Cl_2$Saltren represents tris(3,5-dichlorosalicylidene-2-iminoethyl)amine (**I***d*). The present trivalent metal complexes, prepared according to [1]

[1] $M(NO_3)_3 + H_3X$—Saltren + 3NaOAc → M(X—Saltren) + $3NaNO_3$ + 3HOAc

are expected to have structures represented by the following:

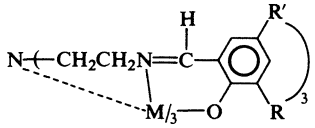

## Experimental

*Chemicals*

Tris(2-aminoethyl)amine was purchased from Ames Laboratories, Inc., salicylaldehyde was a J. T. Baker product, and the substituted salicyladehydes were obtained from the Eastman Kodak Co. The hydrated lanthanide metal nitrates were obtained from Alfa Inorganics Inc. These chemicals and all solvents were used without further purification.

*Physical measurements*

Elemental analyses were performed by Guelph Chemical Laboratories, Inc., Guelph. Infrared spectra were recorded for Nujol mulls between KBr plates (4000–400 $cm^{-1}$ region) and polythene plates (500–100 $cm^{-1}$ region) using Beckman Acculab-6 and Perkin-Elmer 180 spectrophotometers, respectively. A Cary 14 spectrophotometer was used to obtain the electronic spectral data, either as mulls on filter paper or in dimethylsulfoxide using 10 cm cells and ca. $10^{-2}$ *M* solutions. Proton nmr spectra were obtained by Dr. A. Woon-Fat on a Bruker WH-60 FT instrument using dimethylsulfoxide-$d_6$ solutions with TMS as internal standard. Conductivity measurements were made on dimethylsulfoxide solutions with a Beckman Model RC-18A conductance bridge and a cell with platinized electrodes and a cell constant of 0.20.

*Preparation of the complexes*

A solution of the Schiff base ligands (1.0 mmol), hydrated metal nitrate (1.0 mmol), and sodium acetate (1.0 mmol) in absolute ethanol/2,2-dimethoxypropane was stirred and refluxed overnight. The precipitated product was collected by

[1]Permanent address: Department of Chemistry, University of Dacca, Dacca-2, Bangladesh.

0008-4042/82/050667-06$01.00/0

©1982 National Research Council of Canada/Conseil national de recherches du Canada

Can. J. Chem. Downloaded from www.nrcresearchpress.com by 210.87.254.6 on 09/06/12
For personal use only.

TABLE 1. Analytical data for the Schiff base complexes

| Compound[a] | Colour | Calcd. C | Calcd. H | Calcd. N | Found C | Found H | Found N |
|---|---|---|---|---|---|---|---|
| Co(3,5-$Cl_2$Saltren) | Dark green | 45.0 | 2.9 | 7.8 | 44.2 | 3.0 | 7.5 |
| Sc(3,5-$Cl_2$Saltren) | Greenish yellow | 45.9 | 2.9 | 7.9 | 46.0 | 3.0 | 7.9 |
| Y(3,5-$Cl_2$Saltren) | Yellow | 43.2 | 2.8 | 7.5 | 43.6 | 3.0 | 7.7 |
| Pr(3,5-$Cl_2$Saltren) | Greenish yellow | 40.4 | 2.6 | 7.0 | 40.1 | 2.8 | 6.9 |
| Nd(3,5-$Cl_2$Saltren) | Yellow | 40.2 | 2.6 | 6.9 | [b] | [b] | [b] |
| Eu(3,5-$Cl_2$Saltren) | Yellow | 39.8 | 2.6 | 6.9 | 40.1 | 2.4 | 6.9 |
| Gd(3,5-$Cl_2$Saltren)[c] | Yellow | 37.9 | 3.2 | 6.6 | 37.8 | 2.5 | 6.7 |
| Dy(3,5-$Cl_2$Saltren)[d] | Yellow | 36.9 | 3.1 | 6.4 | 36.7 | 2.6 | 6.6 |
| Ho(3,5-$Cl_2$Saltren) | Yellow | 40.2 | 2.8 | 7.0 | 39.5 | 2.5 | 6.9 |
| Yb(3,5-$Cl_2$Saltren) | Yellow | 38.8 | 2.5 | 6.7 | 38.5 | 2.6 | 6.4 |
| La(5-ClSaltren) | Yellow | 46.5 | 3.5 | 8.0 | 46.9 | 3.6 | 8.6 |
| La(5-$NO_2$Saltren)[d] | Yellow | 41.4 | 3.9 | 12.5 | 41.5 | 3.6 | 12.6 |

[a]Ligands are shown in **I***b*, **I***c*, and **I***d*.
[b]Erratic low values obtained, but ir and integrated nmr spectra were satisfactory.
[c]Analyses fit for $2H_2O$.
[d]Analyses fit for $3H_2O$.

filtration, washed with absolute ethanol, then dried over $P_4O_{10}$ for 3 h *in vacuo* at 100°C. The analytical data for the new complexes are given in Table 1. The complexes do not melt, but char at temperatures above 290°C.

## Results and Discussion

A series of lanthanide metal complexes of the potentially heptadentate trianionic Schiff base ligands (**I***d*) has been prepared as an extension of our earlier work (3) on M(3,5-$Cl_2$Saltren) (M = Cr, Fe, La). For comparative purposes, other metal complexes of **I***d*, namely for M = Sc, Y and Co, as well as lanthanum complexes of **I***b* and **I***c* were also synthesized. The instability of ligand **I***a* toward hydrolysis prevented isolation of the analogous lanthanide metal complexes. We had noted earlier that related Schiff base ligands obtained by the condensation of tren with β-diketones are even more susceptible to hydrolysis of the azomethine linkages; however, the *in situ* isolation of lanthanide shift reagents of this type was reported (4) during the present investigation. Other workers have also recently described the preparation and properties of several first-row metal (**III**) complexes of ligands **I***a* and **I***c*; in particular, X-ray analysis has established essentially octahedral [$M(N_3O_3)$] geometries for M(5-ClSaltren) (M = Cr, Mn, and Fe) (5). The present work focuses on the spectroscopic characterization of the lanthanide complexes Ln(3,5-$Cl_2$Saltren) (Ln = La, Pr, Nd, Eu, Gd, Dy, Ho, Yb) with some comparative data being provided for the complexes M(3,5-$Cl_2$Saltren) (M = Cr, Fe, Co, Sc, and Y).

The new complexes have low solubilities in common organic solvents, necessitating the use of dimethylsulfoxide for solution measurements. Such solutions are non-conducting, with molar conductance values of less than 1 mho $cm^2$, confirming the neutral formulation of the complexes. The mass spectrum of La(3,5-$Cl_2$Saltren) showed the parent ion corresponding to the monomer but attempts to obtain the mass spectra of the other lanthanide metal complexes proved unsatisfactory. In spite of the attempts to dehydrate the complexes by using 2,2-dimethoxypropane as a reagent and by drying the products *in vacuo*, the presence of lattice water was indicated in a few cases by elemental analysis (Table 1) and broad infrared bands at ca. 3400 $cm^{-1}$. The existence of lattice water was verified by other workers (5) in the X-ray analyses of M(5-ClSaltren)·$3H_2O$ (Cr, Mn, and Fe).

### *Infrared studies*

The bands near 1600 $cm^{-1}$ associated with the ν(C=N) and ν(C=C) stretching frequencies change in profile in the complexes as compared to those observed for the isolated ligands, with the significant lowering in frequency of the main band also indicating coordination via the azomethine nitrogen atom. The trianionic nature of the ligands in the complexes is shown by the absence of the broad weak hydroxyl bands (3600–2200 $cm^{-1}$) displayed by the free ligands. All of the complexes showed very similar infrared spectra above 500 $cm^{-1}$ and, therefore, far-infrared spectra were recorded (to 100 $cm^{-1}$) in an attempt to assign ν(Ln—O) and ν(Ln—N) vibrational modes. There is a paucity of such assignments in the literature, though it appears that ν(Ln—O) and ν(Ln—N) might be expected in the 500–300 $cm^{-1}$ and 300–200 $cm^{-1}$ regions, respectively (6). Some confirmation of this expectation was obtained by recording the far-infrared spectra of two known lanthanide metal complexes of 8-hydroxyquinoline, whose donor atom environments are similar to those in

Can. J. Chem. Downloaded from www.nrcresearchpress.com by 210.87.254.6 on 09/06/12
For personal use only.

TABLE 2. Far infrared bands for Ln(3,5-$Cl_2$Saltren)[a]

| | |
|---|---|
| La | 420s, 408m, 376s, 336m, 302m, 262s, 202s, 160m |
| Pr | 419s, 406m, 374s, 336m, 307sh, 301m, 260s, 202s, 155bs |
| Nd | 422s, 408m, 376s, 338m, 310sh, 302m, 266m, 204bvs, 170s |
| Eu | 420s, 410s, 377s, 340m, 303m, 270m, 203s, 162s |
| Gd | 423vs, 412s, 380vs, 343s, 306s, 276vs, 204vs, 162vs |
| Dy | 424s, 413m, 381ms, 344m, 316m, 306s, 278s, 205m, 164m |
| Ho | 424s, 410m, 380m, 340m, 315m, 306s, 277s, 200m, 160m |
| Yb | 427vs, 412s, 383vs, 348m, 317sh, 310vs, 284vs, 206vs, 166vs, 152s |
| *Related complexes* | |
| $H_3$3,5-$Cl_2$Saltren | 433bm, 375bs, 295bs, 130vs |
| Cr(3,5-$Cl_2$Saltren) | 476vs, 425m, 366m |
| Fe(3,5-$Cl_2$Saltren) | 470b,sh, 450vs, 415m, 395m, 327b,s, 284m |
| Sc(3,5-$Cl_2$Saltren) | 462sh, 450vs, 440bvs, 413m, 395s, 343m, 327vs, 302s, 260s, 245m, 218s, 205m, 192wm, 134m |
| Y(3,5-$Cl_2$Saltren) | 424s, 412m, 380s, 343m, 306s, 280s, 220s, 167m |
| Hoxin | 460m, 191m |
| Fe(oxin)$_3$[b] | 360(α), 308, 297(β) |
| Al(oxin)$_3$[b] | 466, 455, 444(α); 418, 402(β) |
| Eu(oxin)$_3$ | 484vs, 365bs, 260vm, 195bvs |
| Eu(OPr$^i$)$_3$[c] | 525, 490, 451, 410, 373 |

[a]Bands of medium or stronger intensity only are tabulated.
[b]Values taken from ref. 9.
[c]Values taken from ref. 10(*a*).

our Schiff base ligand of interest. For Nd(oxin)$_3$ and Eu(oxin)$_3$, prepared according to Aly (7), bands near 485 cm$^{-1}$ and 365 cm$^{-1}$ that do not occur in the spectrum of 8-hydroxyquinoline may be assigned to ν(Ln—O). The band near 200 cm$^{-1}$, of greatly increased intensity as compared to the 191 cm$^{-1}$ band in 8-hydroxyquinoline, may more tentatively be assigned to a ν(Ln—N) mode (8). Such assignments are comparable to those made previously for M(oxin)$_3$ (M = Al, Fe, Co) (9). Similarly, comparison of the far-infrared spectra of the Ln(3,5-$Cl_2$Saltren) complexes with the spectra of the uncoordinated ligand and of lighter metal complexes (Table 2, Fig. 1) allows the tentative assignment of ν(Ln—O) and ν(Ln—N) vibrational modes. Several strong metal-sensitive bands in the 300–450 cm$^{-1}$ region are probably associated with ν(Ln—O) since lanthanide metal isopropoxides and β-diketonates also show strong bands in the same range (6, 10). Of the bands at lower frequency, those near 270 cm$^{-1}$ and 200 cm$^{-1}$ appear to be likely candidates for the ν(Ln—N) modes (6). Although the complexes M(3,5-$Cl_2$Saltren) (M = Sc, Cr, Co, Fe) are undoubtedly six-coordinate (5), the apparent decrease in frequency of the far-infrared bands associated with ν(Ln—O) and ν(Ln—N) nevertheless does not allow a choice in assigning either six- or seven-coordination to these new lanthanide complexes. A comparison of ν(M—O) and ν(M—N) modes between the lighter elements and the lanthanide elements is invalidated by the great difference in covalency expected in the metal complexes.

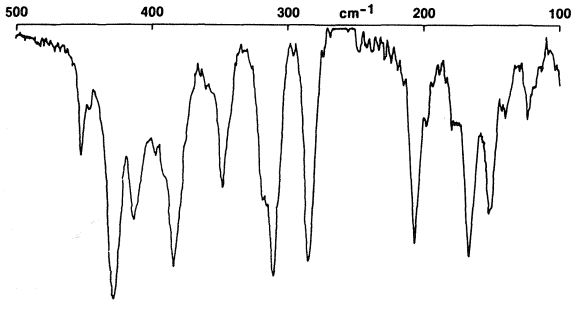


FIG. 1. Far-infrared spectrum of Yb(3,5-$Cl_2$Saltren).

*Electronic transitions*

An intense intraligand transition occurs for all of the M(3,5-$Cl_2$Saltren) complexes at ca. 26 000 cm$^{-1}$, with the slight metal dependence signifying the charge-transfer origin of the band. Solid-state spectra show a prominent shoulder centered near 23 000 cm$^{-1}$ which obscures observations of either *d–d* or *f–f* transitions in this region. Strong bands observed near 18 000 cm$^{-1}$ for the iron(III) complexes of ligands **I** are probably also of charge-transfer (phenol → iron(III)) type (11), but the weaker shoulder near 18 000 cm$^{-1}$ for the chromium(III) complexes of **I** may be the expected (11) $\nu_1$ transition for octahedral chromium(III) complexes since no shoulder to the 26 000 cm$^{-1}$ band is found for the Sc(3,5-$Cl_2$Saltren) and La(3,5-$Cl_2$Saltren) complexes. Similarly, the weak band at 16 400 cm$^{-1}$ observed in the solid state spectrum of Co(3,5-$Cl_2$Saltren) may be attributed to the octahedral transition expected (5, 11) in this region, since X-ray analysis has confirmed this geometry for

Can. J. Chem. Downloaded from www.nrcresearchpress.com by 210.87.254.6 on 09/06/12
For personal use only.

TABLE 3. Hypersensitive transitions for Ln(3,5-$Cl_2$Saltren)

| Ln | Ground term | Excited term | $Ln_{aq}$ | Observed[a] |
|---|---|---|---|---|
| Pr | $^3H_4$ | $^3P_2$, $^3P_1 + {}^1I_6$<br>$^3P_0$, $^1D_2$ | 17 300–<br>23 200[b] | 19 900<br>20 200<br>20 500 |
| Nd | $^4I_{9/2}$ | $^2P_{1/2}$<br>$^4G_{5/2,7/2}$ | 23 400<br>17 500<br>17 460 | [c] |
| Eu | $^7F_{0,1,2}$ | $^5D_{0,1,2}$ | 16 920<br>21 500 | None[d] |
| Gd | $^8S_{7/2}$ | $^6PIDG$ | [e] | (35 700)[e]<br>(40 000)[e] |
| Dy | $^6H_{15/2}$ | $^6F_{11/2}$ | 7 700 | 7 750 |
| Ho | $^5I_8$ | $^5G_6$, $^3G_6$ | 22 100<br>27 700 | 21 750 |
| Yb | $^2F_{7/2}$ | $^2F_{5/2}$ | 10 300 | 10 280<br>10 580 |

[a]All complexes have a ligand band at ca. 26 000 $cm^{-1}$ in DMSO, and additionally a shoulder in the 22 700–25 600 $cm^{-1}$ region in the solid state.
[b]Four peaks are observed in this region.
[c]Several peaks are observed, see Fig. 2. The pattern of peaks is distinctly different from those observed for either $Nd(NO_3)_3 \cdot 5H_2O$ or $Nd_2O_3$.
[d]Bands observed by fluorescence spectroscopy, see text.
[e]Assignments are tentative, broad multiplets in ultraviolet region expected.

M(5-ClSaltren)$\cdot 3H_2O$ (M = Cr, Mn, Fe) (5). The absence of a shoulder to the intense 26 000 $cm^{-1}$ ($\varepsilon \approx 2 \times 10^3$ $mol^{-1}$ L $cm^{-1}$) band for dimethylsulfoxide solutions of the Ln(3,5-Saltren) complexes doubtless implies an increase in coordination number upon dissolution, since the complexes are also insoluble in other common organic solvents.

Changes in the intensity and fine structure of certain "hypersensitive" absorption bands in the absorption spectra of trivalent lanthanide complexes have been related to changes in the symmetry of the ligand field around the lanthanide ions (12). Accordingly, the occurrence of such *f–f* transitions was observed in the solid state for the Ln(3,5-$Cl_2$Saltren) complexes to allow a comparison with those bands reported for the aqueous $Ln^{3+}$ ions (Table 3). A qualitative indication of significant covalency in the ligand-to-metal bonds, as compared to the aquo ions, is given by calculations of the nephelauxetic parameter β for the complexes. For example, the red shift of 350 $cm^{-1}$ for the Ho(3,5-$Cl_2$Saltren) complex represents a nephelauxetic effect of 0.98. More quantitative information on the degree of covalency and site symmetry in the complexes via a comparison of oscillator strengths of these hypersensitive bands is precluded by the low solubility of the complexes, even in dimethylsulfoxide.

The coordination number of neodymium has been related to the shape and intensity of the hypersensitive transition, $^4I_{9/2} \rightarrow {}^4G_{5/2}$, $^2G_{7/2}$, which occurs near 17 000 $cm^{-1}$ (12, 13). Thus, $Nd(NO_3)_3 \cdot 5H_2O$, known to be 10-coordinate (14), shows a single solid state visible band at 17 400 $cm^{-1}$. A prominent shoulder at 17 500 $cm^{-1}$ to the more intense 17 300 $cm^{-1}$ band is observed in the visible spectrum of Nd(oxin)$_3$. An assignment of either 6- or 7-coordination is possible for this 8-hydroxyquinoline complex by comparison with the spectral profiles of tri-β-diketonate complexes (and their adducts) studied by Karraker (13). Because of the similarity in donor atom environment between ligands **I** and 8-hydroxyquinoline, the spectrum of Nd(3,5-$Cl_2$Saltren) was expected to be similar. Although the shoulders on the high energy side of the hypersensitive transition centered at 17 000 $cm^{-1}$ (see Fig. 2) signify a low coordination number, the more extensive splitting indicates a lower symmetry site for the $Nd^{3+}$ ion. Whether or not this low symmetry environment results only from the (expected) trigonal field imposed by a pseudooctahedral environment or from the additional asymmetry due to coordination by the apical nitrogen atom cannot be ascertained from the visible spectra. An X-ray analysis of a Ln(3,5-$Cl_2$Saltren) complex has been initiated in order to answer the question of apical nitrogen coordination. The observance of less extensive splitting of the $^4I_{9/2} \rightarrow {}^4G_{5/2}$, $^2G_{7/2}$ transition for Nd(3,5-ClSaltren) in dimethylsulfoxide solution is compatible with an increase in coordination number. It is

Can. J. Chem. Downloaded from www.nrcresearchpress.com by 210.87.254.6 on 09/06/12
For personal use only.

Can. J. Chem. Downloaded from www.nrcresearchpress.com by 210.87.254.6 on 09/06/12
For personal use only.

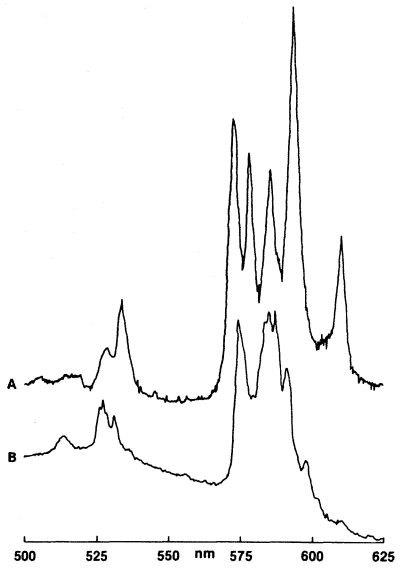


FIG. 2. Visible absorption spectrum of Nd(3,5-$Cl_2$Saltren): *A*, solid state; *B*, dimethylsulfoxide solution.

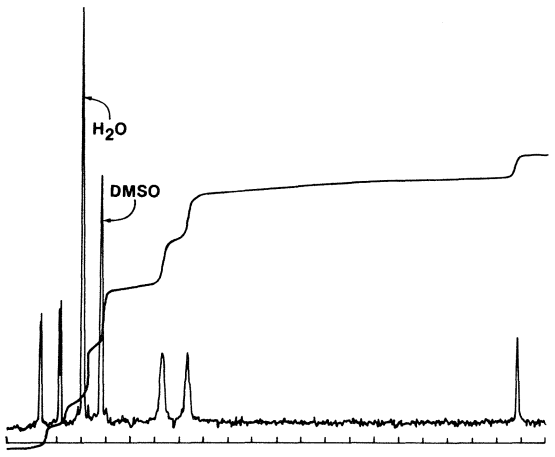


FIG. 3. Proton nmr spectrum of Eu(3,5-$Cl_2$Saltren) in dimethylsulfoxide-$d_6$ solution.

worth noting that an asymmetric tetramethylurea complex of neodymium, $Nd(tmu)_5(F_3CSO_3)_3$, also presumably either 6- or 7-coordinate, shows similar splitting of this hypersensitive band (15).

Hypersensitive transitions in europium complexes are often observed by fluorescence spectroscopy, with information on the local symmetry of the $Eu^{3+}$ ion coming from the number of $^5D_0 \rightarrow {}^7F_J$ transitions. For example, the single $^5D_0 \rightarrow {}^7F_1$ transition observed at 17 000 $cm^{-1}$ is compatible with other evidence for octahedral coordination in $Eu(tmu)_6(CF_3SO_3)_3$ (15). A lower symmetry site for the europium ion in Eu(3,5-$Cl_2$Saltren) is implied by the presence of several peaks in the 16 000–17 800 $cm^{-1}$ region. These peaks are superimposed upon a broad fluorescence band centred at 20 000 $cm^{-1}$ which is also observed for the other Ln(3,5-$Cl_2$Saltren) complexes. Consideration of the possible allowed components for the $^5D_J \rightarrow {}^7F_J$ transitions in the feasible crystal field symmetries (16) does not allow an unambiguous assignment of the coordination number in Eu(3,5-$Cl_2$Saltren).

TABLE 4. $^1$H nmr spectra for (3,5-$Cl_2$Saltren)

| | Assignments, δppm[a,b] | | | |
|---|---|---|---|---|
| Ln | N—$CH_2$ | —$CH_2$N= | Ar—H | N=C—H |
| H | 2.92 | 3.70 | (7.00– 7.60) | 8.40 |
| La | 2.95 | 3.68 | (7.30– 7.60) | 8.03 |
| Pr | 1.51 | −10.32 | 9.33 13.40 | 25.90 |
| Nd | 4.54 | −1.11 | 9.01 10.43 | 24.84 |
| Eu | −0.21 | −1.40 | 4.44 5.30 | −16.85 |

[a]Satisfactory integration obtained for all spectra.
[b]Peaks due to undeuterated dimethylsulfoxide occur at 2.52 for the free ligand and in the range 2.52–2.59 for the lanthanide complexes.

### $^1$*H nmr studies*

Proton nuclear magnetic resonance spectra were recorded for the Ln(3,5-$Cl_2$Saltren) complexes in order to characterize the ligating ability of the ligand. As indicated for the diamagnetic lanthanum complex in Table 4, coordination of the azomethine nitrogen atom results in an upfield shift of the azomethine proton, with the magnitude of the shift being comparable to a solvent shift (3). For the paramagnetic praseodymium, neodymium, and europium compounds, well-resolved spectra are observed (Table 4, Fig. 3) which exhibit large pseudocontact shifts (17). As expected from the distance–shift relationship, the azomethine proton undergoes the greatest shift, with a shielding difference of about 42 ppm between the signals for the europium (upfield) and the two other lanthanide complexes (downfield). The well-resolved resonance peaks due to the ethylene and aromatic protons ($^4J$ = 2.9 Hz for the Eu case) indicate a rigid chelated structure with potential, after modification to improve solubility and eliminate proton peaks, for applications as lanthanide shift reagents. Investigations are underway with suitably modified analogous ligands.

### Acknowledgments

This work was funded by the Natural Sciences and Engineering Research Council of Canada via an operating grant to E.C.A. and a CIDA Research Associateship to A.M.

1. (*a*) C. MEALLI and E. C. LINGAFELTER. Chem. Commun. 885 (1970); (*b*) M. G. B. DREW. Coord. Chem. Rev. **24**, 179 (1977); (*c*) M. G. B. DREW. Prog. Inorg. Chem. **23**, 65 (1977).
2. (*a*) S. AFSHAR and J. I. BULLOCK. Inorg. Chim. Acta, **38**, 145 (1980); (*b*) R. C. MEHROTRA, P. N. KAPOOR, and J. M. BATWARA. Coord. Chem. Rev. **31**, 67 (1980).
3. A. MALEK, G. C. DEY, A. NASREEN, T. A. CHOWDHURY, and E. C. ALYEA. Synth. React. Inorg. Met-Org. Chem. **9**, 145 (1979).
4. K. C. BROOKS and R. E. SIEVERS. Second Chemical Congress of the North American Continent, Las Vegas, Nevada, Aug. 24–29, 1980. Inorg. Abstr. 235.
5. (*a*) D. F. COOK, D. CUMMINS, and E. D. MCKENZIE. J. Chem. Soc. Dalton, 1369 (1976); (*b*) N. W. ALCOCK, D. F. COOK, E. D. MCKENZIE, and J. M. WORTHINGTON. Inorg. Chim. Acta, **38**, 107 (1980).
6. (*a*) Vibrational spectra of transition-element compounds. *In* Specialist Periodical Reports. Spectroscopic properties of inorganic and organometallic compounds. Vols. 6–12; (*b*) E. BARANIAK, R. ST. L. BRUCE, H. C. FREEMAN, N. J. HAIR, and J. JAMES. Inorg. Chem. **15**, 2226 (1976); (*c*) N. N. SPECA, N. M. KARAYANNIS, and L. L. PYTLEWSKI. Inorg. Chim. Acta, **6**, 639 (1972).
7. H. F. ALY, F. M. ABDEL KERIM, and A. T. KANDIL. J. Inorg. Nucl. Chem. **33**, 4340 (1971).
8. J. R. FERRARO, L. J. BASILE, and D. L. KOVACIC. Inorg. Chem. **5**, 391 (1966).
9. R. LARSSON and O. ESKILSSON. Acta Chem. Scand. **22**, 1067 (1968).
10. (*a*) L. M. BROWN and K. S. MAZDIYASNI. Inorg. Chem. **9**, 2783 (1970); (*b*) R. C. MATHUR, S. S. L. SURANA, and S. P. TANDON. Z. Naturforsch. **30**b, 207 (1975).
11. A. B. P. LEVER. Inorganic electronic spectroscopy. Elsevier, London. 1968.
12. K. B. YATSIMIRSKII and N. K. DAVIDENKO. Coord. Chem. Rev. **27**, 223 (1979).
13. D. G. KARRAKER. Inorg. Chem. **6**, 1863 (1967).
14. I. M. RUMANOVA, G. F. VOLODINA, and N. V. BELOV. Crystallography (Soviet Phys.), **9**, 545 (1965).
15. G. VICENTINI and L. B. ZINNER. J. Inorg. Nucl. Chem. **42**, 1510 (1980).
16. S. P. SINHA and E. BUTTER. Mol. Phys. **16**, 285 (1969).
17. B. C. MAYO. Chem. Soc. Rev. **1**, 49 (1972–73).

Can. J. Chem. Downloaded from www.nrcresearchpress.com by 210.87.254.6 on 09/06/12
For personal use only.

Can. J. Chem. Downloaded from www.nrcresearchpress.com by 210.87.254.5 on 09/06/12
For personal use only.



# Electrophilic cyclization of polyene allylsilanes. Synthesis of albicanyl acetate

ROSEMARY J. ARMSTRONG, FRANCIS L. HARRIS,[1] AND LARRY WEILER[2]

*Department of Chemistry, University of British Columbia, Vancouver, B.C., Canada V6T 1Y6*

Received December 28, 1981

ROSEMARY J. ARMSTRONG, FRANCIS L. HARRIS, and LARRY WEILER. Can. J. Chem. **60**, 673 (1982).

The allylsilanes **5** (*a*, R = 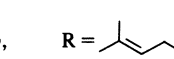 ; *b*, R = 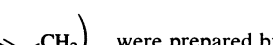 ) were prepared by a nickel(II) catalyzed coupling of trimethylsilylmethylmagnesium chloride with the enol phosphate of the corresponding β-keto esters. Stannic chloride and mercuric trifluoroacetate effected a cyclization of **5**. The product from **5***b* was converted into the marine natural product, albicanyl acetate (**1**).

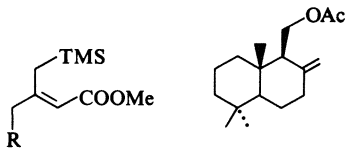


**5** **1**

ROSEMARY J. ARMSTRONG, FRANCIS L. HARRIS et LARRY WEILER. Can. J. Chem. **60**, 673 (1982).

On a préparé les allylsilanes **5** (*a*, R = 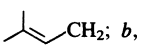 ; *b*, R = 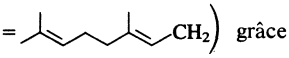 ) grâce à un couplage, catalysé par le nickel(II), du chlorure de triméthylsilylméthylmagnesium avec le phosphate de l'énol des β-cétoesters correspondants. Le chlorure stannique et le trifluoroacétate mercurique ont un effet sur la cyclisation du composé **5**. On a transformé le produit obtenu à partir du composé **5***b* en acétate d'albicanyle (**1**), un produit naturel marin.

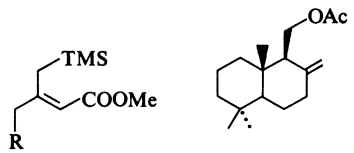


**5** **1**

[Traduit par le journal]

Recent studies on the synthesis of allylic silanes and their cyclization (1) prompt us to report our results on the synthesis of carboxylated allylsilanes and their cyclization which has led to a synthesis of the marine sesquiterpene, albicanyl acetate (**1**) (2). In 1975, Fleming and co-workers found that the allylsilane **2** cyclized cleanly to the exocyclic product **3** (eq. [1]) (3). We were intrigued about the possibility of extending this concept to the cyclization of polyolefinic esters and acids.

[1] 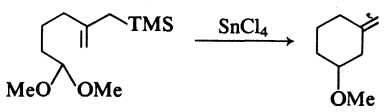


**2** **3**

The esters **5***a* and **5***b* were synthesized from methyl acetoacetate as shown in eq. [2]. The β-keto esters **4** (4) were prepared by the alkylation of the dianion of methyl acetoacetate (5) with γ,γ-dimethylallyl bromide and geranyl bromide respec-

[2] 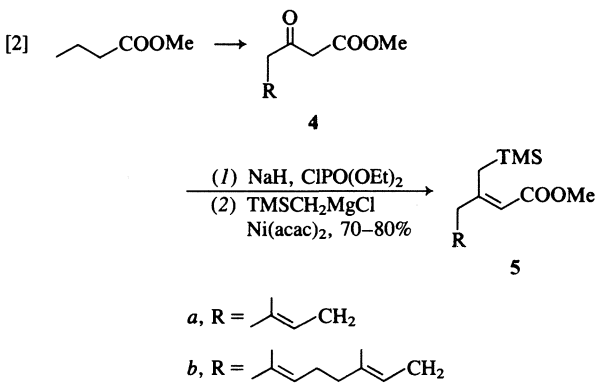


[1]Permanent address: Department of Chemistry, California State University, Northridge, CA 91330, U.S.A.

[2]Author to whom correspondence may be addressed.

0008-4042/82/050673-03$01.00/0

©1982 National Research Council of Canada/Conseil national de recherches du Canada

Can. J. Chem. Downloaded from www.nrcresearchpress.com by 210.87.254.5 on 09/06/12
For personal use only.

tively. Compounds **4***a* and **4***b* were converted into the *Z*-enol phosphates (6) in 95–100% yield. The enol phosphates were reacted with trimethylsilylmethylmagnesium chloride and nickel(II) bisacetylacetonate catalyst[3] (7) to give mainly the *Z*-allylsilanes **5** in 70–80% yield. The stereoselectivity was estimated from the $^1$H nmr of **5***a* (*E*/*Z* = 1:20) and **5***b* (*E*/*Z* < 1:20). In addition we have prepared the *E*-enol phosphate from β-keto ester **4***b*[4] and coupled it with trimethylsilylmethylmagnesium chloride using $Ni(acac)_2$ catalyst to give **5***b* in 76% yield (*E*/*Z* = 7:3). The stereospecificity in this coupling is very different from that recently reported by Casey *et al.* for β-halo enoate esters (8).

We have studied a variety of electrophilic cyclizations of **5** and at this time note the results with Lewis acids and mercuric trifluoroacetate. Treatment of a $CH_2Cl_2$ solution of ester **5***a* with stannic chloride at 0°C gave the exocyclic alkene **6** (E = H) in ca. 90% yield. A gc analysis of the crude reaction product showed that ratio of exocyclic to endocyclic product was 7:1. Prolonged exposure of the reaction mixture to stannic chloride lead to isomerization of **6** (E = H) to the endocyclic β,γ-unsaturated compound. The ester **5***a* gave the organomercury product **6** (E = HgCl) in 84% yield on cyclization with mercury trifluoroacetate in nitromethane followed by an aqueous brine workup (9).

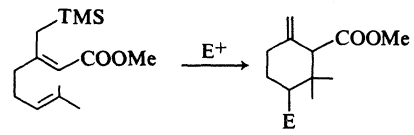


**5***a* **6**, E = H or HgCl

Cyclization of **5***b* (>95% *Z*) in $CH_2Cl_2$ with stannic chloride at −56°C gave the 9β- and 9α-isomers **7** (E = H) in almost quantitative yield. The ratio of 9β-**7**/9α-**7** as determined by gc was 4:1. The structure of the major isomer was determined by reduction ($LiAlH_4$), chromatographic purification (10), and acetylation ($Ac_2O$, py, DMAP) to give (±)-albicanyl acetate (**1**) in 70% yield. The synthetic albicanyl acetate was identical to a natural sample (2) in spectral and chromatographic comparisons. The mercuric trifluoroacetate cyclization (9) of **5***b* gave a mixture of 9β- and 9α-**7** (E = HgCl) and monocyclic product **8**. The mixture could be purified by flash chromatography (10) to give 55–65% of the bicyclic products **7** (E = HgCl) and ca. 10% of **8**. The bicyclic products were analyzed by reduction ($LiAlH_4$) and acetylation ($Ac_2O$, py, DMAP) to give a mixture of (±)-albicanyl acetate (**1**) and its C-9 epimer **9** in a yield of 65–70% (**1**/**9** = 73:27).

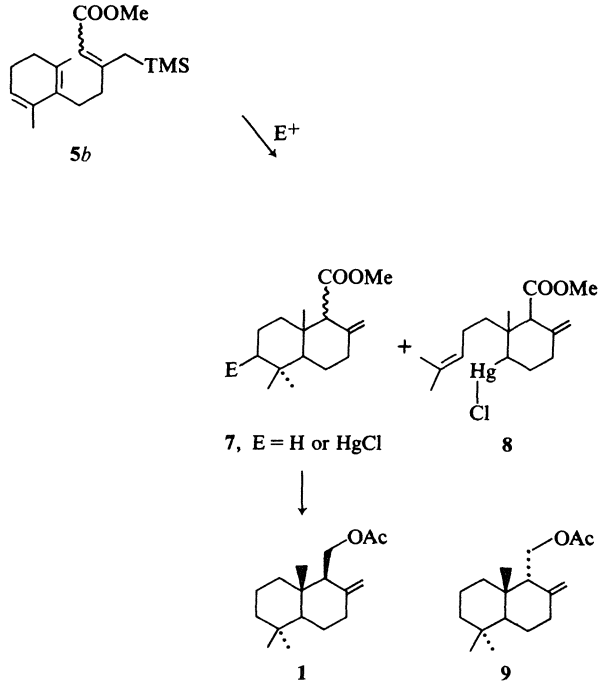


**5***b* **7**, E = H or HgCl **8** **1** **9**

The mixture of **5***b* containing mainly the 2*E* isomer (*E*/*Z* = 7:3) was cyclized with mercuric trifluoroacetate, reduced, and acetylated as above in 85% overall yield. A vpc analysis of the acetates showed that the ratio of **1**/**9** was 18:82. Thus the $Hg^{2+}$ cyclization of the 2*E* and 2*Z* isomers of **5***b* is stereospecific and it would appear that the 9β-ester partially isomerizes to the 9α-ester under the cyclizing conditions or in the hydride reduction.

In summary the allylsilane activates conjugated esters in polyene cyclizations and they can be used to selectively produce exocyclic alkenes in electrophilic cyclizations initiated by protons or mercuric trifluoroacetate.[5]

[3]The coupling of β-phosphoryloxy alkenoate esters with Grignard reagents can be effected with Cu(I) or Ni(II) catalysts (J. P. Barnier, F. L. Harris, and L. Weiler, unpublished results). This extends the utility of our earlier reported alkene synthesis (ref. 6).

[4]The *E*-enol phosphates of β-keto esters can be prepared from the corresponding β-keto esters using triethylamine or 4-dimethylaminopyridine as base and a small amount of HMPA in the solvent system (F. W. Sum, Ph.D. Thesis, University of British Columbia, Vancouver, B.C., 1979 and W. McKay, F. W. Sum, and L. Weiler, unpublished results).

[5]All new compounds were characterized by ir, nmr, mass spectroscopy, and high resolution mass measurement or elemental analysis.

**Acknowledgements**

We are grateful to the Natural Sciences and Engineering Research Council of Canada for financial support, to Professor R. J. Andersen and J. Hellou for spectra and samples of albicanyl acetate, and to Professor E. J. Corey for details on their mercuric trifluoroacetate cyclization (ref. 9). One of us (R.J.A.) is grateful to the Canadian Commonwealth Scholarship and Fellowship Plan for the award of a graduate scholarship.

1. (*a*) T. K. Sarkar and N. H. Andersen. Tetrahedron Lett. 3513 (1978); (*b*) L. R. Hughes, R. Schmid, and W. S. Johnson. Bioorganic Chem. **8**, 513 (1979); (*c*) I. Fleming and A. Pearce. J. Chem. Soc. Perkin Trans. I, 251 (1981).
2. (*a*) J. Hellou. M. Sc. Thesis, University of British Columbia, Vancouver, B.C., 1980; (*b*) J. Hellou, J. E. Thompson, and R. J. Andersen. Tetrahedron. In press.
3. I. Fleming, A. Pearce, and R. L. Snowden. J. Chem. Soc. Chem. Commun. 182 (1976).
4. F. W. Sum and L. Weiler. Tetrahedron, **37**, Supplement 1, 303 (1981).
5. S. N. Huckin and L. Weiler. J. Am. Chem. Soc. **96**, 1082 (1974).
6. F. W. Sum and L. Weiler. Can. J. Chem. **57**, 1431 (1979).
7. T. Hayashi, Y. Katsuro, and M. Kumada. Tetrahedron Lett. **21**, 3915 (1980).
8. C. P. Casey, C. R. Jones, and H. Tukada. J. Org. Chem. **46**, 2089 (1981).
9. (*a*) E. J. Corey, M. A. Tius, and J. Das. J. Am. Chem. Soc. **102**, 1742 (1980); (*b*) J. Am. Chem. Soc. **102**, 7612 (1980).
10. W. C. Still, M. Kahn, and A. Mitra. J. Org. Chem. **43**, 2923 (1978).

# Total synthesis of racemic 2-desoxystemodinone and stemodinol; the identity of natural "stemodinol" with stemarin

Ronald B. Kelly, Mary Lou Harley, and Sandra J. Alward

*Department of Chemistry, University of New Brunswick, P.O. Box 5050, Saint John, N.B., Canada E2L 4L5*

AND

Percy S. Manchand

*Chemical Research Department, Hoffmann-La Roche Inc., Nutley, NJ 07110, U.S.A.*

Received December 11, 1981

Ronald B. Kelly, Mary Lou Harley, Sandra J. Alward, and Percy S. Manchand. Can. J. Chem. **60**, 675 (1982).

Total syntheses of the naturally occurring diterpenoid 2-desoxystemodinone (**3**) and the diterpenoid structure **2** ("stemodinol") are described. The synthetic diterpenoid **2** was not identical to an authentic sample of "stemodinol". The authentic sample was found to be stemarin to which structure **2** had been erroneously assigned in the literature. It would appear that the diterpenoid represented by **2** has not been isolated from natural sources.

---

Ronald B. Kelly, Mary Lou Harley, Sandra J. Alward et Percy S. Manchand. Can. J. Chem. **60**, 675 (1982).

On décrit la synthèse totale du diterpènoïde naturel désoxy-2 stémodinone (**3**) et celle du diterpènoïde ayant la structure **2** ("stémodinol"). Le diterpène synthétique **2** ne correspond pas tout à fait à un échantillon authentique du "stémodinol". On a trouvé que l'échantillon authentique est de la stémarine à laquelle on a attribué par erreur la structure **2** dans la littérature. Il semble donc que le diterpène représenté par la structure **2** n'est pas d'origine naturelle.

[Traduit par le journal]

Recently we described (1) a total synthesis of the structurally unique diterpenoid stemarin (**1**) (2). This synthesis featured photoaddition of allene to an α,β-unsaturated ketone and two subsequent skeletal rearrangements. At the same time (1) we anticipated the completion of syntheses of stemodinol (**2**) (3) and related terpenoids (3, 4) and alphidicolin (5) by a similar strategy.[1] We now wish to describe syntheses of (±)-stemodinol (**2**) and the related diterpenoid (±)-2-desoxystemodinone (**3**) (2) as anticipated.

[1]For syntheses of aphidicolin and the stemodane diterpenoids by entirely different approaches see refs. 6 and 7 respectively.

0008-4042/82/050675-03$01.00/0

©1982 National Research Council of Canada/Conseil national de recherches du Canada

Can. J. Chem. Downloaded from www.nrcresearchpress.com by 210.87.254.5 on 09/06/12
For personal use only.

**Acknowledgements**

We are grateful to the Natural Sciences and Engineering Research Council of Canada for financial support, to Professor R. J. Andersen and J. Hellou for spectra and samples of albicanyl acetate, and to Professor E. J. Corey for details on their mercuric trifluoroacetate cyclization (ref. 9). One of us (R.J.A.) is grateful to the Canadian Commonwealth Scholarship and Fellowship Plan for the award of a graduate scholarship.

1. (*a*) T. K. Sarkar and N. H. Andersen. Tetrahedron Lett. 3513 (1978); (*b*) L. R. Hughes, R. Schmid, and W. S. Johnson. Bioorganic Chem. **8**, 513 (1979); (*c*) I. Fleming and A. Pearce. J. Chem. Soc. Perkin Trans. I, 251 (1981).
2. (*a*) J. Hellou. M. Sc. Thesis, University of British Columbia, Vancouver, B.C., 1980; (*b*) J. Hellou, J. E. Thompson, and R. J. Andersen. Tetrahedron. In press.
3. I. Fleming, A. Pearce, and R. L. Snowden. J. Chem. Soc. Chem. Commun. 182 (1976).
4. F. W. Sum and L. Weiler. Tetrahedron, **37**, Supplement 1, 303 (1981).
5. S. N. Huckin and L. Weiler. J. Am. Chem. Soc. **96**, 1082 (1974).
6. F. W. Sum and L. Weiler. Can. J. Chem. **57**, 1431 (1979).
7. T. Hayashi, Y. Katsuro, and M. Kumada. Tetrahedron Lett. **21**, 3915 (1980).
8. C. P. Casey, C. R. Jones, and H. Tukada. J. Org. Chem. **46**, 2089 (1981).
9. (*a*) E. J. Corey, M. A. Tius, and J. Das. J. Am. Chem. Soc. **102**, 1742 (1980); (*b*) J. Am. Chem. Soc. **102**, 7612 (1980).
10. W. C. Still, M. Kahn, and A. Mitra. J. Org. Chem. **43**, 2923 (1978).

# Total synthesis of racemic 2-desoxystemodinone and stemodinol; the identity of natural "stemodinol" with stemarin

Ronald B. Kelly, Mary Lou Harley, and Sandra J. Alward

*Department of Chemistry, University of New Brunswick, P.O. Box 5050, Saint John, N.B., Canada E2L 4L5*

AND

Percy S. Manchand

*Chemical Research Department, Hoffmann-La Roche Inc., Nutley, NJ 07110, U.S.A.*

Received December 11, 1981

Ronald B. Kelly, Mary Lou Harley, Sandra J. Alward, and Percy S. Manchand. Can. J. Chem. **60**, 675 (1982).

Total syntheses of the naturally occurring diterpenoid 2-desoxystemodinone (**3**) and the diterpenoid structure **2** ("stemodinol") are described. The synthetic diterpenoid **2** was not identical to an authentic sample of "stemodinol". The authentic sample was found to be stemarin to which structure **2** had been erroneously assigned in the literature. It would appear that the diterpenoid represented by **2** has not been isolated from natural sources.

---

Ronald B. Kelly, Mary Lou Harley, Sandra J. Alward et Percy S. Manchand. Can. J. Chem. **60**, 675 (1982).

On décrit la synthèse totale du diterpènoïde naturel désoxy-2 stémodinone (**3**) et celle du diterpènoïde ayant la structure **2** ("stémodinol"). Le diterpène synthétique **2** ne correspond pas tout à fait à un échantillon authentique du "stémodinol". On a trouvé que l'échantillon authentique est de la stémarine à laquelle on a attribué par erreur la structure **2** dans la littérature. Il semble donc que le diterpène représenté par la structure **2** n'est pas d'origine naturelle.

[Traduit par le journal]

Recently we described (1) a total synthesis of the structurally unique diterpenoid stemarin (**1**) (2). This synthesis featured photoaddition of allene to an α,β-unsaturated ketone and two subsequent skeletal rearrangements. At the same time (1) we anticipated the completion of syntheses of stemodinol (**2**) (3) and related terpenoids (3, 4) and alphidicolin (5) by a similar strategy.[1] We now wish to describe syntheses of (±)-stemodinol (**2**) and the related diterpenoid (±)-2-desoxystemodinone (**3**) (2) as anticipated.

[1]For syntheses of aphidicolin and the stemodane diterpenoids by entirely different approaches see refs. 6 and 7 respectively.

0008-4042/82/050675-03$01.00/0

©1982 National Research Council of Canada/Conseil national de recherches du Canada

Can. J. Chem. Downloaded from www.nrcresearchpress.com by 210.87.254.105 on 09/06/12
For personal use only.

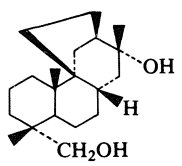

1

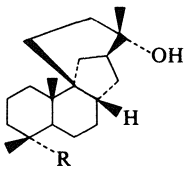

2 R = $CH_2OH$
3 R = $CH_3$
12 R = $CH_2OTs$

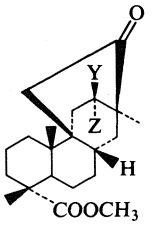

4 Y = H, Z = OH
5 Y = OH, Z = H

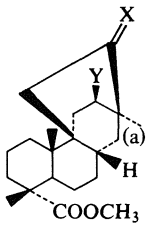

6 X = $S(CH_2)S$, Y = OH
7 X = H, H, Y = OH
8 X = H, H, Y = OTs

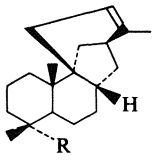

9 R = $COOCH_3$
10 R = $CH_2OH$

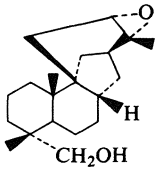

11

During our synthesis of stemarin (**1**) (1) we encountered a pair of epimeric keto alcohols, **4** and **5**. The former was chosen for conversion into stemarin on the basis of stereochemical considerations and it was predicted (1), on the same basis, that **5** could readily be converted into stemodinol (**2**). The validity of this prediction has now been demonstrated by the successful conversion of **5** into **2** and **3** as described in the sequel.[2]

The keto alcohol **5** (mp 191°C; spectral properties similar to **4** (1)) was converted, quantitatively, into the thioketal **6** (mp 177–178°C; nmr δ: 3.17 (m, 4H, ethylene of ketal)) which, on treatment with Raney nickel, afforded (97%) the alcohol **7** (mp 130°C; ir: 3500 (OH) and 1705 (ester) $cm^{-1}$; nmr δ: 3.56 (m, 1H, H—C—OH)). The latter was converted into the gummy tosylate **8** (nmr δ: aromatic protons 7.20–7.85) in which the tosylate group was *anti* and periplanar to the bond (a), the required stereoalignment for the desired rearrangement (*vide infra*).

When **8** was heated at 60°C in DMSO in the presence of methyl sulfinyl carbanion (8), it was transformed, by migration of bond (a) and elimination of hydrogen, into the olefin **9** (oil; ir (film): 1730 (ester) and 1650 (olefin) $cm^{-1}$; nmr δ: 1.55 (d, $J$ = 2 Hz, 3H, vinylic methyl and 4.94 (m, H, vinylic proton)), which was reduced quantitatively with $LiAlH_4$ to the olefinic alcohol **10** (oil; ir (film): 3350 (OH) and 1625 (olefin) $cm^{-1}$; nmr δ: 3.07 and 3.38 (doublets, $J$ = 11 Hz, 1H each, $CH_2$—OH)).

Epoxidation of **10** with *m*-chlorobenzoic acid gave the oily epoxide **11** (68%; nmr δ: 1.27 (s, 3H, methyl attached to oxirane ring)). The oxirane ring was assigned the α-configuration on the basis of conversion of **11** into 2-desoxystemodinone (**3**) (2) (*vide infra*). Finally, reduction of **11** with $LiAlH_4$ afforded the racemic diterpenoid **2** (mp 160°C; ir: 3510 and 3350 (OH) $cm^{-1}$; nmr δ: 0.82, 1.00 and 1.11 (singlets, 3H each, tertiary methyls), 3.07 and 3.37 (doublets, $J$ = 11Hz, 1H each, $CH_2$—OH)).

The synthetic diterpenoid (**2**) was clearly *not identical* with a sample of "stemodinol" from natural sources. Eventually, by comparison with authentic stemarin (**1**), it was discovered that the sample of naturally occurrring stemodinol (3) which we received was in fact stemarin (**1**).[3] To the best of our knowledge the diterpenoid having structure **2** ("stemodinol") has not been isolated from natural sources.

We were now faced with the necessity of demonstrating the validity of structure **2** for our synthetic diterpenoid, a task which was complicated by our inability to produce crystals of **2** or its derivatives suitable for X-ray crystallographic analysis. Eventually this task was accomplished in the following manner. The tosylate **12** of **2** was reduced with $LiAlH_4$ and the product (**3**) was shown to be identical (ir, nmr, ms, and silica gel tlc) with an authentic sample of the naturally occurring 2-desoxystemodinone (2), the structure of which has been unequivocally shown to be **3**.[4] The assignment of the $CH_2OH$ group in **2** to the α-orientation follows from the fact that **2** and stemarin have been synthesized from common intermediates (1). Thus, the conversion of **2** to **3** proves that structure **2** is correct for our synthetic diterpenoid and constitutes a total synthesis of 2-desoxystemodinone (**3**).

**Acknowledgments**

We thank the Natural Sciences and Engineering

[2]Throughout, the ir spectra (in Nujol unless specified) and the nmr spectra (in $CDCl_3$) are entirely consistent with assigned structures. Satisfactory elemental analyses were obtained for all crystalline compounds and correct molecular ions were found in the mass spectra of the remaining compounds.

[3]Professor C. D. Hufford, University of Mississippi, University, Mississippi, concurs with the results of our comparison.

[4]Details to be published elsewhere.

Can. J. Chem. Downloaded from www.nrcresearchpress.com by 210.87.254.105 on 09/06/12
For personal use only.

Research Council of Canada for a grant awarded to R.B.K. and for a Postgraduate Scholarship awarded to M.L.H.

1. R. B. KELLY, M. L. HARLEY, and S. J. ALWARD. Can. J. Chem. **58**, 755 (1980).
2. P. S. MANCHAND and J. F. BLOUNT. J. Chem. Soc. Chem. Commun. 894 (1975).
3. C. D. HUFFORD, R. O. GUERRERO, and N. J. DOORENBOS. J. Pharm. Sci. **65**, 778 (1976).
4. P. S. MANCHAND, J. D. WHITE, H. WRIGHT, and J. CLARDY. J. Am. Chem. Soc. **95**, 2705 (1973).
5. K. M. BRUNDRET, W. DALZIEL, B. HESP, J. A. J. JARVIS, and S. NEIDLE. J. Chem. Soc. Chem. Commun. 1027 (1972).
6. (*a*) B. M. TROST, Y. NISHIMURA, K. YAMAMOTO, and S. S. MCELVAIN. J. Am. Chem. Soc. **101**, 1328 (1979); (*b*) J. E. MCMURRY, A. ANDRUS, G. M. KSANDER, J. H. MUSSER, and M. A. JOHNSON. J. Am. Chem. Soc. **101**, 1330 (1979); (*c*) E. J. COREY, M. A. TIUS, and J. DAS. J. Am. Chem. Soc. **102**, 1742 (1980); (*d*) R. E. IRELAND, J. D. GODFREY, and S. THAISRIVONGS. J. Am. Chem. Soc. **103**, 2446 (1981).
7. (*a*) E. J. COREY, M. A. TIUS, and J. DAS. J. Am. Chem. Soc. **102**, 7612 (1980); (*b*) E. E. VAN TAMELEN, J. G. CARLSON, R. K. RUSSEL, and S. R. ZAWACKY. J. Am. Chem. Soc. **103**, 4615 (1981).
8. E. J. COREY and M. CHAYKOVSKY. J. Am. Soc. **87**, 1345 (1965).

Can. J. Chem. Downloaded from www.nrcresearchpress.com by 210.87.254.105 on 09/06/12
For personal use only.

# The microwave spectrum, harmonic force field, structure, and dipole moment of propiolyl chloride[1]

R. WELLINGTON DAVIS[2] AND M. C. L. GERRY

*Department of Chemistry, The University of British Columbia, 2036 Main Mall, Vancouver, B.C., Canada V6T 1Y6*

Received October 1, 1981

R. WELLINGTON DAVIS and M. C. L. GERRY. Can. J. Chem. **60**, 679 (1982).

The microwave spectra of four isotopic species of propiolyl chloride, HCCCOCl, have been measured for their ground and $v_9 = 1$ excited vibrational states. Values for the rotational constants, quartic centrifugal distortion constants, chlorine nuclear quadrupole coupling constants, and the molecular dipole moment have been obtained. The centrifugal distortion constants have been combined with vibrational wavenumbers from the literature to calculate an approximate harmonic force field. Effective and ground state average structures of the most abundant isotopic species, $H^{12}C^{12}C^{12}C^{16}O^{35}Cl$, are presented.

R. WELLINGTON DAVIS et M. C. L. GERRY. Can. J. Chem. **60**, 679 (1982).

On a mesuré les spectres micro ondes de quatre espèces isotopiques de chlorure de propiolyle, HCC≡COCl, dans les états vibrationnels fondamental et excité, $v_9 = 1$. On a obtenu les valeurs suivantes: les constantes de rotation, les constantes de distorsion centrifuge quartique, les constantes de couplage quadrupolaire nucléaire du chlore et le moment dipolaire moléculaire. On a combiné les constantes de distorsion centrifuge aux nombres d'ondes vibrationnelles, obtenues dans la littérature, afin de calculer un champ de force hamonique approximatif. On présente la structure moyenne réelle à celle à l'état fondamental de l'espèce isotopique la plus abondante: $H^{12}C^{12}C^{12}C^{16}O^{35}Cl$.

[Traduit par le journal]

## Introduction

The acid halide derivatives of simple carboxylic acids have been extensively studied using microwave spectroscopy. The molecules include the acid fluorides and acid chlorides of formic acid (1, 2), acetic acid (3, 4), cyclopropanecarboxylic acid (5, 6), and propionic acid (7, 8). A logical and interesting extension is to the corresponding derivatives of propiolic (propynoic) acid, one of the simplest planar carboxylic acids. These molecules are of especial interest as the parent propiolic acid has a very large acid dissociation constant (9, 10) compared to those of aliphatic, olefinic, or aromatic carboxylic acids. At 20°C, for example, the acid dissociation constants of the three-carbon propionic and propiolic acids are $1.35 \times 10^{-5}$ and $1.36 \times 10^{-2}$ respectively. This difference has been attributed to the strong electron-withdrawing properties of the ethynyl group (11) relative to those of other hydrocarbon substituents. As well, the propiolyl halides are the simplest acid halides in which the carbonyl bond is conjugate to a carbon–carbon triple bond. Therefore it would not be surprising if the —COX groups in the propiolyl halides had somewhat different structures from those found for other acid halides.

This paper deals with the microwave spectrum and structure of one such derivative: propiolyl chloride. Several recent reports have dealt with its synthesis and with other spectroscopic investigations. Augdahl *et al.* (12) prepared propiolyl chloride from the parent acid by halogenation with 1,1-dichlorodimethyl ether, recorded the infrared and Raman spectra and assigned all vibrational fundamentals. Balfour, Grieg, and Visaisouk described a synthesis from propiolic acid and phosphorus pentachloride (13). Subsequently Balfour *et al.* analysed the vibrational spectrum of propiolyl chloride-*d* (14) and observed the near ultraviolet spectra of the normal and deuterated species (15). Two rather incomplete normal coordinate analyses have been made for propiolyl chloride. In the first study the mean amplitudes of vibration were reported without details of the corresponding force field (16). A second analysis gave values for the force constants but unfortunately did not use non-redundant symmetry coordinates (17). Finally, a preliminary account of the microwave spectrum has been published (18).

The rotational spectra of a few molecules structurally similar to propiolyl chloride have been investigated. These have included the spectra of propiolic acid (19, 20) and propiolyl fluoride (21), both of which were shown to be planar. The corresponding aldehyde, propynal, was first studied by Howe and Goldstein (22) who assigned a few low $J$ lines of the normal isotopic species and measured the dipole moment. A complete structure for propynal was later determined by Costain and

[1]Work supported by the Natural Sciences and Engineering Research Council of Canada.

[2]Present address: Department of Chemistry, Memorial University of Newfoundland, St. John's, Nfld., Canada A1B 3X7.

0008-4042/82/060679-11$01.00/0

©1982 National Research Council of Canada/Conseil national de recherches du Canada

Can. J. Chem. Downloaded from www.nrcresearchpress.com by 210.87.254.6 on 09/06/12
For personal use only.

Can. J. Chem. Downloaded from www.nrcresearchpress.com by 210.87.254.6 on 09/06/12
For personal use only.

Morton (23). Their microwave results showed that the carbon chain in propynal has a bend of approximately 1.5°. This result has since been confirmed by a combination of the microwave results with electron diffraction data (24). The deviation from linearity, if any, of the carbon chains of other propiolyl-type molecules is an interesting problem which has not previously received attention.

In the present study of propiolyl chloride four isotopic species have been investigated. Their spectra have been analysed to yield values for the rotational constants, quartic centrifugal distortion constants, and nuclear quadrupole coupling constants. The molecular dipole moment has also been obtained. Using an assumed structure for the ethynyl group the remaining structural parameters have been calculated from the ground state effective moments of inertia. Further, the centrifugal distortion constants have been combined with existing vibrational data to determine an approximate force field. Again, having assumed a structure for the ethynyl group, the average rotational constants have been used to calculate the average structure in the ground vibrational state.

## Experimental methods

The samples of normal propiolyl chloride and propiolyl chloride-*d* were both kindly supplied by Dr. W. J. Balfour. They had been prepared by the reaction of propiolic acid and $PCl_5$ (13). Since propiolyl chloride readily decomposes at room temperature the samples were stored at liquid nitrogen temperature; for manipulations on a vacuum line the storage vessel was held at dry ice temperature.

Transitions were measured in the frequency regions 12.5–18 and 26.5–40 GHz, using a 100 kHz Stark modulated spectrometer with a 10 ft X-band cell. All measurements were made with the Stark cell wrapped in dry ice, with sample pressures of 0.3–3.0 Pa. Under these conditions the sample was quite stable in the cell. Although the infrared and Raman spectra of these samples showed the presence of an $OPCl_3$ impurity (14), this molecule was too involatile in these conditions to be detected in the microwave spectrum.

## Observed spectra and assignments

The spectrum of propiolyl chloride is very rich, and has both *a*- and *b*-type transitions with roughly equal intensities. The transitions show chlorine quadrupole hyperfine structure. The initial assignments were of the $J = 6 \leftarrow 5$ and $7 \leftarrow 6$ *a*-type R branches, which gave preliminary rotational constants. From these constants more accurate predictions were made, and the bootstrap procedure described previously was then used to assign an increasing number of transitions (21). Spectra were assigned for the ground vibrational states of both normal and deuterated isotopic species containing $^{35}Cl$ and $^{37}Cl$. In addition, for all species except $DCCCO^{37}Cl$, transitions were assigned for an excited vibrational state. From relative intensities of the ground and excited state transitions the vibration was deduced to be at $150 \pm 50$ cm$^{-1}$, in good agreement with the measured frequency of the $\nu_9$ fundamental at 157 cm$^{-1}$ (12). In all cases the frequency fit was the chief criterion for the assignments, confirmed by the hyperfine structure.

The entire measured spectra were analysed, first for the nuclear quadrupole coupling constants, and then for the rotational and centrifugal distortion constants, using the methods described in the following section. Some representative observed transitions, along with their assignments and the splittings calculated using the derived quadrupole coupling constants, are given in Table 1. Table 2 contains the frequencies of all the observed rotational transitions with nuclear quadrupole hyperfine structure removed, along with their centrifugal distortion contributions.

## Analysis of the spectra

*1. Nuclear quadrupole coupling*

The chlorine nuclear quadrupole coupling could be accounted for using first-order theory (25). A least-squares fit was made of the observed splittings to the coupling constants $\chi_{aa}$ and $\chi_{bb} - \chi_{cc}$. The results are in Table 3, where account is taken of the fact that

$$\chi_{aa} + \chi_{bb} + \chi_{cc} = 0.$$

*2. Rotational and centrifugal distortion constants*

After the hyperfine structure had been subtracted from each rotational transition using the coupling constants of Table 3, the resulting unsplit line frequencies were then used to calculate the rotational constants and quartic centrifugal distortion constants. The *A* reduction of Watson's Hamiltonian in the $I^r$ representation (26) equation [1] below, was used; no sextic constants were required to fit the data.

$$[1]\quad \mathcal{H} = A\hat{J}_a^2 + B\hat{J}_b^2 + C\hat{J}_c^2 - \Delta_J\hat{J}^4 - \Delta_{JK}\hat{J}^2\hat{J}_a^2 - \Delta_K\hat{J}_a^4 - 2\delta_J\hat{J}^2(\hat{J}_b^2 - \hat{J}_c^2) - \delta_K\{\hat{J}_a^2(\hat{J}_b^2 - \hat{J}_c^2) + (\hat{J}_b^2 - \hat{J}_c^2)\hat{J}_a^2\}$$

Here $A$, $B$, $C$ are rotational constants; $\Delta_J$, $\Delta_{JK}$, $\Delta_K$, $\delta_J$, $\delta_K$ are quartic centrifugal distortion constants; $\hat{J}_a, \hat{J}_b, \hat{J}_c$ are components of the total angular momentum $\hat{J}$. For most species studied the data were used to obtain values for the rotational constants and all the quartic centrifugal distortion constants. For the $HCCCO^{37}Cl$ and $DCCCO^{35}Cl$ excited states, however, there were insufficient data available to perform centrifugal distortion analyses. In these latter two cases the distortion on

Can. J. Chem. Downloaded from www.nrcresearchpress.com by 210.87.254.6 on 09/06/12
For personal use only.

each line was assumed to be the same as that calculated for the corresponding ground state transition, and was subtracted from the measured frequencies; the resulting frequencies were fit to the three rotational constants. The rotational and centrifugal distortion constants so determined are given in Table 4.

*3. Dipole moment*

Because both *a*- and *b*-type transitions were observed the components $\mu_a$ and $\mu_b$ are non-zero. Since the molecule is planar (see later), $\mu_c$ is zero. The values of $\mu_a$ and $\mu_b$, and hence the total dipole moment $\mu$, were determined using the Stark effects of the $M = 0$ component of the $3_{03} \leftarrow 2_{02}$ transition and the $M = 5$ and 6 components of the $6_{24} \leftarrow 6_{15}$ transition. In all three cases the Stark effects were second order, and were measured in the high field limit (with the Stark energies much bigger than the quadrupole energies). The spacing of the Stark electrode in the cell was measured using the $1 \leftarrow 0$ transition of OCS and Muenter's value of its dipole moment (27). Linear plots were obtained for the frequency shifts vs. the square of the electric field; their slopes are in Table 5. Also in Table 5 are the derived values of $\mu_a$, $\mu_b$, and $\mu$, along with estimated outside uncertainty limits. The most probable direction of $\mu$, on electronegativity grounds, is in Fig. 1.

*4. The harmonic force field and structure*

*(a) The effective structure*

The ground state principal moments of inertia and inertial defects of the four isotopic species of propiolyl chloride studied are given in Table 6. The ground state inertial defects are small positive numbers which show only small isotopic variations and therefore confirm that the molecule has a planar structure.

The limited isotopic data obtained for propiolyl chloride precluded the calculation of a full substitution structure. Therefore, in an initial structural refinement, a crude ground state effective geometry was calculated. Values for five bond lengths and four angles are required to define the structure of propiolyl chloride; the four angles can be chosen as ∠(H—C≡C), ∠(C≡C—C), ∠(C—C=O), and ∠(C—C—Cl). As no deviation from linearity has been found for an ethynyl group it is reasonable to assume that ∠(H—C≡C) = 180°; this reduces the number of structural parameters to be determined to eight. Table 6 contains values for twelve ground state principal moments of inertia. Because the molecule is planar, however, only eight of these (two for each isotope) are independent. Therefore further assumptions are required to derive a meaningful structure. Since the C—H and C≡C distances have been found to be nearly identical in a wide range of acetylenic molecules (23, 28–39) values of 1.057 ± 0.002 Å and 1.206 ± 0.003 Å were initially assumed for these bond lengths; only for fluoroacetylene (29) do the C—H and C≡C distances lie outside these ranges.

TABLE 1. Representative transitions (MHz) of $HCCCO^{35}Cl$ used in the nuclear quadrupole coupling analyses

| $F'^a$ | $F^a$ | Observed frequency | Observed splitting | Calculated splitting |
|---|---|---|---|---|
| $5_{33}-4_{32}$ | | | | |
| 5.5 | 4.5 | 27061.58 | −1.39 | −1.39 |
| 4.5 | 3.5 | 27062.35 | −0.62 | −0.62 |
| 6.5 | 5.5 | 27063.75 | 0.78 | 0.79 |
| 3.5 | 4.5 | 27064.55 | 1.58 | 1.56 |
| $8_{17}-8_{08}$ | | | | |
| 6.5 | 6.5 | 29539.16 | −2.78 | −2.76 |
| 9.5 | 9.5 | 29540.01 | −1.93 | −1.94 |
| 7.5 | 7.5 | 29543.79 | 1.85 | 1.84 |
| 8.5 | 8.5 | 29544.62 | 2.68 | 2.67 |
| $8_{36}-8_{27}$ | | | | |
| 6.5 | 6.5 | 28811.38 | −1.72 | −1.72 |
| 9.5 | 9.5 | 28811.90 | −1.20 | −1.20 |
| 7.5 | 7.5 | 28814.24 | 1.14 | 1.14 |
| 8.5 | 8.5 | 28814.76 | 1.66 | 1.66 |
| $10_{19}-10_{1,10}$ | | | | |
| 8.5 | 8.5 | 39196.00 | −2.13 | −2.13 |
| 11.5 | 11.5 | 39196.51 | −1.62 | −1.60 |
| 9.5 | 9.5 | 39199.70 | 1.57 | 1.55 |
| 10.5 | 10.5 | 39200.22 | 2.09 | 2.08 |

[a]Here $F$ and $F'$ are the labels for the initial and final states respectively.

Using the assumed ethynyl group geometry a series of effective structures was calculated for propiolyl chloride. The choice of "best" structure is subjective, however, because different results were obtained when either the *A* and *B* or, alternatively, the *B* and *C* rotational constants were used in the fit. Therefore the effective structure, given in the first column of Table 7, should be regarded with detachment; it was obtained using the ground state *A* and *B* rotational constants and assuming further that ∠(C≡C—C) = 180° and *r*(C—C) = 1.435 Å. When only the geometry of the ethynyl group was constrained somewhat different results were obtained. For example, by fitting the *A* and *B* rotational constants *r*(C—C), *r* (C=O), and *r*(C—Cl) distances of 1.430 Å, 1.200 Å, and 1.764 Å resulted; the corresponding values derived from a fit to the *B* and *C* rotational constants were 1.450 Å, 1.188 Å, and 1.760 Å. Further calculations showed that, with the present data set, the *r*(C—C) and *r*(C=O) distances are highly correlated; isotopic substitution of the carbonyl group would probably alleviate this difficulty. In both of these latter refinements very similar values were obtained for

TABLE 2. Observed rotational transitions (MHz) of propiolyl chloride

| Transition | Observed[a] frequency | Distortion correction | Deviation | Transition | Observed[a] frequency | Distortion correction | Deviation |
|---|---|---|---|---|---|---|---|
| | | | *HCCCO$^{35}$Cl (ground vibrational state)* | | | | |
| $3_{0,3}-2_{0,2}$ | 15422.13 | −0.08 | −0.00 | $9_{2,8}-9_{1,9}$ | 35659.32 | −2.68 | 0.00 |
| $5_{1,4}-4_{1,3}$ | 28253.37 | −0.63 | −0.05 | $9_{3,7}-9_{2,8}$ | 31534.94 | −2.77 | −0.02 |
| $5_{3,3}-4_{3,2}$ | 27062.95 | −0.24 | 0.04 | $9_{3,6}-9_{2,7}$ | 17688.25 | −1.30 | 0.04 |
| $6_{1,6}-5_{1,5}$ | 28261.22 | −0.28 | −0.04 | $10_{1,9}-10_{1,10}$ | 39198.13 | −4.41 | 0.01 |
| $6_{1,5}-5_{1,4}$ | 33278.70 | −0.91 | 0.02 | $10_{2,8}-10_{1,9}$ | 29159.19 | −7.33 | 0.01 |
| $6_{2,5}-5_{2,4}$ | 31341.46 | −0.58 | −0.02 | $11_{2,9}-11_{1,10}$ | 34607.49 | −9.36 | −0.00 |
| $6_{2,4}-5_{2,3}$ | 34666.16 | −1.33 | −0.07 | $11_{4,8}-11_{3,9}$ | 36028.24 | −4.17 | 0.01 |
| $6_{3,4}-5_{3,3}$ | 32497.22 | −0.62 | −0.02 | $11_{5,6}-11_{4,7}$ | 35100.25 | 1.50 | 0.00 |
| $6_{3,3}-5_{3,2}$ | 33252.92 | −0.90 | −0.03 | $12_{4,8}-11_{5,7}$ | 34666.84 | −14.20 | 0.01 |
| $6_{1,6}-5_{0,5}$ | 29075.06 | −0.12 | 0.01 | $12_{3,9}-12_{2,10}$ | 27689.11 | −12.11 | 0.05 |
| $7_{1,6}-6_{1,5}$ | 37944.99 | −1.14 | 0.04 | $13_{5,8}-13_{4,9}$ | 30293.78 | 6.19 | 0.01 |
| $7_{2,6}-6_{2,5}$ | 36214.00 | −0.89 | 0.01 | $14_{3,11}-14_{3,12}$ | 38123.23 | −23.72 | −0.03 |
| $7_{3,5}-6_{3,4}$ | 37873.60 | −1.14 | −0.02 | $14_{3,11}-14_{2,12}$ | 38913.77 | −21.48 | 0.01 |
| $7_{3,4}-7_{2,5}$ | 17312.08 | 0.20 | 0.04 | $14_{5,9}-14_{4,10}$ | 28405.37 | 5.62 | 0.02 |
| $7_{4,3}-7_{3,4}$ | 29105.35 | −1.34 | 0.02 | $15_{4,11}-15_{3,12}$ | 31099.80 | −22.69 | 0.01 |
| $8_{0,8}-7_{0,7}$ | 37251.45 | −0.56 | 0.03 | $15_{5,10}-15_{4,11}$ | 27570.16 | 1.46 | 0.01 |
| $8_{1,8}-7_{1,7}$ | 37140.16 | −0.59 | −0.06 | $15_{6,9}-14_{7,8}$ | 27673.54 | −9.29 | 0.05 |
| $8_{1,8}-7_{0,7}$ | 37355.33 | −0.47 | 0.04 | $16_{4,12}-16_{3,13}$ | 36529.52 | −32.50 | 0.03 |
| $8_{1,7}-7_{2,6}$ | 38796.04 | −2.33 | 0.04 | $16_{5,11}-16_{4,12}$ | 28174.53 | −6.97 | −0.01 |
| $8_{2,6}-7_{3,5}$ | 31381.27 | −4.12 | 0.01 | $17_{5,12}-17_{4,13}$ | 30418.62 | −19.81 | −0.01 |
| $8_{1,7}-8_{0,8}$ | 29541.94 | −2.90 | −0.02 | $17_{6,11}-17_{5,12}$ | 34636.11 | 15.24 | −0.00 |
| $8_{3,6}-8_{2,7}$ | 28813.10 | −1.85 | −0.04 | $18_{5,13}-18_{4,14}$ | 34294.39 | −36.16 | −0.02 |
| $8_{3,5}-8_{2,6}$ | 16954.97 | −0.11 | 0.02 | $18_{6,12}-18_{5,13}$ | 32962.61 | 9.42 | −0.02 |
| $8_{4,5}-8_{3,6}$ | 32032.24 | −2.16 | −0.04 | $18_{7,11}-17_{8,10}$ | 36321.78 | −21.78 | −0.03 |
| $8_{4,4}-8_{3,5}$ | 27423.15 | −0.12 | 0.04 | $20_{6,14}-20_{5,15}$ | 34165.71 | −24.00 | 0.00 |
| | | | *HCCCO$^{35}$Cl ($v_9$ = 1 excited vibrational state)* | | | | |
| $6_{1,5}-5_{1,4}$ | 33332.71 | −0.83 | 0.03 | $11_{4,8}-11_{3,9}$ | 36094.39 | −4.11 | 0.00 |
| $6_{2,4}-5_{2,3}$ | 34753.68 | −1.25 | −0.03 | $13_{5,8}-13_{4,9}$ | 30126.37 | 6.05 | −0.01 |
| $6_{3,3}-5_{3,2}$ | 33337.35 | −0.81 | 0.02 | $15_{5,10}-15_{4,11}$ | 27527.17 | 0.96 | 0.00 |
| $7_{2,6}-6_{2,5}$ | 36267.03 | −0.77 | −0.03 | $16_{5,11}-16_{4,12}$ | 28243.55 | −7.64 | −0.04 |
| $7_{3,4}-7_{2,5}$ | 17265.02 | 0.17 | 0.00 | $17_{5,12}-17_{4,13}$ | 30619.49 | −20.53 | 0.03 |
| $8_{0,8}-7_{0,7}$ | 37279.27 | −0.52 | −0.00 | $17_{6,11}-17_{5,12}$ | 34426.43 | 14.64 | −0.00 |
| $8_{1,8}-7_{1,7}$ | 37170.36 | −0.55 | −0.04 | $18_{6,12}-18_{5,13}$ | 32842.36 | 8.39 | 0.02 |
| $8_{1,8}-7_{0,7}$ | 37380.14 | −0.43 | 0.05 | $19_{6,13}-19_{5,14}$ | 32717.54 | −5.06 | 0.00 |
| $8_{3,5}-8_{2,6}$ | 16939.57 | −0.15 | 0.01 | $20_{6,14}-20_{5,15}$ | 34340.11 | −25.68 | −0.01 |
| | | | *HCCCO$^{37}$Cl (ground vibrational state)* | | | | |
| $5_{1,4}-4_{1,3}$ | 27716.53 | −0.62 | −0.03 | $8_{1,8}-7_{1,7}$ | 36485.07 | −0.61 | −0.02 |
| $6_{0,6}-5_{0,5}$ | 28149.22 | −0.28 | 0.05 | $8_{4,5}-8_{3,6}$ | 31797.02 | −2.04 | 0.01 |
| $6_{1,6}-5_{1,5}$ | 27757.83 | −0.29 | −0.02 | $8_{4,4}-8_{3,5}$ | 27430.51 | −0.05 | −0.07 |
| $6_{1,5}-5_{1,4}$ | 32666.33 | −0.91 | −0.01 | $8_{0,8}-7_{1,7}$ | 36374.41 | −0.71 | −0.06 |
| $6_{2,5}-5_{2,4}$ | 30755.84 | −0.56 | 0.04 | $8_{1,8}-7_{0,7}$ | 36711.66 | −0.47 | −0.01 |
| $6_{2,4}-5_{2,3}$ | 33963.76 | −1.30 | −0.01 | $8_{1,7}-7_{2,6}$ | 37959.35 | −2.40 | −0.04 |
| $6_{3,4}-5_{3,3}$ | 31863.00 | −0.56 | 0.09 | $9_{1,8}-9_{0,9}$ | 33757.47 | −3.53 | −0.03 |
| $6_{1,6}-5_{0,5}$ | 28596.52 | −0.11 | 0.02 | $9_{2,8}-9_{1,9}$ | 35015.11 | −2.51 | −0.03 |
| $7_{0,7}-6_{0,6}$ | 32361.13 | −0.40 | 0.04 | $9_{3,7}-9_{2,8}$ | 31055.48 | −2.53 | −0.00 |
| $7_{1,7}-6_{1,6}$ | 32140.30 | −0.43 | −0.03 | $11_{2,9}-11_{1,10}$ | 33741.53 | −9.24 | −0.03 |
| $7_{1,6}-6_{1,5}$ | 37270.77 | −1.14 | 0.04 | $12_{4,8}-11_{5,7}$ | 33076.32 | −14.04 | 0.03 |
| $7_{2,6}-6_{2,5}$ | 35546.13 | −0.87 | 0.02 | $13_{3,10}-13_{2,11}$ | 32125.13 | −16.72 | 0.02 |
| $7_{3,4}-6_{3,3}$ | 38558.10 | −1.75 | 0.08 | $15_{4,11}-15_{3,12}$ | 30143.61 | −21.48 | 0.02 |
| $7_{0,7}-6_{1,6}$ | 31913.76 | −0.56 | 0.01 | $16_{4,12}-16_{3,13}$ | 35329.74 | −31.54 | 0.02 |
| $7_{1,6}-6_{2,5}$ | 31928.92 | −1.96 | −0.02 | $17_{5,12}-17_{4,13}$ | 29721.53 | −17.05 | −0.04 |
| $7_{3,4}-7_{2,5}$ | 17281.11 | 0.31 | 0.04 | $18_{5,13}-18_{4,14}$ | 33242.33 | −33.35 | −0.03 |
| $7_{4,4}-7_{3,5}$ | 31376.17 | −2.27 | 0.00 | $18_{6,12}-18_{5,13}$ | 33008.99 | 12.98 | 0.00 |
| $7_{4,3}-7_{3,4}$ | 29048.37 | −1.34 | 0.11 | $19_{6,13}-19_{5,14}$ | 32450.44 | 1.04 | 0.02 |
| $8_{0,8}-7_{0,7}$ | 36600.92 | −0.57 | −0.13 | $20_{6,14}-20_{5,15}$ | 33520.17 | −18.48 | 0.00 |
| | | | *HCCCO$^{37}$Cl ($v_9$ = 1 excited vibrational state)* | | | | |
| $7_{1,7}-6_{1,6}$ | 32168.07 | −0.42 | −0.05 | $8_{1,8}-7_{1,7}$ | 36514.92 | −0.62 | 0.02 |
| $7_{0,7}-6_{0,6}$ | 32385.71 | −0.44 | 0.04 | $8_{0,8}-7_{1,7}$ | 36407.26 | −0.72 | 0.03 |
| $8_{0,8}-7_{0,7}$ | 36628.65 | −0.57 | −0.04 | | | | |

Can. J. Chem. Downloaded from www.nrcresearchpress.com by 210.87.254.6 on 09/06/12
For personal use only.

TABLE 2. (*Concluded*)

| Transition | Observed[a] frequency | Distortion correction | Deviation | Transition | Observed[a] frequency | Distortion correction | Deviation |
|---|---|---|---|---|---|---|---|
| | | | *DCCCO$^{35}$Cl (ground vibrational state)* | | | | |
| $6_{0,6}-5_{0,5}$ | 27220.32 | −0.29 | 0.01 | $8_{1,8}-7_{0,7}$ | 35525.23 | −0.51 | 0.01 |
| $6_{1,5}-5_{1,4}$ | 31431.45 | −0.87 | −0.04 | $9_{0,9}-8_{0,8}$ | 39489.08 | −0.85 | −0.09 |
| $6_{2,5}-5_{2,4}$ | 29565.57 | −0.57 | −0.03 | $9_{2,7}-8_{3,6}$ | 35045.08 | −5.15 | 0.05 |
| $6_{2,4}-5_{2,3}$ | 32426.90 | −1.20 | −0.09 | $9_{3,7}-9_{2,8}$ | 30367.90 | −2.62 | 0.01 |
| $7_{0,7}-6_{0,6}$ | 31286.97 | −0.42 | 0.02 | $9_{5,4}-9_{4,5}$ | 39408.38 | −4.19 | 0.01 |
| $7_{1,7}-6_{1,6}$ | 31028.19 | −0.45 | 0.02 | $12_{2,10}-12_{1,11}$ | 36649.99 | −10.56 | −0.01 |
| $7_{1,6}-6_{1,5}$ | 35957.32 | −1.15 | 0.04 | $15_{5,10}-15_{4,11}$ | 28519.27 | 4.02 | 0.00 |
| $7_{2,6}-6_{2,5}$ | 34205.01 | −0.88 | 0.03 | $16_{4,12}-16_{4,13}$ | 32007.70 | −25.29 | −0.02 |
| $7_{3,4}-6_{3,3}$ | 36737.71 | −1.63 | 0.06 | $16_{5,11}-16_{4,12}$ | 27899.78 | −0.72 | 0.01 |
| $7_{1,7}-6_{0,6}$ | 31578.78 | −0.30 | 0.02 | $17_{5,12}-17_{4,13}$ | 28608.40 | −9.35 | 0.01 |
| $7_{2,6}-7_{1,7}$ | 26517.39 | −1.20 | −0.00 | $17_{6,11}-17_{5,12}$ | 37485.52 | 13.51 | −0.01 |
| $7_{3,4}-7_{2,5}$ | 17897.98 | 0.03 | 0.04 | $18_{5,13}-18_{4,14}$ | 30801.18 | −21.96 | −0.02 |
| $7_{0,7}-6_{1,6}$ | 30736.36 | −0.57 | 0.01 | $18_{6,12}-18_{5,13}$ | 35031.99 | 13.26 | −0.00 |
| $8_{0,8}-7_{0,7}$ | 35376.25 | −0.61 | 0.02 | $19_{5,14}-19_{4,15}$ | 34464.80 | −37.75 | 0.00 |
| $8_{1,8}-7_{1,7}$ | 35233.36 | −0.64 | −0.05 | $19_{6,13}-19_{5,14}$ | 33415.47 | 7.53 | −0.01 |
| $8_{0,8}-7_{1,7}$ | 35084.42 | −0.74 | 0.01 | $20_{6,14}-20_{5,15}$ | 33059.76 | −4.69 | 0.02 |
| | | | *DCCCO$^{35}$Cl ($v_9$ = 1 excited vibrational state)* | | | | |
| $6_{0,6}-5_{0,5}$ | 27242.71 | −0.29 | 0.06 | $7_{3,4}-6_{3,3}$ | 36841.02 | −1.63 | 0.05 |
| $6_{2,5}-5_{2,4}$ | 29616.06 | −0.57 | −0.01 | $8_{0,8}-7_{0,7}$ | 35404.30 | −0.61 | −0.01 |
| $6_{3,4}-5_{3,3}$ | 30589.93 | −0.63 | −0.10 | $8_{1,8}-7_{1,7}$ | 35264.57 | −0.64 | −0.03 |
| $7_{0,7}-6_{0,6}$ | 31311.83 | −0.43 | 0.02 | $8_{1,8}-7_{0,7}$ | 35548.60 | −0.51 | −0.01 |
| $7_{2,6}-6_{2,5}$ | 34258.96 | −0.88 | 0.03 | | | | |
| | | | *DCCCO$^{37}$Cl (ground vibrational state)* | | | | |
| $6_{0,6}-5_{0,5}$ | 26753.09 | −0.22 | 0.06 | $9_{1,9}-8_{1,8}$ | 38729.39 | −0.65 | −0.03 |
| $6_{1,5}-5_{1,4}$ | 30861.99 | −0.79 | −0.01 | $9_{0,9}-8_{1,8}$ | 38651.73 | −0.73 | 0.02 |
| $6_{2,5}-5_{2,4}$ | 29026.61 | −0.46 | −0.02 | $10_{3,8}-10_{2,9}$ | 32634.75 | −3.47 | −0.04 |
| $6_{2,4}-5_{2,3}$ | 31796.35 | −1.08 | 0.00 | $12_{2,10}-12_{1,11}$ | 35816.05 | −10.38 | −0.02 |
| $6_{3,3}-5_{3,2}$ | 30477.66 | −0.65 | −0.06 | $14_{3,11}-14_{2,12}$ | 33761.33 | −18.81 | 0.06 |
| $7_{0,7}-6_{0,6}$ | 30749.08 | −0.31 | 0.00 | $14_{5,9}-14_{4,10}$ | 30153.18 | 6.19 | 0.05 |
| $7_{1,7}-6_{1,6}$ | 30486.19 | −0.34 | 0.03 | $15_{4,11}-15_{3,12}$ | 27043.66 | −15.00 | 0.01 |
| $7_{2,6}-6_{2,5}$ | 33587.34 | −0.72 | 0.02 | $15_{5,10}-15_{4,11}$ | 28446.86 | 5.31 | 0.01 |
| $7_{3,5}-6_{3,4}$ | 34930.36 | −0.89 | −0.02 | $17_{5,12}-17_{4,13}$ | 28191.16 | −7.20 | −0.03 |
| $7_{3,4}-6_{3,3}$ | 36013.11 | −1.38 | 0.05 | $17_{6,11}-17_{5,12}$ | 37565.51 | 14.86 | −0.06 |
| $8_{0,8}-7_{0,7}$ | 34766.45 | −0.44 | 0.06 | $18_{5,13}-18_{5,14}$ | 30130.00 | −19.56 | −0.01 |
| $8_{1,8}-7_{1,7}$ | 34619.95 | −0.48 | −0.04 | $18_{6,12}-18_{5,13}$ | 35074.66 | 15.54 | 0.00 |
| $8_{1,8}-7_{0,7}$ | 34921.53 | −0.33 | −0.10 | $19_{6,13}-19_{5,14}$ | 33328.16 | 10.79 | 0.07 |
| $8_{3,5}-8_{2,6}$ | 17089.68 | 0.05 | 0.01 | $20_{5,15}-20_{4,16}$ | 38179.02 | −52.89 | −0.00 |
| $9_{0,9}-8_{0,8}$ | 38806.98 | −0.62 | 0.03 | $20_{6,14}-20_{5,15}$ | 32754.35 | −0.58 | −0.03 |

[a]Hypothetical unsplit line frequencies.

the ∠(C≡C—C): 179.4° from the fit to the *A* and *B* rotational constants and 179.3° from the fit to the *B* and *C* constants (here an angle less than 180° indicates that the ethynyl group is bent away from the C—Cl bond and towards the C=O bond whereas in propynal the opposite was observed (23)). It was felt that a force field refinement and average structure calculation would be useful to determine whether this apparent bend of the carbon chain was an artifact caused by zero point vibrational effects. These calculations are described in the following two sections of this paper.

TABLE 3. Chlorine nuclear quadrupole coupling constants of propiolyl chloride

| Species | $\chi_{aa}$ (MHz) | $\chi_{bb}$ (MHz) | $\chi_{cc}$ (MHz) |
|---|---|---|---|
| HCCCO$^{35}$Cl | −20.56(6)[a] | −3.21(8) | 23.77(8) |
| HCCCO$^{37}$Cl | −16.80(12) | −1.68(13) | 18.48(13) |
| DCCCO$^{35}$Cl | −16.43(15) | −7.20(18) | 23.63(18) |
| DCCCO$^{37}$Cl | −14.43(32) | −4.14(33) | 18.57(33) |

[a]Errors cited are standard errors.

*(b) The harmonic force field*

To determine the average structure of propiolyl chloride it is necessary to calculate the harmonic contributions to the vibration–rotation α-constants from the harmonic force field. Although strictly speaking a complete force field is required, in practice it is sufficient to have good values for the more important force constants. In this work we have calculated an approximate force field by combining the available vibration wavenumbers

Can. J. Chem. Downloaded from www.nrcresearchpress.com by 210.87.254.6 on 09/06/12
For personal use only.

Can. J. Chem. Downloaded from www.nrcresearchpress.com by 210.87.254.6 on 09/06/12
For personal use only.

TABLE 4. Rotational constants and centrifugal distortion constants of propiolyl chloride in ground and excited vibrational states

| Parameter | HCCCO$^{35}$Cl | | HCCCO$^{37}$Cl | | DCCCO$^{35}$Cl | | DCCCO$^{37}$Cl |
|---|---|---|---|---|---|---|---|
| | Ground state | $v_9 = 1$ state | Ground state | $v_9 = 1$ state | Ground state | $v_9 = 1$ state | ground state |
| $A$ (MHz) | 7190.0143(30)[a] | 7190.3397(90) | 7111.7135(87) | 7113.41(79) | 7075.1763(54) | 7072.40(21) | 6990.1164(88) |
| $B$ (MHz) | 3149.2440(10) | 3158.1194(85) | 3084.7668(30) | 3093.18(21) | 2943.0992(34) | 2951.8115(82) | 2885.5642(39) |
| $C$ (MHz) | 2186.7459(11) | 2188.0389(66) | 2148.3505(20) | 2149.635(30) | 2075.4480(26) | 2076.8132(55) | 2039.4673(30) |
| $\Delta_J$ (kHz) | 1.2066(69) | 1.171(60) | 1.197(15) | [b] | 1.080(23) | [b] | 0.99(25) |
| $\Delta_{JK}$ (kHz) | −4.790(28) | −5.30(39) | −5.338(81) | [b] | −3.413(58) | [b] | −4.30(14) |
| $\Delta_K$ (kHz) | 22.69(11) | 24.0(15) | 23.86(41) | [b] | 20.73(25) | [b] | 24.06(68) |
| $\delta_J$ (kHz) | 0.4948(21) | 0.463(19) | 0.4837 | [b] | 0.4174(44) | [b] | 0.4042(62) |
| $\delta_K$ (kHz) | 2.325(30) | 2.91(33) | 2.19(10) | [b] | 2.501(70) | [b] | 2.45(11) |
| Std. deviation of fit (MHz) | 0.031 | 0.033 | 0.050 | 0.061 | 0.038 | 0.056 | 0.047 |
| No. of transitions | 50 | 18 | 38 | 5 | 32 | 9 | 30 |

[a]Errors cited are standard errors.
[b]Centrifugal distortion corrections assumed to be equal to those of the corresponding ground state.

TABLE 5. The dipole moment of propiolyl chloride

| Transition | $10^5 \times \Delta\nu/E^{2a}$ Observed | Calculated |
|---|---|---|
| $3_{03}, M = 0 \leftarrow 2_{02}, M = 0$ | −0.642(3)[b] | −0.642 |
| $6_{24}, M = 5 \leftarrow 6_{15}, M = 5$ | 1.941(9) | 1.961 |
| $6_{24}, M = 6 \leftarrow 6_{15}, M = 6$ | 3.104(23) | 3.074 |

$\mu_a = 2.044(25)$[c] Debye
$\mu_b = 1.790(25)$ Debye
$\mu = 2.717(35)$ Debye

[a]Measured in MHz V$^{-2}$ cm$^2$.
[b]Standard errors.
[c]Estimated outside limits of error.

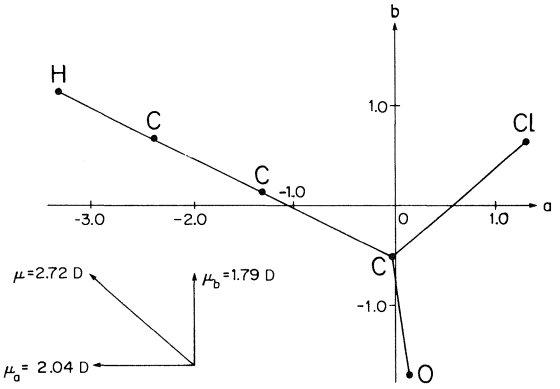


FIG. 1. The ground state average structure and dipole moment of H$^{12}$C$^{12}$C$^{12}$C$^{16}$O$^{35}$Cl in its principal in inertial axis system.

(12, 14, 15) with the centrifugal distortion constants. The chosen non-redundant symmetry coordinates, which transform as $9A' + 3A''$ in the point group $C_s$, are given in terms of the internal displacement coordinates in Table 8. The structure used was the effective structure of Table 7.

From the infrared spectrum of the gas (12) a complete set of vibrational wavenumbers was available for normal propiolyl chloride although the assignment of $\nu_5$ (H—C≡C in plane bend) was considered uncertain. Except for $\nu_7$, which showed a complex hot band structure, these wavenumbers were used directly with no corrections for anharmonicity being made; the Raman liquid value was adopted for $\nu_7$. Unfortunately the results for propiolyl chloride-*d* were less clear cut, partly because a weaker spectrum was obtained. For this species $\nu_{10}$ was not observed and gas phase values for $\nu_9$ and $\nu_{12}$ were unavailable (14). Because the corresponding gas and liquid values for the normal species were quite different the $\nu_9$ Raman liquid value for propiolyl chloride-*d* was discarded; instead, a value was taken from the ultraviolet spectrum (15). Additionally, $\nu_{12}$ for the deuterated species was taken to be 2 cm$^{-1}$ lower in the gas than

Can. J. Chem. Downloaded from www.nrcresearchpress.com by 210.87.254.6 on 09/06/12
For personal use only.

TABLE 6. Ground state inertial parameters[a] of propiolyl chloride

| Parameter | Value | |
|---|---|---|
| | $HCCCO^{35}Cl$ | $HCCCO^{37}Cl$ |
| $I_a^0$ | 70.28901(3)[b] | 71.06290(9) |
| $I_b^0$ | 160.47629(5) | 163.83053(16) |
| $I_c^0$ | 231.11006(12) | 235.24048(22) |
| $\Delta_0$ | 0.34477(13) | 0.34704(29) |
| | Value | |
| Parameter | $DCCCO^{35}Cl$ | $DCCCO^{37}Cl$ |
| $I_a^0$ | 71.42988(5) | 72.29908(9) |
| $I_b^0$ | 171.71660(20) | 175.14045(24) |
| $I_c^0$ | 243.50357(31) | 247.79951(36) |
| $\Delta_0$ | 0.35709(37) | 0.35998(44) |

[a]Calculated from the rotational constants of Table 4 using a conversion factor of 505379.0 uÅ². All parameters given are in uÅ².
[b]Errors quoted are standard errors.
[c]$\Delta_0 = I_c^0 - I_b^0 - I_a^0$.

TABLE 7. The structure of propiolyl chloride

| Parameter | Effective ($r_0$) value[a] | Average ($r_z$) value[b] |
|---|---|---|
| r(C—H)(Å) | 1.056[c] | 1.055[c] |
| r(C≡C)(Å) | 1.208[c] | 1.207[c] |
| r(C—C)(Å) | 1.435[c] | 1.4415[d] |
| r(C=O)(Å) | 1.207 | 1.1988(40)[e] |
| r(C—Cl)(Å) | 1.753 | 1.7587(37) |
| ∠(H—C≡C)(deg) | 180.0[c] | 180.0[c] |
| ∠(C≡C—C)(deg) | 180.0[c] | 179.58(22)[f] |
| ∠(C—C=O)(deg) | 124.9 | 125.19(30) |
| ∠(C—C—Cl)(deg) | 113.0 | 112.42(23) |

[a]Obtained by fitting ground state $A$ and $B$ rotational constants of Table 4.
[b]Ground vibrational state.
[c]Assumed.
[d]Value found by trial and error. See text.
[e]Numbers in parentheses are five standard errors. These are arbitrary error limits, and may underestimate the total errors in these parameters.
[f]The ethynyl group is bent away from the C—Cl bond.

in the liquid (observed shift for the normal species is 3 $cm^{-1}$) and, as for the normal species, the Raman liquid value was adopted for $\nu_7$. Except for $\nu_6$ (D—C≡C in-plane bend) the wavenumbers used for the remaining propiolyl chloride-*d* fundamentals were the reported gas infrared values (14). The previous assignment of $\nu_6$ to a band at 522 $cm^{-1}$ (14) seemed unlikely for several reasons. Firstly, this band showed no appreciable gas-to-liquid frequency shift whereas for normal propiolyl chloride (12) and propynal (40) the Raman liquid values are 20–25 $cm^{-1}$ higher than the gas infrared values. As well, the force field calculations suggested that $\nu_6$ and $\nu_{11}$ (D—C≡C out-of-plane bend) should be nearly degenerate and should occur at a somewhat higher frequency. Notably, a gas infrared band observed at 547 $cm^{-1}$ (assigned to $\nu_{11}$) is seen in the liquid at 570 $cm^{-1}$. No other band shows this behaviour; tentatively therefore $\nu_6$ and $\nu_{11}$ have been taken to be degenerate.

The force constants obtained in the present analysis are given in Table 9. Because of the limited data available the values of several force constants were fixed by analogy with other related molecules, reflecting structural differences (41, 42), and others were constrained to zero. In addition, the corresponding force constants defining the in-plane and out-of-plane H—C≡C and C≡C—C deformations were assumed to be equal. The values obtained for the various force constants appear reasonable in light of results for the related molecules acetylene (43), propyne (44), phosgene (41), and formic acid (45, 46); the value obtained for $F_{44}$ (C—C stretching force constant) does, however, appear low in comparison to the corresponding 5.50 mdyn $Å^{-1}$ value obtained for propyne (44).

Tables 10 and 11 demonstrate how well the present force field reproduces the observed data. Table 10 shows that the fit for the vibrational wavenumbers, with the possible exception of $\nu_9$, is satisfactory. Table 11 shows that the fit is also very good for the centrifugal distortion constants. Finally, a good harmonic force field should accurately predict the values of the ground and excited state inertial defects; the results of Table 12 show that this is the case here and, further, that the isotopic dependence of the ground state inertial defects is well accounted for. Although the results obtained are very pleasing, the force field given in Table 9 should be regarded as a preliminary result; with the many assumptions made, including the neglect of anharmonicity, it is evident that the uncertainties given in Table 9 underestimate the total errors in these parameters.

### *(c) The average structure*

The harmonic force field of Table 9 was used to calculate the harmonic parts of the α constants, and hence the ground state average rotational constants of the four isotopic species studied; these are given in Table 13. Because the inertial defects calculated using these $A_z$, $B_z$, and $C_z$ values are essentially zero (see Table 13), all twelve rotational constants were used to determine the ground state average structure. Again, since only eight of these were independent, it was necessary to assume a structure for the ethynyl group. The r(C—H) bond length was taken to be 1.055 Å ($r_s$ and $r_z$ values for propynal are 1.055 Å (23) and 1.054 Å (24) respectively) and the $r$(C≡C) length was taken to be 1.207 Å ($r_s$ and $r_z$ values for propynal are 1.209 Å (23) and 1.205 Å (24) respectively). The results of a least-

TABLE 8. Internal coordinates and symmetry coordinates of propiolyl chloride

*Internal coordinates*[a]

| | | |
|---|---|---|
| *A'* block | $r_1 = r(C—H) = 1.056$ Å; | $r_2 = r(C{\equiv}C) = 1.208$ Å |
| | $r_3 = r(C—C) = 1.435$ Å; | $r_4 = r(C{=}O) = 1.207$ Å |
| | $r_5 = r(C—Cl) = 1.752$ Å; | $\theta_1 = \angle(H—C{\equiv}C) = 180°$ |
| | $\theta_2 = \angle(C{\equiv}C—C) = 180°$; | $\theta_3 = \angle(C—C{=}O) = 124.9°$ |
| | $\theta_4 = \angle(O{=}C—Cl) = 113.0°$; | $\theta_5 = \angle(C—C—Cl) = 122.2°$ |
| *A"* block | $\alpha_1 = \delta(CCOCl)$[b]; $\alpha_2 = \angle(H—C{\equiv}C) = 180°$ | |
| | $\alpha_3 = \angle(C{\equiv}C—C) = 180°$ | |

*Symmetry coordinates*

| | |
|---|---|
| *A'* block | $S_1 = \Delta r_1$ |
| | $S_2 = \Delta r_2$ |
| | $S_3 = \Delta r_4$ |
| | $S_4 = \Delta r_3$ |
| | $S_5 = \Delta r_5$ |
| | $S_6 = \Delta\theta_1$ |
| | $S_7 = (1/\sqrt{2})(\Delta\theta_3 - \Delta\theta_5)$ |
| | $S_8 = (1/\sqrt{6})(2\Delta\theta_4 - \Delta\theta_3 - \Delta\theta_5)$ |
| | $S_9 = \Delta\theta_2$ |
| *A"* block | $S_{10} = \Delta\alpha_2$ |
| | $S_{11} = \Delta\alpha_1$ |
| | $S_{12} = \Delta\alpha_3$ |

[a]The molecular structure is the effective structure of Table 7.
[b]The internal coordinate $\alpha_1$ defines the *A"* deformation of the CCOCl group.

TABLE 9. The harmonic force field of propiolyl chloride

| Species | Force constants[a] | | |
|---|---|---|---|
| *A'* | $F_{11} = 5.943(94)$[b] | | |
| | $F_{22} = 15.79(29)$ | | |
| | $F_{33} = 12.70$[c]; | $F_{34} = 1.50$; | $F_{35} = 0.50$ |
| | $F_{44} = 4.66(13)$; | $F_{45} = 0.15$; | $F_{48} = -0.84(5)$ |
| | $F_{55} = 3.03$ | | |
| | $F_{66} = 0.263(6)$[d]; | $F_{69} = 0.096(20)$[d] | |
| | $F_{77} = 0.844(27)$; | $F_{79} = 0.040(8)$ | |
| | $F_{88} = 1.249(22)$; | $F_{89} = -0.093(9)$ | |
| | $F_{99} = 0.218(9)$[d] | | |
| *A"* | $F_{10,10} = 0.263(6)$; | $F_{10,12} = 0.096(20)$ | |
| | $F_{11,11} = 0.689(15)$ | | |
| | $F_{12,12} = 0.218(3)$ | | |

[a]Bond stretching force constants in mdyn Å$^{-1}$; stretch–bend interaction force constants in mdyn rad$^{-1}$; angle bending force constants in mdyn Å rad$^{-2}$.
[b]Uncertainties cited are standard errors in units of the last significant figures.
[c]No error cited indicates a constrained force constant. Force constants not cited were constrained to zero.
[d]The corresponding force constants defining the *A'* and *A"* H—C≡C and C≡C—C deformations were assumed to be equal. Specifically, the constraints made were: $F_{66} = F_{10,10}$; $F_{69} = F_{10,12}$, and $F_{99} = F_{12,12}$.

squares fit to the ground state average rotational constants are given in the last column of Table 7. They are shown pictorially in Fig. 1. In the structural refinements the ∠(C—C≡C) was not constrained and *r*(C—C) was varied by trial and error (at 0.0005 Å increments) to find the best fit: isotopic variations in the bond lengths were ignored. The standard deviation of the fit to the twelve rotational constants of Table 13 was 0.008 MHz, not significantly larger than the errors quoted for the effective ground state constants of Table 4; in view of the limited isotopic data available, however, this small standard deviation may not be meaningful. As well, because possible systematic errors have been ignored the least-squares standard errors almost certainly underestimate the total errors in the structural parameters; the uncertainties quoted in Table 7 represent five standard errors but do not indicate outside limits of error.

### 5. *Comments on the structure of propiolyl chloride*

Although the present results for propiolyl chloride are not definitive it is nevertheless interesting to compare the structures of propiolyl chloride and some related molecules; this has been done in Table 14. The results of Table 14 suggest that the

Can. J. Chem. Downloaded from www.nrcresearchpress.com by 210.87.254.6 on 09/06/12
For personal use only.

Can. J. Chem. Downloaded from www.nrcresearchpress.com by 210.87.254.6 on 09/06/12
For personal use only.

TABLE 10. Observed and calculated vibrational wavenumbers ($cm^{-1}$) of propiolyl chloride

| | $HCCCO^{35}Cl$ | | $DCCCO^{35}Cl$ | |
|---|---|---|---|---|
| Vibration | Observed[a] | Deviation | Observed[b] | Deviation |
| $A'$ $\nu_1$ | 3326 | −11.1 | 2609 | 7.8 |
| $\nu_2$ | 2131 | −8.2 | 2000 | 8.9 |
| $\nu_3$ | 1767 | −3.6 | 1772 | 1.6 |
| $\nu_4$ | 1003 | 0.0 | 994 | −5.9 |
| $\nu_5$ | 696 | −3.3 | 653 | 3.9 |
| $\nu_6$ | 655 | −1.4 | 547 | −0.6 |
| $\nu_7$ | 478 | 2.1 | 472 | 1.1 |
| $\nu_8$ | 414 | 3.6 | 404 | −1.2 |
| $\nu_9$ | 157 | 5.2 | 147 | 2.8 |
| $A''$ $\nu_{10}$ | 703 | 3.2 | (664)[c] | — |
| $\nu_{11}$ | 665 | 1.4 | 547 | 3.8 |
| $\nu_{12}$ | 224 | −2.3 | 214 | −2.2 |

[a]Taken from Augdahl *et al.* (12). The observed wavenumbers are gas infrared values except for $\nu_7$ which is a Raman liquid value. In the fits the uncertainty of $\nu_3$ was taken to be 1.5%; all other fundamentals were given uncertainties of 1% of the measured value.
[b]The observed wavenumbers are mostly gas infrared values (14); $\nu_7$ is a Raman liquid value and $\nu_{12}$ is an estimated gas phase value (216 $cm^{-1}$ in the Raman spectrum of the liquid (14)). A value for $\nu_9$ was taken from the ultraviolet spectrum (15). In the fits $\nu_6$ and $\nu_{11}$ were assumed to be degenerate but were given low weights; see text. In the fits $\nu_3$, $\nu_6$, and $\nu_{11}$ were given uncertainties of 2%, 5%, and 5% respectively; all other fundamentals were assigned uncertainties of 1% of the measured value.
[c]Calculated value. No experimental value was available.

TABLE 11. Observed and calculated centrifugal distortion constants (kHz) of propiolyl chloride

| | Value | | |
|---|---|---|---|
| Parameter | Observed[a] | Calculated[b] | Uncertainty[c] |
| *$HCCCO^{35}Cl$* | | | |
| $\Delta_J$ | 1.207 | 1.212 | 0.021 |
| $\Delta_{JK}$ | −4.790 | −4.717 | 0.084 |
| $\Delta_K$ | 22.69 | 22.61 | 0.33 |
| $\delta_J$ | 0.4948 | 0.4911 | 0.0063 |
| $\delta_K$ | 2.325 | 2.195 | 0.090 |
| *$DCCCO^{35}Cl$* | | | |
| $\Delta_J$ | 1.080 | 1.022 | 0.092 |
| $\Delta_{JK}$ | −3.41 | −3.408 | 0.23 |
| $\Delta_K$ | 20.7 | 21.28 | 1.0 |
| $\delta_J$ | 0.417 | 0.4082 | 0.018 |
| $\delta_K$ | 2.50 | 2.424 | 0.28 |
| *$HCCCO^{37}Cl$* | | | |
| $\Delta_J$ | 1.197 | 1.201 | 0.060 |
| $\Delta_{JK}$ | −5.34 | −5.164 | 0.32 |
| $\Delta_K$ | 23.9 | 23.12 | 1.6 |
| $\delta_J$ | 0.484 | 0.4859 | 0.029 |
| $\delta_K$ | 2.19 | 2.006 | 0.40 |
| *$DCCCO^{37}Cl$* | | | |
| $\Delta_J$ | 0.99 | 1.020 | 1.00 |
| $\Delta_{JK}$ | −4.30 | −3.933 | 0.56 |
| $\Delta_K$ | 24.1 | 21.89 | 2.7 |
| $\delta_J$ | 0.404 | 0.4072 | 0.025 |
| $\delta_K$ | 2.45 | 2.172 | 0.44 |

[a]Experimental values from Table 4.
[b]Values calculated using the force field of Table 9.
[c]Uncertainties used in the force field refinement. For $HCCCO^{35}Cl$ the cited uncertainties are three standard errors; for the other isotopes the assigned uncertainties represent four standard errors.

TABLE 12. Observed and calculated inertial defects ($uÅ^2$) of propiolyl chloride

| Species | Observed[a] | Calculated[b] | Deviation |
|---|---|---|---|
| | *Ground vibrational state* | | |
| $HCCCO^{35}Cl$ | 0.3448(1)[c] | 0.3436 | 0.0012 |
| $HCCCO^{37}Cl$ | 0.3470(3) | 0.3460 | 0.0011 |
| $DCCCO^{35}Cl$ | 0.3571(4) | 0.3560 | 0.0011 |
| $DCCCO^{37}Cl$ | 0.3600(4) | 0.3587 | 0.0013 |
| | *$v_9$ = 1 excited state* | | |
| $HCCCO^{35}Cl$ | 0.662(1) | 0.652 | 0.010 |
| $HCCCO^{37}Cl$ | 0.669(14) | 0.668 | 0.001 |
| $DCCCO^{35}Cl$ | 0.676(2) | 0.683 | −0.007 |

[a]Calculated from the rotational constants of Table 4.
[b]The vibrational part of the inertial defect calculated using the force field of Table 9.
[c]Errors cited are standard errors.

TABLE 13. Ground state average rotational constants (MHz) of propiolyl chloride[a]

| | Value | |
|---|---|---|
| Parameter | $HCCCO^{35}Cl$ | $HCCCO^{37}Cl$ |
| $A_z$ | 7175.153 | 7097.163 |
| $B_z$ | 3145.260 | 3080.869 |
| $C_z$ | 2186.696 | 2148.287 |

| | Value | |
|---|---|---|
| Parameter | $DCCCO^{35}Cl$ | $DCCCO^{37}Cl$ |
| $A_z$ | 7060.482 | 6975.728 |
| $B_z$ | 2939.564 | 2882.102 |
| $C_z$ | 2075.455 | 2039.460 |

[a]Obtained using the effective ground state rotational constants of Table 4 and the force field of Table 9.

C=O bond in propiolyl chloride is shorter than that in propynal. This is reasonable in view of results for $H_2CO$ (47), HCOCl (2), and $Cl_2CO$ (48) where C=O bond lengths of 1.207 Å ($r_z$), 1.188 Å ($r_s$), and 1.179 Å ($r_z$) have been obtained; as well, for $CH_3CHO$ (49) and $CH_3COCl$ (50) the corresponding values are 1.207 Å ($r_z$) and 1.185 Å ($r_z$). Therefore the C=O bond in propiolyl chloride might be expected to be 0.010–0.020 Å shorter than that in propynal; the results of Table 14, albeit imprecise, support this hypothesis. More marked are the variations in the C—Cl lengths; essentially identical bond distances have been determined for formyl chloride and propiolyl chloride while that found for acetyl chloride is somewhat longer. Kagarise (51) suggested that electronegative substituents should lower the contribution of nonbonded resonance structures such as $RCO^+Cl^-$; therefore the longest C—Cl bond would be expected for acetyl chloride because of the presence of the "electron-donating" methyl group. Similar arguments have been used to explain the trend in

TABLE 14. The structures of propiolyl chloride and related molecules[a]

| Parameter | Value | | | |
|---|---|---|---|---|
| | HCCCOCl[b] | HCCCHO | HCOCl | $CH_3COCl$ |
| $r$(C—H) (Å) | 1.055 | 1.054(7) | | |
| $r$(C≡C) (Å) | 1.207 | 1.205(6) | | |
| $r$(C—C) (Å) | 1.442 | 1.449(2) | | |
| $r$(C=O) (Å) | 1.199(4) | 1.212(5) | 1.188(2) | 1.185(3) |
| $r$(C—Cl) (Å) | 1.759(4) | | 1.760(2) | 1.796(2) |
| ∠(C—C=O) (deg) | 125.2(3) | 124.2(2) | | 127.2(6) |
| ∠(C—C—Cl) (deg) | 112.4(2) | | | 111.6(6) |
| ∠(C≡C—C) (deg) | 179.6(2)[c] | 178.6(3)[d] | | |
| Reference | This work | ref. 24 | ref. 2 | ref. 50 |

[a]The HCOCl structure is an $r_s$ structure. The other structures are $r_z$ structures.
[b]Structure taken from Table 7.
[c]Ethynyl group bent away from C—Cl bond.
[d]Ethynyl group bent away from C=O bond.

the acid dissociation constants of the parent carboxylic acids (11). On this basis one might expect the C—Cl bond in propiolyl chloride to be slightly shorter than that found in formyl chloride; this very simple argument neglects, however, possible conjugative effects in propiolyl chloride. The remaining bond lengths in propiolyl chloride and propynal are apparently nearly equal.

In the case of the bond angles in acetyl chloride and propiolyl chloride it is seen that the ∠(C—C—Cl) is essentially identical in both molecules; the ∠(C—C=O) is in each case about 14° larger. Apparently the carbon chain in propiolyl chloride is more nearly linear than that found in propynal. Although this may be an experimental artifact the $r_0$ structure calculations lead to the same conclusion. More precise structural results for propiolyl chloride would require additional isotopic data.

## Acknowledgements

We thank W. J. Balfour and S. Visaisouk for the samples of propiolyl chloride and propiolyl chloride-*d* used in this work.

1. R. F. MILLER and R. F. CURL, JR. J. Chem. Phys. **34**, 1847 (1961).
2. H. TAKEO and C. MATSUMURA. J. Chem. Phys. **64**, 4536 (1976).
3. L. PIERCE and L. C. KRISHER. J. Chem. Phys. **31**, 875 (1959).
4. K. M. SINNOTT. J. Chem. Phys. **34**, 851 (1961).
5. H. N. VOLLTRAUER and R. H. SCHWENDEMAN. J. Chem. Phys. **54**, 268 (1971).
6. K. P. R. NAIR and J. E. BOGGS. J. Mol. Struct. **33**, 45 (1976).
7. O. L. STIEFVATER and E. B. WILSON, JR. J. Chem. Phys. **50**, 5385 (1969).
8. H. KARLSSON. J. Mol. Struct. **33**, 227 (1976).
9. G. H. MANSFIELD and M. C. WHITING. J. Chem. Soc. 4761 (1956).
10. J. GUILLEME and B. WOJTKOWIAK. Bull. Soc. Chim. Fr. 3007 (1969).
11. C. K. INGOLD. Structure and mechanism in organic chemistry. 2nd ed. Cornell University Press, Ithaca. 1969. pp. 1110–1116.
12. E. AUGDAHL, E. KLOSTER-JENSEN, and A. ROGSTAD. Spectrochim. Acta A, **30**, 399 (1974).
13. W. J. BALFOUR, C. C. GRIEG, and S. VISAISOUK. J. Org. Chem. **39**, 725 (1974).
14. W. J. BALFOUR, R. H. MITCHELL, and S. VISAISOUK. Spectrochim. Acta A, **31**, 967 (1975).
15. W. J. BALFOUR and S. VISAISOUK. J. Mol. Spectrosc. **80**, 117 (1980).
16. A. ROGSTAD and S. J. CYVIN. Acta Chem. Scand. **27**, 2304 (1974).
17. W. J. BALFOUR and M. K. PHIBBS. Spectrochim. Acta, Part A, **35**, 385 (1979).
18. R. W. DAVIS, M. C. L. GERRY, S. VISAISOUK, and W. J. BALFOUR. Chem. Phys. Lett. **26**, 561 (1974).
19. D. G. LISTER and J. K. TYLER. Spectrochim. Acta, Part A, **28**, 1423 (1972).
20. R. W. DAVIS and M. C. L. GERRY. J. Mol. Spectrosc. **59**, 407 (1976).
21. R. W. DAVIS and M. C. L. GERRY. J. Mol. Spectrosc. **57**, 118 (1975).
22. J. A. HOWE and J. H. GOLDSTEIN. J. Chem. Phys. **23**, 1223 (1955).
23. C. C. COSTAIN and J. R. MORTON. J. Chem. Phys. **31**, 389 (1959).
24. M. SUGIE, T. FUKUYAMA, and K. KUCHITSU. J. Mol. Struct. **14**, 333 (1972).
25. C. FLANAGAN and L. PIERCE. J. Chem. Phys. **38**, 2963 (1963).
26. J. K. G. WATSON. *In* Vibrational spectra and structure, a series of advances. Vol. VI. *Edited by* J. R. Durig. Elsevier, New York. 1977. pp. 1–89.
27. J. S. MUENTER. J. Chem. Phys. **48**, 4544 (1968).
28. W. J. LAFFERTY and R. J. THIBAULT. J. Mol. Spectrosc. **14**, 79 (1964).
29. J. K. TYLER and J. SHERIDAN. Trans. Faraday Soc. **59**, 2661 (1963).
30. H. JONES, M. TAKAMI, and J. SHERIDAN. Z. Naturforsch. Teil A, **33**, 156 (1978).
31. H. JONES, J. SHERIDAN, and O. L. STIEFVATER. Z. Naturforsch. Teil A, **32**, 866 (1977).
32. W. J. LAFFERTY and J. J. RITTER. J. Mol. Spectrosc. **38**, 181 (1971).
33. R. TRAMBARULO and W. GORDY. J. Chem. Phys. **18**, 1613 (1950).
34. M. C. L. GERRY and T. M. SUGDEN. Trans. Faraday Soc. **61**, 2091 (1965).

Can. J. Chem. Downloaded from www.nrcresearchpress.com by 210.87.254.6 on 09/06/12
For personal use only.

35. E. C. THOMAS and V. W. LAURIE. J. Chem. Phys. **44**, 2602 (1966).
36. L. F. THOMAS, J. S. HEEKS, and J. SHERIDAN. Arch. Sci. **10**, 180 (1957).
37. A. J. ALEXANDER, H. W. KROTO, and D. R. WALTON. J. Mol. Spectrosc. **62**, 175 (1976).
38. L. J. NUGENT, D. E. MANN, and D. R. LIDE, JR. J. Chem. Phys. **36**, 965 (1962).
39. A. P. COX, I. C. EWART, and W. M. STIGLIANI. J. Chem. Soc. Faraday Trans. II, **71**, 504 (1975).
40. P. KLABOE and G. KREMER. Spectrochim. Acta, Part A, **33**, 947 (1977).
41. J. H. CARPENTER and D. F. RIMMER. J. Chem. Soc. Faraday Trans. II, **74**, 466 (1978).
42. P. D. MALLINSON, D. C. MCKEAN, J. H. HOLLOWAY, and I. A. OXTON. Spectrochim. Acta, Part A, **31**, 143 (1975).
43. G. STREY and I. M. MILLS. J. Mol. Spectrosc. **59**, 103 (1976).
44. J. L. DUNCAN, D. C. MCKEAN, and G. D. NIVELLINI. J. Mol. Struct. **32**, 255 (1976).
45. R. L. REDINGTON. J. Mol. Spectrosc. **65**, 171 (1977).
46. R. W. DAVIS, A. G. ROBIETTE, M. C. L. GERRY, E. BJARNOV, and G. WINNEWISSER. J. Mol. Spectrosc. **81**, 93 (1980).
47. J. L. DUNCAN. Mol. Phys. **28**, 1177 (1974).
48. M. NAKATA, K. KOHATA, T. FUKUYAMA, and K. KUCHITSU. J. Mol. Spectrosc. **83**, 105 (1980).
49. T. IIJIMA and S. TSUCHIYA. J. Mol. Spectrosc. **44**, 88 (1972).
50. S. TSUCHIYA and T. IIJIMA. J. Mol. Struct. **13**, 327 (1972).
51. R. KAGARISE. J. Am. Chem. Soc. **77**, 1377 (1955).

Can. J. Chem. Downloaded from www.nrcresearchpress.com by 210.87.254.6 on 09/06/12
For personal use only.

# Coordination compounds of indium. Part 39. Some neutral adducts of $In_2Br_4$ and $In_2I_4$

MICHAEL J. TAYLOR,[1] DENNIS G. TUCK,[2] AND LUIS VICTORIANO
*Department of Chemistry, University of Windsor, Windsor, Ont., Canada N9B 3P4*

Received May 19, 1981

MICHAEL J. TAYLOR, DENNIS G. TUCK, and LUIS VICTORIANO. Can. J. Chem. **60**, 690 (1982).

The neutral indium(II) compounds $In_2X_4(Et_3P)_2$, $In_2X_4(TMED)_2$, and $In_2X_4(TMED)_2C_6H_6$ (X = Br, I; TMED = *N,N,N',N'*-tetramethylethylenediamine) have been prepared by the reaction of $InX_2$ and donor in benzene or toluene. With several other neutral donors, and in all systems involving $InCl_2$, decomposition to $In^0$ is the predominant process. Analysis of the vibrational spectra demonstrates that these structures involve $X_2In–InX_2$ kernels. Slight revisions are proposed to previous discussions of the infrared spectra of $In_2X_6^{2-}$ anions.

MICHAEL J. TAYLOR, DENNIS G. TUCK et LUIS VICTORIANO. Can. J. Chem. **60**, 690 (1982).

On a préparé les composés neutres de l'indium(II) $In_2X_4(Et_3P)_2$, $In_2X_4(TMED)_2$ et $In_2X_4(THED)_2$ $C_6H_6$ (X = Br, I; TMED = *N,N,N',N'*-tétraméthyléthylènediamine) en faisant réagir $InX_2$ avec un donneur dans le benzène ou le toluène. La décomposition en $In^0$ est la réaction principale avec plusieurs autres donneurs neutres et dans tous les systèmes qui impliquent $InCl_2$. L'analyse des spectres de vibration démontre que ces structures font intervenir les noyaux $X_2In–InX_2$. On propose une légère revision des discussion antérieures des spectres infrarouges des anions $In_2X_6^{2-}$.

[Traduit par le journal]

## Introduction

In a number of previous publications from this laboratory we have commented on the dearth of information on the chemistry of the lower oxidation states of indium. Recent papers have described the development of synthetic routes to a number of neutral (1), cationic (2), and anionic (3) complexes of indium(I) and there does not seem to exist any barrier now, in principle, to the extension of such work to related systems. On the other hand, the chemistry of indium(II) still presents a number of challenging problems. The neutral dihalides are generally formulated as ionic dimers of mixed oxidation state, and a simple route to the preparation of these compounds (4) also lead to the development of synthetic routes to the first anionic complexes $In_2X_6^{2-}$ (5). These anionic species are structurally similar to the digallium salts which were reported some time ago (6), and for which structural information is available from X-ray crystallography (7, 8).

We now report the preparation of a small number of neutral adducts of the indium dihalides, which on the basis of the vibrational spectra are believed to contain indium–indium bonds. Again these are similar to the gallium analogues which were reported recently by Worrall *et al.* (9), although it appears that the symmetry and coordination number at the metal may not be the same for both sets of compounds.

[1]Permanent address: Department of Chemistry, University of Auckland, Auckland, New Zealand.

[2]To whom all correspondence should be addressed.

## Experimental

### *General*

Spectroscopic and analytical procedures were as described previously (1). Indium dihalides were prepared from indium metal and indium trihalides (3). *N,N,N',N'*-Tetramethylethylenediamine (TMED) and other ligands were the commercially available materials used without further purification. Solvents were refluxed in sodium/benzophenone and distilled from the blue ketyl. All operations were performed in an atmosphere of pure, dry nitrogen.

### *Preparative*

The same general method was used in each case, with isolation procedures which varied according to the particular system. Approximately 2–3 mmol of the dihalide (calculated as the dimer) was placed in a Schlenk flask and 30–40 m of benzene syringed in through a rubber septum. The resultant suspension was frozen in liquid nitrogen, and a four-fold excess of monodentate, or two-fold excess of bidentate, ligand syringed in; solid ligands were dissolved in the minimum amount (5–10 mL) of benzene for this purpose. The liquid nitrogen cooling bath was removed, and the system stirred as soon as the melting of the solvent allowed. Magnetic stirring was continued for 20 min after the solvent had completely melted.

### *Isolation procedures*

*$InBr_2$/TMED:* The white suspension was filtered and the solid collected and dried. Analysis established the composition $InBr_2$(TMED) for this material. The mother liquors were allowed to stand over a period of 72 h, when large crystals (1.5 × 0.5 × 0.5 cm) were obtained, with further smaller (1 × 1 × 2 mm) crystals being obtained from the residual liquid after 24 h. These crystals had the composition $In_2Br_4(TMED)_2C_6H_6$ (see Table 1 for analytical results).

*$InI_2$/TMED:* A red colour, believed to indicate the presence of InI, was still apparent after stirring at room temperature for 2.5 h, and the mixture was therefore refluxed for 2 h. The yellow solid which separated on cooling was collected and dried, and found to have the composition $InI_2$(TMED). The filtrate was concentrated to 20 mL and a viscous brown liquid settled out on standing. This oil was separated and treated with 10 mL of light

0008-4042/82/060690-05$01.00/0
©1982 National Research Council of Canada/Conseil national de recherches du Canada

Can. J. Chem. Downloaded from www.nrcresearchpress.com by 210.87.254.5 on 09/06/12
For personal use only.

Can. J. Chem. Downloaded from www.nrcresearchpress.com by 210.87.254.5 on 09/06/12
For personal use only.

ligroin (40–60°C bp) to yield a sticky yellow solid which was exhaustively pumped at room temperature. Analysis showed the composition of this material to be $In_2I_4(TMED)_2C_6H_6$.

*$InBr_2/Et_3P$:* When these two substances reacted in toluene at −40°C, a deep red solution initially formed but this rapidly changed colour, becoming yellow at about −20°C, and at room temperature, appreciable decomposition to the metal was noted. Addition of cold light ligroin to the solution at −20°C produced a white precipitate which was collected and dried; analysis gave the empirical formula $InBr_2 \cdot Et_3P$. The instability of this material prevented further investigation; in particular the infrared and Raman spectra presented no identifiable features.

*$InI_2/Et_3P$:* The green reaction mixture was concentrated to 20 mL by evaporation; after 2–3 h the orange crystalline material which was deposited was collected and dried. Further material was obtained by addition of light ligroin to the solution. Analysis showed this solid material to be $InI_2 \cdot Et_3P$.

*Other reactions*

Reactions between benzene solutions of $InBr_2$ and the ligands $Et_3N$, pyridine, 2,2′-bipyridine, and dimethylsulphoxide all gave indium metal in yields of 90% or larger, according to the disproportionation reaction

$$3InX_2 \rightarrow In^0 + 2InX_3$$

In the case of $InBr_2/Et_3P$, a substance of stoichiometry $InBr_3 \cdot 2Et_3P$ was recovered from the mother liquor, while $InBr_2 + Ph_3P$ yielded 100% InBr according to

$$In_2Br_4 \rightarrow InBr + InBr_3$$

Similar behaviour was observed with $InI_2$ and $Et_3N$, pyridine, 2,2′-bipyridine, $Ph_3P$, and bis(diphenylphosphino)ethane.

All attempts to make chloro-derivatives by the above methods from $InCl_2$ and a number of neutral donors resulted in disproportionation to indium metal.

## Results and discussion

*General*

The presence of coordinated ligands is apparent from the analytical results, and from infrared spectroscopy. The ir spectrum of neat TMED has bands *inter alia* at 1040 and 1275 $cm^{-1}$, which are shifted to 1025 and 1295 $cm^{-1}$ in the complexes, suggesting that they are related to the vibrations of the donor atom (10). Similarly bands at 1230 and 975 $cm^{-1}$ in the spectrum of $Et_3P$ (11) shift to 1265 and 995 $cm^{-1}$ in the complexes. $^1H$-nmr spectra of the products in deuteroacetonitrile also confirmed the presence of the ligands, without adding to our knowledge of the structures of the complexes. The magnetic susceptibilities of the solid materials (0.01–0.05 BM at 25°C) established them as diamagnetic. Rapid decomposition in suitable solvents prevented the measurement of molar conductivities.

TABLE 1. Analytical results[a]

| Compound | % In | % halogen |
|---|---|---|
| $In_2Br_4(Et_3P)_2$ | 29.0(29.3) | 41.0(40.7) |
| $In_2Br_4(TMED)_2$ | 32.7(29.4)[b] | 39.2(40.9)[b] |
| $In_2Br_4(TMED)_2C_6H_6$ | 26.8(26.7) | 37.3(37.2) |
| $In_2I_4(Et_3P)_2$ | 24.1(23.6) | 52.1(52.2) |
| $In_2I_4(TMED)_2$ | 23.6(23.7) | 52.9(52.4) |
| $In_2I_4(TMED)_2C_6H_6$ | 22.2(21.9) | 48.4(48.5) |

[a] Figures in parentheses indicate theoretical compositions.
[b] See text for discussion of these analyses.

Sharp aromatic resonances (7.20 ppm downfield from TMS) confirmed the presence of benzene in those products formulated as $In_2X_4(TMED)_2C_6H_6$. Neither nmr nor vibrational spectroscopy throws any light on the mode of interaction of benzene in the solid phase of such compounds, and only minor changes in other frequencies were noted on comparing analogous solvated and non-solvated compounds. This may indicate that the benzene is merely trapped in the crystal lattice with no strong interactions towards the metal centre, and in keeping with this, the crystalline materials slowly lose benzene and disintegrate on standing in an atmosphere of dry nitrogen, which frustrated attempts at X-ray structural analysis.

*Vibrational spectroscopy*

In view of the above results, we conclude that the most obvious structural analogues of these compounds are the $Ga_2Cl_4L_2$ compounds reported by Worrall *et al.* (9), and shown to involve Ga—Ga bonding. The presence of In—In bonds in the corresponding indium(II) anionic complexes also provides further indication of a metal–metal bonded structure, and in the absence of X-ray crystallographic data (see above) we now justify the formulation of the present compounds as In—In bonded dimers on the basis of vibrational spectroscopy.

As a preliminary, we first report some necessary revision to the previously published results for the $In_2X_6^{2-}$ anions. Despite the earlier report (5), we now find that these compounds dissolve in $CH_3CN$ with only slight decomposition, and that addition of $Et_2O$ yields good crystalline material. The vibrational spectra of these products are similar to those of the untreated materials, except that the highest frequency infrared features, at 332 $cm^{-1}$ for Cl, 235 $cm^{-1}$ for Br, and 186 $cm^{-1}$ for I, have disappeared; an additional feature is also observed at 135 $cm^{-1}$ for $In_2I_6^{2-}$. We suggest that such absorptions are actually due to tetrahaloindate(III) anion impurities (12). The simplified spectra of the $In_2X_6^{2-}$ anions are summarized in Table 2, from which it is clear that it is no longer necessary to invoke Fermi resonance in order to explain the spectra (cf. ref. 5). Other infrared frequencies, and the Raman spectra, which remain unchanged in the newly purified materials, are not affected. These

TABLE 2. The revised infrared spectra of $In_2X_6^{2-}$ anions, as $Bu_4N^+$ salts (in $cm^{-1}$)

| $In_2Cl_6^{2-}$ | $In_2Br_6^{2-}$ | $In_2I_6^{2-}$ | Assignment | Description |
|---|---|---|---|---|
| 292s | 207s | 162s | $E_u$ | ν(In—X) |
| 284sh | 185s | 135s | $A_{2u}$ | ν(In—X) |

revisions must have some effect on the values of the force constants and potential energy distributions, but do not change the general conclusions reached earlier about the $X_3In—InX_3^{2-}$ structure of these anions.

The Raman and ir features of $In_2X_4L_2$ (X = Br, I; L = TMED, $Et_3P$) are detailed in Table 3. The most prominent feature in the spectra of each of the $In_2X_4$ complexes is a strong Raman line which appears at 141 $cm^{-1}$ in $In_2Br_4(TMED)_2$, at 110 $cm^{-1}$ in $In_2I_4(TMED)_2$, at 116 $cm^{-1}$ in $In_2I_4(Et_3P)_2$. These values agree well with the frequencies for ν(In—In) in the corresponding anionic species $In_2X_6^{2-}$ (5), and the shift of this stretching mode with changes in net charge or coordination number follows the pattern already established for the analogous $Ga_2X_4$ species (9).

*Triethylphosphine complexes*

Once the presence of a metal-to-metal bond has been established, various ionic structures can be ruled out, but even then a number of different structural possibilities must be considered for the TMED complexes; we return to this point below. A structural formulation is most easily made in the case of $In_2I_4(Et_3P)_2$. The mutual exclusion rule identifies the species as centrosymmetric, and on this basis we propose a structure of $C_{2h}$ skeletal symmetry shown in Fig. 1. The vibrational representation for the stretching modes of this $In_2X_4P_2$ kernel is $3A_g + B_g + A_u + 2B_u$, in which the g-modes are Raman-active and all u-modes infrared-active. It was not possible to obtain satisfactory spectra for $In_2Br_4(Et_3P)_2$ (see Experimental), but the vibrational spectrum of $In_2I_4(Et_3P)_2$, given in Table 3, shows the ν(In—In) vibration, together with bands which are reasonably attributed to the four In—I stretching modes.

The assignment of phosphorus-to-metal stretching frequencies has generally raised some difficulties. Shobatake and Nakamoto (13) used metal isotope techniques for $NiX_2(Et_3P)_2$ and thus located ν(Ni—P) near 270 $cm^{-1}$. The spectra of $InX_3(R_3P)_2$ (X = Cl, Br, or I; R = Me or Et) did not reveal any obvious ν(In—P) modes (14), but a single-crystal study of $InCl_3(Me_3P)_2$ lead to the identification of the totally symmetric modes of this molecule, with ν(In—P) being assigned at 135 $cm^{-1}$ (15). This frequency seems rather low in terms of mass considerations, when compared to values of 307 $cm^{-1}$ for ν(In—Si) in $In(SiMe_3)_3$ (16), of 370–380 $cm^{-1}$ for ν(In—S) in a series of toluene-3,4-dithiol derivatives of indium (17), and of 319–339 $cm^{-1}$ for this mode in $InX_3 \cdot 2Et_2S$ (X = Cl, Br) (18). The situation is undoubtedly complicated by the possibility of mixing modes of like symmetry. The present spectra contain bands at 376 m (ir) and 333 m $cm^{-1}$ (R), shown elsewhere (13) to be δ(CCP) modes of the coordinated ligand. This leaves a weak ir band at 254 $cm^{-1}$, which we tentatively assign to ν(In—P).

*N,N,N′,N′-Tetramethylethylenediamine complexes*

In the TMED series, we first consider the In—halogen stretching region, where in all cases two Raman and two non-coincident ir features are found (Table 3). This suggests the presence of a centrosymmetric $In_2X_4$ unit, which requires the $In_2X_4N_4$ kernel to adopt a conformation similar to that in the $Et_3P$ analog. Inspection of the In—N stretching region, as defined by Mertz *et al.* (19), might argue against the presence of a centre of symmetry since all four features are coincident, or nearly so, but in the context of the above discussion, we attribute this to a lowering of the overall molecular symmetry caused by the hydrocarbon framework of the ligand.

The frequencies of coordinated TMED have been reported previously (20), and we assume that the ligand is functioning as a bidentate donor in the present complexes, as implied by the presence of four ν(In—N) frequencies. This requires the indium atoms in $In_2X_4(TMED)_2$ to be five-coordinate, and the shift in the ν(In—In) frequency from 116 $cm^{-1}$ in $In_2I_4(Et_3P)_2$ to 110 $cm^{-1}$ in $In_2I_4(TMED)_2$ is consistent with an increase in coordination number from four to five. This conclusion, and the identification of a centrosymmetric $In_2I_4$ unit, reveal notable differences between these indium complexes and the gallium compounds $Ga_2Cl_4(dioxane)_2$, in which the dioxane is monodentate, the metal atoms are four-coordinate, and the molecular symmetry approximately $C_{2v}$ (9). We note in this context that some examples of five-coordination at tin are known for Sn—Sn bonded compounds (21).

The mode of coordination of *N,N,N′,N′*-tetramethylethylenediamine requires some comment. As already noted, the expected bidentate coordination seems to be confirmed by the number of bands observed in the 350–500 $cm^{-1}$ region of the spec-

Can. J. Chem. Downloaded from www.nrcresearchpress.com by 210.87.254.5 on 09/06/12
For personal use only.

Can. J. Chem. Downloaded from www.nrcresearchpress.com by 210.87.254.5 on 09/06/12
For personal use only.

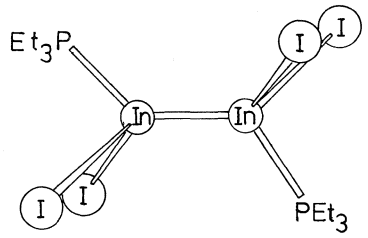


trum (ν(In—N)). This still leaves at least three possibilities to consider: (*a*) terminal TMED, (*b*) intermolecular bridging, and (*c*) intramolecular bridging. The second possibility can be rejected in view of the results for the 700–900 $cm^{-1}$ region of the infrared spectrum. Chelate-type diamines display two bands, assigned as $CH_2$ rocking vibrations at approximately 810 and 770 $cm^{-1}$, while intermolecular bridging leads to a *trans* conformation in the diamine, with ir bands at 870 and 790 $cm^{-1}$ (10, 20). Our materials show bands at 770w and 790s, implying a *cis* or *gauche* conformation of bidentate TMED, and the structures are accordingly written as $X_2$(TMED)InIn(TMED)$X_2$.

Some spectral features still remain unexplained after this analysis. Several of these can be ascribed to small amounts of impurities, as is the case of $In_2Br_4(TMED)_2C_6H_6$ where a Raman line at 197 $cm^{-1}$, and an ir feature at 236 $cm^{-1}$, point to the presence of $InBr_4^-$. Perhaps more interesting is the strong Raman line found at 129 $cm^{-1}$ in the spectrum of $In_2Br_4(TMED)_2$. The intensity and position of this feature suggest the presence of a second metal–metal bonded species, with the frequency of this vibration affected either by a higher coordination number, or by an increase of negative charge, or both. As can be seen from Table 1, the analyses for this material do not agree particularly well with the presumed composition, so that the presence of some unidentified second compound in the crude material is not unreasonable. Our interpretation has also neglected the presence of bending modes, which will be responsible for some of the features still unexplained in the assignments in Table 3.

*Reaction pathway*

Although the reaction is apparently the single addition of neutral ligand to indium dihalide, two significant factors must be recognized. The first is that few of the $InX_2^-$ ligand combinations investigated do in fact yield the desired product, and that in most cases disproportionation to $In^0$ and presumably $In^{III}$ species predominates. The second is that a deep-red or orange colour is formed on the

TABLE 3. Vibrational spectra of $In_2X_4L_2$ (in $cm^{-1}$)

| $In_2Br_4(TMED)_2$ | | $In_2Br_4(TMED)_2C_6H_6$ | | $In_2I_4(TMED)_2$ | | $In_2I_4(TMED)_2C_6H_6$[b] | $In_2I_4(Et_3P)_2$ | | Assignment[a] |
|---|---|---|---|---|---|---|---|---|---|
| Infrared | Raman | Infrared | Raman | Infrared | Raman | Infrared | Infrared | Raman | |
| 488m | 490m | 487m | 492m | 480m | | 486ms | | | |
| 460w, br | 461w | 462w | 468w | 458w | | 466w | | | ν(In—N) |
| 440m | 441vw | 442m | 445vw | 436m | | 443ms | | | |
| 397vw | 397w | 398vw | 385vw, br | 378w | | 380w | | | |
| 362vw | 368vw | 367vw | | 362vw | | 354w | 254vw | | Unassigned |
| | | | | | | | | | ν(In—P)? |
| | | | | | | 200m, br | | | Unassigned |
| | 233vw | | 240m | 220m | 211w | | | 202w | |
| 210s | | 210s | | 160m | | 172m | 178vs | | ν(In—X), |
| 190s, br | | 192s, br | | 144m | | 148s | 152vs | | $A_g + B_g + A_u + B_u$ |
| | 188w | | 175w | | 137m | | | 169w | |
| | 141s | | 139s | | 110s | | | 116s | ν(In—In), $A_g$ |
| 152s, br | 155sh | 153m, br | | | | | | | |
| 128m | 129s | 128m | | 130sh | | 106s | | | Bending modes |
| 103m | 86m | 102m | 86m | | | 95sh | | | |

[a] All species were assigned on the basis of $C_{2h}$ symmetry for the $In_2X_4$ kernel.
[b] Raman data not available.

addition of either anionic (5) or neutral ligands (this work) to solutions of indium dihalide, which is compatible with the establishment of the equilibrium

$$In_2X_4 \rightleftharpoons InX + InX_3.$$

Since very little is known about the solution chemistry of indium(I) or indium(II) compounds in aromatic solvents, we are presently unable to rationalize these various observations, and work on these and related problems is continuing.

### Acknowledgement

This work was supported by a grant from the Indium Corporation of America. One of us (M.J.T.) thanks the University of Auckland for the award of a sabbatical leave.

1. J. J. Habeeb and D. G. Tuck. J. Chem. Soc. Dalton Trans. 1815 (1975).
2. M. J. Taylor, D. G. Tuck, and L. Victoriano. J. Chem. Soc. Dalton Trans. 928 (1981).
3. J. J. Habeeb and D. G. Tuck. J. Chem. Soc. Dalton Trans. 866 (1976).
4. B. H. Freeland and D. G. Tuck. Inorg. Chem. **15**, 475 (1976).
5. B. H. Freeland, J. L. Hencher, D. G. Tuck, and J. G. Contreras. Inorg. Chem. **15**, 2144 (1976).
6. C. A. Evans, K.-H. Tan, S. P. Tapper, and M. J. Taylor. J. Chem. Soc. Dalton Trans. 988 (1973).
7. K. L. Brown and D. Hall. J. Chem. Soc. Dalton Trans. 1843 (1973).
8. M. Khan, C. Oldham, M. J. Taylor, and D. G. Tuck. Inorg. Nucl. Chem. Lett. **16**, 469 (1980).
9. J. C. Beamish, R. W. H. Small, and I. J. Worrall. Inorg. Chem. **18**, 220 (1979).
10. K. Nakamoto. Infrared spectra of inorganic and coordination compounds. 3rd ed. Wiley-Interscience, New York. 1978.
11. J. H. S. Green. Spectrochim. Acta, **24A**, 137 (1968).
12. D. M. Adams. Metal–ligand and related vibrations. E. Arnold, London. 1967.
13. K. Shobatake and K. Nakamoto. J. Am. Chem. Soc. **92**, 3332 (1970).
14. A. J. Carty, T. Hinsperger, and P. M. Boorman. Can. J. Chem. **48**, 1959 (1970).
15. G. A. Ozin. J. Chem. Soc. A, 1307 (1970).
16. H. Bürger and U. Goetze. Angew. Chem. Int. Ed. **8**, 140 (1969).
17. D. G. Tuck and M. K. Yang. J. Chem. Soc. A, 214 (1971).
18. C. A. Evans and M. J. Taylor. J. Chem. Soc. A, 1343 (1969).
19. K. Mertz, W. Schwartz, B. Eberwein, J. Weidlein, H. Hess, and H. D. Hausen. Z. Anorg. Chem. **429**, 99 (1977).
20. L. Maresca, G. Natide, and G. Rizzardi. Inorg. Chim. Acta, **38**, 53 (1980).
21. M. J. Taylor. Metal-to-metal bonded states of the main group elements. Academic Press, New York. 1975. pp. 82–88.

Can. J. Chem. Downloaded from www.nrcresearchpress.com by 210.87.254.5 on 09/06/12
For personal use only.

# Neutral complexes of the indium dihalides

IAN SINCLAIR AND IAN J. WORRALL

*Department of Chemistry, The University of Lancaster, Bailrigg, Lancaster LA1 4YA, England*

Received August 25, 1981

IAN SINCLAIR and IAN J. WORRALL. Can. J. Chem. **60**, 695 (1982).

The neutral complexes $In_2X_4 \cdot 2L$ (X = Cl, Br, I; L = 1,4-dioxan, tetrahydropyran, tetrahydrofuran, tetrahydrothiophene), $In_2X_4 \cdot 2L$ (X = Br, I; L = dimethylsulphide), $In_2X_4 \cdot 4L$ (X = Cl, Br, I; L = piperidine, piperazine, morpholine), and $In_2X_4 \cdot 4L$ (X = Br, I; L = pyridine, dimethylsulphoxide) have been prepared. Solid state Raman spectra indicate that the compounds contain indium–indium bonds.

IAN SINCLAIR et IAN J. WORRALL. Can. J. Chem. **60**, 695 (1982).

On a préparé les complexes neutres $In_2X_4 \cdot 2L$ (X = Cl, Br, I; L = dioxanne-1,4 tétrahydropyranne, tétrahydrofuranne, tétrahydrothiophène), $In_2X_4 \cdot 2L$ (X = Br, I; L = sulfure de diméthyle), $In_2X_4 \cdot 4L$ (X = Cl, Br, I; L = pipéridine, pipérazine, morpholine) et $In_2X_4 \cdot 4L$ (X = Br, I; L = pyridine, diméthylsulfoxyde). Les spectres Raman à l'état solide indiquent que ces composés contiennent des liaisons In–In.

[Traduit par le journal]

## Introduction

Although the gallium halides $Ga_2X_4$ are ionic mixed oxidation state compounds they react with many ligands to form neutral gallium–gallium bonded complexes (1, 2). Recent crystal structure determinations have confirmed the presence of these bonds in $Ga_2X_4 \cdot 2$dioxan (X = Cl, Br) (1, 3) and $Ga_2Br_4 \cdot 2$pyridine (4). The use of the structurally similar indium and thallium dihalides to prepare neutral metal–metal bonded complexes of these elements is a logical extension to the gallium work and we here report the preparation of a number of neutral indium compounds which appear to be similar to their gallium analogues and contain indium–indium bonds.

A survey of previous work suggests that the indium dihalides are capable of forming both ionic and neutral complexes; aniline complexes of stoichiometry $InX_2 \cdot 2$aniline have been formulated In(aniline)$_4^+InX_4^-$ (5) and Russian workers have proposed that metal–metal bonds are present in the complexes $InX_2 \cdot 3NH_3$, $InX_2 \cdot 4NH_3$, $InI_2 \cdot 3EtNH_2$, and $InI_2 \cdot$bipy$\cdot 2EtNH_2$ (bipy = 2,2′-bipyridyl) although no structural evidence has been reported in support of these formulations (6). Very recently Tuck *et al.* (7) have reported the preparation of a number of ionic complexes with macrocyclic ligands and in the same paper state that they have prepared the neutral compounds, e.g. $In_2I_4 \cdot 2PEt_3$ and $In_2Br_4 \cdot 2$(tmen) (tmen = *NNN′N′*-tetramethylethylenediamine) although no details were given.[1]

## Experimental

*Purification of ligands and solvents*

Pyridine, piperidine, and morpholine were refluxed over KOH for 24 h and fractionally distilled from BaO. 1,4-Dioxan, dimethyl sulphide, tetrahydropyran, tetrahydrofuran, and tetrahydrothiophene were refluxed over LiH for 24 h and fractionally distilled. Dimethylsulphoxide was passed down a column of freshly activated alumina and fractionally distilled from BaO. Diethyl and xylene were refluxed over sodium wire for 24 h and fractionally distilled.

*Preparation of $In_2Br_4$ complexes*

(*a*) Dimethyl sulphide, dimethylsulphoxide, tetrahydrofuran, and tetrahydrothiophene complexes: A vial of powdered indium dibromide was opened in a nitrogen-filled dry-box and transferred to a round bottomed flask. The flask was evacuated on a vacuum line, cooled with liquid nitrogen, and ligand condensed on to the halide. This procedure was adopted for the preparation of most complexes. As the ligand melted the mixture was mechanically stirred; an orange compound, thought to be InBr, was initially precipitated and this reacted slowly to produce a colourless solution. On removal of excess ligand a white powder remained.

(*b*) Tetrahydropyran complex: A large excess of tetrahydropyran was condensed on to $InBr_2$ over a period of 2 h. The temperature was allowed to rise to the melting point of the ligand and the solution stirred for 1–2 min until a solution formed. This was then solidified by freezing and the excess ligand removed from the solid; a yellow powder remained. If the described conditions were not strictly adhered to then disproportionation to InBr and the soluble $InBr_3$ complex occurred.

(*c*) Morpholine and piperidine complexes: A large excess of ligand was condensed on to $InBr_2$ and the mixture slowly allowed to warm up to room temperature. After removal of excess ligand a white powder remained.

(*d*) Pyridine complex: This was prepared by the same method as described for the morpholine complex but the reaction temperature was maintained at −30°C. Above this temperature indium metal was deposited. The reaction yielded a white solid which was stable once the excess pyridine had been removed.

(*e*) Tetrahydrofuran complex: Excess ligand was condensed on to $InBr_2$, the mixture was shaken for 20 min and stirred for a further 4 h and after the removal of excess ligand a white solid remained.

(*f*) 1,4-Dioxan complex: The direct addition of this ligand to $InBr_2$ invariably produced InBr and $InBr_2 \cdot$dioxan. However, the complex was successfully prepared by the following indirect method: dry nitromethane was added to $InBr_2$, the orange solid, which initially formed slowly dissolved on stirring and on removal of the excess nitromethane a glassy substance remain-

[1]Full details are now given in the preceding paper (16).

0008-4042/82/060695-04$01.00/0

©1982 National Research Council of Canada/Conseil national de recherches du Canada

Can. J. Chem. Downloaded from www.nrcresearchpress.com by 210.87.254.42 on 09/06/12
For personal use only.

Can. J. Chem. Downloaded from www.nrcresearchpress.com by 210.87.254.42 on 09/06/12
For personal use only.

TABLE 1. Analytical data*

| Complex | Found | | | | Calcd | | | |
|---|---|---|---|---|---|---|---|---|
| | In | Cl | Br | I | In | Cl | Br | I |
| $In_2Cl_4$.2dioxan | 42.2 | 25.7 | — | — | 41.9 | 25.9 | — | — |
| $In_2Br_4$.2dioxan | 31.4 | — | 44.5 | — | 31.6 | — | 44.1 | — |
| $In_2I_4$.2dioxan | 25.1 | — | — | 55.1 | 25.1 | — | — | 55.6 |
| $In_2Cl_4$.2THP | 42.2 | 26.0 | — | — | 42.2 | 26.1 | — | — |
| $In_2Br_4$.2THP | 32.0 | — | 44.2 | — | 31.8 | — | 44.3 | — |
| $In_2I_4$.2THP | 25.1 | — | — | 55.9 | 25.3 | — | — | 55.8 |
| $In_2Cl_4$.2THF | 44.5 | 27.3 | — | — | 44.5 | 27.5 | — | — |
| $In_2Br_4$.2THF | 33.0 | — | 45.6 | — | 33.1 | — | 46.1 | — |
| $In_2I_4$.2THF | 25.9 | — | — | 57.2 | 26.1 | — | — | 57.6 |
| $In_2Cl_4$.2THT | 41.6 | 26.5 | — | — | 41.9 | 25.9 | — | — |
| $In_2Br_4$.2THT | 31.9 | — | 43.9 | — | 31.7 | — | 44.1 | — |
| $In_2I_4$.2THT | 25.1 | — | — | 55.4 | 25.1 | — | — | 55.6 |
| $In_2Br_4$.2DMS | 33.9 | — | 47.2 | — | 34.1 | — | 47.5 | — |
| $In_2I_4$.2DMS | 26.9 | — | — | 58.7 | 26.7 | — | — | 58.9 |
| $In_2Br_4$.4pyridine | 26.7 | — | 37.1 | — | 26.5 | — | 36.9 | — |
| $In_2I_4$.4pyridine | 21.8 | — | — | 47.7 | 21.8 | — | — | 48.1 |
| $In_2Cl_4$.4piperidine | 32.3 | 19.7 | — | — | 32.3 | 19.9 | — | — |
| $In_2Br_4$.4piperidine | 25.7 | — | 35.5 | — | 25.8 | — | 35.9 | — |
| $In_2I_4$.4piperidine | 21.2 | — | — | 47.5 | 21.3 | — | — | 47.1 |
| $In_2Cl_4$.4piperazine | 32.9 | 19.8 | — | — | 32.2 | 19.8 | — | — |
| $In_2Br_4$.4piperazine | 25.6 | — | 36.0 | — | 25.7 | — | 35.8 | — |
| $In_2I_4$.4piperazine | 21.1 | — | — | 46.6 | 21.2 | — | — | 46.9 |
| $In_2Cl_4$.4morpholine | 31.9 | 19.4 | — | — | 31.9 | 19.7 | — | — |
| $In_2Br_4$.4morpholine | 25.7 | — | 35.4 | — | 25.6 | — | 35.6 | — |
| $In_2I_4$.4morpholine | 21.0 | — | — | 46.9 | 21.1 | — | — | 46.7 |
| $In_2Br_4$.4DMSO | 26.5 | — | 36.8 | — | 26.6 | — | 37.1 | — |
| $In_2I_4$.4DMSO | 21.6 | — | — | 47.8 | 21.8 | — | — | 48.4 |

*THP = tetrahydropyran, THF = tetrahydrofuran, THT = tetrahydrothiophene, DMS = dimethylsulphide, DMSO = dimethylsulphoxide.

ed. 1,4-Dioxan was then condensed on to the glass and a white solid formed; this was dried under vacuum.

(*g*) Piperazine complex: A dilute xylene solution of piperazine was added to a suspension of $InBr_2$ in xylene in an atmosphere of dry nitrogen. A white precipitate formed which was separated from the liquid by centrifugation. The white solid was washed with xylene and ether and dried under vacuum.

*Preparation of chloride and iodide complexes*

The preparative methods are very similar. In most reactions a precipitate initially formed and this is thought to be the monohalide, i.e. yellow (InCl) in chloride reactions and purple (InI) in iodide reactions. In the case of $In_2Cl_4$ we were unable to prepare complexes with pyridine, dimethylsulphide, or dimethylsulphoxide since decomposition to metal always occurred.

The indium dihalides were prepared from indium metal and indium trihalides (8–10).

*Raman spectra*

Spectra were recorded on solid samples using an Anaspec 81 L spectrometer and radiation of wavelength 541.5 nm. Spectra could only be obtained on two chloride compounds since the others decomposed in the laser beam even at very low power. Data are given in Table 2 together with the ions $In_2X_6^{2-}$ (12) in the range 100–400 $cm^{-1}$.

*Analytical data*

Indium was determined by atomic absorption spectrophotometry and halogen by Volhard's method. Data are given in Table 1.

## Results and discussion

Analytical results show that two types of compound are formed with stoichiometry $In_2X_4 \cdot 2L$ and $In_2X_4 \cdot 4L$; the former with O and S donors and the latter with N donors (with one exception: dimethylsulphoxide). The same stoichiometries have been reported by Brewer *et al.* for the analogous gallium compounds (11).

The possibility that the complexes have simple ionic structures of the type, e.g. $InL_4^+InX_4^-$ can be ruled out since the characteristic strong bands of the $InX_4^-$ ions are absent in their Raman spectra (Table 2). Conductivity measurements could not be obtained due to the instability of the complexes in the solvents used; however, such measurements have proved to be unreliable in some of the gallium analogues, e.g. conductivity measurements show that $Ga_2Cl_4 \cdot 2$dioxan is ionic in nitrobenzene solution whereas the solid state structure is covalent (1, 11).

The Raman spectra (in the range 100–400 $cm^{-1}$) of all known gallium–gallium species with ethane-like structures each consist of one very intense band together with a smaller number of weaker bands. The very intense band is associated with the gallium–gallium stretching mode and the weaker bands with gallium–halogen modes. In addition the position of the very intense bands in neutral complexes is very similar to observed bands in the parent halides; e.g. $Ga_2Cl_6^{2-}$ 233 $cm^{-1}$, $Ga_2Cl_4$·-

TABLE 2. Raman spectra of complexes in the range 100–400 $cm^{-1}$*

| Complex | ν ($cm^{-1}$) |
|---|---|
| $In_2Cl_4$.2dioxan | *177*vs 322w 338m |
| $In_2Cl_4$.2THT | 136w 144w *169*vs 208w 216w 317w 337w |
| $In_2Cl_6^{2-}$ (12) | *174*vs 289m 325m |
| $In_2Br_4$.2dioxan | *123*vs 150w 202w |
| $In_2Br_4$.2THT | *139*vs 200w 245w |
| $In_2Br_4$.2THP | 112w 119w *144*vs 160w 175w 197w 228w 247w |
| $In_2Br_4$.2THF | *140*vs 225w 247w |
| $In_2Br_4$.2DMS | 110m *139*vs 200w |
| $In_2Br_4$.4pyridine | 115w *128*vs 142w 162w 170w 180w 192w 214w |
| $In_2Br_4$.4piperidine | *138*s 202w 238w |
| $In_2Br_4$.4piperazine | *143*vs 169m 190w 203w 222w 238w |
| $In_2Br_4$.4morpholine | *143*vs 200w 213w 221w |
| $In_2Br_4$.4DMSO | *147*vs 160w 229w 251w |
| $In_2Br_6^{2-}$ (12) | *139*vs 202w 244w |
| $In_2I_4$.2dioxan | *102*vs 138w 155w 183w |
| $In_2I_4$.2THT | *110*vs 149w 210w |
| $In_2I_4$.2THP | *112*vs 140w 148w 157w 175w 191w 203w |
| $In_2I_4$.2THF | *108*vs 144w 155w 190w 237w |
| $In_2I_4$.2DMS | *102*vs 160w |
| $In_2I_4$.4pyridine | *107*s |
| $In_2I_4$.4piperidine | *107*vs 152w 187w 224w |
| $In_2I_4$.4piperazine | *104*s 200w |
| $In_2I_4$.4morpholine | *104*vs 121w 131w 169w |
| $In_2I_4$.4DMSO | 102w *108*s 131m 151m 164w 183w 197w 208w 237w |
| $In_2I_6^{2-}$ (12) | *108*vs 152w 210w |

*vs = very strong, s = strong, m = medium, w = weak.

2dioxan 238 $cm^{-1}$; $Ga_2Br_6^{2-}$ 164 $cm^{-1}$, $Ga_2Br_4$·2dioxan 169 $cm^{-1}$, $Ga_2Br_4$·2pyridine 168 $cm^{-1}$ (1, 2). It is seen in Table 2 that the indium–halide complexes conform to a similar pattern and we therefore conclude that they have similar indium–indium bonded structures.

Band assignment is necessarily speculative due to the absence of X-ray crystallographic data and attempts to grow suitable crystals have so far been unsuccessful. In addition we were unable to measure low frequency infrared spectra. However, the very close similarity (with few exceptions) in the position of the very strong bands (italics in Table 2) compared with those observed for the parent anions $In_2X_6^{2-}$ (12), and in view of the recent assignments by Tuck *et al.* (16) for analogous bromide and iodide complexes we assign the strong bands to $\nu_{In—In}$. The positions of the intense bands are remarkably similar for each set of complexes, falling in the range 173 ± 4 $cm^{-1}$ for the chloride series, 143 ± 4 $cm^{-1}$ for the bromide series (excluding the dioxan and pyridine complexes), and 105 ± 5 $cm^{-1}$ for the iodide series. This constancy is perhaps surprising in view of (*a*) the apparent difference in coordination about indium in $In_2X_4$·2L and $In_2X_4$·4L and, (*b*) the large shifts observed in the mixed halide ions, e.g. $In_2Cl_4Br_2^{2-}$, $\nu_{In—In}$ = 163 $cm^{-1}$ and $In_2Cl_4I_2^{2-}$, $\nu_{In—In}$ = 147 $cm^{-1}$ (13). To fully explain these facts it is necessary to consider the mixing of the various modes and this is not possible with the available data. Mixing effects in analogous gallium systems have been previously discussed (1, 14).

The remaining higher bands are assigned to metal–halogen modes and their numbers will depend upon the symmetry of the molecules and their environments within the crystal, which are unknown. Of the three neutral gallium complexes of known structure, $Ga_2X_4$·2dioxan (X = Cl, Br) have $C_1$ symmetry and $Ga_2Br_4$·2pyridine $C_{2h}$, and their Raman spectra reflect these symmetry differences. No attempt is made here to deduce the symmetry of the indium complexes from the number of higher bands since these are generally of weak intensity and it is possible that in some cases not all bands have been observed (e.g. only the strong band was observed for $In_2I_4$·4pyridine), whilst in others an excess of bands may be due to trace impurities (e.g. in $In_2Br_4$·4pyridine the band at 180 $cm^{-1}$ may be due to $InBr_3$·3pyridine and the band at 192 to $InBr_4^-$).

Ligand bands were observed for all complexes and it is thought that the mode of coordination of morpholine is via nitrogen since the N—H frequency is lowered from 3340 $cm^{-1}$ in morpholine to 3286–3296 $cm^{-1}$ (15) in the complexes.

Since spectroscopic data provide strong evidence for the occurrence of indium–indium bonds in both 4:1 and 2:1 complexes we propose that both types are neutral and the 4:1 contains five coordi-

Can. J. Chem. Downloaded from www.nrcresearchpress.com by 210.87.254.42 on 09/06/12
For personal use only.

nate indium and has the structure

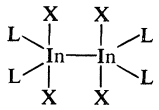

and the 2:1 complexes are expected to be isostructural with their gallium analogues i.e.

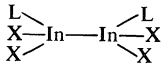

Ligand strength appears to be the dominant factor here since all of the nitrogen donors examined and dimethylsulphoxide form 4:1 complexes whilst the weaker oxygen and sulphur donors form 2:1 complexes.

A comparison between the complexes formed by the similar sized ligands, dioxan and morpholine, emphasizes this point where 2:1 adducts are formed by the former and 4:1 by the latter.

**Acknowledgements**

We thank Mr. A. Boardman for discussions and Professor D. G. Tuck for delaying publication of his paper to enable us to publish simultaneously.

1. J. C. Beamish, R. W. H. Small, and I. J. Worrall. Inorg. Chem. **18**, 220 (1979).
2. A. Boardman and I. J. Worrall. Unpublished results.
3. R. H. W. Small and I. J. Worrall. Acta Crystallogr. In press.
4. R. W. H. Small and I. J. Worrall. Acta Crystallogr. In press.
5. P. L. Goggin and I. J. McColm. J. Inorg. Nucl. Chem. **28**, 2501 (1966).
6. A. P. Kochetkova and O. N. Gilrayov. Zh. Neorg. Khim. **11**, 1239 (1966).
7. M. J. Taylor and D. G. Tuck. J. Chem. Soc. Dalton, 928 (1981).
8. J. H. R. Clark and R. E. Hester. Inorg. Chem. **8**, 1113 (1969).
9. P. H. L. Walter, J. Kleinberg, and E. Griswald. J. Inorg. Nucl. Chem. **19**, 223 (1961).
10. J. E. Davies, L. G. Waterworth, and I. J. Worrall. J. Inorg. Nucl. Chem. **36**, 805 (1974).
11. S. M. Ali, F. M. Brewer, J. R. Chadwick, and G. Garton. J. Inorg. Nucl. Chem. **9**, 124 (1959).
12. B. H. Freeland, J. L. Hencher, D. G. Tuck, and J. G. Contreras. Inorg. Chem. **15**, 2144 (1976).
13. I. Sinclair. Ph.D. Thesis, University of Lancaster, England. 1980.
14. C. A. Evans, K. H. Tan, S. P. Tapper, and M. J. Taylor. J. Chem. Soc. Dalton, 988 (1973).
15. G. Marcotrigiano and G. C. Pellacani. Spectrochim. Acta, **31A**, 1865 (1975).
16. M. J. Taylor, D. G. Tuck, and L. Victoriano. Can. J. Chem. **60**, 690 (1982).

Can. J. Chem. Downloaded from www.nrcresearchpress.com by 210.87.254.42 on 09/06/12
For personal use only.

# The electronic structure of cyclopentadienylindium

C. S. LIN AND DENNIS G. TUCK
*Department of Chemistry, University of Windsor, Windsor, Ont., Canada N9B 3P4*

Received July 20, 1981

C. S. LIN and DENNIS G. TUCK. Can. J. Chem. **60**, 699 (1982).

CNDO calculations have been carried out for the molecule $InC_5H_5$ of $C_{5v}$ symmetry. Overlap populations were calculated and compared with those for related species. The bonding between In and the organic moiety can be described as essentially a covalent interaction involving mainly indium 5*s* and 5*p* orbitals with ring $p_\pi$ orbitals. A lone pair on indium is a dominant feature of the structure, and is largely responsible for a (calculated) dipole moment of 4.75 D. The calculated orbital energies are compared with experimental photoelectron spectra.

C. S. LIN et DENNIS G. TUCK. Can. J. Chem. **60**, 699 (1982).

On a effectué des calculs CNDO pour la molécule de $InC_5H_5$ de symétrie $C_{5v}$. On a calculé le recouvrement des populations et on les a comparé à celui des espèces apparentées. On peut décrire la liaison entre In et la portion organique comme étant essentiellement une interaction covalente impliquant principalement les orbitales 5*s* et 5*p* de l'indium avec les orbitales $p_\pi$ du cycle. Le trait dominant de la structure est le doublet libre de l'indium, et il est grandement responsable d'un moment dipolaire (calculé) de 4,75 D. On a comparé les énergies calculées des orbitales aux spectres photoélectroniques expérimentaux.

[Traduit par le journal]

## Introduction

Cyclopentadienylindium (CpIn), first prepared by Fischer and Hofmann (1) in 1957, is a molecule of some interest for at least two reasons. The first, and the more readily disposed of, is that it is the only readily accessible indium(I) compound which is soluble in common organic solvents, and as such is a useful starting point in the synthesis of indium(I) complexes (2, 3). The second reason is more apposite to this paper; the compound presents an interesting problem in structure and bonding, and the nature of the latter has been the subject of some discussion.

The structure of the molecule in the gas phase has been unambiguously established by the precise electron diffraction study of Shibata, Bartell, and Gavin (4). The results of their work are summarised in Fig. 1, which shows that the molecule indeed has the half-sandwich pentahapto-ligand structure originally postulated by Fischer (1, 5). In the crystalline state, the CpIn molecules line up in an almost linear head-to-tail fashion (6). Bartell *et al.* (4) have reviewed the various attempts to explain the bonding in this molecule (and in the isostructural (7) thallium species). The Fischer and Hofmann representation involves donation from the $\pi$-orbitals of $C_5H_5^-$ into the vacant 5*p* orbitals of $In^+$. Cotton and Reynolds (8) proposed an ionic structure, but Bartell *et al.* showed that this was incorrect, and in fact carried out overlap integral calculations which supported a covalent description of the In—$C_5H_5$ bonding.

In two recent publications, Cradock and Duncan (9) and Egdell, Fragala, and Orchard (10) have reported the He(I) and He(II) photoelectron spectrum of CpIn, with results which are in good agreement. The interpretation is based upon earlier studies of transition metal cyclopentadienyl sandwich compounds, which we believe to be an inappropriate model for CpIn. The present paper reports the results of CNDO calculations which lead to an analysis of the bonding and the electronic properties of the molecule.

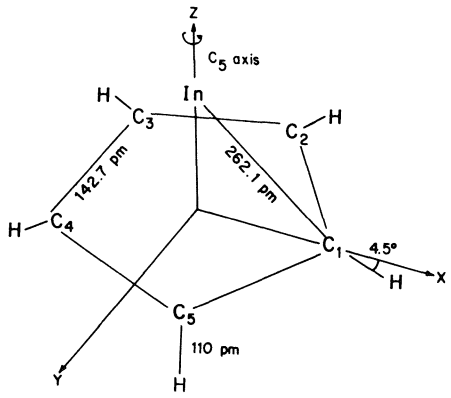


FIG. 1. Structural parameters and coordinate system for cyclopentadienylindium.

## Experimental

*Calculations and results*

Molecular orbitals and corresponding orbital energies were calculated by using the CNDO computer programme of Rinaldi (11), without optimization with respect to the molecular geometry. The theory (12), and the parameters used in the programme, are standard and well-documented and are not detailed here. The bond distances and angles used in this calculation are

0008-4042/82/060699-04$01.00/0
©1982 National Research Council of Canada/Conseil national de recherches du Canada

Can. J. Chem. Downloaded from www.nrcresearchpress.com by 210.87.254.6 on 09/06/12
For personal use only.

TABLE 1. Approximate descriptions of highest occupied molecular orbitals of CpIn[a]

| M.O. | Description | | |
|---|---|---|---|
| | In | C | H |
| $\psi_{14}$ | $0.89(s) + 0.43(z)$ | | |
| $\psi_{13}$ | $0.40(x)$ | $0.57(z_1) + 0.18(z_2 + z_5) - 0.46(z_3 + z_4)$ | |
| $\psi_{12}$ | $0.40(y)$ | $+ 0.55(z_2 - z_5) + 0.34(z_3 - z_4)$ | |
| $\psi_{11}$ | | $0.13(s_1) - 0.11(s_3 + s_4) - 0.44(x_1) + 0.17(x_2 + x_5) - 0.21(x_3 + x_4) - 0.20(y_2 - y_5) + 0.32(y_3 - y_4)$ | $-0.36(s_1) - 0.11(s_2 + s_5) + 0.29(s_3 + s_4)$ |
| $\psi_{10}$ | | $0.12(s_2 - s_5) - 0.20(x_2 - x_5) + 0.32(x_3 - x_4) + 0.23(y_1) - 0.37(y_2 + y_5)$ | $- 0.34(s_2 - s_5) - 0.22(s_3 - s_4)$ |
| $\psi_9$ | | $0.29(x_2 - x_3 + x_4 - x_5) + 0.44(y_1) - 0.26(y_2 + y_5)$ | $- 0.21(s_2 - s_5) + 0.33(s_3 - s_4)$ |
| $\psi_8$ | | $0.10(s_1) + 0.27(x_1) - 0.31(x_2 + x_5) + 0.18(x_3 + x_4) - 0.13(y_2 - y_5) + 0.39(y_3 - y_4)$ | |
| $\psi_7$ | $0.27(s) - 0.21(z)$ | $+ 0.42(z_1 + z_2 + z_3 + z_4 + z_5)$ | |

[a]Atomic orbitals with coefficients less than 0.10 are omitted.

derived from the work of Bartell *et al.* (4); the values and the coordinate axes adopted are shown in Fig. 1.

The CNDO molecular orbital scheme gives rise to fourteen occupied orbitals; Table 1 lists the top seven of these with approximate descriptions. Electron densities in the atomic orbitals, and gross atomic electronic densities, are given in Table 2, and the breakdown of the overlap population in Table 3.

*Dipole moment*

The dipole moment of CpIn in toluene solution (approximately 0.01 mol $L^{-1}$) was determined on a WTW DM-01 instrument at a sample temperature of 40°C. The experimental value was $2.2 \pm 0.2$ D.

## Discussion

### *Bonding*

Table 2 demonstrates the conspicuous absence of ionic character in the bonding. The negative charge on the indium atom is only 0.059e, with the positive charges spread almost evenly among other atoms. Although the five carbon atoms are coplanar, the geometry of the molecule induces the conventional carbon π atomic orbitals ($2p_z$) to mix with the $2s$, $2p_x$, and $2p_y$ orbitals to some extent in order to bond with the indium and hydrogen atoms. As the result of indium–carbon bond formation, a slight build-up of electron density occurs in the space between indium and the plane of carbon atoms, as indicated by the values for $2p_z$ in Table 2. These densities are obviously siphoned off from carbon–carbon and carbon–hydrogen bonds, but since the shift is small, the effect on the ring σ-bonds is apparently negligible.

TABLE 2. Electron densities in atomic orbitals, and gross atomic electron densities, in CpIn

| Orbital | Electron density | | |
|---|---|---|---|
| | In | C | H |
| $s$ | 1.7773 | 0.9998 | 0.9956 |
| $p_x + p_y$ | 0.7364 | 1.9689 | — |
| $p_z$ | 0.5453 | 1.0238 | — |
| Sum | 3.0590 | 3.9927 | 0.9956 |

TABLE 3. Overlap population distribution in CpIn

| | Indium | | |
|---|---|---|---|
| | $5sp_z$ | $5p_x + 5p_y$ | Sum |
| Carbon | | | |
| $2s + 2p_x + 2p_y$ | 0.44 | 0.14 | 0.58 |
| $2p_z$ | 0.33 | 0.25 | 0.58 |
| Sum | 0.77 | 0.39 | — |

In order to analyze the results of the calculations, the overlap population $q_{kl}$ defined by Mulliken (13) was computed, with the following results.

(*a*) Bonding in the hydrocarbon ring. The overlap population for the C—C bond is 0.88, to be compared with the value of 0.55 for the C—C single bond in ethane (14). The resultant ratio of 1.60 is only fractionally lower than the comparable value of 1.67 for benzene, and quite close to that for the C—C bonds in the graphite ring (1.525). Bartell *et al.* (4) obtained a value of 1.40 by considering the equivalent resonance structures of CpIn. The overlap population in the C—H bonds of CpIn is 0.67, which is practically the same as the value of 0.678 for C—H in ethane (14).

The CNDO calculations of Del Bene and Jaffé (15) place the lowest π electron ionisation potential of cyclopentadiene, $e_1(\pi)$, at 9.94 eV. The calculated ionisation potential for the corresponding molecular orbitals in CpIn ($\psi_{12}$, $\psi_{13}$) is 12.54 eV. The difference of 2.60 eV gives a rough estimate of the additional binding energy for an electron in $e_1(\pi)$ due to the bonding of the ring to indium.

(*b*) Indium–carbon bond. Molecular geometry dictates that, in the first approximation, an $sp_z$

Can. J. Chem. Downloaded from www.nrcresearchpress.com by 210.87.254.6 on 09/06/12
For personal use only.

Can. J. Chem. Downloaded from www.nrcresearchpress.com by 210.87.254.6 on 09/06/12
For personal use only.

hybrid on the indium atom be bonded to the totally symmetric σ and π symmetry orbitals of the hydrocarbon ($\psi_7$, $\psi_{14}$), while the $5p_x$ and $5p_y$ orbitals are bonded to the doubly degenerate symmetry orbitals $e_1(\psi_{12}, \psi_{13})$. Although the differentiation between the σ and π atomic orbitals is not strictly valid because of the geometry of the molecule, the above bonding scheme is still essentially correct and is indeed substantiated by the CNDO calculations.

The lone pair ($\psi_{14}$; see below) accounts for 1.566e and 0.365e of the total electron densities of 1.777e and 0.545e in the $5s$ and $5p_z$ atomic orbitals of indium. Since this lone pair contributes little to the In—$C_5H_5$ bonding, only 0.211e and 0.18e in these respective atomic orbitals participate in the bonding to the organic group. By comparison, the entire electron density (0.368e) in both $5p_x$ and $5p_y$ is involved in the bonding ($\psi_{12}$, $\psi_{13}$). Despite the lower electron density available for bonding from the $sp_z$ hybrid, Table 3 shows that this orbital contributes twice as much towards the overlap population as do $5p_x + 5p_y$. In fact, it accounts for two-thirds of the total overlap population (i.e. bonding) between indium and $C_5H_5$, which is to be expected since in this system the $sp_z$ hybrid is what is traditionally regarded as a σ atomic orbital and overlaps effectively with the π orbitals of the hydrocarbon. This observation confirms the view of Bartell *et al.* (4) that an $sp_z$ hybrid on the metal plays an important role in the indium–carbon bonding. Table 3 also shows the σ atomic orbitals ($2s$, $2p_x$, $2p_y$) of the carbon atoms participating as strongly in the bonding to indium as do the $2p_z$ orbitals.

Overall then, while there is a slight shift of electron density from the σ-bonds of the cyclopentadienyl into the indium–carbon bond, as shown by the values for $2p_z$ in Table 2, there is virtually no interatomic transfer of electron density, so that the bonding is essentially covalent in nature. The metal–ring bonding involves both σ- and π-interactions, with the former predominating (Table 3).

(*c*) Lone pair on indium. The highest occupied orbital in the CNDO molecular orbital scheme ($\psi_{14}$) represents a large lone pair (1.93e) on the indium atom, pointing diametrically away from the Cp ring. It is predominantly $5s$ in character with approximately 18% contribution from $5p_z$ and only 3.5% from all other atoms. In fact, it is this lone pair of electrons which contributes most to the calculated molecular electric dipole moment of 4.75 D; since there is practically no transfer of electron densities between atoms, the component of dipole moment arising from the charges amounts to only 0.67 D, with the remaining 4.08 D coming from the lone pair. The theoretical value is much higher than the experimental value of 2.2 ± 0.2 D, not an unusual situation in CNDO calculations. The presence of a large lone pair has formed the basis for earlier discussions of certain aspects of the chemistry of CpIn (16, 17).

*Ionisation potentials*

Table 4 compares the experimental values for the ionisation potentials of CpIn with those derived from the CNDO calculations. The agreement is within the limits normally placed upon such calculations, with the differences ranging from about 1 eV for a lone pair orbital to several eV for a bonding molecular orbital, often increasing with the binding energy. This calculation brought forth two questions inherent to the interpretation of experimental photoelectron spectra on the basis of Koopman's theorem.

Firstly, while our CNDO calculation identifies the lowest ionisation potential of this molecule with the lone pair ($\psi_{14}$) on the metal atom, both Cradock and Duncan (9), and Egdell *et al.* (10) interpret this peak as originating from the doubly degenerate $e_1(\pi)$ of the organic moiety. These authors (9, 10)

TABLE 4. Some ionisation potentials of CpIn

| Ionisation potential (eV) | | Molecular orbital[c] |
|---|---|---|
| Expt.[a] | CNDO[b] | |
| 8.28 | 9.34 | $\psi_{14}$ |
| 9.23 | 12.54 | $\psi_{12}, \psi_{13}$ |
| 12.89 | 16.76, 16.31 | $\psi_8, \psi_9, \psi_{10}, \psi_{11}$ |
| 16.26 | | |
| 16.95 | | |

[a] From ref. 10.
[b] Present work.
[c] See Table 1 for further details.

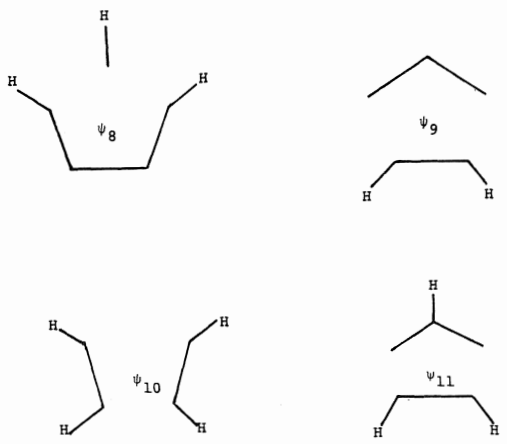


FIG. 2. Bonding schemes of $\psi_8$–$\psi_{11}$.

based their interpretation on the photoelectron spectra of transition element metallocenes (18, 19). Symmetry consideration certainly would indicate that in a *sandwich* complex the lone pair on In should be exclusively *s* in character, and that the lowest ionisation potential should be for the removal of an electron from an $e_1(\pi)$ molecular orbital, but the same argument also clearly indicates that the bonding and electronic structure of indium in CpIn is so fundamentally different from that in a sandwich complex as to render invalid any interpretation of the spectrum of one system on the basis of the other.

Although several lines of argument can be cited to support our assignments, a CNDO calculation on a molecule of this complexity may well not be definitive (see below), and additional information is needed for clarification. The $C_{5v}$ symmetry of this molecule results in a number of pairs of molecular orbitals being doubly degenerate; the last column of Table 4 lists six such examples. Since these orbitals are partially responsible for the bonding in the framework of the cyclopentadienyl group (see Table 1), the removal of an electron from any one of them, and especially from $\psi_{12}$ or $\psi_{13}$, is likely to result in a loss of planarity in the $C_5$ ring of the resultant ion. This loss of co-planarity could induce a strong interaction among all the ionic states,[1] with consequent removal of the double degeneracies. It follows that Koopman's theorem cannot be expected to give a reliable description of the photoelectron spectra of a molecule of this type. A rigorous study taking into account these interactions is beyond the scope of CNDO, and must await more sophisticated calculations.

[1]The authors are grateful to a referee for pointing this out.

**Acknowledgements**

This work was supported by Operating grants from the Natural Sciences and Engineering Research Council of Canada. We thank Mr. Luis Victoriano for the measurement of the dipole moment of CpIn.

1. E. O. Fisher and H. P. Hofmann. Angew. Chem. **69**, 639 (1957).
2. J. J. Habeeb and D. G. Tuck. J. Chem. Soc. Dalton, 1815 (1975).
3. J. J. Habeeb and D. G. Tuck. J. Chem. Soc. Chem. Commun. 600 (1975).
4. S. Shibata, L. S. Bartell, and R. M. Gavin. J. Chem. Phys. **41**, 717 (1964).
5. E. O. Fisher. Angew. Chem. **69**, 207 (1957).
6. E. Frasson, F. Menegus, and C. Panattoni. Nature, **199**, 1087 (1963).
7. J. K. Tyler, A. P. Cox, and J. Sheridan. Nature, **183**, 1182 (1959).
8. F. A. Cotton and L. T. Reynolds. J. Am. Chem. Soc. **80**, 269 (1958).
9. S. Cradock and W. Duncan. J. Chem. Soc. Faraday Trans. II, **74**, 194 (1978).
10. R. G. Egdell, I. Fragala, and A. F. Orchard. J. Electron Spectrosc. Relat. Phenom. **14**, 467 (1978).
11. D. Rinaldi. QCPE **11**, 290 (1975).
12. J. A. Pople, D. P. Santry, and G. A. Segal. J. Chem. Phys. **43**, S129 (1965).
13. R. S. Mulliken. J. Chem. Phys. **23**, 1833 (1955).
14. J. A. Pople and G. A. Segal. J. Chem. Phys. **43**, S136 (1965).
15. J. Del Bene and H. H. Jaffé. J. Chem. Phys. **48**, 4050 (1968).
16. J. G. Contreras and D. G. Tuck. Inorg. Chem. **12**, 2596 (1973).
17. J. G. Contreras and D. G. Tuck. J. Organomet. Chem. **66**, 405 (1974).
18. S. Evans, M. L. H. Green, B. Jewitt, A. F. Orchard, and C. F. Pygall. J. Chem. Soc. Faraday Trans. II, **68**, 1847 (1972).
19. S. Evans, M. L. H. Green, B. Jewitt, and A. F. Orchard. J. Chem. Soc. Faraday Trans. II, **70**, 356 (1974).

Can. J. Chem. Downloaded from www.nrcresearchpress.com by 210.87.254.6 on 09/06/12
For personal use only.

# An electron spin resonance study of organomercury radical complexes with *ortho*-quinones and vitamin C

DOUGLAS WEIR, DOUGLAS A. HUTCHINSON, JUDY RUSSELL, AND JEFFREY K. S. WAN

*Department of Chemistry, Queen's University, Kingston, Ont., Canada K7L 3N6*

Received August 20, 1981

DOUGLAS WEIR, DOUGLAS A. HUTCHINSON, JUDY RUSSELL, and JEFFREY K. S. WAN. Can. J. Chem. **60**, 703 (1982).

Photochemical and thermal reactions of *ortho*-quinones and organomercury lead to the formation of a series of quinone–HgR$^{\bullet}$ radical complexes. Hyperfine splittings due to $^{199}$Hg isotope were resolved for the 3,5-di-*t*-butylbenzoquinone complexes. Photochemical reactions of vitamin C in ethanol with a number of mercuric salts produce a paramagnetic intermediate which is assigned to the ion-pair involving the ascorbate radical anion and the mercuric ion. In di-*n*-butyl mercury, photolysis of vitamin C leads to the formation of a radical complex similar to those of quinone–HgR$^{\bullet}$ but with a much smaller hyperfine coupling constant for $^{199}$Hg. A simple theoretical model using some MO calculations on the π system of these organometal–quinone radical complexes, which include the metal atom, was developed to account for the systematic experimental observations.

DOUGLAS WEIR, DOUGLAS A. HUTCHINSON, JUDY RUSSELL et JEFFREY K. S. WAN. Can. J. Chem. **60**, 703 (1982).

Les réactions photochimiques et thermiques des orthoquinones avec des organomercuriques conduisent à la formation d'une série de complexes radicalaires du type quinone–$^{\bullet}$HgR. On a résolu les dédoublements hyperfins provoqués par l'isotope $^{199}$Hg des complexes de la di-*tert*-butyl-3,5 benzoquinone. Les réactions photochimiques de la vitamine C dans l'éthanol avec un certain nombre de sels mercuriques produisent un intermédiaire paramagnétique identifié comme étant la paire d'ions provenant de l'anion radical ascorbate et l'ion mercurique. La photolyse de la vitamine C dans le di-*n*-butyl mercure conduit à la formation d'un complexe radicalaire semblable à ceux observées pour quinones–$^{\bullet}$HgR mais avec une constante de couplage hyperfin beaucoup plus faible pour le $^{199}$Hg. On a développé un modèle théorique simple, faisant appel à des calculs d'OM sur le système π de ces complexes radicalaires organométalliques–quinones et impliquant l'atome de métal, afin de tenir compte des observations expérimentales systématiques.

[Traduit par le journal]

## Introduction

In the past few years we have studied extensively the interactions of quinones and other dicarbonyl compounds with organometals, including the uranyl (1), the organomercury (2), the group IVB organometals (3), and the group VIB and group VIIB metal carbonyls (4). In many cases where chemically induced dynamic electron polarization can be detected (1, 3), the additional parameter of the spin–lattice relaxation time of the organometallic radical complexes affords supporting arguments of the extent of spin–orbit coupling of the heavy metal which contributes to the *g*-factor shifts. In order to understand the relative contributions to the *g*-shift, we have chosen here some model organomercury radical complex systems for further investigation. The photochemical reactions between quinones and organomercury are in themselves rather interesting, particularly due to the biological implication of organomercury compounds. In that regard we have also studied the reactions between organomercury and vitamin C (ascorbate) by esr spectroscopy. Ascorbate contains a carbonyl group and two adjacent hydroxylic groups and ascorbate is readily oxidized to a relatively stable free radical anion whose structure has been determined using esr spectroscopy and theoretical calculations (5). In this paper we report a systematic investigation of a number of organomercury–quinone radical complexes by esr and a simple theoretical approach, using some MO calculations on the π electron system of these organometal–quinone complexes which include the metal atom, to obtain some qualitative understanding of the *g*-factor shifts. The ability of vitamin C (ascorbate) to form radical complexes with some organomercury compounds is also illustrated in this report.

## Experimental

Procedures for sample preparations and the photochemical generations of the organometal radical complexes are similar to the method described previously (3). Electron spin resonance spectra were recorded on a Bruker 420 X-band spectrometer with a 100 kHz field modulation. The magnetic field was monitored by a Bruker nmr oscillator and the microwave frequency was measured by a Hewlett-Packard 5432 frequency counter. Magnetic field calibration was made using the potassium naphthalene ion-pair in THF as an external standard. All chemicals were used as received. THF was distilled twice over sodium and stored over sodium wire. The light source was a 200 W super pressure Hg lamp.

## Results and Discussion

### *1. The photochemical reactions of quinones with organomercury*

The photochemical reaction of organomercury compounds with *o*-quinones in THF gives unique

0008-4042/82/060703-07$01.00/0

©1982 National Research Council of Canada/Conseil national de recherches du Canada

Can. J. Chem. Downloaded from www.nrcresearchpress.com by 210.87.254.105 on 09/06/12
For personal use only.

Can. J. Chem. Downloaded from www.nrcresearchpress.com by 210.87.254.105 on 09/06/12
For personal use only.

radical esr spectra. The radicals were relatively unstable at high temperatures. Among a number of quinones studied, no reaction was observed with acenaphthenequinone. With tetrachloro- and tetrabromo-*o*-benzoquinones the reaction required light to initiate but the photochemical reaction proceeded too rapidly with immediate destruction of any possible radical complexes, leaving only the esr spectra of the semiquinone radical anions observable. Organomercury radical complexes were observed for phenanthroquinone (PQ), 1,2-naphthoquinone (NQ), camphoroquinone (CQ), and 3,5-di-*t*-butyl-*o*-benzoquinone (DTBQ).

In the case of DTBQ reacting with dibenzyl mercury, the radical complex formed is relatively stable, even at room temperature. A typical esr spectrum of the benzyl mercury – DTBQ radical complex is shown in Fig. 1. The radical has a very low *g*-factor ($g = 1.9994$) and exhibits an esr spectrum which is composed of a strong central doublet of a proton hyperfine splitting of 2.70 G due to the *meta*-proton from the DTBQ moiety, and a pair of weak doublets of 22.7 G due to the interactions with the $^{199}Hg$ isotope (16.84%, $I = 1/2$). The other $^{201}Hg$ isotope (13.24%, $I = 3/2$) was not resolved in the spectrum. Although the hyperfine splittings from the benzyl protons in the organomercury moiety were not resolved, the identification of the radical complex with the following structure (**1**) is reasonable and consistent with previous assignments (2). For most of the other organomercury–quinone radical complexes studied, the $^{199}Hg$ splittings are very difficult to resolve. The observed esr parameters of the various organomercury–quinone radical complexes are given in Table 1.

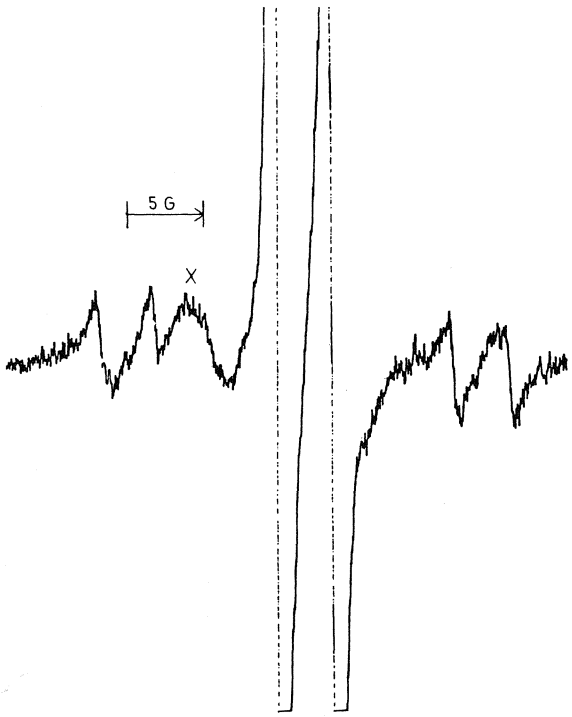


FIG. 1. The esr spectrum of the $DTBQ^{-\cdot}HgCH_2Ph$ complex in THF at −60°C. × marks the $DTBQ^{-\cdot}$ radical anion signal.

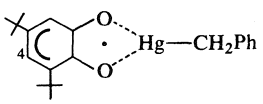


**1**

The observations of these radical complexes were sensitive to the reaction temperatures. With the noted exception of the benzyl mercury – DTBQ complex, temperatures above −50°C lead to rapid decomposition of the complexes. On the other hand, temperatures below −80°C inhibit the formation of the complexes. The best resolution in the esr spectra of the radical complexes was obtained for the 1,2-naphthoquinone complexes (Fig. 2).

The experimental esr parameters of the 1,2-naphthoquinone radical complexes with a variety of organometals are listed in Table 2. It is seen that for the mercury and the uranyl complexes the *g*-factor shift is large and negative as compared to other metals. Furthermore, the mercury complex has larger proton coupling constants but there is little change in the *g*-factors or proton coupling constants as the organic group on the mercury is varied. These observations will be discussed in more detail in section 4.

There are two possible mechanisms leading to the formation of these organomercury–quinone radical complexes. The first one involves a primary electron transfer process followed by secondary processes as outlined below:

$$[1] \quad Q + R_2Hg \xrightarrow[\text{or } \Delta]{h\nu} Q^{-\cdot} + R_2Hg^{+\cdot}$$

$$[2] \quad R_2Hg^{+\cdot} \rightarrow RHg^{+} + R^{\cdot}$$

$$[3] \quad RHg^{+} + Q^{-\cdot} \rightarrow RHg\text{–}Q^{\cdot}$$

In a previous study (2) of the exchange reaction between the quinone – alkali metal ion-pairs and methylmercury chloride, a similar radical ion mechanism has been proposed. Another earlier study (6) also suggested an electron transfer mechanism in the formation of complexes between DTBQ and triethylgermyl mercury. Direct spectroscopic evidence, however, is still lacking since the detection of the reactive $R_2Hg^{+\cdot}$ radical ion has yet to be achieved. On the other hand, it may be feasible to carry out the photochemical reaction at 77 K with an aim to trap pairwise the radical ions involved in

TABLE 1. The esr parameters of some quinone–HgR• complexes in THF

| Quinone | Dibenzyl–Hg | Diphenyl–Hg | $T$ (°C) |
|---|---|---|---|
| 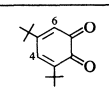 | $g$ = 1.9994±0.0001<br>$a_4^H$ = 2.70±0.05 G<br>$a^{199Hg}$ = 22.7 G | $g$ = 1.9993<br>$a_4^H$ = 2.69 G | −60 |
| 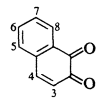 | $g$ = 1.9985<br>$a_4^H$ = 5.52 G<br>$a_6^H = a_8^H$ = 1.70 G<br>$a_3^H = a_5^H$ = 0.49 G<br>$a_7^H$ = 0.18 G | $g$ = 1.9981<br>$a_4^H$ = 5.60 G<br>$a_6^H = a_8^H$ = 1.66 G<br>$a_3^H = a_5^H$ = 0.54 G | −80 |
| 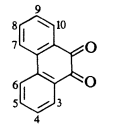 | $g$ = 2.0008 | $g$ = 2.0004 | −60 |
| 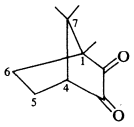 | $g$ = 1.9963<br>$a_4^H$ = 2.78 G<br>$a_{5,6}^H$(*exo*) = 3.05 G<br>$a_7^{CH_3}$(*anti*) = 0.54 G | $g$ = 1.9959 | −80 |

the primary electron transfer process [1]. Similar experiments have indeed been successfully performed with the quinone–organotin systems (7).

Until the electron transfer mechanism is unequivocally established, we must also consider the second possible mechanism which involves mainly the decomposition of the organomercury:

[4] $R_2Hg \xrightarrow[\text{or } \Delta]{h\nu} RHg^\bullet + R^\bullet$

[5] $RHg^\bullet + Q \rightarrow RHg\text{–}Q^\bullet$

The decomposition of $R_2Hg$ has been shown to involve free radicals in a CIDNP study (8) but it was recognized that the intermediate RHg• radical is likely to undergo further decomposition to yield R• and Hg with a rate constant greater than $10^9$ $s^{-1}$. This means that reaction [5] must proceed faster than $10^{-9}$ s which is most unlikely as the reaction in solution is probably at least diffusion-controlled.

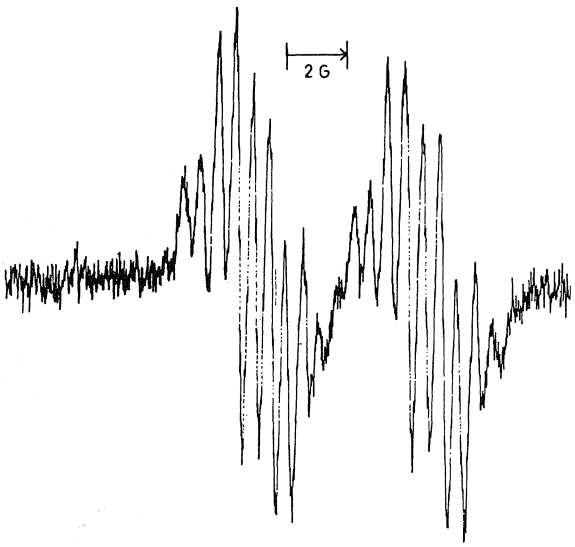


FIG. 2. The esr spectrum of the $NQ^{-\bullet}HgICH_3$ complex in THF at −80°C.

*2. The thermal reactions of quinones in di-*n*-butyl mercury solution*

In a separate series of investigation, liquid di-*n*-butyl mercury was used as solvent for the quinones. The thermal reaction proceeded well at 25°C leading to the esr observation of the radical complex which was found to be stable at room temperature for at least several hours. The thermal reaction involved three different quinones, PQ, NQ, and DTBQ and the corresponding radical complexes are given in Table 3. Among these three quinones PQ gave the weakest concentration of the radical complex. Both NQ and DTBQ gave very strong esr signals with $^{199}Hg$ splittings (Fig. 3). The $^{199}Hg$ coupling constant in these complexes is only about 6 G, much smaller compared to the 22 G observed in the DTBQ–$HgCH_2Ph^\bullet$ complex. This suggests that the Hg—O bonds are weaker in the quinone – aliphatic mercury complexes than those in the quinone – aromatic mercury.

*3. The reactions of vitamin C with mercury(II) salts*

Vitamin C contains functional groups which are structurally similar to *ortho*-quinones. When a degassed ethanol solution of L(+)-ascorbic acid (vitamin C) was photolysed within the esr micro-

Can. J. Chem. Downloaded from www.nrcresearchpress.com by 210.87.254.105 on 09/06/12
For personal use only.

TABLE 2. Electron spin resonance parameters of some NQ–organometal radical complexes in solution[a]

| Organometal | $g$-Factor | $a_4^H$ (G) | $a_{6,8}^H$ (G) | $a_{3,5}^H$ (G) | $a_7^H$ (G) | Solvent | Reference |
|---|---|---|---|---|---|---|---|
| Hg–$CH_2Ph$ | 1.9985 | 5.52 | 1.70 | 0.49 | 0.18 | THF | This work |
| Hg–Ph | 1.9981 | 5.60 | 1.66 | 0.54 | — | THF | This work |
| Hg–$CH_3$ | 1.9982 | 5.58 | 1.70 | 0.56 | — | THF | This work |
| Hg–$CH_2I$ | 1.9983 | 5.61 | 1.70 | 0.54 | — | THF | This work |
| Sn–$Ph_3$ | 2.0049 | 5.30 | 1.45 | 0.30 | — | Toluene | This work |
| Pb–$Ph_3$ | 2.0039 | 4.90 | 1.10 | 0.26 | — | Toluene | This work |
| Tl–$Ph_2$ | 2.0033 | 4.27 | 1.4 | — | — | MTHF | 18 |
| $Mn(CO)_4$ | 2.0040 | 4.22 | 1.55 | — | — | Toluene | 19 |
| $(UO_2H)^{2+}$ | 1.9950 | 4.92 | 1.68 | 0.73 | 0.73 | THF | 1 |

[a]For the proton numbering system, see Table 1.

TABLE 3. Electron spin resonance parameters of some quinone and vitamin C complexes with $n$-butyl mercury in liquid di-$n$-butyl mercury at 25°C

| | | |
|---|---|---|
| DTBQ* | $g$ = 1.9994 | $a_4^H$ = 2.87 G<br>$a^{199Hg}$ = 6.2 G |
| NQ* | $g$ = 1.9999 | $a_5^H$ = 5.26 G<br>$a_6^H = a_7^H = a_8^H$ = 1.24 G |
| PQ | $g$ = 1.9999 | — |
| Vitamin C | $g$ = 1.9884 | $a_4^H$ = 5.84 G |

*For proton numbering system, see Table 1.

wave cavity, a doublet signal with $g$ = 2.0057 and coupling constant of 1.85 G was observed (Fig. 4*a*). This is assigned to the ascorbate radical anion, consistent with literature reports (9). When a mercuric salt was added to the solution and again photolysed the ascorbate signal disappeared and in its place a new single line spectrum was observed (Fig. 4*b*). In all cases the $g$-factor of the new radical is slightly lower (2.0054, 2.0053, 2.0051 for Hg-$(SCN)_2$, $HgBr_2$, and $HgCl_2$, respectively) than the ascorbate radical anion value. In all the above three systems grey precipitate due to colloidal mercury appeared after prolonged irradiation. With mercuric acetate the precipitate appeared immediately upon irradiation and therefore no esr signal was detected. The new radical species formed in these mercuric salt systems were not thermally stable and they decayed immediately when the irradiation was terminated. The fact that colloidal mercury was formed upon prolonged irradiation points to the photoredox nature of the "complexation" in which successive electron transfer steps occurred (17). The radical complex observed is thus probably an ion-pair similar to that observed by Stegmann and co-workers (10) in the vitamin C – $Ph_2T10H$ system. The fact that the $g$-factor shift was so small from the free radical anion ruled out the drastic ring-opening in the complex. In the absence of observable $^{199}Hg$ hyperfine splitting and a significant $g$-shift, whether the ion-pair is a

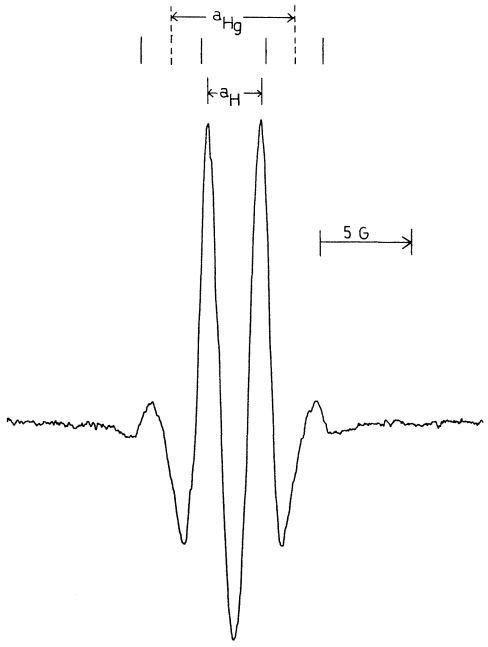


FIG. 3. The second derivative esr spectrum of vitamin C – $n$-butyl mercury in liquid di-$n$-butyl mercury at 25°C.

contact-pair or a solvent-separated pair cannot be established at this time.

When organomercury was added to an ethanol solution of vitamin C, photolysis failed to produce any observable mercury radical complexes. Since more stable mercury – quinone radical complexes have been obtained by using di-$n$-butyl mercury as solvent, the same technique was applied to the vitamin C system. There was no observable thermal reaction of vitamin C in liquid di-$n$-butyl mercury. However, upon irradiation of the system two doublet esr signals were observed. One set of the doublet at lower field can be identified as the well-known ascorbate radical anion, while the doublet at higher field with parameters $g$ = 1.9884 and $a_H$ = 5.84 G is typical for an organomercury

Can. J. Chem. Downloaded from www.nrcresearchpress.com by 210.87.254.105 on 09/06/12
For personal use only.

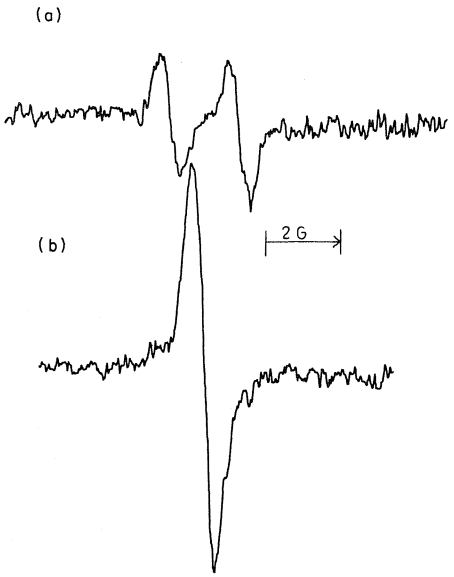


FIG. 4. The esr spectra at 25°C of (*a*) ascorbate radical anion in ethanol and (*b*) when a mercuric salt $Hg(SCN)_2$ was added.

radical complex to vitamin C. The larger proton coupling constant in the C-4 position of the ascorbate moiety is consistent with other observations involving T1–ascorbate complexes (10). These organomercury – ascorbate radical complexes probably have a structure similar to those of quinone–organomercury complexes, but the mercury–ascorbate complexes are much less thermally stable than the quinone analog.

### *4. Some theoretical considerations on the g-factor shifts of metal – quinone radical complexes*

In our systematic study of an extensive series of organometal – quinone radical complexes, we have found that while the uranyl and the organomercury complexes have very low $g$-factors, many of the other metal–quinone complexes have $g$-factors equal to or above the free electron value. For the uranyl–quinone complexes, we were able to obtain a good agreement with the experimental results by using a spin–orbit coupling model to account for the $g$-shifts (1). With a more extensive series of organomercury–quinone and mercury – vitamin C radical complexes reported in this paper, it is interesting to develop a simple theoretical model to account for their trend in $g$-factor shifts. In order to understand the relative contributions to the $g$-shift from the spin–orbit coupling of the metal and from the $d$–$p_\pi$-bonding mechanism proposed earlier for group IVB-substituted methyl and ethyl radicals (11, 12), we have performed some simple calculations on the $\pi$ electron system of these organometal–quinone complexes which include the metal atom.

We began by applying the elegant formulation on **G** tensor by Stone (13) and also followed his arguments in the treatment of the odd electron $\pi$ MO which is expressed as a linear combination of $p_z$ AO's. The final approximate expression for the $g$-factor of the metal–quinone complexes is

$$[6]\quad g \simeq g_e - \frac{4}{3\,\Delta\varepsilon_n}\sum_a |c_{an}|^2\zeta_a$$

where $g_e$ is the free electron $g$-factor and $\zeta_a$ is the spin–orbit coupling parameter, obtainable from spectroscopic results; all other symbols have their conventional meanings.

The energy differences for the atomic C $^3P_2$, $^3P_1$, $^3P_0$ levels are obtained from Moore (14); in atomic units the results are

$$\varepsilon(^3P_2) - \varepsilon(^3P_0) = 1.982 \times 10^{-4}$$

$$\varepsilon(^3P_1) - \varepsilon(^3P_0) = 0.7472 \times 10^{-4}$$

If the $^3P_2$, $^3P_1$, and $^3P_0$ are assigned the respective spin–orbit coupling parameters $\zeta_2$, $\zeta_1$, $\zeta_0$ with splittings $(1/2)\zeta_2$, $-(1/2)\zeta_1$, $-\zeta_0$, then

$$(1/2)\zeta_2 + \zeta_0 = 1.982 \times 10^{-4}$$

$$-(1/2)\zeta_1 + \zeta_0 = 0.7472 \times 10^{-4}$$

and

$$(5/2)\zeta_2 - (3/2)\zeta_1 - \zeta_0 = 0$$

The weighted average is $\zeta_C = 1.254 \times 10^{-4}$. A similar procedure for the oxygen atom gives $\zeta_O = 7.144 \times 10^{-4}$. The procedure for $Hg(..6s^16p^1)$ is somewhat different because the $^3P_1$ and $^1P_1$ levels can interact but the $^3P_2$ and $^3P_0$ levels have the same state vectors for Russell Saunders and *jj* couplings. Thus $\varepsilon(^3P_2) - \varepsilon(^3P_0)$ can be equated to $(3/2)\zeta_{Hg}$; from Moore (14) the result is $\zeta_{Hg} = 194.342 \times 10^{-4}$.

The coefficients $c_{an}$ of eq. [6] are estimated by a Hückel method; the Hg $6p_z$ orbital is included in the description of the $\pi$ states. The orbital energies $\varepsilon_n$ and coefficients $c_{an}$ are then obtained from eq. [7]:

$$[7]\quad (\gamma_a + x_n)c_{an} + \sum_{b\neq a} y_{ab}c_{bn} = 0$$

The parameters $\gamma_a$, $x_n$, and $y_{ab}$ are defined in terms of the atomic integrals $\alpha_a$, bond integrals $\beta_{ab}$, the standard carbon atomic integral $\alpha_C$, and standard benzene bond integral $\beta_B$ as follows:

$$[8]\quad \gamma_a = (\alpha_a - \alpha_C)/\beta_B;$$

$$x_n = (\alpha_C - \varepsilon_n)/\beta_B;$$

Can. J. Chem. Downloaded from www.nrcresearchpress.com by 210.87.254.105 on 09/06/12
For personal use only.

TABLE 4. Calculated and experimental results for $g - g_e$ for some quinone–organomercury radical complexes

| Radical | Calculated $(g - g_e)\Delta\varepsilon_n$ | Calculated $(g - g_e)$; for $\Delta\varepsilon_n = 0.25$ | Experimental $g - g_e$ R = benzyl in THF | Experimental $g - g_e$ R = butyl in di-*n*-butyl Hg |
|---|---|---|---|---|
| DTBQ–HgR· | −0.00093 | −0.00372 | −0.0029 | −0.0029 |
| NQ–HgR· | −0.00086 | −0.00344 | −0.0038 | −0.0024 |
| PQ–HgR· | −0.00087 | −0.00348 | −0.0015 | −0.0024 |

and

$$y_{ab} = \beta_{ab}/\beta_B \simeq \langle a|b\rangle/\langle a|b\rangle_B$$

where $\langle a|b\rangle_B$ is the value for benzene with a CC bond length of 1.397 Å.

A value of −2.505 eV is assigned to $\beta_B$ from the spectroscopic data. The negative of the ionization energy differences for O and C is assigned to $\alpha_O - \alpha_C$; a value of 0.9417 is then obtained for $\gamma_O$. The spectroscopic data for Hg allows one to write the following

$$\varepsilon_\infty - (\varepsilon(\mathrm{Hg}6s6p) - \zeta) = 5.76997 \text{ eV};$$

$$\varepsilon_\infty - (\varepsilon(\mathrm{Hg}6s6p) + (1/2)\zeta) = 4.97675 \text{ eV}$$

for the $^3P_0$ and $^3P_2$ levels. Consequently the $6p$ ionization energy of Hg is $\varepsilon_\infty - \varepsilon(\mathrm{Hg}6s6p) = 5.24116$ eV, from which $\gamma_{Hg} = -2.402$. The inner products of eq. [8] are evaluated from Slater orbitals for C and O. The radial part $R_{6p}(r)$ of the Hg $6p_z$ orbital is constructed from $(R_{31}(\rho_3) + cR_{53}(\rho_5))/(1 + c^2 + 2C(R_{31}, R_{53}))$, where $R_{31}$ and $R_{53}$ are associated Laguerre polynomials of the arguments

$$\rho_n = 2\,Zr/n,$$

$r$ in atomic units. The values $Z = 7.0$ and $c = 0.4$ are obtained by fitting $R_{6p}(r)$ to the Hg $6p$ wavefunction of Hay, Wadt, Kahn, and Bobrowicz (15).

It is convenient to rewrite eq. [6] as

$$[9] \quad g - g_e \simeq -\frac{4}{3\Delta\varepsilon_n}(w_{\mathrm{Hg},n}\zeta_{\mathrm{Hg}} + w_{O,n}\zeta_O + w_{C,n}\zeta_C)$$

where $w_{\mathrm{Hg},n}$, $w_{O,n}$, and $w_{C,n}$ respectively are the sums of the squares of the Hg, O, and C atom coefficients of the odd electron π MO $|n\rangle$. In order to determine the orbital for the odd electron, the number of electrons in the π system needs to be known. For the DTBQ–HgR· radical complex, the six aromatic C atoms and the two O atoms each contribute an electron to the π system. In the valence region of Hg there are seven electrons: four from the O atom lone pairs, two from Hg itself, and one from the R moiety bonded to Hg. Three $sp^2$ hybrids around Hg can accommodate six of the seven electrons so the remaining one is in the π system. From these arguments one concludes that the π system contains nine electrons; thus the odd electron is in the fifth πMO. Similarly NQ–HgR· complex contains thirteen electrons in the π system; the odd electron is in the seventh πMO. PQ–HgR· has a π system with seventeen electrons; the odd electron is in the ninth πMO. The results produced by these arguments, and the experimental $g$-shifts are shown in Table 4.

Although the calculated results for $(g - g_e)\Delta\varepsilon_n$ are negative, $g - g_e$ can be positive or negative depending on the signs of $\Delta\varepsilon_n$. For a semiquinone we follow Stone (16) and recognize that the most important contributing orbitals are occupied σMO's. Thus, after an average energy approximation is introduced, $\Delta\varepsilon_n$ is negative and $g - g_e$ is positive. When the quinone–HgR· complex is formed, the Hg atom has many unoccupied orbitals near the highest filled MO. An average energy approximation should now give a positive $\Delta\varepsilon_n$ and hence a negative $g - g_e$. In this way a qualitative understanding of the $g$-factor shifts is obtained for the metal–quinone complex.

A quantitative assessment of the experimental results is much more difficult to obtain from this simple model. The $\Delta\varepsilon_n$ term, however, should be comparable for all the quinone-HgR· complexes. The Hg spectroscopic data suggest that a value of ~1/4 atomic unit is reasonable for $\Delta\varepsilon_n$. As seen in Table 4 this does give reasonable $g$-shifts and they are in fair agreement with the experimental shifts obtained in the di-*n*-butyl mercury systems. In THF solvent with dibenzyl mercury, the NQ complex appeared to disagree with the predicted trend among the series of three quinone complexes. Our simple model is not capable of accounting for the solvent and other experimental effects which may result from using THF as solvent. Also we would refrain from applying this simple model quantitatively to the ascorbate–mercury radical complexes, as neither the π electron system nor the exact nature of the three oxygen atoms of the ascorbate in the interaction with the mercury would be comparable to the quinone systems.

Can. J. Chem. Downloaded from www.nrcresearchpress.com by 210.87.254.105 on 09/06/12
For personal use only.

Can. J. Chem. Downloaded from www.nrcresearchpress.com by 210.87.254.105 on 09/06/12
For personal use only.

We shall now turn to the $g$-factors of other organometal–quinone radical complexes. The respective $g$-factors for the $Ph_3Sn$— and $Ph_3Pb$— complexes with DTBQ are 2.0038 and 2.0032. The positive shifts of 0.0015 and 0.0009 here indicate that the Sn and Pb atoms coordinate to the quinone more loosely than does a Hg atom. In the absence of additional structural information it is plausible to assume a trigonal bipyramidal arrangement of the two O—Pb and three Ph—Pb bonds about Pb and the same arrangement for Sn. In such an arrangement the $\pi$ system contains two more electrons than the quinone–HgR$^\cdot$ complexes. In the valence region about Pb there are eleven electrons: four from Pb itself, three from the attached phenyl groups, and four from the two O atom lone pairs. The trigonal bipyramidal $sp^3d$ hybridization scheme gives $d_{3z^2-r^2}$ and three $sp^2$ hybrids to the $\sigma$ system and $p_z$ to the $\pi$ system: the $\sigma$ system contains four orbitals and the $\pi$ system contains one. Thus eight of the eleven valence electrons are accommodated in the $\sigma$ system and the remaining three are distributed in the $\pi$ system. Since the quinone moiety contains eight $\pi$ electrons there are a total of eleven electrons in the $\pi$ system. The odd electron occupies the sixth $\pi$MO in contrast to the fifth $\pi$MO for the nine $\pi$ electron quinone–HgR$^\cdot$ complex.

It is instructive to compare the Hg and O atom coefficients for the fifth and sixth $\pi$MO's of the HgR complex determined by eq. [7]. For the fifth $\pi$MO the respective Hg and O atom coefficients are 0.1313 and 0.4526; the corresponding numbers for the sixth $\pi$Mo's are 0.0725 and 0.1293. These results point the way to a reduced role for the metal atom in the Sn and Pb complexes. Conceivably the metal atom coefficient could have been lowered to the point where the binding to the quinone is slight and the occupied $\sigma$MO's of the quinone are more important than the unoccupied orbitals of the metal atom. This would produce a negative $\Delta\varepsilon_n$ and thus a positive $g - g_e$, as observed in the experiments.

We must re-emphasize that our simple model is developed mainly to account for some of the experimental observations among a large number of metal–quinone radical complexes investigated in this laboratory. The results of the calculations do favor a significant $g$-factor shift for the complexes involving the HgR moiety, and they also suggest that the other tin and lead complexes have much smaller $g$ shifts. Such a simple model does provide a qualitative understanding of some of the important esr parameters and as such is a valuable tool for the experimentalists.

## Acknowledgments

This research is supported by the Natural Sciences and Engineering Research Council of Canada and by the School of Graduate Studies and Research, Queen's University.

1. J. W. M. deBoer, K. S. Chen, Y. C. Chung, and J. K. S. Wan. J. Am. Chem. Soc. **101**, 5425 (1979); D. A. Hutchinson, K. S. Chen, J. Russell, and J. K. S. Wan. J. Chem. Phys. **73**, 1862 (1980).
2. K. S. Chen, R. T. Smith, and J. K. S. Wan. Can. J. Chem. **56**, 2503 (1978).
3. J. K. Kochi, K. S. Chen, and J. K. S. Wan. Chem. Phys. Lett. **73**, 557 (1980); K. S. Chen, T. Foster, and J. K. S. Wan. J. Phys. Chem. **84**, 2473 (1980); K. S. Chen, J. K. S. Wan, and J. K. Kochi. J. Phys. Chem. **85**, 1726 (1981).
4. K. A. M. Creber and J. K. S. Wan. J. Am. Chem. Soc. **103**, 2101 (1981); Chem. Phys. Lett. **81**, 453 (1981); D. Weir and J. K. S. Wan. J. Organomet. Chem. **220**, 323 (1981).
5. G. P. Laroff, R. W. Fessenden, and R. Schuler. J. Am. Chem. Soc. **94**, 9062 (1972); C. Thomson. J. Mol. Struct. **67**, 133 (1980).
6. G. A. Abakumov, E. N. Gladyshev, N. S. Vyazankin, G. A. Razuvaev, P. Ya. Bayushkin, and V. A. Muraev. J. Organomet. Chem. **64**, 327 (1974).
7. S. Emori, D. Weir, and J. K. S. Wan. Chem. Phys. Lett. **84**, 512 (1981).
8. R. Benn. Rev. Chem. Intermed. **3**, 45 (1979).
9. Y. Kirino. Chem. Lett. 153 (1974) and references therein.
10. H. B. Stegmann, K. Scheffler, and P. Schuler. Angew. Chem. Int. Ed. **17**, 365 (1978).
11. J. H. Mackey and D. E. Wood. Mol. Phys. **18**, 783 (1970).
12. T. Kawamura and J. K. Kochi. J. Am. Chem. Soc. **94**, 648 (1972).
13. A. J. Stone. Proc. R. Soc. A**271**, 424 (1963).
14. C. E. Moore. Atomic energy levels. NBS Washington. 1945.
15. P. J. Hay, W. R. Wadt, L. R. Kahn, and F. W. Bobrowicz. J. Chem. Phys. **69**, 984 (1978).
16. A. J. Stone. Mol. Phys. **6**, 509 (1963).
17. V. Balzani and V. Carassiti. Photochemistry of coordination compounds. Academic Press, New York. 1970; S. Emori, M. C. Depew, and J. K. S. Wan. Photobiochem. Photobiophys. **3**, 53 (1981).
18. H. B. Stegmann, K. B. Ulmschneider, and K. Scheffler. J. Organomet. Chem. **101**, 145 (1975).
19. T. Foster, K. S. Chen, and J. K. S. Wan. J. Organomet. Chem. **184**, 113 (1980).

# Synthesis and properties of some spin labeled long chain aliphatic acids

D. GALA, R. SCHULTZ, AND R. KREILICK

*Department of Chemistry, University of Rochester, Rochester, NY 14627, U.S.A.*

Received October 9, 1981

D. GALA, R. SCHULTZ, and R. KREILICK. Can. J. Chem. **60**, 710 (1982).

We have synthesized and characterized a series of spin labeled aliphatic acids with variable chain lengths between the nitroxide radicals and the carboxylic group. These molecules should be of general utility in labeling a variety of substrates which can react with the free carboxylic acid group. Variable temperature esr studies have been conducted with some of these molecules to characterize molecular motion as a function of solvent viscosity.

D. GALA, R. SCHULTZ et R. KREILICK. Can. J. Chem. **60**, 710 (1982).

On synthétisé et caractérisé une série d'acides aliphatiques portant un marqueur de spin et l'on a fait varié la longueur de la chaîne entre les radicaux nitroxydes et groupement carboxylique. Les molécules devraient être d'une utilité générale pour marquer un grand nombre de substrats qui peuvent réagir avec le groupement acide carboxylique libre. On a effectué des études de rpe à température variable à l'aide de ces molécules afin de caractériser leur mouvement moléculaire en fonction de la viscosité du solvant.

[Traduit par le journal]

Can. J. Chem. Downloaded from www.nrcresearchpress.com by 210.87.254.42 on 09/06/12
For personal use only.

## Introduction

The electron spin resonance (esr) spectra of spin labeled molecules have been used to investigate motional correlation times of a variety of biologically important compounds (1). Nitroxide radicals are generally the label of choice because extensive theoretical work has been conducted to relate experimental spectra to motional correlation times (2). The motional correlation times may depend on steric interactions between the labeled reporter group and a biological substrate. If the nitroxide group can be attached to a drug molecule or enzyme with a variable length connecting chain, one is able to monitor changes in molecular correlation times as a function of the length of the spacer group between the drug or enzyme and the nitroxide label (3). Through analysis of changes in molecular motion as a function of the spacer group's length one can obtain information about the structure of a binding site. If the spacer group is short compared to the depth of the binding site, the nitroxide label's motion will be inhibited by steric interactions with the substrate while longer spacers may allow the nitroxide to extend out of the binding site resulting in greater mobility of the labeled group. If one determines the motional correlation time as a function of the length of the spacer group one obtains a measure of the depth of the binding site.

We have synthesized a group of spin labels in which a nitroxide label is bound to a carboxylic acid functional group via a variable length aliphatic chain (Fig. 1). The carboxylic acid groups of these molecules can be used to form either ester or amide linkages with a variety of different substrates. We have used these molecules to spin label both morphine and codeine through formation of ester linkages at the 3 and 6 positions. The labeled acids should prove to be of general utility in the synthesis of a variety of other types of labeled drugs or enzymes. The labeled molecules were synthesized by three related techniques. In method A (Fig. 1) the half ester, half acid chloride of a dicarboxylic acid was allowed to react with the amino group of 2,2,6,6-tetramethyl-4-aminopiperidine-1-oxy to form a molecule with both an amide and ester group. The ester was subsequently hydrolysed to form the desired product. In method B the acid function of the half ester of a dicarboxylic acid was condensed with the amino group of the nitroxide radical through use of *N*,*N'*-dicyclohexylcarbodiimide (DCC). Hydrolysis of the ester group again led to the formation of the desired labeled acid. In method C a dicarboxylic acid was directly condensed with the amino group of the nitroxide radical using DCC as a coupling reagent. The spin labeled acids were characterized by their ir spectra, their nmr spectra (after reduction of the nitroxide group), and by their esr spectra. A variable temperature esr study was conducted with two of the labeled acids to determine changes in motional correlation times as a function of solvent viscosity and the chain length of the spacer group.

## Methods and experimental

The spin labeled acids were synthesized by three different techniques. The choice of technique for a given molecule was dictated by availability of starting materials and the overall yield of the product. The three reaction schemes are illustrated in Fig. 1. The half esters of dibasic acids with $n$ = 2–4, 7 were commercially available, while only the diacids were available

0008-4042/82/060710-06$01.00/0

©1982 National Research Council of Canada/Conseil national de recherches du Canada

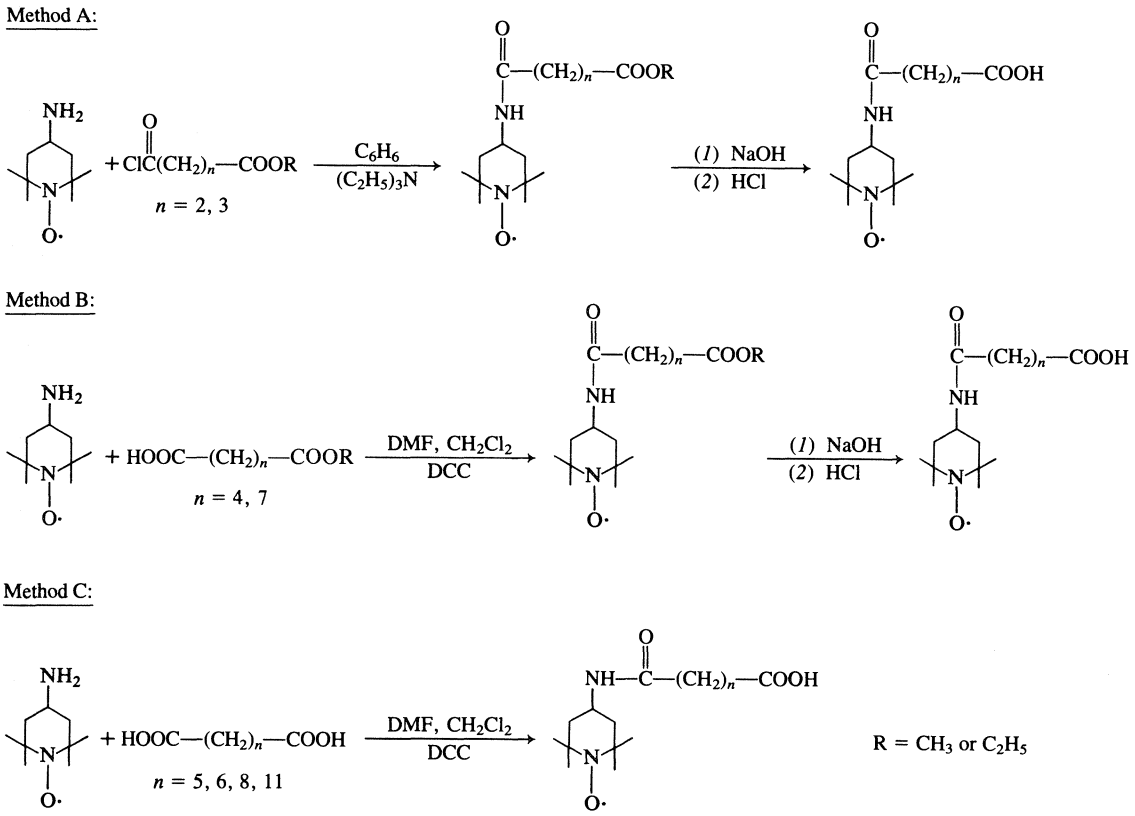


FIG. 1. Reaction schemes for synthesis of the spin labeled acids.

for the other chain lengths. The diacids can react with two molecules of the nitroxide label to yield a biradical and the yield of the desired product was lower than that from molecules in which one of the carboxylic acid groups was blocked with an ester linkage. Synthesis of the half esters of these molecules could have been carried out but the overall yield after this additional reaction would have been comparable to the yield obtained when the diacid was used directly.

All of the diacids and half acid esters were obtained from Aldrich Chemical Co. and used without further purification. The 2,2,6,6-tetramethyl-4-aminopiperidine-1-oxy was synthesized by the technique of Rozantsev (4). Illustrations of the techniques used in the various reaction sequences are given below.

*Method A: reaction of half ester, half acid chlorides (*n = *2, 3) with the nitroxide radical*

A solution of 0.23 g (1.4 mmol) of the nitroxide radical in 1 mL of dry benzene was slowly added to a stirred solution of 0.22 g (1.4 mmol) of ethylsuccinyl chloride in 1 mL of dry benzene and 0.5 mL of triethylamine (TEA) held at 0°C. The reaction mixture was allowed to come to room temperature and stirred for an additional 12 h. Thin-layer chromatography (silica gel, $CH_2Cl_2$ or EtOAc) indicated completion of the reaction. Two milliliters of benzene were added to the reaction mixture and the TEA·HCl was removed by filtration. The TEA·HCl was washed with two 5-mL aliquots of ether and these washings were combined with the original filtrate. The filtrate was evaporated to dryness under vacuum to yield 0.4 g (95%) of a red oil. This oil (spin labeled ethylsuccinate) was saponified without further purification. Attempts at washing the oil with water resulted in lower yields. The spin labeled ethylsuccinate (0.33 g, 1.09 mmol) was dissolved in 5 mL of 95% ethanol and a solution containing 0.80 g (20 mmol) of NaOH in a minimum amount of 50% ethanol was added. This solution was refluxed for 18 h and then the solvent was removed by vacuum evaporation. The resulting solid was dissolved in 20 mL of 2 *N* NaOH and this solution was washed with two 5-mL aliquots of chloroform. The solution was cooled to 0°C and the pH was adjusted to 2 by addition of 1 *N* HCl. The acidified solution was extracted with 20-mL aliquots of chloroform and two 20-mL aliquots of EtOAc. The combined extracts were dried over anhydrous $MgSO_4$ and the solvent was removed under reduced pressure to yield an orange solid. Recrystallization of this material from EtOAc and petroleum ether gave 0.24 g (80%) of yellow-orange spin labeled acid (mp 154–157°C). The overall yield for the two reactions to produce the desired product was 76%. In cases in which the half methyl ester of a dibasic acid was used as an initial reactant, methanol was used in place of ethanol in the saponification.

*Method B: reaction of half ester, half acids (*n = *4, 7) with the nitroxide radical*

A dicyclohexyl carbodiimide (DCC) solution containing 5.19 g (25 mmol) in 10 mL of $CH_2Cl_2$ was added to a stirred solution of 3.56 g (22.5 mmol) of mono-methyladipate in 5 mL of $CH_2Cl_2$ at 0°C. A white solid formed in about 15 min. A solution of 3.8 g (22 mmol) of the nitroxide radical in 10 mL of $CH_2Cl_2$ was slowly added to this mixture while the temperature was maintained at 0°C. The temperature was allowed to rise to room temperature

Can. J. Chem. Downloaded from www.nrcresearchpress.com by 210.87.254.42 on 09/06/12
For personal use only.

Can. J. Chem. Downloaded from www.nrcresearchpress.com by 210.87.254.42 on 09/06/12
For personal use only.

and the mixture was stirred for 24 h. The precipitate was filtered, washed with two 10-mL aliquots of $CH_2Cl_2$, and the filtrate was vacuum evaporated to yield a thick red oil. This oil was dissolved in chloroform and quickly washed with 15 mL of water, 15 mL of 5% $NaHCO_3$, two additional 15-mL aliquots of water, and dried over anhydrous $MgSO_4$. Thin-layer chromatographic examination (silica gel, $CHCl_3$, EtOAc, and $CH_3OH$) showed that more than one component was present in this solution. The solution was concentrated under reduced pressure and the resulting red oil was separated on a silica gel column using either EtOAc or 10% $CH_3OH$ in $CH_2Cl_2$ as eluant to obtain 6.25 g (90%) of the spin labeled adipic acid methyl ester as a thick red oil. The ester was saponified using the general technique described under method A.

*Method C: reaction of diacids (n = 5, 6, 8, 11) with the nitroxide radical*

A solution of DCC (5.64 g, 27 mmol, in a minimum volume of dry DMF) was added to a stirred solution of 6.18 g (38 mmol) of pimelic acid in 10 mL of dry DMF at 0°C. A white crystalline precipitate formed in about 45 min. At this point 4.5 g (26 mmol) of the nitroxide radical in 5 mL $CH_2Cl_2$ was slowly added at 0°C. The reaction mixture was stirred at room temperature for 48 h and the white precipitate was removed by filtration. The precipitate was washed with three 10-mL aliquots of $CHCl_3$ and the combined filtrate was concentrated under vacuum. The resulting thick red oil was dissolved in 90 mL of $CHCl_3$ and insoluble white crystals were removed by filtration. The solution was extracted with three 60-mL aliquots of 10% NaOH and the NaOH extracts were combined, cooled to 0°C, and the pH was adjusted to 2 by titration with concentrated HCl. The acidified solution was extracted with four 60-mL aliquots of chloroform and two 60-mL aliquots of EtOAc. The extracts were washed separately with three 30-mL aliquots of water, dried over anhydrous $MgSO_4$, combined, and the solvent was removed by vacuum evaporation to yield 3.75 g (46%) of an orange-red solid (mp 105–121°C). Thin-layer chromatographic examination (silica gel, $CHCl_3$, EtOAc, $CH_3OH$, and 6% $CH_3OH$ in $CH_2Cl_2$) showed this solid to contain small amounts of impurity. The mixture was separated on a silica gel column with either 6% or 10% $CH_3OH$ in $CH_2Cl_2$ which yielded 2.05 g (25%) of the product. After evaporation of the eluant from the column one always obtained a thick red oil. Addition of about 5 mL of EtOAc to this oil yielded a crystalline product, mp 114–117°C. Recrystallization from EtOAc and petroleum ether yields pure spin labeled pimelic acid, mp 118–121°C.

*Nuclear magnetic resonance spectra*

In order to obtain high resolution nmr spectra of the molecules for analytical purposes, it is necessary to reduce the nitroxide radical to a hydroxyl amine. The reduction was carried out in an nmr sample tube in which 30 to 50 mg of a given spin label was dissolved in 1 mL of DMSO-$d_6$. A solution (15 μL) of 85% hydrazine was added as the reducing agent. The reduction led to formation of gas bubbles ($N_2$) and loss of color from the solution. The reaction was complete in 3–5 h and the nmr spectra were taken. All of the nmr spectra showed the following general characteristics: a sharp singlet with a shoulder (1.12 to 1.18 δ) from the 12 methyl protons on the piperidine ring, a broad doublet (7.8 to 8.0 δ) from the amide proton, and a group of overlapped lines (1.2 to 2.2 δ) whose area corresponded to the protons in the methylene chain. Addition of 0.25 mL of $CDCl_3$ to the solution revealed an additional peak from the single carboxylic acid proton (8.1–8.15 δ).

*Properties of specific labels*

*Compound* ***1***, $n = 2$, prepared by method A; yield 76%; mp 154–157°C; ir (KBr): 3475, 3000, 2960, 1740, 1645, 1555 $cm^{-1}$; nmr δ: 1.1 (12 H), 7.9 (1 H); *Anal.* calcd. for $C_{13}H_{23}N_2O_4 \cdot 1/2H_2O$: C 55.74, H 8.60, N 9.98; found: C 56.29, H 8.54, N 9.89.

*Compound* ***2***, $n = 3$, prepared by method A; yield 73%; mp 117–120°C; ir (KBr); 3460, 3000, 1710, 1625, 1575 $cm^{-1}$; nmr δ: 1.1 (12 H), 7.8 (1 H); *Anal.* calcd. for $C_{14}H_{25}N_2O_4 \cdot 1/2H_2O$: C 57.32, H 8.92, N 9.54; found: C 57.64, H 8.83, N 9.36.

*Compound* ***3***, $n = 4$, prepared by method B; yield 55%; mp 99–101°C; ir (KBr): 3340, 2970, 2880, 1695, 1610, 1560 $cm^{-1}$; nmr δ: 1.1 (12 H), 7.7 (1 H); *Anal.* calcd. for $C_{15}H_{27}N_2O_4$: C 60.18, H 9.09, N 9.36; found: C 60.19, H 9.15, N 9.20.

*Compound* ***4***, $n = 5$, prepared by method C; yield 25%; mp 118–121°C; ir (KBr): 3395, 2960, 2890, 1730, 1640, 1550 $cm^{-1}$; nmr δ: 1.15 (12 H), 7.4 (1 H); *Anal.* calcd. for $C_{16}H_{29}N_2O_4$: C 61.32, H 9.33, N 8.94; found: C 60.83, H 9.45, N 8.78.

*Compound* ***5***, $n = 6$, prepared by method C; yield 28%; mp 103–105°C; ir (KBr): 3360, 2950, 2880, 1710, 1620, 1565 $cm^{-1}$; nmr δ: 1.0 (12 H), 7.7 (1 H); *Anal.* calcd. for $C_{17}H_{31}N_2O_4 \cdot 1/2H_2O$: C 60.69, H 9.58, N 8.32; found: C 60.61, H 9.55, N 8.31.

*Compound* ***6***, $n = 7$, prepared by method B; yield 42%; mp 98–99°C; ir (KBr): 3380, 3340, 2940, 2860, 1720, 1630, 1560 $cm^{-1}$; nmr δ: 1.15 (12 H), 7.65 (1 H); *Anal.* calcd. for $C_{18}H_{33}N_2O_4$: C 63.31, H 9.74, N 8.20; found: C 63.41, H 9.88, N 8.16.

*Compound* ***7***, $n = 8$, prepared by method C, catalytic amounts of 4-dimethylpyridine were used in this reaction; yield 25%; mp 99–101°C; ir (KBr): 3350, 2935, 2860, 1700, 1610, 1565 $cm^{-1}$; nmr δ: 1.1 (12 H), 7.7 (1 H); *Anal.* calcd. for $C_{19}H_{35}N_2O_4$: C 64.19, H 9.92, N 7.88; found: C 63.74, H 10.14, N 7.67.

*Compound* ***8***, $n = 11$, prepared by method C, catalytic amounts of 4-dimethylpyridine were used in this reaction; yield 26%; mp 114–116°C; ir (KBr): 3380, 3320, 2935, 2860, 1720, 1630, 1560 $cm^{-1}$; nmr δ: 1.2 (12 H), 7.5 (1 H); *Anal.* calcd. for $C_{22}H_{41}N_2O_4$: C 66.46, H 10.36, N 7.05; found: C 66.17, H 10.67, N 6.95.

## Electron spin resonance spectra

The esr spectra of this group of radicals in solution at room temperature were essentially identical ($A(N) = 16.2$ G; $g = 2.005$ in 50:50 methanol–ethanol). Variable temperature studies of two of the radicals ($n = 2$ and 11) were conducted to obtain information about the rotational motion of the labels as a function of the viscosity of the solvent. Figure 2 shows spectra of these two radicals at a series of temperatures while Fig. 3 shows plots of the ratio of intensities of the high field to center line and the low field to center line as a function of temperature. The signal intensities are inversely proportional to the square of the linewidth and measurement of relative intensities gives a good measure of line broadening produced by incomplete averaging of anisotropic interactions. If the molecules tumble isotropically so that the components of the dipolar and $g$ anisotropy are averaged equally, one expects to observe the greatest broadening in the high field ($m = -1$) line, the second greatest broadening in the low field ($m = 1$) line, and the least broadening in the center line ($m = 0$) (5). The experimental results show the greatest broadening in the high field line, the second greatest broadening in the center line, and the least broadening in the low field line (Fig. 3).

Can. J. Chem. Downloaded from www.nrcresearchpress.com by 210.87.254.42 on 09/06/12
For personal use only.

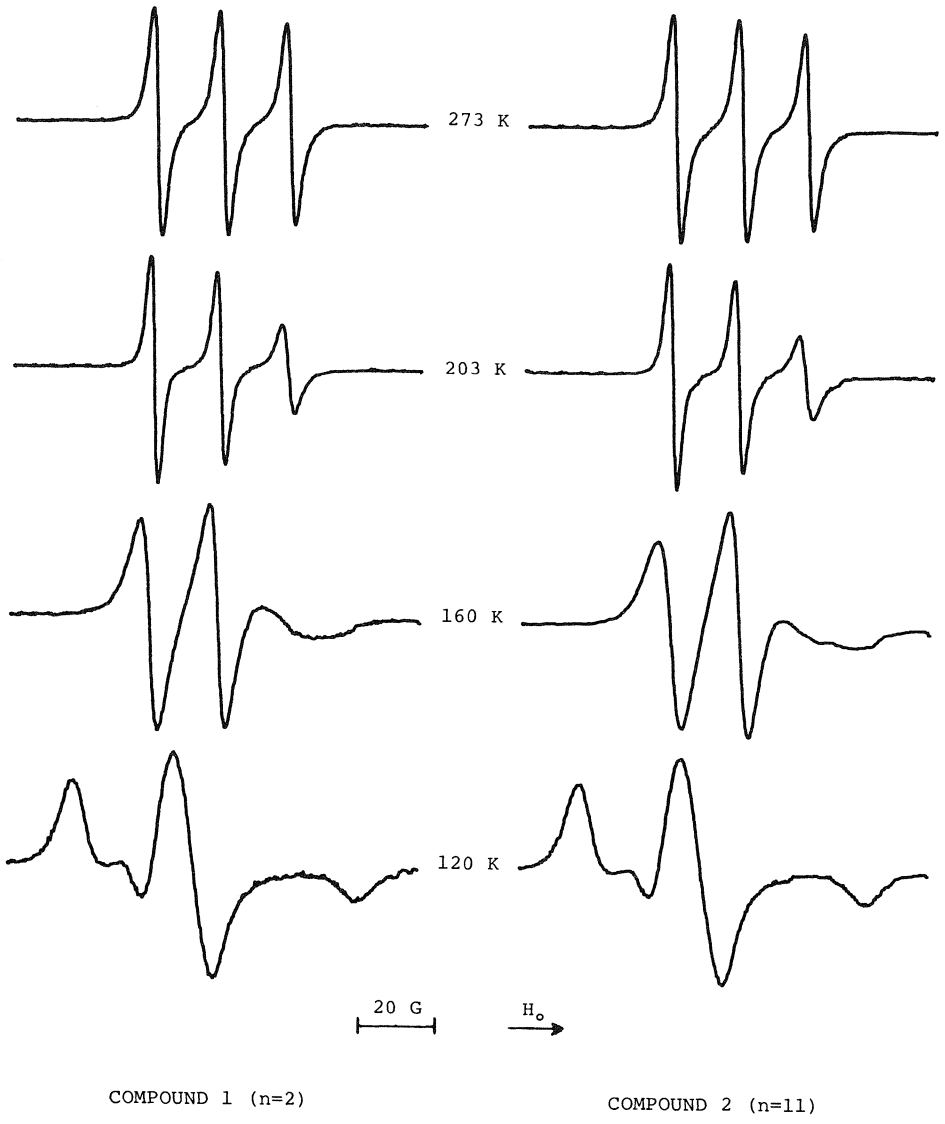


FIG. 2. The esr spectra of compound **1** ($n$ = 2) and compound **8** ($n$ = 11) in 50:50 methanol–ethanol as a function of temperature.

This type of behavior is observed when rotation around the $x$ axis (defined by the N—O bond direction) is preferred over rotation around the other two axes (6) (Fig. 4). The $x$ axis is roughly colinear with the direction (long axis) of the aliphatic connecting chain if this chain extends out into solution and is not wrapped back around the radical. This type of motion is often observed from labels with long chains which are introduced into lipid bilayers where motion around the long axis is much more facile than rotation around the other axes. The motion of the longer chain molecules ($n$ = 11) appears to be slightly slower than that of the short chain acid ($n$ = 2) at a given temperature, which may reflect differences in the steric bulk or configuration of the connecting chain. One cannot obtain values for motional correlation times from the simple formulas used for isotropic rotation and a complete lineshape analysis would be necessary to determine accurate correlation times.

## Conclusions

A group of spin labeled long chain aliphatic acids has been synthesized and characterized by their ir and esr spectra, by elemental analysis, and by the nmr spectra of hydroxyl amines formed by reduction of the radicals. The esr results indicate that molecules preferentially rotate around the $x$ mo-

Can. J. Chem. Downloaded from www.nrcresearchpress.com by 210.87.254.42 on 09/06/12
For personal use only.

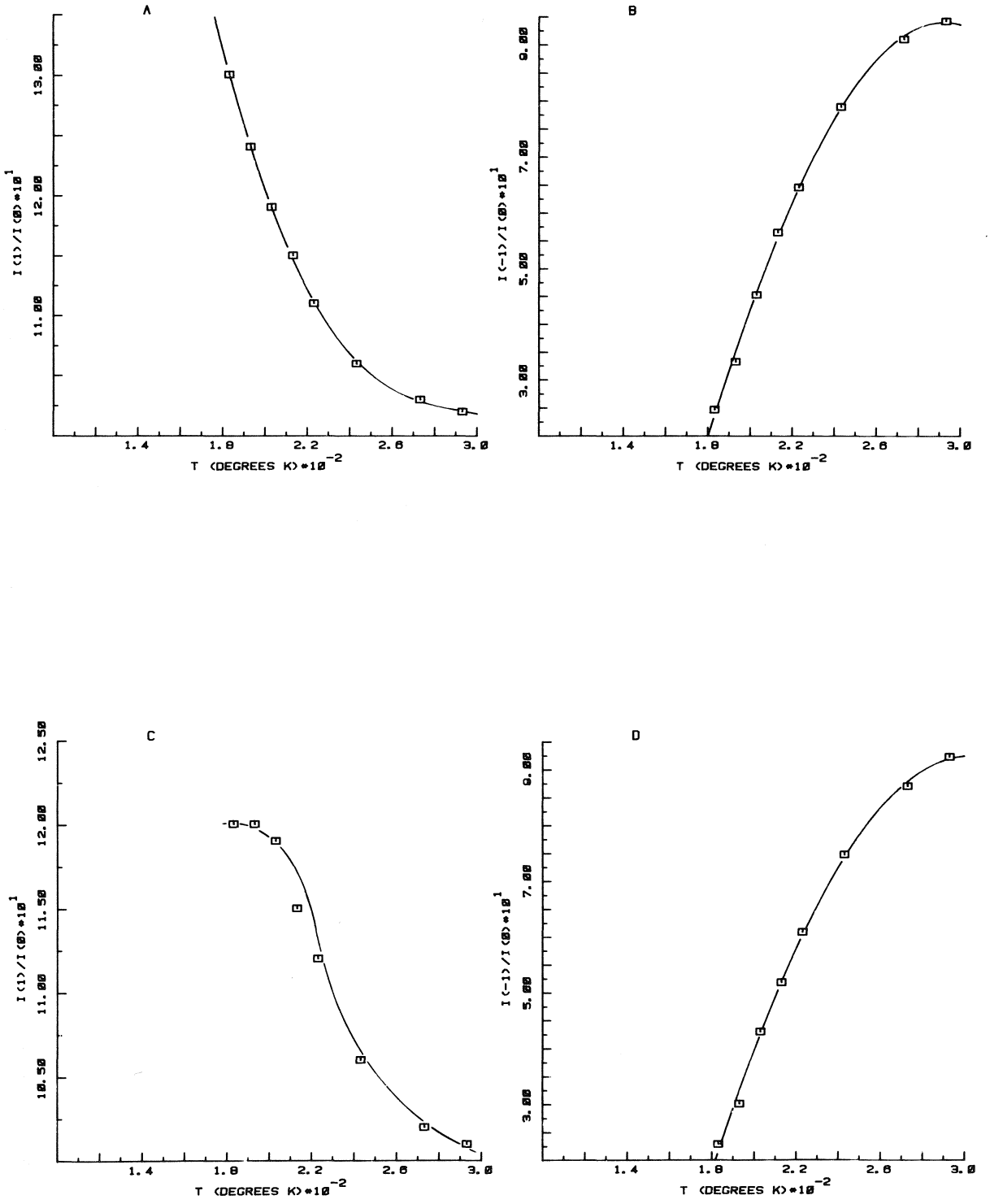


FIG. 3. Plots of the ratio of signal intensities as a function of temperature. A: Compound **1** ($n = 2$) low field line/center line. B: Compound **1** ($n = 2$) high field line/center line. C: Compound **8** ($n = 11$) low field line/center line. D: Compound **8** ($n = 11$) high field line/center line.

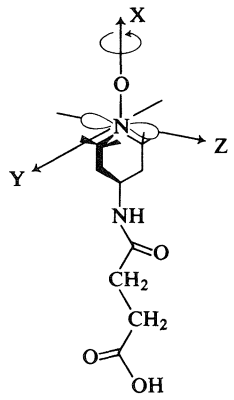


FIG. 4. Schematic representation of axis of preferred rotation for this group of spin labels.

lecular axis. These molecules should be of use as starting material for a variety of spin labeling studies. These spin labels can readily be attached to the head groups of lipids for studies of labeled membranes. The molecules can also be attached to a variety of drug molecules and some enzymes. We have used this group of molecules to produce spin labeled derivatives of both morphine and codeine. The synthesis and properties of these labeled opiates will be reported in a later paper.

**Acknowledgement**

This work was supported in part by N.I.H. grant DA-01733.

1. L. J. BERLINER (*Editor*). Spin labeling, theory and applications. Vols. 1 and 2. Academic Press, New York. 1976 and 1979; A. D. KEITH, M. SHARNOFF, and G. E. COHN. Biochim. Acta, **300**, 379 (1973); B. J. GAFFNEY and C. J. MCNAMEE. Methods Enzymol. **32B**, 161 (1974).
2. J. A. FREED. Ann. Rev. Phys. Chem. **23**, 265 (1972).
3. J. C. HSIA and L. H. PIETTE. Arch. Biochem. Biophys. **129**, 296 (1969); L. J. BERLINER and S. S. WONG. J. Biol. Chem. **249**, 1668 (1974).
4. E. G. ROZANTSEV. Free nitroxyl radicals. Plenum Press, New York. 1970.
5. J. H. FREED. J. Chem. Phys. **41**, 2077 (1964); S. A. GOLDMAN. G. V. BRUNO, and J. H. FREED. J. Phys. Chem. **76**, 1858 (1972).
6. G. B. BIRRELL, S. P. VAN, and O. H. GRIFFITH. J. Am. Chem. Soc. **95**, 2451 (1973); G. B. BIRRELL, O. H. GRIFFITH, and D. FRENCH. J. Am. Chem. Soc. **95**, 8171 (1973).

Can. J. Chem. Downloaded from www.nrcresearchpress.com by 210.87.254.42 on 09/06/12
For personal use only.

# The basicity of phosphines

TIM ALLMAN[1] AND RAM G. GOEL[2]

*Guelph-Waterloo Centre for Graduate Work in Chemistry, Guelph, Ont., Canada N1G 2W1*

Received July 27, 1981

TIM ALLMAN and RAM G. GOEL. Can. J. Chem. **60**, 716 (1982).

The basicities of the triarylphosphines $P(4\text{-}XC_6H_4)_3$ (X = Cl, F, H, $CH_3$, $CH_3O$, $(CH_3)_2N$), $P(3\text{-}CH_3C_6H_4)_3$, and $P(2\text{-}CH_3C_6H_7)_3$ as well as the trialkylphosphines $P(t\text{-}Bu)_3$ and $PCy_3$ have been measured by the nitromethane titration method. The range of basicity available by aryl substitution is very large, being $pK_a = 8.65$ for X = $(CH_3)_2N$ to 1.03 for X = Cl. The most basic phosphine is $P(t\text{-}Bu)_3$ whose $pK_a = 11.40$. The measured basicities correlate well with $\sigma_p$, $\sigma^\phi$, and ν as well as with the lone pair ionisation potentials of the triarylphosphines. Generally the $^1H$, $^{31}P$, and $^{13}C$ nmr spectral parameters of the free and protonated phosphines do not correlate well with $pK_a$.

TIM ALLMAN et RAM G. GOEL. Can. J. Chem. **60**, 716 (1982).

Utilisant la méthode de titration au nitrométhane, on a mesuré les basicités de triarylphosphines $P(4\text{-}XC_6H_4)_3$ (X = Cl, F, H, $CH_3$, $CH_3O$, $(CH_3)_2N$), $P(3\text{-}CH_3C_6H_4)_3$ et $P(2\text{-}CH_3C_6H_7)$ et des trialkylphosphines $P(tert\text{-}Bu)_3$ et $PCy_3$. L'éventail des basicités disponibles pour la substitution des groupes aryles varie de $pK_a = 8{,}65$ pour X = $(CH_3)_2N$ à 1,03 pour X = Cl. La phosphine la plus basique est la $P(tert\text{-}Bu)_3$ dont le $pK_a = 11{,}40$. Les basicités mesurées sont en bon accord avec $\sigma_p$, $\sigma^\phi$ et ν ainsi qu'avec les potentiels d'ionisation des paires libres des triarylphosphines. D'une façon générale, les paramètres des spectres rmn du $^1H$, du $^{13}C$ et du $^{31}P$ des phosphines libres et protonées ne sont pas en accord avec les $pK_a$.

[Traduit par le journal]

## Introduction

Tertiary phosphines form stable complexes (1–4) with many main group Lewis acids as well as with transition metals in their various oxidation states. Due to very useful catalytic properties (5) of a number of phosphine complexes of transition metals, tertiary phosphines have become very widely studied ligands.

By analogy with the bonding of metal carbonyls, it has long been proposed that phosphines can act as σ donors as well as π acceptors (6–11). To test this hypothesis and to evaluate the electronic effects of phosphines on the properties of their complexes, tertiary phosphines with a variety of substituents on phosphorus have been synthesised and the electronic effects in their complexes have been investigated (1–4).

Tolman has proposed an empirical electronic parameter, ν, based on substituent group contributions, $\chi_i$, derived from the CO stretching frequency belonging to the $A_1$ mode of the complexes $Ni(CO)_3PR_3$ (7). These are intended to be a quantitative measure of electronic effects.

Other workers (8–13) have used the inductive and mesomeric effects of the substituents attached to phosphorus to infer the electronic effects of phosphines. For example, the magnitude of $^1J$(M—P) for complexes of tungsten(0) (8) and platinum(II) (9) with the phosphines $PR_nPh_{3-n}$ (R = alkyl, Ph = phenyl) increases as $n$ decreases but the opposite is true for some mercury(II) complexes (10). From these results it has been concluded (8–10) that the magnitude of $^1J(^{183}W—^{31}P)$ or $^1J(^{195}Pt—^{31}P)$ increases with decreasing basicity whereas the $^1J(^{199}Hg—^{31}P)$ values vary in the opposite manner. Using a Hammett-type relationship, Kabachnik and co-workers (14) have derived the substituent parameters $\sigma^\phi$ which have also been used as a measure of electronic effects of phosphines. It has been shown (15) that the reactivity of the complexes $IrCl(CO)L_2$ (L = triarylphosphine) toward oxidative addition of methyl iodide is linearly dependent upon the $\sigma^\phi$ values for the substituents at phosphorus.

Phosphines, like amines, are also Brønsted bases and the electronic effects of the substituents on the metal–phosphorus bond can be quantitatively measured in terms of the basicity of the phosphines toward a proton. It has been shown (16) that the half neutralisation potentials (HNP) for the water-insoluble phosphines in a non-aqueous solvent can be accurately correlated with their aqueous basicities. The $pK_a$ values for a number of trialkyl phosphines have been determined by this method (16).

As part of a systematic investigation of the electronic and steric effects in the phosphine complexes of $d^8$ and $d^{10}$ metals, the metal–phosphorus nuclear spin–spin couplings and/or metal–phosphorus stretching frequencies for the platinum(II) (17), mercury(II) (18), cadmium(II) (19), and silver(I) (20) complexes of tri-*tert*-butylphosphine,

[1]Present address: Department of Chemistry and Chemical Engineering, University of Saskatchewan, Saskatoon, Sask., Canada S7N 0W0

[2]To whom all correspondence should be addressed.

0008-4042/82/060716-07$01.00/0

©1982 National Research Council of Canada/Conseil national de recherches du Canada

Can. J. Chem. Downloaded from www.nrcresearchpress.com by 210.87.254.105 on 09/06/12
For personal use only.

TABLE 1. Basicity, $^1H^a$ and $^{13}C$ nmr data

| | Compound | $pK_a$ | $^1J$(P—H)[a] (Hz) | $\delta(^1H)^a$ (ppm) | $^1J$(P—C) (Hz) | $\delta(^{13}C)_{C_1}$ (ppm) | $\Sigma\sigma\phi'$ |
|---|---|---|---|---|---|---|---|
| I | $P(t\text{-}C_4H_9)_3$ | 11.40 | 443 | 5.21 | −33.9 | 34.7[g] | −4.65 |
| II | $P(c\text{-}C_6H_{11})_3$ | 9.65 | 455 | 5.11 | −28.8 | 30.6 | −3.57 |
| III | $P(4\text{-}(CH_3)_2NC_6H_4)_3$ | 8.65 | 494 | 8.27 | −5.9 | 124.9 | −3.51 |
| IV | $P(4\text{-}CH_3OC_6H_4)_3$ | 4.57 | 494 | 8.32 | −8.7 | 133.7 | −2.22 |
| V | $P(4\text{-}CH_3C_6H_4)_3$ | 3.84 | 509 | 8.33 | −10.0[c] | 134.2[c] | −2.16 |
| VI | $P(3\text{-}CH_3C_6H_4)_3$ | 3.30 | 494 | 8.42 | −12.3 | 137.1 | −1.65 |
| VII | $P(2\text{-}CH_3C_6H_4)_3$ | 3.08 | 491 | 8.83 | −11.44[d] | 142.5[c] | — |
| VIII | $P(C_6H_5)_3$ | 2.73 | 504 | 8.50 | −12.51[e] | 137.4 | −1.77 |
| IX | $P(4\text{-}FC_6H_4)_3$ | 1.97 | 512[b] | [b] | −11.5 | 132.5 | −0.96 |
| X | $P(4\text{-}ClC_6H_4)_3$ | 1.03 | 499 | 8.44 | −14.8 | 134.9 | −0.87 |

[a]These values are for the protonated phosphines in $CF_3CO_2H$. All other nmr data are for the free phosphines in solution.
[b]$^1J$(P—H) value taken from $^{31}P$ spectrum.
[c]Reference 38.
[d]Reference 37.
[e]Reference 36.
[f]Reference 14.
[g]Reference 39.

Can. J. Chem. Downloaded from www.nrcresearchpress.com by 210.87.254.105 on 09/06/12
For personal use only.

tricyclohexylphosphine, and a number of substituted triarylphosphines have been examined in this laboratory. The most significant finding of these investigations is that, contrary to conclusions arrived at from earlier studies, the magnitude of $^1J$(M—P) for the *para* substituted triarylphosphine complexes of platinum(II) (17) as well as mercury(II) (18*g*) and cadmium(II) (19*b*) halides increase with increasing electron releasing power of the aryl group. It is therefore evident that $^1J$(M—P) is not simply related to the electron-donating abilities of phosphines, which are more reliably measured by their basicities towards a proton. Thus, the dependence of the spectral parameters and other properties of the complexes can be evaluated quantitatively from the knowledge of the relative $pK_a$ values of the phosphines. The $pK_a$ values for the ten phosphines used in the nmr studies have been determined in the present work. Correlations between the phosphine basicity and the $^1H$, $^{31}P$, and $^{13}C$ nmr spectral parameters of the phosphines as well as the $^1J(^{31}P—^1H)$ values for the protonated phosphines have also been examined. The topic of substituent contributions to the $^{31}P$ chemical shift has been dealt with by others (41).

## Results and discussion

### *(a) Basicities of phosphines*

The $pK_a$ values for the ten phosphines examined in this study are given in Table 1 along with some of their $^1H$ and $^{13}C$ nmr data. The $pK_a$ values for $P(c\text{-}C_6H_{11})_3$ and $P(4\text{-}CH_3OC_6H_4)_3$ are in good agreement with the values reported by Streuli (16*a*).

For the triarylphosphines the order of basicity is found to be the same as the order of the Hammett $\sigma_p$ and $\sigma_m$ parameters (21) for the substituents on the phenyl groups. $P(4\text{-}FC_6H_4)$ is found to be slightly more basic than $P(4\text{-}ClC_6H_4)_3$. This can be attributed to the more efficient conjugation of the non-bonding electrons on fluorine with the ring. In spite of the powerful inductive effect of fluorine, a significant amount of electron density is donated back to the ring. The three tritolylphosphines are all more basic than triphenylphosphine and their $pK_a$ values occur within a small range. The higher basicities of $P(4\text{-}CH_3OC_6H_4)_3$ and $P(4\text{-}(CH_3)_2\text{-}NC_6H_4)_3$ are expected because of the known electron donating abilities of the substituents. The two trialkylphosphines are significantly more basic than most of the triarylphosphines. They are, in fact, the most basic phosphines whose $pK_a$'s have been measured to date. The very high value for $P(t\text{-}C_4\text{-}H_9)_3$ compared to $P(c\text{-}C_6H_{11})_3$ is consistent with the greater electron-donating ability of the *t*-butyl groups.

It should be noted here that these results are not entirely consistent with some previous work, particularly with respect to the $pK_a$ value for $P(4\text{-}ClC_6H_4)_3$. Goetz and Sidhu (22) measured the $pK_a$'s of two classes of phosphines, $P(C_6H_5)_2(4\text{-}XC_6H_4)$ and $P(4\text{-}XC_6H_4)_3$, by a titration method using HCl in 80% ethanol/water. For the first class they found a good correlation between Hammett's constants and the measured $pK_a$ values. The latter class gave the order of decreasing basicity ($P(4\text{-}CH_3OC_6H_4)_3 > P(4\text{-}ClC_6H_4)_3 > P(C_6H_5)_3$, which is different from ours.

Using a different technique, Hopkins and coworkers (23) also studied several symmetrical 4-substituted triarylphosphines. Using an infrared technique, they measured the equilibrium constant

for eq. [1] by observing the free and H-bonded ν(OH) bands in dilute $CS_2$ solution.

[1] $F_3C\langle\bigcirc\rangle O{-}H + PAr_3 \overset{K}{\rightleftharpoons} F_3C\langle\bigcirc\rangle O{-}H\text{---}:PAr_3$

The rationale was that the more basic phosphines would H-bond more extensively to the phenol. This experiment gave an order of decreasing basicity of $P(4\text{-}CH_3OC_6H_4)_3 \gg P(4\text{-}CH_3C_6H_4)_3 > P(4\text{-}ClC_6H_4)_3 > P(C_6H_5)_3$.

While it is difficult to criticise the methodology of the former study, the latter is open to various interpretations. One possible explanation for the deviation of Hopkins' order from ours is that the substituents which are themselves capable of H-bonding (—Cl and —$OCH_3$) are doing so and raising the apparent basicities of the phosphines. In support of our study is one in which the equilibrium in the reaction of phosphines and tritylperchlorate (eq. [2]) was

[2] $Ar_3P + Ar_3{}^+C + ClO_4{}^- \leftrightharpoons Ar_3P^+{-}CAr_3 + ClO_4{}^-$

studied (24). The more basic phosphines shifted the reaction to the right to give an order of decreasing basicity:

$$P(4\text{-}CH_3C_6H_4)_3 > P(C_6H_5)_3 > P(4\text{-}ClC_6H_4)_3$$

Also in support of our work, and more directly comparable, is a protonation study by Grim and Yankowsky (11). They were able to qualitatively assign basicities to eighteen triarylphosphines based on whether the doublet due to the phosphonium proton could be seen by $^1H$ nmr after bubbling HBr(g) through $CH_2Cl_2$ solutions of the phosphines. Their results are consistent with our study; the phosphonium proton was most easily observed with the most basic phosphines.

Correlations of the basicities of phosphines with Hammett's $\sigma_m$, parameters (22) and to Tafts σ* parameters (16*b*) have been demonstrated. Correlations using these constants are not possible, however, when the groups attached to phosphorus are mixed alkyl–aryl or are not organic. The basicities of these other phosphines can be correlated with Kabachnik's $\sigma^\phi$ constants (14). These values are proportional to Hammett's σ constants for substituted aromatic groups but also include a wide range of alkyl, alkoxy, and halide groups. Because these constants are derived from the ionisation of phosphorus acids they should, at least in principle, be better constants to use with phosphorus compounds.

The correlation between $pK_a$ and $\sigma^\phi$ for the phosphines in this study is excellent (see Fig. 1). Mastryukova and Kabachnik (14) have pointed out that the data of Henderson and Streuli fall on one line when $\sigma^\phi$ is used rather than the three lines obtained when $pK_a$ is plotted vs. σ* (16*b*).

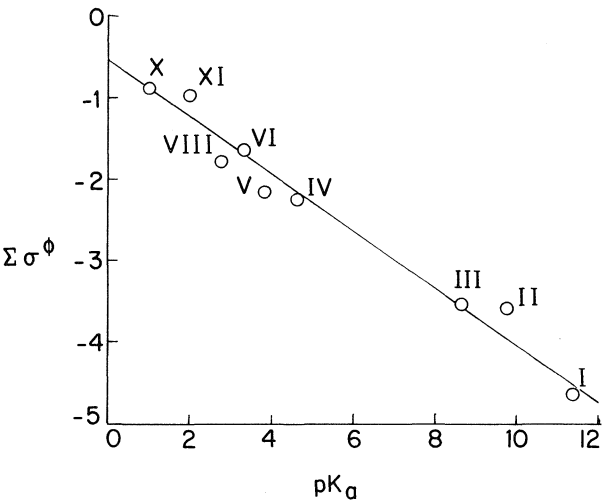


FIG. 1. Plot of Kabachnik's $\Sigma\sigma^\phi$ vs. $pK_a$. Numbers correspond to those in the tables.

$$\Sigma\sigma^\phi = -0.351pK_a - 0.540,$$
$$r = -0.986.$$

Tolman has proposed constants for the phosphines, $\chi_i$, which also reflect the changes in basicity very well (7*a*). In his paper Tolman gives a plot of $\chi_i$ vs. $\sigma^\phi$ which shows significant deviation from linearity in the region of low basicity, particularly in the region where the phosphites are found. As shown in Fig. 2, for the phosphine used in this study the correlation between $pK_a$ and $\chi_i$ is linear, probably because the range of basicities of our phosphines is smaller.

It is reasonable that the phosphorus lone pair ionisation potential (IP) should reflect the variations with ring substitution that we have seen by these other techniques. The lone pair IP of several 4-substituted triarylphosphines have been determined recently by ultraviolet photo-electron spectroscopy. Weiner and Lattman (25) found a good correlation between lone pair IP and $\sigma_p$ but point out that this implies that there are no major changes in hybridisation at phosphorus through the series. Another study (26) corroborates this by showing that while there may be good correlations within a series of closely related phosphines, it is not a good technique for determining the relative basicities of very different phosphines such as $PCl_3$ and $(P(C_6H_5)_3$. Indeed, while the IP of all the triarylphosphines used in this study correlate well with $pK_a$ (Fig. 3), the point for $P(t\text{-}C_4H_9)_3$ is far from the line. The C—P—C angle in the triarylphosphines is probably close to the 103.0° of $P(C_6H_5)_3$ (27) while the angle in $P(t\text{-}C_4H_9)_3$ is larger at 109° (26, 28).

Can. J. Chem. Downloaded from www.nrcresearchpress.com by 210.87.254.105 on 09/06/12
For personal use only.

Can. J. Chem. Downloaded from www.nrcresearchpress.com by 210.87.254.105 on 09/06/12
For personal use only.

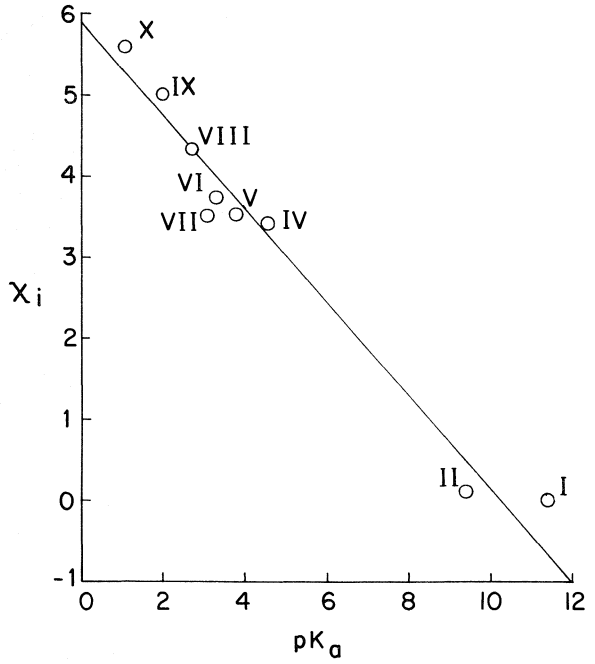


FIG. 2. Plot of Tolman's $\chi_i$ parameters vs. p$K_a$. Numbers correspond to those in the tables.

$\chi_i = -0.577pK_a + 5.90$,

$r = -0.960$

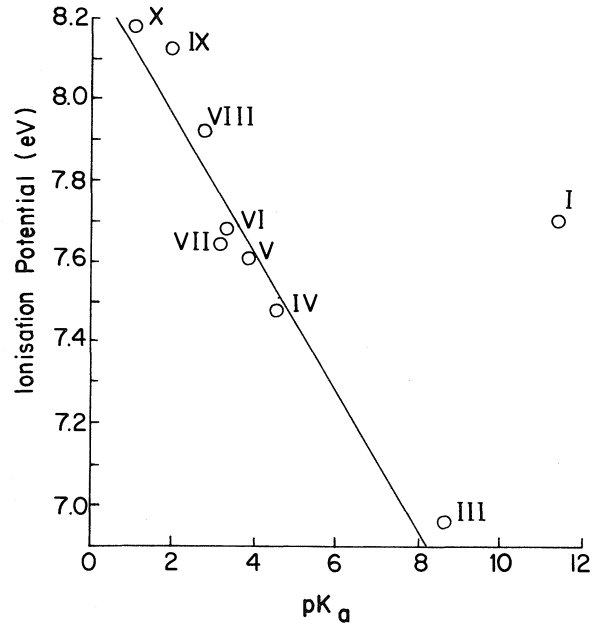


FIG. 3. Plot of phosphorus lone pair ionisation potential vs. p$K_a$. Numbers correspond to those in the tables. The point for *I* is not included in the regression line.

IP $= -0.163pK_a + 8.29$,

$r = 0.978$

*(b) Nuclear magnetic resonance data*

*(i) $^1J$(P—H) in the protonated phosphines*

Previous workers have generated the phosphonium ions by dissolving the phosphines in very strongly acid media such as 100% $H_2SO_4$ (12) or $HSO_3F$ (13) or by bubbling HBr(g) through solutions of the phosphines in $CH_2Cl_2$. We find that the ions can be observed easily in trifluoroacetic acid solution. The nmr data for these ions are given in Table 1.

The coupling constants decrease slightly in the triaryl series with increasing basicity as do the chemical shifts, but the correlation is poor. In light of the wide range of basicity in this series the small range of $^1J$(P—H) is surprising. The two trialkylphosphines give coupling constants that are significantly lower than the others. However, these data are consistent with those from previous studies (11–13); some selected data are presented in Fig. 4. It can be seen clearly that $^1J$(P—H) decreases with increasing basicity (decreasing $\Sigma\sigma^\phi$) of the phosphine or phosphite. Put it in another way, $^1J$(P—H) increases with increasing electronegativity of the substituents in a reasonably smooth manner. This trend is indeed well known for $^1J$(C—H) in various organic compounds. For example, $^1J$(C—H) decreases in the series $HCF_3 > HCCl_3 > HCBr_3 > HCI_3$. These results are consistent with Bent's rule (29) which states that *p* character tends towards the orbitals with the most electronegative substituents. Because the sum of *s* character of the carbon orbitals must be exactly 1,

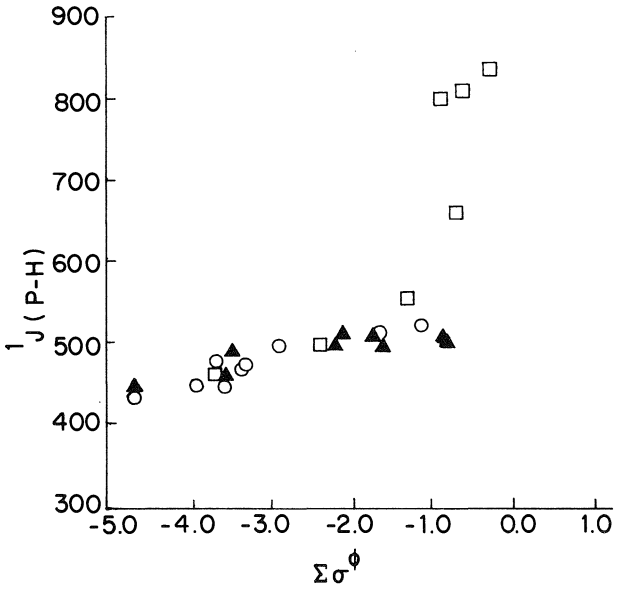


FIG. 4. Plot of $^1J$(P—H) of the protonated phosphines vs. p$K_a$. ▲, this study; ○, ref. 14, □, ref. 13.

Can. J. Chem. Downloaded from www.nrcresearchpress.com by 210.87.254.105 on 09/06/12
For personal use only.

the C—H bond will have more *s* character in $HCF_3$ than in $HCCl_3$. The higher coupling constant implies that the Fermi contact mechanism is dominant in determining these coupling constants (30, 31). Extension of this reasoning to organophosphines is probably sound because no multiple bonding between phosphorus and hydrogen is possible and it has generally been accepted that M—H coupling is explained by this mechanism (32). Supporting this view is the observation that $^1J$(P—H) correlates well with the calculated charges on phosphorus and hydrogen in some protonated phosphites (33).

*(ii)* $^1$J*(P—C) in the free phosphines*

The observed trend in $^1J$(P—C) is not as easily explained. The Fermi contact term, although important, has been found to contribute less as the coupled atoms become heavier and where there is multiple bonding between them (34). If it is assumed that the sign of the coupling constant is merely a label defining the origin of the coupling and that it is the magnitude of the coupling constant that is important, then the trend in $^1J$(P—C) vs. p$K_a$ is not explicable in terms of changes in the Fermi contact term. Rehybridisation of phosphorus in accordance with Bent's rule would increase the *s* character of the P—C bond with increasing basicity of the phosphine thus giving a higher $^1J$(P—C). We see the opposite trend in the triaryl phosphine data in Fig. 5. These changes in the C—P—C angle are likely to be small, if indeed they do exist. So far, there are not enough crystallographic data to know. Much larger changes in hybridisation can be forced by including the phosphorus atom in a heterocyclic ring or by replacing an aryl group by cyclohexyl or *t*-Bu. It has been found that changes in $^1J$(P—C) are consistent with rehybridisation at phosphorus and the Fermi contact mechanism in such ring systems (35).

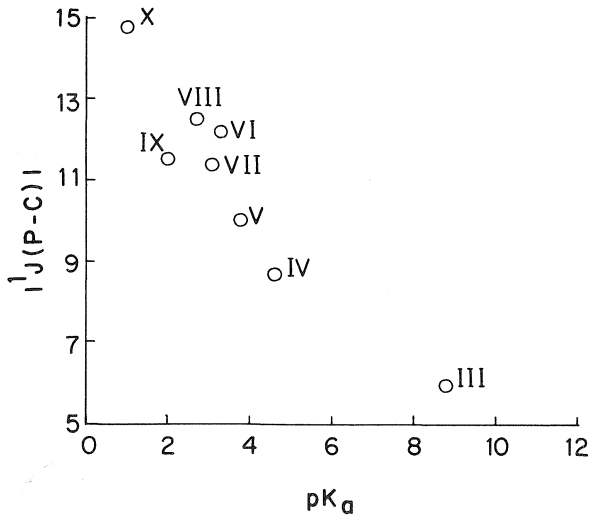


FIG. 5. Plot of $|^1J$(P—C)| vs. p$K_a$ for the triarylphosphines. Numbers correspond to those in the tables.

What can be learned from this is that the interpretation of coupling constants is by no means easy. The other factors in the Fermi contact expression, the electron density at the nucleus and the triplet excitation energy, can only be guessed at and the contributions of the orbital and dipolar mechanisms are unknown. It is likely that several contributions to the coupling constant are changing through the aryl phosphine series and not all in the same direction, thus, giving a correlation of $^1J$(P—C) with p$K_a$ which probably means very little by itself.

## Conclusions

We have shown that substituents on the phenyl rings of triarylphosphines can bring about large changes in the basicities of these phosphines. They should be useful for studies where electronic changes without significant concurrent steric changes are desired. The measured basicities correlate well with $\sigma_p$, $\sigma^\phi$, and $\nu$ as well as with the lone pair ionisation potentials for members of a series of similar phosphines. Generally, the nmr spectral parameters do not correlate well with the measured basicities and do not provide an alternate method of determining basicities. Of all the methods devised to date the nitromethane titration appears to be the most consistent and reasonable method for the measurement of basicities of phosphines.

## Experimental section

*(a) Materials*

Triphenylphosphine from Eastman Kodak was recrystallised twice from hot ethanol and dried *in vacuo*. Tris(4-dimethylaminophenyl) phosphine from Strem Chemicals was purified by recrystallisation from hot benzene under $N_2$. Tricyclohexylphosphine was used as received from Pressure Chemical Co. Tri-*tert*-butylphosphine was prepared as previously reported (40). All other phosphines were prepared as described in (*b*). Purity of each phosphine was established by melting point and $^1$H and $^{31}$P nmr spectral measurements and, except for tri-*tert*-butylphosphine and tricyclohexylphosphine, by elemental analysis. Trifluoroacetic acid from Eastman Kodak was distilled onto molecular sieves and stored in a desiccator. Reagent grade nitromethane and perchloric acid were used as received.

*(b) Synthesis of triarylphosphines*

The preparation of $P(4\text{-}ClC_6H_4)_3$ is described as a representative procedure for the preparation of the triarylphosphines. All glassware was oven-dried and flushed with dry dinitrogen before use. The starting material, 1-bromo-4-chlorobenzene (100 g, 0.52 mol) was dissolved in ~ 100 mL of reagent grade THF from a freshly opened bottle. This solution was slowly added to a 500 mL 3-necked flask containing magnesium turnings (12.7 g, 0.52 mol) and THF (~ 50 mL). The reaction started spontaneously after about 2–3 min. The reagent solution was added continu-

TABLE 2. Analytical data[a]

| | Compound | Melting point (°C) | C Calcd. | C Found | H Calcd. | H Found | δ($^{31}$P) (ppm) | δ($^{1}$H)$_{CH_3}$[b] (ppm) |
|---|---|---|---|---|---|---|---|---|
| I | P(*t*-$C_4H_9$)$_3$ | 27–29 | — | — | — | — | 56.7 | 3.12[c] |
| II | P(*c*-$C_6H_{11}$)$_3$ | 76–77 | — | — | — | — | 8.8 | — |
| III | P(4-$(CH_3)_2NC_6H_4$)$_3$ | 265–270 | 73.6[d] | 73.7 | 7.7 | 7.4 | −11.7 | 3.07 |
| IV | P(4-$CH_3OC_6H_4$)$_3$ | 135–137 | 71.6 | 71.0 | 6.0 | 6.0 | −10.6 | 3.78 |
| V | P(4-$CH_3C_6H_4$)$_3$ | 145–148 | 82.9 | 82.7 | 7.0 | 7.0 | −8.3 | 2.34 |
| VI | P(3-$CH_3C_6H_4$)$_3$ | 103–104 | 82.9 | 83.2 | 7.0 | 6.7 | −5.3 | 2.29 |
| VII | P(2-$CH_3C_6H_4$)$_3$ | 125–127 | 82.9 | 82.9 | 7.0 | 6.9 | −27.8 | 2.38 |
| VIII | P($C_6H_5$)$_3$ | 80 | 82.4 | 82.2 | 5.8 | 5.9 | −6.3 | — |
| IX | P(4-$FC_6H_4$)$_3$ | 80–81 | 68.4 | 68.5 | 3.8 | 3.6 | −9.3[e] | — |
| X | P(4-$ClC_6H_4$)$_3$ | 100–101 | 59.1 | 59.4 | 3.3 | 3.3 | −8.7 | — |

[a]The analytical data are in agreement with those in ref. 41.
[b]These methyl shifts are included because they are diagnostic and show significant shifts on coordination of the phosphine. All the aryl phosphines showed aromatic multiplets around δ = 7. The spectrum of **II** was an unresolved and very complex multiplet between δ = 1.0 and δ = 3.0.
[c]$^3J$(P—H) = 9.5 Hz.
[d]%N = 10.7 (calcd.) 11.2 (found).
[e]Quartet. $^5J$(P—F) = 4.4 Hz.

ously at a rate necessary to maintain reflux. The total time of addition was about 1 h. Using the same dropping funnel, a solution of $PCl_3$ (23.9 g, 0.17 mol, 15.2 mL) in 50 mL THF was prepared and added slowly, also at a rate necessary to maintain reflux. Up to this point all reactions were done under dry nitrogen. Enough water was added to produce two layers in the flask and the organic layer was removed and filtered. The aqueous portion was extracted twice with 50 mL portions of diethyl ether which were also filtered and added to the first organic portion. The aqueous portion was discarded and the organic solution was evaporated. The residue, which had a definite orange colour, was recrystallised from hot ethanol repeatedly until a white crystalline product was obtained. Elemental analyses were performed by Guelph Chemical Laboratory, Guelph, Ontario. Analytical data are given in Table 2 which also contains the $^{31}$P—{$^1$H} and $^1$H nmr data.

*(c) Determination of basicities*

The method of Streuli (16) was modified to suit the equipment and materials available in our laboratory. A solution of $HClO_4$ (0.2 *M*), prepared by adding reagent grade 70% $HClO_4$ (8.4 mL) to $CH_3NO_2$ (500 mL), was deoxygenated by bubbling dry $N_2$ through it for 30 min. Titrations were performed using a 5 mL self-filling burette attached to a source of $N_2$. The phosphines (~ 1 mmol per determination) were dissolved in $CH_3NO_2$ (100 mL) and the titration was followed using a Chemtrix digital pH–mV meter with a combination glass–calomel electrode. The best results were obtained when the electrode was allowed to sit in nitromethane a few hours before the titrations were performed. The endpoint was determined from a derivative plot and the half neutralisation potential (HNP) was recorded. Three separate determinations were made for each phosphine. Triphenylphosphine was used as a standard instead of diphenylguanidine. The difference, HNP(triphenylphosphine) − HNP(phosphine), was calculated. The ΔHNP used by Streuli is merely this value plus 573 mV which is the ΔHNP of triphenylphosphine when diphenylguanidine is used as a reference. This new value can now be used in the equation

$$pK_a = 10.12 - 0.0129(\Delta HNP)$$

where

$$pK_a = -\log_{10}[H^+][PR_3]/[HPR_3^+]$$

The value HNP(triphenylphosphine) was determined daily before the titrations. Tri-*tert*-butylphosphine, tricyclohexylphosphine, and tris(4-dimethylaminophenyl)phosphine were titrated under an atmosphere of oxygen-free nitrogen using deoxygenated solvent. The others were titrated in air. Smaller amounts (~ 0.3 mmol) of tricyclohexylphosphine and tris(4-dimethylaminophenyl)phosphine were used because of their low solubility in nitromethane.

Because of the possible ambiguity about the site of protonation of P(H-$(CH_3)_2NC_6H_4$)$_3$ the titration was continued past the first endpoint. A second equivalence point was found at four times the volume of titrant as for the first. Clearly the first endpoint was from the protonation of the phosphorus atom and the second was from the protonation of the nitrogen atoms.

The reproducibility of the titrations was equivalent to ± 0.05 $pK_a$ units.

*(d) Nuclear magnetic resonance measurements*

*(i) Measurements of $^1J$(P—H)*

The phosphonium ions were generated by dissolving the phosphines in dry trifluoroacetic acid to give clear colourless solutions. High phosphine concentrations tended to promote exchange of the phosphonium protons so that solutions were no more concentrated than necessary to observe the doublet due to the phosphonium proton. The $^1J$(P—H) values for the phosphonium ions of all the phosphines except tris(4-fluorophenyl)-phosphine were determined from their $^1$H nmr spectra measured at ambient temperature with a Varian T-60 nmr spectrometer using TMS as the internal reference. The $^1J$(P—H) value for protonated tris(4-fluorophenyl)phosphine was obtained from its $^{31}$P nmr spectrum run on a Bruker WP-60 FT nmr spectrometer using 85% $H_3PO_4$ as external reference.

*(ii) Spectra of the free phosphines*

All spectra but two ($^{13}$C of **VI** and **X**) were recorded on a Bruker WP-60 FT nmr spectrometer. The other two spectra were run on a Bruker WH-400 FT nmr spectrometer to remove the peak overlap which made assignments impossible in the low field spectra. The $^1$H and $^{13}$C spectra were run in $CDCl_3$ (aryl phosphines) or $C_6D_6$ (alkyl phosphines) using the deuterium lock and internal TMS as a reference. All $^{31}$P spectra were measured on concentrated $CH_2Cl_2$ solutions to which 10% v/v $C_6D_6$ was added to provide a deuterium lock. A capillary of 85% $H_3PO_4$ was used as an external reference. $^{13}$C and $^{31}$P spectra were proton decoupled using a broad band decoupler. All shifts are reported in the same sense; that is, positive shifts are to high frequency of the reference.

Can. J. Chem. Downloaded from www.nrcresearchpress.com by 210.87.254.105 on 09/06/12
For personal use only.

## Acknowledgement

We gratefully thank the Natural Sciences and Engineering Research Council of Canada for financial support of this project.

1. G. BOOTH. Adv. Inorg. Chem. Radiochem. **6**, 1 (1964).
2. C. A. MCAULIFFE. Transition metal complexes of phosphorus, arsenic and antimony ligands. MacMillan, London. 1973.
3. O. STELZER. Top. Phosphorus Chem. **9**, 1 (1977).
4. C. A. MCAULIFFE and W. LEVASON. Phosphine, arsine and stibine complexes of the transition elements. Elsevier, Amsterdam. 1979.
5. R. F. HECK. Organotransition metal chemistry. Academic Press, New York. 1974.
6. (*a*) J. CHATT. Nature. **165**, 637 (1950); (*b*) J. CHATT and A. A. WILLIAMS. J. Chem. Soc. 3061 (1951).
7. (*a*) C. A. TOLMAN. J. Am. Chem. Soc. **92**, 2953 (1970); (*b*) C. A. TOLMAN. Chem. Rev. **77**, 313 (1977) and references cited therein.
8. (*a*) S. O. GRIM, D. A. WHEATLAND, and W. MCFARLANE. J. Am. Chem. Soc. **89**, 5573 (1967); (*b*) S. O. GRIM, R. M. SINGER, A. W. JOHNSON, and F. J. RANDAL. J. Coord. Chem. **8**, 121 (1978).
9. S. O. GRIM, R. L. KEITER, and W. MCFARLANE. Inorg. Chem. **6**, 1133 (1967).
10. (*a*) S. O. GRIM, P. J. LUI, and R. L. KEITER. Inorg. Chem. **13**, 342 (1974); (*b*) S. O. GRIM, D. P. SHAH, C. K. HAAS, J. M. RESSNER, and P. H. SMITH. Inorg. Chim. Acta, **36**, 139 (1979).
11. S. O. GRIM and A. W. YANKOWSKY. J. Org. Chem. **42**, 1236 (1977).
12. W. MCFARLANE and R. F. M. WHITE. J. Chem. Soc. Chem. Commun. 744 (1969).
13. G. A. OLAH and C. MCFARLAND. J. Org. Chem. **34**, 1832 (1969).
14. T. A. MASTRYUKOVA and M. I. KABACHNIK. Russ. Chem. Rev. **38**, 795 (1969) and references cited therein.
15. W. H. THOMPSON and C. T. SEARS, JR. Inorg. Chem. **16**, 769 (1977).
16. (*a*) C. A. STREULI. Anal. Chem. **32**, 985 (1960); (*b*) W. A. HENDERSON and C. A. STREULI. J. Am. Chem. Soc. **82**, 5791 (1960).
17. R. G. GOEL. Inorg. Nucl. Chem. Lett. **15**, 437 (1979).
18. (*a*) E. C. ALYEA, S. A. DIAS, R. G. GOEL, and W. O. OGINI. Can. J. Chem. **55**, 4227 (1977); (*b*) E. C. ALYEA, S. A. DIAS, R. G. GOEL, W. O. OGINI, P. PILON, and D. W. MEEK. Inorg. Chem. **17**, 1697 (1978); (*c*) T. ALLMAN, R. G. GOEL, and P. PILON. Can. J. Chem. **57**, 91 (1979); (*d*) R. G. GOEL, W. P. HENRY, and W. O. OGINI. Can. J. Chem. **57**, 762 (1979); (*e*) T. ALLMAN, R. G. GOEL and P. PILON. Spectrochim. Acta, **35A**, 923 (1979); (*f*) T. ALLMAN and R. G. GOEL. Inorg. Nucl. Chem. Lett. **15**, 199 (1979); (*g*) T. ALLMAN and R. G. GOEL. Abstract. 18th General Assembly of Gessellschaft Deutscher Chemiker. Berlin, September 10–14, 1979.
19. (*a*) R. G. GOEL and W. O. OGINI. Inorg. Chem. **16**, 1968 (1977); (*b*) R. G. GOEL, W. P. HENRY, and R. C. SRIVASTAVA. Inorg. Chem. **20**, 1727 (1981).
20. (*a*) R. G. GOEL and P. PILON. Inorg. Chem. **17**, 2876 (1978); (*b*) R. G. GOEL and T. G. M. M. DIKHOFF. Abstract. XX International Conference on Coordination Chemistry, Calcutta. December 10–14, 1979.
21. N. B. CHAPMAN and J. SHORTER (*Editors*). Advances in linear free energy relationships. Plenum, London. 1972. pp. 28, 29.
22. M. GOETZ and A. SIDHU. Justus Liebigs Ann. Chem. **682**, 71 (1968).
23. H. P. HOPKINS, H. S. RHEE, C. T. SEARS, K. C. NAINAN, and W. H. THOMPSON. Inorg. Chem. **16**, 2884 (1977).
24. M. BJORØY, B. B. SAUNDERS, S. ESPERAS, and J. SONGSTAD. Phosphorus, **6**, 83 (1976).
25. M. A. WEINER and M. LATTMAN. J. Org. Chem. **40**, 1292 (1975).
26. M. F. LAPPERT, J. B. PEDLEY, B. T. WILKINS, O. STELZER, and V. UNGER. J. Chem. Soc. Dalton, 1207 (1975).
27. T. B. DEBIES, J. W. RABALAIS. Inorg. Chem. **13**, 308 (1974).
28. K. J. MOYNIHAN, C. CHIEH, and R. G. GOEL. Acta. Crystallogr. B**35**, 3060 (1979).
29. H. A. BENT. Can. J. Chem. (*a*) **38**, 1235 (1960); (*b*) J. Chem. Ed. **37**, 616 (1960).
30. F. W. WEHRLI and T. WIRTHLIN. Interpretation of carbon-13 spectra. Heyden and Son Ltd., London. 1978.
31. D. M. GRANT and W. M. LITCHMAN. J. Am. Chem. Soc. **87**, 3994 (1965).
32. C. J. JAMESON and H. S. GUTOWSKI. J. Chem. Phys. **51**, 2790 (1969).
33. L. J. VANDE GRIEND, J. G. VERKADE, J. F. M. PENNINGS, and H. M. BUCK. J. Am. Chem. Soc. **99**, 2459 (1977).
34. R. E. WASYLISHEN. Ann. Rev. Nucl. Magn. Reson. Spectrosc. **7**, 245 (1977).
35. G. A. GRAY and S. E. CREMER. Chem. Commun. 451 (1974).
36. T. BUNDGAARD and H. J. JAKOBSEN. Acta Chem. Scand. **26**, 2548 (1972).
37. S. SORENSON, R. S. HANSEN, and H. J. JAKOBSEN. J. Am. Chem. Soc. **94**, 5900 (1972).
38. L. F. JOHNSON and W. C. JANKOWSKI. Carbon-13 nmr Spectra. Wiley, Toronto. 1972.
39. B. E. MANN. J. Chem. Soc. Perkin II, 30 (1975).
40. E. C. ALYEA, G. T. FEY, and R. G. GOEL. J. Coord. Chem. **5**, 143 (1976).
41. S. O. GRIM and A. W. YANKOWSKY. Phosphorus sulphur. **3**, 191 (1977) and references cited therein.

Can. J. Chem. Downloaded from www.nrcresearchpress.com by 210.87.254.105 on 09/06/12
For personal use only.

# Synthesis of 4,5-disubstituted imidazoles

GERRY KAVADIAS,[1] BING LUH, AND ROGER SAINTONGE
*Bristol Laboratories of Canada, 100 Industrial Boulevard, Candiac, P.Q., Canada J5R 1J1*

Received September 10, 1981

GERRY KAVADIAS, BING LUH, and ROGER SAINTONGE. Can. J. Chem. **60**, 723 (1982).

Introduction of a triphenylmethyl group on the nitrogen of imidazole-4,5-dicarboxylic acid esters or 4,5-dihydroxymethylimidazole resulted in deactivation of the functional group adjacent to the protecting group and allowed reactions to take place preferably or exclusively on the other functional group. Thus, dimethyl 1-triphenylmethylimidazole-4,5-dicarboxylate (**2**), on treatment with hydrazine and methylamine produced methyl 4-hydrazinocarbonyl-1-triphenylmethylimidazole-5-carboxylate (**3***a*) and methyl 4-methylaminocarbonyl-1-triphenylmethylimidazole-5-carboxylate (**3***b*), respectively. Reduction of **2** with lithium borohydride gave methyl 4-hydroxymethyl-1-triphenylmethylimidazole-5-carboxylate (**4***a*). Treatment of 4,5-dihydroxymethyl-1-triphenylmethylimidazole (**5***a*), with trimethylacetyl chloride and with acetic anhydride afforded 5-hydroxymethyl-4-trimethylacetoxymethyl-1-triphenylmethylimidazole (**6***a*), and 4-acetoxymethyl-5-hydroxymethyl-1-triphenylmethylimidazole (**6***c*), respectively. Oxidation of **5***a* with activated manganese dioxide produced the monoaldehydes **9** and **10** in a ratio of 11:1. A new mild process for deprotection of *N*-triphenylmethylimidazoles, compatible with acid sensitive groups in the molecule, is reported. The synthesis of several 4,5-disubstituted imidazoles is also described.

GERRY KAVADIAS, BING LUH et ROGER SAINTONGE. Can. J. Chem. **60**, 723 (1982).

L'introduction d'un groupe triphénylméthyle sur l'azote des esters de l'acide imidazoledicarboxylique-4,5 ou du dihydroxyméthyl-4,5 imidazole, provoque la désactivation du groupe fonctionnel voisin du groupe protecteur et induit des réactions préférentielles ou exclusives au niveau de l'autre groupe fonctionnel. Dans ces conditions, le triphénylméthyl-1 imidazoledicarboxylate-4,5 de méthyle réagit avec l'hydrazine ou la méthylamine pour donner soit l'hydrazinocarbonyl-4 triphenylméthyl-1 imidazolecarbonylate-1 de méthyle (**3***a*) ou le méthylaminocarbonyl-4 triphenylméthyl-1 imidazole carboxylate-5 de méthyle (**3***b*). Le composé **2**, en présence de borohydrure de lithium, conduit à l'hydroxyméthyl-4 triphénylméthyl-1 imidazolecarboxylate-5 de méthyle (**4***a*). Le dihydroxyméthyl-4,5 triphenylméthyl-1 imidazole (**5***a*) réagit avec le chlorure de triméthylacétyle ou l'anhydride acétique pour donner soit l'hydroxyméthyl-5 triméthylacetoxyméthyl-4 triphénylméthyl-1 imidazole (**6***a*) ou l'acétoxyméthyl-4 hydroxyméthyl-5 triphénylméthyl-1 imidazole (**6***c*). L'oxydation du composé **5***a* par le dioxyde de manganèse fournit les monoaldéhydes **9** et **10** dans un rapport de 11:1. On rapporte une nouvelle méthode de déprotection douce des *N*-triphénylméthylimidazoles qui est compatible avec les groupes sensibles aux acides. On décrit également la synthèse de plusieurs imidazoles substitués en positions 4 et 5.

[Traduit par le journal]

In a research project directed toward the syntheses of novel histamine H-2 receptor antagonists as potential antiulcer agents, structurally related to cimetidine (1), 4,5-disubstituted imidazoles of the general structure **1** were needed as intermediates.

Most syntheses of 4,5-disubstituted imidazoles are based on ring closure of α-diketones, α-hydroxy-, α-halogeno- or (under reducing conditions) α-oximinoketones. All these suffer from deficiencies such as difficulties in the syntheses of starting materials and low yields. Furthermore, the applicability of these processes is limited to the syntheses of products that can survive the vigorous conditions involved in the ring-closing step (2). It seemed of interest to investigate the possibility of an alternative synthesis which would utilize viable sources of starting materials with a preformed imidazole ring. This paper describes the synthesis of 4,5-heterodisubstituted imidazoles from the readily available dimethyl 4,5-imidazole dicarboxylate (**1**) and from 4,5-dihydroxymethyl imidazole (**5***b*).

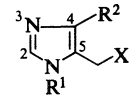

**1**

$R^1$ = H; $R^2$ = $CO_2CH_3$, $CH_2OH$, CN, CHO, $CONHCH_3$, $CONHNH_2$, CH=CHCN; X = Cl, Br

The ester groups in **1** and the hydroxymethyl groups in **5***b* are chemically equivalent and therefore chemical modifications of these molecules invariably yield symmetrically disubstituted products. It appeared to us that the presence of a bulky triphenylmethyl group at the 1-position of dimethyl imidazole-4,5-dicarboxylate (compound **2**) would hinder reactions on the neighboring ester at C-5, thus permitting reactions to take place preferentially at the other ester group. For similar reasons, the reactivities of the hydroxymethyl groups in the protected diol **5***a* were expected to be influenced by the presence of the triphenylmethyl group.

The reactions of the protected ester **2** with nucleophiles are shown in Scheme 1. Treatment of dimethyl imidazole-4,5-dicarboxylate (3) with tri-

[1]To whom all correspondence should be addressed.

0008-4042/82/060723-07$01.00/0
©1982 National Research Council of Canada/Conseil national de recherches du Canada

Can. J. Chem. Downloaded from www.nrcresearchpress.com by 210.87.254.40 on 09/06/12
For personal use only.

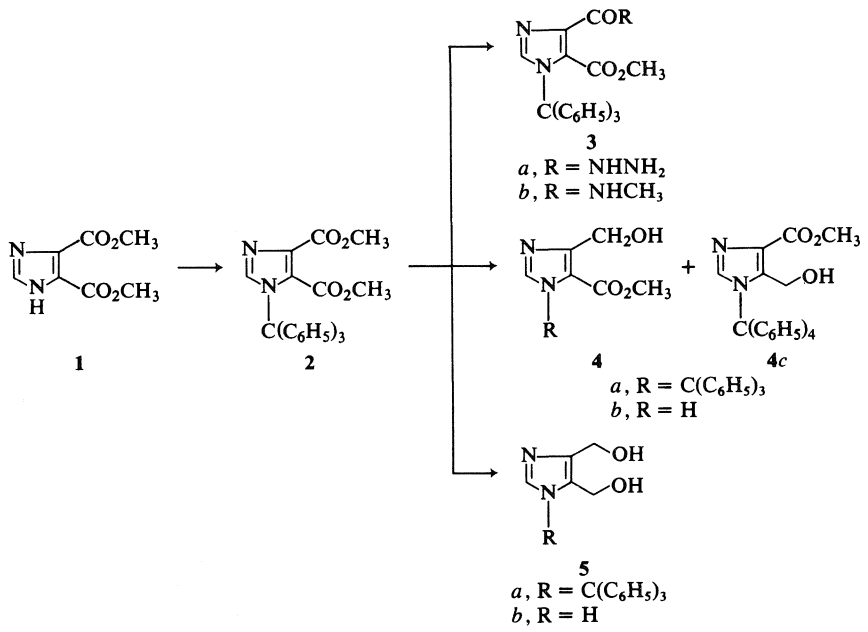


SCHEME 1

phenylmethyl chloride in dimethylformamide in the presence of triethylamine (4, 5) provided a 93% yield of dimethyl 1-triphenylmethylimidazole-4,5-dicarboxylate (**2**). When **2** was treated with a large excess of hydrazine (24 equiv.) in ethanol, the monohydrazide **3***a* was obtained in 94% yield. It is pertinent to note that similar reaction with the unprotected diester **1** yielded exclusively imidazole-4,5-dicarboxylic acid dihydrazide (6). Reaction of **2** with a large excess of methylamine in tetrahydrofuran–ethanol solvent mixture was also regiospecific and produced the monoamide **3***b*, exclusively. It was also possible to reduce one of the ester groups in **2** and produce the corresponding monoester. Thus, treatment of **2** with lithium borohydride in diglyme gave a 62% yield of the monoesters **4***a* and **4***c* in a ratio of 10:1, which upon removal of the triphenylmethyl group yielded the monoester **4***b*.

That the triphenylmethyl group in **3***a*, **3***b*, and **4***a* was correctly assigned to the nitrogen atom adjacent to the carboxymethyl group was supported by $^1$Hmr spectroscopy. The methyl groups of dimethyl imidazole-4,5-dicarboxylate (**1**) experienced the same chemical shift and appeared as a singlet at δ 3.8 (see Table 1). In compound **2**, the methyl groups appeared as sharp singlets at δ 3.87 (same region as in **1**) and 3.17. Due to the shielding influence of the triphenylmethyl group these resonance peaks were assigned to the methyl protons of the carboxymethyl groups at C-4 and C-5, respectively. The $^1$Hmr spectra of **3***a*, **3***b*, and **4***a* revealed that the sharp singlet at lower field (δ 3.8) had disappeared, while the singlet at higher field (δ 3.1–3.2) remained. Thus, the carboxymethyl group of these products must be adjacent to the triphenylmethyl group.

4,5-Dihydroxymethyl-1-triphenylmethylimidazole (**5***a*) was also found to be a viable intermediate for the synthesis of 4,5-heterodisubstituted imidazoles. The triphenylmethyl group in **5***a* appreciably decreased the reactivity of the adjacent hydroxyl group thus allowing reactions to take place preferably at the other hydroxyl group. Although the blocked diol **5***a* could be obtained from **5***b* by reaction with triphenylmethyl chloride, the difficulties involved in the preparation of **5***b* (7) by reduction of **1** with lithium aluminum hydride (mainly because of the extremely low solubilities of **1** in the permissible solvents) makes this process less desirable. It was found more convenient to prepare **5***a* by reduction of the diester **2** with lithium aluminum hydride in tetrahydrofuran. The high solubilities of **2** in THF and ether and the easily removable protective group makes this process attractive for the synthesis of **5***b* on a preparative scale.

It was possible to protect one of the hydroxyl groups in **5***a* while the other remained free for subsequent reactions (Scheme 2). Thus, treatment of **5***a* with trimethylacetyl chloride and with acetic anhydride produced the monoesters **6***a* (79%) and **6***c* (90%), respectively. When **6***a* was treated with thionyl chloride the chloride hydrochloride **7** was

Can. J. Chem. Downloaded from www.nrcresearchpress.com by 210.87.254.40 on 09/06/12
For personal use only.

Can. J. Chem. Downloaded from www.nrcresearchpress.com by 210.87.254.40 on 09/06/12
For personal use only.

TABLE 1. Nuclear magnetic resonance spectra of certain imidazole derivatives[a]

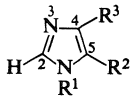

| Compound | H-2 | $R^1$ | $R^2$ | $R^3$ | Solvent |
|---|---|---|---|---|---|
| **1** | (7.93) | H | $CO_2CH_3$ (3.83) | $CO_2CH_3$ (3.83) | DMSO-$d_6$ |
| **2** | (7.55) | Tr[c] (7.1–7.5) | $CO_2CH_3$ (3.17) | $CO_2CH_3$ (3.87) | $CDCl_3$ |
| ***3a*** | [b] | Tr (7.1–7.5) | $CO_2CH_3$ (3.0) | $CONHNH_2$ | DMSO-$d_6$ |
| ***3b*** | [b] | Tr (7.1–7.5) | $CO_2CH_3$ (3.20) | $CONHCH_3$ (2.91, d, $J$ = 5) | $CDCl_3$ |
| ***4a*** | [b] | Tr (7.1–7.4) | $CO_2CH_3$ (3.17) | $CH_2OH$ (4.83) | $CDCl_3$ |
| ***4b*** | (7.62) | H | $CH_2OH$ (4.65) | $CO_2CH_3$ (3.87) | DMSO-$d_6$, $D_2O$ |
| ***5a*** | [b] | Tr (7.2–7.5) | $CH_2OH$ (3.95) | $CH_2OH$ (4.65) | $CDCl_3$ |
| ***5b*** | (7.7) | H | $CH_2OH$ (4.63) | $CH_2OH$ (4.63) | $D_2O$ |
| ***6a*** | [b] | Tr (7.1–7.5) | $CH_2OH$ (4.0) | $CH_2O-\overset{O}{\overset{\|}{C}}-CMe_3$ (5.15) (1.18) | $CDCl_3$ |
| ***6b*** | (7.43) | H | $CH_2OH$ (4.7) | $CH_2O\overset{O}{\overset{\|}{C}}CMe$ (5.03) (1.1) | $CDCl_3$ |
| ***6c*** | [b] | Tr (7.1–7.5) | $CH_2OH$ (4.6, d, $J$ = 6) | $CH_2O\overset{O}{\overset{\|}{C}}-CH_3$ (5.13) (2.08) | $CDCl_3$ |
| ***6d*** | [b] | Tr (7.1–7.5) | $CH_2O\overset{O}{\overset{\|}{C}}CH_3$ (4.53) (1.63) | $CH_2O\overset{O}{\overset{\|}{C}}CH_3$ (5.07) (2.07) | $CDCl_3$ |
| **9** | [b] | Tr (7.1–7.5) | $CH_2-OH$ (3.95, d, $J$ = 6) (4.75, t, $J$ = 6) | CHO (10.0) | $CDCl_3$ |
| **10** | [b] | Tr (7.1–7.5) | CHO (9.3) | $CH_2OH$ (4.75, d, $J$ = 6) (4.20, t, $J$ = 6) | $CDCl_3$ |

[a]Recorded at 60 MHz. Values expressed as ppm (δ). All spectra appeared as sharp singlets, unless otherwise noted. The coupling constants are recorded in Hz.
[b]Appeared in the region 7.1–7.5 together with the aromatic protons.
[c]Tr = $C(C_6H_5)_3$.

obtained in good yield (83.5%). Treatment of **7** with sodium azide in aqueous ethanol afforded a 91% yield of the azide ***8a***. The reaction of **7** with sodium ethanethiolate in water gave a good yield (75%) of the thioether ***8b***.

Oxidation of the diol ***5a*** with activated manganese dioxide (8) in boiling chloroform, conditions similar to those previously employed by Kelley and co-workers for the oxidation of an analogous product (5), gave a mixture of the isomeric monoaldehydes **9** and **10** in which compound **9** was the predominant isomer (92%). Several transformations of **9** giving rise to a variety of 4,5-heterodisubstituted imidazoles are apparent (Scheme 3). Thus, the reaction of **9** with ammonia in methylene chloride in the presence of activated manganese dioxide (8), a process described by Gilman (9), gave rise to the cyanocompound **11**. Treatment of **11** with thionyl chloride afforded **12** which on reaction with sodium 2-aminoethanethiolate produced **13**.

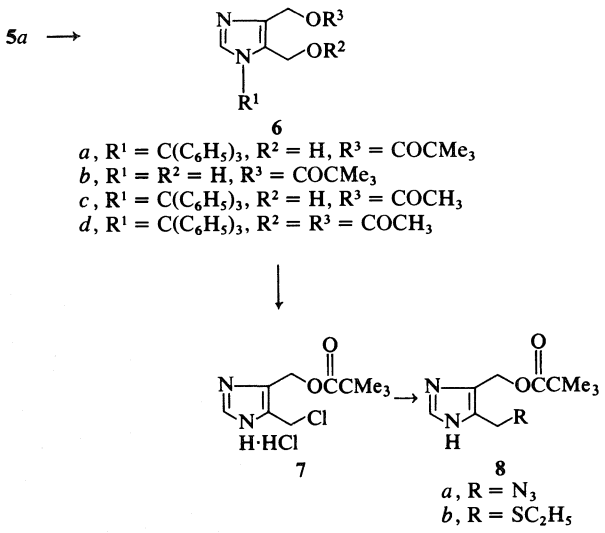


SCHEME 2

Extension of the side chain in **9** was possible by reaction of **9** and diethylcyanomethylphosphonate (10) giving rise to a mixture of the olefins **14** and **15** in a ratio of 2:1.

The assignment of structures for compounds **6***a*, **6***c*, and **9** as having the hydroxymethyl group next to the nitrogen atom carrying the triphenylmethyl group was made on the basis of $^1$Hmr studies. Examination of Table 1 reveals that the methylene groups in 4,5-dihydroxymethylimidazole (**5***b*) experience the same chemical shift and appear as a sharp singlet at δ 4.63. In 4,5-dihydroxymethyl-1-triphenylmethylimidazole (**5***a*), the methylene group at C-4 resonated in the same field as those in **5***b* and appeared as a singlet at δ 4.65 whereas the methylene group at C-5 was shifted to higher field and appeared as a singlet at δ 3.95. The $^1$Hmr spectra of **6***a*, **6***c*, and **9** revealed that the sharp singlet for the methylene of the hydroxymethyl group at δ 4.65 had disappeared, while the singlet in the region of δ 3.95 remained.

Excellent results were obtained in deblocking *N*-triphenylmethylimidazoles (i.e., compound **11***a*) using dilute hydrochloric acid solutions as has already been reported (4, 5). However, equally good results were obtained by simply refluxing ethanolic solutions of blocked imidazoles in the presence of water and a small amount of acetic acid. This process is compatible with acid-sensitive groups in the molecule. Compounds **4***b*, **5***b*, and **6***b* were prepared by this method in high yields.

In summary, we have shown that the commercially available imidazole-4,5-dicarboxylic acid can be conveniently converted to valuable and otherwise not easily accessible 4,5-disubstituted imidazoles by simple chemical processes.

## Experimental

The infrared spectra were recorded on a Unicam SP-200G grating ir spectrophotometer. The $^1$Hmr spectra were determined on a Varian EM 360 spectrometer using tetramethylsilane (for solutions other than deuterium oxide) and sodium 4,4-di-

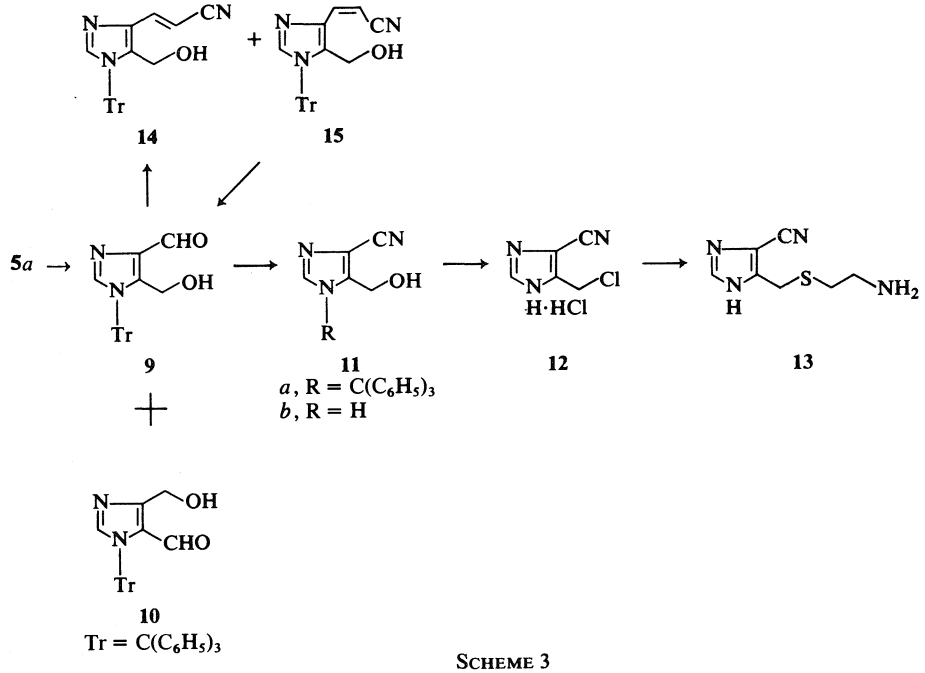


SCHEME 3

Can. J. Chem. Downloaded from www.nrcresearchpress.com by 210.87.254.40 on 09/06/12
For personal use only.

Can. J. Chem. Downloaded from www.nrcresearchpress.com by 210.87.254.40 on 09/06/12
For personal use only.

methyl-4-silapentane-1-sulfonate (for solutions of deuterium oxide) as internal standards. Melting points are uncorrected and were determined on an electrothermal melting point apparatus. The analyses were performed by Micro-Tech Laboratories, Skokie, IL. Thin layer chromatography (tlc) was carried out on pre-coated silica gel plates (E. Merck F-254). Reaction yields refer to products which showed a single spot on tlc plates.

*Dimethyl imidazole-4,5-dicarboxylate (**1**)*

This compound was prepared by a described procedure (3*b*). Recrystallization twice from water provided pure sample, mp 206–207°C. (lit., (3*a*), mp 200–202°C).

*Dimethyl 1-triphenylmethylimidazole-4,5-dicarboxylate (**2**)*

This compound was prepared according to the procedure described in the literature (4, 5) for the synthesis of *N*-triphenylmethylimidazoles. Thus, a mixture of dimethyl imidazole-4,5-dicarboxylate (11.0 g, 60 mmol), dry triethylamine (10.4 mL, 78 mmol), and dry dimethylformamide (75 mL) was blanketed with nitrogen and stirred at room temperature. To this mixture was added 19.5 g (70 mmol) of triphenylmethyl chloride in one lot. Soon after the addition, a white precipitate was formed; to facilitate stirring an additional 40 mL of dimethylformamide was added. The reaction was monitored by tlc on silica plates using 5% methanol in methylene chloride as eluent and was complete after 2 h. After stirring for an additional 2 h, the reaction mixture was poured over a mixture of crushed ice and water (600 mL). The solids were collected and washed with water. The partly dried product was dissolved in methylene chloride and the solution washed several times with water to eliminate unreacted diester **1**, dried, and evaporated. The residue was dissolved in $CHCl_3$ (50 mL), the solution diluted with petroleum ether (100 mL, bp 30–60°C), and the resultant solution allowed to crystallize at room temperature. The solids were collected by filtration to give 19.5 g of **2**, mp 202–205°C. The mother liquor was evaporated at reduced pressure and the residue was recrystallized from the same solvent system as above to provide an additional 4.5 g of **2** which were combined with the first crop to a total of 24 g (93%); ir (Nujol): 1720 $cm^{-1}$. *Anal.* calcd. for $C_{26}H_{22}N_2O_4$: C 73.22, H 5.19, N 6.57; found: C 73.24, H 5.52, N 6.57.

*Methyl 4-hydrazinocarbonyl-1-triphenylmethylimidazole-5-carboxylate (**3**a)*

To a stirred suspension of **2** (0.5 g, 1.18 mmol) in ethanol (2 mL) was added 0.9 mL (0.91 g, 28.4 mmol) of anhydrous hydazine and the reaction mixture stirred at room temperature for 40 min. Removal of the solvent by evaporation and recrystallization of solid residue from ethanol yielded 0.47 g (94%) of **3***a*, mp 240–242°C (decomp.); ir (Nujol): 3300, 1720, 1670, 1620, 1570 $cm^{-1}$. *Anal.* calcd. for $C_{25}H_{22}N_4O_3$: C 70.40, H 5.20, N 13.14; found: C 70.15, H 5.16, N 13.18.

*Methyl 4-methylaminocarbonyl-1-triphenylmethylimidazole-5-carboxylate (**3**b)*

A solution of **2** (1.0 g, 2.34 mmol) in tetrahydrofuran–ethanol solvent mixture (1:1, 45 mL) was saturated with methylamine (gas) and the reaction mixture stirred at room temperature for 48 h. The reaction was monitored by tlc on silica plates using ether–benzene (1:1) as eluent; after 48 h, the spot for **2** ($R_f$ 0.4) disappeared and a new spot of $R_f$ 0.24 (**3***b*) appeared. The reaction mixture was evaporated at reduced pressure. The solid residue was dissolved in acetone–chloroform mixture (1:10) and filtered through a pad of silica (4 cm long × 3.5 cm id) and the silica washed with the same solvent mixture (50 mL). The combined filtrate and washings were evaporated, the residue triturated with acetone–ether (1:2, 15 mL) and the crystalline material collected to give 0.85 g (85%) of **3***b* mp 211–213°C; ir (Nujol): 3380 (NH), 1730, 1680, 1570 $cm^{-1}$. *Anal.* calcd. for $C_{26}H_{23}N_3O_3$: C 73.30, H 5.44, N 9.87; found: C 73.09, H 5.34, N 9.78.

*Methyl 4-hydroxymethyl-1-triphenylmethylimidazole-5-carboxylate (**4**a)*

To a solution of sodium borohydride (0.57 g, 15 mmol) in dry diglyme (25 mL) was added anhydrous lithium bromide (1.3 g, 15 mmol) and the suspension was placed under a slow stream of nitrogen and stirred at room temperature for 30 min. To this mixture was added the diester **2** (2.13 g, 5 mmol) and the reaction mixture stirred at 25°C for 7 h, stored at 0°C overnight, and then stirred at 25°C for 5 h more. The reaction mixture was poured into cold water (200 mL) and the precipitate collected by filtration and washed with water. The solids were dissolved in methylene chloride, the solution extracted with water, dried, and evaporated to give 1.8 g of a syrup. Analysis of this product on tlc (silica, 10% MeOH–$CH_2Cl_2$) showed one major spot of $R_f$ 0.51 (**4***a*) and three minor spots of $R_f$ 0.46 (diol), 0.62, and 0.77 (**2**). The crude product was chromatographed on Alumina Act. II (Alumina Fluka for chromatography type 507C) (column size 13 × 1.8 cm id). Elution with ether–benzene (1:1) mixture removed the unreacted diester (0.32 g); subsequent elution with 2% methanol in methylene chloride gave 1.2 g (62%) of product which on tlc showed a major spot for **4***a* and a minor one of $R_f$ 0.62 (presumably the isomer of **4***a*). Further elution with 4% methanol in methylene chloride gave 0.2 g of the diol **5***a*.

The major fraction (**4***a* plus isomer) without further purification was used in the next reaction. A sample was recrystallized from 80% ethanol to afford **4***a*, mp 162–163°C; ir ($CHCl_3$): 3300, 1720 $cm^{-1}$. *Anal.* calcd. for $C_{25}H_{22}N_2O_3$: C 75.35, H 5.54, N 7.03; found: C 75.28, H 5.53, N 7.05.

*Methyl 4(5)-hydroxymethylimidazole-5(4)-carboxylate (**4**b)*

A solution of **4***a* (0.6 g) in 80% ethanol (10 mL) and glacial acetic acid (0.5 mL) was stirred under reflux for 45 min. Removal of the solvent by evaporation *in vacuo* left a solid which was partitioned between water (10 mL) and ether–hexane mixture (1:1, 10 mL). The organic phase containing triphenyl carbinol was separated and discharged; the aqueous phase was evaporated under reduced pressure to give 0.21 g (90%) of **4***b*. Recrystallization from ethanol yielded the analytical sample, mp 171–172°C. *Anal.* calcd. for $C_6H_8N_2O_3$: C 46.15, H 5.16, N 17.94; found: C 46.13, H 5.16, N 17.95.

*4,5-Dihydroxymethyl-1-triphenylmethylimidazole (**5**a)*

Dimethyl 1-triphenylmethylimidazole-4,5-dicarboxylate (58 g, 0.136 mol) was added in small portions to a stirred mixture of 9 g (0.237 mol) of lithium aluminum hydride in 1 L of dry tetrahydrofuran at 0°C under a nitrogen atmosphere. After the addition was completed (30 min) the cooling bath was removed and stirring was continued at room temperature for 3 h. The reaction mixture was cooled to 0°C and treated successively with 60 mL of water, 60 mL of 15% aqueous sodium hydroxide, and 60 mL of water. It was then filtered and the inorganic salts were washed with tetrahydrofuran. The combined filtrate and washings were evaporated under reduced pressure. The residue was dissolved in methylene chloride, the solution was washed with water, dried, and evaporated to give 38 g (75%) of **5***a*, mp 192–193°C; on tlc (silica, 10% methanol – methylene chloride), this product showed a single spot of $R_f$ 0.4. *Anal.* calcd. for $C_{24}H_{22}N_2O_2$: C 77.81, H 5.99, N 7.56; found: C 77.84, H 6.15, N 7.44.

In a larger scale experiment, the yield of **5***a* was 85%.

*4,5-Dihydroxymethylimidazole (**5**b)*

To a solution of **5***a* (1 g, 2.7 mmol) in 80% ethanol (10 mL) was added glacial acetic acid (0.5 mL) and the solution was refluxed

Can. J. Chem. Downloaded from www.nrcresearchpress.com by 210.87.254.40 on 09/06/12
For personal use only.

for 1.5 h. Removal of the solvent *in vacuo* left a solid residue which was partitioned between water and ether. The ether phase containing triphenyl methanol was separated and discharged; the aqueous phase was evaporated to dryness at reduced pressure to give 0.33 g (98.5%) of crystalline **5***b*. Recrystallization from ethanol afforded the analytical sample, mp 165–166°C (lit. (7) mp 162–163°C).

*5-Hydroxymethyl-4-trimethylacetoxymethyl-1-triphenylmethylimidazole (**6**a)*

To a suspension of **5***a* (29.6 g, 80 mmol) in dry methylene chloride (250 mL) was added 8.3 g (124 mmol) of dry pyridine and the mixture, protected from moisture, was cooled in an ice bath while stirring. A solution of 10.25 g (85 mmol) of trimethylacetyl chloride in 100 mL of methylene chloride was added dropwise. After the addition was completed (10 min), the reaction solution was stirred at room temperature for 2.5 h and then stored at 0°C overnight. The reaction mixture was washed with water (3 × 200 mL), dried, and evaporated under reduced pressure to give a syrup which on tlc (silica, 10% acetone in methylene chloride) showed one major spot for **6***a* ($R_f$ 0.45), a minor spot for unreacted **5***a* ($R_f$ 0) and three other unidentified minor spots ($R_f$ 0.62, 0.82, and 0.92). This product was dissolved in acetone – methylene chloride solvent mixture (1:10, 200 mL) and the solution filtered through a pad of silica (10 cm × 4 cm id) and the silica bed washed with the same solvent system (200 mL). By this treatment, the unreacted **5***a* was removed. The filtrate and washings were combined and evaporated to give 31 g of crystalline product. Recrystallization from benzene (70 mL) – petroleum ether (175 mL, bp 90–120°C) afforded 21.6 g (59.5%) of **6***a*, mp 157–159°C. The mother liquor was evaporated and the residue was chromatographed on silica using acetone–chloroform solvent mixture (1:10) as eluent to provide an additional 7 g of **6***a*. The two crops were combined to a total yield of 28.6 g (79%); ir ($CHCl_3$): 3580, 1720 $cm^{-1}$. *Anal.* calcd. for $C_{29}H_{30}N_2O_3$: C 76.62, H 6.65, N 6.16; found: C 77.03, H 6.49, N 6.16.

*4(5)-Hydroxymethyl-5(4)-trimethylacetoxymethylimidazole (**6**b)*

To a solution of **6***a* (2.0 g, 4.4 mmol) in 80% ethanol (20 mL) was added glacial acetic acid (1 mL) and the resultant solution was heated under reflux for 1 h and then evaporated to dryness at reduced pressure. The residue was chromatographed on a wet column of silica (12 cm × 1.8 cm id) using 5% methanol in chloroform as eluent to give 0.89 g (95%) of **6***b* as a syrup which crystallized on standing. This product showed on tlc (silica, 10% MeOH – $CH_2Cl_2$) a single spot of $R_f$ 0.2. Recrystallization from methylene chloride – ether solvent mixture afforded the analytical sample, mp 97–99°C: ir ($CHCl_3$): 3200, 1720 $cm^{-1}$. *Anal.* calcd. for $C_{10}H_{16}N_2O_3$: C 56.59, H 7.60, N 13.20; found: C 56.55, H 7.62, N 13.15.

*4-Acetoxymethyl-5-hydroxymethyl-1-triphenylmethylimidazole (**6**c)*

To a suspension of **5***a* (0.925 g, 2.5 mmol) in 5 mL of methylene chloride was added 0.4 mL (5 mmol) of dry pyridine and 0.3 mL (3.2 mmol) of acetic anhydride and the mixture stirred at room temperature for 3 h. Methylene chloride (50 mL) was added and the resultant solution was washed with water (3 × 50 mL), dried, and filtered. Removal of the solvent *in vacuo* gave 1.0 g of solids which on tlc (silica, 10% acetone in chloroform) showed a major spot of $R_f$ 0.23 (**6***c*) and two minor spots of $R_f$ 0 and 0.4 (**5***a*). This product was purified by column chromatography on silica using acetone–chloroform mixture (1:3) as eluent to provide 0.92 (90%) of crystalline **6***c*. Recrystallization from ethanol afforded the analytical sample, mp 192–193°C; ir ($CHCl_3$): 3580, 3460, 1727 $cm^{-1}$. *Anal.* calcd. for $C_{26}H_{24}N_2O_3$: C 75.70, H 5.86, N 6.79; found: C 75.60, H 5.85, N 6.80.

*5(4)-Chloromethyl-4(5)-trimethylacetoxymethylimidazole hydrochloride (**7**)*

A mixture of **6***a* (5.0 g, 11 mmol) and thionyl chloride (25 mL) was stirred at 23°C for 10 min and then heated under reflux for 30 min. Removal of the excess thionyl chloride *in vacuo* left a syrupy residue which partly solidified on trituration with ether (50 mL). The ether was removed by evaporation. The residue was dissolved in 95% ethanol (5 mL), the solution was diluted with ether (60 mL) and allowed to crystallize at room temperature. The crystalline product was collected, washed with ether, and dried to give 2.15 g (83.5%) of **7**, mp 275–280°C (decomp.); $^1$Hmr ($CD_3OD$–$CD_3COCD_3$) δ: 1.2 (s, 9H, $CMe_3$), 5.03 (s, 2H, $CH_2Cl$), 5.37 (s, 2H, $CH_2O$), 9.17 (s, 1H, H-2). *Anal.* calcd. for $C_{10}H_{15}ClN_2O_2 \cdot HCl$: C 44.96, H 6.04, N 10.49, Cl 26.14; found: C 44.81, H 5.94, N 10.47, Cl 25.60. In a larger scale experiment, the yield of **7** was 90%.

*5(4)-Azidomethyl-4(5)-trimethylacetoxymethylimidazole (**8**a)*

To a solution of sodium azide (0.52 g, 8 mmol) in 4 mL of aqueous ethanol (50%) was added a solution of **7** (0.534 g, 2 mmol) in 2 mL of 90% ethanol. After stirring at room temperature for 18 h the reaction mixture was diluted with water (10 mL) and extracted with methylene chloride (4 × 10 mL). The combined extracts were washed with water, dried, and evaporated to give 0.45 g (91%) of **8***a* as a syrup which crystallized on trituration with ether. This product showed on tlc (silica, 5% MeOH – $CH_2Cl_2$) a single spot of $R_f$ 0.35. Recrystallization from ether afforded the analytical sample, mp 88.5–89°C; ir (Nujol): 2100 ($N_3$) 1730 $cm^{-1}$ (CO); $^1$Hmr ($CDCl_3$) δ: 1.17 (s, 9H, $COMe_3$), 4.43 (s, 2H, $CH_2N_3$), 5.13 (s, 2H, $CH_2O$), 7.70 (s, 1H, H-2). *Anal.* calcd. for $C_{10}H_{15}N_5O_2$: C 50.62, H 6.37, N 29.52; found: C 50.26, H 6.42, N 29.63.

*4(5)-Ethylthiomethyl-5(4)-trimethylacetoxymethylimidazole (**8**b)*

Ethanethiol (0.6 mL, 8 mmol) was added to 1 mL of 4 *N* aqueous sodium hydroxide and the solution was placed under a nitrogen atmosphere and cooled in an ice bath. To this solution was added 0.534 g (2 mmol) of **7** and the reaction mixture was stirred at room temperature for 2 h. The solvent was removed by evaporation and the residue partition between water and methylene chloride. The organic phase after drying was evaporated to dryness, and the residue was chromatographed on silica gel (10 g) using 5% methanol in methylene chloride as eluent to give 0.396 g (75%) of **8***b* as an oil; ir (neat): 1710 $cm^{-1}$; $^1$Hmr ($CDCl_3$) δ: 1.17 (s, 9H $CMe_3$), 1.20 and 2.50 (t and q for $SCH_2CH_3$), 3.80 (s, 2H, $CH_2S$—), 5.10 (s, 2H, $CH_2O$), 7.67 (s, 1H, H-2). The hydrochloride salt of **8***b* had mp 147–149°C. *Anal.* calcd. for $C_{12}H_{20}N_2O_2 \cdot HCl$: C 49.22, H 7.23, N 9.57; found: C 49.18, H 7.19, N 10.15.

*4-(5-Hydroxymethyl-1-triphenylmethyl)imidazolecarboxaldehyde (**9**) and 5-(4-hydroxymethyl-1-triphenylmethyl)imidazolecarboxaldehyde (**10**)*

The procedure described by Kelley and co-workers (5) for the synthesis of 4-(*N*-triphenylmethyl)imidazole carboxaldehyde was used as follows. A mixture of 29.2 g (73.5 mmol) of **5***a* and 47 g (540 mmol) of activated manganese dioxide (8) and 1 L of dry and ethanol-free chloroform was refluxed with mechanical stirring for 1.5 h. Fresh manganese dioxide (47 g) was added and refluxing continued for an additional 1.5 h. The hot reaction mixture was filtered through a Celite pad and the solids were washed with chloroform (300 mL). The combined filtrate and washings were evaporated *in vacuo* and the residue was triturated with ether (100 mL). The solids were collected to give 25 g of crude product which on tlc (silica, 10% acetone – $CHCl_3$) showed 3 spots of $R_f$ values 0.50 (major, **9**), 0.23 (minor, **10**), and 0. The crude product was chromatographed on a silica column

Can. J. Chem. Downloaded from www.nrcresearchpress.com by 210.87.254.40 on 09/06/12
For personal use only.

(700 g), eluted successively with methylene chloride, 5% acetone – methylene chloride, and 10% acetone – methylene chloride to give 17.9 g (62%) of crystalline **9**. The analytical sample obtained by recrystallization from methylene chloride had mp 177.5–178.5°C; ir ($CHCl_3$): 3350, 1675 $cm^{-1}$. *Anal.* calcd. for $C_{24}H_{20}N_2O_2$: C 78.24, H 5.47, N 7.60; found: C 77.85, H 5.60, N 7.43. Further elution of the column with 1:1 acetone – methylene chloride solvent mixture gave 1.6 g (5.5%) of the isomer **10**, mp 160–164°C; ir ($CHCl_3$); 3350, 1660 $cm^{-1}$. *Anal.* calcd. for $C_{24}H_{20}N_2O_2$: C 78.24, H 5.47, N 7.60; found: C 77.39, H 5.50, N 7.58.

*4-Cyano-5-hydroxymethyl-1-triphenylmethylimidazole (**11**a)*

A described general procedure (9) was used as follows. To a solution of 1.3 g (3.36 mmol) of **9** in 60 mL methylene chloride was added 2.6 g molecular sieves (type 4A) and the mixture was stirred at room temperature. Ammonia (gas) was bubbled into the reaction mixture for 10 min then 2.6 g of activated manganese dioxide (8) was added and the mixture was stirred at room temperature for 2 h while the bubbling of ammonia was maintained. The reaction mixture was filtered and the solids were washed with methylene chloride (50 mL). The combined filtrate and washings were evaporated to give 1.3 g of an oil which crystallized from methylene chloride – ether mixture to give 0.52 g of **11***a*, mp 170–172°C. From the mother liquor, after evaporation and crystallization of the residue as above, an additional 0.17 g of **11***a* was obtained. The two crops were combined to a total yield of 0.69 g (48%); ir (Nujol): 3350, 2240 $cm^{-1}$; $^1$Hmr ($CDCl_3$–$CD_3OD$) δ: 7.4 (m, 16H, ArH and H-2), 3.85 (s, 2H, $CH_2$). *Anal.* calcd. for $C_{24}H_{19}N_3O$: C 78.88, H 5.24, N 11.50; found: C 78.28, H 5.24, N 11.55.

*4(5)-Cyano-5(4)-hydroxymethylimidazole hydrochloride (**11**b)*

To a solution of **11***a* (2.14 g, 5.45 mmol) in methanol (25 mL) was added 2.5 *N* hydrochloric acid (4, 5) (12 mL) and the resulting solution was heated at 40°C for 1 h and then evaporated under reduced pressure. The solid residue was dissolved in water (15 mL) and the solution extracted with ether (2 × 20 mL). The aqueous phase was evaporated to dryness to give 0.82 g (94%) of **11***b* as a solid. Recrystallization from an ethanol–ether solvent mixture afforded the analytical sample mp 180–182°C; ir (Nujol): 2200 (CN) $cm^{-1}$; $^1$Hmr (DMSO-$d_6$) δ: 4.98 (s, 2H, $CH_2O$), 8.04 (s, 1H, H-2). *Anal.* calcd. for $C_5H_5N_3O$·HCl: C 37.63, H 3.16, N 26.33; found: C 37.52, H 3.18, N 26.22.

*5(4)-Chloromethyl-4(5)-cyanoimidazole hydrochloride (**12**)*

A mixture of 1.6 g (4.4 mmol) of **11***a* and 35 mL of thionyl chloride was refluxed for 20 h. The reaction mixture was evaporated to dryness and flashed with chloroform (3 × 20 mL). The residue was extracted with ether (3 × 45 mL) and methylene chloride (25 mL) and the organic extracts were discharged. The solid product was collected to give 0.44 g (56%) of **12**; ir (Nujol): 2600, 2220 $cm^{-1}$; $^1$Hmr ($D_2O$) δ: 8.83 (s, 1H, H-2), 4.95 (s, 2H, $CH_2$). *Anal.* calcd. for $C_5H_4N_3Cl$·HCl: C 33.73, H 2.83, N 23.61; found: C 33.54, H 2.81, N 23.62.

*4(5)-Cyano-5(4)-[(2-aminoethyl)thiomethyl]imidazole (**13**)*

To a solution of 2 *N* sodium ethoxide in ethanol (7 mL) was added a solution of 0.785 g (5 mmol) of 2-aminoethanethiol hydrochloride in 7 mL of ethanol and the mixture was placed under a nitrogen atmosphere and stirred at −10°C for 25 min. To this mixture was added dropwise over a period of 15 min a solution of 0.63 g (3.5 mmol) of **12** in 7 mL ethanol. After the addition of **12** was completed, the cooling bath was removed and the reaction mixture stirred at room temperature for 4 h. Removal of the solvent by evaporation left a residue which was purified by chromatography on a column of Rexyn 102 resin ($NH_4^+$ form, 10 cm long × 2 cm id). The column was eluted successively with water (50 mL), 0.1 *N* ammonium hydroxide (50 mL), and 0.2 *N* ammonium hydroxide (50 mL). The fractions of eluent containing the product were combined and evaporated to give 0.25 g (42.5%) of **13** as a syrup. This product showed on tlc (silica, ammonia–methanol–water, 0.5:9:0.5) a single spot of $R_f$ 0.7; $^1$Hmr ($D_2O$) δ: 7.66 (s, 1H, H-2), 3.90 (s, 2H, $CH_2S$), 2.86 (m, 4H, $SCH_2CH_2N$). *Anal.* calcd. for $C_7H_{10}N_4S$: C 46.13, H 5.53, S 17.59; found: C 46.09, H 5.49, S 17.49.

*Preparation of compounds **14** and **15***

A mixture of 0.811 g of 50% sodium hydride – oil suspension (16.9 mmol) and 20 mL of dry benzene was cooled in an ice bath while stirring under an atmosphere of nitrogen. To this mixture was added dropwise 1.43 mL (8.85 mmol) of diethylcyanomethylphosphonate and, after the addition was completed, the mixture stirred at 0°C for 5 min. This solution was transferred into a dropping funnel and added dropwise to a stirred solution of 2.96 g (8.05 mmol) of the aldehyde **9** in 260 mL of dry benzene at 45°C. After the addition was completed, the reaction mixture was stirred at 45°C for 20 min under a nitrogen atmosphere. After cooling to room temperature, the reaction solution was washed with brine (200 mL), the organic phase separated, and the aqueous phase extracted with chloroform (50 mL). The combined extracts were washed with brine, dried, and evaporated to give 1.9 g (61%) of a syrup. This product showed on tlc (silica, ether) two spots of $R_f$ 0.38 (*trans*-isomer **14**) and 0.23 (*cis*-isomer **15**). The ratio of *trans*- to *cis*-isomer in the mixture was 2:1 as determined by $^1$Hmr. The two isomers were separated by chromatography on a column of silica gel (150 g) eluted successively with ether, ether – methylene chloride mixture (1:1), and methylene chloride. The *trans*-isomer **14** had mp 171–172°C; ir ($CHCl_3$): 3570 (OH), 2220 (CN), 1620 (C=C) $cm^{-1}$; $^1$Hmr ($CDCl_3$) δ: 7.53 (d, 1H, C=CH, $J$ = 16 Hz), 7.3 (m, 16H, ArH and H-2), 6.00 (d, 1H, C=CH, $J$ = 16 Hz), 4.06 (d, 2H, $CH_2OH$, $J$ = 6 Hz on exchange with $D_2O$ gives a singlet), 1.45 (t, 1H, OH, $J$ = 6 Hz, disappears on exchange with $D_2O$). *Anal.* calcd. for $C_{26}H_{21}N_3O$: C 79.77, H 5.40, N 10.73; found: C 79.69, H 5.39, N 10.79. The *cis*-isomer **15** had mp 181–182°C; ir ($CHCl_3$): 3570 (OH), 2220 (CN), 1625 (C=C) $cm^{-1}$; $^1$Hmr ($CDCl_3$) δ: 7.24 (m, 17H, ArH, H-2 and *CH*=CHCN), 5.24 (d, 1H, C=*CH*CN, $J$ = 11.8 Hz), 4.07 (s, 2H, $CH_2OH$). *Anal.* calcd. for $C_{26}H_{21}N_3O$: C 79.77, H 5.40, N 10.73; found; C 79.78, H 5.41, N 10.80.

1. Drugs of the future. **1** (1), 13 (1976) and references therein.
2. M. R. GRIMMETT. Advances in heterocyclic chemistry. Vol. 12. Academic Press, New York. 1970. p. 103.
3. (*a*) R. A. BAXTER and F. S. SPRING. J. Chem. Soc. 233 (1945); (*b*) N. B. VINOGRADOVA and N. V. KROMOV-BORISOV. Metody Poluch. Khim. Reactivov. Prep. **14**, 40 (1966), Chem. Abstr. **67**, 3033 (1967); (*c*) H. SHUBERT, S. HOFFMANN, V. UHLIG, H. E. POLSTER, P. HELD, and M. KLEPEL. Z. Chem. **16**, 483 (1976). Chem. Abstr. **86**, 139937 (1977).
4. (*a*) M. BERNABÉ and A. BURGER. J. Med. Chem. **14**, 883 (1971); (*b*) A. BURGER, M. BERNABÉ, and P. W. COLLINS. J. Med. Chem. **13**, 33 (1970).
5. J. L. KELLEY, C. A. MILLER, and E. W. MCLEAN. J. Med. Chem. **20**, 721 (1977).
6. J. NEMATOLLAHI, W. GUESS, and J. AUTIAN. J. Med. Chem. **9**, 660 (1966).
7. F. FARINA. Anales Real. Soc. Espan. Fis. Y. Quinn (Madrid) **49B**, 599 (1953); Chem. Abstr. **48**, 4524*d* (1954).
8. I. M. GOLDMAN. J. Org. Chem. **34**, 1979 (1969).
9. N. W. GILMAN. Chem. Commun. 733 (1971).
10. W. S. WADSWORTH, JR. and W. D. EMMONS. J. Am. Chem. Soc. **83**, 1733 (1961).

# Molecular orbital structures of sulfones

RUSSELL J. BOYD[1] AND JEFFREY P. SZABO
*Department of Chemistry, Dalhousie University, Halifax, N.S., Canada B3H 4J3*

Received October 6, 1981

RUSSELL J. BOYD and JEFFREY P. SZABO. Can. J. Chem. **60**, 730 (1982).

*Ab initio* molecular orbital calculations are reported for several cyclic and acyclic sulfones. The geometries of $XSO_2Y$, where X, Y = H, F, or $CH_3$ are optimized at the STO-3G* level. Similar calculations are reported for the smallest cyclic sulfone, thiirane-1,1-dioxide, as well as the corresponding sulfoxide, thiirane-1-oxide, and the parent sulfide, thiirane. Where comparison with experiment is possible, the agreement is satisfactory. In order to consider the possibility of substantial differences between axial and equatorial S—O bonds in the gas phase, as observed in the crystal structure of 5*H*,8*H*-dibenzo[*d*,*f*][1,2]-dithiocin-1,1-dioxide, STO-3G* calculations are reported for a six-membered ring, thiane-1,1-dioxide, and a model eight-membered ring. Limited geometry optimization of the axial and equatorial S—O bonds in the chair conformations of the six- and eight-membered rings leads to bond lengths of 1.46 Å with the difference being less than 0.01 Å.

RUSSELL J. BOYD et JEFFREY P. SZABO. Can. J. Chem. **60**, 730 (1982).

On rapporte des calculs *ab initio* d'orbitales moléculaires relatifs à plusieurs sulfones cycliques et acycliques. Au niveau STO-3G*, on a amélioré les géométrie de $XSO_2Y$ où X, Y = H, F ou $CH_3$. On rapporte des calculs analogues pour la sulfone cyclique la plus petite, le thiiranne dioxyde-1,1, ainsi que pour le sulfoxyde correspondant, le thiiranne oxyde-1, et le sulfure apparenté, le thiiranne. L'accord est satisfaisant là où il a été possible d'établir des comparaisons. On rapporte des calculs STO-3G* pour les cycles à 6 chaînons, thianne dioxyde-1,1 et pour un cycle modèle à 8 chaînons dans le but d'envisager la possibilité de différences notables entre les liaisons S—O axiales et équatoriales en phase gazeuse telles qu'observées dans la structure du crystal du 5*H*,8*H*-dibenzo[*d*,*f*][1,2]dithiocinne dioxyde-1,1. Une optimisation limitée de la géométrie des liaisons S—O axiales et équatoriales de la forme chaise des cycles à 6 et à 8 chaînons conduit à des longueurs de liaison de 1,46 Å, avec une différence inférieure à 0,01 Å.
[Traduit par le journal]

## Introduction

The crystal structure (1) of 5*H*,8*H*-[*d*,*f*][1,2]-dithiocin-1,1-dioxide indicates that the eight-membered ring is a pseudo-chair in which the "pseudo-axial" S—O bond is significantly shorter (1.352 Å vs. 1.475 Å) than its "pseudo-equatorial" analogue. Somewhat smaller differences have been observed (2) for $\gamma$-$SO_3$ in the solid state. In this paper we consider the possibility of similar anomalies in the gas phase. To this end, we have carried out extensive *ab initio* molecular orbital (MO) calculations on cyclic and acyclic sulfones.

## Method

Standard single determinant *ab initio* molecular orbital theory, according to which closed-shell species are treated by the spin-restricted Hartree-Fock (RHF) procedure (3), has been used throughout. All calculations were carried out using the Gaussian 76 program (4) on a CDC CYBER 170-720 computer. The STO-3G* basis set (5) in which a manifold of five *d*-type functions, consisting of one second-order Gaussian each, is added to the minimal STO-3G basis set for second row atoms has been used. The minimal STO-3G basis set (6) has been used for hydrogen and first-row elements. We have chosen the STO-3G* basis set because previous studies (5, 7–9) have demonstrated the importance of including *d* functions on second-row atoms in hypervalent molecules. Moreover, the STO-3G* basis set offers a convenient compromise between minimal (5) and larger *sp* basis sets (5, 9) on the one hand and extended plus polarization basis sets (9, 10) on the other.

Geometry optimization was carried out for each molecule. In a few cases model geometries were assumed or part of the molecule was constrained to the experimental structure. For example, model methyl groups, $r$(CH) = 1.09 Å and $\angle$HCH = 109.5°, were adopted to reduce the requirements for computer time. Except where noted otherwise, all calculated structures reported in this paper should be within 0.002 Å and 0.2° of their true theoretical (at the STO-3G* level) geometries. In many cases the geometrical parameters have been determined to within 0.001 Å and 0.1°.

### *Acyclic sulfones*

In order to establish the reliability of *ab initio* calculations on sulfones at the STO-3G* level we begin our discussion with some simple molecules which contain the $SO_2$ functional group. The calculated equilibrium geometries of $XSO_2Y$, where X, Y = H, F, or $CH_3$, are illustrated in Fig. 1. The theoretical geometries are compared with the available (11) gas phase structural data in Table 1. In agreement with experimental evidence (11, 12) and semi-empirical MO calculations (13), the lowest

[1]To whom all correspondence should be addressed.

0008-4042/82/060730-05$01.00/0
©1982 National Research Council of Canada/Conseil national de recherches du Canada

Can. J. Chem. Downloaded from www.nrcresearchpress.com by 210.87.254.6 on 09/06/12
For personal use only.

Can. J. Chem. Downloaded from www.nrcresearchpress.com by 210.87.254.6 on 09/06/12
For personal use only.

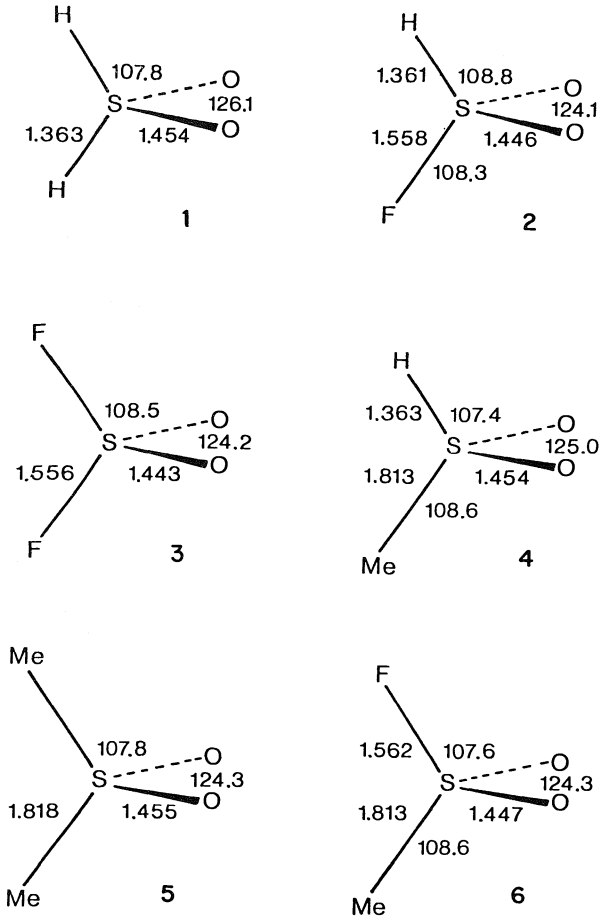


FIG. 1. STO-3G* equilibrium geometries of $XSO_2Y$ molecules.

TABLE 1. Comparison of calculated and experimental geometries[a] of acyclic sulfones

| Molecule[b] | Geometrical parameter | STO-3G* | Microwave spectroscopy | Electron diffraction |
|---|---|---|---|---|
| **3** | *r*(SO) | 1.443 | 1.405[c] | 1.397[c] |
| | *r*(SF) | 1.556 | 1.530 | 1.530 |
| | ∠OSO | 124.2 | 124.0 | 122.6 |
| | ∠FSO | 108.5 | 108.3 | 108.6 |
| **5** | *r*(SO) | 1.455 | 1.431 | 1.435 |
| | *r*(SC) | 1.818 | 1.777 | 1.771 |
| | ∠OSO | 124.3 | 121.0 | 119.7 |
| | ∠CSC | 98.5 | 103.3 | 102.6 |
| **6** | *r*(SO) | 1.447 | | 1.410 |
| | *r*(SF) | 1.562 | | 1.561 |
| | *r*(SC) | 1.813 | | 1.759 |
| | ∠OSO | 124.3 | | 123.1 |
| | ∠FSO | 107.6 | | 106.2 |
| | ∠CSF | 96.3 | | 98.2 |

[a]Bond lengths in Å, angles in deg.
[b]Structures are identified in Fig. 1.
[c]Experimental data from ref. 11 and references therein.

energy conformations of the methyl sulfones (**4**, **5**, and **6**) have a staggered arrangement about the C—S bonds. The agreement between the calculated and observed geometries of **3**, **5**, and **6** is satisfactory and is quite typical of calculations at the STO-3G and STO-3G* levels (5, 10, 14, 15). Two features of the calculated bond lengths are worth noting: all bonds are over-estimated, by about 0.03 Å on average, and the effect of substituents is qualitatively reproduced.

The STO-3G* total energies of the simple sulfones are listed in Table 2. From the computed energies of the eclipsed conformers at the bond lengths and angles of the equilibrium geometries we estimate the barriers to rigid rotation[2] of **4**, **5**, and **6** to be 2.0, 2.3, and 1.8 kcal/mol, respectively.[3] These values are low but in qualitative agreement with the observed barriers of 3.4 (12) and 2.5 (17) in **5** and **6**, respectively. The low value obtained for **6** relative to **4** is contrary to the trends observed for substituted ethanes where replacement of a H atom by a F atom raises the barrier (18). However, not all barriers are raised by fluorine substitution. For example, the observed barriers (18) in $CH_3$—CHO and $CH_3$—CFO are 1.16 and 1.04 kcal/mol, respectively. Similarly the barriers of 1.70 and 1.56 kcal/mol in $CH_3$—$SiH_3$ and $CH_3$—$SiH_2F$, respectively, are consistent with the trends observed here for the theoretical barriers of the sulfones. Unfortunately sulfone **4** has not been reported.

With reference to the net atomic charges listed in Table 2 we observe that the effect of fluorine substitution on the S and O charges in the series $H_nSO_2F_{2-n}$ and $(CH_3)_nSO_2F_{2-n}$ is essentially additive. Similar additivity relationships are apparent for the $(CH_3)_nSO_2H_{2-n}$ series. The charges listed in Table 2 are based on the Mulliken population analysis procedure (19). We conclude this section by emphasizing that the additivity of net charges at the STO-3G* level is not complemented by a corresponding set of bond additivity rules.

*Cyclic sulfones*

Before discussing the question of anomalous S—O bond lengths in cyclic sulfones we consider the smallest cyclic sulfone, namely, thiirane-1,1-dioxide **7**. The STO-3G* equilibrium geometry of **7** is shown in Fig. 2 together with the equilibrium

[2]Our estimate, which corresponds to geometric model B of Radom and Pople (16), would be slightly lower for flexible rotation.

[3]The barrier for simultaneous rotation of the two methyl groups of **5** is estimated to be 6.0 kcal/mol whereas the value of 2.3 kcal/mol given above is for the rotation of a single methyl group.

Can. J. Chem. Downloaded from www.nrcresearchpress.com by 210.87.254.6 on 09/06/12
For personal use only.

TABLE 2. Total energies (au) and net atomic charges of acyclic sulfones

| Molecule | Point group | Total energy[a] | Net atomic charges[b] | | |
|---|---|---|---|---|---|
| **1** | $C_{2v}$ | −542.00088 | +0.33(S) | −0.25(O) | +0.08 (H) |
| **2** | $C_s$ | −639.52895 | +0.41(S)<br>+0.11(H) | −0.22(O) | −0.07(F) |
| **3** | $C_{2v}$ | −737.05271 | +0.52(S) | −0.20(O) | −0.06(F) |
| **4**[c] | $C_s$ | −580.60169 | +0.36(S)<br>+0.08($H_1$) | −0.26(O)<br>+0.09($H_2$) | −0.19(C) |
| **5**[d] | $C_{2v}$ | −619.19996 | +0.40(S)<br>+0.09($H_1$) | −0.27(O)<br>+0.08($H_2$) | −0.19(C) |
| **6**[e] | $C_s$ | −678.12893 | +0.45(S)<br>−0.19(C) | −0.23(O)<br>+0.10($H_1$) | −0.08(F)<br>+0.10($H_2$) |

[a]1 au = 627.5095 kcal/mol = 2625.502 kJ/mol.
[b]Subscripts on atoms are identified in Fig. 1.
[c]Total energy of the eclipsed conformer ($C_s$) is −580.59854 au. $H_1$ is bonded to S.
[d]Total energies of the half-eclipsed ($C_s$) and fully eclipsed ($C_{2v}$) conformers are −619.19637 and −619.19046 au, respectively. $H_1$ lies in the CSC plane.
[e]Total energy of the eclipsed conformer ($C_s$) is −678.12603 au. $H_1$ lies in the FSC plane.

structures of the corresponding sulfoxide **8**, thiirane-1-oxide, and sulfide **9**, thiirane. The total energies and the net atomic charges at the STO-3G* geometries are listed in Table 3. The long C—C bond of **7** relative to the short C—C bonds in

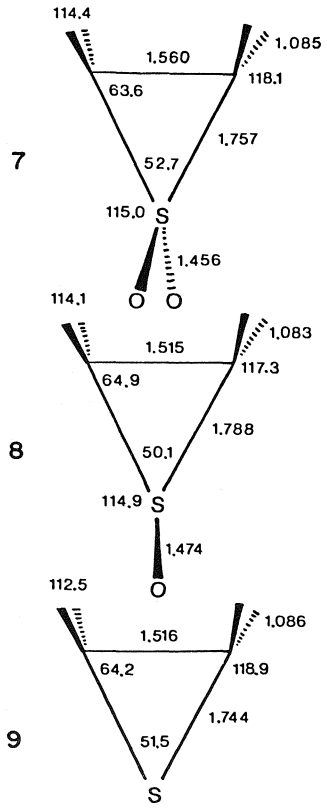


FIG. 2. STO-3G* equilibrium geometries of three-membered rings. In structure **8** the hydrogen atoms on the oxygen side of the CSC plane are designated as $H_2$.

TABLE 3. Total energies (au) and net atomic charges of cyclic sulfones and related compounds

| Molecule | Total energy | Net atomic charges[a] | | |
|---|---|---|---|---|
| **7** | −617.98137 | +0.35(S)<br>+0.09(H) | −0.24(O) | −0.12(C) |
| **8** | −544.15393 | +0.27(S)<br>+0.09($H_1$) | −0.31(O)<br>+0.08($H_2$) | −0.14(C) |
| **9** | −470.31829 | +0.01(S) | −0.13(C) | +0.06(H) |
| **10** | −733.76626 | +0.38(S)<br>−0.12($C_1$) | −0.29($O_1$)<br>−0.10($C_2$) | −0.28($O_2$)<br>−0.10($C_3$) |
| **11** | −1163.13389 | +0.34($S_1$)<br>−0.27($O_2$)<br>−0.07($C_3$)<br>−0.14($C_6$) | +0.09($S_2$)<br>−0.13($C_1$)<br>−0.07($C_4$) | −0.26($O_1$)<br>−0.05($C_2$)<br>−0.05($C_5$) |

[a]Subscripts on atoms are identified in Figs. 2 and 3.

**8** and **9** agrees with the microwave spectroscopic values of 1.590 (20), 1.504 (21), and 1.492 Å (22), respectively. The lengthening of the S—O bond in **8** relative to **7** is less pronounced at the STO-3G* level than in the experimental structures (1.483 for **8** vs. 1.439 Å for **7**). The major discrepancy occurs for the C—S bond of **9**. The microwave values are 1.731, 1.822, and 1.819 Å for **7**, **8**, and **9**, respectively. We note that **7**, **8**, and **9** form a sequence in which the S atom is modified in a regular fashion. Successive removal of the two O atoms converts the hypervalent S atom of **7** to the divalent S atom of **9**.

With a minimal basis set it is essential to include *d* orbitals on hypervalent S atoms in order to obtain reasonable bond lengths. For divalent S, the STO-3G values of the S—H bond lengths are in better agreement with experiment than the STO-3G* values. In general the effect of including *d* orbitals on S in a minimal basis set is to shorten H—S and

Can. J. Chem. Downloaded from www.nrcresearchpress.com by 210.87.254.6 on 09/06/12
For personal use only.

C—S bonds in acyclic divalent molecules by about 0.01 to 0.02 Å. This is apparent from the work of Collins *et al.* (5) on $H_2S$ and $CH_3SH$ where the calculated H—S, C—S, and S—H bond lengths are in better agreement with experiment at the STO-3G level than at the STO-3G* level. Our results on **9** show a similar but somewhat greater effect: 1.773 (STO-3G) vs. 1.744 Å (STO-3G*) for the C—S bond. In the case of disulfides, —S—S—, we have found that the effect of including *d* orbitals on S is an order of magnitude greater than in divalent sulfides involving hydrogen and/or first-row atoms (23). Although we will not discuss the three-membered rings further, we should point out that Hoffmann *et al.* (24) have reported a detailed analysis of the bond lengths of these molecules. On the basis of extended Hückel calculations they propose a bonding picture in which the molecules are described as complexes of an ethylene with S, SO, or $SO_2$.

Two larger systems have been considered. As an example of a six-membered ring we chose thiane-1,1-dioxide (thiacyclohexane-1,1-dioxide) (**10**) (see Fig. 3). Starting with a model geometry, $r$(CS) = 1.82, $r$(CC) = 1.53, $r$(CH) = 1.09, bond angles approximately 109.5° and dihedral angles near 180°, we carried out a limited geometry optimization for the axial and equatorial S—O bonds in the chair conformation. Our conclusion is that the STO-3G* optimized bond lengths for our model geometry are 1.46 Å and that the differences are less than 0.01 Å.

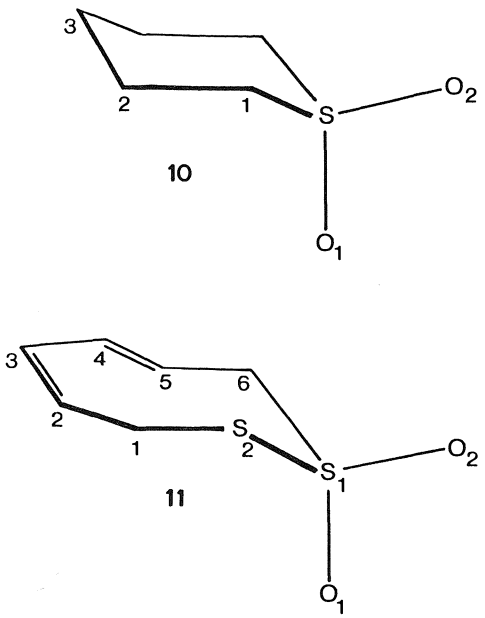


FIG. 3. Structural formulas of six- and eight-membered rings containing the sulfone functional group.

Thus the axial *and* equatorial S—O bonds of **10** are predicted to be essentially equal in the gas phase. The computed total energy and net atomic charges of **10** are listed in Table 3. We observe a slightly greater charge on the axial O atom than on the equatorial O atom and a small increase in the polarity of the S—O bonds relative to the three-membered ring **7**.

The molecule mentioned in the Introduction contains a S atom adjacent to the sulfone group. In order to determine the effect of an adjacent S atom we chose an eight-membered ring **11** as a convenient model. With the coordinates of the atoms in the ring chosen from the crystallographic data of Wahl *et al.* (1), the S—O bond lengths were optimized. As in the case of **10**, the optimized bond lengths turned out to be 1.46 Å with the difference being less than 0.01 Å. Thus, even when we include a S atom adjacent to the sulfone functional group, we find no significant difference between the axial and equatorial S—O bonds. On the strength of the *ab initio* calculations reported in this paper we do not expect anomalies in the gas phase similar to those reported (1, 2) in the solid state on the basis of X-ray diffraction studies. If such anomalies exist then they are presumably associated with crystal packing forces. Here we should like to point out that a X-ray crystal structure determination (25) of 4,4,-*a*-dihydro-5,7-dimethylpyrido[1,2-*d*][1,5,2]dithiazine-1,1,3,3-tetroxide indicates that the S—O bonds of the sulfone functional group are essentially identical. Moreover, the same molecule contains a second $SO_2$ group adjacent to a N atom. The second $SO_2$ group, like the first, contains two essentially equal S—O bonds. And finally we should like to mention that complementary calculations (26, 27) on the importance of *d*-functions in the basis set and the deformability of sulfur moities when crystal forces are present have been reported. In conclusion, we do not expect axial and equatorial S—O bond lengths to differ significantly in the gas phase.

**Acknowledgements**

We would like to thank Professor D. N. Harpp for drawing our attention to this problem and for helpful correspondence. Useful discussions with Professors J. S. Grossert and T. S. Cameron are gratefully acknowledged. J.P.S. would like to thank the Natural Sciences and Engineering Research Council of Canada (NSERC) and the Atlantic Provinces Council on the Sciences for assistantships. The financial support of NSERC and the provision of excellent computing facilities by the Computer Centre of Dalhousie University are gratefully acknowledged.

1. G. H. WAHL, JR., J. BORDNER, D. N. HARPP, and J. G. GLEASON. Acta Crystallogr. B **29**, 2272 (1973).
2. W. S. MCDONALD and D. W. J. CRUICKSHANK. Acta Crystallogr. **22**, 48 (1967).
3. C. C. J. ROOTHAAN. Rev. Mod. Phys. **23**, 69 (1951).
4. J. S. BINKLEY, R. A. WHITEHEAD, P. C. HARIHARAN, R. SEEGER, and J. A. POPLE. QCPE, **11**, 368 (1978).
5. J. B. COLLINS, P. VON R. SCHLEYER, J. S. BINKLEY, and J. A. POPLE. J. Chem. Phys. **64**, 5142 (1976).
6. W. J. HEHRE, R. F. STEWART, and J. A. POPLE. J. Chem. Phys. **51**, 2657 (1969).
7. (*a*) H. B. SCHLEGEL, S. WOLFE, and K. MISLOW. J. Chem. Soc. Chem. Commun. 246 (1975); (*b*) I. H. HILLIER and V. R. SAUNDERS. Mol. Phys. **22**, 193 (1971); (*c*) L. J. AARONS, I. H. HILLIER, and M. F. GUEST. J. Chem. Soc. Faraday Trans. II, **70**, 167 (1974).
8. R. J. BOYD, A. GUPTA, R. F. LANGLER, S. P. LOWNIE, and J. A. PINCOCK. Can. J. Chem. **58**, 331 (1980).
9. A. SCHMIEDEKAMP, D. W. J. CRUICKSHANK, S. SKAARUP, P. PULAY, I. HARGITTAI, and J. E. BOGGS. J. Am. Chem. Soc. **101**, 2002 (1979).
10. N. C. BAIRD and K. F. TAYLOR. Can. J. Chem. **59**, 814 (1981).
11. I. HARTGITTAI. Sulphone molecular structures. Lecture notes in chemistry. Vol. 6. Springer-Verlag, West Berlin. 1978.
12. H. L. CLEVER and E. F. WESTRUM. J. Phys. Chem. **74**, 1309 (1970).
13. G. ROBINET, F. CRASNIER, J.-F. LABARRE, and C. LEIBOVICI. Theoret. Chim. Acta, **25**, 259 (1972).
14. J. S. BINKLEY, J. A. POPLE, and W. J. HEHRE. J. Am. Chem. Soc. **102**, 939 (1980).
15. M. D. NEWTON, W. A. LATHAN, W. J. HEHRE, and J. A. POPLE. J. Chem. Phys. **52**, 4064 (1970).
16. L. RADOM and J. A. POPLE. J. Am. Chem. Soc. **92**, 4786 (1970).
17. E. J. JACOB and D. R. LIDE. J. Chem. Phys. **54**, 4591 (1971).
18. J. P. LOWE. Prog. Phys. Org. Chem. **6**, 1 (1968).
19. R. S. MULLIKEN. J. Chem. Phys. **23**, 1833, 1841 (1955).
20. Y. NAKANO, S. SAITO, and Y. MORINO. Bull. Chem. Soc. Jpn. **43**, 368 (1970).
21. S. SAITO. Bull. Chem. Soc. Jpn. **42**, 663 (1969).
22. G. L. CUNNINGHAM, JR., A. W. BOYD, R. J. MYERS, and W. D. GWINN. J. Chem. Phys. **19**, 676 (1951).
23. R. J. BOYD and R. RAMANI. To be published.
24. R. HOFFMANN, H. FUJIMOTO, J. R. SWENSON, and C.-C. WAN. J. Am. Chem. Soc. **95**, 7644 (1973).
25. J. S. GROSSERT, M. H. BHARADWAJ, R. F. LANGLER, T. S. CAMERON, and R. E. CORDES. Can. J. Chem. **56**, 1183 (1978).
26. P. G. MEZEY and A. KAPUR. Can. J. Chem. **58**, 559 (1980).
27. S. HUZINAGA and M. YOSHIMINE. J. Chem. Phys. **68**, 4486 (1978).

Can. J. Chem. Downloaded from www.nrcresearchpress.com by 210.87.254.6 on 09/06/12
For personal use only.

# The solvolysis of *trans*-1,2-diphenyl-2-phenylthio[1-$^{13}$C]vinyl tosylate in anhydrous or aqueous acetic acid

CHOI CHUCK LEE, CHARLES Y. FIAKPUI, AND J. WILSON QUAIL

*Department of Chemistry and Chemical Engineering, University of Saskatchewan, Saskatoon, Sask., Canada S7N 0W0*

Received July 30, 1981

CHOI CHUCK LEE, CHARLES Y. FIAKPUI, and J. WILSON QUAIL. Can. J. Chem. **60**, 735 (1982).

The acetolysis of *trans*-1,2-diphenyl-2-phenylthiol[1-$^{13}$C]vinyl tosylate (**2**-OTs-1-$^{13}$C) under anhydrous conditions (HOAc–$Ac_2O$–NaOAc) gave *trans*-1,2-diphenyl-2-phenylthio[1,2-$^{13}$C]vinyl acetate (**2**-OAc-1,2-$^{13}$C) as product. The label was scrambled equally over C-1 and C-2 and there was no detectable amount of *cis*-product. These results are consistent with the involvement of an intermediate sulfur-bridged thiirenium ion in the reaction. Solvolysis of **2**-OTs-1-$^{13}$C in 70% HOAc – 30% $H_2O$ containing 3 equiv. of NaOAc gave 1,2-diphenyl-2-phenylthio[1,2-$^{13}$C]ethanone (α-phenyl-α-(phenylthio)acetophenone) (**5**-1,2-$^{13}$C) and 1,2-diphenyl[1,2-$^{13}$C]ethanone (desoxybenzoin) (**6**-1,2-$^{13}$C) as major and minor products, respectively. The $^{13}$C-label in both of these ketones was again equally distributed over C-1 and C-2. Further studies with unlabeled **2**-OTs showed that its solvolysis in aqueous HOAc gave, besides ketones **5** and **6**, some benzil and diphenyl disulfide. It was also found that **6**, benzil, and diphenyl disulfide were derived from the initial product **5**. A possible mechanism for these conversions is proposed.

CHOI CHUCK LEE, CHARLES Y. FIAKPUI et J. WILSON QUAIL. Can. J. Chem. **60**, 735 (1982).

L'acétolyse du tosylate de diphényl-1,2 phénylthio-2 vinyle [$^{13}$C-1] *trans* (OTs-**2** $^{13}$C-1) dans des conditions anhydres (AcOH–$Ac_2O$–AcONa) conduit l'acétate (AcO-**2** $^{13}$C-1,2) de diphényl-1,2 phénylthio-2 vinyle [$^{13}$C-1,2] *trans*. Le marqueur est réparti également entre C-1 et C-2 et il n'y pas de produit *cis*. Ces résultats sont en accord avec la participation d'un ion thiirénium intermédiaire ayant un soufre en position de pont au cours de la réaction. La solvalyse du tosylate (**2**-OTs $^{13}$C-1) dans une solution aqueuse de AcOH à 70% contenant 3 équivalents de AcONa conduit à la diphényl-1,2 phenylthio-2 éthanone [$^{13}$C-1,2] (α-phenyl α-(phénylthio) acétophénone) (**5**-$^{13}$C-1,2) comme produit majoritaire et à la diphényl-1,2 éthanone [$^{13}$C-1,2] (déoxybenzoine) (**6**-$^{13}$C-1,2) comme produit secondaire. Le marqueur $^{13}$C dans ces deux cétones se distribue également entre $C_1$ et $C_2$. Des études plus poussées avec un tosylate **2**-OTs non marqué révèlent que la solvolyse dans AcOH aqueux donne en plus des cétones **5** et **6**, un disulfure de benzyle et un disulfure de diphényle. On a également trouvé que ces disulfures proviennent du produit initial **5**. On propose un mécanisme qui explique ces transformations.

[Traduit par le journal]

The possible involvement of the sulfur-bridged thiirenium ion, such as **1**, as a reaction intermediate in the addition of sulfenyl derivatives to alkynes or in the solvolysis of 2-arylthiovinyl sulfonates has been reviewed by Modena and co-workers (1, 2). Among the evidence in support of **1** was the finding that a labeled substrate such as *trans*-1,2-diphenyl-2-phenylthio[1-$^{14}$C]vinyl brosylate (**2**-OBs-1-$^{14}$C), when treated in $CHCl_3$ saturated with gaseous $BF_3$, gave the cyclized product, 2,3-diphenylbenzo[*b*]-thiophene (**3**), which showed that substantial equilibration of the two ethylenic carbon atoms has taken place (3, 4).

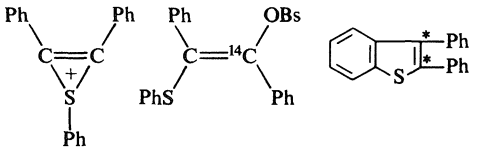


**1** **2**-OBs-1-$^{14}$C **3**

In addition to the study on the formation of **3** from **2**-OBs-1-$^{14}$C, effected in the absence of any nucleophile, a demonstration of the complete scrambling of the label between C-1 and C-2 in the substitution product from a labeled 2-arylthiovinyl sulfonate would give further support to the thiirenium ion as a reaction intermediate. Thus we have undertaken an investigation on the solvolysis of *trans*-1,2-diphenyl-2-phenylthio[1-$^{13}$C]vinyl tosylate (**2**-OTs-1-$^{13}$C) in anhydrous or aqueous HOAc.

The synthesis of **2**-OTs-1-$^{13}$C was carried out using procedures analogous to those employed in the preparation of **2**-OBs-1-$^{14}$C (4) as outlined in Scheme 1. Modena and co-workers (4) have shown that the **2**-OBs-1-$^{14}$C synthesized in this way was *trans* and that the label was located solely at C-1. The $^{13}$C nmr spectrum of the labeled **2**-OTs-1-$^{13}$C, showing an intense C-1 absorption at 144.0 ppm, also confirmed that the $^{13}$C-label was located solely at C-1.

In preliminary experiments with ordinary **2**-OTs, solvolysis in HOAc–$Ac_2O$ (9:1 by volume) containing 3 equiv. of NaOAc gave the acetate product, the $^1$H nmr spectrum of which showed a single peak for the $CH_3$ protons of the acetate group, indicating the formation of only the *trans*-isomer, **2**-OAc (5–7). In the solvolysis of **2**-OTs-1-$^{13}$C, the acetate product was reduced with $LiAlH_4$ to give a mixture of *erythro*- and *threo*-1,2-diphenyl-2-phenylthio[1,2-$^{13}$C]ethanol (**4**-1,2-$^{13}$C) for $^{13}$C nmr analy-

0008-4042/82/060735-06$01.00/0

©1982 National Research Council of Canada/Conseil national de recherches du Canada

Can. J. Chem. Downloaded from www.nrcresearchpress.com by 210.87.254.42 on 09/06/12
For personal use only.

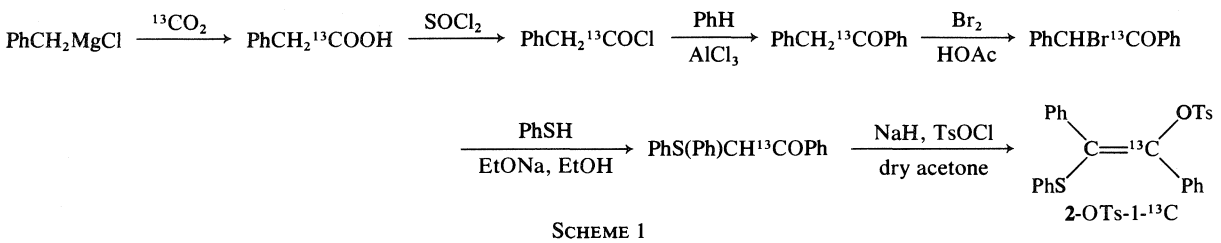


SCHEME 1

sis. It was intended that a quantitative measurement of the $^{13}C$ contents at C-1 and C-2 might be carried out using the method of relative intensities with respect to a suitable internal standard as was done in the reaction of triphenyl[2-$^{13}C$]vinyl or trianisyl[2-$^{13}C$]vinyl bromide with HOAc–AgOAc (8, 9). In these studies (8, 9) the sum of some of the aromatic absorptions of the triphenylvinyl system or the $CH_3O$ absorption of the trianisylvinyl system, which contained $^{13}C$ in its natural abundance, was used as the internal standard for the quantitative $^{13}C$ determination.

In the present work, the $^{13}C$ nmr spectrum of the unlabeled **4** from the reduction of **2**-OAc is shown in Fig. 1*A*. The C-1 and C-2 absorptions of the major diastereomer appear at 74.8 and 59.4 ppm, respectively, while those of the minor diastereomer appear at 76.1 and 60.9 ppm. Probably, the *erythro* isomer, with the OH and PhS groups as well as the two phenyl groups *trans* in the antiperiplanar conformation, constituted the major component, since the *threo* isomer would have the two phenyl groups *gauche* in the antiperiplanar conformation. The $^{13}C$ nmr spectrum of **4**-1,2-$^{13}C$ from the **2**-OAc-1,2-$^{13}C$ derived from the solvolysis of **2**-OTs-1-$^{13}C$, with about 20% $^{13}C$ enrichment, in HOAc–$Ac_2O$ containing 3 equiv. of NaOAc at 148 ± 2°C for 10 h, is given in Fig. 1*B*. It is seen that the intensities of the C-1 and C-2 absorptions are essentially the same in the spectrum of the unlabeled **4** as well as in the spectrum of **4**-1,2-$^{13}C$. These results indicate that the $^{13}C$-label is distributed essentially equally over C-1 and C-2, and it is not necessary to use an internal standard for the calculations as was done with the labeled triphenylvinyl and trianisylvinyl systems (8, 9). The same equal distribution of the label over C-1 and C-2 was observed when similar acetolyses of **2**-OTs-1-$^{13}C$ in HOAc–$Ac_2O$–NaOAc at 148 ± 2°C were carried out for 4 or 7 instead of 10 h. In all of these three experiments, the reaction likely had reached completion since the specific rate constant for the acetolysis of **2**-OTs in the presence of added NaOAc at 151°C was reported to be $81.3 \times 10^{-5}$ $s^{-1}$ (7). The finding that the scrambling of the label over C-1 and C-2 did not change with reaction time would suggest that the acetolysis product was stable when heated under anhydrous conditions in HOAc–$Ac_2O$–NaOAc. The present results on the equal distribution of the label over C-1 and C-2 in the substitution product, the formation of the *trans*-acetate with no detectable amount of the *cis*-isomer, and the earlier observation of Modena and co-workers (3, 4) on the equilibration of the label over the two ethylenic carbons in the cyclized product **3** all are consistent with and hence provide support for the thiirenium ion as a reaction intermediate (1, 2).

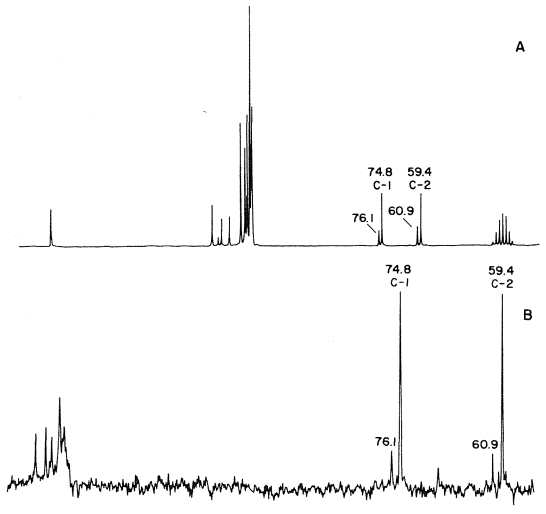


FIG. 1. $^1H$-decoupled $^{13}C$ nmr spectra in acetone-$d_6$ of the mixture of *erythro*- and *threo*-1,2-diphenyl-2-phenylthioethanols (**4**) derived from the reduction of ordinary *trans*-1,2-diphenyl-2-phenylthiovinyl acetate (2-OAc) (*A*), and of the mixture of *erythro*- and *threo*-1,2-diphenyl-2-phenylthio[1,2-$^{13}C$]ethanols (**4**-1,2-$^{13}C$) derived from the acetolysis of 20% enriched **2**-OTs-1-$^{13}C$ in HOAc–$Ac_2O$–NaOAc (*B*). (The chemical shifts in Figs. 1 and 2 were measured using the center peak of the acetone-$d_6$ absorptions at 28.05 ppm as internal reference.)

In previous work in this laboratory on solvolytic studies with labeled triphenylvinyl and trianisylvinyl bromides, one of the solvent systems employed was 70% HOAc – 30% $H_2O$ (by volume) (10, 11). In the present work, 70% HOAc – 30% $H_2O$ (to be called 70% HOAc or aqueous HOAc) was also utilized in solvolytic studies with **2**-OTs-1-$^{13}C$. The chief product from the reaction of **2**-OTs

Can. J. Chem. Downloaded from www.nrcresearchpress.com by 210.87.254.42 on 09/06/12
For personal use only.

TABLE 1. Relative yields of PhS(Ph)CHCOPh (**5**), $PhCH_2COPh$ (**6**), and PhS(Ph)C=C(OAc)Ph (**2**-OAc) from the reaction of *trans*-1,2-diphenyl-2-phenylthiovinyl tosylate (**2**-OTs) in 70% HOAc at 148 ± 2°C

| Expt. | Additional reagent | Reaction time (h) | Relative yields (%)[a] | | |
|---|---|---|---|---|---|
| | | | **5** | **6** | **2**-OAc |
| 1 | None | 6 | 90 | 10 | — |
| 2 | None | 96 | 50 | 50 | — |
| 3 | NaOAc (3 equiv.) | 4 | 95 | 5 | — |
| 4 | NaOAc (3 equiv.) | 7 | 93 | 7 | — |
| 5 | NaOAc (3 equiv.) | 24 | 89 | 11 | — |
| 6 | NaOAc (30 equiv.) | 24 | 67 | Trace | 33[b] |
| 7 | $HClO_4$[c] | 72 | 62 | 38 | — |

[a]Based on the $^1H$ nmr absorptions of the C-2 H's of **5** and **6** and the acetate H's of **2**-OAc.
[b]This would be the amount of **2**-OAc that survived under the conditions of Expt. 6. When only 3 equiv. of NaOAc was employed, apparently any **2**-OAc that might have been formed was likely all hydrolyzed to **5**.
[c]5.0 mL of 70% $HClO_4$ added to 50 mL of 70% HOAc – 30% $H_2O$.

in 70% HOAc was α-phenyl-α-(phenylthio)acetophenone (1,2-diphenyl-2-phenylthioethanone) (**5**). No acetate product, **2**-OAc, was detectable except when the reaction was carried out in the presence of a large excess of NaOAc. Interestingly, another product, usually a minor one, was obtained along with **5**, and it was identified as desoxybenzoin (1,2-diphenylethanone) (**6**). The relative yields of these products from solvolyses of **2**-OTs in aqueous HOAc under different conditions are given in Table 1. It is seen from Table 1 that the extent of formation of **6** rose with increasing reaction time, and furthermore, the presence of NaOAc or $HClO_4$, respectively, apparently could decrease or increase its formation.

When the labeled **2**-OTs-1-$^{13}C$ was solvolyzed in 70% HOAc in the presence of 3 equiv. of NaOAc at 148 ± 2°C for 4 h (conditions of Expt. 3, Table 1), followed by $LiAlH_4$ reduction of the product mixture, the major product, ketone **5**-1,2-$^{13}C$, was converted to the mixture of *erythro*- and *threo*-alcohols **4**-1,2-$^{13}C$ and the minor product, ketone **6**-1,2-$^{13}C$, was converted to1,2-diphenyl[1,2-$^{13}C$]-ethanol (**7**-1,2-$^{13}C$). The expanded aliphatic region of the $^{13}C$ nmr spectrum of the mixture of alcohols, **4**-1,2-$^{13}C$ and **7**-1,2-$^{13}C$, obtained from this experiment, is given in Fig. 2*B*, while the $^{13}C$ nmr spectrum of the unlabeled **7** is shown in Fig. 2*A*. From the essentially equal intensities of the C-1 and C-2 absorptions, it may be concluded that the $^{13}C$-label is distributed equally over C-1 and C-2 in both the major and minor products, ketones **5**-1,2-$^{13}C$ and **6**-1,2-$^{13}C$. Similar results indicating an equal distribution of the label over C-1 and C-2 in both **5**-1,2-$^{13}C$ and **6**-1,2-$^{13}C$ were also observed when **2**-OTs-1-$^{13}C$ was solvolyzed in 70% HOAc in the presence of 3 equiv. of NaOAc at 148 ± 2°C for 7 or 24 h (conditions of Expts. 4 and 5, Table 1).

Since the scrambling of the label over C-1 and C-2 remained the same in both **5**-1,2-$^{13}C$ and **6**-1,2-$^{13}C$, even though the relative amount of **6** that was formed was higher with a longer reaction time (Table 1), it is possible that the minor product, **6**-1,2-$^{13}C$, was formed from the initial product, **5**-1,2-$^{13}C$. It has also been noted from Table 1 that the formation of **6** was favored by the presence of a strong acid, and the *p*-toluenesulfonic acid liberated during the solvolysis of **2**-OTs could be such an acid. In some control experiments, ketone **5** in 70% HOAc containing 1 equiv. of TsOH was heated at 148 ± 2°C for 24 and 74 h, and indeed it was found that about 10 and 20%, respectively, of the ketone **5** was converted to desoxybenzoin (**6**), confirming the idea that **6** could be formed from the initial product **5**.

The detection of **5** and **6** as described above were based chiefly on the absorptions in the aliphatic regions of their $^1H$ and $^{13}C$ nmr spectra. On a closer examination of the carbonyl region of some of the $^{13}C$ nmr spectra of the products from the solvolysis of **2**-OTs in aqueous HOAc, such as the product from Expt. 7, Table 1, which contained some added $HClO_4$, besides the absorptions at 194.8 and 197.7 ppm attributable to the carbonyl groups of **5** and **6**, respectively, there was a third peak at 194.6 ppm, which was very near the 194.8 ppm absorption of **5**. It was shown subsequently that this third component was due to the carbonyl absorption of benzil. The presence of benzil among the products has actually been observed previously in the decomposition in $CH_3NO_2$ of *trans*-1,2-diphenyl-2-phenylthiovinyl and *trans*-1,2-diphenyl-2-*p*-tolylthiovinyl 2,4,6-trinitrobenzenesulfonates (12).

Since benzil was most readily observed in Expt. 7 (Table 1) with $HClO_4$ present in the reaction mixture, there is the possibility that benzil was derived from the oxidation of benzoin. It is known

Can. J. Chem. Downloaded from www.nrcresearchpress.com by 210.87.254.42 on 09/06/12
For personal use only.

Can. J. Chem. Downloaded from www.nrcresearchpress.com by 210.87.254.42 on 09/06/12
For personal use only.

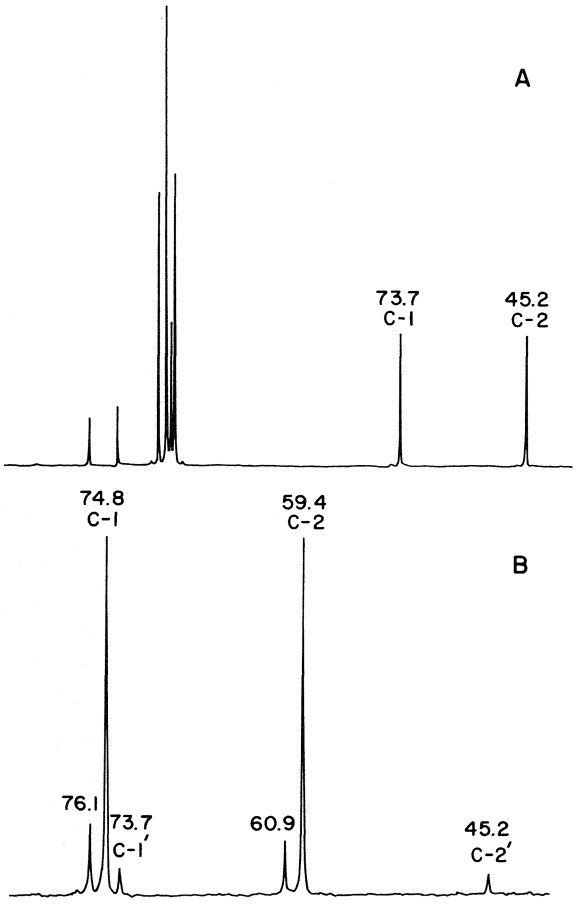


FIG. 2. $^1$H-decoupled $^{13}$C nmr spectra in acetone-$d_6$: *A* is the spectrum of ordinary 1,2-diphenylethanol (**7**); *B* is the expanded aliphatic region of the mixture of *erythro*- and *threo*-alcohols **4**-1,2-$^{13}$C and the alcohol **7**-1,2-$^{13}$C derived from the solvolysis of **2**-OTs-1-$^{13}$C in 70% HOAc in the presence of 3 equiv. of NaOAc at 148 ± 2°C for 4 h; the peaks marked C-1′ and C-2′ are due to **7**-1,2-$^{13}$C.

that vinyl sulfides (thioenol ethers) can be hydrolyzed to give ketones (13, 14). The enol form of **5** would be a thioenol ether and its hydrolysis would give rise to benzoin. Thus under the conditions of solvolysis of **2**-OTs in 70% HOAc, some benzoin might be formed and it in turn might be converted to benzil and desoxybenzoin (**6**). To test this possibility, ketone **5** in 70% HOAc containing 1 equiv. of TsOH and 1 equiv. of benzoin was heated at 148 ± 2°C for 24 h, but there was no significant increase in the 10% conversion of **5** to **6** which was observed in a similar control experiment without the presence of benzoin. Even when **5** in 70% HOAc containing 1 equiv. each of TsOH, benzoin and $C_6H_5SH$, the latter being added as a possible reducing agent, was treated in the same way at 148 ± 2°C for 24 h, there was again no significant increase in the conversion of **5** to **6**. Hence it must be concluded that the desoxybenzoin (**6**) obtained as a minor product in the present studies did not arise from benzoin.

Besides **5**, **6**, and benzil, diphenyl disulfide has also been obtained as another product in the solvolysis of **2**-OTs in aqueous HOAc. In the work with **2**-OTs-1-$^{13}$C, the solvolysis products were treated with $LiAlH_4$ to give the alcohols **4**-1,2-$^{13}$C and **7**-1,2-$^{13}$C. Purification of these alcohols involved their passage through an alumina column. The unwanted materials were first eluted with a mixture of petroleum ether and ether before the desired alcohols were eluted with ether alone. It was from the petroleum ether – ether eluate that diphenyl disulfide was first detected. This disulfide has also been reported previously as among the products from the decomposition of *trans*-1,2-diphenyl-2-phenylthiovinyl 2,4,6-trinitrobenzenesulfonate in $CH_3NO_2$ (12) and from the solvolysis of *trans*-2-phenylthio-1,2-di-*p*-tolylvinyl 2,4,6-trinitrobenzenesulfonate in acetone–methanol (6). When 1.0 g of **2**-OTs in 50 mL of 70% HOAc was heated at 148 ± 2°C for 96 h, the products, **5**, **6**, benzil, and diphenyl disulfide, respectively, were isolated in yields of 22, 21, 11, and 13%. When ketone **5** in 70% HOAc containing 1 equiv. of TsOH was heated at 148 ± 2°C for 72 h, desoxybenzoin (**6**), benzil, and diphenyl disulfide were also obtained, indicating that these products resulted from subsequent reactions of the initial product **5**.

From the above results, it can be concluded that the solvolysis of **2**-OTs in 70% HOAc gave, via the thiirenium ion **1**, α-phenyl-α-(phenylthio)acetophenone (**5**) as the initial product. With labeled **2**-OTs-1-$^{13}$C as substrate, the label would be scrambled equally over C-1 and C-2. Upon being heated in the reaction mixture, part of the initial product **5** could be converted to desoxybenzoin (**6**), benzil, and diphenyl disulfide. To account for the formation of **6**, benzil, and diphenyl disulfide from **5**, a possible mechanism as given in Scheme 2 may be tentatively suggested. The processes outlined in Scheme 2 would be consistent with the finding that acidic and aqueous conditions are necessary to bring about these conversions. A key step is the suggestion that the phenylthio group of a second molecule of **5** could act as a reducing agent on a protonated **5** to give rise eventually to desoxybenzoin (**6**) and the sulfonium ion **8**. A nucleophilic displacement by $H_2O$ on ion **8** would give diphenyl disulfide and benzoin, with the latter being oxidized to benzil. Under the conditions of the present solvolytic studies with **2**-OTs, a possible oxidizing agent could be the liberated sulfonic acid. Indeed a test experiment has shown that some benzil was

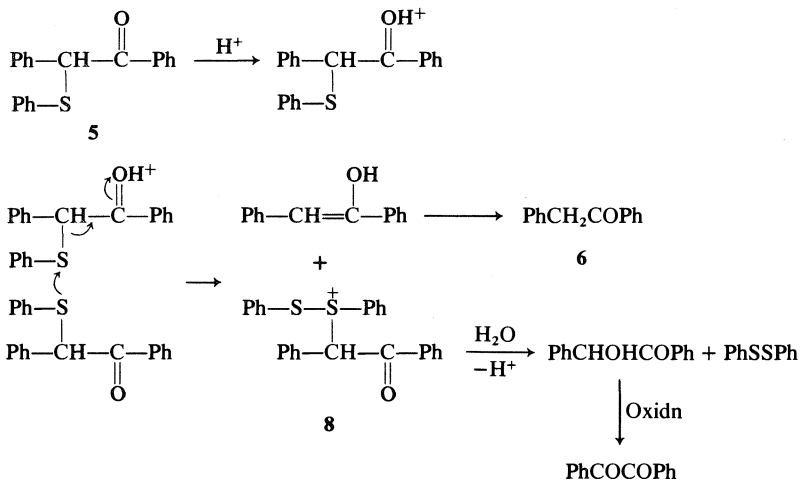

SCHEME 2

isolated after a mixture of benzoin and TsOH was heated in 70% HOAc. The processes responsible for the formation of **6**, benzil, and diphenyl disulfide could, of course, be much more complex than the reactions outlined in Scheme 2. It has been found, for example, that in the solvolysis of β-aminovinyl sulfonates (15), an oxygen–sulfur cleavage in the sulfonate group via

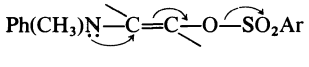

as a transition state gave benzil as one of the products. Such a process conceivably could also play a role in the solvolysis of β-phenylthiovinyl sulfonates.

## Experimental

trans-*1,2-Diphenyl-2-phenylthio[1-*$^{13}$*C]vinyl tosylate (2-OTs-1-*$^{13}$*C)*

**2**-OTs-1-$^{13}$C was synthesized using a series of reactions as given in Scheme 1. The various steps involved were similar to those already reported in the literature (4, 16). The procedures for the steps leading to the carbonyl-labeled desoxybenzoin from $^{13}CO_2$ were essentially the same as those employed for the preparation of the carbonyl-labeled desoxyanisoin (16). The remaining reactions were carried out using procedures described by Modena and co-workers (4), with slight modifications involving the use of HOAc (16) instead of $CCl_4$ (4) as solvent in the bromination of the desoxybenzoin, and the use of *p*-toluenesulfonyl chloride instead of *p*-bromobenzenesulfonyl chloride in the final step to give the tosylate instead of the brosylate. The desired product, **2**-OTs-1-$^{13}$C, after crystallization from dichloromethane–pentane, melted at 140–141°C (lit. (7) mp 139–140°C), $^1$H nmr δ($CDCl_3$) 2.30 ($CH_3$, s, 3H), 6.80–7.60 (arom., m, 19H).

*Acetolysis under anhydrous conditions*

In a typical experiment, a mixture of 400 mg (0.87 mmol) of **2**-OTs-1-$^{13}$C (about 20% $^{13}$C enrichment) and 210 mg (2.6 mmol) of NaOAc in 30 mL of HOAc–$Ac_2O$ (9:1 by volume) in a sealed tube was heated in an oil bath at 148 ± 2°C for 10 h. The resulting material was poured into $H_2O$ and extracted 3 times with $CHCl_3$. The extract was washed successively with $H_2O$, a $NaHCO_3$ solution, and then $H_2O$. After drying over $MgSO_4$, removal of the solvent gave about 250 mg of crude product. In preliminary trials with ordinary **2**-OTs, the crude product was crystallized from methanol to give 50–55% yields of *trans*-1,2-diphenyl-2-phenylthiovinyl acetate (**2**-OAc), mp 88°C (lit. (7) mp 86°C), $^1$H nmr δ($CDCl_3$) 1.90 ($CH_3$, s, 3H), 6.90–7.80 (arom., m, 15H).

The crude acetate product from the labeled **2**-OTs-1-$^{13}$C was reduced twice successively (9, 17) with $LiAlH_4$ in anhydrous ether to give the mixture of *erythro*- and *threo*-1,2-diphenyl-2-phenylthio[1,2-$^{13}$C]ethanol (**4**-1,2-$^{13}$C). The **4**-1,2-$^{13}$C obtained after the $LiAlH_4$ treatments was purified by passage through a 30 cm × 2 cm diameter column packed with adsorption alumina. The unwanted material was first eluted with a 7:3 mixture of petroleum ether (bp 40–60°C) and ether before the product, **4**-1,2-$^{13}$C, was recovered by elution with ether. The $^{13}$C nmr spectrum of the *erythro*- and *threo*-alcohols, **4**-1,2-$^{13}$C, obtained from this experiment, is given in Fig. 1*B*, while the spectrum of the unlabeled **4** from the reduction of ordinary **2**-OAc is shown in Fig. 1*A*.

*Solvolysis in 70% HOAc – 30% $H_2O$*

In a typical experiment, a mixture of 300 mg (0.65 mmol) of **2**-OTs-1-$^{13}$C and 160 mg (2.0 mmol) of NaOAc in 50 mL of 70% HOAc in a sealed tube was heated in an oil bath at 148 ± 2°C for 4 h. The resulting material was worked up as described in the acetolysis under anhydrous conditions to give 200 mg of oil as crude product. Preliminary experiments with unlabeled **2**-OTs showed that under these conditions the crude product contained α-phenyl-α-(phenylthio)acetophenone (**5**) and desoxybenzoin (**6**) in a relative ratio of 95:5.

The crude product from the reaction with **2**-OTs-1-$^{13}$C was dissolved in ether and pentane was added to precipitate out unwanted materials which may contain some unreacted tosylate. After the removal of the precipitate and evaporation of the solvent, the residual oil containing **5**-1,2-$^{13}$C and **6**-1,2-$^{13}$C was treated once with $LiAlH_4$ in anhydrous ether to give the *erythro*- and *threo*-alcohols, **4**-1,2-$^{13}$C, and 1,2-diphenyl[1,2-$^{13}$C]ethanol (**7**-1,2-$^{13}$C), which were recovered after purification through an alumina column as described earlier. The aliphatic region of the $^{13}$C nmr spectrum of the mixture of labeled alcohols obtained in this experiment is shown in Fig. 2*B*, while the $^{13}$C nmr spectrum of a pure sample of ordinary **7** is given in Fig. 2*A*.

Can. J. Chem. Downloaded from www.nrcresearchpress.com by 210.87.254.42 on 09/06/12
For personal use only.

The identification of ketones **5** and **6** in various experiments with ordinary **2**-OTs were based on their $^1H$ and $^{13}C$ nmr spectra, and these spectral data are as follows: α-phenyl-α-(phenylthio)acetophenone (**5**), $^1H$ nmr δ($CDCl_3$) 5.85 (CH, s, 1H), 7.15–7.65 (arom., m, 13H), 7.80–8.15 (arom., m, H *ortho* to CO, 2H); $^{13}C$ nmr δ($CDCl_3$) 60.3 (CH), 128.0, 128.1, 128.9, 133.1, 133.4 (arom.), 134.1, 135.7, 136.6 (quat. arom.), 194.8 (CO). Desoxybenzoin (**6**), $^1H$ nmr δ($CDCl_3$) 4.25 ($CH_2$, s, 2H), 7.20–7.60 (arom., m, 8H), 7.90–8.20 (arom., m, H *ortho* to CO, 2H); $^{13}C$ nmr δ($CDCl_3$) 45.6 ($CH_2$), 126.9, 128.7, 129.6, 133.2 (arom.), 134.3, 136.2 (quat. arom.), 197.7 (CO).

*Product determinations*

A solution of 1.00 g (2.2 mmol) of **2**-OTs in 50 mL of 70% HOAc in a sealed tube was heated at 148 ± 2°C for 96 h. The resulting material was poured into $H_2O$ and extracted with ether. The extract was washed with a $NaHCO_3$ solution and then with $H_2O$. After drying over $MgSO_4$, removal of the solvent gave 0.55 g of crude products which were separated by passage through an alumina column. The first fraction was eluted with a 6:1 (by volume) mixture of petroleum ether (bp 40–60°C) and ether to give 60 mg (13%) of diphenyl disulfide, mp 56–58°C (lit. (12) mp 55–58°C); its mass spectrum showed the molecular ion at *m/e* 218 as expected. The second fraction was eluted with a 3:1 mixture of petroleum ether – ether to give 90 mg (21%) of desoxybenzoin (**6**) which melted alone or on admixture with an authentic sample at 50°C. Its $^1H$ and $^{13}C$ nmr absorptions are given in the preceding section. The third fraction was eluted with a 2:1 mixture of petroleum ether – ether to give 150 mg (22%) of α-phenyl-α-(phenylthio)acetophenone (**5**), mp 82–83°C (lit. (18) mp 83–84°C). Again its $^1H$ and $^{13}C$ nmr absorptions are given in the preceding section. The fourth fraction was eluted with a 1:1 mixture of petroleum ether – ether to give 50 mg (11%) of benzil which melted alone or on admixture with an authentic sample at 95°C, $^1H$ nmr δ($CDCl_3$) 7.30–7.80 (arom., m, 6H), 7.90–8.20 (arom., m, H *ortho* to CO, 4H).

When a mixture of 1.40 g (4.6 mmol) of ketone **5** and 90 mg (4.7 mmol) *p*-toluenesulfonic acid in 50 mL of 70% HOAc in a sealed tube was heated at 148 ± 2°C for 72 h, after the usual work up, separation of the products through the alumina column gave 180 mg (18%) of diphenyl disulfide, 300 mg (33%) of desoxybenzoin (**6**), and 100 mg (10%) of benzil.

When a mixture of 1.00 g (4.7 mmol) of benzoin and 2.70 g (14 mmol) of TsOH in 50 mL of 70% HOAc in a sealed tube was heated at 148 ± 2°C for 72 h, the usual work up and product separation gave 200 mg (20%) of benzil.

## Acknowledgments

Valuable information on the synthesis of the labeled substrate provided by Professor G. Modena, some preliminary work carried out by Dr. E. C. F. Ko, and the financial support given by the Natural Sciences and Engineering Research Council of Canada are sincerely acknowledged.

1. G. Modena and U. Tonellato. Adv. Phys. Org. Chem. **9**, 185 (1971).
2. G. Capozzi, V. Lucchini, and G. Modena. Rev. Chem. Intermediates, **2**, 347 (1979).
3. G. Capozzi, G. Melloni, G. Modena, and U. Tonellato. Chem. Commun. 1520 (1969).
4. G. Capozzi, G. Melloni, and G. Modena. J. Chem. Soc. C, 3018 (1971).
5. G. Capozzi, G. Melloni, and G. Modena. J. Chem. Soc. C, 2625 (1970).
6. G. Modena and U. Tonellato. J. Chem. Soc. B, 381 (1971).
7. G. Modena and U. Tonellato. J. Chem. Soc. B, 1569 (1971).
8. F. H. A. Rummens, R. D. Green, A. J. Cessna, M. Oka, and C. C. Lee. Can. J. Chem. **53**, 314 (1975).
9. M. Oka and C. C. Lee. Can. J. Chem. **53**, 320 (1975).
10. C. C. Lee and E. C. F. Ko. Can. J. Chem. **56**, 2459 (1978).
11. C. C. Lee, E. C. F. Ko, and Z. Rappoport. Can. J. Chem. **58**, 2369 (1980).
12. G. Modena and U. Tonellato. J. Chem. Soc. B, 374 (1971).
13. T. Mukaiyama, K. Kamio, S. Kobayashi, and H. Takei. Bull. Chem. Soc. Jpn. **45**, 3723 (1972).
14. B. M. Trost, K. Hiroi, and S. Kurozumi. J. Am. Chem. Soc. **97**, 438 (1975).
15. A. Burighel, G. Modena, and U. Tonelatto. J. Chem. Soc. Perkin II, 1021 (1973).
16. C. C. Lee and M. Oka. Can. J. Chem. **54**, 604 (1976).
17. C. C. Lee, A. J. Cessna, B. A. Davis, and M. Oka. Can. J. Chem. **52**, 2679 (1974).
18. G. Capozzi, G. Melloni, and G. Modena. J. Chem. Soc. C, 2621 (1970).

Can. J. Chem. Downloaded from www.nrcresearchpress.com by 210.87.254.42 on 09/06/12
For personal use only.

# Effect of hydrogen bonding on the π-electronic absorption spectra of some bicyclic secondary amines

TAPAN GANGULY AND SUKHENDU B. BANERJEE[1]

*Optics Department, Indian Association for the Cultivation of Science, Jadavpur, Calcutta 700032, India*

Received June 25, 1981

TAPAN GANGULY and SUKHENDU B. BANERJEE. Can. J. Chem. **60**, 741 (1982).

Spectral shift and change in the intensity of electronic absorption bands of bicyclic molecules, 1,2,3,4-tetrahydroquinoline (THQ) and 1,2,3,4-tetrahydroisoquinoline (THIQ), on hydrogen bond formation in binary and ternary solutions were investigated. Roles of factors contributing to the spectral changes such as change in configuration of the molecules and σ–π interaction are discussed in this paper.

TAPAN GANGULY et SUKHENDU B. BANERJEE. Can. J. Chem. **60**, 741 (1982).

Dans cet article on examine en détail le décalage spectral et le changement dans l'intensité des bandes d'absorption des molécules bicycliques 1,2,3,4-tétrahydroquinoline (THQ) et 1,2,3,4-tétrahydroisoquinoline (THIQ) suivant la formation de le liaison hydrogène en solutions binaires et ternaires.

On discute les rôles des facteurs comme le changement dans la configuration des molécules et l'interaction σ–π contribuants aux changements mentionnés ci-dessus.

Can. J. Chem. Downloaded from www.nrcresearchpress.com by 210.87.254.6 on 09/06/12
For personal use only.

## Introduction

Several authors have discussed hydrogen bonding in secondary amines acting either as proton donors (1, 2) or as proton acceptors (3–5). The present work concerns the hydrogen bonding behaviour and π-electronic absorption spectra of 1,2,3,4-tetrahydroquinoline (THQ) and 1,2,3,4-tetrahydroisoquinoline (THIQ) in binary and ternary solutions in *n*-heptane and dioxane. The infrared absorption of the molecules in *n*-heptane and dioxane was also measured to get corroborative evidence about intermolecular hydrogen bond. Both these molecules, THQ and THIQ, are bicyclic secondary amines with the NH-group in the ring that has non-aromatic bonds. The hydrogen bonding in such molecules has not been studied earlier. It was felt that study of π-electronic spectral changes effected through intermolecular hydrogen bond formation might provide useful information about change in configuration of the molecules and σ–π conjugation. In this paper the results are described.

## Experimental

Chemically pure compounds of THQ (ρ = 1.055 g/mL; bp 251°C) and THIQ (ρ = 1.0642 g/mL; bp 232°C) supplied by Fluka, Switzerland and dioxane supplied by Messers British Drug House, London were used after distillation under reduced pressure. The solvent *n*-heptane, obtained from E. Merck, was of spectroscopic purity and was used without further purification. The electron absorption spectra were measured with a Hilger U.V. spectrophotometer. Infrared spectra were recorded with a Beckman IR-2OA Spectrophotometer fitted with a grating monochromator. The experimental details were as described earlier (6). The spectral data and the measured thermodynamic quantities are given in Tables 1–4.

[1]To whom all correspondence should be addressed.

## Calculations

Dioxane and *n*-heptane were the proton acceptor and the inert solvent respectively. The concentration of dioxane was increased in steps and in every step the concentration of THQ or THIQ was kept fixed at a very low value ($\sim 10^{-4}$–$10^{-5}$ mol/L) compared to that of dioxane.

The association equilibrium constant ($K$) was calculated by the equation described by Ketelaar *et al.* (7)

$$[1]\quad \frac{1}{\varepsilon - \varepsilon_f} = \frac{1}{C}\,\frac{1}{\varepsilon_b - \varepsilon_f}\,\frac{1}{K} + \frac{1}{\varepsilon_b - \varepsilon_f}$$

where ε = apparent molar extinction coefficient for THQ in solution in which dioxane concentration is $C$, $\varepsilon_f$ = molar extinction coefficient of the non-hydrogen bonded molecule and $\varepsilon_b$ = molar extinction coefficient for the hydrogen bonded molecule. All these extinction coefficients refer to a given frequency. Molar extinction coefficient $\varepsilon_b$ for the hydrogen bonded species was calculated for every frequency from [2] which can be readily deduced from [1].

$$[2]\quad \varepsilon_b = \varepsilon + \frac{\varepsilon - \varepsilon_f}{KC}$$

The hydrogen-bonded curves were obtained by plotting $\varepsilon_b$ against ν (in $cm^{-1}$) (6, 8, 9).

On plotting $1/(\varepsilon - \varepsilon_f)$ against $1/C$, straight lines were obtained and upon extrapolating them to the point $1/(\varepsilon - \varepsilon_f) = 0$, the values of $K$ were obtained.

The free energy ($\Delta F$), the energy of hydrogen bond formation ($\Delta H$), and the $f$-values were calcu-

0008-4042/82/060741-06$01.00/0

©1982 National Research Council of Canada/Conseil national de recherches du Canada

Can. J. Chem. Downloaded from www.nrcresearchpress.com by 210.87.254.6 on 09/06/12
For personal use only.

TABLE 1. Frequency shift on hydrogen bond formation (frequency in $cm^{-1}$)

| System | Transition | $\nu_f$* | $\nu_b$† | $\delta\nu = \nu_b - \nu_f$ | Mean $\delta\nu$ |
|---|---|---|---|---|---|
| THQ | I | 33212 | 33102 | (−110) | (−110) |
| | II | 39987 | 39828 | (−159) | |
| | | 40310 | 40148 | (−162) | (−162) |
| | | 40638 | 40473 | (−165) | |
| THIQ | I | 37582 | 37582 | 0 | 0 |
| | | 36485 | 36485 | 0 | 0 |

*Free species.
†Bonded species.

TABLE 2. Change of intensity with proton acceptor (dioxane) concentration

| Proton donor concentration (mol/L) | Temperature (K) | Proton acceptor concentration (dioxane) (mol/L) | $\int \varepsilon d\nu$ |
|---|---|---|---|
| THQ | | 0 | $1.07 \times 10^7$ |
| $1.584 \times 10^{-4}$ | 302 | 0.1 | $1.17 \times 10^7$ |
| (Transition I) | | 0.3 | $1.25 \times 10^7$ |
| | | 0.5 | $1.33 \times 10^7$ |
| | | Hydrogen-bonded (calculated) | $1.41 \times 10^7$ |
| THQ | | 0 | $4.85 \times 10^7$ |
| $1.584 \times 10^{-5}$ | 302 | 0.08 | $5.53 \times 10^7$ |
| (Transition II) | | 0.2 | $5.54 \times 10^7$ |
| | | 0.3 | $6.38 \times 10^7$ |
| | | 0.5 | $6.61 \times 10^7$ |
| | | Hydrogen-bonded (calculated) | $7.00 \times 10^7$ |
| THIQ | | 0 | $1.68 \times 10^6$ |
| $1.598 \times 10^{-4}$ | 303.5 | 0.08 | $1.69 \times 10^6$ |
| (Transition I) | | 0.3 | $1.71 \times 10^6$ |
| | | 0.4 | $1.76 \times 10^6$ |
| | | Hydrogen-bonded (calculated) | $1.79 \times 10^6$ |

TABLE 3. Equilibrium constants ($K$) and thermodynamic parameters of the systems of THQ and THIQ with dioxane and $n$-heptane

| | | $K$ ($L\ mol^{-1}$) | | | | |
|---|---|---|---|---|---|---|
| System | Temperature (K) | Transition I | Transition II | Mean | $-\Delta F$ (kcal $mol^{-1}$) | $-\Delta H$ (kcal $mol^{-1}$) |
| THQ | 302 | 3.72 | 3.72 | 3.72 | 0.785 | |
| | 313 | 3.10 | 3.41 | 3.25 | 0.730 | 2.49 |
| | 323.5 | 2.96 | 2.69 | 2.825 | 0.665 | |
| THIQ | 303.5 | 2.83 | — | 2.83 | 0.625 | |
| | 315.5 | 2.62 | — | 2.62 | 0.597 | 1.22 |
| | 323.0 | 2.50 | — | 2.50 | 0.586 | |

lated from the familiar relations,

[3] $\Delta F = -RT \ln K$

[4] $\Delta H = -\dfrac{R\,\mathrm{d} \ln K}{\mathrm{d}(1/T)}$

and

[5] $f = 4.32 \times 10^{-9} \int \varepsilon d\nu$

A plot of $R \ln K$ versus $1/T$ yielded straight lines whose slope gave $\Delta H$. The method of least-squares was used for calculating $\Delta H$ and $K$.

## Results and discussion

In $n$-heptane solution THQ exhibits two systems of absorption bands in the regions 2750 Å to 3170 Å and 2320 Å to 2620 Å (Fig. 1 (*a*) and (*b*)). When the

TABLE 4. Measured oscillator strengths of free and hydrogen bonded molecules

| System | Transition | $f_f$* | $f_b$† | $f_b/f_f$ | $\Delta f = f_b - f_f$ |
|---|---|---|---|---|---|
| THQ | I (2750 Å–3170 Å) | 0.046 | 0.061 | 1.326 | 0.015 |
| | II (2320 Å–2620 Å) | 0.209 | 0.302 | 1.444 | 0.093 |
| THIQ | I (2500 Å–2760 Å) | 0.007 | 0.008 | 1.142 | 0.001 |

*Free species.
†Bonded species.

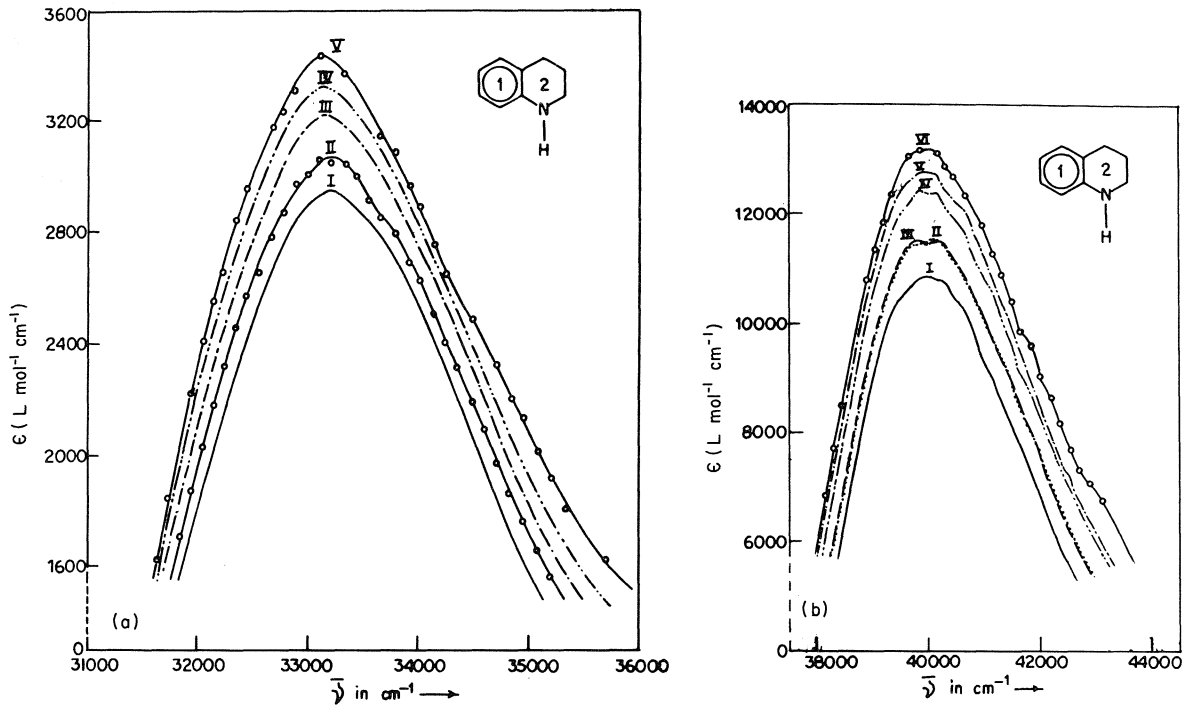


FIG. 1(*a*). Ultraviolet absorption curves for THQ (at 302 K) (transition I). ($1.584 \times 10^{-4}$ mol $L^{-1}$ THQ in *n*-heptane). *I*, $c_{dioxane} = 0$; *II*, $c_{dioxane} = 0.1$ mol $L^{-1}$; *III*, $c_{dioxane} = 0.3$ mol $L^{-1}$; *IV*, $c_{dioxane} = 0.5$ mol $L^{-1}$; *V*, hydrogen bonded curve (only the upper portions of the curves near the peaks are shown). (*b*). Ultraviolet absorption curves for THQ (at 302 K) (transition II). ($1.584 \times 10^{-5}$ mol $L^{-1}$ THQ in *n*-heptane); *I*, $c_{dioxane} = 0$; *II*, $c_{dioxane} = 0.08$ mol $L^{-1}$; *III*, $c_{dioxane} = 0.2$ mol $L^{-1}$; *IV*, $c_{dioxane} = 0.3$ mol $L^{-1}$; *V*, $c_{dioxane} = 0.5$ mol $L^{-1}$; *VI*, hydrogen bonded curve (only the upper portions of the curves near the peaks are shown).

proton acceptor solvent dioxane is added to the binary solution of THQ in *n*-heptane, bands of the both absorption systems shift towards the longer wavelength side (Table 1). The observed red shifts of the two systems are characteristic of a $\pi^* \leftarrow \pi$ transition and both systems may be logically assigned to such transition. Moreover, probability of excitation of a nitrogen non-bonding electron to $\pi$-orbital of the aromatic ring will not be high because the nitrogen atom is in the non-aromatic ring 2 and separated by a bond from the aromatic ring 1 (inset in Fig. 1). In the spectrum of THIQ in *n*-heptane one $\pi$-electronic band system in the region 2500 Å to 2760 Å is observed (Fig. 2) and the bands do not undergo any red shift worth noting when dioxane is added to the THIQ–*n*-heptane solution. For THQ the integrated absorption $\int \varepsilon d\nu$ increases, with the addition of proton acceptor dioxane (Table 2), tending to a constant value at high dioxane concentration (>0.5 mol/L). The corresponding change in the case of THIQ is, however, very small. Since *n*-heptane comprises the bulk of the ternary solution in which the relative concentration of dioxane is low, the effect of change of polarity, without H-bonding, will not be of any great significance and the observed spectral changes should presumably be attributed to intermolecular hydrogen bonding involving THQ (or THIQ) and dioxane molecules. The linear graph obtained from the plot of $1(\varepsilon - \varepsilon_f)$ versus $1/C$ (Figs. 3 and 4)

Can. J. Chem. Downloaded from www.nrcresearchpress.com by 210.87.254.6 on 09/06/12
For personal use only.

Can. J. Chem. Downloaded from www.nrcresearchpress.com by 210.87.254.6 on 09/06/12
For personal use only.

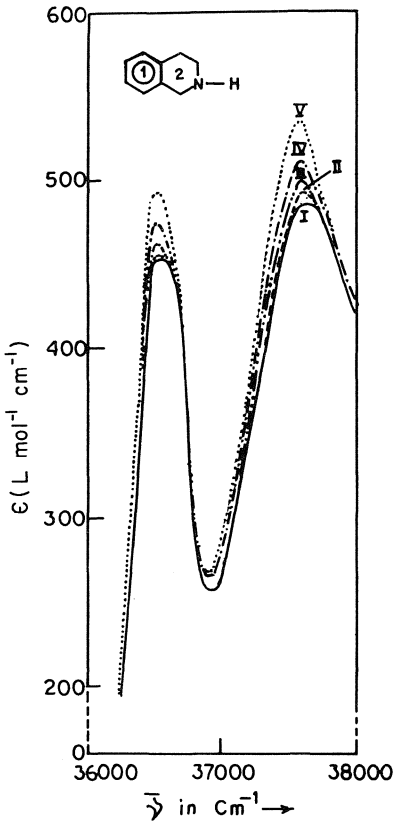


FIG. 2. Ultraviolet absorption curves for THIQ (at 303.5 K) (transition I) ($1.598 \times 10^{-4}$ mol $L^{-1}$ THIQ in *n*-heptane). *I*, $c_{dioxane} = 0$; *II*, $c_{dioxane} = 0.08$ mol $L^{-1}$; *III*, $c_{dioxane} = 0.3$ mol $L^{-1}$; *IV*, $c_{dioxane} = 0.4$ mol $L^{-1}$; *V*, hydrogen bonded curve (only the upper portions of the curves near the peaks are shown).

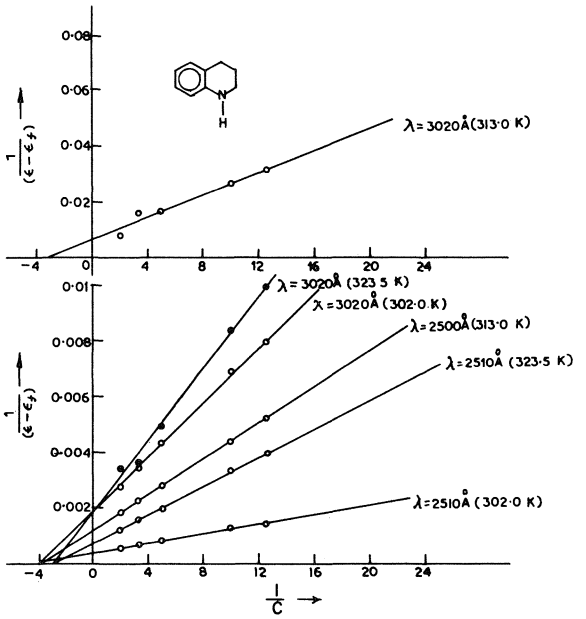


FIG. 3. Plot of $1/(\varepsilon - \varepsilon_f)$ vs. $1/C$ for the determination of *K* in the THQ system.

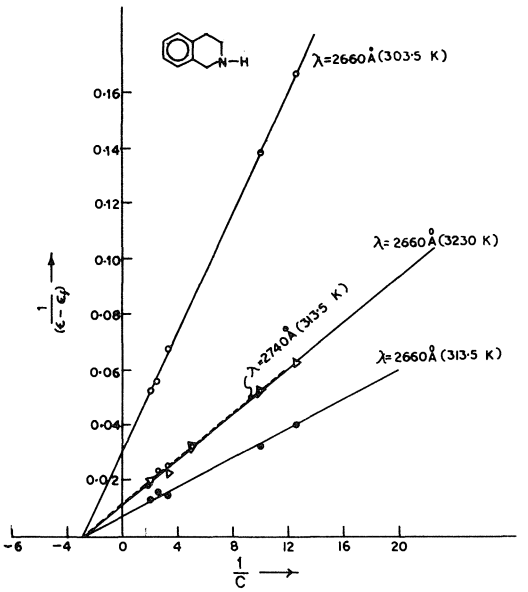


FIG. 4. Plot of $1/(\varepsilon - \varepsilon_f)$ vs. $1/C$ for the determination of *K* in the THIQ system.

further indicates occurrence of 1:1 hydrogen bonded complex.

To get complementary evidence of an intermolecular N—H···O bond, the infrared spectra of THQ and THIQ in *n*-heptane and dioxane were recorded and the absorption curves are presented in Fig. 5(*a*) and (*b*). For THQ in *n*-heptane solution (Fig. 5(*a*)) the free ν(N—H) band can be located at 3430 $cm^{-1}$. When dioxane is added to the solution a second band which may be reasonably assigned to vibration of bonded N—H, appears at 3380 $cm^{-1}$ (Fig. 5(*a*)). In the presence of an excess amount of dioxane in the ternary mixture, this band predominates over the 3430 $cm^{-1}$ band whose intensity becomes vanishingly small. In the infrared spectra of THIQ, the free ν(N—H) band is at 3320 $cm^{-1}$. This value of free ν(N—H) for THIQ in which the N—H group is in the non-aromatic ring and separated from the aromatic ring by intervening bonds, is closer to the value expected for an aliphatic amine (10). Addition of dioxane results in a small but finite red shift of 20 $cm^{-1}$, indicating formation of intermolecular bond, though weak, between THIQ and dioxane.

From Table 4 it is seen that for THQ and THIQ, the oscillator strength of bonded molecules ($f_b$) is larger than that of free molecules ($f_f$). However, some interesting points are brought to light if the enthalpy of hydrogen bond and the change in intensity of absorption, expressed as $f_b/f_f$ or $\Delta f$, for

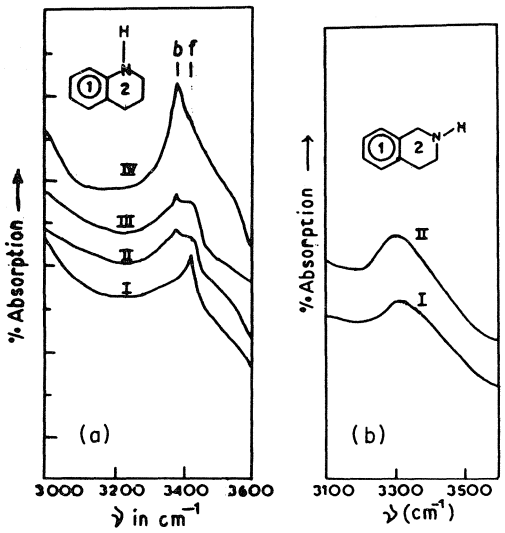


FIG. 5(*a*). Infrared absorption curves for THQ (at 298 K) (1.58 × $10^{-2}$ mol $L^{-1}$ THQ in *n*-heptane): *I*, $c_{dioxane} = 0$; *II*, $c_{dioxane} = 0.5$ mol $L^{-1}$; *III*, $c_{dioxane} = 0.6$ mol $L^{-1}$; *IV*, excess dioxane. (*b*). Infrared absorption curves for THIQ (at 298 K) (1.59 × $10^{-2}$ mol $L^{-1}$ THIQ in *n*-heptane): *I*, $c_{dioxane} = 0$; *II*, excess dioxane.

THQ, THIQ, and *o*-toluidine, a primary amine, presented in Table 5 are examined. Taking up first the molecules of THQ and *o*-toluidine, it is seen that the energy of the hydrogen bond ($\Delta H$) in the case of THQ is nearly half of that in the case of *o*-toluidine. This is as expected because secondary amines are known to be much weaker hydrogen bonding agents than primary amines (11, 12). Interestingly, the increase in *f*-value is much greater for the weaker hydrogen bonding THQ molecule than for the *o*-toluidine molecule. The spectral shifts observed for the two molecules are of comparable magnitude.

The alicyclic ring in tetraline is known to have cyclohexene-like distorted chair structure (13). According to Aroney and Le Fèvre (14), with the valencies of the nitrogen atom disposed pyramidally and the C—C—C angles tetrahedral, a chair structure need be considered for piperidine molecule, where the N—H bond may be axial or equatorial, and they had concluded that piperidine in benzene solution contains 80% or more of the axial form. The non-aromatic ring 2 of THQ (inset in Fig. 1(*a*)) could be assumed to have a similar structure and the π-character of the non-bonding electrons on N-atom should be different from that of the toluidine molecule where the nitrogen atom, as in aniline, uses $sp^2$ orbitals. From proton magnetic resonance studies Booth (15) actually proposed for THQ a mixture of rapidly inverting half-chair structure and made the tentative suggestion that equal proportions of axial and equatorial

TABLE 5. Comparison of enthalpy of hydrogen bond and change in *f*-value for THQ, THIQ, and *o*-toluidine

| System | $-\Delta H$ (kcal $mol^{-1}$) | $f_b/f_f$ | $\Delta f$ |
|---|---|---|---|
| THQ | 2.49 | 1.326 (Transition I) | 0.015 |
| | | 1.444 (Transition II) | 0.093 |
| *o*-Toluidine (6) | 4.92 | 1.178 (Transition I) | 0.007 |
| | | 1.360 (Transition II) | 0.077 |
| THIQ | 1.22 | 1.142 (Transition I) | 0.001 |

conformations might be present. In connection with the changes observed in the spectrum of THQ in *n*-heptane–dioxane solution several possibilities deserve attention. The intermolecular hydrogen bond may bring about change in conformational equilibrium of the THQ molecule with the N—H bond tending to deviate from the axial position. As the intensification of the spectra indicates larger resonance or larger participation of nitrogen nonbonding electrons of the alicyclic-like ring in the π-electronic system of ring 1 (inset in Fig. 1 (*a*)), it appears that the lone pair electrons may possibly have gained some *p*-character consequent upon the new conformation in which the C—NH group may be more coplaner with the ring 1 so that the nitrogen atom is favourably placed to allow for large overlap of lone pair with carbon $p\pi$-electrons. Further, since the formation of intermolecular hydrogen bond leads to an increase in σ-electron density on the nitrogen atom (6, 8, 9, 16, 17), another contributing factor may be increased σ–π interaction, whose role in explaining spectral characteristics of bicyclic molecules has been stressed by previous authors (18, 19).

The situation is different in THIQ (inset in Fig. 2) in which the N—H group is away from the aromatic ring 1 separated by intervening bonds and is shielded by charge clouds of hydrogen atoms on both sides. In this molecule the weak intermolecular hydrogen bond resulting from addition of dioxane to *n*- heptane–THIQ solution produces no noticeable spectral shift or intensification of the spectrum.

1. A. B. SANNIGRAHI and A. K. CHANDRA. J. Phys. Chem. **67**, 1106 (1963).
2. S. B. SHAH and A. S. N. MURTHY. Indian J. Chem. **13**, 664 (1975).
3. M. A. SILFKIN. Charge transfer interactions of biomolecules. Academic Press, New York. 1971.

Can. J. Chem. Downloaded from www.nrcresearchpress.com by 210.87.254.6 on 09/06/12
For personal use only.

4. ED. B. PULLMAN. Molecular association in biology. Academic Press, New York. 1968.
5. R. FOSTER. Organic charge transfer complexes. Academic Press, New York. 1968.
6. T. GANGULY and S. B. BANERJEE. Indian J. Phys. **51**B, 392 (1977).
7. J. A. A. KETELAAR, C. VAN DE STOLPE, A. GOUDSMIT, and W. DZCUBAS. Rec. Trav. Chim. **71**, 1104 (1952).
8. H. BABA and S. SUZUKI. J. Chem. Phys. **35**, 1118 (1961).
9. T. GANGULY and S. B. BANERJEE. Spectrochim. Acta, **34**A, 617 (1978).
10. L. J. BELLAMY. The infrared spectra of complex molecules. Chapman and Hall, London. 1975. p. 281.
11. S. N. VINOGRADOV and R. H. LINNELL. Hydrogen bonding. Van Nostrand Reinhold Company, New York, Cincinnati, Toronto, London, Melbourne, 1971. p. 32.
12. L. H. THOMAS. Trans. Faraday Soc. **62**, 328 (1966).
13. E. L. ELIEL. Stereochemistry of carbon compounds. Tata McGraw-Hill Publishing Company Ltd., New Delhi. 1975. p. 239.
14. M. ARONEY and R. J. W. LE FÈVRE. J. Chem. Soc. 3002 (1958).
15. H. BOOTH. J. Chem. Soc. 1841 (1964).
16. S. SUZUKI and H. BABA. J. Chem. Phys. **38**, 349 (1963).
17. T. GANGULY and S. B. BANERJEE. Indian J. Pure Appl. Phys. **18**, 793 (1980).
18. V. E. MERKEL, Ber Bunsenges. Phys. Chem. **69**, 716 (1965).
19. A. K. SARKAR, S. CHAKRAVORTI, P. K. MALLICK, and S. B. BANERJEE. Spectrosc. Lett. **10**(8), 619 (1977).

Can. J. Chem. Downloaded from www.nrcresearchpress.com by 210.87.254.6 on 09/06/12
For personal use only.

# Large hydrophobic interactions with clearly defined geometry. A dimeric steroid with catalytic properties

J. PETER GUTHRIE, PATRICIA A. CULLIMORE, ROBERT S. MCDONALD, AND STELLA O'LEARY

*Department of Chemistry, University of Western Ontario, London, Ont., Canada N6A 5B7*

Received May 27, 1981

J. PETER GUTHRIE, PATRICIA A. CULLIMORE, ROBERT S. MCDONALD, and STELLA O'LEARY. Can. J. Chem. **60**, 747 (1982).

The steroid dimer α,α′-bis(17β-(4′-imidazolyl)-11-keto-5α-androstan-3β-amino)-*p*-xylene, **3**, has been synthesized by reductive amination of 17β-(4′-imidazolyl)-5α-androstane-3,11-dione by *p*-xylenediamine in the presence of sodium cyanoborohydride, and by reductive amination of terephthalaldehyde by 3β-amino-17β-(4′-imidazolyl)-5α-androstan-11-one. The second method is stereochemically unambiguous; the first is not. Compound **3** acts as a catalyst for the hydrolysis of 3-arylpropionate esters of 3-hydroxy-4-nitrobenzoic acid. For the phenanthryl propionate the rate enhancement relative to imidazole is 200-fold, and the rate enhancement relative to the hypothetical rate for the propionate reacting with the steroid by the same transition state geometry is 3000-fold. The slope of a plot of log $k_{corr}$ vs. π for the reaction of **3***b* with aryl propionate esters was 0.83; the corresponding slope for **12** was 0.39. This provides a design parameter for the construction of artificial enzymes.

J. PETER GUTHRIE, PATRICIA A. CULLIMORE, ROBERT S. MCDONALD et STELLA O'LEARY. Can. J. Chem. **60**, 747 (1982).

On a synthétisé le α,α′-bis-((imidazolyl-4′)-17β céto-11 5α-androstane amino-3β) *p*-zylène, **3**, par amination réductrice de la (imidazolyl-4′)-17β 5α-androstanedione-3,11 par la *p*-xylènediamine en présence de cyanoborohydrure de sodium et par amination réductrice du téréphtalaldéhyde par l'amino-3β (imidazolyl-4′)-17β 5α-androstanone-11.

La deuxième méthode est stéréochimiquement sans ambiguité; la première ne l'est pas. Le composé **3** est un catalyseur pour l'hydrolyse des esters aryl-3 propionates de l'acide hydroxy-3 nitro-4 benzoique. Dans le cas du phénanthryl-3 propionate l'augmentation de la vitesse relative à l'imidazole est égale à 200 alors qu'elle est égale à 3000 par rapport au propionate qui réagirait avec le stéroïde en passant par un état de transition qui aurait la même géométrie. La pente de la courbe de log $k_{corr}$ en fonction π pour la réaction du composé **3***b* avec les esters arylpropionates est de 0,83; la pente correspondante est de 0,39 pour le composé **12**. Ceci fournit un paramètre de conception pour la construction d'enzymes artificiels.

[Traduit par le journal]

## Introduction

We have previously (1) reported studies of the imidazolyl steroid, **1**, which can act as a catalyst, in aqueous solution, for active esters **2***a–d*, and which shows a marked specificity for esters with a hydrophobic acyl group, such as **2***b–d*, with **2***d* being the best substrate found so far. Careful analysis of the kinetic behavior of these reactions showed that there was a potential rate enhancement, due to favorable hydrophobic interactions between steroid and ester, of as much as 156-fold for a phenanthrene ring interacting with the steroid, but that much of this was masked by unavoidable rate-retarding steric effects in the vicinity of the reaction center, so that only a 3.6-fold rate enhancement was observable. In related studies of enolization catalyzed by **1** (2) it was found that the same hydrophobic effect was present and the steric retardation was less, so that more of the potential effect became apparent; in fact a 110-fold rate enhancement relative to imidazole was directly observable.

A clear conclusion from these experiments was that in order to get a large rate enhancement for ester hydrolysis, a greater area of hydrophobic contact between substrate and catalyst was essential. A conceptually simple way to achieve such an increased area of contact would be to use dimeric steroids such as **3** or **4**, with two steroid moieties linked by a *p*-xylylene bridge. Space filling models (CPK) suggested that this sort of dimeric steroid would allow a phenanthryl (or smaller) aromatic system to intercalate snugly, but without crowding or strain.

Clearly, **4** is the more desirable catalyst, because the additional amines allow for more positive charges at the pH where the imidazolyl groups are catalytically active (ca. pH 8) and so allow greater solubility in water. Unfortunately, serious difficulties were encountered in trying to prepare **4** from **1**, and it seemed advisable to study a more accessible steroid, in order to test the validity of our hypothesis that a dimeric steroid would show much larger rate effects.

As anticipated, **3** was relatively accessible by reductive amination as shown in Scheme 1. Preliminary studies, using the material prepared by this route, showed that it was indeed much more effective as a catalyst for the hydrolysis of esters **2***b–d* than **1**, although it was only very sparingly soluble in water. Unfortunately, the high resolution nmr spectrum gave grounds for profound suspicion that it was not stereochemically homogeneous; see Fig. **1**(b). The 100 MHz $^1$H nmr spectrum taken at the time this work was carried out showed only a slight splitting of the signal attributed to the xylene

0008-4042/82/060747-18$01.00/0

©1982 National Research Council of Canada/Conseil national de recherches du Canada

Can. J. Chem. Downloaded from www.nrcresearchpress.com by 210.87.254.105 on 09/06/12
For personal use only.

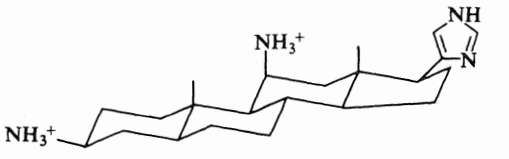

1

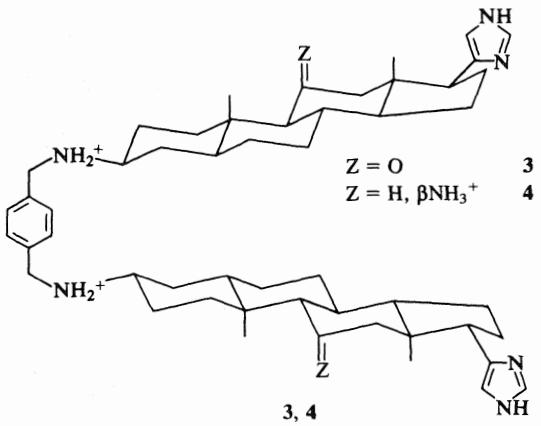

Z = O 3
Z = H, βNH$_3^+$ 4

3, 4

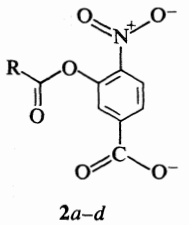

2a–d

CH$_3$ = R 2a
CH$_2$CH$_2$ = R 2b
CH$_2$CH$_2$ = R 2c
CH$_2$CH$_2$ = R 2d

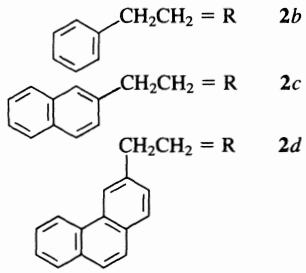

aromatic CH protons. These studies have had to be regarded as preliminary because of doubts about the stereochemical nature and purity of the dimer at the 3-positions of the steroid residues. Nonetheless it was possible to examine the pH dependence of the kinetic behavior of the material prepared in this way, and to study the catalytic properties of this dimer as a model for the stereochemically unambiguous material.

It appeared necessary to prepare **3** by a different route, free of stereochemical ambiguity. This has now been accomplished, by the route shown in Scheme 2. We will refer to the material prepared according to Scheme 1 as **3***a*, and material prepared according to Scheme 2(b) as **3***b*. We are now able to report the results of studies of the reactions of **3***a* and **3***b* with **2***a*–*d*.

This work leads to large hydrophobic effects for which there is very little structural uncertainty. It is our hope that these results will be of interest both to other students of enzyme models, and also to those concerned with the theory of hydrophobic interactions.

## Results

*Synthesis of* **3**a

Reductive amination, using sodium cyanoborohydride, served to link *p*-xylenediamine, **5**, with 17β-imidazolyl-5α-androstane-3,11-dione, **6** (prepared as previously described (4)), to give the dimeric steroid, **3**. This material was isolated as the tetrahydrochloride salt, and was purified by chromatography. The purified material was chromatographically homogeneous, and had an nmr spectrum consistent with the anticipated structure, except that a spectrum recorded at 100 MHz showed splitting of the signal from the phenyl ring protons. In a symmetrical dimer of constitution **3***a* these protons would all be equivalent. It therefore appears that either we have a mixture of compounds or one of the amines was generated with axial and one with equatorial geometry. The salt was of limited, though adequate, solubility in water, but the solubility decreased markedly as the pH was raised above 6.

*Kinetics with* **3**a

The kinetics were carried out under pseudo-first-order or approximately pseudo-first-order conditions; it was sometimes necessary to have a ratio of reagent concentrations closer to unity than is desirable in order to maintain an adequate absorbance change. Most kinetics were done with steroid in excess, although for PPA-HNB[1] as substrate some runs were done with substrate in excess. Considerations discussed in an accompanying paper (3) suggest that in some cases our treatment of the data is oversimplified; unfortunately it is not possible to apply the more sophisticated methods recently developed for this purpose to the data reported in the present paper, because the data were recorded some years ago before our laboratory was equipped with digitizing data-capture apparatus, and consequently the number of data points is too small.

The experimental conditions and the parameters describing the data are contained in Table 1. As is shown in Fig. 2, there is a concentration dependence for the apparent second-order rate constants for the larger substrates, which means that true values can only be determined at rather low concentrations. The limiting concentration, below which the rate constant is independent of reagent concentrations, is a function of the nature of the substrate and in particular of the size of the hydrophobic portion of the substrate. We attribute this behavior to aggregation and/or precipitation of steroid by substrate. The inherent reactivity of the

[1]Abbreviations used: monomer = **12**; dimer = **3**; ACE-HNB = **2***a*, HCA-HNB = **2***b*, NPA-HNB = **2***c*, PPA-HNB = **2***d*.

Can. J. Chem. Downloaded from www.nrcresearchpress.com by 210.87.254.105 on 09/06/12
For personal use only.

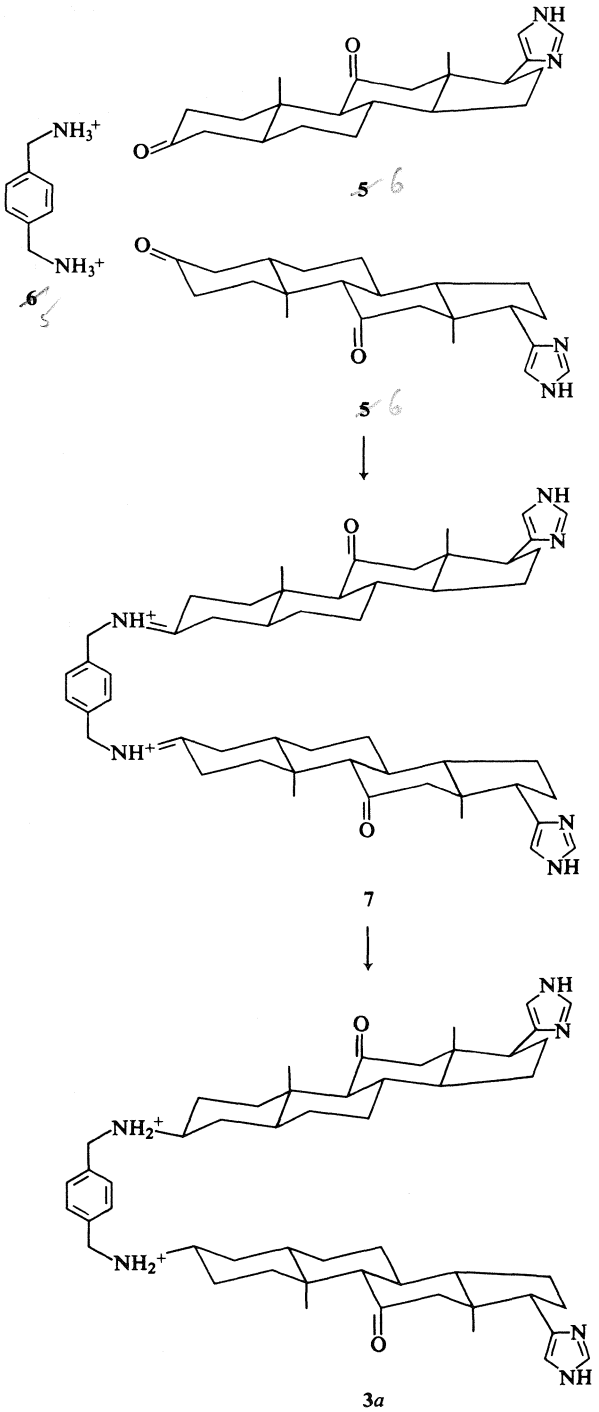

3a

SCHEME 1

three substrates, as measured by rate of reaction with imidazole, is identical.

The apparent rate constant for reaction of the steroid with an aryl ester substrate is expected to be a function of pH as a result of protonation of the imidazole groups. As a working hypothesis we have assumed that the two imidazole groups in **3** act independently, and that both have the same $pK_a$ as imidazole itself (or the imidazole in **1**). This leads to the following equation for the observed rate constant (provided that both the amino groups remain fully protonated, i.e. pH ≦ 8.

$$[1] \quad k_{obs} = k(1 + K/[H^+])/([H^+]/2K + 1 + K/2[H^+])$$

where $k$ is the rate constant per free imidazole of **3**, and $K$ is the microscopic ionization constant for an imidazolium group in **3**. The available data at three pH values are fitted by this equation using the measured $pK_a$ value for **1**, which is essentially the same as for imidazole, and a value for $k$ picked to give the best fit. For NPA-HNB the data are in reasonable accord with this simple picture, although unfortunately the precision is not high enough for a stringent test. For PPA-HNB the rate constants at pH values higher than 7.1 actually decrease with increasing pH; see Table 1. We interpret this to mean that we were not working at low enough concentrations at these higher pH values, and that with a lower net charge on the dimeric steroid, the critical concentration below which aggregation would interfere with the kinetics was lower than the accessible limit in concentration when these experiments were done.

*Synthesis of* **3**b

The synthesis is outlined in Scheme 2(b): corticosterone was converted to **8** as previously described (4). In order to obtain **9** by a Birch reduction it was necessary to increase the solubility of **8** in nonpolar aprotic solvents. Compound **8** itself is very soluble in methanol, but only sparingly soluble in THF or other ether solvents. Accordingly **8** was alkylated using benzyl chloride to give a mixture of isomeric *N*-benzyl derivatives. These could be separated by crystallization, but the mixture was generally used for the reduction. The benzylated material was, as expected, quite adequately soluble in THF for our purposes, and was submitted to reduction by a solution of sodium in liquid ammonia. When the reaction was judged to be complete on the basis of tlc analysis, excess sodium was destroyed using ammonium chloride. Work-up gave **9** contaminated with **8** and some of the overreduced material with a 3-hydroxyl group. Although **9** could be crystallized, it proved easier to perform the purification at the next stage of the synthesis. The stereochemistry of the reduction followed the expected course, giving the α-isomer, as judged by the $^{13}C$ nmr. The chemical shift of C-19 is very sensitive to the stereochemistry at carbon-5 (5). Compound **9** was readily converted to the oxime **10**, which could be crystallized to give

Can. J. Chem. Downloaded from www.nrcresearchpress.com by 210.87.254.105 on 09/06/12
For personal use only.

Can. J. Chem. Downloaded from www.nrcresearchpress.com by 210.87.254.105 on 09/06/12
For personal use only.

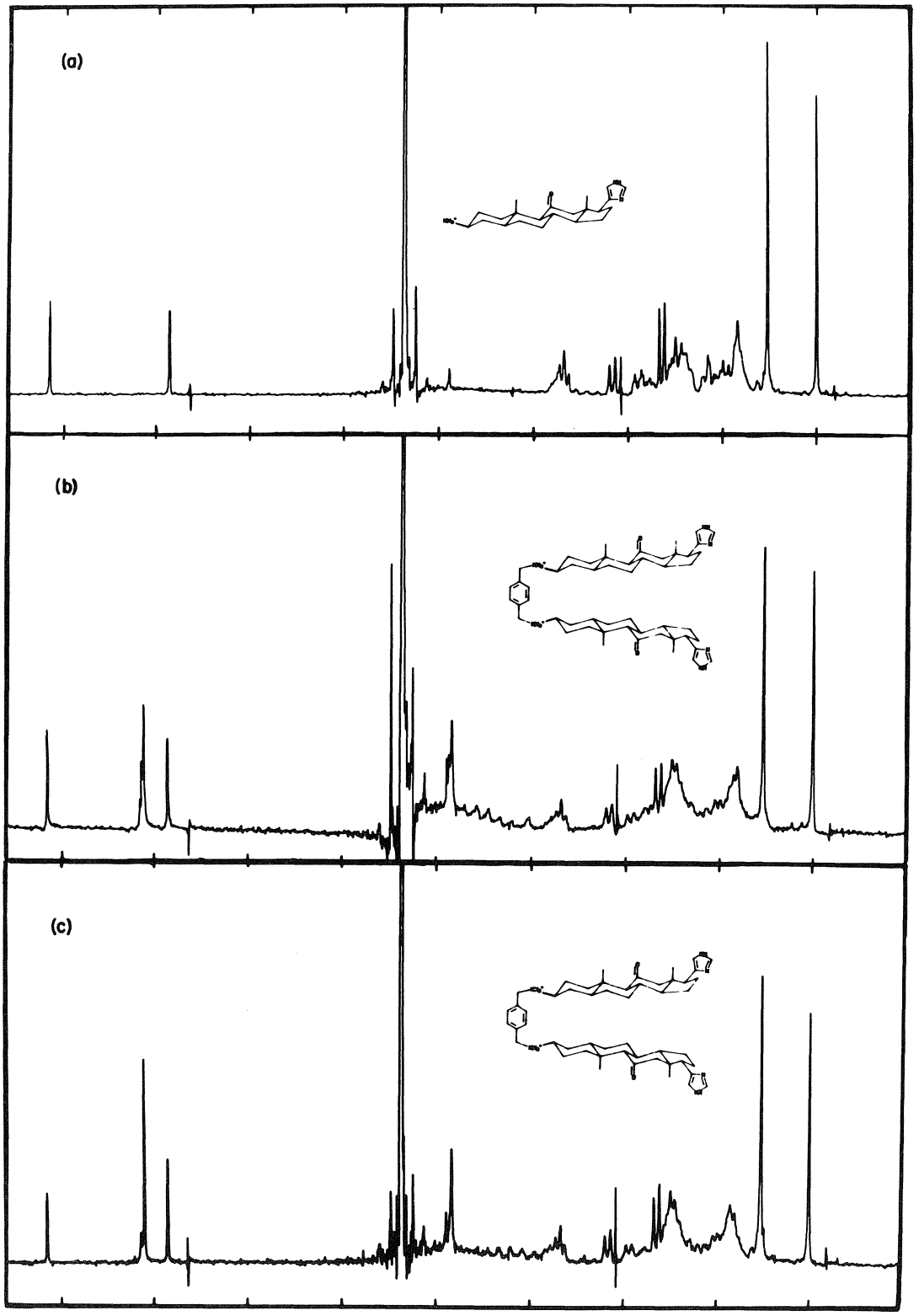


FIG. 1. 200 MHz $^1$H nmr spectra of (a) **12**; (b) **3***a*; and (c) **3***b*.

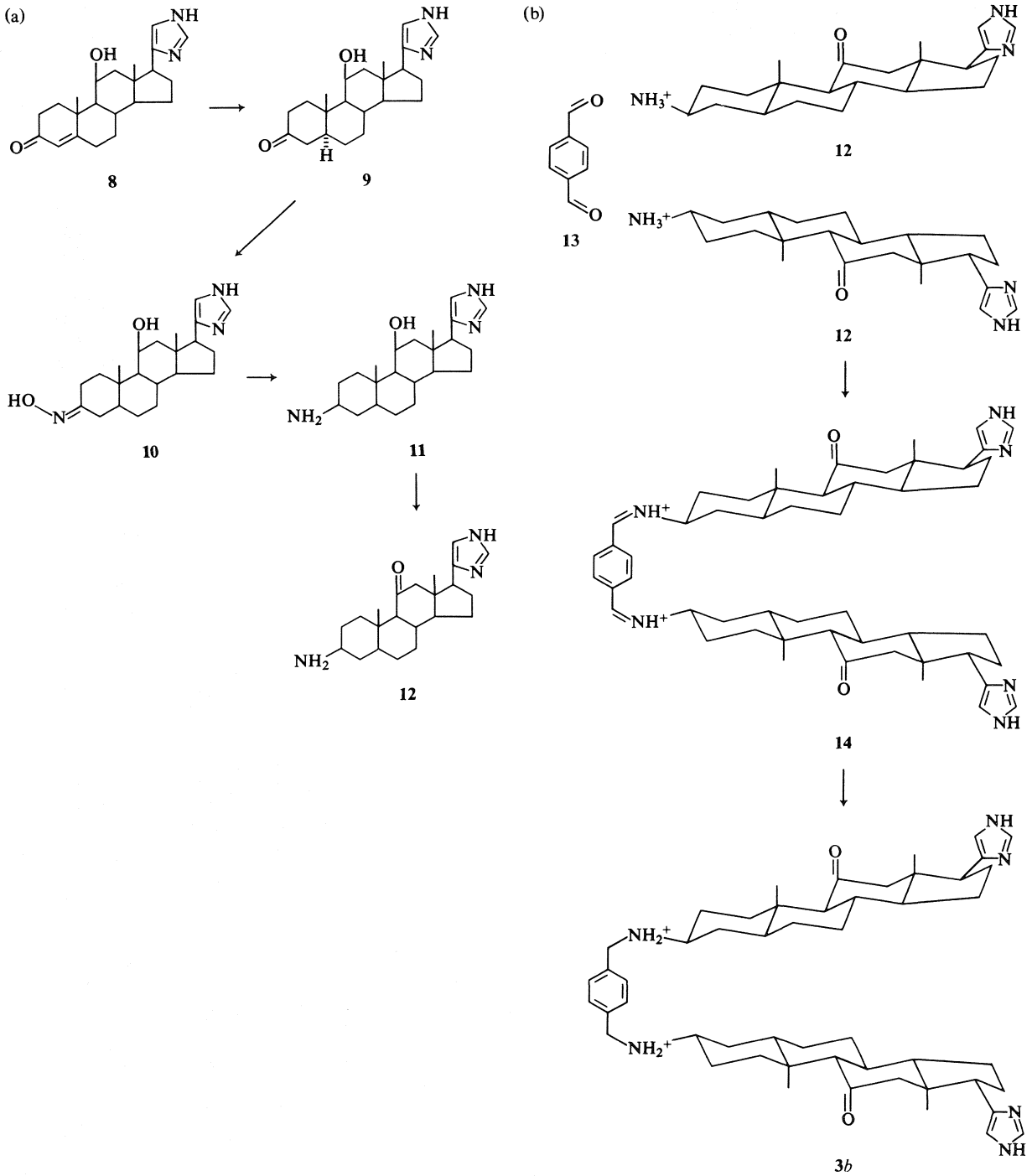


SCHEME 2

material free of C=C-containing contaminants. Reduction of the oxime using sodium – *n*-propanol gave **11**, which was purified by low pressure chromatography. This reaction is expected (6) to give the 3-β (equatorial) amine.

The stereochemistry was confirmed by examination of the 200 MHz $^1$H nmr spectrum of the DCl salt of **12** in $D_2O$, which showed a broad signal at 3.6 δ attributed to the C(3)-H, with $\Delta\nu_{1/2} \simeq 30$ Hz. There is a one-proton triplet overlapping this signal

Can. J. Chem. Downloaded from www.nrcresearchpress.com by 210.87.254.105 on 09/06/12
For personal use only.

TABLE 1. Kinetics of reaction of HNB esters with nucleophiles in aqueous solution (3.2% acetonitrile, v/v), 25°C, $\mu = 0.1$ $M$ (KCl), in 0.01 $M$ phosphate (pH 7.1) or 0.01 $M$ Tris (pH 7.5 and 8.0) buffer. Data were fitted to $A = a_1 + a_2 \exp(-a_3 t) + a_4 t$, with the term $a_4 t$ included only when necessary

| | pH | $10^5$[Catalyst] ($M$) | $10^5$[Ester] ($M$) | $a_1$ | $a_2$ | $10^3\, a_3$ ($s^{-1}$) | $a_4$ | $\sigma$[a] | $k_2$ ($M^{-1}\, s^{-1}$) |
|---|---|---|---|---|---|---|---|---|---|
| (a) | Uncatalyzed hydrolysis of NPA-HNB | | | | | | | | |
| | 7.1 | — | 2.0 | 0.42 | −0.108 | 0.000997 | | 0.0014 | |
| (b) | Imidazole catalyzed hydrolysis of NCA-HNB | | | | | | | | |
| | 7.1 | 1000 | 3.0 | 0.130 | −0.091 | 0.520±0.005 | | 0.0010 | 0.520±0.005 |
| | 7.1 | 2000 | 5.0 | 0.191 | −0.155 | 1.033±0.013 | | 0.0019 | 0.517±0.007 |
| | | | | | | | | Av.[b] | 0.518±0.002 |
| (c) | Imidazole catalyzed hydrolysis of NPA-HNB | | | | | | | | |
| | 7.1 | 1000 | 2.0 | 0.095 | −0.061 | 0.540±0.012 | | 0.0015 | 0.540±0.012 |
| | 7.1 | 1330 | 2.0 | 0.094 | −0.062 | 0.730±0.012 | | 0.0012 | 0.548±0.008 |
| | | 2000 | 3.0 | 0.126 | −0.095 | 1.077±0.013 | | 0.0011 | 0.538±0.007 |
| | | | | | | | | Av.[b] | 0.542±0.005 |
| (d) | Imidazole catalyzed hydrolysis of PPA-HNB | | | | | | | | |
| | 7.1 | 4000 | 3.43 | 0.124 | −0.080 | 2.23±0.05 | | 0.0011 | 0.558±0.013 |
| | | 2000 | 2.28 | 0.117 | −0.039 | 1.25±0.12 | | 0.0029 | 0.625±0.058 |
| | | | | | | | | Av.[b] | 0.562±0.020 |
| (e) | Dimer plus HCA-HNB | | | | | | | | |
| | 7.1 | 10.0 | 0.20 | 0.093 | −0.057 | 0.026±0.001 | | 0.0030 | 2.48±0.12[c] |
| | | 20.0 | 0.40 | 0.174 | −0.0118 | 0.043±0.001 | | 0.0028 | 2.12±0.05[c] |
| | | | | | | | | Av.[b] | 2.17±0.18 |
| (f) | Dimer plus NPA-HNB | | | | | | | | |
| | 7.1 | 96.8 | 2.0 | 0.114 | −0.038 | 0.773±0.100 | | 0.0054 | 7.98±1.03[d] |
| | | 73.3 | 1.5 | 0.146 | −0.075 | 0.483±0.025 | | 0.0048 | 6.60±0.33[d] |
| | | 100.0 | 2.0 | 0.131 | −0.036 | 0.763±0.047 | | 0.0024 | 7.63±0.47[d] |
| | | 80.0 | 1.5 | 0.106 | −0.032 | 0.695±0.047 | | 0.0022 | 8.68±0.58[d] |
| | | 60.0 | 1.0 | 0.092 | −0.026 | 0.818±0.062 | | 0.0019 | 13.63±1.03[d] |
| | | 40.0 | 0.80 | 0.433 | −0.160 | 0.555±0.025 | | 0.0082 | 13.88±0.63[d] |
| | | 20.0 | 0.40 | 0.242 | −0.112 | 0.395±0.007 | | 0.0019 | 19.75±0.33 |
| | | 15.0 | 0.30 | 0.178 | −0.084 | 0.328±0.010 | | 0.0027 | 21.88±0.67 |
| | | 10.0 | 0.20 | 0.117 | −0.058 | 0.195±0.007 | | 0.0020 | 19.50±0.67 |
| | | 2.0 | 1.0 | 0.234 | −0.157 | 0.220±0.007 | 0.0000369 | 0.0066 | 22.00±0.67 |
| | | 1.0 | 1.0 | 0.158 | −0.103 | 0.170±0.007 | 0.0000360 | 0.0052 | 17.00±0.67 |
| | | | | | | | | Av.[b] | 20.0±1.62 |
| | 7.5 | 2.0 | 1.0 | 0.234 | −0.204 | 0.232±.003 | 0.0000884 | 0.0012 | 23.17±0.33 |
| | | 1.0 | 1.0 | 0.123 | −0.074 | 0.263±.008 | 0.0000696 | 0.0010 | 26.33±0.83 |
| | | | | | | | | Av.[b] | 23.67±1.55 |
| | 8.0 | 20.0 | 0.100 | 0.128 | −0.044 | 1.620±0.057 | | 0.0027 | 47.7±2.8 |
| | | 10.0 | 0.100 | 0.129 | −0.070 | 0.502±0.018 | | 0.0027 | 50.2±1.8 |
| | | 10.0 | 0.100 | 0.114 | −0.056 | 0.442±0.015 | | 0.0021 | 44.2±1.5 |
| | | 1.0 | 1.00 | 0.097 | −0.067 | 0.710±0.018 | 0.000250 | 0.0006 | 76.7±1.8 |
| | | 1.0 | 1.00 | 0.126 | −0.074 | 0.658±0.025 | 0.000230 | 0.0013 | 65.8±2.5 |
| | | 1.0 | 1.00 | 0.093 | −0.055 | 1.078±0.043 | 0.000267 | 0.0030 | 107.8±4.3 |
| | | 1.0 | 1.00 | 0.148 | −0.117 | 0.337±0.015 | 0.000120 | 0.0012 | 33.7±1.5 |
| | | 1.0 | 1.00 | 0.111 | −0.086 | 0.295±0.012 | 0.000122 | 0.0051 | 29.5±1.2 |
| | | 0.5 | 1.00 | 0.172 | −0.112 | 0.470±0.022 | 0.000350 | 0.0022 | 47.0±2.2 |
| | | 0.5 | 1.00 | 0.174 | −0.110 | 0.492±0.025 | 0.000386 | 0.0023 | 49.2±2.5 |
| | | 0.5 | 1.00 | 0.076 | −0.046 | 0.362±0.023 | 0.000266 | 0.0010 | 36.2±2.3 |
| | | 0.5 | 1.00 | 0.084 | −0.056 | 0.312±0.012 | 0.000164 | 0.0009 | 31.2±1.2 |
| | | | | | | | | Av.[b] | 43.2±15.4 |
| (g) | Dimer plus PPA-HNB | | | | | | | | |
| | 7.1 | 16.7 | 0.343 | 0.149 | −0.049 | 0.272±0.008 | | 0.0022 | 16.3±0.5[d] |
| | | 23.3 | 0.457 | 0.253 | −0.084 | 0.245±0.013 | | 0.0057 | 10.5±0.6[d] |
| | | 10.0 | 0.343 | 0.160 | −0.042 | 0.307±0.010 | | 0.0017 | 30.7±1.0[d] |
| | | 1.0 | 0.343 | 0.120 | −0.043 | 0.622±0.117 | 0.000047 | 0.0022 | 181.3±34.0 |
| | | 0.667 | 0.343 | 0.080 | −0.022 | 0.412±0.035 | 0.000030 | 0.0019 | 120.0±10.2 |
| | | 1.0 | 0.457 | 0.119 | −0.038 | 0.533±0.063 | 0.000041 | 0.0044 | 116.7±13.9 |
| | | 1.0 | 0.307 | 0.109 | −0.035 | 0.610±0.052 | 0.000057 | 0.0022 | 197.6±16.8 |
| | | 1.0 | 0.307 | 0.132 | −0.031 | 0.588±0.037 | 0.000038 | 0.0018 | 191.6±12.0 |
| | | 1.33 | 0.409 | 0.145 | −0.028 | 0.673±0.067 | 0.000050 | 0.0026 | 164.6±16.3 |
| | | | | | | | | Av.[b] | 152.7±38.0 |

Can. J. Chem. Downloaded from www.nrcresearchpress.com by 210.87.254.105 on 09/06/12
For personal use only.

TABLE 1. (*continued*)

| pH | $10^5$[Catalyst] ($M$) | $10^5$[Ester] ($M$) | $a_1$ | $a_2$ | $10^3\,a_3$ ($s^{-1}$) | $a_4$ | $\sigma^a$ | $k_2$ ($M^{-1}\,s^{-1}$) |
|---|---|---|---|---|---|---|---|---|
| 7.5 | 1.98 | 1.02 | 0.140 | −0.062 | 1.66±0.13 | 0.000212 | 0.0024 | 162.4±13.0 |
| | 0.994 | 1.02 | 0.096 | −0.042 | 0.97±0.12 | 0.000122 | 0.0022 | 95.4±11.5 |
| | 0.795 | 1.02 | 0.093 | −0.043 | 1.19±0.11 | 0.000137 | 0.0019 | 116.5±10.8 |
| | | | | | | | Av.[b] | 121.7±32.3 |
| 8.0 | 10.0 | 1.02 | 0.095 | −0.029 | 0.402±0.070 | | 0.0052 | 39.4±6.9 |
| | 1.0 | 1.02 | 0.094 | −0.037 | 1.092±0.082 | 0.000192 | 0.0034 | 107.0±8.0 |
| | 1.0 | 1.02 | 0.125 | −0.046 | 0.628±0.008 | | 0.0059 | 61.6±8.2 |
| | 1.0 | 1.02 | 0.111 | −0.042 | 1.567±0.188 | 0.000230 | 0.0024 | 152.6±18.5 |
| | 0.5 | 1.02 | 0.088 | −0.026 | 0.607±0.078 | 0.000229 | 0.0016 | 59.5±7.7 |
| | | | | | | | Av.[b] | 80.2±32.3 |

[a]Estimate of the uncertainty in the data based on scatter about the least-squares lines. $\sigma^2$ = (weighted sum of squares of residuals)/(degrees of freedom). A value of $\sigma$ = 0.002 is expected for absorbance values in the range encountered in these experiments.
[b]Weighted average.
[c]Corrected for the uncatalyzed hydrolysis, assuming that NPA-HNB and HCA-HNB undergo uncatalyzed hydrolysis at the same rate at pH 7.1 (as they do at pH 8 (1)).
[d]Not included in the calculation of the average.

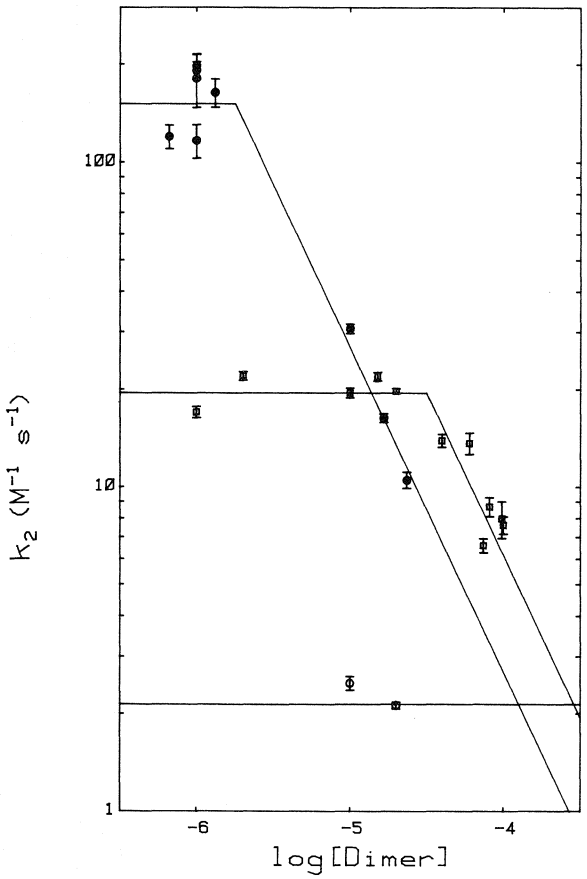


FIG. 2. Concentration dependence of rate constants for the reaction of **3** with HCA-HNB (○), NPA-HNB (□), and PPA-HNB (●). log $k_2$ as a function of log [steroid dimer concentration].

so that $\Delta\nu_{1/2}$ is imprecise, but it is unquestionably > 20 Hz, and ≫ 8 Hz, the value expected if the $NH_3^+$ were axial (7). Thus the stereochemistry is as desired. The C(3)-H was not distinguishable from the mass of skeletal proton signals in the spectrum of the neutral molecule in $CD_3OD$. In the spectrum of the DCl salt in $D_2O$ this peak is well resolved from the skeletal proton signals, but is almost coincident with a triplet; these two signals integrate for a total of 2 protons. There is also a one-proton doublet at 3.07 δ and a two-proton doublet at 2.56 δ; the latter may actually be the two central peaks of an AB quartet. These signals had been seen earlier in the spectrum of 17β-(4-imidazolyl)-5α-androstane-3,11-dione (4), but had not been as well separated or resolved at 100 MHz. Other steroids in this series, lacking the 11-keto group, did not show this pattern of three low-field signals.

Oxidation of **11** by $Cr^{VI}$ in acetic acid, with alkaline work-up by the procedure of Mueller and DiPardo (8), gave **12**, which could be crystallized from acetonitrile. After various trials at reductive dimerization, it was found best to prepare the diimine by reaction in benzene–ethanol, with azeotropic removal of water, followed, after removal of solvent, by reduction in DMF using sodium cyanoborohydride and trifluoroacetic acid. The crude dimer was purified by low pressure chromatography. It was homogeneous by tlc, and gave clean $^1H$ and $^{13}C$ nmr spectra. The molecular ion could be seen in the mass spectrum, although it was rather weak, and gave the expected exact mass.

*Kinetics with* **3**b

For all reactions we have given the parameters for empirical equations which describe the data; in each case the fit was by weighted least squares (9). Despite the fact that we could fit the data reasonably well by a suitable equation, it frequently happened, as will be described below, that there is no theoretical justification for the form of equation used, so that the parameters have no simple interpretation. We report these parameters as a way of summarizing the empirical facts concisely, since the primary data are voluminous.

Can. J. Chem. Downloaded from www.nrcresearchpress.com by 210.87.254.105 on 09/06/12
For personal use only.

Can. J. Chem. Downloaded from www.nrcresearchpress.com by 210.87.254.105 on 09/06/12
For personal use only.

*Monomer and ACE-HNB*

The conditions for these reactions are shown in Table 2; it will be apparent that the reactions are second order because the concentrations of monomer and ester are comparable. Although the data could be fitted reasonably well to an integrated first-order equation, with parameters given in Table 2, the fit was not ideal and there was no theoretical justification for the use of this equation. The difficulty is that there is a competing uncatalyzed hydrolysis, and also hydrolysis of the acetyl imidazole formed from reaction of monomer with ester, leading to regeneration of catalyst.

$$\text{Ester} \xrightarrow{k_1} \text{acid} + \text{aryloxide}$$

$$\text{Steroid} + \text{ester} \xrightarrow{k_2} \text{acylimidazole} + \text{aryloxide}$$

$$\text{Acylimidazole} \xrightarrow{k_3} \text{acid} + \text{steroid}$$

In the absence of a closed-form integrated rate law which could be fitted to the observable data, a new method for extracting the rate constants is required. In an accompanying paper (3) we report two methods for accomplishing this task. In one, numerical integration is used to provide calculated absorbance values corresponding to a set of parameters, and to allow numerical evaluation of the derivatives needed for least-squares refinement of the parameters. Another method uses numerical differentiation of the original data to give a curve from which the rate constants can be extracted. It was concluded that the second method, based on differentiation of the absorbance time curve, was generally preferable.

In the present case we calculate the quantity:

$$[2] \quad z = (\mathrm{d}x/\mathrm{d}t)/(a - x) = k_1 + k_2 (b - y)$$

where $x$ = absorbance − initial absorbance; $a$ = total change in absorbance at completion; $b$ = initial concentration of imidazole; $y$ = concentration of acylimidazole. In calculating the slope, $\mathrm{d}x/\mathrm{d}t$, one must compromise between taking slopes from few points, and accepting high noise levels, and taking slopes involving more points and inevitably smoothing out some of the information, particularly at the beginning of the reaction where we are especially interested in the instantaneous slope. We have generally compromised on 5 or 7 points per instantaneous slope. In several cases we examined the consequences of varying the number of points used to ensure that no major changes in the results would ensue. Inevitably $z$ has large uncertainties at long times where both numerator and denominator are small.

For the situation of ACE-HNB and monomer a plot of $z$ vs. $t$ shows a fall in $z$ followed by a rise to approximately the initial value. From the initial value of $z$,

$$z_0 = k_1 + k_2 b$$

we can determine $k_2$ given $k_1$ and $b$. From the position of the minimum in $z$, $k_3$ can be determined, since we have shown (10) that

$$[3] \quad k_3 = [(A_\infty - A_{\min})/\Delta\varepsilon][(z_0 - k_1)/b] \; [(z_0 - k_1)/(z_0 - z_{\min}) - 1]$$

The value so calculated for $k_2$ was $0.823 \pm 0.021$ $M^{-1}$ $s^{-1}$ (weighted average); for $k_3$ the weighted average was $1.45 \pm 0.15 \times 10^{-4}$ $s^{-1}$. The value for $k_1$ used in these calculations was that measured previously in this laboratory (1). The decline in $z$ from its initial value to the minimum did not obey first-order kinetics since both ester and steroidal imidazole concentrations were changing during the time required by this process. Therefore no simple fit of a curve to the data was possible.

*Monomer plus HCA-HNB*

The conditions for these experiments are as given in Table 2; all runs were under pseudo-first-order conditions. For these reactions, fitting the data to the appropriate integrated equation gave the parameters listed in Table 2. The weighted average value for $k_2$ is $1.37 \pm 0.06$ $M^{-1}$ $s^{-1}$;

*Monomer plus NPA-HNB*

The conditions for these reactions are given in Table 2. For all reactions, the conditions are pseudo-first-order, and the data would be fitted to the simple exponential form of the integrated rate equation. The weighted average value of $k_2$ was $2.04 \pm 0.38$ $M^{-1}$ $s^{-1}$.

*Monomer plus PPA-HNB*

All of the reactions were studied under pseudo-first-order conditions, as described in Table 2. For all of these reactions the second-order rate constant could be calculated from the least-squares parameters. There is a disturbing scatter to the values, and we sought for any trend with concentration, but careful scrutiny shows that the range of scatter is the same at high or low ester concentrations, and for high or low monomer concentrations. The weighted average value was $5.42 \pm 1.36$ $M^{-1}$ $s^{-1}$.

*Dimer plus HCA-HNB*

These reactions were all studied with ester in excess; the conditions are specified in Table 2. It is not proper to assume that the uncatalyzed reaction

Can. J. Chem. Downloaded from www.nrcresearchpress.com by 210.87.254.105 on 09/06/12
For personal use only.

is pseudo-zero-order during the time that the acylation reaction is occurring because the latter reaction is not fast enough relative to hydrolysis. Nonetheless, the data could be fitted reasonably well to a simple exponential plus linear equation, and the corresponding parameters are given in Table 2. Analysis of the data by our derivative treatment led to values for the rate constants. In the present case, a plot of $z$ vs. $t$ showed a decline to a constant value with no apparent recovery at longer times during the period for which the reaction was followed. This corresponds to establishment of a steady state. It is a fair approximation to take the approach to steady state as pseudo-first-order, and this allows a simple analysis of the data. As we have shown (3):

$$[4]\quad z = k_1 + k_2 b - [k_2^2 ab/(k_2 a + k_3)] + [k_2^2 ab/(k_2 a + k_3)]\exp[-(k_2 a + k_3)t] = z_{\text{final}} + \Delta z \exp(-\kappa t)$$

where:

$$\Delta z = k_2^2 ab/(k_2 a + k_3)$$

$$\kappa = k_2 a + k_3$$

Then

$$k_2 = \sqrt{\kappa \Delta z/ab}$$

$$k_3 = \kappa - k_2 a$$

$$k_1 = z_0 - k_2 b$$

An advantage of this approach is that it gives an independent estimate for $k_1$, which can be measured in a separate experiment, and so provides a test of internal consistency. As is shown in Table 2, there is some scatter, but the data give $k_2 = 12.36 \pm 1.36$, $k_1 = 8.3 \pm 1.3 \times 10^{-6}$ s$^{-1}$, and $k_3 = 1.10 \pm 0.43 \times 10^{-4}$ s$^{-1}$. Direct measurement (1) gives $k_1 = 8.7 \times 10^{-6}$ s$^{-1}$, in satisfactory agreement.

*Dimer plus NPA-HNB*

These data were treated in the same way as for the dimer plus HCA-HNB reactions. The first run was clearly aberrant and was not included in the averaging. The rate constants obtained were $k_2 = 95 \pm 19\ M^{-1}$ s$^{-1}$ and $k_1 = 3.7 \pm 1.9 \times 10^{-5}$ s$^{-1}$. This latter value somewhat deviates from the directly measured value of $1.11 \times 10^{-5}$ s$^{-1}$. However, the $k_1$ value calculated is actually a small difference between two large numbers, $z_0$ and $k_2 b$, so that it is inherently imprecise and subject to systematic errors. An alternative estimate can be made from the steady-state value of $z$, since $k_3$ was not distinguishable from zero in these experiments. (The value calculated from eq. [4] was negative.) The steady-state value of $z$ was $1.35 \pm 0.36 \times 10^{-5}$ s$^{-1}$, an average of 7 values. This value agrees reasonably well with the directly measured value of $k_1$.

*Dimer plus PPA-HNB*

The conditions for these experiments are given in Table 2. Runs at ester concentrations near $10^{-5}$ $M$ led to rate constants not much larger than were obtained for NPA-HNB, leading to suspicions that aggregation of the substrate or aggregation of substrate and dimer was leading to spuriously low reactivity. Accordingly reactions were carried out under pseudo-first-order conditions with $10^{-7}$ $M$ substrate and $10^{-6}$ $M$ dimer. These experiments were at the limit of the barely possible with our instrumentation, and required use of a digitizer to give a ten-fold amplification by longer data sampling, in addition to using ten-centimeter cells. We were severely limited by artefacts, generally involving bubble formation on the optical surfaces. In order to get information from this very noisy kind of experiment we did multiple runs, nine in all, and sought ways to average the replicate runs.

Plots using data to 10 000 s and a uniform scale were constructed for the 8 runs, and showed that in almost all cases the absorbance change was over in 5000 s, and had the form expected for a simple exponential; i.e. first-order behavior. One run showed a continuous increase in absorbance to a much larger overall absorbance change than could be rationalized in terms of the known extinction coefficient. Another showed an anomalously slow change, with much less absorbance change in the usual time period than the rest of the experiments. These two runs were deleted from the set. The total absorbance change was small, and there was considerable variation in the final absorbance value; in order to pool the data into one set, it was necessary to put them on a common scale. This was done by calculating the final absorbance for each run as the average of the observed absorbance values from 5000 to 10 000 s, and then calculating the difference between this final value and the observed value for times less than 5000 seconds, (absorbance$_\infty$ − absorbance$_t$). These differences were pooled into one large data set, which could then be fitted by least squares. Since the scatter in the data is considerable, and we recognize that we are at the limits of our techniques, we have examined the range of rate constants which might be consistent with the data by drawing the extreme lines which could fall within the range of the experimental points plotted in first-order fashion; see Fig. 3. In effect we are taking the scatter as a measure of the

Can. J. Chem. Downloaded from www.nrcresearchpress.com by 210.87.254.105 on 09/06/12
For personal use only.

TABLE 2. Kinetics of reaction of monomer, **12**, and dimer, **3*b***, with HNB esters in aqueous solution (3.2% acetonitrile, v/v), $\mu = 0.1\ M$ (KCl), 0.01 *M* Tris buffer, pH 8.0, 25°C. Data were fitted to $A = a_1 + a_2 \exp(-a_3 t) + a_4 t$, with the term $a_4 t$ included only when necessary

| | | Parameters for the equation fitting the data | | | | | | |
|---|---|---|---|---|---|---|---|---|
| $10^5$[Catalyst] | $10^5$[Substrate] | $a_1$ | $a_2$ | $10^3 a_3$ ($s^{-1}$) | $a_4$ | $\sigma^a$ | $k_2$ ($M^{-1}\,s^{-1}$) | Comments |
| (a) Monomer plus ACE-HNB | | | | | | | | |
| 9.69 | 9.77 | 4.368 | −3.891 | 0.0794 | | 0.0014 | 0.828±0.029 | $k_2$ calculated using derivatives, method 1 |
| 9.69 | 19.30 | 8.235 | −7.588 | 0.0689 | | 0.0064 | 0.815±0.019 | |
| 9.69 | 4.88 | 2.378 | −1.954 | 0.0857 | | 0.0022 | 0.880±0.058 | $k_3 = 1.45\pm0.15 \times 10^{-4}\,s^{-1}$ |
| | | | | | | | Av. 0.823±0.021 | |
| (b) Monomer plus HCA-HNB | | | | | | | | |
| 9.69 | 0.468 | 0.521 | −0.218 | 0.130 | | 0.0015 | 1.34±0.01 | $k_2$ calculated from the least-squares parameters |
| 9.69 | 0.937 | 0.792 | −0.459 | 0.132 | | 0.0014 | 1.36±0.01 | |
| 9.69 | 1.873 | 1.282 | −0.911 | 0.129 | | 0.0016 | 1.33±0.01 | |
| 9.69 | 0.468 | 0.518 | −0.227 | 0.144 | | 0.0027 | 1.49±0.01 | |
| 9.69 | 0.937 | 0.822 | −0.482 | 0.132 | | 0.0020 | 1.36±0.01 | |
| 9.69 | 1.873 | 1.275 | 0.934 | 0.130 | | 0.0018 | 1.34±0.01 | |
| | | | | | | | Av. 1.37±0.06 | |
| (c) Monomer plus NPA-HNB | | | | | | | | |
| 9.69 | 0.975 | 0.725 | −0.454 | 0.224 | | 0.0033 | 2.31±0.02 | $k_2$ calculated from least-square parameters |
| 9.69 | 0.975 | 0.734 | −0.444 | 0.225 | | 0.0032 | 2.32±0.02 | |
| 9.69 | 1.95 | 1.468 | −1.189 | 0.362 | | 0.012 | 3.74±0.07 | |
| 9.69 | 0.488 | 0.491 | −0.193 | 0.194 | | 0.0030 | 2.00±0.02 | |
| 9.69 | 0.975 | 0.748 | −0.435 | 0.195 | | 0.0021 | 2.01±0.01 | |
| 9.69 | 1.95 | 1.476 | −1.195 | 0.342 | | 0.0064 | 3.52±0.03 | |
| 9.69 | 0.488 | 0.521 | −0.186 | 0.194 | | 0.0023 | 2.02±0.01 | |
| 9.69 | 0.975 | 0.738 | −0.416 | 0.204 | | 0.0026 | 2.72±0.01 | |
| 9.69 | 1.95 | 1.462 | −1.178 | 0.347 | | 0.012 | 3.58±0.05 | |
| 9.69 | 0.488 | 0.505 | −0.176 | 0.152 | | 0.0033 | 1.56±0.02 | |
| 9.69 | 0.488 | 0.523 | −0.195 | 0.177 | | 0.0040 | 1.82±0.02 | |
| 9.01 | 0.468 | 2.351 | −2.032 | 0.177 | | 0.0007 | 1.96±0.02 | |
| 9.00 | 0.467 | 4.475 | −2.102 | 0.174 | | 0.0002 | 1.93±0.01 | |
| 8.99 | 0.234 | 5.595 | −1.074 | 0.167 | | 0.0002 | 1.86±0.01 | |
| 8.99 | 0.117 | 6.123 | −0.549 | 0.150 | | 0.0002 | 1.67±0.01 | |
| 8.98 | 0.117 | 6.558 | −0.522 | 0.167 | | 0.0001 | 1.86±0.01 | |
| | | | | | | | Av. 2.04±0.38 | |
| (d) Monomer plus PPA-HNB | | | | | | | | |
| 0.969 | 0.104 | 0.792 | −0.581 | 0.0534 | | 0.0046 | 4.40±0.13 | $k_2$ calculated using least-squares parameters |
| 0.969 | 0.104 | 0.733 | −0.463 | 0.0464 | | 0.0014 | 3.67±0.11 | |
| 0.967 | 0.104 | 1.160 | −0.402 | 0.0371 | | 0.0016 | 2.71±0.12 | |
| 0.967 | 0.104 | 1.298 | −0.477 | 0.0380 | | 0.0009 | 2.81±0.11 | |
| 9.91 | 0.184 | 1.539 | −0.834 | 0.536 | | 0.0026 | 5.40±0.04 | |
| 9.93 | 0.105 | 0.842 | −0.422 | 0.474 | | 0.0025 | 4.78±0.04 | |
| 9.90 | 0.184 | 1.636 | −0.799 | 0.532 | | 0.0020 | 5.36±0.04 | |
| 9.89 | 0.105 | 1.995 | −0.467 | 0.566 | | 0.0012 | 5.72±0.06 | |

Can. J. Chem. Downloaded from www.nrcresearchpress.com by 210.87.254.105 on 09/06/12
For personal use only.



TABLE 2. (*continued*)

| $10^5$[Catalyst] | $10^5$[Substrate] | Parameters for the equation fitting the data $a_1$ | $a_2$ | $10^3 a_3$ ($s^{-1}$) | $a_4$ | $\sigma^a$ | $k_2$ ($M^{-1}\,s^{-1}$) | Comments |
|---|---|---|---|---|---|---|---|---|
| 9.68 | 0.475 | 0.697 | −0.323 | 0.280 | | 0.0081 | 2.89±0.07 | |
| 9.69 | 0.242 | 0.402 | −0.095 | 0.419 | | 0.0088 | 4.33±0.16 | |
| 9.69 | 0.484 | 0.690 | −0.317 | 0.300 | | 0.013 | 3.10±0.08 | |
| 9.69 | 0.725 | 0.718 | −0.351 | 0.698 | | 0.0038 | 7.20±0.07 | |
| 9.69 | 0.395 | 0.569 | −0.223 | 0.675 | | 0.0024 | 6.97±0.06 | |
| 9.69 | 0.483 | 0.573 | −0.275 | 0.676 | | 0.0029 | 6.98±0.06 | |
| 9.69 | 0.593 | 0.646 | −0.317 | 0.688 | | 0.0026 | 7.11±0.05 | |
| | | | | | | | Av. 5.42±1.36 | Weighted average |
| (e) Dimer plus HCA + HNB | | | | | | | | |
| 0.116 | 1.12 | 0.429 | −0.151 | 0.260 | $4.78 \times 10^{-5}$ | 0.0018 | 11.83±1.56 | $k_2$ calculated using derivatives, method 2 |
| 0.116 | 2.25 | 0.632 | −0.406 | 0.237 | $1.01 \times 10^{-4}$ | 0.0015 | 7.70±0.84 | $k_1 = 8.3\pm1.3 \times 10^{-6}\ s^{-1}$ |
| 0.116 | 2.25 | 0.549 | −0.180 | 0.339 | $0.833 \times 10^{-4}$ | 0.0009 | 8.84±1.02 | $k_3 = 1.10\pm0.43 \times 10^{-4}\ s^{-1}$ |
| 0.116 | 2.25 | 0.795 | −0.341 | 0.221 | $0.911 \times 10^{-4}$ | 0.0017 | * | *This run showed systematic deviations at |
| 0.116 | 2.25 | 0.475 | −0.161 | 0.392 | $0.938 \times 10^{-4}$ | 0.0012 | 8.88±1.00 | short times and was not used for the |
| 0.116 | 4.50 | 1.365 | −1.098 | 0.177 | $1.55 \times 10^{-4}$ | 0.0019 | 5.68±0.58 | derivative treatment |
| 0.116 | 2.25 | 0.618 | −2.364 | 0.248 | $8.24 \times 10^{-5}$ | 0.0011 | 7.11±0.83 | |
| | | | | | | | Av. 7.36±1.76 | |
| (f) Dimer plus NPA-HNB | | | | | | | | |
| 0.116 | 1.17 | 0.869 | −0.576 | 1.86 | $6.08 \times 10^{-5}$ | 0.0049 | 263±28* | $k_2$ calculated using derivatives, method 2 |
| 0.116 | 2.34 | 0.941 | −0.408 | 1.74 | $9.49 \times 10^{-5}$ | 0.0049 | 130±14 | |
| 0.116 | 1.17 | 1.003 | −0.715 | 1.25 | $5.39 \times 10^{-5}$ | 0.0019 | 126±13 | *This value was not used in calculating the |
| 0.116 | 2.34 | 0.950 | −0.482 | 2.09 | $9.76 \times 10^{-5}$ | 0.0037 | 115±12 | average |
| 0.116 | 1.17 | 0.951 | −0.635 | 1.15 | $7.18 \times 10^{-5}$ | 0.0017 | 113±12 | Treatment leads to $k_1 = 3.7\pm1.9 \times 10^{-5}$ |
| 0.116 | 2.34 | 0.939 | −0.413 | 1.79 | $9.25 \times 10^{-5}$ | 0.0036 | 122±14 | $s^{-1}$, but $k_3$ is indistinguishable from zero |
| 0.232 | 2.34 | 1.792 | −0.758 | 2.29 | $13.2 \times 10^{-5}$ | 0.0037 | 141±15 | |
| 0.058 | 0.585 | 1.151 | −0.850 | 3.83 | $2.47 \times 10^{-5}$ | 0.0027 | 89±9 | |
| | | | | | | | Av. 115±19 | |
| (g) Dimer plus PPA-HNB | | | | | | | | |
| 0.116 | 1.09 | 0.932 | −0.451 | 1.50 | $6.70 \times 10^{-5}$ | 0.0066 | 189±24 | $k_2$ calculated using derivatives, method 2 |
| 0.116 | 2.18 | 0.756 | −0.270 | 1.70 | $9.40 \times 10^{-5}$ | 0.0075 | 200±22 | |
| 0.116 | 2.18 | 1.281 | −0.467 | 1.57 | $1.21 \times 10^{-5}$ | 0.0052 | 192±21 | $k_1$ and $k_3$ were not defined by the data but |
| 0.058 | 0.545 | 0.655 | −0.185 | 0.619 | $2.11 \times 10^{-5}$ | 0.0038 | 216±26 | $z_{final} = 1.52\pm0.25 \times 10^{-5}\ s^{-1} \geq k_1$ |
| 0.058 | 0.545 | 0.938 | −0.291 | 0.727 | $2.55 \times 10^{-5}$ | 0.0023 | 216±23 | |
| 0.116 | 0.0109 | | 0.030 | 0.393 | | 0.0044 | 339±33* | 7 runs combined as described in the text |
| | | | | | | | (337±262)** | |
| | | | | | | | | *Errors in rate constant calculated from least-squares treatment |
| | | | | | | | | **Errors in rate constant calculated from the extreme lines passing through the data |

[a] $\sigma = \sqrt{(\text{weighted sum of squared residuals})/(\text{number of degrees of freedom})}$

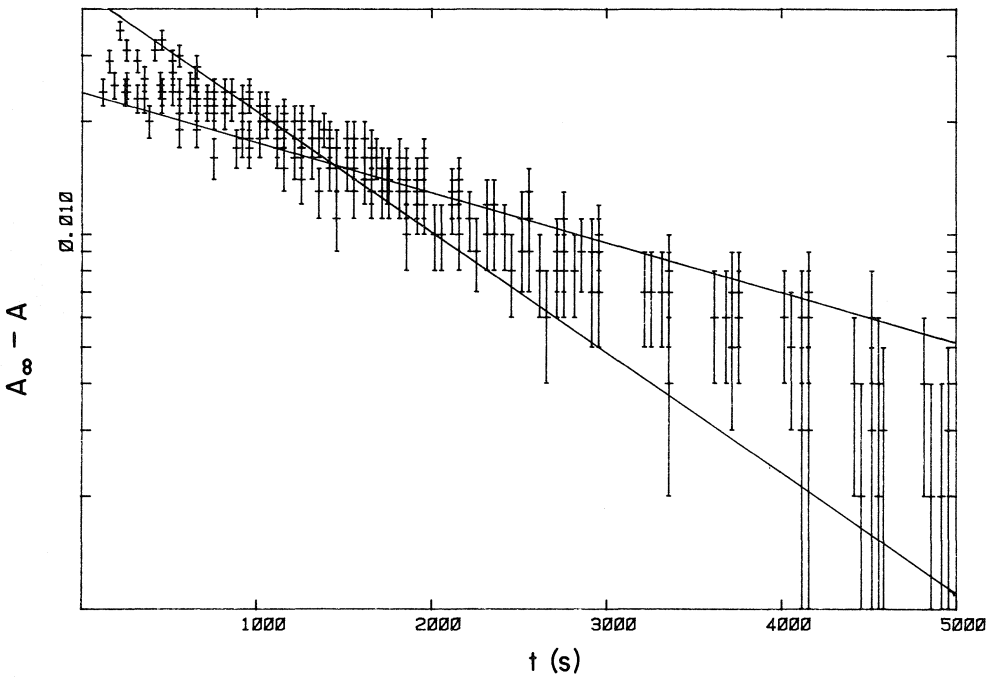


FIG. 3. Reaction of **3***b* with PPA-HNB. Pooled data from seven replicate runs. The extreme lines fitting the data are shown. Error bars are calculated assuming an uncertainty of ± 0.002 in absorbance.

true uncertainty in the data and are calculating possible error limits to supplement the probable error limits suggested by least squares. This approach leads to limits of $265 < k_2 < 639$. Taking the least-squares rate constant as the best estimate, and the higher value for the error implied by these limits, we conclude that $k_2 = 377 \pm 262\ M^{-1}\ s^{-1}$.

Although we believe that we have satisfactorily extracted the rate constant for the reaction of dimer and PPA-HNB, this treatment is necessarily less convincing than we would prefer. The value obtained is roughly consistent with the rest of our results, as will be seen below, and with the conclusion that unambiguous results can only be obtained at the very low concentrations used, or else at still lower concentrations which at present are not experimentally feasible.

## Discussion

*Stereochemistry of* **3**a

In planning the synthesis of **3**, we were guided by reports that the normal stereochemical result of reductive amination of a steroidal 3-one using cyanoborohydride is generation of an equatorial amine (10). Although this indeed seems to be the case for simple reductive aminations, it does not appear to have been so for the reaction of interest. A possible rationalization which presents itself for reductive amination leading to a 3α-amino residue is that the first reductive amination might follow the predicted course, but that the second might well involve reaction of a dimeric molecule which, if the conformation were one with the two steroids in contact, would not allow the reducing agent to attack the iminium ion from the α-surface, thus forcing reaction to occur from the β-surface.

*Kinetics with* **3**a

An approximate measure of the hydrophobic rate enhancement can be obtained by calculating the ratio of the rate constants at pH 7.1 for the reactions of **3** and imidazole with each substrate. When the logarithms of these ratios are plotted vs. the π (11) hydrophobicity parameter a straight line is obtained (Fig. 4). This simple treatment ignores the possibility of reaction by a nonhydrophobically-stabilized transition state (1), but seems appropriate for the rather crude kinetics and sizeable rate enhancements obtained in these experiments. The slope of the plot is 0.77, which is substantially larger than the value obtained for **1**, namely 0.47 (1). The intercept of the plot corresponds to $k_{rel} = 0.095$, a value considerably less than 1.0; we interpret this to mean that if a substrate with no hydrophobic binding group, i.e. the propionate ester, were to react with the same geometry as for the arylpropionate esters, it would be much slower to react with the steroid than with imidazole in the

Can. J. Chem. Downloaded from www.nrcresearchpress.com by 210.87.254.105 on 09/06/12
For personal use only.

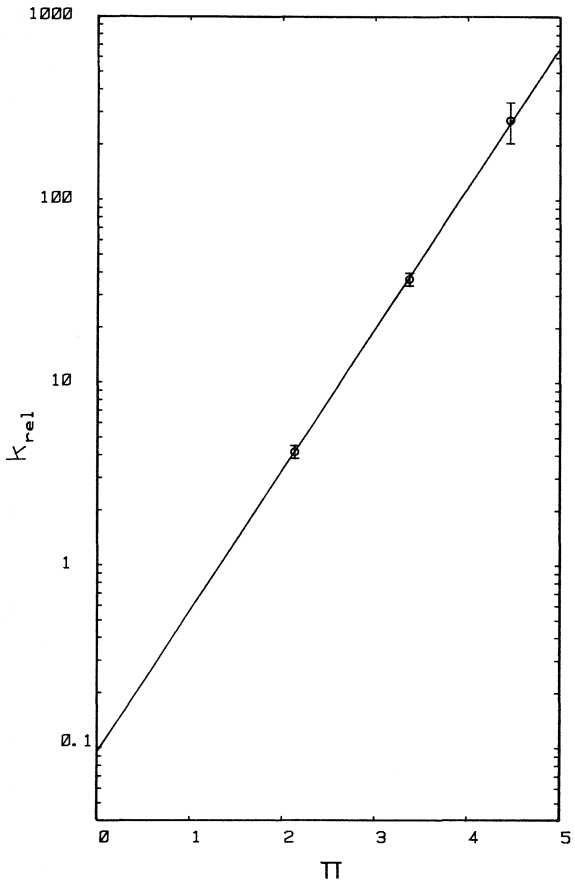


FIG. 4. Relative rate constants (imidazole as standard) for **3** reacting at pH 7.1 with HCA-HNB, NPA-HNB, and PPA-HNB, as a function of $\pi$, the hydrophobicity parameter. The line is fitted by least squares, and has slope = 0.77 and intercept = 0.095.

model reaction. Inspection of molecular models supports this interpretation, since in addition to intermolecular crowding there is an eclipsing interaction of the two methylenes linking aryl and acyl groups (1). This eclipsing interaction, which cannot be avoided if covalent attack and hydrophobic contact are both to occur, destabilizes the transition state and cancels part of the potential hydrophobic stabilization. Although a long extrapolation is involved, it appears that the observed rate enhancement for PPA-HNB of 273-fold for **3** relative to imidazole is only a part of the potential which would be realized if there were no strain, and that this potential could be as large as $10^3$–$10^4$. We observe a value for the rate enhancement of 2900-fold, if we take the intercept from Fig. 3 as the reference point; and 273-fold if we take the rate constant for imidazole as the reference point. As we have argued before (1), we think the former value is the better measure of the potential hydrophobic effect.

Interpretation of the kinetics results with **3***a* is subject to various caveats, since the conditions used were often not truly pseudo-first order, the steroid was of uncertain stereochemistry, and the solutions may not have been sufficiently dilute (because of the impossibility of using lower concentrations). Nevertheless, the experiments do show that markedly larger rate enhancements are available using a dimeric steroid than could be obtained using a monomeric steroid. Furthermore, they serve as guides to the concentration ranges which are likely to be possible for simple kinetic behavior, and demonstrate that the simplest expectations about pH dependence appear to be correct.

*Stereochemistry of* **3**b

This synthesis, although more roundabout, has led to a material which is unambiguously of the desired stereochemistry, since the key stereochemical point, the configuration at C-3, is established by a reaction which is well known to be very stereoselective (6), and the stereochemistry could be confirmed by nmr spectroscopy. As shown in Fig. 1(b), the nmr of **3***b* is consistent with the conclusion that it is homogeneous since there is no sign of splitting of the signal attributed to the benzene ring protons although, despite chromatography and crystallization, there appears to be a small amount of impurity present; this was revealed by the 200 MHz spectrum, but was not apparent at 100 MHz.

*Kinetics with* **3**b

Drawing on the work with the closely related material, **3***a*, which was studied initially, we can confidently expect that experiments at pH 8 will give near maximal rate constants for reaction of dimer and substrates. The conditions were chosen to allow direct comparison with the previous studies of **1**. Because there are important electrostatic interactions in the transition states from **1** and **2***a–d* (1) which are missing in the analogous transition states from **3***b* and **2***a–d*, because of the change from 11-β-amino to 11-keto, we have also studied the reactions of the analogous monomeric steroid **12**. The rate constants evaluated in this work, Table 2, can be analyzed to give a measure of the hydrophobic stabilization of the transition state.

We have previously argued (1) that the imidazolyl steroids always have accessible to them the option of reacting with the substrates in conformations where there is little contact between the steroid and the hydrophobic portion of the substrate, and that such a reaction mode should have a

Can. J. Chem. Downloaded from www.nrcresearchpress.com by 210.87.254.105 on 09/06/12
For personal use only.

Can. J. Chem. Downloaded from www.nrcresearchpress.com by 210.87.254.105 on 09/06/12
For personal use only.

rate constant very similar to that for the acetate, for which hydrophobic stabilization is not possible. The apparent rate constant for a substrate with a hydrophobic acyl substituent is then the sum of a contribution for transition states with no hydrophobic stabilization, and one with hydrophobic stabilization. The latter transition state is favored by the lowering in free energy consequent upon having hydrocarbon residues in contact with each other, freeing water molecules from contact with hydrocarbon, but is disfavored by certain forms of strain, chiefly eclipsing interactions, which must be introduced to satisfy the geometrical constraints for simultaneous hydrophobic interaction and nucleophilic attack.

When we plot the logarithms of the rate constants for reaction of the monomer with HCA-HNB, NPA-HNB, and PPA-HNB, all corrected by subtracting the rate constant for reaction with ACE-HNB to allow for the nonhydrophobically-stabilized contribution, we find that there is a plausibly linear relationship with the $\pi$ parameter (11). For the rate constants for reaction of the dimer, we first divide by 2 to correct for the statistical factor favoring the dimer, and then correct for the nonhydrophobic transition state by subtracting the rate constant for the reaction with ACE-HNB, which is assumed to be the same as that for the monomer. At the accessible concentrations of **3***b* its contribution to the rate of reaction of ACE-HNB would be undetectable. When the logarithms of these corrected rate constants are plotted as a function of $\pi$ we find another linear relationship. In Fig. 5, both sets of data are plotted; the lines were determined by weighted least squares with the condition imposed that the lines have a common intercept. In imposing the condition of a common intercept we are assuming that for both reactions the same imidazole nitrogen is used and that the geometries of the transition states for the reactions of the esters would be identical (1). This is the simpler assumption, although it is possible that the more hindered imidazole nitrogen plays a more important part in the reactions of **3***b* than in those of **12**. The lines are in satisfactory, though not marvellous, accord with the data. It should be noted that despite the very low concentrations which were used for the experiments involving dimer and PPA-HNB, it remains possible that we have not reached concentrations low enough to give the true rate constant. Since the points for dimer plus HCA-HNB and NPA-HNB imply a steeper line and a larger rate constant for PPA-HNB, this is a serious source of concern. The slopes of the lines are 0.40 for the monomer and

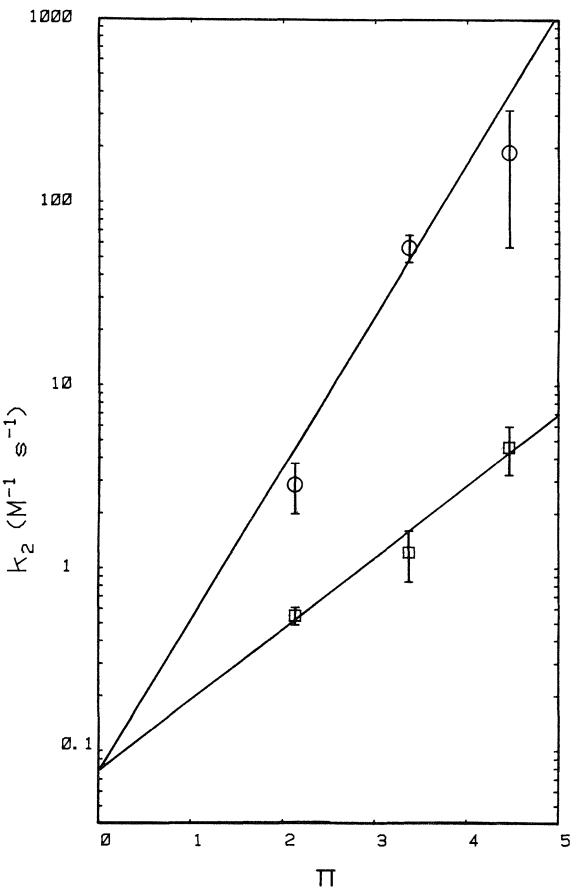


FIG. 5. Corrected second-order rate constants for the reaction of **12** and **3***b* with **2***b*–*d*, as a function of $\pi$. The lines were fitted by least squares with the imposed constraint of a common intercept; the intercept corresponds to $k_{corr} = 0.078$; slope for **3***b* = 0.83; slope for **12** = 0.39. (□) Reaction of **12** with **2***b*–*d*; (○) reaction of **3***b* with **2***b*–*d*.

0.83 for the dimer. The fact that the line for the dimer has a slope twice as great as that for the monomer is in accord with expectation, since twice as much of the surface area of the aromatic ring should be removed from contact with water by the dimer.

A further complication is that these steroidal imidazoles have two imidazole nitrogens, which differ in degree of steric hindrance, and also in suitability for reaction with hydrophobic stabilization. For the best hydrophobic stabilization of the transition state, molecular models suggest that the more hindered nitrogen (N-3 of the imidazolyl group) must react. Studies with an analog of **1**, in which N-1 of the imidazolyl group was isopropylated and unable to react, showed that such a steroid was markedly less reactive than **1** itself, and therefore that **1** reacts almost exclusively at the less hindered nitrogen (1). By analogy we conclude that

Can. J. Chem. Downloaded from www.nrcresearchpress.com by 210.87.254.105 on 09/06/12
For personal use only.

**12** reacts at the less hindered nitrogen. We cannot tell which nitrogen is used by **3*b***, but can state, based on examination of models, that for either **12** or **3*b***, hydrophobic contacts are better if reaction occurs by the more hindered nitrogen. Since the hydrophobic stabilization is clearly much larger for **3*b*** than for **12**, it is possible that the fraction of reaction involving the more hindered nitrogen is greater, and thus that the slope of the plot of the logarithm of the corrected rate constant vs. $\pi$ could be greater than twice that for the monomer, and the intercept smaller than that for the monomer.

The intercept of the plots in Fig. 5 is interpreted as the logarithm of the rate constant for reaction with a hypothetical substrate with no hydrophobic binding group by a transition state geometrically identical to that used by the substrates with aromatic binding groups. It is thus an accessible but very improbable transition state for the reaction of the propionate ester. If we use this hypothetical rate constant as our reference point, we can easily calculate the potential rate enhancement, from hydrophobic stabilization, as 2800-fold for phenanthryl as binding group. The actual rate enhancement can be calculated using the rate constant for the observed reaction of imidazole as reference point as 200-fold. This clearly bears out the expectations which led to the synthesis of **3*b***.

There is only a small amount of ambiguity possible concerning the geometry of the transition state for the reaction of **3*b*** with PPA-HNB. The size of the rate enhancements observed, compared to the behavior seen with **1** and **12**, absolutely requires that the phenanthrene ring be interacting with two steroid residues. The imidazole nitrogen must be attacking the ester carbonyl at the transition state. These constraints plus the very limited amount of rotational freedom in substrate and nucleophile specify the transition state within strict bounds, even if they do not completely specify it.

We conclude that hydrophobic binding with an area equivalent to the upper and lower surfaces of phenanthrene, which is by simple geometry similar to the total surface area of benzene, is sufficient to give a stabilization equivalent to ca. 3000-fold in rate constant. This provides a suitable design parameter for any one wishing to construct an artificial enzyme. The major defect of **3*b*** as an enzyme model is its very low solubility, which leads to severe difficulties in performing experiments and makes many experiments impossible. We are encouraged by the present results to continue our efforts to prepare **4**, which should be at least as good as a catalyst, and much more soluble in water.

## Experimental

*Methods*

Nuclear magnetic resonance spectra were recorded using Varian XL-200, XL-100, HA-100, and T-60 spectrometers, generally in $CD_3OD$ with tetramethylsilane as internal standard. For spectra in $D_2O$, the sample was converted to its DCl salt and evaporated several times from $D_2O$ to remove exchangeable protons and excess DCl. For these spectra the solvent (HOD) peak was used as internal standard; since the concentrations were low ($\simeq$ 5 mg per 0.3 mL) and no excess DCl was present, the solvent peak will not be perturbed. The $^{13}C$ nmr spectra were run for many of the steroids synthesized in this project. From the noise decoupled and off-resonance decoupled spectra it was possible to make a partial assignment of the spectra (12). It was, in general, not possible to make a complete assignment and the results, given in Table 3, indicate this ambiguity. For **3*b*** there were further problems, because the sample was rather small and the solvent peaks caused more serious interference than for the other compounds. Nevertheless, although only a very partial assignment was possible, it is clear that peaks assigned to carbons well removed from the linking xylyene group were essentially unperturbed relative to the monomer. Infrared spectra were recorded using a Beckman Acculab 4 spectrophotometer. Mass spectra were recorded on a Varian MAT 311A spectrometer. Low-pressure chromatography of intermediates in the synthesis of **3*b*** was carried out using Glenco apparatus, including linear-gradient mixing chambers, at a gauge pressure of ca. 13 psi; the column packing was Merck Silica PF254. Thin-layer chromatography was on plates coated with Merck Silica GF254 or on Analtech Silica Gel GF precoated tlc plates. Imidazole-containing compounds were detected on tlc plates by spraying with a freshly prepared solution of diazotized sulfanilic acid in aqueous methanol.

*Materials*

Sodium cyanoborohydride (Aldrich) was purified according to Borch *et al.* (10). Acetonitrile for kinetics solutions was purified by passage through a column of Woelm neutral alumina, Grade I. Tetrahydrofuran was dried by distillation from sodium/benzophenone ketyl. Distilled water was redistilled from alkaline permanganate in an all-glass apparatus.

p-*Xylenediamine*

Phthalamide was converted to its potassium salt following the Organic Syntheses procedure (13). Potassium phthalimide, 14.2 g (76.4 mmol), was suspended in 200 mL dry DMF and stirred for 15 min while protected from moisture. Then $\alpha,\alpha'$-dibromo-*p*-xylene (Aldrich), 10 g (37.9 mmol), was added cautiously in portions. When all of the dibromide had been added the mixture was heated at 65°C with rapid stirring for 90 min, then allowed to cool to room temperature and stirred for 2 days. Thin-layer chromatography showed no remaining dibromide. The mixture was poured into a separatory funnel containing water and $CHCl_3$; the product proved to be almost insoluble in $CHCl_3$ and was isolated by filtration. Yield 14.3 g, 95%; mp 276–278°C (lit. (14) mp 279–280°C; (15) mp 272–273°C). The diphthalimide, 13 g (33 mmol), in 100 mL ethanol and 10 mL hydrazine hydrate (200 mmol) was heated at reflux for 5.5 h (a further 50 mL ethanol was added after 0.5 h because the mass became too thick to stir) and let stand at room temperature overnight. The ethanol was evaporated *in vacuo*, 50 mL of water was added and evaporated to remove excess hydrazine, and then the solid mass was treated with 100 mL 2 *N* HCl, with stirring and warming at 60°C for 15 min. Filtration yielded 14.5 g phthalhydrazide, mp 342–343°C (lit. (16) mp 342–344). The filtrate was concentrated to about 100 mL, cooled, and filtered to give 3.0 g *p*-xylenediamine dihydrochloride, mp > 360°C; nmr

TABLE 3. $^{13}C$ nmr spectral data for imidazolyl steroids in $CD_3OD$; δ relative to TMS[a]

| Compound | Carbon 1 | 2 | 3 | 4 | 5 | 6 | 7 | 8 | 9 | 10 | 11 |
|---|---|---|---|---|---|---|---|---|---|---|---|
| **8** | 35.8(a) | 34.6(a) | 202.3 | 122.5 | 176.6 | 34.1(a) | 33.3(a) | 33.3(a) | 58.0 | 40.7 | 68.5 |
| *N*-benzyl-**8**[c] | 35.1(b) | 34.6(b) | 200.8 | 122.4 | 176.6 | 34.1(b) | 33.3(b) | 33.3(b) | 58.2 | 40.7 | 68.5 |
| **11** | 37.0(c) | 32.0(f) | 51.8 | 38.4(e) | 48.0 | 29.5(f) | 33.8(f) | 33.4 | 60.0(g) | 38.7 | 68.5 |
| **12** | 36.3(j) | 31.6(h) | 51.7 | 38.1(j) | 46.6(1) | 29.3(h) | 33.7(h) | 39.1 | 65.4 | 37.3(j) | 212.1 |
| **3***b*[d] | 37.7(?) | ? | ? | ? | 47.2(?) | 29.4(?) | ? | 39.1(?) | 65.4 | 36.8(?) | — |

| Compound | Carbon 12 | 13 | 14 | 15 | 16 | 17 | 18 | 19 | 2′ | 4′ | 5′ |
|---|---|---|---|---|---|---|---|---|---|---|---|
| **8** | 47.9 | 43.9 | 58.0 | 27.2(c) | 25.3(b) | 50.3 | 15.8 | 21.8 | 135.0[b] | ? | 120.0[b] |
| *N*-benzyl-**8** | 48.1 | 43.8 | 58.2 | 27.1(d) | 25.3(d) | 51.5 | 15.8 | 21.4 | 137.6 | 138.5(?) | 117.5 |
| **11** | 47.8 | 44.1 | 58.9(g) | 27.3(h) | 25.4(h) | 50.2 | 15.9(i) | 15.6(i) | 135.4 | 136.9 | 120.8 |
| **12** | 56.9 | 48.7 | 55.8 | 27.8(m) | 24.8(m) | 49.2(1) | 14.3 | 12.6 | 135.9 | 137.3 | 118.9 |
| **3***b* | 56.9 | 48.7(?) | 55.8 | 27.8(m) | 24.8(m) | 49.2(?) | 14.3 | 12.6 | 135.8 | 139.3(?) | ? |

[a]Letters in parentheses represent sets of signals which could not be assigned unambiguously from the noise-decoupled and off-resonance-decoupled spectra.
[b]Broadened by tautomerism of the imidazole ring.
[c]In addition signals could be seen for the benzylic $CH_2$ (51.9) aromatic quarternary carbon (144.0 (?)), and aromatic CH's (128.4, 129.0, 129.8).
[d]In addition a peak assignable to aromatic CH's was seen at 129.9.

Can. J. Chem. Downloaded from www.nrcresearchpress.com by 210.87.254.105 on 09/06/12
For personal use only.

($D_2O$): 4.33 (4H), 7.64 (4H). Concentration of the mother liquor gave a second crop of yellowish crystals, 1.95 g, and then a third crop of 1.0 g. Total yield 6 g, 85%.

*α,α′-Bis(17β-(4-imidazolyl)-11-keto-5α-androstan-3β-amino)-p-xylene,* **3**

*p*-Xylenediamine dihydrochloride (151 mg; 0.722 mmol) and 120 mg NaOAc (1.46 mmol) were dissolved in 30 mL methanol; then 17-β-(4-imidazolyl)-androstane-3,11-dione (4), 509 mg (1.44 mmol), in 5 mL methanol was added with stirring; then sodium cyanoborohydride, 104 mg (1.64 mmol), was added. The solution was stirred for 36 h. Thin-layer chromatographic analysis suggested that the reaction was incomplete, so 10 mg diamine (0.05 mmol) and 8.6 mg NaOAc (0.1 mmol) were added and stirring continued for another 36 h. Concentrated HCl, 4 mL, was added to destroy excess reducing agent; the mixture was filtered and the precipitate rinsed with methanol. The filtrate was partitioned between water and ethyl acetate. On addition of base the aqueous layer deposited a gummy precipitate. This was filtered off and the filtrate was extracted using ethyl acetate – methanol. The extracts were evaporated and the residue and the gummy precipitate were taken up in methanol and acidified with HCl. The solution was filtered and evaporated to dryness to give the crude hydrochloride salt of the dimer. The salt would not crystallize, so it was taken up in methanol, basified using KOH, and adsorbed onto 1 g silicic acid (Mallinkrodt 2847). Chromatography at atmospheric pressure on 10 g silicic acid, starting in ether and moving in a step gradient to 20% methanol in ether, gave fractions which were predominantly dimer with traces of contaminants. These fractions were pooled, concentrated, and converted to the hydrochloride salt.

*17β-(N-Benzyl-4′-imidazolyl)-11β-hydroxy-4-androsten-3-one,* N-*benzyl-***8**

Compound **8** (prepared from corticosterone (Sigma Chemical Co.) as previously described (4)), 10 g; (28 mmol), dissolved in 90 mL methanol, was treated with 3.3 mL (29 mmol) benzyl chloride and 2.44 g (29 mmol) sodium bicarbonate at reflux until tlc analysis (80:20 $CHCl_3$–$CH_3OH$) showed that the reaction was over. The solution was filtered through sintered glass and evaporated. The residue was purified by low-pressure chromatography, eluting with 90:10 $CHCl_3$–$CH_3OH$, to give 6.26 g *N*-benzyl-**8**, and 1.8 g *N*-benzyl-**8** contaminated by benzyl methyl ether. The latter fraction was purified by partitioning between $CHCl_3$ and a large volume of aqueous 2 *N* $H_2SO_4$. The combined aqueous layers were basified (concentrated $NH_3$) and extracted using ethyl acetate; evaporation of the organic extracts, after drying ($Na_2SO_4$), gave 0.87 g *N*-benzyl-**8**. The total yield of *N*-benzyl-**8** was 7.13 g, 57%. A small portion of *N*-benzyl-**8** was purified by crystallization giving two different materials, which were identified as positional isomers. Crystallization from toluene–cyclohexane gave material of mp 223.5–226.5°C (dec); ir ($CHCl_3$), $\nu_{C=O}$: 1665 $cm^{-1}$; $^1H$ nmr, δ: 7.64 (br s), 6.86 (br s, imidazole ring protons), 7.28 (m, phenyl protons), 5.69 (s, C(4)-H), 5.19 (s, benzylic methylene protons), 4.36 (m, C(11)-H), 1.48 (s, C(19)-$H_3$), 0.80 (s, C(18)-$H_3$), 2.76–0.58 (steroid skeletal protons). The second isomer crystallized from $CHCl_3$; mp 153–160°C (dec); $^1H$ nmr, δ: 8.97 (s), 7.88 (s, imidazole ring protons), 7.42 (s, phenyl protons), 5.66 (s, C(4)-H), 5.41 (s, benzylic methylene protons), 4.36 (m, C(11)-H), 1.46 (s, C(19)-$H_3$), 0.82 (s, C(18)-$H_3$), 2.88–0.72 (steroid skeletal protons); ms (70 eV) *m/e*: 444.27723 (calcd. for $C_{29}H_{36}N_2O_2$: 444.27766).

*17β-(4′-Imidazolyl)-5α-androstan-11β-ol-3-one,* **9**

The isomeric mixture of *N*-benzyl-**8**, 2.82 g (6.3 mmol), dissolved in 100 mL of dry THF, was added dropwise to a solution of sodium, 0.64 g (27.2 mmol) dissolved in 400 mL distilled liquid ammonia. Stirring was continued after addition was complete, and samples of the mixture were analyzed by tlc (80:20 $CHCl_3$–$CH_3OH$). When the reaction was judged to be complete, $NH_4Cl$, 2.0 g (37 mmol), was added and the ammonia was allowed to evaporate. The residue was partitioned between ethyl acetate and 1 *N* aqueous $NH_3$. The organic layers were combined, dried over $Na_2SO_4$, and evaporated to give 2.24 g crude product, which was found to be contaminated by **8**. A small portion was purified by crystallization from methanol, mp 261–263.5°C (dec); $^1H$ nmr ($CD_3OD$), δ: 7.54 (s), 6.77 (s, imidazole ring protons), 4.32 (m, C(11)-H), 1.30 (s, C(19)-$H_3$), 0.78 (s, C(18)-$H_3$), 2.76–0.58 (steroid skeletal protons); ms (70 eV) *m/e*: 356.24636 (calcd. for $C_{22}H_{32}N_2O_2$: 356.24636).

*3-Oximino-17β-(4′-imidazolyl)-5α-androstan-11β-ol,* **10**

Crude **9**, 1.4 g (3.9 mmol), and hydroxylamine hydrochloride, 1.4 g (20 mmol), were dissolved in 15 mL pyridine and allowed to react at room temperature. Analysis by tlc, 80:20 $CHCl_3$–

Can. J. Chem. Downloaded from www.nrcresearchpress.com by 210.87.254.105 on 09/06/12
For personal use only.

$CH_3OH$, showed that reaction was complete by the time the reagents were completely dissolved. Although two isomeric products were detected, the initial product at room temperature was more than 90% one material. Heating led to equilibration of the two products. The reaction mixture was partitioned between $CHCl_3$ and 1 *N* aqueous $NH_3$. The combined organic extracts were dried ($Na_2SO_4$) and evaporated to give 1.16 g crude product. This could be crystallized from methanol to give white flakes, mp 183–185°C; $^1$H nmr, δ: 7.53 (s), 6.77 (s, imidazole ring protons), 4.29 (m, C(11)-H), 1.15 (s, C(19)-$H_3$), 0.75 (s, C(18)-$H_3$), 2.76–0.45 (steroid skeletal protons); ms (70 eV) *m/e*: 371.25748 (calcd. for $C_{22}H_{33}N_3O_2$: 371.25726).

*3β-Amino-17β-(4'-imidazolyl)-5α-androstan-11β-ol,* ***6***

Pure **5**, 0.249 g (0.67 mmol), suspended in 15 mL *n*-propanol, was treated with 0.61 g (40 equiv.) sodium, added in portions. When analysis by tlc, 80:20 $CHCl_3$–$CH_3OH$, showed that the reduction was complete, the solution was cooled, and partitioned between $CH_2Cl_2$ and 1 *N* aqueous $NH_3$. The organic extracts were dried ($Na_2SO_4$) and evaporated. The crude product was purified by low pressure chromatography, eluting with 80:20 $CHCl_3$–$CH_3OH$ to which had been added 2% $NH_3$. The yield of **11** after chromatography was 0.22 g; crystallization from methanol gave material of mp 153–154.5°C; $^1$H nmr, δ: 7.53 (s), 6.77 (s, imidazole ring protons), 4.30 (m, C(11)-H), 1.05 (s, C(19)-$H_3$), 0.72 (s, C(18)-$H_3$), 2.83–0.58 (steroid skeletal protons); ms (70 eV) *m/e*: 357.27793 (calcd. for $C_{22}H_{36}N_3O$: 357.27799).

*3β-Amino-17β-(4'-imidazolyl)-5α-androstan-11-one,* ***12***

Compound **11**, 0.240 g (0.67 mmol), dissolved in 14 mL glacial acetic acid, was treated with 0.62 mL (1.24 mmol) 2 *N* aqueous $H_2SO_4$, followed by 0.4 mL (0.8 mmol) Jones reagent. The reaction was followed by tlc, 1 *N* $NH_3$ in $CH_3OH$. When no more **11** was detectable, 0.5 mL 2-propanol was added to quench residual $Cr^{VI}$. The reaction was then worked up using the method of Mueller and DiPardo (8) which avoids the usual difficulties encountered with alkaline $Cr^{III}$ solutions. Partitioning between $CH_2Cl_2$ and 1 *N* aqueous $NH_3$, drying of the organic extracts, and evaporation gave 0.229 g (96%) crude product. Crystallization from acetonitrile gave crystals which charred on heating; ir ($CHCl_3$) $\nu_{C=O}$: 1703 $cm^{-1}$; $^1$H nmr in $CD_3OD$, δ: 7.57 (s), 6.82 (s, imidazole ring protons), 2.96 (t, $J$ = 9 Hz), 2.46 (d, $J$ = 12 Hz), 2.12 (d, $J$ = 11 Hz, skeletal protons perturbed by the 11-keto group), 1.02 (s, C(19)-$H_3$), 0.42 (s, C(18)-$H_3$), 3.18–0.60 (steroid skeletal protons); $^1$H nmr of the DCl salt in $D_2O$ at 200 MHz, δ: 9.03 (s), 7.74 (s, imidazolium ring protons), 3.6 (broad, $\Delta\nu_{1/2} \simeq$ 30 Hz, C(3)-αH), 3.59 (t, $J$ = 10 H), 3.07 (d, $J$ = 12 Hz), 2.56 (d, $J$ = 12 Hz, skeletal protons perturbed by the 11-keto group), 1.43 (s, C(19)-$H_3$), 0.91 (s, C(18)-$H_3$), 2.9–1.5 (steroid skeletal protons); ms (70 eV) *m/e*: 355.26186 (calcd. for $C_{22}H_{33}N_3O$: 355.26234).

*α,α'-Bis(17β-(4'-imidazolyl)-11-keto-5α-androstan-3β-amino)-p-xylene,* **3***b*

A three-necked flask fitted with a thermometer, stopper, and a Soxhlet extractor charged with 3A molecular sieves was charged with 70 mL of a 70:30 mixture of absolute ethanol and dry benzene. The mixture was refluxed for several hours to dry the system, and then purified **12**, 0.100 g (0.28 mmol), and terephthalaldehyde (Aldrich, recrystallized before use), 0.018 g (0.13 mmol), were added. The reaction mixture was refluxed for 24 h; during this time a white solid precipitated. The solvent was then removed by evaporation and replaced with dry DMF. (Karl Fischer titration using a Photovolt Aquatest II water meter showed 0.02% water.) Sodium cyanoborohydride, 0.365 g (0.58 mmol), was added and the suspension was stirred for a few minutes. Trifluoroacetic acid was then added dropwise until a clear solution was obtained; the total volume added was about 70 μL. The solution was partitioned between $CH_2Cl_2$ and 2 *N* aqueous $H_2SO_4$. The aqueous extracts were neutralized using $NaHCO_3$, made basic with $NH_3$, and extracted using $CH_2Cl_2$. The organic extracts were dried ($Na_2SO_4$) and evaporated to give 0.103 g crude product (90%). Purification by low-pressure chromatography using 0.3 *M* $NH_3$ in $CH_3OH$ as eluant gave pure ***3b***, but the recovery after chromatography was only about 22%. Compound ***3b*** charred without melting; $^1$H nmr in $CD_3OD$ at 100 MHz, δ: 7.56 (s), 6.80 (s, imidazole ring protons), 7.34 (s, phenyl protons), 6.80 (s, benzylic methylene protons), 2.96 (br t, $J$ = 9 Hz), 2.50 (d, $J$ = 12 Hz), 2.14 (d, $J$ = 12 Hz, skeletal protons perturbed by the 11-keto group), 1.02 (s, C(19)-$H_3$), 0.41 (s, C(18)-$H_3$), 3.12–0.58 (steroid skeletal protons); $^1$H nmr of the DCl salt in $D_2O$ at 200 MHz, δ: 9.05 (s), 7.73 (s, imidazolium ring protons), 7.98 (s, xylylene ring protons), 4.71 (s, benzylic $CH_2$), 3.6 (broad peak plus a triplet with $J$ = 10 Hz, C(3)-H plus a proton perturbed by the 11-keto group), 3.07 (d, $J$ = 12 Hz), 2.54 (d, $J$ = 12 Hz, skeletal protons perturbed by the 11-keto group), 1.44 (s, C(19)-$H_3$), 0.91 (s, C(18)-$H_3$), 2.9–1.5 (steroid skeletal protons); ms (70 eV): the molecular ion could be seen at *m/e* 812 although it was rather weak; its *Exact Mass* could be determined as *m/e*: 812.57102; calcd. for $C_{52}H_{72}N_6O_2$: 812.57164. Two major fragments were determined; *m/e*: 458.31733 (calcd. for $C_{30}H_{40}N_3O$: 458.31712), and *m/e*: 354.25385 (calcd. for $C_{22}H_{32}N_3O$: 354.25452).

*Substrates*

Compounds **2***a–d* were prepared as previously reported (1), and purified by crystallization. All showed satisfactory nmr spectra (recorded in acetone-$d_6$).

*Kinetics*

Reactions were followed using a Gilford Model 240 spectrophotometer, with the cell compartment temperature maintained at 25.0 ± 0.1°C using a Braun Thermomix II circulator for experiments with ***3a*** or a Neslab Exacal 300 circulator for experiments with ***3b***. For dilute solutions, 10-cm cells were used with a Gilford Model 2470 sample chamber. For more concentrated solutions, 1-cm cells were used. Hamilton microsyringes, 10 μL or 100 μL, were used for measuring volumes less than 1 mL. Reactions were initiated by adding the required volume of substrate solution to an equilibrated solution containing buffer, nucleophile, and the amount of acetonitrile needed to give a final concentration of 3.2% v/v. The pH of each reaction solution was measured at the end of the reaction.

Stock solutions of substrates were prepared in acetonitrile. The reaction solvent was aqueous buffer, pH 7.1, 7.5, or 8.0, ionic strength 0.097 *M*, with 0.0097 *M* phosphate or 0.0097 *M* Tris, and 3.2% acetonitrile. These conditions are the same as were used for the studies of steroid **1** (1). Reaction of the substrates was followed by monitoring the formation of the 3-hydroxy-4-nitrobenzoate dianion at 420 nm. For experiments involving ***3b***, data were collected using a digitizer constructed in this department, and stored on punched paper tape.

A $10^{-4}$ *M* stock solution of ***3a*** was prepared by dissolving 5.00 mg dimer as the tetrahydrochloride, $KH_2PO_4$ (68.17 mg), and KCl (290.0 mg), in 45 mL glass-distilled water, and adjusting the pH to 7.00 with sodium hydroxide. The solution was then diluted to 50.0 mL. Kinetics solutions were prepared by dilution from this stock.

A stock solution of ***3b***, $1 \times 10^{-4}$ *M* in pH 7 phosphate buffer was prepared. To our surprise this solution was not completely clear, but showed slight turbidity which became noticeable as the pH was adjusted from the initial low value; this became apparent about pH 6.7. No such turbidity was seen at this concentration of ***3a***. Since much of the available supply of dimer ***3b*** was in this solution, and the insoluble material was, and remained, very finely divided, we went ahead and used it as a

stock, mixing well before removing a sample for dilution. For kinetics this solution was diluted at least 50- and generally 100-fold into pH 8 buffer. No visible turbidity was ever detected in the diluted solutions. When Tris buffer was used, solutions were never kept more than one week.

## Acknowledgments

We thank Dr. J. B. Stothers of this department for assistance with $^{13}C$ spectroscopy. Financial assistance from the Natural Sciences and Engineering Research Council of Canada and the Alfred P. Sloan Foundation is gratefully acknowledged.

1. J. P. GUTHRIE and Y. UEDA. Can. J. Chem. **54**, 2745 (1976).
2. J. P. GUTHRIE and S. O'LEARY. Can. J. Chem. **53**, 2150 (1975).
3. J. P. GUTHRIE. Can. J. Chem. **60**, 765 (1982).
4. J. P. GUTHRIE. Can. J. Chem. **50**, 3993 (1972).
5. J. L. GOUGH, J. P. GUTHRIE, and J. B. STOTHERS. J. Chem. Soc. Chem. Commun. 979 (1972).
6. C. W. SHOPPEE, D. E. EVANS, H. C. RICHARDS, and G. H. R. SUMMERS. J. Chem. Soc. 1649 (1956).
7. J. E. BRIDGEMAN, P. C. CHERRY, A. S. CLEGG, J. M. EVANS, Sir E. R. H. JONES, A. KASAL, V. KUMAR, G. D. MEAKINS, Y. MORISAWA, E. E. RICHARDS, and P. D. WOODGATE. J. Chem. Soc. C, 250 (1970); R. GLASER and E. J. GABBAY. J. Org. Chem. **35**, 2907 (1970).
8. R. H. MUELLER and R. M. DIPARDO. J. Org. Chem. **42**, 3210 (1977).
9. P. R. BEVINGTON. Data reduction and error analysis for the physical sciences. McGraw-Hill, New York. 1969.
10. R. F. BORCH, M. D. BERNSTEIN, and H. D. DURST. J. Am. Chem. Soc. **93**, 2897 (1971).
11. T. FUJITA, J. IWASA, and C. HANSCH. J. Am. Chem. Soc. **86**, 5175 (1964); M. S. TUTE. Adv. Drug Res. **6**, 1 (1971).
12. J. W. BLUNT and J. B. STOTHERS. Org. Magn. Reson. **9**, 439 (1977).
13. P. L. SALZBERG and J. V. SUPNIEWSKI. Org. Synth. Coll. Vol. 1, 119 (1937).
14. F. LUSTIG. Chem. Ber. **28**, 2987 (1895).
15. M. A. ABISHEV, V. A. GUSINSKAYA, and T. V. BATRAHOVA. Bull. Acad. Sci. USSR, Div. Chem. Sci. 2010 (1970).
16. R. C. WEAST (*Editor*), Handbook of Chemistry and Physics, 48th ed. Chemical Rubber Co, Cleveland, OH. 1967.

Can. J. Chem. Downloaded from www.nrcresearchpress.com by 210.87.254.105 on 09/06/12
For personal use only.

# Determination of rate constants when analytical integration of the rate law is not possible: approaches based on numerical differentiation and numerical integration

J. PETER GUTHRIE

*Department of Chemistry, University of Western Ontario, London, Ont., Canada N6A 5B7*

Received May 27, 1981

J. PETER GUTHRIE. Can. J. Chem. **60**, 765 (1982).

Two methods for deriving rate constants from absorbance–time data when the rate laws cannot be integrated in closed form are presented, and their use illustrated. One method uses least-squares fitting to the curve obtained by numerical integration of the rate law. The other involves analysis of the numerically evaluated derivative with respect to time of the absorbance–time curve. This allows calculation of rate constants in a direct fashion, either from the initial and minimum values of a function of the derivative or by fitting the decrease in the value of this function to a first-order rate equation when this is suitable. The advantages and disadvantages of the methods are discussed. The illustrations are from recent studies of the reactions of steroidal imidazoles with aryl esters. The derivative method appears to be superior, and of potentially wide utility.

J. PETER GUTHRIE. Can. J. Chem. **60**, 765 (1982).

On présente deux méthodes de dérivation des constantes de vitesse à partir des données d'absorption en fonction du temps lorsqu'il est impossible d'intégrer les lois de vitesse de façon convenable; on illustre ces méthodes. Une méthode utilise l'ajustment des moindres carrés à la courbe obtenue par l'intégration numérique de la loi de vitesse. L'autre implique une analyse numérique de la dérivée, évaluée en fonction du temps, de la courbe d'absorption vs temps. Ceci permet de calculer directement les constantes de vitesse soit à partir des valeurs initiales et minimales d'une fonction de la dérivée ou en ajustant la diminution de la valeur de cette fonction à une équation de première ordre si c'est approprié. On discute des avantages et des inconvénients de ces méthodes. Les exemples d'application portent sur des études récentes des réactions d'imidazoles stéroidaux avec des esters aryliques. La méthode de la dérivée semble supérieure et d'une grande utilité potentielle.

[Traduit par le journal]

Can. J. Chem. Downloaded from www.nrcresearchpress.com by 210.87.254.105 on 09/06/12
For personal use only.

## Introduction

Although integrated forms for various rate laws are given in standard textbooks (1, 2), considerations of practicality strongly favor the use of first order or pseudo-first order kinetics whenever possible. The rational basis for this deep seated prejudice is shown by the fact that for any network of first order processes, it is possible to derive an analytical solution, although this may be of well nigh intractable complexity if the network is not small (1–3). No such analytical solution is possible for networks of higher order reactions, or even for many simple cases of mixed first and second order reactions. We recently stumbled upon one such deceptively simple situation, where the rate law for the situation symbolized below:

[1] $A \xrightarrow{k_1} P_1 + P_2$

[2] $A + B \xrightarrow{k_2} C + P_1$

[3] $C \xrightarrow{k_3} B + P_2$

is given by:

[4] $dx/dt = k_2(a - x)(b - y) + k_1(a - x)$

[5] $dy/dt = k_2(a - x)(b - y) - k_3 y$

where $a$ is the initial concentration of A, $b$ is the initial concentration of B, $x$ is the concentration of $P_1$, and $y$ is the concentration of C. Astonishingly enough this simple set of equations is quite intractable to integration, and remains so even if $k_3 = 0$.

We have developed two methods for extracting rate constants from data for such reaction systems, which we feel will be of some general usefulness. Accordingly we report the methods here with illustrative examples taken from the studies reported in the accompanying paper (7), in which the need for these methods arose. This paper is concerned with the methodology for solving such kinetics problems.

## Mathematical methods

One response to this situation of rate laws which cannot be integrated in closed form, i.e. in terms of well-known standard functions, is to attempt numerical integration (9, 10). We have tried this approach, and found that it is indeed possible to achieve reasonable simulations of the observed behavior, but the approach is not fully satisfactory for determination of the kinetic parameters by least squares, as will be discussed below. We have also developed methods for determining rate constants from the data by first calculating the instantaneous rates of reaction at each data point, and then deducing the rate constants from the differential forms of the rate law.

0008-4042/82/060765-07$01.00/0

©1982 National Research Council of Canada/Conseil national de recherches du Canada

Can. J. Chem. Downloaded from www.nrcresearchpress.com by 210.87.254.105 on 09/06/12
For personal use only.

One is faced with a general problem in extracting rate constants for a system such as the present one in that calculation of the observable values, here absorbance as a function of time, requires specification of more parameters than could be defined by the observed curve. Intuitively it is clear that a straight line is specified by two parameters, and that data which, with some degree of scatter, lie distributed about a straight line allow determination of two parameters but no more. Similarly an exponential curve is specified by three parameters, and data distributed about an exponential curve allow determination of three parameters but no more. For any set of data there is a very limited number of parameters which can be determined by fitting an equation to the data. Since concentrations of reagents, rate constants, initial absorbances, etc. all affect the observable quantity, and almost all are invariably only approximately known, it is very likely that more theoretically significant numerical values are required to calculate a set of data than there are parameters which can be determined by fitting to the data. In the case of reactions described by reactions [1]–[3], numerical calculation requires that one specify not less than seven quantities, none of which is known exactly, and all of which will affect the quality of the fit. These quantities are: the two initial concentrations, the three rate constants, the initial absorbance, and the change in extinction coefficient for conversion of the starting material into the product. However, the experimental data imply a curve which is not sufficiently complicated to define seven parameters. The actual number of parameters defined by the curve is hard to state reliably in the absence of an analytical expression fitting it well, but three or four parameters give fairly good fits. If an analytical expression were known, it might have, say, four parameters, which were functions of the seven theoretical quantities.

The least-squares procedure for fitting an equation to data requires derivatives for $(y_{obs} - y_{calcd})$ with respect to each of the parameters (4, 5). If no analytical form of the integrated rate law is available it is possible to determine these derivatives analytically by determining $(y_{obs} - y_{calcd})$ for the current set of parameters, and then for a set where one parameter is changed by a small amount, say 1%. The change in $(y_{obs} - y_{calcd})$ divided by the change in the parameter is an approximation to the derivative with respect to that parameter. This must then be done for each parameter. Each value of $y_{calcd}$ needed for this calculation must be determined by numerical integration from the differential form of the rate law. We have written a computer program in FORTRAN, using a modified form of the Euler method (6) to perform the integration and evaluate the calculated absorbance at each time for which a value was recorded. In this method the value of a concentration $C_n$ at one time is used to calculate the value at a later time $C_{n+1}$ as:

$$C_{n+1} = C_n + (1/2)[(dC/dt)_n + (dC/dt)_{n+1}]\Delta t$$

The procedure can be iterated to give an improved value, but two iterations seems to be sufficient. Least-squares fitting was carried out using the Marquardt algorithm (4), which leads to more rapid convergence when the initial estimates for the parameters are not close to the best values. The calculations were carried out on a Xitan microcomputer. The quality of the fit was tested in two ways. The first involved calculating $\sqrt{[\Sigma(y_{obs} - y_{calcd})^2 \times (\text{weight})/(\text{degrees of freedom})]}$, which Deming (5) calls $\sigma_{ext}$ and which is a measure of the scatter of points about the line fitted to them; for a good fit it should be comparable to the anticipated experimental error in the points. The second involved plotting the results on a Hewlett-Packard 7225A plotter, for visual examination of the fit.

A disadvantage of numerical integration as a basis for least-squares fitting is that it is very hard to see which parts of the data actually define the individual rate constants.[1] This may be contrasted with the situation seen for example in first order kinetics, where it is quite clear that data from late in the reaction, say the ninth or tenth half-lives, principally determine the infinity value; that data from the first part of the reaction principally determine the initial value, and the initial slope, which depends both on the rate constant and on the total change in the quantity being followed; and that the rate constant is determined by data defining the curvature between the initial and final lines, over the first two–three half-lives which are followed. For data of high precision, later stages of the reaction will contribute to defining the rate constant. For reactions following the mechanism of [1]–[3], when integration in closed form is not possible, it is clear that $k_1$ and $k_3$ will be most important at long times, and that $k_1$ and/or $k_2$ will be important at short times, but it is not easy to see which portion of the data define which rate constant, even when all three rate constants are important, and even more when one may be unimportant. By contrast we may

[1]NOTE ADDED IN PROOF: Since this manuscript was accepted for publication, we became aware of a paper (11) which addressed the problem of which parts of a set of data determine particular parameters, for systems where all of the parameters are specified by the data.

consider a closely related situation where integration in closed form is possible. For the system described by reactions [1]–[3], if [B] ≫ [A] so that [B] was essentially constant, then $k_3$ would not matter, the kinetics would be simple and the rate law would become

$$OD = OD_0 + (a\Delta\varepsilon)\{1 - \exp[-(k_1 + k_2 b)t]\}$$

Here six theoretical quantities would still be required to specify the observed OD–time curve, namely: two concentrations, $a$ and $b$; two rate constants, $k_1$ and $k_2$; the initial OD, and the change in extinction coefficient. However, these would be grouped into three parameters which could be determined from the data. This situation, that numerical integration must use all of the theoretically required quantities, without grouping them into composite parameters, means that there is no obvious way to tell whether a particular rate constant is actually specified by the data. As we will see there can easily be cases where there is strong covariance of parameters, so that least-squares fitting can lead to values quite different from the optimum if a parameter which is not well determined by the data is allowed to vary. Furthermore, numerical integration is a rather slow procedure, and the least-squares method based upon it converges slowly in our experience.

A simpler method, which leads to a convenient solution to this problem, involves calculation of instantaneous derivatives from the experimental absorbance–time data. This calculation is practical if one has many points (generally 200 per run in the present case) and the data are in computer readable form so that the calculations can all be done automatically. There are problems of noise which pose limitations for this approach, and one must compromise between taking slopes from few points, and accepting high noise levels, and taking slopes involving more points and inevitably smoothing out some of the information, particularly at the beginning of the reaction where we are especially interested in the instantaneous slope. In the present case we calculate the quantity:

$$[6] \quad z = (dx/dt)/(a - x) = k_1 + k_2 (b - y)$$

Inevitably this quantity becomes very noisy at long times where both numerator and denominator are small. It is also inevitable that uncertainties in "$a$" have serious effects on "$z$" and quantities derived from it. However, this error becomes major only for long times as $(a - x)$ becomes small. We have found that in many cases the derivative method leads to a convenient solution, and allows one to see what part of the data define the derived rate constants.

One must recognize that there are also disadvantages to the derivative method. In the case where the decrease in $z$ is second order we really use only a small part of the data; the early points to estimate $z_0$, and points around the minimum to estimate $z_{min}$ and $t_{min}$. Since the calculated derivatives have substantial errors, quantities calculated from them are necessarily imprecise. Set against these disadvantages are the advantages of a more direct extraction of rate constants, and the possibility of a more intuitive recognition of whether the rate constants are truly determined by the data.

In applying the derivative method, two situations can be recognized which require different treatment of the data. If only one of the two reagent concentrations, [A] and [B], changes appreciably during the time that $z$ decreases to its minimum, the kinetics for this decline will be pseudo-first order. If it is [B] which is constant, then the kinetics will be simple and can be dealt with by traditional methods. If both change, then the kinetics will be second order and intractable. If $z$ is either constant after the minimum has been reached or else increases slowly, then a linear approximation will lead to useful simplification in the case where the decrease to the minimum is pseudo-first order in [A]. The increase must be slow enough that the steady state approximation remains good if this is to be a useful approach.

Listings of the computer programs DERIV3 and RIGLSQ6 have been deposited as supplementary material.[2] These programs were written in Small Systems Services FORTRAN IV.

## Results

In a study reported in the accompanying paper (7) of the reaction of the steroidal imidazoles, **1** and **2**, with a variety of substrates of general formula **3**, we were forced to study the kinetics under conditions where the concentrations of both reagents were comparable, and the rate of the uncatalyzed reaction was comparable with the rate of the bimolecular reaction of interest. In some cases regeneration of the nucleophile, $k_3$, was clearly important, in other cases it clearly was not. Thus the situation described above arose, and we were faced with the problem of extracting the values for $k_2$ which were the object of the exercise.

[2]Copies of the supplementary material may be obtained, at a nominal charge, from the Depository of Unpublished Data, CISTI, National Research Council of Canada, Ottawa, Ont., Canada K1A 0S2.

Can. J. Chem. Downloaded from www.nrcresearchpress.com by 210.87.254.105 on 09/06/12
For personal use only.

Can. J. Chem. Downloaded from www.nrcresearchpress.com by 210.87.254.105 on 09/06/12
For personal use only.

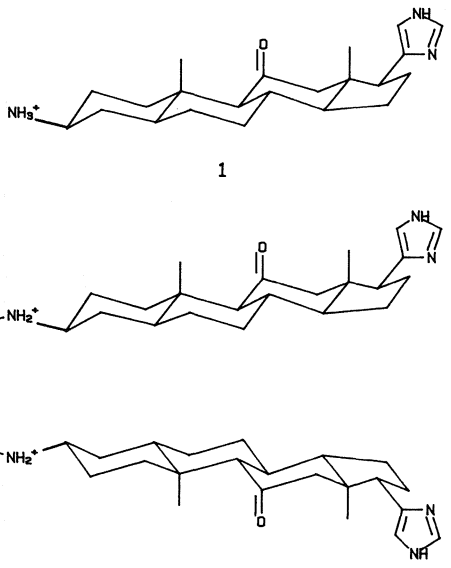

1



2

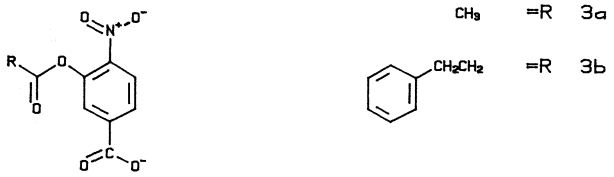

3a, b

The first case considered involves the reaction of **1** and ACE-HNB.[3] Despite the fact that the kinetics were known to be complex, it was possible to get plausible fits to either a first order or a second order integrated rate law by non-linear least squares (4, 5), as shown in Figs. 1 and 2.

Least-squares fitting making use of numerical integration can be employed, and also leads to a plausible fit as shown in Fig. 3.

It turned out that the values obtained for the parameters were strongly dependent upon the number and the identity of the parameters allowed to vary. Figure 3 shows the results when $[A]_0$, $k_2$, and $k_3$ were determined by least-squares, while the other four quantities were held constant. Very similar fits were obtained when $[A]_0$, $k_1$, $k_2$, and $k_3$ were determined by least-squares, but then $k_1$ rose to a value three times the independently measured value (8) and $k_2$ fell, with only a small change in the quality of the fit; see Table 1. As one would expect for this behavior, the correlation coefficient (4) for

[3]Abbreviations used: ACE-HNB = acetyl hydroxynitrobenzoate, **3***a*; HCA-HNB = hydrocinammoyl hydroxynitrobenzoate, **3***b*.

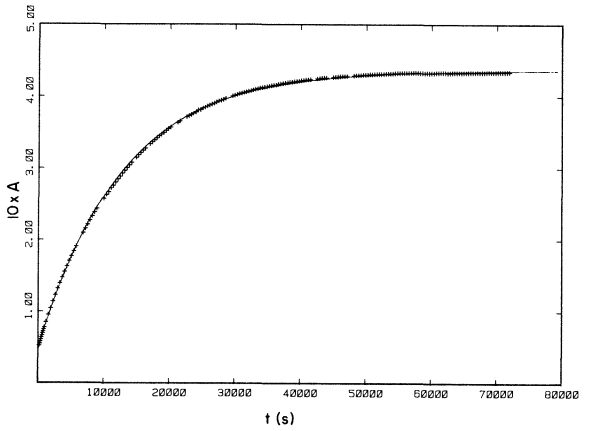


FIG. 1. Reaction of $9.77 \times 10^{-5}$ *M* ACE-HNB with $9.69 \times 10^{-5}$ *M* **1** fitted to a first order integrated rate law; $y = a_1 + a_2 \exp(-a_3 t)$, with $a_1 = 4.37$, $a_2 = -3.89$, $a_3 = 0.0000798$.

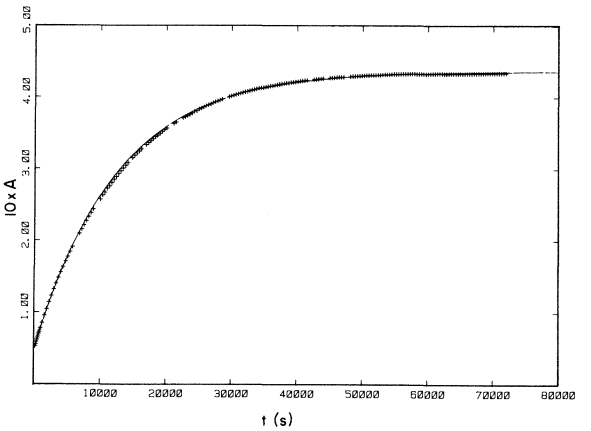


FIG. 2. Reaction of $9.77 \times 10^{-5}$ *M* ACE-HNB with $9.69 \times 10^{-5}$ *M* **1** fitted to a second order integrated rate law; $y = a_1 + a_2[\exp(a_3 t) + 1]/[\exp(a_3 t) + a_4]$, with $a_1 = 0.476$, $a_2 = 3.894$, $a_3 = 7.95 \times 10^{-5}$, $a_4 = 0.0158$.

$k_1$ and $k_2$ from the least-squares fit was large and negative: $-0.9982$. To obtain the observed infinity value the product of $[A]_0$ and $\Delta\varepsilon$ had to be decreased by 8%; whether $\Delta\varepsilon$ was decreased by this amount or held to the experimental value (7) while $[A]_0$ was allowed to vary made little difference in the quality of the fit; see Table 1.

Finally it is possible to apply the derivative method; in this case a plot of $z$ vs. $t$, e.g., Fig. 4 shows a fall in $z$ followed by a rise to approximately the initial value. The initial value of $z$, $z_0$, is equal to $k_1 + k_2 b$; if $k_1$ and $b$ are known then $k_2$ can be calculated. In effect we are using initial rates to determine $k_2$, with an extrapolation procedure to give an improved estimate for the initial rate. From the position of the minimum it is possible to deduce

TABLE 1. Various sets of parameters for the reactions of **1** with ACE-HNB

| $[A]_0$ | $[B]_0$ | $A_0$ | $\Delta\varepsilon$ | $k_1$ | $k_2$ | $k_3$ | $\sigma_{ext}$ |
|---|---|---|---|---|---|---|---|
| (*a*) Least-squares by numerical integration: values in italics were determined by least-squares; the others were held constant | | | | | | | |
| *9.00 × 10⁻⁵* | 9.69 × 10⁻⁵ | 0.477 | 43200 | 1.19 × 10⁻⁵ | *0.761* | *3.19 × 10⁻⁴* | 0.0019 |
| *9.01 × 10⁻⁵* | 9.69 × 10⁻⁵ | 0.477 | 43200 | *3.01 × 10⁻⁵* | *0.554* | *1.88 × 10⁻⁴* | 0.0018 |
| *9.77 × 10⁻⁵* | 9.69 × 10⁻⁵ | 0.477 | 39830 | *3.14 × 10⁻⁵* | *0.541* | *1.95 × 10⁻⁴* | 0.0018 |
| (*b*) Derivative method | | | | | | | |
| 9.77 × 10⁻⁵ | 9.69 × 10⁻⁵ | 0.477 | 39830 | 1.19 × 10⁻⁵ | 0.823 | 1.45 × 10⁻⁴ | |

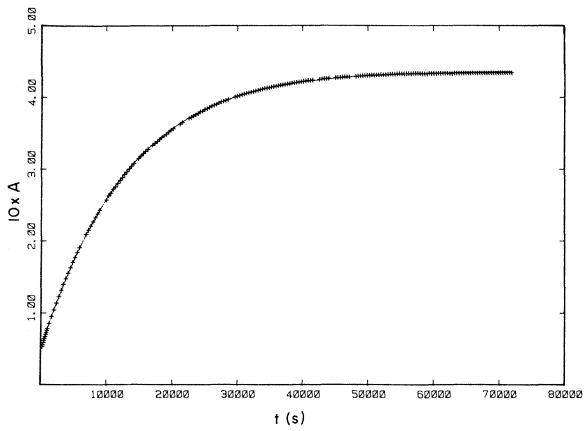


FIG. 3. Reaction of 9.77 × $10^{-5}$ *M* ACE-HNB with 9.69 × $10^{-5}$ *M* **1** fitted by least-squares using numerical integration; held constant were $[B]_0 = 9.69 \times 10^{-5}$ *M*, $10 \times A_0 = 0.477$, $\Delta\varepsilon = 4320$, $k_1 = 1.19 \times 10^{-5}$; determined by least-squares were $[A]_0 = 9.00 \times 10^{-5}$ *M*, $k_2 = 0.761$ $M^{-1}$ $s^{-1}$, and $k_3 = 3.19 \times 10^{-4}$ $s^{-1}$.

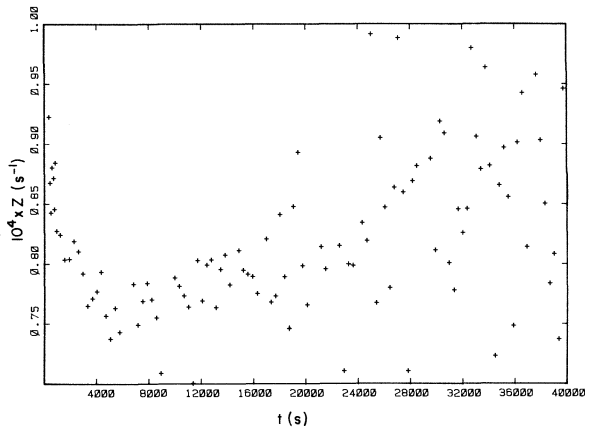


FIG. 4. Reaction of 9.77 × $10^{-5}$ *M* ACE-HNB with 9.69 × $10^{-5}$ *M* **1**. Plot of $z = (dA/dt)/(\Delta A_\infty - \Delta A_t)$; $10 \times \Delta A = 4.368$, $10 \times A_0 = 0.477$.

a value for $k_3$. At the minimum:

[7] $$dy/dt = 0.0 = k_2(a - x_{min})(b - y_{min}) - k_3 y_{min}$$

[8] $$y_{min} = -(z_{min} - k_1 - k_2 b)/k_2 = (z_0 - z_{min})/k_2$$

[9] $$k_3 = k_2(a - x_{min})(b - y_{min})/y_{min} = [(A_\infty - A_{min})/\Delta\varepsilon][(z_0 - k_1)/b][(z_0 - k_1)/(z_0 - z_{min}) - 1]$$

The value for $k_1$ used in these calculations was that measured previously in this laboratory (8). The decline in $z$ from its initial value to the minimum did not obey first order kinetics since both ester and steroidal imidazole concentrations were changing during the time required by this process. Therefore no simple fit of a curve to the data was possible. Using the experimental value for $k_1$ (8), and the values for $k_2$ and $k_3$ derived from the $z$ vs. $t$ curve as described above, as well as independent values for the concentrations, extinction coefficients, and initial absorbance, we calculated the curve in Fig. 5 by numerical integration.

Another situation arose in the reaction of **2** with HCA-HNB (7), where the ester was in excess. The data could be fitted to eq. [10]:

[10] $$Abs = a_1 + a_2 \exp(-a_3 t) + a_4 t$$

see Fig. 6. However, this was not a very satisfactory way to handle the data because the contribution of $k_2 b$ to the observed rate was rather close to the contribution of $k_1$. The data could be fitted by least squares using our numerical integration procedure with the results shown in Fig. 7.

For this fit three parameters were allowed to vary: $[A]_0$, $k_2$, and $k_3$. Allowing $k_1$ to vary as well made little change in either the parameters or the quality of the fit. Analysis of the data by our derivative treatment led to values for the rate constants. In the present case, a plot of $z$ vs. $t$, Fig. 8, showed a decline to a constant value with no apparent recovery at longer times during the period for which the reaction was followed. This corresponds to the establishment of a steady state. The following analysis would also apply if there were a slow increase in $z$ after the decrease to the minimum. It is a fair approximation to take the ap-

Can. J. Chem. Downloaded from www.nrcresearchpress.com by 210.87.254.105 on 09/06/12
For personal use only.

Can. J. Chem. Downloaded from www.nrcresearchpress.com by 210.87.254.105 on 09/06/12
For personal use only.

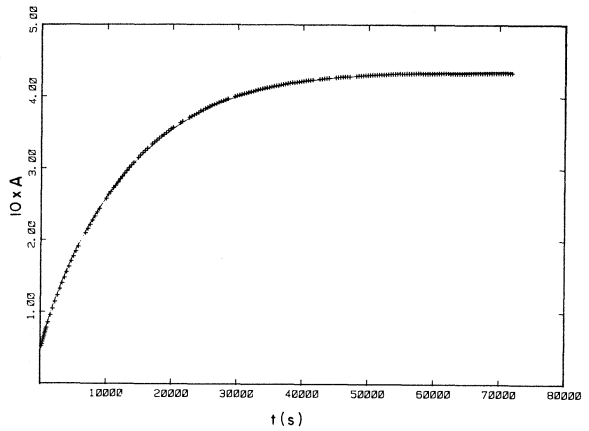


FIG. 5. Reaction of $9.77 \times 10^{-5}$ $M$ ACE-HNB with $9.69 \times 10^{-5}$ $M$ **1**. The curve is drawn by numerical integration using parameters based on the derivative method. $[A]_0 = 9.77 \times 10^{-5}$ $M$, $[B]_0 = 9.69 \times 10^{-5}$ $M$, $10 \times A_0 = 0.477$, $\Delta\varepsilon = 3983$, $k_1 = 1.19 \times 10^{-5}$ s$^{-1}$, $k_2 = 0.823$, $k_3 = 1.45 \times 10^{-4}$ s$^{-1}$.

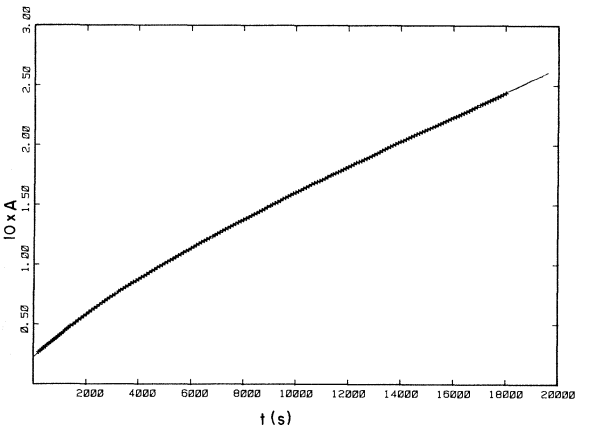


FIG. 6. Reaction of $2.25 \times 10^{-5}$ $M$ HCA-HNB with $1.16 \times 10^{-6}$ $M$ **2** in 10 cm cells, fitted to the equation $y = a_1 + a_2 \exp(-a_3 t) + a_4 t$, with $a_1 = 0.632$, $a_2 = -0.406$, $a_3 = 2.37 \times 10^{-4}$, and $a_4 = 1.01 \times 10^{-4}$.

proach to steady state as first order, since at the time that the minimum value in $z$ is attained, only about 20% of the ester has reacted, and this allows a simple analysis of the data. Equation [5] becomes:

$$[11] \quad dy/dt = k_2 a(b - y) - k_3 y = k_2 ab - (k_2 a + k_3)y$$

After integration

$$[12] \quad y = [k_2 ab/(k_2 a + k_3)]\{1 - \exp[-(k_2 a + k_3)t]\}$$

$$[13] \quad z = k_1 + k_2 b - [k_2^2 ab/(k_2 a + k_3)] + [k_2^2 ab/(k_2 a + k_3)]\{\exp - [(k_2 a + k_3)t]\} = z_{\text{final}} + \Delta z \exp(-\kappa t)$$

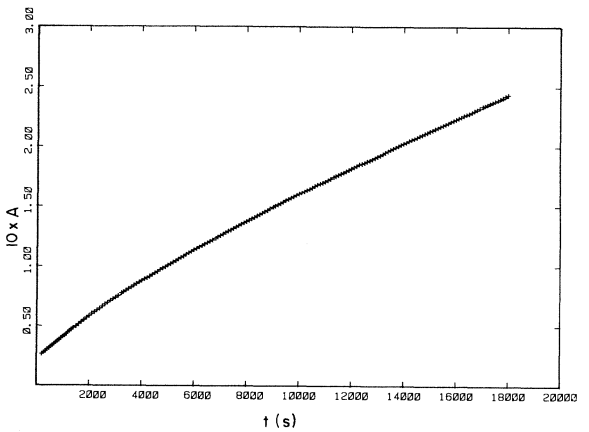


FIG. 7. Reaction of $2.25 \times 10^{-5}$ $M$ HCA-HNB with $1.16 \times 10^{-6}$ $M$ **2** in 10 cm cells, fitted by least-squares using numerical integration; held constant were $[B]_0 = 1.16 \times 10^{-6}$ $M$, $10 \times A_0 = 0.233$, $\Delta\varepsilon = 4320$, and $k_1 = 9.74 \times 10^{-6}$ s$^{-1}$; fitted by least-squares were $[A]_0 = 2.37 \times 10^{-5}$ $M$, $k_2 = 7.53$ $M^{-1}$ s$^{-1}$, and $k_3 = 4.33 \times 10^{-5}$ s$^{-1}$.

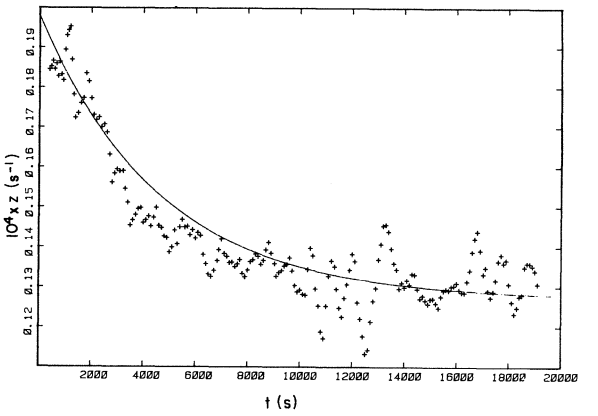


FIG. 8. Reaction of $2.25 \times 10^{-5}$ $M$ HCA-HNB with $1.16 \times 10^{-6}$ $M$ **2** in 10 cm cells, derivative plot; $z$ was calculated using $10 \times \Delta A_\infty = 9.72$ and $10 \times A_0 = 0.233$. The line was fitted by least-squares $z = a_1 + a_2 \exp(-a_3 t)$, with $a_1 = 0.127$, $a_2 = 0.074$, and $a_3 = 0.000201$.

where

$$\Delta z = k_2^2 ab/(k_2 a + k_3)$$
$$\kappa = k_2 a + k_3$$

Then

$$[14] \quad k_2 = \sqrt{\kappa \Delta z / ab}$$

$$[15] \quad k_3 = \kappa - k_2 a$$

$$[16] \quad k_1 = z_0 - k_2 b$$

An advantage of this approach is that it gives an independent estimate for $k_1$, which can be measured in a separate experiment, and so provides a test of internal consistency. $\Delta z$ can be as large as

$k_2b$ for $k_3$ negligibly small and can be zero if $k_3 \gg k_2a$. Thus the magnitude of $z_0$ relative to $k_1$ gives an idea of how well $k_2b$ is defined by $z_0$, and the magnitude of $\Delta z$ relative to $k_2b$ gives an idea of how well $k_3$ is defined. The smallest possible value for $z_{final}$, when $k_3 \simeq 0$, is $k_1$; thus if $z_{final}$ does not fall close to $k_1$ one cannot expect $k_1$ to be well defined by the data. Similarly if $z_0 \gg k_1$, so that it is mostly determined by $k_2b$, one cannot expect $k_1$ to be well defined by eq. [16]. Figure 9 shows that numerical integration based on rate constants derived as just described gives a satisfactory fit to the data.

Figure 9 also illustrates an interpretational hazard when calculating absorbance–time curves from parameters calculated indirectly, and not by direct fitting to the data. For this reaction error analysis based on the least-squares fit to the $z$ vs. $t$ plot leads to $k_1 = 1.07 \pm 0.10 \times 10^{-5}$ s$^{-1}$. If this value is used (Fig. 9*b*) the fit looks rather poor. On the other hand if a value for $k_1 = 1.04 \times 10^{-5}$ s$^{-1}$ is used (Fig. 9*a*) the fit looks excellent. The difference is much less than the uncertainty in $k_1$.

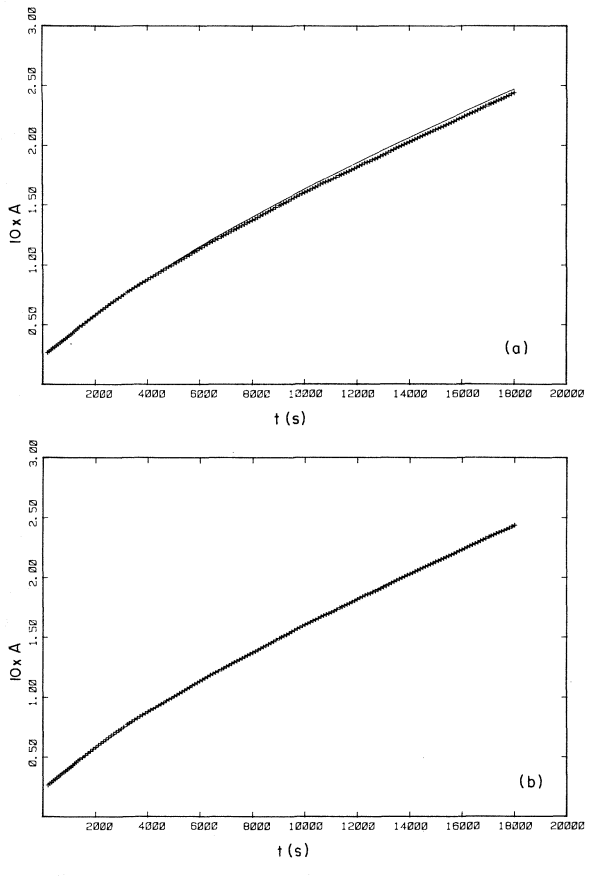


FIG. 9. Reaction of $2.25 \times 10^{-5}$ *M* HCA-HNB with $1.16 \times 10^{-6}$ *M* **2** in 10 cm cells, line calculated by numerical integration using parameters from the derivative fit; $[A]_0 = 2.25 \times 10^{-5}$ *M*, $[B]_0 = 1.16 \times 10^{-6}$ *M*, $10 \times A_0 = 0.233$, $\Delta\varepsilon = 4320$, $k_2 = 7.70$ $M^{-1}$ s$^{-1}$, $k_3 = 4.47 \times 10^{-5}$ s$^{-1}$, and $k_1 = 1.07 \times 10^{-5}$ s$^{-1}$ (9*a*) or $1.04 \times 10^{-5}$ s$^{-1}$ (9*b*).

Various methods for determining parameters by fitting procedures based on numerical integration of rate laws have been reported (9, 10); the method reported here is convenient for simple reaction systems but not unique. We are not aware of any report of approaches analogous to the derivative method reported here.

## Conclusions

When it is not possible to obtain an integrated rate law in analytical form, either of the methods described in this paper can be used to obtain the rate constants. We prefer to use the derivative method although sometimes it may be preferable to use least-squares based on numerical integration. In the latter case one must be very careful because the parameters in the least-squares fit need not all be specified by the data, and may show striking covariance.

## Acknowledgment

Financial assistance from the Natural Sciences and Engineering Research Council of Canada is gratefully acknowledged.

1. A. A. FROST and R. G. PEARSON. Kinetics and mechanism. Wiley, New York. 1961.
2. Z. G. SZABO. *In* Comprehensive chemical kinetics. Vol. 2. *Edited by* C. H. Bamford and C. F. H. Tipper. Elsevier, Amsterdam. 1969. pp. 1–80.
3. A. IKAI and C. TANFORD. J. Mol. Biol. **73**, 145 (1973).
4. P. R. BEVINGTON. Data reduction and error analysis for the physical sciences. McGraw-Hill, New York. 1969.
5. W. E. DEMING. Statistical adjustment of data. Dover. 1964.
6. H. MARGENAU and G. M. MURPHY. The mathematics of physics and chemistry. 2nd ed. Van Nostrand, Princeton, NJ. 1956.
7. J. P. GUTHRIE, P. A. CULLIMORE, R. S. MCDONALD, and S. O'LEARY. Can. J. Chem. **60**, 747 (1982).
8. J. P. GUTHRIE and Y. UEDA. Can. J. Chem. **54**, 2745 (1976).
9. K. B. WIBERG. *In* Investigations of rates and mechanisms of reactions. 3rd ed. Part I. *Edited by* E. S. Lewis, Wiley-Interscience, New York. 1974. p. 764.
10. P. W. HEMKER. *In* Analysis and simulation of biochemical systems. *Edited by* H. C. Hemker and B. Hess. Elsevier, Amsterdam. 1972. p. 59.
11. M. WASNER, G. CZERLINSKI, and M. PRINS. Comput. Biol. Med. **5**, 105 (1975).

Can. J. Chem. Downloaded from www.nrcresearchpress.com by 210.87.254.105 on 09/06/12
For personal use only.

# Flow $^1$H nmr study of the rapid nucleophilic addition of amino acids to 4-formylpyridine

LIANG K. TAN AND MICHAEL COCIVERA[1]

*The Guelph–Waterloo Centre for Graduate Work in Chemistry, Department of Chemistry, University of Guelph, Guelph, Ont., Canada N1G 2W1*

Received June 26, 1981

LIANG K. TAN and MICHAEL COCIVERA. Can. J. Chem. **60**, 772 (1982).

Rapid addition of primary amino acids and imidazole to 4-formylpyridine to form carbinolamine intermediates in water has been studied by means of stopped-flow $^1$H nuclear magnetic resonance spectroscopy. The equilibrium constant $K_n$ for this process was determined using stopped-flow uv spectroscopy. For the amino acid D,L-alanine and its derivatives, D,L-alanine methyl ester and D,L-alanylglycine, $K_n$ does not appear to correlate with $K_a$, the acid dissociation constant. Values of $k_n$, the addition rate constant, appear to be independent of pH and buffer concentration for these nucleophiles. The limited data indicate that the variation in rates of nucleophilic addition to 4-formylpyridine cannot be accounted for in terms of p$K_a$, $K_n$ or related to systematic changes in structure of the nucleophile. As a group, the primary amino acid D,L-alanine and its derivatives have comparable $k_n$ values within a factor of two in spite of their different p$K_a$ values. Imidazole, an aromatic secondary diamine, has a $k_n$ value that is 10 to 20 times larger than these primary amines and has a relatively small $K_n$ value. At the same time, its $k_n$ value is comparable to that found previously for sarcosine, a secondary acyclic amino acid having substantially larger p$K_a$ and $K_n$ values. The nucleophilic addition step of the primary amino acid and derivatives is rapid relative to the subsequent dehydration and prototropic shift steps. It occurs in a pH range at which pyridine nitrogen protonation is negligible.

LIANG K. TAN et MICHAEL COCIVERA. Can. J. Chem. **60**, 772 (1982).

Faisant appel à la spectrocopie de rmn du $^1$H à flux stoppé, on a étudié l'addition rapide des acides aminés primaires et de l'imidazole sur la formyl-4 pyridine en vue d'obtenir les intermédiaires du type carbinolamine dans l'eau. On a déterminé la constante d'équilibre $K_n$ de cette réaction en utilisant la spectroscopie uv découlement à flux stoppé. Dans le cas de D,L-alamine et de ses dérivés, l'ester méthylique de la D,L-alanine et de la D,L-alanylglycine, il n'existe pas de relation en $K_n$ et $K_a$, la constante de dissociation de l'acide. Les valeurs de $K_n$, la constante de vitesse d'addition, semblent être indépendantes du pH et de la concentration du tampon de ces nucléophiles. Des données limitées indiquent que la variation de vitesse de l'addition nucléophile sur la formyl-4 pyridine ne peut être reliée à p$K_a$, à $K_n$ ou à des changements systématiques apparents dans la structure du nucléophile. En tant que groupe, l'acide aminé primaire D,L-alanine et ses dérivés ont des valeurs de $k_n$ qui sont comparables puisqu'elles ne varient pas plus que du simple au double même si les valeurs de leur p$K_a$ sont différentes. L'imidazole, une diamine secondaire aromatique, a une valeur de $k_n$ qui est de 10 à 20 fois plus élevée que celles des amines primaires, alors que son $K_n$ est relativement faible. En même temps, la valeur de $k_n$ est comparable à celle trouvée antérieurement pour la sarcosine, un acide aminé secondaire acyclique ayant des valeurs de p$K_a$ et $K_n$ nettement plus élevées. L'étape d'addition nucléophile de l'acide aminé primaire et des ses dérivés est rapide par rapport aux étapes de déshydratation et de glissement protopiques subséquentes. Elle se produit dans un domaine de pH où la protonation de l'azote de la pyridine est négligeable.

[Traduit par le journal]

## Introduction

Nucleophilic addition of amino acids to 4-formylpyridine (FPY) and its analogues has been used as a model reaction to probe the details of enzymatic reactions involving pyridoxal phosphate (1–3). These studies indicate that imine formation proceeds through a tetrahedral intermediate (1). At high pH equilibration between the aldehyde and this intermediate is rapid relative to the subsequent dehydration step (1, 2) and it has been possible to measure the equilibrium constant for a variety of nucleophiles (2, 4). Measurement of the rate of addition has been reported only for secondary amines for which the reaction with FPY does not proceed beyond the carbinolamine intermediate (2).

In the present paper, we report rate data for the rapid addition of primary amino acids to FPY to form carbinolamine intermediates (CA), which do, in fact, undergo subsequent dehydration. By means of stopped-flow nmr it has been possible to measure the exchange broadened proton nmr resonance of the aldehyde proton of FPY from which $k_n$ and $k_{-n}$ can be calculated for the equilibrium

[1] 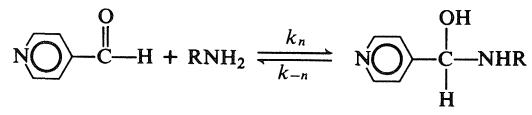


FPY CA

in which $RNH_2$ is alanine (ALN), alanine methyl ester (AME), and alanylglycine (AGY). The details of the subsequent steps are to be reported in the following paper.

## Experimental

*Chemicals*

4-Formylpyridine (FPY) was vacuum distilled and stored over molecular sieves at −25°C. Imidazole was recrystallized

[1]To whom all correspondence should be addressed.

0008-4042/82/060772-06$01.00/0

©1982 National Research Council of Canada/Conseil national de recherches du Canada

Can. J. Chem. Downloaded from www.nrcresearchpress.com by 210.87.254.105 on 09/06/12
For personal use only.

Can. J. Chem. Downloaded from www.nrcresearchpress.com by 210.87.254.105 on 09/06/12
For personal use only.

twice from benzene. Diazobicyclooctane (DABCO) was sublimed at reduced pressure. Benzyl alcohol, spectrograde acetonitrile, D,L-alanine (ALN), D,L-alanine methyl ester hydrochloride (AME), and D,L-alanylglycine (AGY) were used without purification. The last two compounds were stored at −25°C. The oxazolidine of 4-acetylpyridine was prepared from 4-acetylpyridine (vacuum distilled) and 2-amino-2-methyl propanol-ol as described previously (5). Deionized water was distilled in an all-glass apparatus.

*Solutions*

In order to avoid possible heavy metal catalyzed reactions of FPY, $1 \times 10^{-4}$ *M* sodium ethylenediamine tetraacetate was included in all solutions. To reduce the possibility of decomposition of FPY and AME, which are not stable for long periods at high pH, these compounds were added only after the solutions had been brought close to the desired pH value; then the final minor pH adjustments were made. Solutions were buffered with imidazole, phosphate, or DABCO at an ionic strength of 1.3 *M* (KCl). A Radiometer PHM 63 digital pH-meter was used. The pD value was obtained by adding 0.4 to the pH meter reading of the $D_2O$ solution (6).

*Exchange reaction*

Proton exchange data were obtained at 30°C by measuring the line width of the broadened signal of the aldehyde proton of FPY relative to that for the signal due to the aromatic protons of benzyl alcohol, which was used as an internal reference to monitor changes in chemical shift and magnetic field homogeneity. Stopped-flow was employed to measure the nmr spectra (7, 8) because CA undergoes dehydration at a substantial rate as described in the following paper (8*c*). To conserve material, the line width was measured as a function of time during this dehydration reaction. Consequently, the exchange rate and, therefore, the line width was time-dependent since it is related to the concentration of FPY and amino acid as described below. The concentration of these reactants at the time of each line width measurement was simulated using rate constants and rate equations presented in the following paper (8*c*).

*Equilibria*

The acid dissociation equilibrium constant $K_a$ for the amino acids in $H_2O$ were measured at 30°C and an ionic strength of 1.3 *M* (KCl) by titration to half neutralization with standardized NaOH. In the case of AME, nmr was used to verify that no significant hydrolysis had occurred during the measurement.

The equilibrium constant for hydration of FPY, $K_h$ ($\mu = 1.3$ *M* KCl) in $H_2O$ and $K_h'$ in $D_2O$, was determined by measuring the areas of the proton nmr signals due to the aldehyde proton of FPY and the corresponding proton of the hydrate of FPY. For these measurements solutions were buffered with phosphate and DABCO in the pH range 6.5 to 8.7 and in the pD range 8.0 to 9.7.

The equilibrium constant $K$ for the addition step to form carbinolamine was determined at 30 ± 1°C as described previously (4) using a D-110 Durrum stopped-flow spectrophotometer equipped with an oscilloscope. The reaction was followed as a function of time over a period of 20 ms at a wavelength of 280 nm. Extrapolation to zero time gave the absorbance of aldehyde remaining at equilibrium. The absorbances of nucleophiles and CA at this wavelength were also taken into account in this determination.[2] The molar absorptivity of CA is assumed to be the same as that for the structurally similar oxazolidine of 4-acetylpyridine.[3] The $pK_a$ of CA for each nucleophile was estimated according to the previous method (5, 9) by adjusting the $pK_a$ value for the corresponding nucleophile for substituent effects using $\sigma^*$ values.[4] The $pK_a$ values obtained in $H_2O$ and 5.4, 3.4, and 3.7 for CA derived from ALN, AME, and AGY, respectively. The rate of addition of each amino acid is too fast to be measured by stopped-flow uv. For ALN and AGY, $K$ was determined at pH 10.2 (0.200 *M* DABCO). For AME $K$ was determined at pH 7.5 (0.100 *M* imidazole); at this pH ester hydrolysis is not an important factor during the period of the determination. For each nucleophile four concentrations were employed. The value for $K$ does not take hydration of the aldehyde into account, i.e., $K$ = [CA]/[N] ([aldehyde] + [hydrate]) in which [N] is the nucleophile free base concentration. The equilibrium constant $K_n$ based on eq. [1] is calculated using the expression $K_n = K(1 + K_h)$.

## Results and discussion

Figure 1 illustrates the 100 MHz proton nmr spectra in $D_2O$ at pD 9.7 (0.400 *M* DABCO, $\mu = 1.3$ *M* KCl) at 30°C: (*A*) 0.604 *M* FPY; and (*B*) mixture of 0.302 *M* FPY and 0.100 *M* AGY. Only the portion of the spectrum downfield from the HDO signal is illustrated. In Fig. 1*A* the signals labeled *a* and *h* are due to the aldehyde proton of FPY and the corresponding proton of the hydrate of FPY, respectively. The reference signal is labeled *r*. The remaining signals are due to the ring protons of the aldehyde and its hydrate. Note in Fig. 1*B* that signal *a* is broadened but has not shifted. Furthermore, the position and width of signal *h* appears unaffected by the presence of AGY. These results permit two conclusions. First, the equilibrium given by eq. [1] is fast enough to affect the nmr line shape and is in the slow exchange category since the position of signal *a* does not change (10). If the exchange were fast relative to δ, the chemical shift between the two exchanging sites, the signals of the two sites would coalesce to form one signal having a weighted chemical shift (10). Thus in contrast with Fig. 1*B*, the broadened signal should have been observed upfield from signal *a* by about 0.64 ppm,[5] for fast exchange. Second, the hydration equilibrium is slow on the nmr time scale since both the aldehyde and hydrate signals are observed in Fig. 1*A*. Furthermore, the presence of AGY does not increase the line width of the hydrate signal

[2]Molar absorptivities of AME and AGY are found to be 0.04 and 0.19 $M^{-1}$ cm$^{-1}$ respectively at λ 280 nm, μ 1.3 *M* (KCl), and 30°C; molar absorptivity of ALN is negligible under these conditions.

[3]Molar absorptivity of oxazolidine of 4-acetylpyridine is found to be 11.6 ± 1.0 $M^{-1}$ cm$^{-1}$ at λ 280 nm, μ 1.3 *M* (KCl), and 30°C.

[4]Since $\sigma^*$ for $-CH_2Py$ is not available, it is obtained from $pK_a$ values for 4-(dimethyl amino methyl)pyridine ($pK_a = 7.66$) and trimethylamine ($pK_a = 9.81$), giving a value of 0.65.

[5]This value is calculated assuming the chemical shift for the carbinolamine is about the same as that for the hydrate, as has been found previously (see ref. 8*a*). A comparable value is estimated by the method of Shoolery (see ref. 11).

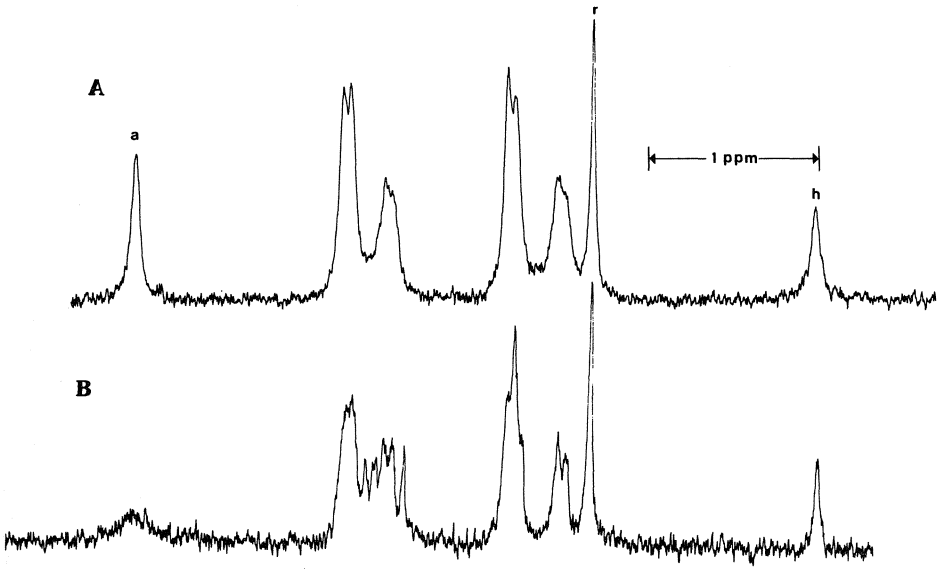


FIG. 1. Partial $^1H$ nmr spectra at 100 MHz in $D_2O$ at pD 9.7 buffered by 0.400 *M* DABCO at 30°C with 1.3 *M* ionic strength. Magnetic field increases from left to right. About 20% acetonitrile was used as an internal lock signal. *A*. portion of the spectrum downfield from the lock signal for a solution containing 0.602 *M* FPY; *B*. same region for a reaction mixture containing 0.301 *M* FPY and 0.100 *M* AGY initially, scan starts immediately after the flow of the liquid is stopped and takes about 4 min to complete. Assignment of signals: *a*, aldehyde proton of FPY; *h*, corresponding proton for hydrated FPY; *r*, ring protons of benzyl alcohol used as an internal line width and chemical shift reference; unlabeled signals are due to the ring protons of the aldehyde and hydrate forms of FPY in *A*, plus product in *B*. During the measurement of the aldehyde proton resonance very little dehydration has occurred.

and, therefore, does not increase the rates for hydration/dehydration. Consequently, the excess line width of the aldehyde signal has no contribution from the hydration reaction.[6]

As a result, the excess line width observed for the aldehyde signal in $D_2O$ in the presence of AGY appears to be due solely to the addition reaction [1], and $k_n$ and $k_{-n}$ are calculated using the analysis for slow exchange between two sites (5, 8*b*, 10). In this case the excess line width in rad/s is equal to $1/\tau_{FPY}$, and $1/\tau_{FPY} = k_n[AGY]$ since $\tau_{FPY}$ is the average lifetime for the aldehyde proton. [AGY] is the concentration of AGY free base. For these calculations, the excess line width has been corrected for variations in magnetic field homogeneity by means of an internal reference line width (benzyl alcohol) as described previously (5). The corresponding signal due to CA is not observed because it is small and broad (about 1/5 the area for the signal due to the aldehyde proton of FPY). Consequently the value for $k_{-n}$ is calculated using the value for $K_n$ and $k_n$. Consistent with slow exchange is the fact that $\delta\tau$ is 5, in agreement with the requirement that $\delta\tau$ should be about 4 or larger (10).[7]

When $H_2O$ is the solvent, the excess line width again appears to be due to slow exchange for AGY, ALN, and AME addition to FPY. However, at low pH the signal shift calculated on the basis of fast exchange is small (around 0.1 ppm or less) because the concentration of nucleophile free base is low under the conditions employed. Consequently the chemical shift measurements do not provide conclusive information about the exchange rate. As a result, the solvent deuterium isotope effect is used to decide between slow and fast exchange at low pH.

For fast exchange in $H_2O$, the ratio $(k_n^{H_2O}/k_n^{D_2O})$ is 31 and 25 for AGY at pH 7.4 and 7.5, respectively.[8] There appears to be no precedent for such large

[6]On the other hand, this hydration reaction is fast relative to the dehydration of CA, i.e., both the addition and hydration equilibria for FPY are maintained during the dehydration of CA.

[7]For this calculation, the value for $\delta$ is 2520 rad/s (see footnote 5) and $\tau$ is calculated using $1/\tau = k_n[AGY] + k_{-n}$ (see refs. 5 and 10).

[8]For this calculation, the chemical shift $\delta$ between the signals of the two sites is estimated as described above. The uncertainty in the chemical shift is unlikely to exceed 0.5 ppm. Consequently, the error in $k_n$ for $H_2O$ solvent is unlikely to exceed 25%. The line width for CA in the absence of exchange is assumed to be equal to the one for the hydrate of FPY since aldehyde–hydrate exchange is slow at this pH.

Can. J. Chem. Downloaded from www.nrcresearchpress.com by 210.87.254.105 on 09/06/12
For personal use only.

Can. J. Chem. Downloaded from www.nrcresearchpress.com by 210.87.254.105 on 09/06/12
For personal use only.

solvent deuterium isotope effects. For example, for the analogous reaction involving hydrolysis of *meta*- and *para*-substituted 2,2,2-trifluoro-*N*-methylacetanilides via a carbinolamine intermediate none of the various steps in the mechanism is found to have a solvent isotope effect that exceeds 3.0 (12). Similar results are found for hydrolysis of *para*-substituted benzoylimidazoles (12). Consequently, when $H_2O$ is the solvent it appears that the excess line width in the presence of AGY is due to slow exchange rather than fast exchange. In view of the close similarity in structure between the three nucleophiles, we conclude that the slow exchange interpretation also applies at low pH for ALN and AME.

Imidazole also undergoes nucleophilic addition to FPY; however, the rate is fast relative to the chemical shift δ between the signals due to the two exchanging sites because the line width and the position of the broadened signal depend on the concentration of imidazole at pH 8.2. Because the equilibrium constant for the addition appears to be small and the concentration of imidazole could not be increased conveniently above 0.8 *M*, only a semiquantitative value for $K_n$ and δ were obtained by successive approximation using eq. [1] and $\delta_C - \delta_{FPY} = p\delta$ in which $p$ is the proton fraction for CA and $\delta_C$ is the chemical shift of the coalescence signal. As a result, the values for $k_n$ must also be considered to be semiquantitative.

To determine $k_n$ for the amino acid nucleophiles when imidazole is used to buffer the solutions, it is necessary to include the effect of the imidazole equilibrium on the line width of the aldehyde signal as well as on the concentration of the amino acid free base. Because nucleophilic substitution at the tetrahedral carbon atom of CA is expected to be substantially slower than nucleophilic addition to the aldehyde carbon, addition by amino acid and imidazole can be treated as separate competitive exchange processes. Consequently, the contribution to the line width made by each exchange process is additive (10). This consideration also applies to the aldehyde–hydrate exchange, whose contribution increases as the pH increases. As discussed above, to calculate $k_n$ from this excess line width, it is necessary to know the concentration of amino acid free base in equilibrium with its corresponding CA. In the presence of imidazole, this concentration was calculated by including the imidazole addition equilibrium as well as the two acid–base equilibria. If the concentration of amino acid free base is not adjusted in this manner, the $k_n$ value calculated from the excess line width is about 18 and 26% larger than the ones listed in Table 1 for AGY and AME, respectively.

Values for $K_n$, $k_n$, and $k_{-n}$ are listed in Table 1 along with the $pK_a$ for each nucleophile. As has been found previously, there appears to be no direct correlation between $K_n$ and $K_a$ (4, 5). In agreement with our $K_n/(1 + K_h)$ values of 2.3[9] and 0.3 $M^{-1}$ for ALN and imidazole, respectively,[10] Sander and Jencks measured values of 2.1[9] and 0.3 $M^{-1}$, respectively (4).

Values of $k_n$ listed in Table 1 are calculated using a linear dependence between $1/\tau$ and the concentration of nucleophile. Temperature jump studies of the addition of sarcosine and piperazine to FPY indicate both a linear and nonlinear term for $1/\tau$ (2); however, a ten-fold variation in nucleophile concentration was possible in these studies, and the nonlinearity becomes apparent at the high concentrations. In the present study a maximum of only about a four-fold variation in concentration was possible because of the limitations in accuracy of nmr line width measurements for this system. Within these limitations, a nonlinear term was not observed. In addition, the nature and concentration of the buffer appear to have no effect on the rate of addition. Thus, varying the concentration of imidazole or DABCO from 0.4 *M* to 0.8 *M* had no effect on the value of $k_n$ for the amino acid nucleophiles. Likewise comparison of the results for phosphate vs. imidazole or imidazole vs. DABCO in Table 1 indicates no dependence on the nature of the buffer. Similar results have been found previously for the addition of various α-nucleophiles to a variety of ketones (5, 7, 8*b*).

Correlation between $k_n$ or $k_{-n}$ and $K_a$ or $K_n$ for the various nucleophiles is not apparent in Table 1. Considering only the amino acids including sarcosine for which the $pK_a$ is 10.03 and $K_n$ is 5.0 $M^{-1}$ (2*b*), the rate constants again do not appear to correlate with either $K_a$ or $K_n$. Thus a plot of log $k_n$ or log $k_{-n}$ vs. $pK_a$ or log $K_n$ is not linear. For this consideration, we calculate an average $k_n$ value of about $5 \times 10^4$ $M^{-1}$ $s^{-1}$ for sarcosine assuming $1/\tau$ has a linear dependence on the nucleophile concentration for data at pH 10.65 (2*b*).

This value of $k_n$ for sarcosine is about 10 times the one for ALN despite the fact that both amino

[9]These values differ from the one obtained kinetically (see ref. 1*a*).

[10]Although there are several reports concerning $K_h$ none refers to the conditions employed in our study. Furthermore, there is quite a spread in values, ranging from 1.28 to 0.67 (see refs. 2*a*, 4, and 14). For these reasons, we have determined the value listed in Table 1 as described above.

TABLE 1. Equilibrium and kinetic data for nucleophilic addition to 4-formylpyridine at 30°C and $\mu = 1.3\ M$ (KCl)

| Nucleophile[a] | $pK_a$ | $K_n$ ($M^{-1}$) | pH[b] | Buffer | $k_n \times 10^{-3}$ [c] ($M^{-1}\ s^{-1}$) | $k_{-n} \times 10^{-3}$ ($s^{-1}$) |
|---|---|---|---|---|---|---|
| | | *Solvent $H_2O$* | | | | |
| Alanylglycine | 8.28 | 4.7±0.7[d] | 7.5 | Phosphate | 2.1±0.3 | 0.45 |
| | | | 7.7 | Imidazole | 2.0±0.2 | 0.43 |
| | | | 9.2 | DABCO | 2.3±0.4 | 0.49 |
| Alanine methyl ester | 8.05 | 1.8±0.1[e] | 6.7 | Imidazole | 2.0±0.4 | 1.1 |
| | | | 7.0 | Imidazole | 1.5±0.3 | 0.83 |
| | | | 7.3 | Imidazole | 1.5±0.3 | 0.83 |
| | | | 8.0 | Imidazole | 2.0±0.4 | 1.1 |
| Alanine | 10.02 | 4.4±0.7[d] | 8.1 | Imidazole | 5.7±0.8 | 1.3 |
| | | | 8.2 | DABCO | 4.9±0.9 | 1.1 |
| | | | 9.2 | DABCO | 4.1±0.7 | 0.93 |
| Imidazole | 7.24 | 0.6[f] | 7.0 | | 40 | 69 |
| | | | 7.8 | | 35 | 61 |
| | | | 8.2 | | 31±7 | 52 |
| $H_2O$ | | 0.93±0.1[g] | | | | |
| | | *Solvent $D_2O$* | | | | |
| Alanylglycine | 8.84[h] | 3.94[i] | 7.5[j] | Phosphate | 2.4±0.4 | 0.54 |
| | | | 9.7 | DABCO | 1.4±0.2 | 0.35 |
| $D_2O$ | | 0.63±0.1[k] | | | | |

[a]FPY aldehyde concentration, 0.07 to 0.18 *M*. Nucleophile total concentration after mixing, including all degrees of protonation had values between 0.02 and 0.09 *M* for $k_n$ measurement. Total buffer concentrations: 0.20 *M* phosphate; 0.4 to 0.8 *M* DABCO and imidazole includes all degrees of protonation.
[b]pH after mixing. Value varied only by 0.02 unit during dehydration.
[c]Average of 5 to 12 determinations over various buffer concentrations as indicated in footnote *a*.
[d]Average of four determinations in the concentration range 0.1 to 0.3 *M* nucleophile including all degrees of protonation.
[e]Average of four determinations in concentration range 0.1 to 0.4 *M* nucleophile including all degrees of protonation.
[f]Estimated from the effect of imidazole concentration on chemical shift of the coalescence signal, see text. The value of δ used to calculate $k_n$ is estimated to be 2.90 ppm.
[g]$K_h$ = [hydrate]/[aldehyde], average of 18 determinations in the pH range 6.5 to 8.7.
[h]Calculated using $pK_a$ in $H_2O$ and the relation $pK_a(D_2O) = pK_a(H_2O) + 0.56$ found for the anilinium ion (see refs. 6 and 13).
[i]Calculated as $K(1 + K_h')$ in which $K_h'$ is the hydration constant in $D_2O$ solvent.
[j]pD. Average of pD 7.4 and 7.5 data.
[k]Average of five determinations in the pD range 8.0 to 9.7.

acids have nearly identical values for $pK_a$ and $K_n$. On the other hand, piperazine, whose second $pK_a$ is about the same as the one for sarcosine, has been found to add to FPY 20 to 40 times faster than sarcosine with a $K_n$ of about 10 times the value for sarcosine (2). Comparison of the data for AGY indicates that there is little or no solvent deuterium isotope effect. This result is similar to that for the analogous reaction in which hydroxide ion adds to substituted *N*-methyltrifluoroacetanilides to form a tetrahedral intermediate. For this system the solvent ($H_2O/D_2O$) deuterium isotope effect is about 1.3 for the addition step (12).

In summary the limited data for the rates of nucleophilic addition to FPY indicate that the variations cannot be accounted for in terms of $pK_a$, $K_n$, or related to systematic changes in structure of the nucleophile. As a group, the primary amino acid and its derivatives, ALN, AME, and AGY, have comparable $k_n$ values within a factor of 2 in spite of their different $pK_a$ values. Imidazole, an aromatic secondary diamine, has a $k_n$ value that is 10 to 20 times larger than these primary amines and has a relatively small $K_n$ value. At the same time, its value is comparable to that for sarcosine, a secondary acyclic amino acid having substantially larger $pK_a$ and $K_n$ values. But the sarcosine rates are 20 to 40 times smaller than those for piperazine, a cyclic, nonaromatic diamine (2). In view of these variations in rates with structure of the nucleophile, it seems that primary amino acids are more suitable for model studies of the details of the addition step involving pyridoxal phosphate. Since the $pK_a$ of FPY is 4.77 (15), the rapid rate of addition of the primary amino acid and derivatives to FPY at high pH could mean that protonation of the ring nitrogen of pyridoxal in the apoenzyme of transaminase need not be a requirement for the addition step. Subsequent protonation may occur prior to the prototropic shift as has been suggested earlier (1*d*). The details of the subsequent steps involving these amino acids and FPY are to be reported in the following paper.

**Acknowledgement**

This work has been supported in part by a grant from the Natural Sciences and Engineering Research Council of Canada.

Can. J. Chem. Downloaded from www.nrcresearchpress.com by 210.87.254.105 on 09/06/12
For personal use only.

1. (*a*) T. C. FRENCH and T. C. BRUICE. Biochem. **3**, 1589 (1964); (*b*) D. S. AULD and T. C. BRUICE. J. Am. Chem. Soc. **89**, 2098 (1967); (*c*) J. R. MALEY and T. C. BRUICE. J. Am. Chem. Soc. **90**, 2843 (1968); (*d*) J. R. MALEY and T. C. BRUICE. Archive Biochem. Biophys. **136**, 187 (1970).
2. (*a*) H. DIEBLER and R. N. F. THORNELEY. J. Am. Chem. Soc. **95**, 896 (1973); (*b*) R. N. F. THORNELEY and H. DIEBLER. J. Am. Chem. Soc. **96**, 1072 (1974).
3. D. E. METZLER, M. I. IKAWA, and E. E. SNELL. J. Am. Chem. Soc. **76**, 648 (1954).
4. E. G. SANDERS and W. P. JENCKS. J. Am. Chem. Soc. **90**, 6154 (1968).
5. L. K. TAN and M. COCIVERA. Can. J. Chem. **58**, 1929 (1980).
6. P. K. GLASOE and F. A. LONG. J. Phys. Chem. **64**, 188 (1960).
7. M. COCIVERA and A. EFFIO. J. Am. Chem. Soc. **98**, 7371 (1976).
8. (*a*) M. COCIVERA, C. A. FYFE, A. EFFIO, S. P. VAISH, and H. E. CHEN. J. Am. Chem. Soc. **98**, 1573 (1976); (*b*) V. MALATESTA and M. COCIVERA. J. Org. Chem. **43**, 1737 (1978); (*c*) L. K. TAN and M. COCIVERA. Can. J. Chem. **60**, 778 (1982).
9. J. CLARK and D. D. PERRIN. Q. Rev. **18**, 295 (1964).
10. J. POPLE, W. SCHNEIDER, and H. BERNSTEIN. High resolution nuclear magnetic resonance. McGraw-Hill, New York. 1959. Chapt. 10.
11. J. N. SHOOLERY. No. 2. Technical Information Bulletin, Varian Associates, Palo Alto, CA. 1959.
12. R. L. SCHOWEN. Progress in physical organic chemistry. *Edited by* A. Streitwieser, Jr. and R. W. Taft. J. Wiley and Sons, New York. 1972. pp. 317–329.
13. H. OHTAKI and M. MAEDA. Z. Naturforsch. **27**B, 571 (1972).
14. Y. POCKER, J. E. MEANY, and B. J. NIST. J. Phys. Chem. **71**, 4509 (1967).
15. K. NAKAMOTO and A. E. MARTELL. J. Am. Chem. Soc. **81**, 5857 (1959).

Can. J. Chem. Downloaded from www.nrcresearchpress.com by 210.87.254.105 on 09/06/12
For personal use only.

# Amino acid addition to 4-formylpyridine and its quaternized salt: transamination

LIANG K. TAN AND MICHAEL COCIVERA[1]

*The Guelph-Waterloo Centre for Graduate Work in Chemistry, Department of Chemistry, University of Guelph, Guelph, Ont., Canada N1G 2W1*

Received June 26, 1981

LIANG K. TAN and MICHAEL COCIVERA. Can. J. Chem. **60**, 778 (1982).

Flow and stopped-flow $^1H$ nuclear magnetic resonance spectroscopy of aqueous solutions have been used to study the reaction between 4-formylpyridine or 4-formyl-1-methylpyridinium iodide and D,L-alanine as well as its methyl ester and D,L-alanylglycine. Because resolved signals can be observed for the alanyl-$CH_3$-proton resonance of the amine, the aldimine, and the ketimine, the time dependence of each species was followed, and the sequence of steps leading to transamination could be studied. As was found previously with alanine, the conversion of aldimine to ketimine appears to be too slow to be detected when 4-formylpyridine is reacted with alanine (pH range to 10) or alanyl methyl ester (pH range 7 to 8). For these systems reaction proceeds until an equilibrium between aldimine and reactants is established. Because the equilibrium constant for the addition step is measured separately, the constant for the equilibrium $K_d$ between carbinolamine and aldimine could be determined. The rate constants for the forward and reverse steps of this equilibrium are independent of buffer but depend on pH. For alanylglycine between pH 7.2 and 7.7, the same process was found to occur. However between pH 8.2 and 10.1, the aldimine derived from this amine undergoes a prototropic shift to form the corresponding ketimine with a rate constant that depends on the concentration of DABCO at each pH. Thus, the change from α-carboxylate anion of alanine (or other amino acids studied previously) to the uncharged α-amide of alanylglycine causes a distinct increase in the rate of prototropic shift when 4-formylpyridine is the electrophile. For the more reactive 4-formyl-1-methylpyridinium iodide, aldimine to ketimine conversion was found to occur for alanine and alanylglycine. During reaction of the latter, a broad nmr signal occurs. This signal may be due to the dihydropyridine structure suggested for an intermediate detected spectrophotometrically for the reaction involving alanine or glycine.

LIANG K. TAN et MICHAEL COCIVERA. Can. J. Chem. **60**, 778 (1982).

On a utilisé la spectroscopie de rmn du $^1H$ en solution aqueuse à écoulement et à flux stoppé, pour étudier la réaction entre la formyl-4 pyridine ou l'iodure de formyl-4 méthyl-l pyridinium et la D,L-alanine, son ester méthylique et la D,L-alanylglycine. En raison du fait que l'on peut observer des signaux résolus pour la résonance du proton $CH_3$ de l'alanyle de l'acide aminé, de l'aldimine et de la cétimine, on a pu étudier l'évolution de chaque espèce en fonction du temps et on a pu déterminer la succession d'étapes conduisant à la transamination. Tel que trouvé antérieurement avec l'alanine, la transformation de l'aldémine en cétimine semble être trop lente pour être décelée lorsque la formyl-4 pyridine réagit avec l'alanine (pH allant jusqu'à 10) ou l'ester méthylique de l'alanine (pH allant de 7 à 8). Pour ces systèmes, la réaction évolue jusqu'à un équilibre entre l'aldimine et les réactifs. On peut déterminer la constante d'équilibre $K_d$ entre la carbinolamine et l'aldimine puisque la constante d'équilibre de l'étape d'addition est mesurée séparément. Les constantes de vitesse des étapes directe et inverse de cet équilibre ne dépendent pas du tampon, mais dépendent du pH. On a trouvé que dans le cas de l'alanylglycine, la même réaction se produit à un pH compris entre 7,2 et 7,7. Cependant à un pH compris entre 8,2 et 10,1 l'aldimine provenant de cet amine subit un glissement prototropique pour conduire à la cétimine correspondante avec une constante de vitesse qui dépend de la concentration en DABCO à chaque pH. Ainsi, le passage de l'anion carboxylate de l'analine (ou d'autres acides aminés étudiés.

[Traduit par le journal]

## Introduction

Model systems consisting of pyridoxal analogues have been used to probe the mechanism of enzyme catalysed transamination involving amino acids (1–3). Since the model reaction consists of a number of steps, some of which involve species not detectable by uv–visible spectrophotometric techniques, we have undertaken a flow and stopped-flow $^1H$ nmr study of nucleophilic addition of amino acids to 4-formylpyridine (FPY) and 4-formyl-1-methylpyridinium iodide (FMP) in $H_2O$ and $D_2O$ at 30°C. In the previous paper (4), line width measurements were used to obtain $k_n$ and $k_{-n}$ for the forward and reverse steps of the rapid pre-equilibrium in which the carbinolamine intermediate (CA) is formed as shown in Scheme 1. In this scheme Py denotes the pyridyl group and R, the carboxylate or substituted carboxyl group.

The purpose of the present paper is to report the results of a study of the subsequent reactions involving dehydration of CA to form aldimine which in some cases (depending on the amino acid and pH) undergoes a prototropic shift to form the *syn* (SKM) and *anti* (AKM) ketimine. Alanine (ALN), alanine methyl ester (AME), and alanylglycine (AGY) were used as nucleophiles to determine the effect of the three forms of the α-carboxyl group. Time-dependent nmr spectra provide information about the values for the rate constants for the steps following the pre-equilibrium indicated in the scheme. Values are dependent on pH and the nature of the α-carboxyl group. For example, $k_{ps}$ and $k_{pa}$ are too small at pH 7 to 8 to detect the ketimine for any of the amino acids except for AGY

[1]To whom all correspondence should be addressed.

0008-4042/82/060778-09$01.00/0

©1982 National Research Council of Canada/Conseil national de recherches du Canada

Can. J. Chem. Downloaded from www.nrcresearchpress.com by 210.87.254.40 on 09/06/12
For personal use only.

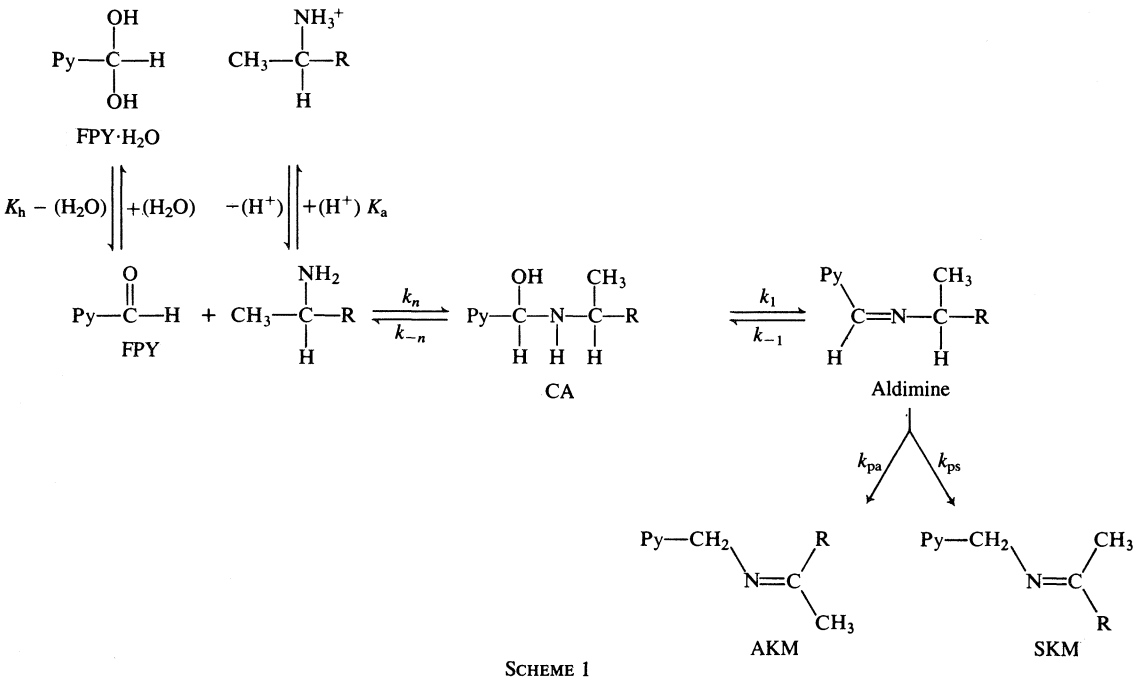

SCHEME 1

at large buffer concentrations. The aldimine slowly decays for AGY but the ketimine is not detected below pH 7.7, perhaps because it hydrolyzes. At higher pH, around 9.5, SKM and AKM are observed for AGY but not for the other amino acids. In previous work, which included only amino acids and no peptides, the prototropic shift was not observed when FPY was used (1*a*).

When the more reactive aldehyde FMP is used, SKM and AKM are observed for the nucleophiles ALN and AGY. In the case of AGY, the prototropic shift appears to occur via an intermediate that is associated with a broadened $^1$H nmr signal. In the corresponding uv–visible study of the reaction between FMP and ALN or glycine, an intermediate was also detected and suggested to be the dihydropyridine tautomer of the carbanion derived from the aldimine by removal of the proton α to the carboxylate group (1*c*). This structure has also been suggested for an intermediate observed spectrophotometrically in an enzymatic reaction involving serine transhydromethylase and alanine (5).

## Experimental

*Chemicals*

4-Formylpyridine (FPY) was vacuum distilled and stored over molecular sieves at −25°C. Imidazole was recrystallized twice from benzene. Diazabicyclooctane (DABCO) was sublimed at reduced pressure. Dimethylsulfoxide (DMSO) was purified by partial crystallization at 5°C and stored over molecular sieves. *t*-Butyl alcohol was distilled prior to use. Spectrograde acetonitrile, D,L-alanine (ALN), D,L-alanine methyl ester (AME) hydrochloride, and D,L-alanylglycine (AGY) were used without purification. The last two compounds were stored at −25°C. 4-Aminomethylpyridine was distilled under reduced pressure. 4-Formyl-1-methylpyridinium iodide (FMP) was prepared from FPY and methyl iodide in dry benzene. The orange–red product was washed with ether, dried, and hydrated in air. The hydrate is a stable pale yellow crystalline material melting at 110–112°C; mp 114–116°C was found previously (6). Deionized water was distilled in an all-glass apparatus prior to use.

*Solutions*

In order to avoid possible heavy metal catalyzed reaction of FPY and FMP, $1 \times 10^{-4}$ *M* sodium ethylene diamine tetraacetate was included in all solutions. To reduce the possibility of decomposition of FPY and AME, which are not stable for long periods at high pH, these compounds were added only after the solutions had been brought close to the desired pH value; then the final minor pH adjustments were made. FMP undergoes side reactions as discussed below. Solutions were buffered with imidazole, sodium phosphate, and DABCO at an ionic strength of 1.3 *M* (KCl). A Radiometer PHM 63 digital pH-meter was used. For $D_2O$ solution, pD was obtained by adding 0.4 to the meter reading (7). Equilibrium constants were measured previously (4).

*Kinetic measurements*

Rate data were obtained by measuring the time dependence of $^1$H nmr spectra at 100 MHz using a Varian HA 100-15 spectrometer equipped with a stopped-flow system described earlier (8). Equal volumes of reactant solutions were mixed at 30 ± 0.3°C. The change in pH after mixing was followed as a function of time. In most cases, there was an immediate drop of 0.1 to 0.4 pH units, depending on the initial pH. After this initial decrease, the pH remained constant to within ±0.03 pH units

Can. J. Chem. Downloaded from www.nrcresearchpress.com by 210.87.254.40 on 09/06/12
For personal use only.

during the dehydration and subsequent reaction steps. For each of these steps, the nmr signals due to the product and reactant could be observed in the $CH_3$-region of the spectrum upfield from the $H_2O$ internal lock signal. Thus, the $CH_3$-proton resonance of the amino acid and corresponding $CH_3$-signals of the aldimine and ketimine (*syn* and *anti*) were observed, and their time dependences were obtained by repetitive scanning of each signal. $CH_3$-proton resonance of DMSO or *t*-butyl alcohol served as the chemical shift and intensity internal reference.

## Results and discussion

### *4-Formylpyridine*

Figure 1 illustrates the proton resonance region upfield from the internal $H_2O$ lock signal at 30°C for: *A*, a solution containing 0.100 *M* AGY at pH 9.7 buffered with 0.400 *M* DABCO and an ionic strength of 1.3 *M* (KCl); *B* and *C*, reaction mixture containing initial concentrations of 0.412 *M* FPY and 0.100 *M* AGY at different stages of reaction as indicated in the figure caption.

Assignment of the signals is given in the figure caption. Figure 1*B* illustrates that the $CH_3$-proton resonance of AGY (doublet)[2] and the corresponding $CH_3$-proton resonances of the aldimine (doublet)[3] and the *syn* and *anti* isomers of the ketimine (singlets) are clearly resolved. Thus, by repetitive scanning of each resonance, it has been possible to follow the time dependence of each species as illustrated in Fig. 2.

Figure 2 indicates that the aldimine decomposition rate is sufficiently slower than its formation so that these two reactions can be treated separately. Furthermore the *syn* and *anti* isomers of the ketimine appear to react very slowly. These general features apply when AGY is used as the nucleophile in the pH range 8.2 to 10.1. The rate of formation of the ketimine decreases as the pH decreases so that the ketimine is not observed in the pH range 7.2 to 7.7 (except at pH 7.7 with 0.6 *M* DABCO). Under these conditions, the equilibrium between CA and aldimine (Scheme 1) is attained.

The spectra observed for ALN in the pH range 8.1 to 10.3 and AME in the pH range 6.7 to 8.0 are similar to Fig. 1*B* except that the *syn* and *anti* isomers of the ketimine are not observed, i.e., the prototropic shift is very slow for these nucleophiles. AME could not be studied above pH 8.0 because ester hydrolysis becomes significant. Thus we cannot rule out the possibility that the prototropic shift could have an appreciable rate for this nucleophile at higher pH. At any rate, it is clear that ALN does not undergo this reaction whereas AGY does. The absence of any significant conversion of aldimine to ketimine has been reported for reaction of a variety of amino acids (including ALN) with FPY (1*a*). Consequently, the results for AGY are generally in contrast with those for amino acids.

As with AGY at low pH, the equilibria in Scheme

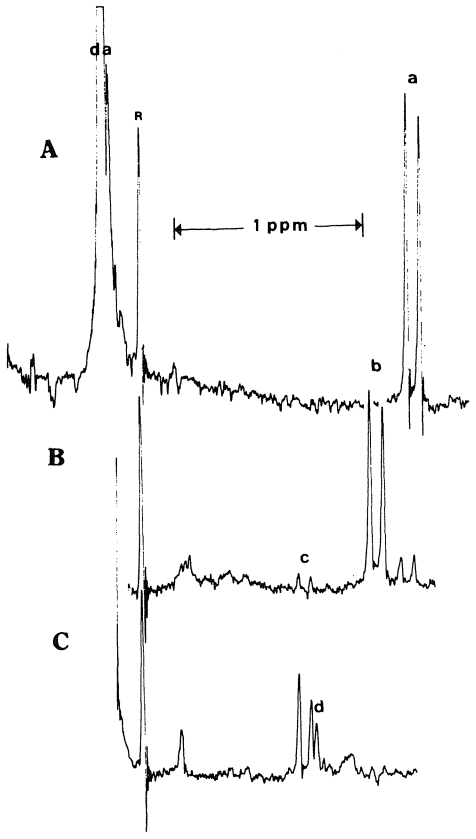


FIG. 1. Partial $^1H$ nmr spectra at 100 MHz obtained upfield from the $H_2O$ lock signal at pH 9.7, 30°C, and 1.3 *M* ionic strength (KCl) using static spinning samples. Magnetic field increases from left to right: *A*, aqueous solution containing 0.100 *M* AGY and 0.400 *M* DABCO; *B*, same as *A* except 0.412 *M* FPY present initially, doublet *a* recorded 1.9 min after mixing; *C*, same as *B*; the two signals labeled *c* were recorded 34 min after mixing. Assignment and chemical shift (relative to TMS) of signals: *a*, $CH_3$-proton of AGY, doublet, 1.32 ppm (this chemical shift is pH dependent, decreasing from 1.57 to 1.28 ppm as the pH is increased from 7.2 to 10.1, respectively); *b*, corresponding $CH_3$-protons of the aldimine derived from AGY, doublet, 1.37 ppm (the corresponding aldimine derived from ALN and AME occurs at 1.35 and 1.38 ppm, respectively); *c*, ketimine $CH_3$-protons, *anti*-singlet, 1.79 ppm and *syn*-singlet, 1.74; *R*, $CH_3$-protons of DMSO (internal reference), singlet 2.62 ppm; *da*, protons of DABCO; and *d*, unidentified product, this signal ultimately becomes the largest in the region of the spectrum.

[2]This doublet also contains a contribution from the corresponding $CH_3$-proton resonance of CA. However, the exchange process involving CA and AGY does not affect line width or position, as might be anticipated since the chemical shift between the exchanging sites is probably small.

[3]The isomers of the aldimine do not give separate $CH_3$-proton signals. Presumably the double bond is separated from the $CH_3$-group by too many bonds to have an effect.

Can. J. Chem. Downloaded from www.nrcresearchpress.com by 210.87.254.40 on 09/06/12
For personal use only.

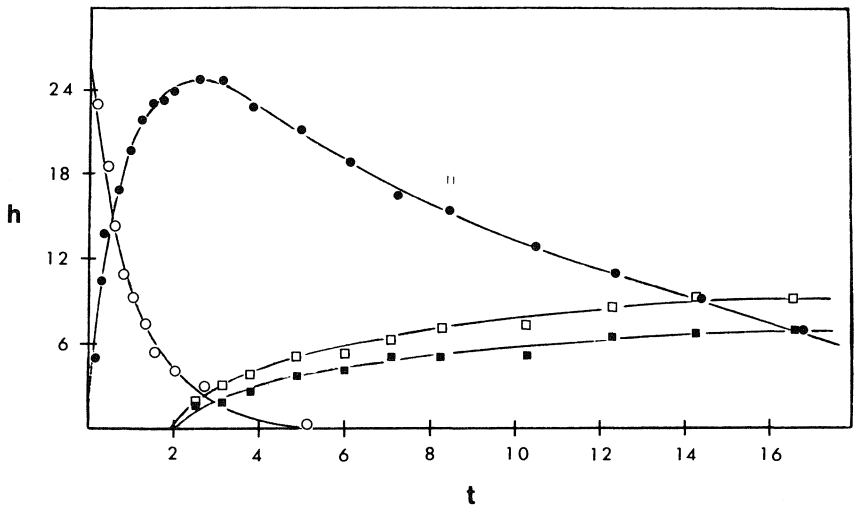


FIG. 2. Time dependence for the $CH_3$-proton signal heights of species occurring during the reaction after mixing at 30°C and ionic strength 1.3 *M* (KCl). Solution contains 0.401 *M* FPY and 0.100 *M* AGY initially at pH 9.7 buffered by 0.400 *M* DABCO. Symbols: *h*, height of signal; *t*, time in min; ○, AGY; ●, aldimine; □, *anti* ketimine; ■, *syn* ketimine. The lines, which have no theoretical significance, are drawn merely to aid in following the behavior of each species. Assignment of *syn* and *anti* isomer is based on ref. 14.

1 are attained with ALN and AME at all pH values employed; and $K_1 = k_1/k_{-1}$, the constant for the equilibrium between CA and the aldimine, can be calculated from the ratio of the signal intensities for the amino acid and its corresponding aldimine using $K_a$ and $K_n$ values reported in the preceding paper (4). Values of $K_1$ for ALN listed in Table 1 indicate that the nmr data provide reasonably precise values over a wide range of pH. When imidazole is the buffer, $K_n'$ for the addition of imidazole to FPY is also included in the calculation of $K_1$ (4). Comparison of the ALN values indicates that $K_1$ is the same when either DABCO or imidazole is the buffer. The average $K_1$ values for ALN, AME, and AGY are 101 ± 15, 93 ± 16, and 66 ± 10, respectively.

For the ALN–FPY system, comparison of our equilibrium data with previous work is possible. A value of 270 $M^{-1}$ has been reported for the equilibrium constant for the overall equilibrium, ALN + FPY ⇌ aldimine (1*a*). Correction of this value by multiplying by the factor ($K_h$ + 1) to take into account the equilibrium hydration of FPY gives a value of 520 $M^{-1}$ which agrees well with our value of 450 $M^{-1}$ calculated as $K_nK_1$. The value of $K_h$, the equilibrium constant for hydration of FPY, is 0.93 (4).[4]

For the cases in which the $K_1$ equilibrium occurs, $k_1$ and $k_{-1}$ have been calculated from time dependence for the amino acid signal decay or the aldimine signal growth using

$$[1] \quad \ln\left(\frac{[N_T] - [N_T]_e}{[N_T]_0 - [N_T]_e}\right) = -(k_1 + k_{-1})\beta t$$

TABLE 1. Equilibrium and kinetic data for dehydration of carbinolamine of the ALN–FPY system in $H_2O$ at 30°C and ionic strength 1.3 *M* (KCl)[a]

| pH[b] | [Buffer][c] (total), *M* | [FPY][d] (total), *M* | $K_1$ | $k_1 + k_{-1}$ ($s^{-1}$) |
|---|---|---|---|---|
| | *Imidazole* | | | |
| 8.1 | 0.800 | 0.202 | 103.2±0.2[e] | [f] |
| | *DABCO* | | | |
| 8.2 | 0.400 | 0.183 | 146.4±6.3 | [f] |
| | | 0.300 | 94.5±1.9 | [f] |
| | 0.600 | 0.304 | 109.4±4.0 | [f] |
| 9.2 | 0.400 | 0.201 | 108.0±17.9 | 3.3±0.2 |
| | 0.600 | 0.201 | 123.1±19.9 | 3.4±0.6 |
| | 0.800 | 0.305 | 117.0±3.0 | 3.6±0.7 |
| 9.5 | 0.400 | 0.204 | 83.2±4.6 | 2.2±0.2 |
| 9.6 | 0.600 | 0.202 | 104.7±13.5 | 2.1±0.2 |
| | 0.800 | 0.202 | 99.4±6.9 | 2.4±0.3 |
| 10.1 | 0.600 | 0.202 | 88.8±11.7 | 1.3±0.2 |
| | 0.800 | 0.202 | 96.8±2.8 | 1.4±0.1 |
| 10.3 | 0.400 | 0.202 | 115.0±1.0 | 1.1±0.1 |
| | | 0.300 | 83.5±0.4 | 0.8±0.1 |
| | 0.600 | 0.203 | 90.9±8.6 | 1.0±0.1 |
| | 0.800 | 0.202 | 101.2±0.3 | 0.9±0.1 |

[a] Total initial concentration of ALN after mixing is 0.100 *M*, includes all degrees of protonation. The free base concentration of ALN was used in calculation.
[b] pH after mixing.
[c] Total concentration after mixing, includes all degrees of protonation.
[d] Total initial concentration after mixing, includes its hydrate form.
[e] A correction was made for the formation of adduct between imidazole and FPY (see text).
[f] Unmeasurable, because the net increase/decrease of the signal heights is small due to a large concentration of protonated ALN.

[4] A number of studies of the hydration of FPY do not agree on the value for $K_h$. Consequently we have determined $K_h$ under our experimental conditions (see ref. 4).

Can. J. Chem. Downloaded from www.nrcresearchpress.com by 210.87.254.40 on 09/06/12
For personal use only.

TABLE 2. Equilibrium and kinetic parameters for reaction steps indicated in Scheme 1

| Nucleophile | $pK_a$[a] | pH range | $k_n \times 10^{-3}$ [a] ($M^{-1}$ $s^{-1}$) | $K_1$ | $k_1^+ \times 10^{-7}$ [g] ($M^{-1}$ $s^{-1}$) | $k_1^0$ ($s^{-1}$) | $k_1^+K_a$ ($s^{-1}$) | $(k_1^{H_2O}/k_1^{D_2O})$[h] |
|---|---|---|---|---|---|---|---|---|
| Alanine | 10.02 | 9.2–10.3[b] | 5.0 | 100±15[e] | 350 | 1.0 | 0.33 | |
| Alanylglycine | 8.28 | 7.2–10.0[c] | 2.1 | 66±10[f] | 3.9 | 0.05 | 0.20 | 3.0 |
| Alanine methyl ester | 8.05 | 6.7–8.0[d] | 1.7 | 93±16[e] | 2.7 | 0.96 | 0.20 | |
| Imidazole | 7.24 | 7.0–8.2 | 33 | | | | | |

[a]Reference 4.
[b]Five pH values for dehydration step.
[c]Seven pH values for dehydration step.
[d]Four pH values for dehydration step.
[e]Average of at least 33 determinations.
[f]Average of 18 determinations for three pH values over pH range 7.2 to 7.7.
[g]Correlation coefficient 0.97 or greater.
[h]Obtained at pH and pD 7.4 using $pK_a = 8.84$ for AGY in $D_2O$ and adding 0.4 to pH meter reading to obtain pD; see refs. 4 and 7.

Can. J. Chem. Downloaded from www.nrcresearchpress.com by 210.87.254.40 on 09/06/12
For personal use only.

in which β is $K_aK_n[FPY]/(K_aK_n[FPY] + [H^+] + K_a)$, $[N_T]$ is the total concentration of the nucleophile at time $t$ including all degrees of protonation, the subscripts 0 and e denote initial and equilibrium values, and [FPY] is the equilibrium concentration of the aldehyde at time $t$ based on the hydration and nucleophilic addition equilibria (Scheme 1). In this treatment protonation of CA has not been included because the $pK_a$ of protonated CA is estimated to be substantially lower than the pH employed (4). Equation [2], in which β is time dependent, must be used because the rapid pre-equilibrium provides significant concentrations of FPY and CA; and, therefore, the time dependence cannot be treated as either a pure first order or second order process. Similar expressions have been employed in previous nmr studies, and it was found that this approximation causes less than a 10% error provided the concentration of one reactant is at least twice that of the other (8*c*), as is the case in the present study. In practice, values for $(k_1 + k_{-1})$ listed in Table 1 were calculated using a linear regression program written for a Hewlett-Packard HP-65 calculator.[5] The errors and scatter indicated in this table for ALN are typical of the data for AME and AGY, also. Each value is an average of three to five determinations. The $(k_1 + k_{-1})$ values are independent of DABCO concentration but increase as the pH decreases. Similar behavior is observed for AME in the pH range 6.7 to 8.0 with imidazole.[5] As discussed above, AGY was used in two pH ranges (7.2–7.7 and 8.2–10.1) and equilibration with the aldimine could be observed only at the lower pH range, presumably because the aldimine–ketimine conversion is very slow in this pH range. Thus in this pH range $(k_1 + k_{-1})$ was calculated according to eq. [1]; in the higher range, $k_1$ was calculated according to a similar equation in which the $k_{-1}$ step was excluded. Over both pH ranges, $k_1$ for AGY appears to be independent of buffer concentration (0.20 to 0.35 *M* phosphate, 0.40 to 0.80 *M* imidazole, and 0.40 to 0.80 *M* DABCO) but dependent on pH, increasing as the pH decreases.[6] Consequently for the three nucleophiles, ALN, AGY and AME, the dehydration/hydration of CA appears to depend on the concentration of hydronium ion. Values of $k_1^+$ listed in Table 2 are obtained by linear regression using the equation, $k_1 = k_1^0 + k_1^+[H_3O^+]$. For ALN and AME the correlation coefficient is greater than 0.99; and for AGY it is greater than 0.98. The intercept $k_1^0$ for ALN is substantially larger than the values for the other two nucleophiles. The reason for this difference is not clear. On the other hand, the large variation in $k_1^+$ values for the nucleophiles may be related to protonation of CA as has been suggested by French and Bruice (1*a*). Thus the $k_1^+$ values in Table 2 have the same meaning as the $k_1/K_a''$ values reported by these workers who define $k_1$ and $K_a''$ to be the dehydration rate constant and the acid dissociation constant, respectively, for $CAH^+$, the protonated form of CA. Comparison with this previous work is possible only for ALN for which a $k_1/K_a''$ value of $2.5 \times 10^8$ $M^{-1}$ $s^{-1}$ was reported. The large difference between this value and the one in Table 2 probably results because the kinetic analysis used in the previous work did not include hydration of FPY.[7]

In spite of this difference in magnitude, the two studies agree that the rate of dehydration of $CAH^+$ makes a significant contribution to the overall rate of formation of the aldimine. Furthermore it ap-

[5]Equation [1] represents an additional approximation since the term $(k_1 + k_{-1})$ should really be $(k_1 + k_{-1}/\beta)$. A correction for this approximation is made by calculating $k_1$ as $\beta K_1 (k_1 + k_{-1})/(\beta K_1 + 1)$. This correction is small for ALN and AGY, a maximum of about 10% at low pH. However, the maximum correction is about 56% for AME.

[6]For AME $K_1$ and $(k_1 + k_{-1})$ data were obtained for 22 pH and buffer concentration combinations in the pH range 6.7 to 8.0. For AGY, data were obtained for 18 and 14 pH and buffer concentration combinations in the pH ranges 7.2 to 7.7 and 8.2 to 10.1 respectively.

[7]For the same reason, their equilibrium constant for ALN + FPY ⇌ CA differs from our value, which agrees with the one determined by Sanders and Jencks (see refs. 4 and 9).

Can. J. Chem. Downloaded from www.nrcresearchpress.com by 210.87.254.40 on 09/06/12
For personal use only.

pears this rate is about the same for the three nucleophiles, i.e., $k_1^+K_a''$, the first order rate constant for dehydration of $CAH^+$, has nearly the same value despite the difference in the $pK_a$ values of the nucleophiles. For this consideration, the absolute value of $k_1^+K_a''$ for each $CAH^+$ cannot be determined accurately because the acid dissociation constant $K_a''$ is not known for these intermediates, although it may be estimated as described previously (10). Nevertheless, using $pK_a$ data in Table 2, one can calculate $k_1^+K_a$, which is expected to be proportional to $k_1^+K_a''$. The $k_1^+K_a$ values listed in Table 2 are all nearly identical. This similarity would indicate that $CAH^+$ dehydrates at nearly the same rate for the three nucleophiles if the difference between $K_a$ and $K''$ were due to identical substituent effects in the three cases.

In contrast, the intercept $k_1^0$, which can be assigned to dehydration of the unprotonated carbinolamine, depends on the nature of the nucleophile with AGY having a substantially smaller value than the other two. It would be useful to have results for other nucleophiles to determine the factors affecting this step. As indicated in Table 2, the solvent deuterium isotope effect for $k_1$ has been determined at only one pH–pD value. In view of the complications involved in the interpretation of solvent deuterium isotope effects (11), any discussion seems premature.

Although imidazole appears to add to FPY (4, 9), there is no evidence to indicate that formation of the imidazole–FPY adduct enhances the rate of aldimine formation for the various nucleophiles. In addition, our results give no indication that imidazole adds to the aldimine to form a complex similar to the one observed during the reaction between pyridoxal and α-aminophenylacetic acid (12).

For the AGY–FPY system at low pH, the aldimine slowly decays after equilibrium between this imine and CA has been attained. Because this decay is slow under these conditions, it was not followed to completion. Nevertheless, a sufficient fraction of the reaction was followed to indicate that it is first order in aldimine and that the first order rate constant increases as the concentration of imidazole is increased. The signals due to the expected *syn* and *anti* ketimine products, which are observed at high pH (see below), are not observed in this pH range, presumably because ketimine formation is rate limiting.[8] Consequently, although it seems likely that ketimine formation is the main reaction for the aldimine, the possible occurrence of competing reactions cannot be ruled out. For this reason, the values for the first order rate constants are not listed for this pH range. They are about a factor of 200 smaller than the values at pH 9.7 with DABCO buffer as discussed below.

At high pH in the range 8.2 to 10.1, evidence for the prototropic shift for the system AGY–FPY is more conclusive. As indicated in Figs. 1 and 2, the *syn* and *anti* isomers of the ketimine are observed. Although aldimine to ketimine interconversion has been observed when more reactive electrophiles such as FMP (1*c*) and 4-formyl-3-hydroxypyridine (1*b*) are used, this process was not detected previously when FPY was reacted with amino acids (1*a*). While it is interesting to speculate about the reasons for the effectiveness of the peptide relative to the amino acids in promoting this step, other systems should be studied to obtain more information.

Both isomers react at a slower rate than they are formed. Presumably this decomposition involves hydrolysis of the ketimine to form pyruvoylglycine and 4-aminomethylpyridine, neither of which are detected. Our failure to detect 4-aminomethylpyridine is due to the fact that its signals occur in the same regions as other stronger signals. Pyruvoylglycine undergoes ring closure under basic conditions to form γ-hydroxypyrrolidone carboxylic acid (13). Although several signals having suitable time dependences are observed, none has been assigned conclusively to this acid. Consequently, because the products have not been identified and because the rates are very slow, kinetic studies of the reaction of ketimine have not been pursued.

On the other hand, the slow rate of decay of ketimine in comparison with its growth permits the measurement of $k_{pa}/k_{ps}$, which is assumed to be equal to the AKM/SKM ratio of $CH_3$-proton signal intensities.[9] Because this ratio was found to be constant over the time the reaction was followed, we cannot decide if the prototropy occurs under kinetic or thermodynamic control. Previous work with the glycine–pyruvate system indicates that the rate of forward and reverse steps of the *syn–anti* equilibrium is comparable to the nmr time scale at nucleophile concentrations larger than those used in the present study (15). For the AGY–FPY system, the line width of the *syn* and *anti* signals gives no indication of an exchange process. Values of $k_{pa}/k_{ps}$ ratio listed in Table 3 are averages over the reaction period.

[8]At higher pH, ketimine decomposition is rate limiting. The transition appears to occur around pH 7.7 since ketimine can be detected only when DABCO concentration is 0.6 *M* and greater, see below.

[9]Assignment of *syn* and *anti* $CH_3$-proton resonance signals is based on ref. 14.

Can. J. Chem. Downloaded from www.nrcresearchpress.com by 210.87.254.40 on 09/06/12
For personal use only.

Because the rate of conversion of aldimine to ketimine is slower than the dehydration of CA, the decay of the aldimine was studied using static spinning samples. Analysis according to first order reaction provides values for the sum of the rate constants ($k_{ps} + k_{pa}$) that are listed in Table 3. These values depend on pH and total DABCO concentration. However, this dependence appears to be more complicated than a first order dependence on buffer concentration because the intercept is negative, the value increasing with pH until it is positive at pH 10.1. This behavior may indicate a nonlinear dependence on buffer concentration. Unfortunately, it is not possible to test this behavior by using buffer concentrations lower than 0.4 *M* because the pH cannot be controlled adequately below this concentration. Consequently, because of the limited buffer concentration range employed, a detailed nonlinear analysis is not reported here. Suffice it to say that the limited data can be fit to the equation, $(k_{pa} + k_{ps}) = k_p'[\text{DABCO}]_T + k_p''[\text{DABCO}]_T^2$. This equation is used assuming that catalysis by hydroxide ion may be neglected. Because the error due to this approximation is not known and only three concentrations are employed at each pH, the calculated values should be considered semiquantitative and sufficient only to indicate trends. For each pH, plots of $(k_{pa} + k_{ps})/[\text{DABCO}]_T$ vs. $[\text{DABCO}]_T$ are linear with correlation coefficients of 0.98 or greater. The value for $k_p'$ increases as the pH increases and the general base catalytic constant, $k_p^{GB}$, which is obtained as $k_p'(K_a + [H_3O^+])/K_a$, has a value of 0.32 ± 0.02 $M^{-1}$ min$^{-1}$ in the pH range 9.2 to 10.1. General base catalysis has also been observed in aldimine–ketimine conversions in studies of more active aldehydes such as FMP or 3-hydroxy-4-formylpyridine (1*b*,*c*). For these systems, it has been suggested that the base is involved in removal of the methine proton of the aldimine. A similar mechanism is consistent with the present results.

TABLE 3. Kinetic data for ketimine formation of the AGY–FPY system in $H_2O$ at 30°C and ionic strength 1.3 *M* (KCl)

| pH[a] | [DABCO][b] (*M*) | [FPY][c] (*M*) | $k_{pa}$[d] / $k_{ps}$ | $(k_{ps} + k_{pa}) \times 10^2$ (min$^{-1}$) |
|---|---|---|---|---|
| 7.7[e] | 0.800 | 0.416 | 1.4±0.1 | 1.3±0.0 |
| 8.2 | 0.400 | 0.201 | 1.4±0.1 | 1.8±0.1 |
| | | 0.361 | 1.3±0.1 | 1.9±0.1 |
| | | 0.409 | 1.4±0.0 | 1.8±0.0 |
| | 0.600 | 0.414 | 1.3±0.0 | 4.4±0.6 |
| | 0.800 | 0.408 | 1.4±0.1 | 6.9±0.5 |
| 9.2 | 0.400 | 0.315 | 1.4±0.0 | 7.2±0.6 |
| | | 0.407 | 1.3±0.0 | 7.1±0.3 |
| | 0.600 | 0.420 | 1.3±0.0 | 11.3±0.9 |
| | 0.800 | 0.406 | 1.3±0.1 | 16.2±0.7 |
| 9.7 | 0.400 | 0.412 | 1.3±0.1 | 10.4±0.8 |
| | 0.600 | 0.419 | 1.3±0.0 | 16.3±0.8 |
| | 0.800 | 0.411 | 1.3±0.0 | 22.0±0.8 |
| 10.1 | 0.400 | 0.403 | 1.4±0.1 | 12.7±0.2 |
| | 0.600 | 0.306 | 1.3±0.1 | 17.9±0.7 |
| | | 0.409 | 1.4±0.1 | 18.7±1.3 |
| | 0.800 | 0.409 | 1.3±0.1 | 24.7±0.3 |

[a]pH after mixing.
[b]Total concentration after mixing, includes all degrees of protonation.
[c]Total initial concentration of FPY after mixing, includes its hydrate form. The total initial concentration of AGY after mixing is 0.100 *M* for all runs, includes all degrees of protonation.
[d]Obtained from the ratio of the $CH_3$-proton signal height of AKM and SKM. Each value is an average of 3 mean values from 3 runs. Each mean value from each run is the average of several ratios at different time.
[e]At this pH, using concentrations of DABCO lower than 0.6 *M* leads to no formation of ketimine.

The value for $k_p''$ decreases as the pH increases from 8.2 to 10.1, at which the value is very close to zero. Although the data are semiquantitative, this trend appears real. A mechanism to account for this behavior is not obvious. In the study of the transamination reaction involving α-aminophenylacetic acid and pyridoxal, catalysis by imidazole was found to depend on the square of the imidazole concentration at low concentration but not at high concentration of imidazole (12). This behavior was interpreted as evidence for a preequilibrium formation of a complex of aldimine with imidazole and imidazolium ion followed by an intracomplex bifunctional acid–base catalysis of the prototropic shift. Complex formation does not appear to apply to the AGY–FPY system because there is no evidence that the rate becomes independent of DABCO concentration at high concentration. On the other hand, complex formation is not necessarily needed for bifunctional catalysis. For example, termolecular terms determined in the enolization of ketones have been attributed to bifunctional acid–base catalysis (16). The DABCO results are not strongly indicative of bifunctional catalysis because $k_p''$ does not exhibit the expected dependence on pH, i.e., a maximum value should be observed when pH equals p$K_a$ (9.4) of DABCO. Instead, the value decreases monotonically as pH increases from 8.2 to 10.1. This effect could not be studied below pH 8.2 because there is no clear indication that ketimine formation is the only path available to the aldimine, i.e., as mentioned above, the reaction is slow and ketimine is not observed below pH 7.7. Even at this pH, ketimine can be detected only when the DABCO concentration is 0.6 *M* or greater, indicating that ketimine may not be formed faster than it is hydrolysed below this concentration. Consequently in this pH range there is no certainty that the decay of aldimine leads solely to ketimine.

### *4-Formyl-1-methylpyridinium iodide*

The reaction of 4-formyl-1-methylpyridinium iodide (FMP) with ALN or AGY could not be

Can. J. Chem. Downloaded from www.nrcresearchpress.com by 210.87.254.40 on 09/06/12
For personal use only.

studied quantitatively because FMP decomposes in the pH range employed (pH 9–10). The rate of this decomposition appears to increase with increase in FMP concentration as well as buffer and nucleophile concentrations. Thus this decomposition competes with nucleophilic addition by ALN or AGY. The FMP concentration dependence indicates that this decomposition may not be important at the concentrations employed in previous studies (1*c*). At any rate, because the nmr study requires FMP concentrations in the range 0.1 to 0.4 M, this reaction becomes important. Therefore, the nmr study has been used to obtain only qualitative information.

First we find that FMP is extensively hydrated so that the aldehyde proton resonance cannot be detected. This hydration has been alluded to previously (1*c*). The rate of hydration/dehydration appears to be slow on the nmr time scale because the position and width of the hydrate methine proton resonance are not affected when the nucleophile is added. Since, by analogy to FPY, nucleophilic addition to the aldehyde form of FMP is expected to be sufficiently rapid to cause line broadening, an increase in line width and/or a change in position of the hydrate signal is expected if hydration/dehydration is also rapid. With available information it is not possible to decide whether dehydration of the hydrate or dehydration of CA is the rate limiting step in aldimine formation.

Although reasonably precise first order rates of formation of aldimine can be obtained based on the time dependence of the $CH_3$-proton resonance of the amino acids, their meaning is unclear because FMP, whose concentration is usually three times that for the amino acid, disappears completely while about 20% of the amino acid remains at the end of the reaction.

Qualitatively it appears that ketimine formation occurs according to Scheme 1, but the concentration of the aldehyde form of FMP is very low. In addition, in the case of ALN–FMP, the hydrolysis of the ketimine is clearly established by detection of the $CH_3$-proton resonance of pyruvate anion. Identification of this signal supports the previous evidence that pyruvate anion is formed as a result of hydrolysis of ketimine derived from ALN (1*c*). Based on intensities, it appears that about a 50% conversion of ALN to pyruvate ion occurs at pH 9.6 in the presence of DABCO in about 30 min, compared with 78% in about 5 h at half neutralization of ALN in the absence of DABCO reported previously (1*c*).

For AGY–FMP, the reaction mechanism appears similar; however, the signal due to the hydrolysis product has not been assigned for the reasons mentioned in the previous section. In Fig. 3, the $CH_3$-region of the spectrum for the AGY–FMP system obtained 17 min after mixing illustrates the appearance of a broad signal in addition to those due to the aldimine and AGY. This broad signal occurs in the presence of DABCO or imidazole[10] in the pH range 9 to 10. It decays more rapidly in the presence of DABCO, but the rate appears to be substantially slower than the hydrolysis rate of the ketimine of ALN. An unambiguous assignment of this signal cannot be made. However, it is possible that this signal may be associated with the dihydropyridine structure (DHP) in eq. [2] suggested earlier to account for the absorbance maxima observed at 500 and 600 nm for the FMP–glycine

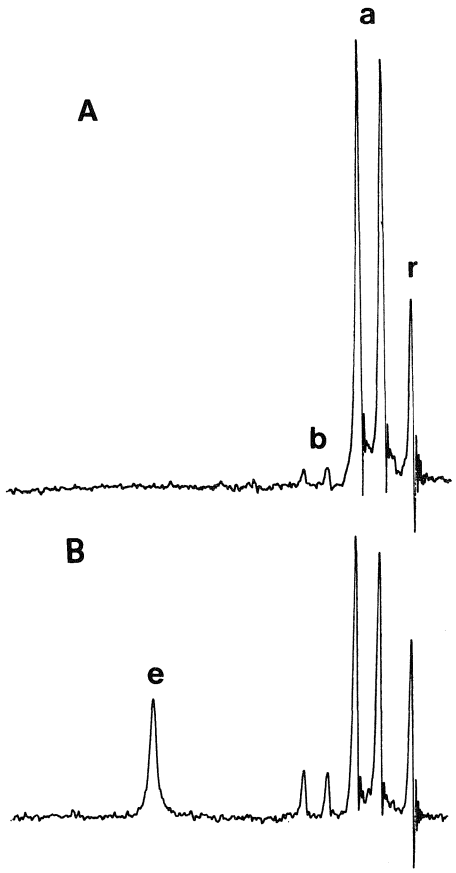


FIG. 3. Partial $^1H$ nmr spectrum of an aqueous reaction mixture containing 0.400 *M* FMP and 0.200 *M* AGY at pH 9.5. Except for the gain, the nmr conditions are identical to those for Fig. 1 as are the labels. This figure is photographically reduced less than Fig. 1 and the chemical shift between signals *e* to *r* is 0.77 ppm. In addition, *r* denotes the $CH_3$-proton resonance of *t*-butyl alcohol, and *e* is not identified conclusively, see text. *A*, Scan is started immediately after mixing, and *r* is recorded 60 s after start; *B*, scan started 17.4 min after mixing.

[10]The pH drop is 0.1 and 0.3 in the presence of DABCO and imidazole, respectively.

and FMP–ALN systems, respectively (1*c*). Thus, the signal may be due to the DHP methyl group attached to the $sp^2$ hybridized carbon. It is broadened because of restricted rotation about the carbon–nitrogen bond. The fact that this signal decays more rapidly in the presence of DABCO than in the presence of imidazole may indicate that conversion of DHP to ketimine is acid catalyzed, i.e.,

[2] 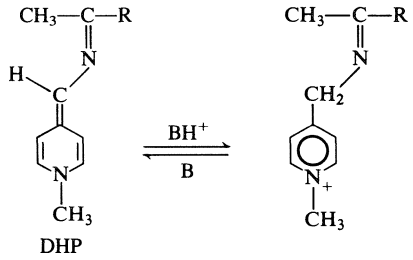


since the fraction of acid form of imidazole ($pK_a$ = 7.24) is very small in this pH range whereas it is appreciable for DABCO ($pK_a$ = 9.40).

For the ALN–FMP system detection of a corresponding signal has not been established conclusively, although some very weak signals have been observed. This result does not necessarily contradict those of the spectrophotometric study (1*c*) since a large molar absorptivity would permit detection of DHP at concentrations too small for nmr detection in a single scan. In addition the enhanced reactivity of ALN vs. AGY may have several factors: (*1*) the negative charge of the α-carboxylate reduces the stability of DHP and the corresponding ketimine resulting in more rapid conversion to hydrolysis product (pyruvate anion); (*2*) unreacted ALN acts as a general acid catalyst in eq. [2].

**Acknowledgement**

This study has been supported in part by a grant from the Natural Sciences and Engineering Research Council of Canada.

1. (*a*) T. C. French and T. C. Bruice. Biochem. **3**, 1589 (1964); (*b*) D. S. Auld and T. C. Bruice. J. Am. Chem. Soc. **89**, 2098 (1967); (*c*) J. R. Maley and T. C. Bruice. J. Am. Chem. Soc. **90**, 2843 (1968); (*d*) J. R. Maley and T. C. Bruice. Archive Biochem. Biophys. **136**, 187 (1970).
2. (*a*) H. Diebler and R. N. F. Thorneley. J. Am. Chem. Soc. **95**, 896 (1973); (*b*) R. N. F. Thorneley and H. Diebler. J. Am. Chem. Soc. **96**, 1072 (1974).
3. D. E. Metzler, M. I. Ikawa, and E. E. Snell. J. Am. Chem. Soc. **76**, 648 (1954).
4. L. K. Tan and M. Cocivera. Can. J. Chem. **60**, 772 (1982).
5. L. V. Shirch and W. T. Jenkins. J. Biol. Chem. **239**, 3801 (1964).
6. G. M. Steinberg, E. J. Poziomek, and B. E. Hackley, Jr. J. Org. Chem. **26**, 368 (1961).
7. (*a*) P. K. Glasoe and F. A. Long. J. Phys. Chem. **64**, 188 (1960); (*b*) H. Ohtaki and M. Maeda. Z. Naturforsch. **27B**, 571 (1972).
8. (*a*) M. Cocivera and A. Effio. J. Am. Chem. Soc. **98**, 7371 (1976); (*b*) C. A. Fyfe, M. Cocivera, S. Damji, T. Hostetter, D. Sproat, and J. O'Brien. J. Magn. Reson. **23**, 377 (1976); (*c*) V. Malatesta and M. Cocivera. J. Org. Chem. **43**, 1737 (1978).
9. E. G. Sanders and W. P. Jencks. J. Am. Chem. Soc. **90**, 6154 (1968).
10. (*a*) J. Clark and D. D. Perrin. Q. Rev. **18**, 295 (1964); (*b*) D. D. Perrin. Dissociation constants of organic bases in aqueous solution. Butterworths, London. 1965.
11. R. L. Schowen. Progress in physical organic chemistry. *Edited by* A. Streitwieser, Jr. and R. W. Taft. J. Wiley and Sons. New York. pp. 317–329.
12. T. C. Bruice and R. M. Topping. (*a*) J. Am. Chem. Soc. **85**, 1480 (1963); (*b*) **85**, 1488 (1963).
13. S-C J. Fu, V. E. Price, and J. P. Greenstein. Arch. Biochem. Biophys. **31**, 83 (1951); (*b*) S-C J. Fu and J. P. Greenstein. Arch. Biochem. Biophys. **32**, 365 (1951).
14. G. J. Karabatsos and R. A. Taller. Tetrahedron, **24**, 3923 (1968).
15. D. Leussing and C. K. Stanfield. J. Am. Chem. Soc. **86**, 2805 (1964).
16. (*a*) E. S. Hand and W. P. Jencks. J. Am. Chem. Soc. **97**, 6221 (1975); (*b*) A. F. Hegarty and W. P. Jencks. J. Am. Chem. Soc. **97**, 7188 (1975).

Can. J. Chem. Downloaded from www.nrcresearchpress.com by 210.87.254.40 on 09/06/12
For personal use only.

# Diamagnetic metal ion – nucleoside interactions in solution as studied by $^{15}N$ nuclear magnetic resonance

G. W. BUCHANAN[1]

*Ottawa–Carleton Institute for Research and Graduate Studies in Chemistry, Carleton University, Ottawa, Ont., Canada K1S 5B6*

AND

J. B. STOTHERS

*Department of Chemistry, The University of Western Ontario, London, Ont., Canada N6A 5B7*

Received October 9, 1981

G. W. BUCHANAN and J. B. STOTHERS. Can. J. Chem. **60**, 787 (1982).

$^{15}N$ nuclear magnetic resonance chemical shifts are shown to be highly sensitive to site-selective diamagnetic metal ion binding for the nucleosides adenosine, cytidine, and guanosine. Conclusions regarding preferred complexation sites are compared with results derived from other physical measurements, and with expectations based on electron density calculations.

G. W. BUCHANAN et J. B. STOTHERS. Can. J. Chem. **60**, 787 (1982).

On a montré que quelques ions diamagnétiques induisent sélectivement des grandes changements des déplacements chimiques dans l'rmn de l'azote-15 pour les nucléosides adenosine, cytidine et guanosine. Les conclusions concernant les sites d'attachement préferés sont comparés avec les résultats d'autres méthodes physiques et avec les calculs basés sur les densités électroniques.

## Introduction

The importance of metal ion interactions with nucleotide components is now well recognized. Subtle features of metal – nucleic acid binding are deemed responsible for the toxic behaviour of some metal complexes and the antineoplastic behaviour of others (1).

Among the available techniques which have been applied in this field are Raman and Raman difference spectroscopy (2), as well as $^{1}H$, $^{13}C$, $^{31}P$, $^{7}Li$, and $^{35}Cl$ nmr (3). For the mononucleotide AMP, $^{15}Nmr$ has recently been used to study paramagnetic $Mn^{+2}$ binding, via $T_1$ and linewidth measurements (4). No changes in $^{15}N$ chemical shifts, however, were apparent upon binding, although the [Mn]/[AMP] ratio was relatively low.

By contrast, no studies have been reported using $^{15}Nmr$ to monitor *nucleoside* – metal ion binding, despite the fact that ions such as $Hg^{+2}$ are known to form complexes of high stability with nucleosides, and the primary binding sites have often been postulated to be one or more of the nitrogen sites of the nucleoside bases (3).

We wish to report that large chemical shift changes are found in the $^{15}N$ spectra of nucleosides on addition of up to one molar equivalent concentration of $HgCl_2$ and $Zn(NO_3)_2$, and that additional information regarding nitrogen site selectivity is thus available. Dimethyl sulfoxide has been used as solvent, since relatively high concentrations of metal ions and nucleosides can be achieved in this medium.

[1]Author to whom correspondence should be addressed.

## Results and discussion

Specifically, the nucleosides adenosine **1**, cytidine **2**, and guanosine **3** have been examined in the presence of $HgCl_2$, $Zn(NO_3)_2$, and $Ba(NO_3)_2$.

The $^{15}N$ chemical shifts for the nucleosides

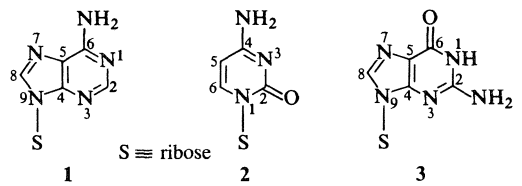


**1** **2** **3**

themselves in DMSO-$d_6$ solution have been reported previously (5), and our data (Table 1) are in excellent agreement with the earlier work.

Our choice of metal ions was made for several reasons. Firstly, there is general agreement (6–10) that $HgCl_2$ binds strongly to endocyclic ring nitrogens of nucleosides in DMSO solution. Our studies, therefore, were aimed mainly at establishing the degree of perturbation of the $^{15}Nmr$ spectra due to the binding interactions. Furthermore $Hg^{+2}$ classifies as a "soft" metal ion species, its bonding being more covalent in nature than that for "harder" metals.

The $Zn^{+2}$ ion was chosen since it also has a known affinity for endocyclic nitrogens of nucleosides (11, 12), but is otherwise "harder" than $Hg^{+2}$. Finally $Ba^{+2}$ was selected as an example of a "hard" ion, its mode of bonding normally being ionic rather than covalent.

The effects of added $HgCl_2$ and $Zn(NO_3)_2$, up to one molar equivalent, on the $^{15}N$ resonances of the

0008-4042/82/060787-05$01.00/0

©1982 National Research Council of Canada/Conseil national de recherches du Canada

Can. J. Chem. Downloaded from www.nrcresearchpress.com by 210.87.254.42 on 09/06/12
For personal use only.

Can. J. Chem. Downloaded from www.nrcresearchpress.com by 210.87.254.42 on 09/06/12
For personal use only.

TABLE 1. $^{15}N$ Chemical Shifts ($\delta_N$ from $NH_3$) ± 0.1 ppm*

| Compound | N-1 | N-3 | N-7 | N-9 | $NH_2$ |
|---|---|---|---|---|---|
| **1** (0.50 *M*) | 234.5 | 221.4 | 239.4 | 168.4 | 80.2 |
| **2** (0.75 *M*) | 152.1 | 206.7 | | | 93.0 |
| **3** (0.50 *M*) | 146.2 | 164.8 | 246.0 | 169.0 | 72.3 |

*DMSO-$d_6$ solutions.

three nucleosides are shown in Figs. 1–6. In all cases, $Ba(NO_3)_2$ induced maximal shift changes of less than 0.3 ppm, and accordingly these results are not plotted.

(a) *Adenosine: $HgCl_2$ addition*

Results in Fig. 1 show that the N-1 resonance of adenosine is most affected by $HgCl_2$ addition, there being a 9.5 ppm *upfield* shift upon addition of 1 molar equivalent of $Hg^{+2}$. The N-7 resonance experiences a minor upfield shift also (1.2 ppm), while the remaining three $^{15}N$ resonances for N-3, N-9, and the $NH_2$ are shifted downfield on addition of 1 molar equivalent $HgCl_2$.

In this context it is interesting to recall the results of protonation of adenosine, also in DMSO solution, using TFA as a proton source (5). It was found that the N-1 $^{15}N$ resonance shifted *upfield* by 72.6 ppm after 1.6 equivalents of TFA were added. By contrast, all other $^{15}N$ resonances were affected to a much lesser extent, and all were shifted downfield, the values being 1.9, 3.3, 8.2, and 9.9 ppm for N-3, N-7, N-9, and the $NH_2$ respectively (5).

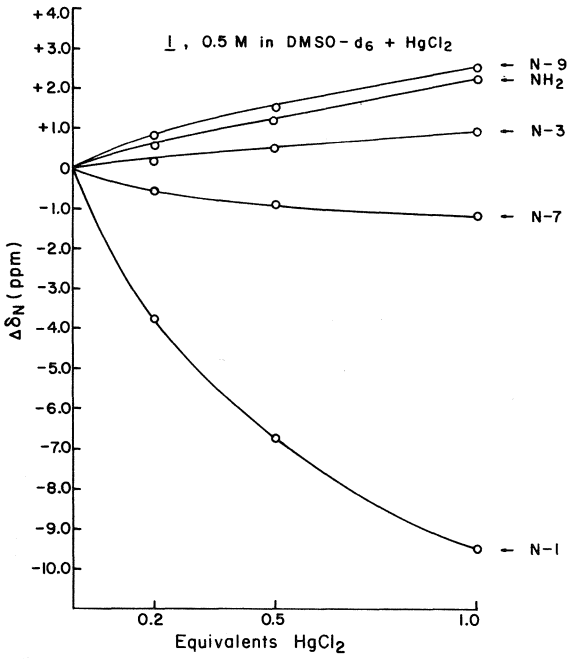


FIG. 1. $^{15}N$ chemical shift changes as a function of added metal ion. + sign denotes increased δ value (downfield shift); − sign denotes decreased δ value (upfield shift); **1** + $HgCl_2$.

For pyridine, protonation induces an upfield shift of about 97 ppm in the $^{15}N$ resonance (5). Thus the upfield shift of N-1 of adenosine can be taken as evidence for this position being the preferred protonation site.

Similarly, one can argue that N-1 is the preferred site of mercuration in adenosine. The fact that N-7 also shifts upfield upon $HgCl_2$ addition suggests that N-1 is not, however, an exclusive complexation site. For the remaining three nitrogens of **1**, the smaller downfield shifts are most likely due to the involvement of these positions in conjugation with a metallated N-1 (or N-7) site (5).

It is interesting to compare these conclusions with theoretical predictions (13) of preferred binding sites of adenosine, based on electron density calculations. Results of these calculations are depicted below, with the circled numbers indicating, in order, the preferred complexation sites.

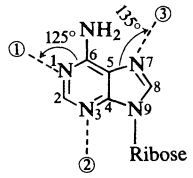


For mercuration and protonation, N-1 does indeed appear to be the preferred site. There is, however, an experimental preference for N-7 over N-3 as the second most likely mercuration site, in contrast to the predictions of the theory.

(b) *Adenosine: $Zn(NO_3)_2$ addition*

As is shown in Fig. 2, the induced $^{15}N$ shifts upon $Zn(NO_3)_2$ addition are largest for the N-7 site (upfield by 7.5 ppm after 1 molar equivalent added). The N-1 resonance is also shifted upfield, but to a smaller extent (1.6 ppm). The N-3 and N-9 resonances are essentially unaffected, while the $NH_2$ is deshielded by 1.4 ppm.

Based on these data, one is led to suggest that $HgCl_2$ and $Zn(NO_3)_2$ solutions with adenosine may contain *different mixes* of N-1 vs. N-7 metallated complexes, the N-1 site being preferred by $Hg^{+2}$, while $Zn^{+2}$ prefers N-7.

It is instructive to note that previous studies (3) of adenosine–$HgCl_2$ and $Zn(NO_3)_2$ complexes, which made use of $^1H_1$, $^{13}C$, and Raman difference spectra, suggested that this is indeed true, although no distinction between relative nitrogen site preferences was possible.

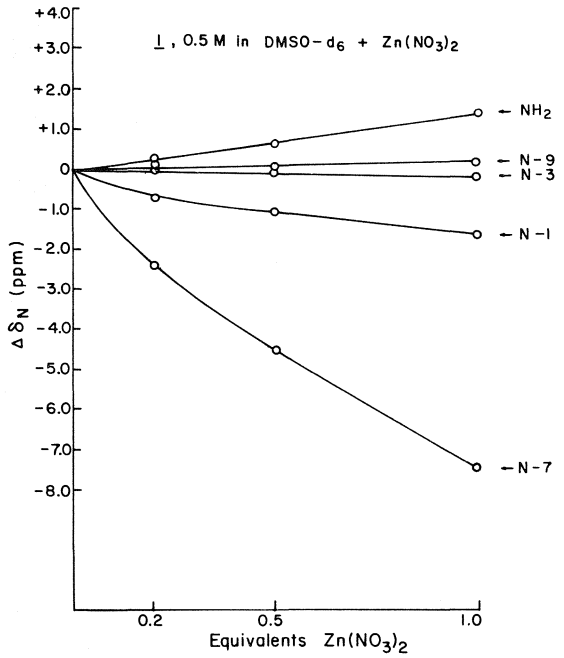


FIG. 2. 1 + $Zn(NO_3)_2$.

Another explanation for the upfield shifts of both N-1 and N-7 of **1** upon metalation is the possible formation of a dimetalated species, as shown below.

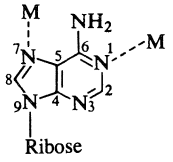


The existence of such a complex has recently been suggested by Farrell (14) for adenosine complexes with $Pt^{II}$. If such a species did exist, however, one might expect more nearly equivalent upfield shifts for N-1 and N-7 of **1** upon addition of the metal ions.

(c) *Adenosine: $Ba(NO_3)_2$ addition*

Raman difference and $^{13}$Cmr spectra of adenosine in the presence of "hard" metal species such as $Ba(NO_3)_2$ indicate no binding (3), and the negligible $^{15}$N chemical shift changes induced upon addition of this salt are consistent with this situation.

(d) *Cytidine: $HgCl_2$ and $Zn(NO_3)_2$ addition*

For cytidine, the primary binding site is calculated (13) to be a chelated position between the carbonyl oxygen and N-3 as shown below.

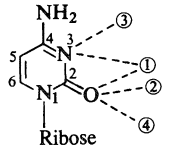


The large upfield shifts at N-3 of **2** induced by both $HgCl_2$ and $Zn(NO_3)_2$, as shown in Figs. 3 and 4 respectively, are consistent with a binding site which preferentially involves this nitrogen. The accompanying downfield shift of the $NH_2$ upon complexation is reminiscent of the effect of protonation (5), where it was postulated that the deshielding of this nitrogen was due at least in part to its interaction with the complexed N-3 position via resonance donation, as depicted below for metalated cytidine.

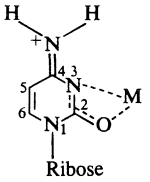


The N-1 resonance of **2** experiences an upfield shift which is less than 10% of that seen for the N-3 absorption. The fact that it is upfield however, suggests that N-1 is also a metalation site, although to rather a minor extent.

Once again it is interesting to compare the effects of metalation with protonation. Upon addition of 1.6 equivalents of TFA, the N-3 resonance of cytidine shifts upfield by 64.8 ppm, while the $NH_2$ is deshielded by 20.8 ppm, and N-1 undergoes a minor shielding of 2.9 ppm (5). This ratio of 22.4 :

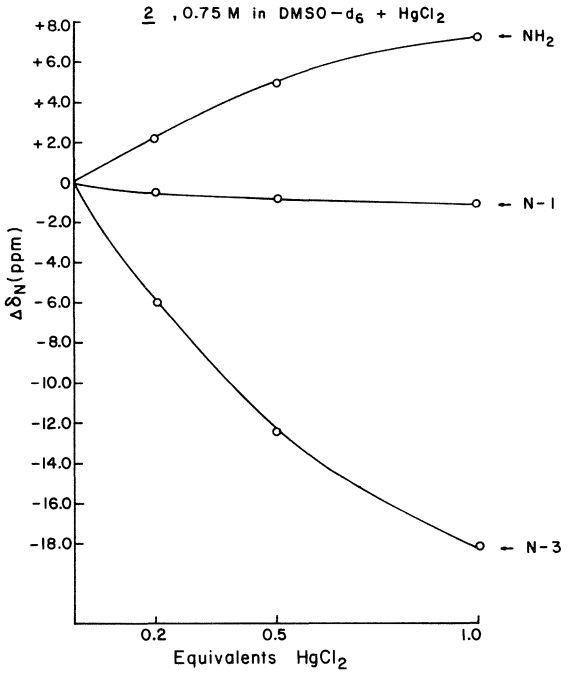


FIG. 3. 2 + $HgCl_2$.

Can. J. Chem. Downloaded from www.nrcresearchpress.com by 210.87.254.42 on 09/06/12
For personal use only.

Can. J. Chem. Downloaded from www.nrcresearchpress.com by 210.87.254.42 on 09/06/12
For personal use only.

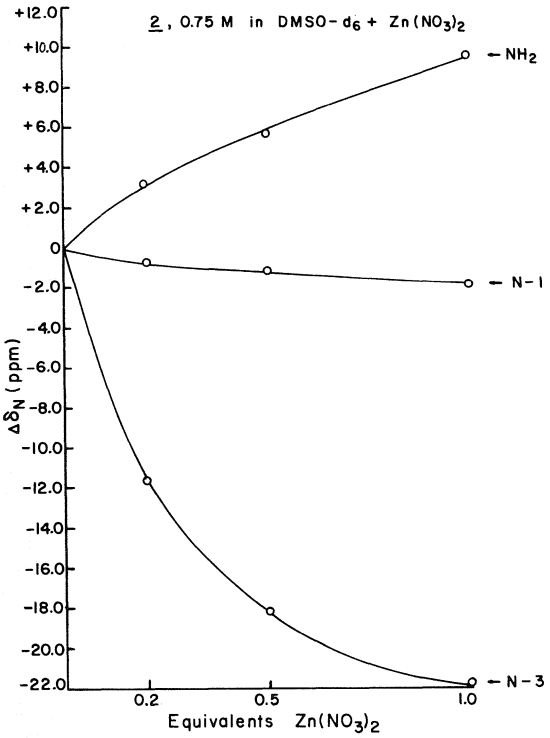


FIG. 4. 2 + $Zn(NO_3)_2$.

7.2 : 1.0 for the induced $^{15}N$ shifts upon protonation is remarkedly similar to the mercuration shift ratio, namely 18.0 : 7.4 : 1.0 (Fig. 3) and the directions of individual induced shifts are the same for protonation and mercuration.

It is unfortunate that the protonation work (5) did not include data for 1.0 equivalent of TFA added, so that highly detailed quantitative comparisons with metalation are not meaningful here.

For $Zn(NO_3)_2$ addition to cytidine (Fig. 4), the induced shifts are somewhat larger than for $HgCl_2$, but the trends are similar.

(e) *Cytidine: $Ba(NO_3)_2$ addition*

We find that $Ba(NO_3)_2$ appears not to bind at a nitrogen of cytidine since no appreciable induced $^{15}N$ shifts are apparent. This result is in agreement with previous conclusions (8), drawn from $^{13}Cmr$ and Raman data, that $Ba^{+2}$ binds preferentially to the carbonyl oxygen of cytidine.

Generally, the earlier results (3) indicate that the site of attachment of metal ions to cytidine depends on the nature of the metal ion. "Hard" metals such as $Ba^{+2}$ bind to the carbonyl oxygen, while soft metals and $H^+$ bind to N-3. In the case of $Zn^{+2}$, binding at both N-3 and the carbonyl oxygen has been suggested.

From the $^{15}N$ results herein, one can conclude that there is certainly N-3 binding for $Hg^{+2}$ and $Zn^{+2}$, while attachment of $Ba^{+2}$ to the carbonyl oxygen does not perturb the magnetic environment at any of the nitrogen atoms enough to influence their chemical shifts.

(f) *Guanosine: $HgCl_2$ and $Zn(NO_3)_2$ addition*

The induced $^{15}N$ shifts (Figs. 5 and 6) clearly show that N-7 is the preferred nitrogen for $Hg^{+2}$ and $Zn^{+2}$ complexation. The pronounced upfield shifts of N-7 are reminiscent of its shift upon protonation (5), as are the directions and magnitudes of the minor changes seen for the remaining four nitrogens.

For guanosine, the primary binding site is calculated (13) to be a chelated position involving the carbonyl oxygen and N-7 as shown below.

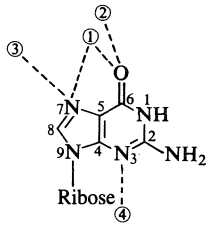


The minor upfield shifts seen for N-3 of **3** upon metalation are consistent with this site being a potential, but less favored, site of complexation than N-7.

(g) *Guanosine: $Ba(NO_3)_2$ addition*

The lack of pronounced $^{15}N$ shift changes upon $Ba^{+2}$ addition indicates that primary $Ba^{+2}$ complexation is not at nitrogen. Presumably this "hard"

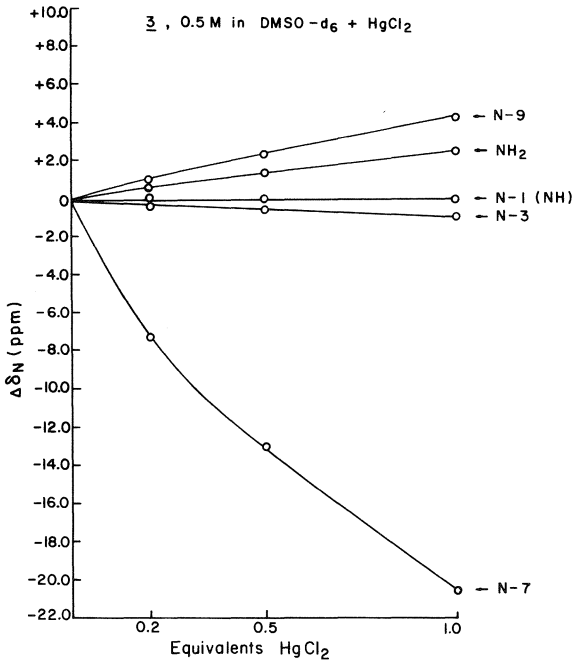


FIG. 5. 3 + $HgCl_2$.

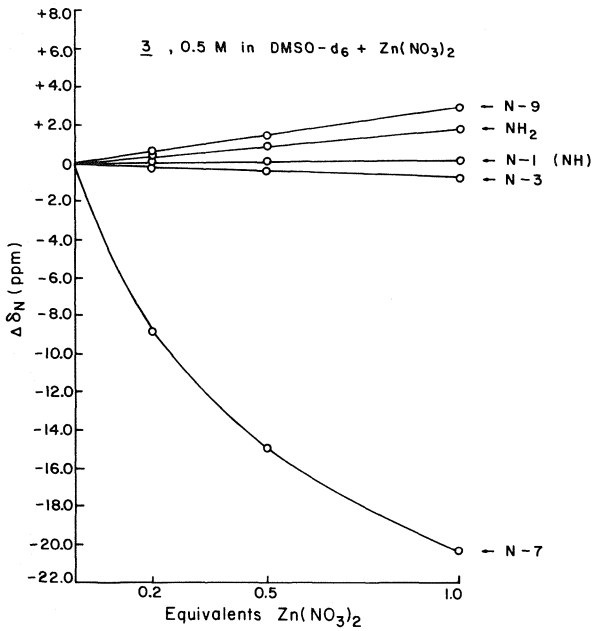


FIG. 6. 3 + $Zn(NO_3)_2$.

ion prefers the carbonyl oxygen, but no $^{13}C$ or Raman data are presently available to check this point.

## Conclusions

It is apparent from this work that $^{15}N$mr chemical shift changes provide a useful addition to the available methods for monitoring metal ion – nucleoside binding. There appears to be a general upfield shift for metalated nitrogen, and the preferred sites of mercuration in the three nucleosides studied here parallel the well-established protonation sites.

Further work in this area using $^{15}N$ relaxation times could be envisaged by analogy to that recently carried out for nucleotide – paramagnetic ion interactions (4).

Extension to aqueous solutions is planned, although the lower solubilities of the materials in aqueous media will retard experiments somewhat. Based on $^{13}C$ and Raman spectra (11, 15) it has been suggested, however, that, with the exception of N-1 of guanosine, similar complexes are formed between these nucleosides and metal ions in $H_2O$ as in DMSO solution.

## Experimental

(a) *Materials*

Samples of adenosine, cytidine, and guanosine were obtained from Sigma Chemical Company, St. Louis, MO 63178, U.S.A. and were used without further purification.

Mercuric chloride was Fisher Certified ACS grade and used without additional purification, as were $Ba(NO_3)_2$ and $Zn(NO_3)_2$. Dimethylsulfoxide-$d_6$ was purchased from Stohler Isotope Chemicals, Montreal 101, Quebec, Canada, and Merck, Sharp & Dohme of Canada Ltd., Pointe Clair – Dorval, Quebec.

(b) *Spectra*

For all resonances except those of protonated nitrogens, natural abundance $^{15}N$ spectra were obtained on a Bruker WH-400 nmr spectrometer at a frequency of 40.54 MHz using facilities at the Southwestern Ontario High Field NMR Centre, Guelph, Ontario. Sample size was 10 mm, and spectra were recorded using inverse gated $^1H$ decoupling in order to eliminate effects of differential nuclear Overhauser effects. Typical pulse angles were 40° and delay times of 30 s were employed. Satisfactory signal to noise ratios were obtained after 300–500 scans. Typical spectral widths were 12 000 Hz.

$^{15}N$ chemical shifts for the protonated nitrogens were obtained on a Varian XL-200 spectrometer at 20.27 MHz. The refocussed INEPT sequence (16, 17) was used. Employing $^1J_{NH} = 91$ Hz, the delays were $\tau = 2.75$ ms ($\frac{1}{4}J$) and $\Delta = 4.12$ ms ($\frac{3}{8}J$), and the $\pi/2$ pulses were 26 μs for $^{15}N$ and 40.5 μs for $^1H$ respectively. A recycle time of 2 s was used. Samples were run in 10 mm tubes.

Chemical shifts were measured relative to external saturated aqueous $NH_4Cl$ and then converted to the standard $^{15}N$ scale in ppm relative to $NH_3$ using a conversion constant of +27.3 ppm (18).

Linewidths of nitrogen resonances did not increase appreciably upon metalation, indicating that the rate of exchange between metalated and free nucleoside is fast on the nmr timescale.

## Acknowledgements

We thank the Natural Sciences and Engineering Research Council of Canada for financial support and Ms. Mary Ellen Sturgeon for technical assistance.

1. B. ROSENBERG. Cancer Chemother. Rep. **59**, 539 (1975).
2. S. MANSY, T. E. WOOD, J. C. SPROULES, and R. S. TOBIAS. J. Am. Chem. Soc. **96**, 1762 (1974).
3. L. G. MARZILLI, B. DE CASTRO, J. P. CARADONNA, R. C. STEWART, and C. P. VAN VUUREN. J. Am. Chem. Soc. **102**, 916 (1980).
4. G. C. LEVY and J. J. DECHTER. J. Am. Chem. Soc. **102**, 6191 (1980).
5. V. MARKOWSKI, G. R. SULLIVAN, and J. D. ROBERTS. J. Am. Chem. Soc. **99**, 714 (1977).
6. S. SHIMOKAWA, H. FUKUI, J. SOHMA, and K. HOTTA. J. Am. Chem. Soc. **95**, 1777 (1973).
7. T. YAKONO, S. SHIMOKAWA, and J. SOHMA. J. Am. Chem. Soc. **97**, 3837 (1975).
8. L. G. MARZILLI, R. C. STEWART, C. P. VAN VUUREN, B. DE CASTRO, and J. P. CARADONNA. J. Am. Chem. Soc. **100**, 3967 (1978).
9. L. S. KAN and N. C. LI. J. Am. Chem. Soc. **92**, 4823 (1970).
10. K. W. JENNETTE, S. J. LIPPARD, and D. A. UCKO. Biochem. Biophys. Acta, **402**, 403 (1975).
11. L. G. MARZILLI. Prog. Inorg. Chem. **23**, 255 (1977).
12. D. J. HODGSON. Prog. Inorg. Chem. **23**, 211 (1977).
13. D. PERATHIA, A. PULLMAN, and B. PULLMAN. Theoret. Chim. Acta, **43**, 207 (1977).
14. N. FARRELL. J. Chem. Soc. Commun. 1014 (1980).
15. Y. H. CHAO and D. R. KEARNS. J. Am. Chem. Soc. **99**, 6425 (1977).
16. G. A. MORRIS and R. FREEMAN. J. Am. Chem. Soc. **101**, 760 (1979).
17. G. A. MORRIS. J. Am. Chem. Soc. **102**, 428 (1980).
18. G. C. LEVY and R. L. LICHTER. Nitrogen-15 nuclear magnetic resonance spectroscopy. Wiley–Interscience, New York, NY. 1979. p. 32.

Can. J. Chem. Downloaded from www.nrcresearchpress.com by 210.87.254.42 on 09/06/12
For personal use only.

# Charge distributions and chemical effects. XXVII. Molecular energies of carbonyl compounds and ethers, a calculation involving the charges of the bond-forming atoms

S. FLISZÁR AND M. T. BÉRALDIN

*Département de Chimie, Université de Montréal, Montréal (Qué), Canada H3C 3V1*

Received June 26, 1981

S. FLISZÁR and M. T. BÉRALDIN. Can. J. Chem. **60**, 792 (1982).

Energy calculations are presented for carbonyl compounds and ethers by applying the equation $\varepsilon_{ij} = \varepsilon_{ij}^0 + a_{ij}\Delta q_i + a_{ji}\Delta q_j$ which describes individual bond contributions in terms of electronic charge increments $\Delta q$ at the bond-forming atoms $i$ and $j$, relative to atomic charges in selected reference bonds with energies $\varepsilon_{ij}^0$. At a molecular level, the sum $\Sigma_i\Sigma_j a_{ij}\Delta q_i$ accounts for virtually the entire energy variations due to charge redistributions accompanying isodesmic structural changes. Coulomb-type interactions between nonbonded atoms play only a minor role in that respect. Using charges derived from $^{13}C$ and $^{17}O$ nmr shift-charge correlations, calculated and experimental energies agree within 0.16 kcal/mol (average deviation).

S. FLISZÁR et M. T. BÉRALDIN. Can. J. Chem. **60**, 792 (1982).

Les énergies d'une série d'aldéhydes, de cétones et d'éthers ont été calculées au moyen de l'équation $\varepsilon_{ij} = \varepsilon_{ij}^0 + a_{ij}\Delta q_i + a_{ji}\Delta q_j$ décrivant la contribution individuelle de chaque lien en termes des variations de charges $\Delta q$ des atomes liés $i$ et $j$, par rapport aux charges atomiques d'un lien de référence d'énergie $\varepsilon_{ij}^0$. Au niveau moléculaire, la somme $\Sigma_i\Sigma_j a_{ij}\Delta q_i$ représente la presque totalité de la variation d'énergie due aux redistributions électroniques accompagnant les changements de structure isodesmiques. Les interactions Coulombiennes entre atomes non liés ne jouent qu'un rôle très secondaire. A l'aide de charges déduites de corrélations avec les déplacements chimiques en rmn pour les noyaux $^{13}C$ et $^{17}O$, le calcul conduit à un bon accord avec les énergies expérimentales, l'erreur moyenne étant de 0.16 kcal/mol.

## Introduction

The simplest "theoretical" description of a molecule, its structural formula featuring the chemical bonds, still represents the single most valuable "material" support for the discussion of a number of problems regarding chemical transformations and molecular properties. Because of the undisputed qualities of this type of description, much can be gained (namely, in simplicity) with the use of a theoretical approach retracing the essential features linked to the concept of chemical bonds.

While, of course, a molecule is a distinct entity which can be characterized in a number of manners, the constituent atoms retain much of their "atomic" properties. In fact, a molecule can be considered as a collection of "atoms" with energies differing from their free state values (1–3). These energy differences are, for each individual atom, a measure for the process of becoming part of the molecule and contain a portion of the molecular binding energy. Alternatively, in an entirely equivalent description, molecules can be regarded as assemblies of "chemical bonds" whose energies depend in a subtle way on the bond-forming atoms, namely, on their electron populations (2). This type of description, resulting from an appropriate energy partitioning, leads to a bond by bond insight into the various factors contributing to the stability of a molecular edifice and appears to be most suited for its analysis in terms of electron distributions.

Fascinating new information can be extracted in this way. For example, in the study (2) of linear and branched paraffins and in compounds containing chair or boat cyclohexane rings it appeared that 0.001 electron (= 1 me) added to hydrogen stabilized a CH bond by 0.632 kcal/mol whereas 1 me added to carbon had a stabilizing effect of 0.247 on a CH bond and of 0.488 kcal/mol on a CC bond. It follows therefrom that any electron enrichment on carbon atoms at the expense of electron populations at the hydrogen atoms results in a gain in molecular stability, which is well reflected in comparisons between isomers or conformers. In the present study, we examine carbon–oxygen bonds in ethers and carbonyl compounds, in order to learn how these and the remaining parts of the molecules are affected by intramolecular electron redistributions accompanying structural changes. While consideration is given to the theoretical interpretation of the energetic aspects related to the individual bonds, we also offer comparisons with experimental results, namely, with enthalpies of formation.

## Bond energies

The following considerations apply to molecules at equilibrium, in their hypothetical vibrationless state at 0 K. The portion of the total atomization energy associated with the *ij* bond (i.e., the "bond energy" $\varepsilon_{ij}$) is given by eq. [1] (2)

0008-4042/82/060792-09$01.00/0

©1982 National Research Council of Canada/Conseil national de recherches du Canada

Can. J. Chem. Downloaded from www.nrcresearchpress.com by 210.87.254.5 on 09/06/12
For personal use only.

Can. J. Chem. Downloaded from www.nrcresearchpress.com by 210.87.254.5 on 09/06/12
For personal use only.

[1] $$\varepsilon_{ij} = K_i^{\text{mol}} Z_i(\partial\varepsilon_{ij}/\partial Z_i) + K_j^{\text{mol}} Z_j(\partial\varepsilon_{ij}/\partial Z_j) + (K_i^{\text{at}} - K_i^{\text{mol}})\, V_{\text{ne}}(\text{free atom } i)/v_i + (K_j^{\text{at}} - K_j^{\text{mol}}) V_{\text{ne}}(\text{free atom } j)/v_j$$

where $Z_i$ is the nuclear charge of atom $i$, $v_i$ the number of atoms attached to it, and $V_{\text{ne}}$ its nuclear–electronic potential energy. For isolated atoms, the $K_i^{\text{at}}$ constants are $E_i^{\text{at}}/V_{\text{ne}}$(free atom $i$) with $E_i^{\text{at}}$ = energy of atom $i$. Similarly, $K_i^{\text{mol}}$ is $E_i^{\text{mol}}/V(i, \text{mol})$ where $E_i^{\text{mol}}$ is the energy of an atom $i$ being part of a molecule and $V(i, \text{mol})$ the total (nuclear–electronic and nuclear–nuclear) potential energy involving nucleus $Z_i$. Detailed numerical analyses have indicated that the $K_i^{\text{mol}}$'s are, indeed, constants for the individual atoms, regardless of hybridization or type of bonding in a molecule (3, 4). They are most conveniently deduced from Hartree–Fock total energies, $E$, and the orbital energies ($\nu$ = orbital occupation) of homonuclear diatomics, by means of eq. [2].

[2] $$(3 - 1/K_i^{\text{mol}})\, E = \Sigma\nu\varepsilon^{\text{orb}}$$

When applied to isolated atoms, eq. [2] permits the calculation of $K_i^{\text{at}}$. The validity of eq. [1] is determined only by the validity of apportioning the molecular atomization energy into bonded and nonbonded terms, i.e., ultimately, by the very existence of chemical bonds (2). Equation [2], on the other hand, is exact in Hartree–Fock theory provided, of course, that all quantities are evaluated at equilibrium geometry (3, 5). The $K_i^{\text{at}}$ and $K_i^{\text{mol}}$ constants, deduced from the appropriate Hartree–Fock calculations (3, 6, 7), are indicated in Table 1.

The $\partial\varepsilon_{ij}/\partial Z_i$ derivatives for use in eq. [1] can be extracted from SCF calculations, by means of eq. [3].

[3] $$Z_i\Sigma_j(\partial\varepsilon_{ij}/\partial Z_i) \simeq V_{\text{ne}}(\text{free atom } i) - V(i, \text{mol})$$

This approximation (2) is certainly valid when the interactions between nonbonded atoms are much smaller than those between bonded atoms. With the selection of a convenient set of "model" bonds, we only need to calculate a limited number of "reference" derivatives, $\partial\varepsilon_{ij}^0/\partial Z_i$, which correspond to the $\varepsilon_{ij}^0$ energies of the reference bonds, e.g., the CC and CH bonds of ethane. The results (Appendix I) are indicated in Table 1.

Using now these results, derived from [5*s*3*p*|3*s*] calculations, we deduce the corresponding theoretical $\varepsilon_{ij}^0$ energies by means of eq. [1]. Of course, any error in their evaluation leads to systematic deviations which are magnified by the number of their occurrence in a molecule. An empirical refinement, using experimental atomization energies, yields the "best" $\varepsilon_{ij}^0$'s which are compared in Table 2 with their theoretical counterparts.

TABLE 1. Theoretical parameters for use in eq. [1]

| Parameter (au) | Source |
|---|---|
| $K_H^{\text{at}} = K_H^{\text{mol}} = 1/2$ | References 2, 3 |
| $K_C^{\text{at}} = 0.4276$ | Clementi and Roetti (6), eq. [2] |
| $K_C^{\text{mol}} = 0.4287$ | Reference 3 |
| $K_O^{\text{at}} = 0.4201$ | Clementi and Roetti (6), eq. [2] |
| $K_O^{\text{mol}} = 0.4213$ | Cade and Wahl (7), eq. [2] |
| $E$ (free at. C) = −37.8558 | From the sum, $-\Sigma$IP, of the ionization potentials (8), using 1 au = 27.2106 eV |
| $E$ (free at. O) = −75.1102 | |
| $\partial\varepsilon_{CH}/\partial Z_H = 0.153$ | Ethane, ref. 2 |
| $\partial\varepsilon_{CH}/\partial Z_C = 0.027$ | Ethane, ref. 2 |
| $\partial\varepsilon_{CC}/\partial Z_C = 0.012$ | Ethane, ref. 2 |
| $\partial\varepsilon_{CO}^0/\partial Z_C = -0.049$ | Diethylether, Appendix I |
| $\partial\varepsilon_{CO}^0/\partial Z_O = 0.036$ | Diethylether, Appendix I |
| $\partial\varepsilon_{CO}^0/\partial Z_C = -0.077$ | Acetone, Appendix I |
| $\partial\varepsilon_{CO}^0/\partial Z_O = 0.071$ | Acetone, Appendix I |

TABLE 2. Energy terms of selected reference bonds

| Reference molecule | Bond | Energy ($\varepsilon_{ij}^0$), kcal/mol: Theor. (eq. [1]) | "Best" |
|---|---|---|---|
| Ethane | CC | 69.3 | 69.63 |
| Ethane | CH | 106.9 | 106.81 |
| Diethylether | CO | 80 | 79.78 |
| Acetone | CO | 181 | 179.40 |

The partial derivatives $\partial\varepsilon_{ij}^0/\partial Z_i$, which are bound to the conditions set by the Hellmann–Feynman theorem used for deriving eq. [1] (implying, namely, constant electron densities), are valid only for the molecules to which they refer. This, of course, holds also for the $\varepsilon_{ij}^0$ energies: they cannot be simply transferred to other molecules. Indeed, the simple transfer of bonds from one molecule to another implies transferring the bond-forming atoms, including their electron clouds, at the sacrifice of preserving molecular electroneutrality (2). The appropriate charge renormalization leads to the following expression for the energy contribution of an *ij* bond (2)

[4] $$\varepsilon_{ij} = \varepsilon_{ij}^0 + a_{ij}\Delta q_i + a_{ji}\Delta q_j$$

where $\Delta q_i$ and $\Delta q_j$ are the increments in net atomic charge with respect to the charges of the atoms $i$ and $j$ in the reference bond. The sum over all the *ij* bonds gives the "bonded" contribution to the energy of atomization, i.e.,

[5] $$\Delta E_a^{*\text{bonds}} = \Sigma\varepsilon_{ij}^0 + \Sigma_i\Sigma_j a_{ij}\Delta q_i$$

TABLE 3. Calculation of $a_{ij}$ (eq. [6])

| Atom | $N_i$ (e) | $\partial E_i/\partial N_i$ | $\partial^2 E_i/\partial N_i^2$ | $r_{ij}$ (Å) | $a_{ij}$ (au) |
|---|---|---|---|---|---|
| H (1*s*) | 1.0117 | −0.195 | | 1.08 (CH) | $a_{HC} = -1.007$ |
| C (2*s*) | 1.44 | −0.735 | 0.45 | 1.08 (CH) | $a_{CH} = -0.394$ |
| | | | | 1.53 (CC) | $a_{CC} = -0.777$ |
| | | | | 1.43 (CO) | $a_{CO} = -1.135$ (ether) |
| C (2*p*) | 1.97 | −0.200[a] | 0.37 | 1.08 (CH) | $a_{CH} = -0.276$ (carbonyl-C) |
| | | | | 1.53 (CC) | $a_{CC} = -0.659$ (carbonyl-C) |
| | | | | 1.22 (CO) | $a_{CO} = -1.182$ (carbonyl-C) |
| O (2*p*) | 4.023 | −0.316 | 0.50 | 1.22 (CO) | $a_{OC}$[b] $= -1.065$ (carbonyl-O) |
| | 3.995 | −0.331 | | 1.43 (CO) | $a_{OC}$[c] $= -0.804$ (ether) |

[a]The selection of the appropriate $\partial E_i/\partial N_i$ derivatives presents no difficulties for $sp^3$ carbon and oxygen atoms because *ab initio* population analyses clearly show the involvement of 2*s* electrons in the former case (2) and of 2*p* electrons in the latter (14). At carbonyl-C atoms, however, mainly 2*p* populations are affected by substitution. The appropriateness of this choice for $\partial E_i/\partial N_i$ is discussed in the text.
[b]Value for acetone. The $a_{OC}$'s for carbonyl groups must be recalculated for each compound of interest, using eq. [6].
[c]For the more negative oxygens, we find $a_{OC} = -0.800$ au (see text).

featuring the effects due to changes in net atomic charges with respect to the charges of the atoms forming the reference bonds. The $a_{ij}$'s are given by the formula (2)

$$[6] \quad a_{ij} = \frac{1}{v_i}\frac{K_{Av}^{mol}}{K_i^{mol}}\left[\left(\frac{\partial E_i}{\partial N_i}\right)^0 - \frac{1}{2}\left(\frac{\partial^2 E_i}{\partial N_i^2}\right)^0 \Delta q_i\right] - K_{Av}^{mol} Z_j^{eff} < r_{ij}^{-1} >^0$$

in which $v_i$ is the number of atoms bonded to $i$ and $K_{Av}^{mol}$ is the molecular average of the $K_i^{mol}$'s, which can be taken at 3/7. Moreover, $Z_i^{eff}$ is the effective nuclear charge of atom $j$, in the spirit of the Politzer–Parr electron partitioning into core and valence region (9), e.g., $Z^{eff}(C) \simeq 4$ and $Z^{eff}(O) \simeq 6$ au. Finally, $< r_{ij}^{-1} >^0$ is the average inverse distance from nucleus $i$ to the $N_j$ electrons of atom $j$, which is approximated by the inverse internuclear distance $(r_{ij}^{-1})_{nn}$. The first and second derivatives of the energy of atom $i$ with respect to its population $N_i$ are conveniently obtained from SCF-Xα theory (10). For hydrogen and $sp^3$ carbon atoms, the appropriate values are those of ref. 2. The results for C and O 2*p* electrons were deduced using the "frozen core" α values given by Schwarz (11), i.e., $\alpha_C = 0.75928$ and $\alpha_O = 0.74447$ (Table 3).[1]

So far, we have deduced the theoretical parameters required for numerical applications of eqs. [4] and [5], namely, the reference bond terms $\varepsilon_{ij}^0$ (Table 2) and the $a_{ij}$ coefficients (Table 3). We now must find a convenient way to determine the $\Delta q_i$'s which are also required in the study of molecular energies using eqs. [4] and [5].

### Approximations for $\Delta q_i$

Atomic charges can, in principle, be derived from molecular wave functions using an appropriate partitioning scheme, but this is a horse of another color (12). In practice, under favorable conditions, one can take advantage of $^{13}C$ and $^{17}O$ nmr information. For $sp^3$ carbon atoms it was shown that a linear shift–charge relationship is remarkably accurate (13) and, moreover, that the theoretical charges satisfying it correspond to the same definition as those satisfying eq. [5] (2). Hence, using charges deduced from $^{13}C$ nmr data, eq. [5] was found to agree with experimental energies within 0.16 kcal/mol (average derivation).

Following the same approach, we use the relationship (2)

$$[7] \quad \Delta q_C = -0.148\ \delta_C \text{ (me)}$$

where $\delta_C$ is the shift relative to the atom chosen as reference in the calculation of $\Delta q_C$. Interestingly, the same relation applies, at least as a valid approximation, also to the α-carbons in ethers and to carbonyl-C atoms provided, of course, that the references are chosen in an appropriate manner. This point is verified by comparisons with experimental results (given below) but in this case our knowledge concerning the precision of eq. [7] is limited by the accuracy of the experimental data used in this type of verification. Furthermore, *ab initio* calculations on ether oxygen atoms indicate that the $\Delta q_O/\delta_O$ slope is ~1.8 times that of the $\Delta q_C/\delta_C$ slope determined under identical conditions, giving (14)

$$[8] \quad \Delta q_O(\text{ether}) = -0.267\delta_O \text{ (me)}$$

Finally, for carbonyl oxygen atoms we use

$$[9] \quad \Delta q_O(\text{carbonyl}) = 2.7\ \delta_O \text{ (me)}$$

In contrast with eqs. [7] and [8] which are based on theoretical electron populations, this relationship is deduced from, and justified by, a numerical

[1]We thank Dr. B. N. McMaster, who carried out these SCF-Xα calculations.

Can. J. Chem. Downloaded from www.nrcresearchpress.com by 210.87.254.5 on 09/06/12
For personal use only.

Can. J. Chem. Downloaded from www.nrcresearchpress.com by 210.87.254.5 on 09/06/12
For personal use only.

analysis involving experimental energies, as explained further below: while not ranking at the same degree of confidence as eqs. [7] and [8], eq. [9] appears to represent at least a reasonable approximation.[2]

For the hydrogen atoms, we deduce the sum $\Sigma\Delta q_H$ from the condition $\Sigma_i q_i = 0$. The result is

$$[10]\quad \Sigma\Delta q_H = -(\Sigma\Delta q_{C\alpha} + \Sigma\Delta q_{C\neq\alpha} + \Sigma\Delta q_O) - (n_{C\alpha}q_{C\alpha}^0 + n_O q_O^0) - (n_{C\neq\alpha}q_C^0 + n_H q_H^0)$$

where Cα and C≠α stand for C atoms adjacent to, viz. nonadjacent to oxygen and $n_i$ is the number of $i$ atoms in the molecule. Finally, $q_{C\alpha}^0$ and $q_O^0$ are for acetone or diethylether, whichever is the appropriate reference, and $q_C^0$, $q_H^0$ are the ethane C and H net charges, 35.1 and −11.7 me, respectively (2). The sum $n_{C\alpha}q_{C\alpha}^0 + n_O q_O^0$ gives $2q_{C\alpha}^0 + q_O^0 \simeq 67.7$ me for diethylether and $q_{C\alpha}^0 + q_O^0 \simeq -7.2$ me for acetone, from charge normalization (Appendix II).

Attention must be given to the difference $\Delta q_{C\alpha}^0 = q_{C\alpha}^0 - q_C^0$. Indeed, for CO bonds the reference is $q_{C\alpha}^0$ but in calculations of CC and CH bonds, including those involving α-carbons, the appropriate reference is $q_C^0$. $\Delta q_{C\alpha}^0$ cannot be simply deduced from the appropriate $^{13}C$ nmr shifts, as oxygen appears to introduce an "extra" downfield shift at α-carbons, estimated at ~ 41.7 ppm in the case of the ethers (16). Assuming here that this shift, which could be due in part of the electric field of the oxygen dipole, is not primarily a carbon charge effect, we estimate the latter by subtracting tentatively 41.7 ppm from the observed α-carbon-shifts (60, viz. 199 ppm from ethane for diethylether (16) and acetone (17), respectively). It turns out that the $\Delta q_{C\alpha}^0 \simeq -2.7$ (ether) and $\Delta q_{C\alpha}^0 \simeq -23$ me (acetone) values obtained in this fashion (eq. [7]) are reasonable: atomization energies calculated with these $\Delta q_{C\alpha}^0$ values differ from their experimental counterparts by ~0.35 kcal/mol (average deviation). A refinement involving experimental energies yields, as described below, $\Delta q_{C\alpha}^0 = -3.84$ me for diethylether and −21.1 me for acetone. Of course, not too much importance should be attached to these estimates since they may, in part, correct for minor uncertainties associated with the $a_{ij}$'s, with eqs. [7]–[9], and with the evaluation of vibrational and thermodynamic data used in this analysis. Clearly, the difficulties are now in the evaluation of fraction of kcal/mol uncertainties, thus preventing us temporarily from further improving the calculations. This is best seen by examining experimental results.

[2] *Ab initio* calculations (14) reveal that carbonyl oxygen atoms behave quite like ethylenic $sp^2$ carbons, in that any increase of electronic charge is reflected in an upfield shift. For the latter, the charge/shift slope is ~ −11.7 times that of alkane carbon atoms (15) giving $\Delta q_C \simeq 1.7\delta_C$, a result which is of the same order as that expressed by eq. [9].

### Comparisons with experimental energies

In addition to the energy $\Delta E_a{}^{*\text{bonds}} = \Sigma\varepsilon_{ij}$ contributed by the chemical bonds, we also consider the small "nonbonded" part, $\Delta E_{nb}{}^* = -E_{nb}{}^*$, of the atomization energy:

$$[11]\quad \Delta E_a{}^* = \Delta E_a{}^{*\text{bonds}} - E_{nb}{}^*$$

Regarding $E_{nb}{}^*$, Del Re (18) has shown that a valid approximation in σ systems is Coulombic in nature, i.e.

$$[12]\quad E_{nb}{}^* = (1/2)\sum_{kl}^{nb} q_k q_l / r_{kl}$$

where $q_k$ and $q_l$ are the net charges of nonbonded atoms at a distance $r_{kl}$. For carbonyl compounds, results derived from eq. [12] should be interpreted with some reservations and are used on a tentative basis.

So far we have considered molecules in their hypothetical vibrationless state. Actual molecules, at some temperature $T$, contain zero-point (ZPE) and thermal vibrational energies ($E_{vibr}$). These were deduced from experimental and calculated fundamental frequencies ν, i.e., in the harmonic oscillator approximation,

$$[13]\quad \text{ZPE} = N_{Av}(1/2)\Sigma_i h\nu_i$$

and, using Einstein's function,

$$[14]\quad E_{vibr} = N_{AV}\Sigma_i h\nu_i \exp(-h\nu_i/kT)/[1 - \exp(-h\nu_i/kT)]$$

Interpolation formulas had to be used in cases for which no or insufficient spectral data are presently available (Table 4). With these results and the

TABLE 4. Zero-point and heat-content energies (kcal mol$^{-1}$)[a]

| Molecule | ZPE | $H_T - H_0$ | Estimated ZPE + $H_T - H_0$ |
|---|---|---|---|
| $CH_3CHO$ | 33.58 | 3.07 | |
| $(CH_3)_2CO$ | 50.59 | 4.00 | |
| $(C_2H_5)_2CO$ | 86.68 | 4.84 | |
| $(CH_3)_2O$ | 49.91 | 2.74 | 52.55 (−0.10) |
| $CH_3OC_2H_5$ | 65.75 | 4.11 | 70.19 (0.33) |
| $CH_3OiC_3H_7$ | 82.74 | 4.92 | 87.83 (0.17) |
| $(C_2H_5)_2O$ | 82.82 | 4.94 | 87.83 (0.07) |
| $C_2H_5OiC_3H_7$ | 99.59 | 5.81 | 105.47 (0.07) |
| $(iC_3H_7)_2O$ | 116.65 | 6.67 | 123.11 (−0.21) |
| Tetrahydropyran | 88.83 | 4.04 | |
| 1,4-Dioxane | 74.61 | 3.87 | |

[a]Results deduced from eqs. [13] and [14] using the vibrational analyses of acetaldehyde and acetone (20*a*) and diethylketone (20*b*). For the ethers, the ir and Raman spectra are taken from refs. 20*c* and 20*d*, for dimethylether. The "estimated" values are deduced from the approximation ZPE + $H_T - H_0$ = 52.55 + 17.64($n_C$ − 2); the differences between these estimates and those based on spectroscopic evidence are given in parentheses.

Can. J. Chem. Downloaded from www.nrcresearchpress.com by 210.87.254.5 on 09/06/12
For personal use only.

appropriate enthalpies of formation of the gaseous atoms (19), $\Delta H_f^0$ $(A_i)$ = 170.89 (C), 52.09 (H), and 59.54 kcal/mol (O), one relates the atomization energies $\Delta E_a$* to the standard molecular enthalpies of formation, $\Delta H_f^0$ (298.15, gas), by means of the formula

$$[15]\quad \Delta E_a^* = \Sigma n_i[\Delta H_f^0\ (A_i) + 5RT/2] + \mathrm{ZPE} + (H_T - H_0) - \Delta H_f^0$$

in which $H_T - H_0 = E_{vibr} + 4RT$ is the increase in enthalpy of non-linear molecules due to their warming up from $T = 0$ to $T = T$. Eqs. [13]–[15] are instrumental in the calculation of "experimental" $\Delta E_a$* energies.

The theoretical sums $\Sigma\varepsilon_{ij}$ can be deduced from bond by bond calculations of the individual $\varepsilon_{ij}$'s (eq. [4]). A detailed example is worked out in Appendix III. For homologous series, like those studied here, it is easy and convenient to derive general formulas. For the carbonyl compounds listed below we obtain

$$[16]\quad \Sigma_i\Sigma_j a_{ij}\Delta q_i = \lambda_1\Sigma N_{CC}\delta_C + \lambda_2\Sigma\delta_{C\neq\alpha} + \lambda_3\delta_{C\alpha} + \lambda_4\delta_O + n_C a_{HC} q_H^0 + \Delta q_{C\alpha}^0\,(a_{C\alpha C}N_{CC}^{\alpha} + a_{C\alpha H}N_{CH}^{\alpha} - a_{HC}) - a_{HC}q_O^0$$

where[3] $\lambda_1 = a_{CC} - a_{CH} = 0.0356$, $\lambda_2 = 4a_{CH} - a_{HC} = 0.0529$, and $\lambda_3 = 2a_{C\alpha H} + a_{CO} - a_{HC} = 0.0675$ kcal mol$^{-1}$ ppm$^{-1}$ (using eq. [7] and 1 au = 627.51 kcal/mol). Because of the large variations of $\Delta q_O$, $a_{OC}$ (eq. [6]) and $\lambda_4 = a_{OC} - a_{HC}$ must be calculated in each case of interest. $a_{OC}$ varies between −1.081 au ($CH_3CHO$) and −1.041 au ($iC_3H_7COiC_3H_7$). $N_{CC}$ is the number of CC bonds formed by the C atom whose shift is $\delta_C$, $N_{CC}^{\alpha}$ and $N_{CH}^{\alpha}$ are the number of CC, viz. CH, bonds involving α carbons. Similarly, one obtains for dialkylethers that

$$[17]\quad \Sigma_i\Sigma_j a_{ij}\Delta q_i = \lambda_1\Sigma N_{CC}\delta_C + \lambda_2\Sigma\delta_{C\neq\alpha} + \lambda_3'\Sigma\delta_{C\alpha} + \lambda_4'\delta_O + (n_C - 2)a_{HC}q_H^0 + \Delta q_{C\alpha}^0\,(a_{CC}\Sigma N_{CC}^{\alpha} + a_{CH}\Sigma N_{CH}^{\alpha} - 2a_{HC}) - a_{HC}q_O^0$$

with $\lambda_1$ and $\lambda_2$ as above and $\lambda_3' = 3a_{CH} + a_{CO} - a_{HC} = 0.1217$ kcal mol$^{-1}$ ppm$^{-1}$. $\lambda_4' = 2a_{OC} - a_{HC}$ is 0.1007 kcal mol$^{-1}$ ppm$^{-1}$ for $a_{OC} = -0.804$ au ($\delta_O < 0$) or 0.0994 kcal mol$^{-1}$ ppm$^{-1}$ for $a_{OC} = -0.800$ ($\delta_O > 0$). Equations [16] and [17] enable an empirical evaluation of the respective $\Delta q_{C\alpha}^0$'s (−21.1 and −3.84 me for acetone and diethylether, respectively) and, therefrom, of $q_O^0$ (−21.2 for acetone and 5.18 me for diethylether, as indicated in Appendix II). The appropriate shift values are reported in Table 5.

[3]The $a_{C\alpha C} - a_{C\alpha H} = a_{CC} - a_{CH}$ term appearing in this calculation does not depend on $\partial E/\partial N$. A possible error associated with this derivative in the treatment of carbonyl-C atoms would result in a constant error for all carbonyl compounds and, hence, in a distortion in the estimate of $\varepsilon_{CO}^0$.

TABLE 5. $^{13}C$ and $^{17}O$ nmr results[a] for use in eqs. [16] and [17]

| Molecule | $\Sigma N_{CC}\delta_C$ | $\Sigma\delta_{C\neq\alpha}$ | $\Sigma\delta_{C\alpha}$ | $\delta_O$ |
|---|---|---|---|---|
| $CH_3CHO$ | 19.8 | 25.3 | −5.5 | 23.0 |
| $C_2H_5CHO$ | 57.6 | 30.1 | −3.3 | 10.5 |
| $nC_3H_7CHO$ | 103.1 | 57.0 | −3.5 | 20.0 |
| $(CH_3)_2CO$ | 44.4 | 44.4 | 0 | 0 |
| $CH_3COC_2H_5$ | 84.9 | 52.9 | 1.2 | −11.5 |
| $CH_3COnC_3H_7$ | 135.8 | 81.9 | 1.5 | −6.0 |
| $CH_3COiC_3H_7$ | 158.8 | 81.0 | 4.0 | −12.0 |
| $(C_2H_5)_2CO$ | 128.8 | 61.6 | 4.2 | −22.0 |
| $CH_3COnC_4H_9$ | 198.6 | 113.1 | 2.0 | −6.0 |
| $(iC_3H_7)_2CO$ | 264.2 | 113.6 | 10.5 | −34.0 |
| $(CH_3)_2O$ | 0 | 0 | −12.4 | −59.0 |
| $CH_3OC_2H_5$ | 10.7 | 8.9 | −6.6 | −29.0 |
| $CH_3OnC_3H_7$ | 48.5 | 22.3 | 1.2 | −35.0 |
| $CH_3OiC_3H_7$ | 46.0 | 32.0 | −3.3 | −8.5 |
| $(C_2H_5)_2O$ | 19.2 | 19.2 | 0 | 0 |
| $(nC_3H_7)_2O$ | 94.0 | 45.2 | 13.6 | −10.0 |
| $(iC_3H_7)_2O$ | 78.4 | 68.8 | 4.8 | 46.0 |
| $(nC_4H_9)_2O$ | 187.6 | 97.2 | 9.6 | −13.5 |
| $(sC_4H_9)_2O$ | 168.2 | 86.1 | 16.7 | −35.0 |
| Tetrahydropyran | | 63.2 | 4.6 | −6.0 |
| 1,4-Dioxane | | | 7.6 | −16.0 |

[a]The $\delta_{C\neq\alpha}$ data (16, 21*a*) are relative to ethane (5.8 ppm from TMS) and the $\delta_{C\alpha}$ shifts are from acetone for carbonyl compounds (21*a*), viz. diethylether for the ethers (16). The $^{17}O$ shifts (16, 17) are relative to acetone and diethylether for the carbonyl compounds and ethers, respectively. The $\Sigma N_{CC}\delta_C$ term includes both, $\delta_{C\alpha}$ and $\delta_{C\neq\alpha}$. The tetrahydropyran and 1,4-dioxane $^{13}C$ data are taken from Stothers (21*a*) and the $^{17}O$ results are extracted from ref. 21*b*.

The calculation of $\Delta E_a$*$^{bonds}$ (eq. [5]) is now straightforward. An estimate of the small non-bonded contributions is obtained from eq. [12] and the approximations outlined in Appendix II. The theoretical atomization energies $\Delta E_a$* derived in this fashion are seen to agree within ~0.16 kcal/mol (average deviation) with their counterparts deduced from experimental results using eq. [15] (Table 6). While this sort of agreement prevents us from retracing minor uncertainties associated with our approximations, it also appears that reliable predictions can be made in a number of cases (Table 7).

The quality of calculated enthalpies rests, of course, largely with the approximations involved in the estimate of ZPE + $H_T - H_0$ energies. The use of vibrational energies constructed on the basis of regular group increments may be regarded acceptable in simple cases like those investigated here.[4] It remains, however, that one should refrain from extrapolations in highly crowded systems until these are adequately supported by spectroscopic evidence. With these reservations in mind, our predicted $\Delta H_f^0$ values should represent reasonably good estimates.

[4]Similar situations are described for saturated hydrocarbons (22).

TABLE 6. Comparison between calculated and experimental energies of atomization (kcal/mol) of selected aldehydes, ketones, and ethers

| Molecule | $\Delta H_f^0$ (298.15, gas)[a] | ZPE + $H_T - H_0$[b] | $\Sigma\varepsilon_{ij}^0$ | $\Sigma_i\Sigma_j a_{ij}\Delta q_i$ | $E_{nb}$* | $\Delta E_a$* Calcd. | $\Delta E_a$* Exptl. |
|---|---|---|---|---|---|---|---|
| $CH_3CHO$ | −39.73±0.12 | 36.65 | 676.25 | −0.78 | −0.30 | 675.77 | 675.69 |
| $C_2H_5CHO$ | −45.45±0.21 | 54.95 | 959.50 | 10.17 | −0.36 | 970.03 | 970.34 |
| $nC_3H_7CHO$ | −48.98±0.34 | 73.25 | 1242.75 | 19.26 | −0.75 | 1262.76 | 1262.76 |
| $(CH_3)_2CO$ | −51.90±0.12 | 54.59 | 959.50 | 16.85 | −0.07 | 976.42 | 976.43 |
| $CH_3COC_2H_5$ | −57.02±0.20 | 72.89 | 1242.75 | 27.19 | −0.45 | 1270.39 | 1270.48 |
| $CH_3COnC_3H_7$ | −61.92±0.26 | 91.19 | 1526.00 | 37.52 | −0.42 | 1563.94 | 1564.30 |
| $CH_3COiC_3H_7$ | −62.76±0.21 | 91.19 | 1526.00 | 38.75 | −0.55 | 1565.30 | 1565.14 |
| $(C_2H_5)_2CO$ | −61.65±0.21 | 91.52 | 1526.00 | 37.42 | −0.92 | 1564.34 | 1564.36 |
| $CH_3COnC_4H_9$ | −66.96±0.28 | 109.49 | 1809.25 | 48.82 | −0.55 | 1858.62 | 1858.27 |
| $(iC_3H_7)_2CO$ | −74.40±0.28 | 128.12 | 2092.50 | 60.60 | −1.85 | 2154.95 | 2154.97 |
| $(CH_3)_2O$ | −43.99±0.12 | 52.55 | 800.42 | −3.33 | −0.05 | 797.14 | 797.07 |
| $CH_3OC_2H_5$ | −51.72±0.16 | 70.19 | 1083.67 | 9.56 | −0.09 | 1093.32 | 1093.07 |
| $CH_3OnC_3H_7$ | −56.82±0.26 | 87.83 | 1366.92 | 19.35 | −0.25 | 1386.52 | 1386.43 |
| $CH_3OiC_3H_7$ | −60.24±0.23 | 87.83 | 1366.92 | 22.82 | −0.12 | 1389.86 | 1389.85 |
| $(C_2H_5)_2O$ | −60.26±0.19 | 87.83 | 1366.92 | 22.45 | −0.17 | 1389.54 | 1389.87 |
| $(nC_3H_7)_2O$ | −69.85±0.40 | 123.11 | 1933.42 | 41.92 | −0.47 | 1975.81 | 1976.00 |
| $(iC_3H_7)_2O$ | −76.20±0.54 | 123.11 | 1933.42 | 48.97 | −0.29 | 1982.68 | 1982.35 |
| $(nC_4H_9)_2O$ | −79.82±0.27 | 158.39 | 2499.92 | 61.95 | −0.73 | 2562.60 | 2562.50 |
| $(sC_4H_9)_2O$ | −86.26±0.41 | 158.39 | 2499.92 | 68.22 | −0.58 | 2568.72 | 2568.94 |
| Tetrahydropyran | −53.39±0.24 | 92.87 | 1506.18 | 50.95 | −0.49 | 1557.62 | 1557.45 |
| 1,4-Dioxane | −75.51±0.17 | 78.48 | 1312.86 | 39.59 | −0.29 | 1352.74 | 1352.62 |

[a]Extracted from ref. 30.
[b]For the carbonyl compounds, an increment of 18.3 kcal/mol was assumed for each added $CH_2$ group with respect to the closest "parent" compound, in line with results obtained for the parent hydrocarbons (22).

TABLE 7. Predicted enthalpies of formation (298.15 K, gas) (kcal/mol)[a]

| Molecule | $\Sigma N_{CC}\delta_C$ | $\Sigma\delta_{C\neq\alpha}$ | $\Sigma\delta_{C\alpha}$ | $\delta_O$ | $\Sigma\varepsilon_{ij}^0$ | $\Sigma_i\Sigma_j a_{ij}\Delta q_i$ | $E_{nb}$* | $\Delta E_a$* | $\Delta H_f^0$ |
|---|---|---|---|---|---|---|---|---|---|
| $CH_3OnC_4H_9$ | 95.4 | 48.4 | −0.8 | −35.0 | 1650.17 | 29.55 | −0.37 | 1680.09 | −62.21 |
| $CH_3OiC_4H_9$ | 110.0 | 50.1 | 6.7 | −36.5 | 1650.17 | 30.93 | −0.34 | 1681.44 | −63.56 |
| $CH_3OsC_4H_9$ | 88.0 | 40.2 | 2.2 | −15.0 | 1650.17 | 32.16 | −0.28 | 1682.61 | −64.73 |
| $CH_3OnC_5H_{11}$ | 142.3 | 71.7 | −0.5 | −34.0 | 1933.42 | 39.99 | −0.49 | 1973.90 | −67.75 |
| $CH_3OiC_5H_{11}$ | 163.7 | 86.3 | −2.2 | −36.0 | 1933.42 | 41.11 | −0.45 | 1974.98 | −68.83 |
| $CH_3OsC_5H_{11}$ | 122.6 | 47.4 | 8.0 | −23.0 | 1933.42 | 41.06 | −0.39 | 1974.87 | −68.72 |
| $C_2H_5OnC_3H_7$ | 56.2 | 31.9 | 6.8 | −4.8 | 1650.17 | 32.17 | −0.32 | 1682.66 | −64.78 |
| $C_2H_5OiC_3H_7$ | 50.7 | 42.9 | 2.6 | 21.5 | 1650.17 | 35.59 | −0.22 | 1685.98 | −68.10 |
| $C_2H_5OnC_4H_9$ | 103.5 | 58.2 | 4.9 | −8.0 | 1933.42 | 42.09 | −0.44 | 1975.95 | −69.80 |
| $C_2H_5OiC_4H_9$ | 117.7 | 59.7 | 12.2 | −7.5 | 1933.42 | 43.61 | −0.41 | 1977.44 | −71.29 |
| $C_2H_5OsC_4H_9$ | 94.3 | 51.3 | 8.5 | 18.0 | 1933.42 | 45.35 | −0.35 | 1979.12 | −72.97 |
| $nC_3H_7OiC_3H_7$ | 88.7 | 55.9 | 9.4 | 17.5 | 1933.42 | 45.46 | −0.37 | 1979.25 | −73.10 |

[a]The estimated ZPE + $H_T - H_0$ energies are 105.47 and 123.11 kcal/mol, respectively, for the $C_5H_{12}O$ and $C_6H_{14}O$ ethers, using the approximation indicated in Table 4. The nmr data are taken from ref. 16.

## Conclusions

The atomization energy of a vibrationless molecule, a true molecular property describing chemical binding, is largely controlled by an energy term reflecting the effects of atomic charges. This is best seen in comparisons between isomers, e.g. $C_2H_5$-CHO vs. $(CH_3)_2CO$ or $nC_3H_7CHO$ vs. $CH_3$-$COC_2H_5$, where the charge redistributions accompanying the structural changes account for virtually the entire variations in molecular energies. Nonbonded Coulomb interactions play only a minor role in that respect.

The effect of adding 0.001 electron (i.e., $\Delta q_i = -1$ me) to an atom is given by theory (eq. [4]): the $a_{ij}$'s (eq. [6]) indicate that 1 me added to hydrogen stabilizes a CH bond by 0.632 kcal/mol, whereas 1 me added to carbon stabilizes a CC bond by 0.488, a CH bond by 0.247, an ether-CO bond by 0.712 and a carbonyl-CO bond by 0.742 kcal/mol. Similarly, an electron enrichment of 1 me at an oxygen atom stabilizes an ether-CO bond by ~0.505 and a carbonyl-CO bond by ~0.668 kcal/mol, the precise values depending on the oxygen net charges. These results answer a number of questions regarding charge-related energy effects. Consider, for example, a charge decrease of 1 me at a hydrogen atom in favor of a carbonyl oxygen atom, causing a loss in stability of 0.632 kcal/mol at the CH bond involved

Can. J. Chem. Downloaded from www.nrcresearchpress.com by 210.87.254.5 on 09/06/12
For personal use only.

Can. J. Chem. Downloaded from www.nrcresearchpress.com by 210.87.254.5 on 09/06/12
For personal use only.

and a gain of 0.668 kcal/mol at the CO bond, for a net gain of 0.036 kcal/mol. This example shows that, *under circumstances which can be evaluated from the* $a_{ij}$*'s, a transfer of electronic charge accompanying isomerization can result in a relatively small change in total stability while the "location" of a certain portion of the overall stability is shifted from one part of the molecule to another*. Of course, this type of reasoning applies only to comparisons involving molecules at equilibrium. With this understanding, the example just presented could apply to a comparison between, say, propanal and propanone, the latter compound being the more stable one (by ~6.1 kcal/mol in $\Delta E_a$* energy), which is largely, but not exclusively, traced back to an electron enrichment at the oxygen atom of the ketone at the expense of electronic charge at the hydrogen atoms. In a way, *the alkyl hydrogen atoms play the role of a reservoir of electronic charge which, under appropriate circumstances depending on molecular geometry, is called upon for stabilizing bonds other than CH bonds, with a net gain in molecular stability*. (This conclusion holds whenever the sum $\Sigma_j a_{ij}$, measuring the stabilization of all the bonds formed by atom $i$ by an electronic charge added to it, is more negative than $a_{HC}$). So, for example, if we are asked why adamantane is more stable than twistane (by 9.1 kcal/mol in $\Delta E_a$* energy), the answer is that the largest part by far of this energy difference is due to the fact that adamantane has less electrons on the H atoms and, consequently, more on the C atoms, than twistane. It is certainly pleasing that this new insight derives *exclusively* from basic and clearly identified physical concepts, namely (*i*) the Politzer–Parr partitioning of molecular energies in terms of "atomic-like contributions" (23) which emphasizes the dependence of atomic and molecular energies upon the electrostatic potentials at the nuclei; (*ii*) the relationships between energy components (1, 3), of which Politzer's approximations (4) are an important part and, finally, (*iii*) the reduction of the problem of molecular energies to its electrostatic aspects, featuring the role of local charges (2).

The single most important difficulty encountered in our approach rests with the accurate calculations of atomic charges. If it was not for this reason, the calculation of the $\Sigma_i \Sigma_j a_{ij} \Delta q_i$ terms would, indeed, be very simple. Presently, the calculations are still somewhat involved because we have to resort to normalization procedures in order to make up for the lack of a comprehensive knowledge of atomic charges. In turn, the use of general formulas, in which hydrogen charges do not appear explicitly, makes it possible to describe large classes of compounds in terms of atoms other than hydrogen, whose charges can be extracted from correlations with nmr shifts. While lacking the elegance of a purely theoretical approach, the judicious use of carefully established charge–nmr shift correlations fulfills its goals, although the significance or generality of such correlations is presently not known. Fortunately, encouraging theoretical progress is being made in the area of charge calculations: since it became clear that the CH polarity in simple alkanes is (13, 24) $C^+H^-$ (at variance with most results derived from Mulliken population analyses), new powerful and realistic methods (25) are converging toward this type of result which is part of the present charge analyses. Extention of the present theory to other classes of molecules (alcohols, acetals, etc.) can be envisaged as a powerful means of studying large molecules of biological interest, which would normally lie outside the range of computational feasibility. This hope seems justified by the close agreement between calculated and experimental energies, for a body of ~80 molecules (0.16 kcal/mol, average deviation).

**Acknowledgements**

We express our gratitude to the National Research Council of Canada for financial assistance, and to "Le Centre de Calcul de l'Université de Montréal" for generous computer time.

1. S. Fliszár and M. T. Béraldin. J. Chem. Phys. **72**, 1013 (1980).
2. S. Fliszár. J. Am. Chem. Soc. **102**, 6946 (1980).
3. S. Fliszár, M. Foucrault, M. T. Béraldin, and J. Bridet. Can. J. Chem. **59**, 1974 (1981).
4. P. Politzer. J. Chem. Phys. **64**, 4239 (1976); P. Politzer. J. Chem. Phys. **70**, 1067 (1979); T. Anno. J. Chem. Phys. **72**, 782 (1980).
5. R. G. Parr and S. R. Gadre. J. Chem. Phys. **72**, 3669 (1980).
6. E. Clementi and C. Roetti. At. Data Nucl. Data Tables, **14**, 177 (1974).
7. P. E. Cade and A. C. Wahl. At. Data Nucl. Data Tables, **13**, 339 (1974).
8. C. E. Moore. Natl. Stand. Ref. Data Ser. US Natl. Bur. Stand. NSRDS-NBS 34 (1970).
9. P. Politzer and R. G. Parr. J. Chem. Phys. **64**, 4634 (1976).
10. J. C. Slater. The self-consistent field for molecules and solids. Vol. 4. McGraw-Hill, Kuala-Lumpur. 1974.
11. K. Schwarz. Phys. Rev. B: Solid State, **5**, 2466 (1972).
12. A. Julg. Top. Curr. Chem. **58**, 1 (1975); V. H. Smith Jr. Phys. Scr. **15**, 147 (1977).
13. S. Fliszár, A. Goursot, and H. Dugas. J. Am. Chem. Soc. **96**, 4358 (1974); G. Kean, D. Gravel, and S. Fliszár. J. Am. Chem. Soc. **98**, 4749 (1976); S. Fliszár. Can. J. Chem. **54**, 2839 (1976).
14. M. T. Béraldin, E. Vauthier, and S. Fliszár. Can. J. Chem. **60**, 106 (1982).

15. H. HENRY and S. FLISZÁR. J. Am. Chem. Soc. **100**, 3312 (1978).
16. C. DELSETH and J. P. KINTZINGER. Helv. Chim. Acta, **61**, 1327 (1978).
17. C. DELSETH and J. P. KINTZINGER. Helv. Chim. Acta, **59**, 466 (1976); **59**, 1411 (1976).
18. G. DEL RE. Gazz. Chim. Ital. **102**, 929 (1972).
19. D. R. STULL and G. C. SINKE. Adv. Chem. Ser. No. **18** (1956).
20. (*a*) P. COSSEE and J. H. SCHACHTSCHNEIDER. J. Chem. Phys. **44**, 97 (1966). (*b*) Z. BURIC and P. J. KRUEGER, Spectrochim. Acta, **30**A, 2069 (1974). (*c*) R. G. SNYDER and G. ZERBI. Spectrochim. Acta, **23**A, 391 (1967). (*d*) K. HAMADA and H. MORISHITA. Z. Physik. Chem. **97**, 295 (1975).
21. (*a*) J. B. STOTHERS. Carbon-13 nmr spectroscopy. Academic Press, New York. 1972; (*b*) T. SUGAWARA, Y. KAWADA, M. KATOH, and H. IWAMURA. Bull. Chem. Soc. Jpn. **52**, 3391 (1979).
22. S. FLISZÁR and J. L. CANTARA. Can. J. Chem. **59**, 1381 (1981).
23. P. POLITZER and R. G. PARR. J. Chem. Phys. **61**, 4258 (1974).
24. R. H. PRITCHARD and C. W. KERN. J. Am. Chem. Soc. **91**, 1631 (1969); M. S. GORDON and W. ENGLAND. J. Am. Chem. Soc. **94**, 5168 (1972); K. B. WIBERG and J. J. WENDOLOSKI. J. Comput. Chem. **2**, 53 (1981).
25. K. B. WIBERG. J. Am. Chem. Soc. **102**, 1229 (1980); R. F. W. BADER, S. G. ANDERSON, and A. J. DUKE. J. Am. Chem. Soc. **101**, 1389 (1979).
26. T. H. DUNNING. J. Chem. Phys. **53**, 2823 (1970).
27. G. KEAN. M.Sc. Thesis, Université de Montréal, Montréal. 1974.
28. J. S. BINKLEY, R. A. WHITESIDE, P. C. HARIHARAN, R. SEEGER, J. A. POPLE, W. J. HEHRE, and M. D. NEWTON. Program 368, Quantum Chemistry Program Exchange, University of Indiana, Chemistry Department, Bloomington, IN 47401.
29. S. FLISZÁR, G. KEAN, and R. MACAULAY. J. Am. Chem. Soc. **96**, 4353 (1974).
30. J. D. COX and G. PILCHER. Thermochemistry of organic and organometallic compounds. Academic Press, New York. 1970.

## Appendix I

The $\partial\varepsilon_{ij}/\partial Z_i$ derivatives were deduced from eq. [3], using the atomic ground state energies and the appropriate $K^{at}$ values (Table 1) giving the free atom values $V_{ne} = -88.5309$ (C) and $-178.7912$ au (O). For the α carbons in diethylether ($\Delta q_C = -3.84$ me) and acetone ($\Delta q_C = -21.1$ me) we calculate $\partial\varepsilon_{ij}/\partial Z_i = \partial\varepsilon_{ij}{}^0/\partial Z_i + a_{ij}\Delta q_i/K_i{}^{mol}Z_i$ (from eqs. [1] and [4]), giving $2\partial\varepsilon_{CH}/\partial Z_C + \partial\varepsilon_{CC}/\partial Z_C = 0.0683$ au (diethylether) and $2\partial\varepsilon_{CC}/\partial Z_C = 0.0368$ au (acetone). The nuclear–nuclear repulsions, $\Sigma_{j\neq i}Z_j/r_{ij}$, deduced from STO-3G optimized geometries, are 9.8107 (α-C of diethylether), 9.2843 (ether-O), 9.1275 (acetone-α-carbon) and 6.3853 au (acetone-O). With these values, eq. [3] gives $\partial\varepsilon_{CO}{}^0/\partial Z_C = -[24.6342 + V_{ne}\,(C, mol)/Z_C]$ and $\partial\varepsilon_{CO}{}^0/\partial Z_O = -[15.8166 + V_{ne}\,(O, mol)/2Z_O]$ for diethylether, as well as $\partial\varepsilon_{CO}{}^0/\partial Z_C = -[23.9195 + V_{ne}\,(C, mol)/Z_C]$ and $\partial\varepsilon_{CO}{}^0/\partial Z_O = -[28.7342 + V_{ne}\,(O, mol)/Z_O]$ for acetone.

The theoretical results were obtained from GTO $(9s\,5p|6s) \rightarrow [5s\,3p|3s]$ calculations using Dunning's exponents (26) and optimum contraction vectors (27), i.e. 42111 for C(*s*) and O(*s*), 311 for C(*p*), O(*p*), and 222 for H(*s*). The "Gaussian 76" program (28) was used. The $V_{ne}\,(i, mol)/Z_i = 1/r$ results are $-24.4910$ (α-C), $-31.6277$ (O) for diethylether, and $-23.7504$ (α-C), $-28.7351$ au (O) for acetone, but a rescaling is necessary before they can be used in eq. [4] together with "experimental" free atom values. This rescaling involves experimental total energies of ethane ($-79.8439$), dimethylether ($-155.0922$), and acetone ($-193.2336$ au), as well as calculated $\gamma = (V_{ne} + 2V_{nn})/E_{mol}$ ratios (3), i.e., respectively, $\gamma = 2.3192$, 2.3459, and 2.3424. Using the appropriate $V_{nn}$ values, i.e., in the same order, 42.2663, 83.8112, and 119.0759 au, we estimate the corresponding $V_{ne}$ energies on a scale approaching the experimental one and find $V_{ne} = -269.7066$ (ethane), $-531.4532$ (dimethylether), and $-690.7822$ au (acetone). Next, we calculate the nuclear–electronic potential energy for each individual atom of this set of molecules and collect the contributions of atoms of the same chemical species. For example, $\Sigma V_{ne}(C) = -403.6756$, $\Sigma V_{ne}(H) = -54.2347$ and $V_{ne}(O) = -229.8811$ au are, respectively, the total contributions of the C, H, and O atoms in acetone. Their sum is scaled as follows to match the total $V_{ne}$ value estimated above from the experimental energy, $403.6756f_C + 54.2347f_H + 229.8811f_O = 690.7822$. Similarly, using the appropriate results for ethane and dimethylether (3), we write $228.1297f_C + 40.0624f_H = 269.7066$ and $252.6870f_C + 49.6558f_H + 226.7787f_O = 531.4532$. The $f_C = 1.0038$ and $f_O = 1.0025$ factors deduced in this fashion are used to rescale the $V_{ne}\,(i, mol)$ results indicated above (giving, e.g., $V_{ne} = -24.5841$ for the α-carbon in diethylether), which are now used in eq. [3] for obtaining the $\partial\varepsilon_{ij}/\partial Z_i$ derivatives. Because of the uncertainties (0.02%) in the γ's, we have also explored the results by assuming ethane, dimethylether, and acetone γ values of 2.3188, 2.3455, 2.3421 and 2.3197, 2.3461, 2.3426, satisfying the constraint that the energy of acetone is correctly reproduced. The selected average $f_C = 1.00386$ and $f_O = 1.00243$ factors give the results reported in Table 1. The point is that this rescaling which did not involve diethylether in a first place also yields the correct $\varepsilon_{CO}{}^0$ energy for this molecule. For comparison, using only $[5s3p|3s]$ results, including $V_{ne}(C, at) = -87.9484$ and $V_{ne}\,(O, at) = -177.8148$ au, we obtain (eq. [3]) that $\partial\varepsilon_{CH}{}^0/\partial Z_H = 0.121$, $\partial\varepsilon_{CH}{}^0/\partial Z_C$

Can. J. Chem. Downloaded from www.nrcresearchpress.com by 210.87.254.5 on 09/06/12
For personal use only.

Can. J. Chem. Downloaded from www.nrcresearchpress.com by 210.87.254.5 on 09/06/12
For personal use only.

$= 0.025$, $\partial\varepsilon_{CO}^0/\partial Z_C = 0.013$, $\partial\varepsilon_{CO}^0/\partial Z_C = -0.042$, $\partial\varepsilon_{CO}^0/\partial Z_O = 0.058$ (ether), $\partial\varepsilon_{CO}^0/\partial Z_C = -0.074$, and $\partial\varepsilon_{CO}^0/\partial Z_O = 0.123$ au (acetone), revealing that the main distortion occurs in the evaluation of the oxygen atoms.

A final assessment of the precision of eq. [1] and the validity of the approximation, eq. [3], for deducing $\partial\varepsilon_{ij}/\partial Z_i$ values must await considerably more sophisticated *ab initio* results. So far we have only established the general validity of our approach within the limits of the uncertainties associated with the *ab initio* evaluation of the various energy components. Our rescaling is made to remain internally consistent with the detailed features of the *ab initio* results on which they are based and has the merit that the resulting molecular energies and their components are set on the same footing as the energies of the isolated atoms, which are taken at their experimental values. The overall consistency of our results can thus, as it should, be demonstrated at a level which is close to experimental accuracy. It remains, however, that this rescaling still represents a delicate procedure because of the extreme accuracy required.

## Appendix II

The calculation of the carbon and oxygen net charges is straightforward, using eqs. [7]–[9] and the appropriate references $q_{C\alpha}^0$, $q_O^0$ and $q_{C\neq\alpha}^0 =$ 35.1 me. The charges of C atoms other than adjacent to O closely parallel those of the parent hydrocarbons (16, 17) and it seems reasonable to anticipate a similar behavior also for the H atoms attached to them. In alkanes, the H and C charges are monotonically related one to another, with different lines for primary and secondary atoms. These lines are easily deduced using the "inductive" charges (28, Table 2, 13) with $q_C^0$ (ethane) = 35.1 me and $n = -4.4122$, which insures the correct scaling of atomic charges, giving (in me units) 35.1 (C), −11.70 (H) for ethane, 33.64 (C), −12.10 (H) for propane-$CH_3$, 32.37 (C), −12.47 (H) for isobutane-$CH_3$, and 31.20 (C), −13.05 (H) for neopentane-$CH_3$. For $CH_2$ charges, it is found: 33.48 (C), −14.09 (H) for propane, 32.28 (C), −14.62 (H) for butane, and 30.82 (C), −15.01 (H) for the central $CH_2$ of *n*-pentane. In this manner it follows for di-*tert*-butylether ($\delta_{C\neq\alpha} = 26.0$ ppm from ethane) that $q_{C\neq\alpha} = 31.25$ and $q_H = -13.02$ me, on the average. Moreover ($\delta_{C\alpha} = 7.7$ ppm from the α-C of diethylether), $q_{C\alpha} = q_{C\alpha}^0 - 1.14$ and ($\delta_O = 69.5$ ppm from diethylether) $q_O = q_O^0 - 18.56$ me. It follows from charge normalization that $q_O^0 + 2\,q_{C\alpha}^0 \simeq 67.7$ me. Similarly, one obtains for acetone ($\delta_{C\neq\alpha} = 22.2$ ppm from ethane) that $q_{C\neq\alpha} = 31.81$, $q_H = -9.40$ and $q_{C\alpha}^0 + q_O^0 \simeq -7.2$ me. With the appropriate $\Delta q_{C\alpha}^0 = q_{C\alpha}^0 - q_C^0$ values determined from eqs. [16] and [17], we find $q_{C\alpha}^0 \simeq 31.26$ and $q_O^0 \simeq 5.18$ me for diethylether and $q_{C\alpha}^0 \simeq 14.0$ and $q_O^0 \simeq -21.2$ me for acetone. The charges of H atoms attached to α-carbons are deduced from charge normalization. This admittedly crude (but realistic) assignment of H charges is straightforward in most cases and a comparison of the trends in the sets of molecules studied here facilitates their reasonable, balanced assessment. The important point is that the uncertainties associated with these estimates (usually $< 0.1$ me) have virtually no effect on the evaluation of nonbonded interaction (eq. [12]).

## Appendix III

The following example illustrates the use of eq. [4]. For di-*n*-propylether, $\delta_O = -10.0$ ppm gives $\Delta q_O = 2.67$ and $q_O = 7.85$ me; $\delta_{C\alpha} = 6.8$ ppm gives $\Delta q_{C\alpha} = 1.01$ and $q_{C\alpha} = 30.25$ me. These $\Delta q_O$ and $\Delta q_C$ values, relative to the reference which is diethylether, are used in the calculation of the CO contributions, giving $\varepsilon_{CO} = 79.15$ kcal/mol. For the β and γ C atoms, the shifts (relative to ethane) are 17.6 and 5.0 ppm, respectively, giving $\Delta q_{C\beta} = -2.60$ and $\Delta q_{C\gamma} = -0.74$ me, i.e., $q_C = 32.50$ (β) and 34.36 me (γ). With these $\Delta q_C$'s, eq. [4] gives $\varepsilon_{CC} =$ 71.26 kcal/mol. For the $C_\alpha$—$C_\beta$ bond, we use again $\Delta q_{C\beta} = -2.60$ me, and $\Delta q_C = 30.25 - 35.1 = -4.85$ me relative to ethane for the α-carbon, and obtain $\varepsilon_{CC} = 73.265$ kcal/mol. The $\Delta q_C = -4.85$ me value is also used in the calculation of the corresponding $\varepsilon_{CH}$ contributions. The total net charge on C and O amounts to 202.07 me, meaning that the average H charge is −14.434 me, i.e., $\Delta q_H = -2.734$ me relative to ethane, for an average $a_{HC}\Delta q_H$ contribution of 1.727 kcal/mol. The calculation of all the $\varepsilon_{CH}$'s is now straightforward and the sum of all $\varepsilon_{ij}$'s can be derived without the detailed knowledge of the distribution of charges among the individual H atoms.

# The Lewis acid complexes of α,β-unsaturated carbonyl and nitrile compounds. A nuclear magnetic resonance study

RONALD F. CHILDS,[1] D. LINDSAY MULHOLLAND, AND ALAN NIXON
*Department of Chemistry, McMaster University, Hamilton, Ont., Canada L8S 4M1*

Received July 20, 1981

RONALD F. CHILDS, D. LINDSAY MULHOLLAND, and ALAN NIXON. Can. J. Chem. **60**, 801 (1982).

1:1 Complexes of a range of Lewis acids with crotonaldehyde (**1**) have been systematically investigated by $^1H$ and $^{13}C$ nmr spectroscopy. Lewis acids employed were: $BF_3$, $BCl_3$, $BBr_3$, $SnCl_4$, $TiCl_4$, $SbCl_5$, $AlCl_3$, $EtAlCl_2$, $Et_2AlCl$, $Et_3Al_2Cl_3$, and $Et_3Al$. Chemical shift changes in $^1H$ nuclei remote from the Lewis acid group were found to be remarkably regular and consistent. The study has been extended to tiglaldehyde (**2**), pent-3-en-2-one (**3**), cyclohexenone (**4**), methyl crotonate (**5**), and crotonitrile (**6**) and the relationships between the chemical shift differences associated with complexation of these have been explored.

RONALD F. CHILDS, D. LINDSAY MULHOLLAND et ALAN NIXON. Can. J. Chem. **60**, 801 (1982).

On a étudié d'une façon systématique des complexes 1:1 de divers acides de Lewis avec le crotonaldéhyde (**1**) en faisant appel à la rmn du $^1H$ et du $^{13}C$. On a utilisé les acides de Lewis suivants: $BF_3$, $BCl_3$, $BBr_3$, $SnCl_4$, $TiCl_4$, $SbCl_5$, $AlCl_3$, $EtAlCl_2$, $Et_2AlCl$, $Et_3Al_2Cl_3$ et $Et_3Al$. On a trouvé que les changements dans les déplacements des $^1H$ qui sont loins de l'acide de Lewis sont très réguliers et consistants. On a étendu l'étude au tiglaldéhyde (**2**), à la pentène-3 one-2 (**3**) à la cyclohexène-2 one (**4**), au crotonate de méthyle (**5**) et au crotonitrile (**6**); on a étudié les relations entre les différences de déplacements chimiques associés avec la complexation.

[Traduit par le journal]

## Introduction

Many reactions of unsaturated carbonyl and nitrile compounds are catalysed by Lewis acids. These include, for example, catalysed Diels–Alder reactions (1), alternating copolymerizations (2), the ene reaction (3), [2 + 2] cycloadditions (4), linear additions (5), aldol condensations (6), and several photoreactions (7). Despite the obvious importance of these catalysed reactions there is not yet a satisfactory explanation of how these reactions proceed and in particular what factors determine the course of the reaction. Take for example the competing catalysed Diels–Alder and alternating copolymerization reactions. Suggestions have been put forward to account for the Lewis acid catalysis of both of these reactions (8, 9). However, none of these suggestions can satisfactorily account for the reaction of butadiene with acrylonitrile which can give predominantly either the Diels–Alder product or alternating copolymer depending on the choice of Lewis acid.

The initial step in catalysis of these reactions by a Lewis acid appears to be complexation of the unsaturated carbonyl or nitrile compounds with the Lewis acid. Complexes of this type have been studied by a wide variety of techniques and it is generally accepted that bonding takes place through the electronegative atoms, oxygen or nitrogen, in the class of Lewis bases studied here (10). Subsequently, the base which has been activated by complexation undergoes attack by another reactant in the component mixture. The structure and properties of the intermediate complex appear to be crucial in determining reactivity and selectivity. The possibility that the charge distribution within the complex could significantly affect the chemistry of these systems led us to investigate this property in particular. Despite limitations, nmr remains one of the few methods available for the investigation of charge distribution in organic molecules (11). We have therefore undertaken and report here a systematic study of the $^1H$ and $^{13}C$ nmr spectra of a series of these complexes with the expectation that the chemical shifts observed at remote nuclei would provide a reasonably reliable indication of the relative charge induced on the base as a whole. It should be noted that the nmr spectra of some complexes of α,β-unsaturated carbonyl compounds have been reported previously under a variety of conditions (12–14).

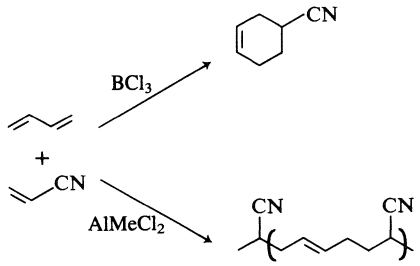


## Results

The unsaturated bases used in these studies are the aldehydes, crotonaldehyde **1** and tiglaldehyde

[1]Author to whom correspondence may be addressed.

0008-4042/82/060801-08$01.00/0
©1982 National Research Council of Canada/Conseil national de recherches du Canada

Can. J. Chem. Downloaded from www.nrcresearchpress.com by 210.87.254.5 on 09/06/12
For personal use only.

2; ketones, pent-3-en-2-one **3** and cyclohex-2-enone **4**; ester, methyl crotonate **5**; and nitrile, crotononitrile **6**.

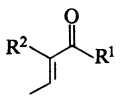

**1** $R^1 = R^2 = H$
**2** $R^1 = H$, $R^2 = CH_3$
**3** $R^1 = CH_3$, $R^2 = H$
**5** $R^1 = OCH_3$, $R^2 = H$

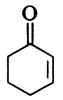

**4**

**6**

These bases were selected as examples of important classes of compounds which undergo the type of catalysed reactions above. For the most part, these bases also have readily and unambigously assignable signals in their nmr spectra. The exception to this is **4**; however, in this case the vinyl signals can be clearly differentiated. Most of the complexes derived from these bases were also sufficiently stable at −20°C for study. The acids used in this study were $BF_3$, $BCl_3$, $BBr_3$, $SbCl_5$, $TiCl_4$, $SnCl_4$, $AlCl_3$, and various ethylaluminum chlorides. Methylene chloride and chloroform (for some $^{13}C$ spectra) were employed as solvents. It is known that these solvents do not react with the Lewis acids (15).

The 1:1 complexes were prepared by adding a known weight of the base to a cooled solution of the Lewis acid (~ 0.3 *M*) in an nmr tube.

The data obtained are given in Tables 1–8. In each case the difference in chemical shift between the complex and the free base is quoted (Δδ = δ complex − δ free base; Δδ is positive for a downfield shift).

TABLE 1. $^1H$ chemical shift differences (Δδ) of crotonaldehyde **1** on complexation with various Lewis acids[a]

| | Proton Δδ (ppm) | | | |
|---|---|---|---|---|
| Lewis acid | H1 | H2 | H3 | H4 |
| $BBr_3$ | 0.11 | 0.93 | 1.49 | 0.51 |
| $BCl_3$ | −0.65 | 0.85 | 1.35 | 0.49 |
| $SbCl_5$ | 0.17 | 0.78 | 1.32 | 0.48 |
| $AlCl_3$ | −0.20 | 0.76 | 1.23 | 0.47 |
| $EtAlCl_2$[b,c] | −0.20 | 0.77 | 1.25 | 0.47 |
| $BF_3$ | −0.27 | 0.74 | 1.17 | 0.44 |
| $EtAlCl_2$[b,c,d] | −0.17 | 0.67 | 1.15 | 0.38 |
| $Et_3Al_2Cl_3$[b] | −0.15 | 0.69 | 1.14 | 0.39 |
| $TiCl_4$ | 0.03 | 0.60 | 1.03 | 0.36 |
| $Et_2AlCl$[b,c] | −0.15 | 0.55 | 0.91 | 0.30 |
| $SnCl_4$ | 0.02 | 0.50 | 0.87 | 0.29 |
| $Et_3Al$[b,c] | −0.34 | 0.42 | 0.63 | 0.23 |

[a]In ppm (± 0.01). Chemical shifts of uncomplexed base are: δ = 9.47 (d, 1H, H1), 6.10 (ddq, 1H, H2), 6.93 (m, 1H, H3), 2.02 (dd, 3H, H4). Δδ is positive for a downfield shift. Approximately 0.3 *M* solution in dichloromethane at −20°C, unless otherwise stated.
[b]At −60°C. Chemical shifts of uncomplexed base: δ = 9.84 (H1), 6.12 (H2), 6.98 (H3), 2.05 (H4), at this temperature.
[c]Written in monomeric form for simplicity.
[d]2:1 in crotonaldehyde–$EtAlCl_2$.

TABLE 2. $^1H$ chemical shift differences (Δδ) of tiglaldehyde **2** on complexation with various Lewis acids[a]

| | Proton Δδ (ppm) | | | |
|---|---|---|---|---|
| Lewis acid | H1 | 2-$CH_3$ | H3 | H4 |
| $BBr_3$ | 0.09 | 0.37 | 1.54 | 0.48 |
| $BCl_3$ | −0.06 | 0.34 | 1.43 | 0.45 |
| $SbCl_5$ | 0.14 | 0.34 | 1.36 | 0.44 |
| $Et_2AlCl$[b] | −0.15 | 0.18 | 0.92 | 0.28 |
| $Et_3Al$[b] | −0.39 | 0.16 | 0.72 | 0.28 |

[a]In ppm (± 0.01). Chemical shifts of uncomplexed base are: δ = 9.37 (d, 1H, H1), 1.71 (m, 3H, 2-$CH_3$), 6.64 (qq, 1H, H3), 1.98 (dm, 3H, H4). Approximately 0.3 *M* solution in dichloromethane at −20°C, unless otherwise stated.
[b]At −60°C. Chemical shifts of uncomplexed base: δ = 9.38 (H1), 1.73 (2-$CH_3$), 6.69 (H3), 1.99 (H4). Acid written in monomeric form for simplicity.

TABLE 3. $^1H$ chemical shift differences (Δδ) of pent-3-en-2-one **3** on complexation with various Lewis acids[a]

| | Proton Δδ (ppm) | | | |
|---|---|---|---|---|
| Lewis acid | 1-$CH_3$ | H2 | H3 | H4 |
| $BBr_3$ | 0.86 | 1.03 | 1.36 | 0.47 |
| $BCl_3$ | 0.80 | 0.95 | 1.26 | 0.42 |
| $SbCl_5$ | 0.80 | 0.83 | 1.12 | 0.39 |
| $Et_2AlCl$[b] | 0.46 | 0.54 | 0.81 | 0.25 |
| $SnCl_4$ | 0.46 | 0.45 | 0.69 | 0.22 |
| $Et_3Al$[b] | 0.31 | 0.38 | 0.60 | 0.18 |

[a]In ppm (± 0.01). Chemical shifts of uncomplexed base are: δ = 2.22 (s, 3H, 1-$CH_3$), 6.04 (dq, 1H, H2), 6.84 (m, 1H, H3), 1.91 (dd, 3H, H4). Approximately 0.3 *M* solution in dichloromethane at −20°C, unless otherwise stated.
[b]At −60°C. Chemical shifts of uncomplexed base: δ = 2.26 (1-$CH_3$), 6.03 (H2), 6.89 (H3), 1.94 (H4). Acid written in monomeric form for simplicity.

## Discussion

### *Crotonaldehyde complexes*

The 2-, 3-, and 4-proton resonances of crotonaldehyde were all found to be shifted downfield on complexation. The magnitude of the shift of the H3 resonance of **1** on complexation was observed to be greatest, while those of H2 and H4 were found to be smaller but linearly related to those of H3. This is clearly shown in Fig. 1 where the Δδ's of H2 and H4 are plotted against Δδ H3 as the Lewis acid is varied. The complexation-induced shift of H1 appears to vary randomly.[2]

There are several possible conformations for the

[2]It is important to be sure of the identity of the Lewis acid with which complexation is occurring. The coincidence of all the resonance shifts obtained with the pairs of acids $AlCl_3$ and $EtAlCl_2$ suggests that, under these reaction conditions, complexation of crotonaldehyde was taking place to the same Lewis acid species, i.e., $AlCl_3$, because of disproportionation. Disproportionation of $EtAlCl_2$ on reaction with Lewis bases has been previously reported (12).

Can. J. Chem. Downloaded from www.nrcresearchpress.com by 210.87.254.5 on 09/06/12
For personal use only.

Can. J. Chem. Downloaded from www.nrcresearchpress.com by 210.87.254.5 on 09/06/12
For personal use only.

TABLE 4. $^1$H chemical shift differences (Δδ) of cyclohex-1-enone **4** on complexation with various Lewis acids[a]

| | Proton Δδ (ppm) | |
|---|---|---|
| Lewis acid | H2 | H3 |
| $BBr_3$ | 1.37 | 1.32 |
| $BCl_3$ | 1.20 | 1.22 |
| $SbCl_5$ | 1.20 | 1.09 |
| $BF_3$ | 0.84 | 1.04 |
| $Et_2AlCl$[b] | 0.60 | 0.76 |
| $SnCl_4$ | 0.60 | 0.71 |
| $Et_3Al$[b] | 0.44 | 0.58 |

[a]In ppm (± 0.01). Chemical shifts of uncomplexed base are: δ = 5.96 (dt, 1H, H2), 7.02 (dt, 1H, H3). Approximately 0.3 *M* solution in dichloromethane at −20°C, unless otherwise stated.
[b]At −60°C. Chemical shifts of uncomplexed base: δ = 5.98 (H2), 7.08 (H3). Acid written in monomeric form for simplicity.

TABLE 5. $^1$H chemical shift differences (Δδ) of methyl crotonate **5** on complexation with various Lewis acids[a]

| | Proton Δδ (ppm) | | | |
|---|---|---|---|---|
| Lewis acid | H2 | H3 | H4 | $OCH_3$ |
| $BBr_3$ | 1.28 | 0.94 | 0.39 | 0.66 |
| $BCl_3$ | 1.14 | 0.87 | 0.38 | 0.63 |
| $SbCl_5$ | 1.02 | 0.77 | 0.34 | 0.60 |
| $BF_3$ | 0.68 | 0.70 | 0.28 | 0.51 |
| $TiCl_4$ | 0.54 | 0.60 | 0.24 | 0.51 |
| $Et_2AlCl$[b] | 0.40 | 0.51 | 0.17 | 0.34 |
| $SnCl_4$ | 0.41 | 0.43 | 0.17 | 0.28 |
| $Et_3Al$[b] | 0.19 | 0.38 | 0.13 | 0.28 |

[a]In ppm (± 0.01). Chemical shifts of uncomplexed base are: δ = 5.84 (dq, 1H, H2), 6.97 (m, 1H, H3), 1.87 (dd, 3H, H4), 3.67 (s, 3H, $OCH_3$). Approximately 0.3 *M* solution in dichloromethane at −20°C, unless otherwise stated.
[b]At −60°C. Chemical shifts of uncomplexed base: δ = 5.86 (H2), 7.00 (H3), 1.90 (H4), 3.69 ($OCH_3$). Acid written in monomeric form for simplicity.

TABLE 6. $^1$H chemical shift differences (Δδ) of crotononitrile **6** on complexation with various Lewis acids[a]

| | Proton Δδ (ppm) | | |
|---|---|---|---|
| Lewis acid | H2 | H3 | H4 |
| $BBr_3$ | 0.69 | 0.99 | 0.40 |
| $BCl_3$ | 0.63 | 0.95 | 0.38 |
| $SbCl_5$ | 0.53 | 0.85 | 0.35 |
| $BF_3$ | 0.44 | 0.75 | 0.28 |
| $Et_2AlCl$[b] | 0.37 | 0.60 | 0.21 |
| $SnCl_4$ | 0.30 | 0.50 | 0.22 |
| $Et_3Al$[b] | — | 0.46 | 0.16 |

[a]In ppm (± 0.01). Chemical shifts of uncomplexed base are: δ = 5.38 (dq, 1H, H2), 6.77 (m, 1H, H3), 1.91 (dd, 3H, H4). Approximately 0.3 *M* solution in dichloromethane at −20°C, unless otherwise stated.
[b]At −60°C. Chemical shifts of uncomplexed base: δ = 5.41 (H2), 6.80 (H3), 1.94 (H4). Acid written in monomeric form for simplicity.

TABLE 7. $^{13}$C chemical shift differences (Δδ) of crotonaldehyde **1** on complexation with various Lewis acids[a]

| | Carbon Δδ (ppm) | | | |
|---|---|---|---|---|
| Lewis acid | C1 | C2 | C3 | C4 |
| $BF_3$ | 8.3 | −3.3 | 26.1 | 3.1 |
| $BCl_3$ | 6.8 | −3.7 | 31.7 | 4.3 |
| $SbCl_5$ | 6.9 | −4.0 | 27.6 | 3.7 |
| $Et_2AlCl$[b] | 9.4 | −2.0 | 20.1 | 2.3 |
| $SnCl_4$ | 7.8 | −2.8 | 19.2 | 2.3 |

[a]In ppm (± 0.01). Chemical shifts of uncomplexed base are: δ = 194.7 (C1), 134.4 (C2), 155.2 (C3), 19.0 (C4). As approximately 0.3 *M* solution in dichloromethane at −20°C.
[b]Acid written in monomeric form for simplicity.

TABLE 8. $^{13}$C chemical shift differences (Δδ) of methyl crotonate **5** on complexation with various Lewis acids[a]

| | Carbon Δδ (ppm) | | | | |
|---|---|---|---|---|---|
| Lewis acid | C1 | C2 | C3 | C4 | $OCH_3$ |
| $BCl_3$ | 8.0 | −5.0 | 17.7 | 2.2 | 7.6 |
| $SbCl_5$ | 5.7 | −3.9 | 14.6 | 1.8 | 6.3 |
| $Et_2AlCl$[b] | 6.3 | −3.1 | 11.6 | 1.0 | 4.5 |
| $SnCl_4$ | 4.8 | −2.5 | 9.4 | 0.9 | 4.0 |

[a]In ppm (± 0.1). Chemical shifts of uncomplexed base are: δ = 167.3 (C1), 122.2 (C2), 145.4 (C3), 18.3 (C4), 51.6 ($OCH_3$). As approximately 0.3 *M* solution in dichloromethane at −20°C.
[b]Acid written in monomeric form for simplicity.

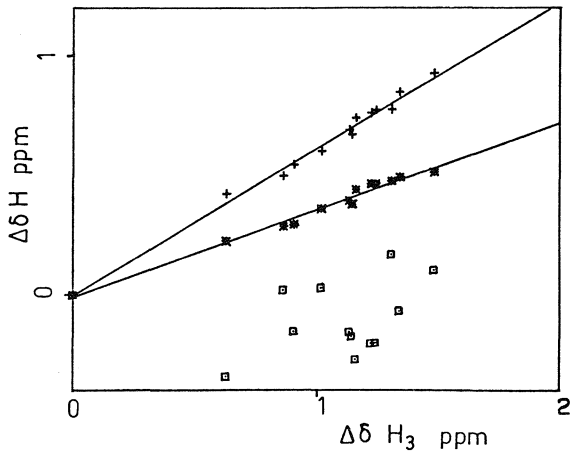


FIG. 1. $^1$H chemical shift differences of the protons of crotonaldehyde, **1**, versus the 3-proton chemical shift difference on complexation with various Lewis acids. (+, Δδ H2/Δδ H3; *, Δδ H4/Δδ H3; ⊡, Δδ H1; Δδ H3.)

complexes of **1**, see eq. [1]. Crotonaldehyde itself adopts the *s-trans* conformation and it is likely that the same conformational preference is maintained on complexation. O-protonated crotonaldehyde exists in the C, O-*E* configuration and, because the Lewis acids used here are larger than a proton, it is most probable that the same configuration is pre-

ferred. As such it will be noted that the Lewis acid is *syn* to the aldehydic proton and removed spatially from the remaining protons of the crotonaldehyde. It is possible that local anisotropy effects are important in determining the chemical shift of H1 in the Lewis acid complexes.

A similar regularity of induced chemical shift was found with the $^{13}C$ nmr spectra of these complexes, Fig. 2.[3] (The number of acids used in this study was less than that used for the $^{1}H$ nmr work because of limited solubility of some of the complexes.) The shifts of the carbonyl carbon resonances appear to be random and unrelated to the corresponding shifts of the C3 resonance.

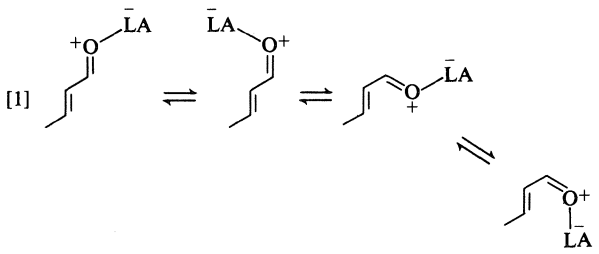


A noteworthy feature of the $^{13}C$ chemical shifts is the upfield shift of the C2 resonance on complexation. This shift is linearly related to the shifts of C3 and C4 but is in the opposite direction. $^{13}C$ chemical shift differences have been taken to give an indication of the change in electron density (11) and therefore it appears that electron density is increased at C2 on complexation but reduced particularly at C3 and somewhat at C4. Similar upfield shifts of C2 resonances have been reported for unsaturated esters (16), ketones (17), ethers (18), and imines (19) on complexation or protonation.

Not only are the Lewis-acid induced chemical shift differences of the $^{13}C$ and $^{1}H$ resonances of crotonaldehyde linearly related within each series but linear relationships also occur between the two series, Fig. 3.[3] Apart from the C1 and H1 resonances, a good correlation exists between the carbon and proton chemical shift differences of the 2, 3, and 4 positions. The slopes of the lines vary considerably, C2/H2 = $-3.6 \pm 0.8$; C3/H3 = $22 \pm 3$; C4/H4 = $8 \pm 2$. There are both theoretical arguments and some empirical evidence to suggest that, at least within related series of compounds, there are linear relationships between both induced $^{1}H$ and $^{13}C$ chemical shifts and charge (20). Specific values for $\Delta\delta^{13}C/\Delta\delta^{1}H$ vary but are usually found to be ca. 16. The slope parameters of the linear relationships reported here for specific carbon–proton pairs differ greatly from this value. It follows that carbon and proton chemical shift differences cannot both be taken as reliable indicators of charge induced at a specific site. This problem is highlighted by the difference in sign between the chemical shift differences of C2 and H2.

If, as seems likely, the carbon chemical shifts are more directly related to charge, the linear relationship between proton and carbon chemical shift differences is a useful result as it allows the prediction of carbon chemical shift differences based on the measurement of proton chemical shift differences. Direct $^{13}C$ measurements are limited in many cases because of poor solubility of the complexes.

It has been suggested that there is a correlation between the algebraic difference ($\Delta\delta$ C3 − $\Delta\delta$ C2) and $\Delta\delta$ C1 for a number of related complexes of unsaturated carbonyl compounds (21). No such relationship was found here for the Lewis acid complexes of crotonaldehyde.

*Extension to other bases*

The effect of various Lewis acids on the $^{1}H$ nmr spectrum of tiglaldehyde follows a very similar pattern to that described above. A similar linear relationship exists between the $\Delta\delta$'s of H4 and the 2-$CH_3$ group with $\Delta\delta$'s of H3, and again there appears to be no correlation of the shifts of H1. In Fig. 4 the $\Delta\delta$'s of the various H's in tiglaldehyde are plotted against those of corresponding $\Delta\delta$'s of crotonaldehyde. Slopes are $0.92 \pm 0.04$, $1.03 \pm 0.07$, and $0.90 \pm 0.18$ for the lines due to H1, H3, and H4 respectively. The closeness to unity of these slopes indicates that the systems are behaving almost identically.

While such parallel behavior might be expected between the two aldehydes, it also exists between crotononitrile, **6**, and crotonaldehyde, Fig. 5.[3] Thus the shifts induced on the H2, H3, and H4 resonances of crotononitrile are also linearly related to those of the corresponding $^{1}H$ resonances of crotonaldehyde as the Lewis acid is varied. In this case the slope of the line is $0.66 \pm 0.15$.

The ketones **3** and **4** differ in behavior from the aldehydes and crotononitrile. Cyclohexenone is the simplest system to examine initially as it has to exist in an *s-trans* conformation because of its ring structure. In this case, plotting $\Delta\delta$ H3 of cyclohexenone against $\Delta\delta$ H3 of crotonaldehyde again leads to a straight line (slope = $0.88 \pm 0.11$) which goes

[3]Figs. 2, 3, 5, 7, 8, 9 are available as supplementary material, at a nominal charge, from the Depository of Unpublished Data, CISTI, National Research Council of Canada, Ottawa, Ont., Canada K1A 0S2. Slopes, intercepts, and correlation coefficients are summarized in Table 9.

Can. J. Chem. Downloaded from www.nrcresearchpress.com by 210.87.254.5 on 09/06/12
For personal use only.

TABLE 9. Slopes, intercepts, and correlation coefficients for induced chemical shift changes

| Figure | y-Axis Compound | y-Axis Resonance | x-Axis Compound | x-Axis Resonance | Slope | y Intercept (ppm) | Correlation coefficient (r) |
|---|---|---|---|---|---|---|---|
| 1 | **1** | H2 | **1** | H3 | 0.61 | −0.003 | 0.995 |
| 1 | **1** | H4 | **1** | H3 | 0.36 | −0.009 | 0.991 |
| 2 | **1** | C2 | **1** | C3 | −0.13 | −0.000(4) | 0.961 |
| 2 | **1** | C4 | **1** | C3 | 0.14 | −0.151 | 0.992 |
| 3 | **1** | C2 | **1** | H2 | −3.6 | −0.015 | 0.946 |
| 3 | **1** | C3 | **1** | H3 | 22.3 | −0.092 | 0.995 |
| 3 | **1** | C4 | **1** | H4 | 8.3 | −0.064 | 0.995 |
| 4 | **2** | H1 | **1** | H1 | 0.92 | −0.017 | 0.999 |
| 4 | **2** | H3 | **1** | H3 | 1.03 | 0.019 | 0.998 |
| 4 | **2** | H4 | **1** | H4 | 0.90 | 0.014 | 0.997 |
| 5 | **6** | H2 | **1** | H2 | 0.73 | −0.033 | 0.981 |
| 5 | **6** | H3 | **1** | H3 | 0.66 | −0.015 | 0.985 |
| 5 | **6** | H4 | **1** | H4 | 0.75 | −0.012 | 0.984 |
| 6 | **4** | H2 | **1** | H2 | 1.81 | −0.327 | 0.966 |
| 6 | **4** | H3 | **1** | H3 | 0.88 | −0.007 | 0.996 |
| 7 | **3** | H2 | **1** | H2 | 1.32 | −0.185 | 0.999 |
| 7 | **3** | H3 | **1** | H3 | 0.90 | −0.011 | 0.994 |
| 7 | **3** | H4 | **1** | H4 | 0.88 | −0.010 | 0.994 |
| 8 | **5** | H2 | **1** | H2 | 2.14 | −0.725 | 0.975 |
| 8 | **5** | H3 | **1** | H3 | 0.63 | −0.037 | 0.989 |
| 8 | **5** | H4 | **1** | H4 | 0.77 | −0.031 | 0.982 |
| 9 | **5** | H2 | **4** | H2 | 1.17 | −0.320 | 0.997 |

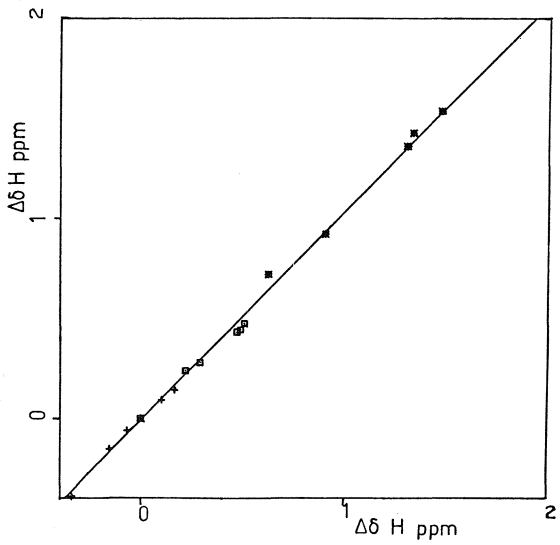


FIG. 4. $^1$H chemical shift differences of the protons of tiglaldehyde, **2**, versus the $^1$H chemical shift difference of the corresponding protons of crotonaldehyde, **1**, on complexation with various Lewis acids. (For clarity, only the 3-proton line has been drawn.) (+, Δδ H1; ⊡ Δδ H4; * Δδ H3.)

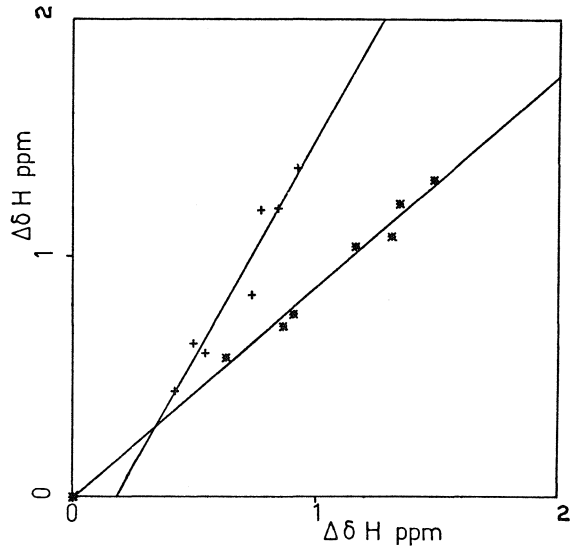


FIG. 6. $^1$H chemical shift differences of the protons of cyclohex-2-enone, **4**, versus the $^1$H chemical shift differences of the corresponding protons of crotonaldehyde, **1**, on complexation with various Lewis acids. (+, Δδ H2; *, Δδ H3.)

through the origin (Fig. 6). On the other hand, the corresponding points of the H2 Δδ's do not lie on this line. A linear relationship still exists but there is a much greater sensitivity to the change of Lewis acid (slope = 1.80 ± 0.22). The line correlating the H2 resonances no longer goes through the origin.

Azzarro and co-workers (13) have shown that the $BF_3$ complex of cyclohexenone exists in two conformations with approximately equal proportions of each. The barrier to interconversion of these two conformations is sufficiently low that, at the temperature used for our studies, it is not possible to detect separate signals from each. However, the Lewis acid grouping in **4** (*E*) is close to H2 and a

Can. J. Chem. Downloaded from www.nrcresearchpress.com by 210.87.254.5 on 09/06/12
For personal use only.

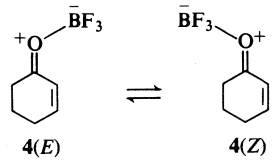

4(*E*) 4(*Z*)

through-space deshielding of this proton might be anticipated (13).

Pentenone shows a similar but diminished pattern of behavior to that of cyclohexenone, Fig. 7.[3] The Δδ's of H3 and H4 are linearly related to those of H3 and H4 crotonaldehyde (slope = 0.90 ± 0.13). However, the Δδ plot of the H2 resonance is steeper than the others and does not go through the origin. In this case the deviation of the plot of the Δδ's of the H2 resonances from the normal Δδ line is less than that observed with cyclohexenone, due to the greater conformational freedom of this complex. It is known that the pentenone itself can exist in both *s-cis* and *s-trans* conformations. It is likely that pentenone when complexed with a Lewis acid exists in three of the four possible conformations. It has not been possible to freeze out interconversions between these conformations to determine which is preferred. In one of these conformations a through-space deshielding of H2 could occur.

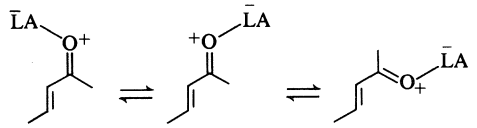

Additional support for the suggestion that the anisotropy of the Lewis acid can affect the resonance position of H2 comes from an analysis of the results obtained with methyl crotonate **5**, Fig. 8.[3] Once more as the Δδ's of methyl crotonate proton resonances are plotted against the corresponding crotonaldehyde values the Δδ's of the H3 and H4 resonances exhibit a linear relationship (slope = 0.63 ± 0.16) while the Δδ's of the H2 resonances show a very much steeper linear relationship which does not go through the origin (slope = 2.14 ± 0.20). Consideration of the possible conformations of the complexed methyl crotonate indicates that only two are reasonable.

The "U" conformation of the complexed ester should be of higher energy as has been established in the case of the protonated carboxylic acids (22). The other two sickle and "W" conformations both

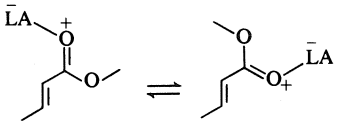

TABLE 10. Lewis acid scale based on Δδ-values of H3 resonances of various bases[a]

| Lewis acid | Relative power |
|---|---|
| $BBr_3$ | 1.00±0.005 |
| $BCl_3$ | 0.93±0.02 |
| $SbCl_5$ | 0.85±0.03 |
| $AlCl_3$[b] | 0.82 |
| $BF_3$[d] | 0.77±0.02 |
| $EtAlCl_2$[b] | 0.77 |
| $TiCl_4$ | 0.66±0.03 |
| $Et_2AlCl$ | 0.59±0.03 |
| $SnCl_4$[c] | 0.52±0.04 |
| $Et_3Al$ | 0.44±0.02 |

[a]Derived from values in Tables 1–6 and from slope parameters quoted in text. Values were obtained from six Lewis bases except where stated.
[b]Crotonaldehyde was the only Lewis base employed.
[c]Values obtained with all Lewis bases except tiglaldehyde.
[d]Values obtained with all Lewis bases except tiglaldehyde and pentenone.

have strong steric interactions between the H3 proton and the group on the adjacent oxygen. Therefore it is likely that the H2 nucleus of **5** is in close proximity to the Lewis acid and is further deshielded as a result.

The suggestion of a similar origin for the effects of the Δδ's of the H2 proton resonances of cyclohexenone and methyl crotonate is confirmed by the linear relationship which exists between them, Fig. 9.[3] It is interesting that no anomalous deshielding of the C2 resonances of the Lewis acid complexes of methyl crotonate is observed.

## Conclusions

A remarkable feature of the above results is the regularity of the linear relationships which exist for the Lewis acid induced shifts of the H3, H4, C3, and C4 resonances of all the bases. The induced shifts of nuclei closer to the site of bonding with the Lewis acid (H1 and C1) appear to be influenced by local anisotropy, the signals of the remote atoms (H3, C3, H4, and C4) are not significantly affected by this and therefore both the $^1H$ and $^{13}C$ nuclei seem to reflect the change in electron distribution associated with complexation. Although the Δδ $^1H$ values in **1** and **2** show little, if any, correlation with the Δδ values of other protons, they are not random. This is demonstrated by the good correlation between the Δδ $^1H$ values for these two bases. Complexation-induced shifts of the C2 and H2 atoms are also regular but appear to be comprised of two components, viz., through-bond and through-space deshielding, with the magnitude of the latter component being determined by conformation.

If indeed a linear relationship exists between

Can. J. Chem. Downloaded from www.nrcresearchpress.com by 210.87.254.5 on 09/06/12
For personal use only.

Can. J. Chem. Downloaded from www.nrcresearchpress.com by 210.87.254.5 on 09/06/12
For personal use only.

induced charge and chemical shift difference, even if the constant of proportionality differs for specific nuclei, then it follows that the choice of Lewis acid influences only the magnitude of the atomic charges induced on the bases and not their distribution.

With all the bases used in this study, linear relationships were found for the shifts induced by complexation with Lewis acids. This means it is possible to set up a Lewis acid scale based upon any or all of these bases in which the acids are ranked on the basis of the magnitude of the induced shift of the H3 resonance. Such a scale is shown in Table 10. The order of Lewis acids, so obtained, is at considerable variance with that found by another group whose results were obtained by deducing complex formation constants from enthalpy measurements (14). It remains to be seen whether reactivity and/or regioselectivity in catalyzed reactions of these bases will follow any such scale.

The bases used here vary in their response to complexation with a Lewis acid. This is shown by the various slope parameters found in plotting $\Delta\delta$ H3 of a particular base against the comparable shift difference of crotonaldehyde. These slope parameters do not necessarily reflect the basicity of the Lewis base, but are to be indicative of the relative charge induced at the 3-position. They could therefore be of importance in predicting reactivity after complexation.

## Experimental

*General*

A number of $^1$H nmr spectra were obtained on a Varian HA-100 spectrometer operating at 100 MHz and fitted with a variable temperature probe controlled by a Varian V-6040 controller. Chemical shifts were measured using a Varian V-4315 frequency counter relative either to TMS or $CH_2Cl_2$ and to a precision of $\pm$ 0.01 ppm. The remaining $^1$H nmr spectra were recorded on a Bruker WP.80 Pulsed Fourier Transform spectrometer operating at 80 MHz. Where the use of TMS as an internal standard was impractical, shifts were measured relative to $CH_2Cl_2$ (HA-100) or to the central resonance of $CHDCl_2$ (WP.80) and were estimated relative to TMS by adding 5.40 ppm. No significant difference in chemical shifts was observed for repeat runs with separately-prepared samples or by using different instruments.

$^{13}$C spectra were obtained on either a Bruker WH.90 or a Bruker WH.80 Pulsed Fourier Transform spectrometer operating at 22.6 MHz and 20.1 MHz respectively. All spectra were obtained at 253 K except those containing alkyl aluminums, which were run at 213 K.

*Materials*

The Lewis bases, which are commercially available materials, were distilled and stored over activated 4A molecular sieves. A further distillation *in vacuo* immediately before use afforded compounds which were >99.5% pure by gas chromatography and in which no impurities were observed by $^1$H nmr. All manipulations were carried out under an atmosphere of dry nitrogen.

The liquid Lewis acids were distilled under reduced pressure. Early fractions were discarded. Later fractions were sealed in small dry glass ampoules until required. Again, all manipulations were carried out under an atmosphere of dry nitrogen. Gaseous Lewis acids ($BF_3$, $BCl_3$) were distilled from trap to trap in a dry glass vacuum line.

Methylene chloride was purified by the method of Jones and Wood (23).

*Preparation of nmr samples*

The nmr samples were prepared under dry nitrogen by adding an appropriate quantity of Lewis base through a rubber septum cap to a solution of Lewis acid in methylene chloride which was cooled to 195 K, except in the case of the gaseous Lewis acids, $BF_3$ and $BCl_3$, which were dispensed in a precalibrated vacuum line system. The stoichiometry of the resulting solution was such that there was a 10 to 100% excess of the Lewis acid present. $^1$H and $^{13}$C nmr spectra were recorded at −20°C, or at −60°C in the case of alkylaluminums to minimize side reactions. Complete complex formation was checked by comparing samples with different ratios of Lewis acid to the base. Only in the case of crotononitrile was there any question about the completeness of the reaction; however, under the conditions used here more than 95% of the base was complexed.

## Acknowledgement

This work was supported by the Natural Sciences and Engineering Research Council of Canada.

1. (*a*) P. YATES and P. EATON. J. Am. Chem. Soc. **82**, 4436 (1960); (*b*) G. I. FRAY and R. ROBINSON. J. Am. Chem. Soc. **83**, 249 (1961); (*c*) H. W. THOMPSON and D. G. MELILLO. J. Am. Chem. Soc. **92**, 3218 (1970); (*d*) M. KAKUSHIMA, J. ESPINOSA, and Z. VALENTA. Can. J. Chem. **54**, 3304 (1976); (*e*) M. KAKUSHIMA and D. G. SCOTT. Can. J. Chem. **57**, 1399 (1979); (*f*) M. KAKUSHIMA. Can. J. Chem. **57**, 2564 (1979); (*g*) M. KAKUSHIMA, L. ALLAIN, R. A. DICKINSON, P. S. WHITE, and Z. VALENTA. Can. J. Chem. **57**, 3354 (1979); (*h*) M. KAKUSHIMA, J. DAS, G. R. REID, P. S. WHITE, and Z. VALENTA. Can. J. Chem. **57**, 3356 (1979).
2. H. HIRAI. J. Polym. Sci. Macromol. Rev. **11**, 47 (1976).
3. H. M. R. HOFFMANN. Angew. Chem. Int. Ed. Engl. **8**, 556 (1969); B. B. SNIDER. J. Org. Chem. **39**, 255 (1974).
4. B. B. SNIDER. J. Org. Chem. **41**, 3061 (1976).
5. S. M. MAKIN. Pure Appl. Chem. **47**, 173 (1976).
6. T. MUKAIYAMA. Angew. Chem. Int. Ed. Engl. **16**, 817 (1977).
7. (*a*) T. SATO, S. YOSHIIE, T. IMAMURA, K. HASEGAWA, M. MIYAHARA, S. YAMAMURA, and O. ITO. Bull. Chem. Soc. Jpn. **50**, 2714 (1977); (*b*) T. SATO, S. YAMAGUCHI, and H. KANEKO. Tetrahedron Lett. 1863 (1979).
8. (*a*) W. KURAN, S. PASYNKIEWICZ, and Z. FLORJANCZYK. Makromol. Chem. **154**, 71 (1972); (*b*) W. KURAN, S. PASYNKIEWICZ, Z. FLORJANCZYK, and E. LUSZTYK. Makromol. Chem. **177**, 2627 (1976).
9. K. N. HOUK. *In* Pericyclic reactions. Vol. 2. Academic Press, New York. 1977.
10. (*a*) V. N. SOKOLOV, V. N. PAVLYUCHENKO, G. P. KONDRATENKOV, and G. A. BALAEV. J. Gen. Chem. USSR, **42**, 946 (1972); (*b*) K. C. MALHOTRA and D. S. KATOCH. Aust. J. Chem. **27**, 1413 (1974); (*c*) P. N. GATES, E. J. MCLAUCHLAN, and E. F. MOONEY. Spectrochim. Acta, **21**, 1445 (1965); (*d*) N. F. SALAKHUTDINOV, I. K. KOROBEINICHEVA, and V. A. KOPTYUG. J. Org. Chem. USSR, **15**, 1304 (1979); (*e*) M. RABINOVITZ and A. GRINVALD. J. Am.

Chem. Soc. **94**, 2724 (1972); J. Chem. Soc. Perkin Trans. II, 514 (1973); (*f*) B. MARCOS, J. AMAUDRUT, and C. DEVIN. J. Chem. Res. (S), 166 (1977); (*g*) A. K. BOSE and P. R. SRINIVASAN. Tetrahedron Lett. 1571 (1975); (*h*) D. P. N. SATCHELL and R. S. SATCHELL. Chem. Rev. **69**, 251 (1969); (*i*) M. AZZARO, J.-F. GAL, S. GERIBALDI, A. GREC-LUCIANO, and C. CALLERI. J. Chem. Res. (S), 134, (1979); (*j*) R. J. GILLESPIE and J. S. HARTMAN. Can. J. Chem. **46**, 3799 (1968); (*k*) J. S. HARTMAN and J. M. MILLER. Adv. Inorg. Chem. Radiochem. **21**, 147 (1978); (*l*) T. L. BROWN and M. KUBOTA. J. Am. Chem. Soc. **83**, 331 (1961); (*m*) J. LAANE and T. L. BROWN. Inorg. Chem. **3**, 148 (1964).

11. M. J. LOOTS, L. R. WEINGARTEN, and R. H. LEVIN. J. Am. Chem. Soc. **98**, 4571 (1976), and references therein.
12. A. NIXON and R. F. CHILDS. J. Polym. Sci. Polym. Chem. Ed. **18**, 1499 (1980).
13. (*a*) C. PARIS, G. TORRI, L. ELEGANT, and M. AZZARO. Bull. Soc. Chim. Fr. 1449 (1974); (*b*) J. TORRI and M. AZZARO. Bull. Soc. Chim. Fr. II-283 (1978).
14. J. BRUNN and C. BECK. Z. Chem. **17**, 296 (1977).
15. E. M. ARNETT and C. PETRO. J. Am. Chem. Soc. **100**, 5408 (1978).
16. J. BRUNN, R. RADEGLIA, B. LEWANSCHECK, and S. PEUST. Z. Phys. Chem. **258**, 681 (1977).
17. A. FRATIELLO, R. KUBO, and S. CHOW. J. Chem. Soc. Perkin Trans. II, 1205 (1976).
18. A. FRATIELLO, R. KUBO, D. LIU, and G. VIDULICH. J. Chem. Soc. Perkin Trans. II, 1415 (1975).
19. M. ALLEN and J. D. ROBERTS. Can. J. Chem. **59**, 451 (1981).
20. D. G. FARNUM. Adv. Phys. Org. Chem. **11**, 123 (1975).
21. R. RADEGLIA. Z. Chem. **18**, 389 (1978).
22. G. A. OLAH, A. M. WHITE, and D. H. BRIEN. *In* Carbonium ions. Vol. IV. Wiley-Interscience, New York. 1973. p. 1697.
23. D. E. H. JONES and J. L. WOOD. J. Chem. Soc. A, 1448 (1966).

Can. J. Chem. Downloaded from www.nrcresearchpress.com by 210.87.254.5 on 09/06/12
For personal use only.

# Lewis acid adducts of α,β-unsaturated carbonyl and nitrile compounds. A calorimetric study

RONALD F. CHILDS,[1] D. LINDSAY MULHOLLAND, AND ALAN NIXON
*Department of Chemistry, McMaster University, Hamilton, Ont., Canada L8S 4M1*

Received July 20, 1981

RONALD F. CHILDS, D. LINDSAY MULHOLLAND, and ALAN NIXON. Can. J. Chem. **60**, 809 (1982).

Enthalpies of complexation of the α,β-unsaturated Lewis bases crotonaldehyde, **1**; methyl crotonate, **2**; mesityl oxide, **3**; and crotononitrile, **4**; with each of the Lewis acids $SnCl_4$, $TiCl_4$, $SbCl_5$, and $BCl_3$ were measured in solution in $CH_2Cl_2$. The results indicate that while a qualitative agreement exists in the ranking of Lewis acids for each of the Lewis bases, there is only a modest quantitative correlation. Similarly, when compared with an nmr-derived Lewis acid scale, the enthalpies were found to agree with the qualitative ranking of Lewis acids, but exhibited only a poor correlation.

RONALD F. CHILDS, D. LINDSAY MULHOLLAND et ALAN NIXON. Can. J. Chem. **60**, 809 (1982).

On a mesuré, en solution dans le $CH_2Cl_2$, les enthalpies de complexation des bases de Lewis α,β-non saturées, crotonaldehyde (**1**), crotonate de méthyle (**2**), oxyde de mésityle (**3**) et crotononitrile (**4**) avec chacun des acides Lewis suivants: $SnCl_4$, $TiCl_4$, $SbCl_5$ et $BCl_3$. Les résultats indiquent que des accords qualitatifs permettent d'ordonner chaque acide de Lewis pour chacune des bases de Lewis; toutefois la corrélation quantitative n'est que modeste. De la même manière, si on compare les enthalpies avec une échelle d'acide de Lewis dérivée de la rmn, on peut qualitativement ordonner les acides de Lewis mais la corrélation est faible.
[Traduit par le journal]

Can. J. Chem. Downloaded from www.nrcresearchpress.com by 210.87.254.40 on 09/06/12
For personal use only.

Lewis acids are used to catalyse a variety of synthetically useful reactions of α,β-unsaturated carbonyl and nitrile compounds. In a previous paper we have reported a systematic examination of the nmr spectra of the complexes formed between some of these unsaturated bases and Lewis acids and have proposed an acid scale which, it was suggested, reflected the amount of charge induced at C3 of the base on complexation (1).

There has been much discussion about and many attempts at correlating Lewis acid/Lewis base interactions (2). These include, among others, the hard/soft concepts introduced by Pearson (3), the donor/acceptor numbers of Gutmann (4), Drago's E/C equation (5), and theoretical treatments of Mulliken and Pearson (6) and Klopman (7). The equilibrium constant or the heat of reaction is generally used to measure the strength of a Lewis acid/base reaction.

In our attempts to quantify the catalytic effects of Lewis acids on the reactions of unsaturated carbonyls and nitriles, it seemed of interest to compare the nmr-based scale mentioned above with the strength of the acid/base interaction. As complex formation was essentially complete for nearly all the systems we had studied it seemed appropriate to base such a comparison on the heats of reaction. There have been some previous reports of the measurement of the $\Delta H$ for reaction of unsaturated bases with Lewis acids (8) but insufficient for a meaningful comparison with our nmr-based scale. We report here a range of calorimetric measurements of these systems and examine the correlations with the nmr scale.

[1]Author to whom correspondence may be addressed.

## Results and discussion

### *Calorimetric measurements*

Ideally the enthalpy measured should be that of the interaction of the acid and base in the gas phase. However, since solvation energies are likely to be small in inert solvents, the gas phase conditions can be approximated by taking the heat of molecular complexation to be the difference in molar heats of solution of the base in a solution of the Lewis acid and that in the same solvent with no acid present (4, 9–11).

The solution calorimeter used was a modified version of a design of Arnett and Petro (10). The precision of the calorimeter was checked by measuring the enthalpy of reaction of water with $FSO_3H$ (measured $-12.23 \mp 0.08$ kcal/mol, literature $-12.2 \mp 0.1$ (12) and $-11.95 \mp 0.04$ kcal/mol (13)). Further checks were made by measuring the heat of solution of various bases in a $SbCl_5/C_2H_4Cl_2$ solution and comparing with literature values.

Methylene chloride was used as the solvent with the unsaturated carbonyl and nitrile compounds of interest in this study. This solvent is inert to the Lewis acids used. The bases used were crotonaldehyde, **1**; methyl crotonate, **2**; mesityl oxide, **3**; and crotononitrile, **4**. The heats of reaction of each of these bases with $BCl_3$, $SbCl_5$, $TiCl_4$, and $SnCl_4$ were measured and the results shown in Table 1.

0008-4042/82/060809-04$01.00/0
©1982 National Research Council of Canada/Conseil national de recherches du Canada

TABLE 1. Enthalpies of complexation ($\Delta H$) of α,β-unsaturated bases with various Lewis acids[a]

| Lewis base | $-\Delta H$ (kcal/mol) $BCl_3$ | $SbCl_5$ | $TiCl_4$ | $SnCl_4$ | $-\Delta H_2$[c] |
|---|---|---|---|---|---|
| Crotonaldehyde | 24.4±0.3 | 21.2±0.4 | 14.0±0.6 | 12.2±0.4 | 0.78±0.3 |
| Methyl crotonate | 19.9±0.4 | 18.0±0.4 | 13.6±0.7 | 6.1±0.3 | 0.64±0.05 |
| Mesityl oxide | 25.4±0.3 | 24.3±0.5 | 17.9±0.3 | 12.1±0.2 | 0.60±0.02 |
| Crotononitrile | 19.2±0.2 | 15.3±0.3 | 11.5±0.3 | (5.6±0.2)[b] | 0.60±0.04 |

[a]As defined by equation given in Experimental. In dichloromethane solution at 295 K.
[b]Value corrected for incomplete complexation. Measured value = 3.8 ± 0.1 kcal/mol.
[c]Heat of solution of base in $CH_2Cl_2$.

*Nature of complexes formed*

Before discussing these heats of reaction it is important to establish the nature of the complexes formed. In all measurements the Lewis acid was held in excess and 1:1 complexes were formed (1). Checks were made for complete complexation by running $^1H$ nmr spectra at 25°C on solutions of comparable concentrations to those used in the calorimetry. In all but one case, variation of the acid to base ratio did not alter the chemical shifts of the resonances of the base indicating that the base was essentially completely complexed.

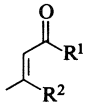

1 $R^1 = R^2 = H$
2 $R^1 = OCH_3$, $R^2 = H$
3 $R^1 = R^2 = CH_3$

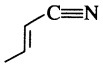

4

The one exception was crotononitrile and $SnCl_4$, where considerable variation was detected, Table 2. From a plot of $1/\Delta\delta$ of H3 against the reciprocal of the Lewis acid concentration (Fig. 1), the equilibrium constant was found to be 5.31 L $mol^{-1}$.[2] The value of the equilibrium constant found here for **4** and $SnCl_4$ corresponds well with that reported by Brown and Kubota (14) for benzonitrile/$SnCl_4$ ($K$ = 4.17 L $mol^{-1}$).

Under the calorimetric conditions used the magnitude of the equilibrium constant between **4** and $SnCl_4$ is such that only some 58% of **4** would be complexed. This contrasts markedly with the $^1H$ nmr measurements at −20°C reported earlier (1) where it appeared that essentially all of **4** was complexed. The entropy term for this equilibrium was found to be −16 eu. Using the linear enthalpy/entropy relationship of Laane and Brown (15), a value of −22 eu might be expected.

*Enthalpy correlations*

Plots of the enthalpies of reaction of the Lewis acids with the Lewis bases against the nmr-derived scale (1) are shown in Fig. 2. Each of the bases shows a qualitative correlation between the enthalpies and nmr rating of the Lewis acids. In each case the ranking of the Lewis acids is the same. However, with the exception of mesityl oxide, the correlations are not very good quantitatively.

If the nmr scale we advanced previously is indeed indicative of the amount of positive charge

TABLE 2. Lewis acid concentrations and chemical shift differences for the complexation of crotononitrile **4** with $SnCl_4$[a]

| $[SnCl_4]$ ($M$) | [**4**] ($M$) | $\delta_3$ (ppm) | $\Delta\delta_3$ (ppm) |
|---|---|---|---|
| 0.205 | 0.06 | 6.97 | 0.20 |
| 0.410 | 0.06 | 7.03 | 0.27 |
| 0.615 | 0.06 | 7.07 | 0.30 |
| 0.820 | 0.06 | 7.08 | 0.31 |

[a]3-H shift of free base is δ 6.77.

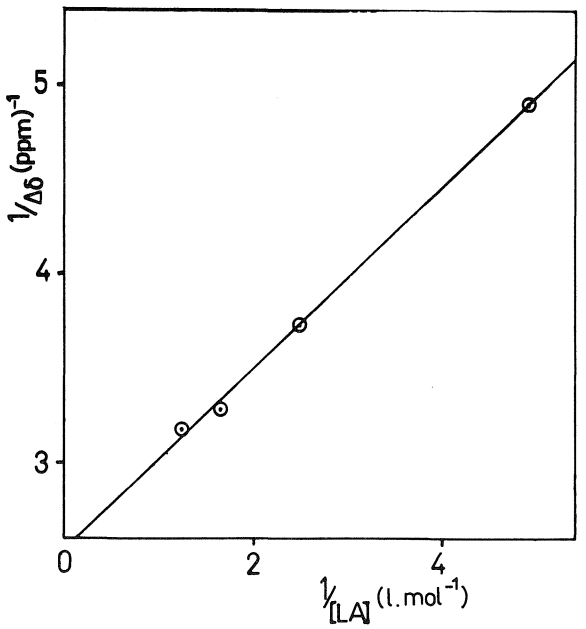


FIG. 1. Plot of $1/\Delta\delta$ of the $^1H$ chemical shift of H3 of crotononitrile versus $1/[SnCl_4]$.

[2]Δδ is the chemical shift of the fast exchange average of a resonance due to the complex and the free base measured relative to the chemical shift of the free base.

Can. J. Chem. Downloaded from www.nrcresearchpress.com by 210.87.254.40 on 09/06/12
For personal use only.

Can. J. Chem. Downloaded from www.nrcresearchpress.com by 210.87.254.40 on 09/06/12
For personal use only.

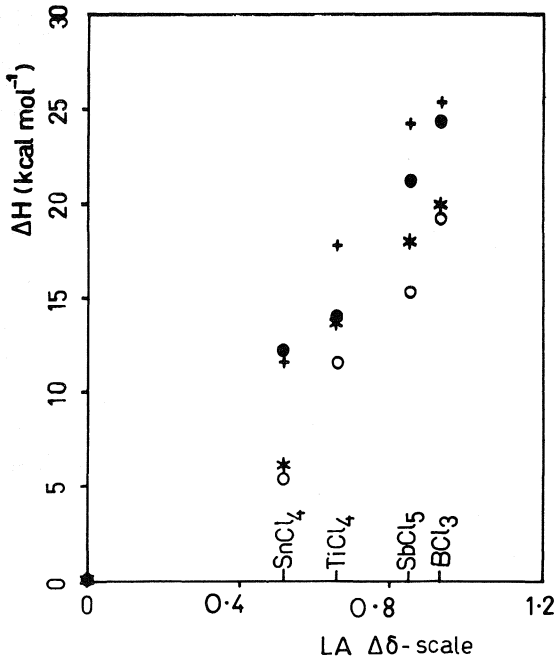


FIG. 2. Plots of the enthalpy of reaction of Lewis acids with crotonaldehyde (●); mesityl oxide (+); methyl crotonate (★); and crotononitrile (○) against nmr Lewis acid scale.

induced on the carbon framework of these unsaturated bases on complexation, then qualitatively this is related to the heat of formation of the complexes. It should be stressed, however, that the Lewis acids selected for this study are all simple inasmuch as they are monomeric in solution. No correlation would be anticipated with dimeric systems such as $Al_2Br_6$ or the alkylaluminum halides unless allowance was made for the heats of dissociation of the Lewis acids.

In the nmr work it was found that each base had a different sensitivity (slope parameter) to change of the Lewis acid. Thus crotonaldehyde was much more sensitive to change of the Lewis acid than pent-3-en-2-one. Crotononitrile was found to be the least sensitive. There appears to be no correlation between the calorimetric data presented in this paper and these base slope parameters. As can be seen from Fig. 2, the slopes of the $\Delta H$ vs. nmr scale plots for all the bases used are qualitatively the same.

In conclusion, it remains to be seen whether the parameters measured for these Lewis acid complexes of the unsaturated bases can be used to predict reactivity in their catalysed reactions.

## Experimental

*General*

All materials were purified as described previously (1). The $^1$H nmr spectra were obtained on a Bruker WP 80 Fourier Transform spectrometer operating at 80 MHz equipped with a Bruker B-VT 1000 variable temperature controller. Samples were run at 25°C in $CD_2Cl_2$ as solvent.

*Equilibrium measurements for crotononitrile/$SnCl_4$*

A series of samples of **4** (0.04 *M*) in $CD_2Cl_2$ (0.3 mL) were prepared and $SnCl_4$ added to them such that the acid concentration varied between 0.2 to 0.8 *M*. The $^1$H nmr chemical shifts of **4** were measured at 25°C and are shown in Table 1. The equilibrium constant was estimated from a slightly modified Benesi–Hildebrand plot (16). The slope is given by $1/\Delta\delta oK$ (where $\Delta\delta o$ is the chemical shift of the complex relative to the free base) and the intercept is given by $1/\Delta\delta o$. The slope was $0.48 \mp 0.02$ mol/L and intercept $2.55 \mp 0.05$ giving a value of $K = 5.31 \mp 0.19$ L mol$^{-1}$ (16). All other combinations of Lewis acids – bases used in this study gave invariant chemical shift differences on comparable changes of the Lewis acid concentration.

*The calorimeter* employed was based on the design by Arnett and Petro (10) with the following modifications. The calorimeter vessel was reduced in size to approximately 125 mL. As a result, the volume of solvent used could be reduced to 60 mL. The bottom of the vessel was made flat except for a V-shaped indentation which acted as a bearing for the Teflon tip of the stirrer. This allowed better immersion of the glass probes containing the thermistor and heaters. The reduction in volume of solvent caused an increase in sensitivity of the calorimeter, decreasing the heat input for balance and calibration runs. For the balance and calibration heaters, Philips metal film precision resistors type MR 25 F (50 ohm) were used. These were in series and mounted in 5 mm od Pyrex glass tubes partially filled with liquid paraffin as a heat transfer fluid. The resistance of these heaters was carefully monitored during use, but heat transfer was found to be so effective that no significant change in resistance took place even with prolonged use. Two 12-V lead–acid accumulators acted as power supplies. These were independently connected to the balance and calibration heaters and the applied voltage was measured using a digital multimeter (Keithley 169). The duration of the calibration heating cycle was measured to 0.01 s using an interconnected digital timer.

*Calorimetric procedure*

The dried calorimeter vessel was charged with dried $CH_2Cl_2$ (60 mL) and blanketed with nitrogen. The Lewis acid was added to the calorimeter with a syringe so as to give a 0.2 to 0.3 *M* solution. (At least two completely independent runs were carried out for each acid/base combination with different acid concentrations being used in each.) The calorimeter was balanced by adjusting the balance heater at ca. 25°C and a series of at least eight electrical calibrations was conducted.

The Lewis base (5–20 mg) was added using a weighed 25 μL syringe. The enthalpies quoted in Table 2 are the arithmetic

TABLE 3. Enthalpy of complexation of crotonaldehyde with $SbCl_5$[a]

| Run | Electrical calibration[b] | Wt. sample (mg) | $\Delta H_1$ (kcal/mol) |
|---|---|---|---|
| 1 | 0.1083±0.0016 | 7.27 | 21.20 |
| | | 8.13 | 21.57 |
| | | 7.50 | 22.06 |
| | | 7.57 | 22.16 |
| 2 | 0.1068±0.0028 | 7.31 | 21.81 |
| | | 4.33 | 22.47 |
| | | 6.29 | 22.37 |
| | | 6.49 | 22.15 |

[a]At 298 K with $SbCl_5$ dissolved in 60 mL $CH_2Cl_2$.
[b]In units of calories per centimeter pen deflection. Each calibration is a mean of 8 measurements.

mean of at least six injections carried out over two separate runs. A typical set of results is shown in Table 3. To obtain the heat of complexation a separate experiment was conducted in which no Lewis acid was added to the calorimeter and the heat of solution subtracted from the previous value. ($\Delta H_{compl.} = \Delta H_1 - \Delta H_2$ where $\Delta H_{compl.}$ = heat of complexation; $\Delta H_1$ = heat of solution of base in $CH_2Cl_2$ containing the Lewis acid; $\Delta H_2$ = heat of solution of base in $CH_2Cl_2$ solution.) A further set of electrical calibrations was carried out at the end of the run.


1. R. F. CHILDS, D. L. MULHOLLAND, and A. NIXON. Can. J. Chem. **60**, 801 (1982).
2. W. B. JENSEN. Chem. Rev. **78**, 1 (1978).
3. R. G. PEARSON. J. Am. Chem. Soc. **85**, 3533 (1963).
4. (*a*) V. GUTMANN and R. SCHMID. Coord. Chem. Rev. **12**, 263 (1974); (*b*) V. GUTMANN. Coord. Chem. Rev. **15**, 207 (1975).
5. R. S. DRAGO and B. B. WAYLAND. J. Am. Chem. Soc. **87**, 3571 (1965).
6. R. S. MULLIKEN and W. B. PEARSON. Molecular complexes: a lecture and reprint volume. Wiley–Interscience, New York, NY. 1969.
7. (*a*) G. KLOPMAN. J. Am. Chem. Soc. **90**, 223 (1968); (*b*) *In* Sigma molecular orbital theory. *Edited by* O. Sinanoğlu and K. B. Wiberg. Yale University Press, New Haven, Conn. 1970. pp. 115–120; (*c*) *In* Chemical reactivity and reaction paths. *Edited by* G. Klopman. Wiley–Interscience, New York, NY. 1974. Chapt. 4.
8. J. BRUNN and C. BECK. Z. Chem. **17**, 296 (1977).
9. T. F. BOLLES and R. S. DRAGO. J. Am. Chem. Soc. **87**, 5015 (1965).
10. E. M. ARNETT and C. PETRO. J. Am. Chem. Soc. **100**, 5402 (1978).
11. G. OLOFSSON, I. LINDQVIST, and S. SUNNER. Acta Chem. Scand. **17**, 259 (1963).
12. E. M. ARNETT, R. P. QUIRK, and J. J. BURKE. J. Am. Chem. Soc. **92**, 1260 (1970).
13. G. W. RICHARDS and A. A. WOOLF. J. Chem. Soc. A, 470 (1968).
14. T. L. BROWN and M. KUBOTA. J. Am. Chem. Soc. **83**, 331 (1961).
15. J. LAANE and T. L. BROWN. Inorg. Chem. **3**, 148 (1964).
16. H. A. BENESI and J. H. HILDEBRAND. J. Am. Chem. Soc. **71**, 2703 (1944).


Can. J. Chem. Downloaded from www.nrcresearchpress.com by 210.87.254.40 on 09/06/12
For personal use only.

## ADDITIONS AND CORRECTIONS/AJOUTS ET CORRECTIONS

Vol. 58, 1980

**J. A. Howard and S. B. Tong.** Metal complexes as antioxidants. 7. A kinetic and product study of the reaction of tertiary alkylperoxy radicals with cobalt(II) acetylacetonate.

Page 1962. This paper should have been Part 8 in the series on metal complexes as antioxidants. In addition, the acetophenone and α-cumyl alcohol yields for the fourth entry in Table 3 are back-to-front. Thus the alcohol yield should have been 0.033 *M* and the acetophenone yield 0.002 *M*.

Vol. 59, 1981

**J. A. Howard, J. B. Bennett, and G. Brunton.** Absolute rate constants for hydrocarbon autoxidation. 30. On the self-reaction of the α-cumylperoxy radical in solution.

Page 2253. In the discussion section of the paper the corrected ratio of $[PhCMe_2{}^{36}O_2{}^{\bullet}]/[PhCMe_2O_2{}^{\bullet}]$ should have been 0.015 and not 0.05 and Nangia and Benson's estimated of $\Delta H_{16}{}^{0}$ was $-20.2$ kcal mol$^{-1}$ and not $-10.2$ kcal mol$^{-1}$.

**Vincenzo Malatesta and Angelo Mugnoli.** The crystal and molecular structure of *N*,*N*′-ethylenebis(benzoylacetoniminato)-nickel(II).

Page 2766. The value for β in both the English and French abstracts should be β = 96.68(2)°; the value given in the text requires no correction.

# *Ab initio* SCF MO calculations on the reactions of OH radical with pyridine and pyridinium ion

M. C. ANTHONY, W. L. WALTZ, AND P. G. MEZEY

*Department of Chemistry and Chemical Engineering and the Saskatchewan Accelerator Laboratory, University of Saskatchewan, Saskatoon, Sask., Canada S7N 0W0*

Received October 30, 1981

M. C. ANTHONY, W. L. WALTZ, and P. G. MEZEY. Can. J. Chem. **60**, 813 (1982).

Relative energies of various products formed in the reaction of pyridine and pyridinium ion with the hydroxyl radical are calculated using non-empirical SCF MO techniques. The favourable electron delocalization in the *meta*-products, rather than the electrophilic character of the OH radical is the determining factor of relative stabilities. Calculated energy barriers along approximate reaction paths correlate with the available experimental information.

M. C. ANTHONY, W. L. WALTZ et P. G. MEZEY. Can. J. Chem. **60**, 813 (1982).

On a calculé les énergies relatives des divers produits qui se forment au cours de la réaction de la pyridine et de l'ion pyridium avec le radical hydroxyle en faisant appel à des techniques OM SCF non empiriques. Le facteur qui détermine les stabilités relatives est la délocalisation favorable des électrons dans les produits meta plutôt que le caractère électrophile du radical OH. Les barrières d'énergies calculées le long des coordonnées approximatives de la réaction sont en bon accord avec les informations expérimentales disponibles.

[Traduit par le journal]

## Introduction

Within recent years, a very large number of experimental investigations have focused on the reactions of hydroxyl radical in aqueous media with nitrogen heterocyclic materials (1). This interest has been engendered in part by the recognition of the general importance of such reactions with respect to radiation biology and chemistry and some nonradiolytic biological processes (refs. 2–4 and references therein). Theoretical calculations pertaining to nitrogen heterocyclic compounds have provided useful insight into the processes associated with tautomerization and protonation (5–10). In this report, theoretical methods have been used to study the reaction of OH with one of the simplest of such heterocyclic compounds, namely pyridine and its protonated form, pyridinium ion. Whereas ground and excited states of pyridine and pyridinium ion have been studied earlier using theoretical methods (11–13), to our knowledge no such studies on reactions with OH radical have been reported.

The choice of this system is appropriate from the perspective that considerable, recent experimental information is available concerning the reactions of hydroxyl radical with pyridine, substituted pyridines, and related benzene systems (14–19). Investigations have also been undertaken into the effects associated with protonation and metal ion complexation (16, 17, 20–22). Such effects can be quite marked as exemplified by the observation that pyridine is about a hundred times more reactive towards OH than is its protonated form (16, 20). For pyridine systems and related benzene entities, their reactions with hydroxyl radical lead in general to OH addition at the aromatic ring to yield radical species. There can be a considerable level of specificity as to the reaction site, even though in some cases the second-order rate constants for these reactions approach values usually characteristic of diffusion-controlled processes. For example, pyridine with four possible reaction sites (nitrogen; carbons at the *ortho*, *meta*, and *para* positions) has an overall reaction rate constant of $4.5 \times 10^9\ M^{-1}\ s^{-1}$ (20), and in situ radiolysis–esr results indicate that OH addition occurs at the *meta* positions to an extent of 80% or more. A recent study involving time-resolved measurements using pulse radiolysis and final product analysis has corroborated this finding (19).

In the interpretation of the site specificity for pyridine systems and substituted benzene compounds, emphasis has been placed on the electrophilic character of OH and on the assumed preference of reaction at the least electron deficient positions of the aromatic ring. On this basis, reaction at the nitrogen position would seem to be quite favorable. Aside from the results of an earlier pulse radiolysis – optical absorption investigation (16), the more recent reports have not provided indications of reaction at the pyridine nitrogen (18, 19). The foregoing suggests that other factors must contribute to the site selection.

To approach this aspect from a new perspective, we have undertaken theoretical calculations on various model reactions and on the stabilities of the

0008-4042/82/070813-07$01.00/0

©1982 National Research Council of Canada/Conseil national de recherches du Canada

Can. J. Chem. Downloaded from www.nrcresearchpress.com by 210.87.254.40 on 09/06/12
For personal use only.

Can. J. Chem. Downloaded from www.nrcresearchpress.com by 210.87.254.40 on 09/06/12
For personal use only.

isomeric radical products. The OH addition to pyridine and its protonated form has been analysed in terms of the energetic stability, and points along the theoretical potential energy surface have been calculated near the assumed reaction paths. While possible effects due to solvent interaction have not been studied, the results are nevertheless in agreement with the experimental observations with regard to the specificity of OH addition and to the relative order of reactivity between pyridine and pyridinium ion.

## Method of calculations

In analyzing the site-specificity of OH addition to both pyridine and its protonated form, the total energies of all the isomeric hydroxypyridine radicals formed in these reactions have been calculated using an *ab initio* SCF MO method. In the calculations, the geometry of the intermediate radical has been assumed to be tetrahedral. A similar assumption has been employed by Imamura and Hirao (23) in a study on benzene systems. For our calculations, experimental parameters (24) have been taken for the geometry of pyridine, and the same geometry has been used as the initial guess for geometry optimization and for all the hydroxypyridine radicals. The series of neutral, ionic, and radical species studied in this work are shown in Fig. 1, and the specific numbering of atoms in the four most important species is given in Fig. 2.

For the reaction path calculations, all the parameters in the reactants and products are optimised and are given in Figs. 3 and 4. Using these optimised parameters, total energies as functions of both C—OH and C—H bond lengths have been calculated along assumed reaction paths, keeping the rest of the geometrical parameters fixed.

An STO-3G minimal basis set was used in all the RHF and UHF calculations using versions of either the Gaussian70 (25) or the MonsterGauss (26) programs, modified for the 36 bit computerword of the DEC-2060 computer of the University of Saskatchewan.[1]

## Results and discussion

Addition of OH to pyridine and to pyridinium ion can occur at four different positions of the ring. The remaining two positions in the ring can be treated as symmetrically identical to one of these positions.

[1]An efficient integral package, utilizing all 36 bits for the storage of integral labels has been developed (27) that will double the maximum size of molecules which can be studied with the new versions of these programs. The new programs will enable us to extend our studies to larger models, using larger, e.g. 4-31G, basis sets.

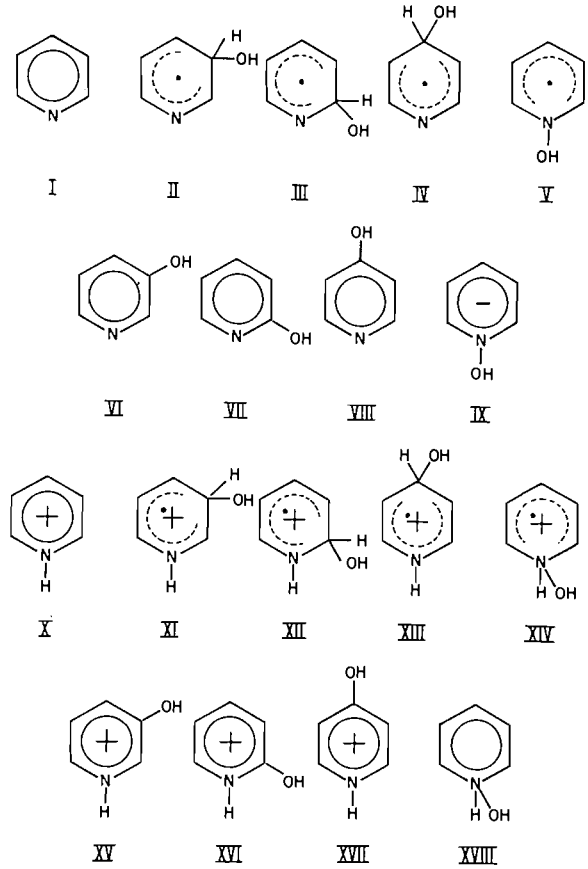


FIG. 1. Molecules, ions, and radicals studied.

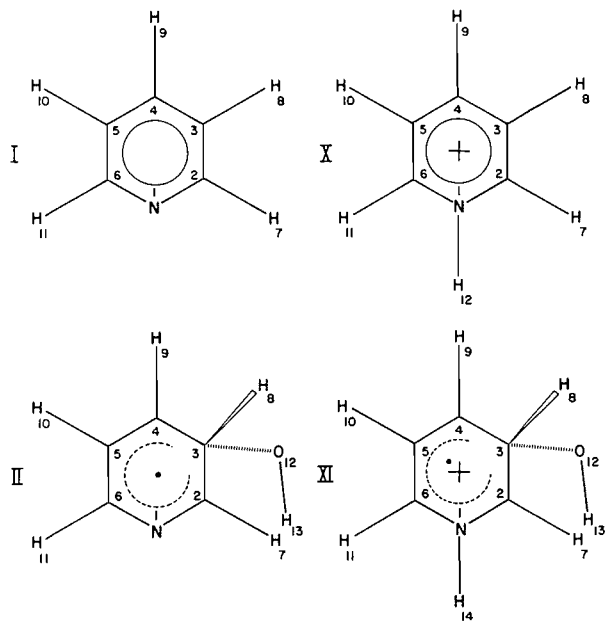


FIG. 2. Numbering of the atoms in species **I**, **X**, **II**, and **XI**.

Can. J. Chem. Downloaded from www.nrcresearchpress.com by 210.87.254.40 on 09/06/12
For personal use only.

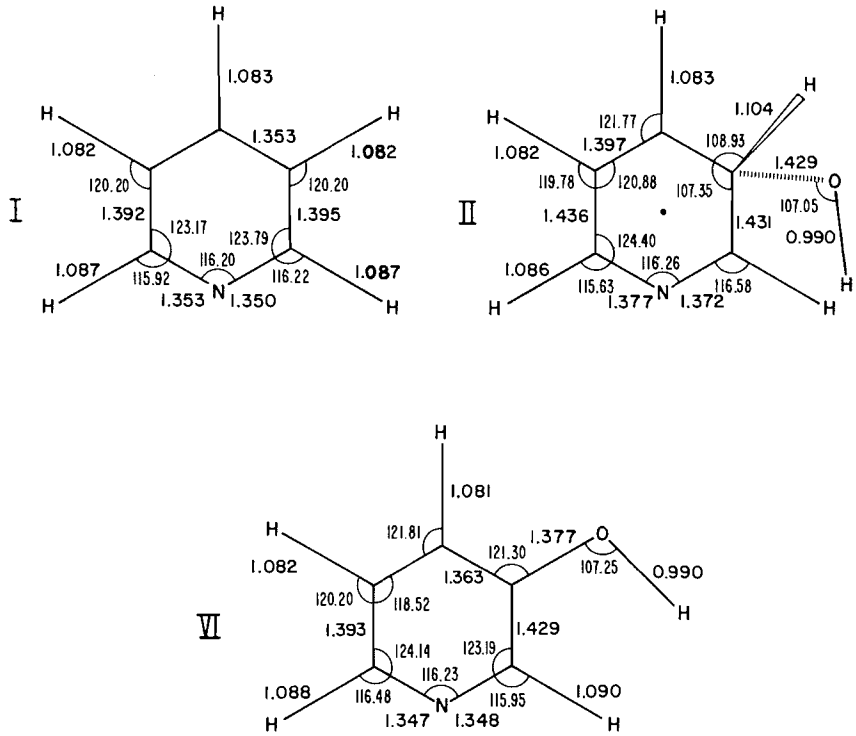


FIG. 3. Optimum geometrical parameters for species **I**, **II**, and **VI**.

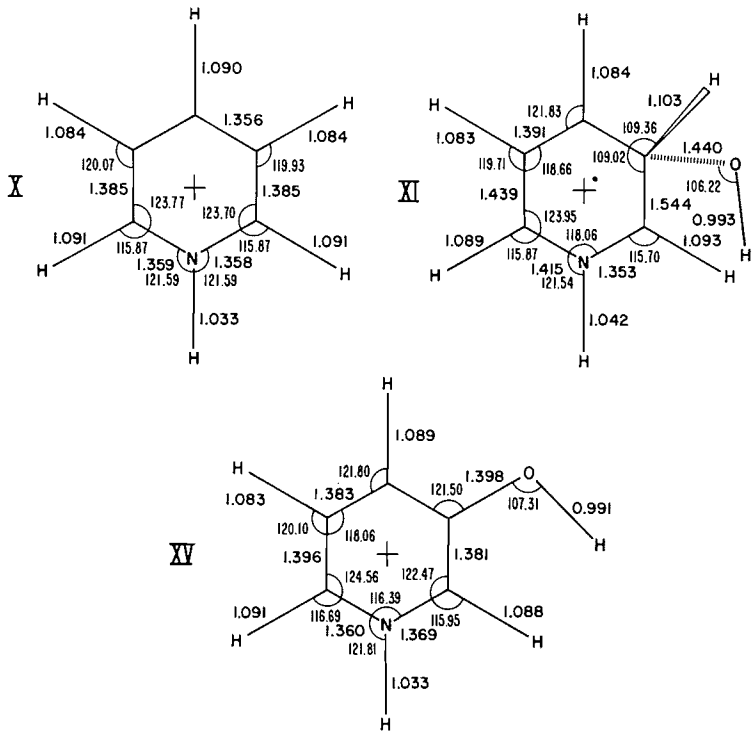


FIG. 4. Optimum geometrical parameters for species **X**, **XI**, and **XV**.

Can. J. Chem. Downloaded from www.nrcresearchpress.com by 210.87.254.40 on 09/06/12
For personal use only.

In earlier studies, the electronic charge distribution has been regarded as the dominant factor in explaining site-specificity of OH addition. The calculated gross charges on all these ring atoms are given in Table 1 (note that not all digits listed in the tables are physically significant, nevertheless they are quoted for the sake of numerical comparisons within the theoretical models). The order of electron density on these atoms is calculated as N > *meta*-C > *para*-C > *ortho*-C. If the specificity of OH addition to ring atoms of pyridine is associated primarily with electrophilicity, as suggested by earlier studies, then its addition to N atom is expected to be the most favoured process. Experimentally this has not been found to be so.[2] According to our calculations of the total energies, the *meta* position is the most preferred site (in agreement with experiment) with nitrogen being the site of second preference. The calculated total energies of all the isomeric hydroxypyridine radicals are given in Table 2. Based upon these energy values, the preferential order for OH addition at the different positions of the ring is *meta*-C > N >> *para*-C > *ortho*-C. For the carbon-based sites, the order appears to be in accord with the reported experimental observations (18, 19).[3] Given this and the calculated lower bound for the corresponding activation energy (see later), an experimental re-examination of the apparent lack of reaction at the nitrogen site may be warranted.

Total energies of the various products of OH addition to pyridinium ion are given in Table 3. By comparing these energy values, the order of site preference for OH addition to protonated pyridine can be given as *meta*-C >> *para*-C > *ortho*-C > N. Evidently, by protonation of pyridine, the selectivity of OH addition changes considerably as now addition to N atom is the least favoured position in contrast to nitrogen being the second preferred site in the unprotonated form. In both cases the *meta* position is the most favourable site. In the protonated form, this preference is much more pronounced. Similarly, it is also found amongst the non-radicals, **VI–IX** and **XV–XVIII**, that the two *meta* compounds (**VI** and **XV**) and the nitrogen-based OH adduct (**IX**) are of the lowest total energy as shown in Tables 2 and 3. It should be noted, however, that the calculated wavefunction for negative ion **IX** is *not* a stable solution of the closed shell Hartree–Fock equations, since the HOMO energy is positive. Such positive HOMO energies, although inconclusive in the strict sense, often indicate a physical instability of the system. Even if the ion does exist, the calculated energy value is less reliable than the rest of the calculated total energies.

With regard to the site-specificity, it is germane to note that among the radical species, the only two forms with calculated atomic spin densities of consistently alternating signs along the molecular skeleton are the two *meta*-substituted species, **II** and **XI**. Such sign alternation of spin densities indicates a high degree of delocalization of the odd electron, which shows an apparent correlation with the exceptional stability of the *meta*-species. The calculated spin densities of **II** and **XI** are listed in Table 4. The favourable delocalization in the meta hydroxypyridine radical (**II**) is also indicated by the calculated dipole moment which is smallest for this

TABLE 1. Gross charges on pyridine (**I**) and pyridinium ion (**X**)

| | Molecule/ion | |
|---|---|---|
| Atom[a] | **I** | **X** |
| 1 | 7.24133 | 7.24559 |
| 2 | 5.96543 | 5.86847 |
| 3 | 6.07125 | 6.04579 |
| 4 | 6.05135 | 5.96480 |
| 5 | 6.07171 | 6.04487 |
| 6 | 5.96595 | 5.86962 |
| 7 | 0.92655 | 0.85053 |
| 8 | 0.92702 | 0.85994 |
| 9 | 0.92655 | 0.85634 |
| 10 | 0.92750 | 0.85980 |
| 11 | 0.92535 | 0.85086 |
| 12 | — | 0.68339 |

[a]For the number sequence, see Fig. 2.

TABLE 2. Calculated electronic and total energies of pyridine and different isomeric hydroxypyridine radicals and molecules

| Molecules/ radicals | Electronic energy (au) | Total energy (au) |
|---|---|---|
| **I** | −449.54088 | −243.63840 |
| **II** (*meta*) | −609.81489 | −317.98024 |
| **III** (*ortho*) | −630.37346 | −317.52033 |
| **IV** (*para*) | −631.09525 | −317.59866 |
| **V** (N)[a] | −613.13425 | −317.90943 |
| **VI** (*meta*) | −592.40234 | −317.46054 |
| **VII** (*ortho*) | −594.26303 | −317.43222 |
| **VIII** (*para*) | −595.36195 | −317.45357 |
| **IX** (N)[b] | −616.01537 | −317.65202 |

[a]Radical **V** shows an extremely flat potential along the N pyramidal inversion coordinate. The results in the table refer to the optimum oxygen out-of-plane angle of 28.7°; however, the planar form ($E_{el}$ = −612.21048 au, $E_{tot}$ = −317.90456 au) lies only 3 kcal/mol above this form.
[b]Ion **IX** has one more H atom than molecules **VI–VIII**.

[2]While it was suggested in an earlier study that OH attack at the nitrogen site may occur (16), more recent investigations give no definite indications of this occurrence (18, 19).

[3]In the text of ref. 19, the order is given as quoted above, although in the abstract, the positions of *para* and *ortho* are reversed.

Can. J. Chem. Downloaded from www.nrcresearchpress.com by 210.87.254.40 on 09/06/12
For personal use only.

TABLE 3. Calculated electronic and total energies of pyridinium ion and different protonated isomeric hydroxypyridine radicals and ions.

| Molecules/ radicals | Electronic energy (au) | Total energy (au) |
|---|---|---|
| **X** | −459.31072 | −244.07547 |
| **XI** (*meta*) | −621.56217 | −318.39339 |
| **XII** (*ortho*) | −642.52921 | −318.05854 |
| **XIII** (*para*) | −643.10825 | −318.10854 |
| **XIV** (N) | −648.92842 | −317.84385 |
| **XV** (*meta*) | −603.93059 | −317.88954 |
| **XVI** (*ortho*) | −606.36012 | −317.87152 |
| **XVII** (*para*) | −606.82134 | −317.88684 |
| **XVIII** (N)[a] | −648.93099 | −317.84642 |

[a]Molecule **XVIII** has one more H atom than ions **XV–XVII**.

TABLE 4. Atomic spin densities for **II** and **XI**

| | Atomic spin density | |
|---|---|---|
| Atom[a] | **II** | **XI** |
| 1 | −0.7763 | −0.6575 |
| 2 | +0.9782 | +0.8698 |
| 3 | −0.2355 | −0.2315 |
| 4 | +0.9471 | +0.9225 |
| 5 | −0.8452 | −0.7922 |
| 6 | +0.9083 | +0.7971 |
| 7 | −0.0752 | −0.0668 |
| 8 | +0.0890 | +0.0911 |
| 9 | −0.0738 | −0.0721 |
| 10 | +0.0597 | +0.0565 |
| 11 | −0.0675 | −0.0600 |
| 12 | +0.0916 | +0.0994 |
| 13 | −0.0004 | −0.0011 |
| 14 | — | +0.0449 |

[a]For the number sequence, see Fig. 2.

species (**II**: 1.48 D, **III**: 6.56 D, **IV**: 5.14 D, **V**: 1.53 D).

These results suggest that the most preferred products for OH addition to pyridine and to pyridinium ion can be given by reactions [1] and [2].

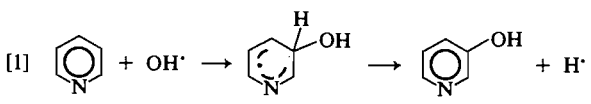


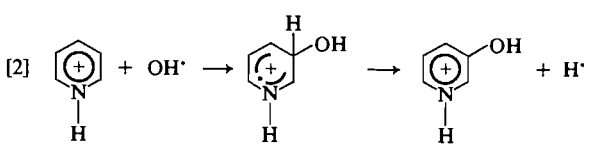


Although the two dehydrogenation reactions, which are portrayed as being subsequent to the OH additions, have not been observed experimentally, we have nevertheless considered them for the sake of completeness to the theoretical model. Approximate reaction paths have been calculated for all four reaction steps in reactions [1] and [2]. The total energies at the equilibrium (optimized) geometries of all species involved in the above equations are listed in Table 5. The calculated total energies along the approximate reaction paths are shown in Figs. 5–8. Since the reaction paths themselves are not fully optimized, the calculated activation energies, $E_A$, are less accurate than the net energy differences, $\Delta E$:

TABLE 5. Total energies of the completely optimized molecules, radicals, and ions

| Species | Total energy (au) |
|---|---|
| **I** | −243.63840 |
| **II** | −318.04995 |
| **VI** | −317.47048 |
| **X** | −244.07547 |
| **XI** | −318.46263 |
| **XV** | −317.90411 |
| OH | −74.36489 |
| H | −0.46658 |

[3] **I** + OH → **II**
$E_A \cong$ 11 kcal/mol, $\Delta E$ = 29 kcal/mol

[4] **X** + OH → **XI**
$E_A \cong$ 16 kcal/mol, $\Delta E$ = 14 kcal/mol

[5] **VI** + H → **II**
$E_A \cong$ 7 kcal/mol, $\Delta E$ = 71 kcal/mol

[6] **XV** + H → **XI**
$E_A \cong$ 14 kcal/mol, $\Delta E$ = 58 kcal/mol

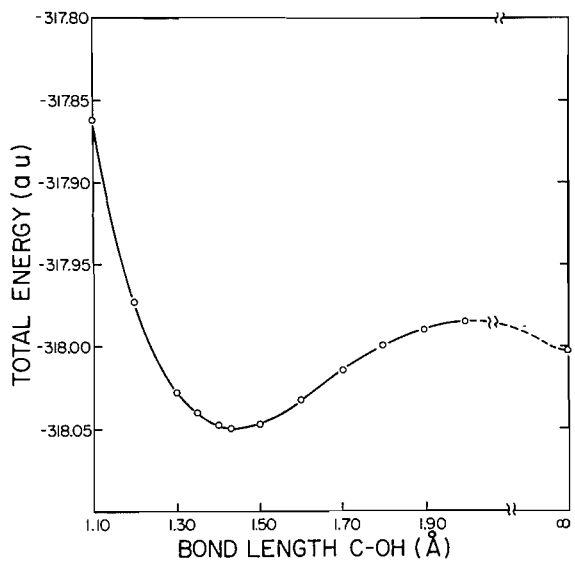


FIG. 5. Calculated approximate energy profile for the reaction of pyridine (**I**) with hydroxyl radical. The assumed reaction path is along the C—O stretching coordinate.

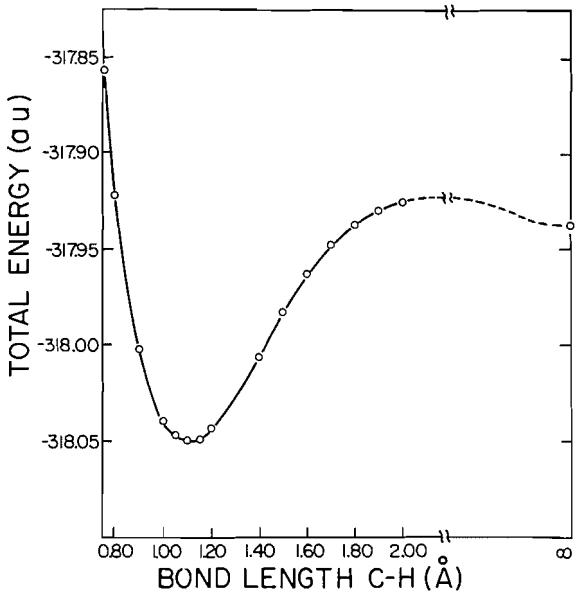


FIG. 6. Calculated approximate energy profile for the reaction of 3-hydroxypyridine (**VI**) with H atom. The assumed reaction path is along the C—H stretching coordinate.

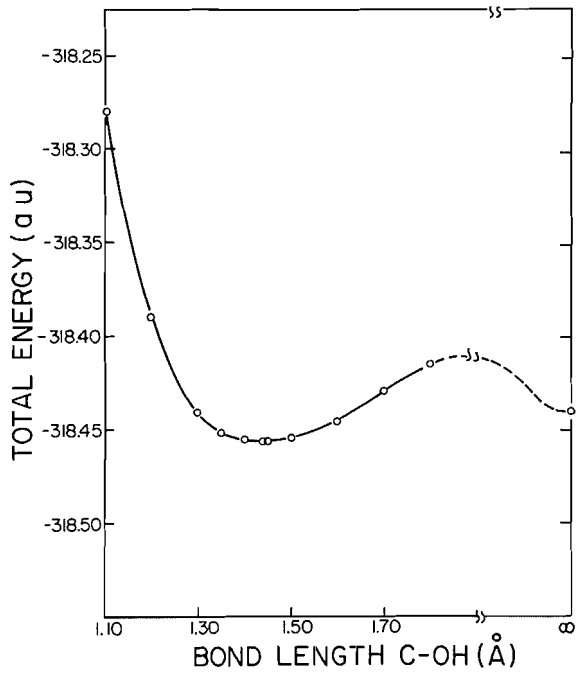


FIG. 7. Calculated approximate energy profile for the reaction of pyridinium ion (**X**) with hydroxyl radical. The assumed reaction path is along the C—O stretching coordinate.

The above results also provide information on the activation energy for the **I** + ·OH → **V** process. Since the total energy of the N-based OH-adduct **V** lies more than 44 kcal/mol above that of the *meta* adduct **II**, the activation energy for the **I** + ·OH → **V** process must be at least 15 kcal/mol, which is certainly larger than that of the **I** + ·OH → **II** process.

The above reactions correspond to processes proceeding from *right to left* along the approximate reaction profiles shown in Figs. 5–8, where a linear approach along the direction of the corresponding chemical bond has been assumed. That is, they refer to hydroxyl or hydrogen *addition* processes. The calculated approximate activation energies are consistently lower for neutral pyridine than for the pyridinium ion. This result is in good agreement with conclusions drawn from experiments, indicating a higher degree of reactivity towards OH for pyridine as compared to pyridinium ion. The corresponding reactions of H atom with hydroxypyridine (**VI** and **XV**) have not apparently been investigated experimentally; however, H atom has been found to be more reactive towards pyridine than pyridinium ion (28).

The calculated protonation energies for the closed-shell species are as follows:

[7] **I** + $H^+$ → **X**
$\Delta E$ = 274 kcal/mol

[8] **VI** + $H^+$ → **XV**
$\Delta E$ = 269 kcal/mol

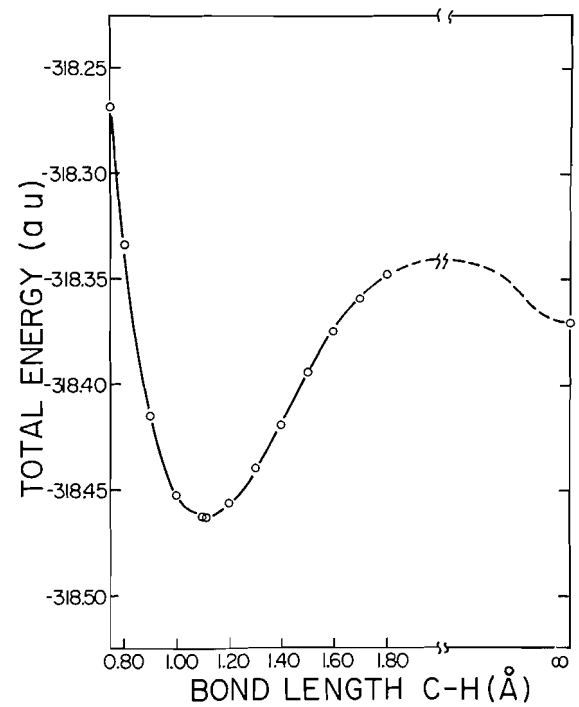


FIG. 8. Calculated approximate energy profile for the reaction of 3-hydroxypyridinium ion (**XV**) with H atom. The assumed reaction path is along the C—H stretching coordinate.

Can. J. Chem. Downloaded from www.nrcresearchpress.com by 210.87.254.40 on 09/06/12
For personal use only.

[9] **VII** + $H^+ \rightarrow$ **XVI**
$\Delta E$ = 275 kcal/mol

[10] **VIII** + $H^+ \rightarrow$ **XVII**
$\Delta E$ = 272 kcal/mol

The protonation energies are the largest for **I** and **VII**. The three carbon-based OH adducts show similar protonation energies with the largest difference being about 6 kcal/mol. Although, as pointed out above, the calculated results for ion **IX** are unreliable, the energy values suggest that protonated form **XVIII** is much more stable than **IX**.

All these calculated protonation energies are significantly lower than those calculated for various thymine and cytosine tautomers (at least by 8 kcal/mol with respect to thymine and by 16 kcal/mol with respect to cytosine tautomers [8]). Protonated forms of the above nucleotide bases and their tautomeric forms are apparently more stable than protonated forms of the above pyridine derivatives.

## Conclusions

Relative stabilities, atomic spin densities, and approximate reaction paths have been calculated for various neutral, ionic, and radical species involved in the reactions of neutral and protonated pyridines with the OH radical. The *meta* product is clearly favored among both neutral and protonated pyridine species. As opposed to earlier suggestions, the site specificity of OH radical addition is not determined solely by the electrophilic character of OH, and by the assumed preference of reaction at the least electron deficient ring positions. Rather, the advantageous delocalization of the odd electron in the *meta*-species appears to play a major role in determining the order of relative stabilities and product preference.

With the new, extended versions of the two *ab initio* programs (27), capable of handling larger (e.g. 4-31G) bases for the molecules studied and also for larger models, further studies are in preparation.

## Acknowledgment

The continuing financial support of the Natural Sciences and Engineering Research Council of Canada is gratefully acknowledged. The authors are indebted to Dr. E. C. Hass for stimulating discussions.

1. (*a*) L. M. Dorfman and G. E. Adams. Natl. Stand. Ref. Data Sec. U.S. Natl. Bur. Stand. NSRDS-NBS46, 1973; (*b*) Farhataziz and A. B. Ross. Natl. Stand. Ref. Data Sec. U.S. Natl. Bur. Stand. NSRDS-NBS59. 1977.
2. L. S. Meyers, Jr. and E. Kay. Int. J. Radiation Oncology Biol. Phys. **5**, 1055 (1979).
3. G. E. Adams. Adv. Rad. Chem. **3**, 125 (1972).
4. R. L. Willson. *In* Oxygen free radicals and tissue damage, CIBA Foundation Symposium 65. Excerpta Medica, Amsterdam. 1979. pp. 19–42.
5. J. D. Goddard, P. G. Mezey, and I. G. Csizmadia. Theor. Chim. Acta, **39**, 1 (1975).
6. P. G. Mezey and J. J. Ladik. Theor. Chim. Acta, **52**, 129 (1979).
7. P. G. Mezey, J. J. Ladik, and M. Barry. Theor. Chim. Acta, **54**, 251 (1980).
8. E. C. Hass, P. G. Mezey, and J. J. Ladik. Theor. Chim. Acta, **60**, 283 (1981).
9. Y. Nishimura, M. Tsuboi, S. Kato, and K. Morokuma. J. Am. Chem. Soc. **103**, 1354 (1981).
10. J. S. Kwiatkowski. Acta Phys. Pol. A**55**, 923 (1979).
11. G. F. Tantardini and M. Simonetta. Internat. J. Quantum Chem. **20**, 705 (1981).
12. A. G. Motten, E. R. Davidson, and A. L. Kwiram. J. Chem. Phys. **75**, 2603 (1981).
13. A. G. Motten and A. L. Kwiram. J. Chem. Phys. **75**, 2608 (1981).
14. M. Anbar, D. Meyerstein, and P. Neta. J. Phys. Chem. **70**, 2660 (1966).
15. P. Neta and L. M. Dorfman. Adv. Chem. Ser. **81**(1), 222 (1968).
16. B. Cercek and M. Ebert. Trans. Faraday Soc. **67**, 1687 (1967).
17. M. Simić and M. Ebert. Int. J. Radiat. Phys. Chem. **3**, 259 (1971).
18. S. Steenken and P. O'Neill. J. Phys. Chem. **82**, 372 (1978).
19. N. Selvarajan and N. V. Raghavan. J. Phys. Chem. **84**, 2548 (1980).
20. H. Cohen and D. Meyerstein. J. Chem. Soc. Dalton, 1976 (1976).
21. W. L. Waltz, R. J. Woods, and K. D. Whitburn. Photochem. Photobiol. **28**, 681 (1978).
22. M. Z. Hoffman, D. W. Kimmel, and M. G. Simic. Inorg. Chem. **18**, 2479 (1979).
23. A. Imamura and K. Hirao. Bull. Chem. Soc. Jpn. **52**, 287 (1979).
24. P. G. Sammes (*Editor*). Comprehensive organic chemistry. Vol. 4. Pergamon Press, Oxford. 1979. p. 4.
25. W. J. Hehre, W. A. Lathan, R. Ditchfield, M. D. Newton, and J. A. Pople. Q.C.P.E. 236, Indiana University, Bloomington, IN.
26. R. E. Kari. Dec. version of program Monstergauss. Laurentian University, Subdury, Ont. Original program written by R. Poirier and M. Peterson.
27. P. G. Mezey. GAUS36 Integral Program, University of Saskatchewan.
28. M. Anbar, Farhataziz, and A. B. Ross. Natl. Stand. Ref. Data Ser. U.S. Natl. Bur. Stand. NSRDS-NBS51. 1975.

Can. J. Chem. Downloaded from www.nrcresearchpress.com by 210.87.254.40 on 09/06/12
For personal use only.

# Marine natural products: highly functionalized steroids (12β-hydroxy-24-norcholesta-1,4,22-trien-3-one and 12β-acetoxy-24-norcholesta-1,4,22-trien-3-one) from the sea raspberry, *Gersemia rubiformis*

JOHN F. KINGSTON AND ALEX G. FALLIS

*Department of Chemistry, Memorial University of Newfoundland, St. John's, Nfld., Canada A1B 3X7*

Received October 14, 1981

JOHN F. KINGSTON and ALEX G. FALLIS. Can. J. Chem. **60**, 820 (1982).

Two new $C_{26}$ steroid $\Delta^{1,4}$-dien-3-ones **5** and **6** with 12β oxygen functions have been isolated from the soft coral *Gersemia rubiformis* and their structures elucidated from their spectral data and chemical transformations.

JOHN F. KINGSTON et ALEX G. FALLIS. Can. J. Chem. **60**, 820 (1982).

On a isolé les deux nouveaux stéroides en $C_{26}$, **5** et **6**, du type hydroxy-12β diène-$\Delta^{1,4}$ one-3, à partir des coraux mous *Gersemia rubiformis* et on a élucidé leur structure en se basant sur des données spectrales et des transformations chimiques.

[Traduit par le journal]

## Introduction

As part of our investigation of local marine natural products we have examined a number of marine invertebrates inhabiting the cold waters off Newfoundland and Labrador. These studies have included several soft corals of the order Alcyonacea (Phylum Cnidaria (Coelenterata), Class Anthozoa, Subclass Octocorallia) and one of these, the sea raspberry, *Gersemia rubiformis* (Pallas) has afforded novel steroids possessing a vinyl side chain and/or a cross conjugated dienone functionality in ring A (1, 2), such as structure **1**. Warm water relatives of these species have provided a rich source of various natural products including sesqui- and diterpenes (3) and compounds related to **1** have been identified in a South Pacific alcyonacean coral (4), a Hawaiian telestacean octocoral (5), and a Mediterranean gorgonian coral (6).

In spite of the wide distribution of $C_{26}$ 3β-hydroxy sterols in marine invertebrates (7) more highly functionalized skeletons are less common, although the dienone **2** has been isolated from a sponge (8) and recently the peroxide **3** was identified in a nudibranch and a sea pen (9). A rare example of a $C_{12}$ hydroxylated marine steroid, the polyoxygenated compound 24-methylcholestan-3β,5α,6β,12β,25-pentol 25-monoacetate (**4**), was found in an alcyonacean coral (10). We report herein the isolation from *Gersemia rubiformis* and structure elucidation of two unusual $C_{26}$ steroids, 12β-hydroxy-24-norcholesta-1,4,22-trien-3-one (**5**) and its acetate **6**. In addition to the rare $C_{12}$ oxygen functionality they comprise the first examples of marine steroids of more than 21 carbons which incorporate the $\Delta^{1,4}$-dien-3-one functionality in ring A.

## Results and discussion

Samples of *Gersemia rubiformis* collected at Admiral's Cove and Bay Bulls, Newfoundland were freeze dried and extracted with acetone. Fractionation of the extract by column chromatography and several tlc steps afforded the alcohol **5** and acetate **6** in 0.009% and 0.008% of the dry weight of the animal.

The molecular formula for the alcohol $C_{26}H_{38}O_2$ was established by high resolution mass spectrometry. The infrared absorptions at 1660, 1620, and 1595 $cm^{-1}$ were characteristic of the presence of the cross conjugated C-3 ketone in ring A (1) as was the uv spectrum ($\lambda_{max}$ 244 nm, $\varepsilon$ = 12 000). The $^1H$ nmr spectrum contained a pattern typical of $\Delta^{1,4}$-dien-3-ones (1) and was assigned as follows. A doublet at δ 7.03 ($J$ = 10 Hz), representing the single proton at C-1, was coupled with a second proton at C-2 which appeared as a doublet of doublets at δ 6.22 ($J$ = 10, 2 Hz). The C-4 proton appeared as a broadened singlet at δ 6.07 ($W_{1/2}$ = 4 Hz) due to coupling with the C-2 proton and the C-6 methylene function. The presence of an hydroxyl group was indicated by the infrared absorption at 3400–3600 $cm^{-1}$ and the large $M - 18$ peak at $m/e$ 364 corresponding to loss of water from the parent ion in the mass spectrum. The secondary nature of the alcohol was established from the signal of the proton on the hydroxyl carbon in the $^1H$ nmr spectrum which appeared at δ 3.40 as a doublet of doublets ($J$ = 10, 5 Hz) and confirmed by the doublet assigned to this carbon at δ 78.6 in the off-resonance $^{13}C$ nmr spectrum. An additional multiplet at δ 5.35 in the $^1H$ nmr spectrum representing two protons suggested the presence of an additional disubstituted double bond and singlets at

0008-4042/82/070820-05$01.00/0

©1982 National Research Council of Canada/Conseil national de recherches du Canada

Can. J. Chem. Downloaded from www.nrcresearchpress.com by 210.87.254.6 on 09/06/12
For personal use only.

Can. J. Chem. Downloaded from www.nrcresearchpress.com by 210.87.254.6 on 09/06/12
For personal use only.

δ 0.74 (3H) and δ 1.20 (3H) were assigned to the C-18 and C-19 methyl groups respectively. In the 400 MHz spectrum the C-21 methyl group appeared as a doublet ($J$ = 6 Hz) at δ 1.02, while the C-25 and C-26 methyl groups gave rise to a common doublet ($J$ = 6 Hz) at δ 0.95 representing six hydrogens. A single proton multiplet at δ 2.25 was assigned to the C-24 proton; irradiation at this frequency caused the doublet at δ 0.95 to collapse to a singlet and resulted in partial collapse of the vinyl proton multiplet at δ 5.35. These experiments demonstrated that this double bond was adjacent to two secondary methyl groups and requires that the olefin function be located in the side chain at C-22. The correctness of this assignment was confirmed by ozonolysis of the acetate **6** to give, amongst other products, iso-butyraldehyde which was characterized as its 2,4-DNP derivative and identified by comparison with an authentic sample. This double bond gave rise to a weak infrared absorption at 970 $cm^{-1}$ consistent with the *trans* configuration.

Since the side chain contains no secondary positions, the alcohol function must be in the steroid ring system. The position of this group was determined as follows. Hydrogenation of **5** over 5% Pd/C afforded a 3:1 ratio of **7** and **8**. The mass spectrum established the molecular formula $C_{26}H_{44}O_2$ and displayed a base peak at $m/e$ 271 corresponding to loss of water plus a saturated $C_7H_{15}$ side chain confirming that the hydroxyl function was attached to a ring position, either C-6, 7, 11, 12, 15, or 16. Oxidation of **5** with Jones' reagent afforded the diketone **9** whose infrared spectrum contained a new carbonyl absorption at 1705 $cm^{-1}$ typical of a cyclohexanone. In addition, the ultraviolet spectrum was unchanged from the starting material and unaffected by addition of base. These data ruled out part structures **10** and **11** and eliminated positions 15 and 16 from further consideration. Thus the alcohol substituent must be located at either C-11 or C-12. It was anticipated that an 11-keto function should significantly deshield the olefinic C-1 proton and this was shown to be the case by the preparation of trione **12** from 11α-hydroxyprogesterone by dehydrogenation with DDQ followed by Jones' oxidation. In this 11-keto compound the C-1 proton doublet occurred at δ 7.68, while in contrast, this signal for **9** appeared at δ 6.85. Thus the hydroxyl group was not located at C-11 and could be tentatively assigned to C-12.

Steroids possessing C-12 ketones and 17-alkyl side chains undergo a characteristic mass spectral fragmentation involving ring D loss and hydrogen transfer from C-20 to the C-12 ketone, resulting in a

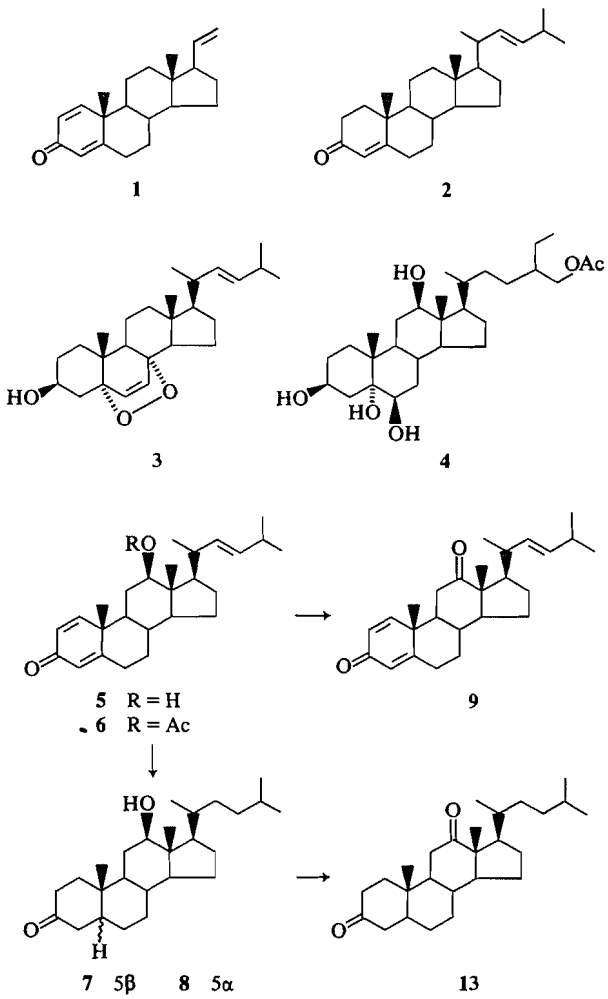


fragment corresponding to loss of the side chain plus 40 mass units (11). This fragment is masked in **9** due to the dominant loss of ring A by bisallylic cleavage to give an ion at $m/e$ 122 typical of $\Delta^{1,4}$-3-ketosteroids. When the reduced keto-alcohols **7** and **8** were oxidized with Jones' reagent to the 3,12-diketone **13**, the mass spectrum of this material displayed, as the largest fragment, $C_{16}H_{23}O_2$ from loss of the side chain plus 40 mass units thereby establishing the location of the oxygen functionality at C-12.

The stereochemistry of the hydroxyl group was ascertained from the $^1H$ nmr spectrum of **5**. The C-12 proton appeared at δ 3.40 as a doublet of doublets due to one axial–axial coupling ($J$ = 10 Hz) and one axial–equatorial coupling ($J$ = 5 Hz) with the C-11 hydrogens, and thus established that this proton was axial and hence the hydroxyl group equatorial (β).

Can. J. Chem. Downloaded from www.nrcresearchpress.com by 210.87.254.6 on 09/06/12
For personal use only.

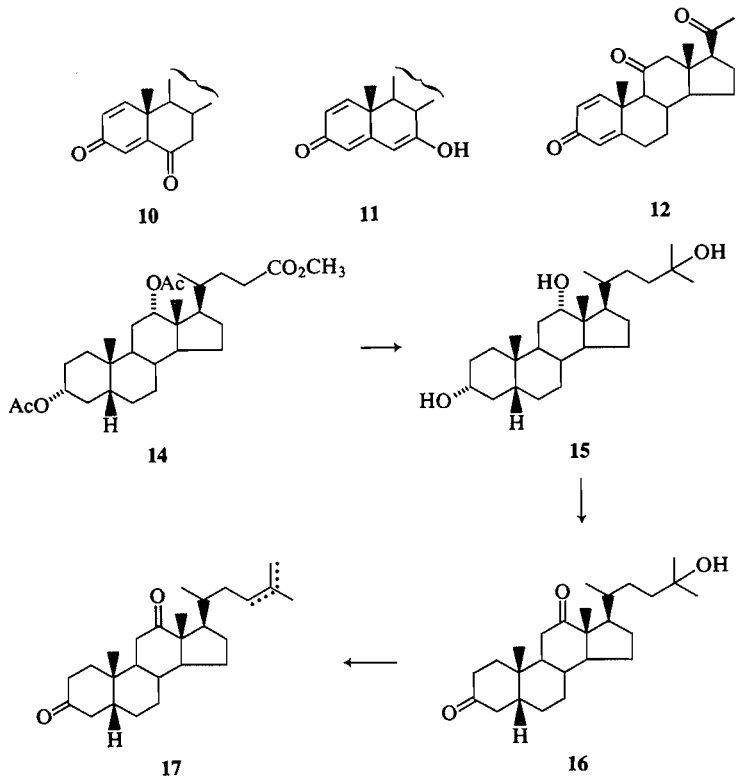


Final confirmation of the correctness of the structural assignment was provided by synthesis of an authentic sample of the 5β isomer of **13** as follows. The triester **14** was treated with excess methyllithium to give the triol **15** which was oxidized with Jones' reagent to the 3,12-diketoalcohol **16**. Elimination of water proceeded smoothly at room temperature in acetic acid containing $BF_3 \cdot Et_2O$. The resulting mixture of olefins **17** was hydrogenated over 5% Pd/C to provide the desired 24-nor-5β-cholesta-3,12-dione which was identical with the major isomer of **13**, separated by glc, prepared from the natural product.

The acetate **6** displayed characteristic infrared carbonyl absorption at 1735 $cm^{-1}$ and a methyl singlet at δ 2.09 in the $^1H$ nmr spectrum. The C-12 proton appeared at δ 4.60 as a doublet of doublets ($J$ = 5, 10 Hz) and the mass spectrum displayed a tiny molecular ion (*m/e* 424), and a large fragment at *m/e* 364 due to loss of acetic acid. The remaining spectral data were similar to those of the alcohol **5**. Treatment of **5** with acetic anhydride in pyridine afforded **6** which was identical in all respects with the naturally occurring acetate.

## Experimental

Melting points were determined in capillary tubes with a Thomas–Hoover Uni-Melt apparatus or a Fisher–Johns melting point apparatus and are uncorrected. Infrared spectra were recorded on a Perkin–Elmer 237B grating spectrophotometer, and were calibrated with the 2850 and 1601 $cm^{-1}$ bands of polystyrene film. Ultraviolet spectra were recorded on a Perkin–Elmer 202 uv–visible spectrophotometer and were calibrated with the 279.4 nm band of a Holmium oxide filter. Proton magnetic resonance spectra were measured at 80 MHz with a Bruker Model WP80 spectrometer employing a chloroform lock. Signal positions are reported in ppm downfield from tetramethylsilane (δ scale) as an internal standard, the number of protons, multiplicity, coupling constants, and proton assignments are indicated in parentheses. The 400 MHz spectrum was recorded on the Bruker WH 400 spectrometer at the University of Alberta. Mass spectra were determined on a Hitachi Perkin–Elmer RMU 6E or Varian MAT 311A instrument using an ionization energy of 70 eV. Gas–liquid chromatographic analyses were conducted on a Hewlett–Packard 402B gas chromatograph equipped with a column (3 m × 6 mm id) containing 1.5% OV-17 supported on Gas Chrom Q using helium as the carrier gas. Thin-layer chromatographic analyses were carried out on commercial pre-coated silica gel plates with fluorescent indicator (Eastman Kodak Silica gel 13181). Preparative thin-layer chromatography was conducted on 20 × 20 cm glass plates coated with silica gel $PF_{254+366}$ type 60 (E. Merck).

Solutions in organic solvents were dried over anhydrous magnesium sulphate and stripped of solvent with a Büchi rotary evaporator connected to a water aspirator.

*Isolation of 12β-hydroxy-24-norcholesta-1,4,22-trien-3-one (5) and 12β-acetoxy-24-norcholesta-1,4,22-trien-3-one (6)*

Samples of *Gersemia rubiformis* were collected at Admiral's Cove and Bay Bulls, Newfoundland. The acetone extract of the freeze dried animals was fractionated by liquid chromatography on silica gel using a stepped gradient of hexanes/chloroform/

Can. J. Chem. Downloaded from www.nrcresearchpress.com by 210.87.254.6 on 09/06/12
For personal use only.

2-propanol. The acetate **6** and alcohol **5** were contained in separate fractions which eluted with chloroform/2-propanol (97:3). Fractions rich in the alcohol were subjected to further column chromatography on silica gel (toluene/acetone, 9:1) followed by preparative tlc on alumina (toluene/acetone, 3:1). Final purification by preparative tlc on silica gel (hexanes/2-propanol, 9:1) afforded the alcohol **5** as a colourless oil (0.009% of dry weight); uv (MeOH)$\lambda_{max}$: 244 nm, $\varepsilon$ = 12 000; ir ($CHCl_3$) $\nu_{max}$: 3600–3400 (O—H), 1660 (C=O), 1620, 1595 (C=C), 970 (C=C—H) $cm^{-1}$; $^1H$ nmr ($CDCl_3$, 400 MHz) $\delta$: 0.74 (3H, s, C-18 methyl), 0.95 (6H, d, $J$ = 6 Hz, C-25 and C-26 methyls), 1.02 (3H, d, $J$ = 6 Hz, C-21 methyl), 1.20 (3H, s, C-19 methyl), 2.25 (1H, m, C-24 H), 3.40 (1H, dd, $J$ = 5, 10 Hz, C-12 H), 5.35 (2H, m, —CH=CH—), 6.07 (1H, s, $W_{1/2}$ = 4 Hz, C-4 H), 6.22 (1H, dd, $J$ = 10, 2 Hz, C-2 H), 7.03 (1H, d, $J$ = 10 Hz, C-1 H); $^{13}C$ nmr ($CDCl_3$) $\delta$: 186.2 (C-3), 168.5 (C-5), 155.2 (C-1), 136.3, 132.3 (C-22, C-23), 127.8, 124.2 (C-2, C-4), 78.6 (C-12), 57.2, 53.5, 51.1, 48.1, 43.4, 37.7, 34.4, 33.1, 32.9, 32.4, 31.2, 24.2, 24.0, 22.7, 22.6, 22.4, 18.7, 8.6; ms *m/e* (%): 382(1), 364(39), 349 (11), 321(45), 267(23), 243(22), 122(49), 121(100). *Exact Mass* calcd. for $C_{26}H_{38}O_2$: 382.2872; found: 382.2867.

Fractions rich in the acetate were purified by column chromatography on silica gel (toluene/acetone, 9:1) and preparative tlc on alumina (toluene/acetone, 9:1) and silica gel (hexanes/2-propanol, 19:1) to afford the acetate **6** as a colourless oil (0.008% of dry weight); uv (MeOH) $\lambda_{max}$: 244, $\varepsilon$ = 11 800; ir ($CHCl_3$) $\nu_{max}$: 1735 (C=O, acetate), 1660 (C=O), 1620, 1600 (C=C), 970 (C=C—H) $cm^{-1}$; $^1H$ nmr ($CDCl_3$, 80 MHz) $\delta$: 2.09 (3H, s, acetate Me), 4.60 (1H, dd, $J$ = 5, 10 Hz, C-12 H), 5.3 (2H, m, —CH=CH—), 6.05 (1H, bs, $W_{1/2}$ = 5 Hz, C-4 H), 6.20 (1H, dd, $J$ = 10, 2 Hz, C-2 H), 6.94 (1H, d, $J$ = 10 Hz, C-1 H); ms *m/e* (%): 424(1), 364(59), 349(15), 321(63), 267(26), 243(24), 122(61), 121(100).

Both the alcohol **5** and acetate **6** were accompanied by a C-27 homolog present as about 5% of the mixture which was separated from the main $C_{26}$ compound by glc.

*Acetylation of 5*

The alcohol **5** (3.0 mg, 8.1 μmol) was treated with acetic anhydride (0.5 mL) in pyridine (0.5 mL) at 23°C for 18 h. Water (5 mL) was added and the resulting mixture was extracted with chloroform (2 × 5 mL). The chloroform extract was washed with water (5 mL) and dried ($MgSO_4$). The solvent was removed under reduced pressure and the resulting crude product purified by preparative tlc on alumina (toluene/acetone, 4:1) to afford the acetate **6** (3.0 mg, 90%) identical to the naturally occurring compound by chromatographic (tlc, glc) and spectral ($^1H$ nmr, ir, uv, ms) comparison.

*Ozonolysis of 6*

Ozone was bubbled for 20 min through a solution of **6** (5.0 mg, 12 μmol) in 2-propanol (3 mL) at −78°C. Dimethyl sulphide (50 μL, 670 μmol) was added and the resulting solution was warmed to 0°C before a solution (2 mL, 0.1 *M*, 200 μmol) of 2,4-dinitrophenylhydrazine in phosphoric acid and ethanol (12) was added. After standing for 18 h at 23°C the resulting precipitate was collected by filtration, dissolved in chloroform (20 mL), and dried over $MgSO_4$. The crude product obtained by removal of the chloroform was fractionated by preparative tlc on silica gel (toluene/2-propanol, 98:2). One of the fractions obtained ($R_f$ 0.60–0.65) was the 2,4-dinitrophenylhydrazone of isobutyraldehyde (1.2 mg, 42%), identical by tlc, mixture melting point, and all spectral data with an authentic sample.

*Hydrogenation of 5*

A solution of **5** (16.5 mg, 43.2 μmol) in ethyl acetate (5 mL) was hydrogenated at atmospheric pressure over 5% Pd/C (7.2 mg) at 23°C for 19 h. After removal of the catalyst and solvent the crude product was purified by preparative tlc on silica gel (toluene/ethyl acetate, 9:1) to afford a 3:1 mixture (glc) of **7** and **8** as a clear oil (11.4 mg, 68%); ir ($CHCl_3$) $\nu_{max}$: 3600–3400 (O—H), 1705 (C=O) $cm^{-1}$; $^1H$ nmr ($CDCl_3$) $\delta$: 2.0–2.8 (4H, bm, —$CH_2COCH_2$—), 3.4 (1H, m, C-12 H); ms *m/e* (%): 388(1), 370(57), 355(7), 299(28), 272(31), 271(100), 247(28). *Exact Mass* calcd. for $C_{26}H_{44}O_2$: 388.3341; found: 388.3366.

*Jones' oxidation of 5*

A solution of **5** (5.5 mg, 14 μmol) in acetone (1 mL) was treated with 3 drops of Jones' reagent and stirred for 10 min at 23°C. Water (10 mL) was added and the resulting mixture was extracted with chloroform (3 × 10 mL). The chloroform extract was dried over $MgSO_4$ and the solvent removed under reduced pressure. The crude product obtained was purified by preparative tlc on silica gel (toluene/acetone, 85:15) to afford **9** (2.9 mg, 53%); uv (MeOH) $\lambda_{max}$: 244 nm, $\varepsilon$ = 12 000, no change with addition of aqueous NaOH; ir ($CHCl_3$) $\nu_{max}$: 1705, 1660 (C=O), 1620, 1600 (C=C) $cm^{-1}$; $^1H$ nmr ($CDCl_3$) $\delta$: 5.28 (2H, m, —CH=CH—), 6.08 (1H, bs, $W_{1/2}$ = 4 Hz, C-4 H), 6.23 (1H, dd, $J$ = 10, 2 Hz, C-2 H), 6.85 (1H, d, $J$ = 10 Hz, C-1 H); ms *m/e* (%): 380(21), 311(13), 269(28), 259(19), 177(28), 161(43), 147(31), 135(70), 122(29), 121(100). *Exact Mass* calcd. for $C_{26}H_{36}O_2$: 380.2715; found: 380.2726.

*Jones' oxidation of 7 and 8*

The mixture of **7** and **8** (8.0 mg, 20.6 μmol) obtained from the hydrogenation of **5** was oxidized with Jones' reagent as described above. The crude product obtained was purified by preparative tlc on silica gel (toluene/acetone, 9:1) to afford **9** (6.0 mg, 75%); ir ($CHCl_3$) $\nu_{max}$: 1705 $cm^{-1}$; ms, *m/e* (%): 386(100), 371(5), 287(11), 261(16), 247.1686(68) ($M^+$ − side chain − 40 mu, $C_{16}H_{23}O_2$, calcd. 247.1698), 121(12). *Exact Mass* calcd. for $C_{26}H_{42}O_2$: 386.3185; found: 386.3174.

*24-Nor-5β-cholesta-3α,12α,24-triol (15)*

A solution of 5β-cholanic acid-3α,12α-diol diacetate methyl ester (**14**) (269 mg, 0.550 mmol Steraloids) in ether (20 mL) was cooled to 0°C under an atmosphere of nitrogen. A solution of methyllithium (1.7 *M*, 5 mL, 8.5 mmol) in ether was added dropwise over a period of 5 min with stirring. The resulting cloudy solution was stirred at 0°C for 15 min, warmed to 23°C for 15 min, and cooled again to 0°C before the addition of 20 mL of water. Ether was added to bring the volume of the organic phase to 100 mL and this phase was washed with water until neutral to litmus (3 × 5 mL), and dried over $MgSO_4$. Removal of the solvent afforded **15** (221.7 mg, 98%), mp 82–85°C, which was used in the next step without further purification; ir ($CHCl_3$) $\nu_{max}$: 3700–3300 (O—H) $cm^{-1}$, no carbonyl; $^1H$ nmr ($CDCl_3$) $\delta$: 3.55 (1H, m, C-3 H), 3.97 (1H, m, C-12 H); ms *m/e* (%): 388(26), 370(29), 355(13), 352(16), 332(21), 314(56), 273(29), 271(16), 255(58), 97(100). *Exact Mass* calcd. for $C_{26}H_{44}O_2$ ($M^+ - H_2O$): 388.3341; found: 388.3331.

*24-Hydroxy-24-nor-5β-cholesta-3,12-dione (16)*

Jones' reagent was added dropwise with stirring to a solution of the triol **15** (990.7 mg, 0.224 mmol) in acetone (2 mL) until a deep orange colour persisted. After stirring for 15 min water (10 mL) was added and the resulting mixture was extracted with chloroform (3 × 20 mL). The crude product obtained after drying ($MgSO_4$) and solvent removal was purified by preparative tlc on silica gel (toluene/acetone, 4:1) to afford **16** (54.3 mg, 60%), mp 157–158°C; ir ($CHCl_3$) $\nu_{max}$: 3700–3300 (O—H), 1705 (C=O) $cm^{-1}$; ms *m/e* (%): 402(9), 387(15), 384(97), 328(100), 315(16), 297(12), 96(22). *Exact Mass* calcd. for $C_{26}H_{42}O_3$: 402.3134; found: 402.3123.

*$\Delta^{23}$- and $\Delta^{24}$-24-nor-5β-cholesten-3,12-dione (17)*

A solution of **16** (22.5 mg, 56.0 μmol) in glacial acetic acid (2 mL) at 23°C was treated with boron trifluoride etherate (0.5 mL) and the resulting solution was stirred for 1 h before dilution with chloroform (30 mL). Enough aqueous NaOH (1 *M*) was added, with vigorous shaking, to bring the aqueous phase to pH 8. The phases were separated and the organic phase was washed with water (20 mL) and dried over $MgSO_4$. The crude product obtained by removal of the solvent was purified by preparative tlc on silica gel (toluene/acetone, 9:1) to afford the mixture of dehydrated products **17** (13.0 mg, 61%), mp 138–140°C; ir ($CHCl_3$) $\nu_{max}$: 1705 (C=O) $cm^{-1}$, no O—H; $^1H$ nmr ($CDCl_3$) δ: 5.12 (~1–2H, m, olefinic H); ms *m/e* (%): 384(100), 328(24), 315(36), 297(31), 273(26). *Exact Mass* calcd. for $C_{26}H_{40}O_2$: 384.3028; found: 384.3039.

*24-Nor-5β-cholesta-3,12,-dione (13)*

The mixture of olefins **17** (5.7 mg, 15 μmol) was hydrogenated for 18 h at atmospheric pressure over 5% Pd/C (10 mg) in ethyl acetate (5 mL). The crude product obtained after removal of the catalyst and solvent was purified by preparative tlc on silica gel (toluene/acetone, 9:1) to afford the crystalline 5β isomer of **13**, mp 133–134°C; chromatographic (tlc) and spectral data were identical to the mixture of 5α and 5β-**13** obtained from the natural product; glc was identical to the 5β isomer. *Exact Mass* calcd. for $C_{26}H_{42}O_2$: 386.3185; found: 386.3185.

## Acknowledgements

We are grateful to Memorial University of Newfoundland, and the Natural Sciences and Engineering Research Council of Canada for financial support of this research; W. Snedden and D. Jamieson for high resolution mass spectra; H. J. Liu (University of Alberta) for 400 MHz nmr spectra; C. Jablonski for $^1H$ nmr spectra, and B. Gregory for fruitful discussions.

1. J. F. KINGSTON, B. GREGORY, and A. G. FALLIS. J. Chem. Soc. Perkin Trans. I, 2064 (1979); Tetrahedron Lett. 4261 (1977).
2. J. F. KINGSTON, A. S. NG, G. GALLACHER, and A. G. FALLIS. Marine Chem. In press.
3. B. TURSCH, J. C. BRAEKMAN, D. DALOZE, and M. KAISIN. *In* Marine natural products: chemical and biological perspectives. Vol. 2. *Edited by* P. J. Scheuer. Academic Press, New York. 1978. pp. 247–296.
4. M. D. HIGGS and D. J. FAULKNER. Steroids, **30**, 379 (1977).
5. R. A. Ross and P. J. SCHEUER. Tetrahedron Lett. 4701 (1979).
6. G. CIMINO, B. DESIDERIO, S. DESTEFANO, and G. SODANO. Experientia, **35**, 298 (1979).
7. L. J. GOAD. *In* Marine natural products: chemical and biological perspectives. Vol. 2. *Edited by* P. J. Scheuer. Academic Press, New York. 1978. pp. 75–172.
8. Y. M. SHEIKH and C. DJERASSI. Tetrahedron, **20**, 2095 (1974).
9. R. J. STONARD, J. C. PETROVICH, and R. J. ANDERSEN. Steroids, **36**, 81 (1980).
10. J. M. MOLDOWAN, W. L. TAN, and C. DJERASSI. Steroids, **26**, 107 (1975).
11. H. BUDZIKIEWICZ and C. DJERASSI. J. Am. Chem. Soc. **84**, 1430 (1962); C. DJERASSI and L. TOKES. J. Am. Chem. Soc. **88**, 536 (1966).
12. L. F. FIESER and M. FIESER. Reagents for organic synthesis. Vol. 1. John Wiley and Sons, New York. 1967. p. 330.

Can. J. Chem. Downloaded from www.nrcresearchpress.com by 210.87.254.6 on 09/06/12
For personal use only.

# Synthesis of cedranoid sesquiterpenes. II. Functionalization at carbon 12[1]

PETER YATES AND KENNETH E. STEVENS

*Lash Miller Chemical Laboratories, University of Toronto, Toronto, Ont., Canada M5S 1A1*

Received October 9, 1981

PETER YATES and KENNETH E. STEVENS. Can. J. Chem. **60**, 825 (1982).

Dimethyl 6,6-dimethyl-7-oxotricyclo[3.2.1.$0^{2,8}$]octane-1,8-dicarboxylate (**6**) undergoes homoconjugate addition with lithium diphenylcuprate to give dimethyl 3-hydroxy-4,4-dimethyl-*exo*-8-phenyl-*cis*-bicyclo[3.3.0]oct-2-ene-1,2-dicarboxylate (**12***a*), which on monodecarboxymethylation, ozonolysis, and esterification with diazomethane gives dimethyl 6,6-dimethyl-7-oxo-*cis*-bicyclo-[3.3.0]octane-1,*exo*-2-dicarboxylate (**15**). Reaction of **6** with diethylaluminum cyanide gives dimethyl *exo*-8-cyano-3-hydroxy-4,4-dimethyl-*cis*-bicyclo[3.3.0]oct-2-ene-1,2-dicarboxylate (**16**), which on hydrolysis and esterification with diazomethane also gives **15**. Sensitized photolysis of dimethyl 5-oxo-6,6-dimethylbicyclo[2.2.2]octa-2,7-diene-2,3-dicarboxylate (**19**) gives dimethyl 4,4-dimethyl-3-oxotricyclo[3.2.1.$0^{2,8}$]oct-6-ene-1,8-dicarboxylate (**20**), which on reduction with lithium in ammonia gives dimethyl 6,6-dimethyl-7-oxobicyclo[3.3.0]oct-3-ene-1,*exo*-2-dicarboxylate (**31**); conversion of **31** to its 2-ene isomer **32** followed by catalytic hydrogenation gives **15** and its *endo*-2 epimer **33**.

PETER YATES et KENNETH E. STEVENS. Can. J. Chem. **60**, 825 (1982).

Le diméthyl-6,6 oxo-7 tricyclo[3.2.1.$0^{2,8}$] octanedicarboxylate-1,8 de méthyle (**6**) subit une addition homoconjuguée du diphénylcuprate de lithium pour donner l'hydroxy-3 diméthyl-4,4 phényl-8-*exo* bicyclo[3.3.0] octène-2 dicarboxylate-1,2-*cis* de méthyle (**12***a*) qui par monodécarboxyméthylation, ozonolyse et estérification par le diazométhane conduit au diméthyl-6,6 oxo-7 bicyclo[3.2.0] octanedicarboxylate-1,2-*exo* de méthyle (**15**). La réaction de **6** avec du cyanure de diéthylaluminium fournit le cyano-8-*exo* hydroxy-3 diméthyl-4,4 bicyclo[3.3.0] octène-2 dicarboxylate-1,2-*cis* de méthyle (**16**) qui, par hydrolyse et estérification par le diazométhane, conduit aussi à **15**. La photolyse sensibilisée de l'oxo-5 diméthyl-6,6 bicyclo[2.2.2] octadiène-2,7 dicarboxylate-2,3 de méthyle (**19**) fournit le diméthyl-4,4 oxo-3 tricyclo[3.2.1.$0^{2,8}$] octène-6 dicarboxylate-1,8 de méthyle (**20**) qui, par réduction par le lithium dans l'ammoniac, conduit au diméthyl-6,6 oxo-7 bicyclo[3.3.0] octène-3 dicarboxylate-1,2-*exo* de méthyle (**31**); la conversion de **31** dans son isomère ène-2 (**32**), suivie par une hydrogénation catalytique, conduit à **15** et à son épimère 2-*endo* (**33**).

[Traduit par le journal]

The cedranoid sesquiterpenes are a group of naturally occurring compounds and their congeners that have the tricyclo[5.3.1.$0^{1,5}$]undecane skeleton, of which the simplest members are α-cedrene (**1**) and cedrol (**2**) (2).[2] A variety of more highly oxygenated compounds have also been isolated, such as laccishellolic acid (**3**) (4) and shellolic acid (**4**) (5).

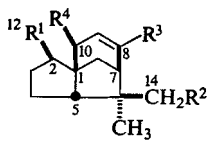

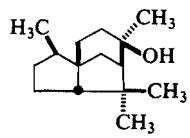

**1** $R^1 = R^3 = CH_3$, $R^2 = R^4 = H$

**3** $R^1 = R^3 = CO_2H$, $R^2 = H$, $R^4 = OH$

**4** $R^1 = R^3 = CO_2H$, $R^2 = R^4 = OH$

**2**

Several total syntheses of compounds **1** and **2** have been achieved (6, 7), but none of compounds **3** and **4**. We have recently designed a new synthesis of (±)-cedrol (**2**) that it was hoped could subsequently be elaborated to provide syntheses of the more highly oxygenated cedranoid sesquiterpenes, including **3** and **4** (1, 8). This synthesis (Scheme 1) has as key steps the photochemical oxa-di-π-rearrangement of the bicyclo[2.2.2]octenone **5** to the tricyclo[3.2.1.$0^{2,8}$]octanone **6** and reaction of lithium dimethylcuprate with the latter to give the homoconjugate addition product **7** [cf. ref. 9]. The bicyclo[3.3.0]octanone **7** was converted in five steps to the β-diketone **8**, which had earlier been prepared by Stork and Clarke by a different route and transformed into cedrol (**2**) (6). The desired elaboration of this approach requires the incorporation of oxygenated functions at C-12 and C-14 in **8** and appropriate manipulations of the ketonic functions at C-8 and C-10. We report now on progress

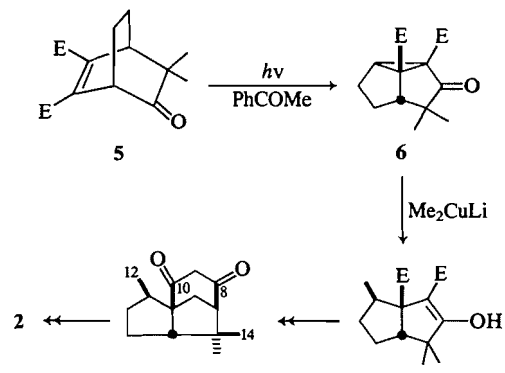

**5** **6** **8** **7**

SCHEME 1 (E = $CO_2Me$)

[1]For a preliminary account of part of this work, see ref. 1.

[2]At least four systems of numbering of the cedrene skeleton have been used; that in **1** is in accord with the IUPAC rules (3).

0008-4042/82/070825-10$01.00/0

©1982 National Research Council of Canada/Conseil national de recherches du Canada

Can. J. Chem. Downloaded from www.nrcresearchpress.com by 210.87.254.5 on 09/06/12
For personal use only.

Can. J. Chem. Downloaded from www.nrcresearchpress.com by 210.87.254.5 on 09/06/12
For personal use only.

towards the attainment of the first of these objectives.

With the intention of introducing a latent carboxylic acid group in place of the C-12 methyl group of **8**, we first attempted to effect the homoconjugate addition of a vinyl group to **6** by treatment with lithium divinylcuprate reagents. However, the use of a large variety of reagents and conditions that had previously been used for the conjugate addition of a vinyl group to α,β-unsaturated carbonyl compounds (see Experimental) failed to effect homoconjugate addition.[3] Nor could such addition be effected with lithium diisobutylhex-1-enylmethylalanate (12) or with the potassium or thallous derivatives of diethyl malonate (9, 13). Attempted homoconjugate addition of an allyl group with allytrimethylsilane and titanium tetrachloride (14) led instead to homoconjugate addition of chloride ion to give **9**, which showed the typical strong ir bands at 6.06 and 6.21 μm of the enolized β-keto ester system of homoconjugate addition products from **6**. We subsequently found that the same product is formed in the presence of titanium tetrachloride alone. The failure to add an allyl group indicates that, while the ethylenic bond of allyltrimethylsilane may be relatively nucleophilic (15), chloride ion is a much better nucleophile under the conditions used. It is possible that in the case of conjugate addition to α,β-unsaturated ketones (14), conjugate addition of chloride also occurs, but is reversible.

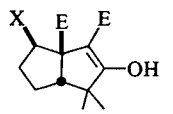


**9** X = Cl, E = $CO_2Me$
**10** X = Br, E = $CO_2Me$

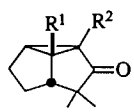


**11***a* $R^1 = (C_6H_5C{\equiv}C)_2COH$, $R^2 = CO_2Me$
**11***b* $R^1 = CO_2Me$, $R^2 = (C_6H_5C{\equiv}C)_2COH$

The recent report (16*a*; see, however, ref. 16*b*) of the homoconjugate addition of Grignard reagents to spiroactivated cyclopropane rings (9) led us to investigate the reaction of **6** with phenylethynylmagnesium bromide in ether. At 2°C a voluminous white precipitate formed immediately and work-up gave two products in approximately equal amounts. When the reaction was conducted at −75°C for 9 hours and then at 2°C for 11 hours, one of these products was formed almost exclusively. This was shown to be a homoconjugate addition product by strong bands in its ir spectrum at 6.06 and 6.19 μm (*vide supra*) and identified as the hydrogen bromide adduct **10**. It was prepared independently by treatment of **6** with hydrogen bromide in dichloromethane. While the other product was not fully characterized, it is tentatively assigned structure **11***a* or **11***b* on the basis of the of the following spectroscopic data and mechanistic considerations. Its ir spectrum with a single band in the carbonyl-stretching region at 5.79 μm suggested that opening of the cyclopropane ring had not occurred; this spectrum also showed a band at 3.07 μm attributable to a strongly hydrogen-bonded hydroxyl group. Its $^1H$ nmr spectrum showed that only one methyl ester group remained (δ 3.67 ppm (s, 3H)) and that two phenyl groups had been incorporated into the molecule. We suggest that the keto and C-1 ester groups or the two ester groups of **6** act as a powerful bidentate ligand and that the precipitate is a magnesium bromide complex of **6** or **10**, either of which could lead to **10** on work-up. As in the precipitation of magnesium bromide from Grignard reagents by dioxane (17), bis(phenylethynyl)magnesium remains in solution and reacts with uncomplexed **6** at 2°C, but not at −75°C. Weight is lent to these suppositions by the observation that treatment of **6** with a solution of bis(phenylethynyl)magnesium, prepared by the addition of dioxane to a solution of phenylethynylmagnesium bromide, at 4°C gives exclusively **11***a* (or **11***b*).

Eventually success was achieved in the introduction of a carboxylic acid function into **6** by the route shown in Scheme 2. Reaction with lithium diphenylcuprate led to homoconjugate addition of a phenyl group to give **12**, whose ir spectrum showed strong bands at 6.09 and 6.25 μm. Life was still not without its complications, however, since the $^1H$ nmr spectrum of this product showed that it was a ~2:1 mixture of the methyl and ethyl esters **12***a* and **12***b* (see Experimental). The ethyl ester **12***b* is considered to be formed by exchange of ethoxide for methoxide in the C-2 ester group of **12***a*; the ethoxide ion most probably has its origin in a slow reaction of phenyllithium with ether, for the phenyllithium was obtained commercially as a solution in ether and benzene (30:70).[4] It is of interest that although reaction of **6** with lithium dimethylcuprate gives, together with the homoconjugate product, small amounts of two stereoisomeric bicyclo[3.2.1]octan-3-ones formed by reduction (8), there

[3]In the course of other work (10) it has recently been observed that lithium divinylcuprate reagents fail to effect conjugate addition of a vinyl group to cholest-4-en-3-one, although this compound undergoes conjugate addition with lithium dimethyl- and diethylcuprate (11).

[4]Compare the slow reaction of *n*-butyllithium with tetrahydrofuran to give butane, ethylene, and the lithium enolate of acetaldehyde (18).

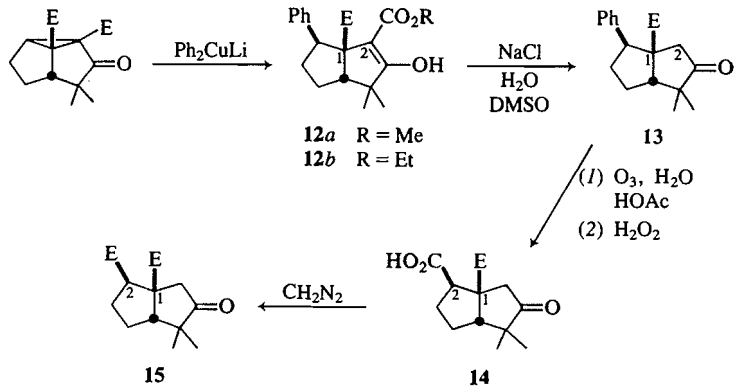


SCHEME 2 (E = $CO_2Me$)

was no evidence for the formation of reduction products in the case of its reaction with lithium diphenylcuprate; this was unexpected since the two cuprates have similar reactivities towards α,β-unsaturated ketones (19). Attempts to separate **12***a* and **12***b* were unsuccessful and the mixture was therefore subjected to monodecarboalkoxylation with sodium chloride in aqueous dimethyl sulfoxide (20) to give the single product **13**. This showed in its ir spectrum a single band in the carbonyl-stretching region at 5.80 μm as expected. Its $^1H$ nmr spectrum showed two one-proton doublets ($J$ = 19 Hz) at δ 2.46 and 3.60 ppm, characteristic of the C-2 protons in this system (cf. the corresponding decarbomethoxylation product from **7**: δ 2.09 (d, 1H) and 3.35 ppm (d, 1H) ($J$ = 20 Hz)); the signal of the methyl ester protons appears at δ 3.21 ppm as a result of shielding of these protons by the phenyl group. This shielding is in accord with the *exo* configuration assigned at C-8 in **12** and **13**, which is also based on analogy with the configuration established at this carbon in **7** (8). Ozonolysis of **13** in aqueous acetic acid followed by oxidative work-up (cf. ref. 21) gave the carboxylic acid **14**, which was characterized as the diester 15. The ir spectrum of this had a single peak in the carbonyl-stretching region at 5.78 μm, and its $^1H$ nmr spectrum included two three-proton singlets at δ 3.67 and 3.71 ppm and two one-proton doublets at δ 2.34 and 3.62 ppm ($J$ = 19 Hz). The *exo* configuration of **14** and **15** at C-2 follows from their formation from **13** and is corroborated by the synthesis of the C-2 epimer of **15** (*vide infra*).

A second route from **6** to **15** is shown in Scheme 3; this process involved homoconjugate addition to **6** and proceeded more expeditiously and in better yield than by the route of Scheme 2. Reaction of **6** with diethylaluminum cyanide in toluene gave the nitrile **16** (cf. ref. 22). The introduction of a nitrile group into the product was signalled by a band at 4.46 μm in its ir spectrum and a singlet at δ 120.0 ppm in its sford $^{13}C$ nmr spectrum. The presence of the enolized β-keto ester was vouchsafed by strong bands at 6.01 and 6.17 μm in their spectrum of the product and a one-proton singlet at δ 10.52 ppm in its $^1H$ nmr spectrum. Attempts to convert **16** directly to **15** led to complex mixtures of products, and this transformation was therefore carried out in two steps. Decarboxylation as before gave **17** and treatment of this with boiling methanol containing sulfuric acid (cf. ref. 23) gave **15** as the major product, identical with the product obtained by the route in Scheme 2. A minor product was also formed in this reaction and is assigned structure **18** on the basis of its origin and its spectra. Its ir spectrum showed bands at 5.62 (m) and 5.79 (s) μm assigned to the carbonyl-stretching vibrations of the five-membered cyclic imide and five-membered cyclic ketonic groups together with an N—H stretching band at 3.02 μm. Its $^1H$ nmr spectrum showed two one-proton doublets at δ 2.38 and 3.22 ppm ($J$ = 19 Hz) indicating that the bicyclo[3.3.0]-octan-3-one system was intact, and a broad one-proton singlet at δ 8.69 ppm (absent after $D_2O$ treatment) confirming the presence of an NH group; this spectrum also revealed the absence of methoxyl protons. The conversion of **17** to **15** and **18** most probably occurs by the pathways shown in Scheme 4 (cf. ref. 24).

A third approach to **15** was undertaken in an entirely different fashion.[5] Irradiation of the dienone **19**, the precursor of **5** (8), with acetophenone as photosensitizer gave one major and two minor products (Scheme 5). The major product was identified by its spectra and further transformations (*vide infra*) as the di-π-methane rearrangement product **20**. Its ir spectrum showed a single band in the carbonyl-stretching region at 5.77 μm. Its $^1H$

[5]We thank Miss Shirley Stiver for suggesting this route.

Can. J. Chem. Downloaded from www.nrcresearchpress.com by 210.87.254.5 on 09/06/12
For personal use only.

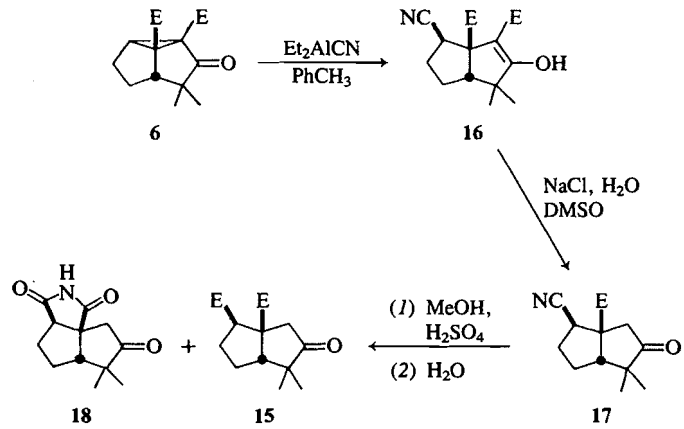


SCHEME 3 (E = $CO_2Me$)

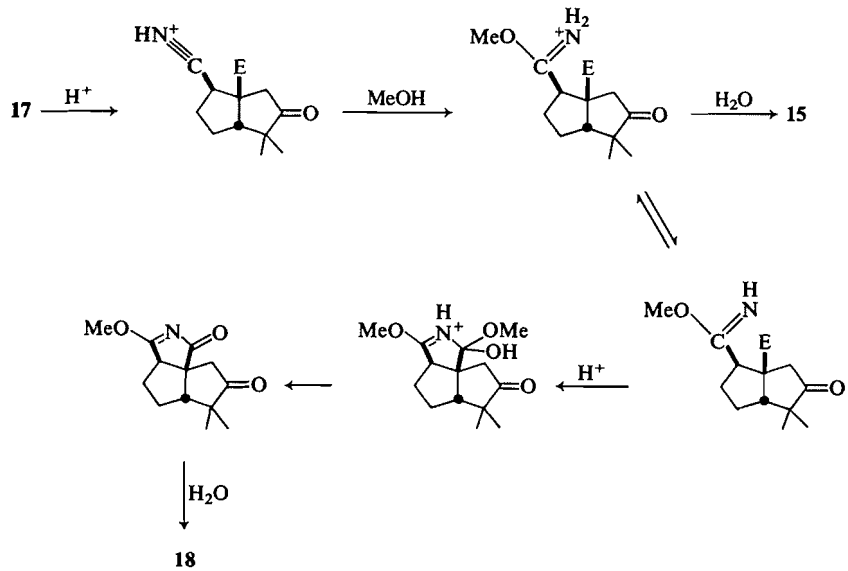


SCHEME 4 (E = $CO_2Me$)

nmr spectrum (in deuteriochloroform) showed two two-proton multiplets at δ 3.5–3.7 and 5.7–6.0 ppm; the former is assigned to the C-2 and C-5 protons, and the latter to the olefinic protons. In benzene–deuteriochloroform the higher field multiplet was resolved into a one-proton singlet at δ 3.62 ppm, assigned to the C-2 proton, and a one-proton doublet at δ 3.38 ppm ($J$ = 2.5 Hz), assigned to the C-5 proton; the lower field multiplet was resolved into a one-proton doublet at δ 5.74 ppm ($J$ = 5.5 Hz), assigned to C-7 and a one-proton doublet of doublets at δ 5.51 ppm ($J$ = 5.5, 2.5 Hz), assigned to C-6. The observed coupling constants are in excellent agreement with those observed for a C-3 methylene analogue of **20** (25). One of the minor products is considered to arise by an oxa-di-π-methane rearrangement in analogous fashion to the formation of **6** and to have structure **21**. Its ir and $^1H$ nmr spectra were similar to those of **20**, the latter spectrum (in deuteriochloroform) showing two two-proton multiplets at δ 3.4–3.7 ppm and

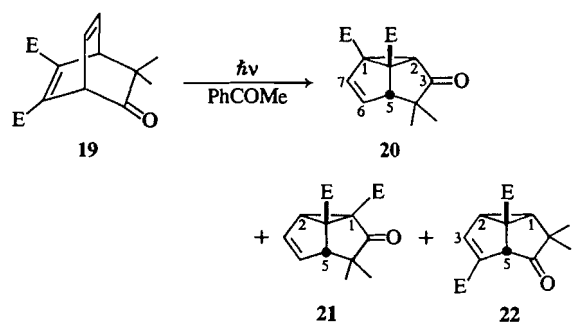


SCHEME 5 (E = $CO_2Me$)

Can. J. Chem. Downloaded from www.nrcresearchpress.com by 210.87.254.5 on 09/06/12
For personal use only.

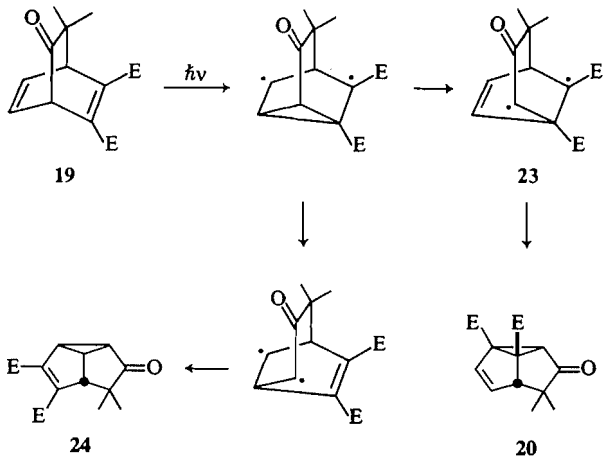


SCHEME 6 (E = $CO_2Me$)

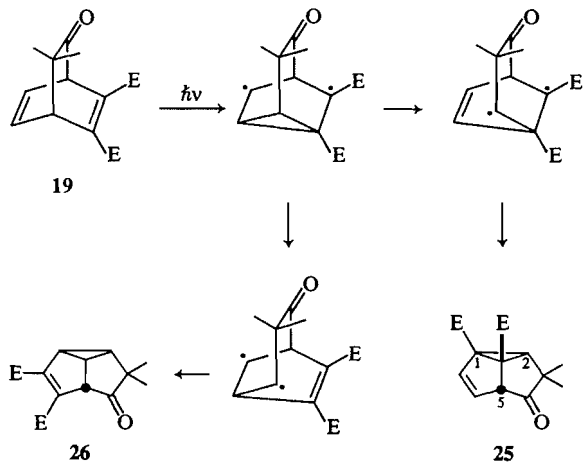


SCHEME 7 (E = $CO_2Me$)

5.6–5.95 ppm.[6] We shall return subsequently to the proposed structure **22** of the other minor product.

Compound **19** is capable of giving four different di-π-methane rearrangement products, **20** and **24–26** (Schemes 6 and 7), and two different oxa-di-π-methane rearrangement products, **21** and **28** (Schemes 8 and 9) (26).

The preference of bicyclo[2.2.2]octadienone derivatives to undergo di-π-methane rather than oxa-di-π-methane rearrangements has been observed previously, but there has been little discussion concerning its origin. The suggestion has been made that this is due to preemptive homoconjugation of the diene moiety, based on the observation that the $n \rightarrow \pi^*$ absorption band of **29** is lower in intensity than that of **30** (27). It may be noted that benzobicyclo[2.2.2]octadienone derivatives, in which the homoconjugate interaction between the aromatic π system and the olefinic double bond is expected to be reduced relative to that in bicyclo[2.2.2]octadienone derivatives without the benzene ring, undergo oxa-di-π-methane rearrangement on triplet-sensitized irradiation (28). The regioselectivity of both the di-π-methane rearrangement of **19** leading to **20** and its oxa-di-π-methane rearrangement leading to the minor product **21** may be interpreted in terms of the greater stabilization of diradicals **23** (Scheme 6) and **27** (Scheme 8) relative to the related diradicals that lead to other di-π-methane and oxa-di-π-methane rearrangement products, respectively. Similar directing influences have been proposed to account for the observed regioselectivity in di-π-methane rearrangements of 5,6-benzo-2-azabicyclo[2.2.2]-5,7-dien-3-one derivatives (29; cf. also ref. 25).

The spectra of the other minor product did not correspond with expectation for any of the other possible primary products **24–26** and **28**. Its ir spectrum showed bands at 5.81 (s) and 6.19 (w) μm suggestive of an α,β-unsaturated carbonyl group. Its $^1H$ nmr spectrum showed a one-proton doublet ($J$ = 2.5 Hz) at δ 6.83 ppm: this proton is coupled with a proton that gives rise to a doublet of doublets at δ 2.99 ppm ($J$ = 2.5, 7.5 Hz), which is also coupled with a proton giving rise to a doublet at δ 2.69 ppm ($J$ = 7.5 Hz); in addition a one-proton singlet appeared at δ 4.29 ppm. On the basis of these data this product is considered to have structure **22**, with assignment of the proton signals referred to above to the C-3, C-2, C-1, and C-5

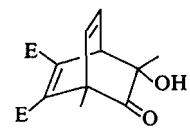


29

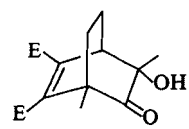


30

protons, respectively. This product may arise from a secondary photochemical reaction of the primary product **20** as shown in Scheme 10. A closely related thermal transformation has been reported (30).

We return now to the conversion of **20** to **15**. This was effected by the route shown in Scheme 11. Reduction with lithium in liquid ammonia and ether cleaved the C-1—C-2 bond to give **31**; the crude product was oxidized with sodium dichromate and sulfuric acid since some reduction of the ketonic group also occurred. The product was obtained as a single epimer at C-2, which is considered to be the

[6]This structure is preferred over structure **25** (*vide infra*), because the latter would be expected to give rise in its $^1H$ nmr spectrum to C-2 and C-5 proton signals with more widely separated chemical shifts, with the C-2 proton signal at higher field and the C-5 proton signal at lower field.

Can. J. Chem. Downloaded from www.nrcresearchpress.com by 210.87.254.5 on 09/06/12
For personal use only.

Can. J. Chem. Downloaded from www.nrcresearchpress.com by 210.87.254.5 on 09/06/12
For personal use only.

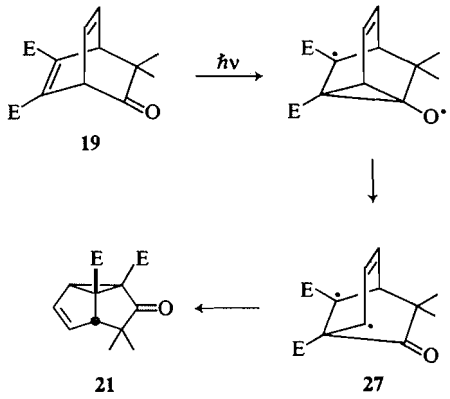


SCHEME 8 (E = $CO_2Me$)

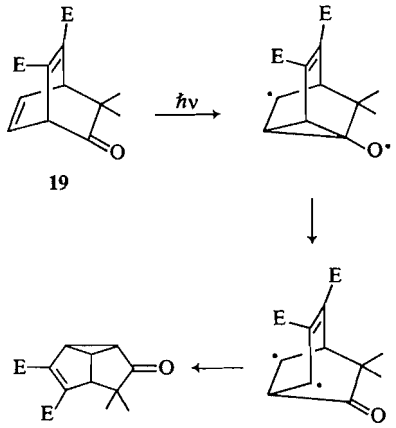


SCHEME 9 (E = $CO_2Me$)

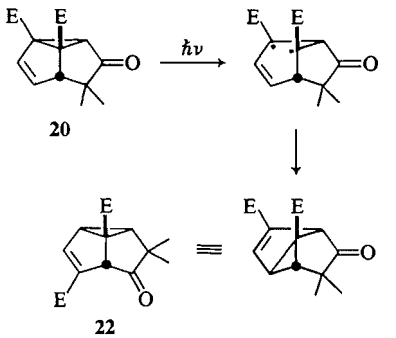


SCHEME 10 (E = $CO_2Me$)

more stable *exo* epimer **31**. Its ir spectrum showed a carbonyl-stretching band at 5.78 μm and its $^1H$ nmr spectrum showed two one-proton doublets ($J$ = 18.5 Hz) at δ 2.20 and 3.02 ppm, characteristic of the C-8 protons in this system, and a two-proton multiplet at δ 5.8 ppm arising from the olefinic protons. Treatment of **31** with methanolic sodium methoxide gave the isomeric α,β-unsaturated ester **32**, whose ir spectrum included a strong band at 5.83 μm and a weak band at 6.13 μm. Its $^1H$ nmr spectrum showed a one-proton triplet ($J$ = 2 Hz) at δ 6.89 ppm, assigned to the C-3 proton. Catalytic hydrogenation of **32** over palladium/carbon in methanol at atmospheric pressure gave exclusively **15**, identical with the diester obtained by the routes in Schemes 2 and 3. Hydrogenation over platinum in cyclohexane gave mixtures of **15** and a new compound, assigned the C-2 epimeric structure **33**.[7] The reaction was exceedingly capricious and the product mixture had variable ratios of **33** and **15**, ranging up to 19:1. The ir and $^1H$ nmr spectra of the two epimers were very similar; a critical difference in the latter spectra was that in the spectrum of **33** the lower field doublet of the two one-proton doublets ($J$ = 19 Hz) at δ 2.14 and 3.18 ppm arising from the C-8 protons exhibited a further small coupling ($J \sim 1$ Hz). This signal is assigned to the *exo* C-8 proton and the additional coupling is attributed to $^4J$ long range coupling with the proton at C-2. Examination of molecular models shows that the "W" relationship between the *exo* C-8 and C-2 protons required for such $^4J$ coupling (31) is possible only if the C-2 proton has the *exo* configuration, i.e., the ester group at C-2 has the *endo* configuration. Molecular models also show that delivery of hydrogen to **32** would be expected to occur from the less hindered *exo* face, leading to **33**. The exclusive formation of **15** in some cases and its formation in variable amounts in others may be due to epimerization of **33** by adventitious acid or base or by the catalyst itself (32).

We have thus attained our objective of functionalization of the carbon designed to become *exo* C-12 in the cedranoid sesquiterpenes by three different methods. The last method has provided in

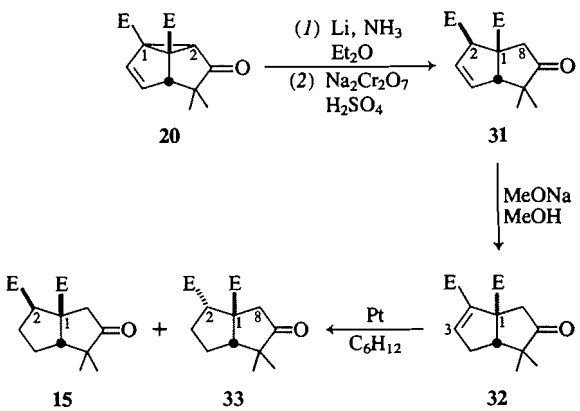


SCHEME 11 (E = $CO_2Me$)

[7]This product was not entirely freed of **15** and was obtained as a solid with a wide melting range.

Can. J. Chem. Downloaded from www.nrcresearchpress.com by 210.87.254.5 on 09/06/12
For personal use only.

addition a potential route to *endo* C-12 functionalized cedranoid sesquiterpenes, which also have been obtained from natural sources.

## Experimental

Melting points were determined on a Fisher–Johns apparatus and are uncorrected. The ir spectra were taken in $CHCl_3$ solution and the $^1H$ and $^{13}C$ nmr spectra in $CDCl_3$ solution. Analytical thin layer chromatography was carried out on 0.25 mm silica gel Q6-F plates from Quantum Industries. Preparative thin layer chromatography was carried out on 20 × 20 cm plates coated with 0.5 mm, 1 mm, or 2 mm silica gel layers (Merck Kieselgel 60 $PF_{254}$ containing gypsum). Medium pressure liquid chromatography was carried out on a Merck silica gel 60 prepacked column (Size B) operated at a pressure of ~5 psi. Solutions were dried over magnesium sulfate and concentrated on a Büchi "Rotovapor < R >" rotary evaporator under water aspirator pressure. Solvents used for work-ups and chromatography were either distilled or were of ACS Reagent Grade quality.

*Attempted homoconjugate addition of an alkenyl group to dimethyl 6,6-dimethyl-7-oxotricyclo[3.2.1.0$^{2,8}$]octane-1,8-dicarboxylate (**6**)*[8]

*(i). With lithium divinylcuprate reagents*

A solution of vinyllithium in tetrahydrofuran (THF) (1.56 *M*; 0.70 mL, 1.09 mmol) was added to a cold (−45°C), stirred slurry of cuprous iodide (109 mg, 0.57 mmol) in ether (4 mL) containing isopropyl sulfide (260 μl, 212 mg, 1.79 mmol) under argon (33). The mixture was warmed to −15°C to −20°C for 15 min, and then rapidly cooled to −75°C, producing a light grey-green solution containing some black solid. A solution of **6** (8) (99 mg, 0.37 mmol) in ether (1 mL) was added. The mixture was stirred at −75°C for 10 min and at 4°C overnight, and then 50% saturated aqueous $NH_4Cl$ (10 mL) was added. The layers were separated, and the aqueous phase was extracted with ether (2 × 10 mL). The combined organic solutions were washed with saturated aqueous $NH_4Cl$ (10 mL), dried, and concentrated to give a yellow oil (68 mg). No vinyl proton signals were apparent in the $^1H$ nmr spectrum of this material, which consisted mostly of unconsumed **6**. Attempted reaction in tetrahydrofuran produced the same result.

The following reagents (34) also failed to effect homoconjugate addition of a vinyl group to **6**: $LiCu(CH{=}CH_2)$ in ether or THF, $LiCu(CH{=}CH_2)_2$ in ether or $THF/(CH_3)_2S$, $LiCu(CH{=}CH_2)_2$ in ether/$(n\text{-}C_4H_9)_3P$, $LiCu(CH{=}CH_2)_2{\cdot}P(n\text{-}C_4H_9)_3$ in ether or THF/pentane, $LiCu[C{\equiv}CC(CH_3)_2OCH_3](CH{=}CH_2)$ in ether or THF, $LiCu[C{\equiv}CCH_2N(CH_3)_2](CH{=}CH_2)$ in triethylamine, $LiCu(CH_3)(CH{=}CH_2)$ in ether or THF, $CH_2{=}CHMgBr/CuI$ in THF, $(CH_2{=}CH)_4(CH_3)Cu_3Mg_2Br_2$ in THF.

*(ii). With lithium diisobutylhex-1-enylmethylalanate*

A solution of diisobutylaluminum hydride in toluene (25% by weight; 265 μL, 0.42 mmol) was added to a stirred solution of 1-hexyne (48 μL, 34 mg, 0.41 mmol) in toluene (5.0 mL) under nitrogen at room temperature. The resulting solution was warmed to 40–60°C for 45 min and then cooled to 0°C. A solution of methyllithium – lithium bromide complex in ether (1.33 *M*; 310 μL, 0.41 mmol) was added, producing a white gelatinous precipitate and a colorless solution. The mixture was stirred at 0°C for 20 min and was then allowed to warm to room temperature. A solution of **6** (100 mg, 0.38 mmol) in toluene (10 mL) was added, and the mixture was stirred at room temperature for 22 h. Ice (~15 g) was added, followed by aqueous 10% HCl (10 mL). The mixture was stirred for 1 h, the layers were separated, and the aqueous phase was extracted with ether (2 × 10 mL). The organic phases were combined, washed with saturated aqueous NaCl (10 mL), dried, and concentrated to give a yellow oil (97 mg), which was found to be **6** almost exclusively.

*Reaction of **6** with titanium tetrachloride. Formation of dimethyl* exo*-8-chloro-3-hydroxy-4,4-dimethyl-*cis*-bicyclo[3.3.0]oct-2-ene-1,2-dicarboxylate (**9**)*[8]

Titanium tetrachloride (100 μL, 0.91 mmol) was added to a stirred solution of **6** (202 mg, 0.76 mmol) in dichloromethane (4.0 mL) under nitrogen. The solution was stirred for 30 min, remaining homogeneous but gradually turning deep red. Saturated aqueous $NH_4Cl$ (10 mL) was added, and the resulting mixture was extracted with ether (2 × 10 mL). The combined ethereal extracts were dried and concentrated to give **9** (212 mg, 0.70 mmol, 92%) as a pale yellow powder. Crystallization from pentanes gave large, white crystals, mp 102–104°C; ir $\lambda_{max}$: 5.80, 6.06, 6.21 μm; $^1H$ nmr δ: 1.08 (s, 3H), 1.12 (s, 3H), 1.2–2.3 (m, 4H), 2.7–3.1 (m, 1H), 3.65 (s, 3H), 3.75 (s, 3H), 4.2–4.5 (m, 1H), 11.93 (s, 1H); ms *m/e*: 304 (3), 303 (*M* + 1; 3), 302 (8). *Anal.* calcd. for $C_{14}H_{19}O_5Cl$: C 55.54, H 6.33, Cl 11.71; found: C 55.70, H 6.44, Cl 11.72.

Treatment of **6** with allyltrimethylsilane and titanium tetrachloride in dichloromethane (14) gave **9** in good yield as the only product.

*Reaction of **6** with phenylethynylmagnesium bromide. Formation of **10** and **11**a or **11**b*[8]

A solution of ethylmagnesium bromide in ether (1.75 *M*; 240 μL, 0.42 mmol) was added to a stirred solution of phenylacetylene (46 μL, 0.42 mmol) in ether (2.0 mL) under nitrogen. The clear homogeneous solution was stirred at room temperature for 30 min and then cooled to 2°C. A solution of **6** (100 mg, 0.38 mmol) in ether (1.0 mL) was added, producing a large amount of white precipitate. The mixture was stirred for 1 h at 2°C, after which aqueous 10% HCl (10 mL) was added. The resulting mixture was shaken with ether (20 mL), and the ethereal layer was washed with saturated aqueous NaCl (10 mL), dried, and concentrated to give a yellow oil (122 mg). The $^1H$ nmr spectrum of this oil showed it to contain phenylacetylene and a ~1:1 mixture of **10** and **11***a* or **11***b* (*vide infra*).

*Reaction of **6** with hydrogen bromide. Formation of dimethyl* exo*-8-bromo-3-hydroxy-4,4-dimethyl-*cis*-bicyclo[3.3.0]-oct-2-ene-1,2-dicarboxylate (**10**)*

Anhydrous hydrogen bromide was bubbled slowly into a cold (0°C), stirred solution of **6** (419 mg, 1.58 mmol) in dichloromethane (20 mL). After 2.5 h analytical thin layer chromatography indicated that no **6** remained. The solution was poured onto ice (~40 g). When all the ice had melted the layers were separated, and the aqueous phase was extracted with dichloromethane (2 × 10 mL). The combined organic solutions were washed with water (10 mL), saturated aqueous $NaHCO_3$ (10 mL), and saturated aqueous NaCl (10 mL). They were dried and concentrated to give a white powder (508 mg). Crystallization from pentanes – ethyl acetate (2:1 v/v) gave **10** (397 mg, 1.14 mmol, 72%) as white crystals, mp 112.5–115.5°C; ir $\lambda_{max}$: 5.80, 6.06, 6.19 μm; $^1H$ nmr δ: 1.12 (s, 3H), 1.16 (s, 3H), 1.3–2.5 (m, 4H), 2.75–3.15 (m, 1H), 3.74 (s, 3H), 3.83 (s, 3H), 4.25–4.60 (m, 1H), 11.02 (s, 1H); $^{13}C$ nmr δ: 19.9 (q), 27.4 (t), 27.9 (q), 38.1 (t), 44.3 (s), 51.3 (q), 52.0 (q), 55.1 (d), 56.6 (d), 65.3 (s), 99.4 (s), 170.8 (s), 173.7 (s), 182.4 (s); ms *m/e*: 348 (1), 346 (1). *Anal.* calcd. for $C_{14}H_{19}O_5Br$: C 48.43, H 5.52, Br 23.01; found: C 48.41, H 5.52, Br 23.01.

*Reaction of **6** with bis(phenylethynyl)magnesium. Formation of **11**a or **11**b*[8]

Dioxane (0.8 mL, 9.38 mmol) was added to a solution of phenylethynylmagnesium bromide prepared by the reaction of a

[8]These experiments were conducted under rigorously anhydrous conditions under a positive pressure of argon or nitrogen.

Can. J. Chem. Downloaded from www.nrcresearchpress.com by 210.87.254.5 on 09/06/12
For personal use only.

solution of ethylmagnesium bromide in ether (0.81 *M*; 11.2 mL, 9.07 mmol) with a solution of phenylacetylene (1.0 mL, 9.11 mmol) in ether (20 mL) under nitrogen. After 30 min the mixture was filtered under nitrogen through a sintered glass frit. The filtrate was titrated as 0.09 *M* in bis(phenylethynyl)magnesium.

A solution of **6** (50 mg, 0.19 mmol) was added with stirring to this solution (2.5 mL, 0.23 mmol), cooled to 4°C under nitrogen. After 4 h aqueous 10% HCl (10 mL) was added, and the resulting mixture was washed with ether (20 mL). The organic layer was washed with saturated aqueous NaCl (10 mL), dried, and concentrated to give a yellow oil (65 mg). This contained only a small amount of phenylacetylene, little or no **6**, and a single major product tentatively identified as **11***a* or **11***b*; ir $\lambda_{max}$: 3.07 (m), 5.79 μm; $^1$H nmr δ: 0.94 (s, 3H), 1.39 (s, 3H), 3.67 (s, 3H), 6.85–7.64 (m, > 10H).

*Methyl 4,4-dimethyl-3-oxo-*exo*-8-phenyl-*cis*-bicyclo[3.3.0]-octane-1-carboxylate (**13**)*

A solution of phenyllithium in ether–benzene (30:70 v/v) (1.9 *M*; 12.0 mL, 22.8 mmol) was added over ~20 min to a cold (5°C), stirred slurry of cuprous iodide (2.18 g, 11.4 mmol) in ether (20 mL) under argon.[8] Stirring for 1 h at 0–5°C gave a homogeneous dark green solution of lithium diphenylcuprate. A solution of **6** (1.00 g, 3.76 mmol) in ether (15 mL) was added and stirring was continued for 4 h. Aqueous 10% HCl (25 mL) was added to the cold solution, and the resulting mixture was stirred for a further 30 min and then suction-filtered. The layers of the filtrate were separated and the aqueous phase was extracted with ether (3 × 10 mL). The organic phases were combined and washed with saturated aqueous $NaHCO_3$ (10 mL), 1 *M* aqueous $Na_2S_2O_3$ (10 mL), and saturated aqueous $NH_4Cl$ (10 mL) made slightly basic by the addition of concentrated aqueous $NH_3$. The organic solution was dried and concentrated to give a yellow oil (1.76 g). The $^1$H nmr spectrum of this material included two singlets at δ 11.2 and 11.4 ppm, in a ratio of ~2:1, which are assigned to the enolic protons of **12***a* and **12***b*, respectively. This spectrum also showed a singlet at δ 3.18 ppm, assigned to the C-1 carbomethoxy groups of both **12***a* and **12***b*, a singlet at δ 3.78 ppm, assigned to the C-2 carbomethoxy group of **12***a*, and a quartet ($J$ = 7 Hz) at δ 4.25 ppm, assigned to the carboethoxy group of **12***b*. The ir spectrum of this crude product showed strong bands at 5.83, 6.09, and 6.25 μm.

This material was stirred and heated (96°C) in dimethyl sulfoxide (8 mL) containing water (500 μL, ~27.8 mmol) and sodium chloride (413 mg, 7.1 mmol) for 6 h. The mixture was allowed to cool to room temperature and was then diluted with water (20 mL). The resulting solution was extracted with ether (4 × 10 mL). The ethereal extracts were combined, washed with water (5 × 10 mL), dried, and concentrated to leave a yellow solid (1.22 g). Crystallization from ether gave **13** (521 mg); medium pressure liquid chromatography of the mother liquors with hexanes – ethyl acetate (7:1 v/v) as eluent gave a further quantity of **13** (175 mg; total: 696 mg, 2.43 mmol, 65% from **6**). Further recrystallizations from 10% ethyl acetate – pentanes gave **13**, mp 125–127°C; ir $\lambda_{max}$: 5.80 μm; $^1$H nmr δ: 1.02 (s, 3H), 1.08 (s, 3H), 1.2–2.5 (m, 5H), 2.46 (d, $J$ = 19 Hz, 1H), 2.8–3.2 (m, 1H), 3.21 (s, 3H), 3.60 (d, $J$ = 19 Hz, 1H), 7.21 (s, 5H); $^{13}$C nmr δ: 18.9 (q), 27.3 (q), 29.7 (t), 31.3 (t), 46.4 (t), 49.0 (s), 51.7 (q), 57.2 (s), 57.8 (d), 59.9 (d), 127.0 (d), 127.6 (d), 128.1 (d), 139.6 (s), 175.8 (s), 219.9 (s); ms *m/e*: 286 (62). *Anal.* calcd. for $C_{18}H_{22}O_3$: C 75.50, H 7.74; found: C 75.27, H 7.77.

*Dimethyl 6,6-dimethyl-7-oxo-*cis*-bicyclo[3.3.0]octane-1,*exo*-2-dicarboxylate (**15**)*

Ozonized oxygen was bubbled through a solution of **13** (207 mg, 0.72 mmol) in glacial acetic acid (21.5 mL) and water (3.5 mL) for 3 h at room temperature. The solution eventually acquired a very faint blue color. It was allowed to stand at room temperature for 2 h, treated with 30% hydrogen peroxide (0.5 mL), and then allowed to stand at room temperature overnight. The solvents were removed by distillation (0.5 Torr) at room temperature, and the residue was dissolved in a mixture of ether (20 mL) and ethyl acetate (10 mL). The solution was extracted with saturated aqueous $NaHCO_3$ (3 × 10 mL). The basic extracts were combined, and made strongly acidic by the addition of concentrated $H_2SO_4$, and extracted with ethyl acetate (3 × 10 mL). The latter extracts were combined, washed with saturated aqueous NaCl, dried, and concentrated to give a colorless oil (130 mg). Molecular distillation (100°C/0.1 Torr) gave **14** (85 mg, 0.33 mol, ~46%) as a colorless oil containing trace impurities; ir $\lambda_{max}$: 2.7–4.0 (br), 5.73 μm; $^1$H nmr δ: 1.02 (s, 3H), 1.08 (s, 3H), 1.6–3.0 (m, 6H), 2.35 (d, $J$ = 19.5 Hz, 1H), 3.59 (d, $J$ = 19.5 Hz, 1H), 3.70 (s, 3H), 10.80 (br s, 1H); $^{13}$C nmr δ: 19.6 (q), 27.3 (q), 28.9 (t), 29.2 (t), 46.1 (t), 48.6 (s), 52.5 (q), 54.2 (s), 57.5 (d), 58.5 (d), 176.0 (s), 178.5 (s), 220.2 (s).

Ethereal diazomethane was added to a cold (0°C) stirred solution of crude **14** (72 mg, ~0.28 mmol) in methanol (5 mL) until the yellow color of the reagent persisted. The solution was allowed to stand at room temperature until all the diazomethane had evaporated. Concentration of this solution gave **15** (76 mg, ~0.28 mmol, ~100%). Preparative thin layer chromatography with elution with 2:1 cyclohexane – ethyl acetate ($R_f$ 0.46), followed by sublimation (70°C/0.05 Torr), and crystallization from ethyl acetate – pentanes gave **15** as a white solid, mp 63–65°C; ir $\lambda_{max}$: 5.78 μm; $^1$H nmr δ: 1.04 (s, 3H), 1.09 (s, 3H), 1.3–2.4 (m, 4H), 2.34 (d, $J$ = 19 Hz, 1H), 2.4–3.0 (m, 2H), 3.62 (d, $J$ = 19 Hz, 1H), 3.67 (s, 3H), 3.71 (s, 3H); $^{13}$C nmr δ: 19.6 (q), 27.3 (q), 29.0 (t), 29.4 (t), 46.2 (t), 48.5 (s), 51.8 (s), 52.4 (q), 54.1 (s), 57.7 (d), 58.4 (d), 172.7 (s), 176.0 (s), 219.6 (s); ms *m/e*: 268 (13). *Anal.* calcd. for $C_{14}H_{20}O_5$: C 62.67, H 7.51; found: C 62.85, H 7.59.

*Dimethyl* exo*-8-cyano-3-hydroxy-4,4-dimethyl-*cis*-bicyclo-[3.3.0]oct-2-ene-1,2-dicarboxylate (**16**)*[8]

A solution of diethylaluminum cyanide in toluene (1.57 *M*; 4.8 mL, 7.54 mmol) was added by means of a syringe equipped with a wide bore needle to **6** (995 mg, 3.74 mmol) in a round-bottomed flask equipped with a magnetic stirring bar, septum, and nitrogen inlet. The resulting solution was stirred at room temperature for exactly 2 h. It was then poured cautiously into a mixture of aqueous 10% HCl (50 mL) and ice (50 g). The resulting mixture was stirred for 1 h and extracted with ether (3 × 20 mL). The combined organic extracts were washed with saturated aqueous NaCl (10 mL), dried, and concentrated to give a white powder. Crystallization from ethyl acetate gave **16** (609 mg, 2.08 mmol, 56%). Further recrystallization gave white crystals, mp 135–137.5°C; ir $\lambda_{max}$: 4.46 (w), 6.01, 6.17 μm; $^1$H nmr δ: 1.12 (s, 3H), 1.17 (s, 3H), 1.30–3.05 (m, 6H), 3.79 (s, 3H), 3.83 (s, 3H), 10.52 (s, 1H); $^{13}$C nmr δ: 19.7 (q), 28.2 (q), 29.1 (t), 32.6 (t), 40.1 (d), 44.4 (s), 51.4 (q), 52.5 (q), 58.6 (d), 61.8 (s), 100.2 (s), 120.0 (s), 169.7 (s), 173.9 (s), 181.0 (s); ms *m/e*: 294 (*M* + 1; 7), 293 (9). *Anal.* calcd. for $C_{15}H_{19}O_5N$: C 61.42, H 6.53, N 4.78; found: C 61.32, H 6.49, N 4.69.

*Methyl* exo*-8-cyano-4,4-dimethyl-3-oxo-*cis*-bicyclo[3.3.0]-octane-1-carboxylate (**17**)*

A mixture of **16** (303 mg, 1.03 mmol) and NaCl (86 mg, 1.47 mmol) in dimethyl sulfoxide containing water (175 μL, 9.72 mmol) was stirred and heated (94°C) under nitrogen for 5 h. After cooling, the mixture was extracted with ether (30 mL), and the extract was washed with water (4 × 10 mL). The ethereal solution was dried and concentrated. The residual oil was molecularly distilled (107°C/0.025 Torr) to give **17** (166 mg, 0.71 mmol, 69%) as a colorless, viscous oil; ir $\lambda_{max}$: 4.46 (w), 5.85 μm; $^1$H nmr δ: 1.06 (s, 6H), 1.25–2.35 (m, 4H), 2.25 (d, $J$ = 19.5 Hz, 1H), 2.55–3.1 (m, 2H), 3.62 (d, $J$ = 19.5 Hz, 1H), 3.91 (s, 3H);

Can. J. Chem. Downloaded from www.nrcresearchpress.com by 210.87.254.5 on 09/06/12
For personal use only.

$^{13}$C nmr δ; 19.3 (q), 26.9 (q), 29.7 (t), 32.1 (t), 42.0 (d), 45.0 (t), 48.6 (s), 53.2 (q), 55.5 (s), 57.6 (d), 119.1 (s), 174.2 (s), 217.6 (s); ms *m/e*: 235 (16). *Anal.* calcd. for $C_{13}H_{17}O_3N$: C 66.36, H 7.28, N 5.95; found: C 66.18, H 7.19, N 5.97.

*Reaction of* ***17*** *with methanol and concentrated sulfuric acid. Formation of* ***15*** *and* ***18***

A mixture of **17** (197 mg, 0.84 mmol), methanol (16 mL), and concentrated $H_2SO_4$ (5.4 mL) was stirred and heated (90°C) for 26 h under nitrogen. After the mixture had cooled to room temperature, water (20 mL) was added and the methanol was removed by distillation at reduced pressure (15 Torr). The residue was extracted with ether (5 × 10 mL). The combined ethereal extracts were washed with saturated aqueous $NaHCO_3$ (10 mL) and saturated aqueous NaCl (10 mL), dried, and concentrated to give a colorless oil (136 mg). Repeated extraction of the aqueous phases with ether gave an additional quantity of crude product (31 mg). Crystallization from a mixture of toluene and pentanes gave crude **18** (19 mg, 0.09 mmol, 11%). Further crystallization gave pure **18**, mp 153.5–154.5°C; ir $\lambda_{max}$: 3.02 (m), 5.62 (m), 5.79, 7.46 (m), 8.61 (m) μm; $^1$H nmr δ: 1.06 (s, 3H), 1.29 (s, 3H), 1.6–2.3 (m, 4H), 2.38 (d, $J$ = 19 Hz, 1H), 2.5–3.1 (m, 2H), 3.22 (d, $J$ = 19 Hz, 1H), 8.69 (br s, 1H); ms *m/e*: 221 (45). *Mol. Wt.* calcd. for $C_{12}H_{15}O_3N$: 221.1052; found (ms): 221.1048.

Concentration of the original mother liquor followed by molecular distillation (90°C/0.05 Torr) gave **15** (92 mg, 0.34 mmol, 41%), mp 63–65°C, whose spectra were identical with those of the sample of **15** prepared from **13** (*vide supra*).

*Sensitized photolysis of* ***19****. Formation of dimethyl 4,4-dimethyl-3-oxotricyclo[3.2.1.0$^{2,8}$]oct-6-ene-1,8-dicarboxylate (****20****), 21, and 22*

A solution of **19** (1.10 g, 4.17 mmol) in acetophenone (freshly distilled; 110 mL) was degassed with nitrogen for 3 h. The solution was then irradiated in a Rayonet–Srinivasan–Griffin Photochemical Reactor equipped with eleven low pressure 350 nm RPR lamps for 34 h. The solvent was removed by distillation at 0.25 Torr. The oily residue was chromatographed (medium pressure liquid chromatography with hexanes – ethyl acetate (5:1 v/v) as eluent; fraction size ~10 mL) to give:

| | | |
|---|---|---|
| fraction | 24 | **21** (20 mg, 0.08 mmol, 2%) |
| | 25 | **20** and **21** |
| | 26–30 | **20** (540 mg, 2.05 mmol, 49%) |
| | 31–33 | **20** and **22** |
| | 34–37 | **22** (52 mg, 0.20 mmol, 5%) |

Samples of compounds **20–22** for analysis were recrystallized from ethyl acetate – hexanes.

Compound **20**, mp 84–85°C; ir $\lambda_{max}$: 5.77 μm; $^1$H nmr δ: 0.95 (s, 3H), 1.27 (s, 3H), 3.5–3.7 (m, 2H), 3.80 (s, 6H), 5.7–6.0 (m, 2H); δ ($C_6H_6$/$CDCl_3$): 0.78 (s, 3H), 1.12 (s, 3H), 3.38 (d, $J$ = 2.5 Hz, 1H), 3.48 and 3.50 (two s, 6H), 3.62 (s, 1H), 5.51 (dd, $J$ = 5.5, 2.5 Hz, 1H), 5.74 (d, $J$ = 5.5 Hz, 1H); $^{13}$C nmr δ: 17.9 (q), 25.4 (q), 47.7 (d), 52.6 (q), 52.8 (q), 53.7 (s), 56.4 (s), 58.0 (d), 62.6 (s), 127.4 (d), 136.5 (d), 167.1 (s), 168.3 (s), 209.0 (s); ms *m/e*: 264 (5). *Anal.* calcd. for $C_{14}H_{16}O_5$: C 63.63, H 6.10; found: C 63.50, H 6.25.

Compound **21**, mp 71–72.5°C; ir $\lambda_{max}$: 5.76 μm; $^1$H nmr δ: 0.97 (s, 3H), 1.35 (s, 3H), 3.4–3.7 (m, 2H), 3.73 (s, 3H), 3.76 (s, 3H), 5.6–5.95 (m, 2H); $^{13}$C nmr δ: 17.7 (q), 24.8 (q), 46.5 (d), 52.5 (q), 52.9 (q), 56.0 (s), 56.3 (d), 56.5 (s), 64.4 (s), 127.0 (d), 136.7 (d), 165.7 (s), 169.0 (s), 206.1 (s); ms *m/e*: 264 (7). *Anal.* calcd. for $C_{14}H_{16}O_5$: C 63.63, H 6.10; found: C 63.49, H 6.13.

Compound **22**, mp 88.5–89.5°C; ir $\lambda_{max}$: 5.75, 5.81, 6.19 (w) μm; $^1$H nmr δ: 1.21 (s, 3H), 1.23 (s, 3H), 2.69 (d, $J$ = 7.5 Hz, 1H), 2.99 (dd, $J$ = 7.5, 2.5 Hz, 1H), 3.74 (s, 3H), 3.76 (s, 3H), 4.29 (s, 1H), 6.83 (d, $J$ = 2.5 Hz, 1H); $^{13}$C nmr δ: 25.8 (q), 29.2 (q), 43.7 (d), 46.1 (d), 48.4 (s), 50.1 (s), 51.8 (q), 52.1 (q), 57.4 (d), 134.0 (s), 141.7 (d), 161.9 (s), 170.8 (s), 210.0 (s); ms *m/e*: 264 (1). *Anal.* calcd. for $C_{14}H_{16}O_5$: C 63.63, H 6.10; found: C 63.57, H 6.13.

*Dimethyl 6,6-dimethyl-7-oxo-*cis*-bicyclo[3.3.0]oct-3-ene-1,*exo*-2-dicarboxylate (****31****)*[8]

Lithium wire (37 mg, 5.33 mmol) was added to a stirred solution of **20** (282 mg, 1.07 mmol) in ether (5 mL) and liquid ammonia (10 mL) under nitrogen. After ~40 min, all the lithium appeared to have reacted, and after a further 20 min, solid ammonium chloride was added. The ammonia was allowed to evaporate at room temperature, after which water (10 mL) was added. The phases were separated and the aqueous layer was extracted with ether (3 × 10 mL). The combined ethereal solutions were washed with saturated aqueous NaCl, dried, and concentrated to leave a colorless oil (217 mg). This was dissolved in benzene (5 mL), and the solution was stirred for 6 h with 10 mL of a solution of sodium dichromate dihydrate (1.2 g, 4.03 mmol) in acetic acid (5 mL), concentrated $H_2SO_4$ (6 mL), and water (19 mL). The phases were separated and the aqueous phase was extracted with ether (3 × 10 mL). The combined organic solutions were washed with water (10 mL), saturated aqueous $NaHCO_3$ (2 × 10 mL), and saturated aqueous NaCl (10 mL), dried, and concentrated to give **31** (92 mg, 0.35 mmol, 33%) as a colorless oil, which crystallized on standing. Recrystallization from ethyl acetate – hexanes gave white crystals, mp 72–73°C; ir $\lambda_{max}$: 5.78 μm; $^1$H nmr δ: 1.06 (s, 3H), 1.09 (s, 3H), 2.20 (d, $J$ = 18.5 Hz, 1H), 3.02 (d, $J$ = 18.5 Hz, 1H), 3.3–3.5 (m, 1H), 3.69 (s, 3H), 3.81 (s, 3H), 4.3–4.5 (m, 1H), 5.6–6.0 (m, 2H); $^{13}$C nmr δ: 22.1 (q), 26.3 (q), 41.5 (t), 47.9 (s), 52.0 (q), 52.9 (q), 55.2 (s), 58.4 (d), 65.2 (d), 128.4 (d), 131.4 (d), 171.6 (s), 175.7 (s), 218.7 (s); ms *m/e*: 266 (5). *Anal.* calcd. for $C_{14}H_{18}O_5$: C 63.15, H 6.81; found: C 62.96, H 6.85.

*Dimethyl 6,6-dimethyl-7-oxo-*cis*-bicyclo[3.3.0]oct-2-ene-1,2-dicarboxylate (****32****)*[8]

Compound **31** (68 mg, 0.26 mmol) ws stirred at room temperature under nitrogen for 1 h in a solution prepared by the reaction of sodium (15 mg, 0.65 mg atom) with methanol (2 mL). The resulting solution was poured into water (10 mL), and the mixture was extracted with ether (3 × 10 mL). The ethereal extracts were combined, washed with saturated aqueous NaCl (10 mL), dried, and concentrated to give **32** (56 mg, 0.21 mmol, 81%) as a colorless oil, which crystallized on standing. Purification by preparative thin layer chromatography with elution with cyclohexane – ethyl acetate (2:1 v/v) gave **32** ($R_f$ 0.41), which crystallized from ethyl acetate – pentanes (~1:10 v/v) to give white needles, mp 84–85°C; ir $\lambda_{max}$: 5.78, 5.83, 6.13 (w) μm; $^1$H nmr δ: 1.06 (s, 3H), 1.11 (s, 3H), 2.39 (d, $J$ = 20 Hz, 1H), 2.4–3.2 (m, 2H), 3.56 (d, $J$ = 20 Hz, 1H), 3.77 (s, 3H), 6.89 (t, $J$ = 2 Hz, 1H); $^{13}$C nmr δ: 20.6 (q), 26.6 (q), 34.5 (t), 42.9 (t), 48.8 (s), 51.8 (q), 52.9 (q), 57.0 (d), 58.1 (s), 138.8 (s), 145.2 (d), 163.9 (s), 174.5 (s), 219.3 (s); ms *m/e*: 266 (6). *Anal.* calcd. for $C_{14}H_{18}O_5$: C 63.14, H 6.81; found: C 62.86, H 6.83.

*Catalytic hydrogenation of* ***32****. Formation of dimethyl 6,6-dimethyl-7-oxo-*cis*-bicyclo[3.3.0]octane-1-*endo*-2-dicarboxylate (****33****) and* ***15***

Compound **32** (17 mg, 0.06 mmol) was hydrogenated at atmospheric pressure over platinum (22 mg) in cyclohexane (3 mL) for 3 h at room temperature. The catalyst was filtered off and the filtrate was concentrated to give a colorless oil (9 mg) which solidified on standing. Sublimation (< 90°C/0.1 Torr) gave **33** (8 mg, 0.03 mmol, 50%) as a white solid, which was crystallized from pentanes – ethyl acetate;[7] ir $\lambda_{max}$: 5.78 μm; $^1$H nmr δ: 1.03 (s, 3H), 1.06 (s, 3H), 1.5–2.2 (m, 4H), 2.14 (d, $J$ = 19 Hz, 1H), 2.4–3.0 (m, 2H), 3.18 (dd, $J$ = 19, ~1 Hz, 1H), 3.69 (s, 3H), 3.82 (s, 3H); ms *m/e*: 268 (16).

Similar hydrogenation of **32** (12 mg) over 10% palladium/carbon (5.5 mg) in methanol (4 mL) gave a product (11 mg) whose $^1$H nmr spectrum showed it to be **15**; the presence of **33** could not be detected.

## Acknowledgments

We thank the Natural Sciences and Engineering Research Council of Canada for support of this work and Messrs. Baldev Gambhir and Nick Plavac for assistance in obtaining the $^{13}$C nmr spectra.

1. K. E. Stevens and P. Yates. J. Chem. Soc. Chem. Commun. 990 (1980).
2. G. Stork and R. Breslow. J. Am. Chem. Soc. **75**, 3291 (1953); P. A. Plattner, A. A. Eschenmoser, W. Keller, H. Kläui, S. Meyer, and M. Rosner. Helv. Chim. Acta, **36**, 1875 (1953); P. A. Plattner, A. Fürst, S. Meyer, and W. Keller. Helv. Chim. Acta, **37**, 266 (1954); J. Simonsen and D. H. R. Barton. The terpenes. Vol. III. 2nd ed. Cambridge University Press. 1952. pp. 75–88; P. Yates. Structure determination. W. A. Benjamin, New York. 1967. pp. 1–37.
3. J. Meinwald and Y. C. Meinwald. Adv. Alicyclic Chem. **1**, 1 (1966).
4. A. N. Singh, A. B. Upadhye, M. S. Wadia, V. V. Mhaskar, and Sukh Dev. Tetrahedron, **25**, 3855 (1969).
5. P. Yates and G. F. Field. J. Am. Chem. Soc. **82**, 5764 (1960); Tetrahedron, **26**, 3135 (1970); P. Yates, P. M. Burke, and G. F. Field. Tetrahedron, **26**, 3159 (1970).
6. G. Stork and F. H. Clarke, Jr. J. Am. Chem. Soc. **77**, 1072 (1955); J. Am. Chem. Soc. **83**, 3114 (1961).
7. E. J. Corey, N. N. Girotra, and C. J. Mathew. J. Am. Chem. Soc. **91**, 1557 (1969); T. G. Crandall and R. G. Lawton. J. Am. Chem. Soc. **91**, 2127 (1969); E. Demole, P. Enggist, and C. Borer. Helv. Chim. Acta, **54**, 1845 (1971); E. J. Corey and R. D. Balanson. Tetrahedron Lett. 3153 (1973); E. G. Breitholle and A. G. Fallis. Can. J. Chem. **54**, 1991 (1976); J. Org. Chem. **43**, 1964 (1978).
8. P. Yates and K. E. Stevens. Tetrahedron. In press.
9. S. Danishefsky. Acc. Chem. Res. **12**, 66 (1979).
10. F. M. Walliser and P. Yates. J. Chem. Soc. Chem. Commun. 1025 (1979); P. Yates and F. M. Winnik. Can. J. Chem. **59**, 1641 (1981).
11. R. E. Ireland and G. Pfister. Tetrahedron Lett. 2145 (1969); D. C. Muchmore. Org. Synth. **52**, 109 (1972); T. Akiyama, D. Pedder, J. V. Silverton, J. I. Seeman, and H. Ziffer. J. Org. Chem. **49**, 3675 (1975).
12. K. F. Bernady, M. B. Floyd, J. F. Poletto, and M. J. Weiss. J. Org. Chem. **44**, 1438 (1979); K. F. Bernady, J. F. Poletto, and M. J. Weiss. Tetrahedron Lett. 765 (1975).
13. M. E. Kuehne and R. Hafter. J. Org. Chem. **43**, 3702 (1978).
14. A. Hosomi and H. Sakurai. J. Am. Chem. Soc. **99**, 1673 (1977).
15. I. Fleming. Chem. Ind. London, 449 (1975).
16. (*a*) T. Livinghouse and R. V. Stevens. J. Chem. Soc. Chem. Commun. 754 (1978); (*b*) R. V. Stevens, G. S. Bissachi, L. Goldsmith, and C. E. Strouse. J. Org. Chem. **45**, 2708 (1980).
17. W. Schlenk and W. Schlenk, Jr. Chem. Ber. **62**, 920 (1929); C. R. Noller and W. R. White. J. Am. Chem. Soc. **59**, 1354 (1937); E. C. Ashby. Bull. Soc. Chim. Fr. 2133 (1972).
18. R. B. Bates, L. M. Kroposki, and D. E. Potter. J. Org. Chem. **37**, 560 (1972).
19. H. O. House and J. M. Wilkins. J. Org. Chem. **43**, 2443 (1978).
20. A. P. Krapcho and A. J. Lovey. Tetrahedron Lett. 957 (1973).
21. G. Fronza, C. Fuganti, and P. Grasselli. Tetrahedron Lett. 2941 (1978); G. Criegee and H. Hover. Chem. Ber. **93**, 2521 (1960).
22. W. Nagata and M. Yoshioka. Org. React. **25**, 255 (1977).
23. R. Adams and A. F. Thol. Org. Synth. Coll. Vol. I, 270 (1932); cf. F. L. James and W. H. Bryan. J. Org. Chem. **23**, 1225 (1958).
24. P. L. Compagnon and M. Miocque. Ann. Chim. Paris, [14] **5**, 23 (1970) and references quoted therein.
25. R. T. Luibrand and E. M. Fujinari. J. Org. Chem. **45**, 958 (1980).
26. S. S. Hixson, P. S. Mariano, and H. E. Zimmerman. Chem. Rev. **73**, 531 (1973); W. G. Dauben, G. Lodder, and J. Ipaktschi. Topics Curr. Chem. **54**, 73 (1975); K. N. Houk. Chem. Rev. **76**, 1 (1976).
27. H.-D. Becker, B. Ruge, B. W. Skelton, and A. H. White. Aust. J. Chem. **32**, 1687 (1979); H.-D. Becker and B. Ruge. J. Org. Chem. **45**, 2189 (1980).
28. L. N. Domelsmith, P. D. Mollere, K. N. Houk, R. C. Hahn, and R. P. Johnson. J. Am. Chem. Soc. **100**, 2959 (1978).
29. L. A. Paquette and R. H. Meisinger. Tetrahedron Lett. 1479 (1970); M. Kuzuya, M. Ishikawa, T. Okuda, and H. Hart. Tetrahedron Lett. 523 (1979); H. Hart and G. M. Love. J. Am. Chem. Soc. **95**, 4592 (1973).
30. H. Prinzbach, H. Hagemann, J. H. Hartenstein, and R. Kitzing. Chem. Ber. **98**, 2201 (1965).
31. M. Barfield and B. Chakrabarti. Chem. Rev. **69**, 757 (1969).
32. P. N. Rylander. Organic synthesis with noble metal catalysts. Academic Press, New York, NY. 1973. Chapt. 5.
33. R. D. Clark and C. H. Heathcock. Tetrahedron Lett. 1713 (1974).
34. H. O. House, C. Chu, J. M. Wilkins, and M. J. Umen. J. Org. Chem. **40**, 1460 (1975); O. P. Vig, J. C. Kapur, and S. D. Sharma. J. Indian Chem. Soc. **45**, 734 (1968); E. J. Corey and R. L. Carney. J. Am. Chem. Soc. **93**, 7318 (1971); R. L. Cargill, D. F. Bushey, P. D. Ellis, S. Wolff, and W. C. Agosta. J. Org. Chem. **39**, 573 (1974); J. Hooz and R. B. Layton. Can. J. Chem. **48**, 1626 (1970); E. J. Corey, D. Floyd, and B. H. Lipshutz. J. Org. Chem. **43**, 3418 (1978); D. B. Ledlie and G. Miller. J. Org. Chem. **44**, 1006 (1979); G. H. Posner, C. E. Whitten, J. J. Sterling, and D. J. Brunelle. Tetrahedron Lett. 2591 (1974); P. M. Wege, R. D. Clark, and C. H. Heathcock. J. Org. Chem. **41**, 3144 (1976); F. Leyendecker, J. Drouin, and J.-M. Conia. Nouv. J. Chim. **2**, 271 (1978).

Can. J. Chem. Downloaded from www.nrcresearchpress.com by 210.87.254.5 on 09/06/12
For personal use only.

# Ene-type adducts from the reaction of 4-phenyl-1,2,4-triazoline-3,5-dione with β-alkyl *s-cis* enones[1]

NORMAN ROBERT HUNTER,[2] BERT PAUL KRAWCHUK, AND JANICE DEBORAH SHILOFF[3]

*Department of Chemistry, University of Manitoba, Winnipeg, Man., Canada R3T 2N2*

Received July 8, 1980[4]

NORMAN ROBERT HUNTER, BERT PAUL KRAWCHUK, and JANICE DEBORAH SHILOFF. Can. J. Chem. **60**, 835 (1982).

The adducts from the reaction of 4-phenyl-1,2,4-triazoline-3,5-dione with a number of α,β-unsaturated ketones have been isolated and characterized. The reaction generally proceeds with migration of the double bond to the β,γ-position and is highly chemoselective towards reaction with enones which have, or can assume, an *s-cis* conformation.

NORMAN ROBERT HUNTER, BERT PAUL KRAWCHUK et JANICE DEBORAH SHILOFF. Can. J. Chem. **60**, 835 (1982).

On a isolé et caractérisé les adduits provenant de la réaction de la phényl-4 triazoline-1,2,4 dione-3,5 avec un certain nombre de cétones α,β non saturées. La réaction procède généralement par la migration de la liaison double vers la position β,γ et elle est très chémosélective vis-à-vis les énones qui ont, ou qui peuvent prendre, une conformation *s-cis*.

[Traduit par le journal]

## Introduction

Recently Sammes (2) reviewed the photocatalysed enolization reaction which occurs for a wide variety of phenones. In many cases the dienol formed in the photoenolization process has sufficient stability to be observed spectroscopically, and in other cases the dienol has been trapped in a Diels–Alder cycloaddition reaction with an appropriate dienophile (3). Our interest in the photoenolization of α,β-enones (4) led us to attempt the trapping of transient dienols from β-alkyl α,β-unsaturated ketones with a reactive dienophile. We chose to study (+)-pulegone (see Table 1, compound **4**) since it does not undergo deconjugation upon photolysis.[5] At the outset of our investigation, there was no evidence of a dienol formed upon photolysis of β-alkyl α,β-enones but we anticipated that if a dienol were formed it could be trapped with a highly reactive dienophile such as 4-phenyl-1,2,4-triazoline-3,5-dione (PTAD)[6] (Scheme 1).

PTAD has been shown to be one of the most reactive dienophiles known (for a summary of the use of triazolinediones as dienophiles see ref. 7) and seemed to be an appropriate choice for the trapping experiments.

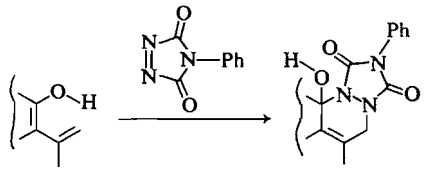

SCHEME 1

When these trapping experiments were attempted, however, it soon became apparent that the product (a mixture of diastereomers **12***a* and **12***b*, see Table 1) did not arise from a route involving that outlined in Scheme 1, but rather via an ene reaction involving ground state (+)-pulegone.

The ene reaction has been studied thoroughly and reviewed for both the inter- and intramolecular cases (refs. 8 and 9, respectively). However, only one case of a probable ene reaction of a β-alkyl α,β-enone (specifically isophorone) has been reported in the literature (10). The results of the PTAD – (+)-pulegone reaction prompted us to investigate the reaction of PTAD with a variety of other β-alkyl enones.[7] Pirkle and Stickler (11) had earlier observed the ene reaction of PTAD with alkenes. Corey and Snider (12) have also used PTAD as an enophile in a synthesis of prostaglandins, and Magnus and co-workers (13) have recently reported the reaction of PTAD with allylsilanes.

## Results and discussion

A total of eleven different β-alkyl α,β-enones

[1]A portion of this work appeared as a preliminary communication (1).

[2]Author to whom enquiries should be addressed.

[3]Taken in part from the M.Sc. thesis of J. D. S., August, 1977.

[4]Revision received December 2, 1981.

[5]N. R. Hunter, unpublished studies.

[6]Shortly after our trapping attempts Tada and Miura (5) demonstrated the existence of a transient dienol from several β-disubstituted α,β-enones by a deuterium exchange and low temperature infrared studies. Subsequently, Noyori *et al.* (6) reported the isolation of a stable dienol from photolysis of 1-acetylcyclooctene.

[7]Subsequent to the completion of this study, Professor T. R. Hoye, University of Minnesota, informed us of his investigation of the reaction of PTAD with a number of α,β-unsaturated ketones and esters. The results of his study, which is complimentary to ours, have been reported recently (24). We thank Professor Hoye for his exchange of information.

0008-4042/82/070835-05$01.00/0

©1982 National Research Council of Canada/Conseil national de recherches du Canada

Can. J. Chem. Downloaded from www.nrcresearchpress.com by 210.87.254.5 on 09/06/12
For personal use only.

Can. J. Chem. Downloaded from www.nrcresearchpress.com by 210.87.254.5 on 09/06/12
For personal use only.





TABLE 1. Adducts from the reaction of 4-phenyl-1,2,4-triazoline-3,5-dione with α,β-enones

| Enone | PTAD adduct[a] | Yield (%)[b] | Melting point (°C) | Infrared ($cm^{-1}$) | $^1H$ nmr (ppm) | Mass spectrum (*m/e*) | Analysis[c] |
|---|---|---|---|---|---|---|---|
| | | 79 | 120–121 | 3350<br>1782<br>1718<br>1605 | 1.88, 3H, bs<br>2.27, 3H, s<br>5.05, 1H, s<br>5.20, 1H, m<br>5.35, 1H, s<br>7.35, 5H, s<br>7.80, 1H, bs | 273 ($M^+$)<br>230<br>187<br>43 | C: 62.02 (61.53)<br>H: 5.65 (5.53)<br>N: 15.38 (15.38) |
| 1 | 9 | | | | | | |
| | | 75 | 180–181 | 3350<br>1780<br>1715<br>1668<br>1600 | 1.5–2.1, 6H, m<br>2.13, 3H, s<br>5.00, 1H, bs<br>7.05, 1H, s<br>7.35, 5H, s<br>7.80, 1H, bs | 299 ($M^+$)<br>178<br>177<br>123 | C: 63.98 (64.20)<br>H: 5.71 (5.72)<br>N: 14.22 (14.04) |
| 2 | 10 | | | | | | |
| | | 78 | 177–178.5 | 3350<br>1780<br>1720<br>1600 | 1.80, 3H, s<br>4.95, 1H, s<br>5.30, 1H, bs<br>7.40, 5H, bd<br>8.95, 1H, bs | 313 ($M^+$)<br>244<br>201<br>188<br>77 | C: 65.22 (65.16)<br>H: 6.25 (6.11)<br>N: 13.38 (13.41) |
| 3 | 11 | | | | | | |
| | **12***a*, *b* | 62 | | | | | C: 65.88 (66.04)<br>H: 6.60 (6.47)<br>N: 13.01 (12.84) |
| | 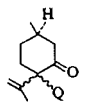 | | 184–186 | 3350<br>1780<br>1720<br>1715 (sh)<br>1605 | 1.00, 3H, d ($J = 4$ Hz)<br>1.80, 3H, bs<br>2.2–2.7, 6H, m<br>4.97, 1H, d<br>5.23, 1H, bs<br>7.35, 5H, s<br>8.40, 1H, bs | 327 ($M^+$)<br>151<br>81 | |
| 4 | **12***a*, *b*[d] | **12***a* | | | | | |
| | | | 153–155 | 3350<br>1780<br>1720<br>1600 | 1.00, 3H, d ($J = 4$ Hz)<br>1.85, 3H, bs<br>2.1–2.7, 6H, m<br>5.03, 1H, s<br>5.32, 1H, bs<br>7.35, 5H, s<br>8.50, 1H, bs | 327 ($M^+$)<br>151<br>81 | |
| | | **12***b* | | | | | |
| | | 55 | 171–173 | 3350<br>1780<br>1715<br>1675 | 1.70, 3H, s<br>1.95, 3H, d ($J = 2$ Hz)<br>2.30, 2H, t ($J = 6$ Hz)<br>2.70, 2H, t ($J = 6$ Hz)<br>4.87, 1H, bs<br>5.15, 1H, q ($J = 2$ Hz)<br>5.90, 1H, bs<br>7.33, 5H, s<br>8.55, 1H, bs | 325 ($M^+$)<br>296<br>149 | C: 66.45 (66.46)<br>H: 5.83 (5.85)<br>N: 13.01 (12.92) |
| 5 | 13 | | | | | | |

Can. J. Chem. Downloaded from www.nrcresearchpress.com by 210.87.254.5 on 09/06/12
For personal use only.

TABLE 1. (*Concluded*)

| Enone | PTAD adduct[a] | Yield (%)[b] | Melting point (°C) | Infrared ($cm^{-1}$) | $^1H$ nmr (ppm) | Mass spectrum (*m/e*) | Analysis[c] |
|---|---|---|---|---|---|---|---|
| | 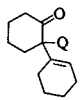 | 50 | 228–230 | 3350<br>1778<br>1720 (sh)<br>1705<br>1602 | 1.5–2.8, 16H, m<br>5.67, 1H, bs<br>7.35, 5H, s<br>8.75, 1H, bs | 353 ($M^+$)<br>177 | C: 66.86 (67.99)<br>H: 6.54 (6.56)<br>N: 11.79 (11.89) |
| **6** | **14** | | | | | | |
| | | 40 | 182–183.5 | 3350<br>1775<br>1705 (vs)<br>1600 | 1.71, 6H, s<br>2.43, 4H, bs<br>7.20, 1H, s<br>7.37, 5H, bs<br>9.10, 1H, bs | 299 ($M^+$)<br>177<br>123 | C: 64.53 (64.20)<br>H: 5.86 (5.72)<br>N: 14.18 (14.04) |
| **7** | **15** | | | | | | |
| 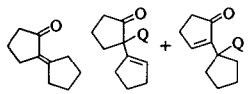 | | 42 | 172–174 | 3350<br>1775<br>1740<br>1705<br>1600 | 1.6–2.2, 4H, m<br>2.2–2.8, 8H, m<br>5.75, 0.6H, bs<br>7.33, 5.4H, bs<br>8.90, 1H, bs | 325 ($M^+$)<br>149 | C: 66.62 (66.45)<br>H: 6.16 (5.89)<br>N: 13.06 (12.91) |
| **8** | **16**[e] **17**[e] | | | | | | |

[a] Q– = 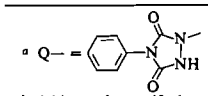

[b] Yields are for purified products and have not been optimized.
[c] Experimental (calculated).
[d] **12***a* and **12***b* were obtained as a diastereomeric mixture which was separated on a silica gel column.
[e] **16** and **17** were inseparable. The ratio of **16**/**17** by nmr was approximately 3:2.

Can. J. Chem. Downloaded from www.nrcresearchpress.com by 210.87.254.5 on 09/06/12
For personal use only.

were chosen for our investigation of their reaction with PTAD. These compounds were either prepared according to literature procedures or obtained commercially (see Experimental). For each compound used in the study a standard reaction procedure was used as described in the Experimental.

The yield for each adduct is recorded in Table 1 and is based on an analytically pure sample obtained by recrystallization of the crude reaction mixture. No attempt has been made to optimize the yield for individual reactions. Yields of 75 to 80% are readily obtained after one recrystallization. All of the structures assigned to the adducts are in complete agreement with the spectral and analytical data which are summarized in the table.

In contrast to the compounds listed in the table the other three enones chosen (3-methylcyclohex-2-en-1-one, 3,3,5-trimethylcyclohex-2-en-1-one, and 3-phenylbut-3-en-2-one) were recovered unreacted after treatment with PTAD under standard conditions.

These results, coupled with the observation that piperitenone (**5**) reacts only at the enone site which has an *s-cis* methyl, indicate the preferential reactivity of PTAD with the β-methyl group of those compounds which have, or can assume, an *s-cis* geometry. The reaction of acetylcyclohexene (**2**) with PTAD gave the adduct **10** which could arise from a regular ene reaction as first reported by Pirkle and Stickler (11).

Our results of the reaction of PTAD with enones (and those of Hoye[7]) reveal that the reaction proceeds with a high degree of regioselectivity. Thus, the acyclic case (**1**) and the exocyclic cyclohexenones (**3**, **4**, **5**, and **6**) all react with the introduction of the PTADH moiety at the α-position and movement of the double bond out of conjugation (cf. **9**, **11**, **12***a*, **12***b*, **13**, and **14**).

In contrast, however, the isopropylidenecyclopentanone (**7**) reacts with opposite regiochemistry (cf. **15**) where the double bond moves into conjugation in the five membered ring and the PTADH functionality becomes attached at the original β-carbon of the enone system. Similarily, but less efficiently, the enone **8** yields **17**. This latter example is the only case where a mixture of double bond isomers was obtained.

From a mechanistic point of view one can speculate about several possible modes of reaction of PTAD with these enones. Such mechanistic speculation, however, must account for several unique features of the reaction. Firstly, the high degree of site selectivity whereby, with the exception of compounds **10**, **15**, and **17**, the PTADH moiety becomes attached to the α-position to the carbonyl can be explained by a normal ene reaction (Scheme 2) with a secondary orbital overlap between the carbonyl group of the enone and the carbonyl–nitrogen system of the PTAD. The formation of compounds **10**, **15**, and **17** can then be considered to arise from a normal ene reaction leading to the thermodynamically more stable conjugated enone. This argument is particularly cogent for compounds **15** and **17**. A second observation which must be explained is the necessity for an *s-cis* conformation of the β-alkyl group in the enone. Once again the normal ene reaction (Scheme 2) may be used to explain the reactivity observed. For systems where the β-alkyl group cannot adopt an *s-cis* conformation the secondary overlap explained above is not possible in any interaction which would lead to an ene reaction of the β-alkyl group.

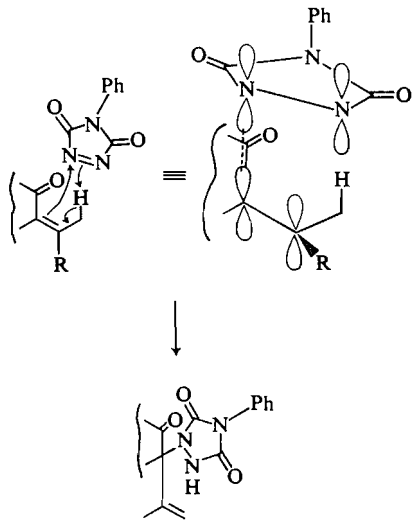


SCHEME 2

The necessity of an *s-cis* conformation of the enones represents a parallel between our results and the recently reported reaction of singlet oxygen with α,β-unsaturated ketones and lactones (14). (For recent discussions of the mechanism of the singlet oxygen ene reaction see refs. 15 and 16.) It is worth noting here that Greene has reported on the mechanism of the ene reaction and cycloaddition of triazolinediones with simple alkenes (25).

As a result of our investigation, a new method for introduction of a nitrogen functionality at the α-position of a ketone is possible. This reaction has potential application both for effecting deconjugation of α,β-enones and also for selective oxidation of these compounds.

Can. J. Chem. Downloaded from www.nrcresearchpress.com by 210.87.254.5 on 09/06/12
For personal use only.

## Experimental

The infrared spectra were recorded on a Perkin–Elmer Model 700 spectrometer as methylene chloride solutions. Proton magnetic resonance spectra were recorded on a Varian Anaspect EM 360 spectrometer using deuterochloroform as solvent and tetramethylsilane as internal standard. Chemical shifts are recorded as values in ppm relative to TMS ($\delta_{TMS} = 0$ ppm). Mass spectra were measured with a Finnigan 1015 quadrupole mass spectrometer. Melting points were determined on a Fisher–Johns melting point apparatus. Column chromatography was done utilizing Camag DSF-5 silica gel containing 5% calcium sulfate. All organic extracts were dried over magnesium sulfate and solvents were removed *in vacuo* using a rotary evaporator. Solvents were used as obtained from commercial sources. Elemental analyses were done by Chemalytics Inc., Tempe, Arizona.

*4-Phenyl-1,2,4-triazoline-3,5-dione (PTAD)*

4-Phenyltriazole (prepared according to Cookson *et al.* (17)) was oxidized to PTAD using *N*-bromosuccinimide according to the procedure of Wamhoff and Wald (18).

*Enones for PTAD–adduct formation*

Isopropylidenecyclopentanone (**7**) was prepared by condensation of acetone and cyclopentanone according to the literature procedure (19). Isopropylidenecyclohexanone (**3**) was prepared from ethyl 2-cyclohexanone carboxylate (Aldrich) according to the procedure of Mukherjii *et al.* (20). 2-Cyclopentylidenecyclopentanone (**8**) was prepared from cyclopentanone following the literature method (21). The procedure of Reese (22) was used to prepare 2-cyclohexylidenecyclohexanone (**6**) from 2-(1-cyclohexyl) cyclohexanone (23). Mesityl oxide (**1**), 1-acetyl-1-cyclohexene (**2**) and (+)-Pulegone (**4**) were obtained from Aldrich Chemical Company. Piperitenone (**5**) was obtained as a gift from Dr. J. J. Beereboom, Pfizer Inc., Groton, Connecticut.

*Typical procedure for the preparation of PTAD–enone adducts*

*Reaction of PTAD with piperitenone (5): formation of adduct 13*

To a solution of piperitenone (1.50 g, 10.0 mmol) in 15 mL of ethyl acetate at ambient temperature was added 1.75 g (10.0 mmol) of 4-phenyl-1,2,4-triazoline-3,5-dione. The reaction mixture was placed in the refrigerator at ~3°C for 2 h. At the end of that time the bright red color of PTAD had disappeared. After filtration to remove a small amount of white precipitate, pentane (10 mL) was added with stirring and the resulting precipitate was filtered, washed with cold benzene (20 mL), and dried under suction. The crude product was recrystallized from a small volume of ethyl acetate to give the adduct **13** (1.79 g, 5.51 mmol; 55%) with mp 171–173°C. Complete spectral data for **13** is recorded in the table.

All other adducts were prepared and purified in a similar way with the only variable being the reaction time (20 min to 1 day).

## Acknowledgements

Dr. J. J. Beereboom is thanked for a generous gift of piperitenone. Dr.'s Jim Charlton and Ted Edwards are thanked for discussion concerning possible mechanisms for the reaction. The University of Manitoba Research Board and the Natural Sciences and Engineering Research Council of Canada (formerly the National Research Council) are thanked for financial support.

1. J. D. Shiloff and N. R. Hunter. Tetrahedron Lett. 3773 (1976).
2. P. G. Sammes. Tetrahedron, **32**, 405 (1976).
3. E. Block and R. Stevenson. J. Chem. Soc. Perkin Trans. I, 308 (1973); M. Pfau, E. W. Sarver, and N. D. Heindal. Bull. Soc. Chim. Fr. 183 (1973).
4. J. D. Shiloff and N. R. Hunter. Can. J. Chem. **57**, 3301 (1979).
5. M. Tada and K. Miura. Bull. Chem. Soc. Jpn. **49**, 713 (1976).
6. R. Noyori, H. Inoue, and M. Kato. Bull. Chem. Soc. Jpn. **49**, 3673 (1976).
7. M. E. Burrage, R. C. Cookson, S. S. Gupte, and I. D. R. Stevens. J. Chem. Soc. Perkin Trans. II, 1325 (1975).
8. H. M. R. Hoffman. Angew Chem. Int. Ed. Engl. **8**, 566 (1969); J. M. Conia and P. LePerchec. Synthesis, 1 (1976); E. C. Keung and H. Alper. J. Chem. Educ. **49**, 97 (1972).
9. W. Oppolzer and V. Snieckus. Angew. Chem. Int. Ed. Engl. **17**, 476 (1978).
10. A. Cornélis, P. Laszlo, and C. Pasquet. Tetrahedron Lett. 4335 (1973).
11. W. H. Pirkle and J. C. Stickler. J. Chem. Soc. Chem. Commun. 761 (1967).
12. E. J. Corey and B. B. Snider. Tetrahedron Lett. 3091 (1973).
13. A. Gopalan, R. Moerck, and P. Magnus. J. Chem. Soc. Chem. Commun. 548 (1979).
14. H. E. Ensley, R. U. C. Carr, R. S. Martin, and T. E. Pierce. J. Am. Chem. Soc. **102**, 2836 (1980).
15. L. B. Harding and W. A. Goddard III. J. Am. Chem. Soc. **102**, 439 (1980).
16. M. Orfanopoulos and L. M. Stephenson. J. Am. Chem. Soc. **102**, 1418 (1980).
17. R. C. Cookson, S. S. Gupte, I. D. R. Stevens, and C. T. Watt. Org. Synth. **51**, 121 (1971).
18. H. Wamhoff and K. Wald. Org. Prep. Proced. Int. **7**, 251 (1975).
19. R. Cornubert and C. Borrell. Bull. Soc. Chim. Fr. **47**, 958 (1935).
20. S. M. Mukherjii, R. B. Gaudhi, and O. P. Vig. J. Indian Chem. Soc. **33**, 853 (1956).
21. I. E. Dolgii, A. P. Meshcheryakou, and I. B. Shvedova. Izv. Akad. Nauk SSSR Ser. Khim. **9**, 2135 (1968); Chem. Abstr. **70**, 774292z (1969).
22. J. Reese. Chem. Ber. **75**, 384 (1942).
23. E. Wenkert, S. K. Bhattacharya, and E. M. Wilson. J. Chem. Soc. 5617 (1964.)
24. T. R. Hoye, K. J. Bottorff, A. J. Caruso, and J. F. Dellaria. J. Org. Chem. **45**, 4287 (1980).
25. C. A. Seymour and F. D. Greene. J. Am. Chem. Soc. **102**, 6384 (1980).

# Réactivité carbanionique de l'enchainement $P^V—CH_2—CH_2—S—$. Application à la synthèse d'un nouveau type de coordinats phosphorylés tétradentés

MONIQUE SAVIGNAC ET PAUL CADIOT

*Laboratoire de Recherche de Chimie Organique, École Nationale Supérieure de Chimie de Paris, 11, rue P. et M. Curie, 75005 Paris, France*

ET

FRANÇOIS MATHEY

*Équipe SNPE–CNRS, 2-8, rue Henry Dunant, B.P. 28, 94320 Thiais, France*

Reçu le 30 juin 1981

MONIQUE SAVIGNAC, PAUL CADIOT et FRANÇOIS MATHEY. Can. J. Chem. **60**, 840 (1982).

La metallation par le *tert*-butyllithium de composés comportant l'enchaînement $P^V—CH_2—CH_2—SR$ se traduit par l'élimination du groupe SR (R = H, $CH_3$) qui est suivie de l'addition du *tert*-BuLi. L'application de cette réaction d'élimination–addition aux oxydes de phosphines fonctionnels $(C_6H_5)_2P(O)CH_2Z$ (Z = CN, COOEt) a permis de synthétiser des composés γ-diphosphorylés fonctionnels originaux. Ceux-ci se dissocient en milieu basique suivant un mécanisme inverse à celui de leur formation qui a été mis en évidence par réaction du mélange réactionnel sur le *para*-chlorobenzaldéhyde pour donner le *para*-chlorocinnamate d'éthyle.

MONIQUE SAVIGNAC, PAUL CADIOT, and FRANÇOIS MATHEY. Can. J. Chem. **60**, 840 (1982).

The *tert*-butyllithium metallation of compounds containing the group $P^V—CH_2—CH_2—SR$ proceeds by elimination of the group SR (R = H, $CH_3$) followed by addition of *tert*-BuLi. Application of this addition–elimination reaction to functionalized phosphine-oxides $\phi_2P(O)CH_2Z$ (Z = CN, COOEt) leads to the synthesis of γ-diphosphorylated compounds. These dissociate in basic medium following a mechanism which is the reverse of their formation as shown by treatment of the reaction mixture with *p*-chlorobenzaldehyde to give ethyl *p*-chlorocinnamate.

[Journal Translation]

Jusqu'à ce jour les composés β-thioéthylphosphorés ont fait l'objet de travaux limités à la préparation (1) et l'emploi en chimie de coordination (2) de β-thioéthylphosphines. À la suite de nos résultats sur les propriétés de ces coordinats trivalents (2*a*) nous avons entamé une étude des propriétés des espèces tétracoordinées correspondantes, oxydes et sulfures.

## A. *Réactivité anionique des sulfures de β-thioéthyldiphényl phosphines*

En présence de soufre élémentaire la β-thioéthyldiphényl phosphine (1*a*) **1** est convertie en sulfure **2** dont la méthylation conduit au thioéther **3** avec des rendements élevés.

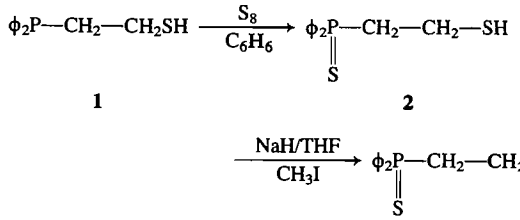

**1** **2** **3**

La métallation en position α du groupe thiophosphoryle des composés **2** et **3** nécessite l'emploi d'une base forte. Le *n*-butyllithium dans le tétrahydrofuranne (THF) nous ayant donné des résultats peu interprétables, nous lui avons substitué le complexe *tert*-butyllithium – TMEDA dans l'hexane. L'addition soit de **2** soit de **3** au complexe *tert*-BuLi/TMEDA à −40°C provoque l'apparition immédiate d'une coloration orangée-vif stable jusqu'à 0°C. Après hydrolyse et traitement en parallèle des deux réactions, un même composé **7** est obtenu correspondant pour **2** à la substitution du groupe —S—H par le groupe *tert*-BuLi et pour **3** à la substitution du groupe —$SCH_3$ par le même groupe *tert*-BuLi. La formation d'un même composé **7** à partir de **2** ou de **3** trouve probablement son origine dans un mécanisme d'élimination–addition représenté sur le schéma suivant:

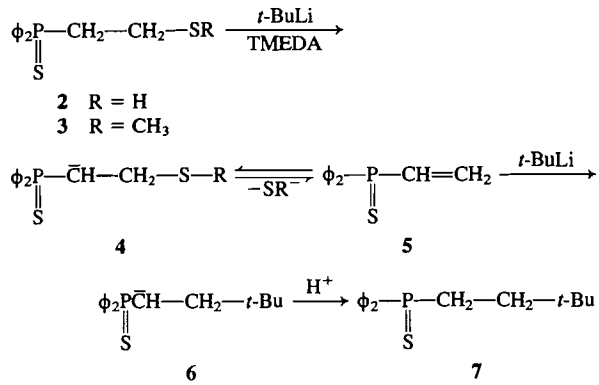

**2** R = H
**3** R = $CH_3$

**4** **5** **6** **7**

À la formation de l'anion lithien **4** succède l'apparition du vinylique **5** par élimination d'un

0008-4042/82/070840-05$01.00/0

©1982 National Research Council of Canada/Conseil national de recherches du Canada

Can. J. Chem. Downloaded from www.nrcresearchpress.com by 210.87.254.42 on 09/06/12
For personal use only.

Can. J. Chem. Downloaded from www.nrcresearchpress.com by 210.87.254.42 on 09/06/12
For personal use only.

anion thiolate ($S^{2-}$ ou $RS^-$), elle-même suivie de l'addition nucléophile du *tert*-BuLi pour engendrer un nouveau carbanion **6** dont la protonation fournit **7**. La vinylphosphine **5** est soumise à une réaction réversible d'élimination–addition qui est déplacée vers la formation de **6** par consommation progressive de **5** par le *tert*-BuLi.

Des additions identiques sur le même type de composé ont déjà été décrites (3). D'autre part la réversibilité de l'addition des anions thiolates sur les composés vinyliques du phosphore a également été mise en évidence lorsque ceux-ci sont substitués en α par un groupe attracteur (4).

Nous avons vérifié que le processus d'élimination–addition est indépendant de la température (entre −60° et −10°C); en outre l'étape d'addition du *tert*-BuLi doit être plus rapide que l'étape d'élimination puisque lorsqu'on opère en défaut de *tert*-BuLi (1 mole au lieu des deux moles nécessaires) on récupère après hydrolyse un mélange de **7** et de produit de départ (**2** ou **3**). L'anion α-lithié **6** peut être alkylé **8** ou carbonaté **10** (3).

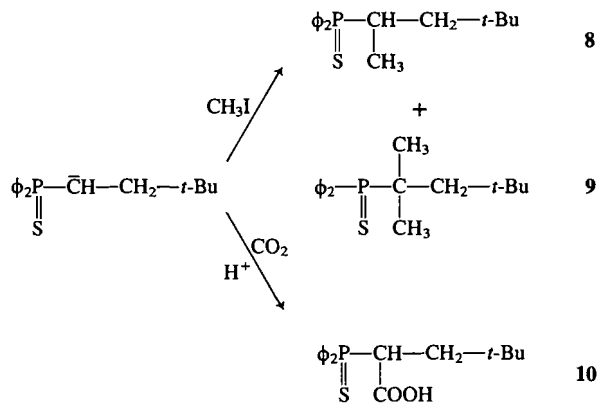

Le produit brut de méthylation **8** contient une petite quantité de produit diméthylé **9** (environ 5%) dont la présence est décelée par spectrométrie de masse.

La présence de **9** peut être attribuée à la formation d'un nouvel anion en α du phosphoré **11** résultant d'un échange entre **6** et **8**.

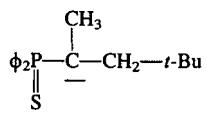

**11**

B. *Application de l'élimination–addition à la préparation de composés γ-diphosphorylés fonctionnels*

Les résultats précédents ont été étendus à la préparation de nouvelles espèces diphosphorylées de formule générale **13** dont à notre connaissance aucune synthèse n'avait été décrite.

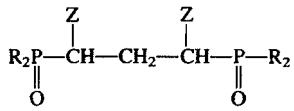

**13**

*a* R = ϕ Z = CN
*b* R = ϕ Z = COOEt
*c* R = EtO Z = COOEt

Le précurseur fonctionnel **14** est un phosphonate ou une phosphine susceptible de donner dans des conditions douces (NaH/THF) l'anion correspondant **15**. La condensation de cet anion **15** sur le

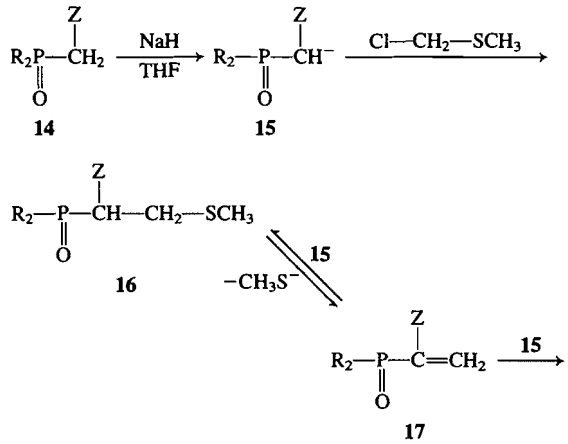

chlorométhylthiométhyléther conduit à **16** générateur en milieu basique du dérivé vinylique **17** sur lequel le précurseur anionique **15** vient s'additionner pour conduire après protonation à l'espèce **13**.

Dans cette réaction c'est l'anion **15** qui induit l'élimination de **16** en **17**, puis le thiométhylate de sodium formé l'entretient, la rendant irréversible. Lorsque Z = COOEt, le composé **13***b* ou **13***c* représente le produit unique; lorsque Z = CN on isole également une faible quantité du composé β-sulfuré **16***a*. Sa présence confirme la réversibilité des processus concurrents d'addition du méthylthiolate et de l'anion **15***a*.

Les composés **13** sont isolés sous la forme d'un mélange sensiblement équimoléculaire de deux diastéréoisomères **13** (α + β). Dans le cas de **13***a* un des diastéréoisomères **13**α (α correspond au dias-

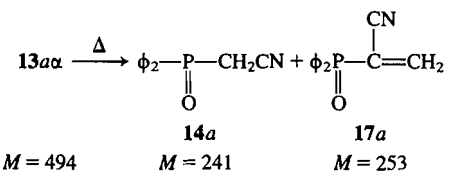

**14***a* **17***a*

$M = 494$ $M = 241$ $M = 253$

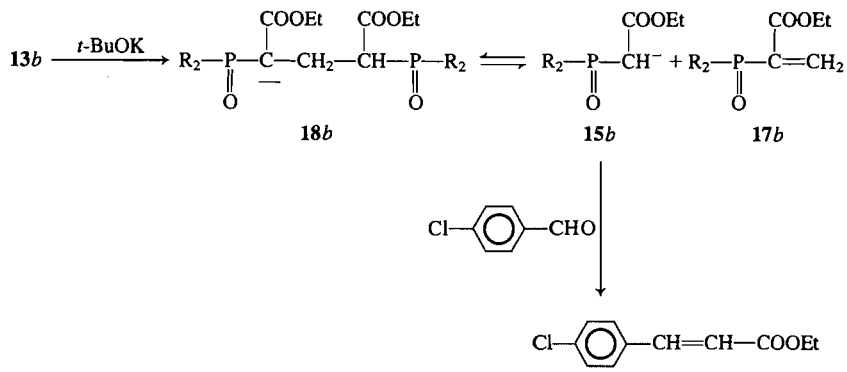


téréoisomère le moins déblindé en rmn $^{31}P$) est isolable par cristallisation dans l'acétate d'éthyle. Il a été complétement caractérisé (rmn: $^{1}H$, $^{31}P$, $^{13}C$; sm; analyse).

En spectrométrie de masse l'interprétation la plus plausible de sa décomposition consiste en une dissociation inverse du processus de formation.

Ce schéma de dissociation a été également vérifié avec **13***b* et **13***c*.

C. *Interconversion en milieu basique des composés isomères γ-diphosphorylés* ***13*** α,β

La réaction a été étudiée sur le mélange de diastéréoisomères **13***b* (α + β). En présence de *tert*-BuOK dans le THF, le mélange des deux diastéréoisomères conduit aux monanions **18***b* qui se dissocient réversiblement en phosphoré vinylique **17***b* et anion **15***b*. Cette dissociation inverse du processus de formation est pleinement confirmée en piègeant l'anion **15***b* par le *p*-chlorobenzaldéhyde. On obtient comme seul produit de réaction le *p*-chlorocinnamate d'éthyle "*trans*"; quant à **17***b* il polymérise.[1]

Cette réaction consomme préférentiellement un des diastéréoisomères. Après hydrolyse on récupère du produit de départ non transformé qui n'est plus un mélange équimoléculaire de diastéréoisomères mais contient très majoritairement l'un deux. Ce nouveau mélange traité par le *tert* BuOK dans le THF redonne le mélange équimoléculaire initial résultant de l'action de NaH sur **14**. Il n'y a donc pas d'influence notable du contre-ion sur le processus d'interconversion. Il semble que l'un des isomères de **13***b* soit préférentiellement métallé par *tert* BuOK pour des raisons stériques ou de solubilité ce qui expliquerait sa consommation préférentielle.

Dans le cas des diastéréoisomères **13***a* nous observons un phénomène d'interconversion identique; le diastéréoisomère pur **13***a*α mis en solution dans le THF en présence de *tert* BuOK subit une interconversion rapide pour donner le mélange équimoléculaire des diastéréoisomères **13***a* (α + β).

D. *Isomérisation du composé γ-diphosphorylé* ***13***a*α en milieu acide*

Le diastéréoisomère **13***a*α s'isomérise en milieu acide en un mélange équimoléculaire des diastéréoisomères α et β. Cette équilibration a été réalisée en 24 h à 20°C en solution chloroformique ou en une heure en solution faiblement acétique de chlorure de méthylène. Dans le chlorure de méthylène pur cette transformation est quasiment inexistante au bout d'une semaine. Il est vraisemblable que l'acide chlorhydrique toujours présent dans $CHCl_3$ ou l'acide acétique conduisent à la protonation de la fonction nitrile suivie de l'épimérisation progressive du carbone porteur du groupe fonctionnel.

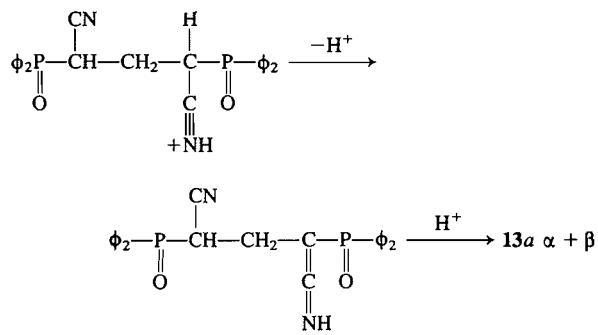


E. *Conformation du diastéréoisomère* ***13***a*α*

La conformation du diastéréoisomère **13***a*α peut être définie par étude de son spectre de rmn $^{13}C$. En solution dans $CDCl_3$ les carbones en α du phos-

[1]Un essai de préparation de **17***b* a été effectué en adaptant le mode opératoire correspondant à la préparation du méthyl-2 (diéthylphosphono)acrylate (4). L'action du formaldéhyde sur l'oxyde de diphénylphosphino-méthyl carbéthoxyéthyl par chauffage pendant 8 h conduit après traitement à l'alcool correspondant qui par déshydratation en présence d'APTS fournit le composé vinylique **17***b*. Il n'a jamais pu être isolé car il polymérise spontanément lors de sa purification.

Can. J. Chem. Downloaded from www.nrcresearchpress.com by 210.87.254.42 on 09/06/12
For personal use only.

Can. J. Chem. Downloaded from www.nrcresearchpress.com by 210.87.254.42 on 09/06/12
For personal use only.

phore porteurs des groupes nitriles apparaissent (31, 65 ppm) sous la forme d'un doublet de doublet ($^1J_{PC}$ = 60,3 Hz et $^3J_{PC}$ = 8,2 Hz). A l'examen des courbes liant l'angle dièdre C—C—C—P au $^3J_{PC}$ (5) nous aurions dans notre cas un angle dièdre de 130°. Une disposition rigoureusement "*trans*" des groupes fonctionnels $P_1$ et CH(CN)—$P_2$ autour de la liaison CH(CN)—$CH_2$ correspondrait environ à $^3J_{PC}$ de 15 Hz comme on aurait pu également le supposer sur la base d'argument purement stérique. Nous proposons donc une certaine stabilisation de la disposition "*cis*" par interaction de l'azote du groupe nitrile avec le phosphore positif du phosphoryle.

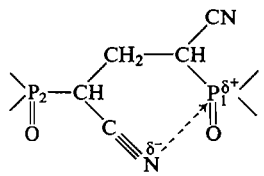

L'étude ir en solution dans le chloroforme des vibrations $\nu_{C\equiv N}$ dans $CH_3CN$, **14***a*, **13***a* va dans le sens de cette interprétation:

| | $\nu_{C\equiv N}$ cm$^{-1}$ | $\Delta\nu$ |
|---|---|---|
| $CH_3CN$ | 2291 | |
| **14***a* | 2252 | 39 |
| **13***a* | 2241 | 11 |

L'importance de cet abaissement supplémentaire nous semble difficile à expliquer par un simple effet inductif à travers quatre liaisons carbone–carbone mais est en faveur d'une intéraction directe à travers l'espace du type de celle figurée sur le schéma.

*Conclusion*

L'étude des espèces β-thioéthylphosphines tétracoordinées a permis de dégager deux faits importants: (*i*) une généralisation du phénomène d'élimination–addition en milieu basique sur les dérivés comportant l'enchaînement $P^V$—$CH_2$—$CH_2$—Nu; et (*ii*) du point de vue synthètique il ouvre la voie à la préparation de nouvelles molécules originales γ-diphosphorylées par un processus relativement simple.

## Partie expérimentale

Les spectres rmn $^1$H sont enregistrés sur Varian T 60 et XL 100; le tetraméthylsilane (TMS) est utilisé comme référence interne; le solvant est $CDCl_3$ sauf lorsque le contraire est précisé.

*Sulfure du diphénylphosphino-2 éthanethiol 2*

Il est préparé par addition du diphénylphosphino-2 éthanethiol (**1**) (10 g) à une suspension de soufre en fleur en quantité équimoléculaire dans le benzène à 0°C. Après retour à température ambiante en 30 min, le solvant est évaporé et l'huile est reprise par l'éther de pétrole (30–60°C). L'huile cristallise; *m* = 8,7 g (Rdt = 80%).

*Méthylation du sulfure de diphénylphosphino-2 éthanethiol 3*

Le sulfure de diphénylphoshino-2 éthanethiol (2 g; 0,0071 mol) dans 20 mL de THF est ajouté à une suspension de 0,35 g (0,0071 mol + 5%) d'hydrure de sodium dans 30 mL de THF. Le mélange est agité 1 h à température ambiante, puis 1,1 g (0,0071 mol + 5%) d'iodure de méthyle dans 10 mL de THF sont ajoutés. Après une heure d'agitation à température ambiante, la solution est hydrolysée (20 mL), puis extraite par l'éther éthylique (3 × 50 mL). Après séchage et évaporation on obtient 1,8 g de **3** (86,7%). Ce produit est utilisé brut; rmn $^1$H, δ: 1,83 (s, $CH_3$), 2,6 ($(CH_2)_2$), 7,4 (massif Ph) ppm.

*Réaction du sulfure de diphénylphosphino-2 éthanethiol avec le* tert-*butyllithium*

Au complexe *t*-BuLi/TMEDA (15,5 cm$^3$/2,59 g; 0,0213 mol) préalablement formé dans 40 mL d'hexane, on ajoute à −40°C, 2 g (0,0071 mol) de **2** en solution dans un minimum de $C_6H_6$ (~10 mL). Une coloration orangée-vif se développe. La métallation est poursuivie pendant 1 h à −40°C.

A. *Hydrolyse*

On additionne à la solution ramenée à température ambiante 30 mL d'une solution aqueuse d'HCl (3 *N*). On extrait à l'éther éthylique (3 × 50 mL), lave au carbonate, sèche et évapore. On obtient 1,25 g de sulfure diméthyl-1,1 diphénylphosphino-3 butane **7** (58%, *F* = 136°C); rmn $^1$H, δ: 0,9 (s, $C(CH_3)_3$), 1,4 (m, $CH_2$), 2,4 (m, $CH_2$), 7,8 (m, Ph) ppm. *Anal.* calc. pour $C_{18}H_{23}PS$: C 71,25; H 7,61; P 10,26%; trouvé: C 71,3; H 7,5; P 9,7%.

B. *Méthylation*

À la solution ramenée à température ambiante, on additionne un large excès de $CH_3I$ (4 g, 0,028 mol). On agite la solution jusqu'à décoloration totale (~1 h), hydrolyse par HCl 3 *N* (30 mL), puis extrait à l'éther (3 × 50 mL). Le produit brut est purifié par chromatographie sur colonne de silice (hexane/$Et_2O$ 80:20). On obtient 0,6 g (Rdt 25%) de sulfure de diphénylphosphino-1 triméthyl-1,3,3 butane, **8** (*F* = 110°C); rmn $^1$H, δ: 0,7 (s, $C(CH_3)_3$), 1,29 (q, $J_{HP}$ = 20 Hz, $J_{HH}$ = 6,7 Hz, $CH_3$), 1,44 (m, $CH_2$), 2,74 (m, CH), 7,72 (m, Ph) ppm; *m/e*: 316(M). *Anal.* calc. pour $C_{19}H_{25}PS$: C 72,15; H 7,9; P 9,8%; trouvé: C 71.9; H 7,8; P, 9,4%.

C. *Carbonatation*

Dans un verre de Dewar contenant de l'éther saturée de $CO_2$ par de la carboglace sèche, on additionne rapidement la solution du carbanion, puis abandonne une nuit. Le lendemain on décante, lave la phase aqueuse à l'éther (3 × 50 mL), acidifie ($H_2SO_4$ concentré), puis extrait à l'éther éthylique (3 × 50 mL), sèche et on concentre: on obtient un produit cristallisé blanc **10** qui est comparé à un échantillon authentique préparé selon la référence 3.

*Réaction du sulfure de diphénylphosphino-2 éthanethiométhyl éther avec le* tert-*butyllithium*

Au complexe *t*-BuLi/TMEDA (9,2 cm$^3$/1,5 g; 0,0123 mol) préalablement formé dans 40 mL d'hexane, on additionne à −40°C 1,8 g (0,0061 mol) de sulfure de diphényl phosphino-2 éthanethiométhyl ether en solution dans le minimum de $C_6H_6$ (~10 mL). La solution prend une coloration orangée-vif. On l'abandonne 1 h à −40°C.

A. *Hydrolyse*

Cette solution est hydrolysée par HCl 3 *N* (30 mL), puis extraite à l'éther éthylique. Après dessication et évaporation du

solvant, on obtient un composé cristallisé ayant les mêmes caractéristiques physiques que le sulfure de diméthyl-1,1 diphénylphosphino-3 butane **7**; $m$ = 0,67 g (35%).

B. *Méthylation*

On laisse la solution remonter à la température ambiante, puis on ajoute un large excès de $CH_3I$. La solution est agitée jusqu'à décoloration complète et hydrolysée par HCl 3 *N* (30 mL), puis extraite par l'éther éthylique (3 × 50 mL). Le produit brut obtenu est purifié par chromatographie sur colonne de silice (hexane/$Et_2O$ 80:20); $m$ = 0,22 g (12%). Il présente les mêmes caractéristiques physiques que **8**.

*Préparation des oxydes de diphosphines* ***13***

*Mode opératoire général*

Nous le décrivons pour R = Ph, Z = COOEt; **13***b*: 14,4 g (0,05 mol) d'oxyde de diphénylphosphinométhyl carbéthoxyéthyl **14***b* dans 50 mL de THF sont ajoutés à température ambiante à une suspension de 2,4 g (0,05 mol + 5%) de NaH dans 20 mL de THF. Après 30 min d'agitation à température ambiante, on additionne 4,83 g (0,05 mol) de chlorométhylthiométhyl ether dans 10 mL de THF. Le mélange réactionnel est progressivement chauffé à 65°C, un abondant précipité de NaCl apparait. Après 3 h à 64°C on hydrolyse (40 mL) et extrait à l'éther éthylique (3 × 50 mL). Le produit brut obtenu est purifié par chromatographie sur colonne de silice (acétate d'éthyle). On obtient un mélange de diastéréoisomères; $m$ = 4 g (Rdt = 42%), $F$ = 154°C; rmn $^1$H, δ: 0,65 (t, $CH_3$), 2,3 (m, $CH_2$), 3,5 (m, $CH_2(CH_3—CH_2)$ et CH), 7,35 (massif Ph) ppm; rmn $^{31}$P, δ: +27,0, + 28,3 ppm; *m/e*: 588 (M). *Anal.* calc. pour $C_{33}H_{34}P_2O_6$: C 67,34; H 5.78; P 10.54%; trouvé: C 67,0; H 5,77; P 9,90%.

*Pour R = Ph, Z = CN* ***13***a *(0,05 mol)*

Par chromatographie sur colonne de silice (acétate d'éthyle) on sépare en tête **16***a*: $m$ = 1,1 g; $F$ = 140°C; rmn $^1$H, δ: 2,18 (s, S—Me), 2,78 (m, $CH_A$—SMe), 3,15 (m, $CH_B$—SMe), 3,68 (m, CH), 7,8 (m, Ph) ppm; rmn $^{31}$P, δ: +23,82 ppm; *m/e*: 301 (M). *Anal.* calc. pour $C_{16}H_{16}NOPS$: C 63,78; H 5,3; P 10,29%; trouvé: C 63,56; H 5,22; P 9,66%. Puis **13***a* pur par cristallisation dans l'acétate d'éthyle: $m$ = 4,15 g, $F$ = 260°C; rmn $^1$H, δ: 2,3 (m, $CH_2$), 3,94 (m, CH), 7,7 (m, Ph) ppm; rmn $^{31}$P, δ: +24,8, +26,1 ppm; *m/e*: 494 (H). *Anal.* calculé: C 70,44; H 4,85; P 12,55%; trouvé: C 70,17; H 4,82; P 11,93%.

*R = EtO, Z = COOEt* ***13***c *(0,05 mol)*

Purification par chromatographie sur colonne de silice (acétate d'éthyle); $m$ = 4,18 g (Rdt = 56%); rmn $^1$H; δ: 1,43 (m, $CH_3$), 2,48 (m, $CH_2$), 3,11 (m, CH), 4,19 (m, $CH_2—CH_3$) ppm; *m/e*: 460 (M).

*Equilibration en milieu basique des composés diphosphorylés* ***13***b

A une suspension de 0,56 g de *t*-BuOK dans 20 mL de THF on additionne un mélange de 2,94 g (0,005 mol) de **13***b* et de 0,830 g (0,0625 mol) de *para*-chlorobenzaldéhyde en solution dans 50 mL de THF. La solution devient limpide puis un précipité apparaît progressivement ($Ph_2P—\overset{\overset{O}{\|}}{O}K$). On hydrolyse par 30 mL d'eau, puis extrait par l'éther éthylique (3 × 50 mL). Après dessication et évaporation on obtient 0,2 g de *para*-chlorocinnamate d'éthyle. Après purification le *para*-chlorocinnamate d'éthyle est comparé à un échantillon authentique.


1. (*a*) J. R. Geigy. A. G. Fr. 1,401, 930, Chem. Abstr. **63**, 116 15h (1965); (*b*) D. L. Dubois, W. H. Myers et D. W. Meek. J. Chem. Soc. Dalton Trans. 1011 (1975); (*c*) D. Brown, R. J. Cross et D. Millinston. J. Chem. Soc. Dalton Trans. 334 (1976); (*d*) M. Ciampolini, P. Dapporto, N. Nardi et F. Zanobini. Inorg. Chim. Acta, **45**, L239 (1980); (*e*) J. Ludvik et J. Podlahova. J. Inorg. Nucl. Chem. **40**, 967 (1978).
2. (*a*) M. Savignac, P. Cadiot et F. Mathey. Inorg. Chim. Acta, **45**, L43 (1980); (*b*) G. Doyle. J. Organometal. Chem. **101**, 85 (1975); A. R. Sanger, C. G. Lobe et J. E. Weiner-Fedorak. Inorg. Chim. Acta, **53**, L123 (1981).
3. (*a*) D. J. Peterson. J. Org. Chem. **31**, 950 (1966), et références citées; (*b*) E. Zbiral. Synthesis, 775 (1974).
4. M. F. Semmelhack, J. C. Tomesch, M. Czarny et S. Boettger. J. Org. Chem. **43**, 1259 (1978).
5. (*a*) C. A. Kingsbury et D. Thoennes. Tetrahedron Lett. **35**, 3037 (1976); (*b*) J. Thiem and B. Meyer. Org. Magn. Reson. **11**, 1 (1978); (*c*) L. D. Quin, M. J. Gallagher, G. T. Cunkle et D. B. Chesnut. J. Am. Chem. Soc. **102**, 3136 (1980).


Can. J. Chem. Downloaded from www.nrcresearchpress.com by 210.87.254.42 on 09/06/12
For personal use only.

# Concerning the conformational distribution in isopropylcyclopropane

TED SCHAEFER AND RUDY SEBASTIAN
*Department of Chemistry, University of Manitoba, Winnipeg, Man., Canada R3T 2N2*
AND
RODERICK E. WASYLISHEN
*Department of Chemistry, University of Winnipeg, Winnipeg, Man., Canada R3B 2E9*

Received August 12, 1981

TED SCHAEFER, RUDY SEBASTIAN, and RODERICK E. WASYLISHEN. Can. J. Chem. **60**, 845 (1982).

A partial analysis of the 400 MHz $^1$H nmr spectrum of isopropylcyclopropane yields 8.6 ± 0.2 Hz for the vicinal proton–proton coupling constant between a cyclopropyl proton and the methine proton of the isopropyl group. The fractional population of the *s-trans* conformer is estimated as 0.65 ± 0.10 at 300 K, in reasonable agreement with molecular mechanics and INDO MO computations of the energies of the *gauche* and *trans* forms.

The conformational preference of this molecule is similar to that in *n*-butane and in vinylcyclopropane but contrasts with that in biisopropyl and bicyclopropyl.

TED SCHAEFER, RUDY SEBASTIAN et RODERICK E. WASYLISHEN. Can. J. Chem. **60**, 845 (1982).

Une analyse partielle du spectre rmn du $^1$H à 400 MHz de l'isopropylcyclopropane permet d'établir à 8.6 ± 0.2 Hz la constante de couplage vicinale entre un proton du cyclopropane et le proton méthine du groupe isopropyle. On évalue à 0.65 ± 0.10 la fraction de la population dans la conformation *s-trans*; cette valeur est en bon accord avec des calculs de mécanique moléculaire et INDO MO des énergies des formes *gauche* et *trans*.

La préférence conformationnelle de cette molécule se rapproche de celles du *n*-butane et du vinylcyclopropane mais elle diffère de celles observées avec le biisopropyl et le bicyclopropyl.

[Traduit par le journal]

## Introduction

The electronic and conformational properties of many cyclopropane derivatives have been studied (1, 2). An exception is isopropylcyclopropane (IPCP) for which an empirical force-field (3) predicts the *trans* conformation, **1**, as 380 cal/mol (1 cal ≡ 4.184 J) more stable than either of the two *gauche* forms, **2**. Apparently the only experimental data are the Raman spectra in the liquid and solid phases (4). These are interpreted to mean that only one conformation is present in both phases, probably **1**.

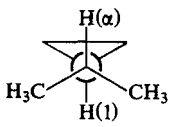


**1**

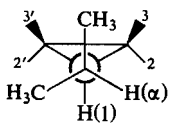


**2**

Here the $^1$H nmr spectrum at 400 MHz is analyzed in enough detail to yield the vicinal coupling, $^3J$, between the methine proton of the isopropyl group and the ring proton. Its magnitude places limits on the conformer distribution.

## Experimental

A 3 mol% solution of IPCP (Chemical Samples Co.) in benzene-$d_6$ was degassed by the freeze–pump–thaw technique and sealed into a 5 mm od nmr sample tube. At 305 K and 100.00 MHz the methyl protons resonate at 6.19 ppm upfield of $C_6H_6$, which itself resonates at 7.15 ppm to low field of internal tetramethylsilane. Accordingly, allowing for small temperature and concentration variations, $\delta_{CH_3}$ is 0.96 ± 0.02 ppm. Decoupling experiments on a WH90 spectrometer did not yield tractable spectra.

The $^1$H nmr spectrum was obtained on a WH400 (University of Guelph) spectrometer at 297 K, utilizing four 20 μs pulses, an acquisition time of 6.55 s, a sweep width of 2500 Hz with 16384 real points and quadrature phase detection. The centerband occurred at 400.1348 MHz. Homonuclear decoupling experiments were also performed.

INDO MO FPT (5) computations utilized an Amdahl 470/V7 system.

## Results and discussion

### *Spectral analysis*

The linewidth of the observed peaks was about 0.8 Hz, part of which at least arises from long-range couplings over four and five bonds. Of the 50 observed peaks, 45 were used in a 12-spin iterative analysis with the computer program NUMARIT (6). The 2084 calculated transitions occurred as 175 groups, each group spanning 0.05 Hz. In all, 289 transitions were assigned to observed peaks. Starting parameters were taken from those for very similar compounds, like 2-hydroxyethyl- and 2-bromoethylcyclopropane (7). The two *cis* vicinal couplings in the $CH_2CH_2$ fragment were set at 9.1 and 9.3 Hz (7), the latter for the protons *trans* to the isopropyl group. These couplings were not allowed to vary during the iteration.

The spectral parameters in Table 1 are probably

0008-4042/82/070845-03$01.00/0
©1982 National Research Council of Canada/Conseil national de recherches du Canada

Can. J. Chem. Downloaded from www.nrcresearchpress.com by 210.87.254.5 on 09/06/12
For personal use only.

Can. J. Chem. Downloaded from www.nrcresearchpress.com by 210.87.254.5 on 09/06/12
For personal use only.

accurate to 0.2 Hz, about 6 times their standard deviations. The couplings interior to the cyclopropyl moiety lie within about 0.1 Hz of those observed for closely related molecules (7). Figure 1 displays the observed and calculated spectra for the unique cyclopropyl proton and the pair of protons *cis* to it, H-2.

*Conformational distribution*

The crucial parameter is $^3J_{1\alpha} \equiv {}^3J = 8.6_4 \pm 0.2_2$ Hz (error is six times the standard deviation). The derived fractional populations, $P_t$ and $P_g$, of the *trans* and *gauche* conformers are most sensitive to the value of $^3J_t$ in **1**. This can be seen as follows.

If the *gauche* conformers each have the same entropy as the *trans* form, then $P_t/P_g = 0.5 \exp(-\Delta H^0/RT)$ and $P_t + P_g = 1$. The observed $^3J$ is related to $P_t$ by $P_t = (8.6_4 - J_g)/(J_t - J_g)$. It is easy to show that, for 2.0 Hz $\leq J_g \leq$ 3.0 Hz, $P_t$ varies by 0.04 at most for a given $J_t$ in the range 8.6 Hz $\leq J_t \leq$ 13.0 Hz. Accordingly, a reliable $J_t$ is needed, estimates being made as follows.

$^3J$(H, $CH_3$) in a cyclopropane derivative is 6.2 Hz (8). An INDO MO FPT calculation, using a standard geometry (9) for the methyl group, the electron diffraction geometry for the cyclopropane fragment (10), and 1.54 Å for the exocyclic C—C bond, gives $J_t = 17.0$ and $J_g = 2.47$ Hz. Adjustment of these numbers to $J_t = 13.6$, $J_g = 2.5$ Hz or to 14.5 and 2.1 Hz, reproduces the observed coupling. Again, a standard geometry for the isopropyl group, together with the geometry above, yields INDO values of $J_t = 16.9$ and $J_g = 2.30$ Hz. In many compounds, INDO overestimates $J_t$ rather more than $J_g$. For example, in propene $(J_t + 2J_g)/3$ is 6.47 Hz whereas $J_t$ and $J_g$ are calculated (11) as 16.2 and 3.2 Hz.

In alkyl derivatives of ethene (12), it was estimated that a *lower* limit of $J_t$ is 11.1 Hz. The orbital used by a carbon atom in cyclopropane to bond to an alkyl carbon atom is very nearly $sp^2$ hybridized (7, 13, 14), implying that $J_t$ in IPCP is not less than 11.1 Hz. In *trans*-butadiene and *s-trans*-vinyl cyclopropane $J_t$ is thought to be 11.0 Hz and $J_g$ is then 1.85 Hz (15, 16). In 1,1,2,2-tetraphenylethane, $J_t$ is 11.3 Hz (17).

If, then, in IPCP 2.0 Hz $\leq J_g \leq$ 3.0 Hz and 11.0 $\leq J_t \leq$ 13.0 Hz, one has $0.56 \leq P_t \leq 0.74$. It is probable that $P_t = 0.65 \pm 0.10$.

These estimates assume "rigid" *gauche* and *trans* conformers insofar as averaging over torsional states (18, 19) *within* the conformers is ignored. The barriers to interconversion of the conformers are calculated as about 3 kcal/mol (3) so that at 300 K the simple approach may underestimate $P_t$ by as much as 0.05 (20). A variable temperature study would have to include the averaging procedure in a classical or quantum mechanical way (20). For reasons of spectral complexity, such a study should be done on the compound in which all but the two relevant protons are replaced by deuterium nuclei.

Molecular mechanics (3) favor the *trans* form by 380 cal/mol, whereas the present INDO results have this preference as 720 cal/mol. These numbers, if taken as enthalpies, give $P_t$ as 0.49 and 0.65, respectively. The INDO approximation of MO theory finds a reasonable conformational preference for phenylcyclopropane (2). The empirical force-field method (3) yields the dihedral angle as 52° in the *gauche* form. Such a number suggests $J_g$ as closer to 3 than to 2 Hz, implying $P_t$ as nearer 0.7

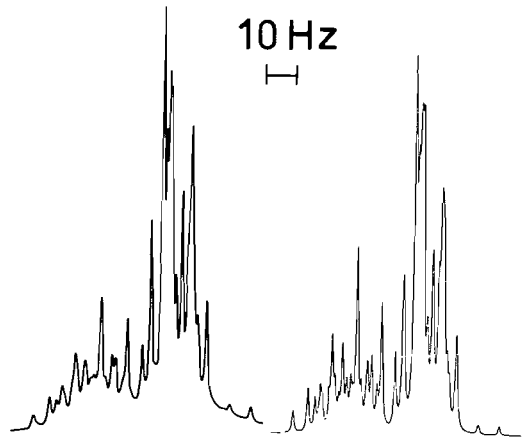


FIG. 1. The observed and calculated spectra of H-1 and H-2 (see **2** in text) at 400.135 MHz for a 3 mol% solution of isopropylcyclopropane in benzene-$d_6$. The calculated spectrum takes the parameters in Table 1 and assumes a linewidth, $\Delta\nu_{1/2}$, of 0.80 Hz. A $\Delta\nu_{1/2}$ of 1.0 Hz for H-1 produces closer agreement for this proton. Much of the width may arise from long-range coupling to the methyl protons. The digital resolution is 0.153 Hz/point. H-2 is more shielded than H-1 by 26.3 Hz.

TABLE 1. Spectral parameters for isopropylcyclopropane in benzene-$d_6$ at 297 K and 400.135 MHz

| Parameter[a,b] | Value | Parameter[a] | Value |
|---|---|---|---|
| $\nu_{CH_3}$ | −3.302(30) | $^3J_{12}$ | 8.250(29) |
| $\nu_a$ | −111.093(24) | $^3J_{13}$ | 4.969(27) |
| $\nu_1$ | −234.585(21) | $^3J_{23'}$ | 5.525(24) |
| $\nu_2$ | −260.901(20) | $^3J_{22'}$ | 9.1 |
| $\nu_3$ | −391.781(20) | $^3J_{33'}$ | 9.3 |
| $^3J_{(\alpha,CH_3)}$ | 6.714(18) | $^2J_{23}$ | −4.303(22) |
| $^3J_{1,\alpha}$ | 8.637(36) | Root mean square error | 0.169 |

[a] The numbers in parentheses give the standard deviations in the last two significant figures.
[b] The shifts are in Hz relative to an arbitrary zero. Approximate shifts in Hz at 400.135 MHz relative to internal TMS are obtained by *addition* of 384.1 Hz. H-3 therefore resonates upfield of TMS by about 0.02 ppm.

than 0.55 (a $P_t$ of 0.65 also fits $J_t = 11.5$ and $J_g = 3.3$ Hz).

From the detailed nmr and infrared studies of biisopropyl and bicyclopropyl by Lüttke and coworkers (21–23), it follows that the *gauche* forms are favored by enthalpies of about 0.1 kcal/mol. By way of contrast, for IPCP the *trans* conformation is distinctly favored by an energy similar to the energies favoring the *trans* forms in *n*-butane and vinylcyclopropane ($^3J$ in the latter is 8.3 Hz near room temperature (24), and is 8.6 Hz in IPCP). For an extensive discussion of the torsional potentials in all these compounds, see (3).

The INDO MO dipole moments are $\mu_t = 0.07_3$ and $\mu_g = 0.08_5$ D, suggesting that solvent perturbations of the conformational equilibrium are small for IPCP.

**Acknowledgments**

We are grateful to R. Lenkinski and the University of Guelph for help in obtaining the nmr spectra at 400 MHz, to S. R. Salman and K. Marat for preliminary experiments at lower frequencies, and to the Natural Sciences and Engineering Research Council of Canada for financial assistance. We thank a referee for helpful comments.

1. J. D. Odom, Z. Szafran, S. A. Johnston, Y. S. Li, and J. R. Durig. J. Am. Chem. Soc. **102**, 7173 (1980), and references therein.
2. W. J. E. Parr and T. Schaefer. J. Am. Chem. Soc. **99**, 1033 (1977), and references therein.
3. H. Braun and W. Lüttke. J. Mol. Struct. **31**, 97 (1976).
4. A. B. Nease and C. J. Wurrey. J. Raman Spectrosc. **9**, 107 (1980).
5. P. A. Dobosh. Quantum Chemistry Program Exchange, **11**, 141 (1979).
6. A. R. Quirt and J. S. Martin. J. Magn. Reson. **5**, 318 (1971); J. S. Martin, A. R. Quirt, and K. F. Worvill. The nmr program library, Daresbury Laboratory, Daresbury, U.K.
7. K. B. Wiberg, D. E. Barth, and P. H. Scherthler. J. Am. Chem. Soc. **38**, 378 (1973).
8. J-L. Pierre, M. Vidal, P. Arnaud, and Cl. Gey. Bull. Soc. Chim. Fr. 1544 (1970).
9. J. A. Pople and M. S. Gordon. J. Am. Chem. Soc. **89**, 4253 (1967).
10. O. Bastiansen, F. N. Fritsch, and K. Hedberg. Acta Crystallogr. **17**, 538 (1964).
11. G. E. Maciel, J. W. McIver, Jr., N. S. Ostlund, and J. A. Pople. J. Am. Chem. Soc. **92**, 4497 (1970).
12. A. A. Bothner-By, C. Naar-Colin, and H. Günther. J. Am. Chem. Soc. **84**, 2748 (1962).
13. N. Muller and D. E. Pritchard. J. Chem. Phys. **31**, 768 (1959); **31**, 1471 (1959).
14. F. J. Weigert and J. D. Roberts. J. Am. Chem. Soc. **89**, 5962 (1967).
15. R. T. Hobgood and J. H. Goldstein. J. Mol. Spectrosc. **12**, 76 (1964).
16. H. Günther, H. Klose, and D. Wendisch. Tetrahedron, **25**, 2047 (1969).
17. D. A. Dougherty, K. Mislow, J. F. Blount, J. B. Wooten, and J. Jacobus. J. Am. Chem. Soc. **99**, 6149 (1977).
18. K. G. R. Pachler and P. L. Wessels. J. Mol. Struct. **68**, 145 (1980).
19. T. A. Wildman. Chem. Phys. Lett. **75**, 383 (1980).
20. V. M. S. Gil and A. J. C. Varandas. J. Magn. Reson. **43**, 28 (1981).
21. A. de Meijere, W. Lüttke, and F. Heinrich. Justus Liebigs Ann. Chem. 306 (1974).
22. H. Braun and W. Lüttke. J. Mol. Struct. **28**, 391 (1975).
23. F. Heinrich and W. Lüttke. Chem. Ber. **110**, 1246 (1977).
24. G. Schrumpf. Tetrahedron Lett. 2571 (1970).

Can. J. Chem. Downloaded from www.nrcresearchpress.com by 210.87.254.5 on 09/06/12
For personal use only.

# Kinetics of the oxidation of diphenyl sulfide with hydrogen peroxide catalyzed by sodium metavanadate[1]

YOSHIRO OGATA[2] AND KAZUSHIGE TANAKA

*Department of Applied Chemistry, Faculty of Engineering, Nagoya University, Chikusa-ku, Nagoya, Japan*

Received April 6, 1981[3]

YOSHIRO OGATA and KAZUSHIGE TANAKA. Can. J. Chem. **60**, 848 (1982).

The oxidation of diphenyl sulfide ($Ph_2S$) by hydrogen peroxide in the presence of a catalytic amount of sodium metavanadate ($NaVO_3$) has been studied kinetically by means of iodometry of hydrogen peroxide. The reaction rate is expressed as: $v = k[NaVO_3]_{st}[Ph_2S]^2$, when the concentration of catalyst is very low and $[Ph_2S]_0/[H_2O_2]_0 > 2$, where $[\ ]_{st}$ and $[\ ]_0$ mean stoichiometric and initial concentration, respectively. The effective oxidant may consist of polymeric as well as monomeric peroxyvanadate in view of the effect of concentration of catalyst on the rate. The main oxidizing species at low concentration of catalyst seems to be diperoxyvanadate $VO_5^-$. The rate constant $k_2$ in $v = k_2[Ph_2S]^2$ tends to decrease with initial concentration of $H_2O_2$, which is present in excess of the catalyst. A probable mechanism for the oxidation is discussed.

YOSHIRO OGATA et KAZUSHIGE TANAKA. Can. J. Chem. **60**, 848 (1982).

Faisant appel à l'iodométrie du peroxyde d'hydrogène, on a réalisé une étude cinétique de l'oxydation du sulfure de biphényle ($Ph_2S$) par le peroxyde d'hydrogène en présence d'une quantité catalytique de métavanadate de sodium ($NaVO_3$). On exprime la vitesse de la réaction par l'équation: $v = k[NaVO_3]_{st}[Ph_2S]^2$, lorsque la concentration du catalyseur est très faible et lorsque $[Ph_2S]_M/[H_2O_2]_0 > 2$ où $[\ ]_{st}$ et $[\ ]_0$ signifiient respectivement les concentrations stochiométriques et initiales. L'oxydant effectif peut être le peroxyvanadate sous la forme polymérisée aussi bien que sous la forme monomère compte tenu de l'effet de la concentration du catalyseur sur la vitesse. Pour une faible concentration du catalyseur, l'oxydant principal semble être de dipéroxyvanadate $VO_5^-$. La constante de vitesse $k_2$ dans l'expression $v = k_2[Ph_2S]^2$ tend à diminuer avec la concentration initiale de $H_2O_2$ qui est en excès par rapport au catalyseur. On discute du mécanisme probable de l'oxydation.

[Traduit par le journal]

## Introduction

Vanadic acid is converted to its peroxy acids on treatment with $H_2O_2$. Beg and Ahmad (1) have reported on the kinetics and mechanism of epoxidation of maleic and fumaric acids by $H_2O_2$ catalyzed by sodium orthovanadate, in which the main oxidant is monoperoxyvanadic acid $H_3VO_5$. On the other hand, Modena and co-workers have reported the oxidation of sulfides with *tert*-butyl hydroperoxide (2) or $H_2O_2$ (3) in the presence of bis(acetylacetonato) oxovanadium(IV) $VO(acac)_2$ in alcohol (ROH) as solvent, where the main oxidant is said to be complexed monoperoxyvanadic acid $VO(OR)_2OOH$ produced by conversion of $VO(OR)_3$. These reports, however, paid little attention to the rate of diperoxyvanadic acid.

The treatment of metavanadate with $H_2O_2$ produces peroxy acids consisting mainly of diperoxyvanadate $VO_5^-$ and polymeric peroxyvanadate (4), so that these peroxyvanadates may participate in this oxidation. The present paper describes the rate data and some factors influencing the rate for the $NaVO_3$-catalyzed oxidation of diphenyl sulfide by hydrogen peroxide in 98 wt.% methanol (with 2 wt.% water).

[1] $Ph_2S + H_2O_2 \xrightarrow{NaVO_3} Ph_2SO + H_2O$

## Results and discussion

### *Peroxyvanadate*

Generally, metavanadate ion is known to exist mainly as $V_3O_9^{3-}$ in neutral solution (5). The ion $V_3O_9^{3-}$ is converted to monoperoxyvanadate ion $VO_3^+$ and diperoxyvanadate ion $VO_5^-$ on treatment with hydrogen peroxide as follows (6).

[2a] $V_3O_9^{3-} \xrightarrow{3\,H_2O_2,\ 6H^+} 3\,VO(O_2)^+$

[2b] $V_3O_9^{3-} \xrightarrow{6\,H_2O_2} 3\,VO(O_2)_2^-$

Here, the formation of $VO_5^-$ is influenced by $[H^+]$ (see eq. [3]). But the main species present in the system with $< 0.015\ M$ $H_2O_2$ seems to be $VO_5^-$ based on the fact that the color of the reaction mixture is yellow, that no decomposition of $H_2O_2$ is observed on standing for ca. 8 h at 25°C, and that the rate becomes first-order with respect to substrate ($Ph_2S$) by addition of strong acid ($H_2SO_4$) as stated later.

The identification of $VO_3^+$ and $VO_5^-$ by means of polarography and uv spectroscopy failed because of the complex reaction at the electrode (7) and partial overlapping of the spectra (8), respectively.

[1]Contribution No. 289.
[2]Author to whom all correspondence should be addressed.
[3]Revision received August 26, 1981.

0008-4042/82/070848-05$01.00/0
©1982 National Research Council of Canada/Conseil national de recherches du Canada

Can. J. Chem. Downloaded from www.nrcresearchpress.com by 210.87.254.40 on 09/06/12
For personal use only.

Can. J. Chem. Downloaded from www.nrcresearchpress.com by 210.87.254.40 on 09/06/12
For personal use only.

*Kinetics*

The oxidation of diphenyl sulfide gave diphenyl sulfoxide together with a small amount of diphenyl sulfone (eq. [1]). Most of our kinetic experiments were done under conditions in which the formation of diphenyl sulfone was negligible; i.e., in the presence of a large excess of sulfide over $H_2O_2$. The rate was followed by iodometry of active oxygen, since the rate constants $k_2$ (in $v = k_2[Ph_2S]^2$) calculated by the iodometry were practically in agreement with those calculated on the basis of the consumption of $Ph_2S$, determined by means of glc; i.e., $6.52 \times 10^{-4}\ M^{-1}\ s^{-1}$ (by iodometry) and $6.15 \times 10^{-4}\ M^{-1}\ s^{-1}$ (by glc).

Though vanadate is a weak oxidant, diphenyl sulfide is oxidized by neither metavanadate nor $H_2O_2$ alone in this solvent (98 wt.% methanol) at 25°C. The spontaneous decomposition of $H_2O_2$ is negligible under these conditions.

The effect of initial concentration of diphenyl sulfide on the rate was examined, the results being shown in Table 1. The rate is expressed as $v = k_2[Ph_2S]^2$, if $[Ph_2S]_0/[H_2O_2]_0 > 2$ and $[H_2O_2]_0 \sim 1.15 \times 10^{-2}\ M$. This result is different from that of sodium tungstate, where the rate expression $v = k_1[Ph_2S]$ is observed. The term $[Ph_2S]^2$ in the rate expression suggests that peroxyvanadate and diphenyl sulfide form a 1:1 coordination complex, $(VO_5{-}Ph_2S)^-$, which may act as a strong oxidant for $Ph_2S$.

If $[Ph_2S]_0$ is lower than $2 \times 10^{-2}\ M$, further oxidation giving a considerable amount of $Ph_2SO_2$ occurs, by which the rate constant decreases.

*Effects of concentration of catalyst and $H_2O_2$*

The effect of the initial concentration of sodium metavanadate $[NaVO_3]_0$ relative to that of $H_2O_2$, which is in large excess to $NaVO_3$, is shown in Fig. 1. The rate constant ($k_2$ in $v = k\,[Ph_2S]^2$) increases with $[NaVO_3]_0$, but the increase is not linear after $5 \times 10^{-4}\ M$ $NaVO_3$. This fact suggests that polymeric diperoxyvanadate, which is a weaker oxidant, may exist in analogy to polymeric vanadate; the extent of polymerization of vanadate is known to increase with its concentration (4).

The effect of the initial concentration of hydrogen peroxide is shown in Fig. 2. As apparent from the figure, the rate constant decreases gradually with increasing $[H_2O_2]_0$. The rate expression $v = k_2[Ph_2S]^2$ is valid at $[Ph_2S]_0/[H_2O_2]_0 > 2$, but when $[Ph_2S]_0/[H_2O_2]_0 < 1/2$, little reaction occurs.

If $[Ph_2S]_0/[H_2O_2]_0 < 2$ and $[H_2O_2]_0$ is kept constant, the rate constant $k_2$ increases with the concentration of $Ph_2S$. These results suggest the presence of a complex consisting of $H_2O_2$, $Ph_2S$, and $VO_5^-$ at the transition state. We found that there is no effect of $[H_2O_2]_0$ on the rate constant, if sodium tungstate is used instead of sodium metavanadate; hence the interaction between hydrogen peroxide and peroxyvanadate is characteristic of vanadate and it may be ascribed to the hydrogen-bonded association of $H_2O_2$ with peroxyvanadate. Since diperoxyvanadate $VO_5^-$ seems to be a highly charge-delocalized anion (3), it is possible that it may associate with $H_2O_2$ more readily than peroxytungstate. In analogy to $H_2O_2$, the addition of a small amount of water to the reaction system retards the rate markedly; for example, $6.52 \times 10^{-4}$

TABLE 1. Rate data[a] for $NaVO_3$-catalyzed oxidation of $Ph_2S$ with $H_2O_2$ at 25°C in 98 wt.% MeOH

| Initial concn. × $10^3$ $M$ | | | |
|---|---|---|---|
| $[NaVO_3]_0$ | $[H_2O_2]_0$ | $[Ph_2S]_0$ | $k_2 \times 10^4\ M^{-1}s^{-1}$ |
| 0.5 | 4.06 | 30 | 7.30 |
| 0.5 | 4.10 | 25 | 7.60 |
| 0.5 | 5.83 | 30 | 6.95 |
| 0.5 | 6.02 | 25 | 6.46 |
| 0.5 | 11.4 | 25 | 5.09 |
| 0.5 | 11.6 | 30 | 5.36 |
| 0.5 | 11.8 | 35 | 5.19 |
| 0.5 | 11.7 | 40 | 5.18 |
| 1.0 | 11.3 | 25 | 6.52 |
| 1.0 | 11.3 | 30 | 7.06 |
| 1.0 | 11.6 | 35 | 7.11 |
| 1.0 | 11.6 | 40 | 6.92 |

[a] $v = k_2[Ph_2S]^2$.

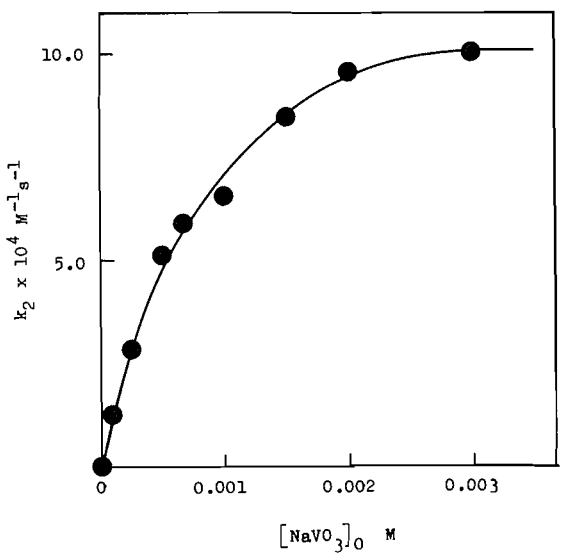


FIG. 1. Effect of $[NaVO_3]_0$ on $k_2$ ($M^{-1}\ s^{-1}$) for $NaVO_3$-catalyzed oxidation of $Ph_2S$ with $H_2O_2$ in 98 wt.% MeOH at 25°C. $[Ph_2S]_0 = 2.5 \times 10^{-2}\ M$, $[H_2O_2]_0 = 1.20 \times 10^{-2}\ M$.

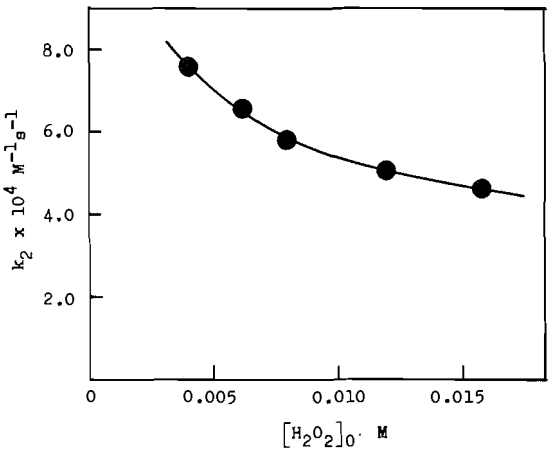


FIG. 2. Effect of $[H_2O_2]_0$ on $k_2$ ($M^{-1}$ $s^{-1}$) for $NaVO_3$-catalyzed oxidation of $Ph_2S$ with $H_2O_2$ in 98 wt.% MeOH at 25°C. $[Ph_2S]_0 = 2.5 \times 10^{-2}$ $M$, $[NaVO_3]_0 = 0.5 \times 10^{-3}$ $M$.

$M^{-1}$ $s^{-1}$ in 98 wt.% MeOH–$H_2O$ and $3.69 \times 10^{-4}$ $M^{-1}$ $s^{-1}$ in 96 wt.% MeOH–$H_2O$. This fact also supports the deactivation of peroxyvanadate with hydrogen-bonded association. It is known that $VO_5^-$ is converted to other peroxyvanadates such as $HV(O)(O_2)_3^{2-}$ or $HV(O)_2(O_2)_2^{2-}$ etc. by an increase of $[OH^-]$ (6). Since $H_2O_2$ is almost neutral (very weak acid), $VO_5^-$ does not seem to be converted to the above peroxyvanadates by a large excess of $H_2O_2$. On the other hand, though $VO_5^-$ is converted to $VO_3^+$ by an increase of $[H^+]$, the conversion into $VO_3^+$ is negligible at this acidity, since there is no change of the rate order and no decomposition of $H_2O_2$ is observed on addition of $H_2SO_4$ (see below).

*Effects of additives*

Effects of additives ($H_2SO_4$, $Ph_2SO$, and $H_2O$) are shown in Table 2. The rate constants did not vary on addition of $4.0 \times 10^{-3}$ $M$ diphenyl sulfoxide. On addition of $1.5 \times 10^{-3}$ $M$ sulfuric acid to the reaction mixture, the rate expression becomes $v = k_1[Ph_2S]$, i.e., not second-order, but first-order in the substrate. The addition of $H_2SO_4$ makes the decomposition of $H_2O_2$ appreciable, and it changes the color of the reaction mixture from yellow to orange. These facts suggest that monoperoxyvanadate is a main oxidizing agent under acidic conditions, as will be explained below.

(a) Monoperoxyvanadate $VO_3^+$ is red and diperoxyvanadate $VO_5^-$ is yellow (9). The observed change of colors to orange by addition of $H_2SO_4$ is ascribed to the increasing content of $VO_3^+$.

(b) Modena and co-workers have reported that the $H_2O_2$ oxidation and the decomposition of $H_2O_2$ occur via $VO(OR)_2OOH$, which is equivalent to $VO_3^+$, according to the equation:

$$VO_3^+ + 2\,RO^- \xrightarrow{H^+} VO(OR)_2OOH.$$

The rate of oxidation by $VO(OR)_2OOH$ is first-order in substrate just like our $H_2SO_4$–$NaVO_3$–$H_2O_2$ oxidation. Hence, the main oxidant in the $H_2SO_4$–$NaVO_3$–$H_2O_2$ system may be $VO_3^+$.

(c) There is an equilibrium between monoperoxyvanadate and diperoxyvanadate, as shown in eq. [3], and the equilibrium constant has been reported (10).

[3] $$VO_3^+ + H_2O_2 \rightleftarrows VO_5^- + 2H^+$$

The increase of the acidity shifts the equilibrium to the left, thus $[VO_3^+]$ increases, so that the main oxidizing species in strong acid solution would be $VO_3^+$. An increase of $H_2SO_4$ concentration over $1.5 \times 10^{-3}$ $M$ resulted in the rapid decomposition of $H_2O_2$, thus leading to inaccurate rate constants, while addition of $2.8 \times 10^{-3}$ $M$ NaOH inhibited the reaction. The oxidation in the range between $1.5 \times 10^{-3}$ $M$ $H_2SO_4$ and $2.8 \times 10^{-3}$ $M$ NaOH gave a complex rate expression because of the participation of mono- and diperoxyvanadium complexes.

On addition of $H_2O$ to the reaction mixture, the rate constant becomes small. This fact supports the deactivation of peroxyvanadate with hydrogen-bonded association as stated above.

*Mechanism*

The above facts suggest the following mechanism for the oxidation in neutral 98 wt.% methanol at very low concentrations of sodium metavanadate with negligible concentration of polyperoxyvanadates.

[4] $$VO_5^- + nH_2O_2 \underset{\text{fast}}{\overset{K_{n,a}}{\rightleftharpoons}} (VO_5^-)(H_2O_2)_n$$

[5] $$(VO_5^-)(H_2O_2)_n + Ph_2S \underset{\text{fast}}{\overset{K_{n,b}}{\rightleftharpoons}} (VO_5\text{–}Ph_2S)^-(H_2O_2)_n$$

[6] $$(VO_5\text{–}Ph_2S)^-(H_2O_2)_n + Ph_2S \xrightarrow[k_n]{\text{slow}} Ph_2SO + (VO_4\text{–}Ph_2S)^-(H_2O_2)_n$$

[7] $$(VO_4\text{–}Ph_2S)^-(H_2O_2)_n + H_2O_2 \xrightarrow{\text{fast}} (VO_5\text{–}Ph_2S)^-(H_2O_2)_n + H_2O$$

Equation [4] shows the hydrogen-bonded association of $H_2O_2$ with $VO_5^-$. In view of the rate equation, this aggregated complex seems to form a 1:1 coordination complex with diphenyl sulfide (eq.

Can. J. Chem. Downloaded from www.nrcresearchpress.com by 210.87.254.40 on 09/06/12
For personal use only.

Can. J. Chem. Downloaded from www.nrcresearchpress.com by 210.87.254.40 on 09/06/12
For personal use only.

TABLE 2. Effect[a] of additives for $NaVO_3$-catalyzed oxidation of $Ph_2S$ with $H_2O_2$ at 25°C in 98 wt.% MeOH

| Additive | × $10^3$ $M$ $[NaVO_3]_0$ | × $10^3$ $M$ $[H_2O_2]_0$ | $k_1$[b] × $10^5$ $s^{-1}$ |
|---|---|---|---|
| $H_2SO_4$ (1.5) | 0.5 | 11.8 | 8.80 |
| $H_2SO_4$ (1.5) | 0.5 | 35.5 | 8.60 |
| $H_2SO_4$ (1.5) | 0.5 | 48.4 | 8.44 |
| | | | $k_2$[c] × $10^4$ $M^{-1}$ $s^{-1}$ |
| $Ph_2SO$ (4.0) | 1.0 | 11.4 | 6.57 |
| $H_2O$ (3.0)[d] | 1.0 | 11.5 | 4.84 |
| $H_2O$ (4.0)[d] | 1.0 | 11.5 | 3.69 |
| None | 1.0 | 11.3 | 6.52 |

[a] $[Ph_2S]_0 = 2.5 \times 10^{-2}$ $M$.
[b] $v = k_1[Ph_2S]$.
[c] $v = k_2[Ph_2S]^2$.
[d] Weight %.

[5]) and this complex seems to react with another molecule of diphenyl sulfide to give diphenyl sulfoxide (eq. [6]). The bulky $Ph_2S$ molecule would permit the second molecule of $Ph_2S$ to attack on the peroxy oxygen atom but not on the vanadium atom. Since monoperoxyvanadate seems to be unstable in this system, $(VO_4–Ph_2S)^-(H_2O_2)_n$ formed in eq. [6] would be rapidly converted to $(VO_5–Ph_2S)^-(H_2O_2)_n$ by excess $H_2O_2$ (eq. [7]).

This mechanism involving a rate-determining attack of complex $(VO_5–Ph_2S)^-(H_2O_2)_n$ on diphenyl sulfide to form diphenyl sulfoxide leads to a rate expression as follows.

$$[8] \quad v = \sum_{i=0}^{n} k_i[(VO_5–Ph_2S)^-(H_2O_2)_i][Ph_2S] = \sum_{i=0}^{n} k_i K_{i,a} K_{i,b}[H_2O_2]^i[VO_5^-][Ph_2S]^2$$

Here, $K_{0,a} = 1$ and $k_i$ represents the $i$th rate constant, $K_{i,a}$ the $i$th equilibrium constant of eq. [4], and $K_{i,b}$, the $i$th equilibrium constant of eq. [5]. Since $NaVO_3$ reacts rapidly with $H_2O_2$ and since the uv spectrum of peroxyvanadates does not change with increasing concentration of $H_2O_2$ which is present in excess of the catalyst, $NaVO_3$ may be completely converted to peroxyvanadates (mainly $VO_5^-$). Hence, the stoichiometric initial concentration of $NaVO_3$ is approximated as: $[NaVO_3]_0 \simeq [VO_5^-]_{st}$. On the other hand, the association of $VO_5^-$ with $H_2O_2$ at various molar ratios is expressed as:

$$[9] \quad [VO_5^-]_{st} = \sum_{i=0}^{n} K_{i,a}[H_2O_2]^i[VO_5^-]$$

Introduction of eq. [9] into eq. [8] leads to

$$[10] \quad v = \sum_{i=0}^{n} k_i K_{i,a} K_{i,b}[H_2O_2]^i\{[VO_5^-]_{st} - \sum_{i=1}^{n} K_{i,a}[H_2O_2]^i[VO_5^-]\}[Ph_2S]^2$$

Also, the reactivity of free $VO_5^-$ is much reduced by association with $H_2O_2$, i.e.,

$$k_0K_{0,b} \gg k_1K_{1,a}K_{1,b}[H_2O_2] + \cdots + k_nK_{n,a}K_{n,b}[H_2O_2]^n;$$

consequently,

$$\sum_{i=0}^{n} k_iK_{i,a}K_{i,b}[H_2O_2]^i \simeq k_0K_{0,b}$$

Hence,

$$[11] \quad v \simeq k_0K_{0,b}\{[VO_5^-]_{st} - \sum_{i=1}^{n} K_{i,a}[H_2O_2]^i[VO_5^-]\} \times [Ph_2S]^2 = k_2[Ph_2S]^2$$

This expression is consistent with the experimental results. The apparent rate constant $k_2$ decreases with increasing $[H_2O_2]_0$, since the concentration or the sum of concentrations of associated peroxyvanadates, i.e.,

$$\sum_{i=1}^{n} K_{i,a}[H_2O_2]^i[VO_5^-]$$

increases with $[H_2O_2]_0$.

On the other hand, in the presence of $H_2SO_4$, the following mechanism may be operating as a main pathway as stated above.

$$[12a] \quad V_3O_9^{3-} + 3H_2O_2 + 6H_2SO_4 \rightleftarrows 3VO_3^+ + 6H_2O + 6HSO_4^-$$

$$[12b] \quad VO_3^+ + Ph_2S \rightarrow VO_2^+ + Ph_2SO$$

But the direct oxidation with acidic $H_2O_2$ and spontaneous decomposition of $H_2O_2$ render the reaction kinetics complex. It has been reported (10) that both peroxy species $VO_3^+$ and $VO_5^-$ participate in the oxidation of iodide ion in the $[H^+]$ range of 0.1–1.0.

## Experimental

*Materials*

Methanol was purified by fractionation (bp 66–67°C) and it was used as 98 wt.% solvent to make the oxidation system homogeneous. Diphenyl sulfide was purified by vacuum distillation (bp 118–119°C, 4 Torr). Sodium metavanadate was of commercial, guaranteed reagent grade, quality.

*Kinetics*

A mixture of $NaVO_3$ and $H_2O_2$ in 98 wt.% MeOH was kept standing at 25°C for 5 min, then the reaction was started by addition of $Ph_2S$. Aliquots were taken out at appropriate intervals of time, and their peroxide contents were determined iodometrically. The concentrations of $Ph_2S$ were calculated based on the $H_2O_2$ concentration after subtraction of metavanadate concentration. The consumption of $Ph_2S$ was measured by glc (a Yanagimoto G 180 gas chromatograph with FID) with a column (2.5 mm × 1 m) packed with PEG 20M.

## Acknowledgments

The authors wish to thank Mr. M. Inaishi for his

assistance in preparation of the manuscript and to Mitsubishi Gas Chem. Co. for their gift of 90% $H_2O_2$.

1. M. A. BEG and I. AHMAD. J. Org. Chem. **42**, 1590 (1977).
2. R. CURICI, F. DI FURIA, R. TESTI, and G. MODENA. J. Chem. Soc. Perkin Trans. II, 752 (1974).
3. (*a*) O. BORTOLINI, F. DI FURIA, P. SCRIMIN, and G. MODENA. J. Mol. Catal. **7**, 59 (1980); (*b*) F. DI FURIA and G. MODENA. *In* Fundamental research in homogeneous catalysis. Vol. 3. *Edited by* M. Tsutsui. Plenum Press, New York. 1979. p. 433.
4. C. F. BELL and K. A. K. LOTT. Modern approach to inorganic chemistry. 2nd ed. London. 1966.
5. (*a*) P. Z. DULLBERG. Z. Phys. Chem. **45**, 129 (1903); (*b*) K. SCHILLER and E. THILO. Z. Anorg. Allg. Chem. **310**, 261 (1961); (*c*) R. A. ROBINSON and D. A. SINCLAIR. J. Chem. Soc. 642 (1934).
6. GMELIN, **48**, V[B], 162.
7. I. M. KOLTHOFF and E. P. PARRY. J. Am. Chem. Soc. **73**, 5315 (1951).
8. O. BORTOLINI, F. DI FURIA, G. MODENA, and P. SCRIMIN. J. Mol. Catal. **9**, 323 (1980).
9. M. ORHANOVIC and R. G. WILKINS. J. Am. Chem. Soc. **89**, 278 (1967).
10. F. SECCO. Inorg. Chem. **19**, 2722 (1980).

Can. J. Chem. Downloaded from www.nrcresearchpress.com by 210.87.254.40 on 09/06/12
For personal use only.

# Synthesis and vibrational study of a 1:1 stoichiometric complex of hydronium tetrafluoroborate and 1,4,7,10,13,16-hexaoxacyclooctadecane (18-crown-6)

ROBERT CHÊNEVERT,[1] ANDRÉ RODRIGUE, MARIE PIGEON-GOSSELIN, AND RODRIGUE SAVOIE[1]

*Département de chimie et Centre de recherche sur les atomes et les molécules, Université Laval, Québec (Qué.), Canada G1K 7P4*

Received September 18, 1981

ROBERT CHÊNEVERT, ANDRÉ RODRIGUE, MARIE PIGEON-GOSSELIN, and RODRIGUE SAVOIE. Can. J. Chem. **60**, 853 (1982).

The macrocyclic ether 1,4,7,10,13,16-hexaoxaoctadecane (18-crown-6) has the remarkable property of being able to transfer the hydronium ($H_3O^+$) ion from an aqueous solution to an organic medium. This property has been used to synthetize a 1:1 stoichiometric complex of this ether with hydronium tetrafluoroborate. This complex is very stable (mp 145°C) and dissolves readily, without decomposition, in solvents such as $CHCl_3$. The presence of the $H_3O^+$ and $BF_4^-$ ions in the complex has been confirmed by chemical analysis, and by $^1H$ nmr, Raman, and ir spectroscopy. The vibrational spectra indicate that a conformational change of the crown ether takes place in the complex over the temperature range −50°C to −100°C. The symmetry of the crown ether, which appears to be relatively high at room temperature, is considerably reduced below the transition temperature.

ROBERT CHÊNEVERT, ANDRÉ RODRIGUE, MARIE PIGEON-GOSSELIN et RODRIGUE SAVOIE. Can. J. Chem. **60**, 853 (1982).

L'éther macrocyclique 1,4,7,10,13,16-hexaoxaoctadécane (18-crown-6) possède la propriété remarquable de pouvoir transférer l'ion hydronium ($H_3O^+$) d'une solution aqueuse à un milieu organique. Cette propriété a été utilisée pour préparer un complexe de stoéchiométrie 1:1 de l'éther avec le tétrafluoroborate d'hydronium. Ce complexe très stable (pf 145°C) se dissout sans décomposition dans des solvants tels que le $CHCl_3$. La présence des ions $H_3O^+$ et $BF_4^-$ dans le complexe a été démontrée par analyse chimique, et par spectroscopie $^1H$ rmn, ir et Raman. Les spectres de vibration ont mis en évidence dans le complexe un changement de conformation de l'éther dans le domaine de température s'étendant approximativement de −50°C à −100°C. La symmétrie de l'éther couronne, assez élevée à température ambiante, serait fortement diminuée au-dessous de la température de transition.

## Introduction

Macrocyclic polyethers have a remarkable complexing ability, not only for alkali metal ions, but also for ammonium (1), guanidinium (2), and sulfonium ions (3), as well as for mercury and cadmium halides (4). Evidence of complexation between crown ethers and diazonium and benzoyl cations has also been reported (5). These cyclic ethers further form complexes with neutral organic molecules such as dimethyl acetylenedicarboxylate (6), thiourea (7), acetonitrile (8), and nitro compounds (9). Izatt and co-workers (10) have characterized a complex between hydronium perchlorate and dicyclohexyl-18-crown-6 (*cis-syn-cis* isomer) by infrared spectroscopy. We report here on the formation and characterization of a 1:1 stoichiometric complex between hydronium tetrafluoroborate and 1,4,7,10,13,16-hexaoxacyclooctadecane (18-crown-6, hereafter referred to as EOc6, as it corresponds to a cyclic hexamer of ethylene oxide).

## Experimental

The complex studied here was first obtained during a study of the complexation of nitronium tetrafluoroborate by the cyclic ether EOc6 in tetrahydrofuran; addition of water produced a precipitate which was later identified as the complex reported here. It was later discovered that the complex could be prepared in a more straightforward manner, by the addition of fluoroboric acid (40%) to a solution of the crown ether in tetrahydrofuran. In contrast to most hydronium salts which have low melting points and are highly hygroscopic, the crown ether hydronium complex as well as the oxonium complex described previously (10) are very stable to moisture and can be kept indefinitely at room temperature. The melting temperature of $EOc6.H_3O^+.BF_4^-$ (145°C) is much higher than that of the ligand (40°C).

The one-to-one stoichiometry of the $H_3O^+.BF_4^-$ and EOc6 components in the complex was established by dissolution of the salt in water followed by titration of the acid content by NaOH 1 *N* with phenolphthalein as an indicator. Elemental analysis for C, H, and F was consistent with the suggested formulation ($C_{12}H_{27}O_7BF_4$; calcd: C 38.94, H 7.35, F 20.53; found: C 39.20, H 7.33, F 20.77).

The Raman spectra were recorded on a microcomputer-controlled Spex Model 1400 spectrometer (11), using the 514.5 nm exciting line from a Spectra Physics Model 165 argon ion laser. The measurements were taken by steps of 1 $cm^{-1}$, with an integration time typically set at 1.5 s per point. The spectral slit width was generally adjusted to 1 $cm^{-1}$ and the laser power at the sample was fixed at 450 mW. The polycrystalline solid complex as well as the solutions were studied in glass capillary cells. For low-temperature measurements, down to −100°C, the sample cell was fixed in the center of an evacuated cylindrical jacket and cooled with a flow of cold nitrogen gas. The spectra at liquid nitrogen temperature were obtained with the sample cell placed in a copper holder fixed at the tip of a cold finger in a liquid nitrogen cryostat.

In the infrared study, Nujol and hexachlorobutadiene mulls contained between Irtran-4 windows were used. The spectra were recorded on a Perkin-Elmer Model 621 spectrophotometer, at a scanning speed of 0.4 $cm^{-1}$/s and a spectral slit width of 3 $cm^{-1}$. The low-temperature spectra were obtained with the same mulls as above, using a conventional liquid nitrogen cryostat.

[1]To whom correspondence should be addressed.

0008-4042/82/070853-09$01.00/0

©1982 National Research Council of Canada/Conseil national de recherches du Canada

Can. J. Chem. Downloaded from www.nrcresearchpress.com by 210.87.254.5 on 09/06/12
For personal use only.

Can. J. Chem. Downloaded from www.nrcresearchpress.com by 210.87.254.5 on 09/06/12
For personal use only.

In both the infrared and Raman studies, the temperature was monitored by a copper–constantan thermocouple linked to a Fluke digital thermometer. In each case the temperature was maintained within ±3°C of any desired value, either by adding controlled amounts of liquid nitrogen to the cryostat in the infrared, or by adjusting the flow on coolant gas in the Raman experiments. The frequencies reported in this study are believed to be accurate to ±2 $cm^{-1}$ for sharp peaks, the infrared spectrometer having been calibrated with a standard indene solution and the Raman instrument with a neon discharge lamp.

The $^1H$ nmr spectra were taken on a Bruker HX-90 (90 MHz) with tetramethylsilane as an internal standard or, for $^{13}C$, on a Bruker WP-80 spectrometer working at 20 MHz.

The microanalyses were performed by Dr. C. Daessle, Organic Microanalysis, Montreal.

## Results and discussion

The EOc6 ether was found to be able to transfer the hydronium tetrafluoroborate ion pair from an aqueous phase to an organic medium (dichloromethane, chloroform, tetrahydrofuran). To the best of our knowledge, this is the first observation of a direct liquid–liquid phase transfer of the hydronium ion from an aqueous solution to an organic phase. This process is obviously of great interest and work is continuing along that line. Preliminary results indicate that other cyclic ethers, such as dicyclohexyl-18-crown-6, dibenzo-18-crown-6, and 15-crown-5 also share the complexing ability of EOc6 towards the $H_3O^+$ ion, although it appears more difficult to isolate complexes of definite composition with these other ethers.

The Raman spectra of the complex in solution and as a polycrystalline powder are reproduced in Fig. 1, together with the spectrum of the uncomplexed ether which is shown for comparison purposes. The infrared spectra of mulled samples of the complex have also been recorded and the frequencies of the observed bands are given in Table 1, along with those of the Raman peaks.

The $^1H$ nmr spectrum of the EOc6.$H_3O^+$.$BF_4^-$ complex in solution in $CDCl_3$ contains only two peaks; the first at 3.77 ppm is slightly shifted with respect to that of the free ether (3.67 ppm), whereas the second consists of a sharp singlet near 11 ppm and is characteristic of the $H_3O^+$ ion (12). The latter, which is not present in the corresponding spectrum of the deuterated complex, has an integrated area which is consistent with the presence of the three hydrogen atoms of the hydronium ion. On the other hand, the proton decoupled $^{13}C$ nmr spectrum of the complex in solution in $CDCl_3$ contains but a very sharp singlet at 70.10 ppm, slightly shifted from the signal obtained from the uncomplexed ether (70.76 ppm). The relative simplicity of the nmr spectra suggests for the complex in solution a rather soft structure, the $H_3O^+$ ion being able to move around so that the six oxygen atoms of the ether share equally, on the average, the possible hydrogen bonds formed between the hydronium ion and the ligand.

The ionic nature of the EOc6.$H_3O^+$.$BF_4^-$ complex is confirmed by its infrared and Raman spectra, which also provide some information on its structure. It is helpful in this regard to compare the vibrational spectra of the complex with that of the uncomplexed cyclic ether, in both the crystalline state and in chloroform solution.

The molecular structure of the uncomplexed hexaether in the crystal departs significantly from the regular ($D_{3d}$) crown conformation (13). It assumes a rectangular shape of symmetry $C_i$, with three different kinds of —O—$CH_2$—$CH_2$—O— units. This low symmetry is reflected in the Raman spectrum (Fig. 1*A*, see also ref. 14), which is appreciably more complicated than those of various crystalline polyether complexes, such as KSCN, RbSCN, and CsCN (15), in which the ether adopts the $D_{3d}$ conformation (16). The same is true of the KBr complex, which has also been extensively studied by infrared spectroscopy (15, 17, 18).

The Raman spectrum of EOc6 dissolved in $CHCl_3$ (Fig. 1*B*) closely resembles that in $CH_3OH$ (14). Simplification of the spectrum occurs upon dissolution, even after taking into account the general broadening of the bands. It therefore appears that the molecule, on the average, has a more symmetrical structure in solution, although this structure probably fluctuates widely between various different conformations. The absence in the Raman spectrum of the solute of the strong band present at 414 $cm^{-1}$ in the spectrum of the solid is worth mentioning, as it may be characteristic of the rectangular structure adopted by the ether in the crystal.

The presence of the $H_3O^+$ ion in the crystalline complex, as well as in the solution in $CHCl_3$, is readily established from the characteristic bands of the hydronium ion (see, for example, ref. 19 and references cited therein) present in the infrared spectra. The two stretching modes ($\nu_1$ and $\nu_3$) give a very strong and broad band centered at 2850 $cm^{-1}$ (Fig. 2), whereas the asymmetric bending mode ($\nu_4$) occurs near 1650 $cm^{-1}$. The band due to the symmetric bending mode ($\nu_2$), which normally occurs near 1100 $cm^{-1}$, is overlapped by a very strong band of the $BF_4^-$ ion. However, its first overtone gives a characteristic band at 2150 $cm^{-1}$. These frequencies are almost identical to those found in the dicyclohexyl-18-crown-6.$H_3O^+$.$ClO_4^-$ complex (10), whose structure is probably quite

Can. J. Chem. Downloaded from www.nrcresearchpress.com by 210.87.254.5 on 09/06/12
For personal use only.

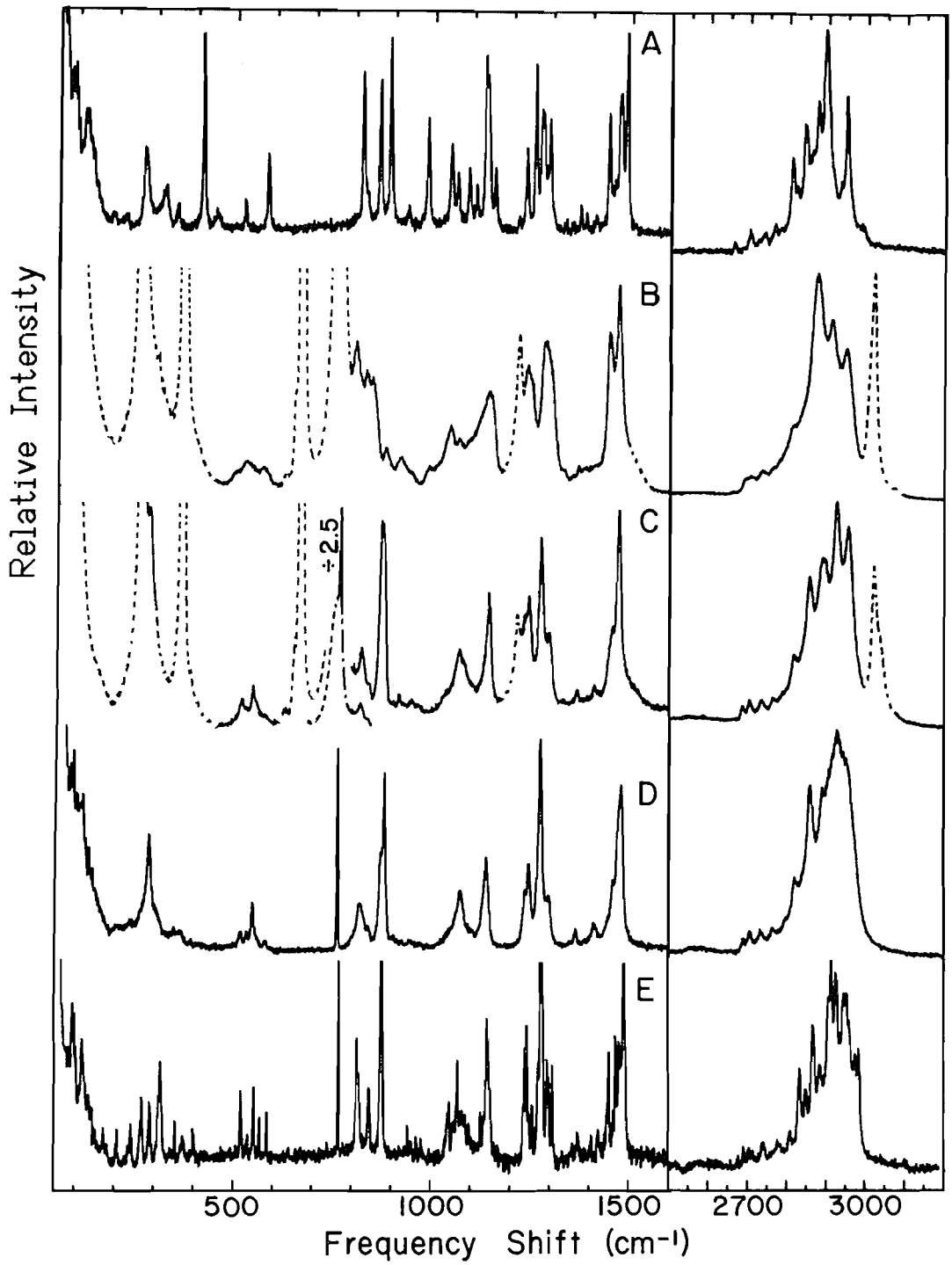


FIG. 1. Raman spectra at 25°C of the 18-crown-6 ether (*A*) as a polycrystalline powder and (*B*) in solution in $CHCl_3$. Corresponding spectra of the 18-crown-6.$H_3O^+$.$BF_4^-$ complex (*C*) in solution in $CHCl_3$ and as a polycrystalline powder at (*D*) 25°C and (*E*) −190°C. Scattering by $CHCl_3$ is indicated by dotted lines.

Can. J. Chem. Downloaded from www.nrcresearchpress.com by 210.87.254.5 on 09/06/12
For personal use only.

TABLE 1. Vibrational frequencies ($cm^{-1}$) of the observed bands in the spectra of the 18-crown-6 ether (EOc6) and its complex with hydronium tetrafluoroborate*

| Raman | | | | | Infrared | |
|---|---|---|---|---|---|---|
| EOc6 | | $EOc6.H_3O^+.BF_4^-$ | | | $EOc6.H_3O^+.BF_4^-$ Mulls | |
| | | | Solid | | | |
| Solid 25°C | Solution $CHCl_3$ 25°C | Solution $CHCl_3$ 25°C | 25°C | −190°C | 25°C | −195°C |
| | | 3037 m,b | | | | |
| 2990 w,sh | | | | 2987 s | | |
| | | | | 2977 m | | |
| | | | | 2961 sh | | |
| | | 2955 s | 2954 s,sh | 2955 s | | |
| 2948 s | 2950 s | | | 2949 s | | |
| 2932 vw | | 2926 vs | 2930 vs,b | 2929 s | 2925 s | |
| | 2912 s | | | 2917 s | | |
| | | | | 2909 sh | | |
| 2894 vs | | 2891 s | 2891 s | 2887 m | | |
| 2874 m | 2875 vs | | | 2870 s | 2875 m | |
| 2859 vw | | 2857 s | 2859 s | 2852 m | | |
| | | | | | 2850 vs,vb | 2700 s,vb |
| 2841 m | | | | 2837 s | 2835 m | |
| 2821 vw | 2815 w,sh | 2818 w | 2822 m | 2812 w | | |
| 2809 m | | | | | | |
| | | | 2797 vw,sh | 2785 vw,sh | | |
| 2781 vw | | | | 2780 w | | |
| 2765 w | 2764 vw,sh | 2765 w | 2765 w | | | |
| 2736 w | 2736 w | 2736 w | 2735 w | 2742 w | | |
| | | | | 2715 w | | |
| 2702 w | 2707 w | 2706 w | 2707 w | 2707 w | | |
| | 2693 w | 2688 w | 2690 w | 2693 w | | |
| 2662 w | 2662 vvw | | | | | |
| | | | 2580 w,vb | | | 2395 w,b |
| | | | | | 2155 m,b | 2180 m |
| | | | | | | 1820 w,b |
| | | | | | 1650 w,b | 1650 w,b |
| 1489 s | | | 1481 s | 1489 s | | 1485 m |
| 1486 sh | | | | | | |
| 1473 m | 1471 s | 1473 s | 1476 sh | 1477 sh | 1476 m | 1481 w,sh |
| 1470 m | | | | | | 1471 w,sh |
| | | | | 1468 m | | 1467 m |
| | | 1458 m,sh | 1462 w,sh | | 1459 m | 1459 w |
| | 1447 m | | | 1450 m | | 1448 w |
| 1443 m | | | | | 1439 w | 1442 m |
| | | | | | | 1428 m |
| 1412 vw | | 1411 w | 1416 w | 1423 vw | | 1419 vw,sh |
| | | | | | | 1405 m |
| 1386 w | | | | | | 1394 w,sh |
| 1371 w | 1370 vw | 1368 w | 1368 w | 1373 w | | 1371 w,sh |
| | | | | | | 1359 m |
| | | | | | 1356 m | 1355 s |
| | | | | 1308 m | | 1306 m |
| | | 1297 m | 1300 w,sh | 1298 m | | 1297 m |
| 1293 m | 1286 m,b | | | 1294 m | 1292 m | 1292 s |
| | | | | 1282 sh | | 1287 w |
| 1276 m | | 1276 s | 1276 s | 1278 s | 1277 sh | 1277 vvw |
| 1273 m | | | 1268 vw,sh | 1271 sh | | 1271 vvw |
| 1258 s | | | | 1257 w | 1253 m | 1256 m |
| | 1248 sh | 1246 m | 1248 m | 1248 w | | 1248 m |
| | | | | 1243 m | 1242 sh | 1242 m |
| 1234 m | 1239 m | 1237 sh | 1239 w | 1237 m | | 1237 sh |
| 1215 vw | | | | | | |
| 1154 m | | | | 1150 sh | | 1154 sh |
| | | | | | | 1148 m |

TABLE 1. (*Concluded*)

| Raman | | | | | Infrared | |
|---|---|---|---|---|---|---|
| EOc6 | | EOc6.$H_3O^+$.$BF_4^-$ | | | EOc6.$H_3O^+$.$BF_4^-$ Mulls | |
| | Solution | Solution | Solid | | | |
| Solid 25°C | $CHCl_3$ 25°C | $CHCl_3$ 25°C | 25°C | −190°C | 25°C | −195°C |
| | 1143 m,b | 1144 m | 1141 m | 1143 m | 1143 m | 1140 m |
| 1134 s,sh | | | | 1134 vw | | |
| 1130 s | | | | 1126 w | | 1131 m |
| 1108 w | | | 1106 vw | | | 1112 sh |
| | | | | 1096 vw | | 1097 vs,b |
| 1088 m | | | | 1086 vw | 1090 vs,b | |
| | | 1078 sh | 1075 m | 1078 vw | | 1080 vs |
| | 1067 vw | 1070 m | | 1068 m | | |
| 1060 w | | | | 1056 vw | | 1051 vs,b |
| 1043 m | 1045 w | | | 1045 w | 1040 vs,b | 1036 vs |
| 984 s | 991 vw | | | | | |
| | | | | | 974 m | 976 s |
| | | 967 vw | | 963 vw | | 962 s |
| | 948 vw,sh | 948 vw | 948 vw | 950 vw | 950 m | 949 m |
| | | | | 942 vw | | 941 s |
| 935 w | | | | | | 932 sh |
| | | | | | | 922 m |
| | 920 w | 917 vw | 907 vw | | | 916 vw,sh |
| 888 s | 881 w | | 883 s | | | |
| 863 s | | 874 s | 874 m,sh | 875 s | | 872 w |
| | 847 m | 840 vw,sh | 843 vw | 844 m | 843 m | 842 s |
| 829 w,sh | 832 w | | | | 835 w,sh | |
| 819 s | | 823 w | 821 m | 818 sh | 821 m | 817 sh |
| | | | | 813 m | | 813 s |
| | 804 m | | | | 801 w,sh | |
| | | 765 s | 765 s | 767 s | | 766 vw |
| | | | | | 721 w | 724 w |
| | | | | | 613 w | |
| 578 m | | 578 vw | 582 w | 586 m | | 582 w |
| | 572 w | | | 567 m | 573 w | |
| | | 548 w | 549 m | 552 m | | |
| | | | 536 w | 535 w | 538 w | 534 w |
| 520 w | 529 w | 520 w | 520 w | 520 m | 516 w | 519 m |
| | 504 vw,sh | | | | | |
| 450 w | | | | | | |
| 414 s | | | | 399 w | | |
| | | | | 374 w | | |
| | | | 369 w | 368 sh | | |
| 349 w | | | 351 w | 341 vw | | |
| 318 w | | | | 316 m | | |
| | | | 307 w,vb | 311 sh | | |
| | | 283 m | 287 s | 289 m | | |
| 268 m | | | 268 sh | 269 m | | |
| | | | | 265 sh | | |
| | | | 242 vw | 241 w | | |
| 218 vw | | | 208 vw | 205 w | | |
| 188 vw | | | | 177 vw | | |
| | | | | 171 w | | |
| | | | | 139 sh | | |
| | | | | 131 sh | | |
| 118 m | | | 120 w | 123 m | | |
| | | | 90 w | 94 s | | |
| 84 m | | | | 83 w | | |
| | | | | 60 s | | |
| | | | | 54 s | | |

*s = strong, m = medium, w = weak, b = broad, v = very, sh = shoulder.

Can. J. Chem. Downloaded from www.nrcresearchpress.com by 210.87.254.5 on 09/06/12
For personal use only.

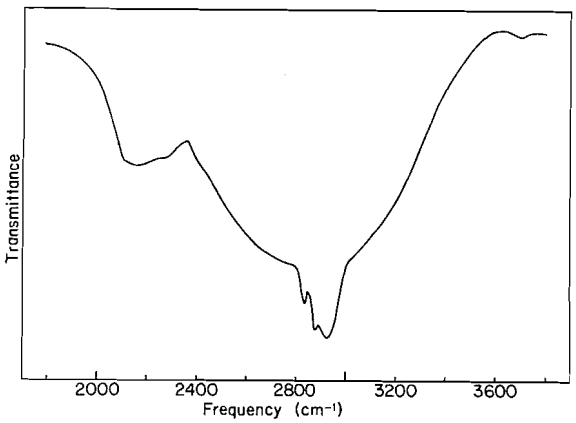


FIG. 2. High-frequency region of the infrared spectrum of 18-crown-6. $H_3O^+.BF_4^-$ complex mulled in hexachlorobutadiene at 28°C, showing the strong band of $H_3O^+$ near 2850 $cm^{-1}$.

similar to that of the complex discussed here. Raman bands due to the weak $H_3O^+$ scatterer were not detected in the Raman spectra of the complex, although this ion has been shown to give a measurable Raman spectrum in various acids (19, 20). It should also be mentioned that the solid monohydrate of tetrafluoroboric acid, $HBF_4.H_2O$, is ionised ($H_3O^+.BF_4^-$) in its crystalline form (21).

The vibrational frequencies of the tetrahedral $BF_4^-$ ion are well known from previous spectroscopic studies of this species in aqueous solution, molten salts (22), and crystalline salts of alkaline metals (23). The very sharp peak due to the totally symmetric stretching mode ($\nu_1$) is particularly evident at 765 $cm^{-1}$ in the Raman spectra of the EOc6 complex (Fig. 1 *C–E*), even in the case of the $CHCl_3$ solution where it emerges from a broader peak due to the solvent. This mode is normally infrared-inactive, but it is responsible for a very weak band detectable in the infrared spectrum at liquid nitrogen temperature. This points to a slight departure from tetrahedral symmetry in the solid, at least at low temperature.

The symmetric bending mode ($\nu_2$) of $BF_4^-$ gives but a weak peak at 369 $cm^{-1}$ in the spectrum of the solid at room temperature. At liquid nitrogen temperature, however, this band is split into a doublet at 368/374 $cm^{-1}$. This probably results from the anisotropy of the local field surrounding the $BF_4^-$ ions in the solid, which also suggests some distortion of these ions in an asymmetric environment. The $\nu_4$ bending mode, which normally occurs in the 520–535 $cm^{-1}$ range, is difficult to single out in the present study due to the presence of other bands from the ether in this same region. The weak band present at 536 $cm^{-1}$ in both the infrared and Raman spectra most likely belongs to this vibration, but it is not possible to establish whether the nearby peaks at 520 and 550 $cm^{-1}$ in the Raman are components of this triply degenerate mode or if they belong to the ether.

The asymmetric stretching mode of the tetrafluoroborate ion ($\nu_3$) is responsible for a very strong absorption band in the 1100 $cm^{-1}$ region of the infrared spectrum. As in crystalline $KBF_4$, $RbBF_4$, and $CsBF_4$ (23), this band is characterized by a submaximum near 1040 $cm^{-1}$ and a very strong reflection shoulder on its high frequency side. This region of the spectrum is extremely complex, due to the interaction between $\nu_3$ and the first overtone of $\nu_4$, and because of the presence of the $\nu_2$ bending mode of the $H_3O^+$ and a strong band from the cyclic ether. The $\nu_3$ band of $BF_4^-$ is weak in the Raman spectrum of the complex, and it cannot be singled out from other bands in this region.

Comparison of the spectrum of the ether complex in solution in $CHCl_3$ (Fig. 1*C*) with that of a solution of the uncomplexed ether (Fig. 1*B*), shows that a noticeable sharpening of the Raman bands occurs upon complexation, along with intensity changes, particularly in the 1450 and 2900 $cm^{-1}$ region. This indicates that the structure of the complex is relatively more rigid than that of the uncomplexed ether and, also, that the conformation of the ether in the complex is modified with respect to the average conformation of the free molecule. On the other hand, the Raman spectra of the complex in solution (Fig. 1*C*) and in the crystalline state (Fig. 1*D*) are very similar, which means that the $EOc6.H_3O^+.BF_4^-$ units have basically the same structure in both conditions. One also notices that the Raman bands of the crystalline complex at room temperature are generally broader than those of the crystalline cyclic ether (Fig. 1*A*). Although the exact significance of this observation is not clear, the possibility that some degree of disorder exists in the crystalline complex cannot be discarded.

The room temperature Raman spectrum of the $EOc6.H_3O^+.BF_4^-$ crystalline complex is very similar to those of various complexes in which the ether is known to have the regular crown geometry of $D_{3d}$ symmetry (14, 15, 24). However, some extra bands are observed in the present case, which suggest some departure from this ideal conformation. For example, whereas three Raman-active modes ($A_{1g} + 2E_g$) are predicted, and generally observed in other spectra, for the $CH_2$ twisting modes in the 1330–1400 $cm^{-1}$ region, at least four bands are present in this region of the spectrum of the hydronium complex. One also notes a splitting of the skeletal breathing mode, which gives a doublet at 874/883 $cm^{-1}$ in the present case, as compared to a singlet in the 860–870 $cm^{-1}$ region

Can. J. Chem. Downloaded from www.nrcresearchpress.com by 210.87.254.5 on 09/06/12
For personal use only.

Can. J. Chem. Downloaded from www.nrcresearchpress.com by 210.87.254.5 on 09/06/12
For personal use only.

with other compounds. Departure from the $D_{3d}$ symmetry is even more evident when the infrared spectra are compared. Those of the very symmetric complexes, such as that with KBr, in which the $K^+$ ion is located at the center of the crown ether cavity, contain but two major bands in the 800–1000 $cm^{-1}$ region (15, 17), whereas two doublets are observed at 820/842 and 949/973 $cm^{-1}$ in the spectrum of the hydronium complex. This type of splitting is too important to be explained by an intermolecular vibrational coupling effect and, also, unlikely to be caused by a purely crystalline field perturbation.

The vibrational spectra of the hydronium complex at liquid nitrogen temperature (Fig. 1*E* and Table 1) differ markedly from those at room temperature. The vibrational bands are much sharper at low temperature and the number of components in each region of the spectrum is considerably increased. Although the observed spectral changes occur gradually with the lowering of the temperature, they mostly take place in the range −55°C to −95°C (Fig. 3). The modifications of the spectra can only be interpreted in terms of a lowering of the symmetry of the ether molecules at low temperature. This, in turn, is most likely accompanied by a change in the structure of the crystal.

It is possible, using known structural data, to build a satisfactory model of the EOc6.$H_3O^+$.$BF_4^-$ complex, which would be consistent with its vibrational spectra. EOc6 is known to be a particularly good complexing agent for metal ions, which interact with its oxygen atoms. When the ionic radius of the metal is appropriate, such as with $K^+$, the ether adopts the $D_{3d}$ conformation and the ion sits at the center of the molecular cavity. Larger ions, such as $Cs^+$ and $Rb^+$, are displaced from the mean plane of the ether, although the latter retains its $D_{3d}$ conformation, whereas with a smaller ion such as $Na^+$ the ether folds itself around the positively charged particle (16). Assuming an average dimension for the EOc6 molecule in its $D_{3d}$ conformation (16) and for the $H_3O^+$ ion ($r$(O—H) = 1.02 Å, ∠ H—O—H = 110°), one finds that the hydronium ion can fit easily within the ether cavity. However, it is to be expected in this case that the $H_3O^+$ ion will orient itself so as to form three OH···O hydrogen bonds, using alternate oxygen atoms of the ether. These three atoms can be those above the mean plane of the ether, as shown in Fig. 4, or the three below, this latter possibility being probably more favorable in view of the relative orientation of the lone pairs on these atoms. It is also possible that both types of complex exist at room temperature, given the relative broadness of the vibrational bands noted above.

The $BF_4^-$ ion is obviously associated electrically with the EOc6.$H_3O^+$ complex and it is likely that, at least in solution, it will take a position so as to maximize its interactions with the hydrogen atoms of the $H_3O^+$ ion. This is most easily done through the cavity of the host ether, with the resulting $H_3O^+$.EOc6.$BF_4^-$ aggregate being best described as a "crown ether-separated ion pair", analogous to the $RNH_3^+$. crown ether.$A^-$ complexes obtained with primary amines (25). The vibrational spectra indicate that the $BF_4^-$ ion in the complex is little distorted from tetrahedral symmetry, contrary to the situation which prevails with isolated $M^+BF_4^-$ ion pairs isolated in rare gas matrices (26). This suggests that the $H_3O^+$–$BF_4^-$ interactions in the complex are not very directional in nature, which may result in the molecular rotation of the $BF_4^-$ ions being relatively free in solution and even in the room temperature solid.

We have mentioned above that the hydronium ion is small enough to fit into the cavity of the crown ether. In fact, it would fit very loosely into this cavity when the crown ether is in its $D_{3d}$ conformation. In this case, assuming equivalent linear hydrogen bonds between the $H_3O^+$ ion and three alternate oxygen atoms of the ether, the O····O distances in the complex can be estimated at 2.95 Å. Such a large value would only be consistent with very weak hydrogen bonds, which could not account for the stability of the complex. Moreover, using known relations between the ν(O—H) frequency and the O····O distances in H-bonded systems (19, 27), the 2850 $cm^{-1}$ value for the room temperature solid leads to an approximate distance of 2.65 Å.

There are many ways in which the O····O distances between the $H_3O^+$ ion and the cyclic ether can be diminished. First, one can consider the case where the ether would essentially retain its $D_{3d}$ geometry, with the hydronium ion moving about in the cavity so as to form at any given time two strong and one weak hydrogen bonds. In this situation, there would be two different types of oxygen atoms in the ether molecule, those which are statistically H-bonded with the hydronium ion, and the other three which are not involved in hydrogen bond formation. The symmetry of the ether molecule would then be statistically $C_{3v}$. Also possible is a symmetric distortion of the ether, in which three alternate oxygen atoms are forced towards each other, which would also lower the symmetry of the complex to $C_{3v}$. This type of symmetry is interesting because it would be consistent with the room temperature vibrational spectra of the complex, which suggest a structure of relatively high symmetry, related to the $D_{3d}$ conformation of the ether

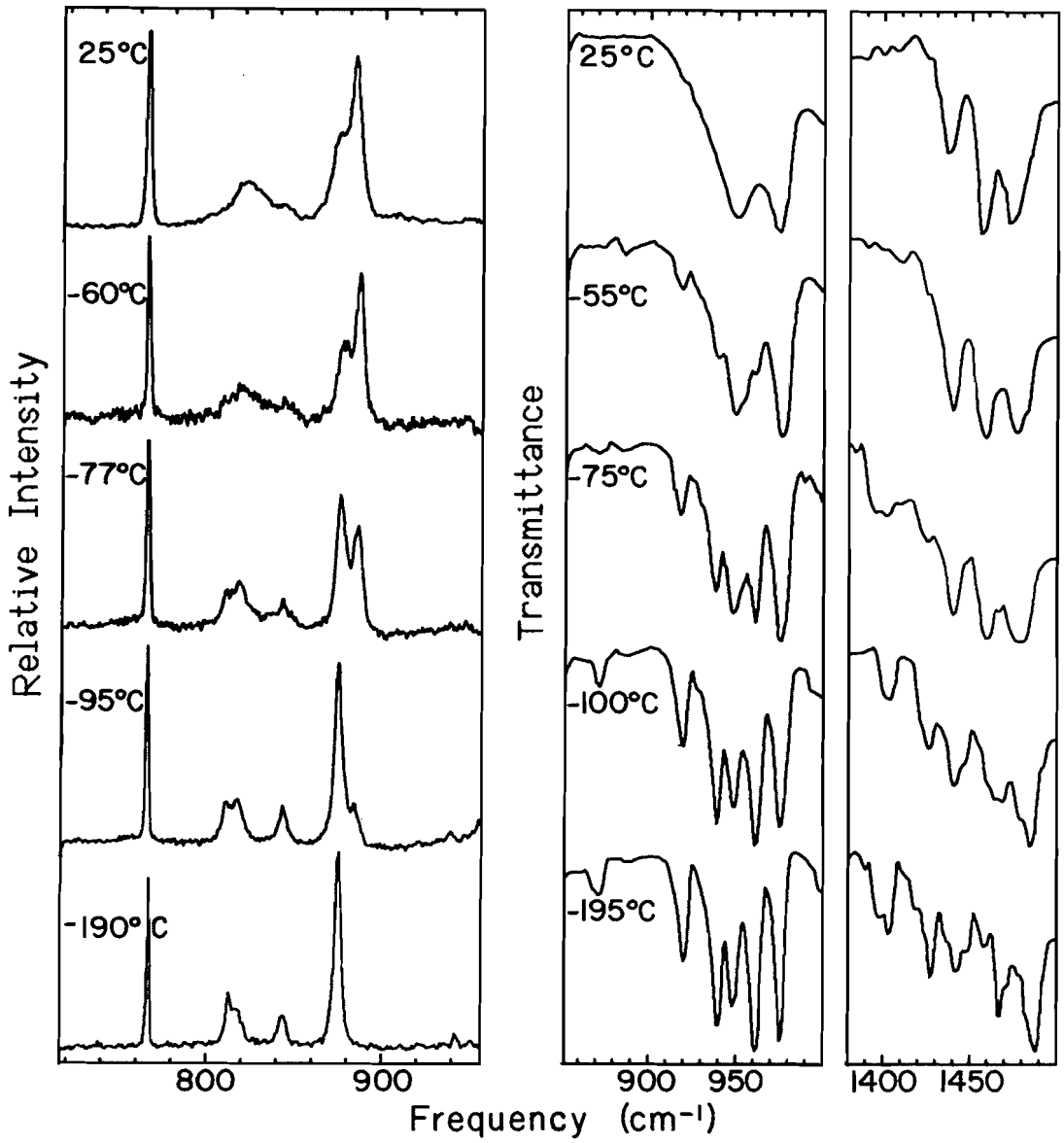


FIG. 3. Selected regions of the Raman (left) and infrared (right) spectra of the 18-crown-6.$H_3O^+$.$BF_4^-$ complex as a function of temperature.

moiety. The extra bands observed in the spectra could be readily explained on this basis, as the predicted number of active vibrational components would be approximately doubled by a lowering of the ether symmetry to $C_{3v}$. For example, whereas three non-coincident Raman- ($A_g + 2E_g$) and infrared- ($A_{2u} + 2E_u$) active modes are predicted for each of the $\delta(CH_2)$ (1430–1500 $cm^{-1}$ region), $\omega(CH_2)$ (1330–1430 $cm^{-1}$ region), and $tw(CH_2)$ (1230–1330 $cm^{-1}$ region) modes in the case of a $D_{3d}$ conformation, six coincident infrared- and Raman-active components ($2A_1 + 4E$) are expected in each region for a molecule of $C_{3v}$ symmetry.

From a theoretical point of view, lowering the symmetry of the crown ether molecule from $D_{3d}$ to $C_{3v}$ by bringing three of the six oxygen atoms closer together is not energetically favorable. This type of perturbation would force the other three oxygen atoms in the molecule to be pushed outwards, and bring strain into the cycle as the torsion angle about the C—C bonds increases from their ideal 60° value and that about the C—O bonds gets smaller than 180°. The strain brought into the cycle would then have to be more than compensated by the extra stability resulting from the formation of the three hydrogen bonds, each with an energy of ~7 kcal

Can. J. Chem. Downloaded from www.nrcresearchpress.com by 210.87.254.5 on 09/06/12
For personal use only.

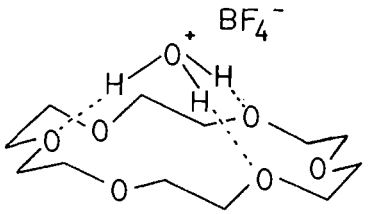


FIG. 4. Schematic representation of the 18-crown-6.$H_3O^+$.$BF_4^-$ complex.

$mol^{-1}$, as deduced from the frequency of the ν(O—H) stretching mode (27). The changes observed in the spectra upon lowering the temperature point to a very low symmetry of the crown ether moiety below the transition temperature. In the present scheme, it would seem that lowering the temperature causes the O···O distances to become shorter (the ν(O—H) frequency decreases to 2700 $cm^{-1}$), which results in the strain in the cyclic ether ring becoming more important than the gain in stability resulting from the formation of the three hydrogen bonds. At this point some folding of the ether molecule would take place, thus lowering the symmetry of the complex, possibly to $C_s$. In this low symmetry, all of the fundamental vibrations of the ether become simultaneously infrared- and Raman-active, which would account for the complexity of the vibrational spectra in the low temperature phase of the crystal. The very sharp lines in the spectra at liquid nitrogen temperature indicate that, whatever the structure of the crystal, it is not disordered as seems to be the case in the higher temperature modification.

The strange behavior of the 874/883 $cm^{-1}$ Raman doublet with temperature (Fig. 3) is noteworthy. The fact that one of the two components appears to grow at the expense of the other with decreasing temperature suggests a shift of equilibrium between two different conformers which would be simultaneously present in the solid at room temperature. This, however, is not supported by the other features in the spectra. These suggest only a gradual change of conformation of the complex as the temperature is lowered. In most cases, new bands gradually appear in the spectra upon going through the transition, and the disappearance of the 883 $cm^{-1}$ Raman band appears to be accidental. It is possible that the splitting of the skeletal breathing mode at high temperature is caused by Fermi resonance between this mode and an overtone or combination mode involving a low frequency skeletal bending mode.

It should finally be mentioned that a slow conformational change has been shown to occur between −90°C and −140°C in a complex of 18-crown-6 with $Cs^+BF_4^-$ (28). However, due to the size and spherical shape of the $Cs^+$ ion, it is doubtful that this change is in any way related to that observed here with the hydronium complex.

**Acknowledgements**

We acknowledge the financial support of this work from the Natural Sciences and Engineering Research Council of Canada and the Ministère de l'Education du Québec.

1. J. M. TIMKO, R. C. HELGESON, M. NEWCOMB, G. W. GOKEL, and D. J. CRAM. J. Am. Chem. Soc. **96**, 7097 (1974).
2. J. M. LEHN, P. VIERLING, and R. C. HAYWARD. J. Chem. Soc. Chem. Commun. 296 (1979).
3. T. J. VAN BERGEN and RICHARD M. KELLOGG. J. Am. Chem. Soc. **99**, 3882 (1977).
4. G. WULFSBERG and A. WEISS. J. Chem. Soc. Dalton, 1640 (1977).
5. G. W. GOKEL and D. J. CRAM. J. Chem. Soc. Chem. Commun. 481 (1973).
6. J. GOLDBERG. Acta Crystallogr. B**31**, 754 (1975).
7. C. J. PEDERSEN. J. Org. Chem. **36**, 1690 (1971).
8. G. W. GOKEL and D. J. CRAM. J. Org. Chem. **39**, 2446 (1974).
9. F. VÖGTLE, W. M. MÜLLER, and E. WEBER. Chem. Ber. **113**, 1130 (1980).
10. R. M. IZATT, B. L. HAYMORE, and J. J. CHRISTENSEN. J. Chem. Soc. Chem. Commun. 1308 (1972).
11. R. SAVOIE, B. BOULÉ, G. GENEST, and M. PÉZOLET. Can. J. Spectrosc. **24**, 112 (1979).
12. V. GOLD, J. L. GRANT, and K. P. MORRIS. J. Chem. Soc. Chem. Commun. 397 (1976).
13. J. D. DUNITZ and P. SEILER. Acta Crystallogr. B**30**, 2739 (1974).
14. H. SATO and Y. KUSUMOTO. Chem. Lett. Chem. Soc. Jpn. 635 (1978).
15. M. FOUASSIER and J.-C. LASSEGUES. J. Chim. Phys. **75**, 865 (1978).
16. P. SEILER, M. DOBLER, and J. D. DUNITZ. Acta Crystallogr. B**30**, 2744 (1974); M. DOBLER and R. P. PHIZACKERLEY. Acta Crystallogr. B**30**, 2746 (1974); B**30**, 2748 (1974).
17. J. DALE and P. O. KRISTIANSEN. Acta Chem. Scand. **26**, 1471 (1972).
18. R. M. COSTES, G. FOLCHER, P. PLURIEN, and P. RIGNY. Inorg. Nucl. Chem. Lett. **12**, 13 (1976).
19. B. DESBAT and P. V. HUONG. Spectrochim. Acta, **31**A, 1109 (1975).
20. P. A. GIGUÈRE, C. MARTEL, and S. TURRELL. Chem. Phys. Lett. **56**, 231 (1978).
21. D. MOOTZ and M. STEFFEN. Z. Krist. **154**, 306 (1981).
22. A. S. QUIST, J. B. BATES, and G. E. BOYD. J. Chem. Phys. **54**, 4896 (1971).
23. J. B. BATES and A. S. QUIST. Spectrochim. Acta, **31**A, 1317 (1975).
24. R. D. MCLACHLAN. Spectrochim. Acta, **30**A, 2153 (1974).
25. F. WADA, Y. WADA, K. KIKUKAWA, and T. MATSUDA. Bull. Chem. Soc. Jpn. **54**, 458 (1981).
26. R. L. HUNT and B. S. AULT. Spectrochim. Acta, **37**A, 63 (1981).
27. G. C. PIMENTEL and A. L. MCCLELLAN. The hydrogen bond. Reinhold Publ. Corp., New York. 1960. pp. 85–87.
28. J. KRANE, J. DALE, and K. DAASVATN. Acta Chem. Scand. B**34**, 59 (1980).

Can. J. Chem. Downloaded from www.nrcresearchpress.com by 210.87.254.5 on 09/06/12
For personal use only.

# Complexes moléculaires d'hétérocycles soufrés et oxygénés. Étude spectrophotométrique de bandes de transfert de charge multiples

JEAN-PAUL CANSELIER,[1] SERGE DOMENECH, ŠTEFAN STANKOVSKY[2] ET (AVEC LA COLLABORATION TECHNIQUE DE) SABINE GAUTIER

*Institut du Génie Chimique, Institut National Polytechnique, Chemin de la Loge, 31078 Toulouse Cédex, France*

Reçu le 28 août 1981

JEAN-PAUL CANSELIER, SERGE DOMENECH, ŠTEFAN STANKOVSKY et SABINE GAUTIER. Can. J. Chem. **60**, 862 (1982).

Comme dans le cas des donneurs benzéniques, les spectres électroniques d'absorption des complexes moléculaires formés par les hétérocycles pentagonaux soufrés ou oxygénés, simples ou condensés, avec le TCNE (ou la DDQ) font apparaître le plus souvent deux bandes de transfert de charge. Dans de nombreux exemples étudiés, la détermination précise des fréquences d'absorption nécessite une méthode de résolution. Les résultats obtenus sont utilisés dans des corrélations avec les potentiels d'ionisation des donneurs d'une part, et avec la réfringence des solvants apolaires d'autre part.

JEAN-PAUL CANSELIER, SERGE DOMENECH, ŠTEFAN STANKOVSKY, and SABINE GAUTIER. Can. J. Chem. **60**, 862 (1982).

As with benzenoid donors, the electronic absorption spectra of the molecular complexes of simple or condensed sulfur or oxygen-containing five-membered heterocycles with TCNE (or DDQ) often show two charge-transfer bands. In many cases, the knowledge of the actual frequencies requires a technique of resolution. The results so obtained are correlated with the ionization potentials of donors on the one hand, and the refractivity of nonpolar solvents on the other hand.

## 1. Introduction

L'étude physico-chimique des hétérocycles soufrés (en particulier celle des thiophènes condensés) trouve des applications dans l'hydrodésulfuration des résidus pétroliers lourds. Les travaux que nous avons entrepris sur le caractère aromatique de ce type d'hétérocycles (1, 2) et, parallèlement, sur l'adsorption de certains de ces composés sur un catalyseur d'hydrodésulfuration (3) sont maintenant poursuivis par l'examen de leur pouvoir donneur d'électrons. Celui-ci se manifeste entre autres dans la formation de complexes moléculaires faibles, dont le spectre électronique d'absorption présente une ou plusieurs bandes supplémentaires, appelées "bandes de transfert de charge" (4–7). Selon la théorie de Mulliken et Person (6), les fréquences de transfert de charge $\nu_{TC}$ donnent lieu à une corrélation avec les potentiels d'ionisation $I_D$ des donneurs pour les complexes d'un même accepteur, ou avec les affinités électroniques $E_A$ des accepteurs lorsqu'on travaille sur un seul donneur:

$$[1] \quad h\nu_{TC} = I_D - E_A + (G_0 - G_1) + \frac{\beta_0^2 + \beta_1^2}{I_D - E_A + (G_0 - G_1)}$$

$G_0$ représente l'énergie résultant des interactions de non-liaison entre A et D et $G_1$ l'énergie d'attraction coulombienne[3] entre $A^-$ et $D^+$. Les intégrales $\beta_i$, ayant la dimension d'une énergie, peuvent être explicitées par un calcul de perturbation du second ordre (6, 7).

D'après une autre approche, partant de la théorie des orbitales moléculaires (8), la bande de transfert de charge de plus basse fréquence observée a pour origine une transition entre la plus haute orbitale occupée (H.O.) du donneur et la plus basse orbitale vacante (B.V.) de l'accepteur, les niveaux d'énergie correspondants n'étant pratiquement pas perturbés par la formation du complexe. Bien qu'approximatives, ces justifications théoriques vont nous permettre une analyse des spectres de transfert de charge surtout en ce qui concerne le nombre et la nature des transitions observées.

## 2. Résultats expérimentaux. Traitement des bandes multiples

Les donneurs d'électrons considérés sont des hydrocarbures et des hétérocycles appartenant aux familles A à F (composés modèles et dérivés substitués **1** à **28** avec X = $CH_2$, O, S; Y = $CH_2$, S) (cf. Tableau 1), certains composés aromatiques de référence comportant un, deux ou trois cycles bénzéniques (**29** à **42**), et quelques donneurs saturés à paire électronique libre: **43** à **47**.

Nous avons choisi d'autre part des accepteurs d'électrons bien connus et figurant parmi les plus puissants répertoriés jusqu'ici (7, 9): le tétracyanoéthylène (TCNE), qui offre de plus l'avantage

[1]Correspondance à adresser à J. P. Canselier.

[2]Adresse actuelle: Laboratoire de Chimie Organique, Université Technique Slovaque, Janska 1, 88037 Bratislava, Tchécoslovaquie.

[3]Mulliken (6) et Foster (7) prennent des conventions de signes opposées concernant $G_0$ et $G_1$; nous adoptons ici celle de Foster.

0008-4042/82/070862-10$01.00/0

©1982 National Research Council of Canada/Conseil national de recherches du Canada

Can. J. Chem. Downloaded from www.nrcresearchpress.com by 210.87.254.42 on 09/06/12
For personal use only.

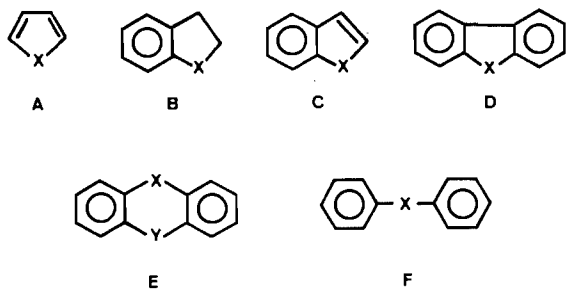


d'être incolore, et la dichloro-2,3 dicyano-5,6 benzoquinone (DDQ).

*(a) Mesure de $\lambda_{max}$*

Les spectres des complexes moléculaires en solution ont été enregistrés à l'aide d'un spectrophotomètre Beckman DBG. Les mesures ont été effectuées dans trois principaux solvants: le dichlorométhane, le chloroforme et le tétrachlorure de carbone. Malgré certains résultats interprétés en termes d'interactions spécifiques avec les hydrocarbures benzéniques (10, 11) ce dernier solvant nous paraît être le seul solvant non polaire capable de dissoudre suffisamment les composés polycycliques et les accepteurs d'électrons.

Les longueurs d'onde des bandes de transfert de charge avec le TCNE mesurées au(x) maximum(s) d'absorption apparent(s) ($\lambda_{max}$) sont rassemblées dans le tableau 1, qui renferme aussi certaines données tirées de la littérature.

Le tableau 2 rassemble les mesures effectuées sur les complexes de la DDQ dans le dichlorométhane et dans le tétrachlorure de carbone. La DDQ présente un maximum d'absorption à 388 nm (dans $CH_2Cl_2$) qui perturbe dans de nombreux cas la deuxième bande de transfert de charge (bande de plus haute fréquence).

Les valeurs de $\lambda_{max}$ sont données à 2 nm près environ:[4] en nombre d'ondes, cet écart correspond à une incertitude comprise entre 0,05 kK (à 650 nm) et 0,15 kK (à 350 nm). L'examen du tableau 1 montre cependant qu'entre différents auteurs les écarts sont parfois supérieurs à 2 nm.

*(b) Prévision des bandes multiples*

Une étude préliminaire de la structure électronique $\pi$ (selon Hückel) des donneurs et des accepteurs envisagés (13, 42) a montré que les deux H.O. des composés de types C et D sont assez proches en énergie ($\Delta\chi_i < 0{,}25\beta$). Les dérivés benzéniques mono- ou disubstitués possèdent la même propriété. Les deux H.O. des composés A et F sont un peu plus espacées, mais, seuls parmi les donneurs $\pi$ envisagés ici, le benzène et l'hexaméthylbenzène, plus symétriques (groupe $D_{6h}$), présentent une dégénérescence de leurs plus hauts niveaux énergétiques, les orbitales correspondantes appartenant à la représentation irréductible $E_{1g}$. Par ailleurs, d'après la spectroscopie de photoélectrons dans l'ultraviolet (SPU), les deux premiers potentiels d'ionisation des composés A à F, souvent assez rapprochés, font bien intervenir des orbitales moléculaires (o.m.) $\pi$ (Tableau 1).

En revanche les deux B.V. du TCNE et de la DDQ sont relativement éloignées (42*b*) de sorte que les transitions les moins énergétiques susceptibles de produire les bandes de transferts de charge doivent mettre en jeu deux o.m. du donneur et une seule o.m. de l'accepteur. Effectivement la majorité des complexes du TCNE considérés laissent apparaître deux bandes de transfert de charge inégalement espacées, même sur l'échelle des nombres d'ondes. Si l'on se réfère aux structures cristallines connues (7, 43), les associations ainsi formées ne possèdent pas en général un haut degré de symétrie, et l'application du critère de symétrie ne diminue pas le nombre de bandes prévu par la théorie (42*b*). L'unique maximum apparent observé avec les donneurs **7**, **12**, **18**, **19**, **22**, **30–32** et **42** recouvre donc deux bandes.

*(c) Forme et résolution des bandes de transfert de charge*

Dans l'analyse des spectres les bandes symétriques sont généralement représentées par des courbes de Gauss ou de Lorentz–Cauchy comportant trois paramètres: les coordonnées $x_0$ et $y_0$ (nombre d'ondes et densité optique) du maximum et la largeur à mi-hauteur $\Delta x_{\frac{1}{2}}$. La principale différence entre les deux représentations réside dans l'importance en surface des traînées latérales, beaucoup plus grande avec le modèle de Lorentz–Cauchy.

En fait, les bandes de transfert de charge, telles qu'on les observe en solution, constituent l'enveloppe d'une structure fine due à la vibration d'élongation totalement symétrique ("respiration") du complexe. Elles résultent donc de la combinaison de courbes gaussiennes élémentaires, généralement considérées comme symétriques sur l'échelle des fréquences (44). Si la fréquence de respiration est assez élevée, les niveaux vibrationnels excités de l'état électronique fondamental sont très peu peuplés et les courbes élémentaires représentent des transitions vibrationnelles $0 \rightarrow v'$ (principe de Franck–Condon). La bande enveloppe sera, par conséquent, très dissymétrique. Au contraire, si la

[4]Les bandes étant larges, la détermination de leur sommet est effectuée par la méthode du point milieu (41).

Can. J. Chem. Downloaded from www.nrcresearchpress.com by 210.87.254.42 on 09/06/12
For personal use only.

TABLEAU 1. Complexes moléculaires du TCNE: longueurs d'onde aux maximums d'absorption apparents

| No | Composé donneur | $\lambda_{max}$ (nm) Solvant $CH_2Cl_2$ | Solvant $CHCl_3$ | Solvant $CCl_4$ | $I_D$ (eV) |
|---|---|---|---|---|---|
| 1 | Furanne | 310; 448 (12)[a] | 450<br>450 (13) | 295; 445 (14)<br>445 (12) | 8,89; 10,30 (26–28) |
| 2 | Thiophène | 383; 448 (15) | 399 (13) | 387; 445 (12)<br>390; 445 (14)<br>390 | 8,90; 9,49 (26–28) |
| 3 | Méthyl-2 thiophène | 408; 497 (15) | 410; 500 (16) | 397; 485 (12)<br>398; 489 | 8,32; 8,96 (28) |
| 4 | Méthyl-3 thiophène | 410; 478 (15) | | 419 (12) | 8,54; 9,11 (28) |
| 5 | Bromo-2 thiophène | 371; 470 (15) | 370; 474 (16) | 370; 472 (12) | 8,50; 9,41 (28) |
| 6 | Bromo-3 thiophène | 375; 450 (12) | | 395; 435 | 9,00; 9,51 (28) |
| 7 | Indane | | | 425; 470 | 8,46; 9,04 (29) |
| 8 | Dihydro-2,3 benzofuranne | | | 389; 550 | 8,22; 9,09 (30) |
| 9 | Méthyl-2 dihydro-2,3 benzofuranne | 400; 571 | | 403; 576 | |
| 10 | Dihydro-2,3 benzothiophène | | | 402; 622 | |
| 11 | Indène | 423; 542 | 430; 542 (13) | 420; 538 | 8,20; 8,95 (31, 32) |
| 12 | Benzofuranne | 457 | 458<br>465 (13) | 457 | 8,60; 8,95 (31, 32) |
| 13 | Benzothiophène | 480; 530 | 480; 545<br>477; 528 (13) | 462; 536 | 8,20; 8,76 (31, 32) |
| 14 | Méthyl-2 benzothiophène | | | 492 | 8,08; 8,50 (32) |
| 15 | Bromo-2 benzothiophène | | | 473 | 8,35; 8,74 (32) |
| 16 | Bromo-3 benzothiophène | 445; 540 | 445; 548 | 430; 535 | 8,35; 8,90 (32) |
| 17 | Fluorène | 567 (17)<br>570 (18) | 419; 567 (13) | 406; 569 | 7,93; 8,80 (33, 34) |
| 18 | Dibenzofuranne | 508<br>500 (18) | 517<br>498 (13) | 512 | 8,35; 8,50 (33) |
| 19 | Dibenzothiophène | 554<br>550 (18) | 560<br>550 (13) | 550<br>550 (12) | 8,01; 8,36 (33) |
| 20 | Bromo-2 dibenzothiophène | | 548 | 543 | |
| 21 | Dibromo-2,8 dibenzothiophène | | 527 | | |
| 22 | Dihydro-9,10 anthracène | | | 439 | |
| 23 | Xanthène | | | 577 | |
| 24 | Thioxanthène | | | 622 | |
| 25 | Thianthrène | | | 470; 602 | |
| 26 | Diphénylméthane | 410 (19) | | 420 (20) | 9,10; 11,80 (34) |
| 27 | Oxyde de diphényle | 495 (19) | 380; 504 | 367; 498 | 8,32 (35) |
| 28 | Sulfure de diphényle | 370; 585 (21) | | 375; 582 | 7,88; 9,20 (35) |
| 29 | Benzène | 384 (17)<br>387 (19) | 388 (22)<br>391 (13, 24) | 383 (23) | 9,24 (36) |
| 30 | Toluène | 406 (17)<br>411 (19) | 414 (22)<br>415 (24) | 409 | 8,80; 9,00 (37) |
| 31 | Cyclohexylbenzène | 413 (19) | | 419 | |
| 32 | Tétraline | 454 | | 444 | |
| 33 | Hexaméthylbenzène | 544 (25)<br>545 (17) | | 532<br>534 (23) | 7,86 (37) |
| 34 | Anisole | 507 (17) | | 381; 504 | 8,42; 9,23 (36) |
| 35 | *p*-Diméthoxybenzène | | | 377; 631 | 7,90; 9,25 (36) |
| 36 | *p*-Méthylthioanisole | | | 650 | 7,80; 8,72 (38) |
| 37 | Thioanisole | 380; 572 (21) | | 380; 566 | 8,07; 9,28 (36) |
| 38 | Diphényle | 498 (19)<br>500 (17) | 505 (13) | 387; 501<br>500 (23) | 8,25; 9,08 (27, 33, 34) |
| 39 | Naphtalène | 429; 550 (17)<br>429; 552 | 432; 560<br>431; 555 (22) | 425; 549 | 8,20; 8,88 (31, 36) |
| 40 | Méthyl-1 naphtalène | | 440; 592 (22) | 428; 578 | |
| 41 | Méthyl-2 naphtalène | | 458; 579 (22) | 450; 565 | |
| 42 | Phénanthrène | 536<br>532 (18) | 541<br>535 (13) | 529<br>526 (23) | 7,90; 8,15 (33, 34) |
| 43 | Sulfure de diméthyle | | | 482 | 8,68 (39) |
| 44 | Oxétanne | | | 331 | 9,92 (40) |
| 45 | Thiétanne | | | 489 | 8,65 (39) |
| 46 | Oxolanne (Tétrahydrofuranne) | | | 336 | 9,80 (40) |
| 47 | Thiolanne (Tétrahydrothiophène) | | 510 (16) | 507 | 8,41 (39)<br>8,55 (40) |

[a]Les valeurs de $\lambda_{max}$ soulignées sont définitives (cas d'une bande unique ou de deux bandes suffisamment séparées). Les numéros entre parenthèses se réfèrent à la bibliographie.

Can. J. Chem. Downloaded from www.nrcresearchpress.com by 210.87.254.42 on 09/06/12
For personal use only.

TABLEAU 2. Complexes moléculaires de la DDQ: longueurs d'onde aux maximums d'absorption apparents

| No | Composé donneur | $\lambda_{max}$ (nm) Solvant $CH_2Cl_2$ | Solvant $CCl_4$ |
|---|---|---|---|
| **2** | Thiophène | 453 (15)[a] | |
| **9** | Méthyl-2 dihydro-2,3 benzofuranne | 649 | |
| **10** | Dihydro-2,3 benzothiophène | 672 | |
| **11** | Indène | | 450; 588 |
| **12** | Benzofuranne | | 512[b] |
| **13** | Benzothiophène | | 495; 590[c] |
| **14** | Méthyl-2 benzothiophène | | 530; 630[c] |
| **17** | Fluorène | 623 (18) | 610 |
| **18** | Dibenzofuranne | 575 (18) | 562 |
| **19** | Dibenzothiophène | 598 | 582 |
| | | 598 (45) | |
| | | 600 (18) | |
| **20** | Bromo-2 dibenzothiophène | 582 | |
| **31** | Cyclohexylbenzène | 472 | |
| **33** | Hexaméthylbenzène | 620 | |
| **38** | Diphényle | | 557 |
| **39** | Naphtalène | | 455; 601 |
| **42** | Phénanthrène | 582 (18) | 565 |

[a]cf. Tableau I(*a*).
[b]Sommet très aplati.
[c]Epaulement.

fréquence de respiration est basse ($\bar{\nu} = 115\,cm^{-1}$ pour le complexe mésitylène–TCNE, par exemple (45)) la possibilité de transitions $1 \rightarrow 0$, $1 \rightarrow 1$, ... et même $2 \rightarrow 0$, $2 \rightarrow 1$, ... diminuera la dissymétrie de la bande observée. Le facteur $B$ de Briegleb et Czekalla (46) caractérise la dissymétrie des bandes de transfert de charge:

$$[2] \quad B = \frac{\bar{\nu}_h - \bar{\nu}_1}{2(\bar{\nu}_{max} - \bar{\nu}_1)}$$

$\bar{\nu}_{max}$, $\bar{\nu}_h$ et $\bar{\nu}_1$ désignent respectivement les nombres d'ondes au maximum d'absorption et à mi-hauteur ($\bar{\nu}_h > \bar{\nu}_1$).

La représentation par des courbes de Gauss asymétriques a été utilisée par Jørgensen (47) en spectrophotométrie des complexes métalliques. Le modèle de Fraser et Suzuki (48), plus complet, a été préféré par certains auteurs (24, 49).

Afin d'identifier les paramètres des bandes élémentaires, nous avons choisi pour notre part un algorithme fondé sur la méthode des moindres carrés associée à l'utilisation d'une fonction de référence, et que préconisent d'ailleurs Fraser et Suzuki (48*b*). Le facteur $B$ est alors imposé et pris identique pour les deux transitions d'un même complexe.[5] Il reste donc à identifier trois paramètres par bande: la hauteur, la position du sommet et la largeur relative, et l'algorithme consiste à modeler les bandes expérimentales sur la courbe de référence au moyen de trois transformations ponctuelles: une translation et deux affinités.

La fonction de référence choisie doit être la plus représentative possible des bandes à séparer. Nous avons retenu comme références les bandes de plus basse fréquence données par les complexes **28**–TCNE et **37**–TCNE en raison de la similitude structurale de ces donneurs avec de nombreux composés étudiés (présence du motif $C_6H_5$—S ou $(C_6H_5)_2S$) ainsi que les bandes uniques des complexes du TCNE avec les donneurs **33** et **47**. La méthode de résolution est présentée en annexe. A titre d'illustration, nous avons représenté sur la figure 1 les spectres expérimentaux et calculés des complexes **13**–TCNE et **19**–TCNE.

Nous avons examiné systématiquement l'influence de la fonction de référence sur le traitement de 60 spectres. Les valeurs des paramètres obtenues à l'aide des quatre fonctions de référence, pour les deux exemples de la figure 1, sont consignées dans le tableau 3. L'écart quadratique moyen entre le spectre expérimental et le spectre calculé[6] est voisin dans ces deux cas de $5 \times 10^{-3}$. L'abscisse d'un sommet est déterminée à 0,2 kK près et l'écart sur $\bar{\nu}$ ne dépasse pas cette valeur. Les hauteurs $h_1$ et $h_2$ sont plus sensibles au choix du modèle. Les nombres d'ondes de transfert de charge $\bar{\nu}_{max}$ obtenus après résolution sont rassemblés dans le tableau 4.

[5]Contrairement à ce que considèrent certains auteurs, la valeur de $B$ est souvent légèrement inférieure à 1,19 et varie quelque peu suivant le complexe examiné.

[6]Pour l'ensemble des spectres calqués sur la fonction de référence **37**–TCNE, les valeurs limites de $S_{min}$ sont $1{,}35 \times 10^{-3}$ et $1{,}25 \times 10^{-2}$ (cf. Annexe).

Can. J. Chem. Downloaded from www.nrcresearchpress.com by 210.87.254.42 on 09/06/12
For personal use only.

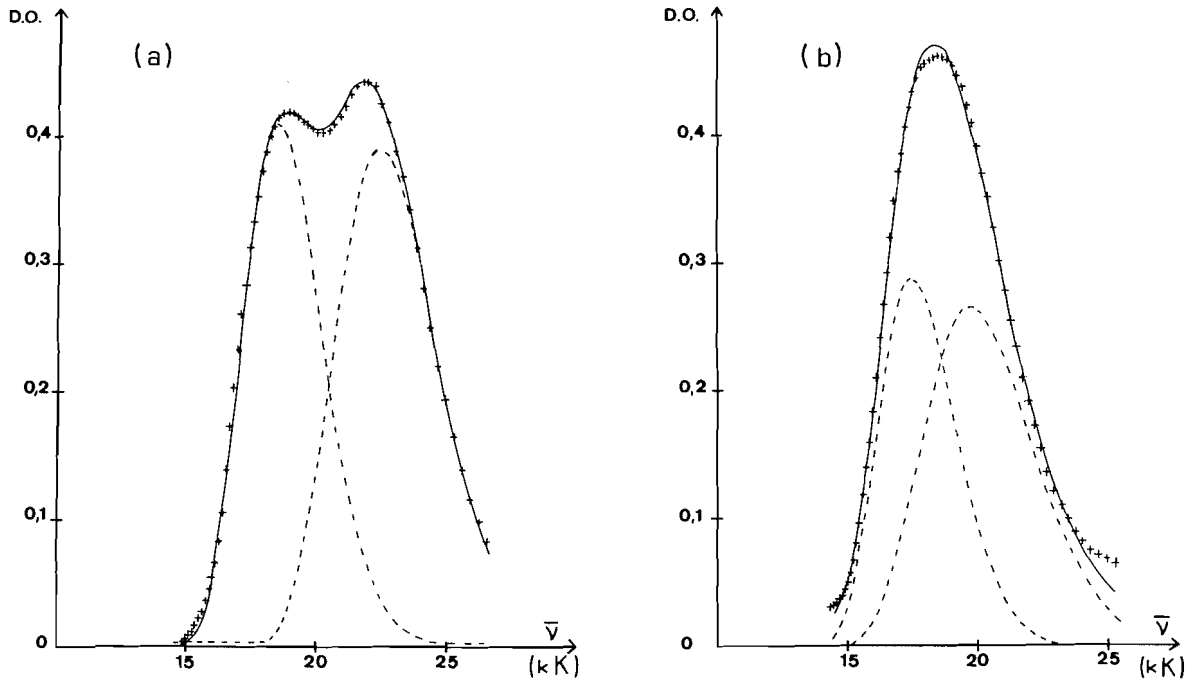


FIG. 1. Résolution de bandes multiples (référence: **37**–TCNE); +++: spectre expérimental discrétisé; ---: bandes élémentaires calculées; ———: spectre calculé; (a) complexe benzothiophène–TCNE (solvant $CCl_4$); (b) complexe dibenzothiophène–TCNE (solvant $CCl_4$).

TABLEAU 3. Influence de la fonction de référence sur les paramètres de quelques bandes de transfert de charge dans $CCl_4$

| Complexe | Fonction de référence (B) | $S_{min} \times 10^3$ | $h_1$ | $\bar{\nu}_1$ (kK) | $h_2$ | $\bar{\nu}_2$ (kK) |
|---|---|---|---|---|---|---|
| **13**–TCNE | **28**–TCNE (1,17) | 4,67887 | 0,417 | 18,40 | 0,362 | 22,30 |
| | **33**–TCNE (1,08) | 5,30585 | 0,383 | 18,25 | 0,392 | 22,10 |
| | **37**–TCNE (1,15) | 4,33759 | 0,406 | 18,25 | 0,387 | 22,25 |
| | **47**–TCNE (1,15) | 4,59803 | 0,404 | 18,30 | 0,361 | 22,05 |
| **19**–TCNE | **28**–TCNE | 8,78735 | 0,266 | 17,40 | 0,268 | 19,40 |
| | **33**–TCNE | 7,65690 | 0,115 | 17,20 | 0,368 | 18,95 |
| | **37**–TCNE | 7,59986 | 0,285 | 17,35 | 0,263 | 19,50 |
| | **47**–TCNE | 3,17512 | 0,250 | 17,00 | 0,335 | 19,20 |

## 3. Interprétation et discussion

*(a) Corrélation des fréquences de transfert de charge avec les premiers potentiels d'ionisation des donneurs*

Les premiers potentiels d'ionisation verticaux des donneurs étudiés, mesurés par spectroscopie de photoélectrons uv (SPU), figurent dans le tableau 1. L'incertitude sur cette grandeur, souvent inférieure ou égale à 0,05 eV, peut atteindre 0,1 eV, notamment lorsque les pics sont mal séparés, ce qui nécessiterait une résolution.

Nous avons appliqué la relation [1] sous l'une des formes simplifiées suivantes:

$$[1'] \quad h\nu_{TC} = I_D - C_1 + \frac{C_2}{I_D - C_1}$$

$$[1''] \quad h\nu_{TC} = aI_D - b$$

aux séries de valeurs obtenues au cours de ce travail et trouvées dans la littérature. Les paramètres $C_1$, $C_2$, $a$ et $b$ ainsi identifiés sont rassemblés dans le tableau 5. La figure 2 illustre graphiquement certains de ces résultats. On s'aperçoit immédiatement que le traitement des données par le modèle [1'] n'apporte guère d'amélioration par rapport à l'équation [1'']. Les complexes étudiés dans le

Can. J. Chem. Downloaded from www.nrcresearchpress.com by 210.87.254.42 on 09/06/12
For personal use only.

Can. J. Chem. Downloaded from www.nrcresearchpress.com by 210.87.254.42 on 09/06/12
For personal use only.

TABLEAU 4. Fréquences de transfert de charge après résolution[a]

| No | Composé donneur | $(\bar{\nu}_{max})_1$ (kK) | $(\bar{\nu}_{max})_2$ (kK) | $\Delta\bar{\nu}$ (kK) |
|---|---|---|---|---|
| | *Accepteur: TCNE* | | | |
| **2** | Thiophène | 22,20 | 26,25 | 4,05 |
| **4** | Méthyl-3 thiophène | 21,15 | 24,75 | 3,60 |
| **6** | Bromo-3 thiophène | 22,25 | 27,05 | 4,80 |
| **7** | Indane | 21,05 | 24,50 | 3,45 |
| **8** | Dihydro-2,3 benzofuranne | 18,50 | 25,85 | 7,35 |
| **11** | Indène | 18,45 | 24,20 | 5,75[b] |
| | | 18,65 | 24,20 | 5,55 |
| **12** | Benzofuranne | 19,80 | 23,50 | 3,70[b] |
| | | 19,75 | 23,45 | 3,70[c] |
| | | 19,70 | 23,45 | 3,75 |
| **13** | Benzothiophène | 18,05 | 22,10 | 4,05[b] |
| | | 17,95 | 21,90 | 3,95[c] |
| | | 18,30 | 22,30 | 4,00 |
| **14** | Méthyl-2 benzothiophène | 17,30 | 21,10 | 3,85 |
| **15** | Bromo-2 benzothiophène | 18,35 | 21,90 | 3,55 |
| **16** | Bromo-3 benzothiophène | 18,40 | 23,25 | 4,85[b] |
| | | 18,20 | 23,05 | 4,85[b] |
| | | 18,65 | 23,60 | 4,95 |
| **18** | Dibenzofuranne | 18,60 | 20,65 | 2,05[b] |
| | | 18,25 | 20,75 | 2,50 |
| **19** | Dibenzothiophène | 17,25 | 19,40 | 2,15[b] |
| | | 17,35 | 19,45 | 2,10 |
| **22** | Dihydroanthracène | 22,30 | 24,70 | 2,40 |
| **25** | Thianthrène | 16,55 | 21,75 | 5,20 |
| **27** | Oxyde de diphényle | 20,15 | 26,95 | 6,80 |
| **30** | Toluène | 23,15 | 26,15 | 3,00 |
| **31** | Cyclohexylbenzène | 22,15 | 25,25 | 3,10 |
| **32** | Tétraline | 20,95 | 23,75 | 2,80 |
| **38** | Diphényle | 19,90 | 26,05 | 6,15 |
| **39** | Naphtalène | 17,95 | 23,45 | 5,50[c] |
| | | 18,30 | 23,60 | 5,30 |
| **41** | Méthyl-2 naphtalène | 17,65 | 22,70 | 5,05 |
| **42** | Phénanthrène | 17,00 | 19,70 | 2,70 |
| | *Accepteur: DDQ* | | | |
| **12** | Benzofuranne | 17,60 | 21,45 | 3,85 |
| **13** | Benzothiophène | 16,70 | 20,60 | 2,90 |
| **19** | Dibenzothiophène | 15,90 | 17,85 | 1,95[b] |
| | | 16,00 | 18,10 | 2,10 |
| **42** | Phénanthrène | 15,85 | 18,35 | 2,50 |

[a] Solvant $CCl_4$ sauf mention contraire.
[b] Solvant $CH_2Cl_2$.
[c] Solvant $CHCl_3$.

dichlorométhane au cours de ce travail donnent franchement une droite de pente égale à l'unité. Ce cas mis à part, il n'apparaît pas de différence notable entre nos résultats d'une part et la totalité des points issus de ce travail et de la littérature d'autre part. On a affaire à première vue à une dispersion quasi-statistique provenant des incertitudes expérimentales et du grand nombre de points considéré. Les irrégularités constatées ne dépendent pas de l'accepteur (voir ci-dessous) et ne sont pas imputables au solvant; la corrélation entre les nombres d'ondes (en kK) observés dans le tétrachlorure de carbone et ceux obtenus dans le dichlorométhane est en effet meilleure que celle de la figure 2:

[3] $\bar{\nu}_{CCl_4} = \bar{\nu}_{CH_2Cl_2} + 0{,}14$ (32 points; $\rho = 0{,}997$)

Le regroupement des donneurs par familles paraît difficile; on remarque toutefois que les points correspondant aux donneurs *n* (**43** à **47**) sont bien alignés. Mais certains autres donneurs se placent très près de cette droite, ce qui ne suffit évidemment pas à prouver leur caractère *n*. Finalement, pour distinguer l'écart théorique à la corrélation d'une part, de la dispersion d'origine expérimentale d'autre part, il vaut sans doute mieux s'intéresser aux points les plus éloignés de la droite des moindres carrés: on découvre alors sans surprise la position de **33**, le plus fort donneur π envisagé ici, et pour lequel l'approximation de Mulliken peut ne plus être suffisante.

De la relation [1″] on tire l'écart théorique $\Delta\bar{\nu}$ entre les sommets des bandes relatives à un même donneur:

$$[4] \quad \Delta\bar{\nu} = \frac{a}{hc} . \Delta I_D$$

ou

$$[4'] \quad \Delta\bar{\nu}(\text{kK}) = 8{,}066\, a . \Delta I_D(\text{eV})$$

L'exploitation des 24 résultats concernant l'ensemble des donneurs étudiées dans $CCl_4$ au cours de ce travail conduit à la droite de régression d'équation:

$$[4''] \quad \Delta\bar{\nu}(\text{kK}) = 7{,}530\, \Delta I_D(\text{eV}) \quad (\rho = 0{,}952)$$

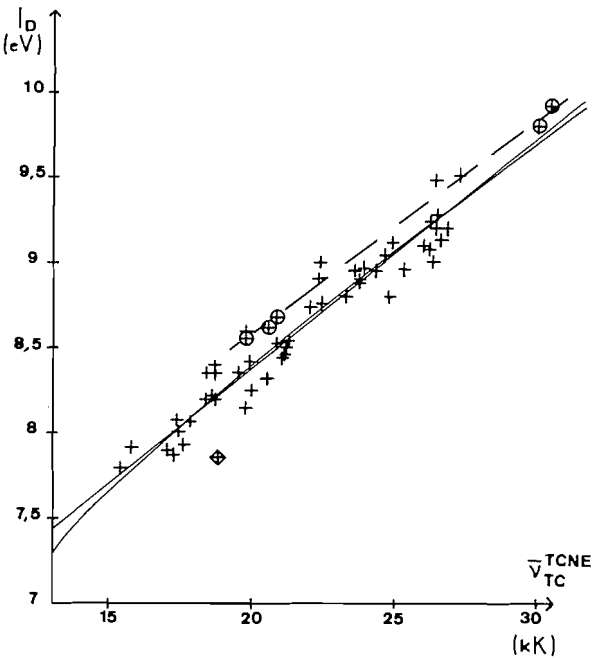


FIG. 2. Corrélation $\bar{\nu}_{TC}^{TCNE} = f(I_D)$; solvant $CCl_4$, ce travail; ⊕ donneurs *n*; ⊕ donneur **33**.

TABLEAU 5. Paramètres $C_1$ et $C_2$ de la corrélation [1'] $a$ et $b$ de la corrélation [1''] (énergies exprimées en eV)

| Accepteur | Solvant | Origine | Nombre de points | $C_1$ (eV) | $C_2$ (eV)[2] | $a$ | $b$ | $\rho$[a] |
|---|---|---|---|---|---|---|---|---|
| TCNE | $CCl_4$ | Ce travail (tous donneurs) | 56 | 6,16 | 0,52 | 0,91 | 5,13 | 0,966 |
| | $CCl_4$ | Ce travail (donneurs n) | 5 | | | 0,97 | 5,86 | 0,999 |
| | $CCl_4$ | Ce travail + littérature | 80 | 6,21 | 0,64 | 0,85 | 4,66 | 0,971 |
| | $CH_2Cl_2$ | Ce travail | 10 | 6,03 | 0,04 | 1,00 | 6,05 | 0,974 |
| | $CH_2Cl_2$ | Littérature | 38 | 6,29 | 0,87 | 0,83 | 4,47 | 0,956 |
| | $CHCl_3$ | Ce travail | 11 | 6,28 | 0,56 | 0,91 | 5,23 | 0,972 |
| | $CHCl_3$ | Littérature | 10 | 6,39 | 0,94 | 0,83 | 4,50 | 0,961 |
| DDQ | $CH_2Cl_2$ | Ce travail + littérature | 11 | 6,58 | 0,79 | 0,72 | 3,76 | 0,878 |
| | $CCl_4$ | Ce travail + littérature | 10 | 6,56 | 0,78 | 0,77 | 4,19 | 0,898 |

[a] Coefficient de corrélation des droites d'équation [1''].

on constate que l'erreur commise sur la pente est inférieure à 3% (8,066 $a$ = 7,340). Cette étude confirme ainsi que les deux bandes de transfert de charge observées sur un même spectre (éventuellement après résolution) proviennent bien des H.O. 1 et 2 du donneur.

*(b) Influence de l'affinité électronique de l'accepteur*

Le dernier terme de la relation [1] est petit devant les autres. Appliquée à un seul donneur formant des complexes avec deux accepteurs A et A', cette égalité devient, $G_1$ étant approximativement constant:

$$[5] \quad \bar{\nu}_{TC}{}^{A} - \bar{\nu}_{TC}{}^{A'} = \frac{1}{hc}(E_{A'} - E_A)$$

Les travaux de Page et coll. (50) et de Chen et Wentworth (51) ont permis d'établir une liste d'affinités électroniques absolues pour les accepteurs d'électrons. Si l'on admet pour le TCNE la valeur mesurée ($E_{TCNE}$ = 2,88 eV (50)), nos résultats spectrophotométriques dans le tétrachlorure de carbone conduisent à:

$$E_{DDQ} = 3{,}08\ \text{eV}$$

Avec le même point de départ ($E_{TCNE}$) et à l'aide de valeurs de $\lambda_{max}$ dans le dichlorométhane tirées en grande partie de la littérature (Tableaux 1 et 2), on trouve:

$$E_{DDQ} = 3{,}14\ \text{eV}$$

Les valeurs ainsi obtenues sont très voisines de celles recalculées par Chen et Wentworth (51) à l'aide de la corrélation [1] ($E_{TCNE}$ = 2,77 eV; $E_{DDQ}$ = 3,13 eV).

*(c) Influence du solvant*

Les spectres des complexes formés par quatre des donneurs avec le TCNE ont été pris dans une gamme de solvants assez étendue en polarité et en polarisabilité, eu égard à la réactivité du TCNE.

Les donneurs choisis correspondent à trois cas de spectres différents: une seule bande (**29**), deux bandes partiellement résolues (**13** et **16**) et deux bandes donnant un seul maximum apparent (**19**). Les résultats relatifs au benzène (**29**) sont tirés en partie de la littérature. Les équations publiées par Davis (52) et par Rao (53) dans des mises au point récentes, pour rendre compte des interactions soluté–solvant non spécifiques, soulignent la complexité des phénomènes mis en jeu.

Examinons si l'effet de solvant sur la fréquence de transfert de charge $\nu_{max}$ peut être traduit par la formule de McRae (54):

$$[6] \quad \bar{\nu}_{max} - \bar{\nu}_{max}{}^{0} = (AL_0 + B)\frac{n^2 - 1}{2n^2 + 1} + C\left(\frac{\varepsilon - 1}{\varepsilon + 2} - \frac{n^2 - 1}{n^2 + 2}\right)$$

$\bar{\nu}_{max}{}^{0}$ caractérise le complexe à l'état gazeux; $n$ et $\varepsilon$ désignent respectivement l'indice de réfraction et la constante diélectrique du solvant. $(AL_0 + B)$ et $C$ sont des constantes. Dans le cas des solvants non polaires ($n^2 \simeq \varepsilon$) cette relation se réduit à:

$$[6'] \quad \bar{\nu}_{max} - \bar{\nu}_{max}{}^{0} = (AL_0 + B)\frac{n^2 - 1}{2n^2 + 1}$$

Les droites obtenues sont représentées sur la figure 3 et les valeurs des paramètres $(AL_0 + B)$ et $\bar{\nu}_{max}{}^{0}$ sont rassemblées dans le tableau 6. On peut admettre comme incertitudes 0,5 kK sur la pente et 0,1 kK sur l'ordonnée à l'origine, sauf pour $\bar{\nu}_2$ de **16** où l'incertitude est environ deux fois plus grande.

Dans les cas étudiés ici l'influence du solvant est identique sur les deux bandes, ce qui confirme l'interprétation faisant intervenir plusieurs états électroniques d'un même complexe. Les complexes

Can. J. Chem. Downloaded from www.nrcresearchpress.com by 210.87.254.42 on 09/06/12
For personal use only.

Can. J. Chem. Downloaded from www.nrcresearchpress.com by 210.87.254.42 on 09/06/12
For personal use only.

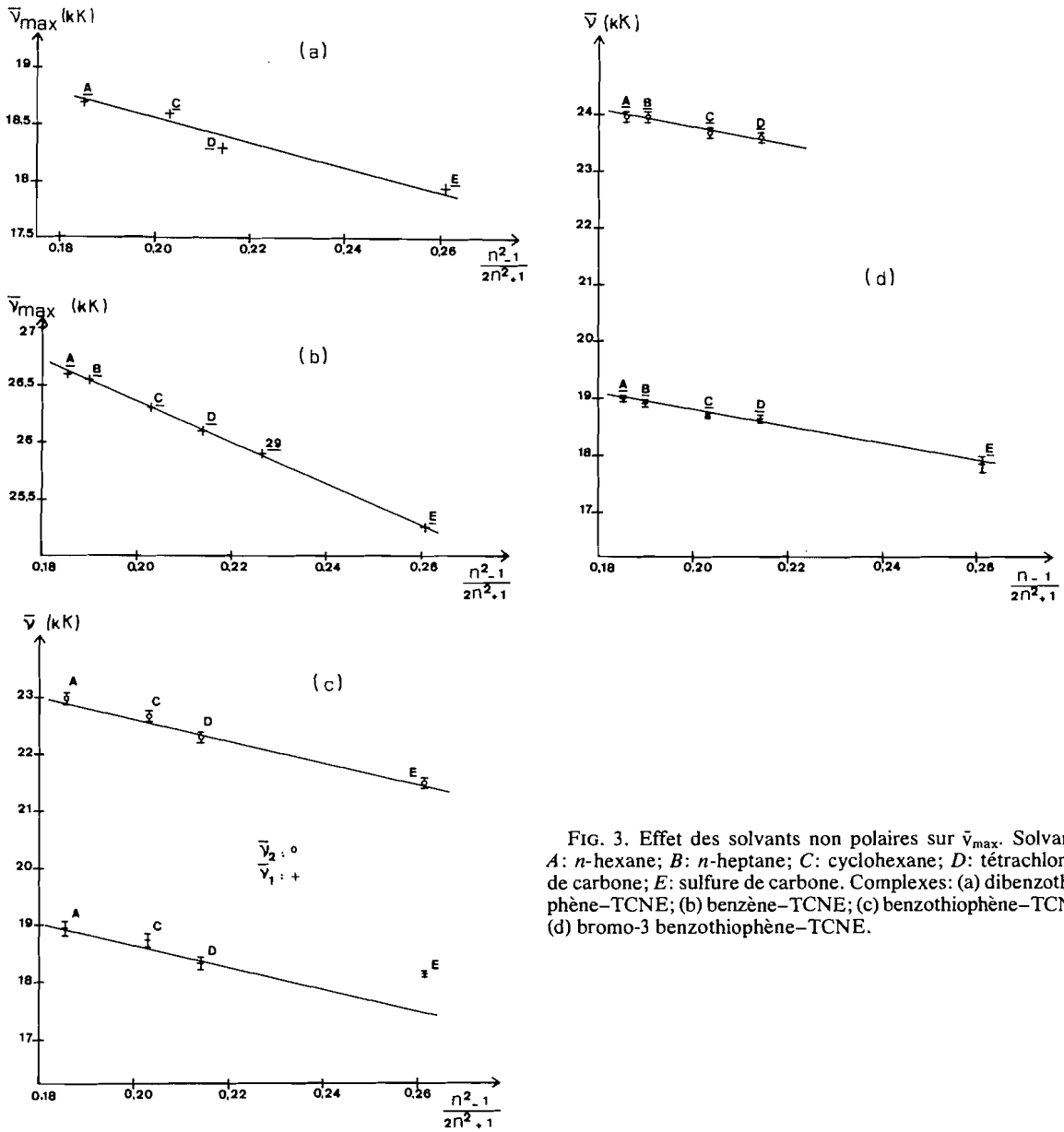


FIG. 3. Effet des solvants non polaires sur $\bar{\nu}_{max}$. Solvants: *A*: *n*-hexane; *B*: *n*-heptane; *C*: cyclohexane; *D*: tétrachlorure de carbone; *E*: sulfure de carbone. Complexes: (a) dibenzothiophène–TCNE; (b) benzène–TCNE; (c) benzothiophène–TCNE; (d) bromo-3 benzothiophène–TCNE.

des hétérocycles soufrés conjugés se comportent donc exactement comme ceux des hydrocarbures aromatiques (55, 56): le déplacement bathochrome observé dans les solvants non polaires, et augmentant avec la réfringence du solvant, est caractéristique des solutés non polaires (forces de dispersion) ou des solutés peu polaires, dont le moment dipolaire augmente de l'état fondamental à l'état excité (forces d'induction).[7]

[7]La comparaison de ces résultats avec ceux rassemblés par Trotter (57) semble bien montrer que la compression interne et l'effet de champ ne sont que le côté pile et le côté face d'une même réalité.

On peut appliquer la relation [1″] aux fréquences $\nu_{max}^0$ calculées et s'apercevoir que ces grandeurs se classent normalement aux incertitudes expérimentales près, en fonction des potentiels d'ionisation ($a = 1{,}03$; $b = 5{,}81$; $\rho = 0{,}98$).

Essayons maintenant de déterminer $C$ par voie graphique, il suffit pour cela de tracer:

$$[6''] \quad \bar{\nu}_{max} - (AL_0 + B)\frac{n^2-1}{2n^2+1} = f\left[\left(\frac{\varepsilon-1}{\varepsilon+2}\right) - \left(\frac{n^2-1}{n^2+2}\right)\right]$$

TABLEAU 6. Influence du solvant sur $\bar{\nu}_{max}$

| No | Composé donneur | $AL_0 + B$ (kK) | $\nu_{max}^0$ (kK) |
|---|---|---|---|
| **13** | Benzothiophène | $\bar{\nu}_1$: −19 | 22,45 |
| | | $\bar{\nu}_2$: −19 | 26,5 |
| **16** | Bromo-3 benzothiophène | $\bar{\nu}_1$: −15 | 21,7 |
| | | $\bar{\nu}_2$: (−15) | 26,9 |
| **19** | Dibenzothiophène | −11 | 20,75 |
| **29** | Benzène | −18 | 29,9 |

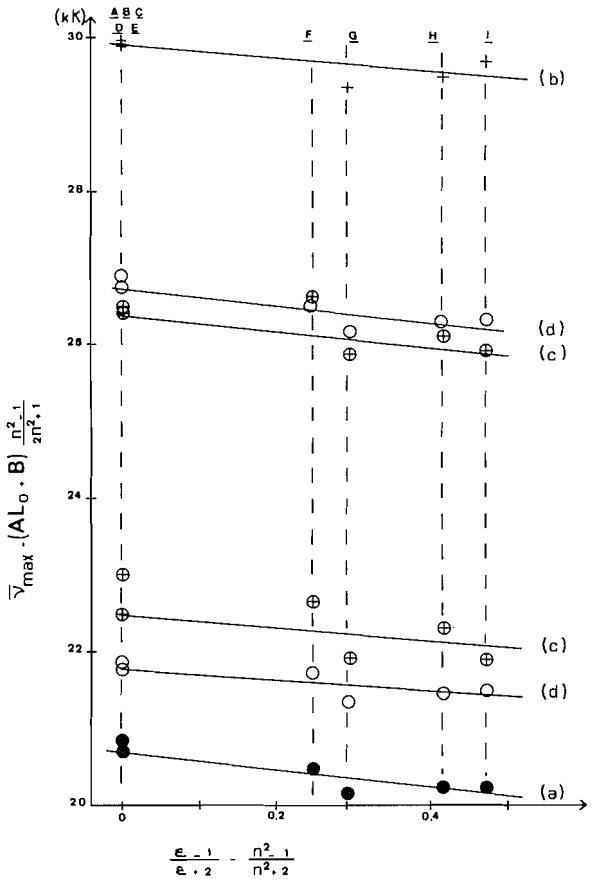


FIG. 4. Effet des solvants polaires sur $\bar{\nu}_{max}$. Solvants: *F*: dibromo-1,2 éthane, *G*: chloroforme, *H*: tétrachloro-1,1,2,2 éthane, *I*: dichlorométhane. Complexes (voir Fig. 3).

Au vu de la figure 4, on constate que les solvants halogénés saturés conduisent à des valeurs faiblement négatives de $C$ ($C \simeq -0{,}5$ kK) comme dans le cas du complexe naphtalène–TCNE (56). Ceci s'explique par le fait que le deuxième terme de la relation [6] rend compte des interactions soluté–solvant du type dipôle de solvant – dipole de soluté (forces d'orientation) et que le paramètre $C$ peut s'exprimer en fonction des moments dipolaires du complexe à l'état fondamental ($\mu_f$) et à l'état excité ($\mu_e > \mu_f$) selon

$$[7] \quad C = \frac{2\mu_f(\mu_f - \mu_e)}{a^3}$$

$a$ représente le rayon de la cavité du solvant.

On ne peut donc pas conclure à une solvatation spécifique des complexes dans ce groupe de solvants. On peut estimer au contraire que la structure électronique des complexes étudiés n'est pratiquement pas influencée par des milieux continus comme ceux considérés ici.

**Remerciements**

Les auteurs remercient Monsieur le Professeur Gilot pour l'intérêt qu'il a porté à ce travail et pour les discussions fructueuses auxquelles ces résultats ont donné lieu.

1. P. CASSOUX et J. P. CANSELIER. Bull. Soc. Chim. Fr. 2379 (1974); J. P. CANSELIER et P. CASSOUX. J. Mol. Struct. **39**, 301 (1977).
2. J. P. CANSELIER et C. CLEMENT. J. Chim. Phys. **75**, 880 (1978); **76**, 699 (1979).
3. S. DOMENECH, B. GILOT et R. GUIRAUD. J. Chim. Phys. **76**, 873 (1979).
4. G. BRIEGLEB. Elektronen Donator-Akzeptor Komplexe. Springer Verlag, Berlin. 1961.
5. L. J. ANDREWS et R. M. KEEFER. Molecular complexes in organic chemistry. Holden-Day, San Francisco. 1964.
6. R. S. MULLIKEN et W. B. PERSON. Molecular complexes: a lecture and reprint volume. Wiley–Interscience, New York. 1969.
7. R. FOSTER. Organic charge-transfer complexes. Academic Press, Londres. 1969.
8. M. J. S. DEWAR et A. R. LEPLEY. J. Am. Chem. Soc. **83**, 4560 (1961).
9. E. A. NECHAEV. Zh. Fiz. Khim. **51**, 30 (1977) (édit. internat., p. 16).
10. R. ANDERSON et J. M. PRAUSNITZ. J. Chem. Phys. **39**, 1225 (1963).
11. D. R. ROSSEINSKY et H. KELLAWI. J. Chem. Soc. A, 1207 (1969); A. AHMED. J. Chem. Soc. Faraday Trans. I, **69**, 541 (1973).
12. G. G. ALOISI, S. SANTINI et G. SAVELLI. J. Chem. Soc. Faraday Trans. I, **71**, 2045 (1975).
13. A. R. COOPER, C. W. P. CROWNE et P. G. FARRELL. Trans. Faraday Soc. **62**, 18 (1966).
14. Z. YOSHIDA et T. KOBAYASHI. Tetrahedron, **26**, 267 (1970).
15. G. G. ALOISI et S. PIGNATARO. J. Chem. Soc. Faraday Trans. I, **69**, 534 (1973).
16. R. ABU-EITTAH et F. AL SUGEIR. Can. J. Chem. **54**, 3705 (1976).
17. R. E. MERRIFIELD et W. D. PHILLIPS. J. Am. Chem. Soc. **80**, 2778 (1958).
18. T. K. MUKHERJEE. J. Phys. Chem. **73**, 3442 (1969).
19. W. HANSTEIN, H. J. BERWIN et T. G. TRAYLOR. J. Am. Chem. Soc. **92**, 829 (1970).
20. S. SANTINI, G. REICHENBACH, S. SORRISO et A. CECCON. J. Chem. Soc. Perkin Trans. II, 1056 (1974).
21. G. G. ALOISI, S. SANTINI et S. SORRISO. J. Chem. Soc. Faraday Trans. I, **70**, 1908 (1974).
22. A. R. LEPLEY. J. Am. Chem. Soc. **86**, 2545 (1964).
23. G. BRIEGLEB, J. CZEKALLA et G. REUSS. Z. Phys. Chem. N.F. **30**, 333 (1961).

Can. J. Chem. Downloaded from www.nrcresearchpress.com by 210.87.254.42 on 09/06/12
For personal use only.

Can. J. Chem. Downloaded from www.nrcresearchpress.com by 210.87.254.42 on 09/06/12
For personal use only.

24. D. D. HOLDER et C. C. THOMPSON. J. Chem. Soc. Chem. Commun. 278 (1972).
25. H. KURODA, M. KOBAYASHI, M. KINOSHITA et S. TAKEMOTO. J. Chem. Phys. **36**, 457 (1962).
26. V. VON NIESSEN, W. P. KRAEMER et L. S. CEDERBAUM. J. Electron. Spectrosc. Relat. Phenom. **8**, 179 (1976).
27. J. H. D. ELAND. Int. J. Mass Spectrom. Ion Phys. **2**, 471 (1969).
28. A. D. BAKER, D. BETTERIDGE, N. R. KEMP et R. E. KIRBY. Anal. Chem. **42**, 1065 (1970).
29. F. BROGLI, E. GIOVANNINI, E. HEILBRONNER et R. SCHURTER. Chem. Ber. **106**, 961 (1973).
30. J. M. BEHAN, F. M. DEAN et R. A. W. JOHNSTONE. Tetrahedron, **32**, 167 (1976).
31. M. H. PALMER et S. M. KENNEDY. J. Chem. Soc. Perkin Trans. II, 1893 (1974).
32. C. GUIMON, M. F. GUIMON, G. PFISTER-GUILLOUZO, P. GENESTE, J. L. OLIVÉ et S. N. UNG. Phosphorus Sulfur, **5**, 341 (1979).
33. B. RUŠČIĆ, B. KOVAĆ, L. KLASINC et H. GUSTEN. Z. Naturforsch. Teil A, **33**, 1006 (1978).
34. M. J. S. DEWAR, E. HASELBACH et S. D. WORLEY. Proc. R. Soc. London, Ser. A, **315**, 431 (1970).
35. G. BUEMI, S. PIGNATARO et G. SPUNTA. Z. Naturforsch. Teil A, **32**, 292 (1977).
36. H. BOCK et G. WAGNER. Tetrahedron Lett. 3713 (1971); H. BOCK, G. WAGNER et J. KRONER. Chem. Ber. **105**, 3850 (1972).
37. J. P. MAIER et E. HEILBRONNER. Electron spectroscopy: theories, techniques and applications. *Edité par* C. R. Brundle et A. D. Baker. Academic Press, Londres. 1976.
38. F. BERNARDI, G. DISTEFANO, A. MANGINI, S. PIGNATARO et G. SPUNTA. J. Electron Spectrosc. Relat. Phenom. **7**, 457 (1975).
39. R. GLEITER et J. SPANGET-LARSEN. Topics Curr. Chem. **86**, 139 (1974).
40. G. LEVY. Thèse de Doctorat d'Etat, Université de Toulouse, 1976.
41. M. MERCIER et P. DUMONT. Chim. Thér. 274 (1971).
42. (*a*) R. ZAHRADNIK, C. PARKANY, V. HORÁK et J. KOUTECKÝ. Collect. Czech. Chem. Commun. **28**, 776 (1963); (*b*) J. P. CANSELIER. Thèse de Doctorat d'Etat, Institut National Polytechnique de Toulouse, 1980.
43. C. K. PROUT et B. KAMENAR. *Dans* Molecular complexes. Vol. 1. *Edité par* R. Foster. Elek Science, Londres. 1973. p. 151.
44. J. T. BELL et R. E. BIGGERS. J. Mol. Spectrosc. **18**, 247 (1965); T. KURUCSEV. J. Chem. Educ. **55**, 128 (1978).
45. J. P. LARKINDALE et D. J. SIMKIN. J. Chem. Phys. **56**, 3730 (1972).
46. G. BRIEGLEB et J. CZEKALLA. Z. Phys. Chem. N.F. **24**, 37 (1960).
47. C. K. JØRGENSEN. Acta Chem. Scand. **8**, 1495 (1954).
48. (*a*) R. D. B. FRASER et E. SUZUKI. Anal. Chem. **38**, 1770 (1966); **41**, 37 (1969); **41**, 935 (1969); (*b*) Physical principles and techniques of protein chemistry, Partie C. Academic Press, New York. 1973. Chapt. 21. p. 301.
49. E. HASELBACH et M. ROSSI. Helv. Chim. Acta, **59**, 2635 (1976); M. ROSSI. Thèse, Université de Bâle, 1975; H. SAKURAI et M. KIRA. J. Am. Chem. Soc. **97**, 4879 (1975); M. ROSSI, U. BUSER et E. HASELBACH. Helv. Chim. Acta, **59**, 1039 (1976); R. GSCHWIND. Thèse, Université de Bâle, 1979.
50. A. L. FARRAGHER et F. M. PAGE. Trans. Faraday Soc. **63**, 2369 (1967); F. M. PAGE et G. C. GOODE. Negative ions and the magnetron. Wiley–Interscience, New York. 1969.
51. E. C. M. CHEN et W. E. WENTWORTH. J. Chem. Phys. **63**, 3183 (1975).
52. K. M. C. DAVIS. *Dans* Molecular association. Vol. 1. *Edité par* R. Foster. Academic Press, Londres. 1975. p. 151.
53. C. N. R. RAO. Chem. Soc. Rev. **5**, 297 (1976).
54. E. G. MCRAE. J. Phys. Chem. **61**, 562 (1957).
55. E. M. VOIGT. J. Phys. Chem. **70**, 598 (1966).
56. J. AIHARA, M. TSUDA et H. INOKUCHI. Bull. Chem. Soc. Jpn. **42**, 1824 (1969).
57. P. J. TROTTER. J. Chem. Phys. **46**, 2736 (1968).

## Annexe. Méthode de résolution des bandes

La fonction de référence est traitée en premier lieu. Le spectre enregistré (linéaire en $\lambda$) est discrétisé à intervalles de 5 nm. Ces données sont converties en nombres d'ondes et subissent une première interpolation quadratique qui espace régulièrement les abscisses (0,1 kK): deux interpolations sont pratiquées ultérieurement de façon que la fonction de référence en coordonnées réduites comporte 101 points équidistants en abscisses, le sommet de la courbe coïncidant avec le point 51.

Le spectre à résoudre est alors introduit sous forme discrétisée; les abscisses sont transformées comme plus haut au moyen de la première interpolation. Ce spectre est assimilé à la somme de deux courbes[8] présentant le même rapport $B$. Un premier calcul est réalisé à partir de six paramètres d'essai (hauteur, position et largeur des bandes) et des deux paramètres fixes qui caractérisent la ligne de base, supposée linéaire (densités optiques aux deux extrémités). On utilise la méthode des moindres carrés appliquée aux fonctions non linéaires (méthode de Gauss–Newton); l'écart quadratique moyen $S$ est minimisé au sixième chiffre significatif près au cours d'un calcul itératif. Une convergence plus probable et plus rapide est assurée par l'intervention d'un facteur de relaxation et d'un facteur d'échelle eux-mêmes optimisés au fur et à mesure des itérations.

Un tableau[9] présente en détail des exemples de résultats obtenus. $S_{min}$ est la valeur minimale de $S$ pour laquelle on arrête le calcul, et le paramètre de largeur $(\Delta\bar{\nu}_{\frac{1}{2}})_i$ de la bande $i$ représente en fait la largeur à mi-hauteur de cette bande (en kK) divisée par la largeur à mi-hauteur de la bande de référence $(\Delta\bar{\nu}_{\frac{1}{2}})_{réf}$ exprimée en abscisses réduites (unités arbitraires).

[8]Nous ne traitons pas l'extrémité de la bande présente vers le bleu et appartenant au spectre d'un des réactifs. La pente en est très grande et le nombre de points insuffisant. C'est pourquoi nous avons discrétisé les spectres à partir d'une longueur d'onde au-delà de laquelle l'influence de cette bande est négligeable.

[9]Déposé au C.N.R.C. comme données supplémentaires, qui peuvent être obtenues à un prix nominal, en s'adressant au Dépôt de données non publiées, ICIST, Conseil national de recherches du Canada, Ottawa, Ont., Canada K1A 0S2.

# Synthesis of (±)-lineatin by the photochemical cycloaddition of allene to anhydromevalonolactone

WILLIAM R. MCKAY, JIM OUNSWORTH, PHAIK-ENG SUM, AND LARRY WEILER[1]

*Department of Chemistry, University of British Columbia, Vancouver, B.C., Canada V6T 1Y6*

Received October 14, 1981

WILLIAM R. MCKAY, JIM OUNSWORTH, PHAIK-ENG SUM, and LARRY WEILER. Can. J. Chem. **60**, 872 (1982).

(±)-Lineatin (**1**), the aggregation pheromone of an ambrosia beetle, was synthesized in five steps from anhydromevalonolactone (**5**) in 10% overall yield. The key step in the synthesis was a photochemical cycloaddition of **5** and allene. This photolysis produced two regioisomers (ca. 3:2) and efforts to improve the regioselectivity by varying the photolysis conditions or substituents on the allene were unsuccessful.

**1** **5**

WILLIAM R. MCKAY, JIM OUNSWORTH, PHAIK-ENG SUM et LARRY WEILER. Can. J. Chem. **60**, 872 (1982).

Nous avons préparé la ±-linéatine (**1**), la phéromone d'aggrégation d'une abeille de type Ambrosia, en réalisant une synthèse en 5 étapes à partir de l'anhydromévalonolactone (**5**) avec un rendement global de 10%. L'addition photochimique du composé **5** sur une allène est l'étape principale de cette synthèse. Cette photolyse conduit à deux régioisomères (environ 3:2) et nous avons vainement tenté d'améliorer la régiosélectivité en changeant les conditions d'hydrolyse ou en faisant varier les substituants sur l'allène.

**1** **5**

[Traduit par le journal]

Female ambrosia beetles, *Trypodendron lineatum*, produce an attractant aggregation pheromone while boring into fallen timber and cut lumber. The active pheromone, called lineatin, was isolated from frass and its structure was proposed to be **1** or **2** (1). Subsequently, Borden *et al.* reported three

**1** **2**

very low yielding syntheses of the pheromone which allowed them to demonstrate that lineatin in fact has structure **1** (2). Recently, Slessor *et al.* (3) and Mori and Sasaki (4) have reported more efficient syntheses of **1** and both groups have been able to resolve one of their synthetic intermediates to provide the optically active pheromone. In this paper we report a short synthetic route to lineatin (**1**) and offer some observations on the photochemical addition of allenes to α,β-unsaturated lactones.

A major challenge in the synthesis of **1** is the construction of the unusual tricyclic acetal skeleton. Our retrosynthetic analysis of this problem is shown in Scheme 1. The critical point in the synthesis of an intermediate such as **3** appeared to be the construction of a cyclobutane with the correct regio- and stereochemistry. We also considered the cyclobutanone **4** derived by oxidation of **3** as a potential synthetic intermediate, since it was expected that reduction of the ketone in **4** should occur preferentially from the *exo* face to yield **3**. This route would only require a regioselective cyclobutanone formation. Finally we sought a synthetic route starting from anhydromevalonolactone (**5**) because of its ready availability (see below).

A convenient method to construct cyclobutane rings employs a [2 + 2] cycloaddition. Although ketenes can be added to trisubstituted olefins, they are not known to add to electron deficient olefins (5) such as **5**. Therefore we chose to investigate a photochemical [2 + 2] reaction of **5** and an appropriate alkene to generate the desired cyclobutane. Photolysis of lactone **5** and ethylene gave the cycloadduct **6** in 70% yield (eq. [1]) (6). Indeed a number of alkenes undergo a photochemical [2 + 2] cycloaddition to α,β-unsaturated lactones (6*b*).

[1]Author to whom correspondence may be addressed.

0008-4042/82/070872-09$01.00/0

©1982 National Research Council of Canada/Conseil national de recherches du Canada

Can. J. Chem. Downloaded from www.nrcresearchpress.com by 210.87.254.42 on 09/06/12
For personal use only.

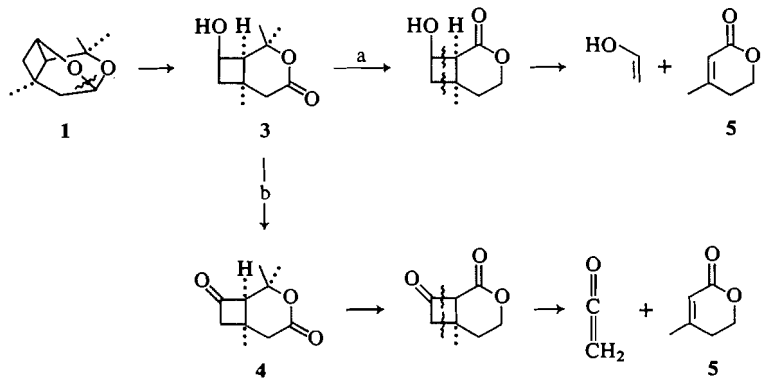

SCHEME 1. Possible retrosynthetic analyses for lineatin (**1**)

Unfortunately there are very few reports on the cycloaddition of heteroatom substituted alkenes to conjugated lactones. The photolysis of **5** and vinyl acetate gave only 4% of the adduct **7** (2). For these reasons, we considered the cycloaddition of allene and **5** as the key step in the synthetic plan.

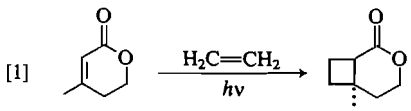

There are a number of examples of the photochemical [2 + 2] cycloaddition of allene to α,β-unsaturated ketones and aldehydes (7). In all cases the methylenecyclobutane produced has the *cis* stereochemistry for cyclic olefinic starting materi-

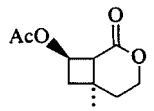

als, and in almost all cases the regioselectivity is that shown in eq. [2] (7). This is precisely the stereochemistry we would require to synthesize a cyclobutanone such as **4** from lactone **5**. Before the initiation of this work we were not aware of any photochemical addition of allene or its derivatives to an α,β-unsaturated lactone. During the course of our work Baker *et al.* reported an intramolecular

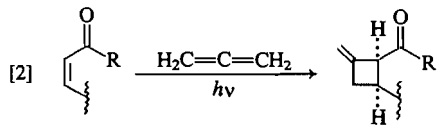

photolysis of a substituted allene and a lactone (8) (see below).

Anhydromevalonolactone (**5**) was conveniently synthesized from methyl vinyl ketone (6*b*, 9, 10). This procedure involves the dehydration of mevalonolactone by distillation from potassium bisulfate (6*b*). Usually the crude dehydration product was a mixture of α,β- and β,γ-unsaturated lactones. This mixture could be isomerized to the α,β-isomer **5** by redistillation from potassium bisulfate or more conveniently by a $RhCl_3$ catalyzed isomerization (11).

Irradiation (Vycor filter) of an acetone solution of lactone **5** and allene gave a mixture of 1:1 cycloaddition products in approximately 80% yield. The photolysis products could not be separated by thin layer or column chromatography. However, two components in the mixture were barely separable by capillary column gas chromatography. The ratio of the two products was ca. 3:2. In addition, the 270 MHz $^1H$ nmr spectrum of the photolysis product had two methyl singlets at δ 1.26 and 1.24 (relative intensity ca. 3:2). The photoadducts were not epimerized by base, thus each contained a *cis* fused cyclobutane. The structures of the photoadducts were determined from the following two ozonolysis experiments. First, ozonolysis of the photolysis mixture in methanol gave **8** and **9**; the ester **8** was the major product. Ozonolysis of the photolysis mixture in dichloromethane gave the cyclobutanones **9** and **10**. The

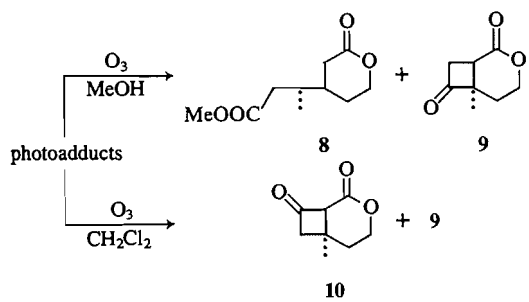

Can. J. Chem. Downloaded from www.nrcresearchpress.com by 210.87.254.42 on 09/06/12
For personal use only.

Can. J. Chem. Downloaded from www.nrcresearchpress.com by 210.87.254.42 on 09/06/12
For personal use only.

cyclobutanone **10**, although difficult to purify, was the major compound.

The results from the ozonolysis experiments and the failure of base to epimerize the adducts prove that the major photolysis product is the desired methylenecyclobutane **11** but a substantial amount of the isomeric methylenecyclobutane **12** is produced in the photolysis (eq. [3]). The low selectivity surprised us in view of the wealth of examples demonstrating the regioselective addition of allene to a variety of α,β-unsaturated ketones and aldehydes (7). It was clear that our photolysis conditions were different from those for enone additions, hence the photolysis in eq. [3] may be occurring by a different mechanism than the enone examples

[3] 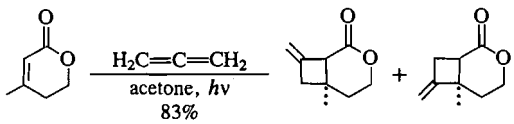


5 11 12

3:2

(eq. [2]). For example, the enone photolyses are usually carried out in ether or hydrocarbon solvents with a Pyrex filter (7). Presumably the enone is excited by direct irradiation and the reaction may proceed through the π,π* triplet (12). In the photolysis of lactone **5** (eq. [3]) the acetone is acting as a triplet sensitizer. Because the π,π* triplet of an α,β-unsaturated ester is of higher energy than the n,π* triplet (13) it may be that the lactone photolysis involves the n,π* triplet. A second possibility is that both types of photolysis reactions involve the same triplet but that the oxygen of the lactone changes the shape of the frontier orbitals involved and thus the regioselectivity of attack.

However, before these arguments are taken too far we should note that the photochemical cycloaddition of allene to 3-methylcyclohexenone gives a 4:1 mixture of regioisomers (eq. [4]) (14). In addition, Baker *et al.* have recently reported an intramolecular photolysis of an allenic α,β-unsaturated lactone to give two regioisomeric products (eq. [5]) (8). However, photolysis of the allenic enone in eq. [6] is highly regioselective (15). Thus the factors controlling the regioselectivity in these reactions are very subtle.

[4] 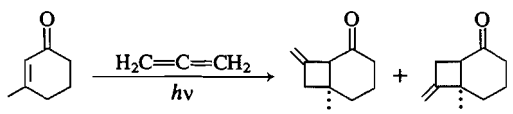


4:1

The summary of several experiments which were carried out in an effort to improve the regioselectivity in the photolysis (eq. [3]) is given in

[5] 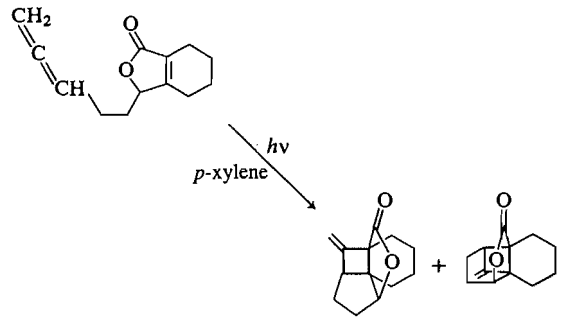


2.5:1

Table 1. The ratio of the regioisomers **11**:**12** was determined by 270 MHz $^1$H nmr. The tertiary methyl group in these isomers has a resonance at δ 1.26 and 1.24 respectively. First we note that the ratio of **11**:**12** did not change significantly with

[6] 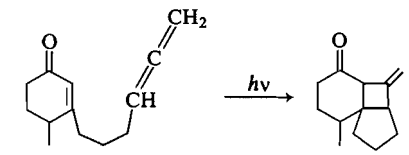


temperature (runs 1 and 2) or using xanthone as a triplet sensitizer (run 3). Finally in runs 4–6 the polarity of the solvent was varied. In dichloromethane and dichloroethane solvents the regioselectivity was essentially the same as in pure acetone. However in methanol solvent (run 4) the regioselectivity did change but in the wrong direction. In addition the total yield of photoadducts was substantially lower in methanol (run 4). We were unable to improve the regioselectivity in eq. [3] by altering the photolysis conditions.

TABLE 1. Photolysis of lactone **5** and allene

| Run | Solvent | Sensitizer | Temperature (°C) | Yield (%)[a] | **11**:**12**[c] |
|---|---|---|---|---|---|
| 1 | Acetone | | 25 | 82 | 5:3 |
| 2 | Acetone | | −78 | 83[b] | 3:2 |
| 3 | Dichloromethane | 0.07% Xanthone | −78 | 60 | 4:3 |
| 4 | Methanol | 10% Acetone | −78 | 27 | 2:3 |
| 5 | Dichloroethane | 20% Acetone | −78 | 100[b] | 3:2 |
| 6 | Dichloromethane | 10% Acetone | −35 | 74 | 3:2 |

[a]Yields are for chromatographed product except where noted.
[b]Crude yield.
[c]Ratios were determined by nmr.

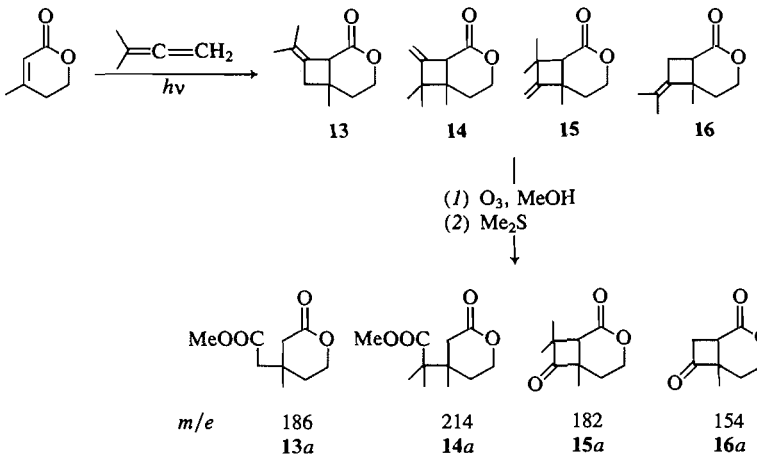


[7]

Then we turned to a study of the photochemical [2 + 2] cycloaddition of substituted allenes to lactone **5**. Since our synthetic plan involved eventual oxidative cleavage of the exocyclic double bond in the methylenecyclobutane, if the exocyclic carbon bore a substituent it would be lost in such a reaction. Phenylallene and 3,3-diphenylallene polymerized when photolyzed in acetone solutions of **5**. At −78°C, 3,3-dimethylallene did not undergo a photochemical addition to the conjugated lactone **5** in acetone. However, at 0°C a photochemical cycloaddition did occur to produce the adducts **13–15** (eq. [7]). The structures of these adducts were determined by ozonolysis of the photolysis mixture in methanol and gas chromatography – mass spectroscopic analysis of the products.

The mixture of photoadducts was ozonized as above and the mixture of products obtained was separated into three peaks by gc and these peaks had parent ions at *m/e* 186, 214, and 182. We could not detect any gc fraction with *m/e* 154 in the mixture. The ratio of the three components (by gc) in the ozonolysis mixture was **13***a*:**14***a*:**15***a* = 16:24:51. The product from the desired isomer **13** was the minor one. All of our efforts to control the regioselectivity in the photochemical cycloaddition were thwarted.

Since the adducts **11** and **12** could not be easily separated we continued the synthesis with the mixture of isomers as follows. On treatment with excess methyllithium, **11** and **12** gave the diols **17** and **18** in almost quantitative yield. These diols were oxidized (16) to the lactones **19** and **20** in 70–75% yield, which were then ozonized to give the keto lactones **21** and **22** in ca. 70% yield. Diisobutylaluminum hydride reduction of **21** and **22** followed by an acid work-up gave a mixture of (±)-lineatin (**1**) and its isomer **2** in a crude yield of 95%. The crude product could be distilled at 110°C/20 Torr. It has been shown that the isomer **2** has no biological activity (17) and the mixture of **1** and **2** is attractive to *T. lineatum* in field trapping studies.[2] In addition, these two products, **1** and **2**, were readily separated by column chromatography; however, their high volatility led to significant loss of material. Nonetheless, pure (±)-lineatin (**1**) could be isolated in 23% yield and the isomer **2** in 13.5% yield.

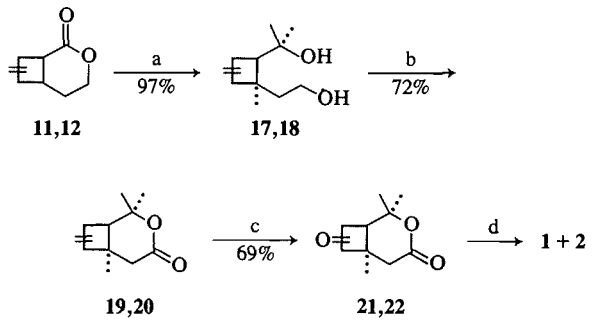


(a) MeLi, $Et_2O$, 0°C; (b) $CrO_3 \cdot 2py$, $CH_2Cl_2$;
(c) $O_3$, $CH_2Cl_2$, −78°C, then $Me_2S$, −78°C → 25°C; (d) DIBAL, then $H^+$

SCHEME 2. Synthesis of (±)-lineatin (**1**)

It is clear from the earlier structural (1) and synthetic studies (3, 4) on lineatin that the 100 MHz $^1H$ nmr spectral data was not sufficient evidence to differentiate structures **1** and **2**. Experiments with nmr shift reagents were also inconclusive (1). The 270 MHz $^1H$ nmr spectra of **1** and **2** are sufficiently resolved (Figs. 1 and 2) that decoupling experiments can be carried out and an essentially complete assignment of the $^1H$ nmr spectra of **1** and **2** obtained (Table 2). A summary of the coupling constants obtained from the decoupling experiments is given in Table 3. The chemical shifts in lineatin (Table 2) are within the range of values

[2]J. A. McLean and T. Shore. Unpublished results, 1979.

Can. J. Chem. Downloaded from www.nrcresearchpress.com by 210.87.254.42 on 09/06/12
For personal use only.

Can. J. Chem. Downloaded from www.nrcresearchpress.com by 210.87.254.42 on 09/06/12
For personal use only.

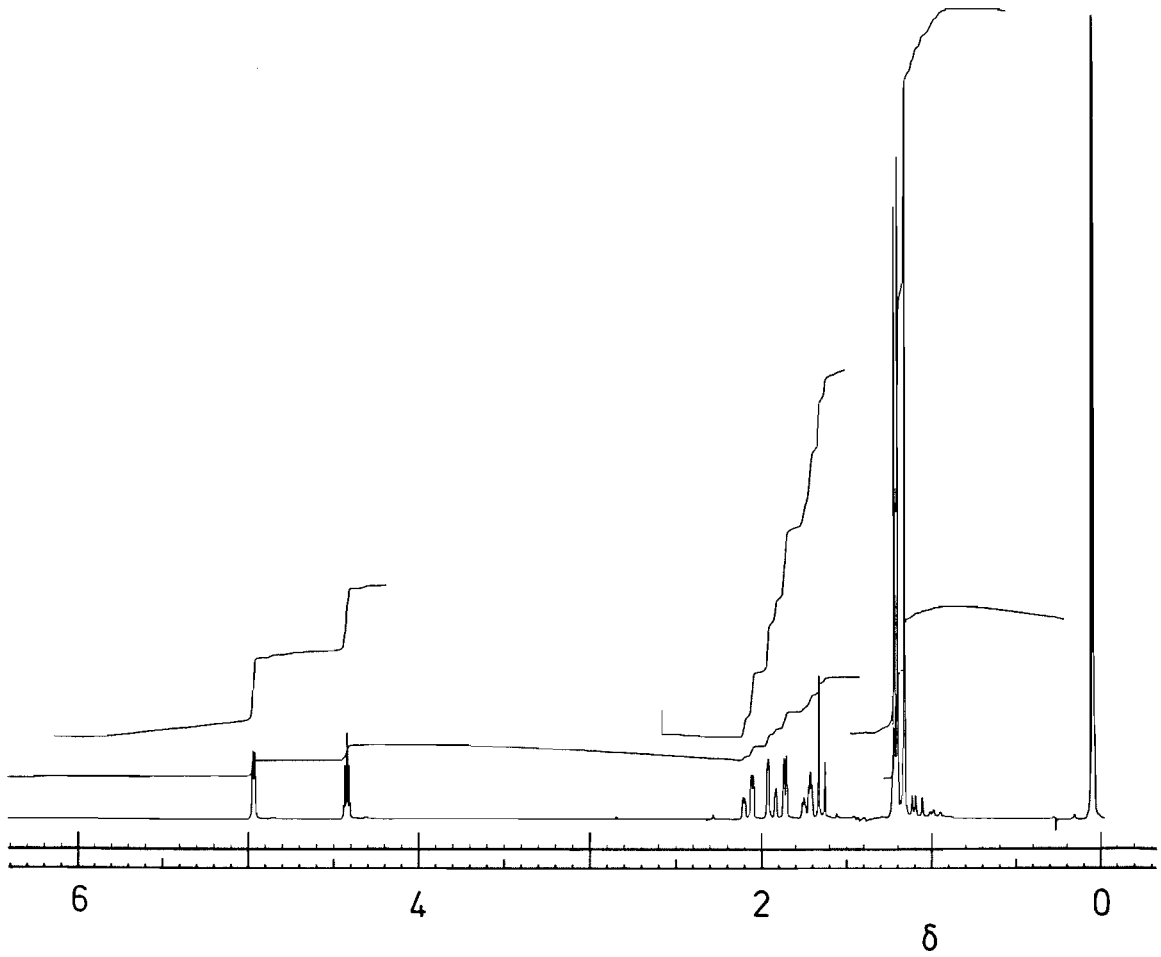


FIG. 1. 270 MHz $^1$H nmr spectrum of lineatin (**1**).

found in model systems. On the other hand there are some unusual shifts in the isomer **2** (Table 2). First $\delta_{5a}$ is rather low for a cyclobutyl methylene hydrogen. Models indicate that **2** adopts a conformation in which $H_{5a}$ and methyl(b) are forced rather close together. Thus we would suggest that the low chemical shift of $H_{5a}$ in **2** is due to a van der Waals deshielding (18) of $H_{5a}$ by the methyl(b). Incidentally we use this same argument to assign the lowest-field methyl singlet to b. The second unusual chemical shift in **2** is the very high field resonance of $H_{8a}$ which may be due to a shielding effect of 0–9 (See ref. 18, p. 80).

The coupling constants in **1** and **2** (Table 3) also show some differences which highlight the structural differences between **1** and **2**. In lineatin (**1**) we find a long range coupling between $H_{6b}$ and $H_{8b}$, and in **2** there is a long range coupling between $H_4$ and $H_6$. In each molecule the hydrogens involved in

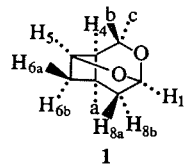


1

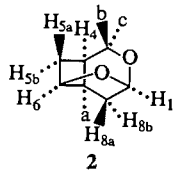


2

TABLE 2. 270 MHz $^1$H nmr chemical shift assignments of **1** and **2**[a,c]

| Lineatin (**1**) | | Isolineatin (**2**) | |
|---|---|---|---|
| $H_1$ | 4.93 (d, $J$ = 4) | $H_1$ | 5.32 (d, $J$ = 4) |
| $H_4$ | 1.83 (d, $J$ = 4) | $H_4$ | 1.9 (m) |
| $H_5$ | 4.38 (t, $J$ = 4) | $H_{5a}$ | 2.35 (ddd, $J$ = 13, 9, 4) |
| $H_{6a}$ | 1.61 (d, $J$ = 10.5) | $H_{5b}$ | 1.9 (m) |
| $H_{6b}$ | 1.69 (dt, $J$ = 10.5, 4) | $H_6$ | 3.93 (t, $J$ = 4) |
| $H_{8a}$ | 2.04 (dd, $J$ = 12, 4) | $H_{8a}$ | 1.33 (dd, $J$ = 12, 4) |
| $H_{8b}$ | 1.91 (dd, $J$ = 12, 4) | $H_{8b}$ | 2.09 (d, $J$ = 12) |
| a | 1.12 | a | 1.08 |
| b | 1.17[b] | b | 1.39 |
| c | 1.16[b] | c | 1.23 |

[a]Chemical shifts are given in ppm (δ) from TMS in $CCl_4$ and coupling constants in Hz.
[b]These assignments may be reversed.
[c]All assignments were verified by decoupling experiments.

Can. J. Chem. Downloaded from www.nrcresearchpress.com by 210.87.254.42 on 09/06/12
For personal use only.

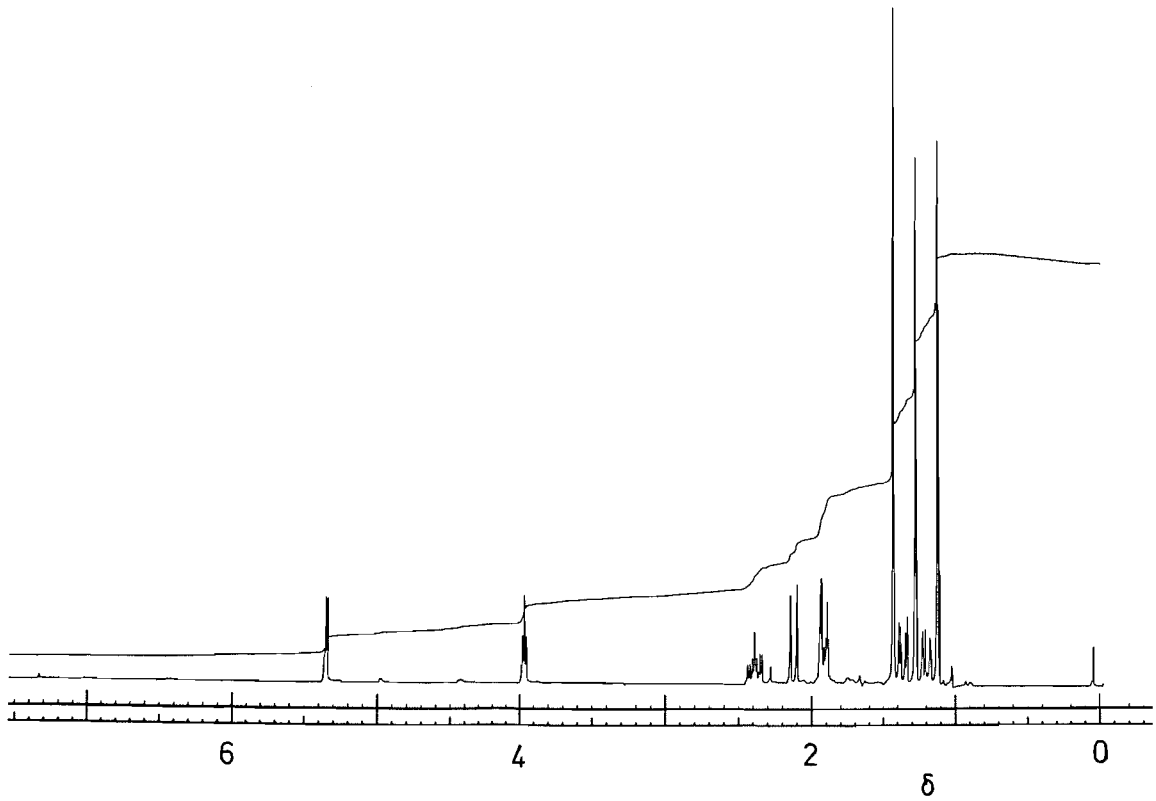


FIG. 2. 270 MHz $^1$H nmr spectrum of isolineatin (**2**).

TABLE 3. Proton coupling constants in **1** and **2**[a]

| Lineatin (**1**) | Isolineatin (**2**) |
|---|---|
| $J_{1,8a} = 4$ | $J_{1,8a} = 4$ |
| $J_{1,8b} = 0$ | $J_{1,8b} = 0$ |
| $J_{4,5} = 4$ | $J_{4,5a} = 9$ |
| $J_{5,6a} = 0$ | $J_{5a,6} = 4$ |
| $J_{5,6b} = 4$ | $J_{5b,6} = 0$ |
| $J_{6a,6b} = 10.5$ | $J_{5a,5b} = 13$ |
| $J_{8a,8b} = 12$ | $J_{8a,8b} = 12$ |
| $J_{6b,8b} = 4$ | $J_{4,6} = 4$ |

[a]Coupling constants are given in Hz.

the long range coupling and the intervening carbons can adopt a *W* configuration (19). Hence we find that the high-field $^1$H nmr data can be used to differentiate structures **1** and **2**.

## Experimental

*General*

Unless otherwise stated the following are implied. Gas–liquid chromatography (glc) was performed on a Hewlett Packard Model 5831A gas chromatograph, using a 6 ft × 1/8 in. column of 3% OV 17 on Chromosorb W. The 60 MHz proton nuclear magnetic resonance spectra were recorded on a Varian Associates Model T-60, the 100 MHz spectra were recorded on a Varian Associates Model HA-100 or Model XL-100, and the 270 MHz spectra were recorded on a homebuilt high resolution nmr spectrometer consisting of an Oxford Instruments' 63.4 KG magnet. Chemical shifts in ppm are reported using δ scale with tetramethylsilane (TMS) as internal reference. Signal multiplicity, integrated area, and coupling constants are indicated in parentheses. Infrared spectra were recorded on either a Perkin–Elmer model 700 or 710B spectrophotometer. Solution spectra were performed using a sodium chloride solution cell of 0.2 mm thickness. Absorption positions are given in $cm^{-1}$ and are calibrated by means of the 1601 $cm^{-1}$ band of polystyrene. Low resolution mass spectra were determined on a Varian/Mat model CH4B mass spectrometer. High resolution mass measurements were obtained using Kratos-AEI model MS902 or model MS50 instrument. The gc–ms data were obtained with a Hewlett Packard 5700 gc interfaced with a Varian/Mat 777 mass spectrometer. Microanalyses were performed by Mr. P. Borda, Microanalytical Laboratory, University of British Columbia, Vancouver.

Analytical thin layer chromatography (tlc) plates and preparative tlc plates were prepared from silica gel GF-254 from E. Merck Co. Preparative tlc plates were of about 1 mm in thickness. Column chromatography was carried out with 100–200 mesh silica gel from Davision Chemical or with 230–400 mesh silica gel from BDH according to the procedure of Still *et al.* (20). Plates were visualized under long and short wavelength ultraviolet radiation and were developed by iodine.

Solvents and reagents used were of either Reagent grade or Certified grade. Solvents were distilled before use. The petroleum ether used was of boiling range ca. 30–60°C. Dry solvents or reagents, where indicated, were prepared as follows: ethyl ether (ether) and tetrahydrofuran (THF) by refluxing over lithium aluminum hydride followed by distillation; dichloromethane

Can. J. Chem. Downloaded from www.nrcresearchpress.com by 210.87.254.42 on 09/06/12
For personal use only.

($CH_2Cl_2$) by distillation from phosphorus pentoxide; pyridine by distillation from barium oxide followed by storage over potassium hydroxide pellets; acetone by distillation from and storage over anhydrous magnesium sulfate; and methanol by refluxing over magnesium methoxide followed by distillation.

Methyllithium (in ethyl ether) was obtained from Aldrich Chemical Company, Inc., and standardized by titration against 1.0 *M tert*-butanol in benzene using 1,10-phenanthroline as indicator.

*3-Methyl-5-hydroxy-2-pentenoic acid δ-lactone (5) (6a)*

A mixture of 10.4 g (80 mmol) of mevalonolactone and 13.6 g of potassium hydrogen sulfate was heated under vacuum for 1 h and distilled at 72–78°C/0.9 Torr to give 8.0 g of colorless liquid. The nmr of the distilled liquid showed it to be a mixture of dehydrated products. The mixture of products was refluxed with 0.2 g (0.76 mmol) of rhodium(III) chloride trihydrate (11) in ethanol (50 mL) for 24 h, allowed to cool, then diluted with water and extracted with dichloromethane. The dichloromethane extract was dried over anhydrous magnesium sulfate, filtered, and the solvents removed under reduced pressure to give 8.0 g (89%) of 3-methyl-5-hydroxy-2-pentenoic acid δ-lactone (**5**). This material was shown to be 94% pure by glc. The spectral data below were the same as those reported for this compound (6*a*); ir ($CHCl_3$): 1650 and 1725 $cm^{-1}$; nmr ($CDCl_3$) δ: 2.01 (br s, 3H), 2.37 (t, $J$ = 6 Hz, 2H), 4.33 (t, $J$ = 6 Hz, 2H), and 5.73 (m, 1H); mass spectrum *m/e* (relative intensity): 41(10), 53(12), 54(44), 55(11), 82(100) and 112(59).

*Photoaddition of 3-methyl-5-hydroxy-2-pentenoic acid δ-lactone (5) to allene*

A solution of 17.8 g (0.445 mol) of allene and 10.0 g (0.089 mol) of 3-methyl-5-hydroxy-2-pentenoic acid δ-lactone (**5**) in 200 mL of degassed acetone was irradiated with a 450 W Hanovia high pressure mercury arc at −78°C for 4 h through a Vycor filter. At the end of the irradiation the solvent was removed by distillation under reduced pressure to give 12.2 g (90%) of crude product. This product was purified by flash column chromatography (20) using silica gel (230–400 mesh) and a mixture of petroleum ether and ethyl acetate (3:2, v/v) as eluent to give 11.3 g (83%) of a mixture of photoadducts: 1-methyl-7-methylene-4-oxa-*cis*-bicyclo[4.2.0]octan-5-one (**11**) and 1-methyl-8-methylene-4-oxa-*cis*-bicyclo[4.2.0]octan-5-one (**12**). The material was shown to be a 3:2 mixture of **11** and **12** respectively by 270 MHz nmr and by glc (using a 23.2 m × 0.28 mm id whisker-walled column coated with Carbowax 20 M).[3] Since separation of the individual components of the photoadduct mixture was very difficult, the sequence was carried through on the mixture. The fraction isolated by the above chromatography was further distilled at 120°C/0.8 Torr (Kugelrohr) and was characterized by the following; ir ($CHCl_3$): 1725 $cm^{-1}$; nmr ($CDCl_3$) δ: 1.25 (s, 3H), 1.8 (m, 2H), 2.6 (m, 1H), 2.95 (m, 1H), 3.4 (m, 1H), 4.4 (m, 2H), and 4.9 (m, 2H); mass spectrum: (*a*) high resolution calcd. for $C_9H_{12}O_2$: 152.0838; found 152.0845 amu; (*b*) low resolution *m/e* (relative intensity): 41(13), 67(10), 77(27), 79(39), 91(20), 93(100), 94(24), 95(10), 107(21), 109(22), 124(15), 137(30), and 152(40). *Anal.* calcd. for $C_9H_{12}O_2$: C 71.03, H 7.95; found: C 70.77, H 8.16.

*Addition of methyllithium to photoadducts 11 and 12*

A solution of 8.0 g (52.60 mmol) of photoadducts **11** and **12** in ca. 20 mL of anhydrous ethyl ether was added dropwise to an ice-cooled flask containing 120 mL (210 mmol) of 1.75 *M* methyllithium in ethyl ether. The mixture was stirred at 0°C for 2 h and the excess methyllithium was decomposed with a saturated aqueous solution of ammonium chloride. The ether layer was separated and the aqueous layer extracted several times with ethyl acetate. The combined extracts were dried over anhydrous magnesium sulfate, filtered, and the solvents were removed under reduced pressure to give 9.35 g (97%) of a mixture of diols **17** and **18** which could not be separated by tlc. The crude mixture was pure enough for the next reaction. A small sample of the mixture of products was chromatographed on a 20 × 20 cm silica gel coated plate, thickness 1 mm, using a mixture of ethyl acetate and petroleum ether (7:1, v/v) as eluent. A thick colorless oil was isolated and characterized by the following data; ir ($CHCl_3$): 1680, 3420, and 3620 $cm^{-1}$; nmr ($CDCl_3$) δ: 1.23 (s, 3H), 1.30 + 1.33 (ss, 6H), 1.8–2.4 (m, 4H), 2.6 (m, 1H), 3.7 (br m, 2H), and 4.8 (br m, 2H); mass spectrum: (*a*) high resolution calcd. for $C_{11}H_{20}O_2$: 184.1463; found: 184.1462 amu; (*b*) low resolution *m/e* (relative intensity): 41(45), 43(100), 53(13), 55(33), 59(95), 67(24), 79(27), 83(72), 85(36), 86(32), 105(19), 107(34), 111(59), 121(49), 123(30), 135(60), 151(34), and 166(15) (P − $H_2O$).

*Oxidation of mixture of diols 17 and 18*

A sample of 31.2 g (312 mmol) of chromium trioxide was added to a stirred solution of 49.32 g (624 mmol) of anhydrous pyridine (16) in ca. 30 mL of anhydrous dichloromethane. The chromium trioxide – pyridine complex was stirred at room temperature for 25 min. Then a solution of 9.20 g (50 mmol) of the mixture of diols **17** and **18** in ca. 5 mL of anhydrous dichloromethane was added in one portion. A tarry, black precipitate separated immediately. After stirring for 4.5 h at room temperature, the solution was decanted from the reaction, and the dichloromethane removed under reduced pressure. The residue was diluted with ethyl ether and the reaction flask rinsed several times with ethyl ether. The combined ether layers were filtered through a bed of Celite, washed with ice-cold dilute hydrochloric acid, aqueous sodium bicarbonate solution, brine, dried over anhydrous magnesium sulfate, and filtered. The solvents were removed under reduced pressure to give 7.60 g (84%) of a mixture of 2,2,6-trimethyl-8-methylene-3-oxa-*cis*-bicyclo[4.2.0]octan-4-one (**19**) and 2,2,6-trimethyl-7-methylene-3-oxa-*cis*-bicyclo[4.2.0]octan-4-one (**20**). The crude products were purified by column chromatography using silica gel (100–200 mesh) and a mixture of petroleum ether and ethyl acetate (2:3, v/v) as eluent. The fraction isolated from this chromatography was homogeneous by tlc analysis, and was shown to be a 3:2 mixture of **19** and **20** by nmr and glc (using a 23.4 m × 0.28 mm id whisker-walled column coated with Silar 10C).[3] Since separation of the individual components from the mixture was very difficult, the next sequence of steps was carried through on the mixture. The mixture from the chromatography was further distilled at 100°C/1.0 Torr (Kugelrohr) to afford 6.5 g (72%) of a mixture of **19** and **20** which was characterized by ir ($CHCl_3$): 1680 and 1725 $cm^{-1}$; nmr ($CDCl_3$) δ: 1.35, 1.42 and 1.47 (ss, 9H), 2.4 (m, 5H), and 4.9 (m, 2H); mass spectrum: (*a*) high resolution calcd. for $C_{11}H_{16}O_2$: 180.1150; found: 180.1158 amu; (*b*) low resolution *m/e* (relative intensity): 41(33), 43(69), 79(77), 80(90), 93(32), 109(24), 121(20), 123(31), 125(31), 139(14), 165(10), and 180(17). *Anal.* calcd. for $C_{11}H_{16}O_2$: C 73.30, H 8.95; found: C 73.10, H 8.95.

*Ozonolysis of alkenes 19 and 20*

A stream of ozone and oxygen was bubbled through a solution of 6.93 g (38.5 mmol) of a mixture of compounds **19** and **20** in ca. 250 mL of anhydrous dichloromethane at −78°C until the solution turned blue. Excess dimethylsulfide was added slowly. The reaction mixture was allowed to stir at −78°C for 20 min, warmed slowly to room temperature, washed with water, dried over anhydrous magnesium sulfate, and filtered. The solvents

[3]We wish to thank Professor A. C. Oehlschlager and Dr. H. Pierce, Jr., Department of Chemistry, Simon Fraser University, Burnaby, B.C., Canada, for the glc analysis of this compound.

Can. J. Chem. Downloaded from www.nrcresearchpress.com by 210.87.254.42 on 09/06/12
For personal use only.

were removed under reduced pressure to give 6.27 g (89%) of crude product which was purified by column chromatography using silica gel (100–200 mesh) and a mixture of petroleum ether and ethyl acetate (1:1, v/v) as eluent. The fraction isolated from this chromatography gave 4.8 g (69%) of a mixture of 2,2,6-trimethyl-3-oxa-*cis*-bicyclo[4.2.0]octan-4,8-dione (**21**) and 2,2,6-trimethyl-3-oxa-*cis*-bicyclo[4.2.0]octan-4,7-dione (**22**). The mixture of products could not be separated by tlc and was characterized by the following spectral data; ir ($CHCl_3$): 1730 and 1785 $cm^{-1}$; nmr ($CDCl_3$) δ: 1.32 and 1.40 (ss, 3H), 1.53 (s, 6H), and 2.2–3.2 (m, 5H); mass spectrum: (*a*) high resolution calcd. for $C_{10}H_{14}O_3$: 182.0943; found: 182.0953 amu; (*b*) low resolution *m/e* (relative intensity): 40(27), 41(60), 42(20), 43(78), 44(38), 51(10), 53(32), 54(17), 55(33), 59(10), 67(35), 68(47), 69(30), 70(14), 77(14), 79(30), 81(53), 82(26), 83(28), 95(25), 96(100), 97(79), 98(42), 123(46), 125(89), 126(23), 141(19), 167(8), and 182(6).

*(±)-Lineatin (1) and 3,3,7-trimethyl-2,9-dioxatricyclo-[4.2.1.0$^{4,7}$]nonane (isolineatin) (2)*

A solution of 5.0 g (27.5 mmol) of a mixture of ketones **21** and **22** in anhydrous ether (100 mL) was cooled to −60°C and a solution of 60 mL (1.0 *M* in hexane, 60 mmol) of diisobutylaluminum hydride in hexane was added dropwise under nitrogen. The reaction mixture was stirred at −60°C for 1 h, and saturated ammonium chloride (100 mL) was added. The reaction mixture was warmed to 0°C and acidified by dilute hydrochloric acid. Stirring was continued for an additional 1 h and the mixture was extracted several times with ether. The combined extracts were washed with aqueous sodium bicarbonate solution, dried over anhydrous magnesium sulfate, filtered, and the solvents removed under reduced pressure to give 4.3 g (95%) of crude product. The material was shown to be a 1.6:1 mixture of 3,3,7-trimethyl-2,9-dioxatricyclo[3.3.1.0$^{4,7}$]nonane (**1**) (±-lineatin) and 3,3,7-trimethyl-2,9-dioxatricyclo[4.2.1.0$^{4,7}$]nonane (**2**) (isolineatin) by glc. Purification was achieved by flash column chromatography (20) using silica gel (230–400 mesh) and a mixture of petroleum ether and ethyl ether (3:2, v/v) as eluent. Two components were isolated from this chromatography, and these were, in order of elution, (±)-lineatin (**1**) (1.05 g, 23%) and 3,3,7-trimethyl-2,9-dioxatricyclo[4.2.1.0$^{4,7}$]nonane (**2**) (0.615 g, 13.5%). All the spectral data of compound **1** were similar to those published by MacConnell *et al.* for (±)-lineatin (**1**) and **2** (1). This synthetic (±)-lineatin (**1**) was distilled at 110°C/20 Torr (Kugelrohr) and was characterized by; ir ($CCl_4$): 838, 875, 905, 920, 960, 1000, 1020, 1078, 1100, 1125, 1170, 1185, 1210, 1225, 1245, 1318, 1345, 1365, 1380, 1385, 1455, 1470, 2880, 2940, and 2975 $cm^{-1}$; nmr (100 MHz, $CCl_4$) δ: 1.08 (s, 3H), 1.12 (s, 3H), 1.14 (s, 3H), 1.55–2.1 (m, 5H), 4.34 (t, $J$ = 4 Hz, 1H), and 4.86 (d, $J$ = 3.5 Hz, 1H); nmr (270 MHz, $CCl_4$) δ: 1.12 (s, 3H), 1.16 (s, 3H), 1.17 (s, 3H), 1.61 (d, $J$ = 10.5 Hz, 1H), 1.69 (dt, $J$ = 10.5, 4 Hz, 1H), 1.83 (d, $J$ = 4 Hz, 1H), 1.91 (dd, $J$ = 12, 4 Hz, 1H), 2.04 (dd, $J$ = 12, 4 Hz, 1H), 4.38 (t, $J$ = 4 Hz, 1H), and 4.93 (d, $J$ = 4 Hz, 1H); mass spectrum: (*a*) high resolution calcd. for $C_{10}H_{16}O_2$: 168.1150; found: 168.1148 amu; (*b*) low resolution *m/e* (relative intensity): 41(44), 43(43), 55(44), 69(34), 83(58), 85(100), 96(84), 97(47), 107(68), 109(51), 111(85), 125(56), 140(12), 153(8), and 168(10). *Anal.* calcd. for $C_{10}H_{16}O_2$: C 71.39, H 9.59; found: C 71.52, H 9.76.

3,3,7-Trimethyl-2,9-dioxatricyclo[4.2.1.0$^{4,7}$]nonane (**2**) was distilled (Kugelrohr) at 110°C/20 Torr and was characterized by the following spectral data; ir ($CCl_4$): 660, 700, 850, 895, 905, 925, 938, 960, 970, 980, 990, 1000, 1018, 1040, 1050, 1080, 1100, 1115, 1140, 1160, 1178, 1195, 1205, 1220, 1238, 1255, 1295, 1300, 1325, 1345, 1360, 1365, 1382, 1435, 1455, 1470, 2875, 2950, and 2980 $cm^{-1}$; nmr (100 MHz, $CCl_4$) δ: 1.03 (s, 3H), 1.19 (s, 3H), 1.34 (s, 3H), 1.7–2.45 (m, 5H), 3.86 (t, $J$ = 4 Hz, 1H), and 5.23 (d, $J$ = 4 Hz, 1H); nmr (270 MHz, $CCl_4$) δ: 1.08 (s, 3H), 1.23 (s, 3H), 1.39 (s, 3H), 1.33 (dd, $J$ = 12, 4 Hz, 1H), 1.9 (m, 2H), 2.09 (d, $J$ = 12 Hz, 1H), 2.35 (ddd, $J$ = 13, 9, 4 Hz, 1H), 3.93 (t, $J$ = 4 Hz, 1H), and 5.32 (d, $J$ = 4 Hz, 1H); mass spectrum: (*a*) high resolution calcd. for $C_{10}H_{16}O_2$: 168.1150; found: 168.1152 amu; (*b*) low resolution *m/e* (relative intensity): 41(37), 43(30), 55(23), 67(13), 69(37), 71(17), 79(14), 81(18), 83(14), 91(45), 92(29), 93(13), 95(22), 97(16), 105(16), 107(22), 109(100), 120(15), 125(15), 124(60), 125(20), 130(16), 166(6), and 168(1). *Anal.* calcd. for $C_{10}H_{16}O_2$: C 71.39, H 9.59; found: C 71.19, H 9.59.

*Photoaddition of 3-methyl-5-hydroxy-2-pentenoic acid δ-lactone (5) to 3,3-dimethylallene*

A solution of 0.73 g (10.7 mmol) of 3,3-dimethylallene (Aldrich) and 0.80 g (7.13 mmol) of 3-methyl-5-hydroxy-2-pentenoic acid δ-lactone (**5**) in 30 mL of degassed acetone was irradiated with a 450 W Hanovia high pressure mercury arc at 0°C for 4 h through a Vycor filter. At the end of the irradiation the solvent was removed under reduced pressure to give 1.55 g of crude product. This product was purified by flash chromatography (20) using silica gel (230–400 mesh) and a mixture of ethyl acetate and petroleum ether (1:3, v/v) as eluent to give 0.69 g (53%) of a mixture of photoadducts. This mixture was found to contain three main components by glc in the ratio 13:20:65. These were subsequently shown by the following ozonolysis experiment to correspond to compounds **13**, **14**, and **15** respectively.

*Ozonolysis of alkenes 13, 14, and 15*

A stream of ozone and oxygen was bubbled through a solution of 0.25 g (1.4 mmol) of a mixture of compounds **13**, **14**, and **15** in 25 mL of anhydrous methanol at −78°C until the solution turned blue. Excess dimethylsulfide was added slowly. The reaction mixture was allowed to stir at −78°C for 20 min, warmed slowly to room temperature, washed with water, dried over anhydrous magnesium sulfate, and filtered. The solvents were removed under reduced pressure to give 0.14 g (ca. 50% yield) of a mixture of compounds. This mixture was shown by gc–ms to contain compounds with *m/e* 186(13*a*), 214(**14***a*), and 182(**15***a*) in the ratio 16:24:51 (glc ratios) respectively.[4]

## Acknowledgements

We are grateful to the Natural Sciences and Engineering Research Council of Canada (NSERC) and the Science Council of British Columbia for financial support of this work. One of us (J.O.) is grateful to NSERC for the award of a graduate fellowship.

1. J. G. MacConnell, J. H. Borden, R. M. Silverstein, and E. Stokkink. J. Chem. Ecol. **3**, 549 (1977).
2. J. H. Borden, J. R. Handley, B. D. Johnston, J. G. MacConnell, R. M. Silverstein, K. N. Slessor, A. A. Swigar, and D. T. W. Wong. J. Chem. Ecol. **5**, 681 (1979).
3. K. N. Slessor, A. C. Oehlschlager, B. D. Johnston, H. D. Pierce, Jr., S. K. Grewal, and L. K. G. Wickremesinghe. J. Org. Chem. **45**, 2290 (1980).
4. K. Mori and M. Sasaki. Tetrahedron, **36**, 2197 (1980).
5. (*a*) R. W. Holder. J. Chem. Educ. **53**, 81 (1976); (*b*) R. Huisgen and L. A. Feiler. Chem. Ber. **102**, 3444 (1969).
6. (*a*) R. C. Gueldner, A. C. Thompson, and P. A. Hedin. J. Org. Chem. **37**, 1854 (1972); (*b*) H. Kosugi, S. Seki-

[4]We wish to thank Professor F. S. Abbott and Mr. R. Burton, Pharmacy, U.B.C., for this gc–ms analysis.

GUCHI, R. SEKITA, and H. UDA. Bull. Chem. Soc. Jpn. **49**, 520 (1976).
7. (*a*) P. E. EATON. Tetrahedron Lett. 3695 (1964); (*b*) E. J. COREY, J. D. BASS, R. LEMAHIEU, and R. B. MITRA. J. Am. Chem. Soc. **86**, 5570 (1964); (*c*) K. WIESNER. Tetrahedron, **31**, 1655 (1975), and references therein; (*d*) R. B. KELLY, M. L. HARLEY, and S. J. ALWARD. Can. J. Chem. **58**, 755 (1980), and references therein; (*e*) G. MARINI-BETTOLO, S. P. SAHOO, G. A. POULTON, T. Y. R. TSAI, and K. WIESNER. Tetrahedron, **36**, 719 (1980), and references therein.
8. W. R. BAKER, P. D. SENTER, and R. M. COATES. J. Chem. Soc. Chem. Commun. 1011 (1980).
9. J. W. CORNFORTH, R. H. CORNFORTH, A. PELTER, M. G. HORNING, and G. POPJAK. Tetrahedron, **5**, 311 (1959).
10. R. A. ELLISON and P. K. BHATNAGAR. Synthesis, 719 (1974).
11. (*a*) T. HUDLICKY and T. KUTCHAN. Tetrahedron Lett. **21**, 691 (1980); (*b*) J. ANDRIEUX, D. H. R. BARTON, and H. PATIN. J. Chem. Soc. Perkin Trans. I, 359 (1977).
12. (*a*) P. E. EATON. Acc. Chem. Res. **1**, 50 (1968); (*b*) P. DE MAYO. Acc. Chem. Res. **4**, 41 (1971).
13. J. R. SCHEFFER and R. A. WOSTRADOWSKI. J. Org. Chem. **37**, 4317 (1972).
14. D. K. M. DUC, M. FETIZON, I. HANNA, A. OLESKER, C. PASCARD, and T. PRANGE. J. Chem. Soc. Chem. Commun. 1209 (1980).
15. D. BECKER, Z. HAREL, and D. BIRNBAUM. J. Chem. Soc. Chem. Commun. 377 (1975).
16. R. RATCLIFFE and R. RODEHORST. J. Org. Chem. **35**, 4000 (1970).
17. J. H. BORDEN, A. C. OEHLSCHLAGER, K. N. SLESSOR, L. CHONG, and H. D. PIERCE, JR. Can. J. Entomol. **113**, 1099 (1980).
18. L. M. JACKMAN and S. STERNHILL. Applications of nuclear magnetic spectroscopy in organic chemistry. 2nd ed. Pergamon Press Ltd., Headington Hill Hall, Oxford, England. 1969. p. 70.
19. K. B. WIBERG, G. M. LAMPMAN, R. P. CIULA, D. S. CONNOR, P. SCHERTLER, and J. LAVANISH. Tetrahedron, **21**, 2749 (1965).
20. W. C. STILL, M. KAHN, and A. MITRA. J. Org. Chem. **43**, 2923 (1978).

Can. J. Chem. Downloaded from www.nrcresearchpress.com by 210.87.254.42 on 09/06/12
For personal use only.

# Clathrate and other solid phases in the tetrahydrofuran–water system: thermal conductivity and heat capacity under pressure

RUSSELL G. ROSS[1] AND PER ANDERSSON
*Department of Physics, University of Umeå, 901 87 Umeå, Sweden*

Received September 15, 1981

RUSSELL G. ROSS and PER ANDERSSON. Can. J. Chem. **60**, 881 (1982).

Solid phases in the tetrahydrofuran–water (THF–$H_2O$) system were investigated in the temperature range 100–260 K and at pressures up to 1.5 GPa. Thermal conductivity, $\lambda$, and heat capacity per unit volume, $\rho c_p$, were measured, using the transient hot-wire method. We made measurements on solid phases having nominal compositions THF·17$H_2O$, THF·7.1$H_2O$, and THF·4.6$H_2O$, which we refer to as phases $\alpha$, $\beta$, and $\gamma$, respectively. Phase $\alpha$ is known to be a structure II clathrate hydrate, and $\lambda$ for this phase was found to be similar to other crystalline solids which are glass-like in relation to their thermal properties. Low-energy excitations are known to be relevant to the properties of glass-like solids, and, in the case of phase $\alpha$, were probably rotational vibrations of the THF guest molecules. Phase $\beta$ was similar, and we inferred that it was probably a structure I clathrate hydrate. Phase $\gamma$ behaved nearly like a normal crystal phase at low temperatures, but $\lambda$ became almost independent of temperature near melting. At 1.1 GPa and 130 K, we found evidence that phase $\alpha$ transformed, on pressurization, to a metastable modification which may be a new high-density form of clathrate hydrate. The astrophysical implications of our results were mentioned briefly.

RUSSELL G. ROSS et PER ANDERSSON. Can. J. Chem. **60**, 881 (1982).

On a étudié les phases solides dans le système tétrahydrofuranne–eau (THF–$H_2O$) dans un intervalle de température allant de 100 à 260 K et des pressions allant jusqu'à 1,5 GPa. On a mesuré la conductivité thermique, $\lambda$, et la capacité calorifique par unité de volume, $\rho c_p$, en utilisant la méthode du fil chaud transitoire. Nous avons effectué ces mesures sur des phases solides ayant des compositions nominales de THF·17$H_2O$, THF·7,1$H_2O$ et THF4,6$H_2O$ que nous désignons respectivement comme phases $\alpha$,$\beta$ et $\gamma$. On sait que la phase $\alpha$ a une structure II d'hydrate de clathrate et on a trouvé que, pour cette phase, $\lambda$ est semblable à celui d'autres solides cristallins qui ressemblent à des verres si l'on tient compte de leurs propriétés thermiques. On sait que les excitations de faible énergie sont reliées aux propriétés des solides ressemblant à des verres et, dans le cas de la phase $\alpha$, ce sont probablement des vibrations–rotations des molécules-hôtes de THF. La phase $\beta$ est semblable et nous en déduisons qu'elle a probablement une structure I d'hydrate de clathrate. La phase $\gamma$ se comporte presque comme une phase cristalline normale à basse température, mais $\lambda$ devient presqu'indépendant de la température au voisinage du point de fusion. A 1,1 GPa et 130 K, nous avons trouvé des indications à l'effet que la phase $\alpha$ se transforme, sous pression, en une forme métastable qui peut être une nouvelle forme d'hydrate de clathrate à haute densité. Nous mentionnons brièvement les implications astrophysiques de nos résultats.

[Traduit par le journal]

## 1. Introduction

We report here the first detailed measurements of the thermal properties of a clathrate hydrate. The properties we measured were thermal conductivity and heat capacity per unit volume. The system we studied was tetrahydrofuran–water (THF–$H_2O$), and we investigated three intermediate solid phases occurring at different compositions. One of these phases is known to be a clathrate hydrate, and we found evidence to suggest that a second one is as well. By way of introduction, our aim in the present section is to provide information both on clathrate hydrates, and on thermal properties of nonmetallic solids. Structural disorder, and its effects, will be a recurring theme.

### *1.1 Clathrate hydrates*

Clathrate solids (1) are a class of multi-component solid phase in which the major component, the host, encages individual guest molecules of the minor component(s). When the host is $H_2O$, the resulting clathrate solids are referred to as clathrate hydrates. Various properties of clathrate hydrates have been described in a detailed review by Davidson (2) on which the present introductory remarks are based. We consider here only binary systems yielding simple clathrate hydrates in which guest molecules of a single chemical species are encaged by a structure of $H_2O$ molecules of the host. The host molecules are hydrogen-bonded to each other, and form structures which may be described as "ice-like". A guest molecule may be considered to undergo relatively free rotational vibrations within its cage (3).

For almost all clathrate hydrates studied to date, the host molecules have a crystal structure which is of either one of two types, referred to as structure I and structure II. Structure I clathrate hydrates have been found for guest molecules (or atoms) up to about 0.53 nm in diameter, and structure II for guest molecules having diameters in the range 0.56–0.66 nm. Some examples are known where

[1]Permanent address: School of Mathematics and Physics, University of East Anglia, Norwich NR4 7TJ, U.K.

0008-4042/82/070881-12$01.00/0
©1982 National Research Council of Canada/Conseil national de recherches du Canada

Can. J. Chem. Downloaded from www.nrcresearchpress.com by 210.87.254.40 on 09/06/12
For personal use only.

Can. J. Chem. Downloaded from www.nrcresearchpress.com by 210.87.254.40 on 09/06/12
For personal use only.

guest molecules of about 0.55 nm diameter can form clathrate hydrates of either structure I or II. Structure I clathrate hydrates may be formed in principle in the range of composition from $M \cdot 5\frac{3}{4}H_2O$ to $M \cdot 7\frac{2}{3}H_2O$, where M represents a guest molecule. This compositional range reflects varying degrees of occupancy by guest molecules of the two sizes of cage available in the host structure. Structure II clathrate hydrates always seem to occur in a very narrow range of composition near $M \cdot 17H_2O$. This composition corresponds to full occupancy of large cages only.

The clathrate-forming system under investigation here is THF–$H_2O$. One reason for selecting this system was that samples were easy to prepare. Under normal conditions of temperature and pressure, THF is a liquid and binary samples can be prepared by simple mixing weighed amounts of the components. Guest species which are gaseous under normal conditions of temperature and pressure cannot be handled using our present experimental arrangements. In addition, the THF–$H_2O$ system has been relatively thoroughly investigated by previous workers. Dyadin *et al.* (4) determined the phase diagram over the whole range composition, at temperatures 240–320 K and at pressures up to 0.9 GPa. Figure 1 has been drawn to show the essential features of their results. They detected four intermediate solid phases at nominal compositions $THF \cdot 17H_2O$, $THF \cdot 7.1H_2O$, $THF \cdot 4.6H_2O$, and $THF \cdot 2.2H_2O$. For convenience, we shall refer to these phases as α, β, γ, and δ, respectively. Phases α, β, and γ were investigated in the present work. Phase α is known to be a structure II clathrate hydrate (5) which probably has a precise composition (6) $THF \cdot 16.86H_2O$. The existence of a structure II clathrate hydrate in this system is consistent with the structural generalizations previously described, since the diameter of the THF molecule is about 0.59 nm. However, Fig. 1 shows that phase α is stable only at a fairly low pressure. The possibility of the formation of other clathrate hydrate structures at high pressures will be considered later. Phases β and γ, for which no structural data are available, have been assigned (4) an experimental uncertainty of $\pm 0.3H_2O$ in composition, and are asserted to have a narrow range of composition. It can be seen from Fig. 1 that, at suitable pressures, all phases α, β, and γ can be formed by the procedure of congruent freezing of a liquid solution. We generally followed such a procedure in order to obtain the simplification of a single-phase solid sample.

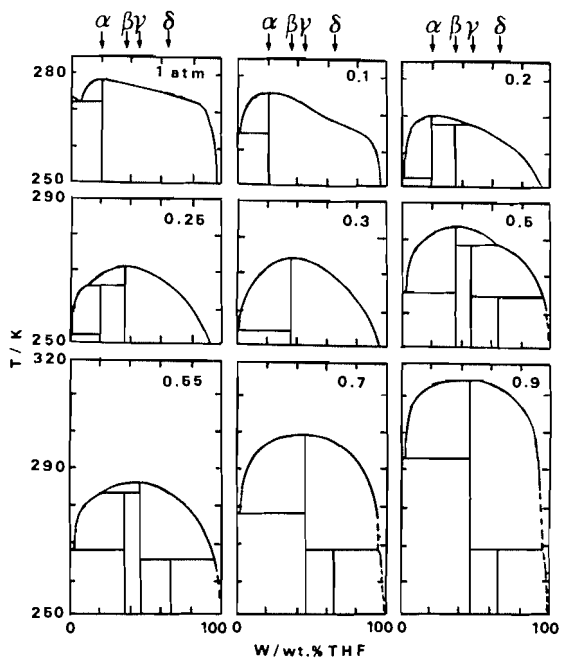


FIG. 1. Phase diagram of THF–$H_2O$ system, after Dyadin *et al.* (4). Solid phases have nominal compositions $THF \cdot nH_2O$ with $n$ = 17, 7.1, 4.6, and 2.2 for phases α, β, γ, and δ, respectively. Pressure for each isobaric section in GPa (except at 1 atm).

### *1.2 Thermal properties of nonmetallic crystals and glasses*

We now describe some simple and basic ideas in connection with the thermal properties of nonmetallic solids, in particular, molecular solids. It is well-known that specifically molecular properties exhibited in the gas phase are modified to a relatively small extent on transition to a solid phase. We shall therefore assume, in connection with the crystallography of molecular solids, that molecules may be regarded as the effective structural units.

We may distinguish several different types of internal motion in a molecular solid. One type of motion will be associated with the collective movement of the whole molecules and will correspond to the plane-wave solutions familiar from an elementary analysis of the lattice dynamics of a simple solid. The acoustic modes of the resulting dispersion relation should be of importance for the conduction of heat. Lattice optic modes and intramolecular vibrations also need to be taken into account, in principle.

In discussing the thermal conductivity, λ, it is usual to start with the Debye formula (7)

$$[1] \quad \lambda = \frac{1}{3} Cvl$$

In eq. [1], $C$ is the heat capacity per unit volume, $v$ the phonon velocity, and $l$ the phonon mean free

Can. J. Chem. Downloaded from www.nrcresearchpress.com by 210.87.254.40 on 09/06/12
For personal use only.

path. An expression of the form of eq. [1] should pertain for each of the lattice modes of vibration, but in practice we shall ignore optic modes by using the argument that they are expected to have a negligibly small phonon velocity. Although no detailed theoretical model (8) has yet been developed specifically for the thermal conductivity of complex molecular solids, it seems reasonable to assume that eq. [1] may be applied, and that only the acoustic modes carry heat. Thermal resistivity will arise from processes which scatter phonons. We shall present evidence which suggests that, in a clathrate hydrate, such processes may include motion of guest molecules.

As a preliminary to a more detailed view of the thermal conductivity of a molecular solid, we consider first the simplest possible analysis (7) for two idealized materials: a structurally-perfect crystalline solid of monatomic basis, and a structurally-disordered glass. We shall use eq. [1] to predict the form of $\lambda(T)$, where $T$ is the temperature.

For the structurally-perfect crystal, the thermal resistivity at high temperatures is considered to arise entirely from three-phonon umklapp processes. The density of other phonons with which a given phonon can interact is taken to be $\propto T$, from the high-temperature limit of the Planck distribution function, so $l \propto 1/T$. The heat capacity is taken to be constant at its classical value, and the temperature dependence of $v$ is ignored. The resulting theoretical prediction is $\lambda \propto 1/T$, and a more detailed treatment (9) gives the same result. The prediction is expected to be valid for $T \gtrsim$ the Debye temperature, $\theta_D$. As is well-known, the predicted form of $\lambda(T)$ is found in practice for many real crystals, including some molecular crystals (10).

For a glass, on the other hand, a common approximation is to take $l$ to be a temperature-independent constant, the value of which is fixed at a relatively small value as a result of structural disorder. Three-phonon umklapp processes are considered to make a negligible contribution to the total thermal resistivity. The temperature dependence of $v$ is ignored, and $C(T)$ is assumed to be described by a Debye model. The temperature dependence of $\lambda$ is then predicted to be similar to that of $C$, i.e., $\lambda$ increases modestly with $T$. Real glasses show approximately the predicted behaviour.

Even for the very simplest models, an outstanding difference to be emphasized between a perfect crystal and a glass is in the sign of $d\lambda/dT$; negative for a perfect crystal ($d \ln \lambda/d \ln T = -1$), and positive for a glass. It is also found empirically that $\lambda$(glass) is relatively small and close to $\lambda$(liquid) (11), whereas $\lambda$ usually shows a dramatic increase on freezing to a normal crystalline phase (8).

Recently, thermal properties of glasses at low temperature have been the subject of considerable experimental and theoretical investigation; see ref. 12 and references cited therein. In particular, for the thermal conductivity, a plateau at about 10 K is found to be superposed on a general increase of $\lambda$ with $T$. This and other features of the thermal properties are generally considered to be associated with the existence of low-energy, localized excitations, but detailed theoretical interpretation of the plateau is still controversial (12–14).

A related but somewhat surprising result which is by now established is that there are essentially-crystalline solids whose thermal properties are very similar to those just described for glasses. Such solids are also known to exhibit some form of structural disorder, and will be referred to here as glass-like (in relation to thermal properties). Data on the thermal properties of these solids has recently been summarized by Ackerman *et al.* (15). Further relevant references are refs. 16 to 18. As for glasses, appropriate localized excitations are invoked (15) to account for the observed thermal properties of glass-like solids.

From the discussion in section 1.1, we might expect that a clathrate hydrate would be a glass-like solid, and we shall present evidence to support this view. We shall further attempt to associate the low-energy excitations, relevant to the thermal conductivity, with the rotational vibrations of the guest molecules. Since our experiments were made at $T > 100$ K, our results complement those of previous investigations (15) which were mainly concerned with very low temperature conditions. A preliminary report of some of our results has already appeared (19).

### *1.3 Thermal conductivity of a two-phase system*

Methods for estimating the thermal conductivity of a two-phase mixture must also be mentioned briefly. This topic has been discussed by Parrott and Stuckes (7). In general, we tried to ensure that our sample was single-phase, but sometimes we were fairly sure that a second phase was present. In the latter case, we assumed that the thermal conductivity of the mixture could be calculated using the formula due to Maxwell. The input data required in the calculation were the thermal conductivities of each of the phases, and their volume fractions. The result was probably a good approximation when the volume fraction of one of the phases was small, but less satisfactory when the volume fractions of the two phases were nearly equal.

Can. J. Chem. Downloaded from www.nrcresearchpress.com by 210.87.254.40 on 09/06/12
For personal use only.

## 2. Experimental details

The thermal conductivity, $\lambda$, and the heat capacity per unit volume, $\rho c_p$, were measured simultaneously using the transient hotwire method. $c_p$ is the specific heat capacity at constant pressure, and $\rho$ is the mass density. Details of the method have been given elsewhere (10). Measurements were made in the temperature range $T = 100$–$260$ K and at pressures $P = 0.1$–$1.5$ GPa. Such ranges exceed, to a modest degree, those of the known phase diagram (4) (Fig. 1). Our investigation was concentrated on phases $\alpha$, $\beta$, and $\gamma$.

Samples were prepared by mixing at room temperature and pressure weighed quantities of spectroscopic grade THF and doubly-distilled water. A sample of liquid solution was poured into the Teflon cell of our piston-cylinder high pressure apparatus, and frozen, normally congruently, by cooling at the appropriate pressure. Overall compositions were calculated using the measured weights of the components.

Accuracy was $\pm 3\%$ in $\lambda$ and $\pm 10\%$ in $\rho c_p$.

## 3. Results

Our results for congruent freezing temperatures of phases $\alpha$, $\beta$, and $\gamma$ agreed to within 2 K with the known phase diagram (4). In all cases, we observed about 4 K supercooling, followed by an arrest. Such behaviour indicates unambiguously that a first-order liquid $\rightarrow$ solid transition occurred on cooling, and excludes the possibility of glass formation.

Data for $\lambda$ and $\rho c_p$ are shown in Figs. 2–6. There are no previous results available for comparison. Equations were fitted where appropriate, and the resultant coefficients are given in Tables 1 and 2.

We also made measurements for the liquid-phase solutions, but for simplicity these data have been omitted from the figures. In addition, for technical reasons discussed elsewhere (20), our measurements for liquids are less accurate than for solids. We can, however, obtain approximate values for the ratio $\lambda$(solid)/$\lambda$(liquid) at congruent freezing, and the results were values 1.07, 1.04, and 1.20 in connection with phases $\alpha$, $\beta$, and $\gamma$ respectively.

We investigated a number of solid samples under various conditions, according to the following outline:

(*i*) All samples had a composition at or near that expected for phase $\alpha$, $\beta$, or $\gamma$.

(*ii*) For each of these phases, we made isobaric measurements under conditions of thermodynamic equilibrium at the pressure we employed for congruent freezing, which was 0.1, 0.3, or 0.55 GPa for phase $\alpha$, $\beta$, or $\gamma$ respectively. For phase $\gamma$, isobaric measurements were also made at pressures of 0.91 and 1.4 GPa. The former pressure is known from the phase diagram (Fig. 1) to correspond to thermodynamic equilibrium, and it appears from our measurements that the latter pressure does as well. Results for isobaric measurements under conditions of themodynamic equilibrium are described in section 3.1.

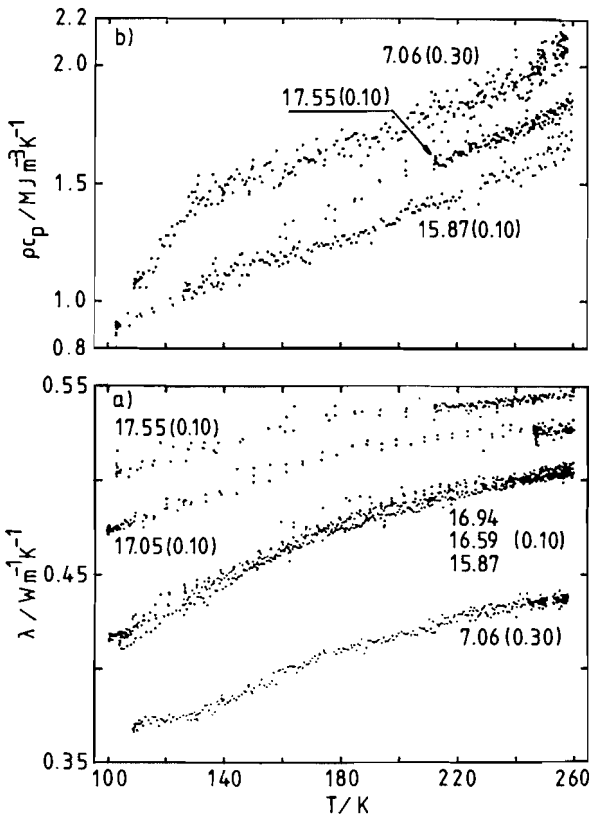


FIG. 2. Isobaric temperature dependence of (*a*) thermal conductivity $\lambda$ and (*b*) heat capacity per unit volume $\rho c_p$. Data for samples of composition THF·$n$H$_2$O at pressure $P$/GPa labelled $n(P)$.

(*iii*) In another series of experiments, samples of composition appropriate to each of phases $\alpha$, $\beta$, and $\gamma$ were cooled at the pressure employed for congruent freezing, and then pressurized isothermally at 130 K to about 1.5 GPa. At 1.1 GPa, there was evidence that phase $\alpha$ transformed to what we shall call phase $\alpha'$. Results for isothermal compression at 130 K are described in section 3.2.

(*iv*) Phases $\alpha'$ and $\beta$ were probably metastable at 1.4 GPa and low temperatures, and reliable measurements could only be made up to 200 K. Results for isobaric measurements on these metastable phases are described in sections 3.2.4 and 3.2.2 respectively.

(*v*) Phases $\alpha$ and $\beta$ could be compressed under equilibrium conditions at 240 K, and the corresponding results for isothermal measurements are described in section 3.3

### *3.1 Isobaric measurements under conditions of thermodynamic equilibrium*

#### *3.1.1 Phase* $\alpha$

Figure 2(*a*) includes data for $\lambda(T)$ at 0.1 GPa for samples having compositions near THF·17H$_2$O.

Can. J. Chem. Downloaded from www.nrcresearchpress.com by 210.87.254.40 on 09/06/12
For personal use only.

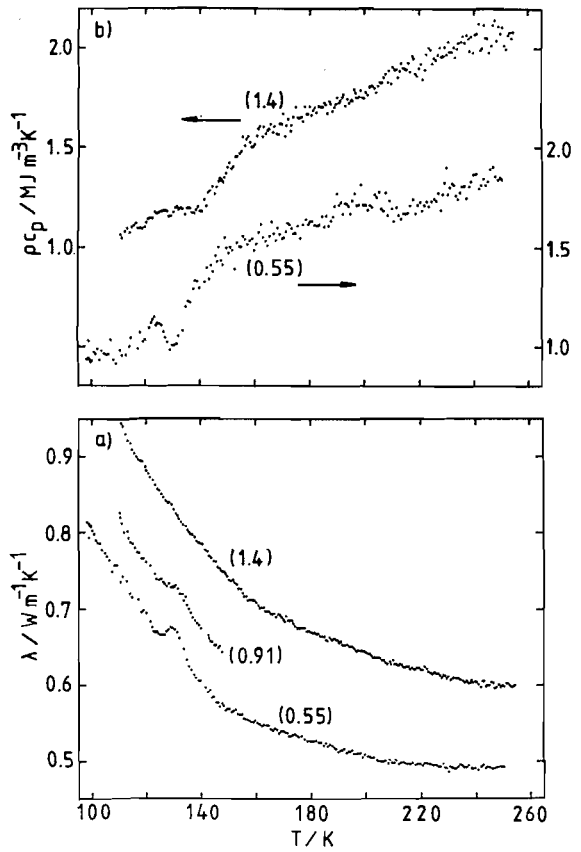


FIG. 3. Isobaric temperature dependence of (*a*) thermal conductivity $\lambda$ and (*b*) heat capacity per unit volume $\rho c_p$ for sample of composition THF·4.60$H_2O$. Pressure in GPa given in parentheses.

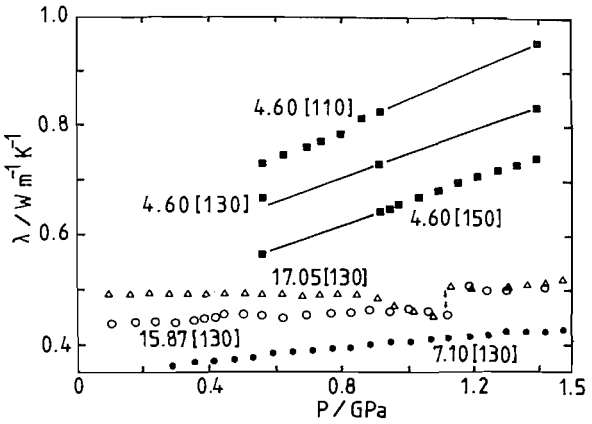


FIG. 4. Isothermal pressure dependence of thermal conductivity $\lambda$. Data for samples of composition THF·$n$$H_2O$ at temperature $T$/K labelled $n$[$T$].

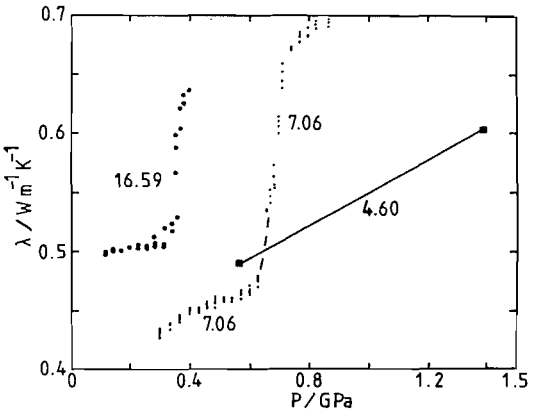


FIG. 5. Isothermal pressure dependence of thermal conductivity $\lambda$ at 240 K. Data for samples of composition THF·$n$$H_2O$ labelled $n$.

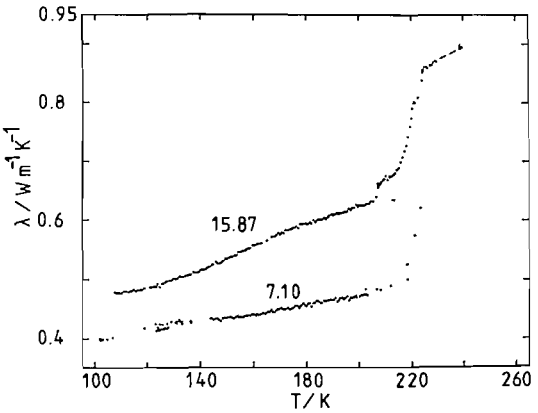


FIG. 6. Isobaric temperature dependence of thermal conductivity $\lambda$ at 1.4 GPa. Data for samples of composition THF·$n$$H_2O$ labelled $n$.

The figure shows that $\lambda(T)$ had the same general form for all these samples, and that it was similar to that for a glass.

The measured values of $\lambda(T)$ were essentially identical for samples in the range of composition from THF·15.87$H_2O$ to THF·16.94$H_2O$. Since phase $\alpha$ is known (6) to have a narrow range of composition at about THF·16.9$H_2O$, these samples should consist either of phase $\alpha$ or of phase $\alpha$ + a small proportion of a THF-rich phase. For $T \gtrsim$ 170 K, the THF-rich phase will consist (4, 21) of liquid solution, whereas at lower temperatures it is most likely to be pure solid THF. The normal freezing point of pure THF is 164.76 K (22). Whether solid or liquid, the presence of a small proportion of THF-rich phase should have a very small effect on $\lambda$. This is because the THF-rich phase is expected to have a value of $\lambda$ quite close to that of phase $\alpha$. It was stated earlier that we found $\lambda$(phase $\alpha$)/ $\lambda$(liquid) $\approx$ 1.07 for liquid solution of the same composition as phase $\alpha$. In the case of pure solid THF, $\lambda \approx 0.65$ W m$^{-1}$ K$^{-1}$ at 130 K and low

Can. J. Chem. Downloaded from www.nrcresearchpress.com by 210.87.254.40 on 09/06/12
For personal use only.

TABLE 1. Isobaric temperature dependence of thermal conductivity $\lambda$ for samples of composition $THF{\cdot}nH_2O$ fitted to equations of form $\lambda/(W\ m^{-1}\ K^{-1}) = A + B(T/K) + C(T/K)^2$

| $n$ | $A$ | $B$ | $C$ | $P$/GPa | $T$/K |
|---|---|---|---|---|---|
| 17.55 | 0.449 | $0.066 \times 10^{-2}$ | $-0.114 \times 10^{-5}$ | 0.10 | 102–260 |
| 17.05 | 0.383 | $0.111 \times 10^{-2}$ | $-0.215 \times 10^{-5}$ | 0.10 | 99–260 |
| 16.94, 16.59, 15.87 | 0.279 | $0.162 \times 10^{-2}$ | $-0.288 \times 10^{-5}$ | 0.10 | 100–260 |
| 7.06 | 0.234 | $0.139 \times 10^{-2}$ | $-0.235 \times 10^{-5}$ | 0.30 | 130–260 |

TABLE 2. Isothermal pressure dependence of thermal conductivity $\lambda$ for samples of composition $THF{\cdot}nH_2O$ fitted to equations of form $\lambda/(W\ m^{-1}\ K^{-1}) = D + E(P/GPa) + F(P/GPa)^2$

| $n$ | $D$ | $E$ | $F$ | $T$/K | $P$/GPa |
|---|---|---|---|---|---|
| 17.05 | 0.493 | −0.001 | — | 130 | 0.10–0.80 |
| 17.05 | 0.435 | 0.006 | — | 130 | 1.1 –1.5 |
| 15.87 | 0.436 | 0.025 | — | 130 | 0.10–1.0 |
| 15.87 | 0.475 | 0.019 | — | 130 | 1.2 –1.4 |
| 7.10 | 0.336 | 0.089 | −0.018 | 130 | 0.30–1.5 |
| 4.60 | 0.577 | 0.269 | — | 110 | 0.55–1.4 |
| 4.60 | 0.529 | 0.219 | — | 130 | 0.55–1.4 |
| 4.60 | 0.451 | 0.211 | — | 150 | 0.55–1.4 |
| 16.59 | 0.495 | 0.039 | — | 240 | 0.10–0.28 |
| 7.06 | 0.404 | 0.109 | — | 240 | 0.30–0.63 |
| 4.60 | 0.424 | 0.141 | — | 240 | 0.55–1.4 |

pressure.[2] From the data shown in Fig. 2, there was no evidence that freezing of the THF-rich phase, which probably occurred at about 170 K, had any significant effect on the measured value of $\lambda$. We therefore conclude that $\lambda(T)$ for phase $\alpha$ is closely approximated by the data shown in Fig. 2(*a*) for samples in the range of composition from $THF{\cdot}15.87H_2O$ to $THF{\cdot}16.94H_2O$.

Similarly, samples of composition $THF{\cdot}17.05H_2O$ and $THF{\cdot}17.55H_2O$ were expected to contain a small proportion of ice Ih, but, by contrast, the presence of the latter should have a relatively large effect on $\lambda$ since $\lambda$(ice Ih)/$\lambda$(phase $\alpha$) $\approx$ 5. To show this effect in more detail, we can estimate $\lambda$ for a two-phase mixture using the Maxwell formula (7). At a temperature of about 250 K, we take $\lambda$(phase $\alpha$) $\approx$ 0.5 W m$^{-1}$ K$^{-1}$ from present work, and $\lambda$(ice Ih) $\approx$ 2.5 W m$^{-1}$ K$^{-1}$ from previous work (23). We ignore any difference of density (6) between the two phases. An increase of molecular concentration by $0.5H_2O$ above the exact composition of phase $\alpha$ then implies a volume ratio (ice Ih):(phase $\alpha$) $\approx$ 1:35. Use of the Maxwell formula then yields a corresponding increase in $\lambda$ of 5%, which was about what was observed experimentally. Supporting evidence for the presence of ice Ih in the sample of composition $THF{\cdot}17.55H_2O$ was our observation of a response in $\lambda(T)$, as usually found for a phase transition, at the temperature of the (phase $\alpha$)–(ice Ih)–(liquid) eutectic.

*3.1.2 Phase* $\beta$

Figure 2(*a*) also includes data for $\lambda(T)$ at 0.3 GPa for a sample of composition $THF{\cdot}7.1H_2O$, which we assumed consisted entirely of phase $\beta$. As for phase $\alpha$, the form of $\lambda(T)$ for phase $\beta$ is similar to that for a glass.

*3.1.3 Phase* $\gamma$

Figure 3 shows our results along various isobars for a sample of composition $THF{\cdot}4.6H_2O$, which we assumed consisted entirely of phase $\gamma$. The form of $\lambda(T)$ for phase $\gamma$ is evidently very different from that for phases $\alpha$ and $\beta$ (Fig. 2), and closer to what would be expected for a normal crystalline phase. At 0.55 GPa, a weak maximum in $\lambda(T)$, and minimum in $\rho c_p(T)$, were detected at a temperature of about 130 K. These features became less pronounced with increasing pressure. We shall argue later that they can most plausibly be regarded as an artifact of the transient hot-wire method. Our results at 260 K indicated that the region of stability of phase $\gamma$ in the phase diagram (Fig. 1) can be extended to at least 1.4 GPa at this temperature.

*3.2 Isothermal compression at 130 K, and metastability*

Figure 4 shows our results for isothermal compression of phases $\alpha$, $\beta$, and $\gamma$ at a temperature of 130 K. Only data for $\lambda(P)$ are shown. With an exception to be noted in the following paragraph, $\rho c_p$ had a value of about 1 MJ m$^{-3}$ K$^{-1}$ for all phases and $P$–$T$ conditions indicated in Fig. 4.

*3.2.1 Phase* $\alpha$

We begin with a consideration of samples of composition $THF{\cdot}15.87H_2O$ and $THF{\cdot}17.05H_2O$, which were both expected to consist mostly of phase $\alpha$. Both of these samples showed evidence for a phase transition (which we have referred to as $\alpha \rightarrow \alpha'$) at a pressure of about 1.1 GPa, but discussion of this transition is deferred until later (section 3.2.4). The phase $\alpha \rightarrow \alpha'$ transition was accompanied by an increase of about 25% in $\rho c_p$.

Our first concern is with $\lambda(P)$ at pressures up to 1.1 GPa. It seems reasonable to conclude from section 3.1 that $\lambda(P)$ shown in Fig. 4 for the sample of composition $THF{\cdot}15.87H_2O$ closely represented the behaviour of phase $\alpha$. For reasons which will become apparent shortly, this composition was deliberatly selected so that we could be quite sure that the sample did not include any ice. A small proportion of THF-rich second phase was expected to be present in this sample, but we conclude that it would have a small effect on the total $\lambda$. The

[2] R. G. Ross and P. Andersson. Unpublished work.

Can. J. Chem. Downloaded from www.nrcresearchpress.com by 210.87.254.40 on 09/06/12
For personal use only.

argument in support of this conclusion was given earlier in discussing $\lambda(T)$ for this sample; namely, that $\lambda$ for the THF-rich second phase which was present was close to that for phase $\alpha$. At 130 K, the THF-rich second phase was most likely to be pure solid THF, although there is no direct evidence for this from the known phase diagram (Fig. 1). For solid THF at 130 K and low pressures, $\lambda \approx 0.65$ W m$^{-1}$ K$^{-1}$ and $d\lambda/dP \approx 0.79$ W m$^{-1}$ K$^{-1}$ GPa$^{-1}$.[2]

The constitution of the sample of composition THF·17.05$H_2O$ was considered earlier (section 3.1.1), where we concluded that it almost certainly contained a small proportion of ice as a second phase. The main evidence from our experiments for such a mixture of phases in this sample was that calculations using the Maxwell formula yielded about the same composition dependence of $\lambda$ as was observed experimentally.

We shall now attempt to show that the presence of a small proportion of ice phase in this sample is consistent with the observed form of $\lambda(P)$. The main point to be emphasized is that $\lambda$(ice Ih)/$\lambda$(phase $\alpha$) $\approx$ 5. Thus, even a relatively small proportion of ice Ih can have a relatively large effect on the total $\lambda$, and its pressure dependence. Ice Ih is known (23) to have a negative value of $d\lambda/dP$. Figure 4 and Table 2 show that $d\lambda/dP$ for the sample of composition THF·17.05$H_2O$ was very small, and in fact slightly negative, at pressures up to about 0.8 GPa. This behaviour was probably caused by the ice Ih phase present. Furthermore, in the pressure range 0.8–1.1 GPa, $\lambda$ decreased relatively rapidly with pressure. Such a decrease could be due to a gradual transformation of the ice Ih second phase to one or more of the high pressure modifications, such as ice III or ice V. The latter are known (23) to have absolute values of $\lambda$ which are smaller than that of ice Ih by a factor about 2. However, there are no data available to provide direct evidence for transitions from ice Ih to other modifications on pressurization at 130 K.

*3.2.2 Phase* $\beta$

Figure 4 and Table 2 include data for $\lambda(P)$ at 130 K for a sample of composition THF·7.1$H_2O$, which we assumed consisted entirely of phase $\beta$. $d\lambda/dP$ was positive, and there was no evidence for any phase transition at pressures up to the maximum of 1.5 GPa. The phase diagram (Fig. 1) leads us to expect that phase $\beta$ was probably metastable with respect to other phases for $P \gtrsim 0.6$ GPa. When phase $\beta$ was warmed at a pressure of 1.5 GPa, we found the form of $\lambda(T)$ which is shown in Fig. 6 for the sample of composition THF·7.1$H_2O$. Up to a temperature of about 200 K, this form is similar to that found for phase $\beta$ at a pressure of 0.3 GPa (Fig. 2). At higher temperatures, $\lambda$ increased rapidly, probably due to a transition to an equilibrium configuration of phases. A consequence was internal damage to the cell, and termination of the run at this point.

*3.2.3 Phase* $\gamma$

A sample of composition THF·4.6$H_2O$ was assumed to consist entirely of phase $\gamma$. Low-temperature pressurization experiments were carried out for this sample at temperatures of 110 and 150 K. These temperatures were selected so as to be below and above the weak maximum in $\lambda(T)$ which we found for phase $\gamma$ at about 130 K (Fig. 3). The resultant isothermal measurements showed no significant difference between the two temperatures. These measurements, together with data deduced from Fig. 3, yield the results for phase $\gamma$ shown in Fig. 4 and Table 2.

*3.2.4 Phase* $\alpha'$

We now return to a consideration of the behaviour of phase $\alpha$ in the region of 1.1 GPa at 130 K. Figure 4 shows that $\lambda$ increased discontinuously by about 10%, and we also found that $\rho c_p$ increased discontinuously by about 25%. In addition, thermocouple response in the cell indicated evolution of heat, on increase of pressure. In our type of experiments, such observations are normally associated with a first-order phase transition. We shall therefore assume that at a pressure of about 1.1 GPa, phase $\alpha$ transformed to what we have referred to as phase $\alpha'$. It is recognized that phase $\alpha'$ may be single-phase but metastable, or perhaps consist of a mixture of phases, and we now examine some possibilities for the latter.

The phase diagram (Fig. 1) suggests that phase $\alpha$ was probably metastable with respect to other phases for $P \gtrsim 0.3$ GPa. Thus, under conditions of thermodynamic equilibrium and at, say, 0.9 GPa, phase $\alpha$ would be expected to dissociate to yield phase $\gamma$ + an ice phase. The latter would be expected to be ice VI, on the basis of the known phase diagram for ice (24). The same mixture of phases should be the stable equilibrium configuration for $P \gtrsim 1.1$ GPa, since we have found (Fig. 3) that phase $\gamma$ is stable up to at least 1.4 GPa. Let us suppose that phase $\alpha'$ is actually a mixture of phase $\gamma$ + ice VI. At 130 K and 1.4 GPa, $\lambda$(phase $\gamma$) $\approx$ 0.84 W m$^{-1}$ K$^{-1}$ from present work, and we estimate $\lambda$(ice VI) $\approx$ 3 W m$^{-1}$ K$^{-1}$ from previous work (23, 25). The value of $\lambda$ for phase $\gamma$ gives a lower limit for $\lambda$(mixture), whatever the volume fractions in the mixture we have supposed to exist. If we take the volume fraction of phase $\gamma$ to be 0.44, as suggested by the phase diagram, the Maxwell

Can. J. Chem. Downloaded from www.nrcresearchpress.com by 210.87.254.40 on 09/06/12
For personal use only.

formula (7) yields $\lambda$(phase $\gamma$ + ice VI) $\approx$ 1.9 W m$^{-1}$ K$^{-1}$. All predictions of $\lambda$(mixture) which involve phase $\gamma$ are substantially larger than the value 0.51 W m$^{-1}$ K$^{-1}$ found experimentally for phase $\alpha'$. We conclude, therefore, that phase $\alpha'$ is very unlikely to consist of a mixture of phase $\gamma$ and ice VI. A similar conclusion is reached if we assume phase $\alpha$ to undergo a less probable dissociation to give a mixture of phase $\beta$ + ice VI, in equal volume fractions. If we take $\lambda$(phase $\beta$) $\approx$ 0.42 W m$^{-1}$ K$^{-1}$, from present work, the Maxwell formula then yields $\lambda$(phase $\beta$ + ice VI) $\approx$ 1 W m$^{-1}$ K$^{-1}$. The final result is that no phase mixture suggested by the phase diagram yields an estimate for $\lambda$(mixture) which is close to the value found experimentally for phase $\alpha'$.

It seems to us most likely that phase $\alpha'$ was a single phase, formed by a first-order transition from phase $\alpha$ on pressurization, but probably metastable with respect to a mixture of phase $\gamma$ and ice VI. When phase $\alpha'$ was pressurized to 1.42 GPa, cooled to 110 K, and then warmed, we obtained the results which are included in Fig. 6 for the sample of composition THF·15.87$H_2O$. We found $d\lambda/dT$ for this sample to be positive, up to temperatures of about 200 K, so from the form of $\lambda(T)$ phase $\alpha'$ must be included in the same group as phases $\alpha$ and $\beta$. For $T > 200$ K, $\lambda$ increased rapidly, probably in the course of a transition to an equilibrium configuration of phases. A consequence was internal damage to the cell, and termination of the run at this point.

*3.3 Isothermal compression at 240 K*

Results for pressurization of various samples at a temperature of 240 K are shown in Fig. 5. In all cases, we expected that the system was close to thermodynamic equilibrium.

*3.3.1 Phase* $\alpha$

For the sample of composition THF·16.59$H_2O$, pressure was increased until there was evidence that a phase transformation had taken place, as indicated by the rapid increase of $\lambda$ shown in Fig. 5 at a pressure of about 0.3 GPa. According to the phase diagram (Fig. 1), the transformation to be expected is a compositional dissociation of phase $\alpha$ to yield phase $\beta$ + a high pressure ice, presumably ice III (24). With the assumption that this dissociation indeed occurred, we may estimate $\lambda$ for the resulting mixture, using the Maxwell formula. We assume the volume fraction of ice III to be 0.45, and take $\lambda$(phase $\beta$) $\approx$ 0.44 W m$^{-1}$ K$^{-1}$ (Fig. 2, sample THF·7.06$H_2O$) and $\lambda$(ice III) $\approx$ 1.0 W m$^{-1}$ K$^{-1}$ (25). The resulting prediction for the mixture is $\lambda$ = imentally.

*3.3.2 Phase* $\beta$

Results for the pressurization of phase $\beta$ at 240 K are also shown in Fig. 5. The rapid increase of $\lambda$ for pressures greater than about 0.6 GPa we associate with a compositional dissociation of phase $\beta$. According to the phase diagram (Fig. 1), we expect phase $\beta$ to dissociate at about this pressure to yield phase $\gamma$ + a high pressure ice modification. At a pressure of 0.8 GPa, the latter should almost certainly be ice VI (24). We shall again use the Maxwell formula, at this pressure, to calculate $\lambda$ for the assumed mixture. From Fig. 5, we take an interpolated value, $\lambda$(phase $\gamma$) $\approx$ 0.52 W m$^{-1}$ K$^{-1}$ (sample of composition THF·4.6$H_2O$), and $\lambda$(ice VI) $\approx$ 1.7 W m$^{-1}$ K$^{-1}$ (23). The phase diagram (Fig. 1) indicates that ice VI should be the dispersed phase, and, although the density of phase $\gamma$ is not known, we estimate the volume fraction of ice VI as about 0.21. The Maxwell formula then yields the value $\lambda$(mixture) $\approx$ 0.68 W m$^{-1}$ K$^{-1}$, compared with 0.69 W m$^{-1}$ K$^{-1}$ found experimentally.

## 4. Discussion

All of the solid phases we have investigated in the THF–$H_2O$ system have interesting and somewhat unusual thermal properties. We shall be concerned with discussing mainly the temperature and pressure (volume) dependences of $\lambda$.

$\lambda(T)$ for phases $\alpha$, $\alpha'$, or $\beta$ is similar to that for a glass (12) or for a glass-like solid (15). An obvious assumption is that this behaviour arises from structural disorder, at least for phase $\alpha$ which is known to be a structure II clathrate hydrate. Our experiments did not extend to sufficiently low temperatures to determine whether or not a plateau in $\lambda$ exists for a clathrate hydrate.

The only data for $\lambda$ for clathrate hydrates are due to Stoll and Bryan (26). These workers measured the magnitude of $\lambda$ for a propane hydrate (structure II) and a methane hydrate (structure I). In both cases, they found $\lambda \approx 0.4$ W m$^{-1}$ K$^{-1}$ at a temperature of 275 K. The pressure was of order 1 MPa for the propane hydrate and 10 MPa for the methane hydrate. The temperature dependence of $\lambda$ was not determined.

The results available from our work and that of Stoll and Bryan (26) lead to the preliminary conclusion that $\lambda$ for a clathrate hydrate always has a value of about 1/2 W m$^{-1}$ K$^{-1}$ near 300 K and at low pressures. If such uniformity in the magnitude of $\lambda$ indeed exists generally for clathrate hydrates, then it may correspond to a similar uniformity which is known to pertain for glasses (12) and other glass-like solids (15).

Both the magnitude of $\lambda$, and its temperature dependence, suggest that phase $\beta$ should be regarded as a clathrate hydrate. If so, it is probably structure I, on the basis of composition, although

Can. J. Chem. Downloaded from www.nrcresearchpress.com by 210.87.254.40 on 09/06/12
For personal use only.

no structural data are available. In fact, phase β is only stable under pressure (Fig. 1). As suggested by Dyadin *et al.* (4), structure II may become less stable than structure I under pressure, even for a guest molecule having a diameter as large as that of THF (0.59 nm). The largest diameter of guest molecule previously known to form a structure I clathrate hydrate was about 0.55 nm (2), but this was at low pressure.

We shall now discuss each phase in more detail.

*4.1 Phase α*

We have tried a number of mathematical forms to fit our data for $\lambda(T)$ of phase α. The results are shown in Figs. 7 and 8. We keep in mind that this structure II clathrate hydrate can probably be appropriately regarded as a glass-like solid (15).

We first made use of eq. [1]. If we take the mean free path $l$ and the velocity $v$ to be independent of $T$, then all of the temperature dependence of λ must come from $C$. As described in section 1.2, it is reasonable to take only the acoustic modes into account, so we use a model for $C$ since our measured $C$ values probably included additional contributions from optic and intramolecular modes. Figure 7 shows that a relatively poor fit is obtained using an Einstein model for $C$, with Einstein temperature $\theta_E = 190$ K. The root-mean-square deviation, $F$, was $6.3 \times 10^{-3}$ W m$^{-1}$ K$^{-1}$. Indistinguishable results were obtained using the high-temperature approximation for a Debye model, with $\theta_D = 248$ K. Evidently, the temperature dependence of λ is not well approximated by the temperature dependence of $C$.

If we assume $\lambda \sim T^n$, then Fig. 7 shows that a better fit is obtained ($F = 3.2 \times 10^{-3}$ W m$^{-1}$ K$^{-1}$). We get $n = 0.22$, but have no independent means of estimating this exponent. An exponent of about 0.6 may be deduced for the glass-like solid $KFeF_3$ (17). If we use eq. [1] and write $(vl) \sim T^m$, then Fig. 7 shows that we can obtain a good fit to the data ($F = 2.5 \times 10^{-3}$ W m$^{-1}$ K$^{-1}$), which is not surprising since there are three parameters. We used an Einstein model for $C(T)$. The parameters had values $\theta_E = 91$ K and $m = 0.17$. According to this fitting procedure, the product $vl$, and presumably $l$, decreased with decreasing $T$. This is contrary to the likely variation if some form of phonon–phonon interaction determined the thermal resistivity. Moreover, the corresponding change of $l$ of about 18% from 100 to 260 K evidently cannot be accounted for by linear thermal expansion, which is only (3) ~1% over this range of temperature.

An interesting and somewhat surprising result is shown in Fig. 8. Empirically, we find that the form $\lambda \sim \exp(-T_0/T)$ provides a good fit to the data ($F = 3.3 \times 10^{-3}$ W m$^{-1}$ K$^{-1}$). The characteristic temperature, $T_0$, required to fit the data turns out to be about 37 K, and we now examine the significance of this value.

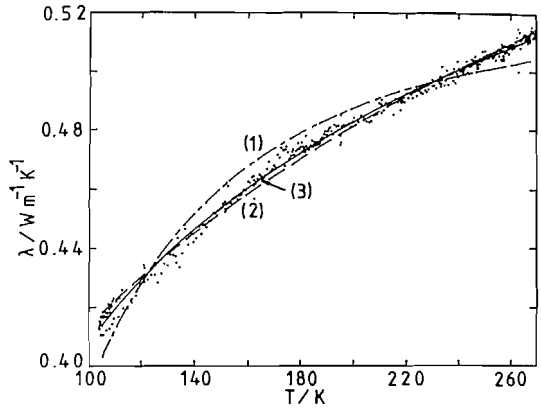


FIG. 7. Isobaric data for thermal conductivity λ of sample of composition THF·16.59$H_2O$ at 0.10 GPa fitted to equations of form: (*1*) $C(T)$, (*2*) $T^n$, (*3*) $C(T)\,(vl)^m$.

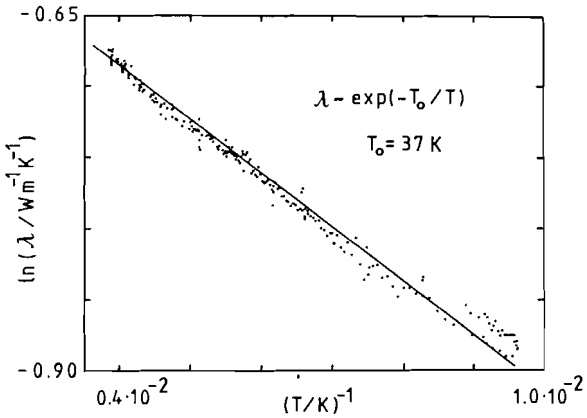


FIG. 8. Isobaric data for thermal conductivity λ of sample of composition THF·16.59$H_2O$ at 0.10 GPa fitted to equation of form ln (λ/W $m^{-1}$ K$^{-1}$) ~ $(-T_0/T)$.

In recent far-infrared spectroscopic measurements on phase α at low temperatures, Bertie and Jacobs (3) found that a principal absorption assigned to rotational vibrations of the THF molecules occurred at a wave number of about 25 cm$^{-1}$. The corresponding energy, expressed in terms of temperature, is $T_{RV} = 36$ K. Whilst the agreement between this temperature and $T_0$ may be fortuitous, it strongly suggests to us that rotational vibrations of the guest molecules have a predominant influence on the conduction of heat. Since the localized guest molecules obey Maxwell–Boltzmann statistics (27) the degree of excitation of rotational vibrations will be $\propto \exp(-T_{RV}/T)$, which is similar to $\lambda(T)$. Thus, it appears that heat

Can. J. Chem. Downloaded from www.nrcresearchpress.com by 210.87.254.40 on 09/06/12
For personal use only.

transport in this clathrate hydrate occurs by lattice vibrations which couple, perhaps inelastically (13, 14), with the rotational vibrations of the THF guest molecules, and that $\lambda$ is proportional to the degree of excitation of these vibrations. We infer that rotational vibrations of THF guest molecules are probably a specific example of low-energy excitations of the general type expected (15) to affect the thermal properties of glass-like solids.

We now consider $\lambda$ of phase $\alpha$ under pressure, in particular the volume dependence, $g = (\partial \ln \lambda / \partial \ln \rho)_T$. As described above in section 3.1.2, $\lambda(P)$ was quite sensitive to the presence of a small proportion of ice Ih in the sample. We concluded that our best estimate, at 130 K, of $\lambda(P)$ for phase $\alpha$ was obtained for the sample of composition $THF \cdot 15.87H_2O$. Thus, we obtained $(\partial \ln \lambda / \partial P)_T = 0.058\ GPa^{-1}$ for phase $\alpha$, as may be deduced from Table 2. Whalley (28) has estimated that the compressibility of a structure II clathrate hydrate will be 1.162 times that of ice Ih, and we take the compressibility of ice Ih to be $0.11\ GPa^{-1}$ (29). Putting these results together we obtain $g = 0.45$ for phase $\alpha$. This result for $g$ supersedes the estimate given previously (19), where, in a preliminary report, we failed to take adequate account of the influence of a small proportion ice Ih in the measured value of $(\partial \lambda / \partial P)_T$.

This value of $g$ for phase $\alpha$ is very small in magnitude. Normal (8) and plastic (30) crystal phases usually have $g$ values in the range 5–10. $g$ is usually in the range 1–4 for liquids and glasses (8, 31), with the smallest magnitude previously recorded being 0.65 for quartz glass (8). The glass-like solid phase $\alpha$ evidently has a value of $g$ similar to glasses and liquids. If, as suggested above, the thermal resistivity of phase $\alpha$ is closely connected with the rotational vibrations of the THF guest molecules, the latter might be expected to be relatively insensitive to pressure in a clathrate hydrate. On the other hand, the host structure is "ice-like", and ice Ih is known (23) to have a negative value of $g$. Slack (32) has discussed this behaviour of ice Ih in terms of a transverse acoustic mode which dominates thermal conduction, and which softens under pressure. Data for the pressure dependence of transverse and longitudinal sound velocities would be necessary to apply Slack's type of analysis to phase $\alpha$.

*4.2 Phase* $\beta$

Lack of other data precludes detailed discussion of this phase. It was argued above that phase $\beta$ is probably a structure I clathrate hydrate. If so, then Whalley (28) has estimated that the compressibility should be 1.135 times that of ice Ih. Combined with our data at 130 K, we estimate $g = 2.5$ for phase $\beta$, a value similar to glasses and liquids (8, 31).

*4.3 Phase* $\gamma$

$\lambda(T)$ for phase $\gamma$ was very different from that for phases $\alpha$ and $\beta$, as may be seen by comparing Figs. 2 and 3. The structure of phase $\gamma$ is not known. It is presumably not a clathrate hydrate, on the basis of composition. There was no evidence for "clathrate-like" behaviour from our measurements of $\lambda(T)$. Moreover, as described above, $\lambda$(solid)/$\lambda$(liquid) was much larger for phase $\gamma$ than for phase $\alpha$ or $\beta$, and closer to values found previously (8) in connection with normal crystal phases.

Except for the weak maxima in $\lambda(T)$ near 130 K, we found that for $T \lesssim 160$ K the data shown in Fig. 3 could be approximated with reasonable accuracy by $\lambda \sim T^n$ with $n = -0.8$. As described in section 1, we expect $n = -1$ for a normal crystal phase, where the thermal resistivity arises entirely from three-phonon umklapp processes. At higher temperatures, $\lambda$ gradually became nearly independent of $T$ for phase $\gamma$. This may indicate the effect of some form of structural disorder.

We now consider the weak maximum in $\lambda(T)$, and weak minimum in $\rho c_p(T)$, shown in Fig. 3 at about 130 K. Sandberg and Bäckström (11) observed such behaviour previously, and concluded that it was an artifact of the transient hot-wire method. Specifically in relation to a glass, they argued that at the glass transition the energy of the heat pulse of the hot-wire method would be shared. If such sharing took place between the phonon field and the "hole" field of the glass, the observed peak in $\lambda$ would result. There seems no reason why the "hole" field of the glass could not be generalized to include other thermally-activated structural rearrangements in a crystal. This would be necessary if the explanation advanced by Sandberg and Bäckström (11) is to be applied to phase $\gamma$, where there is no evidence for a glass transition. At $P = 0.55$ GPa, the deviation from near-normal crystal behaviour started at a temperature (160 K) about 30 K higher than the weak maximum in $\lambda(T)$ (130 K). Even if structural disorder began to be activated at about 130 K, $d\lambda/dP$ was about the same above and below this temperature (Fig. 4).

From Fig. 4 and Table 2 it may be deduced that $d \ln \lambda / dP \approx 0.35\ GPa^{-1}$ for phase $\gamma$ in the temperature range 110–150 K. There are no data or estimates for the compressibility of phase $\gamma$, but if we assume the value which has been estimated (33) for ice VI we obtain $g = 4.7$ for phase $\gamma$. This is a larger value of $g$ than for phases $\alpha$ or $\beta$, but still relatively small for a normal crystal phase (8). If structural

Can. J. Chem. Downloaded from www.nrcresearchpress.com by 210.87.254.40 on 09/06/12
For personal use only.

disorder existed in phase γ it would tend to reduce $g$ below a value typical for a normal crystal phase.

*4.4 Phase α′*

The evidence we found for a transition from phase α at 1.1 GPa and 130 K was described in section 3.2.4. The temperature dependence of λ for phase α′, shown in Fig. 6, suggests that it may be a clathrate hydrate. If so, it presumably arises from a densification of the host lattice of the structure II clathrate hydrate, perhaps by a rearrangement analogous to the formation of the high pressure ices (24). No precedent for this suggestion is known from previous studies of clathrate hydrates (2).

*4.5 Astrophysical implications*

We would like to mention briefly that our results may have astrophysical implications. Low-density satellites, such as Ganymede and Callisto, are considered to be icy bodies. Structural models of these satellites (34) depend to some degree on calculations of heat flow. One such calculation (35) took into account preliminary laboratory data for λ of high pressure ice modifications, but not more recent results (23, 25). If significant quantities of a clathrate hydrate were present, as might perhaps be the case for Titan (35), our results suggest that heat-flow calculations would be significantly affected. For example, if we take $\lambda(\text{clathrate}) \approx \frac{1}{2}$ W $m^{-1}$ $K^{-1}$, then $\lambda(\text{ice Ih})/\lambda(\text{clathrate}) \approx 5$ at 250 K and ≈ 15 at 100 K.

## 5. Conclusions

The structure II clathrate hydrate, phase α, has been found to have a thermal conductivity λ similar to that of other glass-like crystalline solids. The temperature dependence of λ indicated that rotational vibrations of THF guest molecules were probably closely connected with the thermal resistivity. If so, such vibrations provide a specific example of a low-energy excitation affecting the thermal properties of a glass-like solid (15). The thermal resistivity was relatively insensitive to density.

Phase β was probably a structure I clathrate hydrate, stable only under pressure. The thermal properties of phase β were similar to those of phase α.

There was no evidence that phase γ was a clathrate hydrate. The thermal properties of this phase indicated that three-phonon umklapp processes were the main mechanism for thermal resistivity at low temperatures. Near melting, the thermal resistivity became nearly independent of temperature, which was perhaps connected with structural disorder.

There was evidence that, on pressurization at 130 K, phase α transformed at 1.1 GPa to a metastable modification of the same composition (phase α′). Phase α′ showed characteristics which indicated that it was probably a clathrate hydrate. If so, it must be considered to be a new high-density form of clathrate hydrate, perhaps involving a host structure having some similarities to high pressure ice modifications.

## Acknowledgments

This work was supported by the Swedish Natural Science Research Council. We are grateful to Dr. D. W. Davidson of the National Research Council of Canada for suggesting this investigation.

1. N. G. Parsonage and L. A. K. Staveley. Disorder in crystals. Clarendon Press, Oxford. 1978.
2. D. W. Davidson. *In* Water: a comprehensive treatise. Vol. 2. *Edited by* F. Franks. Plenum, New York. 1973. pp. 115–234.
3. J. E. Bertie and S. M. Jacobs. J. Chem. Phys. **69**, 4105 (1978).
4. Yu. A. Dyadin, P. N. Kuznetsov, I. I. Yakovlev, and A. V. Pyrinova. Dokl. Chem. **208**, 9 (1973).
5. D. F. Sargent and L. D. Calvert. J. Phys. Chem. **70**, 2689 (1966).
6. S. R. Gough and D. W. Davidson. Can. J. Chem. **49**, 2691 (1971).
7. J. E. Parrott and A. D. Stuckes. Thermal conductivity of solids. Pion, London. 1975.
8. G. A. Slack. *In* Solid state physics. Vol. 34. *Edited by* H. Ehrenreich, F. Seitz, and D. Turnbull. Academic Press, New York. 1979. pp. 1–71.
9. M. Roufosse and P. G. Klemens. Phys. Rev. B**7**, 5379 (1973).
10. R. G. Ross, P. Andersson, and G. Bäckström. Mol. Phys. **38**, 377 (1979).
11. O. Sandberg and G. Bäckström. J. Pol. Sci.: Pol. Phys. Ed. **18**, 2123 (1980).
12. D. P. Jones, N. Thomas, and W. A. Phillips. Philos. Mag. B**38**, 271 (1978).
13. W. Dietsche and H. Kinder. Phys. Rev. Lett. **43**, 1413 (1979).
14. A. R. Long, A. F. Cattell, and A. M. MacLeod. J. Non-cryst. Solids, **35/36**, 1149 (1980).
15. D. A. Ackerman, D. Moy, R. C. Potter, A. C. Anderson, and W. N. Lawless. Phys. Rev. B**23**, 3886 (1981).
16. G. A. Slack. Phys. Rev. **134**, A1268 (1964).
17. Y. Suemune. J. Phys. Soc. Jpn. **19**, 2234 (1964).
18. G. A. Slack, D. W. Oliver, G. D. Brower, and J. D. Young. J. Phys. Chem. Solids, **38**, 45 (1977).
19. R. G. Ross, P. Andersson, and G. Bäckström. Nature, **290**, 322 (1981).
20. R. G. Ross and P. Andersson. Mol. Cryst. Liq. Cryst. **69**, 145 (1981).
21. W. Hayduk, H. Laudie, and O. H. Smith. J. Chem. Eng. Data, **18**, 373 (1973).
22. B. V. Lebedev, I. B. Rabinovich, V. I. Milov, and V. Ya. Lityagov. J. Chem. Thermodyn. **10**, 321 (1978).
23. R. G. Ross, P. Andersson, and G. Bäckström. J. Chem. Phys. **68**, 3967 (1978).
24. P. V. Hobbs. Ice physics. Clarendon Press, Oxford. 1974.

25. R. G. Ross, P. ANDERSSON, and G. BÄCKSTRÖM. High temp. High Pressures, **9**, 87 (1977).
26. R. D. STOLL and G. M. BRYAN. J. Geophys. Res. **84**, 1629 (1979).
27. J. A. REISSLAND. The physics of phonons. Wiley, London. 1973.
28. E. WHALLEY. J. Geophys. Res. **85**, 2539 (1980).
29. A. J. GOW and T. C. WILLIAMSON. J. Geophys. Res. **77**, 6348 (1972).
30. J. WIGREN and P. ANDERSSON. Mol. Cryst. Liq. Cryst. **59**, 137 (1980).
31. O. SANDBERG. Ph. D. thesis. University of Umeå, Sweden. 1980.
32. G. A. SLACK. Phys. Rev. B**22**, 3065 (1980).
33. G. P. JOHARI and E. WHALLEY. J. Chem. Phys. **64**, 4484 (1976).
34. E. M. PARMENTIER and J. W. HEAD. J. Geophys. Res. **84**, 6263 (1979).
35. M. J. LUPO and J. S. LEWIS. Icarus, **40**, 157 (1979).

Can. J. Chem. Downloaded from www.nrcresearchpress.com by 210.87.254.40 on 09/06/12
For personal use only.

# A kinetic and surface study of the oxidation of ethane by nitrous oxide and by oxygen over manganese(III) oxide

CRAIG FAIRBRIDGE[1]

*Department of Chemistry, Lakehead University, Thunder Bay, Ont., Canada P7B 5E1*

AND

ROBERT ANDERSON ROSS

*Alcan International Limited, Kingston Laboratories, Box 8400, Kingston, Ont., Canada K7L 4Z4*

Received August 13, 1981

CRAIG FAIRBRIDGE and ROBERT ANDERSON ROSS. Can. J. Chem. **60**, 893 (1982).

The kinetics of the nitrous oxide/ethane and oxygen/ethane reactions on manganese(III) oxide have been studied from 573 to 673 K and from 523 to 593 K, respectively. The apparent activation energy for carbon dioxide formation was $130 \pm 4$ kJ mol$^{-1}$ in both reactions while that for nitrogen formation in the nitrous oxide/ethane reaction changed from $106 \pm 4$ kJ mol$^{-1}$, 573–613 K, to $133 \pm 4$ kJ mol$^{-1}$, 623–673 K. The kinetic results for both reactions fit the same rate equation:

$$r = \frac{kap_{C_2H_6}bp_x}{(1 + ap_{C_2H_6} + bp_x)^2} \cdot (p_{C_2H_6}p_x)$$

where $p_x$ represents either $p_{N_2O}$ or $p_{O_2}$. The rate-controlling step has been associated with the interaction of adsorbed species on the catalyst surface while both ethane and the oxidising gas appear to be directly involved in further steps in the mechanism. Samples were analysed routinely by scanning electron microscopy, X-ray powder diffraction, and infrared spectroscopy. Electron spectroscopy results from samples treated in various ways with hydrocarbon/oxidant mixtures gave O(1*s*) values from 528.7 to 529.7 eV which are indicative of binding energies usually associated with chemisorbed oxygen. No N(1*s*) spectrum was obtained from catalysts exposed to hydrocarbon/nitrous oxide mixtures, in agreement with the absence of bands in the infrared which are usually associated with nitrates or nitrogen/oxygen complexes. A binding energy value of 406.5 eV was measured in the comparable N(1*s*) spectrum of a catalyst used at 623 K for the oxidation of ethane by nitric oxide — a result which confirms conclusions from previous surface studies on the same system using infrared spectroscopy.

CRAIG FAIRBRIDGE et ROBERT ANDERSON ROSS. Can. J. Chem. **60**, 893 (1982).

La cinétique des réactions entre le protoxyde d'azote et l'ethane et entre l'oxygène et l'éthane a été étudiée sur l'oxyde de manganèse (III) à 573 jusqu'à 593 K respectivement. La valeur de l'énergie apparente d'activation du dioxyde de carbone était $130 \pm 4$ kJ mol$^{-1}$ dans les deux réactions, pendant que la valeur originelle de $106 \pm 4$ kJ mol$^{-1}$, 573–613 K, pour la formation de l'azote dans la réaction du protoxyde d'azote avec l'éthane augmentait à $133 \pm 4$ kJ mol$^{-1}$, 623–673 K. Les valeurs cinétiques pour les deux réactions s'accordent avec la même équation de vitesse:

$$r = \frac{kap_{C_2H_6}bp_x}{(1 + ap_{C_2H_6} + bp_x)^2} \cdot (p_{C_2H_6}p_x)$$

dans laquelle $p_x$ représente $p_{N_2O}$ ou $p_{O_2}$. Le procédé du contrôle de vitesse semble être lié avec l'interaction des éléments adsorbés sur la surface catalytique; mais l'influence directe de l'éthane aussi que celle du gaz oxydant apparément ne se manifeste que pendant les étapes suivantes du mécanisme. Un microscope électronique explorant, la diffraction de rayons X des poudres et la spéctroscopie infrarouge ont été utilizés dans une analyse courante des échantillons. Les résultats d'une analyse par la spéctroscopie électronique obtenus pour des échantillons traîtés de diverses manières par des mélanges des carbures d'hydrogène et d'un agent oxydant représentent les valeurs O(1*s*) de 528.7 à 529.7 eV, caractéristiques pour les énergies de liaison normalement associées avec l'oxygène absorbé chimiquement. Des catalyseurs exposés aux mélanages de la carbure d'hydrogène et du protoxyde d'azote ne produisaient pas de spêctre N(1*s*) et cela s'accorde avec l'absence des bandes normalement associées avec les nitrates ou les complexes nitrogène–oxygène en analyse par la spéctroscopie infrarouge. La valeur de l'énergie de liaison de 406.5 eV était obtenue en mesurant un spectre N(1*s*) comparable d'un catalyseur utilisé pendant l'oxydation de l'éthane par l'oxyde nitrique à 623 K cette valeur est en accord avec les résultats des analyses infrarouge executées auparavant à l'étude des surfaces d'un système identique.

## Introduction

In previous, related studies the kinetics of the nitrous oxide/carbon monoxide reaction were evaluated on several transition metal oxides (1–5) and the reaction mechanism held to involve the adsorption and reaction of carbon monoxide with surface oxygen followed by the formation of a surface carbonate. In a similar way, investigations of the water–gas shift reaction over manganese(II) oxide led to the proposal that the rate-controlling step was associated with the reducing action of adsorbed carbon monoxide on a surface oxygen species (6). Further, the decomposition of nitrous oxide on manganese oxides has been explained by a redox-

[1]Present address: Energy Research Laboratories, Energy Mines and Resources Canada, 555 Booth Street, Ottawa, Ont., Canada K1A 0G1.

0008-4042/82/070893-05$01.00/0

©1982 National Research Council of Canada/Conseil national de recherches du Canada

Can. J. Chem. Downloaded from www.nrcresearchpress.com by 210.87.254.6 on 09/06/12
For personal use only.

Can. J. Chem. Downloaded from www.nrcresearchpress.com by 210.87.254.6 on 09/06/12
For personal use only.

type mechanism which would be enhanced by conditions which preserve the 3+ oxidation state of the metal (7).

Those features of the surface chemical properties of manganese oxides which appeared to contribute to catalysis were most recently investigated in a kinetic study of the reaction of nitric oxide with ethane over manganese(III) oxide (8). A contiguous investigation of the oxidation of ethane by both oxygen and nitrous oxide is reported here with the experimental rate data supplemented by structure analysis including the results of electron spectroscopic measurements on selected catalyst samples.

## Experimental

*Apparatus and procedure*

A quartz reactor and Pyrex flow system (9) were used for the kinetic studies in conjunction with a Hewlett-Packard Research Chromatograph Model 5754B. Nitrogen, oxygen, carbon dioxide, nitrous oxide, ethane, and water were analysed by a thermal conductivity bridge using stainless steel columns 244 × 0.32 cm od packed with 61 cm Carbosieve B and 183 cm Poropak T. The column oven was temperature programmed with a 2 min post-injection interval at 353 K followed by a 60 K $min^{-1}$ rise to 443 K where the temperature was maintained for 5 min prior to recycling.

Surface areas were determined by application of the BET theory to low-temperature krypton adsorption (77 K, $\sigma$ = 21.5 Å$^2$).

The experimental conditions for which reaction rates were not influenced by internal or external diffusion were determined in the usual way by altering space velocity, catalyst mass, and particle size (10). Hence, kinetic measurements were conducted at a total flow rate of 350 $dm^3$ $min^{-1}$ (NTP) on 1.0 g catalyst samples, <37 μm maximum diameter with surface area 15.5 $m^2$ $g^{-1}$, and were recorded as the rate of nitrogen or carbon dioxide production after steady catalyst activity had been attained and at less than 15% total conversion to products. The temperature regions adopted for kinetic measurements were defined at the high end by the maximum of 15% conversion and at the low end by the reasonable limits of detection of nitrogen and carbon dioxide on the gas chromatograph, $>10^{-4}$ mol $L^{-1}$. The only products observed were nitrogen, carbon dioxide, and water in the nitrous oxide/ethane reaction, and carbon dioxide and water in the oxygen/ethane reaction. Because of the tailing involved in the water peak in the chromatogram, the area under the peak, and hence the water concentration, could not be estimated with acceptable accuracy.

Infrared spectra were obtained using KBr pellets (0.5% w/w) with a Beckman IR-12 Spectrophotometer.

X-ray photoelectron spectra were obtained on a Vacuum Generator Limited ESCA-3 spectrometer using Al $K_\alpha$ radiation. A 50 eV electron analyzer pass energy was used. Samples were run as powders, mounted on double-sided tape and the spectra were corrected for charging by reference to the C(1*s*) line at 284.0 eV.

*Materials*

Manganese(III) oxide was prepared and analysed as described previously (11). No change in the nature of the catalyst was observed from XRD, scanning electron microscopy, chemical analysis, or surface area measurements after reaction.

Ethane (99.0%) and oxygen (99.99%) were supplied by Matheson of Canada Ltd. Carbon dioxide (99.5%), nitrogen (99.99%), and helium (99.995%) were obtained from Canadian Liquid Air Ltd. and nitrous oxide (99.9%) from Liquid Carbonic Ltd. The water in the gas saturators was distilled and de-ionized prior to use.

## Results

*Reaction rate orders*

Rate order measurements based upon the rates of nitrogen, $r_1$, or carbon dioxide, $r_2$, formation were determined at 623 K for the $N_2O/C_2H_6$ reaction and at 573 K for the $O_2/C_2H_6$ reaction.

*Nitrous oxide/ethane*

With the partial pressure of ethane held constant at 2.66 kPa, the effects of the partial pressure of nitrous oxide on $r_1$ and $r_2$ were observed and the results plotted as ln (rate) against ln (partial pressure), Fig. 1. A reaction rate order of 0.8 was obtained with respect to nitrous oxide partial pressure from 0.665 to 5.32 kPa.

The effects of variations in ethane partial pressure were observed with the partial pressure of nitrous oxide held at 2.66 kPa. A reaction rate order of 0.7 was obtained from 0.665 to 3.325 kPa and, as indicated in Fig. 1, a rate order of 0.2 was determined from 3.325 to 5.32 kPa.

With both ethane and nitrous oxide partial pressures held constant at 2.66 kPa, the effects on the rates of the partial pressures of the products, nitrogen and carbon dioxide, were observed from 0.333 to 5.32 kPa. In both cases, the reaction rate order was zero. Similarly, the addition of from 0.04 to 1.5 kPa of water vapour had no effect upon the reaction rates.

The experimental rate of reaction was therefore represented by the expressions:

$$[1] \quad r = k p_{N_2O}^{0.8} p_{C_2H_6}^{0.7}$$

for $0.665 < p_{C_2H_6} < 3.325$ kPa and

$$[2] \quad r = k p_{N_2O}^{0.8} p_{C_2H_6}^{0.2}$$

for $3.325 < p_{C_2H_6} < 5.32$ kPa where $r$ and $k$ represent either $r_1$ and $k_1$ or $r_2$ and $k_2$.

*Oxygen/ethane*

The dependence of the reaction rate, $r_2$, on variations in the oxygen partial pressure from 0.665 to 5.32 kPa was examined with ethane partial pressure maintained at 2.66 kPa. At 573 K, a reaction rate order of 0.5 was obtained, Fig. 1. With the partial pressure of oxygen held at 2.66 kPa, the rate order with respect to ethane partial pressure was 0.6 from 0.665 to 2.66 kPa and 0.85 from 2.66 to 5.32 kPa. The experimental reaction rate was not affected by variations in the carbon dioxide or water vapour partial pressures as in the nitrous

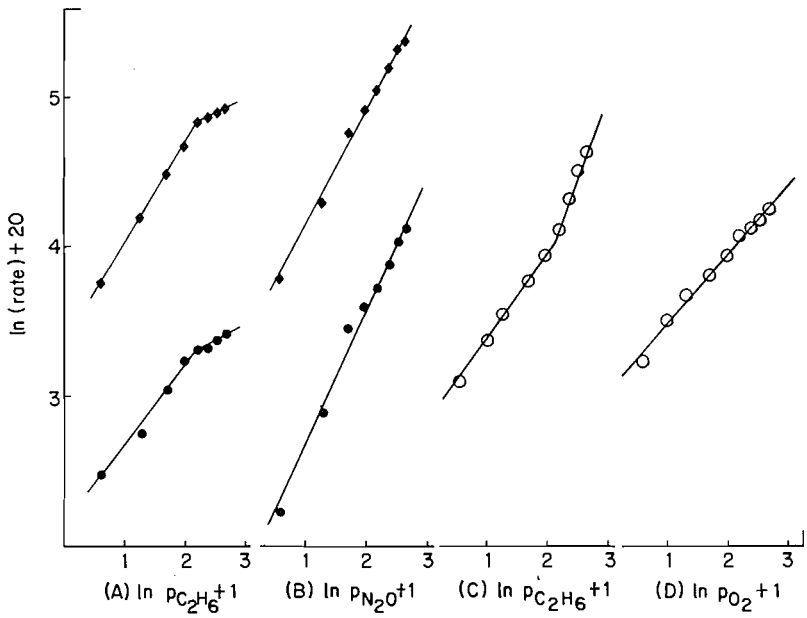


FIG. 1. Nitrogen (◆) and carbon dioxide (● in *A* and *B*, ○ in *C* and *D*) rate dependency on variations in the partial pressure of ethane (*A*) and nitrous oxide (*B*) in the $N_2O/C_2H_6$ catalytic reaction over $Mn_2O_3$ at 623 K; and ethane (*C*) and oxygen (*D*) in the $O_2/C_2H_6$ reaction at 573 K.

oxide/ethane reaction. The experimental reaction rate was therefore expressed as:

$$[3] \quad r_2' = k_2' p_{O_2}^{0.5} p_{C_2H_6}^{0.6}$$

where $0.665 < p_{C_2H_6} < 2.66$ kPa and

$$[4] \quad r_2' = k_2' p_{O_2}^{0.5} p_{C_2H_6}^{0.85}$$

where $2.66 < p_{C_2H_6} < 5.32$ kPa.

*Temperature effects*

*Nitrous oxide/ethane*

Steady catalytic activity was obtained after 2 h exposure to the standard mixture of 2.66 kPa each of nitrous oxide and ethane at 673 K. Reaction rate constants were calculated by integration of the rate equation [1] as a function of concentration from 673 to 573 K. Two apparent activation energies were obtained using $r_1$, namely 133 ± 4 kJ mol$^{-1}$ from 673 to 623 K and 106 ± 4 kJ mol$^{-1}$ from 613 to 573 K, Fig. 2. The pre-exponential factors were $6.35 \times 10^8$ and $3.27 \times 10^6$ mol L m$^{-2}$ s$^{-1}$, respectively.

*Oxygen/ethane*

After catalyst pretreatment with 2.66 kPa oxygen and 2.13 kPa ethane at 593 K for 3 h, the rate of carbon dioxide formation was determined from 593 to 523 K at 10 K intervals. Rate constants were calculated from the integrated form of eq. [3] and plotted in the Arrhenius fashion, Fig. 2. The results lay on the same straight line as those for the rate of carbon dioxide formation in the nitrous oxide/ethane reaction. The apparent activation energy was 130 ± 4 kJ mol$^{-1}$ and the pre-exponential factor, $9.72 \times 10^7$ mol L m$^{-2}$ s$^{-1}$.

*Infrared spectra*

The infrared spectra of the catalysts after reaction with nitrous oxide/ethane or oxygen/ethane were similar to those observed previously for samples of manganese(III) oxide after catalysis in the nitric oxide/ethane reaction (8). However, a major difference was the absence of any nitrate bands in the spectra. Peaks were noted at 615(s), 490(s), 425(m), and 350(m) cm$^{-1}$ which may possibly suggest the presence of some $Mn_3O_4$ phase as a surface trace since both chemical analysis and XRD indicated no apparent change from the original $Mn_2O_3$ composition.

*X-ray photoelectron spectroscopy*

O(1*s*) spectra on the fresh, unreacted manganese oxide gave a binding energy value of 528.7 eV. Samples exposed to 2.66 kPa each of ethane and nitrous oxide from 573 to 673 K in a kinetic temperature cycle gave an O(1*s*) value of 529.0 eV while 529.5 eV was obtained for the binding energy in a catalyst sample after exposure to the standard mixture of ethane and oxygen in a cycle from 523 to 593 K. All of these energy values are close to that expected for chemisorbed oxygen in metal oxides

Can. J. Chem. Downloaded from www.nrcresearchpress.com by 210.87.254.6 on 09/06/12
For personal use only.

Can. J. Chem. Downloaded from www.nrcresearchpress.com by 210.87.254.6 on 09/06/12
For personal use only.

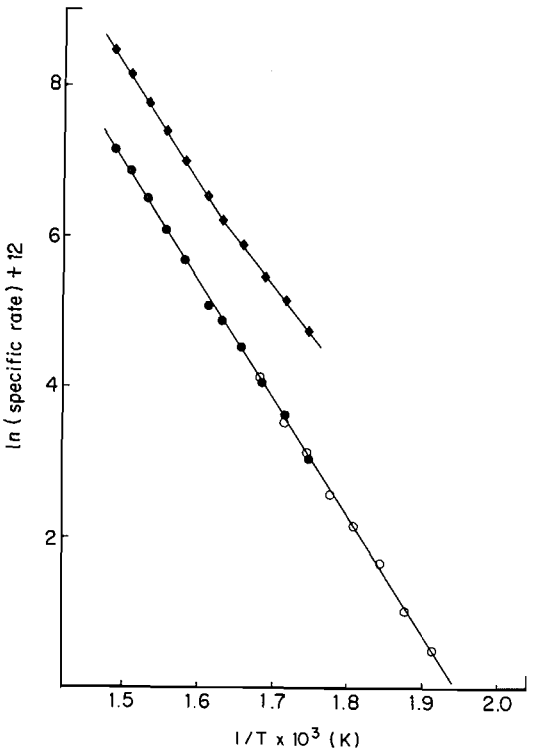


FIG. 2. Arrhenius plots for the $N_2O/C_2H_6$ (◆, $r_1$; ●, $r_2$) and $O_2/C_2H_6$ (○, $r_2$) catalytic reactions over $Mn_2O_3$.

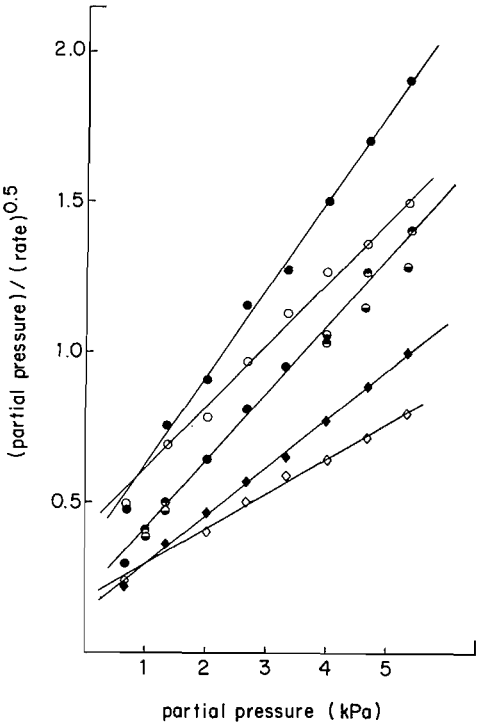


FIG. 3. Reduced plots corresponding to eq. [5] for the nitrous oxide (◇, $r_1$; ○, $r_2$) and ethane (◆, $r_1$; ●, $r_2$) rate orders in the $N_2O/C_2H_6$ reaction; and for the oxygen (◓, $r_2$) and ethane (◒, $r_2$) rate orders in the $O_2/C_2H_6$ reaction over $Mn_2O_3$.

and significantly less than an O(1*s*) value of 532–533 eV which usually characterises the presence of molecular oxygen (12).

Only two of the catalyst samples tested gave N(1*s*) spectra. Catalyst exposed to 2.66 kPa each of ethane and nitric oxide at 623 K, steady state, gave a binding energy of 406.5 eV and a sample used in a cycle from 573 to 673 K with the same gases before cooling to room temperature gave an N(1*s*) value of 406.4 eV.

Manganese(IV) oxide was not detected in any sample and it is difficult to distinguish between manganese(II) and manganese(III) oxides using this technique solely because the Mn/O intensities are similar in the two oxides (13). X-ray diffraction and chemical analysis confirmed that the metal was present as $Mn_2O_3$ in all bulk samples.

## Discussion

Several plausible mechanistic schemes were evaluated by computer tests of the rate order results in many kinetic expressions related mainly to the Langmuir–Hinshelwood model (14, 15). The significance of such statistical criteria in the evaluation of the step-by-step nature of the catalytic process has been frequently analysed (16–18) and recently reviewed (19). The approach has been adopted here to obtain a broad guide to the interpretation of the kinetic results.

Only one kinetic expression clearly accommodated the rate order data. It was the same for both reactions:

$$[5]\quad r = \frac{kap_{C_2H_6}bp_x}{(1 + ap_{C_2H_6} + bp_x)^2}(p_{C_2H_6}p_x)$$

where $p_x$ represents the partial pressure of nitrous oxide or oxygen and $a$ and $b$ are adsorption coefficients. As shown in Fig. 3, plots of $p/r^{0.5}$ versus $p$ were linear for both nitrogen and carbon dioxide rate order results in the nitrous oxide/ethane reaction and for the carbon dioxide results in the oxygen/ethane reaction. A similar kinetic expression was evaluated previously for the nitric oxide/ethane reaction (8). It may be interpreted to represent an irreversible bimolecular reaction between reactive species adsorbed on the same type of site (20). The reaction rate is proportional to the probability that the reactants are adsorbed on neighbouring sites, and thus also proportional to the product of the fraction of surface covered by each reactant, $\theta_{C_2H_6}$ and $\theta_{N_2O}$ or $\theta_{O_2}$. The $(p_{C_2H_6}p_x)$ multiplier term in eq. [5] suggests that additional

Can. J. Chem. Downloaded from www.nrcresearchpress.com by 210.87.254.6 on 09/06/12
For personal use only.

interactions involve nitrous oxide and ethane or oxygen and ethane in the appropriate reaction.

On a test/reject basis (6), surface mechanisms consistent with eq. [5] were formulated:

*Nitrous oxide/ethane*

[6] $N_2O_{(g)} = N_2O_{(ads)}$

[7] $C_2H_{6(g)} = C_2H_{6(ads)}$

[8] $C_2H_{6(ads)} + N_2O_{(ads)} + [O] \rightarrow C_2H_{5(ads)} + [OOH] + N_2$

[9] $C_2H_6 + [OOH] \rightarrow H_2O + C_2H_{5(ads)} + [O]$

[10] $2C_2H_{5(ads)} + 13N_2O \rightarrow 4CO_2 + 5H_2O + 13N_2$

with an overall stoichiometry:

[11] $C_2H_6 + 7N_2O \rightarrow 2CO_2 + 3H_2O + 7N_2$

*Oxygen/ethane*

[12] $O_{2(g)} = O_{2(ads)}$

[13] $C_2H_{6(g)} = C_2H_{6(ads)}$

[14] $C_2H_{6(ads)} + O_{2(ads)} + [\ ] \rightarrow C_2H_{5(ads)} + [OOH]$

[15] $C_2H_6 + [OOH] \rightarrow H_2O + C_2H_{5(ads)} + [O]$

[16] $2C_2H_{5(ads)} + [O] + 6O_2 \rightarrow 4CO_2 + 5H_2O + [\ ]$

with an overall stoichiometry:

[17] $2C_2H_6 + 7O_2 \rightarrow 4CO_2 + 6H_2O$

Previous studies of ethane oxidation over nickel(II) oxide have indicated that the hydrocarbon was adsorbed prior to surface reaction with preadsorbed oxygen while chemisorption of ethane on iron(III) and nickel(II) oxides was shown to involve C—H bond rupture to give a $C_2H_{5(ads)}$ species (21). The rate-determining step in the oxidation of ethane over nickel(II) oxide was thought to be either the adsorption of ethane as a $C_2H_5$ radical or the interaction of adsorbed oxygen with gas phase or adsorbed ethane through attack at the C—H bond (22). In the homogeneous oxidation of ethane by oxygen the formation of $C_2H_5$ and $HO_2$ radicals was postulated as the initial step (23); indeed, peroxide species are often formed in gas phase hydrocarbon oxidation reactions.

It seems likely then that the rate-limiting step in the oxidation of ethane over manganese(III) oxide involves the formation of an adsorbed $C_2H_5$ species, which may occur through the interaction of adsorbed ethane with adsorbed nitrous oxide or oxygen, eqs. [8] or [14]; or through the action of a surface peroxide radical on gas phase or weakly adsorbed ethane, eqs. [9] or [15].

The apparent activation energies are in good agreement with those determined for the nitrous oxide/carbon monoxide reaction, 493 to 573 K (3), the decomposition of isopropyl alcohol, 483 to 638 K (11), and the dehydration of formic acid, 523 to 573 K (24), all over similar manganese oxide catalysts. These reactions, together with the water–gas shift reaction (6), all appear to involve both $Mn^{2+}$ and $Mn^{3+}$ reactive surface species in the catalytic cycle. The same species may also occur in the present reactions, as well as in the oxidation of ethane by nitric oxide (8).

**Acknowledgements**

We are pleased to thank the Natural Sciences and Engineering Research Council, Ottawa and Imperial Oil Limited, Sarnia for financial support and Dr. David K. Creber and Mr. Robert Lazier for supplying the ESCA spectra.

1. B. W. KRUPAY and R. A. Ross. J. Catal. **50**, 220 (1978).
2. B. W. KRUPAY and R. A. Ross. Z. Physik. Chem. Neue Folge. **106**, 83 (1977).
3. B. W. KRUPAY and R. A. Ross. Can. J. Chem. **56**, 10 (1978).
4. B. W. KRUPAY and R. A. Ross. Can. J. Chem. **56**, 2447 (1978).
5. B. W. KRUPAY and R. A. Ross. Can. J. Chem. **57**, 718 (1979).
6. B. W. KRUPAY and R. A. Ross. Can. J. Chem. **51**, 3520 (1973).
7. A. CIMINO and V. INDOVINA. J. Catal. **17**, 54 (1970).
8. R. A. ROSS and C. FAIRBRIDGE. Can. J. Chem. **59**, 2232 (1981).
9. D. V. FIKIS, W. J. MURPHY, and R. A. Ross. Can. J. Chem. **56**, 2530 (1978).
10. C. N. SATTERFIELD. Mass transfer in heterogeneous catalysis. M.I.T. Press. 1970.
11. E. F. MCCAFFREY, D. G. KLISSURSKI, and R. A. Ross. J. Catal. **26**, 380 (1972); Can. J. Chem. **49**, 3778 (1971).
12. M. W. ROBERTS. Adv. Catal. **29**, 55 (1980).
13. J. C. CARVER, G. K. SCHWERTZER, and T. A. CARLSON. J. Chem. Phys. **57**, 573 (1972).
14. K. H. YANG and O. A. HOUGEN. Chem. Eng. Prog. **46**, 146 (1950).
15. O. A. HOUGEN and K. M. WATSON. Chemical process principles. Part III. Wiley, New York and London. 1966.
16. M. BOUDART. A.I.Ch.E.J. **2**, 62 (1956).
17. S. W. WELLER. Chemical reaction engineering reviews. *Edited by* H. M. Hulbert. Am. Chem. Soc., Washington, D.C. (1975).
18. L. BERÁNEK. Catal. Rev. Sci. Eng. **16**, 1 (1977).
19. R. W. MAATMAN. Adv. Catal. **29**, 97 (1980).
20. P. H. EMMETT (*Editor*). Catalysis. Vol. V. Reinhold, New York. 1954.
21. W. J. THOMAS. Trans. Faraday Soc. **53**, 1124 (1957); **55**, 624 (1959).
22. Y-F. YU YAO and J. T. KUMMER. J. Catal. **28**, 124 (1973).
23. R. I. MOSHKINA, S. S. POLYAK, N. A. SOKOLOVA, I. F. MASTEROVOI, and A. B. NALBANOYAN. Int. J. Chem. Kin. **XII**, 315 (1980).
24. B. W. KRUPAY and R. A. Ross. J. Catal. **39**, 369 (1975).

# Développement d'un détecteur à plasma micro-onde pour chromatographie en phase gazeuse

GILLES CHEVRIER, TOSHIHIKO HANAI, KHANH-CHI TRAN ET JOSEPH HUBERT[1]

*Département de chimie, Université de Montréal, C.P. 6210, Succ. A, Montréal (Qué.), Canada H3C 3V1*

Reçu le 20 novembre 1981

GILLES CHEVRIER, TOSHIHIKO HANAI, KHANH-CHI TRAN et JOSEPH HUBERT. Can. J. Chem. **60**, 898 (1982).

Le développement d'un détecteur à émission atomique comme détecteur de chromatographie en phase gazeuse a été décrit. Un plasma micro-onde d'hélium à pression atmosphérique généré à l'aide d'un dispositif appelé Surfatron a été utilisé comme source d'atomisation et d'excitation. Les caractéristiques d'opération de ce détecteur ont été définies et ses performances analytiques pour l'analyse du carbone, chlore, brome et iode ont été déterminées. Des limites de détection de l'ordre du pg/s ont été obtenues et les domaines de linéarité du détecteur couplé à une colonne en silice s'étendent sur trois ordres de grandeur en concentration.

GILLES CHEVRIER, TOSHIHIKO HANAI, KHANH-CHI TRAN, and JOSEPH HUBERT. Can. J. Chem. **60**, 898 (1982).

The development of an atomic emission detector for gas chromatography is described. An atmospheric pressure microwave helium plasma generated with an original device called Surfatron was used as an atomization and excitation source. The characteristics of operation are defined and the analytical performances for carbon, chlorine, bromine, and iodine analyses are measured. Detection limits are in the order of pg/s and the dynamic range of the detector covers three orders of magnitude.

## Introduction

La grande complexité d'échantillons d'origine environnementale ou biologique associée au développement de colonnes chromatographiques à très grande résolution a nécessité le développement de nouveaux détecteurs sélectifs en chromatographie en phase gazeuse. Plusieurs détecteurs sélectifs ont été développés et utilisés, leur principale limitation vient de leur manque de flexibilité: seul un nombre restreint d'éléments sont détectables et la détection d'un autre élément nécessite souvent l'achat d'un autre détecteur.

Un détecteur qui ne possède pas ces limitations a été décrit par McCormack *et al.* (1). Ce détecteur est basé sur la spectroscopie d'émission atomique et la source d'atomisation et d'excitation est un plasma d'argon induit par micro-onde. Plusieurs auteurs ont étudié des détecteurs similaires en utilisant des plasmas d'argon à diverses pressions ou d'hélium sous pression réduite (2–5). L'étude la plus complète des performances de ce détecteur à plasma sous pression réduite a été faite par Van Dalen *et al.* (6). En 1977, Beenakker (7) a rapporté quelques performances analytiques d'un plasma d'hélium à pression atmosphérique induit par micro-onde à l'aide d'une nouvelle cavité ($TM_{010}$). Les limites de détection obtenues sous conditions non chromatographiques étaient généralement supérieures à celles obtenues précédemment. Le même type de plasma mico-onde a été utilisé par d'autres auteurs (8–12) comme source d'excitation d'un détecteur chromatographique.

Plusieurs problèmes concernant l'opération de ces détecteurs ont été rapportés: la sensibilité du plasma au solvant organique utilisé en chromatographie, le dépôt de carbone sur les tubes de décharge du plasma et le couplage entre la cavité dans laquelle le plasma est généré et le générateur micro-onde.

En 1979, nous avons rapporté le développement d'un nouveau système de génération de plasma micro-onde à pressions réduites et atmosphérique basé sur la propagation d'une onde de surface (13); ce dispositif appelé Surfatron permet d'obtenir des plasmas stables d'argon, d'hélium ou d'azote à pression atmosphérique. Les premières applications comme détecteur de chromatographie ont été rapportées (14).

Dans cet article, les conditions optimales d'utilisation et les performances analytiques de ce détecteur en chromatographie en phase gazeuse sont rapportées pour quatre éléments en termes de limite de détection, sélectivité et domaine de linéarité.

## Partie expérimentale

Le schéma du montage expérimental utilisé est représenté à la figure 1.

1. *Système chromatographique*

Un chromatographe en phase gazeuse (FM Scientific Corporation 810R-15) a été modifié pour l'utilisation d'une colonne capillaire en silice (HP, Phase stationnaire SE-30, 12 m, diamètre intérieur 0,2 mm). L'injecteur a été modifié pour permettre l'injection de tout l'échantillon sur la colonne. A la sortie de la colonne un raccord en T permet d'augmenter le débit d'hélium. L'extrémité de la colonne capillaire est placée à des distances de 2 à 5 mm en arrière du plasma dans le tube à décharge. Un système d'injection continue basé sur l'évaporation d'un produit volatil contenu dans un tube capillaire a été adapté au système chromatographique. Ce système sert à repérer la

[1]Auteur à qui toute correspondance doit sera adressée.

0008-4042/82/070898-06$01.00/0

©1982 National Research Council of Canada/Conseil national de recherches du Canada

Can. J. Chem. Downloaded from www.nrcresearchpress.com by 210.87.254.105 on 09/06/12
For personal use only.

Can. J. Chem. Downloaded from www.nrcresearchpress.com by 210.87.254.105 on 09/06/12
For personal use only.

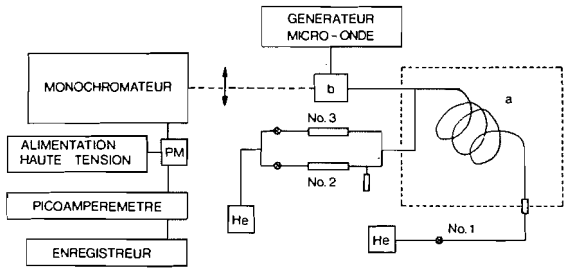


FIG. 1. Schéma du montage expérimental. (a) Colonne capillaire en silice; (b) plasma d'hélium; (c) tube d'évaporation.

longueur d'onde d'émission de l'analyte et à effectuer le travail d'optimisation. Les débits d'hélium dans le chromatographe (≃1 mL/min) (No. 1) et dans le circuits No. 2 et No. 3 (Fig. 1) peuvent être ajustés indépendamment.

2. *Système de détection*

Le Surfatron utilisé, représenté à la figure 2, est refroidi à l'air comprimé sec. Le tube de décharge est constitué de tubes de quartz de différents diamètres internes. Pour la partie chromatographique, on a utilisé un tube de 2,8 mm de diamètre interne et de 6,0 mm de diamètre externe.

Le plasma est amorcé à l'aide d'une bobine Tesla en faisant passer dans le tube de décharge un débit d'hélium d'environ 25 mL/min. La puissance du générateur est ensuite ajustée à 90 W. Le coupleur et la longueur de la cavité sont ajustés de façon à minimiser la puissance réfléchie (≃ 0 W). Il est à souligner que cet ajustement se fait au début et ne change pas durant les manipulations. La longueur d'onde du spectrophotomètre est ajustée en injectant de manière continue un produit volatil par l'intermédiaire du circuit de gaz No. 2 (Fig. 1).

Un générateur à micro-onde Microtron 200, Mark III (Electromedical Supplies, England) capable de produire jusqu'à 200 W de puissance à 2,45 GHz a été utilisé. Le plasma est observé axialement et son image est formée sur la fente d'entrée du monochromateur à l'aide d'une lentille en quartz ($f$ = 10 cm). Un grossissement de 4 a été utilisé. Un monochromateur Spex modèle 1800-2 de 0,75 m de distance focale équipé d'un réseau à 1200 traits/mm "blazé" à 500 nm, un photomultiplicateur Hamamatsu R-446, une alimentation haute tension Hamner (modèle N-4035), un picoampèremètre Keithley (modèle 410) et un enregistreur Brinkmann (modèle 2541) ont été utilisés. Les fentes d'entrée et de sortie étaient fixées à 40 μm.

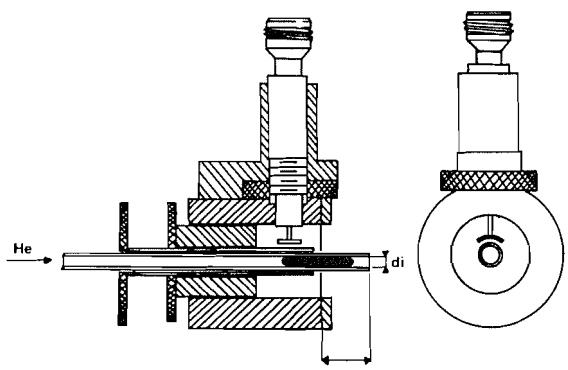


FIG. 2. Schéma du Surfatron.

*Mode opératoire pour l'optimisation du détecteur*

Pour pouvoir étudier l'effet de différents paramètres sur l'intensité du signal analytique, on a placé dans le circuit No. 2 (Fig. 1) un tube capillaire de 1,2 mm de diamètre intérieur et de 10 cm de longueur contenant un composé halogéné ($CCl_4$, $C_6H_5Cl$, $CH_2Br_2$ ou $C_3H_7I$). En faisant passer un débit d'hélium constant au-dessus de ce capillaire, on entraîne une quantité constante d'analyte vers le plasma. Pour un tube à décharge de 2,8 mm de diamètre interne et un débit d'hélium au-dessus du tube capillaire de 17 mL/min, le taux d'évaporation est de 21 nL/min de $CCl_4$ liquide à 19°C. Ceci conduit à une concentration de 0,03% (volume de $CCl_4$ gazeux/volume d'hélium) de $CCl_4$ dans le plasma pour un débit total d'hélium de 17 mL/min. En conservant le débit au-dessus du tube capillaire constant et en faisant varier le débit d'hélium (No. 3, Fig. 1), on fait varier la concentration et le temps de séjour de l'analyte dans le plasma.

Pour déterminer les limites de détection, les domaines de linéarité et les sélectivités, on a injecté 20 nL d'une solution d'un produit contenant l'analyte dans le dodécane. L'ensemble des produits incluant le solvant, passe directement dans le plasma à la sortie de la colonne.

## Résultats et discussion

1. *Optimisation*

Les principaux paramètres qui affectent les performances analytiques du détecteur sont: le débit du gaz plasmagène, la puissance d'opération, le diamètre intérieur ($d_i$) et la position ($l$) du tube à décharge dans le Surfatron (Fig. 2). Pour cette étude, une quantité constante de $CCl_4$ a été entraînée vers le plasma par évaporation sous un débit d'hélium de 17 mL/min et a été mélangée à une quantité variable d'hélium. L'intensité émise par le chlore (479,5 nm) a été mesurée pour diverses conditions expérimentales.

1. a. *Position du tube à décharge*

La position du tube à décharge ($l$, Fig. 2) affecte la stabilité du plasma d'hélium. Les débits minimum limites d'opération du plasma pour une position et une puissance donnée sont rapportés sur la figure 3. Pour une puissance de 90 W, le plasma ne peut pas être entretenu à des débits inférieurs à 40 mL/min, si la longueur $l$ n'est pas au moins de 2 cm. Cette distance peut être plus courte, si l'on augmente le débit. Cet effet n'a pas encore été rapporté lors des études antérieures et il a été établi que l'instabilité du plasma provient de la rétrodiffusion de l'air vers le plasma. Ceci a été mis en évidence par l'augmentation des bandes moléculaires du système $N_2$ lorsqu'on diminue $l$ pour un débit donné ou le débit pour une valeur de $l$ donnée. La rétrodiffusion de l'air change les caractéristiques du plasma, qui devient un plasma mixte hélium–air et par conséquent affecte le couplage entre le plasma et le générateur. Si l'on réajuste le couplage en diminuant le débit d'hélium, on peut conserver un plasma pour un débit d'hélium nul, il s'agira

Can. J. Chem. Downloaded from www.nrcresearchpress.com by 210.87.254.105 on 09/06/12
For personal use only.

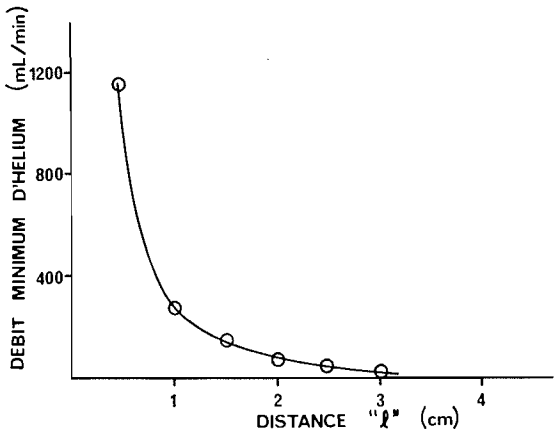


FIG. 3. Stabilité du plasma en fonction de la position du tube à décharge. Puissance: 90 W, $d_i = 2{,}8$ mm.

alors d'un plasma d'air. Par la suite ce paramètre ($l$) a été fixé à 3 cm, ce qui a permis d'opérer à des débits d'hélium de 20 mL/min et plus.

1. b. *Puissance*

La variation du signal net émis par le chlore en fonction de la puissance est rapportée à la figure 4. Pour le domaine de puissance étudié, le fond continu et le bruit ne varient pas. Une augmentation de plus de 50% du signal est obtenu lorsqu'on passe de 100 à 150 W. Une opération du plasma à plus haute puissance améliorera donc la sensibilité et les limites de détection; cependant pour fins de comparaison avec des études antérieures, notre étude a été faite à 90 W. Le même effet a été observé pour le carbone, le brome et l'iode.

1. c. *Débit d'hélium et diamètre du tube à décharge*

L'influence de ces deux paramètres est illustrée sur les figures 5 et 6. Pour un tube à décharge donné, on observe généralement une augmentation rapide, un maximum et une décroissance du signal

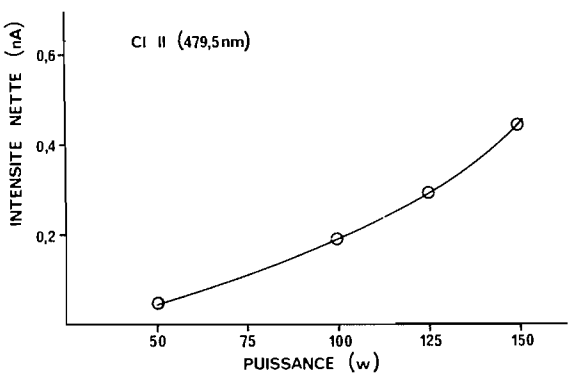


FIG. 4. Effet de la puissance sur le signal net émis par le chlore. $d_i = 2{,}8$ mm, l = 3,0 cm, débit d'hélium 21,5 mL/min.

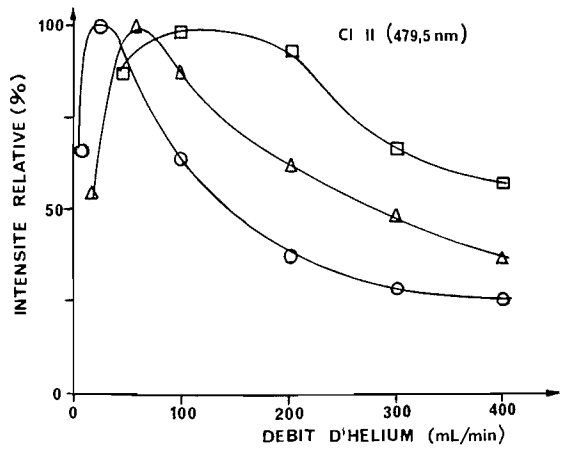


FIG. 5. Effet du débit d'hélium et du diamètre du tube à décharge sur le signal émis par le chlore. ○ $d_i = 1{,}5$ mm; Δ $d_i = 2{,}8$ mm; □ $d_i = 4{,}5$ mm.

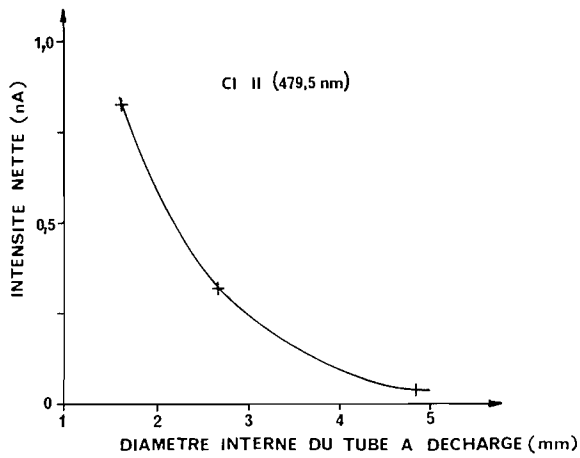


FIG. 6. Effet du diamètre interne du tube à décharge sur l'intensité émise par le chlore.

émis par l'analyte en fonction du débit. A très faibles débits (20 mL/min pour un tube de 3 mm de diamètre interne), le plasma est peu stable et l'excitation est peu efficace. Une augmentation de débit d'une part stabilise le plasma et favorise l'excitation, et d'autre part diminue la concentration en analyte et le temps de séjour de l'analyte dans le plasma. La superposition de ces effets entraîne une augmentation rapide de l'intensité émise, suivie d'une décroissance rapide à forts débits.

Ce comportement se retrouve également pour le carbone et les autres halogènes. Le débit correspondant au maximum d'émission pour le carbone est généralement inférieur à celui des halogènes. Ceci provient probablement du fait que la raie utilisée pour le carbone est une raie atomique facile à exciter.

TABLEAU 1. Limites de détection

| Elément | Raie | Longueur d'onde (nm) | Limite de détection[a] (pg/s) | Limite de détection[b] absolue (pg) |
|---|---|---|---|---|
| C | I | 247,9 | 2–5 | 14–38 |
| Cl | II | 479,5 | 2–4 | 9–124 |
| Br | II | 470,5 | 7–12 | 37–565 |
| I | I | 206,2 | 0,2–2 | 1–12 |

[a]La limite de détection est définie comme la masse d'analyte par unité de temps qui produit un signal égal à 2 fois l'écart-type sur l'intensité du fond continu.
[b]La limite de détection absolue est égale au produit de note [a] par la largeur à la base du pic chromatographique (15).

Lorsqu'on change le diamètre interne du tube à décharge, l'allure globale de la courbe de variation de l'intensité relative émise par l'analyte en fonction du débit demeure la même. On note cependant qu'en diminuant le diamètre du tube de décharge, le maximum est déplacé vers des débits plus faibles et que ce maximum devient plus étroit. Le déplacement du maximum peut être expliqué par la plus grande stabilité du plasma dans un tube à décharge de petit diamètre, donc par une meilleure excitation à faible débit. L'excitation est liée au temps de séjour dans le plasma et une augmentation de débit d'hélium se traduit par une augmentation de la vitesse de passage de l'analyte dans le plasma. Pour un tube à décharge de faible diamètre la vitesse du gaz qui produit une émission maximale est de l'ordre de 20 cm/s ($d_i$ = 1,55 mm, débit de 25 mL/min) et on retrouve sensiblement la même vitesse pour le maximum observé avec un tube de plus grand diamètre ($d_i$ = 2,8 mm, débit de 75 mL/min). Pour le tube de petit diamètre, une augmentation de débit de 5 mL/min au voisinage du maximum se traduit par une augmentation de vitesse de plus de 18% et donc par une diminution du temps de séjour. La même variation de débit pour un tube de plus grand diamètre (2,8 mm) se traduit par une augmentation de vitesse de 1%. Cette faible diminution explique la plus grande largeur du maximum observé pour ce tube à décharge. L'importance du temps de séjour a également été mise en évidence en enregistrant les variations d'intensité du signal du carbone présent sous forme d'impuretés dans l'hélium ordinaire en fonction du débit d'hélium. Un maximum d'émission a été observé vers 75 mL/min ($d_i$ = 3 mm), ce qui correspond à des vitesses de l'ordre de 15 cm/s.

Sur la figure 6, on a représenté la variation de l'intensité nette mesurée au maximum d'émission pour divers tubes à décharge à 90 W. On constate que l'utilisation d'un tube à décharge plus petit permet d'obtenir une intensité plus forte avec un fond continu et un bruit constant. Cependant la durée de vie du tube à décharge diminue et par la suite nous avons utilisé un tube à décharge de 2,8 mm de diamètre pour nous permettre de faire l'ensemble des mesures avec le même tube.

Le même type de comportement a été observé lorsqu'on injecte le même échantillon dans le chromatographe en phase gazeuse en faisant varier les divers paramètres précédents.

2. *Performances analytiques*

Les performances analytiques ont été mesurées en mode chromatographique, la puissance a été fixée à 90 W, le tube à décharge avait 2,8 mm de diamètre interne et de débit d'hélium total était compris entre 20 et 30 mL/min.

2. a. *Limite de détection*

Les limites de détections pour une cinquantaine de composés de structure moléculaire et de volatilité différentes ont été mesurées. Les valeurs obtenues sont résumées au tableau 1.[2] Ces limites de détection sont inférieures ou équivalentes à celles obtenues par d'autres auteurs (6–11). Il faut cependant souligner que ces valeurs ne sont qu'indicatives et peuvent être réduites en diminuant le diamètre du tube à décharge et/ou en augmentant la puissance. Les limites de détection sont également moins dépendantes de la structure de la molécule comme il avait été observé précédemment (14) et ceci provient d'un meilleur contrôle du plasma.

2. b. *Domaine de linéarité et sélectivité*

Les domaines de linéarité du détecteur pour les divers éléments ont été mesurés et sont rapportés au tableau 2. Le domaine de linéarité pour la plupart des éléments est de l'ordre de $10^3$, ce qui est du même ordre de grandeur que celui obtenu pour des détecteurs similaires (11, 12). La limite supérieure du domaine de linéarité est due à la capacité de la colonne de silice et non au plasma.

La sélectivité du détecteur par rapport au carbone a été mesurée et les valeurs obtenues sont

[2]L'ensemble des valeurs obtenues est disponible et peut être obtenu à un prix nominal, en s'adressant au Dépôt de données non publiées, ICIST, Conseil national de recherches du Canada, Ottawa, (Ont.), Canada K1A 0S2.

Can. J. Chem. Downloaded from www.nrcresearchpress.com by 210.87.254.105 on 09/06/12
For personal use only.

TABLEAU 2. Domaine de linéarité et sélectivité

| Elément | Domaine de linéarité | Sélectivité par rapport au carbone[a] |
|---|---|---|
| C | $10^3$ | — |
| Cl | $10^3$ | 600 |
| Br | $1{,}5 \times 10^3$ | 1100 |
| I | $15 \times 10^3$ | 800 |

[a]La sélectivité est le rapport de l'intensité du signal produit par un atome-gramme de l'élément X (Cl, Br ou I) sur l'intensité du signal produit par un atome-gramme de carbone. Les hydrocarbures utilisés comme références sont le cumène et l'éthylbenzène.

rapportées au tableau 2. Ces valeurs sont comparables à celle obtenues avec des montages optiques équivalents et peuvent être améliorées par l'utilisation de fentes plus petites sur le système dispersif, par l'utilisation d'un monochromateur à plus haute résolution ou par de la modulation de longueur d'onde (16).

Des exemples de chromatogrammes obtenus pour des mélanges de produits organiques en utilisant le détecteur aux longueurs d'onde du carbone, chlore, brome et iode sont représentés à la figure 7.

Ces chromatogrammes ont été obtenues en mode séquentiel, notre système optique ne nous permettant pas une analyse simultanée à plusieurs longueurs d'onde.

Le système qui a été décrit, ne présente pas le problème associé à divers modes de génération de plasmas micro-ondes (1–12), à savoir l'instabilité du couplage entre le générateur et le plasma avec le temps. Les conditions d'ajustement du Surfatron sont uniques et reproductibles d'une manipulation à l'autre. Ce système contrairement aux autres systèmes décrits précédemment peut également être opéré avec une puissance réfléchie de zéro dans des conditions expérimentales très variées (gaz plasmagène, débit, diamètre de tube à décharge et puissance différents).

Les variations du signal émis en fonction du débit du gaz plasmagène ont été étudiées sur un plus grand intervalle de débits et de diamètre de tube à décharge par rapport aux études antérieures ou parallèles (6, 8, 11). Un diamètre ($d_i$) de 3 mm a été trouvé comme étant le meilleur compromis entre la durée de vie du tube à décharge et des limites de détection acceptables.

Aucun maximum du rapport signal sur fond continu en fonction de la puissance a été observé pour les quatres éléments étudiés, contrairement à l'étude d'Estes *et al.* (11). Cette différence provient du plus petit tube à décharge (0,5 mm) utilisée par ces auteurs.

Les performances analytiques décrites rendent ce détecteur intéressant pour des applications où

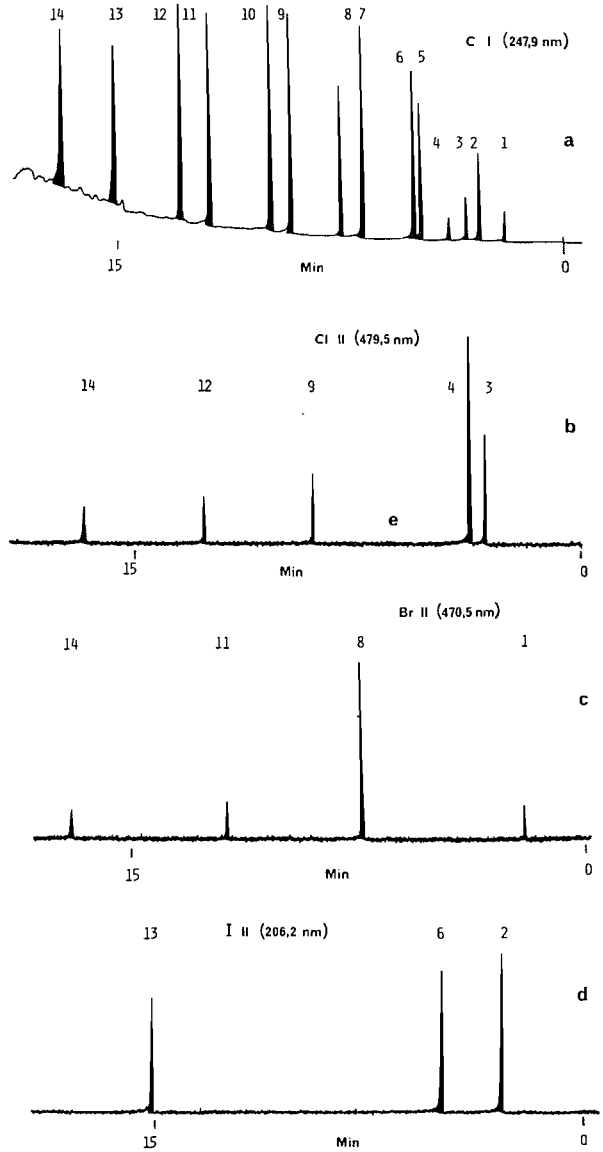


FIG. 7. Chromatogrammes d'un mélange de produits organiques. (a) Détection du carbone; (b) détection du chlore; (c) détection du brome; (d) détection de l'iode. Produits: bromoéthane (1), iodoéthane (2), 1,4-dichloroéthane (3), tétrachlorure de carbone (4), 2,2,4-triméthylpentane (5), iodopropane (6), toluène (7), 1,4-dibromoéthane (8), chlorobenzène (9), ethylbenzène (10), bromobenzène (11), 4-chlorotoluène (12), iodobenzène (13), 3-chlorobromobenzène (14). Colonne: Silice WCOT, OV-101, 20 m, di = 0.25 mm.

une grande variété d'éléments peuvent être présents dans des mélanges complexes séparées par chromatographie gazeuse. La grande sélectivité de ce détecteur et la possibilité de travailler en mode d'analyse multiéléments séquentielle ou simultanée constituent les principaux avantages de ce détecteur.

Can. J. Chem. Downloaded from www.nrcresearchpress.com by 210.87.254.105 on 09/06/12
For personal use only.

Les limites de détection obtenues pour une grande variété de composés peuvent être améliorées par augmentation de la puissance du plasma et par diminution des diamètres des tubes de décharge.

**Remerciements**

Nous remercions le CRSNG pour son soutien financier (Octrois A-1036 et RD-161). L'un d'entre nous (G.C.) remercie la compagnie Alcan pour l'obtention d'une bourse d'étude. Nous remercions M. K. Sotomaru de la compagnie Gasukuro Kogo, Tokyo, Japan pour le don de la colonne OV-101.

1. A. J. McCormack, S. C. Tong et W. D. Cooke. Anal. Chem. **37**, 1470 (1965).
2. C. A. Bache et D. J. Lisk. Anal. Chem. **43**, 950 (1971).
3. R. M. Dagnall, T. S. West et P. Whitehead. Analyst, **98**, 647 (1973).
4. Y. Talmi. Anal. Chim. Acta, **74**, 107 (1975).
5. F. A. Serravello et T. H. Risby. Anal. Chem. **47**, 2141 (1975).
6. J. P. J. Van Dalen, P. A. de Lezenne-Coulander et L. de Galan. Anal. Chim. Acta, **94**, 1 (1977).
7. C. I. M. Beenakker. Spectrochim. Acta Part B, **32**, 173 (1977).
8. B. D. Quimby, P. C. Uden et R. M. Barnes. Anal. Chem. **50**, 1903 (1978).
9. B. D. Quimby, M. F. Delaney, P. C. Uden et R. M. Barnes. Anal. Chem. **51**, 875 (1979).
10. K. Tanabe, H. Haraguchi et K. Fuwa. Spectrochim. Acta Part B, **36**, 633 (1981).
11. S. A. Estes, P. C. Uden et R. M. Barnes. Anal. Chem. **53**, 1829 (1981).
12. H. A. Dingjan et H. J. de Jong. Spectrochim. Acta Part B, **36**, 325 (1981).
13. J. Hubert, M. Moisan et A. Ricard. Spectrochim. Acta Part B, **33**, 1 (1979).
14. T. Hanai, S. Coulombe, M. Moisan et J. Hubert. Development in atomic plasma spectrochemical analyses. *Edité par* R. Barnes. Heyden. 1981.
15. J. Sevcik. Detectors in gas chromatography. Elsevier, Amsterdam. 1976. p. 8.
16. P. M. Houpt. Anal. Chim. Acta, **86**, 129 (1976).

Can. J. Chem. Downloaded from www.nrcresearchpress.com by 210.87.254.105 on 09/06/12
For personal use only.

# Nuclear analogs of β-lactam antibiotics. XV.[1] Synthesis of 6-substituted 2-methylpenem-3-carboxylic acids

YASUTSUGU UEDA,[2] ALAIN MARTEL,[2] JEAN-PAUL DARIS, BERNARD BELLEAU, AND MARCEL MÉNARD

*Bristol Laboratories of Canada, 100 Industrial Boulevard, Candiac, P.Q., Canada J5R 1J1*

Received November 2, 1981

YASUTSUGU UEDA, ALAIN MARTEL, JEAN-PAUL DARIS, BERNARD BELLEAU, and MARCEL MÉNARD. Can. J. Chem. **60**, 904 (1982).

The synthesis of 6-substituted 2-methylpenem-3-carboxylic acids is described. The dianion **6** was prepared *in situ* from 2-methylpenem-3-carboxylic acid (**5**) by the addition of two equivalents of *n*-butyllithium in THF at −78°C. This dianion reacted with deuterated acetic acid, acetone, acetaldehyde, benzaldehyde, and methyl thiomethylsulfonate to give 6-deuterio-, 6-(2′-hydroxy-2′-propyl)-, 6-(1′-hydroxyethyl)-, 6-(1′-hydroxybenzyl)-, 6-methylthio-2-methylpenem-3-carboxylic acids and their sodium or potassium salts, **7–11**, respectively. The stereochemistry of the products is also discussed.

YASUTSUGU UEDA, ALAIN MARTEL, JEAN-PAUL DARIS, BERNARD BELLEAU et MARCEL MÉNARD. Can. J. Chem. **60**, 904 (1982).

On décrit la synthèse d'acides méthyl-2 penèmecarboxyliques-3 substitués en position 6. On a préparé le dianion **6** *in situ* à partir de l'acide méthyl-2 penèmecarboxylique-3 (**5**) par l'addition de deux équivalents de *n*-butyllithium dans le THF à −78°C. Les réactions de ce dianion avec l'acide acétique deutéré, l'acétone, l'acétaldehyde, le benzaldéhyde et le thiométhylsulfonate de méthyle conduisent respectivement aux acides deutéro-6, (hydroxy-2 propyl-2)-6, (hydroxy-1′ éthyl)-6, (hydroxy-1′ benzyl)-6 et méthylthio-6 méthyl-2 penèmecarboxyliques-3 (**7–11**) aussi qu'à leurs sels de sodium ou de potassium. On discute aussi de la stéréochimie des produits.

[Traduit par le journal]

Naturally occurring carbapenem antibiotics, isolated from *streptomyces* species, were shown to differ markedly from the classical penicillins and cephalosporins in the composition of their side chain at position 6: thienamycin (**1**) (1) and the olivanic acids (**2**) (2) possess a 1-hydroxyethyl moiety while PS-5 (**3**) (3) and carpetimycins (or C-19393) (**4**) (4) carry a simple ethyl group and a 2-hydroxypropyl group respectively as a substituent.

In order to assess the influence of the side chain on the biological activity of the analogous penems, members of a new class of totally synthetic antibiotics (5), we prepared a series of 6-substituted penem-3-carboxylic acids (6). In this paper[3] we report the most direct and most desirable approach to 6-substitution: a one-step introduction of the 6-substituent onto a preformed 6-unsubstituted 2-substituted penem-3-carboxylic acid by metallation and subsequent reaction with electrophiles.

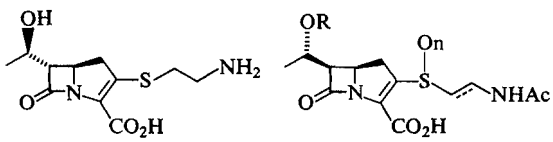

**1**



**2** (R = H, $SO_3H$)

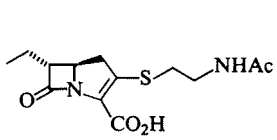

**3**

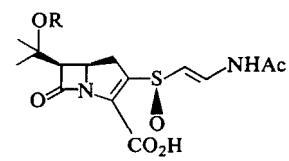

**4** (R = H, $SO_3H$)

Although metallation of monocyclic β-lactams is well documented (7–9) and this method has been used in the total synthesis of thienamycin (10) and in the synthesis of 6-substituted penem acids (5*e*, 6*c*), a direct metallation on 6-unsubstituted penem acid has not been reported. Furthermore, electrophilic additions to enolates of the penam and the cephem nuclei have been achieved (11, 12) but, because of the lability of the penem system, especially toward strong bases, it was generally assumed (5*e*) that such a process would not be possible with the penem nucleus.

The dianion **6** was prepared from 2-methylpenem-3-carboxylic acid (**5**) (6*a*) by the addition of two equivalents of *n*-butyllithium in the presence or absence of diisopropylamine (2 equiv.) in THF at −78°C. This species was stable enough at −78°C to react with a variety of electrophiles to give the 6-substituted penem acids. Thus, the dianion, so prepared, reacted with $CD_3CO_2D$, acetone, acetaldehyde, benzaldehyde, or methyl thiomethylsul-

[1]For Part XIV see ref. 17.

[2]Authors to whom correspondence may be addressed.

[3]Following papers will describe the synthesis of 6-substituted penems where the 6-substituents are introduced at an earlier stage in the sequence. See also ref. 6*c*.

0008-4042/82/070904-06$01.00/0

©1982 National Research Council of Canada/Conseil national de recherches du Canada

Can. J. Chem. Downloaded from www.nrcresearchpress.com by 210.87.254.6 on 09/06/12
For personal use only.

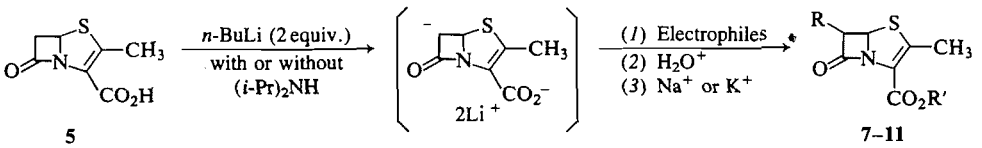


5 6 7–11

SCHEME 1

fonate to yield 6-substituted 2-methylpenem-3-carboxylic acids or the corresponding sodium or potassium salts, **7–11**, in 6–60% yield. Most of the penem acid products were immediately converted to their sodium or potassium salts, **8***a*, **9**, **10**, and **11***a*. 6-(1′-Hydroxyethyl) or 6-(1′-hydroxybenzyl) derivatives could not be isolated in the acid form without serious decomposition.

The infrared spectrum of each product showed a strong β-lactam carbonyl band in the 1750–1793 $cm^{-1}$ region. The ultraviolet spectrum of each product exhibited a maximum at around 300 nm. These data indicated that the penem ring system had been retained.

Examination of the $^1$Hmr spectrum of each product revealed that the reaction of this dianion with the above electrophiles produced a mixture of *cis* and *trans* 6-substituted penem acids or the corresponding salts. The *cis–trans* ratio varied from 4:1 to 3:7 as listed in Table 1. The relative stereochemistry at C5—C6 of each product was determined based on the fact that *cis* β-lactam coupling constants (~4 Hz) were larger than *trans* coupling constants (~2 Hz) (13). Deuterated acetic acid, acetaldehyde, and methyl thiomethylsulfonate gave the *cis* isomers as the major product. Among these, the smallest electrophile, $CD_3CO_2D$, produced the highest ratio of the *cis* isomer (80% *cis*). This preferential formation of the sterically more hindered *cis* isomers is quite unusual, although there are a few examples in similar systems (8, 12). However, when bulkier electrophiles such as acetone were employed, steric hindrance between the incoming electrophile and the thiazoline ring was large enough to force the electrophile to come from the other side of the thiazoline group, yielding the *trans* isomer as the major product. In the case of benzaldehyde the situation was well balanced, giving a 1:1 mixture of *cis* and *trans* isomers. Two diastereomers were found in the *trans* isomer and only one diastereomer in the *cis* isomer.

Although acetone and methyl thiomethylsulfonate gave a mixture of *cis* and *trans* isomers, we were able to isolate each pure *trans* isomer (**8***b* and **11***b*) in the acid form by crystallization.

It is worth mentioning that the aldol condensation of the dianion **6** with acetaldehyde gave only a single diastereomer of *cis*-6-(1′-hydroxyethyl)-penem as was the case for benzaldehyde. In both cases, the other diastereomer was not detected on the scale on which our reactions were performed. We presumed this diastereomer was a *cis-R**[4] isomer because we expected that in the transition state depicted by **12** (14), **12***a* will form in preference to **12***b* because of the severe repulsive interaction between the R-group of the electrophiles and the thiazoline ring in **12***b* (11). This *cis-R** stereochemistry in the product was unambiguously confirmed by total synthesis of both isomers (*cis-R**, **9***a* and *cis-S**, **9***b*)[5] from *N-tert*-butyldimethyl-(*cis-R** and *cis-S**)-3-(1′-hydroxyethyl-4-tritylthioazetidin-2-ones (**13***a* and **13***b*) (6*c*). This will be reported in a forthcoming publication.[6]

R = Me or Ph

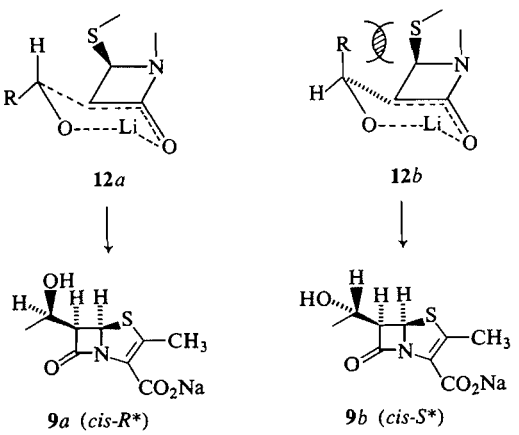


SCHEME 2

[4]All compounds described here are racemic. All structural formulae and stereochemical designations refer to the enantiomer related to natural products, such as the penicillins and thienamycin.

[5]Examination of $^1$Hmr spectra of the two diastereomers **9***a* and **9***b* revealed that although $J_{6-1'}$ or $\delta_{6-H}$ were not different enough to allow the two isomers to be distinguished from one another, $\delta_{1'-Me}$ was distinctly different for the two compounds. The signal for *cis-R** methyl (1.23 ppm) appeared at higher field than the signal for *cis-S** methyl (1.31 ppm).

[6]See footnote 3.

Can. J. Chem. Downloaded from www.nrcresearchpress.com by 210.87.254.6 on 09/06/12
For personal use only.

Can. J. Chem. Downloaded from www.nrcresearchpress.com by 210.87.254.6 on 09/06/12
For personal use only.

TABLE 1. 6-Substituted 2-methylpenem-3-carboxylic acids and their salts **7–11**

| Penems | Electrophiles | R | R′ | Yield (%) | *cis*/*trans*[a] |
|---|---|---|---|---|---|
| **7** | $CD_3CO_2D$ | D | H | 60 | 4/1 |
| **8***a* | $CH_3COCH_3$ | | K | 26 | 3/7 |
| **8***b* | $CH_3COCH_3$ | | H | 23 | *trans* only |
| **9** | $CH_3CHO$ | | Na | 9 | *cis* major |
| **10** | PhCHO | | K | 20 | 1/1 |
| **11***a* | $CH_3SSO_2CH_3$ | $CH_3S$ | K | 28 | 5/3 |
| **11***b* | $CH_3SSO_2CH_3$ | $CH_3S$ | H | 6 | *trans* only |

[a]À *cis*/*trans* ratio was determined from integration of C5–H signals in the $^1$Hmr spectra.

Since the aldol condensation with acetaldehyde, unlike the reaction with benzaldehyde, did not give a sufficient amount of the *trans* isomer, after isolation as the sodium salt, we were unable to measure the *cis*–*trans* ratio in the product. An attempt to obtain more of the *trans* isomer using $ZnCl_2$, a chelate stabilizing agent which is known to change the stereochemistry of aldol products (14*a*), was not successful. No penem product was isolated in this reaction.

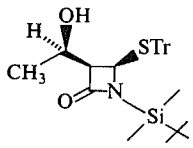

**13***a*

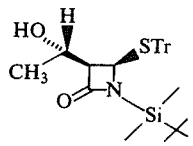

**13***b*

A major acidic by-product in the reaction with acetaldehyde was identified as 5-methylthiazole-4-carboxylic acid (**14**) based on a singlet at 2.63 ppm which was assigned to 5-Me protons and a broad singlet at 8.63 ppm, assigned to 2-H. More of this thiazole **14** was found when the crude product was left in the acid form. This indicates that the thiazole **14** may have formed during the work-up by the acid-catalyzed decomposition of the penem nucleus or by the retro [2 + 2] process as shown in Scheme 3 (5*a*). Separation of sodium salt **9** from the crude product (which was contaminated with thiazole sodium salt **15**) was achieved in two ways. The

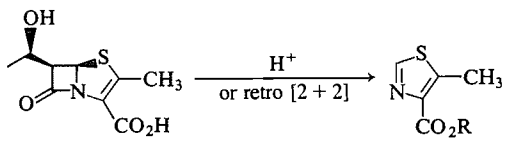

**16** → (H$^+$ or retro [2 + 2]) → **14**: R = H; **15**: R = Na

SCHEME 3

first involved several steps as shown in Scheme 4. A mixture of the crude material was converted to the *p*-nitrobenzyl esters, **17** and **18**, which were separated by chromatographic means. Catalytic hydrogenation of **17** gave the corresponding sodium salt **9**. Alternatively, the salt **9** precipitated out without contamination of thiazole **15** by addition of sodium 2-ethylhexanoate to the crude acid in EtOAc. When $Et_2O$ was used as a solvent, both salts (**9** and **15**) precipitated.

We also attempted the direct introduction of 6-substituents on the methoxymethyl ester of **5** by the method described above using, in this case, one equivalent of *n*-butyllithium in the presence of diisopropylamine (with or without HMPA). In this experiment, we expected that the monoanion, generated *in situ*, would react more cleanly with electrophiles to give 6-substituted penem esters. In fact this reaction gave a complex mixture in which the desired product was not detected. This is presumably due to the fact that lithium diisopropylamide reacts, in the absence of HMPA, with the α,β-unsaturated ester moiety to give the Michael adduct (15). The deprotonation at the γ-position of this unsaturated ester moiety also creates more complications in the reaction with LDA-HMPA.

In summary, we have described here the synthesis of 6-substituted 2-methylpenem-3-carboxylic acids by direct metallation on 6-unsubstituted penem acid followed by the reaction with electrophiles, producing a mixture of *cis* and *trans* isomers, the ratio varying from *cis*-major to *trans*-major.

## Experimental

Melting points were determined on a Gallenkamp melting point apparatus and are not corrected. The infrared spectra were recorded on a Perkin–Elmer 267 Grating Infrared spectrophotometer.

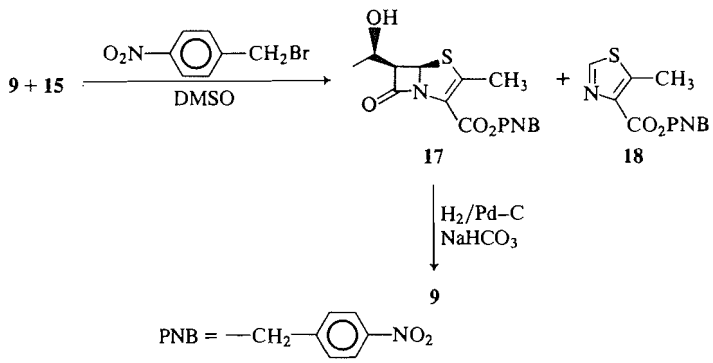


SCHEME 4

The $^1$H nuclear magnetic resonance spectra were taken with either a Varian EM-360A (60 MHz) or a Varian CFT-20 (80 MHz) nmr spectrometer. Tetramethylsilane (for solution other than deuterium oxide) and sodium 4,4-dimethyl-4-silapentane-1-sulfonate (for solutions of deuterium oxide) were used as internal standards and chemical shifts are reported in parts per million (δ) relative to the internal standards.

The ultraviolet spectra were recorded on either an Unicam SP-800 or SP 8-100 uv spectrophotometer. Tetrahydrofuran was freshly distilled from $LiAlH_4$.

Commercial $CH_3CHO$ was distilled prior to use. Diisopropylamine was distilled from $CaH_2$ and stored over NaOH. *n*-Butyllithium in hexane (Aldrich) and $CD_3CO_2D$ (99.5%, MSD) were used as supplied. 2-Methylpenem-3-carboxylic acid (**5**) was prepared as described before (6*a*). Methyl thiomethylsulfonate was prepared by the procedure of Slusarchyk *et al.* (16).

*6-Deuterio-2-methylpenem-3-carboxylic acid (7)*

To a stirred solution of 2-methylpenem-3-carboxylic acid (**5**) (50 mg, 0.27 mmol) in THF (10 mL) was added at −78°C under a nitrogen atmosphere a solution of *n*-butyllithium in hexane (1.66 *M*, 0.36 mL, 0.60 mmol). After a half minute, $CD_3CO_2D$ (0.4 mL, a large excess) was injected. The yellow reaction mixture was stirred (−78°C, $N_2$) for 5 min and then diluted with EtOAc (15 mL). This was washed with brine (×2), dried ($Na_2SO_4$), and evaporated, yielding 45 mg of yellow solid. This solid was rinsed with a small amount of anhydrous $Et_2O$ to obtain 30 mg (0.16 mmol, yield 60%) of the title compound **7** as a mixture of the *cis* and *trans* isomers in a ratio of 4:1. This material was contaminated with a small amount of **5**, mp 113–117°C (dec.); ir (KBr disc) $\nu_{max}$: 2400–3100 ($CO_2H$), 1775 (β-lactam), and 1670 ($CO_2H$) cm$^{-1}$; uv (EtOH) $\lambda_{max}$: 262 (ε 4330) and 305 nm (ε 6680); $^1$Hmr (acetone-$d_6$; CFT-20) δ: 2.34 (3H, s, 2-Me), 3.41 (1/5 H, dt, $J_{6-5\,trans}$ = 2 Hz, $J_{H-D}$ = 2 Hz, H-6), 3.81 (4/5 H, dt, $J_{6-5\,cis}$ = 4 Hz, $J_{H-D}$ = 2 Hz, H-6), and 5.71 ppm (1H, 2d, $J_{5-6\,cis}$ = 4 Hz and $J_{5-6\,trans}$ = 2 Hz, H-5; the both isomers appeared at the same place). The signals for **5** appeared at 3.40 (dd, $J$ = 2 Hz, $J_{gem}$ = 16.5 Hz, H-6) and 3.85 ppm (dd, $J$ = 4 Hz, $J_{gem}$ = 16.5 Hz, H-6).

*Potassium 6-(2′-hydroxy-2′-propyl)-2-methylpenem-3-carboxylate (8a)*

To a solution of diisopropylamine (0.098 mL, 0.699 mmol) in THF (2 mL) *n*-butyllithium in hexane (1.6 *M*, 0.44 mL, 0.70 mmol) was added at −78°C under a nitrogen atmosphere and stirred (−78°C, $N_2$) for 30 min. To this solution was added a solution of 2-methylpenem-3-carboxylic acid (**5**) (116 mg, 0.627 mmol) in THF (4 mL) and the mixture was stirred for 5 min at −78°C, followed by successive addition of diisopropylamine (0.098 mL; 0.699 mmol) and *n*-butyllithium in hexane (1.6 *M*, 0.44 mL, 0.70 mmol) at −78°C. It was then stirred for 10 min at −78°C and treated rapidly with acetone (5 mL). After 10 min at −78°C, it was acidified (pH 2) with 1% HCl, diluted with EtOAc (40 mL), and the organic layer was washed with brine (3 × 20 mL), dried ($Na_2SO_4$), and evaporated to give a crude residue which was taken up in $CH_2Cl_2$. The crude acid (yield 90 mg) was dissolved in cold methylisobutylketone (2 mL) and treated dropwise with a solution of potassium 2-ethylhexanoate in *n*-BuOH (50%). After addition of anhydrous $Et_2O$, it gave 36.4 mg (0.13 mmol, yield 20.6%) of the title compound as a mixture of the *cis* and *trans* isomers in a ratio of 7:3; ir (Nujol mull) $\nu_{max}$: 3600–3100 (OH), 1765 (β-lactam), and 1582 (—$CO_2^-$) cm$^{-1}$; uv (EtOH) $\lambda_{max}$: 257 (ε 3920) and 300 nm (ε 4020); $^1$Hmr (DMSO-$d_6$) δ: 1.32, 1.35 (2s, di-Me), 1.40, 1.47 (2s, di-Me), 2.34 (3H, s, $CH_3$), 3.50 (br s, OH), 3.62 (d, $J_{6-5\,trans}$ = 2 Hz, H-6), 3.93 (d, $J_{6-5\,cis}$ = 4 Hz, H-6), 5.55 (1 × 7/10 H, d, $J_{5-6\,trans}$ = 2 Hz, H-5), and 5.60 ppm (1 × 3/10 H, d, $J_{5-6\,cis}$ = 4 Hz, H-5).

trans-*6-(2′-Hydroxy-2′-propyl)-2-methylpenem-3-carboxylic acid (8b)*

To a stirred solution of 2-methylpenem-3-carboxylic acid (**5**) (50 mg, 0.27 mmol) in THF (4 mL) diisopropylamine (0.08 mL, 0.58 mmol) was added at 0–5°C under a nitrogen atmosphere. The mixture was cooled to −78°C and *n*-butyllithium (0.38 mL, 1.6 *M* in hexane, 0.60 mmol) was added. After 5 min at −78°C, acetone (0.5 mL) was injected into this orange mixture. The resulting yellow mixture was stirred for 10 min at −78°C. This was neutralized with 0.1 *N* HCl (12 mL) and extracted with EtOAc (3 × 20 mL). The EtOAc extracts were washed with brine, dried ($Na_2SO_4$), and evaporated to yield 59 mg of a crude oil. This oil was extracted with $Et_2O$, removing the insoluble material to give 53 mg of an oily solid. This was characterized by $^1$Hmr as a mixture of the *cis* and *trans* isomers in a ratio of 7:3; $^1$Hmr ($CDCl_3$) δ: 3.75 (7/10 H, d, $J$ = 1.5 Hz, 6-$H_{trans}$), 4.00 (3/10 H, d, $J$ = 4 Hz, 6-$H_{cis}$), 5.62 (d, $J$ = 1.5 Hz, 5-$H_{trans}$) and 5.70 ppm (d, $J$ = 4 Hz, 5-$H_{cis}$). This oily solid was triturated with a small amount of $CHCl_3$ and $Et_2O$ to yield 15 mg (0.062 mmol, yield 23%) of the title compound **8*b*** as white crystals, mp 117–121°C; ir (Nujol mull) $\nu_{max}$: 3500 (OH), 1765 (β-lactam), and 1660 ($CO_2H$) cm$^{-1}$; uv (EtOH) $\lambda_{max}$: 265 (ε 3400) and 309 nm (ε 5700); $^1$Hmr (acetone-$d_6$) δ: 1.30 (3H, s, 2′-$CH_3$), 1.35 (3H, s, 2′-$CH_3$), 2.35 (3H, s, 2-$CH_3$), 3.77 (1H, d, $J$ = 1.8 Hz, 6-H), and 5.63 ppm (1H, d, $J$ = 1.8 Hz, 5-H).

*Sodium* cis-*6-(1′-hydroxyethyl)-2-methylpenem-3-carboxylate (9)*

To a stirred solution of 2-methylpenem-3-carboxylic acid (**5**) (1.00 g, 5.40 mmol) in THF (80 mL) *n*-butyllithium (7.00 mL, 1.6 *M* in hexane, 11.2 mmol) was added dropwise at −78°C under a nitrogen atmosphere. After 1 min $CH_3CHO$ (1.2 mL) was added to this reddish mixture and the resulting pale yellow

Can. J. Chem. Downloaded from www.nrcresearchpress.com by 210.87.254.6 on 09/06/12
For personal use only.

Can. J. Chem. Downloaded from www.nrcresearchpress.com by 210.87.254.6 on 09/06/12
For personal use only.

mixture was stirred (−78°C, $N_2$) for 10 min. To this mixture was added saturated $NH_4Cl$ (100 mL) followed by brine (50 mL). The aqueous layer was collected and washed with EtOAc (2 × 60 mL). This aqueous layer, mixed with EtOAc (60 mL), was cooled in an ice-bath and acidified carefully with a cold 0.1 *N* HCl solution (120 mL), saturated with NaCl, and extracted quickly with EtOAc (3 × 60 mL). The EtOAc extracts were washed with brine, dried ($Na_2SO_4$), and evaporated to reduce the volume to ca. 25 mL. To this was added sodium 2-ethylhexanoate in *n*-BuOH (10% w/w, 2.1 mL) and the precipitate was collected by a centrifuge and washed with EtOAc to yield 123 mg (0.490 mmol, yield 9.1%) of the title compound **9** as a yellow powder; ir (Nujol mull) $\nu_{max}$: 3350 (OH), 1750 (β-lactam), and 1590 ($CO_2Na$) $cm^{-1}$; uv ($H_2O$) $\lambda_{max}$: 252 (ε 4200) and 297 nm (ε 3400); $^1$Hmr ($D_2O$) δ: 1.23 (3H, d, $J$ = 6 Hz, 1′-$CH_3$), 2.28 (3H, s, 2-$CH_3$), 3.85 (1H, dd, $J_{6-5\,cis}$ = 4 Hz, $J_{6-1'}$ = 8 Hz, 6-H), and 5.65 ppm (1H, d, $J_{5-6\,cis}$ = 4 Hz, 5-H).

To the supernatant solution was added $Et_2O$ and the precipitate was collected by a centrifuge and washed with $Et_2O$ to give 145 mg of a mixture of the title compound **9** and sodium 5-methylthiazole-4-carboxylate (**15**) as a white solid; $^1$Hmr ($D_2O$) δ: thiazole peaks at 2.63 (3H, s, 5-Me) and 8.63 ppm (1H, s, 2-H). This material was purified as follows.

The material containing **9** and **15** (total 201 mg) was converted to the mixture of the corresponding *p*-nitrobenzyl ester by treating it with *p*-nitrobenzyl bromide (104 mg, 0.9 mmol) in dimethylsulfoxide (2 mL) at room temperature overnight (21 h). The crude products were separated by preparative tlc (E. Merck silica gel 60F-254, benzene–$Et_2O$ 1:1), collecting 40 mg (0.14 mmol) of *p*-nitrobenzyl 5-methylthiazole-4-carboxylate (**18**) as white crystals (fast moving band), mp 128–130°C; ir (Nujol mull) $\nu_{max}$: 1720 (ester), 1603, 1520 ($NO_2$), and 1350 ($NO_2$) $cm^{-1}$; uv (EtOH) $\lambda_{max}$: 256 nm (ε 12 500); $^1$Hmr ($CDCl_3$) δ: 2.80 (3H, s, 5-$CH_3$), 5.47 (2H, s, —$CH_2$—), 7.53–7.68–8.15–8.30 (2H, $A_2'B_2'$, aromatic H's), and 8.60 ppm (1H, br s, 2-H); and 41 mg (0.11 mmol) of **17** as white crystals (slow moving band), mp 140–143°C; ir (Nujol mull) $\nu_{max}$: 3400 (OH), 1770 (β-lactam), and 1705 (ester) $cm^{-1}$; uv (EtOH) $\lambda_{max}$: 265 (ε 12 000) and 309 nm (ε 9200); $^1$Hmr ($CDCl_3$) δ: 1.25 (3H, $J$ = 6 Hz, 1′-$CH_3$), 2.40 (3H, s, 2-$CH_3$), 3.78 (1H, dd, $J_{6-5}$ = 4 Hz, $J_{6-1'}$ = 9 Hz, 6-H), 4.35 (1H, m, 1′-H), 5.03–5.27–5.37–5.60 (2H, AB type, —$CH_2$Ar), 5.61 (1H, d, $J_{5-6}$ = 4 Hz, 5-H), and 7.52–7.67–8.13–8.24 ppm (2H, $A_2'B_2'$, aromatic H's).

A solution of **17** (40 mg, 0.11 mmol) in THF (4 mL) was mixed with $Et_2O$ (8 mL), $H_2O$ (4 mL), $NaHCO_3$ (9.5 mg, 0.11 mmol), and 30% Pd–Celite (45 mg; Engelhard) and hydrogenated at room temperature ($H_2$, 30 psi) for 3 h. After filtration of the catalyst over Celite, the filtrate and the washings were combined. The aqueous layer was washed once with $Et_2O$ and lyophilized to yield 24 mg (0.096 mmol, yield 87%) of the title compound (**9**) as a greyish powder; ir (Nujol mull) $\nu_{max}$: 3350 (OH), 1760 (β-lactam), and 1585 ($CO_2Na$) $cm^{-1}$; uv ($H_2O$) $\lambda_{max}$: 297 (ε 3000) and 254 nm (ε 2900); $^1$Hmr (DMSO-$d_6$) δ: 1.03 (3H, d, $J$ = 6 Hz, 1′-$CH_3$), 2.20 (3H, s, 2-$CH_3$), 3.53 (1H, dd, $J$ = 4 Hz, $J$ = 9 Hz, 6-H), 3.9 (1H, m, 1′-H), and 5.40 ppm (1H, d, $J$ = 4 Hz, 5-H).

*Potassium 6-(1′-hydroxybenzyl)-2-methylpenem-3-carboxylate (**10**)*

To a solution of diisopropylamine (0.084 mL, 0.599 mmol) in THF (2 mL) was added at −78°C under a nitrogen atmosphere 1.6 *M* *n*-butyllithium in hexane (0.380 mL, 0.608 mmol) and stirred (−78°C, $N_2$) for 30 min. To this solution was added dropwise a solution of 2-methylpenem-3-carboxylic acid (**5**) (100 mg, 0.54 mmol) in THF (6 mL) and the mixture stirred for 5 min at −78°C, followed by successive addition of diisopropylamine (0.084 mL, 0.599 mmol) and 1.6 *M* *n*-butyllithium in hexane (0.380 mL, 0.608 mmol). It was then stirred for 7 min at −78°C and treated rapidly with benzaldehyde (0.3 mL). The mixture was allowed to react at −78°C for 20 min. It was acidified with 1% HCl (pH ≃ 2), diluted with EtOAc (40 mL), washed with $H_2O$–brine (1:1, 3 × 20 mL) and brine (1 × 20 mL). It was dried over $Na_2SO_4$ and evaporated to give a residue which was dissolved in methylisobutylketone (2 mL). This was treated dropwise with a solution of potassium 2-ethylhexanoate in *n*-BuOH to give 35 mg (0.11 mmol, yield 20%) of the title compound **10** as a diastereomeric mixture (*cis*–*trans* ≃ 1:1); ir (Nujol mull) $\nu_{max}$: 3600–3100 (OH), 1760 (β-lactam), and 1590 ($CO_2K$) $cm^{-1}$; uv ($H_2O$) $\lambda_{max}$: 262 (ε 5100) and 296 nm (ε 3000); $^1$Hmr (DMSO-$d_6$) δ: 2.35 (3H, 2s, $CH_3$), 3.65 (br s, OH), 3.90 (m, H-6), 4.25 (dd, $J_{6-5\,cis}$ = 4 Hz, $J_{6-1'}$ = 10 Hz, H-6), 5.0 (m, H-1′), 5.35 (d, $J_{5-6\,cis}$ = 4 Hz, H-5), 5.45 (d, $J_{5-6\,trans}$ = 1.5 Hz, H-5), 5.57 (d, $J_{5-6\,trans}$ = 1.5 Hz, H-5), and 7.95 ppm (5H, s, aromatic H's).

*Potassium 6-methylthio-2-methylpenem-3-carboxylate (**11**a)*

A solution of 2-methylpenem-3-carboxylic acid (**5**) (100 mg, 0.54 mmol) in THF (5 mL) was added dropwise to a cold (−78°C) THF (2 mL) solution of lithium diisopropylamide, made from diisopropylamine (0.084 mL, 0.599 mmol) and 1.6 *M* *n*-butyllithium – hexane (0.380 mL, 0.608 mmol). The mixture was stirred for 7–8 min, followed by successive addition of diisopropylamine (0.084 mL, 0.599 mmol) and 1.6 *M* *n*-butyllithium – hexane (0.380 mL, 0.608 mmol). It was then stirred for 7 min at −78°C and treated rapidly with methyl thiomethylsulfonate (0.30 mL, excess). The mixture was allowed to react at −78°C for 5 min. It was acidified with 1% HCl (pH ≃ 2), diluted with EtOAc (40 mL), washed with 1:1 $H_2O$–brine (3 × 20 mL) and then brine (20 mL). The organic solution was dried ($Na_2SO_4$) and evaporated to give a residue which was dissolved in cold methylisobutylketone (2 mL). To this solution was added dropwise a solution of potassium 2-ethylhexanoate in *n*-BuOH (50% w/w). The precipitate was collected to yield 40 mg (0.15 mmol, yield 28%) of the title compound **11***a* as a 5:3 mixture of *cis* and *trans* isomers, mp 115–120°C (dec.); ir (Nujol mull) $\nu_{max}$: 1770 (β-lactam) and 1600 ($CO_2K$) $cm^{-1}$; uv ($H_2O$) $\lambda_{max}$: 252 (ε 4200) and 297 nm (ε 3700); $^1$Hmr (DMSO-$d_6$) δ: 2.25 (s, $SCH_3$), 2.33 (s, $CH_3$), 2.37 (s, $SCH_3$), 3.42 (br s, OH), 4.72 (1H, d, $J_{6-5\,trans}$ = 1.5 Hz, H-6), 4.87 (1H, d, $J_{6-5\,cis}$ = 4 Hz, H-6), 5.57 (1H, d, $J_{5-6\,trans}$ = 1.5 Hz, H-5), and 5.85 ppm (1H, d, $J_{5-6\,cis}$ = 4 Hz, H-5).

trans-*6-Methylthio-2-methylpenem-3-carboxylic acid (**11**b)*

Diisopropylamine (1.16 g, 11.4 mmol) was added at 5°C to a solution of 2-methylpenem-3-carboxylic acid (**5**) (1.00 g, 5.40 mmol) in THF (800 mL). The mixture was cooled to −78°C and treated with 2.52 *M* *n*-butyllithium – hexane (4.4 mL, 11.1 mmol). After stirring at −78°C for 5 min, methyl thiomethylsulfonate (750 mg, 5.90 mmol) was added and it was stirred at −78°C for an additional 10 min. Then the reaction mixture was poured into a saturated $NH_4Cl$ solution, extracted with $CH_2Cl_2$, acidified to pH 3 with dilute HCl, and again extracted with $CH_2Cl_2$. The organic extracts were washed with brine, dried ($MgSO_4$), and evaporated to give a mixture of *cis*- and *trans*-6-methylthio-2-methylpenem-3-carboxylic acids. However, crystallization from $Et_2O$ afforded 75 mg (0.32 mmol, yield 6%) of the pure *trans* isomer **11***b*, mp 109–112°C; ir ($CH_2Cl_2$) $\nu_{max}$: 1793 (β-lactam) and 1681 ($CO_2H$) $cm^{-1}$; uv (EtOH) $\lambda_{max}$: 303 nm (ε 4348); $^1$Hmr ($CDCl_3$) δ: 2.24 (3H, s, —$SCH_3$), 2.37 (3H, s, —$CH_3$), 4.56 (1H, d, $J$ = 1.6 Hz, H-6), and 5.49 ppm (1H, d, $J$ = 1.6 Hz, H-5).

## Acknowledgements

We would like to thank Professor T. Durst of the University of Ottawa for helpful discussions, Dr. T. Conway for part of the preliminary experiments,

and C. Damas and J. Lajeunesse of these laboratories for technical assistance during the course of this work.

1. (*a*) G. ALBERS-SCHÖNBERG, B. H. ARISON, O. D. HENSENS, J. HIRSHFIELD, K. HOOGSTEEN, E. A. KACZKA, R. E. RHODES, J. S. KAHAN, F. M. KAHAN, R. W. RATCLIFFE, E. WALTON, L. J. RUSWINKLE, R. B. MORIN, and B. G. CHRISTENSEN. J. Am. Chem. Soc. **100**, 6491 (1978); (*b*) J. S. KAHAN, F. M. KAHAN, R. GOOGELMAN, S. A. CURRIE, M. JACKSON, E. O. STAPLEY, T. W. MILLER, A. K. MILLER, D. HENDLIN, S. MOCHALES, S. HERNANDEZ, H. B. WOODRUFF, and J. BIRNBAUM. J. Antibiot. **32**, 1 (1979).
2. (*a*) A. G. BROWN, D. F. CORBETT, A. J. EGLINGTON, and T. T. HOWARTH. Chem. Commun. 523 (1977); (*b*) D. F. CORBETT, A. J. EGLINGTON, and T. T. HOWARTH. Chem. Commun. 954 (1977); (*c*) A. G. BROWN, D. F. CORBETT, A. J. EGLINGTON, and T. T. HOWARTH. J. Antibiot. **32**, 961 (1979).
3. (*a*) K. OKAMURA, S. HIRATA, Y. OKUMURA, Y. FUKAGAWA, Y. SHIMAUCHI, K. KOUNO, T. ISHIKURA, and J. LEIN. J. Antibiot. **31**, 480 (1978); (*b*) K. YAMAMOTO, T. YOSHIOKA, Y. KATO, N. SHIBAMOTO, K. OKAMURA, Y. SHIMAUCHI, and T. ISHIKURA. J. Antibiot. **33**, 796 (1980).
4. (*a*) M. NAKAYAMA, A. IAWASAKI, S. KIMURA, T. MIZOGUCHI, S. TANABE, A. MURAKAMI, I. WATANABE, M. OKUCHI, H. ITOH, Y. SAITO, F. KOBAYASHI, and T. MORI. J. Antibiot. **33**, 1388 (1980); (*b*) S. HARADA, S. SHINAGAWA, Y. NOZAKI, M. ASAI, and T. KISHI. J. Antibiot. **33**, 1425 (1980).
5. (*a*) I. ERNEST, J. GOSTELI, C. W. GREENGRASS, W. HOLICK, D. E. JACKMAN, H. R. PFAENDLER, and R. B. WOODWARD. J. Am. Chem. Soc. **100**, 8214 (1978); (*b*) M. LANG, K. PRASAD, W. HOLICK, J. GOSTELI, I. ERNEST, and R. B. WOODWARD. J. Am. Chem. Soc. **101**, 6296 (1979); (*c*) I. ERNEST, J. GOSTELI, and R. B. WOODWARD. J. Am. Chem. Soc. **101**, 6301 (1979); (*d*) H. R. PFAENDLER, J. GOSTELI, and R. B. WOODWARD. J. Am. Chem. Soc. **101**, 6306 (1979); (*e*) H. R. PFAENDLER, J. GOSTELI, and R. B. WOODWARD. J. Am. Chem. Soc. **102**, 2039 (1980).
6. (*a*) M. MÉNARD and G. CARON (Bristol-Myers Co.). U.S. Patent No. 4,155,912 (1979); (*b*) Y. UEDA (Bristol-Myers Co.). U.S. Patent No. 4,182,711 (1980); (*c*) M. MÉNARD and A. MARTEL (Bristol-Myers Co.). U.S. Patent No. 4,272,437 (1981).
7. (*a*) T. DURST and M. J. LEBELLE. Can. J. Chem. **50**, 3196 (1972); (*b*) T. DURST, R. VAN DEN ELZEN, and R. LEGAULT. Can. J. Chem. **52**, 3206 (1974).
8. J. P. DEPRÈS, A. E. GREENE, and P. CRABBÉ. Tetrahedron Lett. 2191 (1978).
9. S. KANO, T. EBATA, K. FUNAKI, and S. SHIBUYA. Synthesis, 746 (1978).
10. (*a*) D. B. R. JOHNSTON, S. M. SCHMITT, F. A. BOUFFARD, and B. G. CHRISTENSEN. J. Am. Chem. Soc. **100**, 313 (1978); (*b*) F. A. BOUFFARD, D. B. R. JOHNSTON, and B. G. CHRISTENSEN. J. Org. Chem. **45**, 1130 (1980).
11. F. DININNO, T. R. BEATTIE, and B. G. CHRISTENSEN. J. Org. Chem. **42**, 2960 (1977).
12. J. A. AIMETTI and M. S. KELLOGG. Tetrahedron Lett. 3805 (1979).
13. P. V. DEMARCO and R. NAGARAJAN. *In* Cephalosporins and penicillins: chemistry and biology. *Edited by* E. H. Flynn. Academic Press, New York. 1972. pp. 330–340.
14. (*a*) H. O. HOUSE, D. S. CRUMRINE, A. Y. TERANISHI, and D. OLMSTEAD. J. Am. Chem. Soc. **95**, 3310 (1973); (*b*) W. A. KLESCHICK, C. T. BUSE, and C. H. HEATHCOCK. J. Am. Chem. Soc. **99**, 247 (1977); (*c*) P. FELLMAN and J. E. DUBOIS. Tetrahedron, **34**, 1349 (1978).
15. J. L. HERMANN, G. R. KIECZYKOWSKI, and R. H. SCHLESSINGER. Tetrahedron Lett. 2433 (1973).
16. W. A. SLUSARCHYK, H. E. APPLEGATE, P. FUNKE, W. KOSTER, M. S. PUAR, M. YOUNG, and J. E. DOLFINI. J. Org. Chem. **38**, 943 (1973).
17. A. MARTEL *et al*. Can. J. Chem. **60**, 942 (1982).

Can. J. Chem. Downloaded from www.nrcresearchpress.com by 210.87.254.6 on 09/06/12
For personal use only.

Page 910. The second sentence after reaction [5] on the left hand column of p. 914 should read "$PA(C_6H_5F) - PA(C_6H_6) = +1.4$ kcal $mol^{-1}$ and $PA(C_6H_5Cl) - PA(C_6H_6) = +0.7$ kcal $mol^{-1}$."

ERRATA

# A comparison of the relative binding energies of $H^+$ and $NO^+$ to aromatic and haloaromatic bases by high pressure mass spectrometry

JOHN A. STONE, DENA E. SPLINTER, AND SOON YAU KONG

*Department of Chemistry, Queen's University, Kingston, Ont., Canada K7L 3N6*

Received October 2, 1981

JOHN A. STONE, DENA E. SPLINTER, and SOON YAU KONG. Can. J. Chem. **60**, 910 (1982).

Proton transfer equilibria ($B_1H^+ + B_2 \rightleftharpoons B_1 + B_2H^+$) and $NO^+$ transfer equilibria ($B_1NO^+ + B_2 \rightleftharpoons B_1 + B_2NO^+$) have been studied for the following bases B, benzene, toluene, *o*-, *m*-, and *p*-xylene. $NO^+$ transfer equilibria for fluoro- and chlorobenzene have also been studied. Pulsed electron beam, high-pressure ion source mass spectrometry has been used to obtain the equilibrium constant $K$ and hence the free energy changes $\Delta G^0$ and from van't Hoff plots, $\Delta H^0$ and $\Delta S^0$. Entropy changes are in general much smaller for $NO^+$ transfer than for $H^+$ transfer but the magnitude of the changes in the proton affinity and $NO^+$ affinity of toluene caused by a fluorine substituent is about the same, even though the absolute value of the proton affinity is greater by a factor of 4. The position of the F substituent on toluene has a marked effect on proton affinity but no effect on $NO^+$ affinity. The latter appears to be responsive only to the inductive effect.

JOHN A. STONE, DENA E. SPLINTER et SOON YAU KONG. Can. J. Chem. **60**, 910 (1982).

On a étudié les équilibres de transfert du proton ($B_1H^+ + B_2 \rightleftharpoons B_1 + B_2H^+$) et les équilibres de transfert du $NO^+$ ($B_1NO^+ + B_2 \rightleftharpoons B_1 + B_2NO^+$) dans les bases B suivantes: benzène, toluène, *o*-, *m*- et *p*-xylène. On a également étudié les équilibres de transfert de $NO^+$ pour les fluoro et chlorobenzènes. On a utilisé le faisceau d'électrons pulsés d'un spectromètre de masse à source d'ions à haute pression pour obtenir la constante d'équilibre $K$ et par la suite les variations d'énergie libre $\Delta G^0$; les courbes de Van't Hoff fournissent le $\Delta H^0$ et $\Delta S^0$. Les variations d'entropie sont en général plus faibles pour le transfert de $NO^+$ que pour celui du $H^+$ mais l'ordre de grandeur des variations de l'affinité du proton et du $NO^+$ pour le toluène, provoqué par le substituant fluor est environ le même, même si la valeur absolue de l'affinité du proton est plus grande d'un facteur de 4. La position du fluor comme substituant sur le toluène a un effet marqué sur l'affinité du proton mais n'en a aucun sur l'affinité du $NO^+$. Ce dernier semble être responsable uniquement de l'effet inductif.

[Traduit par le journal]

## Introduction

Our understanding of substituent effects in solution chemistry has been considerably aided by thermodynamic data obtained from measurements of gas phase ion–molecule equilibria (1). Most gas phase studies have concentrated on proton transfer equilibria although a growing body of information is becoming available for electrophilic reactions involving other cations (2, 3).

Liquid phase electrophilic aromatic substitution has a long experimental history but arguments concerning the actual reaction mechanism still prevail. It is now widely accepted that the transition state is a σ-bonded complex (arenium ion) (4) but there are arguments in favour of a π-bonded transition state in certain cases (5). Although these arguments have been criticized on the grounds that they are based on experimental artefacts (6), the controversy has not been fully resolved. Comparisons of the thermodynamic properties of stable σ and π complexes in the gas phase in the absence of solvent should aid in the understanding of the properties of such transients in solution.

Experimental results and theoretical calculations agree that the stable, protonated aromatics observed in the gas phase are σ bonded (7, 8). In contrast, nitrosated benzene, $C_6H_6NO^+$, formed by transfer of $NO^+$ from nitrosated methylnitrite to benzene, is a π complex which is clearly distinguishable from protonated nitrosobenzene, $C_6H_5NOH^+$ (9). The main evidence in favour of π bonding is the demonstrated ability of $C_6H_6NO^+$ to transfer $NO^+$ rather than $H^+$ to the stronger base pyridine. The experiments were conducted at low pressure ($\sim 10^{-6}$ Torr) in an ion cyclotron resonance (icr) spectrometer. We have confirmed this behaviour in a high pressure ($\sim 1$ Torr) photoionization mass spectrometer (10). Reents and Freiser have recently determined standard free energy changes at 300 K for $NO^+$ transfer equilibria for a large and diverse series of bases (11). Correlations were found between basicity towards $NO^+$ ($\Delta G^0$) and proton affinity ($\Delta H^0$) for several classes of compounds. In discussion of the binding between $NO^+$ and the bases they assumed that entropy changes in such reactions are small. In this paper we report a confirmation of this assumption.

A major argument for π-complex participation in the rate-determining step of aromatic electrophilic substitution reactions in solution is the relatively small effect of ring substituents compared with the effects observed for σ complexes (4). The presence of anomalous substituent effects on ion–molecule reaction rates in the gas phase has also been ascribed to π-complex formation (12). It is, therefore, of value to make further comparisons of

0008-4042/82/070910-06$01.00/0

©1982 National Research Council of Canada/Conseil national de recherches du Canada

proton affinities (σ bonding) with $NO^+$ affinities (π bonding). For the reasons given below we have chosen to study benzene, halobenzenes, toluene, and the three fluorotoluenes.

We have recently determined by high pressure mass spectrometry the proton affinities of $C_6H_6$, $C_6H_5F$, and $C_6H_5Cl$ (13) and shown, in agreement with Lau and Kebarle (14), that proton affinity *decreases* in the order $C_6H_5F > C_6H_5Cl > C_6H_6$. Evidently stabilization of the ion by π donation from halogen situated *para* to the protonation site more than compensates for electron withdrawal by the inductive-field effect. We have examined the $NO^+$ affinity of this group of compounds to determine whether a similar behaviour is observed for π complexes.

The energetically favoured protonation site in toluene is *para* to $CH_3$ (15). The location of a substituent on the toluene ring is therefore expected to have a marked effect on proton affinity whereas for a π complex, whose binding site involves at least two ring C atoms, a different effect of the same substituent might be expected. We have investigated substituent positional effects on the proton affinities (PA) and $NO^+$ affinities (NOA) of *o*-, *m*-, and *p*-fluorotoluene. Neither of these sets of data has been previously reported.

## Experimental

The two high pressure mass spectrometers, one a quadrupole (10) and the other a magnetic sector instrument (16), used in this study have been described previously. The field-free source of the quadrupole photoionization instrument (10) has been replaced by a simple electron impact source, modeled on one previously described (13). The lower LiF window has been replaced by a blank, stainless steel flange and the upper one by a similar flange containing a slit fabricated from razor blades of dimensions 1.5 × 0.05 $mm^2$. The flanges are sealed by gold "O" rings. Ionization is by 500 eV electrons and the electron beam may be pulsed on and off by removal and application of a blocking potential on the first of two electron beam defining electrodes which is −90 V with respect to the filament (13). The vacuum system of this instrument has also been modified to give differential pumping. The source is now separated from the ion-focusing lenses and quadrupole mass analyzer by a stainless steel skimmer plate with a 2 mm circular orifice which is placed 1.5 cm from the ion exit slit. The analyzer side is pumped by a 4 in. diffusion pump while the original 6 in. pump evacuates the ion source housing. The vacuum in the analyzer section is less than $5 \times 10^{-6}$ Torr when the ion source pressure is 1 Torr.

The nitric oxide (Matheson) and methane (Matheson 99.99%) were not dried since water has a much lower basicity towards both $NO^+$ and $H^+$ than any of the compounds used. Benzene (J. T. Baker, Ultrex) and toluene, the fluorotoluenes and the halobenzenes (all Aldrich) were of the highest purity available and were used as received.

Only the quadrupole instrument was used for the $NO^+$ studies. The heated 1 L glass reservoir was filled with NO at 760 Torr and 20 μL of a binary liquid mixture of aromatic compounds of accurately known composition together with 5 μL of carbon tetrachloride were injected and allowed to equilibrate. The carbon tetrachloride was added to attach electrons and reduce the rate of ambipolar diffusion (16). The gaseous mixture was passed into the ion source via a heated all metal valve. Helium was also bled into the source via a separate valve so that the total pressure in the source might be varied independently of the sample pressure. The equilibrium thermodynamic data obtained are independent of the total pressure (range 0.5–1.5 Torr), the NO/He ratio, the molar ratio of the two bases and the amount of sample.

Proton transfer equilibrium measurements were made on both the magnetic and quadrupole instruments, the equilibrium thermodynamic data obtained being identical within experimental error. The buffer gas employed was $CH_4$ rather than the He/NO mixture, otherwise the method for the study of both $NO^+$ and $H^+$ complexes was the same

## Results and discussion

### *Proton affinities of toluene and the fluorotoluenes*

Equilibria of the form

[1] $B_1H^+ + B_2 \rightleftharpoons B_1 + B_2H^+$

were studied to determine the equilibrium constant $K$ from the known ratio of concentrations of neutrals $[B_1]/[B_2]$ and the measured ion current ratio at long residence times, $i_{B_2H^+}/i_{B_1H^+}$ (13). Determination of $K$ leads to $\Delta G^0 = -RT \ln K$. The $\Delta G^0$ values for equilibria between *o*- and *p*-fluorotoluene and toluene are large so an intermediate standard, methyl formate, was employed. The use of this standard limited measurements to high temperature where proton bound dimer formation is not a problem. Entropy changes, $\Delta S^0$, for proton transfer equilibria are in general very small (< 2 cal $K^{-1}$ $mol^{-1}$) for the types of compounds employed and they can be calculated with reasonable accuracy by statistical thermodynamics from changes in external rotational symmetry numbers (17, 18). Relative proton affinities defined as $\Delta H^0$ for reaction [1] were determined from $\Delta H^0 = \Delta G^0 + T\Delta S^0$.

The difference in proton affinity between toluene and methylformate is 1.9 kcal $mol^{-1}$ (high pressure measurements at 600 K (14, 18) and 1.0 kcal $mol^{-1}$ (icr measurements at ~300 K (17)). The discrepancy is substantial. As shown in Table 1, the present value of 1.3 kcal $mol^{-1}$ for an intermediate temperature of 478 K lies between the two literature values which may signify that for this particular system the entropy change upon protonation is not accurately given by calculated changes in symmetry numbers alone or that there is mass discrimination in either or both of the high and low pressure techniques.

The measured reproducibility for the results shown in Table 1 is better than ±0.1 kcal $mol^{-1}$ for $\Delta G^0$ values below 2 kcal $mol^{-1}$ and ±0.2 kcal $mol^{-1}$ for those above. The results are invariant with

TABLE 1. Standard free energy changes for the reaction $B_1H^+ + B_2 \rightleftharpoons B_1 + B_2H^+$ and calculated differences in proton affinity for bases B; $B_2$ is situated above $B_1$

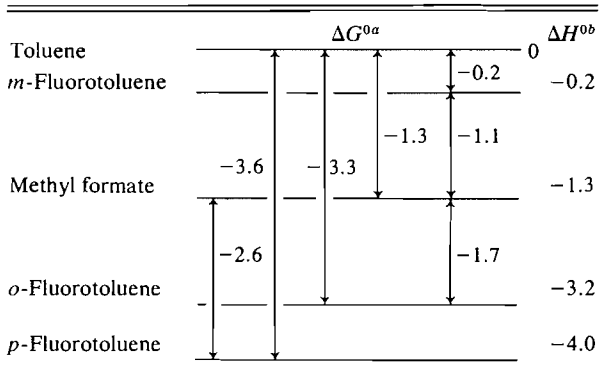


[a]Units kcal mol$^{-1}$. Basicity increases in the upward direction (478 K).
[b]Proton affinity relative to that of toluene. Units kcal mol$^{-1}$.

change in neutral concentration ratio but for the measurement of the large $\Delta G^0$ values the range over which this ratio could be varied and equilibrium still be observed was very limited.

A ring-fluorine substituent on toluene, no matter what its position, decreases the proton affinity in contrast to the increase observed for benzene (13). The position of the substituent does, however, have a very marked effect, both *ortho*- and *para*-fluorine causing a large decrease while a *meta*-fluorine has little effect.

Toluene protonates in the *para* position although *ortho* protonation is energetically only slightly less favoured (15). It is therefore not surprising that *p*-F-toluene has the lowest proton affinity since the protonation site will necessarily change and become *ortho* to methyl but *meta* to fluorine. In this position the latter substituent is electron attracting (19). *o*-F-Toluene presumably protonates *para* to $CH_3$ and *meta* to F and the proton affinity of toluene is consequently again lowered considerably although not quite to the same extent as for the *para*-substituted compound.

Only in *m*-F-toluene are canonical structures involving $\pi$-resonance contributions from fluorine available to enhance the stabilization of the protonated form when protonation is either *para* or *ortho* to $CH_3$ (**I** and **II**). **II** may be favoured by a lessening of the destabilizing inductive effect with distance between F and the tetrahedral ring carbon atom.

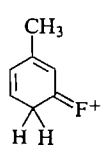


**I**

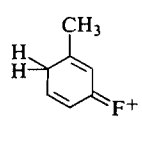


**II**

The observed substituent effects in the fluorotoluene are not a simple superposition of individual effects, but are qualitatively in agreement with expectations.

*$NO^+$ affinities*

NO has been studied as a potentially useful chemical ionization reagent gas (20). Since abundant yields of the association ion $MNO^+$ were observed for internal olefins and dienes M, at pressures in the range 0.5–1.0 Torr it is surprising that NO containing small concentrations of aromatics under CI conditions yielded $MNO^+$ ions as the major product only for compounds with ionization potentials close to that of NO (9.26 eV) (21). When M has a lower ionization potential, charge transfer yielding $M^+$ was the major reaction. Probably the presence of a repeller field, an ion source temperature of 100–200°C and a low pressure (0.5 Torr) did not allow time for collisional stabilization of the initially formed, excited $MNO^+$ complexes. At low pressures only the charge-transfer reaction

[2] $NO^+ + M \rightleftharpoons NO + M^+$

is observed by icr although $MNO^+$ may be readily formed by transfer from nitrosated methylnitrite (11).

The only ions observed in the present work in He/NO mixtures (10–60% NO) at pressures from 0.5 to 1.5 Torr and temperatures around 45°C are $He^+$, $NO^+$, and $(NO)_2^+$. $NO^+$ constitutes more than 90% of the total ion intensity and $(NO)_2^+$ less than 1%. When the electron beam is pulsed, charge transfer from $He^+$ to NO is observed, the lifetime of the $He^+$ being exceedingly short. The presence of a very small amount (~0.1 mol%) of an alkyl or halo-aromatic leads to the rapid disappearance of $NO^+$, the only observed products being $MNO^+$ and for some compounds, a very small amount of $M^+$ (< 2%). The amount of the latter increases to a small extent with increasing temperature but it is only present in significant yields (< 10% total ionization) for one compound *p*-F-toluene and that at 220°C. The reaction scheme is

[3] $M + NO^+ \rightleftharpoons MNO^{+*}$

[4*a*] $MNO^{+*} \xrightarrow{M} MNO^+$

[4*b*] $MNO^{+*} \rightarrow M^+ + NO$

Approximate pseudo second-order rate constants for the disappearance of $NO^+$ may be obtained from the slopes of linear plots such as the one shown in Fig. 1. Values obtained are in the range $1–6 \times 10^{-10}$ cm$^3$ molecule$^{-1}$ s$^{-1}$. All the aromatics employed have ionization potentials within 8 kcal mol$^{-1}$ of that of NO and even though the reaction to

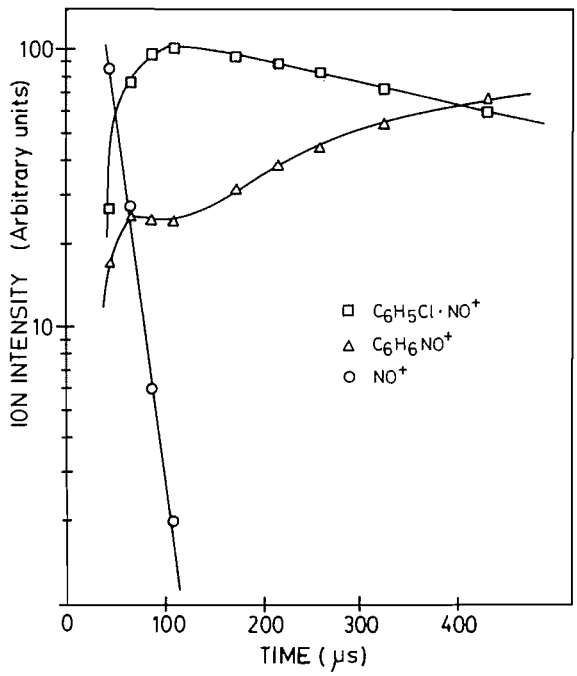


FIG. 1. The variation of ion intensities with time for a mixture containing 0.5 Torr He, 0.5 Torr NO, $5 \times 10^{-4}$ Torr $C_6H_5Cl$, and $2 \times 10^{-5}$ Torr $C_6H_6$ (350 K, 50 μs electron pulse).

form $MNO^+$ does not occur with 100% efficiency, charge transfer is not a significant alternate channel. The dissociation of $MNO^{+*}$ to M and $NO^+$ is efficient.

Provided that the equilibrium constant is not too large ($\Delta G^0 < 5$ kcal $mol^{-1}$), a judicious choice of relative concentrations for two aromatic compounds allows the attainment of equilibrium at long ion residence times (Fig. 2). The equilibrium constant for the reaction

[5] $C_6H_5FNO^+ + C_6H_5Cl \rightarrow C_6H_5F + C_6H_5ClNO^+$

calculated using the invariant ratio of ion currents at long residence times, is constant with change of relative concentrations of $C_6H_5F$ and $C_6H_5Cl$ by at least a factor of 5. The enthalpy change ($\Delta H^0$) is obtained from the temperature dependence of the equilibrium constant (Fig. 3). The results obtained are presented in Table 2 while in Table 3, the $\Delta G^0$ values obtained by Reents and Freiser (11) for toluene, benzene, and the halobenzenes at low pressure are compared with the present values which were obtained by extrapolation of the van't Hoff plots to 298 K since the lowest operating temperature with the present instrumentation is 328 K.

The ordering of the basicities is the same under low (icr) and high pressure conditions and the internal consistency is good for each method. The

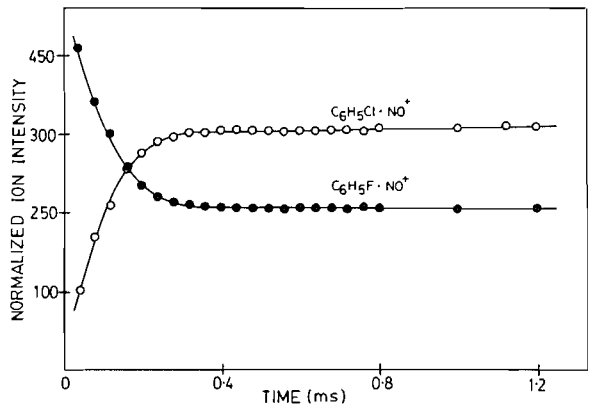


FIG. 2. The normalized ion yields for a mixture containing 0.53 Torr He, 0.20 Torr NO, $7 \times 10^{-4}$ Torr $C_6H_5Cl$, and $3 \times 10^{-3}$ Torr $C_6H_5F$ (328 K, 50 μs pulse).

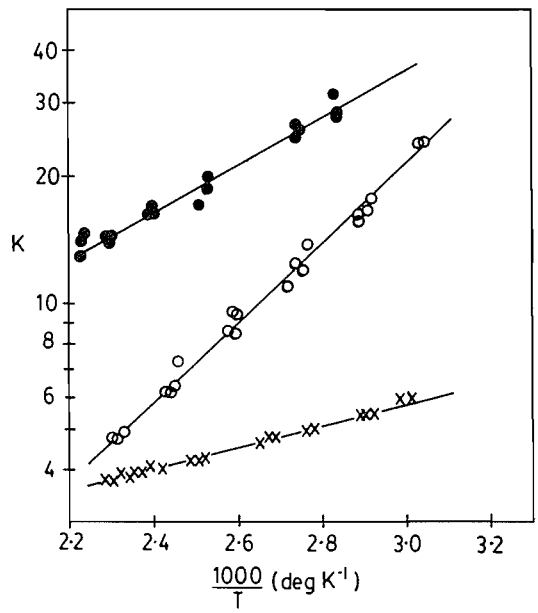


FIG. 3. van't Hoff plots of equilibrium constants for reactions $B_1NO^+ + B_2 \rightleftharpoons B_1 + B_2NO^+$: ($B_1$, $B_2$): × ($C_6H_5F$, $C_6H_5Cl$); ○ ($C_6H_5F$, $C_6H_6$); ● ($C_6H_5Cl$, $C_6H_6$).

absolute values do differ somewhat and it is a little disturbing that $\Delta G^0$ differs by almost a factor of 2 for the only pair ($C_6H_5F/C_6H_5Cl$) for which direct determinations were made at both pressures. We plan to investigate a wider range of compounds to determine whether there is a significant difference between the results obtained by the two methods. There will be limitations to this range since we find from preliminary experiments that, as with proton transfer equilibrium measurements, there can be complications due to further solvation when polar molecules are investigated. For example, nitrobenzene readily forms $(C_6H_5NO_2)_2NO^+$.

TABLE 2. Standard enthalpy changes (kcal $mol^{-1}$) and standard entropy changes (cal $K^{-1}$ $mol^{-1}$, in parentheses) for the reaction $B_1NO^+ + B_2 \rightleftharpoons B_1 + B_2NO^+$; $B_2$ is situated above $B_1$

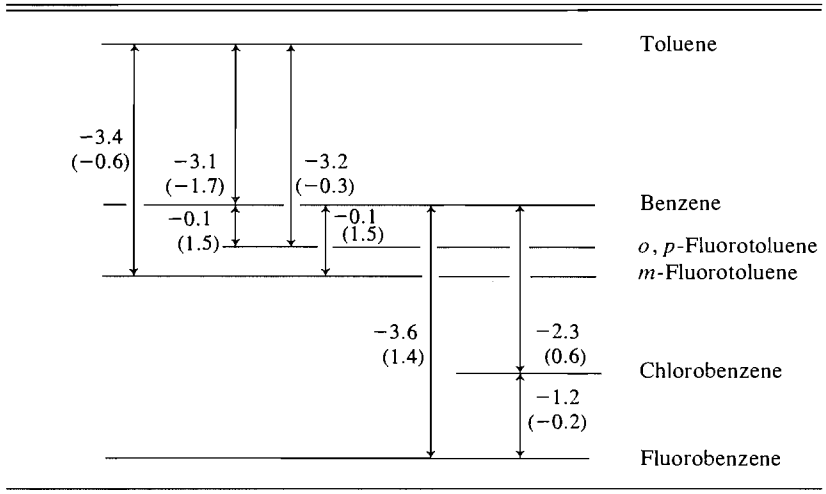


TABLE 3. Standard free energy changes for the reaction $B_1NO^+ + B_2 \rightleftharpoons B_1 + B_2NO^+$

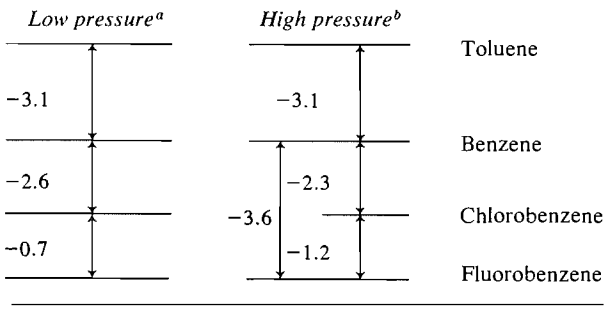


[a]Reference 11, 298 K.
[b]This work, extrapolation to 298 K. Units: kcal $mol^{-1}$. Basicity increases in the upward direction.

By analogy with the definition of proton affinity (PA), the nitric oxide cation affinity (NOA) of a compound M will be defined as the enthalpy change for the reaction

[5] $MNO^+ \rightarrow M + NO^+$

The differences and similarities between NOA and PA values are immediately obvious when data from Tables 1 and 2 and ref. 13 are compared. (In the latter reference the relevant data are: $PA(C_6H_5F)$ $PA(C_6H_6) = +0.7$ kcal $mol^{-1}$.) (*i*) The stabilizing effect of a $CH_3$ group for the $\pi$ complex is less than 50% that for the $\sigma$ complex (NOA(toluene) − NOA(benzene) = 3.1 kcal $mol^{-1}$, PA(toluene) − PA(benzene) = 8.4 kcal $mol^{-1}$ (14)). (*ii*) An F substituent raises PA(benzene) by 1.4 kcal $mol^{-1}$ but NOA is decreased by 3.6 kcal $mol^{-1}$. A Cl substituent behaves similarly but its effect on both PA and NOA is less than that of F. (*iii*) An F substituent decreases NOA(toluene) by roughly the same extent as that of benzene. This decrease is practically independent of position whereas, as discussed earlier, the effect on PA is very sensitive to the position of the substituent.

In the $\sigma$ complex the proton forms a covalent bond with a ring carbon whose character changes from $sp^2$ to $sp^3$. The positive charge is delocalized over the ring and is subject to stabilization or destabilization by both substituent-inductive and resonance effects. Bonding in $MNO^+$ will mainly involve overlap of the vacant $2\pi$ antibonding orbital of $NO^+$ with the highest filled aromatic orbital ($E_{1b}$) in benzene, the most stable structure presumably having $C_{6v}$ symmetry with nitrogen closest to the ring. Fluorine shows an electron-withdrawing effect in destabilizing both the benzene and toluene $NO^+$ complexes. We therefore agree with Reents and Freiser that the electron-donating or -withdrawing ability of the substituent is the important parameter in deciding the stability of the $\pi$ complex (11). Resonance effects are not of significance.

It is interesting to note that although the PA values of the molecules studied are more than four times the NOA values (NOA(toluene) ~49 kcal $mol^{-1}$ (11)), the absolute value of the effect of a halogen substituent is as great on NOA as on PA.

*Entropy changes in $NO^+$ transfer equilibria*

All the entropy changes shown in Table 3 are small, the only ones that are significantly different from zero involve benzene. Entropy changes for proton transfer equilibria between benzene and the halobenzenes are about three times larger than for

$NO^+$ and in the opposite direction, i.e., there is an increase in entropy when $C_6H_6$ (rotational symmetry number $\sigma = 12$) becomes $C_6H_7^+$ ($\sigma = 2$) (13). The nitrosation of $C_6H_6$ seems to consistently give a decrease in entropy of 0.6–1.5 cal $K^{-1}$ $mol^{-1}$ which cannot be accounted for by appropriate statistical calculations with reasonable and consistent geometries for the complexes. It is to be noted that the ladder of entropies is not very self-consistent even allowing for a reproducibility of $\pm 0.4$ in entropy difference measurements. Entropy determinations, unlike enthalpy determinations, are very sensitive to any mass discrimination in ion sampling from the source or in the analysis system. At the moment we can only conclude that the entropy changes in $NO^+$ transfer equilibria are very small.

**Acknowledgement**

The authors thank the Natural Sciences and Engineering Research Council of Canada for financial support.

1. R. W. TAFT. *In* Proton transfer reactions. *Edited by* E. F. Caldin and V. Gold. Chapman and Hall, London. 1975. p. 31.
2. P. KEBARLE. Ann. Rev. Phys. Chem. **28**, 445 (1977).
3. A. W. CASTLEMAN, P. M. HOLLAND, T. D. MARK, K. I. PETERSON, R. G. KEESEE, and N. LEE. Proc. 28th Ann. Conf. Mass Spec. and Allied Topics. New York 1980. pp. 68–69.
4. J. MARCH. Advanced organic chemistry. 2nd ed. McGraw-Hill. 1977.
5. G. A. OLAH. Acc. Chem. Res. **4**, 240 (1971).
6. D. V. BANTHORPE. Chem. Rev. **70**, 295 (1970).
7. J. F. WOLF, J. L. DEVLIN, D. J. DEFREES, R. W. TAFT, and W. J. HEHRE. J. Am. Chem. Soc. **98**, 5097 (1976).
8. W. C. ERMLER and R. S. MULLIKEN. J. Am. Chem. Soc. **100**, 1647 (1978).
9. W. D. REENTS and B. S. FREISER. J. Am. Chem. Soc. **102**, 271 (1980).
10. J. A. STONE, M. S. LIN, and J. VARAH. Can. J. Chem. **59**, 2412 (1981).
11. W. D. REENTS and B. S. FREISER. J. Am. Chem. Soc. **103**, 2791 (1981).
12. D. A. CHATFIELD and M. M. BURSEY. J. Am. Chem. Soc. **98**, 6492 (1976).
13. D. K. BOHME, J. A. STONE, R. S. MASON, R. S. STRADLING, and K. R. JENNINGS. Int. J. Mass Spec. Ion Phys. **37**, 283 (1981).
14. Y. K. LAU and P. KEBARLE. J. Am. Chem. Soc. **98**, 7452 (1976).
15. J. L. DEVLIN, J. F. WOLFE, R. W. TAFT, and W. J. HEHRE. J. Am. Chem. Soc. **98**, 1990 (1976).
16. P. KEBARLE. *In* Interactions between ions and molecules. *Edited by* P. Ausloos. Plenum Press, New York. 1974. p. 459.
17. J. F. WOLF, R. H. STALEY, I. KOPPEL, M. TAAGEPERA, R. T. MCIVER, J. L. BEAUCHAMP, and R. W. TAFT. J. Am. Chem. Soc. **99**, 5417 (1977).
18. R. YAMDAGNI and P. KEBARLE. J. Am. Chem. Soc. **98**, 1320 (1976).
19. J. F. WOLF, J. L. DEVLIN, D. J. DEFREES, R. W. TAFT, and W. J. HEHRE. J. Am. Chem. Soc. **98**, 5097 (1976).
20. D. F. HUNT and T. M. HARVEY. Anal. Chem. **47**, 2136 (1975).
21. N. EINOLF and B. MUNSON. Int. J. Mass Spec. Ion Phys. **9**, 141 (1972).

# The pressure dependence of the rate of isomerization of cyclopropane at 897 K

HIROSHI FURUE AND PHILIP D. PACEY

*Department of Chemistry, Dalhousie University, Halifax, N.S., Canada B3H 4J5*

Received December 15, 1980[1]

HIROSHI FURUE and PHILIP D. PACEY. Can. J. Chem. **60**, 916 (1982).

The isomerization of cyclopropane has been studied in a flow reactor at 897 K and from 4 to 406 Torr. The pressure dependence of the rate constants from this work and from the literature have been compared with predictions obtained from two models based on the theory of Yau and Pritchard and from three RRKM models. The collisional deactivation efficiency was found to generally decline with increasing temperature. The average energy removed per collision was calculated by the method of Tardy and Rabinovitch and was found to have values from 15 to 23 kJ mol$^{-1}$ at 897 K. Combining the results of this work with data from the literature from 690 to 1038 K, the limiting high pressure rate constants follow the relation $\log k_\infty = 15.50 \pm 0.14 - (276.0 \pm 2.1 \text{ kJ mol}^{-1})/2.3RT$.

HIROSHI FURUE et PHILIP D. PACEY. Can. J. Chem. **60**, 916 (1982).

L'isomérisation du cyclopropane a été étudiée à 897 K, à des pressions comprises entre 4 et 406 Torr et en réacteurs dynamiques. On a comparé les résultats avec les prédictions de la théorie RRKM, en utilisant trois hypothèses différentes pour la structure du complexe activé, et avec les prédictions de la théorie de Yau et Pritchard. La probabilité de désactivation collisionelle diminue aux hautes températures. L'énergie moyenne transférée par collision est entre 15 et 23 kJ mol$^{-1}$ à 897 K, selon la méthode de Tardy et Rabinovitch. Les paramètres d'Arrhénius à la limite de hautes pressions, en tenant compte des résultats antérieurs entre 690 et 1038 K, sont $\log A = 15{,}50 \pm 0{,}14$ et $E_A = 276{,}0 \pm 2{,}1$ kJ mol$^{-1}$.

## Introduction

The isomerization of cyclopropane has played an important part in the study of unimolecular reactions. Because it is a reasonably clean reaction system, it was the subject of early, successful experimental investigations (1, 2). In turn, because of the availability of the experimental data, it was one of the first reactions used to test RRKM theory (3, 4). It has now been the subject of at least 20 experimental studies (1, 2, 5–22) and at least three RRKM models (3, 4, 23).

Despite this impressive body of work, some questions remain. RRKM models which were developed to reproduce the fall-off of the rate constant at low pressures at one temperature have been found to be unsuccessful at other temperatures (4). It has been suggested (16, 17) that this is caused by a decline in β, the efficiency of collisions in removing excess vibrational energy, as the temperature increases. The evidence for this is strong for collisions of cyclopropane with small molecules like He, for which β is said to fall from 0.08 at 771 K (16) to 0.006 at 1175 K (20). The evidence is weaker for collisions of cyclopropane with itself, where β is said to fall from unity at 771 K to 0.5 ± 0.05 at 973 K (17).

When one examines the experimental data, certain strengths and weaknesses are evident. Most studies (1, 2, 7, 8, 17) agree that the Arrhenius parameters at the high pressure limit are in the following ranges: $\log_{10} A$ (s$^{-1}$) = 15.2–15.5, $E_A$ = 272–276 kJ mol$^{-1}$. For the rate constants themselves, reliable, limiting high pressure values, $k_\infty$, based on extrapolation of data from a number of pressures, have been obtained between 718 K and 773 K (1, 2, 5, 7). There have been six recent studies of the pressure dependence of the rate at higher temperatures (17–22), but the pressure ranges were narrow and the authors did not extrapolate their data to determine $k_\infty$. In the studies of the collision efficiency at high temperatures (16, 18, 20, 22), $k_\infty$ was calculated starting with the above Arrhenius parameters determined at lower temperatures. Even these relatively precise Arrhenius parameters can lead to an uncertainty in $k_\infty$ at 1000 K of 50%.

The purpose of the present work is to study the reaction at high pressures and high temperatures using a flow system. Such a system can provide activation energies (24) and reaction orders (25), d ln $k$/d ln $P$, with a precision of 2 or 3%. This precision is not better than that of the activation energy quoted above, so experiments were restricted to a single temperature, 897 K. At this temperature the pressure has been varied by two orders of magnitude. The data from this study, together with data from the literature, are compared with the predictions of RRKM theory, using three different structures for the activated complex, and with the predictions of a newer theory due to Yau and Pritchard (26). These comparisons are achieved by making horizontal and vertical adjustments to theoretical and experimental plots of log $k$ versus log $P$. As explained in the discussion, this comparison provides estimates of $k_\infty$ and β. Values of $k_\infty$ are compared with literature values in the form of an

[1]Revision received December 8, 1981.

0008-4042/82/070916-05$01.00/0

©1982 National Research Council of Canada/Conseil national de recherches du Canada

Can. J. Chem. Downloaded from www.nrcresearchpress.com by 210.87.254.40 on 09/06/12
For personal use only.

Arrhenius plot and the temperature dependence of β is examined.

## Experimental

A general description of the apparatus has been given elsewhere (24, 25, 27). Quartz flow reactor tubes of 2 and 8 mm inside diameter were heated by a 45 cm long, Nichrome-wound resistive furnace. For the 2 mm reactor, a thermocouple was placed inside a coaxial quartz tube of 8 mm inside diameter, but for the 8 mm reactor it was placed in a 4 mm outside diameter tube positioned along the reactor axis. The platinum/platinum–13% rhodium thermocouple was calibrated against the melting point of gold.

Product concentrations were analyzed in a gas chromatograph with a 2 m, 10% silicone oil on Chromosorb W column at 0°C. Cyclopropane (Matheson) was degassed at nitrogen-boiling and isopentane-melting temperatures. It contained about 0.3% propylene as an impurity.

## Results

Experiments have been performed from 3.9 to 406 Torr, the useful range of the Bell and Howell 4-366-0006-03MO pressure transducer employed. Rate constants, $k$, were calculated from measured yields of propylene. At pressures above 100 Torr it was necessary to increase the calculated rate constant by from 3 to 10% because of the effect of incomplete radial heat transfer (27). The values of $k$ obtained are shown in Fig. 1.

## Discussion

The data were compared to the predictions of RRKM theory for three activated complex structures: Model *a* (ref. 23), Model *b* (ref. 20), and Model *c* (ref. 4). Most details of these models are given in the appropriate references. For Model *a*, the vibrational frequencies (in $cm^{-1}$) in the complex were chosen as 3056(6), 1452(3), 1116(5), 640(2), and 530(4). The degeneracies are given in parentheses. The density of states in the biradical intermediate, included in ref. 23, was omitted here, because it was found to have little influence (23). The properties of the reactant were obtained from ref. 28. All vibrations were assumed to be harmonic. The hard sphere collision diameter was taken as 0.44 nm, as found at 773 K in ref. 17. Calculations were performed using an extended version of the Bunker–Hase RRKM program (29). Densities of reactant states were calculated using the Whitten–Rabinovitch technique. Numbers of activated complex states were obtained by a direct count. The integration was carried out over a range of 120 kJ $mol^{-1}$ above the barrier height with a step size of 1.6 kJ $mol^{-1}$.

Results of these calculations are shown as the smooth curves in Fig. 1. It is clear that all of the models lead to a high pressure, limiting rate constant, $k_\infty$, less than that indicated by the experimental data.

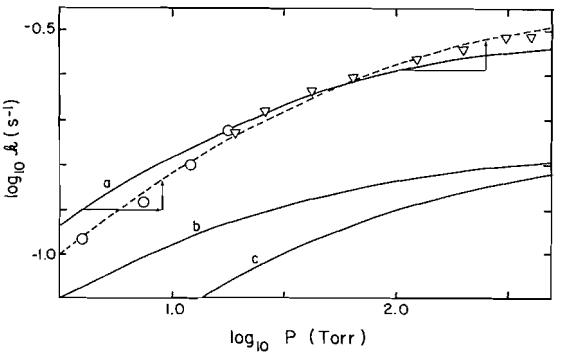


FIG. 1. Experimental and theoretical values of $k$ at 897 K; ▽, data from 2 mm id reactor; ○, data from 8 mm id reactor; *a*, *b*, *c*, predicted by Models *a*, *b*, *c*, respectively, --- curve *a* shifted horizontally and vertically to improve the fit.

The theoretical curves were then shifted vertically and horizontally to improve the fit with experiment. The dotted curve shows the result of shifting curve *a*. This procedure has been used previously for RRKM curves in this laboratory (25), for Kassel curves by Powell (30), and for analytical fits to RRKM curves by Troe (31). A shift to the right by an amount ε corresponds to a decrease of ε in log β; an upwards shift, to an increase in log $k_\infty$. The change in β assumes that β is constant within the experimental pressure range. The vertical shift involves an apparent contradiction: to change $k_\infty$ it is necessary to change either the pre-exponential factor or the activation energy in the RRKM model itself. This introduces two conceptual difficulties. Firstly, the structure of the complex for the shifted curve must be different from the structure for the original curve. This difficulty cannot be avoided; some complexes cannot fit all the data. Secondly, changing the structure of the complex can shift the fall-off to higher or lower pressures. In other words, a vertical shift may entail a horizontal shift; the two dimensions are not independent. This difficulty can be avoided if the pre-exponential factor, $A$, and activation energy, $E_A$, are changed simultaneously in such a way that they induce equal and opposite horizontal shifts. In ref. 4 it was shown that multiplying $A$ by γ leads to a horizontal shift of log γ. Similarly, increasing $E_A$ by δ leads to a horizontal shift of $-\theta\delta/(2.3RT)$. Here θ was shown to be approximately 0.24 for cyclopropane (4). The shifts are equal and opposite, then, when $\log \gamma = \theta\delta/(2.3RT)$. For example, in Fig. 1, curve *c* can be shifted upward without affecting the horizontal

Can. J. Chem. Downloaded from www.nrcresearchpress.com by 210.87.254.40 on 09/06/12
For personal use only.

Can. J. Chem. Downloaded from www.nrcresearchpress.com by 210.87.254.40 on 09/06/12
For personal use only.

axis if $E_A$ is decreased by 7.9 kJ mol$^{-1}$ and log $A$ is decreased by 0.11. In summary, the method illustrated in Fig. 1 has conceptual limitations, but it does provide a means of comparing experimental data with the results of sophisticated theoretical calculations.

A similar method was used to compare the data with the results of the theory of Yau and Pritchard (26), which uses different expressions for the rates of energy transfer and reaction by energized molecules. Model *d* is the same as that proposed for cyclopropane in ref. 26, but with the collision diameter changed to 0.44 nm. Model *e* has the Arrhenius parameters changed so that no vertical adjustment is required at 764 and 897 K.

Adjusted values of $k_\infty$, determined from vertical shifts, depended only slightly on the structure of the complex used to obtain the theoretical curves. For example, the values of $k_\infty$ obtained from Fig. 1 were 0.363, 0.368 and 0.369 s$^{-1}$, after adjustment of curves *a*, *b* and *c*, respectively. Model *d* yielded 0.361 s$^{-1}$. By a least-squares fit of the data of Fig. 1 to an expression of the form (32),

$$[1] \quad k^{-1} = k_\infty^{-1} + aP^{-\alpha}$$

where $a$ and $\alpha$ are adjustable parameters, $k_\infty$ was found to be $0.353 \pm 0.012$ s$^{-1}$. (Here the uncertainty is a standard deviation, $a = 15.6 \pm 0.9$, and $\alpha = 0.62 \pm 0.03$. Points were given a weighting proportional to $k^2$.) The two methods of extrapolation are in substantial agreement.

Figure 2 shows an Arrhenius plot for $k_\infty$. For the results of refs. 5, 7, 18, 19, and this work, the values shown were obtained by the procedure illustrated in Fig. 1. For refs. 10, 14, and 15, values of $k_\infty$ were taken from the original articles. For refs. 1, 2, 6, and 8, quoted values of $k$ have been multiplied by the value of $k_\infty/k$ calculated for the experimental pressure and temperature using Model *c*. This model was selected as, without adjusting the original value of $\beta$, it came closest to reproducing the pressure dependence observed at 718 (7), 764 (5) and 897 K. The five highest temperature points were obtained from experiments in shock tubes (14, 15, 18, 19), for which temperatures are difficult to calculate and for which adjustments of $k$ to $k_\infty$ are greater. For these reasons, data from shock tube experiments at even higher temperatures have been omitted.

The straight line in Fig. 2 was obtained from the most extensive set of experimental data (8). The Arrhenius parameters for this line are given in the first row of Table 1. Arrhenius parameters for a fit to all the points in Fig. 2 are given in the second line of the table.

The activated complex theory expressions for $k_\infty$ according to the three RRKM models (before any vertical adjustments) have been differentiated to obtain the following parameters:

$$[2] \quad E_A = -R(\mathrm{d} \ln k_\infty / \mathrm{d}T^{-1})$$

$$[3] \quad A = k_\infty \exp(E_A/RT)$$

$$[4] \quad C = \mathrm{d}E_A/\mathrm{d}T$$

The values of the parameters determined at 750 K are quoted in Table 1. The values of $\log_{10} A$ and $E_A$

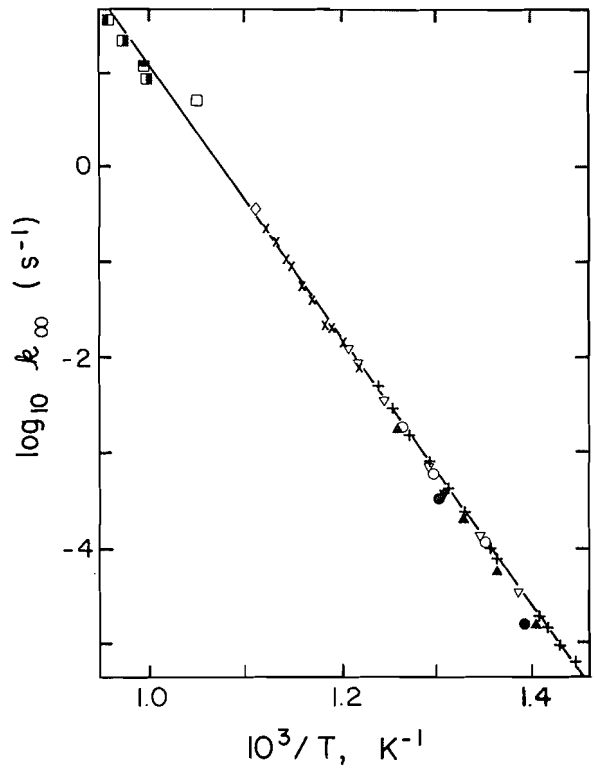


FIG. 2. Arrhenius plot of $k_\infty$: ○, ref. 1; ▲, ref. 2; ▼, ref. 5; ▽, ref. 6; ●, ref. 7; +, ref. 8; ×, ref. 10; ◨, ref. 14; □, ref. 15; ◧, ref. 18; ◒, ref. 19; ◇, this work. The straight line is a least-squares fit to the points from ref. 8.

TABLE 1. Temperature dependence of $k_\infty$

| Source | $\log_{10} A^a$ (s$^{-1}$) | $E_A{}^a$ (kJ mol$^{-1}$) | $C^a$ (J mol$^{-1}$ K$^{-1}$) |
|---|---|---|---|
| Experimental results | | | |
| Ref. 8 | 15.45 | 274.3 | 0 |
| All data linear | 15.50±0.14 | 276.0±2.1 | 0 |
| Predictions for three activated complex structures | | | |
| Model *a* (ref. 23) | 15.45 | 274.0 | 8 |
| Model *b* (ref. 20) | 15.25 | 275.4 | 11 |
| Model *c* (ref. 4) | 15.07 | 272.2 | 5 |
| Parameters for method of ref. 26 | | | |
| Model *d* | 15.27 | 274.5 | 0 |
| Model *e* | 16.76 | 295.5 | 0 |

[a]Where $C = 0$, the Arrhenius plot was assumed to be straight. Where $C \neq 0$, the parameters quoted are for $T = 750$ K. Quoted uncertainties are standard deviations.

TABLE 2. Collision efficiencies and average energy removed per collision

| $T$ (K) | Average reaction order | Model $a$ | | Model $b$ | | Model $c$ | | Model $d$ | Model $e$ |
|---|---|---|---|---|---|---|---|---|---|
| | | $\beta^a$ | $\langle\Delta E\rangle^b$ | $\beta^a$ | $\langle\Delta E\rangle^b$ | $\beta^a$ | $\langle\Delta E\rangle^b$ | $\beta^a$ | $\beta^a$ |
| 718[c] | 1.2 | 0.81 | $\geq 20$ | 0.34 | 15 | 0.43 | 17 | 0.11 | 1.20 |
| 764[d] | 1.33 | 0.48 | 17 | 0.19 | 10 | 0.27 | 13 | 0.063 | 0.69 |
| 897 | 1.25 | 0.45 | 23 | 0.21 | 15 | 0.21 | 16 | 0.060 | 0.69 |

[a]Determined from horizontal adjustments, as in Fig. 1, of curves predicted by Models $a$ to $e$.
[b]kJ mol$^{-1}$. Calculated from $\beta$, the average order of reaction and $\langle E^+\rangle$, using the results of ref. 34 for a stepladder model.
[c]From the data of ref. 7.
[d]From the data of ref. 5.

for Model $a$ are the closest to those observed experimentally. The positive values of $C$ indicate that these models predict a slight upward curvature of the Arrhenius plot. This curvature would be too small to be detected experimentally.

The Arrhenius parameters for Model $e$, quoted in Table 1, are too large to be reasonable. This is caused by the fact that the points in Fig. 2 at 764 K and 897 K are 0.14 log units low and 0.07 units high, respectively, compared to the straight line.

Values of $\beta$ determined from the horizontal shifts required in Fig. 1 and from similar fits to the data of refs. 5 and 7 are quoted in Table 2.

The values of $\beta$ were found to be greatest from Model $e$. This was expected, as this model had the largest value of $A$ (4). The values of $\beta$ for Models $b$ and $c$ did not follow the order of the values of $A$. This is caused by the greater values of $E_A$ and $C$ in Model $b$. (Forst (33) has shown that a large value of $C$ requires a smaller value of $\beta$.) Model $d$ also gives lower values of $\beta$, as was noted when the model was originally developed (26).

Table 2 also shows that $\beta$ declines in most cases with increasing temperature. This confirms the recent experimental findings of Rabinovitch and co-workers (16, 17, 20–22) and the theoretical predictions of Tardy and Rabinovitch (34) and of Troe (31). The decline is clearest from 718 to 764 K.

The above-mentioned theories also indicate that it is possible to determine $\langle\Delta E\rangle$, the average energy removed per collision, from measurements of $\beta$ and the order. The theory of Tardy and Rabinovitch requires the assumption of a model for deactivation of reactant molecules and a calculation of $\langle E^+\rangle$, the average energy of reacting molecules above the barrier height in the second order regime. They recommend the use of a stepladder model of deactivation for efficient deactivators like cyclopropane. Values of $\langle E^+\rangle$ have been obtained by numerical integration of the expression,

$$[5]\quad \langle E^+\rangle = \frac{\int_{E_0}^{\infty} (E - E_0)N(E)\exp(-E/RT)\mathrm{d}E}{\int_{E_0}^{\infty} N(E)\exp(-E/RT)\mathrm{d}E}$$

where $E$ is the energy, $E_0$, the barrier height, and $N(E)$, the density of states. Using the quasi-universal graphs in ref. 34, values of $\langle\Delta E\rangle$ have been calculated and are listed in Table 2.

Rabinovitch and co-workers (16, 17, 21) have recently found evidence for a decline in $\langle\Delta E\rangle$ with increasing temperature in the isomerization of 1,1-cyclopropane-$d_2$. They measured rate constants and kinetic isotope effects and compared their data with the predictions of a modified RRKM calculation, based on a structure for the activated complexes like the present Model $b$. At 773 K, they found $\langle\Delta E\rangle \approx 40$ kJ mol$^{-1}$. This is greater than the values in Table 2 at 718 and 764 K. The method of Rabinovitch and co-workers, involving a competition between isotopically distinct reaction channels, is a more powerful method for finding $\langle\Delta E\rangle$ than the present method. We do not have an explanation of the difference in the results, but we note that, when $\beta$ approaches unity, as at low temperatures, any uncertainty in $\beta$ leads to a substantially greater uncertainty in $\langle\Delta E\rangle$. At 973 K Rabinovitch and co-workers (21) found $\langle\Delta E\rangle \approx 22$ kJ mol$^{-1}$. This is in satisfactory agreement with the results of the present work at 897 K.

**Acknowledgements**

The authors wish to thank Dr. C. R. Masson of the Atlantic Research Laboratory, National Research Council of Canada, for assistance with the calibration of the thermocouple and the Natural Sciences and Engineering Research Council of Canada for a grant in support of this work.

1. T. S. CHAMBERS and G. B. KISTIAKOWSKY. J. Am. Chem. Soc. **56**, 399 (1934).
2. E. S. CORNER and R. N. PEASE. J. Am. Chem. Soc. **67**, 2067 (1945).
3. D. W. SETSER and B. S. RABINOVITCH. Can. J. Chem. **40**, 1425 (1962).
4. G. M. WIEDER and R. A. MARCUS. J. Chem. Phys. **37**, 1835 (1962).
5. H. O. PRITCHARD, R. G. SOWDEN, and A. F. TROTMAN-DICKENSON. Proc. R. Soc. A**217** 563 (1953).
6. R. H. LINDQUIST and G. K. ROLLEFSON. J. Chem. Phys. **24**, 725 (1956).
7. E. W. SCHLAG and B. S. RABINOVITCH. J. Am. Chem. Soc. **82**, 5996 (1960).

Can. J. Chem. Downloaded from www.nrcresearchpress.com by 210.87.254.40 on 09/06/12
For personal use only.

8. W. E. FALCONER, T. F. HUNTER, and A. F. TROTMAN-DICKENSON. J. Chem. Soc. 609 (1961).
9. G. L. PRATT. J. Chem. Soc. 6050 (1963).
10. B. R. DAVIS and D. S. SCOTT. Ind. Eng. Chem. Fund. **3**, 20 (1964).
11. E. A. DORKO, D. B. MCGHEE, C. E. PAINTER, A. J. CAPONECCHI, and R. W. CROSSLEY. J. Phys. Chem. **75**, 2526 (1971).
12. J. N. BRADLEY and M. A. FREND. Trans. Faraday Soc. **67**, 72 (1971).
13. E. V. WAAGE and B. S. RABINOVITCH. J. Phys. Chem. **76**, 1695 (1972).
14. P. JEFFERS, D. LEWIS, and M. SARR. J. Phys. Chem. **77**, 3037 (1973).
15. J. A. BARNARD, A. T. COCKS, and R. J. Y. LEE. J. Chem. Soc. Faraday Trans. I, **70**, 1782 (1974).
16. I. E. KLEIN, B. S. RABINOVITCH, and K. H. JUNG. J. Chem. Phys. **67**, 3833 (1977).
17. I. E. KLEIN and B. S. RABINOVITCH. J. Phys. Chem. **82**, 243 (1978); Chem. Phys. **35**, 439 (1978).
18. D. K. LEWIS, S. E. GIESLER, and M. S. BROWN. Int. J. Chem. Kinet. **10**, 277 (1978).
19. W. TSANG. Int. J. Chem. Kinet. **10**, 599 (1978).
20. E. KAMARATOS, J. F. BURKHALTER, D. G. KEIL, and B. S. RABINOVITCH. J. Phys. Chem. **83**, 984 (1979).
21. V. V. KRONGAUZ, M. E. BERG, and B. S. RABINOVITCH. Chem. Phys. **47**, 9 (1980).
22. J. F. BURKHALTER, E. KAMARATOS, and B. S. RABINOVITCH. J. Phys. Chem. **84**, 476 (1980).
23. M. C. LIN and K. J. LAIDLER. Trans. Faraday Soc. **64**, 927 (1968).
24. P. D. PACEY. Can. J. Chem. **53**, 2742 (1975).
25. P. D. PACEY and J. H. WIMALASENA. J. Phys. Chem. **84**, 2221 (1980).
26. A. W. YAU and H. O. PRITCHARD. Can. J. Chem. **56**, 1389 (1978).
27. H. FURUE and P. D. PACEY. J. Phys. Chem. **84**, 3139 (1980).
28. T. SHIMANOUCHI. Tables of molecular vibrational frequencies, consolidated volume I. U.S. Dept. of Commerce, Washington. 1972.
29. D. L. BUNKER and W. L. HASE. Quantum Chemistry Program Exchange, **10**, 234 (1974).
30. R. E. POWELL. J. Chem. Phys. **30**, 724 (1959).
31. J. TROE. J. Phys. Chem. **83**, 114 (1979).
32. I. OREF and B. S. RABINOVITCH. J. Phys. Chem. **72**, 4488 (1968).
33. W. FORST. J. Phys. Chem. **83**, 100 (1979).
34. D. C. TARDY and B. S. RABINOVITCH. J. Chem. Phys. **48**, 1282 (1968).

Can. J. Chem. Downloaded from www.nrcresearchpress.com by 210.87.254.40 on 09/06/12
For personal use only.

# A reactive lactonic dienophile – 3-carbethoxy-5,5-dimethyl-2(5*H*)-furanone. Application to the synthesis of a monoterpenoid lactone

HSING-JANG LIU, ERIC N. C. BROWNE, AND PURUSHOTTAM R. PEDNEKAR

*Department of Chemistry, University of Alberta, Edmonton, Alta., Canada T6G 2G2*

Received November 2, 1981

HSING-JANG LIU, ERIC N. C. BROWNE, and PURUSHOTTAM R. PEDNEKAR. Can. J. Chem. **60**, 921 (1982).

In contrast to the low dienophilicity generally observed for α,β-unsaturated lactones, the title compound **2** is shown to be a reactive dienophile. Under stannic chloride catalysis, it undergoes Diels–Alder reaction regio- and stereoselectively with a variety of dienes at room temperature. The synthesis of (±)-*o*-mentha-1,3-dien-1→8-olide (**20**) has been achieved by a two-step sequence using lactone ester **2**. Addition of **2** to 1-acetoxy-1,3-butadiene afforded epimeric acetoxy lactones **12** and **13** which were converted to the monoterpenoid lactone **20** by treatment with lithium iodide dihydrate in collidine.

HSING-JANG LIU, ERIC N. C. BROWNE et PURUSHOTTAM R. PEDNEKAR. Can. J. Chem. **60**, 921 (1982).

Alors que les lactones, α,β-non saturées ne sont généralement pas de bons dièmophiles, le composé **2** est un dièmophile réactif. Sous l'effet de la catalyse acide du chlorure stanneux, il subit, à la température ambiante, une réaction de Diels–Alder régio- et stéréo-sélective avec divers dièmes. On a réalisé la synthèse du (±)-*o*-menthadiène-1,3 olide-1→8 (**20**) en deux étapes à partir de la lactone ester **2**. L'addition de **2** à l'acétoxy-1 butadiène-1,3 fournit les acétoxy lactones épimères **12** et **13** qui peuvent être transformées dans la lactone **20** par traitement avec le dihydrate de l'iodure de lithium dans la collidine.

[Traduit par le journal]

Although α,β-unsaturated esters and carboxylic acids have long been characterized as reactive dienophiles and have been widely used as such in organic synthesis (1), the Diels–Alder reaction of the corresponding lactones has not been extensively studied in spite of its potential utility as a more direct approach to useful intermediates. Possibly this is due to the expectation of a low level of reactivity for such compounds. In one known example (2), addition of 2,3-dimethyl-1,3-butadiene to coumarin was effected in only 22% yield under severe conditions while butadiene and isoprene failed to react. Fortunately, the reactivity of an α,β-unsaturated lactone should be enhanced, as predicted by the Alder rule (3), by introduction of an additional electron-withdrawing substituent to the potentially dienophilic double bond. For instance, γ,γ-dimethylaconic acid has been shown to be a useful dienophile which reacts efficiently with isoprene at high temperature (4). In our experience as well (5–7), the addition of a carbalkoxy substituent can produce a substantial increase in reactivity relative to the unsubstituted parent system. Our interest in lactonic dienophiles stems from a projected synthesis of the citrus bitter principal limonin (1) (8, 9). Carbethoxy activated lactone **2** would be a useful synthon for the introduction of the A′ ring. A close examination of the Diels–Alder characteristics of **2** (reactivity, orientation, and stereochemistry of adducts) is warranted prior to proceeding toward the ultimate objective of employing **2** in a Diels–Alder approach to limonin.

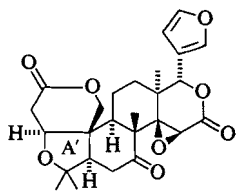

**1**

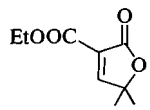

**2**

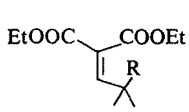

**3** R = H
**4** R = Br

Lactone ester **2**[1] was prepared in 67% yield from the known diester **3** (11) by bromination with *N*-bromosuccinimide followed by the cyclization of the resulting bromide **4** using silver oxide in aqueous tetrahydrofuran. Interestingly, a more economical procedure proved to be the pyrolytic cyclization of bromide **4** to give lactone ester **2** in 51% overall yield. In general, lactone ester **2** was found to react efficiently with a variety of dienes under stannic chloride catalysis.[2] The reaction occurred readily in ether at room temperature to give adducts in good yield (Table 1) with the exception of furan which produced only addition product **14**. With unsymmetrically substituted dienes (Entries 2 and 4–6), the adducts were found to be those predicted on the basis of the normal rules

[1]After the completion of this work, the preparation of the corresponding methyl ester was described using similar procedures (10).

[2]Under similar conditions, two other Lewis acids were briefly examined as potential catalysts. Boron trifluoride etherate gave virtually no reaction while reactions catalyzed by ferric chloride proved to be very slow relative to those catalyzed by stannic chloride.

0008-4042/82/070921-05$01.00/0

©1982 National Research Council of Canada/Conseil national de recherches du Canada

Can. J. Chem. Downloaded from www.nrcresearchpress.com by 210.87.254.42 on 09/06/12
For personal use only.

Can. J. Chem. Downloaded from www.nrcresearchpress.com by 210.87.254.42 on 09/06/12
For personal use only.

TABLE 1. Diels–Alder reactions of lactone ester **2**

| Entry | Diene[a] | Time(h)[b] | Adduct(s) (ratio) | % Yield |
|---|---|---|---|---|
| 1 | | 6 | 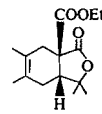 **5** | 91 |
| 2 | | 3 | 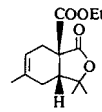 **6** | 86 |
| 3 | | 0.25 | 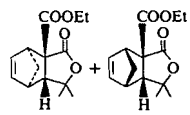 **7** + **8** (20:1)[d] | 100 |
| 4 | | 24 | 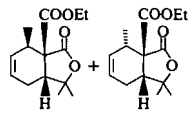 **9** + **10** (7:3)[e] | 75 |
| 5 | | 22 | 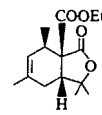 **11** | 93 |
| 6 | | 24[c] | 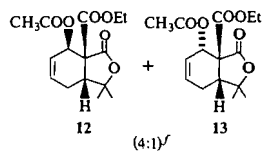 **12** + **13** (4:1)[f] | 60 |
| 7 | | 19 | 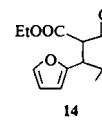 **14** | 89 |

[a]In each case 20 equiv. of diene was used except for that of 1-acetoxyl-1,3-butadiene in which 10 equiv. was used.
[b]Unless otherwise specified, reactions were performed in ether at ambient temperature using stannic chloride (0.5 equiv.) as a catalyst.
[c]This reaction was carried out at 0°C using 1 equiv. of stannic chloride.
[d]Separation was effected by column chromatography on silica gel.
[e]Separation was effected by flash chromatograph (12).
[f]Inseparable mixture was obtained. The ratio was based on the $^1$Hmr spectrum of the mixture.
[g]A single product was obtained, the stereochemistry of which could not be readily assigned.

(*ortho* and *para*) governing the orientation of Diels–Alder addition (1). In cases where differing secondary orbital overlap (13) would affect the stereochemistry of the adducts (Entries 3–6), experimental results showed a strong preference of the diene to overlap with one carbonyl over the other.

Several aspects of the structural assignments should be discussed. With respect to the orientation of the adducts derived from unsymmetrical dienes, assignments in cases of **9–13** were easily made since in each case the signal which was readily assigned to the ring junction proton appeared as a doublet of doublets in the $^1$Hmr indicating the presence of two protons on the adjacent carbon. Assignment of the regiochemistry of adduct **6** was concluded after comparison of the $^{13}$Cmr spectrum with those of the structurally related compounds **15** and **16**, the structures of which have been rigorously established (7). The adduct **6** showed two triplets at δ 28.1 and 27.1 for the two carbocyclic methylene carbons similar to the cor-

Can. J. Chem. Downloaded from www.nrcresearchpress.com by 210.87.254.42 on 09/06/12
For personal use only.

responding carbons (δ 29.0 and 28.7) in compound **15** and in marked contrast to the signals at δ 33.1 and 24.2 observed in isomer **16**.

With regard to the stereochemical assignments, the ring junction stereochemistry of all the adducts follows from the *cis*-principle (1) for which no violations have been observed. The complete stereochemistry of cyclopentadiene adducts **7** and **8** was further deduced as follows. Examination of Dreiding models showed the lactone ring junction proton should be shielded by the double bond in structure **7** while in structure **8** this proton should not be affected (14). Examination of the $^1$Hmr spectrum of the major adduct showed a signal at δ 2.37 which was assignable to the ring junction proton while the corresponding proton in the minor isomer showed a relatively normal shift of δ 2.92 (δ 2.66–3.29 for other compounds in this series). In cases of adducts **9–13** which are conformationally flexible, the complete stereochemistry could not be assigned without ambiguity by spectroscopic analysis. A number of chemical methods were attempted[3] but were not succesful. The depicted stereochemistry of these compounds was tentatively assigned based mainly on the results obtained for cyclopentadiene, which indicated that the Diels–Alder reaction proceeded with a preferential secondary overlap of the diene with the ester carbonyl rather than the lactone carbonyl.

This report enlarges the scope of application of Diels–Alder reactions to the synthesis of lactone-containing systems and further demonstrates the advantage of using an activated dienophile to prepare useful adducts from relatively less reactive dienophile systems. A simple application of this particular dienophile (**2**) to the synthesis of natural products is illustrated by the two-step synthesis of

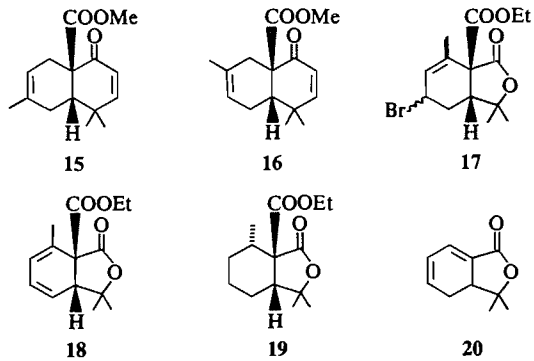


**15** **16** **17**

**18** **19** **20**

*o*-mentha-1,3-dien-1→8-olide (**20**), a monoterpene lactone isolated from the urine of the koala bear (*Phascolarctos cinereus*) (15). The mixture of the epimeric acetoxy lactones **12** and **13**, prepared in 60% yield from **2** and 1-acetoxy-1,3-butadiene, was treated with lithium iodide dihydrate in collidine at reflux for 1 h. Racemic *o*-menthane lactone **20** was isolated in 50% yield and showed spectroscopic properties identical to those reported for the levorotatory natural compound (15).

## Experimental

*General*

Melting points were determined on a Kofler hot stage apparatus and are uncorrected. Elemental analyses were performed by the microanalytical laboratory of this department. The ir spectra were recorded on a Nicolet 7-199 FT-IR spectrophotometer and, except where otherwise stated, were obtained on solutions in chloroform. The $^1$Hmr spectra were recorded on a Varian HA-100, Bruker WH-200, or WH-400 spectrometer and, except where otherwise stated, were obtained on solutions in carbon tetrachloride with tetramethylsilane as internal reference. The $^{13}$Cmr spectra were recorded on a Bruker WP-60/Nicolet BNC-12 system or a Bruker WH-400 spectrometer and were obtained on solutions in deuteriochloroform using tetramethylsilane as internal reference. Mass spectra (ms) were recorded using A.E.I. model MS12 or MS50 mass spectrometers. Unless stated otherwise, anhydrous magnesium sulfate was used for drying organic solutions.

*Ethyl 4-bromo-2-carbethoxy-4-methyl-2-pentenoate (4)*

Diester **3** (5.14 g, 24 mmol) was dissolved in carbon tetrachloride (50 mL) under an argon atmosphere and *N*-bromosuccinimide (4.7 g, 26.4 mmol) was added followed by benzoyl peroxide (100 mg, 0.41 mmol). The mixture was heated at reflux for 1 h, cooled to room temperature, filtered, and concentrated to give the crude bromo ester **4** (7.55 g). A portion of this material (1.114 g) was purified by column chromatography on silica gel. Elution with 15% ether in petroleum ether gave pure bromo ester **4** (936 mg; 91% yield); ir: 1733 (C=O) and 1643 (C=C) cm$^{-1}$; $^1$Hmr δ: 6.95 (s, 1H, —CH=), 4.20, 4.18 (both q, 2H each, $J$ = 7 Hz each, 2 × —$OCH_2$—), 1.91 (s, 6H, 2 × —$CH_3$), 1.31, and 1.29 (both t, 3H each, $J$ = 7 Hz each, 2 × —$OCH_2CH_3$). *Anal.* calcd. for $C_9H_{12}O_3Br$: C 45.07, H 5.85, Br 27.26; found: C 45.06, H 5.93, Br 27.44.

*3-Carbethoxy-5,5-dimethyl-2(5H)-furanone (2)*

Crude bromo ester **4** (2.84 g, ~9.7 mmol) was dissolved in

[3]In one approach, both compounds **9** and **10** were converted, via bromide **17**, to diene **18** (>60% yield; ir (neat): 1768, 1742, 1729, 1640, 1600, and 1995 cm$^{-1}$; $^1$Hmr ($CDCl_3$) δ: 5.84–6.18 (complex, 2H, —C(=)CH—CH=), 5.55 (dd, 1H, $J$ = 8, $J'$ = 6 Hz, =CH—CH—), 4.15 (q, 2H, $J$ = 7 Hz, —$OCH_2$—), 3.38 (d, 1H, $J$ = 6 Hz, —CH—), 1.94 (s, 3H, =C(—)—$CH_3$), 1.47 (s, 3H, —$CH_3$), 1.21 (t, 3H, $J$ = 7 Hz, —$OCH_2CH_3$), and 1.18 (s, 3H, —$CH_3$); ms $M^+$ 250.1202 (calcd. for $C_{14}H_{18}O_4$: 250.1203)) by allylic bromination (*N*-bromosuccinimide (1 equiv.) and α,α′-azodiisobutyronitrile (trace) in refluxing carbon tetrachloride; 1 h) and dehydrobromination (1,5-diazabicyclo[4.3.0]non-5-ene in refluxing benzene; 8 h). In an attempt to prepare compound **19** to compare with the dihydro-derivative of **9** or **10**, catalytic hydrogenation of **18** resulted only in the saturation of the disubstituted double bond even under severe conditions (e.g. Pt in EtOAc; $H_2$; 1500 psi). The transformation of **9** and **10** to the same diene **18** nevertheless serves to confirm their epimeric relationship and orientation.

Can. J. Chem. Downloaded from www.nrcresearchpress.com by 210.87.254.42 on 09/06/12
For personal use only.

tetrahydrofuran (50 mL) and water (25 mL). Silver oxide (2.48 g, 10.67 mmol) was added. After stirring for 48 h at room temperature, the reaction mixture was filtered and tetrahydrofuran was removed under reduced pressure. The aqueous solution was extracted with methylene chloride. The extracts were washed with water, dried, and concentrated. Column chromatography on silica gel eluting with 50% ether in petroleum ether gave lactone ester **2** (1.12 g; 67% yield from diester **3**); mp 68–70°C (ether); ir: 1763 (C=O), 1714 (C=O), and 1638 (C=C) $cm^{-1}$; $^1$Hmr δ: 8.06 (s, 1H, —CH=), 4.24 (q, 2H, $J$ = 7 Hz, —$OCH_2$—), 1.52 (s, 6H, 2 × —$CH_3$), and 1.35 (t, 3H, $J$ = 7 Hz, —$OCH_2CH_3$); $^{13}$Cmr δ: 167.1, 160.4, 124.6, 83.5, 61.7, 25.0, and 14.1; ms $M^+$ 184.0744 (calcd. for $C_9H_{12}O_4$: 184.0735). *Anal.* calcd. for $C_9H_{12}O_4$: C 58.69, H 6.57; found: C 58.76, H 6.66.

A less expensive method was found to be the pyrolytic cyclization of the crude bromo ester **4**. Lactone ester **2** was produced directly on attempted distillation of **4** (70.8 g) at 1 Torr. The fraction collected at 128°C was pure lactone ester **2** (15.9 g). Additional **2** (4.8 g) was obtained by column chromatography of the combined lower boiling fractions (102–120°C). The total yield was 51% from diester **3**.

*Diels–Alder reactions of lactone ester 2*

The reactions were carried out using the general procedure illustrated below with 2,3-dimethyl-1,3-butadiene. Temperature and time of reactions as well as quantities of dienes and stannic chloride relative to **2** are noted in Table 1.

Lactone ester **2** (500 mg, 2.71 mmol) was dissolved in ether (25 mL) under an argon atmosphere. The solution was chilled to 0°C and stannic chloride (354 mg, 1.36 mmol) was added. A dense white precipitate was observed immediately. After 5 min, 2,3-dimethyl-1,3-butadiene (6.13 mL, 54.3 mmol) was added and stirring was continued for 6 h at room temperature. Water (20 mL) was added and the resulting mixture was extracted with methylene chloride. The extracts were washed with water, dried, filtered, and concentrated. Column chromatography on silica gel eluting with 10–20% ether in petroleum ether gave adduct **5** (657 mg; 91% yield); ir: 1769 (C=O) and 1736 (C=O) $cm^{-1}$; $^1$Hmr δ: 4.16 (q, 2H, $J$ = 7 Hz, —$OCH_2$—), 2.84 (dd, 1H, $J$ = 7, $J'$ = 3 Hz, —CH—), 2.63, 2.22 (both d, 1H each, $J$ = 16 Hz each, —$CH_2$—), 1.78–2.12 (complex, 2H, —$CH_2$CH—), 1.68 (s, 6H, 2 × =$CCH_3$), 1.43 (s, 3H, —$CH_3$), 1.28 (t, 3H, $J$ = 7 Hz, —$OCH_2CH_3$), and 1.24 (s, 3H, —$CH_3$); $^{13}$Cmr δ: 174.6, 171.0, 125.4, 125.1, 85.9, 62.1, 56.2, 47.3, 34.5, 30.1, 29.4, 23.9, 19.0, 18.8, and 14.0; ms $M^+$ 266.1516 (calcd. for $C_{15}H_{22}O_4$: 266.1518). *Anal.* calcd. for $C_{15}H_{22}O_4$: C 67.65, H 8.33; found: C 67.37, H 8.36.

The adducts **6–14** showed the following spectral data.

Compound **6**; mp 43–44°C (ether – petroleum ether); ir: 1767 (C=O) and 1736 (C=O) $cm^{-1}$; $^1$Hmr δ: 5.46 (m, 1H, —CH=), 4.18 (q, 2H, $J$ = 7 Hz, —$OCH_2$—), 2.98 (dd, 1H, $J$ = 7, $J'$ = 2 Hz, —CH—), 2.87, 2.22 (both md, 1H each, $J$ = 14 Hz each, =$CHCH_2$—), 1.84–2.12 (complex, 2H, —$CH_2$CH—), 1.72 (s, 3H, —$CH_3$), 1.46 (s, 3H, —$CH_3$), 1.29 (t, 3H, $J$ = 7 Hz, —$OCH_2CH_3$), and 1.24 (s, 3H, —$CH_3$); $^{13}$Cmr δ: 174.6, 170.6, 133.2, 118.4, 86.0, 62.1, 53.5, 46.6, 29.8, 28.1, 27.1, 23.4, 23.2, and 14.0; ms $M^+$ 252.1368 (calcd. for $C_{14}H_{20}O_4$: 252.1361). *Anal.* calcd. for $C_{14}H_{20}O_4$: C 66.65, H 7.99; found: C 66.76, H 8.28.

Compound **7**; ir: 1761 (C=O) and 1726 (C=O) $cm^{-1}$; $^1$Hmr δ: 6.13–6.34 (complex, 2H, —CH=CH—), 4.16 (q, 2H, $J$ = 7 Hz, —$OCH_2$—), 3.38 (m, 1H, =CHCH—), 3.01 (br s, 1H, =CHCHCH—), 2.37 (s, 1H, —CH—), 1.54 (s, 3H, —$CH_3$), 1.51 (m, 2H, —$CH_2$—), 1.43 (s, 3H, —$CH_3$), and 1.29 (t, 3H, $J$ = 7 Hz, —$OCH_2CH_3$); ms $M^+$ 250.1206 (calcd. for $C_{14}H_{18}O_4$: 250.1205). *Anal.* calcd. for $C_{14}H_{18}O_4$: C 67.18, H 7.25; found: C 67.18, H 7.04.

Compound **8**; ir: 1762 (C=O) and 1732 (C=O) $cm^{-1}$; $^1$Hmr δ: 6.29 (ddd, 1H, $J$ = 6, $J'$ = 3, $J''$ = 1 Hz, =CH—), 6.17 (dd, 1H, $J$ = 6, $J'$ = 4 Hz, =CH—), 4.23 (q, 2H, $J$ = 7 Hz, —$OCH_2$—), 3.38 (m, 1H, =CHCH—), 3.02 (m, 1H, =CHCH—CH—), 2.92 (d, 1H, $J$ = 4 Hz, —CH—), 1.68 (m, 2H, —$CH_2$—), 1.45 (s, 3H, —$CH_3$), 1.34 (s, 3H, —$CH_3$), and 1.33 (t, 3H, $J$ = 7 Hz, —$OCH_2CH_3$); ms $M^+$ 250.1205 (calcd. for $C_{14}H_{18}O_4$: 250.1205). *Anal.* calcd. for $C_{14}H_{18}O_4$: C 67.18, H 7.25; found: C 67.26, H 7.13.

Compound **9**: ir: 1770 (C=O) and 1728 (C=O) $cm^{-1}$; $^1$Hmr δ: 5.78 (m, 1H, —CH=), 5.62 (ddd, 1H, $J$ = 10, $J'$ = 3, $J''$ = 2 Hz, —CH=), 4.16 (q, 2H, $J$ = 7 Hz, —$OCH_2$—), 2.66 (dd, 1H, $J$ = 7, $J'$ = 5 Hz, —$CH_2$CH—), 2.53 (mq, 1H, $J$ = 7 Hz, =CHCH—), 2.36, 1.92 (both md, 1H each, $J$ = 16 Hz each, =$CHCH_2$—), 1.35 (s, 3H, —$CH_3$), 1.30 (s, 3H, —$CH_3$), 1.28 (t, 3H, $J$ = 7 Hz, —$OCH_2CH_3$), and 1.20 (d, 3H, $J$ = 7 Hz, —$CHCH_3$); $^{13}$Cmr δ: 174.0, 170.0, 131.8, 125.8, 84.5, 61.7, 58.1, 48.1, 33.5, 29.8, 23.8, 22.4, 15.6, and 14.1; ms $M^+$ 252.1361 (calcd. for $C_{14}H_{20}O_4$: 252.1362).

Compound **10**; ir: 1768 (C=O) and 1730 (C=O) $cm^{-1}$; $^1$Hmr δ: 5.88 (m, 1H, =$CHCH_2$—), 5.70 (ddd, 1H, $J$ = 8, $J'$ = 3, $J''$ = 2 Hz, =CH—), 4.21 (q, 2H, $J$ = 7 Hz, —$OCH_2$—), 2.79 (dd, 1H, $J$ = 8, $J'$ = 3 Hz, —$CH_2$CH—), 2.69 (dq, 1H, $J$ = 7, $J'$ = 2 Hz, —$CHCH_3$), 2.33, 2.01 (both m, 1H each, —$CH_2$—), 1.35 (s, 3H, —$CH_3$), 1.30 (s, 3H, —$CH_3$), 1.30 (d, 3H, $J$ = 7 Hz, —$CHCH_3$), and 1.30 (t, 3H, $J$ = 7 Hz, —$OCH_2CH_3$); $^{13}$Cmr δ: 173.0, 172.0, 135.1, 127.5, 84.4, 62.1, 61.8, 50.9, 34.9, 30.9, 25.2, 24.0, 15.0, and 14.1; ms $M^+$ 252.1362 (calcd. for $C_{14}H_{20}O_4$: 252.1362).

Compound **11**; ir: 1772 (C=O) and 1730 (C=O) $cm^{-1}$; $^1$Hmr δ: 5.31 (m, 1H, —CH=), 4.15 (q, 2H, $J$ = 7 Hz, —$OCH_2$—), 2.69 (dd, 1H, $J$ = 7, $J'$ = 6 Hz, —$CH_2$CH—), 2.53 (m, 1H, =CHCH—), 2.22 (dd, 1H, $J$ = 16, $J'$ = 7 Hz, —CHH—), 1.97 (dd, 1H, $J$ = 16, $J'$ = 6 Hz, —CHH—), 1.76 (s, 3H, —$CH_3$), 1.36 (s, 3H, —$CH_3$), 1.29 (s, 3H, —$CH_3$), 1.28 (t, 3H, $J$ = 7 Hz, —$OCH_2CH_3$), and 1.17 (d, 3H, $J$ = 7 Hz, —$CHCH_3$); $^{13}$Cmr δ: 174.1, 169.9, 133.7, 125.4, 84.4, 61.5, 58.1, 48.6, 34.2, 29.8, 27.6, 23.8, 23.0, 15.9, and 14.1; ms $M^+$ 266.1517 (calcd. for $C_{15}H_{22}O_4$: 266.1520).

Compounds **12** and **13**; ir (neat): 1769 (C=O) and 1740 (C=O) $cm^{-1}$; ms $M^+$ 296.1261 (calcd. for $C_{15}H_{20}O_6$: 296.1260). *Anal.* calcd. for $C_{15}H_{20}O_6$: C 60.81, H 6.75; found: C 60.79, H 6.88. The $^1$Hmr ($CDCl_3$) of the inseparable mixture showed two sets of signals integrated to a ratio of 4:1; major set (**12**) δ: ~6.01–6.25 (complex, 2H, —CH=CH—), 5.98 (d, 1H, $J$ = 4 Hz, —OCH—), 4.25 (q, 2H, $J$ = 7 Hz, —$OCH_2$), 3.14 (dd, 1H, $J$ = 9, $J'$ = 6 Hz, —$CHCH_2$—), ~2.46–1.98 (complex, 2H, —$CH_2$—), 2.04 (s, 3H, —$COCH_3$), 1.57 (s, 3H, —$CH_3$), 1.45 (s, 3H, —$CH_3$), and 1.30 (t, 3H, $J$ = 7 Hz, —$OCH_2CH_3$); minor set (**13**) δ: ~6.01–6.25 (complex, 2H, —CH=CH—), 5.81 (d, 1H, $J$ = 5 Hz, —OCH—), 4.28 (q, 2H, $J$ = 7 Hz, —$OCH_2$—), 3.29 (dd, 1H, $J$ = 8, $J'$ = 4 Hz, —$CHCH_2$—), ~2.46–1.98 (complex, 2H, —$CH_2$—), 2.09 (s, 3H, —$COCH_3$), 1.46 (s, 3H, —$CH_3$), 1.38 (s, 3H, —$CH_3$), and 1.30 (t, 3H, $J$ = 7 Hz, —$OCH_2CH_3$).

Compound **14**; ir: 1781 (C=O) and 1737 (C=O) $cm^{-1}$; $^1$Hmr δ: 7.35 (dd, 1H, $J = 2, J' < 1$ Hz, =CHO—), 6.30 (dd, 1H, $J = 4$, $J' = 2$ Hz, —C*H*=CHO—), 6.19 (dd, 1H, $J = 4$, $J' < 1$ Hz, —CH=C—), 4.21 (q, 2H, $J = 7$ Hz, —$OCH_2$—), 3.90 (s, 2H, —CHCH—) 1.64 (s, 3H, —$CH_3$), 1.31 (t, 3H, $J = 7$ Hz, —$OCH_2CH_3$), and 1.10 (s, 3H, —$CH_3$); ms $M^+$ 252.1002 (calcd. for $C_{13}H_{16}O_5$: 252.0998). *Anal.* calcd. for $C_{13}H_{16}O_5$: C 61.90, H 6.39; found: C 62.09, H 6.45.

*(±)-o-Mentha-1,3-dien-1→8-olide (20)*

Lithium iodide dihydrate – collidine reagent (1.28 *N*) was freshly prepared by the sequential addition of lithium iodide (514 mg, 3.84 mmol) and water (138 μL, 7.68 mmol) to 2,4,6-collidine (3.05 mL). A mixture of acetoxy lactones **12** and **13** (152 mg, 0.51 mmol) was dissolved in this reagent (2.3 mL) under an argon atmosphere. The resulting solution was heated at reflux with stirring for 1 h. After cooling to room temperature, the reaction mixture was acidified with ice-cold 5% aqueous hydrochloric acid and extracted with ether. The extracts were washed with ice-cold aqueous hydrochloric acid and water, dried, filtered, and concentrated. Flash chromatography (12) of the residue on silica gel eluting with 5% ether in petroleum ether gave racemic *o*-menthane lactone **20** (42 mg; 50% yield); ir (neat): 1749 (C=O), 1664, and 1570 (C=C) $cm^{-1}$; $^1$Hmr ($CDCl_3$) δ: 6.89 (m, 1H, —C=CH—), 6.06–6.24 (complex, 2H, —CH=CH—), 2.98 (m, 1H, —CH—), 2.12–2.46 (complex, 2H, —$CH_2$—), 1.54 (s, 3H, —$CH_3$), and 1.36 (s, 3H, —$CH_3$); ms *m/e*: 164.0837 ($M^+$; 22.59%; calcd. for $C_{10}H_{12}O_2$: 164.0837), 106.0427 (95.21%; $C_7H_6O$), 105.0351 (100%; $C_7H_5O$), 78.0492 (43.03%; $C_6H_6$), and 77.0375 (20.35%; $C_6H_5$).

## Acknowledgments

We are grateful to the Natural Sciences and Engineering Research Council of Canada and the University of Alberta for financial support.

1. A. S. Onishchenko. Diene synthesis. Israel Program for Scientific Translation, Jerusalem, 1964.
2. R. Adams, W. D. McPhee, R. B. Carlin, and Z. W. Wicks. J. Am. Chem. Soc. **65**, 356 (1943).
3. J. Sauer. Angew. Chem. Int. Ed. Engl. **6**, 16 (1967).
4. S. Torii, T. Oie, H. Tanaka, J. D. White, and T. Furuta. Tetrahedron Lett. 2471 (1973).
5. H. J. Liu and E. N. C. Browne. Tetrahedron Lett. 2919 (1977).
6. H. J. Liu and E. N. C. Browne. Can. J. Chem. **57**, 377 (1979).
7. H. J. Liu and E. N. C. Browne. Can. J. Chem. **59**, 601 (1981).
8. D. Arigoni, D. H. R. Barton, E. J. Corey, O. Jeger, L. Cagliotti, S. Dev. P. G. Ferrini, E. R. Glazier, A. Melera, S. K. Pradhan, K. Schaffner, S. Sternhell, J. F. Templeton, and S. Tobinga. Experientia, **16**, 41 (1960).
9. S. Arnott, A. W. Davie, J. M. Robertson, G. A. Sim, and D. G. Watson. Experientia, **16**, 49 (1960).
10. T. Gulbrandsen and P. Kolsaker. Acta Chem. Scand. B, **34**, 305 (1980).
11. A. C. Cope, C. M. Hofmann, C. Wyckoff, and E. Hardenbergh. J. Am. Chem. Soc. **63**, 3452 (1941).
12. W. C. Still, M. Kahn, and A. Mitra. J. Org. Chem. **43**, 2923 (1978).
13. R. B. Woodward and R. Hoffmann. Angew. Chem. Int. Ed. Engl. **8**, 781 (1969).
14. L. M. Jackman and S. Sternhell. Applications of nuclear magnetic resonance spectroscopy in organic chemistry, 2nd ed. Pergamon Press, Oxford, England. 1969. pp. 230–231.
15. I. A. Southwell. Tetrahedron Lett. 1885 (1975).

Can. J. Chem. Downloaded from www.nrcresearchpress.com by 210.87.254.42 on 09/06/12
For personal use only.

# Stéréochimie de diéthylphosphono carbéthoxy-4 pyrrolidines. Étude par rmn du proton à haut champ (250 MHz) et du carbone ($^{13}$C)

C. RABILLER[1]

*Laboratoire Chimie Organique Physique E.R.A. C.N.R.S. 315, U.E.R. Chimie, 2 Rue de la Houssinière, 44072 Nantes, France*

ET

A. DEHNEL ET G. LAVIELLE

*Laboratoire de Synthèse Organique, U.E.R. de Sciences Fondamentales et Appliquées, 45046 Orléans, France*

Reçu le 4 juin 1981

C. RABILLER, A. DEHNEL et G. LAVIELLE. Can. J. Chem. **60**, 926 (1982).

Une série de diéthylphosphono-2 carbéthoxy-4 pyrrolidines est étudiée par rmn du proton (à 250 MHz) et du carbone ($^{13}$C). L'étude des déplacements chimiques permet d'établir les configurations alors que l'analyse des constantes de couplages $^3J_{HH}$, $^3J_{PH}$ et $^3J_{PC}$ conduit à préciser les conformations privilégiées adoptées par ces cycles. Un bon accord est observé entre les relations de dépendance angulaire liant ces différentes constantes de couplage aux angles dièdres.

C. RABILLER, A. DEHNEL, and G. LAVIELLE. Can. J. Chem. **60**, 926 (1982).

A series of 2-diethylphosphono 4-carbethoxy pyrrolidines has been studied by 250 MHz $^1$H nmr and $^{13}$C nmr. A study of the chemical shifts allows us to establish the structures and the analysis of the $^3J_{HH}$, $^3J_{PH}$ and $^3J_{PC}$ coupling constants leads to designation of preferred conformations for these rings. Good agreement is noted between the angular dependence of these coupling constants and the dihedral angles.

[Journal translation]

Une nouvelle méthode de synthèse régio et stéréospécifique (1*a*) permet d'accéder à une série de diéthylphosphono-pyrrolidines diversement substituées du type:

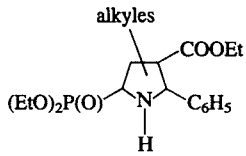


Afin de pouvoir étudier le mécanisme de formation de ces composés, il était important de connaitre les dispositions relatives des différents substituants. En effet, l'anion azaallylique de départ pouvait se présenter sous quatre configurations (1*b*, *c*): *cis–trans*, *trans–trans*, *trans–cis* et *cis–cis*.

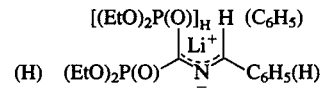


La réaction ne conduisant qu'à un seul diastéréoisomère, on devait pouvoir démontrer la structure de l'anion de départ et préciser la stéréochimie de cette condensation. Par ailleurs ce type de molécule présente la particularité de posséder un groupement (O)P·(OEt)$_2$. Or, des travaux antérieurs ont montré l'existence de relations de dépendances angulaires des couplages $^3J_{PH}$ (2, 3) et $^3J_{PC}$ (3 à 9). Il était intéressant de confronter ces résultats à ceux obtenus dans cette série et d'obtenir des informations sur les conformations adoptées par ces cycles.

[1]Auteur à qui toute correspondance sera adressée.

## Résultats

La liste ainsi que la structure des composés étudiés est décrite dans le tableau 1. La substitution du cycle pyrrolidinique par les groupements (O)P-(OEt)$_2$, COOEt et $C_6H_5$ implique l'existence théorique de quatre diastéréoisomères dont 3 seulement ont été mis en évidence.

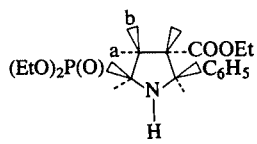


I

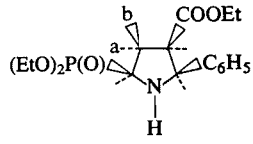


II

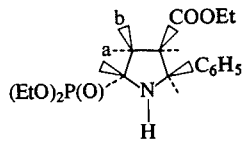


III

Les paramètres rmn sont rassemblés dans les tableaux 2 (déplacements chimiques δ $^1$H), 3 (constantes de couplage $J_{^1H^1H}$ et $J_{^1H^{31}P}$), 4 (déplacements chimiques δ $^{13}$C) et 5 (constantes de couplage $J_{^{13}C-^{31}P}$).

La grande majorité des spectres protoniques sont analysables au 1er ordre à la condition d'utiliser un spectrographe à haut champ (250 MHz).

0008-4042/82/070926-08$01.00/0

©1982 National Research Council of Canada/Conseil national de recherches du Canada

Can. J. Chem. Downloaded from www.nrcresearchpress.com by 210.87.254.40 on 09/06/12
For personal use only.

TABLEAU 1. Structure des phosphonato pyrrolidines étudiées

| Type du composé | | Substituants | | | | |
|---|---|---|---|---|---|---|
| | | | 3 | | | |
| Diastéréoisomère | No | 2 | b | a | 4 | 5 |
| 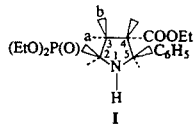 I | I-*1*, II-*1* | H | H | H | H | H |
| | I-*2*, II-*2* | Me | H | H | H | H |
| | I-*3*, II-*3* | H | H | Me | H | H |
| | II-*4* | H | H | H | Me | H |
| 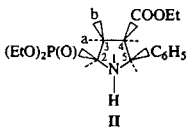 II | II-*5* | H | H | H | H | Me |
| | II-*6* | Me | H | Me | H | H |
| | II-*7* | Me | H | H | Me | H |
| | II-*8* | H | H | Me | Me | H |
| | II-*9*<br>III-*9* | H | H | Me | H | Me |
| 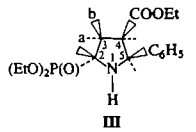 III | I-*10*, II-*10* | H | Me | Me | H | H |
| | II-*11* | H | H | | | H |
| | I-*12*, II-*12*, III-*12* | H | | | H | H |

TABLEAU 2. Déplacements chimiques (δ $^1$H/TMS) des protons des phosphano pyrrolidines. Solvant: $CDCl_3$ ($c \sim 1$ mol/L)

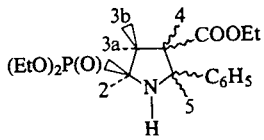

| | | | | | | COO Et* | | | (O)P·(OEt)$_2$* | |
|---|---|---|---|---|---|---|---|---|---|---|
| | | | | | | | $\delta_{CH_2}$ | | $\delta_{CH_3}$ | |
| | $\delta_2$ | $\delta_{3a}$ | $\delta_{3b}$ | $\delta_4$ | $\delta_5$ | $\delta_{CH_3}$ | (A) | (B) | (A) | (B) |
| I-*1* | 3,69 | 2,39 | 2,44 | 2,95 | 4,43 | 1,18 | 4,05 | 4,16 | 1,36 | 1,35 |
| II-*1* | 3,48 | 2,26 | 2,55 | 3,32 | 4,52 | 0.78 | 3,51 | 3,66 | 1,38 | 1,36 |
| I-*2* | 1,53 (Me) | 2,02 | 2,73 | 3,05 | 4,58 | 1,12 | 4,05 | 4,05 | 1,35 | 1,33 |
| II-*2* | 1,45 (Me) | 1,88 | 2,83 | 3,50 | 4,79 | 0,78 | 3,49 | 3,62 | 1,38 | 1,36 |
| I-*3* | 3,30 | 1,12 (Me) | 2,90 | 3,02 | 4,58 | 1,21 | 4,08 | 4,16 | 1,34 | 1,32 |
| II-*3* | 3,09 | 1,20 (Me) | 2,90 | 2,90 | 4,56 | 0.77 | 3,54 | 3,65 | 1,34 | 1,36 |
| II-*4* | 3,55 | 1,85 | 2,92 | 1,44 (Me) | 4,00 | 0,79 | 3,49 | 3,58 | 1,36 | 1,35 |
| II-*5* | 3,68 | 2,28 | 2,52 | 3,04 | 1,64 (Me) | 0,87 | 3,60 | 3,70 | 1,40 | 1,37 |
| II-*6* | 1,34 (Me) | 1,08 (Me) | 3,16 | 3,05 | 4,74 | 0,85 | 3,48 | 3,62 | 1,39 | 1,37 |
| II-*7* | 1,54 (Me) | 1,61 | 3,31 | 1,58 (Me) | 4,36 | 0,78 | 3,46 | 3,61 | 1,41 | 1,38 |
| II-*8* | 3,20 | 1,09 (Me) | 3,16 | 1,34 (Me) | 4,07 | 0,81 | 3,51 | 3,57 | 1,37 | 1,37 |
| II-*9* | 3,32 | 1,19 (Me) | 2,87 | 2,64 | 1,72 (Me) | 0,88 | 3,60 | 3,69 | 1,39 | 1,36 |
| III-*9* | 3,83 | 1,23 (Me) | 2,94 | 3,06 | 1,89 (Me) | 0,95 | 3,78 | 3,78 | 1,36 | 1,36 |
| I-*10* | 3,25 | 1,20 (Me) | et 1,41 (Me) | 2,82 | 4,57 | 1,18 | 4,04 | 4,16 | 1,34 | 1,32 |
| II-*10* | 3,06 | 1,34 (Me) | et 1,36 (Me) | 3,12 | 4,38 | 0,85 | 3,76 | 3,76 | 1,35 | 1,35 |
| II-*11* | 3,74 | | 3,23 | — | 4,13 | 0,84 | 3,56 | 3,56 | 1,38 | 1,38 |
| I-*12* | 3,53 | | cyclohexyle | 3,11 | 4,63 | 1,19 | 4,07 | 4,14 | 1,34 | 1,30 |
| II-*12* | 2,99 | | cyclohexyle | 3,28 | 4,32 | 0,83 | 3,69 | 3,74 | 1,39 | 1,39 |
| III-*12* | 3,72 | | cyclohexyle | 3,41 | 4,80 | 0,88 | 3,76 | 3,80 | 1,35 | 1,36 |

*Les protons méthylènes du groupement carbéthoxy sont non-équivalents ainsi que les éthoxy du groupe phosphono.

Can. J. Chem. Downloaded from www.nrcresearchpress.com by 210.87.254.40 on 09/06/12
For personal use only.

Can. J. Chem. Downloaded from www.nrcresearchpress.com by 210.87.254.40 on 09/06/12
For personal use only.

TABLEAU 3. Constantes de couplage $J_{HH}$ et $J_{HP}$ ( Hz) pyrrolidines étudiées; solvant $CDCl_3$*

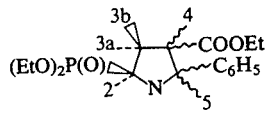


| No | $^3J_{2-3a}$ | $^3J_{2-3b}$ | $^2J_{3a-3b}$ | $^3J_{3a-4}$ | $^3J_{3b-4}$ | $^3J_{4-5}$ | $^2J_{P-H^2}$, $^3J_{P-H^2}$ | $^3J_{P-H^{3a}}$ | $^3J_{P-H^{3b}}$ |
|---|---|---|---|---|---|---|---|---|---|
| I-*1* | 8,8 | 7,4 | −13,0 | 8,0 | 8,8 | 8,0 | 2,4 | 2,5 | 20,5 |
| II-*1* | 6,8 | 11,2 | −12,9 | 9,2 | 8,4 | 9,2 | 4,8 | 2,3 | 16,5 |
| I-*2* | — | — | −12,9 | 10,0 | 8,4 | 9,5 | 15,2 ($^3$J) | 19,5 | 14,7 |
| II-*2* | — | — | −12,7 | 7,9 | 10,0 | 9,8 | 15,2 ($^3$J) | 1,6 | 15,0 |
| I-*3* | — | 7,1 | 6,9 ($^3$J) | 9,1 | — | 7,7 | 2,2 | — | 21,6 |
| II-*4* | 6,5 | 11,4 | −12,6 | — | — | — | 4,8 | 2,1 | 17,0 |
| II-*5* | 7,0 | 10,7 | −13,0 | 7,6 | 8,4 | — | 5,6 | 3,6 | 16,6 |
| II-*6* | — | — | 6,6 ($^3$J) | — | 11,2 | 10,0 | 16,0 ($^3$J) | — | 13,5 |
| II-*7* | — | — | −13,4 | — | — | — | 15,0 ($^3$J) | 3,7 | 17,4 |
| II-*9* | — | 10,5 | 6,5 ($^3$J) | — | 9,5 | — | 2,7 | — | 14,5 |
| I-*10* | — | — | — | — | — | 10,8 | 8,8 | — | — |
| II-*10* | — | — | — | — | — | 6,9 | 16,7 | — | — |
| II-*11* | — | 11,8 | — | — | — | — | 1,5 | — | 16,5 |
| I-*12* | — | — | — | — | — | 9,0 | 8,3 | — | — |
| II-*12* | — | — | — | — | — | 6,0 | 17,8 | — | — |
| III-*12* | — | — | — | — | — | 5,7 | 11,5 | — | — |

*Le couplage entre les hydrogènes non équivalents du méthylène de $CH_3$—$CH_2$—COO est de l'ordre de −10,7 Hz par ailleurs, on mesure également $^3J_{P-O-CH_2}$ ~ 7 à 8 Hz et $^3J_{P-O-CH_3}$ ~ 0,3 Hz.

TABLEAU 4. Déplacements chimiques des carbones (δ $^{13}$C/TMS); solvant $CDCl_3$*

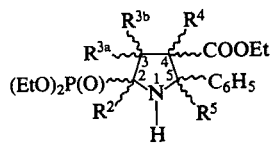


| No | $\delta_{C^2}$ | $\delta_{C^3}$ | $\delta_{C^4}$ | $\delta_{C^5}$ | $\delta_{R^2}$ | $\delta_{R^{3a}, R^{3b}}$ | $\delta_{R^4}$, $\delta_{R^5}$ | COOEt $\delta_{CO}$ | COOEt $\delta_{CH_2}$ | COOEt $\delta_{CH_3}$ |
|---|---|---|---|---|---|---|---|---|---|---|
| I-*1* | 53,4 | 31,1 | 51,7 | 66,6 | — | — | — | 173,3 | 60,7 | 14,1 |
| II-*1* | 54,5 | 30,0 | 49,6 | 65,6 | — | — | — | 172,0 | 60,1 | 13,6 |
| I-*2* | 58,9 | 39,7 | 53,1 | 64,6 | 24,5 (Me) | — | — | 173,0 | 60,4 | 14,1 |
| II-*2* | 59,8 | 36,2 | 48,6 | 63,0 | 22,5 (Me) | | — | 171,7 | 60,0 | 13,6 |
| I-*3* | 61,2 | 37,5 | 56,9 | 63,7 | — | 15,7 (Me) | — | 172,1 | 60,4 | 14,3 |
| II-*3* | 61,4 | 38,3 | 58,4 | 64,3 | — | 17,6 (Me) | — | 171,5 | 60,3 | 13,7 |
| II-*4* | 53,7 | 37,9 | 54,9 | 74,2 | — | — | 24,3 (□)‡ | 173,9 | 60,3 | 13,5 |
| II-*5* | 53,1 | 29,4 | 56,3 | 67,7 | — | — | 31,0 (△) | 172,0 | 60,1 | 13,6 |
| II-*6* | 62,2 | 39,5 | 56,9 | 61,3 | 14,0 (Me) | 17,6 (Me) | — | 171,3 | 60,1 | 13.7 |
| II-*7* | 59,5 | 45,9 | 54,5 | 71,8 | 22,7 (Me) | — | 25,7 (□) | 174,3 | 60,3 | 13,6 |
| II-*8* | 60,1 | 40,2 | 58,1 | 73,3 | — | 12,5 (Me) | 19,3 (□) | 173,6 | 60,3 | 13,6 |
| II-*9* | 59,9 | 39,0 | 65,7 | 65,3 | — | 17,3 (Me) | 30,0 (△) | 171,3 | 60,2 | 13,7 |
| III-*9* | 57,8 | 37,1 | 62,2 | 66,5 | — | 14,1 (Me) | 30,0 (△) | 170,9 | 60,1 | 13,9 |
| I-*10* | 65,4 | 45,2 | 63,2 | 64,0 | — | 25,4 (Me) 25,8 (Me) | — | 171,7 | 60,2 | 14,3 |
| II-*10* | 66,1 | 47,2 | 62,1 | 64,8 | — | 22,0 (Me) 31,7 (Me) | | 171,4 | 59,8 | 13,8 |
| II-*11* | 55,0 | 39,3 | 59,1 | 71,2 | — | 20,6-22,4-23,6 32,2 (cyclohexyle) | | 172,4 | 60,3 | 13,6 |
| | | | | | | 22,8, 23,1, 25,9 | | 172,6 | 60,4 | 14,2 |
| I-*12* | 63,4 | 50,3 | 60,8 | 64,5 | — | 31,8†, 33,2† (cyclohexyle) | | | | |
| II-*12* | 67,9 | 52,5 | 57,9 | 65,6 | — | 23,7, 24,7, 25,4, 30,9† 39,4‡ (cyclohexyle) | | 171,8 | 59,7 | 13,7 |
| III-*12* | 64,3 | 51,1 | 56,4 | 63,7 | — | 23,3, 24,1, 25,8, 32,7* 33,3† (cyclohexyle) | | 171,4 | 59,8 | 13,7 |

*Les déplacements des carbones du groupe (O)P $(OEt)_2$ sont pratiquement constants, ainsi:
$\delta^{13}CH_3$ ~ 16,5–16,7 ppm, $\delta^{13}CH_2$ ~ 62–63 ppm } Les 2 groupes OEt sont diastéréotopiques.
†Carbones $C^{3a}$ et $C^{3b}$ du cyclohexyle. L'attribution de ces carbones est effectuée sur la base de l'existence de couplages $^3J_{P-C-C-C}$.
‡(□), (△) Déplacements chimiques de méthyles respectivement en position 4 et 5.

Can. J. Chem. Downloaded from www.nrcresearchpress.com by 210.87.254.40 on 09/06/12
For personal use only.

TABLEAU 5. Constantes de couplage $^{n}J_{^{13}C^{31}P}$ (en Hz) des phosphonopyrrolidines (solvant $CDCl_3$); $^{2}J_{P-O-CH_2} \sim -6$ à $-8$ Hz*

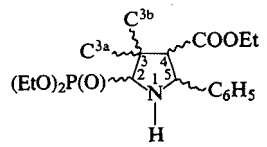


| No | $^{1}J_{PC^2}$ | $^{3}J_{PC^4}$ | $^{3}J_{PC^5}$* | $^{3}J_{PC^{3a}}$† et $^{3}J_{PC^{3b}}$† |
|---|---|---|---|---|
| **I**-*1* | 169,0 | 9,0 | 15,0 | — |
| **II**-*1* | 166,5 | 13,5 | 18,5 | — |
| **I**-*2* | 172,7 | 4,6 | 9,3 | — |
| **II**-*2* | 168,2 | 13,3 | 13,6 | — |
| **I**-*3* | 167,0 | 9,2 | 14,9 | 6 |
| **II**-*3* | 163,5 | 14,8 | 18,0 | ~ 0 |
| **II**-*4* | 167,0 | 13,5 | 18,1 | — |
| **II**-*5* | 165,4 | 11,8 | 15,0 | — |
| **II**-*6* | 167,8 | 15,2 | 16,8 | 7,6 |
| **II**-*7* | 167,0 | 12,0 | 16,5 | — |
| **II**-*8* | 165,1 | 15,0 | 16,2 | ~ 0 |
| **II**-*9* | 166,5 | 14,9 | 18,0 | ~ 0 |
| **III**-*9* | 153,6 | 2,5 | 4,2 | 4,6 |
| **I**-*10* | 162,3 | 8,6 | 14,8 | 9 et ~ 0 |
| **II**-*10* | 166,2 | 6,1 | 21,4 | ~ 0 |
| **II**-*11* | 168,5 | 14,0 | 12,0 | ~ 0 |
| **I**-*12* | 160,5 | 6,1 | 11,9 | 8,7 et 3,3 |
| **II**-*12* | 154,2 | 6,3 | 20,9 | 4,9 et 4,8 |
| **III**-*12* | 162,4 | 7,5 | 10,1 | 7 et ~ 0 |

*On mesure le couplage $^{2}J_{P-C^2-CH_3}$ pour les composés **I**-*2* (7,6 Hz) **II**-*2* (6,0 Hz), **II**-*6* (~ 0 Hz), **II**-*7* (5,6 Hz).
†Le signe des constantes de couplage $^{1}J_{PC}$, $^{3}J_{PCCC}$ et $^{3}J_{PCNC}$ est positif (17).

L'attribution des signaux de résonance des atomes de carbone ($^{13}C$) ne pose pas de problème particulier et leur distinction s'effectue en comparant les spectres $^{13}C$ des diverses pyrrolidines et en considérant les valeurs relatives des couplages $J_{^{13}CH}$ et $J_{^{13}CP}$.

A. *Configuration des pyrrolidines étudiées. Étude des déplacements chimiques*

1. *Stéréochimie au niveau de la liaison $C^4$—$C^5$*

Les déplacements chimiques du proton constituent un excellent critère pour l'attribution structurale des cycles à 5 chainons (10, 11). Ainsi, on peut aisément déterminer les positions relatives du phényle et du COOEt en considérant les déplacements des protons méthylènes et méthyles de la fonction ester éthylique (voir tableau 2).

On observe en effet une remarquable constance des valeurs de $\delta_{CH_2}$ et de $\delta_{CH_3}$ au sein de deux séries:

série **I** $\delta_{CH_3} \sim 1{,}1$ à $1{,}2$ ppm
$\delta_{CH_2} \sim 4{,}05$ à $4{,}16$ ppm

série **II**, **III** $\delta_{CH_3} \sim 0{,}8$ à $0{,}9$ ppm
$\delta_{CH_2} \sim 3{,}5$ à $3{,}8$ ppm

Compte tenu de l'anisotropie magnétique du groupe phényle, on en déduit que dans la série **I**, la disposition des deux substituants est *trans* et *cis* dans les séries **II** et **III** (12). Cette observation est confirmée par l'analyse des déplacements du carbone $\delta$ $^{13}C$ (voir tableau 3) bien que les effets soient relativement moins importants que dans le cas du proton.

2. *Influence des méthyles sur les protons et les carbones: établissement des structures **I**-1 à 3 et **II**-1 à 9*

Il est maintenant bien établi que sauf cas particuliers (10, 11), un substituant en *cis* d'un proton vicinal déplace celui-ci à champ fort, alors que l'effet inverse est produit si le substituant se situe en *trans*.

Par ailleurs, il faut noter que les effets de plusieurs substituants sont additifs (10) et c'est ainsi que pour le composé **II**-*7* diméthylé en 2 et 4, on trouve une différence de déplacement chimique $\Delta\delta_{H^3}$ (**II**-*7*) = $\delta_{H^{3b}} - \delta_{H^{3a}} = 1{,}7$ ppm. Une telle valeur ne peut s'expliquer que si les deux méthyles se situent en *cis* l'un par rapport à l'autre, ce qui nous permet de conclure à une disposition *cis* des trois autres substituants ($C_6H_5$, COOEt et (O)P·$(OEt)_2$).

La comparaison du $|\Delta\delta_{H^3}$ (**II**-*7*)| aux valeurs $|\Delta\delta_{H^3}$ (**I**-*1*)| = 0,05 ppm $|\Delta\delta_{H^3}$ (**II**-*1*)| = 0,29 ppm ainsi que des résultats antérieurs (11) concernant l'influence d'un méthyle sur les protons vicinaux, nous permettent de déduire que le composé **II**-*1* possède la même structure que celle de **II**-*7*. On établit ainsi de proche en proche la structure **II** pour les pyrrolidines **II**-*2*, **II**-*3*, **II**-*4*, **II**-*5*, **II**-*6*, **II**-*8*, **II**-*9* (voir tableau 6) et **I** pour les pyrrolidines **I**-*1*, **I**-*2*, **I**-*3*. Par ailleurs, si nous utilisons les incréments structuraux déterminés dans la série **II** à partir des

TABLEAU 6. Influence des méthyles sur les déplacements des protons du cycle pyrrolidinique

| Composé | $\alpha(n)$ | $\beta$-$n(m)$ *A* et *S** | $\gamma$-$n(m)$ *A* et *S** |
|---|---|---|---|
| **I**-*2* | — | −0,37 $\beta$-2(3) *S*<br>+0,29 $\beta$-2(3) *A* | +0,10 $\gamma$-2(4) *A*<br>+0,15 $\gamma$-2(5) *S* |
| **I**-*3* | +0,46 ($\alpha$-3) | −0,39 $\beta$-3(2) *S*<br>+0,07 $\beta$-3(4) *A* | +0,15 $\gamma$-3(5) *S* |
| **II**-*2* | — | −0,38 $\beta$-2(3) *S*<br>+0,28 $\beta$-2(3) *A* | +0,18 $\gamma$-2(4) *S*<br>+0,27 $\gamma$-2(5) *S* |
| **II**-*3* | +0,35 ($\alpha$-3) | −0,39 $\beta$-3(2) *S*<br>−0,42 $\beta$-3(4) *S* | +0,04 $\gamma$-3(5) *S* |
| **II**-*4* | — | −0,41 b-4(3) *S*<br>+0,37 $\beta$-4(3) *A*<br>−0,52 $\beta$-4(5) *S* | +0,07 $\gamma$-4(2) *S*<br>+0,02 $\gamma$-5(3) *A*<br>−0,03 $\gamma$-5(3) *S* |
| **II**-*5* | | −0,28 $\beta$-5(4) *S* | +0,20 $\gamma$-5(2) *S* |

*$\beta$-$n(m)$, $\alpha$-$n(m)$ représentent les influences d'un méthyle en position $n$ sur un proton situé en $m$ sur le cycle. *A* et *S* indique la disposition relative *anti* ou *syn* du méthyle et du proton.

Can. J. Chem. Downloaded from www.nrcresearchpress.com by 210.87.254.40 on 09/06/12
For personal use only.

TABLEAU 7. Valeurs calculées des déplacements chimiques protoniques (en ppm/THS) des pyrrolidines diméthylées (valeurs expérimentales entre paranthèses)

| No | $\delta_{H^2}$ | $\delta_{H^{3a}}$ | $\delta_{H^{3b}}$ | $\delta_{H^4}$ | $\delta_{H^5}$ |
|---|---|---|---|---|---|
| **II-*6*** | — | — | 3,18 (3,16) | 3,08 (3,05) | 4,83 (4,74) |
| **II-*7*** | — | 3,20 (3,31) | 1,47 (1,61) | — | 4,27 (4,36) |
| **II-*8*** | 3,16 (3,20) | — | 3,27 (3,16) | — | 4,04 (4,07) |
| **II-*9*** | 3,29 (3,32) | — | 2,92 (2,87) | 2,62 (2,64) | — |

TABLEAU 8. Influence des méthyles sur les déplacements chimiques des carbones ($^{13}C$, valeurs en ppm)

| No | $\alpha(n)$ | $\beta$-$n(m)$* | $\alpha$-$n(m)$ |
|---|---|---|---|
| **I-*2*** | $\alpha(2) = 5,4$ | $\beta$-2 (3) = 8,6 | $\gamma$-2 (4) = 1,4 |
| **I-*3*** | $\alpha(3) = 6,4$ | $\beta$-3 (2) = 7,8 | $\gamma$-2 (5) = −2 |
| | | $\beta$-3 (4) = 5,2 | $\gamma$-3 (5) = −2,9 |
| **II-*2*** | $\alpha(2) = 5,3$ | $\beta$-2 (3) = 6,2 | $\gamma$-2 (4) = −1 |
| **II-*3*** | $\alpha(3) = 8,3$ | $\beta$-3 (2) = 6,9 | $\gamma$-2 (5) = −2,6 |
| | | $\beta$-3 (4) = 8,8 | $\gamma$-3 (5) = −1,3 |
| **II-*4*** | $\alpha(4) = 5,3$ | $\beta$-4 (3) = 7,9 | $\gamma$-4 (2) = −0,8 |
| **II-*5*** | $\alpha(5) = 2,1$ | $\beta$-4 (5) = 8,4 | $\gamma$-5 (3) = −0,6 |
| | | $\beta$-5 (4) = 6,7 | $\gamma$-5 (2) = −1,4 |

*$\beta$-$n(m)$ ou $\gamma$-$n(m)$ se rapportent à l'influence d'un méthyle en position $n$ sur le carbone $C^m$ du cycle.

TABLEAU 9. Valeurs calculés des déplacements chimiques ($\delta$ $^{13}C$ en ppm/TMS) des pyrrolidines dimethylées (valeurs expérimentales entre parenthèses)

| No | $\delta_{C^2}$ | $\delta_{C^3}$ | $\delta_{C^4}$ | $\delta_{C^5}$ |
|---|---|---|---|---|
| **II-*6*** | 66,7 (62,2)* | 45,2 (39,5)* | 57,4 (56,9) | 61,7 (61,3) |
| **II-*7*** | 59,0 (59,5) | 44,1 (45,9) | 53,9 (54,5) | 72,0 (71,8) |
| **II-*8*** | 60,6 (60,1) | 46,2 (40,2)* | 63,7 (58,1)* | 72,7 (73,3) |
| **II-*9*** | 60,0 (59,9) | 37,7 (39,0) | 65,1 (65,7) | 64,8 (65,3) |

*Le mauvais accord observé dans ce cas est attribuable à l'intéraction de deux méthylés en *cis* portés par des carbones voisins (18). Ainsi pour les composés **II-*6*** et **II-*8***, ce fait se traduit par un abaissement d'environ 4,5 à 5 ppm des $\delta$ $^{13}C$ des carbones impliqués.

dérivés monométhylés (tableau 6) au calcul théorique des déplacements des dérivés diméthylés (voir tableau 7) on s'aperçoit que l'accord avec les valeurs expérimentales est excellent. Cette observation constitue une preuve supplémentaire de l'analogie structurale des composés considérés et indique de surcroit une grande homogénéité conformationnelle. De plus une approche similaire réalisée sur les déplacements du carbone ($\delta$ $^{13}C$) conduit aux mêmes conclusions (voir tableaux 8 et 9).

### 3. *Structures de* I-10, II-10, I-12, II-12, III-12 *et III*-9

L'analyse structurale des composés **I-*10*** et **II-*10*** est plus délicate en ce sens que l'utilisation des incréments de déplacement chimique conduit à des résultats difficilement interprétables et laisse supposer des variations sensibles de conformation (voir discussion sur les conformations).

L'étude comparée des déplacements $^{13}C$ des méthyles 3a et 3b (composés **I-*10*** et **II-*10***) à ceux des méthyles des autres composés de la série permet d'attribuer les structures compte tenu de l'effet stérique $\gamma$. Ainsi les valeurs respectives $\delta_{CH_3{}^{3a}}$ et $\delta_{CH_3{}^{3b}} = 25,4$ et 25,8 ppm (pour **I-*10***), 22,0 et 31,7 ppm (pour **II-*10***), indiquent que les groupes $O{=}P(OEt)_2$ et COOEt sont en *trans* dans le 1er cas en *cis* dans le second.

De la même façon, on peut déduire les structures de **I-*12*** et **II-*12***, en considérant les valeurs de $\delta_{C^{3a}}$ et $\delta_{C^{3b}}$ (carbones du cyclohéxyle). Le faible écart $|\delta_{C^{3a}} - \delta_{C^{3b}}|$ mesuré pour **III-*12*** indique une structure *trans* du COOEt par rapport au $O{=}P(OEt)_2$. Pour le composé **III-*9*** la valeur de $\delta_{CH_3{}^{3a}}$ (**III-*9***) = 14,1 ppm montre que les deux groupements $O{=}P{-}(OEt)_2$ et COOEt sont situés en *trans*. Dans ces conditions, la position de ce méthyle par rapport à ces deux substituants reste à déterminer. Les valeurs des couplages $^3J_{PC^4}$ et $^3J_{PC^5} \sim 2,5$ et 4,2 Hz (tableau 5) indiquent que le phosphore de **III-*9*** est essentiellement axial (8) ce qui est en plein accord avec la constatation selon laquelle $^1J_{PC}$ est plus faible dans un composé à phosphore axial que dans un composé à phosphore équatorial (7, 13)[2] ainsi:

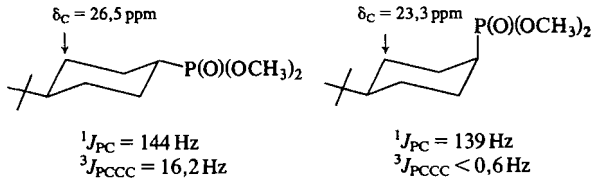


$^1J_{PC} = 144$ Hz, $^3J_{PCCC} = 16,2$ Hz

$^1J_{PC} = 139$ Hz, $^3J_{PCCC} < 0,6$ Hz

Or, nous avons $^1J_{PC^2}$ (**III-*9***) = 153,6 Hz et $^1J_{PC^2}$ (**II-*9***) = 166,5 Hz.

Une autre indication intéressante réside dans l'interaction $\gamma$ du phosphore axial produisant un effet diamagnétique sur les carbones (7, 13) (voir schéma ci-dessus). Le fait que pour **II-*9*** et **III-*9***, on mesure respectivement $\delta_{C^4} = 65,7$ et 62,2 ppm nous

[2]L'un des rapporteurs nous a fait remarquer que le plus grand couplage $^3J_{PNCC}$ connu a été mesuré dans le composé suivant couplage, notablement plus grand que celui observé dans notre cas est probablement à mettre sur le compte de la conjugaison existant entre les atomes impliqués.

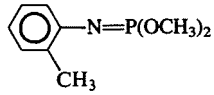


$^3J_{PNCC} = 22,7$ Hz

TABLEAU 10. Angles dièdres (en degrés) calculés à partir des relations de Karplus

| No | $PC^2—C^3H^{3a}$ (*trans*) | $PC^2—C^3H^{3b}$ (*cis*) | $H^2C^2—C^3H^{3a}$ (*cis*) | $H^2C^2—C^3H^{3b}$ (*trans*) | $PC^2—C^3C^4$ | $PC^2—NC^5$ |
|---|---|---|---|---|---|---|
| **II**-*1* | −84 | 41 | 38 | 159 | 153 | 162 |
| **II**-*2* | −86 | 47 | — | — | 152 | 135 |
| **II**-*4* | −85 | 39 | 41 | 161 | 153 | 152 |
| **II**-*5* | −81 | 41 | 37 | 156 | 146 | 140 |
| **II**-*6* | — | 52 | — | — | 161 | 147 |
| **II**-*7* | −80 | 38 | — | — | 147 | 145 |
| **II**-*9* | — | 49 | — | 154 | 159 | 151 |
| **II**-*10* | — | — | — | — | 127 | 170 |
| **II**-*11* | — | 41 | — | 165 | 158 | 130 |
| **II**-*12* | — | — | — | — | 127 | 166 |
| **I**-*1* | −97 | 21 | 21 | 136 | 136 | 140 |
| **I**-*2* | −167 | −48 | — | — | 121 | 120 |
| **II**-*3* | — | 11 | — | 134 | 137 | 140 |
| **II**-*10* | — | — | — | | 135 | 139 |
| **II**-*12* | — | — | — | — | 127 | 123 |
| **III**-*9* | — | — | — | — | −113 | −87 |
| **III**-*12* | — | — | — | — | −131 | −123 |

amène aux conclusions suivantes pour **III**-*9*: (*i*) le groupement $O{=}P(OEt)_2$ est axial, et (*ii*) la différence de déplacement entre le $\delta_{C^4}$ (**II**-*9*) et le $\delta_{C^4}$ (**III**-*9*) indique que pour ces deux dérivés, la seule différence structurale tient à la position du phosphore. En conséquence le méthyl 3 est situé en *trans* du COOEt et en *cis* du $O{=}P(OEt)_2$. Notons également la valeur du déplacement δ $^{13}C$ pour le méthyle 5. Si le composé possédait la structure **I** ce méthyle serait blindé relativement au même méthyle dans la structure **II**-*9* ce qui n'est pas le cas. Cette interprétation est par ailleurs confirmée par les valeurs des déplacements chimiques protoniques observés pour **III**-*9* (tableau 2).

4. *Structure* ***II***-11

On montre aisément que la pyrrolidine **II**-*11* possède la structure **II** et que la jonction pyrrolidine/cyclohexane est *cis*. En effet le proton $H^3$ est équatorial vis à vis du cyclohexane (du fait de l'absence de couplage diaxial avec l'un des protons de ce cycle), dans ces conditions la jonction des deux cycles est nécessairement *cis*. Par ailleurs, on mesure $^3J_{H^2H^3}$ = 11,8 Hz (tableau 3): $H^2$ et $H^3$ adoptent donc une disposition *trans*–diaxiale.

B. *Constantes de couplage et analyse conformationnelle. Étude des couplages* $^3J_{HH}$, $^3J_{PH}$, $^3J_{PC}$

Nous avons élucidé la stéréochimie des pyrrolidines étudiées essentiellement à l'aide des déplacements chimiques $^1H$ et $^{13}C$. L'étude des constantes de couplage doit nous permettre de préciser plus particulièrement les conformations adoptées par ces cycles. Par ailleurs, nous disposons d'un ensemble de constantes de couplage du type $^3J_{H-H}$, $^3J_{P-H}$, $^3J_{P-C}$, or pour ces trois couplages, différents auteurs ont établi des relations de dépendance angulaire. Il était donc intéressant de comparer les résultats obtenus à l'aide de chacune de ces relations. Dans une série de nicotines, Pitner et coll. (14, 15) ont établi les relations

[A] $^3J_{H-H} = 7{,}8 \cos^2 \phi + 2 \quad (0° < \phi < 90°)$

[B] $^3J_{H-H} = 10{,}5 \cos^2 \phi + 2 \quad (90° < \phi < 180°)$

Pour les pyrazolines Pudovik et coll. (2) ont déterminé:

[C] $^3J_{P-C-C-H} = 22 \cos \phi \quad (0° < \phi < 90°)$

[D] $^3J_{P-C-C-H} = -(1 + 21 \cos \phi + \cos 2\phi) \pm 1 \quad (90° < \phi < 180°)$

De la même façon, Thiem et Meyer (8) ont calculé:

[E] $^3J_{P-C-C-C} = 7{,}35\text{-}1{,}76 \cos \phi + 7{,}86 \cos 2\phi \quad (0 < \phi < 180°)$

(ϕ représente l'angle dièdre existant entre les atomes couplés.)

Les angles calculés à l'aide de chacune de ces relations et des couplages impliqués sont rassemblés dans le tableau 10. Si nous remarquons que l'on doit théoriquement avoir les égalités suivantes:

$$|PC^2—C^3C^4| = |H^2C^2—C^3H^{3b}|_{(trans)} = |PC^2—C^3H^{3b}|_{(cis)} + 120° = |H^2C^2—C^3H^{3a}|_{(cis)} + 120°$$

on constate que l'accord entre les angles calculés, sans être parfait, donne indubitablement des indications précieuses sur les conformations.

En effet dans la série des isomères **II**, l'influence des méthyles se fait peu sentir et le phosphore adopte une position essentiellement équatoriale

Can. J. Chem. Downloaded from www.nrcresearchpress.com by 210.87.254.40 on 09/06/12
For personal use only.

Can. J. Chem. Downloaded from www.nrcresearchpress.com by 210.87.254.40 on 09/06/12
For personal use only.

($PC^2$—$C^3C^4$ ~ 150°). Les composés **II**-*10* et **II**-*12* disubstitués en position 3 s'écartent notablement de ce type de conformation, comme nous l'avions supposé lors de l'étude des déplacements chimiques. Contrairement à la majorité des dérivés **II** la substitution du cycle par des méthyles sur les dérivés **I** introduit des variations importantes de conformation. Ainsi pour **I**-*2* (méthylé en 2) le groupement $P(O)(OEt)_2$ est préférentiellement axial. Cette constatation confirme par ailleurs les structures: les composés **II** sont entièrement *cis* ($OP(OEt)_2$, COOEt et $C_6H_5$) alors que les isomères **I** différent de ces derniers par la position du COOEt. Dans le premier cas, les trois substituants *cis* tendent à adopter dans tous les cas une disposition hors du cycle (encombrement minimum) alors que dans le second cas l'introduction d'un méthyle est suffisante pour que l'un des substituants se place axiallement. On note également une tendance similaire dans la série **III**. Par ailleurs, l'examen du tableau 10 indique une bonne concordance entre les angles obtenus à l'aide des couplages $^3J_{PH}$ et $^3J_{HH}$. Par contre les écarts assez importants entre ces résultats et ceux calculés avec les couplages $^3J_{PCCC}$ semblent montrer que la relation [E] soit à modifier quelque peu. De plus cette relation devient inapplicable dans le cas de couplages $^3J_{PCNC}$. En effet les valeurs de $^3J_{PCNC}$ sont plus élevées que celles de $^3J_{PCCC}$ et laissent à penser que les hétéroatomes pourraient avoir un effet sur la valeur de $^3J_{CP}$. Ainsi $^3J_{PCNC}$ (**II**-*10*) = 21,4 Hz alors que le couplage $^3J_{PC}$ maximum observé pour un angle de 180° est de 16,2 Hz (13*a*, *b*). Il est probable cependant qu'une relation de dépendance angulaire doit également gouverner en partie ce couplage. Si nous admettons que pour un cycle à cinq chainons, l'angle diédre maximum a une valeur de 170° environ (16), la valeur $^3J_{PCNC}$ (**II**-*10*) = 21,4 Hz pourrait être attribuable à cet angle. L'introduction de ces valeurs dans la relations [E] conduit à la relation corrigée [F]:

$$[F] \quad {}^3J_{PCNC} = 12{,}25 - 1{,}76 \cos \phi + 7{,}86 \cos 2\phi$$

qui permet le calcul des angles $PC^2$—$NC^5$.

Il est raisonnable d'admettre la relative validité de cette relation ainsi que la dépendance angulaire de ce couplage dans la mesure où l'angle $PC^2$—$NC^5$ calculé pour **III**-*9* est de 87°. Le phosphore occupe en conséquence une position axiale ce qui est un excellent agrément avec nos conclusions concernant les déplacements chimiques δ $^{13}C$ (voir chapitre précédent).

## Conclusion

Les déplacements chimiques δ $^{13}C$ et δ $^1H$ ont permis d'établir les structures des pyrrolidines isomères **I**, **II**, **III**. Les analogies structurales constatées confirment les résultats de synthèse. Ainsi dans la série **II**, les groupes phosphono, carbéthoxy et phényle sont situés en *cis*. Ce fait montre deux choses:

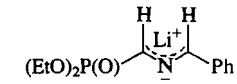


(*1*) L'anion azaallylique a réagi sous la forme *trans–trans*

(*2*) La forme *cis–cis* qui conduirait également à des composés à phényl et phosphore en *cis*, ne semble pas suffisamment stable dans nos conditions pour être envisagée.

Ce résultat est en accord avec les données de la littérature qui montrent que la confirmation *trans–trans* est en général prépondérante (1*b*).

Bien que non concertée, la réaction est stéréospécifique et conduit à un composé peu stable qui peut-être isomérisé. Par ailleurs connaissant les configurations, nous avons pu préciser les conformations privilégiées adoptées par ces cycles à l'aide des constantes de couplage. La bonne concordance observée entre les résultats obtenus par analyse des déplacements δ $^1H$ et δ $^{13}C$ et ceux donnés par les couplages confirme toutes les conclusions avancées au sein de la série **II**.

## Partie expérimentale

*Synthèse des pyrrolidines*

La synthèse de ces différents cycles est décrite dans la référence 1*a*.

*Spectres rmn*

(a) *Résonance $^1H$*

Les spectres sont enregistrés sur spectrographe Cameca à 250 MHz fonctionnant en onde continue. L'analyse des spectres est réalisable dans presque tous les cas au 1er ordre sauf pour **II**-*3* **II**-*8* et **III**-*9*. Pour ces composés les spectres sont très complexes (recouvrement de massifs) et très fortement couplés. Nous n'avons pas effectué d'analyse au 2ème ordre. Les déplacements chimiques donnés pour ces trois composés sont donc approximatifs.

Les déplacements chimiques des protons de tous les autres produits et les constantes de couplage $J_{HH}$ sont respectivement précis à ± 0,01 ppm et 0,1 Hz près. Les solutions utilisées sont concentrées à 1 *M*/L environ dans $CDCl_3$.

(b) *Résonance du $^{13}C$*

Les spectres $^{13}C$ sont enregistrés sur spectrographe Varian XL.100.12 opérant en transformée de Fourier et équipé d'une sonde de 8 mm. Les solutions utilisées sont concentrées à 1 *M*/L environ dans $CDCl_3$. Les déplacements chimiques sont précis à 0,1 ppm près.

1. (*a*) A. DEHNEL et G. LAVIELLE. Tetrahedron Lett. **21**, 1315 (1980); (*b*) TH. KAUFFMANN. Angew. Chem. Int. Ed. Engl. **13**, 627 (1979); (*c*) H. H. FREEDMAN, V. R. SANDEL et B. P. THILL. J. Am. Chem. Soc. **89**, 1762 (1967).
2. YU. YU. SAMITOV, R. D. GAREEV, L. A. STABROVSKAYA et A. N. PUDOVIK. Zh. Obshch. Khim. **42**, 1227 (1972).

3. YU. YU. SAMITOV, A. A. MUSINA, R. M. AMINOVA, M. A. PUDOVIK, A. I. KHAYAROV et M. D. MEDVEDEVA. Org. Magn. Reson. **13**, 163 (1980).
4. L. D. QUIN, M. J. GALLAGHER, G. T. CUNKLE et D. B. CHESNUT. J. Am. Chem. Soc. **102**, 3136 (1980).
5. G. W. BUCHANAN et C. BENEZRA. Can. J. Chem. **54**, 231 (1976).
6. G. W. BUCHANAN et F. G. MORIN. Can. J. Chem. **57**, 21 (1979).
7. G. W. BUCHANAN et J. H. BOWEN. Can. J. Chem. **55**, 604 (1977).
8. J. THIEM et B. MEYER. Org. Magn. Reson. **11** (1), 50 (1978).
9. L. D. QUIN et L. LITTLEFIELD. J. Org. Chem. **43**, 3508 (1978).
10. D. DANNEELS et M. ANTEUNIS. Org. Magn. Reson. **6**, 617, (1974).
11. M. ANTEUNIS et D. DANNEELS. Org. Magn. Reson. **7**, 345, (1975).
12. A. HIRSHFELD et W. TAUB. Tetrahedron, **28**, 1275 (1972).
13. G. W. BUCHANAN et F. G. MORIN. (*a*) Can. J. Chem. **58**, 530 (1980); (*b*) Org. Magn. Reson. **14**, 517 (1980).
14. T. P. PITNER, W. B. EDWARDS III, R. L. BASSFIELD et J. F. WHIDBY. J. Am. Chem. Soc. **100**, 246, (1978).
15. J. F. WHIDBY, W. B. EDWARDS III et T. PITNER. J. Org. Chem. **44**, 794, 1979.
16. J. W. EMSLEY, J. FEENEY et L. H. SUTCLIFFE. Prog. Nucl. Magn. Reson. Spectrosc. **5**, 212 (1969).
17. W. MCFARLANE. Proc. R. Soc. London, Ser A. **306**, 185 (1968).
18. D. K. DALLING et D. M. GRANT. J. Am. Chem. Soc. **89**, 6612 (1967).

Can. J. Chem. Downloaded from www.nrcresearchpress.com by 210.87.254.40 on 09/06/12
For personal use only.

# The crystal structure of bis(μ-trichloroacetato-*O*,*O'*)-bis[dimethyltin(IV)] and its relationship to other μ-acetato derivatives

THOMAS BIRCHALL[1] AND JAMES P. JOHNSON[2]

*Department of Chemistry and Institute for Materials Research, McMaster University, 1280 Main Street West, Hamilton, Ont., Canada L8S 4M1*

Received September 3, 1981

THOMAS BIRCHALL and JAMES P. JOHNSON. Can. J. Chem. **60**, 934 (1982).

The X-ray crystal structre of bis(μ-trichloroacetato-*O*,*O'*)-bis[dimethyltin(IV)] has been determined: $R' = 0.0518$. The crystals were monoclinic, space group $P2_1/c$, $a = 10.223(3)$ Å, $b = 7.539(2)$ Å, $c = 12.711(4)$ Å, $\beta = 97.76(2)$ and $Z = 2$. The molecular structure consists of a planar $(CH_3)_2Sn$—$Sn(CH_3)_2$ unit with the tin atoms bridged asymmetrically by two trichloroacetato groups to give each tin atom five coordination.

THOMAS BIRCHALL et JAMES P. JOHNSON. Can. J. Chem. **60**, 934 (1982).

On a déterminé la structure cristalline du bis(μ-trichloroacétato-*O*,*O'*)-bis[diméthyl étain(IV)] par diffraction des rayons X: $R' = 0{,}0518$. Les cristaux sont monocliniques, groupe d'espace $P2_1/c$, $a = 10{,}223(3)$, $b = 7{,}539(2)$, $c = 12{,}711(4)$ Å, $\beta = 97{,}76(2)$ et $Z = 2$. La structure moléculaire comporte une unité $(CH_3)_2Sn$—$Sn(CH_3)_2$ plane dont les atomes d'étain sont reliés d'une façon asymétrique aux deux groupes trichloroacétato; la coordination de chaque étain est de cinq.

[Traduit par le journal]

## Introduction

The preparation and spectroscopic properties of a series of bis(μ-haloacetato-*O*,*O'*)-bis[dimethyltin(IV)] compounds have been reported by us (1). The spectroscopic data were interpreted in terms of a tetramethylditin(IV) moiety in which the two tin atoms were bridged by two acetato ligands, thus completing the five coordinate environment about each tin. It was concluded that the changes observed in the spectroscopic data were associated with the nature of the substituted acetato ligand in the axial positions, and that only minor changes would be observed in the $(CH_3)_2Sn$—$Sn(CH_3)_2$ framework which constitutes the equatorial plane. Infrared, Raman, and Mössbauer data suggested that the average Sn—O bond length increases as the electronegativity of the R substituent on the acetato ligand increases.

Preliminary X-ray crystallographic data have been reported for the monochloroacetato (2) and the trifluoroacetato (3) derivatives and here we report the structure of the trichloroacetato compound and make a comparison between all three structures. The compounds are confirmed as being five coordinate in the solid state, with the acetato groups bridging the two tin atoms in an asymmetric fashion. The spectroscopic data are evaluated in light of the crystallographic data.

## Experimental

The preparation of the title compound has already been described (1). Crystals suitable for an X-ray study were obtained from the reaction product at 0°C and mounted in a thin quartz tube for examination.

*Crystal data*

$C_8H_{16}Cl_6O_4Sn_2$ mw = 622.27

Monoclinic, $a = 10.223(3)$ Å, $b = 7.539(2)$ Å, $c = 12.711(4)$ Å, $\beta = 97.76(2)°$, $U = 970.7(5)$ Å$^3$, $Z = 2$, $D_m = 2.06(2)$ g cm$^{-3}$, $D_c = 2.13$ g cm$^{-3}$, $F(000) = 588$, $\lambda(Mo - K_\alpha) = 0.719\,69$ Å, and $\mu(Mo - K_\alpha) = 34$ cm$^{-1}$.

The unit cell parameters were obtained from a least-squares refinement of 15 well centred reflections with $17.96° < 2\theta < 29.71°$. Zero and first layer precession photographs showed the systematic absence $0k0$ ($k$ odd), and $h0l$ ($l$ odd) indicating the space group $P2_1/c$ (No. 14) (4) and the structure was successfully refined in this space group.

*X-ray intensity measurements*

An almost spherical crystal of radius 0.15 mm sealed in a dry quartz capillary was mounted on a Syntex $P2_1$ diffractometer for data collection. Intensities were measured with graphite-monochromated radiation, using a $\theta$–$2\theta$ scan, for a total of 2560 reflections with $0 \le h \le 13$, $-1 \le k \le 9$, $-16 \le l \le 16$, and $3.23° \le 2\theta \le 55.13°$: equivalent reflections were averaged and the systematically absent reflections were removed from the data set. Of these 2051 reflections, 725 were "unobserved", i.e. had intensities less than $3\sigma$, where $\sigma$ is the error based on counting statistics. Two standard reflections (2, 3, −1); (2, 1, −4) were measured every 50 reflections and these showed a small but significant variation during data collection because of surface decomposition. The data were divided into three batches for refinement, each set with a different scale factor. A spherical absorption correction was necessary since $\mu(Mo - K_\alpha)R = 0.5$.

*Structure determination and refinement*

The positional parameters of the tin atom in the asymmetric unit were obtained from a three-dimensional Patterson synthesis, and were used to phase the initial structure-factor calculations. Least-squares refinement, using the locally written program CUDLS, of positional and isotropic thermal parameters of the tin atom gave a $R^1$ index of 0.39. The positional parameters of the remaining atoms were located by a difference-Fourier synthesis. By varying the coordinates and anisotropic temperature factors of all atoms the $R^1$ index dropped to 0.073 and a

[1]To whom all correspondence should be addressed.

[2]Present address, Department of Chemistry, University of Waterloo, Waterloo, Ont., Canada.

0008-4042/82/070934-05$01.00/0

©1982 National Research Council of Canada/Conseil national de recherches du Canada

Can. J. Chem. Downloaded from www.nrcresearchpress.com by 210.87.254.105 on 09/06/12
For personal use only.

Can. J. Chem. Downloaded from www.nrcresearchpress.com by 210.87.254.105 on 09/06/12
For personal use only.

weighting scheme was then imposed on the data set along with a secondary extinction correction,

$$F^* = F[1 + 0.542 \times 10^{-6} \times \beta\ (2\theta)F^2]^{1/2}$$

given by Larson (5). The refinement converged at $R = 0.0527$ and

$$R' = \{[\Sigma\omega(|F_o| - |F_c|)^2/\Sigma|F_o|^2]^{1/2}\} = 0.0518$$

where

$$\omega = [\sigma^2 + (0.027F_o)^2]^{-1}$$

$\sigma$ being the standard error in $F_o$ derived from counting statistics. The maximum value of shift over error was 0.004 for the $x$ coordinate of the tin atom, and the average shift over error for all variables was 0.0009. The final value of

$$[\Sigma\omega(|F_o| - |F_c|)^2/(N_F - N_p)]^{1/2} = 1.08$$

where $N_F$ = number of reflections and $N_P$ = number of refined parameters (= 94). This indicates that the model accounts for all structurally significant information in the observed structure factors. A final electron-difference map did not reveal the positions of the hydrogen atoms of the methyl groups. The largest feature was a peak of 1 e Å$^{-3}$ within 1 Å of the tin atoms along the Sn—Sn axis, with a minimum of $-1$ e Å$^{-3}$ at the centre of symmetry of the molecule. All other features were $\pm 0.5$ e Å$^{-3}$ with random distribution throughout the cell. Atomic scattering factors corrected for anomalous dispersion were taken from ref. 4.

The final positional co-ordinates of the atoms in the asymmetric unit are given in Table 1, bond lengths and bond angles in Table 2. Anisotropic temperature (Table 3) and structure factors have been deposited on supplementary information and are available on request.[3]

TABLE 1. Atomic coordinates (× $10^4$)

| Atom | $x/a$ | $y/b$ | $z/c$ |
|---|---|---|---|
| Sn | 4489(1) | 1610(1) | 187(1) |
| Cl(1) | 8115(3) | 384(3) | 3300(3) |
| Cl(2) | 9442(2) | 2440(5) | 5017(2) |
| Cl(3) | 9100(3) | 3845(4) | 2902(2) |
| O(1) | 2963(5) | 41(7) | 964(5) |
| O(2) | 6255(5) | 2341(7) | 4779(4) |
| C(1) | 7078(7) | 3407(12) | 4088(6) |
| C(2) | 8399(7) | 2547(12) | 3821(7) |
| C(3) | 2984(8) | 2187(14) | 4094(7) |
| C(4) | 5157(9) | 1986(12) | 6609(7) |

TABLE 2. Bond lengths (Å) and bond angles (deg) for $(CH_3)_4Sn_2(O_2CCCl_3)_2$

| Bond | Length | Bonds | Angle |
|---|---|---|---|
| Sn—O(1) | 2.285(6) | Sn—Sn—O(1) | 85.1(1) |
| Sn—O(2) | 2.332(5) | Sn—Sn—O(2) | 83.5(1) |
| Sn—Sn | 2.711(1) | Sn—Sn—C(3) | 121.9(3) |
| Sn—C(3) | 2.131(9) | Sn—Sn—C(4) | 120.5(2) |
| Sn—C(4) | 2.126(9) | C(3)—Sn—C(4) | 117.6(4) |
| C(1)—O(1) | 1.234(10) | Sn—O(1)—C(1) | 120.9(5) |
| C(1)—O(2) | 1.255(9) | Sn—O(2)—C(1) | 120.2(5) |
| C(1)—C(2) | 1.576(11) | O(1)—C(1)—O(2) | 129.5(7) |
| C(2)—Cl(1) | 1.769(9) | O(1)—C(1)—C(2) | 115.0(7) |
| C(2)—Cl(2) | 1.736(8) | O(2)—C(1)—C(2) | 115.4(7) |
| C(2)—Cl(3) | 1.751(9) | C(1)—C(2)—Cl(1) | 111.0(5) |
| | | C(1)—C(2)—Cl(2) | 105.9(5) |
| | | C(1)—C(2)—Cl(3) | 110.7(6) |
| | | Cl(1)—C(2)—Cl(2) | 109.6(5) |
| | | Cl(1)—C(2)—Cl(3) | 109.0(5) |
| | | Cl(2)—C(2)—Cl(3) | 110.6(4) |

*Estimated standard deviations in parentheses.

## Discussion

The molecular structure consists of independent $(CH_3)_4Sn_2(O_2CCCl_3)_2$ units, one of which is shown in Fig. 1. As has been found for the other structures of this type (2, 3, 6), the $C_2Sn$—$SnC_2$ unit is planar with a tin—tin bond of 2.711(1) Å which can be compared to the sum of the covalent radii, 2.80 Å. The $H_3C$—Sn bond lengths average 2.127(8) Å and are of normal length. The coordination about each tin atom is completed by two oxygen atoms, one above and one below the $C_2$—Sn—Sn—$C_2$ plane from two trichloroacetato ligands. Each tin is then five coordinate, there being no other significant interactions. These Sn—O distances, 2.286(6) Å and 2.333(5) Å, are significantly different so that the trichloroacetato ligand bridges the two tin atoms in an asymmetric fashion. Because of this one might have expected that the C(1)—O bonds within the trichloroacetato ligand would also be of different lengths. The values are 1.235(11) Å and 1.251(9) Å, and are not significantly different.

In the equatorial plane about each tin atom, the mutual repulsions between the two methyl groups and the bulky $(CH_3)_2Sn$ group results in a closing down of the C—Sn—C angle from 120° to 117.6(4)°. A consequence of the trichloroacetato ligand having a bite which is smaller than the tin–tin distance (2.711 Å) is that the Sn—Sn—O angles are significantly less than 90° and the O(1)—C(1)—O(2) angle is much greater than 120°. These effects have been observed for the analogous trifluoroacetato molecule (3).

A comparison of the structure of the title compound with the monochloro (2) and trifluoroacetato (3) complexes and with $(C_6H_5)_4Sn_2(O_2CCH_3)_2$ (6) reveals some interesting trends. Table 4 summarises the more important parameters for these four structures. The tin–tin distances are relatively short at ~2.7 Å and essentially invariant in all four molecules as are the tin–carbon (methyl or phenyl) distances. This invariance in bond lengths in the $C_2Sn$—$SnC_2$ framework is consistent with the lack of any changes in the $^{119}$Sn Mössbauer isomer shifts or in the $^1$H nmr parameters which we reported earlier (1).

[3]Complete set of data is available, at a nominal charge, from the Depository of Unpublished Data, CISTI, National Research Council of Canada, Ottawa, Ont., Canada K1A 0S2.

TABLE 3. Temperature factors ($\times 10^4$) in the form exp $(-2\pi^2\Sigma\Sigma U_{ij}H_iH_ja_i^*a_j^*)$

| Atom | $U_{11}$ | $U_{22}$ | $U_{33}$ | $U_{12}$ | $U_{13}$ | $U_{23}$ |
|---|---|---|---|---|---|---|
| Sn | 416(5) | 316(4) | 494(4) | 1(3) | 147(2) | −3(3) |
| Cl(1) | 693(16) | 639(16) | 1203(23) | 127(13) | 360(15) | −342(16) |
| Cl(2) | 589(15) | 1132(23) | 820(20) | 192(16) | −81(14) | 90(17) |
| Cl(3) | 735(16) | 904(20) | 887(19) | 157(14) | 524(14) | 191(15) |
| O(1) | 552(32) | 343(32) | 747(40) | −58(27) | 342(29) | −24(28) |
| O(2) | 452(30) | 320(27) | 610(34) | 44(25) | 279(27) | −53(26) |
| C(1) | 369(37) | 456(43) | 409(39) | 95(40) | 103(32) | −58(40) |
| C(2) | 395(42) | 468(47) | 593(52) | 90(38) | 130(38) | −80(42) |
| C(3) | 423(45) | 700(63) | 654(59) | −70(43) | −28(41) | −155(49) |
| C(4) | 762(60) | 547(59) | 483(50) | 133(45) | 62(44) | 150(42) |

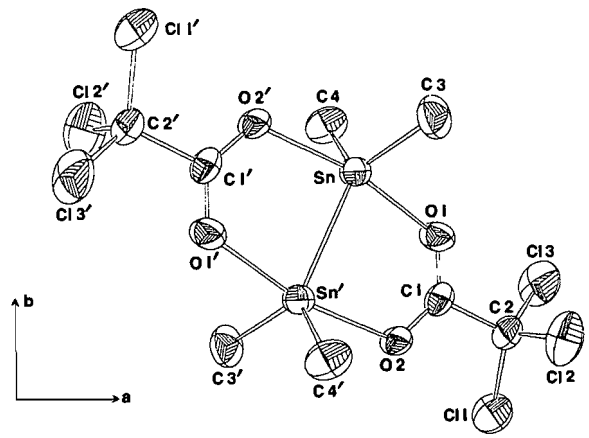


FIG. 1. A view of bis(μ-trichloroacetato-*O*,*O*′)-bis[dimethyltin(IV)] down the *c* axis.

Systematic changes are noted in the C—O and Sn—O bond lengths across this series of compounds, and we had predicted, based on ir spectroscopic data, that the $CCl_3$ derivative would have the most asymmetric C—O bond distances while the $CH_2Cl$ and $CF_3$ compounds would be the most symmetric (1). This does not appear to be the case and it is the $CCl_3$ derivative which appears the most symmetric. Undoubtedly the $\nu_{C-O}$ vibrations are strongly influenced by the Sn—O interactions and cannot be considered in isolation.

The variations in the Sn—O bond lengths for the three $(CH_3)_4Sn_2(O_2CR)_2$ compounds are, however, significantly greater than the errors on these distances. It would appear that the Sn—O(2) bond length is invariant at 2.34 Å while the Sn—O(1) distances are 2.241(7) Å, 2.286(6) Å, and 2.319(4) Å in the $CH_2Cl$, $CCl_3$, and $CF_3$ compounds, respectively. Thus the $CF_3$ derivative is the most symmetrically bonded with the longest average Sn—O bond length at 2.332 Å while the $CH_2Cl$ is the most asymmetric but with the shortest average Sn—O bond length at 2.285 Å.

These average tin–oxygen distances are consistent with the $^{119}$Sn Mössbauer quadrupole coupling constants which we have already reported (1). The longer the average Sn—O distance, the greater is the quadrupole coupling constant. Based upon data for series of trimethyltin carboxylates, it was suggested (7, 8) that the Mössbauer quadrupole coupling constants reflected the asymmetry in the tin–oxygen distances. In these molecules, the carboxylate ligand bridges the $(CH_3)_3Sn$ moieties intermolecularly with one short and one long Sn—O bond. These different bond lengths were attributed to an increase in double bond character of one C—O bond at the expense of the other C—O bond of the carboxylate as the electronegativity of the R group increases. If such were the case, then one might expect a corresponding difference in the Sn—O distances in related organo-tin carboxylates as R becomes more electronegative. For the series of trimethyltin carboxylates the difference in Sn—O bond distances does increase from 0.186(5) Å to 0.281(21) Å as the R group is changed from $CH_3$ to $CF_3$ (8), which supports the above suggestion about the quadrupole coupling constants (7, 8). However, in the tetramethylditin carboxylates reported here the difference in the two Sn—O bond lengths decreases as the ligand electronegativity increases (0.108(10), $-CH_2Cl$; 0.047(8), $-CCl_3$; 0.026(6), $-CF_3$).

Although the type of carboxylate bridge is quite different in these two series of compounds, the concept of partial contributions to the Mössbauer quadrupole splittings appears valid in the two series (9). It seems reasonable to conclude that with increasing electronegativity of the R group, the average Sn—O distance will also increase and that this will be manifested in larger quadrupole splittings, though the Sn—O distances may not be different. In the trimethyltin carboxylates the average Sn—O distance increases from 2.298(5) Å for R = $CH_3$ to 2.318(21) Å for R = $CF_3$ and although this increase is not statistically significant, it does parallel the increase observed in the tetramethyl-

Can. J. Chem. Downloaded from www.nrcresearchpress.com by 210.87.254.105 on 09/06/12
For personal use only.

TABLE 4. A summary of bond lengths and bond angles for $(CH_3)_4Sn_2(O_2CR)_2$ and $(C_6H_5)_4Sn_2(O_2CCH_3)_2$

| Bond | Length | | | |
|---|---|---|---|---|
| | $CH_2Cl$[a] | $CCl_3$[b] | $CF_3$[c] | $CH_3$[d] |
| Sn—Sn | 2.691(2) | 2.711(1) | 2.707(1) | 2.69(1) |
| Sn—O(1) | 2.241(7) | 2.285(6) | 2.319(4) | 2.25(2) |
| Sn—O(2) | 2.349(7) | 2.332(5) | 2.345(4) | 2.25(2) |
| Sn—C(3) | 2.112(14) | 2.131(9) | 2.100(10) | 2.15(2) |
| C(1)—O(1) | 1.27(2) | 1.234(10) | 1.218(12) | 1.31(4) |
| C(1)—O(2) | 1.25(2) | 1.255(9) | 1.251(12) | 1.20(4) |
| **Bonds** | **Angle** | | | |
| | $CH_2Cl$[a] | $CCl_3$[b] | $CF_3$[c] | $CH_3$[d] |
| Sn—Sn—O(1) | 86.3(3) | 85.1(1) | 84.6(2) | 84.2 |
| Sn—Sn—O(2) | 82.4(3) | 83.5(1) | 83.8(2) | 84.5 |
| O(1)—C(1)—O(2) | 125.5(10) | 129.5(7) | 129.9(6) | 125.6 |
| C(2)—C(1)—O(1) | 112.5(13) | 115.0(7) | 115.9(8) | 113.2 |
| C(2)—C(1)—O(2) | 122.0(14) | 115.4(7) | 114.2(8) | 121.3 |

[a]Reference 2.
[b]This work.
[c]Reference 3.
[d]Reference 6, $(C_6H_5)_4Sn_2(O_2CCH_3)_2$.

ditin series discussed here. These asymmetries are a common feature in organotin carboxylates. The Sn—O distances, being nearly equal in the tetramethylditin series, are larger for the trimethyltin series and largest for the tribenzyltin acetate where the Sn—O distances are 2.14(2) Å and 2.65(2) Å (10). In tricyclohexyltin acetate the Sn—O distances are 2.12(3) Å and 2.95(4) Å and this compound is best regarded as an example of a monomeric four-coordinate tin compound (11). The bonding scheme in the tetramethylditin carboxylates does not appear to be explicable in terms of a localised bonding arrangement of the carboxylate ligand and we must look elsewhere for an explanation of the trends in Sn—O distances.

In all of these molecules the Sn—Sn—O angles are all significantly less than 90° and while there are small changes in these values as $R$ is varied, we attach little significance to them. They are undoubtedly the result of the bite of the acetato ligand being less than the tin–tin distance of 2.7 Å. The more interesting angles are those about C(1) of the acetato group. That the O(1)—C(1)—O(2) angles are greater than 120° is not surprising in view of the constraints imposed by the bite of the acetato ligand as mentioned above. In the $CCl_3$ and $CR_3$ derivatives this angle is nearly 130° with the C(2)—C(1)—O(1) and C(2)—C(1)—O(2) angles being equal at ~115°. The $CH_2Cl$ derivative is somewhat different in having a smaller O(1)—C(1)—O(2) angle at 125.5°, but more surprising is the fact that the other two angles at C(1) are not equal, one being 122.0° and the other 112.5°. A similar situation exists in the $(C_6H_5)_4Sn_2(O_2CCH_3)_2$ molecule though in this case the structure is not as well refined and large errors in the angles ($3\sigma = 8.4°$) were quoted (6). There is no obvious reason for such a distortion in this molecule. On the other hand, in the monochloroacetato complex the strong repulsions between the Cl and O(2) would open up the C(2)—C(1)—O(2) angle to the observed value; the chlorine atom is in the same plane as all of the other atoms of the monochloroacetato group except the hydrogens (2). One might have expected that the chlorine atom would move out of this plane in order to relieve the repulsions and allow the ligand to bridge symmetrically. That it does not do so must be because the observed arrangement can pack much more efficiently in the crystal. This arrangement is aided by hydrogen-bonded interactions between the hydrogens of the $CH_2Cl$ group and the oxygens of neighbouring molecules. The position of the hydrogen atoms of the $CH_2Cl$ group were deduced from chemical considerations and correspond to a peak of 0.5 e $Å^{-3}$ in the final difference synthesis. The orientation of the —$CH_2Cl$ group is such as to allow for one hydrogen atom from two different $CH_2Cl$ groups to form hydrogen bonds of length 3.06 Å to the oxygen atom forming the long Sn—O bond in a third molecule.

The most symmetrically bonded ligand is the trifluoroacetato group and it has been noted that the fluorines of this ligand are either disordered or rotating in the crystal (3). Calculation of bond valences for the atoms in the trifluoroacetato group, using the method of Brown and Shannon

Can. J. Chem. Downloaded from www.nrcresearchpress.com by 210.87.254.105 on 09/06/12
For personal use only.

(12), showed that one of the oxygen atoms was short of this normal bond valence of two and that this could be made up at least partially by two additional interactions to hydrogens of adjacent methyl groups (3) giving hydrogen bonds of 3.2 Å. There was also evidence for hydrogen bonded interactions to the fluorines of the $CF_3$ groups which aided the keying together of the molecules in the crystal. In the case of the trichloroacetato group, the $CCl_3$ group cannot rotate, partly because of the size of the chlorines and possibly also because of hydrogen bonded interactions which occur between these atoms and the methyl hydrogens. Repulsions are minimised by a slight rotation of the $CCl_3$ group so that none of the chlorines lie in the plane of the C—$CO_2$ atoms, and the C(2)—C(1)—O angles remain equal.

**Acknowledgement**

The Natural Sciences and Engineering Research Council of Canada is thanked for financial assistance.

1. T. Birchall and J. P. Johnson. Can. J. Chem. **57**, 160 (1979).
2. R. Faggiani, J. P. Johnson, I. D. Brown, and T. Birchall. Acta Crystallogr. B**34**, 3742 (1978).
3. R. Faggiani, J. P. Johnson, I. D. Brown, and T. Birchall. Acta Crystallogr. B**35**, 1227 (1979).
4. International Tables for X-Ray Crystallography. Vol. 1. Kynoch Press, Birmingham, 1962.
5. A. C. Larson. Acta Crystallogr. **23**, 664 (1967).
6. G. Bandoli and D. A. Clemante. Chem. Commun. 311, (1971).
7. C. Poder and J. R. Sams. J. Organomet. Chem. **19**, 67 (1969).
8. H. Chin and B. R. Penfold. J. Cryst. Mol. Struct. **3**, 285 (1973).
9. G. M. Bancroft, V. G. K. Das, F. K. Sham, and M. G. Clark. J. Chem. Soc. Dalton Trans. 643 (1976).
10. N. W. Alcock and R. E. Timms. J. Chem. Soc. A, 1873 (1968).
11. N. W. Alcock and R. E. Timms. J. Chem. Soc. A, 1876 (1968).
12. I. D. Brown and R. Shannon. Acta Crystallogr. A**29**, 266 (1973).

Can. J. Chem. Downloaded from www.nrcresearchpress.com by 210.87.254.105 on 09/06/12
For personal use only.

Can. J. Chem. Downloaded from www.nrcresearchpress.com by 210.87.254.40 on 09/06/12
For personal use only.



# The structures of phyllanthostatin 1 and phyllanthoside from the Central American tree *Phyllanthus acuminatus* Vahl[1]

GEORGE R. PETTIT,[2] GORDON M. CRAGG, DEVENS GUST, PETER BROWN,[3] AND JEAN M. SCHMIDT

*Cancer Research Institute and Department of Chemistry, Arizona State University, Tempe, AZ 85287, U.S.A.*

Received January 28, 1982

GEORGE R. PETTIT, GORDON M. CRAGG, DEVENS GUST, PETER BROWN, and JEAN M. SCHMIDT. Can. J. Chem. **60**, 939 (1982).

A new antineoplastic glycoside, phyllanthostatin 1, and the related glycoside, phyllanthoside, have been isolated from the Central American tree, *Phyllanthus acuminatus* Vahl. The structures of phyllanthostatin (**1***a*) and phyllanthoside (**1***b*) were completely assigned by analyses of spectral data, principally by high resolution (400 MHz) nmr. In addition to exhibiting activity against the National Cancer Institute's P388 lymphocytic leukemia, phyllanthoside was found to possess a curative level of activity against the murine B16 melanoma.

GEORGE R. PETTIT, GORDON M. CRAGG, DEVENS GUST, PETER BROWN et JEAN M. SCHMIDT. Can. J. Chem. **60**, 939 (1982).

On a isolé d'un arbre de l'Amérique Centrale, le *Phyllanthus acuminatus* Vahl, un nouveau glycoside antinéoplastique, la phyllanthostatine 1, et le glycoside apparenté phyllanthoside. L'analyse des données spectrales obtenues principalement par la rmn à haute résolution (400 MHz) a permis d'établir complètement les structures de la phyllanthostatine (**1***a*) et du phyllanthoside (**1***b*). En plus de montrer une activité contre la leucémie lymphocytique P388 de l'Institut National du Cancer, on a trouvé que le phyllanthoside possède une certaine activité curative contre mélanoma B-16 de la murine.

[Traduit par le journal]

The Euphorbiaceae family is rich in plants with a long history of human medicinal applications (2, 3). The Euphorbiaceae genus *Phyllanthus* (about 600 species ranging from free floating aquatic forms to trees) contains several species that have been employed in the primitive treatment of cancer (4, 5). Because of the U.S. National Cancer Institute's (NCI) exploratory plant evaluation program, in collaboration with the U.S. Dept. of Agriculture (USDA), the roots of a tree believed[4] to be *P. brasiliensis* Muell were collected about a decade ago in Costa Rica. An ethanol extract of the original collection was found to inhibit growth of the NCI murine P388 lymphocytic leukemia (PS system), and the Kupchan group (6) isolated and partially characterized a PS active glycoside termed phyllanthoside from a 1974 re-collection. We now report the isolation of a new anticancer glycoside designated phyllanthostatin 1 (**1***a*, 52% life extension against the PS leukemia) and a substance spectroscopically identical to phyllanthoside (**1***b*)[5] from the roots of *P. acuminatus* Vahl,[4] re-collected (1978) in Costa Rica. Structure elucidation of these unusual 1 → 2 linked disaccharides (**1***a*, **1***b*) has been accomplished. Also we are pleased to note that phyllanthoside (**1***b*) has exhibited a curative level (at 8 mg/kg with an average 62–74% life extension over the dose range 4–16 mg/kg) of antineoplastic activity against the NCI murine B16 melanoma and is presently being considered for eventual human clinical trial.

The chipped roots (81.5 kg) of *P. acuminatus* were processed by a convenient new technique[6] for initial plant and animal extraction involving the use of methylene chloride – methanol (1:1) at ambient temperatures (7). After extraction enough water

[1]Antineoplastic Agents 73. For part 72 refer to ref. 1.

[2]Author to whom correspondence should be addressed.

[3]The study reported herein is dedicated to the memory of Professor P. Brown who passed away March, 1981.

[4]Later, information was uncovered by Drs. J. Duke and R. Spjut of the USDA indicating *P. brasiliensis* does not extend into Central America. A detailed study of the taxonomic problem by Dr. Spjut has revealed (private communication) that the plant collection provided for the original isolation of phyllanthoside was in actuality the very closely related Central American *P. acuminatus* Vahl. Thus the re-collections (about 150 kg of root from Costa Rica) of this plant, kindly provided by Dr. J. Duke and employed in the present investigation, have been identified as *P. acuminatus*.

[5]Unfortunately, no specimens of phyllanthoside or phyllanthocin remain from the original separations. Part of the large scientific and medical loss was due to Prof. M. Kupchan's untimely death in 1976.

[6]Developed by one of us (G.R.P.) with Drs. D. L. Doubek and D. L. Herald. Application of the safer (for personnel) methylene chloride (in place of chloroform) for most solvent partition and chromatographic procedures has been summarized with pertinent references as part of another study (7*a*).

0008-4042/82/070939-03$01.00/0

©1982 National Research Council of Canada/Conseil national de recherches du Canada

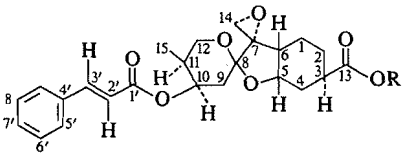

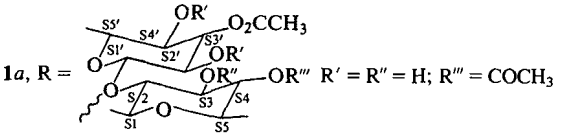

**1***a*, R = R′ = R″ = H; R‴ = $COCH_3$

*b*, **1***a*, R′ = R‴ = H; R″ = $COCH_3$

*c*, **1***a*, R′ = R″ = R‴ = $COCH_3$

*d*, R = $CH_3$

*e*, R = H

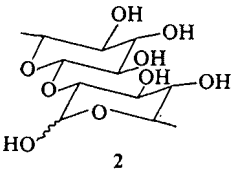

**2**

was added to separate the methylene chloride phase. The latter fraction[7] (475 g) was partitioned using the sequence 9:1 → 4:1 → 3:2 methanol–water with ligroin → carbon tetrachloride → methylene chloride (7, 8). Combination of the carbon tetrachloride (44 g) and methylene chloride (210 g) fractions followed by gel permeation (Sephadex LH-20, methanol) and repeated silica gel (98:2:0.1 chloroform–methanol–water) column chromatography of a 38 g aliquot afforded 0.24 g of pure (by hplc, μ-Porasil column with 97:3.0:0.2 methylene chloride – methanol–water) phyllanthostatin 1 (**1***a*) as an amorphous solid, mp 125–126°C; $[\alpha]_D^{26}$ −3.6° (*c* 0.83, $CHCl_3$); $\lambda_{max}$(MeOH) (log ε): 216 (4.19), 222 (4.12), and 277 (4.29) nm; ir (KBr) $\nu_{max}$: 3450, 1755, 1740, 1710, 1640, 1452, 1380, 1310, 1245, 1170, 1075, and 770 $cm^{-1}$; FD ms *m/e*: 805 ($M^+$ + H). Additional silica gel chromatography of PS active fractions yielded 0.6 g of pure (by hplc, as above) **1***b* as an amorphous solid with the following characteristics: mp 125–127°C; $[\alpha]_D^{22}$ +16.9° (*c* 0.71, $CHCl_3$); $\lambda_{max}$(MeOH) (log ε): 216 (4.25), 222 (4.19), and 277 (4.34) nm; ir (KBr) $\nu_{max}$: 3475, 1750, 1735, 1710, 1640, 1452, 1380, 1311, 1253, 1173, 1080, and 770 $cm^{-1}$; FD ms *m/e*: 805 ($M^+$ + H). Comparison of spectral data with that recorded for authentic phyllanthoside (**1***b*) indicated that both are identical.[5]

The complete structures of phyllanthostatin 1 and phyllanthoside were deduced by interpreting the $^{13}C$ nmr (22.63 MHz, $CDCl_3$), $^1H$ nmr (400 MHz, $CDCl_3$), and EI high resolution and FD mass spectra.[8] Although the structure of glycoside **1***b* was not previously known, Kupchan *et al.* (6) reported structural studies of two degradation products which proved very useful in the present study. Methanolysis of glycoside **1***b* gave an aglycone (phyllanthocin (**1***d*) by X-ray crystallographic analysis) and a disaccharide, $C_{12}H_{22}O_9$. Acid hydrolysis of the disaccharide yielded 6-deoxy-D-glucose and spectral evidence suggested that the disaccharide portion contained two acetate groups.

Examination of the $^1H$ and $^{13}C$ nmr results for **1***a* and **1***b* indicated that these potent antineoplastic plant constituents have identical aglycones and differ only in the disaccharide portion. Both glycosides afforded identical peracetates (**1***c*, mp 122–126°C, $[\alpha]_D^{24}$ +26.3° (*c* 1.1, $CHCl_3$)) and were readily interconverted via an acetyl shift upon standing at room temperature for periods exceeding 24 h in 90% aqueous ethanol.[9] Thus, glycosides **1***a* and **1***b* differ only in the location of one acetyl group on the disaccharide unit and consist of aglycone **1***e* joined via an ester linkage to a diacetylated 6-deoxy-D-glucose disaccharide. In addition, the $^3J_{HH}$ coupling constants of ~8 Hz measured for both anomeric protons of glycosides **1***a* and **1***b* indicated β-linkages at the anomeric centers. At this point only location of the three 6-deoxy-D-glucose ester groups and position of the disaccharide linkage of **1***a* and **1***b* remained to be solved.

The $^1H$ nmr spectrum of phyllanthoside (**1***b*) exhibited two 6-deoxy-D-glucose ring proton resonances at δ 4.78 and 4.90 ppm. The ca. 1 ppm downfield shift of these resonances from the usual positions for such protons clearly indicated attachment to carbon atoms bearing ester groups (9). And $^1H$ nmr decoupling studies revealed that these two ester linkages were at S-3 and S-3′. The $^{13}C$ and $^1H$ nmr results showed that the third ester linkage was at S-1 (S-1: $^{13}C$ 92.06, $^1H$ 5.50, d, $J$ = 8.1 Hz; S-1′: $^{13}C$ 103.84, $^1H$ 4.00, d, $J$ = 7.8 Hz). Similar

[7]The NCI PS in vivo and in vitro lymphocytic leukemia bioassays were employed to guide each step of the separation.

[8]The spectral data were quite consistent with the assigned structures and will be summarized in a future complete report. Elemental analytical results were also consistent with structures **1***b* and *c*. The instrumental analyses were conducted using Varian-MAT 731, Bruker WH-90, and Bruker WH-400 instruments. We are pleased to thank Drs. R. R. Inners, P. D. Ellis, J. A. McCloskey, and J. Witschel, Jr. for expert assistance with these measurements.

[9]More polar products resulting from hydrolysis of the acetates are also formed. Similar interconversion occurs with solutions of the compounds in 0.9% saline containing 5% ethanol.

Can. J. Chem. Downloaded from www.nrcresearchpress.com by 210.87.254.40 on 09/06/12
For personal use only.

Can. J. Chem. Downloaded from www.nrcresearchpress.com by 210.87.254.40 on 09/06/12
For personal use only.

studies of phyllanthostatin (**1***a*) indicated that the ester linkages were at S-1, *S-4*, and S-3′. Because chemical (acetylation) evidence suggested that glycosides **1***a* and **1***b* differed only in the location of an acetate group, the ester at S-3 in phyllanthoside and S-4 in phyllanthostatin 1 must be acetate. Furthermore, treatment of phyllanthoside with cellulase in an acetate buffer (pH 5.0) yielded a monoacetyl derivative. Here $^1$H nmr studies of this derivative showed that the S-3′ proton resonance was shifted upfield ca. 1 ppm, whereas resonances for the aglycone and the other glucose protons remained essentially unchanged. Accordingly, the second acetate group resides at S-3′ in both glycosides **1***a* and **1***b* and the aglycone must be linked to the disaccharide at S-1.

The final structural question concerned the nature of the disaccharide linkage. Because carbon atoms S-1 and S-3 in phyllanthoside (**1***b*) and S-1 and S-4 in phyllanthostatin (**1***a*) bear ester groups, the 6-deoxy-D-glucose units must, by elimination, be linked 1 → 2. This rather unusual linkage was confirmed by the following experiments. Methanolysis (0.1 *M* sodium methoxide in methanol) of phyllanthoside gave aglycone methyl ester **1***d* and disaccharide **2** (6), mp 217–219°C; $[\alpha]_D^{26}$ −3.3° (*c* 1.51, $H_2O$); $^1$H nmr (100 MHz, $D_2O$) δ: 1.27 and 1.31 (6H, d, $J$ = 6 Hz, 6,6′-$CH_3$), 3.06–4.12 (9H, m), 4.67 (d, $J$ = 8 Hz), 5.4 (d, $J$ = 4 Hz) ppm. Acetylation (acetic anhydride in pyridine) yielded a peracetate whose $^1$H nmr spectrum featured two methyl group doublets at δ 1.18 and 1.22, acetate methyl resonances at 2.00–2.20, a three-proton multiplet at 3.40–4.05, a group of resonances from 4.55–5.6, and an α-anomeric proton ($^3J_{HH}$ = 3 Hz) at 6.29 ppm. The resonance at 6.29 ppm was assigned to S-1. The low-field resonances at 4.55–5.6 ppm were attributed to S-1′ plus the protons of the acetate-bearing ring carbon atoms which experienced an expected (9) downfield shift, relative to the parent disaccharide. The three protons appearing at 3.40–4.05 ppm correspond to S-5, S-5′, and the proton on the carbon involved in the anomeric linkage to the second sugar. Proton decoupling experiments showed resonances at 3.55 and 3.93 ppm which belong to S-5 and S-5′ and a doublet of doublets at 3.90 coupled to the resonance at 6.29 ppm which must arise from S-2. Therefore the anomeric linkage at S-2 was confirmed and the phyllanthostatin 1 (**1***a*) and phyllanthoside (**1***b*) structural assignments were completed.

We have also found that *P. acuminatus* contains a series of antineoplastic glycosides related to **1***a* and **1***b* and the structures of these new and potentially useful cancer chemotherapeutic agents are presently under investigation.

## Acknowledgments

We gratefully acknowledge assistance provided by Contract NO1-CM-97297 with the Division of Cancer Treatment, NCI, National Institutes of Health, DHW, Grant Nos. CA16049-06 and 07 awarded by the National Cancer Institute, DHW, Mrs. Mary Dell Pritzlaff, the Olin Foundation (Spencer T. and Ann W.), the Fannie E. Rippel Foundation, and the National Science Foundation Regional Facility at the University of South Carolina (CH78-18723). We are also pleased to thank Drs. M. I. Suffness, J. D. Douros, M. E. Wall, C. L. Herald, D. L. Herald, Mr. H. Taylor, Miss M. S. Pettit, and Mr. R. Booze for very helpful assistance.

1. G. R. PETTIT, Y. KAMANO, Y. FUJII, C. L. HERALD, M. INOUE, P. BROWN, D. GUST, K. KITAHARA, J. M. SCHMIDT, D. L. DOUBEK, and C. MICHEL. J. Nat. Prod. In press.
2. J. M. WATT and M. G. BREYER-BRANDWIJK. The medicinal and poisonous plants of southern and eastern Africa. 2nd ed. E. S. Livingstone Ltd., London. 1962. p. 426.
3. J. F. MORTON. Major medicinal plants. C. C. Thomas, Springfield, IL. 1977. pp. 193, 366.
4. J. L. HARTWELL. Lloydia, **32**, 153 (1969).
5. R. W. SPJUT and R. E. PERDUE. Cancer Treatment Reports, **60**, 979 (1976).
6. S. M. KUPCHAN, E. J. LAVOIE, A. R. BRANFMAN, B. Y. FEI, W. M. BRIGHT, and R. F. BRYAN. J. Am. Chem. Soc. **99**, 3199 (1977).
7. (*a*) G. R. PETTIT, Y. FUJII, J. A. HASLER, J. M. SCHMIDT, and C. MICHEL. J. Nat. Prod. Submitted; (*b*) G. R. PETTIT and G. M. CRAGG. Biosynthetic products for cancer chemotherapy. Vol. 2. Plenum Publishing Corp., New York. 1978; (*c*) G. R. PETTIT and R. H. ODE. Biosynthetic products for cancer chemotherapy. Vol. 3. Plenum Publishing Corp., New York. 1979.
8. J. M. SCHMIDT and G. R. PETTIT. Experientia, **34** 659 (1978).
9. L. D. HALL. Adv. Carbohyd. Chem. **19**, 51 (1964).

# Nuclear analogs of β-lactam antibiotics. XIV. Synthesis of penems via (4-tritylthio-2-azetidinon-1-yl)triphenylphosphoranylideneacetates

ALAIN MARTEL,[1] PIERRE DEXTRAZE, JEAN-PAUL DARIS, ROGER SAINTONGE, PHILIPPE LAPOINTE, TERRY T. CONWAY, IVO MONKOVIC, GERRY KAVADIAS, YASUTSUGU UEDA, PATRICK ELIE, SHAM PATIL, GILLES CARON, JAMES L. DOUGLAS, MARCEL MÉNARD, AND BERNARD BELLEAU[2]

*Bristol Laboratories of Canada, 100 Industrial Boulevard, Candiac, P.Q., Canada J5R 1J1*

Received December 11, 1981

ALAIN MARTEL, PIERRE DEXTRAZE, JEAN-PAUL DARIS, ROGER SAINTONGE, PHILIPPE LAPOINTE, TERRY T. CONWAY, IVO MONKOVIC, GERRY KAVADIAS, YASUTSUGU UEDA, PATRICK ELIE, SHAM PATIL, GILLES CARON, JAMES L. DOUGLAS, MARCEL MÉNARD, and BERNARD BELLEAU. Can. J. Chem. **60**, 942 (1982).

The preparation of (4-tritylthio-2-azetidinon-1-yl)triphenylphosphoranylideneacetates from 4-acetoxyazetidin-2-one is described. They are easily converted to mercuric or silver mercaptides. These mercaptides are acylated with a wide variety of acylating agents and cyclized to 2-substituted penem-3-carboxylates.

ALAIN MARTEL, PIERRE DEXTRAZE, JEAN-PAUL DARIS, ROGER SAINTONGE, PHILIPPE LAPOINTE, TERRY T. CONWAY, IVO MONKOVIC, GERRY KAVADIAS, YASUTSUGU UEDA, PATRICK ELIE, SHAM PATIL, GILLES CARON, JAMES L. DOUGLAS, MARCEL MÉNARD et BERNARD BELLEAU. Can. J. Chem. **60**, 942 (1982).

On décrit la préparation des (tritylthio-4 azètidinone-2 yl-1) triphénylphosphoranylidèneacétates à partir de l'acétoxy-4 azétidinone-2. On les transforme facilement en sulfures de mercure ou d'argent. On acyle ces sulfures avec une grande variété d'agents acylants et on les cyclise en pénèmecarboxylates-3 substitués en position 2.

[Traduit par le journal]

In connection with our continuing effort in modified β-lactam antibiotics (1) the penicillin–cephalosporin hybrid nature of the penem nucleus **1** looked especially attractive to us. The "Wittig route" to the penems, as devised by Woodward (2), was ingenious but too restrictive: the potential substituents on the nucleus must be introduced early in a long sequence, which severely limits the preparation of a series of analogs (3). Consequently we searched for a more versatile modification of the approach.[3] A recent publication by Farmitalia (4) has since described a similar approach to the synthesis of penems.

We considered that a building block such as **3**, with a sulfur protecting group that (a) allows introduction of $R^2$ through acylation at sulfur, (b) could potentially allow introduction of $R^3$ (e.g. hydroxyethyl) through anion generation at C(3),[4] and (c) is commercially available and devoid of asymmetric centers, would possess the required versatility. We found that a trityl group fulfilled all the above requirements as a sulfur protecting group.

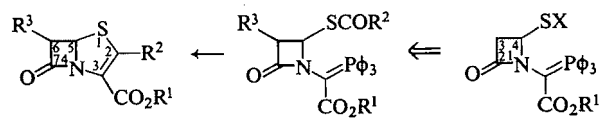

**1** **2** **3**

SCHEME 1

In this paper we describe the preparation of penems substituted in position 2 via (1) synthesis of 4-tritylthioazetidinonylphosphorane carboxylic acids (**8**) protected by two alcohol residues, (2) transformation of **8** to heavy metal mercaptides **9** (M = Ag, Hg), (3) their reaction with various acylating agents, and (4) their cyclization followed by deprotection.

Nucleophilic displacement of the acetoxy group of azetidinone **4** is well known (5). Reaction with sodium triphenylmethyl mercaptide gave a high yield (90%) of crystalline 4-triphenylmethylthio-2-azetidinone (**5**). *N*-substitution with two glyoxylic acid esters ($R^1$ = *p*-nitrobenzyl and trimethylsilylethyl), reaction with thionyl chloride, and then with triphenylphosphine following well documented procedures[4] afforded the key intermediates **8** (66% and 68% overall from **5** for the respective esters). Whereas both carboxylic acid protecting groups were found suitable for conversion to 2-substituted penems, the trimethylsilylethyl ester

[1]Author to whom correspondence may be addressed.

[2]McGill University.

[3]This work is part of a Bristol-Myers patent filed on September 21, 1979 (see ref. 3*c*); it was also presented at the ACS Annual Meeting held in New York City, August 23–28, 1981.

[4]See ref. 2*c*, and references cited therein.

0008-4042/82/070942-03$01.00/0

©1982 National Research Council of Canada/Conseil national de recherches du Canada

Can. J. Chem. Downloaded from www.nrcresearchpress.com by 210.87.254.6 on 09/06/12
For personal use only.

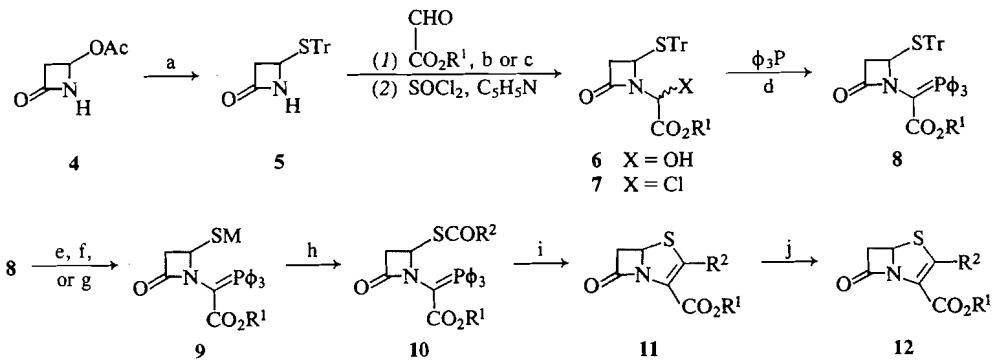

**11***a* $R^1$ = *p*-nitrobenzyl; $R^2$ = CH=CHNOMe
**11***b* $R^1$ = $(CH_2)_2Si(CH_3)_3$; $R^2$ = $(CH_2)_3CN$
**11***c* $R^1$ = $(CH_2)_2Si(CH_3)_3$; $R^2$ = $(CH_2)_3SCN$
**11***d* $R^1$ = *p*-nitrobenzyl; $R^2$ = $CH_2OCH$=NOMe
**11***e* $R^1$ = *p*-nitrobenzyl; $R^2$ = $CH_2SCH_3$

**12***a* $R^1$ = Na; $R^2$ = CH=CHNOMe
**12***b* $R^1$ = K; $R^2$ = $(CH_2)_3CN$
**12***c* $R^1$ = K; $R^2$ = $(CH_2)_3SCN$
**12***d* $R^1$ = Na; $R^2$ = $CH_2OCH$=NOMe
**12***e* $R^1$ = H; $R^2$ = $CH_2SCH_3$

(a) TrSNa (0.85 equiv.), MeOH/$H_2O$ 1:1, 20°C, 4H; (b) refluxing benzene; (c) benzene, 20°C, triethylamine; (d) refluxing benzene, 2,6-lutidine; (e) $AgNO_3$ (1.1 equiv., 0.15 *M* in MeOH), pyridine (1.1 equiv.), $CH_3OH$, 20°C, 2h and 5°C, 1h; (f) $Hg(OAc)_2$ (1 equiv.), MeOH/$CH_2Cl_2$ 1:1, 5°C, 2h; (g) $AgNO_3$ (4 equiv.), diethyl ether/water 1:1, tri-*n*-butylamine (1.3 equiv.) 20°C, 20 min; (h) $R^2COX$, pyridine, $CH_2Cl_2$, 0°C, 15–20 min; (i) refluxing benzene or toluene; (j) $H_2$, 30% Pd/Celite, THF, diethyl ether, $NaHCO_3$ (1.1 equiv.), $H_2O$ ($R^1$ = *p*-nitrobenzyl) and tetrabutylammonium fluoride, THF, 0°C, ($R^1$ = trimethylsilylethyl), potassium ethylhexanoate.

TABLE 1. Spectral data and yields[a]

| Compound | $^1$Hmr, 80 MHz, δ[b] | Infrared,[c] $cm^{-1}$ | Ultraviolet,[d] nm (ε) | Yields |
|---|---|---|---|---|
| **12***a* | 8.01, (1H, d, *J* = 9.0), 7.72 (1H, d, *J* = 15.7), 6.36 (1H, dd, *J* = 9.9, 15.7), 5.76 (1H, dd, *J* = 3.6, 2.9), 3.93 (>3H, m), 3.78 (<1H, d, *J* = 3.6), 3.56 (1H, dd, *J* = 16.9, 2.0), ($D_2O$) | 1750<br>1600 | 357 (8325)<br>300 (9200)<br>275 (10300) | 7.5% |
| **12***b* | 5.72 (1H, dd, *J* = 3.6, 1.7), 3.83 (1H, dd, *J* = 16.7, 3.6), 3.47 (1H, dd, *J* = 16.7, 1.7), 3.30–1.79 (6H, m), ($D_2O$) | 2250<br>1765<br>1610 | 306 (6875)<br>258 (4810) | 46% |
| **12***c* | 5.75 (H, dd, *J* = 3.6, 1.8), 3.87 (1H, dd, *J* = 16.8, 3.6), 3.48 (1H, dd, *J* = 16.8, 1.8) 3.31–2.50 (4H, m), 2.22 (2H, m), ($D_2O$) | 2150<br>1765 | 306 (6875)<br>254 (3786) | 34% |
| **12***d* | 7.63 (0.55 H, t, *J* = 5.3), 7.06 (0.45 H, t, *J* = 4.0), 5.78 (1H, dd, *J* = 3.6, 1.8), 5.07, 3.90, 4.53 (1H, part of ABq, *J* = 15.2), 4.44 (0.9 H, d, *J* = 4.0), 4.25 (1.1 H, d, *J* = 5.3), 3.91 (3H, s), 3.88 (1H, dd, *J* = 16.8, 3.6), 3.55 (1H, dd, *J* = 16.8, 1.8), ($D_2O$) | 1765<br>1620 | 307 (5500)<br>253 (3674) | 21% |
| **12***e* | 5.33 (1H, dd, *J* = 2.0, 3.8), 3.58 (2H, ABq, *J* = 13.5), 3.48 (1H, dd, *J* = 16.1, 3.8), 3.10 (1H, dd, *J* = 16.1, 2.0), 2.63 (bs), 1.75 (3H, s), (DMSO-$d_6$) | 1780<br>1657 | 315 (5600)<br>260 (3600) | 5.8% |

[a] Yields (**11** to **12**).
[b] Chemical shifts, δ, in ppm relative to internal TMS. Coupling constants, *J*, in Hz.
[c] Recorded in Nujol.
[d] Recorded in $H_2O$.

Can. J. Chem. Downloaded from www.nrcresearchpress.com by 210.87.254.6 on 09/06/12
For personal use only.

of **8** was the candidate of choice particularly for 6-substitution.[5]

Acylation of the key intermediate at sulfur was achieved through its conversion to metal mercaptides. Reaction of **8** with silver nitrate (6) or mercuric acetate (7) precipitated the corresponding silver (85%, $R^1$ = *p*-nitrobenzyl; 100%, $R^1$ = trimethylsilylethyl) or mercuric (91%, $R^1$ = *p*-nitrobenzyl) mercaptides **9** in high yield.[6] These mercaptides were found to be stable solids that could be stored for months without any sign of alteration; they are soluble in some organic solvents and readily acylated.

Acylation of the mercaptides **9** was found to be a simple process that can be carried out under a wide variety of conditions depending on the nature and stability of the substituents on the acylating moiety. The acylating species can vary from simple acid chlorides (8) to anhydrides, mixed anhydrides ($R^2CO_2OCOR$, $R^2CO_2SO_2CH_3$), or Vilsmeier complexes ($R^2CO_2CH{=}\overset{+}{N}Me_2\bar{Cl}$), thus making possible the synthesis of penems **11** with a wide variety of functional groups in the substituent at position 2. The phosphoranes **10***a–e*, so obtained, were thermally cyclized to penems (**11***a–e*) (2) in refluxing toluene ($R^1$ = *p*-nitrobenzyl) or benzene ($R^1$ = trimethylsilylethyl). The acid protecting groups were finally cleaved with appropriate reagents ($R^1$ = *p*-nitrobenzyl: $H_2$/30% Pd/Celite or sodium dithionite; $R^1$ = trimethylsilylethyl: tetrabutylammonium fluoride) and gave penems **12** ($R^1$ = H, K, or Na) in reasonable yields (see Table 1).

[5]The methodology for the preparation of 2,6-disubstituted penems from intermediates **8** will be the subject of a following paper.

[6]The mercaptide **9** (M = Ag, $R^1$ = *p*-nitrobenzyl) can also be obtained in high yield (78% to 93%) by treatment (in MeOH) of the corresponding 4-acetylthio-2-azetidinonephosphorane **10** ($R^2$ = $CH_3$) with $AgNO_3$ under basic (DBU, $Na_2CO_3$) or nucleophilic basic (pyrrolidine) conditions (for preparation of **10** see ref. 2*d*).


## Acknowledgements

We would like to thank the following for their technical assistance: Jean Collerette, Henry Wong, Carol Bachand, Bing Luh, Jean Lajeunesse, and Pierre Rivest.



1. T. W. Doyle, J. L. Douglas, B. Belleau, T. T. Conway, C. F. Ferrari, D. E. Horning, G. Lim, B. Y. Luh, A. Martel, M. Ménard, L. R. Morris, and M. Misiek. Can. J. Chem. **58**, 2508 (1980).
2. (*a*) R. B. Woodward. Acta Pharm. Suec. **14** (Suppl.), 23 (1977); (*b*) R. B. Woodward. *In* Recent advances in the chemistry of β-lactam antibiotics. *Edited by* J. Elks. The Chemical Society, London. 1977. Chapt. 18.; (*c*) I. Ernest, J. Gosteli, C. W. Greengrass, W. Holick, D. E. Jackman, H. R. Pfaendler, and R. B. Woodward. J. Am. Chem. Soc. **100**, 8214 (1978); (*d*) M. Lang, K. Prasad, W. Holick, J. Gosteli, I. Ernest, and R. B. Woodward. J. Am. Chem. Soc. **101**, 6296 (1979); (*e*) I. Ernest, J. Gosteli, and R. B. Woodward. J. Am. Chem. Soc. **101**, 6301 (1979); (*f*) H. R. Pfaendler, J. Gosteli, and R. B. Woodward. J. Am. Chem. Soc. **102**, 2039 (1980).
3. (*a*) M. Ménard and G. Caron (Bristol-Myers Co.). U.S. Patent No. 4,155,912 (1979); (*b*) Y. Ueda (Bristol-Myers Co.). U.S. Patent No. 4,182,711 (1980); (*c*) M. Ménard and A. Martel (Bristol-Myers Co.). U.S. Patent No. 4,262,437 (1981); (*d*) M. Ménard and A. Martel (Bristol-Myers Co.). U.S. Patent No. 4,282,150 (1981).
4. A. Longo, P. Lombardi, C. Gandolfi, and G. Francesci. Tetrahedron Lett. 355 (1981).
5. K. Klauss, D. Grimm, and G. Prossel. Justus Leibigs Ann. Chem. 539 (1974).
6. F. I. Caroll, H. M. Dickson, and M. E. Wall. J. Org. Chem. **30**, 33 (1965), and references cited therein.
7. R. Lattrell. Angew. Chem. Int. Ed. Engl. **12**, 926 (1973).
8. Y. Hamashima. *In* Recent advances in the chemistry of β-lactam antibiotics. *Edited by* J. Elks. The Chemical Society, London. 1977. Chapt. 24. pp. 245–246.


Can. J. Chem. Downloaded from www.nrcresearchpress.com by 210.87.254.6 on 09/06/12
For personal use only.

# One-electron photooxidation of carbazole in the presence of carbon tetrachloride. Part I. Carbon tetrachloride and ethanol used as reaction media

BOGUMIL ZELENT[1] AND GILLES DUROCHER

*Département de Chimie, Université de Montréal, C.P. 6210, Succ. A, Montréal (Qué.), Canada H3C 3V1*

Received July 29, 1981

*This paper is dedicated to Professor Camille Sandorfy on the occasion of his 60th birthday*

BOGUMIL ZELENT and GILLES DUROCHER. Can. J. Chem. **60**, 945 (1982).

The photochemical reaction products of carbazole with carbon tetrachloride in ethanol have been isolated and identified along with photoproducts in the irradiated solution of carbazole in pure $CCl_4$ using water and ethanol added after the irradiation. This allowed us to discuss the complex mechanism of secondary photochemical changes in the carbazole–$CCl_4$ system. We propose that the electron transfer from carbazole to $CCl_4$ molecule in the excited CT complex, $^1(C^{\delta+}\cdots CCl_4^{\delta-})^*$, is the primary photochemical reaction followed by an heterolytic dissociation of a C—Cl bond which gives rise to the primary photoproducts in the solvent cage $[C^{+\cdot}Cl^-\dot{C}Cl_3]$. Secondary photochemical reactions initiate transformation of the radical cation of carbazole in the solvent cage giving rise to the following intermediate species:

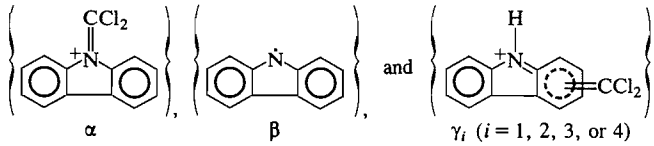


α β $\gamma_i$ ($i$ = 1, 2, 3, or 4)

The probability of formation and further transformations of these transient products: α, β, and $\gamma_i$, depends strongly on the nature of the reaction media. Thermodynamically stable products are formed depending on the reaction media; (carboethoxy)carbazoles, (carbo-*N*-carbazyl)carbazoles, and carbazole – carboxylic acids can serve as a proof for the formation of the above listed intermediates. All the results reported on the secondary photochemical reactions strongly support the electron-transfer primary mechanism used to explain the fluorescence quenching of carbazole by $CCl_4$.

These results also explain the changes observed in the fluorescence spectrum of carbazole when the ethanol solution of carbazole in the presence of $CCl_4$ is irradiated.

BOGUMIL ZELENT et GILLES DUROCHER. Can. J. Chem. **60**, 945 (1982).

Nous avons isolé et identifié les produits de la réaction photochimique entre le carbazole et le tétrachlorure de carbone d'abord dans l'éthanol comme solvant mais aussi dans le $CCl_4$ pur utilisé comme solvant pendant l'irradiation alors que l'eau et l'éthanol étaient ajoutées au $CCl_4$ après l'irradiation. Ceci nous a permis de discuter du mécanisme complexe des réactions photochimiques secondaires dans le système carbazole–$CCl_4$. Nous proposons que l'étape photochimique primaire soit le transfert électronique du carbazole au $CCl_4$ par l'intermédiaire d'un complexe de transfert de charge excité $^1(C^{\delta+}\cdots CCl_4^{\delta-})^*$ suivi par une dissociation hétérolytique d'un lien C—Cl donnant lien à l'apparition des photoproduits primaires $[C^{+\cdot}Cl^-\dot{C}Cl_3]$ dans la cage du solvant. Par réactions photochimiques secondaires, les espèces intermédiaires suivantes seraient formées dans la cage du solvant:

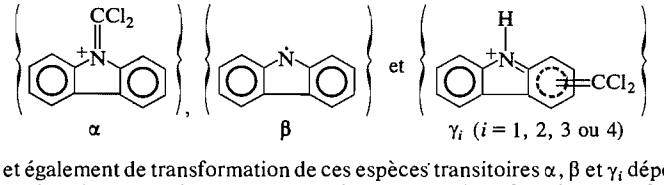


α β $\gamma_i$ ($i$ = 1, 2, 3 ou 4)

La probabilité de formation et également de transformation de ces espèces transitoires α, β et $\gamma_i$ dépend beaucoup de la nature des milieux réactionnels. La nature des photoproduits thermodynamiquement stables formés est en fonction de la nature du milieu réactionnel. Les molécules de (carboéthoxy)carbazoles, de (carbo-*N*-carbazyl)carbazoles et d'acides carbazole – carboxylique formées démontrent bien l'importance des espèces transitoires ci-haut mentionnées dans l'élaboration du mécanisme réactionnel. Tous les résultats obtenus sur les réactions photochimiques secondaires sont en accord avec un mécanisme primaire impliquant un phototransfert électronique lequel mécanisme est responsable pour la désactivation de la fluorescence du carbazole en présence de $CCl_4$. Ces résultats expliquent également les modifications observées dans le spectre de fluorescence du carbazole dans l'éthanol en présence de $CCl_4$ au cours de l'irradiation.

## Introduction

Carbon tetrachloride is a well-known fluorescence quencher of various aromatic electron donors (1–6). The mechanism of quenching is most commonly connected with the photochemical reaction in which $CCl_4$ participates as an electron acceptor, favorable conditions being created by the distinctive electron affinity of $CCl_4$ (2.12 eV) (7) and comparatively low C—Cl bond energy (231.2 kJ $mol^{-1}$) (8).

The electron transfer mechanism has proved to

[1]On leave from the Department of Chemistry, University of Gdańsk, 80-952 Gdańsk, Poland.

0008-4042/82/080945-12$01.00/0

©1982 National Research Council of Canada/Conseil national de recherches du Canada

Can. J. Chem. Downloaded from www.nrcresearchpress.com by 210.87.254.105 on 09/06/12
For personal use only.

Can. J. Chem. Downloaded from www.nrcresearchpress.com by 210.87.254.105 on 09/06/12
For personal use only.

explain the fluorescence quenching of carbazole in non-polar solvents (1) whereas in hydrogen bonding solvents like ethanol, the fluorescence quenching decay rate did not follow the usual correlation with the ionization potential of the first excited singlet donor state (2). Carbazole cation-radicals have been observed when alcoholic solutions of carbazole were irradiated into the $^1L_b$ or the $^1L_a$ states of the carbazole molecule and the number of these radicals was found to increase in the presence of $CCl_4$ (9). The explanation of the fluorescence quenching mechanism of carbazole by $CCl_4$ in alcoholic solvents requires more extended studies. Therefore it became interesting to study the photochemical reaction in the carbazole–$CCl_4$ system in ethanol as the reaction medium. In this paper we made an attempt to discuss the photochemical reaction mechanisms responsible for all the photochemical substituted carbazoles obtained and identified when a $CCl_4$ solution of carbazole is irradiated in presence of ethanol or when ethanol or water were added to the photolite after irradiating the carbazole molecules in pure $CCl_4$.

## Results and discussion

When an ethanol solution of carbazole ($1 \times 10^{-4}$ *M*) in the presence of $CCl_4$ (0.1 *M*) is irradiated in its longwave absorption band, the typical carbazole fluorescence disappears and new fluorescence emissions appear at approximately 375, 400, and 425 nm as can be seen in Fig. 1. The excitation spectra of these new emissions are shifted to the red compared to the excitation spectrum of carbazole. This, coupled to the fact that the charge transfer exciplex "carbazole–$CCl_4$" was found to be non-emissive (2), strongly suggests that these new fluorescence emissions might be due to photochemical products.

As our studies progressed we discovered that photoproducts created in the carbazole–$CCl_4$ system are of the transient character and are stable only in pure $CCl_4$ medium, but when ethanol or water are present they easily undergo further transformation giving as a result, proper mono- and di-substituted derivatives of carbazole: (carboethoxy)carbazoles, (carbo-*N*-carbazyl)carbazoles, and carbazole – carboxylic acids.

Table 1 shows the photoproducts identified from the photoreaction of carbazole with $CCl_4$ in ethanol as a solvent (first column) and also in pure $CCl_4$ (second and third columns). These photoproducts were obtained and identified when the solution was first irradiated in pure $CCl_4$ followed by additions of ethanol or water.

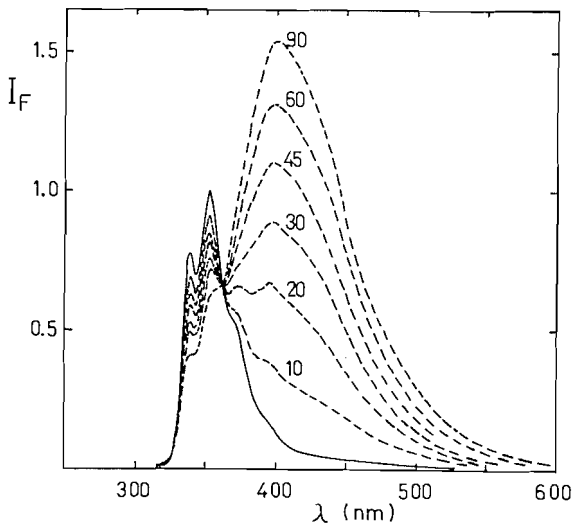


FIG. 1. Fluorescence spectra of an ethanol solution of carbazole ($1 \times 10^{-4}$ *M*) in the presence of $CCl_4$ (0.1 *M*) before irradiation (—), and after the specified time of irradiation in seconds (---). The excitation wavelength was fixed at 320 nm.

We found that derivatives of carbazole, namely mono-substituted in positions 1 and 3, and di-substituted in positions 1 and 6 or 3 and 9(N), are the main products obtained from the photochemical reaction of carbazole with $CCl_4$.

Considering the well-known photophysical results (1, 2, 5–7, 10) and also the photochemical reaction products obtained, we propose the following primary photophysical and photochemical processes:

[1] $\quad C + h\nu \rightarrow {}^1C^*$

[2] $\quad {}^1C^* \rightarrow C + h\nu_F$

[3] $\quad {}^1C^* + CCl_4 \rightsquigarrow {}^3C^* + CCl_4$
$\qquad\qquad\qquad\qquad\quad \rightsquigarrow C + CCl_4$

[4] $\quad {}^1C^* + CCl_4 \rightsquigarrow {}^1(C^{\delta+} \cdots CCl_4{}^{\delta-})^*_{solv}$
$\qquad\qquad\qquad\qquad\quad \rightsquigarrow {}^3C^* + CCl_4$

[5] $\quad {}^1(C^{\delta+} \cdots CCl_4{}^{\delta-})^*_{solv} \rightsquigarrow {}^1C^* + CCl_4$
$\qquad\qquad\qquad\qquad\quad \rightsquigarrow C + CCl_4$

[6] $\quad {}^1(C^{\delta+} \cdots CCl_4{}^{\delta-})_{solv} \rightsquigarrow \{C^+ \cdot Cl^- CCl_3\}_{solv}$

The energy loss into the singlet state manifold may proceed through emission of radiation (reaction [2]) or radiationless processes via the external spin–orbital coupling with $CCl_4$ molecule, internal conversion (reaction [3]) or via complexation (reactions [4] and [5]). Furthermore, when transient excited CT complex is formed, electron transfer may occur from carbazole molecule to $CCl_4$ molecule. It is followed by an heterolytic dissociation of

TABLE 1. Photochemical reaction products of carbazole in the presence of $CCl_4$

| No. | Compound | Reaction medium† | | |
|---|---|---|---|---|
| | | $CCl_4$ in $C_2H_5OH$ | $CCl_4$ ($C_2H_5OH$) | $CCl_4$ ($H_2O$) |
| C | Carbazole | s | s | s |
| 1 | Hexachloroethane | b | b | b |
| 2 | *N*-(Trichloroethylene)carbazole* | b | b | b |
| 3 | 1-Chlorocarbazole | | b | b |
| 4 | *N*-(Carboethoxy)carbazole | b | b | |
| 5 | 1-(Carboethoxy)carbazole | a | a | |
| 6 | 2-(Carboethoxy)carbazole | b | b | |
| 7 | 3-(Carboethoxy)carbazole | a | a | |
| 8 | 4-(Carboethoxy)carbazole | a | b | |
| 9 | 3,9-Di(carboethoxy)carbazole* | b | b | |
| 10 | 1,3-Di(carboethoxy)carbazole* | b | b | |
| 11 | 1,6-Di(carboethoxy)carbazole* | b | b | |
| 12 | 1,8-Di(carboethoxy)carbazole* | b | | |
| 13 | 3,6-Di(carboethoxy)carbazole | b | b | |
| 14 | 3,5-Di(carboethoxy)carbazole* | b | | |
| 15 | Carbazole-1-carboxylic acid | b | b | a |
| 16 | Carbazole-3-carboxylic acid | b | b | a |
| 17 | *N,N'*-Carbodicarbazyl* | | b | a |
| 18 | 1-(Carbo-*N*-carbazyl)carbazole* | | b | a |
| 19 | 3-(Carbo-*N*-carbazyl)carbazole* | | b | a |
| 20 | 3,9-Di(carbo-*N*-carbazyl)carbazole* | | b | a |
| 21 | 1,6-Di(carbo-*N*-carbazyl)carbazole* | | b | a |

*New compound.
†a: main product of the reaction studied (chemical yields between 5 and 20%); b: other product of the reaction studied (chemical yields below 5%); s: remaining substrate.

a C—Cl bond giving rise to the possible primary products in the solvent cage (reaction [6]).

The secondary products obtained and identified along with the data published (11–20) allow us to propose the following mechanism of transformation of the carbazole radical cation in the solvent cage:

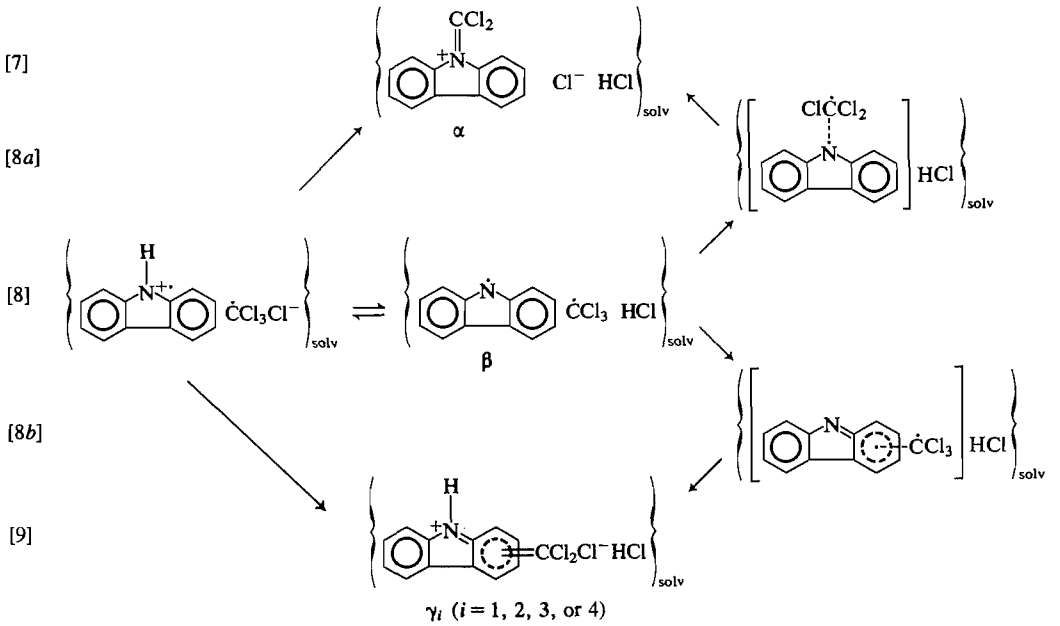


Can. J. Chem. Downloaded from www.nrcresearchpress.com by 210.87.254.105 on 09/06/12
For personal use only.

Can. J. Chem. Downloaded from www.nrcresearchpress.com by 210.87.254.105 on 09/06/12
For personal use only.

The electron densities calculated for the carbazole molecule show that among a variety of mesomeric structures of the radical-cation, the 1, 3, 6, 8, and 9(N) positions are likely to be favored (11, 12). This was later confirmed by the analysis of the electrochemical oxidation products of carbazole and its substituted derivatives (12, 13). Radical recombination reactions [7] and [9] in the solvent cage then become very probable, giving the intermediate ionic products α and $\gamma_i$ (mainly with $i = 1$ or 3). The presence of chlorine ion in the solvent cage makes possible the transformation of the radical-cation of carbazole to carbazyl radical β. A similar reaction has already been discussed in the literature (21). But since the N—H and H—Cl bond energies are nearly the same at 431 kJ mol$^{-1}$ (14), reaction [8] is probably reversible (15). However, radicals β and $CCl_3$ appearing close to each other in the solvent cage can immediately react with themselves. This reaction can occur with the participation of the ring or the nitrogen in radical β. If the ring is involved (reaction [8*b*]) then the transient products $\gamma_i$ are formed. On the other hand, because of steric hindrance, reaction [8*a*] can only occur through an activated complex which dissociates to cation α and chloride ion after the electron transfer has taken place into the complex. Reaction of radical $CCl_3$ and radical β with simultaneous chlorine atom split off is another way that the nitrogen atom can be involved (reaction [10]).

[10] 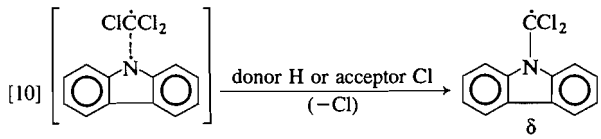


Reaction [10], in which radical δ is formed, is supposedly more probable outside the solvent cage where the presence of chlorine atom acceptor or/and hydrogen atom donor facilitates its occurrence.

*N*-(Trichloroethylene)carbazole (**2**) found among the products of the photochemical reaction probably forms when radical δ reacts with radical $CCl_3$ following the pattern of reaction [11]. Because of steric hindrance, reaction of radicals δ and $CCl_3$ is only possible when accompanied by the cleavage of at least one C—Cl bond. So this reaction occurs when acceptor Cl or/and donor H is present.

In pure $CCl_4$ as well as in polar medium, product **2** forms with low yield. However, this compound is the main product of the reaction in 3-methylpentane non-polar medium which favours radical reactions. This fact supports the assumed radical mechanism of reactions [10] and [11]. In addition to reaction

[11] δ + $\dot{C}Cl_3$ 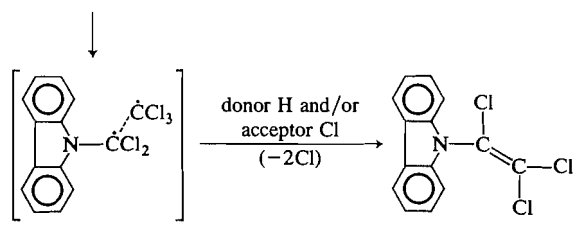


**2**

[10], it has also been suggested that radical δ can be formed from cation α when electron donor is present (22).

Along with the possibilities of transformation of the carbazole radical cation in the solvent cage discussed above, the substitution reactions of the carbazole radical cation with chloride ion or chlorine atom probably take place in this reaction medium. Such reactions are suggested by the formation of chloroderivatives of carbazole. We have found 1-chlorocarbazole (**3**) among the products. Substitution reactions between aromatic radical cations and chloride ions are known in the literature (23). On the other hand, $CCl_4$ is the reaction medium in which chlorine atoms are easily generated (8, 19).

[12] 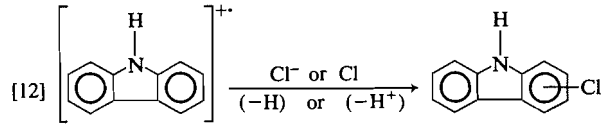


Carbon tetrachloride or trichloromethyl radical can be hydrogen acceptors while the chloride ions can serve as proton acceptors in reaction [12].

The carbon tetrachloride medium favours the chain photochemical reaction mechanism initiated by electron transfer from the electron donor to the $CCl_4$ molecule (16, 20, 24). The great photochemical activity of carbazole in $CCl_4$ can also be explained by chain reaction initiated by $CCl_3$ radicals in the presence of $CCl_4$. Comparatively low C—Cl bond energy in the $CCl_4$ molecule makes possible the participation of $CCl_4$ in the reaction as a hydrogen acceptor, the reaction scheme is as follows:

[13] **C** + $\dot{C}Cl_3$ $\xrightarrow{CCl_4}$ 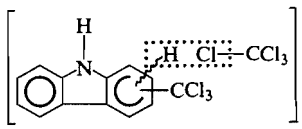


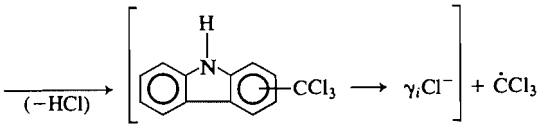

Can. J. Chem. Downloaded from www.nrcresearchpress.com by 210.87.254.105 on 09/06/12
For personal use only.

In the reaction above, the sum of bond energies undergoing splitting is smaller than the sum of energies of new bonds formed (14). Therefore reaction [13] might be an additional source of $Cl^-\gamma_i$ intermediates.

The reaction of $CCl_3$ radicals with $\alpha$ and $\gamma_i$ cations in $CCl_4$ explains the formation mechanism of di-substituted transient products (reactions [14] to [19]).

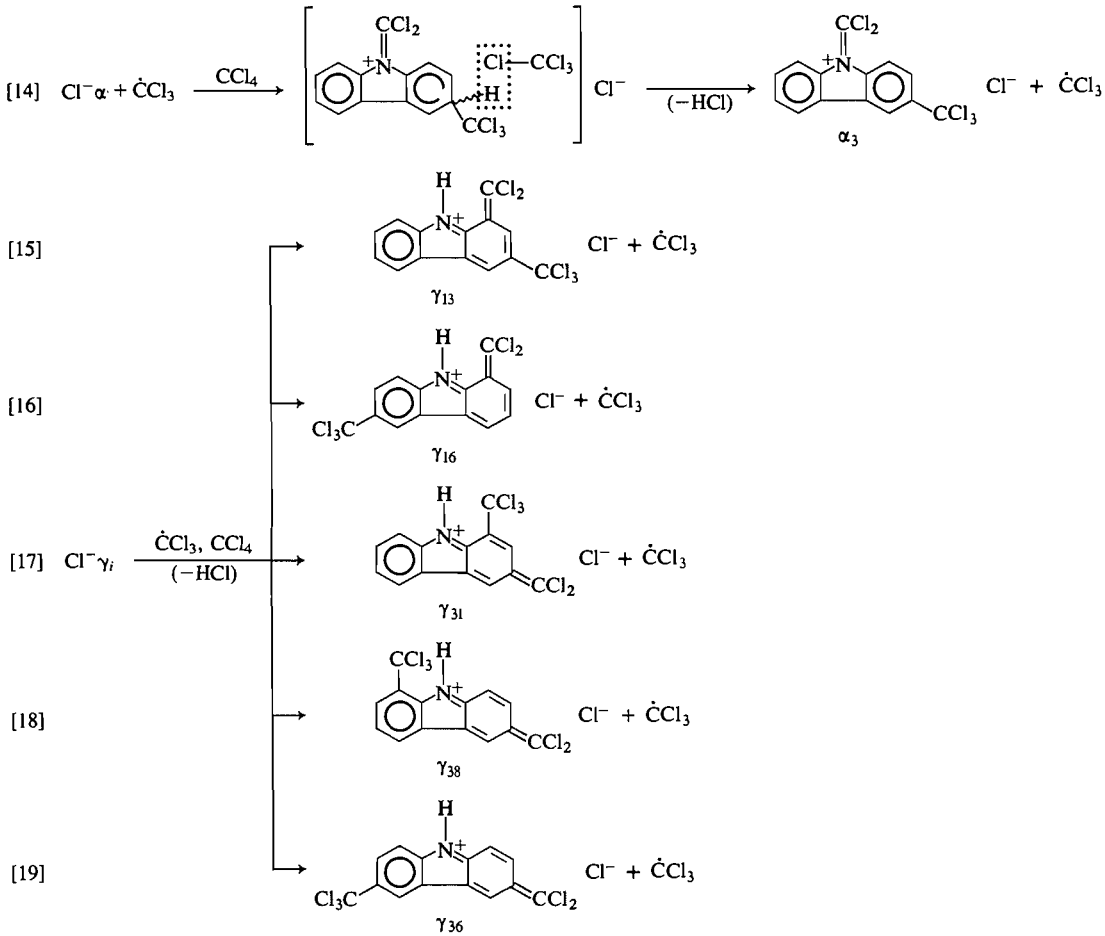


The closing chain reaction might be

[20] $\mathbf{C} + \dot{C}Cl_3 \longrightarrow \beta + CHCl_3$

[21] [22] $\beta + \dot{C}Cl_3 \rightarrow \alpha Cl^-$, $\gamma_i Cl^-$

[23] $2\dot{C}Cl_3 \longrightarrow C_2Cl_6$

**1**

In pure $CCl_4$, ionic products $\alpha$ and $\gamma_i$ can undergo further reactions with carbazole molecules resulting in the correspondingly $\alpha'$ and $\gamma_i'$ monocations. The reaction scheme is as follows:

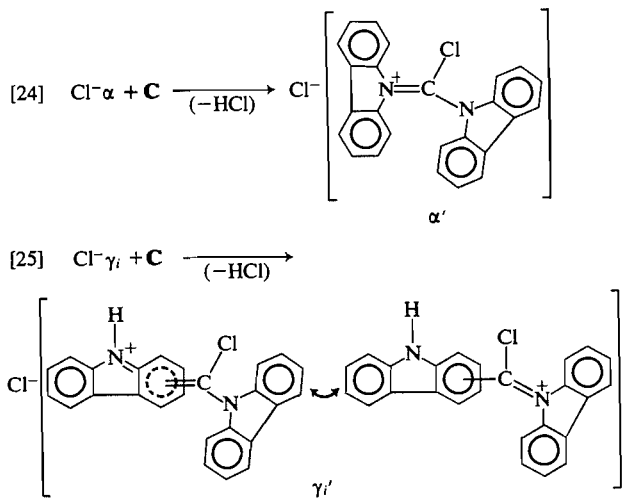

Can. J. Chem. Downloaded from www.nrcresearchpress.com by 210.87.254.105 on 09/06/12
For personal use only.

The mechanism proposed above for the photochemically initiated reaction in the carbazole–$CCl_4$ system has been strongly supported by a collection of data achieved while studying the reaction products. This will now be described more extensively.

*Use of water after irradiation*

If we add water to the photolysis solution, transient products, showing significant stability in pure $CCl_4$, undergo easy hydrolysis resulting in corresponding (carbo-*N*-carbazyl)carbazole and carbazole – carboxylic acids (see Table 1).

The hydrolysis of intermediates $\alpha'$ and $\gamma_i'$ partially explains the formation mechanism of *N*,*N*′-carbodicarbazyl (**17**), 1-(carbo-*N*-carbazyl)carbazole (**18**), and 3-(carbo-*N*-carbazyl)carbazole (**19**) according to the following scheme:

[26] $Cl^-\alpha' \xrightarrow[(-2\,HCl)]{H_2O}$ 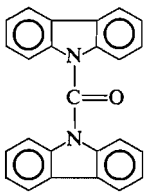

**17**

[27] $Cl^-\gamma_i' \xrightarrow[(-2\,HCl)]{H_2O}$ 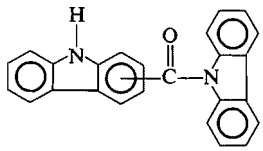

**18, 19**

Intermediates $\gamma_i$, being the precursors of carbazole-1-carboxylic acid (**15**), and carbazole-3-carboxylic acid (**16**), easily undergo further transformation in the presence of water until the proper acid chlorides [**A**], which are of intermediate character, are formed (reaction [28]), this transformation being followed by the formation of the acids (reaction [29]). The labile acid chlorides formed from intermediates $\gamma_i$ can also undergo reaction with carbazole thus acting as additional source of products **18** and **19** (reaction [30]).

[28] $Cl^-$ 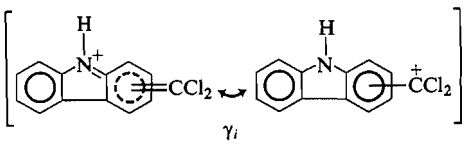

$\gamma_i$

$H_2O\,|\,(-2\,HCl)$

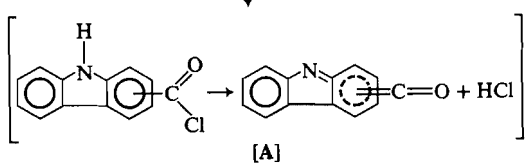

**[A]**

[29] 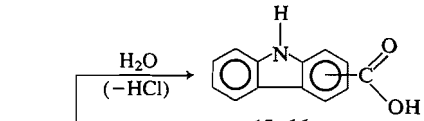

**15, 16**

[30] 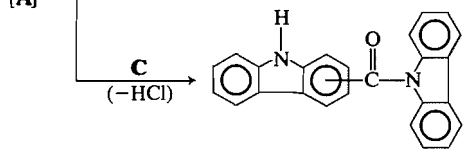

Intermediate α present in the reaction medium undergoing the reaction with water can give rise to not only mono-substituted but also to di-substituted (carbo-*N*-carbazyl)carbazoles. During the first step of the reaction, cation α undergoes transformation in the presence of water until *N*-(carbochloro)-carbazole as an intermediate product [**B**] is formed (reaction [31]). Then [**B**] can undergo reaction with carbazole leading to the formation of **17** (reaction [33]) or **18** and **19** (reaction [34]). In the presence of water it should also undergo reaction resulting in the formation of unstable carbazole-*N*-carboxylic acid which presumably decomposes to carbazole and carbon dioxide (25), reaction [32].

[31] $Cl^-\alpha \xrightarrow[(-2\,HCl)]{H_2O}$ 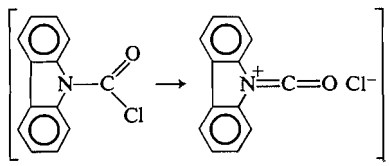

**[B]**

[32] 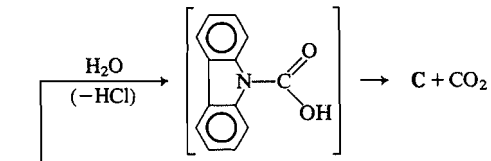

[33] **17**

[34] 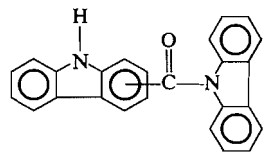

Intermediate [**B**] formed in the reaction medium can also undergo reaction with products **17**, **18**, and **19** present, thus explaining the formation of 3,9-di(carbo-*N*-carbazyl)carbazole (**20**), and 1,6-di-(carbo-*N*-carbazyl)carbazole (**21**), (reactions [35]–[37]). The formation of 1,3- and 3,6-di-substituted (carbo-*N*-carbazyl)carbazoles is less probable.

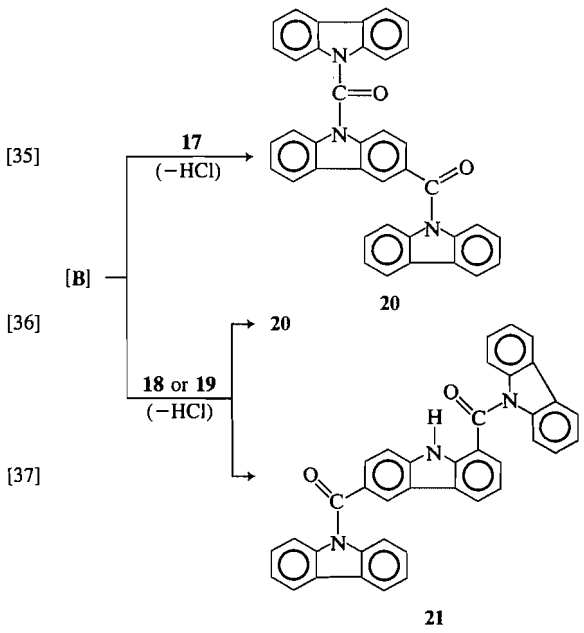

The remaining part of carbazole present among the products of photolysis is efficiently used in reactions [30], [33], and [34]. This can be observed by TLC method.

Probably di-substituted (carbo-*N*-carbazyl)carbazoles can also be formed in another way. If intermediates $\alpha'$ and $\gamma_i'$, formed in the reactions [24] and [25] undergo reactions with the transient product $\alpha$, these reactions lead to the corresponding di-cations, mainly to 1,6- and 3,9-di-substituted carbazole derivatives. These di-cations undergoing hydrolysis would explain the second way in which products **20** and **21** are formed. But it is presently difficult to estimate to what extent these reactions contribute to the formation of the above mentioned products.

Intermediate di-substituted monocations in the presence of water probably undergo transformations to proper carbazole – dicarboxylic acids. We did not manage to isolate these compounds.

*Use of ethanol after irradiation*

If we add ethanol to the photolysis solution, the transient products formed in pure $CCl_4$ undergo reactions with alcohol, and mono- and di-substituted (carboethoxy)carbazoles are formed as a result. As ethanol contains traces of water, (carbo-*N*-carbazyl)carbazoles as well as carboxylic acids appear but with significantly lower yield than in the case when water is used (Table 1). In the reaction discussed there exists a probability of the participation of water from the surface of silica gel used as a filling of chromatographic column.

*N*-(carboethoxy)carbazole (**4**) appearing among the products when ethanol is added after irradiation, as well as *N*-cyanocarbazole found when the irradiated solution was saturated with ammonia gas (22) confirm the formation of transient $\alpha$ cation in the system of carbazole–$CCl_4$. The reaction mechanism between $\alpha$ cation and ethanol to give product **4** can be suggested as follows:

[38] $Cl^-\alpha \xrightarrow[(-HCl)]{C_2H_5OH}$

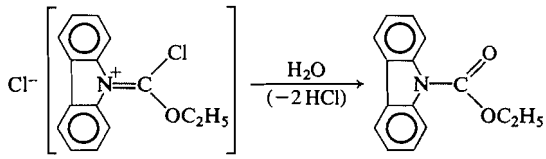

**4**

[39] $Cl^-\alpha \xrightarrow[(-2HCl)]{H_2O} [B] \xrightarrow[(-HCl)]{C_2H_5OH} \mathbf{4}$

If intermediate $\alpha$ reacts first with an ethanol molecule (or two molecules) and then with the water molecule, the reaction results directly in **4** (reaction [38]), but when $\alpha$ reacts with the water molecule first, the transient product appearing in the reaction should be [**B**] which can undergo transformation in the presence of an excess of ethanol, mainly to **4** (reaction [39]). But when compared to the other products in this reaction, **4** is formed with relatively low yield.

Similar pattern exists for the reaction of transient products $\gamma_i$ in the presence of ethanol during which 1-(carboethoxy)carbazole (**5**), 2-(carboethoxy)carbazole (**6**), 3-(carboethoxy)carbazole (**7**), and 4-(carboethoxy)carbazole (**8**) are formed (reactions [40] and [41]):

[40] $Cl^-\gamma_i \xrightarrow[(-HCl)]{C_2H_5OH}$

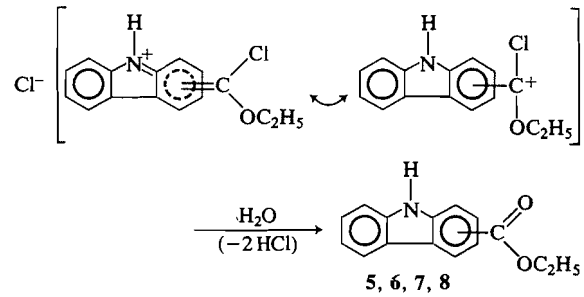

**5, 6, 7, 8**

[41] $Cl^-\gamma_i \xrightarrow[(-2HCl)]{H_2O} [A] \xrightarrow[(-HCl)]{C_2H_5OH}$ **5, 6, 7, 8**

Products **5**, **6**, **7**, and **8** confirm the existence of intermediates $\gamma_i$ in the system carbazole–$CCl_4$ when irradiated. On the other hand di-substituted (carboethoxy)carbazoles: 3,9-di(carboethoxy)car-

Can. J. Chem. Downloaded from www.nrcresearchpress.com by 210.87.254.105 on 09/06/12
For personal use only.

Can. J. Chem. Downloaded from www.nrcresearchpress.com by 210.87.254.105 on 09/06/12
For personal use only.

bazole (**9**), 1,3-di(carboethoxy)carbazole (**10**), 1,6-di(carboethoxy)carbazole (**11**), and 3,6-di(carboethoxy)carbazole (**13**) found among the products indicate that di-substituted cations are formed alongside with transient mono-substituted α and $\gamma_i$ when the carbazole–$CCl_4$ system is irradiated. The probable mechanism of formation of di-substituted intermediates, as a result of the reactions between α and $\gamma_i$ and $CCl_3$ radicals in the presence of $CCl_4$, was described by reactions [14] to [19].

The formation of **9**, **10**, **11**, and **13** can be assessed as follows:

[42] $Cl^-\alpha_3 \xrightarrow[(-6\,HCl)]{C_2H_5OH(H_2O)}$ **9**

[43] $Cl^-\gamma_{13\text{ or }31} \xrightarrow[(-6\,HCl)]{C_2H_5OH(H_2O)}$ **10**

[44] $Cl^-\gamma_{16\text{ or }38} \xrightarrow[(-6\,HCl)]{C_2H_5OH(H_2O)}$ **11**

[45] $Cl^-\gamma_{36} \xrightarrow[(-6\,HCl)]{C_2H_5OH(H_2O)}$ **13**

*Use of ethanol as a solvent*

When ethanol is used as a solvent of carbazole in the presence of $CCl_4$, the secondary photochemical transformation is significantly changed in comparison with the reactions in pure $CCl_4$ described above.

The polar reaction medium favours the formation of ionic intermediates in the solvent cage which is supported by the products found in this reaction (Table 1).

Intermediates α and $\gamma_i$ which have appeared during irradiation can immediately undergo further reactions ([38] to [41]) which result in the formation of all the mono-substituted (carboethoxy)carbazoles. So, active participation of ethanol in the reaction medium probably eliminates reactions [14]–[19] leading to di-substituted cations. Furthermore, reactions of intermediates α and $\gamma_i$ with carbazole molecules become less probable (reactions [24], [25]).

Attention should be paid to the fact that *N*-(carboethoxy)carbazole is formed with comparatively lower yield than 1-(carboethoxy)carbazole and 3-(carboethoxy)carbazole. This can be observed when TLC method is used. This fact suggests that the ethanol medium mainly favours the formation of intermediates $\gamma_i$ which can be the result of both reactions [9] and [13]. When ethanolic solution of carbazole with $CCl_4$ was irradiated the mono(carboethoxy)carbazoles, formed during irradiation, also undergo photochemical reactions in the presence of $CCl_4$. This leads to di-substituted (carboethoxy)carbazoles, **9**, **10**, **11**, **12**, **13**, and **14** these being formed from the corresponding intermediate products (reaction [46]).

[46] 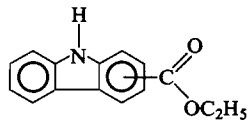

$\xrightarrow{CCl_4,\ h\nu}$ $\{\text{intermediate products}\}_{solv}$

$\xrightarrow[(-n\,HCl)]{C_2H_5OH(H_2O)}$ **9** + **10** + **11** + **12** + **13** + **14** + ···

Reaction [46] can be used as a method of photochemical synthesis of di(carboethoxy)carbazoles.

The mechanism of one-electron photooxidation of carbazole in the presence of carbon tetrachloride already suggested by us in a recent paper (22) has been extended above and strongly supported by the qualitative study of the various reaction products obtained.

## Fluorescence spectra

We are now in a good position to explain the new fluorescence emissions observed when ethanol solutions of carbazole in the presence of $CCl_4$ are irradiated (Fig. 1). We showed in Table 2 the wavelength of the maximum fluorescence intensity for a series of (carboethoxy)carbazoles. Obviously, the new fluorescence band at about 400 nm appearing in Fig. 1 during irradiation of the solution might be a complex mixture of the (carboethoxy)-carbazole fluorescences. The spectroscopy and the

Can. J. Chem. Downloaded from www.nrcresearchpress.com by 210.87.254.105 on 09/06/12
For personal use only.

TABLE 2. Fluorescence maxima of a series of (carboethoxy)carbazole molecules in ethanol at room temperature excited at 320 nm

| Molecules | $\lambda_{max}$ (F) (nm) |
|---|---|
| Carbazole | 352 |
| *N*-(Carboethoxy)carbazole | 328 ($\lambda_{exc}$ = 310) |
| 1-(Carboethoxy)carbazole | 397 |
| 2-(Carboethoxy)carbazole | 404 |
| 3-(Carboethoxy)carbazole | 362 |
| 4-(Carboethoxy)carbazole | 430 |
| 3,9-Di(carboethoxy)carbazole | 336 |
| 1,3-Di(carboethoxy)carbazole | 398 |
| 1,6-Di(carboethoxy)carbazole | 383 |
| 1,8-Di(carboethoxy)carbazole | 372 |
| 3,6-Di(carboethoxy)carbazole | 351 |
| 3,5-Di(carboethoxy)carbazole | 400 |

photophysics of all these molecules are now being studied in our laboratory.

## Experimental

*Apparatus*

$^1$H-nmr spectra were measured with a Bruker WH-90 spectrometer operating at 90 MHz. Chemical shift values are given in a δ scale with respect to TMS as an internal standard. Infrared spectra were recorded on a Perkin-Elmer 710B infrared spectrophotometer and mass spectra were taken with an AE1 MS902 mass spectrometer.

The absorption spectra were recorded on a Cary 14 spectrophotometer using a 10 mm optical path cell. The emission spectra were recorded on a fluorescence spectrophotometer Model SF-1 "Fluorispec" (Baird-Atomic, INC; Cambridge, MA). All solutions examined in fluorescence were first degassed by the well-known freeze–thaw method.

*Materials*

Carbazole was an Eastman Organic chemical and was used without any further purification. Carbon tetrachloride from American Chemicals was of spectrograde quality and it was washed with a saturated sodium carbonate solution and then repeatedly with water, dried with calcium chloride and $P_2O_5$, and redistilled. Ethanol was purified by refluxing with concentrated sulfuric acid (4 mL $H_2SO_4$/1000 mL solvent) for 24 h and then was distilled twice before use.

Benzene and petroleum ether were distilled before use.

*General procedure*

Carbazole solutions (0.005 *M*) in pure $CCl_4$ or 0.1 *M* $CCl_4$ in ethanol were deoxygenated with oxygen-free argon and irradiated in a Pyrex Hanovia immersion-well reactor for 1 h with an Hanovia 679A36; 450 W medium-pressure mercury lamp. Hydrogen chloride generated during these reactions was neutralized with sodium carbonate. 1% sodium carbonate water solution or ethanol with sodium carbonate were added to the irradiated solution of carbazole in pure $CCl_4$. But only sodium carbonate was added to the irradiated carbazole solution with $CCl_4$ in ethanol. Solutions containing ethanol were mixed and then the sediment was separated by filtration. The remaining solutions were concentrated. The solution containing water (biphase system) was shaken, and then the $CCl_4$ was evaporated under vacuum. The remaining products not dissolved in water were precipitated at the bottom of the flask. Then water was decanted and products were dried using a stream of air.

The photochemical products were then analysed by TLC detected by uv (using Eastman-Kodak TLC plates, silica gel 13181) and separated by column chromatography. The columns were packed with silica gel (Kieselgel 60, Merck, particle size 0.040–0.063 mm). Developing systems consisted of petroleum ether (low-boiling fraction) and ethyl ether or benzene and ethanol. Identified products have been listed in Table 1 and their $R_f$ values on TLC plates with silica gel in Table 3.

*Spectral characteristics of the photochemical products*

*Hexachloroethane* (**1**): single crystals, unobserved by TLC. This compound is going down first on the chromatographic column. The product has been identified by comparison with the infrared and mass spectra of an authentic sample.

N-*(Trichloroethylene)carbazole* (**2**): was identified as described previously (22).

*1-Chlorocarbazole* (**3**): colorless crystalline solid; $^1$H-nmr ($CDCl_3$) δ 7.09–7.53 (m, 5H, arom), 7.92, 8.01, 8.10 (3s, 2H, arom), 8.28 (s, 1H, N—H), ($d_6$-acetone) 7.10–7.70 (complex m, 5H, arom), 8.04–8.20 (m, 2H, arom), ~10.65 (s, broad band, 1H, N—H).

Infrared (film) $\tilde{\nu}_{max}$ 3400 (s, N—H), 1620 (w), 1600 (m), 1555 (m), 1485 (m), 1445 (s), 1415 (s), 1360 (vw), 1325 (m), 1310 (m), 1260 (w), 1220 (w), 1200 (vw), 1175 (m), 1125 (m), 1020 (m), 920 (w), 845 (w), 790 (vw), 770 (w), 730 (vs) cm$^{-1}$.

Mass spectrum (70 eV) (mol wt for $C_{12}H_8NCl$ 201.66), *m/e* 203 ($M^+$, 33.7), 201 ($M^+$, 100), 166 (42), 165 (29.4), 164 (26.2), 138 (42), 137 (11.7).

N-*(Carboethoxy)carbazole* (**4**): white crystalline solid; $^1$H-nmr ($CDCl_3$) δ 1.56 (t, *J* = 7 Hz, 3H, methyl), 4.60 (q, *J* = 7 Hz, 2H, methylene), 7.27–7.58 (m, 4H, arom), 7.94–8.04 (m, 2H, arom), 8.27–8.37 (m, 2H, arom).

Infrared (film) $\tilde{\nu}_{max}$ 3040–2830 (m), 1730 (vs, C=O), 1590 (w), 1480 (m), 1455 (m), 1440 (vs), 1420 (m), 1390 (s), 1365 (vs), 1335 (s), 1320 (vs), 1295 (vs), 1245 (s), 1215 (s), 1200 (vs), 1100 (s), 1040 (s), 1005 (m), 920 (m), 840 (m), 750 (vs), 740 (vs), 705 (s) cm$^{-1}$.

Mass spectrum (70 eV) (mol wt for $C_{15}H_{13}NO_2$ 239.28), *m/e* 239 ($M^+$, 41.5), 180 (59.6), 167 (100), 166 (62.8), 140 (37.2), 139 (24.8).

*1-(Carboethoxy)carbazole* (**5**): white crystalline solid; $^1$H-nmr ($CDCl_3$) δ 1.48 (t, *J* = 7 Hz, 3H, methyl), 4.50 (q, *J* = 7 Hz, 2H, methylene), 7.16–7.57 (m, 4H, arom), 8.05, 8.14, 8.22, 8.31 (2d, 3H, arom), 9.97 (s, 1H, N—H), ($d_6$-acetone) 10.78 (s, broad band, 1H, N—H); ir and ms are the same as described previously (22).

*2-(Carboethoxy)carbazole* (**6**): white crystalline solid; $^1$H-nmr ($CDCl_3$) δ 1.44 (t, *J* = 7 Hz, 3H, methyl), 4.43 (q, *J* = 7 Hz, 2H, methylene), 7.21–7.50 and 7.90–8.20 (2m, 3H and 4H, arom), 8.25 (s, 1H, N—H), ($d_6$-acetone) 10.63 (s, 1H, N—H).

Infrared (film) $\tilde{\nu}_{max}$ 3400 (s, N—H), 1685 (vs, C=O), 1620 (s), 1490 (w), 1450 (m), 1435 (s), 1375 (w), 1350 (w), 1330 (m), 1315 (w), 1285 (m), 1260 (m), 1210 (m), 1080 (w), 1015 (w), 980 (vw), 860 (m), 825 (w), 810 (vw), 760 (vw), 735 (vs), 710 (s) cm$^{-1}$.

Mass spectrum (70 eV) (mol wt for $C_{15}H_{13}NO_2$ 239.28), *m/e* 239 ($M^+$, 100), 211 (28.7), 194 (72), 166 (39.3), 139 (22.3).

*3-(Carboethoxy)carbazole* (**7**): white crystalline solid; $^1$H-nmr ($CDCl_3$) δ 1.45 (t, *J* = 7 Hz, 3H, methyl), 4.44 (q, *J* = 7 Hz, 2H, methylene), 7.18–7.48 (m, 4H, arom), 8.08, 8.18 (2s, 2H, arom), 8.82 (s, 1H, arom), 8.41 (s, 1H, N—H), ($d_6$-acetone) 10.74 (s, broad band, 1H, N—H); ir and ms are the same as described previously (22).

*4-(Carboethoxy)carbazole* (**8**): white crystalline solid; $^1$H-nmr ($CDCl_3$) δ 1.49 (t, *J* = 7 Hz, 3H, methyl), 4.54 (q, *J* = 7 Hz, 2H, methylene), 7.19–7.93 (complex m, 6H, arom), 8.82, 8.91 (2s, 1H, arom), 8.30 (s, 1H, N—H), ($d_6$-acetone) ~10.73 (s, 1H, N—H).

TABLE 3. $R_f$ values of the photoproducts in the carbazole–$CCl_4$ system

| | Developing system† (v/v) | | | | | | |
|---|---|---|---|---|---|---|---|
| | | PE–EE | | | | B–EE | B–E |
| No.* | PE | 100:1 | 20:1 | 5:1 | B | 10:1 | 2:1 |
| C | 0.03 | 0.05 | 0.13 | 0.40 | 0.76 | 0.80 | |
| 2 | 0.68 | 0.76 | 0.82 | 0.88 | 0.89 | 0.90 | |
| 3 | 0.18 | 0.26 | 0.42 | 0.70 | 0.82 | 0.86 | |
| 4 | 0.06 | 0.24 | 0.52 | 0.77 | 0.75 | 0.85 | |
| 5 | 0.03 | 0.10 | 0.28 | 0.54 | 0.67 | 0.80 | |
| 6 | | | 0.02 | 0.08 | 0.23 | 0.48 | |
| 7 | | | 0.03 | 0.11 | 0.27 | 0.54 | |
| 8 | | | 0.05 | 0.20 | 0.49 | 0.70 | |
| 9 | | 0.03 | 0.14 | 0.42 | 0.45 | 0.82 | |
| 10 | | | 0.06 | 0.25 | 0.40 | 0.75 | |
| 11 | | | | 0.13 | 0.19 | 0.59 | |
| 12 | | 0.06 | 0.23 | 0.61 | 0.45 | 0.84 | |
| 13 | | | | | 0.05 | 0.25 | |
| 14 | | | | | 0.06 | 0.29 | |
| 15 | | | | | | | 0.20 |
| 16 | | | | | | | 0.28 |
| 17 | 0.07 | 0.23 | 0.50 | 0.73 | 0.83 | 0.87 | |
| 18 | | 0.06 | 0.12 | 0.41 | 0.73 | 0.84 | |
| 19 | | | | 0.04 | 0.29 | 0.51 | |
| 20 | | | 0.07 | 0.33 | 0.69 | 0.87 | |
| 21 | | | | 0.06 | 0.47 | 0.75 | |

*Notation of compounds is the same as in Table 1.
†B: benzene; PE: petroleum ether; E: ethanol; EE: ethyl ether.

Infrared (Nujol film) $\tilde{\nu}_{max}$ 3350 (s, N—H), 1690 (vs, C=O), 1590 (m), 1430 (m), 1395 (m), 1360 (m), 1330 (w), 1320 (m), 1305 (vs), 1285 (m), 1270 (vs), 1225 (w), 1180 (s), 1150 (m), 1135 (s), 1110 (m), 1085 (m), 1020 (m), 1010 (m), 745 (s), 730 (m), 720 (vs) $cm^{-1}$.

Mass spectrum (70 eV) (mol wt for $C_{15}H_{13}NO_2$ 239.28), *m/e* 239 ($M^+$, 100), 211 (23.7), 195 (10.7), 194 (63.7), 193 (2.2), 167 (19.7), 166 (41.4), 165 (9.1), 164 (5.7), 139 (21.4).

*3,9-Di(carboethoxy)carbazole* (**9**): white crystalline solid; $^1$H-nmr ($CDCl_3$) δ 1.45 and 1.57 (2t, $J$ = 7 Hz, 6H, methyl), 4.44 and 4.62 (2q, $J$ = 7 Hz, 4H, methylene), 7.25–7.65 and 8.0–8.45 (2m, 2H, and 4H, arom), 8.67 (s, 1H, arom).

Infrared (film) $\tilde{\nu}_{max}$ 1730 (vs, C=O), 1695 (vs, C=O), 1610 (w), 1585 (m), 1475 (m), 1440 (s), 1420 (s), 1380 (w), 1360 (s), 1330 (m), 1310 (m), 1295 (m), 1275 (w), 1230 (vs), 1190 (s), 1090 (s), 1040 (m), 1010 (s), 915 (w), 885 (w), 760 (m), 745 (m), 730 (m), 700 (m) $cm^{-1}$.

Mass spectrum (70 eV) (mol wt for $C_{18}H_{17}NO_4$ 311.34), *m/e* 311 ($M^+$, 50.3), 266 (11.7), 239 (29.1), 238 (25.9), 210 (13.5), 194 (100), 193 (25.8), 167 (27.7), 166 (48.2), 165 (40.4), 164 (31.2), 139 (33.3), 138 (26.9).

*1,3-Di(carboethoxy)carbazole* (**10**): white crystalline solid; $^1$H-nmr ($CDCl_3$) δ 1.47 and 1.49 (2t, $J$ = 7 Hz, 6H, methyl), 4.46 and 4.51 (2q, $J$ = 7 Hz, 4H, methylene), 7.20–7.60 (m, 3H, arom), 8.10, 8.18 (2s, 1H, arom), 8.78 (d, $J$ = 1.8 Hz, 1H, arom), 8.98 (s, 1H, arom), 10.16 (s, 1H, N—H), ($d_6$-acetone) 11.16 (s, 1H, N—H).

Infrared (Nujol film) $\tilde{\nu}_{max}$ 3360 and 3320 (s, N—H), 1695 (s, C=O), 1670 (vs, C=O), 1620 (vw), 1595 (s), 1565 (w), 1385 (m), 1355 (m), 1325 (s), 1305 (s), 1260 (vs), 1230 (s), 1210 (s), 1200 (s), 1180 (s), 1140 (w), 1110 (w), 1090 (m), 1060 (s), 1015 (m), 1000 (w), 900 (w), 780 (w), 760 (m), 715 (s) $cm^{-1}$.

Mass spectrum (70 eV) (mol wt for $C_{18}H_{17}NO_4$ 311.34), *m/e* 311 ($M^+$, 65.3), 267 (3.8), 266 (27.5), 265 (100), 239 (1.5), 238 (7.6), 237 (16.2), 220 (2.9), 210 (3), 294 (1), 293 (5), 292 (8.4), 165 (7.6), 164 (12.3), 44 (8.8).

*1,6-Di(carboethoxy)carbazole* (**11**): white crystalline solid; $^1$H-nmr ($CDCl_3$) δ 1.44 and 1.47 (2t, $J$ = 7 Hz, 6H, methyl), 4.42 and 4.44 (2q, $J$ = 7 Hz, 4H, methylene), 7.25–7.60 and 8.05–8.40 (2 complexes m, 5H, arom), 8.82 (d, $J$ = 1.8 Hz, 1H, arom).

Infrared (Nujol film) $\tilde{\nu}_{max}$ 3370 (s, N—H), 1700 (s, C=O), 1670 (s, C=O), 1615 (w), 1595 (s), 1490 (m), 1415 (m), 1355 (m), 1335 (m), 1300 (s), 1260 (vs), 1245 (vs), 1215 (s), 1200 (s), 1180 (m), 1145 (s), 1115 (m), 1100 (vs), 1060 (m), 1020 (m), 755 (m), 735 (m), 715 (m) $cm^{-1}$.

Mass spectrum (70 eV) (mol wt for $C_{18}H_{17}NO_4$ 311.34), *m/e* ($M^+$, 100), 267 (8.4), 266 (43.7), 265 (99.7), 239 (2.5), 238 (7.5), 237 (13.5), 220 (44.7), 210 (3.2), 194 (3.7), 193 (16), 192 (17.5), 165 (8.8), 164 (28), 44 (14.3).

*1,8-Di(carboethoxy)carbazole* (**12**): white crystalline solid.

Infrared (film) $\tilde{\nu}_{max}$ 3410 (w, N—H), 2950–2820 (s), 1685 (s, C=O), 1595 (m), 1490 (m), 1465 (m), 1450 (w), 1425 (m), 1360 (m), 1290 (w), 1265 (vs), 1200 (vs), 1160 (m), 1140 (vs), 1080 (m), 1010 (w), 740 (m), 715 (m) $cm^{-1}$.

Mass spectrum (70 eV) (mol wt for $C_{18}H_{17}NO_4$ 311.34), *m/e* 311 ($M^+$, 100), 296 (22.2), 267 (9.5), 266 (16.6), 265 (14), 220 (19), 194 (23.3), 193 (79), 192 (16.4), 165 (14.4), 164 (28.2).

*3,6-Di(carboethoxy)carbazole* (**13**): white crystalline solid; $^1$H-nmr ($CDCl_3$) δ 1.45 (t, $J$ = 7 Hz, 6H, methyl), 4.44 (q, $J$ = 7 Hz, 4H, methylene), 7.41 and 7.50 (2s, 2H, arom), 8.13 and 8.23 (2d, $J$ = 1.8 Hz, 2H, arom), 8.87 (d, $J$ = 1.8 Hz, 2H, arom), 8.49 (s, 1H, N—H).

Infrared (Nujol film) $\tilde{\nu}_{max}$ 3300 (s, N—H), 1685 (vs, C=O), 1615 (w), 1595 (w), 1350 (m), 1300 (m), 1280 (m), 1260 (s), 1225 (m), 1210 (m), 1090 (m), 1015 (m), 755 (m), 710 (s) $cm^{-1}$.

Mass spectrum (70 eV) (mol wt for $C_{18}H_{17}NO_4$ 311.34), *m/e*

Can. J. Chem. Downloaded from www.nrcresearchpress.com by 210.87.254.105 on 09/06/12
For personal use only.

Can. J. Chem. Downloaded from www.nrcresearchpress.com by 210.87.254.105 on 09/06/12
For personal use only.

311 ($M^+$, 100), 267 (10.3), 266 (65.9), 265 (1.3), 239 (5.2), 238 (26.8), 237 (2.1), 210 (10.9), 194 (3.3), 193 (12.4), 192 (4.4), 165 (6.8), 164 (11.1), 44 (14).

*3,5-Di(carboethoxy)carbazole* (**14**): white crystalline solid; $^1$H-nmr ($CDCl_3$) δ 1.52 and 1.54 (2t, $J$ = 7 Hz, 6H, methyl), 4.43 and 4.52 (2q, $J$ = 7 Hz, 4H, methylene), 7.15–8.55 (complex m, 5H, arom), 9.54 (s, 1H, arom).

Infrared (film) $\bar{\nu}_{max}$ 3260 (s, N—H), 2950–2800 (s), 1700 (vs, C=O), 1675 (vs, C=O), 1605 (s), 1595 (s), 1555 (w), 1440 (w), 1390 (w), 1375 (w), 1355 (m), 1310 (s), 1280 (s), 1270 (s), 1240 (vs), 1160 (s), 1140 (m), 1125 (m), 1100 (m), 1015 (m), 755 (w), 735 (m), 710 (m) cm$^{-1}$.

Mass spectrum (70 eV) (mol wt for $C_{18}H_{17}NO_4$ 311.34), *m/e* 311 ($M^+$, 100), 267 (12.7), 266 (68.8), 265 (0.8), 239 (6.1), 238 (23.8), 237 (1.4), 210 (6.0), 194 (6.4), 193 (14.7), 192 (17.5), 165 (10.4), 164 (13.7), 44 (15.5).

*Carbazole-1-carboxylic acid* (**15**): white crystalline solid; $^1$H-nmr ($CDCl_3$) δ 7.26–7.55 (m, 4H, arom), 8.07–8.38 (m, 3H, arom), ~9.92 (s, 1H, N—H); ($d_6$-acetone) 10.76 (s, 1H, N—H).

Infrared (film) $\bar{\nu}_{max}$ 3395 (s, N—H), 1660 (s, C=O), 1610 (m), 1590 (m), 1480 (m), 1420 (s), 1300 (s), 1250 (m), 1215 (m), 1200 (m), 1130 (m), 1100 (m), 1055 (w), 1010 (w), 915 (w), 850 (w), 810 (w), 745 (vs), 715 (s) cm$^{-1}$.

Mass spectrum (70 eV) (mol wt for $C_{13}H_9NO_2$ 211.22), *m/e* 211 ($M^+$, 52.5), 194 (19.8), 193 (100), 166 (17.7), 165 (69.5), 139 (18.4), 138 (19.5).

*Carbazole-3-carboxylic acid* (**16**): white crystalline solid; $^1$H-nmr ($CDCl_3$) δ 7.20–7.55 (m, 4H, arom), 8.11 and 8.15, 8.25 (s, s, and 2d, $J$ = 1.8 Hz, 2H, arom), 8.90 (s, 1H, arom), 8.38 (s, 1H, N—H).

Infrared (film) $\bar{\nu}_{max}$ 3375 (m, N—H), 1665 (vs, C=O), 1615 (m), 1595 (vs), 1570 (m), 1480 (m), 1435 (m), 1400 (s), 1320 (s), 1295 (m), 1260 (s), 1230 (s), 1210 (m), 1190 (m), 1120 (m), 1010 (w), 920 (w), 900 (w), 810 (w), 765 (m), 750 (m), 735 (m), 710 (s) cm$^{-1}$.

Mass spectrum (70 eV) (mol wt for $C_{13}H_9NO_2$ 211.22), *m/e* 211 ($M^+$, 100), 194 (48.2), 193 (47.8), 166 (36.2), 165 (39.0), 164 (25.2), 139 (30.5), 138 (14.2).

*N,N'-Carbodicarbazyl* (**17**): white crystalline solid; $^1$H-nmr ($CDCl_3$) δ 7.26–7.42 (m, 12H, arom), 8.0–8.14 (m, 4H, arom).

Infrared (film) $\bar{\nu}_{max}$ 1695 (vs, C=O), 1590 (w), 1470 (m), 1445 (s), 1430 (m), 1365 (s), 1335 (w), 1320 (s), 1300 (m), 1290 (s), 1230 (w), 1205 (s), 1170 (m), 1145 (m), 1110 (w), 1090 (w), 1020 (w), 925 (w), 825 (m), 760 (w), 740 (vs), 710 (s) cm$^{-1}$.

Mass spectrum (70 eV) (mol wt for $C_{25}H_{16}N_2O$ 360.42), *m/e* 360 ($M^+$, 17.0), 194 (46.8), 166 (100), 140 (23.4), 139 (11.3).

*1-(Carbo-N-carbazyl)carbazole* (**18**): white crystalline solid; $^1$H-nmr ($CDCl_3$) δ 7.12–7.45 and 7.49–7.79 (2 complexes m, 10H, arom), 8.01–8.22 (m, 4H, arom), 8.31, 8.39 (2s, 1H, arom), 9.75 (s, 1H, N—H), ($d_6$-acetone) 7.22–7.78 (complex m, 11H, arom), 8.11–8.33 (m, 3H, arom), 8.46, 8.55 (2s, 1H, arom), 10.91 (s, 1H, N—H).

Infrared (film) $\bar{\nu}_{max}$ 3420 (m, N—H), 1650 (s, C=O), 1615 (w), 1595 (m), 1480 (m), 1470 (m), 1445 (s), 1435 (s), 1420 (m), 1350 (m), 1320 (s), 1310 (s), 1290 (s), 1270 (s), 1250 (w), 1210 (s), 1165 (w), 1145 (m), 1130 (m), 1105 (m), 1090 (m), 1055 (w), 945 (w), 920 (w), 830 (w), 800 (w), 770 (m), 740 (vs), 710 (s) cm$^{-1}$.

Mass spectrum (70 eV) (mol wt for $C_{25}H_{16}N_2O$ 360.42), *m/e* 360 ($M^+$, 10.6), 194 (100), 166 (78.7), 139 (51).

*3-(Carbo-N-carbazyl)carbazole* (**19**): white crystalline solid; $^1$H-nmr ($CDCl_3$) δ 7.24–8.13 (complex m, 14H, arom), 8.55 (s, 1H, arom), 8.40 (s, 1H, N—H), ($d_6$-acetone) 7.14–7.90 (m, 11H, arom), 8.10–8.27 (m, 3H, arom), 8.64 (s, 1H, arom), 10.91 (s, 1H, N—H).

Infrared (Nujol film) $\bar{\nu}_{max}$ 3400 (m, N—H), 1660 (s, C=O), 1620 (w), 1595 (m), 1570 (w), 1465 (m), 1435 (s), 1350 (s), 1320 (s), 1300 (m), 1275 (m), 1240 (m), 1220 (m), 1210 (m), 1185 (w), 1140 (m), 1120 (m), 1055 (w), 1010 (w), 930 (w), 840 (w), 815 (m), 760 (w), 745 (s), 710 (s) cm$^{-1}$.

Mass spectrum (70 eV) (mol wt for $C_{25}H_{16}N_2O$ 360.42), *m/e* 360 ($M^+$, 8.5), 194 (100), 166 (31.9), 139 (22).

*3,9-Di(carbo-N-carbazyl)carbazole* (**20**): white crystalline solid; $^1$H-nmr ($CDCl_3$) δ 7.26–7.65 (complex m, 16H, arom), 7.92–8.12 (m, 6H, arom), 8.54 (s, 1H, arom).

Infrared (Nujol film) $\bar{\nu}_{max}$ 1700 (vs, C=O), 1670 (s, C=O), 1615 (w), 1595 (m), 1435 (vs), 1350 (s), 1330 (w), 1315 (vs), 1290 (vs), 1275 (m), 1235 (m), 1220 (m), 1205 (s), 1190 (w), 1165 (m), 1145 (m), 1110 (w), 1090 (w), 1075 (w), 1020 (m), 915 (w), 885 (w), 870 (w), 820 (m), 765 (m), 740 (vs), 710 (s) cm$^{-1}$.

Mass spectrum (70 eV) (mol wt for $C_{38}H_{23}N_3O_2$ 553.63), *m/e* 553 ($M^+$, 11.2), 387 (95.0), 194 (26.7), 167 (23.3), 166 (100), 165 (20.8), 164 (13.3), 140 (12.5), 139 (10), 138 (6.7).

*1,6-Di(carbo-N-carbazyl)carbazole* (**21**): white crystalline solid; $^1$H-nmr ($CDCl_3$) δ 7.14–7.82 (complex m, 15H, arom), 7.94–8.22 (m, 5H, arom), 8.35, 8.42 (2s, 1H, arom), 8.51 (s, 1H, arom), 9.87 (s, 1H, N—H), ($d_6$-acetone) 11.01 (s, 1H, N—H).

Infrared (film) $\bar{\nu}_{max}$ 3410 (m, N—H), 1670 (vs, C=O), 1660 (vs, C=O), 1615 (m), 1595 (s), 1570 (m), 1485 (s), 1475 (s), 1445 (vs), 1435 (vs), 1420 (s), 1345 (s), 1315 (vs), 1290 (vs), 1270 (vs), 1250 (w), 1235 (w), 1210 (vs), 1170 (w), 1140 (s), 1120 (m), 1105 (m), 1095 (m), 1055 (m), 1020 (w), 940 (w), 925 (vw), 895 (vw), 860 (vw), 830 (w), 815 (vw), 795 (w), 780 (w), 745 (vs), 710 (s) cm$^{-1}$.

Mass spectrum (70 eV) (mol wt for $C_{38}H_{23}N_3O_2$ 553.63), *m/e* 553 ($M^+$, 5.7), 387 (41.7), 194 (100), 193 (10), 166 (45.8), 165 (20), 164 (10.8), 140 (10), 139 (24.2), 138 (5).

## Conclusion

The following scheme describes the complex mechanism of photochemical reactions in the carbazole–$CCl_4$ system in pure $CCl_4$ as well as in ethanol as the reaction media:

$$^1(C^{\delta+}\cdots CCl_4^{\delta-})^* \rightarrow [C^+\,{}^\bullet Cl^-\,\dot{C}Cl_3] \rightarrow \alpha, \beta, \text{and } \gamma_i \rightarrow \text{products}$$

The electron transfer from the electronically excited carbazole molecule to $CCl_4$ molecule in the excited CT complex is the primary photochemical reaction followed by the primary photoproducts in the solvent cage. The radical cation of carbazole undergoes transformations in the presence of chloride ion and trichloromethyl radical in the solvent cage giving radical β and cations α and $\gamma_i$. Following that, depending upon the reaction media used, intermediates α, β, and $\gamma_i$ undergo further transformation to proper thermodynamically stable products. This mechanism of one-electron photooxidation of carbazole in the presence of carbon tetrachloride was strongly supported by a qualitative study of the various reaction products obtained.

## Acknowledgements

The authors appreciate the financial support of the National Research Council of Canada and the "Ministère de l'Éducation du Québec, FCAC". Thanks are also due to Professor Denis Gravel of the Chemistry Department, Université de Mont-

réal, for many valuable discussions about this paper.

1. A. AHMAD and G. DUROCHER. Can. J. Spectrosc. **26**(1), 19 (1981).
2. A. AHMAD and G. DUROCHER. Photochem. Photobiol. **34**, 573 (1981).
3. G. LESSARD and G. DUROCHER. Can. J. Spectrosc. **23**, 130 (1978); J. Phys. Chem. **82**, 2812 (1978); Photochem. Photobiol. **29**, 399 (1979).
4. W. R. WARE and C. LEWIS. J. Chem. Phys. **57**, 3546 (1972).
5. R. O. LOUFTY and A. C. SOMERSALL. Can. J. Chem. **54**, 760 (1976).
6. J. KLEIN, V. P. PLAZANET, and G. LAUSTRIAT. J. Chim. Phys. **67**, 302 (1970); J. KLEIN and G. LAUSTRIAT. J. Chim. Phys. **67**, 310 (1970).
7. D. SAPERSTEIN and E. LEVIN. J. Chem. Phys. **62**, 3560 (1975).
8. J. R. BEWS and CH. GLIDEWELL. J. Mol. Struct. **71**, 287 (1981).
9. V. I. SKVORTSOV and M. V. ALFIMOV. Opt. Spectrosc. **41**, 284 (1976).
10. M. BAILLET and G. DUROCHER. J. Phys. Chem. To be published; R. SOLARO, E. CHIELLINI, and A. LEDWITH. J. Chem. Soc. Chem. Commun. 580 (1980); 583 (1980); U. LANDMAN, A. LEDWITH, D. G. MARSCH, and D. J. WILLIAMS. Macromolecules, **9**, 833 (1976); L. P. ELLINGER. Advances in macromolecular chemistry. Vol. 1. *Edited by* W. M. Pasika, Academic Press, NY. 1968. p. 169.
11. I. FISCHER-HJALMARS and M. SUNDBOM. Acta Chem. Scand. **22**, 607 (1968).
12. J. F. AMBROSE and R. F. NELSON. J. Electrochem. Soc. **115**, 1159 (1968).
13. J. F. AMBROSE, L. L. CARPENTER, and R. F. NELSON. J. Electrochem. Soc. **122**, 876 (1975).
14. S. L. MUROV. Handbook of photochemistry. Marcel Dekker, Inc., New York. 1973.
15. E. J. LAND. Prog. React. Kinet. **3**, 371 (1965).
16. T. LATOWSKI and B. ZELENT. Rocz. Chem. **48**, 831 (1974); **51**, 1883 (1977).
17. T. LATOWSKI and K. WYRZYKOWSKA. Rocz. Chem. **49**, 833 (1974).
18. K. WYRZYKOWSKA, M. GRODOWSKI, K. WEISS, and T. LATOWSKI. Photochem. Photobiol. **28**, 311 (1978).
19. T. IWASAKI, T. SAWADA, M. OKUYAMA, and H. KAMADA. J. Phys. Chem. **82**, 371 (1978); Photographic Sci. Eng. **22**, 312 (1978).
20. T. LATOWSKI and B. ZELENT. J. Org. Chem. **20**, 3559 (1979).
21. A. LEDWITH and M. SAMBHI. J. Chem. Soc. Chem. Commun. 64 (1965); V. A. BOROVKOVA, KH. S. BAGDASAR'YAN, V. F. PIKEL'NI, V. A. KOLOSOV, and YU. I. KIRYUKHIN. Dokl. Adad. Nauk SSSR, **224**(3), 616 (1975).
22. B. ZELENT and G. DUROCHER. J. Org. Chem. **46**, 1496 (1981).
23. A. J. BARD, A. LEDWITH, and H. J. SHINE. Adv. Phys. Org. Chem. **13**, 155 (1976).
24. T. LATOWSKI and E. SIKORSKA. Rocz. Chem. **42**, 1063 (1968).
25. J. MARCH. Advanced organic chemistry. McGraw-Hill Book Company, 1977. p. 807.

Can. J. Chem. Downloaded from www.nrcresearchpress.com by 210.87.254.105 on 09/06/12
For personal use only.

# Calcul des déplacements chimiques par la méthode des perturbations finies au niveau INDO avec GIAO et approximation de London. I. $^{13}C$ et $^{1}H$

E. VAUTHIER ET S. ODIOT

*Service de Spectroscopie Moléculaire en Milieu Condensé, Laboratoire de Recherches Physiques associé au C.N.R.S., Université Pierre et Marie Curie, 4, place Jussieu, Tour 22, 75230 Paris Cedex 05, France*

ET

F. TONNARD

*Département de Physique Cristalline et Chimie Structurale, E.R.A. au C.N.R.S. No 15, Université de Rennes, Campus de Beaulieu, Avenue du Général Leclerc, 35031 Rennes, France*

Reçu le 30 juillet 1981

E. VAUTHIER, S. ODIOT et F. TONNARD. Can. J. Chem. **60**, 957 (1982).

Un formalisme pour le calcul de σ dans le cadre de la méthode des perturbations finies est développé en gardant hermitienne la matrice de perturbation au premier ordre en ***B***. Le formalisme de σ est séparé en termes de contributions mono, di, triatomiques et l'importance des densités électroniques des liaisons proches et lointaines est mise en évidence. Les déplacements chimiques du $^{13}C$ ne dépendent que très peu des liaisons lointaines contrairement au $^{1}H$. Un calcul de la constante d'écran sur une série de 16 carbones $sp$, $sp^2$, donne une précision moyenne de 5 ppm pour le noyau $^{13}C$.

E. VAUTHIER, S. ODIOT, and F. TONNARD. Can. J. Chem. **60**, 957 (1982).

A formalism for the calculation of σ in the finite perturbation method is developed by keeping hermitian the first order perturbed matrix in ***B***. The σ formalism is separated into mono, di, and triatomic terms, and the importance of the electron densities of neighboring and remote bonds is shown. $^{13}C$ chemical shifts depend only slightly on the remote bonds in contrast to those for $^{1}H$. A calculation of the screening constant for a series of 16 $sp$ and $sp^2$ carbons gives an average precision of 5 ppm for the $^{13}C$ nuclei. [Journal translation]

## Introduction

Le calcul a priori des constantes d'écran en résonance magnétique nucléaire (rmn) présente un grand intérêt dans la mesure où la précision du calcul est suffisante. Pour le $^{13}C$, par exemple, une précision de ~1 ppm faciliterait considérablement l'identification de structures organiques. Les méthodes de calcul présentement employées reproduisent les déplacements chimiques du $^{13}C$ avec une précision moyenne n'excédant pas ~10 ppm dans la majorité des cas (1).

Quatre formalismes de calcul sont actuellement utilisés, soit (*i*) la méthode Hartree–Fock couplée (CHF) (2, 3), (*ii*) la méthode des perturbations finies (FPM) (4), (*iii*) la théorie des perturbations classique de Pople (5) et, finalement (*iv*), la méthode des variations (6, 7). Les calculs CHF en *ab initio* conduisent à des résultats qui dépendent du choix de l'origine des axes moléculaires (8). Aussi, pour pallier cet inconvénient majeur, Ditchfield a introduit des orbitales atomiques jauge invariantes (GIAO) (9). Ce formalisme, récemment appliqué sur des composés du lithium (10), a également été adapté à la méthode "Extended Hückel" (EHT) et conduit ainsi au calcul de déplacements chimiques avec une précision moyenne de ~15 ppm pour le $^{13}C$ et de ~0,5 ppm pour $^{1}H$ (11). Par ailleurs, la méthode classique de Pople a été utilisée par Webb sur une base GIAO aux niveaux CNDO/S et INDO (12–17), avec une précision moyenne sur le $^{13}C$ de ~10 ppm dans une série de coumarines (12) et de ~8 ppm dans une série d'éthyléniques méthylés (14). Dans le formalisme variationnel de Stephen (18) et Didry et Guy (7), Aminova *et al.* (19) a introduit les orbitales GIAO ce qui a conduit, aux niveaux EHT et INDO, à une précision moyenne de ~10 ppm pour le $^{13}C$ et de ~26 ppm pour $^{1}H$.

La méthode des perturbations finies utilisée ici est due à Pople *et al.* (4). Elle a donné lieu à des calculs *ab initio* avec (20, 21) ou sans GIAO (22). Pour le proton, un calcul LEMAO-5G (21) donne une précision moyenne (sur 9 valeurs) de l'ordre de 0,7 ppm et de 10 ppm pour le $^{13}C$. Ce formalisme a aussi été utilisé au niveau INDO (23–26) afin d'éviter le coût excessif des calculs *ab initio*. Les premiers travaux (23) découlent d'une application stricte des approximations INDO lors du développement du formalisme, ce qui entraîne l'élimination de la perturbation due au champ magnétique dans les éléments de la matrice de Fock. De plus, dans ce formalisme INDO, il s'introduit des approximations CNDO dans l'expression des éléments de matrice $G_{\mu\nu}$. Plus récemment, Garber *et al.* (26), toujours dans un cadre INDO et en évitant, pour la première fois, l'approximation de London, ne néglige plus l'effet important du champ magné-

0008-4042/82/080957-13$01.00/0

©1982 National Research Council of Canada/Conseil national de recherches du Canada

Can. J. Chem. Downloaded from www.nrcresearchpress.com by 210.87.254.5 on 09/06/12
For personal use only.

tique. Toutefois, les approximations INDO détruisent dans son formalisme le caractère nécessairement hermitique de la matrice $H$.

Nous avons donc repris l'écriture de ce formalisme avec les approximations INDO sur une base de GIAO et avec l'approximation de London, en conservant la condition d'hermiticité. Le rôle des interactions lointaines, traduites par des intégrales à trois centres dans les termes dia et paramagnétiques, n'a pas été clairement démontré (26), à l'exception du proton pour le terme paramagnétique (11). Aussi, l'un des buts de notre travail est-il de mettre en évidence l'importance de ces liaisons lointaines en ne faisant aucune approximation dans le calcul des intégrales tricentriques et d'étudier leurs effets relatifs sur le déplacement chimique du $^{13}C$ et du $^{1}H$. Nous montrons, enfin, que l'amélioration apportée au formalisme par le maintien de la condition d'hermiticité des matrices se traduit par une précision moyenne égale à 5 ppm pour le $^{13}C$.

## Théorie

En présence d'un champ magnétique externe $\boldsymbol{B}$ et du moment magnétique $\mu_M$ d'un noyau résonnant $M$, l'hamiltonien électronique d'une molécule à couche complète s'écrit, en unités atomiques

$$(\boldsymbol{B}, \mu_M) = \sum_k \boldsymbol{H}_k + \sum_{k<l} 1/r_{kl}$$

où $H_k$ est l'opérateur monoélectronique $= \frac{1}{2}[\boldsymbol{P}_k + (1/c)\boldsymbol{A}_k]^2 + V_k$ et $\boldsymbol{A}_k = \frac{1}{2}\boldsymbol{B}\Lambda\boldsymbol{r}_k + \mu_M\Lambda\boldsymbol{r}_{Mk}/r_{Mk}^3$ est le potentiel vecteur au point repéré par le vecteur $\boldsymbol{r}_k$ dans un système d'axes moléculaires.

La fonction d'onde $\psi(\boldsymbol{B}, \mu_M)$ est un déterminant de Slater construit sur des orbitales moléculaires $\phi_i$, combinaisons linéaires d'orbitales atomiques (GIAO).

$$\phi_i = \sum_\nu C_{\nu i}\chi_\nu \text{ avec } \chi_\nu = \chi_\nu^0\left(\exp -\frac{i}{c}\,\boldsymbol{A}_\nu\cdot\boldsymbol{r}\right) \quad \text{et} \quad \boldsymbol{A}_\nu = \tfrac{1}{2}\boldsymbol{B}\Lambda\boldsymbol{R}_\nu$$

où $\boldsymbol{R}_\nu$ repère la position du centre porteur de l'orbitale $\chi_\nu$ et $\chi_\nu^0$ est l'orbitale atomique en absence de $\boldsymbol{B}$. La fonction d'onde $\psi(\boldsymbol{B}, \mu_M)$ est la solution de l'équation

$$\mathcal{H}(\boldsymbol{B}, \mu_M)\psi(\boldsymbol{B}, \mu_M) = E(\boldsymbol{B}, \mu_M)\psi(\boldsymbol{B}, \mu_M)$$

L'énergie Hartree Fock perturbée, $\boldsymbol{E}(\boldsymbol{B}, \mu_M)$ se met sous la forme classique $E(\boldsymbol{B}, \mu_M) = \Sigma_{\mu\nu}\boldsymbol{P}_{\mu\nu}H_{\mu\nu} + \frac{1}{2}\Sigma_{\mu\nu}\boldsymbol{P}_{\mu\nu}G_{\mu\nu}$ avec

$$H_{\mu\nu} = \left\langle \chi_\nu \left| \frac{1}{2}\left(\boldsymbol{P} + \frac{1}{c}\boldsymbol{A}\right)^2 + V \right| \chi_\nu \right\rangle$$

[1] $$G_{\mu\nu} = \sum_{\eta\sigma} P_{\eta\sigma}[(\mu\nu|\eta\sigma) - \tfrac{1}{2}(\mu\sigma|\eta\nu)]$$

$$(\mu\nu|\eta\sigma) = \iint \chi_\mu^*(1)\chi_\nu(1)\frac{1}{r_{12}}\chi_\eta^*(2)\chi_\sigma(2)\,d\tau_1\,d\tau_2$$

*Expression des éléments matriciels* $H_{\mu\nu}$

Il est connu que

[2] $$H\chi_\nu = H\chi_\nu^0\left(\exp -\frac{i}{c}\boldsymbol{A}_\nu\cdot\boldsymbol{r}\right)$$

$$= \left(\exp -\frac{i}{c}\boldsymbol{A}_\nu\cdot\boldsymbol{r}\right)\left\{\frac{1}{2}\left[\boldsymbol{P} + \frac{1}{c}(\boldsymbol{A} - \boldsymbol{A}_\nu)\right]^2 + V\right\}\chi_\nu^0$$

$$= \left(\exp -\frac{i}{c}\boldsymbol{A}_\nu\cdot\boldsymbol{r}\right) H_\nu\chi_\nu^0$$

Un élément $H_{\mu\nu}$ devient ainsi

Can. J. Chem. Downloaded from www.nrcresearchpress.com by 210.87.254.5 on 09/06/12
For personal use only.

[3] $$H_{\mu\nu} = \int \left[ \exp \frac{i}{c} (A_\mu - A_\nu) \cdot r \right] \chi_\mu^{0*} H_\nu \chi_\nu^0 \, d\tau$$

$$H_\nu \chi_\nu^0 = H^0 \chi_\nu^0 - \frac{i}{2c} B \cdot r_\nu \Lambda \nabla \chi_\nu^0 - \frac{i}{c} \mu_M \frac{r_M \Lambda \nabla}{r_M^3} \chi_\nu^0 + \frac{1}{2c^2} \sum_{\alpha\beta} \left( \frac{r_\nu \cdot r_M \delta_{\alpha\beta} - r_{\nu\alpha} r_{M\beta}}{r_M^3} \right) \chi_\nu^0 \mu_{M\alpha} B_\beta$$

Où $$r_\nu = r - R_\nu$$

Il est important de remarquer que l'énergie perturbée $E(B \cdot \mu_M)$ est une quantité réelle (27) et qu'en conséquence, la matrice $H_{\mu\nu}$ doit rester hermitienne. Cette condition d'hermiticité impose que l'on doit avoir constamment $\int \chi_\mu^* H \chi_\nu \, d\tau = \int \chi_\nu (H\chi_\mu)^* \, d\tau$. Or, les approximations usuelles pour l'estimation des éléments $H_{\mu\nu}$ peuvent détruire cette condition d'hermiticité. Ainsi en est-il de l'approximation de London: $r = \frac{1}{2}(R_\mu + R_\nu)$ qui détruit (5) l'hermiticité même au niveau *ab initio*. Les approximations de la méthode INDO détruisent aussi, à elles seules, l'hermiticité. Dans ce présent travail, qui fait appel à la fois à l'approximation de London et aux approximations INDO, il y a donc lieu, selon Pople (5), de retenir dès à présent la partie hermitienne de $H_{\mu\nu}$ dans le formalisme général, soit (28)

$$[H_{\mu\nu}] \text{ herm} = \tfrac{1}{2}[H_{\mu\nu} + H_{\nu\mu}^*]$$

Partant de [3] on obtient

[4] $$H_{\nu\mu}^* = \int \left[ \exp \frac{i}{c} (A_\mu - A_\nu) \cdot r \right] \chi_\nu^0 \left\{ (H^0 \chi_\mu^0)^* + \frac{i}{2c} B \cdot r_\mu \Lambda \nabla \chi_\mu^{0*} + \frac{i}{c} \mu_M \cdot \frac{r_M \Lambda \nabla}{r_M^3} \chi_\mu^{0*} + \frac{1}{2c^2} \sum_{\alpha\beta} \left( \frac{r_\mu r_M \delta_{\alpha\beta} - r_{\mu\alpha} r_{M\beta}}{r_M^3} \right) \chi_\mu^{0*} \mu_{M\alpha} B_\beta \right\}$$

En ajoutant [3] à [4] après développement de l'exponentielle et en adoptant des $\chi_\mu^0$ réels, on trouve:

$$|H_{\mu\nu}|_{\text{herm}} = \int \chi_\mu^0 H^0 \chi_\nu^0 \, d\tau + \frac{i}{4c} B \left\{ \int \chi_\mu^0 ((R_\mu - R_\nu) \Lambda r) H^0 \chi_\nu^0 \, d\tau + \int \chi_\nu^0 ((R_\mu - R_\nu) \Lambda r) H^0 \chi_\mu^0 \, d\tau \right\} - \frac{i}{4c} B \left\{ \int \chi_\mu^0 (r_\nu \Lambda \nabla) \chi_\nu^0 \, d\tau - \int \chi_\nu^0 (r_\mu \Lambda \nabla) \chi_\mu^0 \, d\tau \right\} + \text{termes en } \mu, \mu B, \text{ etc. ...}$$

A ce niveau, l'introduction de l'approximation de London dans l'expression précédente donne pour l'élément de matrice perturbé par la composante $B_\alpha$ du champ l'expression suivante

[5] $$[H_{\mu\nu}(B_\alpha)]_{\text{herm}} = H_{\mu\nu}^0 + \frac{i}{2c} B_\alpha (R_\mu \Lambda R_\nu)_\alpha H_{\mu\nu}^0 - \frac{i}{4c} B_\alpha \left\{ \int \chi_\nu^0 l_\alpha^\nu \chi_\nu^0 \, d\tau - \int \chi_\nu^0 l_\alpha^\mu \chi_\mu^0 \, d\tau \right\}$$

avec $l_\alpha^\mu = (r_\mu \Lambda \nabla)_\alpha$.

Cette dernière équation représente la base pour nos calculs de déplacements chimiques.

*Expressions des éléments* $G_{\mu\nu}$

Sur une base GIAO, dans le cadre des approximations INDO, les parties réelle r et imaginaire i des $G_{\mu\nu}$ (eq. [1]) s'écrivent dans les trois éventualités suivantes

$\mu \in A, \ \nu \in A, \ \mu \neq \nu$

$$G_{\mu\nu}^r = P_{\mu\nu}^r \{ \tfrac{3}{2}(\mu^0\nu^0|\mu^0\nu^0) - \tfrac{1}{2}(\mu^0\mu^0|\nu^0\nu^0) \}$$
$$G_{\mu\nu}^i = P_{\mu\nu}^i \{ \tfrac{1}{2}(\mu^0\mu^0|\nu^0\nu^0) - \tfrac{1}{2}(\mu^0\nu^0|\mu^0\nu^0) \}$$

$\mu \in A, \ \nu \in B$

$$G_{\mu\nu}^r = -\tfrac{1}{2} P_{\mu\nu}^r (\mu^0\mu^0|\nu^0\nu^0)$$
$$G_{\mu\nu}^i = \tfrac{1}{2} P_{\mu\nu}^i (\mu^0\mu^0|\nu^0\nu^0)$$

$\mu = \nu \in A$

$$G_{\mu\mu}^i = 0$$

Can. J. Chem. Downloaded from www.nrcresearchpress.com by 210.87.254.5 on 09/06/12
For personal use only.

La partie réelle est alors donnée par

$$[6] \quad G^{r}_{\mu\mu} = \left\{ \sum_{B}^{\text{tous les atomes}} \sum_{\eta \in B} P^{r}_{\eta\eta}(\mu^0\mu^0|\eta^0\eta^0) \right\} - \frac{1}{2} P^{r}_{\mu\mu}(\mu^0\mu^0|\mu^0\mu^0) - \frac{1}{2} \sum_{\eta \neq \mu}^{A} P^{r}_{\eta\eta}(\mu^0\eta^0|\eta^0\mu^0)$$

Il convient de relever que cette équation [6] diffère de l'équation [A-5] de la référence 23 par la présence du dernier terme qui s'annule *seulement* dans les approximations CNDO. Les éléments $G_{\mu\nu}$ sont donnés en fonction des paramètres $F^0$, $F^2$, $G^1$ classiques (29) dans l'appendice I.

*Tenseur d'écran* $\sigma^{M}_{\alpha\beta}$

Sur la base des équations déduites ci-haut, notamment les éqs. [5] et [6] qui correspondent à un développement plus rigoureux du formalisme FPM, il devient maintenant possible de donner des expressions rigoureuses pour le tenseur d'écran.

L'énergie Hartree–Fock perturbée est

$$E(\boldsymbol{B}, \mu_M) = \sum_{\mu\nu} P_{\mu\nu} \{ [H_{\mu\nu}(\boldsymbol{B}, \mu_M)]_{\text{herm}} + \tfrac{1}{2} G_{\mu\nu}(\boldsymbol{B}) \}$$

Par définition, l'expression de la constante d'écran pour un noyau $M$ est

$$\sigma^{M}_{\alpha\beta} = \left[ \frac{\partial^2 E(\boldsymbol{B}, \mu_M)}{\partial B_\beta \partial \mu_{M_\alpha}} \right] \mu_M = \boldsymbol{B} = 0$$

Les GIAO étant indépendantes de $\mu_M$, Pople (4) a montré que l'on peut appliquer le théorème de Hellman–Feymann à cette méthode variationnelle sur $\boldsymbol{B}$, pour obtenir la première dérivée par rapport à $\mu_{M_\alpha}$ (30). Pour la dérivée seconde, on obtient

$$\sigma^{M}_{\alpha\beta} = \lim_{\mu = B = 0} \left\{ \sum_{\mu\nu} \frac{\partial P_{\mu\nu}(B_\beta)}{\partial B_\beta} \left\{ \frac{1}{2} \int \chi^*_\mu \frac{\partial}{\partial \mu_{M_\alpha}} H \chi_\nu \, d\tau + \frac{1}{2} \int \chi_\nu \frac{\partial}{\partial \mu_{M_\alpha}} (H\chi_\mu)^* \, d\tau \right\} \right.$$
$$\left. + \sum_{\mu\nu} P_{\mu\nu}(\boldsymbol{B}) \frac{\partial}{\partial B_\beta} \left\{ \frac{1}{2} \int \chi^*_\mu \frac{\partial}{\partial \mu_M} H \chi_\nu \, d\tau + \frac{1}{2} \int \chi_\nu \frac{\partial}{\partial \mu_{M_\alpha}} (H\chi_\mu)^* \, d\tau \right\} \right\}$$

Les perturbations apportées par $\mu$ et $\boldsymbol{B}$ étant imaginaires, les coefficients perturbés sont imaginaires et les parties réelle et imaginaire de $P_{\mu\nu}$ s'écrivent

$$P^{r}_{\mu\nu} = 2 \sum_{i}^{occ} (C^{r}_{\mu i} C^{r}_{\nu i} + C^{i}_{\mu i} C^{i}_{\nu i}); \quad P^{i}_{\mu\nu} = 2 \sum_{i}^{occ} (C^{r}_{\mu i} C^{i}_{\nu i} - C^{i}_{\mu i} C^{r}_{\nu i})$$

Une fois effectuées les dérivations, on obtient

$$\sigma^{M}_{\alpha\beta} = \sum_{\mu\nu} \left[ \frac{\partial P_{\mu\nu}(B_\beta)}{\partial B_\beta} \right]_{B_\beta = 0} (\text{intégrales 1}) + \sum_{\mu\nu} P_{\mu\nu}(O) \ (\text{intégrales 2})$$

La dérivée $[\partial P_{\mu\nu}(B_\beta)/\partial B_\beta]_{B_\beta=0}$ est calculée numériquement selon la méthode des perturbations finies (4) par la formule approchée suivante

$$\left[ \frac{\partial P_{\mu\nu}(B_\beta)}{\partial B_\beta} \right]_{B_\beta = 0} \simeq \frac{1}{2h_\beta} [P_{\mu\nu}(h_\beta) - P_{\mu\nu}(-h_\beta)]$$

où $h_\beta$ est une petite valeur attribuée à $B_\beta$.

En remarquant que $F^{r}_{\mu\nu}(-h_\beta) = F^{r}_{\mu\nu}(h_\beta)$ et $F^{i}_{\mu\nu}(-h_\beta) = -F^{i}_{\mu\nu}(h_\beta)$, on montre que $C^{r}_{\mu i}(-h_\beta) = C^{r}_{\mu i}(h_\beta)$ et $C^{i}_{\mu i}(-h_\beta) = -C^{i}_{\mu i}(h_\beta)$, ce qui entraîne

$$\left[ \frac{\partial P^{r}_{\mu\nu}(B_\beta)}{\partial B_\beta} \right]_{B_\beta = 0} = 0 \quad \text{et} \quad \left[ \frac{\partial P^{i}_{\mu\nu}(B_\beta)}{\partial B_\beta} \right]_{B_\beta = 0} = \frac{P^{i}_{\mu\nu}(h_\beta)}{h_\beta}$$

Can. J. Chem. Downloaded from www.nrcresearchpress.com by 210.87.254.5 on 09/06/12
For personal use only.

L'expression rigoureuse du tenseur d'écran est alors

$$[7]\quad \sigma^M_{\alpha\beta}=\frac{1}{2c^2}\sum_{\mu\nu}P_{\mu\nu}(O)\left\{\int \chi^0_\mu \frac{\boldsymbol{r}_\nu\cdot\boldsymbol{r}_M\delta_{\alpha\beta}-r_{\nu\alpha}r_{M\beta}}{r_M^3}\,\chi^0_\nu\,d\tau-(R_\nu\wedge R_\mu)_\beta\int\chi^0_\mu\frac{l^M_\alpha}{r_M^3}\chi^0_\nu\,d\tau\right.$$
$$\left.-\int\chi^0_\mu(\boldsymbol{R}_{\mu\nu}\wedge\boldsymbol{r}_\nu)_\beta\frac{l^M_\alpha}{r_M^3}\chi^0_\nu\,d\tau\right\}+\frac{1}{c}\sum_{\mu\nu}\frac{P^{i}_{\mu\nu}(h_\beta)}{h_\beta}\int\chi^0_\mu\frac{l^M_\alpha}{r_M^3}\chi^0_\nu\,d\tau$$

où $\boldsymbol{R}_{\mu\nu}=\boldsymbol{R}_\nu-\boldsymbol{R}_\mu$. L'expression du tenseur moyen avec l'approximation de London s'écrit

$$[8]\quad \sigma^M=\frac{1}{3c^2}\sum_{\mu\nu}P_{\mu\nu}(O)\int\chi^0\frac{\boldsymbol{r}_\nu\cdot\boldsymbol{r}_M}{r_M^3}\chi^0_\nu\,d\tau-\frac{1}{6c^2}\sum_{\mu\nu}\sum_{\alpha=x,y,z}P_{\mu\nu}(O)(R_\nu\wedge R_\mu)_\alpha$$
$$\times\int\chi^0_\mu\frac{l^M_\alpha}{r_M^3}\chi^0_\nu\,d\tau+\frac{1}{3c}\sum_{\mu\nu}\sum_{\alpha=x,y,z}\frac{P^{i}_{\mu\nu}(h_\alpha)}{h_\alpha}\int\chi^0_\mu\frac{l^M_\alpha}{r_M^3}\chi^0_\nu\,d\tau$$

On a démontré (1) que l'approximation de London ne détruit pas le caractère "gauge invariant" de $\sigma^M$. Les $P^{i}_{\mu\nu}(h_\alpha)$ seront obtenus en résolvant l'équation de Roothan $Fc=\varepsilon Sc$ avec une petite valeur $h_\alpha$ pour $B_\alpha$ (voir Appendice I).

Afin de mettre en évidence les contributions relatives des différentes densités électroniques au déplacement chimique du $^{13}C$ et $^1H$ nous séparerons l'équation [8] en contributions électroniques mono, di, ou tricentriques (11, 23, 26) et développons comme suit les différentes contributions (eq. [9]).

$$[9]\quad \sigma^M=\sigma^d(M)+\sigma^d(KK)+\sigma^p(M)+\sigma^p(KK)+\sigma^d(MK)+\sigma^d_0(MK)+\sigma^p_0(MK)$$
$$+\sigma^d(M,A,B)+\sigma^d_0(M,A,B)+\sigma^p_0(M,A,B)$$

avec

$$\sigma^d(M)=\frac{1}{3c^2}\sum_{\mu\nu}^{M}P_{\mu\nu}(O)\left\langle\chi^{0M}_\mu\left|\frac{1}{r_M}\right|\chi^{0M}_\nu\right\rangle;\quad \sigma^d(KK)=\frac{1}{3c^2}\sum_{\mu\nu}^{K\neq M}P_{\mu\nu}(O)\left\langle\chi^{0K}_\mu\left|\frac{\boldsymbol{r}_K\cdot\boldsymbol{r}_M}{r_M^3}\right|\chi^{0K}_\nu\right\rangle$$

$$\sigma^p(M)=\frac{1}{3c}\sum_{\mu\nu}\sum_\alpha\frac{P^{i}_{\mu\nu}(h_\alpha)}{h_\alpha}\left\langle\chi^{0M}_\mu\left|\frac{l^M_\alpha}{r_M^3}\right|\chi^{0M}_\nu\right\rangle$$

$$\sigma^p(KK)=\frac{1}{3c}\sum_{\mu\nu}^{K\neq M}\sum_\alpha\frac{P^{i}_{\mu\nu}(h_\alpha)}{h_\alpha}\left\langle\chi^{0K}_\mu\left|\frac{l^M_\alpha}{r_M^3}\right|\chi^{0K}_\nu\right\rangle$$

$$\sigma^d(MK)=\frac{1}{3c^2}\sum_{\mu}^{K\neq M}\sum_{\nu}^{M}P_{\mu\nu}(O)\left\langle\chi^{0K}_\mu\left|\frac{1}{r_M}\right|\chi^{0M}_\nu\right\rangle+\frac{1}{3c^2}\sum_{\mu}^{M}\sum_{\nu}^{K\neq M}P_{\mu\nu}(O)\left\langle\chi^{0M}_\nu\left|\frac{\boldsymbol{r}_K\cdot\boldsymbol{r}_M}{r_M^3}\right|\chi^{0K}_\nu\right\rangle$$

$$\sigma^d_0(MK)=-\frac{1}{6c^2}\sum_\alpha\sum_{\mu}^{K\neq M}\sum_{\nu}^{M}P_{\mu\nu}(O)(R_\nu\wedge R_\mu)_\alpha\left\langle\chi^{0K}_\mu\left|\frac{l^M_\alpha}{r_M^3}\right|\chi^{0M}_\nu\right\rangle$$
$$-\frac{1}{6c^2}\sum_\alpha\sum_{\mu}^{M}\sum_{\nu}^{K\neq M}P_{\mu\nu}(O)(R_\nu\wedge R_\mu)_\alpha\left\langle\chi^{0M}_\mu\left|\frac{l^M_\alpha}{r_M^3}\right|\chi^{0K}_\nu\right\rangle$$

$$\sigma^p_0(MK)=\frac{1}{3c}\sum_\alpha\sum_{\mu}^{K\neq M}\sum_{\nu}^{M}\frac{P^{i}_{\mu\nu}(h_\alpha)}{h_\alpha}\left\langle\chi^{0K}_\mu\left|\frac{l^M_\alpha}{r_M^3}\right|\chi^{0M}_\nu\right\rangle+\frac{1}{3c}\sum_\alpha\sum_{\mu}^{M}\sum_{\nu}^{K\neq M}\frac{P^{i}_{\mu\nu}(h_\alpha)}{h_\alpha}\left\langle\chi^{0M}_\mu\left|\frac{l^M_\alpha}{r_M^3}\right|\chi^{0K}_\nu\right\rangle$$

Can. J. Chem. Downloaded from www.nrcresearchpress.com by 210.87.254.5 on 09/06/12
For personal use only.

$$\sigma^{d}(M,A,B) = \frac{1}{3c^2} \sum_{A}^{\neq M} \sum_{B}^{\neq M} \sum_{\mu}^{A} \sum_{\nu}^{B \neq A} P_{\mu\nu}(O) \left\langle \chi_{\mu}^{0A} \left| \frac{r_B \cdot r_M}{r_M^3} \right| \chi_{\nu}^{0B} \right\rangle$$

$$\sigma_{o}^{d}(M,A,B) = -\frac{1}{6c^2} \sum_{\alpha} \sum_{A}^{\neq M} \sum_{B}^{\neq M} \sum_{\mu}^{A} \sum_{\nu}^{B \neq A} P_{\mu\nu}(O)(R_\nu \wedge R_\mu)_\alpha \left\langle \chi_{\mu}^{0A} \left| \frac{l_\alpha^M}{r_M^3} \right| \chi_{\nu}^{0B} \right\rangle$$

$$\sigma_{o}^{p}(M,A,B) = \frac{1}{3c} \sum_{\alpha} \sum_{A}^{\neq M} \sum_{B}^{\neq M} \sum_{\mu}^{A} \sum_{\nu}^{B \neq A} \frac{P_{\mu\nu}^{i}(h_\alpha)}{h\alpha} \left\langle \chi_{\mu}^{0A} \left| \frac{l_\alpha^M}{r_M^3} \right| \chi_{\nu}^{0B} \right\rangle$$

Dans ces expressions, les indices supérieurs d et p repèrent, respectivement, les parties dia- et para-magnétiques. L'indice inférieur o représente un terme qui dépend de l'origine des coordonnées. Il est à noter que les sommes $\sigma_o^d(MK) + \sigma_o^p(MK)$ et $\sigma_o^d(M,A,B) + \sigma_o^p(M,A,B)$ sont indépendantes de l'origine des coordonnées. Afin de calculer l'éq. [9], il est nécessaire d'évaluer toutes les intégrales (Appendice II).

## Modalités de calcul[1]

Afin de tenir compte d'un effet d'environnement moléculaire différent pour chaque atome, nous avons modifié les exposants de Slater $\zeta_{MM}$ dans les intégrales portant sur σ par la formule classique.

$$\zeta_{MM} = [Z^+ - 0{,}35\,(P_{MM} - Z_{MM})]/n^+$$

avec $Z^+$ = charge nucléaire effective, $n^+$ = nombre quantique effectif, $P_{MM}$ = population électronique totale de la couche de valence et $Z_{MM}$ = charge de cœur. Pour $^1$H la valeur 0,35 a été remplacée par 0,31 conformément aux règles de Slater.

Pour le proton et le carbone, afin de pallier l'erreur introduite par l'approximation de London, nous avons modifié les paramètres $\beta_H^0$ et $\beta_C^0$ classiques INDO. Ceux-ci ont été paramétrisés selon la méthode de Garber *et al.* (26) sur la série $CH_4$, $C_2H_6$, $C_2H_4$ et $C_2H_2$, ce qui a conduit à $\beta_H^0 = -14{,}31$ et $\beta_C^0 = -16{,}57$ eV. Ces paramètres représentent les meilleures valeurs dans le cadre de l'approximation de London.[3] Tous les autres paramètres sont standards (29), ainsi que les géométries (31).

## Résultats

La comparaison entre les déplacements chimiques calculés et observés (Tableau 1) indique une erreur moyenne de 5,6 ppm sur 15 composés couvrant un domaine de ~145 ppm. Ce résultat se compare avantageusement aux calculs *ab initio* LEMAO-5G avec invariance de jauge (21) qui donnent lieu à une erreur moyenne de 10,2 ppm sur la même série de composés.

On constate également que le propène et le propyne sont bien reproduits par notre calcul, alors que les calculs *ab initio* sans GIAO conduisent à un ordre renversé des déplacements chimiques (22).

Nos résultats illustrent un fait bien connu, à savoir que le terme diamagnétique local $\sigma^d(M)$ est pratiquement constant alors que le terme paramagnétique local $\sigma^p(M)$ subit de fortes variations. Par contre, un fait moins connu a trait à la somme des terms $\sigma^d(MK) + \sigma_o^d(MK) + \sigma_o^p(MK)$ décrivant l'effet de la densité électronique de première liaison, somme dont les variations peuvent atteindre ~8 ppm et qui ne peut donc pas être négligée. Ceci permet de comprendre que parmi les nombreuses corrélations (34) entre charges atomiques et déplacements chimiques, les meilleures sont celles décrites par Fliszar et coll. (35). En effet, ces dernières tiennent explicitement compte de ces contributions, en utilisant des charges de type Mulliken incluant une considération appropriée des populations de recouvrement. La validité de corrélations entre déplacements chimiques et charges atomiques, représentant, elles, des propriétés strictement locales, est illustrée par nos résultats qui montrent que les liaisons lointaines ne participent que très peu à la constante d'écran d'éléments lourds tel que le $^{13}$C.

Ce dernier point mérite une attention particulière. Ainsi convient-il d'évaluer l'importance des intégrales à trois centres, soit la somme des termes $\sigma^d(M,A,B) + \sigma_o^d(M,A,B) + \sigma_o^p(M,A,B)$ qui représente la contribution à l'écran du $^{13}$C des densités électroniques lointaines. Pour visualiser l'effet des densités autres que celles dues au premiers voisins, nous avons dressé le tableau 2 pour l'éthylène et le

[1]Programme Fortran NMR CINDO-80.[2]

Ce programme calcule $\sigma^M$ sous la forme décrite ci-dessus pour les noyaux $^1$H, $^{13}$C, $^{15}$N, $^{17}$O, $^{19}$F en version INDO ou CNDO (IBM version, 10 000 cards, 35 atoms, 120 OA, 1050 K bytes of central memory, 78 000 K bytes of direct access memory).

[2]Le programme est disponible sur demande adressée au premier auteur.

[3]La paramérisation a été effectuée en n'utilisant que les premiers termes de l'équation [9]; ceci est une approximation justifiée a posteriori pour le $^{13}$C.

Can. J. Chem. Downloaded from www.nrcresearchpress.com by 210.87.254.5 on 09/06/12
For personal use only.

Can. J. Chem. Downloaded from www.nrcresearchpress.com by 210.87.254.5 on 09/06/12
For personal use only.



TABLEAU 1. Constante d'écran du $^{13}C$ dans quelques hydrocarbures[a]

| Molécules | $\sigma^d(M)$ | $\sigma^d(KK)$ | $\sigma^p(M)$ | $\sigma^p(KK)$ | $\sigma^d(MK)$ | $\sigma^d_\delta(MK)$ | $\sigma^p_\delta(MK)$ | $\sigma_{calc}$ | $\delta^{CH_4 b}_{calc}$ | $\delta^{CH_4}_{exp}$ | $\delta^{CH_4}_{calc} - \delta^{CH_4}_{exp}$ |
|---|---|---|---|---|---|---|---|---|---|---|---|
| $\overset{*}{C}H_4$ | 57,81 | 3,58 | −51,51 | −0,0 | 20,89 | 0,0 | 0,17 | 30,94 | 0 | 0 | 0 |
| $\overset{*}{C}H_3—CH_3$ | 57,57 | 3,62 | −52,18 | −0,07 | 17,55 | 0,0 | −0,04 | 26,44 | −4,5 | −8,0[c] | 3,5 |
| $CH\equiv\overset{*}{C}H$ | 58,14 | 4,96 | −129,48 | 6,34 | 23,58 | 0,0 | −4,69 | −41,14 | −72,1 | −76,1[c] | 4,0 |
| $CH_3—\overset{*}{C}\equiv CH$ | 57,82 | 5,56 | −137,63 | 6,17 | 20,88 | 0,22 | −5,02 | −51,98 | −82,9 | −87,8[c] | 4,9 |
| $CH_3—C\equiv\overset{*}{C}H$ | 58,57 | 4,83 | −131,48 | 6,03 | 23,45 | −0,18 | −2,24 | −41,01 | −71,9 | −72,1[c] | 0,2 |
| $CH_3—\overset{*}{C}\equiv C—CH_3$ | 58,22 | 5,40 | −139,63 | 5,82 | 20,79 | 0,28 | −2,73 | −51,86 | −82,8 | −75,9[d] | 6,9 |
| $CH_2=\overset{*}{C}H_2$ | 57,81 | 4,04 | −171,41 | 2,16 | 19,38 | 0,0 | −3,37 | −91,39 | −122,2 | −125,1[e] | 2,9 |
| $CH_3—\overset{*}{C}H=CH_2$ | 57,14 | 4,97 | −181,71 | 2,56 | 16,14 | 0,59 | −4,71 | −105,07 | −136,0 | −135,4[e] | 0,6 |
| $CH_3—CH=\overset{*}{C}H_2$ | 58,21 | 3,80 | −169,57 | 1,75 | 19,36 | 0,0 | −1,05 | −87,50 | −118,4 | −117,3[e] | 1,1 |
| 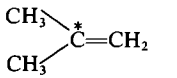 | 57,28 | 4,34 | −184,47 | 3,07 | 13,03 | 0,97 | −4,22 | −109,97 | −140,9 | −143,5[e] | 2,6 |
| 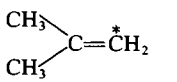 | 58,32 | 3,81 | −173,88 | 1,56 | 19,33 | 0,0 | −0,04 | −90,89 | −121,8 | −112,1[e] | 9,7 |
| $CH_3—\overset{*}{C}H=CH—CH_3$ | 57,77 | 4,08 | −180,40 | 2,18 | 16,19 | 0,0 | −1,56 | −101,73 | −132,6 | −125,7[d] | 6,9 |
| $CH_3—CH=\overset{*}{C}H—CH_3$ (*cis* / *trans*) | 57,78 | 4,07 | −179,04 | 2,29 | 16,17 | 0,0 | −1,62 | −100,34 | −131,3 | −127,1[d] | 4,2 |
| 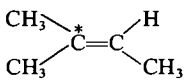 | 57,52 | 4,20 | −186,55 | 2,64 | 13,04 | 0,0 | −1,42 | −110,57 | −141,5 | −133,7[e] | 7,8 |
| 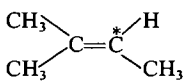 | 58,02 | 3,93 | −181,88 | 1,80 | 16,15 | 0,85 | −0,86 | −101,96 | −132,9 | −121,0[e] | 11,9 |
| 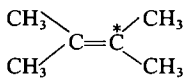 | 57,74 | 4,08 | −188,11 | 2,34 | 13,02 | 0,98 | −0,82 | −110,7 | −141,7 | −123,9[d] | 17,8 |
| | | | | | | | | | | | $\Sigma = 83,8/15 = 5,6$ |

[a] Valeurs en ppm; géométrie standard (31); *noyau résonnant.
[b] Un signe négatif signifie un déblindage.
[c] Référence 23.
[d] Référence 32, en utilisant $\delta^{CH_4}_{TMS} = +2,3$ ppm.
[e] Référence 33 en utilisant $\delta^{CH_4}_{TMS} = +2,3$ ppm.

Can. J. Chem. Downloaded from www.nrcresearchpress.com by 210.87.254.5 on 09/06/12
For personal use only.





TABLEAU 2. Contribution relative des diverses densités électroniques au déplacement chimique du $^{13}C$ en ppm

| Molécules | $\sigma^d(M)$ | $\sigma^d(KK)$ | $\sigma^p(M)$ | $\sigma^p(KK)$ | $\sigma^d(MK)$ | $\sigma^d_o(MK)$ | $\sigma^p_o(MK)$ | $\sigma^d(M,A,B)$ | $\sigma^d_o(M,A,B)$ | $\sigma^p_o(M,A,B)$ | $\sigma_{calc}$ | $\delta^{CH_2=CH_2}_{calc}$ | $\delta^{CH_2=CH_2}_{exp}$ | Colonne no 9 + 10 + 11 |
|---|---|---|---|---|---|---|---|---|---|---|---|---|---|---|
| $CH_2=\overset{*}{C}H_2$ | 57,81 | 4,04 | −171,41 | 2,16 | 19,38 | 0 | −3,37 | 1,55 | 1,19 | −1,19 | −89,85 | 0 | 0 | 1,55 |
| $CH_3-\overset{*}{C}H=CH_2$ | 57,14 | 4,97 | −181,71 | 2,56 | 16,14 | 0,59 | −4,71 | 3,14 | 4,47 | −4,16 | −101,57 | −11,7 | −10,3 | 3,45 |
| $CH_3-CH=\overset{*}{C}H_2$ | 58,21 | 3,80 | −169,57 | 1,75 | 19,36 | 0,0 | −1,05 | 1,13 | 4,05 | −3,47 | −85,79 | 4,0 | 7,8 | 1,71 |
| $\overset{*}{C}H_3-CH=CH_2$ | 60,47 | 3,05 | −61,33 | −1,61 | 14,0 | −6,97 | 12,81 | 2,95 | 8,62 | −6,14 | 25,85 | 115,7 | 104,1 | 5,43 |

TABLEAU 3. Contributions relatives des densités électroniques pour les protons du propène

| | $\sigma^d(M)$ | $\sigma^d(KK)$ | $\sigma^p(M)$ | $\sigma^p(KK)$ | $\sigma^d(MK)$ | $\sigma^d_o(MK)$ | $\sigma^p_o(MK)$ | $\sigma^d(M,A,B)$ | $\sigma^d_o(M,A,B)$ | $\sigma^p_o(M,A,B)$ | $\delta_{calc}$ | $\delta^{CH_2=CH_2}_{calc}$ | $\delta^{CH_2=CH_2}_{exp}$[a] | $\delta_{calc}-\delta_{exp}$ |
|---|---|---|---|---|---|---|---|---|---|---|---|---|---|---|
| $H_{H}\!>\!C\!=\!C<^{H}_{\overset{*}{H}}$ | 21,17 | 6,14 | 0 | −5,93 | 15,60 | 0,0 | 0,0 | 2,81 | −0,74 | 0,30 | 39,05 | 0 | 0 | 0 |
| $CH_3>C\!=\!C<^{H_7}_{\overset{*}{H}_5}$ | 21,18 | 5,99 | 0 | −6,14 | 15,70 | 0,0 | 0,0 | 3,09 | 3,52 | −3,37 | 39,97 | 0,92 | 0,44 | 0,48 |
| $CH_3>C\!=\!C<^{H_7}_{\overset{*}{H}_6}$ | 21,31 | 6,32 | 0 | −6,28 | 15,67 | 0,0 | 0,0 | 2,78 | 3,01 | −2,87 | 39,93 | 0,88 | 0,53 | 0,35 |
| $CH_3>C\!=\!C<^{\overset{*}{H}_7}_{H_6}$ | 21,80 | 6,33 | 0 | −6,48 | 15,26 | 0,0 | 0,0 | 1,85 | 2,47 | −2,96 | 38,27 | −0,78 | −0,31 | 0,47 |

[a]Référence 39.

TABLEAU 4. Mise en évidence[a] de l'importance des densités électroniques lointaines pour le déplacement chimique du $^1H$

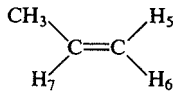

| | $H_5$ | $H_7$ | $CH_2{=}CH_2$ | $H_6$ |
|---|---|---|---|---|
| Déplacements chimiques calculés sans les termes $\sigma^d(M,A,B)+\sigma^d_o(M,A,B)+\sigma^p_o(M,A,B)$ | 0,25 | −0,08 | 0 | 0,04 |
| Déplacements chimiques expérimentaux[b] | 0,44 | −0,31 | 0 | 0,53 |
| Déplacements chimiques calculés avec les termes $\sigma^d(M,A,B)+\sigma^d_o(M,A,B)+\sigma^p_o(M,A,B)$ | 0,92 | −0,78 | 0 | 0,88 |

[a]Un déplacement chimique négatif signifie un déplacement à champ faible.
[b]Référence 39.

propène. Une telle analyse des effets lointains n'a pas encore été rapportée bien que des "effets lointains" aient été occasionnellement invoqués (26) pour expliquer les écarts entre le calcul et l'observation. Nos résultats indiquent clairement que, sur une échelle de variations de ~220 ppm pour le $^{13}C$, les liaisons lointaines ne participent que très peu à la constante d'écran. L'importance de leur contribution, qui est faible au départ, est encore atténuée dans une échelle établie pour des atomes de même type (e.g., les carbones $sp^2$) en se référant à un des membre de cette classe.

Ces résultats conduisent à une conclusion qu'il convient de relever. La faible contribution des intégrales à trois centres impliquant les atomes lointains suggère que les termes prépondérants relèvent des distributions électroniques locales, ce qui justifie à posteriori l'existence de corrélations entre déplacements chimiques et charges atomiques pour des classes de composés bien définies. Bien entendu, la présence de tout atome (même lointain) est reflétée dans la fonction d'onde moléculaire et c'est en participant à l'établissement des charges atomiques qu'elle se manifeste. De plus, le peu d'influence des centres lointains justifie en partie le modèle du solvaton (36), récemment utilisé par Jallah-Heravi et Webb (37).

Ces considérations, basées sur des calculs concernant les atomes de carbone, sont également valables pour l'oxygène et l'azote (38). Pour l'hydrogène, cependant, il en est tout autrement.

Les constantes d'écran des noyaux du propène et de l'éthylène $^1H$ ont été calculées en retenant l'éq. [9] dans son entier, en utilisant les géométries standards ainsi que les paramètres $\beta^0_H = -14{,}31$ et $\beta^0_C = -16{,}37$ eV (Tableau 3). La précision moyenne, ~0,4 ppm, est comparable à celle obtenue par Ducasse (11) pour une plus grande série de composés. Le fait le plus frappant est l'importance des intégrales à trois centres dans le calcul de $\sigma$.

Le calcul sans intégrales à trois centres donne un ordre aléatoire des déplacements chimiques du $^1H$ (Tableau 4), alors que l'inclusion de ces intégrales rétablit pratiquement l'ordre des résonances, en ce sens que le proton $H_7$ est calculé comme résonnant à champ faible par rapport à l'éthylène. Ceci montre bien que le $^1H$ est extrêmement sensible à la présence de toutes les liaisons dans la molécule et non pas seulement en ce qui a trait à la première liaison. Aussi le $^1H$ sera extrêmement sensible au solvant.

*Conclusion*

Le calcul des déplacements chimiques du $^{13}C$ et du $^1H$ dans une série d'hydrocarbures a été effectué dans le cadre de la méthode des perturbations finies en maintenant l'invariance de jauge, ce qui représente une condition essentielle. Le formalisme utilisé conserve, tout au long des approximations de London et INDO, le caractère hermitien de la matrice des $H_{\mu\nu}$ perturbée par le champ magnétique extérieur et, de plus, tient explicitement compte des intégrales à trois centres.

La précision obtenue pour le $^{13}C$ est supérieure à celle d'autres calculs, même *ab initio*, ne respectant pas les conditions mentionnées ci-dessus. Elle passe, en effet, de ~10 à ~5 ppm en valeur moyenne en se rapprochant ainsi des conditions requises pour l'identification de structures difficiles à atteindre par les moyens classiques et, notamment, pour permettre de distinguer des effets conformationnels.

L'analyse des contributions "atomiques" et "de liaison" à la constante d'écran indique clairement que le $^{13}C$ est pratiquement insensible aux modifications de structure électronique des atomes et

Can. J. Chem. Downloaded from www.nrcresearchpress.com by 210.87.254.5 on 09/06/12
For personal use only.

liaisons lointains, en justifiant ainsi la faiblesse des effets de solvant. De plus, on justifie ainsi le rôle essentiel de la charge locale du carbone incluant une partie de la densité électronique des liaisons dans lesquelles il est engagé et, par conséquent, l'existence de relations entre déplacements chimiques et charges atomiques.

Il n'en est pas de même pour le proton, très sensible aux liaisons lointaines, dont les contributions sont tout aussi importantes que celles des contributions locales: toutes les intégrales à trois centres doivent être retenues. Il en découle que le choix des données expérimentales choisies en vue de comparaisons avec la théorie doit être, dans ce cas, particulièrement critique et judicieux en raison des effets de solvant.

**Remerciements**

Les auteurs remercient S. Fliszar de l'Université de Montréal pour de nombreuses et fructueuses discussions.

1. E. VAUTHIER. Thèse, Université de Paris VII, 1980.
2. R. M. STEVENS, R. M. PITZER et W. N. LIPSCOMB. J. Chem. Phys. **38**, 550 (1963).
3. W. N. LIPSCOMB. Advances in magnetic resonance. Vol. 2. *Édité par* J. S. Waugh. Academic Press, New York. 1966. p. 137.
4. J. A. POPLE, J. W. MCIVER et N. S. OSTLUND. J. Chem. Phys. **49**, 2960 (1968).
5. J. A. POPLE. J. Chem. Phys. **37**, 53 (1962).
6. J. TILLIEU. Ann. Phys. Paris, Tome 2. **471**, 631 (1957).
7. J. R. DIDRY et J. GUY. C.R. Acad. Sci. **239**, 1203 (1954).
8. W. N. LIPSCOMB, M.T.P. International Review of Science, Physical Chemistry, Serie 1, Vol. 1. *Édité par* W. B. Brown. Butterworths University Park Press, London. 1972. p. 167.
9. R. DITCHFIELD. Mol. Phys. **27**, 789 (1974).
10. F. RIBAS PRADO, G. GIESSNER-PRETTRE, J. P. DAUDEY, A. PULLMAN, J. F. HINTON, G. YOUND et D. HARPOL. J. Magn. Reson. **37**, 431 (1980).
11. L. DUCASSE. Thèse, Université de Bordeaux I, no. d'ordre 677, 1980.
12. G. I. GRIGOR et G. A. WEBB. Org. Magn. Reson. **9**, 477 (1977).
13. K. A. K. EBRAHEEM et G. A. WEBB. Org. Magn. Reson. **9**, 241 (1977).
14. M. JALLALI et G. A. WEBB. Org. Magn. Reson. **11**, 34 (1978).
15. K. A. K. EBRAHEEM et G. A. WEBB. Org. Magn. Reson. **18**, 70 (1977).
16. K. A. K. EBRAHEEM, G. A. WEBB et M. WITANWSKY. Org. Magn. Reson. **11**, 27 (1978).
17. K. A. K. EBRAHEEM et G. A. WEBB. J. Magn. Reson. **25**, 399 (1977).
18. M. J. STEPHEN. Proc. R. Soc. London, Ser. A, **242**, 264 (1957).
19. R. M. AMINOVA, H. I. ZOROATSKAYA et YU. SAMITOV. J. Magn. Reson. **33**, 497 (1979).
20. R. DITCHFIELD et P. D. ELLIS. Chem. Phys. Lett. **17**, 342 (1972).
21. R. DITCHFIELD. Chem. Phys. Lett. **15**, 203 (1972).
22. R. DITCHFIELD, D. P. MILLER et J. A. POPLE. J. Chem. Phys. **54**, 4186 (1971).
23. P. D. ELLIS, G. E. MACTEL et J. W. MCIVER. J. Am. Chem. Soc. **94**, 4069 (1978).
24. M. KONDO, I. ANDO, R. CHUJO et A. NISHIOKA. J. Magn. Reson. **24**, 315 (1976).
25. V. GALASSO. Org. Magn. Reson. **12**, 318 (1979).
26. A. R. GARBER, P. D. ELLIS, K. SEIDMAN et K. SCHADE. J. Magn. Reson. **34**, 1 (1979).
27. J. I. MUSHER. Advances in magnetic resonance. Vol. 2. *Édité par* J. S. Waugh. Academic Press, New York. 1966. p. 117.
28. E. MERZBACKER. Quantum mechanics. John Wiley, New York et London. 1970. p. 147.
29. J. A. POPLE et D. L. BEVERIDGE. Approximate molecular orbital theory. McGraw Hill, New York. 1970. p. 81.
30. R. DITCHFIELD. J. Chem. Phys. **56**, 5688 (1972).
31. J. A. POPLE et M. GORDON. J. Am. Chem. Soc. **89**, 4253 (1967).
32. F. BRETMAYER et W. VOELTER. $^{13}C$ nmr spectroscopy. Verlag Chemie, Germany. 1974. p. 129 ou 127.
33. J. B. STOTHERS. Carbon-13 nmr spectroscopy. Academic Press, New York. 1972.
34. G. J. MARTIN, M. L. MARTIN et S. ODIOT. Org. Magn. Reson. **7**, 2 (1975), et références citées.
35. H. HENRI et S. FLISZAR. J. Am. Chem. Soc. **100**, 3312 (1978); S. FLISZAR, A. GOURSOT et H. DUGAS. J. Am. Chem. Soc. **96**, 4358 (1974); S. FLISZAR. Can. J. Chem. **54**, 2839 (1976).
36. A. A. GERMER. Theor. Chim. Acta, **34**, 245 (1974).
37. M. JALLAH-HERAVI et G. A. WEBB. Org. Magn. Reson. **13**, 116 (1980).
38. E. VAUTHIER, S. ODIOT, S. FLISZAR et F. TONNARD. Soumis pour publication.
39. EMSLEY, FEENEY et SUTCLIFFE. High resolution nuclear resonance spectroscopy. Vol. 2. Pergamon Press, London. 1966.
40. J. GUY, A. SALES et J. R. DIDRY. J. Phys. Rad. **23**, 149 (1962).
41. R. M. PITZER, C. W. KERN et W. N. LIPSCOMB. J. Chem. Phys. **37**, 267 (1962).
42. H. ICHIMURA et A. RANK. J. Chem. Phys. **59**, 5720 (1973).
43. B. ALDER, S. FERNBACK et M. RUTENBERG. Methods in computational physics. Vol. 2. Academic Press, New York. 1963. p. 1.
44. J. LEGRAS. Précis d'analyse numérique. Dunod, Paris. 1963.
45. T. TOKUHIRO, B. R. APLEMAN, G. FRANKEL, P. K. PEARSON et C. W. KERN. J. Chem. Phys. **57**, 20 (1972).

## Appendice I

*Eléments de la matrice de Fock:* $F_{\mu\nu}(B_\alpha) = H_{\mu\nu}(B_\alpha) + G_{\mu\nu}(B_\alpha)$ *corrigé au premier ordre en* **B** *dans l'approximation de London et les paramètres INDO:* $\alpha = x, y, z$

On distingue les parties réelle r des parties imaginaire i.

Can. J. Chem. Downloaded from www.nrcresearchpress.com by 210.87.254.5 on 09/06/12
For personal use only.

Can. J. Chem. Downloaded from www.nrcresearchpress.com by 210.87.254.5 on 09/06/12
For personal use only.

$H_{\mu\nu}(B_\alpha) \Rightarrow$

(a) $\mu \in A,\ \nu \in A,\ \mu \neq \nu$

$$H^{r}_{\mu\nu} = H^{0}_{\mu\nu} = 0$$

$$H^{i}_{\mu\nu} = -\frac{1}{4c} B_\alpha \{\langle \chi^{0A}_\mu | l^A_\alpha | \chi^{0A}_\nu \rangle - \langle \chi^{0A}_\nu | l^A_\alpha | \chi^{0A}_\mu \rangle\};\ l^A_\alpha = (r_A \Lambda \nabla)_\alpha$$

(b) $\mu = \nu \in A$

$$H^{r}_{\mu\mu} = H^{0}_{\mu\mu};\ H^{i}_{\mu\mu} = 0$$

(c) $\mu \in A,\ \nu \in B$

$$H^{r}_{\mu\nu} = H^{0}_{\mu\nu} = \tfrac{1}{2}(\beta^0_A + \beta^0_B) S_{\mu\nu}$$

$$H^{i}_{\mu\nu} = \frac{1}{2c} B_\alpha (R_\mu \Lambda R_\nu)_\alpha H^{0}_{\mu\nu} - \frac{1}{4c} B_\alpha \{\langle \chi^{0A}_\mu | l^B_\alpha | \chi^{0B}_\nu \rangle - \langle \chi^{0B}_\nu | l^A_\alpha | \chi^{0A}_\mu \rangle\}$$

$G_{\mu\nu}(B_\alpha) \Rightarrow$

(a) $\mu \in A,\ \nu \in A,\ \mu \neq \nu$

$$G^{r}_{sp} = \tfrac{1}{2} P^{r}_{sp}(G^1 - F^0);\ G^{r}_{P_\alpha P_\beta} = \tfrac{1}{2} P^{r}_{P_\alpha P_\beta}(\tfrac{11}{25} F^2 - F^0)$$

$$G^{i}_{sp} = \tfrac{1}{2} P^{i}_{sp}(F^0 - \tfrac{1}{3} G^1);\ G^{i}_{P_\alpha P_\beta} = \tfrac{1}{2} P^{i}_{P_\alpha P_\beta}(F^0 - \tfrac{1}{5} F^2)$$

(b) $\mu = \nu \in A$

$$G^{r}_{2s2s} = (P^{r}_{AA} - \tfrac{1}{2} P^{r}_{2s2s})\gamma_{AA} + \sum_{B \neq A} \gamma_{AB} P^{r}_{BB} - \tfrac{1}{6} G^1 (P^{r}_{AA} - P^{r}_{2s2s})$$

$$G^{r}_{xx} = (P^{r}_{AA} - \tfrac{1}{2} P^{r}_{xx})\gamma_{AA} + \sum_{B \neq A} \gamma_{AB} P^{r}_{BB} + \tfrac{2}{25} F^2 P^{r}_{xx} - \tfrac{1}{6} G^1 P^{r}_{2s2s} - \tfrac{7}{50} F^2 (P^{r}_{yy} + P^{r}_{zz})$$

$$G^{i}_{\mu\mu} = 0$$

(c) $\mu \in A,\ \nu \in B$

$$G^{r}_{\mu\nu} = -\tfrac{1}{2} P^{r}_{\mu\nu} \gamma_{AB};\ G^{i}_{\mu\nu} = \tfrac{1}{2} P^{i}_{\mu\nu} \gamma_{AB}$$

## Appendice II

*Evaluation des intégrales nécessaires sur une base d'orbitales atomiques de Slater*

*1. Intégrales à deux centres*

Afin de réduire au maximum les temps de calcul de ces intégrales nous avons calculé les intégrales à deux centres dans un système de coordonnées elliptiques. Toutes ces intégrales ont été tabulées à la référence 1. Dans le système d'axe choisi les intégrales

$$\left\langle \chi^K_\mu \left| \frac{\mathbf{r}_K \cdot \mathbf{r}_M}{r^3_M} \right| \chi^K_\nu \right\rangle \quad \text{et} \quad \left\langle \chi^M_\mu \left| \frac{\mathbf{r}_K \cdot \mathbf{r}_M}{r^3_M} \right| \chi^K_\nu \right\rangle$$

sont une somme d'intégrales du type

$$I_{mn}(k,b) = \int_1^\infty d\xi \int_{-1}^{+1} \xi^m \eta^n (\xi + \eta)^{-1} e^{-k\xi} e^{-b\eta} d\eta$$

qui peuvent être calculées analytiquement selon la méthode de Guy *et al.* (40) et exprimées en termes d'intégrales auxiliaires $A_n(y)$ et $B_n(y)$ bien connues

$$A_n(y) = \int_1^\infty x^n e^{-yx} dx \quad \text{et} \quad B_n(y) = \int_{-1}^{+1} x^n e^{-yx} dx$$

Can. J. Chem. Downloaded from www.nrcresearchpress.com by 210.87.254.5 on 09/06/12
For personal use only.

Les intégrales

$$\left\langle \chi_\mu^K \left| \frac{r_M \wedge \nabla}{r_M^3} \right| \chi_\nu^K \right\rangle$$

apparaissent dans la littérature (41) et nous avons développé les formules générales données par l'auteur afin de les obtenir sous une forme plus programmable (1).

Pour les intégrales

$$\left\langle \chi_\mu^M \left| \frac{r_M \wedge \nabla}{r_M^3} \right| \chi_\nu^K \right\rangle$$

l'opérateur $r_M \wedge \nabla$ est développé sur le centre $K$ (42) et exprimées en termes des $I_{mn}(k, b)$ puis en termes des $A_n(y)$ et $B_n(y)$. Toutes les autres intégrales sont reportées dans la littérature (26) ou aisément calculables.

*2. Intégrales à trois centres*

Pour les intégrales du type

$$\left\langle \chi_\mu^A \left| \frac{r_B \cdot r_C}{r_C^3} \right| \chi_\nu^B \right\rangle \quad \text{et} \quad \left\langle \chi_\mu^A \left| \frac{l_\alpha^C}{r_C^3} \right| \chi_\nu^B \right\rangle$$

nous avons utilisé la technique de transformation d'une STO en terme d'une GTO au moyen de la transformée de Laplace (43)

$$\int (\exp - \alpha r_a) = \frac{\alpha}{2\pi^{1/2}} \int_0^\infty s^{-3/2} \left( \exp - \frac{\alpha^2}{4s} \right) (\exp - s r_a^2)\, \mathrm{d}s$$

Nous avons d'abord obtenu

$$[10] \quad \int (\exp - s_1 r_a^2) \frac{r_b r_c}{r_c^3} (\exp - s_2 r_b^2)\, \mathrm{d}\tau$$

$$= 2\pi \left( \exp - \frac{s_1 s_2}{s_1 + s_2} \overline{AB}^2 \right) \left[ \frac{3}{s_1 + s_2} \int_0^1 t^2 [\exp - (s_1 + s_2)\overline{PC}^2 t^2]\, \mathrm{d}t + \frac{2s_1}{s_1 + s_2} \boldsymbol{AB} \cdot \boldsymbol{PC} \right.$$

$$\left. \times \int_0^1 t^2 [\exp - (s_1 + s_2)\overline{PC}^2 t^2]\, \mathrm{d}t - 2\overline{PC}^2 \int_0^1 t^4 [\exp - (s_1 + s_2)\overline{PC}^2 t^2]\, \mathrm{d}t \right.$$

avec $\overline{AB}_\alpha = A_\alpha - B_\alpha$, $PC_\alpha = P_\alpha - C_\alpha$, $P_\alpha = (s_1 A_\alpha + s_2 B_\alpha)/(s_1 + s_2)$.

Puis en terme de STO nous avons obtenu

$$[11] \quad \int (\exp - \alpha_a r_a) \frac{r_b r_c}{r_c^3} (\exp - \alpha_b r_b)\, \mathrm{d}\tau = \alpha_a \alpha_b [3/2(1, -3/2, -3/2, -3) + \overline{AB}^2(1, 1/2, -3/2, -2)$$

$$+ \boldsymbol{AB} \cdot \boldsymbol{BC}(1, -1/2, -3/2, -2) - \overline{AB}^2(2, 1/2, -3/2, -2) - 2\boldsymbol{AB} \cdot \boldsymbol{BC}(2, -1/2, -3/2, -2)$$

$$- \overline{BC}^2(2, -3/2, -3/2, -2)]$$

où la notation $(m,n,l,p)$ signifie:

$$(m,n,l,p) = \int_0^1 \int_0^1 \int_0^\infty t^{2m} u^m (1-u)^l z^p \left[ \exp - \frac{1}{4} \left( \frac{\alpha_a^2}{u} + \frac{\alpha_b^2}{1-u} \right) \frac{1}{z} \right]$$

$$\times \{\exp - [u(1-u)AB^2 + t^2(u^2 AB^2 + 2u\, \boldsymbol{AB} \cdot \boldsymbol{BC} + BC^2)]z\}\, \mathrm{d}t\, \mathrm{d}u\, \mathrm{d}z$$

$z. \in |0, \infty|$, $u. \in |0, 1|$, $t. \in |0, 1|$

L'expression de $(m,n,l,p)$ peut être simplifiée en écrivant

$$p_1 = ua + b;\ a = A - B;\ b = B - C;\ f = u(1-u)\overline{AB}^2;\ g = \frac{1}{4}\left[\frac{\alpha_a^2}{u} + \frac{\alpha_b^2}{1-u}\right]$$

et on obtient seulement une double quadrature

$$(m,n,l,p) = 2\int_0^1 u^n(1-u)^l g^{(p+1)/2} \int_0^1 \frac{t^{2m}}{(f+p_1^2t^2)^{(p+1)/2}} K_{p+1}[2\sqrt{g(f+p_1^2t^2)}]\,dt\,du$$

où $K$ est la fonction de Bessel modifiée de seconde espece. Afin d'éviter la manipulation de grands nombres dans l'ordinateur on peut utiliser la fonction de Bessel réduite $k_\nu(z)$ définie par $k_\nu(z) = K_\nu(z)z^\nu$. Nous n'avons rencontré que des valeurs négatives pour $p$. Dans ces conditions on obtient

$$[12]\quad (m,n,l,p) = \frac{2^{|p|}}{2^{2|p+1|}} \int_0^1 u^n(1-u)^l \frac{1}{g^{|p+1|}} \int_0^1 t^{2m} k_{|p+1|}(2\sqrt{g(f+p_1^2t^2)})\,dt\,du$$

L'expression [12] conduit à une double quadrature numérique qui a été faite par une méthode Gauss Legendre (44) à 32 points pour l'intégration sur $t$ et à 14 points pour l'intégration sur $u$. Les intégrales

$$\left\langle \chi_\mu^A \left| \frac{l_\alpha^c}{r_c^3} \right| \chi_\nu^B \right\rangle$$

ont été reportées par Tokuhiro (45). L'auteur trouve

$$[13]\quad \int e^{-ar_a} \frac{l_\alpha^c}{r_c^3} e^{-br_b}\,d\tau = -2ab(1,-1/2,-1/2,-1)\Gamma_\alpha \quad \text{avec} \quad \Gamma_\alpha = (\boldsymbol{B}\wedge\boldsymbol{A} + \boldsymbol{A}\wedge\boldsymbol{C} + \boldsymbol{C}\wedge\boldsymbol{B})_\alpha$$

Les intégrales portant sur des STO, $2s$, $2px$, $2py$, $2pz$ ont été calculées par dérivation des formules [11] et [13].

*3. Vérification du programme d'ordinateur NMR CINDO-80*

Nous avons programmé indépendamment le formalisme des intégrales à 2 et 3 centres. En utilisant le formalisme des intégrales à 3 centres $\langle A|C|B\rangle$ nous avons reproduit les valeurs numériques des intégrales à deux centres avec une précision absolue de 0,005.

Can. J. Chem. Downloaded from www.nrcresearchpress.com by 210.87.254.5 on 09/06/12
For personal use only.

# The ultraviolet and visible absorption spectra of berberrubine

ZVONIMIR GAŠPAREC
*The Faculty of Pharmacy and Biochemistry, University of Zagreb, Zagreb, Yugoslavia*

ŠEBOJKA KOMORSKY-LOVRIĆ
*OUR "Ljekarne", Zagreb, Yugoslavia*

AND

MILIVOJ LOVRIĆ
*Center for Marine Research, "Ruder Bošković" Institute, Zagreb, Yugoslavia*

Received October 8, 1981

ZVONIMIR GAŠPAREC, ŠEBOJKA KOMORSKY-LOVRIĆ, and MILIVOJ LOVRIĆ. Can. J. Chem. **60**, 970 (1982).

The absorption spectra of berberrubine in the visible and uv spectral range were recorded. The measurements were made in four different solvents (water, absolute methanol, absolute ethanol, and absolute propanol) changing the acidity and the alkalinity of the solutions in the wide range from pH 2 to pH 13 by the addition of HCl and KOH. The experimental and theoretical results, derived by simple Hückel MO calculations, were compared and discussed.

ZVONIMIR GAŠPAREC, ŠEBOJKA KOMORSKY-LOVRIĆ et MILIVOJ LOVRIĆ. Can. J. Chem. **60**, 970 (1982).

On a enregistré les spectres d'absorbtion de la berberrubine dans le visible et l'uv. On a effectué ces mesures dans quatre solvants différents (eau, méthanol, éthanol et propanol) et on a fait varier le pH de 2 à 13 par addition de HCl ou de KOH aux solutions. On compare et on discute des résultats expérimentaux et des valeurs théoriques obtenues par des calculs simples OM de Hückel.

[Traduit par le journal]

Berberrubine belongs to the group of protoberberinic alkaloids (Fig. 1). It has been, so far, isolated only from *Berberis vulgaris* L., family Berberidaceae (1), but as early as 1903 Berkurst and Frerichs (2) had synthesized it from berberine chloride by pyrolysis at 200°C with urea.

The alkaloids of the berberine group are known to form complexes with biologically important macromolecules, such as alcohol dehydrogenase from horse liver (3) and some nucleic acids (4). In the spectrophotometric study of these interactions it was first necessary to determine the absorption properties of the alkaloids. Recently, Pavelka and co-workers have published several papers dealing with the ultraviolet and visible absorption (5, 6) and fluorescence (7) spectra of protoberberinic alkaloids. The authors have paid much attention to berberrubine because of some of its special properties. Unfortunately, their measurements were done only in 96% ethanol solution at undefined pH.

The aim of this work is to report the results of the measurements of the absorption spectra of berberrubine in four different solvents with pH of the solutions changing in the range between 2 and 13. Besides, some simple Hückel MO calculations were performed for berberine and its derivatives jatrorhizine, berberrubine, and jatrorubine and the results will be compared with present and previously published (9, 10) experimental spectroscopic data. The calculations were made for all three possible ionic forms of these alkaloids (quaternary amine cation, carbinolic, and open amino-aldehydic forms) in order to gain a better understanding of the possible ionic transformation of berberrubine under the influence of acid or base.

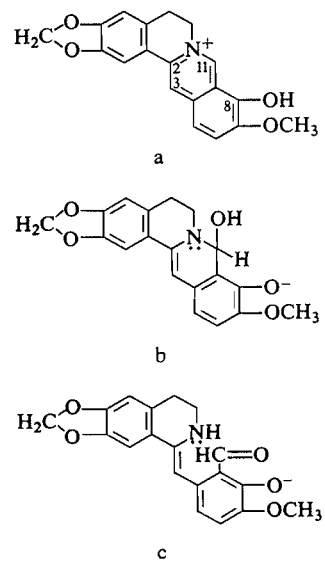


FIG. 1. The structural formulae of berberrubine; (a) the quaternary amine form (the numbers assign certain carbon atoms), (b) the carbinolic form, (c) the open amino-aldehydic form.

0008-4042/82/080970-06$01.00/0
©1982 National Research Council of Canada/Conseil national de recherches du Canada

Can. J. Chem. Downloaded from www.nrcresearchpress.com by 210.87.254.42 on 09/06/12
For personal use only.

Can. J. Chem. Downloaded from www.nrcresearchpress.com by 210.87.254.42 on 09/06/12
For personal use only.

## Experimental

For the preparation of solutions, the following chemicals were used: absolute methanol, absolute ethanol, absolute propanol, KOH, HCl (all p.a. "Merck"), distilled water, and berberrubine chloride synthesized in our laboratory. The purity of berberrubine was checked by thin-layer chromatography (stationary phase Stahl's silica-gel and mobile phase 15% solution of $NH_4OH$ in methanol). Stock solutions of berberrubine, KOH, and HCl in all four solvents were prepared. Four series (20 solutions each) of $5 \times 10^{-5}$ (mol $dm^{-3}$) berberrubine chloride were prepared. The concentrations of HCl and KOH added varied from $2.5 \times 10^{-5}$ to 0.5 (mol $dm^{-3}$). In every series there was one solution in which neither HCl nor KOH was added. The pH measurements were performed by a E 603 Metrohm Herisau pH-meter with a combined glass–calomel electrode. The pH-values of the alcoholic solutions were measured directly in the absolute alcohols. A Carl Zeiss Jena Universal spectrophotometer with 1 cm glass vessels and a PMQ II Zeiss-Opton spectrophotometer with 1 cm quartz vessels were used for the measurements in the visible and ultraviolet spectral ranges, respectively. All the measurements were done at room temperature.

Hückel MO calculations were performed according to Streitwieser's suggestion (12) that $h$ values for $N^+$ and N: are 2 and 1.5, respectively, and that the $k$ value for the CN bond is equal to unity. Besides, the influence of the undissociated OH group in jatrorhizine, berberrubine, and jatrorubine, which is supposed to exist in the strongly acidic solutions of these alkaloids, is neglected. Under this assumption, all four alkaloids in strongly acidic medium possess the same aromatic structure. The appearance of possible carbinolic or amino-aldehydic forms is supposed to happen only after the dissociation of hydroxy groups in these alkaloids. The recommended (12) $h$ and $k$ values for O: and C—O bonds are 2 and 1, respectively.

## Results

In Table 1, the positions of the absorption maxima and corresponding extinction coefficients of berberrubine in four solvents are presented. The disappearance of the absorption maxima at 441–450 and 348–359 (nm) and the appearance of three new maxima at 328–333, 380–399, and 490–516 (nm) in the basic solutions can be noted. The number and the positions of the absorption maxima do not change further in strongly alkaline solutions. The choice of the solvent has significant influence on the absorption spectra causing the bathochromic shifts of all the peaks except the third one. The results of the measurements in ethanolic solutions are in agreement with the results of Pavelka and Smekal (5). Some small differences have probably arisen from the fact that their measurements were done in the mixed solvent.

In Fig. 2, the absorption spectrum of berberrubine in aqueous solutions in the uv spectral range is given as an example.

In Table 2, the experimental spectroscopic data for berberine (9), jatrorhizine (10), and jatrorubin (11) are compiled. Compared with the results of berberrubine, this table shows that the spectral

TABLE 1. The absorption maxima of berberrubine

| Solvent | $\lambda_{max}$ nm ($\varepsilon$) | | | | pH | Addition | Color |
|---|---|---|---|---|---|---|---|
| | $B_a$ | $B_b$ | $L_a$ | $L_b$ | | | |
| Water | 235(28 000) | 268(25 500) | — 348(19 000) | — 441(1400) | 3.05 | HCl | lime-yellow |
| | 235(29 000) | 268(25 000) | — 348(19 300) | — — | 5.03 | — | orange |
| | 235(31 000) | 268(24 000) | 330(11 000) — | 380(12 000) — | 490(1200) 8.52 | KOH | rose |
| | 235(31 000) | 268(24 300) | 330(12 000) — | 380(12 100) — | 490(1250) 12.70 | KOH | red |
| Methanol | 238(26 500) | 278(23 600) | — 355(17 400) | — 447(1350) | — 0.63 | HCl | yellow |
| | 238(27 100) | 278(24 000) | 328(11 000) — | 392(12 000) 447(1050) | 513(800) 5.96 | — | orange |
| | 238(27 000) | 278(23 000) | 328(13 000) — | 392(14 000) — | 513(1100) 9.23 | KOH | rose |
| | 238(27 000) | 278(22 500) | 328(12 500) — | 392(15 800) — | 513(1240) 13.62 | KOH | red |
| Ethanol | 240(30 000) | 276(25 000) | — 356(18 000) | — 450(1500) | — 0.95 | HCl | yellow |
| | 240(28 300) | 276(26 000) | — 356(16 000) | — 450(1000) | — 5.85 | — | orange |
| | 240(29 400) | 276(27 100) | 329(10 000) — | 396(13 000) — | 516(1200) 9.55 | KOH | red |
| | 240(29 100) | 276(26 700) | 329(11 100) — | 396(12 200) — | 516(1000) 13.68 | KOH | red |
| Propanol | 240(22 000) | 278(19 000) | — 359(13 500) | — 450(1900) | — 1.13 | HCl | yellow |
| | 240(25 000) | 278(17 400) | 332(9 600) — | 399(9 400) — | 516(1000) 6.25 | — | rose |
| | 240(24 000) | 278(18 000) | 330(10 000) — | 399(10 000) — | 516(1110) 7.91 | KOH | red |
| | 240(23 000) | 278(16 000) | 330(9 800) — | 399(11 000) — | 516(1240) 13.82 | KOH | red |

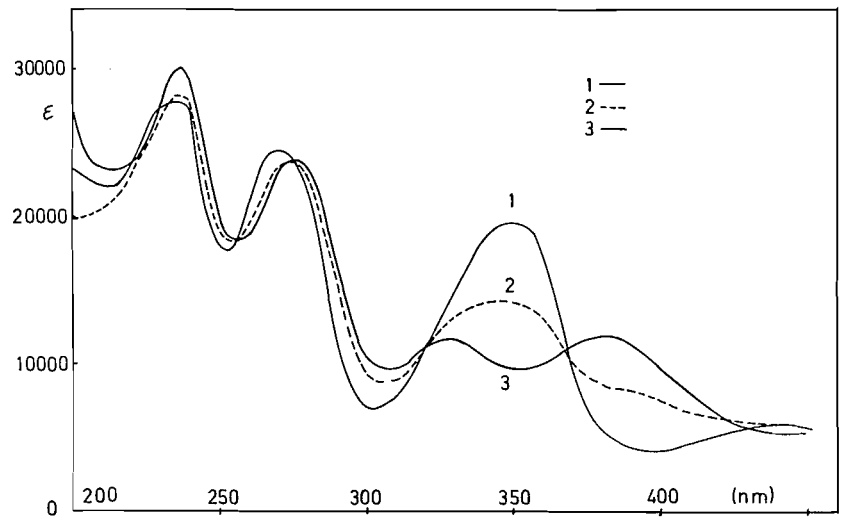


FIG. 2. The absorption spectra of water solutions of berberrubine (uv spectral range); (1) pH = 5.03; (2) pH = 6.51; (3) pH = 8.52.

changes in the solutions of jatrorhizine, jatrorubine, and berberrubine are in principle similar, but jatrorhizine exhibits an additional maximum at about 240 nm instead of the one at 330 nm. Differences appear in strongly alkaline ethanol and propanol solutions of jatrorhizine (where the maximum in the visible spectral range disappears, which is similar to the behaviour of berberine in all alcoholic solutions containing larger concentrations of alkali) and in propanol solution of jatrorubin where the maximum at 460 nm exists in parallel with that at 540 nm. As berberine does not possess an OH group, its spectral changes are less dramatic, but the similarity between the spectra of all four alkaloids in strongly acidic media must be noted.

The results of Hückel MO calculations (eigenvalues, total energies, resonance energies, bond orders and lengths, $\pi$-charges, etc.) are available on request.[1] Here we shall report only general theoretical characteristics of the investigated molecules. In the quaternary amine ions an extraordinarily high positive charge appears on the carbon atom in the neighborhood of the $N^+$ atom (C11) which enables these alkaloids to undergo nucleophilic substitution on this site (berberine +0.331 net charge, jatrorhizine +0.326, berberrubine +0.327, and jatrorubine +0.323). The positive charge on the N atom in all four molecules is bigger than that on the C11 atom, but the difference is small and can be compensated by possible polarization of $\sigma$ N—C bonds. The carbinolic molecules of all alkaloids still possess a small positive charge on nitrogen and its neighboring (C2) atom, but a negative charge on the C3 atom. These charges become even greater if open amino-aldehydic forms occur, but in this case an additional and large positive charge appears on the aldehydic carbon atom (C11) because the aldehydic bond seems to be highly polarized. So, from the point of view of charge distribution in the molecule, the appearance of the open aldehydic ionic form seems to be unlikely under the conditions which prefer nucleophilic substitution.

After the dissociation, the jatrorhizinic and berberrubinic hydroxy groups do not have the same negative charge (jatrorhizine −0.901 net charge, berberrubine −0.887, jatrorubine −0.901 and −0.886, respectively). The latter one contributes more to the annihilation of positive charge on the nitrogen and C2 atoms. That is why we can expect that between these two hydroxy groups in jatrorubine the berberrubinic one will dissociate first.

The values for the bond lengths (13, 14) are in agreement with some experimental data (18, 19). Except for jatrorubine, all the alkaloids have the longest bond between the quinolinic and benzenoid parts of the molecule, which can be considered as proof of a certain charge separation between these two parts.

If the $\beta$ part of the total energy of $\pi$ electrons, divided by the number of $\pi$ electrons ($E_\beta$/el.) is chosen as the criterion for stability of a certain ionic form, we can see that the most stable form of berberine is its quaternary amine form and the most unstable its carbinolic form. For jatrorhizine, berberrubine, and jatrorubine, under the same crite-

[1]Copies of the Supplementary Material are available at a nominal charge from the Depository of Unpublished Data, CISTI, National Research Council of Canada, Ottawa, Canada, K1A 0S2.

Can. J. Chem. Downloaded from www.nrcresearchpress.com by 210.87.254.42 on 09/06/12
For personal use only.

Can. J. Chem. Downloaded from www.nrcresearchpress.com by 210.87.254.42 on 09/06/12
For personal use only.

rion, the most stable is the quaternary amine form with dissociated hydroxy groups and the most unstable form is again the carbinolic one. If the criterion is resonance energy per electron ($E_R^*$/el., calculated after Milun *et al.* (17)), the most stable form for all four alkaloids is their open aminoaldehydic form, but the carbinolic forms of berberine and jatrorhizine are as stable as their quaternary amine ions while in the other two alkaloids the carbinolic form is less stable than their quaternary amine ions with dissociated hydroxy groups. This could be a reason why only berberine and jatrorhizine exhibit the appearance of the carbinolic ionic form in some strongly alkaline alcoholic solutions. From these criteria it also appears that the carbinolic form of berberrubine is unlikely to be expected.

In Table 3 the values of the energy separations between the frontier orbitals of all four alkaloids are given. In the parentheses are the positions of the absorption maxima corresponding to these energy separations ($B_b$, $L_b$, and $L_a$). These values were calculated with the parameters reported by Zahradnik and Koutecký (15*b*) for pyridine-type resonance molecules. The parameters probably do not fit exactly for the molecules under our consideration so that the analyses of theoretical absorption spectra must be made under the assumption that $B_b$ and $L_a$ bands are fairly accurate and that $L_b$ is always about 60 nm too small (see Table 2). Looking first at berberine we notice that theory predicts the $B_b$ and $L_b$ bands of the carbinolic form to be shifted hypsochromically for 26 and 32 nm, respectively, while the $L_a$ band stays almost untouched in comparison to their quaternary amine form. The experimental results (9) (Table 2) show that there are no spectral changes in water solutions, but in strongly alkaline alcoholic solutions the extinction coefficients of $B_b$ and $L_b$ decrease (especially of the latter band so that color of the solution totally vanishes). The hypsochromic shifts of the maxima can hardly be noted. On the other hand, our simple MO calculations did not give us the values of theoretical extinction coefficients, so that we have to accept the observed spectral changes as proof of appearance of the carbinolic form. The theoretical spectra of jatrorhizine, berberrubine, and jatrorubine show that the influence of dissociation of the hydroxy group manifests itself in the bathochromic shift of all maxima, but this shift is not large. The influence of the jatrorhizinic group is greater than of the berberrubinic one, but if both of them dissociate (in jatrorubine) the effect is approximatively the sum of both effects. Carbinolic forms of these alkaloids shift all the peaks hypsochromically. On the contrary, for the

TABLE 2. The absorption maxima of berberine (9), jatrorhizine (10), and jatrorubine (11)

| Solvent | $\lambda_{max}$ nm | | | | | | | | | | | | | Addition |
|---|---|---|---|---|---|---|---|---|---|---|---|---|---|---|
| | Berberine | | | Jatrorhizine | | | | Jatrorubine | | | | | | |
| Water | 227 | 262 | 346 | 422 | 224 | — | 274 | 340 | — | 425 | — | 226 | 274 | — | 348 | — | 445 | — | HCl |
| | 227 | 262 | 346 | 422 | 224 | — | 274 | 340 | — | 425 | — | 226 | 276 | — | 350 | — | — | — | — |
| | 227 | 262 | 346 | 422 | 227 | 238 | 262 | 348 | 372 | — | 457 | 228 | 276 | 325 | — | 380 | — | 480 | KOH ≤ 0.05 *M* |
| | 227 | 262 | 346 | 422 | 230 | 244 | 290 | — | 370 | — | 457 | 228 | 276 | 324 | — | 380 | — | 490 | KOH > 0.05 *M* |
| Methanol | 230 | 266 | 349 | 431 | 226 | 238 | 264 | 350 | — | 433 | — | 224 | 278 | — | 350 | — | 450 | — | HCl |
| | 230 | 266 | 349 | 431 | 226 | 240 | 265 | 350 | — | 433 | — | 220 | 278 | — | 350 | — | 450 | — | — |
| | 230 | 266 | 349 | 431 | 230 | 248 | — | — | 388 | — | 487 | 220 | 278 | 325 | — | 390 | — | 505 | KOH ≤ 0.05 *M* |
| | — | (266)* | 349 | — | 220 | 248 | — | — | 386 | — | 487 | 220 | 278 | 325 | — | 395 | — | 510 | KOH > 0.05 *M* |
| Ethanol | 236 | 266 | 351 | 431 | 228 | 242 | 264 | 348 | — | 436 | — | 226 | 278 | — | 350 | — | 448 | — | HCl |
| | 236 | 266 | 351 | 431 | 228 | 242 | 264 | 348 | 404 | 436 | — | 220 | 285 | — | 350 | — | — | 505 | — |
| | 236 | 266 | 351 | 431 | 230 | 248 | — | — | 398 | — | 500 | 220 | 278 | 330 | — | 385 | — | 505 | KOH ≤ 0.05 *M* |
| | — | (266)* | 351 | — | — | 248 | — | — | 375 | — | — | 220 | 278 | 324 | — | 395 | — | 505 | KOH > 0.05 *M* |
| Propanol | 238 | 268 | 352 | 431 | — | 240 | 264 | 352 | — | 440 | — | 220 | 278 | — | 355 | — | 464 | — | HCl |
| | 238 | 268 | 352 | 431 | — | 242 | 266 | 354 | 417 | — | — | 236 | 276 | 320 | — | 400 | — | 490 | — |
| | 238 | 268 | 352 | 431 | — | 248 | — | 362 | 404 | — | 518 | 226 | 278 | 326 | — | 400 | — | 540 | KOH ≤ 0.05 *M* |
| | — | (268)* | 352 | — | — | — | 260 | — | 400 | — | — | 220 | 276 | 320 | — | 385 | 460 | 540 | KOH > 0.05 *M* |

*Very small peak.

TABLE 3. The energy separations between the boundary orbitals

| Compound | Ionic forms* | $\overline{\Delta E\binom{m, m+2}{m-1, m+1}}(\beta)(B_b; L_b)$ (nm) | $\Delta E(m, m+1)(\beta)(L_a)$ (nm) |
|---|---|---|---|
| Berberine | 1 | 1.278 (268; 363) | 0.966 (347) |
| | 2 | 1.475 (242; 331) | 0.950 (352) |
| | 3 | 1.173 (284; 384) | 0.686 (453) |
| Jatrorhizine | 1a | 1.278 (268; 363) | 0.966 (347) |
| | 1b | 1.241 (274; 370) | 0.912 (362) |
| | 2 | 1.422 (249; 339) | 0.967 (347) |
| | 3 | 1.124 (292; 394) | 0.670 (461) |
| Berberrubine | 1a | 1.278 (268; 363) | 0.966 (347) |
| | 1b | 1.255 (271; 368) | 0.952 (351) |
| | 2 | 1.365 (256; 349) | 0.950 (352) |
| | 3 | 1.160 (286; 387) | 0.720 (445) |
| Jatrorubine | 1a | 1.278 (268; 363) | 0.966 (347) |
| | 1c | 1.201 (280; 378) | 0.918 (361) |
| | 2 | 1.372 (255; 348) | 0.968 (347) |
| | 3 | 1.136 (290; 392) | 0.689 (452) |

*Legend: 1, the quaternary amine cation; 1a, the quaternary amine cation with undissociated -OH group; 1b, the quaternary amine dipole with dissociated -OH group; 1c, the quaternary amine anion with both -OH groups dissociated; 2, the carbinolic form; 3, the open amino-aldehydic form.

open amino-aldehydic form, the theoretical analysis predicts the probability of two strong absorption maxima in the visible spectral range and only one (beside $B_a$) in the uv range (and this prediction is based on energy separation and not only on correlation parameters). A similar prediction is valid for amino-aldehydic forms of all four alkaloids, so that we can safely say that no significant amount of this form appears in any of the solutions.

## Discussion

According to Gadamer's theory (16), the quaternary amine cations are in equilibrium with their carbinolic (which appears as the result of $OH^-$ or $OR^-$ group attachment on a C atom in the neighborhood of the $N^+$ atom) and open amino-aldehydic forms (which appears as the further step of molecular rearrangement) (8). This theory was criticized in at least two comprehensive review articles (15*a*, *c*) and the main criticism was given to the lack of experimental support for the existence of the open amino-aldehydic form, except in several special cases. As their authors have pointed out, the spectroscopic measurements which were performed to confirm this theory not only failed to do so in many cases (15*a*), but are in principle incapable of doing so because of their low sensitivity which does not enable them to detect the presence or absence of the open amino-aldehydic form in trace amounts (15*c*). The intention of our Hückel MO calculations was to analyse the probable spectroscopic and electronic characteristics of all three ionic forms of our alkaloids. The comparison of theoretical and experimental spectroscopic data could be used for predictions about the significant appearance of certain forms in the measured system.

The experimental results for berberrubine show three theoretically unpredicted details: (a) the influence of the undissociated hydroxy group (theoretically neglected) is manifest in a bathochromic shift for $L_b$ of about 20 nm (compared with $L_b$ of berberine), (b) the influence of dissociation of the hydroxy group is also about 20 nm bigger than predicted, and (c) instead of a simple bathochromic shift, the $L_a$ band undergoes splitting into two smaller bands, one shifted towards longer and another to the shorter wave lengths. All these differences (especially the last one) can be attributed to the probable differences between absorption maxima/energy splitting correlation parameters for simple amino and both amino and oxy substituted aromatic compounds. Besides, the literature about uv and visible absorption spectra (19) of other substituted aromatic compounds shows that the influence of substituent frequently can manifest itself in the splitting of the original aromatic band into two or more less intensive bands. In the light of probable smaller electron exchange between benzenoid and quinolinic parts of these molecules, we can postulate, although rather nonexactly, that the absorption bands $B_a$ and $B_b$ are more influenced by the electronic conditions in the benzenoid part of molecule while the bands $L_a$ and $L_b$ are more influenced by the quinolinic part. Under this assumption, we can expect that the dissociation of the berberrubinic hydroxy group will act towards splitting the $L_a$ band (which is more sensitive to substituent) and this can be seen in Table 1 for

Can. J. Chem. Downloaded from www.nrcresearchpress.com by 210.87.254.42 on 09/06/12
For personal use only.

Can. J. Chem. Downloaded from www.nrcresearchpress.com by 210.87.254.42 on 09/06/12
For personal use only.

berberrubine and in Table 2 for jatrorubine (moreover, from this assumption we can recognize the berberrubinic group in jatrorubine to be dissociated, which is in agreement with our expectation on the basis of MO diagrams of jatrorubine), while the dissociation of the jatrorhizinic group will split the $B_b$ band as can be seen in Table 2 for jatrorhizine where the additional peak at 240 nm appears, but the $L_a$ and $L_b$ bands are only bathochromically shifted. Nevertheless, except in the case of ethanolic and propanolic strongly alkaline solutions of jatrorhizine, where the experimentally noted criterion for carbinolic form appearance (the vanishing of absorption maxima in the visible range) is satisfied, in all other cases we are not able to note any spectral change which could, according to our theoretical predictions, be attributed to the carbinolic form appearance, but all the changes can be described solely by hydroxylic group dissociation.

In the light of the above discussion, the analysis of present spectroscopical results for berberrubine can, finally, be summarized in the following manner.

(a) In strongly acidic media, berberrubine exhibits four absorption maxima $B_a$ (235–240 nm), $B_b$ (268–278), $L_a$ (348–359), and $L_b$ (441–450 nm), which can be attributed to the quaternary amine ionic form.

(b) In all alkaline solutions, the $L_b$ band shifts bathochromically to 490–516 nm, the $L_a$ band splits into two smaller bands, the first one at about 330 nm and the second one between 380 and 399 nm, while the $B_a$ and $B_b$ bands do not change. This spectral rearrangement can be attributed to the dissociation of the hydroxy group in the molecule.

(c) The appearance of neither carbinolic nor open amino-aldehydic forms of berberrubine was noted in any of the investigated solutions. While the latter is unlikely to exist, because of the charge distribution in the molecule, the possibility of existence of the former cannot be rejected, at least in more strongly alkaline conditions than investigated. The dissociation of the hydroxy group does not change the positive charge on the active C11 carbon atom, but only neutralizes slightly the positive charges on the nitrogen and C2 atoms. The only way that dissociation can prevent the nucleophilic attack on the C11 atom would be if we suppose that two or more berberrubine dipole molecules form ionic pairs or clusters in which the C11 sites will be unapproachable. The probable ionic pairs are usually blamed for weak solubility of berberrubine in slightly alkaline solutions.

(d) The choice of solvent can influence the position of absorption maxima. The hypsochromic shift is proportional to polarity of the solvent. The pH of a pure solution of berberrubine (when neither HCl nor KOH was added) changes from 5.03 in water to 6.25 in absolute propanol, which can be connected with the changes in $pK_a$ values of these four solvents. The color of the solutions and the absorption spectra of berberrubine in pure solutions show that only in propanol is its hydroxy group totally dissociated while in other solutions both forms are still in comparable concentrations. The solutions of berberrubine can serve as a kind of pH indicator because it changes its color throughout the whole pH range.

**Acknowledgements**

This work was supported in part by the Self Management Council for Scientific Research of S. R. Croatia. The authors wish to thank to Dr. N. Trinajstić, Dr. S. Sabljić, and Dr. R. D. Allendoerfer for their kind help and useful discussions during the preparation of this work.

1. E. SPATH and N. POLGAR. Monatsh. Chem. **52**, 117 (1929).
2. H. BERKURST and G. FRERICHS. Apoth. Ztg. **18**, 697 (1903).
3. E. SEBE, S. ABE, N. MURASE, and H. SUGAYA. J. Chin. Chem. Soc. **15**, 146 (1968).
4. M. KLIMEK and L. HNILICA. Arch. Biochem. Biophys. **81**, 105 (1959).
5. S. PAVELKA and E. SMEKAL. Collect. Czech. Chem. Commun. **41**, 3157 (1976).
6. S. PAVELKA and J. KOVAR. Collect. Czech. Chem. Commun. **41**, 3654 (1976).
7. E. SMEKAL and S. PAVELKA. Stud. Biophys. **64**, 184 (1977).
8. B. SKINNER. J. Chem. Soc. 832 (1950).
9. K. WEBER and Z. GAŠPAREC. Croat. Chem. Acta, **38**, 143 (1966).
10. Z. GAŠPAREC and K. WEBER. Croat. Chem. Acta, **39**, 175 (1967).
11. Š. KOMORSKY-LOVRIĆ and Z. GAŠPAREC. Croat. Chem. Acta, **54**, 97 (1981).
12. A. STREITWIESER. Molecular orbital theory. John Wiley and Sons Inc., New York. 1966.
13. C. A. COULSON and A. GOLEBIEWSKI. Proc. Phys. Soc. **78**, 1310 (1961).
14. T. AUNO, M. ITO, R. SHIMADA, A. SADO, and W. MIZUSHIMA. Bull. Chem. Soc. Jpn. **30**, 638 (1957).
15. (*a*) D. BEKE. Adv. Heterocycl. Chem. **1**, 167 (1966); (*b*) R. ZAHRADNIK and J. KOUTECKÝ. Adv. Heterocycl. Chem. **5**, 205 (1969); (*c*) J. W. BUNTING. Adv. Heterocycl. Chem. **25**, 151 (1979).
16. J. GADAMER. J. Prakt. Chem. **82**, 817 (1911).
17. M. MILUN, Ž. SOBOTKA, and N. TRINAJSTIĆ. J. Org. Chem. **37**, 139 (1972).
18. G. JONES (*Editor*). Quinolines. Vol. 1. J. Wiley and Sons Inc., London. 1977.
19. Sadtler standard spectra, uv and vis. spectral range. Sadtler Corp. 1970.

# Introduction of 9-fluorenylmethyloxycarbonyl, trichloroethoxycarbonyl, and benzyloxycarbonyl amine protecting groups into O-unprotected hydroxyamino acids using succinimidyl carbonates[1]

ALENKA PAQUET

*Food Research Institute, Canada Department of Agriculture, Ottawa, Ont., Canada, KIA 0C6*

Received August 12, 1981

ALENKA PAQUET. Can. J. Chem. **60**, 976 (1982).

9-Fluorenylmethyl succinimidyl, pentachlorophenyl, and benzotriazole-1-yl carbonates were prepared and their reactivity with L-serine and L-serine benzyl ester was compared. The most efficient reagent, 9-fluorenylmethyl succinimidyl carbonate, was used for the preparation of 9-fluorenylmethyloxycarbonyl derivatives of other hydroxyamino acids and hydroxyamino acid esters in high yields. The use of trichloroethyl and benzyl succinimidyl carbonates for an efficient conversion of hydroxyamino acids and their esters into the corresponding *N*-trichloroethoxycarbonyl and benzyloxycarbonyl derivatives is described.

ALENKA PAQUET. Can. J. Chem. **60**, 976 (1982).

On a préparé les carbonates de fluorènyl-9 methylsuccinimidile, de pentachlorophényle et de benzotriazolyle-1 et on a comparé leur réactivité vis-à-vis la L-sérine et son ester benzylique. On a utilisé le réactif le plus efficace, le carbonate du fluorènyl-9 méthylsuccinimidile, pour préparer avec d'excellents rendements des dérivés fluorènyl-9 méthyloxycarbonyles d'autres acides hydroxyaminés et de leurs esters. On décrit l'utilisation des carbonates de trichloroéthyle et de benzyle succinimidile pour la transformation efficace des acides hydroxyaminés et de leurs esters en dérivés *N*-trichloroéthoxycarbonyle et benzyloxycarbonyle correspondants.

[Traduit par le journal]

Amino acids bearing urethane-type protecting groups are commonly used in peptide synthesis because they can be coupled without racemization. Except for *N-tert*-butoxycarbonylamino acids, they are usually prepared using the alkoxycarbonyl chloride under Schotten–Baumann conditions. An alternative reagent which does not require the presence of base is the mixed carbonate containing a substituted phenolic group (1) and more recently the succinimidyl group (1–3). New protecting groups are continually being proposed for use in peptide and general organic chemistry, and methods for their introduction are necessary. This paper describes a new method of preparing 9-fluorenylmethyloxycarbonyl (Fmoc-),[2] trichloroethoxycarbonyl (Tec-), and benzyloxycarbonyl (Z-) amino acids with particular attention to the hydroxyamino acids using succinimidyl carbonates as reagents and the free amino acids or amino acid esters as substrates. The possibility of using other carbonates was also examined.

The Fmoc group (4) which is labile to secondary amines is being promoted for use both in solid phase (5, 6) and solution (7) peptide synthesis, particularly because it eliminates the need for a potentially harmful acid deprotection cycle. Fmoc-amino and hydroxyamino acid derivatives have been obtained using Fmoc-chloride in the presence of aqueous sodium carbonate (8). Fmoc-amino acid esters have been obtained by subsequent esterification (4, 8). The Tec group is an attractive protecting group as it can be cleaved by zinc in acetic acid (9) or organic solvents (10, 11) leaving other functional groups unaffected. However, it has been little used in peptide chemistry possibly because of the uncertainty over its stability to hydrogenolytic conditions (12). It also has been reported that an attempt to convert serine into Tec-Ser-OH using trichloroethoxycarbonyl chloride in the presence of 1 *N* sodium hydroxide failed (11).

Mixed carbonates have been obtained by reaction of alkyl chloroformates with alcohols in pyridine (1) and more recently with the thallium salt of *N*-hydroxysuccinimide in organic solvents (3). But thallium salts are toxic and their preparation involves handling of the unstable and toxic thallium ethoxide. We have now found that the dicyclohexylammonium salts of alcohols, which are readily obtained by mixing the two components in an organic solvent, serve as well for the preparation of mixed carbonates from alkyl chloroformates. Thus 9-fluorenylmethyl, trichloroethyl, and benzyl succinimidyl carbonates **1**, **4**, and **5** were prepared in high yields in this manner. As well, 9-fluorenylmethyl pentachlorophenyl carbonate **2** and benzo-

[1]Contribution No. 473 from the Food Research Institute, Agriculture Canada, Ottawa, Ont., Canada.

[2]*Abbreviations*: nmr, nuclear magnetic resonance, ir, infrared. Other abbreviations are those recommended by the IUPAC–IUB Commission on Biochemical Nomenclature J. Biol. Chem. **247**, 977–983 (1972). Amino acid symbols represent the L-isomers.

0008-4042/82/080976-05$01.00/0

©1982 National Research Council of Canada/Conseil national de recherches du Canada

Can. J. Chem. Downloaded from www.nrcresearchpress.com by 210.87.254.105 on 09/06/12
For personal use only.

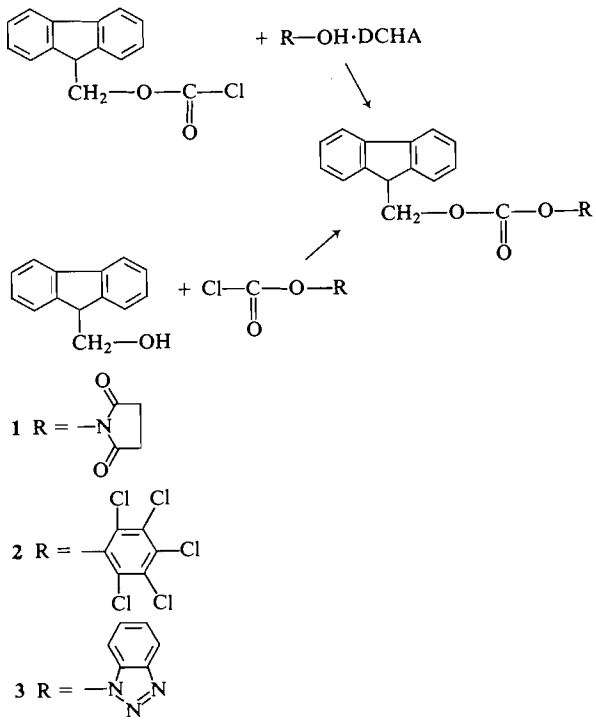


triazole-1-yl carbonate **3** were obtained from 9-fluorenylmethyloxycarbonyl chloride and the dicyclohexylammonium salt of the corresponding alcohols.

Succinimidyl carbonate **1** was also obtained by the reverse procedure, namely by reaction of 9-fluorenylmethanol with succinimidyl chloroformate. Again, the dicyclohexylammonium instead of the thallium salt (3) of *N*-hydroxysuccinimide served for the preparation of the chloroformate using phosgene. We found a literature procedure (13) to be a convenient source for 9-fluorenylmethanol.

9-Fluorenylmethyl carbonates **1–3** were reacted with one equivalent of L-serine in a water–acetone mixture in the presence of one equivalent of sodium bicarbonate, and with serine benzyl ester hydrochloride in chloroform in the presence of 1.5 equivalents of triethylamine. Under these conditions, the succinimidyl carbonate **1** gave excellent yields of Fmoc-Ser-OH and Fmoc-Ser-OBzl, the pentachlorophenyl carbonate **2** gave no Fmoc-Ser-OH and a moderate yield of the ester, and the benzotriazole-1-yl carbonate **3** gave an excellent yield of the ester but only a moderate yield of the acid derivative. The results are given in Table 1. On this basis, the succinimidyl carbonate **1** was chosen for further study. It reacted smoothly with valine and valine methyl ester giving the Fmoc-derivatives in

TABLE 1. Reactivity of reagents **1–3** with serines

| | H-Ser-OH | | H-Ser-OBzl | |
|---|---|---|---|---|
| Reagent | Time (h) | Yield (%) | Time (h) | Yield (%) |
| **1** | 2 | 87 | 2 | 87 |
| **2** | 48 | — | 48 | 50 |
| **3** | 48 | 64 | 2 | 89 |

good yields. Other amino acid derivatives prepared are described in Table 2. The results demonstrate that the use of 9-fluorenylmethyl succinimidyl carbonate is indeed a good alternative to the use of the chloroformate for the preparation of Fmoc-derivatives. It has the advantage that it eliminates the possibility that the mixed anhydride might form during the acylation reaction. The mixed anhydride could give rise to some protected dipeptide in addition to the desired *N*-protected amino acid, a side-reaction encountered in the original synthesis of benzoylglycine (14, 15).

The pentachlorophenyl carbonate **2** also proved unsatisfactory for acylating valine and valine methyl ester, 50% of **2** being recovered even after 72 h.

Using the same conditions as for the preparation of the Fmoc-derivatives, trichloroethyl succinimidyl carbonate **4** and benzyl succinimidyl carbonate **5** gave good yields of the corresponding derivatives when reacted with hydroxyamino acids and esters. The compounds prepared are described in Tables 3 and 4.

All amino acid derivatives obtained gave correct elemental analyses, exhibited absorptions at 3420 (N—H), 1695–1710 (urethane carbonyl), and 1510 (urethane C—N) $cm^{-1}$ in ir and showed amide proton signals in nmr spectra. This served as a proof that the amino group was acylated.

## Experimental

Melting points (uncorrected) were taken by the capillary method. The nmr spectra were recorded on a Varian T-60 spectrometer in deuterochloroform unless stated otherwise. The ir spectra were obtained with a Beckman-IR-20 spectrometer in chloroform. Optical rotations were determined on Perkin–Elmer model 141 polarimeter. Solutions were dried over $Na_2SO_4$.

9-Fluorenylmethanol was prepared according to the literature (13) or purchased from Fluka, A. G. Buchs, Switzerland. Amino acids and their esters were purchased from Sigma Chemical Company (Saint Louis, Missouri, USA). Serine benzyl ester hydrochloride and tyrosine benzyl ester were prepared as indicated in the literature (16).

*N*-Protected amino acid esters with the exception of tyrosine esters were prepared as shown for the preparation of Fmoc-Ser-OBzl. *N*-Protected tyrosine ester derivatives were synthesized as described for the preparation of Fmoc-Tyr-OBzl.

Can. J. Chem. Downloaded from www.nrcresearchpress.com by 210.87.254.105 on 09/06/12
For personal use only.

Can. J. Chem. Downloaded from www.nrcresearchpress.com by 210.87.254.105 on 09/06/12
For personal use only.

TABLE 2. *N*-(9-Fluorenylmethyloxycarbonyl)-amino acid derivatives

| Compound | Solvent for recrystallization | Yield % | Melting point °C | $[\alpha]_D^{26}$[a] | Molecular formula | Nmr data (δ) |
|---|---|---|---|---|---|---|
| Fmoc-Ser-OH | $CH_2Cl_2$–hexane | 89 | 86–88[b] | +14.8° | — | [f] |
| Fmoc-Ser-OBzl | $CH_2Cl_2$–hexane | 87 | 97[c] | +1.3° | — | [f] |
| Fmoc-Ser-$OCH_3$ | Benzene | 90 | 128 | +4.0° | $C_{19}H_{19}NO_5$ | 2.4 (1H, m), 3.8 (3H, s), 3.9 (2H, m), 4.4 (4H, m), 5.8 (1H, m), 7.2–7.9 (8H, m) |
| Fmoc-Thr-OH·DCHA | AcOEt–$Et_2O$ | 95 | 165 | +9.8° | $C_{31}H_{42}N_2O_5$ | Not taken |
| Fmoc-Tyr-$OCH_3$ | $CH_2Cl_2$–hexane | 88 | 120–122[d] | +3.4° | $C_{25}H_{23}NO_5$ | 3.06 (2H, m), 3.76 (3H, s), 4.1–4.9 (4H, m), 5.4 (1H, m), 6.93 (4H, m), 7.33–7.93 (8H, m) |
| Fmoc-Tyr-OBzl | $CHCl_3$–EtOH | 86 | 152 | −11.3° | $C_{31}H_{27}NO_5$ | Not taken |
| Fmoc-Val-OH[g] | $CH_2Cl_2$ – pet. ether | 86 | 144[e] | +4.6° | — | [f] |
| Fmoc-Val-$OCH_3$ | $CH_2Cl_2$ – pet. ether | 90 | 95 | −5° | $C_{21}H_{23}NO_4$ | 0.96 (6H, dd), 2.1 (1H, m), 3.8 (3H, s), 4.3 (4H, m), 5.3 (1H, m), 7.3–7.9 (8H, m) |

Elemental analyses of all compounds gave satisfactory results (C ± 0.21, H ± 0.06, N ± 0.21).
[a]Determined in AcOEt except for Fmoc-Thr-OH·DCHA (DMF).
[b]Literature (8) mp 86–88°C, $[\alpha]_D^{23-25}$ +14.9° (ethyl acetate).
[c]Literature (8) mp 97–98°C, $[\alpha]_D^{23-25}$ +1.4° (ethyl acetate).
[d]126–127°C on Koffler block.
[e]Literature (8) mp 143–144°C, $[\alpha]_D^{23-25}$ +4.8° (ethyl acetate).
[f]In accord with data in literature (8).
[g]Prepared from 1.

TABLE 3. *N*-Trichloroethoxycarbonylamino acid derivatives

| Compound | Solvent for recrystallization | Yield % | Melting point °C | $[\alpha]_D^{25}$[a] | Molecular formula | Nmr data (δ) |
|---|---|---|---|---|---|---|
| Tec-Ser-OH | $H_2O$ | 67 | 115 | +11.7° | $C_6H_8Cl_3NO_5$ | 3.73 (2H, m), 4.13 (m, 1H), 4.80 (2H, s), 7.71 (1H, broad s) |
| Tec-Ser-OBzl | — | 90 | Amorphous[b] | Not taken | $C_{13}H_{14}Cl_3NO_5$ | 2.63 (1H, m), 4.08 (2H, m), 4.58 (1H, m), 4.8 (2H, s), 5.30 (2H, s), 6.23 (1H, m), 7.46 (5H, s) |
| Tec-Tyr-OBzl | $CH_3Cl_2$–$Et_2O$ | 85 | 112 | −9.3° | $C_{19}H_{18}NCl_3O_5$ | 3.1 (2H, m), 4.9–4.63 (3H, m and s), 5.03 (2H, s), 5.66 (1H, m), 8.3 (4H, m), 7.38 (5H, s) |
| Tec-Val-OH | $CH_2Cl_2$–hexane | 79 | 85 softens[c] 95 melts | −4.1° | — | 1.0 (6H, dd), 2.2 (1H, m), 4.3 (1H, m), 4.8 (2H, s), 5.63 (1H, m) |

[a]Determined in ethyl acetate except for Tec-Val-OH (ethanol).
All compounds gave satisfactory elemental analyses (C ± 0.09; H ± 0.18; N ± 0.02) except for Tec-Ser-OBzl (*Anal.* calcd.: C 42.13, H 3.80, N 3.78; found: C 41.16, H 4.27, N 3.57).
[b]Attempts to recrystallize the compound resulted in decomposition.
[c]Literature (11) mp 80.5–81°C; $[\alpha]_D^{25}$ −3.2° (ethanol).

TABLE 4. *N*-Benzyloxycarbonylamino acid derivatives

| Compound | Yield % | Melting point °C | $[\alpha]_D^{26}$ |
|---|---|---|---|
| Z-Thr-OH | 70 | 102–103[a] | −5.5° (4% aq. acetic acid) |
| Z-Ser-OH | 78[e] | 120[b] | +5.7° (acetic acid) |
| Z-Ser-$OCH_3$ | 90 | Oil[c] | −12.6° (methanol) |
| Z-Tyr-OBzl | 92 | 119[d] | −14.3° (methanol) |

[a]Literature (17) 103–104°, $[\alpha]_D^{28}$ −5.5° (4% aq. acetic acid).
[b]Literature (18) 119–120°, $[\alpha]_D$ +5.8° (acetic acid).
[c]Literature (19) 33–35°, $[\alpha]_D^{20}$ −13.2° (methanol).
[d]Literature (20) 118–119°, $[\alpha]_D$ −13.9° (methanol).
[e]92% yield was obtained using 2 equivalents of **4**.

*Dicyclohexylammonium salts*

To 0.01 mol each of *N*-hydroxysuccinimide (in acetone), pentachlorophenol (in ether), and 1-hydroxybenzotriazole (in ethyl acetate), 0.01 mol of dicyclohexylamine was added. The mixtures were stirred overnight, the precipitates isolated by filtration, washed with cold solvents used for preparation, and thoroughly dried. Elemental analyses of all products gave satisfactory results (C ± 0.38, H ± 0.02, N ± 0.03). *N*-Hydroxysuccinimide·DCHA 95%; Pentachlorophenol·DCHA, 87%; 1-hydroxybenzotriazole·DCHA, 86% yield.

*Succinimidyl chloroformate*

To a stirred suspension of 5.96 g (20 mmol) of *N*-hydroxy-

Can. J. Chem. Downloaded from www.nrcresearchpress.com by 210.87.254.105 on 09/06/12
For personal use only.

succinimide·DCHA in methylene chloride (100 mL) at −30°C was added liquified phosgene (20 mL) under a stream of nitrogen. The reaction was stirred for 4 h at −5°C and the excess of phosgene was removed at room temperature with a stream of nitrogen in a well vented fume-hood. Methylene chloride was added, the mixture was cooled to −2°C, the precipitate was filtered off and washed with cold methylene chloride. The combined filtrate and washings were washed with a cold 10% solution of sodium bicarbonate, water, dried, and the solvent was evaporated giving 2.85 g (80%) of the title compound; ir: 1740–1760 (chloride carbonyl), 1790–1800, and 1820 (imide carbonyl) $cm^{-1}$.

*9-Fluorenylmethyl succinimidyl carbonate (1)*

*A. From 9-fluorenylmethyl chloroformate and N-hydroxysuccinimide·DCHA salt*

To a stirred solution of 14.06 g of Fmoc-chloride (54.4 mmol) in chloroform (100 mL) was added 16.12 g (54.4 mmol) of *N*-hydroxysuccinimide·DCHA salt in portions. The stirring was continued overnight, the precipitate was filtered off and washed with chloroform. The filtrate and washings were combined and washed with 1/3 of the volume each of 10% citric acid, 10% sodium bicarbonate, and water, and dried. The solvent was distilled off *in vacuo* and the residue was recrystallized from chloroform–ether giving 16.5 g (90%) of the title compound, mp 151°C. *Anal.* calcd. for $C_{19}H_{15}NO_5$: C 67.65, H 4.48, N 4.15; found: C 67.85, H 4.60, N 4.05.

*B. From 9-fluorenylmethanol and succinimidyl chloroformate*

To a stirred solution of 7.22 g (36.8 mmol) of 9-fluorenylmethanol and 2.9 g (36.8 mmol) of pyridine in methylene chloride (7.5 mL) was added 6.54 g (36.8 mmol) of succinimidyl chloroformate in methylene chloride (6.5 mL) under cooling with tap water. The stirring was continued for 5 h at room temperature. Ice-water was added, and the organic layer was washed with 1/3 of the volume each of 10% hydrochloric acid (2 times), saturated sodium bicarbonate (2 times), water, and dried. Solvent was removed *in vacuo* and the residue recrystallized from chloroform–ether giving 8.95 g (72%) of the compound **1**, which was identical with the product obtained by method A (identical mp and ir spectra).

*9-Fluorenylmethyl pentachlorophenyl carbonate (2)*

This compound was obtained from 2.58 g (10 mmol) of Fmoc-chloride and 4.47 g (10 mmol) of pentachlorophenol DCHA salt as described for the synthesis A of ester **1**. Crystallization of the product from chloroform afforded 4.0 g (82%) of the title compound, mp 162–164°C. *Anal.* calcd. for $C_{21}H_{11}O_3Cl_5$: C 51.62, H 2.26, Cl 36.28; found: C 51.64, H 2.20, Cl 36.10.

*9-Fluorenylmethyl benzotriazole-1-yl carbonate (3)*

This compound was p ep red from 2.59 g (8.2 mmol) of 1-hydroxybenzotriazol DCHA salt and 2.12 g (8.2 mmol) of fluorenylmethyl chloroformate in methylene chloride (15 mL) as described for the synthesis of ester **1** giving 2.42 g (83%) yield, mp 180°C. *Anal.* calcd. for $C_{21}H_{15}N_3O_3$: C 70.58, H 4.23, N 11.75; found: C 70.76, H 4.39, N 11.17.

*Trichloroethyl succinimidyl carbonate (4)*

This compound was obtained from trichloroethyl chloroformate and the DCHA salt of *N*-hydroxysuccinimide as indicated for preparation of carbonate **1** (method A). Yield, 89%; mp 114–115°C (lit. (3) mp 113°C).

*Benzyl succinimidyl carbonate (5)*

This synthesis was carried out from benzyl chloroformate and the DCHA salt of *N*-hydroxysuccinimide as shown for the preparation of carbonate **1**. Yield, 90%; mp 80–81°C (lit. (2) mp 79–81°C).

N-*(9-Fluorenylmethyloxycarbonyl)*-L-*serine*

To a stirred solution of 525 mg (5 mmol) of L-serine and 420 mg (5 mmol) of sodium bicarbonate in a mixture of water (7 mL) and acetone (7 mL) was added 1.68 g (5 mmol) of reagent **1**. After stirring overnight the mixture was acidified to pH 2 with concentrated hydrochloric acid and acetone was removed *in vacuo*. The product was taken up in chloroform and washed with 0.1 *N* HCl and water. The combined organic phases were dried, evaporated *in vacuo*, and the residue was crystallized.

N-*Trichloroethoxycarbonyl*-L-*serine*

To a stirred solution of 526 mg (5 mmol) of L-serine and 420 mg (5 mmol) of sodium bicarbonate in water (10 mL) and tetrahydrofurane (5 mL) was added 1.45 g (5 mmol) of reagent **4**. The mixture was stirred overnight, acidified with concentrated hydrochloric acid, the organic solvent was distilled off, and the aqueous layer was extracted with chloroform (3 × 5 mL). The combined extracts were washed with water, dried, and evaporated *in vacuo*, and the crude product was recrystallized.

N-*Trichloroethoxycarbonyl*-L-*valine*

This compound was obtained from 117 mg (1 mmol) of L-valine and (1 mmol) of carbonate **4** as shown for the synthesis of Tec-Ser-OH.

N-*Benzyloxycarbonyl*-L-*serine*

To a stirred solution of 525 mg (5 mmol) of L-serine and 420 mg (5 mmol) of sodium bicarbonate in a mixture of water (7 mL) and acetone (7 mL) was added 1.24 g (5 mmol) of ester **5**. The mixture was stirred overnight, acetone was removed *in vacuo*, and the solution was washed twice with methylene chloride (3 mL). The aqueous layer was acidified to pH 2.5 by concentrated hydrochloric acid and extracted with ethyl acetate (3 × 5 mL). The combined ethyl acetate layers were washed with water, dried, solvent removed *in vacuo*, and the residue recrystallized.

N-*(9-Fluorenylmethyloxycarbonyl)*-L-*threonine*

This compound was prepared from 119 mg (1 mmol) of L-threonine and 337 mg (1 mmol) of reagent **1** following the procedure described for the preparation of Fmoc-Ser-OH. It was crystallized as its DCHA salt by adding 181 mg (1 mmol) of dicyclohexylamine to the crude product in ethyl acetate. The mixture was stirred for 2 h, the volume was reduced *in vacuo*, ether was added, and the crystalline product was separated by filtration.

*9-Fluorenylmethyloxycarbonyl*-L-*valine*

This derivative was obtained from 117 mg (1 mmol) of L-valine and 337 mg (1 mmol) of reagent **1** using the procedure described for Fmoc-Ser-OH.

N-*(9-Fluorenylmethyloxycarbonyl)*-L-*serine benzyl ester*

A solution of 232 mg (1 mmol) of L-serine benzyl ester hydrochloride, 0.21 mL of triethylamine (1.5 mmol), and 337 mg (1 mmol) of ester **1** in methylene chloride (5 mL) was stirred at room temperature for 2 h. The mixture was washed with 0.1 *N* hydrochloric acid and water, the organic phase was dried, and the residue was recrystallized after removal of the solvent.

N-*(9-Fluorenylmethyloxycarbonyl)*-L-*tyrosine benzyl ester*

A solution of 271 mg (1 mmol) of tyrosine benzyl ester and 337 mg (1 mmol) of compound **1** in chloroform (5 mL) was stirred at room temperature overnight. The mixture was washed with water (3× 1 mL) and dried. The solvent was removed *in vacuo* and the residue was recrystallized.

## Acknowledgements

The author thanks Mr. M. Bergeron for technical assistance and Mr. G. Morris (Analytical Services,

C.B.R.I., Agriculture Canada) for carrying out the microanalyses. The author is grateful for the invaluable comments from one of the referees.

1. M. BODANSZKY, Y. S. KLAUSNER, and M. A. ONDETTI. *In* Peptide synthesis. 2nd ed. J. Wiley, New York. 1976. p. 32.
2. H. GROSS and L. BILK. Ann. Chem. **725**, 212 (1969).
3. A. PAQUET. Can. J. Chem. **57**, 2775 (1979).
4. L. A. CARPINO and G. Y. HAN. J. Org. Chem. **37**, 3404 (1972).
5. J. MEIENHOFER, M. WAKI, E. P. HEIMER, T. J. LAMBROS, R. C. MAKOFSKE, and C.-D. CHANG. Int. J. Peptide Protein Res. **13**, 35 (1979).
6. E. ATHERTON, C. J. LOGAN, and R. C. SHEPPARD. J. Chem. Soc. Perkin Trans. I, 538 (1981).
7. A. BODANSZKY, M. BODANSZKY, N. CHANDRAMOULI, J. Z. KWEI, J. MARTINEZ, and J. C. TOLLE. J. Org. Chem. **45**, 72 (1980).
8. C.-D. CHANG, M. WAKI, M. AHMAD, J. MEIENHOFER, E. O. LUNDELL, and J. D. HAUG. Int. J. Peptide Protein Res. **15**, 59 (1980).
9. T. B. WINDHOLZ and D. B. R. JOHNSTON. Tetrahedron Lett. 2555 (1967).
10. H. YAJIMA, H. WATABANE, and M. OKAMOTO. Chem. Pharm. Bull. (Tokyo) **19**, 2185 (1971).
11. J. F. CARSON. Synthesis, 268 (1981).
12. R. GEIGER and W. KÖNIG. *In* The peptides. Vol. 3. *Edited by* E. Gross and J. Meienhofer. Academic Press, New York. 1981. p. 27.
13. C. J. COLLINS. J. Am. Chem. Soc. **70**, 2418 (1948).
14. T. CURTIUS. J. Prakt. Chem. **24**, 239 (1881); **26**, 145 (1882).
15. T. WIELAND and R. SEHRING. Ann. Chem. **569**, 122 (1950).
16. J. P. GREENSTEIN and M. WINITZ. *In* Chemistry of the amino acids. Vol. 2. J. Wiley, New York. 1961. p. 928.
17. R. B. MERRIFIELD. J. Biol. Chem. **232**, 43 (1958).
18. E. BAER and J. MAURUKAS. J. Biol. Chem. **212**, 25 (1955).
19. C. H. HASSAL and J. O. THOMAS. J. Chem. Soc. C, 1495 (1968).
20. R. WADE and F. BERGEL. J. Chem. Soc. C, 592 (1967).

Can. J. Chem. Downloaded from www.nrcresearchpress.com by 210.87.254.105 on 09/06/12
For personal use only.

# Étude comparée de trois antibiotiques ionophores: X.537 A (lasalocide), A.23187 (calcimycine) et X.14547 A. Complexation des cations IA et IIA, transport de $Ca^{++}$

JEAN BOLTE, COLETTE DEMUYNCK ET GEORGES JEMINET

*Laboratoire de Chimie Organique Biologique, E.R.A. 392 du C.N.R.S., Université de Clermont II, B.P. 45, 63170 Aubiere, France*

ET

JEAN JUILLARD ET CLAUDE TISSIER

*Laboratoire des Interactions Soluté–Solvant, Université de Clermont II, B.P. 45, 63170 Aubiere, France*

Reçu le 5 octobre 1981

JEAN BOLTE, COLETTE DEMUYNCK, GEORGES JEMINET, JEAN JUILLARD et CLAUDE TISSIER. Can. J. Chem. **60**, 981 (1982).

Nous avons déterminé par une méthode potentiométrique, la stoechiométrie et la stabilité des associations formées dans le méthanol, entre ces trois ionophores naturels et les cations alcalins et alcalino-terreux. Avec les alcalins, ils forment des complexes neutres de stoechiométrie 1:1 pour X.537 A et A.23187, 2:1 pour X.14547 A. Des complexes de plus grande stabilité sont obtenus avec les divalents, correspondant à des associations 1:1 chargées et 2:1 neutres. A.23187 et X.14547 A ont un comportement comparable quant aux séquences de formation des deux types de complexes mais les constantes sont beaucoup plus élevées pour le premier cité. Pour X.537 A, l'existence du complexe 2:1 n'est pratiquement pas décelable par la méthode utilisée, sauf dans le cas du magnésium.

Nous avons également étudié le transport du calcium par ces ionophores dans une cellule modèle: phase aqueuse/phase chloroformique/phase aqueuse. Nous tentons de relier les flux ioniques obtenus aux constantes d'équilibre précédentes.

JEAN BOLTE, COLETTE DEMUYNCK, GEORGES JEMINET, JEAN JUILLARD, and CLAUDE TISSIER. Can. J. Chem. **60**, 981 (1982).

Using a potentiometric method, both the stoechiometry and the stability of complexes formed in methanol between the three natural ionophores and cations $I_A$ and $II_A$ have been obtained. With alkali metal ions, neutral complexes of stoechiometry 1:1 for X.537 A and A.23187, 2:1 for X.14547 A are formed. Complexes of higher stability are obtained with alkaline-earth cations, corresponding to two types of association; 1:1 charged and 2:1 neutral. A.23187 and X.14547 A show similar behaviour as far as the sequence of formation of these two complexes is concerned, but the stability constants are higher for the first one. For X.537 A, the existence of a 2:1 complex is not detectable by our method, except for magnesium.

Calcium transport by these ionophores through a cell such as: aqueous phase/chloroformic phase/aqueous phase has also been studied. An attempt is made to relate ionic fluxes to the preceding equilibrium constants.

## Introduction

L'étude des phénomènes de transport cationique à travers les membranes connaît un développement important. Celui-ci est lié, en particulier, à la découverte de nouveaux antibiotiques, dont la propriété fondamentale est de s'associer spécifiquement aux cations alcalins ou alcalino-terreux, et de permettre sous cette forme, le passage de ces cations à travers les phases membranaires. Ces ionophores (1) d'origine bactérienne sont devenus, de ce fait, des outils d'exploration très utilisés en biologie expérimentale (2). Ils présentent des structures polydentées macrocycliques neutres (peptides, depsipeptides, macrotétrolides) (3) ou en chaîne ouverte (acides carboxyliques polyéthers) (4).

Au fil des années, ce deuxième groupe d'ionophores a pris une grande importance en raison du nombre de représentants qui ont été isolés. Actuellement, plus de soixante composés de ce type sont connus; ce sont essentiellement des transporteurs biologiques des cations alcalins et notamment de $K^+$, quelques composés transportent cependant plus sélectivement $Ca^{++}$ ou $Mg^{++}$, pour cette raison ils offrent un intérêt particulier. Les principaux connus à ce jour sont X.537 A (lasalocide) (5), A.23187 (calcimycine) (6), X.14547A (7) et ionomycine (8). Dans ce travail, nous nous intéresserons aux trois premiers mentionnés (Fig. 1).

Le mécanisme du transport membranaire d'un cation, par l'intermédiaire d'un transporteur, peut être discuté en considérant les grandes étapes suivantes: (*1*) formation d'une association transporteur–cation, soit en solution, soit à l'interface membrane–solution; (*2*) diffusion du complexe liposoluble à travers la membrane; (*3*) dissociation du complexe à l'autre interface ou dans la solution; (*4*) diffusion en retour du transporteur vers le premier interface. L'efficacité globale du transport semble déterminée, pour l'essentiel, par les étapes (*1*) et (*3*) (9); celles-ci présentent une similitude avec les processus correspondants de formation et de dissociation des complexes en milieu homogène qui sont plus faciles à étudier.

Ces observations d'un caractère général, permettent de comprendre la motivation des études

0008-4042/82/080981-09$01.00/0

©1982 National Research Council of Canada/Conseil national de recherches du Canada

Can. J. Chem. Downloaded from www.nrcresearchpress.com by 210.87.254.40 on 09/06/12
For personal use only.

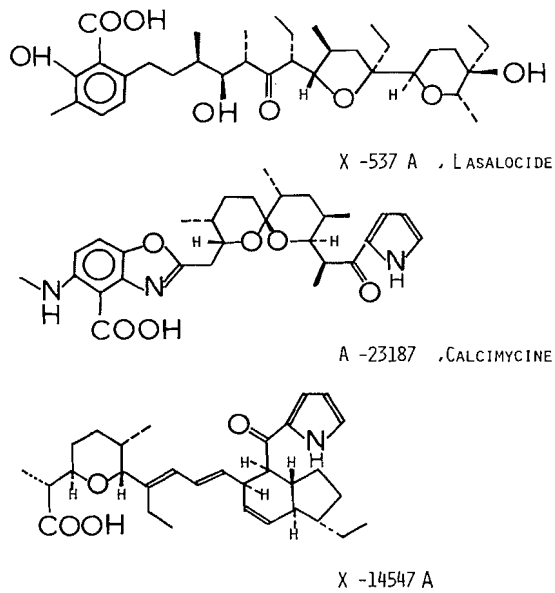


FIG. 1. Structure des trois ionophores étudiés.

entreprises depuis quelques années dans le domaine de la complexation et du transport des cations.

Pour le cas des deux ionophores X.537 A (10) et A.23187 (11), on a peu, jusqu'à présent, examiné dans le détail les équilibres de complexation en milieu homogène; par ailleurs, les études de transport sont généralement effectuées dans des membranes biologiques (mitochondries, reticulum sarcoplasmique, etc.) ou des bicouches artificielles, dans des zones de pH peu étendues, qui rendent difficiles des comparaisons entre ces transporteurs naturels. L'ionophore X.14547 A n'a fait l'objet d'aucune étude.

Dans un travail précédent, nous avons déterminé la stabilité des associations de A.23187 avec les cations alcalins et alcalino-terreux, dans le méthanol à 25°C (12). Le choix du solvant est imposé par l'insolubilité des composés dans l'eau; la plupart des études en milieu homogène sont généralement effectuées dans le méthanol, considéré comme le solvant protique le plus proche de l'eau. Nous poursuivons ici ces mesures, dans les mêmes conditions, en examinant le cas des ionophores X.537 A et X.14547 A. Nous utilisons une méthode complexométrique classique qui consiste à suivre le pH de la solution, lors du dosage de l'antibiotique par une base, ceci en présence ou non d'ions métalliques; les méthodes de calcul faisant intervenir la fonction de formation de Bjerrum permettent de préciser les différents complexes qui se forment (12), et d'apporter des compléments aux résultats antérieurs de Degani et Friedman (13) en ce qui concerne X.537 A.

Dans la suite de ce travail, nous nous intéressons plus précisément au transport de $Ca^{++}$ d'une phase aqueuse de départ à une phase aqueuse d'arrivée, à travers une "membrane liquide épaisse" constituée par du chloroforme qui contient l'un des ionophores. La comparaison des flux ioniques permet de discuter les aptitudes respectives des trois transporteurs. Les résultats obtenus, fonctions du pH des phases aqueuses, sont reliés aux constantes d'équilibre mesurées dans le méthanol.

## Partie expérimentale

*Obtention des ionophores*

X.537 A (ou lasalocide) est disponible commercialement (Sigma) sous la forme de son sel de sodium, il a été traité pour obtenir l'acide libre. A.23187 (ou calcimycine) est isolé à partir d'une culture en fermenteur de la souche de *Streptomyces chartreusis* NRRL 3882, selon un procédé qui a été décrit (12).

L'antibiotique X.14547 A est isolé à partir d'une souche de *Streptomyces antibioticus* NRRL 8167. La culture de la souche est réalisée en fermenteur de 20 L, dans le milieu suivant pour 1 litre d'eau: glucose 10 g, mélasses de sucrerie 20 g, soyoptim 5 g, $CaCO_3$ 2 g, extrait de levure Mérieux 1 g. Le pH de départ est ajusté à 7,2. On utilise l'antimousse B Rhône-Poulenc. On maintient la quantité d'air dissous à 90%. L'agitation est de 620 tours/min à 27°C. Après 6 jours de culture, on sépare le mycelium par centrifugation. Le jus est extrait trois fois par l'acétate d'éthyle, le mycelium finement broyé est extrait deux fois à l'éthanol. Les différentes solutions organiques sont concentrées à l'évaporateur cyclone. Le résidu total est repris par HCl 0,1 *N*, puis extrait à l'éther. L'huile brunâtre résiduelle est purifiée par chromatographie sur colonne (kieselgel 60 Merck, 70–230 mesh ASTM) avec un gradient d'élution cyclohexane–éther puis cyclohexane – acétate d'éthyle. La structure de l'antibiotique ainsi isolé a été vérifiée par comparaison de ses propriétés physiques avec celles d'un échantillon authentique fourni généreusement par le docteur J. W. Westley, à l'aide des techniques suivantes: spectrométrie de masse I.E., polarimétrie, spectroscopies infrarouge et uv–visible, rmn $^1H$ et $^{13}C$. Les résultats obtenus sont en accord avec ceux publiés (21).

*Mesures complexométriques dans le méthanol*

Les solvants et réactifs utilisés, la technique des mesures potentiométriques ainsi que le traitement des valeurs ont été présentés dans la référence 12.

*Mesures du transport de $Ca^{++}$*

La cellule utilisée est un tube en U (Fig. 2). Les valeurs de flux mesurées sont fonctions des conditions expérimentales (forme de la cellule, agitation, température, concentrations relatives cation–ionophore). Pour cette étude comparative, un protocole très bien défini a été suivi.

La cellule est thermorégulée 25.0 + 0.1°C par une circulation d'eau. Diamètre intérieur du tube: 11 mm. Volumes des phases A et C: 4 mL, de la phase B: 9 mL. Agitation des phases A et C par des agitateurs constitués d'une baguette de verre (diamètre 3 mm), terminée par une pale rectangulaire de 6 × 3 mm, mue par un petit moteur électrique synchrone tournant à 600 tours/min. Le bas de la pale est situé à 20 mm de l'interface eau/chloroforme. La phase B est agitée par un barreau magnétique cylindrique (diamètre 2 mm, hauteur 10 mm), tournant à 600 tours/min.

Can. J. Chem. Downloaded from www.nrcresearchpress.com by 210.87.254.40 on 09/06/12
For personal use only.

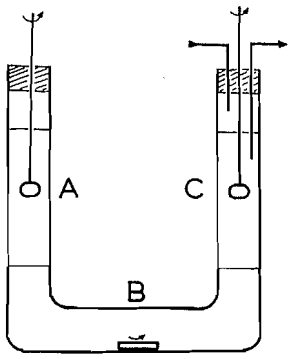


FIG. 2. Schéma de la cellule de transport utilisée.

Les solutions aqueuses sont tamponnées par un mélange tricine–triéthanolamine $10^{-2}$ *M* ou tricine – hydroxyde de tétraméthyl ammonium pour les pH supérieurs à 8. La phase aqueuse d'arrivée contient un indicateur de $Ca^{++}$, l'arsenazo III (Fluka) à la concentration $2 \times 10^{-4}$ *M* ce qui permet un dosage en continu du cation grâce à un système à circulation passant dans la cuve d'un spectrophotomètre (Beckman DU 8), lecture à 650 nm. La concentration du calcium dans cette phase ne dépasse jamais $4 \times 10^{-5}$ *M*; lorsque cette valeur est atteinte, la solution est renouvelée, le pH est toujours maintenu à 7,0. La solution aqueuse de départ contient $Ca(ClO_4)_2$ (Merck) à la concentration $10^{-2}$ *M*, le pH est mesuré avec une précision de 0,02 unités. La phase B est constituée de chloroforme, préalablement saturé d'eau, qui contient l'ionophore à la concentration $4 \times 10^{-4}$ *M*. En l'absence d'ionophore, aucun apport de calcium n'est observé dans la phase C.

On mesure le flux d'ions $Ca^{++}$ exprimé en mol $s^{-1}$ $cm^{-2}$. Au cours de l'expérience, ce flux augmente d'abord en fonction du temps puis reste constant. La première période correspond à l'établissement du régime quasi-stationnaire.

Chaque point des courbes a, b, c de la figure 3 est obtenu dans les conditions où le flux est constant. Le spectrophotomètre muni d'un calculateur donne une valeur du flux toutes les 5 min; la durée de chaque expérience, pour un pH donné, est comprise entre 1 h et 4 h. La précision sur la mesure du flux est de l'ordre de 5%.

## Résultats

### A. *Complexation des cations alcalins et alcalino-terreux dans le méthanol*

Si l'on désigne respectivement par $M^+$ et $M^{++}$ le cation alcalin et alcalino-terreux, par AH l'ionophore carboxylique sous sa forme protonée; les différents équilibres mis en évidence au cours de cette étude s'écrivent:

avec $H^+$ [1] $AH \rightleftharpoons A^- + H^+$

avec $M^+$ [2] $A^- + M^+ \rightleftharpoons AM$

[3] $A^- + AH + M^+ \rightleftharpoons A_2HM$

avec $M^{++}$ [4] $A^- + M^{++} \rightleftharpoons AM^+$

[5] $2A^- + M^{++} \rightleftharpoons A_2M$

Dans ce qui suit, les constantes de formation $\beta_1$–$\beta_5$ correspondent aux équilibres [1]–[5].

#### 1. *X.537 A (lasalocide)*

Les résultats obtenus pour les deux séries de cations sont rassemblés dans les tableaux 1 et 2 où figurent également les résultats précédemment acquis pour A.23187 (12). Pour X.537 A, la constante de formation $\beta_5$ du complexe 2:1 avec les cations divalents, est le plus souvent très faible et hormis dans le cas du magnésium, il n'a pas été possible d'obtenir la valeur numérique de cette constante.

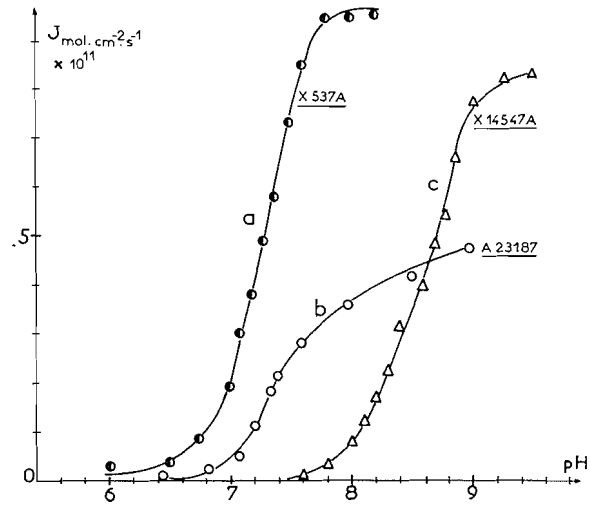


FIG. 3. Variations du flux ionique en fonction du pH du compartiment de départ.

Sur la figure 4 sont reportées les courbes de titrage de l'antibiotique en présence des divers cations métalliques. Pour calcium, strontium et baryum on note une formation quasi-totale du complexe 1:1, $AM^+$ qui correspond au premier palier. La neutralisation de l'antibiotique restant par la base correspond au second palier. A ce niveau, le fait que les courbes représentatives du dosage soient alors confondues est significatif; il n'y a pour aucun de ces cations de formation notable de sel complexe 2:1, $A_2M$.

Dans le cas du magnésium par contre, le calcul

TABLEAU 1. Constantes de formation $\beta_2$ des sels complexes 1:1 (éq. [2]) avec les cations monovalents, dans le méthanol à 25,0°C (échelle molaire)

| | X.537 A (lasalocide) | | A.23187 (calcimycine) |
|---|---|---|---|
| Cation | $\log \beta_2$[a] | $\log \beta_2$[b] | $\log \beta_2$[c] |
| $H^+$ | 8,23 | 7,6 | 10,94 |
| $Li^+$ (0,78 Å)[d] | 1,44 | 1,68 | 4,1 |
| $Na^+$ (0,98 Å) | 2,61 | 2,57 | 3,4 |
| $K^+$ (1,33 Å) | 3,45 | 3,58 | 2,4 |
| $Rb^+$ (1,49 Å) | 3,39 | 3,56 | 2,0 |
| $Cs^+$ (1,65 Å) | 3,36 | 3,43 | 1,9 |

[a]Nos valeurs.
[b]Référence 13.
[c]Référence 12.
[d]Rayon ionique de Goldschmidt.

Can. J. Chem. Downloaded from www.nrcresearchpress.com by 210.87.254.40 on 09/06/12
For personal use only.

Can. J. Chem. Downloaded from www.nrcresearchpress.com by 210.87.254.40 on 09/06/12
For personal use only.

TABLEAU 2. Constantes de formation des complexes avec les cations alcalino-terreux (éqs. [4] et [5]), dans le méthanol à 25,0°C (échelle molaire)

| | X.537 A (lasalocide) | | | X.14547 A | | A.23187 (calcimycine) | |
|---|---|---|---|---|---|---|---|
| Cation | log $\beta_4$[a] | log $\beta_4$[b] | log $\beta_5$[a] | log $\beta_4$[a] | log $\beta_5$[a] | log $\beta_4$[c] | log $\beta_5$[c] |
| $Mg^{++}$ (0,78 Å)[d] | 4,12 | 3,83 | 6,07 | 4,77 | 7,61 | 7,6 | 15,9 |
| $Ca^{++}$ (1,06 Å) | 4,88 | 4,57 | | 4,80 | 7,89 | 8,2 | 16,2 |
| $Sr^{++}$ (1,27 Å) | 5,60 | 5,47 | | 4,05 | 6,52 | 6,7 | 14,2 |
| $Ba^{++}$ (1,43 Å) | 6,58 | 6,46 | | 3,63 | 6,10 | 6,2 | 12,4 |

[a]Nos valeurs.
[b]Référence 13.
[c]Référence 12.
[d]Rayon ionique de Goldschmidt.

par des méthodes déjà décrites (12) a permis d'accéder aux deux constantes de formation ($\beta_4$ et $\beta_5$).

On peut remarquer sur les tableaux 1 et 2, le bon accord entre nos résultats et ceux de Degani et Friedman (13), si l'on tient compte du fait que la méthode utilisée est différente. Une divergence existe en ce qui concerne le p$K_a$ de l'acide (éq. [1]); la valeur obtenue ici 8,23 peut être comparée à celle de l'acide salicylique dans le même milieu 7,79 (14); un affaiblissement de cet ordre de grandeur de l'acidité pouvait être attendu du fait de la substitution du cycle aromatique.

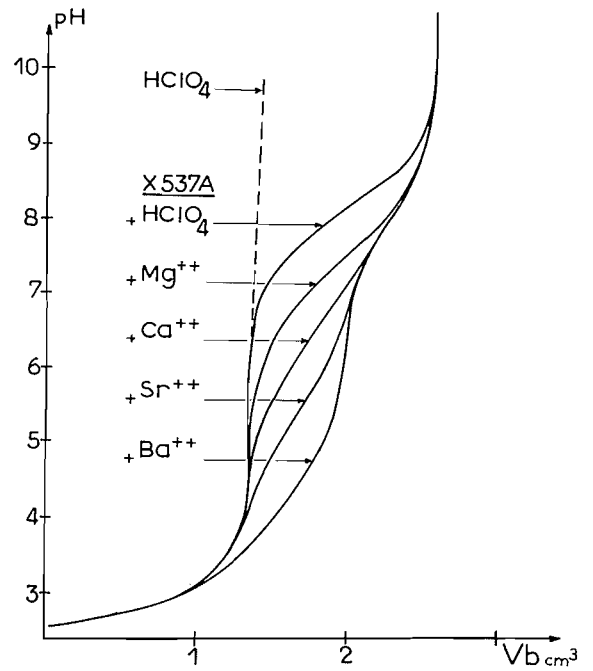


FIG. 4. Courbes de titrages de l'ionophore X.537 A (lasalocide) en présence d'acide perchlorique par le méthoxyde de tétrabutylammonium, ceci en l'absence et en présence des divers perchlorates alcalins: pH en fonction du volume de solution basique $V_b$ ajouté.

2. *X.14547 A*

La constante de dissociation de la fonction acide carboxylique mesurée (p$K_a$ = 10.22) est voisine de celle obtenue précédemment pour des antibiotiques ionophores polyéthers du même groupe spécifiques des alcalins: grisorixine, 10.24; nigéricine, 10.32; alborixine, 10.29 (15); qui présentent un groupement terminal substitué analogue, il s'agit d'un acide propionique 2-tétrahydropyranyl di- ou trisubstitué sur le cycle.

Pour ce composé, les courbes obtenues en potentiométrie avec les cations alcalino-terreux sont facilement interprétées si l'on prend en considération les équilibres [4] et [5], les valeurs $\beta_4$ et $\beta_5$ correspondantes sont mentionnées dans le tableau 2. Une certain nombre d'essais ont été effectués avec les cations alcalins, ils ont permis de montrer que la complexation de $Li^+$ est pratiquement inexistante, celles de $K^+$ et $Rb^+$ par contre bien que faibles, ne sont pas totalement négligeables. Le traitement des données conduit à privilégier la formation de complexe AH $A^-$ $M^+$ (éq. [3]). Les résultats obtenus sont particulièrement probants avec $Rb^+$ (log $\beta_3$ = 5.2 ± 0.1), $K^+$ donne une constante de formation du même ordre de grandeur mais avec une incertitude plus grande.

B. *Transport de $Ca^{++}$ à travers une membrane liquide*

Dans les expériences effectuées, à l'aide d'un système à trois phases, eau/chloroforme/eau, le pH du compartiment aqueux de départ varie entre 5,0 et 9,0. L'ensemble des résultats obtenus pour $Ca^{++}$, dans des conditions expérimentales identiques (voir Partie expérimentale) est représenté sur la figure 3. Nous pouvons affirmer que les trois ionophores étudiés présentent une aptitude à transporter l'ion calcium à travers une membrane liquide chloroformique, ce transport dépend du pH. Considérons l'exemple de X.537 A (courbe a), à pH < 6 le flux de calcium est inférieur à $10^{-12}$ mol $s^{-1}$ $cm^{-2}$ qui est la limite inférieure de sensibilité de

TABLEAU 3. Flux ioniques exprimés en mol $s^{-1}$ $cm^{-2}$ pour $Ca^{++}$, dans une cellule à trois phases eau/$CHCl_3$/eau

| Ionophore | $J_{max} \times 10^{11}$ | $pH_{1/2}$[a] | $pK_a$ (MeOH) |
|---|---|---|---|
| X.537 A (lasalocide) | 10,2 | 7,3 | 8,23 |
| A.23187 (calcimycine) | 5,2 | 7,5 | 10,94 |
| X.14547 A | 8,2 | 8,6 | 10,22 |

[a] $pH_{1/2}$ = pH pour lequel $J = J_{max}/2$.

notre méthode. $J$ augmente jusqu'à atteindre une valeur limite $J_{max}$ pour pH > 7,8. Le même type de courbe sigmoïde est obtenue pour les deux autres composés, mais dans des zones de pH différentes. X.14547 A (courbe c) diffère des deux autres ionophores en ce qui concerne la zone de pH du transport très déplacée vers les domaines basiques. A noter que dans le cas de la calcimycine (courbe b) la valeur $J_{max}$ est entachée d'imprécision en raison de la faible solubilité du complexe calcique aux pH élevés qui tend à cristalliser à l'interface eau–chloroforme. Pour chacune des courbes, on définit une valeur $pH_{1/2}$ correspondant au point où le flux est égal à $J_{max}/2$ (Tableau 3). Cette valeur ne varie pas sensiblement suivant les conditions expérimentales (cellule, agitation, concentrations en $Ca^{++}$ et ionophore), contrairement à celle de $J_{max}$ qui en dépend.

## Discussion

Les trois antibiotiques étudiés ont fait l'objet de déterminations cristallographiques aux rayons X sur les acides libres ou leurs sels complexes, la conformation des squelettes et le mécanisme d'encagement des cations se trouvent donc précisés à l'état solide. A cet égard, X.537 A a donné lieu à de nombreux travaux sur différents complexes avec $Ag^+$ (16), $Ba^{++}$ (17) et $Na^+$ sous la forme monomère (10) ou dimère (18) et sur l'acide libre cristallisé avec une molécule de méthanol (19). La structure de A.23187 a été élucidée sur son acide libre (6), le complexe dimérique avec $Ca^{++}$ a également été étudié (20). On ne dispose actuellement que d'une seule étude cristallographique, concernant un dimère particulier (21), pour X.14547 A. Ces données structurales sont complétées par des mesures spectroscopiques en solution, par résonance magnétique nucléaire dans différents solvants pour X.537 A (22) et A.23187 (23). On ne discutera pas dans le détail, les résultats qui ont été acquis dans ce domaine.

La connaissance de la stabilité thermodynamique des associations avec des cations de différentes tailles, dans une même série, apporte des éléments d'information supplémentaires concernant la nature des associations en solution. C'est ce point que nous nous proposons de développer en relation avec les études structurales citées.

*Complexation des alcalins*

Pour X.537 A, l'ordre d'association s'écrit $Cs^+ \sim Rb^+ \sim K^+ > Na^+ \gg Li^+$, il n'y a pas de spécificité marquée pour un cation, comme dans le cas de la grisorixine ou la monensine (12), par ailleurs le maximum de stabilité observé pour $K^+$ n'excède pas 3,5 ($\log \beta_2$). Deux éléments structuraux se conjugent pour entraîner cette sélectivité médiocre: la longueur trop faible de la chaîne complexante et les irrégularités qui existent dans la disposition des sites oxygènes donneurs. La structure du sel de sodium, étudiée par Chiang et Paul (10) fait apparaître assez clairement ces deux points.

Quant à la calcimycine, une inversion véritable s'opère dans la séquence: $Li^+ > Na^+ > K^+ > Rb^+ \sim Cs^+$. Seul $Li^+$ (0,78 Å) doit pouvoir se loger dans la cavité ménagée par la molécule repliée dont l'existence est mise en évidence dans la structure cristalline de l'acide libre (6). On note une constante très faible pour $K^+$: 2,4 ($\log \beta_2$).

Il s'agit ici de la première étude de complexes des alcalins avec X.14547 A. Le type de complexes obtenus est différent des deux ionophores précédents; il implique la participation d'une molécule d'acide et de son anion dans une association 2:1 avec le cation, telle qu'on l'a déjà observée dans la structure cristalline avec l'ion R(+) bromo-4 phényl-1 éthyl ammonium (21). Cette différence de comportement est très vraisemblablement liée à la structure particulière du composé. L'examen des modèles moléculaires montre qu'une conformation repliée de la chaîne ne laisse pas apparaître une cavité complexante permettant l'accueil d'un cation, ce qui est dû en particulier à la géométrie de la molécule, imposée par le groupement *trans*-butadiényle et la conformation bloquée du tétrahydroindane; seule des associations du type 2:1 semblent possibles à réaliser si l'on se réfère à l'étude cristallographique (21).

*Complexation des alcalino-terreux*

Sur la figure 5 sont comparées les constantes de formation des complexes 1:1 et 2:1, correspondant aux équilibres

[4] $A^- + M^{++} \rightleftharpoons AM^+$

et

[6] $AM^+ + A^- \rightleftharpoons A_2M$

A.23187 a déjà été discutée (12), cette molécule qui présente un nombre faible de degrés de liberté de rotation dans sa chaîne est remarquablement construite pour s'associer à $Ca^{++}$ et $Mg^{++}$, dans un

Can. J. Chem. Downloaded from www.nrcresearchpress.com by 210.87.254.40 on 09/06/12
For personal use only.

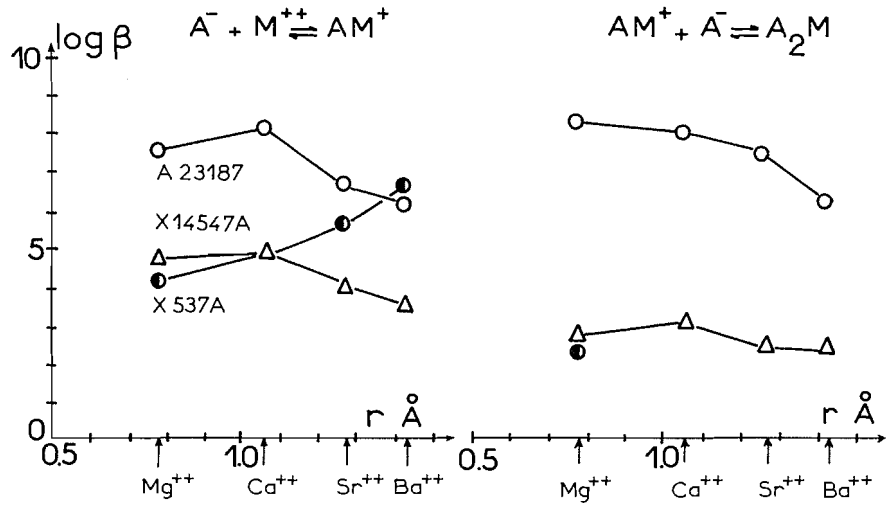


FIG. 5. Constantes de formations successives, dans le méthanol, des complexes des ions alcalino-terreux avec les trois ionophores: log $\beta_4$ et $\beta_6$ en fonction du rayon ionique de ces ions.

mécanisme en deux étapes bien définies. En effet, si on considère les constantes de formation successives, on peut noter qu'elles sont pour chacun des cations étudiés, du même ordre de grandeur. Ceci est assez inhabituel; le plus souvent, comme il est observé ici pour X.14547 A, les constantes de stabilité décroissent au fur et à mesure qu'augmentent le nombre de coordinats participants au complexe. Pour ces deux ionophores la séquence de formation des deux types de complexes est analogue: $Ca^{++} \sim Mg^{++} > Sr^{++} > Ba^{++}$, mais les constantes de stabilité sont beaucoup plus grandes dans le cas de A.23187. Si on possède des informations sur la structure des complexes 2:1 à l'état solide avec $Ca^{++}$ (20) et $Mg^{++}$ (24) ou en solution (23) pour cet ionophore, aucune étude n'a encore été effectuée pour les complexes analogues de X.14547 A. La différence essentielle, déjà soulignée pour ce composé, réside dans la partie centrale de la chaîne *trans*-butadiène qui est totalement différente du spirocétale de A.23187 qui porte et oriente convenablement les deux "bras" où sont situés les sites de complexations et amorce ainsi la formation d'une cavité complexante.

Pour X.14547 A, le complexe 1:1 avec les cations divalents est suffisamment stable pour être pris en compte dans les calculs, ce n'est pas le cas avec les cations monovalents: l'interaction avec les sites de coordination est plus forte avec les cations doublements chargés.

Pour X.537 A, l'association croit d'une manière monotone en fonction de la taille du cation $Ba^{++} > Sr^{++} > Ca^{++} > Mg^{++}$, et pratiquement le complexe 2:1 ne se forme pas dans le méthanol, hormis pour $Mg^{++}$. Il paraît pourtant nécessaire que la charge du métal divalent soit neutralisée dans le complexe pour que le cation puisse migrer à travers la barrière membranaire. De fait, la situation n'est sans doute pas la même dans un milieu apolaire, comme le chloroforme étudié plus loin, ou l'hexane dans lequel Degani et Friedman (13) ont montré que le complexe 2:1 se formait de façon exclusive. Cette tendance à une formation préférentielle du complexe 1:1 en solvant protique, soulignée également par Chiang et Paul (10), peut être rapprochée du fait que dans la structure cristalline du sel 2:1 étudiée avec $Ba^{++}$ (17), une des molécules du ligande joue un rôle privilégié (intervention de six sites coordinants) par rapport à l'autre (intervention de deux sites coordinants).

Pour les trois ionophores, les p$K_a$ des groupements acide carboxylique d'une part et les constantes d'associations avec les cations alcalino-terreux d'autre part diffèrent. Le degré de formation de chacun des complexes varient donc de façon très spécifique avec le pH dans le méthanol, comme cela apparaît sur la figure 6, pour $Ca^{++}$. On notera que dans les domaines de concentrations choisis: pour A.23187 la formation du complexe 1:1 est faible et présente un maximum vers pH ~ 4; elle est beaucoup plus importante pour X.14547, avec un maximum voisin de pH 8. Pour X.537 A, elle est totale à partir d'un pH de l'ordre de 7. Le complexe 2:1 se forme à très bas pH pour A.23187 alors que pour X.14547 A il apparaît vers pH 8.

Les mesures effectuées en phase homogène, dans le méthanol, font ainsi apparaître une nette disparité de comportement de ces trois ionophores avec les cations divalents. On peut se demander comment cette différence se traduit dans un pro-

Can. J. Chem. Downloaded from www.nrcresearchpress.com by 210.87.254.40 on 09/06/12
For personal use only.

Can. J. Chem. Downloaded from www.nrcresearchpress.com by 210.87.254.40 on 09/06/12
For personal use only.

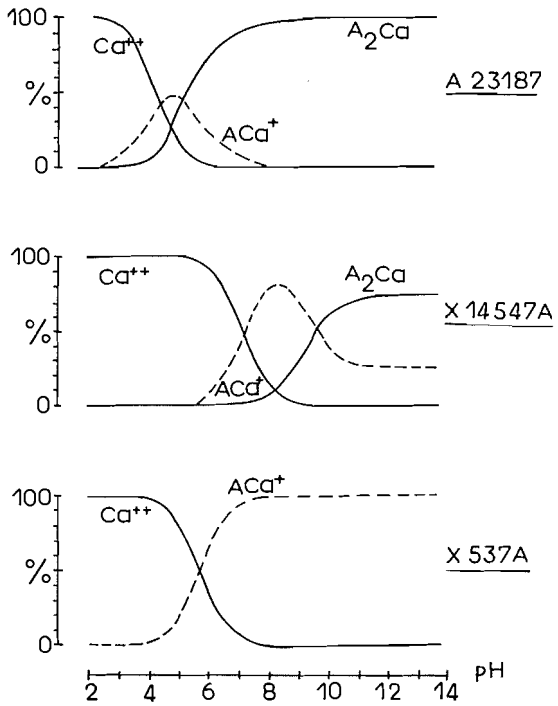


FIG. 6. Courbes de formation, dans le méthanol, des complexes du calcium avec les trois ionophores, en fonction du pH.

cessus de transport membranaire. Nous avons abordé ce problème avec différents types de membranes. Dans le présent travail nous apportons des éléments de réponse dans le cas d'une "membrane épaisse liquide" constituée par du chloroforme. Le cation examiné est $Ca^{++}$ dont l'activité biologique est liée à son mouvement transmembranaire, mouvement que les biologistes ont abondamment étudié ces dernières années en se servant précisément des ionophores X.537 A et A.23187.

*Transport de $Ca^{++}$ à travers une phase chloroformique*

Les variations de flux observées (Fig. 3), pour les trois ionophores étudiés, montrent clairement que la dissociation de la fonction acide est une des étapes importantes du transport. Dans la mesure où les trois phases sont agitées, nous pensons que les processus de diffusion peuvent être négligés et seuls les phénomènes intervenant aux interfaces sont pris en compte. Le fait que les flux observés pour divers ionophores puissent être très différents conforte cette hypothèse. Dans toutes les expériences effectuées, le pH du compartiment d'arrivée est maintenu constant, ce qui autorise une analyse des résultats en se référant seulement au premier compartiment aqueux où a lieu l'extraction du cation par l'ionophore. Dans la succession des équilibres envisageables à l'interface eau/chloroforme, schématisés sur la figure 7 pour un processus limite simple, on voit que la dissociation du transporteur constitue l'étape d'initiation du transport. Les $pK_a$ des ionophores ne sont pas connus à l'interface; nous sommes amenés à supposer qu'il existe une corrélation entre ceux-ci et ceux mesurés dans le méthanol; nous avons fait la même démarche pour les constantes des réactions correspondant aux étapes 2 et 3.

Après l'étude de Reusch et Cussler (25), Kirch et Lehn (26), puis Lamb *et al.* (27) ont pu pour des macrocycles neutres de synthèse, en utilisant une cellule du même type que la nôtre, montrer qu'il existe une relation entre vitesses de transport des cations alcalins et alcalino-terreux et constantes d'associations mesurées dans le méthanol. Dans le cas des transporteurs à fonction dissociable, une étude a été réalisée pour la monensine (28), les auteurs utilisent une cellule à diaphragme imprégné d'octanol. Notre approche expérimentale est différente, la phase intermédiaire chloroformique est agitée, par ailleurs cette étude implique un ionophore carboxylique et un cation divalent, le nombre d'étapes à prendre en considération est nécessairement plus élevé que pour tous les travaux précédemment cités. Il est également vraisemblable que les mécanismes diffèrent d'un ionophore à l'autre. Nous pouvons seulement faire ici, comparant les ionophores deux à deux, un certain nombre de remarques qui découlent de l'examen des tableaux 2 et 3 pour l'ion $Ca^{++}$ et des figures 3 et 5.

A.23187 et X.14547 A ont des $pK_a$ très voisins, ils devraient présenter des valeurs de $pH_{1/2}$ proches si la déprotonation de l'acide était l'étape détermi-

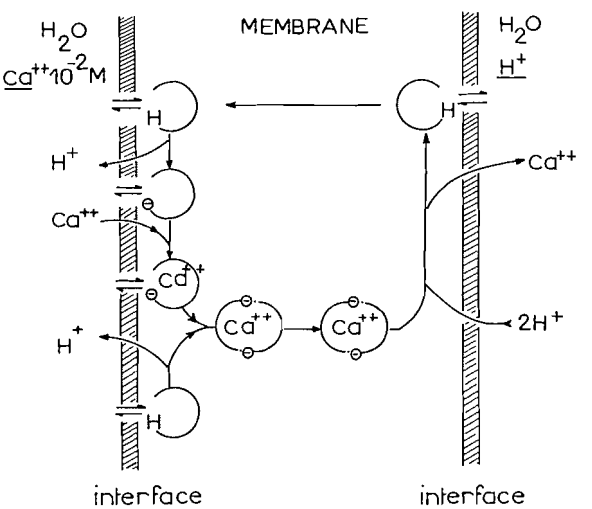


FIG. 7. Schéma limite possible pour l'extraction d'un ion $Ca^{++}$ à l'interface eau/chloroforme (les processus de libération de $Ca^{++}$ à l'autre interface sont en cours d'étude).

Can. J. Chem. Downloaded from www.nrcresearchpress.com by 210.87.254.40 on 09/06/12
For personal use only.

nante; en fait, le premier ionophore a une valeur $pH_{1/2}$ très nettement inférieure ce qui s'explique par des constantes de formation des complexes $\beta_4$ et $\beta_5$ nettement plus élevées. X.14547 A et X.537 A présentent des constantes $\beta_4$ du même ordre de grandeur, leur $pK_a$ diffère nettement; ceci se retrouve sur les valeurs de $pH_{1/2}$ qui varient dans le même sens. A.23187 et X.537 A ont des $pH_{1/2}$ très voisins bien que leurs $pK_a$ soient différents ainsi que leurs constantes $\beta_4$. Les grandeurs $\log \beta_7 = pK_a - \log \beta_4$ représentatives de l'équilibre

[7] $AH + M^{++} \rightleftharpoons AM^{+} + H^{+}$

sont par contre voisines pour les deux ionophores (respectivement 2,7 et 3,8); ceci suggère que la formation du complexe 1:1 à partir de l'acide protonné serait l'étape limitante dans le transport. De nouvelles expériences sont en cours pour vérifier cette hypothèse.

Un certain nombre d'études ont été effectuées dans des membranes beaucoup plus proches de la membrane biologique. Kafka et Holtz (29) utilisent des bicouches de phosphatidylcholine dans lesquelles ils incorporent A.23187 ou X.537 A; les deux composés transportent $Ca^{++}$, mais avec une efficacité supérieure pour A.23187. Caswell et Pressman (30) aboutissent à la même conclusion en utilisant des vésicules reconstitués du réticulum sarcoplasmique. Nous avons fait l'observation inverse: le flux maximum atteint est supérieur pour X.537 A. Dans la cellule à "membrane liquide épaisse" utilisée, seuls les échanges ioniques aux interfaces interviennent dans la cinétique globale du transport, la diffusion du complexe n'étant pas à considérer du fait de l'agitation du compartiment central. Il est vraisemblable que dans le cas d'une membrane bicouche, la vitesse de translocation du complexe formé, d'un interface à l'autre, doit intervenir dans la cinétique globale du transport, de ce fait, les valeurs $J_{max}$ obtenues avec ces deux types de membranes ne sont pas nécessairement comparables.

Wulf et Pohl (31) ont étudié d'une manière approfondie le transport de $Ca^{++}$ par A.23187 dans des bicouches de phosphatidylcholine. Il est intéressant de noter que le flux mesuré est multiplié par 5 lorsque le pH augmente de 6 à 8, ce qui est en bon accord avec nos observations dans la membrane chloroformique, tant du point de vue de l'augmentation du flux que de la zone de pH. Il semble donc que nous puissions, dans une certaine mesure, utiliser notre technique simple pour modéliser le comportement de ces ionophores dans une membrane biologique. X.537 A et A.23187 apparaissent alors comme des transporteurs de $Ca^{++}$ intéressants compte tenu de leur zone de pH efficace, ceci a été amplement prouvé par les études biologiques. Il nous paraît, par contre, peu probable que X.14547 A soit un transporteur efficace de $Ca^{++}$, au pH physiologique.

NOTE: Pendant la soumission de ce travail, une intéressante étude concernant le transport des ions alcalins par des ionophores carboxyliques de synthèse, dans une membrane épaisse liquide, a été publiée dans ce journal (32).

**Remerciement**

Ce travail a été effectué dans le cadre de la RCP 80/605 du C.N.R.S.

1. B. C. PRESSMAN, E. J. HARRIS, W. S. JAGGER et J. H. JOHNSON. Proc. Natl. Acad. Sci. U.S.A. **58**, 1949 (1967).
2. P. W. REED. Methods Enzymol. **55**, 435 (1979).
3. W. SIMON, W. E. MORF et P. CH. MEIER. Struct. Bonding (Berlin), **16**, 113 (1973).
4. J. W. WESTLEY. Adv. Appl. Microbiol. **22**, 177 (1977).
5. J. W. WESTLEY, R. H. EVANS, T. WILLIAMS et A. STEMPEL. J. Chem. Soc. Chem. Commun. 71 (1970).
6. M. O. CHANEY, P. Y. DEMARCO, N. D. JONES et J. C. OCCOLOWITZ. J. Am. Chem. Soc. **96**, 1932 (1974).
7. J. W. WESTLEY, R. M. EVANS, C. M. LIU, T. HERMANN et J. F. BLOUNT. J. Am. Chem. Soc. **100**, 6784 (1978).
8. W. C. LIU, D. S. SLUSARCHYK, G. ASTLE, W. J. TREJO, W. E. BROWN et E. MEYERS. J. Antibiot. **31**, 815 (1978).
9. J. M. LEHN. Struct. Bonding (Berlin), **16**, 1 (1973).
10. C. C. CHIANG et I. C. PAUL. Science, **196**, 1441 (1977).
11. D. R. PFEIFFER, R. W. TAYLOR et H. A. LARDY. Ann. N.Y. Acad. Sci. **307**, 402 (1978).
12. C. TISSIER, J. JUILLARD, G. JEMINET et M. DUPIN. J. Chim. Phys. **76**, 611 (1979).
13. H. DEGANI et H. L. FRIEDMAN. Biochemistry, **24**, 5022 (1974).
14. C. L. DE LIGNY, P. F. M. LUIKX, M. REBACH et A. A. VIENECKE. Recl. Trav. Chim. Pays-Bas, **79**, 699 (1960).
15. Y. POINTUD, J. JUILLARD, G. JEMINET et L. DAVID. J. Chem. Soc. Faraday Trans I, **77**, 1 (1981).
16. C. A. MAIER et I. C. PAUL. J. Chem. Soc. Chem. Commun. 181 (1971).
17. S. M. JOHNSON, J. HERRIN, S. J. LIU et I. C. PAUL. J. Chem. Soc. Chem. Commun. 172 (1970).
18. C. D. SMITH, W. L. DUAX et S. FORTIER. J. Am. Chem. Soc. **100**, 6725 (1978).
19. J. M. FRIEDMAN, D. L. ROUSSEAU, C. SHEN, C. C. CHIANG, E. N. DUESLER et I. C. PAUL. J. Chem. Soc. Perkin Trans. I, 835 (1979).
20. G. D. SMITH et W. L. DUAX. J. Am. Chem. Soc. **98**, 1578 (1976).
21. J. W. WESTLEY, R. H. EVANS, L. H. SELLO, N. TROUPE, C. M. LIU et J. F. BLOUNT. J. Antibiot. **32**, 100 (1979).
22. (*a*) D. J. PATEL et C. SHEN. Proc. Natl. Acad. Sci. U.S.A. **73**, 1786 (1976); (*b*) C. SHEN et D. J. PATEL. Proc. Natl. Acad. Sci. U.S.A. **73**, 4277 (1976).
23. M. J. O. ANTEUNIS. Bioorg. Chem. **6**, 1 (1977).
24. M. ALLEAUME, Y. BARRANS et G. JEMINET. Acta Crystallogr. B. Soumis.
25. C. F. REUSCH et E. L. CUSSLER. A.I. Ch. E. J. **19**, 736 (1973).

26. M. KIRCH et J. M. LEHN. Angew. Chem. Int. Ed. Engl. **14**, 555 (1975).
27. J. D. LAMB, J. J. CHRISTENSEN, J. L. OSCARSON, B. L. NIELSEN, B. W. ASAY et R. M. IZATT. J. Am. Chem. Soc. **102**, 6820 (1980).
28. E. M. CHOY, D. F. EVANS et E. L. CUSSLER. J. Am. Chem. Soc. **96**, 7085 (1974).
29. M. S. KAFKA et R. W. HOLTZ. Biochim. Biophys. Acta, **426**, 31 (1976).
30. A. H. CASWELL et B. C. PRESSMAN. Biochem. Biophys. Res. Commun. **49**, 292 (1972).
31. J. WULF et W. G. POHL. Biochim. Biophys. Acta, **465**, 471 (1977).
32. T. M. FYLES, V. A. MALIK-DIEMER et D. M. WHITFIELD. Can. J. Chem. **59**, 1734 (1981).

Can. J. Chem. Downloaded from www.nrcresearchpress.com by 210.87.254.40 on 09/06/12
For personal use only.

# Aryl radicals from hexazadienes and tetrazenes

DONALD MACKAY AND DEANE DOUGLAS MCINTYRE

*Guelph–Waterloo Centre for Graduate Work in Chemistry, University of Waterloo, Waterloo, Ont., Canada N2L 3G1*

Received September 29, 1981

DONALD MACKAY and DEANE DOUGLAS MCINTYRE. Can. J. Chem. **60**, 990 (1982).

Aryl radicals are produced from both ends of the hexazadienes **1** and **2** and from the tetrazene **3**, either thermally or photolytically. They attack aromatic compounds in the nucleus, the yield of biaryl being in the range 40–70%, though it can be made nearly quantitative by using *m*-dinitrobenzene as an additive. The aryl radicals also oxidize 2-propanol to acetone, the reduction products being the halogenobenzene and 1,2-diacetylhydrazine.

Photolysis of **1** goes mainly by way of the tetrazene **3**, and this may also be a significant pathway in the thermal reaction. Azodiacetyl is an intermediate in the thermal reaction of **1** with 2-propanol and may be generally so in all its reactions.

Radical induced decomposition is believed to be important in the reactions of **1**, **2**, and **3**, and it is probably responsible for the formation of 1-acetyl-1-arylhydrazines, routinely produced in yields of up to 25%.

---

DONALD MACKAY et DEANE DOUGLAS MCINTYRE. Can. J. Chem. **60**, 990 (1982).

On a préparé des radicaux aryles à partir des deux extrêmités des hexadiènes **1** et **2** et à partir du tétrazène **3** soit thermiquement ou photochimiquement. Ils attaquent les composés aromatiques au niveau du noyau, le rendement en dérivés biaryles étant de l'ordre de 40 à 70%. Ce rendement peut être quantitatif si on utilise le *m*-dinitrobenzène comme additif. Les radicaux aryles oxydent également le propanol-2 en acétone, avec comme produits de réduction l'halogénobenzène et la diacétyl-1,2 hydrazine.

La photolyse du composé **1** se fait principalement au moyen du tétrazène **3** et ceci peut constituer également un mécanisme important dans la réaction thermique. L'azodiacétyle est un intermédiaire dans la réaction thermique du composé **1** avec le propanol-2 et il peut en être ainsi dans toutes ses réactions.

On pense que la décomposition induite par les radicaux est importante dans les réactions des composés **1**, **2** et **3** et qu'elle est probablement responsable de la formation des acétyl-1 aryl-1 hydrazines, produits couramment avec des rendements allant jusqu'à 25%.

[Traduit par le journal]

## Introduction

The thermal decomposition of linear N to N unsaturated polyaza compounds, like that of simple azo compounds, is expected to yield radicals. There is a common presumption, which is generally but not invariably true, that the more N atoms there are in the system the less stable it is. Thus polyaza compounds with more than four contiguous N atoms are expected to decompose more easily than tetrazenes or triazenes.

Pentazadienes (1), hexazadienes (2) (there is no record anywhere of a heptaza compound), and octazatrienes (3) have all been known for over 70 years, though since then there have been relatively few references to their chemistry. In many of the reactions described radical pathways are either not involved or are not clearly established. Examples in which nitrogen–nitrogen homolysis has been demonstrated are found for 1,3,5-tri-*p*-tolyl-1,4-pentazadiene both by a product study of its thermolysis in cumene (4), and by the observation of a CIDNP effect in $CHCl_3$ at 70°C (5), and for other pentazadienes by their ability to initiate polymerization (6–8). Octazatriene homolysis was inferred in the case of 1,8-di-*p*-tolyl-3,6-diphenyl-1,4,7-octazatriene by its reaction with cumene (9), and in the case of the tetraphenyl analogue by the successful polymerization of ethylene (8).

One hexazadiene has been used as a polymerization initiator (8) but, in the only other papers describing this class of compounds (10, 11), no reactions are reported which are unambiguously homolytic in nature.

Recently we carried out a crystal determination on 1,6-di-*p*-chlorophenyl-3,4-diacetyl-1,5-hexazadiene (**1**) (12), which showed that its *N*-acetyl groups had an unusually high degree of single bond character in the C to N bond (1.403 Å) and of double bond character in the C to O bond (1.200 Å). This led to the prediction that the acetyl group should be very electrophilic, which was verified by its ability to form esters from alkoxides and phenoxides and acetamide derivatives from primary and secondary amines; the amine reactions showed very high selectivity, particularly to steric factors. In all these and in the hydrolysis reactions described by earlier workers (10) heterolytic cleavage of **1** is obviously involved. Since no product studies have been carried out in any reaction of a hexazadiene where homolysis might be likely, we decided to extend our work with **1** in that direction.

We report here on the efficient production of *p*-chloro- and *p*-bromophenyl radicals by thermolysis and photolysis both of the hexazadienes **1** and **2**, and of the tetrazene **3** whose chemistry is interconnected with that of **1** in some of these reactions.

0008-4042/82/080990-10$01.00/0

©1982 National Research Council of Canada/Conseil national de recherches du Canada

Can. J. Chem. Downloaded from www.nrcresearchpress.com by 210.87.254.6 on 09/06/12
For personal use only.

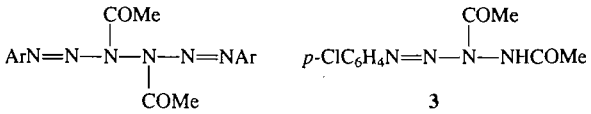

1 Ar = $p$-$ClC_6H_4$
2 Ar = $p$-$BrC_6H_4$

## Results and discussion

The hexazadienes **1** and **2**, prepared by the coupling of two equivalents of the diazonium solution with one of diacetylhydrazine (10, 12), are extraordinarily stable once purified. Samples of **1** remain unaffected indefinitely at room temperature, even in an open atmosphere and unprotected from light. Its stability in solution to acids (10) and to hindered secondary amines (12) has been noted. It has a half-life of several hours in refluxing benzene (though it accelerates thereafter), and of almost 5 minutes in refluxing chlorobenzene.

Though 1-aryl-3,4-diacetyl-1-tetrazenes have been implicated as intermediates in the formation of hexazadienes (10), **3** is the first example of such a compound isolated and characterized. It crystallizes as a monohydrate in excellent yield when a solution of $p$-chlorophenyldiazonium chloride is added to a carbonate solution of one equivalent of diacetylhydrazine.[1] It also is stable to ambient conditions but decomposes very much more rapidly in solution than the hexazadienes; immediate and copious evolution of nitrogen is observed when a solution in benzene is heated.

Dilute solutions (usually 0.025 *M*) of **1** or **2** were completely decomposed in refluxing benzene (80°C) or chlorobenzene (131°C), or in bromobenzene (also at 131°C). Quantitative analysis of the yields of the major products, the biaryls and diacetylhydrazine, were determined by high resolution gas–liquid chromatography (glc).

The coupled products obtained in benzene were $p$-chlorobiphenyl from **1** and $p$-bromobiphenyl from **2**. In chlorobenzene **1** and **2** gave all three 4′-halo-chlorobiphenyls and the analogous 4′-halo-bromobiphenyls in bromobenzene. Yields were in the range of 40–70%. The absence of other significant coupling products, and in particular the *o*:*m*:*p* isomer ratios observed in chlorobenzene and bromobenzene, are unmistakeably diagnostic of the involvement of $p$-chloro- and $p$-bromophenyl radicals (13, 14).

[1]It crystallizes out in fact much more rapidly than **1**, which can cause problems in the synthesis of the latter. On occasion we had to resort to making **1** in a laboratory in which **3** had never been prepared or worked with.

The tetrazene **3** was also decomposed (a much faster reaction) in both refluxing benzene and chlorobenzene. The isomer ratios from the latter solvent are again indicative of $p$-chlorophenyl radical reactions, though the $o$-ratio is rather higher and the $p$-ratio lower than in the corresponding reaction of **1** in chlorobenzene (Table 1).

The yields of biaryls and their isomer ratios from thermolysis of **1–3** in chlorobenzene and bromobenzene are shown in Table 1, along with the yields and ratios from related thermolyses to be discussed later.

The following compounds were not detected (< 1%, glc) in the pyrolysis reactions: $p$-chlorophenyl azide and 1-$p$-chlorophenyl-3-acetyltriazene,[2] $p,p'$-dichloroazobenzene, 1,2-di-$p$-chlorophenylhydrazine, $p$-chloroaniline, $p$-chloroacetanilide, and 1-$p$-chlorophenyl-5-methyltetrazole, an expected hydrolysis product of **3** (10) (by which route it was synthesized), or of 1-$p$-chlorophenyl-4-acetyltetrazene (15).

Since the biaryls and diacetylhydrazine are the major products, the main overall process must be the dehydrogenation of the initially formed arylcyclohexadienyl radicals (13, 14) by one or more intermediates containing the *N*,*N*′-diacetyl fragment (reaction [1]).

[1] $ArC_6H_5Z\cdot \xrightarrow{[O]} ArC_6H_4Z + (MeCONH)_2$

A plausible set of steps leading to these products from both the hexazadiene **1** and the tetrazene **3**, are shown in reactions [2]–[12]. Reactions [2][3] and [8] suppose only spontaneous fission of substrate. If induced fission also occurs, as appears to be the case for **1** at least, many other decomposition pathways are possible. Of those leading to biaryls[4,5] the processes involving the diazanyl radical **6** (from reactions [6] or [8]), or the cyclohexadienyl radical **5** (from reaction [3]) are probably important examples; these are shown in reactions [9]–[12]. Indeed [11] and [12] between them, in chain reac-

[2]The triazene was shown in a control experiment to be stable to the reaction conditions. These two products are quantitatively formed in the reaction of **1** with nucleophiles (10, 12).

[3]We reject as unlikely the one-step decomposition of the hexazadiene to 2 Ar· + 2 $N_2$ + MeCON=NCOMe.

[4]Another route to biaryls of course, is the disproportionation of 2 moles of the arycyclohexadienyl radical to biaryl and cyclohexadiene; this is significant only if oxidation or trapping of the radical cannot intervene (see later discussion).

[5]Attack of Ar· on **1** or **3** would give the symmetrical biaryl. In view of the high reactivity and hence low concentration of such radicals this reaction is unlikely in dilute solution. No $p,p'$-dichlorobiphenyl was obtained when **1** was decomposed in benzene.

Can. J. Chem. Downloaded from www.nrcresearchpress.com by 210.87.254.6 on 09/06/12
For personal use only.

TABLE 1. Yields (%) of products of thermolysis of **1**, **2**, and **3** in various solvents

| Reagent | Solvent | Biaryl Yield[a] | Biaryl Isomer ratio *o* | *m* | *p* | $(MeCONH)_2$[b] | $ArNNH_2(COMe)$[b,c] **9** | Other |
|---|---|---|---|---|---|---|---|---|
| **1** | $C_6H_6$ | 62 | | | | | 13 | |
| | $C_6H_5Cl$ | 67 | 50.5 | 27.7 | 21.8 | 60 | 27 | |
| | $C_6H_5Br$ | | | | | | | |
| | (*i*) untreated | 60 | 51.1 | 31.3 | 17.6 | | 25 | |
| | (*ii*) added *m*-$C_6H_4(NO_2)_2$ | 93 | 53.9 | 28.3 | 17.8 | >90 | <5 | |
| | (*iii*) $N_2$ | 25 | 58.9 | 25.5 | 15.6 | | 9 | |
| | (*iv*) $O_2$ | 38 | 56.4 | 27.4 | 16.2 | | | |
| | $C_6H_5I$ | | 52.6 | 30.5 | 16.9 | | | |
| | $C_6H_5Me$ | | 53.2 | 23.5 | 23.3 | | | $PhCH_2CH_2Ph$[d] |
| | $(C_6H_5)_2$ | | 43.8 | 25.1 | 31.1 | | | |
| | $C_6H_5OMe$ | | | | | | | |
| | (*i*) untreated | | 62.5 | 18.2 | 19.3 | | | |
| | (*ii*) 1 equiv. $AlCl_3$ added | | 63.9 | 19.6 | 16.5 | | | |
| | None | | | | | | | |
| | (*i*) glc injection | 0.9 | | | 100 | | | $C_6H_5Cl$(8) |
| | (*ii*) sand reaction | 0.4 | | | 100 | | | |
| | $Me_2CHOH$ | | | | | 99 | Trace | $Me_2CO$, $C_6H_5Cl$(81), $pClC_6H_4N_3$ (0.2) |
| **2** | $C_6H_5Cl$ | 49 | 53.3 | 29.4 | 17.3 | | | |
| | $C_6H_5Br$ | 77 | 53.3 | 29.2 | 17.5 | | | |
| | $C_6H_5I$ | | 50.9 | 30.8 | 18.3 | | | |
| | None: glc injection | 1.7 | | | 100 | | | $C_6H_5Br$ (7) |
| | $Me_2CHOH$ | | | | | | | $C_6H_5Br$ (90) |
| **3** | $C_6H_5Cl$ | 60 | 61.2 | 24.6 | 14.2 | | | |

[a]Based on $[ArN{=}NN(COMe)]_2 + 2\ C_6H_5Z \rightarrow 2\ ArC_6H_4Z$ and on $ArN{=}NN(COMe)NHCOMe + C_6H_5Z \rightarrow ArC_6H_4Z$.
[b]Not routinely estimated, but always present.
[c]Based on $[ArN{=}NN(COMe)]_2 \rightarrow ArN(COMe)NH_2$.
[d]< 5% of total yield of *p*-chloromethylbiphenyls.

tions together with [3], could account completely for the formation of biaryl from **1** and **3**.

The spontaneous or induced decomposition of **1** or **3** (reactions [2], [8], [9], [11], [12]) produces aryl radicals, directly if loss of $N_2$ is concerted with fission, or otherwise by way of unstable aryldiazenyl radicals $ArN_2^{\cdot}$. Evidence in favour of the latter can be found in the decomposition of 1,3,5-tri-*p*-tolyl-1,4-pentazadiene (5). If the radicals $ArN_2^{\cdot}$ are involved we assume that loss of $N_2$ precedes attack on the solvent by reaction [3].

[2] $(ArN{=}N{-}N(COMe){-})_2$
**1**(Ar = $pClC_6H_4$)

$ArN_2^{\cdot}$ ↓ or $Ar^{\cdot} + N_2$ } + $ArN{=}N{-}N(COMe){-}\dot{N}COMe$

**4**

[3] $Ar^{\cdot} + C_6H_5Z \rightarrow$ **5**

[4] **4** + **5** → Ar–(Z)–C + $ArN{=}N{-}N(COMe){-}NHCOMe$
**3** Ar = $p$-$ClC_6H_4$

[5] **4** + $C_6H_5Z$ → **5** + $N_2$ + MeCON=NCOMe
(or **4** → $Ar^{\cdot}$ + $N_2$ + MeCON=NCOMe, followed by [3])

[6] MeCON=NCOMe + **5** → Ar–(Z)–C + $MeCONH\dot{N}COMe$
**6**

[7] **6** + **5** → Ar–(Z)–C + MeCONHNHCOMe

[8] **3** → $ArN_2^{\cdot}$ ↓ or $Ar^{\cdot} + N_2$ } + **6**

[9] **6** + **1** → $ArN_2^{\cdot}$ (or $Ar^{\cdot} + N_2$) + MeCON=NCOMe + **3**

[10] **6** + **3** → MeCONHNHCOMe + **4**

[11] **5** + **1** → Ar–(Z)–C + $ArN_2^{\cdot}$ (or $Ar^{\cdot} + N_2$) + **3**

[12] **5** + **3** → Ar–(Z)–C + $ArN_2^{\cdot}$ (or $Ar^{\cdot} + N_2$)
+ MeCONHNHCOMe

Can. J. Chem. Downloaded from www.nrcresearchpress.com by 210.87.254.6 on 09/06/12
For personal use only.

Can. J. Chem. Downloaded from www.nrcresearchpress.com by 210.87.254.6 on 09/06/12
For personal use only.

Certainly they do not attack the solvent to form N to C bonds, since neither azo compounds nor the related diarlyhydrazines were detected in the reactions.

Reaction [3] normally provides the only route to the cyclohexadienyl radical **5** in radical arylations, but reaction [5] suggests another mechanism by which formation of **5** might become possible, the driving force being the creation of two stable molecules (Scheme 1). This could be a concerted reaction between **4** and ArH (Scheme 1), or a two-step process with **4** first decomposing to the aryl radical, followed by reaction [3].

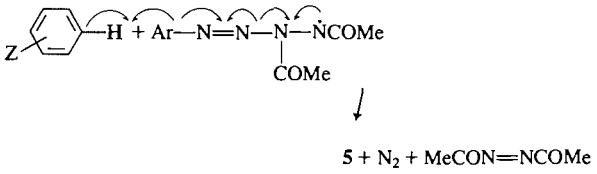


SCHEME 1

The oxidation of **5** to biaryl can take place either by a neutral molecule or by encounter with another radical. An example of the former is reaction [6], in which the dehydrogenating power of an azodicarbonyl compound is utilized. So too are reactions [11] and [12], in the induced decomposition, the radical source (**1** or **3**) being the oxidizing agent. The analogous oxidation of the phenylcyclohexadienyl radical by benzoyl peroxide in benzene has been shown to be significant even in dilute solution (16). Oxidation of **5** by another radical is exemplified by reactions [4] and [7]. Processes of this type are very important in radical arylations where induced decomposition of the radical source is absent. They have ample precedent in the unimolecular decomposition of diaroyl peroxides in aromatic solvents (13, 14, 16).

Examination of reactions [2]–[12] shows that two stable intermediates have been invoked, the tetrazene **3** and azodiacetyl. These may, but need not, be independent of each other. For example, in the unimolecular decomposition of **1** the sequence [2], [4], [8], [7], and in its induced decomposition the sequence [11], [12], involve only **3**. Similarly azodiacetyl only is produced in the sequence [2], [5], [6], [7] when **1** decomposes unimolecularly. Reaction [9] of course produces both, as do sequences like [2], [4], [5], [6]. In the decomposition of **3** azodiacetyl could be involved, as in sequence [8], [10], [5].

While both intermediates are probably involved in thermolysis of **1**, we believe azodiacetyl is of greater importance than the tetrazene.

This choice is made on the basis of the different isomer ratios found in the thermolysis of **1** and **3** in chlorobenzene. The tetrazene **3** gives *o* and *p* ratios of 61 and 14% and a total dichlorobiphenyl yield of 60%. If the thermolysis of **1**, which gives *o* and *p* ratios of 51 and 22% and a total biaryl yield of 67%, goes only by way of **3**, and the latter again gives a 60% biaryl yield, then it follows that the first oxidation step in the thermolysis (reaction [4] in the sequence [2], [3], [4]) affords an *o* and *p* ratio of 43 and 29%. This amount of divergence from the normal spread of *o*/*p* ratios, produced by other sources of aryl radicals, has not been observed in any other work and we regard it as quite unlikely.[6]

We tried to detect the intermediacy of azodiacetyl by allowing a solution of **1** in refluxing chlorobenzene to decompose in the presence of a large excess of cyclopentadiene, in the hope that the latter might trap the azo compound as its known adduct **7** (17). Much polymeric material from the diene was formed, and a reduced yield of biaryl, but no trace of **7** or its product of thermal rearrangement **8** (17) could be detected by glc analysis. Azodiacetyl is evidently more efficiently trapped by **5** than by the diene at this temperature. Using the diene, however, in the reaction of **1** with 2-propanol at 83°C (described below), the involvement of azodiacetyl was established, and so it is reasonable that it can also be an intermediate in the reactions in aromatic solvents.

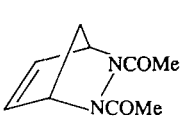


7

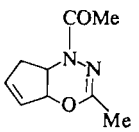


8

Photolysis of **1** or **3** also yields aryl radicals. Decomposition in benzene or chlorobenzene at 10°C with a medium pressure mercury lamp gave diacetylhydrazine and biaryl; the yields and isomer ratios are shown in Table 2. The lower temperature allowed the reaction of **1** to be monitored by $^1$H nmr spectroscopy for the presence of the thermally labile azodiacetyl or tetrazene. While the former could not be conclusively detected, the tetrazene was seen to be the major coproduct of the first arylation step, an observation consistent with the closeness of the isomer ratios in the photolysis of **1** and **3** in chlorobenzene (cf. the thermolysis results). Concentrations of **3** greater than 60% of theoretical (determined by $^1$H nmr analysis) were obtained before separation of solids made further analysis

[6]The spread of ratios between **1** and **3** is quite large but is within the range observed in arylations with different radical sources in other reported work (14).

TABLE 2. Yields (%) of products[a] of photolysis[b] of **1** and **3** in benzene and chlorobenzene

| | | Biaryl | | | |
|---|---|---|---|---|---|
| | | | Isomer ratios | | |
| Reagent | Solvent | Yield[c] | *o* | *m* | *p* |
| **1** | $C_6H_6$ | 65 | | | |
| | $C_6H_5Cl$ | 43 | 62.7 | 24.4 | 12.9 |
| **3** | $C_6H_6$ | 82 | | | |
| | $C_6H_5Cl$ | 48 | 66.5 | 21.0 | 12.5 |

[a]1,2-Diacetylhydrazine and 1-acetyl-1-arylhydrazine also produced but yields not determined.
[b]450 W lamp.
[c]Measured as for Table 1.

unreliable (Table 3). Work-up of a partially reacted solution gave a slightly impure sample of **3**.

Though the yields of biaryls in the reactions described were moderate to good they showed some degree of variation among themselves, even with duplicate runs on the same system.[7] A limiting factor in the success of the reaction is, of course, the ability of the cyclohexadienyl radical **5** to get oxidized to biaryl before it either disproportionates to the cyclohexadiene and biaryl or couples to the tetrahydroquaterphenyl (13, 14). This problem has been addressed in great detail in diaroyl peroxide chemistry, particularly by Hey and by Williams, and their co-workers. They found that a range of N=O containing additives (nitrobenzene, *m*-dinitrobenzene, nitrosobenzene, azoxybenzene) greatly improved the yield of biaryl and aroic acid (the coproduct of the oxidation–reduction), without being chemically changed themselves (18, 19). The use of nitrobenzene in the decomposition of benzoyl peroxide in benzene was examined in detail (19). It was shown that "the nitro group effect" operates by trapping the very reactive phenylcyclohexadienyl radical, probably by σ-bond addition

TABLE 3. Proportions (%)[a] of **1**, **3**, and other Me-containing products from photolysis[b] of **1** in benzene

| Initial [1] | Time (min) | 1 | 3 | Other |
|---|---|---|---|---|
| 0.26 *M* | 10 | 84 | 12 | 4 |
| | 25 | 81 | 14 | 5 |
| | 45 | 68 | 25 | 7 |
| | 62 | 64 | 27 | 9 |
| | 90 | 44 | 39 | 17 |
| 0.13 *M* | 10 | 75 | 21 | 4 |
| | 25 | 63 | 29 | 8 |
| | 62 | 17 | 63 | 20 |

[a]Determined by integration of Me region of $^1H$ nmr spectrum.
[b]100 W lamp.

[7]The isomer ratios, however, remained constant (± 1.6%).

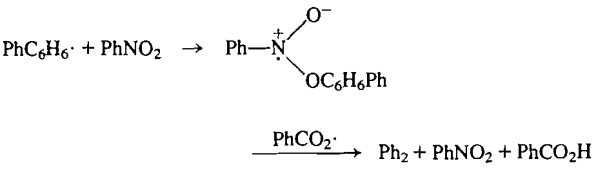


SCHEME 2

at nitro oxygen (Scheme 2), the new, more stable, radical being capable of survival till encounter with the benzoyloxy radical gives benzoic acid, biphenyl, and recovered nitrobenzene.

This approach to optimizing yields has not to our knowledge been applied to arylations from radical sources other than peroxides, but the principle should be equally applicable. In reactions of **1**, radicals such as **4** and **6** take the place of the benzoyloxy radical. We repeated the thermolysis of **1** in bromobenzene with 0.67 molar equivalent of *m*-dinitrobenzene and obtained yields of >90% of both the chlorobromobiphenyls and diacetylhydrazine.

The isomer ratio was not significantly changed and is thus independent of yield, a point firmly established in peroxide work (20). Gas–liquid chromatography showed that the dinitrobenzene was recovered, and though its amount was not measured, the nearly quantitative nature of the arylation establishes that its role must again have been strictly catalytic. This result suggests that reactions like [4] and [7] are important, and that induced decomposition alone (reactions [11], [12]) cannot be responsible for biaryl formation.

Degassing the solution and maintenance of a nitrogen atmosphere during the decomposition of **1** in bromobenzene caused a large reduction in the yield of biaryl, with an increase in the amount of material appearing in the late stages of the chromatogram. Thus oxygen has a beneficial effect in the reactions in untreated solvents, explaining the slight variations of yields in the latter. High oxygen levels were deleterious, since decomposition of **1** in bromobenzene in the presence of the dispersed gas gave a reduction in yield and the appearance of many new products in the chromatogram. This result is at variance with others involving diaroyl peroxides (20, 21), where a dramatic increase in biaryl yields and a reduction of side products was clearly demonstrated. Oxidative degradation of **1** is presumably a competing process.

The hexazadienes were also decomposed in other representative monosubstituted benzenes. Isomer ratios were determined, but not yields, though glc again showed that in all cases the biaryls and diacetylhydrazine were by far the major products. These results are also shown in Table 1.

Can. J. Chem. Downloaded from www.nrcresearchpress.com by 210.87.254.6 on 09/06/12
For personal use only.

Can. J. Chem. Downloaded from www.nrcresearchpress.com by 210.87.254.6 on 09/06/12
For personal use only.

Both **1** and **2** gave very similar results in iodobenzene; there is a notable absence of any steric effect, even for attack of the *p*-bromophenyl radical at the *o*-position. A similar isomer distribution is reported in the decomposition of the corresponding diaroyl peroxides in iodobenzene, but radical displacement of iodine was also observed leading to the aryl iodides (22). We did not look for these in our reactions.

In the reaction of **1** in toluene there was very little side chain attack, less than 5% of that of ring substitution where the isomer ratios were similar to those observed in the halogenated benzenes. *p*-Chlorobenzoyl peroxide attacks the side chain of toluene more extensively (11%), but substitution ratios have not been reported (23). In biphenyl **1** gave the expected monochloroterphenyls, in a ratio predictably low in the *o*-isomer, and similar to that found in the benzoyl peroxide reaction (24).

In our earlier work with **1** it was shown to be a mild and selective acetylating agent for primary and secondary amines (12). We considered that it might also function as an acetylating agent towards an electron-rich aromatic nucleus in the presence of a Friedel–Crafts catalyst. In fact with anisole containing $AlCl_3$ there was no evidence of the formation of methoxyacetophenones. The methoxybiphenyls were produced in the normal free radical ratio, similarly observed without the catalyst and noted by others (20).

2-Propanol was chosen as a readily oxidizable solvent in which **1** might be expected to react readily by aryl (or other) radical abstraction. The oxidation of ethanol by **1** has already been demonstrated, though a mechanism was not determined (10). Radical oxidation of 2-propanol has been effected by benzoyl peroxide, both phenyl and benzoyloxy radicals being involved (25), as well as by other radical sources (26, 27). Reaction of **1** was rapid at the bp of the alcohol, giving acetone (not estimated), chlorobenzene (81%), and diacetylhydrazine (99%). Similar reaction of **2** gave bromobenzene (90%). Since the products are equally consistent with an ionic mechanism, we tried to prove the involvement of radicals by repeating the oxidation in an equimolar mixture of alcohol and chlorobenzene. A low yield (21%) of the three dichlorobiphenyls was obtained in the normal isomer ratio for radical attack.[8] Since this isomer mixture was rapidly obtained at a temperature (83°C) at which **1** itself reacts very slowly, the presumption is that *p*-chlorophenyl radicals are generated by reaction with the alcohol. The stoicheiometry of the oxidation is thus described by [13] and the mechanism must operate mainly by induced decomposition. Reasonable sets of steps are shown in reactions [14]–[20].

[13] $\mathbf{1} + 2\,Me_2CHOH \rightarrow 2\,C_6H_5Cl + 2\,N_2 + MeCONHNHCOMe + 2\,Me_2CO$

[14] $Ar\cdot + Me_2CHOH \rightarrow ArH + Me_2\dot{C}OH$

[15] $Me_2\dot{C}OH + \mathbf{1} \rightarrow Me_2CO + ArH + N_2 + ArN{=}N{-}\underset{\displaystyle COMe}{\underset{|}{N}}{-}\dot{N}COMe$ (**4**)

[16] $\mathbf{4} + Me_2CHOH \rightarrow ArH + N_2 + MeCON{=}NCOMe + Me_2\dot{C}OH$

(or $\mathbf{4} \rightarrow Ar\cdot + N_2 + MeCON{=}NCOMe$, followed by [14])

[17] $Me_2\dot{C}OH + MeCON{=}NCOMe \rightarrow Me_2CO + MeCONH\dot{N}COMe$ (**6**)

[18] $\mathbf{6} + Me_2CHOH \rightarrow MeCONHNHCOMe + Me_2\dot{C}OH$

[19] $\mathbf{4} + Me_2CHOH \rightarrow \mathbf{3} + Me_2\dot{C}OH$

[20] $Me_2\dot{C}OH + \mathbf{3} \rightarrow Me_2CO + ArH + N_2 + \mathbf{6}$

Initiation by, for example, the aryl radicals (reaction [14]) gives the 2-hydroxy-2-propyl radical which with **1** gives **4**, but which is regenerated by reaction of **4** with alcohol (reaction [16], in a one- or two-step process). The sequence [15], [16] is thus a chain process completing the reduction of both equivalents of aryl radicals and the oxidation of one equivalent of alcohol. The other product, azodiacetyl, completes the oxidation of alcohol by the repeating sequence [17], [18] which involves the radical **6**. Alternatively **4** can react with alcohol to give **3** and the 2-hydroxy-2-propyl radical (reaction [19]); these react to product and **6**, which with alcohol completes the chain (reactions [20], [18]). Thus a sequence involving azodiacetyl ([15]–[18]) or one involving tetrazene ([15], [19], [20], [18]) is possible, but we made no attempt to assess the relative contributions of these. However, we were able to confirm the involvement of azodiacetyl at least, by repeating the oxidation in the presence of cyclopentadiene. The glc analysis of the products showed the formation of both the adduct **7** and its thermal isomer **8**. The amounts were not estimated.

Consistently reported in yields of 10–25% in Tables 1, 2, and 3 is the formation of 1-acetyl-1-*p*-chloro(or -bromo)phenylhydrazine (**9**) in thermal and photolytic reactions of **1**, **2**, or **3**. It was absent, or almost so, only in the reaction of **1** with 2-propanol, and with chlorobenzene in the presence of *m*-dinitrobenzene, where the yields of

[8]Even in the absence of added chlorobenzene the amount generated in the alcohol oxidation was sufficient to allow the formation of a detectable mixture of the dichlorobiphenyls.

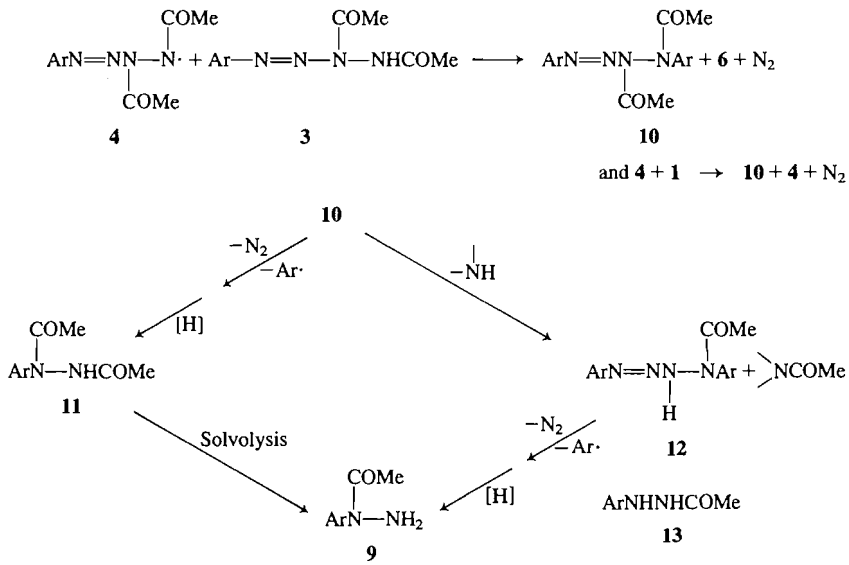


SCHEME 3

chlorophenyl-containing products were very high.

No obvious simple pathway to this product is apparent, involving as it does overall aryl migration to an acetyl-bearing nitrogen, followed by *N*-acetyl cleavage β to the aryl group. Spontaneous aryl migration in **1** or **3** is possible but is much less likely than an intermolecular aryl transfer from **1** or **3** to a suitable *N*,*N*′-diacetyl containing nitrogen-centred radical. By far the best candidate is the radical **4** and we propose that the key intermediate generated is the (presumably) unstable 1,4-diaryl-3,4-diacetyl-1-tetrazene (**10**). Its formation from **4** and possible reactions leading from it to **9** are shown in Scheme 3.

A sequence of spontaneous or induced homolysis of **10**, followed by hydrogen abstraction by the resulting radical ArN(COMe)NCOMe, would give the *N*,*N*′-diacetylarylhydrazine (**11**). However, **11** does not seem a probable precursor for **9**. It is difficult to imagine a mechanism for the transformation **11** → **9** except one of selective solvolysis, which would require a more reactive nucleophile than any likely to be present in the reaction.

We propose that deacetylation of **10** occurs directly to give **12**. The acetyl group on the nitrogen α to the azo group is expected to be highly electrophilic (12), and a mild nucleophile should be capable of displacing it. The nucleophile must be a basic nitrogen derivative, though certainly not *p*-chloroaniline, since both it and its acetyl derivative were not reaction products.[9] Conversion of **12** → **9**[10] would again involve radical decomposition and hydrogen abstraction of the resulting radical ArN(COMe)NH·.

Since **9** is the only reaction product containing both the aryl and diacetylhydrazine fragments we thought that it might be the major product when **1** was decomposed in the absence of solvent. Injection of an ethereal solution of **1** in the inlet of the gas chromatogram (250°C, a temperature at which **1** explodes in the condensed state) indeed gave **9** (25%) as well as diacetylhydrazine (24%) as by far the major simple products, though the yield is no greater than in other decomposition reactions. Chlorobenzene (8%), not otherwise routinely tested for, was also a product; so too was *p*,*p*′-dichlorobiphenyl, in very low yield, but significantly free of the *o*- or *m*-isomers. It must arise by the induced decomposition: $p$-$ClC_6H_4$· + **1** → ($p$-$ClC_6H_4)_2$ + $N_2$ + **4**. Pyrolysis of **1** at 150°C, dispersed thinly on the surface of sand, gave an almost identical result.

Though we have not succeeded in isolating **9**, its identity has been clearly established. Work-up of the photolysate of **1** in benzene gave a fraction very rich in **9** (glc). The $^1H$ nmr of this fraction showed a strong absorption in the acetyl region as well as the expected *p*-chlorophenyl splitting pattern. A gc–ms analysis showed it had a mol. wt. of 184 (based

[9]A variety of basic products may be involved since no other peak of major significance in the glc chromatogram was unaccounted for.

[10]The alternative decomposition of **12** → $ArN_3$ + ArNHCOMe would be analogous to the solvolysis pathway observed for **1** with bases to give $ArN_3$ + ArN=NNHCOMe (10, 12). However, in the latter reaction the triazenyl anion is the leaving group and has a resonance stabilization not matched by the anilide anion.

Can. J. Chem. Downloaded from www.nrcresearchpress.com by 210.87.254.6 on 09/06/12
For personal use only.

Can. J. Chem. Downloaded from www.nrcresearchpress.com by 210.87.254.6 on 09/06/12
For personal use only.

on $^{35}Cl$), one Cl atom (isotope ratio), and one acetyl group (strong $M - 42$ peaks); the products from the sand pyrolysis also showed a very intense peak at *m/e* 184. We were able to rule out the other monoacetyl isomer **13**, since an authentic sample of it had a shorter glc retention time, thus confirming the structure as **9**. An attempt to synthesize **9**, by acetylation of 1-*p*-chlorophenyl-2-formylhydrazine followed by acid hydrolysis, gave a mixture of mono and diacyl *p*-chlorophenylhydrazines of which **9** was one (glc coinjection with a pyrolysis reaction mixture).

## Experimental

Melting points are uncorrected. Infrared spectra were recorded on a Beckman IR-10 spectrometer. Nuclear magnetic resonance spectra were obtained on a Perkin–Elmer R12B ($^1H$) or a Bruker WP-80 ($^1H$, $^{13}C$) spectrometer, and are referred against internal tetramethylsilane. All gas–liquid chromatographic analyses were carried out on a Hewlett–Packard 5830 or 5840A Chromatograph with flame ionization detection and He or $N_2$ as carrier gas; glass columns 6 ft × 1/8 in. id with an Aue packing of Carbowax 20M on Chromosorb W were used. Gas chromatographic – mass spectrometric measurements were made on a Hewlett–Packard 5992 instrument. Conventional mass spectra were run on a Varian MAT-CH7.

*Starting materials and reference compounds*

Solvents were dried by conventional methods, but were not degassed for most routine decompositions. For reactions done in the absence of oxygen the solvent was first refluxed to expel all gases and an atmosphere of $N_2$ then maintained during the decomposition.

*Hexazadienes 1 and 2*

These were prepared as described earlier (10, 12).

*1-p-Chlorophenyl-3,4-diacetyl-1-tetrazene (3)*

A freshly prepared solution (150 mL) of *p*-chlorophenyldiazonium chloride from *p*-chloroaniline (12.7 g, 0.10 mol), sodium nitrite (6.9 g, 0.10 mol), and 12 *M* hydrochloric acid (50 mL) was added to a stirred ice-cold solution (300 mL) containing 1,2-diacetylhydrazine (11.6 g, 0.10 mol) and sodium carbonate (50 g), covered with diethyl ether (100 mL; it efficiently removes colored impurities and dissolves very little of the product at this temperature). There was rapid separation of **3** as the colorless crystalline hydrate. Stirring was continued for 15 min, the whole was filtered, the product washed with water and dried, finally, in a vacuum desiccator over phosphorus pentoxide; $^1H$ nmr analysis showed it to be the monohydrate (16 g, 65%).

A purified sample of **3** could not be obtained crystalline and free of solvent. In solvents not rigorously dried it formed the hydrate, and from anhydrous solvents containing ether the solid obtained showed ether in its $^1H$ nmr spectrum. Prolonged evacuation was without effect on the bound solvents. Solutions of **3** could be dried with magnesium perchlorate and gave water-free spectra, but evaporation of such solutions gave a gummy residue.

It was best recrystallized from undried chloroform-pentane as the monohydrate, which melted with decomposition at 90°; ν(anhydrous $CHCl_3$): 3405 (NH), 1720 (C=O) $cm^{-1}$; $^1H$ nmr ($CDCl_3$) δ: 8.05 (1H, s, NH), 7.3–7.6 (4H, m, $ClC_6H_4$), 2.60 (3H, s, N(3)—$COCH_3$), 2.17 (3H, s, N(4)—$COCH_3$); $^{13}C$ nmr ($CDCl_3$) δ: 170.4, 168.4 (C=O), 146.1 (C1), 135.7 (C4), 129.4 (C3), 123.8 (C2), 22.0 ($CH_3$), 20.5 ($CH_3$). *Anal.* calcd. for $C_8H_{11}ClN_4O_2 \cdot H_2O$: C 44.05, H 4.80, N 20.54; found: C 43.92, H 4.78, N 20.49%.

*p*-Chlorobiphenyl was prepared from *p*-chloroaniline by the Gomberg–Hey reaction (28). *p*-Bromo-*p'*-chlorobiphenyl was obtained by bromination of *p*-chlorobiphenyl in acetic acid, and *p,p'*-dichlorobiphenyl by chlorination of biphenyl in acetic acid (29); *p,p'*-dibromobiphenyl was obtained in an analogous manner (30).

1-Acetyl-2-*p*-chlorophenylhydrazine (15) was made from *p*-chlorophenylhydrazine and one equivalent of acetic anhydride.

*Gas–liquid chromatographic analyses*

Biphenyl was used as an internal standard for all glc analyses.

In the case of the *p,p'*-dihalogenated biphenyls the linearity of response (signal area) over a 10-fold range of concentrations ($10^{-3}$–$10^{-2}$ *M*, greater than that encountered in the experimental work) was established; the standard deviation for six trials was 1.6%. It is known that for halogenated biphenyls the FID response shows almost no variation between different isomers (31). Thus the calibration for all isomers was based on results from standard solutions of the *p,p'*-isomer and biphenyl.

1,2-Diacetylhydrazine gave a nonlinear FID response especially at very low concentrations. A calibration curve was determined using ten standard solutions spanning the concentration range of interest. In most of the decomposition reactions the diacetylhydrazine separated out of the solution. Addition of methanol to give a homogeneous solution was necessary before the glc determination was carried out. The yield of diacetylhydrazine was not determined in all reactions.

For the determination of 1-acetyl-1-*p*-chlorophenylhydrazine (**9**) the isomeric 1-acetyl-2-*p*-chlorophenylhydrazine (**13**) was used. It was assumed they would have the same FID response.

*Determination of half-life of 1*

A solution of **1** and dimethyl phthalate (as internal standard) (0.26 *M* each) in benzene in an nmr tube was immersed in refluxing benzene and the proton spectrum run at intervals. A first order plot became nonlinear after a few hours, showing that the reaction was accelerating. The half-life was about 6.4 h.

In refluxing chlorobenzene the half-life was less than 5 min.

The half-life of **3** in refluxing benzene could not be readily determined since evolution of nitrogen began almost immediately on warming.

*Thermolyses*

The thermal decompositions in solution were carried out using 20 mL of ca. 0.025 *M* solutions of **1**, **2**, or **3**, at suitable temperatures: benzene 80°C, chlorobenzene, bromobenzene, iodobenzene, 131°C; anisole, 100°C; biphenyl, 190°C; 2-propanol, 83°C. The reactions were followed by observing the disappearance of the acetyl methyl singlets in the $^1H$ nmr spectrum.

Where yields were determined a known weight of biphenyl was added to the solution after completion of the reaction.

In the case of the reaction of **1** with benzene and chlorobenzene the final solutions were evaporated and the hexane-soluble portions of the residue worked up to give *p*-chlorobiphenyl and *p,p'*-dichlorobiphenyl. These were crystallized from methanol and identified by mixture mp.

*Photolyses*

Irradiation by a 100 or a 450 W Hanovia medium pressure mercury immersion lamp was used through quartz walls.

Routinely solutions 0.026 *M* (reactor volume 250 mL) in **1** or **3** were photolyzed (450 W) at a temperature of about 10°C. Samples were periodically removed and monitored in the aliphatic region by $^1H$ nmr spectroscopy. The complete decomposition required about 6 h for **1** and 2 h for **3**.

Can. J. Chem. Downloaded from www.nrcresearchpress.com by 210.87.254.6 on 09/06/12
For personal use only.

*Work-up of products of photolysis of 1 in benzene*

The photolysate from complete reaction of **1** (2.0 g) in benzene (250 mL) was evaporated to dryness and the residue extracted with refluxing pentane (2 × 100 mL). The pentane solution afforded 1.0 g (52%) of almost pure *p*-chlorobiphenyl; recrystallized from methanol it had mp and mixture mp 144–145°C. The pentane-insoluble fraction was then extracted with refluxing ether (2 × 100 mL) which yielded a residue (0.72 g) which had both aromatic and methyl (several peaks) absorption in its $^1$H nmr spectrum. A major component was **9** (δ 2.0), which was established by gc–ms evidence, as described later. The pentane- and ether-insoluble residue contained diacetylhydrazine, which was isolated as the insoluble product obtained on addition of chloroform.

*Detection of 3 as intermediate in photolysis of 1*

A total of 4 mL of a solution of **1** (0.15 *M*) in benzene was divided among seven 5-mm nmr tubes arrayed around the 100 W lamp. Photolysis was carried out and the proton spectrum was periodically checked using different tubes randomly. After 1 1/2 hours the balance between **3** and accumulating by-products was judged to be optimal and the reaction was stopped. The combined solutions were set aside whereupon crystallization of a small amount of material soon occurred. The $^1$H nmr spectrum of the crystals showed them to consist of the tetrazene **3** (δ(Me) 2.60 and 2.17, and the characteristic water peak at ca. 2.7) contaminated by a small amount of diacetylhydrazine.

*Kinetic analysis of photolysis of 1 in benzene (see Table 3)*

A 5-mm nmr tube containing a solution of **1** (0.26 *M*) in benzene was irradiated by the 100 W lamp as described above. Integration at suitable intervals of the methyl region of the proton spectrum enabled the proportions of **1**, **3**, and all other methyl-containing products to be determined. After the midpoint of the reaction separation of solid precluded further analysis.

The experiment was repeated at half the concentration (0.13 *M*). In this case the solution remained clear till after 80% of the reaction was complete. As expected this reaction was much slower, but the relative proportions of products were essentially unchanged.

The estimated error in the analysis was about ± 3%.

*Effect of additives or catalysts on 1*

In the decomposition of **1** in bromobenzene the following variations were carried out (substrate concentration as before): (*i*) 0.67 mol of *m*-dinitrobenzene included; (*ii*) solvent first degassed by refluxing, then $N_2$ atmosphere maintained during reaction; (*iii*) $O_2$ passed through solution during reaction.

In the anisole reaction the decomposition was carried out both without catalyst and with 3 mol of $AlCl_3$.

*Azodiacetyl trapping experiments*

(*i*) A solution of **1** in chlorobenzene was heated in the usual manner (131°C) except that cyclopentadiene (10 mL) was added dropwise with stirring during the course of the reaction. The glc analysis failed to detect the presence of either of the adducts **7** or **8** (17).

(*ii*) The experiment was repeated using refluxing 2-propanol as solvent. Both adducts **7** and **8** were observed in the glc, their identity being confirmed by coinjection with authentic samples of the adducts.

*Identification of 1-acetyl-1-p-chlorophenylhydrazine (9)*

Refluxing of *p*-chlorophenylhydrazine with ethyl formate for 30 min gave the 2-formyl derivative (70%), mp 185.5–186.5°C (lit. (32) mp 186–187°C).

The formyl derivative (0.10 g) was heated with acetic anhydride (1 mL) for 1 hour. Evaporation and examination of the residue by $^1$H nmr spectroscopy showed it consisted of a mixture of products. The mixture was hydrolyzed by heating it in 1 *N* $H_2SO_4$ (25 mL) for 15 min at 100°C, neutralized with $Na_2CO_3$, and extracted with ether. Gas–liquid chromatography of the extract showed a mixture having one peak with the same retention time as the major, otherwise unidentified, product obtained in the thermolysis and photolysis reactions; coinjection with a worked-up sample rich in this product (from a photolysis reaction as described above) gave a single peak. The retention time was longer than that of synthetic 1-acetyl-2-*p*-chlorophenylhydrazine.

The enriched sample was also subjected to gc–ms analysis which showed the product to have a parent peak at *m/e* 184 ($^{35}$Cl), one chlorophenyl ring (isotope ratio), and an acetyl group (strong peak at *m/e* 142). In the mass spectrum of the pyrolysate from the sand reaction, the peak at *m/e* 184 was the most intense. The combination of glc and ms evidence thus establishes the product as **9**.

*Decompositions without solvent*

(*i*) *Gas-liquid chromatographic injection*

A 3 μL sample of a solution of **1** (0.025 *M*) in ether containing biphenyl as internal standard was introduced into the injection port (250°C) of the gas chromatograph; the chromatogram was run under the usual operating conditions.

(*ii*) *Pyrolysis on sand*

Clean sand (20 g) was added to a solution of **1** (0.50 g, 1.27 mmol) in dichloromethane (20 mL) and the solvent removed on a rotary evaporator. The coated sand was then heated at 150°C under a Dry-Ice condenser until the reaction was judged to be complete (15 min, by which time the surface of the sand was very discolored). The product was extracted with ether, and the solution and ethereal washings from the condenser combined. Internal standard was added and the solution analyzed in the usual way.

## Acknowledgements

We thank the Natural Sciences and Engineering Research Council of Canada and the University of Waterloo for financial assistance. We also thank Dr. R. E. Clement of this department for helpful discussions on the gc–ms analysis.

1. H. Goldschmidt and V. Badl. Chem. Ber. **22**, 933 (1889); H. von Pechmann and L. Frobenius. Chem. Ber. **27**, 703 (1894).
2. K. A. Hofmann and H. Hock. Chem. Ber. **44**, 2946 (1911).
3. A. Wohl and H. Schiff. Chem. Ber. **33**, 274 (1900); **35**, 1900 (1902).
4. H. Minato and M. Oku. Bull. Chem. Soc. Jpn. **38**, 1529 (1965).
5. J. Hollaender and W. P. Neumann. Angew. Chem. Intl. Ed. Engl. **9**, 804 (1970).
6. J. E. Wiklatz. U.S. Pat. Nos. 2530497 (1950) and 2564632 (1951).
7. W. Hall and L. Seed. Jpn. Pat. No. 11791 (1960).
8. J. C. McGowan and L. Seed. Brit. Pat. No. 834332 (1960).
9. H. Minato, M. Oku, and S. H-P. Chan. Bull. Chem. Soc. Jpn. **39**, 1049 (1966).
10. J. P. Horwitz and V. A. Grakauskas. J. Am. Chem. Soc. **79**, 1249 (1957).
11. W. Theilacker and E. C. Fintelman. Chem. Ber. **91**, 1597 (1958).
12. D. Mackay, D. D. McIntyre, and N. J. Taylor. J. Org. Chem. In press.

13. G. H. WILLIAMS. Homolytic aromatic substitution. Pergamon Press, Oxford. 1960. Chapt. 4.
14. W. A. PRYOR. Free radicals. McGraw Hill Inc., New York. 1966. Chapt. 16.
15. O. DIMROTH and G. DE MONTMOLLIN. Chem. Ber. **43**, 2904 (1910).
16. G. B. GILL and G. H. WILLIAMS. J. Chem. Soc. 995 (1965).
17. D. MACKAY, J. A. CAMPBELL, and T. D. SAUER. Can. J. Chem. **50**, 371 (1972).
18. D. H. HEY, M. J. PERKINS, and G. H. WILLIAMS. Chem. Ind. 83 (1963).
19. G. B. GILL and G. H. WILLIAMS. J. Chem. Soc. 880 (1966).
20. R. T. MORRISON, J. CAZES, N. SAMKOFF, and C. A. HOWE. J. Am. Chem. Soc. **84**, 4152 (1962).
21. M. EBERHARDT and E. L. ELIEL. J. Org. Chem. **27**, 2289 (1962).
22. D. L. BRYDON and J. I. G. CADOGAN. J. Chem. Soc. C, 819 (1968).
23. J. K. HAMBLING, D. H. HEY, and G. H. WILLIAMS. J. Chem. Soc. 487 (1962).
24. J. I. G. CADOGAN, D. H. HEY, and G. H. WILLIAMS. J. Chem. Soc. 794 (1954).
25. S. KATO and F. MASHIO. Chem. Abstr. **51**, 11288h (1957); **51**, 14387f (1957).
26. S. J. COHEN and J. NICHOLSON. J. Org. Chem. **30**, 1162 (1965).
27. D. MACKAY, U. F. MARX, and W. A. WATERS. J. Chem. Soc. 4793 (1964).
28. J. ELKS, J. W. HAWORTH, and D. H. HEY. J. Chem. Soc. 1284 (1940).
29. F. R. SHAW and E. E. TURNER. J. Chem. Soc. 285 (1932).
30. R. SCHOLL and V. NEOVIUS. Chem. Ber. **44**, 1987 (1911).
31. B. BØE and E. EGAAS. J. Chromatogr. **180**, 127 (1979).
32. W. BAKER, W. D. OLLIS, and V. D. POOLE. J. Chem. Soc. 3389 (1950).

Can. J. Chem. Downloaded from www.nrcresearchpress.com by 210.87.254.6 on 09/06/12
For personal use only.

# $^{13}C$ nuclear magnetic resonance and Raman investigations of aqueous carbon dioxide systems

THERESA M. ABBOTT,[1] GERALD W. BUCHANAN, PEETER KRUUS, AND KEITH C. LEE[2]

*Department of Chemistry, Carleton University, Ottawa, Ont., Canada K1S 5B6*

Received September 17, 1981

THERESA M. ABBOTT, GERALD W. BUCHANAN, PEETER KRUUS, and KEITH C. LEE. Can. J. Chem. **60**, 1000 (1982).

$^{13}C$-nmr spectra of carbon dioxide in water are reported for a wide range in pH. Chemical shifts were determined for the following species: $CO_2(g)$, $CO_2(aq)$, $HCO_3^-(aq)$, $CO_3^{2-}(aq)$. A linear relationship was found between the shift of the $^{13}C$ line and the fraction of carbonate ion calculated to be present, as well as between the ratio of the area under the 1067 $cm^{-1}$ (carbonate) Raman peak to the sum of the area under the 1067 $cm^{-1}$ and 1017 $cm^{-1}$ (bicarbonate) peaks and the fraction carbonate.

THERESA M. ABBOTT, GERALD W. BUCHANAN, PEETER KRUUS et KEITH C. LEE. Can. J. Chem. **60**, 1000 (1982).

On rapporte les spectres de rmn du $^{13}C$ du bioxyde de carbone dans l'eau et à des pH très variés. On a déterminé les déplacements chimiques des espèces suivantes: $CO_2(g)$, $CO_2(aq)$, $HCO_3^-(aq)$, $CO_3^{2-}(aq)$. On a trouvé une relation linéaire entre le déplacement des pics du $^{13}C$ et la fraction de l'ion carbonate qui existe d'après les calculs; on a aussi décelé une relation linéaire entre le rapport de la surface du pic Raman à 1067 $cm^{-1}$ (carbonate) sur la somme des surfaces des pics à 1067 et 1017 $cm^{-1}$ (bicarbonate) et la fraction carbonate.

[Traduit par le journal]

## Introduction

Carbon dioxide is of vital interest in the chemistry of natural waters, both with regard to inorganic (e.g. refs. 1–3) and biochemical (e.g. ref. 4) aspects. The species and reactions involved are usually taken to be the following:

[1] $CO_2(g) \rightleftharpoons CO_2(aq)$

[2] $CO_2(aq) + H_2O \rightleftharpoons H_2CO_3(aq)$

[3] $H_2CO_3(aq) \rightleftharpoons H^+(aq) + HCO_3^-(aq)$

[4] $HCO_3^-(aq) \rightleftharpoons H^+(aq) + CO_3^{2-}(aq)$

[5] $K^+(aq) + CO_3^{2-}(aq) \rightleftharpoons (KCO_3)^-(aq)$

The existence of the species $H_2CO_3(aq)$ has been postulated due to kinetic considerations (5, 6). No actual spectroscopic evidence of this species seems to exist, and quantum mechanical calculations suggest that it is not a stable species in the gas phase (7, 8). Stable species with two hydroxyl groups on one carbon are also rare in organic chemistry.

Even if $H_2CO_3(aq)$ were a stable species rather than a transition state, it would be present only in a very small amount relative to $CO_2(aq)$ due to the low value of the equilibrium constant in [2] (5). In calculations, $CO_2(aq)$ and $H_2CO_3(aq)$ are often considered together (1) as

[6] $$[H_2CO_3^*(aq)] = [H_2CO_3(aq)] + [CO_2(aq)] \simeq [CO_2(aq)]$$

The square brackets indicate concentration in mol $L^{-1}$ ($M$).

Reactions [3] and [4] involve only proton transfers and have rapid reaction rates, with relaxation times of the order of $10^{-9}$ s (9). This is less than the characteristic time for nmr measurements, but greater than that for Raman spectroscopy. Thus nmr will average the $^{13}C$ over its environments as the species $CO_3^{2-}(aq)$, $HCO_3^-(aq)$, and possibly $H_2CO_3(aq)$. Raman spectroscopy will however differentiate between these species.

The ion pairing reaction [5] is shown for the $K^+$ and $CO_3^{2-}$ ions, as this is the most likely equilibrium to be of consequence in the studies reported here. Equilibria involving divalent cations are of more importance in natural waters (3), and the $HCO_3^-$ ion would also be involved in such equilibria (10, 11). It is not certain whether Raman spectroscopy would distinguish between species such as $CO_3^{2-}$ and $K^+$. $CO_3^{2-}$ as the influence of the neighbouring $K^+$ may not be sufficient to change the vibrational modes of $CO_3^{2-}$ significantly. The presence of $K^+$ next to $CO_3^{2-}$ would affect the chemical shift of $^{13}C$, but again the magnitude of this effect is not known.

Considering the importance of the carbon dioxide – water system, it is surprising that only one $^{13}C$-nmr study has been carried out on it (12). Some $^{13}C$ nmr, however, has been used to study the enzyme catalysis of reactions [2] and [3] (4). Raman studies have been carried out previously on this system (13–15).

A more thorough $^{13}C$-nmr study is reported here, with the nmr results evaluated in the context of the

[1]Present address: CIL Inc., P.O. Box 10, Montreal, P.Q., Canada H3C 2R3.

[2]Defense Research Establishment Ottawa, Shirley's Bay, Ottawa, Ont., Canada K1A 0Z4.

0008-4042/82/081000-07$01.00/0

©1982 National Research Council of Canada/Conseil national de recherches du Canada

Can. J. Chem. Downloaded from www.nrcresearchpress.com by 210.87.254.105 on 09/06/12
For personal use only.

Can. J. Chem. Downloaded from www.nrcresearchpress.com by 210.87.254.105 on 09/06/12
For personal use only.

TABLE 1. Samples for $^{13}C$-nmr analysis

| Sample No. | pH | $C_c/M$ | $\%CO_3^{2-}$* | δ/ppm† |
|---|---|---|---|---|
| 1‡ | 11.86 | 0.53 | 99 | 169.5 |
| 2§ | 10.66 | 0.45 | 86 | 167.3 |
| 3‡ | 10.56 | 0.48 | 83 | 167.0 |
| 4‡ | 10.21 | 0.46 | 70 | 166.3 |
| 5 | 10.00 | 0.48 | 65 | 164.1 |
| 6§ | 9.90 | 0.42 | 61 | 164.2 |
| 7§ | 9.73 | 0.41 | 45 | 163.7 |
| 8§ | 9.57 | 0.40 | 36 | 163.2 |
| 9‡ | 9.39 | 0.42 | 27 | 163.9 |
| 10§ | 9.17 | 0.39 | 19 | 163.0 |
| 11‡ | 8.61 | 0.40 | 6 | 163.2 |
| 12 | 11.44 | 0.050 | 90 | 168.4 |
| 13 | 10.87 | 0.050 | 69 | 166.4 |
| 14 | 10.60 | 0.049 | 54 | 165.3 |
| 15 | 10.39 | 0.049 | 42 | 164.8 |
| 16 | 10.27 | 0.049 | 35 | 164.0 |
| 17 | 10.27 | 0.048 | 35 | 164.0 |
| 18‡ | 10.10 | 0.048 | 49 | 163.9 |
| 19 | 9.97 | 0.049 | 21 | 163.4 |
| 20§ | 9.94 | 0.048 | 52 | 164.2 |
| 21 | 9.78 | 0.049 | 14 | 162.6 |
| 22 | 9.58 | 0.049 | 10 | 162.3 |
| 23 | 8.43 | 0.049 | 3 | 161.7 |
| 24 | 7.43 | 0.048 | 0.4 | 161.5 |
| 25 | >11 | 6 | 100 | 170.3 |
| 26 | <7 | 0.015 | 0 | 125.9 |
| 27 | <7 | 0.065 | 0 | 125.9 |
| 28 | <7 | 0.7 | 0 | 125.9, 124.5 |
| 29‡ | 0.031 *M* in Na | 0.035 | 0 | 125.9, 161.3 |
| 30‡ | 0.023 *M* in Na | 0.035 | 0 | 125.9, 161.3 |
| 31‡ | 0.022 *M* in $NH_4$ | 0.030 | 0 | 125.9, 161.3, 151.5¶ |
| 32‡ | 0.011 *M* in Na | 0.020 | 0 | 125.9, 151.5¶ |
| 33‡ | 276 K | 0.030 | 0 | 125.8, 161.6 |
| 34‡ | 315 K | 0.030 | 0 | 125.9, 161.2 |

*Calculated with eqs. [7] to [12].
†±0.2 ppm (from TMS).
‡Sample in half $H_2O$.
§Sample in water.
¶Unstable with time.

assumed speciation reactions [1] to [5]. The discussion is supported by further Raman data and speciation calculations.

## Experimental

$^{13}C$ nmr spectra were determined at 25.16 MHz using a Varian XL-100-12 spectrometer equipped with a Nicolet TT-100 Fourier Transform data system. Chemical shifts were measured relative to an external methanol capillary and were converted to the TMS scale using a value of 49.3 ppm for the $^{13}C$ shift of neat methanol (16). Spectral widths were 5000 Hz and 8 K data points were employed. Typically the pulse angle was 45° and the pulse delay, 1 s. In nearly all cases, standard 5 mm tubes were used, but thick-walled 8 mm tubes were used for some samples when pressures above 1 atm (up to 10 atm) were present (samples 27, 28 in Table 1). Spectra were taken at 305 ± 2 K in nearly all cases.

Samples with a pH > 7 were made up by mixing the appropriate amounts of solutions of $K_2CO_3$ and HCl (samples 1 to 24 in Table 1). Samples with total carbon dioxide content $C_c$ of the order of 0.5 *M* (samples 1 to 11) were made up with natural $K_2CO_3$ (Fisher Certified Reagent), but a small amount (< 10%) of $^{13}C$-enriched $K_2CO_3$ (90% $^{13}C$ Merck, Sharp and Dohme) was added to some of these samples. Lower concentration samples (12 to 24) were made up with isotope-enriched $K_2CO_3$.

The stock solution of isotope-enriched $K_2CO_3$ was made up in $D_2O$ as deuterium is required as a frequency lock for $^{13}C$ spectra on the XL-100. Thus many of the samples were primarily in $D_2O$. Some ordinary water was present from the HCl solution, but this was usually a small amount as concentrated (> 1 *M*) acid was used. Measurements of pH (or pD) were taken on a Fisher Accumet Model 620 with an E-5A electrode. For samples 1 to 24, the pH was taken at 305 K. There is an increase of 0.10 in the pH at 305 K as compared to the 293 K value for most solutions.

Samples with pH < 7 (26 to 34) were prepared by introducing a sample of water (26 to 28) or a solution of base (NaOH or $NH_4OH$, 20 to 34) into an nmr tube, attaching the tube to a vacuum system, freezing the contents by immersing the tube end in liquid nitrogen, evacuating the system, subliming measured amounts of $^{13}C$-enriched $CO_2$ gas (90% $^{13}C$ Merck, Sharp and Dohme) into the tube, sealing the tube with a glass-blowing torch, and removing it to allow for equilibration. It was not possible to measure the pH of these sealed samples; approximate concentrations are given in Table 1.

Samples for Raman spectrometry (Table 2) were also made up in nmr tubes by the method described for nmr samples 1 to 24.

Can. J. Chem. Downloaded from www.nrcresearchpress.com by 210.87.254.105 on 09/06/12
For personal use only.

TABLE 2. Summary of Raman results

| Sample | pH | $C_c/M$ | % Area* | $\%CO_3^{2-}$ Expl† | $\%CO_3^{2-}$ Calcd§ |
|---|---|---|---|---|---|
| 35 | 11.55 | 0.50 | 100 | 100 | 97 |
| 36 | 10.55 | 0.47 | 78 | 86 | 79 |
| 37 | 9.81 | 0.43 | 38 | 52 | 43 |
| 38 | 9.50 | 0.42 | 26 | 39 | 28 |
| 39 | 9.01 | 0.41 | 11 | 18 | 11 |
| 40 | 7.64 | 0.40 | 5 | 8 | 0.5 |
| 41‡ | 8.23 | 0.50 | 2 | 4 | 2 |
| 42‡ | 9.79 | 0.50 | 39 | 53 | 43 |
| 43‡ | 11.09 | 0.50 | 87 | 93 | 93 |

*% of area under 1060 $cm^{-1}$ (see Fig. 1), ±2%.
†% Area modified by scattering coefficients from ref. 14.
‡Na rather than K salt.
§Using eqs. [7] to [12].

Ordinary $K_2CO_3$ and water were used; the presence of deuterium introduces an extra line (due to $DCO_3^-$) into the spectrum. Only samples with $C_c \simeq 0.5\ M$ were prepared, as 0.05 $M$ samples would have insufficient scattering for reasonable resolution. A Jobin-Yvon Raman HG2S spectrometer with a CR-4 or CR-12 ion laser was used. Curve resolution of the spectra (Fig. 1) was done using the curve-resolving program of the Nicolet 1180 system computer. A Lorentz–Gaussian distribution (20% Gaussian) was used to form the resolved peaks. Spectra were taken at room temperature (293 ± 2 K).

## Results and discussion

*(a) Positions of nmr lines (acidic range)*

Table 1 indicates the $^{13}C$ shifts for various samples using the $\delta_c$ scale relative to TMS = 0. Spectra of the liquid portion of samples 26 and 27 ($CO_2$ in $D_2O$) show a line at 125.9 ± 0.1 ppm. The major species present must be $CO_2$(aq) in these samples. Patterson and Ettinger (12) report 125 ppm for $CO_2$(aq), and Stothers (16) quotes it as 124.2. A change of solvent (to $H_2O$) does not change the peak position to a noticeable extent. The position is also relatively insensitive to temperature (samples 26 to 34).

The spectrum of sample 28 (high pressure $CO_2$) taken with part of the gas phase observed showed an additional peak at 124.5 ppm. This must correspond to $CO_2$(g).

The spectra for samples 29 and 30 are shown in Fig. 2. With a greater amount of base (sample 29), the magnitude of the $HCO_3^-$(aq) peak at 161.3 ppm is increased relative to the $CO_2$(aq) peak at 125.9 ppm. Quantification of peak sizes and $CO_2/HCO_3^-$ ratios cannot be easily done since accurate analysis of the sample contents was not possible for the sealed samples, and since the magnitudes of the $^{13}C$ peaks are not necessarily proportional to the concentrations. The 161.3 ppm position for $HCO_3^-$(aq) found here compares well with the 161 ppm in ref. 12 and 160.0 ppm in ref. 16. Again there is little temperature dependence for this resonance (samples 33, 34).

Separate peaks exist for $CO_2$(aq) and $HCO_3^-$(aq) as the kinetics of exchange between these species (reactions [2], [3]) is relatively slow (6). Use of an enzyme such as carbonic anhydrase speeds up the kinetics so that line broadening is present (4), but coalescence of lines is not achieved.

The $H_2CO_3$(aq), if present as an equilibrium species (7), is present in very small quantities relative to $CO_2$(aq). Extrapolation of the peak positions of $CO_3^{2-}$(aq) (at 169.5 ppm) and $HCO_3^-$(aq) (at 161.3 ppm), suggests that the $H_2CO_3$(aq) peak should be at about 153 ppm. Such a peak would be so small relative to the $CO_2$(aq) peak (of the order of 1:600) that it would not be observable with the XL-100. The presence of $H_2CO_3$(aq) should, in principle, shift the position of the $HCO_3^-$(aq) peak from 161.3 towards 153 ppm due to the rapid exchange (reaction [3]). However, as $H_2CO_3$(aq) would never be present to an appreciable extent relative to $HCO_3^-$(aq), then such a shift would not be observable in practise.

Peaks were observed at 151.5 ppm in several samples such as 31 and 32. As indicated in Fig. 2, the 151.5 ppm peaks were observed when both the 125.9 and 161.3 ppm peaks were present (sample 31) and with only the 125.9 ppm present (sample 32). This 151.5 ppm peak was, however, not stable with time. After the tubes had aged for a month, it was no longer observable. A species such as $H_2CO_3$ may have been formed on the glass surface in the procedure used for preparation of such sam-

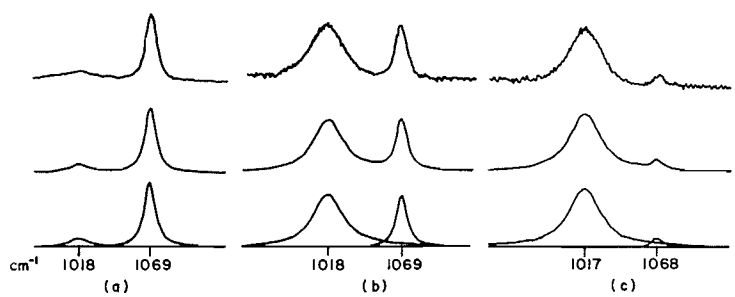


FIG. 1. Examples of Raman spectra and curve resolution: (*a*) sample 36, Table 2, (*b*) sample 38, (*c*) sample 40.

Can. J. Chem. Downloaded from www.nrcresearchpress.com by 210.87.254.105 on 09/06/12
For personal use only.

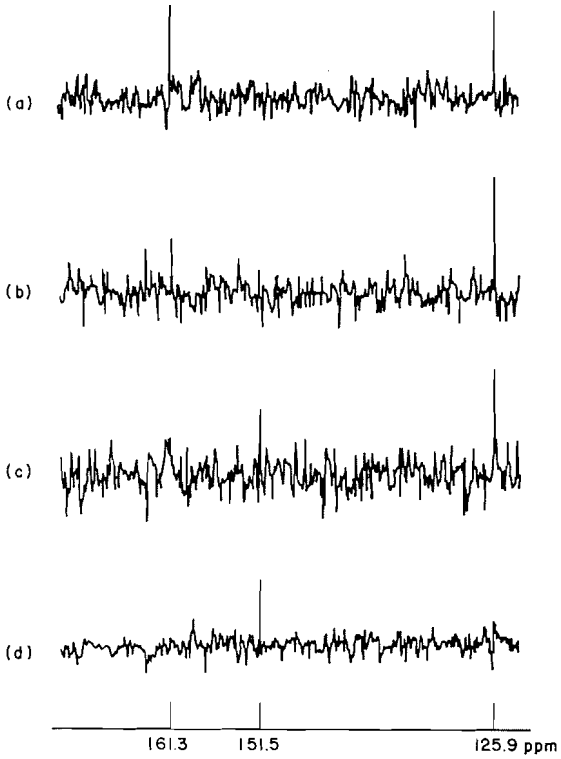


FIG. 2. Examples of $^{13}$C-nmr spectra: (*a*) sample 29, Table 1, (*b*) sample 30, (*c*) sample 31, (*d*) sample 32.

ples, and the equilibration time for such species may be greater than the allowed-for day or two. Non-equilibrium conditions in aqueous carbon dioxide systems are not unknown (e.g. ref. 17).

*(b) Calculation of concentrations of species*

A discussion of the experimental results from Raman and $^{13}$C-nmr spectroscopy of basic solutions involves quantitative analysis of the concentrations of $HCO_3^-$(aq) and $CO_3^{2-}$(aq). The pH, the total concentration of carbon dioxide species, $C_c$, and the concentration of other ions ($K^+$, $Cl^-$), $C_I$, are known in these samples.

Stumm and Morgan (1) give the basic equations for such a calculation for an ideal state, where concentrations equal activities:

$$[7] \quad [CO_3^{2-}] = C_c \left[ \frac{[H^+]^2}{K_1 K_2} + \frac{[H^+]}{K_2} + 1 \right]^{-1}$$

$$[8] \quad [HCO_3^-] = C_c \left[ \frac{[H^+]}{K_1} + \frac{K_2}{[H^+]} \right]^{-1}$$

$$[9] \quad [H_2CO_3^*] = C_c \left[ 1 + \frac{K_1}{[H^+]} + \frac{K_1 K_2}{[H^+]^2} \right]^{-1}$$

Here $[H_2CO_3^*]$ is defined by eq. [6] and the equilibrium constants $K_1$, $K_2$ are defined by [10] and [11] below.

Relationships [7–9] can be used for non-ideal systems if $K_1$, $K_2$ are taken to be concentration equilibrium constants, i.e.

$$[10] \quad K_1 = K_{1,c} = K_{1,a}/K_{1,y} = K_{1,a} \frac{1}{y_{H^+} y_{HCO_3^-}}$$

$$[11] \quad K_2 = K_{2,c} = K_{2,a}/K_{2,y} = K_{2,a} \frac{y_{HCO_3^-}}{y_{H^+} y_{CO_3^{2-}}}$$

Here $y$ is used to denote the activity constants on the molar scale. $K_{1,a}$ and $K_{2,a}$ are the activity equilibrium constants for reactions [3] and [4], and are thus invariant with concentrations and/or ionic strengths. The concentration equilibrium constants $K_{1,c}$ and $K_{2,c}$ are not invariant.

The molar activity coefficients $y$ can be calculated using several equations (18). Here an equation similar to that of Davies (18) was used.

$$[12] \quad \log_{10} y_i = -A z_i^2 \left( \frac{\sqrt{I}}{1+\sqrt{I}} - 0.2I \right)$$

Here $I$ is the ionic strength, $z_i$ the charge type of the $i$th species, and $A$ the Debye–Hückel constant (18). The Debye–Hückel limiting law and the Guntelberg equation (as [12] but with no $0.2I$ term) were also tested.

Calculations were done on a computer using iteration. First the $y_i$ were assumed to be unity and [7], [8], and [9] were used to calculate the concentrations with $[H^+] = 10^{-pH}$. The ionic strength was obtained from these results and the $y_i$ calculated using [12]. New equilibrium constants $K_1$ and $K_2$ were then obtained from [10] and [11] and $[H^+]$ set as $10^{-pH}/y_{H^+}$. A revised set of concentrations were calculated and the same procedure repeated until no further change occurred in the concentrations.

Some examples of results are shown in Table 3. The activity coefficients $y_{HCO_3^-}$ for the 0.05 *M* solutions agree to two significant figures with those in ref. 19. Those for the 0.5 *M* solutions are higher (0.72 as compared to 0.57 in ref. 19). The $y_{CO_3^{2-}}$ at high ionic strength compare reasonably with those calculated for surface sea water (3) (0.27 compared to 0.20). They are, however, vastly different to the experimental value (0.02) quoted in ref. 3.

Activity coefficients obtained from one experimental method are not always applicable to consideration of speciation using another method (9). The Raman and $^{13}$C-nmr data probably have insufficient resolution to differentiate between free $CO_3^{2-}$ and $CO_3^{2-}$ in the form of an ion pair. Conductivity and electromotive force experiments would, however,

Can. J. Chem. Downloaded from www.nrcresearchpress.com by 210.87.254.105 on 09/06/12
For personal use only.

TABLE 3. Examples of results of speciation calculation

| Sample | pH | $C_C/M$ | $C_I/M$ | $y_{HCO_3^-}$ | $y_{CO_3^{2-}}$ | $C_{H_2CO_3}$ | $C_{HCO_3^-}$ | $C_{CO_3^{2-}}$ | $\%CO_3^{2-}$ |
|---|---|---|---|---|---|---|---|---|---|
| 5 | 10.00* | 0.48 | 1.2 | 0.72 | 0.27 | $3 \times 10^{-5}$ | 0.20 | 0.28 | 59 |
| 20 | 9.94* | 0.048 | 0.120 | 0.76 | 0.42 | $4 \times 10^{-6}$ | 0.023 | 0.025 | 52 |
| 17 | 10.27* | 0.048 | 0.120 | 0.75 | 0.32 | $1 \times 10^{-6}$ | 0.014 | 0.034 | 70 |
| 17 | 10.27† | 0.048 | 0.120 | 0.76 | 0.34 | $3 \times 10^{-6}$ | 0.031 | 0.017 | 35 |

*$T = 305$ K, $K_2 = 5.32 \times 10^{-11}$.
†$K_2 = 1.28 \times 10^{-11}$.

exclude ion paired $CO_3^{2-}$ from being considered as $CO_3^{2-}$(aq). Thus values of $y_{CO_3^{2-}}$ should be considerably lower for emf and conductivity experiments than those relevant for Raman and $^{13}$C-nmr.

*(c) Raman spectra*

Raman spectroscopy of carbon dioxide in water is discussed in some detail in refs. 13–15. Here only the region around 1000 $cm^{-1}$ is of interest. As shown in Fig. 1, this region contains the 1067 $cm^{-1}$ ($CO_3^{2-}$) and the 1017 $cm^{-1}$ ($HCO_3^-$) bands.

Recent work on sulfuric acid (20) suggests that such bands can be further resolved to give separate, but overlapping, peaks for free and ion paired species. It was not attempted to resolve the peaks as shown in Fig. 1 further to test whether this could be the case for $HCO_3^-$ and $CO_3^{2-}$ lines. This may be possible in further, more extensive spectroscopic work. The degree of ion pairing in the solutions should be significant. A solution 0.5 $M$ in $K_2CO_3$ should have 53% of the $CO_3^{2-}$ in the form $(K^+ \cdot CO_3^{2-})^{-1}$, while a solution 0.5 $M$ in $KHCO_3$ should have 33% of $HCO_3^-$ as $(K^+ \cdot HCO_3^-)^0$ if ion pairing constants for the sodium salts (21) are assumed valid also for the potassium salts.

Figure 3 shows the ratio of the 1067 $cm^{-1}$ area to the sum of the 1067 $cm^{-1}$ and 1017 $cm^{-1}$ areas as plotted versus the percentage of $CO_3^{2-}$ as calculated using the procedure in (*b*). It is probably somewhat fortuitous that the plot is so close to a linear relation (correlation coefficient 0.996) as the scattering coefficients of these two bands are not necessarily equal.

Using the results in ref. 14, the scattering coefficient of the 1067 $cm^{-1}$ line is calculated to be 1.80 times that of the 1017 $cm^{-1}$ line. When this ratio is used, the relation in Fig. 3 is not as linear. The 1.80 ratio used was derived from intensity–concentration curves measured relative to the 459 $cm^{-1}$ band of $CCl_4$. However, in a previous publication (13), it is apparent that scattering from the 1067 $cm^{-1}$ band is more intense, but seemingly only by a factor of about 1.4 rather than 1.8.

The effect of the equation used to calculate the percentage of $CO_3^{2-}$ is shown in Fig. 3 to be of vital importance. Equation [12] appears to be quite reasonable for the calculation of $y$'s relevant to Raman spectroscopy, but it may be very misleading for $y$'s useful to an experimental method such as conductivity.

If $H_2CO_3$(aq) exists, then some signs of it should be apparent in Raman spectra at high $CO_2$ pressures; this was not observed (15).

*(d) Nuclear magnetic resonance spectra in the high pH range*

The position of the $^{13}$C peak for $CO_3^{2-}$(aq) seems to be at 169.5 ppm. This compares with 171 ppm reported in ref. 12 and 170.0 ppm in ref. 16. Sample 25, 6 $M$ in $K_2CO_3$, showed a peak at 170.3 ppm, but in such a concentrated solution (ion-to-water ratio 2:5) a very different environment from a more dilute solution should be expected to be present.

Figure 4 shows a plot of the resonance position for the 0.5 $M$ solutions as a function of the percentage $CO_3^{2-}$. As the exchange in reaction [4] is rapid, the shift would be 161.3 ppm for 0% $CO_3^{2-}$ (100% $HCO_3^-$), and 169.5 ppm for 100% $CO_3^{2-}$. It should vary linearly between these extremes as the chemi-

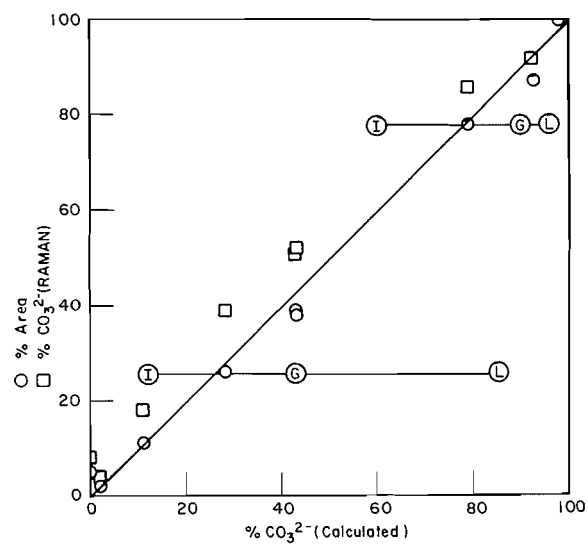


FIG. 3. Percentage area ○ and percentage of $CO_3^{2-}$ from Raman □ versus percentage $CO_3^{2-}$ calculated (data from Table 2). Ⓘ, Calculated percentage of $CO_3^{2-}$ assuming $y = 1.0$; Ⓖ, assuming $y$ follows the Guntelberg equation; Ⓛ, assuming $y$ follows the Debye–Hückel limiting law.

Can. J. Chem. Downloaded from www.nrcresearchpress.com by 210.87.254.105 on 09/06/12
For personal use only.

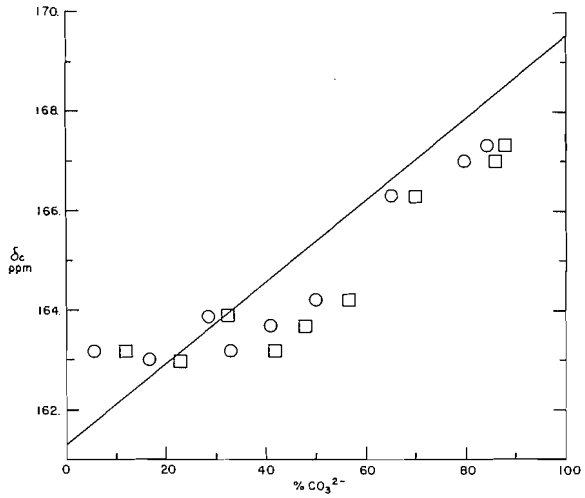


FIG. 4. $^{13}C$ chemical shift versus percent $CO_3^{2-}$ for $C_c \simeq 0.5\,M$ (samples 1–4, 6–11 in Table 1). ○, calculated percentage of $CO_3^{2-}$ ($K_2 = 5.32 \times 10^{-11}$), □ percentage of $CO_3^{2-}$ interpolated from Raman data as shown in Fig. 3.

cal shift would be the concentration average of the two values. Figure 4 shows points where the percentage of $CO_3^{2-}$ is given both as that calculated from eq. [12] and as that obtained by interpolation of a percentage of $CO_3^{2-}$ versus pH curve constructed from the Raman data in Table 2.

Neither set of points gives a particularly good fit to a linear relation (correlation coefficient 0.919). The Raman-derived percentage $CO_3^{2-}$ points have not been corrected for a change in temperature (293 K to 305 K) or for the presence of some $D_2O$ in the nmr samples (1 to 11). Such corrections would not change the positions of the points very much, and would increase the percentage of $CO_3^{2-}$ and bring most points even further off the curve.

The deviations are possibly due to ion pairing. It is likely that the presence of a $K^+$ ion would shift the $CO_3^{2-}$ signal towards the direction of the $HCO_3^-$, i.e. upfield, and also the $HCO_3^-$ signal upfield. The magnitudes of such shifts can not be determined on the basis of the data currently available.

Relatively dilute samples can be used for nmr studies if $^{13}C$-enriched material is used. A series of solutions with $C_c \simeq 0.05\,M$ (samples 12 to 24) were thus studied. For such lower ionic strength solutions, calculation of $y$'s through eq. [12] would be more meaningful and effects such as ion pairing would be smaller. Figure 5 shows that the calculated percentage of $CO_3^{2-}$ is for this case not quite as sensitive to the form of the equation used for $y$.

When the usual value of the dissociation constant for $HCO_3^-$ at 305 K is used ($5.32 \times 10^{-11}$), then as can be seen from Fig. 5, a plot of chemical shift versus the percentage of $CO_3^{2-}$ is definitely non-linear. The samples were, however, made up in $D_2O$, and according to ref. 22, the p$K$ of an acid with p$K \simeq 10$ is 0.62 units higher in $D_2O$. When a value $1.28 \times 10^{-11}$ is used for $K_2$, then the points approximate a linear relationship quite well (correlation coefficient 0.997). Table 3 indicates how large an effect a change in the $K_2$ value has on the calculated percentage of $CO_3^{2-}$ when pH $\simeq$ p$K_2$ (sample 17).

The uncertainty in the points in Fig. 5 is about $\pm 0.2$ ppm in the chemical shift and up to $\pm 5\%$ in the percentage of $CO_3^{2-}$. The temperature-control on the XL-100 can vary up to $\pm 2$ K, and such variations can change the value of $K_2$ by several percent.

## Conclusions

The $^{13}C$ nmr shifts of the various species present in a carbon dioxide – water system are as follows: $CO_2$ 124.5 ppm, $CO_2$(aq) 125.9 ppm, $HCO_3^-$(aq) 161.3 ppm, $CO_3^{2-}$(aq) 169.5 ppm. An unstable species with a shift of 151.5 ppm was also detected.

The $^{13}C$ nmr and Raman spectra obtained for samples at various pH are in agreement with the kinetics and equilibria assumed for the carbon dioxide – water system. No direct evidence of the species $H_2CO_3$(aq) was obtained.

Activity coefficients of relevance to these experimental methods can be obtained with reasonable accuracy from an equation such as the Davies equation, even at high ion strengths (> 1).

Further $^{13}C$-nmr studies of aqueous carbonate solutions seem promising as a means of increasing

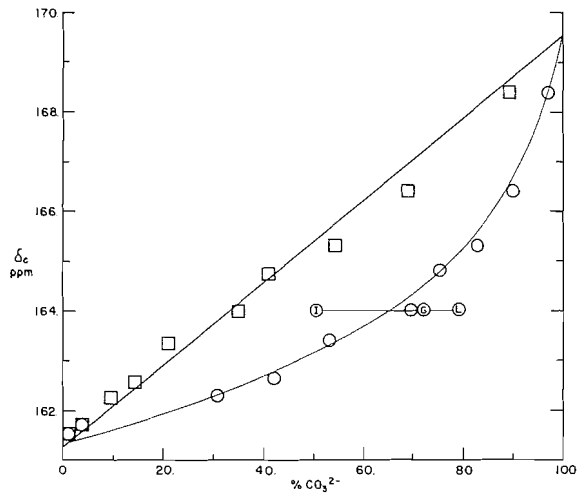


FIG. 5. $^{13}C$ chemical shift versus calculated percentage of $CO_3^{2-}$ for $C_c \simeq 0.5\,M$ (samples 12–17, 19, 21–24 in Table 1) ○, $K_2 = 5.32 \times 10^{-11}$; □, $K_2 = 1.28 \times 10^{-11}$. Ⓘ, $y = 1$; Ⓖ, $y$ from Guntelberg; and Ⓛ, $y$ from the limiting law.

understanding of speciation in such systems. It is necessary to make allowances for changes in equilibrium constants in these systems if heavy water is used.


## Acknowledgements

Aid in the experimental work from Ms. M. J. McGuire, Dr. W. A. Adams, and Ms. M. J. Bell is gratefully acknowledged. Financial support was provided through Environment Canada contract 0SS3-0174 and Natural Sciences and Engineering Research Council of Canada grants.



1. W. STUMM and J. J. MORGAN. Aquatic chemistry, Wiley-Interscience, 1970.
2. H. GAMSJAGER and F. REITERER. Environment international, **2**, 419 (1979).
3. S. D. MORTON and G. I. LEE. J. Chem. Ed. **45**, 513 (1968).
4. I. SIMONSSON, B. H. JONSSON, and S. LINDSKOG. Eur. J. Biochem. **93**, 409 (1979).
5. R. C. PATEL, R. J. BOE, and G. ATKINSON. J. Solution Chem. **2**, 357 (1973).
6. D. M. KERN. J. Chem. Ed. **37**, 14 (1960).
7. B. JONSSON, G. KARLSTROM, H. WENNERSTROM, and B. ROOS. Chem. Phys. Lett. **41**, 317 (1976).
8. B. JONSSON, G. KARLSTROM, and H. WENNERSTROM. J. Am. Chem. Soc. **100**, 1658 (1978).
9. L. W. GREEN, P. KRUUS, and M. J. MCGUIRE. Can. J. Chem. **54**, 3152 (1976).
10. R. C. PATEL, F. GARLAND, and G. ATKINSON. J. Solution Chem. **4**, 161 (1975).
11. M. P. RYAN and J. E. BAUMAN. Inorg. Chem. **17**, 3329 (1978).
12. A. PATTERSON and R. ETTINGER. Z. Elektrochem. **64**, 98 (1960).
13. A. R. DAVIS and B. G. OLIVER. J. Solution Chem. **1**, 329 (1972).
14. B. G. OLIVER and A. R. DAVIS. Can. J. Chem. **51**, 698 (1973).
15. Y. K. SZE, W. A. ADAMS, and A. R. DAVIS. *In* Chemistry and physics of aqueous gas solutions. Electrochemical Society. 1975. p. 42.
16. J. B. STOTHERS. Organic chemistry. Vol. 24. Carbon-13 NMR spectroscopy. Academic Press. 1972.
17. C. BROSSET. Swedish water and air polution research institute. B540 (1980).
18. R. A. ROBINSON and R. H. STOKES. Electrolyte solutions. Revised edition, Butterworths, London. 1968.
19. K. S. PITZER and J. C. PEIPER. J. Phys. Chem. **84**, 2396 (1980).
20. R. A. COX, U. L. HALDNA, K. L. IDLER, and K. YATES. Can. J. Chem. **59**, 2591 (1981).
21. F. S. NAKAYAMA. J. Phys. Chem. **74**, 2726 (1970).
22. E. HÖGFELDT and J. BIGELEISEN. J. Am. Chem. Soc. **82**, 15 (1960).


Can. J. Chem. Downloaded from www.nrcresearchpress.com by 210.87.254.105 on 09/06/12
For personal use only.

# $^1H$ and $^{13}C$ nuclear magnetic resonance study of the complexation of uranyl ion with malic acid

M. TERESA NUNES[1]

*Laboratório Nacional de Engenharia e Tecnologia Industrial, Sacavem, Portugal and Centro de Química Estrutural, Complexo I, IST, Av.Rovisco Pais, 1096 Lisboa, Portugal*

VICTOR M. S. GIL

*Departamento de Química, Universidade de Aveiro, Portugal and Centro de Química (INIC), Coimbra, Portugal*

AND

ANTÓNIO V. XAVIER

*Departamento de Química e Biotecnia, FCT, UNL and Centro de Química Estrutural, Complexo I, IST, Av.Rovisco Pais, 1096 Lisboa, Portugal*

Received September 4, 1981

M. TERESA NUNES, VICTOR M. S. GIL, and ANTÓNIO V. XAVIER. Can. J. Chem. **60**, 1007 (1982).

A full pH range $^1H$ and $^{13}C$ nmr study was performed of the complexation of $UO_2^{2+}$ with malic acid, for variable concentrations and molar ratios. Spectral evidence for the existence of at least five complexes was found, and their stoichiometry and dependence on pH were investigated. Information on the conformation of the bound ligand molecules was also obtained.

M. TERESA NUNES, VICTOR M. S. GIL et ANTÓNIO V. XAVIER. Can. J. Chem. **60**, 1007 (1982).

On a étudié la rmn du $^1H$ et du $^{13}C$ à tous les pH des produits de complexation de $UO_2^{2+}$ avec l'acide maléique à des concentrations et des rapports molaires variables. On a obtenu des preuves spectrales de l'existence d'au moins cinq complexes et on a étudié leur stoichiométrie et l'influence du pH. On a également obtenu des informations sur la conformation des ligands.

[Traduit par le journal]

## Introduction

The interaction of uranyl ion with malic acid has been previously studied by potentiometric (1–4), polarographic (4, 5), spectrophotometric (1, 4, 6, 7), and polarimetric (8) methods. It has been found that, in equimolar solutions and for the pH region 2–4, a binuclear complex involving tridentate chelation is formed (as has also been shown for the solid by ir spectroscopy (9)); at pH > 4 this dimer seems to react further with hydroxyl ions to form ternuclear species (1, 2). Dimerization and trimerization constants have been reported (2, 10).

The nmr proton coupling constants and chemical shifts obtained for the binuclear complex 1:1 (0.2 *M* solution at pH = 3) gave indication about the type of dimer present (11), thus confirming the structure previously postulated by Rajan and Martell (3): OH groups of the ligands acting as bridges between the U atoms (**1**, or its isomer of $C_s$ symmetry)

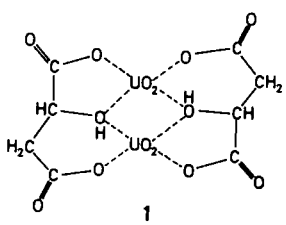

**1**

the ligand being in a conformation close to $c_1$

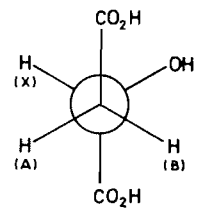

$c_1$

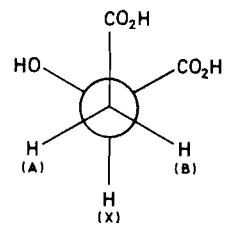

$c_2$

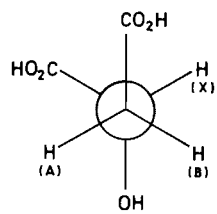

$c_3$

The pH range from 3 to 5.6 has also been investigated by proton nmr spectroscopy, using equimolar solutions (0.16 and 0.2 *M*); as a result, the simultaneous existence of three complexes was suggested (4): the monomer ($UO_2$) Mal, the dimer (**1**) and another dimer (**2**)

[1]Author to whom correspondence may be addressed at the Laboratório Nacional de Engenharia e Technologia Industrial, Estrada Nacional No. 10, 2685 Sacavem, Portugal.

0008-4042/82/081007-12$01.00/0

©1982 National Research Council of Canada/Conseil national de recherches du Canada

Can. J. Chem. Downloaded from www.nrcresearchpress.com by 210.87.254.105 on 09/06/12
For personal use only.

Can. J. Chem. Downloaded from www.nrcresearchpress.com by 210.87.254.105 on 09/06/12
For personal use only.

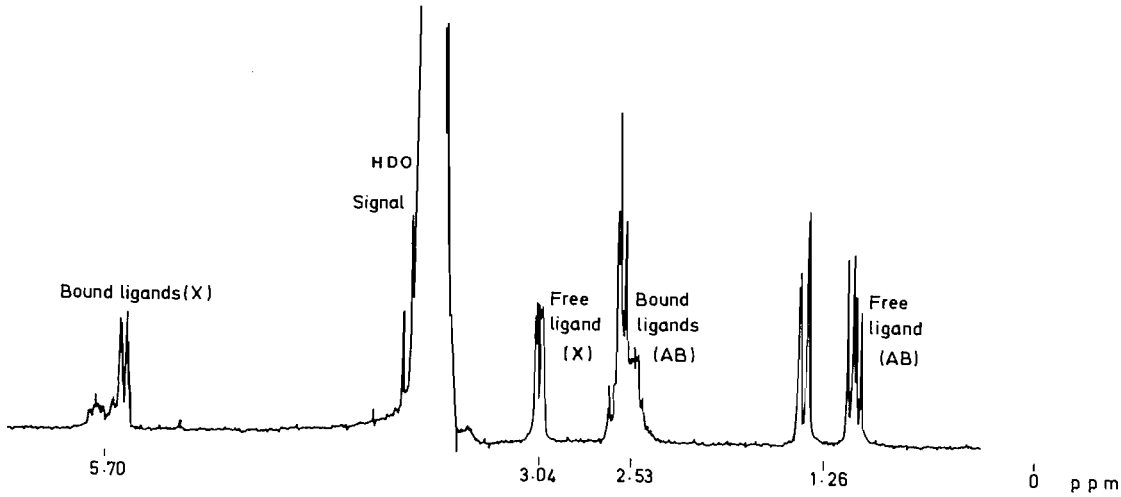


FIG. 1. Bound and free ligand $^1H$ spectra of a 1:2 (metal/ligand) solution.

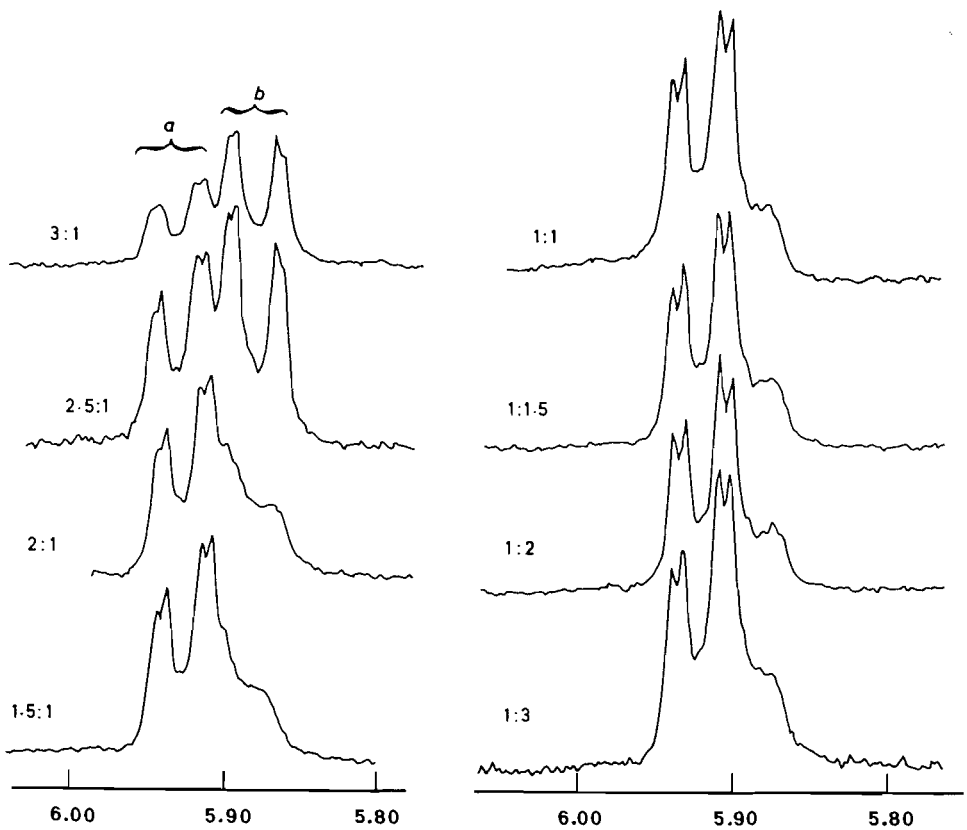


FIG. 2. X sub-spectra of bound ligand for pH* = 2.7, for variable metal/ligand ratios.

Can. J. Chem. Downloaded from www.nrcresearchpress.com by 210.87.254.105 on 09/06/12
For personal use only.

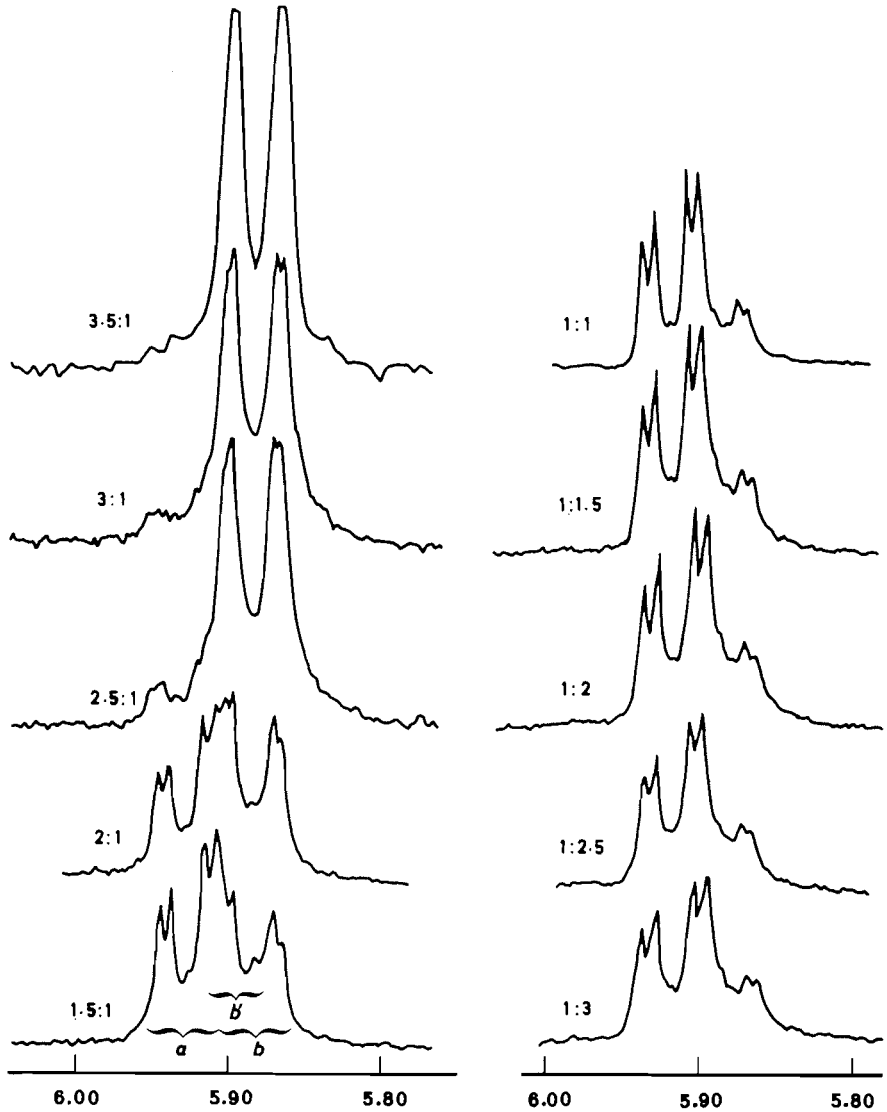


FIG. 3. X sub-spectra of bound ligand for pH* = 3.9, for variable metal/ligand ratios.

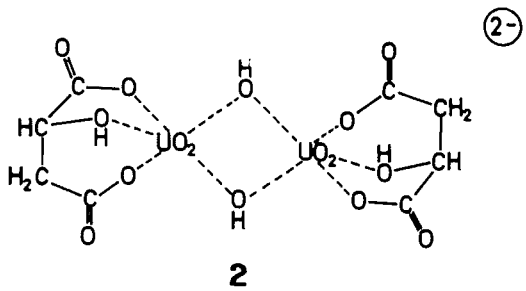


2

corresponding to an hypothesis proposed by Feldman *et al.* (1, 2, 11) and requiring $c_2$ as the ligand conformation.

Aiming at a clarification of the number and structure of the complexes, we report in this paper a full pH range study using $^1H$ and $^{13}C$ nmr spectroscopy. It being a very complicated system, due in particular to the hydrolysis of $UO_2(H_2O)_n^{2+}$ with the resulting formation of polynuclear species, we have only partly succeeded, and this on account of the great stability of the complexes formed and their being, in general, in sufficiently slow exchange for different spectra to be observed for different species.

## Experimental

$D_2O$ solutions (0.5 *M*), prepared from commercially available

Can. J. Chem. Downloaded from www.nrcresearchpress.com by 210.87.254.105 on 09/06/12
For personal use only.

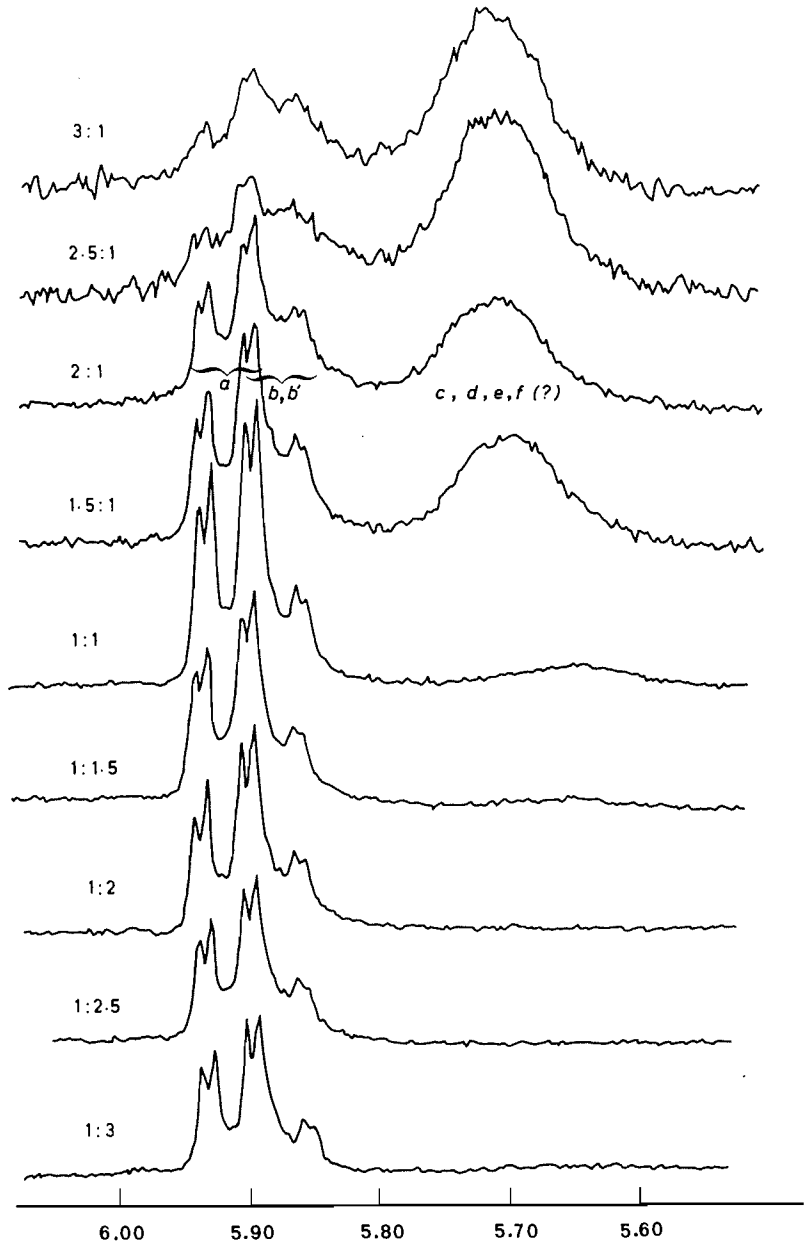


FIG. 4. X sub-spectra of bound ligand for pH* = 5.2, for variable metal/ligand ratios.

pure uranyl nitrate and (L) – malic acid, were standardized by gravimetry and potentiometry, respectively. The solutions actually used were obtained by dilution of those parent solutions and the pH was adjusted with NaOD and DCl; the pH* values quoted are the direct meter readings.

The $^1H$ spectra were recorded on a Bruker CXP-300 nmr spectrometer and in a JEOL PS-100 spectrometer in the Fourier transform mode. The $^{13}C$ spectra were run with proton decoupling on the JEOL spectrometer. *tert*-Butanol ($\delta = 1.23$) and *p*-dioxan ($\delta = 67.40$) were used as internal references, respectively, for $^1H$ and $^{13}C$ resonances. Unless otherwise specified, the measurements were done at 293 K.

## Results and discussion

### *$^1H$ nuclear magnetic resonance spectra*

The methylene and methine protons of malic acid give rise to an ABX spectrum, at 300 MHz. Depending on pH, from 2.7 to 10.7, and on the uranyl/malic acid molar ratio, at least seven different X signals of bound ligand are identified, besides that of free ligand when in excess (the case of 1:*n* molar ratios with $n \gtrsim 1.5$ for pH $\lesssim 9.5$ and $n \gtrsim 1$ for pH $\simeq 10.5$); the AB sub-spectra of bound species

Can. J. Chem. Downloaded from www.nrcresearchpress.com by 210.87.254.105 on 09/06/12
For personal use only.

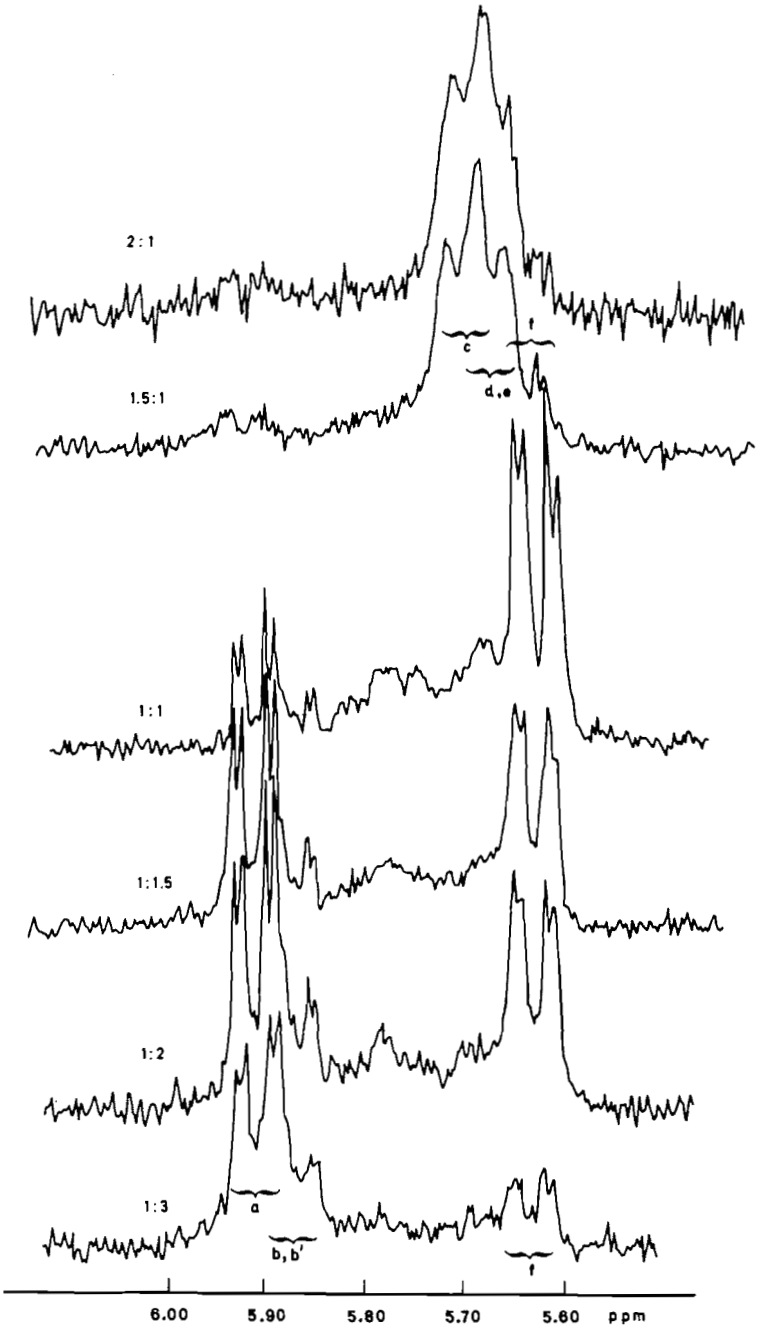


FIG. 5. X sub-spectra of bound ligand for pH* = 6.7, for variable metal/ligand ratios.

are in part suppressed. This AB pattern lies about 1.3 ppm to low field of the mid point of the AB sub-spectrum of free ligand; the low-field shift of the X signals upon complexation ranges from about 2.6 to 2.8 ppm. A typical full spectrum is shown in Fig. 1.

The fact that different spectra are observed for different species means that, at room temperature, they are undergoing exchange processes that are slow in the nmr time scale. However, some of the X-signals can be exchange broadened, the degree of broadening depending on pH and molar ratio.

Figures 2–6 show the X sub-spectra of bound ligand for pH* values ranging from 2.7 to 7.9 and

Can. J. Chem. Downloaded from www.nrcresearchpress.com by 210.87.254.105 on 09/06/12
For personal use only.

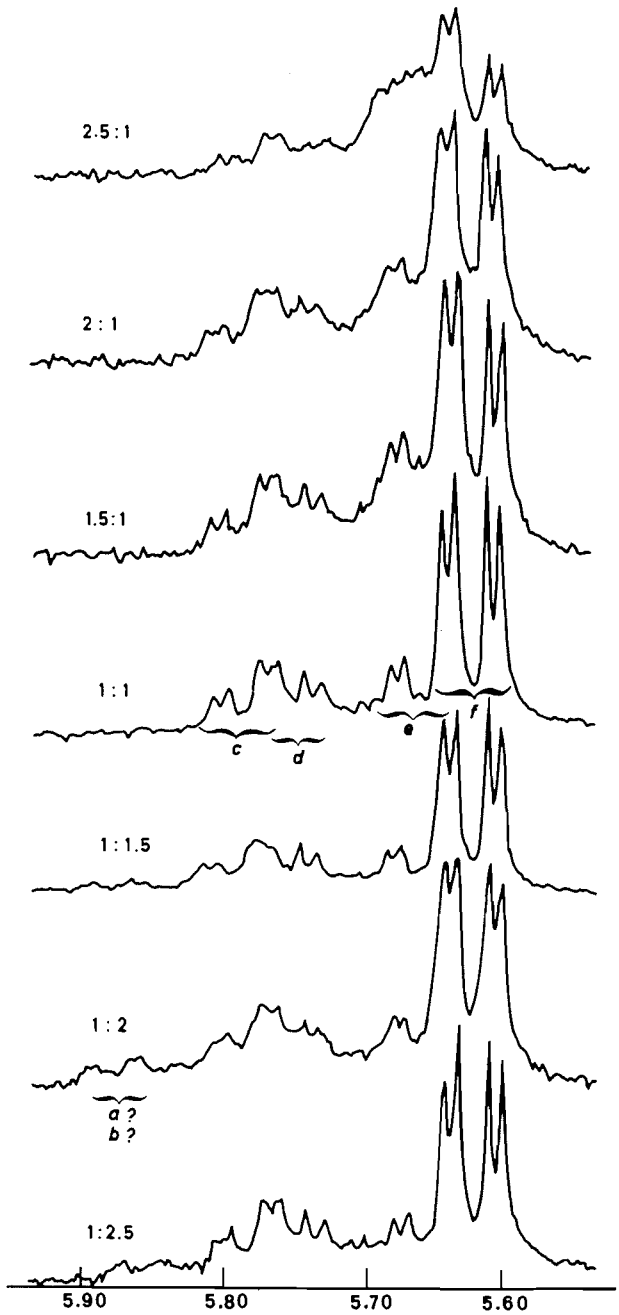


FIG. 6. X sub-spectra of bound ligand for pH* = 7.9, for variable metal/ligand ratios.

for variable molar ratios (usually, from 3:1 to 1:3); Fig. 7 shows the X signals obtained for three solutions (1:1, 1:1.5, and 1:2) at pH = 10.7. The total concentration of the complexing species ($UO_2^{2+}$ + malic acid) was kept constant (0.075 *M*), so that Job's plots based on the spectral intensities could be constructed, as shall be discussed later.

Two quartets a and b are clearly identified at pH* = 2.7 (Fig. 2) and pH* = 3.9 (Fig. 3); another less resolved signal (b') can be detected in the latter case. Quartet a is dominant for molar ratios from 1:3 up to 2:1, b becoming dominant for higher molar ratios, specially at pH* = 3.9.

At pH* = 5.2, quartets a and b remain, but a very broad signal at 5.66 ppm appears for molar ratios $n$:1 with $n \geq 1$ (Fig. 4). On increasing the pH of these solutions to pH* = 6.7, the broad signal sharpens (c, d, e), while the intensities of the a and b quartets greatly decrease (Fig. 5). However, for higher ligand contents these quartets become intense again; at the same time, a well defined quartet at high field is detected (f).

For pH* = 7.9, the intensities of signals a and b become very weak, and three other weak and partially superposed quartets, c, d, and e are detected, as well as the intense quartet f at higher field (Fig. 6). At pH* = 10.7, the major difference is the appearance of a new signal, g, to the high field side of quartet f (Fig. 7).

The ligands responsible for signals c, d, e, and f in Fig. 5 seem to be in intermediate exchange at pH* = 5.2, thus accounting for the broad peak observed. At pH* = 7.9, the various signals are still relatively broad due to exchange; this is confirmed by the effect of lowering the temperature on the sharpness of the signals. This is also observed at higher pH; Fig. 8 shows the spectrum obtained for pH* = 9.5 at 273 K. Similarly, exchange processes may be responsible for the low-field shift of the resonances of species a with the increase of the population of b (see Figs. 2–4).

The effect of exchange is also revealed in Fig. 9 where the 100 MHz spectra of a 1:1 solution of pH* = 5.5 at 293 and 343 K are compared. Whereas the a quartet broadens, the hump due presumably to c, d, e, and f sharpens into a well defined quartet. Further work is in progress on the details of the exchange processes in such a complex system.

From a comparison of the intensities of the a, b, f, and g X-signals, in various conditions, we may immediately conclude that they arise from four different complexes and not from nonequivalent ligand moieties in a smaller number of complexes. The remaining three X-signals (c, d, and e) are too weak to enable a conclusion on whether they correspond to three other less abundant complexes or to two or even just one; in the latter case, three magnetically nonequivalent malate ligands should be present per molecule.

Can. J. Chem. Downloaded from www.nrcresearchpress.com by 210.87.254.105 on 09/06/12
For personal use only.

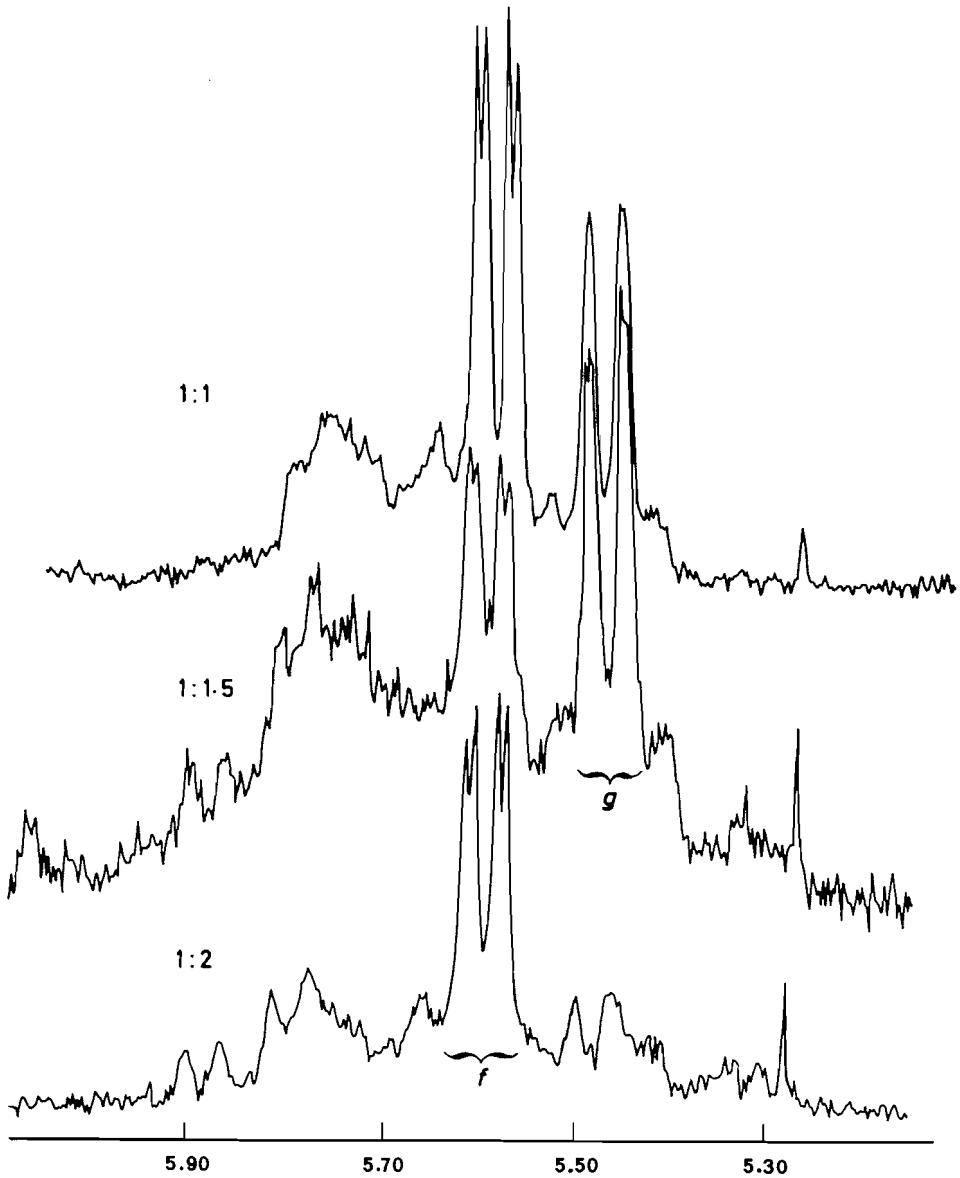


FIG. 7. X sub-spectra of bound ligand for pH* = 10.7, for variable metal/ligand ratios.

From the intensities of the X-signals in Figs. 2–6 (and that for free ligand when in excess), the concentrations of species a, b, f, and g are estimated as a function of molar ratio. The corresponding Job's plots for a and b at pH* = 2.7, for a at pH* = 6.7, for f at pH* = 7.9, and for g at pH* = 10.7, are given in Figs. 10 and 11. We must be cautious when drawing conclusions from these curves. In fact, Job's method is only expected to give directly the stoichiometry of a given complex when other complexes (or other equilibria) are present, if certain conditions are met. In particular, it is necessary that the solution of the complex under study having a maximal concentration has the other species in sufficiently smaller concentration. These are approximately the conditions in the study of complexes a and b at low pH (Figs. 2 and 3) and f at pH* $\simeq$ 8 (Fig. 6). Thus, Job's plots such as those of Fig. 10 confirm that a, the dominant complex in an equimolar solution at low pH, is a 1:1 complex, as previously reported (actually 2:2) (3, 11); this complex is accompanied by another species b of

Can. J. Chem. Downloaded from www.nrcresearchpress.com by 210.87.254.105 on 09/06/12
For personal use only.

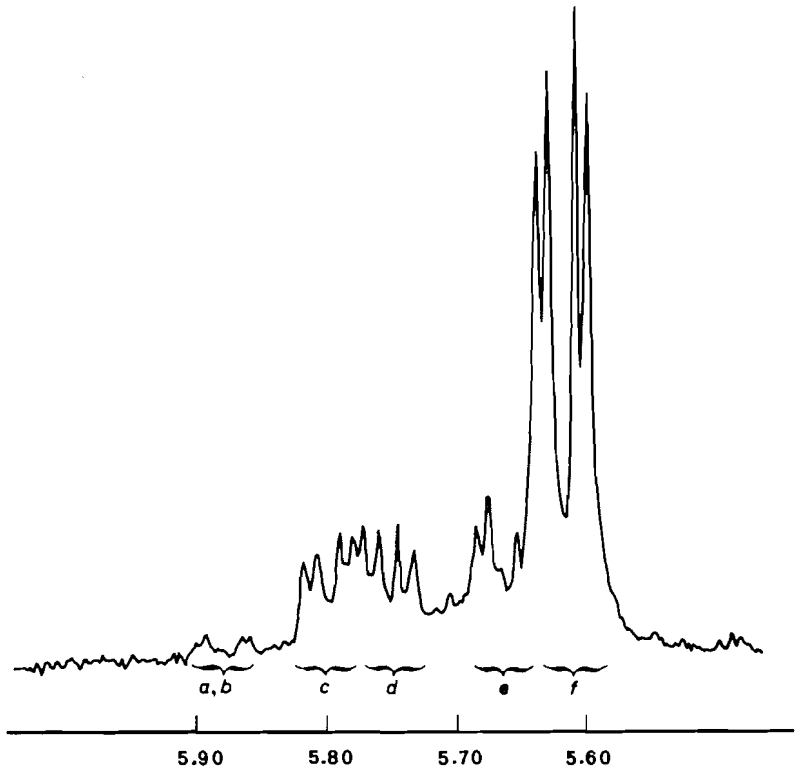


FIG. 8. X sub-spectra of bound ligand of a 1:2 (metal/ligand) solution for pH* = 9.5 at 273 K.

TABLE 1. $^1$H chemical shifts (ppm) and coupling constants (Hz) of the complexes identified

| Complex† | $\delta_A$ (or $\delta_B$) | $\delta_B$ (or $\delta_A$) | $\delta_X$ | $^2J_{AB}$ | $^3J_{AX} + {}^3J_{BX}$ | $^3J_{AX}$ (or $^3J_{BX}$) | $^3J_{BX}$ (or $^3J_{AX}$) |
|---|---|---|---|---|---|---|---|
| a (pH* = 2.75) | 2.54 | 2.48 | 5.93 | (−) 17.65 | 12.51 | 2.38 | 10.13 |
| | (2.62)‡ | (2.52)‡ | (5.91)‡ | ((−) 17.7)‡ | (12.9)‡ | (1.5±0.2)‡ | (11.4)‡ |
| a′ (pH* = 6.70) | 2.54 | 2.48 | 5.91 | (−) 16.91 | 13.20 | 1.53 | 11.71 |
| b′ | — | — | 5.90 | — | 14.70 | — | — |
| b | 2.55 | 2.44 | 5.88 | (−) 16.91 | 12.51 | 0.90 | 11.61 |
| c | — | — | 5.80 | — | 13.24 | — | — |
| d | — | — | 5.76 | — | 13.97 | — | — |
| e | — | — | 5.66 | — | 14.71 | — | — |
| f | 2.59 | 2.52 | 5.63 | (−) 16.91 | 13.24 | 1.64 | 11.60 |
| g | 2.43 | 2.33 | 5.49 | (−) 16.91 | 13.23 | 1.27 | 11.97 |

†The results are for: a 1:1 solution, pH* = 2.75. a′ 1:3 (metal/ligand) solution, pH* = 6.70, $T$ = 280 K. b 2.5:1 (metal/ligand) solution, pH* = 3.91. b′ 1.5:1 (metal/ligand) solution, pH* = 3.91. c, d, e 1:2 (metal/ligand) solution, pH* = 7.48, $T$ = 277 K. f 1:1.5 (metal/ligand) solution, pH* = 7.94. g 1:1.5 (metal/ligand) solution, pH* = 10.75, $T$ = 273 K.
‡1:1 solution, pH* 2–4, 100 MHz spectra (ref. 11).

composition $n$:1, with $n \gtrsim 2.5$. From the f curve in Fig. 11 it may be inferred that complex f is another 1:1 compound.

The conditions mentioned above are not present for pH* = 6.7 (Fig. 5) and pH* = 10.7 (Fig. 7). Accordingly, the maximal concentration of a is found in a solution of molar ratio $n$:1, with $n \simeq 1.5$ (Fig. 11). Also, the stoichiometry of complex g could not be obtained from a Job's plot, because there is always a large concentration of f and, in addition, it was not possible to run spectra for higher contents of $UO_2^{2+}$ at pH* ≃ 11, due to precipitation.

Dilution of a 1:2 solution of pH* ≃ 6.7 by a factor of 50 does not show significant change of the relative populations of complexes a and f. This suggests that they have the same degree of polymerization (2:2). The pH dependence of the relative

Can. J. Chem. Downloaded from www.nrcresearchpress.com by 210.87.254.105 on 09/06/12
For personal use only.

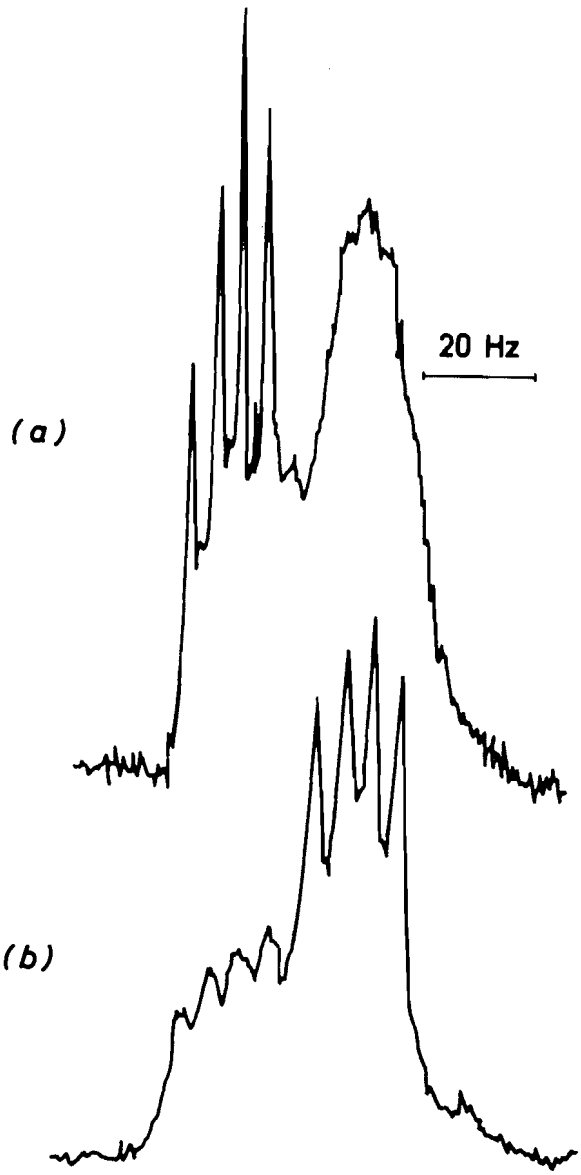


FIG. 9. 100 MHz X sub-spectra of a 1:1 solution for pH* = 5.5 at: (a) 293 K; (b) 343 K.

populations of a and f is compatible with these two complexes being an acid species and its conjugate base in slow exchange.[2] The fact that their equilibrium is slow in the nmr time scale may be due to a conformational modification linked with the protonation, f possibly being caused by a geometric isomerization of a. A different result is observed for pH* = 10.7 with respect to f and g, the former having a higher degree of polymerization.

Figures 12–14 show the relative populations of the various complexes detected for molar ratios of 2:1; 1:1, and 1:2 as a function of pH.

By choosing appropriate conditions, the full ABX analysis of the spectra of the a, b, f, and g complexes could be performed. In the case of the less intense signals b′, c, d, and e only a partial analysis could be done. The $^1H$ nmr parameters for the various complexes are given in Table 1. From the values of the vicinal coupling constants we see that in all complexes the ligand conformation is such that an approximately *trans* and a *gauche* arrangement of H atoms is present. This excludes conformation $c_2$ proposed by Feldman *et al.* (1, 2, 11).

*$^{13}C$ nuclear magnetic resonance spectra*

The solutions used for $^{13}C$ spectra were about 100 times as concentrated as those for $^1H$ data. In these conditions and for pH ranging from 3.0 to 10.1 only three distinct spectra of bound ligand were identified, besides that of free ligand for molar ratios 1:*n* with $n \gtrsim 1.5$. At pH* = 3.0 and for a 2:1 solution (1.50 *M* : 0.75 *M*) two separate ligand spectra are found and attributed to complexes a and b. For pH* in the range ~ 5 (solution 1:1) to ~ 7 (solution 1:2) signals attributed to complex a are observed (the spectrum of complex b is much too weak to be observed) and another spectrum assigned to complex f is clearly identified. At pH* ≃ 10 only spectrum f is observed. The assignment of the peaks was made by comparison with the spectra for various molar ratios and/or pH. The relative abundance of a and f is very sensitive to pH in the region of pH* = 6.3 (if they are an acid–base conjugate pair, then $pK_a \simeq 6.3$).

The $^{13}C$ chemical shifts (in ppm) for a 2:1 (1.50 *M* : 0.75 *M*) metal/ligand solution at pH* = 3.0 relative to the malate ion are to low field as follows

| $^-O_2C$ | $CH_2$ | CH(OH) | $CO_2^-$ |
|---|---|---|---|
| Complex a 5.7 (or 5.5) | 1.76 | 13.71 (or 14.20) | 8.3 (or 8.5) |
| Complex b 5.5 (or 5.7) | 1.76 | 14.20 (or 13.71) | 8.5 (or 8.3) |

It has been assumed that the relative position of the carboxylic peaks observed for the free ligand is retained on complexation; otherwise, the shifts for the β $CO_2H$ groups would be 4.6 and 4.4 and those for α 9.4 and 9.6, respectively, for complexes a and b.

For a 1:2 (0.75 *M* : 1.50 *M*) solution at pH* = 6.3,

[2]The authors thank one of the referees for calling their attention to this interpretation.

Can. J. Chem. Downloaded from www.nrcresearchpress.com by 210.87.254.105 on 09/06/12
For personal use only.

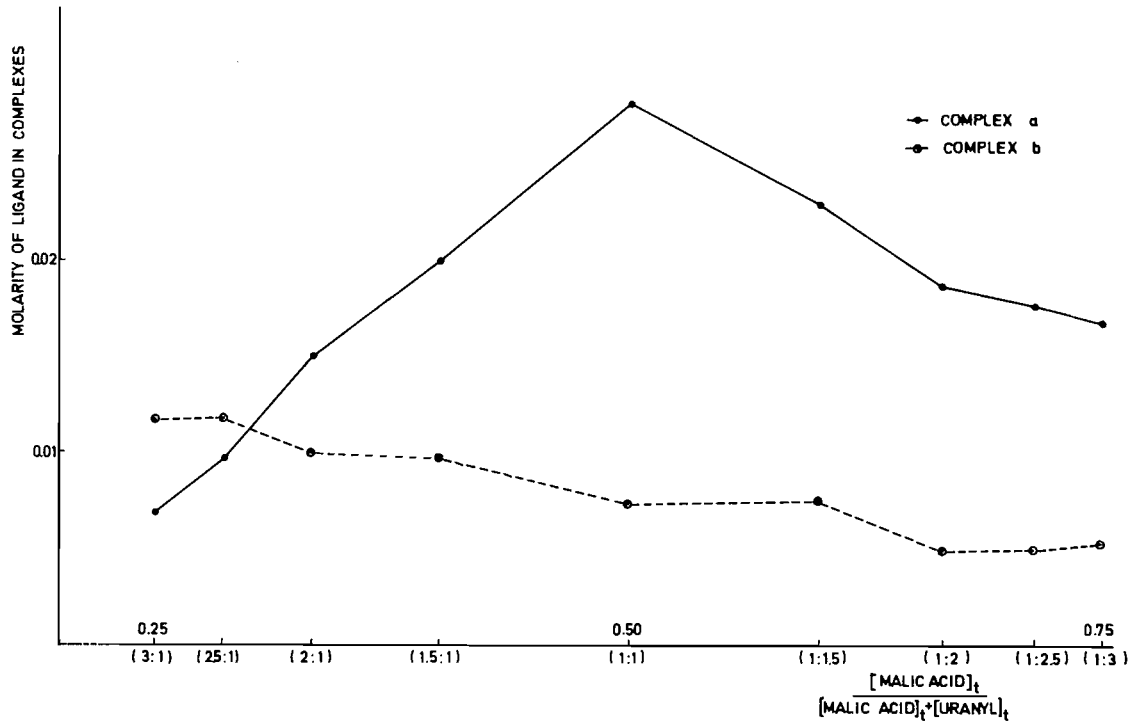


FIG. 10. Job's plots for a and b complexes at pH* = 2.7.

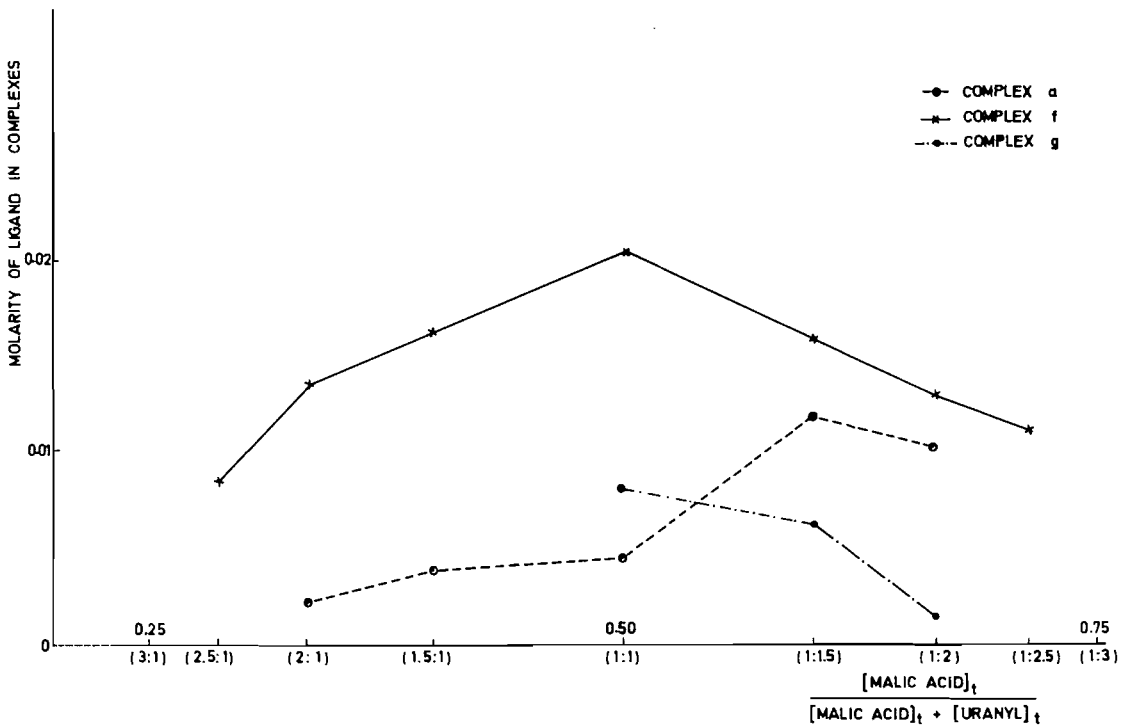


FIG. 11. Job's plots for complex a at pH* = 6.7, complex f at pH* = 7.9 and complex g at pH* = 10.7.

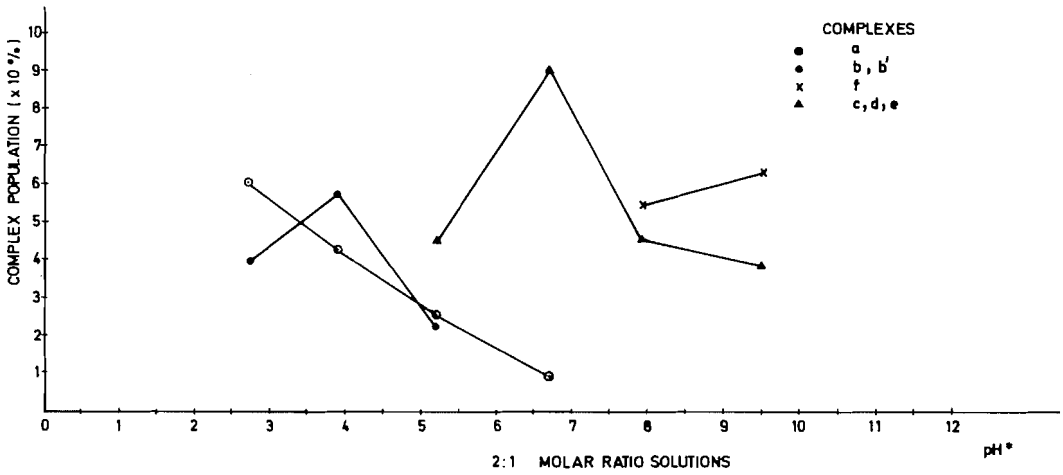


FIG. 12. Relative populations of the complexes for a 2:1 (metal/ligand) molar ratio as a function of pH.

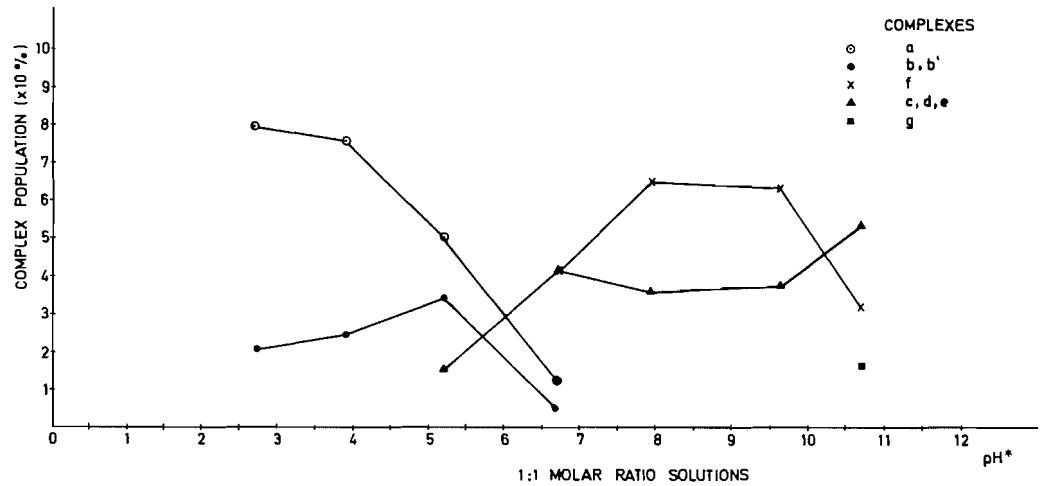


FIG. 13. Relative populations of the complexes for a 1:1 molar ratio as a function of pH.

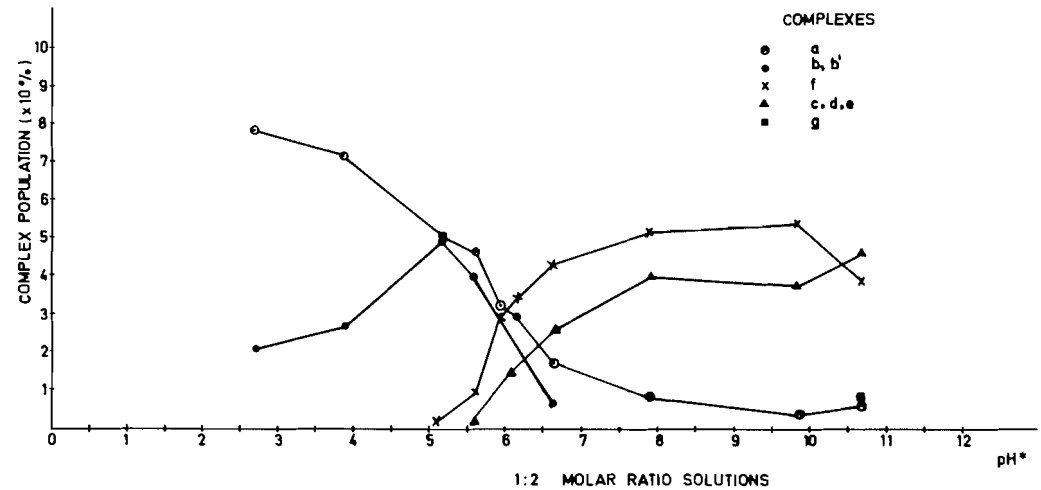


FIG. 14. Relative populations of the complexes for a 1:2 (metal/ligand) molar ratio as a function of pH.

Can. J. Chem. Downloaded from www.nrcresearchpress.com by 210.87.254.105 on 09/06/12
For personal use only.

the values are

| | $^{-}O_2C$ | $CH_2$ | CH(OH) | $CO_2^{-}$ |
|---|---|---|---|---|
| Complex a | 4.6 | 1.63 | 12.56 | 7.9 |
| Complex f | 5.5 | 1.88 | 13.77 | 9.4 |

The observed difference in the shifts for complex a is probably due to exchange processes as already discussed.

The big low-field shift of the methyne $^{13}C$ nucleus in comparison with $^{13}CH_2$ is a clear indication of involvement of the OH group of malic acid in complexation. The shifts of carboxylic $^{13}C$ nuclei of a and b with respect to the $CO_2H$ groups of the acid are consistent with participation of both groups in bonding to $UO_2^{2+}$. The similitude of shifts for complexes f and a, at pH* = 6.3, suggests that the same conclusion applies to complex f.

## Conclusion

We may thus conclude the following.

(*a*) At low pH values (approximately 2–4), uranyl and malic acid form at least two complexes. One is a 1:1 compound (a) and the other has a higher content of uranyl (b). The ligand is tridentate in both, but its conformation is not $c_2$; the HH coupling constants indicate a conformation close to $c_1$, or $c_3$. This is consistent with the existence of a 2:2 complex with structure **1**, as previously reported (3, 11) (ligand in conformation close to $c_1$) or its isomer of symmetry $C_s$, and a 2:1 complex of similar structure, for instance **3**,

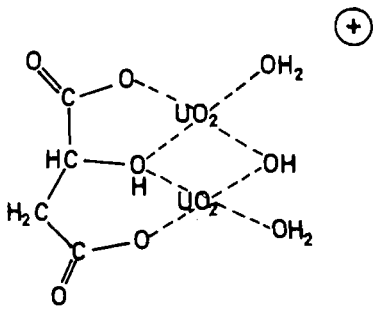


**3**

although other hypothesis (for instance 4:2 complexation as for Mo(VI)–malic acid (12)) cannot be ruled out.

(*b*) At pH from ~ 5 to about 10, at least two further complexes are formed, the most abundant of which is another 1:1 species (f). This seems to be a polynuclear complex (2:2) as indicated by dilution studies. The ligand is again tridentate, with a conformation close to $c_1$ or $c_3$. This complex might be a conjugate base of the acidic species appearing at low pH.

(*c*) At pH ≃ 11 a new complex is formed of stoichiometry difficult to ascertain. Again, the conformation of the ligand is one having two H nuclei in a *trans* orientation ($c_1$ or $c_3$).

Work is in progress regarding a complete clarification of this complex system, as well as of the various exchange phenomena present.

1. I. FELDMAN, J. R. HAVILL, and W. F. NEUMAN. J. Am. Chem. Soc. **76**, 4726 (1954).
2. I. FELDMAN, C. A. NORTH, and H. B. HUNTER. J. Phys. Chem. **64**, 1224 (1960).
3. K. S. RAJAN and A. E. MARTELL. J. Inorg. Nucl. Chem. **26**, 1927 (1964).
4. I. KHALIL, M. M. PETIT-RAMEL, and C. CHAPELET-BARBIER. Can. J. Chem. **56**, 1919 (1978).
5. W. F. NEUMAN, J. R. HAVILL, and I. FELDMAN. J. Am. Chem. Soc. **73**, 3593 (1951).
6. I. FELDMAN and W. F. NEUMAN. J. Am. Chem. Soc. **73**, 2312 (1951).
7. I. FELDMAN and J. R. HAVILL. J. Am. Chem. Soc. **76**, 2114 (1954).
8. M. DEODATA AZEVEDO, R. GOMES DA COSTA, and M. TERESA VILHENA. Rev. Port. Quim. **15**, 35 (1973).
9. Y. Y. KHARITONOV and Z. M. ALIKHANOVA. Sov. Radiochem. **6**, 680 (1964).
10. E. CAMPI and M. C. GINNARO. Ann. Chim. (Roma), **11–12**, 761 (1974).
11. J. PEDROSA and V. M. S. GIL. J. Inorg. Nucl. Chem. **36**, 1803 (1973).
12. M. CADIOT and B. VIOSSAT. Rev. Chim. Miner. **6**, 327 (1969).

Can. J. Chem. Downloaded from www.nrcresearchpress.com by 210.87.254.105 on 09/06/12
For personal use only.

# The design and synthesis of nonpeptide compounds as mimics of a conformation of methionine-enkephaline

PATRICE C. BELANGER, CLAUDE DUFRESNE, JOHN SCHEIGETZ, AND ROBERT N. YOUNG

*Medicinal Chemistry Department, Merck Frosst Laboratories, P.O. Box 1005, Pointe-Claire/Dorval, P.Q., Canada H9R 4P8*

JAMES P. SPRINGER

*Merck Sharp & Dohme Research Laboratories, P.O. Box 2000, Rahway, NJ 07065, U.S.A.*

AND

GARY I. DMITRIENKO

*The Guelph–Waterloo Center for Graduate Work In Chemistry, Waterloo Campus, Department of Chemistry, University of Waterloo, Waterloo, Ont., Canada N2L 3G1*

Received September 29, 1981

PATRICE C. BELANGER, CLAUDE DUFRESNE, JOHN SCHEIGETZ, ROBERT N. YOUNG, JAMES P. SPRINGER, and GARY I. DMITRIENKO. Can. J. Chem. **60**, 1019 (1982).

A model for the active conformation of methionine-enkephalin containing a β-turn was derived from computer modeling. Using a *trans*-perhydronaphthalene as a structural template and a mimic of the β-turn, target compounds were designed and synthesized. Thus, a key intermediate, *trans*-3-oxo-5β-formamidomethyl-8a-phenylmethylperhydronaphthalene, was prepared by two different routes from cyclohexanone.

The addition of a methionine-like side-chain to this key intermediate was best achieved by a reaction with the anion of methyl 2-trimethylsilyl-4-methylthiobutanoate. This led to the preparation of an *exo*-tetrasubstituted double bond in high yield. Subsequent addition of tyrosine through coupling with the 5β-aminomethyl group provided the desired perhydronaphthalene mimics of met-enkaphalin.

---

PATRICE C. BELANGER, CLAUDE DUFRESNE, JOHN SCHEIGETZ, ROBERT N. YOUNG, JAMES P. SPRINGER et GARY I. DMITRIENKO. Can. J. Chem. **60**, 1019 (1982).

A l'aide d'un ordinateur, on a déduit un modèle de la conformation active de la méthionine-encéphaline contenant une hélice β. Utilisant le perhydronaphtalène-*trans* comme modèle de structure et une imitation de l'hélice β, on a proposé et synthétisé les composés cibles. Ainsi on a préparé un intermédiaire principal, l'oxo-3 formamidométhyl-5 β phénylméthyl-8a perhydronaphtalène par deux voies différentes, en partant de la cyclohexanone.

L'addition de la méthionine, comme chaîne latérale, sur cet intermédiaire principal se fait mieux par une réaction avec l'anion du triméthylsilyl-2 méthyl-4 thiobutanoate de méthyle. Ceci conduit à la préparation d'une double liaison *exo*-tétrasubstituée avec un rendement élevé. L'addition subséquente de la tyrosine à travers le couplage avec le groupe aminométhyl-5 β conduit au perhydronaphtalène désiré qui est une réplique de la mét-encéphaline.

[Traduit par le journal]

## Introduction

In the realm of compounds that act on the central nervous system to combat pain, the opiate alkaloids (for example, morphine) have been the preeminent drugs for many years. More recently, the discovery and characterization of the naturally occuring opiate receptor agonists, the enkephalins, has renewed interest in this field (1), increasing the hope that analogs of the enkephalins would lead to drugs having reduced side-effects while maintaining a high analgesic activity.

We felt that it should be possible to design nonpeptide compounds which would mimic the enkephalins, which would be less conformationally mobile and could therefore interact specifically with the enkephalin receptors. To do this it was necessary to derive a model of what we perceived to be the active conformation for the enkephalins. Many conformational studies have been published using nmr (2, 3), fluorescence (4), theoretical studies (5–7), and more recently X-ray studies (8). Some of the conformations proposed can be correlated with synthetic opiates (9, 10). However, among the many published studies which derived "active conformations" for the enkephalins there has been no real consensus. Most do agree that the tyrosine group is very important and that the molecule is bent on itself in a β-turn. The glycines are generally thought to be positioning groups and the phenylalanine aromatic system is considered to be important for activity.

We have derived a model of the bioactive conformer of enkephalins, shown in Fig. 1, based on a combination of structure–activity relationships for the enkephalins and for the opiates, computer modeling, and comparisons with the opiates. A key feature of this model is the presence of a β-turn which adds rigidity to the flexible enkephalin

0008-4042/82/081019-11$01.00/0

©1982 National Research Council of Canada/Conseil national de recherches du Canada

Can. J. Chem. Downloaded from www.nrcresearchpress.com by 210.87.254.40 on 09/06/12
For personal use only.

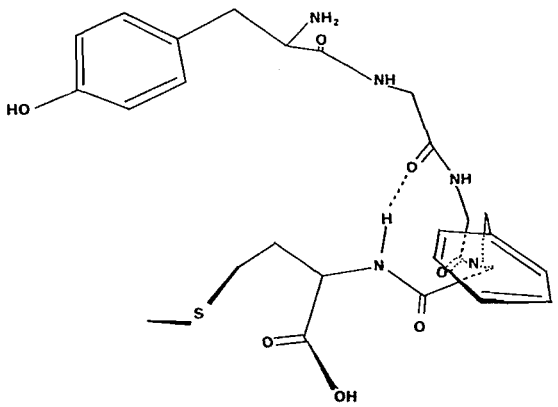

FIG. 1.

backbone and also acts as a template positioning the key groups (the tyrosine and the phenylalanine's phenyl group) in space as is found in very active opiates (e.g. morphine, etorphine). The modeling studies carried out on this conformer have revealed it to be a low energy conformer.

Using this model we sought to design novel rigid nonpeptide mimics of the enkephalins with the aid of the Merck Modeling System and the compare (superimposition) program. The β-turn in the model, with its hydrogen bond between gly$^2$ and met$^5$, makes a 10-membered ring and thus one of our most interesting structures derived by computer modeling was based on a perhydronaphthalene backbone. The perhydronaphthalene could serve to position the key groups in space as does the β-turn in the enkephalin model (Fig. 2). We therefore chose **1** as our target.

## Results and discussion

In our synthetic strategy to **1** it was considered expedient to prepare the *E* and *Z* olefin isomers, and as the addition of the tyrosine moiety to the perhydronaphthalene backbone would create diastereomers, a total of four isomers of the final

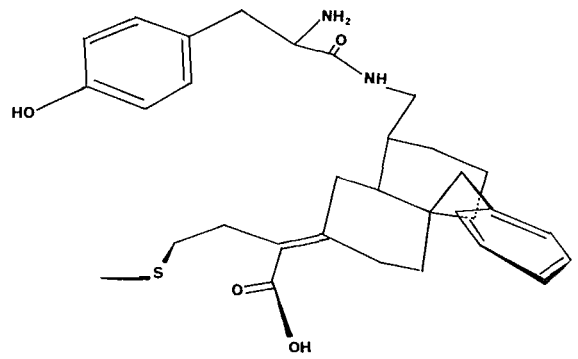

FIG. 2.

system were expected. Thus the preparation of **1** had to be achieved in as efficient and stereospecific a manner as possible. A potential difficulty was to ensure the *trans* ring junction and diaxial orientation of side chains. Strategic analysis identified the amino ketone **2***a* or a derivative such as **2***b* as key intermediates to **1**.

Compound **2***b* was prepared via two routes from cyclohexanone. The first route is outlined in Scheme 1. The key C-5 substituent was introduced via a Vilsmeier–Haack formylation reaction (11).

Cyclohexanone (**3**) was converted to 2-phenylmethylcyclohexanone (**4**) via alkylation of the pyrrolidine enamine with phenylmethylchloride following the method of Stork *et al.* (12). Subse-

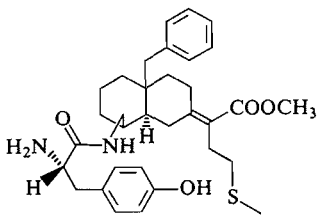

**1**

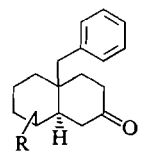

**2**

*a* R = $NH_2$
*b* R = NHCHO
*c* R = $N_3$

quent Robinson annellation (13) with methyl vinyl ketone provided 1,2,3,5,6,7,8,8a-octahydro-3-oxo-8a-phenylmethylnaphthalene (**5**). Treatment with methyl orthoformate gave the dienolether **6** which upon Vilsmeier– Haack formylation (11) provided the 5-formyl derivative **7***a* and thence the oxime **7***b* in 26% overall yield from **5** utilizing conditions similar to those developed by Yoshikoshi and co-workers (11) in their synthesis of (±) bulnesol. Thus the functionality at C(3) and C(5) were in place and it remained to introduce the required *trans* stereochemistry at the ring junction and the β-configuration at C(5). It was felt that hydrogenation of **7***b* would be nonselective whereas if a β-substituent were present at C(3), then a stereospecific reduction could be expected (14). As the oxime function led to complications in subsequent steps, it was converted to the nitrile **8** via treatment with trichloroacetonitrile (15). Hydrolysis of the enolether provided a mixture of olefinic ketones **9** which formed a single enolacetate **10**. Compound **10** was smoothly reduced by sodium borohydride to provide 5-cyano-3β-hydroxy-1,2,3,4,6,7,8,8a-octahydro-8a-phenylmethylnaphthalene (**11**). The β stereochemistry was assigned by analogy with the work of Heathcock and Kelly (16) in their β-eudesmol synthesis. Despite many trials, selective hydrogenation of the double bond could not be achieved. Hydrogenation over 10% palladium on

Can. J. Chem. Downloaded from www.nrcresearchpress.com by 210.87.254.40 on 09/06/12
For personal use only.

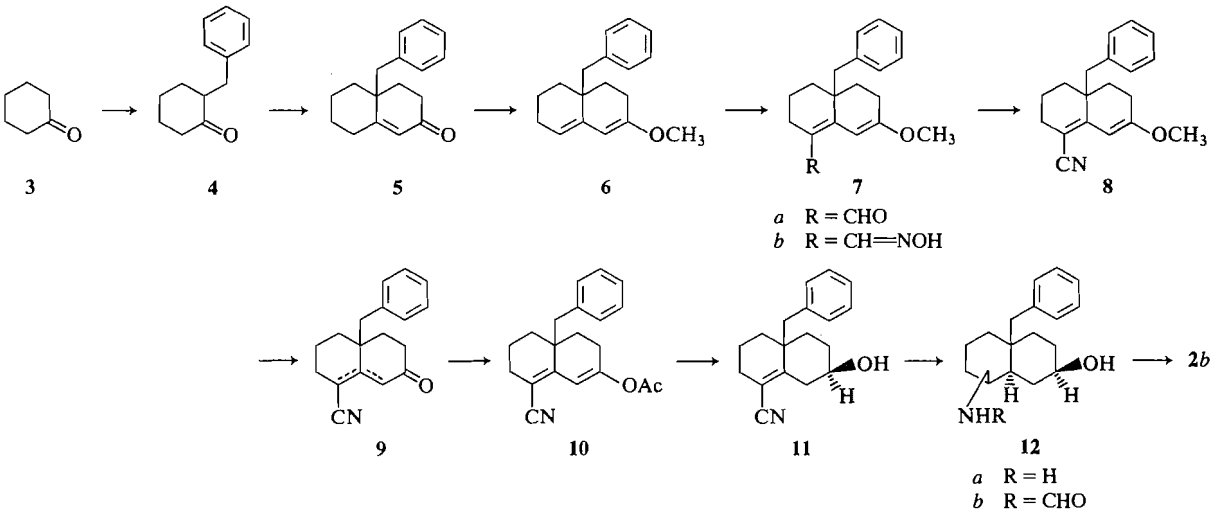


SCHEME 1

charcoal provided the aminoalcohol **12***a* contaminated with some material where the aromatic ring had been reduced. Compound **12***a* was converted to its *N*-formyl derivative **12***b* and the alcohol was oxidized with the Sarett reagent as modified by Ratcliffe and Rodehorst (17) to provide the crystalline *N*-formylketone **2***b*.

Due to the partial reduction of the aromatic ring in the hydrogenation step and also due to difficulties anticipated in scaling up the synthesis, an alternative route to **2***b* was devised and is summarized in Scheme 2.

Thus, following a scheme similar to that utilized by Marshall *et al.* (14, 18) in their synthesis of β-eudesmol, **5** was converted to the deconjugated ketal **13**. Hydroboration of **13** provided, after oxidative work-up, a mixture of *cis*-fused alcohols, **14** and **15**, plus small amounts of ketal cleavage products in a ratio of approximately 25:70:5. The desired alcohol **15** could be readily purified by chromatography or the mixture could be used as such for the subsequent oxidation ($CrO_3$·2pyr) to provide the *cis*-fused ketone **16** which, on reaction with methylenetriphenylphosphorane in the presence of excess base, first isomerized the ring junction to **17** and then effected the methylene addition. This provided the ketal olefin **18**, readily purified at this point, in 44% overall yield from **5**.

Hydroboration of **18** occurred exclusively from the α-face to provide, after oxidative work-up, the primary alcohol **19***a*, which was converted to the crystalline mesylate **19***b* (60% yield from **18**). Treatment of **19***b* with sodium azide in DMF provided the azide **20** plus the exocyclic olefin **18** in ca. 4:6 mixture. After chromatographic separation, the olefin **18** could be recycled. Reduction (LAH),

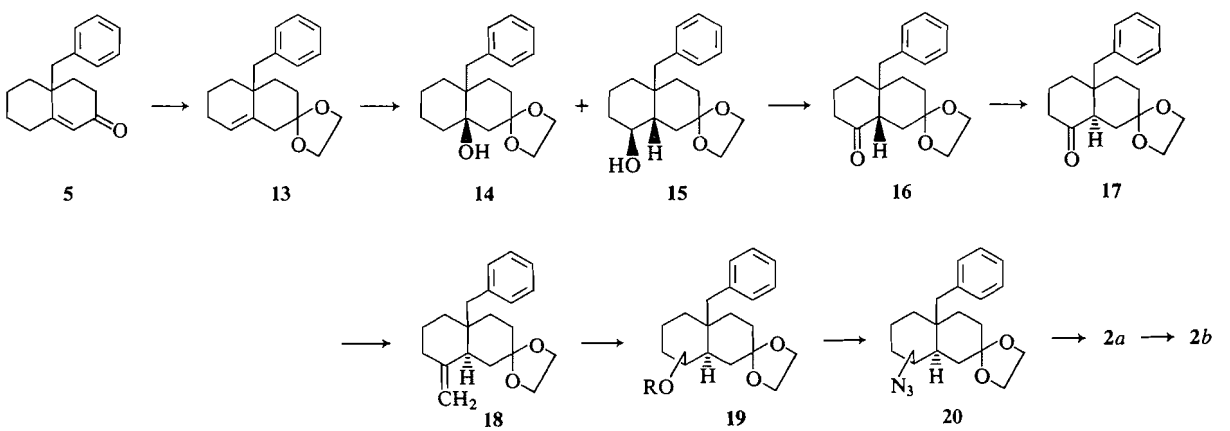


SCHEME 2

Can. J. Chem. Downloaded from www.nrcresearchpress.com by 210.87.254.40 on 09/06/12
For personal use only.

Can. J. Chem. Downloaded from www.nrcresearchpress.com by 210.87.254.40 on 09/06/12
For personal use only.

hydrolysis, and formylation of the ketal provided the *N*-formyl ketone **2***b* identical to that obtained from the previous route.

Having the required perhydronaphthalene backbone in hand, attention was directed towards the attachment of the side chain at C(3). Several possible methods were explored. Addition via a Reformatsky reaction was considered but was rapidly set aside when it was found that the dehydration of model compound proved to be nonspecific and led to mixtures of conjugated and deconjugated olefins under acidic conditions.

As it is known that endocyclic β,γ-unsaturated esters should be more stable than the exocyclic α,β-unsaturated isomers in cases such as these (19), a more specific method was sought. It was felt that the Wadsworth–Emmons phosphonate modification of the Wittig reaction (20) could provide a direct introduction of the side chain. Thus ethyl-2-diethylphosphono-4-methylthiobutyrate (**21**), readily prepared by alkylating triethylphosphonoacetate with methyl-β-chloroethyl sulfide, was found to react at best sluggishly (80–100°C, 18 h) with **2***b* or **2***c* when reacted with sodium hydride in dimethoxyethane. The mixture of *E* and *Z* adducts **22***a* or **22***b* were obtained only in rather poor yield (40–50%) and always with varying amounts of β,γ-unsaturated by-products **23***a* or **23***b*, probably due to base catalyzed isomerization of the products under these harsh conditions.

The possibility of utilizing α-trimethylsilylesters to effect the olefination was explored (21, 22). This method has not been used previously to prepare tetrasubstituted olefins but seemed worthy of investigation despite the reported failure of α,α-bistrimethylsilylesters to react with ketones (23).

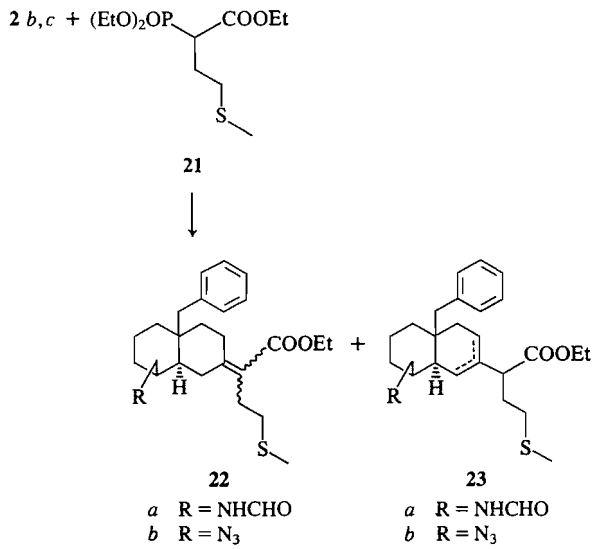


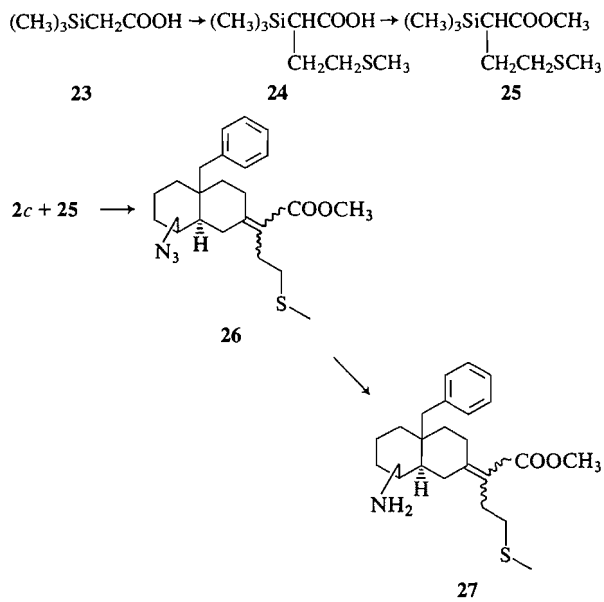


SCHEME 3

As shown in Scheme 3, alkylation of the dianion of α-trimethylsilylacetic acid **23** with β-methylthioethyl chloride and subsequent esterification of **24** led to **25** in good yield. Treatment of **25** at 0°C with one equivalent of lithium diisopropylamide (LDA) followed by cooling to −78°C and addition of the azido ketone **2***c* effected a rapid and efficient (80–90% yield) reaction to provide the desired mixture of *E* and *Z* α,β-unsaturated esters **26***a*, **26***b* with no detectible traces of deconjugated by-products. The isomers were not separable at this point. Reduction of the azide was thought to be potentially a problem due to the other functionality present in the molecule. It was found that aluminium amalgam effected a clean but rather inefficient conversion of **26***a*, **26***b* to the *E* and *Z* mixture of amines **27***a*, **27***b* (42–50%). However, somewhat surprisingly, the reduction could be very cleanly effected in high yield (90%) by hydrogenation over Adams catalyst. The resultant amines could now be readily separated via column chromatography to provide the pure crystalline amines **27***a* (less polar) and **27***b* (more polar) in a 1:1 mixture.

The relative stereochemistry and ultimate proof of structure of the series was obtained via an X-ray structure determination on **27***a*, which is shown in Figure 3. Thus the less polar isomer has the *E* stereochemistry for the side chain and the more polar isomer has the *Z* stereochemistry. The rigid nature of the two cyclohexane rings with chair conformations in the *trans* perhydronaphthalene system forces the functional groups on the periphery into specific conformations. Because of a 1,3

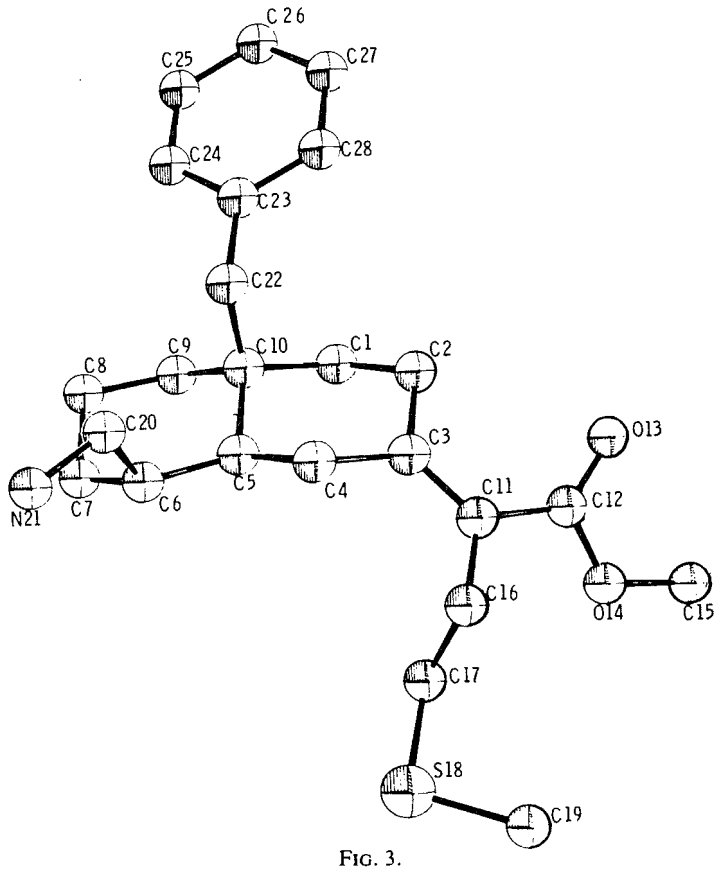


FIG. 3.

diaxial interaction C(20) and C(22) are pushed away from each other. This is clearly seen by examining the torsional angles C(8)—C(7)—C(6)—C(20) and C(10)—C(5)—C(6)—C(20) which are 79° and −77°, respectively, compared to ± 60° for an ideal chair geometry. In addition the phenyl group is forced away from the perhydronaphthalene system so that the torsional angle C(5)—C(10)—C(22)—C(23) is 176°. Also because of a nonbonded interaction between the equatorial H(2b) and O(13) the ester cannot fully conjugate with the exocyclic double bond but is twisted with a torsional angle for C(3)—C(11)—C(12)—O(13) at 37°.

It is interesting to observe that the considerable deformation of the bond angles had been predicted by our computer modeling studies (24) but prior to determining the X-ray structure, we felt that the modeling program had exaggerated this effect.

The final conversion to the target structures was achieved via DCC coupling (25) of **27***a* and **27***b* to *N*-*t*-BOC-tyrosine to provide the *N*-protected adducts in good yields (88% and 91%, respectively) as mixtures of diastereomers. These diastereomeric pairs could be separated in each case via hplc to provide the four pure isomers **28***a*–*d*. Acid treatment in each case liberated the amino function and gave the final four isomeric target molecules directly as the hydrochloride salts **1***a*–*d*. Attempts to obtain crystalline material from these products, suitable for X-ray analysis, were unsuccessful.

These compounds have all been tested in the $^3$H-Naloxone Binding Assay (26) and, unfortunately, were found to have only weak binding activity. The possibility remains that the tyrosine side chain in these molecules does not adopt the predicted, desired conformation at the receptor site. In addition, the drastic changes done by approximating the β-turn with a perhydronaphthalene could also explain these biological results.

## Conclusion

It would therefore seem that our model has failed to accurately mimic the enkephalin active conformation. Of course activity can be affected by very subtle changes and it is possible that the steric requirements of the perhydronaphthalene unit are not tolerated by the opiate receptor. It is notable that subsequent experiments (27) have demonstrated that enkephalin derivatives where the carbonyl of the glycine 3-residue is reduced to a

Can. J. Chem. Downloaded from www.nrcresearchpress.com by 210.87.254.40 on 09/06/12
For personal use only.

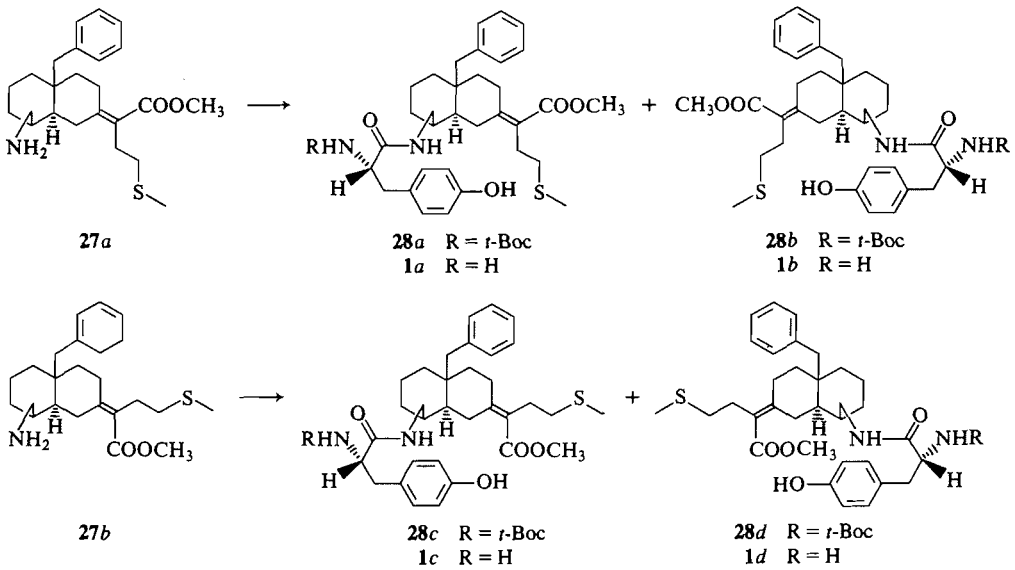


methylene group have been shown to be inactive and thus it would appear that the β-turn portion of the enkephalins has significance in binding with the receptor, rather than merely acting as a template. Thus mimics such as ours which replace these hydrophilic amide bonds with more hydrophobic methylene groups may introduce an unacceptable degree of lipophilicity into this region of the receptor.

## Experimental

Melting points were taken on a Thomas Hoover apparatus in open capillary tubes and are uncorrected. Infrared spectra were recorded on a Perkin–Elmer 267 grating spectrophotometer. A Varian EM-360 spectrometer was used to record nmr spectra. Proton chemical shifts are relative to tetramethylsilane (TMS) as internal standard. Elemental analyses were performed by Dr. C. Daesslé of Montreal or by Galbraith and Associates, Knoxville, TN. The low resolution mass spectral analyses were performed by the Morgan–Schaffer Corporation, Montreal. A Syntex $P2_1$ automatic four-circle diffractometer was used to collect the X-ray diffraction data.

All reactions as well as column chromatography were monitored routinely with the aid of thin layer chromatography (tlc) using precoated 0.25 mm silica gel plates (Eastman Kodak) or silica gel GF plates (Analtech).

*1-Pyrrolidino-1-cyclohexene*

1-Pyrrolidino-1-cyclohexene was prepared according to the method of Stork *et al.* (12); bp 70°C/15 Torr.

*2-Benzylcyclohexanone (4)*

To 1-pyrrolidino-1-cyclohexene (238 g; 1.58 mol) dissolved in dioxane (1 L) was added benzyl chloride (277 g; 2.19 mol) and the mixture was refluxed 16 h. Water (250 mL) was then added and reflux was continued for 2.5 hours more. The dioxane was removed under vacuum and the aqueous phase was extracted four times with ether (4 × 500 mL). The combined extracts were washed with 5% aqueous hydrochloric acid (50 mL), and with water (50 mL), then dried ($Na_2SO_4$) and concentrated to an oily residue that was distilled to yield **4** (163 g; 55%), bp 105°C/0.5 Torr; ir (film) $\nu_{max}$: 1700 (C=O) $cm^{-1}$; $^1$Hmr ($CDCl_3$) δ: 1.2–2.6 (10H, m), 3.20 (1H, m), 7.13 (5H, s, aromatic).

*1,2,3,5,6,7,8,8a-Octahydro-3-oxo-8a-phenylmethylnaphthalene (5)*

Ketone **4** (550 g; 2.92 mol) in ether (2 L) was added to a solution of potassium hydroxide (33 g; 0.59 mol) in absolute ethanol (110 mL) maintained at 0°C. It was followed by the dropwise addition of methyl vinyl ketone (242 g; 2.92 mol) over a period of 4 hours. After warming to room temperature, water (1 L) was added and the organic layer was separated, washed with water, dried ($Na_2SO_4$), and concentrated to an oil. The residue was distilled to give 345 g (49%) of α,β-unsaturated ketone **5**, bp 155°C/0.5 Torr, which solidified on standing; mp 74–75°C; ir (KBr) $\nu_{max}$: 1660 (C=O), 1610 (C=C) $cm^{-1}$; $^1$Hmr ($CDCl_3$) δ: 2.80 (2H, s, benzylic $CH_2$), 5.72 (1H, s, H4), 7.10 (5H, s, aromatic). *Anal.* calcd. for $C_{17}H_{20}O$: C 84.95, H 8.38; found: C 85.39, H 8.49.

*5-Formyl-1,2,6,7,8,8a-hexahydro-3-methoxy-8a-phenylmethylnaphthalene (7a)*

Ketone **5** (1.06 g; 0.005 mol) was dissolved in trimethylorthoformate (7 mL) at room temperature and the solution was cooled in an ice–water bath. *p*-Toluenesulfonic acid (10 mg) was added and stirring was continued for 3 hours. Pyridine (20 mL) was added and the mixture was evaporated under high vacuum to provide crude dienol ether **6** as a brown oil which was used directly in the next reaction; $^1$Hmr ($CDCl_3$) δ: 2.80 (2H, s, benzylic $CH_2$), 3.70 (3H, s, $OCH_3$), 6.43 (1H, s, H4), 7.20 (5H, s, aromatic and H5).

Phosphorous oxychloride (0.9 mL; 9.6 mmol) was added to an ice-cooled solution of dimethylformamide (3 mL) in methylene chloride (8 mL). Dienol ether **6** from the previous reaction (1 g; crude) in methylene chloride (15 mL) was added over 15 min. The mixture was stirred at room temperature under nitrogen for 4 hours. A 20% solution of sodium acetate was added and the mixture was stirred for 30 min, then extracted with methylene chloride. The organic layers were successively washed with 10% aqueous sodium bicarbonate and with water, then dried ($Na_2SO_4$) and concentrated *in vacuo* to a brown oil, which on treatment with ether yielded crystalline **7a** (400 mg; 34% yield). Recrystallization from ether gave an analytical sample, mp 117–120°C; ir (KBr) $\nu_{max}$: 1650 (C=O), 1610 (C=C) $cm^{-1}$; $^1$Hmr

Can. J. Chem. Downloaded from www.nrcresearchpress.com by 210.87.254.40 on 09/06/12
For personal use only.

Can. J. Chem. Downloaded from www.nrcresearchpress.com by 210.87.254.40 on 09/06/12
For personal use only.

($CDCl_3$) δ: 2.87 (2H, s, benzylic $CH_2$), 3.80 (3H, s, OMe), 6.47 (1H, s, H4), 7.20 (5H, s, aromatic), 10.27 (1H, s, CHO). *Anal.* calcd. for $C_{19}H_{22}O_2$: C 80.81, H 7.85; found: C 80.68, H 7.91.

*Oxime of* 7a

The 5-formyl derivative *7a* (0.141 g; 0.5 mmol) was dissolved in methanol (4 mL) and pyridine (0.1 mL). Hydroxylamine hydrochloride (0.10 g) was added and the mixture was stirred at room temperature for 30 min. Water (10 mL) was added and the resulting oxime *7b* (0.11 g; 76%) was filtered off, washed with water, and air-dried; mp 146–147°C; ir (KBr) $\nu_{max}$: 3300 (OH), 1650 (C=N), 1620 (C=C) $cm^{-1}$; $^1$Hmr ($CDCl_3$) δ: 2.77 (2H, s, benzylic $CH_2$), 3.67 (3H, s, $OCH_3$), 5.80 (1H, s, H4), 7.20 (5H, s, aromatic), 8.43 (1H, s, —C*H*=NOH). *Anal.* calcd. for $C_{19}H_{23}NO_2$: C 76.73, H 7.80, N 4.71; found: C 76.83, H 7.73, N 4.53.

*5-Cyano-1,2,6,7,8,8a-hexahydro-3-methoxy-8a-phenylmethylnaphthalene (8)*

The oxime *7b* (600 mg; 2.02 mmol) was dissolved in trichloroacetonitrile (2 mL) and the solution was stirred at room temperature for 30 min. The mixture was stripped to dryness under high vacuum, leaving a brown oil which was taken up in $CCl_4$, filtered, and concentrated to an oil. This oil was taken up in ether, washed with 5% sodium hydroxide and with water. The organic layer was dried ($Na_2SO_4$) and evaporated to dryness to yield cyano derivative **8** (500 mg; 85% yield), mp 106–107°C; ir (KBr) $\nu_{max}$: 2210 (C≡N) $cm^{-1}$; $^1$Hmr ($CDCl_3$) δ: 2.80 (2H, s, benzylic $CH_2$), 3.72 (3H, s, OMe), 5.83 (1H, s, H4), 7.20 (5H, s, aromatic). *Anal.* calcd. for $C_{19}H_{21}NO$: C 81.68, H 7.58, N 5.01; found: C 81.71, H 7.70, N 5.08.

*Enol acetate of* ***10***

The cyano derivative **8** (184 mg; 0.66 mmol) was dissolved in tetrahydrofuran (2 mL) and concentrated hydrochloric acid (0.5 mL) was added. The mixture was stirred at room temperature for 1 hour. The mixture was taken up in methylene chloride (100 mL) and washed with water (10 mL). The organic phase was dried ($Na_2SO_4$) and concentrated to dryness to give a pale yellow oil (175 mg) which was used directly in the next reaction. Spectroscopic analysis indicated that the product **9** was largely in the enolic form; ir (film) $\nu_{max}$: 2200 (CN), 1720 (CO), 1670 (C=O conj.), 1625 (C=C) $cm^{-1}$; $^1$Hmr ($CDCl_3$) δ: 2.73 (2H, s, benzylic $CH_2$), 5.97 (1H, s, olefinic CH), 7.17 (5H, s, aromatic), 7.57 (1H, broad, OH of enol).

Compound **9** (175 mg from previous reaction) was dissolved in benzene (5 mL) and acetyl chloride (1 mL) was added, followed by the addition of triethylamine (5 drops). The mixture was kept for 28 h in the refrigerator, then was poured onto water and extracted with methylene chloride. The organic phase was dried ($Na_2SO_4$), and concentrated under vacuum to yield a yellowish oil. Purification by preparative tlc (hexane–ether 1:1 v/v) gave 0.128 g of colorless oil that crystallized on standing. Triturated in ether, **10** melted at 115–116°C; ir (KBr) $\nu_{max}$: 2050 (CN), 1765 ($OCOCH_3$), 1655 (C=C) $cm^{-1}$; $^1$Hmr ($CDCl_3$) δ: 2.17 (3H, s, OAc), 2.80 (s, 2H, benzylic $CH_2$), 6.4 (1H, m, H4), 7.2 (5H, s, aromatic). *Anal.* calcd. for $C_{20}H_{21}NO_2$: C 78.15, H 6.87, N 4.56; found: C 77.75, H 6.75, N 4.72.

*5-Cyano-3β-hydroxy-1,2,3,4,6,7,8,8a-octahydro-8a-phenylmethylnaphthalene (11)*

Enol acetate **10** (0.391 g; 1.28 mmol) dissolved in a mixture of tetrahydrofuran (8 mL), ethanol (7 mL), and water (1.5 mL) was cooled under nitrogen, to −3°C. Sodium borohydride (0.5 g) was added and the mixture was stirred overnight. A solution of 5% sodium hydroxide (2 mL) was added and the mixture was diluted with brine (20 mL) and extracted with methylene chloride (150 mL). The organic phase was washed with water, dried ($Na_2SO_4$), and evaporated to dryness. The oily residue was purified by preparative tlc (ether–hexane 7:3 v/v). Extraction of the major band yielded a colorless oil which crystallized on standing. Trituration in a small volume of ether gave 0.26 g (76%) of **11**, mp 102–104°C; ir (KBr) $\nu_{max}$: 3450 (OH); 2210 (CN), 1620 (C=C) $cm^{-1}$; $^1$Hmr ($CDCl_3$) δ: 2.87 (2H, d, benzylic $CH_2$), 3.70 (1H, broad, C*H*OH), 7.20 (5H, m, aromatic). *Anal.* calcd. for $C_{18}H_{21}NO$: C 80.86, H 7.92, N 5.24; found: C 80.79, H 8.16, N 5.27.

*3β-Hydroxy-6β-formamidomethyl-8a-phenylmethyl-*trans*-perhydronaphthalene (12*b*)*

Cyano derivative **11** (0.205 g; 0.77 mmol) was dissolved in glacial acetic acid (25 mL) and hydrogenated at 30 psi over 5% platinum on charcoal (0.133 g) for 2 hours. The catalyst was filtered off through Celite and washed with absolute ethanol (100 mL). The filtrate was concentrated *in vacuo* to yield the amino derivative **12***a* (200 mg) as a pale oil that was used for the next step; ir (film) $\nu_{max}$: 3400 (NH and OH) $cm^{-1}$; $^1$Hmr ($CDCl_3$) δ: 2.82 (2H, m, benzylic $CH_2$), 3.68 (1H, broad, CHOH), 7.18 (5H, s, aromatic).

Crude **12***a* (195 mg; 0.71 mol) dissolved in formic acid (5 mL) and acetic formic anhydride (2 mL) was heated on a steam bath for 30 min. The mixture was evaporated to dryness and taken up in methylene chloride. The resulting solution was washed with 5% sodium hydroxide, with water, dried ($Na_2SO_4$), and evaporated giving the diformyl compound (222 mg) as a pale yellow oil; ir (KBr) $\nu_{max}$: 3300 (NH), 1720 (OCHO), 1660 (NCHO) $cm^{-1}$; $^1$Hmr ($CDCl_3$) δ: 2.78 (2H, s, benzylic $CH_2$), 4.93 (1H, m, CHOCO), 7.17 (5H, s, aromatic), 8.03 (1H, s, OCHO), 8.15 (1H, s, NCHO).

The crude diformyl intermediate isolated above (0.222 g) was dissolved in methanol (5 mL) and 5% aqueous bicarbonate (2 mL) was added. The reaction mixture was stirred at room temperature for 3 hours. It was then taken up in methylene chloride and the organic phase was washed with water, dried ($Na_2SO_4$), and concentrated to give **12***b* as a pale yellow oil which solidified on standing. Trituration in ether gave 168 mg (72% from **11**) of crystalline **12***b*, mp 212–213°C; ir (KBr) $\nu_{max}$: 3300 (OH), 1660 (NCHO) $cm^{-1}$; $^1$Hmr ($CDCl_3$) δ: 2.50 (1H, d, $J$ = 14 Hz, benzylic CH), 3.00 (1H, d, $J$ = 14 Hz, benzylic CH), 3.65 (1H, broad m, =C*H*OH), 7.20 (5H, s, aromatic), 8.15 (1H, s, NCHO). *Anal.* calcd. for $C_{19}H_{27}NO_2$: C 75.71, H 9.02, N 4.65; found: C 75.41, H 9.24, N 4.89.

*6β-Formamidomethyl-3-oxo-8a-phenylmethyl-*trans*-perhydronaphthalene (2*b*)*

The hydroxy derivative **12***b* (0.15 g; 0.5 mmol) was added as a solution in dry pyridine (3 mL) to a mixture made up by adding chromium trioxide (0.5 g) to a solution of pyridine (0.8 mL) in methylene chloride (30 mL). The mixture was stirred at room temperature under nitrogen for 2 hours. The methylene chloride solution was decanted off from the brown gum which had deposited. The gum was washed with methylene chloride (6 × 50 mL) and the combined extracts were washed with 5% sodium hydroxide, water, dried ($Na_2SO_4$), and evaporated to dryness to yield a residue that was purified by preparative tlc (ether–methanol 95:5 v/v) to give pure **2***b*, mp 193–195°C (0.12 g; 81%) after trituration with ether; ir (KBr) $\nu_{max}$: 3300 (NH), 1710 (C=O), 1665 (NHCHO) $cm^{-1}$; $^1$Hmr ($CDCl_3$) δ: 2.83 (2H, s, benzylic $CH_2$), 6.35 (1H, broad, —N*H*CHO), 7.23 (5H, s, aromatic), 8.20 (1H, s, —NHC*H*O). *Anal.* calcd. for $C_{19}H_{25}NO_2$: C 76.21, H 8.41, N 4.68; found: C 76.00, H 8.64, N 4.65.

*3-Ethylenedioxy-1,2,3,4,6,7,8,8a-octahydro-8a-phenylmethylnaphthalene (13)*

Ketone **5** (50 g; 0.208 mol) was refluxed in benzene (1 L) with ethylene glycol (50 mL) and *p*-toluenesulfonic acid monohydrate (1 g) for 18 h under a Soxhlet containing calcium hydride.

Can. J. Chem. Downloaded from www.nrcresearchpress.com by 210.87.254.40 on 09/06/12
For personal use only.

The solution was washed with water (500 mL), 1 *N* sodium hydroxide (100 mL), water (500 mL), dried ($Na_2SO_4$), and concentrated. The residue was taken up in ether (50 mL) and left to crystallize. The resulting crystals were filtered and washed with hexane, providing 31.5 g of **13**. The mother liquors, recycled through the above procedure, yielded a further 14.7 g for a total yield of 46.2 g (77%), mp 91–93°C; $^1$Hmr ($CDCl_3$) δ: 2.80 (2H, m, benzylic $CH_2$), 3.87 (4H, s, $CH_2CH_2$), 5.40 (1H, m, olefinic H), 7.10 (5H, s, aromatic). *Anal.* calcd. for $C_{19}H_{24}O_2$: C 80.24, H 8.50; found: C 80.47, H 8.71.

*3-Ethylenedioxy-5*β*-hydroxy-8a-phenylmethyl-*cis-*perhydronaphthalene (**15**)*

To a solution of olefin **13** (21 g; 74 mmol) in anhydrous tetrahydrofuran (100 mL) cooled at 0°C was added dropwise and under nitrogen a solution of diborane in tetrahydrofuran (150 mL of 1 *M* solution). The reaction mixture was stirred at room temperature for 3 hours. It was then cooled to 0°C and methanol (30 mL) was added slowly. Sodium hydroxide (50 mL, 1 *N*) was then added, followed by the addition of 30% hydrogen peroxide (20 mL). The excess hydrogen peroxide was destroyed by adding a solution of sodium bisulfite until no peroxide was detected by starch iodide paper. The mixture was then extracted three times with methylene chloride and the combined extracts were washed with water and dried ($Na_2SO_4$). Concentration under vacuum gave crude **15** (27.3 g) which was used as such for the next step.

A sample of the crude mixture was purified by preparative tlc (ether–hexane 70:30 v/v) to yield the desired alcohol **15** as an oil and the tertiary alcohol **14** also as an oil. The ratio of **15** to **14** was 3:1.

Secondary alcohol **15**; ir (film) $\nu_{max}$: 3450 ($OH^-$), 1604 (aromatic) $cm^{-1}$; $^1$Hmr ($CDCl_3$) δ: 2.80 (2H, s, benzylic $CH_2$), 3.93 (4H, s, ethylenedioxy protons), 7.17 (5H, s, aromatic).

Tertiary alcohol **14**; ir (film) $\nu_{max}$: 3520 (OH), 1601 (aromatic) $cm^{-1}$; $^1$Hmr ($CDCl_3$) δ: 2.83 (1H, d, $J$ = 14 Hz, benzylic CH), 3.13 (1H, d, $J$ = 14 Hz, benzylic CH), 4.00 (4H, s, ethylenedioxy protons), 7.17 (5H, s, aromatic).

*3-Ethylenedioxy-5-oxo-8a-phenylmethyl-*cis-*perhydronaphthalene (**16**)*

Crude **15** (27.3 g; 0.09 mol) dissolved in acetone (500 mL) was oxidized by adding slowly 55 mL of 1.15 *M* Jones reagent (28). After stirring at room temperature for 30 min, ether (250 mL) was added. The two layers were separated and the organic layer was washed with dilute sodium hydroxide and with water, dried ($Na_2SO_4$), and concentrated to a residue that solidified on standing (26.2 g). The crude **16** was used as such in the following step.

A 200 mg sample was purified by preparative tlc (ether–hexane 1:1 v/v). Recrystallized from methanol, pure *cis*-**16** had mp 117–118°C; ir (KBr) $\nu_{max}$: 1705 (C=O), 1602 (aromatic) $cm^{-1}$; $^1$Hmr ($CDCl_3$) δ: 2.57 (2H, AB quartet, $J_{A,B}$ = 14 Hz, benzylic $CH_2$), 3.84 (4H, s, ethylenedioxy protons), 7.17 (5H, s, aromatic). *Anal.* calcd. for $C_{19}H_{24}O_3$: C 75.97, H 8.05; found: C 76.24, H 8.24.

*3-Ethylenedioxy-5-oxo-8a-phenylmethyl-*trans-*perhydronaphthalene (**17**)*

Purified *cis*-ketone **16** (670 mg; 2.2 mmol) and sodium methoxide (100 mg) in methanol (20 mL) were refluxed under nitrogen for 2.5 hours. The mixture was poured into water (10 mL), extracted with chloroform (3 × 10 mL), washed with brine, dried ($Na_2SO_4$), and evaporated to dryness. The residue was chromatographed on preparative tlc (ether–hexane 70:30 v/v) to yield the *trans* isomer **17** (440 mg) and the *cis* isomer **16** (180 mg). Recrystallized from methanol, the *trans* isomer **17** had mp 119–120°C; ir (KBr) $\nu_{max}$: 1703 (C=O), 1602 (aromatic) $cm^{-1}$; $^1$Hmr ($CDCl_3$) δ: 2.57 (2H, AB quartet, $J_{A,B}$ = 14 Hz, benzylic protons), 3.97 (4H, s, ethylenedioxy protons), 7.20 (5H, m, aromatic protons). *Anal.* calcd. for $C_{19}H_{24}O_3$: C 75.97, H 8.05; found: C 75.42, H 7.84.

*3-Ethylenedioxy-5-methylene-8a-phenylmethyl-*trans-*perhydronaphthalene (**18**)*

A. *Preparation from compound **17***

*trans*-Ketone **17** (50 mg; 0.17 mmol) was added at −78°C to the ylid formed by reacting at 0°C triphenylmethylphosphonium bromide (800 mg; 2 mmol) with *n*-butyllithium (0.7 mL of 2.4 *M* solution in hexane). The mixture was stirred 15 min at −78°C and then allowed to warm to room temperature for 1 hour. It was poured into water, extracted with ether, and the organic extracts were washed with water, dried ($Na_2SO_4$), concentrated *in vacuo*, and purified by preparative tlc, eluting with ether–hexane (50:50 v/v). The resultant oil was triturated with hexane and, after recrystallization from hexane, **18** melted at 75–77°C; ir (KBr) $\nu_{max}$: 3080, 1645, and 898 (exocyclic methylene) $cm^{-1}$; $^1$Hmr ($CDCl_3$) δ: 2.60 (2H, s, benzylic $CH_2$), 3.95 (4H, s, ethylenedioxy), 4.52 and 4.83 (2H, two broad s, $=CH_2$), 7.17 (5H, s, aromatic). *Anal.* calcd. for $C_{20}H_{26}O_2$: C 80.49, H 8.78; found: C 80.51, H 8.54.

B. *Preparation from compound **16***

The crude **16** (26 g) from the previous reaction dissolved in THF (100 mL) was added over 10 min, under $N_2$, to an ice-cold solution of methylenetriphenylphosphorane (0.219 mol) (previously prepared by stirring together for 1 hour at room temperature in THF (400 mL) potassium *tert*-butoxide (29.4 g; 0.262 mol) and methyltriphenylphosphonium bromide (78.1 g; 0.219 mol)).

The reaction mixture was warmed to room temperature, then refluxed for 20 min. It was then cooled, poured into water (500 mL), and extracted with dichloromethane (3 × 250 mL). The organic layer was washed with brine (500 mL), dried ($Na_2SO_4$), and concentrated. The residue was partitioned between 400 mL of hexane and 400 mL of 75% aqueous methanol. The lower phase was washed with another 400 mL of hexane. The combined hexane layers were dried ($Na_2SO_4$) and reduced to dryness to give a residue (23.3 g) which was purified by column chromatography on silica gel. Elution with 10% ether–hexane yielded pure **18** (11.1 g; 43.5% based on **13**), mp 75–77°C.

*Mesylate of 3-ethylenedioxy-5*β*-hydroxymethyl-8a-phenylmethyl-*trans-*perhydronaphthalene (**19**a)*

Under $N_2$ atmosphere, 150 mL of 1 *M* borane in THF was added dropwise over 15 min to an ice-cold solution of *trans* olefin **18** (20.4 g; 68.4 mmol) in dry THF (100 mL). The mixture was stirred at room temperature for 1.5 hours, cooled in an ice–water bath, and 30 mL of methanol was added dropwise to decompose excess borane. Sodium hydroxide (1 *N*, 30 mL) and then 30% hydrogen peroxide (20 mL) were added, each over a period of 15 min. After stirring for 15 min at 0°C, a solution of sodium sulfite (18 g) in water (100 mL) was added dropwise to decompose excess peroxide. The mixture was extracted with methylene chloride (3 × 500 mL). The organic layer was washed with water, dried ($Na_2SO_4$), and evaporated. The crude residue was chromatographed on silica gel eluting with 2.5% methanol–chloroform, to yield **19***a* (13.6 g, 63%); ir (KBr) $\nu_{max}$: 3400 (OH), 1600 (aromatic) $cm^{-1}$; $^1$Hmr ($CDCl_3$) δ: 2.60 (2H, AB quartet; $J_{A,B}$ = 14 Hz, benzylic), 3.67 (2H, m, $—CH_2O$), 3.90 (4H, s, ethylenedioxy), 7.17 (5H, s, aromatic); *m/e*: 316 ($M^+$).

To an ice-cold solution of the alcohol derivative **19***a* (6.8 g; 21.5 mmol) in pyridine (100 mL) was added methanesulfonyl chloride (3.7 g; 32 mmol). The mixture was stored at 0°C for 3 days, then was evaporated to dryness *in vacuo* and the residue was partitioned between ether and water. The organic layer was

Can. J. Chem. Downloaded from www.nrcresearchpress.com by 210.87.254.40 on 09/06/12
For personal use only.

washed with water, dried ($Na_2SO_4$), and evaporated to provide the solid mesylate **19***b*, mp 121–126°C (8.1 g; 95%). Recrystallization from cyclohexane raised the mp to 141–143°C; ir (KBr) $\nu_{max}$: 1350, 1175 ($SO_2$) $cm^{-1}$; $^1$Hmr ($CDCl_3$) δ: 2.58 (2H, AB quartet, $J_{A,B}$ = 14 Hz, benzylic $CH_2$), 2.97 (3H, s, $OSO_2CH_3$), 3.97 (4H, s, ethylenedioxy), 4.25 (2H, m, —$CH_2O$), 7.17 (5H, s, aromatic); *m/e*: 394 ($M^+$). *Anal.* calcd. for $C_{21}H_{30}SO_5$: C 63.93, H 7.66, S 8.12; found: C 64.00, H 7.73, S 8.11.

*5β-Azidomethyl-3-ethylenedioxy-8a-phenylmethyl-*trans*-perhydronaphthalene (20)*

A mixture of mesylate **19***b* (8.5 g; 21.5 mmol), sodium azide (17 g; 262 mmol), and 100 mL of DMF was heated in an oil bath preheated to 125°C, under $N_2$ for 1 hour. The mixture was poured into water and extracted with ether. The organic layer was washed with water, dried ($Na_2SO_4$), and evaporated to give a mixture (5.8 g) which was chromatographed on silica gel, eluting with 10% ether – *n*-hexane to give regenerated olefin **18** (3.1 g; 49%) and the desired azide **20** (2.0 g; 28%), which crystallized on standing, mp 88–89°C; ir (KBr) $\nu_{max}$: 2100 ($N_3$) $cm^{-1}$; $^1$Hmr ($CDCl_3$) δ: 2.63 (2H, AB quartet, $J_{A,B}$ = 14 Hz, benzylic $CH_2$), 3.43 (2H, m, $CH_2N_3$), 3.97 (4H, s, ethylenedioxy), 7.17 (5H, s, aromatic). *Anal.* calcd. for $C_{20}H_{27}N_3O_2$: C 70.35, H 7.97, N 12.30; found: C 70.39, H 8.15, N 12.00.

*5β-Aminomethyl-3-oxo-8a-phenylmethyl-*trans*-perhydronaphthalene (2*a*)*

To a suspension of LAH (1.0 g; 26 mmol) in THF (150 mL) was added the azide **20** (3.5 g; 10.3 mmol) in THF (25 mL). After stirring under $N_2$ for 30 min at room temperature, the reaction was quenched with water (0.5 mL), 15% NaOH (0.5 mL), and water (1.5 mL). The mixture was filtered and the filtrate concentrated to yield crude 5β-aminomethyl-3-ethylenedioxy-8a-phenylmethyl-*trans*-perhydronaphthalene (3.4 g) which was taken up in methanol (150 mL), water (10 mL) and concentrated HCl (5 mL). This mixture was heated under $N_2$ for 30 min at 70°C, then stirred at room temperature for 30 min. The resultant crystals were filtered and washed with ether to yield **2***a* (3.0 g; 64% from **20**), mp 285°C (dec.); ir (KBr) $\nu_{max}$: 1710 (C=O) $cm^{-1}$; $^1$Hmr (DMSO-$d_6$) δ: 2.2–3.2 (6H, m, $CH_2$—CO—$CH_2$ and —$CH_2$—$NH_2$), 7.27 (5H, s, aromatics). *Anal.* calcd. for $C_{18}H_{25}NO.HCl$: C 70.22, H 8.51, N 4.55, Cl 11.51; found: C 69.93, H 8.88, N 4.46, Cl 11.41.

*3-Oxo-5β-formamidomethyl-8a-phenylmethyl-*trans*-perhydronaphthalene (2*b*)*

To the HCl salt **2***a* (210 mg; 0.77 mmol) in formic acid (10 mL) was added formic acetic anhydride (5 mL) and sodium bicarbonate (500 mg). The reaction mixture was refluxed overnight, then concentrated *in vacuo*, diluted with methylene chloride, washed with sodium bicarbonate, dried ($Na_2SO_4$), and concentrated *in vacuo*, to yield a residue which was purified by preparative tlc (5% methanol–chloroform). Recrystallization from methylene chloride – hexane yielded **2***b*, mp at 198–199°C.

This material, compared to the formyl derivative prepared by Scheme 1, was found to be identical and had mixture mp 197–199°C.

*5β-Azidomethyl-3-oxo-8a-phenylmethyl-*trans*-perhydronaphthalene (2*c*)*

The ketal **20** (9.5 g; 28.7 mmol) was dissolved in methanol (200 mL) and 3 *N* hydrochloric acid (50 mL) was added slowly. The mixture was stirred at room temperature for a period of 2.5 hours. The resultant crystals were filtered off to yield **2***c* (7.6 g, 89%), mp 155–157°C; ir (KBr) $\nu_{max}$: 2100 ($N_3$), 1690 (C=O) $cm^{-1}$; $^1$Hmr ($CDCl_3$) δ: 2.77 (2H, AB quartet; *J* = 14 Hz, benzylic), 3.47 (2H, m, $CH_2N_3$), 7.17 (5H, s, aromatic). *Anal.* calcd. for $C_{18}H_{23}N_3O$: C 72.70, H 7.79, N 14.13; found: C 72.90, H 7.76, N 13.91.

*Ethyl-2-diethylphosphono-4-methylthiobutyrate (21)*

Triethylphosphonoacetate (4.4 g; 20 mmol) was added slowly to a suspension of sodium hydride (0.95 g of 50% dispersion in oil) in dimethylformamide (15 mL). Methylthioethylchloride (4.4 g; 40 mmol) was then added and the resulting mixture was heated overnight at 80°C. A precipitation of sodium chloride occurred after three hours. The reaction mixture was cooled, filtered, and evaporated to dryness. The residue was then distilled to yield first unreacted triethylphophonoacetate: bp 105°C/0.5 Torr and then **21**; bp 127–135°C/0.5 Torr (2.8 g; 42% yield); ir (film) $\nu_{max}$: 1735 (C=O) $cm^{-1}$; $^1$Hmr ($CDCl_3$) δ: 1.37 (9H, m, $3CH_3$), 2.17 (3H, s, $SCH_3$), 2.5 (4H, m), 3.03 (1H, m), 4.2 (6H, m, $3CH_2$). *Anal.* calcd. for $C_{11}H_{23}PO_5S$: C 44.28, H 7.77, S 10.75; found: C 44.09, H 7.80, S 10.70.

*Z- and E-3-(3'-Methylthio-1'-carbomethoxypropylidin-1'-yl)-5β-formamidomethyl-8a-phenylmethyl-*trans*-perhydronaphthalene (22*a*)*:

To sodium hydride (25 mg; 50% dispersion in mineral oil, 0.54 mmol) suspended in dimethoxyethane (5 mL) at 0°C under $N_2$ was added ethyl 2-diethylphosphono-4-methylthiobutyrate (150 mg; 0.5 mmol). After stirring for 30 min, the mixture was cooled to −78°C and ketone **2***b* (30 mg; 0.1 mmol) in dimethoxyethane (2 mL) was added. The mixture was stirred at −78°C for 1 hour and then warmed to an internal temperature of 80°C for 6 hours. The mixture was poured into water and extracted with ether. The organic layer was washed with water, dried ($Na_2SO_4$), and concentrated *in vacuo* to yield a residue (197 mg) that was chromatographed on a preparative tlc plate, eluting with 2% methanol–chloroform. The product, $R_f$ = 0.2 (19 mg; 43%), was a mixture of desired **22***a* and of isomer **23***a* as could be determined by the presence of two carbonyl absorptions at 1685 $cm^{-1}$ and 1735 $cm^{-1}$ respectively in the ir spectrum.

*Z- and E-3-(3'-Methylthio-1-carbomethoxy propylidinyl)-5β-azidomethyl-8a-phenylmethyl-*trans*-perhydronaphthalene (22*b*)*:

To a suspension of sodium hydride (47 mg; 50% dispersion in mineral oil; 1 mmol) in dimethoxyethane (5 mL) at 0°C under $N_2$ was added **21** (300 mg; 1 mmol). After stirring for 30 min, ketone **2***c* (27 mg; 0.1 mmol) in DMF (1 mL) was added. The reaction mixture was heated at 80°C for 4 hours. It was then poured into water and extracted with ether. The organic layer was washed with water, dried ($Na_2SO_4$), and concentrated *in vacuo*. The residue was chromatographed on a preparative tlc plate, eluting with ether–hexane 1:5 v/v to give 18 mg (41%) of a mixture of **22***b* and **23***b* as a yellowish oil. The presence of a mixture was again demonstrated by ester absorptions of equal intensity at 1730 $cm^{-1}$ and 1700$^{-1}$.

*Methyl 2-trimethylsilyl-4-methylthiobutyrate (25)*

To a solution of diisopropylamine (128 g; 1.27 mol) in anhydrous THF (1 L) cooled to 0°C was added dropwise over 20 min *n*-butyllithium (557 mL of 2.28 *M* in hexane). The mixture was stirred for 30 min at 0°C. α-Trimethylsilylacetic acid (**23**) (76.3 g; 0.58 mol) dissolved in anhydrous THF (100 mL) was then added dropwise over a period of 15 min and the resulting mixture was stirred at 0°C for 30 min. 2-Methylthioethylchloride (67 g; 0.60 mol) was then added dropwise over 15 min. The reaction mixture was refluxed for 70 h, then was cooled to room temperature and poured into 1.5 liters of water. The organic layer was removed and the aqueous layer was further washed with ether. The aqueous layer was acidified with 20% citric acid and extracted several times with ether. These ether extracts were washed with water, dried ($Na_2SO_4$), and evaporated to give a crude residue that was distilled under vacuum to provide **24**, bp 130°C/0.2 Torr (27 g; 23% yield); $^1$Hmr δ: 0.1 (9H, s,

Can. J. Chem. Downloaded from www.nrcresearchpress.com by 210.87.254.40 on 09/06/12
For personal use only.

—$SiMe_3$), 2.1 (3H, s, $SCH_3$), 10.3 (1H, b, exchanged by $D_2O$, COOH).

The acid was esterified ($CH_2N_2$, excess) in ether. The resulting solution was washed with sodium bicarbonate (5%), dried ($Na_2SO_4$), concentrated, and purified by preparative hplc (5% ether–hexane) to give 19 g (69%) of methyl-2-trimethylsilyl-4-methylthiobutyrate **25**; ir (KBr) $\nu_{max}$: 1712 $cm^{-1}$; $^1$Hmr ($CDCl_3$) δ: 0.15 (9H, s, $SiMe_3$), 2.07 (3H, s, $SCH_3$), 3.67 (3H, s, $COOCH_3$). *Anal.* calcd. for $C_9H_{20}SSiO_2$: C 49.04, H 9.15, S 14.55; found: C 49.23, H 9.18, S 14.32.

*3-(3'-Methylthio-1'-carbomethoxypropylidinyl)-5β-azidomethyl-8a-phenylmethylperhydronaphthalene (**26**)*

To a solution of diisopropylamine (4.75 mL; 36 mmol) in tetrahydrofuran (100 mL) at 0°C under $N_2$ was added a 2.2 *M* solution of *n*-butyl lithium in hexane (16.36 mL; 36 mmol). The mixture was stirred at 0°C for 15 min and then cooled at −78°C. Ester **25** (8 g; 36.4 mmol) dissolved in 10 mL tetrahydrofuran was added over 5 minutes. The resulting mixture was stirred for 20 min at −78°C and then ketone **2***c* (5.23 g; 17.6 mmol) in 40 mL tetrahydrofuran was added dropwise over a period of 10 min. The reaction mixture was stirred at −78° for another 10 min, and was allowed to warm to room temperature. The mixture was poured into water and extracted with ether. The organic phase was washed successively with 3 *N* hydrochloric acid and with water, dried ($Na_2SO_4$), and evaporated to dryness to yield a pale yellow oil which was chromatographed on silica gel. Elution with 5% ether–hexane gave successively methyl ester **25** (5.2 g), and the mixture of *E* and *Z* isomers of the desired product **26** (7.2 g; 96%); ir (NaCl) $\nu_{max}$: 2100 ($N_3$), 1705 (C=O) $cm^{-1}$; $^1$Hmr ($CDCl_3$) δ: 2.13 (3H, s, $SCH_3$), 2.60 (4H, s, $CH_2CH_2$), 3.50 (2H, m, $CH_2N_3$), 3.73 (3H, s, $OCH_3$), 7.17 (5H, s, aromatic); *m/e*: 427 (weak, $M^+$), 399 (M − $N_2$), 384 (M − $HN_3$).

*Z and E Isomers of 3-(3'-methylthio-1'-carbomethoxypropylidinyl)-5β-aminomethyl-8a-phenylmethyl-*trans*-perhydronaphthalene (**27**a and **27**b)*

The *Z* and *E* mixture of azide **26** (7.5 g; 17.6 mmol) was dissolved in methanol (300 mL) and hydrogenated in a Parr hydrogenator at 30 psi for one hour over platinum oxide (500 mg). The reaction mixture was filtered through Celite and concentrated *in vacuo* to yield an oil which was chromatographed on silica gel. Elution with methanol–chloroform – aqueous ammonia (2000:40:5 v/v/v) gave the *E* isomer (3.6 g) and the *Z* isomer (3.4 g) successively (99% combined yield). The *E* isomer **27***a* recrystallized from ether gave an analytical sample, mp 96.5–97.5°C; ir (KBr) $\nu_{max}$: 1705 ($COOCH_3$), 1610, 3350 ($NH_2$) $cm^{-1}$; $^1$Hmr ($CDCl_3$) δ: 2.10 (3H, s, $SCH_3$), 2.53 (4H, s, —$CH_2CH_2S$—), 3.75 (3H, s, $OCH_3$), 7.07 (5H, s, aromatic); *m/e*: 401 ($M^+$), 386 (M − $CH_3$), 370 (M − $OCH_3$), 354 (M − $SCH_3$), 340 (base peak, M − $CH_2SCH_3$), 310 (M − $CH_2C_6H_5$). *Anal.* calcd. for $C_{24}H_{35}NO_2S$: C 71.78, H 8.78, N 3.49, S 7.98; found: C 71.89, H 8.92, N 3.42, S 7.69.

The *Z* isomer **27***b* recrystallized from ether gave an analytical sample, mp 104–106°C; ir (KBr) $\nu_{max}$: 1705 ($COOCH_3$), 1610, 3350 ($NH_2$) $cm^{-1}$; $^1$Hmr ($CDCl_3$) δ: 2.10 (3H, s, $SCH_3$), 2.53 (4H, s, —$CH_2CH_2S$—), 3.73 (3H, s, $OCH_3$), 7.07 (5H, s, aromatic); *m/e*: 401 ($M^+$), 386, 370, 354, 340 (base peak), 310. *Anal.* calcd. for $C_{24}H_{35}NO_2S$: C 71.78, H 8.78, N 3.49, S 7.98; found: C 71.93, H 8.89, N 3.43, S 7.71.

*X-ray structure determination of **27**a*

Suitable crystals of **27***a* for single crystal X-ray diffraction experiments formed from ether containing traces of chloroform. Preliminary diffraction experiments indicated that the space group was *P*1 with $a$ = 11.029(4) Å, $b$ = 13.460(4), $c$ = 8.709(2), α = 97.80(2)°, β = 110.34(2), and γ = 68.78(2) for $Z$ = 2. Of the 3061 reflections collected using CuKα radiation (λ = 1.5418 Å), 2624 were observed and corrected for Lorentz and polarization effects. Application of direct methods (29) and tangent formula recycling procedures (30) provided initial coordinates for all nonhydrogen atoms. After refinements and Fourier calculations hydrogens were placed and refined. The function $\Sigma w(|F_o| - |F_c|)^2$ was minimized with full matrix least squares techniques (31) to give an unweighted residual factor of 0.077. Tables 1, 2, and 3 contain the final atomic coordinates and temperature parameters, bond distances, and bond angles, respectively.[1]

*The coupling of **27**a with* N-t-*BOC-tyrosine*

A solution of the *E* isomer **27***a* (2.63 g; 6.56 mmol), *t*-BOC tyrosine (3.72 g; 13.2 mmol), dicyclohexylcarbodiimide (2.72 g; 15 mmol), and 1-hydroxybenzotriazole (2.03 g; 15 mmol) in methylene chloride (140 mL) was stirred at room temperature overnight. The reaction mixture was diluted with ether and was then filtered. The cake was washed with ether. The combined filtrates were washed with 20% citric acid, with 5% sodium bicarbonate, and with water. After drying over sodium sulfate, the solution was evaporated to a foam (6.08 g).

The mixture of diastereoisomers was separated by chromatography on silica gel eluting with a mixture of 1% butanol–chloroform to yield the desired coupled products **28***a* and **28***b*. The less polar isomer, arbitrarily assigned structure **28***a* (1.78 g; 44% yield), was a glass, mp 104–106°C. The more polar isomer, arbitrarily assigned structure **28***b* (1.85 g, 45% yield), was a glass, mp 106–108°C.

**28***a*: ir (KBr) $\nu_{max}$: 3350 (NH amide), 1700, 1665 $cm^{-1}$; $^1$Hmr ($CDCl_3$) δ: 1.40 (9H, s, —$C(CH_3)_3$), 2.10 (3H, s, $SCH_3$), 2.55 (4H, broad s, —$CH_2CH_2$—S—), 3.73 (3H, s, $OCH_3$), 4.13 (1H, m, tyrosyl methyne), 5.33 (b d, exchanged by $D_2O$, $J$ = 8 Hz, tyrosyl NH—BOC), 5.53 (1H, broad, NH amide, exchanged by $D_2O$), 6.80 (4H, $A_2B_2$ quartet, tyrosyl aromatics), 7.10 (5H, s, aromatics), 7.85 (s, 1H, OH, exchanged by $D_2O$).

**28***b*: ir (KBr) $\nu_{max}$: 3340, 1700, 1660 $cm^{-1}$; $^1$Hmr ($CDCl_3$) δ: 1.37 (9H, s, —$C(CH_3)_3$), 2.07 (3H, s, $SCH_3$), 2.53 (4H, b, $CH_2CH_2S$), 3.68 (3H, s, $OCH_3$), 4.18 (1H, m, tyrosyl methyne), 5.20 (1H, d, $J$ = 8 Hz, tyrosyl—NH—BOC, exchanged by $D_2O$), 5.97 (1H, broad, NH amide, exchanged by $D_2O$), 6.77 (4H, $A_2B_2$ quartet, tyrosyl aromatics), 7.07 (5H, s, aromatics), 7.97 (s, 1H, OH, exchanged by $D_2O$).

*The coupling of **27**b with* N-t-*BOC tyrosine*

Similarly, reacting the *Z* isomer **27***b* (2.5 g) with *t*-BOC tyrosine (3.46 g), dicyclohexylcarbodiimide (2.53 g), and 1-hydroxybenzotriazole (1.9 g) in methylene chloride (125 mL) afforded after extraction with ether 5.7 g of a crude mixture of diastereoisomers that was separated by chromatography on silica gel.

**28***c*: (less polar diastereoisomer), 1.5 g (39%) as a glass, mp 100–104°C; ir (KBr) $\nu_{max}$: 3350, 1700, 1660 $cm^{-1}$; $^1$Hmr ($CDCl_3$) δ: 1.40 (9H, s, *t*-Bu), 2.08 (3H, s, $SCH_3$), 2.57 (4H, broad s, $CH_2CH_2S$), 3.67 (3H, s, $OCH_3$), 4.17 (1H, m, tyrosyl methyne), 5.23 (1H, $J$ = 8 Hz, d, NH—BOC, exchanged by $D_2O$), 6.17 (1H, b, amide NH, exchanged by $D_2O$), 6.80 (4H, $A_2B_2$ quartet, $J_{AB}$ = 8 Hz, tyrosyl aromatic), 7.05 (5H, s, aromatic), 7.85 (1H, b s, OH, exchanged by $D_2O$).

**28***d*: (more polar diastereoisomer), 1.22 g (31%) as a glass, mp 108–111°C; ir (KBr) $\nu_{max}$: 3350, 1700, 1660 $cm^{-1}$; $^1$Hmr ($CDCl_3$) δ: 1.40 (9H, s, *t*-Bu), 2.07 (3H, s, $SCH_3$), 2.53 (4H, b s, $CH_2CH_2S$), 3.67 (3H, s, $OCH_3$), 4.2 (1H, m, tyrosyl methyne), 5.13 (1H, d, $J$ = 8 Hz, NH—BOC exchanged by $D_2O$), 5.90 (1H, b s, NH amide, exchanged by $D_2O$), 6.80 (4H, $A_2B_2$ quartet, $J_{AB}$ = 8 Hz, tyrosyl aromatic), 7.07 (5H, s, aromatic), 7.40 (1H, b s, OH, exchanged by $D_2O$).

[1]Tables 1, 2, and 3 are available, at a nominal charge, from the Depository of Unpublished Data, CISTI, National Research Council of Canada, Ottawa, Ont., Canada K1A 0S2.

Can. J. Chem. Downloaded from www.nrcresearchpress.com by 210.87.254.40 on 09/06/12
For personal use only.

*The four isomers of* trans-*methyl-2-(decahydro-4β-(phenylmethyl)-8β-(L-tyrosylaminomethyl)-2-naphthalenylidene)-4-(methylthio)butanoate HCl monohydrate* **1**a–d

The blocked derivatives **28***a–d* dissolved in chloroform (25 mL) were saturated with anhydrous hydrogen chloride and the resulting mixtures were stirred at room temperature for one hour. In each case the excess hydrogen chloride was blown off with a stream of nitrogen and the chloroform solution was washed with sodium bicarbonate and with water. The organic phase was dried over sodium sulfate and evaporated to dryness, leaving a residue which was purified by preparative hplc, eluting with 3% methanol–chloroform. The resulting derivative was taken up in chloroform, treated with hydrogen chloride, and evaporated to dryness. The residue was triturated in ether and filtered. Thus **28***a* (1.68 g) gave **1***a* (1.37 g; 89%), mp 154–156°C, $[\alpha]_D^{22}$ 0 (*c* 1.0, MeOH); ir (KBr) $\nu_{max}$: 3500–2600 ($NH_3^+$), 1700, 1670 $cm^{-1}$; $^1$Hmr ($CDCl_3$) (on free base) δ: 2.10 (3H, s, $SCH_3$), 2.57 (4H, s, $CH_2CH_2S$), 3.73 (3H, s, $OCH_3$), 3.80 (3H, $NH_2$ and OH, exchanged by $D_2O$), 6.90 (4H, $A_2B_2$ quartet, $J = 8$ Hz, tyrosyl aromatics), 7.13 (5H, s, aromatic), 7.45 (1H, b, amide NH, exchanged by $D_2O$); *m/e*: 564 ($M^+$), 503 ($M^+ - CH_2SCH_3^+$). *Anal.* calcd. for $C_{33}H_{44}N_2O_4S.HCl.\frac{1}{2}H_2O$: C 64.83, H 7.71, N 4.65; found: C 64.95, H 7.59, N 4.59.

Similarly **28***b* (1.77 g) gave **1***b* (1.30 g; 80%), mp 162–164°C, $[\alpha]_D^{22}$ +67.7° (*c* 1.0, MeOH); ir (KBr) $\nu_{max}$: 3500–2600 ($NH_3^+$), 1700, 1670 $cm^{-1}$; $^1$Hmr ($CDCl_3$) (on free base) δ: 2.10 (3H, s, $SCH_3$), 2.57 (4H, s, $CH_2CH_2S$), 3.73 (3H, s, $OCH_3$), 3.70 (3H, $NH_2$ and OH, exchanged by $D_2O$), 6.87 (4H, $A_2B_2$ quartet, $J = 8$ Hz, tyrosyl aromatic), 7.10 (5H, s, aromatic), 7.40 (1H, b s, NH amide, exchanged by $D_2O$); *m/e*: 546 ($M^+$), 503 ($M^+ - CH_2SCH_3$). *Anal.* calcd. for $C_{33}H_{44}N_2O_4S.HCl.\frac{1}{2}H_2O$: C 64.83, H 7.71, N 4.65; found: C 64.53, H 7.58, N 4.54.

Similarly, **28***c* (1.5 g) gave **1***c* (0.75 g; 54%), mp 149–151°C, $[\alpha]_D^{22}$ −17.1° (*c* 1.0, MeOH); ir (KBr) $\nu_{max}$: 3500–2600 ($NH_3^+$), 1700, 1670 $cm^{-1}$; $^1$Hmr ($CDCl_3$) (free base) δ: 2.10 (3H, s, $SCH_3$), 2.57 (4H, s, $CH_2CH_2S$), 3.73 (3H, s, $OCH_3$), 3.70 (3H, $NH_2$ and OH, exchanged by $D_2O$), 6.87 (4H, $A_2B_2$ quartet, $J = 8$ Hz, tyrosyl aromatic), 7.10 (5H, s, aromatic), 7.40 (1H, b s, NH amide, exchanged by $D_2O$), 7.47 (1H, b s, NH amide, exchanged by $D_2O$); *m/e*: 564 ($M^+$), 503 ($M - CH_2SCH_3$). *Anal.* calcd. for $C_{33}H_{44}N_2O_4S.HCl$: C 65.92, H 7.54, N 4.66; found: C 65.78, H 7.62, N 4.50.

Similarly, **28***d* (1.15 g) gave **1***d* (0.750 g; 54%), mp 157–160°C, $[\alpha]_D^{22}$ +79.1° (*c* 1.0, MeOH); ir (KBr) $\nu_{max}$: 3500–2600 ($NH_3^+$), 1700, 1670 $cm^{-1}$; $^1$Hmr ($CDCl_3$) (free base) δ: 2.13 (3H, s, $SCH_3$), 2.57 (4H, s, $CH_2CH_2S$), 3.60 (3H, $NH_2$ and OH, exchanged by $D_2O$), 3.70 (3H, s, $OCH_3$), 6.87 (4H, $A_2B_2$ quartet, $J = 8$ Hz, tyrosyl aromatic), 7.13 (5H, s, aromatic), 7.57 (1H, b s, NH amide, exchanged by $D_2O$); *m/e*: 546 ($M^+$), 503 ($M - CH_2SCH_3$). *Anal.* calcd. for $C_{33}H_{44}N_2O_4S.HCl.\frac{1}{2}H_2O$: C 64.83, H 7.71, N 4.65; found: C 65.33, H 7.86, N 4.48.

## Acknowledgments

The authors wish to thank Dr. P. Gund and G. M. Smith (Merck Sharp & Dohme Research Laboratories, Rahway, New Jersey) for their help and discussions regarding the Merck Modeling System, and Dr. F. M. Robinson (Merck Sharp & Dohme Research Laboratories, Rahway, New Jersey) for useful and frequent discussions on analgesics.

1. Opiates and endogeneous opioid peptides. Elsevier/North-Holland Biomedical Press, Amsterdam, The Netherlands. 1976.
2. M. A. Khaled, M. M. Long, W. D. Thompson, R. J. Bradley, G. B. Brown, and D. W. Urry. Biochem. Biophys. Res. Commun. **76**, 224 (1977).
3. C. R. Jones, V. Garsky, and W. A. Gibbons. Biochem. Biophys. Res. Commun. **76**, 619 (1977).
4. P. W. Schiller, C. F. Yam, and M. Lis. Biochemistry, **16**, 1831 (1977).
5. J. L. De Coen, C. Humblet, and M. H. J. Koch. FEBS Lett. **73**, 38 (1977).
6. Y. Isogai, G. Nemethy, and H. A. Scheraga. Proc. Natl. Acad. Sci. U.S.A. **74**, 414 (1977).
7. F. A. Gorin and G. R. Marshall. Proc. Natl. Acad. Sci. U.S.A. **74**, 5179 (1977).
8. T. L. Blundell, L. Hearn, I. J. Tickle, R. A. Palmer, B. A. Morgan, G. D. Smith, and J. F. Griffin. Science, **205**, 220 (1979).
9. A. S. Horn and J. R. Rogers. J. Pharm. Pharmacol. **29**, 257 (1977).
10. A. F. Bradbury, D. G. Smyth, and C. R. Snell. Nature, **260**, 165 (1976).
11. M. Kato, H. Kosugi, and A. Yoshikoshi. Chem. Commun. 185 (1970).
12. G. Stork, R. Terrell, and J. Szmuszkovicz. J. Am. Chem. Soc. **76**, 2029 (1954).
13. J. W. Cornforth and R. Robinson. J. Chem. Soc. 1855 (1949).
14. J. A. Marshall, M. T. Pike, and R. D. Carroll. J. Org. Chem. **31**, 2933 (1966).
15. T. L. Ho and C. M. Wong. J. Org. Chem. **38**, 2241 (1973).
16. C. H. Heathcock and T. R. Kelly. Tetrahedron, **24**, 1801 (1968).
17. R. Ratcliffe and R. Rodehorst. J. Org. Chem. **35**, 4000 (1970).
18. J. A. Marshall and M. T. Pike. Tetrahedron Lett. 3107 (1965).
19. K. H. Fung, K. J. Schmalzl, and R. N. Mirrington. Tetrahedron Lett. 5017 (1969).
20. W. S. Wadsworth, Jr. and W. D. Emmons. J. Am. Chem. Soc. **83**, 1733 (1961).
21. P. A. Grieco, C. L. J. Wang, and S. D. Burke. Chem. Commun. 537 (1975).
22. H. Taguchi, K. Shimoji, H. Yamamoto, and H. Nozaki. Bull. Chem. Soc. Jpn. **47**, 2529 (1974).
23. S. L. Hartzell and M. W. Rathke. Tetrahedron Lett. 2737 (1976).
24. P. Gund, J. D. Andose, J. B. Rhodes, and G. M. Smith. Science, **208**, 1425 (1980).
25. J. C. Sheehan and G. P. Hess. J. Am. Chem. Soc. **77**, 1067 (1955).
26. C. B. Pert, S. H. Snyder, and E. L. May. Exp. Ther. **196**, 316 (1976).
27. M. Szelke. International Narcotic Research Conference, North Falmouth, Mass., June 11–15 (1978).
28. K. Bowden, I. M. Heilbron, E. R. H. Jones, and B. C. L. Weedon. J. Chem. Soc. 39 (1946).
29. P. Main, S. E. Hull, L. Lessinger, G. Germain, J. Declercq, and M. M. Woolfson. MULTAN 78, A system of computer programs for the automatic solution of crystal structures from X-ray diffraction data. Universities of York, England, and Louvain, Belgium. 1978.
30. J. Karle. Acta Crystallogr. Sect. B, **24**, 182 (1968).
31. J. M. Stewart, G. J. Kruger, H. L. Ammon, C. Dickinson, and S. R. Hall. The X-ray system, version of June, 1972, TR-192, University of Maryland, College Park, Maryland.

# Enzymes in organic synthesis. 23.[1] Effects of organic solvents on horse liver alcohol dehydrogenase-catalyzed oxidation

J. Bryan Jones and Harold M. Schwartz

*Department of Chemistry, University of Toronto, Toronto, Ont., Canada M5S 1A1*

Received November 2, 1981

J. Bryan Jones and Harold M. Schwartz. Can. J. Chem. **60**, 1030 (1982).

The effects have been evaluated of up to 50% (v/v) of methanol, *tert*-butyl alcohol, dimethylsulfoxide, sulfolane, acetonitrile, dimethylformamide, *N*-methyl-2-pyrrolidone, hexamethylphosphoramide, acetone, 2-butanone, tetrahydrofuran, dimethoxyethane, diglyme, and dioxane on horse liver alcohol dehydrogenase (HLADH)-catalyzed oxidation of the representative alcohol substrate cyclohexanol. With the exception of dimethylsulfoxide and dimethylformamide, all solvents tested are suitable for use as cosolvents with HLADH in the oxidative and reductive directions.

J. Bryan Jones et Harold M. Schwartz. Can. J. Chem. **60**, 1030 (1982).

Utilisant des concentrations de solvant allant jusqu'à 50% (v/v), on a étudié l'effet du méthanol, du *tert*-butanol, du diméthylsulfoxyde, du sulfolane, de l'acétonitrile, du diméthylformamide, de la *N*-méthylpyrrolidone-2, de l'hexaméthylphosphoramide, de l'acétone, de la butanone-2, du tétrahydrofuranne, du diméthoxyéthane, du diglyme et de la dioxanne sur l'oxydation d'un alcool typique, le cyclohexanol, catalysée par la dehydrogénase d'alcool du foie de cheval (DAFC). A l'exception du diméthylsulfoxyde et du diméthylformamide, tous les solvants utilisés peuvent servir de cosolvants à la DAFC aussi bien pour l'oxydation que pour la réduction.

[Traduit par le journal]

Most of the compounds and intermediates encountered in organic synthesis are hydrophobic in nature and do not dissolve to any significant extent in water. Accordingly, for the full potential of enzymes in organic synthesis to be realized, it is necessary to induce sufficient solubility of hydrophobic compounds in the aqueous media preferred by enzymes to ensure that such organic substrates are readily accessible to the enzymic catalysts. The most convenient general method for achieving this goal is by the addition of water-miscible organic solvents to the reaction medium and we are currently surveying this topic (1*a*–*d*) in order to identify the most suitable organic cosolvents for preparative-scale applications of enzymes.

Alcohol dehydrogenases, which catalyze alcohol oxidations and ketone reductions of central asymmetric synthetic importance via the reaction pathway depicted in eq. [1][2], are among the most useful

[1] $\rangle CHOH + NAD^+ \rightleftharpoons \rangle C{=}O + NADH + H^+$

enzymes of current value for preparative-scale reactions (1*f*). In this paper, we report on the effects of various solvents on the catalytic activity of HLADH-catalyzed oxidation of its representative alcohol substrate, cyclohexanol.

[1]For Part 22, see ref. 1*a*. Abstracted from the Ph.D. thesis of H.M.S., University of Toronto (1979).

[2]Abbreviations used: $NAD^+$ and NADH, oxidized and reduced forms respectively of nicotinamide adenine dinucleotide; HLADH, horse liver alcohol dehydrogenase; DMSO, dimethylsulfoxide; DMF, dimethylformamide; NMP, *N*-methyl-2-pyrrolidone; HMPA, hexamethylphosphoramide; THF, tetrahydrofuran.

## Results

As in the reductive mode study carried out previously (1*a*), a range of common water-miscible protic and aprotic solvents of different polarities was considered. The solvents used were, protic: methanol and *tert*-butyl alcohol; aprotic: DMSO, sulfolane, acetonitrile, DMF, NMP, HMPA, acetone, 2-butanone, THF, dimethoxyethane, diglyme, and dioxane. The effects of up to 50% of each cosolvent on HLADH-catalyzed oxidation were evaluated using cyclohexanol as representative substrate. The oxidations were carried out in 0.1 *M* glycine – NaOH buffer pH 9.0 at 0.5 m*M* $NAD^+$ and 1, 5, and 25 m*M* cyclohexanol concentrations. The relative activities recorded, based on initial velocities, are summarized in Table 1. While all solvents have a deleterious influence at their highest concentrations, HLADH is seen to be remarkably tolerant of many of the added solvents when operating in its oxidation mode. The worst cosolvents are DMSO and DMF, both of which inhibit strongly at low concentrations. The most remarkable effects are seen with NMP, HMPA, and diglyme, in the presence of which the activity of the enzyme is actually increased initially. Attempts to identify the nature of the generally inhibitory effects of the solvents using Lineweaver–Burk and Dixon analyses (2) of the Table 1 data were inconclusive, with nonlinear plots being obtained in each case.

## Discussion

As for the analogous study on HLADH-catalyzed reduction (1*a*), the solvents were chosen to en-

0008-4042/82/081030-04$01.00/0

©1982 National Research Council of Canada/Conseil national de recherches du Canada

Can. J. Chem. Downloaded from www.nrcresearchpress.com by 210.87.254.42 on 09/06/12
For personal use only.

TABLE 1. Relative rates of HLADH-catalyzed oxidation of cyclohexanol in the presence of different organic cosolvents[a]

| Cosolvent (ε) | 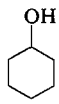 (m*M*) | Relative rate[b] in cosolvent 1% | 5% | 10% | 20% | 30% | 40% | 50% |
|---|---|---|---|---|---|---|---|---|
| Protic | | | | | | | | |
| Methanol | 1 | 38 | 13 | 6 | <0.1 | | | |
| (32.7) | 5 | 56 | 28 | 12 | 6 | | | |
| | 25 | 82 | 51 | 28 | 14 | | | |
| *tert*-Butyl | 1 | 63 | 39 | 28 | 14 | | | |
| alcohol (12.5) | 5 | 62 | 41 | 30 | 16 | | | |
| | 25 | 62 | 40 | 29 | 15 | | | |
| Aprotic | | | | | | | | |
| DMSO (46.7) | 5 | 4 | 1[c] | | | | | |
| Sulfolane (43.3) | 1 | 41 | 23 | 21 | 18 | 11 | 7 | |
| | 5 | 78 | 58 | 48 | 35 | 29 | 19 | |
| | 25 | 93 | 75 | 62 | 45 | 36 | 23 | |
| Acetonitrile | 1 | 52 | 14 | 13 | | | | |
| (37.5) | 5 | 52 | 38 | 18 | | | | |
| | 25 | 70 | 37 | 23 | | | | |
| DMF (36.7) | 1 | 7 | 4[c] | | | | | |
| | 5 | 7 | 4 | | | | | |
| | 25 | 11 | 5 | | | | | |
| NMP (32.0) | 1 | 97 | 89 | 68 | 47 | 27 | 12 | |
| | 5 | 109 | 105 | 84 | 56 | 31 | 13 | |
| | 25 | 92 | 83 | 81 | 52 | 25 | 9 | |
| HMPA (30.0) | 1 | 129 | 126 | 120 | 109 | 97 | 65 | 17 |
| | 5 | 102 | 111 | 113 | 107 | 64 | 51 | 26 |
| | 25 | 107 | 122 | 140 | 137 | 117 | 60 | 43 |
| Acetone (20.7) | 1 | 44 | 25 | 14 | 7 | 4 | | |
| | 5 | 60 | 35 | 25 | 13 | 13 | | |
| | 25 | 64 | 46 | 34 | 22 | 9 | | |
| 2-Butanone | 1 | 35 | 23 | 20 | 17 | | | |
| (18.5) | 5 | 36 | 27 | 20 | 16 | | | |
| | 25 | 32 | 29 | 24 | 16 | | | |
| THF (7.6) | 1 | 22 | 11 | 6 | 2 | 1 | | |
| | 5 | 29 | 16 | 9 | 7 | 1 | | |
| | 25 | 32 | 23 | 21 | 11 | 1 | | |
| Dimethoxyethane | 1 | 77 | 50 | 39 | 24 | 12 | 9 | |
| (7.2) | 5 | 80 | 42 | 34 | 24 | 14 | 7 | |
| | 25 | 82 | 49 | 40 | 27 | 15 | 6 | |
| Diglyme | 1 | 100 | 87 | 82 | 55 | 37 | 20 | |
| | 5 | 105 | 90 | 74 | 54 | 28 | 15 | |
| | 25 | 89 | 86 | 69 | 50 | 31 | 14 | |
| Dioxane (2.2) | 1 | 71 | 41 | 39 | 21 | 16 | 8 | |
| | 5 | 70 | 47 | 35 | 21 | 12 | 7 | |
| | 25 | 77 | 53 | 36 | 25 | 12 | 6 | |

[a]Determined in 0.1 *M* glycine – NaOH buffer pH (app) 9.0, 0.5 m*M* in $NAD^+$ at 25°C.
[b]Relative to initial velocity of 100 in absence of organic cosolvent.
[c]Intermediate activities were observed at 2 and 3% organic solvent levels.

compass as broad a range of the common, water-miscible, solvents as possible. Both protic and aprotic solvents were considered, with dielectric constant used as the guide to polarity. The choice of protic solvents was restricted to methanol and *tert*-butyl alcohol since the other common alcohol solvents were themselves substrates. However, with the enzyme operating in its oxidation mode, the ketone solvents acetone and 2-butanone, excluded in the reductive study (1*a*) because they were substrates, could now be evaluated.

Cyclohexanol was selected as the substrate since

Can. J. Chem. Downloaded from www.nrcresearchpress.com by 210.87.254.42 on 09/06/12
For personal use only.

Can. J. Chem. Downloaded from www.nrcresearchpress.com by 210.87.254.42 on 09/06/12
For personal use only.

its behaviour with HLADH is representative of organic alcohol substrates in general (1*e*) and the mechanism of its HLADH-catalyzed oxidation has been thoroughly investigated (3). Cyclohexanol has a relatively low $K_m$ of 0.7 m*M* (3*a*) thus permitting facile evaluation of its oxidation at saturating levels. Furthermore, above a 5 m*M* concentration, substrate activation takes place (3*a*). In order to determine the effects of cosolvents under differing kinetic conditions, the cyclohexanol concentration values selected for the current study were set at a value close to the $K_m$ (1 m*M*) at the beginning of the substrate activation range (5 m*M*), and at 25 m*M*, a level ensuring considerable substrate activation. A saturating concentration (0.5 m*M*) of the $NAD^+$ coenzyme was employed throughout.

For each cosolvent studied, the initial oxidation velocities were determined in glycine–NaOH buffers of pH 9.0, the normal preparative-scale pH for oxidation reactions (1*f*). Neither the apparent pH's of the assay solutions (4), nor the reaction rates, were sufficiently affected by the added organic solvents to require corrections to be made to the raw data. While additions of organic cosolvents do affect the pH optima of enzymes, the deviations induced at the solvent concentrations employed in this study are seldom >0.5 pH units (1*a*, *c*, *d*).

For each cosolvent, the concentration was increased progressively until the enzyme retained ~15% or less of its initial activity, a level selected as representing the effective lower limit of activity in any practical preparative-scale use of HLADH.

The enzymic activities were determined by monitoring the 340 nm absorbance charges of the coenzyme. When methanol, HMPA, and acetonitrile were present, increases in the 340 nm absorption occurred even when the substrate was not present. For methanol, this substrate-independent rate is likely due to its slow HLADH-catalyzed oxidation to formaldehyde (5, 6). The effect of HMPA may be due to its known affinity for electrophiles (7), which would result in the formation of an addition complex with $NAD^+$ (8). The effect on $NAD^+$ of acetonitrile is probably the result of nucleophilic addition of the trace of cyanide which is present even in doubly distilled acetonitrile (9). The relative activity rates of Table 1 have been corrected for these nonenzymic solvent-induced rates.

The Table 1 data show that HLADH is remarkably tolerant of added cosolvents when operating in its oxidation mode. This is in sharp contrast to the situation observed for HLADH-catalyzed reduction, where the enzyme was found to be much more sensitive to the presence of cosolvents (1*a*). Of the Table I solvents, the only strong inhibitors at low concentration levels are DMSO and DMF. Their deleterious effects were expected since both are known to coordinate to the catalytically essential zinc ion at the active site (10). For all of the other cosolvents tested, HLADH retains significant activity at concentration levels as high as 20% (v/v), with sulfolane and NMP remaining viable up to 40% (v/v). HMPA is the most remarkable of all, with preparatively useful enzyme activity levels being retained even in 50% (v/v) solutions.

Another feature which distinguishes the oxidation situation from that of reduction is the pronounced enhancement of HLADH activity induced by several of the cosolvents. For HLADH-catalyzed reduction of cyclohexanone, only one instance of a modest rate increase, in 5% HMPA solution, was observed. In contrast, for the oxidation reactions of the current study, each of NMP, HMPA, and diglyme stimulated the enzymic activity over a range of different concentration levels. The effect is most dramatic for HMPA, where the normal aqueous solution activity of the enzyme is exceeded within the cosolvent concentration range of 1–30% (v/v). The behaviour of the enzyme in HMPA solutions, being stimulated at lower, and inhibited at higher, concentrations resembles the response of HLADH to imidazole (11), a modifier which can bind to the active site zinc ion (12). The solvent-mediated protein conformation changes (13) responsible for this activation phenomenon are clearly catalytically much more effective in the oxidation than the reduction direction. Again, as noted in the previous reductive solvent effects study (1*a*), no correlation of the inhibitory power of a solvent with its dielectric constant, nor its aprotic or protic character, is evident from the Table 1 results.

In the reductive mode study (1*a*), Lineweaver–Burk and Dixon plot analyses provided useful information on the nature of the inhibition by most of the solvents studied. It is unfortunate that similar analyses of the Table 1 data did not give interpretable plots since the literature data on the influence of solvents on HLADH-catalyzed oxidations is very limited. To our knowledge, detailed studies have been performed only for methanol, which forms a ternary $E{\cdot}NAD^+{\cdot}MeOH$ complex (14), and DMSO, a competitive inhibitor which acts by binding to the active site zinc ion (10, 15, 16).

For some solvents, increasing the substrate concentration affords partial protection against the inactivation process. These include methanol, sulfolane, acetonitrile, HMPA, acetone, and THF. For the other solvents, substrate concentration changes have little effect on the activity at any one cosolvent concentration.

Can. J. Chem. Downloaded from www.nrcresearchpress.com by 210.87.254.42 on 09/06/12
For personal use only.

*Summary of solvent effects on HLADH-catalyzed oxidation and reduction*

The presence of high concentrations of organic cosolvents is generally deleterious to HLADH activity. However, the effects are considerably more adverse for the reductive reaction (1*a*). In fact, HLADH is remarkably tolerant of high organic solvent concentrations in its oxidative mode.

DMSO and DMF are strongly inhibitory in both directions and should not be used as cosolvents. Also, the common solvents that are potential substrates must clearly be excluded. These include primary and secondary alcohols (methanol, ethanol, 2-propanol) in oxidation reactions, and ketones (acetone, 2-propanone) for the reductive direction. Those solvents that interact with the coenzyme should also be avoided if possible. Methanol, HMPA, and acetonitrile are in this category for both oxidative and reductive directions, although they are suitable for short- to medium-term reactions involving rapidly transformed substrates. The peroxide contaminants of the ethereal solvents THF, dimethoxyethane, diglyme, and dioxane may also cause problems during long-term use.

The most innocuous solvents for general use in HLADH-catalyzed oxidations appear to be *tert*-butyl alcohol, sulfolane, NMP, and acetone. The corresponding list for reduction is ethanol, *tert*-butyl alcohol, and sulfolane. Unfortunately, sulfolane and NMP are not very effective cosolvents for hydrophobic substrates. However, *tert*-butyl alcohol provides a good balance of hydrophobic and hydrophilic properties and should be a good general cosolvent for many substrates in either catalytic direction. For substrates with unique characteristics or unusual combinations of functional groups, the general recommendations made above may not give optimum results. In such cases, data provided by the current and previous (1*a*) studies will aid the selection of the most suitable cosolvent for any individual substrate. Also, it should always be borne in mind that it is not necessary to achieve complete substrate solubility. Satisfactory reaction rates will result as soon as sufficient substrate is accessible to the enzyme. These levels are often attained when only a small proportion of the substrate has been brought into solution.

## Experimental

HLADH, prepared by the method of Roy and Nishikawa (17), was generously donated by Hoffmann-La Roche. The enzyme may also be purchased from Sigma. The solvents were purified as described previously (1*a*) and were redistilled immediately prior to use, as was cyclohexanol.

*Relative rate studies*

These were carried out by the general procedure described for the previous HLADH-catalyzed reduction study (1*a*) at 25°C in 0.1 *M* glycine – NaOH buffer pH 9.0 containing varying proportions of cosolvent, $5.00 \times 10^{-4}$ *M* in $NAD^+$, $9.92 \times 10^{-8}$ *M* in HLADH, and with cyclohexanol concentrations of 1.0, 5.0, and $25.0 \times 10^{-3}$ *M*. The initial oxidation rates were determined from the rate of increase in optical density at 340 nm. The relative rates are recorded in Table 1. Those obtained in methanol, HMPA, and acetonitrile solutions have been corrected for the nonenzymic, solvent-induced, reactions.

## Acknowledgements

We thank NSERC for their generous financial support and Hoffmann-La Roche, Nutley, New Jersey, for their much appreciated and continuing aid. We are also grateful to Drs. G. Sanyal and T. H. Maren (University of Florida) for providing details of their work on the cyanide content of acetonitrile in advance of publication (9).

1. (*a*) J. B. Jones and H. M. Schwartz. Can. J. Chem. **60**, 335 (1982); (*b*) J. B. Jones and M. M. Mehes. Can. J. Chem. **57**, 2245 (1979); (*c*) D. H. Pliura and J. B. Jones. Can. J. Chem. **58**, 2633 (1980), and references therein; (*d*) J. B. Jones and D. H. Pliura. Can. J. Chem. **59**, 2921 (1980), and references therein; (*e*) A. J. Irwin, K. P. Lok, K. W-C. Huang, and J. B. Jones. J. Chem. Soc. Perkin Trans. I, 1636 (1978); (*f*) J. B. Jones and J. F. Beck. Tech. Chem. N.Y. **10**, 107 (1976).
2. M. Dixon and E. C. Webb. Enzymes. 2nd ed. Longmans, London. 1964.
3. (*a*) K. Dalziel and F. M. Dickinson. Biochem. J. **180**, 491 (1966); (*b*) K. Dalziel. *In* The enzymes. Vol. 11. 3rd ed. *Edited by* P. D. Boyer. Academic, New York. 1975. pp. 1–60.
4. H. Gutfreund. Enzymes, physical principles. Wiley–Interscience, London. 1972.
5. J. C. Mani, R. Pietruszko, and H. Theorell. Arch. Biochem. Biophys. **140**, 52 (1970).
6. R. L. Brooks and J. D. Shore. Biochemistry, **10**, 3855 (1971).
7. H. Normant. Angew. Chem. Int. Ed. Engl. **6**, 1046 (1967).
8. J. F. Biellmann, C. Lapinte, E. Haid, and G. Weimann. Biochemistry, **18**, 1212 (1979).
9. G. Sanyal. Biochim. Biophys. Acta. Submitted.
10. R. L. Perlman and J. Wolff. Science, **160**, 317 (1968).
11. P. A. Collins, C. S. Hanes, and J. T-F. Wong. Can. J. Biochem. **56**, 1016 (1978).
12. C. I. Brändén, H. Jörnvall, H. Eklund, and B. Furugren. *In* The enzymes. Vol. 11. 3rd ed. *Edited by* P. D. Boyer. Academic, New York. 1975.
13. P. M. Hinckle and J. F. Kirsch. Biochemistry, **9**, 4633 (1970).
14. C. C. Wratten and W. W. Cleland. Biochemistry, **4**, 2442 (1965).
15. E. Bignetti, G. L. Rossi, and E. Zeppezauer. FEBS Lett. **100**, 17 (1979).
16. (*a*) B. V. Plapp, H. Eklund, and C. I. Brändén. J. Mol. Biol. **122**, 22 (1978); (*b*) H. Eklund and C. I. Brändén. J. Biol. Chem. **254**, 3458 (1979).
17. S. K. Roy and A. H. Nishikawa. Biotechnol. Bioeng. **21**, 775 (1979).

# Electron and cation transport in fluid dimethyl ether: effects of density and temperature

NORMAN GEE AND GORDON R. FREEMAN

*Chemistry Department, University of Alberta, Edmonton, Alta., Canada T6G 2G2*

Received October 13, 1981

NORMAN GEE and GORDON R. FREEMAN. Can. J. Chem. **60**, 1034 (1982).

The effect of molecular electric dipole moment $D$ on charge transport in fluids was examined by measurement of electron and ion mobilities in dimethyl ether ($D$ = 1.3 D) and comparing them with the behavior in hydrocarbons. The fluid density was varied continuously from that of the normal vapor to that of the normal liquid, passing through the critical region. The density normalized mobility $n\mu_e$ of electrons in dimethyl ether vapor at low densities is 30-fold smaller than that in propane, although for the cations $n\mu_+$ in the ether is only 1.4-fold smaller than that in the alkane. The permanent dipole moment of the ether dominates the scattering of low energy electrons but not that of cations. The electron momentum transfer cross section is roughly 33% larger than that predicted by the Altshuler point dipole model, and has a minimum at ~0.12 eV. The energy gained from the electric field is removed mainly through inelastic collisions, even in the thermal energy range.

Molecular clustering decreases both electron and ion mobilities, but the effect on the former is much larger due to the greater change in reduced mass. The extent of electron quasilocalization in the dense vapor of dimethyl ether is four times greater than that in nonpolar hydrocarbons. Electrons form relatively stable localized states in the liquid at $n/n_c > 2.0$. Ion mobility undergoes a transition from "density control" to "viscosity control" with increasing density in the low density liquid. Viscosity control is operative at $n/n_c > 2.4$.

NORMAN GEE et GORDON R. FREEMAN. Can. J. Chem. **60**, 1034 (1982).

On a étudié l'effet du moment dipolaire électrique moléculaire $D$ sur le transport de charge dans les fluides en mesurant les mobilités des électrons et des ions dans l'éther méthylique ($D$ = 1,3 D) et en les comparant avec leur comportement dans les hydrocarbures. On a fait varier la densité du fluide d'une façon continue à partir de celle de la vapeur normale à celle du liquide normal en passant par la région critique. La mobilité normalisée pour la densité, $n\mu_e$, des électrons dans la vapeur d'éther à de faibles densités est 30 fois plus petite que celle dans le propane, bien que le valeur de $n\mu_+$ des cations soit 1,4 fois plus petit dans l'éther que dans l'alcane. Le moment dipolaire permanent de l'éther domine la dispersion des électrons de faible énergie mais pas celle des cations. La section droit de transfert du momentum de l'électron est approximativement 33% plus grande que celle prédite par le modèle du point dipolaire de Altshuler et il a un minimum à ~0,12 eV. L'énergie gagnée à partir du champ électrique est enlevée principalement à travers les collisions non élastiques, même dans le domaine d'énergie thermique.

L'entassement moléculaire diminue les mobilités des électrons et des ions, mais l'effet du premier est plus grand à cause d'une plus grande variation de la masse réduite. Le taux de quasilocalisation de l'électron dans la vapeur dense d'éther est 4 fois plus grand que celui dans les hydrocrabures non polaires. Les électrons forment des états localisés relativement stables dans le liquide à $n/n_c >$ 2,0. La mobilité des ions subit une transition du "contrôle de densité" au "contrôle de viscosité" avec une augmentation de la densité dans le liquide de faible densité. Le contrôle de viscosité est opérant à $n/n_c > 2,4$.

[Traduit par le journal]

## Introduction

Electrons in dense gases can be localized in several ways. The electrons can be ephemerally localized by density fluctuations; this transitory localization occurs in the heavier noble gases argon (1) and xenon (2) as well as in all hydrocarbons studied to date (3–10). These hydrocarbons range from methane (3), which is the simplest alkane, and ethene (5) the simplest alkene, to more complex structures such as benzene and toluene (10). Quasilocalization occurs to a similar extent in all these compounds and the density normalized mobility $n\mu$ decreases by a factor up to three or so. However, in helium (11–15), nitrogen (16), carbon dioxide (17), and ammonia (18, 19), much stronger localization processes occur. The electron mobility decreases by factors up to several orders of magnitude and may approach that of heavy ions. The mobility transition in helium is attributed to bubble formation, due to the strong electron–helium repulsive interaction. In carbon dioxide it is attributed to electron attachment to the molecules, in a multibody process; in ammonia attachment to molecular clusters (incipient solvation) is invoked. The difference between the extent of localization in ammonia and that in hydrocarbons is presumably caused by the larger dipole moment of the former. Ammonia has a dipole moment of 1.47 D (20). The largest dipole moment of the previously studied hydrocarbons was that of isobutene, 0.49 D (20). To clarify the role of dipole moment in the localization process, the mobilities of electrons and ions have been studied in dimethyl ether, which has a dipole moment of 1.3 D (20).

## Experimental

Dimethyl ether (Matheson, 99.87%) was further purified in a grease-free, glass, vacuum line. Transfer of the gas from the cylinder to the vacuum line was effected through a length of flexible stainless steel tubing welded to the cylinder valve at one end and to a Kovar-glass seal at the other. About 50 cm$^3$ of liquid ether was purified at a time. The sample was degassed by trap-to-trap distillation, the receiver being cooled by liquid

0008-4042/82/081034-10$01.00/0

©1982 National Research Council of Canada/Conseil national de recherches du Canada

Can. J. Chem. Downloaded from www.nrcresearchpress.com by 210.87.254.40 on 09/06/12
For personal use only.

Can. J. Chem. Downloaded from www.nrcresearchpress.com by 210.87.254.40 on 09/06/12
For personal use only.

nitrogen and continually open at the back to the vacuum system. The ether was then transferred to a bulb containing potassium hydroxide pellets and held overnight as a liquid at 195 K (Dry Ice/acetone). It was then degassed again, transferred onto freshly activated molecular sieves (Davison 3A), and held overnight at 195 K. It was then treated with four fresh potassium mirrors for 1 day each at 195 K. Two different procedures were then used. Process *A*: the ether was held on a fifth mirror for 2–8 weeks at 195 K prior to use. Process *B*: the sample was transferred onto a liquid sodium–potassium alloy (20% sodium) and stirred gently for 4 weeks at 270 K prior to use.

Other experimental details are described in refs. 2, 3, 7, and 21. Ion and electron mobilities were obtained from times of flight (7), except for electrons in liquid ether at $T < 355$ K. In the latter instance electron capture interfered with the time of flight measurement, so a conductance method was used (22). Both methods were used at 372 K and conductance gave a mobility value 11% higher than that from time of flight. The free ion yields needed in the conductance method were measured at the same temperatures, as described in ref. 22.

Densities at $n > 3 \times 10^{20}$ molecules/cm$^3$ were obtained from ref. 23; those at $n < 1 \times 10^{20}$ were calculated from the van der Waals equation (24). Intermediate densities were obtained by graphical interpolation. The critical parameters are $T_c = 400$ K, $P_c = 52$ atm, and $n_c = 3.55 \times 10^{21}$ molecules/cm$^3$ (23, 24).

Dielectric constants of the liquid were obtained from refs. 25 and 26. The experimental values could be fitted to Onsager's equation (ref. 27, p. 26) using a dipole moment of 1.4 D. This moment is 8% larger than the gas phase value (1.3 D), and agrees with the trend noted in diethyl ether, for which the dipole moment in benzene solvent was found to be 6% higher than that in the vapor (ref. 27, p. 48).

## Results

Mobilities of the electrons and ions were measured over wide ranges of density, temperature, and electric field strength. Conditions were varied from those of the normal liquid and vapor to that of the supercritical fluid.

### *Electrons*

The density normalized mobility of electrons, $n\mu_e$, in the low density vapor is plotted in Fig. 1 for several temperatures. The mobility increases with temperature and with field strength. The threshold field $(E/n)_{thr}$ increases slightly with temperature, being ~3 Td at 252 K and ~5 Td at 466 K, where Td = $10^{-17}$ V cm$^2$/molecule. Earlier measurements near 295 K gave $n\mu_e$ values 20–30% (29) and ~10% (30) higher than the present ones (Fig. 1).

At $E/n > 20$ Td the mobility decreases (Fig. 1). The temperature coefficient of $n\mu_e$ is smaller at high fields than at low fields.

Increasing the vapor density along the vapor–liquid coexistence curve up to ~$2 \times 10^{20}$ molecules/cm$^3$ has little effect upon $n\mu_e$ (Fig. 2). At higher densities $n\mu_e$ decreases and $(E/n)_{thr}$ increases.

The value of $n\mu_e$ passes through a minimum near the critical density (Fig. 3), increases to a low maximum in the liquid phase at $n/n_c \approx 1.4$, then decreases rapidly at higher densities. The shape of the curve is an intermediate to those observed previously in ethane (4) and cyclopropane (6). However, the low density value of $n\mu_e$ in dimethyl ether is 50-fold lower than those for ethane and cyclopropane.

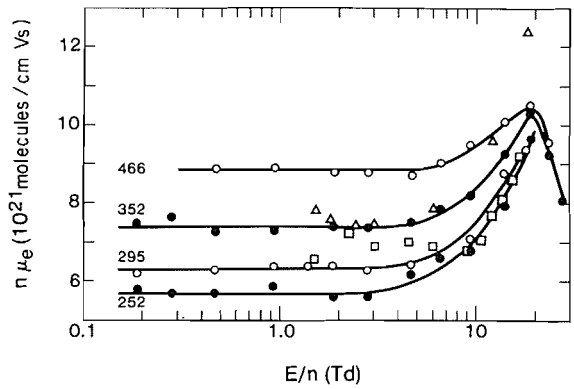


FIG. 1. Density normalized plot of electron mobility against field strength in low density dimethyl ether vapor. Circles, $n = 3.32 \times 10^{19}$ molecules/cm$^3$, numbers labelling curves are $T$ (K). △, 293 K, 6–80 ($10^{16}$ molecules/cm$^3$), ref. 29; □, 297 ± 3 K?, ~5 × $10^{18}$ molecules/cm$^3$?, ref. 30. Td = $10^{-17}$ V cm$^2$/molecule.

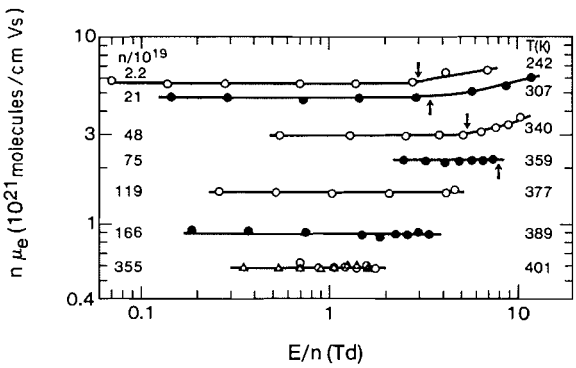


FIG. 2. Effect of density on $n\mu_e$ in the coexistence vapor. The arrows indicate approximate values of $(E/n)_{thr}$. The supercritical gas ($n = 355 \times 10^{19}$, $T = 401$) was approached both from the gas (○) and liquid (△) phases.

The temperature coefficient of $\mu_e$ increases with density at $n > 1 \times 10^{20}$ molecules/cm$^3$ (Figs. 4 and 5). The coefficient in the low density gas is approximately equivalent to an Arrhenius $E_\mu$ of 2 kJ/mol, which increases to 4 kJ/mol at $2 \times 10^{20}$ molecules/cm$^3$ and ~50 kJ/mol at $36 \times 10^{20}$ (Table 1).

In the coexistence liquid phase $\mu_e$ and its temperature coefficient increase steadily with temperature (Figs. 4 and 6).

### *Cations*

The relative variation of $n\mu_+$ with density in the

Can. J. Chem. Downloaded from www.nrcresearchpress.com by 210.87.254.40 on 09/06/12
For personal use only.

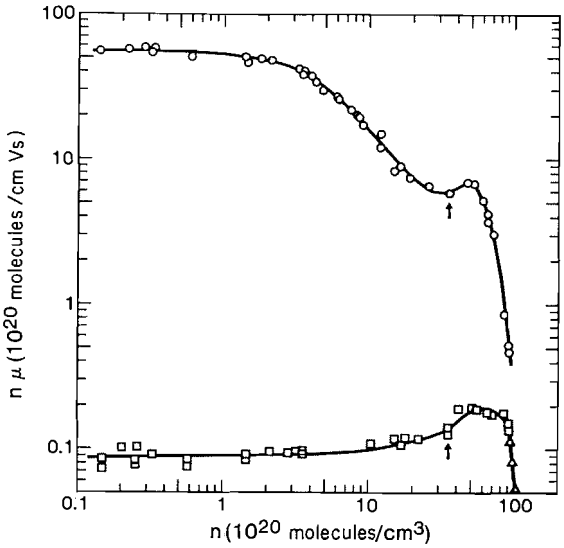


FIG. 3. Effect of density on the density normalized mobilities of thermal electrons (○) and cations (□) in the coexistence vapor and liquid. The arrows mark the critical density $n_c$. The ether was purified by process *B*. △, cations in liquid, ref. 26.

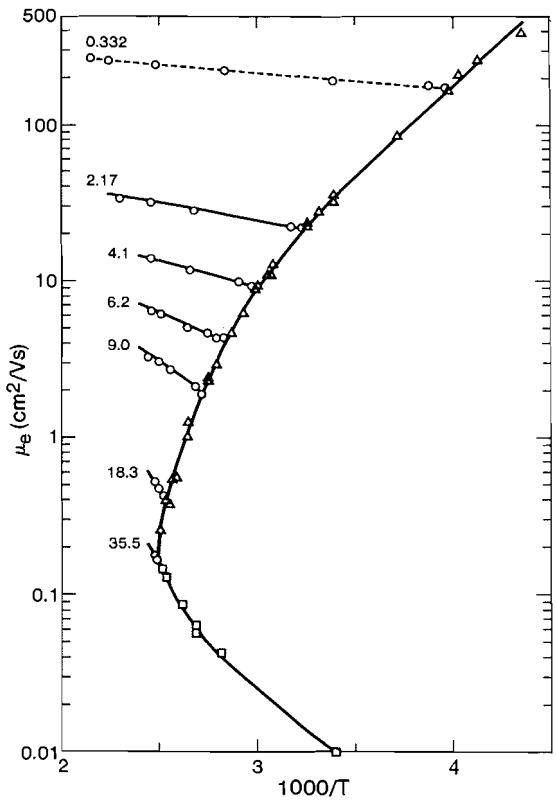


FIG. 4. Arrhenius plots of $\mu_e$ in the gas at several constant densities (○). The numbers labelling the curves are $n/10^{20}$. The dashed line near the top was calculated from eq. [1] or [10], using the appropriate electron scattering cross sections in Fig. 11. The sample with $6.2 \times 10^{20}$ molecules/cm³ contained 0.08 mol% of methanol. △, coexistence vapour; □, coexistence liquid.

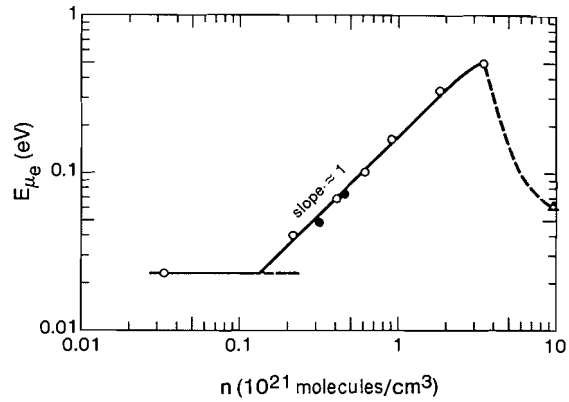


FIG. 5. $E_{\mu_e}$ as a function of fluid density. ○, vapor, Fig. 4; ●, vapor, dash–dot lines in Fig. 7; △, liquid, ref. 26.

coexistence liquid and dense gas was much smaller than that for electrons (Fig. 3). The value of $n\mu_+$ does not decrease with increasing density in the coexistence gas phase, but rather increases slightly at $n/n_c > 0.3$. The near constancy of $n\mu_+$ up to the critical density is similar to the behavior in nonpolar hydrocarbon vapors (21, 31) and the value of $n\mu_+$ is similar to that for cyclopentane (21).

There is a small maximum in $n\mu_+$ at $n/n_c \approx 1.5$, as there is for $n\mu_e$ (Fig. 3), and as there is for cations in nonpolar hydrocarbons. There is also a slight maximum in $\mu_+$ itself at $T$ just below $T_c$ in the liquid phase (Fig. 6); such a maximum was observed previously only for the cyclic hydrocarbons (21, 31, 32).

The temperature coefficient of $\mu_+$ in the constant density vapor increased with density (Fig. 6 and Table 1). The apparent values of $E_\mu$ are similar for cations and electrons at a given density (Table 1), although the values of $n\mu_+$ are nearly three orders of magnitude smaller than those of $n\mu_e$.

*Effect of impurity on apparent value of* $\mu_e$

Ether purified by process *A* (Experimental section) gave low values of mobilities in the coexistence vapor when $n > 2 \times 10^{20}$ molecules/cm³; at $n > 1 \times 10^{21}$ molecules/cm³ only a heavy ion mobility could be measured. Extending the potassium mirror treatment to 3 months increased the mobility values in this material to those obtained in ether from process *B* (Fig. 3). Longer treatment with mirror or alloy did not further increase the mobilities.

The impurity effect in the dense vapor was greatest near the coexistence curve. Heating the gas at constant density reduced the effect of the impurity (Fig. 7). The Arrhenius temperature coefficient of the apparent mobility in $10.8 \times 10^{20}$ molecules/cm³ near the coexistence curve is ~150 kJ/mol, while that at $4.6 \times 10^{20}$ is 100 kJ/mol. This

TABLE 1. Temperature coefficients of thermal electron and ion mobilities in dimethyl ether vapor at different densities

| $n$ ($10^{19}$ molecules/cm$^3$) | $\frac{n}{n_c}$ | Electrons $T_{range}$ (K) | Electrons $E_{\mu_e}$ (kJ/mol) | Ions $T_{range}$ (K) | Ions $E_{\mu_+}$ (kJ/mol) |
|---|---|---|---|---|---|
| 3.32 | 0.0094 | 252–466 | 2 | 252–454 | 2 |
| 21.7 | 0.061 | 310–434 | 4 | 311–434 | 3 |
| 31.4 | 0.088 | | | 322–432 | 4 |
| 41 | 0.115 | 336–406 | 7 | | |
| 62 | 0.175 | 353–406 | 10 | | |
| 90 | 0.254 | 368–408 | 16 | | |
| 108 | 0.304 | | | 377–405 | 9 |
| 183 | 0.515 | 396–404 | 33 | 394–404 | 31 |
| 355 | 1.00 | 401–403 | 50±10 | 400–404 | 68±10 |

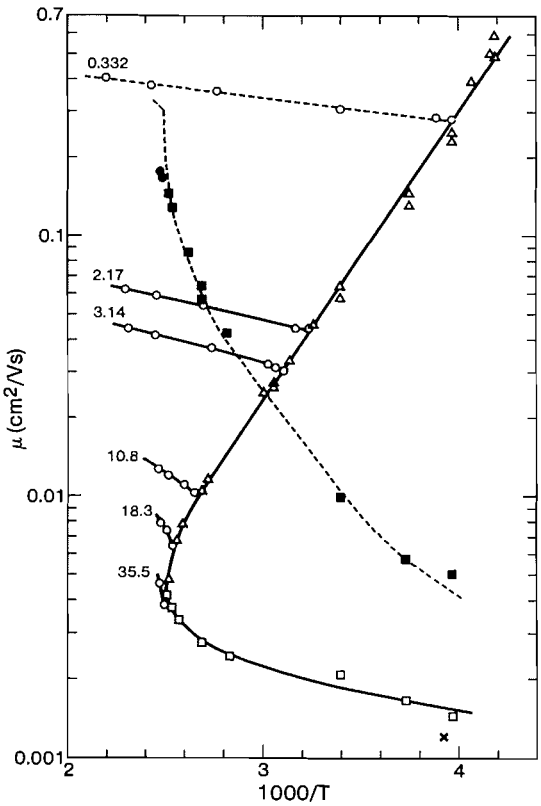


FIG. 6. Arrhenius plots of cation (open symbols) and electron (■) mobilities. The symbols have the same meanings as in Fig. 4, except ×, ion in liquid, ref. 26. The dashed line through the upper gas isochore was calculated from eq. [10], using the ion cross sections in Fig. 13. The dashed line through the liquid phase electron mobilities was calculated from eqs. [4]–[9].

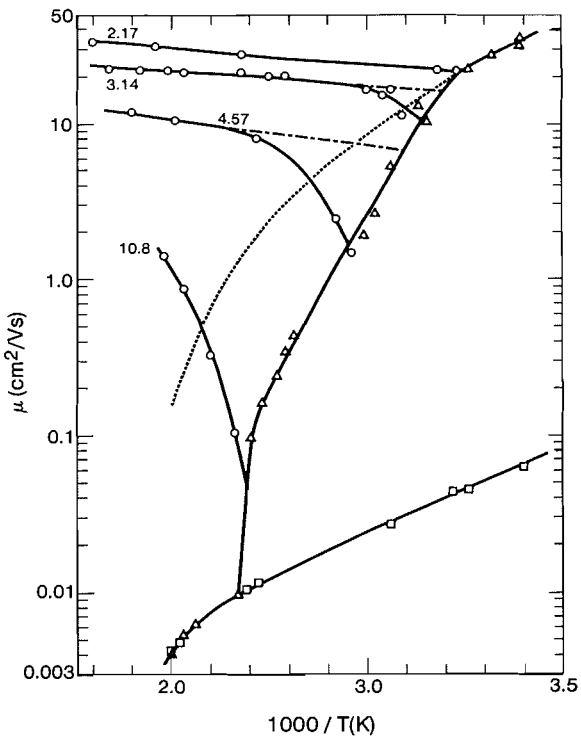


FIG. 7. Arrhenius plot illustrating the effect of an impurity in the dense gas. Ether from process *A*. The symbols have the same meanings as in Fig. 4, except □ = $\mu_{ion}$ in coexistence gas; ---, $\mu_e$ from Fig. 4. ·····, joins the high temperature end of an isochore to the temperature on the dashed line where the saturated vapor has the isochoric density.

behavior suggests $e^- + S \rightleftharpoons S^-$, where $S^-$ only forms in association with a cluster of ether molecules. The clusters are destroyed by heating the vapor at constant density. The temperature coefficients obtained from the dash–dot lines in Fig. 7 agree with those in the clean sample (Fig. 5), so an unclustered S does not interfere with $\mu_e$. This conclusion is supported by the absence of an impurity effect at low vapor densities.

Traces of methanol and carbon dioxide were detected in the unpurified ether by mass spectral analysis (33).[1] Small amounts of methanol or carbon dioxide were therefore added to purified (process *B*) ether to measure their effect on $\mu_e$. A sample

[1]Probable impurities are methanol, carbon dioxide, and methyl formate.

Can. J. Chem. Downloaded from www.nrcresearchpress.com by 210.87.254.40 on 09/06/12
For personal use only.

with $n = 6.2 \times 10^{20}$ molecules/cm$^3$ containing 0.08 mol% methanol gave curved traces of electron current against time, but the estimated mobilities were the same as those expected from pure samples (Figs. 3 and 4). The main effect of methanol was to scavenge electrons at the lower field strengths, thereby decreasing the $E/n$ range over which $\mu_e$ could be measured.

Addition of 0.015 and 0.04 mol% of carbon dioxide caused $\mu_e$ along the coexistence curve to decrease at $T \gtrsim 320$ K (Fig. 8, $n \gtrsim 3 \times 10^{20}$ molecules/cm$^3$), while 0.24% caused the electron signal to disappear. The Arrhenius temperature coefficient in the gas at $n = 8.5 \times 10^{20}$ containing 0.04% carbon dioxide was 120 kJ/mol near the coexistence curve (Fig. 8). This behavior is similar to that obtained with dimethyl ether from process $A$, so it is concluded that process $A$ left a trace of carbon dioxide in the ether.

Examples of oscilloscope traces obtained with pure and impure ethers are shown in Fig. 9. The presence of carbon dioxide caused the signal trace to become curved, which is the usual effect of electron scavengers, but the product of the signal decay time and the field strength increased, which

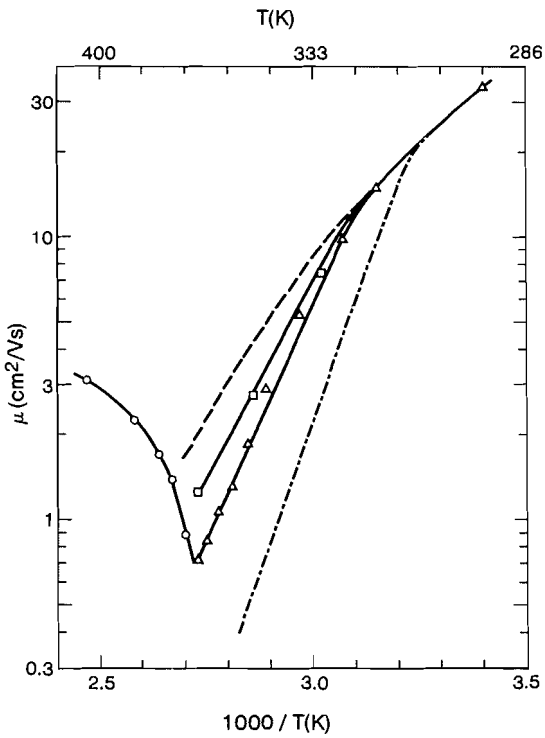


FIG. 8. Effect of carbon dioxide upon electron mobility in dimethyl ether vapor. Ether, coexistence vapor: -·-·-, process $A$; ---, process $B$; □, $B$ + ~0.015 mol% $CO_2$; △, $B$ + ~0.04% $CO_2$; ○, $n = 8.5 \times 10^{20}$, $B$ + ~0.04% $CO_2$.

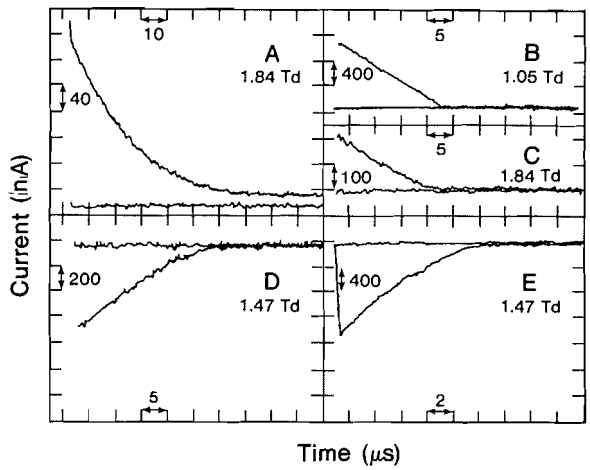


FIG. 9. Oscilloscope traces illustrating the current–time signals in pure and impure ether vapors at 12.5 kV/cm ($E/n \approx$ 1–2 Td). Radiation dose $\approx 1 \times 10^{10}$ eV/g. The values of $T$(K) are: $A$, 356; $B$, 377; $C$, 356; $D$, 370; $E$, 387. The ether purities are: $A$, process $A$ (dirtiest); $B$, process $B$ (cleanest); $C$–$E$, process $B$ + 0.04% $CO_2$. Signals $A$–$C$ are coexistence vapors, while $D$ and $E$ are for temperatures above the coexistence curve.

is the opposite of the usual scavenger effect. In the pure ether, trace $B$ Fig. 9, $t_dE/n = 2.2$ ($10^{-22}$ s V cm$^2$/molecule), while in the impure ethers, traces $A$ and $C$, $t_dE/n = 8.8$ and 3.2 units, respectively. However, heating the impure gas to remove it from the coexistence region reduced the value of $t_dE/n$: trace $D$, 370 K, $t_dE/n = 3.8$ units; trace $E$, 387 K, $t_dE/n = 1.5$ units.

To check the effect of the third listed possible impurity in the unpurified ether (33), ~0.003 mol% of methyl formate was added to process $B$ ether at $n = (4–9) \times 10^{20}$. The electrons were completely scavenged.

## Discussion

### *Electrons*

#### *1. Low density gas*

##### *(a) Scattering cross sections*

In the low density coexistence vapor $n\mu_e$ is nearly independent of density (Fig. 3). Similar behavior was found in nonpolar vapors (1–10). In the alkane series ethane (4), propane (6), $n$-pentane (8), and $n$-hexane (9) the $n\mu_e$ values decrease with increasing molecular size or mean polarizability. The presence of a permanent dipole moment $D$ decreases $n\mu_e$ as well, with $n\mu_e \propto D^{-2}$ for point dipoles (34). Thus, while propane, propene, and dimethyl ether have similar mean polarizabilities (ref. 20, section 14207), their respective dipole moments increase and values of $n\mu_e$ decrease in the order listed (Table 2). The values of $D$ and $n\mu_e$ in low density ammonia vapor are similar to those in

Can. J. Chem. Downloaded from www.nrcresearchpress.com by 210.87.254.40 on 09/06/12
For personal use only.

TABLE 2. Molecular properties and average momentum transfer cross sections

| Compound | $\bar{\alpha}^a$ ($10^{-30}$ m$^3$) | $D^b$ (D) | $n\mu_e{}^c$ ($10^{22}$ molecules/cm V s) | $\sigma_{av,e}{}^d$ ($10^{-19}$ m$^2$) | $n\mu_+{}^e$ ($10^{19}$ molecules/cm V s) | $\sigma_{av,+}{}^f$ ($10^{-19}$ m$^2$) |
|---|---|---|---|---|---|---|
| $CH_3CH_2CH_3$ | 6.2 | 0.084 | 15[g] | 0.84 | 1.9[i] | 33 |
| $CH_3CHCH_2$ | 6.0 | 0.37 | 5.4[g] | 2.4 | 1.7[i] | 38 |
| $CH_3OCH_3$ | 5.2 | 1.30 | 0.55 | 21 | 1.0 | 58 |
| $NH_3$ | 2.3 | 1.47 | 0.5[h] | 28 | 2.1[j] | 47 |

[a]Mean polarizability, ref. 20, section 14207.
[b]Electric dipole moment, ref. 20.
[c]Low density coexistence vapor.
[d]Equation [1], 298 K, $\sigma_{av,e} = \langle v \rangle / \langle v/\sigma_m \rangle$.
[e]298 K.
[f]Equation [10], 298 K, $\sigma_{av,+} = \langle v^3\sigma_m \rangle / \langle v^3 \rangle$.
[g]Reference 6.
[h]Reference 19.
[i]Reference 48.
[j]Reference 28.

dimethyl ether, although the former is a much smaller molecule (Table 2). Electron scattering by the ether and ammonia is therefore dominated at low energies by interaction with the permanent dipole moments.

The momentum transfer cross section $\sigma_m$ as a function of electron velocity $v$ was extracted from the temperature dependence of $n\mu_e$ at low densities. The procedure was to fit the measured set of ($n\mu_e$, $T$) values to eq. [1] (36, 37).

$$[1] \quad n\mu_e = (5.23 \times 10^{-14}/T^{2.5}) \times \int_0^\infty (v^3/\sigma_m) \exp(-3.30 \times 10^{-12} v^2/T) dv$$

As a first trial, the point-dipole scattering cross sections of Altshuler (34) were used:

$$[2] \quad \sigma_m(\text{Alt}) = (8\pi/3)(eD/\hbar v)^2$$

where $h = 2\pi\hbar$ is Planck's constant. The calculated values of $n\mu_e$ so obtained were roughly 33% too high (Fig. 10). Multiplying the Altshuler cross sections by 1.33 gave approximately correct values of $n\mu_e$, but the temperature coefficient was too small. By adjusting the cross sections to obtain a best-fit to the experimental $n\mu_e$ values, the curve depicted with open circles in Fig. 11 was obtained.

The energy range to which the curve fitting is most sensitive is that near the maximum of the integrand in eq. [1]. Over the present temperature range, 252–466 K, the most sensitive energy range is ~0.03–0.18 eV, and the integrand peaks at 0.09–0.12 eV. The integrand $F$ is plotted for 359 K in Fig. 11; it displays the relative contributions of electrons at different energies to the drift of the swarm.

The cross sections at $\varepsilon > 0.15$ eV were chosen so that the curve would smoothly join earlier results for $\varepsilon \geq 1$ eV (38).

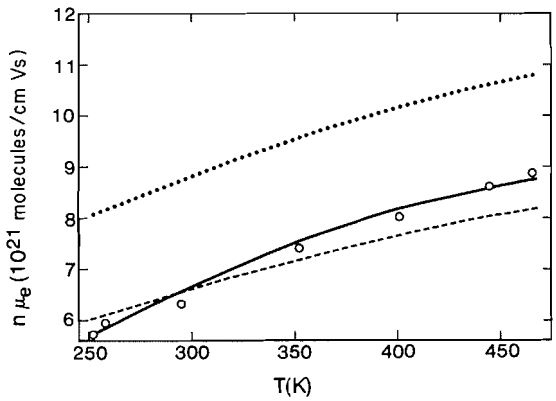


FIG. 10. Comparison of calculated and experimental (○) values of $n\mu_e$ in gaseous dimethyl ether. $n = 3.32 \times 10^{19}$ molecules/cm$^3$. The lines were calculated from eq. [1] and the following cross sections: ..., eq. [2]; ---, eq. [2] × 1.33; ———, curve —○—○— in Fig. 11.

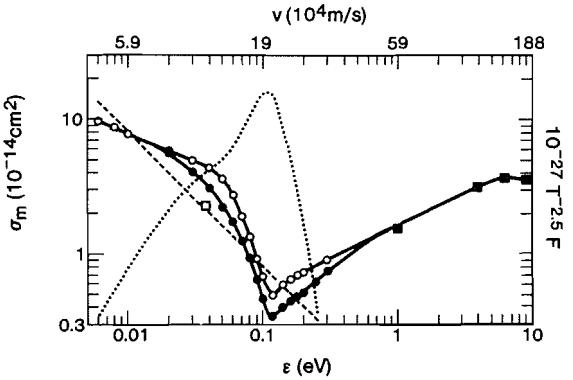


FIG. 11. Electron momentum transfer cross sections $\sigma_m$ of low density gaseous dimethyl ether. ○, from eq. [1]; ●, from eq. [10]; □, ref. 29; ■, ref. 38. The mean deviation between the present calculated and experimental mobilities was 1%; ----, Altshuler charge-point dipole cross sections (34); ···, $10^{-27} T^{-2.5}F$, where $F = (v^3/\sigma_m) \exp(-3.3 \times 10^{-12} v^2/T)$, at 359 K. $F$ is inversely proportional to the probability of a scattering event, weighted for the velocity distribution at a given $T$.

Can. J. Chem. Downloaded from www.nrcresearchpress.com by 210.87.254.40 on 09/06/12
For personal use only.

Can. J. Chem. Downloaded from www.nrcresearchpress.com by 210.87.254.40 on 09/06/12
For personal use only.

*(b) Field effect*

At $E/n > 3$ Td in the low density gas at 252 K the electrons gain more energy from the field than they lose by collisions with the dimethyl ether molecules. The electrons become heated and $n\mu_e$ increases (Figs. 1 and 2). For two other molecules of similar size, propane and propene, the threshold fields at 250 K are 0.09 and 0.3 Td, respectively (39). The threshold drift velocities $v_d^{thr}$ in propane, propene, and dimethyl ether are 1.4, 1.5, and 1.6 km/s, respectively. The ratio of $v_d^{thr}$ to the speed of low frequency sound $c_0$ in the gas is an indicator of the contribution of inelastic processes to the electron scattering: $v_d^{thr}/c_0 \lesssim 1$ when elastic scattering dominates (2–5, 40). The value of $c_0$ is given by (41):

$$[3] \quad c_0 = (\gamma kT/M)^{1/2}$$

where $\gamma$ is the heat capacity ratio,[2] $k$ is Boltzmann's constant, and $M$ is the molecular mass. At 250 K this gives $c_0 = 232$, 236, and 225 m/s in propane, propene, and dimethyl ether; the respective values of $v_d^{thr}/c_0$ are 6.0, 6.4, and 7.1. Thus inelastic collisions dominate the electron energy loss processes near thermal energies in these three gases.

It should be mentioned that the mobility is limited by the momentum transfer collisions even when inelastic collisions govern the electron energy.

*2. Dense gas and liquid*

In many nonpolar and slightly polar gases the values of $n\mu_e$ decrease at high densities to reach a minimum at a density roughly half that of the critical fluid (1–10). The ratio of the value of $n\mu_e$ at low densities to the minimum value in the dense gas is typically 2–3. Anion formation in nitrogen (16) and carbon dioxide (17) increases the ratio to $\gtrsim 100$. The ratio in ammonia is 40 at $T/T_c = 0.99$ and $n/n_c = 0.3$ (19). By analogy with the optical absorption of localized electrons that was observed in dense vapors of ammonia (43) and water (44), the low mobility in dense ammonia vapor was attributed to electron localization in van der Waals clusters of molecules. In dimethyl ether the ratio is 9 (Fig. 3). The behavior is intermediate between those in nonpolar gases and that in ammonia. The greater degree of electron localization in dense ammonia vapor may be attributed to a tendency of the electron to be attracted to the H—N protons.

As the density is increased through and past $n_c$ the value of $n\mu_e$ increases, goes through a maximum at $n/n_c = 1.4$, then decreases (Fig. 3). In the liquid, electron transport is a stronger function of temperature than of density. The liquid phase electron mobilities (Fig. 6) can be analyzed using the two-state model of electron transport widely applied to dielectric liquids (6, 26, 45). The relevant equations have been discussed (26, 45) and are simply listed here. The electron mobility $\mu_e$ is given by

$$[4] \quad \mu_e = (1 - \chi)\mu^0_{il} \exp(-E_{il}/kT) + \chi\mu^0_h$$

where $\chi$ is the fraction of electrons in the high mobility state with mobility $\mu^0_h$. $\mu^0_{il}$ and $E_{il}$ are respectively the pre-exponential factor and activation energy of mobility in the localized (ion-like) state.

$$[5] \quad \chi = \int_{-\infty}^{\infty} N(E)[1 + \exp(E/kT)]^{-1}\, dE$$

$$[6] \quad N(E) = \pi^{1/2}\sigma^{-1} \exp[-(E - E_0)^2/\sigma^2]$$

$$[7] \quad E_0 = E(O) - aT$$

$$[8] \quad \sigma = \sigma(O) + bT$$

$$[9] \quad \mu^0_h = \mu^0_{ref} (d_{ref}/d_T)^2 (T_{ref}/T)$$

where $N(E)dE$ is the fraction of localized states that lie at energies between $E$ and $E + dE$ from the high mobility state, $E_0$ is the center of the transition energy distribution, $\sigma$ is the dispersion parameter, and $d_{ref}$ is the liquid density at $T_{ref}$. Equations [7]–[9] are adequate at $E \gg kT$. The mobilities of electrons in the two states must be different and the electrons must spend an appreciable time in each of the two states. The parameters $\mu^0_{il}$ and $E_{il}$ can be estimated from the liquid-phase ion mobility (26). The dashed line through the liquid-phase electron mobility results in Fig. 6 was calculated using $\mu^0_{il} = 0.01$ cm$^2$/V s, $E_{il} = 0.04$ eV, $E_0 = 0.60 - 0.00085T$, $\sigma = 0.168$ eV, and $\mu^0_{ref} = 2.6$ cm$^2$/V s at $T_{ref} = 296$ K. Agreement is good except near the critical point.

*Ions*

*1. Low density gas*

When the most important interaction between the ion and the gas molecule is the polarization force, $n\mu_+$ is solely a function of the average polarizability $\bar{\alpha}$ and the reduced mass of the ion–molecule pair (46). The temperature independent polarization limit can be obtained from the diffusion expression derived by Maxwell in 1866 (47). For the small $C_1$ to $C_4$ hydrocarbons, the low density coexistence vapor values of $n\mu_+$ are approximately temperature independent (48). The values are a function of $(\bar{\alpha}M_r)^{1/2}$ (Fig. 12), although they are about half those predicted by the theory.

[2] $\gamma$ from heat capacities in ref. 24, p. D-162.

Can. J. Chem. Downloaded from www.nrcresearchpress.com by 210.87.254.40 on 09/06/12
For personal use only.

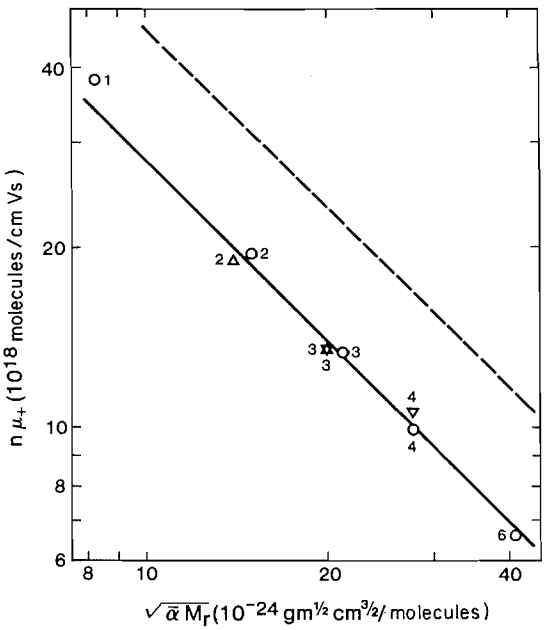


FIG. 12. Density-normalized ion mobility plotted against the square root of the product of average polarizability and reduced mass. The symbols represent: ○, *n*-alkanes; △, alkenes; and ▽, cyclopropane and isobutane. The numbers beside the symbols indicate the number of carbon atoms in the molecule. The dashed line indicates the $n\mu_+$ values expected at the polarization limit (ref. 46). The average polarizabilities are from ref. 20, section 14207, $M_r$ is taken to be the molecular mass and $n\mu_+$ values are from refs. 31 and 48.

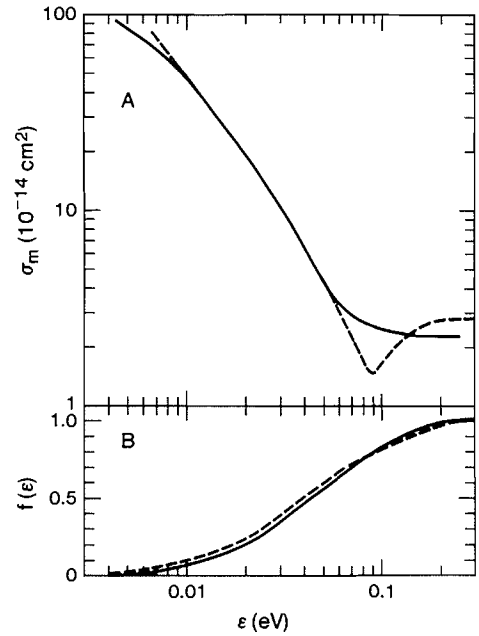


FIG. 13. *A*: Cation-momentum transfer cross-sections $\sigma_m$ of low density gaseous dimethyl ether. ———, chosen through attempting to have no minimum in the curve; ---, obtained when the foregoing restriction was removed. The two curves give equivalent matchings of the experimental ($n\mu_+$, *T*) data. *B*; $f(\varepsilon)$ at 353 K. $f(\varepsilon)$ is the fraction of the integral in eq. [10] that has been contributed by ions of kinetic energies up to ε. The full and dashed curves correspond to those in *A*.

The dimethyl ether value of $n\mu_+ = 9 \times 10^{18}$ at $(\bar{\alpha}M_r)^{1/2} = 19.9 \times 10^{-24}$ is below the $C_3$ hydrocarbon points. This is due to the much larger dipole moment in dimethyl ether, 1.3 D, compared to the next largest value of 0.3 D for propene.

In analogous fashion to the electrons, the temperature dependence of $n\mu_+$ at constant *n* can be used to extract the energy dependence of the ion–molecule momentum transfer cross-section. The mobility equation of ref. 49 was used:

$$[10] \quad n\mu_+ = \frac{\dfrac{3e}{8M_r}\sqrt{\pi}\left(\dfrac{2kT}{M_r}\right)^{5/2}}{\displaystyle\int_0^\infty v^5\sigma_m \exp(-M_r v^2/2kT)\,dv}$$

where $M_r$ is the ion–molecule reduced mass and $\sigma_m$ is the ion–molecule momentum transfer cross-section. The experimental set of ($n\mu_+$,*T*) was matched to a set of ($\sigma_m$, ε) values through iterative calculations. A $\sigma_m$ curve obtained in this manner is not unique, and two curves that give equivalent fits to the mobilities are shown in Fig. 13*A*. The full curve was obtained by attempting to have no minimum in $\sigma_m$ in the manner used for monomeric $CO_3^-$ ions in $N_2$ gas (48). The dashed curve was obtained when the foregoing restriction was removed, and it has a minimum in $\sigma_m$ at 0.09 eV. Curves intermediate between these would also be possible. Another source of information would be needed to choose between them.

The function $f(\varepsilon)$ in Fig. 13*B* shows the fraction of the integral in eq. [10] that has been contributed by the ions in the swarm with energies up to ε. Ions at energies between those corresponding to $f(\varepsilon) \approx 0.1$ and 0.9 make the major contribution to transport of the swarm. At 353 K this energy range is ~0.012–0.12 eV; $f(\varepsilon) = 0.5$ at 0.042 eV, which is $1.4kT$.

The value of $n\mu_+$ in dimethyl ether at 298 K is approximately half those in propane, propene-(48), and ammonia (28) (Table 2). The average ion scattering cross section of ammonia is only 20% smaller than that of dimethyl ether (Table 2); most of the mobility difference is due to the smaller mass of the former.

The average electron scattering cross-section of dimethyl ether is 25 times greater than that of propane, whereas the average cation cross-sections differ by a factor of only 1.8 (Table 2).

Can. J. Chem. Downloaded from www.nrcresearchpress.com by 210.87.254.40 on 09/06/12
For personal use only.

It has been suggested that for polar gases eq. [10] should also be used for electrons (35, 42). Use of eq. [10] leads to lower cross-sections (solid circles in Fig. 11) than does eq. [1]. At $\varepsilon \leq 0.01$ eV the same cross-sections could be used in either equation. The average cross-section at 295 K is $2.13 \times 10^{-14}$ cm$^2$ from eq. [1] and $1.90 \times 10^{-14}$ cm$^2$ from eq. [10], in agreement with the earlier observation that eq. [10] gives average cross-sections ~13% lower than eq. [1] (35).

References 35 and 42 also offer useful discussions of molecular structure effects in charge scattering.

*2. Dense gas and liquid*

At $n \lesssim 1 \times 10^{21}$ molecules/cm$^3$ the value of $n\mu_+$ is nearly independent of $n$ in the coexistence vapor (Fig. 3); the slight increase with increasing $n$ is due to the concomitant increase of temperature. At $n \gtrsim 1 \times 10^{21}$ molecules/cm$^3$ the value of $n\mu_+$ increases more rapidly with $n$ (Fig. 3). The increase may be attributed to the mutual interference of the long range, attractive potentials when the ion interacts with more than one molecule at a time.

The value of $n\mu_+$ passes through a maximum at $n \approx 6 \times 10^{21}$ molecules/cm$^3$ and decreases at higher densities (Fig. 3). The steep decrease occurs at $n > 2.4n_c$ for cations, whereas for electrons it occurs at $n > 1.7n_c$ (Fig. 3). The decrease of $n\mu_e$ is due to the increasing stability of the localized state of the electron, whereas $n\mu_+$ decreases due to molecular crowding when the average free distance between molecules is much smaller than the molecular diameter. The van der Waals diameter of dimethyl ether is $3.9 \times 10^{-8}$ cm (ref. 24, calculated from $b/4$), whereas the Wigner–Seitz diameter at $>2.4n_c$ is $<6.2 \times 10^{-8}$ cm (estimated by assuming that the average volume available per molecule is spherical); the mean free distance between molecules at these densities is $< 0.6d_{vdw}$.

Viscosities $\eta$ have not been reported for dimethyl ether, but by analogy with the behavior in hydrocarbons (48) one may assume that in the liquid phase at $\eta/\eta_c > 2$, the ion mobility is approximately proportional to $\eta^{-1}$. In the low density region where $n\mu_+$ is constant, the mobility is limited by ion collisions with single molecules. In the high density region where $\eta\mu_+$ is nearly constant the mobility is limited by multibody interactions and liquid dynamics. The transition region corresponds to $0.3 \lesssim n/n_c \lesssim 2.0$ and $0.5 \lesssim \eta/\eta_c \lesssim 3$, where the critical fluid is denoted by the subscript c (48).

The temperature coefficient of $\mu_+$ in the dense vapor over a small temperature range near the coexistence curve is large (Table 1). The effect is attributed to clustering of molecules about the ion:

[11] $M^+ + M \rightleftharpoons M_2^+$

[12] $M_2^+ + M \rightleftharpoons M_3^+$

and so on

which are equivalent to

[13] $M^+ + mM \rightleftharpoons M_{m+1}^+$

The clusters are largest in number and size in the dense gas near the coexistence curve. Heating the gas at constant density removes it from the coexistence region and decreases the average size of the clusters, thereby increasing the mobility. A larger cluster has a larger reduced mass and a larger collision diameter, both of which decrease $\mu$. The Arrhenius temperature coefficient ~68 kJ/mol of ions in ether at $n_c$ near $T_c$ corresponds to the energy of evaporation of several molecules from each cluster.

The value of $n\mu_+$ in the coexistence vapor increases slightly in the dense vapor, instead of decreasing as one might expect from the clustering (Fig. 3). The evidence for clustering is the large temperature coefficients (Fig. 6 and Table 1). The effects of increased reduced mass and hard core radius are more than compensated by the mutual interference of the charge–dipole attractive potentials when the ion interacts with more than one gas molecule at a time.

*Effect of carbon dioxide on the value of $\mu_e$*

A trace of carbon dioxide has no effect on $n\mu_e$ in the low density gas. In the dense gas at temperatures near the coexistence curve carbon dioxide decreases the mobility. Heating the gas at constant density reduces the effect. This behavior is characteristic of transient capture of electrons by molecular clusters that contain a $CO_2$ molecule.

[11] $e^- + (CO_2)M_n \rightleftharpoons (CO_2^-)M_n$

where $M_n$ is a van der Waals cluster of $n$ molecules of M. The large temperature coefficient $E_{\mu_e} = 120$ kJ/mol near the coexistence curve, for $n = 8.5 \times 10^{20}$ with 0.04% $CO_2$, implies that the capturing clusters are quite large. The value of $n$ in $M_n$ is probably $> 10$. The behavior is similar to, but more marked than, quasilocalization in the denser pure ether vapour.

*Summary*

The scattering of electrons in low density polar gases is dominated by the magnitude of the dipole moment. A large dipole moment also enhances quasilocalization of the electrons in the dense gas and localization in the dense liquid. By contrast, the cation mobility in fluid dimethyl ether is only about 40% lower than that in propane at the same density $n$. The dipole moment has a much smaller effect upon ion transport in these fluids.

## Acknowledgements

We would like to thank the Natural Sciences and Engineering Research Council of Canada for financial assistance, and the personnel of the Radiation Research Center for aid with the electronics.

1. G. R. Freeman and S. S.-S. Huang. Phys. Rev. A**20**, 2619 (1979).
2. S. S.-S. Huang and G. R. Freeman. J. Chem. Phys. **68**, 1355 (1978).
3. N. Gee and G. R. Freeman. Phys. Rev. A**20**, 1152 (1979).
4. N. Gee and G. R. Freeman. Phys. Rev. A**22**, 301 (1980).
5. N. Gee and G. R. Freeman. Phys. Rev. A**23**, 1390 (1981).
6. N. Gee and G. R. Freeman. Rad. Phys. Chem. **15**, 267 (1980).
7. T. Wada and G. R. Freeman. Can. J. Chem. **57**, 2716 (1979).
8. I. György and G. R. Freeman. J. Chem. Phys. **70**, 4769 (1979).
9. S. S.-S. Huang and G. R. Freeman. Can. J. Chem. **56**, 2388 (1978).
10. S. S.-S. Huang and G. R. Freeman. J. Chem. Phys. **72**, 2849 (1980).
11. J. L. Levine and T. M. Sanders, Jr. Phys. Rev. **154**, 138 (1967).
12. H. R. Harrison, L. M. Sander, and B. E. Springett. J. Phys. B**6**, 908 (1973).
13. A. Bartels. (*a*) Phys. Lett. **45**A, 491 (1973); (*b*) Appl. Phys. **8**, 59 (1975).
14. J. A. Jahnke, M. Silver, and J. P. Hernandez. Phys. Rev. B**12**, 3420 (1975).
15. K. W. Schwarz and B. Prasad. Phys. Rev. Lett. **36**, 878 (1976).
16. T. Wada and G. R. Freeman. J. Chem. Phys. **72**, 6726 (1980).
17. H. Lehning. Phys. Lett. **28**A, 103 (1968).
18. P. Krebs and M. Wantschik. J. Phys. Chem. **84**, 1155 (1980).
19. P. Krebs, V. Giraud, and M. Wantschik. Phys. Rev. Lett. **44**, 211 (1980).
20. H. Stuart. Landolt-Börnstein Zahlenwerte und Funktion. I. band 3 teil. *Edited by* A. Eucken and K. H. Hellwege. Springer-Verlag, Berlin. 1951. Section 14206.
21. S. S.-S. Huang and G. R. Freeman. J. Chem. Phys. **70**, 1538 (1979).
22. J.-P. Dodelet and G. R. Freeman. Can. J. Chem. **50**, 2667 (1972).
23. E. Cardoso and A. A. Coppola. J. Chim. Phys. **20**, 337 (1923).
24. R. C. Weast (*Editor*). Handbook of Chemistry and Physics. 57th ed. CRC Press, Cleveland, OH. 1976. p. D-178.
25. J. Marsden and O. Maass. Can. J. Res. B**13**, 296 (1934).
26. J. P. Dodelet and G. R. Freeman. Can. J. Chem. **53**, 1263 (1975).
27. C. P. Smyth. Dielectric behavior and structure. McGraw-Hill, New York. 1955.
28. E. S. Sennhauser and D. A. Armstrong. Can. J. Chem. **56**, 2337 (1978).
29. T. L. Cottrell, W. J. Pollock, and I. C. Walker. Trans. Faraday Soc. **64**, 2260 (1968).
30. L. G. Christophorou and A. A. Christodoulides. J. Phys. B**2**, 71 (1969).
31. S. S.-S. Huang and G. R. Freeman. J. Chem. Phys. **72**, 1989 (1980).
32. N. Gee and G. R. Freeman. Can. J. Chem. **58**, 1490 (1980).
33. W. Braker and A. L. Mossman. Matheson data book, Matheson gas products. New Jersey. 1971. p. 221.
34. S. Altshuler. Phys. Rev. **107**, 114 (1957).
35. O. H. Crawford, M. Dalgarno, and P. B. Hays. Mol. Phys. **13**, 181 (1967).
36. L. S. Frost and A. V. Phelps. Phys. Rev. **136**, A1538 (1964).
37. G. R. Freeman, I. György, and S. S.-S. Huang. Can. J. Chem. **57**, 2626 (1979).
38. F. Schmieder. Z. Elektrochem. **36**, 700 (1930).
39. N. Gee and G. R. Freeman. To be published.
40. B. V. Paranjape. Phys. Rev. A**21**, 205 (1980).
41. E. Hausmann and E. P. Slack. Physics. Van Nostrand, New York. 1944. p. 412.
42. W. R. Garrett. Mol. Phys. **24**, 465 (1972).
43. R. Olinger, U. Schindewolf, A. Gaathon, and J. Jortner. Ber. Bunsen. Phys. Chem. **75**, 690 (1971).
44. A. Gaathon, G. Czapski, and J. Jortner. J. Chem. Phys. **58**, 2648 (1973).
45. J.-P. Dodelet, K. Shinsaka, and G. R. Freeman. Can. J. Chem. **54**, 744 (1976).
46. E. W. McDaniel and E. A. Mason. The mobility and diffusion of ions in gases. J. Wiley and Sons, New York. 1973. p. 146.
47. J. C. Maxwell. Philos. Trans. CLVII, May 1866. *In* Collected papers of J. C. Maxwell. Vol. II. *Edited by* W. D. Niven, Cambridge. 1890. p. 59.
48. N. Gee and G. R. Freeman. Can. J. Chem. **59**, 2988 (1981).
49. F. W. Morrison, G. R. Akridge, H. W. Ellis, R. Y. Pai, E. W. McDaniel, L. A. Viehland, and E. A. Mason. J. Chem. Phys. **63**, 2238 (1975).

Can. J. Chem. Downloaded from www.nrcresearchpress.com by 210.87.254.40 on 09/06/12
For personal use only.

# Arene carbonyl rhodium(I) complexes

MAURICIO VALDERRAMA

*Department of Inorganic Chemistry, Institute of Chemical Sciences, Catholic University of Chile, Santiago, Chile*

AND

LUIS A. ORO[1]

*Department of Inorganic Chemistry, University of Zaragoza, Zaragoza, Spain*

Received August 26, 1981

MAURICIO VALDERRAMA and LUIS A. ORO. Can. J. Chem. **60**, 1044 (1982).

The arene carbonyl rhodium complexes, $[Rh(C_6Me_6)(CO)_2]PF_6$ and $[Rh(C_6Me_6)(CO)PPh_3]PF_6$, have been prepared by treating the dimeric complexes, $[RhCl(CO)_2]_2$ and $[RhCl(CO)PPh_3]_2$, with $AgPF_6$ in the presence of hexamethylbenzene. The reaction of $[Rh(C_6Me_6)(CO)_2]PF_6$ with tetrafluorobenzobarrelene affords $[Rh(C_6Me_6)(TFB)]PF_6$. On the other hand, the reaction of [Rh(arene)$(CO)_2]PF_6$ with a stoichiometric amount of triphenylphosphine gives [Rh(arene)$(CO)PPh_3]PF_6$ (arene = $C_6Me_6$ or $C_6H_3Me_3$), whereas with excess of this ligand $[Rh(CO)(PPh_3)_3]PF_6$ is formed. The related $[Rh(C_6Me_6)(CO)P(p\text{-}MeC_6H_4)_3]PF_6$ derivative has also been prepared.

The reactivity of both hexamethylbenzene carbonyl rhodium complexes has been examined. The addition of bipyridine to solutions of $[Rh(C_6Me_6)(CO)L]PF_6$ (L = CO or $PPh_3$) causes the immediate displacement of the coordinated hexamethylbenzene. Their reactions with the nucleophiles, acetylacetonate, tropolonate, or pyrazolate in the presence of triethylamine afford neutral derivatives of the type $[RhA(CO)L]_x$ (L = CO or $PPh_3$; A = acac or trop, $x = 1$; A = pz, $x = 2$).

MAURICIO VALDERRAMA et LUIS A. ORO. Can. J. Chem. **60**, 1044 (1982).

On a préparé les complexes $[Rh(C_6Me_6)(CO)_2]PF_6$ et $[Rh(C_6Me_6)(CO)PPh_3]PF_6$ en faisant réagir les complexes $[RhCl(CO)_2]_2$ et $[RhCl(CO)PPh_3]_2$ avec $AgPF_6$ en présence d'hexaméthylbenzène. La réaction du $[Rh(C_6Me_6)(CO)_2]PF_6$ avec le tétrafluorobenzobarrèlène fournit le $[Rh(C_6Me_6)(TFB)]PF_6$. Par ailleurs, la réaction du [Rh(arène)$(CO)_2]PF_6$ avec une quantité stoichiométrique de triphénylphosphine donne le [Rh(arène)$(CO)PPh_3]PF_6$ (arène = $C_6Me_6$ ou $C_6H_3Me_3$), alors qu'avec un excès de ce ligand, il y a formation de $[Rh(CO)(PPh_3)_3]PF_6$. On a aussi préparé le dérivé $[Rh(C_6Me_6)(CO)P(p\text{-}MeC_6H_4)_3]PF_6$ apparenté.

On a étudié la réactivité des deux complexes hexaméthylbenzène rhodium carbonyle. L'addition de bipyridine à des solutions de $[Rh(C_6Me_6)(CO)LPF_6]$ (L = CO ou $PPh_3$) provoque le déplacement immédiat de l'hexaméthylbenzène coordonné. Leurs réactions avec des nucléophiles comme l'acétylacétonate, le tropolonate ou le pyrazolate, en présence de triéthylamine, conduit à des dérivés neutres du type $[RhA(CO)L]_x$ (L = CO ou $PPh_3$; A = acac ou trop, $x = 1$; A = pz, $x = 2$).

[Traduit par le journal]

## Introduction

In recent years several types of arene rhodium(I) derivatives have been described. In particular cationic complexes of the types [Rh(arene)(diolefin)]A (1–5), [Rh(arene)$(C_2H_4)_2$]A (1, 2), [Rh(arene) (diphos)]A (6), and [Rh(arene)$\{P(OPh)_3\}_2$]A (1, 7) have been reported.

Furthermore, the tetraphenylborate group or diphosphine ligands can be coordinated to the metal by $\pi$-interaction of an arene ring with formation of complexes of the type $RhL_2PhBPh_3$ ($L_2$ = diolefin (8, 9), phen (10), diphos (11); L = $C_2H_4$ (8), $PR_3$ (8, 12, 13), $P(OR)_3$ (7, 14, 15)), or $[Rh(diphos)]_2A_2$ (16, 17). The crystal structures of some of these complexes show the rhodium atom $\pi$-bonded to the arene ring but in no case is the arene planar (4, 7, 11, 15).

As far as we know, no arene carbonyl rhodium complexes have hitherto been described in the literature. We now report the synthesis and properties of $[Rh(C_6Me_6)(CO)_2]PF_6$, **1**, $[Rh(C_6Me_6)(CO)PPh_3]PF_6$, **2**, and other related complexes.

[1]To whom all correspondence should be addressed.

## Experimental

The C and H analyses were made with a Perkin-Elmer 240 microanalyzer. Infrared spectra were recorded on a Perkin-Elmer 567 spectrophotometer (over the range 4000–200 $cm^{-1}$) using Nujol mulls between KBr discs or in dichloromethane solution between NaCl plates. Conductivities were measured in ca. $5 \times 10^{-4}$ *M* acetone solutions with a Philips 9501/01 conductimeter and the decomposition temperature with a Buchi apparatus. $^1$Hmr spectra were recorded on a Varian XL-100 instrument relative to tetramethylsilane.

All reactions were carried out under a dry argon atmosphere and solvents were dried and distilled prior to use. The starting dimer $[RhCl(CO)_2]_2$ was purchased from Strem Chemical Co. Tetrafluorobenzobarrelene (TFB) was prepared according to literature procedure (18).

*Preparation of complexes*

*$[Rh(C_6Me_6)(CO)_2]PF_6$*

A slurry of 200 mg (0.52 mmol) of $[RhCl(CO)_2]_2$, 169 mg (1.04 mmol) of hexamethylbenzene, and 263 mg (1.04 mmol) of $AgPF_6$ in acetone was stirred for 1 h at room temperature. The AgCl was removed by filtration through kieselguhr and the pale-yellow solution obtained was evaporated to dryness. The solid thus obtained was crystallized from dichloromethane–diethyl-ether (311 mg; 65% yield). *Anal.* calcd. for $C_{14}H_{18}F_6O_2PRh$: C 36.07, H 3.89; found: C 35.81, H 3.91; mp 130°C. $\Lambda_M(Me_2CO)$: 127 $ohm^{-1}$ $cm^2$ $mol^{-1}$. The $^1$Hmr in $(CD_3)_2CO$ shows the presence of the coordinated arene (δ: 2.62, Me) along with free $C_6Me_6$.

0008-4042/82/081044-04$01.00/0

©1982 National Research Council of Canada/Conseil national de recherches du Canada

Can. J. Chem. Downloaded from www.nrcresearchpress.com by 210.87.254.42 on 09/06/12
For personal use only.

Can. J. Chem. Downloaded from www.nrcresearchpress.com by 210.87.254.42 on 09/06/12
For personal use only.

*[Rh(C$_6$Me$_6$)(CO)PPh$_3$]PF$_6$*

The complex was prepared by two methods:

(*i*) The addition of a stoichiometric amount of triphenylphosphine (19.8 mg; 0.07 mmol) to a solution of [Rh(C$_6$Me$_6$)(CO)$_2$]PF$_6$ (35.2 mg; 0.07 mmol) in dichloromethane produced the immediate evolution of carbon monoxide. The solution obtained was stirred at room temperature for 1 h, evaporated to a small volume, and crystallized by addition of diethylether (16 mg; 30% yield).

(*ii*) [RhCl(CO)PPh$_3$]$_2$ (19) (85.7 mg; 0.1 mmol) was treated with AgPF$_6$ (50.6 mg; 0.2 mmol) and hexamethylbenzene (32.5 mg; 0.2 mmol) in acetone. The mixture was stirred for 1 h at room temperature and evaporated to dryness. The addition of 25 mL of dichloromethane and the filtration through kieselguhr gave a yellow solution which was evaporated to a small volume and crystallized by adding diethylether (62.1 mg; 44% yield).

In both cases, a yellow–orange microcrystalline solid was obtained. *Anal.* calcd. for C$_{31}$H$_{33}$F$_6$OP$_2$Rh: C 53.16, H 4.74; found: C 53.08, H 4.38; mp 190–192°C. $\Lambda_M$(Me$_2$CO): 129 ohm$^{-1}$ cm$^2$ mol$^{-1}$. The $^1$Hmr in (CD$_3$)$_2$CO show the presence of the coordinated arene (δ: 2.46, Me) along with free C$_6$Me$_6$.

*[Rh(C$_6$H$_3$Me$_3$)(CO)PPh$_3$]PF$_6$*

[RhCl(CO)]$_2$ (77.8 mg; 0.2 mmol) was treated with 101.1 mg (0.4 mmol) of AgPF$_6$ and 0.06 mL (slight excess) of 1,3,5-trimethylbenzene in acetone. The mixture was stirred for 1 h at room temperature and evaporated to dryness. The residue obtained was extracted with 30 mL of dichloromethane and filtered off through kieselguhr. To the yellow filtrate was added the stoichiometric amount of triphenylphosphine and the solution was stirred for 30 min. Partial evaporation and addition of diethylether gave a yellow-brownish microcrystalline solid (142.5 mg; 54% yield). *Anal.* calcd. for C$_{28}$H$_{27}$F$_6$OP$_2$Rh: C 51.08, H 4.13; found: C 51.75, H 3.65; mp 138–140°C.

*[Rh(C$_6$Me$_6$)(CO)P(p-MeC$_6$H$_4$)$_3$]PF$_6$*

The addition of a stoichiometric amount of P(*p*-MeC$_6$H$_4$)$_3$ (30.4 mg; 0.1 mmol) to a solution of [Rh(C$_6$Me$_6$)(CO)$_2$]PF$_6$ (46.6 mg; 0.1 mmol) in dichloromethane involved the evolution of carbon monoxide. The solution obtained was stirred under reflux for 1 h, evaporated to a small volume, and crystallized by addition of diethylether (67.6 mg; 91% yield). *Anal.* calcd. for C$_{34}$H$_{39}$F$_6$OP$_2$Rh: C 55.00, H 5.29; found: C 54.12, H 5.19; mp 178–180°C. $\Lambda_M$(Me$_2$CO): 129 ohm$^{-1}$ cm$^2$ mol$^{-1}$. The $^1$Hmr in (CD$_3$)$_2$CO shows the presence of [Rh(C$_6$Me$_6$)(CO)P(*p*-MeC$_6$H$_4$)$_3$]$^+$ (δ: 2.42, Me (arene) and 2.24, Me (phosphine)) and [Rh(CO)P(*p*-MeC$_6$H$_4$)$_3${(CD$_3$)$_2$CO}$_x$]$^+$ (δ: 2.38, Me (phosphine)).

*[Rh(C$_6$Me$_6$)(TFB)]PF$_6$*

[Rh(C$_6$Me$_6$)(CO)$_2$]PF$_6$ (46.6 mg; 0.1 mmol) was treated with an excess of TFB (45.2 mg; 0.2 mmol) in dichloromethane under reflux for 2 h. A small quantity of orange solid was separated by filtration and the yellow solution obtained was evaporated to ca. 3–4 mL. A pale-yellow solid was crystallized by adding diethylether (54.2 mg; 85% yield). *Anal.* calcd. for C$_{24}$H$_{24}$F$_{10}$PRh: C 45.30, H 3.80; found: C 45.58, H 3.77; mp 235°C. $\Lambda_M$(Me$_2$CO): 135 ohm$^{-1}$ cm$^2$ mol$^{-1}$. $^1$Hmr ((CD$_3$)$_2$CO) δ: 5.2–5.3 (CH); 3.7–3.9 (CH=CH), and 2.52 (Me).

The orange solid obtained in small yield (1%) was identified as [Rh(TFB)$_2$]PF$_6$ (20).

## Results and discussion

### *Preparation and properties of [Rh(C$_6$Me$_6$)(CO)$_2$]PF$_6$*

The dimeric complex [RhCl(CO)$_2$]$_2$ reacts in acetone with AgPF$_6$ and hexamethylbenzene:

[1] (1/2)[RhCl(CO)$_2$]$_2$ + AgPF$_6$ + C$_6$Me$_6$ → [Rh(C$_6$Me$_6$)(CO)$_2$]PF$_6$ + AgCl

**1**

The isolated complex **1** show a yellow or light olive–green colour depending on the precipitation conditions. The CH$_2$Cl$_2$ solution ir shows two ν(CO) strong bands at 2095 and 2045 cm$^{-1}$, characteristic of a *cis*-dicarbonyl structure (21, 22). In fact, the crystal structure of the related complex [Rh(C$_6$H$_5$Me){P(OPh)$_3$}$_2$]ClO$_4$ (7) shows a P(1)—Rh—P(2) angle of 90.07°. Solid-state infrared measurements on **1** show absorptions in the carbonyl region at 2100 s, 2080 w,sh, 2050 s, 2020 w,sh, and 2010 w cm$^{-1}$, along with the characteristic bands of uncoordinated PF$_6^-$ (840 vs, 560 s cm$^{-1}$) (23, 24).

The presence of the PF$_6^-$ anion seems to be important. Thus, although the formation of [Rh(C$_6$Me$_6$)(CO)$_2$]ClO$_4$ can be observed by a reaction similar to [1], when AgClO$_4$ was used instead of AgPF$_6$, the perchlorate complex was too unstable to be isolated in the solid state. The $^1$Hmr spectrum shows the presence of the following equilibrium

[2] [Rh(C$_6$Me$_6$)(CO)$_2$]PF$_6$ + *x*(CD$_3$)$_2$CO ⇄ [Rh(CO)$_2${(CD$_3$)$_2$CO}$_x$]PF$_6$ + C$_6$Me$_6$

displaced towards the right (58% for a saturated solution).

The reaction of **1** with tetrafluorobenzobarrelene (TFB) (18) in dichloromethane under reflux leads to the displacement of the carbon monoxide, with the formation of [Rh(C$_6$Me$_6$)(TFB)]PF$_6$, **3**. Although the bubbling of carbon monoxide (1 atm, room temperature) through solutions of [Rh(diolefin)L$_2$]A complexes usually lead to the formation of several types of cationic carbonyl derivatives (L = group Vb ligands) (13, 20–22, 25), no reaction was observed when complex **3** was treated with carbon monoxide. This behaviour is in contrast with the carbonylation reaction observed for [Rh(C$_6$H$_5$Me){P(OPh)$_3$}$_2$]ClO$_4$, where [Rh(CO)$_3${P(OPh)$_3$}$_2$]ClO$_4$ (7) was formed.

Addition of acetonitrile to dichloromethane solutions of **1** shows the existence of the equilibrium

[3] [Rh(C$_6$Me$_6$)(CO)$_2$]PF$_6$ + 2MeCN ⇄ [Rh(MeCN)$_2$(CO)$_2$]PF$_6$ + C$_6$Me$_6$

that can be detected by infrared spectroscopy. The equilibrium can be partially shifted towards the right by addition of an excess of acetonitrile. Even in pure acetonitrile, the solution infrared spectrum shows the presence of [Rh[(MeCN)$_2$(CO)$_2$]PF$_6$ (ν(CO): 2090 and 2020 cm$^{-1}$) as the major product, along with [Rh(C$_6$Me$_6$)(CO)$_2$]PF$_6$ (ν(CO): 2110 and

Can. J. Chem. Downloaded from www.nrcresearchpress.com by 210.87.254.42 on 09/06/12
For personal use only.

2055 $cm^{-1}$). Nevertheless, the addition of diethylether to the acetonitrile solution of **1**, causes the precipitation of $[Rh(MeCN)_2(CO)_2]PF_6$ (1) as a single product.

The reaction of complex **1** with 2,2′-bipyridine in dichloromethane leads to the immediate displacement of the arene group, with the formation of $[Rh(bipy)(CO)_2]PF_6$ (21).

The reaction of **1** with some nucleophiles was also examined. Thus, acetylacetone, tropolone, and pyrazole, in the presence of triethylamine react with **1** to give the previously reported neutral derivatives, Rh(acac)$(CO)_2$ (26), Rh(trop)$(CO)_2$ (27), and $[Rh(pz)(CO)_2]_2$ (28):

[4] $[Rh(C_6Me_6)(CO)_2]PF_6 + HA + NEt_3 \rightarrow [RhA(CO)_2]_x + HNEt_3PF_6$,

where A = acac or trop, $x = 1$; A = pz, $x = 2$.

No reaction was observed when excess of perchloric acid was added to Rh(trop)$(CO)_2$ in the presence of hexamethylbenzene. On the contrary, under the same conditions Rh(trop)(COD) (29) reacts according to reaction [5].

[5] $Rh(trop)(COD) + HClO_4 + C_6Me_6 \rightarrow [Rh(C_6Me_6)(COD)]ClO_4 + Htrop$

When reaction [1] was performed with other arenes with less methyl substituents, e.g. $C_6H_3Me_3$, the formation of the corresponding arene carbonyl complexes was observed spectroscopically (e.g. $[Rh(C_6H_3Me_3)(CO)_2]PF_6$,[2] ν(CO): 2100 and 2035 $cm^{-1}$ ($CH_2Cl_2$)), but the products were not isolated.

All attempts to prepare the complex $Rh(CO)_2PhBPh_3$, related to the well-known Rh(diolefin)$PhBPh_3$ derivatives (8), by reaction of $[RhCl(CO)_2]_2$ with $NaBPh_4$ in polar solvents were unsuccessful.

*Preparation and properties of [Rh(arene)(CO)(triarylphosphine)]$PF_6$*

The reaction of $[RhCl(CO)PPh_3]_2$ (19) with $AgPF_6$ and hexamethylbenzene in acetone leads to the formation of **2**.

[6] $(1/2)\ [RhCl(CO)PPh_3]_2 + AgPF_6 + C_6Me_6 \rightarrow [Rh(C_6Me_6)(CO)PPh_3]PF_6 + AgCl$

**2**

An alternative and competitive route is the reaction of $[Rh(arene)(CO)_2]PF_6$ (arene = $C_6Me_6$ or $C_6H_3Me_3$) with a stoichiometric amount of $PPh_3$, whereas with excess of the ligand, $[Rh(CO)(PPh_3)_3]PF_6$ is formed (reaction [7]).

[7] $[Rh(arene)(CO)_2]PF_6 \xrightarrow{+\ PPh_3} [Rh(arene)(CO)PPh_3]PF_6$

$\xrightarrow{+\ 2\ PPh_3} [Rh(CO)(PPh_3)_3]PF_6$

These complexes were isolated as a stable yellow–orange microcrystalline solid that behaves as 1:1 electrolyte in acetone. The $^1$Hmr of the complexes show a high dissociation of the coordinated $C_6Me_6$ (73% for a saturated solution) while the $C_6H_3Me_3$ derivative is completely dissociated in deuteroacetone. The ir show absorptions characteristic of uncoordinated $PF_6^-$ and coordinated CO (ν(CO): 2015 $cm^{-1}$, $C_6Me_6$; 2005 $cm^{-1}$, $C_6H_3Me_3$ ($CH_2Cl_2$)). On the other hand, the related complex $[Rh(C_6Me_6)(CO)P(p\text{-}MeC_6H_4)_3]PF_6$ (ν(CO): 2010 $cm^{-1}$ ($CH_2Cl_2$)) has also been prepared in dichloromethane according to reaction [7], but refluxing conditions were used.

Complex **2** reacts with 2,2′-bipyridine with the formation of $[Rh(bipy)(CO)PPh_3]PF_6$ (21). The latter complex shows a strong carbonyl absorption at 1985 $cm^{-1}$, whilst the $[Rh(CO)(PPh_3)_3]PF_6$ complex shows it at 2030 $cm^{-1}$.

As expected, complex **2** reacts with acetylacetone, tropolone, and pyrazole in the presence of triethylamine to give Rh(acac)$(CO)PPh_3$ (26), Rh(trop)$(CO)PPh_3$ (30), and $[Rh(pz)(CO)PPh_3]_2$ (31).

[2]In $(CD_3)_2CO$ the $^1$Hmr show that the arene is completely dissociated.

**Acknowledgements**

We thank "Pontificia Universidad Católica de Chile (DIUC)" and "Programa de Cooperación con Iberoamérica, Ministerio de Educación y Ciencia, España" for financial support.

1. R. R. Schrock and J. A. Osborn. J. Am. Chem. Soc. **93**, 3089 (1971).
2. M. Green and T. A. Kuc. J. Chem. Soc. Dalton Trans. 832 (1972).
3. P. T. Draggett, M. Green, and S. F. W. Lowrie. J. Organomet. Chem. **135**, C60 (1977).
4. M. R. Thompson, C. S. Day, V. W. Day, R. I. Mink, and E. L. Muetterties. J. Am. Chem. Soc. **102**, 2979 (1980).
5. R. Uson, L. A. Oro, C. Foces-Foces, F. H. Cano, A. Vegas, and M. Valderrama. J. Organomet. Chem. **215**, 241 (1981).
6. (*a*) J. Halpern, A. S. C. Chan, D. D. Riley, and J. J. Pluth. Adv. Chem. Ser. **173**, 16 (1979); (*b*) J. M. Townsend and J. F. Blount. Inorg. Chem. **20**, 269 (1981).
7. (*a*) R. Uson, P. Lahuerta, J. Reyes, and L. A. Oro. Transition Met. Chem. **4**, 332 (1979); (*b*) R. Uson, P. Lahuerta, J. Reyes, L. A. Oro, C. Foces-Foces, F. H. Cano, and S. Garcia-Blanco. Inorg. Chim. Acta, **42**, 75 (1980).
8. R. R. Schrock and J. A. Osborn. Inorg. Chem. **9**, 2339 (1970).
9. L. A. Oro, E. Pinilla, and M. L. Tenajas. J. Organomet. Chem. **148**, 81 (1978).
10. G. Mestroni, G. Zassinovich, and A. Camus. J. Organomet. Chem. **140**, 63 (1977).

11. P. ALBANO, M. ARESTA, and M. MANASSERO. Inorg. Chem. **19**, 1069 (1980).
12. P. R. BROOKES. J. Organomet. Chem. **43**, 415 (1972).
13. L. A. ORO, J. V. HERAS, K. A. OSTOJA-STARZEWSKI, P. S. PREGOSIN, A. MANRIQUE, and M. ROYO. Transition Met. Chem. **6**, 1 (1981).
14. M. J. NOLTE, G. GAFNER, and L. M. HAINES. J. Chem. Soc. Chem. Commun. 1406 (1969).
15. M. J. NOLTE and G. GAFNER. Acta Crystallogr. B**30**, 738 (1974).
16. J. HALPERN, D. P. RIELEY, A. S. C. CHAN, and J. J. PLUTH. J. Am. Chem. Soc. **99**, 8055 (1977).
17. A. MIYASHITA, A. YASUDA, H. TANAKA, K. TORIUMI, T. ITO, T. SOUCHI, and R. NOYORI. J. Am. Chem. Soc. **102**, 7932 (1980).
18. A. J. TOMLINSON and A. G. MASSEY. J. Organomet. Chem. **8**, 321 (1967).
19. D. F. STEELE and T. A. STEPHENSON. J. Chem. Soc. A, 2161 (1972).
20. R. USON, L. A. ORO, M. VALDERRAMA, and C. CLAVER. Synth. React. Inorg. Met. Org. Chem. **9**, 577 (1979).
21. C. COCEVAR, G. MESTRONI, and A. CAMUS. J. Organomet. Chem. **35**, 389 (1972).
22. R. USON, L. A. ORO, C. CLAVER, and M. A. GARRALDA. J. Organomet. Chem. **105**, 365 (1976).
23. O. A. SERRA, M. PERRIER, V. K. L. OSORIO, and Y. KAWANO. Inorg. Chim. Acta, **17**, 135 (1976).
24. B. R. JAMES, R. H. MORRIS, and K. J. REIMER. Can. J. Chem. **55**, 2353 (1977).
25. R. R. SCHROCK and J. A. OSBORN. J. Am. Chem. Soc. **93**, 2397 (1971).
26. F. BONATI and G. WILKINSON. J. Chem. Soc. 3156 (1964).
27. M. VALDERRAMA and L. A. ORO. J. Organomet. Chem. **218**, 241 (1981).
28. N. F. BORKETT and M. I. BRUCE. J. Organomet. Chem. **65**, C51 (1974).
29. M. VALDERRAMA, H. RAFART, and L. A. ORO. Transition Met. Chem. **6**, 221 (1981).
30. J. G. LEIPOLDT, L. D. C. BOK, S. S. BASSON, and H. MEYER. Inorg. Chim. Acta, **42**, 105 (1980).
31. R. USON, L. A. ORO, M. A. CIRIANO, M. T. PINILLOS, A. TIRIPICCHIO, and M. TIRIPICCHIO CAMELLINI. J. Organomet. Chem. **205**, 247 (1981).

Can. J. Chem. Downloaded from www.nrcresearchpress.com by 210.87.254.42 on 09/06/12
For personal use only.

# Magnetic and spectroscopic studies of structure and bonding in hexafluorophosphate and hexafluoroarsenate complexes of copper(II)

RAYMOND M. MORRISON[1] AND ROBERT C. THOMPSON

*Department of Chemistry, The University of British Columbia, Vancouver, B.C., Canada V6T 1Y6*

Received October 14, 1981

RAYMOND M. MORRISON and ROBERT C. THOMPSON. Can. J. Chem. **60**, 1048 (1982).

Complexes of composition $CuL_4(EF_6)_2$ (where L is pyridine, 3-methylpyridine, or 4-methylpyridine and E is P or As) have been prepared and characterized by epr, electronic and infrared spectroscopic, and magnetic susceptibility studies. Results are consistent with elongated tetragonal–octahedral structures with coordinated anions. The coordinating strength of $PF_6^-$ is estimated to be less than that of $AsF_6^-$ and both are considered weaker than perchlorate. Analysis of the epr data indicates significant metal to heterocyclic ligand $\pi$-electron delocalization, the extent and nature of which depends on the orientation of the heterocyclic ring in the $CuL_4$ chromophore. Analysis of infrared data suggests that the intensities of the $\nu_1$ and $\nu_2$ vibrations as they occur in $EF_6^-$ complexes generally provide an indication of the strength of metal–anion interactions.

RAYMOND M. MORRISON et ROBERT C. THOMPSON. Can. J. Chem. **60**, 1048 (1982).

On a préparé des complexes de formule $CuL_4(EF_6)_2$ (où L = pyridine, méthyl-3 pyridine ou méthyl-4 pyridine et E = P ou As) et on les a caractérisé par des études de rpe, de spectroscopie infrarouge et de susceptibilité magnétique. Les résultats sont en accord avec des structures tétragonales–octahédriques allongées avec des anions coordonés. On évalue la force de coordination de $PF_6^-$ comme étant inférieure à celle de $AsF_6^-$ et on considère ces deux forces plus faibles que celle du perchlorate. L'analyse des données de la rpe indique une délocalisation importante de l'électron $\pi$ du ligand hétérocyclique par rapport au métal. La nature et le taux de cette délocalisation dépendent de l'orientation de l'hétérocycle dans le chromophore $CuL_4$. L'analyse des données infrarouges suggère que les intensités des vibrations $\nu_1$ et $\nu_2$ telles qu'elles se produisent dans les complexes de $EF_6^-$ constituent généralement une indication de la force des interactions métal–anion.

[Traduit par le journal]

## Introduction

Through the synthesis and study of pyridine and methylpyridine complexes containing hexafluorophosphate and hexafluoroarsenate it has been possible to examine the coordinating tendencies of these very weakly basic anions (1–6). The $PF_6^-$ and $AsF_6^-$ ions have been shown to be non-coordinated in complexes of composition $M(4mpy)_8(H_2O)_2(EF_6)_2$ (where 4mpy is 4-methylpyridine and M is Co or Ni) (4) and $M(py)_6(EF_6)_2$ (where py is pyridine and M is Co or Ni) (2, 3) and in the complexes $Co(py)_4(EF_6)_2$ and $Co(4mpy)_4(EF_6)_2$ (3, 5). Complexes in which these anions are definitely coordinated to metal ions are less common. On the basis of a single crystal X-ray structure study of $Ni(4mpy)_4(PF_6)_2$ and some vibrational spectral studies it was concluded that the diamagnetic $Ni(py)_4(EF_6)_2$ and $Ni(4mpy)_4(EF_6)_2$ complexes have structures involving essentially square planar $NiL_4$ units with anions which, although not fully coordinated, are nonetheless held in axial positions by weak metal–anion interactions(6). The strongest evidence for conventional anion coordination has been found for a low temperature form of $Ni(py)_4(AsF_6)_2$ (6).

The copper(II) complex, $Cu(py)_4(PF_6)_2$, was the first compound of this general type to have been prepared and studied in any great detail (1). Good evidence for conventional anion coordination, or at least "semi-coordination", was obtained from a combination of electronic, epr, and infrared spectral studies. As an extension of this earlier work and to obtain a more thorough comparison of the coordinating properties of $PF_6^-$ and $AsF_6^-$ with those of more basic anions we report here the synthesis and study of a series of copper(II) complexes of the type $CuL_4(EF_6)$ (where L is py, 4mpy, or 3mpy). Structure and metal–ligand bonding in these compounds have been examined primarily through electronic and epr spectroscopy. In addition, to complement our earlier studies in which we established infrared criteria for non-coordinated anions in $EF_6^-$ complexes (4), we have examined the infrared spectra for the effects of increased metal–anion interactions on the fundamental vibrations of the $EF_6^-$ moieties.

## Experimental

*Preparations*

Tetrakis(pyridine)copper(II) hexafluorophosphate and hexafluoroarsenate were prepared using procedures similar to that described previously for the preparation of $Cu(py)_4(PF_6)_2$ (2). Copper(II) nitrate trihydrate (4.8 g) was dissolved in 50 mL water and 16 mL pyridine. A filtered aqueous solution of $NH_4PF_6$ (6.5 g in 150 mL water) or $KAsF_6$ (9.2 g in 250 mL water) was added. A blue-mauve powder precipitated immediately.

[1]Present address: C.A.N.M.E.T., 555 Booth Street, Ottawa, Ont., Canada K1A 0G1.

0008-4042/82/081048-07$01.00/0

©1982 National Research Council of Canada/Conseil national de recherches du Canada

TABLE 1. Electronic spectra and magnetic moments

| Complex | Energies of band maxima ($10^3$ cm$^{-1}$) Diffuse reflectance | Nujol mull | $CH_2Cl_2$ solution[a] | Magnetic moment (BM)[b] 100 K | 200 K | 300 K |
|---|---|---|---|---|---|---|
| $Cu(py)_4(AsF_6)_2$ | 18.2 | 18.7 | | 1.84 | 1.88 | 1.87 |
| $Cu(py)_4(PF_6)_2$ | 18.4 | 18.7 | | 1.84 | 1.86 | 1.86 |
| $Cu(3mpy)_4(AsF_6)_2$ | 18.9 | 19.4 | 18.9(73) | 1.93 | 1.92 | 1.90 |
| $Cu(4mpy)_4(AsF_6)_2$ | 18.9 | 19.6 | 18.9(71) | 1.84 | 1.86 | 1.89 |
| $Cu(3mpy)_4(PF_6)_2$ | 18.9 | 19.4 | 19.0(77) | 1.88 | 1.87 | 1.86 |
| $Cu(4mpy)_4(PF_6)_2$ | 19.1 | 19.6 | 19.0(69) | 1.85 | 1.89 | 1.90 |

[a] Molar absorptivities, ε, in parentheses.
[b] $\mu_{eff} = 2.828\,((\chi_m - \text{t.i.p.})T)^{1/2}$ where $\chi_m$ is the molar magnetic susceptibility corrected for the diamagnetism of all atoms and t.i.p. is the temperature independent paramagnetism calculated from t.i.p. = $4N\beta^2/10Dq$.

After 1/2 h of stirring, the precipitate was filtered, washed with a solution of 5 mL pyridine in 50 mL water, and dried "in vacuo" for 48 h. The infrared spectra of the materials showed the presence of non-coordinated pyridine. Heating at 40°C under vacuum for 24 h gave the desired $Cu(py)_4(EF_6)_2$ products as mauve powders.

*Anal.* calcd. for $CuC_{20}H_{20}N_4P_2F_{12}$: C 35.86, H 3.01, N 8.36; found: C 35.68, H 3.02, N 8.45. *Anal.* calcd. for $CuC_{20}H_{20}N_4As_2F_{12}$: C 31.70, H 2.66, N 7.39; found: C 31.51, H 2.57, N 7.27.

Tetrakis(4-methylpyridine)copper(II) hexafluorophate and hexafluoroarsenate were prepared as described above except that the solutions used were four times more dilute. The more dilute solutions were required in these preparations to avoid contamination of products by nitrate. Precipitates were filtered, washed, dried "in vacuo" for 48 h, and finally heated to 40°C under vacuum for 24 h as before. The final products were obtained as mauve powders.

*Anal.* calcd. for $CuC_{24}H_{28}N_4P_2F_{12}$: C 39.71, H 3.89, N 7.72; found: C 39.68, H 3.88, N 7.91. *Anal.* calcd. for $CuC_{24}H_{28}N_4As_2F_{12}$: C 35.42, H 3.47, N 6.88; found: C 35.57, H 3.47, N 7.00.

In the preparations of tetrakis(3-methylpyridine)copper(II) hexafluorophosphate and hexafluoroarsenate, the reagents, $Cu(NO_3)_2 \cdot 3H_2O$, 3-$CH_3C_5H_4N$, and $NH_4PF_6$ (or $KAsF_6$), were mixed as described for the preparation of the pyridine complexes. In this instance, however, instead of immediate precipitation occurring, a two-liquid phase system developed with an upper weakly coloured aqueous phase and a more dense and strongly coloured, blue–purple, oily phase. After the reaction flask was allowed to stand for one week, blue–purple crystals formed in the oily phase. The crystals have been characterized as having the composition $Cu(3mpy)_6(H_2O)_2(EF_6)_2$ (7). When these crystals were ground up and dried under vacuum for 24 h, the desired $Cu(3mpy)_4(EF_6)_2$ compounds were obtained as mauve powders.

*Anal.* calcd. for $CuC_{24}H_{28}N_4P_2F_{12}$: C 39.71, H 3.89, N 7.72; found: C 39.67, H 3.91, N 7.67. *Anal.* calcd. for $CuC_{24}H_{28}N_4As_2F_{12}$: C 35.42, H 3.47, N 6.88; found: C 35.31, H 3.46, N 6.86.

Elemental analyses were done by P. Borda of the Department of Chemistry, The University of British Columbia.

*Spectroscopic and magnetic measurements*

Magnetic susceptibility measurements, electronic spectroscopy, and infrared spectroscopy were done as described previously (5). The equipment and methods used in the epr studies have also been described before (8).

## Results and discussion

### *Electronic spectra and magnetic susceptibilities*

The complexes exhibit electronic spectra consisting of a single broad assymmetrical band in the visible region with band maxima around 18 000 to 19 000 cm$^{-1}$. The spectra are consistent with either a square-coplanar $CuN_4$ chromophore (and non-coordinated anions) or with an elongated tetragonal–octahedral ligand field as would be obtained in a structure involving four neutral ligands forming a square plane about copper with anions coordinated in axial positions (9). The epr data presented below provide clear support for the second structural type.

The energies of the visible band maxima are given in Table 1. In each instance where a solution spectrum was recorded (the py complexes were not sufficiently soluble in dichloromethane), there is excellent agreement with the corresponding diffuse reflectance spectrum, thus indicating retention of the solid state molecular structure on dissolution. The extinction coefficients (67 to 77 $M^{-1}$ cm$^{-1}$) are similar to those observed earlier for other tetragonally elongated $CuL_4X_2$ complexes (8). The mull spectra consistently show higher energy maxima than the diffuse reflectance spectra. This phenomenon was observed previously (8), where it was suggested that the relative intensities of different components of the visible band could be different in the two phases. Whatever the cause of this difference between mull and reflectance spectra, its presence requires that comparisons between complexes always be made on the same phase. The spectrum of $Cu(py)_4(PF_6)_2$ at room temperatures has been reported previously as a Kel-F mull (band maximum at 19 100 cm$^{-1}$ (2)) and as a powder by diffuse reflectance (band maximum at 18 300 cm$^{-1}$ (1)). Our diffuse reflectance spectrum agrees well with the earlier report. Although our spectra are broad we could find no clear indication of the shoulders previously reported at 16 200 cm$^{-1}$ and 16 700 cm$^{-1}$ in the mull and reflectance spectra respectively. We have prepared complexes of com-

position $Cu(3mpy)_6(H_2O)_2(EF_6)_2$ and $Cu(4mpy)_8(H_2O)_2(EF_6)_2$ (7) which have absorptions in the region of these reported shoulders and it is possible that impurities of species analogous to these were present in the samples of $Cu(py)_4(PF_6)_2$ reported earlier. In the present work we found it necessary to remove traces of water and free pyridine (detected by ir spectra) by heating to about 40°C under vacuum. This precaution does not appear to have been taken in the previous work.

In polarized, single-crystal, electronic spectral studies on related complexes, Hathaway *et al.* have found that of the three electronic transitions possible in $D_{4h}$ symmetry, $^2B_{1g} \rightarrow {}^2A_{1g}$, $^2B_{1g} \rightarrow {}^2B_{2g}$, and $^2B_{1g} \rightarrow {}^2E_g$ ($\Delta E_{z^2}$, $\Delta E_{xy}$, and $\Delta E_{xz,yz}$ respectively), the last forms the highest energy component of the visible band and a shift in the position of this transition to higher energy as a result of increasing tetragonal distortion results in an overall shift in the visible band (10). The position of the visible band maximum thus provides a measure of the degree of tetragonal distortion in complexes of this type and this has been used previously to rank the coordinating abilities of a number of polyatomic anions (8). The band maxima in the diffuse reflectance spectra of the $Cu(py)_4(EF_6)_2$ complexes are higher in energy than observed in other $Cu(py)_4X_2$ complexes and clearly indicate greater tetragonal distortion than in, for example, the corresponding perchlorate and fluorosulfate complexes (8). This is consistent with the weaker basicity associated with the $PF_6^-$ and $AsF_6^-$ anions. The energy of the band maxima in the 3mpy and 4mpy complexes is consistently higher than in the corresponding py complexes consistent with the greater basicity of the methylpyridine ligands. Moreover, it is interesting to note that in comparing $PF_6^-$ complexes with corresponding $AsF_6^-$ complexes the band maxima are approximately the same or slightly higher in energy for $PF_6^-$, suggesting a slightly higher degree of tetragonality and weaker anion basicity in these complexes. This could possibly account for our earlier observation that while $Ni(py)_4(AsF_6)_2$ has a low temperature form in which the anions are fully coordinated to nickel, the corresponding $PF_6^-$ complex appears to exist only in the form in which the anions are not fully coordinated (6).

Magnetic susceptibilities were measured at about 10 different temperatures over the range 80 to 300 K for each of the complexes. Values of $\mu_{eff}$ at three temperatures interpolated from plots of $\mu_{eff}$ vs. $T$ are given in Table 1. The moments which are essentially temperature independent are of a magnitude normally observed for magnetically dilute copper(II) complexes. Variations of magnetic moments for different complexes are not sufficiently great to permit an evaluation of the effects of tetragonal distortion on magnetic moments.

*Electron paramagnetic resonance*

The general features of the epr spectra of all six complexes are the same and may be illustrated by the discussion which follows for $Cu(3mpy)_4(AsF_6)_2$. The room temperature dichloromethane solution spectrum consists of four lines arising from copper nuclear hyperfine interaction (Fig. 1). At liquid nitrogen temperature two regions of absorption occur centred at $g_{||}$ and $g_\perp$. As seen in Fig. 2, nuclear hyperfine splitting of $g_{||}$ is observed with two of the four components clearly resolved and the other two obscured by the $g_\perp$ peak. The splitting of $g_\perp$ is not resolved because of superimposed nitrogen hyperfine coupling and because of the relatively smaller magnitude of $A_\perp$ compared to $A_{||}$. Although exchange coupling normally broadens the epr spectrum of copper(II) complexes in the solid state to an extent that hyperfine data is masked (11), such is not the case here. The epr spectrum of the room temperature powdered sample (Fig. 3) is very similar to that of the frozen solution spectrum. This phenomenon has been observed before (12–14); however, it is not common.

The epr parameters, calculated employing equations which include magnetic hyperfine coupling to second order (15), are listed in Table 2 (together with data for related $Cu(py)_4X_2$ complexes for comparison (8)). The complexes are listed in order of increasing $\Delta E_{xz,yz}$ and therefore increasing tetragonality. The isotropic $g_0$ and $A_0$ values were calculated from the room temperature solution spectra and the $g_{||}$ and $A_{||}$ values were obtained

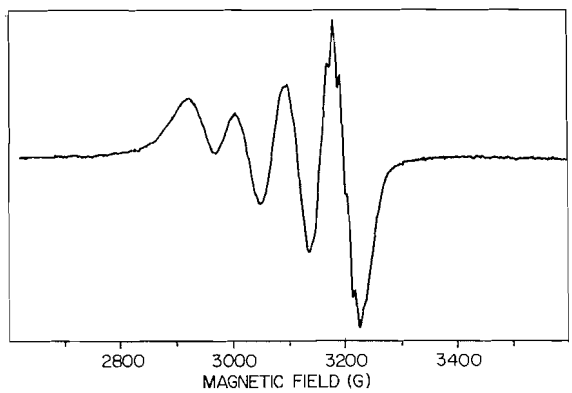


FIG. 1. Tetrakis(3-methylpyridine)copper(II) hexafluoroarsenate in dichloromethane; epr spectrum at room temperature.

TABLE 2. Electron paramagnetic resonance[a] and bonding[b] parameters

| Complex[c] | $g_{\|\|}$ | $g_\perp$ | $g_0$ | $\|A_{\|\|}\| \times 10^4$ ($cm^{-1}$) | $\|A_\perp\| \times 10^4$ ($cm^{-1}$) | $\|A_0\| \times 10^4$ ($cm^{-1}$) | $K \times 10^4$ ($cm^{-1}$) | $\alpha$ | $\beta$ | $\delta$ |
|---|---|---|---|---|---|---|---|---|---|---|
| $Cu(py)_4(Tos)_2$[d,e] | 2.260 | 2.062 | 2.128 | 183 | 6 | 65 | 110 | 0.92 | 0.79 | 0.84 |
| $Cu(py)_4(SO_3F)_2$[d] | 2.253 | 2.054 | 2.121 | 186 | 17 | 73 | 116 | 0.91 | 0.79 | 0.81 |
| $Cu(py)_4(ClO_4)_2$[d] | 2.263 | 2.040 | 2.114 | 181 | 25 | 77 | 117 | 0.89 | 0.82 | 0.72 |
| $Cu(py)_4(BF_4)_2$[d] | 2.256 | 2.043 | 2.114 | 184 | 25 | 78 | 118 | 0.89 | 0.81 | 0.75 |
| $Cu(py)_4(AsF_6)_2$ | 2.232 (2.239) | 2.052 (~2.07) | 2.112 | 187 (193) | 24 | 78 | 118 | 0.88 | 0.78 | 0.85 |
| $Cu(py)_4(PF_6)_2$ | 2.235 (2.239) | 2.068 (~2.06) | 2.124 | 198 (193) | 21 | 80 | 124 | 0.90 | 0.76 | 0.95 |
| $Cu(3mpy)_4(AsF_6)_2$ | 2.218 (2.228) | 2.052 (~2.04) | 2.107 | 202 (192) | 19 | 80 | 118 | 0.91 | 0.73 | 0.83 |
| $Cu(4mpy)_4(AsF_6)_2$ | 2.224 (2.239) | 2.062 (~2.06) | 2.116 | 197 (183) | 25 | 82 | 123 | 0.89 | 0.76 | 0.93 |
| $Cu(3mpy)_4(PF_6)_2$ | 2.222 (2.228) | 2.064 (~2.04) | 2.117 | 202 (192) | 24 | 83 | 125 | 0.90 | 0.75 | 0.94 |
| $Cu(4mpy)_4(PF_6)_2$ | 2.217 (2.239) | 2.064 (~2.06) | 2.115 | 207 (183) | 20 | 82 | 123 | 0.91 | 0.73 | 0.93 |

[a] Values in parentheses were obtained from room temperature powder spectra. Other values from $CH_2Cl_2$ solutions.
[b] Bonding parameters $K$, $\alpha$, $\beta$, and $\delta$ obtained from solution epr parameters.
[c] Complexes are listed in order of increasing tetragonality as estimated by the solution $\Delta E_{xy,yz}$ values. See text.
[d] Data obtained from ref. 8. A systematic error in unit conversion leading to incorrect $A_{\|}$ and $A_\perp$ values in ref. 8 has been corrected here.
[e] Tos is $p$-$CH_3C_6H_4SO_3$.

from the frozen solution spectra. The values of $A_\perp$ and $g_\perp$ were obtained from the equations $3A_0 = A_{\|} + 2A_\perp$ and $3g_0 = g_{\|} + 2g_\perp$ (16). For comparison, values of $g_{\|}$, $g_\perp$, and $A_{\|}$ have been estimated from the room temperature powder spectra and these are also given in Table 2. We note that, as a consequence perhaps of exchange coupling, the values of $g_{\|}$ are consistently greater in the solid state spectra while $A_{\|}$ is generally smaller. The accuracy of the $g_\perp$ determination is too low to permit any meaningful comparison.

The fact that these complexes exhibit two $g$-value spectra in which the lowest $g$-value is equal to or greater than 2.04 is consistent according to Hathaway and Billings (17), with an elongated tetragonal–octahedral environment about copper in which the unpaired electron occupies the $d_{x^2-y^2}$ orbital in the ground electronic state. We note also that there are small but significant differences in the epr parameters between $Cu(py)_4(PF_6)_2$ and $Cu(py)_4(AsF_6)_2$ (and similarly for the 3mpy and 4mpy complexes). This is not consistent with a structural formulation involving square-coplanar $CuL_4^{2+}$ moieties with non-coordinated anions but instead supports the elongated tetragonal–octahedral structure.

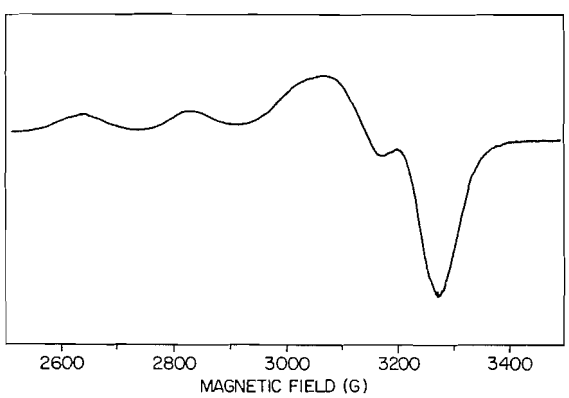


FIG. 2. Tetrakis(3-methylpyridine)copper(II) hexafluoroarsenate in dichloromethane; epr spectrum at liquid nitrogen temperature.

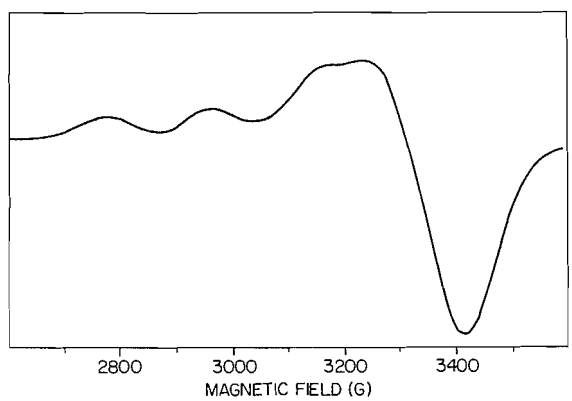


FIG. 3. Tetrakis(3-methylpyridine)copper(II) hexafluoroarsenate; epr spectrum of powdered sample at room temperature.

In our earlier studies of the epr spectra of some $Cu(py)_4X_2$ complexes (8) we noted that as the coordinating strength of the anion decreases, and therefore the tetragonality of the complex increases, the value of $g_\perp$ decreases. It is clear from the present work that this trend does not continue into the $PF_6^-$ and $AsF_6^-$ series of compounds. In spite of the fact that these anions are less basic than $ClO_4^-$, for example, the value of $g_\perp$ tends to be greater in all cases. As stated in the earlier paper, a decrease in $g_\perp$ would be expected to occur with increasing tetragonality only in the absence of a significant decrease in electron delocalization from copper (relatively larger increase in the magnitude of the orbital reduction factor). Moreover, we note that on going from complexes containing the relatively more strongly coordinating fluorosulfate and tosylate anions to those containing $PF_6^-$ and $AsF_6^-$ anions, the value of $g_\parallel$ decreases and $A_\parallel$ increases. This, in fact, parallels the findings of Antosic *et al.* (16) who investigated the epr parameters of weak complexes of copper(II) β-ketoenolates with chloroform. To try to understand more fully the observed variations in the epr parameters we have evaluated bonding parameters for all of the complexes under discussion.

Using the notation and equations of Gersmann and Swalen (18) and the methods of Herring *et al.* (19) (modified to suit $D_{4h}$ symmetry), the magnetic parameters are:

$$[1]\quad g_\parallel = g_e - (8\lambda/\Delta E_{xy})(\alpha^2\beta^2)$$

$$[2]\quad g_\perp = g_e - (2\lambda/\Delta E_{xz,yz})(\alpha^2\beta^2)$$

$$[3]\quad A_\parallel = -K - \frac{4}{7}\alpha^2 P - 2\lambda\alpha^2 P \times \left(\frac{4\beta^2}{\Delta E_{xy}} + \frac{3}{7}\frac{\delta^2}{\Delta E_{xy,yz}}\right)$$

$$[4]\quad A_\perp = -K + \frac{2}{7}\alpha^2 P - \frac{22}{14}\frac{\lambda\alpha^2\delta^2}{\Delta E_{xz,yz}} P$$

The Fermi contact term can be obtained from

$$[5]\quad -K = \frac{1}{3}[(A_\parallel + 2A_\perp) - P[(\Delta g_\parallel + 2\Delta g_\perp)]$$

and $\alpha^2$ from

$$[6]\quad \alpha^2 = \frac{7}{4P}\left[-A_\parallel - K + P\left(\Delta g_\parallel + \frac{3}{7}\Delta g_\perp\right)\right]$$

where $\Delta g_\parallel = g_\parallel - 2.0023$ and $\Delta g_\perp = g_\perp - 2.0023$ and the signs of $A_\parallel$ and $A_\perp$ are taken to be negative (19). The following parameter values were used: $\lambda = -828\,cm^{-1}$ and $P = 360 \times 10^{-4}\,cm^{-1}$. The value of $\Delta E_{xz,yz}$ was taken as the position of the band maximum in the solution spectrum of each complex (diffuse reflectance for the $Cu(py)_4(EF_6)_2$ complexes) and for $\Delta E_{xy}$ the value $13.5 \times 10^3\,cm^{-1}$ was used for all complexes. The assumption that $\Delta E_{xy}$ should be approximately the same for all complexes is reasonable in that variations of axial substituents should have relatively little effect on this transition since neither the $d_{xy}$ nor the $d_{x^2-y^2}$ orbital has a $Z$ component. Moreover, changing the in-plane ligand in this series of complexes should also have little effect since differences in ligand field parameters for analogous pyridine and methyl–pyridine complexes have been shown previously to be small (4). The value of $13.5 \times 10^3\,cm^{-1}$ was estimated by assuming $\Delta E_{xy} = 10\,Dq$ (octahedral) (20) and by obtaining the latter from the measured $10\,Dq$ for $[Ni(py)_6]^{2+}$ (4) and the "ligand field $g$-parameters" for $Cu^{2+}$ and $Ni^{2+}$ (21).

The bonding parameters α, β, δ, and $K$ were calculated as described previously (19) and are given in Table 2. Uncertainties in these parameters resulting from the fact that they are obtained from epr results at two different temperatures (8) and as a consequence of having to assume values of $P$ and $\Delta E_{xy}$ should not significantly affect their relative values and hence comparisons from one compound to another should be valid. We estimate that the measured parameters $\Delta g_0$, $A_0$, $\Delta g_\parallel$, and $A_\parallel$ are obtained from the epr spectra with an uncertainty of less than 2%. This gives rise to a maximum error of approximately ±0.04 in the α and β parameters and 0.07 in the δ parameter. We note that α, which measures σ-bonding, is constant within experimen-

TABLE 3. Infrared spectra,[a] selected bands for pyridine and 4-methylpyridine

| | Band | |
|---|---|---|
| Assignment[b] | $Cu(py)_4(PF_6)_2$ | $Cu(py)_4(AsF_6)_2$ |
| 8a | 1609 s | 1611 s |
| 6a | 642 m | 650 m, 642 m |
| 16b | 440 s, 430 w | 440 s, 430 w |

| | Band | |
|---|---|---|
| Assignment[c] | $Cu(4mpy)_4(PF_6)_2$ | $Cu(4mpy)_4(AsF_6)_2$ |
| 8a | 1620 s | 1620 s |
| 19a | 1512 m | 1512 m |
| 9a | 1241 m | 1241 m |
| 1 | [d] | [d] |
| 10b + 12 | [e] | 810 s |
| 6a | [f] | [d] |

[a] In $cm^{-1}$. Abbreviations as in Table 4. Samples as Nujol mulls.
[b] Assignment as in ref. 3.
[c] Assignment as in ref. 4.
[d] Not observed.
[e] Possibly obscured by $\nu_3(T_{1u})$ of $PF_6^-$.
[f] Possibly obscured by $\nu_4(T_{1u})$ of $PF_6^-$.

TABLE 4. Infrared spectra,[a] anion bands

| Complex | Assignments ($O_h$ upper and $C_{4v}$ lower) | | | | | | |
|---|---|---|---|---|---|---|---|
| | $\nu_1(A_{1g})$ | $\nu_2(E_g)$ | | $\nu_3(T_{1u})$ | | $\nu_4(T_{1u})$ | |
| | $A_1$ | $A_1$ | $B_1$ | $A_1$ | $E$ | $A_1$ | $E$ |
| $Cu(py)_4(PF_6)_2$ | 742 ms | [b] | [c] | 852 vs | 828 s | 551 s, asy | |
| $Cu(4mpy)_4(PF_6)_2$ | 740 ms | [b] | [c] | 850 vs, br | | 555 s, asy | |
| $Cu(3mpy)_4(PF_6)_2$ | 740 s | [b] | [c] | 830 vs, br | | 553 s, asy | |
| $Cu(py)_4(AsF_6)_2$ | 675 ms | 556 s | 579 w | 705 vs, br | | 395 s, br | |
| $Cu(4mpy)_4(AsF_6)_2$ | 670 s | 552 s | 579 w | 705 vs, br | | 397 s, br | |
| $Cu(3mpy)_4(AsF_6)_2$ | 669 s | 549 s | 578 w | 705 vs, br | | 395 s, br | |

[a] In $cm^{-1}$. Abbreviations: s = strong, m = medium, w = weak, br = broad, asy = assymetric, v = very. Samples as Nujol mulls.
[b] Not observed. May be obscured by $\nu_4$.
[c] Not observed.

tal error throughout the series. The parameter which measures in-plane π-bonding, β, is measurably smaller than unity consistent with the presence of metal–ligand π-electron delocalization. Moreover, there appears to be a marginal decrease in the β values with increasing tetragonality.

It seems reasonable to expect that out-of-plane π-bonding will experience greater sensitivity to variations in the nature of the axial ligands than in-plane π-bonding. Unfortunately, the out-of-plane π-bonding parameter, δ, is the least precisely measured. Nevertheless, it is clear from the data in Table 2 that the variation in δ over the series is large and exceeds the range permitted by the uncertainty in δ. Some interesting comparisons may be made between individual complexes. The δ value for $Cu(py)_4(PF_6)_2$ is measurably greater than that of $Cu(py)_4(ClO_4)_2$. Since the tetragonality of the hexafluorophosphate complex is greater than that of the perchlorate, one might have expected the former compound to show stronger metal–pyridine bonding and hence more, rather than less, electron delocalization. A possible explanation for the poor out-of-plane π-bonding in the hexafluorophosphate derivative is that, in this compound, the anions are sufficiently weakly coordinated that the pyridine rings are able to adopt an orientation such that the angles between the planes of the rings and the $CuN_4$ plane are near 90°. Such a ring orientation, which has been observed in the analogous $Ni(4mpy)_4(PF_6)_2$ complex (6), would result in poor orbital overlap between pyridine π-orbitals and the metal $d_{xz}$ and $d_{yz}$ orbitals. In contrast, it seems likely that in the perchlorate derivative (and also probably in the tetrafluoroborate and sulfonate derivatives), the anions are sufficiently strongly bonded to the metal that the angles that the planes of the pyridine rings make with the $CuN_4$ plane are closer to 45°. Ring orientation of this type, which has been seen in the related $Cu(py)_4(CF_3CO_2)_2$ (22, 23) and Ni(3,5-dimethylpyridine)$_4(ClO_4)_2$ (24) complexes, would be more favourable to out-of-plane π-bonding. Finally we note that the other two hexafluorophosphate complexes studied here and the $Cu(4mpy)_4(AsF_6)_2$ complex also have δ values which suggest ring orientations which disfavour out-of-plane π-bonding.

*Infrared spectroscopy*

The infrared spectra of all complexes showed the absence of water and free heterocyclic ligand; moreover, bands arising primarily from anion vibrations and those arising from coordinated neutral ligand vibrations were usually easily distinguished. Infrared bands reported previously at 600 and 407 $cm^{-1}$ for $Cu(py)_4(PF_6)_2$ (2) are due to non-coordinated pyridine and were seen in this work in freshly precipitated samples but not in the final (dried at 40°C under vacuum) product. Otherwise our spectrum of $Cu(py)_4(PF_6)_2$ is in good agreement with the previously published data (1, 2). Some selected stereochemically sensitive pyridine and 4-methylpyridine bands are listed in Table 3 for comparison with earlier tabulations (3, 4). Frequencies assigned to the fundamental vibrations of the anions are listed in Table 4.

Free $EF_6^-$ anions have $O_h$ symmetry and should exhibit only two infrared absorptions, $\nu_3(T_{1u})$ and $\nu_4(T_{1u})$. Other transitions such as $\nu_1(A_{1g})$ and $\nu_2(E_g)$ are formally forbidden in $O_h$ symmetry (1). In complexes where the anions are formally non-coordinated, there may be some breakdown of these rules; it was found earlier that such complexes are characterized by spectra which show strong $\nu_3$ bands (possibly split by up to 25 $cm^{-1}$), strong and unsplit $\nu_4$ and, sometimes, weak $\nu_1$ or $\nu_2$ bands (4). In complexes where the anions are formally coordinated through one fluorine atom to the metal the anion symmetry can be no higher than $C_{4v}$. Under these circumstances the vibrational modes alter.

The formerly forbidden $\nu_1$ mode becomes allowed ($A_1$ symmetry), $\nu_2$ splits into $A_1$ and $B_1$ (the latter forbidden in infrared), $\nu_3$ and $\nu_4$ both split into formally allowed transitions of $A_1$ and $E$ symmetry. Two additional infrared-active $E$ modes derived from $\nu_5$ and $\nu_6$ (in $O_h$ symmetry) are also predicted in $C_{4v}$ symmetry; however, these bands are expected to be at low frequencies and possibly because of this or interference with other ligand vibrations these have not been observed in earlier work (1, 2) or in the present study. In summary, then, the presence of coordinated $EF_6^-$ groups should be indicated by strong and split $\nu_3$ and $\nu_4$ vibrations and medium to strong $\nu_1$ and $\nu_2$ bands.

These criteria for anion coordination were applied previously, to conclude that $Cu(py)_4(PF_6)_2$ contains "semi-coordinated" anions (1) and that the $Ni(py)_4(EF_6)_2$ and $Ni(4mpy)_4(EF_6)_2$ complexes contain weakly interacting anions (4, 6). These criteria for anion coordination are clearly met in the copper complexes studied in the present work (Table 4). In all complexes, $\nu_3$ is very broad or split, $\nu_4$ is assymetric (evidence for unresolved splitting) in the $PF_6^-$ compounds and relatively broad in the $AsF_6^-$ complexes. In all complexes, $\nu_1$ and $\nu_2$ are medium to strong in intensity.

Comparing the infrared spectra of the copper complexes studied here with those of analogous $CoL_4(EF_6)_2$ and $NiL_4(EF_6)_2$ complexes, it seems that the most sensitive test of anion coordination involves the $\nu_1(A_{1g})$ and $\nu_2(E_g)$ transitions. These bands are weak or not observed in the cobalt complexes where the anions are non-coordinated. In the nickel complexes, where weak anion coordination is present these bands appear with medium intensity and in the copper complexes, where even stronger anion coordination is evident, the bands are generally more intense, $\nu_2$ being split into strong $A_1$ and weak $B_1$ components in the hexafluoroarsenate complexes.

**Acknowledgements**

Financial assistance from the Natural Sciences and Engineering Research Council of Canada and the Natural, Applied and Health Sciences Committee (U.B.C.) is gratefully acknowledged. R.M.M. thanks the University Awards Committee for a MacMillan Family Fellowship.

1. S. A. BELL, J. C. LANCASTER, and W. R. MCWHINNIE. Inorg. Nucl. Chem. Lett. **7**, 405 (1971).
2. H. G. MAYFIELD and W. E. BULL. J. Chem. Soc. A, 2279 (1971).
3. R. M. MORRISON and R. C. THOMPSON. Inorg. Nucl. Chem. Lett. **12**, 937 (1976).
4. R. M. MORRISON and R. C. THOMPSON. Can. J. Chem. **56**, 985 (1978).
5. R. M. MORRISON, R. C. THOMPSON, and J. TROTTER. Can. J. Chem. **57**, 135 (1979).
6. R. M. MORRISON, R. C. THOMPSON, and J. TROTTER. Can. J. Chem. **58**, 238 (1980).
7. R. M. MORRISON. Ph.D. Thesis, University of British Columbia, Vancouver, B.C. 1980.
8. C. S. ALLEYNE and R. C. THOMPSON. Can. J. Chem. **52**, 348 (1974).
9. B. J. HATHAWAY. J. Chem. Soc. Dalton, 1196 (1972).
10. B. J. HATHAWAY, D. E. BILLINGS, P. NICHOLLS, and I. M. PROCTER. J. Chem. Soc. A, 319 (1969).
11. B. HATHAWAY, M. DUGGAN, A. MURPHY, J. MULLANE, C. POWER, A. WALSH, and B. WALSH. Coord. Chem. Rev. **36**, 267 (1981).
12. H. A. KUSKA, F. M. D'ITRI, and A. I. POPOV. Inorg. Chem. **5**, 1272 (1966).
13. J. R. WASSON, C. TRAPP, C. I. SHYR, and D. SMITH. J. Chem. Phys. **49**, 5197 (1968).
14. D. M. L. GOODGAME, M. GOODGAME, P. J. HAYWARD, and G. W. RAYNER-CANHAM. Inorg. Chem. **7**, 2447 (1968).
15. B. BLEANY. Phil. Mag. **42**, 441 (1951).
16. S. ANTOSIK, N. M. D. BROWN, A. A. MCCONNELL, and A. L. PORTE. J. Chem. Soc. A, 545 (1969).
17. B. J. HATHAWAY and D. E. BILLINGS. Coord. Chem. Rev. **5**, 143 (1970).
18. H. R. GERSMANN and J. D. SWALEN. J. Chem. Phys. **36**, 3221 (1962).
19. F. G. HERRING, J. M. PARK, S. J. RETTIG, and J. TROTTER. Can. J. Chem. **57**, 2379 (1979).
20. J. H. HUHEEY. Inorganic chemistry. Principles of structure and reactivity. Harper and Row, New York. 1978. p. 385.
21. B. N. FIGGIS. Introduction to ligand fields. Interscience, New York. 1966. p. 244.
22. J. A. PRETORIUS and J. C. A. BOEYENS. J. Inorg. Nucl. Chem. **40**, 1745 (1978).
23. S. J. PRADILLA, H. W. CHEN, F. W. KOKNAT, and J. P. FACKLER. J. Inorg. Chem. **18**, 3519 (1979).
24. F. MADAULE-AUBRY and G. M. BROWN. Acta. Crystallogr. B**24**, 745 (1968).

# Rearrangement of 10-acetoxy-10-vinylcamphene

NANCY LAMB, THOMAS MONEY, STEVEN J. RETTIG, AND JAMES TROTTER

*Department of Chemistry, University of British Columbia, 2036 Main Mall, Vancouver, B.C., Canada V6T 1Y6*

Received December 2, 1981

NANCY LAMB, THOMAS MONEY, STEVEN J. RETTIG, and JAMES TROTTER. Can. J. Chem. **60**, 1055 (1982).

Treatment of 10-acetoxy-10-vinylcamphene with $BF_3$ or $HClO_4$ results in rearrangement to a bicyclo[3.2.1]octane derivative in preference to 5-*endo*-trigonal cyclization. Alkaline hydrolysis of this bicyclooctane yields a diol, crystals of which are orthorhombic, $a = 9.571(1)$, $b = 12.416(1)$, $c = 18.860(2)$ Å, $Z = 8$, space group $C222_1$. The structure was solved by direct methods and was refined by a full-matrix least-squares procedure to $R = 0.035$ and $R_w = 0.044$ for 930 reflections with $I \geq 3\sigma(I)$. The structure analysis has unambiguously identified the diol as 2,3-dimethyl-4-vinylbicyclo[3.2.1]octan-2,3-diol.

NANCY LAMB, THOMAS MONEY, STEVEN J. RETTIG et JAMES TROTTER. Can. J. Chem. **60**, 1055 (1982).

Sous l'action du $BF_3$ ou du $HClO_4$, l'acétoxy-10 vinyl-10 camphène se transpose en un dérivé du bicyclo[3.2.1] octane plutôt que de subir une cyclisation 5-*endo* trigonale. L'hydrolyse alcaline de ce dérivé fournit un diol dont les cristaux sont orthorombiques, $a = 9,571(1)$, $b = 12,416(1)$, $c = 18,860(2)$ Å, $Z = 8$, groupe spatial $C222_1$. On a résolu la structure par des méthodes directes et on l'a affinée par la méthode des moindres carrés (matrice complète) jusqu'à des valeurs de $R = 0,035$ et $R_w = 0,044$ pour 930 réflexions avec $I \geq 3\sigma(I)$. Cette analyse permet d'attribuer sans ambiguité la structure du diol: diméthyl-2,3 vinyl-4 bicyclo[3.2.1] octanediol-2,3.

[Traduit par le journal]

## Introduction

The key step in a recent attempt to synthesize the former structure (**10**) (1) of (−)-albene[1] involved cyclization of 10-acetoxy-10-vinylcamphene, **8**, derived from 9-bromocamphor, **1** (cf. Scheme 1). Treatment of **8** with $HClO_4/CHCl_3$ or $BF_3/CH_2Cl_2$ led to the formation of a crystalline hydroxyacetate, **11**, in 25% yield.[2] The nmr, ir, and mass spectrum of **11** indicated the presence of

$>CHCH{=}CH_2$, $CH_3{-}\overset{|}{\underset{|}{C}}{-}$, and $CH_3{-}\overset{|}{\underset{|}{C}}{-}OAc$

groups and led us to suspect that rearrangement of the bicyclo[2.2.1]heptane skeleton of **3** had occurred. Alkaline hydrolysis of **11** provided a crystalline diol, **12**, whose structure has been established by X-ray crystallographic analysis.

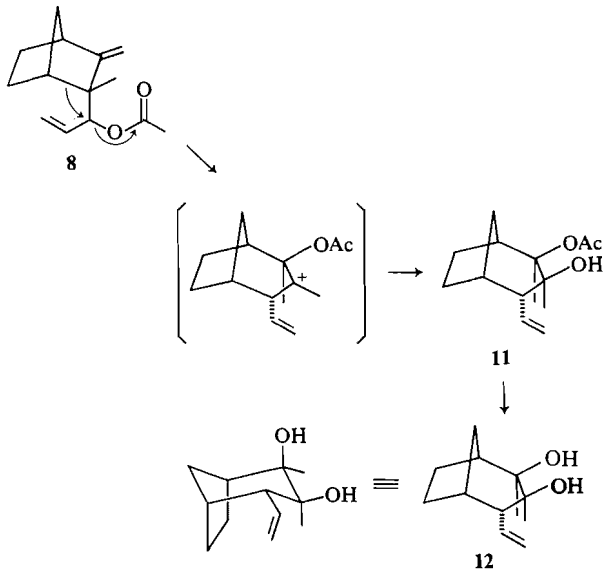


SCHEME 1

[1]During the course of this work a new structure (**13**) for (−)-albene was established by chemical and X-ray crystallographic evidence (2).

[2]The isomeric hydroxyacetate structure is not, of course, excluded by our evidence.

## Experimental

Unless otherwise stated the following are implied. Melting points (mp) were determined on a Kofler micro heating stage or a Thomas Hoover capillary melting point apparatus and are uncorrected. Gas chromatography was carried out on either a Hewlett-Packard model 5831A gas chromatograph using 6 ft × 1/8 in. columns and nitrogen as carrier gas, or a Varian Aerograph model 90-P with 5 ft × 1/4 in. columns and helium as carrier gas. Carrier gas flow rate for 1/4 in. columns was about 60 mL/min and for 1/8 in. columns about 35 mL/min. The 60 MHz nmr spectra were recorded on a Varian Associates model T-60 and 100 MHz spectra were recorded on a Varian Associates model HA-100 or XL-100. Signal positions are given in δ with tetramethylsilane (TMS) as an internal reference. Signal multiplicity and integrated area are indicted in parentheses. Infrared spectra were recorded on a Perkin-Elmer 137 spectrophotometer and optical rotations were measured with either a Perkin-Elmer model 141 or 241 MC polarimeter. Low resolution mass spectra were recorded on a Varian/Mat model CH4B mass spectrometer and high resolution mass spectra were determined on the AE1 model MS902 or model MS50 instrument. Microanalyses were performed by Mr. P. Borda, Microanalytical Laboratory, University of British Columbia, Vancouver. All the solvents used for nmr, ir, and optical rotations were of Spectral grade.

*(+)-9-Acetoxycamphor, 2 (3)*

A mixture of (+)-9-bromocamphor, **1** (4) (8.08 g, 34.9 mmol) and potassium acetate (16.3 g, 165.4 mmol) in dry hexamethyl-

0008-4042/82/081055-07$01.00/0

©1982 National Research Council of Canada/Conseil national de recherches du Canada

Can. J. Chem. Downloaded from www.nrcresearchpress.com by 210.87.254.40 on 09/06/12
For personal use only.

Can. J. Chem. Downloaded from www.nrcresearchpress.com by 210.87.254.40 on 09/06/12
For personal use only.

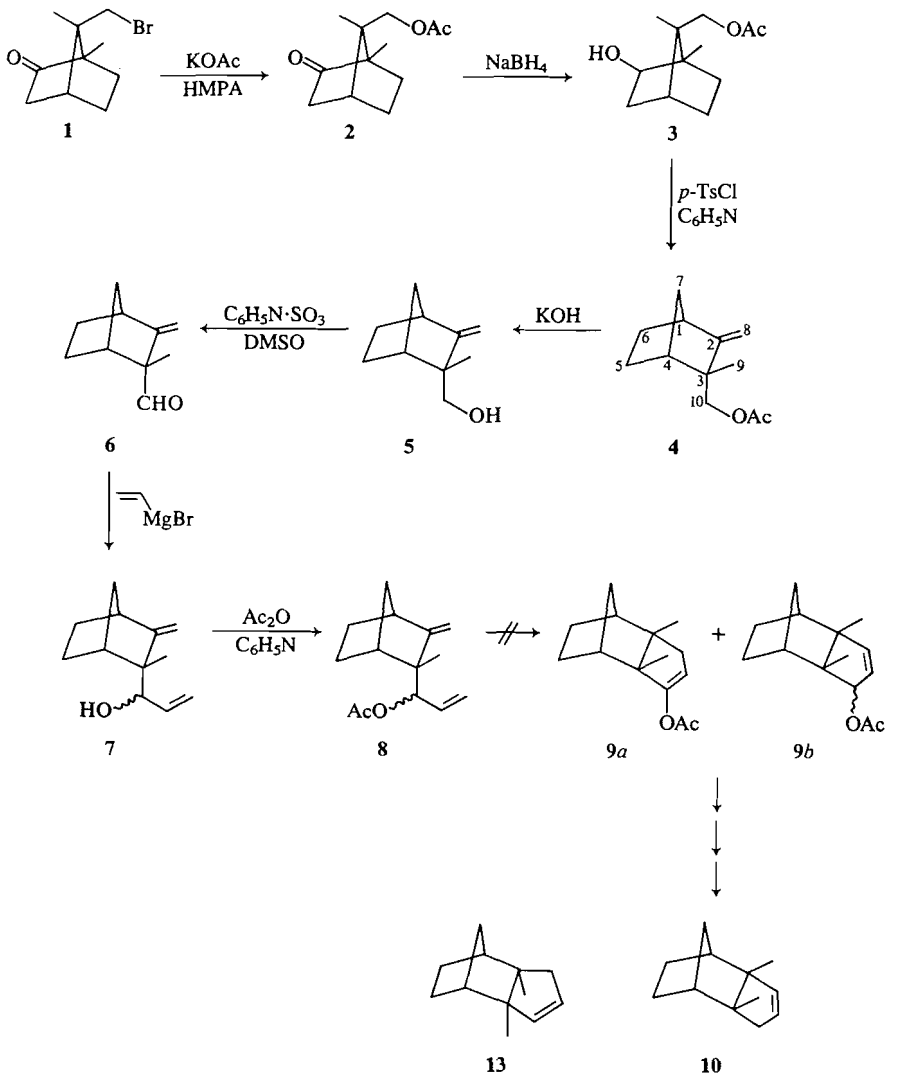


1 2 3 4 5 6 7 8 9a 9b 10 13

phosphoramide[3] was refluxed under nitrogen for 24 h. Addition of water, extraction with ether, and work-up in the usual way gave a brown oil (7.27 g) which was purified by column chromatography (silica gel) followed by distillation (bp 66–68°C, 0.04 Torr; lit. (3) bp 123°C (5 Torr)) to provide (+)-9-acetoxycamphor, **2**, as a colorless oil (6.55 g, 86% yield), $[\alpha]_D^{30}$ + 53.2° (c 0.88, $CHCl_3$); δ($CCl_4$), 4.15 and 3.90 (two doublets, 2 H, $J$ = 12 Hz, – $CH_2OAc$), 2.01 (singlet, 3H, $CH_3COO$—), 0.92 and 0.90 (two singlets, 6 H, tertiary methyls); $\nu_{max}$ ($CCl_4$), 2950 and 2900 (broad, medium, CH), 1750 (sharp, strong, C=O), 1240 $cm^{-1}$ (broad, strong, C—O—C); *m/e* 210 ($M^+$), 167, 164, 150, 137, 122, 108, 107, 95, 93, 79, 67, 43 (base peak). Fw calcd. for $C_{12}H_{18}O_3$: 210.1256; found (high resolution mass spectrometry): 210.1251. *Anal.* calcd. for $C_{12}H_{18}O_3$: C 68.54, H 8.63; found: C 68.59, H 8.80.

*10-Acetoxycamphene, 4*

A solution of (+)-9-acetoxycamphor, **2** (3.71 g, 17.7 mmol), in ethanol was added slowly with stirring to a mixture of sodium borohydride (1.92 g, 50.9 mmol) and ammonium chloride (1.59 g, 29.7 mmol) in 95% ethanol at 0°C. The reaction mixture was then stirred at room temperature for 30 min before dilute hydrochloric acid was added. Usual work-up provided a mixture of 9-acetoxyisoborneol, **3**, and 9-acetoxyborneol as a colorless oil (3.43 g), which was used in the subsequent Wagner–Meerwein rearrangement without purification.

The crude reduction product was treated with *p*-toluenesulphonyl chloride (3.9 g, 20 mmol) in refluxing dry pyridine for 15 h. Work-up in the usual fashion provided a yellow oil (2.87 g) which was distilled (36–38°C, 1.2 Torr) to afford 10-acetoxycamphene, **4**, as a colorless oil (1.92 g, 56% overall yield); δ($CCl_4$), 4.82 and 4.57 (two broad singlets, 1 H each, $=CH_2$), 3.90 (broad signal, 2 H, $—CH_2OAc$), 2.70 (broad multiplet, 1 H, half-width 8 Hz, bridgehead allylic methine), 2.00 (singlet, 3 H, $CH_3COO$—), 1.07 (singlet, 3 H, tertiary methyl); $\nu_{max}$($CCl_4$), 2950 and 2850 (sharp, medium CH), 1755 (sharp, strong, C=O), 1660 (broad, weak, C=C), 1240 (broad, strong, C—O—C), 895 $cm^{-1}$ (broad, medium, $=CH_2$); *m/e* 194 ($M^+$), 134, 121 (base peak), 106, 93, 91, 89, 87, 43. Fw calcd. for $C_{12}H_{18}O_2$: 194.1306;

[3]Acetic acid was previously used as solvent in this reaction (3).

Can. J. Chem. Downloaded from www.nrcresearchpress.com by 210.87.254.40 on 09/06/12
For personal use only.

found (high resolution mass spectrometry): 194.1305. *Anal.* calcd. for $C_{12}H_{18}O_2$: C 74.19, H 9.34; found: C 74.10, H 9.33.

*10-Hydroxycamphene, 5*

A mixture of 10-acetoxycamphene, **4** (1.9 g, 10 mmol), and potassium hydroxide (2.0 g, 35 mmol) in 95% ethanol (15 mL) was refluxed for 4 h. Dilution with water, extraction with ether, work-up in the usual way gave yellow crystals (1.37 g) which were sublimed (bath temperature 110°C, atmospheric pressure) and subsequently recrystallized from petroleum ether (30–60) to provide 10-hydroxycamphene, **5**, as colorless needles, mp 93–95°C (sealed tube); $[\alpha]_D^{25}$ +88.6° (c 1.00, $CHCl_3$); δ($CCl_4$), 4.75 and 4.44 (two broad signals, 1 H each, $=CH_2$), 3.49 and 3.35 (two doublets, 2 H, $J$ = 11 Hz, $—CH_2OH$), 2.67 (broad multiplet, 1 H, half-width, 7 Hz, bridgehead allylic methine), 1.07 (singlet, 3 H, tertiary methyl); $\nu_{max}$($CCl_4$), 3700 (sharp, medium, non-hydrogen-bonded OH), 3500 (broad, medium, hydrogen-bonded OH), 1670 (sharp, medium, C=C), 1045 and 1025 (broad, strong, C—O), 890 $cm^{-1}$ (sharp, strong, $=CH_2$); *m/e* 152 ($M^+$), 124, 122, 121 (base peak), 93, 91, 79, 77. Fw calcd. for $C_{10}H_{16}O$: 152.1201; found (high resolution mass spectrometry): 152.1203. *Anal.* calcd. for $C_{10}H_{16}O$: C 78.90, H 10.59; found: C 78.60, H 10.47.

*10-Oxocamphene, 6*

A solution of dry pyridine (32 mL, 400 mmol) in carbon tetrachloride (25 mL) was cooled to 0°C under nitrogen while chlorosulphonic acid (4.6 mL, 8 g, 69.4 mmol) was slowly added with stirring. The white solid formed was allowed to warm up to room temperature over 15 min, washed with *n*-hexane, and dissolved in dry dimethylsulphoxide (DMSO). A solution of (+)-10-hydroxycamphene, **5** (4.2 g, 27.6 mmol), in dry DMSO (30 mL) and dry triethylamine (55 mL, 40 g, 395 mmol) was added. The reaction mixture was stirred at room temperature for 2 h, then quenched with water and extracted with ether. Work-up in the usual way followed by distillation (35°C, 40 Torr) provided aldehyde **6** as a pale yellow liquid (2.7 g) which was homogenous on glc (3% SE 30, Varaport 30; 115°C) and tlc (silica gel) and exhibited nmr spectral data consistent with structure **6**; δ($CCl_4$), 9.50 (singlet, 1H, —CHO), 4.84 and 4.44 (two broad singlets, 1 H each, $=CH_2$), 2.70 (broad signal, 1 H, half-width 7 Hz, bridgehead allylic methine), 1.02 (singlet, 3 H, tertiary methyl).

Aldehyde **6** was used without purification in the Grignard reaction described below.

*10-Hydroxy-10-vinylcamphene, 7*

Magnesium turnings (1.3 g, 54 mmol) and a crystal of iodine were vigorously stirred in dry THF. The reaction flask was fitted with a dry ice – acetone condenser and a solution of vinyl bromide (about 10 g, 100 mmol) in dry THF was added over 30 min. After all the magnesium had dissolved the yellow suspension was stirred for 1 h before the condenser was removed and excess vinyl bromide was allowed to evaporate. A solution of crude 10-oxocamphene, **6**, (2.6 g, 17 mmol) in dry THF was added over 10 min and the mixture stirred at room temperature for 15 h. Acidification with dilute ammonium chloride, extraction with ether, and work-up in the usual way gave a yellow oil (3.1 g), which on distillation (43–45°C, 0.03–0.04 Torr) provided 10-hydroxy-10-vinylcamphene, **7**, as a colorless oil (2.5 g, 83% yield); δ($CCl_4$), 5.92 (doublet of doublets of doublets, 1 H, $J_{AM}$ = 10 Hz, $J_{BM}$ = 17 Hz, $J_{MX}$ = 4 Hz, $—CH_XOH—CH_M{=}CH_AH_B$), 5.33 (doublet of doublets of doublets, 1 H, $J_{AB}$ = 2 Hz, $J_{BM}$ = 17 Hz, $J_{BX}$ = 2 Hz, $—CH_XOH—CH_M{=}CH_AH_B$), 5.15 (doublet of doublets of doublets, 1 H, $J_{AM}$ = 10 Hz, $J_{AB}$ = 2 Hz, $J_{AX}$ = 2 Hz, $—CH_XOH—CH_M{=}CH_AH_B$), 4.87 and 4.79 (two broad singlets, 2 H, $—CH_2$), 4.09 (doublet of multiplets, 1 H, $J_{MX}$ = 4 Hz, $J_{AX}$ = 2 Hz, $J_{BX}$ = 2 Hz, $CH_XOH—CH_M{=}CH_AH_B$), 2.68 (broad signal, 1 H, half-width 8 Hz, bridgehead allylic methine), 0.95 (singlet, 3 H, tertiary methyls); $\nu_{max}$($CCl_4$), 3650 (broad, medium, OH), 3100, 2900, and 2830 (sharp, strong, CH), 1660 (broad, medium, C=C), 995 and 930 (broad, strong, $—CH{=}CH_2$), 900 $cm^{-1}$ (broad, strong, $—C{=}CH_2$); *m/e* 178 ($M^+$), 160, 150, 122, 121 (base peak), 105, 94, 93, 91, 79, 77. Fw calcd. for $C_{12}H_{18}O$: 178.1358; found (high resolution mass spectrometry): 178.1352.

*10-Acetoxy-10-vinylcamphene, 8*

10-Hydroxy-10-vinylcamphene, **7** (2.36 g, 14 mmol), was treated with acetic anhydride (3.22 g, 31.5 mmol) in refluxing dry pyridine (15 mL) for 15 h. Work-up in the usual way gave a brown oil (3.13 g) which was distilled (49–53°C, 0.01 Torr) to provide 10-acetoxy-10-vinylcamphene, **8**, as a colorless oil (2.53 g, 84% yield). $[\alpha]_D^{25}$ +17.7 (c 1.13, $CHCl_3$); δ($CCl_4$), 5.84 (doublet of doublets of doublets, 1 H, $J$ = 16, 10, 5 Hz, $—CHOAc—CH{=}CH_2$), 5.30 (multiplet, 2 H, $—CH{=}CH_2$), 5.14 (multiplet, 1 H, allylic $—CHOAc$), 4.73 and 4.62 (two broad singlets, 1 H each, $=CH_2$), 2.69 (broad signal, 1 H, half-width 8 Hz, bridgehead allylic methine), 2.03 (singlet, 3 H, $CH_3COO—$), 1.04 (singlet, 3 H, tertiary methyl); $\nu_{max}$($CCl_4$), 3130, 2900 and 2850 (sharp, medium, CH), 1750 (sharp, strong, C=O), 1650 (broad, weak, C=O), 1240 (broad, strong, C—O—C), 980, 970, 940 and 925 (broad, medium $—CH{=}CH_2$), 895 $cm^{-1}$ (sharp, medium, $—C{=}CH_2$); *m/e* 220 ($M^+$), 194, 161, 160, 145, 132, 122, 121 (base peak), 93, 89, 43. Fw calcd. for $C_{14}H_{20}O_2$: 220.1464; found (high resolution mass spectrometry): 220.1464.

*Cyclization of 10-acetoxy-10-vinylcamphene, 8, with perchloric acid*

A solution of 10-acetoxy-10-vinylcamphene, **8** (274 mg, 1.25 mmol) in chloroform was cooled by a dry ice – carbon tetrachloride bath. Perchloric acid (70%) (six drops) was added and the reaction mixture was stirred at −20°C for 1 h. It was then allowed to warm up to room temperature and stirred for 4 h. Usual aqueous work-up afforded a yellow oil (326 mg) which was purified by column chromatography (silica gel (activity grade III), elution with ether:petroleum ether (1:4)) to provide acetate **11** as colorless crystals (74 mg), mp 85–89°C (hot stage); δ($CCl_4$), 5.96 (doublet of doublets of doublets, 1 H, $J$ = 17, 12, 6 Hz, olefinic proton), 5.06 (doublet of triplets, 1 H, $J$ = 17, 2 Hz, olefinic proton), 3.25 (multiplet, 1 H, allylic methine), 2.04 (singlet, 3 H, $CH_3COO—$), 1.50 and 1.03 (two singlets, 3 H each, methyls); $\nu_{max}$($CCl_4$), 3600 (sharp, medium, non-hydrogen-bonded OH), 3500 (broad, weak, hydrogen-bonded OH), 1745 (sharp, strong, C=O), 1640 (sharp, weak, C=C), 1240 (broad, strong, C—O—C), 910 $cm^{-1}$ (broad, medium, =CH); *m/e* 238 ($M^+$), 195, 178, 153, 137, 135, 107, 106, 98, 79, 67, 43 (base peak). *Anal.* calcd. for $C_{14}H_{22}O_3$: C 70.65, H 9.30; found: C 70.37, H 9.17.

*Cyclization of 10-acetoxy-10-vinylcamphene, 8, with boron trifluoride*

10-Acetoxy-10-vinylcamphene, **8** (200 mg, 0.94 mmol), was dissolved in methylene chloride (100 mL). Boron trifluoride gas was bubbled through the solution until it was saturated and the reaction mixture was stirred at room temperature for another 10 min. Aqueous work-up gave a yellow oil (195 mg) which was purified by column chromatography (silica gel, activity grade III) followed by short-path distillation (130–150°C, 5 Torr) to provide colorless crystals (42.5 mg) which showed spectral data identical to those of acetate **11**.

Hydrolysis of the crystalline product **11** with potassium hydroxide in refluxing ethanol (95%) provided pale yellow needles which were purified by preparative glc (207 DEGS, Chromosorb W; 110°C) to provide colorless needles of diol **12**, mp 78–84°C; δ($CCl_4$), 5.91 (doublets of doublets, 1 H, $J$ = 16, 11, 4 Hz, olefinic proton), 5.06 (doublet of multiplets, $J$ = 11 Hz,

Can. J. Chem. Downloaded from www.nrcresearchpress.com by 210.87.254.40 on 09/06/12
For personal use only.

olefinic proton), 5.02 (doublet of multiplets, $J$ = 16 Hz, olefinic proton), 1.13 and 1.06 (two singlets, 3 H each, tertiary methyls); $\nu_{max}(CCl_4)$, 3500 (broad, strong, OH), 3100 (sharp, weak), and 2850 (broad, strong) (CH), 1645 (sharp, medium, C=C), 985 and 915 $cm^{-1}$ (broad, strong, =CH); *m/e* 196 ($M^+$), 178, 163, 153 (base peak), 137, 135. *Anal.* calcd. for $C_{12}H_{20}O_2$: C 73.43, H 10.27; found: C 73.42, H 10.20.

*X-ray crystallographic analysis of* **12**

A crystal ca. 0.46 × 0.38 × 0.30 mm in size was mounted in a general orientation. Unit-cell parameters were refined by least-squares on 2 sin θ/λ values for 25 reflections measured on a diffractometer with Mo Kα radiation (λ = 0.71073 Å). Crystal data at 22°C are:

$C_{12}H_{20}O_2$ fw = 196.30

Orthorhombic, $a$ = 9.571(1), $b$ = 12.416(1), $c$ = 18.860(2) Å, $V$ = 2241.2(4) Å$^3$, $\rho_m$ = 1.15 (by flotation in aqueous KI), $Z$ = 8, $\rho_c$ = 1.164 g $cm^{-3}$, $F(000)$ = 864, $\mu$(Mo Kα) = 0.43 $cm^{-1}$. Absent reflections: $hkl$, $h + k \neq 2n$, and $00l$, $l \neq 2n$ uniquely indicate the space group $C222_1$ ($D_2^5$, No. 20).

Intensities were measured with graphite-monochromatized Mo Kα radiation on an Enraf-Nonius CAD4-F diffractometer. An ω–2θ scan at 1.12–6.71° $min^{-1}$ over a range of (0.55 + 0.35 tan θ) degrees in ω (extended by 25% on both sides for background measurement) was employed. Data were measured to 2θ = 52°. The intensities of three check reflections, measured every 3600 s throughout the data collection, remained constant to within 3%.

After data reduction, no absorption correction was made in view of the low value of μ. Of the 1253 independent reflections measured, 930 (74.2%) had intensities greater than 3σ($I$) above background where $\sigma^2(I) = S + 2B + (0.04(S - B))^2$ with $S$ = scan count and $B$ = background count.

The structure was solved by direct methods, the coordinates of the oxygen and carbon atoms being determined from an $E$-map. After full-matrix least-squares refinement of the non-hydrogen atoms with anisotropic thermal parameters to $R$ = 0.085, a difference map gave the positions of all 20 hydrogen atoms which were refined with isotropic thermal parameters in subsequent least-squares cycles. The hydroxyl hydrogen atoms were both found to be twofold disordered and in view of both equal peak heights on the difference map and physical considerations discussed below, the site occupancies were kept fixed at 0.5. In the final stages of refinement, the thermal parameters of H(02a) and H(02b) were not refined since whenever the temperature factors of all four disordered hydrogen atoms were refined, at least two of them refined to negative values. The absolute configuration of **12** is determined by that known for the chiral precursor **8**. The scattering factors of ref. 5 were used for non-hydrogen atoms and those of ref. 6 for hydrogen atoms. The weighting scheme, $w = 1/\sigma^2(F)$, where $\sigma^2(F)$ is derived from the previously defined $\sigma^2(I)$, gave uniform average values of $w(|F_o| - |F_c|)^2$ over ranges of $|F_o|$ and was employed in the final stages of refinement. Convergence was reached at $R$ = 0.035 and $R_w$ = 0.044 for 930 reflections with $I \geq 3\sigma(I)$. For all 1253 reflections $R$ = 0.059 and $R_w$ = 0.047. The function minimized was $\Sigma w(|F_o| - |F_c|)^2$, $R = \Sigma||F_o| - |F_c||/\Sigma|F_o|$ and $R_w = (\Sigma w(|F_o| - |F_c|)^2/\Sigma w|F_o|^2)^{1/2}$.

On the final cycle of refinement the mean and maximum parameter shifts corresponded to 0.07 and 0.65 σ respectively. The maximum shift/error was associated with the $z$ coordinate of disordered H(01a). The mean error in an observation of unit weight was 1.362. A final difference map showed maximum fluctuations of ±0.23 e Å$^{-3}$. The final positional and thermal parameters appear in Tables 1 and 2[4] respectively. Measured and calculated structure factors have been placed in the Depository of Unpublished Data.[4]

The ellipsoids of thermal motion for the non-hydrogen atoms are shown in Fig. 1. The thermal motion has been analysed in terms of the rigid-body modes of translation, libration, and screw motion (7). The rms standard error in the temperature factor σ$U_{ij}$ (derived from the least-squares analysis) is 0.0015 Å$^2$. Analysis of all non-hydrogen atoms gave rms $\Delta U_{ij}$ = 0.0022 Å$^2$ and physically reasonable rigid-body parameters. The appropriate bond distances have been corrected for libration (7, 8), using shape parameters $q^2$ of 0.08 for all atoms involved. Corrected bond lengths appear in Table 3 along with the uncorrected values; corrected bond angles do not differ by more than 1σ from the uncorrected values given in Table 4. Intra-annular torsion angles defining the conformations of the seven-, six-, and five-membered rings of the bicyclo[3.2.1]octane system are listed in Table 5. Distances and angles involving hydrogen atoms and a complete list of torsion angles (Tables 6–8) are included as supplementary material.[4]

TABLE 1. Final positional (fractional × $10^5$, H × $10^4$) and isotropic thermal parameters ($U$ × $10^3$ Å$^2$) with estimated standard deviations in parentheses

| Atom | $x$ | $y$ | $z$ | $U_{eq}/U_{iso}$ |
|---|---|---|---|---|
| O(1) | 54342(22) | 37269(20) | 67899(12) | 55 |
| O(2) | 63954(25) | 45319(17) | 56761(11) | 52 |
| C(1) | 70884(30) | 22922(24) | 69436(15) | 51 |
| C(2) | 69009(27) | 34618(23) | 66904(12) | 43 |
| C(3) | 71693(25) | 35948(20) | 58717(12) | 36 |
| C(4) | 65726(26) | 26187(21) | 54550(11) | 38 |
| C(5) | 68125(27) | 15232(22) | 58164(16) | 47 |
| C(6) | 83489(36) | 12976(28) | 60200(21) | 61 |
| C(7) | 85186(36) | 17940(28) | 67637(19) | 61 |
| C(8) | 60983(34) | 15455(26) | 65397(15) | 54 |
| C(9) | 69881(28) | 26684(27) | 46789(14) | 51 |
| C(10) | 75000(42) | 18835(39) | 42944(22) | 75 |
| C(11) | 77678(44) | 42374(31) | 71397(18) | 63 |
| C(12) | 87044(32) | 38440(26) | 56941(16) | 48 |
| H(1) | 6954(29) | 2256(21) | 7435(18) | 59( 8) |
| H(4) | 5555(28) | 2757(22) | 5451(13) | 42( 7) |
| H(5) | 6413(30) | 956(24) | 5485(13) | 50( 8) |
| H(6a) | 8464(42) | 528(35) | 6037(18) | 87(11) |
| H(6b) | 8986(37) | 1468(29) | 5704(20) | 67(10) |
| H(7a) | 8744(38) | 1276(30) | 7148(19) | 77(10) |
| H(7b) | 9228(34) | 2303(26) | 6795(16) | 55( 8) |
| H(8a) | 5119(39) | 1817(26) | 6497(17) | 72(10) |
| H(8b) | 6075(39) | 835(30) | 6808(19) | 81(10) |
| H(9) | 6870(38) | 3332(31) | 4429(19) | 75(11) |
| H(10a) | 7691(40) | 2019(32) | 3787(20) | 83(11) |
| H(10b) | 7695(66) | 1149(48) | 4544(27) | 154(23) |
| H(11a) | 7661(28) | 4988(27) | 6936(15) | 50( 7) |
| H(11b) | 7532(41) | 4244(28) | 7628(20) | 76(10) |
| H(11c) | 8709(41) | 3986(28) | 7137(17) | 66(10) |
| H(12a) | 8797(30) | 3963(23) | 5133(16) | 58( 8) |
| H(12b) | 8923(40) | 4534(31) | 5882(20) | 83(11) |
| H(12c) | 9376(41) | 3349(36) | 5860(22) | 91(13) |
| H(O1a)′ | 5214(41) | 3820(34) | 7177(23) | 13(10) |
| H(O1b)′ | 5447(79) | 4259(66) | 6536(44) | 82(28) |
| H(O2a)′ | 5843(53) | 4766(43) | 5891(28) | 25 |
| H(O2b)′ | 6516(47) | 4667(36) | 5268(26) | 25 |

*$U_{eq}$ = (1/3) trace ($U_{diag}$), primed atoms have occupancy 0.5.

[4]The structure factor table, Table 2 (anisotropic thermal parameters) and other material mentioned in the text are available, at a nominal charge, from the Depository of Unpublished Data, CISTI, National Research Council of Canada, Ottawa, Canada K1A 0S2.

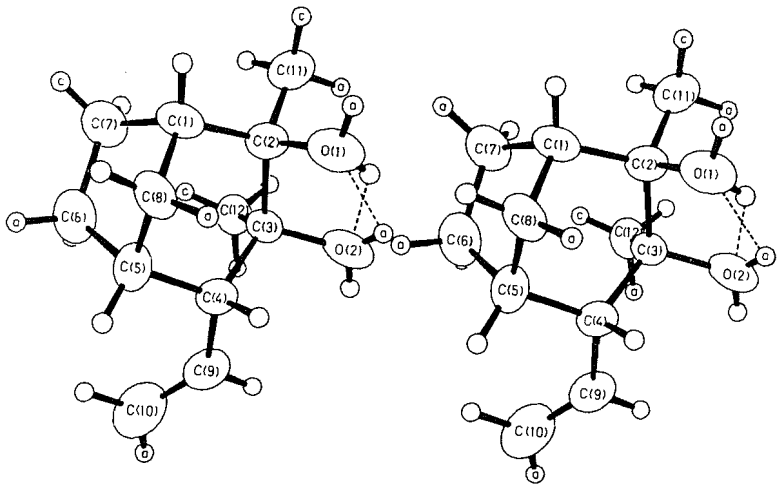


FIG. 1. Stereoscopic view of **12** showing crystallographic numbering and the disordered hydroxyl protons. 50% probability thermal ellipsoids are shown for the non-hydrogen atoms and hydrogen atoms have been assigned arbitrarily small thermal parameters for the sake of clarity.

TABLE 3. Bond lengths (Å) with estimated standard deviations in parentheses

| | Length | | | Length | |
|---|---|---|---|---|---|
| Bond | Uncorr. | Corr. | Bond | Uncorr. | Corr. |
| O(1)—C(2) | 1.454(3) | 1.460 | C(3)—C(12) | 1.538(4) | 1.543 |
| O(2)—C(3) | 1.428(3) | 1.434 | C(4)—C(5) | 1.539(4) | 1.546 |
| C(1)—C(2) | 1.539(4) | 1.546 | C(4)—C(9) | 1.518(3) | 1.522 |
| C(1)—C(7) | 1.540(5) | 1.545 | C(5)—C(6) | 1.545(4) | 1.550 |
| C(1)—C(8) | 1.529(4) | 1.535 | C(5)—C(8) | 1.526(4) | 1.531 |
| C(2)—C(3) | 1.574(3) | 1.580 | C(6)—C(7) | 1.541(5) | 1.546 |
| C(2)—C(11) | 1.528(4) | 1.530 | C(9)—C(10) | 1.310(5) | 1.312 |
| C(3)—C(4) | 1.553(3) | 1.560 | | | |

TABLE 4. Bond angles (deg) with estimated standard deviations in parentheses

| Bonds | Angle (deg) | Bonds | Angle (deg) |
|---|---|---|---|
| C(2)—C(1)—C(7) | 114.5(2) | C(2)—C(3)—C(12) | 113.0(2) |
| C(2)—C(1)—C(8) | 110.2(2) | C(4)—C(3)—C(12) | 113.4(2) |
| C(7)—C(1)—C(8) | 101.4(3) | C(3)—C(4)—C(5) | 114.2(2) |
| O(1)—C(2)—C(1) | 106.6(2) | C(3)—C(4)—C(9) | 111.1(2) |
| O(1)—C(2)—C(3) | 105.1(2) | C(5)—C(4)—C(9) | 115.1(2) |
| O(1)—C(2)—C(11) | 108.1(2) | C(4)—C(5)—C(6) | 114.4(2) |
| C(1)—C(2)—C(3) | 112.6(2) | C(4)—C(5)—C(8) | 108.2(2) |
| C(1)—C(2)—C(11) | 111.1(2) | C(6)—C(5)—C(8) | 102.0(3) |
| C(3)—C(2)—C(11) | 112.9(2) | C(5)—C(6)—C(7) | 104.7(3) |
| O(2)—C(3)—C(2) | 104.7(2) | C(1)—C(7)—C(6) | 105.5(3) |
| O(2)—C(3)—C(4) | 108.3(2) | C(1)—C(8)—C(5) | 100.3(2) |
| O(2)—C(3)—C(12) | 106.0(2) | C(4)—C(9)—C(10) | 127.0(4) |
| C(2)—C(3)—C(4) | 110.8(2) | | |

## Results and discussion

The structure analysis unambiguously identifies **12** as 2,3-dimethyl-4-vinylbicyclo[3.2.1]octan-2,3-diol, having the absolute configuration (1*R*,2*S*,3*R*,-4*R*,5*S*). The geometry of the bicyclo[3.2.1]octane system is in good agreement with that observed previously (9, 10). The mirror symmetry of the bicyclo[3.2.1]octane system is slightly disrupted by the asymmetric substitution of the C(2)—C(3)—C(4) fragment, but is retained within experimental error in the unsubstituted portion of the molecule. The bond between tetrasubstituted atoms C(2) and

Can. J. Chem. Downloaded from www.nrcresearchpress.com by 210.87.254.40 on 09/06/12
For personal use only.

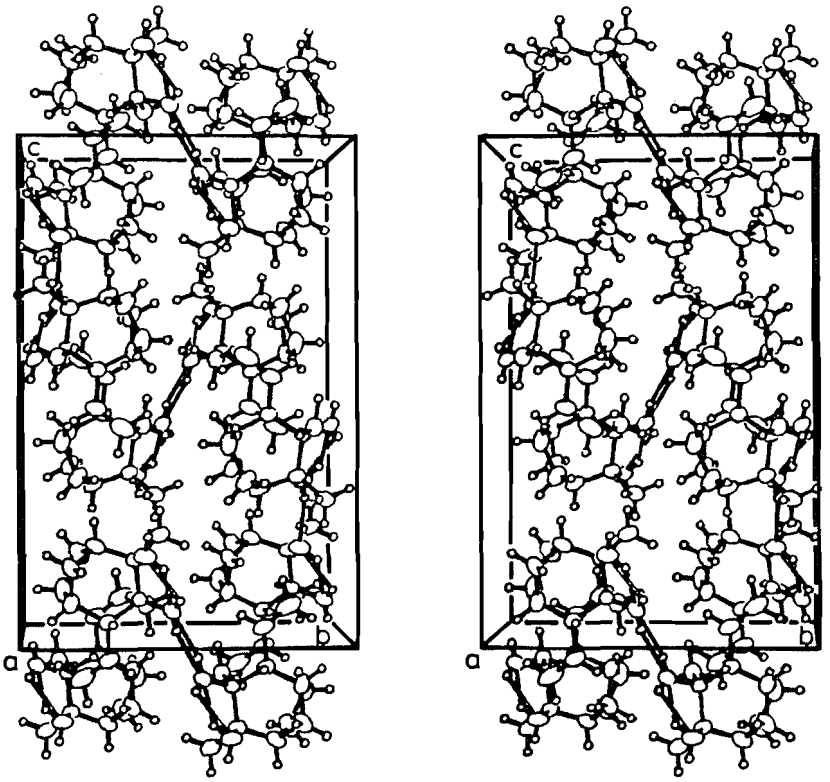


FIG. 2. Stereoscopic view down the *a* axis of the structure of **12**.

C(3), 1.580(3) Å, is significantly longer than the C(3)—C(4) bond of 1.560(3) Å. Other deviations from mirror symmetry involve bond angles at C(1), C(5), C(2), and C(4) in the six-membered ring and intra-annular torsion angles involving the C(1)—C(2), C(5)—C(4), C(2)—C(3), and C(3)—C(4) bonds (see Tables 4 and 5), in each case the difference between corresponding values not exceeding 2.0°. The C(2)—O(1) distance of 1.460(3) Å is significantly longer than the less sterically crowded C(3)—O(2) bond of 1.434(3) Å. The five-, six-, and seven-membered rings comprising the bicyclo-[3.2.1]octane system have envelope, distorted chair, and distorted boat conformations respectively. Other bond lengths and angles in the molecule are as expected.

In each molecule there is an intramolecular O—H···O hydrogen bond (O(1)···O(2) = 2.502(3) Å) involving either H(01b) (O···H = 1.89(9) Å, O—H···O = 131(7)°) or H(02a) (O···H = 2.17(5) Å, O—H···O = 109(5)°). Molecules are each linked to two others by intermolecular O—H···O hydrogen bonds (O(1)—H(01a)···O(1)(1 − *x*, *y*, 3/2 − *z*), O···O = 2.805(4), O···H = 2.05(5) Å, O—H···O = 168(4)°; O(2)···H(02b)—O(2) (*x*, 1 − *y*, 1 − *z*), O···O = 2.803(4), O···H = 2.04(5) Å, O···H—O = 160(4)°) forming continuous chains which spiral about the twofold screw axes along *c*. Molecules in these chains must alternately have the "a" and "b" OH positions occupied. If any two adjacent molecules were to have the same OH positons occupied, unrealistically short intermolecular H···H distances would result (H(01a)···H(01a) = 1.29(9)

TABLE 5. Intra-annular torsion angles (deg), standard deviations in parentheses

| Atoms | Value (deg) |
|---|---|
| C(7)—C(1)—C(2)—C(3) | 55.3(3) |
| C(1)—C(2)—C(3)—C(4) | 38.8(3) |
| C(2)—C(3)—C(4)—C(5) | −40.5(3) |
| C(3)—C(4)—C(5)—C(6) | −52.7(3) |
| C(4)—C(5)—C(6)—C(7) | 87.4(3) |
| C(5)—C(6)—C(7)—C(1) | 0.9(3) |
| C(2)—C(1)—C(7)—C(6) | −88.2(3) |
| C(8)—C(1)—C(2)—C(3) | −58.2(3) |
| C(1)—C(2)—C(3)—C(4) | 38.8(3) |
| C(2)—C(3)—C(4)—C(5) | −40.5(3) |
| C(3)—C(4)—C(5)—C(8) | 60.2(3) |
| C(4)—C(5)—C(8)—C(1) | −72.6(3) |
| C(2)—C(1)—C(8)—C(5) | 73.0(3) |
| C(8)—C(1)—C(7)—C(6) | 30.4(3) |
| C(7)—C(1)—C(8)—C(5) | −48.6(3) |
| C(6)—C(5)—C(8)—C(1) | 48.3(3) |
| C(8)—C(5)—C(6)—C(7) | −29.1)3) |
| C(5)—C(6)—C(7)—C(1) | 0.9(3) |

Can. J. Chem. Downloaded from www.nrcresearchpress.com by 210.87.254.40 on 09/06/12
For personal use only.

or H(02b)···H(02b) = 1.31(9) Å). This implies equal occupancy of the disordered OH sites.

Thus we can conclude that treatment of dieneacetate **8** with $HClO_4$ or $BF_3$ results in rearrangement and ring expansion to the bicyclo[3.2.1]octane framework (cf. Scheme 1). The failure of **8** to provide the required tricyclic product **9** is probably due to the fact that this would involve an unfavorable 5-*endo*-trigonal cyclization reaction (11). As a result we are currently investigating an alternative synthetic route to albene, **13**, which involves a more favorable 5-*endo*-digonal cyclization reaction.

## Acknowledgments

We thank the Natural Sciences and Engineering Research Council of Canada for financial support and the University of British Columbia Computing Centre for assistance.

1. K. Vokac, Z. Samek, V. Herout, and F. Sorm. Tetrahedron Lett. 1665 (1972); P. T. Lansbury and R. M. Boden. Tetrahedron Lett. 5017 (1973).
2. W. Kreiser and L. Janitschke. Tetrahedron Lett. 601 (1978); Chem. Ber. **112**, 408 (1979) and references cited therein.
3. P. C. Guha and S. C. Bhattacharyya. J. Ind. Chem. Soc. **21**, 271 (1944); W. L. Meyer, A. P. Lobo, and R. N. McCarty. J. Org. Chem. **32**, 1754 (1967).
4. H. Nishimitsu, M. Nishikawa, and M. Hagiwara. Proc. Jpn. Acad. **27**, 285 (1951), Chem. Abstr. **46**, 6111 (1952); E. J. Corey, S. W. Chow, and R. A. Scherrer. J. Am. Chem. Soc. **79**, 5773 (1957).
5. D. T. Cromer and J. B. Mann. Acta Crystallogr. Sect. A, **24**, 321 (1968).
6. R. F. Stewart, E. R. Davidson, and W. T. Simpson. J. Chem. Phys. **42**, 3175 (1965).
7. V. Schomaker and K. N. Trueblood. Acta Crystallogr. Sect. B, **24**, 63 (1968).
8. D. W. J. Cruickshank. Acta Crystallogr. **9**, 747 (1956); **9**, 754 (1956); **14**, 896 (1961).
9. F. Brisse, A. Battat, S. Perez, H. Favre, and J.-C. Richer. Acta Crystallogr. Sect. B, **33**, 1503 (1977).
10. K. K. Chacko, S. K. Bhattacharjee, R. Zand, and R. Water. Acta Crystallogr. Sect. B, **34**, 147 (1978).
11. J. E. Baldwin. J. Chem. Soc. Chem. Commun. 734 (1976); 736 (1976); J. E. Baldwin, R. C. Thomas, L. I. Kruse, and L. Silberman. J. Org. Chem. **42**, 3846 (1977).

Can. J. Chem. Downloaded from www.nrcresearchpress.com by 210.87.254.40 on 09/06/12
For personal use only.

# Interaction en milieu eau–dioxane des ions $Cu^{2+}$, $Ni^{2+}$ et $Ag^{+}$ avec les acides furannecarboxylique-2 et tetrahydrofurannecarboxylique-2

EMMANUELLE MICHAUD, GILLES PIVERT, GÉRARD DUC, MICHELLE PETIT-RAMEL[1] ET GERMAINE THOMAS-DAVID

*Laboratoire de Chimie Analytique II, Université Claude Bernard, Lyon I, 43 boulevard du 11 Novembre 1918, 69622 Villeurbanne Cedex, France*

Reçu le 24 septembre 1981

EMMANUELLE MICHAUD, GILLES PIVERT, GÉRARD DUC, MICHELLE PETIT-RAMEL et GERMAINE THOMAS-DAVID. Can. J. Chem. **60**, 1063 (1982).

Les constantes de protonation des acides furanne-2 carboxylique (HFC) et tétrahydrofuranne-2 carboxylique (THFC), puis les constantes de stabilité des complexes 1:1 formés avec le cuivre, le nickel et l'argent, ont été mesurées dans un mélange mixte 50% eau – 50% dioxane ($I$ = 0,1 ($NaNO_3$); $t$ = 25°C). L'étude potentiométrique a été complétée par des mesures spectrophotométriques uv–visible. Les résultats sont discutés et une structure chélate a été mise en évidence pour le système Cu – acide tétrahydrofuranne-2 carboxylique.

EMMANUELLE MICHAUD, GILLES PIVERT, GÉRARD DUC, MICHELLE PETIT-RAMEL, and GERMAINE THOMAS-DAVID. Can. J. Chem. **60**, 1063 (1982).

The protonation constants of furan-2 carboxylic (HFC) and tetrahydrofuran-2 carboxylic (THFC) acids and the stability constants of their copper, nickel and silver 1:1 complexes have been measured in water containing 50% dioxane ($I$ = 0.1 ($NaNO_3$); $t$ = 25°C). Treatment of the potentiometric data has been completed by uv–visible spectrophotometric measurements. The results are discussed and a chelate structure is displayed for the Cu – tetrahydrofuran-2 carboxylic acid system.

## Introduction

Un certain nombre d'antibiotiques naturels, ionophores, cycliques ou non, contiennent plusieurs hétéroatomes susceptibles de coopérer à la complexation d'un cation et, dans ces molécules, les atomes d'oxygène donneurs font partie, soit de cycles tétrahydrofuranne, soit de fractions carbonyle, alcool ou acide carboxylique. Nous nous intéressons particulièrement aux ligands qui contiennent un groupement carboxylique situé en α de l'hétéroatome (l'oxygène) et, dans un premier temps les études sont faites sur des molécules modèles contenant un seul motif furanne ou tétrahydrofuranne, fréquemment rencontrés dans les produits naturels, pour pouvoir, dans un second temps, apprécier l'effet coordinant de structures polycycliques. Les complexes correspondants sont relativement peu étudiés et concernent généralement les espèces formées avec les ions $Mn^{2+}$, $Cu^{2+}$, $Zn^{2+}$, d'intérêt biologique évident (1 à 4). Pour notre part nous avons retenu le cuivre(II), jouant principalement le rôle d'élément de référence, le nickel(II) et l'argent(I) et nous nous proposons, à l'aide du calcul de leurs stabilités thermodynamiques de mettre en évidence la formation éventuelle d'espèces chélatées.

Dans un autre domaine, il faut noter que la stabilité des complexes comme celle du ligand est nettement influencée par la composition du solvant et se traduit en général par un accroissement de stabilité avec la diminution de la constante diélectrique du milieu. En outre, les noyaux furanne et tétrahydrofuranne se révélant peu solubles en solution aqueuse, nous avons utilisé le mélange eau ($D$ = 80) – dioxane ($D$ = 2,2) qui offre une large gamme de constantes diélectriques puisque cet éther cyclique est miscible à l'eau en toutes proportions.

## Partie expérimentale

L'étude systématique des coordinats et des complexes a été réalisée par une méthode protométrique à l'aide d'une chaîne de titration automatique Tacussel. Les cellules de mesure sont thermostatées à 25°C ± 0,1°C. Dans le cas des complexes de l'argent nous avons muni l'électrode au calomel d'une allonge contenant $NaNO_3$ afin d'éviter la précipitation de AgCl. En outre la cellule de travail a été peinte en noir opaque pour prévenir toute réaction photochimique des sels d'argent.

Toutes les mesures sont effectuées en présence de sel neutre ($NaNO_3$ $10^{-1}$ $M$ dans eau – dioxane 50%) de manière à maintenir aussi constants que possible les coefficients d'activité, le potentiel de jonction liquide et la force ionique dans toute l'échelle de pH considérée ($2 < pH < 11$).

L'ensemble des résultats est donné pour un solvant mixte eau – dioxane 50% en volume ce qui correspond à une constante diélectrique voisine de 40.

### 1. *Etalonnage de la chaîne de mesure*

La pente du couple d'électrodes a été déterminée en milieu aqueux avec les solutions étalons de Bates. De plus, la correspondance entre la valeur expérimentale $pH_{exp}$ et le cologarithme de la concentration réelle en protons ($pH_{théorique}$) dépend du milieu, de la force ionique et du couple d'électrodes utilisé. L'étalonnage de la chaîne de mesure a donc été fait dans le milieu mixte sur une série de solutions de titre connu en acide nitrique par addition de soude et donne le ΔpH de correction. Cette valeur est en accord avec les résultats graphiques obtenus par la méthode de Van Uitert et Haas (5).

[1]Auteur à qui toute correspondance doit être adressée.

0008-4042/82/091063-04$01.00/0

©1982 National Research Council of Canada/Conseil national de recherches du Canada

2. *Produit ionique de l'eau*

Nous avons utilisé le même protocole d'étude que Roletto et Zelano et coll. (6 à 8) en calculant, à partir de la mesure du $pH_{exp}$, la concentration en ions $H^+$ théorique de solutions acides et basiques. Pratiquement, ceci est réalisé lors de l'étalonnage en suivant la fem au delà du point d'équivalence. La connaissance des valeurs de $pH_{théor.}$ et pOH permet alors de calculer $pK_e$.

La fem, $E$, de la cellule à 25°C est donnée par l'équation de Nernst:

$$[1] \quad E = E^0 - a\text{pH} + C\,|H^+|$$

$E^0$ est une constante de cellule, $a$ est la pente de la droite d'étalonnage mV/pH et $C|H^+|$ est le potentiel de jonction liquide.

En ce qui concerne ce paramètre $C|H^+|$, Roletto et Zelano ont montré que dans le domaine de concentration étudié, la contribution du potentiel de jonction liquide était négligeable. L'expression [1] devient:

$$[2] \quad \text{En milieu acide } E = E_a^0 - a\ \text{pH}$$

$$[3] \quad \text{En milieu alcalin } E = E_b^0 + a\ \text{pOH}$$

$$[4] \quad pK_e = \text{pH} + \text{pOH}$$

$$[5] \quad pK_e = E_a^0 - E_b^0/a$$

Il suffit alors de déterminer expérimentalement $E_a^0$ et $E_b^0$ à partir des dosages protométriques de solutions d'acide nitrique. Dans nos conditions expérimentales $pK_e = 15{,}22$.

3. *Réactifs*

*Tampons, electrolyte support, base, solvant*

Les solutions tampons de phtalate acide de potassium et de borax sont préparées par pesée et dissolution dans l'eau de produits cristallisés Merck "pro analysis". Le nitrate de sodium est un produit Prolabo R.P. cristallisé. La base est une soude Titrisol Merck préparée dans un mélange 50%eau – 50% dioxane et dosée potentiométriquement par du phtalate acide de potassium. Le dioxane est un produit Prolabo R.P. pour analyse.

*Sels métalliques*

Les cations $Cu^{2+}$, $Ni^{2+}$, sont introduits sous forme de solutions de nitrate titrées par complexométrie EDTA. Le nitrate d'argent est préparé à partir du produit cristallisé Prolabo et la solution dosée électrochimiquement par NaCl à l'aide d'une électrode reversible aux ions $Ag^+$.

*Ligands*

L'acide furannecarboxylique-2 est un produit Prolabo recristallisé et dosé par potentiométrie. L'acide tétrahydrofurannecarboxylique-2 a été préparé par hydrogénation catalytique de l'acide furoïque-2 (9, 10) et sa pureté vérifiée par chromatographie en phase vapeur. La synthèse du produit ainsi que les mesures de pureté ont été faites au laboratoire de Chimie organique Physique de Lyon I par les soins du Docteur F. Chastrette et ses collaborateurs que nous remercions vivement.

## Résultats et discussion

Considérons l'équilibre général:

$$[6] \quad pM + qH + rL \rightleftarrows M_p\,H_q\,L_r$$

où $p$ représente le nombre d'ions métalliques, M, par ligand, L; $q$ le nombre de protons liés par coordinat; $r$ le nombre de coordinats liés par ion métallique.

Pour les ligands, les équilibres d'ionisation peuvent être représentés par les constantes $\beta_{pqr}$ telles que:

$$[7] \quad \beta_{011} = |HL|/|H||L|$$

Pour chaque valeur de pH, on peut calculer le nombre moyen de protons neutralisables $\bar{q}$ par mole de coordinat.

$$[8] \quad \bar{q} = \frac{C_H - h + oh}{C_L}$$

$C_H$ et $C_L$ étant les concentrations molaires totales des constituants H et L, $h$ et $oh$ étant les concentrations libres en protons et en ions hydroxydes.

L'allure de la courbe $\bar{q} = f(\text{pH})$ indépendante de la concentration en ligand permet de prévoir la convergence rapide du processus d'affinement de la constante $\beta_{011}$ (tableau 1).

En ce qui concerne l'étude spectrale des deux acides, dans le domaine uv, un point isosbestique net à 247–248 nm confirme l'ionisation du groupement carboxylique qui provoque un déplacement vers les courtes longueurs d'onde et une diminution de l'intensité d'absorption en relation avec la diminution de résonance des molécules. Le calcul des coefficients d'absorption moléculaire (tableau 1) de chaque forme protonée met en évidence l'influence importante des doubles liaisons du cycle sur l'absorption:

$$[9] \quad \varepsilon_{(HFC)} \gg \varepsilon_{(THFC)}$$

Les constantes de stabilité des complexes ML telles que:

$$[10] \quad M + rL \rightleftarrows ML_r$$

avec:

$$[11] \quad \beta_{10r} = \frac{[ML_r]}{[M][L]_r}$$

ont été déterminées pour plusieurs rapports coordinat/métal. Les courbes de neutralisation ont été tracées en présence d'un excès de ligand et leurs transformées sous forme $\bar{q}_{exp} = f(\text{pH})$ présentent les mêmes caractéristiques de plus en plus nettes de l'argent au cuivre et nickel.

Pour des pH supérieurs à 5, les potentiels d'électrodes deviennent instables et le milieu réactionnel se trouble; il y a alors compétition entre hydrolyse et complexation du métal, la concentration des ions hydroxydes devenant supérieure à celle des ions libres du coordinat.

Pour chaque métal, les courbes de formation $\bar{r} = f(\text{pL})$ restent confondues et tendent vers 1, quel que soit le rapport ligand/métal envisagé; il ne se forme donc qu'un seul complexe ML (tableau 2) à l'exclusion d'autres espèces.

L'absorption dans le domaine visible (maximum à 715 nm pour le cuivre) confirme les résultats

TABLEAU 1. Constantes de protonation et coefficients d'absorption molaire des acides furannecarboxylique-2 (HFC) et tétrahydrofuranne carboxylique-2 (THFC)[a]

| | $\log \beta_{011}$ | | $\log \varepsilon_{011}$ $\lambda$ = 253 nm | | $\log \varepsilon_{001}$ $\lambda$ = 245 nm | |
|---|---|---|---|---|---|---|
| HFC | Nos valeurs 4,41 (0,02) | — | Nos valeurs 4,08 | (3) 4,09 | Nos valeurs 4,05 | (3) 4,05 |
| THFC | 4,96 (0,02) | (1) 4,95 (0,01) | 3,19 | — | 3,15 | — |

[a]Solvant: Eau–dioxane 50%; t = 25°C; $\mu$ = 0,1 $NaNO_3$.

TABLEAU 2. Constantes de stabilité $\log \beta_{101}$ des furoates (HFC) et tétrahydrofuroates (THFC) de cuivre, nickel et argent[a]

| | Cuivre | Nickel | Argent |
|---|---|---|---|
| HFC | 2,39 (0,03) | 1,87 (0,04) | 1,76 (0,03) |
| THFC | 3,47 (0,04) | 2,01 (0,04) | 1,86 (0,02) |

[a]Solvant eau–dioxane 50%; $t$ = 25°C; $\mu$ = 0,1 $NaNO_3$.

potentiométriques relatifs à la distribution des espèces: domaine étroit de variation d'intensité et de fréquence entre le métal libre et le métal complexé correspondant à de faibles perturbations des électrons *d*, donc à des stabilités thermodynamiques relativement peu élevées. A 715 nm on peut facilement calculer l'absorptivité molaire $\varepsilon_{101}$ = 9,5 pour le système Cu–HFC.

La presque totalité des travaux concernant les interactions métal–coordinat avec des ligands contenant un hétéroatome porte davantage sur la comparaison des stabilités selon la nature de l'hétéroatome (soufre, oxygène, azote) que sur son influence dans le phénomène de chélation (1, 11, 12). Pour notre part, nous nous attacherons à montrer la formation possible de chélate en comparant les stabilités thermodynamiques déterminées dans ce travail avec celles des complexes formés avec des ligands modèles linéaires comme les acides chloracétique (I), formique (II), β-chloropropionique (III), acétique (IV) et propionique (V). Comme l'a montré Sigel *et al.* (1), la constante de stabilité $\beta_{101}$ d'un complexe de cuivre, par exemple, est une fonction linéaire de la stabilité protonique $\beta_{011}$ du ligand correspondant (Fig. 1).

Le système Cu–THFC, reporté sur cette figure, fait apparaître un net accroissement de stabilité par rapport à la basicité du groupement carboxylique. Il faut noter que cet écart est cependant moins important que pour le complexe Cu – acide hydroxyacétique (Cu–HOAc) où l'oxygène α-substitué est qualifié de "dur" dans la classification de Pearson (13, 14). Il n'y a donc plus simple complexation mais formation d'un chélate à cinq chaînons dans lequel intervient l'hétéroatome.

Le point figuratif du système Cu–HFC se situe

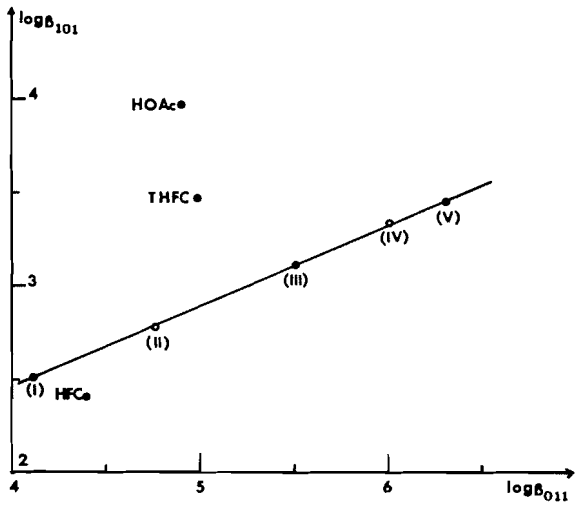


FIG. 1. Relation entre $\log \beta_{101}$ et $\log \beta_{011}$ pour les complexes du cuivre. Acides chloracétique(I) (1), formique(II) (1), β-chloropropionique(III) (1), acétique(IV) (1), propionique(V) (1), hydroxyacétique(HOAC) (1), tétrahydrofuranne(THFC) et furanne(HFC).

sensiblement en dessous de la droite précédente et ne permet donc pas d'avancer la formation d'un cycle de chélation.

D'un point de vue plus général, l'examen du tableau 2 permet d'élargir la discussion sur les valeurs relatives des stabilités des complexes formés.

Le cuivre et le nickel, complexés sous la forme ML, s'inscrivent normalement dans la série d'Irving et Williams (15) applicable aux espèces dans lesquelles les ligands n'occupent pas plus de quatre positions de coordination dans le même plan; la valeur de la constante de stabilité pour l'argent reste la plus faible.

Ces conclusions se retrouvent, en outre, être en excellent accord avec la classification de Pearson: le cuivre et le nickel se situent à la limite des acides de Lewis "durs" et "doux" alors que l'argent reste localisé dans les "doux"; l'oxygène donneur étant une base "dure" les stabilités thermodynamiques ne pourront que décroître dans le sens $Cu^{2+} > Ni^{2+} > Ag^{+}$.

1. H. SIGEL, R. GRIESSER, B. PRISS, D. MCCORMICK et M. JOINER. Arch. Biochem. Biophys. **130**, 514 (1969).
2. H. ERLENMEYER, R. GRIESSER, B. PRISS et H. SIGEL. Helv. Chim. Acta, **51**, 339 (1968).
3. P. LUMME. Suom. Kemistil. B, **33**, 87 (1960).
4. P. LUMME et K. PONKALA. Suom. Kemistil. B, **45**, 52 (1972).
5. L. G. VAN UITERT et C. G. HAAS. J. Am. Chem. Soc. **75**, 451 (1953).
6. E. ROLETTO, V. ZELANO et A. VANNI. Anal. Chim. **69**, 73 (1979).
7. E. ROLETTO, V. ZELANO et A. VANNI. J. Chim. Phys. **74**, 1126 (1977).
8. P. G. DANIELE, G. OSTACOLI et V. ZELANO. Anal. Chim. **65**, 455 (1975).
9. H. WIENHAUS et H. SERGE. Ber. **46**, 1927 (1913).
10. W. E. KAUFMANN et R. ADAMS. J. Am. Chem. Soc. **45**, 3029 (1923).
11. H. J. BLAIS et G. BERTHON. J. Inorg. Nucl. Chem. **41**, 933 (1979).
12. R. ROULET, J. FEUZ et T. VU DUC. Helv. Chim. Acta, **52**, 2154 (1969).
13. R. G. PEARSON. Science, **151**, 172 (1966).
14. R. G. PEARSON. J. Am. Chem. Soc. **85**, 3533 (1963).
15. H. IRVING et R. J. P. WILLIAMS. J. Chem. Soc. **3**, 192 (1953).

# Orientation of the methoxyl group in *cis*- and *trans*-2-methoxy-4-methyl-1,3-dioxanes and related compounds as inferred by $^1H$ and $^{13}C$ nmr spectroscopy. The significance of the "*exo*-anomeric" effect

VANGA S. RAO

*Department of Chemistry, McGill University, Montreal, P.Q., Canada H3A 2A7*

Received September 9, 1981

VANGA S. RAO. Can. J. Chem. **60**, 1067 (1982).

Carbon-13 chemical shifts and $^{13}C—^1H$ couplings are reported for some substituted 2-methoxy-1,3-dioxanes and related tetrahydropyran derivatives. These data, together with nuclear Overhauser enhancement experiments, provided evidence for a favored orientation of the methoxyl group. From an analysis of the $^{13}C$ chemical shifts and the magnitude of vicinal $^{13}C—^1H$ coupling between $—OCH_3$ and H-2, a possible dynamic-equilibrium orientation for the methoxyl group is proposed, and an evaluation of the significance of a "generalized *exo*-anomeric effect" is presented.

VANGA S. RAO. Can. J. Chem. **60**, 1067 (1982).

On rapporte les déplacements chimiques et les constantes de couplage du $^{13}C$ et du $^1H$ des méthoxy-2 dioxannes-1,3 substitués et des dérivés tétrahydropyranniques apparentés. Ces données ainsi que les expériences d'augmentation de l'effet Overhauser nucléaire, confirment l'existence d'une orientation préférentielle du groupe méthoxy. A partir de l'analyse des déplacements chimiques du $^{13}C$ et de la grandeur du couplage vicinal $^{13}C—^1H$ entre le $O-CH_3$ et le H-2, on propose une orientation possible de l'équilibre dynamique du groupe méthoxy et on présente une évaluation de la signification "d'un effet *exo*-anomère généralisé".

[Traduit par le journal]

## Introduction

In a recent publication (1) attention was drawn to a differential shielding influence by a γ-*anti* anomeric oxygen atom on the $^{13}C$ chemical shifts of C-3 and C-5 in aldopyranoses and derivatives, resulting in a larger upfield displacement for C-5 (4–5 ppm). This shielding difference was rationalized by invoking the *exo*-anomeric conformation (2) in which the *p*-type lone pair[1] of the anomeric oxygen (O-1) is oriented *anti* with respect to the C1—O5 bond, thus affecting C-5 more strongly. In extending these observations the diastereoisomeric orthoformates, *cis*- and *trans*-2-methoxy-4-methyl-1,3-dioxanes (5*a*), were prepared and their nmr data were analyzed.

## Results and discussion

### *The question of a "generalized* exo*-anomeric" effect*

The presence of the 4-methyl group in *cis*- and *trans*-2-methoxy-4-methyl-1,3-dioxanes effectively renders these isomers conformationally homogeneous (biased). Thus in the *trans* isomer (**1**) the methoxy group is in the preferred axial position (double anomeric effect) whereas the methyl substituent is in its preferred equatorial position. By contrast, the corresponding *cis* isomer (**2**) has both the methoxy and methyl groups in equatorial orientations. The *cis* isomer, **2**, is particularly well suited for studying what may be termed a "generalized *exo*-anomeric effect". It is conceivable for it to manifest a double *exo*-anomeric effect due to the presence of two equivalent adjacent ring oxygen atoms. As the methoxy group is not spherically symmetrical, in principle it can assume several rotameric states. In the *trans* isomer, **1**, the *exo*-anomeric stabilization should be at a maximum when both lone pairs ($sp^3$) of the exocyclic oxygen can participate simultaneously in the presumed electronic interaction, as in **3**. However, this "Me-inside" rotameric conformation should experience severe steric constraints due to interactions of the O-methyl group with H-4a and H-6a, as well as parallel orientation of $O—CH_3$ with O3—C4 and O1—C6 bonds. It is perhaps unreasonable to

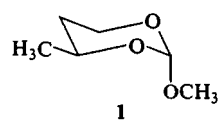

**1**

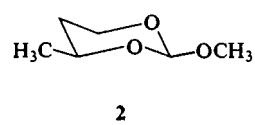

**2**

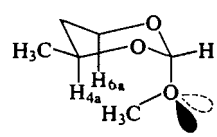

**3**

[1]Although an oxygen atom is conventionally regarded as $sp^3$ hybridized, there is theoretical (3) and experimental (4) evidence to suggest that the lone pairs are directionally nonequivalent, one occupying a higher energy orbital with considerable *p*-character (*p*-type), and the other a lower energy orbital (*s*-type). In the present paper, both concepts are utilized for comparative purposes.

0008-4042/82/091067-06$01.00/0

©1982 National Research Council of Canada/Conseil national de recherches du Canada

Can. J. Chem. Downloaded from www.nrcresearchpress.com by 210.87.254.6 on 09/06/12
For personal use only.

Can. J. Chem. Downloaded from www.nrcresearchpress.com by 210.87.254.6 on 09/06/12
For personal use only.

assume that the *exo*-anomeric stabilization alone could exceed or outweigh these destabilizing repulsive interactions, so as to maintain **1** in the conformation shown in **3**. A more probable conformation, then, is one in which each $sp^3$ lone pair interacts sequentially with the C2—O1 (**4**) and C2—O3 (**5**) bonds in a dynamic process involving an unfavorable eclipsing barrier between the O—Me group and C2—H2 bond. Alternatively, with a $sp^2$ hybridized oxygen, a symmetric conformation for **1** is conceivable in which the O—$CH_3$ and C2—H2 bonds are eclipsed and the *p*-type orbital is oriented symmetrically with respect to the C2—O1 and C2—O3 bonds, forming dihedral angles of ± 30° with these bonds, and lying orthogonal to the C2—H2 bond as shown in the Newman projection **6**. With this stereochemistry, the unfavorable O—$CH_3$ and C2—H2 eclipsing interaction may be more than compensated for by the stabilizing *exo*-anomeric effect, although when θ = ± 30°, the latter would be somewhat weaker. In fact, this orientation for the methoxy group was proposed recently (6) in rationalizing relative rates of hydrogen atom abstraction from some diastereoisomeric orthoesters of types **1** and **2** by the *tert*-butoxy radical.

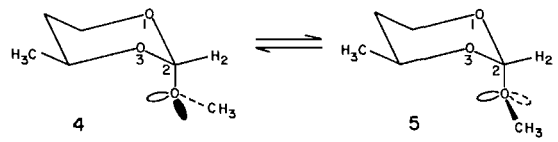


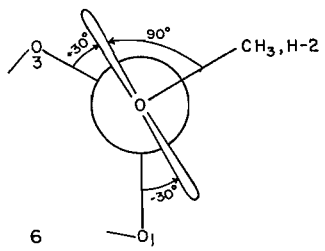


*Nuclear Overhauser enhancement experiments and vicinal $^{13}C$—$^1H$ couplings*

Nuclear magnetic resonance spectral evidence has now been obtained favoring a *cis* relationship between the O—Me and C2—H2 bonds, as in **6**. Thus, saturation of the methoxy protons of **1** resulted in an 18% nuclear Overhauser enhancement in the signal intensity of the methine proton (H-2).[2] This is similar to the level of enhancement observed with aldopyranoses and their derivatives (2*d*, 8). Another measurement was that of three-bond carbon–hydrogen coupling ($^3J_{OCH_3,\ H_2}$) between O—$CH_3$ and H-2, which amounted to 2.2 Hz. It is now well known that measured (9) and calculated (10) carbon–hydrogen vicinal couplings follow an approximate Karplus-type relationship. The observed value of 2.2 Hz appears too low (based on carbohydrate derivatives (11)) for a dihedral angle close to 0° between the O—$CH_3$ and H-2 (6), despite the presence of an additional electronegative oxygen attached to the carbon carrying the coupled proton. Hence, these results are more in accord with an entropy-favorable dynamic equilibrium (analogous to that between **4** and **5**) in which the *p*-type orbital on the exocyclic oxygen is oriented *anti* with respect to the C2—O1 (**7**) and C2—O3 (**8**) bonds, in turn. This conformation then gives dihedral angles of ± 30° between the O—$CH_3$ and C2—H2 and ± 60° between the *p*-type lone pair and C2—H2. As this ± 60° angle between the lone pair and C2—H2 is unfavorable for the

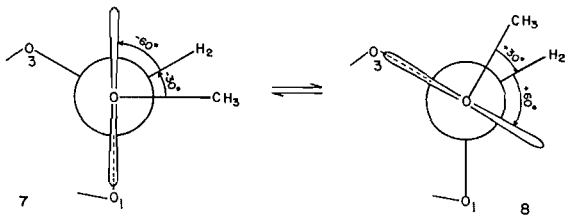


arrangement required (6) to assist homolytic fission of the C2—H2 bond, the geometries in **7** and **8** are consistent with the published results (6).

With the *cis* isomer, **2**, the preferred orientation of the methoxy group, incorporating the *exo*-anomeric effect, would be one in which each of the $sp^3$ lone pairs is *anti* with respect to the C2—O1 and C2—O3 bonds simultaneously (**9**), i.e., an *anti* orientation between O—$CH_3$ and H-2 ("Me-up rotamer"). This is also the conformation for the methoxy group proposed (6) to account for the rate of hydrogen atom abstraction in this molecule relative to **1**. Nuclear Overhauser enhancement (nOe) experiments with **2** showed no significant enhancement in the intensity of the H-2 signal when the O—$CH_3$ protons were saturated, which is taken as evidence that the O—$CH_3$ and H-2 are *trans*, as in **9**. Also, this tends to rule out the possibility of a dynamic equilibrium between two methoxy conformations in this system; one in which the $sp^3$ lone pairs are *anti* with respect to the C2—O1 and C2—H2 bonds, and the other in which they are *anti*

[2]Irradiation of the methine proton (H-2) did not cause any measurable nOe in the methoxy signal intensity. This lack of reciprocity, by analogy with a similar situation (7), may be attributed to spin-rotation and the intramethyl group dipole–dipole relaxation dominating the dipole–dipole contribution to relaxation of the methoxy group.

Can. J. Chem. Downloaded from www.nrcresearchpress.com by 210.87.254.6 on 09/06/12
For personal use only.

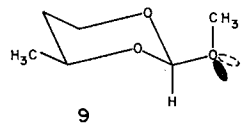

9

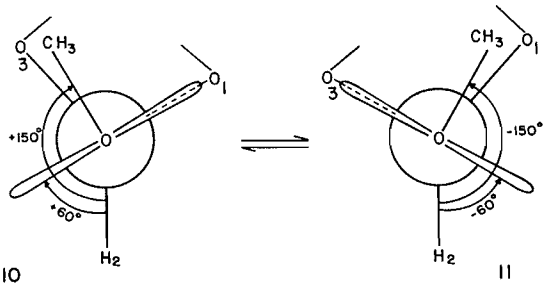

10 11

with respect to the C2—O3 and C2—H2 bonds, passing through an eclipsing barrier between the O—$CH_3$ and C2—H2 bonds. The measured coupling between O—$^{13}CH_3$ and H-2 in **2** ($^3J_{OCH_3, H_2}$) was 3.7 Hz. This is low for an *anti* arrangement between the coupled nuclei, when compared with a coupling of 5–6 Hz between $^{13}C_3$ and $H_1$ in α-D-glucopyranose (9), although the additional oxygen atom on the coupling path in **2** is expected (10) to cause a slight reduction. One way in which the magnitude of the vicinal coupling (3.7 Hz) may be rationalized is by assuming that the *p*-type lone pair on the exocyclic oxygen is oriented *anti* with respect to the C2—O1 and C2—O3 bonds *in turn*, in a dynamic equilibrium which, notably, is without any eclipsing barrier because of the *trans* arrangement between O—$CH_3$ and H-2, which probably represents two extreme ends of a flat bottomed potential energy well. This would then give a dihedral angle of ± 150° (**10** and **11**) between O—$CH_3$ and H-2, which is in better agreement with the $^{13}C$—$^1H$ coupling observed, and ± 60° between the lone pair and H-2, which again is in accordance with the published (6) rates of hydrogen atom abstraction.

### $^{13}C$ *Chemical shifts*

Turning to a consideration of $^{13}C$ chemical shifts, data for 2-alkoxy-1,3-dioxanes **1** and **2** and related compounds are presented in Table 1. The chemical shifts for **1** and **2**, unlike those of aldopyranoses and their derivatives (1) indicate no dramatic γ-*anti* differential shielding effects by the methoxy substituent. An upfield shift attributable to the γ-*anti* exocyclic oxygen in **2**, in comparison with 1,3-dioxane, is only slightly higher for C-6 (2.0 ppm) than for C-4 (1.2 ppm). Thus, reduction in the magnitude of γ-*anti* shielding as compared with aldopyranoses, and also the nearly equal effect observed on C-4 and C-6 by the methoxy substituent in **2** appears to reinforce the proposed dynamic equilibrium between **10** and **11**, because a *p*-type lone pair on the exocyclic oxygen would then be *anti* to the C2—O1 or C2—O3 bond only *half* of the time. The interpretation of the $^{13}C$ chemical shifts for *trans* isomer **1** is complicated by the superposition of γ-*gauche* upfield shifts on C-4 and C-6 by the methoxy substituent and thus of no direct concern in the present context. It is notable, however, that the upfield shifts observed for C-4 and C-6 (Table 1) are approximately of the same magnitude. Also, not surprisingly, they are larger than in cyclohexanes (12), consistent with a closer spatial relationship between the involved atoms across a shorter C–O–C bond sequence in **1** as compared with the longer C–C–C sequence in cyclohexanes. The $^{13}C$ chemical shifts of equatorial 2-methoxy-tetrahydropyran (**12**) (13) and 2-methylthio-tetrahydropyran (**26**) are of special interest in the context of the γ-*anti* upfield shifts observed in **2** (Table 1). That is, when compared with tetrahydropyran (**25**), **12** exhibits no significant differential γ-*anti* upfield shifts by the

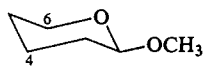

12

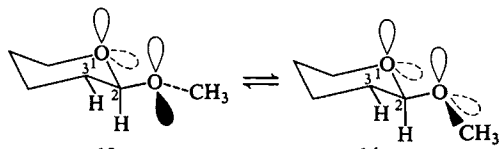

13 14

anomeric —$OCH_3$ for C-6 and C-4, as in **2**, but in contrast to the aldopyranose derivatives (1). The upfield shift on C-6 (1.9 ppm) is about twice that on C-4 (0.7 ppm). Furthermore, the γ-shifts are very nearly of the same magnitude as those in **2**. To account for these observations, an equilibrium between two conformations for the O—$CH_3$ group is envisaged, one in which the O—$CH_3$ bond is *gauche* with respect to C2—O1 and *anti* with respect to the C2—C3 bond (**13**), and the other conformation (**14**) in which these relationships are reversed. Appropriate variations can be realized if the exocyclic oxygen is $sp^2$ hybridized, rather than $sp^3$ as in **13** and **14**. The apparent nonbonded steric interactions in **13** are ($CH_3$:lone-pair), (H:lone-pair), as compared with (lone-pair:lone-pair) and ($CH_3$:H) interactions in **14**. If the lone pairs are considered bigger or nearly equal in size to the hydrogens, a matter of long controversy (14), the

TABLE 1. A comparison of the $^{13}C$ chemical shifts[a] of 1,3-dioxanes and tetrahydropyrans

| Structure | Compound | C-2 | Δ[b] | C-3 | Δ[b] | C-4 | Δ[b] | C-5 | Δ[b] | C-6 | Δ[b] | —$CH_3$ | —$OCH_3$ |
|---|---|---|---|---|---|---|---|---|---|---|---|---|---|
| 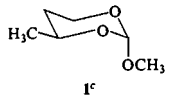 | **1**[c] | 109.0 | | | | 64.0 | | 32.5 | | 58.4 | | 21.5 | 52.7 |
| | | | 15.2 | | | | −8.9 | | −1.3 | | −8.3 | | |
| 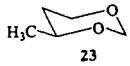 | **23** | 93.8 | | | | 72.9 | | 33.8 | | 66.7 | | | |
| | | | 18.2 | | | | −1.2 | | −1.9 | | −2.0 | | |
| 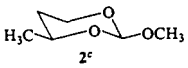 | **2**[c] | 112.0 | | | | 71.7 | | 31.9 | | 64.7 | | 21.3 | 52.7 |
| 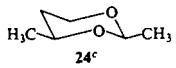 | **24**[c] | 98.9 | | | | 72.7 | | 32.9 | | 66.5 | | 21.7<br>21.3 | |
| 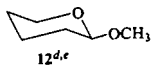 | **12**[d,e] | 104.5 | | 32.3 | | 23.0 | | 25.0 | | 67.3 | | | 57.0 |
| | | | 35.3 | | 5.3 | | −0.7 | | −2.0 | | −1.9 | | |
| | **25**[d,e] | 69.2 | | 27.0 | | 23.7 | | 27.0 | | 69.2 | | | |
| | | | 29.7 | | 3.6 | | −5.2 | | −0.9 | | −9.0 | | |
| 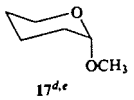 | **17**[d,e] | 98.9 | | 30.6 | | 18.5 | | 26.1 | | 60.2 | | | 55.0 |
| 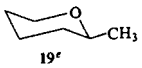 | **19**[e] | 74.9 | | 34.7 | | 24.5 | | 26.8 | | 69.2 | | 22.6 | |
| 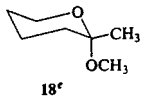 | **18**[e] | 97.5 | | 35.8 | | 18.9 | | 25.1 | | 61.3 | | 23.9 | 47.7 |
| 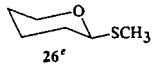 | **26**[e] | 85.1 | | 32.3 | | 24.6 | | 25.9 | | 69.9 | | 14.2 | |

[a]In $CDCl_3$ as solvent and tetramethylsilane as internal reference.
[b]Chemical shift difference (ppm) between 2-unsubstituted and the corresponding 2-substituted compounds for the carbon preceding the Δ symbol.
[c]One-bond $^{13}C—^1H$ coupling constants (Hz): **1**: C-4, H-4 = 140.4; 4-$CH_3$ = 123.6; 2-$OCH_3$ = 140.4; **2**: C-4, H-4 = 138.0; 4-$CH_3$ = 124.2; 2-$OCH_3$ = 140.7; **24**: C-2, H-2 = 156.9; 2, 4-$CH_3$ = 125.8, 125.2.
[d]In $CHFCl_2$ at −130°C.
[e]Reference 13.

Can. J. Chem. Downloaded from www.nrcresearchpress.com by 210.87.254.6 on 09/06/12
For personal use only.

Can. J. Chem. Downloaded from www.nrcresearchpress.com by 210.87.254.6 on 09/06/12
For personal use only.

steric interactions depicted may cancel out, thus allowing for a contribution of **14** as well as **13** to the overall (total) rotamer population, provided the electronic interactions alone[3] do not dictate the conformations in these molecules. However, it is possible for the O—$CH_3$ group to assume a single rotameric state if steric and electronic effects both favor such a conformer. Such a situation can be realized in β-pyranosides. Of the two conformations, **15** and **16**, for methyl β-D-glucopyranoside, **15** is favored by both steric and electronic interactions, although the electronic component ("*exo*-anomeric effect") appears to be viewed as the more important.

$^{13}C$ Chemical shifts of axial 2-methoxy tetrahydropyran (**17**) (Table 1) are complicated by γ-*gauche* upfield influences. It is noteworthy, however, that the γ-*gauche* upfield shift on C-6 (9.0 ppm) is approximately of the same magnitude as that for **1** (8.6 ppm average, C-4, 6). The smaller upfield shift for C-4 (5.2 ppm) is analogous to that in cyclohexanes (12*b*) and in saturated six-membered heterocycles (15). It is also known (12) that geminal substituents experience steric compression, resulting in local ring distortions which manifest themselves as discrepancies in $^{13}C$ chemical shifts (see ref. 14*b*, p. 194) and other nmr parameters to varying degrees within the ring. Such discrepancies (13) are to be noted when the $^{13}C$ chemical shifts of **18** are compared with those of **17** and **19** (Table 1).

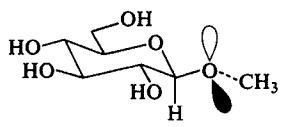


**15**

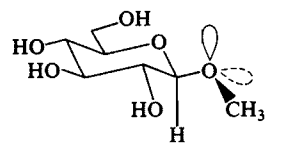


**16**

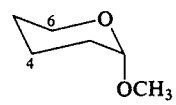


**17**

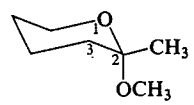


**18**

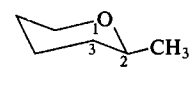


**19**

These discrepancies provide a useful example of the fact that when extending the nmr parameters from one system (e.g., THP and sugars) to another (e.g., 1,3-dioxanes), allowance should be made for intramolecular torsional variations, which can be complex and cause local or total geometries to deviate from the ideal situation. Consider the chemical shifts of **17**, **18**, and **19**. Geminal substitution of C-2 in **19** by an axial methoxy group (giving **18**) causes a 1.3 ppm downfield shift of $CH_3$-2 and a 1.1 ppm downfield shift of C-3. The O$CH_3$ signal of **18** is shifted upfield by 7.3 ppm as compared with the corresponding resonance of **17**, consistent with the *gauche* relationship between the two methyl groups in **18**. If the orientation of the $OCH_3$ group is as shown in **20**, then the observed 1.3 ppm downfield shift on $CH_3$-2 can be rationalized in the following way. There are two effects to be considered. The deshielding β-effect of the exocyclic oxygen, superimposed upon the γ-*gauche* shielding effect of the O-methyl group. As there is an overall downfield shift of 1.3 ppm on $CH_3$-2 the β-effect appears to dominate. The upfield shift of 7.3 ppm experienced by the O$CH_3$ due to the γ-*gauche* interaction with $CH_3$-2 may be considered complementary, thus making it possible to estimate the β-effect by the exocyclic oxygen as 7.3 + 1.3 = 8.6 ppm. Now C-3 should experience the same β-effect, but little influence due to the O—$CH_3$ group, because the latter is in the γ-*anti* arrangement (**20**). Hence, the predicted shift for C-3 is 8.6 ppm downfield, whereas the measured shift is only 1.1 ppm deshielding which, incidentally, is about equal to the observed shift for $CH_3$-2 (1.3 ppm). Hence, it appears necessary to examine another orientation for the $OCH_3$ group, one in which the group may be symmetrically disposed between the $CH_3$-2 substituent and C-3. This arrangement is realized in the conformation shown in **21**. Here, the $OCH_3$ is still *gauche* to $CH_3$-2, but is also *gauche* to C-3, rather than the ring oxygen atom as in **20**. Now, the preceding analysis, used to explain the net 1.3 ppm deshielding observed for $CH_3$-2, may once again be recalled in its entirety to explain the 1.1 ppm downfield shift observed for C-3. The steric requirements of **20** and **21** may not be very different, thus allowing for a substantial contribution of **21** (which is required) to the total rotamer population. Even if molecule **18** exists partly in the ring inverted form, with axial —$CH_3$ and equatorial —$OCH_3$, it appears that a major contribution of the conformation in which the —$OCH_3$ is doubly *gauche* to $CH_3$-2 and the ring C-3 is necessary to rationalize the $^{13}C$

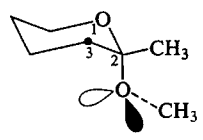


**20**

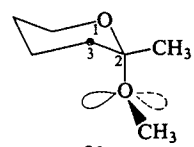


**21**

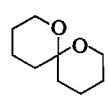


**22**

[3]Another example of the balance between electronic and steric factors is evident in the equilibration of aldoses. It may be recalled in this context that D-glucopyranose exists in aqueous solution as α- and β-anomers in the ratio 36:64, respectively (see ref. 14*a*, p. 160), even though one might have expected the α-anomer to preponderate on the basis of electronic interactions alone. Obviously this ratio is determined by a number of parameters.

Can. J. Chem. Downloaded from www.nrcresearchpress.com by 210.87.254.6 on 09/06/12
For personal use only.

chemical shifts. An interesting extension of **18** is the spiro-bicyclic compound **22**. A re-evaluation of the $^{13}C$ chemical shift data for **22** seems necessary, in view of the preceding analysis for **18** for which the contribution of conformation **21** appears unavoidable. This might then point to a conformation for **22** analogous to that for **21**, in contrast to what has been postulated (13).

*One-bond $^{13}C$—$^{1}H$ coupling constants*

Finally, it may be noted that the magnitude of one-bond coupling between C-2 and H-2 ($^{1}J_{C\text{-}2,\ H\text{-}2}$) in **1** and **2** appears to be related to the C—H bond orientation (9), just as in aldopyranoses and their derivatives. A value of 192.2 Hz is observed when H-2 is equatorial (**1**), whereas the value is 10 Hz smaller for its axial isomer **2** (182.2 Hz). Although these values are larger than those of aldopyranoses, the difference of 10 Hz between the equatorial and axial C—H bonds is in accordance with the orientation effects of lone pairs of the adjacent ring oxygen atoms on the magnitude of these couplings (1). The additional ring oxygen in the 1,3-dioxane derivatives does not affect this difference. Hence, although there are two oxygen atoms in the ring, there is only one axial C—H bond, and only one C—H antibonding orbital for interaction with the adjacent lone pairs of the oxygen atoms. This, incidentally, is in contrast to the situation in *cis*-1,4-dioxane-2,6-diol (1) wherein there is one *anti* lone pair of the adjacent oxygen atom but two degenerate antibonding C—H orbitals. The apparent increase in the $^{1}J_{C\text{-}2,\ H\text{-}2}$ (164.6 Hz) of this diol as compared to the aldopyranoses may have some bearing on this general question. The one-bond coupling between C-6 and H-6e in **2** ($^{1}J_{C\text{-}6,\ H\text{-}6e}$ = 147.2 Hz) is 9.2 Hz larger than that between C-6 and H-6a (138.0 Hz), as expected from the earlier results (1).

## Experimental

4-Methyl-1,3-dioxane (**23**) (*5b*), *cis*-2,4-dimethyl-1,3-dioxane (**24**) (*5b*), and *cis*- and *trans*-2-methoxy-4-methyl-1,3-dioxanes (**2** and **1**) (*5a*) were all prepared by literature procedures, and had physical properties in agreement with the literature.

*Nuclear magnetic resonance spectroscopy*

The $^{13}C$ nmr spectra were recorded at 22.63 MHz with a Bruker WH-90 spectrometer equipped with a B-NC 12 computer and $^{1}H$ nmr spectra were recorded at 200 MHz with a Varian XL-200 spectrometer, using $CDCl_3$ as the solvent. Chemical shifts are reported with reference to tetramethylsilane. The proton-coupled $^{13}C$ spectra were recorded in the "gated" $^{1}H$-irradiation mode with a repetition time ~2.0 s, the decoupling time ~0.6 s and the pulse width 90° (~ 18 μs). A spectral width of 3000 Hz and 8K points were used giving a digital resolution of 0.73 Hz after Fourier transformation (4K real data points).

*Nuclear Overhauser experiments*

A mixture of **1** and **2** (~ 30 mg) in approximately 54:46 ratio in $CDCl_3$ (0.7 mL) solution was freed of oxygen by slow passage of dry nitrogen gas for about two hours. The percent nuclear Overhauser enhancement in the intensity of the methine proton (H-2) was calculated from the intensities of the methine proton (H-2) with and without the irradiating frequency applied to the methoxyl protons. Several irradiating power levels were used, some well below the complete saturation of the signal, and in each case, the methine proton (H-2) was observed and integrated several times. The mean integrated intensities were used for the calculation of the percent nOe.

## Acknowledgements

The author acknowledges the kindness of Prof. A. S. Perlin in providing invaluable assistance in the preparation of this manuscript and, together with McGill University, for financial support during the course of this investigation. The author also expresses his gratitude to L. Ayotte and Dr. F. Sauriol for their generous help in recording the nmr spectra.

1. V. S. Rao and A. S. Perlin. Carbohydr. Res. **92**, 141 (1981).
2. (*a*) A. J. de Hoog, H. R. Buys, C. Altona, and E. Havinga. Tetrahedron, **25**, 3365 (1969); (*b*) A. J. de Hoog and H. R. Buys. Tetrahedron Lett. 4175 (1969); (*c*) R. U. Lemieux, A. A. Pavia, J. C. Martin, and K. A. Watanabe. Can. J. Chem. **47**, 4427 (1969); (*d*) R. U. Lemieux and S. Koto. Tetrahedron, **30**, 1933 (1974); (*e*) G. A. Jeffrey, J. A. Pople, J. S. Binkley, and S. Vishveshwara. J. Am. Chem. Soc. **100**, 373 (1978).
3. (*a*) S. David, O. Eisenstein, W. J. Hehre, L. Salem, and R. Hoffmann. J. Am. Chem. Soc. **95**, 3806 (1973); (*b*) J. O. Williams, J. N. Scarsdale, and L. Schafer. J. Mol. Struct. **76**, 11 (1981).
4. D. A. Sweigart. J. Chem. Educ. **50**, 322 (1973), and references cited.
5. (*a*) E. L. Eliel and F. W. Nader. J. Am. Chem. Soc. **92**, 584 (1970); (*b*) E. L. Eliel and Sr. M. C. Knoeber. J. Am. Chem. Soc. **90**, 3444 (1968).
6. A. L. J. Beckwith and C. J. Easton. J. Am. Chem. Soc. **103**, 615 (1981).
7. R. Rowan III, P. H. Mazzocchi, C. A. Kanagy, and M. Regan. J. Magn. Reson. **39**, 27 (1980).
8. B. Coxon. Carbodhydr. Res. **12**, 313 (1970).
9. J. A. Schwarcz and A. S. Perlin. Can. J. Chem. **50**, 3667 (1972).
10. R. Wasylishen and T. Schaefer. Can. J. Chem. **51**, 961 (1973).
11. G. K. Hamer, F. Balza, N. Cyr, and A. S. Perlin. Can. J. Chem. **56**, 3109 (1978).
12. (*a*) D. M. Grant and B. V. Cheney. J. Am. Chem. Soc. **89**, 5315 (1967); (*b*) D. K. Dalling and D. M. Grant. J. Am. Chem. Soc. **89**, 6612 (1967); (*c*) J. Am. Chem. Soc. **94**, 5318 (1972).
13. N. Pothier, D. D. Rowan, P. Deslongchamps, and J. K. Saunders. Can. J. Chem. **59**, 1132 (1981).
14. (*a*) J. F. Stoddart. Stereochemistry of carbohydrates. Wiley–Interscience, New York. 1971, pp. 55 and 189; (*b*) E. L. Eliel and K. M. Pietrusiewicz. *In* Topics in carbon-13 nmr spectroscopy. Vol. 3. *Edited by* G. C. Levy. Wiley–Interscience, New York. 1979. p. 211.
15. (*a*) G. M. Kellie and F. G. Riddell. J. Chem. Soc. B, 1030 (1971) and ref. 9 cited therein; (*b*) E. L. Eliel, V. S. Rao, and F. G. Riddell. J. Am. Chem. Soc. **98**, 3583 (1976); (*c*) R. L. Willer and E. L. Eliel. J. Am. Chem. Soc. **99**, 1925 (1977).

# The crystal structure of 1-azoniatricyclo[4.4.4.$0^{1,6}$]tetradecane and 1-azoniatricyclo[4.4.3.$0^{1,6}$]tridecane bromides[1]

JOHN M. MCINTOSH AND MASOOD A. KHAN

*Department of Chemistry, University of Windsor, Windsor, Ont., Canada N9B 3P4*

AND

LOUIS T. J. DELBAERE

*Department of Biochemistry, University of Saskatchewan, Saskatoon, Sask., Canada S7N 0W0*

Received October 14, 1981

JOHN M. MCINTOSH, MASOOD A. KHAN, and LOUIS T. J. DELBAERE. Can. J. Chem. **60**, 1073 (1982).

The crystal structures of 1-azoniatricyclo[4.4.4.$0^{1,6}$]tetradecane bromide (**1**) and 1-azoniatricyclo[4.4.3.$0^{1,6}$]tridecane bromide (**2**) are reported. Compound **1**, $C_{13}H_{24}NBr$, crystallizes in space group $P6_3/mmc$ with $a = 8.383$ (2) Å, $c = 10.092$ Å, $\gamma = 120°$, $Z = 2$. Compound **2**, $C_{12}H_{22}NBr$, crystallizes in space group $P6_3/mmc$ with $a = 8.283$ (2) Å, $c = 10.046$ (2) Å, $\gamma = 120°$, $Z = 2$. The crystal structures of **1** and **2** are statistically disordered with both enantiomers occurring in the unit cell. Compound **2** is further disordered with the one five-membered ring and the two six-membered rings of the cation being averaged over the same site in the unit cell.

The structures confirm the previously reported conclusions based on the 400 MHz nmr spectra of **1**.

JOHN M. MCINTOSH, MASOOD A. KHAN et LOUIS T. J. DELBAERE. Can. J. Chem. **60**, 1073 (1982).

On rapporte les structures des cristaux des bromures de azonia-1 tricyclo[4.4.4.$0^{1,6}$] tétradécane (**1**) et de azonia-1 tricyclo[4.4.3.$0^{1,6}$] tridécane (**2**). Le composé **1**, $C_{13}H_{24}NBr$, cristallise dans le groupe d'espace $P6_3/mmc$ avec $a = 8{,}383(2)$ Å et $c = 10{,}092$ Å, $\gamma = 120°$, $Z = 2$. Le composé **2**, $C_{12}H_{22}NBr$ cristallise dans le groupe d'espace $P6_3/mmc$ avec $a = 8{,}283(2)$ Å et $c = 10{,}046(2)$ Å, $\gamma = 120°$, $Z = 2$. Les structures des cristaux **1** et **2** sont statistiquement désordonnées avec les deux énantiomères présents dans la maille élémentaire. Le composé **2** est encore plus désordonné avec le cycle à cinq chaînons et les deux cycles à six chaînons du cation situés en moyenne au dessus du même site de la maille élémentaire.

Les structures confirment les conclusions tirées antérieurement à partir des spectres de rmn à 400 MHz du composé **1**.

[Traduit par le journal]

Recently, one of us reported the synthesis of the tricyclic ammonium salts **1** and **2** (1, 2). The background for the interest in these molecules lies in their application as the basic structural unit of chiral phase-transfer catalysts. In our analysis of the requirements for effective transfer of chirality during such a process (1, 3), it became clear that only salts in which one of the four faces of the tetrahedral nitrogen atom was available for association with an anion would be effective and salts such as **1** and **2** appeared to possess this property. However, to predict the nature and effectiveness of steric and/or polar interactions between these salts which bear further substitution on the exposed face and developing asymmetry in the transition state of the catalyzed reaction, a knowledge of the three-dimensional shape of such molecules is required.

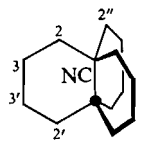


**1** ● = NC′ = $N^+$
**3** ● = NC′ = C

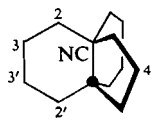


**2** ● = NC′ = $N^+$

While the 400 MHz nmr spectra provided important information regarding the dynamic properties of **1**, especially with regard to its rate of racemization (2), we felt that an X-ray crystallographic structure determination would provide important data upon which the design of substituted materials might be based. The results of the X-ray experiments on **1** and **2** and a brief comparison with **3**, the hydrocarbon analog of **1**, are reported here.

## Experimental

The crystal data for compounds **1** and **2** are given in Table 1. The systematically-absent reflections that occurred for the crystals of **1** and **2** are $hh\bar{2}hl$ ($l = 2n + 1$) and these are consistent with the following three space groups: $P6_3mc$ (No. 186), $P\bar{6}2c$ (No. 190), and $P6_3/mmc$ (No. 194).

All three of these possible space groups contain a three-fold axis which relates the three rings of the cation in both **1** and **2** to each other; i.e. the three rings are crystallographically equivalent. The six-membered rings of **1** have been shown to be present in the chair conformation in solution (2) and this conformation should also be maintained in the crystals. Regardless of whichever of these three space groups is correct, disorder of these rings must be present. Space group $P6_3mc$ (No. 186) contains a mirror plane which passes through the four planar atoms (NC, NC′, C3, C3′) of the six-membered ring chair. Space group $P\bar{6}2c$ (No. 190) contains a mirror plane perpendicular to the plane of these four atoms which would relate these atoms, in equivalent pairs, across this mirror plane (NC .. NC′, C3 .. C3′). Space group $P6_3/mmc$ (No. 194) contains both of these mirror

[1]Azapropellanes as phase-transfer catalysts, part 3. For part 2 see ref. 2.

0008-4042/82/091073-05$01.00/0

©1982 National Research Council of Canada/Conseil national de recherches du Canada

Can. J. Chem. Downloaded from www.nrcresearchpress.com by 210.87.254.105 on 09/06/12
For personal use only.

Can. J. Chem. Downloaded from www.nrcresearchpress.com by 210.87.254.105 on 09/06/12
For personal use only.

TABLE 1. Crystal data for compounds **1** and **2**

| Parameter | Compound 1 | Compound 2 |
|---|---|---|
| Formula | $C_{13}H_{24}NBr$ | $C_{12}H_{22}NBr$ |
| fw | 274.2 | 260.2 |
| Space group | $P6_3/mmc$ | $P6_3/mmc$ |
| $a = b$ (Å) | 8.383 (2) | 8.283 (2) |
| $c$ (Å) | 10.092 (2) | 10.046 (2) |
| $\gamma$ (°) | 120 | 120 |
| $V$ (Å) | 614.2 | 596.9 |
| $Z$ | 2 | 2 |
| $\rho_o$ (g cm$^{-3}$) | 1.47 | 1.46 |
| $\rho_c$ (g cm$^{-3}$) | 1.48 | 1.45 |
| Crystal dimensions (mm) | 0.10 × 0.15 × 0.25 | 0.16 × 0.16 × 0.2 |
| Radiation | $CuK_\alpha$ ($\lambda = 1.5418$ Å) | $MoK_\alpha$ ($\lambda = 0.71069$ Å) |
| 2θ max | 140 | 55 |
| Total reflections measured | 253 | 801 ($-h,k,l$; no. of unique sets = 4; $R(I) = 1.95\%$) |
| No. of unique reflections with net $I > 3\sigma(I)$ | 239 | 244 |
| $R = (\Sigma\|\|F_o\| - \|F_c\|\|/\Sigma\|F_o\|)$ | 0.068 | 0.058 |
| $Rw = (\Sigma W\Delta^2/\Sigma WF_o^2)^{1/2}$ | 0.077 | 0.051 |
| $\mu$(cm$^{-1}$) | 47.5 | 36.1 |
| Min/max absorption corr. | 1.51/2.22 | 1.72/1.92 |

planes. Regardless of whether space group $P6_3mc$ or $P\bar{6}2c$ is used, as a consequence of the mirror plane operating on the other two atoms (C2 and C2′) of the six-membered ring chair, the second (pseudo-) mirror plane is produced by the resulting position of the two equivalent atoms C2″ and C2‴; i.e. the symmetry corresponding to space group $P6_3/mmc$ is produced. Attempted least-squares refinement, in either space group $P6_3mc$ or $P\bar{6}2c$, of crystallographically independent C2 and C2′ atoms results in a very unstable refinement with one of the C2 or C2′ atoms being shifted to a chemically unreasonable location due to the high correlation between the coordinates of these atoms. Only in space group $P6_3/mmc$, where the C2 and C2′ atoms were crystallographically equivalent, was the least-squares refinement well-behaved and a chemically-meaningful result produced. Thus only this space group will be further considered in this paper. As a consequence of the symmetry of this space group, the quaternary nitrogen and carbon atoms of the cations are statistically disordered over the same atomic site (denoted as NC) in the crystal structures. As a consequence, weighted mean scattering factors (4*a*) were used (50% N, 50% C) for this atom position.

Crystals of **1** were colorless hexagonal prisms exhibiting the forms $\{10\bar{1}0\}$ and $\{0001\}$. The crystal data are given in Table 1. A single crystal of **1** was used for the data collection on an Enraf Nonius CAD4F diffractometer. Nickel-filtered $CuK_\alpha$ radiation was employed with an W/2θ scan. A total of 253 reflections were measured of which 239 unique reflections had net $I > 3\sigma(I)$. Observational weights for the reflections were derived from the formula

$$w = 1/(T + (0.02)^2T^2 + r^2B)$$

where $w$ is the derived weight, $T$ is the total peak count, $B$ is the total background counting time ($r = 2$ for this data). Lorentz and polarization corrections as well as an analytical absorption correction (5) were applied.

For **2** the crystals were needle-shaped with hexagonal cross-section. The data were collected on a Syntex P2 diffractometer equipped with a molybdenum X-ray tube and a highly oriented graphite monochromator. The procedure for data collection and processing is described elsewhere (6). A total of 801 reflections (with indices $h, k, l$) were measured and reduced to 244 unique observed data ($I > 3\sigma(I)$). During the data collection, the intensities of three monitor reflections did not change significantly. The data were corrected for Lorentz and polarization effects and an analytical absorption correction was also carried out.

*Structure determination*

The position of the bromide ion in the crystal structure of **1** was determined by inspection of the Patterson map. An $R$ index of 0.326 was obtained for the structure factor calculation based on this anion. A subsequent difference map revealed the positions of the nonhydrogen atoms of the structure. Full matrix least-squares refinement using isotropic temperature factors produced an $R$ index of 0.098. The methylene carbon atoms (C2) are also disordered and have a one-half population parameter throughout the crystal. The disorder of C2 is due to both enantiomers of the molecule being present in the crystal structure, with each of the half-occupied positions of C2 corresponding to one enantiomer. Full matrix anisotropic least-squares analysis of the atomic parameters converged with an $R$ index of 0.068. The final atomic parameters are given in Table 2. Crystallographic computations for **1** were carried out using the XRAY76 System (7) on a DEC 2060 computer at the University of Saskatchewan.

For **2**, the position of the bromide anion was obtained from a sharpened three-dimensional Patterson synthesis. A difference Fourier synthesis based on the bromide ion gave the positions of NC, C2, and C3. The structure was refined isotropically with proper multiplicity and population factors (Table 2) for these atoms to a $R$-value of 0.08. A difference map at this stage clearly indicated the disorder and showed a peak for the C4 atom. Since no separate peak for the C2 position in the five-membered ring could be observed, it was assumed that its displacement from the position of the analogous atoms in the six-membered rings is too small to be visible in the difference map. The parameters of these atoms, including the C4 atom, were refined anisotropical-

Can. J. Chem. Downloaded from www.nrcresearchpress.com by 210.87.254.105 on 09/06/12
For personal use only.

TABLE 2. Atomic parameters

(A) Atomic coordinates[a]

| | Atom | x/a | y/b | z/c | Multiplicity | Population |
|---|---|---|---|---|---|---|
| Compound **1** | Br | 0.6667 (—) | 0.3333 (—) | 0.2500 (—) | 1/12 | 1 |
| | NC | 0.6667 (—) | 0.3333 (—) | 0.6733 (10) | 1/6 | 1 |
| | C2 | 0.4881 (11) | 0.3169 (12) | 0.6214 (10) | 1 | 1/2 |
| | C3 | 0.3127 (—) | 0.1563 (4) | 0.6758 (9) | 1/2 | 1 |
| Compound **2** | Br | 0.6667 (—) | 0.3333 (—) | 0.2500 (—) | 1/12 | 1 |
| | NC | 0.6667 (—) | 0.3333 (—) | 0.6736 (10) | 1/6 | 1 |
| | C2 | 0.4824 (13) | 0.3070 (13) | 0.6243 (8) | 1 | 1/2 |
| | C3 | 0.3088 (—) | 0.1544 (9) | 0.6736 (12) | 1/2 | 2/3 |
| | C4 | 0.3332 (23) | 0.1666 (23) | 0.7500 (—) | 1/4 | 1/3 |

(B) Thermal parameters ($\times 10^3$, $A^2$)[b,c]

| | Atom | $U_{11}$ | $U_{22}$ | $U_{33}$ | $U_{12}$ | $U_{13}$ | $U_{23}$ |
|---|---|---|---|---|---|---|---|
| Compound **1** | Br | 36(—) | 36(—) | 47(1) | 18.1(4) | — | — |
| | NC | 29(—) | 29(—) | 40(6) | 15(2) | — | — |
| | C2 | 25(4) | 33(5) | 46(4) | 16(4) | −4(3) | 1(4) |
| | C3 | 23(—) | 39(3) | 67(5) | 12(2) | −9(—) | −5(2) |
| Compound **2** | Br | 38(—) | 38(—) | 40(1) | 19.1(3) | — | — |
| | NC | 31(—) | 31(—) | 31(4) | 16(1) | — | — |
| | C2 | 38(4) | 45(5) | 61(5) | 23(3) | −12(4) | −1(4) |
| | C3 | 41(4) | 112(—) | 46(6) | 56(9) | −9(6) | 17(12) |
| | C4 | 28(11) | 83(41) | 117(47) | 42(20) | — | — |

[a]The esd of the last digit is given in parentheses.
[b]Standard deviations given in parentheses.
[c]Anisotropic temperature factors are of the form:
$\exp[-2\pi^2(h^2a^{*2}U_{11} + k^2b^{*2}U_{22} + l^2c^{*2}U_{33} + 2hka^*b^*U_{12} + 2hla^*c^*U_{13} + 2klb^*c^*U_{23})]$

ly; ten cycles of full-matrix least-squares refinement converged at a final $R$-value of 0.058.[2] In the final cycle of refinement, the largest shift/error ratio was 0.01 and the final difference map had no features of chemical significance. Least-squares refinement minimized the function $\Sigma w(|F_o| - |F_c|)^2$, unit weights were used in the initial stages of refinement, while in the final cycles of calculation a weighting scheme of the form $w = (1/(\sigma^2(F) + 0.01F^2))$ was employed. Positional and thermal parameters are given in Table 2. All calculations for **2** were performed at the University of Windsor on the IBM 3031. Programs used during the structural analysis include SHELX (Fourier and L.S. refinement calculations) (8), ABSORB (absorption correction) (9), and ORTEP (thermal ellipsoid plotting program) (10). Scattering factors, including anomalous dispersion and correction terms ($\Delta f'$) and ($\Delta f''$) for the bromide ion, were taken from ref. 4*b*.

## Results and discussion

The bond lengths and angles as determined for **1** and **2** are shown in Table 3 and the torsion angles in Table 4. Also included in these tables are the corresponding weighted mean average values for hydrocarbon **3** (11). Perspective drawings of **1** and **2** are given in Fig. 1.

Compound **1** has $C_3$ symmetry and exists as two enantiomers which are interconverted by chair–chair ring inversion of all three six-membered rings. In solution, the barrier to this inversion is 17.6 kcal/mol (12*a*), while in **3** the value is 15.7 (12*b*). The crystal unit cell contains both enantiomers which results in crystal disorder. The bond lengths

TABLE 3. Bond distances and angles[a,b,c]

(A) Bond distances (Å)

| | Length | | |
|---|---|---|---|
| Bond | **1** | **2** | **3** |
| NC—NC′ | 1.55 (1) | 1.54 (2) | 1.556 |
| NC—C2 | 1.53 (1) | 1.51 (1) | 1.551 |
| C2—C3 | 1.52 (1) | 1.45 (1) | 1.531 |
| C3—C3′ | 1.50 (1) | 1.54 (2) | 1.523 |
| C2—C4 | — | 1.74 (2) | — |

(B) Bond angles (degrees)

| | Angle | | |
|---|---|---|---|
| Bond | **1** | **2** | **3** |
| C2—NC—NC′ | 110.1 (5) | 109.1 (8) | 110.9 |
| C2—NC—C2″ | 108.9 (6) | 109.8 (4) | 108.0 |
| NC—C2—C3 | 115.4 (7) | 120.3 (7) | 114.0 |
| C2—C3—C3′ | 111.2 (5) | 110.0 (11) | 110.6 |
| NC—C2—C4 | — | 100.8 (10) | — |

[a]The esd of the last digit is given in parentheses.
[b]The corresponding mean values for hydrocarbon **3** are given.
[c]Symmetry equivalent positions: ′ is $(x, x-y, 3/(2-z))$; ″ is $(1-y, x-y, z)$.

[2]The observed and final calculated structure amplitudes are available at a nominal charge from the Depository of Unpublished Data, CISTI, National Research Council of Canada, Ottawa, Ont., Canada K1A 0S2.

TABLE 4. Torsion angles (degrees)[a,b]

| Bond | Angle 1 | 2 | 3 |
|---|---|---|---|
| C2—NC—NC′—C2′ | 50.5 | 44.8 | 48.8 |
| C3—C2—NC—NC′ | −53.1 | 51.6 | −52.4 |
| C3′—C3—C2—NC | 53.7 | 52.0 | 55.4 |
| C2′—C3′—C3—C2 | −51.2 | −47.3 | −54.6 |

[a]Symmetry equivalent position ′ is $(x, x-y, 3/(2-z))$.
[b]The esd of the last digit is of the same magnitude as in Table 3B.

and angles in **1** are very similar to those in **3** (Table 3). The small differences may seem somewhat surprising when the effect of the positive center and the presence of the bromide ion is contemplated. The mean of the torsion angles in **1** (52.1°) (in **3**, 52.8°) is significantly smaller than those in cyclohexane (55.1°),[3] which indicates a flattening of the ring from the pure chair form. This observation is in accord with the 400 MHz nmr spectrum of **1** which lacks one of the expected coupling constants between the equatorial proton on C2 and the protons on C3 (2). Models indicate that a flattening of the ring would tend to bring the equatorial protons on C2 and C3 close to a 90° relationship, which would cause a vanishingly small coupling between them according to the standard Karplus relationship (14). The decrease in the mean torsion angle is compensated for largely by the NC—C2—C3 bond angle of 115.4(7)° which is significantly larger than the tetrahedral value. Again, this is similar to **3** where the corresponding angle is 114° (11).

The nmr spectra of derivatives of **1** indicate that, in solution, the anion does associate with only the exposed face of the nitrogen atom (2). Similarly, in the crystal of **1**, the bromide ion interacts with this face, the distances being 4.27 Å (NC—Br) and 4.01 Å (C2—Br).

The crystal structure of salt **2** was complicated by the occurrence of severe crystal disorder. It appears that the crystal forces are insufficient to cause a unique lattice structure with the result that the five-membered ring is randomly oriented with respect to the other two rings. As a result, the central methylene group of the five-membered ring shows a 1/3 occupancy in all three rings. In addition, the methylene groups adjacent to the quaternary centers are not resolved between the two ring sizes and are refined as a weighted mean average position. Consequently the accuracy of the bond lengths and angles involving C2 is drastically lowered. This can be seen in the calculated value of the NC—C2—C3 angle of 120.3° and the C2—C4 distance of 1.74 Å. Nevertheless it can be seen that, in general, reducing the size of one of the rings to five atoms causes only minor alterations in the bond lengths and angles of the other six-membered rings.

[3]Calculated from the cyclohexane phase II crystal data given in ref. 13.

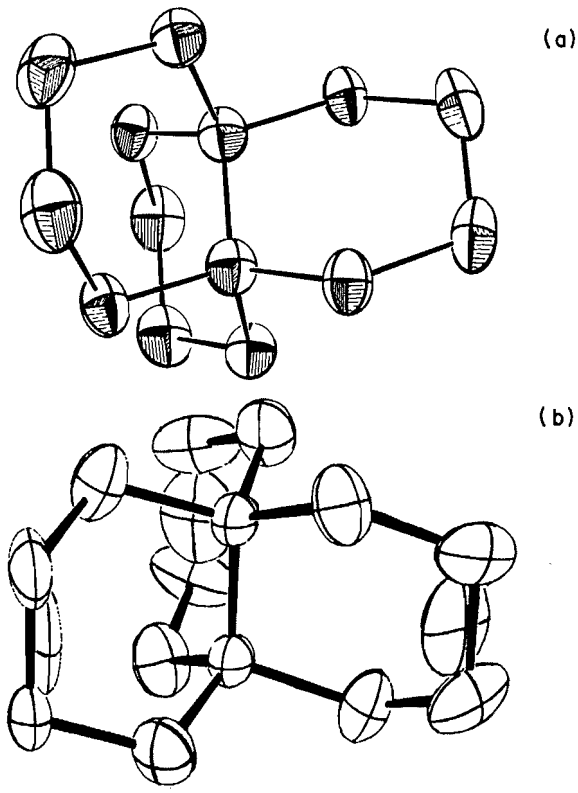


FIG. 1. ORTEP perspective drawings of (a) **1** and (b) **2**.

## Conclusions

The results presented here amply confirm our expectation that salt **1** is in the all-chair form with some small distortion of the bond angles. They also provide a framework upon which the design of substituted materials can be based. The small variations between **1** and **3** are noteworthy in that the presence of a charged atom and counterion might have been expected to have caused larger structural changes. Models indicate that, with appropriate substitution, ring inversion in **1** should become very slow, thus allowing the preparation of optically stable derivatives. Experiments toward that end are currently in progress.

## Acknowledgments

The work described was made possible by funds provided by the Natural Sciences and Engineering Research Council of Canada (to J.M.M.) and the

Can. J. Chem. Downloaded from www.nrcresearchpress.com by 210.87.254.105 on 09/06/12
For personal use only.

Medical Research Council of Canada (to L.T.J.D.) Their support is most gratefully acknowledged.

1. J. M. McINTOSH. Can. J. Chem. **58**, 2604 (1980).
2. J. M. McINTOSH. Tetrahedron. In press.
3. J. M. McINTOSH. Tetrahedron Lett. 403 (1979).
4. International Tables for X-ray Crystallography. Vol. IV. Kynoch Press, Birmingham. 1974. (*a*) p. 73; (*b*) pp. 99, 149.
5. P. COPPENS. Crystallographic computing. *Edited by* F. R. Ahmed. Munksgaard, Copenhagen. 1970. pp. 255–270.
6. M. A. KHAN, R. C. STEEVENSZ, D. G. TUCK, J. G. NOLTES, and P. W. R. CORFIELD. Inorg. Chem. **19**, 3407 (1980).
7. J. M. STEWART. The X-ray system of crystallographic computer programs. Computer Science Center, University of Maryland, College Park, MD. 1976.
8. G. M. SHELDRICK. SHELX. A program for crystal structure determinations. University of Cambridge, England. 1977.
9. D. TEMPLETON and L. TEMPLETON. ABSORB. An analytical absorption correction program. University of California, Berkeley, CA. 1973.
10. C. K. JOHNSON. ORTEP. Report ORNL-3794. Oak Ridge National Laboratory, Oak Ridge, TN. 1965.
11. O. ERMER, R. GERDIL, and J. D. DUNITZ. Helv. Chim. Acta, **54**, 2476 (1971).
12. (*a*) R. W. ALDER and R. J. ARROWSMITH. J. Chem. Res. 2301 (1980); (*b*) H. GILBOA, J. ALTMAN, and A. LOEWENSTEIN. J. Am. Chem. Soc. **91**, 6062 (1969).
13. R. KAHYN, R. FOURME, D. ANDRE, and M. RENAUD. Acta Crystallogr. Ser. B, **29**, 131 (1973).
14. L. M. JACKMAN and S. STERNHELL. Nuclear magnetic resonance spectroscopy in organic chemistry. Pergamon Press, New York. 1969. p. 280ff.

Can. J. Chem. Downloaded from www.nrcresearchpress.com by 210.87.254.105 on 09/06/12
For personal use only.

# Nematic phase nuclear magnetic resonance measurement of the $^{19}F$ chemical shift anisotropy in fluoranil[1]

D. F. R. GILSON[2]

*Department of Chemistry, McGill University, 801 Sherbrooke St. W., Montreal, P.Q., Canada H3A 2K6*

AND

S. BROWNSTEIN

*Division of Chemistry, National Research Council, Ottawa, Ont., Canada K1A 0R6*

Received October 14, 1981

D. F. R. GILSON and S. BROWNSTEIN. Can. J. Chem. **60**, 1078 (1982).

The $^{19}F$ nmr spectra of fluoranil (2,3,5,6-tetrafluoro-*p*-quinone) partially oriented in a phenyl-cyclohexyl type of nematic solvent have been studied as a function of temperature and the anisotropy of the fluorine chemical shift determined. The results, $\sigma_{zz} - \frac{1}{2}(\sigma_{xx} + \sigma_{yy}) = 185$ ppm and $(\sigma_{xx} - \sigma_{yy}) = -41$ ppm are in good agreement with the values obtained for the solid phase.

D. F. R. GILSON et S. BROWNSTEIN. Can. J. Chem. **60**, 1078 (1982).

On a étudié les spectres de rmn du $^{19}F$ du fluoranil (tétrafluoro-2,3,5,6 *p*-quinone) partiellement orienté dans un solvant nématique du type phényl-cyclohexyle, en fonction de la température; on a aussi déterminé l'anisotropie du déplacement chimique du fluor. Les résultats, $\sigma_{zz} - \frac{1}{2}(\sigma_{xx} + \sigma_{yy}) = 185$ ppm et $(\sigma_{xx} - \sigma_{yy}) = -41$ ppm, s'acordent très bien avec les valeurs obtenues dans la phase solide.

[Traduit par le journal]

## Introduction

The anisotropy of the nuclear shielding can be studied by multiple pulse coherent averaging techniques for solid phase samples or by partial orientation of a solute molecule dissolved in a liquid crystal solvent (1). The two methods can provide complementary information since the first will give values of the three principal tensor elements but not their directions (unless a single crystal is used), while the liquid crystal approach gives only differences between the tensor elements but does relate these to the molecular axes. Relatively few molecules, however, have been examined by both methods (1, 2). The first application of the coherent averaging technique to the anisotropy of a fluorine chemical shift was for fluoranil (2,3,5,-6-tetrafluoro-*p*-quinone), where the tensor elements were assigned with the assumption that the direction of greatest shielding is perpendicular to the molecular plane, by analogy with aromatic fluorocarbons (3, 4). Fluoranil has not been examined in a liquid crystal solvent, perhaps because this molecule is one of the strongest $\pi$-acceptor species (5) and can form charge transfer complexes, followed by reaction, with the commonly used nematic solvents. The availability of nematic materials based upon cyclohexyl derivatives rather than aromatic systems has made it possible to determine the chemical shift anisotropy in an oriented phase and to compare the results with those of the coherent averaging method.

## Experimental

A solution of fluoranil, 2% by weight, in a eutectic nematic solvent M1132 was used. This solvent, obtained from B.D.H., consists of a mixture of alkylcyclohexyl-phenyl and -biphenyl cyanides and has a wide temperature range nematic phase. There does not appear to be any chemical reaction with fluoranil. The FT spectra were obtained at different temperatures using a Varian XL-100 spectrometer operating at 94.18 MHz. Temperatures were measured from the proton shift difference in an ethylene glycol sample recorded either immediately before or after obtaining the $^{19}F$ sample spectrum. Fluorine chemical shifts were measured relative to an external trifluoracetic acid capillary but no corrections were applied for any temperature dependence of the reference shift position. Spectra were recorded with and without the reference sample capillary and improved resolution occurred in the latter case but at each temperature both spectra were analysed and the results averaged. Spectral width and memory size were chosen to give a digital resolution of 1.16 data points/Hz with the capillary and 2.048 without the reference. Calculations were performed using an AIM65 microprocessor with BASIC language programs.

## Results and discussion

### *Direct dipole coupling constants and motional constants*

The analysis of the spectrum of an oriented four-spin system with $D_{2h}$ symmetry has been given by Bulthuis *et al.* (6). The spectrum consists of six pairs of lines but the difference between two transitions is small and often indistinguishable. These two transitions, however, are the only ones which involve second order contributions and the

[1]NRCC No. 20012.

[2]Author to whom correspondence may be addressed.

0008-4042/82/091078-03$01.00/0

©1982 National Research Council of Canada/Conseil national de recherches du Canada

Can. J. Chem. Downloaded from www.nrcresearchpress.com by 210.87.254.105 on 09/06/12
For personal use only.

TABLE 1. Direct dipole coupling constants (Hz), motional constants, and chemical shift differences (ppm)

| Temperature °C | $D_{12}$ | $D_{13}$ | $D_{14}$ | $C_{3z^2-r^2}$ | $C_{x^2-y^2}$ | $\Delta\sigma$* |
|---|---|---|---|---|---|---|
| 26 | −907.9 | −101.4 | −77.50 | −0.3156 | −0.0459 | 16.89 |
| 34 | −838.5 | −101.2 | −75.56 | −0.3004 | −0.0372 | 16.14 |
| 44 | −754.1 | −97.31 | −71.16 | −0.2775 | −0.0292 | 14.97 |
| 54 | −636.3 | −87.44 | −62.63 | −0.2404 | −0.0211 | 13.01 |
| 64 | −424.2 | −61.33 | −43.08 | −0.1637 | −0.0120 | 8.88 |

*To high field from trifluoroacetic acid (external). 65.6 ppm in the isotropic phase.

spectra can be solved quite simply to give the three direct dipole coupling constants using the remaining four pairs of lines. Of these the outermost lines were the most intense at all temperatures and therefore all direct dipole coupling constants must have the same sign (negative) and the fluoranil molecule aligns with the principal axis parallel to the liquid crystal director axis. Only the sum of the indirect coupling constants $J_{13} + J_{14}$ is obtainable from the remaining pair of lines. A value of +5 Hz was obtained, which falls within the range of reported values (7, 8).

For molecules with $D_{2h}$ symmetry two motional constants, or orientation parameters, are required to describe the average orientation of the solute molecule. Thus, using Snyder's notation (9), the direct dipole coupling constants are given by eq. [1]

$$[1]\quad D_{ij} = -\frac{K}{\sqrt{5}}\left\{C_{3z^2-r^2}\left(\frac{2(\Delta z_{ij})^2}{r_{ij}^5} - \frac{(\Delta x_{ij})^2}{r_{ij}^5} - \frac{(\Delta y_{ij})^2}{r_{ij}^5}\right) + \sqrt{3}C_{x^2-y^2}\left(\frac{(\Delta x_{ij})^2}{r_{ij}^5} - \frac{(\Delta y_{ij})^2}{r_{ij}^5}\right)\right\}$$

where $K$ is a constant involving the magnetogyric ratio, $r_{ij}$ is the internuclear distance, and $\Delta x_{ij}$, $\Delta y_{ij}$, and $\Delta z_{ij}$ are the components of $r_{ij}$ along coordinate axes in the molecular framework. In the present case all $\Delta z_{ij}$ are zero, $\Delta x_{14} = r_{14}$ and $\Delta y_{12} = r_{12}$. If one internuclear distance, e.g. $r_{12}$, is assumed then there are three parameters, $C_{3z^2-r^2}$, $C_{x^2-y^2}$, and $r_{14}$ to be determined from three direct dipole coupling constants. Alternatively, eq. [1] for each $D_{ij}$ can be recast in terms of the ratio between $r_{12}$ and $r_{14}$ and the motional constants eliminated to give a single eq. [2]

$$[2]\quad D_{13}(1+\rho^2)^{5/2} - D_{14}\rho^5 - D_{12} = 0$$

where $\rho = r_{14}/r_{12}$. A plot of $D_{14}/D_{12}$ versus $D_{13}/D_{12}$ can be used to derive a value for ρ. Figure 1 shows that the magnitudes of the direct dipole coupling constant ratios are such that valid geometrical information can be obtained and, since a straight line plot will fit the data at different orientations,

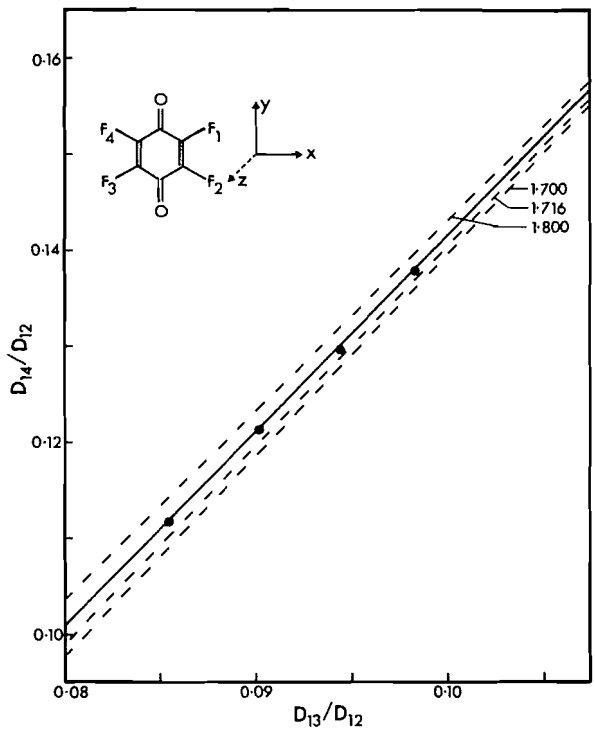


FIG. 1. Plot of $D_{14}/D_{12}$ versus $D_{13}/D_{12}$. The dotted lines are calculated for various values of ρ, including = 1.716, the value obtained from an X-ray crystallographic study. The solid line is a least-squares fit to the points, ρ = 1.746.

the anisotropy in the indirect coupling constants is small (10).

A least-squares fit gave a value of ρ = 1.746, which can be compared with the results of X-ray crystallographic (11) and electron diffraction (12) structure determinations. There is poor agreement between the present results and that obtained in the X-ray study of 1.716. However, the electron diffraction value, ρ = 1.731, is much closer, and is similar to that found in a study of fluoranil in the solid charge transfer complex with perylene (13) of 1.739. Thus the nmr value supports the contention of Schei *et al.* (12) that the reliability of the X-ray

Can. J. Chem. Downloaded from www.nrcresearchpress.com by 210.87.254.105 on 09/06/12
For personal use only.

Can. J. Chem. Downloaded from www.nrcresearchpress.com by 210.87.254.105 on 09/06/12
For personal use only.

investigation is lower than the reported error limits would indicate.

*Anisotropy of the fluorine chemical shift*

The chemical shift difference, $\Delta\sigma$, between the partially oriented and isotropic solutions is given by eq. [3]

$$[3]\quad \Delta\sigma = \frac{2}{3\sqrt{5}} C_{3z^2-r^2}\{\sigma_{zz} - \frac{1}{2}(\sigma_{xx} + \sigma_{yy})\} + \frac{1}{\sqrt{15}} C_{x^2-y^2}\{\sigma_{xx} - \sigma_{yy}\}$$

If only one measurement of this shift difference is made then only a linear relationship between the tensor elements can be derived, but if the dependence of $\Delta\sigma$ upon orientation is known, for example by changing concentration or temperature, then a plot of $\Delta\sigma/C_{3z^2-r^2}$ versus $C_{x^2-r^2}/C_{3z^2-r^2}$ can be used to give $\{\sigma_{z^2} - \frac{1}{2}(\sigma_{xx} + \sigma_{yy})\}$ from the intercept and $\{\sigma_{xx} - \sigma_{yy}\}$ from the slope. However, the values of the motional constants depend upon the assumed internuclear distances and thus the calculated shift anisotropy will reflect the uncertainty in $r_{12}$ and $r_{14}$. Figure 2 shows the plots for the two values of $\rho$, obtained from the direct dipole coupling constant ratios and from the electron diffraction structure, and the shift anisotropy terms are listed in Table 2. The agreement with the results of Mehring *et al.* (4) is quite good and shows that their assumption that the direction of largest shielding is perpendicular to the molecular plane was correct. In comparing the results of solid phase and oriented solution measurements, the possibility of contributions to $\Delta\sigma$ from the change in local environment cannot be excluded. The vibrational spectra of fluoranil in the solid, solution, and vapour phases show only small changes in vibrational frequencies (14) indicating that there are no strong intermolecular interactions in the solid. In the solution phase the possibility exists of charge transfer complex formation between fluoranil and the aromatic regions of the solvent molecules. Such complex formation, however, is probably very slight since the solvent molecules should be poor donors due to steric effects and the cyano substituent causes acceptor rather than donor ability. An attempt to measure the anisotropy of the chemical shift of fluoranil in a charge transfer complex was unsuccessful since addition of hexamethylbenzene to the fluoranil solution resulted in crystallization of the donor–acceptor complex.

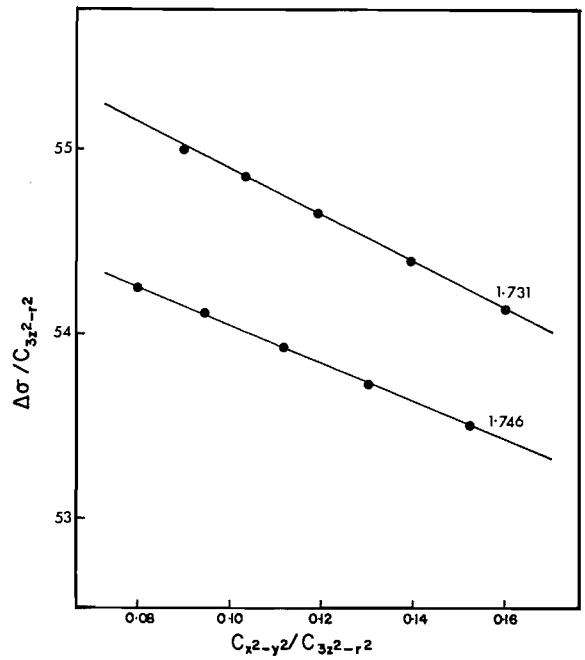


FIG. 2. Plot of $\Delta\sigma/C_{3z^2-r^2}$, ppm, versus $C_{x^2-y^2}/C_{3z^2-r^2}$. The solid lines are least-squares fits for two different values of $\rho$.

TABLE 2. Anisotropy of the chemical shift (ppm)

| $\rho$ | $\sigma_{zz} - \frac{1}{2}(\sigma_{xx} + \sigma_{yy})$ | $(\sigma_{yy} - \sigma_{yy})$ |
|---|---|---|
| 1.746 | 184.6 | −40.5 |
| 1.731 | 187.7 | −45.9 |
| Reference 4 | 175.5 | −51.0 |

**Acknowledgements**

The work at McGill University was supported by grants from the Natural Sciences and Engineering Research Council of Canada. The assistance of Mr. J. Bornais is gratefully acknowledged.

1. B. R. APPLEMAN and B. P. DAILEY. Adv. Magn. Reson. **7**, 231 (1974).
2. M. MEHRING. NMR: basic principles and progress. Vol. 11. Springer Verlag. 1976.
3. M. MEHRING, R. G. GRIFFIN, and J. S. WAUGH. J. Am. Chem. Soc. **92**, 7222 (1970).
4. M. MEHRING, R. G. GRIFFIN, and J. S. WAUGH. J. Chem. Phys. **55**, 746 (1971).
5. R. FOSTER. Organic charge transfer complexes. Academic Press, New York. 1969.
6. J. BULTHUIS, J. GERRITSEN, C. W. HILBERS, and C. MACLEAN. Recl. Trav. Chim. Pays-Bas, **87**, 417 (1968).
7. M. HUDLINKY and H. M. BELL. J. Fluorine Chem. **6**, 201 (1975).
8. V. WRAY, Annu. Rep. NMR Spectrosc. **10B**, (1980).
9. L. C. SNYDER. J. Chem. Phys. **43**, 4041 (1965).
10. J. GERRITSEN, G. KOOPMANS, H. S. ROLLEMA, and C. MACLEAN. J. Magn. Reson. **8**, 20 (1972).
11. A. MERESSE, C. COURSELLE, and N. B. CHANH. Acta Crystallogr. Sect. B, **20**, 524 (1974).
12. H. SCHEI, K. HAGEN, M. TRAETTEBERG, and R. SEIP. J. Mol. Struct. **62**, 121 (1980).
13. A. W. HANSON, Acta Crystallogr. **16**, 1147 (1963).
14. A. GIRLANDO and C. PECILE. J. Chem. Soc. Faraday Trans. II, **71**, 689 (1975).

# Total synthesis of zizaane sesquiterpenes: (−)-khusimone, (+)-zizanoic acid, and (−)-epizizanoic acid

HSING-JANG LIU AND WING HONG CHAN

*Department of Chemistry, University of Alberta, Edmonton, Alta., Canada T6G 2G2*

Received November 23, 1981

HSING-JANG LIU and WING HONG CHAN. Can. J. Chem. **60**, 1081 (1982).

Three sesquiterpenes of the zizaane family, khusimone (**1**), epizizanoic acid (**3**), and zizanoic acid (**2**) have been synthesized in optically active form from the ammonium salt of (−)-*l*-10-camphorsulfonic acid in sixteen, nineteen, and twenty steps respectively.

HSING-JANG LIU et WING HONG CHAN. Can. J. Chem. **60**, 1081 (1982).

Partant de l'acide (−)-*l*-camphresulfonique-10, on a synthétisé dans une forme optiquement active trois sesquiterpènes de la famille du zizaane soit la khusimone (**1**) et les acides zazinoïque (**2**) et épizazinoïque (**3**); ces synthèses requièrent respectivement seize, vingt et dix-neuf étapes.

[Traduit par le journal]

Can. J. Chem. Downloaded from www.nrcresearchpress.com by 210.87.254.42 on 09/06/12
For personal use only.

We wish to report a stereoselective total synthesis of khusimone (**1**) (1, 2), zizanoic acid (**2**) (3) (also known as khusenic acid (4)), and epizizanoic acid (**3**) (5), three tricyclic sesquiterpenes of the zizaane family which have been isolated from the essential oil of vetiver varieties. Zizaane sesquiterpenes have been the subject of considerable synthetic activity and several total syntheses have been accomplished during the last decade (6–13). A successful synthetic approach to this class of natural products must address three principal problems: (*i*) the construction of the tricyclo[6.2.1.$0^{1,5}$]-undecane ring system which is characteristic of the class, (*ii*) installation of an *exocyclic* methylene unit, and (*iii*) control of the stereochemistry, particularly the less stable *trans*-fused hydroindan ring junction. Although the tricyclic ring system has been assembled by a number of elegant approaches, simple solutions to the latter two problems are still in demand.

Khusimone (**1**)[1] was chosen as the primary target of our study because of its considerable importance to the perfume industry and for the possibility of its ready conversion to other members of the zizaane family. Our projected scheme (Scheme 1) would employ an intramolecular photochemical process (**4** → **5**) as a means to control the stereochemistry and facilitate the introduction of the *exocyclic* double bond. Not only does the stereochemistry of the resulting ketone **5** at C-1 and C-6 coincide with that of the two crucial centers, C-5 and C-8 respectively, of the natural products, but the replacement of the ketone carbonyl with a methylene unit (**5** → **7**) via the dehydration of alcohol **6** could

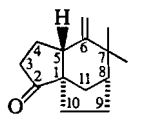

**1**

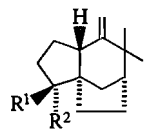

**2** $R^1 = COOH$; $R^2 = H$
**3** $R^1 = H$; $R^2 = COOH$

be expected to proceed without difficulty since the formation of an *endocyclic* double bond by dehydration of **6** would impose additional angular strain to the already strained cyclobutane ring. It was further anticipated that ring expansion of cyclobutanone **8** (derived from olefin **7**) to cyclopentanone **9** followed by cyclization would effectively complete the khusimone synthesis.

Towards this end, several 2-cyclohexenone derivatives of type **4** were prepared and their photochemistry was examined. (−)-α-Campholenic acid (**10**) possessing the same chirality as the natural khusimone (**1**) was obtained in 52% yield from the commercially available *l*-10-camphorsulfonic acid

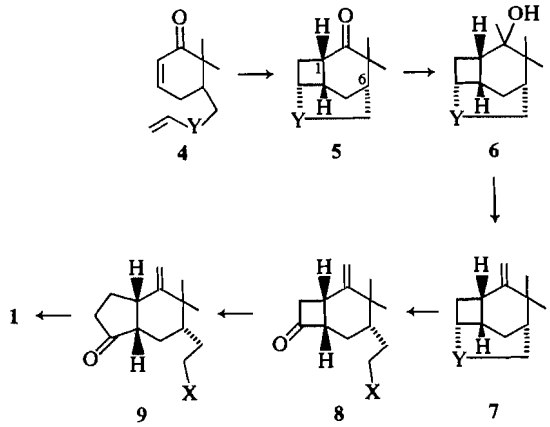

**4** **5** **6** **7** **8** **9** **1**

SCHEME 1

[1](±)-Khusimone has been synthesized previously by Büchi *et al.* (11). For a preliminary account of our work leading to (−)-khusimone, see ref. 14.

0008-4042/82/091081-11$01.00/0

©1982 National Research Council of Canada/Conseil national de recherches du Canada

Can. J. Chem. Downloaded from www.nrcresearchpress.com by 210.87.254.42 on 09/06/12
For personal use only.

ammonium salt by fusion with potassium hydroxide (15). Esterification of acid **10** with potassium carbonate and methyl iodide in refluxing acetone (16) gave a quantitative yield of ester **11** which was subjected to ozonolysis at −78°C in a solution of methylene chloride – methanol (1:1). Reductive work-up using triphenyl phosphine[2] (18) gave keto aldehyde **13** which, without purification,[3] was immediately treated with *p*-toluenesulfonic acid in refluxing benzene to give enone ester **14** (70% yield from **11**).

For the transformation of enone ester **14** to a tricyclic compound of type **5** via an intramolecular photocycloaddition reaction, vinyl ester **15** was an attractive intermediate. Apart from its anticipated ease of preparation from enone ester **14**, the cycloaddition of vinyl ester **15** was expected to proceed in a head-to-tail fashion, well precedented by the addition of vinyl acetate to 2-cyclohexenones by an intermolecular photochemical process,[4] to give product **16** with the desired orientation. The conversion of enone ester **14** into vinyl ester **15** was indeed straightforward. The latter compound was obtained in 60% yield when the former was hydrolyzed with sodium hydroxide and the resulting acid **17** was treated with vinyl acetate in the presence of a catalytic amount of mercuric acetate and concentrated sulfuric acid (22). The attempted photocycloaddition of vinyl ester **15** using a variety of conditions was, however, completely fruitless and resulted in recovery of the starting material. Although the observed unreactivity of vinyl ester **15** remains to be understood, we hoped that the photochemical reaction would take a different course by increasing or reducing its side chain by one atom. Thus, allyl ester **18** was prepared by esterification of acid **17** using allyl bromide and potassium carbonate. Disappointingly, allyl ester **18** was found to be equally unreactive. The photochemistry of enone acetate **19**, which has a shorter side chain than that of vinyl ester **15**, was also examined. This compound was prepared from enone ester **14** in four steps as follows. Enone ester **14** was first reduced to diol **20** (72% yield) by lithium aluminium hydride. Oxidation of **20** with four equiv. of pyridinium chlorochromate (23) afforded keto aldehyde **21** in 69% yield. Treatment of **21** with a slight excess of vinylmagnesium bromide at −78°C followed by acetylation of the resulting ketols **22** with acetic anhydride in pyridine gave an inseparable mixture of two epimeric keto acetates **19** (1:1) in 50% yield. Irradiation of a methanolic[5] solution of keto acetates **19** for 4 h caused the complete disappearance of the starting material. The product which was obtained in 43% yield showed in the ir spectrum the appearance of an absorption band at 1700 $cm^{-1}$ and the absence of the 1675 $cm^{-1}$ band previously observed for the conjugated enone system, suggesting that the photocycloaddition had taken place. This was confirmed by the mass spectrum displaying a molecular ion peak at 236.1419 and by the absence of low field signals for olefinic protons in the nmr spectrum. The nmr spectrum showing three sharp methyl singlets at δ 1.00, 1.21, and 1.95 further suggested that the product was a single compound which might have resulted from selective isomerization or destruction of one epimer of the starting material during the irradiation. The cycloaddition in principle can proceed in two different ways, head-to-tail and head-to-head, to give adducts **23** and **24** respectively. The available spectral data, however, did not permit unambiguous definition of the orientation of the isolated product. Nor did the examination of a Dreiding model reveal the preference of one orientation to the other. The conclusive evidence was provided by the following chemical transformations whereby the structure of the product was found to be as depicted in **24** with the undesired orientation. Hydrolysis of the acetate **24** with aqueous potassium carbonate in refluxing methanol gave the corresponding alcohol **25** which was oxidized with Jones reagent to diketone **26**. When treated with *m*-chloroperbenzoic acid in dichloromethane, diketone **26** underwent selective Baeyer–Villiger oxidation to give lactone **27**. Hydrolysis of **27** with aqueous potassium carbonate in refluxing methanol induced concomitant cyclobutane ring cleavage, apparently by a retro-aldol, giving rise to acid **28**,[6] the structure of which was further confirmed by esterification with diazomethane to give the corresponding methyl ester **30**.

Although it would be of general interest to investigate the photochemistry of other suitable derivatives of keto ester **14** such as **31** and **32** in

[2]Attempted reductive work-up using dimethyl sulfide (17) was proven to be ineffective and a single ozonide **12** (ir (neat): 1750 (C=O) $cm^{-1}$; nmr ($CCl_4$) δ: 5.62 (t, 1H, $J$ = 1 Hz, —OCHO—), 3.58, 1.36, 1.12, and 0.93 (all s, 3H each, 4 × —$CH_3$)) was isolated in 42% yield.

[3]Keto aldehyde **13** was shown to be rather unstable. Attempted purification resulted in substantial loss of material.

[4]For reviews of photocycloaddition reactions, see refs. 19–21.

[5]Similar results were obtained using acetonitrile or benzene as a solvent.

[6]By the reaction sequence, the alternative photochemical product **23** should result in the formation of stable hydroxy acid **29**, and the isolation of acid **28** clearly defines the structures of its precursors as depicted.

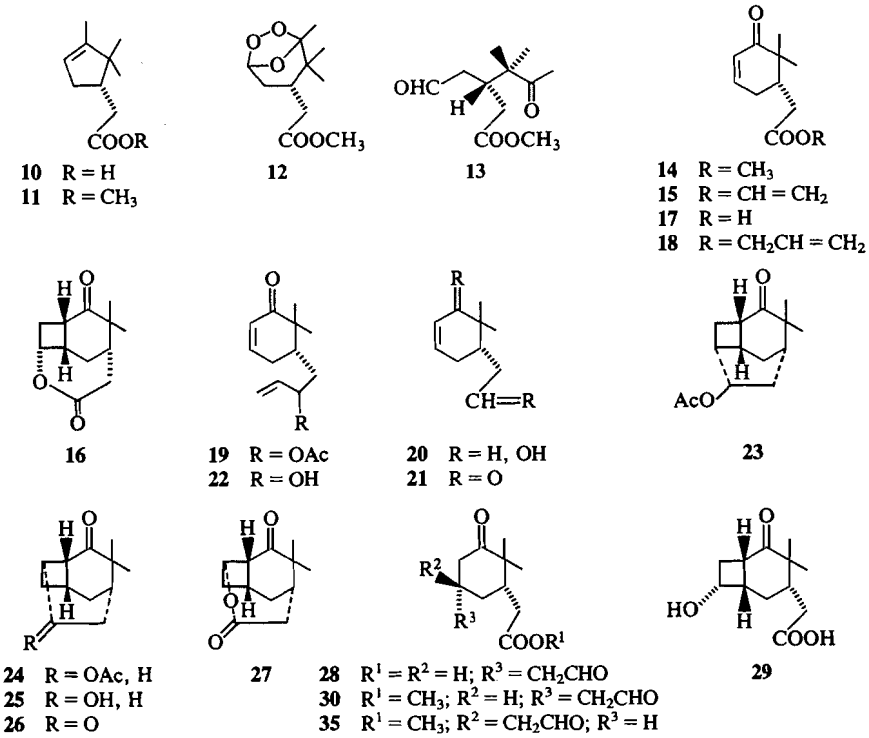


**10** R = H
**11** R = $CH_3$

**12**

**13**

**14** R = $CH_3$
**15** R = $CH=CH_2$
**17** R = H
**18** R = $CH_2CH=CH_2$

**16**

**19** R = OAc
**22** R = OH

**20** R = H, OH
**21** R = O

**23**

**24** R = OAc, H
**25** R = OH, H
**26** R = O

**27**

**28** $R^1 = R^2 = H$; $R^3 = CH_2CHO$
**30** $R^1 = CH_3$; $R^2 = H$; $R^3 = CH_2CHO$
**35** $R^1 = CH_3$; $R^2 = CH_2CHO$; $R^3 = H$

**29**

particular, the large number of steps required for their synthesis as well as for the later modification preclude their efficient application to khusimone (**1**) synthesis. The subsequent studies were focussed on the addition, in a head-to-tail manner, of a latent ketene unit to the carbon–carbon double bond of keto ester **14** by an intermolecular photochemical process. We realized at the outset that such an approach would not allow profound stereochemical control as the addition could take place from both the α and the β face of the molecule and hence adjustment of stereochemistry at a suitable stage would be necessary. This drawback could, however, be compensated to a certain extent as enone **14** could be used directly without modifying its ester side chain.

Vinyl acetate was initially used as a ketene equivalent. Irradiation of enone **14** with a twenty-fold excess of vinyl acetate in benzene for 3 h at room temperature afforded a mixture of inseparable photoadducts in 77% yield. As shown by the subsequent transformation, both regioisomers **33** and **34** were formed in a ratio of approximately 4:1 with the desired isomer **33** predominating. On treatment with sodium methoxide in methanol at room temperature for 30 min, the mixture of photoadducts gave two products readily separable by column chromatography on silica gel. The minor component isolated in 16% yield was deduced to be a mixture of aldehyde **30** and its C-5 epimer **35** resulting, apparently, from the undesired photoadduct **34**. The major component, which was obtained in 67% yield, was shown to be a mixture of diastereomeric alcohols **36**[7] derived from the desired head-to-tail adducts **33**. Jones oxidation of this mixture gave two separable ketones **37** and **38** in a ratio of 5:6 and in a total yield of 67%. Although the ir and mass spectra of these ketones were very similar, distinct differences were observed in their nmr spectra. The geminal methyl groups of the major isomer appeared as a pair of singlets at δ 1.06 and 1.12 whereas the minor isomer showed two singlets at δ 0.97 and 1.21 for the corresponding methyls. The difference in Δδ (0.24 for the minor vs. 0.06 for the major) observed for the *gem*-dimethyl groups of these two compounds allowed us to tentatively assign their stereochemistry as follows. An examination of Dreiding models reveals that in the most stable contributive conformation of compound **37**, which could be represented by **37***a*, one methyl group lies within the deshielding zone of cyclohexanone carbonyl and the other within the shielding zone of cyclobutanone. On the other hand, in the case of compound **38**, whose stable conformation is depicted in formula **38***a*,

[7]Based on previous observations (24), a *cis* ring junction could be readily assigned to each diastereomer.

Can. J. Chem. Downloaded from www.nrcresearchpress.com by 210.87.254.42 on 09/06/12
For personal use only.

Can. J. Chem. Downloaded from www.nrcresearchpress.com by 210.87.254.42 on 09/06/12
For personal use only.

both methyls are distant from the cyclobutanone ring and thus devoid of any serious influence from its carbonyl. A larger $\Delta\delta$ for **37** and a smaller one for **38** are therefore expected and it follows that the minor isomer possesses structure **37** and the major structure **38**. These structural assignments were further supported by the optical rotatory dispersion analysis (25). The minor isomer displayed a positive anomalous single Cotton effect curve and the major showed a negative one. With the aid of models, the octant diagrams corresponding to the most stable conformations of the two diastereomers **37** and **38** are represented by Figs. 1 and 2 respectively. In the case of **37** (Fig. 1), since the large ester side chain occupies the positive octant at upper left position while the four-membered ring and the two methyl groups are more or less equally distributed among the positive and the negative octants, the octant rule predicts unambiguously a positive Cotton effect and indeed this was observed. In contrast, the Cotton effect of isomer **38** (Fig. 2) is less predictable, as the cyclobutanone ring and the ester chain are expected to exert opposing effects while two methyl substituents occupy two adjacent octants. It was especially gratifying to find that the major isomer showed a negative Cotton effect, eliminating its alternative structure of **37** (and thus confirming its structural assignment of **38**). The optical rotation dispersion properties of these two diastereomers are compiled in Table 1 which also summarizes the molecular amplitude of each compound. The observation that compound **37** showed a molecular amplitude far greater than that of **38** was in full support of the above analysis of substitution effect.

The transformation of enone ester **14** into diketones **37** and **38** was improved considerably when 1,1-diethoxyethene (26) was used as a ketene equivalent. Its photocycloaddition to **14** in benzene proceeded in a completely regioselective manner to give an inseparable mixture of at least two diastereomers (four sets of partially superimposed $-OCH_2-$ quartets at the $\delta$ 3.39 region in the nmr spectrum) of the head-to-tail adduct **39** in near-quantitative yield. This mixture when treated with dilute hydrochloric acid in acetone gave, as the only products, diketones **37** and **38** (3:5) in a combined yield of 80%.

Of the two diketones **37** and **38**, only the former is synthetically useful. To enhance the efficiency of synthesis, it is highly desirable to invert the stereochemistry of both ring junction carbons of the latter compound. In principle, this could be directly accomplished by a process of double epimerization, since each of the chiral centers in question is $\alpha$ to a ketone carbonyl. In practice, it was found not to be the case; under a variety of reaction conditions the starting material was recovered intact. The unreactivity of the compound was, however, not totally surprising and could be attributed to its inability to undergo first-stage epimerization at either center to give the corresponding *trans*-fused compound, which is expected to be thermodynamically far less stable (24). An alternative approach which is conceivable for the conversion of diketone

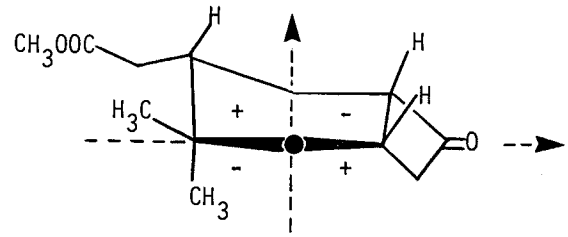


FIG. 1. Octant diagram of diketone **37**.

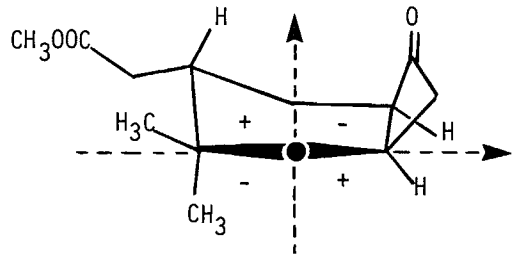


FIG. 2. Octant diagram of diketone **38**.

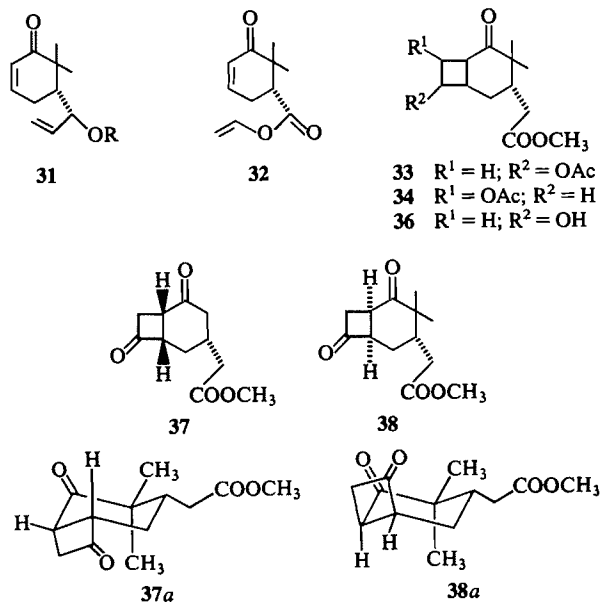

TABLE 1. Optical rotation dispersion properties of diketones **37** and **38**

| Compound | Specific rotation $[\alpha]_D^{25}$ | Molecular rotation $[\phi]_{320}$ | $[\phi]_{278}$ | Molecular amplitude $([\phi]_{320} - [\phi]_{278})/100$ |
|---|---|---|---|---|
| **37** | +119.5° | +17024° | −15679° | +327 |
| **38** | −126.4° | −4164° | +2959° | −71 |

**38** to its diastereomer **37** involves a two-step sequence, dehydrogenation and hydrogenation. This was successfully applied. Although initial attempts to oxidize diketone **38** with standard oxidizing agents such as dichlorodicyanoquinone and selenium dioxide were fruitless, its treatment with pyridinium bromide perbromide in acetic acid induced consecutive bromination and dehydrobromination to give an inseparable mixture of enediones **40** and **41** (ca. 7:1; 66% yield). Reduction of this mixture with zinc dust in acetic acid at room temperature afforded a 3:2 ratio of diketones **37** and **38** in 65% yield.

Before the incorporation of the required *exo*-methylene group into diketone **37**, its cyclobutanone carbonyl was protected. Although standard ketalization conditions ($(CH_2OH)_2$ and *p*-TsOH in refluxing benzene) showed little selectivity, transketalization of diketone **37** with 2-ethyl-2-methyl-1,3-dioxolane at 95°C in the presence of a catalytic amount of *p*-toluenesulfonic acid (27) resulted in the formation of the desired ketal ester **42** in 84% yield. Hydrolysis of **42**[8] with aqueous sodium hydroxide in refluxing methanol followed by treatment of the resulting acid **43** sequentially with sodium hydride[9] (1 equiv.) and methylmagnesium bromide (5 equiv.) at room temperature gave hydroxy acid **45**, which was immediately converted by diazomethane to the corresponding methyl ester **46** (78% yield from **42**). When **46** was exposed to thionyl chloride and pyridine in benzene, it underwent dehydration giving an 89% yield of olefin **47**. The reaction was found to be completely regioselective; no detectable amount of the corresponding endocyclic olefin was produced via the alternative mode of dehydration.

Olefin **47** was subsequently reduced with lithium aluminum hydride in tetrahydrofuran at room temperature to give alcohol **48**. Treatment of this alcohol with phosphorus oxychloride in pyridine afforded chloride **49**, which was hydrolysed with

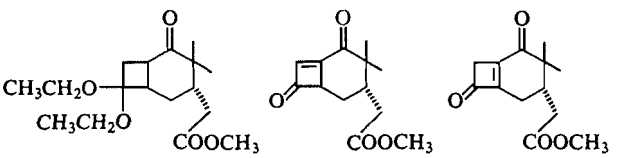

**39** **40** **41**

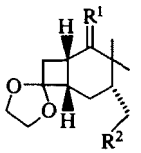

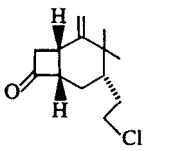

**50**

**42** $R^1 = O$; $R^2 = COOCH_3$
**43** $R^1 = O$; $R^2 = COOH$
**44** $R^1 = CH_3$, OH; $R^2 = C(CH_3)_2OH$
**45** $R^1 = CH_3$, OH; $R^2 = COOH$
**46** $R^1 = CH_3$, OH; $R^2 = COOCH_3$
**47** $R^1 = CH_2$; $R^2 = COOCH_3$
**48** $R^1 = CH_2$; $R^2 = CH_2OH$
**49** $R^1 = CH_2$; $R^2 = CH_2Cl$

aqueous hydrochloric acid in acetone to give keto chloride **50** in 75% yield over three steps.

The transformation of keto chloride **50** to (−)-khusimone (**1**) requires two primary operations: homologation of the cyclobutanone ring and cyclization. Each was accomplished by a single step. Keto chloride **50** was subjected to one-carbon ring expansion with ethyl diazoacetate and boron trifluoride etherate in ether (28, 29). The reaction was found to be complete after 1 h at 0°C and 4 h at room temperature and two isomeric products were obtained in a ratio of 2:1 and a total yield of 86%. Tentative assignment of structure **51** to the major isomer and **52** to the minor[10] was made on the basis of previous findings (29, 30) that the boron trifluoride catalyzed homologation of cycloalkanone with ethyl diazoacetate proceeded, without a single exception, via the preferential migration of the less substituted carbon α to the carbonyl group. When heated at reflux with aqueous sodium hydroxide in refluxing methanol[11] for 40 min, the major isomer

[8]As previously observed for similar systems (6, 8), ketal ester **42** failed to undergo Wittig reaction with methylenetriphenylphosphorane. Its ketone carbonyl also failed to react preferentially with methylmagnesium bromide and methyllithium.

[9]Direct treatment of acid **43** with methylmagnesium bromide produced a substantial quantity of diol **44**.

[10]These assignments were substantiated by the following transformation of the major isomer to (−)-khusimone (**1**).

[11]It was necessary to bring the solution into reflux rapidly using a preheated oil bath. Otherwise a substantial amount of keto ether **53** was formed.

Can. J. Chem. Downloaded from www.nrcresearchpress.com by 210.87.254.42 on 09/06/12
For personal use only.

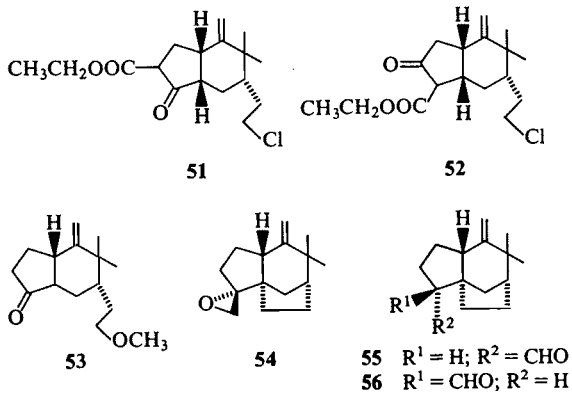


**51**[12] underwent concomitant decarbethoxylation and cyclization to give a 70% yield (−)-khusimone (**1**). The totally synthetic material was shown to be identical in all respects with the natural product.

Following the completion of the (−)-khusimone synthesis, our efforts were directed towards its extension to the synthesis of other zizaane sesquiterpenes possessing the normal fifteen-carbon skeleton. A scheme leading to (+)-zizanoic acid (**2**) and its (−)-epimer **3**[13] was successfully explored as follows.

The synthetic (−)-khusimone was treated with an excess of dimethylsulfonium methylide (31) in tetrahydrofuran. The addition of the ylide occurred exclusively from the sterically less hindered β face of the molecule to give a single epoxide **54** in 52% yield. Upon brief treatment with boron trifluoride etherate in ether at 0°C, epoxide **54** underwent rearrangement with inversion of stereochemistry (32) to give aldehyde **55** in quantitative yield. Jones oxidation of this compound afforded a 77% yield of (−)-epizizanoic acid (**3**). The ir and nmr spectra of the synthetic material were shown to be identical with those of the natural product.

Aldehyde **55** underwent epimerization on treatment with aqueous sodium hydroxide in methanol at room temperature. After 9 h, an equilibrium mixture consisting of five parts of α-epimer **55** and seven parts of β-epimer **56** (47% combined yield) was established. The latter compound was oxidized to (+)-zizanoic acid (**2**) in 86% yield when treated with Jones reagent. The identity of the synthetic and the naturally occurring material was established by comparison of their ir and nmr spectra.

[12]Under the same conditions, the minor ring expansion product gave rise to a complex mixture in which (−)-khusimone (**1**) was absent. These results were in agreement with its structural assignment.

[13]For existing syntheses of these two compounds, see refs. 6–8.

## Experimental

*General*

Melting points were determined on a Kofler hot stage apparatus and are uncorrected. Optical rotations were measured by a Perkin–Elmer 141 polarimeter. The ir spectra were obtained by using a Perkin–Elmer model 457, 337 spectrophotometer and Nicolet 7199 Fourier transform spectrophotometer. Unless otherwise stated, ir samples were run as thin films. The nmr spectra were recorded on Varian A-60, HR-100, and 90 MHz Perkin–Elmer 32 spectrometers. Unless otherwise stated, carbon tetrachloride was used as solvent and tetramethylsilane as internal standard. Mass spectra (ms) were recorded on an AEI MS-50 mass spectrometer. Elemental analyses were performed by the microanalytical laboratory of this department. Jasco ORD/UV-5-SS-20-2 was used to measure optical rotatory dispersion.

*Materials*

Acetone was treated with potassium permanganate, dried over anhydrous potassium carbonate, and distilled. Dichloromethane used for reactions was distilled from phosphorus pentoxide. Methanol was dried over magnesium turnings at elevated temperature for 2 h and distilled. Ether, tetrahydrofuran, 1,2-dimethoxyethane, and benzene were freshly distilled from lithium aluminium hydride. Ozone was generated with a Welsbach ozonator. Ammonium salt of (−)-*l*-10-camphorsulfonic acid was obtained from Aldrich Chemical Company. Silica gel, 0.15–0.33 mm granulation, was used as adsorbent for column chromatography. Thin-layer chromatography was carried out using Merck silica gel G (type 60).

*(−)-α-Campholenic acid (**10**)*

To the fused potassium hydroxide (120 g, 2.14 mol) in a porcelain casserole, was added slowly with stirring the ammonium salt of (−)-*l*-10-camphorsulfonic acid (100 g, 0.40 mol). After the completion of the addition (ca. 25 min), the molten mass was heated for an additional period of 15 min. Upon cooling, the mass was dissolved with water (800 mL). After extraction with ether (200 mL) and dichloromethane (400 mL), the aqueous solution was acidified with ice-cold dilute hydrochloric acid and extracted with ether (300 mL) and dichloromethane (2 × 300 mL). The organic solution was dried ($MgSO_4$) and filtered. After most of the solvent was removed under the reduced pressure, the viscous residue was distilled to give pure acid **10** (35.4 g, 52% yield); bp 97°C/0.65 Torr; $[\alpha]_D^{25}$ −9.0° (*c* 1.1, $CHCl_3$); ir: 3200–2500 and 1708 (acid) $cm^{-1}$; nmr δ: 11.48 (br s, 1H, —COOH), 5.20 (br s, 1H, —HC=), 1.60 (br s, 3H, $CH_3$—CH=), 0.98 (s, 3H, —$CH_3$), and 0.79 (s, 3H, —$CH_3$); ms $M^+$ 168.1142 (calcd. for $C_{10}H_{16}O_2$: 168.1150).

*Methyl α-campholenate (**11**)*

A mixture of α-campholenic acid (**10**) (2.02 g, 12 mmol) and potassium carbonate (4.14 g, 30 mmol) in acetone (20 mL) was stirred at room temperature for 2 h. Methyl iodide (37 mL, 60 mmol) was introduced by syringe and the reaction mixture was refluxed overnight. After most of the solvent was evaporated under the reduced pressure, water was added and the organic product extracted with dichloromethane. The combined organic extracts were dried ($MgSO_4$), filtered, and evaporated to dryness. Bulb-to-bulb distillation (100°C/2 Torr) of the residue gave methyl ester **11** (2.17 g, 100% yield); ir: 1745 (ester) $cm^{-1}$; nmr δ: 5.20 (br s, 1H, —CH=), 1.58 (br s, 3H, $CH_3C$=). 0.98 (s, 3H, —$CH_3$), and 0.75 (s, 3H, —$CH_3$); ms $M^+$ 182.1308 (calcd. for $C_{11}H_{18}O_2$: 182.1306). *Anal.* calcd. for $C_{11}H_{18}O_2$: C 72.49, H 9.95; found: C 72.46, H 10.12.

*5-Carbomethoxymethyl-6,6-dimethyl-2-cyclohexenone (**14**)*

At −78°C, ozone (condition: $E$ = 80 V, air inlet = 8 psi, ozone

Can. J. Chem. Downloaded from www.nrcresearchpress.com by 210.87.254.42 on 09/06/12
For personal use only.

Can. J. Chem. Downloaded from www.nrcresearchpress.com by 210.87.254.42 on 09/06/12
For personal use only.

outlet = 0.06 psi) was allowed to pass through a solution of ester **11** (23.58 g, 0.13 mol) in dichloromethane (65 mL) and methanol (60 mL) until a light blue color was retained. The mixture was warmed up gradually to about −25°C under a nitrogen atmosphere and triphenylphosphine (34 g, 0.13 mol) was added. After removal of the solvent, the crude keto aldehyde **13** (ir: 2840, 2740 (aldehyde), 1735 (ester), and 1705 (ketone and aldehyde) $cm^{-1}$; nmr δ: 9.52 (t, 1H, $J$ = 1.5 Hz, —CHO), 3.59 (s, 3H, —$COOCH_3$), 2.11 (s, 3H, —$COCH_3$), 1.07 (s, 6H, 2 × —$CH_3$); ms $M^+$ 198.1250 (calcd. for $C_{11}H_{18}O_3$: 198.1255)) without purification was dissolved in 100 mL of benzene. To this solution *p*-toluenesulfonic acid (2.58 g, 15 mmol) was added. The resulting mixture was refluxed for 5 h with continuous removal of water using a Dean–Stark water separator. After the solvent was removed *in vacuo* ether was introduced to precipitate triphenylphosphine oxide. Filtration and concentration gave a residue which was subjected to bulb-to-bulb distillation at 100°C/2 Torr. Enone ester **14** (15.6 g, 70% yield) thus obtained showed the following physical data: $[\alpha]_D^{25}$ −65.1° (*c* 2.6, $CHCl_3$); ir: 1675 (α,β-unsaturated ketone), 1735 (ester), 1380 and 1368 (geminal methyls) $cm^{-1}$; nmr δ: 6.75 (m, 1H, —COCH=C*H*—), 5.86 (dt, $J$ = 10, $J'$ = 2 Hz, 1H, —COC*H*=CH—), 3.61 (s, 3H, —$COOCH_3$), 1.11 (s, 3H, —$CH_3$), and 0.94 (s, 3H, —$CH_3$); ms $M^+$ 196.1095 (calcd. for $C_{11}H_{16}O_3$: 196.1100). *Anal.* calcd. for $C_{11}H_{16}O_3$: C 67.32, H 8.22; found: C 67.19, H 8.40.

*5-Carboxymethyl-6,6-dimethyl-2-cyclohexenone (**17**)*

Keto ester **14** (2.94 g, 15 mmol) was dissolved in methanol (60 mL) and 2 *N* aqueous sodium hydroxide (30 mL) was added. The mixture was refluxed for 1.5 h. After cooling to room temperature, it was diluted with water and washed with dichloromethane to remove the nonacidic material. Ice-cold hydrochloric acid was introduced to adjust the acidity of the solution to ca. pH 1. The resulting aqueous solution was extracted with dichloromethane. Combined extracts were dried ($MgSO_4$), filtered, and concentrated to give acid **17** (2.73 g, 100% yield) as an oil; $[\alpha]_D^{25}$ −38.7° (*c* 0.9, $CHCl_3$); ir ($CHCl_3$): 3200–2500, 1708 (acid), and 1673 (α,β-unsaturated ketone) $cm^{-1}$; nmr ($CDCl_3$) δ: 10.65 (br s, 1H, —COOH), 6.82 (m, 1H, —COCH=C*H*—), 5.88 (m, 1H, —COC*H*=CH—), 1.21 (s, 3H, —$CH_3$), and 1.04 (s, 3H, —$CH_3$); ms $M^+$ 182.0945 (calcd. for $C_{10}H_{14}O_3$: 182.0943).

*Vinyl (6,6-dimethyl-5-oxo-3-cyclohexenyl)acetate (**15**)*

Acid **17** (900 mg, 4.94 mmol) was dissolved in vinyl acetate (8 mL) and the solution was stirred for 30 min under a nitrogen atmosphere. Mercuric acetate (20 mg) and concentrated sulfuric acid (3 μL) were added. The reaction mixture was refluxed for 4 h. Ice-cold aqueous sodium bicarbonate solution was added and the organic material extracted with dichloromethane. The combined organic extracts were dried over magnesium sulfate. Filtration and concentration yielded 819 mg of crude product which was chromatographed on silica gel (50 g). Elution with pentane–benzene (1:4) afforded pure ester **15** (610 mg, 60% yield) as an oil; ir: 3080, 1642 (olefins), 1748 (ester), 1670 (α,β-unsaturated ketone), 1390 and 1370 (geminal methyls) $cm^{-1}$; nmr δ: 7.28 (dd, $J$ = 14, $J'$ = 6 Hz, 1H, —OC*H*=$CH_2$), 6.80 (m, 1H, —COCH=C*H*—), 5.89 (dt, $J$ = 10, $J'$ = 2 Hz, 1H, —COC*H*=CH—), 4.83 (dd, $J$ = 14, $J'$ = 2 Hz, 1H, —OCH=C*H*H), 4.55 (dd, $J$ = 6, $J'$ = 2 Hz, 1H, —OCH=C*H*H), 1.12 (s, 3H, —$CH_3$), and 0.96 (s, 3H, —$CH_3$); ms $M^+$ 208.1109 (calcd. for $C_{12}H_{16}O_3$: 208.1100). *Anal.* calcd. for $C_{12}H_{16}O_3$: C 69.21, H 7.74; found: C 69.41, H 7.94.

*Allyl (2,2-dimethyl-3-oxo-4-cyclohexenyl)acetate (**18**)*

Acid **17** (346 mg, 1.9 mmol) was dissolved in acetone (8 mL). To this solution, anhydrous potassium carbonate (690 mg, 5 mmol) was added. The resulting mixture was stirred at room temperature for 2 h before allyl bromide (0.87 mL, 10 mmol) was introduced. After heating at reflux for 5 h, the reaction mixture was poured into water and extracted with dichloromethane. Drying ($MgSO_4$), filtration, and concentration gave the crude product which was purified by column chromatography on silica gel (30 g). Elution with benzene gave the allyl ester **18** (331 mg, 79% yield); ir: 3030, 3010, 1660 (olefins), 1675 (α,β-unsaturated ketone), and 1735 (ester) $cm^{-1}$; nmr δ: 6.86 (m, 1H, —COCH=C*H*—), 5.95 (m, 1H, —COC*H*=CH—), 5.75 (m, 1H, —C*H*=$CH_2$), 5.35 (m, 1H, —CH=C*H*H), 5.15 (m, 1H, —CH=C*H*H), 4.50 (m, 2H, —O$CH_2$CH=$CH_2$), 1.12 (s, 3H, —$CH_3$), and 0.95 (s, 3H, —$CH_3$); ms $M^+$ 222.1261 (calcd. for $C_{13}H_{18}O_3$: 222.1256).

*6,6-Dimethyl-5-(2-hydroxyethyl)-2-cyclohexen-1-ol (**20**)*

At 0°C, to a suspension of lithium aluminum hydride (228 mg, 6 mmol) in tetrahydrofuran (10 mL), was added a solution of enone ester **14** (413 mg, 2.1 mmol) in tetrahydrofuran (2 mL). After 15 min the reaction mixture was allowed to warm up to room temperature and stirred for 5 h. The mixture was treated successively with 0.2 mL of water, 0.2 mL of 3 *N* aqueous sodium hydroxide solution, and again with 0.6 mL of water. The inorganic salt was removed by filtration. Concentration of the filtrate gave diol **20** (257 mg, 72% yield); ir ($CHCl_3$): 3340 (alcohol), 3020 and 1660 (olefin) $cm^{-1}$; nmr ($CDCl_3$) δ: 5.58 (m, 2H, —CH=CH—), 3.83 (br s, 1H, —C*H*OH), 3.60 (m, 2H, —C$H_2$OH), 2.55 (br s, 2H, 2 × —OH), 1.00 (s, 3H, —$CH_3$), and 0.70 (s, 3H, —$CH_3$); ms $M^+$ 170.1307 (calcd. for $C_{10}H_{18}O_2$: 170.1307.

*6,6-Dimethyl-5-(2-oxoethyl)-2-cyclohexenone (**21**)*

To a suspension of pyridinium chlorochromate (2.37 g, 11 mmol) in dichloromethane (26 mL), a solution of diol **20** (470 mg, 2.8 mmol) in dichloromethane (4 mL) was introduced in one portion. The mixture was stirred at room temperature for 2 h and diluted with ether (50 mL). The resulting mixture was passed through a short pad of Florisil. Removal of the solvent under reduced pressure gave keto aldehyde **21** (315 mg, 69% yield); ir: 2730, 1735 (aldehyde), and 1680 (α,β-unsaturated ketone) $cm^{-1}$; nmr δ: 9.70 (m, 1H, —CHO), 6.70 (m, 1H, —COCH=C*H*—), 5.83 (dt, $J$ = 10, $J'$ = 2 Hz, 1H, —COC*H*=CH—), 1.12 (s, 3H, —$CH_3$), and 0.96 (s, 3H, —$CH_3$); ms $M^+$ 166.0997 (calcd. for $C_{10}H_{14}O_2$: 166.0994).

*5-(2-Acetoxy-3-butenyl)-6,6-dimethyl-2-cyclohexenone (**19**)*

At −78°C, to a stirred solution of keto aldehyde **21** (181 mg, 1.1 mmol) in tetrahydrofuran (5 mL) under a nitrogen atmosphere, was added a 1.2 *M* solution of vinylmagnesium bromide in tetrahydrofuran (1 mL, 1.2 mmol). After stirring for 30 min, ice-cold aqueous ammonium chloride solution was added. The resulting solution was extracted with ether. The etherate solution was dried ($MgSO_4$) filtered, and evaporated to dryness to give crude keto alcohol **22** (200 mg) which was dissolved in pyridine (2 mL). To this solution, acetic anhydride (0.5 mL) was added. After stirring at room temperature for 16 h the reaction mixture was concentrated. The residue was chromatographed on silica gel (10 g). Elution with a solution of 2% ether in benzene afforded keto acetates **19** (126 mg, 50% yield from **21**); ir: 1735 (ester), 1675 (α,β-unsaturated ketone), 1395 and 1375 (geminal methyls) $cm^{-1}$; nmr δ: 6.68 (m, 1H, —COCH=C*H*—), 5.80 (dt, $J$ = 10, $J'$ = 3Hz, 1H, —COC*H*=CH—), 5.58 (m, 1H, —C*H*=$CH_2$), 5.20 (m, 2H, —CH=C$H_2$), 5.16 (m, 1H, —CHO—), 2.00, 1.98 (both s, total 3H, $CH_3COO$—), 1.11, 1.08, and 0.94 (all s, total 6H, 2 × —$CH_3$); ms $M^+$ 236.1408 (calcd. for $C_{14}H_{20}O_3$: 236.1413).

Can. J. Chem. Downloaded from www.nrcresearchpress.com by 210.87.254.42 on 09/06/12
For personal use only.

*3-Acetoxy-9,9-dimethyltricyclo[4.3.1.0$^{4,7}$]decan-8-one (24)*

Keto acetates **19** (94 mg, 0.4 mmol) were dissolved in 10 mL of methanol. The solution was placed in a Pyrex tube and irradiated at room temperature using a 450 W Hanovia high-pressure quartz mercury vapor lamp for 4 h. The solution was concentrated and the residue chromatographed on silica gel (9 g). Elution with a solution of 2% ether in benzene gave keto acetate **24** (40 mg, 43% yield) as a colorless liquid; ir: 1735 (ester), 1700 (ketone), 1390 and 1372 (geminal methyls) cm$^{-1}$; nmr δ: 4.84 (m, 1H, —CHO—), 1.95 (s, 3H, $CH_3COO$—), 1.21 (s, 3H, —$CH_3$), and 1.00 (s, 3H, —$CH_3$); ms M$^+$ 236.1419 (calcd. for $C_{14}H_{20}O_3$: 236.1412).

*3-Hydroxy-9,9-dimethyltricyclo[4.3.1.0$^{4,7}$]decan-8-one (25)*

Keto acetate **24** (170 mg, 0.72 mmol) was dissolved in methanol (6 mL) and saturated aqueous potassium carbonate (3 mL) was added. The reaction mixture was refluxed for 1.5 h, poured into water, and extracted with dichloromethane. The extracts were dried ($MgSO_4$), filtered, and concentrated to yield an oily product (120 mg) which was chromatographed on silica gel (10 g). Elution with ether–benzene (3:2) gave keto alcohol **25** (91 mg, 65% yield); ir: 3400 (alcohol) and 1695 (ketone) cm$^{-1}$; nmr δ: 3.78 (m, 1H, —CHO—), 1.12 (s, 3H, —$CH_3$), and 0.98 (s, 3H, —$CH_3$).

*9,9-Dimethyltricyclo[4.3.1.0$^{4,7}$]decane-3,8-dione (26)*

At 0°C, to a solution of keto alcohol **25** (91 mg, 0.46 mmol) in acetone (5 mL) was added 8 *N* Jones reagent (0.3 mL) (33). After stirring at room temperature for 10 min, the mixture was diluted with water and extracted with ether. The organic solution was dried ($MgSO_4$), filtered, and evaporated to dryness. The crude product was chromatographed on silica gel (6 g). Elution with a solution of 2% ether in benzene gave diketone **26** (70 mg, 80% yield); ir: 1695 and 1710 (ketone) cm$^{-1}$; nmr δ: 2.96 (d, $J$ = 2.5 Hz, 2H, —$COCH_2$—), 1.13 (s, 3H, —$CH_3$), and 1.08 (s, 3H, —$CH_3$).

*10,10-Dimethyl-4-oxatricyclo[5.3.1.0$^{5,8}$]decane-3,9-dione (27)*

A mixture of the diketone **26** (80 mg, 0.4 mmol), *m*-chloroperbenzoic acid (259 mg, 1.2 mmol), and sodium bicarbonate (200 mg, 2.0 mmol) in dichloromethane (4 mL) was stirred for three days. A 10% aqueous sodium sulfite solution (5 mL) was added and the resulting solution was extracted with dichloromethane. The combined extracts were washed with aqueous sodium bicarbonate solution. Concentration gave an oil which was chromatographed on silica gel (5 g). Elution with a solution of 10% ether in benzene gave keto lactone **27** (50 mg, 60% yield); ir: 1730 (lactone) and 1705 (ketone) cm$^{-1}$; nmr δ: 5.04 (m, 1H, —CHO—), 1.21 (s, 3H, —$CH_3$), and 1.11 (s, 3H, —$CH_3$); ms M$^+$ 208.1105 (calcd. for $C_{12}H_{16}O_3$: 208.1100).

cis-*3-Carbomethoxymethyl-2,2-dimethyl-5-(2-oxoethyl)cyclohexanone (30)*

Lactone **27** (20 mg, 0.1 mmol) was dissolved in methanol (6 mL). To this solution, saturated aqueous potassium carbonate (3 mL) was added. The reaction mixture was refluxed for 30 min under a nitrogen atmosphere. After cooling to room temperature, it was poured into water and extracted with dichloromethane to remove the nonacidic material. The aqueous solution was acidified with hydrochloric acid and extracted with dichloromethane. Drying ($MgSO_4$), filtration, and concentration yielded acid **28** (10 mg, 45% yield); ir ($CHCl_3$): 3200–2500 (acid), 2730 (aldehyde) and 1705 (carbonyls) cm$^{-1}$; nmr ($CDCl_3$) δ: 11.8 (br s, 1H, —COOH), 9.76 (br s, 1H, —CHO), 1.11 (s, 3H, —$CH_3$), and 1.01 (s, 3H, —$CH_3$); ms M$^+$ 226.1207 (calcd. for $C_{12}H_{18}O_4$: 226.1205).

Acid **28** (10 mg) was dissolved in ether (4 mL). At 0°C, to this solution, diazomethane in ether was added dropwise until the light yellow color was retained. Removal of the solvent gave ester **30** (10 mg, 95% yield); ir: 2730 (aldehyde), 1735 (ester), and 1710 (ketone and aldehyde) cm$^{-1}$; nmr δ: 9.72 (s, 1H, —CHO), 3.62 (s, 3H, —$COOCH_3$), 1.15 (s, 3H, —$CH_3$), and 0.98 (s, 3H, —$CH_3$); ms M$^+$ 240.1362 (calcd. for $C_{13}H_{20}O_4$: 240.1362).

*Photocycloaddition of enone 14 to vinyl acetate*

To a photochemical reaction vessel (34) containing enone ester **14** (2.15 g, 11 mmol) in benzene (50 mL) was added freshly distilled vinyl acetate (21 mL, 0.22 mol). The mixture was irradiated using a 450 W Hanovia high-pressure quartz mercury vapor lamp and a Pyrex filter for 1.5 h. The solution was concentrated and the residue chromatographed on silica gel (300 g) with benzene elution to give 2.37 g (77% yield) of photoadducts **33** and **34**; ir: 1735 (ester) and 1698 (ketone) cm$^{-1}$; nmr δ: 3.61 (s, 3H, —$COOCH_3$), 1.95, 1.96 (both s, total 3H, $CH_3COO$—), and 0.9–1.1 (complex, 6H, 2 × —$CH_3$); ms M$^+$ 282.1462 (calcd. for $C_{15}H_{22}O_5$: 282.1467).

*4-Carbomethoxymethyl-7-hydroxy-3,3-dimethylbicyclo[4.2.0]-octan-2-one (36),* cis-*(30) and* trans-*3-carbomethoxymethyl-2,2-dimethyl-5-(2-oxoethyl)cyclohexanone (35)*

At 0°C, sodium (690 mg, 30 g-atom) was added to methanol (35 mL). After all sodium reacted, a mixture of photoadducts **33** and **34** (3.07 g, 10.87 mmol) was added. The resulting mixture, after stirring at room temperature for 45 min, was carefully poured into ice-cold 3 *N* hydrochloric acid (100 mL) and extracted with dichloromethane. The extracts were dried ($MgSO_4$), filtered, and concentrated to give an oily residue which was chromatographed on silica gel (120 g). Elution with a solution of 50% ether–pentane gave keto aldehydes **30** and **35** (0.42 g, 16% yield); ir: 2730, (aldehyde), 1735 (ester), and 1710 (aldehyde and ketone) cm$^{-1}$; ms M$^+$ 240.1355 (calcd. for $C_{13}H_{20}O_4$: 240.1362). The nmr spectrum of the mixture showed, in addition to one set of signals corresponding to keto aldehyde **30** (*vide supra*), the following signals for compound **35**: δ: 9.72 (s, 1H, —CHO), 3.62 (s, 3H, —$COOCH_3$), 1.03 (s, 3H, —$CH_3$), and 0.98 (s, 3H, —$CH_3$).

Further elution with a solution of ether–pentane (4:1) gave a mixture of diastereomeric alcohols **36** (1.75 g, 67% yield); ir: 3450 (alcohol), 1738 (ester), and 1702 (ketone) cm$^{-1}$; nmr δ: 3.60 (s, 3H, —$COOCH_3$), 3.76 (m, 1H, —CHO—), and 0.90–1.21 (six s, total 6H, 2 × —$CH_3$); ms M$^+$ 240.1355 (calcd. for $C_{13}H_{20}O_4$: 240.1362).

*4-Carbomethoxymethyl-3,3-dimethylbicyclo[4.2.0]octane-2,7-diones (37 and 38)*

At 0°C, to a solution of alcohols **36** (3.2 g, 13.3 mmol) in acetone (30 mL), 8 *N* Jones reagent (ca. 5 mL) was introduced dropwise until the brown color persisted for more than 30 s. The mixture was stirred at room temperature for 30 min. After most of the solvent was removed under reduced pressure, water was added. The resulting aqueous solution was extracted with chloroform. The extracts were washed successively with aqueous sodium bicarbonate solution and aqueous sodium chloride solution and dried ($MgSO_4$). Filtration and concentration yielded 2.6 g of crude product which showed two partially overlapping spots on silica gel thin-layer chromatography. Column chromatography on silica gel (150 g), eluting with a solution of 40% ether in pentane, gave diketone **37** (850 mg, 27% yield); $[\alpha]_D^{25}$ +119.5° (*c* 2.0, $CHCl_3$); ir: 1785 (four-membered ketone), 1738 (ester), and 1710 (ketone) cm$^{-1}$; nmr δ: 3.61 (s, 3H, —$COOCH_3$), 1.21 (s, 3H, —$CH_3$), and 0.97 (s, 3H, —$CH_3$); ms M$^+$ 238.1204 (calcd. for $C_{13}H_{18}O_4$: 238.1205). *Anal.* calcd. for $C_{13}H_{18}O_4$: C 65.53, H 7.61; found: C 65.20, H 7.28.

Can. J. Chem. Downloaded from www.nrcresearchpress.com by 210.87.254.42 on 09/06/12
For personal use only.

Further elution with the same solvent system gave a mixture of **37** and **38** (ca. 1:1; 234 mg, 7% yield). This was followed by pure ketone **38** (1.055 g, 33% yield) as a white solid; mp 127–128°C (ether); $[\alpha]_D^{25}$ −126.4° (*c* 1.4, $CHCl_3$); ir ($CHCl_3$): 1785 (four-membered ketone), 1738 (ester), and 1708 (ketone) $cm^{-1}$; nmr δ: 3.67 (s, 3H, —$COOCH_3$), 1.12 (s, 3H, —$CH_3$), and 1.06 (s, 3H, —$CH_3$); ms $M^+$ 238.1205 (calcd. for $C_{13}H_{18}O_4$: 238.1205). *Anal.* calcd. for $C_{13}H_{18}O_4$: C 65.53, H 7.61; found: C 65.79, H 7.80.

*4-Carbomethoxymethyl-7,7-diethoxy-3,3-dimethylbicyclo-[4.2.0]octan-2-one (**39**)*

To a Pyrex tube containing a solution of enone ester **14** (500 mg, 2.5 mmol) in benzene (12 mL), 1,1-diethoxyethene (4.35 g, 37.5 mmol) was added. The reaction mixture was irradiated at room temperature with a 450 W Hanovia high-pressure quartz mercury vapor lamp for 3 h. The solvent and excess reagent were removed under the reduced pressure. The residue was chromatographed on silica gel (40 g). Elution with a solution of 20% ether in pentane gave a diastereomeric mixture of adducts **39** (750 mg, 96% yield); ir: 1735 (ester) and 1700 (ketone) $cm^{-1}$; nmr δ: 3.61 (s, 3H, —$COOCH_3$), 3.31, 3.33, 3.37, 3.39 (all q, $J$ = 7 Hz each, total 4H, —$OCH_2CH_3$), and ~1.10 (complex, total 12H, 4 × —$CH_3$); ms $M^+$ 312.1943 (calcd. for $C_{17}H_{28}O_5$: 312.1937).

*Diketones **37** and **38** from ketal **39***

Ketal **39** (680 mg, 2.2 mmol) was dissolved in 8 mL of acetone and 2 *N* aqueous hydrochloric acid (4 mL) was added. After stirring at room temperature for 3 h, the solution was diluted with water and extracted with dichloromethane. The combined extracts were dried ($MgSO_4$), filtered, and evaporated to dryness. The crude product was chromatographed on silica gel (40 g). Elution with a solution of 40% ether in pentane gave pure diketones **37** (160 mg, 30% yield) and **38** (260 mg, 50% yield).

*Mixture of $\Delta^{1,8}$- (**40**) and $\Delta^{1,6}$-4-carbomethoxymethyl-3,3-dimethylbicyclo[4.2.0]octene-2,7-dione (**41**)*

To a solution of the diketone **38** (100 mg, 0.42 mmol), in glacial acetic acid (4 mL), pyridinium bromide perbromide (268 mg, 0.84 mmol) was added. The reaction mixture was stirred at room temperature for 16 h. It was cautiously made basic with ice-cold saturated aqueous sodium bicarbonate solution. Extraction with dichloromethane followed by the usual work-up of the extracts gave a thick oil which was chromatographed on silica gel (6 g). Elution with a solution of 25% ether in pentane gave enediones **40** and **41** (65 mg, 66% yield); ir: 1785 (four-membered ketone), 1740 (ester), and 1695 (six-membered ketone) $cm^{-1}$; nmr δ: 5.44 (br s, 0.88 H, —CH=C<), 3.65 (s, 3H, —$COOCH_3$), 3.42 (m, 0.24 H, —$COCH_2$C=), 1.22, 1.28 (both s, total 3H, —$CH_3$), and 1.08 (s, 3H, —$CH_3$); ms $M^+$ 236.1048 (calcd. for $C_{13}H_{16}O_4$: 236.1049).

*Reduction of enediones **40** and **41***

Zinc dust (1 g, 0.015 g-atom) was added to a solution of enediones **40** and **41** (523 mg, 2.21 mmol) in glacial acetic acid (8 mL). The resulting mixture was stirred at room temperature for 5 h. It was then cautiously made basic with ice-cold saturated aqueous sodium bicarbonate solution. Extraction with dichloromethane followed by concentration of the organic solution gave an oily product which was chromatographed on silica gel (30 g). Elution with a solution of 40% ether in pentane afforded diketones **37** (192 mg, 39% yield) and **38** (135 mg, 26% yield).

*4-Carbomethoxymethyl-7,7-ethylenedioxy-3,3-dimethylbicyclo[4.2.0]octan-2-one (**42**)*

Diketone **37** (655 mg, 2.76 mmol) was dissolved in 2-methyl-2-ethyl-1,3-dioxalane (8 mL) and *p*-toluenesulfonic acid (40 mg, 0.26 mmol) was added. The mixture was heated at 95°C (oil bath temperature) for 12 h. After cooling to 0°C, aqueous sodium bicarbonate solution was added. Extraction with dichloromethane followed by the usual work-up of the extracts gave the crude product which was chromatographed on silica gel (30 g). Elution with a solution of 40% ether in benzene gave ketal **42** (650 mg, 84% yield); $[\alpha]_D^{25}$ +71.8° (*c* 1.5, $CHCl_3$); ir: 1735 (ester) and 1715 (ketone) $cm^{-1}$; nmr δ: 3.75 (m, 4H, —$OCH_2CH_2O$—), 3.72 (s, 3H, —$COOCH_3$), 1.06 (s, 3H, —$CH_3$), and 0.96 (s, 3H, —$CH_3$); ms $M^+$ 282.1471 (calcd. for $C_{15}H_{22}O_5$: 282.1467).

*4-Carbomethoxymethyl-7,7-ethylenedioxy-2-hydroxy-2,3,3-trimethylbicyclo[4.2.0]octane (**46**)*

To a solution of ketal **42** (209 mg, 0.74 mmol) in methanol (6 mL) was added 2 *N* aqueous sodium hydroxide (3 mL). The resulting mixture was refluxed for 1 h. After cooling to room temperature, the mixture was poured into ice-cold dilute hydrochloric acid and extracted with dichloromethane. The usual work-up of the extracts gave crude acid **43**. The crude acid was then dissolved in 1,2-dimethoxyethane (10 mL) and cooled to 0°C. Sodium hydride (36 mg, 50% oil dispersion, 0.75 mmol) was added. After the evolution of gas ceased, a 2 *M* solution of methylmagnesium bromide in ether (1.8 mL, 3.6 mmol) was slowly introduced. The mixture was allowed to warm up to room temperature and stirred for 20 h under a nitrogen atmosphere. Saturated aqueous ammonium chloride solution was added and the resulting mixture was extracted with dichloromethane. The combined extracts were dried ($MgSO_4$), filtered, and concentrated to give a mixture of acids **43** and **45** as a light yellow liquid. This acidic material was dissolved in ether (6 mL) and a slight excess of ethereal diazomethane was introduced. The residue obtained upon concentration was chromatographed on silica gel (20 g). Elution with a solution of 40% ether in pentane gave the starting ketal **42** (39 mg, 19% recovery). Further elution with a solution of 50% ether in pentane afforded alcohol **46** (140 mg, 78% yield based on consumed **42**); ir: 3520 (alcohol) and 1735 (ester) $cm^{-1}$; nmr δ: 3.81 (br s, 4H, —$OCH_2CH_2O$—), 3.63 (s, 3H, —$COOCH_3$), 1.10 (s, 3H, —$CH_3$), 0.96 (s, 3H, —$CH_3$), and 0.92 (s, 3H, —$CH_3$); ms $M^+$ 298.1777 (calcd. for $C_{16}H_{26}O_5$: 298.1780). *Anal.* calcd. for $C_{16}H_{26}O_5$: C 64.41, H 8.78; found: C 64.19, H 8.68.

*4-Carbomethoxymethyl-7,7-ethylenedioxy-3,3-dimethyl-2-methylidenebicyclo[4.2.0]octane (**47**)*

To a solution of alcohol **46** (1.5 g, 5.0 mmol) and pyridine (4 mL), in benzene (50 mL), was added a solution of thionyl chloride (1 mL) in benzene (5 mL). The reaction mixture was stirred at room temperature under an atmosphere of nitrogen for 30 min. It was acidified with ice-cold 2 *N* aqueous hydrochloric acid and extracted with dichloromethane. The combined organic extracts were dried ($MgSO_4$), filtered, and concentrated. Column chromatography of the residue on silica gel (80 g), eluting with a solution of 20% ether in pentane, gave olefin **47** (1.176 g, 89% yield); $[\alpha]_D^{25}$ +41.4° (*c* 1.0, $CHCl_3$); ir: 3100, 1630, 890 (olefin), and 1740 (ester) $cm^{-1}$; nmr δ: 4.96 (br s, 1H, —C=C*H*H), 4.78 (br s, 1H, —C=C*H*H), 3.75 (br s, 4H, —$OCH_2CH_2O$—), 3.60 (s, 3H, —$COOCH_3$), 1.10 (s, 3H, —$CH_3$), and 1.03 (s, 3H, —$CH_3$); ms $M^+$ 280.1674 (calcd. for $C_{16}H_{24}O_4$: 280.1674). *Anal.* calcd. for $C_{16}H_{24}O_4$: C 68.55, H 8.63; found: C 68.80, H 8.69.

*7,7-Ethylenedioxy-4-(2-hydroxyethyl)-3,3-dimethyl-2-methylidenebicyclo[4.2.0]octane (**48**)*

To a suspension of lithium aluminium hydride (200 mg, 5.3 mmol) in tetrahydrofuran (20 mL) at 0°C, a solution of ester **47** (1.176 g, 4.2 mmol) in tetrahydrofuran (2 mL) was added. The

Can. J. Chem. Downloaded from www.nrcresearchpress.com by 210.87.254.42 on 09/06/12
For personal use only.

reaction mixture was stirred at room temperature under a nitrogen atmosphere for 16 h. Water (0.2 mL), 3 *N* sodium hydroxide (0.2 mL), and again water (0.6 mL) were successively added. Filtration followed by concentration of the filtrate gave alcohol **48** (1.05 g, 99% yield); $[\alpha]_D^{25}$ +39.2° (*c* 1.3, $CHCl_3$); ir: 3420 (alcohol), 3100 and 1630 (olefin) $cm^{-1}$; nmr δ: 4.91 (s, 1H, —C(—)=C*H*H), 4.27 (s, 1H, —C(—)=C*H*H), 3.74 (br s, 4H, —$OCH_2CH_2O$—), 1.06 (s, 3H, —$CH_3$), and 1.03 (s, 3H, —$CH_3$); ms $M^+$ 252.1730 (calcd. for $C_{15}H_{24}O_3$: 252.1725). *Anal.* calcd. for $C_{15}H_{24}O_3$: C 71.39, H 9.59; found: C 71.70, H 9.66.

*4-(2-Chloroethyl)-7,7-ethylenedioxy-3,3-dimethyl-2-methylidenebicyclo[4.2.0]octane (**49**)*

Alcohol **48** (190 mg, 0.75 mmol) was dissolved in pyridine (2 mL) and cooled to 0°C. Phosphorus oxychloride (0.5 mL) was introduced. The mixture was stirred at room temperature under a nitrogen atmosphere for 16 h and poured into ice-cold water. The resulting mixture was extracted with dichloromethane. The organic solution was dried ($MgSO_4$), filtered, and concentrated to give an oily residue which was chromatographed on silica gel (15 g). Elution with a solution of 10% ether in pentane yielded chloride **49** (150 mg, 75% yield); $[\alpha]_D^{25}$ +29.7° (*c* 0.7, $CHCl_3$); ir: 1630 (olefin) $cm^{-1}$; nmr δ: 4.92 (s, 1H, —C(—)=C*H*H), 4.75 (s, 1H, —C(—)=C*H*H), 4.74 (br s, 4H, —$OCH_2CH_2O$—), 3.50 (m, 2H, —$CH_2Cl$), 1.07 (s, 3H, —$CH_3$), and 1.03 (s, 3H, —$CH_3$); ms $M^+$ 270.1380 and 272.1362 (calcd. for $C_{15}H_{23}OCl$: 270.1386 and 272.1357).

*4-(2-Chloroethyl)-3,3-dimethyl-2-methylidenebicyclo[4.2.0]-octan-7-one (**50**)*

Chloride **49** (120 mg, 0.44 mmol) was dissolved in acetone (4 mL) and 2 *N* aqueous hydrochloric acid (2 mL) was added. After stirring at room temperature for 8 h, the mixture was poured into water and extracted with dichloromethane. Drying ($MgSO_4$), filtration, and concentration gave ketone **50** (100 mg, quantitative yield; $[\alpha]_D^{25}$ +48.6° (*c* 1.3, $CHCl_3$); ir: 1785 (ketone) and 1640 (olefin) $cm^{-1}$; nmr δ: 5.04 (d, *J* = 2 Hz, 1H, —C(—)=C*H*H), 4.91 (d, *J* = 2 Hz, —C(—)=C*H*H), 3.50 (m, 2H, —$CH_2Cl$), 1.16 (s, 3H, —$CH_3$), and 1.11 (s, 3H, —$CH_3$); ms $M^+$ 226.1124 and 228.1090 (calcd. for $C_{13}H_{19}OCl$: 226.1124 and 228.1095).

*8-Carboethoxy-4-(2-chloroethyl)-3,3-dimethyl-2-methylidenebicyclo[4.3.0]nonan-7-one (**51**) and 7-carboethoxy-4-(2-chloroethyl)-3,3-dimethyl-2-methylidenebicyclo-[4.3.0]nonan-8-one (**52**)*

At 0°C, to a solution of ketone **50** (100 mg, 0.46 mmol) in ether (8 mL), was added boron trifluoride etherate (0.12 mL, 1 mmol). After stirring at 0°C for 15 min, ethyl diazoacetate (0.1 mL, 1 mmol) was introduced. The mixture was stirred under a nitrogen atmosphere at 0°C for 1 h and at room temperature for 4 h. Ice-cold saturated aqueous sodium bicarbonate solution was added dropwise. Extraction with dichloromethane followed by the usual work-up of the organic solution gave an oily product which showed two spots in thin-layer chromatography. Their separation was effected by column chromatography on silica gel (10 g). Elution with a solution of 8% ether in pentane afforded keto ester **51** (82 mg, 57% yield); $[\alpha]_D^{25}$ +31.9° (*c* 0.6, $CHCl_3$); ir: 1760 (ketone), 1735 (ester), and 1650 (olefin) $cm^{-1}$; nmr δ: 4.90 (br s, 2H, —C(—)=$CH_2$), 4.12 (q, *J* = 7 Hz, 2H, —$COOCH_2CH_3$), 3.54 (m, 2H, —$CH_2Cl$), 1.24 (s, 3H, —$CH_3$), 1.23 (t, *J* = 7 Hz, 3H, —$COOCH_2CH_3$), and 1.06 (s, 3H, —$CH_3$); ms $M^+$ 312.1490 and 314.1445 (calcd. for $C_{17}H_{25}O_3Cl$: 312.1492 and 314.1462).

Further elution with the same solvent system gave keto ester **52** (42 mg, 29% yield); ir: 1750 (ketone), 1730 (ester), and 1635 (olefin) $cm^{-1}$; nmr δ: 4.98 (s, 1H, —C(—)=C*H*H), 4.72 (s, 1H, —C(—)=C*H*H), 4.14 (q, *J* = 7 Hz, 2H, —$COOCH_2CH_3$), 3.52 (m, 2H, —$CH_2Cl$), 1.25 (t, *J* = 7 Hz, 3H, —$COOCH_2CH_3$), 1.15 (s, 3H, —$CH_3$), and 1.01 (s, 3H, —$CH_3$); ms $M^+$ 312.1488 and 314.1466 (calcd. for $C_{17}H_{25}O_3Cl$: 312.1492 and 314.1463).

*(−)-Khusimone (**1**)*

To a solution of the keto ester **51** (122 mg, 0.39, mmol) in methanol (3 mL) under a nitrogen atmosphere, was added 2 *N* aqueous sodium hydroxide solution (1.5 mL). The resulting solution was immediately brought into reflux using a preheated oil bath. After 40 min, ice-cold water was added. Extraction with dichloromethane, drying ($MgSO_4$), filtration, and concentration gave a solid which was recrystallized from petroleum ether to give (−)-khusimone (**1**) (56 mg, 70% yield); mp 78°C; $[\alpha]_D^{25}$ −108.7° (*c* 2.0, $CHCl_3$); ir ($CHCl_3$): 3140, 1640 (olefin), 1728 (ketone), 1395 and 1360 (geminal methyls) $cm^{-1}$; nmr ($CDCl_3$) δ: 4.84 (br s, 1H, —C(—)=C*H*H), 4.68 (br s, 1H, —C(—)=C*H*H), and 1.06 (s, 6H, 2 × —$CH_3$); ms $M^+$ 204.1514 (calcd. for $C_{14}H_{20}O$: 204.1512).

*2,12-Epoxyzizaene (**54**)*

At 0°C, to a suspension of trimethylsulfonium iodide (100 mg, 0.5 mmol) in tetrahydrofuran (6 mL) under a nitrogen atmosphere, was added a solution of 2 *M* butyllithium in ether (0.16 mL, 0.32 mmol). After stirring at room temperature for 1 h, the mixture was again cooled to 0°C and a solution of (−)-khusimone (**1**) (40 mg, 0.2 mmol) in tetrahydrofuran (4 mL) was added. The resulting mixture was stirred at room temperature for 2.5 h. Water was added and the aqueous solution extracted with dichloromethane. The usual work-up of the extracts gave an oil which was chromatographed on silica gel (6 g). Elution with a solution of 2% ether in pentane gave epoxide **54** (15 mg, 52% based on consumed starting material); ir: 3110 and 1645 (olefin), 1385 and 1365 (geminal methyls) $cm^{-1}$; nmr δ: 4.77 (m 1H, —C(—)=C*H*H), 4.58 (br s, 1H, —C(—)=C*H*H), 2.67 (d, *J* = 12 Hz, 1H, —OC*H*H), 2.53 (d, *J* = 12 Hz, 1H, —OC*H*H), and 1.06 (s, 6H, 2 × —$CH_3$); ms $M^+$ 218.1674 (calcd. for $C_{15}H_{22}O$: 218.1670).

Further elution with a solution of 5% ether in pentane afforded 13 mg of the starting material.

*12-Oxoepizizaene (**55**)*

Epoxide **54** (17.5 mg, 0.08 mmol) was dissolved in ether (4 mL) and cooled to 0°C. Boron trifluoride etherate (0.05 mL, 0.41 mmol) was introduced. The mixture was stirred under a nitrogen atmosphere at 0°C for 1 h, and then at room temperature for 30 min. It was made basic with saturated sodium bicarbonate and extracted with ether. The organic solution was dried ($MgSO_4$), filtered, and concentrated to give aldehyde **55** (17.5 mg, quantitative yield); ir: 2710, 1720 (aldehyde), 1640 (olefin), 1380 and 1360 (geminal methyls) $cm^{-1}$; nmr δ: 9.73 (d, *J* = 2 Hz, 1H, —CHO), 4.80 (s, 1H, —C(—)=C*H*H), 4.60 (s, 1H, —C(—)=C*H*H), 1.10 (s, 3H, —$CH_3$), and 1.06 (s, 3H, —$CH_3$); ms $M^+$ 218.1670 (calcd. for $C_{15}H_{22}O$: 218.1670).

*(−)-Epizizanoic acid (**3**)*

At 0°C, to a solution of the aldehyde **55** (16 mg, 0.073 mmol) in acetone (3 mL), was slowly added 8 *N* Jones reagent until a brown color persisted. The mixture was stirred for 5 min, added to ice-cold aqueous sodium chloride solution (50 mL), and extracted with dichloromethane. The usual work-up of the extracts gave the crude product which was taken up in ether and extracted with saturated sodium bicarbonate. The extracts were

Can. J. Chem. Downloaded from www.nrcresearchpress.com by 210.87.254.42 on 09/06/12
For personal use only.

combined and acidified with hydrochloric acid. This was followed by extraction with dichloromethane. Drying ($MgSO_4$), filtration, and concentration gave (−)-epizizanoic acid (14) (13 mg, 77% yield); mp 110°C (petroleum ether); $[\alpha]_D^{25}$ −1.0° (*c* 1.2, $CHCl_3$); ir ($CHCl_3$): 3200–2500, 1691 (acid), 1638 (olefin), 1380 and 1360 (geminal methyls) $cm^{-1}$; nmr δ: 11.7 (s, 1H, —COOH), 4.75 (s, 1H, —C(—)=C*H*H), 4.56 (s, 1H, —C(—)=C*H*H), 1.08 (s, 3H, —$CH_3$), and 1.05 (s, 3H, —$CH_3$); ms $M^+$ 234.1626 (calcd. for $C_{15}H_{22}O_2$: 234.1619).

*Epimerization of aldehyde 55*

To a solution of aldehyde **55** (13 mg, 0.06 mmol) in methanol (4 mL), was added 2 *N* aqueous sodium hydroxide solution (1 mL). The reaction mixture was stirred at room temperature under a nitrogen atmosphere for 9 h. Saturated aqueous sodium chloride solution was added. The resulting solution was extracted with dichloromethane. Drying ($MgSO_4$), filtration, and concentration gave a mixture of epimeric aldehydes **55** and **56** which was separated by column chromatography on silica gel (5 g). Elution with a solution of 5% ether in petroleum ether gave pure β-aldehyde **56** (2.5 mg), a mixture of α- and β-epimers (1:1; 2 mg), followed by pure α-aldehyde **55** (1.6 mg). β-Aldehyde **56** showed the following spectral data; ir: 2720, 1720 (aldehyde), 1640 (olefin), 1380 and 1360 (geminal methyls) $cm^{-1}$; nmr δ: 9.80 (d, $J$ = 2 Hz, 1H, —CHO), 4.78 (dd, $J = J'$ = 2 Hz, 1H, —C(—)=C*H*H), 4.63 (dd, $J = J'$ = 2 Hz, 1H, —C(—)=C*H*H), and 1.07 (s, 6H, 2 × —$CH_3$); ms $M^+$ 218.1667 (calcd. for $C_{15}H_{22}O$: 218.1670).

*(+)-Zizanoic acid (2)*

At 0°C, to a solution of aldehyde **56** (2.5 mg, 0.011 mmol) in 2 mL of acetone, was added 8 *N* Jones reagent until a brown color persisted. After stirring at room temperature for 15 min, the reaction mixture was added to water and extracted with dichloromethane. The usual work-up of the extracts gave (+)-zizanoic acid (**2**) (2.3 mg, 86% yield); $[\alpha]_D^{25}$ +22.2° (*c* 0.23, $CHCl_3$); ir ($CHCl_3$): 3200–2600, 1701 (acid), 1639 and 891 (olefin) $cm^{-1}$; nmr δ: 4.77 (dd, $J = J'$ = 1.5 Hz, 1H, —C(—)=C*H*H), 4.63 (dd, $J = J'$ = 1.5 Hz, 1H, —C(—)=C*H*H), 2.68 (m, 1H, —C*H*COOH), 1.10 (s, 3H, —$CH_3$), and 1.07 (s, 3H, —$CH_3$); ms $M^+$ 234.1621 (calcd. for $C_{15}H_{22}O_2$: 234.1620).

## Acknowledgements

We wish to thank the Natural Sciences and Engineering Research Council of Canada and the University of Alberta for financial support. We also thank Dr. G. Ohloff for a sample of natural (−)-khusimone, and Prof. A. Yoshikoshi for the ir and nmr spectra of natural zizanoic acid and epizizanoic acid.

1. D. C. Umrani, R. Seshadri, K. G. Gore, and K. K. Chakravarti. Flavour Ind. **1**, 623 (1970).
2. B. Maurer, M. Fracheloud, A. Grieder, and G. Ohloff. Helv. Chim. Acta, **5**, 2371 (1972).
3. F. Kido, H. Uda, and A. Yoshikoshi. Tetrahedron Lett. 2815 (1967); 1247 (1968).
4. I. C. Nigam, H. Komae, G. A. Neville, C. Radecka, and S. K. Pakmikar. Tetrahedron Lett. 2497 (1968).
5. N. Hanayama, F. Kido, R. Sakuma, H. Uda, and A. Yoshikoshi. Tetrahedron Lett. 6099 (1968).
6. F. Kido, H. Uda, and A. Yoshikoshi. Chem. Commun. 1335 (1969).
7. D. F. MacSweeney and R. Ramage. Tetrahedron, **27**, 1481 (1971).
8. F. Kido, H. Uda, and A. Yoshikoshi. J. Chem. Soc. 1775 (1972).
9. A. Deljac, W. D. MacKay, C. S. J. Pan, J. J. Wiesner, and K. Wiesner. Can. J. Chem. **50**, 726 (1972).
10. R. M. Coates and L. Sowerby. J. Am. Chem. Soc. **94**, 5386 (1972).
11. G. Büchi, A. Hauser, and J. Limacher. J. Org. Chem. **42**, 3323 (1977).
12. E. Piers and J. Banville. Chem. Commun. 1138, (1979).
13. A. J. Barker and G. Pattenden. Tetrahedron Lett. 2599 (1981).
14. H. J. Liu and W. H. Chan. Can. J. Chem. **57**, 708 (1979).
15. R. S. Sauers. J. Am. Chem. Soc. **81**, 925 (1959).
16. H. J. Liu and P. C. L. Yao. Can. J. Chem. **55**, 822 (1977).
17. J. J. Pappas and W. P. Keaveney. Tetrahedron Lett. 4273 (1966).
18. O. Loreny and C. R. Parks. J. Org. Chem. **30**, 1976 (1965).
19. P. E. Eaton. Acc. Chem. Res. **1**, 50 (1968).
20. P. G. Bauslaugh. Synthesis, 287 (1970).
21. P. de Mayo. Acc. Chem. Res. **4**, 41 (1971).
22. W. H. Watanabe and L. E. Conlon. J. Am. Chem. Soc. **79**, 2828 (1957).
23. E. J. Corey and J. W. Suggs. Tetrahedron Lett. 2647 (1975).
24. E. J. Corey, J. D. Nass, R. LeMahieu, and R. B. Mitra. J. Am. Chem. Soc. **83**, 4013 (1964).
25. P. Crabbé. Optical rotatory dispersion and circular dichroism in organic chemistry. Holden-day, Inc., San Francisco, CA. 1965.
26. S. M. McElvain and D. Kundigen. Org. Synth. Coll. Vol. III, 506 (1955).
27. H. J. Pauben, B. Löken, and H. J. Ringold. J. Am. Chem. Soc. **76**, 1359 (1954).
28. W. T. Tai and E. W. Warnhoff. Can. J. Chem. **42**, 1333 (1964).
29. H. J. Liu and T. Ogino. Tetrahedron Lett. 4937 (1973).
30. H. J. Liu and S. P. Majumdar. Synth. Commun. **5**, 125 (1975).
31. E. J. Corey and M. Chaykovsky. J. Am. Chem. Soc. **87**, 1353 (1965).
32. N. L. Wendler. *In* Molecular Rearrangement. Vol. 2. *Edited by* P. de Mayo. Interscience Publishers, New York, NY. 1964. Chapt. 16.
33. C. Djerassi, R. R. Engle, and A. Bowers. J. Org. Chem. **21**, 1547 (1956).
34. Z. Valenta and H. J. Liu. Org. Synth. **57**, 113 (1977).

# Formation and reactivity of 1,3-benzodioxol-2-yl, 1,3-benzodioxan-2-yl, and related radicals. A search for an aromatic analog of the radical acetoxy rearrangement (Surzur–Tanner reaction)

FEREIDOON SHAHIDI AND THOMAS T. TIDWELL

*Department of Chemistry, University of Toronto, Toronto, Ont., Canada M5S 1A1*

Received November 6, 1981

FEREIDOON SHAHIDI and THOMAS T. TIDWELL. Can. J. Chem. **60**, 1092 (1982).

Reaction of the 1,3-dioxole, **9**, the 1,3-dioxan, **18**, and the 1,3-dioxepin, **29**, with *tert*-butoxy radicals gave evidence in each case for formation of the corresponding 1,1-dioxyethyl radicals. No conclusive evidence for formation of any of these radicals by cyclization of acetoxyaryl radicals could be obtained. Several of the 1,1-dioxyethyl radicals reacted by rearrangement.

FEREIDOON SHAHIDI et THOMAS T. TIDWELL. Can. J. Chem. **60**, 1092 (1982).

Lors de la réaction du dioxole-1,3 (**9**), du dioxanne-1,3 (**18**) et de la dioxépine-1,3 (**29**) avec les radicaux *tert*-butoxy, on a observé dans chacun des cas la formation des radicaux dioxy-1,1 éthyles correspondants. On n'a pas pu prouver que ces radicaux peuvent être préparés par la cyclisation des radicaux acétoxyaryles. Plusieurs de ces radicaux réagissent en se transposant.

[Traduit par le journal]

1,3-Dioxan-2-yl radicals (**1**) and 1,3-dioxol-2-yl radicals (**2**) have recently been the subject of intense investigation (1, 2). The most common

**1**

**2**

route for formation of these species has been hydrogen atom abstraction from the dioxane or dioxole (e.g. eq. [1]). Rearrangements of 2-acyloxyethyl radicals (the Surzur–Tanner reaction)[1] (3) evidently proceed through transition states resembling **2** as illustrated in eq. [2], but cyclized radical intermediates apparently are not formed in these processes (3).

[1] 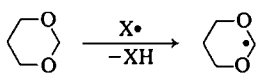

[2] 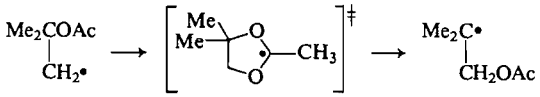

Only recently have there been any studies of the benzo analogs of **1** or **2**. Radical **3** was generated by hydrogen atom abstraction (eq. [3]) and its esr spectrum was observed (1*a*). However, when α-acetoxyphenyl radicals (4) were generated by thermolysis of diacyl peroxides (eq. [4]), no rearrangement to dioxolyl radicals **5** could be detected (4). This rearrangement involves breaking a carbon–oxygen double bond and forming an aryl carbon–oxygen single bond and would be exothermic by about 13 kcal/mol.[2] It was suggested that geometrical constraints prevented favorable orbital overlap in the transition state for cyclization and precluded the rearrangement from occurring.

[3] 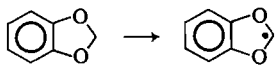

**3**

Recently we have been interested in the formation of substituted furanyl radicals by cyclization reactions involving free radicals (5) and report

[4] 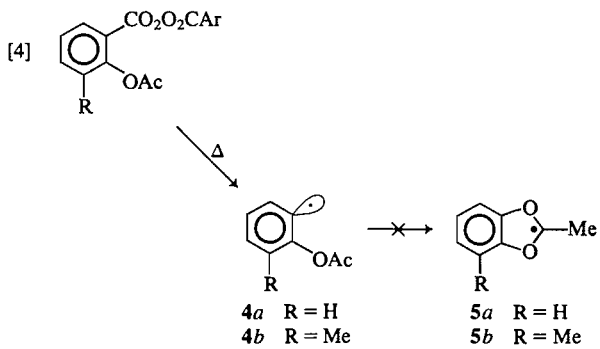

**4***a* R = H
**4***b* R = Me

**5***a* R = H
**5***b* R = Me

herein studies of 1,3-benzodioxan-2-yl and 1,3-benzodioxol-2-yl radicals and attempts to form these species by free radical cyclizations.

## Results and discussion

*tert*-Butyl acetylperoxysalicylate (**6**) (6) appeared to be an attractive source of radical **4***a* in order to test for the possible occurrence of the cyclization to

[1]So named following a suggestion of Barclay *et al.* (17). This reaction was evidently discovered independently by Tanner and Law (3*a*) and Surzur and Teissier (3*f*).

[2]See the Appendix for the basis of this estimate.

0008-4042/82/091092-06$01.00/0

©1982 National Research Council of Canada/Conseil national de recherches du Canada

Can. J. Chem. Downloaded from www.nrcresearchpress.com by 210.87.254.105 on 09/06/12
For personal use only.

Can. J. Chem. Downloaded from www.nrcresearchpress.com by 210.87.254.105 on 09/06/12
For personal use only.

[5] 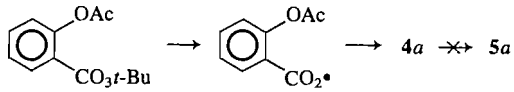


6 7

**5** (eq. [5]). Thermal decomposition of **6** in benzene at 100°C gave the products shown in eq. [6] (the carboxylic acids were isolated by first esterifying with $CH_2N_2$ or $PhCHN_2$). Acetylsalicyclic acid (**8***a*) was found to be converted to salicyclic acid (**8***b*) under the reaction conditions so **8***a* is apparently a precursor to the **8***b* found in the reaction product.

[6] 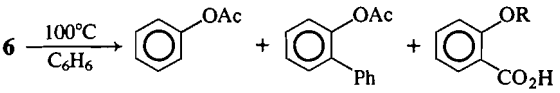


10% 36% **8***a* (R = Ac) 12%
**8***b* (R = H) 42%

Similarly reaction of *o*-bromophenyl acetate with *n*-$Bu_3SnH$ gave phenyl acetate but no cyclized product (eq. [7]). These results confirm the conclu-

[7] 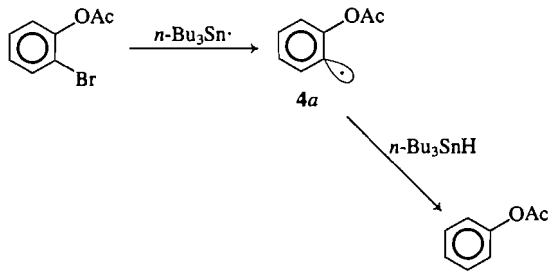


sion of Evanochko and Shevlin (4) that the cyclization of eq. [4] is slow. These authors also concluded (4) that radical **7** has less of a tendency to decarboxylate than $PhC\dot{O}_2$, and the high yields of the nondecarboxylated products **8***a* and **8***b* observed in our work are consistent with this finding.

In order to confirm the postulated stability of **5***a* this radical was generated independently by hydrogen abstraction by *tert*-butoxy radicals from the dioxole **9** (7*a*, *c*). When this reaction was carried out in benzene-$d_6$ the products shown in eq. [8] were identified by gc/ms (gas chromatography/mass spectroscopy) and nmr. The nmr of recovered **9** revealed the presence of deuterium at the methine position (Fig. 1). These products indicate that radical **5***a* was formed; this conclusion was confirmed by observation of the esr spectrum of **5***a* when **9** was photolyzed with *t*-BuOO–*t*-Bu at −110°C: $a^H_{CH_3}$ = 12.41 G, *a* (4 aryl H) = 0.26 G, *g* = 2.00329.[3]

[3]This experiment was carried out by Dr. D. Griller and Dr. K. U. Ingold at the National Research Council, Ottawa.

The source of the deuterium in **9**-*d* is evidently a cyclohexadienyl radical or cyclohexadiene derived from addition of *tert*-butoxy, methyl, or another reactive radical to benzene-$d_6$.

[8] 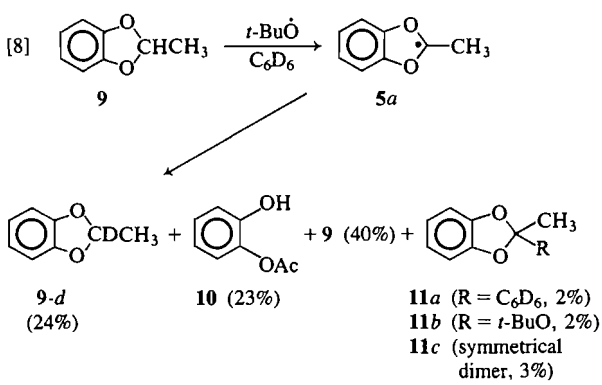


**9**-*d* (24%) **10** (23%) **11***a* (R = $C_6D_6$, 2%)
**11***b* (R = *t*-BuO, 2%)
**11***c* (symmetrical dimer, 3%)

Product **10** apparently arises from decomposition of **11***b* which was observed to occur during gas chromatography. Products **11***a* and **11***b* could arise from combination of **5***a* with $C_6D_6$ or *t*-$Bu\dot{O}$, and **11***c* from dimerization of **5***a*. The fact that these products form indicates a reasonable lifetime for **5***a*.

Our results, and those of Evanochko and Shevlin (4), are all consistent with a greater thermodynamic stability of **5***a* relative to **4***a*. The failure of the rearrangement to occur can be accounted for by the proposal (4) that the geometry of **4***a* does not permit facile bond formation between the singly occupied σ orbital of **4***a* and the bonding π orbital at the carbonyl oxygen. Such geometrical and stereoelectronic constraints on free radical reactions are becoming increasingly well identified (3*d*, 5, 8). Acetoxyalkyl radicals (eq. [2]) are apparently sufficiently less rigid than acetoxyaryl radicals so that rearrangement is feasible.

In selected cases it is possible for a phenyl radical to cyclize with formation of a 5-membered ring, as in the reported example shown in eq. [9] (8). Such

[9] 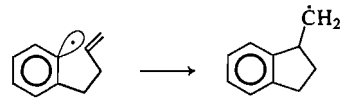


cyclizations involving formation of exocyclic radicals are predicted (8*b*, 9) to be favored, as opposed to reactions such as that of eq. [4], which is not observed, and is predicted not to be favored. The observation (8*a*) that the radical in eq. [10] cyclized

[10] 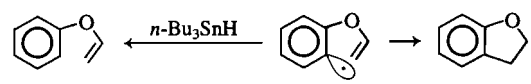


94% <1%

Can. J. Chem. Downloaded from www.nrcresearchpress.com by 210.87.254.105 on 09/06/12
For personal use only.

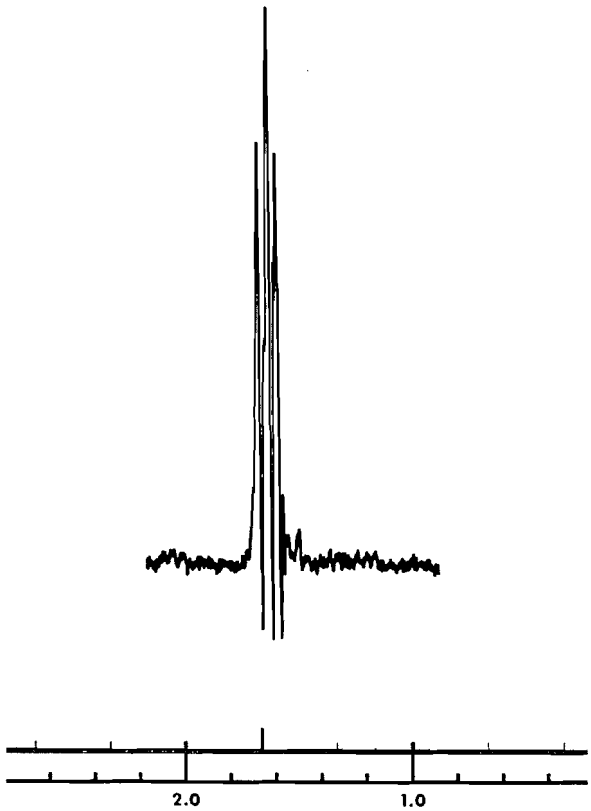


FIG. 1. The $^1H$ nmr absorption of $CH_3$ in a mixture of **9** and **9-*d***.

to the extent of less than 1% is another example of the barrier to formation of endocyclic radicals.

When the homologous acetal **12** was reacted with *tert*-butoxy radicals the only radical visible by esr was **13** (eq. [11]). Evidently formation of the

[11] 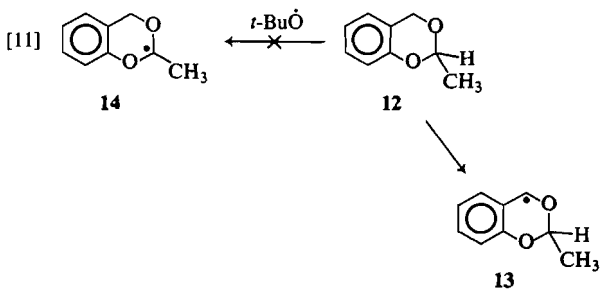


isomeric radical **14** was not competitive with abstraction to give the benzylic radical **13**. An attempt to generate **14** from cyclization of 2-acetoxybenzyl (**15**) also failed. Thus 2-acetoxytoluene (**16**) was reacted with *tert*-butoxy radicals in $C_6D_6$ as shown in eq. [12]. The formation of the dimer **17** indicates formation of **15**, but no evidence of cyclization to **14** was obtained.

[12] 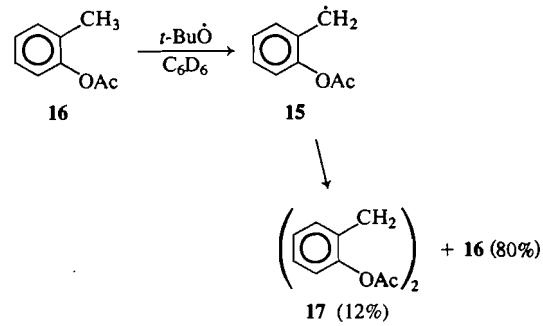


Reaction of **18**, which has no reactive benzylic hydrogens, with *tert*-butoxy radicals led to esr observation of the radical **19** and isolation of the ring opened product **20**. Ring opening of **19** to give the benzylic radical **21** is likely to be exothermic so this path appears plausible.

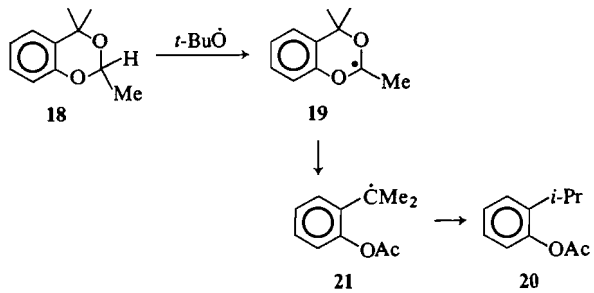


Reaction of **20** with *tert*-butoxy radicals gave the product distribution in eq. [13], as analyzed by

[13] 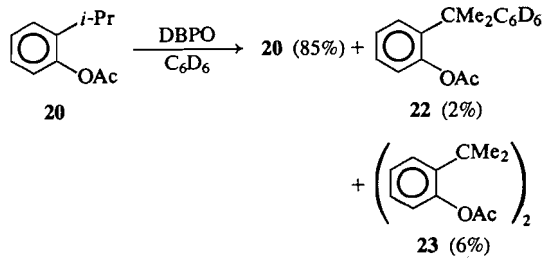


gc/ms. These products indicate that radical **21** was formed, but there is no evidence for cyclization to **19**, in agreement with the observation that **19** rearranges to **21**.

These results suggest that evidence for the formation of the radicals **14** and **19**, or their rearrangement products **15** and **21**, could be obtained if these species were indeed formed from

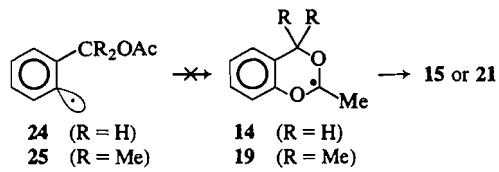

Can. J. Chem. Downloaded from www.nrcresearchpress.com by 210.87.254.105 on 09/06/12
For personal use only.

aryl radicals **24** and **25**. Furthermore, conversion of **24** and **25** to **14** and **19**, respectively, ought to be exothermic. However, treatment of the appropriate aryl halide precursors **26** and **27** with $n$-$Bu_3SnH$

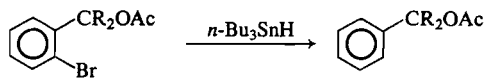


**26** (R = H), **27** (R = Me)

gave only reduction to the unrearranged acetates. Evidently rearrangements to **14** and **19** suffer from sufficiently high kinetic barriers so as not to be able to compete with direct reduction. Rate constants for this latter process are high so the aryl radicals from **26** and **27** are short lived under these conditions.

Generation of the 1,3-dioxepinyl radical **28** was also attempted by reaction of **29** with *tert*-butoxy radicals. No radical was detected by esr, but surprisingly an 85% yield of benzocoumarin (**30**) was identified in the reaction mixture by gc/ms, along with 10% recovered **29**. A reasonable mechanism for the formation of **30** is shown (eq. [14]).

[14]

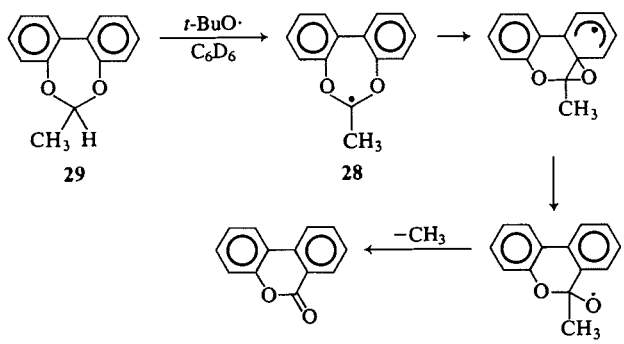


**29** **28** **30**

There is a high propensity for formation of **30** from many precursors, including **31**–**33** (10, 11), but the extensive rearrangement from **28** is certainly one of the most unusual.

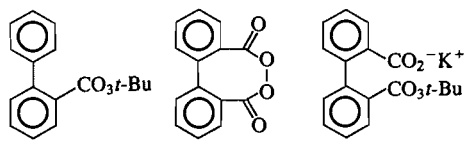


**31** **32** **33**

Radical **34** appeared as a plausible precursor to give an aryl Surzur–Tanner cyclization, and photolysis or thermolysis of the perester **35** did give a high yield of **30** analogous to the reaction of **29**. However, this result does not confirm that acetoxy cyclization has occurred. Reaction of the biphenylpercarboxylate **31** also gave a high yield of **30** (10), but apparently by a route involving homolytic aromatic substitution by an intermediate carboxy radical. Similarly 2′-substituted biphenyl-2-carboxy radicals **36**, generated from peresters or by oxidation of carboxylic acids, also gave **30** by homolytic *ipso* substitution (12).

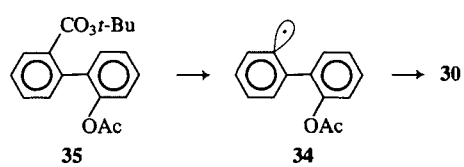


**35** **34**

To test for the path followed by **35** the bromo analog **37** was prepared by the route shown from the lactone **38** and was found to reform this compound as the only lactonic product on decomposition. If a structure **39** analogous to **28** had been

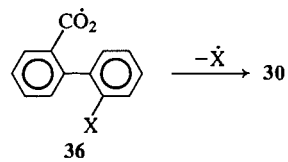


**36**

formed then ring opening to form 2 isomeric lactones would have been expected. It may be concluded that the formation of **28** or **39** by an acetoxy cyclization has yet to be convincingly demonstrated. The mechanism of eq. [14] appears likely for the conversion of **29** to **30**, while the intervention of **28** in the conversion of **34** to **30** is possible but is not established.

In summary it is apparent that intramolecular attack on an acetoxy group by an aryl radical is an elusive process, despite the fact that it is apparently favorable thermochemically. Benzo derivatives of 1,3-dioxol-2-yl and 1,3-dioxan-2-yl radicals display some fascinating reactivity, but confirmation of

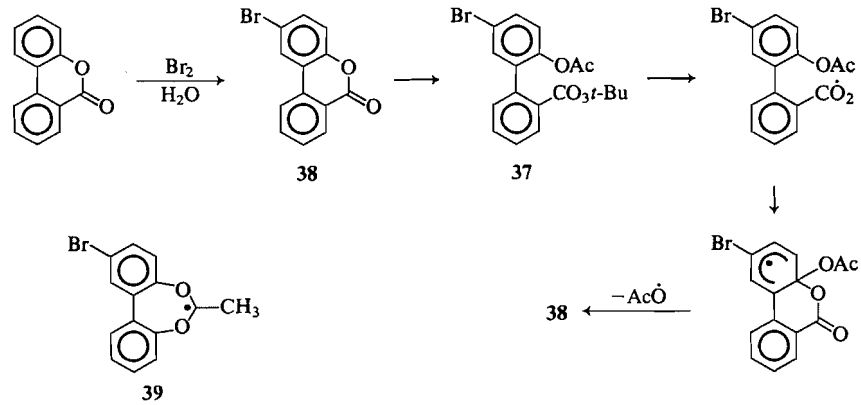


formation of these species by a rearrangement route must await further more inspired study.

## Experimental

Qualitative ir spectra were measured on a Perkin–Elmer 237 instrument. The nmr spectra were recorded on a Varian T-60 spectrometer. Elemental analyses were performed by A. G. Gygli Microanalysis Ltd., Toronto.

*Products from* tert-*butyl acetylperoxysalicylate (6)*

A solution of **6** (1.02 g, 4.0 mmol) in 10 mL benzene was heated 48 h at 100°C in a sealed tube. In separate experiments the reaction product was esterified with $CH_2N_2$ or $PhCHN_2$ and the product analyzed by vpc separation and isolation using a 1.5 m × 4 mm SE-30 column. Products were identified by their nmr spectra and, in the case of 2-acetoxybiphenyl, by its mass spectral molecular weight. Product yields (independent of the method of esterification) were phenyl acetate (10%), salicyclic acid (42%), acetylsalicyclic acid (12%), and 2-acetoxybiphenyl (36%). Methyl and benzyl esters of acetic acid were also isolated and it was found that acetylsalicyclic acid formed salicyclic acid and acetic acid under the reaction conditions.

*Reaction of 2-bromophenyl acetate* (0.43 g) with 0.4 g *n*-$Bu_3$-SnH (Aldrich) by photolysis in 5 mL ether containing 10 mg *t*-BuOO–*t*-Bu gave a product containing 35% phenyl acetate (isolated by vpc) but no **9**.

*2-Methyl-1,3-benzodioxole (9)* was originally prepared by a reported procedure (*7a*) utilizing pyrocatechol and paraldehyde but the reaction was highly irreproducible and gave low or nil yields of product. Therefore a modification of a reported (*7b*) method for preparation of acetals of *o*-dihydroxyaromatics was utilized. A solution of pyrocatechol (11.0 g, 0.10 mol), 1,1-dichloroethane (11.2 g, 0.11 mol), CuO (1.6 g), and $K_2CO_3$ (41.4 g, 0.30 mol) in 120 mL DMF was flushed with $N_2$ and heated at 125°C overnight. The mixture was cooled, poured into ice water, extracted with ether, and the ether layer was extracted once with 3% HCl, eight times with 20% $K_2CO_3$ solution, and once with water. The ether layer was dried with Drierite and evaporated and the product separated by vpc using a 1.5 m × 4 mm 10% SE-30 column at 160°C to give 2.3 g (0.017 mol, 17%) **9** with nmr ($CCl_4$) δ: 1.75 (d, 6, $J$ = 5 Hz, $CH_3$), 6.20 (q, 1, $J$ = 5 Hz, C*H*Me), 6.78 (s, 4, Ar).

*Reaction of 9 with di-*tert-*butyl peroxyoxalate (DBPO) in benzene-*$d_6$

A solution of **9** (0.2 g, 1.5 mmol) in 2 mL $C_6D_6$ with DBPO (0.5 g, 2 mmol) was degassed and sealed in a glass tube and allowed to stand at 25°C for 3 days. The mixture was separated by vpc (4 mm × 2 m 10% SE-30 column) and the products identified by nmr, **9** (40% $d_0$ and 24% $d_1$ by nmr, see Fig. 1), **10** (23%); nmr ($CDCl_3$) δ: 2.48 (s, 3, $CH_3CO$), 5.60 (broad s, 1, OH), 7.1 (m, 4, Ar). The identifications of **11***a–c* are tentative and depend on mass spectral data ($M^+$ peaks for **11***a* and **11***c*, an $M^+ - t$-Bu peak for **11***b*) and an nmr of **11***b* contaminated with **6**; nmr **11** ($CDCl_3$) δ: 1.28 (s, 9, *t*-Bu), 1.68 (s, 3, Me), 6.76 (s, 4, Ar).

*2-Methyl-1,3-benzodioxan (12)*

1,1-Dichloroethane (7.5 g, 0.074 mol) was added to a solution obtained by adding 9.3 g (0.075 mol) *o*-hydroxybenzyl alcohol (Aldrich) in 50 mL DMF to an ice-cooled mixture of 3.6 g (0.15 mol) pentane-washed NaH in 200 mL dry DMF. The resulting solution was heated overnight at 100°C, cooled, poured into ice water, and extracted with ether. The ether layer was washed repeatedly with 10% KOH solution, once with 10% HCl, dried over $MgSO_4$, and evaporated. Separation by vpc gave 0.25 g (1.7 mmol, 2%) **12**, identified by nmr ($CDCl_3$) δ: 1.54 (d, 3, $J$ = 5 Hz, $CH_3$), 4.85 (center of AB quartet of $CH_2$), 5.10 (q, 1, $J$ = 5 Hz, CHMe), 6.7–7.1 (m, 4, Ar).

*Reaction of 2-acetoxytoluene (16) with DBPO* was carried out analogously to the reaction of **9** using $C_6D_6$ as solvent. Formation of 12% **17** was indicated by gc/ms.

*2,4,4-Trimethyl-1,3-benzodioxan (18)* was prepared in 3–5% yields by the same procedure used for **12** from *o*-hydroxycumyl alcohol prepared by reacting excess MeLi in ether with *o*-hydroxyacetophenone. The product **18** was purified by vpc (1.5 mm × 4 m SE-30 at 140°C) and identified by nmr ($CDCl_3$) δ: 1.50 (d, 3, $J$ = 5 Hz, $CHCH_3$), 1.60 (s, 6, $CMe_2$), 5.16 (q, 1, $J$ = 5 Hz, $CHCH_3$), 6.7–7.3 (m, 4, Ar).

*Reaction of 18 with DBPO*

A $C_6H_6$ solution of **18** (0.18 g, 1.0 mmol) and 0.18 g DBPO (0.75 mmol) in dry benzene was sealed in an evacuated tube and let stand at 25°C for 2 days. Analysis of the product by gc/ms revealed the presence of 73% unreacted **18** and 27% *o*-acetoxycumene (**20**).

o-*Acetoxycumene 20* was prepared by reaction of 13.6 g (0.1 mol) *o*-hydroxycumene with 10 mL pyridine and 78 g (1 mol) acetyl chloride in 150 mL ether at 0°C. After one day the reaction mixture was poured into ice water, extracted with ether, and the ether layer washed with 10% HCl, 10% KOH, dried over $MgSO_4$, and evaporated. The product was identified by nmr ($CDCl_3$) δ: 1.10 (d, 6, $J$ = 7 Hz, $CH(CH_3)_2$), 2.32 (s, 3, $CH_3CO$), 3.00 (heptet, 1, $J$ = 7 Hz, $CHMe_2$), 7.0–7.4 (m, 4, Ar).

*2-Bromobenzyl acetate (26) and* n-$Bu_3SnH$

A solution of 2.3 g (10 mmol) **26** (obtained from reaction of Aldrich 2-bromobenzyl bromide and NaOAc) and 3.2 g (11 mmol) *n*-$Bu_3SnH$ (Alfa) in 8 mL benzene with 0.2 g azoisobutyronitrile was heated in a sealed tube at 90°C for 48 h. Distillation of the benzene and then the product showed benzyl acetate as the only volatile product.

*2-Chlorocumyl acetate (27)* was obtained by reaction of

Can. J. Chem. Downloaded from www.nrcresearchpress.com by 210.87.254.105 on 09/06/12
For personal use only.

Can. J. Chem. Downloaded from www.nrcresearchpress.com by 210.87.254.105 on 09/06/12
For personal use only.

*o*-chloroacetophenone with methyllithium, followed by treatment of the isolated 2-chlorocumyl alcohol with KH and acetyl chloride in ether. This was reacted with $n$-$Bu_3SnH$ as described for **26**, and gc/ms analysis of the product showed cumyl acetate as the major volatile product.

*2-Methyl dibenzo[d,f][1,3]dioxepin (29)* was prepared in 6% yield by the same procedure used for **12** from *o,o'*-biphenol (Aldrich). The material was purified by vpc separation on a 6 m SE-30 column, mp 48–49°C, and was identified by nmr ($CDCl_3$) δ: 1.62 (d, 3, $J$ = 5 Hz, $CH_3$), 5.78 (q, 1, $J$ = 5 Hz, C*H*Me), 7.0–7.8 (8, m, Ar).

*Products from 29 and DBPO*

The reaction was carried out with 70 mg (0.5 mmol) **29** and 120 mg (0.5 mmol) DBPO in 1 mL $C_6D_6$ as described for **9**.

*2-Acetoxy-2'*-tert-*butylpercarboxylbiphenyl (35)* was prepared by adding to the known (13) acid chloride of 2-acetoxy-2'-biphenylcarboxylic acid (1.37 g, 5 mmol), in 150 mL ether stirred at 0°C, a solution of 1.0 g (11 mmol) *t*-BuOOH and 1 mL pyridine in 30 mL ether. The mixture was stirred overnight, poured into water, extracted into ether, washed with 10% NaOH and then 10% HCl, dried, and the solvent evaporated. The crude product was chromatographed on a 20 cm silica gel column with 1:1 pentane/ether to give 0.52 g **35** (1.6 mmol, 32%); nmr ($CDCl_3$) δ: 1.12 (s, 9, *t*-Bu), 1.96 (s, 3, $CH_3CO$), 7.2 (m, 8, Ar).

*Products from 35*

Solutions of **35** (0.165 g, 0.5 mmol) in 2 mL of solvent were sealed in evacuated Pyrex tubes and decomposed either thermally (40 h at 110°C) or photochemically (72 h irradiation with a Hanovia medium pressure Hg lamp). The products were analyzed by gas chromatography as shown (±5%):

| | Photochemical | | Thermal |
|---|---|---|---|
| Product | Benzene | Toluene | Benzene |
| *o*-Acetoxybiphenyl | 2 | 9 | 2 |
| 2-(2'-Acetoxyphenyl)benzoic acid | 14 | 11 | 2 |
| **30** | 80 | 80 | 90 |

*2-Acetoxy-5-bromo-2'*-tert-*butylpercarboxybiphenyl (37)* was obtained by a route analogous to **35** beginning with **38** (14), which on reaction with NaOH and $Ac_2O$ gave 2-(2'-acetoxy-5'-bromophenyl)benzoic acid (mp 126–127°C), which on reaction with $SOCl_2$ followed by *t*-BuOOH/pyridine gave **37** as an oil; nmr ($CDCl_3$) δ: 1.23 (s, 9, *t*-Bu), 2.03 (s, 3, Ac), and 7.0–8.0 (m, 7, Ar). *Anal.* calcd. for $C_{19}H_{19}BrO_5$ (mol. wt. 407.27): C 56.03, H 4.70, Br 19.62; found: C 56.52, H 4.36, Br 19.46. Product studies on **37** carried out analogously to **35** gave **38** as the only lactonic product detected, as identified by nmr and mass spectroscopy.

## Acknowledgements

Financial support of the Natural Sciences and Engineering Research Council of Canada is gratefully acknowledged. We thank Drs. Griller and Ingold for the esr studies of **5*a***, **13**, and **19**. Professor J. Warkentin suggested the experiments utilizing **37**.

1. (*a*) C. Gaze, B. C. Gilbert, and M. C. R. Symons. J. Chem. Soc. Perkin Trans. II, 235 (1978); (*b*) C. Gaze and B. C. Gilbert. J. Chem. Soc. Perkin Trans II, 763 (1979); (*c*) G. Brunton, K. U. Ingold, B. P. Roberts, A. L. J. Beckwith, and P. J. Krusic. J. Am. Chem. Soc. **99**, 3177 (1977); (*d*) A. L. J. Beckwith and C. J. Easton. J. Am. Chem. Soc. **103**, 615 (1981); (*e*) V. Malatesta and K. U. Ingold. J. Am. Chem. Soc. **103**, 609 (1981).
2. (*a*) Sh. M. Samirkhanov, S. S. Zlotskii, and D. L. Rakhmankulov. Zh. Org. Khim. **15**, 1815 (1979); (*b*) L. L. Kostyukevich, S. S. Zlotskii, E. Kh. Kravets, V. S. Martem'yanov, and D. L. Rakhmankulov. Zh. Prikl. Khim. (Leningrad), **50**, 2124 (1977).
3. (*a*) D. D. Tanner and F. C. P. Law. J. Am. Chem. Soc. **91**, 7535 (1969); (*b*) A. L. J. Beckwith and P. K. Tindal. Aust. J. Chem. **24**, 2099 (1971); (*c*) A. L. J. Beckwith and C. B. Thomas. J. Chem. Soc. Perkin Trans. I, 861 (1973); (*d*) M. J. Perkins and B. P. Roberts. J. Chem. Soc. Perkin Trans. II, 77 (1975); (*e*) A. L. J. Beckwith and K. U. Ingold. *In* Rearrangement in ground and excited states. *Edited by* P. de Mayo. Academic Press, New York. 1980; (*f*) J.-M. Surzur and P. Teissier. C. R. Acad. Sci. **264**, 1981 (1967).
4. W. T. Evanochko and B. P. Shevlin. J. Org. Chem. **44**, 4426 (1979).
5. C. M. Rynard, C. Thankachan, and T. T. Tidwell. J. Am. Chem. Soc. **101**, 1196 (1979).
6. C. Rüchardt and S. Rochlitz. Justus Liebigs Ann. Chem. 15 (1974).
7. (*a*) G. Slooff. Recl. Trav. Chim. Pays-Bas, **54**, 995 (1935); (*b*) S. McLean and J. Whelan. Can. J. Chem. **51**, 2457 (1973); (*c*) E. R. Cole, G. Crank, and H. T. Hai Minh. Aust. J. Chem. **33**, 675 (1980).
8. (*a*) A. L. J. Beckwith and W. B. Gara. J. Chem. Soc. Perkin Trans. II, 795 (1975); (*b*) A. L. J. Beckwith, C. J. Easton, and A. K. Serelis. J. Chem. Soc. Chem. Commun. 482 (1980); (*c*) A. L. J. Beckwith and G. F. Meijs. J. Chem. Soc. Chem. Commun. 136 (1981); (*d*) A. L. J. Beckwith. Tetrahedron, **37**, 3073 (1981).
9. (*a*) J. E. Baldwin. J. Chem. Soc. Chem. Commun. 734 (1976); (*b*) M. J. Perkins, P. C. Wong, J. Barrett, and G. Dhaliwal. J. Org. Chem. **46**, 2196 (1981).
10. H. Minato, H. Matuszaki, and K. Miwa. Bull. Chem. Soc. Jpn. **41**, 249 (1968).
11. J.-y Koo and G. R. Schuster. J. Am. Chem. Soc. **100**, 4496 (1978).
12. S. A. Glover, S. L. Golding, A. Goosen, and C. W. McCleland. J. Chem. Soc. Perkin Trans. I, 842 (1981).
13. A. Gringauz. J. Pharm. Sci. **65**, 291 (1976).
14. R. Richter. J. Prakt. Chem. **28**, 301 (1883).
15. S. W. Benson, F. R. Cruickshank, D. M. Golden, G. R. Haugen, H. E. O'Neal, A. S. Rodgers, R. Shaw, and D. Walsh. Chem. Rev. **69**, 279 (1969).
16. Z. B. Alfassi and D. M. Golden. J. Phys. Chem. **76**, 3314 (1972).
17. L. R. C. Barclay, D. Griller, and K. U. Ingold. Abstracts OR-WA18. 64th Canadian Chemical Congress, Halifax, N.S. May 31 – June 3, 1981.

## Appendix

The $\Delta\Delta H_f^0$ for the conversion of **4*a*** to **5*a*** at 25°C may be derived from the $\Delta H_f^0$ values for phenyl acetate (−51.4 kcal/mol) and **9** (−55.7 kcal/mol, not corrected for ring strain) calculated by the method of group equivalents (15) and the estimated C—H bond dissociation energies of phenyl acetate to form **4*a*** (110 kcal/mol) and of **9** to form **5*a*** (93 kcal/mol) (16). The latter value applies to H—$CH(OH)CH_3$ and the actual value is probably less.

# Anionic decomposition of an organic peroxide leading to *o*-xylene

FEREIDOON SHAHIDI AND THOMAS T. TIDWELL

*Department of Chemistry, University of Toronto, Toronto, Ont., Canada M5S 1A1*

Received November 6, 1981

FEREIDOON SHAHIDI and THOMAS T. TIDWELL. Can. J. Chem. **60**, 1098 (1982).

Reaction of 1,2-dimethyl-1,2-dihydrophthalic anhydride (**8**) with *t*-BuOONa at 40°C gave *o*-xylene as the only observed product. This reaction is proposed to occur through intermediacy of the anionic peroxide **10** whose conversion to *o*-xylene is calculated to be exothermic by 84 kcal/mol. Extension of this reaction to systems that do not have the possibility for gaining aromatic stabilization was unsuccessful.

FEREIDOON SHAHIDI et THOMAS T. TIDWELL. Can. J. Chem. **60**, 1098 (1982).

L'anhydride de l'acide diméthyl-1,2 dihydro-1,2 phtalique (**8**) réagit avec le *tert*-BuOONa à 40°C en donnant uniquement du *o*-xylène. On pense que cette réaction se produit par l'intermédiaire du peroxyde anionique **10** qui par la transformation en *o*-xylène libèrerait 84 kcal/mol. On a vainement tenté d'étendre cette réaction aux systèmes qui n'ont pas la possibilité d'acquérir la stabilité aromatique.

[Traduit par le journal]

The reactions of peroxides derived from 1,2-dicarboxylic acid systems have been the subject of continuing interest. Examples include reaction of di-*tert*-butylperoxy *meso*-2,3-diphenylsuccinate (**1**), which proceeds with rate limiting scission of one peroxide bond to give the benzylic radical **2**, which gives exclusive formation of *trans*-stilbene (eq. [1]) (1). This general reaction was developed as a general synthetic method for the conversion of 1,2-dicarboxylic acid systems to alkenes (eq. [2] (2).

[1] 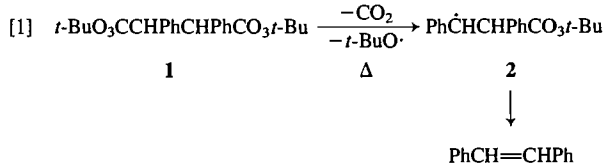


[2] 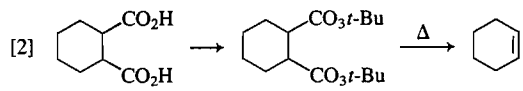


The aromatic analog di-*tert*-butylperoxy phthalate (**3**) was the object of careful study in our laboratory (3), and it was found that, although the free radical reactions of this substrate did not involve direct interaction between the two carboxyl groups, there was evidently a nonradical decomposition of the peroxidic intermediate **4** involved (eq. [3]) as one of the reaction paths followed.

[3] 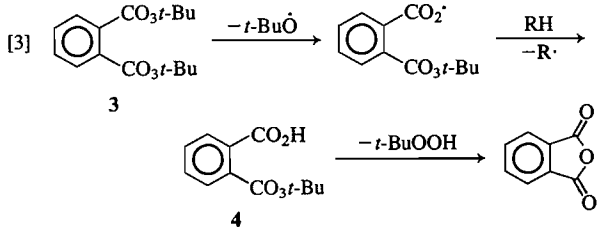


Related studies have dealt with cyclic diacyl peroxides **5–7** derived from 1,2-dicarboxylic acids.

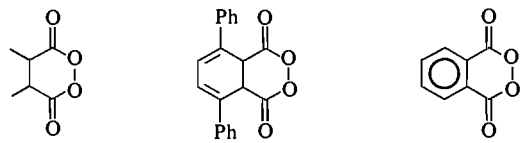


**5** **6** **7**

The study of **5** and several related systems was reported by Dervan and Jones (4), who presented evidence for their thermal decomposition according to eq. [4]. Even though these reactions were

[4] 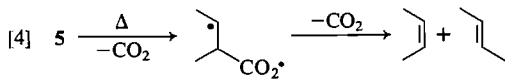


potentially sufficiently exothermic to produce excited states of the product alkenes, the evidence indicated that this did not occur. However, in the reaction of eq. [5] the species **6** was evidently

[5] 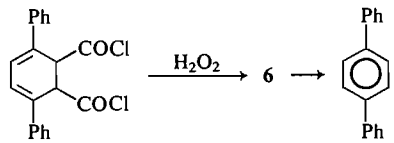


generated and the observation of fluorescence in the reaction indicated that the product terphenyl was formed as an excited singlet (5).

The most recent of a variety of studies of the reactivity of phthalyl peroxide (**7**) involves electron transfer from pyrene (*5b*).

The goal of the present study was to search for a case of concerted reaction of a derivative of a vicinal dicarboxylic acid system. A system of the type **6** appeared to be most appropriate, as the potential for aromatization of the ring would in-

0008-4042/82/091098-03$01.00/0

©1982 National Research Council of Canada/Conseil national de recherches du Canada

Can. J. Chem. Downloaded from www.nrcresearchpress.com by 210.87.254.5 on 09/06/12
For personal use only.

Can. J. Chem. Downloaded from www.nrcresearchpress.com by 210.87.254.5 on 09/06/12
For personal use only.

crease the exothermicity of a bisdecarboxylation. However, the presence of reactive α-hydrogens in **6** and its immediate precursors appeared undesirable because of their potential for facile isomerization to α,β-unsaturated carbonyl derivatives.

## Results and discussion

The anhydride **8**, originally prepared (6*a*) in one of two classic syntheses of cantharidin (6), was selected for study. The preparation followed the established methods, but the yield of **8** from the dibromide **9** was increased to 78% from the previously reported 11% by the use of 1,5-diazabicyclo[5.4.0]undec-5-ene (DBU) as base instead of the previously utilized trimethylamine (6*a*). The hydrolysis of **8** to the corresponding diacid was carried out by the reported procedure (6*a*) but all attempts to convert the diacid or **8** to a diacyl chloride led to isolation of only **8** in every case. Consequently preparation of a cyclic peroxide or bisperester from **8** could not be attempted.

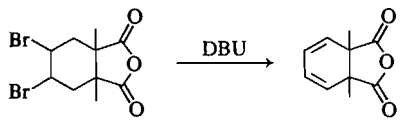


**9** **8**

Reaction of **8** with *t*-BuOONa in a mixed solvent (DME–$CH_2Cl_2$–pentane) at 40°C followed by distillation of the solvent at 60°C and vpc separation of the volatile products led to the isolation of *o*-xylene as the only product derived from **8**. Similarly reaction of **8** with *t*-BuOOK in THF-$d_8$ at 0°C and prompt observation of the nmr spectrum showed signals ascribable to *o*-xylene and *t*-BuOK as the only products. One possible route to these products is shown (eq. [6]). The method of group equivalents (7) predicts the decomposition of the conjugate acid of **10** to $2CO_2$ + *t*-BuOH to be exothermic by about 84 kcal/mol and it would appear that the reaction of eq. [6] would be equally exothermic. Other pathways for the process may be envisaged, including stepwise ionic (eq. [7]) or radical (eq. [8]) routes.

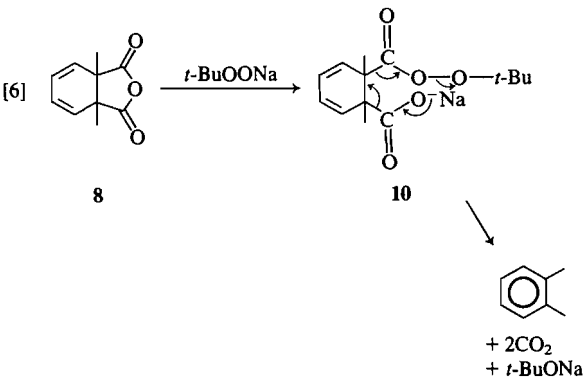


**8** **10**

The powerful driving force for the concerted pathway suggests that this route is favored. The cyclohexadienyl anion and radical formed in eqs. [7] and [8], respectively, would not appear to be sufficiently stabilized to form under these conditions.

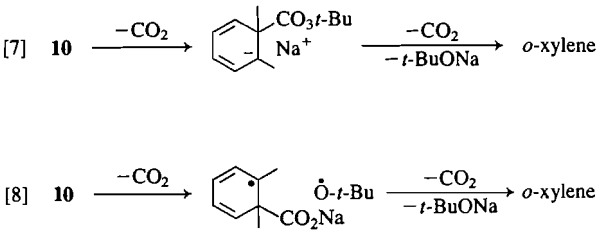


Thus our goal of observing a facile bisdecarboxylation reaction has been met, although in a rather unexpected and novel fashion. The possibility of developing a preparatively useful procedure for biscarboxylation in analogous systems that do not lead to aromatic systems occurred to us, but in several experiments (e.g., eq. [9]) this goal has not yet been realized. Variable amounts of the products **13**–**15** were identified by their nmr spectra, but the inconsistency of the yields suggested that radical-induced decompositions may have been occurring. Comparable results were obtained in benzene or toluene, with or without added KH or $Et_3N$.

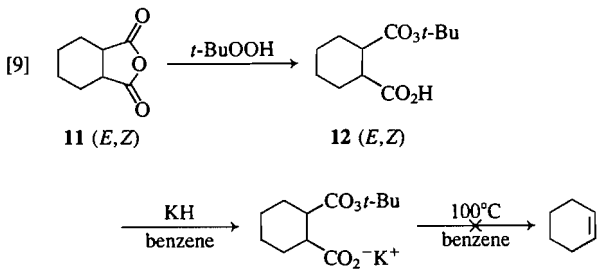


**11** (*E*,*Z*) **12** (*E*,*Z*)

A semiquantitative kinetics determination for decomposition of *E*-**12** gave a rate constant of $5.3 \times 10^{-5}$ $s^{-1}$ at 98.0°C in toluene. Comparison to the value of $6.9 \times 10^{-4}$ $s^{-1}$ at 110°C reported (8) for *tert*-butyl cyclohexanepercarboxylate indicates similar rate limiting steps for these two peresters.

Other anionic decompositions of organic perox-

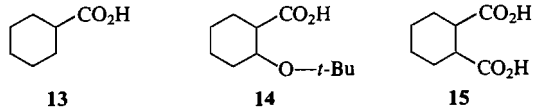


**13** **14** **15**

ides include the reaction of diphenic anhydride (**16**) with *t*-BuOONa yielding lactone as shown in eq. [10] (9). This reaction was proposed to involve the

[10] 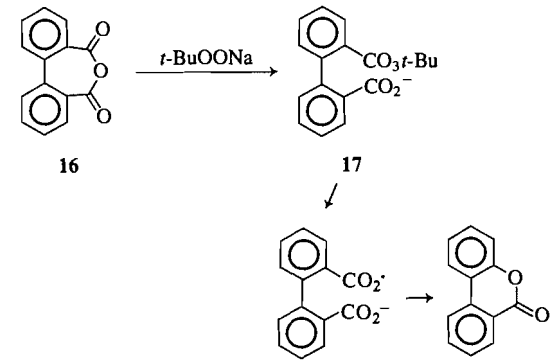


**16** **17**

intermediate **17**, but it may be noted that the reaction conditions (refluxing tetrahydrofuran) would not ordinarily be sufficient to result in homolytic reaction of a model compound such as *tert*-butyl perbenzoate.

Another reported (10) case of anionic decomposition of a peroxide is shown in eq. [11] and may be seen to be closely related to the proposal of eq. [6].

[11] $t\text{-BuOOCMe}_2\text{CO}_2^- \longrightarrow t\text{-BuO}^- + \text{O=CMe}_2 + \text{CO}_2$

## Experimental

Qualitative ir spectra were measured on a Perkin–Elmer 237 instrument. The nmr spectra were recorded on a Varian T-60 spectrometer. Elemental analyses were performed by A. B. Gygli Microanalysis Ltd., Toronto. Dimethoxyethane (DME) was freshly distilled from Na.

*1,2-Dimethyl-1,2-dihydrophthalic anhydride (**8**)*

A mixture of 1.7 g (5.0 mmol) dibromide **9** (*6b*) and 1.52 g (8.6 mmol) DBU (Aldrich) were heated 5 min at 150°C. Sublimation gave 0.69 g (3.9 mmol, 78%) of **8**, mp 64°C (lit. (*6a*) mp 63–67°C); nmr ($CDCl_3$) δ: 1.35 (s, 6, 2Me); 5.5–6.2 (m, 4, $A_2B_2$ pattern of vinyl H).

*Reaction of **8** with t-BuOONa*

A solution of 0.078 g (0.44 mmol) **8** in 5 mL $CH_2Cl_2$ and 3 mL pentane was added dropwise to a mixture of 1 mmol NaH (washed free of oil) and 1 mmol *t*-BuOOH in 15 mL dry DME. The mixture was heated 4 h at 40°C, poured into ice water, and extracted twice with ether. The combined ether layers were washed twice with 10% HCl, dried, and the solvent was distilled away below 60°C. Separation of the residue by vpc using a 3 m × 10 mm OV-17 column gave 36 mg (0.34 mmol, 77%) of *o*-xylene, identified by nmr. Reaction of **8** (1.0 mmol) in 1.0 mL THF-$d_8$ with *t*-BuOOK (1.5 mmol, from *t*-BuOOH and KH) with ice cooling, followed by prompt measurement of the nmr spectrum, gave peaks ascribable to *o*-xylene and a *tert*-butyl signal as the only reactant-derived absorptions.

*E-2-Carbo-*tert*-perbutoxy cyclohexanecarboxylic acid (E-**12**)*

*trans*-1,2-Cyclohexanedicarboxylic anhydride (7.2 g, 50 mmol, Fluka) was added over 0.5 h to a mixture of 50 mmol NaH (washed free of oil with pentane) and 50 mmol *t*-BuOOH in 100 mL dry ether. The solution was stirred 1 h at 25°C, poured into ice water, acidified with HCl, and extracted with ether. After drying and evaporation of solvent there was obtained 9.3 g (38 mmol, 76%) of *E*-**12** which was recrystallized from $CHCl_3$/pentane (10:1), mp 114–116°C (resolidification and remelting at 225–229°C); ir (toluene): 1710 $cm^{-1}$ (C=O of $CO_2H$), 1775 (C=O of $CO_3$-*t*-Bu) $cm^{-1}$; nmr ($CDCl_3$) δ: 1.30 (s, 9, *t*-Bu), 1.4–2.2 (m, 8, $(CH_2)_4$), 2.7 (m, 2, 2 methine H), 10 (broad s, 1, $CO_2H$). *Anal.* calcd. for $C_{12}H_{20}O_5$ (244.29): C 59.00, H 8.25; found: C 58.77, H 8.18.

*Z-2-Carbo-*tert*-perbutoxy cyclohexanecarboxylic acid (Z-**12**)*

This isomer was prepared in the same way as the *E*-isomer from the *Z* anhydride (Aldrich) and recrystallized from $CHCl_3$, mp 196–198°C; ir ($CHCl_3$): 1710 (C=O of $CO_2H$), 1765 (C=O of $CO_3$-*t*-Bu) $cm^{-1}$. nmr ($CDCl_3$) δ: 1.30 (s, 9, *t*-Bu), 1.4–2.0 (m, 8, $(CH_2)_4$), 3.0 (m, 2, 2 methine H), 8.5 (broad s, 1, $CO_2H$). *Anal.* calcd. for $C_{12}H_{20}O_5$ (244.29): C 59.00, H 8.25; found: C 59.18, H 8.26.

*Product studies from* E-**12** *and* Z-**12**

The perester (0.6 g, 2.5 mmol) was dissolved in 10 mL solvent, sealed in a glass tube, and heated at 100°C for 24 h. The product was esterified with $CH_2N_2$ and analyzed by vpc with a 5 m × 3 mm Carbowax column at 130°C and 60 mL/min He flow. Products were isolated and identified by their nmr spectra and mass spectral molecular weights. Authentic samples of the methyl esters of cyclohexanecarboxylic acid and the 1,2-cyclohexanedicarboxylic acids were prepared for comparison. An authentic sample of methyl 2-*tert*-butoxycyclohexanecarboxylate was not available so this identification must be regarded as tentative. The nmr spectrum ($CDCl_3$) of this material from either *E*- or *Z*-**12** showed pairs of closely spaced sharp singlets at δ 1.15 and 3.65 attributable to the *t*-BuO and MeO groups, respectively, of an *E*/*Z* mixture of products from either source.

*Kinetics of decomposition of* E-**12**

Ampules of a 0.064 *M* solution of the perester were removed at intervals from a constant temperature bath at 98.0°C and the disappearance of the perester band at 1775 $cm^{-1}$ was monitored as a function of time using a Perkin–Elmer 180 spectrophotometer. A single run was performed, which gave good first order kinetics ($r = 0.999$).

## Acknowledgements

Financial support by the Natural Sciences and Engineering Research Council of Canada is gratefully acknowledged.

1. L. M. Bobroff, L. B. Gortler, D. J. Sahn, and H. Wiland. J. Org. Chem. **31**, 2678 (1966).
2. E. N. Cain, R. Vukov, and S. Masumune. J. Chem. Soc. Chem. Commun. 98 (1969).
3. D. A. Cable, J. A. Ernst, and T. T. Tidwell. J. Org. Chem. **37**, 3420 (1972).
4. P. B. Dervan and C. R. Jones. J. Org. Chem. **44**, 2116 (1979).
5. (*a*) G. B. Schuster. J. Am. Chem. Soc. **99**, 651 (1977); (*b*) K. A. Horn and G. B. Schuster. J. Am. Chem. Soc. **101**, 7097 (1979).
6. (*a*) K. Ziegler, G. Schenck, E. W. Krockow, A. Siebert, A. Wenz, and H. Weber. Justus Liebigs Ann. Chem. **551**, 1 (1942); (*b*) R. B. Woodward and R. V. Loftfield. J. Am. Chem. Soc. **63**, 3167 (1941).
7. S. W. Benson, F. R. Cruickshank, D. M. Golden, G. R. Haugen, H. E. O'Neal, A. S. Rodgers, R. Shaw, and R. Walsh. Chem. Rev. **69**, 279 (1969).
8. P. Lorenz, C. Rüchardt, and E. Schacht. Chem. Ber. **104**, 3429 (1971).
9. J.-y. Koo and G. B. Schuster. J. Am. Chem. Soc. **100**, 4496 (1978).
10. W. H. Richardson and R. S. Smith. J. Am. Chem. Soc. **91**, 3610 (1969).

Can. J. Chem. Downloaded from www.nrcresearchpress.com by 210.87.254.5 on 09/06/12
For personal use only.

# Ring opening reactions of *N*-substituted-5,6-dihydro-2-methyl-1,4-oxathiin-3-carboxamides

MARSHALL KULKA AND W. A. HARRISON
*Uniroyal Limited, Research Laboratories, Guelph, Ont., Canada N1H 6N3*
Received November 2, 1981

MARSHALL KULKA and W. A. HARRISON. Can. J. Chem. **60**, 1101 (1982).

The amides prepared from 5,6-dihydro-2-methyl-1,4-oxathiin-3-carbonyl chloride **2** and imidamides **4**, carbamimidothioates **4**, 2-benzimidazolamine **7**, 2-benzothiazolamine **12**, and 2-thiazolamine have been studied. The reaction of **2** with imidamides **4** and with carbamimidothioates **4** in the presence of base gave the amides **5**, which when heated in toluene underwent the 1,4-oxathiin ring opening and rearrangement to produce 2-substituted-5-[(2-hydroxyethyl)thio]-6-methyl-4(1*H*)-pyrimidinones **6**. Acylation of 2-benzimidazolamine **7** with **2** yielded the amide **10**. This, in boiling ethanol, ring opened and rearranged to give the compound **11**. The reaction of 2-benzothiazolamine **12** with **2** gave the rearrangement product **14** directly and neither of the possible amides **13** and **15** could be detected. The amide **15** was synthesized by an unambiguous route from 2-aminobenzenethiol and 5,6-dihydro-2-methyl-1,4-oxathiin-3-carbonyl isothiocyanate **3**. It would not undergo ring opening and rearrangement when heated. Acylation of 2-thiazolamine with **2** yielded a mixture from which the amide **19** and the rearrangement ester **18** were separated. Structural assignments are based mainly on nmr, uv, and ir spectral evidence.

MARSHALL KULKA et W. A. HARRISON. Can. J. Chem. **60**, 1101 (1982).

On a étudié les amides préparés à partir du chlorure de dihydro-5,6 méthyl-2 oxathiine-1,4 carbonyle-3 (**2**) et des imidamides **4**, des carbamimidothioates **4**, de la benzimidazolamine-2 (**7**), du benzothiazolamine-2 (**12**) et de la thiazolamine-2. Le composé **2** réagit avec les imidamides **4** et avec les carbamimidothioates **4** en milieu basique en donnant les amides **5**, qui par chauffage dans le toluène, subissent une ouverture du cycle oxathium-1,4 et se transposent en donnant les [(hydroxéthyl-2) thio]-5 méthyl-6 (1*H*)-pyrimidinones-4 (**6**) substitués en position 5. L'acylation de la benzimidazolamine-2 (**7**) avec le composé **2** donne l'amide **10**. Ce dernier dans l'éthanol bouillant subit une ouverture de cycle et une transposition qui conduisent au composé **11**. La benzo-2 thiazolamine **12** réagit avec le composé **2** en donnant le produit de transposition **14** directement et on n'a pas pu déceler les amides **13** et **15** qu'il serait possible d'obtenir. On a synthétisé l'amide **15** selon une méthode non équivoque à partir de l'amino-2 benzènethiol et de l'isothiocyanate de dihydro-5,6 méthyl-2 oxathiine-1,4 carbonyle **3**. Le chauffage de ce composé ne provoque pas d'ouverture de cycle ni de transposition. L'acylation de la thiazolamine-2 avec le composé **2** donne un mélange à partir duquel on isole l'amide **19** et l'ester **18** résultant d'une transposition. On a attribué les structures en s'appuyant principalement sur les spectres de rmn, uv et ir.
[Traduit par le journal]

The discovery in 1966 (1) of the systemic fungicides 5,6-dihydro-2-methyl-*N*-phenyl-1,4-oxathiin-3-carboxamide (VITAVAX®) and its 4,4-dioxide (PLANTVAX®),[1] now used throughout the world to control fungal plant pathogens, has created a great deal of interest in the biological activity and the chemistry of 1,4-oxathiins.

Publications (2, 3) from this laboratory record studies of ring opening reactions of *N*-substituted-5,6-dihydro-2-methyl-1,4-oxathiin-3-carboxamides of the type **1** where X = O and Y = NHR (2), where X = S and Y = NHR (3), and where —C(=X)Y equals 2-pyridyl and 2-pyrimidinyl. In each case, the ring-opening reaction takes place through an attack at the 2-position of the 1,4-oxathiin ring by the nitrogen function followed by rearrangement to form 4(1*H*)-pyrimidinone derivatives.

This paper describes the ring-opening and rearrangement reactions of *N*-substituted-5,6-dihydro-2-methyl-1,4-oxathiin-3-carboxamides of the type **1** where X = NH and Y = alkyl, aryl, alkylthio, and aralkylthio and where —C(=X)Y is 2-benzimidazolyl, 2-benzothiazolyl, and 2-thiazolyl.

Acylation of 2,2,2-trichloroethanimidamide (**4**, Y = $CCl_3$) with 5,6-dihydro-2-methyl-1,4-oxathiin-3-carbonyl chloride (**2**) in the presence of triethylamine gave the amide **5** (Y = $CCl_3$) in 80% yield. When the amide **5** (Y = $CCl_3$) was dissolved in toluene and the solution heated under reflux, the 1,4-oxathiin ring opening and rearrangement occurred to form 5-[(2-hydroxyethyl)thio]-6-methyl-2-(trichloromethyl)-4(1*H*)-pyrimidinone (**6**, Y = $CCl_3$). The amides **5** prepared from **2** and the hydrochlorides of benzeneethanimidamide (**4**, Y = phenylmethyl), benzenemethanimidamide (**4**, Y = phenyl), ethanimidamide (**4**, Y = methyl), and butanimidamide (**4**, Y = propyl) in the presence of aqueous sodium hydroxide were sensitive to heat and no attempts were made to purify them. Instead the crude products were heated in toluene to form the 4(1*H*)-pyrimidinones **6** where Y = phenylmethyl, phenyl, methyl, and propyl respectively. The structural assignments were based on the elemental analysis and on the ir and nmr spectra. It

[1]®Uniroyal's registered trademark.

0008-4042/82/091101-05$01.00/0
©1982 National Research Council of Canada/Conseil national de recherches du Canada

Can. J. Chem. Downloaded from www.nrcresearchpress.com by 210.87.254.5 on 09/06/12
For personal use only.

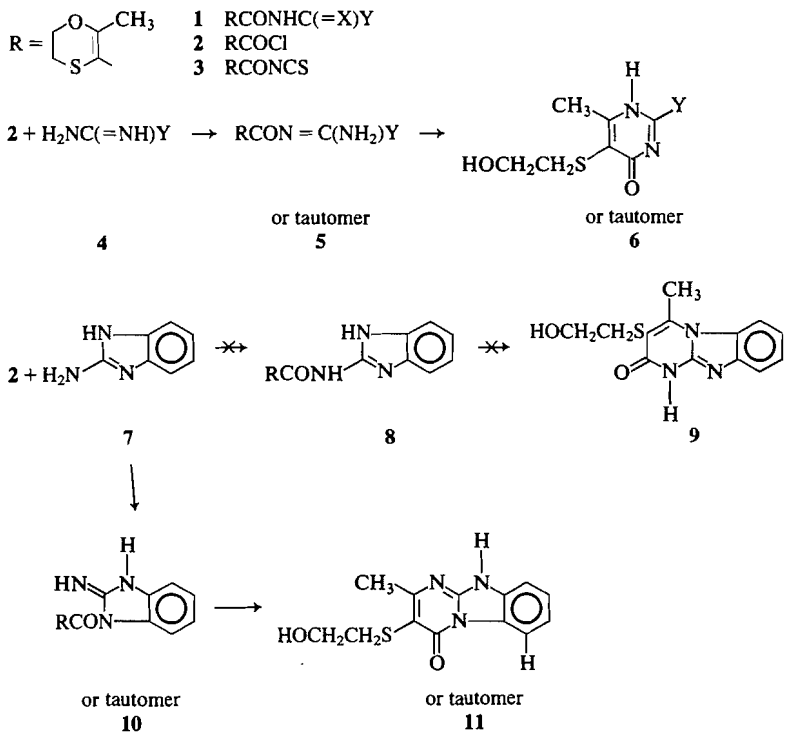


is believed that the compounds **5** exist predominantly in the amino form (RCON=C($NH_2$)Y) in view of the fact that their uv spectra are similar to that of *N*-(1-aminoethylidene)benzamide (**5**, R = phenyl, Y = methyl) which exists in the amino form (4).

5,6-Dihydro-*N*[[(2-chlorophenyl)methylthio]-aminomethylene]-2-methyl-1,4-oxathiin-3-carboxamide (**5**, Y = 2-chlorophenylmethylthio), prepared from **2** and the hydrochloride of 2-chlorophenylmethyl carbamimidothioate (**4**, Y = 2-chlorophenylmethylthio), appeared to be stable and could be recrystallized from boiling methanol. However, when it was heated on the steam bath in toluene it quickly underwent the ring-opening and rearrangement reaction to form the 4(1*H*)-pyrimidinone **6** (Y = 2-chlorophenylmethylthio). Similarly, six other amides **5** (Y = 4-chlorophenylmethylthio, phenylmethylthio, 4-nitrophenylmethylthio, 4-methoxy-3-nitrophenylmethylthio, 1-(2,5-dimethylphenyl)-ethylthio, and 2-methyl-2-propenylthio) were prepared and rearranged to the corresponding **6**. An attempt to rearrange 5,6-dihydro-2-methyl-*N*-[[(1-methylethyl)thio]aminomethylene]-1,4-oxathiin-3-carboxamide (**5**, Y = 1-methylethylthio) to the corresponding 4(1*H*)-pyrimidinone **6** was not successful.

The tautomeric forms of 2-benzimidazolamine (**7**) on acylation with **2** could lead to two amides **8** and **10**, which might undergo the 1,4-oxathiin ring opening and rearrangement to yield the pyrimidinones **9** and **11** respectively. Actually, when 2-benzimidazolamine (**7**) was treated with **2** in the presence of triethylamine only one compound could be isolated (in 70% yield). To this compound was assigned the structure **10**, not **8**, on the basis of the following evidence. In boiling ethanol it quickly changed to a less soluble compound to which the rearrangement structure **11** was assigned. This assignment is based on the fact that the aromatic proton in the 6 position of the nmr spectrum shows a shift of almost 1 ppm downfield from the other aromatic protons. This shift is attributed to the deshielding effect of the 6-proton by the keto group of the 4-pyrimidinone **11**, whereas a similar effect is not possible in the 2-pyrimidinone **9**, which might arise from the amide **8**. The assignments of the structure **11** to the rearrangement product and the structure **10** to the intermediate amide are in agreement with previous assignments (2) to the rearrangement product and its intermediate amide from 2-pyridinamine and **2**.

The reaction of 2-benzothiazolamine (**12**) with **2** yielded only one compound to which the rearrangement structure **14** was assigned on the basis of ir and nmr spectra. Neither of the intermediate amides **13** and **15** could be detected. However, the amide **15** was prepared by an unambiguous route from 2-aminobenzenethiol and 5,6-dihydro-2-methyl-1,4-oxathiin-3-carbonyl isothiocyanate **3** (3) and this amide (**15**) would not undergo rearrange-

Can. J. Chem. Downloaded from www.nrcresearchpress.com by 210.87.254.5 on 09/06/12
For personal use only.

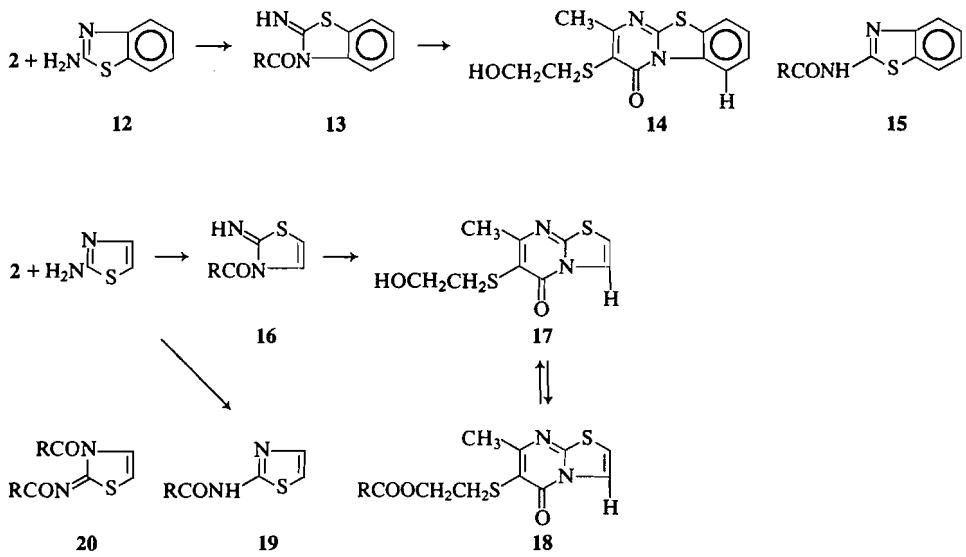


ment even on prolonged heating on the steam bath in toluene in the presence of triethylamine or its hydrochloride. Therefore the amide **15** could not have been the intermediate in the formation of **14**. Further support for the structure **14** comes from the nmr spectra. The aromatic 6-proton is shifted by 1.5 ppm downfield from the other aromatic protons. This is attributed to the deshielding effect by the keto group in the 4-pyrimidinone **14**. A similar effect is not possible in a 2-pyrimidinone structure that might arise from the amide **15**.

The reaction of 2-thiazolamine with the acid chloride **2** was more involved because of the unexpected esterification in addition to the rearrangement reaction. When 2-thiazolamine was treated with **2**, a mixture of two compounds was obtained which was separated by fractional recrystallization from methanol. The more soluble compound was identified as the amide **19** (5, 6) by nmr spectrum, elemental analysis, and by the fact that it was stable and would not rearrange on heating. The less soluble component of the mixture was identified as the ester **18** by elemental analysis, nmr and ir spectra, and by its hydrolysis to the alcohol **17**. The nmr spectra exhibited the aromatic 3-proton shift downfield due to the deshielding of the keto group in not only the ester **18** but also in its hydrolysis product **17**. In another experiment, when 2-thiazolamine was treated with two moles of the acid chloride **2** (instead of one), a 70% yield of the ester **18** was obtained and none of the amide **19** could be isolated. The possibility of the reaction product of 2-thiazolamine and **2** being the bisamide **20** and not the ester **18** was eliminated by evidence from hydrolysis and esterification experiments. Hydrolysis of the ester **18** gave the alcohol **17** which on treatment with **2** gave back the ester **18**. While it is possible that hydrolysis of the bisamide **20** could lead to the alcohol **17** via a rearrangement reaction, the esterification of the alcohol **17** could only lead to the ester **18** and not to the bisamide **20**.

## Experimental

The ir spectra were obtained on Perkin–Elmer 237B or 521 grating spectrometers. The nmr spectra were recorded using an R-20 Hitachi Perkin–Elmer spectrometer and are expressed in ppm (δ values) relative to tetramethylsilane as standard. The uv spectra were obtained on a Varian model G34 spectrophotometer. Melting points were determined on a Gallenkamp melting point apparatus and are uncorrected. The elemental analyses were performed on a Perkin–Elmer 240 elemental analyzer.

*5,6-Dihydro-2-methyl-*N*-(2,2,2-trichloro-1-aminoethylidene)-1,4-oxathiin-3-carboxamide (**5**, Y = $CCl_3$)*

To a solution of 5,6-dihydro-2-methyl-1,4-oxathiin-3-carbonyl chloride (**2**) (2) (prepared from 12 g of the corresponding acid) in toluene (100 mL) was added triethylamine (10 g) followed by 2,2,2-trichloroethanimidamide (**4**, Y = $CCl_3$) (12 g) in toluene (50 mL) keeping the temperature of the reaction mixture below 50°C by cooling occasionally. The reaction mixture was allowed to stand overnight and then the triethylamine hydrochloride was filtered off. The filtrate was concentrated *in vacuo* below 50°C to about 50 mL and allowed to cool. The yellow prisms were filtered, washed, and dried, mp 122–124°C, yield 18.1 g or 80%. The melting point was 125–126°C after recrystallization from methanol; uv ($CH_3OH$) $\lambda_{max}$: 212, 277 nm (ε 7018, 4021); ir (KBr): 3400, 3180, 1640 $cm^{-1}$; nmr ($CDCl_3$) (after standing in $CDCl_3$ solution for 24 h at 34°C): 8.5 (2H, m, $NH_2$), 4.35 (2H, m, $OCH_2$), 2.98 (2H, m, $SCH_2$), 2.50 (3H, m, $CH_3$) (a tautomeric mixture is indicated in a fresh solution). *Anal.* calcd. for $C_8H_9Cl_3N_2O_2S$: C 31.64, H 2.97, N 9.19; found: C 31.78, H 2.92, N 9.22.

*5-[(2-Hydroxyethyl)thio]-6-methyl-2-(trichloromethyl)-4(1*H*)-pyrimidinone (**6**, Y = $CCl_3$)*

A solution of 5,6-dihydro-2-methyl-*N*-(2,2,2-trichloro-1-

Can. J. Chem. Downloaded from www.nrcresearchpress.com by 210.87.254.5 on 09/06/12
For personal use only.

Can. J. Chem. Downloaded from www.nrcresearchpress.com by 210.87.254.5 on 09/06/12
For personal use only.

aminoethylidene)-1,4-oxathiin-3-carboxamide (**5**, Y = $CCl_3$) (8 g) in toluene (50 mL) was heated under reflux for 3 h and then allowed to cool overnight. The white prisms were filtered, washed, and recrystallized from toluene, mp 161–162°C, yield 4.5 g or 56%; nmr (DMSO-$d_6$): 3.55 (2H, m, $OCH_2$), 3.05 (2H, m, $SCH_2$), 2.68 (3H, s, $CH_3$), OH and NH broad. *Anal.* calcd. for $C_8H_9Cl_3N_2O_2S$: C 31.64, H 2.98, N 9.22; found: C 31.91, H 3.01, N 9.17.

*5-[(2-Hydroxyethyl)thio]-6-methyl-2-phenylmethyl-4(1H)-pyrimidinone (**6**, Y = phenylmethyl)*

To a stirred suspension of benzeneethanimidamide (**4**, Y = phenylmethyl) hydrochloride (12 g) in acetone (150 mL) was added portionwise with cooling (below 20°C) a solution of sodium hydroxide (5 g) in water (10 mL). To this reaction mixture was added portionwise with stirring and cooling a solution of the acid chloride **2** (2) (prepared from 10 g of the corresponding acid) in acetone (40 mL) keeping the temperature below 20°C. The reaction mixture was stirred overnight, filtered, and the filtrate distilled *in vacuo*. The residue was extracted with ether, the extract washed with aqueous sodium bicarbonate, and the ether distilled off. The liquid residue was heated on the steam bath for 1 h. The resulting solid product was extracted with dilute hydrochloric acid, the extract filtered, and the filtrate neutralized with solid sodium bicarbonate. The white precipitate was filtered, washed with water, and crystallized from methanol to yield 8.5 g (or 50%) of white crystals melting at 179–180°C; ir (KBr): 3260, 1663 $cm^{-1}$; nmr (DMSO-$d_6$): 7.32 (5H, s, aromatic), 3.86 (2H, s, $CH_2$), 3.46 (2H, m, $OCH_2$), 2.90 (2H, m, $SCH_2$), 2.43 (3H, s, $CH_3$), OH and NH broad. *Anal.* calcd. for $C_{14}H_{16}N_2O_2S$: C 60.86, H 5.84, N 10.14; found: C 60.98, H 5.82, N 10.02.

*5,6-Dihydro-N-[[(2-chlorophenyl)methylthio]aminomethylene]-2-methyl-1,4-oxathiin-3-carboxamide (**5**, Y = 2-chlorophenylmethylthio)*

Solid 2-chlorophenylmethyl carbamimidothioate (**4**, Y = 2-chlorophenylmethylthio) hydrochloride (34 g) was added in portions over 0.5 h to a stirred and ice-cooled (3 to 5°C) solution of the acid chloride **2** (prepared from 22 g of the corresponding acid) in dry toluene (200 mL) and triethylamine (35 g). The stirring was continued at 3 to 5°C for 2 h and then at room temperature overnight. The precipitated triethylamine hydrochloride was filtered and the solvent removed from the filtrate *in vacuo* at room temperature. The residue was dissolved in ether, the solution washed with water, and the ether distilled off. The residue was crystallized from methanol to give light-yellow prisms (28 g or 60%) melting at 105–106°C; uv ($CH_3OH$) $\lambda_{max}$: 215, 268 nm (ε 16 825, 14 085); ir (KBr): 3330, 3240, 1610 $cm^{-1}$; nmr ($CDCl_3$): 8.05 (2H, s, $NH_2$), 7.70 (H, m, aromatic), 7.30 (3H, m, aromatic), 4.60 (2H, s, $SCH_2$), 4.33 (2H, m, $OCH_2$), 2.95 (2H, m, $SCH_2$), 2.40 (3H, s, $CH_3$). *Anal.* calcd. for $C_{14}H_{15}ClN_2O_2S_2$: C 49.04, H 4.41, N 8.16; found: C 49.01, H 4.30, N 8.43.

*Other N-[(substituted)-aminomethylene]-5,6-dihydro-2-methyl-1,4-oxathiin-3-carboxamides* prepared, for which analysis, yields, and nmr spectra are available from the Depository of Unpublished Data[2] are **5** where Y = phenylmethylthio, mp 79–80°C; Y = 4-chlorophenylmethylthio, mp 120–121°C; Y = 4-nitrophenylmethylthio, mp 131–133°C; Y = 4-methoxy-3-nitrophenylmethylthio, mp 105–107°C; Y = α,2,5-trimethylphenylmethylthio, mp 109–110°C; Y = 2-methyl-2-propenylthio, liquid, and Y = 1-methylethylthio, mp 101–103°C.

[2]Photocopies may be obtained at a nominal charge upon request from the Depository of Unpublished Data, CISTI, National Research Council of Canada, Ottawa, Ont., Canada K1A 0S2.

*2-[(2-Chlorophenyl)methylthio]-5-[(2-hydroxyethyl)thio]-6-methyl-4(1H)-pyrimidinone (**6**, Y = 2-chlorophenyl)-methylthio)*

A solution of 5,6-dihydro-*N*-[[(2-chlorophenyl]methylthio]-aminomethylene]-2-methyl-1,4-oxathiin-3-carboxamide (**5**, Y = (2-chlorophenyl)methylthio) (16 g) in toluene (12 mL) was heated on the steam bath for 3 h and then allowed to cool. The white solid was filtered and recrystallized from toluene, mp 134–136°C, yield 10 g or 63%; nmr (DMSO-$d_6$): 7.50 (4H, m, aromatic), 4.50 (2H, s, $SCH_2$), 3.50 (2H, m, $OCH_2$), 2.90 (2H, m, $SCH_2$), 2.52 (3H, s, $CH_3$), OH and NH broad. *Anal.* calcd. for $C_{14}H_{15}ClN_2O_2S_2$: C 49.04, H 4.41, N 8.16; found: C 49.01, H 4.32, N 8.55.

*Other 2-Substituted-5-[(2-hydroxyethyl)thio]-6-methyl-4(1H)-pyrimidinones* prepared for which analysis, yields, and nmr spectra are available from the Depository of Unpublished Data[2] are **6** where Y = phenyl, mp 221–223°C; Y = methyl, mp 151–153°C; Y = propyl, mp 141–143°C; Y = phenylmethylthio, mp 144–145°C; Y = 4-chlorophenylmethylthio, mp 172–173°C; Y = 4-nitrophenylmethylthio, mp 187–189°C; Y = 4-methoxy-3-nitrophenylmethylthio, mp 183–184°C; Y = α,2,5-trimethylphenylmethylthio, mp 148–150°C; and Y = 2-methyl-2-propenylthio, mp 128–130°C.

*2,3-Dihydro-3-(5,6-dihydro-2-methyl-1,4-oxathiin-3-carbonyl)-1H-benzimidazol-2-imine (**10**, R = 5,6-dihydro-2-methyl-1,4-oxathiin-3-yl)*

To a solution of 2-benzimidazolamine (**7**) (6.7 g) in dry acetone (150 mL) and triethylamine (7 g) was added portionwise with stirring a solution of the acid chloride, **2** (prepared from 8.5 g of the corresponding acid), in acetone (25 mL), keeping the temperature below 35°C by occasional cooling. The reaction mixture was stirred for 5 h, cooled to −5°C, filtered, washed with cold acetone and with water, and dried. The white solid weighed 9.7 g (or 70%) and melted at 245–247° dec. Infrared (KBr): 3420, 3100, 1680 $cm^{-1}$; nmr (DMSO-$d_6$): 7.15 (4H, m, aromatic); 4.48 (2H, m, $OCH_2$); 3.18 (2H, m, $SCH_2$), 1.86 (3H, s, $CH_3$), 2NH broad. *Anal.* calcd. for $C_{13}H_{13}N_3O_2S$: C 56.72, H 4.76, N 15.27; found: C 56.61, H 5.13, N 14.95.

*3-[(2-Hydroxyethyl)thio]-2-methylpyrimido[1,2-a]benzimidazol-4(10H)-one (**11**)*

A solution of 2,3-dihydro-3-(5,6-dihydro-2-methyl-1,4-oxathiin-3-carbonyl)-(1*H*)-benzimidazol-2-imine (**10**) (10 g) in 95% ethanol (120 mL) was heated under reflux for 2 h (precipitation began soon after the heating started). The mixture was cooled, filtered, washed, and dried. The white solid (8.5 g or 85%) melted at 254–255° dec. Infrared (KBr): 3400, 1675 $cm^{-1}$; nmr (DMSO-$d_6$): 8.43 (1H, m, aromatic), 7.45 (3H, m, aromatic), 3.55 (2H, m, $OCH_2$), 2.86 (2H, m, $SCH_2$), 2.62 (3H, s, $CH_3$), NH and OH broad. *Anal.* calcd. for $C_{13}H_{13}N_3O_2S$: C 56.72, H 4.76, N 15.27; found: C 57.30, H 4.90, N 14.80.

*3-[(2-Hydroxyethyl)thio]-2-methyl-4H-pyrimido[2,1-b]benzothiazol-4-one (**14**)*

A solution of the acid chloride, **2** (prepared from 12 g of the corresponding acid), in toluene (50 mL) was added to a solution of 2-benzothiazolamine (**12**) (10 g) in toluene (100 mL) and triethylamine (12 g). The temperature went up to 45°C. The reaction mixture was allowed to stand overnight. The precipitate was filtered, washed with methanol, with warm water and with methanol, and dried, mp 144–145°C after recrystallization from ethanol, yield 10 g or 45%. The same results were obtained when the reaction was carried out at 0°C. Infrared (KBr): 3425, 1675 $cm^{-1}$; nmr ($CDCl_3$): 9.05 (H, m, aromatic), 7.55 (3H, m, aromatic), 3.70 (3H, m, $OCH_2$ and OH), 2.98 (2H, m, $SCH_2$), 2.70 (3H, s, $CH_3$); *Anal.* calcd. for $C_{13}H_{12}N_2O_2S_2$: C 53.43, H 4.14, N 9.59; found: C 53.34, H 4.23, N 9.45.

Can. J. Chem. Downloaded from www.nrcresearchpress.com by 210.87.254.5 on 09/06/12
For personal use only.

*N-(2-Benzothiazolyl)-5,6-dihydro-2-methyl-1,4-oxathiin-3-carboxamide (**15**)*

To a solution of 5,6-dihydro-2-methyl-1,4-oxathiin-3-carbonyl isothiocyanate (**3**) (3) (prepared from 12 g of the corresponding acid via the acid chloride **2** and ammonium thiocyanate) in dry toluene (100 mL) was added a solution of 2-aminobenzenethiol (9.5 g) in toluene (15 mL). The reaction mixture was heated at 70–80°C for 4 h to liberate the hydrogen sulfide, then concentrated *in vacuo* to about 60 mL and allowed to cool. The precipitate was filtered and recrystallized from ethanol, golden prisms, mp 173–175°C, yield 11.1 g or 50%; nmr ($CDCl_3$): 9.75 (H, m, NH), 7.82 (2H, m, aromatic), 7.35 (2H, m, aromatic), 4.40 (2H, m, $OCH_2$), 2.90 (2H, m, $SCH_2$), 2.36 (3H, s, $CH_3$). This compound remained unchanged when heated in toluene on the steam bath for 3 h in the presence of triethylamine or triethylamine hydrochloride. *Anal.* calcd. for $C_{13}H_{12}N_2O_2S_2$: C 53.43, H 4.14, N 9.59; found: C 53.19, H 4.17, N 9.50.

*5,6-Dihydro-2-methyl-N-(2-thiazolyl)-1,4-oxathiin-3-carboxamide (**19**) and 2-[(7-methyl-5-oxo-5H-thiazolo[3,2-a]pyrimidin-6-yl)thio]ethyl-5,6-dihydro-2-methyl-1,4-oxathiin-3-carboxylate (**18**)*

A solution of the acid chloride (**2**) (prepared from 12 g of the corresponding acid) in toluene (30 mL) was added portionwise to a solution of 2-thiazolamine (8 g) in toluene (120 mL) and triethylamine (15 g), keeping the temperature below 50°C by occasional cooling. The reaction mixture was allowed to stand at room temperature for 2 days and then filtered. The filtrate was taken to "dryness" *in vacuo* and the residue fractionally crystallized from methanol. The more soluble component (2.8 g) melted at 120–122°C after repeated crystallization from toluene (lit. (5) mp 96–98°C and (6) 114–116°C). Infrared (KBr): 3120, 1655 $cm^{-1}$; nmr ($CDCl_3$): 10.95 (1H, s, NH), 7.45 (1H, m, aromatic), 6.98 (1H, m, aromatic), 4.42 (2H, m, $OCH_2$), 2.98 (2H, m, $SCH_2$), 2.25 (3H, s, $CH_3$). This compound remained unchanged when heated under reflux in toluene in the presence of triethylamine or its hydrochloride. *Anal.* calcd. for $C_9H_{10}N_2O_2S_2$: C 44.63, H 4.16, N 11.57; found: C 44.85, H 4.23, N 11.09.

The less soluble component of the above mixture on recrystallization from methanol and from toluene yielded (1.7 g) the pure ester **18** melting at 140–141°C. In another experiment, when 2-thiazolamine was treated with 2 moles of the acid chloride **2** as above instead of one mole, a 70% yield of the ester **18** was obtained (about half the ester precipitated out of the reaction mixture along with triethylamine hydrochloride). No amide **19** could be found. Infrared (KBr): 1690, 1675 $cm^{-1}$; nmr ($CDCl_3$): 8.00 (1H, m, aromatic), 7.12 (1H, m, aromatic), 4.30 (4H, m, $2OCH_2$), 3.25 (2H, m, $SCH_2$), 2.90 (2H, m, $SCH_2$), 2.68 (3H, s, $CH_3$), 2.30 (3H, s, $CH_3$). *Anal.* calcd. for $C_{15}H_{16}N_2O_4S_3$: C 46.88, H 4.20, N 7.29; found: C 46.74, H 4.26, N 7.30.

*6-[(2-Hydroxyethyl)thio]-7-methyl-5H-thiazolo[3,2-a]pyrimidin-5-one (**17**)*

The ester **18** (10 g) was dissolved in boiling ethanol (200 mL), concentrated hydrochloric acid (25 mL) in water (110 mL) added, and the reaction mixture was heated one hour on the steam bath. Concentration of the reaction mixture to 50 mL, *in vacuo*, neutralization with sodium bicarbonate, and extraction with ether yielded 5 g of white crystals melting at 89–91°C after recrystallization from toluene. Infrared (KBr): 3410, 3065, 1650 $cm^{-1}$; nmr ($CDCl_3$): 8.00 (1H, d, aromatic), 7.25 (1H, d, aromatic), 4.20 (1H, m, OH), 3.68 (2H, m, $OCH_2$), 2.95 (2H, m, $SCH_2$), 2.70 (3H, s, $CH_3$). *Anal.* calcd. for $C_9H_{10}N_2O_2S_2$: C 44.63, H 4.16, N 11.57; found: C 44.69, H 4.09, N 11.58.

This compound (**17**), when treated with the acid chloride **2** and triethylamine, regenerated the ester **18**.

## Acknowledgements

Grateful acknowledgements are made to W. R. Boos, Murray Ross, and Helen Van Veggel for providing analyses and nmr, ir, and uv spectra.

1. (*a*) B. VON SCHMELING and M. KULKA. Science, **152**, 659 (1966); (*b*) B. VON SCHMELING, M. KULKA, D. S. THIARA, and W. A. HARRISON. U.S. Patents 3,249,499 (1966), 3,393,202 (1968), 3,399,214 (1968), and 3,402,241 (1968); Can. patents 787,893 (1968), 791,151 (1968), 824,243 (1970), and 825,665 (1969).
2. M. A. CORBEIL, M. CURCUMELLI-RODOSTAMO, R. J. FANNING, B. A. GRAHAM, M. KULKA, and J. B. PIERCE. Can. J. Chem. **51**, 2650 (1973).
3. M. KULKA. Can. J. Chem. **58**, 2044 (1980).
4. S. CHUA, M. J. COOK, and A. R. KATRITZKY. J. Chem. Soc. Perkin Trans. **II**, 546 (1974).
5. P. TEN HAKEN and B. P. ARMITAGE. Ger. Offen. 2,117,807 (1971); Chem. Abstr. **76**, P24217w (1972).
6. N. N. MEL'NIKOV, N. J. SHVETSOV-SHILOVSKII, N. I. LYALYAKINA, and N. I. RUDNEVA. U.S.S.R. 328,702 (1977); Chem. Abstr. **88**, P 37827t (1978).

# New catalysts and procedures for the dimethoxytritylation and selective silylation of ribonucleosides[1]

GHOLAM H. HAKIMELAHI, ZBIGNIEW A. PROBA, AND KELVIN K. OGILVIE[2]

*Department of Chemistry, McGill University, Montreal, P.Q., Canada H3A 2K6*

Received December 2, 1981

GHOLAM H. HAKIMELAHI, ZBIGNIEW A. PROBA, and KELVIN K. OGILVIE. Can. J. Chem. **60**, 1106 (1982).

Procedures have been developed for the selective formation of (a) 2′,5′-silylated ribonucleosides and (b) 3′,5′-silylated ribonucleosides. These procedures also permit the selective silylation at either the 2′- or 3′-position of dimethoxytritylated ribonucleosides. The procedures involve nitrate or perchlorate ion catalysis for selective reaction at 2′-positions and a combination of silver ion and DABCO or 4-nitropyridine *N*-oxide for selective reaction at the 3′-position. During the course of this work a general and rapid procedure was developed for the preparation and isolation of the 5′-dimethoxytrityl derivatives of the four common ribonucleosides. Silver ion was found to have a marked effect on dimethoxytritylation reactions.

GHOLAM H. HAKIMELAHI, ZBIGNIEW A. PROBA et KELVIN K. OGILVIE. Can. J. Chem. **60**, 1106 (1982).

On a mis au point des méthodes de formation sélective des ribonucléosides silylés en positions 2′ et 5′ et des ribonucléosides silylés en positions 3′ et 5′. Ces méthodes permettent également la silylation sélective en positions 2′ ou 3′ des ribonucléosides diméthoxytritylés. Les méthodes impliquent une catalyse par l'ion nitrate ou l'ion perchlorate pour la réaction sélective en position 2′ et une combinaison de l'ion argent et du DABCO ou du *N*-oxyde de nitro-4 pyridine pour la réaction sélective en position 3′. On a développé, au cours de ce travail, une méthode rapide générale de préparation et de séparation des dérivés diméthoxytrityl-5′ des quatres ribonucléosides ordinaires. On a trouvé que l'ion argent a un effet marqué sur les réactions de diméthoxytritylation.

[Traduit par le journal]

## Introduction

Progress in the chemical synthesis of oligodeoxynucleotides has culminated in the development of automated procedures for the synthesis of gene fragments (1). This success in the deoxy area is due principally to the early establishment of adequate and versatile protecting groups for the amino, hydroxyl, and phosphate functions of the growing chains (2). With the protecting group problem out of the way, successive developments in condensation procedures (3–6) have led to automation of the synthesis using a solid-support procedure.

Ribonucleotides have posed a more difficult challenge in terms of protecting groups. The presence of the 2′-hydroxyl group in ribonucleosides not only requires protection but places serious limitations on the nature of the protecting groups used. During the last few years we have been refining a new approach to the total synthesis of ribonucleotides (7). The approach is based on our development of the alkylsilyl protecting groups for the 2′-position of ribonucleosides (8). During this developmental stage we have used monomethoxytrityl protection of 5′-hydroxyl groups and trichloroethyl protection of phosphates. Amino groups have either been protected with benzoyl groups or left unprotected. Condensations have been effected using the "phosphite–triester" approach. We have recently adapted these developments to a solid-support procedure (*7a*) for ribonucleotide synthesis.

The procedures developed for the synthesis of ribonucleotides possessing the 3′–5′ phosphate bridge have been extended to 2′–5′ linked nucleotides (9). These molecules are of considerable interest because of the implication of 2′–5′ linked oligoadenylates in the interferon process (10). Thus the ready availability of 3′,5′-diprotected ribonucleosides is of importance.

At this stage in the development of a total procedure for ribonucleotide synthesis it became essential to reduce to a minimum the time involved in protection–deprotection of nucleosides and nucleotides. In terms of deprotection of nucleotides we wished to take advantage of the 10-fold reduction in time required to remove a dimethoxytrityl group compared to a monomethoxytrityl group. We also sought to speed up the rate of tritylation and silylation of ribonucleosides and to increase the selectivity of 2′ vs. 3′-silylation. In this report we describe: (1) procedures for the rapid and efficient dimethoxytritylation of ribonucleosides; (2) procedures for the rapid and highly selective 2′-silylation of ribonucleosides, and (3) procedures for the rapid and highly selective 3′-silylation of ribonucleosides.

## Discussion

### *Dimethoxytritylation*

The general procedures for dimethoxytritylation of ribonucleosides (Scheme 1) are based on those originally developed by the Khorana group in the

[1]This manuscript constitutes part XIX in a series on silyl protecting groups in nucleoside and nucleotide chemistry. Part XVIII is ref. 20.

[2]Author to whom correspondence may be addressed.

0008-4042/82/091106-08$01.00/0

©1982 National Research Council of Canada/Conseil national de recherches du Canada

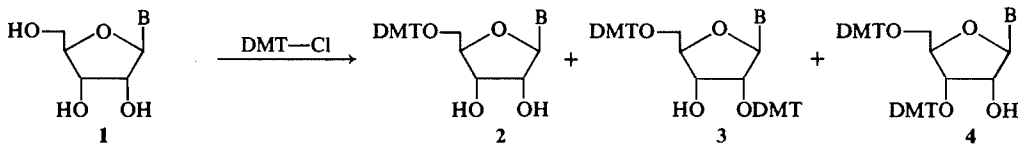


*a* B = uracil
*b* B = adenine
*c* B = *N*-benzoyladenine
*d* B = *N*-benzoylcytidine
*e* B = guanine
*f* B = *N*-benzoylguanine

DMT = dimethoxytrityl

SCHEME 1

deoxy area (11, 12). Two of the desired compounds **2***a* (13) and **2***d* (14) have been described in the literature. By this standard procedure the nucleoside and dimethoxytrityl chloride (DMT-Cl) are dissolved in pyridine and, after about 12 h, products are isolated by chromatography. We found that by using this procedure a mixture of desired product, ditritylated (2′,5′ and 3′,5′) material, *N*-tritylated material, and unreacted starting material was always obtained and that separation of these components was time-consuming.

We observed that a simple change in the procedure led to a much cleaner product mixture which could easily be separated on short column chromatography. Thus the nucleoside was completely dissolved in pyridine or pyridine–DMF (1:1) and dimethoxytrityl chloride was added in eight equal portions (1 per hour) to the solution maintained at 0°C. At the end of the reaction period (9 h) the solvent was concentrated at reduced pressure and mixed with an aqueous sodium bicarbonate solution. If this bicarbonate treatment was eliminated a significant amount of detritylation occurred. The product was then extracted into methylene chloride. Thin-layer chromatography at this point indicated that only a very little by-product was present. Consequently the solution was concentrated and applied to a short silica gel column from which the desired product was rapidly eluted. Yields ranged from 69% for the guanosine derivative **2***f* to 85% for the cytidine derivative **2***d*. The elimination of by-products was particularly evident in the preparation of the adenosine derivative **2***b* in 80% yield. *N*-Tritylation was not a problem in this case. However, *N*-tritylation is a serious problem using the original procedure (8*a*). The only drawback to this modified procedure was the time involved (8–10 h). However, we found that the addition of silver nitrate gave a marked improvement in the rate of product formation.

The use of silver nitrate was based on our initial use of this reagent in the selective silylation of nucleosides to be described below. The results summarized in Table 1 show that the use of silver nitrate caused complete reaction within 1 h leading to yields of **2** ranging from 70% for **2***d* to 95% for **2***f*. The results also show that while ditritylation could be rapidly achieved using silver nitrate catalysis, selective ditritylation occurred only for the uridine case (**3***a* (80%), **4***a* (15%)). It appears that *N*-protection is necessary when using silver nitrate since in a test reaction on adenosine (**1***b*) a significant amount of *N*-tritylation was observed.

Silver ion is the effective catalyst in these reactions. As expected, silver trifluoroacetate gave the same results as silver nitrate, while tetrabutylammonium nitrate was ineffective.

### *Silylations*

#### A. *Selective 2′-silylations*

We have previously described procedures for the silylation of ribonucleosides and their 5′-methoxytrityl derivatives (8). These procedures always lead to a mixture of 2′,5′ and 3′,5′ derivatives in nearly equal amounts. While these isomers can be separated by silica gel chromatography, the yield of the 2′,5′-diprotected compound was lower than desired. We have investigated numerous procedures in an effort to obtain higher yields of the 2′,5′-protected compounds. Most of these procedures, including slow addition of silylating agent at lowered temperature, gave no significant improvement in selectivity. However, the addition of nitrates and perchlorates gave a remarkable improvement in the selectivity of silylation.

The reactions are outlined in Scheme 2 and the results are summarized in Table 2. The general procedure can be illustrated with the silylation of 5′-dimethoxytrityl-*N*-benzoylcytidine (**2***d*). The nucleoside is dissolved in THF after which pyridine (3.7 mmol/mmol $AgNO_3$) and silver nitrate (1.2 mmol/mmol nucleoside) are added and the solution

TABLE 1. Silver nitrate catalysis of dimethoxytritylation reactions*

| Nucleoside | DMT-Cl (mmol) | $AgNO_3$ (mmol) | Pyridine (mmol) | Yield (%) 5′ (**2**) | 2′,5′ (**3**) | 3′,5′ (**4**) |
|---|---|---|---|---|---|---|
| U, **1***a* | 1 | 1 | 5 | 90 | — | — |
| U, **1***a* | 2 | 2 | 10 | | 80 | 15 |
| $A^{Bz}$, **1***c* | 1 | 1 | 5 | 80 | — | — |
| $A^{Bz}$, **1***c* | 2.5 | 2.5 | 10 | 10 | 40 | 40 |
| $C^{Bz}$, **1***d* | 1 | 1 | 5 | 70+ | 10 | 10 |
| $C^{Bz}$, **1***d* | 2 | 2 | 10 | | 45 | 45 |
| $G^{Bz}$, **1***f* | 1 | 1 | 5 | 70 | — | — |
| $G^{Bz}$, **1***f* | 2 | 2 | 10 | 95 | — | — |
| $G^{Bz}$, **1***f* | 5 | 5 | 25 | 10 | 40 | 40 |

*Solvent was THF except for + where THF–DMF (1:1) was used and DMT–Cl was added portionwise in this case only. The time was 1 h in all cases except the last entry for **1***f* where 1.5 h were used. For the general procedure see the Experimental.

is stirred until the silver nitrate is completely dissolved (~ 5 min). At this point *tert*-butyldimethylsilyl chloride (TBDMS-Cl, 1.3 mmol/mmol **2***d*) is added all at once and the resulting mixture is stirred at room temperature for 1.5 h. The mixture is then filtered and the clear solution is mixed with 5% aqueous $NaHCO_3$ to prevent detritylation. The product is extracted into methylene chloride. The products are separated on short column chromatography to yield 5′-DMT-2′-TBDMS-$C^{Bz}$ (**6***d*) in 68% and the 3′-isomer, **8***d*, in 21% yield. These results show very high conversion yields with remarkable selectivity in all cases except for *N*-benzoylguanosine derivatives which will be discussed later.

The scope of the reaction was investigated using the unprotected nucleoside. Treatment of **1** with 2.2 equivalents each of TBDMS-Cl and $AgNO_3$ in THF led to exclusive formation of the 5′-TBDMS derivatives **5** in ~ 95% isolated yields (Table 2) within 3 h. No disilylation was observed in doubling the amounts of reagents (entry 6). However, if the solvent were changed to DMF, a mixture of mono, di, and trisilylated products was obtained. Repeating the original THF reaction but adding 5 equivalents of pyridine gave a rapid and highly selective disilylation. Yields of the 2′,5′-disilyl derivatives **7** were 82–90%.

An interesting contrast exists between guanosine (**1***e*) and *N*-benzoylguanosine (**1***f*). In the former case the reaction showed good selectivity, while in the latter there was very little selectivity. We believe this is due to steric hindrance created by the $N^2$-benzoyl group in the vicinity of the 2′-hydroxyl group. In this regard it may be of interest to note our observations on separating isomeric-protected guanosine derivatives. These isomers have always given us considerable difficulty. However, we have found that in acetone – petroleum ether – triethyl amine (6:5.5:0.5) the 2′,5′-protected compound **6***f* has an $R_f$ of 0.59 while the 3′,5′-isomer **8***f* has an $R_f$ of 0.21. If the triethylamine is eliminated from this solvent, both isomers have an $R_f$ of 0.41. In chloroform–acetone–triethylamine (9:0.5:0.5) compound **6***f* had an $R_f$ of 0.30 while **8***f* was at 0.05. In the absence of triethylamine both had an $R_f$ value of 0.28. This suggests that there may be hydrogen bonding between the 2′-hydroxyl in **8***f* and the 2-amide group. This H-bonding would be destroyed in the presence of triethylamine leading to a more polar structure for **8***f* and a resultant decreased $R_f$ value (stronger absorption). As expected, we were not able to observe a similar effect with the other nucleosides.

Nitrates which are soluble in the reaction medium all give good results. For example, tetrabutylammonium nitrate (entries 33 and 34) gives the same rate and selectivity as silver nitrate. In

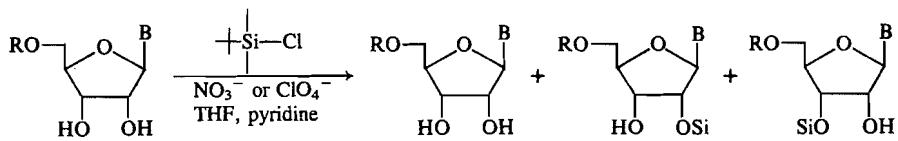


**1**, R = H
**2**, R = DMT
**5**, R = Si
**6**, R = DMT
**7**, R = Si
**8**, R = DMT
**9**, R = Si

*a–f* as in Scheme 1

Si = *tert*-butyldimethylsilyl

SCHEME 2

TABLE 2. Nitrate ion catalysis of silylation reactions*

| Entry | Nucleoside | TBDMS-Cl (mmol) | $AgNO_3$ (mmol) | Base (mmol) | Time (h) | Product (%) 5′ | 2′,5′ | 3′,5′ |
|---|---|---|---|---|---|---|---|---|
| 1 | DMT-U (**2***a*) | 1.3 | 1.2 | py (3.7) | 1.5 | — | 70 | 15 |
| 2 | DMT-A (**2***b*) | 1.3 | 1.2 | py (3.7) | 5 | — | 65 | 21 |
| 3 | DMT-$C^{Bz}$ (**2***d*) | 1.3 | 1.2 | py (3.7) | 1.5 | — | 68 | 20 |
| 4 | DMT-$G^{Bz}$ (**2***f*) | 1.7 | 1.5 | py (5) | 5 | — | 45 | 40 |
| 5 | U (**1***a*) | 2.2 | 2.2 | — | 3 | 98 | — | — |
| 6 | U (**1***a*) | 4 | 4 | — | 3 | 98 | — | — |
| 7 | U (**1***a*) | 2.2 | 2.2 | (DMF) | 3 | 20 | 30 | 10 |
| 8 | U (**1***a*) | 2.2 | 2.2 | py (5) | 1 | — | 90 | 5 |
| 9 | U (**1***a*) | 2.2 | 2.2 | col (5) | 3 | 97 | — | — |
| 10 | U (**1***a*) | 2.2 | — | py (5) | 5 | <10 | — | — |
| 11 | U (**1***a*) | 2.2 | 2.2 | im (4) | 1 | — | 70 | 15 |
| 12 | A (**1***b*) | 2 | 2 | py (5) | 1 | — | 68 | 22 |
| 13 | A (**1***b*) | 2.2 | 2.2 | im (4) | 1 | — | 60 | 20 |
| 14 | A (**1***b*) | 2.2 | — | im (4) | 30 | 25 | 13 | 12 |
| 15 | A (**1***b*) | 2.2 | 2.2 | — | 3 | 95 | — | — |
| 16 | $C^{Bz}$ (**1***d*) | 2.2 | 2.2 | py (5) | 1 | — | 82 | 13 |
| 17 | $C^{Bz}$ (**1***d*) | 2.2 | 2.2 | — | 3 | 95 | — | — |
| 18 | $C^{Bz}$ (**1***d*) | 2.2 | 2.2 | im (4) | 1 | — | 65 | 15 |
| 19 | G (**1***e*) | 2.2 | 2.2 | — | 3 | 95 | — | — |
| 20 | G (**1***e*) | 2.2 | 2.2 | py (5) | 4 | — | 33 | 17 |
| 21 | G (**1***e*) | 2.2 | 2.2 | py (5) | 2 | — | 60 | 35 |
| 22 | $G^{Bz}$ (**1***f*) | 2.2 | 2.2 | — | 4 | 97 | — | — |
| 23 | $G^{Bz}$ (**1***f*) | 2.2 | 2.2 | py (5) | 2 | — | 48 | 40 |
| 24 | $G^{Bz}$ (**1***f*) | 2.2 | 2.2 | im (4) | 3 | — | 50 | 40 |
| 25 | U (**1***a*) | 2.2 | 2.2 | DMAP (5) | 3 | — | 80 | 15 |
| 26 | U (**1***a*) | 2.2 | 2.2 | 4-Acpy (5) | 1 | 98 | — | — |
| 27 | U (**1***a*) | 2.2 | 2.2 | 4-Acpy (5) | 5 | 68 | 30 | — |
| 28 | U (**1***a*) | 2.2 | 2.2 | 4-Acpy (5) | 10 | 35 | 60 | — |
| 29 | U (**1***a*) | 2.2 | 2.2 | 4-Acpy (5) | 15 | — | 94 | 1 |
| 30 | U (**1***a*) | 2 | $KH_2PO_4$ (2) | py (5) | 2 | — | — | — |
| 31 | U (**1***a*) | 2 | $(n\text{Bu})_4NI$ (2) | py (5) | 2 | — | — | — |
| 32 | U (**1***a*) | 2 | $(n\text{Bu})_4NSO_3H$ (2) | py (5) | 2 | 90 | — | — |
| 33 | U (**1***a*) | 2.2 | $(n\text{Bu})_4NNO_3$ (2.2) | py (5) | 1 | — | 87 | 6 |
| 34 | A (**1***b*) | 2 | $(n\text{Bu})_4NNO_3$ (2) | py (5) | 1 | — | 67 | 23 |

*All reactions were carried out in THF except for No. 7 which was in DMF and Nos. 21, 23, and 24 which were carried out in THF–DMF (1:1). Abbreviations used are: py = pyridine, col = collidine, im = imidazole, DMAP = 4-dimethylaminopyridine, and 4-Acpy = 4-acetylpyridine.

another experiment in which adenosine was dissolved in THF–DMF (1:1) along with 2 equivalents each of TBDMS-Cl and potassium nitrate and 5 equivalents of pyridine, compounds **7***b* and **9***b* were produced in a 1.5:1 ratio.

Soluble perchlorates give equally good results in selective silylations (Table 3). Silver perchlorate and $(n\text{Bu})_4NClO_4$ give excellent yields of 2′-silylated derivatives. The use of nitrates and perchlorates as catalysts in silylations is not new (15, 16) but the selectivity described here is unprecedented. Other soluble silver salts such as silver carbonate, silver trifluoroacetate, and silver cyanate have no effect on silylation under these conditions.

Pyridine is required for disilylation to occur. In the absence of pyridine, reaction stops at the 5′-monosilyl stage. Replacing pyridine with the hindered base 2,4,6-trimethylpyridine gives only monosilylation even after 20 h. These results represent an excellent procedure for the highly selective monosilylation of nucleosides.

In a separate experiment one equivalent each of TBDMS-Cl and $AgNO_3$ were mixed together in THF. The mixture was stirred at room temperature and after 30 min the solution was decanted and distilled. The presumed *tert*-butyldimethylsilyl nitrate distilled at 140–142°C (1 atm) and was collected as a pale yellow liquid. This material, TBDMS-$NO_2$, silylated uridine in the presence or absence of pyridine with the same results as described for TBDMS-Cl and $AgNO_3$.

B. *Selective 3′-silylation*

The selective protection of the 3′-position in ribonucleosides cannot be achieved with most common protecting groups. Only acylation has been reported (17) to give high yields of 3′-derivatization. This occurs through migration from the 2′-position and selective crystalization of the 3′-

TABLE 3. Perchlorate ion catalysis of silylation reactions*

| Entry | Nucleoside | TBDMS-Cl (mmol) | $AgClO_4$ (mmol) | Base (mmol) | Time (h) | Product (%) 5′ | 2′,5′ | 3′,5′ |
|---|---|---|---|---|---|---|---|---|
| 1 | U (1*a*) | 2.2 | 2.2 | py (5) | 2 | — | 90 | 7 |
| 2 | DMT-U (2*a*) | 1.3 | 1.2 | py (5) | 2 | — | 75 | 15 |
| 3 | Si-U (5*a*) | 1.3 | 1.2 | py (5) | 2 | — | 90 | 6 |
| 4 | U (1*a*) | 2.2 | 2.2 | — | 2 | 90 | 2 | 2 |
| 5 | A (1*b*) | 2.2 | 2.2 | py (5) | 2 | — | 87 | 8 |
| 6 | DMT-A (2*b*) | 1.3 | 1.2 | py (5) | 4 | — | 70 | 20 |
| 7 | Si-A (5*b*) | 1.3 | 1.2 | py (3) | 2 | — | 80 | 10 |
| 8 | $C^{Bz}$ (1*d*) | 2.2 | 2.2 | py (5) | 2 | — | 90 | 5 |
| 9 | DMT-$C^{Bz}$ (2*d*) | 1.3 | 1.2 | py (5) | 2 | — | 70 | 20 |
| 10 | Si-$C^{Bz}$ (5*d*) | 1.3 | 1.2 | py (3) | 2 | — | 92 | 5 |
| 11 | $G^{Bz}$ (1*f*) | 2.5 | 2.5 | py (6) | 5 | — | 55 | 40 |
| 12 | $G^{Bz}$ (1*f*) | 3 | 3 | — | 2 | 95 | — | — |
| 13 | DMT-$G^{Bz}$ (2*f*) | 1.5 | 1.5 | py (5) | 5 | — | 55 | 42 |
| 14 | Si-$G^{Bz}$ (5*f*) | 1.4 | 1.3 | py (4) | 5 | — | 60 | 35 |
| 15 | U (1*a*) | 2.2 | $(n\text{Bu})_4NClO_4$ (2.2) | py (5) | 2 | — | 90 | 5 |
| 16 | A (1*b*) | 2.2 | $(n\text{Bu})_4NClO_4$ (2.2) | py (5) | 2 | — | 85 | 5 |
| 17 | $C^{Bz}$ (1*d*) | 2.2 | $(n\text{Bu})_4NClO_4$ (2.2) | py (5) | 2 | — | 93 | 4 |

*Reaction conditions are the same as for Table 2 and are described in the Experimental.

isomer from solution. Markiewicz (18) has described a novel bifunctional silylating agent, 1,3-dichloro-1,1,3,3-tetraisopropyl disiloxane which reacts with both the 5′- and 3′-positions. To date there has not been a report of the direct and selective protection of the 3′-position of ribonucleosides using a monofunctional silylating agent. We have developed procedures which accomplish this objective (Scheme 3). A preliminary account of some of these results has appeared (19, 20).

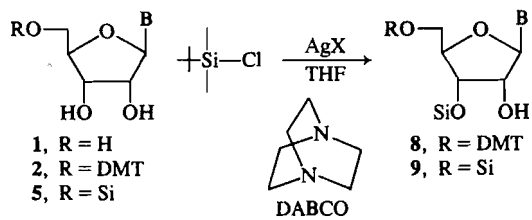


SCHEME 3

Two procedures have been developed. The first involves the silylation of ribonucleosides in the presence of DABCO (1,4-diazabicyclo[2.2.2]-octane) and silver salts. The second procedure employs silver salts with 4-nitropyridine *N*-oxide.

The reaction involving ribonucleosides, TBDMS-Cl, DABCO, and silver salts leads to 3′,5′-di-TBDMS derivatives (**9**) in yields as high as 94% (Table 4). It is apparent from Table 4 that the silver ion is important in the reaction. All soluble silver salts tested ($AgNO_3$, $AgClO_4$, $AgOCOCF_3$) produce excellent selectivity while the salts $(n\text{Bu})_4NNO_3$ and $(n\text{Bu})_4NClO_4$ have no effect. In the absence of DABCO only 5′-silylation occurs. The procedure works equally well with dimethoxytritylated nucleosides (**2**) giving 3′-TBDMS-5′-DMT nucleosides (**8**) in yields of 70–93%.

The reaction with 4-nitropyridine *N*-oxide (Scheme 4) also leads to selective reaction at the 3′-position when silylation is carried out in THF with silver salts and TBDMS-Cl. We have only observed selectivity with the 4-nitropyridine *N*-oxide among those tested (Table 5). The one drawback with this procedure is that the reaction conditions rapidly remove dimethoxytrityl groups (e.g. from **2**). It is interesting to note that 4-nitropyridine (**14**) produces similar results to 4-nitropyridine *N*-oxide (**10**) but in a much slower reaction (10–20 h). This result contrasts with 4-acetylpyridine which gives a slow, but highly selective, silylation at the 2′-position (Table 2, entries 26–29).

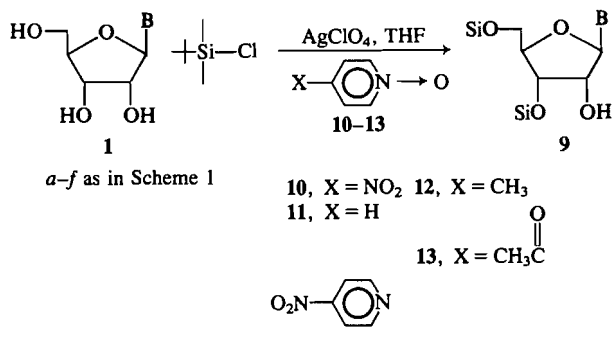


SCHEME 4

TABLE 4*. Selective 3′-silylations with DABCO and $Ag^+$

| Entry | Nucleoside | TBDMS-Cl (mmol) | Salt (mmol) | Time (h) | Products (%) 5′ | 3′,5′ | 2′,5′ |
|---|---|---|---|---|---|---|---|
| 1 | U (**1***a*) | 2.3 | $AgClO_4$ (2.3) | 3 | — | (**9***a*) 90 | (**7***a*) 5 |
| 2 | U (**1***a*) | 2.3 | $AgNO_3$ (2.3) | 3 | — | (**9***a*) 91 | (**7***a*) 3 |
| 3 | U (**1***a*) | 2.3 | $AgOCOCF_3$ (2.2) | 3 | — | (**9***a*) 90 | (**7***a*) 5 |
| 4 | U (**1***a*) | 2.3 | $(n\text{Bu})_4NClO_4$ (2.2) | 10 | (**5***a*) 65 | (**9***a*) 18 | (**7***a*) 2 |
| 5 | U (**1***a*) | 2.3 | $(n\text{Bu})_4NNO_3$ (2.2) | 10 | (**5***a*) 60 | (**9***a*) 25 | (**7***a*) 1 |
| 6 | U (**1***a*) | 2.3 | — | 10 | (**5***a*) 85 | (**9***a*) 2 | — |
| 7 | DMT-U (**2***a*) | 1.3 | $AgClO_4$ (1.2) | 2 | — | (**8***a*) 91 | (**6***a*) 5 |
| 8 | Si-U (**5***a*) | 1.3 | $AgClO_4$ (1.2) | 3 | — | (**9***a*) 90 | (**7***a*) 5 |
| 9 | $C^{Bz}$ (**1***d*) | 2.4 | $AgClO_4$ (2.3) | 3 | — | (**9***d*) 92 | (**7***d*) 3 |
| 10 | $C^{Bz}$ (**1***d*) | 2.4 | $AgNO_3$ (2.3) | 3 | — | (**9***d*) 90 | (**7***d*) 5 |
| 11 | DMT-$C^{Bz}$ (**2***d*) | 1.3 | $AgClO_4$ (1.2) | 3 | — | (**8***d*) 90 | (**6***d*) 5 |
| 12 | A (**1***b*) | 2.4 | $AgClO_4$ (2.3) | 4 | — | (**9***b*) 70 | (**7***b*) 25 |
| 13 | A (**1***b*) | 2.4 | $AgNO_3$ (2.3) | 4 | — | (**9***b*) 70 | (**7***b*) 20 |
| 14 | DMT-A (**2***b*) | 1.3 | $AgClO_4$ (1.2) | 4 | — | (**8***b*) 70 | (**6***b*) 25 |
| 15 | $G^{Bz}$ (**1***f*) | 2.6 | $AgClO_4$ (2.5) | 6 | — | (**9***f*) 60 | (**7***f*) 30 |
| 16 | $G^{Bz}$ (**1***f*) | 2.6 | $AgNO_3$ (2.5) | 6 | — | (**9***f*) 60 | (**7***f*) 35 |
| 17 | DMT-$G^{Bz}$ (**2***f*) | 1.5 | $AgNO_3$ (1.5) | 5 | — | (**8***f*) 30 | (**6***f*) 60 |

*Reactions were carried out in THF with 6 mmol DABCO/mmol of nucleoside, as described in the Experimental.

TABLE 5. Selective 3′-silylation using 4-nitropyridine *N*-oxide*

| Entry | Nucleoside | Salt (mmol) | Catalyst* (mmol) | Time (h) | Products (%) 5′ | 3′,5′ | 2′,5′ |
|---|---|---|---|---|---|---|---|
| 1 | U (**1***a*) | $AgClO_4$ (2.2) | **10** (2.3) | 1.5 | — | (**9***a*) 50 | (**7***a*) 40 |
| 2 | A (**1***b*) | $AgClO_4$ (2.2) | **10** (2.3) | 2 | — | (**9***b*) 89 | (**7***b*) 5 |
| 3 | $C^{Bz}$ (**1***d*) | $AgClO_4$ (2.2) | **10** (2.3) | 2 | — | (**9***d*) 90 | (**7***d*) 8 |
| 4 | $G^{Bz}$ (**1***f*) | $AgClO_4$ (2.5) | **10** (2.6) | 2.5 | — | (**9***f*) 98 | — |
| 5 | $C^{Bz}$ (**1***d*) | $AgClO_4$ (2.2) | **11** (2.3) | 2 | — | (**9***d*) 40 | (**7***d*) 40 |
| 6 | $C^{Bz}$ (**1***d*) | $AgClO_4$ (2.2) | **12** (2.3) | 2 | — | (**9***d*) 40 | (**7***d*) 40 |
| 7 | $C^{Bz}$ (**1***d*) | $AgClO_4$ (3.7) | **13** (3.5) | 60 | (**5***d*) 40 | (**9***d*) 25 | (**7***d*) 18 |
| 8 | $C^{Bz}$ (**1***d*) | $(n\text{Bu})_4NClO_4$ (2.2) | **10** (2.3) | 5 | — | — | — |

*Reactions were carried out in THF (25 mL/mmol of nucleoside) using TBDMS-Cl (2.2 mmol/mmol of **1**) as described in the Experimental.

These selective silylations at the 3′-position apparently involve direct attack at the 3′-position since the 2′-silyl derivatives (e.g. **6** and **7**) appear to be stable under the reaction conditions (i.e., they do not rearrange to the 3′-position). The mechanistic implications of the combination of silver ion and DABCO or 4-nitropyridine *N*-oxide are being explored.

## Conclusion

This report describes procedures for the facile preparation of ribonucleosides protected with two of the most versatile and useful blocking groups, the dimethoxytrityl group and the *tert*-butylmethylsilyl group. The procedures incorporate truly novel catalytic effects leading to highly selective protection at the 2′-position and the unprecedented highly selective silylation at the 3′-position.

## Experimental

*General methods*

Thin-layer chromatographic data ($R_f$ values) are recorded from Merck Kieselgel 60 F 254 analytical sheets. All uv spectra were recorded on a Cary 17 spectrophotometer. Nuclear magnetic resonance spectra were recorded on a Varian T-60A instrument. Infrared spectra were obtained on a Perkin Elmer 297 spectrophotometer. Melting points were determined on a Fisher–Johns melting point apparatus and are reported uncorrected.

Reagent grade pyridine was distilled first from *p*-toluenesulfonyl chloride, redistilled from calcium hydride, and stored over molecular sieves (type 4A). Tetrahydrofuran was refluxed with benzophenone and sodium for at least 3 h and was freshly distilled before use. *N*,*N*-Dimethylformamide (DMF) and 2,4,6-trimethylpyridine were distilled from calcium hydride and stored over molecular sieves (type 4A).

*Short column chromatography*

Short columns of Merck silica gel 60 (230–400 mesh) were packed in glass columns 5 cm in diameter using 10 g of silica gel per gram of crude mixture. Columns were washed first with a low polarity solvent to remove tritanol and other fast-moving impurities. The desired products were then eluted with a more polar solvent. Solvents used are indicated for each preparation described below. Fractions of 15 mL were collected every 5 min using a fraction collector. Contents of fractions were determined by analytical tlc.

*General preparation of 5′-dimethoxytritylnucleosides*

(a) *5′-Dimethoxytrityluridine (**2a**)*

Uridine (**1***a*, 24.4 g, 0.10 mol) was dissolved in pyridine (200

TABLE 6. Properties of protected nucleosides*

| Compound | Melting point (°C) | (EtOH) $\lambda_{max}$ (nm) | $R_f$ (tlc)† |
|---|---|---|---|
| DMT-U **2***a* | 111–112 | 233, 265 | 0.28[a] |
| DMT-A **2***b* | 145–146 | 234, 258 | 0.16[a] |
| DMT-$A^{Bz}$ **2***c* | 113–115 | 234, 261, 284 | 0.14[b] |
| DMT-$C^{Bz}$ **2***d* | 109–111 | 234, 259, 305 | 0.30[a] |
| DMT-$G^{Bz}$ **2***f* | 169–171 | 234, 255(sh), 265, 291 | 0.26[a] |
| 2′,5′-DiDMT-U **3***a* | 144–146 | 231, 265 | 0.41[b] |
| 2′,5′-DiDMT-$A^{Bz}$ **3***c* | 139–141 | 233, 262, 283 | 0.39[b] |
| 2′,5′-DiDMT-$C^{Bz}$ **3***d* | 148–150 | 235, 261, 305 | 0.40[b] |
| 2′,5′-DiDMT-$G^{Bz}$ **3***f* | 158–160 | 233(sh), 261(sh), 281, 295 | 0.79[a], 0.14[c], 0.72[b] |
| 3′,5′-DiDMT-U **4***a* | 136–138 | 231, 265 | 0.32[b] |
| 3′,5′-DiDMT-$A^{Bz}$ **4***c* | 130–131 | 233, 262, 283 | 0.29[b] |
| 3′,5′-DiDMT-$C^{Bz}$ **4***d* | 150–153 | 235, 261, 305 | 0.30[b] |
| 3′,5′-DiDMT-$G^{Bz}$ **4***f* | 154–156 | 233(sh), 261(sh), 281, 295 | 0.71[b], 0.03[c] |
| DMT-$U^{Si}_{OH}$ **6***a* | 100–102 | 233, 265 | 0.22[d] |
| DMT-$A^{Si}_{OH}$ **6***b* | 102–103 | 235, 261 | 0.35[b], 0.57[e] |
| DMT-$^{Bz}_{C}$ $^{Si}_{OH}$ **6***d* | 112–113 | 232, 261, 306 | 0.77[b], 0.75[e] |
| DMT-$^{Bz}_{G}$ $^{Si}_{OH}$ **6***f* | 148–150 | 233, 256(sh), 264, 291 | 0.41[f], 0.59[g], 0.30[h], 0.29[i] |
| DMT-$U^{OH}_{Si}$ **8***a* | 109–110 | 233, 265 | 0.07[d] |
| DMT-$A^{OH}_{Si}$ **8***b* | 172–173 | 235, 261 | 0.28[b], 0.54[e] |
| DMT-$^{Bz}_{C}$ $^{OH}_{Si}$ **8***d* | 110–111 | 232, 261, 306 | 0.48[b], 0.59[e] |
| DMT-$^{Bz}_{G}$ $^{OH}_{Si}$ **8***f* | 140–142 | 233, 265(sh), 264, 291 | 0.41[f], 0.21[g], 0.05[h], 0.28[i] |

*The nmr and ir spectra of all compounds agreed with the reported structures.
†Solvents employed were (a) chloroform–methanol (9:1); (b) chloroform–methanol (9.5:0.5); (c) chloroform–triethylamine (9.5:0.5); (d) hexane–ether (1:3); (e) chloroform–methanol–triethylamine (9.5: 0.5: 0.5); (e) acetone – petroleum ether (6:5.5); (g) acetone – petroleum ether – triethylamine (6:5.5:0.5); (h) chloroform–acetone–triethylamine (9:0.5:0.5); (i) chloroform–acetone (9:0.5).

mL) and kept at 0°C. Dimethoxytrityl chloride (41 g, 0.12 mol) was added in portions (5.1 g, 0.015 mol) during an 8 h period. After an additional 2 h methanol (50 mL) was added and the solution was concentrated at reduced pressure. A 5% $NaHCO_3$ solution (200 mL) was added and the resulting solution was extracted with methylene chloride (500 mL). The methylene chloride solution was washed once with water, then dried over magnesium sulfate and evaporated to leave the crude product.

The residue was washed with chloroform–hexane (1:20, 100 mL) to remove residual pyridine. The residue was then applied to a short column (5 cm diameter) packed with 450 g (10 g/g of crude product) of Merck silica gel 60 (230–400 mesh). The column was washed with ether (500 mL) to remove impurities, followed by ethyl acetate (800 mL). Fractions of 15 mL were collected (fraction collector) every 5 min. The product was recovered from the ethyl acetate fractions which, on evaporation, gave 43.7 g of **2***a* (80%). Compound **2***a* crystallizes from ether: mp 111–112°C. Properties of **2***a* are listed in Table 6.

(b) *5′-Dimethoxytrityladenosine (2*b)

This procedure was very similar to that of (a) except that the solvent consisted of 100 mL each of pyridine and DMF. At the end of the reaction period (10 h) the solution was poured into 2 liters of cold water. A pale yellow precipitate was obtained which was collected by filtration, washed with water, and dried under air. The crude product was dissolved in hot xylene (2500 mL) and, on cooling, the product **2***b* crystallized as a white solid which was collected by filtration and washed with ether (yield 80%, mp 145–146°C). Properties of **2***b* are listed in Table 6.

(c) *5′-Dimethoxytrityl-*N*-benzoylcytidine (2*d)

This procedure was virtually the same as that described for **2***a*, including isolation of the product on short silica gel column chromatography using first chloroform (400 mL) and then chloroform–methanol (9:1, 600 mL) as solvent. The yield of **2***d* was 85% (mp 109–111°C). Properties are listed in Table 6.

(d) *5′-Dimethoxytrityl-*N*-benzoylguanosine (2*f)

This preparation was identical to that described above for **2***d* except that, during short column chromatography of the reaction products, 500 mL of chloroform was used to wash off impurities and the product was recovered in 800 mL of chloroform–methanol (9:1). The yield of **2***f* was 69% and its properties are listed in Table 6.

*Preparation of dimethoxytritylated nucleosides using silver nitrate as catalyst*

The general procedure is outlined for the synthesis of 5′-dimethoxytrityl-*N*-benzoyladenosine (**2***c*). *N*-Benzoyladenosine was dissolved in THF (30 mL/mmol of nucleoside). Pyridine (5 mmol/mmol of **1**), silver nitrate (1 mmol/mmol **1**), and dimethoxytrityl chloride (1 mmol/mmol **1**) were added successively and the mixture was stirred at room temperature for 1 h. The mixture was filtered and the solution added to a 5% sodium bicarbonate solution. The product was extracted into methylene chloride which was dried and evaporated to give **2***c* in an 80% yield.

When the above reaction was repeated except that the amounts of pyridine, silver nitrate, and dimethoxytrityl chloride were doubled, the 2′,5′ and 3′,5′-ditritylated products **3***c* and **4***c* were each obtained in 40% yields. The results for all of the nucleosides are listed in Table 1 and the properties of the products are listed in Table 6.

*Silylation of dimethoxytritylated nucleosides **2** using nitrate (or perchlorate) catalysts*

(a) The standardized procedure can be illustrated by the silylation of 5′-dimethoxytrityladenosine (**2***b*). Compound **2***b* (5.69 g, 10 mmol) was dissolved in THF (100 mL) followed by the addition of pyridine (3 g, 37 mmol) and silver nitrate (2 g, 12 mmol). The solution was stirred (5 min) until all the silver nitrate had dissolved and then *tert*-butyldimethylsilyl chloride (2 g, 13 mmol) was added and the mixture was stirred at room temperature for 5 h. The solution was then filtered into a 5% $NaHCO_3$ solution (100 mL). This solution was extracted with methylene chloride (300 mL) and the extracts were dried and evaporated.

Ether (100 mL) was added to the crude product (6.5 g). The solution was separated from undissolved **2***b* by filtration. The ether solution was concentrated, at reduced pressure without heating, to about 60 mL. During this period the 2′-silylated derivative precipitated and 3 g of **6***b* was collected by filtration. By repeated concentration it has been possible to collect most of the 2′-isomer. However, a more direct procedure is to collect the residue from the remaining ether solution and apply it directly to short column chromatography using chloroform–methanol (9.5:0.5) for elution. The yield of the 2′-isomer **6***b* was 65%, and that of the 3′-isomer **8***b* was 21%. Properties of these compounds are collected in Table 6.

(b) 5′-Dimethoxytrityluridine was silylated using the same procedure. Products **6***a* and **8***a* were obtained in 70% and 15% yields respectively from short column chromatography using ether–hexane (1:1). Properties are listed in Table 6.

(c) 5′-Dimethoxytrityl-*N*-benzoylcytidine was silylated using the standard procedure. Products **6***d* and **8***d* were obtained in 68% and 20% yields respectively after short column chromatography using ether–hexane (3:1). Properties of products are listed in Table 6.

(d) 5′-Dimethoxytrityl-*N*-benzoylguanosine was silylated using the standard procedure except that 1.5 equivalents of silver nitrate and 1.7 equivalents of TBDMS-Cl were used. The products were separated on short column chromatography using chloroform – methylene chloride – triethylamine (9:0.5:0.5). The collected fractions were neutralized by passing them through Dowex 50W × 8 ($H^+$ form) resin. The solvent was evaporated and the individual products were obtained as white solids on precipitation from chloroform with petroleum ether. The 2′-isomer **6***f* was obtained in 45% yield and the 3′-isomer **8***f* in 40% yield. Properties are summarized in Table 6.

*Silylation of nucleosides* **1**

The general procedure is illustrated for the silylation of uridine. Uridine (1 mmol) was dissolved in THF (30 mL). Pyridine (5 mmol) and silver nitrate (2.2 mmol) were added and stirring was continued for 5 min until all silver nitrate had dissolved. TDBMS-Cl (2.2 mmol) was added and the mixture was stirred for 1 h. The solution was collected by filtration and the solvents concentrated to a small volume and applied to 4 tlc plates which were developed in ether–hexane (4:1). The yields are shown in Table 2 for all compounds tested.

For monosilylation the above procedure is repeated exactly except that pyridine is omitted. Yields of the 5′-monosilyl derivatives are collected in Table 2. All silylated compounds were identified by comparison to authentic material (8).

The general procedure described above was employed for all nitrate and perchlorate salts tested. The results of all of these reactions are summarized in Tables 2 and 3. It is important to add the reagents in the order described above. All solvents used in the reactions should be purified by distillation.

*Selective 3′-silylations*

A. *General procedure using DABCO*

The general procedure is much the same as described above. DABCO (0.67 g, 6 mmol/mmol of nucleoside) was dissolved in dry THF (25 mL/mmol nucleoside). Silver nitrate (0.37 g, 2.2 mmol/mmol of nucleoside) was added and the solution was stirred for 5 min. At this point *tert*-butyldimethylsilyl chloride (0.35 g, 2.2 mmol/mmol of nucleoside) was added. After an additional 5 min the nucleoside (1 mmol) was added and stirring continued (for time of reaction, see Table 4). At the end of the reaction period the solution was collected by filtration, diluted with 50 mL of water, and extracted with chloroform (80 mL). The organic layer was dried and concentrated and the products were isolated by short column chromatography.

The results of individual experiments are collected in Table 4.

B. *General procedure using pyridine* N-*oxide*

This procedure is identical to that described in A above except that a pyridine *N*-oxide is used in place of DABCO. The ratio of reagents used and the results of individual experiments are collected in Table 5.

## Acknowledgements

We gratefully acknowledge generous financial support from the Natural Sciences and Engineering Research Council of Canada (NSERCC Strategic Grant) and the Government of Quebec (FCAC).

1. G. Alvarado-Urbina, G. M. Sathe, W-C. Liu, M. F. Gillen, P. D. Duck, and K. K. Ogilvie. Science, **214**, 270 (1981).
2. H. Kossel and H. Seliger. Prog. Chem. Org. Nat. Prod. **32**, 298 (1975).
3. H. G. Khorana. Some recent developments in the chemistry of phosphate esters of biological interest. J. Wiley & Sons, New York. 1961. pp. 93–140.
4. R. L. Letsinger and K. K. Ogilvie. J. Am. Chem. Soc. **89**, 4801 (1967).
5. S. A. Narang, R. Brousseau, H. M. Hsiung, and J. J. Michniewicz. Methods Enzymol. **65**, 610 (1980).
6. R. L. Letsinger, J. L. Finnan, G. A. Heavner, and W. B. Lunsford. J. Am. Chem. Soc. **97**, 3278 (1975).
7. (*a*) K. K. Ogilvie and M. J. Nemer. Tetrahedron Lett. **21**, 4159 (1981); (*b*) K. K. Ogilvie and R. T. Pon. Nucleic Acids Res. **8**, 2105 (1980); (*c*) K. K. Ogilvie, N. Y. Theriault, J-M. Seifert, R. T. Pon, and M. J. Nemer. Can. J. Chem. **58**, 2686 (1980); (*d*) K. K. Ogilvie and M. J. Nemer. Can. J. Chem. **58**, 1389 (1980); (*e*) K. K. Ogilvie and N. Y. Theriault. Can. J. Chem. **57**, 3140 (1979).
8. (*a*) K. K. Ogilvie, A. L. Schifman, and C. L. Penney. Can. J. Chem. **57**, 2230 (1979); (*b*) K. K. Ogilvie, S. L. Beaucage, A. L. Schifman, N. Y. Theriault, and K. L. Sadana. Can. J. Chem. **56**, 2768 (1978).
9. K. K. Ogilvie and N. Y. Theriault. Tetrahedron Lett. 2111 (1979).
10. B. R. G. Williams and I. M. Kerr. Nature, **276**, 88 (1978).
11. K. L. Agarwal, A. Yamazaki, P. J. Cashion, and H. G. Khorana. Angew. Chem. Int. Ed. Engl. **11**, 451 (1972).
12. H. Schaller, G. Weimann, B. Lerch, and H. G. Khorana. J. Am. Chem. Soc. **85**, 3821 (1963).
13. M. Smith, D. H. Rammler, I. H. Goldberg, and H. G. Khorana. J. Am. Chem. Soc. **84**, 430 (1962).
14. D. H. Rammler and H. G. Khorana. J. Am. Chem. Soc. **84**, 3112 (1962).
15. D. J. Ager and I. Flemming. J. Chem. Research (S), 6 (1977).
16. T. J. Barton and C. R. Tully. J. Org. Chem. **43**, 3649 (1978).
17. C. B. Reese and D. R. Trentham. Tetrahedron Lett. 2467 (1965).
18. W. T. Markiewicz. J. Chem. Research (S), 24 (1979).
19. G. H. Hakimelahi, Z. A. Proba, and K. K. Ogilvie. Tetrahedron Lett. **22**, 4775 (1981).
20. G. H. Hakimelahi, Z. A. Proba, and K. K. Ogilvie. Tetrahedron Lett. **22**, 5243 (1981).

# Alkylation of enolate anions with dimethyl 3-bromo-2-ethoxypropenylphosphonate. A convergent cyclopentenone annulation method

EDWARD PIERS AND BRIAN ABEYSEKERA

*Department of Chemistry, University of British Columbia, 2036 Main Mall, University Campus, Vancouver, B.C., Canada V6T 1Y6*

Received December 2, 1981

EDWARD PIERS and BRIAN ABEYSEKERA. Can. J. Chem. **60**, 1114 (1982).

A new, convergent synthesis of 2-cyclopenten-1-ones is reported. Treatment of dimethyl 2-oxopropylphosphonate (**21**) with excess triethyl orthoformate in the presence of ferric chloride hexahydrate provides the enol ether **22**, which upon allylic bromination with *N*-bromosuccinimide yields the allylic bromide **19**. Alkylation of the ketones **24–28** with **19**, followed by mild acid hydrolysis of the resultant products **29–33**, affords the diketo phosphonates **34–38**. When the latter substances are treated with sodium hydride in dimethoxyethane, the corresponding 2-cyclopenten-1-ones **40–44** are formed in good yields.

EDWARD PIERS et BRIAN ABEYSEKERA. Can. J. Chem. **60**, 1114 (1982).

On rapporte une nouvelle synthèse convergente des cyclopentène-2 ones-1. L'oxo-2 propylphosphonate de diméthyle (**21**) réagit avec un excès d'orthoformiate de triéthyle en présence du chlorure ferrique hexahydraté en donnant l'éther énolique **22** qui par bromation allylique avec la NBS conduit au bromure **19**. L'alkylation des cétones **24–28** avec le composé **19** suivie d'une hydrolyse acide douce des produits obtenues (**29–33**) conduit aux dicétophosphonates **34–38**. Ces derniers composés réagissent avec l'hydrure de sodium dans le diméthoxyéthane en donnant les cyclopentène-2 ones-1 correspondantes (**40–44**) avec de bons rendements.

[Traduit par le journal]

## Introduction

Functionalized cyclopentane rings are very commonly found in structurally novel, physiologically active, and/or commercially important natural products. Consequently, it is not surprising to find that, particularly in recent times, a great deal of effort has gone into developing new, efficient methods for synthesizing five-membered ring systems.

The overall annulation scheme represented in general terms by eq. [1] constitutes an important, much employed method for preparing substituted 2-cyclopenten-1-ones. In this process, the (theoretical) combination of a $d^2$ synthon **1** (normal reactivity) (1) with an $a^2$ synthon **2** (reactivity umpolung) (1) results in the formation of a 1,4-diketone system **3**. Subjection of the latter substance to base-promoted intramolecular aldol condensation, followed by dehydration, would provide the desired enone **4**.

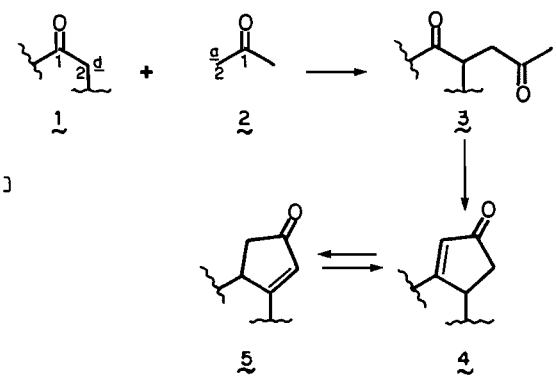

[1]

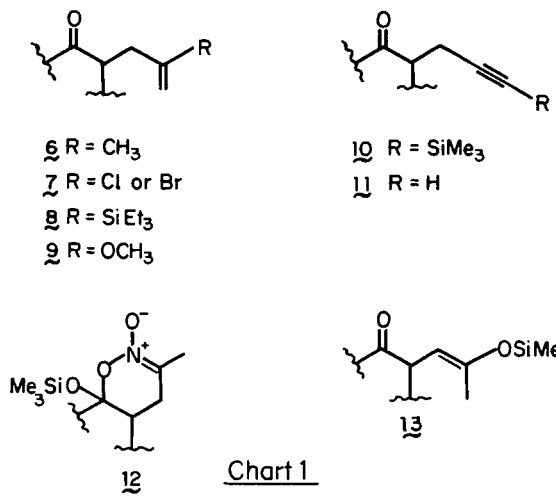


Chart 1

Various species (e.g. enolate anions, enol ethers) corresponding to the $d^2$ synthon **1** are prepared very readily from the corresponding ketone. However, there has been an ongoing search for efficient and generally applicable synthetic equivalents to the $a^2$ synthon **2**, and, thus far, a number of reagents have been employed successfully. For example, alkylation of enolate anions with 3-halo-2-methylpropenes (2–4) 2,3-dihalopropenes (5, 6), 3-iodo-2-(triethylsilyl)propene (7), 3-bromo-2-methoxypropene (8), 3-bromo-1-(trimethylsilyl)-propyne (9–11), or 3-bromopropyne (12) provides the corresponding substances of general structure **6–11**, respectively (see Chart 1). On the other hand, reaction of trimethylsilyl enol ethers with 2-nitropropene in the presence of stannic chloride or

0008-4042/82/091114-08$01.00/0

©1982 National Research Council of Canada/Conseil national de recherches du Canada

Can. J. Chem. Downloaded from www.nrcresearchpress.com by 210.87.254.105 on 09/06/12
For personal use only.

Can. J. Chem. Downloaded from www.nrcresearchpress.com by 210.87.254.105 on 09/06/12
For personal use only.

titanium tetrachloride (13) or with diazoacetone in the presence of cupric acetylacetonate (14) yields compounds of general structures **12** or **13**, respectively.

A diversity of reagents and experimental conditions are involved in converting the appendages in **6–13** into the required acetonyl side chain (cf. **3**): **6**, cleavage of the carbon–carbon double bond by ozonolysis (2, 3) or osmium tetroxide – sodium periodate (2, 4); **7**, hydrolysis of the vinyl halide function with concentrated sulfuric acid (5, 6); **8**, epoxidation with peracid, followed by acid hydrolysis of the resultant epoxy silane (7); **9**, hydrolysis of the enol ether function with aqueous oxalic acid (8); **10** and **11**, hydration of the carbon–carbon triple bond with aqueous acid in the presence of mercuric salts (10–12); **12**, hydrolysis with water – stannic chloride (or titanium tetrachloride) in refluxing dichloromethane (13); **13**, hydrolysis of the trimethylsilyl enol ether with water (14).

In general, the methods for converting **1** into **4**, as summarized above, suffer mainly from two difficulties. Firstly, the conditions required to introduce or unmask the various synthetic equivalents to the $a^2$ synthon **2** often have (or would have) deleterious effects on other functional groups which might be present in the ketonic (or enol ether) substrate. For example, carbon–carbon double or triple bonds and/or acid-sensitive groups[1] would certainly be susceptible to chemical reaction when subjected to many of the reagents and/or conditions summarized above. Secondly, the intramolecular aldol condensation process (**3** → **4**) can be accompanied by an undesirable base-catalyzed isomerization of the initially formed product (**4** ⇆ **5**, see eq. [1]).[2]

A method which circumvents very efficiently the second difficulty mentioned above has been reported by Heathcock and co-workers (16) and is summarized in eq. [2]. Conversion of the keto ester **14** (obtained by alkylation of the requisite ketone with methyl haloacetate) into the corresponding ketal **15**, followed by treatment of the latter substance with 2 equivalents of lithium dimethoxyphosphinylmethide ($LiCH_2PO(OMe)_2$) affords the keto phosphonate **16**. Acid-catalyzed hydrolysis of **16** gives the diketo phosphonate **17**. Treatment of **17** with base (e.g. sodium hydride) effects an intramolecular Horner–Emmons reaction, providing the annulation product **4** in good yield. Importantly, the last step produces in addition to the desired product only the weak base sodium dimethylphosphate, which is incapable of causing isomerization of the initially formed cyclopentenone **4**.

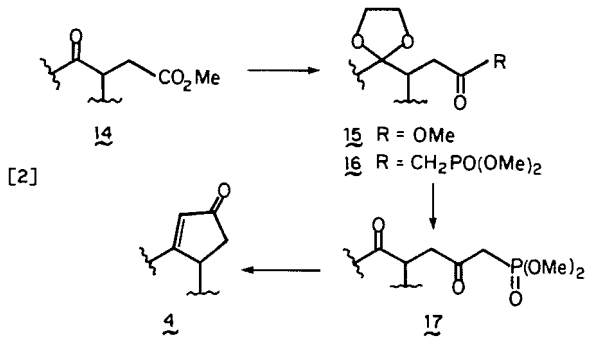


The Heathcock methodology, however, does not eliminate the first drawback mentioned previously. Clearly, the steps involving introduction and removal of the ketal protecting group (formation of **15** and **17**) could readily affect other acid-sensitive groups which might be present in the ketonic substrate. We describe herein an efficient, convergent method for effecting the conversion of **1** into **4** via a route which removes this limitation as well.[3] Essentially, the overall process, summarized in general terms in eq. [3], involves the following steps: (a) treatment of an enolate anion **18** with dimethyl 3-bromo-2-ethoxypropenylphosphonate (**19**) (cf. ref. 18) to provide the alkylation product **20**, (b) hydrolysis of **20** to give the required diketo phosphonate **17**, and (c) intramolecular Horner–Emmons reaction (**17** → **4**).

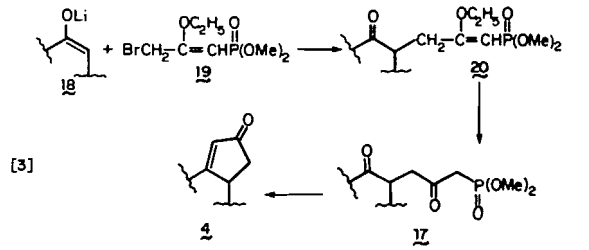


## Results and discussion

### (a) *Preparation of dimethyl 3-bromo-2-ethoxypropenylphosphonate* (19)

The required alkylating agent **19** was prepared efficiently as follows (see Chart 2). Treatment of dimethyl 2-oxopropylphosphonate (**21**) with excess triethyl orthoformate in the presence of a catalytic

[1]For an example of hydration of the triple bond of the propargyl group (cf. **11**) with retention of a ketal moiety, see ref. 12.

[2]Recently, an intramolecular, base-promoted aldol condensation of the type **3** → **4** was achieved without causing subsequent isomerization of the initially formed product (15). See also ref. 3.

[3]For a preliminary report regarding this work, see ref. 17.

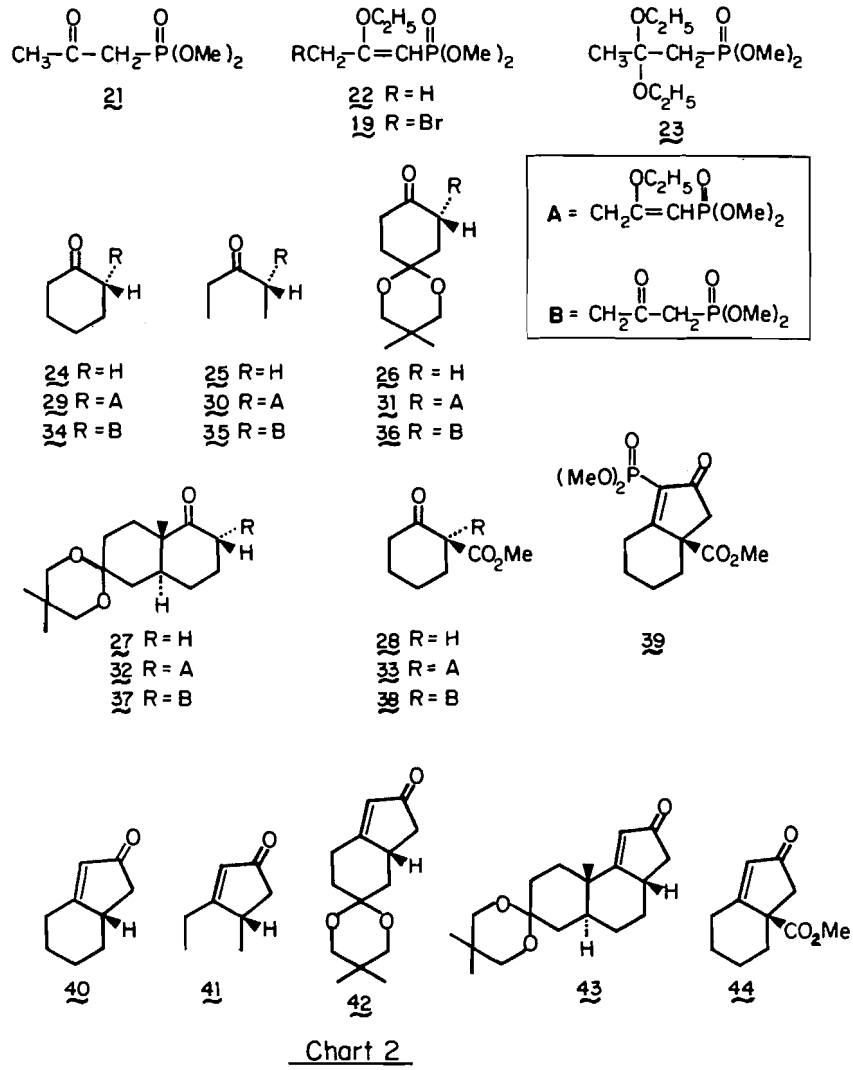


Chart 2

amount of ferric chloride hexahydrate (19) afforded mainly the desired enol ether **22**. In most of the attempts to carry out this transformation, the latter substance was accompanied by small amounts of starting material **21** and variable amounts of a second component which appeared to be dimethyl 2,2-diethoxypropylphosphonate (**23**). Therefore, in each of these cases, a dichloromethane solution of the crude product was treated with an appropriate amount of sodium hydride, which converted **23** into the desired **22** and transformed **21** into the corresponding insoluble (20) sodium salt. Filtration of the resultant mixture, followed by isolation and purification of the product, provided the enol ether **22** in 94% yield.

Allylic bromination of **22** with *N*-bromosuccinimide (21; see also ref. 18) in carbon tetrachloride afforded, after purification of the crude product by column chromatography, dimethyl 3-bromo-2-ethoxypropenylphosphonate (**19**) (76% yield). Although the $^1$H nmr spectra of compounds **22** and **19** indicated that each of these compounds consisted very largely of one isomer, their configuration is not known. However, this point is irrelevant to the synthetic work reported herein, and therefore did not receive further attention.

(b) *Alkylation of the ketones* ***24–27*** *and the keto ester* **28** *with the bromide* **19**

The allylic bromide **19** proved to be an excellent alkylating agent. Thus, when the enolate anion of cyclohexanone was allowed to react with **19** in tetrahydrofuran (THF) (−78°C, 30 min; 0°C, 30 min; room temperature, 30 min), the alkylation product **29** was formed in quantitative yield (see Chart 2). In identical fashion, 3-pentanone (**25**)

Can. J. Chem. Downloaded from www.nrcresearchpress.com by 210.87.254.105 on 09/06/12
For personal use only.

Can. J. Chem. Downloaded from www.nrcresearchpress.com by 210.87.254.105 on 09/06/12
For personal use only.

could be converted quantitatively into the alkylated material **30**. On the other hand, application of this procedure to the keto ketal **26** (22)[4] gave the desired product **31** in mediocre yield (~40%). However, a notable improvement could be realized when 1 equivalent of hexamethylphosphoramide (HMPA) was added to the reaction mixture prior to addition of the alkylating agent **19**. This minor modification led to the formation of **31** in 78% yield. In similar fashion, alkylation (**19**, THF, 1 equivalent of HMPA) of the lithium enolates of the keto ketal **27**[5] and the keto ester **28** afforded good yields of compounds **32** and **33**, respectively. In the case of the transformation of **28** into **33**, a longer reaction time (room temperature, 6 h) was required for completion of the reaction.

It is clear from the experiments summarized above that the bromo compound **19** alkylates enolate anions very efficiently. In this sense, **19** compares favorably with the alkylating reagents involved in the formation of compounds of general structure **6–11** (*vide supra*).

(c) *Hydrolysis of compounds **29–33**. Formation of the diketo phosphonates **34–38***

The crucial step in each of the annulation sequences described herein involved hydrolysis of the enol ether functional group in the side chain of each of the compounds **29–33**. Although this transformation was expected to be straightforward in the case of the alkylation products **29**, **30**, and **33**, the keto ketals **31** and **32** were particularly important examples of the present methodology, since, in each case, the enol ether group would have to be hydrolyzed under conditions which would not affect the ketal function.

When an acetone solution of **29** containing 1 *N* hydrochloric acid was allowed to stir at room temperature for 30 min, the desired diketo phosphonate **34** was obtained in quantitative yield. An identical procedure also effected smooth conversion of **30** into **35**.

An unexpected difficulty arose in connection with attempted hydrolysis of the alkylation product **33**. Thus, subjection of the latter substance to conditions very similar to those employed for **29** and **30** gave, in addition to some of the expected product **38**, a compound which exhibited *m/e* 330 ($M^+$) in the mass spectrum. Although the latter material was not fully characterized, the mass spectral data along with a fairly intense infrared absorption at 1605 $cm^{-1}$ (carbon–carbon double bond stretching vibration) suggested that this substance possessed structure **39**. Apparently, under the reaction conditions, some of the initially formed diketo phosphonate had undergone intramolecular aldol condensation. After some experimentation, it was found that this difficulty could be largely avoided quite simply by carrying out the hydrolysis of **33** with more dilute acid (0.5 *N* hydrochloric acid, acetone, room temperature, 35 min). Although the infrared spectrum of the crude product indicated that these conditions still produced small amounts of the enone **39**, the material thus obtained was sufficiently pure to be used directly for the next step.

With respect to the hydrolysis of the keto ketals **31** and **32**, it was eventually found that conditions similar to those employed for compound **33** (0.5 *N* hydrochloric acid, acetone, room temperature) were quite satisfactory. Under these conditions, the enol ether moiety was, in each case, hydrolyzed smoothly, while the ketal function remained essentially unaffected. In the case of compound **31**, reaction times of up to 2 h left the ketal group intact. Using this procedure, the hydrolysis products **36** and **37** were obtained in high yield (92%, 96%, respectively).

(d) *Intramolecular Horner–Emmons reaction of the diketo phosphonates **34–38***

Cyclization of the diketo phosphonates **34–38** was accomplished by treatment of each of these substances with sodium hydride in dimethoxyethane (DME) (16, 24). In general, the reactions were quite efficient, the yields of the products **40** (8), **41** (25), and **42–44** being 74, 82, 72, 86, and 70% (based on **33**), respectively. Importantly, in accord with previous observations (16), the products **41–43** were very clean and, in each of these cases, there was no indication of isomerization to the corresponding isomeric cyclopentenone.

## Conclusion

The convergent annulation sequence described in this paper would appear to constitute a general, efficient method for the construction of functionalized 2-cyclopenten-1-one systems. It is appropriate to note that, very recently, this method has been employed successfully in an elegant well-designed synthesis of (±)-quadrone, a structurally novel sesquiterpenoid which exhibits antitumor properties (26).

Finally, two additional pertinent items should be mentioned. Firstly, after appearance of our prelim-

[4]We are grateful to Mr. M. Burmeister for supplying a sample of this compound.

[5]This substance was prepared in a straightforward, unambiguous fashion from the Wieland–Miescher ketone (23). Details will be reported elsewhere.

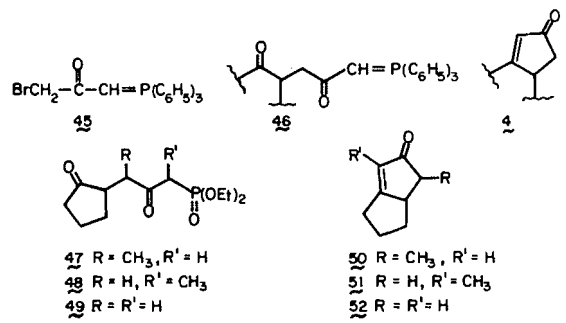


Chart 3

inary report, Altenbach described (27) the alkylation of enolate anions with (bromoacetylmethylene)triphenylphosphorane (**45**) (see Chart 3). Subsequent intramolecular Wittig reaction of the resultant diketo phosphoranes **46** (not isolated) provided the corresponding cyclopentenones **4**. Although, in principle, the Altenbach methodology is very similar to that described in this paper, the reported yields of the annulation products were low (14–39%). Secondly, Pattenden and co-workers have reported (28) very recently that although treatment of the diketo phosphonates **47** and **48** (Chart 3) with sodium hydride in DME at 60°C provided good yields of the bicyclic enones **50** and **51**, respectively, attempted conversion of **49** into **52**[6] under similar conditions failed. Instead, a "tarry mass" was produced. Attempts to transform **49** into **52** using alternative reaction conditions were also unsuccessful.

## Experimental

*General*

Melting points were taken on a Fisher–Johns melting point apparatus and are uncorrected. Distillation temperatures (also uncorrected) refer to the mean air bath temperature during a short path (bulb-to-bulb) distillation. Infrared (ir) spectra were obtained on liquid films or chloroform solutions, employing Perkin Elmer models 710 or 710B spectrophotometers. Proton magnetic resonance ($^1$H nmr) spectra (deuterochloroform solution) were measured using Bruker WP-80 or WH-400 instruments or Varian Associates T-60, HA-100, and/or XL-100 spectrometers. Signal positions are given in $\delta$ units, with tetramethylsilane as the internal standard. Gas–liquid chromatography (glc) was carried out with a Hewlett–Packard model 5832A gas chromatograph. High resolution mass spectrometric measurements were recorded on a Kratos MS-50 mass spectrometer. Microanalyses were carried out by Mr. P. Borda, Microanalytical Laboratory, University of British Columbia, Vancouver, B.C.

The solvents and reagents employed were freshly distilled under an atmosphere of argon as follows: THF and DME from sodium benzophenone ketyl; HMPA from barium oxide; diisopropylamine from calcium hydride; carbon tetrachloride and dichloromethane from phosphorus pentoxide.

*Dimethyl 2-ethoxypropenylphosphonate (22)*

To dimethyl 2-oxopropylphosphonate (**21**) (5.1 g, 37.8 mmol) was added triethyl orthoformate (9.0 g, 60.8 mmol) and ferric chloride hexahydrate (0.2 g). The mixture was stirred briefly and then allowed to stand at room temperature for 3 days. The volatile byproducts and excess triethyl orthoformate were removed under reduced pressure and the residual material was dissolved in 50 mL of dry dichloromethane. The solution was treated with 0.5 g of sodium hydride (washed free of mineral oil with hexane) and the resultant mixture was stirred for 10 min and then filtered. Removal of the solvent from the filtrate, followed by distillation (air bath temperature 80°C/0.05 Torr) of the residual material gave 6.89 g (94%) of the enol ether **22** as a colorless oil; ir (film): 1605, 1250, 1050, 1025 cm$^{-1}$; $^1$H nmr $\delta$: 1.33 (t, 3H, $J$ = 7 Hz, $CH_3CH_2O$), 2.14 (d, 3H, $J_{H-P}$ = 2 Hz, vinyl methyl), 3.65 (d, 6H, $J_{H-P}$ = 11 Hz, $PO(OCH_3)_2$), 3.77 (q, 2H, $J$ = 7 Hz, $CH_3CH_2O$), 4.35 (d, 1H, $J_{H-P}$ = 7 Hz, vinyl proton). *Anal.* calcd. for $C_7H_{15}O_4P$: C 43.30, H 7.79; found: C 43.13, H 7.70. *Exact mass* calcd.: 194.0707; found: 194.0708.

*Dimethyl 3-bromo-2-ethoxypropenylphosphonate (19)*

To a solution of the enol ether **22** (3.0 g, 15.5 mmol) in 150 mL of dry carbon tetrachloride was added 3.1 g (17.4 mmol) of *N*-bromosuccinimide. The well-stirred mixture was heated (reflux) while it was being irradiated with a sun lamp (Westinghouse, 275 W, 110–120 V). After 15 min the reaction mixture was cooled and filtered. The filtrate was concentrated under reduced pressure to a volume of approximately 50 mL and then cooled in an ice-bath to precipitate residual succinimide. The mixture was filtered through a small amount of neutral alumina (Act. I). Removal of the solvent from the filtrate gave a yellow oil which was subjected to column chromatography on silica gel (160 g). Elution of the column with ethyl acetate, followed by distillation (air bath temperature 110°C/0.05 Torr) of the crude oil thus obtained gave 3.2 g (76%) of dimethyl 3-bromo-2-ethoxypropenylphosphonate (**19**) as a colorless oil, which exhibited one peak by glc analysis and one spot by tlc analysis; ir (film): 1605, 1250, 1050–1025 (broad) cm$^{-1}$; $^1$H nmr $\delta$: 1.39 (t, 3H, $J$ = 7 Hz, $CH_3CH_2O$), 3.76 (d, 6H, $J_{H-P}$ = 11 Hz, $PO(OCH_3)_2$), 3.91 (q, 2H, $J$ = 7 Hz, $CH_3CH_2O$), 4.42 (s, 2H, $CH_2Br$), 4.57 (d, 1H, $J_{H-P}$ = 5 Hz, vinyl proton). *Exact Mass* calcd. for $C_7H_{14}{}^{79}BrO_4P$: 271.9813; found: 271.9815.

*Alkylation of the ketones 24–27 and the keto ester 28 with the allylic bromide 19*

(a) *Preparation of compound 29*

To a cold (−78°C) stirred solution of lithium diisopropylamide (LDA) (1.2 mmol) in dry THF (2 mL) under an atmosphere of argon was added 98 mg (1 mmol) of cyclohexanone. The cooling bath was removed and replaced by an ice-water bath, and the solution was allowed to stir for 1 h. The reaction mixture was recooled to −78°C and 330 mg (1.2 mmol) of the alkylating agent **19** was added. After the reaction mixture had been stirred at −78°C for 30 min, at 0°C for 30 min, and at room temperature for 30 min, the THF was removed under reduced pressure. The residual material was dissolved in dichloromethane and the resultant solution was washed twice with brine and dried over anhydrous sodium sulfate. Removal of the solvent under reduced pressure (water aspirator, followed by vacuum pump) gave 290 mg (100%) of the alkylated ketone **29** as a colorless oil. Both tlc and glc indicated that this material consisted of one component; ir (film): 1710, 1605, 1250, 1060–1025 (broad) cm$^{-1}$; $^1$H nmr $\delta$: 1.26 (t, 3H, $J$ = 7 Hz, $CH_3CH_2O$), 1.42–3.06 (diffuse,

[6]For a recent successful synthesis of this substance, see ref. 29.

Can. J. Chem. Downloaded from www.nrcresearchpress.com by 210.87.254.105 on 09/06/12
For personal use only.

Can. J. Chem. Downloaded from www.nrcresearchpress.com by 210.87.254.105 on 09/06/12
For personal use only.

11H), 3.62 (d, 6H, $J_{H-P}$ = 11 Hz, $PO(OCH_3)_2$), 3.72 (q, 2H, $J$ = 7 Hz, $CH_3CH_2O$), 4.36 (d, 1H, $J_{H-P}$ = 7 Hz, vinyl proton). *Exact Mass* calcd. for $C_{13}H_{23}O_5P$: 290.1283; found: 290.1301.

(b) *Preparation of compound* ***30***

This compound was prepared via a procedure identical with that described above. From 86 mg (1 mmol) of 3-pentanone there was obtained, after distillation (air bath temperature 140°C/0.05 Torr) of the crude product, 278 mg (100%) of the alkylated material **30** as a colorless oil, which exhibited one peak by glc analysis and one spot by tlc analysis; ir (film): 1705, 1605, 1250, 1050–1025 (broad) $cm^{-1}$; $^1H$ nmr δ: 1.04 (t, 3H, $J$ = 7 Hz, $CH_3CH_2CO$), 1.12 (d, 3H, $J$ = 6 Hz, secondary methyl), 1.28 (t, 3H, $J$ = 7 Hz, $CH_3CH_2O$), 2.50 (q, 2H, $J$ = 7 Hz, $CH_3CH_2CO$), 2.66–2.98 (diffuse, 3H), 3.66 (d, 6H, $J_{H-P}$ = 11 Hz, $PO(OCH_3)_2$), 3.76 (q, 2H, $J$ = 7 Hz, $CH_3CH_2O$), 4.39 (d, 1H, $J_{H-P}$ = 6 Hz, vinyl proton). *Exact Mass* calcd. for $C_{12}H_{23}O_5P$: 278.1283; found: 278.1277.

(c) *Preparation of compound* ***31***

For the alkylation of the keto ketal **26** (198 mg, 1 mmol) the procedure described above was modified as follows. Just prior to addition of the alkylating agent **19**, HMPA (180 μL, 1 mmol) was added to the reaction mixture (−78°C). After work-up, most of the HMPA was removed from the crude product (air bath temperature ~100°C/0.05 Torr) and the residual oil was subjected to column chromatography on silica gel (10 g). Elution of the column with ethyl acetate gave 304 mg (78%) of the alkylated ketone **31** as a colorless oil which, according to analyses by glc and tlc, consisted of one component; ir (film): 1715, 1610, 1250, 1030 $cm^{-1}$; $^1H$ nmr δ: 0.94, 1.01 (s, s, 3H each, tertiary methyls), 1.30 (t, 3H, $J$ = 6 Hz, $CH_3CH_2O$), ~1.4–3.2 (diffuse, 9H), 3.48 (s, 4H, ketal methylene protons), 3.67 (d, 6H, $J_{H-P}$ = 11 Hz, $PO(OCH_3)_2$), 3.78 (q, 2H, $J$ = 6 Hz, $CH_3CH_2O$), 4.43 (d, 1H, $J_{H-P}$ = 6 Hz, vinyl proton). *Exact Mass* calcd. for $C_{18}H_{31}O_7P$: 390.1808; found: 390.1796.

(d) *Preparation of compound* ***32***

Alkylation of **27** was accomplished via a procedure identical with that described above (preparation of **31**). From 266 mg (1 mmol) of the keto ketal **27**, there was obtained 348 mg (76%) of the alkylated substance **32** as a white solid. Recrystallization (ether–hexane) of a small amount of this material provided an analytical sample, mp 99–100°C; ir ($CHCl_3$): 1705, 1610, 1250, 1060–1020 (broad) $cm^{-1}$; $^1H$ nmr δ: 0.93, 1.02, 1.16 (s, s, s, 3H each, tertiary methyls), 1.32 (t, 3H, $J$ = 7 Hz, $CH_3CH_2O$), ~1.4–3.2 (diffuse, 14H), 3.4–3.6 (m, 4H, ketal methylene protons), 3.72 (d, 6H, $J_{H-P}$ = 11 Hz, $PO(OCH_3)_2$), 3.80 (q, 2H, $J$ = 7 Hz, $CH_3CH_2O$), 4.44 (d, 1H, $J_{H-P}$ = 6 Hz, vinyl proton). *Exact Mass* calcd. for $C_{23}H_{39}O_7P$: 458.2434; found: 458.2412.

(e) *Preparation of compound* ***33***

Alkylation of 2-carbomethoxycyclohexanone (**28**) (156 mg, 1 mmol) was carried out via a procedure very similar to that employed for the preparation of compounds **31** and **32**. However, 1.5 mmol of each of LDA, the allylic bromide **19** (413 mg), and HMPA (270 μL) were employed instead of the quantities indicated above and the reaction mixture was stirred at room temperature for 6 h instead of for 30 min. Distillation (air bath temperature 180°C/0.05 Torr) of the material obtained from the chromatography column afforded 247 mg (71%) of the alkylated keto ester **33** as a colorless oil. Both glc and tlc indicated that this material consisted of one component; ir (film): 1740, 1710, 1610, 1240, 1060–1020 (broad) $cm^{-1}$; $^1H$ nmr δ: 1.28 (t, 3H, $J$ = 7 Hz, $CH_3CH_2O$), ~1.5–2.5 (diffuse, 8H), 3.11, 3.37 (d of d, d of d, 1H each, $J_{H-H}$ = 16 Hz, $J_{H-P}$ = 2 Hz in each case, allylic methylene protons), 3.56–3.84 (a series of partially overlapped signals consisting of: d, 6H, $PO(OCH_3)_2$; s, 3H, $CO_2Me$; q, 2H, $CH_3CH_2O$), 4.40 (d, 1H, $J_{H-P}$ = 5 Hz, vinyl proton). *Exact Mass* calcd. for $C_{15}H_{25}O_7P$: 348.1338; found: 348.1333.

*Hydrolysis of the enol ether functional group of the alkylation products* ***29–33***

(a) *Preparation of compound* **34**

To a stirred solution of compound **29** (290 mg, 1 mmol) in 25 mL of acetone at room temperature was added 0.5 mL of 1 *N* hydrochloric acid. After the resultant mixture had been stirred at room temperature for 30 min, the acid was neutralized by addition of anhydrous potassium carbonate and the acetone was removed under reduced pressure. Dichloromethane was added to the residual material and the organic solution was washed twice with saturated aqueous potassium bicarbonate and then was dried over anhydrous sodium sulfate. Removal of the solvent, followed by distillation (air bath temperature 182°C/0.02 Torr) of the residual oil gave 262 mg (100%) of the diketo phosphonate **34** as a colorless oil, glc and tlc analyses of which indicated that it consisted of one component; ir (film): 1710, 1260, 1030 $cm^{-1}$; $^1H$ nmr δ: ~1.1–2.6 (diffuse, 9H), ~2.75–3.2 (diffuse, 2H), 3.16, 3.36 (d, d, 1H each, $J$ = 14 Hz, —$COCH_2PO$—), 3.72 (d, 6H, $J_{H-P}$ = 11 Hz, $PO(OCH_3)_2$). *Exact Mass* calcd. for $C_{11}H_{19}O_5P$: 262.0970; found: 262.0987.

(b) *Preparation of compound* ***35***

Hydrolysis of the enol ether **30** was accomplished by a procedure identical with that described above. The crude product obtained from 278 mg (1 mmol) of **30** was subjected to column chromatography on 8 g of silica gel. Elution of the column with ethyl acetate, followed by removal (reduced pressure) of the solvent from the appropriate fractions, gave 250 mg (100%) of compound **35** as a colorless oil. Analysis of this material by glc and tlc indicated that it consisted of one component; ir (film): 1710, 1270, 1040 $cm^{-1}$; $^1H$ nmr δ: 1.07 (t, 3H, $J$ = 8 Hz, $CH_3CH_2CO$), 1.08 (d, 3H, $J$ = 8 Hz, secondary methyl group), 2.42–2.88 (m, 3H, $CH_3CH_2CO$ and tertiary proton), 2.90–3.40 (m, 4H, $CH_2COCH_2PO$—), 3.75 (d, 6H, $J_{H-P}$ = 11 Hz, $PO(OCH_3)_2$). *Exact Mass* calcd. for $C_{10}H_{19}O_5P$: 250.0970; found: 250.0965.

(c) *Preparation of compound* ***36***

To a stirred solution of compound **31** (195 mg, 0.5 mmol) in 25 mL of acetone at room temperature was added 0.5 mL of 0.5 *N* hydrochloric acid. After the reaction mixture had been stirred at room temperature for 2 h, it was subjected to a work-up procedure identical with that described above (preparation of compound **34**). The crude product was purified by means of column chromatography on silica gel (8 g). Elution of the column with ethyl acetate, followed by removal (reduced pressure) of the solvent from the appropriate fractions gave 167 mg (92%) of the diketo phosphonate **36** as a colorless oil (one peak by glc analysis and one spot by tlc analysis); ir (film): 1710, 1260, 1025 $cm^{-1}$; $^1H$ nmr δ: 0.98, 1.04 (s, s, 3H each, tertiary methyl groups), ~1.35–3.30 (diffuse, 11H), 3.42–3.64 (m, 4H, ketal methylene protons), 3.81 (d, 6H, $J_{H-P}$ = 11 Hz, $PO(OCH_3)_2$). *Exact Mass* calcd. for $C_{16}H_{27}O_7P$: 362.1494; found: 362.1491.

(d) *Preparation of compound* ***37***

This substance was prepared by hydrolysis of compound **32** via a procedure identical with that described above (preparation of **36**), except that the reaction time was 15 min instead of 2 h. From 229 mg (0.5 mmol) of **32** there was obtained 206 mg (96%) of the diketo phosphonate **37** as a colorless oil which could be crystallized from ether–hexane. Recrystallization provided a pure sample, mp 107–109°C; ir ($CHCl_3$): 1705, 1260, 1030 $cm^{-1}$; $^1H$ nmr (400 MHz) δ: 0.90, 1.03, 1.17 (s, s, s, 3H each, tertiary methyl groups), 1.32–1.85 (diffuse, 8H), 1.94 (d of t, 1H, $J$ = 2, 13 Hz), 2.08 (m, 1H), 2.32–2.43 (m, 2H), 2.97–3.16 (8-line m,

Can. J. Chem. Downloaded from www.nrcresearchpress.com by 210.87.254.105 on 09/06/12
For personal use only.

2H), 3.28–3.65 (m, 6H), 3.80, 3.81 (d, d, 3H each, $J_{H-P}$ = 11 Hz in each case, $PO(OCH_3)_2$). *Exact Mass* calcd. for $C_{21}H_{35}O_7P$: 431.2198; found: 431.2159.

(e) *Preparation of compound 38 (crude)*

To a stirred solution of compound **33** (174 mg, 0.5 mmol) in 15 mL of acetone at room temperature was added 0.5 mL of 0.5 *N* hydrochloric acid. After the resultant mixture had been stirred at room temperature for 35 min, it was subjected to a work-up procedure identical with that described above (preparation of compound **34**). Since the crude product thus obtained contained a small amount of the bicyclic keto ester **39** in addition to the desired product **38**, it was not purified further but was used directly for the next step.

*Intramolecular Horner–Emmons reactions of the diketo phosphonates 34–38*

(a) *Preparation of compound 40*

To a cold (0°C), stirred suspension of sodium hydride (14 mg, 0.6 mmol) in dry DME (2 mL), under an atmosphere of argon, was added, dropwise, a solution of the diketo phosphonate **34** in 1 mL of dry DME. After the reaction mixture had been stirred at room temperature for 30 min, it was warmed to 65°C and kept at that temperature for 1 h. The cooled mixture was poured into aqueous sodium chloride solution and the resultant mixture was extracted thoroughly with ether. The combined extract was washed with water and dried over anhydrous sodium sulfate. Removal of the solvent, followed by distillation (air bath temperature 45°C/0.02 Torr) of the residual oil gave 51 mg (74%) of the bicyclic enone **40** (8) as a colorless liquid (one peak by glc analysis); ir (film): 1700, 1620 $cm^{-1}$; $^1H$ nmr δ: 1.02–2.92 (diffuse, 11H), 5.88 (s, 1H, olefinic proton). *Exact Mass* calcd. for $C_8H_{12}O$: 136.0888; found: 136.0891.

(b) *Preparation of compound 41*

This substance was prepared via a procedure identical with that described above, except that the reaction mixture was stirred at 65°C for 3 h instead of for 1 h. Distillation (air bath temperature 100°C/15 Torr) of the crude product gave 51 mg (82%) of 3-ethyl-4-methyl-2-cyclopenten-1-one (**41**) (25) as a colorless liquid which exhibited one peak by glc analysis; ir (film): 1700, 1610 $cm^{-1}$; $^1H$ nmr δ: 1.20 (t, 3H, $J$ = 7 Hz, $CH_3CH_2$), 1.21 (d, 3H, $J$ = 7 Hz, secondary methyl group), 1.96–2.96 (diffuse, 5H), 5.94 (narrow m, 1H, olefinic proton). *Exact Mass* calcd. for $C_8H_{12}O$: 124.0888; found: 124.0893.

(c) *Preparation of compound 42*

The procedure employed was identical with that used for the preparation of the cyclopentenone **41**, except that the quantities of reactants used were sodium hydride, 9 mg (0.38 mmol) and diketo phosphonate **36**, 118 mg (0.33 mmol). The crude product was subjected to chromatography on 4 g of silica gel. Elution of the column with ethyl acetate produced a light yellow solid which was distilled (air bath temperature 155–160°C/0.05 Torr) to yield 56 mg (72%) of the bicyclo enone **42**. An analytical sample, obtained by recrystallization of this material from ether–hexane, exhibited mp 73–74°C; ir ($CHCl_3$): 1700, 1620 $cm^{-1}$; $^1H$ nmr δ: 1.00, 1.02 (s, s, 3H each, tertiary methyl groups), ~1.2–3.1 (diffuse, 9H), 3.56 (s, 4H, ketal methylene protons), 5.91 (broad s, 1H, olefinic proton). *Exact Mass* calcd. for $C_{14}H_{20}O_3$: 236.1412; found: 236.1422.

(d) *Preparation of compound 43*

This compound was prepared via a procedure identical with that employed for the synthesis of **42**, except that the reaction mixture was maintained at 65°C for 2 h instead of for 3 h. The crude product obtained from 142 mg (0.33 mmol) of the diketo phosphonate **37** was purified by chromatography on 4 g of silica gel. Elution of the column with ethyl acetate – hexane (1:1) gave 86 mg (86%) of the tricyclic enone **43** as a white solid, an analytical sample of which was obtained by recrystallization of this material from ether–hexane, mp 116–117°C; ir ($CHCl_3$): 1680, 1610 $cm^{-1}$; $^1H$ nmr (400 MHz) δ: 0.94, 1.00 (s, s, 3H each, ketal methyl groups), 1.13 (s, 3H, angular methyl group), 1.18 (q of d, 1H, $J$ = 5 Hz, 13 Hz), 1.39–1.67 (diffuse, 6H), 1.73 (q of d, 1H, $J$ = 4, 14 Hz), 1.96 (d of d, 1H, $J$ = 2, 18 Hz), 1.99 (d of t, 1H, $J$ = 3, 13 Hz), 2.18 (m, 1H), 2.34 (d of q, 1H, $J$ = 3, 13 Hz), 2.58 (d of d, 1H, $J$ = 7, 18 Hz), 2.98 (m, 1H), 3.42–3.61 (m, 4H, ketal methylene protons), 5.80 (d, 1H, $J$ = 1.5 Hz, olefinic proton). *Exact Mass* calcd. for $C_{19}H_{28}O_3$: 304.2039; found: 304.2029.

(e) *Preparation of compound 44*

The crude diketo phosphonate **38** (*vide supra*) was subjected to cyclization via a procedure identical with that described above (preparation of **40**), except that the reaction mixture was stirred at 65°C for 2 h instead of for 1 h. Distillation (air bath temperature 110°C/0.05 Torr) of the crude product gave 68 mg (70%, based on the enol ether **33**) of the bicyclic keto ester **44** (colorless oil, one peak by glc analysis and one spot by tlc analysis); ir (film): 1730, 1710, 1625 $cm^{-1}$; $^1H$ nmr δ: ~1.2–2.9 (diffuse, 8H), 2.26, 2.60 (d, d, 1H each, $J$ = 18 Hz, $—CH_2CO$), 3.66 (s, 3H, $CO_2CH_3$), 5.93 (d, 1H, $J$ = 2 Hz, olefinic proton). *Exact Mass* calcd. for $C_{11}H_{14}O_3$: 194.0944; found: 194.0944.

## Acknowledgements

Financial support from the Natural Sciences and Engineering Research Council of Canada and the Natural, Applied, and Health Sciences Grants Committee of the University of British Columbia is gratefully acknowledged. One of us (B.A.) thanks the University of British Columbia for Graduate Fellowships.

1. D. SEEBACH. Angew. Chem. Int. Ed. Engl. **18**, 239 (1979).
2. M. MIYANO and C. R. DORN. J. Org. Chem. **37**, 268 (1972).
3. E. BROWN and M. RAGAULT. Tetrahedron Lett. 1927 (1973).
4. D. A. EVANS, C. L. SIMS, and G. C. ANDREWS. J. Am. Chem. Soc. **99**, 5453 (1977).
5. Y. FUKUYAMA, T. TOKOROYAMA, and T. KUBOTA. Tetrahedron Lett. 4869 (1973).
6. T. CUVIGNY, M. LARCHEVEQUE, and H. NORMANT. Tetrahedron Lett. 1237 (1974).
7. G. STORK and M. E. JUNG. J. Am. Chem. Soc. **96**, 3862 (1974).
8. R. M. JACOBSON, R. A. RATHS, and J. H. MCDONALD III. J. Org. Chem. **42**, 2545 (1977).
9. R. B. MILLER. Synth. Commun. **2**, 267 (1972).
10. D. A. MCCRAE and L. DOLBY. J. Org. Chem. **42**, 1607 (1977).
11. P. E. SUM and L. WEILER. Can. J. Chem. **56**, 2301 (1978).
12. W. G. DAUBEN and D. J. HART. J. Org. Chem. **42**, 3787 (1977).
13. M. MIYASHITA, T. YANAMI, and A. YOSHIKOSHI. J. Am. Chem. Soc. **98**, 4679 (1976).
14. R. M. COATES, L. O. SANDEFUR, and R. D. SMILLIE. J. Am. Chem. Soc. **97**, 1619 (1975).
15. J. E. MCMURRY, A. ANDRUS, G. M. KSANDER, J. H. MUSSER, and M. A. JOHNSON. J. Am. Chem. Soc. **101**, 1330 (1979).
16. R. D. CLARK, L. G. KOZAR, and C. H. HEATHCOCK. Synth. Commun. **5**, 1 (1975).
17. E. PIERS, B. ABEYSEKERA, and J. R. SCHEFFER. Tetrahedron Lett. 3279 (1979).

18. H. NORMANT and G. STURTZ. C. R. Acad. Sci. (Paris), **260**, 1984 (1965).
19. A. MICHAEL and G. H. CARLSON. J. Am. Chem. Soc. **57**, 162 (1935).
20. F. A. COTTON and R. A. SCHUNN. J. Am. Chem. Soc. **85**, 2394 (1963).
21. L. HORNER and E. H. WINKELMANN. Newer methods of preparative organic chemistry. Vol. 3. *Edited by* W. Foerst. Academic Press, New York, NY. 1964. p. 151.
22. J. A. MARSHALL and G. A. FLYNN. Synth. Commun. **9**, 123 (1979).
23. P. WIELAND and K. MIESCHER. Helv. Chim. Acta, **33**, 2215 (1950); S. RAMACHANDRAN and M. S. NEWMAN. Org. Synth. **41**, 38 (1961).
24. P. A. GRIECO and C. S. POGONOWSKI. Synthesis, 425 (1973).
25. J.-M. CONIA and M.-L. LERIVEREND. Bull. Soc. Chim. Fr. 2981 (1970).
26. W. K. BORNACK, S. S. BHAGWAT, J. PONTON, and P. HELQUIST. J. Am. Chem. Soc. **103**, 4647 (1981).
27. H.-J. ALTENBACH. Angew. Chem. Int. Ed. Engl. **18**, 940 (1979).
28. M. J. BEGLEY, K. COOPER, and G. PATTENDEN. Tetrahedron Lett. **22**, 257 (1981).
29. D. K. KLIPA and H. HART. J. Org. Chem. **46**, 2815 (1981).

Can. J. Chem. Downloaded from www.nrcresearchpress.com by 210.87.254.105 on 09/06/12
For personal use only.

# Syntheses of condensed imidazoles by lead tetraacetate oxidation of amidines

S. CHAUDHURY, A. DEBROY, AND M. P. MAHAJAN[1]

*Department of Chemistry, North-Eastern Hill University, Shillong 793 003, India*

Received September 23, 1981

S. CHAUDHURY, A. DEBROY, and M. P. MAHAJAN. Can. J. Chem. **60**, 1122 (1982).

2-Phenylbenzimidazoles, 2-benzylbenzimidazoles, 2-phenyl-1*H*-naphtho[1,2-*d*]imidazole, and 2-benzyl-1*H*-naphtho[1,2-*d*]-imidazole have been synthesized in excellent yields (77–98%) by lead tetraacetate oxidation of suitable *N*-arylbenzamidines, *N*-arylphenylacetamidines, *N*-α-naphthylbenzamidine, and *N*-α-naphthylphenylacetamidine respectively. The mechanism of nitrene insertion and intramolecular competitive nitrene insertion leading to these heterocycles has also been discussed.

S. CHAUDHURY, A. DEBROY et M. P. MAHAJAN. Can. J. Chem. **60**, 1122 (1982).

On a synthétisé, avec d'excellents rendements (77–98%), les composés suivants: phényl-2 benzimidazoles, benzyl-2 benzimidazoles, phényl-2 1*H*-naphtho[1,2-*d*] imidazole et benzyl-2 1*H*-naphtho[1,2-*d*] imidazole par l'oxydation, au moyen du tétraacétate de plomb, des composés suivants convenablement choisis: *N*-arylbenzamidines, *N*-arylphénylacétamidines, *N*-α napthylbenzamidine et *N*-α naphthylphénylacétamidine respectivement. On discute également des mécanismes d'insertion du nitrène et d'insertion intramoléculaire compétitive du nitrène conduisant à ces hétérocycles.

[Traduit par le journal]

Because of the increasing importance of benzimidazoles, a simpler approach to the synthesis of these heterocyclics was thought to be of great value. The procedure for the synthesis of benzimidazoles usually involves the condensation of *o*-phenylenediamine or *o*-nitroaniline with a carboxylic acid derivative. In each case, the cyclization involves coupling at the *o*-phenylene nitrogens.

Since *N*-arylamidines are easily available (1–3), it appeared that substituted amidines could be potential precursors for the synthesis of benzimidazoles, if they could be induced to cyclize by some oxidative means. The formation of benzimidazoles from *N*-arylamidines was first reported by Partridge and Turner and required the prior conversion of *N*-arylamidines to *N*-hydroxy amidines (4). Later on it was found that *N*-arylamidine hydrochlorides could be transformed into benzimidazoles with one mole of sodium hypochlorite and base (5, 6). Often the yields of *N*-chloro derivatives are unsatisfactory, which in turn is reflected in lower yields of benzimidazoles.

We report here the syntheses of various 2-phenyl and 2-benzyl condensed imidazoles, in excellent yields (77–98%), by lead tetraacetate (LTA) oxidation of suitable amidines (Schemes 1–3). The object of the present investigation has also been to explore intramolecular competitive nitrene insertions and the nitrene insertion mechanism leading to these heterocycles.

In the case of LTA oxidation of *N*-*o*-tolylbenzamidine, where there is a possibility of nitrene insertion into both the C—H bond of methyl and the C—H bond of phenyl, insertion takes place exclusively into the C—H bond of phenyl. This is perhaps due to the aromatic stabilization of the benzimidazole ring formed by insertion into the phenyl C—H bond, which is not the case with dihydroquinazoline formed by insertion into the methyl C—H bond (Scheme 2). Similarly, in the case of oxidation of *N*-*m*-chlorophenylbenza-

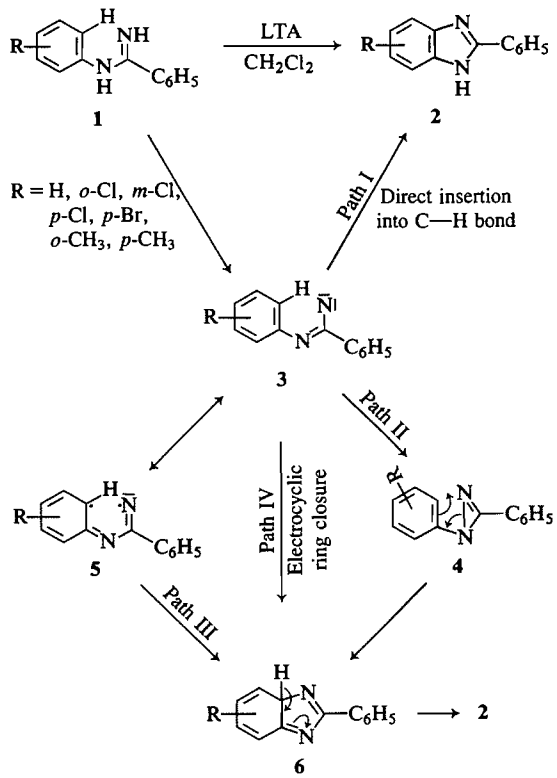


SCHEME 1

[1]Author to whom all correspondence should be addressed.

0008-4042/82/091122-05$01.00/0

©1982 National Research Council of Canada/Conseil national de recherches du Canada

Can. J. Chem. Downloaded from www.nrcresearchpress.com by 210.87.254.6 on 09/06/12
For personal use only.

Can. J. Chem. Downloaded from www.nrcresearchpress.com by 210.87.254.6 on 09/06/12
For personal use only.

midine there exists a possibility of nitrene insertion into the C—H bond either *ortho* or *para* to chlorine. The product formed in this case is 4(7)-chloro-2-phenylbenzimidazole (**7**) confirmed by its superimposable ir spectrum and undepressed mixture melting point with the product obtained by oxidation of *N*-*o*-chlorophenylbenzamidine. This observation indicates that the nitrene insertion has taken place into the C—H bond *ortho* to chlorine (Scheme 2).

In the case of LTA oxidations of *N*-arylphenylacetamidines in refluxing dichloromethane, the yield of the 2-benzylbenzimidazoles was always between 20–30%. The tlc of the reaction mixture, even on addition of excess of LTA (2 equiv.), always showed the presence of unreacted amidine. A number of futile attempts were made to improve the yields of 2-benzylbenzimidazoles, e.g., by carrying out the oxidation (*i*) in refluxing benzene; (*ii*) in acetic acid. In the case of oxidation with LTA/acetic acid, 2-benzylbenzimidazole was not formed at all. It was concluded that the acetic acid was perhaps protonating amidine and inhibiting the attack of nitrogen on lead of LTA. With this in mind pyridine was used as a scavenger for acetic acid and oxidations of *N*-arylphenylacetamidines with LTA/$CH_2Cl_2$/pyridine gave excellent yields (85–98%) of 2-benzylbenzimidazoles.[2]

In the case of LTA oxidations of *N*-arylphenylacetamidines (**8**), there exists a possibility of nitrene insertion into a C—H bond of either of the two phenyl groups. But the intermediate azomethine nitrene (**9**), in this case, appears to be highly selective in undergoing cyclization leading to 2-benzylbenzimidazoles (Scheme 3).

In the case of LTA oxidation of *N*-*o*-tolylphenylacetamidine the product obtained was also that of nitrene insertion into the phenyl C—H bond. The oxidation of *N*-*m*-chlorophenylphenylacetamidine gave the same product as obtained by oxidation of *N*-*o*-chlorophenylphenylacetamidine, indicating again that the nitrene insertion has taken place into the phenyl C—H bond which is *ortho* to chlorine.

This oxidation method was extended to the synthesis of 2-phenyl-1*H*-naphtho[1,2-*d*]imidazole[3] and 2-benzyl-1*H*-naphtho[1,2-*d*]imidazole by the oxidation of *N*-α-naphthylbenzamidine and N-α-naphthylphenylacetamidine with LTA/$CH_2$-

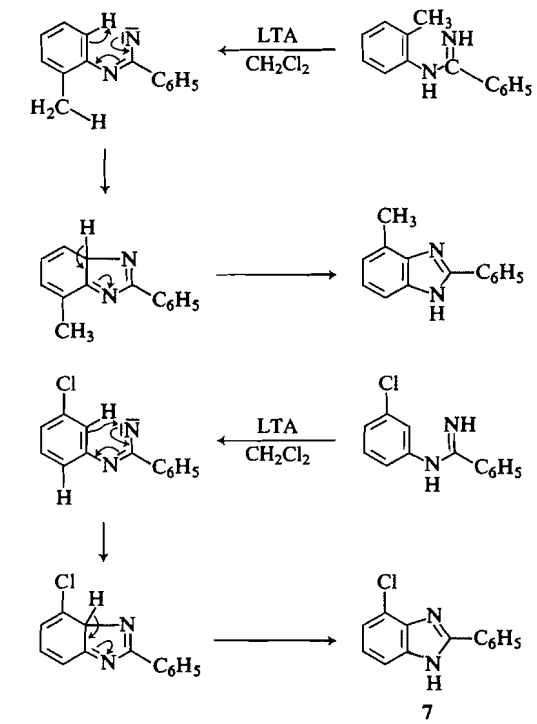


SCHEME 2

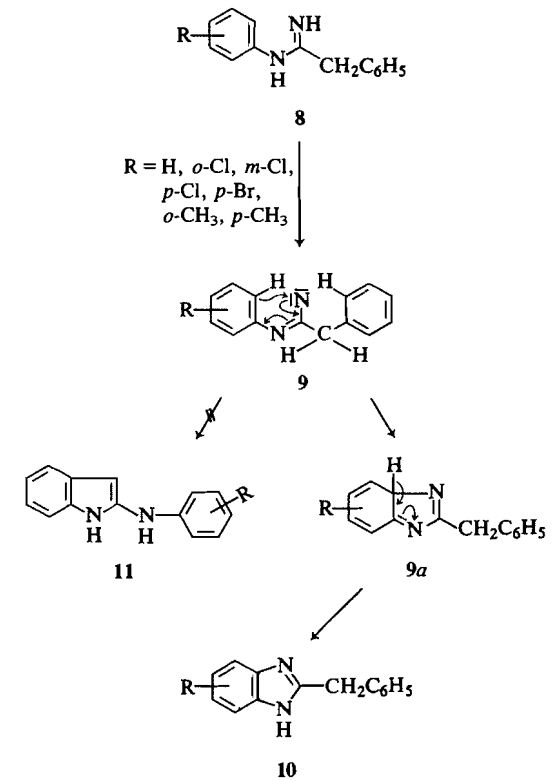


SCHEME 3

[2]Yield of 2-benzylbenzimidazole by the method of Haruki *et al.* (14) is only 36%.

[3]The yield of 2-phenyl-1*H*-naphtho[1,2-*d*]imidazole by the method of Haruki *et al.* (14) is only 24%.

Can. J. Chem. Downloaded from www.nrcresearchpress.com by 210.87.254.6 on 09/06/12
For personal use only.

$Cl_2$/pyridine. It may be mentioned here that LTA oxidation of *N*-α-naphthylbenzamidine in refluxing dichloromethane gave only about 30% of the product and the yield improved tremendously by carrying out the oxidation in the presence of pyridine.

In the case of oxidation of *N*-arylbenzamidines (**1**), the probable intermediate azomethine nitrene (**3**) may lead to 2-phenylbenzimidazoles (**2**) by any of the four paths shown in Scheme 1. The probable intermediate **3** may lead to 2-phenylbenzimidazoles (**2**) by direct insertion of nitrene into the C—H bond (Path I); it may lead to imidazole ring formation by ring expansion of the diazirine intermediate **4** (Path II); the resonance stabilization of the azomethine nitrene **3** may lead to 2-phenylbenzimidazoles via intermediates **5** and **6** (Path III); or the intermediate **3** may, via the electrocyclic ring closure to intermediate **6**, lead to **2** (Path IV).

The biradical mechanism involved in Path III may be ruled out because it has been shown by Lwowski and others that acylnitrenes, to which **3** bears a more than superficial resemblance, insert into C—H as singlets (7–11)

Direct insertion (Path I) may be ruled out of the other alternatives, and the electrocyclic ring closure mechanism (Path IV) favoured, on the basis of the following observations.

(*i*) As already pointed out in the case of LTA oxidations of *N*-arylphenylacetamidines (**8**), there exists a possibility of nitrene insertion into a C—H bond of either of two phenyl groups. Direct nitrene insertion would lead to 2-benzylbenzimidazoles (**10**) or 2-anilinoindoles (**11**), both of which possess aromatic stabilization. But the intermediate **9** appears to be highly selective in undergoing cyclization leading to 2-benzylbenzimidazoles rather than 2-anilinoindoles (Scheme 3). This discrimination between two possible ring closures may be attributed to electron delocalization[4] in an intermediate azomethine nitrene (**9**), indicating the preference for reaction Path IV for the formation of these benzimidazoles via **9***a*.

(*ii*) In the case of oxidation of *N*-*m*-chlorophenylbenzamidine and *N*-*m*-chlorophenylphenylacetamidine, insertion of nitrene takes place *ortho* to chlorine, though insertion at the *para* position should be favoured for steric reasons. This can also be explained by a delocalization mechanism, i.e., Path IV is favoured and insertion at the *ortho* position takes place because of the pull of electrons towards chlorine due to its inductive effect.

[4]This kind of electron delocalization is absent for the formation of 2-anilinoindoles (**11**).

(*iii*) In the case of oxidation of *N*-*o*-tolylbenzamidine the exclusive formation of 4(7)-methyl-2-phenylbenzimidazole can also be explained by this electrocyclic ring closure mechanism (Path IV).

Further work on such reactions in the presence of various 1,3-dipolarophiles, in order to trap the nitrene intermediate and to look into its spin multiplicities, is in progress.

## Experimental

All the mp's are uncorrected. The ir spectra were recorded on a Perkin–Elmer Model 297 ir spectrometer. The nmr traces were recorded on a Varian EM-390 90 MHz nmr spectrometer.

The following *N*-arylbenzamidines and *N*-arylphenylacetamidines, with yields (%), mp (°C), (lit. mp (°C)), and (reference) were prepared by the reported methods (2, 3). *N*-phenylbenzamidine, 75, 113–114 (116) (12); *N*-phenylphenylacetamidine, 70, 134–135 (133–135) (13); *N*-*o*-tolylbenzamidine, 98, 102–103; *N*-*o*-tolylphenylacetamidine, 71, 107–108; *N*-*p*-tolylbenzamidine, 76, 99–100, (100.5–101) (12); *N*-*p*-tolylphenylacetamidine, 84, 117–118 (119) (12); *N*-*o*-chlorophenylbenzamidine, 85, 109–110; *N*-*o*-chlorophenylphenylacetamidine, 42, 109–110 (111–112) (12); *N*-*m*-chlorophenylbenzamidine, 34, 106–107; *N*-*m*-chlorophenylphenylacetamidine, 82, 87–88; *N*-*p*-chlorophenylbenzamidine, 99, 116–119; *N*-*p*-chlorophenylphenylacetamidine, 68, 114–115; *N*-*p*-bromophenylbenzamidine, 65, 115–116; *N*-*p*-bromophenylphenylacetamidine, 57, 119–120; N-α-naphthylbenzamidine, 54, 139–140 (140–142) (14); *N*-α-naphthylphenylacetamidine, 39, 123–124.

*LTA oxidation of* N-*phenylbenzamidine*

To a stirred solution of *N*-phenylbenzamidine (1.96 g, 0.01 mol) in dichloromethane (25 mL) was added LTA (4.88 g, 0.011 mol) in small portions over 15 min. After the complete addition of LTA, the reaction mixture was refluxed for 1½ hours. After careful removal of the solvent, the reaction mixture was treated with hot benzene and filtered. The filtrate was then washed with water and dried over anhydrous sodium sulphate. The solvent was removed under reduced pressure and the 2-phenylbenzimidazole (1.73 g; 89%), obtained on addition of a mixture (1:1) of benzene and hexane to the residue, was recrystallized from a mixture (9:1) of benzene and ethanol; mp. 288–289°C (lit. (14) mp 289–290°C); ir (Nujol) $\nu_{max}$: 3400 (weak broad band, $\nu_{N-H}$), 2960, 2920, 2860 ($\nu_{C-H}$), 1590, 1540, 1495 (v. weak), 1465, 1445 ($\nu_{C=C}$ and $\nu_{C=N}$). (These ir bands are common in all the 2-arylbenzimidazoles reported in this paper). *Anal.* calcd. for $C_{13}H_{10}N_2$: C 80.41, H 5.16, N 14.43%; found: C 80.77, H 5.09, N 13.94%. Mol. Wt. calcd.: 194; found (ms): 194.

Other 2-phenylbenzimidazoles (Table 1, 2–6) were obtained similarly by LTA oxidation of the corresponding *N*-arylbenzamidines.

*LTA oxidation of* N-*phenylphenylacetamidine*

To a stirred solution of *N*-phenylphenylacetamidine (2.10 g; 0.01 mol) in dichloromethane (25 mL) and pyridine (8 mL) was added LTA (4.88 g; 0.011 mol) in small portions in about 15 min. After the complete addition of LTA, the reaction mixture was heated in an oil bath (80–90°C) for 1½ hours. The solvent was then removed under reduced pressure and the residue so obtained was extracted with hot benzene. The benzene extracts were washed with water and dried over anhydrous sodium sulphate. The solvent was then removed under reduced pressure and the 2-benzylbenzimidazole (1.89 g; 90%), obtained on addition of a mixture (1:1) of benzene and hexane, was

Can. J. Chem. Downloaded from www.nrcresearchpress.com by 210.87.254.6 on 09/06/12
For personal use only.

TABLE 1. Condensed 2-phenylbenzimidazoles

| No. | Name of the compound[a,b] | Melting point °C (lit. mp) (ref) | Yield (%) | Nuclear magnetic resonance spectrum (δ)[c] |
|---|---|---|---|---|
| 1. | 2-Phenylbenzimidazole | 288–289 (289–290) (14) | 89 | 3.20 (b, 1H, —N(H)—) and 7.60 (m, 9H, aromatic) |
| 2. | 4(7)Methyl-2-phenylbenzimidazole | 246–247 (247–248) | 77 | 2.45 (s, 3H, $-CH_3$), 3.22 (b, 1H, —N(H)—), and 7.60 (m, 8H, aromatic) |
| 3. | 5(6)Methyl-2-phenylbenzimidazole | 241–242 (241–243) (15) | 77 | 2.42 (s, 3H, $-CH_3$), 3.10 (b, 1H, —N(H)—), and 7.55 (m, 8H, aromatic) |
| 4. | 5(6)Chloro-2-phenylbenzimidazole | 209–210 (210–212) (15) | 83 | 3.65 (b, 1H, —N(H)—) and 7.65 (m, 8H, aromatic) |
| 5. | 4(7)Chloro-2-phenylbenzimidazole | 226–227 | 78 | 2.90 (b, 1H, —N(H)—) and 7.60 (m, 8H, aromatic) |
| 6. | 5(6)Bromo-2-phenylbenzimidazole | 201–202 | 77 | 3.45 (b, 1H, —N(H)—) and 7.65 (m, 8H, aromatic) |
| 7. | 2-Phenyl-1*H*-naphtho[1,2-*d*]imidazole | 213–214 (215–216) (14) | 83 | 3.50 (b, 1H, —N(H)—) and 7.90 (m, 12H, aromatic) |

[a]Satisfactory elemental analysis was found for all these compounds.
[b]All these compounds were recrystallized from a mixture (9:1) of benzene and ethanol.
[c]The nmr spectra were taken in $CDCl_3$ with the minimum amount of added DMSO $d_6$.

TABLE 2. Condensed 2-benzylbenzimidazoles

| No. | Name of the compound[a] | Melting point °C (lit. mp) (ref) | Yield (%) | Nuclear magnetic resonance spectrum ($CDCl_3$) δ: |
|---|---|---|---|---|
| 1. | 2-Benzylbenzimidazole | 182–183 (183–184) (14) | 90 | 4.20 (s, 2H, $-CH_2-$), 5.30 (b, 1H, —N(H)—), and 7.30 (m, 9H, aromatic) |
| 2. | 2-Benzyl-4(7)-methylbenzimidazole | 163 | 98 | 2.50 (s, 3H, $-CH_3$), 4.15 (s, 2H, $-CH_2-$), and 7.35 (m, 9H, aromatic and —N(H)—) |
| 3. | 2-Benzyl-5(6)-methylbenzimidazole | 146–147 | 95 | 2.40 (s, 3H, $-CH_3$), 4.10 (s, 2H, $-CH_2-$), and 7.15 (m, 9H, aromatic and —N(H)—) |
| 4. | 2-Benzyl-4(7)-chlorobenzimidazole | 182 | 88 | 4.22 (s, 2H, $-CH_2-$) and 7.25 (m, 9H, aromatic and —N(H)—) |
| 5. | 2-Benzyl-5(6)-chlorobenzimidazole | 172–173 | 96 | 4.05 (s, 2H, $-CH_2-$) and 7.15 (m, 9H, aromatic and —N(H)—) |
| 6. | 2-Benzyl-5(6)-bromobenzimidazole | 179–180 | 86 | 4.18 (s, 2H, $-CH_2-$) and 7.50 (m, 9H, aromatic and —N(H)—) |
| 7. | 2-Benzyl-1*H*-naphtho[1,2-*d*]imidazole | 185–186 | 81 | 4.10 (s, 2H, $-CH_2-$) and 7.65 (m, 13H, aromatic and —N(H)—) |

[a]Satisfactory elemental analysis was found for all these compounds. All these compounds were recrystallized from benzene.

recrystallized from benzene, mp 182–183°C (lit. (14) mp 183–184°C). *Anal.* calcd. for $C_{14}H_{12}N_2$: C 80.77, H 5.77, N 13.46%; found: C 81.36, H 5.60, N 12.84%.

Other 2-benzylbenzimidazoles (Table 2, 2–6), 2-benzyl-*1H*-naphtho[1,2-*d*]imidazole (Table 2, 7), and 2-phenyl-*1H*-naphtho[1,2-*d*]imidazole (Table 1, 7) were prepared similarly by the LTA/$CH_2Cl_2$/pyridine oxidation of the corresponding *N*-arylphenylacetamidines, *N*-α-naphthylphenylacetamidine, and *N*-α-naphthylbenzamidine respectively.

## Acknowledgements

The authors are grateful to Mr. B. Myrboh and Mrs. Jacob of N.E.H.U., Shillong, for recording of the spectral data.

1. R. L. SHRINER and F. W. NEUMANN. Chem. Rev. **35**, 351 (1944).
2. P. OXLEY and W. F. SHORT. J. Chem. Soc. **69**, 449 (1949).
3. P. OXLEY, M. W. PARTRIDGE, and W. F. SHORT. J. Chem. Soc. 1110 (1947).
4. M. W. PARTRIDGE and H. A. TURNER. J. Chem. Soc. 2086 (1958).
5. V. J. GRENDA, R. E. JONES, G. GAL, and M. SLETZINGER. J. Org. Chem. **30**, 259 (1965).
6. S. PATAI. The chemistry of amidines and imidates. John Wiley & Sons, New York. 1975. p. 321.
7. W. LWOWSKI and T. W. MATTINGLY. J. Am. Chem. Soc. **87**, 1947 (1965).
8. J. S. MCCONAGHY and W. LWOWSKI. J. Am. Chem. Soc. **89**, 2357 (1967).
9. I. BROWN and O. E. EDWARDS. Can. J. Chem. **45**, 2599 (1967).
10. S. YAMADA, S. TERASHIMA, and K. ACHIWA. Chem. Pharm. Bull. Jpn. **13**, 751 (1965).
11. W. LWOWSKI and S. LINKE. Justus Liebigs Ann. Chem. 8 (1977).
12. P. OXLEY and W. F. SHORT. J. Chem. Soc. 149 (1946).
13. F. C. COOPER and M. W. PARTRIDGE. J. Chem. Soc. 259 (1953).
14. E. HARUKI, T. INAIKI, and E. IMOTO. Bull. Chem. Soc. Jpn. **41**, 1361 (1968).
15. J. I. G. CADOGAN, R. MARSHALL, D. M. SMITH, and M. J. TODD. J. Chem. Soc. 2441 (1970).

Can. J. Chem. Downloaded from www.nrcresearchpress.com by 210.87.254.6 on 09/06/12
For personal use only.

# The mechanism of electrochemical reduction of *N*-haloamides in acetonitrile: trapping of intermediate amide anions and father–son protonation[1,2]

DENIS BÉRUBÉ[3] AND JEAN LESSARD

*Département de chimie, Université de Sherbrooke, Sherbrooke (Qué.), Canada J1K 2R1*

Received September 8, 1981

DENIS BÉRUBÉ and JEAN LESSARD. Can. J. Chem. **60**, 1127 (1982).

The electrochemical reduction of *N*-haloamides (ZCONRX) in acetonitrile involves two consecutive one-electron transfers and generates the amide anion. Attempts to trap the intermediate amidyl radical resulting from the first electron transfer were unsuccessful. In the case of the N-*halo*-N-*hydroamides* (R = H), the amide anion formed at the electrode abstracts a proton from an incoming *N*-halo-*N*-hydroamide molecule to give the parent amide and the conjugate base of the *N*-haloamide (father–son protonation). Thus, half of the *N*-halo-*N*-hydroamide reaching the electrode is reduced, the other half being converted to its conjugate base. In acetonitrile–$LiClO_4$ (0.2 *M*) containing 0.2% water, the conjugate base is reducible and the polarograms therefore show two waves (irreversible and diffusion controlled) of *equivalent intensities* due respectively to the reduction of the *N*-halo-*N*-hydroamide and to the reduction of its conjugate base. In the case of the N-*chloro*-N-*alkyl(aryl)amides* (X = Cl, R = alkyl or aryl), the amide anion abstracts a proton from the medium to give the parent amide and anionic species that react with the starting *N*-chloroamide regenerating the amide anion. Hence, the coulometric results are low (≃ 0.5 F/mol). However, in the presence of acetic acid, the reduction consumes 2 F/mol as expected. The *N*-alkylamide anion has been trapped by *N*-alkylation and *N*-acylation. The voltammograms of *N*-chloro-*N*-alkyl(aryl)amides show multiple waves on mercury and platinum due to passivation–adsorption phenomena but a single wave on vitreous carbon.

DENIS BÉRUBÉ et JEAN LESSARD. Can. J. Chem. **60**, 1127 (1982).

La réduction électrochimique des *N*-haloamides (ZCONRX) fait intervenir deux transferts consécutifs d'un électron et conduit à l'anion de l'amide. Le radical amidyl résultant du transfert du premier électron n'a pu être piégé. Dans le cas des N-*halo*-N-*hydroamides* (R = H), l'anion de l'amide est protoné par le *N*-halo-*N*-hydroamide arrivant à l'électrode pour donner l'amide et la base conjuguée du *N*-haloamide (protonation père-fils). Ainsi, la moitié du *N*-halo-*N*-hydroamide atteignant l'électrode est réduite et l'autre moitié est convertie en sa base conjuguée. Dans le milieu acétonitrile–$LiClO_4$ (0.2 *M*) contenant 0.2% d'eau où la base conjuguée du *N*-halo-*N*-hydroamide peut être réduite, les polarogrammes montrent donc deux vagues (irréversibles et contrôlées par la diffusion) d'*intensités égales*; la première est due à la réduction du *N*-halo-*N*-hydroamide et la deuxième à la réduction de sa base conjuguée. Dans le cas des N-*chloro*-N-*alkyl(aryl)amides* (X = Cl, R = alkyl ou aryl), l'anion de l'amide abstrait un proton du milieu pour donner l'amide et des espèces anioniques qui réagissent avec le *N*-chloroamide de départ pour regénérer l'anion de l'amide, ce qui conduit à des coulométries observées faibles (≃ 0.5 F/mol). Cependant, en présence d'acide acétique, la coulométrie est de l'ordre de 2 F/mol tel qu'attendu. L'anion des *N*-alkylamides a été piégé par *N*-alkylation et *N*-acylation. Les voltammogrammes des *N*-chloro-*N*-alkyl(aryl)amides montrent plus d'une vague sur électrodes de mercure et de platine à cause de phénomènes d'adsorption mais ne révèlent qu'une seule vague sur carbone vitreux.

Our previous work (1) on the electrochemical reduction of *N*-haloamides (ZCONRX) led us to the conclusion that the reduction involves two consecutive one-electron steps as described by reactions [1] and [2] and that the intermediate amidyl radical (step [1]) might have been captured by intramolecular hydrogen abstraction. We now report further studies on the mechanism of electroreduction of *N*-halo-*N*-hydroamides (R = H) and *N*-halo-*N*-alkyl(aryl)amides (R = alkyl or aryl) in acetonitrile which show clearly that the reduction leads to the amide anion (reactions [1] and [2]). No evidence for the trapping of the electrochemically generated amidyl radical (step [1]) could be obtained.

$$[1]\quad ZCONRX + e^- \xrightarrow{\text{slow}} ZCO\dot{N}R + X^-$$

$$[2]\quad ZCO\dot{N}R + e^- \xrightarrow{\text{fast}} ZCO\bar{N}R$$

## Results and discussion

### N-*Halo*-N-*hydroamides (ZCONHX)*

#### *Polarographic studies*

*Amperometric titrations*: As reported in the previous paper (1), the polarograms of *N*-halo-*N*-hydroamides show two irreversible and diffusion-controlled reduction waves in methanol as well as in acetonitrile using lithium perchlorate (0.2 *M*) as supporting electrolyte.[4] For instance, in the case of *N*-chlorourethane (NCU) (**1***a*), $(E_{1/2})_1 = -0.60$ V and $(E_{1/2})_2 = -0.96$ V vs. a saturated calomel

[1]Part II in the series "Electroreduction of *N*-haloamides". For part I, see ref. 1.

[2]Taken from the Ph.D. Thesis of D. Bérubé, Université de Sherbrooke, Sherbrooke, Qué, 1979.

[3]NRCC (1977–1978) and Ministère de l'Education du Québec (1975–1976) predoctorate fellow. Present address: Chemistry Division, National Research Council of Canada, Ottawa, Ont., Canada K1A 0R6.

[4]Unless specified otherwise, the acetonitrile–$LiClO_4$ (0.2 *M*) medium contains about 0.2% of water (≃ 0.1 *M*).

0008-4042/82/091127-16$01.00/0

©1982 National Research Council of Canada/Conseil national de recherches du Canada

Can. J. Chem. Downloaded from www.nrcresearchpress.com by 210.87.254.105 on 09/06/12
For personal use only.

Can. J. Chem. Downloaded from www.nrcresearchpress.com by 210.87.254.105 on 09/06/12
For personal use only.

electrode (sce)[5] in methanol and, in acetonitrile, $(E_{1/2})_1 = -0.22$ V and $(E_{1/2})_2 = -1.22$ V (1). *The limiting currents of the two waves are nearly equivalent in both solvents:* $I_1 \simeq I_2$. Upon adding 1 equiv. (or more) of a base such as the methoxide anion, the *N*-halo-*N*-hydroamide (**1**) is converted to its conjugate base **2** (reaction [3])[6] and the first

[3] $\underset{\mathbf{1}}{\text{ZCONXH}} + \text{CH}_3\text{O}^- \longrightarrow \underset{\mathbf{2}}{\text{ZCON}^-\text{X}} + \text{CH}_3\text{OH}$

wave disappears; the limiting current of the second wave is then nearly twice that in the neutral medium ($I \simeq 2I_2$ or $I \simeq I_1 + I_2$). This is illustrated in Fig. 1 (part *A*) in the case of *N*-bromoacetamide (NBA) (**1***b*). When acetic acid is added to the resulting solution (Fig. 1, part *B*), the excess of base is neutralized first, then the addition of about 1 equiv. of acid regenerates the neutral medium with its two equivalent waves ($I_1 \simeq I_2$); the addition of a second equivalent (or more) of acid causes the disappearance of the second wave, the limiting current of the first wave being now nearly twice that in the neutral medium ($I \simeq 2I_1$ or $I \simeq I_1 + I_2$). The lithium salts **2** of some *N*-halo-*N*-hydroamides have been obtained independently as solids (1). When dissolved in acetonitrile–$LiClO_4$ (0.2 *M*), they show the second wave only; upon addition of acetic acid, they behave as the lithium salts obtained *in situ*: compare Fig. 1, part *B*, and Fig. 2.[7]

The amperometric titrations just described show that the first wave must correspond to the reduction of the *N*-halo-*N*-hydroamide **1** and the second wave, to the reduction of its conjugate base **2** as previously proposed (1). However, no explanation was given for the equivalence of the limiting

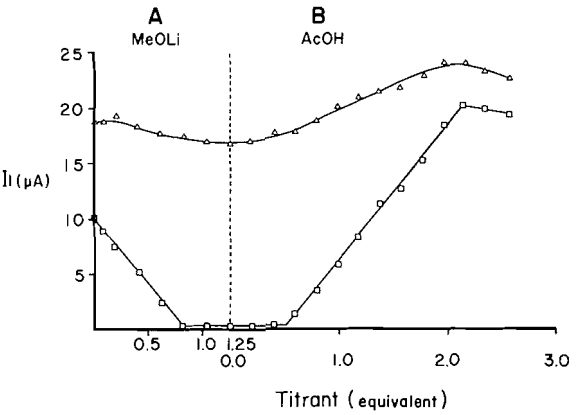


FIG. 1. Amperometric titration of NBA (**1***b*) (3.3 m*M*) in acetonitrile–$LiClO_4$ (0.2 *M*) at 0°C. The addition of lithium methoxide (part A) is followed by that of acetic acid (part B): □, limiting current of the first wave ($I_1$); △, total limiting current ($I_1 + I_2$).

currents of the two waves ($I_1 \simeq I_2$) in a neutral medium (1). The equivalence is due to the fact that the two-electron cleavage of the >N—X bond leads to the amide anion **3** (reaction [4] which is the sum of reactions [1] and [2] where R = H) which then abstracts a proton from an incoming molecule of *N*-halo-*N*-hydroamide **1** to give the parent amide and the conjugate base **2** of the *N*-haloamide **1** (reaction [5]). The amide anion **3** is a much stronger base than **2**[8] and the proton exchange must be fast enough to prevent the incoming molecules of *N*-halo-*N*-hydroamide **1** to reach the electrode (see below). Reaction [5] constitutes a clear-cut example of a *father–son protonation* (4) and other cases of such reactions can be found in the literature (5, 6). Reaction [6] represents the sum of reactions [4]

[4] $\underset{\mathbf{1}}{\text{ZCONHX}} + 2e^- \longrightarrow \underset{\mathbf{3}}{\text{ZCON}^-\text{H}} + \text{X}^-$

[5] $\underset{\mathbf{3}}{\text{ZCON}^-\text{H}} + \underset{\mathbf{1}}{\text{ZCONHX}} \longrightarrow \text{ZCONH}_2 + \underset{\mathbf{2}}{\text{ZCON}^-\text{X}}$

[6] $\underset{\mathbf{1}}{2\text{ZCONHX}} + 2e^- \longrightarrow \text{ZCONH}_2 + \underset{\mathbf{2}}{\text{ZCON}^-\text{X}} + \text{X}^-$

and [5] and it shows clearly that at the first wave potential, only *half* of the *N*-halo-*N*-hydroamide **1** reaching the electrode is reduced, the other half being converted to its conjugate base **2** (not reduced at the first wave level). Similarly, at the second wave potential where the reduction of **2** does occur, only *half* of the *N*-halo derivative **1** reaching the electrode is converted to **2**, the other half being

[5]All the potentials reported in this paper were measured with respect to an aqueous saturated calomel electrode (sce).

[6]The $pK_a$ of $CH_3OH$ is close to 16 and that of ZCONHZ varies between 2.9 and 8.0 in water, 3.6 and 10.2 in 75% ethanol, depending on Z and X (2), so the equilibrium constant of reaction [3] must be large (e.g. $K_{eq.} \simeq 10^8$ for NCU in water) in methanol and acetonitrile as well.

[7]For the amperometric titration of NCU (**1***a*) in methanol (1), it took exactly 1 mol sodium methoxide to generate the conjugate base (disappearance of the first wave) and exactly 1 mol acetic acid to cause the disappearance of the second wave. The titration of the lithium salt **2***a* of NCU in acetonitrile with acetic acid is also exact (Fig. 2). However, in the case of NBA (**1***b*), less than 1 equiv. lithium methoxide (≃ 0.85 equiv.; Fig. 1, part *A*) was needed to convert NBA to its conjugate base **2***b*. This can be accounted for by the partial decomposition of **2***b* (e.g. Hoffmann degradation). Consequently, the amount of acetic acid needed to neutralize **2***b* (Fig. 1, part *B*) was also less than 1 equiv. (≃ 0.8 equiv.). It can be seen from Fig. 1 and Fig. 2 that the total limiting current ($I_1 + I_2$) varies during the titration and this can be attributed to differences in the diffusion coefficients of the *N*-halo-*N*-hydroamide **1** and of its conjugate base **2**.

[8]For instance, the $pK_a$ of $CH_3CONH_2$ is 15 (3) and that of NBA in water is 7.89 (2) which would give $K_{eq} \simeq 10^7$ for reaction [5].

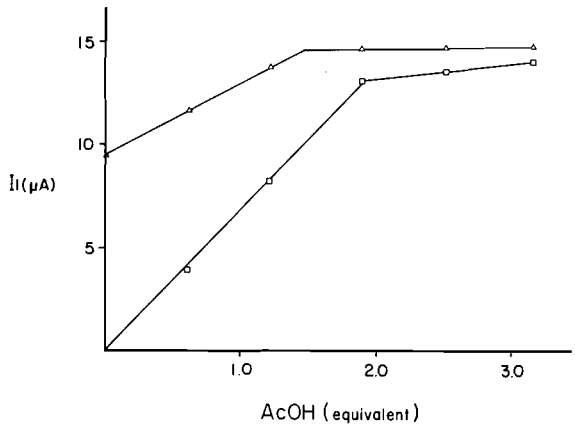


FIG. 2. Amperometric titration of the lithium salt of NCU (1.41 m*M*) in acetonitrile–$LiClO_4$ (0.2 *M*) with acetic acid: □, limiting current of the first wave ($I_1$); △, total limiting current ($I_1 + I_2$).

converted to the electroinactive parent amide $ZCONH_2$. Hence $I_1 \simeq I_2$.

In order to verify that proton exchange (reaction [5]) can be fast in acetonitrile, even when dry, we studied the polarographic behavior of a mixture of *N*-chlorosuccinimide (NCS) (**4**) and *N*-fluorourethane (NFU) (**1***c*) in dry acetonitrile[9] using tetraethylammonium perchlorate (TEAP) (0.1 *M*) as supporting electrolyte. The polarogram of NCS in that medium shows one wave ($E_{1/2} = -0.12$ V) described by reaction [7]. When NFU was added, we could not observe its reduction wave ($E_{1/2} = -1.81$ V) until more than 1 equiv. with respect to NCS had been added. This is because 1 equiv. of NFU is used to protonate the conjugate base of NCS (eq. [8])[10] produced near the electrode (reaction [7]). Reaction [9] represents the sum of reactions [7] and [8] and it shows that when 1 equiv. (or less) of NFU is present, all the incoming NFU is converted to its electroinactive conjugate base.[11] Therefore, the proton-transfer reaction [8] is fast enough to prevent the NFU to reach the electrode.

The effect of the father–son reaction [5] should be eliminated by adding to the medium, in sufficient amount (1 equiv. or more), an acid which is stronger than the *N*-halo-*N*-hydroamide **1**. Indeed, in the case of NCU (**1***a*) with a $pK_a$ of 8.02 (2) and NBA (**1***b*) with a $pK_a$ of 7.89 (2), the addition of 1

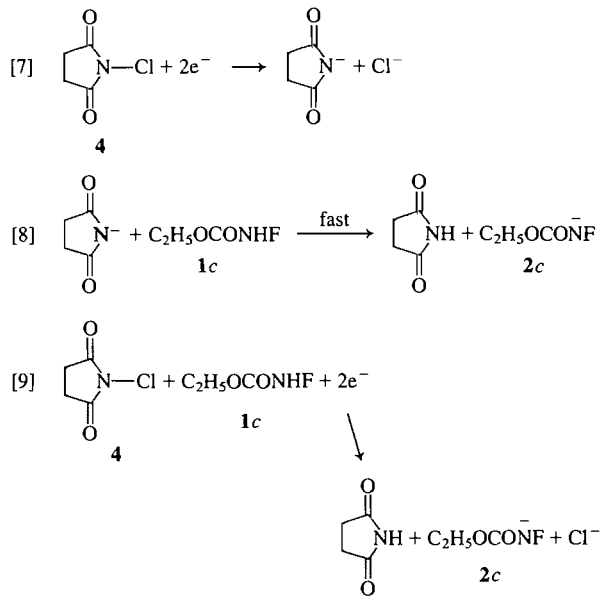


equiv. or more of acetic acid ($pK_a = 4.76$) causes the disappearance of the second wave[12] (due to the reduction of the conjugate bases **2***a* and **2***b*) and a twofold increase in the limiting current of the first wave ($I \simeq 2I_1$), as already pointed out. Thus the effect of the father–son protonation has been suppressed (reaction [10] and/or reaction [11]) and *all* the *N*-halo-*N*-hydroamide reaching the electrode is now reduced as shown by reaction [12] which is the sum of reactions [5] and [10] or the sum of reactions [5], [6], and [11].

*Influence of water*: For the above polarographic studies, the acetonitrile used contained about 0.2% of water (wet acetonitrile) as already indicated. When using dry acetonitrile, the polarograms of NCU (**1***a*) and NBA (**1***b*) showed the first wave only at the same potentials as in wet acetonitrile, the limiting currents being also the same: $I = I_1 \simeq 1/2(I_1 + I_2)$. Thus the father–son protonation (reaction [5]) does take place also in dry acetonitrile in agreement with the fact that the analogous proton exchange reaction [8] was fast in dry acetonitrile. At the second wave level, an ill-defined maximum was observed and, upon adding water, it changed gradually to a well-defined wave when about 0.2%

[9]The water content of dry acetonitrile was ≃ 0.01% (see Experimental section).

[10]NCS has a $pK_a$ of 9.6 (7) and that of NFU is 5.69 (2) which gives, for reaction [8], $K_{eq} \simeq 10^4$ in water.

[11]The electrochemical and chemical behavior of NFU (**1***c*) is, in many respects, different from that of the other *N*-halo-*N*-hydroamides studied and this will be reported and discussed in a forthcoming paper.

[12]In fact, in methanol, the second wave disappears completely (8) but in acetonitrile, it does not disappear entirely as can be seen from Fig. 1, part B, and Fig. 2. According to the $pK_a$ values in water, the conjugate bases **2***a* and **2***b* should be neutralized to an extent of 99.9% or more ($K_{eq} \simeq 1.4–1.8 \times 10^3$) in the presence of 1 equiv. of acetic acid. However, in acetonitrile, and particularly in the double layer region, acetic acid might be a less efficient proton donor towards the conjugate base **2** than expected from the $pK_a$ values in water.

Can. J. Chem. Downloaded from www.nrcresearchpress.com by 210.87.254.105 on 09/06/12
For personal use only.

Can. J. Chem. Downloaded from www.nrcresearchpress.com by 210.87.254.105 on 09/06/12
For personal use only.

[10] $\underset{\mathbf{3}}{\text{ZCO}\bar{\text{N}}\text{H}} + \text{CH}_3\text{COOH} \rightarrow \text{ZCONH}_2 + \text{CH}_3\text{COO}^-$

[11] $\underset{\mathbf{2}}{\text{ZCO}\bar{\text{N}}\text{X}} + \text{CH}_3\text{COOH} \rightleftharpoons \underset{\mathbf{1}}{\text{ZCONHX}} + \text{CH}_3\text{COO}^-$

[12] $\underset{\mathbf{1}}{\text{ZCONHX}} + \text{CH}_3\text{COOH} + 2e^- \rightarrow \text{ZCONH}_2 + \text{CH}_3\text{COO}^- + \text{X}^-$

(or more) water had been added. The fact that the second wave cannot be observed before the reduction of the solvent-supporting electrolyte system ($E_{\text{limit}} \simeq -3.2$ V) when the medium is dry shows that the reduction of the conjugate base **2** becomes easier in the presence of water.[13] Indeed, the insertion of the first electron into the anion **2** should lead to the radical dianion shown in reaction [13] or

[13] $\underset{\mathbf{2}}{\text{ZCO}\bar{\text{N}}\text{X}} + e^- \not\rightarrow [\text{ZCONX}]^{2-\cdot} \rightarrow \text{Products}$

to a transition state closely resembling that radical dianion, a species of high energy. In the presence of a sufficient amount of water (or of a protic solvent), the formation of such an energetic species can be avoided (reaction [14]) and the reduction of the

[14] $\underset{\mathbf{2}}{\text{ZCO}\bar{\text{N}}\text{X}} + \text{H}_2\text{O} + e^- \rightarrow [\text{ZCONHX}]^{-\cdot} + \text{OH}^- \rightarrow \text{ZCO}\dot{\text{N}}\text{H} + \text{X}^-$

conjugate base **2** becomes easier than that of the solvent-supporting electrolyte system. In reaction [14], water could intervene before the electron exchange (solvation or preprotonation of the anion **2**) or during the electron exchange. Reaction [15]

[15] $\underset{\mathbf{2}}{\text{ZCO}\bar{\text{N}}\text{X}} + 2\text{H}_2\text{O} + 2e^- \rightarrow \text{ZCONH}_2 + \text{X}^- + 2\text{OH}^-$

describes the overall two-electron reduction of the conjugate base **2** in the presence of water.

It must be stressed that water is needed in the double layer in order to observe the reduction of the conjugate base **2**. By using TEAP (0.1 *M*) as supporting electrolyte, the polarogram of NCU (**1***a*) showed the first wave only ($E_{1/2} = -0.15$ V) even when the bulk solution did contain as much as 10% of water (the half-wave potential and the limiting current did not change upon the addition of water). Tetraalkylammonium salts are indeed known to render the double layer anhydrous when electrolytic reductions are carried out in an aprotic medium containing water (9). However, the addition of 1 equiv. or more of acetic acid led to a twofold increase of the limiting current (Fig. 3), thus showing that the double layer contains enough acetic acid to suppress the father–son protonation [5]:[14] all the *N*-halo-*N*-hydroamide **1** reaching the electrode is then reduced according to reaction [12].

*Preparative electrolyses*

The exhaustive electrolysis of NCU (**1***a*) in methanol–$LiClO_4$ (0.2 *M*) at −0.7 V and in wet acetonitrile–$LiClO_4$ (0.2 *M*)[4] at −0.3 V, on a mercury or platinum electrode, has been reported to give over 90% of urethane (1), thus showing that the conjugate base **2** can be reduced under these conditions even at potentials near the half-wave potential of the first wave. The lithium salt of NCU (conjugate base **2***a*) has been quantitatively reduced (−1.2 V) to urethane in methanol (1). However, in dry acetonitrile – $LiClO_4$ (0.2 *M*),[9] attempts to reduce this salt at a platinum electrode were unsuccessful: no significant current was observed before the reduction of the solvent–electrolyte system (−3.2 V). These results agree with the above polarographic studies showing that water (or a protic solvent like methanol) is needed in order to observe the reduction of the anion **2** (reaction [15]).

The exhaustive electrolysis of NCU in dry acetonitrile – $LiClO_4$ (0.2 *M*) led to only 25% of the NCU anion **2***a* instead of the expected 50% (reaction [6]) according to polarographic and iodometric analyses. The reaction mixture was treated with sodium bisulfite and urethane was the sole product detected by vapor phase chromatography (vpc) (81% yield). The fact that only 25% of **2***a* was left after the exhaustive electrolysis can be attributed mainly to the thermal and/or photochemical decomposition of **2***a* during the 9 h required for the electrolysis to be completed as shown by a control experiment carried out on the lithium salt of NCU (see Experimental section). Other authors have also observed the decomposition of the NCU anion **2***a* in an aprotic medium (11). In the presence of acetic acid, the exhaustive electrolysis led to the complete consumption of NCU as expected (reaction [12]) and the yield of urethane (the sole product detected by vpc and $^1$H nmr) was 80%. For these experiments in a dry medium, the coulometric determinations gave 1.9 F per mol of NCU consumed, indicating a two-electron reduction of the

[13] The conjugate base **2** is reduced in methanol according to polarographic studies and preparative electrolyses (1).

[14] Acetic acid (0.005 *M*) is far superior than water (up to about 5 *M*) as a proton donor towards anions **2** and/or **3** in acetonitrile–TEAP (0.1 *M*) as would be expected from the p$K_a$ values and from the fact that acetic acid would be expected to be more soluble than water in the double layer. Interestingly, Fry and Reed (10) have found that, in dimethylformamide – tetraethylammonium bromide (0.1 *M*), acetic acid was a less efficient proton donor than water towards carbanions. The protonation of anions **2** and/or **3** probably occurs in the outer Helmholtz layer whereas the more basic carbanions must be reacting in the inner layer.

Can. J. Chem. Downloaded from www.nrcresearchpress.com by 210.87.254.105 on 09/06/12
For personal use only.

N—Cl bond as found previously in methanol and wet acetonitrile (1).

NCU (**1***a*) has been added to olefins (14–18% yield) in electrochemical reductions carried out under very special conditions (1). In a control experiment where no potential was applied, a 1% yield of addition products was obtained (1). These facts were interpreted as evidence of trapping of the electrochemically generated intermediate amidyl radical (reaction [1]) (1). However, in the electrochemical experiment, the resistivity of the catholyte was probably quite high and the temperature of the cathode compartment higher than in the control experiment, which should result in an enhanced yield of thermal addition of NCU. Therefore, the formation of 1,2-addition products in 14–18% yield in the presence of olefins under such conditions cannot be considered as evidence for the capture of the intermediate amidyl radical resulting from the first electron transfer (reaction [1]).

N-*Chloro*-N-*Alkyl(aryl)amides (ZCONRCl)*

The electroreduction of *N*-chloro-*N*-alkyl(aryl)-amides should involve two electrons and lead to the amide anion (see reaction [16] which is the sum of

[16] $ZCONRCl + 2e^- \rightarrow ZCO\bar{N}R + Cl^-$

reactions [1] and [2] where X = Cl, R = alkyl or aryl) as in the case of the *N*-halo-*N*-hydroamides **1** (reaction [4]). However, in contrast to their *N*-hydro analogues, *N*-chloro-*N*-alkyl(aryl)amides do not bear any acidic hydrogen ($pK_a > 20$). As a consequence, a father–son protonation appears unlikely and all the *N*-chloro derivative reaching the electrode should be reduced. Therefore, the voltammograms would be expected to show one wave only and coulometric results should be close to 2 F/mol. However, the voltammograms at a mercury or a platinum electrode did show two waves and, in controlled potential electrolyses (cpe), usually less than 1 F/mol was needed for the nearly complete consumption of the *N*-chloro derivative. We shall discuss first the cpe studies which provide evidence for the two-electron reduction of *N*-chloro-*N*-alkyl(aryl)amides leading to the amide anion (reaction [16]) and then consider the voltammetric studies.

*Controlled potential electrolyses*

The results recorded in Table 1 show that controlled potential electrolysis of *N*-chloro-*N*-alkyl(aryl)amides in acetonitrile–TEAP (0.1 *M*) gives the parent amide as the main reaction product and requires less than 1 F/mol. For instance, the nearly exhaustive electrolysis (more than 98% of active chlorine reduced according to iodometric titration) of *N*-chloro-*N*-methylurethane (**5**) at a mercury or a platinum electrode consumed about 0.5 F/mol only and led to a 90% yield of *N*-methylurethane (entries 1 and 2). A radical chain reaction involving steps [17] and [18] with reaction [19] as the termination step could have explained

[17] $ZCO\dot{N}R + CH_3CN \rightarrow \underset{\text{Parent amide}}{ZCONHR} + \cdot CH_2CN$

[18] $\cdot CH_2CN + ZCONRCl \rightarrow ClCH_2CN + ZCO\dot{N}R$

[19] $2\cdot CH_2CN \rightarrow (CH_2CN)_2$

the low coulometry. However, using appropriate substrates, we did not succeed in capturing the electrochemically generated *N*-alkyl(aryl)amidyl radical (reaction [1]) while the amide anion ([16] = [1] + [2]) has been efficiently trapped. Thus the insertion of the second electron (reaction [2]) must be faster than most of the reactions of amidyl radicals.[15]

*Attempts to trap the electrochemically generated amidyl*: The radical cyclization of *N*-chloro-*N*-methyl-3-cyclohexenecarboxamide (**6**), under a variety of initiating conditions, has been shown to be very efficient giving the bicyclic products **10** and **11** in yields greater than 95% (12, 13). However, its

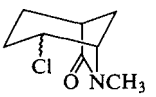


**10** (*exo*)
**11** (*endo*)

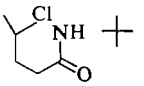


**12**

electrochemical reduction (Table 1, entry 3) did not give any bicyclic products which might have resulted from intramolecular trapping of the amidyl radical; the sole product detected and identified was the parent amide. Therefore, the reduction of the electrochemically generated amidyl must be faster than its intramolecular addition to the double bond. It is therefore not surprising that the electrochemical reduction of *N*-chloro-*N*-methylurethane (**5**) in the presence of a large excess of 1-octene gave the parent amide only (Table 1, entry 1). The radical 1,2-addition of **5** to 1-octene has been achieved upon photochemical initiation (14).

The photolysis of *N*-chloro-*N*-tertiobutylpentanamide (**7**) in benzene was reported to give the 4-chloro derivative **12** in a 43% yield via

[15]The breakage of the *N*-halogen bond to give the amidyl radical and the halide ion (reaction [1]) is most probably concerted with the insertion of the first electron but we cannot exclude the possibility that an *N*-haloamide radical anion is first formed and then breaks down rapidly into the amidyl and the halide anion.

Can. J. Chem. Downloaded from www.nrcresearchpress.com by 210.87.254.105 on 09/06/12
For personal use only.

intramolecular hydrogen abstraction by the amidyl radical generated in the initiation step (15). As seen from Table 1, entries 4 and 5, the electrochemical reduction of **7** gave the parent amide together with a small amount (≤2%) of the 4-chloro derivative **12**. However, about 1% of **12** was already present in the starting *N*-chloroamide **7**. Thus, if any 4-chloro derivative **12** was formed during the electrolyses, the amount produced was negligible and was probably due to thermal and/or photochemical decomposition of the *N*-chloroamide **7**; it did not arise from the electrochemically generated amidyl radical.[16] Indeed, in control experiments in which no potential was applied, we observed the disappearance of **7** after 4 to 5 days at room temperature (iodometric titration) and the formation of **12** in yields ranging from 20% (in the dark) to 50% (in the presence of mercury and not in the dark[17]).

The electrochemical reduction of *N*-chlorobenzanilide (**9**) was then investigated (Table 1, entries 7 to 10). Ford *et al.* (16) had reported the isolation, in a 26% yield, of the head-to-tail dimer **13** resulting from the coupling of two *N*-phenylbenzamidyl radicals when a concentrated solution (2 *M*) of **9** in benzene was treated with dimethyl azobisisobutyrate. The probability of radical coupling should be larger when the radicals are generated at the surface of an electrode than when they are produced in an homogeneous medium where they should be farther apart. However, from the reduction of **9** at a mercury electrode (entries 7 and 8) no dimer could be detected whereas at a platinum electrode (entries 9 and 10) between 1 to 2% of dimer **13** was formed. Thus it appears that the electrochemically generated *N*-phenylbenzamidyl radical might have been trapped to a very small extent. We also studied the photolysis of *N*-chlorobenzanilide (**9**) in acetonitrile–TEAP (0.1 *M*) and obtained 67% of 4′-chlorobenzanilide (**14**) and 12% of 2′-chlorobenzanilide (**15**); no dimer **13** was detected and very little parent amide, if any, was formed (see Experimental section). In contrast, the electroreduction of **9** (Table 1, entries 7 to 10) gave the parent amide in yields ranging from 76 to 84% and small amounts only of **14** (4 to 10%) and **15** (0 to 3%). Therefore, in these electrochemical reductions, the parent amide must have originated from the *N*-phenylbenzamide anion (proton abstraction from the medium) resulting from the two-electron cleavage of the N—Cl bond. Although the ring chlorinated products **14** and **15** could have been formed via a chain reaction involving the *N*-phenylbenzamidyl radical, we believe that the *N*-phenylbenzamide anion is responsible for their formation as illustrated in reaction [20] (father–son chlorination).

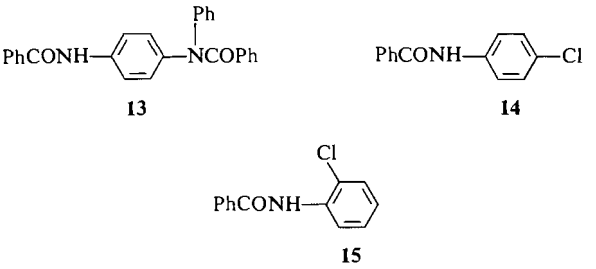


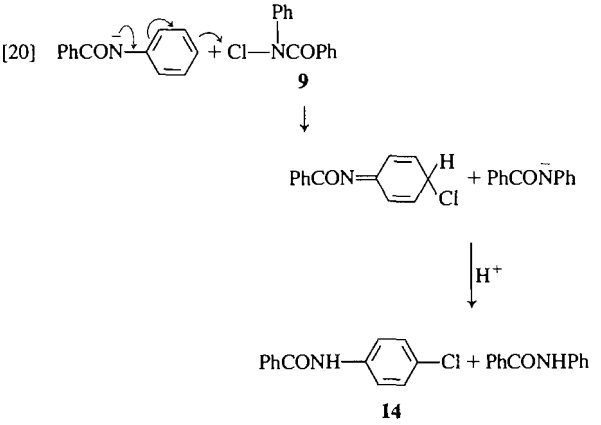


In one electrochemical experiment, 2′,4′-dichlorobenzanilide (**16**) was isolated in a 2% yield (Table 1, entry 10) and it was probably formed by chlorination of the anion derived from **14** (reaction [20]) and/or from **15**.

*Trapping of the amide anion*: In order to confirm unequivocally that the electrochemical reduction of *N*-chloro-*N*-alkylamides does lead to the amide anion (reaction [16]), the latter was trapped by *N*-alkylation and *N*-acylation. Indeed, intermolecular alkylation of amide anions has been reported to lead to *N*-alkylated products whereas alkylation of amides under neutral conditions occurs at oxygen

[16]In ref. 1, we reported that the electrochemical reduction of *N*-chloro-*N*-tertiobutylpentanamide (**7**) at a mercury electrode in acetonitrile–$LiClO_4$ (0.2 *M*) did give the 4-chloro derivative **12** in a 37% yield together with the parent amide (55% yield) and this was considered as evidence for the trapping of the electrochemically generated amidyl radical. In this experiment, a platinum auxiliary electrode had been used. The formation of **12** in significant amount when platinum is used as the auxiliary electrode instead of magnesium is most probably due to the oxidation of some of the *N*-chloro derivative **7** which migrates into the anolyte compartment. Indeed we have shown that the oxidation of **7** at a platinum electrode leads to the formation of the 4-chloro derivative **12** (27%). We are currently studying the electrochemical oxidation of *N*-haloamides.

[17]A grey precipitate was formed as in the experiment reported in ref. 1. However, the latter experiment had been stopped after 24 h, 31% only of *N*-chloroamide **7** had reacted, and the 4-chloro derivative **12** had not been detected.

TABLE 1. Controlled potential electrolysis of *N*-chloro-*N*-alkyl(aryl)amides in acetonitrile–TEAP (0.1 *M*)[a]

| Entry | *N*-Chloroamide | Working electrode | $E^b$ (V) | $n_{app}$ (F/mol) | Electrolysis product(s) | Yield[c] (%) |
|---|---|---|---|---|---|---|
| 1[d] | $C_2H_5OCON(CH_3)Cl$ (5) | Hg | −0.8 | 0.57 | Parent amide | 87 |
| 2[e] | | Pt | −1.0 | 0.49 | Parent amide | 92 |
| 3 | 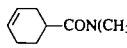 (6) | Hg | −0.8 | 0.59 | Parent amide | 76 |
| 4[f] | $CH_3(CH_2)_3CON(t\text{-}C_4H_9)Cl$ (7) | Hg | −0.3 | 1.33 | Parent amide | 81 |
| | | | | | 4-Chloro deriv. **12** | ≤2[g] |
| 5 | | Pt | −0.8 | 0.81 | Parent amide | 88 |
| | | | | | 4-Chloro deriv. **12** | ≤2[g] |
| 6[h] | 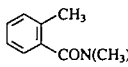 (8) | Pt | −0.8 | 0.87 | Parent amide | 90[i] |
| 7[j] | PhCON(Ph)Cl (9) | Hg | −0.1 | 0.22 | Parent amide | 84 |
| | | | | | 4′-Chlorobenz. **14** | 5 |
| 8 | | Hg | −0.6 | 0.93 | Parent amide | 79 |
| | | | | | 4′-Chlorobenz. **14** | 4 |
| 9 | | Pt | −0.4 | 0.77 | Parent amide | 76 |
| | | | | | Dimer **13** | 2 |
| | | | | | 4′-Chlorobenz. **14** | 5 |
| | | | | | 2′-Chlorobenz. **15** | 3 |
| 10 | | Pt | −0.8 | 0.96 | Parent amide | 76 |
| | | | | | Dimer **13** | 1.5 |
| | | | | | 4′-Chlorobenz. **14** | 10 |
| | | | | | 2′-Chlorobenz. **15** | 1 |
| | | | | | 2′,4′-Dichlorobenz. **16** | 2.5 |

[a]Unless otherwise stated, the electrolyses were carried out at room temperature using a magnesium auxiliary electrode, and were stopped when 2% or less active chlorine was left (iodometric titration). The mixture was treated with sodium bisulfite to remove the residual active chlorine (see Experimental section).
[b]*E* vs sce.
[c]The yields were determined by vpc in entries 1 to 5 and they refer to products isolated by preparative layer chromatography (plc) in entries 7 to 10.
[d]1-Octene was present in large excess (40% solution v/v in acetonitrile–TEAP).
[e]The cell was cooled in an ice bath.
[f]Lithium perchlorate (0.2 *M*) was used as supporting electrolyte.
[g]By $^1$H nmr spectroscopy. Some 4-chloro derivative **12** was already present (1–2%) in the starting *N*-chloroamide 7 according to its $^1$H nmr spectrum.
[h]The electrolysis was carried out at −30°C and was stopped when 21% of active chlorine was still present.
[i]The crude product consisted essentially of the parent amide according to its $^1$H nmr spectrum.
[j]A grey precipitate was formed during the electrolysis.

and requires strong alkylating agents (17). The results reported in Table 2, entries 3 and 4, show that methyl bromide (entry 4) was more efficient than methyl tosylate (entry 3) as a trapping agent for the amide anion. Trapping by *N*-acylation (entry 5) was more efficient than by *N*-alkylation. The parent amides were recovered unchanged when treated with an excess of alkylating or acylating agent under the conditions of the electrolyses and work-up. We hoped that intramolecular trapping would be more efficient than intermolecular trapping. However, the reduction of *N*-chloro-*N*-methyl-α-chloroorthotoluamide (**17**) led to only 31% of *N*-methyllactam **22** (Table 2, entry 6) resulting from intramolecular *N*-alkylation of the amide anion (Scheme 1). The major product isolated was the iminolactone **21** (56%) arising from the cyclization of the parent amide formed during the electrolysis (Scheme 1). Indeed the cyclization of the amide was found to be fairly easy either in solution or in solid state to afford quantitatively the iminolactone hydrochloride **20**[18] (see Experimental section). The iminolactone **21** was isolated after basic work-up. We have also shown that the amide anion generated by treatment with lithium diisopropylamide in dry tetrahydrofuran afforded exclusively and quantitatively the *N*-methyl lactam **22**.[18] Thus it appears that proton abstraction from the medium (SH in Scheme 1) by the amide anion generated electrochemically from the reduction of **17** in acetonitrile – TEAP is about 1.8 times faster than intramolecular alkylation.

*Coulometry*: As can be seen from Table 2, the coulometric results ($n_{app}$) parallel the trapping efficiency, the values ranging from 0.5–0.9 F/mol in the absence of a trapping agent (entries 1 and 2) to

[18]The behavior of *N*-methyl-α-chloroorthotoluamide parallels that of 4-bromo-*N*-cyclohexylbutyramide: the thermal cyclization of the neutral amide was reported to give *N*-cyclohexyliminobutyrolactone hydrobromide while the anion afforded *N*-cyclohexylbutyrolactam (18).

Can. J. Chem. Downloaded from www.nrcresearchpress.com by 210.87.254.105 on 09/06/12
For personal use only.

Can. J. Chem. Downloaded from www.nrcresearchpress.com by 210.87.254.105 on 09/06/12
For personal use only.

TABLE 2. Trapping of the amide anion during the electrolysis, at a platinum electrode, of *N*-chloro-*N*-alkylamides in acetonitrile–TEAP (0.1 *M*)[a]

| Entry | *N*-Chloroamide | Trapping agent[b] | $E^c$ (V) | $n_{app}$ (F/mol) | Yield of parent amide (%) | Product(s) of trapping | Yield (%) |
|---|---|---|---|---|---|---|---|
| 1[d] | $C_2H_5OCON(CH_3)Cl$ (5) | None | −1.0 | 0.49 | 92 | None | |
| 2[e] | 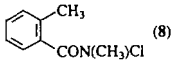 (8) | None | −0.8 | 0.87 | >90 | None | |
| 3 | | $CH_3OTs$ | −1.0 | 0.95 | 68[f] | 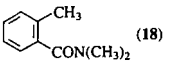 (18) | 15[f] |
| 4 | | $CH_3Br$ | −1.0 | 1.04 | 59[f] | 18 | 29[f] |
| 5[g] | $C_2H_5OCON(CH_3)Cl$ (5) | $C_2H_5OCOCl$ | −1.0 | 1.45 | [h] | $(C_2H_5OCO)_2NCH_3$ (19) | 50[f] |
| 6[i] | 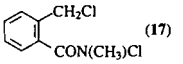 (17) | — | −1.0 | 1.83 | 56[j] | 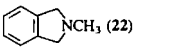 (22) | 31[k] |
| 7[l] | 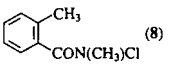 (8) | $CH_3COOH$ | −1.0 | 1.85 | | Parent amide | >90[l] |

[a]See footnote *a* of Table 1.
[b]An excess of more than 8 mol per mol of *N*-chloroamide was used except in the case of acetic acid (entry 7) where 1 equiv. was added.
[c]*E* vs. sce.
[d]Taken from Table 1, entry 2.
[e]Taken from Table 1, entry 6.
[f]By vpc.
[g]The electrolysis was stopped after the consumption of 35% of active chlorine.
[h]Not determined.
[i]The amount of active chlorine still present when the electrolysis was stopped was 10–11%.
[j]The amide was isolated as the iminolactone **21** (see Scheme 1 and Experimental section).
[k]Yield of isolated product.
[l]The crude product consisted of the parent amide according to its $^1H$ nmr spectrum.

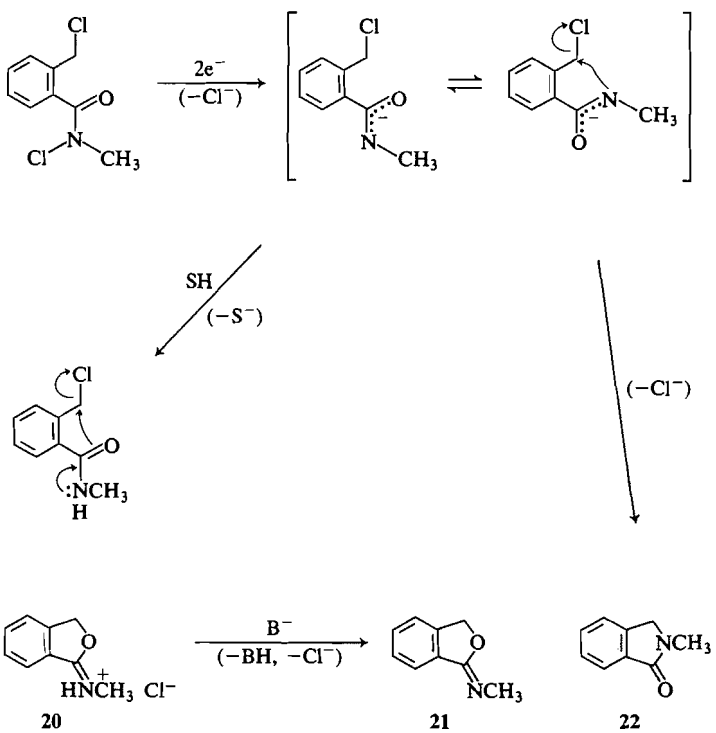


SCHEME 1

Can. J. Chem. Downloaded from www.nrcresearchpress.com by 210.87.254.105 on 09/06/12
For personal use only.

about 1.45 F/mol for the most efficient intermolecular alkylating reaction (entry 5). A value close to the theoretical value of 2 F/mol was obtained when a good proton donor was present: the hydrochloride **20** in entry 6 and acetic acid in entry 7.[19] The fact that the number of coulombs increases as the trapping of the amide anion becomes more efficient or when protons are readily available indicates (*i*) that a secondary reaction must consume the starting *N*-chloroamide and give a non-electroactive compound, and (*ii*) that the amide anion must generate anions or bases responsible for the secondary reaction. Since the parent amide is the main product of the electrochemical reductions reported in Table 1, the amide anion must abstract a proton from the medium, most probably from acetonitrile (SH = $CH_3CN$ in reaction [21]). The acetonitrile anion ($S^- = {}^-CH_2CN$) could react with acetonitrile to give basic polymers ($A^- = (CH_2CN)_n^-$ in reaction [21]) as proposed by Saveant *et al.* (18). An orange-to-brown coloration did appear during all the electrolyses recorded in Table 1 and disappeared upon acidification of the reaction medium. Such a coloration has been observed by Saveant *et al.* (18) in electroreductions where bases were generated and it was attributed to anionic polymeric species generated from acetonitrile. These polymeric species would then react with the starting *N*-chloroamide to give non-electroactive C-chlorinated derivatives (ACl in reaction [22]). Most

[21] $ZCO\bar{N}R + SH \rightarrow ZCONHR + S^- (\rightarrow A^-)$

[22] $ZCONRCl + S^- \text{ (or } A^-) \rightarrow ZCO\bar{N}R + SCl \text{ (or ACl)}$

carbon–chlorine bonds should be electroinactive at the potentials used for the controlled potential electrolyses (from −0.1 to −1.0 V) (20). The amide ion is regenerated in reaction [22] so the consumption of the *N*-chloroamide would involve a chain reaction, hence the low coulometric values or the high coulometric yields observed (e.g. ≃ 400% based on the *N*-chloroamide in entries 1 and 2).[20]

[19]The amide anion has been trapped also by the magnesium ion, a Lewis acid, probably to form the magnesium enolate. Indeed, the reduction of *N*-chloro-*N*-tertiobutylacetamide (**23**), at a mercury electrode ($E$ = −0.45 V), in acetonitrile–TEAP (0.1 *M*) containing 2 equiv. of magnesium perchlorate or using magnesium perchlorate (0.1 *M*) as the supporting electrolyte, gave a coulometry of 1.83 to 1.89 F/mol.

[20]It is interesting to compare the electroreduction of *N*-chlorosuccinimide **4** with that of an *N*-chloro-*N*-alkyl(aryl)-amide. In acetonitrile–TEAP (0.1 *M*), NCS gives a coulometry of 1.85 F/mol both at a mercury and a platinum electrode, thus showing that no secondary reactions consume the starting *N*-chloro compound. This is because the succinimide anion resulting from the two-electron reduction of the N—Cl bond, being much less basic ($pK_a$ = 9.6 (7)) than an amide anion ($pK_a$ = 15–17), presumably cannot abstract a proton from acetonitrile.

The acetonitrile ion itself generated in reaction [21][21] does not appear to be involved to a significant extent in the decomposition of the starting *N*-chloroamide (reaction [22]) since chloroacetonitrile (SCl = $ClCH_2CN$) was not detected; succinonitrile and the *N*-cyano derivative $ZCONRCH_2CN$, respectively the alkylation product of the acetonitrile anion and of the amide anion by chloroacetonitrile, were not detected either. Although residual water can certainly act as a proton source towards the amide anion (SH = $H_2O$ in reaction [21]), its concentration was less than 10% of that of the starting *N*-chloroamide in most of the electrolyses. Furthermore, the attack of the hydroxyde ion on the *N*-chloroamide (reaction [23]) would not con-

[23] $ZCONRCl + HO^- \rightarrow ZCONHR + OCl^-$

tribute to lower the coulometric results since the hypochlorite ion should be reducible in the potential range used.[22] The tetraethylammonium ion could also act as a proton donor towards the electrochemically generated amide anion (reaction [16]) and/or the acetonitrile anion generated in reaction [21] leading to triethylamine and ethylene by a Hoffman elimination (10, 22, 23). However, such a reaction with the supporting electrolyte would not contribute to the low coulometry observed and we did not try to determine if ethylene was evolved or not.

### *Voltammetric studies*

*Polarography*:

As recorded in Table 3, all the *N*-chloro-*N*-alkyl(aryl)amides studied give rise to two waves at a dropping mercury electrode in acetonitrile–TEAP (0.1 *M*). The reduction is truly irreversible ($\alpha n$ values of 0.3 for the first wave and ≃ 0.4 for the ill-defined second wave) as in the case of the *N*-chloro-*N*-hydroamides. The first wave shows passivation–adsorption phenomena (abnormal current–time curve during the lifetime of a drop) and its limiting current, $I_1$, becomes practically independent of the concentration of the *N*-chloroamide for concentrations higher than ca. $5 \times 10^{-4}$ *M* (Fig. 3). The second wave, even if ill-defined due to incipient maxima, is diffusion controlled: the total limiting current, $I_1 + I_2$, increases linearly with concentration (Fig. 3).

The anomalous polarographic behavior obser-

[21]The electrochemically generated acetonitrile anion has been trapped by carbonyl compounds (21).

[22]In fact the water content of the medium had no effect on the coulometric results. Other experimental conditions such as the temperature, the nature of the electrode (Hg or Pt), the electrolyte, and the potential had also little effect on the coulometry.

TABLE 3. Half-wave potentials[a] for the reduction of *N*-chloro-*N*-alkyl(aryl)amides in acetonitrile–TEAP (0.1 *M*)

| Entry | *N*-Chloroamide | Electrode | $(E_{1/2})_1$[b] V vs. sce | $(E_{1/2})_2$[b] V vs. sce |
|---|---|---|---|---|
| 1 | $C_2H_5OCON(CH_3)Cl$ (5) | Hg | −0.13 | −0.40 |
| 2 | | Pt | −0.2 (none) | −1.40 (−0.76) |
| 3 | | C | None | −0.60 (−0.65) |
| 4 | PhCON(Ph)Cl (9) | Hg | −0.11 | −0.35 |
| 5 | | Pt | 0.0 (none) | −0.80 (−0.60) |
| 6[c] | | C | None | −0.70 (−0.70) |
| 7 | $CH_3CON(t\text{-}C_4H_9)Cl$ (23) | Hg | −0.11 | −0.45 |
| 8 | | Pt | −0.30 (none) | −0.75 (−0.90) |
| 9 | $CH_3(CH_2)_3N(t\text{-}C_4H_9)Cl$ (7) | Hg | −0.11 | −0.55 |
| 10 | 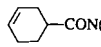 —$CON(CH_3)Cl$ (6) | Hg | −0.13 | −0.40 |

[a]The half-wave potentials were determined by classical dc polarography (mercury electrode) and by linear voltammetry using a rotating disc electrode (platinum and vitreous carbon discs).
[b]For the platinum and vitreous carbon electrodes, values in parentheses were obtained on reverse scan.
[c]In acetonitrile–$LiClO_4$ (0.2 *M*).

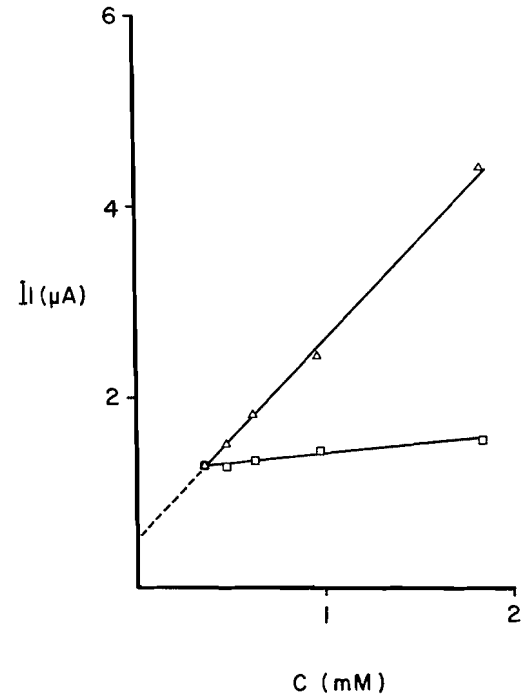


FIG. 3. Variation of the limiting currents (*Il*) with the concentration of *N*-chloro-*N*-methylurethane (**5**) in acetonitrile–TEAP (0.1 *M*): □, limiting current of the first wave ($I_1$); △, total limiting current ($I_1 + I_2$).

ved could be attributed, at least in part, to the presence of electrogenerated strong bases (anions) at the surface of the electrode. Thus, the addition of about 0.5 to 0.6 equiv. of acetic acid did eliminate the passivation–adsorption phenomena and gave only one well-defined, diffusion-controlled, and irreversible wave ($\alpha n = 0.4$) at a potential close to that of the first wave (e.g. −0.18 V and −0.14 V for *N*-chloro-*N*-methylurethane (**5**) and *N*-chloro-*N*-tertiobutylacetamide (**23**) respectively). The use of magnesium perchlorate (0.1 *M*), a Lewis acid, as supporting electrolyte did eliminate also the anomalous polarographic behavior leading to only one well-defined wave at more anodic potentials (e.g. + 0.06 V and +0.14 V for *N*-chloroamides **5** and **23** respectively).[23] In the case of the *N*-chloro-*N*-hydroamides which are quite acidic (although weaker acids than acetic acid) and do act as proton donors in their reduction as already pointed out (reaction [5]), the polarograms show well-defined waves. Finally, the polarographic reduction of *N*-chlorosuccinimide (**4**) in acetonitrile–TEAP (0.1 *M*), which leads to the much less basic succinimide anion (reaction [7]), shows a normal behavior giving only one well-defined, diffusion-controlled, and irreversible wave ($\alpha n = 0.3$) at a potential (−0.12 V) near that of the first wave of the *N*-chloroamides of Table 3.[24]

In relation to the phenomena observed in the polarographic reduction of *N*-chloro-*N*-alkyl(aryl)amides, it is informative to look again at their electrolysis at a mercury electrode, taking *N*-chlorobenzanilide (**9**) as an example (see Table 1, entries 7 and 8). We have already discussed the

[23]Both the addition of acetic acid and the use of magnesium perchlorate as supporting electrolyte caused an increase of the total limiting current: a 20% to 30% increase upon the addition of 0.5 to 0.6 equiv. of acetic acid with no further effect when adding more acid, and a 50% increase in the case of magnesium perchlorate.

[24]The addition of acetic acid had no effect on the position of the wave and on the limiting current. However, the use of magnesium perchlorate (0.1 *M*) as supporting electrolyte did lead to an anodic displacement of the wave ($E_{1/2} = +0.14$ V) and to an increase (≃ 30%) of the limiting current as in the case of *N*-chloro-*N*-tertiobutylacetamide (**23**).

Can. J. Chem. Downloaded from www.nrcresearchpress.com by 210.87.254.105 on 09/06/12
For personal use only.

Can. J. Chem. Downloaded from www.nrcresearchpress.com by 210.87.254.105 on 09/06/12
For personal use only.

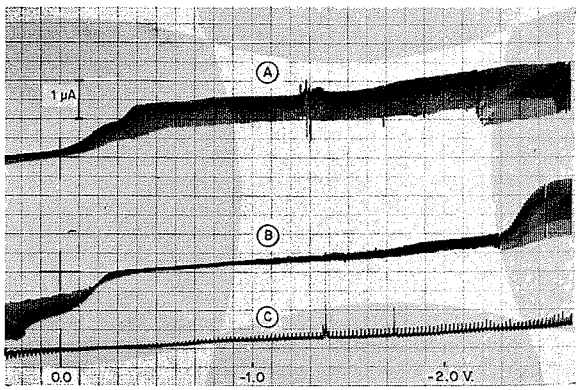


FIG. 4. Electrolysis of *N*-chlorobenzanilide (*9*) at −0.6 V in acetonitrile–TEAP (0.1 *M*) followed by polarography: *A*, before the electrolysis (*C* = 0.4 m*M*); *B*, after the electrolysis; *C*, residual current.

products formed; their yield and relative proportion is about the same whether the electrolysis was carried out at −0.1 V (first wave) (entry 7) or at −0.6 V (second wave) (entry 8). The electrolyses were followed by polarography. We will first consider the electrolysis carried out at −0.6 V. The polarograms of Fig. 4 have been recorded before the electrolysis (polarogram A) and after the complete disappearance of *N*-chloroamide **9** (polarogram B). In polarogram B, the two waves due to the starting *N*-chloroamide have disappeared as expected, a wave due to the reduction of *N*-phenylbenzamide can be seen at $E_{1/2} = -2.3$ V, and an *anodic* wave is present at a potential corresponding to that of the first wave of polarogram A. This anodic wave can be attributed to the oxidation of mercury in the presence of electrogenerated anions (24) and such an oxidation could account for the polarographic phenomena observed at the first wave level.

For the electrolysis carried out at −0.1 V, the coulometric results were very low (Table 1, entry 7) and some current continued to flow through the cell even after the complete disappearance of the substrate **9** (iodometric titration). A grey precipitate was formed. Polarography showed the wave due to the parent amide and the complete disappearance of the second wave. In a control experiment, where an aliquot of the starting cathodic solution was stirred with non-polarized mercury, a grey precipitate was also formed, *N*-chloroamide **9** was completely consumed (iodometric titration), and polarography showed the wave due to the parent amide, the disappearance of the second wave, and a very small current at the first wave level. Therefore, a potential of −0.1 V was not sufficient to prevent the chemical reaction between *N*-chloroamide **9** and mercury. Such chemical reaction with mercury was observed with all the other *N*-haloamide studies (see also ref. 1). This suggests that organomercurials might be involved as intermediates in the electroreduction of *N*-haloamides as described in reactions [24] and [25].

[24] $ZCONRX + Hg^0 \rightarrow ZCONRHgX$

[25] $ZCONRHgX + 2e^- \rightarrow ZCONR^- + Hg^0 + X^-$

Organomercurials have been obtained by allowing mercury to react with allyl or benzyl halides and they have been proposed as intermediates in the electroreduction of organic halides (25–30). It seems that organomercurials derived from *N*-haloamides are not stable, at least in acetonitrile, but this does not rule out their participation as intermediates in the electroreduction of *N*-haloamides.

*Linear sweep voltammetry*:

In order to eliminate the interactions with mercury, we used smooth platinum and vitreous carbon as electrode material. The half-wave potentials obtained by linear sweep voltammetry at a rotating disc electrode are reported in Table 3. The limiting current did increase with the concentration of the *N*-haloamide and the rotation rate ω. Unfortunately, the waves were not reproducible and it was not possible to obtain a linear relationship between the concentration and the limiting current on one hand, and between $\omega_{1/2}$ and the limiting current on the other hand, as expected for diffusion-controlled waves. On smooth platinum, two waves were observed for all the *N*-chloro-*N*-alkyl(aryl)amides studied (Table 3). As seen from Fig. 5, the amplitude of the first wave is small and it disappears almost completely on reverse scan; furthermore the position of

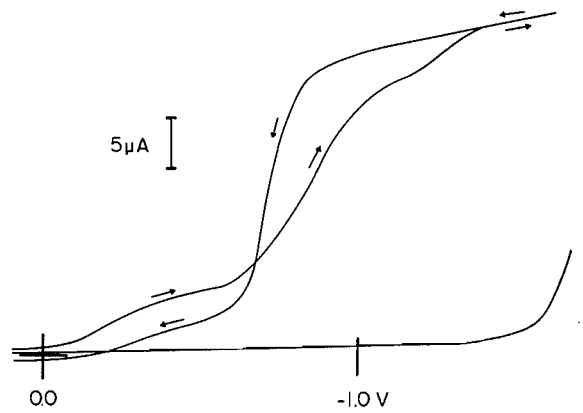


FIG. 5. Linear voltammetry on a platinum rotating disc electrode (ω = 350 rpm) of *N*-chloro-*N*-methylurethane (**5**) in acetonitrile–TEAP (0.1 *M*). The sweep rate was 5 mV/s. The arrows indicate the direction of scanning. The residual current is also indicated.

Can. J. Chem. Downloaded from www.nrcresearchpress.com by 210.87.254.105 on 09/06/12
For personal use only.

the second wave does vary with the direction (forward or backward) of the scan (hysteresis). Holding the potential at the level of the first wave (e.g. at ca. −0.4 V in the case of *N*-chloro-*N*-methylurethane (**5**)) led to zero current after a few minutes so that it was not possible to carry out any electrolysis at potentials close to that of the first wave. On vitreous carbon, however, only one wave was observed and its half-wave potential was practically independent of the direction of the scan (little or no hysteresis) (Table 3). Thus it appears that the multiple waves and hysteresis observed on smooth platinum originates from surface phenomena (adsorption of halide and/or amide ions or of anions derived from amide ions).[25] However, further studies would be needed to fully understand the voltammetric behavior of *N*-chloro-*N*-alkyl-(aryl)amides.

## Experimental

Most of the pertinent general information concerning the analysis of products and starting materials is the same as that given in ref. 1. In addition to an OS-138 (polyphenyl ether, 15%) column, SE-30 (10%) and UCON Polar 50-HB-2000 (5%) columns were used for vapor phase chromatography (vpc); for these three columns (6 ft × 0.25 in.), the support was acid washed and dimethylsilylated Chromosorb W 60/80 mesh. In a few cases, the $^1$H nmr spectra were recorded on a Bruker WP-60 instrument.

*Acetonitrile*

Technical grade acetonitrile was purified by a method described by Mann *et al.* (34). The resulting acetonitrile contained about 0.2% of water. When refluxed for 2 days over calcium hydride then distilled, the water content dropped to below 0.01% (to about 0.003% in many cases) as determined with a coulometric Karl Fisher titrator. Such dry acetonitrile was used immediately after its distillation and transferred into the electrochemical cell with a syringe and under dry nitrogen (sometimes a glove box was used). Regular controls at the end of an electrolysis showed that the medium contained about 0.03% of water when dry acetonitrile was used to start with.

*Electrolytes*

Lithium perchlorate (anhydrous reagent, Alfa inorganics, Co.) was used after drying in a vacuum oven for 24 h at 100°C. Tetraethylammonium perchlorate, prepared from tetraethylammonium bromide and perchloric acid (35), was recrystallized from water until the silver ion test was negative. It was then dried in a vacuum oven for 2 days at 75°C. Magnesium perchlorate (anhydrous reageant, Matheson, Coleman and Bell) was used as such.

[25]Allyl bromides and iodides (31), and 9-fluorenyl and benzyhydryl chlorides and bromides (32) also show multiple waves on platinum and a single wave on vitreous carbon when reduced in acetonitrile or dimethylformamide. The surface effects on platinum have been attributed to adsorption of halide ions (31, 32) or to electrocatalysis from electrode impurities or adventions impurities (32). Merz and Bard (31) have stressed that "surface effects in the reduction of halo compounds at platinum electrodes are a frequent occurrence and deserve further studies".

*Amides*

The commercially available amides were used without further purification. The preparation of *N*-methyl-3-cyclohexenecarboxamide has been reported (13*a*). The other amides were prepared from the corresponding amine and acid chloride (2 mol amine per mol of acid chloride) in ether at 0°C in yields ranging from 70% to 80% after purification. N-*Tertiobutylpentanamide*, mp 47–49°C (lit. (15), 48–49°C). N-*Methylorthotoluamide*, mp 77–78°C (lit. (36), 78–79°C). N-*Tertiobutylacetamide*, mp 97–98°C (lit. (37) 98–99°C). N-*Methyl*-α-*chloroorthotoluamide*, mp 207–209°C (dec.);[26] $\nu_{max}$($CHCl_3$) 3460, 1660, and 1520 cm$^{-1}$; δ($CDCl_3$) 3.01 (d, $J$ = 5 Hz, 3H), 4.83 (s, 2H), 6.37 (m, 1H), and 7.43 ppm (m, 4H); *m/e* 183, 185 (3:1, $M^+$). *Anal.* calcd. for $C_9H_{10}ClNO$: C 58.87, H 5.49, N 7.63; found: C 58.71, H 5.55, N 7.57. 2-Chloromethylbenzoyl chloride was prepared from phtalide according to a published procedure (38): bp 104–105°C, 3 Torr.

Upon heating the solid at 90°C in an oven for 24 h and upon refluxing a solution in chloroform for 2 h, *N*-methyl-α-chloroorthotoluamide was converted quantitatively to N-*methyliminophtalide hydrochloride* (**20**), mp 205–206°C (decour.); $\nu_{max}$($CHCl_3$) 2550 (broad) and 1705 cm$^{-1}$; δ($CDCl_3$) 3.31 (s, 3H), 5.86 (s, 2H), 7.5 to 8.0 (m, 4H), and 9.20 ppm (m, NH). The hydrochloride **20** was dissolved in water. The aqueous solution was made basic by addition of sodium hydroxide then extracted with methylene chloride. The organic phase was washed with brine then dried and the solvent evaporated to give the pure imino lactone **21** identical (ir, $^1$H nmr) to the authentic sample prepared below.

At room temperature, according to $^1$H nmr spectroscopy, 40% of solid amide was converted to the hydrochloride **20** after 1 week and a solution of amide in $CD_3CN$–TEAP (0.1 *M*) gave 30% of hydrochloride **20** after 6 h.

N-*Haloamides*

NCU (**1***a*) (99% active chlorine) was prepared by the sodium hypochlorite method (39) and NBA (**1***b*) was purchased from Aldrich (>99% active chlorine after recrystallization from methylene chloride). Their lithium salts **2***a* and **2***b* were obtained as previously described (1) with appreciable loss of material (≃ 50%). The $^1$H nmr spectrum of **2***a* in $D_2O$ showed the absorptions due to the salt at δ 1.21 (t, $J$ = 7 Hz, 3H) and 4.08 ppm (q, $J$ = 7 Hz, 2H) together with very weak peaks due to urethane.

The preparation of N-*chloro*-N-*methyl*-3-*cyclohexenecarboxamide* (**6**) has been described (13*b*) as well as that of N-*chloro*-N-*tertiobutylpentanamide* (**7**) (1) and N-*chloro*-N-*tertiobutylacetamide* (**23**) (14). N-*Chloro*-N-*methylurethane* (**5**) and N-*chloro*-N-*methylorthotoluamide* (**8**) were prepared by treatment of 0.01 mol of amide in methylene chloride (25 mL) with 0.02 to 0.04 mol of sodium hypochlorite (5% aqueous solution) containing sodium bicarbonate in the dark at 0°C (ice bath), monitoring the reaction by $^1$H nmr spectroscopy. The organic phase was separated, washed with water, dried, and the solvent removed under vacuum in a rotatory evaporator (bath temperature: <30°C): **5**, 87% yield (98% active chlorine); **8**, 98% yield (99% active chlorine).

N-*Chlorobenzanilide* (**9**) was obtained as above but at room temperature and using methanol (150 mL) instead of methylene chloride. Methanol was then partly removed under vacuum, water was added, and the mixture was extracted with methylene chloride. The organic phase was washed with water, dried, and the solvent evaporated under vacuum (≤30°C). The residue was recrystallized from water–methanol (1:1): mp 78–79°C (lit. (40) 78–80°C), 56% yield (99% active chlorine). The recrystallized

[26]This is the melting point of the hydrochloride **20** since the amide cyclizes readily upon heating (see below).

Can. J. Chem. Downloaded from www.nrcresearchpress.com by 210.87.254.105 on 09/06/12
For personal use only.

material was treated with sodium bisulfite to give the parent amide contaminated with some (≃ 0.7%) 4'-chlorobenzanilide (**14**) separated by preparative layer chromatography on silica gel and identified to an authentic sample; no trace of head-to-tail dimer **13** was detected.

N-*Chloro*-N-*methyl*-α-*chloroorthotoluamide* (**17**) was also prepared by treatment of a methylene chloride solution of the amide with excess sodium hypochlorite but in the presence of hydrochloric acid (0.01 mol) instead of sodium bicarbonate: 65% yield (90% active chlorine); $\nu_{max}(CHCl_3)$ 1660 $cm^{-1}$ plus a weak peak at 1760 $cm^{-1}$ (C=O of phtalide); $\delta(CDCl_3)$ 3.25 (s, 3H), 4.54 (s, 2H), and 7.23 ppm (m, 4H) plus a singlet at 5.17 ppm due to the methylene group of phtalide. According to the integration, the molar ratio of phtalide to **17** was 0.11 (≃ 7% by weight). Some parent amide was also present (≤2%).

*Authentic samples*

*Head-to-tail dimer* ***13***: *N*-Phenylparaphenylenediamine (258 mg, 1.40 mmol), triethylamine (287 mg, 2.84 mmol), and benzoyl chloride (417 mg, 2.97 mmol) in dry toluene (35 mL) were heated to reflux for 7.5 h. Chloroform (150 mL) was added and the resulting solution washed successively with 5% hydrochloric acid (100 mL), 4 *N* sodium hydroxide (100 mL), and water (100 mL). The organic phase was dried and the solvent evaporated. Purification of the crude product by preparative layer chromatography (chloroform–methanol 95:5) gave 4-*benzamido*-N-*benzoyldiphenylamine* (**13**) (370 mg, 65% yield), mp 203°C (lit. (16), 203°C); *m/e* 392 ($M^+$).

*4'-Chlorobenzanilide* ***(14)*** *and 2'-chlorobenzanilide* ***(15)***: They were prepared from the corresponding chloroanilines and benzoyl chloride according to the general method described above for the preparation of amides: **14**, mp 192–193°C (lit. (41), 192–193°C); **15**, mp 97–98°C (lit. (42), 99°C).

N,N-*Dimethylorthotoluamide* ***(13)***: It was prepared from dimethylamine and orthotoluyl chloride according to the same general method (100% yield). The analytical sample was obtained by microdistillation at 80–85°C (0.25 Torr): $\nu_{max}(CHCl_3)$ 1630 $cm^{-1}$; $\delta(CDCl_3)$ 2.22 (s, 3H), 2.73 (s, 3H), 3.03 (s, 3H), and 7.03 ppm (narrow m, 4H); *m/e* 163 ($M^+$). *Anal.* calcd. for $C_{10}H_{13}NO$; C 73.59, H 8.03, N 8.58; found: C 73.62, H 8.00, N 8.66.

*Ethyl*-N-*methylazamalonate* ***(19)***: Ethyl azamalonate was prepared from urethane and ethylchloroformate as described by Tompkins and Degering (43): mp 48–49°C (lit. (43), 49–50°C); $\nu_{max}(CHCl_3)$ 3430, 1815, 1780, 1740, and 1500 $cm^{-1}$; $\delta(CDCl_3)$ 1.32 (t, $J$ = 7 Hz, 6H), 4.35 (q, $J$ = 7 Hz, 4H), and 7.68 ppm (m, NH). According to the method of Sheehan and Balhoper (44), ethyl azamalonate (458 mg, 2.84 mmol) was converted to its potassium salt which was then treated with excess methyl iodide. Separation of the crude product by preparative layer chromatography (ether–hexane 1:1) led to the recovery of ethyl azamalonate (184 mg, 40%) and gave the *N*-methyl derivative **19** (201 mg, 40%) as a colorless liquid: $\nu_{max}(CHCl_3)$ 1795, 1745, and 1695 $cm^{-1}$; $\delta(CDCl_3)$ 1.32 (t, $J$ = 7 Hz, 6H), 3.23 (s, 3H), and 4.28 ppm (q, $J$ = 7 Hz, 4H); *m/e* 175 ($M^+$).

N-*Methyliminophtalide* ***(21)***: Phtalide (12.0 g, 89.5 mmol) was added to a saturated solution of methylamine in methanol. After 36 h, evaporation to dryness gave α-hydroxy-*N*-methyltoluamide (14.7 g, 99.5%), mp 123–124°C; $\nu_{max}(CHCl_3)$ 3460, 3360, 1655, and 1535 $cm^{-1}$; δ(acetone-$d_6$) 2.85 (d, $J$ = 5 Hz, and m, $CH_3$ and OH), 4.50 (s, 2H), and 7.28 ppm (m, 4H), no detectable absorption for the NH. To a stirred solution of this hydroxyamide (5.0 g, 30 mmol) in pyridine (50 mL) cooled in an ice bath, solid paratoluenesulfonyl chloride (6.4 g, 33 mmol) was added in small portions in order to keep the temperature of the reaction mixture below 10°C. The solution turned orange, then pink, and a white solid separated out after 15 min. The reaction mixture was stirred at room temperature for 45 min then poured onto crushed ice. Hydrochloric acid was added (300 mL of a 10% solution) and the mixture washed with methylene chloride. The ice-cold aqueous phase was made basic by addition of solid sodium hydroxide (pellets) then extracted with methylene chloride. The organic phase was washed with brine then dried and the solvent was evaporated. Molecular distillation at 70–75°C (0.3 Torr) afforded the imino lactone **21** (3.7 g, 87% yield); $\nu_{max}(CHCl_3)$ 1700 $cm^{-1}$; $\delta(CDCl_3)$ 3.18 (s, 3H), 5.30 (s, 2H), 7.3 to 7.9 ppm (4H); *m/e* 147 ($M^+$). *Anal.* calcd. for $C_9H_9NO$: C 73.45, H 6.16, N 9.52; found: C 72.76, H 6.31, N 9.37. An impurity was formed during distillation according to the $^1H$ nmr spectrum.

N-*Methylphtalimidine* ***(22)***: It was prepared from *N*-methylphtalimide and zinc in acetic acid according to the method described by Brewster *et al.* (45), mp 113–114°C (lit. (45), 114.5–115.5°C); *m/e* 147 ($M^+$).

*Photochemical decomposition of* N-*chlorobenzanilide* ***(9)***

The *N*-chloro derivative **9** (381 mg, 97% active chlorine, 1.54 mmol) in acetonitrile–TEAP (0.1 *M*) (30 mL) was irradiated at 2537 Å in a Vycor cell with a Rayonnet RPR-100 reactor for 2.5 h (negative starch iodide paper test). Water was added and the mixture extracted with ether. The crude product (322 mg) was separated by plc (benzene–chloroform 95:5) to give three fractions consisting respectively of 2'-*chlorobenzanilide* (**15**), mp 96–97°C (44 mg, 12%), 4'-*chlorobenzanilide* (**14**), mp 187–189°C (238 mg, 67%), and benzanilide, mp 162–163°C (23 mg), identified (ir, $^1H$ nmr, tlc) to authentic samples. The amount of benzanilide isolated did correspond to that present in the starting material.

*Electrochemical instrumentation and methods*

All solutions were deoxygenated by bubbling through them dry and oxygen-free nitrogen saturated with acetonitrile. A nitrogen atmosphere was then maintained over the solution throughout the experiments which were carried out at a room temperature (without cooling the cell) unless otherwise stated. All voltammetric analyses and mass electrolyses were carried out using a three electrode system. Potentials were measured with respect to an aqueous saturated calomel electrode (sce) which has been described in ref. 1.

*Voltammetry*: The three electrode potentiostat used was a PAR-174. For the polarograms, the drop time (automatic drop dislodger supplied with the PAR-174) was generally 2 s, the sweep rate was 10 mV/s, and the potential range was 0.0 to −3.0 V. In the case of NBA (1*b*), Nujol was added at the bottom of the cell to isolate the solution from mercury and the cell was cooled in an ice bath (1). For the voltammograms, the platinum or vitreous carbon discs of the rotating electrode (Tacussel type ED1 with controvit speed controller) had a surface of 10 to 20 $mm^2$ and they were polished on a Carbimet-600 paper (Buehler) before each use. Platinum was regularly washed with nitric acid then rinsed with water and dried in an oven. The rotation rates varied from 500 to 5000 rpm.

*Mass electrolyses*: Controlled potential electrolyses (cpe) were performed with a Tacussel type ASA-100 three electrode potentiostat having both a Tacussel type IG-5 integrator and an ammeter connected in series within the auxiliary circuit. A glass cell described by Peltier and Moinet (46) was used with a mercury pool or a platinum plate as the working electrode, and a magnesium bar as the counter electrode. Two auxiliary electrode compartments differing in their length (depth) were used. With the shorter one, the volume of the catholyte varied from 90 to 175 mL and that of the anolyte from 15 to 40 mL; with the longer one, the volume of the catholyte varied between 15 and 25 mL and that of the anolyte, between 5 and 15 mL. The electrolyses were carried out on 2.5 to 7.5 mmol of *N*-haloamide (concentrations ranging from 0.03 to 0.3 *M*). In all electrolyses, a white precipitate of magnesium halide was formed in the anode

Can. J. Chem. Downloaded from www.nrcresearchpress.com by 210.87.254.105 on 09/06/12
For personal use only.

compartment. Since the cell was not cooled, heating of the solution (up to 40°C) was noted at the beginning of the electrolysis when the current density was high. The progress of the electrolysis was followed by iodometry and sometimes by polarography. Unless otherwise specified, the electrolyses were stopped when practically no current was flowing through the cell; about 98% of the starting active chlorine had been consumed by then.

In some cases (Table 1, entry 5, and Table 2, entries 3 to 7), passivation of the electrode did occur towards the end of the electrolysis and it was necessary to apply an anodic potential (+1.2 V) for 1 min to remove the species adsorbed on the electrode, then apply the working potential until passivation occurred again and the procedure was repeated until the electrolysis was completed. The coulometric results ($n_{app}$) are given in Tables 1 and 2 together with the applied potential and the cathode material. The larger the scale the longer was the time required for the electrolyses. The final solutions showed an orange to brown coloration which disappeared when sulfuric or perchloric acid was added. When the electrolysis was stopped, the catholyte and anolyte were combined, the acetonitrile was evaporated, and the residue was treated with a saturated aqueous solution of sodium bisulfite to destroy any residual active halogen. The resulting mixture was extracted with ether (a continuous extraction for 2 days was needed in the case of the urethane derivatives). The organic layer was dried, the solvent evaporated under vacuum or distilled at atmospheric pressure, and the resulting solution transferred into a volumetric flask. Aliquots were used for vpc and other analyses, and for chromatographic (plc) separations. All the products reported were identified to be authentic by ir and $^1$H nmr spectroscopy, vpc and/or tlc, and sometimes by mass spectrometry. The yields reported in Tables 1 and 2 were determined by vpc or plc. A few typical electrolyses are described below.

*Attempt to reduce the lithium salt of NCU (2a) in dry acetonitrile*

A freshly prepared solution of **2a** in dry acetonitrile (45.5 mL of a 0.11 *M* solution, 5.00 mmol) was added to the cathode compartment containing 100 mL of a 0.2 *M* solution of $LiClO_4$ in dry acetonitrile. The anode compartment contained 25 mL of the 0.2 *M* electrolyte solution. The cathode (Pt) potential was increased from −1.4 to −1.8 V during the first 2 h (25 C only were consumed) then to −3.2 V (reduction of the solvent–electrolyte system) for 13 h (436 C were consumed). Iodometric titration showed a loss of 27% of active chlorine. In a control experiment under the same conditions but without applying any potential, the loss of active chlorine after 15 h was 28%. Therefore the loss of active chlorine in the electrochemical experiment was not due to the reduction of **2a** but to its thermal and/or photochemical decomposition. The same work-up was applied to the two experiments: evaporation of the solvent, acidification with dilute sulfuric acid, continuous extraction with ether for 2 days. The vpc analyses (OS-138) showed the presence of urethane and *N*-chlorourethane (**1a**) in the same relative proportions for the two experiments.

*Reduction of* N-*Chloro*-N-*methyl-3-cyclohexenecarboxamide (6) (Table 1, entry 3)*

*N*-Chloroamide **6** (944 mg, 94% active chlorine, 5.11 mmol) was added to the cathode compartment containing 125 mL of a 0.1 *M* solution of TEAP in acetonitrile. The anode compartment contained 25 mL of the 0.1 *M* electrolyte solution. A potential of −0.8 V (Hg cathode) was applied until the current had reached a near zero value (4.5 h, <2% of active active chlorine left, 493 C). The anolyte and catholyte were combined and the solvent was evaporated. The residue was treated with a saturated $NaHSO_3$ solution then extracted with ether. The organic phase was dried, then concentrated in a rotatory evaporator. The resulting solution was transferred into a 50 mL volumetric flask. Analysis by vpc (OS-138) gave a 76% yield of *N*-methyl-3-cyclohexenecarboxamide (parent amide) and showed the presence of about 1% of the bicyclic compounds **10** and **11** which were already present in the starting material in similar quantities. An aliquot was separated by plc to give a pure sample of parent amide, mp 86–87°C, identified (ir, $^1$H nmr) to an authentic sample (13*a*).

*Reduction of* N-*chloro*-N-*methylorthotoluamide (8)*

*In the absence of a trapping agent* (Table 1, entry 6): *N*-Chloroamide **8** (795 mg, 98.5% active chlorine, 4.27 mmol) was added to the cathode compartment containing 15 mL of a 0.1 *M* solution of TEAP in acetonitrile. The anode compartment contained 5 mL of the electrolyte solution. The cell was cooled to −30°C and a potential of −0.8 V (Pt cathode) was applied. After 5.5 h, the current had dropped from 10.0 to 0.6 mA/cm² (327 C). The electrolysis was stopped and 21% of active chlorine was still present according to the iodometric titration. After the usual work-up, the ether solution was evaporated to dryness to afford *N*-methylorthotoluamide (659 mg) with a purity greater than 90% according to the $^1$H nmr spectrum.

*In the presence of methyl tosylate* (Table 2, entry 3): *N*-Chloroamide **8** (765 mg, 98.5% active chlorine, 4.11 mmol) and methyl tosylate (7.0 g, 38 mmol) were added to the cathode compartment containing 40 mL of a 0.1 *M* solution of TEAP in dry acetonitrile. The anode compartment contained 10 mL of the electrolyte solution. A potential of −1.0 V (Pt cathode) was applied until essentially nearly all the active chlorine was consumed (6.5 h, ≤2% of active chlorine left, 397 C). Towards the end of the electrolysis, passivation of the electrode occurred and an anodic potential has to be applied regularly as already described. After the usual work-up, the solvent was removed *in vacuo* and the residue was refluxed for 2 h in methanol–water (9:1, 40 mL) containing potassium iodide (6.4 g, 38 mmol) to convert the excess methyl tosylate into methyl iodide. Water was added and the mixture was extracted with ether. The ether layer was dried and the solvent stripped off in a rotatory evaporator. The $^1$H nmr of the crude product (605 mg) showed the presence of *N*-methylorthotoluamide and N,N-*dimethylorthotoluamide* (**18**) in a 5.7/1.0 molar ratio. The yields of parent amide (68%) and **18** (15%) were determined by vpc (OS-138). An aliquot was separated by plc for identification with authentic samples.

In control experiments, *N*-methylorthotoluamide and methyl tosylate were heated to reflux for 5 h either in the presence of potassium iodide in methanol–water (9:1) or in a 0.1 *M* solution of TEAP in acetonitrile. After the usual work-up, no trace of *N*,*N*-dimethylorthotoluamide (**18**) could be detected in either of the crude products by vpc, tlc, and $^1$H nmr spectroscopy.

The electrolysis and control experiments in the presence of methyl bromide were carried out in a similar way except that it was not necessary to destroy the excess methyl bromide. A green coloration appeared during the electrolysis. The yields are reported in Table 2, entry 4.

*Reduction of* N-*Chlorobenzanilide (9)*

*N*-Chloroamide **9** (701 mg, 99% active chlorine, 2.97 mmol) was added to the cathode compartment containing 40 mL of a 0.1 *M* solution of TEAP in dry acetonitrile. The anode compartment contained 10 mL of the electrolyte solution. A potential of −0.8 V (Pt cathode) was applied and after 3 h the current had dropped from 13.5 to 0.0 mA/cm² (287 C). After the usual work-up, the crude product (565 mg) was separated by plc (benzene–chloroform 95:5) to give *2′,4′-dichlorobenzanilide* (**16**), mp 116–116.5°C (lit. (42), 115–117°C) (2 mg, 2.5%), *2′-chlorobenzanilide* (**15**), mp 95–96°C (6 mg, 1%), *4′-chlorobenzanilide* (**14**), mp 192–192.5°C (71 mg, 10%), and benzanil-

Can. J. Chem. Downloaded from www.nrcresearchpress.com by 210.87.254.105 on 09/06/12
For personal use only.

ide, mp 162–163°C (446 mg, 76%). The most polar fraction was separated again (chloroform–methanol 89:11) to give the head-to-tail dimer **13**, mp 161–162°C (2 mg, 1.5%).

*Reduction of* N-*chloro*-α-*chloro*-N-*methylorthotoluamide* (**17**)

*N*-Chloroamide **17** (622 mg, 90% active chlorine, 2.55 mmol) in 40 mL of a 0.1 *M* solution of TEAP in acetonitrile (anode compartment: 10 mL of the electrolyte solution) was electrolysed at −1.0 V (Pt cathode) until passivation of the electrode (8 h); 89% of active chlorine (2.27 mmol) had been consumed (iodometric titration). The usual work-up procedure was applied except that the aqueous solution was made basic before extracting with ether. The $^1$H nmr spectrum of the crude product (471 mg) showed the presence of the iminolactone **21**, the *N*-methyllactam **22**, and the parent amide in a 1.55/1.00/0.58 molar ratio. Taking the quantity of **22** isolated below as the amount present in the crude product, the yields of **22** and **21** were 31% and 48% respectively (based on 2.27 mmol of **17** reduced). The amount of parent amide in the crude product was 0.41 mmol; assuming that the 0.28 mmol of **17** remaining after the electrolysis was quantitatively converted to the parent amide by sodium bisulfite, the yield of parent amide was 6%. The crude product was dissolved in chloroform and heated to reflux for 2 h to convert the parent amide into the hydrochloride **20** as seen above. The resulting solution was extracted with 5% hydrochloric acid. The organic phase was washed with brine, dried, and the solvent evaporated. Separation of the residue (171 mg) by plc (ether–methanol 99.5:0.5) gave some phtalide (16 mg) present in the starting material and N-*methylphtalimidine* (**22**), mp 111–113°C (104 mg, 31%). The acidic phases (from the extraction with hydrochloric acid) were combined, ice was added, and the mixture was made basic by adding solid sodium hydroxide. It was extracted with methylene chloride. The organic phase was washed with brine, dried, and the solvent was evaporated to afford pure N-*methyliminophtalide* (**21**) (226 mg, 56% yield).

*Cyclization of the anion of* α-*chloro*-N-*methylorthotoluamide*

The amide (108 mg, 0.59 mmol) in dry tetrahydrofuran (15 mL) was added, under argon at −78°C, to a solution of lithium diisopropylamide (0.67 mmol) in THF (4 mL). The addition took 30 min. The mixture was then allowed to warm up to room temperature. Ice was added and the basic medium extracted with methylene chloride. The organic phase was dried and the solvent evaporated to afford pure N-*methylphalimidine* (**22**), mp 110–112°C (88 mg, 100%).

## Acknowledgements

We are grateful to the "Ministère de l'Education du Québec" and to the Natural Sciences and Engineering Research Council of Canada for financial assistance. We thank Professor F. M. Kimmerle for helpful discussions and Y. Couture for carrying out the experiments on the cyclization of *N*-methyl-α-chloroorthotoluamide and its anion.

1. D. Bérubé, J. Caza, F. M. Kimmerle, and J. Lessard. Can. J. Chem. **53**, 3060 (1975).
2. H. Menard and J. Lessard. J. Chem. Eng. Data, **23**, 64 (1978).
3. C. D. Gutsche and D. J. Pasto. Fundamentals of organic chemistry. Prentice-Hall Inc., New Jersey. 1975. p. 181.
4. P. J. Elving. Can. J. Chem. **55**, 3392 (1977).
5. J. J. Eisch and W. Kaska. Chem. Ind. 470 (1961); J. J. Eisch and W. Kaska. J. Org. Chem. **27**, 3745 (1962); E. G. Janzen and J. L. Gerlock. J. Organomet. Chem. **8**, 354 (1967).
6. P. J. Elving and T. E. Cummings. J. Electroanal. Chem. **94**, 123 (1978); T. Wasa and P. J. Elving. J. Electroanal. Chem. **91**, 249 (1978); J. Y. Pape and J. Simonet. Electrochim. Acta, **23**, 445 (1978).
7. J. B. Hendrickson, D. J. Cram, and G. S. Hammond. Organic chemistry. McGraw-Hill Inc., New York. 1979. p. 305.
8. J. Caza. M. Sc. Dissertation. Université de Sherbrooke, Sherbrooke, Québec. 1973.
9. M. M. Baizer and T. Troll. Electrochim. Acta, **20**, 33 (1975).
10. A. J. Fry and R. G. Reed. J. Am. Chem. Soc. **94**, 8475 (1972).
11. N. Torimoto, T. Shingaki, and T. Nagai. J. Org. Chem. **44**, 636 (1979).
12. Y. L. Chow and R. A. Perry. Tetrahedron Lett. **531** (1972); M. E. Kuehne and D. A. Horne. J. Org. Chem. **40**, 1287 (1975).
13. (*a*) P. Mackiewicz, R. Furstoss, B. Waegell, R. Cote, and J. Lessard. J. Org. Chem. **43**, 3746 (1978); (*b*) J. Lessard, R. Cote, P. Mackiewicz, R. Furstoss, and B. Waegell. J. Org. Chem. **43**, 3730 (1978).
14. J. Lessard, M. Mondon, and D. Touchard. Can. J. Chem. **59**, 431 (1981).
15. R. S. Neale, N. L. Marcus, and R. G. Scheppers. J. Am. Chem. Soc. **88**, 3051 (1966).
16. M. C. Ford, L. J. Hunt, and W. A. Waters. J. Chem. Soc. 3529 (1953).
17. J. Zabicky (*Editor*). The chemistry of amides. John Wiley and Sons, New York. 1970. (*a*) pp. 159, 160; (*b*) pp. 734–752.
18. C. J. M. Stirling. J. Chem. Soc. 255 (1960).
19. F. M'Halla, J. Pinson, and J. M. Saveant. J. Electroanal. Chem. **89**, 347 (1978); L. Nadjo and J. M. Saveant. J. Electroanal. Chem. **30**, 41 (1971).
20. M. R. Rifi. *In* Organic electrochemistry. *Edited by* M. M. Baizer. Marcel Dekker, New York. 1973. pp. 282–286.
21. A. J. Bellamy, G. Howat, and I. S. Mackirdy. J. Chem. Soc. Perkin II, 786 (1978).
22. J. L. Webb, C. K. Mann, and H. M. Walborsky. J. Am. Chem. Soc. **92**, 2042 (1970).
23. R. A. De La Tore and J. W. Sease. J. Am. Chem. Soc. **101**, 1687 (1979).
24. O. Manousek and P. Zuman. Coll. Czech. Chem. Commun. **29**, 17 (1964); G. Charlot, J. Badoz-Lambling, and B. Tremillon. Les réactions électrochimiques, Masson, Paris. 1959. p. 75.
25. A. Kirmann and M. Kleene-Peter. Bull. Soc. Chim. Fr. 894 (1957).
26. N. S. Husch and K. B. Oldham. J. Electroanal. Chem. **6**, 34 (1963).
27. S. Wawzonek, R. C. Duty, and J. H. Wagenknecht. J. Electrochem. Soc. **111**, 74 (1964).
28. L. B. Rogers and A. J. Diefenderfer. J. Electrochem. Soc. **114**, 942 (1967).
29. A. J. Fry and D. Herr. Tetrahedron Lett. 1721 (1978).
30. R. B. Yamasaki, M. Tarle, and J. Casanova. J. Org. Chem. **44**, 4519 (1979).
31. A. Merz and A. J. Bard. J. Am. Chem. Soc. **101**, 2959 (1979).
32. F. M. Triebe, K. J. Borhoni, and D. M. Hawley. J. Am. Chem. Soc. **101**, 4637 (1979).
33. C. P. Andrieux, C. Blockman, J. M. Dumas-Bouchiat, and J. M. Saveant. J. Am. Chem. Soc. **101**, 3431 (1979).

34. J. F. O'DONNEL, J. T. AYRES, and C. K. MANN. Anal. Chem. **37**, 1161 (1965).
35. H. O. HOUSE, E. FENG, and N. P. PEET. J. Org. Chem. **36**, 2371 (1971).
36. R. L. VAULX, W. H. PUTERBOUGH, and C. R. HAUSER. J. Org. Chem. **29**, 3514 (1964).
37. J. J. RITTER and P. P. MINIERI. J. Am. Chem. Soc. **70**, 4047 (1948).
38. D. J. BURTON and W. M. KOPPER. J. Org. Chem. **40**, 3026 (1975).
39. C. BACHAND, H. DRIGUEZ, J. M. PATON, D. TOUCHARD, and J. LESSARD. J. Org. Chem. **39**, 3136 (1974).
40. H. YUKI, T. KISHIKAWA, Y. TOHIKA, S. SUZUKI, F. FANO, and S. HAYAKAWA. Chem. Pharm. Bull. **15**, 1123 (1967); Chem. Abstr. **68**, 39304*f* (1968).
41. Beilstein Handbuch der Organischen Chemie, Vol. 12, 1929. p. 612.
42. F. M. FAHMY and H. ABDEL-FADEL. Indian J. Chem. **11**, 440 (1973).
43. L. G. R. TOMPKINS and E. F. DEGERING. J. Am. Chem. Soc. **69**, 2617 (1947).
44. J. C. SHEEHAN and W. A. BALHOPER. J. Am. Chem. Soc. **72**, 2786 (1950).
45. J. H. BREWSTER, A. M. FUSO, L. E. CAROSINO, and B. G. CORMAN. J. Org. Chem. **28**, 498 (1963).
46. D. PELTIER and C. MOINET. Bull. Soc. Chim. Fr. 690 (1969).

Can. J. Chem. Downloaded from www.nrcresearchpress.com by 210.87.254.105 on 09/06/12
For personal use only.

FOR ERRATA SEE
V.61 1983 P. 640



# Some observations on the Pd(II)-catalysed ferrocenylation of acrylonitrile

PATRICK M. HENRY
*Department of Chemistry, Guelph–Waterloo Centre for Graduate Work in Chemistry, Guelph Campus, Guelph, Ont., Canada N1G 2W1*
NITA A. LEWIS
*Department of Chemistry, University of New Brunswick, Fredericton, N.B., Canada E3B 6E2*
AND
HENRY TAUBE
*Department of Chemistry, Stanford University, Stanford, CA 94305 U.S.A.*

Received April 15, 1981

PATRICK M. HENRY, NITA A. LEWIS, and HENRY TAUBE. Can. J. Chem. **60**, 1143 (1982).

The Pd(II)-catalysed alkylation of ferrocene with acrylonitrile has been reinvestigated. We were not able to prepare the 1,1′-bis-(2-cyanovinyl)ferrocene using 1,1′-bis(chloromercuri)ferrocene and Pd(II) under stoichiometric conditions. Using ethanol as solvent, a side-product, 3,3-diethoxypropanenitrile, was obtained. Using methanol, the corresponding 3,3-dimethoxypropanenitrile was produced. Acetonitrile as solvent gave a small amount of the desired product. The reaction of chloromercuriferrocene with acrylonitrile under conditions catalytic in Pd(II) produced the 2-cyanovinylferrocene species. Mixtures of *cis* and *trans* isomers were obtained. The *cis*/*trans* ratio was 20/80, 30/70, and 50/50 in methanol, ethanol, and acetonitrile, respectively. The pure *trans* product was obtained by refluxing the *cis*/*trans* mixture with $I_2/CHCl_3$. The isomers were also separated by chromatography on alumina.

PATRICK M. HENRY, NITA A. LEWIS et HENRY TAUBE. Can. J. Chem. **60**, 1143 (1982).

On a étudié de nouveau l'alkylation, catalysée par le Pd(II), du ferrocène avec l'acrylonitrile. Nous n'avons pas pu préparer le bis(cyano-2 vinyl)-1,1′ ferrocène en utilisant le bis(chloro-mercure)-1,1′ ferrocène et le Pd(II) en quantités stochiométriques. On obtient un produit secondaire, le diéthoxy-3,3 propanenitrile, lorsqu'on utilise l'éthanol comme solvant. Dans le méthanol, on obtient le diméthoxy-3,3-propanenitrile comme produit secondaire. L'utilisation de l'acétonitrile comme solvant permet d'obtenir une faible quantité du produit désiré. Le chloromercureferrocène réagit avec l'acrylonitrile en présence du Pd(II) comme catalyseur en donnant des cyano-2 vinyl ferrocènes. On a obtenu des mélanges d'isomères *cis* et *trans*. Le rapport *cis*/*trans* est de 20/80, 30/70 et 50/50 respectivement dans le méthanol, l'éthanol et l'acétonitrile. On obtient le produit *trans* à l'état pur en portant un mélange d'isomères *cis*/*trans* au reflux avec de l'iode dans le chloroforme. On a également séparé les isomères par chromatographie sur alumine.

[Traduit par le journal]

## Introduction

It has been reported that alkyl and 1,1′-dialkyl substituted ferrocenes may be prepared by the reactions of olefins with chloromercuriferrocene (**1**) or 1,1′-bis(chloromercuri)ferrocene (**2**), respectively, in the presence of lithium chloropalladite. Our repeated attempts to prepare 1,1′-bis(2-cyanovinyl)ferrocene (**3**) by the reaction of the dimercurial (**2**) with acrylonitrile in ethanol showed that the reaction is not as simple as was reported earlier (2).

The yield of product was always extremely low and side reactions, one of which involved the solvent, were found to interfere. All possible combinations of *cis*/*trans* isomeric products were produced for **3** and **4**; these were separated and characterised independently in the case of 2-cyanovinylferrocene, **4**. Since these reactions did not proceed as expected, we wish to report the results of our detailed studies on these systems.

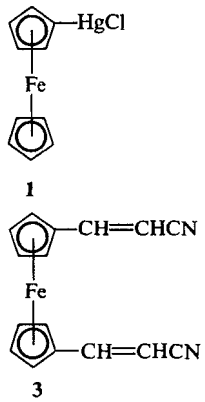


## Experimental

*Chemicals and reagents*

All chemicals were reagent grade and were used as supplied except for the acetonitrile and acrylonitrile which were freshly distilled prior to being used. Solvents were purchased from Baker Chemicals, $PdCl_2$ from Engelhardt or Alfa, ferrocene and

0008-4042/82/091143-05$01.00/0
©1982 National Research Council of Canada/Conseil national de recherches du Canada

Can. J. Chem. Downloaded from www.nrcresearchpress.com by 210.87.254.40 on 09/06/12
For personal use only.

Can. J. Chem. Downloaded from www.nrcresearchpress.com by 210.87.254.40 on 09/06/12
For personal use only.

$HgCl_2$ from BDH. The commercial sample of 1,1'-bis(chloromercuri)ferrocene (**2**) was obtained from Aldrich.

The dimercurial (**2**) was prepared by three different procedures. The first sample was synthesised according to the method of Fish and Rosenblum (3), the second was the commercial sample (Aldrich) and the third was made using the procedure of Rausch *et al.* (4). This third sample was thoroughly extracted with acetone to remove the 1,2-bis(chloromercuri)ferrocene which is a common contaminant. All samples of the dimercurial were found to be insoluble in all common solvents except dimethylformamide or dimethylsulphoxide, and in these media, they were only sparingly soluble. The nmr spectra of all three samples in $d^6$-dmso showed that the dimercurial (**2**) was at least 95% pure.

*Physical measurements*

The nmr measurements were performed on a Varian A60 instrument. All values are quoted in ppm from TMS on the δ scale. Elemental analyses were performed by Guelph Chemical Laboratories Ltd.

*Preparation of palladium(II) chloride stock solutions.* The solutions were 0.10 *M* in Pd(II) and contained sufficient lithium chloride to solubilize the palladium(II) chloride. In acetonitrile, LiCl is sparingly soluble but 1 mol LiCl dissolves along with 1 mol $PdCl_2$ to give a species with the composition $LiPdCl_3$ which spectral evidence suggests is the dimer, $Li_2Pd_2Cl_6$, similar to the species present in acetic acid (ref. 1, p. 15). On the other hand, in methanol and ethanol 2 mol LiCl per mole of $PdCl_2$ are required to dissolve $PdCl_2$. This suggests that the species is largely the monomer, $Li_2PdCl_4$, and a spectral study has supported this supposition (ref. 1, p. 15).

*Reaction of 1,1'-bis(chloromercuri)ferrocene (2) with acrylonitrile using Pd(II) under stoichiometric conditions.* The method used was essentially the same as that of Kasahara *et al.* (2). To 100 mL of the appropriate palladium(II) chloride stock solution was added acrylonitrile (40 mmol, 2.64 mL) and 1,1'-bis(chloromercuri)ferrocene (**2**) (10 mmol, 3.28 g) and the solution was allowed to stir for 16 h at room temperature. The solvent was then allowed to evaporate and the residue was chromatographed on neutral alumina using benzene and chloroform as eluents.

In reactions using methanol or ethanol as solvent, organic oxidation products, 3,3-dimethoxypropanenitrile and 3,3-diethoxypropanenitrile, respectively, were sometimes observed with yields less than 5% based on Pd(II) used in both cases (see Results and discussion). Samples of these materials were also made by leaving out the dimercurial in the above reaction. These samples were purified by distillation and were found to have nmr spectra identical with those of the compounds formed in the presence of the dimercurial. *Anal.* calcd. for $C_5H_9NO_2$: C 52.16, H 7.89, N 12.17; found: C 51.80, H 8.03, N 12.56. *Anal.* calcd. for $C_7H_{13}NO_2$: C 58.71, H 9.17, N 9.78; found: C 58.72, H 9.25, N 10.16.

*Reaction of 1,1'-bis(chloromercuri)ferrocene (2) with acrylonitrile using Pd(II) under catalytic conditions.* To 100 mL of the acetonitrile stock solution acrylonitrile (100 mmol, 7.0 mL), $CuCl_2$ (20 mmol, 2.69 g), and **2** (5 mmol, 3.28 g) were added. The solution was allowed to stir at 30°C for 1 week. The reaction mixture was then diluted with $CH_2Cl_2$ and extracted thrice with 3 *M* HCl to remove the metal salts, then thrice with water. The remaining organic layer was dried over magnesium sulphate, concentrated, and then chromatographed on neutral alumina using hexane/$CH_2Cl_2$ mixtures as eluents. The total yield of 2-cyanovinylferrocene was 15–20% with each of the *cis* and *trans* isomers accounting for about half of the product (see Results and discussion).

*Reaction of chloromercuriferrocene with acrylonitrile under conditions catalytic in Pd(II).* A 10 mL aliquot of the palladium(II) chloride/acetonitrile stock solution was diluted to 100 mL with $CH_3CN$. To this solution acrylonitrile (100 mmol, 7.0 mL), $CuCl_2$ (20 mmol, 2.69 g), and **1** (10 mmol, 4.20 g) were added. To 100 mL of the solvent $PdCl_2$ (1.0 mmol, 0.177 g) and LiCl (2 mmol, 0.08 g) were added. After these compounds had dissolved, acrylonitrile (100 mmol, 7.0 mL), $CuCl_2$ (20 mmol, 2.69 g), and **1** (10 mmol, 4.20 g) were added. The solution was allowed to stir for 24 h and was then worked-up as described for the catalytic mixture in the previous reaction. The *cis*/*trans* isomers separated cleanly on the alumina column if the separation were performed slowly by using a low concentration (2–5%) of $CH_2Cl_2$ in the $CH_2Cl_2$/hexane mixture. The total yield of 2-cyanovinylferrocene was 17–20%; the proportion of each isomer obtained depended on the solvent employed (see Results and discussion). *Anal.* calcd.: C 65.86, H 4.68, N 5.91; found: *cis* C 65.37, H 4.75, N 5.56, *trans* C 65.99, H 4.68, N 6.02.

## Results and discussion

In experiments run under conditions stoichiometric in Pd(II) and using the dimercurial prepared according to the method of Fish and Rosenblum (3), the major product was a volatile liquid. The nmr spectrum and analysis of this material showed it to be 3,3-diethoxypropanenitrile (**5**) (see Fig. 1 and Table 1). The expected quartet due to the protons on the methylene carbon of the ethoxy groups was unexpectedly split to give a doublet of quartets. Since a similar splitting does not occur in the peaks due to the methine proton, this fine structure must be due to the existence of two different diastereomers in solution.

The acetal product (**5**) is that expected from the oxidation of acrylonitrile in the absence of mercurial, by analogy (ref. 1, pp. 133–147) to the oxidation of acrylonitrile in water which gives the product cyanoacetaldehyde (5). The formation of the acetal probably depends on the acidity of the medium since acids are known to inhibit the acetal forming reaction (6). Similar results were obtained using methanol as solvent. In this case, 3,3-dimethoxypropanenitrile (**6**) (see Table 1) was formed. The organic oxidation product could be obtained under the same reaction conditions (stoichiometric in Pd(II)) in the absence of any mercurial. The major products produced in all experiments with mercurial present were intractable polymers.

The reactions of either the commercial sample of the dimercurial (**2**) or the sample prepared according to the method of Rausch *et al.* (4) with acrylonitrile and Pd(II) used in stoichiometric amounts in ethanol did not produce any detectable amounts of the disubstituted product, 1,1'-bis(2-cyanovinyl)ferrocene (**3**). Neither was any of the organic oxidation product observed in experiments with these starting materials, presumably because the trace amounts of acid were greater in these two preparations. The only materials obtained after

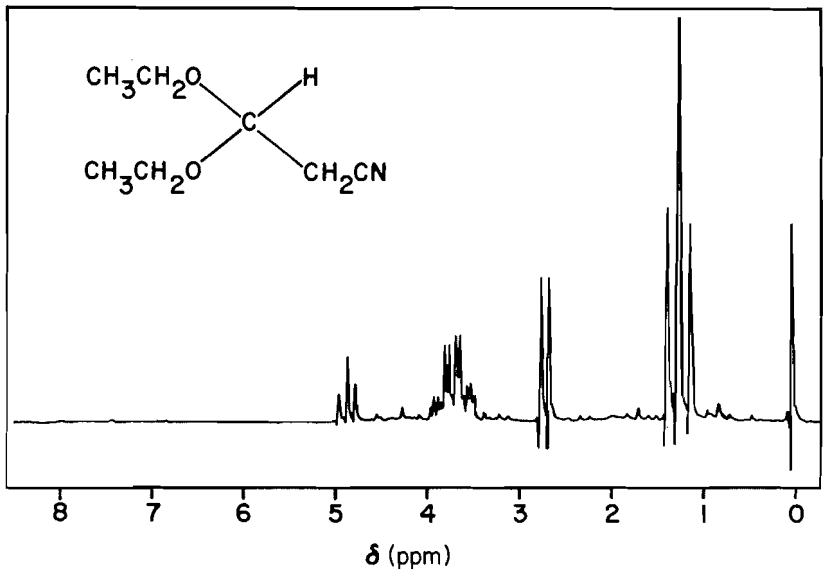


FIG. 1. Proton magnetic resonance spectrum of 3,3-diethoxypropanenitrile showing the existence of the two conformers.

TABLE 1. Proton magnetic resonance shifts of the organic oxidation products[a]

| Compound | Chemical shift (ppm δ) | | | |
|---|---|---|---|---|
| | —C(—H)—[b] | $CH_3$— | —$CH_2$—[c] | —$CH_2CN$[b] |
| 3,3-Dimethoxypropanenitrile $(CH_3O)_2CH_2CN$ | 4.65 (t, 1) | 3.41 (s, 6) | | 2.65 (d, 2) |
| 3,3-Diethoxypropanenitrile $(CH_3CH_2O)_2CHCH_2CN$ | 4.82 (t, 1) | 1.18 (t, 6) | 3.48, 3.52<br>3.60, 3.64<br>3.72, 3.76<br>3.84, 3.88 | 2.66 (d, 2) |

[a]Spectra run in $CDCl_3$ with internal TMS standard.
[b]The coupling constant between the methine proton and the methylene group for both complexes was $J$ = 6 Hz.
[c]Quartet of doublets due to existence of two conformers. Integration gives four protons. See figure.

chromatography on alumina were small amounts of ferrocene and 2-cyanovinylferrocene (**4**) as determined by nmr spectroscopy. Most of the starting material was converted to polymeric materials which could not be removed from the alumina.

Recrystallisation of the product mixture from hexane gave an analytically pure sample of **4**. However, the nmr spectrum had an extra set of peaks which were not reported earlier (2), in the vinyl region (7.36, 7.08(d); 7.05, 6.86(d); and 5.48,

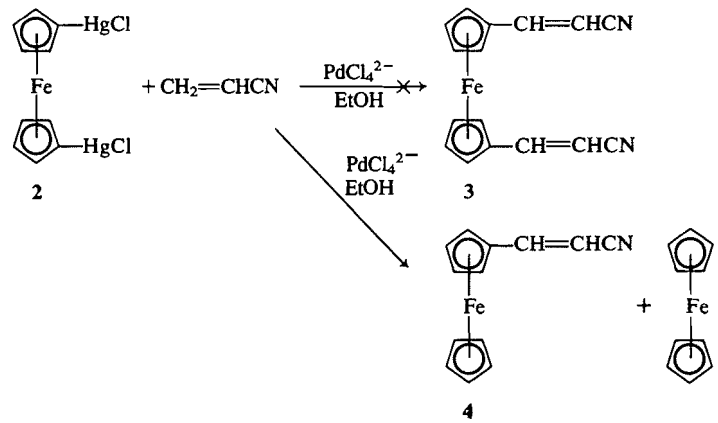


Can. J. Chem. Downloaded from www.nrcresearchpress.com by 210.87.254.40 on 09/06/12
For personal use only.

TABLE 2. Proton magnetic shifts of 2-cyanovinylferrocene derivatives[a]

| Compound | Chemical shift (ppm δ) | | | |
|---|---|---|---|---|
| | Unsubstituted ring | Substituted ring | $Fc-\overset{H_A}{\underset{|}{C}}=$ | $=\overset{H_B}{\underset{|}{C}}-CN$ |
| *cis*-(2-Cyanovinylferrocene) | 4.21 (s, 5) | 4.46 (t, 2)[b]<br>4.85 (t, 2) | 5.17 (d, 1)[c] | 6.96 (d, 1) |
| *trans*-(2-Cyanovinylferrocene) | 4.12 (s, 5) | 4.39 (s, 4) | 5.34 (d, 1)[d] | 7.22 (d, 1) |

[a]The solvent used was $CDCl_3$ with internal TMS standard.
[b]The coupling between the two types of protons on the substituted ring was $J$ = 1.8 Hz.
[c]The coupling constant for *cis*-2-cyanovinyl protons was $J$ = 11.4 Hz.
[d]The coupling constant for *trans*-2-cyanovinyl protons was $J$ = 16.8 Hz.

5.20(d); 5.26, 5.07(d)) which suggested that this compound existed as a mixture of *cis* and *trans* isomers. The total yield of the isomeric mixture of **4**, using either the commercial sample or the sample prepared according to Rausch *et al.* (4), was low, about 3% based on Pd(II).

The use of acetonitrile as solvent produced somewhat different results, although they were the same for all three preparations of the dimercurial. A small amount of material was obtained which had an nmr spectrum consistent with that of the expected product, 1,1′-bis(2-cyanovinyl)ferrocene (**3**) (2). The yield of **3** was about 2% based on Pd(II). The nmr spectrum in the vinyl region indicated that the material was a mixture of *cis*/*cis*, *trans*/*trans*, and *cis*/*trans* isomers. Traces of other products were obtained but these were present in such minute quantities that they could not be identified. Again, the major products were polymers which could not be characterised.

The formation of traces of the monosubstituted product, 2-cyanovinylferrocene (**4**) in the reaction of the dimercurial, **2**, could result from impurities of the monomercurial, **1**. It could also result from demercuration of the dimercurial under the reaction conditions to give the monomercurial, **1**, which could then react with acrylonitrile as usual to give **4**.

There is some analogy for this reaction since palladium(II) acetate can dehalogenate bromo- and iodobenzene (7).

Since the earlier study (2) reported only the *trans* isomers from the preparations of both 1,1′-bis-(2-cyanovinyl)ferrocene (**3**) and 2-cyanovinylferrocene (**4**), we decided to investigate further the reaction leading to the latter product. It had been reported (2) that the reaction of chloromercuriferrocene and acrylonitrile proceeded nicely under conditions catalytic in Pd(II) by using Cu(II) to reoxidise the expensive palladium catalyst.

The yield of 2-cyanovinylferrocene (**4**) obtained under these catalytic conditions was 17–20% based on chloromercuriferrocene used. A small amount (<5%) of unreacted chloromercuriferrocene and diferrocene was also obtained from each preparation. The remainder of the starting material was converted to sparingly soluble polymeric material which would not pass through the alumina column and which defied characterisation.

The product, 2-cyanovinylferrocene, always contained some *cis* isomer, the amount depending on the solvent used in the reaction. The *cis*/*trans* ratio was 20/80, 30/70, and 50/50 in methanol, ethanol, and acetonitrile, respectively. The pure *trans* product could be obtained by refluxing the isomeric mixture in $CHCl_3$ containing $I_2$ for a period of one week.[1] The nmr of the material obtained in this fashion was similar to that reported earlier for the pure *trans* compound (2). This spectrum is anomalous for a monosubstituted ferrocene compound. Normally the peaks for the protons on the substituted rings appear as two triplets but in this spectrum (see Table 2) they are present as a singlet, at 4.39 δ.

The two isomers could also be separated efficiently by chromatography on alumina. The nmr spectrum of the pure *cis* product is given in Table 2. The spectrum is the expected one for a monosub-

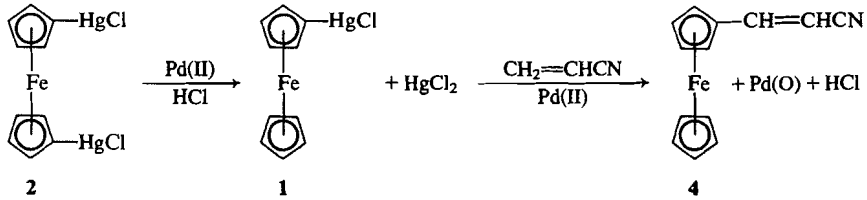


2 1 4

[1]We are grateful to Professor Z. Valenta for this suggestion.

Can. J. Chem. Downloaded from www.nrcresearchpress.com by 210.87.254.40 on 09/06/12
For personal use only.

stituted ferrocene derivative with a singlet for the unsubstituted ring and two triplets for the substituted one. Borovyak *et al.* (8) reported the same results for the nmr spectra of the *cis* and *trans* isomers of **4** prepared by an alternative method (9). In addition, they determined the crystal structure of the *trans* isomer (8).

We attempted to make the complex 1,1′-bis(2-cyanovinyl)ferrocene, **3**, by the catalytic route using $PdCl_2$ and $CuCl_2$ to reoxidise the palladium. In all cases, we obtained only the monosubstituted derivative **4** in surprisingly high yield (about 15–20% based on dimercurial used). This lends support to the idea that demercuration does indeed occur (*vide supra*). The remainder of the starting material was converted to polymeric materials.

The isolation of *cis* products may seem a bit surprising since the olefin arylation reaction usually gives *trans* products (ref. 1, pp. 147–178) but in the case of acrylonitrile, the arylation reaction, for some reason, gives mixtures of *cis* and *trans* isomers (10–12).

**Acknowledgments**

P.M.H. and N.A.L. are grateful to the Natural Sciences and Engineering Research Council of Canada for a Co-op grant in aid of this research. They also thank H.T. for his hospitality, the former during the winter and spring of 1978 while he was on sabbatical leave at Stanford, and the latter during 1977–1979 while she was a post-doctoral fellow in the laboratories of H.T. This work was initiated during that period. We thank Mr. Chris Friesen for the chromatographic separation of the *cis* and *trans* isomers.

1. P. M. HENRY. Palladium catalysed oxidation of hydrocarbons. D. Reidel, Dordrecht, Holland. 1980.
2. A. KASAHARA, T. IZUMI, G. SAITO, M. YODONO, R. SAITO, and Y. GOTO. Bull. Chem. Soc. Jpn. **45**, 895 (1972).
3. R. E. FISH and M. ROSENBLUM. J. Org. Chem. **30**, 1253 (1965).
4. M. D. RAUSCH, L. P. KLEMANN, A. SIEGEL, R. F. KOVAR, and T. H. GUND. Synth. Inorg. Met. Org. Chem. **3**, 193 (1973).
5. J. SMIDT and R. SIEBER. Angew. Chem. **71**, 626 (1959).
6. H.-B. LEE and P. M. HENRY. Can. J. Chem. **54**, 1726 (1976).
7. H. TANAKA, Y. FUJIWARA, I. MORITANI, and S. TERANISHI. Bull. Chem. Soc. Jpn. **48**, 3372 (1975).
8. T. É. BOROVYAK, V. E. SHKLOVER, A. I. GUSEV, S. P. GUBIN, A. A. KORIDZE, and YU. T. STRUCHKOV. Zhur. Strukt. Khim. **11**, 1087 (1970).
9. T. P. VISHNYAKOVA and A. A. KORIDZE. Zh. Obshch. Khim. **39**, 210 (1969).
10. S. DANNO, I. MORITANI, and Y. FUJIWARA. Tetrahedron, **25**, 4819 (1969).
11. R. F. HECK. J. Am. Chem. Soc. **93**, 6896 (1971).
12. J. B. MELPOLDER and R. F. HECK. J. Org. Chem. **41**, 265 (1976).

Can. J. Chem. Downloaded from www.nrcresearchpress.com by 210.87.254.40 on 09/06/12
For personal use only.

# Étude structurale d'aldimines derivées des furanne-, thiophène- et *N*-méthylpyrrolecarboxaldéhydes-2. I. *N*-hétéroarylidèneanilines

PAUL AUDOYE, RENÉ-CHARLES COUMES, ANTOINE GASET ET JEAN-PIERRE GORRICHON[1]

*Laboratoire de Chimie Organique et d'Agrochimie, Ecole Nationale Supérieure de Chimie (INPT), 118, route de Narbonne, 31077 Toulouse Cédex, France*

Reçu le 14 mai 1981[2]

PAUL AUDOYE, RENÉ-CHARLES COUMES, ANTOINE GASET et JEAN-PIERRE GORRICHON. Can. J. Chem. **60**, 1148 (1982).

Nous avons étudié une série de cinq *N*-hétéroarylidèneanilines, nitrées ou non sur l'hétérocycle et dans lesquelles l'hétéroatome peut être O, S ou N—$CH_3$. Les résultats obtenus en uv et en rmn du carbone-treize permettent de penser que, comme pour la benzylidèneaniline, ces molécules ne sont pas entièrement planes. De plus, la rmn du proton montre qu'il n'existe qu'un seul rotamère (ou à la limite un équilibre entre deux rotamères en échange rapide) sur les quatre possibles.

PAUL AUDOYE, RENÉ-CHARLES COUMES, ANTOINE GASET, and JEAN-PIERRE GORRICHON. Can. J. Chem. **60**, 1148 (1982).

We have studied a series of five *N*-heteroarylideneanilines, either nitrated or not on the heterocyclic ring, in which the hetero atom can be O, S or N—$CH_3$. The uv and $^{13}C$ nmr results obtained suggest that these molecules are, as in the case of benzylideneaniline, not entirely planar. In addition, $^1H$ nmr shows that only a single rotamer exists out of the four possibilities (or, at the limit, a rapid equilibrium between two rotamers).

[Journal translation]

## Introduction

Dans le cadre d'une étude des propriétés antibactériennes (1) et antiparasitaires (2) d'aldimines issues d'aldéhydes hétérocycliques et de diverses amines, nous avons été amené à synthétiser des molécules du type:

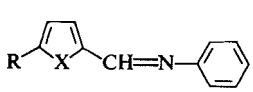

| | | | |
|---|---|---|---|
| R = H | X = O | | 1 |
| | X = S | | 2 |
| | X = N—Me | | 3 |
| R = $NO_2$ | X = O | | 4 |
| | X = S | | 5 |

De nombreuses études structurales ont été menées sur les *N*-benzylidèneanilines (3–10) à l'aide de différentes techniques physicochimiques. De ces divers travaux, on peut conclure que pour ces molécules, seul l'isomère *E* (*anti*) est présent à l'équilibre et que la structure n'est pas plane. Dans le cas de la benzalaniline (4), le plan du noyau benzénique provenant de l'aniline semble être perpendiculaire au plan du reste phényliminique. De plus, il a été proposé (4), en prenant en compte l'énergie électronique de ce composé, que l'hybridation de l'azote est proche du type *sp*.

Les résultats comparables en série hétérocyclique à cinq chaînons sont peu nombreux (11–14) et demeurent peu concluants voire contradictoires. Nous avons donc entrepris l'étude de ces cinq composés en spectroscopies infrarouge, ultraviolette et de résonance magnétique nucléaire du proton et du carbone-13.

## Résultats et discussion

Pour de telles molécules, on peut prévoir deux isomères *E* et *Z* autour de la double liaison >C= N—. Ces molécules présentent quatre isomères de rotation que nous avons représentés dans la figure 1.

La chromatographie en phase gazeuse ne permet de détecter qu'un seul isomère. De plus, dans le cas de la thiénylidèneaniline, **2**, nous avons enregistré une série de spectres ultraviolets après irradiation (de 2 à 60 minutes) à des longueurs d'onde de 254 et 350 nm. Le fait que le spectre n'est pas modifié lors de cette expérience, indique bien que nous sommes en présence d'un seul isomère de ce dérivé. Compte tenu des résultats de la littérature obtenus pour les benzylidineanilines et de l'encombrement stérique, on peut penser qu'il s'agit de l'isomère *E*.

### *Spectrographie infrarouge*

Les fréquences d'absorption $\nu_{C=N}$ et $\nu_{NO_2}$ que nous observons pour les cinq composés étudiés (cf. tableau 1) sont conformes à celles déjà présentés dans la littérature (12, 13, 15). Signalons simplement que la présence du groupement —$NO_2$, si elle n'a que peu d'influence sur la position de la vibration $\nu_{C=N}$, semble affaiblir considérablement l'intensité de la bande d'absorption correspondante.

Il est à noter que Head et Jones (13), ont pu montrer que pour le dérivé **6** (cf. figure 2), la fréquence de la bande d'absorption $\nu_{N-H}$ est en accord avec une liaison N—H...N (et non avec une liaison N—H...π), ce qui renforce l'hypothèse

[1]Auteur auquel doit être adressée toute correspondance.
[2]Révision reçu le 1 décembre 1981.

0008-4042/82/091148-07$01.00/0
©1982 National Research Council of Canada/Conseil national de recherches du Canada

Can. J. Chem. Downloaded from www.nrcresearchpress.com by 210.87.254.5 on 09/06/12
For personal use only.

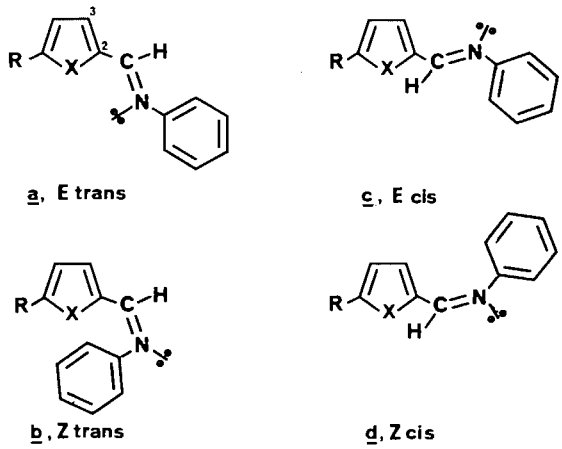


FIG. 1. Isomères de rotation des aldimines 1 à 5. La notation *cis* ou *trans* correspond aux positions *s-cis* ou *s-trans* des doubles liaisons C=N et C(2)=C(3) (intracyclique).

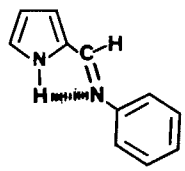

FIG. 2. 2-Pyrrolylméthylèneaniline 6.

d'une seule configuration *E* pour ce type de substrat.

*Spectroscopie ultraviolette*

Le problème de la non coplanéité des composés de la même série que la benzylidèneaniline a été étudié, nous l'avons déjà vu, par divers auteurs avec l'aide de la spectroscopie ultraviolette (3–6). Leurs discussions font intervenir deux modes de participation du groupement azomethine $\rangle CH=N-$ dans la conjugaison de la molécule: d'une part, au moyen des électrons $\pi$ de la double liaison, d'autre part de la paire libre portée par l'atome d'azote.

Si bien que l'on peut s'attendre à trois bandes d'absorption correspondant aux systèmes représentés dans la figure 3. La présence de ces trois bandes dans le spectre uv doit alors confirmer la structure non planaire du composé étudié.

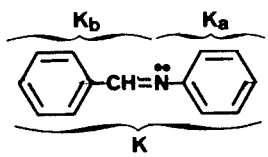


FIG. 3. Types de bandes d'absorption observées en uv pour la benzylidèneaniline.

Nous avons envisagé un travail similaire pour les aldimines **1** à **5**. Les valeurs des maxima d'absorption et des coefficients d'extinction sont rassemblées dans le tableau 1.

Pour les composés non nitrés **1**, **2** et **3**, on constate effectivement l'existence de bandes du type *K*, $K_a$ et $K_b$. Les bandes situées entre 315 et 324 nm représentent le système totalement conjugué. En effet, cette bande disparaît lorsque l'on hydrolyse ces imines en milieu acide. Les bandes comprises entre 287 et 302 nm sont composées et attribuables d'une part à la transition $\pi-\pi^*$ du type de celle des aldéhydes de départ (273–288,5 nm; cf. tableau 2) et d'autre part à la transition $n-\pi^*$ de la paire libre d'électrons de l'atome d'azote telle qu'elle existe dans la molécule d'aniline (286 nm selon réf. 11).

Les bandes correspondantes à la transition $\pi-\pi^*$ de l'aniline (235 nm selon réf. 11) apparaissent à 237 et 240 nm dans le cas des dérivés **1** et **2**. Elle est probablement masquée par l'absorption qui se trouve à 220 nm dans le cas de la *N*-méthyl pyrrolylméthylèneaniline **3**.

On note de plus, dans le cas des composés **2** et **3**, une bande d'absorption respectivement à 269 et 260 nm. Nous pensons qu'elles sont attribuables au système $K_a$ puisqu'on retrouve des bandes de ce type et à des maxima très voisins, aussi bien dans les aldéhydes que dans des imines où la bande *K* de conjugaison totale n'existe pas (cf. tableau 2). Toutefois pour vérifier cette hypothèse et s'assurer qu'il ne s'agit pas d'une bande due à une hydrolyse partielle des composés au cours de la dilution nécessaire à l'enregistrement des spectres uv, nous avons réalisé le spectre du produit **2** à la concentration *M*/1000 dans l'éthanol pour une cuve de 0,1 cm. Le spectre obtenu est identique à celui que donne une solution *M*/20 000 dans une cuve de 1 cm. Après évaporation du solvant, le spectre de rmn du proton, dans le benzène deutérié, ne révèle aucune trace d'hydrolyse.

En ce qui concerne les composés nitrés **4** et **5**, on retrouve les trois types de bandes (cf. tableau 1), mais fortement décalées vers les hautes absorptions par la présence du groupement $-NO_2$. Ainsi dans le cas de la *N*-(nitro-5)thiénylidèneaniline, **5**, on observe le système *K* à 377 nm et le système $K_b$ sous forme d'inflexion à 293 et 340 nm (cf. la *N*-(nitro-5)thiénylidènebenzylamine dans le tableau 2).

*Résonance magnétique nucléaire du proton*

Nous avons enregistré les spectres de rmn du proton à 250 MHz pour les composés **1** à **5**. Pour

Can. J. Chem. Downloaded from www.nrcresearchpress.com by 210.87.254.5 on 09/06/12
For personal use only.

Can. J. Chem. Downloaded from www.nrcresearchpress.com by 210.87.254.5 on 09/06/12
For personal use only.

TABLEAU 1. Caractéristiques ir ($\nu$ en $cm^{-1}$) et uv ($\lambda_{max}$ en nm) pour les composés **1** à **5**

| No | $\nu_{C=N}$ | (réf.) | $\nu_{NO_2}$ | $\lambda_{max}$ (EtOH) ($\varepsilon$) | (réf.) Solvant |
|---|---|---|---|---|---|
| **1** | 1625 | | | | |
| X = O | | | — | 229 (7500); 237 (7200); 287 (12 400); 315 (11 400) | |
| R = H | 1632 | (13) | | 290 (11 000); 319,5 (10 600) | (13) EtOH |
| **2** | 1618 | | — | 223 (8200); 240 (5000); 269 (11 500); 302 (13 150); 322,5 (13 550) | |
| X = S | | | | 270 (9800); 324 (12 100) | (13) EtOH |
| R = H | 1618 | (13) | | 240 (9249); 300 (15 250); 323 (15 260) | (11) MeOH |
| **3** | 1625 | | | | |
| X = N | | | — | 220 (8600); 260 (inflexion); 302 (16 800); 324 (20 300) | |
| Me | 1630 | (12) | | 219 (7300); 287 (8300); 324 (18 400) | (12) EtOH |
| R = H | | | | | |
| **4** | | | 1532 | | |
| X = O | 1622 | | | 279 (9400); 330 ep. (12 500); 358 (15 000) | |
| $R = NO_2$ | | | 1351 | | |
| **5** | | | 1540 | | |
| X = S | 1620 | | | 267 (9600); 293 (inflexion); 340 ep. (8000); 377 (15 000) | |
| $R = NO_2$ | | | 1342 | | |

TABLEAU 2. Caractéristiques ultraviolettes de quelques dérivés aldéhydiques et iminiques d'hétérocycles à cinq chaînons

| Composé | $\lambda_{max}$ (EtOH) en nm ($\varepsilon$) | (réf.) |
|---|---|---|
| Furannecarboxaldéhyde-2 | 227 (3000); 273 (13 200) | (16) |
| Thiophènecarboxaldéhyde-2 | 260 (10 500); 285 (7100) | (16) |
| *N*-méthylpyrrolecarboxaldéhyde-2 | 255 (5250); 288,5 (12 600) | (16) |
| *N*-furfurylidènebenzylamine | 273 (18 800) | (13) |
| *N*-thienylidènebenzylamine | 260 (15 800); 281 (14 000) | |
| *N*-méthylpyrrolylméthylènebenzylamine | 257 (inflexion); 186 (18 200) | |
| *N*-(nitro-5)thiénylidènebenzylamine | 233 (8800); 293 (inflexion); 335 (14 200) | |

TABLEAU 3. Déplacements chimiques (ppm/TMS) et constantes de couplage (Hz) pour les composés **1** à **5**[a]

| No | Formule | δ H(1) | δ H(3) | δ H(4) | δ H(5) | δ H | $^3J_{3-4}$ | $^4J_{3-5}$ | $^3J_{4-5}$ | $^5J_{1-5}$ |
|---|---|---|---|---|---|---|---|---|---|---|
| **1** | 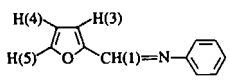 | 8,17 | 6,83 | 6,42 | 7,49 | 7,27 (2H)<br>7,17 (3H) | 3,50 | 0,75[b] | 1,75 | 0,70 |
| **2** | 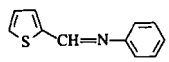 | 8,35 | 7,36 | 7,02 | 7,38 | 7,29 (2H)<br>7,13 (3H) | 3,60 | 1,0[b] | 5,0 | 1,0 |
| **3** | 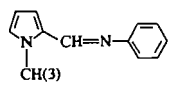 | 8,16 | 6,58 | 6,10 | 6,64 | 7,25 (2H)<br>7,07 (3H)<br>N—$CH_3$: 3.94 | 3,75 | 1,75 | 2,50 | ≤0,4 |
| **4** | 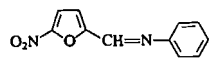 | 8,35 | 7,17 | 7,38 | — | 7,35 (2H)<br>7,24 (3H) | 3,70 | — | — | — |
| **5** | 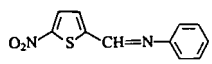 | 8,50 | 7,32 | 7,85 | — | 7,35 (2H)<br>7,22 (3H) | 4,25 | — | — | — |

[a]Spectres enregistrés dans $CDCl_3$.
[b]Valeurs mesurées après irradiation de H(1).

cette valeur du champ magnétique appliqué, les spectres sont tous analysables au premier ordre. Les déplacements chimiques et constantes de couplage que nous en avons déduits, sont rassemblés dans le tableau 3.

Du point de vue des déplacements chimiques, on peut noter que les protons H(3) (cf. tableau 3) de tous les dérivés sont moins déblindés que les mêmes protons dans les aldéhydes correspondants (cf. tableau 4). Ceci montre que l'effet électronique

Can. J. Chem. Downloaded from www.nrcresearchpress.com by 210.87.254.5 on 09/06/12
For personal use only.

TABLEAU 4. Comparaison des effets de déblindage des groupements >C=O et >C=N—

| Composé | δ H(3)[a] | Δδ[b] |
|---|---|---|
| Furanne | 6,34 | — |
| Furannecarboxaldéhyde-2 | 7,33[c] | −0.99 |
| **1** | 6,83 | −0,49 |
| Thiophène | 7,03 | — |
| Thiophènecarboxaldéhyde-2 | 7,75[c] | −0,72 |
| **2** | 7,36 | −0,33 |
| *N*-méthylpyrrole | 6,06[d] | — |
| *N*-méthylpyrrolecarboxaldéhyde-2 | 6,84[d] | −0,78 |
| **3** | 6,58 | −0,52 |

[a]Déplacements chimiques dans le deutériochloroforme.
[b]Δδ = δ H(3) du composé non substitué − δ H(3) du composé substitué en 2.
[c]Référence 17.
[d]Référence 18.

du groupe imine est très inférieur à celui du groupement carbonyle. Toutefois, en comparant les valeurs des déplacements chimiques de ces protons H(3) dans **1**, **2** et **3** avec celles des mêmes protons respectivement dans le furanne, le thiophène et le *N*-méthylpyrrole (tableau 4), on voit qu'il subsiste des déblindages de −0,49, −0,33 et −0,52 ppm. Les protons impliqués se trouvent donc dans le cône de déblindage de la double liaison >C=N—. Si on admet que ce cône d'anisotropie est de la même forme que celui proposé par Karabatsos *et al.* (19) pour le groupement carbonyle (cf. figure 4), on peut en déduire que le rotamère *E trans* (*a* de la figure 1) sera privilégié. De plus, les spectres de rmn du proton des composés **1** et **2** ne changent pas lorsque l'on abaisse la température de l'échantillon à −100°C. Ceci suggère, soit la présence d'un seul rotamère, soit une interconversion rapide entre deux isomères de rotation même à cette température.

Les résultats d'une étude de l'effet Overhauser dans de telles molécules (composés **1** et **3**, tableau 5) sont encore en faveur de cette hypothèse. On observe, en effet, à température ordinaire, des augmentations de surface des signaux traduisant la proximité des protons H(1) et H(3) d'une part, H(1) et H(7–11) d'autre part. Cela exclut totalement la conformation *Z cis* (*d* de la figure 1) et suggère soit la présence du seul rotamère *a* (où ces deux effets existent) soit un équilibre avec un des deux autres

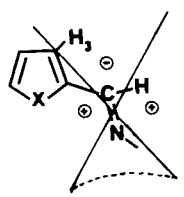


FIG. 4. Cône d'anisotropie de la liaison C=N—.

TABLEAU 5. Effet Overhauser observé dans les composés **1** et **3**

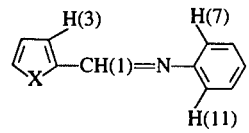


| Proton irradié | Effet (%)[a] sur H(1) | H(3) | H(7–11) | H(4) |
|---|---|---|---|---|
| H(1) | — | 26<br>*22*[b] | 8<br>*15*[b] | 0<br>*0* |
| H(3) | 26<br>*20*[b] | — | 0<br>*0* | — |
| H(7–11) | 7[b]<br>*17* | 0<br>*0* | — | 0<br>*0* |

[a]Exprimé en % d'augmentation du signal initial.
[b]Les chiffres en italique concernent les effets observés pour le composé **1**, les autres ceux du composé **3**.

rotamères *b* ou *c* (dans lesquels un seul des ces effets Overhauser peut être rencontré).

Au sujet des constantes de couplage, il faut surtout remarquer que les couplages lointains ont toujours lieu entre le proton aldiminique H(1) et le proton H(5) sur l'hétérocycle. Nous n'observons pas de constantes $^5J_{H(1)-H(4)}$ même dans les composés nitrés, où la position 5 sur l'hétérocycle est occupée par le groupement nitro. Si on compare ces résultats à ceux obtenus par Roques et coll. (17, 18, 20, 21), sur la stéréospécificité des couplages lontains dans des aldéhydes hétérocycliques, on peut penser que les valeurs $^5J_{H(1)-H(5)}$ = 0,7 et 1,0 Hz observées respectivement pour les furanne- et thiophènealdimines sont en accord avec un rotamère majoritaire X—N *cis* (*a* ou *b* dans la figure 1). Le cas du composé 3 est plus surprenant puisque $^5J_{H(1)H(5)} \leq 0{,}4$ Hz, alors que pour un rotamère N—O *cis* (17) on mesure $^5J_{CHO-H(5)}$ de l'ordre de 1,1 Hz. Si ce composé présente un équilibre entre deux rotamères *cis* et *trans*, on devrait mesurer une constante $^5J_{CHO-H(4)}$ de l'ordre de 0,70 Hz, ce qui n'est pas le cas.

Cette étude des constantes de couplage à longue distance permet de faire des hypothèses quant à l'existence de rotamères uniques ou en équilibre pour ces molécules. Malheureusement, elle n'apporte aucun renseignement sur la structure spatiale de ces dérivés. En effet, selon Bell *et al.*, les torsions des groupements formyles ou aldiminiques ne semblent pas toujours affecter fortement la grandeur du couplage lointain (22). Ceci s'expliquerait, selon ces auteurs, par la participation à la transmission de ce couplage, entre autres d'une contribution π de l'hétérocycle.

Can. J. Chem. Downloaded from www.nrcresearchpress.com by 210.87.254.5 on 09/06/12
For personal use only.





TABLEAU 6. Déplacements chimiques (ppm/TMS) et constantes de couplage (Hz) pour les carbones des imines du type[a]:

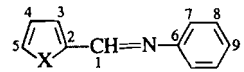


| No | δ C(1) | δ C(2) | δ C(3) | δ C(4) | δ C(5) | δ C de  | δ $CH_3$ | $J_{C(1)-H}$ | $J_{C(2)H}$ | $J_{C(3)H}$ | $J_{C(4)H}$ | $J_{C(5)H}$ |
|---|---|---|---|---|---|---|---|---|---|---|---|---|
| **1** | 147,7 | 152,1 | 116,2 | 112,1 | 145,5 | C(6): 151,3; C(7–11): 129,1<br>C(8–10): 120,9; C(9): 126,2 | — | H(1): 161,75 | H(3): 7,05<br>H(4): 15,25 | H(3): 177<br>H(4) < 3<br>H(5) < 3 | H(4): 177<br>H(3) < 3<br>H(5): 10,7 | H(5): 203<br>H(3): 9,15<br>H(4): 9,15 |
| **2** | 152,8 | 142,8 | 132,2 | 127,7 | 130,2 | C(6): 151,3; C(7–11): 129,0<br>C(8–10): 120,9; C(9): 126,0 | — | H(1): 161,3 | H(3): 7,05<br>H(4): 15,1 | H(3): 167,4<br>H(4): 6,0<br>H(5): 6,0 | H(4): 167,4<br>H(3) < 3<br>H(5) < 3 | H(5): 181,5<br>H(3): 9,1<br>H(4): 9,1 |
| **3** | 150,7 | 130,2 | 118,7 | 108,7 | 129,0 | C(6): 152,8; C(7–11): 129,0<br>C(8–10): 120,7; C(9): 124,9 | 36,7<br>$J_{CH}$: 140,4 | H(1): 157,2 | H(3)[b]<br>H(4)[b] | H(3): 172,4<br>H(4): 6,1<br>H(5): 6,1 | H(4): 172,4<br>H(3): 3,1<br>H(5): 7,7 | H(5): 180<br>H(3)[b]<br>H(4)[b] |
| **4** | 146,4 | 153,3 | 112,9 | 114,5 | 154,1 | C(6): 150,1; C(7–11): 129,5<br>C(8–10): 121,2; C(9): 127,9 | — | H(1): 166,3 | H(3): 6,1<br>H(4): 13,1 | H(3): 187,7<br>H(4): 3,05 | H(4): 183,1<br>H(3) < 3 | H(3): 8,1<br>H(4): 14,1 |
| **5** | 151,2 | 148,9 | 128,6 | 129,6 | 154,1 | C(6): 149,8; C(7–11): 129,5<br>C(8–10): 121,3; C(9): 127,7 | — | H(1): 164,8 | H(3): 6,0<br>H(4): 10,5 | H(3): 177,0<br>H(4): 4,6 | H(4): 178,5<br>H(3) < 3 | H(3): 10,1<br>H(4): 15,0 |

[a]Spectres enregistrés dans $CDCl_3$.
[b]Couplages non visibles sur le spectre à 62,86 MHz.

Can. J. Chem. Downloaded from www.nrcresearchpress.com by 210.87.254.5 on 09/06/12
For personal use only.

*Résonance magnétique nucléaire du carbone-treize*

L'enregistrement des spectres de rmn du $^{13}C$ des composés **1** à **5** a été réalisé à 15,08 MHz en découplage total et à 62,86 MHz sans découplage des protons. Les attributions des déplacements chimiques des divers carbones ont été effectuées à l'aide de données de la littérature (23–27) et au moyen d'irradiations sélectives de certains protons lorsque cela s'avérait nécessaire. Les résultats de cette analyse et les constantes de couplage $J_{^{13}C-H}$ mesurées sont rassemblés dans le tableau 6.

Pour les composés **1** à **3**, si l'on compare les effets du substituant —CH=N— sur les déplacements des divers carbones des hétérocycles, à ceux, déjà connus, du groupement —CH=O, on s'aperçoit (tableau 7) qu'ils se traduisent par un déblindage de tous les carbones quel que soit l'hétéroatome (N—$CH_3$, O ou S), considéré. Ils sont cependant plus faibles sur C(4) que sur C(3) et C(5), ce qui est en accord avec les effets de résonance et les délocalisations de charge attendus entre le substituant et le noyau hétérocyclique. De plus, dans l'ensemble, les effets du groupement —CH=N sont plus faibles que ceux du groupe —CH=O. Ceci pourrait traduire soit une diminution des effets précédemment cités quand on remplace un oxygène par un azote dans la double liaison, soit une noncoplaneité de la molécule, puisque dans ce cas l'atome d'azote serait sollicité par une conjugaison avec le noyau phényle.

Dans le cas des dérivés **4** et **5**, l'effet électroattracteur du groupement —$NO_2$ perturbe considérablement les effets de délocalisation de charge et de résonance au point que le groupement —CH=O a une influence inférieure à celle du groupe imine. Ce phénomène paraît encore en faveur de la noncoplanéité de ces molécules.

Les constantes de couplage $^1J_{^{13}C(n)-H(n)}$, pour les carbones des différents hétérocycles étudiés, ont des valeurs normales, comparables à celles de la littérature (23, 24, 28, 30). Dans tous les cas, la valeur de $^1J_{C-H}$ pour le carbone aldiminique est plus faible et se situe entre 157 et 166 Hz. Cette diminution traduit une augmentation du caractère $sp^2$ du carbone en question (31) en rapport avec la présence de l'azote doublement lié au carbone. On peut aussi noter que c'est le seul carbone qui ne présente pas de couplage à distance avec des hydrogènes. En particulier, il n'est donc pas couplé avec le proton H(3) de l'hétérocycle.

TABLEAU 7. Effet des substituants —CH=N— et —CH=O sur les déplacements chimiques des carbones hétérocycliques des composés **1** à **5**[a]

| No | $\Delta\delta_R$[b] | C(2) | C(3) | C(4) | C(5) |
|---|---|---|---|---|---|
| **1** | —CH=N— | −9,3 | −6,3 | −2,3 | −2,7 |
| | —CH=O[c] | −10,3 | −12,4 | −3,1 | −5,8 |
| **2** | —CH=N— | −17,2 | −4,8 | −0,3 | −4,6 |
| | —CH=O[c] | −18,1 | −9,2 | −0,9 | −9,4 |
| **3** | —CH=N— | −9,1 | −10,9 | −0,9 | −7,9 |
| | —CH=O[d] | −10,3 | −15,7 | −1,2 | −10,3 |
| **4** | —CH=N— | −6,4 | −0,3 | 0 | −0,4 |
| | —CH=O[e] | −4,3 | +0,3 | −5,9 | +0,2 |
| **5** | —CH=N— | −14,2 | −0,2 | −0,3 | −2,9 |
| | —CH=O[f] | −10,7 | +1,9 | +1,7 | −1,4 |

[a]Les valeurs des δ des carbones des hétérocycles non substitués et des aldéhydes sont données en partie expérimentale.
[b]$\Delta\delta_R$ = δ C(*n*) de l'hétérocycle non substitué − δ C(*n*) de l'hétérocycle substitué en 2 (pour les composés **4** et **5**, nous avons considéré que le groupement nitro était en position 5 sur l'hétérocycle non substitué).
[c]Référence 25.
[d]Référence 26.
[e]Référence 28.
[f]Référence 29.

## Partie expérimentale

La synthèse des composés **1** à **5** a déjà été décrite (1, 32). La chromatographie en phase gazeuse est effectuée sur le brut de manipulation sur un appareil Intersmat IGC 120 DFL muni d'une colonne SE 30 de 1,5 m utilisée en isotherme à 180°C avec un débit d'azote de 25 mL/min. La température de l'injecteur et du détecteur est fixée à 240°C.

Les spectres ir ont été réalisés sur un appareil Beckman IR 20 en solution *M*/20 dans le tétrachlorure de carbone pour **1**, **2** et **3** dans le chloroforme à saturation pour **4** et **5**. Les spectres uv ont été enregistrés dans un spectrophotomètre Cary, modèle 15, pour des solutions *M*/20 000 dans l'éthanol avec des cuves de 1 cm. La rmn du proton a été effectuée sur un appareil Cameca 250. Les composés sont solubilisés (environ *M*/20) dans le chloroforme deutérié avec le TMS comme référence interne.

La mesure des effets Overhauser a été effectuée selon la méthode décrite par Bell et Saunders (33), sur des solutions soigneusement filtrées mais non dégazées.

L'enregistrement des spectres de rmn du carbone-treize a été conduit: soit sur un appareil Bruker WP 60 travaillant à 15,08 Mz pour des composés à saturation dans le chloroforme deutérié, avec découplage total des protons; soit sur un appareil Cameca 250 travaillant à 62,86 MHz pour des composés *M*/20 dans le chloroforme deutérié. Dans ce cas, nous n'avons pas utilisé le découplage des protons, de façon à conserver l'information concernant les constantes de couplage $J_{^{13}C-H}$.

Les valeurs des déplacements chimiques des carbones des hétérocycles de base et des aldéhydes utilisés dans le tableau 6 sont données ci-dessous.

*Furanne*: rmn $^{13}C$ à 15,08 MHz, chloroforme deutérié; δ ppm; C(2): 142,8; C(3): 109,8.

*Thiophène*: rmn $^{13}C$ à 15,08 MHz, chloroforme deutérié; δ ppm; C(2): 125,6; C(3): 127,4.

*N-méthylpyrrole*: rmn $^{13}C$ à 25,14 MHz, chloroforme deutérié, réf. 26; δ ppm; C(2): 121,7; C(3): 107,8; $CH_3$: 35,8.

*Nitro-2 furanne*: rmn $^{13}C$ à 25,14 MHz, acétone deutérié, réf. 28; δ ppm; C(2): 153,7; C(3): 114,5; C(4): 112,6; C(5): 146,9.

*Nitro-2 thiophène*: rmn $^{13}C$ à 25,14 MHz, acétone deutérié, réf. 29; δ ppm; C(2): 151,2; C(3): 129,9; C(4): 128,4; C(5): 134,7.

*Furannecarboxaldéhyde-2*: rmn $^{13}C$ à 22,63 MHz, chloroforme deutérié, réf. 25; δ ppm; C(2): 153,1; C(3): 122,2; C(4): 112,9; C(5): 148,6; *C*HO: 178,1.

*Thiophènecarboxaldéhyde-2*: rmn $^{13}C$ à 22,63 MHz, chloroforme deutérié, réf. 25; δ ppm; C(2): 143,7; C(3): 136,6; C(4): 128,3; C(5): 135,6; *C*HO: 183,0.

N-*méthylpyrrolecarboxaldéhyde-2*: rmn $^{13}C$ à 25,14 MHz, chloroforme deutérié, réf. 26; δ ppm; C(2): 131,4; C(3): 123,5; C(4): 109,0; C(5): 131,4; *C*HO: 178,7; *C*$H_3$: 36,2.

*Nitro-5 furannecarboxaldéhyde-2*: rmn $^{13}C$ à 15,08 MHz, chloroforme deutérié; δ ppm; C(2): 151,2; C(3): 112,3; C(4): 120,4; C(5): 153,5; *C*HO: 178,7.

*Nitro-5 thiophènecarboxaldéhyde-2*: rmn $^{13}C$ à 15,08 MHz, chloroforme deutérié; δ ppm; C(2): 145,4; C(3): 126,5; C(4): 128,2; C(5): 152,6; *C*HO: 168,3.


1. R. C. Coumes, A. Gaset, J. P. Gorrichon et G. Michel. Eur. J. Med. Chem. **13**, 527 (1978).
2. P. Gayral, M. C. Rigothier, J. C. Lantier, R. C. Coumes, A. Gaset et J. P. Gorrichon. Eur. J. Med. Chem. **16**, 151 (1981).
3. V. A. Izmailskii et E. A. Smirnov. Zh. Obshch. Khim. **26**, 3042 (1956).
4. N. Ebara. Bull. Chem. Soc. Jpn. **33**, 534 (1960).
5. P. Brocklehurst. Tetrahedron, **18**, 299 (1962).
6. V. A. Izmailskii et Y. A. Fedorov. Dokl. Acad. Nauk SSSR, **158**, 900 (1964).
7. K. Tabei et E. Saito. Bull. Chem. Soc. Jpn. **42**, 1440 (1969).
8. N. Inamoto, K. Kushida, S. Masuda, H. Ohta, S. Satoh, Y. Tamura, K. Tokumaru, K. Tori et M. Yoshida. Tetrahedron Lett. 3617 (1974).
9. J. S. Sandhu, D. Mago et B. J. Wakefield. Tetrahedron Lett. 1092 (1975).
10. J. Scaszar, J. Balog et A. Makary. Acta Phys. Chem. Szeged. **24**, 473 (1978).
11. V. I. Paskii, A. E. Lipkin, N. A. Kabo et V. A. Terent'ev. Zh. Fiz. Khim. **57**, 2733 (1977).
12. R. A. Jones. Aust. J. Chem. **17**, 894 (1964).
13. R. J. Head et R. A. Jones. Aust. J. Chem. **19**, 1747 (1966).
14. D. Mago et J. S. Sandhu. Indian J. Chem. **15B**, 658 (1977).
15. D. Dolphin et A. Wick. Tabulation of infrared spectral data. Wiley–Interscience, New York. 1977.
16. O. H. Wheeler et L. A. Kaplan. Organic electronic spectra. Vols. **1**, **2** et **3**. Interscience Publishers, New York. 1958.
17. C. Jaureguiberry, M. C. Fournie-Zaluski, B. Roques et S. Combrisson. Org. Magn. Reson. **5**, 165 (1973).
18. B. Roques et M. C. Fournie-Zaluski. Org. Magn. Reson. **3**, 305 (1971).
19. G. J. Karabatsos, G. C. Sonnichsen, N. Hsi et D. J. Fenoglio. J. Am. Chem. Soc. **89**, 5067 (1967).
20. B. Roques, S. Combrisson, C. Riche et C. Pascard-Billy. Tetrahedron, **26**, 3555 (1970).
21. B. Roques et S. Combrisson. Can. J. Chem. **51**, 573 (1973).
22. C. L. Bell, S. S. Danyluck et T. Schaeffer. Can. J. Chem. **47**, 3529 (1969).
23. T. F. Page, T. Alger et D. M. Grant. J. Am. Chem. Soc. **87**, 5333 (1962).
24. F. Fringuelli, S. Gronowitz, A. B. Hörnfeldt, L. Johnson et A. Tatichi. Acta Chem. Scand. Ser. B, **28**, 175 (1974).
25. M. T. W. Hearn. Aust. J. Chem. **29**, 107 (1976).
26. R. J. Abraham, R. D. Lapper, K. M. Smith et J. F. Usworth. J. Chem. Soc. Perkin Trans. II, 1004 (1974).
27. R. J. Cushley, R. J. Sykes, C. K. Shaw et H. H. Wasserman. Can. J. Chem. **53**, 148 (1975).
28. S. Gronowitz, I. Johnson et A. B. Hörnfeldt. Chem. Scr. 7, 211 (1975).
29. S. Gronowitz, I. Johnson et A. B. Hörnfeldt. Chem. Scr. 7, 76 (1975).
30. F. J. Weigert et J. D. Roberts. J. Am. Chem. Soc. **90**, 3543 (1968).
31. N. Muller et E. Pritchard. J. Chem. Phys. **31**, 768 (1959).
32. A. Gaset, R. C. Coumes, J. P. Gorrichon, L. Albertini et G. Michel. Fr. Demande, 80.14.172, 1980.
33. R. A. Bell et J. K. Saunders. Can. J. Chem. **48**, 1114 (1970).


Can. J. Chem. Downloaded from www.nrcresearchpress.com by 210.87.254.5 on 09/06/12
For personal use only.

# Utilisation d'une méthode d'ajouts pour la détermination précise des volumes molaires partiels des constituants dans un solvant mixte. Application au système eau–méthanol

PIERRE LETELLIER ET MICHEL BIQUARD

*Laboratoire de Physicochimie des Solutions, Associé au C.N.R.S. no 161, E.N.S.C.P., 11 rue Pierre et Marie Curie, F-75231, Paris, Cedex 05, France*

Reçu le 29 septembre 1981

PIERRE LETELLIER et MICHEL BIQUARD. Can. J. Chem. **60**, 1155 (1982).

La détermination des volumes molaires partiels de l'eau et du méthanol dans leurs mélanges a été effectuée avec précision par une *méthode d'ajouts*. Outre le fait que l'on retrouve bien la grandeur d'excès totale en faisant la somme des volumes molaires partiels caractéristiques de l'eau et du méthanol dans le mélange, cette technique permet de proposer des fonctions polynômiales thermodynamiquement cohérentes pour décrire les variations de volumes molaires partiels des deux composants de la solution. Cette méthode de détermination est utilisable pour caractériser chaque élément dans des solutions qui font intervenir différents solvants et solutés en forte concentration.

PIERRE LETELLIER and MICHEL BIQUARD. Can. J. Chem. **60**, 1155 (1982).

The determination of partial molar volumes of each component in a binary mixture is usually the result of the derivation of the polynomial function which describes the whole excess curve. The accuracy of the present available densimeters (vibrating densimeter Piker type) allows direct access to the values of partial molar volume by a method requiring successive additions of various components. The method of calculation is discussed in this paper and applied for the water–methanol system. Partial molar volumes of water and methanol are calculated for different phase compositions, and each variation is described by polynomial functions which are related to each other by thermodynamic rules. This technique may be extended to mixtures which contain different solvents and highly concentrated solutes.

## Introduction

L'étude des propriétés physicochimiques de solutés à faible concentration dans les milieux mixtes obtenus par le mélange de plusieurs solvants miscibles pose le problème des interactions spécifiques qui s'établissent entre le soluté et chacun des composants du mélange.

Une étude précédente (1) effectuée dans les mélanges eau–diméthylsulfoxyde montre à ce propos que l'on retrouve dans l'expression des volumes molaires partiels à dilution infinie ($\bar{V}_{MX}^{0}$) des halogénures alcalins MX, les propriétés volumétriques partielles des deux cosolvants ($\bar{V}_{H_2O}$, $\bar{V}_{DMSO}$) différemment amplifiées selon l'affinité des sels pour l'un ou l'autre des deux solvants.

La "grandeur molaire d'excès", qui est une grandeur globale caractéristique du milieu (écart à l'idéalité) n'est pas alors adaptée pour décrire les interactions soluté–cosolvants et l'on doit dans ce cas déterminer très précisément les grandeurs molaires partielles individuelles de chacun des constituants de la solution.

Les déterminations sont parfois délicates et le but principal de cet article est de proposer une technique expérimentale simple qui permette d'accéder, avec une grande précision, aux valeurs des grandeurs molaires partielles recherchées. Afin d'illustrer notre propos, nous avons choisi de traiter l'exemple du calcul des volumes partiels pour une série de mélanges eau–méthanol à la température de 25°C. La technique proposée peut bien évidemment être généralisée et appliquée à la mesure d'autres paramètres extensifs (l'enthalpie par exemple) dans des milieux plus complexes (milieux salins, ternaires ...).

## I. Détermination des grandeurs molaires partielles

### *I-1. À partir de la grandeur d'excès*

Dans le cas d'un mélange binaire (mélange de solvant A et de solvant B) la méthode la plus couramment utilisée consiste à calculer tout d'abord la "grandeur molaire d'excès", $Y_E$, pour un grand nombre de mélanges et de décrire ses variations avec la composition du milieu (fraction molaire $X_B$) au moyen d'une fonction polynômiale d'ordre $n$. Celle-ci peut prendre plusieurs formes mais la plus utilisée à cet effet est celle proposée par Redlich et Kister (2) ou Wilson et Scatchard (3, 4)

$$Y_E = X_B(1 - X_B)\left[\sum_{j=0}^{j} a_j(2X_B - 1)^j\right]$$

qui admet comme cas particulier celui des courbes symétriques en ne conservant que les valeurs de $j$ paires. En théorie, l'application des relations habituelles de la thermodynamique, permet à partir des dérivées de la fonction $Y_E$ par rapport à la fraction molaire $X_B$ d'accéder aux propriétés molaires partielles de chacun des deux cosolvants.

0008-4042/82/091155-07$01.00/0

©1982 National Research Council of Canada/Conseil national de recherches du Canada

Can. J. Chem. Downloaded from www.nrcresearchpress.com by 210.87.254.6 on 09/06/12
For personal use only.

Can. J. Chem. Downloaded from www.nrcresearchpress.com by 210.87.254.6 on 09/06/12
For personal use only.

Toutefois cette manière de procèder est sujette à plusieurs difficultés: (a) pour être "paramétrable", la courbe d'excès doit comporter un nombre minimum de points expérimentaux régulièrement espacés sur l'échelle des abscisses. Par exemple, une bonne description de la courbe de variation pour un polynôme d'ordre 6 ne peut s'obtenir qu'à partir d'environ 40 points expérimentaux répartis sur l'échelle des fractions molaires. Lorsque cette condition est remplie, la dérivation (ou la détermination de la tangente) peut alors s'effectuer; mais elle conduit bien souvent à des valeurs généralement erronées pour les parties à faible courbure.[1] De ce fait, même en effectuant un nombre important de mesures, la dérivation de la courbe polynômiale donnera rarement satisfaction sur l'ensemble de la courbe d'excès. (b) Avant de pouvoir procéder à son exploitation, la méthode précédente impose de connaître la totalité de la courbe d'excès ce qui limite généralement le calcul des grandeurs molaires partielles aux solvants totalement miscibles. Sont exclus de ce type de développement les solutés solides moléculaires ou salins, qui entrent cependant dans la composition de nombreux milieux réactionnels de grand intérêt (eau–urée, milieux salins, milieux micellaires ...). (c) La description par le polynôme devient de moins en moins satisfaisante au fur et à mesure que l'on approche des bornes du domaine d'étude.

*I-2. Détermination expérimentale directe*

La méthode de calcul présentée ci-dessous présente l'avantage de résoudre les problèmes évoqués; elle nécessite, en contrepartie, l'acquisition de nombreuses données expérimentales, donc une étude plus longue que celles généralement effectuées pour ce type de mesure.

Si l'on considère le milieu mixte non idéal constitué de $n_A$ moles de solvant A et $n_B$ moles de solvant B de volumes molaires respectivement $V_A^0$ et $V_B^0$, le volume du mélange obtenu est égal à $V = n_A\bar{V}_A + n_B\bar{V}_B$ où $\bar{V}_A$ et $\bar{V}_B$ sont les volumes molaires partiels des cosolvants A et B. La méthode des perturbations que nous proposons consiste à modifier ce mélange par de faibles ajouts de l'un ou de l'autre des constituants et d'en étudier les conséquences sur le volume du milieu.

Si l'on ajoute un nombre de moles $\varepsilon_A$ de solvant A au milieu, le volume total varie et peut s'écrire en attribuant à l'ajout l'essentiel de la perturbation $P_A$ observée sur le volume total:

$$V' = n_A\bar{V}_A + n_B\bar{V}_B + \varepsilon_A P_A$$

$P_A$ intervient comme une grandeur molaire partielle apparente et peut être calculée comme telle.

$$P_A = \frac{V' - V}{\varepsilon_A} = \frac{\Delta V}{\varepsilon_A}$$

La valeur limite de la perturbation $P$ lorsque l'ajout $\varepsilon$ tend vers 0 s'identifie à celle du volume molaire du cosolvant ajouté, tous les autres paramètres étant fixés.

$$[1] \qquad \lim_{\varepsilon_A \to 0} P_A = \bar{V}_A$$

La quantité $P_A$ est facilement calculable pour des additions finies de A à partir des masses volumiques $\rho_x$ des solutions ainsi constituées.

$$[2] \qquad P_A = \frac{n_A M_A + n_B M_B}{\varepsilon_A}\left(\frac{1}{\rho_x} - \frac{1}{\rho_s}\right) + \frac{M_A}{\rho_x}$$

où $\rho_s$ est la masse volumique du solvant étudié, $M_A$ et $M_B$ les masses molaires des cosolvants A et B.

La valeur cherchée $\bar{V}_A$ sera obtenue par extrapolation des valeurs de $P_A$ à "ajout nul".[2] L'étude complète d'un mélange binaire comportera donc pour chaque concentration envisagée l'étude de deux séries d'ajouts. A titre d'exemple nous présentons ci-dessous le cas des mélanges eau–méthanol à 298 K.

## II. Volumes molaires partiels de l'eau et du méthanol dans leurs mélanges

Les solvants eau et méthanol[3] ont été purifiés par distillation et les mesures des masses volumiques ont été réalisées à l'aide d'un densimètre vibratomètre à flux Piker Modèle 03D maintenu à la température constante de 298 K par un thermostat Setaram régulant à $\pm 3 \times 10^{-3}$ K (13).

*II-1. La grandeur molaire d'excès*

Les mélanges eau–méthanol (MeOH) sont connus pour présenter des écarts importants à l'idéalité (5–10). La grandeur d'excès $V_E$ qui caractérise cet

[1] Une régression polynômiale d'ordre supérieur à 1 ne peut en aucun cas décrire avec précision une partie linéaire. Or ces zones, lorsqu'elles existent, sont primordiales car elles correspondent généralement à des solutions diluées d'un des deux constituants dans l'autre.

[2] La loi d'extrapolation à adopter ne pose aucun problème dans ce cas. Les écarts entre la courbe et sa tangente sont des fonctions linéaires de l'incrément imposé tant que celui-ci reste suffisamment faible. Nous avons toujours vérifié expérimentalement que les valeurs de $P$ s'extrapolaient linéairement avec le nombre de moles de solvant ajouté, et que bien souvent les variations du paramètre $P$ étaient suffisamment petites pour que l'incertitude sur $\bar{V}$ reste inférieure à $\pm$ 0,2 cm$^3$ mol$^{-1}$.

[3] La teneur en eau du méthanol après distillation est inférieure à 0,1%.

écart pour le volume peut être calculée classiquement par la mesure de la masse volumique ($\rho_X$) pour chaque solution.

$$V_E = X_A M_A \left(\frac{1}{\rho_X} - \frac{1}{\rho_A{}^0}\right) + X_B M_B \left(\frac{1}{\rho_X} - \frac{1}{\rho_B{}^0}\right)$$

$X_A$ et $X_B$ sont les fractions molaires de A et B dans le mélange; $\rho_A{}^0$ et $\rho_B{}^0$ les masses volumiques de A et B purs.

Les résultats obtenus pour différentes solutions d'eau et de méthanol sont reportés dans le tableau 1.

*II-2. Application de la méthode des perturbations*

Pour chaque mélange indiqué dans le tableau 1 nous avons effectué deux séries d'au moins 5 ajouts d'eau et de méthanol. Afin d'accroître la précision sur les valeurs recherchées nous avons procédé par dilution d'une solution "mère" obtenue à partir d'une addition assez importante de cosolvant (de l'ordre de $\varepsilon_A = 1/20\, n_A$).

Les résultats trouvés pour le milieu $X_{CH_3OH} = 0{,}0446$ sont reportés dans le tableau 2 à titre d'exemple. Des variations tout à fait comparables sont obtenues dans les autres milieux. Les très faibles quantités de produit ajouté permettent d'obtenir une droite d'extrapolation à "ajout nul" pratiquement horizontale pour l'eau et le méthanol.

TABLEAU 1. Volumes d'excès des mélanges eau–méthanol $\rho^0_{eau} = 0{,}997047$ g/cm³; $\rho^0_{MeOH} = 0{,}78555$ g/cm³

| $N_{MeOH}$ | $\rho^*_x$ g/cm³ | $V_E$ cm³mol⁻¹ |
|---|---|---|
| 0 | 0,997047 | 0 |
| 0,0227 | 0,9898 | −0,063 |
| 0,0446 | 0,9830 | −0,119 |
| 0,0978 | 0,9700 | −0,306 |
| 0,1552 | 0,9569 | −0,495 |
| 0,2196 | 0,9422 | −0,671 |
| 0,2930 | 0,9256 | −0,826 |
| 0,3784 | 0,9066 | −0,944 |
| 0,4809 | 0,8836 | −0,977 |
| 0,6077 | 0,8566 | −0,899 |
| 0,7718 | 0,8245 | −0,629 |
| 0,8322 | 0,8134 | −0,482 |
| 0,8750 | 0,8064 | −0,393 |
| 0,9480 | 0,7936 | −0,154 |
| 1,0000 | 0,78555 | 0 |

*La moindre précision donnée sur ces valeurs par rapport à celles reportées dans le tableau 2 peut paraître surprenante. Cette différence tient à notre mode opératoire qui comporte deux étapes distinctes: la première consiste à préparer une masse importante de solvant mixte d'une *manière volumétrique*. La masse volumique de ce liquide peut être déterminée avec une grande précision mais la composition du milieu ainsi préparé n'est pas suffisamment reproductible pour que cette précision ait un sens, c'est pourquoi nous ne donnons dans ce tableau que 4 chiffres caractéristiques (sauf pour les deux milieux purs). La deuxième étape, en revanche, fait intervenir de l'addition de faibles quantités d'eau et de méthanol suivies par *gravimétrie* ce qui permet d'exploiter au maximum les qualités de l'appareil.

TABLEAU 2. Perturbations sur le volume du mélange $X_{MeOH} = 0{,}0446$ de masse volumique $\rho_s = 0{,}983000$ g/cm³ par ajout d'eau et par ajout de méthanol

| Ajout d'eau* $\varepsilon_{H_2O}$ | $\rho_x$ g/cm³ | $\Delta\rho = \rho_x - \rho_s$ $10^6$ g/cm³ | $P_{H_2O}$ cm³·mol⁻¹ |
|---|---|---|---|
| 1,0056 | 0,983223 | 223 | 18,083 |
| 1,6314 | 0,983356 | 356 | 18,089 |
| 2,1739 | 0,983463 | 463 | 18,095 |
| 3,3233 | 0,983720 | 720 | 18,087 |
| 4,0124 | 0,983864 | 864 | 18,087 |
| **Ajout de méthanol*** $\varepsilon_{MeOH}$ | $\rho_x$ g/cm³ | $\Delta\rho = \rho_x - \rho_s$ $10^6$ g/cm³ | $P_{MeOH}$ cm³·mol⁻¹ |
| 0,2163 | 0,981947 | −1053 | 37,676 |
| 0,2380 | 0,981840 | −1160 | 37,684 |
| 0,5604 | 0,980335 | −2665 | 37,620 |
| 0,8794 | 0,978928 | −4072 | 37,542 |
| 1,5336 | 0,976092 | −6908 | 37,519 |

*ε est exprimé en nombre de moles ajoutées pour 1000 g de solvant.

L'incertitude sur les valeurs extrapolées peut être estimée à ± 0.2 cm³·mol⁻¹ (figure 1).

Comme le montre fort bien le tableau 2, la nécessité d'ajouter de très petites quantités d'un des constituants du mélange, conduit à de très faibles variations du paramètre mesuré (voir la colonne Δρ du tableau 2).

La mise en œuvre expérimentale de la méthode proposée ne peut donc être envisagée que si l'on dispose de moyens de mesures suffisamment précis,

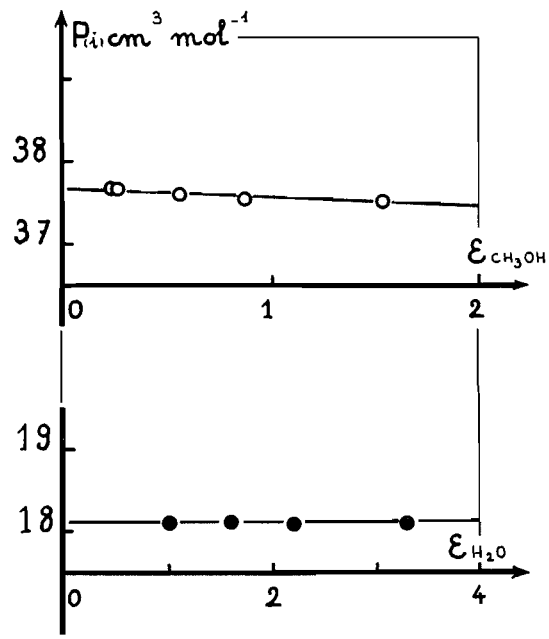


FIG. 1. Variation de la perturbation $P$ lors d'ajouts successifs de méthanol (ou d'eau) dans le milieu hydroalcoolique $X_{CH_3OH} = 0{,}0446$. La quantité ε portée en abscisses correspond au nombre de moles de solvant pur ajouté à 1 kg de mélange eau–méthanol.

Can. J. Chem. Downloaded from www.nrcresearchpress.com by 210.87.254.6 on 09/06/12
For personal use only.

TABLEAU 3. Volumes molaires partiels de l'eau et du méthanol dans les mélanges de ces deux solvants

| $X_{MeOH}$ | $\bar{V}_{H_2O}$ cm³ mol⁻¹ expérimental | $V^*_{H_2O}$ cm³ mol⁻¹ calculé | $\bar{V}_{MeOH}$ cm³ mol⁻¹ expérimental | $V^*_{MeOH}$ cm³ mol⁻¹ calculé |
|---|---|---|---|---|
| 0,000 | 18,06 | 18,06 | 38,42 | — |
| 0,0227 | 18,08 | 18,07 | 38,00 | — |
| 0,0446 | 18,09 | 18,09 | 37,74 | — |
| 0,0978 | 18,14 | 18,07 | 37,68 | — |
| 0,1552 | 18,10 | 18,03 | 37,80 | — |
| 0,2196 | 17,92 | 17,91 | 38,30 | 38,28 |
| 0,2930 | 17,68 | 17,76 | 38,74 | 38,92 |
| 0,3784 | 17,32 | 17,47 | 39,28 | 39,54 |
| 0,4809 | 16,92 | 17,10 | 39,82 | 40,00 |
| 0,6077 | 16,36 | — | 40,20 | 40,42 |
| 0,7718 | 15,58 | — | 40,56 | 40,72 |
| 0,8750 | 14,98 | — | 40,69 | 40,78 |
| 1,0000 | 14,25 | — | 40,78 | 40,78 |

*Les valeurs calculées ont été déterminées au moyen de la relation [3] à partir des valeurs $\bar{V}$ de l'autre cosolvant.

comme c'est le cas ici pour le volume (précision sur la masse volumique $\pm 2 \times 10^{-6}$ g/cm³). Cette restriction liée à la qualité de l'appareillage de mesure limite, dans sa généralité, l'extension de cette méthode à d'autres grandeurs thermodynamiques.

Les volumes molaires partiels de l'eau et du méthanol obtenus par cette méthode pour différents mélanges sont reportés dans le tableau 3.

*Remarque*: La masse volumique du solvant étant connue, la détermination du volume molaire partiel d'un seul des deux constituants est en théorie suffisante pour accéder à la valeur de l'autre.

Avec les notations précédentes, $\bar{V}_B$ peut être calculé connaissant $\bar{V}_A$ par la relation:

$$[3] \quad \bar{V}_B = \frac{X_A}{X_B}\left(\frac{M_A}{\rho_S} - \bar{V}_A\right) + \frac{M_B}{\rho_S}$$

Cette propriété peut effectivement être mise à profit pour éviter un certain nombre de manipulations dans des zones où l'un des deux cosolvants est en excès devant l'autre (on se servira exclusivement de la valeur expérimentale relative au liquide le plus dilué si l'on veut garder au résultat du calcul une précision acceptable).

Nous avons reporté dans le tableau 3 différents résultats obtenus par ce calcul qui montrent l'excellente cohérence entre les valeurs expérimentales et calculées.

*II-3. Discussion sur les valeurs obtenues*

La détermination précise des grandeurs molaires partielles d'excès $\overline{\Delta V} = (\bar{V} - V^0)$ pour chaque cosolvant par des manipulations indépendantes comme celles décrites précédemment, permet de retrouver parfaitement la grandeur d'excès totale.

A l'inverse, et la figure 2 le montre parfaitement, il est difficile de calculer, à partir de la courbe d'excès totale, les valeurs précises des volumes molaires partiels d'excès des constituants du mélange, en particulier lorsque celles-ci présentent des maximums (4, 12).

Comme nous l'avions suggéré dans l'introduction de ce travail, l'utilisation d'une équation polynômiale de type Redlich devrait donc être réservée dans son emploi à la seule description de la courbe expérimentale représentative de la grandeur d'excès. L'exploitation thermodynamique de ce type d'équation (particulièrement les opérations qui mettent en jeu la dérivation), (11) ne peut être entreprise qu'au risque d'attribuer aux grandeurs physiques recherchées des valeurs très imprécises et parfois même assez éloignées de la réalité physique, particulièrement dans le domaine des solutions diluées ($X < 0{,}1$ ou $X > 0{,}9$).

Seule une méthode directe du type de celle que nous proposons permet d'évaluer avec précision ces grandeurs qui peuvent alors être traitées théoriquement dans le cadre d'un modèle de solution.

En revanche, l'opération inverse qui consiste à retrouver la courbe d'excès à partir de la description des variations des deux grandeurs molaires partielles d'excès pour chacun des deux cosolvants est parfaitement licite, à condition bien entendu, de respecter les relations thermodynamiques qui relient ces différentes grandeurs, ce qui sera examiné dans le paragraphe suivant.

## III. Représentations mathématiques. Relations entre les différentes grandeurs d'excès

Comme il a été vu précédemment l'écart à l'idéalité pour le volume d'un mélange de 2 solvants A et B de composition $X_B = x$ peut être caractérisé par le volume d'excès $V_E$:

$$V_E = x(\bar{V}_B - V_B^0) + (1-x)(\bar{V}_A - V_A^0)$$

Can. J. Chem. Downloaded from www.nrcresearchpress.com by 210.87.254.6 on 09/06/12
For personal use only.

Can. J. Chem. Downloaded from www.nrcresearchpress.com by 210.87.254.6 on 09/06/12
For personal use only.

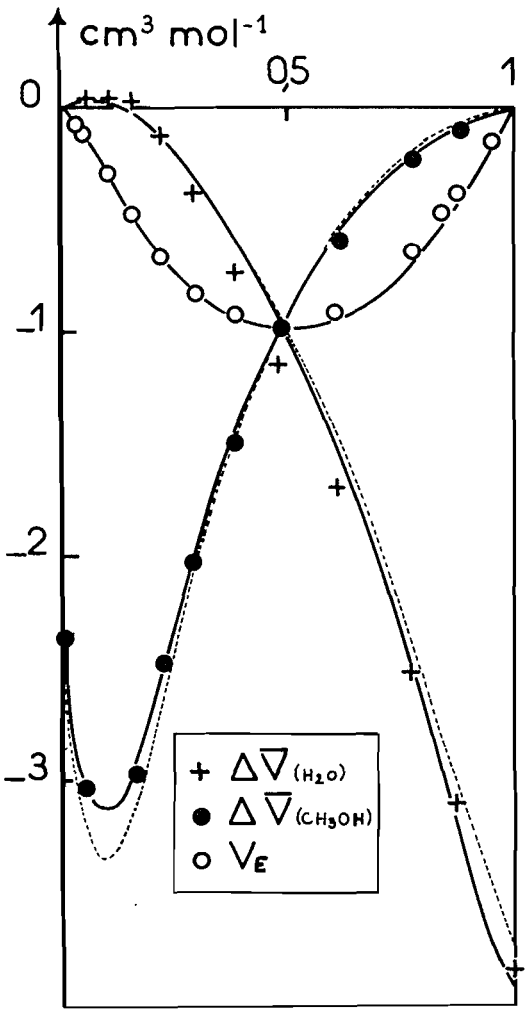


FIG. 2. Variation des grandeurs d'excès individuelles et totale en fonction de la composition du mélange (points expérimentaux). Les courbes, en traits pleins, sont tracées à partir de l'équation [10]. Les courbes de variations des $\Delta\bar{V}_{H_2O}$ et $\Delta\bar{V}_{CH_3OH}$ obtenues par Benson et Kiyo Hara (12) ont été indiquées en traits pointillés. Les principaux écarts, avec nos valeurs expérimentales, apparaissent aux extremums et à proximité des deux liquides purs.

Les valeurs $\bar{V}_B$ et $\bar{V}_A$ étant déterminées expérimentalement pour différents mélanges, il est alors possible de proposer pour leurs variations deux fonctions représentatives $f(x)$ et $h(x)$ dont les propriétés sont résumées ci-dessous.

(a) Pour le cosolvant A:

$$\bar{V}_A - V_A^0 = h(x)\cdot(\bar{V}_A^0 - V_A^0)$$

La fonction $h(x)$ doit s'annuler pour $x = 0$ car A est alors pur ($\bar{V}_A = V_A^0$) et doit être égale à l'unité pour $x = 1$ puisque A est alors infiniment dilué dans B ($\bar{V}_A = \bar{V}_A^0$).

(b) Pour le cosolvant B:

$$\bar{V}_B - \bar{V}_B^0 = f(x)\cdot(V_B^0 - \bar{V}_B^0)$$

La fonction $f(x)$ possède les mêmes bornes que $h(x)$: pour $x = 0, f(0) = 0$, B est infiniment dilué dans A ($\bar{V}_B = \bar{V}_B^0$); pour $x = 1, f(1) = 0$, B est pur ($\bar{V}_B = V_B^0$).

Les fonctions $f(x)$ et $h(x)$ ainsi définies ne sont pas indépendantes car elles doivent satisfaire aux conditions imposées par la loi de Gibbs–Duhem

$$x\,d\bar{V}_B + (1-x)d\bar{V}_A = 0$$

soit en faisant apparaître les fonctions $f(x)$ et $h(x)$

$$df(x) = -\frac{\bar{V}_A^0 - V_A^0}{V_B^0 - \bar{V}_B^0}\cdot\frac{1-x}{x}\,dh(x)$$

Cette équation différentielle, intégrée entre les bornes 0 et $x$ ($f(0) = 0$) conduit à:

$$f(x) = -\frac{\bar{V}_A^0 - V_A^0}{\bar{V}_B^0 - V_B^0}\left[h(x) - \int_0^x \frac{dh(x)}{x}\right]$$

Les variations relatives aux solvants A et B peuvent être représentées à partir d'une seule et même fonction $h(x)$:

$$[4]\quad \bar{V}_A - V_A^0 = (\bar{V}_A^0 - V_A^0)h(x)$$

$$[4']\quad \bar{V}_B - \bar{V}_B^0 = (\bar{V}_A^0 - V_A^0)\left[h(x) - \int_0^x \frac{dh(x)}{x}\right]$$

Les équations [4] et [4'] permettent de retrouver l'expression du volume d'excès:

$$[5]\quad V_E = (\bar{V}_A^0 - V_A^0)\left[h(x) - x\int_0^x \frac{dh(x)}{x}\right] + (\bar{V}_B^0 - V_B^0)x$$

Cette relation peut être écrite sous une forme plus simple en remarquant que les valeurs limites pour les grandeurs molaires partielles de A et B sont liées:

$$[6]\quad V_B^0 - \bar{V}_B^0 = (\bar{V}_A^0 - V_A^0)\left[1 - \int_0^1 \frac{dh(x)}{x}\right]$$

en posant[4]

$$A = \int_0^1 \frac{dh(x)}{x}$$

[4]La relation [6] montre que les grandeurs molaires partielles limites dans un mélange binaire ne sont pas indépendantes une fois la loi de variation définie.

Le volume d'excès prend la forme simple:

$$[7] \quad V_E = (\bar{V}_A^0 - V_A^0) \times \left[ h(x) - x \left( 1 - A + \int_0^x \frac{dh(x)}{x} \right) \right]$$

Le problème réside alors dans le choix de la meilleure fonction $h(x)$ pour décrire simultanément les variations de $\bar{V}_A$, $\bar{V}_B$ et $V_E$.

Pour les mélanges eau–méthanol en l'absence d'un type particulier de variation imposé par le choix d'un modèle de solution une représentation polynômiale de $h(x)$ reste la plus simple à envisager.

Un tel développement ne peut toutefois s'effectuer qu'à l'ordre minimum 2, car la constante $A$ [6] devant être finie, il ne peut exister de termes d'ordre 1 pour $x$ qui conduirait à une valeur infinie pour $A$.

$$[8] \quad h(x) = \sum_{j=2}^{n} a_j x^j$$

Les différentes valeurs des volumes d'excès sont représentées par les équations:

$$[9] \quad \begin{cases} \bar{V}_A - V_A^0 = (\bar{V}_A^0 - V_A^0) \left( \sum_{j=2}^{n} a_j x^j \right) & \text{(a)} \\ \bar{V}_B - \bar{V}_B^0 = (\bar{V}_A^0 - V_A^0) \left[ \sum_{j=2}^{n} a_j x^j - \sum_{j=2}^{n} a_j \frac{j}{j-1} x^{j-1} \right] & \text{(b)} \\ V_E = (\bar{V}_A^0 - V_A^0) \cdot x \left[ \sum_{j=2}^{n} \frac{a_j}{j-1} (1 - x^{j-1}) \right] & \text{(c)} \end{cases}$$

En procédant par ajustements successifs des coefficients des polynômes représentatifs des 3 grandeurs d'excès, il est possible d'obtenir pour $h(x)$ ($x = X_{CH_3OH}$) une forme permettant une description convenable de l'ensemble des courbes expérimentales pour les mélanges eau–méthanol:

$$[10] \quad \begin{cases} \bar{V}_A - V_A^0 = 9{,}77x^2 - 95{,}81x^3 + 238{,}74x^4 - 252{,}2x^5 + 95{,}56x^6 & \text{(a)} \\ \bar{V}_B - \bar{V}_B^0 = -19{,}54x + 153{,}49x^2 - 414{,}13x^3 + 554{,}00x^4 - 368{,}01x^5 + 95{,}56x^6 & \text{(b)} \\ V_E = -2{,}495x - 9{,}77x^2 + 47{,}905x^3 - 79{,}58x^4 + 63{,}05x^5 - 19{,}11x^6 & \text{(c)} \end{cases}$$

Dans le cas le plus général où l'on est conduit à décrire les variations d'une grandeur totale d'excès, caractéristique d'un mélange binaire, au moyen d'une équation de forme polynômiale, l'utilisation de la relation [9c] sous la forme

$$[11] \quad Y_E = (\bar{Y}_A^0 - Y_A^0) \left( x \sum_{j=1}^{n} b_j - \sum_{j=1}^{n} b_j x^{j+1} \right)$$

peut être considérée comme une alternative avantageuse à la description habituelle.

La relation [11], outre le fait qu'elle s'établit très facilement par une régression polynômiale classique d'ordre $n$, met un accent particulier sur la description du comportement d'un des constituants du système ($\bar{X}_A^0 - X_A^0$) lors d'un changement de composition du milieu. Elle permet, et c'est là son avantage principal, d'accéder aux variations des grandeurs d'excès individuelles par simple identification des coefficients des polynômes représentatifs (voir relations [9]).

## Conclusion

Le calcul des grandeurs molaires partielles caractéristiques des produits (solutés et solvants) qui entrent dans la composition de milieux réactionnels n'a généralement été entreprise que dans le cas simple des mélanges binaires à partir des valeurs de grandeurs d'excès.

La méthode expérimentale de détermination que nous proposons, outre le fait qu'elle conduit à des valeurs très précises pour ces paramètres, permet de traiter le cas des solvants mixtes complexes composés à la fois de solvants et de solides dissous, ce qui ne pouvait être envisagé par les techniques précédentes.

Le cas particulier du mélange binaire d'eau et de

Can. J. Chem. Downloaded from www.nrcresearchpress.com by 210.87.254.6 on 09/06/12
For personal use only.

méthanol traité à titre d'exemple montre que la forme des courbes représentatives des variations des grandeurs d'excès individuelles de l'eau et du méthanol, avec la composition du milieu ne pouvait être retrouvée aisément à partir de la courbe d'excès globale (4) et qu'une détermination expérimentale s'imposait.

En revanche, l'opération inverse qui consiste à représenter l'une des variations individuelles au moyen d'une équation polynômiale permet de décrire convenablement l'autre variation individuelle, et bien entendu de retrouver la courbe d'excès globale. La discussion des conditions thermodynamiques auxquelles doivent obéir les différents paramètres mesurés permet de proposer une équation polynômiale représentative des variations des grandeurs d'excès pour les mélanges binaires, dont l'intérêt principal est de pouvoir, lorsqu'elle est établie, accéder aux variations des grandeurs d'excès individuelles par simple identification des coefficients des polynômes représentatifs.

1. P. LETELLIER, R. GABORIAUD et R. SCHAAL. J. Chim. Phys. **77**, 1051 (1980).
2. O. REDLICH et A. T. KISTER. Ind. Eng. Chem. **40**, 345 (1948).
3. G. M. WILSON. J. Am. Chem. Soc. **86**, 127 (1964).
4. G. SCATCHARD. Chem. Rev. **44**, 7 (1949).
5. E. FRIEDMAN et H. A. SCHERAGA. J. Phys. Chem. **69**, 3795 (1965).
6. D. M. ALEXANDER. J. Chem. Eng. Data, **4**, 252 (1959).
7. R. P. RAGOSTI et K. T. R. VARMA. J. Chem. Soc. 2257 (1957).
8. S. Z. MIKHAIL et W. R. KIMEL. J. Chem. Eng. Data, **7**, 358 (1962).
9. R. BATTINO. Chem. Rev. **71**, 5 (1971).
10. K. NAKANISHI. Bull. Chem. Soc. Jpn. **33**, 793 (1960).
11. M. KATO et N. SUZUKI. Bull. Chem. Soc. Jpn. **51**, 1020 (1978).
12. G. C. BENSON et O. KIYO HARA. J. Solution Chem. **9**, 791 (1980).
13. P. PICKER, E. TREMBLAY et C. JOLICŒUR. J. Solution Chem. **3**, 377 (1974).

Can. J. Chem. Downloaded from www.nrcresearchpress.com by 210.87.254.6 on 09/06/12
For personal use only.

# Spectres photoélectroniques de cyclohexène-2 ones-1 diversement substituées en position 3. Correlations avec la réactivité[1]

GENEVIÈVE PFISTER-GUILLOUZO

*Laboratoire de Chimie Théorique et Organique Physique, ERA 895, Avenue Philippon, 64000 Pau, France*

ET

SERGE GERIBALDI ET JEAN-FRANÇOIS GAL

*Laboratoire de Chimie Organique Physique, Université de Nice, IPM, Parc Valrose, 06034 Nice Cedex, France*

Reçu le 7 décembre 1981

GENEVIÈVE PFISTER-GUILLOUZO, SERGE GERIBALDI et JEAN-FRANÇOIS GAL. Can. J. Chem. **60**, 1163 (1982).

Nous avons enregistré les spectres photoélectroniques de 32 cyclohexène-2 ones-1 diversement substituées en 3 ainsi que de 10 acétophénones *para*-substituées. Une attribution de la plupart des bandes de cyclohexénones est proposée et les effets de substituant sur les potentiels d'ionisation des électrons π et de la paire libre de l'oxygène sont discutés. Les relations linéaires entre le potentiel d'ionisation de la paire libre de l'oxygène du carbonyle de ces cétones et les constantes de type $\sigma_p$ ainsi que celles entre les potentiels d'ionisation et les enthalpies de complexation $\Delta H^0$ des cétones avec le trifluorure de bore dans le chlorure de méthylène permettent de supposer que l'interaction conjugative directe entre les substituants et la fonction carbonyle est faible dans la cétone libre et qu'elle devient très importante dans l'état complexé ou protoné. L'existence de deux relations distinctes $\Delta H^0 = f(\mathrm{PI}\ n_O)$ pour les cyclohexénones directement substituées en 3 et les cétones aromatiques montre que ce type de relation ne peut être utilisé pour la comparaison des basicités au sens de Lewis de différents types de cétones; par contre, ces relations peuvent permettre d'apprécier la basicité relative des cétones d'un même type.

GENEVIÈVE PFISTER-GUILLOUZO, SERGE GERIBALDI, and JEAN-FRANÇOIS GAL. Can. J. Chem. **60**, 1163 (1982).

We have recorded the photoelectronic spectra of 32 differently 3-substituted 2-cyclohexen-1-ones as well as those of 10 *para*-substituted acetophenones. Assignment of most of the cyclohexenone bands is made and the substituent effects on the π-electron ionization potentials and of the oxygen lone pair are discussed. The linear relationship between the ionization potential of the carbonyl oxygen lone pair and $\sigma_p$-type constants as well as those between the ionization potentials and the enthalpies of complexation ($\Delta H^0$) of the ketones with $BF_3$ in methylene chloride allows us to propose that the direct conjugative interaction between the substituents and the carbonyl group is weak in the free ketone but becomes very strong in the complexed or protonated state. The existence of two distinct relationships ($\Delta H^0 = f(\mathrm{PI}\ n_O)$ for 3-substituted cyclohexenones and the aromatic ketones indicates that this type of expression cannot be used for the comparison of the Lewis basicities of different types of ketones; on the contrary, these expressions do allow for the comparison of the relative basicities of the same type.

[Journal translation]

## Introduction

Les cétones α,β-éthyléniques constituent une classe de composés dont la réactivité est influencée par la conformation du motif α-énonique et surtout par la nature des substituants fixés sur ce motif. En ce qui concerne les réactions entre ces α-énones et des entités électrophiles, les notions de contrôle de charge ou de contrôle frontalier sont généralement invoquées (1). La connaissance des énergies des dernières orbitales moléculaires occupées de l'entité nucléophile se révèle ainsi une information utile pour la prévision et la compréhension de la réactivité de ces composés. Ces énergies orbitales et les effets consécutifs à une substitution peuvent être estimées si l'on admet la validité du théorème de Koopmans (2) par le biais de la spectroscopie photoélectronique. Deux études détaillées de composés carbonylés non saturés cycliques (3, 4) et un travail exhaustif sur des aldéhydes et des cétones α,β-insaturées substitués par des groupements alkyles (5) ont paru dans ce domaine.

Nous nous proposons dans ce travail d'étudier par spectroscopie photoélectronique les effets de substitution en β dans des séries de cétones α,β-éthyléniques et plus particulièrement les intéractions substituants – foyers nucléophiles (C=C et C=O). Nous tenterons de relier les différents potentiels d'ionisation observés, d'une part aux constantes classiques de substituant et d'autre part à divers paramètres caractéristiques des structures α-énoniques, en particulier aux enthalpies de complexation $\Delta H^0$ de ces cétones avec le trifluorure de bore dans le chlorure de méthylène, paramètres caractérisant la basicité au sens de Lewis de ces composés (6).

Notre choix a porté sur des diméthyl-5,5 cyclohexène-2 ones-1 substituées en 3 par des groupements X ou $p$-$XC_6H_4$, dont le motif cyclique se retrouve dans de nombreux composés naturels ou

[1]Part 12. Applications de la spectroscopie photoélectronique aux propriétés moléculaires. Part 11: C. Guimon, G. Pfister-Guillouzo et M. Begtrup, J. Am. Chem. Soc. Soumis à publication.

0008-4042/82/101163-10$01.00/0

©1982 National Research Council of Canada/Conseil national de recherches du Canada

Can. J. Chem. Downloaded from www.nrcresearchpress.com by 210.87.254.5 on 09/06/12
For personal use only.

Can. J. Chem. Downloaded from www.nrcresearchpress.com by 210.87.254.5 on 09/06/12
For personal use only.

Série 1

| No | X | No | X |
|---|---|---|---|
| **1** | H | **7** | OH |
| **2** | $CH_3$ | **8** | $SC_2H_5$ |
| **3** | Cl | **9** | CN |
| **4** | Br | **10** | $C_6H_5$ |
| **5** | $OCH_3$ | **11** | $NH_2$ |
| **6** | $OC_2H_5$ | **12** | $N(CH_3)_2$ |

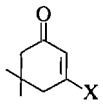

Série 2

| No | X | No | X |
|---|---|---|---|
| **11** | $NH_2$ | **17** | $NHiC_4H_9$ |
| **12** | $N(CH_3)_2$ | **18** | $NHtC_4H_9$ |
| **13** | $N(C_2H_5)_2$ | **19** | $NHnC_5H_{11}$ |
| **14** | $NHCH_3$ | **20** | NH cyclo $C_6H_{11}$ |
| **15** | $NHnC_3H_7$ | **21** | |
| **16** | $NHiC_3H_7$ | **22** | |

Série 3

| No | X | No | X |
|---|---|---|---|
| **23 ≡ 10** | H | **28** | $OCH_3$ |
| **24** | $CH_3$ | **29** | $NH_2$ |
| **25** | Cl | **30** | $C_6H_5$ |
| **26** | Br | **31** | $NO_2$ |
| **27** | F | **32** | CN |

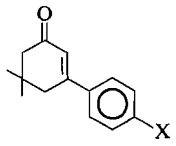

SCHÉMA 1. Cyclohexénones étudiées.

de synthèse d'intérêt biologique ou pharmaceutique. Ce modèle présente l'avantage d'être dans une conformation figée *s-trans*. On élimine ainsi les possibilités d'élargissement ou d'éclatement des bandes des spectres de photoélectrons dues à l'isomérie *s-cis* – *s-trans* (5). Enfin, les atomes d'oxygène et de carbones 1, 2, 3, 4 et 6 étant coplanaires (7), il n'y a pas d'interaction spatiale entre l'orbitale du doublet libre de l'oxygène du carbonyle et l'orbitale π du système conjugué. On peut donc supposer que les variations de structure électronique π n'influenceront qu'indirectement la paire libre du carbonyle, par exemple en modifiant la charge nucléaire effective de l'atome d'oxygène (8).

Les cyclohexénones étudiées ont été scindées en trois séries.

## Techniques expérimentales et calcul théorique

Toutes les cyclohexénones ont été préparées au laboratoire par l'adaptation de méthodes déjà décrites ou par la mise au point de nouvelles voies de synthèse (9, 10).

Les spectres ont été enregistrés sur un spectromètre photoélectronique Perkin–Elmer PS 18 en utilisant comme références les doublets $P_{1/2}$ et $P_{3/2}$ de l'argon et du xénon, ainsi que le pic à 15,60 eV de l'azote. Les raies HeI (584 Å) et HeII (304 Å) ont été utilisées comme source de radiation ionisante. Les potentiels d'ionisation ont été déterminés avec une précision de ± 0,03 eV.

Dans le cas du composé **10**, les énergies orbitales ont été calculées selon la méthode CNDO/S. La géométrie de la molécule a été déduite du spectre microonde de la cyclohexénone (7) et des valeurs standards (11).

Nous avons adopté un angle dièdre de 30° entre les plans du système α-énonique et du noyau benzénique.

## Résultats et discussion

### *Spectres photoélectroniques*

Pour les cyclohexénones directement substituées en 3 (série 1) seuls les trois premiers potentiels d'ionisation verticaux ont pu être mesurés avec précision. A l'exception des composés azotés ou soufrés dont l'hétéroatome du substituant possède une paire libre facilement ionisable, les deux premiers potentiels d'ionisation des cétones de la série 1 peuvent être attribués sans ambiguïté à l'ionisation des électrons de l'orbitale non liante $n_O$ de l'oxygène de la fonction carbonyle et de la combinaison antisymétrique $\pi_-$ entre l'orbitale $\pi_{C=C}$ et l'orbitale $\pi_{C=O}$, la combinaison symétrique $\pi_+$

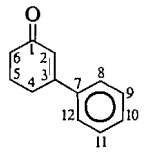

| Distances (Å) | Angles (°) |
|---|---|
| $C_1$—O:1,2241 | ∠612 = 117,746 |
| $C_1$—$C_2$:1,4646 | ∠123 = 121,177 |
| $C_2$—$C_3$:1,3550 | ∠234 = 122,497 |
| $C_3$—$C_4$:1,5057 | ∠345 = 109,589 |
| $C_4$—$C_5$:1,5287 | ∠456 = 109,389 |
| $C_5$—$C_6$:1,5297 | ∠561 = 112,582 |
| $C_3$—$C_7$:1,5200 | ∠378 = 118,751 |
| $C_7$—$C_8$:1,3900 | ∠8712 = 120,000 |
| $C_2$—H:1,0900 | |
| $C_4$—H = $C_5$—H = $C_6$—H = 1,1000 | |
| $C_{arom}$—H = 1,0900 | |

SCHÉMA 2. Géométrie adoptée pour la phényl-3 cyclohexène-2 one-1.

Can. J. Chem. Downloaded from www.nrcresearchpress.com by 210.87.254.5 on 09/06/12
For personal use only.

étant associées à une des bandes du massif non résolu au delà de 11 eV. L'attribution des deux premiers potentiels d'ionisation du composé **1** à 9,24 eV ($n_O$) et à 9,99 eV ($\pi_-$) est en accord avec celle proposée pour l'hexène-2 one-4 (5) et la cyclopentène-2 one-1 (8, 12).

Les valeurs des potentiels d'ionisation des composés de la série 1 sont rassemblées dans le tableau 1. Le spectre du composé **8** est reporté dans la figure 1.

Contrairement à l'hypothèse avancée par certains auteurs (13), l'introduction d'un groupement *gem* diméthyl en position 5 ne semble pas provoquer une altération significative de la planéité du motif α-énonique du composé **1** par rapport à son homologue non diméthylé. En effet, les trois premiers potentiels d'ionisation de la cyclohexène-2 one-1 sont très voisins (9,23, 10,10 et 11,73 eV) de ceux du composé **1**. Comme dans les séries à chaine ouverte (5), l'introduction d'un groupement alkyle supplémentaire sur les carbones éthyléniques provoque une destabilisation des orbitales $n_O$ et $\pi_-$ dans le composé **2** par rapport à **1** (−0,17 eV pour $n_O$ et −0,45 eV pour $\pi_-$). La légère stabilisation de l'orbitale non liante de l'oxygène et la destabilisation des niveaux $\pi_-$ des deux cétones halogénées **3** et **4** par rapport au composé **1** sont en accord avec la nature des effets inductifs attracteurs et mésomères donneurs des halogènes (14). La première bande relativement large des éthers d'énol **5** et **6** est associée à l'ionisation des électrons de l'orbitale non liante du carbonyle et de l'orbitale $\pi_-$ qui ont approximativement la même énergie (15). Cependant, si la destabilisation de l'orbitale $\pi_-$ (−1,04 eV pour **5** et −1,12 eV pour **6**) est en accord avec l'effet d'un groupement alkoxy introduit sur l'éthylène (−1,43 eV en passant de l'éthylène (14) au *n*-butyl vinyl éther (16), la destabilisation observée pour l'orbitale $n_O$ (−0,29 eV et −0,37 eV)

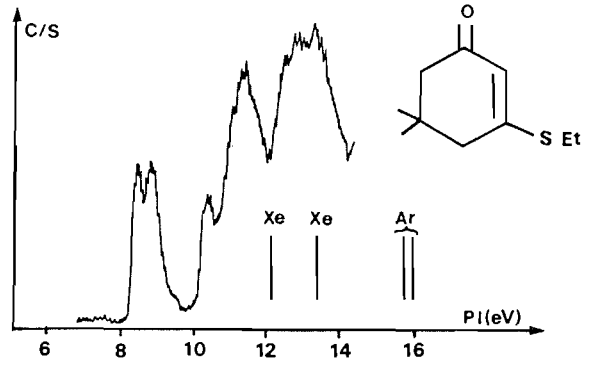


FIG. 1. Spectre photoélectronique (HeI) de l'éthylthio-3 cyclohexènone-2.

TABLEAU 1. Attributions des premiers potentiels d'ionisation des composés de la série 1

| Composés[a] No | X | $n_S$ ou $n_N$ (eV) | $n_O$ (eV) | $\pi_-$ (eV) | PI non attribué (eV) |
|---|---|---|---|---|---|
| **1** | H | | 9,24 | 9,99 | 11,30 |
| **2** | $CH_3$ | | 9,07 | 9,54 | 11,14 |
| **3** | Cl | | 9,35 | 9,73 | 11,30 |
| **4** | Br | | 9,35 | 9,71 | 10,73 |
| **5** | $OCH_3$ | | 8,95 | 8,95 | 11,81 |
| **6** | $OC_2H_5$ | | 8,87 | 8,87 | 11,66 |
| **7** | OH[b] | | 9,45[b] | 9,92[b] | 11,62[b] |
| **8** | $SC_2H_5$ | 8,46 | 8,82 | 10,40 | |
| **9** | CN | | 9,72 | 10,33 | 10,48 |
| **11** | $NH_2$ | 8,55 | 8,55 | 11,05 | |
| **12** | $N(CH_3)_2$ | 7,88 | 8,49 | 10,41 | |

[a]Le composé **10** (X = $C_6H_5$) sera étudié avec la série 3.
[b]Ces potentiels d'ionisation correspondent à ceux d'une forme dicétonique en accord avec Houk *et al.* (15).

par rapport à **1** semble en contradiction avec la stabilisation de nature inductive suggérée par Houk *et al.* (15). L'ensemble de ces résultats (ceux de Houk et les notres) reste cependant homogène si nous tenons compte des variations de l'effet inductif de R des substituants OR pouvant être décrit par les constantes σ* de Taft (17) (tableau 2).

Pour le composé **8**, les différences d'intensité observées lors du passage du rayonnement HeI à HeII (18) permettent d'attribuer le premier potentiel d'ionisation (8,46 eV) à l'ionisation de la paire libre non liante localisée sur l'atome de soufre alors que le second potentiel d'ionisation correspond à l'ionisation de la paire libre $n_O$. La stabilisation de l'orbitale $\pi_-$ (troisième potentiel d'ionisation) s'interprête par l'interaction entre l'orbitale de la paire libre de symétrie π du soufre et l'orbitale $\pi_-$ du motif α-énonique. L'importante interaction conjugative entre le système π et l'hétéroatome entraine une forte destabilisation de l'orbitale $n_O$.

Les effets inductifs (−I) et conjugatif (−R) du groupement CN sont à l'origine des stabilisations des potentiels d'ionisation associés aux orbitales $n_O$ et $\pi_-$ (respectivement 9,72 et 10,33 eV) du composé **9** par rapport à la cyclohexénone non substituée **1**.

TABLEAU 2. Influence des effets polaires de R sur les potentiels d'ionisation des orbitales $n_O$ et $\pi_-$ dans les alkoxy (ou hydroxy)-3 cyclohexénones

| | $n_O$ | | | $\pi_-$ | |
|---|---|---|---|---|---|
| OR | ΔPI (eV) | ΔΔPI[a] (eV) | σ* de R | ΔPI (eV) | ΔΔPI[a] (eV) |
| OH[b] | 0,10 | 0,39 | 0,49 | −0,90 | 0,15 |
| $OCH_3$ | −0,29 | 0,00 | 0,00 | −1,05 | 0,00 |
| $OC_2H_5$ | −0,37 | −0,08 | −0,10 | −1,12 | −0,07 |

[a]Rapporté au $OCH_3$.
[b]Valeurs issues de la ref. 15.

TABLEAU 3. Attribution des trois premiers potentiels d'ionisation des énaminocétones de la série 2 (eV)

| No | Composés X | $n_N - \pi_-$ | $n_O$ | $n_N + \pi_-$ | $\Delta E^a$ |
|---|---|---|---|---|---|
| **11** | $NH_2$ | 8,55 | 8,55 | 11,05 | 2,50 |
| **12** | $N(CH_3)_2$ | 7,88 | 8,49 | 10,41 | 2,53 |
| **13** | $N(C_2H_5)_2$ | 7,64 | 8,27 | 10,10 | 2,46 |
| **14** | $NHCH_3$ | 8,11 | 8,43 | 10,82 | 2,71 |
| **15** | $NHnC_3H_7$ | 8,03 | 8,35 | 10,64 | 2,61 |
| **16** | $NHiC_3H_7$ | 7,94 | 8,32 | 10,50 | 2,56 |
| **17** | $NHiC_4H_9$ | 7,98 | 8,42 | 10,50 | 2,52 |
| **18** | $NHtC_4H_9$ | 7,69 | 8,20 | 10,41 | 2,72 |
| **19** | $NHnC_5H_{11}$ | 8,07 | 8,44 | 10,50 | 2,43 |
| **20** | NH *cyclo* $C_6H_{11}$ | 7,75 | 8,24 | 10,25 | 2,50 |
| **21** | | 7,54 | 8,20 | 10,05 | 2,51 |
| **22** |  | 7,67 | 8,38 | 10,05 | 2,38 |

$^a\Delta E$ (eV) = $(n_N + \pi_-) - (n_N - \pi_-)$

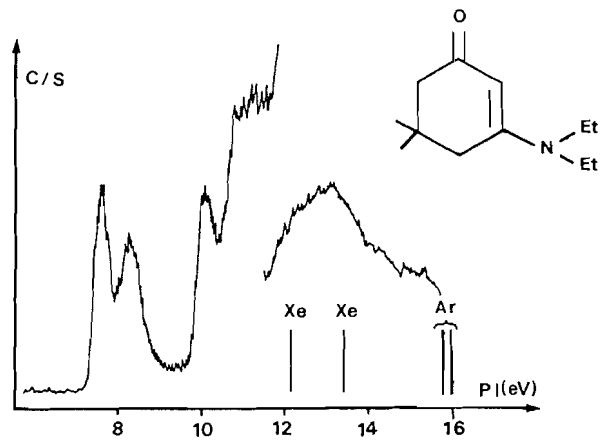


FIG. 2. Spectre photoélectronique (HeI) du diéthylamino-3 cyclohexénone-2.

Pour les énaminocétones **11** et **12**, le premier potentiel d'ionisation est attribuable à l'ionisation d'une orbitale essentiellement localisée sur l'atome d'azote. Si l'on compare le potentiel d'ionisation de la paire libre de l'azote dans le composé **11** et celui de la cyclohexylamine (9,15 eV, réf. 19) ou du composé **12** et celui de la quinuclidine (8,02 eV, réfs. 19, 20) la destabilisation observée (respectivement −0,60 et −0,14 eV) ne peut pas être expliquée par l'effet inductif (−I) du motif α-énonique qui provoquerait une variation inverse. Comme dans le cas des énamines (20), il faut envisager une forte interaction entre la paire libre de l'azote et l'orbitale $\pi_-$ du motif α-énone. Le premier potentiel d'ionisation correspond donc à l'ionisation d'un électron d'une orbitale du type $n_N - \pi_-$. En conséquence, l'orbitale $\pi_-$ du composé **1** se trouve stabilisée dans les énaminones **11** et **12** (respectivement 11,05 eV et 10,40 eV). Cette interaction conjugative entre l'azote et le système π induit comme dans le cas du composé soufré, un effet secondaire de destabilisation de l'orbitale $n_O$ des cétones **11** et **12**.

Les potentiels d'ionisation des énaminones de la série 2 sont attribués par analogie aux composés **11** et **12** (tableau 3). Le spectre du composé **13** est reporté dans la figure 2.

Compte tenu de la précision des mesures, la séparation moyenne ente les orbitales $n_N + \pi_-$ et $n_N - \pi_-$ due à l'interaction entre les orbitales de base $n_N$ et $\pi_-$ est identique pour l'ensemble des composés ($\overline{\Delta E}$ = 2,53 eV). Cette valeur est comparable à celles obtenues pour les *N*,*N*-diméthylamino-1 cyclopentène et cyclohexène (20), pour la *N*,*N*-diméthylaniline (21) et pour le méthyl-2 aza-2 bicyclo[3.2.1] octène-3 (22). On peut donc supposer que l'angle dièdre entre le plan contenant l'axe de la paire libre de l'azote et la liaison $C_3$—N et le plan contenant cette liaison et l'axe de l'orbitale 2*p* de $C_3$ est voisin de zéro pour l'ensemble des composés étudiés ou tout au moins qu'il varie très peu en fonction des substituants alkyles de l'azote. Pour les phényl-3 cyclohexène-2 ones-1 (série 3) (fig. 3) nous n'avons reporté dans le tableau 4 que les quatre premiers potentiels d'ionisation dont les bandes se situent entre 7, 8 et 11 eV. L'attribution est basée sur les observations faites pour la série 1 et sur les données concernant les benzènes substitués (23–28) et en particulier les styrènes (29–31).

Ces attributions sont en accord avec les énergies orbitales calculées en CNDO/S pour la cyclénone **23**: 10,17 eV ($Ph_S - \pi_-$); 10,58 eV ($n_O$); 10,99 eV ($Ph_A$) et 11,77 eV ($\pi_- + Ph_S$).

Dans diverses séries de benzènes disubstitués, McAlduff et coll. (26–28) montrent qu'il existe des relations linéaires entre les potentiels d'ionisation des orbitales associées au noyau phényle et les potentiels d'ionisation de l'orbitale $Ph_S$ des benzènes monosubstitués (26). Ceci est vérifié pour nos composés:

$$\text{PI}\ (Ph_S - \pi_-\ \text{série 3}) = (0{,}769 \pm 0{,}047)\ \text{PI}\left(Ph_S\ X\text{—}\langle\bigcirc\rangle\right) + 1{,}73$$
$$r = 0{,}987 \qquad S = 0{,}08\ \text{eV}$$

L'existence de cette relation, tout en confirmant nos attributions, met en évidence que pour ce système aromatique disubstitué, la sensibilité aux effets de substituant est moins importante que dans le système

Can. J. Chem. Downloaded from www.nrcresearchpress.com by 210.87.254.5 on 09/06/12
For personal use only.

Can. J. Chem. Downloaded from www.nrcresearchpress.com by 210.87.254.5 on 09/06/12
For personal use only.

benzénique par suite de la délocalisation des électrons π du noyau benzénique sur le système α-énonique. L'orbitale $\pi_- + Ph_S$ beaucoup plus localisée sur ce système est encore moins sensible aux effets de substituant que l'orbitale $Ph_S - \pi_-$ comme l'indique la valeur de la pente de la relation suivante:

$$PI\ (\pi_- + Ph_S) = (0{,}687 \pm 0{,}049)\ PI\ (Ph_S - \pi_-) + 4{,}10$$
$$r = 0{,}983 \qquad S = 0{,}06\ eV$$

*Corrélations avec les constantes de substituant*

Ayant une estimation directe de l'effet électonique d'une substitution du squelette α-énonique sur l'énergie de la paire libre de l'oxygène du carbonyle, nous avons cherché à vérifier si cet effet pouvait être corrélé avec les valeurs des constantes de type Hammett. De telles corrélations ont déjà été tentées dans diverses séries de composés carbonylés aromatiques (25, 26, 28). Si nous faisons exception de la cétone **8**, une bonne corrélation est obtenue entre les potentiels d'ionisation attribués à l'orbitale $n_O$ dans la série 1 et les constantes $\sigma_p$ de McDaniel et Brown (32):

$$\text{Série 1}\ PI\ (n_O) = (0{,}852 \pm 0{,}031)\ \sigma_p + 9{,}17$$
$$r = 0{,}995 \qquad S = 0{,}041\ eV$$

L'anomalie observée pour le composé **8** est en partie explicable par le fait que les substituants de type −SR possèdent une "constante" $\sigma_{R^+}$ variable suivant la réaction étudiée (33) et que la constante $\sigma_p$ contient une part non négligeable d'effet de résonance direct entre la fonction et le substituant (34).

Bien que la précision des mesures et le domaine de variations soient faibles dans la série 3, nous obtenons une corrélation correcte:

$$\text{série 3: } PI\ (n_O) = (0{,}362 \pm 0{,}046)\ \sigma_p + 8{,}93$$
$$r = 0{,}949 \qquad S = 0{,}058\ eV$$

Les deux relations précédentes sont représentées dans la figure 4.

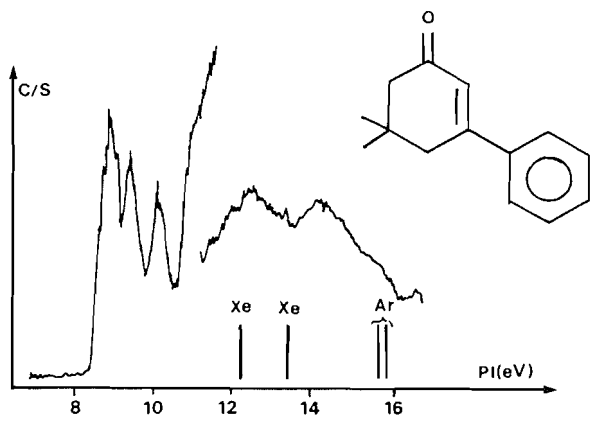


FIG. 3. Spectre photoélectronique de la phényl-3 cyclohexénone-2.

L'introduction d'un groupement phényle entre le substituant et l'enchainement α-énone entraine comme l'on pouvait s'y attendre une atténuation de l'effet de substituant sur l'énergie de la paire libre de l'oxygène. Le rapport des pentes des deux relations précédentes conduit à un facteur d'amortissement du noyau phényle égal à 0,42.

De la même façon, la comparaison des pentes des relations de Hammett pour la série 3 et les acétophénones conduit au coefficient d'amortissement apporté par un relais vinylique introduit entre une fonction carbonyle et le noyau phényle. Bien qu'une relation ait été obtenue par McAlduff (28) pour les acétophénones *para*-substituées, nous avons préféré utiliser une série de valeurs homogènes acquises dans les mêmes conditions expérimentales (tableau 5).

Pour tous les substituants, la relation suivante est obtenue:

$$PI\ (n_O) = (0{,}590 \pm 0{,}060)\ \sigma_p + 9{,}42$$
$$r = 0{,}962 \qquad S = 0{,}079\ eV$$

Le coefficient de transmission du relais vinylique est donc égal à 0,362/0,590 = 0,61. Cette valeur est en accord avec celle mesurée à partir des enthalpies de complexation avec le trifluorure de bore pour les cyclénones de la série 3 et les acétophénones 0,62 (35).

La principale caractéristique des trois relations de Hammett précédentes est qu'elles font intervenir les constantes de type σ. La fonction carbonyle

TABLEAU 4. Attribution des quatre premiers potentiels d'ionisation des cétones de la série 3 (eV)

| Composés | | $n_O$ | $Ph_S - \pi_-$ | $Ph_A$ | $\pi_- + Ph_S$ |
|---|---|---|---|---|---|
| No | X | (eV) | (eV) | (eV) | (eV) |
| **23** | H | 8,90 | 8,90 | 9,43 | 10,14 |
| **24** | $CH_3$ | 8,90 | 8,59 | 9,36 | 10,03 |
| **25** | Cl | 8,95 | 8,67 | 9,76 | 10,03 |
| **26** | Br | 8,93 | 8,57 | 9,68 | 9,98 |
| **27** | F | 8,90 | 8,90 | 9,76 | 10,15 |
| **28** | $OCH_3$ | 8,88 | 8,26 | 9,55 | 9,72 |
| **29** | $NH_2$ | 8,72 | 7,85 | 9,27 | 9,57 |
| **30** | $C_6H_5$ | 8,88 | [a] | [a] | [a] |
| **31** | $NO_2$ | 9,28 | 9,38 | 10,14 | 10,64 |
| **32** | CN | 9,20 | 9,20 | 10,02 | 10,43 |

[a] On observe trois autres bandes à 8,23, 9,21 et 10,19 eV correspondant au squelette du biphényl.

Can. J. Chem. Downloaded from www.nrcresearchpress.com by 210.87.254.5 on 09/06/12
For personal use only.

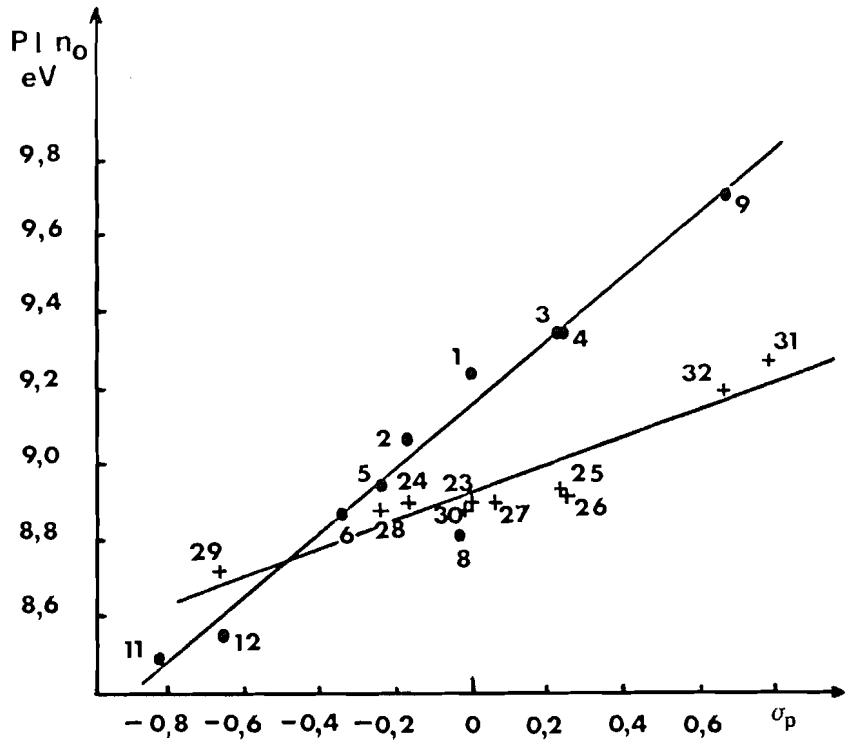


FIG. 4. Relations PI ($n_0$) = $f(\sigma_p)$ pour les séries 1 (●) et 3 (+).

étudiée étant de type −R l'on pouvait espérer un fort effet de conjugaison directe entre la fonction et les substituants de type +R (34) comme nous l'observons lors des relations établies pour les réactions de complexation avec $BF_3$ ou les réactions de protonation (6, 9, 35). Toutefois en phase gazeuse et donc en l'absence de solvatation l'effet de résonance direct dans l'ion radical ne semble pas aussi important que pour l'entité $BH^+$ ou B: $BF_3$ en solution. En ce qui concerne la série 3 et les acétophénones, cette hypothèse est vérifiée par l'existence de relations correctes entre les potentiels d'ionisation et les constantes dites "normales" $\sigma^0$ de Yukawa (36):

$$\text{série 3: PI } (n_0) = (0{,}434 \pm 0{,}053)\,\sigma^0 + 8{,}88 \qquad r = 0{,}944 \quad S = 0{,}057 \text{ eV}$$

$$\text{Acétophénones: PI } (n_0) = (0{,}694 \pm 0{,}078)\,\sigma^0 + 9{,}36 \qquad r = 0{,}953 \quad S = 0{,}087 \text{ eV}$$

Pour les énaminocétones de la série 2, dans l'hypothèse où l'angle dièdre θ varie très peu autour d'une valeur moyenne proche de zéro, le niveau $n_0$ ne devrait donc être influencé en premier lieu que par les effets polaires des substituants H ou alkyles de l'azote quantifiés par les constantes σ* de Taft (17) et Hall (37). En fait, il existe deux droites parallèles représentant les relations PI ($n_0$) = $f$ ($\Sigma\sigma^*$) pour les énaminocétones mono et disubstituées, ce qui permet d'établir la relation unique (figure 5):

$$\text{PI } (n_0) = (1{,}00 \pm 0{,}15)\,\Sigma\sigma^* + 0{,}48n + 7{,}53 \qquad r = 0{,}93 \quad S = 0{,}05 \text{ eV}$$

où $n$ représente le nombre de substituants alkyles de l'azote ($n$ = 0, 1 ou 2) et $\Sigma\sigma^*$ la somme des σ* des substituants H ou alkyles de l'azote. La valeur de 0,48 eV correspond donc à la destabilisation apportée par l'effet d'une alkylation sur le site $NH_2$.

Compte tenu de la précision des mesures (± 0,03 eV) l'écart type de la relation est correct, cependant l'intervention d'un effet stérique de la part des substituants alkyles, modifiant également l'interaction $p$–π n'est pas à exclure dans l'interprétation des déviations.

*Corrélations avec la basicité au sens de Lewis*

Dans la mesure où la labilité de la paire libre d'un

Can. J. Chem. Downloaded from www.nrcresearchpress.com by 210.87.254.5 on 09/06/12
For personal use only.

TABLEAU 5. Potentiels d'ionisation de la paire libre de l'oxygène du carbonyle d'une série d'acétophénones *para* substituées (eV)

| Composés | | | Composés | | |
|---|---|---|---|---|---|
| No | X | $n_0$ (eV) | No | X | $n_0$ (eV) |
| **33** | H | 9,51 | **38** | CN | 9,82 |
| **34** | Cl | 9,52 | **39** | $CH_3$ | 9,38 |
| **35** | Br | 9,55 | **40** | $NO_2$ | 9,98 |
| **36** | $OCH_3$ | 9,20 | **41** | $C_6H_5$ | 9,33 |
| **37** | $NH_2$ | 9,08 | **42** | $COCH_3$ | 9,61 |

hétéroatome (O, N, P...) est le facteur prédominant de l'affinité protonique et où le potentiel d'ionisation peut être considéré comme une mesure de l'aptitude de cette paire à céder ses électrons, de nombreux auteurs se sont attachés à relier ce potentiel d'ionisation à la basicité en phase gazeuse des séries de composés hétéroatomiques (19, 38–43). Ne possédant pas les affinités protoniques des cyclohexénones, nous avons donc tenté de relier les potentiels d'ionisation de la paire libre de l'oxygène du carbonyle des cyclohexénones et des acétophénones à un paramètre s'approchant le plus de la basicité en phase gazeuse à savoir l'enthalpie de complexation des cétones en solution dans le chlorure de méthylène par le trifluorure de bore gazeux. Nous avons démontré que ce paramètre $\Delta H^0$ pouvait être considéré comme une mesure de la basicité au sens de Lewis de ces composés en milieu organique peu solvatant (6, 9, 35). Les valeurs de $\Delta H^0$ pour les cyclohexénones des séries 1 et 3 et pour les acétophénones sont reportées dans le tableau 6.

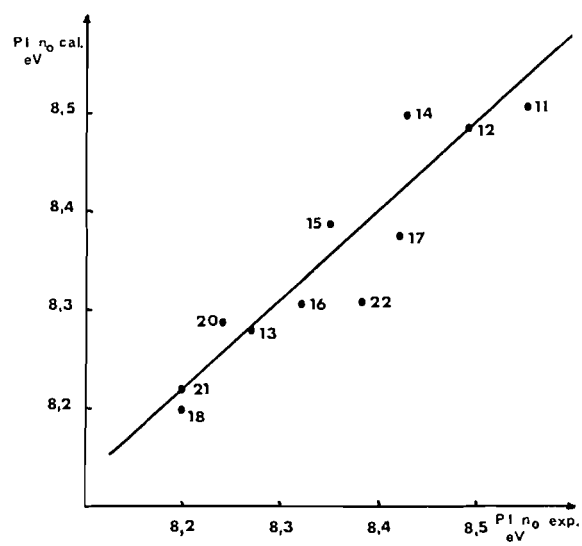


FIG. 5. Energies $n_0$ (calc.) vs. énergies $n_0$ (exp.) pour les énaminocétones (série 2).

Toutes les cétones possédant un groupement $-NH_2$ ou —NHR n'ont pu être étudiées par microcalorimétrie, car les associations intermoléculaires dues à la présence d'une liaison N—H conduisent à des valeurs erronées de $\Delta H^0$.

Nous obtenons une relation $\Delta H^0 = f(\text{PI } n_0)$ unique pour les cyclohexénones de la série 3 et les acétophénones *para*-substituées

$$\Delta H^0 = (20{,}8 \pm 1{,}1)\ \text{PI}\ n_0 - 272{,}30$$
$$r = 0{,}980 \qquad S = 1{,}53\ \text{kJ mol}^{-1}$$

Il semblerait donc que le potentiel d'ionisation de la paire libre de l'oxygène soit une mesure correcte de la basicité au sens de Lewis en milieu organique peu solvatant pour la classe des cétones aromatiques. Par contre, les cyclohexénones de la série 1 ne peuvent être inclues dans cette relation. En excluant les dérivés **5** ($OCH_3$), **6** ($OC_2H_5$) et **12** ($N(CH_3)_2$), nous obtenons une relation de pente et d'ordonnée à l'origine différentes de la précédente:

$$\Delta H^0 = (37{,}1 \pm 2{,}1)\ \text{PI}\ (n_0) - 424{,}81$$
$$r = 0{,}994 \qquad S = 1{,}41\ \text{kJ mol}^{-1}$$

Ainsi, le potentiel d'ionisation PI $n_0$ ne peut être utilisable pour la comparaison des basicités de différents types de cétones; par contre, ces potentiels d'ionisation peuvent permettre de comparer la basicité relative de cétones d'un même type. Les deux relations précédentes sont représentées dans la figure 6.

L'obtention d'une relation linéaire correcte pour la série 1 a nécessité l'exclusion de trois dérivés correspondant à des substituants possédant un important effet mésomère donneur ($N(CH_3)_2$, $OCH_3$, $OC_2H_5$). Les déviations de ces points sont en accord avec le fait que les potentiels d'ionisation ($n_0$) sont fonction des constantes $\sigma_p$ alors que les $\Delta H^0$ sont reliés aux $\sigma_p^+$ (9, 35). L'hypothèse émise précédemment est donc vérifiée, à savoir que l'interaction conjugative directe entre le substituant et la fonction carbonyle est assez faible dans les cyclohexénones et les acétophénones libres et devient très importante dans l'état complexé par $BF_3$. Cette exaltation des effets entre substituant et site basique lors du passage état initial – état final complexé ou protoné a été récemment mise en évidence par Taft et coll. (44) au cours d'une étude sur l'affinité protonique des pyridines substituées. Ces auteurs démontrent que l'énergie d'interaction substituant – pyridine substituée est environ huit fois plus faible que l'interaction substituant – ion pyridinium.

*Corrélations avec les résultats de résonance magnétique nucléaire*

Des corrélations entre les potentiels d'ionisation

Can. J. Chem. Downloaded from www.nrcresearchpress.com by 210.87.254.5 on 09/06/12
For personal use only.

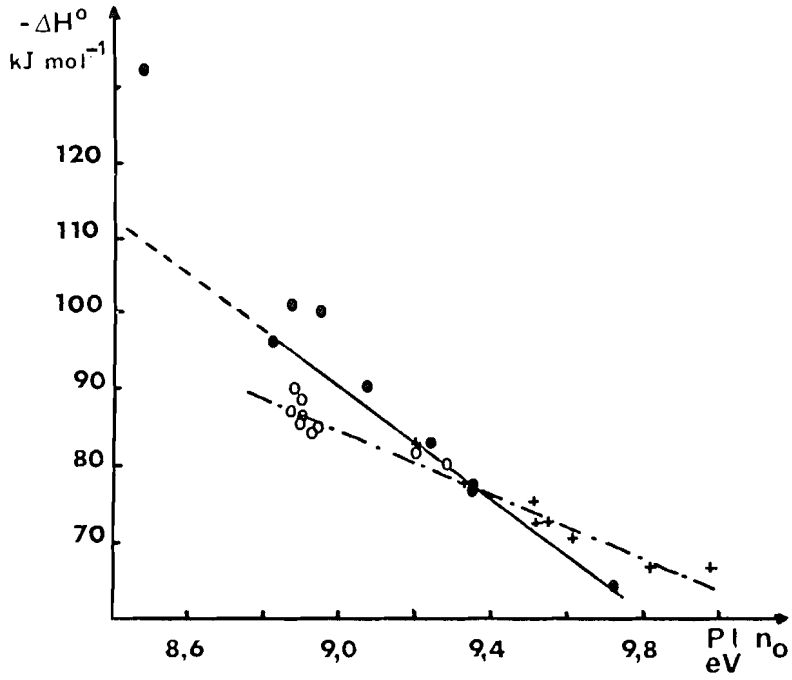


FIG. 6. Relations $\Delta H^0 = f(\text{PI } n_0)$ pour les cyclohexénones de la série 1 (●), et de la série 3 (○) et pour les acétophénones (+).

et des déplacements chimiques de rmn ont déjà été tentées avec succès dans diverses séries de composés carbonylés aromatiques aussi bien en rmn du $^{13}C$ et du $^{15}N$ (26) qu'en rmn protonique (28). Pour les cyclohexénones, nous avons récemment démontré que le déplacement chimique du carbone éthylénique $C_2$ en α de la fonction carbonyle est essentiellement influencé par la densité électronique π de ce carbone, une augmentation de densité entrainant un blindage et inversement (45, 46). Les orbitales $\pi_-$ pour la série 1 et $\pi_+$ PhS pour la série 3 sont celles dans lesquelles il y a la plus forte localisation sur le carbone $C_2$. Si nous faisons exception des composés dans lesquels il existe une très forte interaction entre l'orbitale $\pi_-$ et le doublet libre de l'hétéroatome du substituant (composés **8**, **11** et **12**) il existe effectivement une relation linéaire entre $\delta^{13}C_2$ de la série 1 (tableau 7)

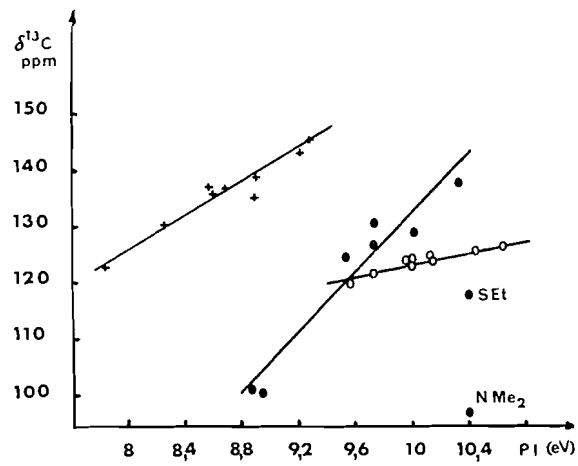


FIG. 7. $\delta^{13}C = f(\text{PI})$ pour le $C_2$ de la série 1 (●) pour le $C_2$ (○) et le $C_7$ (+) de la série 3.

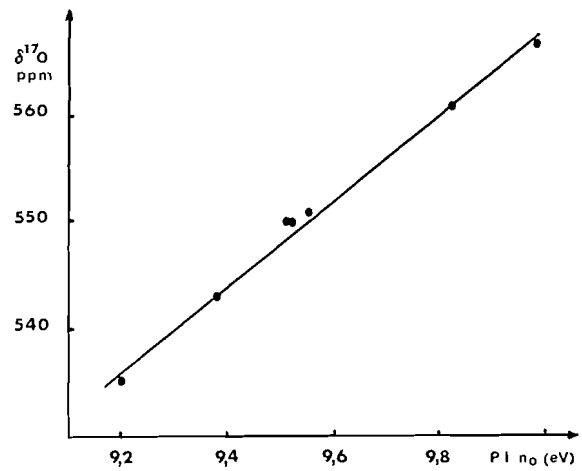


FIG. 8. Relation $\delta^{17}O$ (C=O) $= f(\text{PI } n_0)$ pour les acétophénones *para*-substituées.

TABLEAU 6. Enthalpies de complexation $\Delta H^0$ des cyclohexénones et des acétophénones avec le trifluorure de bore

| Substituants | Série 1 $-\Delta H^0$ kJ mol$^{-1}$ | Série 3 $-\Delta H^0$ kJ mol$^{-1}$ | *p*-X acétophénones $-\Delta H^0$ kJ mol$^{-1}$ |
|---|---|---|---|
| H | 83,58±0,34 | 86,48±0,29 | 75,52±0,15 |
| $CH_3$ | 90,56±0,41 | 88,79±0,28 | 77,82±0,33 |
| $C_6H_5$ | 86,48±0,29 | 87,16±0,33 | 77,03±0,18 |
| F | | 86,06±0,26 | |
| Cl | 77,87±0,33 | 85,41±0,43 | 73,03±0,31 |
| Br | 77,28±0,18 | 84,87±0,34 | 73,09±0,40 |
| $OCH_3$ | 99,89±0,20 | 90,44±0,33 | 83,01±0,43 |
| $OC_2H_5$ | 101,25±0,35 | | |
| $SC_2H_5$ | 96,64±0,80 | | |
| CN | 64,46±0,53 | 82,20±0,55 | 67,08±0,25 |
| $NO_2$ | | 80,29±0,48 | 67,07±0,50 |
| $N(CH_3)_2$ | 132,48±0,47 | | |
| $COCH_3$ | | | 70,58±1,18 |

TABLEAU 7. Déplacements chimiques du $^{13}C$ des cétones des séries 1 et 3 et du $^{17}O$ des acétophénones *para*-substituées

| Substituants | Série 1 $C_2$ (ppm) | Série 3 $C_2$ (ppm) | Série 3 $C_7$ (ppm)[a] | Acétophénones $^{17}O(C{=}O)$ ppm[b] |
|---|---|---|---|---|
| H | 129,07 | 124,37 | 138,96 | 550 |
| $CH_3$ | 125,62 | 123,53 | 136,06 | 543 |
| $C_6H_5$ | 124,37 | 124,00 | 137,71 | |
| F | | 124,15 | 135,14 | 545 |
| Cl | 127,49 | 124,52 | 137,39 | 550 |
| Br | 131,59 | 124,40 | 137,77 | 551 |
| $OCH_3$ | 101,09 | 122,44 | 130,91 | 535 |
| $OC_2H_5$ | 101,54 | | | |
| $SC_2H_5$ | 118,31 | | | |
| CN | 137,83 | 126,34 | 143,63 | 561 |
| $NO_2$ | | 126,77 | 145,56 | 567 |
| $NH_2$ | | 120,75 | 128,42 | 511 |
| $N(CH_3)_2$ | 97,49 | | | |

[a]Référence 9. Déplacements chimiques mesurés dans $CDCl_3$ par rapport au TMS.
[b]Référence 47. Déplacements chimiques mesurés dans le dioxanne par rapport à $H_2O$.

et les potentiels d'ionisation relatifs à l'orbitale $\pi_-$:

$$\delta^{13}C_2 \text{ (série 1)} = (26{,}6 \pm 3{,}7)\ PI\ (\pi_-) - 132{,}55$$
$$r = 0{,}995 \qquad S = 4{,}75 \text{ ppm}$$

Cette relation devient nettement meilleure pour la série 3:

$$\delta^{13}C_2 \text{ (série 3)} = (5{,}40 \pm 0{,}59)\ PI\ (\pi_- + Ph_S) + 69{,}75$$
$$r = 0{,}961 \qquad S = 0{,}54 \text{ ppm}$$

Le même raisonnement peut être tenu pour le potentiel d'ionisation de l'orbitale $Ph_S - \pi_-$ et le carbone $C_7$ en *para* du substituant variable dans la série 3 dont le déplacement chimique est essentiellement fonction de la densité électronique (48):

$$\delta^{13}C_7 \text{ (série 3)} = (11{,}54 \pm 0{,}82)\ PI\ (Ph_S - \pi_-) + 37{,}20$$
$$r = 0{,}985 \qquad S = 1{,}07 \text{ ppm}$$

L'anomalie observée pour le dérivé fluoré a été également rencontrée dans la série des benzamides *para*-substituées (26). Les trois relations précédentes sont schématisées dans la figure 7.

Récemment Fiat et Coll. (47) ont recherché des relations permettant de prévoir et d'interpréter les déplacements chimiques de l'oxygène 17 de la fonction carbonyle des acétophénones. Ils ont pour cela tenté de relier les déplacements chimiques aux constantes de substituants ainsi qu'à divers paramètres

Can. J. Chem. Downloaded from www.nrcresearchpress.com by 210.87.254.5 on 09/06/12
For personal use only.

spectroscopiques et en particulier à la longueur d'onde d'absorption de la transition $n \rightarrow \pi^*$. Ils en concluent que la plus importante contribution à la constante d'écran de l'oxygène est apporté par le terme paramagnétique et à l'intérieur de celui-ci par l'énergie $\Delta E^{-1}{}_{n\rightarrow\pi^*}$. Cependant, d'autres auteurs considèrent que le terme $\langle r^{-3}\rangle$ où $r$ représente le rayon de l'orbitale $2p$ de l'oxygène joue également un rôle dans l'évaluation du terme paramagnétique (49). Nous avons donc recherché une relation entre les déplacements chimiques $\delta^{17}O$ des acétophénones mesurés par Fiat et coll. (47) (tableau 7) et un paramètre lié indirectement à $\langle r^{-3}\rangle$ et à l'énergie de la transition $n \rightarrow \pi^*$ à savoir le potentiel d'ionisation de l'orbitale $2p$ de l'oxygène. Si nous excluons le composé portant le groupement $NH_2$, une excellente corrélation est obtenue (fig. 8):

$$\delta^{17}O \text{ (ppm) acétophénones} = (40{,}5 \pm 1{,}6)\ PI\ (n_O) + 163{,}4$$
$$r = 0{,}996 \qquad S = 1{,}0 \text{ ppm}$$

L'écart observé pour le composé **37** est explicable par l'existence de liaisons hydrogènes dues au groupement $NH_2$ qui ont pour effet de blinder anormalement l'oxygène du carbonyle (47).

Nous avons tenté sans succès d'enregistrer les spectres de rmn de l'oxygène 17 des cyclohexé nones sans enrichissement isotopique, ce qui nous aurait permis de confirmer la validité de la relation $\delta^{17}O = f(PI\ n_O)$ dans la prédiction du déplacement ainsi que dans son interprétation théorique.


1. I. FLEMING. Frontier orbital and organic chemical reactions. Wiley–Interscience, London. 1976.
2. T. KOOPMANS. Physica, **1**, 104 (1934).
3. N. BODOR, M. J. S. DEWAR et Z. MAKSIC. Croat. Chem. Acta, **48**, 9 (1976).
4. W. SCHAEFER, A. SCHWEIG et J. K. CRANDALL. Tetrahedron Lett. 1213 (1974).
5. P. MASCLET et G. MOUVIER. J. Electron Spectrosc. Relat. Phenom. **14**, 77 (1978).
6. J. F. GAL. Thèse d'Etat, Nice (1979).
7. S. A. MANLEY and J. K. TYLER. Chem. Commun. 382 (1970).
8. A. D. BAIN et D. C. FROST. Can. J. Chem. **51**, 1245 (1973).
9. S. GERIBALDI. Thèse d'Etat, Nice (1979).
10. M. AZZARO, S. GERIBALDI et B. VIDEAU. Synthesis, 880 (1981).
11. J. A. POPLE et M. GORDON. J. Am. Chem. Soc. **89**, 4253 (1967).
12. D. CHADWICK, D. C. FROST et L. WEILER. J. Am. Chem. Soc. **93**, 4320 (1971).
13. D. PITEA et G. FAVINI. J. Chem. Soc. Perkin Trans. II, 142 (1972).
14. D. W. TURNER, C. BAKER, A. D. BAKER et C. R. BRUNDLE. Molecular photoelectron spectroscopy. Wiley– Interscience, London. 1970.
15. K. N. HOUK, L. P. DAVIS, G. R. NEWKOME, R. E. DUKE, JR. et R. V. NAUMAN. J. Am. Chem. Soc. **95**, 8364 (1973).
16. R. SUSTMANN et H. TRILL. Angew. Chem. Int. Ed. Engl. **11**, 838 (1972).
17. R. W. TAFT. Steric effects in organic chemistry, *Edited by* M. S. Newman. Wiley, New York. 1956.
18. A. SCHWEIG et W. THIEL. J. Electron Spectrosc. **3**, 27 (1974), et références citées.
19. D. H. AUE, H. M. WEBB et M. T. BOWERS. J. Am. Chem. Soc. **98**, 311 (1976).
20. R. S. BROWN. Can. J. Chem. **54**, 1521 (1976).
21. J. P. MAIER et D. W. TURNER. J. Chem. Soc. Faraday Trans. II, **69**, 521 (1973).
22. G. LAUER, W. SCHÄFER et A. SCHWEIG. Tetrahedron Lett. 3939 (1975).
23. L. ASBRINK, E. LINDHOLM et O. EDQVIST. Chem. Phys. Lett. **5**, 609 (1970).
24. R. EGDELL, J. C. GREEN et C. N. R. RAO. Chem. Phys. Lett. **33**, 600 (1975).
25. C. N. R. RAO. Tetrahedron, **32**, 1521 (1976).
26. E. J. MCALDUFF, B. M. LYNCH et K. N. HOUK. Can. J. Chem. **56**, 495 (1978).
27. E. J. MCALDUFF et T. CHAN. Can. J. Chem. **56**, 2714 (1978).
28. E. J. MCALDUFF. Can. J. Chem. **58**, 622 (1980).
29. J. M. MAIER et D. W. TURNER. J. Chem. Soc. Faraday Trans II, **69**, 196 (1973).
30. J. W. RABALAIS et R. J. COLTON. J. Electron Spectrosc **1**, 83 (1972/73).
31. J. W. RABALAIS. Principles of photoelectron spectroscopy. Wiley–Interscience, London. 1977.
32. D. M. MCDANIEL et H. C. BROWN. J. Org. Chem. **23**, 420 (1958).
33. R. T. C. BROWNLEE, S. EHRENSON et R. W. TAFT. Progr. Phys. Org. Chem. **10**, 1 (1973).
34. C. D. JOHNSON. The Hammett equation. University Press, Cambridge. 1973. p. 27.
35. M. AZZARO, J. F. GAL, S. GERIBALDI et A. DREC-LUCIANO. J. Chem. Res. (S) 134, (M) 1478 (1979).
36. Y. YUKAWA. Conference Euchem. Correlation Analysis in Organic Chemistry, Assisi. 1979.
37. H. K. HALL. J. Am. Chem. Soc. **79**, 5441 (1957).
38. D. W. DAVIS et J. W. RABALAIS. J. Am. Chem. Soc. **96**, 5305 (1974).
39. K. YOSHIKAWA, M. HASHIMOTO et J. MORISHIMA. J. Am. Chem. Soc. **96**, 288 (1974).
40. D. H. AUE, H. M. WEBB et M. T. BOWERS. J. Am. Chem. Soc. **97**, 4136 (1975); **97**, 4137 (1975).
41. M. F. LAPPERT, J. B. PEDLEY, B. T. WILKINS, O. STELZER et E. UNGER. J. Chem. Soc. Dalton Trans. 1207 (1975).
42. M. GRAFFEUIL, J. F. LABARRE, M. F. LAPPERT, C. LEIBOVICI et O. STELZER. J. Chim. Phys. **72**, 799 (1975).
43. R. L. DEKOCK et M. R. BARBACHYN. J. Am. Chem. Soc. **101**, 6516 (1979).
44. M. TAAGEPERA, K. D. SUMMERHAYS, W. J. HEHRE, R. D. TOPSOM, A. PROSS, L. RADOM et R. W. TAFT. J. Org. Chem. **46**, 891 (1981).
45. M. AZZARO, J. F. GAL, S. GERIBALDI et N. NOVO-KREMER. Org. Magn. Reson. **9**, 181 (1981).
46. M. AZZARO, J. F. GAL, S. GERIBALDI et N. NOVO-KREMER. Spectrochim. Acta Part H, **34**, 157 (1978).
47. T. E. ST AMOUR, M. L. BURGAR, B. VALENTINE et D. FIAT. J. Am. Chem. Soc. **103**, 1128 (1981).
48. E. SOLANIOVA, S. TOMA et S. GRONOWITZ. Org. Magn. Reson. **8**, 439 (1976).
49. D. J. SARDELLA et J. B. STOTHERS. Can. J. Chem. **47**, 3089 (1979).


Can. J. Chem. Downloaded from www.nrcresearchpress.com by 210.87.254.5 on 09/06/12
For personal use only.

# Molecular motion and methyl group rotation barriers from $^{13}C$ nmr relaxation times. Podacarpic acid derivatives

HELMUT BEIERBECK,[1] JOHN W. EASTON,[2] AND JOHN K. SAUNDERS
*Departement de chimie, Université de Sherbrooke, Sherbrooke (Qué.), Canada J1K 2R1*
AND
RUSSELL A. BELL
*Chemistry Department, McMaster University, Hamilton, Ont., Canada L8S 4M1*

Received May 14, 1981

HELMUT BEIERBECK, JOHN W. EASTON, JOHN K. SAUNDERS, and RUSSELL A. BELL. Can. J. Chem. **60**, 1173 (1982).

The $^{13}C$ nmr relaxation time data for a number of compounds related to podocarpic acid are presented. The $T_1$ values of these molecules were satisfactorily reproduced by application of Woessner's equations for an asymmetric top assuming that the preferred principal axis of the rotational diffusion tensor was either the preferred principal inertial axis or an axis containing the centre of mass and the heterosubstituent at C-4. The values for hindrance to rotation for the various methyl groups are given and their variations discussed.

HELMUT BEIERBECK, JOHN W. EASTON, JOHN K. SAUNDERS et RUSSELL A. BELL. Can. J. Chem. **60**, 1173 (1982).

On rapporte les temps de relaxation en rmn $^{13}C$ d'un certain nombre de composés apparentés à l'acide podocarpique. On peut reproduire assez fidèlement les valeurs $T_1$ de ces molécules en faisant appel aux équations de Woessner pour un sommet asymétrique en faisant l'hypothèse que l'axe principal préféré par le tenseur de diffusion rotationnelle est soit l'axe principal préféré d'inertie ou un axe comprenant le centre de masse et l'hétérosubstituant en C-4. On rapporte des données relatives à l'empêchement à la rotation de divers groupes méthyles et on les discute.

[Traduit par le journal]

For an asymmetric top molecule the rotational diffusion constants can be obtained from eq. [1]

$$[1]\quad \frac{1}{T_1} = \frac{\hbar^2\gamma_H^2\gamma_C^2}{(r_{C-H})^6}\left[\frac{C_1}{4R_1+R_2+R_3} + \frac{C_2}{4R_2+R_1+R_3} + \frac{C_3}{4R_3+R_1+R_2} + \frac{C_4}{6[R+(R^2-L^2)^{\frac{1}{2}}]} + \frac{C_5}{6[R-(R^2-L^2)^{\frac{1}{2}}]}\right]$$

where $R_1$, $R_2$, and $R_3$ are the respective rotational diffusion rates about the principal axes of the diffusion tensor, $R = 1/3\,(R_1 + R_2 + R_3)$, $L^2 = 1/3\,(R_1R_2 + R_1R_3 + R_2R_3)$ and the $C$'s are geometrical functions defined in ref. 1. The calculation of diffusion constants about the principal axes requires *a priori* that these axes have been defined. The usual method using Woessner's equations is to use the principal axes of inertia of the molecule. This appears to be quite satisfactory, when molecules containing only carbon and hydrogen are studied (2), or when a diffusional axis is coincident with an inertia axis (3, 4). As pointed out by Stilbs and Moseley (5), the assumption that the principal axes of the diffusion and the inertia tensors are coincident may not be valid if heterosubstituents are present when the carbon–heterosubstituent bond is not coincident with a symmetry axis of the molecule. They found that the use of Woessner's equation did not give satisfactory values for relatively concentrated solutions of borneol in $CDCl_3$. Recently we have reported (6) the results for a number of norbornane and adamantane derivatives including borneol where satisfactory agreement was obtained between experimental values and those calculated using Woessner's equation for a symmetric top (1). The best correlation was obtained by assuming that the principal axis of the diffusion tensor passes through the heterosubstituent and the centre of mass of the molecule. In other words, the oxygen is "fixed" by intermolecular interactions whereas the movement of the hydrocarbon portion is controlled by inertial effects which correspond with volume effects. This does not necessarily infer that the centre of mass of the molecule is the origin of the diffusion tensor since the geometrical terms of eq. [1] refer only to direction cosines relative to the various axes. Thus, it is necessary only to define the principal axis of rotation and the direction of two mutually perpendicular axes. This can be seen by comparing monosubstituted benzene and adamantane derivatives. In the former, the principal axis of the diffusion tensor is coincident with the *para* C—H bond and this carbon is found (3) to have a shorter

[1]Permanent address: Centre Régional de RMN, Université de Montréal, Montréal, Québec.

[2]Permanent address: Ryerson Polytechnical Institute, Toronto, Ontario.

0008-4042/82/101173-05$01.00/0

©1982 National Research Council of Canada/Conseil national de recherches du Canada

Can. J. Chem. Downloaded from www.nrcresearchpress.com by 210.87.254.40 on 09/06/12
For personal use only.

TABLE 1. $^{13}C$ nmr $T_1$ data[a] for compounds **1–8** as approximately 1 *M* solutions in $CDCl_3$

| Compound | C-1 | C-2 | C-3 | C-5 | C-6 | C-7 | C-11 | C-13 | C-14 | C-18 | C-19 | C-20 | C-21 | C-22 |
|---|---|---|---|---|---|---|---|---|---|---|---|---|---|---|
| **1** | 0.74 | 0.69 | 0.52 | 1.3 | 0.64 | 0.76 | 1.4 | 0.79 | 1.4 | 1.1 | 0.77 | 2.2 | 2.6 | |
| **2** | 0.75 | 0.69 | 0.62 | 1.4 | 0.76 | 0.75 | 1.4 | 1.1 | 1.4 | 0.83 | — | 1.2 | 2.6 | 3.4 |
| **3** | 0.95 | 0.9 | 0.79 | 1.6 | 0.84 | 0.97 | 1.7 | 1.1 | 1.7 | 1.1 | — | 1.5 | 2.2 | |
| **4** | 1.3 | 1.3 | 1.1 | 2.4 | 1.4 | 1.6 | 2.7 | 1.8 | 2.7 | 1.3 | 2.9 | 2.5 | 3.1 | |
| **5** | 0.55 | 0.59 | 0.43 | 0.94 | 0.58 | 0.56 | 0.99 | 0.69 | 0.96 | 0.66 | — | 1.0 | 1.7 | 2.3 |
| **6** | 0.56 | 0.52 | — | 1.0 | — | — | 1.0 | 0.67 | 0.98 | 0.62 | — | 0.89 | 1.6 | 2.3 |
| **7** | 0.35 | 0.34 | 0.29 | 0.64 | 0.33 | 0.62 | 0.58 | 0.51 | 0.66 | 0.56 | — | 0.89 | 1.6 | 2.1 |
| **8** | 0.84 | 0.87 | 0.66 | 1.5 | 1.3 | 1.6 | 1.6 | 1.0 | 1.7 | 1.0 | — | 0.76 | 2.3 | 3.4 |

[a]In seconds estimated error ± 10%.

$T_1$ than the other carbons since rotation about the principal axis does not modulate this C—H bond vector. In 1-substituted adamantanes, the C—H *endo* bond of the δ carbon is parallel but not coincident with the $C_3$ symmetry axis which is the principal axis of the rotation tensor. This carbon has a shorter $NT_1$ than the other protonated carbons for the same reason (4).

The experimental $^{13}C$ $T_1$ values for the diterpenoid compounds **1** to **8**, which are related to podacarpic acid, are given in Table 1. These compounds were studied as approximately 1 *M* solution in $CDCl_3$. These values imply significant anisotropic motion for these molecules, since $NT_1$ for C-3 and C-13 are less than for other protonated carbons. The $T_1$ values were converted into diffusion constants using eq. [1] and these are recorded in Table 2.

The calculations were performed using two assumptions about the orientation of the principal axes; in the first, (A), the principal axes of the diffusion constant tensor are assumed to be coincident with those of the moments of inertia and in the second, (B), the principal axis of rotation passes through the centre of mass of the molecule and the axial substituent at C-4. For **1**, the rotational constants were also calculated by assuming that the principal axis passes through the centre of mass and the oxygen at C-12. The discrepancy between calculated and experimental was much larger using this last assumption and it was taken to be invalid. This was verified with several other compounds and found to hold true in each case.

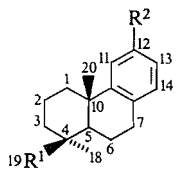


**1** $R^1 = CH_2OH$, $R^2 = OCH_3$
**2** $R^1 = CO_2CH_3$, $R^2 = OCH_3$
**3** $R^1 = CHO$, $R^2 = OCH_3$
**4** $R^1 = CH_3$, $R^2 = OCH_3$
**5** $R^1 = CO_2CH_3$, $R^2 = O_2CCH_3$

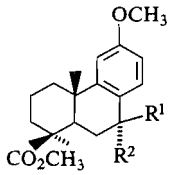


**6** $R^1 + R^2 = O$
**7** $R^1 = OH$, $R^2 = H$

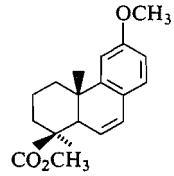


**8**

The calculations using either assumption A or B reproduce satisfactorily the observed variations in the $NT_1$ values for C-3 and C-13 relative to other protonated carbons. There are more subtle variations at carbons 1, 2, 6, and 7 in the calculated values. In most cases the experimental values for these carbons are within experimental error of those calculated by either choice of axes. In fact, with only one or two exceptions, the difference between calculated and experimental value is less than 10% for each carbon in each molecule. The results are not precise enough to distinguish between the two assumptions. Inspection of the illustration of **2** relative to the inertia axes shown in Fig. 1 shows that the principal axis passes in relatively close proximity to the substituent at C-4 and it is therefore not unexpected that the differences between the two assumptions are minimal. Further discussion on the subtle differences is imprudent for at least two reasons. Firstly, the observed values are not sufficiently accurate and secondly, the representation in space of the molecules was obtained from molecular models assuming normal bond angles and bond lengths. X-ray data for these compounds were not available but data (7) from similar compounds show that molecular distortions are present. For example the ring junction at C-5 is flatter than in models with tetrahedral angles of 109.47°. In each compound the observed $T_1$ for C-5 is less than that calculated, which could be indicative of a shorter C—H bond. Any molecular deformation will obviously result in variations in the C—H bond vectors and hence in the $T_1$ values.

The diffusion constant for internal rotation of a

Can. J. Chem. Downloaded from www.nrcresearchpress.com by 210.87.254.40 on 09/06/12
For personal use only.

Can. J. Chem. Downloaded from www.nrcresearchpress.com by 210.87.254.40 on 09/06/12
For personal use only.

TABLE 2. Calculated diffusion constants[a] about the various axes: comparison between calculated and experimental $T_1$ values.

| Compound | Axis[b] | C-1 | C-2 | C-3 | C-5 | C-6 | C-7 | C-11 | C-13 | C-14 | R¹ | R² | R³ |
|---|---|---|---|---|---|---|---|---|---|---|---|---|---|
| **1** | Exp | 0.74 | 0.69 | 0.52 | 1.3 | 0.69 | 0.76 | 1.4 | 0.79 | 1.4 | | | |
| | A | 0.68 | 0.73 | 0.52 | 1.5 | 0.68 | 0.73 | 1.4 | 0.79 | 1.4 | 1.1 | 0.30 | 0.26 |
| | B | 0.70 | 0.70 | 0.52 | 1.4 | 0.71 | 0.73 | 1.4 | 0.80 | 1.4 | 1.1 | 0.32 | 0.26 |
| | C | 0.63 | 0.73 | 0.59 | 1.7 | 0.63 | 0.73 | 1.2 | 0.90 | 1.2 | 1.1 | 0.41 | 0.12 |
| **2** | Exp | 0.75 | 0.69 | 0.62 | 1.4 | 0.76 | 0.75 | 1.4 | 1.1 | 1.4 | | | |
| | A | 0.70 | 0.73 | 0.64 | 1.5 | 0.70 | 0.76 | 1.5 | 1.1 | 1.5 | 0.81 | 0.42 | 0.36 |
| | B | 0.72 | 0.68 | 0.64 | 1.4 | 0.74 | 0.78 | 1.5 | 1.1 | 1.4 | 1.0 | 0.42 | 0.29 |
| **3** | Exp | 0.95 | 0.90 | 0.79 | 1.6 | 0.84 | 0.97 | 1.7 | 1.1 | 1.7 | | | |
| | A | 0.87 | 0.94 | 0.74 | 2.0 | 0.86 | 0.96 | 1.8 | 1.2 | 1.7 | 1.3 | 0.50 | 0.31 |
| | B | 0.92 | 0.85 | 0.75 | 1.8 | 0.94 | 0.96 | 1.7 | 1.2 | 1.7 | 1.3 | 0.48 | 0.34 |
| **4** | Exp | 1.3 | 1.3 | 1.1 | 2.4 | 1.4 | 1.6 | 2.7 | 1.8 | 2.7 | | | |
| | A | 1.3 | 1.4 | 1.1 | 2.8 | 1.3 | 1.4 | 2.8 | 1.8 | 2.8 | 1.8 | 0.69 | 0.64 |
| | B | 1.4 | 1.3 | 1.1 | 2.6 | 1.4 | 1.5 | 2.7 | 1.9 | 2.7 | 2.1 | 0.57 | 0.67 |
| **5** | Exp | 0.55 | 0.59 | 0.43 | 0.94 | 0.58 | 0.56 | 0.99 | 0.69 | 0.96 | | | |
| | A | 0.53 | 0.59 | 0.44 | 1.2 | 0.52 | 0.59 | 1.1 | 0.65 | 1.1 | 1.2 | 0.22 | 0.13 |
| | B | 0.55 | 0.50 | 0.46 | 1.1 | 0.56 | 0.58 | 1.1 | 0.68 | 1.0 | 0.94 | 0.26 | 0.15 |
| **6** | Exp | 0.56 | 0.53 | | 1.0 | | | 1.0 | 0.67 | 0.98 | | | |
| | A | 0.51 | 0.53 | | 1.1 | | | 1.1 | 0.68 | 1.0 | | | |
| | B | 0.55 | 0.50 | | 1.1 | | | 1.0 | 0.69 | 1.0 | 0.91 | 0.31 | 0.13 |
| **7** | Exp | 0.35 | 0.34 | 0.29 | 0.64 | 0.33 | 0.62 | 0.58 | 0.51 | 0.66 | | | |
| | A | 0.32 | 0.33 | 0.30 | 0.71 | 0.33 | 0.71 | 0.65 | 0.51 | 0.64 | 0.36 | 0.23 | 0.15 |
| | B | 0.34 | 0.32 | 0.29 | 0.65 | 0.34 | 0.66 | 0.65 | 0.51 | 0.64 | 0.38 | 0.19 | 0.19 |
| | D | 0.37 | 0.34 | 0.31 | 0.68 | 0.32 | 0.67 | 0.68 | 0.55 | 0.66 | 0.22 | 0.36 | 0.16 |
| **8** | Exp | 0.84 | 0.87 | 0.66 | 1.6 | 1.4 | 1.6 | 1.6 | 1.0 | 1.7 | | | |
| | A | 0.82 | 0.84 | 0.66 | 1.8 | 1.2 | 1.7 | 1.8 | 1.1 | 1.7 | 1.4 | 0.34 | 0.31 |
| | B | 0.86 | 0.78 | 0.66 | 1.8 | 1.6 | 1.6 | 1.6 | 1.1 | 1.6 | 1.2 | 0.44 | 0.34 |

[a] $\times 10^{10}$ $s^{-1}$: estimated error ± 10%.
[b] Axis: principal axis of rotation assumed to be A: principal axis of inertia. B: axis which passes through centre of mass and the substituent at C-4. C: axis which passes through centre of mass and the oxygen at C-12. D: axis which passes through centre of mass and the oxygen at C-7.

methyl group undergoing 120° jumps can be determined from eq. [2] (8), where ρ is $R_{int}/R$ and $A$, $B$, and $C$ are geometrical constants. Equation [2] is valid for isotropic motion.

$$[2] \quad \frac{T_1(CH)}{3T_1(CH_3)} = \left[\frac{A}{6} + \frac{B+C}{6+\rho}\right]$$

For molecules undergoing anisotropic motion equations similar to [2] have been derived (9). A parameter ($V_R$) characterizing the hindrance to rotation (10) can be estimated from the relationship (11) $R_{int} = R_o \exp(-V_R/RT)$ where $R_o = 3/2\ kT/I$ and $I$ is the moment of inertia of the methyl group. In earlier work, we had observed that the value of $V_R$ depends on the number of 1,3 diaxial hydrogen interactions to which the $CH_3$ group is subjected. Furthermore, replacement of one of these axial hydrogens by an OH group had little effect on the value of $V_R$. The $V_R$ values for the methyl groups C-18 and C-20 in compounds **1–8** were calculated and are given in Table 3.

The $V_R$ value for C-18 of compound **4**, with a methyl group at C-4 is 15.6 kJ/mol, which can be compared to the value of 14.4 kJ/mol found in 4,4-dimethyl adamantan-2-one (6). Both compounds have only one 1,3 diaxial $CH_3$ group – hydrogen interaction. The replacement of the axial methyl by a carbomethoxy group does not alter $V_R$ since each of the compounds which contain this group at C-4, with the exception of **8**, has a value of 15.7 ± 0.4 kJ/mol. Inspection of molecular models

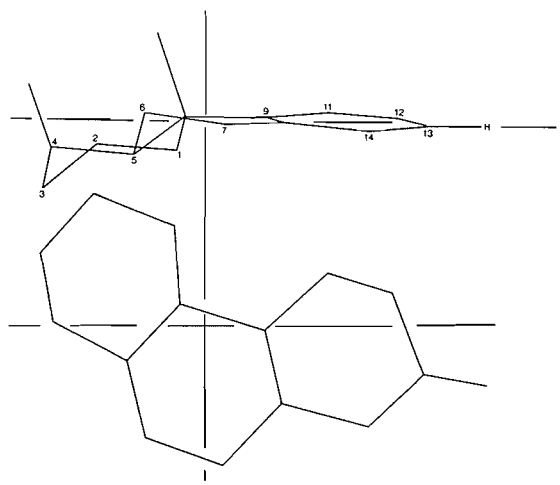

FIG. 1. Representation of **2** relative to the principal inertial axes.

TABLE 3. Internal reorientation diffusion constants ($R_{int}$)[a] and values for the hindrance to rotation ($V_R$)[b] for compounds **1–8**

| | C-18 | | C-19 | | C-20 | |
|---|---|---|---|---|---|---|
| Compound | $R_{int}$ | $V_R$ | $R_{int}$ | $V_R$ | $R_{int}$ | $V_R$ |
| **1** | 5.3 | 13.9 | | | 22.5 | 10.3 |
| **2** | 2.7 | 15.6 | | | 6.2 | 13.5 |
| **3** | 4.0 | 14.6 | | | 8.0 | 12.9 |
| **4** | 2.8 | 15.5 | 17.7 | 11.0 | 14.5 | 11.4 |
| **5** | 2.4 | 15.9 | | | 5.9 | 13.6 |
| **6** | 3.0 | 15.3 | | | 7.8 | 12.9 |
| **7** | 2.2 | 16.1 | | | 4.9 | 14.2 |
| **8** | 3.7 | 14.8 | | | 1.8 | 16.6 |

[a]$\times 10^{10}$ $s^{-1}$: estimated error ± 15%.
[b]kJ/mol: estimated error ± 0.3 kJ/mol.

suggests that the 1,3-interaction between H-6 and C-18 in **8** is more severe than in the other compounds. The two entries with either a $CH_2OH$ or a CHO group at C-4 have a slightly lower barrier.

The $V_R$ value for the methyl group, C-20, shows a more marked dependence on substituent than C-18. As for C-18, the C-20 values for compounds with a $CO_2CH_3$ at C-4 do not vary significantly with the exception of **8**. Compound **8** contains a double bond at C-6,C-7 and thus has one 1,3 diaxial methyl–hydrogen interaction less than the other compounds and thus the hindrance to relation is greater. Replacing a $CO_2CH_3$ by a CHO group only marginally decreases the hindrance to rotation. When a $CH_3$ group is present at C-4, $V_R$ is reduced significantly and this decrease is even more pronounced when a $CH_2OH$ group is present. The accepted explanation of rapidly rotating *syn* diaxial methyl groups is that they turn in a gear wheel type of fashion. This explanation cannot, however, be invoked in the present examples since the rotation rates of C-19 and C-20 are quite different in both compounds **1** and **4**. The $NT_1$ value of C-19 in **1** is within experimental error of that calculated for a rigid carbon and therefore the rate of rotation about the C-4,C-19 bond must be relatively very slow. For **4**, the rotation rate about the C-4,C-19 is more rapid than that about the C-10,C-20 bond.

The $T_1$ values for the two $OCH_3$ groups, when present, are given in Table 1. The absolute values may have a larger error than those for the other carbons since these were not of primary interest for this study. The trends, however, are correct in that the methyl carbon of the carbomethoxy group always has a longer $T_1$ than the aromatic methoxy methyl. Estimation of the hindrance to rotation cannot be performed since rotation about more than one bond is possible. It is to be expected that the rotation about the aromatic carbon–oxygen bond and the carbonyl carbon–oxygen bond would be relatively slow due to overlap of the nonbonding electrons of the oxygen and the $\pi$ system. The difference then will be due to differences in rotation rates about the O—$CH_3$ bonds or a relatively rapid rotation rate about the C-(4)—C(19) bond. The barrier to rotation about a carbon–carbonyl bond is known to be small (12). Whatever the explanation, this difference in $T_1$'s is useful for distinguishing between the two O—$CH_3$ groups.

## Experimental

Carbon-13 relaxation time data were obtained using the inversion recovery methods on a Bruker HX-90 as previously described (6). Sweep widths of 4000 Hz were generally employed. In some cases, much smaller sweep widths were also employed (2000 Hz) in which case the values for the aliphatic and aromatic regions were obtained in separate experiments. The values for the two types of experiments were within experimental error. Errors limits are estimated to be ± 10% in $T_1$ values which give rise to estimated errors of ± 15% in $R$ and ± 0.3 kJ/mol in $V_R$ (6).

The compounds used have all been reported in the literature. Spectral data and melting points corresponded to those reported.[3] The corresponding references are **1** (13), **2** (14), **3** (15), **4**, **6**, **8** (16), **5** (17), and **7** (18).

The chemical shift data for **1–3** (19) and **4** (20) have been reported. The spectra of the remaining compounds were readily assigned using these data and the substituent effects observed for similar compounds (19). The chemical shifts of **1** were verified by use of shift reagent. Carbons 11 and 13 have similar chemical shifts but they can easily be assigned from the coupled spectra (19).

## Acknowledgements

The authors express their appreciation to the Natural Sciences and Engineering Research Council of Canada and the Ministère d'éducation du Québec for generous financial support.

1. D. E. WOESSNER. J. Chem. Phys. **37**, 647 (1962).
2. K. F. KUHLMANN, D. M. GRANT, and R. K. HARRIS. J. Chem. Phys. **52**, 3439 (1970); S. BERGER, F. R. KREISSL, D. M. GRANT, and J. D. ROBERTS. J. Am. Chem. Soc. **97**, 1805 (1975).
3. G. C. LEVY, J. D. CARGIOLI, and F. A. L. ANET. J. Am. Chem. Soc. **95**, 1528 (1973).
4. H. BEIERBECK, R. MARTINO, and J. K. SAUNDERS. Can. J. Chem. **57**, 1224 (1979).
5. P. STILBS and M. E. MOSELEY. J. Magn. Reson. **33**, 209 (1979).
6. H. BEIERBECK, R. MARTINO, and J. K. SAUNDERS. Can. J. Chem. **58**, 102 (1980).
7. R. C. CAMBIE, G. R. CLARK, D. R. CRUMP, and T. N. WATERS. Chem. Commun. 183 (1968).
8. D. E. WOESSNER and B. S. SNOWDEN. Adv. Mol. Relaxation Processes, **3**, 181 (1972).
9. D. E. WOESSNER, B. SNOWDEN, and G. H. MEYER. J. Chem. Phys. **50**, (1969).
10. A. ERICCSON, J. KOWALEWSKI, T. LILJEFORS, and P. STILBS. J. Magn. Res. **38**, 9 (1980).
11. K. F. KUHLMANN and D. M. GRANT. J. Chem. Phys. **55**, 2998 (1971).

[3]J. W. Easton, Ph.D. Thesis, McMaster University, Hamilton, Ont. (1973).

Can. J. Chem. Downloaded from www.nrcresearchpress.com by 210.87.254.40 on 09/06/12
For personal use only.

12. W. TABOR. J. Chem. Phys. **27**, 974 (1957).
13. H. H. ZEISS, C. E. SLIMOWICZ, and V. Z. PASTERNAK. J. Am. Chem. Soc. **70**, 1981 (1948).
14. W. P. CAMPBELL and D. TODD. J. Am. Chem. Soc. **64**, 928 (1942).
15. C. R. BENNETT and R. C. CAMBIE. Tetrahedron, **23**, 927 (1967).
16. C. R. BENNETT, R. C. CAMBIE, and W. R. DENNY. Aust. J. Chem. **22**, 1069 (1969).
17. L. H. BRIGGS, R. C. CAMBIE, R. N. SEEBYE, and A. D. WARTH. Tetrahedron, **7**, 270 (1959).
18. F. WENKERT, P. BEAK, R. W. J. CARNEY, J. W. CHAMBERLIN, D. B. R. JOHNSTON, C. D. ROTH, and A. TAHARA. Can. J. Chem. **41**, 1924 (1963).
19. E. WENKERT, B. L. BUCKWALTER, I. R. BURFITT, M. J. CASIE, H. E. COHLIEB, E. W. HAGAMAN, F. M. SCHELL, P. M. WOVKALICH, and A. ZHELEVA. Top. Carbon-13 NMR Spectrosc. **2**, 81 (1976).
20. T. NISHIDA, I. WAHLBERG, and C. R. ENZELL. Org. Magn. Reson. **9**, 203 (1977).

Can. J. Chem. Downloaded from www.nrcresearchpress.com by 210.87.254.40 on 09/06/12
For personal use only.

# Solvent effects on the tautomeric equilibrium of 2,4-pentanedione

J. N. SPENCER, ERIC S. HOLMBOE, MINDY R. KIRSHENBAUM, DANIEL W. FIRTH, AND PATRICIA B. PINTO

*Department of Chemistry, Franklin and Marshall College, Lancaster, PA 17604, U.S.A.*

Received June 11, 1981

J. N. SPENCER, ERIC S. HOLMBOE, MINDY R. KIRSHENBAUM, DANIEL W. FIRTH, and PATRICIA B. PINTO. Can. J. Chem. **60**, 1178 (1982).

The influence of solvent on the equilibrium position of the tautomeric forms of 2,4-pentanedione was studied by calorimetric and nmr spectroscopic techniques. For solvents such as $CCl_4$ and cyclohexane the intramolecular bond of the enol form persists and bulk solvent effects account for the equilibrium enol–keto content. In solvents such as DMSO, disruption of the intramolecular bond occurs and the percentage of enol falls due to unfavorable entropy changes. The enol intramolecular bond is disrupted by the solvents water and methanol. Enol hydrogen bond formation through self-association and with the solvent accounts for the entropy changes upon enolization in these solvents. The thermodynamic parameters for enolization in neat 2,4-pentanedione are rationalized by the disruption of the enol intramolecular hydrogen bond through consequent polymerization of the enol tautomer.

J. N. SPENCER, ERIC S. HOLMBOE, MINDY R. KIRSHENBAUM, DANIEL W. FIRTH et PATRICIA B. PINTO. Can. J. Chem. **60**, 1178 (1982).

Faisant appel aux techniques de la calorimétrie et de la spectroscopie de RMN, on a étudié l'influence du solvant sur la position à l'équilibre des formes tautomères de la pentanedione-2,4. Dans le cas de certains solvants, tels le $CCl_4$ et le cyclohexane, la liaison intramoléculaire de la forme énolique persiste et les effets d'encombrement du solvant interviennent dans l'équilibre céto–énolique. Dans le cas du DMSO, il se produit une rupture de la liaison intramoléculaire et le pourcentage d'énol diminue beaucoup par suite des variations défavorables de l'entropie. Les solvants, tels le méthanol et l'eau, rompent la liaison intramoléculaire de l'énol. La formation de liaisons hydrogènes par suite d'une auto-association ou d'une association avec le solvant est responsable des variations d'entropie lors de l'énolisation dans ces solvants. On rationnalise les paramètres thermodynamiques de l'énolisation de la pentanedione-2,4 à l'état pur en considérant que la liaison hydrogène intramoléculaire de l'énol est rompue conduisant ainsi à une polymérisation de l'énol tautomère.

[Traduit par le journal]

## Introduction

In contrast to the low enol content of monocarbonyl compounds, the enol form of the tautomeric species of β-diketones generally predominates over the corresponding keto form. Solvent effects on the equilibrium position of β-diketones are pronounced. The enol content of 2,4-pentanedione in $CCl_4$ is 95% at 298 K but falls to 16% in water at 298 K. This report deals with a calorimetric and nmr investigation of solvent effects on the keto–enol equilibrium in 2,4-pentanedione.

## Experimental

The calorimeter and methods of calculation of the enthalpies of solution have been described previously (1, 2).

Spectra of solutions containing 2–4% of 2,4-pentanedione in various solvents were recorded on a Perkin-Elmer 732 90 megaherz nmr spectrometer equipped with a variable temperature accessory. The temperature range was 0 to 80°C. Assignments of the resonance peaks to the tautomeric forms have been reported (3). The ratio of the integrated areas and the peak heights of the resonance signals corresponding to the two tautomeric forms was used to calculate the percentage of enol. The equilibrium constant was calculated as the ratio of mole fraction of enol to keto tautomer. Plots of $\ln k$ vs. $T^{-1}$ were used to find $\Delta H^0$ and $\Delta S^0$. In order to provide as wide as possible variation in the equilibrium constant, data were recorded at temperature intervals of 15–20° over the temperature range. An average of about 10 determinations were made at each temperature using different freshly prepared solutions.

The purification of *N*,*N*-dimethylacetamide (DMA) has been given (4). Fisher Spectranalyzed methanol was fractionally distilled from magnesium under nitrogen atmosphere. Fisher Reagent Grade 2,4-pentanedione was fractionally distilled under reduced pressure. Fisher Spectranalyzed cyclohexane was refluxed over $P_2O_5$ and distilled under nitrogen. Fisher Certified ACS DMSO was refluxed over NaOH pellets and distilled under nitrogen. Fisher Certified ACS $CCl_4$ was refluxed over $P_2O_5$ and distilled under nitrogen. $CCl_4$, DMSO, DMA, and cyclohexane were stored over molecular sieves prior to distillation. Solution preparation was done in a nitrogen atmosphere.

## Results

Enthalpies of solution at infinite dilution are given in Table 1. The results of nmr analysis and comparisons with previously reported parameters for the enolization of 2,4-pentanedione are given in Table 2. The solvation enthalpy of the keto and enol tautomers was calculated by application of the Euler's theorem for homogeneous functions of

TABLE 1. Enthalpies of solution

| Solvent | $\Delta H_s$ (kcal mol$^{-1}$, 298 K) |
|---|---|
| Cyclohexane | +2.33±0.14 |
| $CCl_4$ | +0.77±0.11 |
| DMA | +0.11±0.03 |
| DMSO | +0.46±0.09 |
| Water | +0.42±0.09 |

0008-4042/82/101178-05$01.00/0

©1982 National Research Council of Canada/Conseil national de recherches du Canada

Can. J. Chem. Downloaded from www.nrcresearchpress.com by 210.87.254.5 on 09/06/12
For personal use only.

TABLE 2. Comparison of nmr results from the present study and literature values

| Solvent | $\Delta H^0$ (kcal mol$^{-1}$) | | $\Delta S^0$ (cal deg$^{-1}$ mol$^{-1}$) | | % enol (298 K) | |
|---|---|---|---|---|---|---|
| | Lit. | This work | Lit. | This work | Lit. | This work |
| Gas | −2.1,[a] −2.3[b] | | −1.7,[a] −1.9[b] | | 92,[a] 93.3[b] | |
| Cyclohexane | −3.0[c] | −3.0 | −4.0[c] | −2.9 | 96,[c] 91,[d] | 97 |
| $CCl_4$ | −3.0[c] | −2.5 | −4.4[c] | −2.7 | 95,[c] 96[e] | 95 |
| Neat | −2.8,[c] −2.84[a] | −2.8 | −6.4,[c] −6.7[a] | −6.6 | 82,[c] 80.9[f] | 81 |
| | −2.84,[f] −2.7[d] | | −6.66[f] | | 81,[a] 81.4[d] | |
| Methanol | | −2.7 | | −7.2 | 74[e] | 74 |
| DMA | | −1.9 | | −5.0 | | 66 |
| DMSO | −1.6[c] | −1.8 | −4.3[c] | −5.1 | 63,[c] 62[e] | 62 |
| Water | | −2.7 | | −12.4 | 15.5[g] | 16 |

[a]Reference 5.
[b]Reference 12.
[c]Reference 6, $\Delta S^0$ and % enol at 298 K calculated from the $\Delta H^0$ and % enol reported at 38°C.
[d]Reference 3.
[e]Reference 10, 33°C.
[f]Reference 9, % enol at 33°C.
[g]Reference 13, 20°C.

degree one. The enthalpy of a mixture of keto and enol forms is given by

$$H = X_k\bar{H}_k + \bar{X}_e\bar{H}_e$$

where $X_k$ and $X_e$ are the mole fractions of keto and enol tautomers respectively in a given phase; $\bar{H}_k$ and $\bar{H}_e$ are the enthalpies of the keto and enol tautomers in that phase. The transfer enthalpy from phase β to phase α may be written as

$$[1]\quad H_\alpha - H_\beta = (X_{k\alpha}\bar{H}_{k\alpha} + X_{e\alpha}\bar{H}_{e\alpha}) - (X_{k\beta}\bar{H}_{k\beta} + X_{e\beta}\bar{H}_{e\beta})$$

where $H_\alpha - H_\beta$ is the transfer enthalpy, $\Delta H_{\underset{\beta\to\alpha}{tr}}$, from phase β to phase α. For this study phase β was taken to be the gas phase and phase α the solvent under consideration. Manipulation of eq. [1] gives

$$[2]\quad \Delta H_{\underset{g\to\alpha}{tr}} = (\bar{H}_{k\alpha} - \bar{H}_{kg}) + X_{e\alpha}\Delta H_\alpha{}^0 - X_{eg}\Delta H_g{}^0$$

where $\Delta H_\alpha{}^0$ is the enthalpy change for enolization in solvent α and $\Delta H_g{}^0$ is the enthalpy change in the gas phase. Equation [1] may also be rearranged to give

$$[3]\quad \Delta H_{\underset{g\to\alpha}{tr}} = (\bar{H}_{e\alpha} - \bar{H}_{eg}) - X_{k\alpha}\Delta H_\alpha{}^0 + X_{kg}\Delta H_g{}^0$$

$\Delta H_{\underset{g\to\alpha}{tr}}$ may be calculated from the enthalpy of vaporization of 2,4-pentanedione (5) and the enthalpies of solution given in Table 1. The enthalpy changes in a given solvent, $\Delta H_\alpha{}^0$, $X_{e\alpha}$, and $X_{k\alpha}$ were obtained from nmr analysis; $\Delta H_g{}^0$, $X_{eg}$, and $X_{kg}$ were taken from the literature. Equations [2] and [3] may then be used to calculate $(\bar{H}_{k\alpha} - \bar{H}_{kg})$ and $(\bar{H}_{e\alpha} - \bar{H}_{eg})$. The enthalpies of the keto and enol tautomers in the gas phase, $\bar{H}_{kg}$ and $\bar{H}_{eg}$ were arbitrarily set to zero so that the terms $(\bar{H}_{k\alpha} - \bar{H}_{kg})$ and $(\bar{H}_{e\alpha} - \bar{H}_{eg})$ give the enthalpies of the keto and enol tautomers in the solvent α relative to the gas phase enthalpies. These quantities are given in Table 3 along with the enthalpy and entropy changes, the mole fraction enol as determined from nmr analysis, and the dielectric constant of the solvent. The difference $(\bar{H}_{k\alpha} - \bar{H}_{e\alpha})$ obtained from columns two and three of Table 3 gives the solvation difference between keto and enol tautomers of 2,4-pentanedione in a given solvent. Because the enol form is more stable by 2.2 kcal mol$^{-1}$ in the gas phase it is necessary to add −2.2 kcal mol$^{-1}$ to $(\bar{H}_{k\alpha} - \bar{H}_{e\alpha})$ to obtain $\Delta H_\alpha{}^0$ for the enolization in a given solvent. For example, in cyclohexane the enol form is enthalpically stabilized by solvation interactions over the keto form by −0.8 kcal mol$^{-1}$. Because the enthalpy of the enol form in the gas phase was arbitrarily assigned as zero enthalpy, the enthalpy change for enolization in cyclohexane is −3.0 kcal mol$^{-1}$. Of the 3.0 kcal mol$^{-1}$, 0.8 kcal mol$^{-1}$ is due to solvent interaction to stabilize the enol tautomer. In general, as the dielectric constant of the medium increases the keto tautomer becomes increasingly enthalpically stabilized as does the enol tautomer. However, as subsequent analysis will show, the nature of the solvent interaction which enthalpically stabilizes the two tautomers is different in different bases.

The enthalpy changes given in column four of Table 3 show that with the exceptions of DMA and DMSO, the enthalpy of enolization is more exothermic in solution than in the gas phase. In these solvents interaction with the enol tautomer is greater than with the keto form.

The entropy changes for enolization in $CCl_4$ and cyclohexane are more negative than those in the

Can. J. Chem. Downloaded from www.nrcresearchpress.com by 210.87.254.5 on 09/06/12
For personal use only.

TABLE 3. Thermodynamic parameters for the enolization of 2,4-pentanedione

| Solvent | $\bar{H}_{k\alpha}$ (kcal mol$^{-1}$) | $\bar{H}_{e\alpha}$ (kcal mol$^{-1}$) | $\Delta H^{0a}$ (kcal mol$^{-1}$) | $\Delta S^0$ (cal deg$^{-1}$ mol$^{-1}$) | % enol (298 K) | ε |
|---|---|---|---|---|---|---|
| Gas | 0.0 | 0.0 | | | | |
| Cyclohexane | −6.2 | −7.0 | −3.0±0.3 | −2.9 | 97 | 2.0 |
| $CCl_4$ | −8.2 | −8.5 | −2.5±0.3 | −2.7 | 95 | 2.2 |
| Neat | −9.1 | −9.7 | −2.8±0.3 | −6.6 | 81 | 26 |
| Methanol | | | −2.7±0.3 | −7.2 | 74 | 32.7 |
| DMA | −10.1 | −9.8 | −1.9±0.2 | −5.0 | 66 | 37 |
| DMSO | −9.8 | −9.4 | −1.8±0.2 | −5.1 | 62 | 47 |
| Water | −10.6 | −11.1 | −2.7±0.3 | −12.4 | 16 | 78 |

[a]Error limits were estimated by consideration of the linearity of a ln $K$ vs. $T^{-1}$ plot and the uncertainty in the equilibrium constant. The error in $K$ is ±10%. The uncertainty in the percentage of enol is ±1%.

gas phase. The corresponding enthalpy changes are also more negative but the free energy change is such that the mole fraction of enol in these solvents is slightly greater than that in the gas phase. Thus the greater enthalpy due to to interaction of the enol tautomer with the solvent is sufficient to shift the equilibrium from the gas phase toward greater enol content in these two solvents. The greater interaction enthalpy of the enol tautomer is probably due to a closer approach of solvent molecules which gives stronger Van der Waals interactions. Reeves (3) and Allen and Dwek (6) report no chemical shift for 2,4-pentanedione resonance signals results upon dilution in cyclohexane. This supports a bulk interaction effect by the solvent.

The entropy changes in the solvents other than $CCl_4$ and cyclohexane are considerably more negative than those for gas phase enolization. Only for water as a solvent does it seem possible that these more negative entropy changes could result from structural effects on the solvent molecules. DMSO and DMF have been shown to disrupt intramolecular hydrogen bonds (7, 8) and because DMA is a strong proton acceptor, it seems reasonable that DMA could also disrupt the intramolecular hydrogen bond. The similarity of the thermodynamic functions for DMA and DMSO in Table 3 indicates that the solvent–solute interactions in DMA and DMSO must be similar. The entropy and enthalpy changes in these two solvents can be rationalized by the disruption of the intramolecular hydrogen bond of the enol tautomer and the consequent formation of an intermolecular hydrogen bond with the solvent. The enthalpy terms $\bar{H}_{k\alpha}$ and $\bar{H}_{e\alpha}$ for these solvents thus give the enthalpic stabilization of the keto form which must be primarily due to dipole–dipole interactions and the enthalpic stabilization of the enol form which consists partly of a stabilization due to hydrogen bond formation with the solvent. The mole fraction of enol in these two solvents drops markedly from the gas phase value, due primarily to the unfavorable entropy change. The disruption of the intramolecular bond and consequent reduction of freedom of the solvent molecules by association with the enol tautomer accounts for the unfavorable entropy change. Likewise the less favorable enthalpy change relative to $CCl_4$ and cyclohexane is in part due to the enthalpy required to disrupt the intramolecular hydrogen bond of the enol form.

The enthalpy changes for enolization (Table 3) in water and methanol are identical and similar to those found in $CCl_4$ and cyclohexane. The entropy changes in water and methanol, however, are the most unfavorable for any of the solvents. For water such an unfavorable entropy change is not surprising because of the well-documented structural changes water can undergo. Such structural changes do not seem as likely for methanol but it appears that the large negative entropy changes reflect the disruption of the intramolecular bond of the enol tautomer in both solvents. With water, additional structural changes may also occur, leading to a further entropy reduction. The enthalpy data of columns two and three of Table 3 show that the enol tautomer in water is enthalpically stabilized relative to the keto tautomer in contrast to the situation in the solvents DMA and DMSO. Water molecules must hydrogen bond to the keto tautomer as well as to the enol tautomer. If disruption of the intramolecular bond occurs in water, an additional enthalpic stabilization of the enol tautomer is possible through self-association and through association with the solvent.

Melia and Merrifield (5) have reported enthalpies and entropies of formation for the pure keto and enol tautomers in both liquid and gas phases for 2,4-pentanedione (Table 4). The enthalpy change on passing from the gas phase to pure liquid for the keto tautomer is −9.1 kcal mol$^{-1}$ and that for the enol tautomer is −9.8 kcal mol$^{-1}$. The corresponding entropy changes are −27.8 cal deg$^{-1}$ mol$^{-1}$ for the keto tautomer and −32.8 cal deg$^{-1}$ mol$^{-1}$ for the enol tautomer. The enthalpy of vaporization of the

Can. J. Chem. Downloaded from www.nrcresearchpress.com by 210.87.254.5 on 09/06/12
For personal use only.

TABLE 4. Enthalpies and entropies of formation for 2,4-pentanedione at 298 K[a]

| Phase | $\Delta H_f^0$ (kcal mol$^{-1}$) | $S_{298}^0$ (cal deg$^{-1}$ mol$^{-1}$) |
|---|---|---|
| Enol (l) | −101.89 | 62.4 |
| Keto (l) | −99.00 | 69.1 |
| Enol (g) | −92.10 | 95.2 |
| Keto (g) | −89.90 | 96.9 |
| Equilibrium mixture (l) | −101.34 | 63.7 |
| Equilibrium mixture (g) | −91.92 | 95.3 |

[a]Reference 5.

equilibrium liquid mixture of 2,4-pentanedione may be found from the data given in Table 4, and the mole fractions of enol in gas and liquid phase may be used in eq. [2] to calculate $\bar{H}_{kl} - \bar{H}_{kg}$, the enthalpy of the keto tautomer in the equilibrium liquid mixture minus the enthalpy of the keto tautomer in the gas phase. Equation [3] may be used to calculate the corresponding enthalpy difference for the enol tautomer. The enthalpy changes so calculated are $\bar{H}_{kl} - \bar{H}_{kg} = -9.1$ kcal mol$^{-1}$ and $\bar{H}_{el} - \bar{H}_{eg} = -9.7$ kcal mol$^{-1}$. Thus the interactions experienced by the keto tautomer in the equilibrium liquid mixture relative to the gas phase are nearly the same as the interactions experienced by the keto tautomer in pure liquid keto form. The interactions of the enol tautomer in pure enol or in the liquid equilibrium mixture are also similar. Thus the keto and enol tautomers must find themselves in essentially the same environment in the pure liquid keto and enol forms as in the liquid mixture which consists of both tautomeric forms. The pure enol tautomer is more stable enthalpically than the pure keto tautomer. The entropy of the pure liquid enol tautomer is also lower than that of the pure liquid keto tautomer. These data seem to be consistent only if the intramolecular hydrogen bond of the enol tautomer is disrupted in the liquid equilibrium mixture and in pure enol. The enol form without the intramolecular hydrogen bond would be expected to form an intermolecular hydrogen bond with itself and with the keto form in the equilibrium mixture. If this occurred, the enthalpy and entropy of the enol tautomer could be more negative than that of the keto tautomer. However, intermolecular hydrogen bond formation by the enol to the keto form would be expected to enthalpically stabilize the keto tautomer. This would mean that the enthalpy of the keto form in pure liquid keto would not be the same as that of the keto tautomer in the equilibrium mixture. The most likely way for these considerations to be satisfied is through self-association of the enol tautomer, thus reducing hydrogen bonding to the keto tautomer.

Burdett and Rogers (9) report an upfield shift in the enol hydroxyl and enol α-proton resonance signals of 2,4-pentanedione with increasing temperature. They suggest that an intermolecularly hydrogen bonded species is present and becomes less favored at higher temperatures. Thus their results are consistent with the disruption of the intramolecular hydrogen bond in neat 2,4-pentanedione. Rogers and Burdett (10) also interpret the chemical shift on dilution of 2,4-pentanedione to inter and intramolecularly bonded species.

## Conclusions

The usual rule that is applied to rationalize the effect of solvent on the percentage of enol in a β-diketone is that the enol tautomer is less polar than the keto tautomer and therefore polar solvents stabilize the keto tautomer over the corresponding enol tautomer. In solvents which do not specifically interact with the keto or enol forms, as for example through hydrogen bond formation, the keto form is increasingly stabilized with increasing dielectric constant of the solvent. The interaction which stabilizes the keto form is electrostatic in origin. For these solvents the entropy of enolization should not show much variation from solvent to solvent.

In solvents like DMA and DMSO which can disrupt the intramolecular hydrogen bond, an unfavorable entropy of enolization results. Solvents of this type which can disrupt the intrabond can also stabilize the keto form by electrostatic interactions. Thus the percentage of enol in these solvents will decrease in accordance with increasing dielectric constant, but to a greater extent than expected because of the unfavorable entropy change.

In solvents that can act as hydrogen bond proton donors and acceptors, the keto tautomer is enthalpically stabilized by hydrogen bonding to the carbonyls but is not stabilized as much as the enol tautomer. The entropy of enolization is unfavorable for these solvents, but due to the enthalpic stabilization of the enol tautomer the percentage of enol is greater than would be expected on the basis of dielectric constant.

Powling and Bernstein (11) have correlated sol-

Can. J. Chem. Downloaded from www.nrcresearchpress.com by 210.87.254.5 on 09/06/12
For personal use only.

TABLE 5. Percent enol as a function of the Onsager–Kirkwood dielectric expression

| Solvent | % enol | | |
|---|---|---|---|
| | Observed | Calculated[a] | Δ(obsd. − calcd.) |
| Hexane | 95[b] | 98 | −3 |
| $CCl_4$ | 95 | 94 | +1 |
| Acetone | 75[c] | 77 | −2 |
| Benzene | 89[b] | 93 | −4 |
| Cyclohexane | 97 | 94 | +3 |
| Ether | 95[b] | 90 | +5 |
| DMSO | 62 | 75 | −13 |
| DMA | 66 | 82 | −16 |
| Methanol | 74 | 53 | +21 |
| Ethanol | 82[b] | 69 | +13 |

[a]Percent enol for each solvent was calculated from the least-squares equation obtained by plotting percent enol vs. the Onsager–Kirkwood relation for the first six solvents.
[b]Reference 10 at 33°C.
[c]Reference 6 at 38°C.

vent influence and thermodynamic parameters using the Onsager–Kirkwood theory of solvent interaction. The percentage of enol as a function of the Onsager–Kirkwood dielectric function for those solvents not capable of undergoing hydrogen bonded interactions or disruption of the intramolecular enol hydrogen bond was plotted and the best least-squares fit was made. Table 5 compares the percentage of enol calculated from the fitted data with experiment. For these solvents the fit is good, the percentage of enol drops as the dielectric function increases due to greater stabilization of the keto form by solvent interaction.

The observed values for the percentage of enol in solvents DMA and DMSO which can disrupt the intramolecular hydrogen bond fall below the percentages calculated from the least-squares relation. This is due mainly to the unfavorable entropy change resulting from the disruption of the intrabond by the solvent. Methanol and ethanol, on the other hand, show a higher percentage of enol than that calculated from the least-squares relation. The higher percentage is due to the significant enthalpic stabilization of the enol form due to hydrogen bond formation with these solvents.

## Acknowledgment

Acknowledgment is made to the donors of the Petroleum Research Fund, administered by the American Chemical Society, for support of this research. The authors also acknowledge William Graf and Joe Monteforte for assistance in this work.

1. J. N. SPENCER, J. E. GLEIM, M. L. HACKMAN, C. H. BLEVINS, and R. C. GARRETT. J. Phys. Chem. **82**, 563 (1978).
2. J. N. SPENCER, S. K. BERGER, C. R. POWELL, B. D. HENNING, G. S. FURMAN, W. M. LOFFREDO, E. M. RYDBERG, R. A. NEUBERT, C. E. SHOOP, and D. N. BLAUCH. J. Phys. Chem. **85**, 1236 (1981).
3. L. W. REEVES. Can. J. Chem. **35**, 1351 (1957).
4. J. N. SPENCER, R. C. GARRETT, F. J. MAYER, J. E. MERKLE, C. R. POWELL, M. T. TRAN, and S. K. BERGER. Can. J. Chem. **58**, 1372 (1980).
5. T. P. MELIA and R. MERRIFIELD. J. Appl. Chem. **19**, 79 (1969).
6. G. ALLEN and R. A. DWEK. J. Chem. Soc. B, 161 (1966).
7. J. N. SPENCER, R. S. HARNER, and C. D. PENTURELLI. J. Phys. Chem. **79**, 2488 (1975).
8. J. N. SPENCER, J. R. SWEIGART, M. E. BROWN, R. L. BENSING, T. L. HASSINGER, W. KELLY, D. L. HOUSEL, G. W. REISINGER, D. S. REIFSNYDER, J. E. GLEIM, and J. C. PEIPER. J. Phys. Chem. **81**, 2237 (1977).
9. J. L. BURDETT and M. T. ROGERS. J. Phys. Chem. **70**, 939 (1966).
10. M. T. ROGERS and J. L. BURDETT. Can. J. Chem. **43**, 1516 (1965).
11. J. POWLING and H. J. BERNSTEIN. J. Am. Chem. Soc. **73**, 4353 (1951).
12. W. STROHMEIER and I. HÜHNE. Z. Naturforsh. **7b**, 184 (1952).
13. G. SCHWARZENBACH and E. FELDER. Helv. Chim. Acta, **27**, 1044 (1944).

Can. J. Chem. Downloaded from www.nrcresearchpress.com by 210.87.254.5 on 09/06/12
For personal use only.

# Solvation of heterocyclic nitrogen compounds by methanol and water

J. N. SPENCER, E. S. HOLMBOE, M. R. KIRSHENBAUM, S. W. BARTON, K. A. SMITH, W. S. WOLBACH, J. F. POWELL, AND C. CHORAZY

*Department of Chemistry, Franklin and Marshall College, Lancaster, PA 17604, U.S.A.*

Received October 13, 1981

J. N. SPENCER, E. S. HOLMBOE, M. R. KIRSHENBAUM, S. W. BARTON, K. A. SMITH, W. S. WOLBACH, J. F. POWELL, and C. CHORAZY. Can. J. Chem. **60**, 1183 (1982).

The proton-donating and -accepting abilities of water and methanol to various nitrogen-containing compounds have been determined by calorimetric analysis. Water is a better proton donor than methanol but methanol is a better proton acceptor than water. The interactions by water and methanol at the nitrogens of the diazines follow trends expected from relative proton affinities, p*K*'s, and theoretical calculations. Electrostatic interactions by the diazine nitrogens with pyridine parallel the interactions found for methanol and water at these nitrogens.

J. N. SPENCER, E. S. HOLMBOE, M. R. KIRSHENBAUM, S. W. BARTON, K. A. SMITH, W. S. WOLBACH, J. F. POWELL et C. CHORAZY. Can. J. Chem. **60**, 1183 (1982).

On a déterminé, par l'analyse calorimétrique, les capacités de l'eau et du méthanol d'agir comme accepteurs et donneurs de protons en présence de divers composés azotés. L'eau est un meilleur donneur de proton que le méthanol, mais ce dernier est un meilleur accepteur de proton. Les interactions de l'eau et du méthanol sur les atomes d'azote des diazines suivent les tendances prévues à partir des p*K*, des affinités relatives du proton et de calculs théoriques. Les interactions électrostatiques des atomes d'azote de la diazine avec la pyridine se comparent aux interactions trouvées dans le cas du méthanol et de l'eau sur ces atomes d'azote.

[Traduit par le journal]

## Introduction

The ability of water to act as a proton donor and acceptor is in part responsible for its remarkable solvating properties. The usual methods employed to study proton-donating ability require the preparation of a dilute solution of the donor in an inert solvent which contains a proton acceptor. Because of the difficulty of obtaining accurately known concentrations of water in organic solvents, few measurements of the proton-donating properties of water have been reported. Even for those systems for which measurements can be made, the solvation of water by organic solvents makes difficult the interpretation of actual proton-donating ability. Studies of water acting as a proton acceptor are even more limited because the usual spectroscopic methods which involve measurements in the hydroxyl stretching region are not possible. Similar difficulties are encountered for methanol as a proton acceptor. Solutes which can act as donors and acceptors in solvents which can also behave as donors and acceptors cannot be studied by the usual spectroscopic techniques. Measurements carried out on dilute solutions of water or methanol in suitable solvents do not give information on the behavior of these species when present in bulk. The pure base calorimetric method allows determination of proton-accepting enthalpies in solvents such as water and methanol, and enthalpies of solution allow the determination of the proton-donating abilities of these solvents. In this study, enthalpies due to interactions for the solvents methanol and water acting as donors and acceptors have been determined by calorimetric analysis.

## Experimental

The calorimeters and method of analysis have been previously described (1, 2).

Purifications for NMF (3), DMF (4), pyrrole (1), *N*-methylpyrrole (1), imidazole (5), and methylimidazole (5) have been given. Benzene was refluxed over $P_2O_5$ and fractionally distilled under nitrogen. Pyridine was dried over fresh BaO and fractionally distilled under nitrogen. 1,4-Diazine (pyrazine) was vacuum sublimed, 1,2-diazine (pyridazine) was dried over sieves and distilled under nitrogen, 1,3-diazine (pyrimidine) was Aldrich 99+% and used without further purification. Pyrazole was vacuum sublimed. Methanol was dried over sieves and then twice redistilled under nitrogen. Deionized water was doubly distilled under nitrogen and used immediately.

## Results

Enthalpies of solution for the various solutes and solvents are given in Table 1. Enthalpies of vaporization and sublimation are also given in Table 1.

### *Calculation of enthalpies due to interactions*

The hydrogen bond enthalpy of the N—H proton of imidazole and of *N*-methyl formamide to water and methanol was determined by the pure base calorimetric method (6). The parameters to be used in this calculation for water have been given (2), and the parameters necessary for the calculations for methanol solvent are given in Table 2.

The enthalpies due to interactions by methanol and water at the nitrogens of pyridine and the

0008-4042/82/101183-04$01.00/0

©1982 National Research Council of Canada/Conseil national de recherches du Canada

Can. J. Chem. Downloaded from www.nrcresearchpress.com by 210.87.254.42 on 09/06/12
For personal use only.

Can. J. Chem. Downloaded from www.nrcresearchpress.com by 210.87.254.42 on 09/06/12
For personal use only.

TABLE 1. Enthalpies of solution (kcal mol$^{-1}$, 298 K)

| Solute | Enthalpies of solution in solvent | | | $\Delta H^{0}$[d] |
|---|---|---|---|---|
| | $H_2O$ | $CH_3OH$ | $C_5H_5N$ | |
| Pyrrole | +0.84±0.10 | −0.31±0.01 | −2.01±0.05 | 10.80[e] |
| Methylpyrrole | | +0.87±0.03 | −0.06±0.01 | |
| Imidazole | +3.09±0.01[a] | +1.77±0.02 | +3.01±0.02 | 17.81[f] |
| Methylimidazole | −2.25±0.10 | −1.69±0.06 | +0.18±0.04 | |
| Pyrazole | +3.72±0.17 | +2.56±0.16 | | 16.53[f] |
| NMF | −1.67±0.04 | +0.40±0.01 | | |
| DMF | −3.52±0.04 | −0.06±0.01 | | |
| Benzene | +0.49±0.01[b] | +0.36±0.04 | −0.04±0.01 | 8.09[e] |
| Pyridine | −2.30[c] | −0.96±0.04 | 0.0 | 9.61[e] |
| 1,2-Diazine | −2.10±0.09 | +0.06±0.02 | +0.07±0.03 | 12.78[e] |
| 1,3-Diazine | −2.33±0.03 | +0.30±0.02 | +0.12±0.02 | 11.95[e] |
| 1,4-Diazine | +1.57±0.05 | +3.85±0.13 | +3.86±0.33 | 13.45[e] |

[a] Reference 8.
[b] Reference 9.
[c] Average of enthalpies reported in ref. 10.
[d] Enthalpy of vaporization or sublimation.
[e] Reference 11.
[f] Reference 12.

TABLE 2. Enthalpies due to interactions

| Acid | Base | $\Delta\bar{H}$ (kcal mol$^{-1}$, 298 K) |
|---|---|---|
| Pyrrole (N—H) | $H_2O$ | −2.3 |
| | $CH_3OH$[a] | −3.0 |
| | $C_5H_5N$ | −3.7[c] |
| Imidazole (N—H) | $H_2O$ | −2.7 |
| | $CH_3OH$[a] | −3.8 |
| | $C_5H_5N$ | −4.4 |
| Imidazole ($N_3$) | $H_2O$ | −4.3 |
| | $CH_3OH$ | −4.1 |
| | $C_5H_5N$ | −1.4 |
| Pyridine ($N_1$) | $H_2O$ | −4.3 |
| | $CH_3OH$ | −2.9 |
| 1,2-Diazine ($N_1N_2$) | $H_2O$ | −7.3(−4.0, −3.3)[b] |
| | $CH_3OH$ | −5.0(−2.7, −2.3)[b] |
| | $C_5H_5N$ | −4.6 |
| 1,3-Diazine ($N_1N_3$) | $H_2O$ | −6.7(−3.7, −3.0)[b] |
| | $CH_3OH$ | −4.0(−2.2, −1.8)[b] |
| | $C_5H_5N$ | −3.8 |
| 1,4-Diazine ($N_1N_4$) | $H_2O$ | −4.3(−2.4, −1.9)[b] |
| | $CH_3OH$ | −1.9(−1.0, −0.9)[b] |
| | $C_5H_5N$ | −1.5 |
| NMF (N—H) | $H_2O$ | −2.0[d] |
| | $CH_3OH$ | −2.6 |

[a] For details of the pure base calculations see refs. 2 and 6. The parameters used for methanol per —$CH_2$— are: cavity term 1.6 kcal mol$^{-1}$, dispersion term 2.3 kcal mol$^{-1}$, and dipole-induced-dipole 0.1 kcal mol$^{-1}$.
[b] Estimated stepwise enthalpies due to interactions. The numbers in parentheses refer to the first and second stepwise enthalpy respectively.
[c] Reference 5.
[d] Reference 2.

diazines were obtained by taking the difference between the transfer of benzene from the gas phase to either solvent and the transfer of the nitrogen-containing base from the gas phase to the respective solvent. For example, the transfer enthalpy for benzene from gas phase to water is −7.6 kcal mol$^{-1}$; that of pyridine is −11.9 kcal mol$^{-1}$; the difference between the two transfers, −4.3 kcal mol$^{-1}$, is attributed to interactions at the nitrogen of pyridine. The same transfer for 1,3-diazine, −14.3 kcal mol$^{-1}$, gives an enthalpy due to interactions at the two nitrogens of −6.7 kcal mol$^{-1}$.

The interactions at either nitrogen of the diazines may be due in most part to hydrogen bonded interactions. Due to inductive effects for the diazines, the interaction enthalpy of a second hydrogen bonded species will be less than the first. Thus, the addition of solvating species to the diazines may be considered in a stepwise fashion. The data do not allow an exact division of the total heat produced by solvation of the diazine nitrogens into the heat associated with the stepwise solvation of each nitrogen. However, an estimate of the enthalpies at each nitrogen may be made by consideration of the relative proton affinities (Table 3) of pyridine and the diazines. The PA of pyridine is greater than that of 1,2-diazine; therefore, it would be expected that the enthalpy of interaction for the solvation of the first nitrogen site in 1,2-diazine would be less than that of the solvation of the pyridine nitrogen. For solvation by water the enthalpy due to interactions at the first nitrogen of 1,2-diazine must be less exothermic than −4.3 kcal mol$^{-1}$. The sum of the solvation enthalpies for 1,2-diazine in water is −7.3 kcal mol$^{-1}$. Thus, the solvation enthalpy for the first nitrogen site should be more exothermic than the average solvation enthalpy of the two sites. This gives a range of −4.3 to −3.7 kcal mol$^{-1}$ for the first interaction site on 1,2-diazine. An estimate of −4.0 kcal mol$^{-1}$ for the first interaction enthalpy of water with 1,2-diazine should not be in error by more than 0.3 kcal mol$^{-1}$. Then the enthalpy

TABLE 3. Comparison of interaction enthalpies with other parameters

| Compound | PA[a] | p$K$[b] | $\delta\Delta H$[c] | Water-base interaction enthalpy | |
|---|---|---|---|---|---|
| | | | | THEO[d] | This work |
| Pyridine | 222.0 | 5.23 | 0 | −4.7 | −4.3 |
| 1,2-Diazine | 218.3 | 2.33 | −4.3 | −4.2 | −7.3 (−3.7)[e] |
| 1,3-Diazine | 215.5 | 1.30 | −9.5 | −4.1 | −6.7 (−3.4)[e] |
| 1,4-Diazine | 210.8 | 0.60 | −11.7 | −3.7 | −4.3 (−2.2)[e] |

[a]Reference 13.
[b]Reference 14.
[c]Reference 15. $\delta\Delta H$ measures the proton affinity of the base relative to pyridine.
[d]Reference 16. These calculations are for a 1:1 complex of water and base.
[e]Average enthalpy due to interactions at two nitrogen sites.

due to interaction at the second nitrogen would be $-3.3$ kcal mol$^{-1}$.

For the other diazines the range is too large to provide reliable estimates of the stepwise solvation. If it is assumed that the ratio of interactions at the two nitrogen sites is the same for all the diazines, the 1,2-diazine ratio of stepwise enthalpies may be used to calculate the interaction on 1,3- and 1,4-diazine. The interactions so calculated are given in Table 2.

The interaction enthalpies of methanol and water at the imidazole $N_3$ can be determined by a comparison of the transfers of pyrrole from the gas phase to a given solvent and of imidazole from the gas phase to the same solvent. The gas phase to water transfer for pyrrole is $-10.0$ kcal mol$^{-1}$. If the pyrrole N—H to water hydrogen bond enthalpy, $-2.3$ kcal mol$^{-1}$, is subtracted from this transfer enthalpy, the interaction of the pyrrole ring structure with water, $-7.7$ kcal mol$^{-1}$, is determined.

The transfer from gas phase to water for imidazole is the sum of three terms: the N—H hydrogen bond enthalpy with water, the $N_3$ interaction with water, and the interaction and cavity terms for the pyrrole ring structure of imidazole. The N—H hydrogen bond enthalpy (Table 2) and pyrrole ring structure term are known. Thus, the interaction at $N_3$ may be found by difference. The $N_3$ interaction for imidazole with water and that for methanol with imidazole, similarly determined, are given in Table 2.

## Discussion

The p$K$ for the autoprotolysis of methanol is 16.9 compared to 15.7 for water at 25°C. Comparison of the data for the hydrogen bonding of water and methanol to pyridine and the diazines given in Table 2 shows that water is a better proton donor than methanol. Comparison of the hydrogen bond enthalpies for the N—H of imidazole and *N*-methylformamide to methanol and water (Table 2) shows that methanol is a better proton acceptor than water. It was not possible to obtain the hydrogen bond enthalpy of the pyrrole $N_1$—H to water directly because the model compound to be used in the pure base method, *N*-methylimidazole is not sufficiently soluble in water. However, an estimate of the hydrogen bond enthalpy in water can be made by comparison of the relative proton-donating abilities of imidazole and pyrrole. For hydrogen bonded complexes of imidazole and pyrrole with pyridine, *N*,*N*-dimethylformamide and acetonitrile, the ratio of the pyrrole hydrogen bond strength to that of imidazole is $0.85 \pm 0.01$ (5). Thus if the imidazole–water hydrogen bond is $-2.7$ kcal mol$^{-1}$, the pyrrole hydrogen bond with water may be inferred to be $-2.3$ kcal mol$^{-1}$.

The pyrrole–methanol hydrogen bond enthalpy was determined by direct use of the pure base method. The ratio of the hydrogen bond enthalpy of the pyrrole–methanol complex to that of the imidazole–methanol complex is 0.79, a ratio not far removed from 0.85 (a difference of 0.1 kcal mol$^{-1}$ in either hydrogen bond enthalpy makes the ratio 0.82). This can be taken to mean that the methanol interaction at $N_3$ of imidazole does not substantially alter the hydrogen bond enthalpy for the imidazole $N_1$—H proton.

Table 3 compares proton affinities (PA), and p$K$, of the bases to the observed enthalpies due to interactions at the nitrogens of pyridine, 1,2-diazine, 1,3-diazine, and 1,4-diazine. The theoretical calculations given in the same table correspond to a complex made up of single water molecule and the base. The enthalpies due to interactions given in column 6 of Table 3 correspond to interactions at all sites. The numbers in parentheses (column 6) denote the average interaction enthalpy. The expected trends in enthalpies due to interactions with PA and p$K$ are observed, and the theoretical calculations predict the observed order of interaction enthalpies.

SCF calculations (7) for pyridine and the diazines give no correlation between the total or $\pi$ electron populations and the proton affinities of these bases. The electron populations in the diazines seem to

Can. J. Chem. Downloaded from www.nrcresearchpress.com by 210.87.254.42 on 09/06/12
For personal use only.

Can. J. Chem. Downloaded from www.nrcresearchpress.com by 210.87.254.42 on 09/06/12
For personal use only.

reflect inductive effects of the two nitrogen atoms (7). The favorable alignment of molecular dipole moments accounts for the order of stability of pyridine and the diazine complexes with water given in Table 3.

The interactions of pyridine and the diazines with pyridine are given in Table 2. These interactions were determined by using benzene as a model and attributing differences between the gas phase to pyridine transfers of benzene and the diazines to interactions at the nitrogen. The interactions of pyridine solvent with the diazines are dipolar. The molecule with the largest dipole moment undergoes the strongest interaction. These electrostatic interactions parallel the interactions attributed largely to hydrogen bonding for methanol and water solvent. The imidazole $N_3$ and pyridine nitrogen interactions are very similar enthalpically in pyridine solvent as are the enthalpies due to interactions at these nitrogens in hydrogen bonding solvents.

The solvation of pyrrole, imidazole, pyridine, and the diazines relative to the gas phase is found by using the enthalpies of solution and the enthalpies of sublimation or vaporization in Table 1. This total solvation enthalpy may be divided into an enthalpy due to interactions in the first solvation shell, and an enthalpy due to interactions with the ring structure of the systems studied. The first solvation shell enthalpies are given in Table 2. The enthalpy due to interaction with the ring structure can be found by the difference between the total solvation and the first solvation shell interactions given in Table 2. The diazines are more strongly solvated by water than by methanol because of the greater proton-donating ability of water. Pyrrole and imidazole are more strongly solvated by methanol than by water because of the better proton-accepting abilities of methanol. The difference between the solvation of the ring system in water and methanol is not great for either the pyrrole-type ring structure or the pyridine-type ring structure. Thus, the difference in total solvation is determined largely by the interactions in the first hydration shell. These interactions for methanol and water solvent are principally hydrogen-bonded interactions.

Imidazole is solvated by about 2 kcal $mol^{-1}$ more by water and methanol than is pyrazole. Both imidazole and pyrazole are more strongly solvated by methanol than by water. The transfer enthalpies from water to methanol for imidazole ($-1.32$ kcal $mol^{-1}$) and for pyrazole ($-1.16$ kcal $mol^{-1}$) indicate that the thermodynamic states of the two solutes in methanol and water are similar. Thus, the proximity of the nitrogens of pyrazole must lead to dipole interactions which enthalpically destabilize pyrazole by 2 kcal $mol^{-1}$ relative to imidazole.

The total solvation enthalpies of the diazines by pyridine follow the solvation trends set by methanol and water. This seems to support the contention that the interactions of water with these diazines are determined largely by the dipolar moment of the diazine.

**Acknowledgement**

Acknowledgement is made to the donors of the Petroleum Research Fund, administered by the American Chemical Society, for support of this research. Project SEED also provided support for one student (C.C.).

1. J. N. SPENCER, J. E. GLEIM, M. L. HACKMAN, C. H. BLEVINS, and R. C. GARRETT. J. Phys. Chem. **82**, 563 (1978).
2. J. N. SPENCER, S. K. BERGER, C. R. POWELL, B. D. HENNING, G. S. FURMAN, W. M. LOFFREDO, E. M. RYDBERG, R. A. NEUBERT, C. E. SHOOP, and D. N. BLAUCH. J. Phys. Chem. **85**, 1236 (1981).
3. J. N. SPENCER, R. C. GARRETT, F. J. MAYER, J. E. MERKLE, C. R. POWELL, M. T. TRAN, and S. K. BERGER. Can. J. Chem. **58**, 1372 (1980).
4. J. N. SPENCER, J. R. SWEIGART, M. E. BROWN, R. L. BENSING, T. L. HASSINGER, W. KELLY, D. L. HOUSEL, G. WILLIAM REISINGER, D. S. REIFSNYDER, J. E. GLEIM, and J. C. PEIPER. J. Phys. Chem. **81**, 2237 (1977).
5. J. N. SPENCER, J. E. GLEIM, C. H. BLEVINS, R. C. GARRETT, F. J. MAYER, J. E. MERKLE, S. L. SMITH, and M. L. HACKMAN. J. Phys. Chem. **83**, 2615 (1979).
6. J. N. SPENCER, J. E. GLEIM, C. H. BLEVINS, R. C. GARRETT, and F. J. MAYER. J. Phys. Chem. **83**, 1249 (1979).
7. J. E. DEL BENE. J. Am. Chem. Soc. **99**, 3617 (1977).
8. E. M. WOOLLEY, R. W. WILTON, and L. G. HEPLER. Can. J. Chem. **48**, 3249 (1970).
9. S. J. GILL, N. F. NICHOLS, and I. WADSÖ. J. Chem. Thermodyn. **8**, 445 (1976).
10. E. M. ARNETT, J. J. BURKE, J. V. CARTER, and C. F. DOUTY. J. Am. Chem. Soc. **94**, 7837 (1972); L. SACONNI, P. PAOLETTI, and M. CIAMPOLINI. J. Am. Chem. Soc. **82**, 3828 (1960).
11. J. D. COX and G. PILCHER. Thermochemistry of organic and organometallic compounds. Academic Press, New York. 1970.
12. R. SABBAH. Thermochim. Acta, **41**, 33 (1980).
13. M. MEOT-NER. J. Am. Chem. Soc. **101**, 2396 (1979).
14. A. ALBERT and E. P. SERJEANT. Ionization constants of acids and bases. John Wiley and Sons, Inc., New York. 1962.
15. J. E. DEL BENE. J. Am. Chem. Soc. **99**, 3617 (1977).
16. J. E. DEL BENE. Chem. Phys. **15**, 463 (1976).

# The generation and vibrational spectrum of matrix isolated thioformaldehyde and dideuterothioformaldehyde

M. TORRES, I. SAFARIK, A. CLEMENT, AND O. P. STRAUSZ

*Department of Chemistry, University of Alberta, Edmonton, Alta., Canada, T6G 2G2*

Received October 23, 1981

M. TORRES, I. SAFARIK, A. CLEMENT, and O. P. STRAUSZ. Can. J. Chem. **60**, 1187 (1982).

The photolysis of inert matrix isolated methylene trithiocarbonate at 10 K has been shown to be a clean source of thioformaldehyde. The $CH_2S$ and $CD_2S$ molecules produced this way are indefinitely stable under these conditions and their FTIR spectra could be recorded. A normal coordinate analysis has been carried out and all the normal frequencies of both molecules have been assigned.

M. TORRES, I. SAFARIK, A. CLEMENT et O. P. STRAUSZ. Can. J. Chem. **60**, 1187 (1982).

La photolyse de la matrice inerte de trithiocarbonate de méthylène obtenu à 10 K, a montré qu'elle est une source propre de thioformaldéhyde. Les molécules de $CH_2S$ et de $CD_2S$ obtenues de cette façon sont indéfiniment stables dans ces conditions et on peut enregistrer leurs spectres de IR-TF. On a réalisé une analyse normale de coordonnées et on a identifié toutes les fréquences normales de ces deux molécules.

[Traduit par le journal]

Can. J. Chem. Downloaded from www.nrcresearchpress.com by 210.87.254.5 on 09/06/12
For personal use only.

Thioformaldehyde **1**, although known in its trimer form for decades (1), has only recently been prepared in its pure monomeric form by the thermolysis of methylsulfenyl chloride in the presence of stoichiometric amounts of hydrogen chloride (2). Several other methods have been described for the generation of **1** (3) but most of them are also based on thermolysis, which poses severe constraints on the use of spectroscopic methods of analysis because of the tendency of **1** to trimerize. Infrared studies have been reported in the gas- and argon-matrix phase but in both cases the method of generation, H-abstraction by fluorine atoms (4) and vacuum uv photolysis of $CH_3SH$ (5), resulted in the formation of substantial amounts of by-products that obscure large parts of the spectrum of **1**, and therefore the results are fragmentary. Recently more detailed studies of the spectrum of **1** by laser stark spectroscopy in the 10 μm region (6), and by single rotational level resonance fluorescence (7), have been reported and in parallel developments a force field and the vibrational spectrum have been calculated for **1** by an *ab initio* mo computation (8).

We have recently reported that photolysis of vinylene trithiocarbonates (9) and thioxocarbonates (10) resulted in the extrusion of $CS_2$ and COS and the formation of thiirenes and ketenes, respectively. It appears, therefore, that elimination of $CS_2$, which is reasonably transparent in the 3500–400 $cm^{-1}$ region, is a primary photochemical process of trithiocarbonates and, consequently, methylene trithiocarbonate **2** should be an excellent source compound for the generation of **1**.

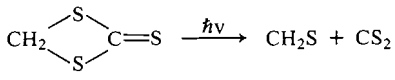


**2** **1**

In the present article we wish to report the generation of thioformaldehyde **1** and dideuterothioformaldehyde **3** by the photolysis of argon-matrix isolated methylene trithiocarbonate **2** and dideuteromethylene trithiocarbonate **4** respectively at 10 K. We have also reexamined the ir spectra of **1** and **3** with the aid of FTIR spectroscopy, allowing the assignment of the ir frequencies of **1** and **3**, and have carried out a normal coordinate analysis.

## Experimental

An Air-Products and Chemicals Inc. Model CS-202 Displex closed-cycle-helium refrigeration system coupled to a high vacuum line was employed as described before (11). The light source was a Hanovia low pressure resonance mercury lamp equipped with a Vycor filter. Mass spectra were recorded on a Metropolitan Vickers MS-12 spectrometer at an ionization potential of 70 eV and ir spectra of matrix isolated species were obtained on a Nicolet 7199 FT infrared spectrophotometer at 1 $cm^{-1}$ resolution.

Methylene trithiocarbonate **3** was prepared as described (12) and purified by sublimation; mp 55–56°C; ms (30°C): 122(70) 76(44.5) 46(100); and methylene trithiocarbonate-$d_2$ **4** (99% *d*) was prepared similarly from diiodomethane (99% *d*, Merck, Sharp and Dohme Canada Ltd.); ms (50°C): 124(38.8) 76(46.1) 48(100).

## Results and discussion

Photolysis of argon-matrix isolated **2** at 10 K and at $\lambda = 254$ nm resulted in the disappearance of the initial ir spectrum, Fig. 1a, and the appearance of a new spectrum, Fig. 1b, in which $CS_2$ could be readily identified by the absorptions at 2180(w), 1528(vs), and the $^{13}CS_2$ satellite at 1479(w) $cm^{-1}$. The remaining absorptions could be clearly identified as thioformaldehyde **1** by the agreement with

0008-4042/82/101187-05$01.00/0

©1982 National Research Council of Canada/Conseil national de recherches du Canada

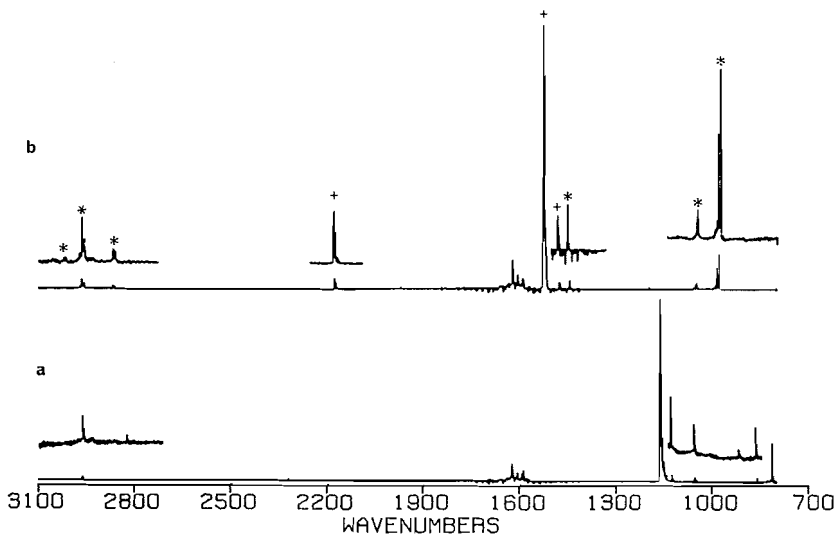


FIG. 1. (*a*) FTIR spectrum of argon-matrix isolated methylene trithiocarbonate **2**. (*b*) After 10 min photolysis at $\lambda = 254$ nm radiation. Bands marked (+) are assigned to $CS_2$ and bands marked (*) are assigned to thioformaldehyde-$d_0$ **1**.

TABLE 1. Observed frequencies of $CH_2S$ ($cm^{-1}$)

| | Frequencies | | | | | | |
|---|---|---|---|---|---|---|---|
| | This work[a] | [b] | [c] | [d] | [e] | [f] | $\Delta\nu$[g] |
| C—H str | 3022–3017 | 3025 | 3028 sh | — | 3024.62 | 3024.6 | −8 |
| | 2965–2958 | 2971 | 2970–2962 | — | 2971.03 | 2971.0 | −6 |
| | 2869–2864 | 2870 | 2874 | — | | | |
| C=S | 1052–1054 | — | 1056–1063 | 1059 | 1059.20 | 1059.2 | −7 |
| $CH_2$ def | 1447 | — | — | — | 1457.3 | 1447.0 | −10 |
| | 982, 980 | | 988–993 | 990 | 990.19 | 990.2 | −10.2 |
| | 992, 988, 986 | | | 991 | 991.01 | 991.0 | −2 |

[a]Argon-matrix photolysis; the strongest band in each group is underlined.
[b]Gas-phase, taken from ref. 4.
[c]Argon-matrix, taken from ref. 5.
[d]Gas-phase, laser stark spectroscopy taken from ref. 6.
[e]Gas-phase, single rotational level resonance fluorescence, taken from ref. 7.
[f]Gas-phase FTIR values, taken from ref. 13.
[g]$\nu_{gas} - \nu_{matrix}$.

those absorptions that have previously been assigned to **1**, Table 1. All the absorptions appeared as doublets, indicating different trapping sites (14). The photolysis proceeded rapidly and cleanly to completion without the formation of other products, in agreement with the mass spectrum of **2** which showed exclusive decomposition into $CS_2$ and **1** under electron impact. The split absorptions of argon-matrix isolated **1** have been reported to be replaced by single absorptions in a nitrogen matrix (5). However, in our case, although nitrogen-matrix experiments resulted in single absorptions for $CS_2$, the splitting of the absorptions for **1** in nitrogen, xenon, or CO matrices remained. In each case only the strongest band, for each fundamental, underlined in Table 1, will be mentioned in the assignments and these have been used in the calculations.

The exclusive formation of $CS_2$ (CS was not detected), and the good agreement between the remaining spectrum and the known $CH_2S$ absorptions leave no doubt that **1** is responsible for the observed spectrum and that **2** is a clean source compound for the photochemical generation of **1**. Similarly, photolysis of dideuteromethylene trithiocarbonate **4** resulted in the formation of $CS_2$ and thioformaldehyde-$d_2$, **3**, Fig. 2, in which a similar matrix effect in the splitting of the $CS_2$ and **3** bands was observed upon changing the host from argon to nitrogen. The observed bands are listed in Table 2.

Thioformaldehyde has a planar structure with $C_{2v}$ symmetry. The six normal vibrations form the representation $3a_1 + b_1 + 2b_2$ and all are ir active.

*C—H stretchings*

Three bands have been observed for **1** in the

Can. J. Chem. Downloaded from www.nrcresearchpress.com by 210.87.254.5 on 09/06/12
For personal use only.

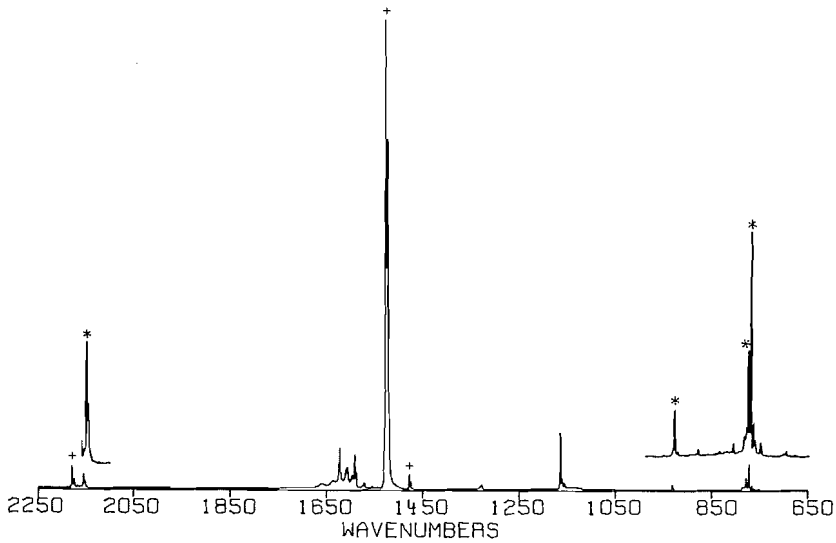


FIG. 2. FTIR spectrum of argon-matrix isolated dideuteromethylene trithiocarbonate **4** after 10 min photolysis with $\lambda = 254$ nm. Bands marked (+) are assigned to $CS_2$, and bands marked (*) are assigned to thioformaldehyde-$d_2$ **3**.

C—H stretching region at 2869(w), 2965(m), and 3017(broad, vw) $cm^{-1}$, in agreement with previous observations, Table 1, whereas in the C—D stretching region **3** featured only a single clear absorption at 2155 $cm^{-1}$; a weak, very broad absorption centered at 2280 $cm^{-1}$ is also tentatively assigned to **3**. The shift upon deuteration, and the similarity between the relative intensities of the 3017 and 2965 $cm^{-1}$ absorptions of **1** (the antisymmetric C—H stretch is weaker than the symmetric one) and those of formaldehyde (15) support Johns and Olson's assignment of these bands to the antisymmetric and symmetric C—H stretches, respectively (4) based on the rotational assignment of the gas phase spectrum. The 2869 $cm^{-1}$ band originally assigned to a $2\nu_6$ by Johns and Olson (4) should be reassigned to a $2\nu_2$, based on the observed $\nu_2$ (7).

*C═S stretch*

In agreement with Jacox and Milligan (5) and Bedwell and Duxbury (6) we have retained the assignment of the 1052 $cm^{-1}$ and the 932 $cm^{-1}$ bands to ν(C═S) in **1** and **3**, respectively. The weakness of these bands contrasts with the very strong ν(C═S) at ~1160 $cm^{-1}$, typical of trithiocarbonates, and also present in the spectra of **2** and **4**.

TABLE 2. Observed frequencies for $CD_2S$[a] ($cm^{-1}$)

| | Frequencies | | | |
|---|---|---|---|---|
| | This work | From ref. 5 | From ref. 13 | Δν[c] |
| C—D str | 2280 (tentative) | — | — | |
| | 2155, 2152 | — | 2158.5 | −3.5 |
| C═S | 932 | 941 | 936.2 | −4.2 |
| $CH_2$ def | 1167[b] | — | 1171.8 | −4.8 |
| | 773 | 779, 783 | 781.2 | −8.2 |
| | 788, 779 | | 757.4 | +22.4 |

[a]Argon-matrix isolated.
[b]Only observed in nitrogen-matrix.
[c]$\nu_{gas} - \nu_{matrix}$.

*C—H deformations*

The symmetric $CH_2$ deformation mode had often been assigned to a band at ~1530 $cm^{-1}$ hidden by the prominent 1528 $cm^{-1}$ $CS_2$ band, although the actual band had never been seen. Recently, Clouthier *et al.* (7) were able to observe the $CH_2$ symmetric deformation mode at 1457 $cm^{-1}$. In argon and xenon matrices the band appears at 1447 $cm^{-1}$, and the fact that the band could not be seen in the nitrogen-matrix experiments in which there is a shift between +2 and +11 $cm^{-1}$ in the position of all the other bands may be due to the fact that the $a_1$ $CH_2$ deformation mode experiences a larger shift of +30 $cm^{-1}$ and becomes hidden in the $^{13}CS_2$ satellite at 1479 $cm^{-1}$. Similarly, upon deuteration no band is observed in the argon-matrix photolysis that could be assigned to the symmetric $CD_2$ def, which is probably obscured by the prominent 1165 $cm^{-1}$ absorption of **2**. However, in nitrogen matrices a distinct absorption could be observed at 1167 $cm^{-1}$, Fig. 3.

For the remaining $CH_2$ deformations, the out-of-plane and the in-plane, there is only one remaining absorption which is apparently split into various bands in the 992–980 $cm^{-1}$ region, Fig. 4. However, in agreement with the recent results of Bedwell and Duxbury (6), Table 1, and on the basis of the splitting as compared to the other bands and their

Can. J. Chem. Downloaded from www.nrcresearchpress.com by 210.87.254.5 on 09/06/12
For personal use only.

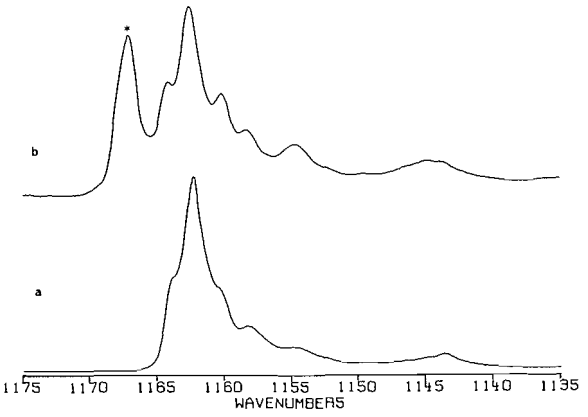


FIG. 3. 1175–1135 $cm^{-1}$ region FTIR spectrum of nitrogen-matrix isolated dideuteromethylene trithiocarbonate (a) after deposition, (b) after 15 min photolysis at $\lambda = 254$ radiation (*, assigned to thioformaldehyde-$d_2$ **3**).

behaviour in different matrices, the presence of two fundamentals is clearly indicated. We have tentatively assigned the strongest to the CH out-of-plane deformation based on the similar situation for formaldehyde (15). These two bands have their counterparts in thioformaldehyde-$d_2$ at 779 and 773 $cm^{-1}$.

*Product rule*

The theoretical Teller–Redlich rule (16) was calculated for thioformaldehyde based on the moments of inertia obtained from the geometrical parameters ($R$(C═S) = 1.6108 Å, $R$(C—H) = 1.0925 Å, and α(HCH) = 116.87°) determined by Johnson *et al.* (17) from the microwave spectra. The values obtained are in very good agreement with the observed values for each symmetry species, Table 3, strongly supporting the assignment.

*Normal coordinate analysis*

The seven internal coordinates used for the calculation are the changes in the three bond lengths ($\Delta r_1$, $\Delta r_2$, $\Delta R$), the changes in the HCH angle and the two HC═S angles ($\Delta\alpha$, $\Delta\beta_1$, $\Delta\beta_2$) and in the angle between the C═S bond and the HCH plane ($\Delta\beta$). The symmetry coordinates constructed with these internal coordinates are as follows:

$$\begin{aligned} a_1 \quad & S_1 = (\Delta r_1 + \Delta r_2)/\sqrt{2} \\ & S_2 = (2\Delta\alpha - \Delta\beta_1 - \Delta\beta_2)/\sqrt{6} \\ & S_3 = \Delta R \\ b_1 \quad & S_4 = \Delta\delta \\ b_2 \quad & S_5 = (\Delta r_1 - \Delta r_2)/\sqrt{2} \\ & S_6 = (\Delta\beta_1 - \Delta\beta_2)/\sqrt{2} \end{aligned}$$

The force field obtained by Jaquet *et al.* (8) for thioformaldehyde by *ab initio* mo methods was used as our initial force field which was then adjusted to fit the observed frequencies of thioformaldehyde-$d_0$ **1** and thioformaldehyde-$d_2$ **3**. The vibrational frequencies were calculated using a computer program (VSEC) written by Schachtschneider (18).

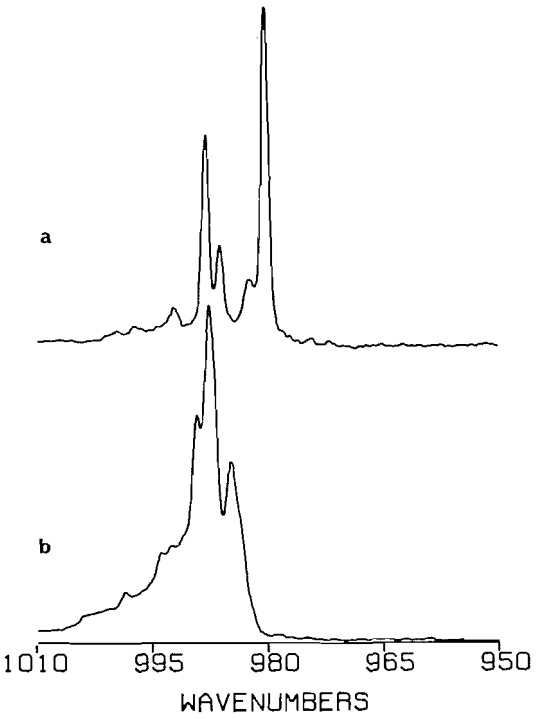


FIG. 4. 1010–950 $cm^{-1}$ region FTIR spectra of methylene trithiocarbonate **2** after $\lambda = 254$ nm photolysis for 10 min (a) argon-matrix (b) nitrogen-matrix.

TABLE 3. Theoretical vs. observed product rule ratios[a]

| Species | Theoretical | Observed |
|---|---|---|
| $a_1$ | 0.511 | 0.519 |
| $b_1$ | 0.788 | 0.789 |
| $b_2$ | 0.568 | 0.586 |

[a]The observed values are slightly higher due to the anharmonicity. When the band was split, due to matrix effects, only the stronger band was used in the calculation.

The calculated normal frequencies together with the observed values are listed in Table 4. The derived force field, in terms of the symmetry coordinates listed above, is given in Table 5, together with the force field from the *ab initio* calculation (8). The off-diagonal elements which can be calculated fairly reliably by *ab initio* methods have not been changed in the iteration with the exception of $F_{56}$. The value given by Jacquet *et al.* is rather low, and the one used in our calculations is in agreement with the relationship $F_{13} = 3^{-1/2}F_{56}$

Can. J. Chem. Downloaded from www.nrcresearchpress.com by 210.87.254.5 on 09/06/12
For personal use only.

TABLE 4. Observed and calculated frequencies for thioformaldehyde-$d_0$ and thioformaldehyde-$d_2$

| Species | | Thioformaldehyde-$d_0$ obs. | calcd. | Relative error, %[a] | Thioformadehyde-$d_2$ obs. | calcd. | Relative error, %[a] |
|---|---|---|---|---|---|---|---|
| $a_1$ | $\nu_1$ | 2965 (m) | 2968 | 0.1 | 2155 (m) | 2149 | 0.3 |
| | $\nu_2$ | 1447 (m) | 1450 | 0.2 | 1167 (m) | 1164 | 0.3 |
| | $\nu_3$ | 1052 (w) | 1057 | 0.5 | 932 (w) | 929 | 0.3 |
| $b_1$ | $\nu_4$ | 980 (s) | 981 | 0.1 | 773 (s) | 773 | — |
| $b_2$ | $\nu_5$ | 3017 (vw) | 3022 | 0.2 | [2280][b] (vvw) | 2243 | — |
| | $\nu_6$ | 988 (s) | 1002 | 1.4 | 779 (s) | 767 | 1.5 |

[a][$\nu$(calc.) − $\nu$(obs.)]/$\nu$(obs.) × 100.
[b]Tentative, not used for the calculation.

TABLE 5. Derived force field

| | Force field | |
|---|---|---|
| | This work | From ref. 8[a] |
| $F_{11}$ | 5.021 | 5.78 |
| $F_{12}$ | 0.221 | 0.22 |
| $F_{22}$ | 6.464 | 7.17 |
| $F_{13}$ | 0.140 | 0.14 |
| $F_{23}$ | −0.261 | −0.29 |
| $F_{33}$ | 0.454 | 0.53 |
| $F_{44}$ | 0.284 | 0.32 |
| $F_{55}$ | 4.882 | 5.59 |
| $F_{56}$ | 0.240 | 0.10 |
| $F_{66}$ | 0.578 | 0.62 |

[a]*ab initio* calculation.

found to be valid in the case of formaldehyde (19). The diagonal force constants are rather different mainly because we could not use anharmonic corrections, but the relative magnitudes agree well with those obtained from the *ab initio* calculation.

After submission of the present manuscript we became aware of a gas-phase FTIR study of thioformaldehyde, **1**, and dideuterothioformaldehyde, **3**, by Mills and co-workers (13). The FTIR gas-phase values have been included in Tables 1 and 2 together with the matrix shift. As seen from the data, the matrix shift is in the range of −3 to −10 $cm^{-1}$ with the exception of $\nu_6$ for $CD_2S$ which has a value of +22 $cm^{-1}$. When splitting of a band occurs in the matrix, $\Delta\nu$'s are computed for the most intense component of the split band.

## Acknowledgments

The authors are grateful to the Natural Sciences and Engineering Research Council of Canada for continuing financial support, to Dr. E. M. Lown for helpful discussions, and to R. Swindlehurst and J. Hoyle for technical assistance.

1. E. E. REID. Organic chemistry of bivalent sulfur. Vol. III. Chemical Publishing Co., Inc., New York, NY. 1960. Chapt. 2.
2. B. SOLOUKI, P. ROSMUS, and H. BOCK. J. Am. Chem. Soc. **98**, 6054 (1976).
3. H. BOCK, B. SOLOUKI, S. MOHMAND, E. BLOCK, and L. K. REVELLE. J. Chem. Soc. Chem. Commun. 287 (1977).
4. J. W. C. JOHNS and W. B. OLSON. J. Mol. Spectrosc. **39**, 479 (1971).
5. M. E. JACOX and D. E. MILLIGAN. J. Mol. Spectrosc. **58**, 142 (1975).
6. D. J. BEDWELL and G. DUXBURY. J. Mol. Spectrosc. **84**, 531 (1980).
7. D. J. CLOUTHIER, C. M. L. KERR, and D. A. RAMSAY. Chem. Phys. **56**, 73 (1981).
8. R. JAQUET, W. KUTZELNIGG, and V. STAEMMLER. Theor. Chim. Acta, **54**, 205 (1980).
9. M. TORRES, A. CLEMENT, H. E. GUNNING, and O. P. STRAUSZ. Nouv. J. Chim. **3**, 365 (1979).
10. M. TORRES, A. CLEMENT, and O. P. STRAUSZ. J. Org. Chem. **45**, 2271 (1980).
11. M. TORRES, A. CLEMENT, J. E. BERTIE, H. E. GUNNING, and O. P. STRAUSZ. J. Org. Chem. **43**, 2490 (1978).
12. J. WORTMANN, G. KIEL, and G. GATTOW. Z. Anorg. Allg. Chem. **376**, 73 (1970).
13. P. H. TURNER, L. HALONEN, and J. M. MILLS. J. Mol. Spectrosc. **88**, 402 (1981).
14. A. J. BARNES. *In* Vibrational spectroscopy of trapped species. *Edited by* H. E. Hallam. Wiley, London. 1973.
15. K. B. HARVEY and J. F. OGILVIE. Can. J. Chem. **40**, 85 (1962).
16. E. B. WILSON, JR., J. C. DELEIUS, and P. C. CROSS. *In* Molecular vibrations. McGraw-Hill, New York. 1955. p. 183.
17. D. R. JOHNSON, F. X. POWELL, and W. H. KIRCHHOFF. J. Mol. Spectrosc. **39**, 136 (1971).
18. J. H. SCHACHTSCHNEIDER. Technical Report No. 57-65, Project #31450, Shell Development, Emeryville, CA.
19. J. L. DUNCAN and P. D. MALLINSON. Chem. Phys. Lett. **23**, 597 (1973).

Can. J. Chem. Downloaded from www.nrcresearchpress.com by 210.87.254.5 on 09/06/12
For personal use only.

# Metal hydride reductions of unsymmetrical cyclic anhydrides. The importance of the antiperiplanar effect on the regioselectivity of these reactions

MARGARET M. KAYSER[1]

*Department of Chemistry, University of Ottawa, Ottawa, Ont., Canada K1N 9B4*

AND

GEORGES WIPFF

*Institut le Bel, Université Louis Pasteur, 1 Rue Blaise Pascal, 67000 Strasbourg, France*

Received November 9, 1981

MARGARET M. KAYSER and GEORGES WIPFF. Can. J. Chem. **60**, 1192 (1982).

A quantum mechanical study by the SCF *ab initio* method of the interaction of $H^-$ with methylsuccinic and 2,2-dimethylsuccinic anhydrides (naked and in the presence of a cation) suggests that nonperpendicular rearside attack cannot be the factor responsible for the regioselectivity of hydride transfer to the more sterically hindered carbonyl group. In this model, the nucleophilic attack at the less hindered carbonyl group is calculated to be of lower energy (with or without cation). Deformation of the planar succinic anhydride ring to the quasi-chair conformation is energetically favoured as it allows the nucleophile to attack both carbonyl functions antiperiplanar to a quasi axial C—H or C—C bond. The attack antiperiplanar to the C—$CH_3$ bond is lower in energy than the attack antiperiplanar to the C—H bond suggesting that the reduction will occur at the sterically more hindered carbonyl group which is in agreement with the experimental findings.

MARGARET M. KAYSER et GEORGES WIPFF. Can. J. Chem. **60**, 1192 (1982).

Une étude, par la méthode SCF *ab initio*, de l'interaction de $H^-$ avec les anhydrides méthyl- et diméthyl-2,2 succiniques (seuls ou en présence d'un cation) suggère que l'attaque non-perpendiculaire ne peut être le facteur responsable de la régiosélectivité du transfert d'hydrure au groupe carbonyle le plus stériquement encombré. Dans ce modèle, on calcule que l'attaque nucléophile sur le groupe carbonyle le moins encombré requiert moins d'énergie (avec ou sans cation). La déformation du cycle plan de l'anhydride succinique en une conformation quasi-chaise est favorisée énergétiquement puisqu'elle permet au nucléophile d'attaquer les deux fonctions carbonyles antipériplanaires jusqu'à une liaison quasi-axiale C—H ou C—C. L'attaque antipériplanaire à la liaison C—H demande moins d'énergie que l'attaque antipériplanaire à la liaison C—H. Ce fait suggère que la réduction se fera sur le carbonyle le plus encombré, ce qui s'accorde avec les résultats expérimentaux.

[Traduit par le journal]

Metal hydride reductions of unsymmetrically substituted cyclic anhydrides (1, 2) and succinimides (3) frequently occur regioselectively at the carbonyl function adjacent to the most highly substituted carbon atom. Greatest selectivity is observed in reductions of *gem*-disubstituted succinic anhydrides and succinimides. In monosubstituted compounds, generally mixtures of the two regioisomers are obtained, although even there reduction occurs preferentially at the carbonyl group next to the substituent. This problem is well illustrated by reduction of 2,2-dimethylsuccinic anhydride and 2-methylsuccinic anhydride (Scheme 1) (2).

It has been suggested that a variety of factors may be involved in controlling regioselectivity of these reactions (2). The intrinsic reactivities of the two carbonyl groups toward the nucleophilic addition (expressed in terms of the size of LUMO coefficients on the carbon atoms of the carbonyl functions) correlate satisfactorily with regioselectivity patterns for a series of substituted succinic anhydrides (4). The observed regioselectivity could also be due to the nonperpendicular, restricted path of nucleophilic approach. This assumption was based on crystallographic analysis (5) and *ab initio* calculations (6, 7) of nucleophilic addition to the carbonyl group. Models of succinic anhydrides (8) and succinimides (9, 10) suggested that the approach of a nucleophile to the β-carbonyl function, along the preferred reaction path, might be effec-

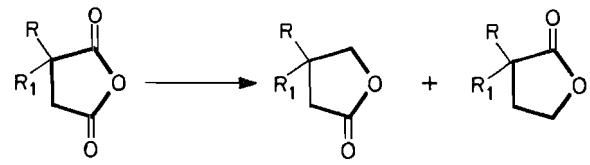


SCHEME 1

[1]Author to whom correspondence should be addressed. Present address: Département de chimie, Université de Moncton, Moncton, N.-B., Canada E1A 3E9.

0008-4042/82/101192-07$01.00/0

©1982 National Research Council of Canada/Conseil national de recherches du Canada

Can. J. Chem. Downloaded from www.nrcresearchpress.com by 210.87.254.42 on 09/06/12
For personal use only.

Can. J. Chem. Downloaded from www.nrcresearchpress.com by 210.87.254.42 on 09/06/12
For personal use only.

tively more hindered by the substituents than the approach to the α-carbonyl group.

The purpose of this paper is to determine if such models (Fig. 1) are theoretically justified and can be used to rationalize and predict regioselectivity of metal hydride reductions, and to present alternative arguments based on ring nonplanarity and the "antiperiplanar effect".

## Results and discussion

*Ab initio* molecular orbital calculations using the programme Gaussian 70 (11) with the standard STO-3G basis set were carried out for methylsuccinic and 2,2-dimethylsuccinic anhydrides and all regioisomeric "supermolecules" (anhydride + $H^-$ and anhydride–proton + $H^-$). To reduce computation costs we have represented compounds **1** and **2** by realistic models based on crystallographic data for the parent succinic anhydride (12) while standard bond lengths and bond angles (13) were used for the substituents. The optimum orientation for the methyl group(s) was found to be fully staggered in the naked molecules **1** and **2** as well as in the "supermolecules" (Fig. 2).

To obtain a qualitative description of the anhydride–$H^-$ "supermolecule" we have scanned a number of points on the potential surface. The choice of positions was guided by the existing knowledge of the geometry of nucleophilic addition to the carbonyl group in formaldehyde. The $H^-\cdots$ C=O distance was maintained constant at 2 Å and the reacting carbonyl group was not pyramidalized.

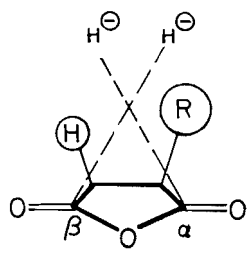


FIG. 1. Model of minimum energy path for $H^-$ approach to the more hindered α-carbonyl group and the less hindered β-carbonyl group suggesting that the attack at the α group is effectively more opened.

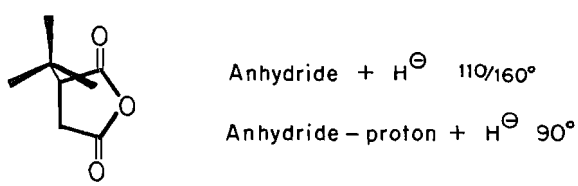


FIG. 2. The optimum orientation of the methyl group(s) in "naked" anhydrides **1**, **2**, and in the corresponding "supermolecules."

*Optimum geometry calculations for anhydride + $H^-$ "supermolecule"*

The calculations of the optimum geometry for hydride attack at the carbonyl group in succinic anhydride show that at the distance $H^-\cdots$C=O of 2 Å the preferred position for the hydride ion is on the bisector of the C=O group at an angle of ca. 110° to the molecular plane (4). Thus although the calculations confirm the nonperpendicular attack they do not predict a shift away from the ring oxygen atom as was suggested in the model (8, 14) (Fig. 3). This may result from the steric repulsion with the H atom(s) protruding above the plane of the ring or from the attractive interaction with the opposite carbonyl's carbon atom.

In the presence of the substituents (Me, Ph) in the position 2, nucleophilic attack occurs at the neighbouring α-, rather than more remote β-carbonyl group. This selectivity has been explained in terms of nonperpendicular rearside attack by a nucleophile (8–10). We have decided to test computationally the validity of such a hypothesis, by calculating the preferred position of $H^-$ attack at the α- and β-carbonyl group in methyl succinic and 2,2-dimethylsuccinic anhydride. No geometry relaxation of the anhydride was allowed, the five membered ring was kept planar, and the distance $H^-\cdots$C=O was fixed at 2 Å. Four values of the angle of attack (90°, 100°, 110°, and 120°) were computed for each point of the scan about the carbon atom of the "reacting" carbonyl group. Five scan points were chosen for the values of angle δ: 120°, 150°, 180°, 210°, and 240° (Fig. 4).

The optimum structures for each regioisomeric "supermolecule" are listed in Table 1. The results show that (a) the nucleophile is shifted away from the methyl substituent rather than from the ring

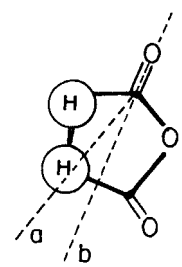


FIG. 3. Projections of the $H^-$ position onto the molecular plane; (a) a shift in space away from the ring oxygen atom suggested in the model for nucleophilic attack on the carbonyl group in succinic anhydrides; (b) the STO-3G calculated $H^-$ position falls directly on the bisector of the carbonyl group.

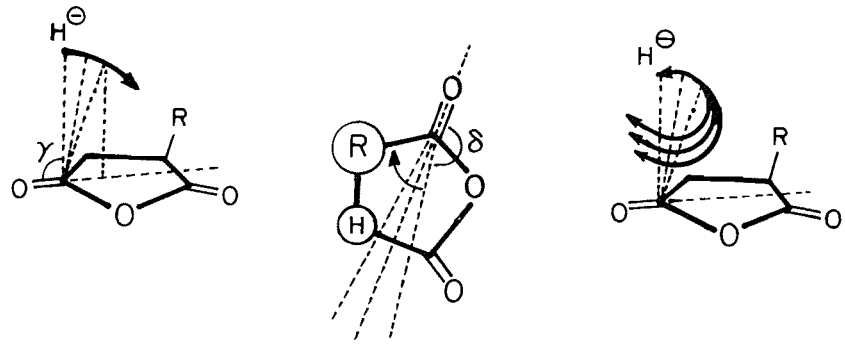

FIG. 4. The search for the optimum geometry for $H^-$ attack on the carbon atom of the carbonyl group in the β regioisomer of the model compound 1*b*. The angle γ between the incoming $H^-$ and the molecular plane varied from 90° to 120° by increments of 10°. The angle δ between $H^-$ projection on the plane of the ring and the C=O bisector varied from 120° to 240° by increments of 10°.

TABLE 1. Optimum geometries for regioisomeric "supermolecules" in the absence of a cation

| Substrate | γ/δ Angle of attack | Energy (au) | ΔE (kcal/mol) |
|---|---|---|---|
| 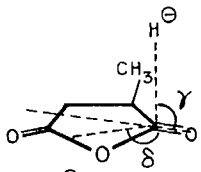 | 110/160 | −412.27477 | 0 |
| 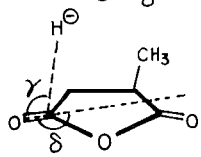 | 110/180 | −412.28321 | −5.3 |
| 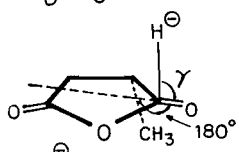 | 110/180 | −412.28203 | −4.6 |
| 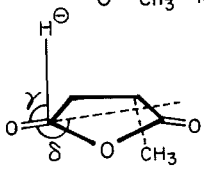 | 110/180 | −412.28077 | −3.8 |
| 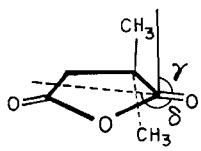 | 110/180 | −450.85135 | 0 |
| 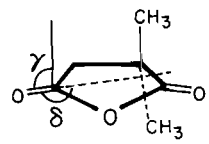 | 110/160 | −450.86150 | −6.4 |

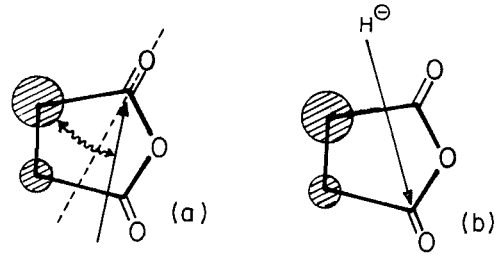

FIG. 5. The path of nucleophilic approach at 2 Å distance is shifted away from the methyl substituent in the attack on the α-carbonyl group, suggesting that in this model the α-carbonyl group is in effect more sterically hindered (a). The attack at the β-carbonyl group is energetically favoured (b).

oxygen atom (Fig. 5); and (b) the attack at the β-carbonyl group is energetically more favourable. These results are inconsistent with both the proposed model for the nucleophilic attack on succinic anhydrides and with the experimentally observed regioselectivity. The discrepancy most likely lies not in the calculations per se but rather in the model chosen for the transition state, particularly with regard to the planarity of the anhydride ring and the carbonyl groups.

*The optimum geometry for anhydride–proton + $H^-$ "supermolecule"*

We should point out that all the above calculations have been performed for hydride ion and naked substrate molecule. Neither solvent nor a cation normally present in the reaction medium were taken into account. Nevertheless, it has been demonstrated that in the absence of cations ($H^+$, $Li^+$, $Na^+$) and protic solvents the isolated carbonyl groups are not reduced (15*a*) by metal hydrides and reductions of conjugated ketones are considerably slower (15*b*). In order to ascertain if our previous result might not be modified when the more realis-

Can. J. Chem. Downloaded from www.nrcresearchpress.com by 210.87.254.42 on 09/06/12
For personal use only.

Can. J. Chem. Downloaded from www.nrcresearchpress.com by 210.87.254.42 on 09/06/12
For personal use only.

TABLE 2. Optimum geometries for regioisomeric "supermolecules" in the presence of a cation

| Substrate | γ Angle of of attack | Energy (au) | ΔE (kcal/mol) |
|---|---|---|---|
| 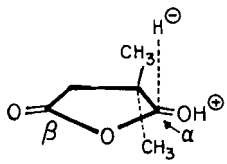 | 90 | −451.50938 | 0 |
| 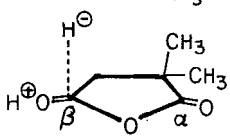 | 90 | −451.51649 | −4.5 |
| 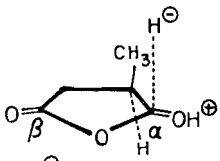 | 90 | −412.93088 | 0 |
| 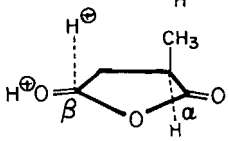 | 90 | −412.93699 | −3.8 |
| 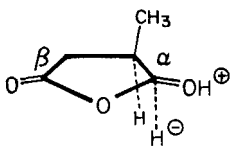 | 90 | −412.93601 | −3.2 |
| 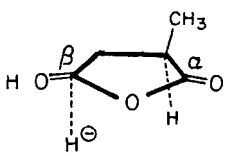 | 90 | −412.93608 | −3.3 |

tic model incorporating a cation is used in computation, we have recalculated all regioisomeric supermolecules with a proton (simulating a cation) coordinated to the oxygen atom of the reacting carbonyl group. The results are summarized in Table 2. The equilibrium structures for the nucleophilic attack on the α- and β-carbonyl groups associated with a cation show that the optimum angle of attack is not 110° but is in fact close to perpendicular. This is in agreement with the results obtained by Anh and Eisenstein (16), who have shown that in model ketones the coordination with a cation favours near perpendicular attack. However, even in the presence of a cation, the attack at the less hindered β-carbonyl group remains energetically preferred, contrary to the experimental findings.

In view of these results we have concluded that the explanation of regioselectivity based on the nonperpendicular, restricted path of nucleophilic approach to the carbonyl function in succinic anhydrides is not adequate and thus the major factor influencing regioselectivity of these reactions has eluded us so far.

*The importance of the antiperiplanar effect*

The studies of Anh and co-workers (17) have suggested that in the nucleophilic addition to the carbonyl group in ketones, the transition state is stabilized if there is a neighbouring bond C—X antiperiplanar to the forming partial bond C—$H^-$ as shown in **3**.

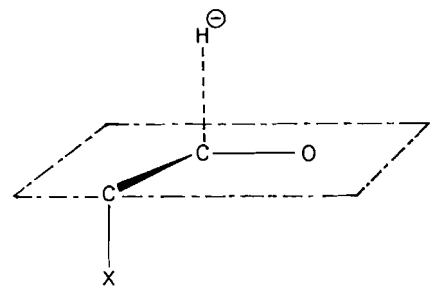

**3**

The greatest stabilization is observed when $\sigma^*_{C-X}$ is low in energy. For example the C—C bond antiperiplanar to C—$H^-$ is favoured over the C—H bond since the energy of $\sigma^*_{C-C}$ is lower than the energy of $\sigma^*_{C-H}$. The authors have proposed that in cyclic ketones, where originally there is no antiperiplanarity possible, flattening of the ring and pyrimidalization at the carbonyl carbon atom occurs in order to achieve antiperiplanar geometry in the transition state (17). This hypothesis rationalized successfully the ratios of axial/equatorial attack in a variety of cyclic ketones.

Does the antiperiplanar effect play a role in the nucleophilic addition to systems other than cyclic ketones? If the original interpretation of the particular stability of the Felkin transition states is correct, then in any nucleophilic addition to a carbonyl function where regio and stereoselectivity may occur, antiperiplanarity between the incipient $H^-$—C bond and an adjacent σ bond of lowest energy should lead to the favoured transition state, other things being equal. Thus antiperiplanarity allows the correct prediction of regioselective reduction at the more hindered function in unsymmetrical diesters and diacids (18) (Fig. 6).

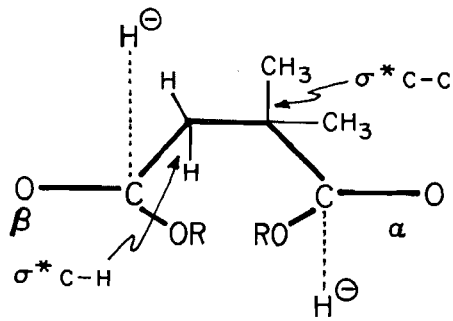


FIG. 6. The attack antiperiplanar to the C—C bond is favoured over the attack antiperiplanar to the C—H bond. Thus the α-carbonyl group is reduced preferentially.

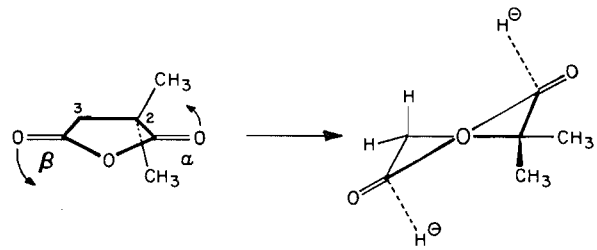


FIG. 7. A deformation of $C_2$ symmetry of the planar ring leads to a quasi-chair conformation. Nucleophilic attack at the α and β carbon atoms can now occur in the antiperiplanar fashion to a C—Me and C—H bond.

At first glance, achieving antiperiplanarity in succinic anhydrides does not appear possible due to the ring angle strain imposed on the planar ring by two trigonal carbon atoms. Crystallographic data have shown that in the crystal form succinic anhydride is indeed almost planar (12). Gas electron diffraction studies of gaseous succinic anhydride (19) suggest deviation from planarity of only 4.8°. Although in succinic anhydride the strain conferred by two trigonal carbon atoms is sufficient to hold the pair of adjacent methylene groups eclipsed in the equilibrium conformation, this may not be the case when succinic anhydride is substituted with larger groups where the ring may be intrinsically nonplanar. Moreover, since the deformation of the ring removes eclipsed interactions in the substrate, releases interactions with the nucleophile, and permits an antiperiplanar attack, the ring nonplanarity may be *enhanced* in the transition state. Upon examination of the model it can be seen that when the ring is twisted as shown in Fig. 7 we obtain a quasi-chair conformation. Now the incipient C—$H^-$ bond is nearly antiperiplanar to the quasi-axial C—C or C—H bond.

A second effect increasing the antiperiplanarity of nucleophilic attack is the pyrimidalization of the carbonyl group. We suggest that this effect is larger in cyclic succinic anhydrides than in open chain ketones or esters because of the strain at the carbonyl carbon atom (C—CO—C angle 110.5°) (19). The situation is analogous to that observed in the inversions at nitrogen (20) and carbanion (21), where the inversion barriers increase with the increasing strain. In addition, it is possible that in a nonsymmetric environment, the carbonyl group may be intrinsically nonplanar (22). The results obtained by Houk and co-workers (23) for model systems show that in the out-of-plane deformation of the carbonyl group the rehybridized π orbital is antiperiplanar to the "axial" C—H or C—Me bonds in the same direction as that which also gives the best antiperiplanar effect in the addition reaction.

As a result, nonplanarity of the anhydride ring increases the possibility of an effective antiperiplanar attack by forcing C—H and C—Me bonds into a pseudo axial orientation and by facilitating pyramidalization of the carbonyl group (Fig. 8) in the direction which permits the best antiperiplanar attack. Thus in methyl and 2,2-dimethylsuccinic anhydrides, nucleophilic attack at the α-carbon atom, antiperiplanar to an "axial" C—Me bond, is expected to be favoured, as is observed experimentally.

Ring flexibility and antiperiplanar effects are supported by 3G calculations carried out on succinic anhydrides and the corresponding supermolecules. We have not included carbonyl pyramidalization in our calculations since the degree of pyramidalization in the transition state, especially in the presence of a cation, is not known.

The calculations carried out for methyl and 2,2-dimethylsuccinic anhydrides show a slight but consistent drop in total energy upon twisting of the molecule into a quasi-chair conformation (Table 3). It should be noted that in the distorted rings, the LUMO coefficients are still more localized on the α than on the β carbon atom (Table 3). Although the fully optimized conformation of the molecules is not for the moment available, these results indicate that the anhydride ring possesses some flexibility and that deformation should not cost much in terms

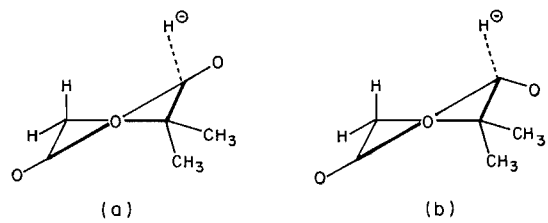


FIG. 8. Nucleophilic attack at planar (a) and pyramidalized (b) carbonyl functions in 2,2-dimethylsuccinic anhydride.

Can. J. Chem. Downloaded from www.nrcresearchpress.com by 210.87.254.42 on 09/06/12
For personal use only.

Can. J. Chem. Downloaded from www.nrcresearchpress.com by 210.87.254.42 on 09/06/12
For personal use only.

TABLE 3. Energies and LUMO coefficients on $C_\alpha$ and $C_\beta$ in planar and distorted 2,2-dimethyl- and methylsuccinic anhydrides

| Molecule | Energy (au) | $E$ (kcal/mol) | LUMO coefficients $C_\alpha$ | $C_\beta$ |
|---|---|---|---|---|
| 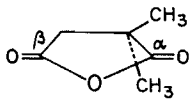 | −450.64620 | 0 | 0.598 | −0.580 |
| 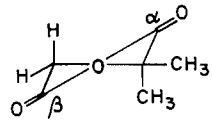 | −450.64699 | −0.5 | 0.564 | −0.553 |
| 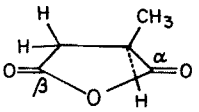 | −412.06665 | 0 | 0.595 | −0.584 |
| 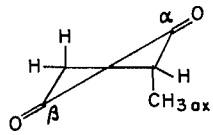 | −412.06724 | −0.4 | 0.560 | −0.556 |
| 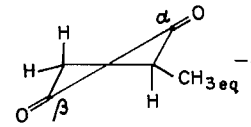 | −412.06696 | −0.2 | 0.564 | −0.554 |

TABLE 4. Energies of the distorted supermolecules

| Supermolecule | Energy (au) | Relative energy $\Delta E$ (kcal/mol) |
|---|---|---|
| 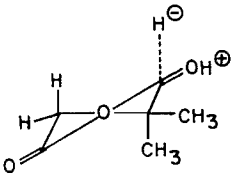 | −451.51913 | −3.3 |
| 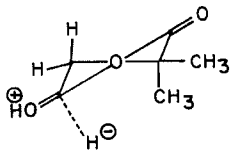 | −451.51383 | 0 |
| 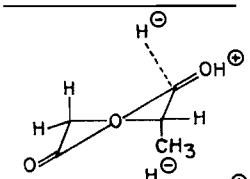 | −412.93939 | −3.5 |
| 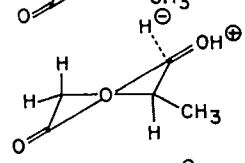 | −412.93989 | −3.8 |
| 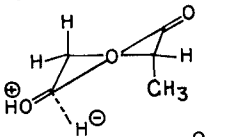 | −412.93391 | 0 |
| 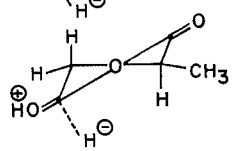 | −412.93935 | −3.4 |

of energy. On the other hand, the distortion of the supermolecules in which hydride attack occurs at the α-carbonyl group is definitely energetically favoured (see Table 4).

Finally, we should point out that in the process of distorting of the substrate molecule into a quasi-chair conformation some of the steric congestion about the α-carbonyl group, which is present in a planar molecule, is now removed. As a result nucleophilic attack at the α-carbonyl function in the quasi-chair conformer is preferred to β-attack in the planar molecule. Thus on the basis of the foregoing calculations we should expect regioselective reduction at the α-carbonyl group, which is in agreement with the experimental findings.

## Conclusion

It appears that in the reduction of unsymmetrical cyclic anhydrides by simple metal hydrides two factors must be taken into consideration: (1) in systems possessing a certain flexibility in which, therefore, some degree of antiperiplanarity may be achieved, attack at the carbonyl function adjacent to the most highly substituted carbon atom should be favoured; (2) in rigorously rigid systems, preferred attack should occur at the least hindered carbonyl group. In other words, in succinic anhydrides in which the ring cannot be distorted to accommodate the antiperiplanar attack by a nucleophile, we should expect reduction at the β-carbonyl function.

In summary, we may conclude that theoretical studies of the reductions of cyclic anhydrides by metal hydrides suggest that the search for any single factor capable of explaining all the regioselectivity patterns is an exercise in futility. So far, four different effects controlling the course of these reductions have been identified, the two reported previously (4):

1. intrinsic reactivity of the carbonyl function
2. chelating effect

and the two discussed in this paper, namely:

3. antiperiplanar effect
4. steric congestion.

It is possible that the same factors affect regioselectivity in reductions of other systems such as, for example, cyclic imides and diesters.

**Acknowledgement**

It is a pleasure to acknowledge Le Ministère français des Affaires Etrangères for the award of a Bourse de Long Séjour to MMK.

1. J. J. BLOOMFIELD and S. L. LEE. J. Org. Chem. **32**, 3919 (1967); D. M. BAILEY and R. E. JOHNSON. J. Org. Chem. **35**, 3575 (1970).
2. M. M. KAYSER and P. MORAND. Can. J. Chem. **56**, 1524 (1978).
3. J. B. WIJNBERG, W. N. SPECKAMP, and H. E. SHOEMAKER. Tetrahedron Lett. 4073 (1974); J. B. WIJNBERG and W. N. SPECKAMP. Tetrahedron Lett. 4035 (1975); J. B. WIJNBERG, H. E. SHOEMAKER, and W. N. SPECKAMP. Tetrahedron, **34**. 179 (1978).
4. M. M. KAYSER and O. EISENSTEIN. Can. J. Chem. **59**, 2457 (1981).
5. H. B. BÜRGI, J. D. DUNITZ, and E. SHEFTER. J. Am. Chem. Soc. **95**, 5065 (1973).
6. H. B. BÜRGI, J. D. DUNITZ, J. M. LEHN, and G. WIPFF. Tetrahedron, **30**, 1563 (1974).
7. H. B. BÜRGI, J. M. LEHN, and G. WIPFF. J. Am. Chem. Soc. **96**, 1956 (1974).
8. M. M. KAYSER and P. MORAND. Tetrahedron Lett. 695 (1979).
9. R. SUESS. Helv. Chim. Acta, **60**, 1650 (1977).
10. R. R. ROSENFIELD, JR. and J. D. DUNITZ. Helv. Chim. Acta, **61**, 2176 (1978).
11. W. J. HEHRE, W. A. LATHAN, R. DITCHFIELD, M. D. NEWTON, and J. A. POPLE. Gaussian 70, QCPE. No. 236, Bloomington, Indiana.
12. M. EHRENBERG. Acta Crystallogr. **19**, 698 (1966); R. DESTRO, G. FILIPINI, C. M. GRAMACCIOLI, and M. SIMONETTA. Acta Crystallogr. Sect. B, **27**, 2023 (1971).
13. J. A. POPLE and D. L. BEVERIDGE. Approximate molecular orbital theory. McGraw Hill, New York. 1970. p. 111; W. J. HEHRE, R. DITCHFIELD, R. E. STEWART, and J. A. POPLE. J. Chem. Phys. **52**, 2769 (1970).
14. J. E. BALDWIN. J. Chem. Soc. Chem. Commun. 738 (1976).
15. (*a*) J. L. PIERRE and H. HANDEL. Tetrahedron Lett. 2317 (1974); (*b*) A. LOUPY, J. SEYDEN-PENNE, and B. TCHOUBAR. Tetrahedron Lett. 1677 (1976).
16. NGUYEN TRONG ANH and O. EISENSTEIN. Nouv. J. Chem. **1**, 61 (1977).
17. J. HUET, Y. MARONI-BARNAUD, NGUYEN TRONG ANH, and J. SEYDEN-PENNE. Tetrahedron Lett. 159 (1976); NGUYEN TRONG ANH and O. EISENSTEIN. Tetrahedron Lett. 155 (1976).
18. M. M. KAYSER and P. MORAND. J. Org. Chem. **44**, 1338 (1979).
19. K. BRENDHOUGEN, M. KOLDENEP FIKKE, and H. M. SEIP. Acta Chem. Scand. **27**, 1101 (1973).
20. J. M. LEHN. Fortsch. Chem. Forsch., Topics Curr. Chem. **15**, 311 (1970).
21. E. D. JEMMIS, V. BUSS, P. v. R. SCHLEYER, and L. C. ALLEN. J. Am. Chem. Soc. **98**, 6483 (1976).
22. C. L. LIOTTA. Tetrahedron Lett. 519 (1975); 523 (1975).
23. N. G. RONDAN, M. N. PADDON-ROW, P. CARAMELLA, and K. N. HOUK. J. Am. Chem. Soc. **103**, 2436 (1981).

Can. J. Chem. Downloaded from www.nrcresearchpress.com by 210.87.254.42 on 09/06/12
For personal use only.

# Metal hydride reductions of unsymmetrically substituted cyclic anhydrides attached to strained ring systems

MARGARET M. KAYSER,[1] JUDITH SALVADOR, AND PETER MORAND
*Department of Chemistry, University of Ottawa, Ottawa, Ont., Canada K1N 9B4*
AND
H. G. KRISHNAMURTY
*Department of Chemistry, University of Delhi, Delhi–110007, India*
Received November 9, 1981

MARGARET M. KAYSER, JUDITH SALVADOR, PETER MORAND, and H. G. KRISHNAMURTY. Can. J. Chem. **60**, 1199 (1982).

A dramatic reversal in regioselectivity is observed in the metal hydride reduction of unsymmetrical cyclic anhydrides such as **2**, **3**, and **4** compared to cyclic anhydrides attached to bridged ring systems (e.g. **1**). The synthesis of model cyclic anhydrides attached to strained rings is described and the ratios of isomeric lactones obtained upon reduction with metal hydride are reported. On the basis of theoretical calculations and, taking into account the intrinsic reactivity of the carbonyl group, the antiperiplanar effect, and steric congestion, an explanation is offered for the regioselectivity observed in the reduction of these compounds.

MARGARET M. KAYSER, JUDITH SALVADOR, PETER MORAND et H. G. KRISHNAMURTY. Can. J. Chem. **60**, 1199 (1982).

On a observé une inversion remarquable de la régiosélectivité dans la réduction par des hydrures métalliques des anhydrides cycliques, tels **2**, **3** et **4**, par opposition aux résultats obtenus avec des anhydrides cycliques attachés à des systèmes cycliques pontés (i.e. **1**). On décrit la synthèse d'anhydrides cycliques modèles attachés à des cycles tendus et on rapporte les proportions de lactones isomères obtenues lors de leurs réductions par les hydrures métalliques. A partir de calculs théoriques et en tenant compte de la réactivité intrinsèque du groupe carbonyle, de l'effet antipériplanaire et de la contrainte stérique, on propose une explication de la régiosélectivité observée lors de la réduction de ces composés.

[Traduit par le journal]

During a recent study of regioselectivity in metal hydride reductions of unsymmetrically substituted cyclic anhydrides we have noted that cyclic anhydrides attached to bridged ring systems such as **1** were reduced selectively at the carbonyl function next to the least substituted carbon atom (1). This observation was surprising in view of the fact that related systems such as **2**, **3**, and **4** are reduced regioselectively at the more hindered carbonyl group (1, 2).

The reversal of regioselectivity observed in the reduction of compound **1** (vs. **2**, **3**, and **4**) was suspected to be related to ring size and/or ring strain in the ring systems to which the anhydride is attached. In order to determine the impact of ring strain/ring size on the regioselectivity of metal hydride reductions, the model anhydrides **5**, **6**, and **7** were synthesized and subsequently reduced with $LiAlH_4$ and $NaBH_4$. Anhydride **7**, the one most closely related to the bridged cyclic system **1**, was reduced selectively at the β-carbonyl function, adjacent to the least substituted carbon atom. A trace amount (constituting < 5%) of the isomeric lactone was detected by glc, isolated by careful chromatography, and identified by proton nmr. Reductions of compounds **5** and **6** yielded mixtures of isomeric lactones in almost equal proportions.

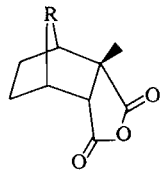

R = $CH_2$; $CH_2CH_2$
**1**

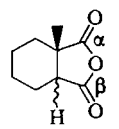

*cis* and *trans*
**2**

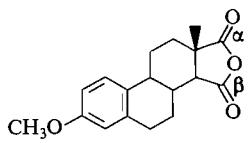

**3**

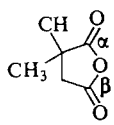

**4**

These results suggest that although the small size

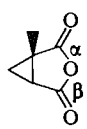

**5**

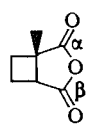

**6**

[1]Author to whom correspondence should be addressed. Present address: Département de chimie, Université de Moncton, Moncton, N.-B., Canada E1A 3E9.

0008-4042/82/101199-08$01.00/0
©1982 National Research Council of Canada/Conseil national de recherches du Canada

Can. J. Chem. Downloaded from www.nrcresearchpress.com by 210.87.254.105 on 09/06/12
For personal use only.

Can. J. Chem. Downloaded from www.nrcresearchpress.com by 210.87.254.105 on 09/06/12
For personal use only.

of the ring attached to the cyclic anhydride, and/or the issuing strain in the system, may in some manner be responsible for diminished selectivity in the reduction of compounds such as **5** and **6**, these effects, per se, cannot explain the high regioselectivity observed in the reduction of bridged compounds **1** and **7**. In this paper we propose that the

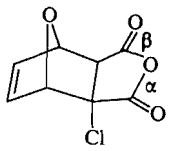

7

most satisfactory interpretation of the results is based on perturbational considerations, stressing the importance of the antiperiplanar effect in the transfer of hydride ion to the carbonyl function in cyclic anhydrides. In cases where antiperiplanar attack is not possible, the fate of the reaction is determined to a great extent by steric factors.

## Experimental results

A. *Synthesis of 1-methylcyclopropane, 1,2-dicarboxylic acid anhydride* **5**, *and 1-methylcyclobutane 1,2-dicarboxylic acid anhydride* **6**

The simplest and most successful method for the preparation of the anhydride **5** proved to be the procedure described by McCoy (3) as outlined in Scheme 1.

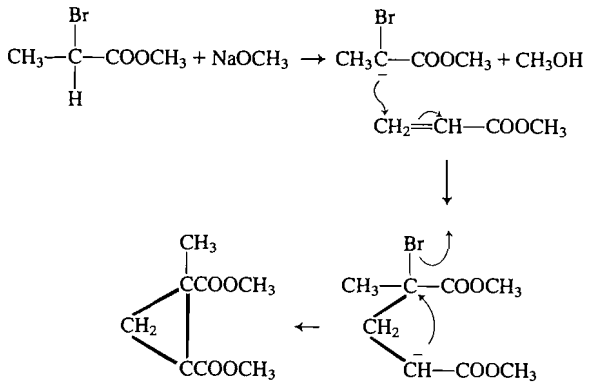

**5** *cis* and *trans*

SCHEME 1

Saponification of this product yielded 62% of the *trans* diacid (4) and 30% of the *cis* diacid which were converted to the anhydrides by treatment with acetic anhydride and separated by sublimation or crystallization.

The synthesis of anhydride **6** in 69% yield was cleanly effected by the photochemical |2 + 2| cycloaddition of ethylene to methylmaleic anhydride (Scheme 2).

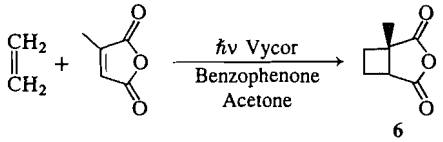

**6**

SCHEME 2

B. *Diels–Alder addition of furan and chloromaleic anhydride* **7**

Diels–Alder adducts derived from furan are generally thermally unstable and susceptible to dissociation with a varying degree of facility. Although furan, a poor diene due to its aromaticity, will not react directly with methyl or dimethyl maleic anhydride (4, 5), it will undergo |4 + 2| cycloaddition with maleic or chloromaleic anhydride simply by stirring the two compounds at room temperature. The commercially available chloromaleic anhydride contains ca. 30% maleic anhydride, which is difficult to remove. We chose to carry out the reaction with this mixture of chloromaleic and maleic anhydrides and to subsequently separate the two adducts (Scheme 3). This was accomplished by hplc or by fractional crystallization. Both **7** and **8** tend to deteriorate upon standing, adduct **8** being considerably more susceptible to decomposition.

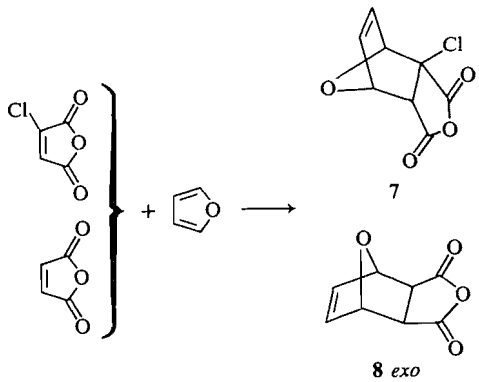

**7**

**8** *exo*

SCHEME 3

In theory, two modes of addition are possible, leading to the formation of an *endo* or an *exo* adduct as shown in Scheme 4. The Diels–Alder adduct of maleic anhydride with furan has been shown to have the *exo* configuration (6). Anet (7) demonstrated by proton nmr study that, under the usual conditions, the addition of furan to maleic

TABLE 1. Metal hydride reductions of model cyclic anhydrides

| Anhydride | Products a | Products b | % Yield lactonic product | Observed ratio a/b |
|---|---|---|---|---|
| 5 | 5a | 5b | 62[a] 60[b] | 55:45 62:38 |
| 6 | 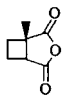 6a | 6b | 80[a] 71[b] | 44:56 43:57 |
| 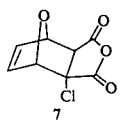 7 | 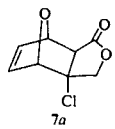 7a | 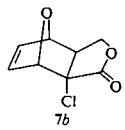 7b | 74[a] 76[b] | trace: 95 |
| 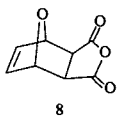 8 | 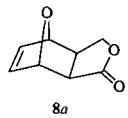 8a | — | 30[b] | |

[a]$LiAlH_4$ reduction.
[b]$NaBH_4$ reduction.

anhydride gives initially the kinetically favoured *endo* product which isomerizes to the more thermodynamically stable *exo* anhydride dissociation and recombination. On the basis of the proton nmr spectrum the addition of chloromaleic anhydride to furan appears to give exclusively the thermodynamically more stable *exo* adduct **7**.

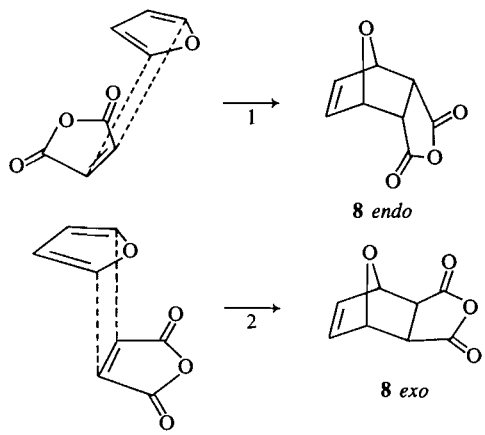


SCHEME 4

The model anhydrides **5**, **6**, and **7** were reduced by $LiAlH_4$ and $NaBH_4$. The various reaction products were isolated and purified as detailed in the experimental section. The results are summarized in Table 1. Reductions by $LiAlH_4$ and $NaBH_4$ gave essentially identical product ratios for each anhydride studied.

The lactone which is more rapidly eluted during glc was in all cases the isomer reduced at the less hindered carbonyl group. The lactones (**5***b*, **6***b*, **7***b*) show a complex multiplet due to two methylene protons at δ 4.2–4.5. The lactones resulting from the reduction of the carbonyl function adjacent to the more highly substituted carbon atom have somewhat longer elution times. The nmr spectra of **5***a* and **6***a* exhibit a characteristic AB quartet for two methylene protons. The structural assignment was confirmed by an independent synthesis of lactone **6***a*, which was prepared by photochemical cycloaddition of ethylene to 4-hydroxy-3-methyl *cis*-crotonic acid lactone **9** (Scheme 5).

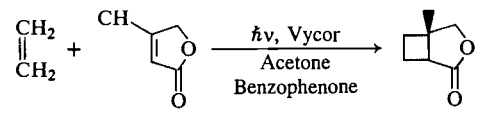


**9** **6a**

SCHEME 5

The minor product isolated by chromatography from the $LiAlH_4$ reduction of the adduct **7** was assumed, on the basis of the nmr spectrum, to be the open form (hydroxy acid) of the lactone **7***a*.

*Results of* ab initio *calculations*

*Ab initio* molecular orbital calculations (8) with a

Can. J. Chem. Downloaded from www.nrcresearchpress.com by 210.87.254.105 on 09/06/12
For personal use only.

Can. J. Chem. Downloaded from www.nrcresearchpress.com by 210.87.254.105 on 09/06/12
For personal use only.

minimum STO-3G basis set were performed for 1-methylcyclopropane 1,2-dicarboxylic acid anhydride **5**, 1-methylcyclobutane 1,2-dicarboxylic acid anhydride **6**, and eight "supermolecules" (anhydride–proton and hydride ion) corresponding to all regioisomers. The geometry for the parent succinic anhydride was obtained from crystallographic data (9). The geometries of compounds **5** and **6** were adapted from the crystallographic data for the related compounds (10) and from MINDO/3 calculations of the relative positions of the atoms in the molecule corresponding to minimum energy (11).

Since full optimization for complicated systems is prohibitively expensive and time-consuming, the choice of the geometries for the "supermolecules" was guided by the existing knowledge of the gross features of nucleophilic attack on the activated (by association with a cation) carbonyl group. In these terms nucleophilic attack occurs at the carbon atom of the carbonyl group activated by a cation (simulated in the calculations by $H^+$). The direction of nucleophilic approach is perpendicular to the plane of the trigonal carbon atom and the distance between nucleophile (simulated by $H^-$) and carbon atom remains fixed at 2 Å (Fig. 1).

In order to obtain information on the nature of the substrate molecules **5** and **6** we examined first the "naked molecules". It is generally accepted that a nucleophile adds to the LUMO $\pi^*$ (lowest unoccupied MO) and specifically to the carbon atom of the carbonyl function (12). The carbon atom where the $\pi^*$ orbital has its maximum amplitude (i.e. highest LUMO coefficient), permitting the best overlap, should be the preferred site for nucleophilic attack. Thus, we have suggested that the size of the LUMO coefficient on the carbon atom reflects the intrinsic reactivity of the carbonyl group (13).

The results of the calculations obtained for anhydrides **5** and **6** are shown in Table 2. In 1-methylcyclopropane 1,2-dicarboxylic acid anhydride **5**, the LUMO coefficient on the carbon atom of the α-carbonyl group is considerably higher than the coefficient on the β-carbonyl group. Hence we should expect a better overlap and consequently higher reactivity at the α-carbonyl function. In 1-methylcyclobutane 1,2-dicarboxylic acid anhydride **6** the two LUMO coefficients are almost identical, and therefore, on the basis of intrinsic reactivity alone, no regioselectivity would be expected. However, as was pointed out before (14), three other factors can influence selectivity of nucleophilic addition: (a) possibility of chelation; (b) antiperiplanar attack; (c) steric hindrance.

The chelating effect is obviously not operative in

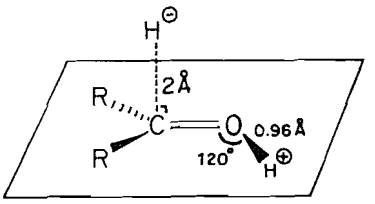


FIG. 1. Geometry of nucleophilic attack (simulated by $H^-$) on activated (by association with a cation simulated by $H^+$) carbonyl group.

systems such as **1**, **5**, **6**, and **7** and can be neglected. On the other hand, the remaining two effects should be examined in relation to our model compounds.

Methylsuccinic and 2,2-dimethylsuccinic anhydride were shown to possess the necessary flexibility to accommodate antiperiplanar attack in the developing transition state (Fig. 2) (14). However, when the anhydride ring is attached to a cyclopropane ring the resistance to torsional motion about the C—C bond is significantly higher. Hence the anhydride ring is rigidly planar and any distortion would require considerable energy input. As a result, antiperiplanar geometry in the supermolecule cannot be achieved and the site of nucleophilic addition will be influenced by the degree of steric hindrance about the two carbonyl functions.

The argument can be extended to 1-methylcyclobutane 1,2-dicarboxylic acid anhydride **6**. It is generally agreed that cyclobutane is puckered with a relatively high barrier to the planar configuration (16). As a result, distortion of the anhydride ring attached to cyclobutane will be energetically unfavourable. Hence in **6**, as in **5**, antiperiplanar attack is not feasible, and we must consider that nucleophilic addition occurs to the planar anhydride ring.

TABLE 2. Comparison between theoretical results (LUMO coefficients) and experimental data (ratio of lactonic products obtained)

| Compound | LUMO coefficients on $C_\alpha$ | LUMO coefficients on $C_\beta$ | Experimental ratio, reduction at $C_\alpha$ | Experimental ratio, reduction at $C_\beta$ |
|---|---|---|---|---|
| 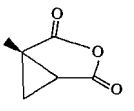 | −0.564 | 0.541 | 62 | 38 |
| 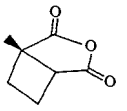 | −0.580 | 0.570 | 43 | 57 |

TABLE 3. Relative energies of isomeric "supermolecules"

| "Supermolecule" | Relative energy $\Delta E$ kcal/mol | "Supermolecule" | Relative energy $\Delta E$ kcal/mol |
|---|---|---|---|
| | 0 | | 0 |
| 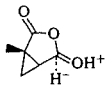 | −0.3 | 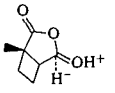 | −0.1 |
| 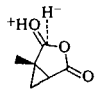 | −6.4 | 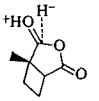 | −1.1 |
| 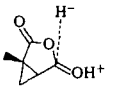 | −6.4 | 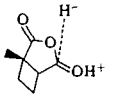 | −5.4 |

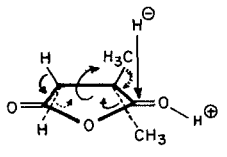

FIG. 2. The transition state is stabilized if there is a neighbouring bond C—X antiperiplanar to the forming partial bond C—$H^-$. The stabilization is greater where X = C than where X = H (15).

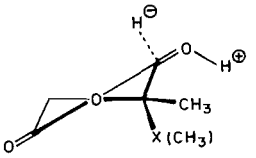

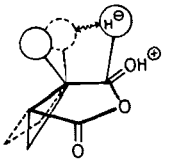

FIG. 3. Superimposed models of compounds **6** and **5**. As the internal angle diminishes from 90° in cyclobutane to 60°C in cyclopropane the substituents (here the anhydride ring and $CH_3$ group) are spread further apart.

The STO-3G calculations carried out for all isomeric supermolecules (formed by substrate–proton and hydride ion) show that in **5** and **6** nucleophilic attack at the ring side of the molecule is unfavourable. As a result $H^-$ adds preferentially to the methyl bearing face of the molecule. We should caution at this point that, since full optimization of the geometry for the supermolecules is not available, the results of these calculations can provide only a rough guideline to the trends in energy changes. With this in mind we may observe that, while in compound **6** preferential attack should occur at the β-carbonyl function, in compound **5** attack at either the α- or β-carbonyl (13) function is equally favourable (Table 3). This difference between **5** and **6** may be due to the fact that, as a result of the diminution of the internal angle, the substituents on the cyclopropane ring are spread further apart. Hence the methyl substituent in **5** is tilted away from the plane of the molecule and interferes less with the approaching nucleophile. This effect is less pronounced in **6** and therefore steric interaction between the nucleophile and the methyl group is more important (Fig. 3).

Although the effects discussed above are small in magnitude, the combination of the higher intrinsic reactivity and diminished steric hindrance at the α-carbonyl group in **5** add up to increased reactivity at that site. In anhydride **6** the intrinsic reactivity of the two carbonyl groups is the same but as the β-carbonyl function is more exposed to nucleophilic attack a slight excess of β-reduction should result. These predictions correlate well with the experimental findings.

The foregoing arguments allow rationalization of the regioselectivity observed in the reduction of bridged compound **1**. It has been demonstrated before that in related compounds such as **10**, hydride addition takes place from the *exo* side (17), as shown in Scheme 6. By analogy, a similar addition mode should apply to the bridged compound **1**. Due to the strain in the tricyclic system, the anhydride ring in **1** is planar and rigid and the position of the methyl substituent is similar to that

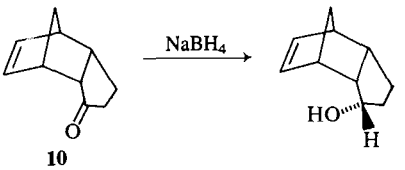

**10**

SCHEME 6

Can. J. Chem. Downloaded from www.nrcresearchpress.com by 210.87.254.105 on 09/06/12
For personal use only.

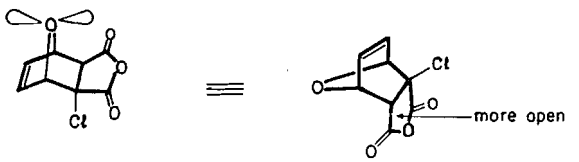


FIG. 4. On the basis of the geometry of this Diels–Alder adduct, the nucleophile should attack the more open (convex) face of the molecule. Therefore the same regioselectivity should be observed as for the *endo* bridged compound **1**.

of the methyl group in planar 2,2-dimethylsuccinic anhydride **4** (10).

Although compound **7** has the *exo* configuration, the structural features dictate that nucleophilic addition should occur from the more open side, i.e. the side on which the chlorine atom is attached (Fig. 4).

The computations performed on planar 2,2-dimethylsuccinic anhydride **4** have shown that the attack at the β-carbonyl function is favoured by −4.5 kcal/mol (14). Hence on the basis of the model calculations, bridged compounds are expected to be reduced preferentially at the β-carbonyl function. This prediction is confirmed by the experimental results.

In summary, it should be underlined that the arguments presented above are the only ones, so far, capable of successful rationalization of all the experimental results.

## Experimental

Melting points were determined on a Thomas–Hoover capillary melting point apparatus and are uncorrected. Infrared spectra were obtained on a Beckman IR-20 spectrophotometer and proton nmr spectra in $CDCl_3$ or DMSO, with TMS as internal standard, on a Varian HA-100 instrument. Tetrahydrofuran was distilled under nitrogen from lithium aluminum hydride into oven-dried flasks containing $LiAlH_4$ or $NaBH_4$.

The general procedures for the reductions were as follows.

(a) Lithium aluminum hydride (0.004 mol) was placed in an oven-dried, three-neck flask into which 60 mL of tetrahydrofuran was subsequently distilled. The flask was fitted with an inlet post for syringes, gas outlet tube, thermometer, and magnetic stirrer. The suspension, swept with a slow stream of nitrogen, was stirred for 15 min at room temperature, then cooled in a dry ice–acetone bath. An anhydride (0.008 mol) dissolved in freshly distilled tetrahydrofuran (40 mL) was injected slowly into the reaction flask. The temperature of the reaction mixture was maintained below −50°C throughout the addition process. The stirred solution was allowed to warm to 0°C over a period of 1½ hours. The flask was then cooled again to −20°C and excess water and 6 *N* HCl were added slowly. The reaction mixture was stirred overnight. The layers were separated and the acidic aqueous layer extracted repeatedly with ether. In some cases liquid/liquid extraction of the aqueous layer with ether was carried out overnight. The combined organic layers were dried, the solvent evaporated, and the product analyzed by proton nmr and using a Gow Mac Series 550 gas chromatograph fitted with an 8 ft, 10% DEGS on Chromosorb column.

(b) Reductions with sodium borohydride were carried out as follows. The suspension of crushed $NaBH_4$ (0.005 mol) in dry tetrahydrofuran (60 mL) was refluxed for 15 min and then cooled in an ice bath. A solution of an anhydride (0.008 mol) in dry tetrahydrofuran (40 mL) was added dropwise to a stirred, ice-cold suspension of $NaBH_4$. The stirring was continued for 2½ hours during which time 2–3 drops of 6 *N* HCl were added to the reaction mixture. After quenching with 6 *N* HCl (to pH 2), excess water was added and stirring continued overnight. The work-up procedure was the same as in the procedure described for $LiAlH_4$ reductions.

*1-Methylcyclopropane 1,2-dicarboxylic acid anhydride* **5**

Anhydride **5** was prepared according to the method of McCoy (3). Commercial sodium methoxide 25% in methanol (Aldrich) was evaporated to dryness on a rotatory evaporator at 50°C (2–3 hours). The solid sodium methoxide was removed from the flask and ground to a fine powder in a glove bag under dry nitrogen. The acrylic ethylester (1.0 mol) and methylbromopropionate (0.5 mol) were treated with sodium methoxide (1.0 mol) added in several small portions, under nitrogen. The temperature of the reaction mixture was kept between 10–30°C by cooling in an ice bath when necessary. After stirring for 1½ hours the reaction was hydrolyzed with a large excess of water and stirred overnight. The organic layer was extracted with water, then with saturated NaCl, dried over $MgSO_4$, and distilled. The yield of pure diester was 46% (10 Torr, 100–108°C). The diester was saponified by refluxing with 50% excess of a 15% aqueous solution of NaOH. After two hours reflux the basic solution was evaporated on a rotatory evaporator. The residue was diluted with water and acidified to pH 2. The acidic mixture was extracted with ether on a continuous liquid–liquid extractor for 36 h. On evaporation of the ether extracts, a mixture of *cis* and *trans* acids was obtained (0.23 mol, 92% yield on the basis of diester). Analysis by $^1H$ nmr showed the ratio *cis*–*trans* to be 67:33.

Alternately 1-methylcyclopropane 1,2-dicarboxylic acid (a mixture of *cis* and *trans*) was prepared under conditions similar to those described by Jonczyk *et al.* (18). α-Chloroacetonitrile (8.95 g, 0.1 mol) was added slowly, with stirring, to a flask containing finely powdered potassium hydroxide (6 g) suspended in benzene (20 mL). The reaction flask was cooled with an ice bath (exothermic reaction). The acrylonitrile (5.3 g, 0.1 mol) was added in small portions to the stirred reaction mixture. The stirring was continued for an additional hour. The mixture was diluted with water and extracted with benzene. The combined organic layers were washed with aqueous sodium chloride solution, dried, and the solvent removed. The oily product (7.0 g) was distilled at 1 Torr. Fraction 1 (2.0 g) collected at 60–70°C was identified as pure *trans* 1-methylcyclopropane 1,2-dinitrile, the second fraction (2.5 g) collected at 110–120°C was pure *cis* 1-methylcyclopropane 1,2-dinitrile. The same reaction run under phase transfer conditions in the presence of the catalyst (benzyltriethylammonium chloride) (19), yielded *trans* dinitrile as the major product (6.0 g) and *cis* dinitrile (2.0 g).

Upon hydrolysis (40% aqueous KOH) of the *trans* isomer, the *trans* diacid was obtained in 25% yield. The hydrolysis of *cis* nitrile under the same conditions gave a mixture of *cis* and *trans* diacids (*cis* 12%, *trans* 15%). The two isomers were separated by fractional crystallization from acetonitrile. The *cis* diacid, mp 133–135°C; $^1H$ nmr $\delta_{DMSO}$: 1.01 (m, 1H), 1.32 (s, 3H), 1.48 (m, 1H), 1.78 (m, 1H); *trans* diacid, mp 163–165°C, $^1H$ nmr $\delta_{DMSO}$: 1.16 (m, 1H), 1.32 (s, 3H), 1.45 (m, 1H), 2.16 (q, 1H).

The mixture of two isomeric diacids was stirred and heated under reflux for ½ hour, with 20% excess acetic anhydride. The unreacted acetic anhydride and acetic acid were removed by distillation under reduced pressure (3 Torr, 35°C). The oily

Can. J. Chem. Downloaded from www.nrcresearchpress.com by 210.87.254.105 on 09/06/12
For personal use only.

Can. J. Chem. Downloaded from www.nrcresearchpress.com by 210.87.254.105 on 09/06/12
For personal use only.

residue was taken up in dry ether. Upon standing in a Dry Ice – acetone bath, the anhydride **5** precipitated as a white crystalline solid. Crystallization from dry ethylacetate – hexane gave a pure sample, mp 45–46°C (lit. (3) mp 45–47°C); ir $\nu_{max}$: 1775 $cm^{-1}$, 1850 $cm^{-1}$ (C=O anhydride); $^1H$ nmr $\delta_{DMSO}$: 1.40 (s, 3H) 1.58 (m, 1H), 1.86 (m, 1H), 2.76 (m, 1H); $\delta_{CDCl_3}$: 1.50 (m, 1H), 1.58 (s, 3H), 1.75 (m, 1H), 2.56 (m, 1H); *m/e*: $M^+$ 126, $(M^+ - CO_2)$ 82.

1-Methylcyclopropane 1,2-dicarboxylic acid anhydride **5** was reduced with $LiAlH_4$ as described in the general procedure. Upon work-up a mixture of two lactones was obtained. The total yield of lactonic product was 62%. Analysis by glc (column temperature 145°C) indicated that lactones **5***a* and **5***b* (corresponding to the second and first peak respectively) were present in the ratio 55:45. The reduction with $NaBH_4$, according to the general procedure, yielded 60% of lactonic product. The ratio of the two lactones was **5***a*/**5***b* = 60:40. Lactones **5***a* and **5***b* were separated by hplc. Lactone **5***a*: ir $\nu_{max}$: 1765 $cm^{-1}$ (lactone CO); $^1H$ nmr $\delta_{CDCl_3}$: 1.15 (m, 2H), 1.41 (s, 3H), 1.86 (m, 1H), 4.16 (q, 2H); *m/e*: $(M - H)^+$ 111, $(M - CH_3)^+$ 97, $(M - CO)^+$ 84. Lactone **5***b*: ir $\nu_{max}$: 1765 $cm^{-1}$ (lactone CO); $^1H$ nmr $\delta_{CDCl_3}$: 1.05 (m, 2H), 1.44 (s, 3H), 2.10 (m, 1H), 4.20 (m, 2H), *m/e*: $M^+$ 112, $(M^+ - CO)$ 84.

*Synthesis of 1-methylcyclobutane 1,2-dicarboxylic acid anhydride* **6**

A solution of citraconic anhydride (1.25 g, 0.01 mol) and benzophenone (0.05 g) in freshly distilled acetone (400 mL), cooled with a cold water jacket (10–15°C), was irradiated with a high pressure mercury arc lamp through a Vycor filter. Ethylene gas was introduced steadily, during the reaction time (6 hours). Evaporation of the solvent under reduced pressure gave a colourless oil (1.5 g). The oil was taken up in dry ether and hexane was added until the solution was cloudy. Upon cooling in a Dry Ice – acetone bath white crystalline anhydride precipitated. The yield of pure product was 69%, mp 63–65°C; ir $\nu_{max}$: 1775 $cm^{-1}$, 1855 $cm^{-1}$ (anhydride CO); $^1H$ nmr $\delta_{CDCl_3}$: 1.55 (s, 3H), 2.48 (m, 4H), 3.23 (m, 1H); *m/e*: $(M^+ - CO_2)$ 96.

1-Methylcyclobutane 1,2-dicarboxylic acid anhydride **6** was reduced with $LiAlH_4$ under the usual conditions. The work-up procedure yielded 65% of lactonic product. Gas-liquid chromatographic analysis revealed two sharp peaks, a product peak of shorter elution time corresponding to the lactone **6***b*, reduced at the β-carbonyl group, and the second peak corresponding to the lactone **6***a*. The ratio of **6***a* to **6***b* was 44:56. The reduction of anhydride **6** by sodium borohydride according to the general procedure gave 71% yield of lactonic product. Analysis by glc (column temperature 150°C) showed the ratio of lactones **6***a*/**6***b* to be 43:57. The two lactones were separated by hplc. Lactone **6***a*: ir $\nu_{max}$: 1765 $cm^{-1}$ (CO lactone); $^1H$ nmr $\delta_{CDCl_3}$: 1.32 (s, 3H), 2.32 (m, 5H), 4.06 (q, 2H); *m/e*: $M^+$ 126, $(M^+ - CH_3)$ 111, $(M^+ - CCH_3)$ 99, $(M^+ - CO_2)$ 82. Lactone **6***b*: ir $\nu_{max}$: 1760 $cm^{-1}$ (CO lactone); $^1H$ nmr $\delta_{CDCl_3}$: 1.36 (s, 3H), 2.20 (m, 4H), 2.72 (m, 1H), 4.24 (m, 2H); *m/e*: $M^+$ 126, $(M^+ - CO_2)$ 82.

*Photocondensation of 4-hydroxy-3-methyl* cis*-crotonic acid lactone* **9** *with ethylene*

A solution of **9** (0.69 g, 0.007 mol) and benzophenone in purified actone, through which ethylene gas was bubbled slowly, was irradiated under the usual conditions. After 5 hours acetone was removed and an oily product (67% yield) purifid by chromatography. The principal product obtained was identical to lactone **6***a* obtained from the reduction of 1-methylcyclobutane 1,2-dicarboxylic acid anhydride **6**. Some unreacted lactone **9** was also recovered; ir $\nu_{max}$: 1760 $cm^{-1}$ (CO lactone); $^1H$ nmr $\delta_{CDCl_3}$: 1.3 (s, 3H), 2.14 (m, 4H), 2.62 (m, 1H), 4.06 (q, 2H); *m/e*: $M^+$ 126.

*Preparation of Diels–Alder adduct* **7**

Freshly distilled furan (20.0 g, 0.28 mol) and chloromaleic anhydride (commercial product, containing 30% of maleic anhydride, 40.82 g, 0.30 mol) dissolved in dry ether (25 mL) were stirred in a darkened flask for 4 hours at room temperature. After being placed in a refrigerator overnight, the first crop (4.26 g) was isolated and identified as pure adduct **8**. After standing for a day in a refrigerator the second crop (4.05 g) was obtained. This was a mixture of **7** and **8**, with **8** being the major component. The third crop (1.12 g) was identified as pure adduct **7**. Subsequently isolated crops (in all, 6.5 g) were shown to be adduct **7** contaminated with **8** and with traces of unidentified polymeric material. The two compounds could be easily separated by hplc. Both adducts **7** and **8** were recrystallized from acetonitrile and ether and analyzed by glc. Adduct **8**: mp 116–117°C dec.; ir $\nu_{max}$: 1770 $cm^{-1}$ and 1850 $cm^{-1}$ (anhydride CO); $^1H$ nmr $\delta_{DMSO}$: 3.34 (s, 2H), 5.34 (m, 2H), 6.6 (m, 2H); *m/e*: $M^+$ 166. Adduct **7**: mp 106–107°C, **7** gave a positive Beilstein's test for halogens and positive halide test after sodium fusion; ir $\nu_{max}$: 1790 $cm^{-1}$ and 1860 $cm^{-1}$ (CO anhydride); $^1H$ nmr $\delta_{DMSO}$: 3.56 (s, 1H), 5.61 (split singlet 2H), 6.86 (m, 2H); *m/e* $(M^+ - Cl)$ 165, $(M^+ - CO)$ 172, $(M^+ - CO_2H)$ 155. The reduction of chloroadduct **7** by $LiAlH_4$ under the conditions described in the general procedure yielded 74% of oily lactonic product. Analysis by glc (column temperature 160°C) showed one major peak and a trace of a second peak as well as small quantities of unidentified impurities. The chromatography on silica gel (hexane–ethylacetate 2:1) gave a pure sample of lactone **7***a*, mp 83–84°C; ir $\nu_{max}$: 1775 $cm^{-1}$ (C=O anhydride); $^1H$ nmr $\delta_{CDCl_3}$: 2.63 (two doublets, 1H), 4.43 (multiplet consisting of two doublets 4.15, 4.30 and three peaks, the middle one split 4.50, 4.64, 4.82, the multiplet corresponding to 2H), 5.03 (s, 1H), 5.17 (s, 1H), 6.62 (s, 2H); *m/e*: $(M^+ - Cl)$ 151.

Chromatography furnished a trace amount of oily compound which appeared to be the opened form of the isomeric lactone **7***b*; $^1H$ nmr $\delta_{CDCl_3}$: 2.78 (s, 1H), 4.57 (s, 2H), 4.94 (s, 1H), 5.28 (s, 1H), 6.56 (s, 2H).

The reduction of chloroadduct with $NaBH_4$ according to the method described in the general procedure gave 76% yield of crude lactonic product. Analysis by glc showed the presence of only one lactone **7***a*. The reduction of the nonchloroadduct **8** with $NaBH_4$ as described in the general procedure gave a poor yield (30%) of lactone **8***a*; ir $\nu_{max}$: 1770 $cm^{-1}$; $^1H$ nmr $\delta_{CDCl_3}$: 2.66 (m, 2H), 4.34 (complex multiplet, 2H), 4.90 (s, 1H), 5.23 (s, 1H), 6.42 (s, 2H); *m/e*: $M^+$ 152.

## Acknowledgement

Financial support from Natural Sciences and Engineering Research Council of Canada (Grant A 1918) is gratefully acknowledged.

1. M. M. KAYSER and P. MORAND. Can. J. Chem. **56**, 1524 (1978).
2. J. J. BLOOMFIELD and S. L. LEE. J. Org. Chem. **32**, 3919 (1967); D. M. BAILEY and R. E. JOHNSON. J. Org. Chem. **35**, 3575 (1970).
3. L. L. MCCOY. J. Am. Chem. Soc. **80**, 6568 (1958).
4. O. DIELS and K. ALDER. Ber. **62**, 554 (1929); O. DIELS and B. OLSEN. J. Prakt. Chem. (2) **156**, 285 (1940).
5. W. C. DAUBEN, C. R. KESSEL, and K. H. TAKEMURA. J. Am. Chem. Soc. **102**, 6893 (1980).
6. R. B. WOODWARD and H. BEAR. J. Am. Chem. Soc. **70**, 1161 (1948).
7. F. A. L. ANET. Tetrahedron Lett. 1219 (1962).
8. W. J. HEHRE, W. A. LATHAM, R. DITCHFIELD, M. D. NEWTON, and J. A. POPLE. Gaussian 70, QCPE No. 236, Bloomington, Indiana.
9. M. EHRENBERG. Acta Crystallogr. **19**, 698 (1966).

10. R. DESTRO, G. FILIPPINI, C. A. GRAMAECIOLI, and M. SIMONETTA. Acta Crystallogr. Sect. B, **25**, 2465 (1969); D. VAN DER HELM, I. N. HSU, and J. M. SIMS. Acta Crystallogr. Sect. B, **28**, 3109 (1972).
11. D. RINALDI. Program GEOMO, Fortran IV version. Laboratoire de Chimie Théorique, Université de Nancy, France.
12. R. G. PEARSON. Symmetry rules for chemical reactions. Wiley–Interscience, New York. 1976. p. 341.
13. M. M. KAYSER and O. EISENSTEIN. Can. J. Chem. **59**, 2457 (1981).
14. M. M. KAYSER and G. WIPFF. Can. J. Chem. **60**, 000 (1982).
15. J. HUET, Y. MARONI-BARNAND, N. T. ANH, and J. SEYDEN-PENNE. Tetrahedron Lett. 159 (1976).
16. T. UEDA and T. SHIMANOUCHI. J. Chem. Phys. **49**, 470 (1968); T. B. MALLOY, JR. and W. J. LAFFERTY. J. Mol. Spectrosc. **54**, 20 (1975).
17. W. L. DILLING and R. A. PLEPYS. J. Org. Chem. **35**, 2971 (1970).
18. A. JONCZYK, A. KWAST, and M. MAKOSZA. Tetrahedron Lett. 541 (1979).
19. A. JONCZYK and M. MAKOSZA. Synthesis, 387 (1976).

Can. J. Chem. Downloaded from www.nrcresearchpress.com by 210.87.254.105 on 09/06/12
For personal use only.

# Thermal degradation of EDTA chelates in aqueous solution

RAMUNAS J. MOTEKAITIS, X. B. COX, III, PATRICK TAYLOR, AND ARTHUR E. MARTELL[1]
*Department of Chemistry, Texas A&M University, College Station, TX 77843, U.S.A.*
AND
BRAD MILES AND TORY J. TVEDT, JR.
*The Dow Chemical Company, Freeport, TX 77541, U.S.A.*
Received January 22, 1982

RAMUNAS J. MOTEKAITIS, X. B. COX, III, PATRICK TAYLOR, ARTHUR E. MARTELL, BRAD MILES, and TORY J. TVEDT, JR. Can. J. Chem. **60**, 1207 (1982).

The thermal degradation of Ca(II), Mg(II), Zn(II), Fe(II), and Ni(II) chelates of EDTA was investigated in alkaline aqueous solution at elevated temperatures (230–310°C). The kinetics of decomposition were followed by nmr, titrimetry, and spectrophotometry. Reaction products were identified through nmr and by gas chromatography. The relative order of degradation rates, as measured by the loss of EDTA, was found to be Mg(II) > Ca(II) > Zn(II) > Fe(II) > Ni(II). The main degradation products formed in the lower temperature range (~250°C) are iminodiacetic acid, hydroxyethyliminodiacetic acid, and ethylene glycol. Higher temperature products are primarily dimethylamine and carbon dioxide. The rates of degradation of Ca(II), Mg(II), and Zn(II) EDTA chelates are considerably enhanced when either phosphate is present or a glass-lined autoclave is employed.

RAMUNAS J. MOTEKAITIS, X. B. COX, III, PATRICK TAYLOR, ARTHUR E. MARTELL, BRAD MILES et TORY J. TVEDT, JR. Can. J. Chem. **60**, 1207 (1982).

On a étudié la dégradation thermique, en solution aqueuse basique et à des températures élevées (230–310°C), des chelates entre l'EDTA et les ions CA(II), Mg(II), Zn(II), Fe(II) et Ni(II). On a déterminé les cinétiques de décomposition par la rmn, la titrimétrie et la spectrophotométrie. On a identifié les produits de la réaction par la rmn et la chromatographie en phase gazeuse. On a trouvé que l'ordre relatif des vitesses de dégradation, telles que mesurées par la perte de EDTA, est le suivant: Mg(II) > Ca(II) > Zn(II) > Fe(II) > Ni(II). Les principaux produits de dégradation formés dans le domaine de basses températures (~250°C) sont l'acide iminodiacétique, l'acide hydroxyéthyliminodiacétique et l'éthylène glycol. Les produits formés à une température plus élevée sont principalement la diméthylamine et le bioxyde de carbone. La présence du phosphate ou l'utilisation d'un autoclave tapissé de verre augmente considérablement les vitesses de dégradation des chelates de l'EDTA avec les ions Ca(II), Mg(II) et Zn(II).
[Traduit par le journal]

## Introduction

The numerous applications of ethylenediaminetetraacetic acid, EDTA, include its use in aqueous solutions at high temperatures for metal oxide solubilization and for maintenance of metal ions in a sequestered state in solution. This specific application is of particular interest to the power industry which employs EDTA formulation for the continuous treatment of boiler water in steam generators to prevent excessive build-up of scale. Since EDTA in this application is used at elevated temperatures, aqueous chemistry of EDTA and its chelates should be studied at high temperatures to understand the various reactions affecting the efficacy of this sequestering agent. Two preliminary publications describe the reactions of EDTA at elevated temperatures in aqueous solution (1, 2). At moderate temperatures, ~ 175°C in alkaline solution, EDTA was found to undergo hydrolytic C—N fission to give iminodiacetic acid (IDA) and hydroxyethyliminodiacetic acid (HEIDA) as the main reaction products (2). The half-life for this first order process at 175°C is 4.5 h at pH = 9.4. At somewhat higher temperatures (2) (200°C) this half-life is reduced to 0.5 h, while a concomitant consecutive reaction involving the further hydrolysis of HEIDA to ethylene glycol and IDA also takes place. At still higher temperatures decarboxylation reactions also occur. Thus at 265°C, the initial hydrolysis products decarboxylate to give *N*-methylglycine and dimethylamine.

Another type of degradation reaction of EDTA chelates at elevated temperatures has been described recently (3). EDTA coordinated to Fe(III) or Cu(II) becomes oxidized to ethylenediamine triacetic acid (ED3A) and glyoxylic acid while the iron(III) is reduced to Fe(II) and copper(II) to Cu(0). The half life for Fe(III)–EDTA at pH 9.3 is about 3 h at 125°C. This redox reaction greatly destabilizes EDTA at temperatures just above the boiling point of water. However, the Fe(II) chelate formed was found to be stable at similar or higher temperatures even for periods exceeding several days.

The purpose of this present work is to determine the thermal stabilities and reaction sequences of representative metal chelates of EDTA under conditions of varying temperature, pH, and in the

[1]To whom all correspondence should be addressed.

0008-4042/82/101207-07$01.00/0
©1982 National Research Council of Canada/Conseil national de recherches du Canada

Can. J. Chem. Downloaded from www.nrcresearchpress.com by 210.87.254.40 on 09/06/12
For personal use only.

Can. J. Chem. Downloaded from www.nrcresearchpress.com by 210.87.254.40 on 09/06/12
For personal use only.

presence and absence of catalysts. The metal ions employed are those that are not easily reduced, so that thermal degradation reactions would be expected to involve hydrolysis and decarboxylation, rather than redox reactions, in contrast to the reactions of the Fe(III) and Cu(II) chelates.

Very little work has been carried out previously on the thermal degradation of EDTA chelates and related compounds. Yakimets *et al.* (4) studied the thermal reactions of several EDTA chelates of reducible and non-easily reducible metal ions, and found a variety of products. By means of ir spectroscopy and gas chromatography, oxalic acid, formaldehyde, and hydrogen were found in the reaction mixture, but no major components were identified. An extensive study (5) of thermal degradation of NTA chelates of Fe(II), Fe(III), Ni(II), Co(II), and Cu(II) also yielded a wide variety of decomposition products.

## Experimental

*Reagents*

All salts, solvents, and reagents were analytical grade materials and were obtained from various major chemical distributors. Doubly distilled, deionized water was used throughout. Solutions were deoxygenated by scrubbing with prepurified grade nitrogen gas which had been passed through an acidic chromous chloride solution. The metal ion – EDTA solutions were prepared from reagent grade $Ca(OH)_2$, $Mg(OH)_2$, $FeSO_4 \cdot 7H_2O$, MgO, ZnO, $Ni(OH)_2$, $Ni(OAc)_2$ (nickel acetate), $NaH_2PO_4$, and NaOH, as needed.

*Kinetics*

The reactions were conducted under an inert atmosphere in a 2 L Parr all-titanium stirred bench autoclave equipped with temperature and pressure sensors and appropriate valves which were manipulated as needed to obtain samples either from the liquid or gaseous phase as the reaction proceeded.

*Product analyses*

The constituents of the liquid phase were determined by nmr measurements of $D_2O$/NaOD solutions. For Ca(II) and Mg(II) chelates unreacted EDTA was generally determined by titration with standard 0.0200 *M* copper(II) solution in acetic acid-acidified solutions with pyrocatechol violet as an indicator. The products formed at high temperatures do not interfere with this determination.

*Instrumentation*

Gas chromatograms were obtained with a microprocessor controlled Hewlett-Packard Model 5830A gas chromatograph equipped with dual TC and FI detectors. For gaseous sample analysis an 8-ft glass column packed with Chromosorb 101/4% was utilized, while liquid samples were run on a 1/8 in. × 10 ft. SS column packed with OV-1. The nmr spectra were recorded with a Varian T-60 spectrometer equipped with a variable temperature probe. The visible spectra were obtained on a Cary Model 14 spectrophotometer equipped with a Himamatsu photomultiplier tube.

## Results and discussion

In general, it was found that the EDTA molecule is considerably stabilized towards thermal and hydrolytic degradation through coordination to metal ions. Also, the decomposition pathways, the decomposition products, and the kinetics of the degradation of coordinated EDTA have been elucidated. Finally, it was found that phosphate and silicate catalyze this decomposition for some metal ions while not for others. In general, the reaction products at a given temperature were found to be the same for all metal ion tested at that temperature.

*Kinetics of EDTA degradation*

Most of the decomposition rates were measured at the relatively high pH of 10.4 for several reasons. At this pH, the EDTA chelates of the divalent metal ions investigated are completely formed, and the species $ML^{2-}$ (where $L^{4-}$ is the $EDTA^{4-}$ anion) is the only major species present in solutions containing equimolar concentrations of metal ion and ligand. The fact that EDTA is used commercially at high pH to prevent scale build-up in steam generators also offers a practical incentive for determining degradation rates in alkaline solution.

The decomposition rates of the chelates were measured by monitoring the concentration of the remaining EDTA. Ca(II) and Mg(II) EDTA rates were followed titrimetrically in acid solution with standard Cu(II) solution. The ferrous EDTA samples were dried, methyl esterified, and subjected to gas chromatographic analysis. Zinc(II)–EDTA sample solutions were evaporated and measured in NaOD/$D_2O$ by nmr. The nickel(II)–EDTA decomposition rate was likewise followed by nmr after pretreatment with excess $CN^-$ to convert the nickel(II) ion into the diamagnetic $Ni(CN)_4^{2-}$ ion.

Table 1 contains a summary of the first order rate constants for the decomposition of EDTA and its Ca(II), Mg(II), Fe(II), and Zn(II) chelates. The data in Table 1 show that metal chelate formation very strongly protects EDTA against hydrolytic degradation. Uncomplexed EDTA was found to decompose quite rapidly at 190°C ($k_{obs} = 0.37\,h^{-1}$), with a half-life at pH = 10.4 of 1.9 h. On the other hand, the Ca(II) chelate is inert under these conditions and requires heating at 310°C to achieve a similar rate of decomposition. Monitoring the reaction at 320°C showed that the rate of thermal decomposition is four times that measured at 307°C. In comparing the decomposition of the Mg(II) chelate at 307°C with that of the Ca(II) chelate at 310°C, it is seen that the Mg(II) rate is about a factor of two higher than the rate of Ca(II)–EDTA. The Fe(II)–EDTA and Zn(II)–EDTA degradation rates were found to be similar to that of Ca(II) after slight differences in temperature in Table 1 are taken into account. Nickel(II)

Can. J. Chem. Downloaded from www.nrcresearchpress.com by 210.87.254.40 on 09/06/12
For personal use only.

TABLE 1. First order rate constants for decomposition of EDTA and its metal chelates at $pH_0 = 10.4$ at various temperatures

| Metal ion | $t$ (°C) | $k_{obs}$ ($h^{-1}$) | Analytical method |
|---|---|---|---|
| None | 190 | 0.37 | Nmr |
| $Ca^{2+}$ | 310 | 0.27 | Titrimetric |
| $Ca^{2+}$ | 320 | 1.1 | Titrimetric |
| $Mg^{2+}$ | 307 | 0.50 | Titrimetric |
| $Fe^{2+}$ | 310 | 0.31 | Gas chromatographic |
| $Fe^{2+}$ | 310 | 0.30 | Spectrophotometric |
| $Zn^{2+}$ | 308 | 0.22 | Nmr |
| $Ni^{2+}$ | 310 | 0.075 | Nmr |

proved to be surprisingly inert, with only about one half the decomposition of the chelate observed at 310°C within the time limitation of the reaction employed.

The trend from the above results can be summarized in terms of a statement of relative rates in decreasing order:

$$\text{None (sodium salt)} > Mg^{2+} > Ca^{2+} \sim Fe^{2+} \sim Zn^{2+} \gg Ni^{2+}$$

The relative rates correlate approximately and inversely with the order of formation constants of the "normal" chelates, designated as $ML^{2-}$. These constants measured at room temperature for $Mg^{2+}$, $Ca^{2+}$, $Fe^{2+}$, $Zn^{2+}$, and $Ni^{2+}$ are respectively 8.8, 10.6, 14.3, 16.4, and 18.5 log units (6).

The inverse stability constant – rate correlation points to a mechanism whereby the predominant pathway near 310°C is a dissociation mechanism resulting in the liberation of the free EDTA anion. The resulting low concentrations of the free ligand may then undergo the type of degradation described previously (1, 2), as follows:

[1] $MEDTA^{2-} \rightleftharpoons M^{2+} + EDTA^{4-}$

[2] $EDTA^{4-} \rightarrow$ decomposition products

In [1] the very low concentration of $EDTA^{4-}$ formed is offered no protection and immediately undergoes rapid degradation. The degree to which equilibrium [1] is shifted is inversely proportional to the magnitude of the stability constant at 310°C. It would be very desirable to know precisely what these values are at 310°C but such information is not available and cannot be measured with techniques currently feasible. Therefore it is necessary to settle for the time being for equilibrium data taken at room temperature. The comparisons made above involve the assumption that the temperature coefficients of stability constants are sufficiently similar to maintain at high temperature the stability order observed at 25°C.

The correlation with inverse stability order described above is very rough and predicts considerably greater differences in decomposition rates of the Ca(II), Fe(II), and Zn(II) chelates on the basis of dissociation tendencies controlled by the stability constants alone (i.e., one would expect the chelates of the transition metal ions to be much more stable than the Ca(II) chelate). For the transition metal ions and the zinc(II) ion, the tendencies to liberate EDTA would be further increased by the tendencies of the metal ions to hydrolyze and precipitate from solution at pH 10. Thus the dissociation reactions may be written as in Table 2.

Through the use of the appropriate solubility products the logarithms of the equilibrium constants of reactions [3]–[5] at pH 10 show that there is considerable difference between the hydroxide precipitation tendencies of the Zn(II) and Fe(II)–EDTA chelates on one hand, and the Ni(II)–EDTA chelate on the other: a consequence of the much higher stability of the Ni(II) chelate. Thus metal hydroxide precipitation is expected to provide an additional driving force for EDTA chelate dissociation and on the basis of the proposed mechanism would increase the degradation rates of the Fe(II) and Zn(II) chelates much more than that of Ni(II), accounting more closely to the observed rate sequence, $Ca^{II} \sim Fe^{II} \sim Zn(II) \gg Ni(II)$.

*Catalysis by glass surface and phosphate ion*

In early experimental runs the use of a Pyrex liner in the autoclave resulted in considerable rate enhancement for calcium(II) and magnesium(II) over those shown in Table 1. For example at 310°C, $k_{obs} = 1.0\ h^{-1}$ for Ca(II)–EDTA, which is almost four times greater than the rate constant determined after the glass liner was removed. For magnesium(II) the rate enhancement was even more dramatic. A measurable rate could not even be obtained near 310°C.

Further investigations revealed that the presence of phosphate ion also enhanced the rates of degradation of EDTA chelates of Mg(II), Ca(II), and Zn(II) but not those of the other metal ions tested. The only explanation for such catalytic behavior is the formation of insoluble Ca(II) and Mg(II) silicates (probably adsorbed on the glass surface) and of Ca(II), Mg(II), and Zn(II) phosphates. Such

TABLE 2. Dissociation reaction with hydroxide precipitation[a]

| Reaction | | $\log k_{eff}^{M(OH)_2}$ |
|---|---|---|
| [3] | $FeL^{2-} \rightleftharpoons L^{4-} + Fe(OH)_2 + 2H^+$ | −8.0 |
| [4] | $ZnL^{2-} \rightleftharpoons L^{4-} + Zn(OH)_2 + 2H^+$ | −8.4 |
| [5] | $NiL^{2-} \rightleftharpoons L^{4-} + Ni(OH)_2 + 2H^+$ | −11.3 |

[a]Solubility products obtained from Smith and Martell (7).

Can. J. Chem. Downloaded from www.nrcresearchpress.com by 210.87.254.40 on 09/06/12
For personal use only.

insoluble phases would free more EDTA from its metal complexes resulting in enhanced reaction rates. Reaction [6] illustrates the postulated ion exchange process for glass

$$[6] \quad CaL^{2-} \xrightarrow[\text{glass}]{H_2O} (CaSiO_4)\downarrow + L^{4-}$$

Since phosphate ion may be studied over a range of conditions, some details of phosphate catalysis were investigated for Ca(II)–EDTA degradation. Table 3 lists the results of rate measurements under various conditions in the absence and presence of phosphate. The data for this table were obtained from kinetic plots obtained by titrimetric analysis of residual EDTA as a function of time. A typical example is illustrated in Fig. 1.

While the initial concentration of the Ca(II)–EDTA chelate was maintained constant at 0.0133 *M*, the phosphate concentration was varied sufficiently to produce a significant variation in the observed pseudo first order rate constants. Although the intended temperature for the comparison was 230°C, the data in Table 3 show some deviation from this value as well as deviations in pH values.

Equations [7] and [8] describe the proposed rate law for Ca(II)–EDTA decomposition in these solutions and reaction [9] gives the concentration of the phosphate trianion in the experimental solution. Assuming that the phosphate does not become inaccessible to the reactants, then the slope of a plot of $k_{obs}$ vs. phosphate levels can be obtained by combining eqs. [9], [10], and [8] to give eq. [11].

The numerical value of $k'$ calculated from a least-squares plot is 69 ± 12. The large scatter results from lack of precise temperature and pH control. In spite of the uncertainties involved, there does appear to be a direct correlation between reaction rate and phosphate anion concentration.

TABLE 3. Initial conditions and pseudo first order rate constants obtained as a function of phosphate concentration, temperature, and pH for the thermal degradation of Ca(II)–EDTA[a]

| Total phosphate | pH[b] | Temperature (°C) | $k_{obs}$ ($h^{-1}$) |
|---|---|---|---|
| 0 | 10.40 | 250[c] | 0[c] |
| 0.00668 | 10.12 | 224 | 0.22±0.01[d] |
| 0.00667 | 10.85 | 226 | 0.31±0.01 |
| 0.00998 | 10.15 | 230 | 0.83±0.05 |
| 0.0133 | 10.17 | 229 | 0.86±0.07 |
| 0.0150 | 10.05 | 230 | 0.93±0.07 |
| 0.020[f] | 10.40 | 228 | 0.28[e] |
| 0.020[f] | 11.2 | 228 | 0.59[e] |
| 0.022[f] | 11.4 | 232 | >1.3[e] |
| 0.022[f] | 9.3 | 230 | 0.19[e] |

[a]$[CaEDTA]_0 = 1.33 \times 10^{-2} M$; $PO_4^{3-}$ added as $KH_2PO_4$.
[b]pH measured at room temperature on the first sample collected for kinetic studies.
[c]No appreciable decomposition had occurred in 14 h at ~20° higher than the temperatures of other systems in this table.
[d]Standard deviations of slope obtained by least squares regression analysis.
[e]Error was evaluated only in terms of the regression coefficient which was > 0.998 in each case.
[f]Phosphate added as phosphoric acid.

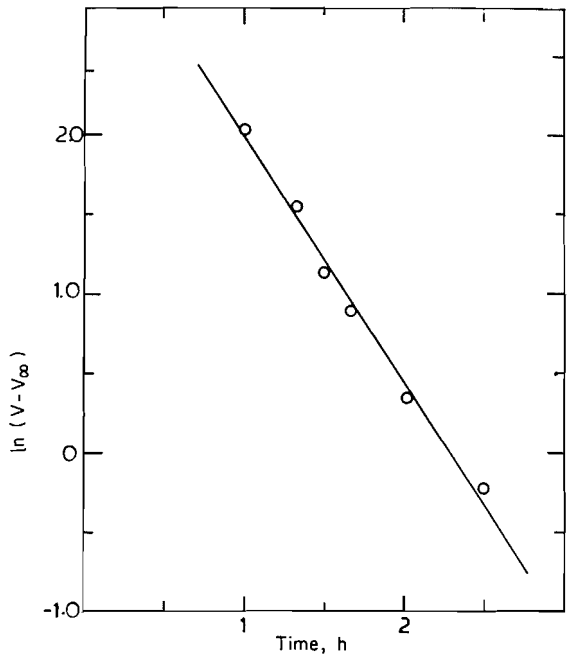


FIG. 1. Logarithm of volume of standard copper(II) solution titrated (measure of residual EDTA) vs. time of samples taken in the thermal degradation of Ca(II)–EDTA in the presence of phosphate at 230°C.

$$[7] \quad d[Ca\text{–}EDTA]/dt = -k_{obs}[Ca\text{–}EDTA]$$

$$[8] \quad k_{obs} = k'[PO_4^{3-}]$$

$$[9] \quad K^H = [HPO_4^{2-}]/[H^+][PO_4^{3-}]$$

$$[10] \quad T_{PO_4} = [PO_4^{3-}] + [HPO_4^{2-}] \approx [HPO_4^{2-}]$$

$$[11] \quad \text{Slope} = k'/K^H[H^+]$$

*Reaction products*

*Ca(II)–EDTA degradation*. At the initial moderately high temperature, nonredox metal chelate reaction products are primarily the result of hydrolytic reactions, as has been clearly shown previously for uncomplexed EDTA (2). The calcium chelate, **1** (Scheme 1), in the presence of 1.5 equiv. of phosphate for example, after about four half-lives at 229°C undergoes the reaction sequence **1** → **2** → **3** + **4** indicated in Scheme 1, yielding predominantly a mixture of hydroxyethyliminodiacetic acid and iminodiacetic acid. A colorless solid found in the reaction mixture dissolves when treated with 6 *M* HCl, but without evolution of gas, and was identified as calcium phosphate (Fig. 2).

When phosphate is absent, the chelate solution must be heated at 300°C to induce decomposition,

Can. J. Chem. Downloaded from www.nrcresearchpress.com by 210.87.254.40 on 09/06/12
For personal use only.

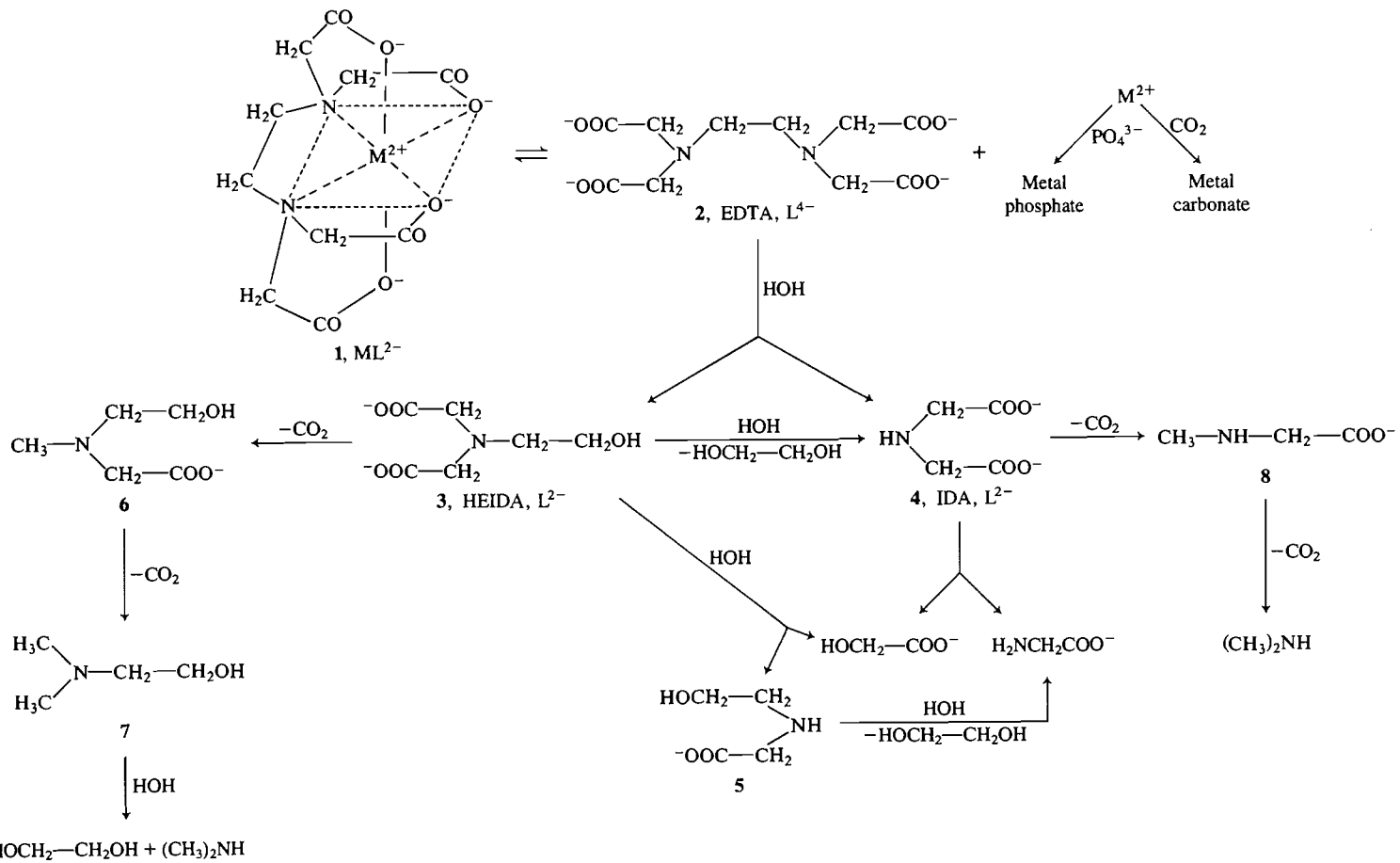


SCHEME 1. Proposed degradation scheme for EDTA chelates of divalent metal ions in the vicinity of 300°C. Final reaction products: carbon dioxide, ethylene glycol; dimethylamine, glycine, glycolic acid (~300°C), **3**, hydroxyethyliminodiacetic acid (HEIDA); **4**, iminodiacetic acid (IDA) (200–230°C); intermediates (300°C) **3**, hydroxyethyliminodiacetic acid (HEIDA); **4**, iminodiacetic acid (IDA); **5**, *N*-hydroxyethylglycine; **6**, *N*-methyl-*N*-hydroxyethylglycine; **7**, *N*,*N*-dimethylethanolamine; **8**, *N*-methylglycine.

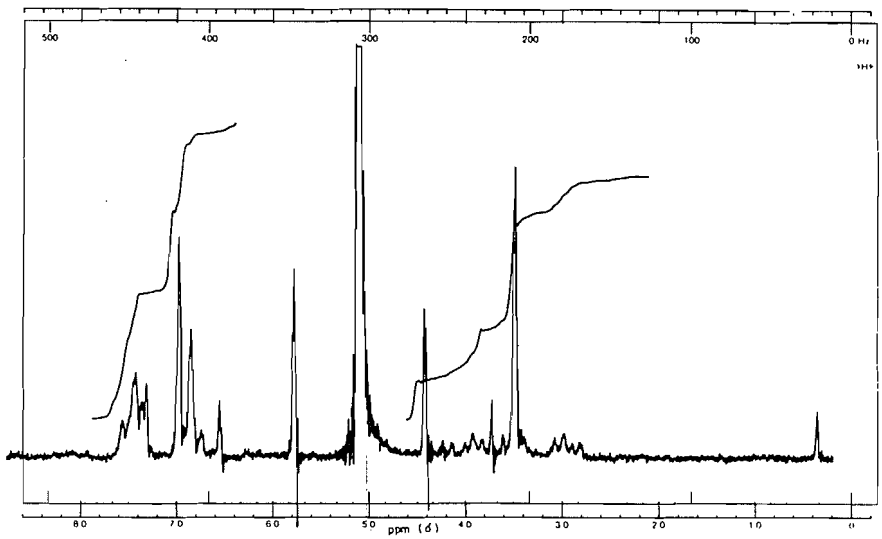


FIG. 2. Nuclear magnetic resonance spectrum of Ca(II)–EDTA solutions after thermal degradation showing the formation of IDA and HEIDA as sole reaction products at 230°C. The low field resonances belong to phenoxide which had been added as an internal standard.

and the degradation reactions proceed far beyond **3** and **4**. The predominant decomposition products found are: dimethylamine, ethylene glycol, and calcium carbonate. The carbonate was inferred from a test with dilute HCl, which produced the evolution of $CO_2$ from the colorless precipitate formed during the reaction. Ethylene glycol was detected by its nmr spectrum at 3.8 ppm, while dimethylamine was isolated in an acid trap from the volatile portion of the reaction. The acid solution was concentrated, made basic, and injected into a gc glass column. A peak at 1.0 min which was duplicated with standard dimethylamine confirmed the assignment.

*Other metal chelates*

Thermal degradation of a sample of Zn(II)–EDTA produced a reaction mixture characterized by the nmr resonances tabulated in Table 4. It is interesting that one of the products appears to be glycolic acid (3.62 or 3.73 ppm). There are at least two types of acetate methylene resonances. Glycine with a $—CH_2—$ resonance at 3.27 ppm, is definitely present. In addition ethylene diamine or substituted ethylenediamine may be present in view of the fact that a resonance was found at 2.80 ppm.

When the spectra of the Fe(II)–EDTA chelate and of the degradation products obtained were compared with those obtained from other metal EDTA chelates near 300°C, they were found to be generally similar, indicating that the distribution of reaction products does not vary much with the type of the metal ion present. A quantitative distinction has not been attempted from the experimental data available at this stage.

TABLE 4. Major nmr resonances of reaction products of Zn(II)–EDTA degradation at 300°C and pH 10

| Chemical shift (ppm)[a] | Assignment |
|---|---|
| 2.30 | $N—CH_3$ |
| 2.43 | EDTA, $NCH_2CH_2N$ |
| 2.80 | EN, $NCH_2CH_2N$ |
| 3.20 | EDTA, $N—CH_2COO^-$ |
| 3.27 | Glycine, $N—CH_2COO^-$ |
| 3.62 or 3.73 | $O—CH_2COO^-$ |
| 3.80 | Ethylene glycol |

[a]Measurements made in strongly basic $D_2O$ solution with a T-60 Varian nmr spectrometer. Chemical shifts relative to trimethylsilylpropanesulfonate.

In summary, tentative reaction pathways illustrated in the reaction scheme are suggested in order to provide a conceptual picture of the interrelationships of the various degradation products which have been shown to be formed in the present metal–EDTA chelate study.

In the complex reaction mixture formed, the metal ion probably distributes between the lower chelating ligands formed, principally IDA and HEIDA, and precipitated metal carbonate (or phosphate). The intermediate products **6** and **7** are inferred by consideration of the reactions known to take place in this system but have not directly been proved to be present in the reaction mixture. They do, however, lead to the known reaction products. The detection by nmr of the *N*-methyl and 2-hy-

Can. J. Chem. Downloaded from www.nrcresearchpress.com by 210.87.254.40 on 09/06/12
For personal use only.

droxyethyl groups provides some further support for their presence.

Work currently in progress is directed at obtaining further details about the complex degradation reactions of EDTA metal chelates reported for the first time in the present paper. These studies involve the quantitative determination of effects of temperature and pH on the stabilities of the chelates of the primary intermediates, IDA and HEIDA, further amplification of the chemistry of phosphate and silicate catalysis, and the exploration of the thermal stabilites in aqueous solution of other aminopolycarboxylic acids and their metal chelates.

**Acknowledgements**

This research was supported by a contract from The Dow Chemical Company to Coordination Chemistry Consultants of College Station. The authors thank the Department of Chemistry of Texas A&M University for the use of laboratory facilities.

1. R. J. MOTEKAITIS, D. HAYES, A. E. MARTELL, and W. W. FRENIER. Can. J. Chem. **57**, 1018 (1979).
2. A. E. MARTELL, R. J. MOTEKAITIS, A. R. FRIED, J. S. WILSON, and D. T. MACMILLAN. Can. J. Chem. **53**, 3471 (1975) and references therein.
3. R. J. MOTEKAITIS, A. E. MARTELL, D. HAYES, and W. W. FRENIER. Can. J. Chem. **58**, 1999 (1980).
4. E. M. YAKIMETS, N. A. BERG, and N. I. KUZ'MENKO. Teploenergetica, **18**, 84 (1971).
5. M. BOOY and T. W. SWADDLE. Can. J. Chem. **55**, 1772 (1976).
6. A. E. MARTELL and R. M. SMITH. Critical stability constants. Vol. 1. Plenum, New York. 1967.
7. R. M. SMITH and A. E. MARTELL. Critical stability constants. Vol. 4. Plenum, New York. 1969.

Can. J. Chem. Downloaded from www.nrcresearchpress.com by 210.87.254.40 on 09/06/12
For personal use only.

# Pyridazino[3,4,5-*de*]phthalazines. II.[1] Synthesis of nitrogen-substituted derivatives

JOHN E. FRANCIS,[2] KARL J. DOEBEL, PAULA M. SCHUTTE, ERNST F. BACHMANN, AND ROBERT E. DETLEFSEN

*Research Department, Pharmaceuticals Division, CIBA-GEIGY Corporation, Ardsley, NY 10502, U.S.A.*

Received September 8, 1981

JOHN E. FRANCIS, KARL J. DOEBEL, PAULA M. SCHUTTE, ERNST F. BACHMANN, and ROBERT E. DETLEFSEN. Can. J. Chem. **60**, 1214 (1982).

The synthesis of a wide variety of 9-substituted-3-oxo-3*H*-2,9-dihydropyridazino[3,4,5-*de*]phthalazines (**11**) was achieved by treatment of 3-substituted-3,4-dihydro-4-oxophthalazine-5-carboxylic esters (**10**) with hydrazine hydrate. These esters were prepared from 3-hydroxyphthalide-7-carboxylic acid (**7**) by two different routes. Under basic conditions, alkylation of 3-oxo-3*H*-2,9-dihydropyridazino[3,4,5-*de*]phthalazine (**1**) gave 9-substituted products. These undergo further alkylation at the 2-position. Some of them were converted to 3-chloro, 3-thiono, and 3-hydrazino compounds by standard methods. Dehalogenation of selected 3-chloro compounds or desulphurization of 3-thiono derivatives gave 1-substituted-1*H*-pyridazino[3,4,5-*de*]phthalazines (**22**), some of which were also prepared by direct alkylation of the parent heterocycle **2** under basic conditions. However, treatment of **2** or its 1-methyl homologue with methyl iodide resulted in products in which nitrogen attached to carbon had been attacked rather than the 1- or 9-position. Treatment of the acid chloride of 3,4-dihydro-4-oxophthalazine-5-carboxylic acid with methyl hydrazine led to 2-methyl-3-oxo-3*H*-2,9-dihydropyridazino[3,4,5-*de*]phthalazine (**21***a*) which was purified by cyanoethylation at the 9-position, recrystallization, and hydrazinolysis of the cyanoethyl group. Biological testing revealed that many of the compounds lowered blood pressure in animal models but none had a sufficient therapeutic ratio of activity vs. side effects to warrant clinical trial.

JOHN E. FRANCIS, KARL J. DOEBEL, PAULA M. SCHUTTE, ERNST F. BACHMANN et ROBERT E. DETLEFSEN. Can. J. Chem. **60**, 1214 (1982).

On a réalisé la synthèse d'une grande variété d'oxo-3 dihydro-2,9 3*H*-pyridazino[3,4,5-*de*] phtalazines (**11**) substituées en position 9 en faisant réagir les esters des acides dihydro-3,4 oxo-4 phtalazine carboxyliques-5 (**10**) substitués en position 3, avec l'hydrate d'hydrazine. On a préparé ces esters de deux façons différentes en partant de l'acide hydroxy-3 phtalidicarboxylique-7 (**7**). Dans des conditions basiques, l'alkylation de l'oxo-3 dihydro-2,9 3*H*-pyridazino[3,4,5-*de*] phtalazine (**1**) donne des produits substitués en position 9. Ces derniers subissent une alkylation plus poussée en position-2. On transforme certains de ces composés en composés chloro-3, thiono-3 et hydrazino-3 par des méthodes usuelles. Par déshalogénation de dérivés chlorés en position 3 ou par désulfurisation des dérivés thiono-3, on obtient des dérivés *1H*-pyridazino[3,4,5-*de*] phtalazines (**22**) substitués en position 1. On a préparé certains de ces composés par alkylation directe de l'hétérocycle **2** apparenté en milieu basique. Cependant, la réaction du composé **2** ou de son homologue méthylé en position 1 avec l'iodure de méthyle conduit à des produits dans lesquels l'attaque se fait de préférence au niveau de l'atome d'azote attaché au carbone plutôt qu'au niveau des positions 1 ou 9. La réaction du chlorure de l'acide dihydro-3,4 oxo-4 phtalazine carboxylique-5 avec la méthylhydrazine conduit à la méthyl-2 oxo-3 dihydro-2,9 3*H*-pyridazino[3,4,5-*de*] phtalazine (**21***a*) que l'on a purifiée par cyanoéthylation en position 9, recristallisation et hydrazinolyse du groupe cyanoéthyle. Les tests biologiques ont révélé que plusieurs de ces composés abaissent la pression sanguine chez les animaux choisis à titre de modèles, mais qu'aucun d'eux n'a un rapport thérapeutique suffisant par rapport aux effets secondaires pour justifier des essais cliniques.

[Traduit par le journal]

In the first publication of this series (1) we illustrated the importance of structure **1** as a key intermediate in the synthesis of the desired compounds **2** and **3**.[3]

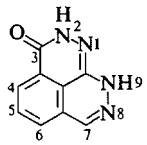

**1**

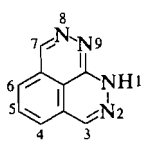

**2**

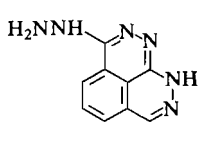

**3**

Just as structure **2** represents an internal *hydrazone* of the drug hydralazine (**4***a*), so **1** represents an internal *hydrazide* derived from 4-hydrazinophthalazine-5-carboxylic acid (**5**).

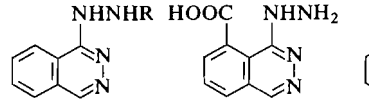

**4***a* R = H
**4***b* R = $COCH_3$
**4***c* R = $COOC_2H_5$

**5**

**6**

Although hydrazones of hydralazine were prepared and studied for their hypotensive activity (2), hydrazides received little attention because attempted preparation of some examples led to con-

[1]Part I of this series is ref. 1.

[2]Author to whom correspondence should be addressed.

[3]Placement of hydrogen at the 9-position in structures **1** and **3** represents one tautomeric form of the structure. In the case of **1** the reason for this assignment will become apparent.

0008-4042/82/101214-19$01.00/0

©1982 National Research Council of Canada/Conseil national de recherches du Canada

Can. J. Chem. Downloaded from www.nrcresearchpress.com by 210.87.254.6 on 09/06/12
For personal use only.

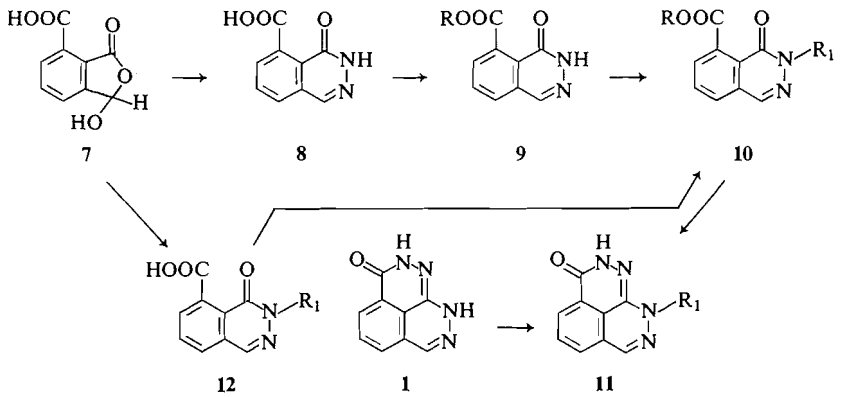

SCHEME 1

densed triazoles which showed no hypotensive activity (2, 3). The first isolated metabolite of hydralazine was not the *N*-acetyl derivative **4***b* as first reported (4) but rather the hydrate of 3-methyl-[1,2,4]-triazolo[3,4-*a*]phthalazine (**6**) (2, 5). The drug todralazine (ecarizine) **4***c*, marketed by Polfa–Pabianice as Binazin®, illustrates that an acylated derivative, albeit a urethane, shows hydralazine-like activity (6). In initial tests, compound **1** showed no activity, but we attributed this possibly to poor absorption. Accordingly, we searched for methods of introducing substituents on one or more of the nitrogens of **1** as a route, not only to a variety of readily absorbed derivatives of **1**, but also to examples of *N*-substituted derivatives of **2** and **3**, thus allowing further exploration of the tricyclic ring system as a possible drug template.

The derivatives of **1** which received our greatest attention were those substituted at the 9-position since they are direct analogs of **1** and potential precursors of *N*-substituted derivatives of **2** and **3**. They were prepared by pathways illustrated in Scheme 1.

As described previously (1), the key intermediate **7** was converted to the phthalazinone acid **8** with aqueous hydrazine in alcohols or acetic acid at reflux. This acid was then esterified to **9**, either the methyl ester **9***a* or the ethyl ester **9***b*, via the acid chloride. Alkylation of the amide nitrogen was accomplished with an alkyl halide in the presence of aqueous sodium hydroxide in an alcohol, or with sodium methoxide in dimethylsulphoxide, or, in two examples, with sodium amide in dimethylsulphoxide. The resulting ester was heated under reflux with aqueous hydrazine to afford the target **11**. Although this route was suitable for alkyl or aralkyl substituted compounds, a more versatile route to **10** involved the reaction of **7** with a monosubstituted hydrazine in alcohol, acetic acid, or water to yield the acid **12** which was then esterified to **10**. This method was used to prepare alkyl-, aryl-, and heterocyclic-substituted products and though often used for the synthesis of 2-aryl-1(2*H*)-phthalazinones (7) it is less commonly illustrated for 2-alkyl-1(2*H*)-phthalazinones (8). Since we have used this method extensively, further explanation for our structure assignments is in order. From 1(2*H*)-phthalazinone, four *N*- or *O*-methylated products can be obtained, all readily differentiated by melting point (9–15). Their structures were only recently confirmed and further characterized by spectroscopy (15–17) and mass spectrometry (18). The only reported method of preparing the *O*-methylated derivative **13** requires conversion of the hydrazide to 1-chlorophthalazine followed by sodium methoxide treatment (9, 10). *O*-Alkylated products are clearly ruled out in our examples since they would react with hydrazine to form structure **1**. In addition, more than two dozen examples of structures **12** (Table 1) and **10** (Table 2) showed strong ir absorption in the range 1640 to 1705 $cm^{-1}$ (Nujol). In the model compounds, it is reported that **14** and **15** show peaks in this region whereas **13** shows two peaks out of this range at 1550 and 1590 $cm^{-1}$ (16). Preparation of the inner salt **15** appears to require a strong alkylating agent under vigorous conditions followed by removal of the proton with base (16) whereas alkylation of the preformed anion or alkylation in the presence of base clearly favours formation of **14** (15, 19–21). The inner salt **15** is converted photochemically in water to the amide **14** but, with acetonitrile as

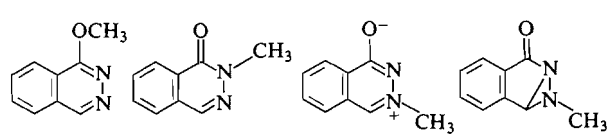

Can. J. Chem. Downloaded from www.nrcresearchpress.com by 210.87.254.6 on 09/06/12
For personal use only.

Can. J. Chem. Downloaded from www.nrcresearchpress.com by 210.87.254.6 on 09/06/12
For personal use only.



TABLE 1. Phthalazinone acids

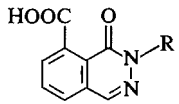

| No. | R | Method | Melting point (°C) | Yield (%) | Recrystallization solvent | Infrared ($cm^{-1}$) ν(C=O) | $^1$Hmr (δ) (DMSO-$d_6$) H at C-1 |
|---|---|---|---|---|---|---|---|
| **12***a* | $-CH_3$ | A | 228–231 | 80[a] | $H_2O$ | 1695, 1800–2200[c] | 8.55 |
| **12***b* | | A | 197–198 | 87[a] | Benzene | 1665, 1705[c] | 8.7 |
| **12***c* | | B | 234–237 | 85[a] | EtOAc | 1655, 1695[c] | 8.7 |
| **12***d* | 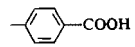 | A | 333–339 dec. | 77[a] | $MeOCH_2CH_2OH$, DMF–$H_2O$ | 1660, 1690, 1715[c] | 8.75 |
| **12***e* | | B | 249–253 | 85[a] | EtOAc, EtOH–$H_2O$ | 1695, 1710[d] | 8.7 |
| **12***f* | $-CH_2CH_2OH$ | A | 165–168 | 59[a] | $H_2O$ | 1640, 1695[c] | 8.55 |
| **12***g* | 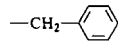 | B | 168–171 | 70[a] | EtOH, benzene–hexane | 1650, 1710[c] | 8.6 |
| **12***h* | 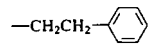 | B | 119–122 | 57[b] | EtOH–$H_2O$ | 1650, 1705[c] | 8.55 |
| **12***i* | 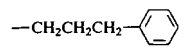 | C | 115–117 | 62[a] | MeOH, benzene–hexane | 1695, 1800–2200[c] | 8.55 |
| **12***j* | 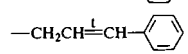 | C | 164–166 | 39[b] | Benzene–hexane | 1705, 1800–2250[c] | 8.6 |
| **12***k* | | A | 273–277 | 86[a] | EtOH–$H_2O$ | 1660, 1695[c] | 8.8 |
| **12***l* | 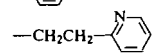 | A | 205–207 | 62[a] | $H_2O$ | 1650, 1690[c] | 8.55 |
| **12***m* | 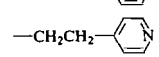 | A | 226–230 | 66[a] | $H_2O$ | 1640, 1700[c] | 8.6 |

[a]Crude yield.
[b]Pure yield.
[c]Taken in Nujol.
[d]Taken in KBr.

Can. J. Chem. Downloaded from www.nrcresearchpress.com by 210.87.254.6 on 09/06/12
For personal use only.



TABLE 2. Phthalazinone esters

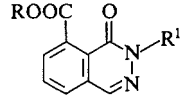

| No. | R | $R^1$ | Method[a] | Melting point (°C) | Yield (%) | Recrystallization solvent | Infrared ($cm^{-1}$) ν(C=O) | $^1$Hmr (δ) (DMSO-$d_6$) H at C-1 |
|---|---|---|---|---|---|---|---|---|
| **10***a* | $CH_3$ | $-CH_3$ | A | 125–126 | 87[b] | $H_2O$ | 1730, 1650[e] | 8.6 |
| **10***b* | $CH_2CH_3$ | $-CH_3$ | B | 103–104.5 | 48[c] | $C_2H_5OH$ | 1730, 1650[e] | 8.6 |
| **10***c* | $CH_2CH_3$ | | B | 150–151 | 90[b] | $C_2H_5OH$ | 1740, 1670[f] | 8.75 |
| **10***d* | $CH_2CH_3$ | 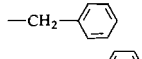 | B | 147–149 | 95[c] | $C_2H_5OH$ | 1740, 1670[e] | 8.6 |
| **10***e* | $CH_3$ | 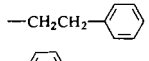 | B | 113–114 | 87[b] | $CH_3OH$ | 1720, 1645[e] | 8.65 |
| **10***f* | $CH_3$ | 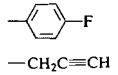 | B | 138–140 | 91[b] | $CH_3OH$ | 1720, 1670[e] | 8.7 |
| **10***g* | $CH_3$ | $-CH_2C{\equiv}CH$ | A | 162–164 | 46[b] | $CH_3OH$ | 1720, 1640[g] | 8.65 |
| **10***h* | $CH_3$ | 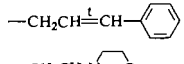 | C | 123–124 | 66[b] | $CHCl_3$–hexane | 1730, 1650[e] | 8.6 |
| **10***i* | $CH_3$ | 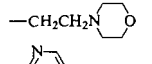 | A | 93–96 | 27[c] | $CCl_4$–$Et_2O$ | 1730, 1650[e] | 8.6 |
| **10***j* | $CH_2CH_3$ | | B | 132–134 | 87[b] | EtOH; EtOAc | 1730, 1665[g] | 8.75 |
| **10***k* | $CH_3$ | 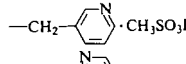 | C<br>D | 178–180 | 32[d]<br>65[d] | MeOH–$Et_2O$ | 1730, 1660[e] | 8.65 |
| **10***l* | $CH_3$ | 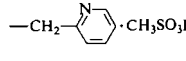 | D | 171–173 | 59[d] | EtOH | 1735, 1660[e] | 8.65 |

[a]Methods: A, from **11** with alkyl halide/NaOH; B, from **14**; C, from **11** with alkyl halide/sodium methoxide; D, from **11** with alkyl halide/$NaNH_2$.
[b]Before crystallization.
[c]Pure.
[d]As free base.
[e]Taken in Nujol.
[f]Taken in $CHCl_3$.
[g]Taken in KBr.

Can. J. Chem. Downloaded from www.nrcresearchpress.com by 210.87.254.6 on 09/06/12
For personal use only.

solvent, the intermediate **16** was isolated, which was readily converted to **14** in acid or water (15). The carbonyl frequency of **16** at 1750 $cm^{-1}$ is out of the range of our phthalazinones. Conversion of **7** to **12***a* (**12**: $R^1 = CH_3$) gave the same product as obtained by saponification of **10***b* (**10**: $R = CH_2CH_3$, $R^1 = CH_3$). The synthesis of **14** from phthalaldehydic acid and methylhydrazine is apparently unreported (22)[4] although 2-(dibromomethyl)-benzoic acid, a phthalaldehydic acid precursor (23), reacts with methylhydrazine in ethanol to give **14** in 75% yield (24). We reacted methylhydrazine with phthalaldehydic acid in refluxing acetic acid and obtained **14** in 81% yield. For further confirmation of the structure, we reacted **9***a* with methyltosylate in refluxing chlorobenzene overnight to obtain the tosylate salt from which the inner salt **17**, an isomer of **10***a* (**10**: $R = R^1 = CH_3$), was obtained by reaction with zinc hydroxide. Our phthalazinone esters (Table 2) display a singlet in the $^1$Hmr spectrum in the range 8.55–8.75 δ (DMSO-$d_6$) whereas **17** has a singlet at slightly lower field (8.8 δ) and the tosylate salt a peak well downfield at 10.2 δ. Structure assignment based on the methyl signals is not well defined as it is for **14** and **15**, since all signals in **10***a* and **17** fall in the range 3.65–4.1 δ. More convincing evidence for the structure of **17** is based on infrared analysis. Structure **10***a* showed strong carbonyl absorption at 1730 $cm^{-1}$ (ester) and 1650 $cm^{-1}$ (hydrazide) in Nujol, whereas **17** showed a strong ester band at 1730 $cm^{-1}$ and bands at 1610 and 1555, not attributable to a cyclic hydrazide. Since the structures of **10** and **12** are now established, the structure assignment of **11** must follow. Many examples of **11** were prepared by direct alkylation of **1**, thus supporting the isomer with H at C-9 as the most reasonable depiction of the basic building block **1**.

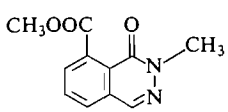

**10***a*

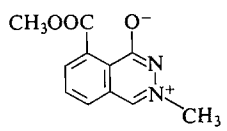

**17**

The conversion of **9** to **11** was done in some examples without purification of **10**, generally in low overall yields. Fortunately, the tricyclic structures were well separated from impurities in an aqueous work-up from which the target compounds separated as bright yellow recrystallizable solids. This ease of preparation was also helpful in those examples prepared from **1**. The anion of **1** was preformed with sodium methoxide in dimethylsulphoxide and the alkyl halide added, whereupon the target compounds were obtained in 18 to 88% yields (Table 3). In most examples, no attempts were made to optimize yields although example **11***a* (**11**: $R^1 = CH_3$) was rerun several times by different routes. It was prepared from 3-dibromomethylphthalic anhydride (1) via **8**, **9***a*, and **10***a* in 74% overall yield, via **12***a* and **10***a* in 33% yield, and in two steps via **1** in 18% yield.

As observed with **1**, the 9-substituted compounds **11** could be converted to the corresponding 3-chloro compounds **18** (Table 6), usually with a phosphoryl chloride/phosphorous pentachloride mixture.

Reaction of **11** with phosphorous pentasulphide in pyridine led to structures of type **19**, as exemplified for $R^1$ = methyl (**19***a*), phenyl (**19***b*), and *N*-morpholinoethyl (**19***c*). Treatment of **18** or **19**

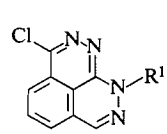

**18**

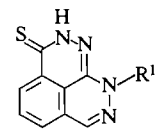

**19**

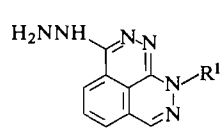

**20**

with hydrazine hydrate produced the hydrazines **20**, illustrated for $R^1$ = methyl (**20***a*), phenyl (**20***b*), and benzyl (**20***c*). Since most tricyclic compounds were soluble in dimethylsulphoxide, the $^1$Hmr spectra were almost all run in DMSO-$d_6$. We noticed in all examples of **19** and in the spectra of **20***c* and the benzylidene hydrazone of **20***b* that the proton at C-4 appeared as a doublet of doublets shifted downfield from the other aromatic protons. This did not appear in any examples of **11** run in DMSO-$d_6$, nor in **20***a*, run in $D_2O$. However, **11***j* (**11**: $R^1 = CH_2CH_2CH_2C_6H_5$) was soluble in $CDCl_3$ and this spectrum showed the shifted doublet of doublets centred at 8.35 δ.

Inferior yields of **11** via direct alkylation of **1** were due in part to a second alkylation occurring at the 2-position. One such compound, **21***f* (**21**: $R^1 = R^2$ = *N*-morpholinoethyl) (Table 4), was isolated as a by-product of the synthesis of **11***g* (**11**: $R^1$ = *N*-morpholinoethyl). Generation of the anion of **11** with sodium methoxide followed by alkyl halide

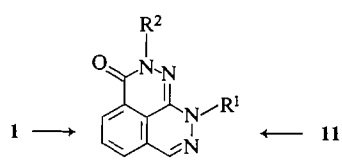

**21**

[4]Several Russian references were unavailable to us in the original form and their abstracts do not mention the method of synthesis of **14**.

Can. J. Chem. Downloaded from www.nrcresearchpress.com by 210.87.254.6 on 09/06/12
For personal use only.

produced other examples of **21**, in which $R^1$ and $R^2$ could be the same or different, in yields as high as 95%. When **1** was treated with two moles of sodium methoxide followed by two moles of alkyl halide, the yields of **21** were generally low with **11** as the principle by-product. The structure assignment of **21** is based on a strong carbonyl band in the infrared in the range 1620–1645 $cm^{-1}$ (Nujol). Also, a sharp singlet at 7.85–8.15 δ in the $^1$Hmr spectrum corresponds to the proton at C-7, comparable to that in examples of **11**, where the range is 7.8–8.1 δ. As observed for **11**, structure **21***b* (**21**: $R^1 = R^2 = CH_3$) shows a doublet of doublets shifted downfield corresponding to the proton at C-4 in $CDCl_3$ but not in DMSO-$d_6$.

In contrast to the usual alkylation, cyanoethylation of **1** proceeds in high yield. With at least two (preferably three) moles of acrylonitrile in 50% aqueous pyridine with a catalytic amount of Triton B, **21***g* (**21**: $R^1 = R^2$ = cyanoethyl) was obtained in yields exceeding 90%. Attempted monocyanoethylation of **1** produced a mixture of **21***g* and **1** and no detectable amount of the expected product. Since cyanoethylation of **9***a* followed by hydrazine hydrate produced only **1** we were frustrated in our attempt to obtain the monocyanoethyl compound, but instead discovered a method for removing the cyanoethyl group cleanly in our series. This was confirmed by smooth conversion of **21***g* to **1** with hydrazine hydrate. The process was not simply a matter of base catalysis, since excess Triton B in one experiment produced partial hydrolysis of one of the cyanoethyl groups of **21***g* to a carboxyethyl group with no loss of the side chain. Acid stability of the group was also evident, since 80% sulphuric acid converted **21***g* to the diamide **21***i* (**21**: $R^1 = R^2$ = carbamoylethyl) in moderate yield. Under the same cyanoethylation reaction conditions, crotononitrile reacted sluggishly with **1** to give a poor yield of the dialkylated product **21***h* and a considerable recovery of starting material.

The decyanoethylation process was used advantageously in the synthesis of the only derivative of **1** in which only the 2-position was substituted. The acid chloride of **8** was reacted with methylhydrazine in hot chlorobenzene in an effort to prepare **21***a* (**21**: $R^1$ = H, $R^2 = CH_3$). Since the reaction of methylhydrazine with acid chlorides or anhydrides to produce mainly 1-acyl-1-methylhydrazines is well documented (25), we obtained the desired product, but contaminated with an impurity not readily removed by crystallization. Thus the crude product was cyanoethylated to **21***j*, recrystallized, and decyanoethylated with hydrazine hydrate to yield pure **21***a*.

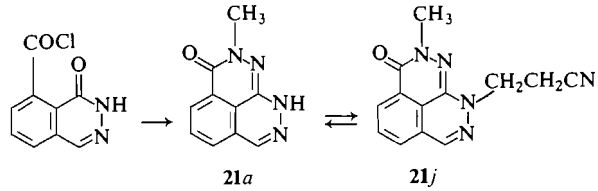


**21***a* **21***j*

Removal of the cyanoethyl group was not only achieved with hydrazine hydrate but also in the following example. When **21***g* was treated with morpholinoethyl chloride in the presence of sodium methoxide in dimethylsulphoxide, the cyanoethyl group at the 9-position was replaced by morpholinoethyl in 35% yield. Proof of the assigned structure **21***e* rested on its conversion to **11***q* by treatment with hydrazine hydrate. Since the yield of **21***e* was mediocre and no attempt was made to isolate other products from the mother liquor, we cannot state that replacement occurs exclusively at position 9. No detailed study of the reaction was made, since products such as **21***e* and **11***q* could be prepared by more straightforward methods. However, the illustrated transformations might find application in the preparation of derivatives of other nitrogen heterocycles.

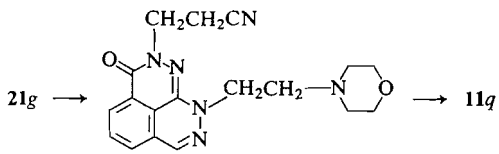


**21***g* → **21***e* → **11***q*

Derivatives of **2**, i.e. **22**, were prepared by dehalogenation of chloro compounds **18**, by desulphurization of **19**, and by direct alkylation of the parent heterocycle **2** (Table 5). Dehalogenation was achieved with red phosphorous in 47% hydriodic acid and desulphurization was done with Raney nickel. Direct alkylation took place when the anion was first generated with base. Cyanoethylation of **2**, as described for **1**, gave the desired product **22***e* (**22**: $R^1$ = cyanoethyl) although in only 24% yield after purification. Treatment of **22***e* with 10% aqueous sodium hydroxide at reflux followed by acidification gave the acid **22***f* (**22**: $R^1$ = carboxyethyl) in 82% yield. Generally the yields on direct alkylation were poor and required column chromatography before recrystallization. From the few

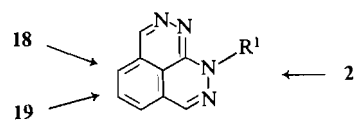


**22**

Can. J. Chem. Downloaded from www.nrcresearchpress.com by 210.87.254.6 on 09/06/12
For personal use only.



TABLE 3. 9-Substituted-3-oxo-3*H*-2,9-dihydropyridazino[3,4,5-*de*]phthalazines

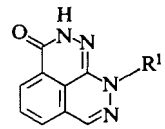

| No. | R | Method[a] | Melting point (°C) | Yield (%) | Recrystallization solvent | Infrared ($cm^{-1}$) ν(C=O), Nujol | $^1$Hmr (δ) (DMSO-$d_6$) H at C-7 |
|---|---|---|---|---|---|---|---|
| **11***a* | $-CH_3$ | A | 292–296 | 75[c] | $CH_3OCH_2CH_2OH$ | 1650 | 7.8 |
| **11***b* | $-CH(CH_3)_2$ | C | 258–259 | 30[b] | EtOH | 1655 | 7.95 |
| **11***c* | $-CH_2CH_2CH_2CH_3$ | D | 189–194 | 56[b] | Benzene | 1640 | 8.0 |
| **11***d* | $-CH_2CH_2OH$ | A | 248–250 | 86[b] | $CH_3OCH_2CH_2OH$ | 1640 | 7.9 |
| **11***e* | $-CH_2CH=CH_2$ | C | 219–222 | 24[c] | EtOH | 1645 | 7.95 |
| **11***f* | $-CH_2CH=CHCH_3$ | C | 238–240 | 25[c] | EtOH–$CH_3OCH_2CH_2OH$ | 1650 | 8.1 |
| **11***g* | | A | 254–257 | 89[b] | DMF | 1655 | 8.1 |
| **11***h* | 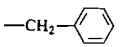 | D | 239–243 | 66[b] | EtOH | 1645 | 8.05 |
| **11***i* | 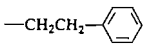 | A | 203–205 | 96[b] | $CHCl_3$ | 1650 | 7.95 |
| **11***j* | 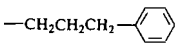 | A | 170–172 | 95[b] | Benzene–hexane | 1650 | 7.95 |
| **11***k* | 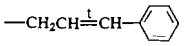 | C | 218–220 | 55[c] | $CH_3OCH_2CH_2OH$ | 1655 | 7.95 |
| **11***l* | $CH_2CH_2N(CH_3)_2$ | C | 197–199 | 19[c] | Benzene | 1650 | 7.95 |
| **11***m* | 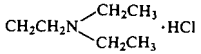 | C | 280 dec. | 35[c] | — | 1650 | 7.8 |
| **11***n* | 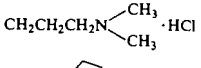 | C | 290 dec. | 5[c] | — | 1645 | 7.7 |
| **11***o* | 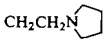 | C | 192–194 | 31[c] | EtOH | 1650 | 7.9 |
| **11***p* | 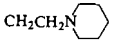 | D | 178–180 | 22[b] | Benzene–cyclohexane | 1645 | 8.0 |
| **11***q* | 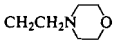 | D | 203–205.5 | 25[b] | $H_2O$ | 1645 | 8.0 |
| **11***r* | 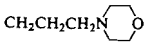 | C | 180–183 | 38[c] | EtOH | 1645 | 7.95 |
| **11***s* | 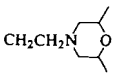 | C | 203–205 | 35[c] | EtOH | 1650 | 8.0 |

Can. J. Chem. Downloaded from www.nrcresearchpress.com by 210.87.254.6 on 09/06/12
For personal use only.



TABLE 3 (*Concluded*)

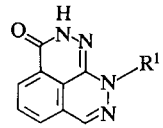

| No. | R | Method[a] | Melting point (°C) | Yield (%) | Recrystallization solvent | Infrared ($cm^{-1}$) ν(C=O), Nujol | $^1$Hmr (δ) (DMSO-$d_6$) H at C-7 |
|---|---|---|---|---|---|---|---|
| **11***t* | 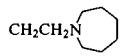 | C | 183.5–186.5 | 55[b] | EtOH | 1655 | 7.95 |
| **11***u* | | B | 261–262 | 8[c] | EtOH | 1650 | 8.2 |
| **11***v* | 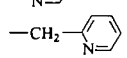 | C | 275.5–276.5 | 18[c] | EtOH | 1650 | 8.1 |
| **11***w* | 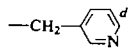 | C | 261–263 | 16[c] | $CH_3OH$ | 1655 | 8.05 |
| **11***x* | 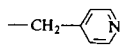 | C | 253–255 | 10[c] | EtOH | 1650 | 8.0 |
| **11***y* | 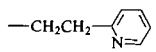 | D | 235–239 | 18[b] | EtOH | 1655 | 7.85 |
| **11***z* | 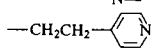 | A | 200.5–203 | 43[c] | EtOH | 1645 | 7.9 |
| **11***aa* | 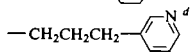 | C | 207–212 | 13[c] | MeOH–$Et_2O$ | 1650 | 7.95 |
| **11***bb* | 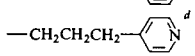 | C | 216–218 | 21[c] | EtOH | 1655 | 8.0 |
| **11***cc* | 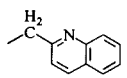 | A | 233 dec. | 50[c] | — | 1650 | 8.2 |

[a]Methods: A, from **12**; B, from **14**; C, from **11**; D, from **1**.
[b]Before recrystallization.
[c]Purified yield.
[d]Methanesulphonate salt.

Can. J. Chem. Downloaded from www.nrcresearchpress.com by 210.87.254.6 on 09/06/12
For personal use only.



TABLE 4. 2,9-Disubstituted-3-oxo-2,9-dihydropyridazino[3,4,5-*de*]phthalazines

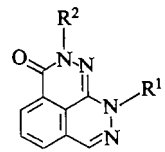

| No. | $R^1$ | $R^2$ | Method[a] | Melting point (°C) | Yield (%) | Recrystallization solvent | Infrared ($cm^{-1}$) $\nu$(C=O) | $^1$Hmr ($\delta$) (DMSO-$d_6$) H at C-7 |
|---|---|---|---|---|---|---|---|---|
| **21***a* | H | $CH_3$ | E | 307–311 | 77[c] | — | 1630, 1655[d] | 7.85 |
| **21***b* | $CH_3$ | $CH_3$ | A<br>B | 195–197 | 24[c]<br>93[b] | $CH_3OH$ | 1640[d]<br>1650[e] | 7.85 |
| **21***c* | $CH_3$ | $CH_2CH_2$-morpholino | B | 176–179 | 65[c] | Benzene | 1645[d] | 7.8 |
| **21***d* | | $CH_2CH_2$-morpholino | B | 162–164.5 | 40[c] | Isopropanol | 1645[d] | 8.15 |
| **21***e* | $CH_2CH_2$-morpholino | $CH_2CH_2CN$ | C | 195–198 | 24[c] | $CH_3OH$ | 1650[d] | 8.05 |
| **21***f* | $CH_2CH_2$-morpholino | $CH_2CH_2$-morpholino | A | 179–182 | 1.5[c] | EtOAc | 1645[d] | 7.95 |
| **21***g* | $CH_2CH_2CN$ | $CH_2CH_2CN$ | A | 188–191.5 | 92[c] | EtOH | 1645[d] | 8.05 |
| **21***h* | $CH(CH_3)CH_2CN$ | $CH(CH_3)CH_2CN$ | A | 168–170 | 29[f] | $CHCl_3$–$Et_2O$ | 1645[d] | 8.0 |
| **21***i* | $CH_2CH_2CONH_2$ | $CH_2CH_2CONH_2$ | D | 234–238 | 58[c] | $H_2O$ | 1620, 1650[d] | 8.0 |
| **21***j* | $CH_2CH_2CN$ | $CH_3$ | E | 187–193 | 34[c] | EtOH | 1640[d] | 7.9 |

[a]Methods: A, alkylation of **1**; B, alkylation of **13**; C, alkylation of **21***g*; D, acid hydrolysis of **21***g*; E, see Experimental.
[b]Before recrystallization.
[c]Analytically pure.
[d]Nujol.
[e]$CHCl_3$.
[f]Conversion yield, pure.

Can. J. Chem. Downloaded from www.nrcresearchpress.com by 210.87.254.6 on 09/06/12
For personal use only.

TABLE 5. 1-Substituted-1*H*-pyridazino[3,4,5-*de*]phthalazines

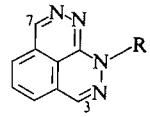

| No. | R | Method[a] | Melting point (°C) | Yield (%) | Recrystallization solvent | $^1$Hmr (δ) (DMSO-$d_6$) H at C-3 | H at C-7 |
|---|---|---|---|---|---|---|---|
| **22***a* | —$CH_3$ | B<br>C | 149–151<br>147–149 | 71[c]<br>66[b] | EtOH | 8.0 | 8.8 |
| **22***b* | | B | 168.5–170 | 50[c] | Benzene | 8.3 | 9.1 |
| **22***c* | 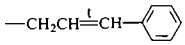 | A | 145–148 | 15[c] | EtOAc | 8.15 | 9.0 |
| **22***d* | 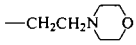 | A | 138–140 | 16[c] | Isopropanol | 8.1 | 8.9 |
| **22***e* | —$CH_2CH_2CN$ | A | 203–206 | 24[c] | Benzene | 8.2 | 9.0 |
| **22***f* | —$CH_2CH_2COOH$ | D | 251.5–253.5 | 35[c] | EtOH–$H_2O$ | 8.1 | 8.95 |
| **22***g* | 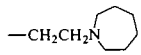 | A | 117–121 | 18[c] | Hexane | 8.1 | 8.95 |
| **22***h* | | B | 198–201 | 40[c] | EtOH | 8.3 | 9.1 |
| **22***i* | 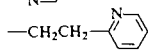 | A | 160–161 | 22[c] | $CH_3OH$ | 8.05 | 8.9 |

[a]Methods: A, direct alkylation of **2**; B, dehalogenation of **18**; C, desulphurization of **19**; D, alkaline hydrolysis of **22***e*.
[b]Yield before recrystallization.
[c]Purified.

TABLE 6. 3-Chloro-9-substituted-9*H*-pyridazino[3,4,5-*de*]phthalazines

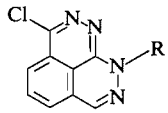

| No. | R | Melting point (°C) | Yield (%) | Recrystallization solvent | $^1$Hmr (δ) (DMSO-$d_6$) H at C-7 | Additional absorptions |
|---|---|---|---|---|---|---|
| **18***a* | —$CH_3$ | 253–255 | 87[a]<br>48[b] | Ethanol | 8.1 | 3.75 (s, $CH_3$), 7.6–8.0 (m, 3*H*, aryl) |
| **18***b* | | 225–228 | 66[b] | Ethanol | 8.4 | 7.45–8.3 (m, 8*H*, aryl) |
| **18***c* | —$CH_2$— | 208–209 | 75[a]<br>38[b] | Benzene | 8.1 | 5.35 (s, $CH_2$), 7.2–8.0 (m, 8*H*, aryl) |
| **18***d* | | 257–258 | 92[a]<br>74[b] | 2-Methoxyethanol | 8.4 | 7.45–8.3 (m, 6*H*, 3 aryl + 3 pyridyl), 8.7 (dd, *H* at 6′) |
| **18***e* | —$CH_2CH_2$ 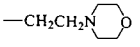 | 207–209 | 56[a] | Benzene | 8.05 | 2.5 (m, 2$CH_2$), 2.8 (t, $CH_2$), 3.5 (m, 2$CH_2$), 4.3 (t, $CH_2$), 7.2–7.9 (m, 3*H*, aryl) |

[a]Crude yield.
[b]Analytically pure.

examples explored it appears that dehalogenation of **18** is the best route to these structures.

In the course of the work, we attempted to build structures **22** as we had done for **11**, in this case by generation of an aldehyde function in the 8-position of a 2-substituted 1(2*H*)-phthalazinone. Attempts to reduce esters or acid chloride functions at the 8-position to an aldehyde such as **23** or an alcohol such as **24** with metal hydrides by standard literature methods gave, at best, low yields of the expected product. In one instance, the reason for the poor yield was clear. Lithium borohydride, a

Can. J. Chem. Downloaded from www.nrcresearchpress.com by 210.87.254.6 on 09/06/12
For personal use only.

reagent not noted for reducing amides (26) reduced the ester **12***d* to the amino alcohol **25** when used in excess. This is reminiscent of the overreduction of esters and lactones with sodium borohydride in the work of Wenkert *et al.* (27) in which ready intramolecular hydride transfer to a neighbouring carbonyl group occurred from an intermediate obtained from a newly formed primary alcohol combined with excess borohydride. A similar rationale could account for the reduction product **25** and the poor yields in our other attempts.

Comparison of **22***a* (**22**: $R^1 = CH_3$) with **2** will serve to illustrate the significant changes in spectral properties caused by alkylation at the 1-position. The uv spectra are almost identical in neutral and acidic ethanol. The spectrum of **2** undergoes a bathochromic shift with base (1) whereas **22***a* remains unchanged. The broad ir absorption at 2800–2200 $cm^{-1}$ in **2** is missing from the spectrum of **22***a* in Nujol. In the $^1$Hmr spectra (DMSO-$d_6$), the low field exchangeable proton of **2** is replaced in **22***a* by a sharp singlet at 3.7 δ due to the *N*-methyl. The aromatic patterns and shifts are identical but the equivalent vinyl protons in **2** are replaced by singlets at 8.0 δ (H at C-3) and 8.8 δ (H at C-7) in **22***a*. The latter signal is missing in 7-substituted compounds such as **18**. The methanesulphonate of **2** shows a singlet corresponding to the two vinyl protons at 8.8 δ ($D_2O$) whereas **22***a* in DCl/$D_2O$ shows separate singlets at 8.9 δ and 9.1 δ.

Reaction of **2** with methyl iodide or ethyl iodide gave stable quaternary salts, but when the methiodide was treated with freshly prepared silver oxide in aqueous methanol, a red solid was obtained, not identical to **22***a*. This red solid formed a yellow methiodide, mp 313–314°C, isomeric with the methiodide derived from **22***a*, mp 207–208.5°C. The methiodide of **22***a* showed $^1$Hmr signals for methyls at 3.8 δ and 4.3 δ (DMSO-$d_6$) and proton singlets at 8.6 δ and 9.7 δ. Since the position of one methyl group is not in doubt, the lower melting methiodide must be structure **26** or, less likely due to steric

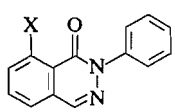

**23** X = CHO
**24** X = $CH_2OH$

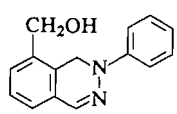

**25**

crowding, **27**. The higher melting methiodide showed equivalent methyl signals at 4.1 δ and a singlet corresponding to two identical vinyl protons at 9.0 δ with an aromatic multiplet centred at 8.0 δ. The spectrum indicates a molecule symmetrical about the C(5)—C(9b)—C(9a) axis. Assignment of structure **28** to the methiodide of **2** and structure **29**

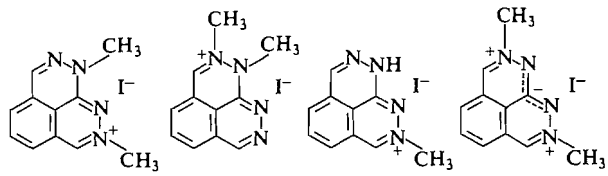

**26** **27** **28** **29**

to the higher melting methiodide derived from **28** accounts for the observed spectral data. The $^1$Hmr patterns of **26** and **28** are virtually identical except for the methyl singlet at 3.8 δ in **26** in place of the broad exchangeable singlet at 13.4 δ in **28**. These results are reminiscent of the two methylation products of 1*H*-naphtho[1,8-*de*]triazine, namely, the expected product **30** and the 2-methylated derivative **31** (28).

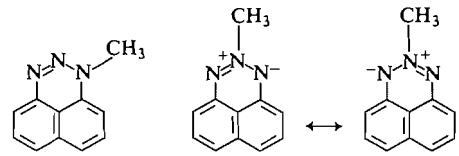

**30** **31**

The unusual inner salt **29** is related to the aminimides (29, 30) except that the ammonium imine is stabilized in a

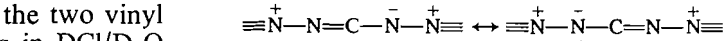

system contained in a flat molecule further stabilized by ring current.

The relative ease with which the phthalazinone esters react with hydrazine to form the tricyclic system deserves comment, particularly in the examples where the nitrogen is substituted. One would not expect to prepare an amidrazone by reaction of an amide with hydrazine, especially a non-enolizable amide. If the reaction involved initial conversion of the ester to the hydrazide followed by intramolecular cyclization, we would have expected to isolate some bicyclic hydrazides, though admittedly we were not looking for them. The reaction of methylhydrazine with the acid chloride of **8** was designed to create a hydrazide in the first stage of the synthesis. This *enolizable* phthalazinone was ring closed only under vigorous conditions and not cleanly. The synthesis of the parent heterocycle **2**, attempted under a variety of conditions (1), suggests that the initial formation of the phthalazinone hydrazone **32** followed by intramolecular attack on the enolizable carbonyl of the phthalazinone moiety is not the major reaction pathway, since most ring closure methods resulted in either intermolecular azine formation or no reaction. Ring closure occurs in nonaqueous highly polar media only under forcing conditions to a

TABLE 7. Antihypertensive activity[a] of selected compounds

| Test model | GPA 1595 | GPA 2079 | GPA 2265 | GPA 3095 | GPA 3166 | 1-Hydrazinophthalazine |
|---|---|---|---|---|---|---|
| Intact anaesthetized cat | 3 iv | 3 iv | 1 id | 3 id | 3 id | |
| Renal hypertensive dog | 1 po | 3 po | Emesis at 20 po | 20 po | 10 po | 10 po |
| Normotensive dog | | 20 po | | Inactive 10–40 po | | 20 po |
| Normotensive anaesthetized dog | | | 10 iv 20 id | Inactive at 30 id | 3 id | 30 id 1 iv |
| Neurogenic hypertensive dog | | | | 40 po | 40 po | 10 po |
| DOCA rat | 100 po | | | Inactive at 100 po | 40 po | 5 po |
| Normotensive rat | 30 po | | | Inactive at 300 po | 100 po | 30 po |
| Spontaneous hypertensive rat | | | | 80 po | | |
| Normotensive cat | | | Emesis at 10 po | | | |
| Normotensive monkey | | | Emesis at 25 po | | | |

[a]Key: Activity reported in mg/kg is the minimal dose tested which produced blood pressure lowering of at least 20%, but not necessarily the minimal effective dose. iv: intravenously; id: intraduodenally; po: orally.

small extent. On the other hand, dilute aqueous hydrazine at reflux was an excellent medium for conversion of **32** to the tricyclic system in good yield and purity. Since hydrazine is a strong nucleophile and the formation of the tricyclic system seems favoured by moderately high dilution in a hydroxylic solvent (water or water/alcohol mixtures) we suggest that the mechanism for the formation of **2** from **32** involves formation of a transient intermediate **34**, which stabilizes itself by

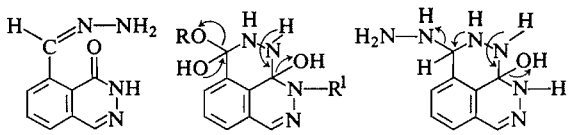

**32** **33** **34**

elimination of hydrazine and water. Similarly, the formation of **11** from **10** involves formation of an intermediate such as **33** which undergoes a double elimination depicted by the arrows to form the highly resonance-stabilized tricyclic system. Furthermore, the distance between the carbonyl carbon atoms of **10** appears optimal for allowing nucleophilic attack by hydrazine to form **33** and subsequently **11**.

## Biological results

Derivatives of the tricyclic system were tested for blood pressure lowering activity, primarily in the acute anaesthetized cat via intraduodenal administration. Secondary screening was done usually in the Goldblatt dog (31). Other models were also used in secondary screening.

Since **3**(*GPA 1595*) (1) was highly active, it was not surprising to find examples of structure **20** also active. The best of the three examples by far was **20***a*, coded as *GPA 2079*. This was highly active in the anaesthetized cat, Goldblatt dog, and the unanaesthetized normotensive dog. Since it was more toxic in mice than *GPA 1595*, it was not further pursued. Many of the 9-substituted derivatives of **1** lowered blood pressure in the anaesthetized cat. The first one to be studied in depth, **11***q* (*GPA 2265*), was also active in the anaesthetized dog but caused emesis in unanaesthetized dogs, cats, and monkeys. Most of the 9-pyridylalkyl compounds were active and the one most thoroughly investigated was **11***w* (*GPA 3166*). This compound was active in anaesthetized cats and dogs, the Goldblatt dog, the DOCA rat, and the neurogenic hypertensive dog (32) with no indication of tolerance on repeated dosage. The drug showed tachycardia in the anaesthetized animals and the Goldblatt dog, but not in the neurogenic dog which suggested that the tachycardia was reflex in origin. Lack of significant autonomic effects suggested a peripheral vasodilator mechanism of action. Further studies in toxicology and pharmacology revealed an unacceptable safety margin and the compound was not pursued clinically. The 9-alkyl and 9-aralkyl deriv-

Can. J. Chem. Downloaded from www.nrcresearchpress.com by 210.87.254.6 on 09/06/12
For personal use only.

Can. J. Chem. Downloaded from www.nrcresearchpress.com by 210.87.254.6 on 09/06/12
For personal use only.

atives of **1** were generally poorly active in the cat, except for the *trans*-cinnamyl derivative **11***k* (*GPA 3095*). This was moderately active in the anaesthetized cat, Goldblatt dog, neurogenic dog, and spontaneous hypertensive rat without tachycardia except slightly in the anaesthetized cat. It was inactive in the anaesthetized dog, DOCA rat, and normotensive rat. Even with micronized preparations, absorption was poor as determined by blood level studies in rats. Since pharmacological dose–response results were variable during repeated testing, possibly due to erratic absorption, the compound was not further investigated. The phthalazinone acids and esters were tested for antiinflammatory activity. The most promising of these, acid **12***j* (*GPA 3273*) was active in the anticarrageenin rat paw test with little ulcerogenic potential, but it failed in secondary screening in the 14-day established adjuvant arthritis screen. None of the compounds in Tables 4, 5, and 6 were sufficiently active in the primary screen to warrant further study.

## Experimental

Melting points (uncorrected) were determined on a Thomas–Hoover capillary apparatus or, if above 250°C, on a Reichart hot stage apparatus. Infrared spectra (ir) reported in wave numbers ($cm^{-1}$) over the 3500–1500 $cm^{-1}$ range for the principal peaks in Nujol (N) or chloroform ($CHCl_3$) were measured on a Perkin–Elmer model 137 calibrated with respect to the 1602 $cm^{-1}$ band of polystyrene or on a model 457 grating instrument. Proton magnetic resonance spectra ($^1$Hmr) were measured on a Varian EM-390 spectrometer in DMSO-$d_6$ unless otherwise stated, with peaks reported in ppm relative to tetramethylsilane as internal standard. Ultraviolet spectra (uv) were recorded on a Cary 14B spectrophotometer in nanometers with ε values in parentheses. All new compounds had microanalytical data for C, H, and N fitting within ±0.3. Additional elements are reported.

*2-Methyl-1(2*H*)-phthalazinone (**16**)*

A mixture of phthalaldehydic acid (18 g) and glacial acetic acid (100 mL) was treated with methyl hydrazine (7.6 mL) and the whole stirred at reflux under nitrogen for 18 h. The resulting solution was concentrated to dryness under water vacuum and the residue taken up in methanol (30 mL), treated with water (30 mL), and refrigerated. After 15 h the precipitated solid was collected, washed with methanol, and air dried. The product (15.5 g, 81%, mp 111–113°C) was recrystallized from cyclohexane (800 mL) to afford pure white crystals, mp 111.5–113°C (14.0 g). Literature mp values: 116°C (20); 111–112°C (10); 105–108°C (14); 114°C (9a); 112–114°C (17, 19). Infrared (N) ν: 1637 (C=O) $cm^{-1}$ (lit. (14) ν: 1645 $cm^{-1}$); $^1$Hmr: 3.8 (s, $CH_3$), 7.8–8.5 (m, 4*H*, aryl), 8.5 (s, vinyl *H*); literature (20) values: 3.71 (s, 3*H*), 8.31 (s, *H*), 7.65–8.30 (m, 4*H*).

*Synthesis of 3-substituted-3,4-dihydro-4-oxophthalazine-5-carboxylic esters **10** (Table 2)*

*Method A. From **9** with alkyl halide/alcohol/aqueous sodium hydroxide*

Methyl 3,4-dihydro-4-oxo-5-phthalazine carboxylate (**9***a*, 2.04 g (1)) was suspended in a solution of methanol (20 mL) and methyl iodide (0.75 mL), treated with 4*N* aqueous sodium hydroxide (2.3 mL), and heated under reflux for 1 h. It was quenched in ice, extracted with benzene, and the benzene extract dried ($Na_2SO_4$) and concentrated to dryness at reduced pressure. The residual solid (1.9 g, mp 113–119°C) was recrystallized from water to constant mp (3 recrystallizations) to afford pure **10***a*, mp 125–126°C; ir ($CHCl_3$): 1740, 1650, 1595; $^1$Hmr: 3.65 (s, $CH_3$—), 3.85 (s, $CH_3$—), 7.75–8.2 (m, 3*H*, aryl), 8.5 (s, vinyl *H*).

*Method B. From **12** via the acid chloride*

3-Methyl-3,4-dihydro-4-oxo-5-phthalazine carboxylic acid (**12***a*, 52 g) was suspended in a mixture of thionyl chloride (125 mL) and chlorobenzene (550 mL) and heated 3 h at reflux. The mixture was cooled and the precipitate collected, washed with benzene, and air dried to give the acid chloride (28.3 g, mp 185–190°C). Evaporation of the filtrate and trituration of the residue with hexane gave a second crop (23.4 g, mp 182–186°C) suitable for the next step. The acid chloride (15 g) was stirred at reflux in absolute ethanol (300 mL) during 18 h, cooled, and the white solid collected, washed with ethanol, and dried to afford the pure ester **10***b* (7.8 g, mp 103–104.5°C); ir (N): 1730, 1650, 1595; $^1$Hmr: 1.3 (t, $CH_3$—C), 3.8 (s, $CH_3$—N), 4.4 (q, $CH_2$), 7.8–8.15 (m, 3*H*, aryl), 8.6 (s, vinyl *H*).

*Method C. From **9** with an alkyl halide/sodium methoxide/dimethyl sulphoxide*

A mixture of methyl 3,4-dihydro-4-oxo-phthalazine-5-carboxylate (**9***a*, 40.8 g), sodium methoxide (12 g), and dimethylsulphoxide (300 mL) was treated dropwise under stirring with 3-chloropropenylbenzene (40 g) in dimethylsulphoxide (50 mL). The mixture was stirred at 80°C for 4 h under moisture exclusion and then quenched in ice and excess 2*N* HCl. The brownish solid was collected, washed with water, and extracted with chloroform. The dried ($Na_2SO_4$) extract was concentrated to dryness, taken up in a minimal quantity of hot methanol, treated with charcoal, and filtered. On cooling, pale yellow crystals (42.3 g, mp 116–121°C) were obtained. One crystallization from methanol and two from chloroform–hexane gave pure **10***h* as white crystals, mp 123–124°C; ir (N): 1730, 1650; $^1$Hmr: 3.95 (s, $CH_3$—O), 4.95 (d, $CH_2$—, $J$ = 5), 6.5 (dt, *CH*, $J$ = 5, 16), 6.7 (d, *CH*, $J$ = 16), 7.25–7.65 (m, 5*H*, benzene ring), 7.85–8.2 (m, 3*H*, aryl), 8.65 (s, vinyl *H*). The coupling constants indicate a *trans* double bond.

*Method D. From **9** with an alkyl halide/lithium amide/dimethylsulphoxide*

To a solution of methyl 3,4-dihydro-4-oxo-phthalazine-5-carboxylate (**9***a*, 40.8 g) in dry dimethylsulphoxide (100 mL) under nitrogen was added lithium amide (5 g) and the mixture stirred 2 h at ambient temperature. Additional lithium amide (5 g) was added followed by 2-picolyl chloride hydrochloride (32.8 g) portionwise. The resulting dark solution was stirred 3 h at ambient temperature under nitrogen, poured into water (1.5 L), and refrigerated 3 days. The precipitated product (35 g, mp 109–112°C) was dissolved in a minimal quantity of methanol, treated with an equimolar amount of methanesulphonic acid and the methanesulphonate salt of **10***l* purified by recrystallization from ethanol, mp 170.5–173°C; ir (N) ν: 1660, 1735 (C=O); $^1$Hmr: 2.55 (s, $CH_3$—S), 3.9 (s, $CH_3O$), 5.75 (s, $CH_2$), 7.8–9.1 (m, 7*H*, aryl + pyridyl), 8.65 (s, vinyl *H*), 14.95 (s, O*H*, exchangeable in $D_2O$).

*Ethyl-3,4-dihydro-4-oxo-phthalazine-5-carboxylate (**9**b)*

To a vigorously stirred solution of thionyl chloride (40 mL) in chlorobenzene (200 mL) was added 3,4-dihydro-4-oxo-phthalazine-5-carboxylic acid (1) (30.4 g) and the whole heated 4 h at reflux under moisture exclusion. The solid was collected on a ground glass filter, washed with benzene, pressed dry, and then transferred to a round bottom 1 L flask containing absolute

Can. J. Chem. Downloaded from www.nrcresearchpress.com by 210.87.254.6 on 09/06/12
For personal use only.

ethanol (305 mL). The mixture was heated at reflux under moisture exclusion 18 h, treated hot with activated charcoal, and filtered. On cooling, off-white crystals were obtained (26.1 g, mp 170–171.5°C) identical to the product obtained by a different route (1) as shown by ir, $^1$Hmr, and mmp.

*Synthesis of 3-substituted-3,4-dihydro-4-oxo-5-phthalazinone carboxylic acids* **12** *(Table 1)*

*Method A. From 3-hydroxyphthalide-7-carboxylic acid and a monosubstituted hydrazine*

A mixture of phenylhydrazine (3.6 mL), 3-hydroxyphthalide-7-carboxylic acid (1) (5.82 g), and glacial acetic acid (100 mL) was stirred 18 h at reflux, concentrated to dryness at reduced pressure, triturated with cold methanol, and collected. The crude acid **12***b* (6.97 g, mp 197–199°C) was recrystallized from benzene to afford pure white crystals, mp 197–198°C; ir (N): 2680, 1705, 1665, 1590; $^1$Hmr: 7.4–7.85 (m, 5*H*, phenyl), 7.9–8.25 (m, 3*H*, aryl), 8.7 (s, vinyl *H*), 13.4 (s, O*H*).

*Method B. From 3-hydroxyphthalide-7-carboxylic acid and a substituted hydrazine salt*

To a stirring solution of *p*-fluorophenylhydrazine hydrochloride (18 g), anhydrous sodium acetate (14.2 g), and glacial acetic acid (1.3 L) was added 3-hydroxyphthalide-7-carboxylic acid (19.4 g) and the mixture stirred 18 h at reflux. The mixture was filtered hot and the filtrate concentrated to one-third volume at reduced pressure and diluted with water. The resulting precipitate (24.2 g, mp 228–234°C) was twice recrystallized from ethyl acetate to afford pure white crystals of **12***c*, mp 234–237°C; ir (N): ~2600, 1695, 1655, 1585; $^1$Hmr: 7.3–8.2 (m, 7*H*, aryl), 8.7 (s, vinyl *H*), 13.3 (s, O*H*). *Anal.* calcd. for $C_{15}H_9N_2O_3F$: F 6.69; found: F 6.63.

*Method C. By hydrolysis of* **10**

A mixture of methyl 3-phenylpropyl-3,4-dihydro-4-oxo-phthalazine-5-carboxylate (**10***m*, 33 g, bp 225°C/2 Torr, prepared from **9***a*) and 2 *N* sodium hydroxide (500 mL) was stirred at reflux for 3 h, cooled, and poured into water (2.5 L). The mixture was extracted with chloroform and the aqueous layer was evaporated at reduced pressure to one-third volume and acidified with 6 *N* HCl under cooling. The mixture was extracted with chloroform, the chloroform layer dried ($Na_2SO_4$), and the material obtained as an oil by evaporation of the solvent at reduced pressure. It was stirred in ethanol at −8°C for 12 h and the solid which formed (**12***i*, 19.7 g, mp 110–112°C) was recrystallized once from methanol and once from benzene–hexane to afford the pure acid (14.2 g), mp 115–117°C; ir (N): ~1910, 1690; $^1$Hmr: 2.15 (m, C*H*$_2$), 2.6 (q, C*H*$_2$, *J* = 7), 4.2 (t, C*H*$_2$, *J* = 7), 7.25–7.45 (m, 5*H*, phenyl), 7.8–8.15 (m, 3*H*, aryl), 8.6 (s, vinyl *H*), 13.35 (s, O*H*).

*Synthesis of 9-substituted-3-oxo-3*H*-2,9-dihydropyridazino-[3,4,5-*de*]phthalazines* **11** *(Table 3)*

*Method A. From* **10**

A mixture of methyl 3-methyl-3,4-dihydro-4-oxophthalazine-5-carboxylate (**10***a*, 95.3 g), hydrazine hydrate (1650 mL), and water (400 mL) was stirred at reflux for 66 h. The mixture was allowed to cool to room temperature and 9-methyl-3-oxo-3*H*-2,9-dihydropyridazino[3,4,5-*de*]phthalazine (**11***a*) was collected, washed with water, and oven dried at reduced pressure. The bright yellow crystals (84 g, mp 292–296°C, 96% yield) were unchanged on recrystallization from 2-methoxyethanol; ir (N): 3130, 1650, 1595, 1555; uv (MeOH, neutral): 218 (21 600), 273.5 (8 900), 299.5 (8 000), 311.0 (7 000), 374.0 (6 000); (MeOH, acid): 253.0 (5 900), 263.0 (6 200), 273.5 (5 900), 300.0 (7 200), 312.0 (7 300), 331.0 (4 700), 364.0 (4 900); $^1$Hmr: 3.55 (s, C*H*$_3$), 7.8 (s, *H* at C-7), 7.7–8.1 (m, 3*H*, aryl), 12.1 (s, N*H*).

*Method B. From* **12**

A mixture of 3-(4-pyridylethyl)-3,4-dihydro-4-oxo-phthalazine-5-carboxylic acid (**12***m*, 64.5 g), thionyl chloride (90 mL), and chlorobenzene (650 mL) was stirred 3 h at reflux under moisture exclusion and then concentrated to dryness at reduced pressure. The residue was treated with absolute methanol (2 L) at reflux for 18 h and then concentrated at reduced pressure to a yellow foam. This material was treated with hydrazine hydrate (800 mL), water (200 mL), and then methanol (300 mL) to produce a homogenous solution. It was heated under stirring and the liquid gradually allowed to distil off at a bath temperature of 130°C. After a further 66 h at this temperature, the mixture was cooled and the yellow solid collected (44 g), washed with water, and then dissolved as well as possible in excess 1 *N* HCl. After filtration to remove 4.4 g of **1**, the solution was made basic with 5% sodium carbonate and the precipitated solid was collected, washed with water, air dried, and recrystallized thrice from ethanol to afford pure **11***z*, mp 200.5–203°C; $^1$Hmr: 3.1 (t, C*H*$_2$, *J* = 5), 4.3 (t, C*H*$_2$, *J* = 5), 7.3 (m, 2 C*H*—C), 7.9 (s, *H* at C-7), 7.75–8.2 (m, 3*H*, aryl), 8.5 (m, 2 C*H*—N), 12.0 (s, N*H*). The free base suspended in warm methanol was treated with an equimolar quantity of methanesulphonic acid, treated with ether to turbidity, refrigerated 90 h, and the *methanesulphonate salt* collected, mp 253–256°C, resolidified and dec. ca. 340°C; ir (KBr): ~2900 (broad), 1660, 1638, 1620, 1600, 1560, 1520, 1503. *Anal.* calcd. for $C_{16}H_{13}N_5O\cdot CH_4O_3S$: S 8.28; found: S 8.28.

*Method C. From* **9**

To a solution of 1 *N* sodium hydroxide (100 mL) in methanol (100 mL) was added *N*-hexamethyleneiminoethyl chloride hydrochloride (20 g) and the resulting mixture added to a solution of methyl 3,4-dihydro-4-oxophthalazine-5-carboxylate (**9***a*, 20.4 g) in methanol (250 mL). Additional 1 *N* sodium hydroxide (100 mL) was added and the whole heated 3 h on a steam bath. It was evaporated to dryness at reduced pressure and the residue triturated with water, extracted with chloroform, and the dried ($Na_2SO_4$) extract concentrated at reduced pressure to a brown oil. This was treated with hydrazine hydrate (420 mL) and water (140 mL) at reflux over 48 h, well cooled, and the precipitate collected, washed with water, and oven dried. The crude yellow solid was triturated with excess 1 *N* HCl, filtered free of impurities, and the filtrate made basic with 20% sodium carbonate solution. The yellow solid which formed was dissolved in chloroform, filtered free of further impurities, and concentrated at reduced pressure to a yellow solid (17.0 g, mp 182–185°C, 55%). Three recrystallizations from ethanol gave pure 3-(*N*-hexamethyleneiminoethyl)-3-oxo-3*H*-2,9-dihydropyridazino-[3,4,5-*de*]phthalazine (**11***t*), mp 183.5–186.5°C; ir(N): 3130, 1655, 1625, 1595. $^1$Hmr: 1.5 (s, 4-C*H*$_2$), 2.5–2.95 (t + m, 3-C*H*$_2$—N), 4.1 (t, C*H*$_2$, *J* = 5), 7.95 (s, *H* at C-7), 7.75–8.15 (m, 3*H*, aryl), 12.0 (s, N*H*).

In examples **11***b*, **11***e*, **11***f*, **11***l*, **11***m*, and **11***x*, the crude solid obtained after hydrazine hydrate treatment was taken up in hot chloroform, filtered free of **1**, evaporated to dryness, and recrystallized. In examples **11***w*, **11***aa*, and **11***bb*, the crude tricyclic compound was converted to the methanesulphonate salt and recrystallized.

*Method D. From* **1**

To a suspension of sodium methoxide (7 g) in dry dimethylsulphoxide (500 mL) was added **1** (18.6 g) and the mixture heated to 60°C. Benzyl bromide (14 mL) was added under stirring and the mixture maintained 2 h at 60°C. The dark mixture was poured into ice water, stirred 0.5 h, and filtered. The dark precipitate was stirred 1 h in ethanol (400 mL) and the resulting tan solid (18.3 g) recrystallized from 2-methoxyethanol with charcoal. On cooling, a first crop (5.3 g) was obtained, combined with a second crop (4.1 g) obtained after 3 days, and recrystallized thrice from ethanol to afford pure 9-benzyl-3-oxo-2,9-dihydropyridazino[3,4,5-*de*]phthalazine (**11***h*), mp 239–243°C; ir (N):

Can. J. Chem. Downloaded from www.nrcresearchpress.com by 210.87.254.6 on 09/06/12
For personal use only.

3150, 1645, 1590, 1550; $^1$Hmr: 5.2 (s, $CH_2$), 7.4 (s, $C_6H_5$), 8.05 (s, *H* at C-7), 7.85–8.2 (m, 3*H*, aryl), 11.9 (s, N*H*).

In examples **11***c*, **11***p*, **11***q*, and **11***y*, the crude product was dissolved in hot ethanol, filtered free of unreacted **1**, and concentrated to dryness before the final crystallization. In addition, **11***p* and **11***y* were dissolved in 1 *N* HCl, filtered free of impurity, and reprecipitated with aqueous sodium carbonate before the final recrystallization.

*3-Chloro-9-phenyl-9*H*-pyridazino[3,4,5-*de*]phthalazine (**18***b*) (Table 6)*

To a stirring mixture of phosphorous pentachloride (6.3 g) in phosphoryl chloride (40 mL) was added 9-phenyl-3-oxo-3*H*-2,9-dihydropyridazino[3,4,5-*de*]phthalazine (**11***g*, 7.8 g) and the mixture stirred 3 h at reflux. It was poured cautiously onto ice, made alkaline with 20% sodium hydroxide solution, and the yellow precipitate collected and washed thoroughly with water. The crude solid was further triturated with warm water (600 mL), refiltered, and recrystallized from boiling ethanol to afford yellow crystals (5.5 g) of pure **18***b*, mp 225–228°C; ir (N): 1620, 1595, 1530. *Anal.* calcd. for $C_{15}H_9ClN_4$: Cl 12.63; found: Cl 12.67.

In example **18***c*, the reaction mixture was quenched instead in ice-cold ether, filtered, and the precipitate recrystallized. In example **18***d*, phosphoryl chloride alone was used as the chlorinating agent. In example **18***c*, the crude product was extracted from the ice-water mixture with chloroform, concentrated, and filtered through a column of Woelm neutral alumina, grade I, before final recrystallization.

*9-Phenyl-3-thiono-3*H*-2,9-dihydropyridazino[3,4,5-*de*]-phthalazine (**19***b*)*

A mixture of phosphorous pentasulphide (2.5 g), dry pyridine (15 mL), and **11***g* (2.6 g) was stirred at reflux under moisture exclusion for 2.5 h. The dark red solution was cooled, poured into ice-cold saturated sodium chloride solution, and stirred 1.5 h. The precipitated thiono compound was collected, washed thoroughly with water, air dried, and recrystallized from ethanol in golden yellow flakes, mp 230–231°C; ir (N): 3150, ~2400 (broad), 1615, 1590, 1560; $^1$Hmr: 7.4–8.25 (m, 7*H*, phenyl + aryl), 8.3 (s, *H* at C-7), 8.6 (dd, *H* at C-4), 13.8 (s, N*H*). *Anal.* calcd. for $C_{15}H_{10}N_4S$: S 11.52; found: S 11.64.

The *9-methyl compound* **19***a*, prepared by the same route, was obtained in 56% yield after one recrystallization from 2-methoxyethanol. Two further recrystallizations did not change the mp of 299–316°C (dec.); ir (N): ~3180, ~2800 (broad), 1620, 1555, 1520; $^1$Hmr: 3.6 (s, $CH_3$), 8.05 (s, *H* at C-7), 7.8–8.15 (2*H*, aryl), 8.45 (dd, *H* at C-4), 14.0 (s, N*H*). *Anal.* calcd. for $C_{10}H_8N_4S$: S 14.83; found: S 14.72.

*9-(*N*-Morpholinoethyl)-3-thiono-3*H*-2,9-dihydropyridazino-[3,4,5-*de*]phthalazine (**19***c*)*

To a solution of **11***q* (29.9 g) in pyridine (250 mL) was added phosphorous pentasulphide (25 g) and the mixture stirred 5 h at reflux. The dark solution was poured into ice-water and the yellow solid collected, washed with water, and pressed dry on the filter. The crude product (15.5 g), mp 200–204°C dec., was suspended in hot chloroform (500 mL), filtered and the filtrate treated with hexane, whereupon a yellow precipitate formed. This material (6.6 g, one spot in tlc) was twice recrystallized from benzene to afford the pure thiono compound **19***c*, mp 202–204°C, resolidified, and remelted 220–222°C; ir (N): ~3150, 1590, 1555; $^1$Hmr: 2.5 (m, 2$CH_2$), 2.7 (t, $CH_2$), 3.55 (m, 2$CH_2$), 4.15 (t, $CH_2$), 7.85–8.1 (m, 2*H*, aryl), 8.15 (s, *H* at C-7), 8.5 (dd, *H* at C-4), 13.9 (s, N*H*). *Anal.* calcd. for $C_{15}H_{17}N_5OS$: S 10.17; found: S 10.15.

*3-Hydrazino-9-methyl-9*H*-pyridazino[3,4,5-*de*]phthalazine (**20***a*)*

To a hot stirring solution of hydrazine hydrate (162 mL) and water (60 mL) was added **19***a* (6.48 g) and the mixture stirred mechanically 20 h at reflux. It was filtered hot and the filtrate evaporated at reduced pressure to dryness. The residual yellow solid was taken up in 3 *N* HCl (400 mL), filtered to remove insoluble material, and the filtrate evaporated to dryness at reduced pressure. It was dissolved in water (100 mL), again filtered free of impurity, and the filtrate concentrated to dryness. The residual solid was dissolved in water (50 mL), ethanol (50 mL) added and, at 70°C under stirring, treated with benzaldehyde (15 mL) in ethanol (50 mL). Water (25 mL) was added, followed by 1 *N* sodium bicarbonate (100 mL), and the mixture stirred 5 min at 70°C. Bicarbonate solution (100 mL) was again added and the whole heated 10 min at reflux. The mixture was cooled and the orange solid collected, washed with water, and treated with excess 2 *N* HCl at the boil (fume hood) until no odour of benzaldehyde remained and a yellow solution was obtained. It was filtered through sintered glass and the clear yellow filtrate concentrated to dryness at reduced pressure. The residual solid was dried in a dessicator over $P_2O_5$ and recrystallized from methanol–ether to give pale yellow crystals of the dihydrochloride of **20***a* (4.4 g), mp ~260°C, gas evolution; ir (N): ~2600 (broad), 1580, 1545, 1510; $^1$Hmr ($D_2O$): 4.05 (s, $CH_3$), 8.15–8.6 (m, 3*H*, aryl), 8.7 (s, *H* at C-7). *Anal.* calcd. for $C_{10}H_{10}N_6 \cdot 2HCl$: Cl 24.70; found: Cl 24.44.

In a similar way, **19***b* was reacted with aqueous hydrazine hydrate followed by benzaldehyde to afford the benzylidene hydrazone of *3-hydrazino-9-phenyl-9*H*-pyridazino[3,4,5-*de*]-phthalazine* in 63% yield, crude. After three recrystallizations from 2-methoxyethanol, it melted in the range 219–222°C; ir (N): 3350, 1615, 1590, 1565, 1550, 1530; $^1$Hmr: 7.3–7.95 (m, 12*H*, aryl), 8.0 (s, *H* at C-7), 8.3 (dd, *H* at C-4, $J$ = 7, 1.5), 8.4 (s, C*H*=N), 11.5 (s, N*H*).

*9-Benzyl-3-hydrazino-9*H*-pyridazino[3,4,5-*de*]phthalazine hydrochloride (**20***c*) from **11***h*

A mixture of phosphorous pentasulphide (25 g), pyridine (250 mL), and **11***h* (28 g) was stirred 3 h at reflux. The dark mixture was poured into ice-water, stirred 2 h, and the precipitated solid collected and recrystallized from 2-methoxyethanol. The resulting product was suspended in chloroform, filtered, and 7 g of crude thiono compound obtained, mp 275–278°C. It was suspended in hydrazine hydrate (300 mL) and water (80 mL), stirred 20 h at reflux, well cooled, and the solid collected, washed with water, taken up in 3 *N* HCl (400 mL), and filtered. The filtrate was concentrated at reduced pressure and the residue recrystallized from methanol to afford the monohydrochloride of **20***c*, mp 270–271°C; ir (N): 3200, ~2800 (broad), 1650, 1585, 1545; $^1$Hmr: 5.3 (s, $CH_2$), 7.2–7.5 (m, 5*H*, phenyl), 8.05–8.15 (m, 2*H*, aryl), 8.2 (s, *H* at C-7), 8.7 (dd, *H* at C-4). *Anal.* calcd. for $C_{16}H_{14}N_6 \cdot HCl$: Cl 10.81; found: Cl 10.92.

*2,9-Dimethyl-3-oxo-3*H*-2,9-dihydropyridazino[3,4,5-*de*]-phthalazine (**21***b*)*

*(a) **21**b from **11**a*

To a suspension of **11***a* (20 g) in dimethylsulphoxide (200 mL) was added sodium methoxide (10 g) and the mixture stirred at 60°C. A thick yellow suspension formed. Methyl iodide (20 mL) was added whereupon the suspension became a clear yellow solution from which a yellow solid gradually precipitated. The mixture was stirred 3 h at 60°C, cooled, washed with dilute aqueous sodium bisulphite followed by water, and air dried. The yellow solid (20 g, mp 191–192°C, sint. 186°C) was recrystallized from methanol to give pure **21***a*, mp 195–196.5°C; ir ($CHCl_3$):

Can. J. Chem. Downloaded from www.nrcresearchpress.com by 210.87.254.6 on 09/06/12
For personal use only.

1650, 1625, 1595, 1555; uv (MeOH): 274.5 (8900), 301.0 (7100), 312.5 (6300), 374.0 (6700), unchanged in acidic or alkaline methanol; $^1$Hmr: 3.5 (s, $CH_3$), 3.6 (s, $CH_3$), 7.85 (s, *H* at C-7), 7.6–8.05 (m, 3*H*, aryl); $^1$Hmr ($CDCl_3$): 3.6 (s, $CH_3$), 3.8 (s, $CH_3$), 7.5–7.95 (m, 3*H* aryl + *H* at C-7), 8.25 (dd, *H* at C-4, $J$ = 8, 1.5).

*(b) **21**b from **1***

In an apparatus consisting of a 4-necked flask, thermometer, dropping funnel, mechanical stirrer, and double jacketed condenser surmounted with a nitrogen T-tube, a suspension of **1** (56 g) in dimethylsulphoxide (700 mL) was treated under stirring with sodium methoxide (36 g), whereupon the internal temperature rose to 34°C. After the weak exotherm subsided, methyl iodide (15 g) was added, whereupon the internal temperature rose to 72°C. After stirring 2 h at ambient temperature, the mixture was poured into ice-water (700 mL) containing a little sodium bisulphite. It was made slightly acidic with HCl, stirred 30 min at 0–5°C, and filtered. The filtrate was extracted with chloroform (3 × 750 mL) and the extract dried ($Na_2SO_4$) and concentrated to dryness. The residual yellow solid (15.1 g), mp 186–189°C, was identical (ir, $^1$Hmr) to **21***b* obtained from **13***a*. Evaporation of the aqueous dimethylsulphoxide layer to dryness followed by extraction with chloroform containing 5% methanol yielded a mixture of **21***b* and **13***a* (10.8 g).

*2,9-Bis-(*N*-morpholinoethyl)-3-oxo-3*H*-2,9-dihydropyridazino-[3,4,5-*de*]phthalazine (**21**f) from **1***

To a suspension of **1** (93 g) in dimethylsulphoxide (600 mL) was added sodium methoxide (29 g) and the mixture raised to 80°C under stirring. *N*-Morpholinoethyl chloride (75 g) was added and the mixture stirred 5 h longer at 80°C, quenched in ice-water (3 L), and the yellow precipitate collected. The wet solid (ca. 100 g) was impure **11***q*. The mother liquor was extracted with chloroform and the organic layer extracted with 2*N* HCl. The acidic layer was made basic with 5% sodium carbonate solution and extracted with chloroform. The dried ($Na_2SO_4$) organic layer was concentrated to 20 g of dark semisolid. It was taken up in a minimum quantity of ethyl acetate and chromatographed on Woelm basic alumina, grade III (400 g), with ethyl acetate as eluent. The second 500 mL fraction, on evaporation at reduced pressure, gave a yellow solid. Recrystallization from ethyl acetate gave pure **21***f* (2.2 g), mp 179–182°C; ir (N): 1645, 1620, 1595, 1540; $^1$Hmr: 2.5 (m, 4C$H_2$), 2.75 (t, 2C$H_2$), 3.55 (m, 4C$H_2$), 4.2 (2 overlapping dd, 2C$H_2$), 7.95 (s, *H* at C-7), 7.75–8.2 (m, 3*H*, aryl).

*2,9-Bis-(cyanoethyl)-3-oxo-3*H*-2,9-dihydropyridazino-[3,4,5-*de*]phthalazine (**21**g)*

A mixture of **1** (55.8 g), 50% aqueous pyridine (500 mL), Triton B (40% in $CH_3OH$, 10 mL), and acrylonitrile (60 mL) was heated 18 h at reflux. It was evaporated at reduced pressure to dryness, taken up in water (700 mL), filtered, and the precipitate (80.4 g, mp 186–192°C) recrystallized three times from ethanol (ca. 40 mL/g) to afford the pure sample, mp 188–191.5°C; ir (N): 2220, 1645, 1590, 1545; $^1$Hmr: 3.1 (q, 2C$H_2$), 4.3 (m, 2C$H_2$), 8.05 (s, *H* at C-7), 7.8–8.25 (m, 3*H*, aryl).

*2,9-Bis-(1-methyl-2-cyanoethyl)-3-oxo-3*H*-2,9-dihydropyridazino[3,4,5-*de*]phthalazine (**21**h)*

A mixture of **1** (18.6 g), crotononitrile (20 mL), Triton B (3 mL), and 50% aqueous pyridine (1 L) was heated 18 h at reflux. The red solution was concentrated to dryness at reduced pressure and the residue triturated with water, cooled, and filtered. The solid was taken up in chloroform, filtered to remove residual **1** (6.5 g), and the filtrate concentrated to dryness at reduced pressure. The residue (14 g) was recrystallized from benzene–hexane with charcoal, then thrice from chloroform–ether to afford the pure product (5.6 g, 29% conversion), mp 168–170°C; ir (N): 2230, 1645, 1625, 1595, 1550; $^1$Hmr: 1.5 (t, 2C$H_3$), 3.1 (2d, 2C$H_2$), 5.0–5.65 (m, 2C*H*), 8.0 (s, *H* at C-7), 7.9–8.35 (m, 3*H*, aryl).

*2,9-Bis-(carbamoylethyl)-3-oxo-3*H*-2,9-dihydropyridazino-[3,4,5-*de*]phthalazine (**21**i)*

A mixture of **21***g* (7.17 g) and 80% sulphuric acid (75 mL) was stirred for 20 h under reflux. The resulting yellow suspension was cooled and quenched in ice. The yellow precipitate (7.1 g, mp 230–235°C) was twice recrystallized from water to afford the pure product, mp 234–238°C; ir (N): 3350, 3150, 1650, 1620, 1575, 1530; $^1$Hmr: 2.55 (m, 2C$H_2$), 4.25 (q, 2C$H_2$), 6.95 (s, N$H_2$), 7.5 (s, N$H_2$), 8.0 (s, *H* at C-7), 7.8–8.2 (m, 3*H*, aryl).

*9-Methyl-2-(*N*-morpholinoethyl)-3-oxo-3*H*-2,9-dihydropyridazino[3,4,5-*de*]phthalazine (**21**c)*

Sodium methoxide (2.5 g) was added to a stirring suspension of **11***a* (6 g) in dimethylsulphoxide (200 mL), heated to 80°C, *N*-(2-chloroethyl)morpholine (6 g) added, and the mixture stirred 5 h at 80°C. The orange solution was quenched in ice-water and extracted with chloroform. The organic layer was extracted with 1*N* HCl (500 mL) and the acidic layer made basic with 5% sodium carbonate, extracted with chloroform, dried ($Na_2SO_4$), and concentrated to dryness to give the crude product (9.3 g, mp 171–174°C). Three recrystallizations from benzene gave the pure sample, mp 176–179°C; ir (N): 1645, 1620, 1595, 1550; $^1$Hmr: 2.5 (dd, 2C$H_2$, $J$ = 5), 2.75 (t, C$H_2$, $J$ = 7), 3.5 (s, $CH_3$), 3.6 (dd, 2C$H_2$, $J$ = 5), 4.1 (t, C$H_2$, $J$ = 7), 7.6–8.05 (m, 3*H*, aryl), 7.8 (s, *H* at C-7).

Under similar conditions, **21***d* was prepared from **11***g*, except that the crude product precipitated directly on quenching in ice-water and was obtained pure after three recrystallizations from isopropanol in 40% yield, mp 162–164.5°C; ir (N): 1645, 1620, 1595, 1550; $^1$Hmr: 2.4 (dd, 2C$H_2$, $J$ = 5), 2.6 (t, C$H_2$, $J$ = 7), 3.5 (dd, 2C$H_2$, $J$ = 5), 4.05 (t, C$H_2$, $J$ = 7), 7.3–8.25 (m, 8*H*, aryl), 8.15 (s, *H* at C-7).

*2-Cyanoethyl-9-(*N*-morpholinoethyl)-3-oxo-3*H*-2,9-dihydro-[3,4,5-*de*]phthalazine (**21**e)*

A mixture of **21***g* (12.0 g), dimethylsulphoxide (300 mL), and sodium methoxide was heated to 60°C under stirring and *N*-(2-chloroethyl)morpholine (10 g) added. It was stirred 4 h at 60°C under moisture exclusion, then poured into ice-water. The resulting solid (7.1 g) was suspended in 1*N* HCl, filtered and the filtrate made basic with 5% sodium carbonate solution, extracted with chloroform and the chloroform layer concentrated to dryness at reduced pressure. The residual solid (5.5 g) was recrystallized from methanol to produce the pure **21***e* (3.45 g), mp 195–198°C; ir (N): 2220, 1650, 1615, 1590, 1545; $^1$Hmr: 2.5 (m, 2C$H_2$), 2.7 (t, C$H_2$, $J$ = 7), 3.05 (t, C$H_2$, $J$ = 7), 3.6 (m, 2C$H_2$), 4.2 (t, C$H_2$, $J$ = 7), 4.3 (t, C$H_2$, $J$ = 7), 8.05 (s, *H* at C-7), 7.8–8.25 (m, 3*H*, aryl).

*Preparation of **11**q from **21**e*

A mixture of **21***e* (1.3 g), hydrazine hydrate (30 mL), and water (7 mL) was stirred 20 h at reflux. It was cooled and the yellow precipitate collected, washed with water, and dried. The product (0.8 g, mp 200–203°C) was recrystallized from water to afford 0.6 g, mp 203–205°C, identical by ir, $^1$Hmr, and mmp to **11***q* prepared from **1**.

*2-Methyl-3-oxo-3*H*-2,9-dihydropyridazino[3,4,5-*de*]-phthalazine (**21**a)*

The acid chloride of 3,4-dihydro-4-oxo-phthalazine-5-carboxylic acid, prepared as described in the synthesis of **9***b* (40 g)

Can. J. Chem. Downloaded from www.nrcresearchpress.com by 210.87.254.6 on 09/06/12
For personal use only.

was suspended in chlorobenzene (250 mL) and methylhydrazine (50 mL) added cautiously. The mixture was stirred at reflux 44 h under moisture exclusion, cooled in an ice bath, and treated cautiously with methanol (200 mL). The crude solid (12.8 g, mp ~300°C dec.) was collected and combined with a second batch (17.3 g) and suspended in 50% aqueous pyridine (900 mL). Acrylonitrile (25 mL) and Triton B (5 mL) were added and the mixture stirred 18 h at reflux. The orange solution was concentrated to dryness at reduced pressure and the residue triturated with water and collected. The crude product (15.2 g) was twice recrystallized from ethanol to afford *9-cyanoethyl-2-methyl-3-oxo-3*H-*2,9-dihydro[3,4,5-*de*]phthalazine* (**21***j*), mp 187–193°C; ir (N) v: 2220 (C≡N), 1640 (C=O); $^1$Hmr: 3.1 (t, C$H_2$, $J$ = 7), 3.65 (s, C$H_3$), 4.2 (t, C$H_2$, $J$ = 7), 7.9 (s, *H* at C-7), 7.7–8.1 (m, 3*H*, aryl). The nitrile **21***j* (7.6 g) was treated with hydrazine hydrate (240 mL) and water (60 mL) under reflux for 18 h, cooled in ice, and the yellow precipitate collected, washed with water, and dried. The product **21***a* was thus obtained analytically pure, mp 307–311°C dec.; ir (N): 3200 (sh), 3100, 1655, 1630, 1605, 1590, 1550; $^1$Hmr: 3.6 (s, C$H_3$), 7.85 (s, *H* at C-7), 7.65–8.05 (m, 3*H*, aryl), 12.1 (s, N*H*).

*1-Methyl-1*H-*pyridazino[3,4,5-*de*]phthalazine* (**22**a)

*Method A. From* **18**a

A mixture of **18***a* (10.8 g), 47% hydriodic acid (150 mL), and red phosphorous (10 g) was stirred at reflux for 23 h, poured into ice-water, and filtered. The filtrate was evaporated to a small volume at reduced pressure, made basic with 5% sodium carbonate solution, and extracted with chloroform. The chloroform layer was dried ($Na_2SO_4$), concentrated to a small volume, and chromatographed on Woelm neutral alumina, grade II, in a 2 inch diameter column. The desired compound fluoresced strongly under long wave (3660 Å) uv light and its progress down the column was determined with a Rayteck model LS-7 handheld lamp. After a forerun, the compound was eluted with chloroform (ca. 2 L). Evaporation of the chloroform left 9.3 g of yellow solid, which was combined with a second run (8.0 g) and recrystallized from ethanol with charcoal to afford pure **22***a* (13.1 g), mp 149–151°C; ir (N): 1615, 1590, 1535; uv (MeOH, neutral or alkaline): 254.0 (6 700), 332.2 (11 400), 341.5 (11 500); uv (MeOH + 0.1 *N* HCl): 2445 (9 300), 253.0 (8 400), 312.5 (9 500), 334.5 (5 900), 348.8 (6 000); $^1$Hmr: 3.7 (s, C$H_3$), 7.45–7.9 (m, 3*H*, aryl), 8.0 (s, *H* at C-3), 8.85 (s, *H* at C-7); $^1$Hmr (DCl/$D_2O$): 4.1 (s, C$H_3$), 8.3–8.65 (m, 3*H*, aryl), 8.9 (s, vinyl *H*), 9.1 (s, vinyl *H*).

*Method B. From* **19**a

The thiono compound **19***a* (1.08 g) was suspended in ethanol (200 mL) and Raney nickel slurried in ethanol (ca. 5 g) added a little at a time as the mixture was agitated with an air-driven stirrer. After addition was complete, the whole was stirred on a steam bath for 1 h. It was filtered hot and the filtrate evaporated at reduced pressure. The residual solid was again dissolved in hot ethanol, refiltered, and concentrated to dryness. The residual yellow solid (0.6 g) was recrystallized from benzene–hexane with charcoal to give 0.4 g of product, mp 147–149°C, identical to **22***a* derived from **18***a* as indicated by tlc, ir, and $^1$Hmr. This substance formed a hydriodide with 47% hydriodic acid, mp 247–248°C dec. (from ethanol–ether); ir (N): ~2700 (broad), 1640, 1580, 1570.

Treatment of **22***a* with methanol and methyl iodide at reflux over 25 h gave a methiodide **29**, mp 207–208.5°C (from methanol–ether); ir (N): 1615, 1595, 1550; $^1$Hmr: 3.8 (s, C$H_3$), 4.3 (s, C$H_3$), 8.1–8.5 (m, 3*H*, aryl), 8.6 (s, *H* at C-3), 9.7 (s, *H* at C-7).

*1-Phenyl-1H-pyridazino[3,4,5-*de*]phthalazine* (**22**b)

A mixture of red phosphorous (6.5 g), 47% hydriodic acid (65 mL), and **18***b* (9.0 g) was stirred 18 h at reflux, poured into ice-water, and filtered. The filtrate was made basic with 5% sodium carbonate and extracted with chloroform. The extract was dried ($Na_2SO_4$) and concentrated to dryness at reduced pressure. The residual crude product (6.5 g) was recrystallized from benzene with charcoal and a first crop of 3.1 g obtained. Addition of hexane to the mother liquor gave an additional 0.7 g. The combined material was recrystallized from benzene to give pure **22***b* (2.9 g), mp 168.5–170°C; ir (N): 1600, 1575, 1520; uv (MeOH, neutral or alkaline): 343.2 (13 400); uv (MeOH + 0.1 *N* HCl): 311.7 (9 900), 336.5 (6 400), 351.0 (7 000); $^1$Hmr: 7.4–8.1 (m, 8*H*, aryl), 8.3 (*H* at C-3), 9.1 (*H* at C-7).

*Method C. From* **2**

*1-(*N-*Morpholinoethyl)-1*H-*pyridazino[3,4,5-*de*]phthalazine* (**22**d)

Sodium methoxide (1.7 g) was added to a suspension of **2** (5.1 g) in dimethylsulphoxide (75 mL), the mixture stirred at 60°C, and *N*-(2-chloroethyl)morpholine (5 g) added under moisture exclusion. After 4 h stirring at 80°C, the red solution was poured into ice-water and extracted with chloroform. The extract was washed with 1 *N* HCl and the aqueous acid layer made basic with 5% sodium carbonate and extracted with chloroform. Evaporation of the dried ($Na_2SO_4$) chloroform yielded 6 g of dark semisolid. This was dissolved in a minimal quantity of 5:1 benzene–dimethylformamide and chromatographed on Woelm neutral alumina, grade I (200 g). The first 150 mL fraction, on evaporation, yielded a yellow solid (3 g, mp 131–135°C). This was combined with material from a second run (6 g) and recrystallized from ethanol with charcoal. The product (7.5 g) was again recrystallized from ethanol and twice from isopropanol to afford the pure sample (4.0 g, 16%), mp 138–140°C; ir (N): 1630, 1605, 1545; $^1$Hmr: 2.5 (m, 2C$H_2$), 2.75 (t, C$H_2$, $J$ = 7), 3.55 (m, 2C$H_2$), 4.35 (t, C$H_2$, $J$ = 7), 7.5–8.0 (m, 3*H*, aryl), 8.1 (s, *H* at C-3), 8.9 (s, *H* at C-7).

*1-(2-Pyridyl)-1*H-*pyridazino[3,4,5-*de*]phthalazine* (**22**h)

A mixture of **18***d* (11.24 g), red phosphorous (8 g), and 47% hydriodic acid (100 mL) was stirred 3 h at reflux, cooled, poured into ice-water, and extracted with chloroform. The dried ($Na_2SO_4$) extract was concentrated to dryness and the residual solid (9.7 g, mp 182–188°C) chromatographed on Woelm basic alumina, grade I (500 g), with chloroform as eluent. The eluted product (6.4 g) was recrystallized twice from ethanol to afford the pure compound, mp 198–201°C, in 40% yield; ir (KBr): 1620, 1585, 1565, 1540; $^1$Hmr: 7.5–8.2 (m, 6*H*, 3 aryl + 3 pyridyl), 8.3 (s, *H* at C-3), 8.8 (m, *H* at C-6 in pyridyl ring), 9.1 (s, *H* at C-7).

The free base was treated with an equimolar amount of methanesulphonic acid in methanol, concentrated to dryness at reduced pressure, taken up in water, filtered, and the filtrate concentrated to dryness. The residual solid was twice recrystallized from isopropanol to afford the methanesulphonate salt of **22***h*, mp 186–189°C; ir (KBr): 1640, 1610, 1595, 1570, 1520. *Anal.* calcd. for $C_{15}H_{13}N_5O_3S$: S 9.34; found: S 9.21.

*1-(*N-*Hexamethyleneiminoethyl)-1*H-*pyridazino[3,4,5-*de*]-phthalazine* (**22**g)

To a suspension of **2** (8.5 g) in methanol (200 mL) was added *N*-(2-chloroethyl)hexamethyleneimine hydrochloride (9.9 g) in methanol (100 mL) followed by 1 *N* sodium hydroxide (100 mL). It was stirred 3 h at reflux and then evaporated to dryness at reduced pressure. The dark residue was chromatographed in 5:1 benzene–dimethylformamide on Woelm neutral alumina, grade I, with 100 mL fractions eluted. The second fraction yielded 5.2 g of yellow solid, which was recrystallized from benzene (20 mL) – hexane (300 mL) with charcoal to afford pure **22***g*, mp 117–121°C; ir (N): 1620, 1600, 1535; $^1$Hmr: 1.55 (s, 4C$H_2$), 2.7 (m, 2C$H_2$—N), 2.9 (t, C$H_2$, $J$ = 7), 4.3 (t, C$H_2$, $J$ = 7), 7.55–8.05 (m, 3*H*, aryl), 8.1 (s, *H* at C-3), 8.95 (s, *H* at C-7).

Can. J. Chem. Downloaded from www.nrcresearchpress.com by 210.87.254.6 on 09/06/12
For personal use only.

By the same method, *1*-trans-*cinnamyl-1*H-*pyridazino[3,4,5-de]phthalazine* was obtained after chromatography in a crude yield of 35%, mp 135–140°C. It was twice recrystallized from ethanol to afford pure **22***c*, mp 147–149°C; ir (N): 1620, 1595, 1530; $^1$Hmr: 4.95 (d, C$H_2$, $J$ = 5), 6.6 (dt, C*H*, $J$ = 5, 16), 6.8 (d, C*H*, $J$ = 16), 7.25–8.05 (m, 8*H*, aryl), 8.15 (s, *H* at C-3), 9.0 (s, *H* at C-7).

*1-(2-Pyridylethyl)-1*H-*pyridazino[3,4,5-de]phthalazine (22i)*

A mixture of **2** (8.5 g), 2-vinylpyridine (20 mL), glacial acetic acid (125 mL), and anhydrous cupric sulphate (50 mg) was stirred 4 h at 135–140°C, then evaporated to dryness at 100°C/12 Torr. The residue was triturated with water, well cooled, and the crude product (6.6 g, mp 150–153°C) twice recrystallized from methanol with charcoal to afford pure **22***i*, mp 160–161°C; ir (N): 1620, 1590, 1565, 1540; $^1$Hmr: 3.3 (dd, C$H_2$, $J$ = 9, 7.5), 4.6 (dd, C$H_2$, $J$ = 9, 7.5), 7.2–7.9 (m, 6*H*, aryl + 3 pyridyl), 8.05 (s, *H* at C-3), 8.55 (dd, *H* at C-6), 8.9 (s, *H* at C-7).

*1-(2-Cyanoethyl)-1*H-*pyridazino[3,4,5-de]phthalazine (22e)*

A mixture of **2** (10.2 g), Triton B (2 mL), acrylonitrile (12 mL), and 50% aqueous pyridine (500 mL) was stirred at reflux for 1 h, concentrated to dryness at reduced pressure, triturated with water, and filtered. The residual solid (10.1 g, mp 195–197°C) was combined with 5.1 g from a one-half scale run, dissolved largely in 400 mL of chloroform, filtered, and the chloroform solution treated with hexane (800 mL) and cooled. The precipitate which formed (12.3 g, mp 197–199°C) was chromatographed on Woelm neutral alumina, grade I (450 g), with ethyl acetate as eluent. After removal of an impurity with 1 L of solvent, acetone was used as eluent and 500 mL fractions taken. Fractions 4 to 7 were combined, concentrated to dryness, and recrystallized from benzene to give pure **22***e* (4.8 g), mp 203–206°C; ir (N): 2250, 1620, 1600, 1540; $^1$Hmr: 3.15 (t, C$H_2$, $J$ = 7), 4.5 (t, C$H_2$, $J$ = 7), 7.45–8.05 (m, 3*H*, aryl), 8.2 (s, *H* at C-3), 8.9 (s, *H* at C-7).

*1-(2-Carboxyethyl)-1*H-*pyridazino[3,4,5-de]phthalazine (22f)*

A mixture of **22***e* (11.15 g) and 10% sodium hydroxide (200 mL) was heated 1 h at reflux. The yellow solution was cooled, acidified to pH 4 with 6 *N* HCl, and the crystalline product which formed (9.7 g, mp 245–247°C) was recrystallized twice from wet ethanol to afford **22***f* (4.2 g), mp 251.5–253.5°C; ir (N): 3300, ~2400 (broad), ~1900 (broad), 1715, 1615, 1595, 1520; $^1$Hmr: 2.8 (t, C$H_2$, $J$ = 7.5), 4.4 (t, C$H_2$, $J$ = 7.5), 7.55–8.0 (m, 3*H*, aryl), 8.1 (s, *H* at C-3), 8.95 (s, *H* at C-7), *OH* of carboxyl not visible.

*8-Hydroxymethyl-2-phenyl-1(2*H*)phthalazinone (24)*

The ester **10***c* (5.9 g) suspended in diglyme (15 mL) was treated portionwise with lithium borohydride (0.6 g) in diglyme (20 mL), the whole heated 4 h at 70°C, cooled, and treated cautiously with water. A pale off-white solid precipitated (4.2 g). It was recrystallized once from methanol and twice from benzene to afford colourless needles, mp 178–180°C; ir ($CHCl_3$): 3450, 1635, 1580; $^1$Hmr: 5.15–5.5 (m, C$H_2$, O*H*), 7.45–7.7 (m, 5*H*, phenyl), 7.7–8.3 (3*H*, aryl), 8.6 (s, vinyl *H*).

When the reaction was carried out with twice the amount of lithium borohydride at 70°C for 6 h, work-up yielded 4.1 g of solid. Two recrystallizations from methanol gave 2.66 g of *8-hydroxymethyl-2-phenyl-1,2-dihydrophthalazine (25)*, mp 122–124°C; ir (N): 3280, 3180, 1595, 1560; $^1$Hmr: 4.6 (d, C$H_2$—O, $J$ = 6), 4.9 (s, C$H_2$ at C-1), 5.3 (t, O*H*), 6.9–7.5 (m, 8*H*, aryl), 8.55 (s, *H* at C-3).

*Phenylhydrazone of 23*

To a stirring solution of phenylhydrazine (25 mL) in ethanol (100 mL) was added 3-hydroxyphthalide-7-carboxaldehyde (1) (3.56 g) and the mixture heated 22 h at reflux. After 1.5 h, a yellow precipitate formed. The mixture was cooled to room temperature and the solid collected, washed thoroughly with ethanol, and twice recrystallized from 2-methoxyethanol to give the pure phenylhydrazone of *8-formyl-2-phenyl-1(2*H*)-phthalazinone* (4.77 g, 70%), mp 264°C; ir (N): 3250, 1645, 1600, 1550, 1530; $^1$Hmr: 6.8–8.7 (m, 13*H*, aryl + *H* at C-4), 9.65 (s, —C*H*=N on C-8), 10.8 (s, N*H*).

*Methanesulphonate of 2*

Treatment of **2** with an equimolar amount of methanesulphonic acid in methanol followed by ether gave the salt, mp 288–293°C dec., after two recrystallizations from dimethylformamide; ir (N): 3280, ~2600 (broad), 1635, 1600, 1500; $^1$Hmr ($D_2O$): 2.9 (s, C$H_3$—S), 8.1–8.5 (m, 3*H*, aryl), 8.8 (s, protons at C-3 and C-7). *Anal.* calcd. for $C_{10}H_{10}N_4O_3S$: S 12.04; found: S 11.96.

*Methiodide of 2 (28)*

A mixture of **2** (5.1 g), methyl iodide (16 mL), and methanol (200 mL) was stirred at reflux under moisture exclusion for 16 h. It was concentrated to dryness at reduced pressure and recrystallized from methanol. This product (5.23 g, mp 269–270.5°C) was twice recrystallized from methanol to yield pure methiodide, mp 279–281°C; ir (N): 1640, 1610, 1585, 1510; $^1$Hmr: 4.3 (s, C$H_3$), 8.15–8.5 (m, 3*H*, aryl), 8.6 (s, C*H*=N—), 9.85 (s, C*H*=$\overset{+}{\text{N}}$=), 13.4 (s, N*H*). *Anal.* calcd. for $C_{10}H_{10}N_4I$: I 40.66; found: I 40.63.

In a similar way, the *ethiodide* was prepared in 60% crude yield and purified by two recrystallizations from ethanol, mp 260–262°C; ir (N): 1640, 1610, 1585, 1510; $^1$Hmr: 1.6 (t, C$H_3$, $J$ = 7), 4.5 (q, C$H_2$, $J$ = 7), 8.1–8.5 (m, 3*H*, aryl), 8.6 (s, C*H*=N—), 9.8 (s, C*H*=$\overset{+}{\text{N}}$=), 13.6 (s, N*H*). *Anal.* calcd. for $C_{11}H_{11}N_4I$: I 38.91; found: I 39.02.

*Conversion of 28 to 29*

Silver nitrate (1.7 g) was dissolved in a minimal quantity of water, treated with 1 *N* sodium hydroxide (10 mL) and then quickly with **28** (3.12 g) dissolved in warm methanol (200 mL). The mixture was stirred at 65°C for 20 min and the dark brown mixture filtered. The filtrate was concentrated to dryness at reduced pressure to a dark red solid. This was taken up in hot chloroform, filtered, and the filtrate evaporated at reduced pressure to a brick red solid, mp ~190°C dec. A portion of this (460 mg) was suspended in methanol (35 mL), treated with methyl iodide (2 mL), and the whole refluxed 32 h under moisture exclusion. The mixture was cooled and filtered and the orange-yellow crystals collected (151 mg), mp 312–315°C dec. The methiodide was recrystallized from dimethylformamide to afford orange-yellow needles, mp 313–314°C dec.; ir (N): ~2500 (broad), 1610, 1580, 1540; $^1$Hmr: 4.1 (s, 2C$H_3$), 7.9–8.25 (m, 3*H*, aryl), 9.1 (s, 2C*H*=$\overset{+}{\text{N}}$=). *Anal.* calcd. for $C_{11}H_{11}N_4I$: I 38.91; found: I 38.78.

*5-Carboxy-3,4-dihydro-2-methyl-4-oxophthalazinium hydroxide, inner salt (17)*

A mixture of **9***a* (41 g), methyl *p*-toluenesulphonate (35 mL), and chlorobenzene (100 mL) was heated under nitrogen at reflux for 18 h, more chlorobenzene added (150 mL), and reflux continued another 30 h. The mixture was filtered hot and the white precipitate collected, washed with chlorobenzene, then cyclohexane, and oven dried under vacuum at 120°C. The *p-toluenesulphonate salt of 17* (66 g, 84%), mp 205–207°C, was analytically pure; ir (N): ~2400 (broad), 1725, 1590, 1570, 1505; $^1$Hmr: 2.3 (s, C$H_3$), 3.95 (s, C$H_3$), 4.4 (s, C$H_3$), 7.4 (q, 4*H*, aryl, 1,4-substituted), 8.25–8.65 (m, 3*H*, aryl), 10.2 (s, C*H*=$\overset{+}{\text{N}}$=), 14.6 (s, O*H*).

The tosylate (7.3 g) in warm water (200 mL) was treated dropwise with 2 *N* sodium hydroxide (10 mL). Zinc acetate dihydrate (2.2 g) in water (20 mL) was added, the whole evaporated at reduced pressure at 70°C to ca. 20 mL, and methanol

(240 mL) added. Some solid (0.6 g) formed at once and a second crop (1.6 g) was obtained after overnight refrigeration. The combined material was recrystallized from water to afford colourless plates (1.45 g) which, after drying at 85°C/0.1 Torr for 20 h, gave pure product, mp 302–305°C dec.; ir (N): 1730, 1610, 1550; $^1$Hmr: 3.8 (s, $CH_3O$), 4.1 (s, $CH_3\overset{+}{N}\equiv$), 7.5–7.9 (m, 3*H*, aryl), 8.8 (s, $CH—\overset{+}{N}\equiv$).

*Additional spectral data*

$^1$*Hmr of* ***11****j* (DMSO-$d_6$): 2.1 (m, $CH_2$), 2.65 (t, $CH_2$), 4.0 (t, $CH_2$), 7.3 (s, $C_6H_5$), 7.95 (s, *H* at C-7), 7.75–8.2 (m, 2*H*, aryl), 11.9 (N*H*); ($CDCl_3$): 2.25 (m, $CH_2$), 2.8 (t, $CH_2$), 4.05 (t, $CH_2$), 7.25 (s, $C_6H_5$), 7.75 (s, *H* at C-7), 7.55–8.0 (m, 2*H*, aryl), 8.35 (dd, *H* at C-4, $J$ = 8, 1.5), 11.4 (N*H*).

## Acknowledgements

The authors are grateful to Mr. A. Clemente and Dr. P. Nicolson for microanalytical data, to Mr. D. Spiegel for uv studies, to Mrs. L. Raabis for $^1$Hmr spectra, and to Miss C. Signor and Miss L. Samoyedna for ir spectra. The cardiovascular test results were supplied by Drs. S. J. Ehrreich, R. Lee, M. Antonaccio, and R. Tanz, anti-inflammatory tests by Mrs. M. L. Graeme, the toxicology results by Dr. R. Katz, and the absorption studies by Dr. G. Lucas. We also thank Dr. R. Rodebaugh for helpful discussions related to the $^1$Hmr data.

1. J. E. Francis, K. J. Doebel, P. M. Schutte, E. C. Savarese, S. E. Hopkins, and E. F. Bachmann. Can. J. Chem. **57**, 3320 (1979).
2. J. Druey and J. Tripod. *In* Antihypertensive agents. *Edited by* E. Schlittler. Academic Press, New York. 1967. Chapt. 6.
3. J. Druey and B. H. Ringier. Helv. Chim. Acta, **34**, 195 (1951).
4. C. D. Douglass and R. Hogan. Proc. Soc. Exptl. Biol. Med. **100**, 446 (1959).
5. S. Edwards and F. H. Marquardt. Hoppe-Seyler's Z. Physiol. Chem. **350**, 85 (1969).
6. S. Biniecki, A. Hasse, J. Izdebski, E. Kesler, and L. Rylski. Bull. Acad. Polon. Sci. Ser. Sci. Chim. **6**, 227 (1958); Chem. Abstr. **52**, 18424f (1958).
7. J. C. E. Simpson. *In* The chemistry of heterocyclic compounds. Vol. 5. *Edited by* A. Weissburger. Interscience Publishers Inc., New York. 1953. Chapt. 13.
8. V. Kolesnikov and E. Bisagni. Chim. Ther. **2**, 250 (1967); Chem. Abstr. **69**, 19105j (1968).
9. S. Gabriel and A. Neumann. Chem. Ber. **26**, 521 (1893).
10. R. von Rothenburg. J. Prakt. Chem. **51**, 140 (1895).
11. S. Gabriel and A. Neumann. Chem. Ber. **26**, 705 (1893).
12. T. Ikeda, S. Kanahara, and K. Aoki. Yakugaku Zasshi, **88**, 521 (1968); Chem. Abstr. **69**, 86934s (1968).
13. A. N. Kost, S. Foldeak, and K. Grabliauskas. Khim.-Farm. Zh. **1**, 43 (1967); Chem. Abstr. **67**, 100090f (1967).
14. A. N. Kost, K. Grabliauskas, V. Vinokurov, and A. Zhakun. J. Prakt. Chem. **312**, 542 (1970); Chem. Abstr. **73**, 98881t (1970).
15. Y. Maki, M. Suzuki, T. Furuta, M. Kawamura, and M. Kuzuya. J. Chem. Soc. Perkin Trans. I, 1199 (1979).
16. N. Dennis, A. R. Katritzky, and M. Ramaiah. J. Chem. Soc. Perkin Trans I, 1506 (1975).
17. M. J. Cook, A. R. Katritzky, A. D. Page, and M. Ramaiah. J. Chem. Soc. Perkin Trans. II, 1184 (1977).
18. N. Dennis, A. R. Katritzky, and M. Ramaiah. J. Indian Chem. Soc. **55**, 1235 (1978).
19. K. Fujii and S. Sato. Annu. Rep. G. Tanabe and Co. Ltd. **1**, 1 (1956); Chem. Abstr. **51**, 6650c (1957).
20. G. Vanags and M. Matskanova. Zh. Obshch. Khim. **26**, 1749 (1956); Chem. Abstr. **51**, 1944f (1957).
21. A. Albert and G. Barlin. J. Chem. Soc. 3129 (1962).
22. Chem. Abstr. **74**, 140376e (1971); **84**, 179558x (1976); **89**, 146857u (1978); **89**, 157617a (1978).
23. E. L. Eliel and D. E. Rivard. J. Org. Chem. **17**, 1252 (1952).
24. H. Sato, S. Horie, N. Sekikawa, and H. Ono. U.S. Patent No. 4,096,143, June 20, 1978.
25. (*a*) R. L. Hinman and D. Fulton. J. Am. Chem. Soc. **80**, 1895 (1958); (*b*) W. J. Theuer and J. A. Moore. J. Org. Chem. **29**, 3734 (1964); (*c*) F. E. Condon. J. Org. Chem. **37**, 3608 (1972); (*d*) N. P. Peet and S. Sunder. J. Org. Chem. **40**, 1909 (1975); (*e*) N. P. Peet, S. Sunder, and R. J. Cregge. J. Org. Chem. **41**, 2733 (1976).
26. R. C. Wade (*Editor*). Sodium borohydride, potassium borohydride: a manual of techniques. Metal Hydrides Inc. 1958. p. 28.
27. E. Wenkert, D. B. R. Johnston, and K. G. Dave. J. Org. Chem. **29**, 2534 (1964).
28. M. J. Perkins. J. Chem. Soc. 3005 (1964).
29. M. Brown. J. Chem. Eng. Data, **12**, 612 (1967).
30. W. J. McKillip, E. A. Sedor, B. M. Culbertson, and S. Wawzonek. Chem. Rev. **73**, 255 (1973).
31. H. Goldblatt. J. Exp. Med. **59**, 347 (1934).
32. K. S. Grimson. Arch. Surg. London, **43**, 284 (1941).

Can. J. Chem. Downloaded from www.nrcresearchpress.com by 210.87.254.6 on 09/06/12
For personal use only.

# The bromination–methanolysis of *N*-acetyl-2,3-dimethylindole[1]

SUSAN F. VICE AND GARY I. DMITRIENKO[2]

*The Guelph–Waterloo Centre for Graduate Work in Chemistry, Waterloo Campus, Department of Chemistry, University of Waterloo, Waterloo, Ont., Canada N2L 3G1*

Received October 15, 1981

SUSAN F. VICE and GARY I. DMITRIENKO. Can. J. Chem. **60**, 1233 (1982).

Bromination of *N*-acetyl-2,3-dimethylindole **11** in the presence of excess methanol at room temperature gave a mixture of products consisting of *cis* and *trans* *N*-acetyl-2,3-dimethoxy-2,3-dimethylindoline **17** and **18**, 3-methoxy-2,3-dimethylindolenine **19**, and *N*-acetyl-3-methoxymethyl-2-methylindole **21**. The same reaction performed at −40°C yielded a mixture of **17**, **18**, and *N*-acetyl-2-methoxy-2-methyl-3-methyleneindoline **22**. Bromination of **11** at low temperature in the presence of 1.5 equivalents of methanol followed by treatment with triethylamine yielded **22** quantitatively. Treatment of **22** with acidic methanol readily gave **21**. The mechanistic implications of these transformations are considered.

SUSAN F. VICE et GARY I. DMITRIENKO. Can. J. Chem. **60**, 1233 (1982).

La bromation du *N*-acétyl diméthyl-2,3 indole **11**, en présence d'un excès de méthanol et à température ambiante, donne un mélange de produits comprenant les *N*-acétyl diméthoxy-2,3 diméthyl-2,3 indolines *cis* et *trans* **17** et **18**, le méthoxy-3 diméthyl-2,3 indolenine **19** et du *N*-acétyl méthoxyméthyl-3 méthyl-2 indole **21**. La même réaction effectuée à −40°C donne un mélange des isomères **17** et **18** et de *N*-acétyl méthoxy-2 méthyl-2 méthylène-3 indoline **22**. La bromation du composé **11** à basse température, en présence de 1,5 équivalent de méthanol, suivie d'une réaction avec la triéthylamine donne quantitativement le composé **22**. Ce dernier, en présence de méthanol acidulé, donne facilement le composé **21**. On considère le mécanisme de ces transformations.
[Traduit par le journal]

In connection with our interest in the development of new methods for the synthetic elaboration of 2,3-dialkylindoles **1**, we have recently reported the preparation of 3-methoxyindolenines **7** by bromination–methanolysis of 2,3-dialkylindoles (1). In the presence of triethylamine the corresponding bromindolenines **3** are moderately stable intermediates. Acidification of a solution of **3** in the presence of methanol has been shown to lead to the rapid formation of the methoxyindolenine **7**. We have argued (1*c*) that the methanolysis process likely proceeds via addition of methanol to the *N*-protonated bromoindolenine **2** to give, after deprotonation, the 2-methoxy-3-bromoindoline **4** (see Scheme 1). $S_N1$ type methanolysis of **4** would yield **6** ($R^1$ = H) which upon loss of methanol would generate the methoxyindolenine **7**.

We felt that an examination of the bromination–methanolysis of an *N*-acyl-2,3-dialkylindole **1** ($R^1$ = Ac) might offer some further insight into the nature of the intermediates involved in such processes. As a result, we have examined the bromination–methanolysis of *N*-acetyl-2,3-dimethylindole **11** and report the results of this investigation herein.

A survey of the literature revealed that the only previous studies of the bromination of *N*-acyl-2,3-

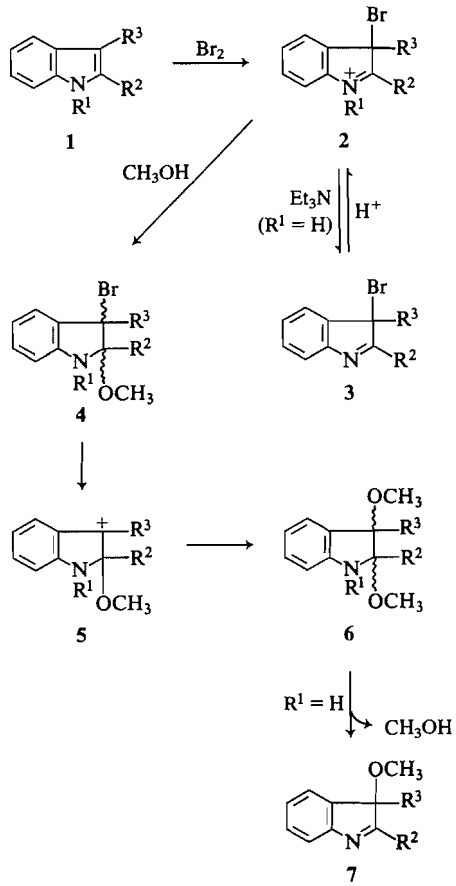


SCHEME 1

[1]Presented in part at the 64th Annual Conference of the Chemical Institute of Canada, Halifax, Canada, May 31–June 3, 1981, Abstract No. ORTA9.

[2]Author to whom communications may be addressed.

0008-4042/82/101233-05$01.00/0

©1982 National Research Council of Canada/Conseil national de recherches du Canada

Can. J. Chem. Downloaded from www.nrcresearchpress.com by 210.87.254.6 on 09/06/12
For personal use only.

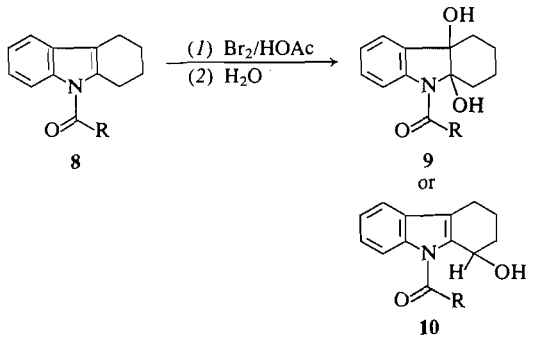


SCHEME 2

dialkylindoles were those reported by Plant and Tomlinson (2).[3] The bromination of several *N*-acetyltetrahydrocarbazoles **8** with bromine in acetic acid followed by addition of water yielded either *N*-acyl-2,3-dihydroxyindolines **9** or C2-side-chain hydroxylated products **10** (2*a*) (see Scheme 2). There was no apparent correlation between the nature of the *N*-acyl group and the nature of the product produced. In all cases products were isolated in low yield. Of the compounds examined by Plant and Tomlinson, *N*-acetyl-2,3-dimethylindole **11** was studied in greatest detail (2*b*). In this case the product of bromination–hydrolysis was *N*-acetyl-2-hydroxymethyl-3-methylindole **12** (see Scheme 3). In addition, a monobrominated product assumed to be *N*-acetyl-2-bromomethyl-3-methylindole **13** was isolated if the hydrolytic step was avoided. Hydrolysis of **13** in the presence of silver oxide yielded **12**, which upon alkaline hydrolysis gave **14**. Some years later, Taylor (3) provided proof for the assigned structure for **14** by an unambiguous synthesis.

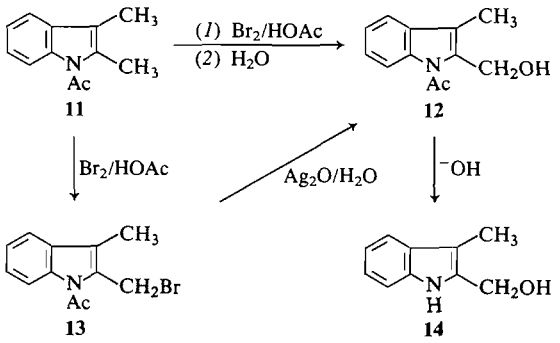


SCHEME 3

The formation of **13** was rationalized as shown in Scheme 4. Bromination of **11** was assumed to give the dibromide **15** which upon elimination of HBr yielded the allylic bromide **16**. Allylic rearrangement of **16** would yield **13** and regenerate the aromatic indole ring system.

In our hands, bromination of **11** in glacial acetic acid as described by Plant and Tomlinson (2*b*) or in methylene chloride gave **13** as the sole product with spectroscopic characteristics compatible with the assigned structure (1*a*). On the other hand, bromination of **11** at room temperature in methanol gave a mixture of products which were separated by column chromatography (Scheme 5). Two of the products were readily recognizable as the dimethoxyindolines **17** and **18**. The proton nmr spectra of the major and minor isomers are compared in Table

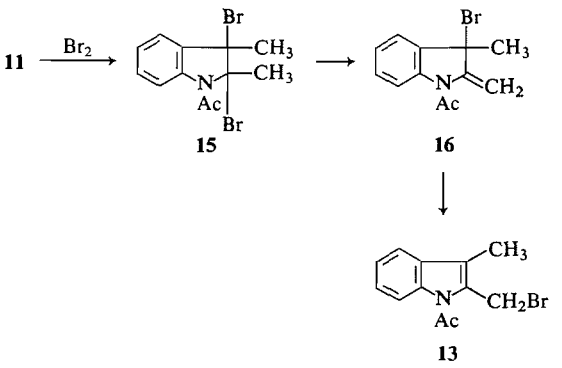


SCHEME 4

1. Although we suspect that the major isomer is the *trans*-product **17** and the minor isomer the *cis*-product **18**, the available data does not allow an unambiguous assignment. A very minor product identified in the mixture was 3-methoxy-2,3-dimethylindolenine **19** arising presumably via deacylation of **17** or **18**. In addition a crystalline product, **A**, with elemental composition $C_{13}H_{15}NO_2$ was isolated in 30% yield. Initially, we felt that **A** was *N*-acetyl-2-methoxymethyl-3-methylindole **20**, derivable, in principle, by methanolysis of **13**.

Since **17** and **18** are structurally analogous to the dihydroxyindolines produced in the bromination–hydrolysis of *N*-acyl tetrahydrocarbazoles, and since the monomethoxylated product **A** seemed to be an analog of **12** produced in the bromination–hydrolysis of **11**, it appeared that no new mechanistic information could be gleaned from our product study of the bromination–methanolysis of **11**. However, when authentic *N*-acetyl-2-methoxymethyl-3-methylindole **20** (see Scheme 6) was prepared by methanolysis of **13** it was found to be not identical with **A**. The similarity of the spectroscopic properties of **A** and **20** clearly required that **A** be the isomeric *N*-acetyl-3-methoxymethyl-2-methylindole **21**. This surprising finding prompted us to explore the bromination–methanolysis process further. We have found that, when the reaction is performed at

[3]For corrections of some of the work described by these authors see ref. 1*a*.

Can. J. Chem. Downloaded from www.nrcresearchpress.com by 210.87.254.6 on 09/06/12
For personal use only.

TABLE 1. Nuclear magnetic resonance spectral data: **17/18***

| | C2 or C3—$CH_3$ | C3 or C2—$CH_3$ | —C(=O)—$CH_3$ | C2 or C3—$OCH_3$ | C3 or C2—$OCH_3$ |
|---|---|---|---|---|---|
| Major isomer | 1.46 | 1.76 | 2.36 | 2.87 | 3.07 |
| Minor isomer | 1.53 | 1.76 | 2.42 | 3.22 | 3.47 |

*All signals quoted are 3 proton singlets and chemical shifts are quoted on the δ scale.

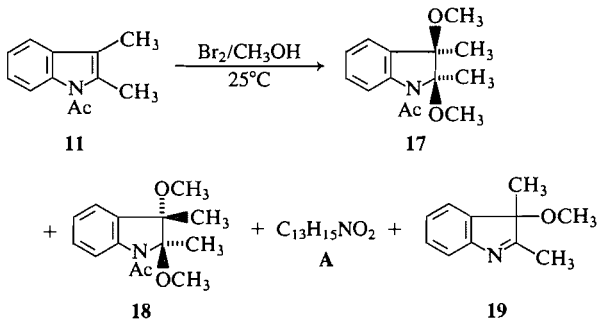


SCHEME 5

low temperature (−40°C), **21** is not observed. Instead, in addition to **17** and **18**, another isomer of **21**, compound **B**, with spectroscopic properties compatible with **22** or **23**, was obtained in 15% isolated yield.

It was also found that **B** was very likely a precursor to **21** in the room temperature bromination–

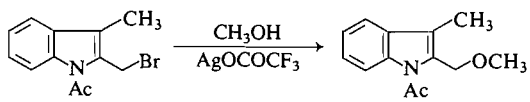


SCHEME 6

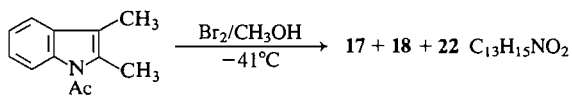


SCHEME 7

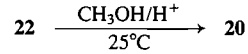


SCHEME 8

methanolysis of **11**, since treatment of **B** at room temperature with *p*-toluenesulfonic acid in methanol gave **21** in good yield. This chemical relationship between **B** and **21** clearly suggested that **B** was **22** and not **23**. This was confirmed by the synthesis of authentic **23** by the reaction of 3-methoxy-2,3-dimethylindolenine with acetic anhydride in pyridine (see Scheme 9). The most notable difference in the proton nmr spectra of **22(B)** and **23** is the fact that the methylene hydrogens in the former case appear as two one-proton singlets at δ 5.17 and 5.68 ppm whereas the methylene hydrogens in the latter case appear as two one-proton doublets ($J$ = 2.0 Hz) at δ 5.10 and 5.38 ppm. In the $^{13}C$ spectra the methylene carbon of **22** appears at 104.5 ppm, significantly downfield from that of **23** at 96.8 ppm, reflecting the expected higher electron density of the β-carbon of the "enamide" system of **23**.

Although the formation of **21** seemed, at first, surprising in light of earlier results on bromination–hydrolysis of *N*-acetyl-2,3-dimethylindole, a re-examination of the mechanism suggested earlier for the bromination–methanolysis of 2,3-dialkyl-

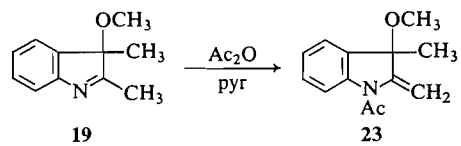


SCHEME 9

indoles suggests that the formation of **21** and **22** can be readily rationalized with a minimum of additional mechanistic assumptions. Thus if the bromination of **11** proceeds as suggested for **1** in Scheme 1 (see Scheme 10), one would expect that in the presence of methanol a C2-methoxy-C3-bromoindoline **25** analogous to **4** would be produced. $S_N1$ type methanolysis of **25** via the stabilized carbonium ion **26** would give the mixture of dimethoxyindolines **17** and **18**. In addition, $E_1$ or possibly $E_2$ type elimination of HBr from **25** would give **22** at low temperature, and acid-catalyzed reaction of **22** with methanol would give the allylic rearrangement product **21** observed in the room temperature bromination–methanolysis of **11**.

Thus all of the observed products can be readily rationalized on the assumption that the 2-methoxy-3-bromoindoline **25** is an intermediate and hence our confidence in the intermediacy of **25** in such processes is bolstered. Furthermore, our confidence in the existence of **25** in the formation of **22** and **17** and **18** suggested that the formation of **22** might be favoured by the use of triethylamine to catalyze $E_2$ type elimination. It was found that bromination of **11** in methanol containing excess triethylamine led to a substantial increase in the ratio of **22** to **17** and **18**. However, under these conditions triethylamine

Can. J. Chem. Downloaded from www.nrcresearchpress.com by 210.87.254.6 on 09/06/12
For personal use only.

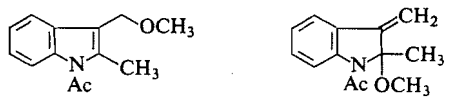


A ≡ 21 B ≡ 22

FIG. 1

catalyzes a reaction between methanol and bromine and as a result a large amount of unreacted **11** remained. Further experimentation has led us to the discovery that **22** can be produced quantitatively from **11** via a two-stage process. Thus treatment of **11** with one equivalent of bromine in methylene chloride in the presence of a limited amount of methanol (1.5 equivalents) at low temperature (−78°C) gives a colourless solution which upon treatment with triethylamine and aqueous work-up yields **22**.

This transformation not only represents a facile route to a relatively rare example of a C3-alkylidene indoline, but, coupled with the facile conversion of **22** to **21**, also represents a potentially simple and efficient route to C3 side-chain functionalization of 2,3-dialkylindoles.[4] Continuing studies in our laboratory are aimed at exploiting the synthetic utility of these transformations in the preparation of more complex indole-derived natural products.

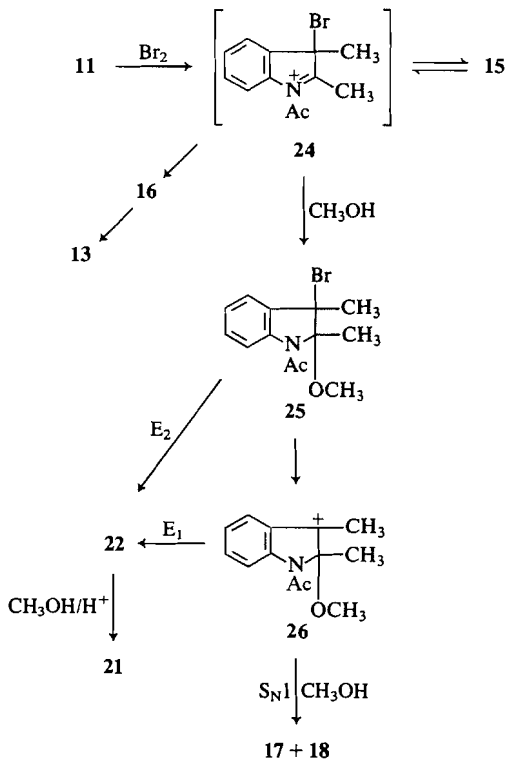


SCHEME 10

[4]For an example of the preparation of a C3-alkylidene indoline by reaction of singlet oxygen with C3-vinylindoles, see ref. 4.

## Experimental

Melting points were determined on a Fisher Mel-temp melting point apparatus and are uncorrected. Infrared spectra were recorded on a Beckman IR-10 spectrometer and the frequency ($cm^{-1}$) of significant peaks is reported. A Beckman Model 35 spectrophotometer was used for uv spectra and wavelengths (nm) of absorption bands are reported followed by extinction coefficients (ε) in parentheses. Nuclear magnetic resonance spectra were recorded on a Varian T-60 or Bruker WP80 spectrometer (chloroform-*d* solvent unless otherwise indicated) and chemical shifts are reported on the δ scale, followed in parentheses by an account of the multiplicity and number of protons concerned. Mass spectra were recorded on a VG-7070 mass spectrometer. Microanalyses were performed by Galbraith Laboratories and Guelph Chemical Laboratories. *N*-Acetyl-2,3-dimethylindole was prepared by the method of Dave and Warnhoff (5).

*Bromination of* N-*acetyl-2,3-dimethylindole* ***11*** *in methylene chloride*

*N*-Acetyl-2,3-dimethylindole **11** (0.510 g; 2.73 mmol) was dissolved in methylene chloride (30 mL) and cooled in an ice bath. A solution of bromine (1.1 equivalents) in methylene chloride (3.8 mL) was added dropwise with stirring in a nitrogen atmosphere. After five minutes the solvent was removed *in vacuo* to yield *N*-acetyl-2-bromoethyl-3-methylindole **13** quantitatively as a homogeneous crystalline solid which soon turned purple upon exposure to a normal atmosphere; uv ($CH_2Cl_2$): 290 (11 480); $^1$H nmr: 2.23 (s, 3, C3—$CH_3$), 2.76 (s, 3, —CO—$CH_3$), 5.01 (s, 2, —$CH_2$—Br), 7.02–7.90 (m, 4, Ar—H). Molecular ions at *m/e* 267 ($m^+$ $^{81}$Br) and *m/e* 265 ($m^+$ $^{79}$Br).

An analogous result was obtained with acetic acid rather than methylene chloride as solvent.

*Methanolysis of* N-*acetyl-2-bromomethyl-3-methylindole*

To a stirred solution of *N*-acetyl-2-bromomethyl-3-methylindole **13** (0.426 g; 1.60 mmol) in methanol (50 mL) was added silver trifluoroacetate (0.365 g; 1.76 mmol). The mixture was stirred for 20 min in a nitrogen atmosphere and then filtered through Celite. The Celite was washed with methylene chloride. The combined filtrate was washed with water and saturated aqueous sodium chloride. The organic phase was dried over anhydrous sodium sulfate and evaporated to dryness on a rotary evaporator to give *N*-acetyl-2-methoxymethyl-3-methylindole in 90% yield as a homogeneous viscous oil which could not be induced to crystallize. Infrared (neat): 1675 (s, C=O); uv MeOH: 237 (16 900), 260 (10 700), 288 (6500), 297 (6370); $^1$H nmr: 2.26 (s, 3, C3—$CH_3$), 2.72 (s, 3, —CO$CH_3$), 3.32 (s, 3, —$OCH_3$), 4.66 (s, 2, C2—$CH_2$), 7.19–7.53 (m, 3, C4,5,6—H), 8.09–8.21 (m, 1, C7—H). *Exact mass* calcd. for. $C_{13}H_{15}NO_2$: 217.1103; found: (ms): 217.1093.

*Preparation of* N-*acetyl-2-methyl-3-methoxymethylindole* ***21***

To a solution of *N*-acetyl-2-methoxy-2-methyl-3-methylene indoline **22** in methylenechloride prepared from *N*-acetyl-2,3-dimethylindole (0.216 g; 1.15 mmol) as described below was added methanol (40 mL) followed by a solution of *p*-toluenesulfonic acid (0.360 g) in methanol (2 mL) at room temperature. After 15 min the mixture was washed with water, 10% aqueous ammonia, and saturated aqueous sodium chloride. Removal of solvent from the dried organic phase *in vacuo* yielded **21** as a crystalline solid in quantitative yield. This material was identical in all respects with material isolated from the room temperature bromination of **11**, mp 55°C.

Can. J. Chem. Downloaded from www.nrcresearchpress.com by 210.87.254.6 on 09/06/12
For personal use only.

Can. J. Chem. Downloaded from www.nrcresearchpress.com by 210.87.254.6 on 09/06/12
For personal use only.

*Preparation of* N-*acetyl-2-methoxy-2-methyl-3-methylene indoline* **22**

To a solution of *N*-acetyl-2,3-dimethylindole **11** (0.101 g; 0.54 mmol) in methylene chloride (40 mL) containing methanol (0.81 mmol, 1.5 equivalents) cooled to −78°C was added dropwise a solution of bromine (0.59 mmol) in methylene chloride (0.76 mL). After 20 min, triethylamine (0.11 mL; 1.5 equivalents) was added and the solution allowed to warm to room temperature. Methylene chloride (20 mL) was added and the organic phase was washed with water and saturated aqueous sodium chloride. Removal of solvent from the dried organic phase *in vacuo* gave a quantitative yield of **22** as a colourless thick oil which could not be induced to crystallize and which darkened rapidly on standing. Infrared (neat): 1665, (N—$COCH_3$); uv ($CHCl_3$): 250 (18 200), 268 (14 400), 317 (3770), 327 (3580); $^1$H nmr: 1.74 (s, 3, C2—$CH_3$), 2.49 (s, 3, —$COCH_3$), 3.03 (s, 3, $OCH_3$), 5.22 (s, 1, =$CH_2$), 5.72 (s, 1, =$CH_2$), 6.96–7.55 (m, 3, C4,5,6—H), 8.36–8.46 (m, H, C7—H). *Exact mass* calcd. for $C_{13}H_{15}NO_2$: 217.1103; found (ms): 217.1100.

*Preparation of* N-*acetyl-3-methoxy-3-methyl-2-methylene-indoline* **23** *from 2,3-dimethyl-3-methoxyindolenine* **19**

To a solution of freshly prepared 2,3-dimethyl-3-methoxy indolenine **19** (1) (0.292 g; 1.68 mmol) in pyridine (2 mL) was added acetic anhydride (1 mL). The solution was heated at 100°C in a nitrogen atmosphere for 19 h. Methylene chloride (20 mL) was added and the solution was washed with water and saturated aqueous sodium chloride solution. The organic phase was dried over anhydrous sodium sulfate and evaporated to dryness on a rotary evaporator.

The residue was chromatographed on silica gel with elution by a 1:1 mixture of ether – petroleum ether (60–80°C) to give **23** as colourless analytically pure crystals, mp 52–54°C, in 42% yield. Infrared ($CHCl_3$): 1657 (C=O); uv (MeOH): 257 (13 400), sh 312 (1500); $^1$H nmr: 1.58 (s, 3, C3—$CH_3$), 2.54 (s, 3, —$COCH_3$), 2.90 (s, 3, —$OCH_3$), 5.10 (d, $J$ = 2 Hz, 1, C2=C$H_2$), 5.38 (d, $J$ = 2 Hz, 1, C2=C$H_2$); ms *m/e* 217 (molecule ion). *Anal.* calcd. for $C_{13}H_{15}NO_2$: C 71.86, H 6.96, N 6.45; found: C 71.94, H 6.89, N 6.58.

*Low temperature bromination – methanolysis of* N-*acetyl-2,3-dimethylindole*

To a cooled (−40°C) solution of **11** (0.538 g; 2.87 mmol) in methanol (175 mL) was added dropwise a solution of bromine (1.0 equivalents) in acetic acid (3.7 mL). After four minutes the solution was poured into cold aqueous (10% v/v) ammonia and the mixture was extracted with methylene chloride. The organic phase was washed with saturated aqueous sodium chloride and dried over anhydrous sodium sulfate. Removal of solvent *in vacuo* yielded a brown oily product (0.76 g). The crude mixture was chromatographed on silica gel with elution by a step-wise gradient of ether – petroleum ether (60–80°C) increasing in ether content in 5% increments at 100-mL intervals from 10% to 50% v/v.

The first material eluted was **11** (0.021 g; 0.11 mmol). Further elution gave **22** (0.093 g; 0.43 mmol) as a colourless oil which darkened on standing, could not be induced to crystallize, and was identical in all respects with the material obtained by stepwise bromination–elimination of **11** described above.

After a number of mixed fractions of **22** and **17** (0.074 g of a 1:4 mixture), pure **17** (0.258 g; 1.04 mmol) was obtained as a crystalline solid, mp 49°C (from petroleum ether (60–80°C)). Infrared (film): 1675 (N$COCH_3$); uv (MeOH): 248 (13 500), 278 sh (2480), 285 sh (1900); $^1$H nmr: 1.46 (s, 3, C3 or C2—$CH_3$), 1.76 (s, 3, C2 or C3—$CH_3$), 2.36 (s, 3, N$COCH_3$), 2.87 (s, 3, C3 or C2—$OCH_3$), 3.07 (s, 3, C2 or C3—$OCH_3$), 6.83–7.70 (m, 4, Ar—H). *Exact mass* calcd. for $C_{14}H_{19}NO_3$: 249.1365; found (ms): 249.1353. *Anal.* calcd. for $C_{14}H_{19}NO_2$: C 67.44, H 7.68, N 5.62; found: C 67.62, H 7.81, N 5.63.

Finally, after a mixed fraction of **17** and **18** (0.109 g, 0.48 mmol), pure **18** (0.060 g; 0.241 mmol) was obtained as a solid, mp 50°C (from petroleum ether (60–80°C)). Infrared (film): 1668 (N—$COCH_3$); uv (MeOH): 250 (11 200), 278 sh (2440), 288 sh (1600); $^1$H nmr: 1.53 (s, 3, C3 or C2—$CH_3$), 1.66 (s, 3, C2 or C3—$CH_3$), 2.42 (s, 3, N$COCH_3$), 3.22 (s, 3, C2 or C3—$OCH_3$), 3.47 (s, 3, C3 or C2—$OCH_3$), 6.98–7.37 (m, 3, C4,5,6—H), 7.91–8.18 (m, 1, C7—H). *Exact Mass* calcd. for $C_{14}H_{19}NO_3$: 249.1365; found (ms): 249.1344. *Anal.* calcd. for $C_{14}H_{19}NO_3$: C 67.44, H 7.68, N 5.62; found: C 67.37, H 7.65, N 5.57.

*Room temperature bromination–methanolysis of* N-*acetyl-2,3-dimethylindole*

To a stirred solution of **11** (1.00 g; 5.35 mmol) in methanol (60 mL) was added dropwise a solution of bromine (1.1 equivalents) in glacial acetic acid (7.6 mL). After 10 min, the mixture was diluted with water (75 mL) and made basic with 10% aqueous ammonia. The mixture was extracted with methylene chloride and the dried organic extract was evaporated to dryness *in vacuo* to yield a brown residue (1.17 g). Part of the crude product (1.09 g) was chromatographed on silica gel with elution by a stepwise gradient of ether – petroleum ether increasing in ether content from 5% to 50% v/v. The first component eluted was the starting material **11** (0.30 g; 1.60 mmol). Further elution gave a mixture of **17** and **21** (0.361 g of a 49:51 mixture) and finally a small fraction (0.007 g) which consisted of a mixture of **18** and **19** in a ratio of 2.8:1.0 as indicated by tlc and nmr analysis.

The mixture of **17** and **21** was chromatographed on silica gel with elution by methylene chloride to give pure **21** as a waxy solid, mp 55°C (white needles from hexane). Infrared ($CHCl_3$): 1700 (C=O); uv: 242 (16 000), 263 (10 300), 289 (4900), 297 (4800); $^1$H nmr: 2.58 (s, 3, C2—$CH_3$), 2.67 (s, 3, C=O—$CH_3$), 3.32 (s, 3, C3—$OCH_3$), 4.50 (s, 2, C3—$CH_2$—), 7.02–8.00 (m, 4, Ar—H); ms *m/e* 217 (molecule ion). *Anal.* calcd. for $C_{13}H_{15}NO_2$: C 71.86, H 6.96, N 6.45; found: C 71.99, H 7.16, N 6.37.

Further elution by methanol – methylene chloride (5:95) gave pure **17** identical in all respects with that obtained from the low temperature bromination–methanolysis.

## Acknowledgements

This work was supported by operating grants from the Natural Sciences and Engineering Research Council of Canada and the University of Waterloo. An NSERC postgraduate scholarship to one of us (S.F.V.) is gratefully acknowledged.

1. (*a*) G. I. DMITRIENKO. Heterocycles, **12**, 1141 (1979); (*b*) G. I. DMITRIENKO, E. A. GROSS, and S. F. VICE. Can. J. Chem. **58**, 808 (1980); (*c*) E. A. GROSS, S. F. VICE, and G. I. DMITRIENKO. Can. J. Chem. **59**, 635 (1981).
2. (*a*) S. G. P. PLANT and M. L. TOMLINSON. J. Chem. Soc. 3324 (1932); (*b*) J. Chem. Soc. 955 (1933).
3. W. I. TAYLOR. Helv. Chim. Acta, **33**, 164 (1950).
4. M. MATSUMOTO and K. KONDO. J. Am. Chem. Soc. **99**, 2393 (1977).
5. V. DAVE and E. W. WARNHOFF. Can. J. Chem. **49**, 1911 (1971).

# Isomerization of acetylenic acids with sodium salt of 1,2-diaminoethane: a one step synthesis of megatomoic acid[1]

S. R. ABRAMS

*Prairie Regional Laboratory, National Research Council of Canada, Saskatoon, Sask., Canada S7N 0W9*

Received December 15, 1981

S. R. ABRAMS. Can. J. Chem. **60**, 1238 (1982).

A number of isomeric tetradecynoic acids were isomerized with the sodium salt of 1,2-diaminoethane. Isomers having the triple bond near the carboxyl group rearranged to *E,Z*-3,5- and *E,E*-3,5-tetradecadienoic acids (**1** and **2**), the former compound being the sex pheromone of the black carpet beetle. Isomers having the triple bond closer to the terminus of the chain afforded some 13-tetradecynoic acid along with **1** and **2**. Delocalized anions **12** and **13** are thought to contribute to the formation of **1** and **2**.

S. R. ABRAMS. Can. J. Chem. **60**, 1238 (1982).

On a isomérisé un certain nombre d'acides tétradécynoïques isomères avec le sel de sodium du diamino-1,2 éthane. Les isomères ayant une triple liaison près du groupe carbonyle se transposent en acides tétradécadiènoiques-*E,Z*-3,5 et *E,E*-3,5 (**1** et **2**). Le premier de ces composés est la phéromone sexuelle de l'abeille de tapis noir. Les isomères ayant une triple liaison tout près de l'extrémité de la chaîne fournissent l'acide tétradécyne-13 oïque ainsi que les acides **1** et **2**. On pense que les anions délocalisés **12** et **13** contribuent à la formation des composés **1** et **2**.

[Traduit par le journal]

## Introduction

Very strong bases isomerize internal triple bonds of hydrocarbons and alkyn-1-ols to the terminal position in high yield. The first successful isomerization reagent, the potassium salt of 1,3-diaminopropane, was discovered by Brown and Yamashita (1, 2). We have developed alternative reagents, the sodium salts of 1,3-diaminopropane (3, 4) or 1,2-diaminoethane,[2] which effect the same transformation and which can be prepared simply, reproducibly, and with greater safety.

In the course of developing a general route for the synthesis of naturally occurring terminally hydroxylated fatty acid derivatives, we sought to extend the use of these reagents to the isomerization of acetylenic acids, anticipating that an internal triple bond would be isomerized to give the terminal acetylenic acid. That is, it was thought that the base would abstract one proton from the carboxylic acid group and another from a carbon next to the triple bond. Protonation would give either the starting acetylenic acid or an allenic isomer. Abstraction by the base of an allenic proton would, after reprotonation, give the allenic acid, the original acetylenic acid, or a positional isomer. In the alkyn-1-ol case, such reversible random rearrangements are rapid with our reagents; the reaction sequence is completed when the terminal triple bond is formed and the relatively acidic acetylenic proton abstracted to give the disodium alkoxide acetylide salt.

Although alkali metal alkyl amides had not previously been employed as isomerization reagents, rearrangements of acetylenic acids with other bases have been carried out. Vigorous treatment with molten alkali results in cleavage of the carbon skeleton (the Varrentrapp reaction) (5). Reaction of 4-hexynoic and 4-pentynoic acids at 120–160°C with 9 *N* potassium hydroxide affords the conjugated 2,4-dienoic acids in good yield (6). Under milder conditions the usual acetylene–allene interconversions are observed; a series of 2-alkynoic acids rearranged by sodium amide in ammonia gives mixtures of 3-alkynoic and 2,3-alkadienoic acids (7). Both potassium carbonate (8) and aqueous sodium hydroxide (9) lead to interconversion of short chain 3-alkynoic, 2,3-alkadienoic, and 2-alkynoic acids.

From the foregoing, base mediated rearrangements of alkynoic acids would be expected to follow a course parallel to that of the acetylenic alcohols. We thus anticipated that isomerization of acetylenic acids with our reagents would proceed rapidly to produce as sole products carboxylic acids containing a terminal triple bond. However, the rearrangement did not take the expected course, but rather followed a novel pathway. We now report a study of alkali metal alkyl amide mediated rearrangements of some isomeric tetradecynoic acids including a one step synthesis of the sex pheromone of the black carpet beetle (Attagenus megatomia), *E,Z*-3,5-tetradecadienoic acid (**1**) (10).

## Results and discussion

The fourteen carbon tetradecynoic acid series was chosen to study triple bond isomerizations because the twelve possible isomers are all easily handled, known compounds (11–13). Interconver-

[1]NRCC No. 20049.

[2]S. R. Abrams. Unpublished results.

0008-4042/82/101238-06$01.00/0

©1982 National Research Council of Canada/Conseil national de recherches du Canada

Can. J. Chem. Downloaded from www.nrcresearchpress.com by 210.87.254.5 on 09/06/12
For personal use only.

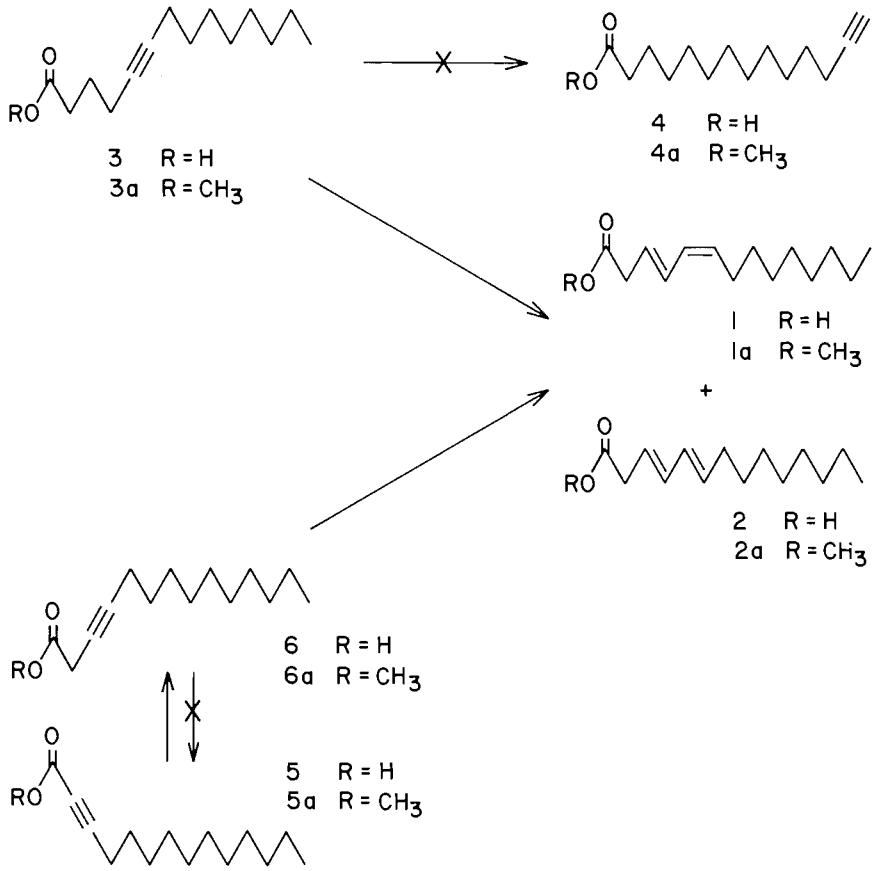


FIG. 1. Products of rearrangement of 2-, 3-, 5-tetradecynoic acid with sodium salt of 1,2-diaminoethane.

sions could be conveniently followed by gas chromatographic analysis of the methyl esters. Isomerizations were carried out by employing a five-fold excess of the sodium salt of 1,2-diaminoethane (DAE) in DAE at 60°C. The reagent was prepared just before use by reaction of sodium hydride with DAE at 60°C for 0.5–1.0 hour.

Isomerization of 5-tetradecynoic acid (**3**) for 2.5 hours gave none of the anticipated 13-tetradecynoic acid (**4**), but rather rearranged smoothly to a 1:1 mixture of two other isomeric compounds (Fig. 1). No intermediate reaction products could be detected by glc. Separation of the crude product by silver resin chromatography gave *E,Z*- and *E,E*-3,5-tetradecadienoic acids (**1** and **2**) in 67% yield. Structure and stereochemistry were established by comparison with published infrared spectra (14), mass spectral and nmr data (15).

To gain further insight into this unusual rearrangement, 2-tetradecynoic acid (**5**) was subjected to the same isomerization conditions. Quenching after 5 minutes, followed by esterification and chromatography, afforded methyl 3-tetradecynoate (*6a*) in 33% yield. The Δ3 isomer, 3-tetradecynoic acid (**6**), prepared independently, was also isomerized for 5 minutes to give a mixture of three components: starting material (50%), and the same two products **1** and **2** (50%, 1:1) isolated from the 5-tetradecynoic acid rearrangement reaction (**1** and **2**). The Δ2 to Δ3 isomerization appears to be irreversible; no 2-tetradecynoic acid was observed in the product of isomerization of 3-tetradecynoic acid. As well, allenic intermediates were not seen, and thus, if formed, must rearrange quickly under the reaction conditions.

To study how far along the carbon skeleton the effect of the carboxyl group extends, tetradecynoic acids with the triple bond closer to the methyl terminus were isomerized (Table 1). 7-Tetradecynoic acid was rearranged cleanly to the same mixture of **1** and **2** observed with the 5-tetradecynoic acid isomerization. Gas–liquid chromatography did not allow distinction between the Δ7- and Δ5-methyl esters. Although 5-tetradecynoic acid

Can. J. Chem. Downloaded from www.nrcresearchpress.com by 210.87.254.5 on 09/06/12
For personal use only.

TABLE 1. Product distributions of rearrangements of isomeric tetradecynoic acids with sodium salt of 1,2-diaminoethane determined by glc analysis of methyl esters

| Triple bond position of starting acetylenic acid | Reaction time (min) | Product distribution (%) | | | | |
|---|---|---|---|---|---|---|
| | | **1** | **2** | **4** | **6** | Other isomeric tetradecynoic acids |
| 2[a] | 5 | 0 | 0 | 0 | 88 | 12 |
| 2 | 120 | 42 | 42 | 0 | 0 | 16 |
| 3 | 5 | 25 | 25 | 0 | 50 | 0 |
| 5[b] | 150 | 43 | 49 | 0 | 0 | 8 |
| 7[c] | 5 | 41 | 38 | 0 | 0 | 21 |
| 9 | 50 | 29 | 31 | 21 | 0 | 19 |
| 11 | 60 | 24 | 18 | 27 | 0 | 21 |
| 13 | 60 | 0 | 0 | 100 | 0 | 0 |

[a]33% isolated methyl 3-tetradecynoate.
[b]67% isolated 1 and 2.
[c]65% isolated 1 and 2.

was not isolated, it seems reasonable to postulate that the normal acetylene–allene interconversions occur and that 7-tetradecynoic acid is isomerized to 5-tetradecynoic acid which, in turn, is rearranged to **1** and **2**. Isomerization of 9-tetradecynoic acid, in which the triple bond at the Δ9 position is equidistant from C-5 and C-13, gave **1**, **2** (60%), and 13-tetradecynoic acid (**4**) (20%). The carboxyl group still affects the course of the rearrangement even when the triple bond starts eight positions away. Isomerization of 11-tetradecynoic acid gave similar results: conversion to 13-tetradecynoic acid was 27% and the 3,5-dienoic acids comprised 42% of the crude reaction mixture. Subjection of 13-tetradecynoic acid to the isomerization conditions left the terminal triple bond unchanged.

Fractions of dienoic acids rich in each isomer were subjected to the isomerization reaction conditions. In each case 70% of the material was recovered. Little change in the ratio of isomers was observed. Thus it appears that the isomers do not interconvert and are stable to the reaction conditions.

Based upon these results it seems likely that the triple bond of the fourteen carbon acid is isomerized along the carbon chain in a random fashion through acetylenic and allenic isomers. There appear to be two thermodynamic minima in the system. One, that was anticipated at the beginning of the study, is the terminal acetylenic acid **4**. Its stability is derived from the presence of acidic protons at each end of the molecule. The second thermodynamic well is the 3,5-dienoic acid system.

The formation of the 3,5-tetradecadienoic acids **1** and **2** may be accounted for by consideration of the relative acidities of the various protons in the postulated intermediate species. It is known that some alkali metal alkyl amides, notably lithium diisopropylamide, abstract two protons from carboxylic acids: one from the COOH and one from the carbon α to the carboxyl group (16). The sodium salt of DAE also appears to abstract the α proton. Reaction of 2,2-dideuterohexadecanoic acid with the sodium salt of DAE, followed by quenching with water, results in complete loss of deuterium. The loss of both deuterium atoms may be due to protonation of the dianion with the solvent 1,2-diaminoethane. Dianions may be contributing species in acetylenic acid rearrangements. Thus, Δ5 isomer **3** may give **7** which could be reprotonated by solvent (Fig. 2). Other possible intermediates may be **8** to **11**. Proton shifts from C-3 to C-5 in **10** and from C-6 to C-4 in **11** would result in extended delocalized pi (π) systems **12** and **13** which should have added stability. Protonation of **12** and **13** at C-2 would give the observed products **1** and **2**. Quenching of dianions **12** and **13** with methyl iodide would be anticipated to introduce a methyl group at C-2 giving **14** and **15** (17).

To test this hypothesis, isomerization of 7-tetradecynoic acid was carried out and the reaction quenched with methyl iodide. Two major products (total 90%, 1:1), each closely followed by minor products (10%, 1:1) were observed in the glc of the esterified reaction mixture. The mass spectra of the two major products were identical with those of **1** and **2**. The fragmentation patterns of **1** and **2** are superimposable: 238 ($M^+$), 179 ($M^+ - COOCH_3$, α-cleavage) and 164 ($M^+ - CH_3COOCH_3$, McLafferty rearrangement). The mass spectra of the two minor components were also superimposable, and consistent with **14** and **15** which are alkylated at C-2: 252 ($M^+$), 193 ($M^+ - COOCH_3$, α-cleavage), and 164 ($M^+ - H_2CCH_3COOCH_3$, McLafferty

Can. J. Chem. Downloaded from www.nrcresearchpress.com by 210.87.254.5 on 09/06/12
For personal use only.

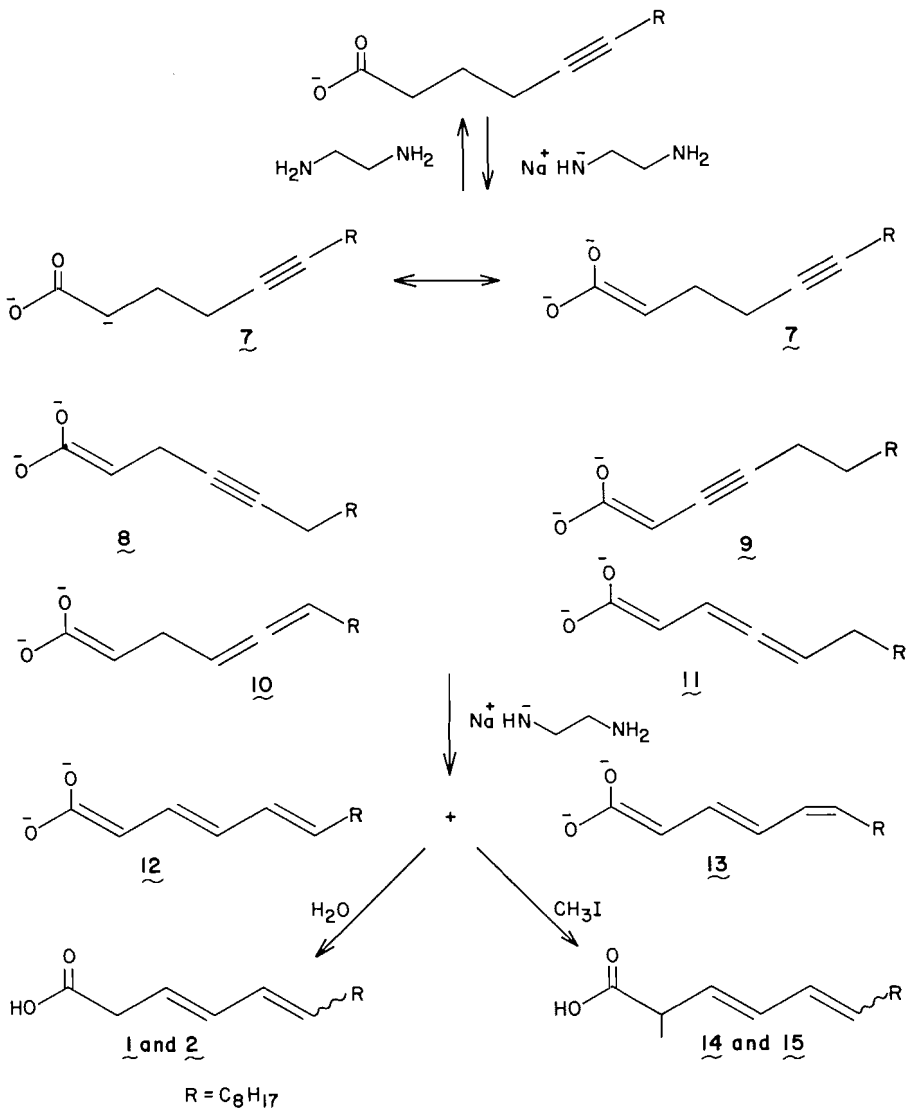


FIG. 2. Postulated intermediates in isomerization of tetradecynoic to 3,5-tetradecadienoic acids.

rearrangement). The peak at *m/z* 164 found in the spectra of the minor compounds and **1** and **2** establishes that alkylation occurs at C-2.

Ionic species having extensive delocalization of the negative charge such as **12** and **13** can only be formed if the starting alkynoic acid has an abstractable proton at C-2. As a further test for the intermediacy of **12** and **13** a 2,2-disubstituted alkynoic acid was prepared and subjected to the isomerization reaction conditions (Fig. 3). Thus, isobutyric acid was treated with two equivalents of lithium diisopropylamide to form the dianion, followed by addition of 1-bromohexadec-7-yne affording 2,2-dimethyloctadec-9-ynoic acid (**16**) according to the method of Cregar (17). Rearrangement of **16** with the sodium salt of 1,2-diaminoethane produced a single isomer, that containing the terminal triple bond, 2,2-dimethyloctadec-17-ynoic acid (**17**).

It appears from the methyl iodide trapping experiment and from the rearrangement of the 2,2-disubstituted alkynoic acid to the terminally substituted isomer that the formation of a delocalized dianion system may be the driving force for the rearrangement of acetylenic to 3,5-dienoic acids. The stereochemistry observed in **1** and **2** is consistent with protonation of **12** and **13**. The barrier for interconversion of **1** and **2** or **12** and **13** must be

Can. J. Chem. Downloaded from www.nrcresearchpress.com by 210.87.254.5 on 09/06/12
For personal use only.

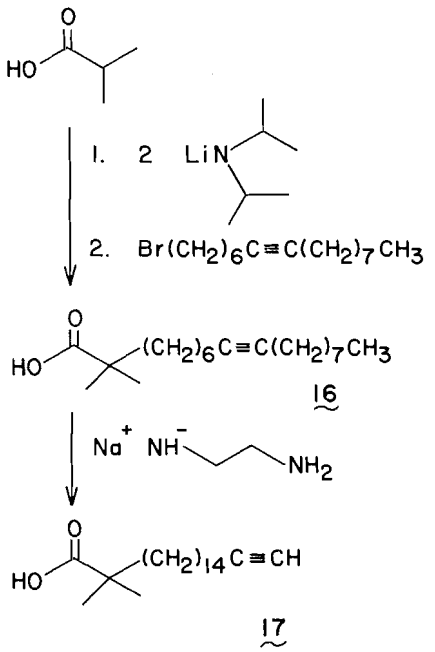


FIG. 3. Synthesis and isomerization of 2,2-dimethyloctadec-9-ynoic acid.

quite high as **1** and **2** did not equilibrate under the reaction conditions.

The rearrangement of a triple bond in the fourteen carbon acetylenic acids affords an improved synthesis of *E,Z*-3,5-tetradecadienoic acid (**1**), megatomoic acid, a component of the sex pheromone of the black carpet beetle (Attagenus megatoma). This insect is a serious pest in stored grain and flour and also attacks fabrics in clothing, rugs, and padding of furniture. The published synthesis of megatomoic acid gives **1** and **2** in 14% yield over 6 steps (15). Rearrangement of either 5- or 7-tetradecynoic acids gives mixtures of **1** and **2** cleanly and in good isolated yield (67% and 65%, respectively).

## Experimental

Infrared spectra were obtained with a Perkin Elmer 237B instrument employing chloroform solutions or neat films. Proton nmr spectra were recorded on an HA-100 spectrometer using deuterochloroform with internal tetramethylsilane as reference. Gas chromatographic separations were carried out on a Varian 3700 instrument with an SP 2100 capillary column (J and W Scientific, 30 m) with a flame ionization detector, and were run isothermally at 160° or 140°C. Acids were converted to methyl esters with diazomethane prior to glc analysis. Mass spectra were recorded on a Finnigan 4000E gc/ms instrument with an Incos 2300 data system and using an SP 2100 column. Mass spectra are reported in mass to charge units (*m/z*) with the relative intensities as percentages of the base peak. Accurate mass measurements were provided by the mass spectrometry laboratory, Psychiatric Research Unit, University of Saskatchewan, with an MS902S instrument with VG console update. Accurate masses were obtained at 1500 resolution and 3 s/decade using accurate mass – low resolution software with PFTBA internal standard. Elemental analyses were performed by Spang Microanalytical Laboratory, Eagle Harbor, Michigan, U.S.A.

The 7 tetradecynoic acids employed in this study are all known compounds. Each was prepared from the corresponding alcohol by Jones oxidation. The 2-, 5-, 7-, 9-, and 11-tetradecyn-1-ols were obtained by alkylation of the appropriate ω-tetrahydropyranyloxy alkyne using lithium amide in dimethoxyethane and alkyl halides as described previously (3). 2-Tetradecyn-1-ol was isomerized with the lithium salt of 1,3-diaminopropane at −11°C for 10 min to give 3-tetradecyn-1-ol (5) (81% conversion); product purified by chromatography over silica gel. Treatment of 2-tetradecyn-1-ol with the sodium salt of 1,3-diaminopropane at 60°C gave 13-tetradecyn-1-ol as previously reported (3).

All rearrangement reactions were carried out using the same experimental conditions, varying only the substrate and reaction time. An isomerization reaction of 7-tetradecynoic acid is described in full.

*Isomerization of 7-tetradecynoic acid*

To a 100 mL flask (flame dried under vacuum), fitted with a magnetic stirring bar and rubber septum through which a slight positive pressure of dry nitrogen was introduced, was added NaH (680 mg, 57% in mineral oil, 17 mmol). The mineral oil was removed with 3 hexane washes and 1,2-diaminoethane (DAE, previously distilled from BaO and stored over molecular sieves, 8 mL) was added. The mixture was stirred and heated at 60°C for 1 h by which time $H_2$ evolution had ceased and a purple solution resulted. A solution of 7-tetradecynoic acid (900 mg, 4 mmol) in DAE (8 mL) was added to the reagent at 60°C. After 5 min the reaction was quenched by addition of ice/water. The mixture was acidified with HCl and was extracted 3 times with ether. The combined extracts were washed with $H_2O$ and NaCl solution, dried over $Na_2SO_4$, filtered, and the solvent evaporated to give 620 mg of product. Gas–liquid chromatographic analysis (160°C) indicated 3 major components in the mixture: methyl tetradecynoates, 12%; **1***a*, 41%; **2***a*, 38%. The crude acidic product was chromatographed over an ion exchange column (Lewatit SP 1080 GR, Merck, $Na^+$ ions replaced by $Ag^+$) eluting with methanol. First to elute was *E,E*-3,5-tetradecadienoic acid (**2**), 180 mg, mp 55.5–57.0°C (plates from petroleum ether), followed by a mixed fraction of 80 mg **1** and **2**, and then by *E,Z*-3,5-tetradecadienoic acid (**1**), 120 mg as an oil. The acids were characterized as the methyl esters: methyl *E,Z*-3,5-tetradecadienoate (**1***a*); ir $\nu_{max}$ (neat film): 1740 (s), 1050 (w), 960 (m), and 940 (m) $cm^{-1}$; $^1H$ nmr δ: 5.2 to 6.7 (m, olefinic H, 4H), 3.68 (s, $OCH_3$, 3H), 3.14 (d, $J$ = 8 Hz, $OCCH_2$, 2H), 2.0 to 2.2 (m, $CH_2C$=, 2H), 1.2 to 1.4 (m, $CH_2$, 12H), and 0.90 (t, $J$ = 6 Hz, $CH_3$, 3H); mass spectrum: 238 ($M^+$, 5.3%), 179 ($M^+$ − $COOCH_3$, 1.6%), 178 ($M^+$ − $HCOOCH_3$, 1.5%), 164 ($M^+$ − $H_3CCOOCH_3$, 5.6%), 79 (81%), 41 (100%). Methyl *E,E*-3,5-tetradecadienoate (**2***a*); ir $\nu_{max}$ (neat film): 1740(s), 980(s) $cm^{-1}$; $^1H$ nmr δ: 5.4 to 6.2 (m, olefinic H, 4H), 3.63 (s, $OCH_3$, 3H), 3.05 (d, $J$ = 8 Hz, $OCCH_2$, 2H), 1.9 to 2.3 (m, $CH_2C$=C, 2H), 1.1 to 1.6 (m, $CH_2$, 12H), 0.88 (t, $J$ = 6 Hz, $CH_3$, 3H); mass spectrum: 238 ($M^+$, 4.3%), 179 ($M^+$ − $COOCH_3$, 1.8%), 178 ($M^+$ − $HCOOCH_3$, 1.2%), 164 ($M^+$ − $H_3CCOOCH_3$, 5.3%), 79 (89%), 41 (100%).

*Attempted isomerizations of* E,E-*3,5-tetradecadienoic acid (2) and of* E,Z-*3,5-tetradecadienoic acid (1)*

A sample of 3,5-tetradecadienoic acids rich in the *E,E*-isomer (86:14), 200 mg, was subjected to the isomerization reaction conditions. After 2 h 140 mg product was recovered, glc analysis gave 78% **2***a* and 13% **1***a*.

Similarly a sample rich in *E,Z*-3,5-tetradecadienoic acid

Can. J. Chem. Downloaded from www.nrcresearchpress.com by 210.87.254.5 on 09/06/12
For personal use only.

Can. J. Chem. Downloaded from www.nrcresearchpress.com by 210.87.254.5 on 09/06/12
For personal use only.

(79:17), 105 mg, was submitted to the reaction conditions for 2 h; 70 mg was recovered. Gas–liquid chromatographic analysis indicated 73% **1***a* and 17% **2***a*.

*Reaction of 2,2-dideuterohexadecanoic acid with the sodium salt of DAE*

To the sodium salt of DAE (7.2 mmol in 4.0 mL DAE) at 60°C was added a solution of 2,2-dideuteropalmitic acid in DAE (300 mg, 1.2 mmol in 3.2 mL DAE). The reaction was quenched after 15 min and worked up to give 300 mg white solid. A small sample was esterified with diazomethane and $^1$H nmr integration of $OCH_3$ to $CH_2CO$ was 3:2 indicating complete exchange of protons for deuterons.

*Isomerization of 7-tetradecynoic acid quenched with methyl iodide*

The isomerization reaction of 7-tetradecynoic acid was repeated using 250 mg Δ7. After 5 min the reaction was cooled in an ice/salt bath and methyl iodide (0.6 mL, 9 equiv.) was added dropwise. After the usual work-up 260 mg product was obtained; glc of the methyl esters at 160°C showed two new products each with slightly longer retention times than **1***a* and **2***a*: methyl tetradecynoates, 11%; **1***a*, 38%; **14***a*, 3.4%; **2***a*, 35%; **15***a*, 3.5%. Mass spectrum of **14***a*: 252 ($M^+$, 5.5%), 193 ($M^+ - COOCH_3$, 6.2%), 192 ($M^+ - HCOOCH_3$, 2.7%), 164 ($M^+ - CH_3COOCH_3$, 3.1%), 81 (94%), 41 (100%); mass spectrum of **15***a*: 252 ($M^+$, 6.0%), 193 ($M^+ - COOCH_3$, 7.4%), 192 ($M^+ - HCOOCH_3$, 2.4%), 164 ($M^+ - CH_3COOCH_3$), 81 (100%). Quenching with a larger excess of methyl iodide led to the same ratios of products.

*2,2-Dimethyloctadec-9-ynoic acid (**16**)*

To a cooled solution of diisopropylamine (1.6 mL, 12 mmol) in dry tetrahydrofuran (THF, distilled from benzophenone ketyl, 50 mL) was added a solution of *n*-butyllithium in hexane (7.0 mL, 14 mmol) maintaining internal temperature less than 0°C. The pale yellow solution was kept at 0°C for 0.5 h, then a solution of isobutyric acid (0.56 mL, 6.0 mmol, distilled from $P_2O_5$) in THF (5 mL) was added. Still at 0°C, after 0.5 h, to the gold solution was added 1-bromohexadec-7-yne (1.6 g, 10 mmol) in THF (10 mL). After warming to ambient temperature and stirring overnight the reaction mixture was poured into ice/dilute HCl and the product extracted 3× with ether. The combined organic phases were washed with NaCl solution, dried over $Na_2SO_4$, filtered, and the solvent evaporated to give 2.8 g product. Filtration over silica gel, eluting first with hexane, gave 550 mg recovered bromide and then with ether gave **16** (1.15 g, 3.7 mmol, 62%) having bp 200°C at 0.1 Torr; ir $\nu_{max}$ (neat film): 3100 (br s), 1700 (s) cm$^{-1}$; $^1$H δ: 2.12 (m, $w_{1/2}$ = 5 Hz, $H_2CC{\equiv}C$, 4H), 1.2–1.6 (m, $w_{1/2}$ = 15 Hz, $CH_2$, 22H), 1.15 (s, $CH_3$, 6H), 0.86 (t, $J$ = 6 Hz, $CH_3$, 3H). *Anal.* calcd. for $C_{20}H_{36}O_2$: C 77.86, H 11.76; found: C 77.46, H 11.79. The methyl ester gave glc retention time 16.7 min at 210°C; mass spectrum *m/z*: 322 ($M^+$, 1%), 102 ($(H_3COCOHC(CH_3)_2)^+$, McLafferty rearrangement, 100%); molecular ion *Exact Mass* calcd.: 322.2872; found: 322.2892.

*2,2-Dimethyloctadec-17-ynoic acid (**17**)*

To the sodium salt of DAE (5.0 mmol in 2.0 mL DAE) at 60°C was added a solution of **16** (250 mg, 0.8 mmol) in DAE (3.0 mL). After 3 h, the reaction was quenched and worked up to give 340 mg crude product. The glc of methyl esters at 210°C gave 2 peaks: retention time 16.7 min (7%) and 17.5 min (92%). The product was distilled at 240°C (0.1 Torr) to give pure **17**, 120 mg (48%); ir $\nu_{max}$ ($CHCl_3$): 3610 (m), 3300 (s), 3100 (br s), 2100 (w), 1700 (s) cm$^{-1}$; $^1$H nmr δ: 2.16 (m, $w_{1/2}$ = 12 Hz, $H_2CC{\equiv}C$, 2H), 1.88 (t, $J$ = 1.5 Hz, $C{\equiv}CH$, 1H), 1.2–1.6 (m, $w_{1/2}$ = 4 Hz, 26H), 1.20 (s, $CH_3$, 6H). *Anal.* calcd. for $C_{20}H_{36}O_2$: C 77.86, H 11.76; found: C 78.27, H 12.14. The methyl ester gave glc retention time 17.5 min at 210°C; mass spectrum *m/z*: 322 ($M^+$, 1%), 102 ($(H_3COCOHC(CH_3)_2)^+$, McLafferty rearrangement, 100%); molecular ion *Exact Mass* calcd.: 322.2872; found: 322.2869.

## Acknowledgements

The author wishes to thank A. P. Tulloch and G. D. Abrams for helpful discussion and A. Christ for technical assistance.

1. C. A. Brown and A. Yamashita. J. Am. Chem. Soc. **97**, 891 (1975).
2. C. A. Brown and A. Yamashita. J. Chem. Soc. Chem. Commun. 959 (1976).
3. S. R. Macaulay. J. Org. Chem. **45**, 734 (1980).
4. S. R. Macaulay. Can. J. Chem. **58**, 2567 (1980).
5. R. G. Ackman, R. A. Dytham, B. J. Wakefield, and B. C. L. Weedon. Tetrahedron, **8**, 239 (1960).
6. E. R. H. Jones, G. H. Whitham, and M. C. Whiting. J. Chem. Soc. 3201 (1954).
7. J. Cymerman Craig and M. Moyle. J. Chem. Soc. 4402 (1963).
8. G. Eglington, E. R. H. Jones, G. H. Mansfield, and M. C. Whiting. J. Chem. Soc. 3197 (1954).
9. R. J. Bushby and G. H. Whitham. J. Chem. Soc. B, 67 (1969).
10. R. M. Silverstein, J. O. Rodin, W. E. Burkholder, and J. E. Gorman. Science, **157**, 85 (1967).
11. F. Masino. Ann. **202**, 172 (1980).
12. N. W. Gilman and B. C. Holland. Chem. Phys. Lipids, **13**, 239 (1974).
13. M. Ya. Kraft and E. G. Popova. Zh. Obshch. Khim. **27**, 906 (1957); Chem. Abstr. **52**, 3675i (1958).
14. H. Fukui, F. Matsunura, A. V. Barak, and W. E. Burkholder. J. Chem. Ecol. **3**, 539 (1977).
15. J. O. Rodin, M. A. Leaffer, and R. M. Silverstein. J. Chem. Educ. **45**, 794 (1964); J. Org. Chem. **35**, 3154 (1970).
16. P. E. Pfeffer, L. S. Silbert, and J. M. Chirinko, Jr. J. Org. Chem. **37**, 451 (1972).
17. L. S. Melvin and B. M. Trost. J. Am. Chem. Soc. **94**, 1790 (1972); P. L. Cregar. J. Am. Chem. Soc. **89**, 2500 (1967).

# The adsorption of tri-*N*-butylphosphate at the benzene–water interface[1,2]

NORMAN H. SAGERT, WOON LEE, AND MICHAEL J. QUINN

*Research Chemistry Branch, Atomic Energy of Canada Limited, Whiteshell Nuclear Research Establishment, Pinawa, Man., Canada R0E 1L0*

Received November 25, 1981

NORMAN H. SAGERT, WOON LEE, and MICHAEL J. QUINN. Can. J. Chem. **60**, 1244 (1982).

Adsorption of tri-*n*-butylphosphate (TBP) at the benzene–water interface was studied as a function of the TBP mole fraction in benzene up to 0.018 and at temperatures from 9 to 29°C. The extent of adsorption was calculated from interfacial tension data obtained by the drop-volume technique. Standard free energies of adsorption from benzene ranged from −20.9 kJ/mol at 9°C to −22.5 kJ/mol at 29°C, giving a standard enthalpy of adsorption of +2.5 kJ/mol. Thus the strong adsorption occurs because of entropy changes. Distribution coefficients for the partition of TBP between benzene and water were measured by gas chromatography, and standard free energies of adsorption from water were derived. They ranged from −44.8 kJ/mol at 9°C to −51.1 kJ/mol at 29°C, with standard enthalpies of adsorption ranging from 74 to 15 kJ/mol over the same temperature range.

Results at higher mole fractions were fitted to various equations of state, after using vapor pressure osmometry (at 37°C) to determine that activity corrections were small. The Schofield–Rideal equation described the results adequately, with $A_0$ close to 1.0 nm² and $i$ close to 1.0 at lower temperatures. These values imply that lateral repulsion between TBP molecules in the adsorbed layer is minimal.

NORMAN H. SAGERT, WOON LEE et MICHAEL J. QUINN. Can. J. Chem. **60**, 1244 (1982).

On a étudié l'adsorption du tri-*n*-butylphosphate (TBP) à l'interface benzène–eau, en fonction de la fraction molaire de TBP dans le benzène, jusqu'à une valeur de 0,018 et à des températures allant de 9 à 29°C. On a calculé le taux d'adsorption à partir des données de tension interfaciale obtenues par la technique du volume de la goutte. Les énergies libres standard d'adsorption à partir du benzène varient de −20,9 kJ/mol à 9°C à −22,5 kJ/mol à 29°C pour une enthalpie standard d'adsorption de +2,5 kJ/mol. Ainsi il se produit une forte adsorption par suite des variations d'entropie. On a mesuré la distribution des coefficients de partage du TBP entre le benzène et l'eau en utilisant la chromatographie en phase gazeuse et on en a déduit les énergies libres standard d'adsorption à partir de l'eau. Elles se situent entre −44,8 kJ/mol à 9°C et −51,1 kJ/mol à 29°C avec des enthalpies standard d'adsorption se situant entre 74 et 15 kJ/mol pour le même intervalle de température.

On a accordé les résultats obtenus pour de plus fortes fractions molaires à différentes équations d'état après avoir utilisé l'osmométrie de la pression de vapeur (à 37°C) pour déterminer que les corrections du coefficient d'activité sont faibles. Pour les basses températures, l'équation de Schofield-Ridéal décrit adéquatement les résultats avec $A_0$ voisin de 1,0 nm² et $i$ voisin de 1,0. Ces valeurs impliquent que la répulsion latérale entre les molécules de TBP dans la couche adsorbée est minimale.

[Traduit par le journal]

## Introduction

As part of a program to study the interfacial properties of solvent extraction systems used in the nuclear industry, we previously studied the adsorption of tri-*n*-butylphosphate (TBP) and the lower trialkylphosphates at the dodecane–water interface (1, 2). That work showed large negative standard free energies of adsorption, as well as fairly large negative enthalpies of adsorption. Recent work by Chifu *et al.* (3, 4) on the adsorption of TBP at the benzene–water interface seemed to show much less negative standard free energies of adsorption, but actual numerical data were not given and enthalpies were not determined. Since there are several reports that indicate significant bonding between alkylphosphates and benzene (5–7), it seemed appropriate to study the thermodynamics of adsorption of TBP at the benzene–water interface. To interpret our results properly, it was necessary to have good values of the distribution ratios of TBP between benzene and water at several temperatures. Hence it was necessary to determine these ratios as well.

## Experimental

The adsorption of TBP at the benzene–water interface was studied by measuring interfacial tensions. For temperatures of 9, 14, 19, 24, and 29°C, up to 50 μmol TBP were added to a system of 50 cm³ water and 50 cm³ benzene, and the system thoroughly equilibrated. At four intermediate temperatures, 11.5, 16.5, 21.5, and 26.5°C, interfacial tensions were measured only in the more dilute region, by adding up to 2.5 μmol TBP to the same water–benzene system. Solutions were not used longer than 72 h. Interfacial tension measurements were made by the drop-volume method using apparatus and procedures that have been described previously (1, 2).

Distribution ratios were measured at 10, 15, 20, 30, and 40°C using procedures that have been described previously (8). Because of the magnitude of these ratios, small amounts of the organic phase in the aqueous phase could have a large effect on the results. Hence, 1.0-cm³ samples of the aqueous phase were withdrawn and centrifuged at 100 Hz for 30 min. The organic phase was diluted by a factor of 100 with pure benzene and then both phases were analyzed for TBP by gas chromatography, using a glass column of 3% nitrile silicone gum OV-225 on Chromosorb G at 220°C.

Osmotic coefficients of TBP in benzene were measured at

[1]AECL No. 7459.

[2]Presented in part at the 4th International Conference on Surface and Colloid Science, Jerusalem, Israel, July 1981.

0008-4042/82/101244-06$01.00/0

©1982 National Research Council of Canada/Conseil national de recherches du Canada

Can. J. Chem. Downloaded from www.nrcresearchpress.com by 210.87.254.40 on 09/06/12
For personal use only.

TABLE 1. Coefficients of eq. [1] for the adsorption of TBP at the benzene–water interface

| $T$ (°C) | $10^3\ C_1$ | $10^3\ C_2$ | $10^4\ C_3$ | $10^5\ C_4$ | $10^4$ standard deviation of fit |
|---|---|---|---|---|---|
| 9.0 | 1.880 477 | −7.439 290 | −5.451 184 | −1.305 762 | 1.54 |
| 14.0 | 2.902 057 | −7.239 576 | −5.313 483 | −1.266 274 | 2.01 |
| 19.0 | 1.424 420 | −8.169 817 | −6.710 180 | −1.840 776 | 0.97 |
| 24.0 | 6.920 264 | −6.222 104 | −4.608 928 | −1.131 525 | 1.16 |
| 29.0 | 6.140 988 | −6.625 637 | −5.195 849 | −1.368 602 | 1.38 |

37°C using a Mechrolab 301A vapor pressure osmometer, modified by substituting a Hewlett-Packard HP419A null voltmeter for the built-in null detector. Zone-refined biphenyl was used as a standard.

The sources and purification of water and TBP have been described previously (1, 2). The benzene was Phillips Research Grade, and before use it was passed through an alumina column.

## Results

Some typical results,[3] at 24°C, for the adsorption of TBP at the benzene–water interface are shown in Fig. 1. These and similar data were fitted to expressions of the form of eq. [1]

$$[1]\quad \gamma = C_1 + C_2 \ln X + C_3 (\ln X)^2 + C_4 (\ln X)^3$$

where $\gamma$ is the interfacial tension in N/m and $X$ is the mole fraction of TBP in the benzene. The values of the constants, $C_i$, obtained by a least-squares fit to eq. [1], are listed in Table 1. Standard deviations of the fit are also given. In the most dilute region of solute mole fraction, the decreases in interfacial tensions, i.e. the interfacial pressures, become linear with solute mole fraction. Some data, shown at only two temperatures for clarity, are plotted in this form in Fig. 2. Within the claimed experimental error of ±50 μN/m (1) for interfacial tensions, and thus ±100 μN/m for $\pi$, these plots may be considered as linear.

Distribution ratios, defined as the concentration of TBP in benzene divided by that in water, are shown in Fig. 3 as a function of TBP concentration in benzene. These distribution ratios are easily extrapolated to zero solute concentration to obtain the distribution coefficient, $K_D$. The values of $K_D$ so obtained, and of the mole fraction distribution coefficients, $K_D^X$, defined in a similar fashion to $K_D$, are listed in Table 2. The errors here are ±5% as a minimum, and may be as large as ±10%, because of the large absolute values of the distribution ratios and attendant difficulties in the gas chromatographic technique.

[3]All the measured distribution ratios and interfacial tensions are available, at a nominal charge, from the Depository of Unpublished Data, CISTI, National Research Council of Canada, Ottawa, Ont., Canada K1A 0S2.

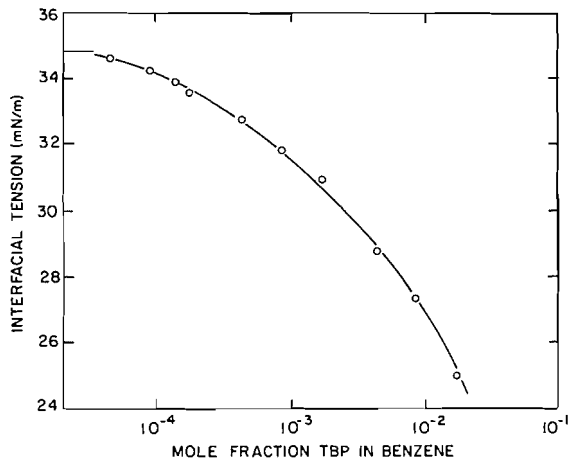


FIG. 1. Interfacial tension at the benzene–water interface as a function of TBP mole fraction in benzene; $T$ = 24°C.

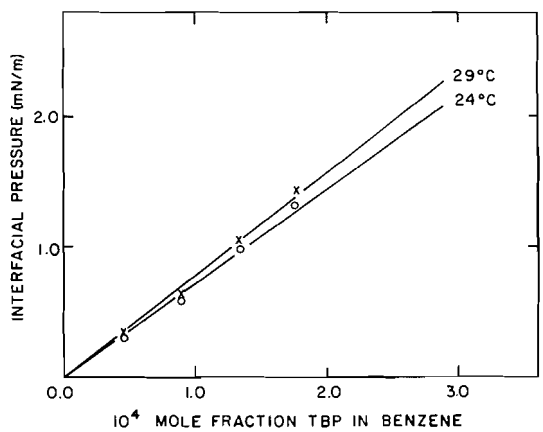


FIG. 2. Interfacial pressure of TBP at the benzene–water interface at 29°C (×) and 24°C (○), as a function of TBP mole fraction in benzene.

The osmotic coefficient for TBP in benzene at 37°C is shown in Fig. 4 as a function of TBP mole fraction. The osmotic coefficient is essentially constant at 1.0 in this low mole-fraction range.

Can. J. Chem. Downloaded from www.nrcresearchpress.com by 210.87.254.40 on 09/06/12
For personal use only.

Can. J. Chem. Downloaded from www.nrcresearchpress.com by 210.87.254.40 on 09/06/12
For personal use only.

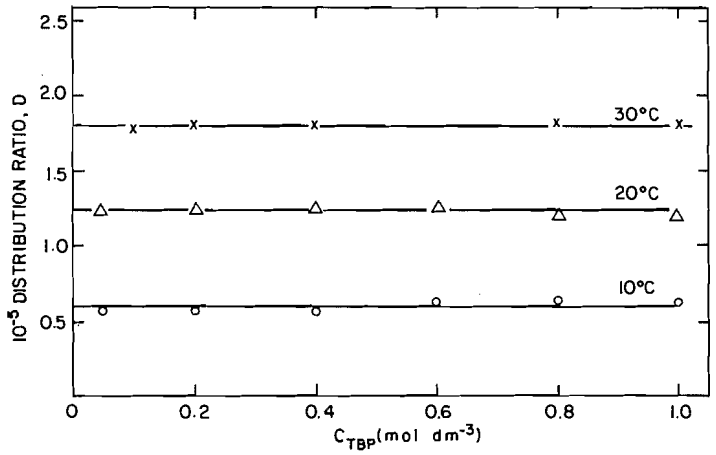


FIG. 3. Distribution ratios, $D$, for TBP between benzene and water at three indicated temperatures.

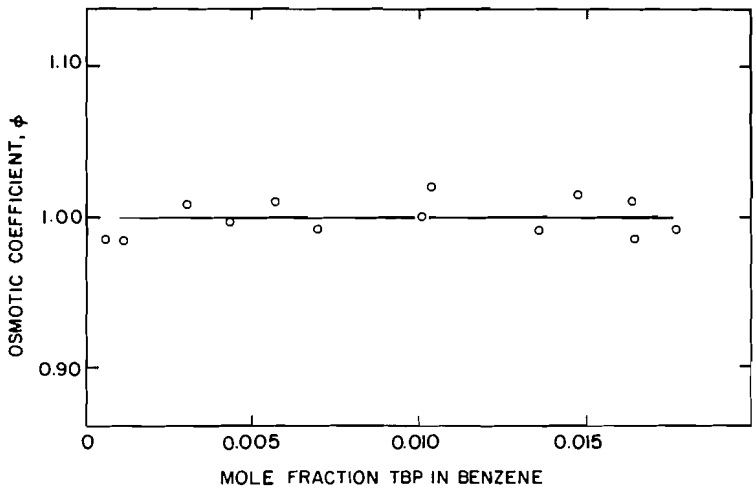


FIG. 4. Osmotic coefficients for TBP in benzene measured by vapor pressure osmometry, $T$ = 37°C.

TABLE 2. Distribution ratios at infinite dilution for TBP transfer from water to benzene

| $T$ (°C) | $10^{-3}\ K_D$ | $10^{-4}\ K_D^X$ |
|---|---|---|
| 10.0 | 6.0 | 2.92 |
| 12.5 | 7.2 | 3.52 |
| 15.0 | 8.8 | 4.31 |
| 17.5 | 10.6 | 5.21 |
| 20.0 | 12.4 | 6.11 |
| 25.0 | 15.4 | 7.62 |
| 30.0 | 17.8 | 8.85 |
| 35.0 | 19.3 | 9.64 |
| 40.0 | 20.4 | $10.2_3$ |

## Discussion

*Thermodynamics of transfer*

The standard free energy of transfer of TBP from water to benzene, $\Delta_\alpha^\beta \bar{G}_1^\ominus$, is given by eq. [2]:

$$[2] \quad \Delta_\alpha^\beta \bar{G}_1^\ominus = \mu_1^{\ominus,\beta} - \mu_1^{\ominus,\alpha} = -RT \ln K_D^X$$

where β and α refer to the benzene and aqueous phases, respectively, and subscript 1 refers to the solute, TBP. The standard states are the hypothetical conditions of unit solute mole fraction and unit activity coefficient (8, 9). From the temperature variation of the standard free energies of transfer, standard enthalpies of transfer, $\Delta_\alpha^\beta \bar{H}_1^\ominus$, may be calculated using eq. [3]:

$$[3] \quad \Delta_\alpha^\beta \bar{H}_1^\ominus = \partial(\Delta_\alpha^\beta \bar{G}_1^\ominus/T)/\partial(1/T)$$

Standard entropies of transfer, $\Delta_\alpha^\beta \bar{S}_1^\ominus$, are then easily obtained. Figure 5 shows a plot of $\Delta_\alpha^\beta \bar{G}_1^\ominus/T$ against $1/T$. This plot has significant curvature, and therefore $\Delta_\alpha^\beta \bar{H}_1^\ominus$ varies with temperature. Table 3 lists values of three thermodynamic functions at selected temperatures. The variations in the standard enthalpy of transfer correspond to a standard heat capacity of $-1300 \pm 200$ J mol$^{-1}$ K$^{-1}$.

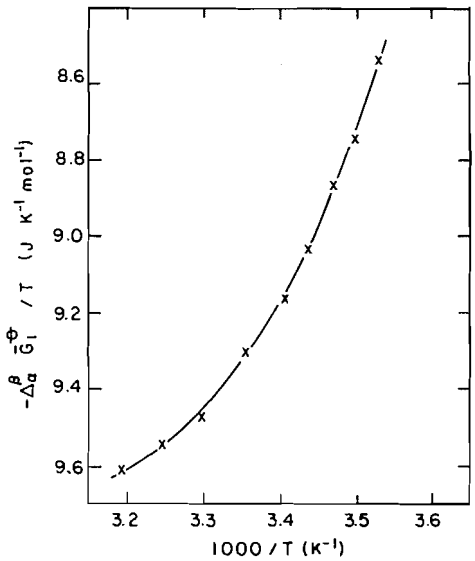


FIG. 5. Determination of the standard enthalpies of transfer of TBP from water to benzene.

TABLE 3. Standard free energies, enthalpies, and entropies of transfer of TBP from water to benzene

| $T$ (°C) | $\Delta_\alpha^\beta \bar{G}^\ominus$ (kJ/mol) | $\Delta_\alpha^\beta \bar{H}^\ominus$ (kJ/mol) | $\Delta_\alpha^\beta \bar{S}^\ominus$ (J K$^{-1}$ mol$^{-1}$) |
|---|---|---|---|
| 15 | −25.57 | 40.2 | 236 |
| 25 | −27.75 | 28.6 | 189 |
| 35 | −29.40 | 16.3 | 148 |

It is instructive to compare the thermodynamic parameters given in Table 3 with similar ones for the transfer of TBP from water to dodecane (8). The standard free energy of transfer of TBP to benzene is much more negative than that to dodecane, reflecting much larger distribution ratios. Weak complexing between TBP and benzene (5–7) could explain the difference. As with dodecane, the standard enthalpy of transfer is positive, indicating that transfer of TBP from water to benzene is opposed enthalpically and takes place only because of the large standard entropy of transfer. The standard enthalpy change at 25°C is equivalent to the breaking of about two hydrogen bonds (10). However, at 35°C it is, perhaps, equivalent to the breaking of only one such bond. The standard entropy of transfer at 30°C is similar to that for the transfer from water to dodecane (8). This is consistent with the commonly accepted picture for "hydrophobic bonding", which attributes the entropy changes largely to the loss of water structure around the hydrocarbon chains as the solute is transferred from water into hydrocarbon (11, 12).

The standard heat capacity of transfer corresponds almost exactly with the negative of the apparent molal heat capacity of three butyl groups in water, as calculated from the additivity relations of Jolicoeur and Lacroix (13). Thus the observed standard heat capacity of transfer can be accounted for by the loss of hydrational heat capacity as the butyl groups are transferred from water to benzene. A larger temperature range was examined in this work than with the dodecane–water system (8), so perhaps it is not surprising that heat capacity effects were not noted in the previous work.

It would be desirable to compare the standard enthalpies of transfer obtained here with those calculated from calorimetric data, since the enthalpy of transfer is simply the difference between the enthalpies of solution in the two phases. The enthalpy of solution of TBP in benzene was determined by Kertes *et al.* (5) to be −1.7 kJ/mol. However, the heat of solution of TBP in water has not been measured because of the low solubility of TBP in water. From our data, we would estimate it as −27 ± 5 kJ/mol at 25°C, somewhat lower than the value of −34 ± 5 kJ/mol deduced previously from the transfer of TBP from water to dodecane. One major difference between measuring enthalpies of transfer directly and obtaining them from calorimetric data is that heats of solution are usually measured in pure phases, whereas in the transfer experiment, the phases are mutually saturated. Since mutual solubilities are much higher in the benzene–water system than in the dodecane–water system, they could be responsible for some of the differences noted.

*Thermodynamics of adsorption*

Standard free energies of adsorption, $\Delta_a\mu^\ominus$, from benzene were calculated from the limiting slopes in Fig. 2 using eq. [4]:

$$[4] \quad \Delta_a\mu^\ominus = -RT \ln (\pi/X)_0$$

where $(\pi/X)_0$ is the limiting slope of the surface pressure $\pi$ against the TBP mole fraction $X$, as both approach zero. The standard states used are unit mole fraction of TBP in benzene, but with unit activity coefficient, and 1.0 mN/m in the surface layer, as used by Aveyard and Briscoe (14, 15). Mole fractions of TBP in the aqueous phases were determined from the distribution coefficients, and standard free energies of adsorption from water were calculated from the same interfacial pressure data. The standard free energies of adsorption from both phases are listed in Table 4. They are somewhat less negative than those for the adsorption of TBP from dodecane or water to the dodecane–water interface (2). This is in accord with evidence that there is some complexing between TBP and benzene (5–7).

Can. J. Chem. Downloaded from www.nrcresearchpress.com by 210.87.254.40 on 09/06/12
For personal use only.

Can. J. Chem. Downloaded from www.nrcresearchpress.com by 210.87.254.40 on 09/06/12
For personal use only.

TABLE 4. Standard free energies of adsorption of TBP at the benzene–water interface

| $T$ (°C) | From benzene (kJ/mol) | From water (kJ/mol) |
|---|---|---|
| 9.0 | −29.90 | −44.82 |
| 11.5 | −20.99 | −45.64 |
| 14.0 | −21.24 | −46.56 |
| 16.5 | −21.62 | −47.59 |
| 19.0 | −21.80 | −48.52 |
| 21.5 | −21.97 | −49.13 |
| 24.0 | −22.08 | −49.72 |
| 26.5 | −22.26 | −50.41 |
| 29.0 | −22.53 | −51.08 |

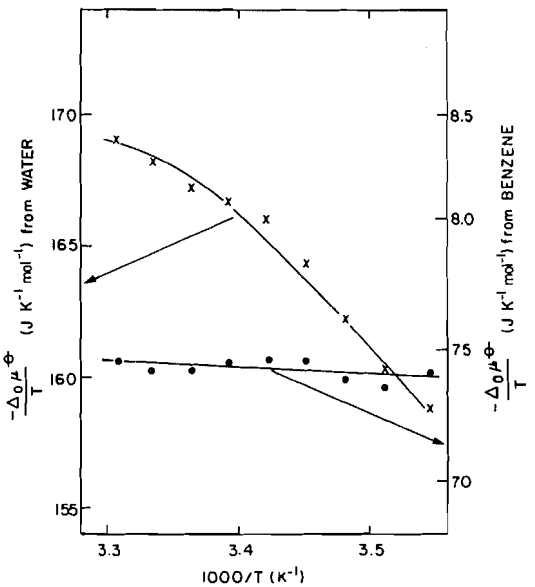


FIG. 6. Determination of the standard enthalpies of adsorption of TBP from benzene (○) and from water (×) to the benzene–water interface.

Standard enthalpies of adsorption, $\Delta_a h^\ominus$, were obtained from the standard free energies of adsorption by using equations analogous to eq. [3]. Plots of $\Delta_a\mu^\ominus/T$ against $1/T$ are shown in Fig. 6, and the derived standard enthalpies and entropies of adsorption are given in Table 5. Since adsorption from both phases involves a positive standard enthalpy of adsorption, adsorption is not favored enthalpically. Adsorption from benzene is only slightly endothermic, whereas adsorption from water is endothermic by an amount equivalent to about two hydrogen bonds at the higher temperatures. However, the overall process must be much more complicated than simply breaking hydrogen bonds, since complexing of TBP with benzene is also involved. It seems that complexing of TBP with benzene begins to occur (5–7) at the same time as the hydrogen bonds with water are broken, when the TBP moves from water to the interface. On moving from the interface into benzene, these two processes are almost balanced.

The positive standard enthalpies of adsorption are, of course, offset by large positive standard entropies of adsorption, $\Delta_a S^\ominus$. For adsorption from the water side, a large fraction of this standard entropy of adsorption is accounted for by the "hydrophobic bonding" involved in transferring the butyl groups from water to benzene (11). This effect has been discussed above. However, there is also a large positive entropy change in going from the bulk to the surface. Since adsorption from dodecane to the dodecane–water interface involves a negative standard entropy of adsorption using the same standard states (12), the standard entropy observed here reflects a loss of benzene structure around the phosphate groups as they approach the interface.

*Surface equation of state*

Surface tension data were fitted to the Schofield–Rideal equation of state (16), eq. [5],

$$[5]\quad \pi(A - A_0) = ikT$$

where $\pi$ is the surface pressure as before, and $i$ and $A_0$ are fitting constants. The area available per molecule, $A$, was calculated from the Gibbs adsorption isotherm using the constants of Table 1, as previously described (1, 2). Activity coefficients of TBP in benzene were taken as 1.0. Values of $i$ and $A_0$ obtained from the least-squares fit are listed in Table 6, and the goodness of the fits is illustrated in Fig. 7. Although $A_0$ is only a fitting constant, it is frequently discussed in terms of the static molecular area of the solute. At the lower temperatures,

TABLE 5. Standard free energies, enthalpies, and entropies of TBP adsorption at the benzene–water interface

| | From benzene | | | From water | | |
|---|---|---|---|---|---|---|
| $T$ (°C) | $\Delta_a\mu^\ominus$ (kJ/mol) | $\Delta_a h^\ominus$ (kJ/mol) | $\Delta_a S^\ominus$ (J K$^{-1}$ mol$^{-1}$) | $\Delta_a\mu^\ominus$ (kJ/mol) | $\Delta_o h^\ominus$ (kJ/mol) | $\Delta_a S^\ominus$ (J K$^{-1}$ mol$^{-1}$) |
| 9.0 | −20.9 | 2.5 | 83 | −44.8 | 74 | 420 |
| 19.0 | −21.8 | 2.5 | 83 | −48.5 | 43 | 310 |
| 29.0 | −22.5 | 2.5 | 83 | −51.1 | 15 | 220 |

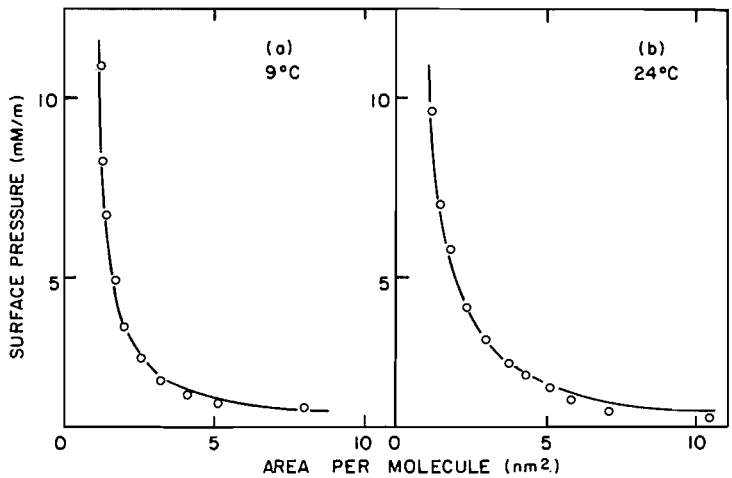


FIG. 7. Fit of surface pressure and area data at 9°C (7*a*) and 24°C (7*b*) to the Schofield–Rideal equation of state, using the constants in Table 6.

TABLE 6. Constants of the Schofield–Rideal equation

| $T$ (°C) | $A_0$ (nm²) | $i$ |
|---|---|---|
| 9 | 0.86±0.02 | 1.09±0.05 |
| 14 | 0.88±0.03 | 1.07±0.07 |
| 19 | 0.59±0.05 | 1.48±0.08 |
| 24 | 0.67±0.07 | 1.59±0.09 |
| 29 | 0.60±0.18 | 1.78±0.19 |

the $A_0$ values are very close to the geometric area of the TBP and the $i$ values are close to 1.0, as is usual for adsorption at a liquid–liquid interface (17). At higher temperatures, the $i$ values become larger than 1.0 and the $A_0$ values become smaller. This behavior corresponds to increased cohesion in the adsorbed layer, somewhat similar to that for ionized adsorbed layers (17). Some of this repulsion can be accounted for by dipole–dipole repulsion in the adsorbed layer (1, 2), or by variation of $A_0$ with coverage.

Attempts were made to use a two-dimensional solution model for the interface (18, 19) and to fit data to the Van der Waals equation of state (20), but these did not result in any improvements in the fit.

## Acknowledgements

We thank R. J. Porth for preparing TBP, and A. S. Kertes, P. R. Tremaine, and our colleagues at the Whiteshell Nuclear Research Establishment for helpful advice.

1. N. H. SAGERT, W. LEE, and M. J. QUINN. Can. J. Chem. **57**, 1218 (1979).
2. N. H. SAGERT and W. LEE. Can. J. Chem. **58**, 2789 (1980).
3. E. CHIFU, Z. ANDREI, and M. TOMOAIA. Ann. Chim. **64**, 869 (1974).
4. Z. ANDREI and E. CHIFU. Stud. Univ. Babes-Bolyai Ser. Chem. **21**, 10 (1976).
5. A. S. KERTES, L. TSIMERING, and F. GRAUER. J. Inorg. Nucl. Chem. **38**, 867 (1976).
6. D. M. PETKOVIĆ and Z. B. MAKSIMOVIĆ. J. Inorg. Nucl. Chem. **38**, 297 (1976).
7. A. APELBLAT. J. Inorg. Nucl. Chem. **42**, 411 (1980).
8. N. H. SAGERT and W. LEE. Can. J. Chem. **58**, 1463 (1980).
9. R. AVEYARD and R. W. MITCHELL. Trans. Faraday Soc. **65**, 2645 (1969).
10. A. V. KARYAKIN and G. A. MURADOVA. Zh. Fiz. Khim. **45**, 1054 (1971) (Russ. J. Phys. Chem. **45**, 591 (1971)).
11. H. S. FRANK and M. W. EVANS. J. Chem. Phys. **13**, 507 (1945).
12. C. TANFORD. The hydrophobic effect: formation of micelles and biological membranes. 2nd ed. John Wiley, New York. 1980. pp. 14–28.
13. C. JOLICOEUR and G. LACROIX. Can. J. Chem. **54**, 624 (1976).
14. R. AVEYARD and B. J. BRISCOE. Trans. Faraday Soc. **66**, 2911 (1970).
15. R. AVEYARD and B. J. BRISCOE. J. Chem. Soc. Faraday I, **68**, 478 (1972).
16. R. K. SCHOFIELD and E. K. RIDEAL. Proc. R. Soc. London A**109**, 57 (1925).
17. R. AVEYARD and B. VINCENT. Prog. Surf. Sci. **8**, 59 (1977).
18. F. M. FOWKES. J. Phys. Chem. **66**, 1863 (1962).
19. E. H. LUCASSEN-REYNDERS. *In* Progress in surface and membrane science. Vol. 10. *Edited by* D. A. Cadenhead and J. F. Danielli. Academic Press, New York. 1976. pp. 253–360.
20. S. ROSS and E. S. CHEN. Ind. Eng. Chem. **57**(7), 40 (1965).

Can. J. Chem. Downloaded from www.nrcresearchpress.com by 210.87.254.40 on 09/06/12
For personal use only.

# Molecular orbital calculations of the ionization potentials and stabilization energies of aminoalkyl radicals[1]

JOHN D. GODDARD

*Division of Chemistry, National Research Council of Canada, Ottawa, Ont., Canada K1A 0R6*

Received September 11, 1981

JOHN D. GODDARD. Can. J. Chem. **60**, 1250 (1982).

A series of aminoalkyl radicals, $H_2NCH_2$, $H(CH_3)NCH_2$, $(CH_3)_2NCH_2$, $H_2NC(CH_3)H$, $H_2NC(CH_3)_2$, and the corresponding amines have been examined by *ab initio* computations. The first vertical ionization potentials of the radicals calculated by the direct SCF method were very low: $H_2NCH_2$ (6.3 eV), $H(CH_3)NCH_2$ (6.0 eV), and $(CH_3)_2NCH_2$ (5.8 eV) and decreased with methyl substitution at nitrogen. The first ionization potentials of $H_2NC(CH_3)H$ and $H_2NC(CH_3)_2$ were predicted to be 5.9 and 5.6 eV respectively. Radical stabilization energies were calculated from SCF results in several basis sets and with several choices of optimized geometries for $R_2NCR_2 + CH_4 \rightarrow R_2NCR_2H + CH_3$. The aminomethyl radical, $H_2NCH_2$, was calculated to be 8 to 10 kcal/mol stabilized relative to methyl. The present calculations predict that methyl substitution at N has a small destabilizing effect on $H_2NCH_2$ which contrasts with recent experiments. The effect of methyl substitution and details of the "three-electron" bond in aminoalkyl radicals are examined qualitatively by orbital interaction diagrams.

JOHN D. GODDARD. Can. J. Chem. **60**, 1250 (1982).

Faisant appel à des calculs *ab initio*, on a étudié une série de radicaux aminoalkyles $H_2NCH_2$, $H(CH_3)NCH_2$, $(CH_3)_2NCH_2$, $H_2NC(CH_3)H$, $H_2Nc(CH_3)_2$ ainsi que les amines correspondantes. Les premiers potentiels d'ionisation verticaux des radicaux, calculés par la méthode directe SCF, sont très faibles $H_2NCH_2$ (6,3 eV), $H(CH_3)NCH_2$ (6,0 eV) et $(CH_3)_2NCH_2$ (5,8 eV) et diminuent lorsque les substituants méthyles sur l'azote augmentent. On a prévu que les premiers potentiels d'ionisation du $H_2NC(CH_3)H$ et du $H_2NC(CH_3)_2$ seraient respectivement de 5,9 et de 5,6 eV. On a calculé les énergies de stabilisation du radical à partir des résultats SCF dans plusieurs ensembles de base et avec plusieurs choix de géométries optimisées pour la réaction $R_2NCR_2 + CH_4 \rightarrow R_2NCR_2H + CH_3$. On a calculé que le radical aminoéthyle est stabilisé par environ 8 à 10 kcal/mol par rapport au méthyle. Les calculs actuels prédisent que le degré de substitution en méthyle au niveau de l'azote a un faible effet déstabilisateur sur le $H_2NCH_2$ qui contraste avec des expériences récentes.

Utilisant les diagrammes d'interactions d'orbitales, on a étudié qualitativement les effets de la substitution du méthyle et les détails de la liaison à "trois électrons" dans les radicaux aminoalkyles.

[Traduit par le journal]

## Introduction

Aminoalkyl radicals, $R_2NCR_2$, represent an interesting series of compounds in that their properties must be strongly influenced by the carbon–nitrogen "three-electron bond". In recent experiments, Griller and Lossing (1), using in part recent thermochemical data on alkyl immonium ions (2), found remarkably large stabilization energies and low first ionization potentials for $H_2NCH_2$, $H(CH_3)NCH_2$, and $(CH_3)_2NCH_2$. The first ionization potential for $(CH_3)_2NCH_2$ of 5.7 eV measured by Griller and Lossing (1) is the lowest yet reported for an organic species. The stabilization energy, $E_s$, of $NH_2CH_2$ was determined to be $10 \pm 2$ kcal/mol in agreement with earlier kinetics experiments (3). However, the dramatic increase in $E_s$ with *N*-methylation as observed by Griller and Lossing (1) ($E_s(H(CH_3)NCH_2) = 17$, $E_s((CH_3)_2NCH_2) = 20$ kcal/mol) was noteworthy. Earlier data (4) suggesting that $(CH_3)_2N$— was stabilizing by 19 kcal/mol had been discounted (3) on the assumption that $E_s$ should *not* be significantly affected by *N*-alkylation. However, in the somewhat related alkyl immonium ions (2), the stabilizations (changes in heterolytic bond dissociation energy) brought about by substitution by —$NH_2$, —$N(CH_3)H$, and —$N(CH_3)_2$ were 94, 107, and 114 kcal/mol, showing a large change upon *N*-methylation.

The unusual properties of aminoalkyl radicals must be due largely to the presence of the "three-electron" bond between C and N. Qualitative aspects of the three-electron bond have been discussed in the literature (5–7, 9). However, *ab initio* computational studies of such bonding are relatively scarce (8–11) and the CN "three-electron" bond has only recently been examined in detail by such methods (11). In the present computational study, *ab initio* SCF calculations in several basis sets were performed for the "three-electron" bonded radicals: $H_2NCH_2$, $H(CH_3)NCH_2$, $(CH_3)_2NCH_2$, $H_2NC(CH_3)H$, and $H_2NC(CH_3)_2$. All species have been geometry-optimized including the amines necessary to determine radical stabilization energies from the reaction:

$$R_2NCR_2 + CH_4 \rightarrow R_2NCHR_2 + CH_3$$

The computed results are analyzed by qualitative MO methods and compared in detail with recent experimental work (1).

[1]NRCC No. 20025.

0008-4042/82/101250-06$01.00/0

©1982 National Research Council of Canada/Conseil national de recherches du Canada

Can. J. Chem. Downloaded from www.nrcresearchpress.com by 210.87.254.42 on 09/06/12
For personal use only.

Can. J. Chem. Downloaded from www.nrcresearchpress.com by 210.87.254.42 on 09/06/12
For personal use only.

## Methods of calculation

All calculations were performed with a modified version (12) of the GAUSSIAN76 program system (13). Geometries were optimized for all molecules at the 4-31G (14) level using energy gradient methods (15). Some species were also geometry-optimized with the minimal STO-3G (16) and the polarized 6-31G* (17) basis sets. Additional calculations with other basis sets including the 6-31G** set (17) were also carried out at the various optimized geometries. Calculations on the radicals employed the unrestricted Hartree-Fock (UHF) method (18). The 4-31G expectation values of $S^2$ at the optimum geometries ranged from 0.7599 to 0.7613 while the value for a doublet is 0.7500. It is anticipated that spin contamination had no significant effects on the calculated geometries. For aminomethyl in the 4-31G basis set, this assumption was explicitly checked by carrying out an RHF calculation including the energy gradients at the UHF-optimized geometry. The value of $S^2$ for the UHF calculation was 0.7600 in this case. The RHF forces at the UHF geometry were all small with the largest less than $8 \times 10^{-3}$ mdyn-Å/radian in magnitude and indicate that reoptimization with an RHF procedure would lead to very minor changes in geometry. In order to set a scale for the orbital interaction diagram vertical first ionization potentials were predicted from the orbital energy of the singly occupied molecular orbital (SOMO) by Koopmans' theorem. More accurate ionization potentials for comparison with the experimental results (1) were calculated by a direct SCF approach (19) involving a separate SCF calculation on the cation at the 4-31G UHF optimized geometry of the radical. Thus, the calculated ionization potentials refer to a strictly vertical process.

## Results and discussion

### *Geometries*

No detailed discussion of the optimized geometries of the amines or aminoalkyl radicals will be presented here. A few points regarding the structures will be noted to the extent that they bear on the probable reliability of the calculated ionization potentials and radical stabilization energies. The 4-31G basis set is well known (e.g. (20)) to underestimate the pyramidality of trivalent nitrogen and this *systematic error* is present in the results of this study *both* for the amines *and* for the aminoalkyl radicals (see Tables 1 and 2). Other geometrical parameters (e.g. the CN bond lengths) are in good agreement with experiment for the amines (within 0.02 Å) and presumably also for the aminoalkyl

TABLE 1. Selected features of the SCF optimized geometries for the amines; *anti* or *gauche* refer to the methyl's conformation with respect to the nitrogen "lone pair"

| Molecule | Basis set | $R$(CN) | $R$(NH) | ∠(HNC) | ∠(CNC) | $R(CH)_{anti}$ / $R(CH)_{gauche}$ | ∠$(NCH)_{anti}$ / ∠$(NCH)_{gauche}$ |
|---|---|---|---|---|---|---|---|
| Methylamine, $CH_3NH_2$ | 4-31G | 1.450 | 0.994 | 116.4 | — | 1.089 / 1.081 | 114.5 / 109.4 |
| | STO-3G | 1.486 | 1.033 | 107.3 | — | 1.093 / 1.089 | 113.8 / 109.2 |
| | 6-31G* | 1.453 | 1.001 | 109.2 | — | 1.091 / 1.084 | 114.8 / 109.2 |
| | Expt.[a] | 1.471 | 1.010 | 110.3 | — | — / — | 113.8 / 109.5 |
| Dimethylamine, $(CH_3)_2NH$ | 4-31G | 1.449 | 0.990 | 114.1 | 116.6 | 1.091 / 1.082 | 113.7 / 109.7 |
| | Expt.[b] | 1.466 | 1.022 | 108.8 | 112.2 | — / — | — / — |
| Trimethylamine, $(CH_3)_3N$ | 4-31G | 1.451 | — | — | 114.2 | 1.093 / 1.081 | 112.9 / 109.7 |
| | STO-3G | 1.485 | — | — | 110.2 | 1.093 / 1.088 | 112.9 / 109.2 |
| | 6-31G* | 1.445 | — | — | 111.9 | 1.095 / 1.084 | 113.0 / 109.8 |
| | Expt.[c] | 1.451 | — | — | 110.9 | 1.109 / 1.008 | 111.7 / 110.1 |
| Ethylamine, $CH_3CH_2NH_2$ | 4-31G | 1.453 | 0.995 | 116.2 | — | — / — | — / — |
| Isopropylamine, $(CH_3)_2CHNH_2$ | 4-31G | 1.459 | 0.996 | 115.8 | — | — / — | — / — |

[a]Reference 29.
[b]Reference 30.
[c]Reference 31.

TABLE 2. Selected features of the SCF optimized geometries for the aminoalkyl radicals

| Radical | Basis set | $R$(CN) | $R$(NH) | ∠(HNC) | ∠(CNC) | $R$(CH) | ∠(HCN) |
|---|---|---|---|---|---|---|---|
| $CH_2NH_2$ | 4-31G | 1.392 | 0.990 | 119.9 | — | 1.071 | 117.1 |
| | STO-3G | 1.444 | 1.031 | 109.6 | — | 1.085 | 115.2 |
| | 6-31G* | 1.402 | 0.999 | 113.4 | — | 1.076 | 115.6 |
| $CH_2N(CH_3)H$ | 4-31G | 1.390 | 0.991 | 117.3 | 121.0 | 1.071 | 117.1 |
| $CH_2N(CH_3)_2$ | 4.31G | 1.392 | — | — | 118.4 | 1.072 | 117.0 |
| | STO-3G | 1.443 | — | — | 112.9 | 1.086 | 114.7 |
| | 6-31G* | 1.393 | — | — | 115.6 | 1.076 | 116.0 |
| $C(CH_3)HNH_2$ | 4-31G | 1.399 | 0.991 | 119.4 | — | 1.074 | 114.9 |
| $C(CH_3)_2NH_2$ | 4-31G | 1.407 | 0.992 | 118.9 | — | — | — |

radicals. In determining the radical stabilization energies from

$$R_2NCR_2 + CH_4 \rightarrow R_2NCR_2H + CH_3$$

at the 4-31G geometries and with various basis sets (4-31G, 6-31G*, 6-31G**), it is implicitly assumed that the errors in having the nitrogen too planar are the same in the amines and aminoalkyl radicals and thus approximately cancel. Some computational evidence for this assumption will be presented in the section on stabilization energies where the results of determining these quantities at STO-3G or 6-31G* geometries (which do *not* suffer from the defect of having the nitrogen too planar) will be given. *Trends* in the stabilization energies will be shown to be independent of the reference geometries and basis sets used in the SCF calculations.

The aminoalkyl radicals are all calculated to be at least slightly nonplanar at both N and C and to adopt nontwisted *anti* conformations:

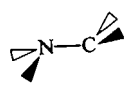

Given the 4-31G basis set's known tendency to underestimate pyramidality, this slight nonplanarity strongly implies that the radicals will be found to be nonplanar experimentally. The predicted geometries agree qualitatively (chair conformation, C and N nonplanar) with suggestions based on esr experiments (21, 22) and semiempirical INDO calculations (21). The methyl substituents on N show a conformation previously seen in methylamine (e.g. (20)) with one long CH bond antiperiplanar to the nitrogen lone pair and two shorter bonds *gauche* to this pair.

A few of the more interesting geometrical parameters are collected in Tables 1 and 2 where some comparisons of the results with different basis sets and with experiment are also given.

## Ionization potentials

Ionization potentials of the aminoalkyl radicals as calculated by Koopmans' theorem and by direct SCF calculations on the radical and cation are given in Table 3. The Koopmans' theorem results which neglect orbital relaxation are not expected to be quantitatively accurate and are ~1.5 eV larger than experiment (1). These values are presented as they provide the orbital energy scale in the qualitative discussion to follow. The direct SCF results are in surprising agreement with experiment (1) being ~0.1 eV larger. The direct SCF method neglects changes in correlation energy between the neutral radical and the closed-shell cation. However, to zeroth order, these species differ only in one singly occupied orbital whereas important correlation effects are due to pairs of electrons. Thus, a direct SCF approach would be expected to yield reliable vertical ionization potentials for the present species. However, the experimental results have previously been assumed to be close to the *adiabatic* values of the ionization potential (25). Methylation at N lowers the first ionization potential by 0.2 to 0.3 eV and follows the experimental trend (1). The same *trend* may be seen in either the Koopmans' theorem or direct SCF results. $H_2NC(CH_3)H$ and $H_2NC(CH_3)_2$, which have not yet been characterized experimentally, are predicted to have low ionization potentials of 5.9 and 5.6 eV respectively. Thus, methylation directly at the carbon radical centre lowers the ionization potential by ~0.1 eV more than methylation at N (e.g. $CH_3(H)NCH_2$ 4-31G ΔSCF 6.04 eV, $NH_2C(CH_3)H$ 4-31G ΔSCF 5.9 eV).

### *Radical stabilization energies*

Radical stabilization energies (in kcal/mol) are reported in Tables 4 and 5. These quantities were calculated from the computed heats of reaction for $R_2NCR_2 + CH_4 \rightarrow R_2NCHR_2 + CH_3$ with several basis sets and geometries. The methyl radical defines a zero on the scale with more stable radicals having negative stabilization energies. In Table 4, the ethyl radical is included for comparison with a very recent experimental determination of its stabi-

Can. J. Chem. Downloaded from www.nrcresearchpress.com by 210.87.254.42 on 09/06/12
For personal use only.

Can. J. Chem. Downloaded from www.nrcresearchpress.com by 210.87.254.42 on 09/06/12
For personal use only.

TABLE 3. Ionization potentials from Koopmans' theorem and direct SCF methods; all calculations were carried out at 4-31G SCF optimized geometries

| Molecule | Basis set | Ionization potential (eV) Koopmans' theorem | ΔSCF |
|---|---|---|---|
| $H_2NCH_2$ | 4-31G | 7.60 | 6.37 |
| | 6-31G* | 7.56 | 6.29 |
| | 6-31G** | 7.57 | 6.30 |
| | Experiment[a] | 6.2±0.1 | |
| $CH_3(H)NCH_2$ | 4-31G | 7.37 | 6.04 |
| | 6-31G* | 7.37 | 5.99 |
| | 6-31G** | 7.38 | 6.00 |
| | Experiment[a] | 5.9±0.1 | |
| $(CH_3)_2NCH_2$ | 4-31G | 7.24 | 5.82 |
| | 6-31G* | 7.27 | 5.80 |
| | Experiment[a] | 5.7±0.1 | |
| $H_2NC(H)CH_3$ | 4-31G | 7.32 | 5.93 |
| | 6-31G* | 7.30 | 5.87 |
| | 6-31G** | 7.31 | 5.88 |
| $H_2NC(CH_3)_2$ | 4-31G | 7.15 | 5.63 |
| | 6-31G** | 7.16 | 5.59 |

[a]Reference 1. The theoretical results are strictly vertical ionization potentials while the experimental results have been assumed to be close to adiabatic values.

TABLE 4. Radical stabilization energies in kcal/mol; all calculations were carried out at 4-31G optimized geometries for the reaction $R\cdot + CH_4 \rightarrow RH + CH_3\cdot$

| Radical | Stabilization energy 4-31G | 6-31G* | 6-31G** |
|---|---|---|---|
| $\dot{C}H_3$[a] | 0.0 | 0.0 | 0.0 |
| $\dot{C}H_2CH_3$ | −3.2 | −2.8 | −2.8 |
| $\dot{C}H_2\ddot{N}H_2$ | −10.3 | −7.9 | −8.2 |
| $\dot{C}H_2\ddot{N}HCH_3$ | −9.7 | −7.6 | −7.8 |
| $\dot{C}H_2\ddot{N}(CH_3)_2$ | −8.9 | −7.1 | —[b] |
| $\dot{C}H(CH_3)\ddot{N}H_2$ | −11.5 | −9.5 | −9.6 |
| $\dot{C}(CH_3)_2\ddot{N}H_2$ | −12.8 | −11.0 | —[b] |

[a]$CH_3$ is taken as zero on the scale with a negative stabilization energy implying greater stability than $CH_3$.
[b]Not calculated at this level.

TABLE 5. Radical stabilization energies in kcal/mol calculated for the reaction $R\cdot + CH_4 \rightarrow RH + CH_3\cdot$; A//B implies basis set A at the optimum geometry for basis set B

| Conditions | Stabilization energy $H_2NCH_2$ | $(CH_3)_2NCH_2$ |
|---|---|---|
| STO-3G//STO-3G | −10.0 | −9.0 |
| 4-31G//STO-3G | −8.9 | −7.4 |
| 6-31G*//STO-3G | −7.8 | −6.9 |
| 4-31G//4-31G | −10.3 | −8.9 |
| 6-31G*//4-31G | −7.9 | −7.1 |
| 6-31G*//6-31G* | −8.2 | −7.5 |
| Experiment (1) | −10±2 | −20±2 |

lization energy. The ethyl radical is predicted to be ~3 kcal/mol more stable than methyl in good agreement with the value of 4.1 ± 1.0 kcal/mol from experiment (23). The aminomethyl radical, $H_2NCH_2$, is predicted to have a stabilization energy of 8 to 10 kcal/mol which also agrees with the values inferred from experiment (1, 3).

The calculated stabilization energies for $CH_2N(CH_3)H$ and $CH_2N(CH_3)_2$ are particularly noteworthy in that they are slightly *less* than that found for $H_2NCH_2$. This calculated trend disagrees with recent experiments (1) which derived a very dramatic increase in stability with *N*-alkylation to $E_s(CH_2N(CH_3)H) = 17$ and $E_s(CH_2N(CH_3)_2) = 20$ kcal/mol. As can be seen from Table 5, the calculated small decrease in stability of dimethylamino-relative to amino- is *not* due to the use of 4-31G optimized geometries (Table 4) as the same trend appears in SCF calculations at STO-3G or 6-31G* optimized geometries. Further discussion of this discrepancy between computation and experiment will be given in the next section.

The *C*-methylated aminoalkyl radicals are predicted to be slightly more stable than either the simple amino or the *N*-methylated amino radicals. Stabilizations of 9.5 to 11.5 and 11.0 to 12.8 kcal/mol are calculated for $C(CH_3)HNH_2$ and $C(CH_3)_2NH_2$. Thus the additional methyls attached to C are stabilizing by 1.0 to 1.5 kcal/mol relative to $H_2NCH_2$.

### *Qualitative molecular orbital considerations and comparisons with experiment*

Figure 1 illustrates an orbital interaction scheme between the HOMO of ammonia, methylamine, and dimethylamine and the SOMO of the methyl radical to give the "one-" and "two-" electron components of the "three-electron" bond. The

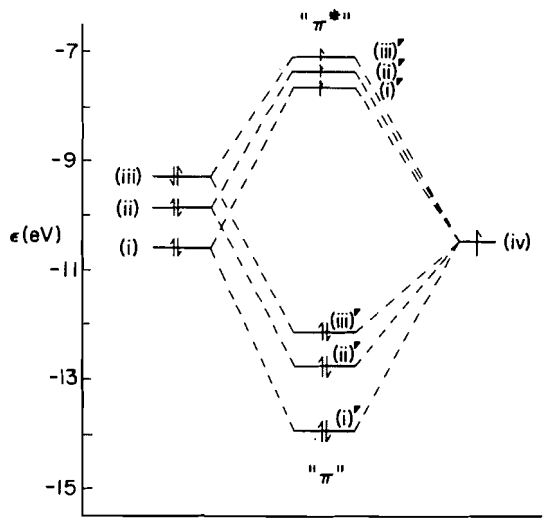


FIG. 1. Orbital interaction diagram for the "three-electron" bond. Orbital energies are from 4-31G calculations for (*i*) ammonia, (*ii*) methylamine, (*iii*) dimethylamine, (*i*)' aminomethyl, (*ii*)' methylaminomethyl, (*iii*)' dimethylaminomethyl, and (*iv*) methyl.

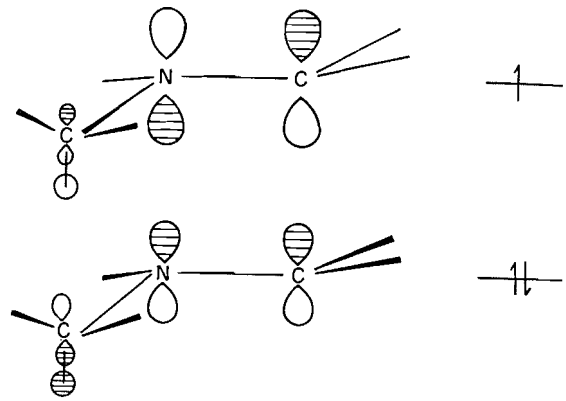


FIG. 2. "π"-type interactions of the methyl group with the "one-" and "two-" electron components of the "three-electron" bond. Orbital phases from the UHF 4-31G α-spin MO.

HOMO of ammonia shifts up with methylation which may be rationalized (e.g. (24)) by a model which considers the methyl group as a pseudo *p* orbital interacting with the *p* component of the nitrogen lone pair. This hyperconjugative interaction results in a lower energy orbital mainly in the methyl group (bonding interaction) and a higher energy (antibonding interaction) consisting mainly of the lone pair. This latter orbital lies at an energy higher than the noninteracting lone pair orbital in ammonia. The increase in energy of the amine HOMO coupled with a constant energy for the methyl SOMO leads to destabilization of both the HOMO (π) and SOMO (π*) orbitals of the aminoalkyl radicals upon methylation at N. Figure 2 shows that at least in the pseudo π system the interactions between the methyl group and the "three-electron" CN bond are destabilizing for the highest two orbitals. The lessened orbital stability in the "three-electron" bond also matches the decreased total stability calculated from the total energies (recall Tables 4 and 5). These trends in radical stabilization energies run contrary to those observed experimentally. However, the decreased stability of the SOMO upon methylation at N matches the experimental decrease in ionization potential. Figures 1 and 2 serve to illustrate an internal consistency in the calculated results. Destabilization in the total energies is reflected in less stable highest molecular orbitals (or vice versa).

The experimental results (1) for the ionization potentials are derived from appearance energies measured by the impact of an energy-resolved electron beam combined with a quadrupole mass spectrometer.

$$AE(R^+) = \Delta H_f(R_1^+) + \Delta H_f(R_2\cdot) - \Delta H_f(R_1R_2)$$

$\Delta H_f(R_1^+)$ were known independently (2) and the $\Delta H_f(R_1R_2)$ estimated by group equivalents. Thus, measurement of the appearance energy, AE, allows a determination of $\Delta H_f(R_2\cdot)$ and the ionization potentials follow from

$$IP(R_2\cdot) = \Delta H_f(R_2^+) - \Delta H_f(R_2\cdot)$$

These ionization potentials have been assumed to be close to the adiabatic values. The agreement between the strictly vertical calculated values (Table 3) and the experimental ones (1) implies either that relaxation energies are small or that the experimental values may be closer to vertical than previously thought. Relaxation effects in changing the CN bond to a true double bond could be substantial. For dimethylaminomethyl, another experiment (26) has yielded an ionization potential of 5.35 eV which is 0.35 eV less than the value in ref. 1. Using this value a radical stabilization energy of only ~14 kcal/mol would follow for $(CH_3)_2NCH_2$. A calculated value (4-31G//STO-3G) for $\Delta E(CH_2OH - CH_2OH^+)$ of 7.2 eV is in the literature (27) which is 0.4 eV *less* than that derived from experiments (1, 28) similar to those performed on the aminoalkyl radicals.

Since the radical stabilization energies were calculated using bond dissociation energies derived from

$$D(R_1H) = \Delta H_f(R_2\cdot) + \Delta H_f(H) - \Delta H_f(R_2H)$$

it is clear that the ionization potentials and radical stabilization energies are strongly interdependent.

Can. J. Chem. Downloaded from www.nrcresearchpress.com by 210.87.254.42 on 09/06/12
For personal use only.

Can. J. Chem. Downloaded from www.nrcresearchpress.com by 210.87.254.42 on 09/06/12
For personal use only.

## Conclusions

The present work predicts strikingly low vertical ionization potentials of aminoalkyl radicals. The dramatic increase in aminoalkyl radical stability with *N*-methylation as observed experimentally is not predicted by the present *ab initio* SCF calculations. Basis set and geometry effects have essentially been ruled out as causes of the discrepancy. Qualitative MO arguments regarding the "three-electron" bond are internally consistent with a small destabilizing effect due to methylation at N. A remaining possibility on the theoretical side would be an unexpected inability of the SCF method to describe the three-electron bond and/or other interactions in the aminoalkyl radicals. Perhaps correlated wave functions are necessary for even a correct low-order description of these species. On the experimental side, there may exist errors in the exact determination of the appearance potentials and in the group-equivalents scheme used to determine certain of the thermochemical data. In addition, the appearance energies do not appear to be strictly adiabatic and thus some inconsistency in their use with the other thermochemical data is possible. The source of the discrepancy between the theoretical calculations and the derived experimental results is not completely clear. Further calculations including correlation effects by configuration interaction or perturbation theory are in order. A direct photoelectron spectrum of the transient radicals would be an invaluable experiment.

## Acknowledgements

The author had valuable discussions with Drs. F. P. Lossing and D. Griller regarding the experimental work on aminoalkyl radicals.

1. D. Griller and F. P. Lossing. J. Am. Chem. Soc. **103**, 1586 (1981).
2. F. P. Lossing, Y.-T. Lam, and A. Maccoll. Can. J. Chem. **59**, 2228 (1981).
3. A. J. Colussi and S. W. Benson. Int. J. Chem. Kinet. **73**, 381 (1969).
4. H. G. Richey, Jr. and D. W. Shull. Tetrahedron Lett. 575 (1976).
5. L. Pauling. J. Am. Chem. Soc. **53**, 3225 (1931).
6. N. C. Baird. J. Chem. Educ. **54**, 291 (1977).
7. R. D. Harcourt. J. Am. Chem. Soc. **102**, 5195 (1980).
8. T.-K. Ha. Chem. Phys. Lett. **30**, 379 (1975).
9. F. Bernardi, N. D. Epiotis, W. Cherry, H. B. Schlegel, M.-H. Whangbo, and S. Wolfe. J. Am. Chem. Soc. **98**, 469 (1976).
10. N. C. Baird and K. F. Taylor. J. Chem. Phys. **72**, 6529 (1980).
11. K. N. Houk. Private communication.
12. M. R. Peterson and R. A. Poirier. MONSTERGAUSS 80. Department of Chemistry, University of Toronto, Toronto, Ont. 1980.
13. J. S. Binkley, R. A. Whiteside, P. C. Hariharan, R. Seeger, J. A. Pople, W. J. Hehre, and M. D. Newton. GAUSSIAN 76. QCPE368. Department of Chemistry, Indiana University, Bloomington, IN. U.S.A.
14. R. Ditchfield, W. J. Hehre, and J. A. Pople. J. Chem. Phys. **54**, 724 (1971).
15. H. B. Schlegel. Ph. D. Thesis. Queen's University, Kingston, Ont. 1975.
16. W. J. Hehre, R. F. Stewart, and J. A. Pople. J. Chem. Phys. **51**, 2657 (1969).
17. P. C. Hariharan and J. A. Pople. Mol. Phys. **27**, 209 (1974); Theoret. Chim. Acta, **28**, 213 (1973).
18. J. A. Pople and R. K. Nesbet. J. Chem. Phys. **22**, 571 (1954).
19. M. E. Schwartz. *In* Modern theoretical chemistry. Vol. 4. *Edited by* H. F. Schaefer III. Plenum, New York. 1977. p. 357.
20. H. B. Schlegel, S. Wolfe, and F. Bernardi. J. Chem. Phys. **67**, 4181 (1977).
21. D. E. Wood and R. V. Lloyd. J. Chem. Phys. **53**, 3932 (1970).
22. A. R. Lyons and M. C. R. Symons. J. Chem. Soc. Faraday Trans. **2**, 502 (1972).
23. A. L. Castelhano, P. R. Marriott, and D. Griller. J. Am. Chem. Soc. **103**, 4262 (1981).
24. P. Avouris and A. R. Rossi. J. Phys. Chem. **85**, 2340 (1981).
25. F. P. Lossing. Private communication.
26. Y. Loguinov, V. V. Takhistov, and L. P. Vatlina. Org. Mass Spectrom. **16**, 239 (1981).
27. W. A. Lathan, L. A. Curtiss, W. J. Hehre, J. B. Lisle, and J. A. Pople. Prog. Phys. Org. Chem. **11**, 175 (1974).
28. F. P. Lossing. J. Am. Chem. Soc. **99**, 7256 (1977).
29. K. Takagi and T. Kojima. J. Phys. Soc. Jpn. **30**, 1145 (1971).
30. J. E. Wollraub and V. W. Laurie. J. Chem. Phys. **48**, 5088 (1968).
31. J. E. Wollraub and V. W. Laurie. J. Chem. Phys. **51**, 1580 (1969).

# Reaction of β-halo α,β-unsaturated ketones with cuprate reagents. Efficient syntheses of β,β-dialkyl ketones and β-alkyl α,β-unsaturated ketones. A synthesis of (*Z*)-jasmone

EDWARD PIERS, KIN FAI CHENG,[1] AND ISAO NAGAKURA

*Department of Chemistry, University of British Columbia, 2036 Main Mall, University Campus, Vancouver, B.C., Canada V6T 1Y6*

Received November 13, 1981

EDWARD PIERS, KIN FAI CHENG, and ISAO NAGAKURA. Can. J. Chem. **60**, 1256 (1982).

Treatment of the 3-halo-2-cyclohexen-1-ones **11–15** and **17** with an excess of lithium dimethylcuprate provided good to excellent yields of the corresponding 3,3-dimethylcyclohexanones **21–24**. Similar reactions involving the β-bromo cyclopentenones **19** and **20** stopped at the monoaddition stage, producing the cyclopentenones **40** and **43**. Reaction of the β-bromo cyclohexenones **12** and **15** with 1.1 equiv. of lithium dimethylcuprate did not effect clean conversion of these substrates into the corresponding 3-methyl-2-cyclohexen-1-ones. When a series of β-bromo enones **12**, **14–19** were allowed to react with the lithium (phenylthio)(alkyl)cuprates **44–47**, the corresponding β-alkyl enones were, in general, produced cleanly and efficiently. However, reaction of 3-bromo-2-methyl-2-cyclopenten-1-one (**19**) with the cuprate reagent **44** gave mainly the β-phenylthio enone **49**. This undesired result could be avoided by employing, in the place of **19**, the β-iodo cyclopentenone **50**, which reacted smoothly with **44** to give a high yield of 2,3-dimethyl-2-cyclopenten-1-one (**40**). Reaction of 3-bromo-2-cyclohexen-1-one (**14**) with 3 equiv. of the mixed vinylcuprate reagent **48** gave 3-(3-butenyl)-2-cyclohexen-1-one (**32**). Alkylation of 1,3-cyclopentanedione with (*Z*)-1-chloro-2-pentene afforded compound **51**, which was converted into the β-bromo enone **52**. Treatment of the latter substance with lithium dimethylcuprate provided (*Z*)-jasmone (**53**).

EDWARD PIERS, KIN FAI CHENG et ISAO NAGAKURA. Can. J. Chem. **60**, 1256 (1982).

Les halo-3 cyclohexène-2 ones-1 (**11–15** et **17**) réagissent avec le diméthylcuprate de lithium en excès en donnant les diméthyl-3,3 cyclohexanones correspondantes avec des rendements variables. Des réactions analogues mettant en jeu les β-bromo cyclopentènones (**19** et **20**) s'arrêtent à l'étape de monoaddition en produisant les cyclopentènones (**40** et **43**). La réaction des β-bromo cyclohexènones (**12** et **15**) avec 1,1 équivalent de diméthylcuprate de lithium n'affectent pas la transformation franche de ces substrats en méthyl-3 cyclohexène-2 ones-1 correspondantes. Quand on fait réagir une série de β-bromo ènones (**12**, **14–19**) avec les (phenylthioalkyl)cuprates de lithium (**44–47**), on obtient en général les β-alkylènones correspondantes d'une manière efficace et pure. Cependant, la bromo-3 méthyl-2 cyclopentène-2 one-1 (**19**) réagit avec le cuprate **44** en donnant principalement la β-phénylthioénone **49**. On peut éviter ce produit indésirable en remplaçant le produit **19** par la β-iodo cyclopentènone **50** qui réagit doucement avec le réactif **44** en donnant avec un excellent rendement la diméthyl-2,3 cyclopentène-2 one-1 (**40**). La bromo-3 cyclohexène-2 one-1 (**14**) réagit avec 3 équivalents du vinylcuprate mixte (**48**) en donnant la (butène-3 yl)-3 cyclohexène-2 one-1 (**32**). L'alkylation de la cyclopentanedione-1,3 avec le (*Z*) chloro-1 pentène-2 conduit au composé **51** que l'on transforme en β-bromo ènone (**52**). Cette dernière réagit avec le diméthylcuprate de lithium en donnant la (*Z*)-jasmone (**53**).

[Traduit par le journal]

## Introduction

The reaction outlined in general terms by eq. [1] has been employed a great deal in organic synthesis, particularly in the very recent past. In this process, a β-substituted α,β-unsaturated ketone **1** reacts with a nucleophilic species (or an electron-transfer reagent) to provide initially the conjugate addition intermediate **2**. If Y is a good leaving group, it will be expelled from this intermediate to provide the product **3**. Thus, in an overall sense, a substitution reaction has occurred and, as such, the β-substituted enone **1** acts as a synthetic equivalent to the unsaturated $a^3$ synthon **5** (normal reactivity) (1). On the other hand, if the initially formed product **3** were to react in a conjugate addition sense with a second equivalent of reagent, the final product would be the ketone **4**. In this case, the

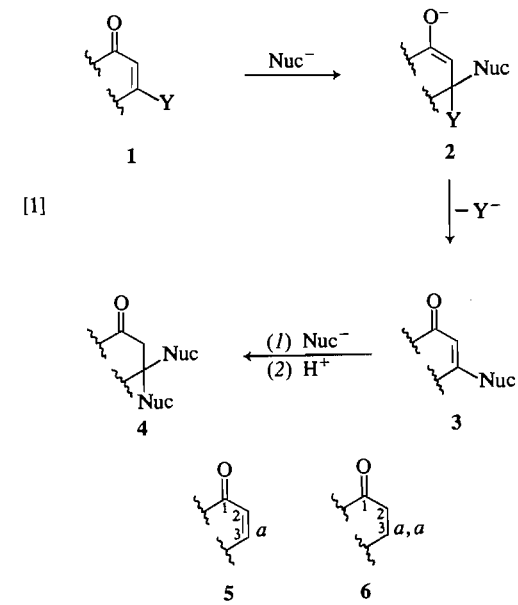


[1]Professor Cheng's contribution to this work was carried out while he was on sabbatical leave from the Department of Chemistry, University of Hong Kong.

0008-4042/82/101256-08$01.00/0

©1982 National Research Council of Canada/Conseil national de recherches du Canada

Can. J. Chem. Downloaded from www.nrcresearchpress.com by 210.87.254.5 on 09/06/12
For personal use only.

TABLE 1. Reaction of β-halo α,β-unsaturated ketones with lithium dimethylcuprate

| Entry | Starting material | Equivalents of $Me_2CuLi$ | Reaction conditions | Product(s) (ratio)[a] | Yield (%)[b] |
|---|---|---|---|---|---|
| 1 | **11** | 3 | 0°C, 1 h | **21** | 82 |
| 2 | **12** | 3 | 0°C, 1 h | **21** | 86 |
| 3 | **13** | 3 | 0°C, 1 h | **21** | 84 |
| 4 | **14** | 3 | 0°C, 1 h | **22** | 74 |
| 5 | **15** | 3 | 0°C, 1 h | **23** | 61 |
| 6 | **17** | 6 | 0°C, 10 min; room temp., 15 min | **24** + **38** (9:1) | 65 |
| 7 | **19** | 3 | 0°C, 1 h | **40** | 56 |
| 8 | **20** | 2 | 0°C, 30 min | **43** | 68 |
| 9 | **12** | 1.1 | 0°C, 10 min | **21** + **25** (10:86)[c] | 86 |
| 10 | **12** | 1.1 | −78°C, 10 min | **21** + **25** (3:97) | 87 |
| 11 | **15** | 1.1 | 0°C, 15 min | **33** | 51[d] |

[a] Where pertinent, the ratio of products was determined by glc.
[b] Yield of distilled product(s).
[c] This product mixture also contained ~4% of the starting material **12**.
[d] Starting material **15** (31%) was recovered.

original β-substituted enone **1** would be serving as the equivalent to the $a^3$–$a^3$ synthon **6**.

With respect to the nature of Y in eq. [1], a variety of functional groups have been employed successfully: chloro (2–19), bromo (14, 16, 20), alkylthio (21–27), alkylsulfinyl (27, 28), acyloxy (29), alkoxy (23, 30), tosyloxy (31, 32), mesyloxy (33), and diethylphosphonoxy (34). It is clear from a perusal of the chemical literature that the synthetic utility of β-chloro enones has been particularly well established, since the chloro substituent has been displaced successfully by a wide variety of oxygen, nitrogen, sulfur, and carbon nucleophiles (2–19). Until recently, however, efficient substitution of the chloro group by *carbon* nucleophiles had been accomplished only when the carbanions were relatively highly stabilized (e.g. conjugate bases of malonic ester derivatives, β-keto esters, trimethylsulfoxonium chloride, etc.). Obviously, the products of these reactions were enones containing highly functionalized substituents at the β carbon. Although the preparation of structurally simpler β-alkyl or β-alkenyl α,β-unsaturated ketones had been accomplished by the reaction of β-chloro enones with dialkyl- or dialkenylcadmium reagents, the yields were generally poor to mediocre (2).

Recently, we described a new, general method for the preparation of β-halo α,β-unsaturated ketones **8** (35). This method, which involved the reaction of 1,3-diketones **7** with triphenylphosphine dihalides in the presence of triethylamine (eq. [2]), not only provided high yields of β-chloro and β-bromo enones, but also constituted the first general procedure for the preparation of cyclic β-iodo α,β-unsaturated ketones, a previously unknown class of compounds. We report herein that cyclic β-halo enones **8**, particularly the bromo and iodo derivatives, react smoothly and efficiently with a variety of organocuprate reagents to produce the corresponding β,β-dialkyl **9** or, more importantly, the corresponding β-alkyl α,β-unsaturated ketones **10**[2,3] (eq. [3]). As such, the β-halo enones **8** serve as excellent synthetic equivalents to the unsaturated $a^3$ synthon **5** and the $a^3$–$a^3$ synthon **6**.

[2] 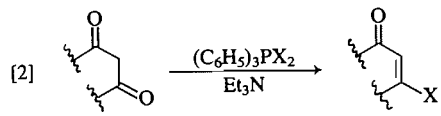

7 8

[3] 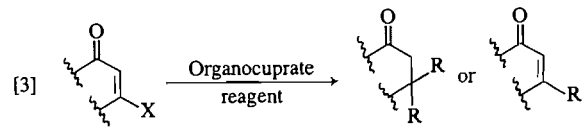

8 9 10

## Results and discussion

### (a) *Reaction of cyclic β-halo enones with lithium dimethylcuprate*

Our initial work in this area involved a brief study of the use of an excess of the reagent lithium dimethylcuprate ($Me_2CuLi$) with the expectation that the β-halo enones would be transformed into the corresponding β,β-dimethyl ketones (cf. **8** → **9**). The results of some of these experiments are summarized in Table 1. Thus, reaction of 3-chloro-5,5-dimethyl-2-cyclohexen-1-one (**11**) (see Chart 1)

[2] For a preliminary account of some of the work reported herein, see ref. 36.

[3] Prior to our initial communication (36), the reaction of β-halo enones with cuprate reagents had not been described. Subsequently, a few examples of the reaction of β-chloro and/or β-bromo enones with lithium dialkylcuprates or related reagents have been reported (5*b*, 13, 14, 16). It should be noted also that similar transformations have been accomplished with β-alkylthio (21–25), β-acetoxy (29), β-alkoxy (23), β-diethylphosphonoxy (34), and β-mesyloxy (33) enones.

Can. J. Chem. Downloaded from www.nrcresearchpress.com by 210.87.254.5 on 09/06/12
For personal use only.

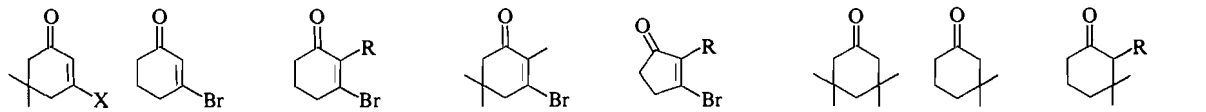

**11** X = Cl
**12** X = Br
**13** X = I

**14**

**15** R = $CH_3$
**16** R = $CH_2CH{=}CH_2$
**17** R = $CH_2CH_2CN$

**18**

**19** R = $CH_3$
**20** R = $CH_2CH{=}CH_2$

**21**

**22**

**23** R = $CH_3$
**24** R = $CH_2CH_2CN$

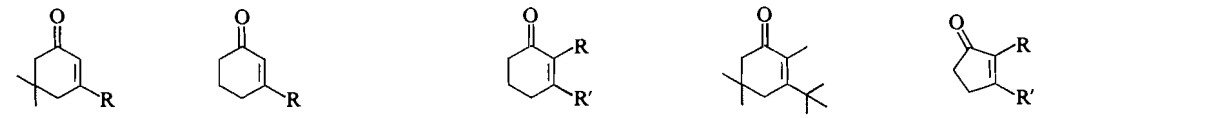

**25** R = $CH_3$
**26** R = *n*-Bu
**27** R = *t*-Bu

**28** R = $CH_3$
**29** R = *n*-Bu
**30** R = *sec*-Bu
**31** R = *t*-Bu
**32** R = $(CH_2)_2CH{=}CH_2$

**33** R = R′ = $CH_3$
**34** R = $CH_3$, R′ = *n*-Bu
**35** R = $CH_3$, R′ = *sec*-Bu
**36** R = $CH_3$, R′ = *t*-Bu
**37** R = $CH_2CH{=}CH_2$, R′ = $CH_3$
**38** R = $CH_2CH_2CN$, R′ = $CH_3$

**39**

**40** R = R′ = $CH_3$
**41** R = $CH_3$, R′ = *n*-Bu
**42** R = $CH_3$, R′ = *t*-Bu
**43** R = $CH_2CH{=}CH_2$, R′ = $CH_3$

with 3 equivalents of $Me_2CuLi$ at 0°C gave an excellent yield of 3,3,5,5-tetramethylcyclohexanone (**21**) (Table 1, Entry 1). Similarly the corresponding β-bromo and β-iodo enones **12** and **13** were also smoothly converted into the ketone **21**, and the substituted cyclohexanones **22** and **23** could be obtained readily from the β-bromo enones **14** and **15**, respectively (Entries 2–5). In contrast, attempted conversion, under identical reaction conditions, of 3-bromo-2-(2-cyanoethyl)-2-cyclohexen-1-one (**17**) into the corresponding β,β-dimethyl cyclohexanone derivative **24** gave only a poor yield (~25%) of a mixture of products, which included, in addition to the expected compound **24**, a significant amount of the enone **38**. However, when a greater excess (6 equiv.) of reagent was employed and the reaction conditions were altered somewhat, a reasonable yield of the desired product **24** (contaminated with a small amount of the enone **38**) was realized (Entry 6). Thus, although these experiments do not constitute an extensive investigation, it appears that substituted 3-halo-2-cyclohexen-1-ones can serve as convenient precursors for the preparation of the corresponding 3,3-dialkylcyclohexanone systems.

In contrast to these results involving six-membered ring substrates, reaction of the β-bromo cyclopentenones **19** and **20** with excess $Me_2CuLi$ did not result in the formation of the corresponding β,β-dimethyl cyclopentanones. Instead, in both cases, the reaction stopped at the monoaddition stage, and the products were identified as the cyclopentenones **40** and **43** (Entries 7, 8). It is thus clear that conjugate addition of $Me_2CuLi$ to 2,3-disubstituted cyclopentenones is not as facile a process as the corresponding reaction involving 2,3-disubstituted cyclohexanones. From a strictly synthetic point of view, it is pertinent to note that the reaction of 2-alkyl-3-bromo-2-cyclopenten-1-ones with $Me_2CuLi$ constitutes an efficient method for preparing 2-alkyl-3-methyl-2-cyclopenten-1-ones. This reaction was subsequently applied to a synthesis of (*Z*)-jasmone (*vide infra*).

In an effort to determine whether or not the reaction of β-bromo cyclohexenones with $Me_2CuLi$ could be controlled so as to produce only the corresponding 3-methyl-2-cyclohexen-1-ones (cf. **8** → **10**), the reactions of the β-bromo enones **12** and **15** with slightly more than 1 equivalent of the cuprate reagent were investigated. When **12** was allowed to react with 1.1 equivalents of $Me_2CuLi$ at 0°C for 10 min, the major product was the desired 3,5,5-trimethyl-2-cyclohexen-1-one (**25**). However, a small amount of starting material was recovered and, in addition, a significant quantity of the "double addition" product **21** was also formed (Entry 9). When the reaction temperature was lowered to −78°C an improvement was noted, but the product still contained a small amount of the tetramethylcyclohexanone **21** (Entry 10). Furthermore, reaction of 3-bromo-2-methyl-2-cyclohexen-1-one (**15**) with 1.1 equivalents of $Me_2CuLi$ at 0°C for 15 min gave only a 51% yield of the desired enone **33**, along with 31% of the starting material (Entry 11). Longer reaction times led to the disappearance of nearly all of the starting material, but also produced small amounts of the trimethylcyclohexanone **23**.

In view of these results, it was decided to investigate the use of a different type of cuprate reagent with the aim of developing a better method for effecting the clean, efficient conversion of cyclic β-bromo enones into the corresponding

Can. J. Chem. Downloaded from www.nrcresearchpress.com by 210.87.254.5 on 09/06/12
For personal use only.

Can. J. Chem. Downloaded from www.nrcresearchpress.com by 210.87.254.5 on 09/06/12
For personal use only.

β-alkyl enones. After some investigation, we found that lithium (phenylthio)(alkyl)cuprate reagents (37, 38) are generally excellent for this purpose, and the next section of this paper describes the results of this study.

*(b) Reaction of cyclic β-bromo enones with lithium (phenylthio)(alkyl)cuprates*

Solutions of the mixed cuprate reagents **44–48** employed in this study were prepared simply by addition of a solution of the appropriate alkyllithium (or vinyllithium) to a stirred suspension of (phenylthio)copper in dry tetrahydrofuran at −20°C (37, 38). The reactions of these reagents with a number of cyclic β-bromo enones were investigated (see Chart 1 and Table 2).

$[C_6H_5SCuR]Li$

**44** R = Me
**45** R = *n*-Bu
**46** R = *sec*-Bu
**47** R = *t*-Bu
**48** R = CH=$CH_2$

In connection with the experiments summarized in Table 2, a number of points should be noted. In some of the experiments involving the cuprate reagents **44–47** (Entries 1–17), the distilled products contained small amounts of starting material (generally <5%). However, in no case were we able to detect any product resulting from further addition to the initially formed β-alkyl enone. Thus, the mixed cuprate reagents **44–47** are, in general, excellent reagents for the conversion of β-bromo enones into the corresponding β-alkyl enones.

TABLE 2. Reaction of β-bromo α,β-unsaturated ketones with lithium (phenylthio)(alkyl)cuprates

| Entry | β-Bromo enone | Cuprate reagent[a] | Reaction temperature (°C)[b] | Product (% yield)[c] |
|---|---|---|---|---|
| 1 | **12** | **44** | 0 | **25** (94) |
| 2 | **14** | **44** | 0 | **28** (82) |
| 3 | **15** | **44** | 0 | **33** (70) |
| 4 | **16** | **44** | 0 | **37** (83) |
| 5 | **17** | **44** | 0 | **38** (76) |
| 6 | **19** | **44** | 0 | **40** (15)[d] |
| 7 | **12** | **45** | −20 | **26** (93) |
| 8 | **14** | **45** | −20 | **29** (84) |
| 9 | **15** | **45** | −20 | **34** (87) |
| 10 | **19** | **45** | −20 | **41** (64) |
| 11 | **14** | **46** | −78 | **30** (91) |
| 12 | **15** | **46** | −20 | **35** (82) |
| 13 | **12** | **47** | 0 | **27** (89) |
| 14 | **14** | **47** | 0 | **31** (87) |
| 15 | **15** | **47** | 0 | **36** (84) |
| 16 | **18** | **47** | 22 | **39** (95) |
| 17 | **19** | **47** | 0 | **42** (89) |
| 18 | **14** | **48** | −78 | **32** (70) |

[a]Cuprate reagents $[C_6H_5SCuR]Li$: **44**, R = Me; **45**, R = *n*-Bu; **46**, R = *sec*-Bu; **47**, R = *t*-Bu; **48**, R = CH=$CH_2$. Relative to the quantities of β-bromo enones used, the following amounts of reagents were employed: **44**, 2.0 equiv. (Entries 1–6); **45–47**, 1.5 equiv. (Entries 7–17); **48**, 3.0 equiv. (Entry 18).
[b]The reaction time was 2.5 h in each case.
[c]Yield of distilled product. In some of the experiments, a small amount (generally <5%) of starting material was recovered.
[d]The major product in this case was 2-methyl-3-phenylthio-2-cyclopenten-1-one (**49**) (see text and Experimental).

Although lithium (phenylthio)(methyl)cuprate (**44**) efficiently transformed the 3-bromo-2-cyclohexen-1-ones **12**, **14**, and **15–17** into the corresponding β-methyl enones (Entries 1–5), a similar reaction of **44** with the β-bromo cyclopentenone **19** afforded 2,3-dimethyl-2-cyclopenten-1-one (**40**) in very poor yield (Entry 6). In fact, the major product of this reaction was the crystalline 2-methyl-3-phenylthio-2-cyclopenten-1-one (**49**), showing that, in this case, phenylthio transfer was more facile than methyl transfer.[4] It was subsequently found, however, that the formation of **49** could be avoided nearly completely by use of the iodo enone **50** in place of the corresponding bromo compound **19**. Thus, treatment of **50** with the cuprate reagent **44** afforded 2,3-dimethyl-2-cyclopenten-1-one (**40**) in high yield.

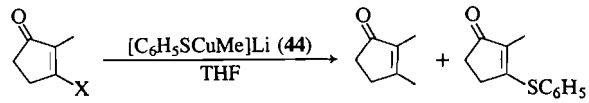


**19** X = Br
**50** X = I

**40**: X = Br 15%; X = I 91%
**49**: 61%; Trace

The reactions involving β-bromo enones and lithium (phenylthio)(*tert*-butyl)cuprate (**47**) proved to be remarkably efficient (Entries 13–17). Although the *tert*-butyl enones **27** (39), **31** (40), and **42** (41) had been prepared previously via entirely different synthetic processes, the yields were generally low. In contrast, the present method provided these substances in excellent yields. Furthermore, even the relatively highly hindered β-bromo enones **15**, **18**, and **19** reacted smoothly with the cuprate reagent **47** to give the corresponding β-*tert*-butyl enones **36**, **39**, and **42** in yields greater than 80%.

Treatment of 3-bromo-2-cyclohexen-1-one (**14**) with 1.3 equiv. of lithium (phenylthio)(vinyl)cuprate (**48**) in tetrahydrofuran at −78°C gave, in addition to starting material, the α,β-unsaturated ketone **32** (ratio ≈7:2, respectively). Clearly, 1,6 addition of the cuprate reagent **48** to the initially formed 3-vinyl-2-cyclohexen-1-one occurred at a rate faster

[4]In general, transfer of the $C_6H_5S$ group was not a problem in these reactions. Although small amounts of the β-phenylthio cycloalkenones were also formed in the experiments summarized in Entries 2–5 and 10, the yields of the desired β-alkyl enones were quite satisfactory.

Can. J. Chem. Downloaded from www.nrcresearchpress.com by 210.87.254.5 on 09/06/12
For personal use only.

than the original 1,4 addition to **14**. Reaction of **14** with 3.0 equiv. of the cuprate reagent **48** provided **32** in 70% yield (Entry 18).

*(c) Synthesis of (Z)-jasmone (53)*[5]

From a structural point of view, (*Z*)-jasmone (**53**) is a relatively simple compound. However, partly because of the fact that this substance is an important compound in the perfume industry and partly because it serves as a convenient synthetic target for testing new synthetic methods aimed at cyclopentenone-type compounds, (*Z*)-jasmone (**53**) has been synthesized many times via many different pathways. Reported here is a simple conversion of 1,3-cyclopentanedione into this natural product.

Alkylation of 1,3-cyclopentanedione with (*Z*)-1-chloro-2-pentene afforded compound **51** (41%) which, upon treatment with triphenylphosphine dibromide in the presence of triethylamine (35), was transformed smoothly (82%) into the β-bromo enone **52**. When the latter substance was allowed to react with $Me_2CuLi$ in ether at 0°C, (*Z*)-jasmone (**53**) was produced in 93% yield.

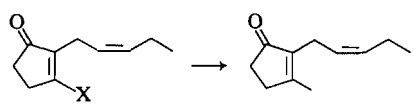

**51** X = OH
**52** X = Br

**53**

## Experimental

*General*

Melting points, which were taken on a Fisher–Johns melting point apparatus, and distillation temperatures are uncorrected. Infrared (ir) spectra were recorded on a Perkin–Elmer model 710 spectrophotometer. Proton magnetic resonance ($^1$H nmr) spectra (deuterochloroform solution) were measured using Varian Associates spectrometers, models T-60 and/or HA-100 or XL-100. Signal positions are given in δ units, with tetramethylsilane as the internal standard. High resolution mass spectrometric measurements were recorded on a Kratos MS-50 mass spectrometer. Gas–liquid chromatography (glc) was carried out with a Hewlett–Packard model 5832A gas chromatograph (analytical) or with a Varian Aerograph model 90-P instrument (preparative). Microanalyses were performed by Mr. P. Borda, Microanalytical Laboratory, University of British Columbia, Vancouver, B.C.

*General procedure for the reaction of β-halo α,β-unsaturated ketones with lithium dimethylcuprate (Table 1)*

To a cold (−78°C), stirred solution of the indicated amount of lithium dimethylcuprate (44) in anhydrous ether (~6–10 mL per mmol of reagent) under an atmosphere of nitrogen was added a solution of 1.0 mmol of β-halo enone (**11–15**, **17**, **19**, **20**) in anhydrous ether (~3 mL). After the resulting solution had been stirred at the designated temperature for the required length of time, it was treated with cold (0°C) saturated aqueous ammonium chloride (~5 mL). The resulting mixture was extracted thoroughly with ether. The combined ethereal extract was washed with brine and dried over anhydrous magnesium sulfate. Removal of the solvent, followed by bulb-to-bulb distillation of the residual oil under reduced pressure (water aspirator or vacuum pump), afforded the product(s).

*Table 1, Entries 1–3*

The product was 3,3,5,5-tetramethylcyclohexanone (**21**) (45); ir (film): 1710 cm$^{-1}$; $^1$H nmr δ: 1.07 (s, 12H), 1.57 (s, 2H), 2.16 (s, 4H).

*Table 1, Entry 4*

The product was 3,3-dimethylcyclohexanone (**22**) (46); ir (film): 1712 cm$^{-1}$; $^1$H nmr δ: 1.07 (s, 6H), 1.46–2.60 (diffuse, 8H).

*Table 1, Entry 5*

The product was 2,3,3-trimethylcyclohexanone (**23**) (47); ir (film): 1710 cm$^{-1}$; $^1$H nmr δ: 0.79, 1.06 (s, s, 3H each), 0.98 (d, 3H, $J$ = 7 Hz), 1.50–2.53 (diffuse, 7H).

*Table 2, Entry 6*

Analysis of the product by glc indicated the presence of two components, in a ratio of 9:1. The minor component was shown to possess retention times identical with those of the enone **37**, which was prepared via another reaction (*vide infra*). The major component, a pure sample of which was collected by preparative glc, was 2-(2-cyanoethyl)-3,3-dimethylcyclohexanone (**24**); ir (film): 2250, 1705 cm$^{-1}$; $^1$H nmr δ: 0.77, 1.13 (s, s, 3H each), 1.30–2.63 (diffuse, 11H). *Anal.* calcd. for $C_{11}H_{17}NO$: C 73.70, H 9.56, N 7.81; found: C 73.44, H 9.50, N 7.60.

*Table 1, Entry 7*

The product was 2,3-dimethyl-2-cyclopenten-1-one (**40**) (48); ir (film): 1700, 1650 cm$^{-1}$; $^1$H nmr δ: 1.70 (broad s, 3H), 2.05 (s, 3H), 2.23–2.66 (diffuse, 4H).

*Table 1, Entry 8*

The product was 2-allyl-3-methyl-2-cyclopenten-1-one (**43**) (49); ir (film): 1700, 1640 cm$^{-1}$; $^1$H nmr δ: 2.04 (s, 3H), 2.30–2.66 (m, 4H), 2.84–3.12 (m, 2H), 4.86–5.24 (m, 2H), 5.58–6.04 (m, 1H).

*Table 1, Entries 9 and 10*

Analysis of the products from these two experiments showed that in each case the minor product exhibited retention times identical with those of 3,3,5,5-tetramethylcyclohexanone (**21**). The product mixture from the experiment summarized in Entry 9 also contained a small amount (4%) of the starting material, bromo enone **12**. In each case, a sample of the major product was isolated by preparative glc and was shown to be 3,5,5-trimethyl-2-cyclohexen-1-one (**25**); ir (film): 1673, 1635 cm$^{-1}$; $^1$H nmr δ: 1.05 (s, 6H), 1.93 (broad s, 3H), 2.20 (broad s, 4H), 5.90 (m, 1H).

*Table 1, Entry 11*

Gas–liquid chromatographic analysis showed that the material obtained from this experiment consisted of the starting material **15** and 2,3-dimethyl-2-cyclohexen-1-one (**33**), a sample of which was collected by preparative glc; ir (film): 1668, 1635 cm$^{-1}$; $^1$H nmr δ: 1.76 (broad s, 3H), 1.90–2.13 (m, 5H), 2.20–2.60 (m, 4H).

*General procedure for the reaction of β-bromo α,β-unsaturated ketones with lithium (phenylthio)(alkyl)cuprates (Table 2)*

To a cold (−20°C) stirred suspension of (phenylthio)copper (38) (for reagent **44**, 2 mmol; for reagents **45–47**, 1.5 mmol; for reagent **48**, 3 mmol) in dry THF (10 mL), under an atmosphere of nitrogen, was added via syringe a required amount of alkyllith-

[5] A perusal of the chemical literature makes it abundantly clear that there is no lack of (*Z*)-jasmone syntheses (see refs. 42 and 43 and citations therein). However, it is difficult to escape the impression that if a person is actively engaged in research in the area of synthetic organic chemistry, then it is "necessary" for him (her) to report at some time during his (her) career a synthesis of this natural product. Described in this brief section of the paper is our (modest) contribution to this area.

Can. J. Chem. Downloaded from www.nrcresearchpress.com by 210.87.254.5 on 09/06/12
For personal use only.

ium or vinyllithium solution (methyllithium in ether, 2 mmol; *n*-butyllithium in hexane, 1.5 mmol; *sec*-butyllithium in cyclohexane, 1.5 mmol; *tert*-butyllithium in pentane, 1.5 mmol; vinyllithium in THF, 3 mmol).[6] The resultant mixture was stirred at −20°C for 15 min and then was cooled to −78°C. A solution of the appropriate β-bromo enone (1 mmol) in 2 mL of THF was added and the reaction mixture was stirred at the indicated temperature for 2.5 h. Methanol (1 mL), saturated aqueous ammonium chloride (0.5 mL), ether (10 mL), and anhydrous magnesium sulfate (4 g) were added sequentially, the resultant mixture was stirred for a few minutes and then was filtered through a short column of silica gel (~ 10–15 g). The column was eluted with ~ 100 mL of ether. Removal of the solvent from the combined eluate, followed by bulb-to-bulb distillation of the residual oil under reduced pressure (water aspirator), afforded the product. In some of the experiments, gas–liquid chromatographic analysis of the product indicated the presence of a small amount (≤ 5%) of starting material. In each of these cases, a pure sample of the desired β-alkyl enone was obtained by preparative glc.

*Table 2, Entry 1*

The product was 3,5,5-trimethyl-2-cyclohexen-1-one (**25**) (*vide supra*).

*Table 2, Entry 2*

The product was 3-methyl-2-cyclohexen-1-one (**28**); ir (film): 1665, 1630 $cm^{-1}$; $^1H$ nmr δ: 1.76–2.57 (diffuse, 6H), 1.97 (s, 3H), 5.87 (m, 1H).

*Table 2, Entry 3*

The product was 2,3-dimethyl-2-cyclohexen-1-one (**33**) (*vide supra*).

*Table 2, Entry 4*

The product was 2-allyl-3-methyl-2-cyclohexen-1-one (**37**) (52); ir (film): 1665, 1630, 985, 895 $cm^{-1}$; $^1H$ nmr δ: 1.80–2.17 (diffuse, 2H), 1.95 (s, 3H), 2.23–2.60 (m, 4H), 3.08 (broad d, 2H, $J$ = 6 Hz), 4.72–5.20 (m, 2H), 5.44–6.17 (m, 1H).

*Table 2, Entry 5*

The product was 2-(2-cyanoethyl)-3-methyl-2-cyclohexen-1-one (**38**); ir (film): 2255, 1662, 1628 $cm^{-1}$; $^1H$ nmr δ: 1.78–2.15 (diffuse, 2H), 2.05 (s, 3H), 2.22–2.66 (diffuse, 8H). *Anal.* calcd. for $C_{10}H_{13}NO$: C 73.59, H 8.02, N 8.57; found: C 73.25, H 8.15, N 8.29.

*Table 2, Entry 6*

The volatile product was 2,3-dimethyl-2-cyclopenten-1-one (**40**) (*vide supra*). The residue from the distillation was purified by column chromatography on silica gel. Recrystallization (ether) of the solid thus obtained gave 2-methyl-3-phenylthio-2-cyclopenten-1-one (**49**) (61%), mp 96–98°C; ir ($CHCl_3$): 1675, 1595 $cm^{-1}$; $^1H$ nmr δ: 1.87 (broad s, 3H), 2.36 (broad s, 4H), 7.33–7.70 (diffuse, 5H). *Anal.* calcd. for $C_{12}H_{12}OS$: C 70.54, H 5.92; found: C 70.25, H 6.00.

*Table 2, Entry 7*

The product was 3-*n*-butyl-5,5-dimethyl-2-cyclohexen-1-one (**26**) (52); ir (film): 1670, 1630 $cm^{-1}$; $^1H$ nmr δ: 1.03 (poorly resolved t, 3H), 1.17 (s, 6H), 1.23–1.86 (diffuse, 4H), 2.04–2.53 (diffuse, 6H), 6.02 (broad s, 1H).

*Table 2, Entry 8*

The product was 3-*n*-butyl-2-cyclohexen-1-one (**29**) (52); ir (film): 1670, 1625 $cm^{-1}$; $^1H$ nmr δ: 0.90 (poorly resolved t, 3H), 1.13–1.63 (diffuse, 6H), 1.70–2.70 (diffuse, 6H), 5.87 (m, 1H).

[6]The solutions of the alkyllithium reagents were purchased from the Alfa Division of Ventron Corporation, while vinyllithium in THF was prepared by the procedure of Seyferth and Weiner (50). These reagents were standardized by the method of Gilman and Cartledge (51).

*Table 2, Entry 9*

The product was 3-*n*-butyl-2-methyl-2-cyclohexen-1-one (**34**); ir (film): 1670, 1627 $cm^{-1}$; $^1H$ nmr δ: 0.98 (poorly resolved t, 3H), 1.10–1.66 (diffuse, 6H), 1.70–2.63 (diffuse, 6H), 1.83 (t, 3H, $J \approx$ 1 Hz). *Anal.* calcd. for $C_{11}H_{18}O$: C 79.52, H 10.91; found: C 79.52, H 10.96.

*Table 2, Entry 10*

The product was 3-*n*-butyl-2-methyl-2-cyclopenten-1-one (**41**) (53); ir (film): 1705, 1645 $cm^{-1}$; $^1H$ nmr δ: 1.13 (poorly resolved t, 3H), 1.33–1.84 (diffuse, 4H), 1.88 (s, 3H), 2.40–2.87 (unresolved m, 6H).

*Table 2, Entry 11*

The product was 3-*sec*-butyl-2-cyclohexen-1-one (**30**) (54); ir (film): 1665, 1620 $cm^{-1}$; $^1H$ nmr δ: 1.01 (t, 3H, $J$ = 6 Hz), 1.25 (d, 3H, $J$ = 7 Hz), 1.33–2.70 (diffuse, 9H), 6.02 (s, 1H).

*Table 2, Entry 12*

The product was 3-*sec*-butyl-2-methyl-2-cyclohexen-1-one (**35**); ir (film): 1667, 1618 $cm^{-1}$; $^1H$ nmr δ: 0.86 (t, 3H, $J$ = 7 Hz), 1.04 (d, 3H, $J$ = 7 Hz), 1.46 (quintet, 2H, $J$ = 7 Hz), 1.74–2.06 (m, 2H), 1.80 (t, 3H, $J$ = 2 Hz), 2.16–2.52 (m, 4H), 2.81 (hextet, 1H, $J$ = 7 Hz). *Exact Mass* calcd. for $C_{11}H_{18}O$: 166.1357; found: 166.1380.

*Table 2, Entry 13*

The product was 3-*tert*-butyl-5,5-dimethyl-2-cyclohexen-1-one (**27**) (39); ir (film): 1672, 1618 $cm^{-1}$; $^1H$ nmr δ: 1.03 (s, 6H), 1.12 (s, 9H), 2.20 (broad s, 4H), 5.97 (broad s, 1H).

*Table 2, Entry 14*

The product was 3-*tert*-butyl-2-cyclohexen-1-one (**31**) (40); ir (film): 1667, 1613 $cm^{-1}$; $^1H$ nmr δ: 1.13 (s, 9H), 1.65–2.53 (diffuse, 6H), 5.97 (broad s, 1H).

*Table 2, Entry 15*

The product was 3-*tert*-butyl-2-methyl-2-cyclohexen-1-one (**36**); ir (film): 1665, 1592 $cm^{-1}$; $^1H$ nmr δ: 1.26 (s, 9H), 1.70–2.10 (diffuse, 2H), 1.93 (t, 3H, $J$ = 2 Hz), 2.12–2.58 (diffuse, 4H). *Anal.* calcd. for $C_{11}H_{18}O$: C 79.52, H 10.91; found: C 79.77, H 10.85.

*Table 2, Entry 16*

The product was 3-*tert*-butyl-2,5,5-trimethyl-2-cyclohexen-1-one (**39**); ir (film): 1662, 1596 $cm^{-1}$; $^1H$ nmr δ: 0.99 (s, 6H), 1.26 (s, 9H), 1.96 (t, 3H, $J \approx$ 2 Hz), 2.20 (s, 2H), 2.28 (q, 2H, $J \approx$ 2 Hz). *Anal.* calcd. for $C_{13}H_{22}O$: C 80.35, H 11.35; found: C 80.45, H 11.31.

*Table 2, Entry 17*

The product was 3-*tert*-butyl-2-methyl-2-cyclopenten-1-one (**42**) (41); ir (film): 1695, 1640 $cm^{-1}$; $^1H$ nmr δ: 1.26 (s, 9H), 1.84 (t, 3H, $J \approx$ 2 Hz), 2.17–2.70 (diffuse, 4H).

*Table 2, Entry 18*

The product was 3-(3-butenyl)-2-cyclohexen-1-one (**32**) (55); ir (film): 1670, 1625, 980, 895 $cm^{-1}$; $^1H$ nmr δ: 1.75–2.80 (diffuse, 10H), 4.84–5.27 (diffuse, 2H), 5.44–6.06 (diffuse, 1H), 5.91 (broad s, 1H).

*Reaction of 3-iodo-2-methyl-2-cyclopenten-1-one (**50**) with lithium (phenylthio)(methyl)cuprate (**44**)*

To a cold (−20°C) stirred solution of the cuprate reagent **44** (2 mmol) in dry THF (10 mL), under an atmosphere of nitrogen, was added a solution of the iodo enone **50** (222 mg, 1.0 mmol) in 2 mL of THF. The reaction mixture was allowed to warm to 0°C and was stirred at this temperature for 2.5 h. Subjection of the reaction mixture to work-up as described above, followed by distillation (air-bath temperature 65–75°C/21 Torr) of the crude product, gave 100 mg (91%) of 2,3-dimethyl-2-cyclopenten-1-one (**40**) (*vide supra*).

*2-[(Z)-2-Pentenyl]-1,3-cyclopentanedione (**51**)*

To an ice-cold solution of 1,3-cyclopentanedione (750 mg,

Can. J. Chem. Downloaded from www.nrcresearchpress.com by 210.87.254.5 on 09/06/12
For personal use only.

7.5 mmol) in 2 *M* aqueous potassium hydroxide (4 mL, 8 mmol) was added (*Z*)-1-chloro-2-pentene (885 mg, 8.5 mmol) and a small amount of copper powder. The reaction mixture was stirred at 0°C for 1 h and then at room temperature for 3.5 h. The reaction mixture was made alkaline by addition of 10% aqueous sodium hydroxide and the resultant solution was washed with ether, cooled to 0°C, and acidified by addition of 3 *N* hydrochloric acid. The resulting mixture was extracted thoroughly with chloroform. The combined extracts were dried over anhydrous magnesium sulfate. Removal of the solvent gave a yellow oil which, upon crystallization from ether, afforded 510 mg (41%) of 2-[(*Z*)-2-pentenyl]-1,3-cyclopentanedione (**51**), mp 135–136°C; $^1$H nmr δ: 0.92 (t, 3H, $J$ = 7.5 Hz), 2.15 (m, 2H), 2.52 (s, 4H), 2.94 (broad d, 2H, $J$ = 6.0 Hz), 5.36–5.54 (m, 2H), 8.62 (broad s, 1H). The $^1$H nmr spectrum clearly indicated that this compound existed very largely in the enol tautomer. *Anal.* calcd. for $C_{10}H_{14}O_2$: C 72.26, H 8.49; found: C 72.06, H 8.45.

*3-Bromo-2-[(Z)-2-pentenyl]-2-cyclopenten-1-one (52)*

To an ice-cold, stirred solution of triphenylphosphine (435 mg, 1.66 mmol) in benzene (10 mL) was added, dropwise, a 1 *M* solution of bromine in dry benzene (1.66 mL, 1.66 mmol). To the resulting suspension was added triethylamine (167 mg, 1.66 mmol) and a solution of 2-[(*Z*)-2-pentenyl]-1,3-cyclopentanedione (**51**) (250 mg, 1.5 mmol) in benzene (8 mL). The reaction mixture was stirred at room temperature for 4 h and was then diluted with 100 mL of ether. The resulting mixture (suspension) was filtered through a short column of neutral, activity II, silica gel. The column was eluted with an additional 200 mL of ether. Removal of the solvent from the combined eluate, followed by distillation (air-bath temperature 105–115°C/0.5 Torr) of the residual oil gave 283 mg (82%) of 3-bromo-2-[(*Z*)-2-pentenyl]-2-cyclopenten-1-one (**52**) as a clear colorless oil; ir (film): 1700, 1625, 1300, 1195 cm$^{-1}$; $^1$H nmr δ: 0.98 (t, 3H, $J$ = 7.5 Hz), 2.18 (m, 2H), 2.52 (m, 2H), 2.82–3.10 (m, 4H), 5.10–5.62 (m, 2H). *Anal.* calcd. for $C_{10}H_{13}BrO$: C 52.41, H 5.73, Br 34.87; found: C 52.16, H 5.55, Br 34.70.

*(Z)-Jasmone (53)*

To a cold (−78°C) stirred solution of lithium dimethylcuprate (1.15 mmol) in anhydrous ether (8 mL), under an atmosphere of nitrogen, was added over a period of 10 min a solution of 3-bromo-2-[(*Z*)-2-pentenyl]-2-cyclopenten-1-one (**52**) (120 mg, 0.52 mmol) in ether (2 mL). The reaction mixture was allowed to warm to 0°C and was stirred at 0°C for 1 h. Saturated aqueous ammonium chloride was added and the resulting mixture was thoroughly extracted with ether. The combined extracts were dried over anhydrous magnesium sulfate. Removal of the solvent under reduced pressure afforded 80 mg (93%) of pure (*Z*)-jasmone (**53**) as a pale yellow oil; ir (film): 1685, 1640, 1440, 1380, 1340, 1300, 1175, 1070 cm$^{-1}$; $^1$H nmr δ: 0.98 (t, 3H, $J$ = 7.5 Hz), 2.06 (s, 3H), 2.02–2.28 (m, 2H), 2.30–2.70 (m, 4H), 2.95 (d, 2H, $J$ = 6.0 Hz), 5.10–5.56 (m, 2H).

## Acknowledgements

Financial support for this work from the Natural Sciences and Engineering Research Council of Canada is gratefully acknowledged.

1. D. Seebach. Angew. Chem. Int. Ed. Engl. **18**, 239 (1979).
2. A. E. Pohland and W. R. Benson. Chem. Rev. **66**, 161 (1966).
3. E. E. van Tamelen, M. P. Seiler, and W. Wierenga. J. Am. Chem. Soc. **94**, 8229 (1972).
4. J. L. Hermann, J. E. Richman, and R. H. Schlessinger. Tetrahedron Lett. 2599 (1973).
5. R. D. Clark and C. H. Heathcock. (*a*) J. Org. Chem. **38**, 3658 (1973); (*b*) J. Org. Chem. **41**, 636 (1976).
6. Y. Tamura, T. Miyamoto, T. Nishimura, J. Eiho, and Y. Kita. J. Chem. Soc. Perkin Trans. I, 102 (1974).
7. J. P. Marino and T. Keneko. J. Org. Chem. **39**, 3175 (1974).
8. Y. Tamura, Y. Sumida, S. Haruki, and M. Ikeda. J. Chem. Soc. Perkin Trans. I, 575 (1975).
9. R. J. Chorvat and R. Pappo. Tetrahedron Lett. 623 (1975); R. J. Chorvat, J. R. Palmer, and R. Pappo. J. Org. Chem. **43**, 966 (1978).
10. E. Vedejs and J. P. Bershas. Tetrahedron Lett. 1359 (1975).
11. J. Druin, F. Layendecker, and J. M. Conia. Tetrahedron Lett. 4053 (1975).
12. D. A. Archer and B. W. Singer. J. Chem. Soc. Perkin Trans. I, 2484 (1976).
13. J. P. Marino and L. J. Browne. J. Org. Chem. **41**, 3629 (1976).
14. J. L. Coke, H. J. Williams, and S. Natarajan. J. Org. Chem. **42**, 2380 (1977).
15. R. J. K. Taylor and I. T. Harrison. Tetrahedron Lett. 4793 (1976).
16. P. A. Wender and S. L. Eck. Tetrahedron Lett. 1245 (1977).
17. C. R. Engel and G. Dionne. Can. J. Chem. **56**, 424 (1978).
18. J. E. McMurry, W. A. Andrus, and J. H. Musser. Synth. Commun. **8**, 53 (1978).
19. M. Gill and R. W. Rickards. Tetrahedron Lett. 1539 (1979).
20. N. Okukado, D. E. Van Horn, W. L. Klima, and E. Negishi. Tetrahedron Lett. 1027 (1978).
21. R. M. Coates and R. L. Sowerby. J. Am. Chem. Soc. **93**, 1027 (1971).
22. E. J. Corey and R. H. K. Chen. Tetrahedron Lett. 3817 (1973).
23. G. H. Posner and D. J. Brunelle. J. Chem. Soc. Chem. Commun. 907 (1973).
24. R. M. Coates and L. O. Sandefur. J. Org. Chem. **39**, 275 (1974).
25. R. B. Gammill and T. A. Bryson. Tetrahedron Lett. 3793 (1975).
26. Y. Ittah and I. Shahak. Synthesis, 320 (1976).
27. T. Nishio and Y. Omote. Synthesis, 390 (1980).
28. T. A. Bryson, R. E. Dardis, and R. B. Gammill. Tetrahedron Lett. 743 (1978).
29. C. P. Casey, D. F. Marten, and R. A. Boggs. Tetrahedron Lett. 2071 (1973).
30. G. A. Molander and H. C. Brown. J. Org. Chem. **42**, 3106 (1977).
31. R. E. Ireland and J. A. Marshall. J. Org. Chem. **27**, 1615 (1962).
32. R. T. Buckler and D. L. Garling. Tetrahedron Lett. 2257 (1978).
33. C. J. Kowalski and K. W. Fields. J. Org. Chem. **46**, 197 (1981).
34. F. W. Sum and L. Weiler. Can. J. Chem. **57**, 1431 (1979); Tetrahedron, **37**, Supplement No. 9, 303 (1981).
35. E. Piers and I. Nagakura. Synth. Commun. **5**, 193 (1975); E. Piers, J. R. Grierson, C. K. Lau, and I. Nagakura. Can. J. Chem. **60**, 210 (1982).
36. E. Piers and I. Nagakura. J. Org. Chem. **40**, 2694 (1975).
37. G. H. Posner, C. E. Whitten, and J. J. Sterling. J. Am. Chem. Soc. **95**, 7788 (1973).
38. G. H. Posner, D. J. Brunelle, and L. Sinoway. Synthesis, 662 (1974).

39. N. F. FIRRELL and P. W. HICKMOTT. J. Chem. Soc. C, 716 (1970).
40. W. G. DAUBEN, G. W. SHAFFER, and N. D. VIETMEYER. J. Org. Chem. **33**, 4060 (1968).
41. T. S. SORENSEN and K. RAJESWARI. J. Am. Chem. Soc. **93**, 4222 (1971).
42. F. NÄF and R. DECORZANT. Helv. Chim. Acta, **61**, 2524 (1978).
43. P.-E. SUM and L. WEILER. Can. J. Chem. **56**, 2301 (1978).
44. H. O. HOUSE, W. L. RESPESS, and G. M. WHITESIDES. J. Org. Chem. **31**, 3128 (1966); H. O. HOUSE and W. F. FISCHER, JR. J. Org. Chem. **33**, 949 (1968).
45. M. S. KHARASCH and P. O. TAWNEY. J. Am. Chem. Soc. **63**, 2308 (1941).
46. B. RICKBORN and M. T. WUESTHOFF. J. Am. Chem. Soc. **92**, 6894 (1970).
47. W. G. DAUBEN, L. SCHUTTE, and E. J. DEVINY. J. Org. Chem. **37**, 2047 (1972).
48. W. F. BERKOWITZ and A. A. OZORIO. J. Org. Chem. **36**, 3787 (1971).
49. K. SISIDO, S. TORII, and M. KAWANISI. J. Org. Chem. **29**, 2290 (1964).
50. D. SEYFERTH and M. A. WEINER. J. Am. Chem. Soc. **83**, 3583 (1961).
51. H. GILMAN and F. K. CARTLEDGE. J. Organomet. Chem. **2**, 447 (1964).
52. J.-M. CONIA and A. LE CRAZ. Bull. Soc. Chim. Fr. 1929 (1960).
53. T. HIYAMA, M. TSUKANAKA, and H. NOZAKI. J. Am. Chem. Soc. **96**, 3713 (1974).
54. G. F. WOODS, P. H. GRISWOLD, JR., B. H. ARMBRECHT, D. I. BLUMENTHAL, and R. PLAPINGER. J. Am. Chem. Soc. **71**, 2028 (1949).
55. J.-M. CONIA and P. BESLIN. Bull. Soc. Chim. Fr. 483 (1969).

Can. J. Chem. Downloaded from www.nrcresearchpress.com by 210.87.254.5 on 09/06/12
For personal use only.

# An iodine-127 Mössbauer study of some chalcogen cations of iodine

THOMAS BIRCHALL[1] AND RONALD D. MYERS

*Department of Chemistry and Institute for Materials Research, McMaster University, 1280 Main Street West, Hamilton, Ont., Canada L8S 4M1*

AND

JACK PASSMORE, W. A. SHANTHA NANDANA, AND GEORGE SUTHERLAND

*Department of Chemistry, University of New Brunswick, P.O. Box 4400, Fredericton, N.B., Canada E3B 5A3*

Received September 16, 1981

THOMAS BIRCHALL, RONALD D. MYERS, JACK PASSMORE, W. A. SHANTHA NANDANA, and GEORGE SUTHERLAND. Can. J. Chem. **60**, 1264 (1982).

The iodine-127 Mössbauer spectra of some chalcogen–iodine cations have been recorded and the Mössbauer parameters are discussed in terms of their known structures. These cations are compared to other cationic species of iodine as well as with a molecular compound of iodine which contains a sulphur–iodine bond.

THOMAS BIRCHALL, RONALD D. MYERS, JACK PASSMORE, W. A. SHANTHA NANDANA et GEORGE SUTHERLAND. Can. J. Chem. **60**, 1264 (1982).

On a enregistré les spectres Mössbauer de l'iode-127 de quelques cations chalcogène–iode et on discute des paramètres Mössbauer en fonction de leurs structures connues. On a comparé ces cations avec d'autres espèces cationiques de l'iode aussi bien qu'avec un composé moléculaire de l'iode qui contient une liaison soufre–iode.

[Traduit par le journal]

## Introduction

Compounds between sulfur and iodine were for a long time thought not to exist (1). However, Passmore and co-workers (2–5) and other (6–9) have recently succeeded in isolating compounds containing sulfur–iodine bonds. Some of these novel compounds have been characterized by X-ray crystallography (2–5, 9) but hitherto very little spectroscopic information on these has appeared. We have recently begun a program to measure the iodine-127 Mössbauer spectra of well characterized compounds and to correlate the data obtained with X-ray crystallographic, and other spectroscopic data in an attempt to gain more detailed information about the nature of bonding at the iodine atom.

We present here iodine-127 Mössbauer spectroscopic data for a number of cationic species in which iodine is bonded to sulfur, and in some cases to selenium (10) and tellurium (11). These results are compared with data obtained for other cationic species of iodine (12), and with those obtained for an organosulfur iodide, the latter being obtained by iodine-129 Mössbauer spectroscopy (13).

## Experimental

The compounds were prepared according to the procedures already described (2–5, 10, 11). Mössbauer spectra ($^{127}$I) were recorded using an Elscint AME-40 drive system operating in the constant acceleration triangular wave form mode. The transmitted radiation was detected by a Harshaw NaI(Tl) scintillation counter and the resulting pulses fed to a Tracor-Northern multichannel analyzer operating in the multiscaling mode. Samples of the compounds containing 30 mg of iodine per cm$^2$ were mixed thoroughly with dried prefluorinated Teflon powder and placed in a 20 mm id threaded Kel-F sample holder. The Zn$^{127m}$Te source (10 mCi) was purchased from New England Nuclear Corporation. Both sample and source were immersed in liquid helium (4.2 K) in a research cryostat manufactured by Janis Research Company. The temperature was monitored by means of a calibrated Allen-Bradley 47 ohm, 1/4 watt carbon resistor, and a Cryogenic Research Company temperature controller. The velocity scale was calibrated using an iron foil absorber and a $^{57}$Co/Rh source. The folded spectra were computer fitted using a previously described program which incorporates full transmission integral procedures (14).

## Results and discussion

The iodine-127 Mössbauer parameters for the compounds studied are summarized in Table 1 and the corresponding spectra of $[S_7I]^+[AsF_6]^-$ and $[Se_2I_4]^+[AsF_6]^-$ are shown in Fig. 1. The isomer shifts of all compounds are negative with respect to the reference compound, KI, and since $\delta R/R$ is negative for $^{127}$I, this means that the *s* electron density at the nucleus is higher in these compounds than in KI. This increase in *s* electron density could be achieved by the removal of *p* electrons from the iodine as a result of bonding to the chalcogen atom, and since *p* electrons shield, their removal would cause an increase in the effective *s* electron density. Also, if the positive charge of these cations resides at the iodine, then the *s* electrons will be contracted more strongly than the *p* electrons, also

[1]To whom all correspondence should be addressed.

0008-4042/82/101264-05$01.00/0

©1982 National Research Council of Canada/Conseil national de recherches du Canada

Can. J. Chem. Downloaded from www.nrcresearchpress.com by 210.87.254.6 on 09/06/12
For personal use only.

TABLE 1. Iodine-127 Mössbauer data for some chalcogen cations of iodine

| Compound | Isomer shift (mm $s^{-1}$) | $e^2q_{zz}Q_g/h$ (MHz) | $\Gamma$ (mm $s^{-1}$) | $\eta$ | $T_a$[a] | $\chi^2$/degree of freedom | $U_p$ | $h_s$ ($h_p = U_p$) | $h_p$ ($h_s = 0$) |
|---|---|---|---|---|---|---|---|---|---|
| $[S_7I][AsF_6]$ | −0.70(3) | −2453(19) | 1.64(10) | — | 1.27(8) | 0.92 | 1.07 | 0.02 | 0.95 |
| $[S_7I][SbF_6]$ | −0.63(2) | −2453(11) | 1.45(7) | — | 0.85(3) | 1.04 | 1.07 | 0.04 | 0.84 |
| $[(S_7I)_4S_4][AsF_6]_6$ | −0.68(2) | −2490(11) | 1.25(6) | — | 3.66(23) | 3.29 | 1.09 | 0.03 | 0.92 |
| $[(S_7I)_2I][SbF_6]_3 \cdot 2AsF_3$ | −0.69(8) | −2453(56) | 1.78(18) | — | 0.14(1) | 1.00 | 1.07 | 0.02 | 0.93 |
| | −0.60(16) | −2490(91) | | | | | 1.09 | 0.05 | 0.79 |
| $[S_2I_4][AsF_6]_2$ | −0.80(3) | −2193(19) | 2.65(13) | 0.70(2) | 1.16(4) | 1.45 | 0.96 | −0.03 | 1.11 |
| $[Se_2I_4][AsF_6]_2$ | −0.53(6) | −2360(37) | 1.68(21) | 0.19(4) | 0.66(8) | 0.83 | 1.03 | 0.06 | 0.67 |
| | −0.53(6) | −2360(35) | 1.77(22) | — | 0.62(7) | 0.85 | | | |
| $[SeI_3][SbF_6]$ | −0.54(8) | −2509(50) | 2.00(30) | — | 0.55(7) | 0.77 | 1.09 | 0.07 | 0.67 |
| $[TeI_3][AsF_6]$ | −0.51(4) | −2026(19) | 1.73(13) | — | 0.76(5) | 1.08 | 0.88 | 0.04 | 0.64 |
| KI | 0 (−0.14)[b] | 0 | 2.35(16) | — | 0.45(1) | 0.95 | — | — | — |
| $I_2$ | −0.49(2) | −2137(11) | 1.99(7) | 0.22(1) | 0.84(2) | 1.22 | 0.93 | 0.05 | 0.61 |
| $[I_2][Sb_2F_{11}]$ | −0.68(1) | −1951(11) | 1.72(7) | 0.19(2) | 0.72(2) | 1.02 | 0.85 | 0.01 | 0.92 |

[a]Dimensionless absorber thickness, see ref. 14.
[b]Isomer shift of KI relative to ZnTe source.
[c]Reference 12.

resulting in a higher $s$ electron density at the iodine nucleus. Both of these effects could be operating simultaneously. What does appear clear is that the binding to iodine is principally of $p$ character and that there is little involvement of the iodine $5s$ electrons in the bonding to the chalcogen atoms.

The compounds which contain the $[S_7I]^+$ unit have structures in which the S—I (exocyclic) distances are nearly constant at 2.355(7) to 2.347(6) Å. Secondary I---F contacts which vary from 2.92 to 2.99(3) Å in these compounds complete an essentially linear S—I---F arrangement. The Mössbauer parameters for the exocyclic iodine in these compounds are essentially the same. The isomer shift of the iodine in these $[S_7I]^+$ cations is more negative than that found for the iodide anion and could be the result of the different charges on the iodine, positive in the former and negative in the latter case. However, the $[S_7I]^+$ cations all show large quadrupole coupling constants, indicating an asymmetric distribution of electrons about the iodine, whereas the iodide anion has a spherical distribution of electrons and hence no quadrupole splitting. Since the quadrupole coupling constants are all negative this indicates that there is an excess of electron density in the $xy$ plane about the iodine atom compared to the $z$ direction which is taken to be along the S—I---F axis.

From the measured values of the quadrupole coupling constants it is usual to estimate the $p$ electron imbalance $U_p$ from expression [1] (15).

$$[1] \quad U_p = \frac{-e^2q_{mol}{}^{127}Q_g/h}{e^2q_{at}{}^{127}Q_g/h}$$

where $e^2q_{at}{}^{127}Q_g/h$ = 2293 MHz (16), and $U_p$ is related to the electron occupation numbers $U_x$, $U_y$, and $U_z$ of the $p_x$, $p_y$, and $p_z$ orbitals by expression [2].

$$[2] \quad U_p = -U_z + 1/2(U_x + U_y)$$

For the $[S_7I]^+$ compounds, $U_p > 1$, indicating that the iodine has had slightly more than one $p$ electron removed from its noble gas valence bond configuration. This removal of $p$ electrons from the iodine is consistent with the observed increase in $s$ electron density compared to the iodide anion. If the assumption is made that $U_p = h_p$, then one can calculate $h_s$ from expression [3],[2] which leads to small positive values for $h_s$ in all cases but one.

$$[3] \quad {}^{127}\delta_{KI} = 3.74h_s - 0.61h_p - 0.12$$ ERRATA

An alternative approach is to assume that there is no $s$ electron contribution to the bond between the iodine and sulfur and one can then use the measured isomer shift to calculate $h_p$ from expression [3]. These calculated values are included in the table and one can see that there is little agreement between the values for $h_p$ calculated from expression [3] and from the measured quadrupole coupling constants. We conclude that these empirical correlations, being based on a rather limited number of compounds, perhaps do not have the general applicability that has been hitherto assumed.

The quadrupole coupling constants are much more negative than those measured for molecular species such as $CH_3I$ and $CF_3I$ (17) and are more like the values found for the central iodine in the

[2]This relationship was recently re-evaluated using the same series of compounds as in ref. 12, but against KI as zero isomer shift.

Can. J. Chem. Downloaded from www.nrcresearchpress.com by 210.87.254.6 on 09/06/12
For personal use only.

Can. J. Chem. Downloaded from www.nrcresearchpress.com by 210.87.254.6 on 09/06/12
For personal use only.

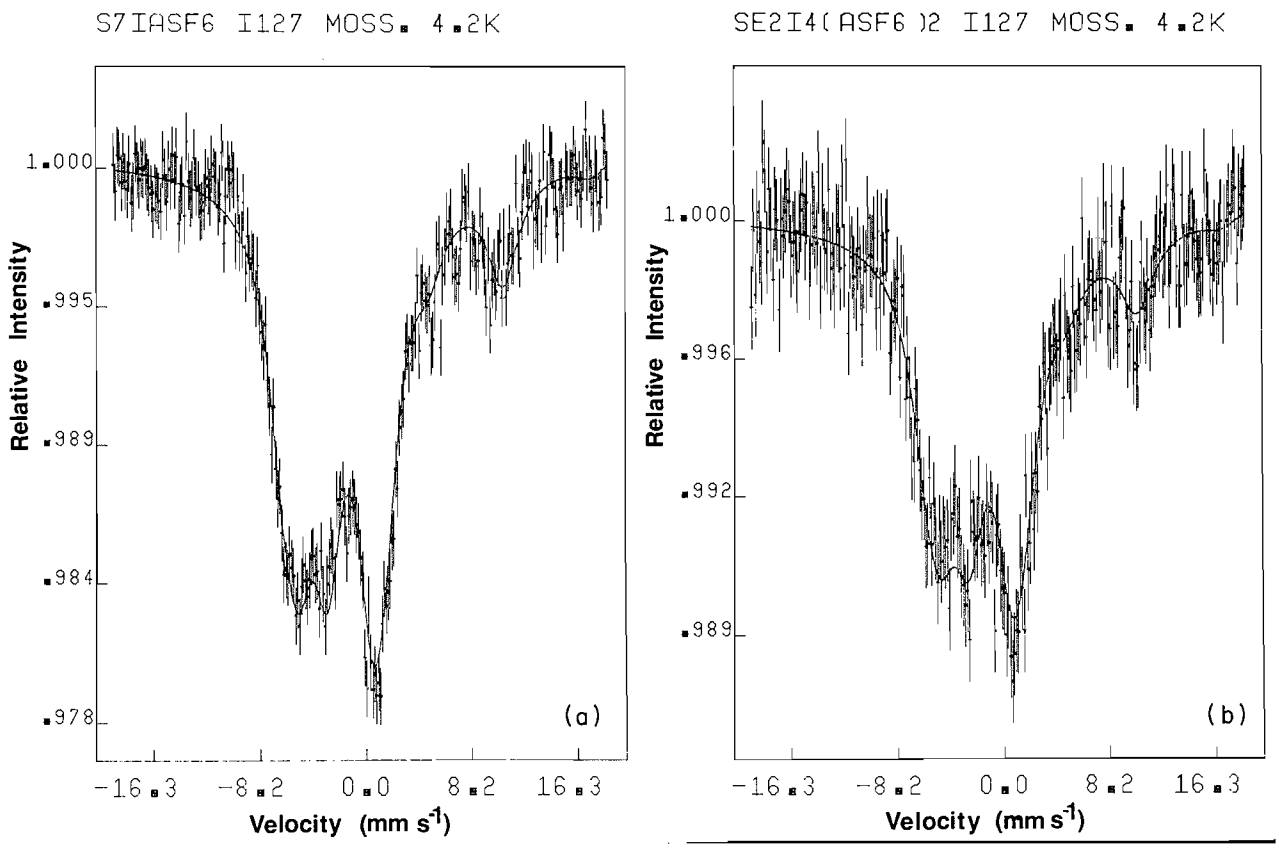


FIG. 1. The iodine-127 Mössbauer spectra at 4.2 K of (*a*) $[S_7I]^+[AsF_6]^-$, (*b*) $[Se_2I_4]^{2+}[AsF_6]_2^-$. The solid lines represent the best fit to the data.

linear $[X—I—Y]^-$ (X, Y = F, Cl, Br, I) compounds (12), being comparable to that of the central iodine in $[I_3]^-$ (18). The secondary I---F interaction in these $[S_7I]^+$ cations is rather long at 2.96 Å, but plays a significant part in influencing the distribution of electrons about the iodine, keeping it in an essentially $sp^3d^2$ hybridised arrangement. Potasek (13) has measured the $^{129}I$ Mössbauer spectrum of RS$^{129}$I (R = *N*-*p*-chlorophenyl-2-(benzyloxycarbonamide)-3-methylbutanamide) and found $^{129}\delta_{ZnTe} = -0.41$ mm s$^{-1}$ and $e^2q_{zz}\,^{129}Q_g/h = -1510$ MHz. After conversion to their iodine-127 equivalents ($^{127}\delta_{ZnTe} = -0.14$ mm s$^{-1}$, and $e^2q_{zz}\,^{127}Q_g/h = -2153$ MHz) (19) their values resemble those found for the RI (R = $CH_3$, $CF_3$, etc.) compounds (17) rather than the cations reported here. This is consistent with the molecular nature of the RI and RSI compounds compared to the charged species discussed here where strong cation–anion interactions occur.

The second iodine site in the compound $[(S_7I)_2I]^{3+}[SbF_6]_3^-\cdot 2AsF_3$ has a slightly less negative isomer shift but similar quadrupole coupling constant compared to the values found for exocyclic iodine atom in the $[S_7I]^+$ cations. This indicates that there is a somewhat lower *s* electron density at the central iodine in $(S_7I)—I—(S_7I)$ than for the $S_7—I$---F iodine. This perhaps indicates that there is less positive charge on this central, bridging iodine than on the exocyclic iodine, since the degree of *p* character in the bonding of these iodines is approximately the same.

X-ray crystallography has shown that $[S_2I_4]^{2+}$-$[AsF_6]_2^-$ has the novel distorted right triangular prismatic structure with one $S_2$ unit asymmetrically bonded to two $I_2$ units: S—S, 1.828(11) Å; $I_1—I_2$, 2.597(2) Å; S—$I_1$, 2.858(6) Å; S—$I_2$, 3.195(6) Å (5). It was of interest to determine $[Se_2I_4]^{2+}$ has a similar structure. We have therefore attempted to fit the spectra of these compounds to two unique iodine sites, but with little success; the Mössbauer fitting program diverges after only a few cycles. Suitable refinement of the spectra occurred when only one site was incorporated in the fitting procedure, and when the value of the asymmetry parameter $\eta$ was allowed to vary in the case of $[S_2I_4]^{2+}$.

Can. J. Chem. Downloaded from www.nrcresearchpress.com by 210.87.254.6 on 09/06/12
For personal use only.

The $\chi^2$ value for the latter refinement is somewhat high, although not unusual, perhaps suggesting that the bulk sample contained a small amount of impurity or decomposition product which, of course, would not be present in the single crystal selected from the material and used for the X-ray analysis. The selenium analog gave a much better spectrum (Fig. 1) and a good fit to the data was obtained: when the value of $\eta$ was allowed to vary a marginally improved fit was obtained. This may be because the asymmetry parameter is compensating for the presence of two slightly different iodine environments which are probably present in the compound. The isomer shifts of the $[S_2I_4]^{2+}$ and $[Se_2I_4]^{2+}$ cations are nearly the same as those found for the exocyclic iodine site in the $[S_7I]^+$-containing species, but in view of the structures of $[S_2I_4]^{2+}$, $[I_2]^+$ may provide a better comparison. We have recently remeasured the $^{127}I$ Mössbauer spectrum of $[I_2][Sb_2F_{11}]$ and obtained more reliable data than those reported earlier (12). Contrary to our original findings, the isomer shift of $[I_2]^+$ is slightly more negative than molecular iodine (see Table 1), indicating that the *s* electron density at the iodine nucleus has increased. Thus although an electron is removed from a $\pi_g^*$ orbital of $I_2$ upon oxidation, the most important contribution to the observed isomer shift is the positive charge on $[I_2]^+$. This positive charge contracts the *s* orbitals of iodine more strongly than the *p* orbitals, thereby causing an effective increase in the *s* electron density at the nucleus, and hence the more negative isomer shift. As was previously reported (12), the quadrupole coupling constant of $[I_2]^+$ is less negative than that of $I_2$. If there are $\pi$ interactions between the $I_2$ and $S_2(Se_2)$ units in the $[S_2I_4]^{2+}$ and $[Se_2I_4]^{2+}$ cations as has been suggested (4) for $[S_2I_4]^{2+}$ then it would be expected that these latter cations would have Mössbauer parameters intermediate to those of $I_2$ and $[I_2]^+$.

While the isomer shift of the $[Se_2I_4]^{2+}$ cation is between those for $I_2$ and $[I_2]^+$, that for the sulfur analogue is much more negative, indicating a higher *s* electron density. In $[S_2I_4]^{2+}$, the iodine quadrupole coupling constant is about the same as that in $I_2$, indicating that the degree of *p* participation in the bonding is the same, but since the *s* electron density is much greater for $[S_2I_4]^{2+}$ than for $I_2$ there must be quite a high residual positive charge on the iodine in the cation. For the selenium analogue the quadrupole constant is much larger, indicating a greater *p* electron imbalance at iodine. The *s* electron density is much lower than for the sulfur analogue which leads us to conclude that, in this cation, there is much less positive charge on the iodine than in the case of the $[S_2I_4]^{2+}$ cation. Presumably there is a better match of orbitals between Se and I than between S and I, allowing the positive charge on the $[Se_2I_4]^{2+}$ cation to be more delocalized.[3] The remaining two cations $[SeI_3]^+$ and $[TeI_3]^+$ may be compared to the isoelectronic group (V) tri-iodides, $AsI_3$, $SbI_3$, and $BiI_3$ whose iodine-129 Mössbauer spectra have been measured (20). In the trigonal pyramidal $[TeI_3]^+$ cation the average Te—I bond is 2.667(1) Å long and the I—Te—I bond angle is 99.90(3)° (11). Secondary contacts between tellurium and fluorine atoms of the anion are also present at 2.88(1) Å completing a pseudo-octahedral geometry around tellurium. $[SeI_3]^+[AsF_6]^-$ (10) is isomorphous and probably isotructural with $[TeI_3]^+[AsF_6]^-$. The structures of the neutral group V tri-iodides, $AsI_3$ (21), $SbI_3$ (22), and $BiI_3$ (22) are similar to that of $[TeI_3]^+[AsF_6]^-$, where secondary contacts from tellurium to fluorine atoms of the anion have been replaced by long interactions from the central metal atom to iodine atoms of adjacent molecules. In $AsI_3$ and $SbI_3$ the arsenic and antimony atoms are significantly displaced from the centres of the iodine octahedra and have three short contacts to iodine at 2.556(4) and 2.68(10) Å respectively. The octahedra are completed by secondary contacts to iodine at 3.50 and 3.316 Å respectively. In $BiI_3$, however, the bismuth atom is situated at the centre of the iodine octahedron (Bi—I, 3.1 Å) so that the lone pair of electrons is stereochemically inactive in this compound. One might then expect similar Mössbauer parameters for these two series of compounds since the same gross structure is observed by both systems and any differences could perhaps be attributed to the difference in charge and/or to the nature of the secondary contacts to iodine. Since the iodine atoms in $[TeI_3]^+$, and presumably also in $[SeI_3]^+$, are nearly the same distance from the central element the spectra were fitted assuming only one iodine environment. The isomer shifts are very similar to those of the other cations reported in Table 1, but are more negative than the shifts for $AsI_3$, $SbI_3$, and $BiI_3$ (mean $-0.34$ mm $s^{-1}$) (20), after these have been converted from their $^{129}I$ values (19). This is probably due to the charge on the cation which contracts the *s* orbitals, thereby increasing the effective *s* electron density.

Okuda *et al.* (23) have reported $^{127}I$ nqr data for $TeI_4$ while Jones and Mauguin (24) have recently

[3]The structure of $[S_2I_4][Sb_2F_{11}]_2$ has recently been determined. The $[Se_2I_4]^{2+}$ cation has an eclipsed $[S_2O_4]^{2-}$-like, $[I_2\overset{+}{S}\overset{+}{S}eI_2]$ structure, consistent with the $^{127}I$ Mössbauer results (26).

Can. J. Chem. Downloaded from www.nrcresearchpress.com by 210.87.254.6 on 09/06/12
For personal use only.

reported the $^{129}I$ Mössbauer spectrum of $TeI_4$ as well as of several other tellurium iodides. The latter workers were able to resolve three independent iodine sites; this finding is consistent with the X-ray crystal structure of $TeI_4$ (25). The terminal iodine atom in $TeI_4$ was found to have a quadrupole coupling constant of 1190 MHz and an isomer shift with respect to the ZnTe source of 0.70 mm $s^{-1}$. The second site which was assigned to the iodine which bridges two tellurium atoms had $e^2q^{129}Q_g/h$ = 600 MHz, $\eta = 1.0$, and the isomer shift was 0.30 mm $s^{-1}$. The final site which corresponds to the iodine atom which bridges three tellurium atoms showed no quadrupole coupling and the isomer shift was 0.40 mm $s^{-1}$. The terminal iodine atoms in $TeI_4$ provide the best comparison with $[TeI_3]^+$ and after conversion to their iodine-127 equivalents, $e^2q^{127}Q_g/h$ = 1700 MHz and the isomer shift with respect to KI is −0.10 mm $s^{-1}$. The isomer shift of the $[TeI_3]^+$ cation is more negative than the neutral compound and this has been attributed to a contraction of the *s* orbitals of the iodine atom in the cation, causing a higher *s* electron density and hence a more negative isomer shift. The quadrupole coupling constant of the iodine atom in $[TeI_3]^+$ is somewhat larger than the converted coupling constant of $TeI_4$. This indicates a larger *p* electron imbalance in the former compound and is caused by the removal of more *p* electron density in $[TeI_3]^+$ probably because of the shorter Te—I bond. The Te—I bond distances in $[TeI_3]^+$ average 2.667 Å (11) while in $TeI_4$ (25) the average terminal Te—I bond distance is 2.768 Å.

The quadrupole coupling constant of $[SeI_3]^+$ is substantially more negative than that of $[TeI_3]^+$, which is consistent with the higher electronegativity of the central atom in the former compound. However, both compounds have quadrupole coupling constants which are significantly larger than those found for the neutral group V tri-iodides. Since the iodine environments are essentially the same in both the neutral and charged species, the larger quadrupole coupling constant in the latter compounds must be a consequence of the positive charge and smaller size of the group VI cation compared to the isoelectronic group V neutral species. Both of these factors contribute to the shorter M—I bond observed in the cationic species, creating a larger electric field gradient and hence more negative quadrupole coupling constant in the cations. The Mössbauer parameters of $[TeI_3]^+$ and $[SeI_3]^+$ clearly indicate that there is considerable *p* character in the M—I bonds.

## Conclusion

The iodine-127 Mössbauer spectra of a number of novel chalcogen–iodine cations have been measured. The data clearly indicate that the nature of the bonding between the group VI atom and iodine is of essentially *p* character. It was also concluded that empirical correlations based on the hyperfine parameters and established earlier, perhaps do not have general applicability. The Mössbauer data discussed are consistent with the known structures of the compounds as established by X-ray crystallography.

## Acknowledgement

The Natural Sciences and Engineering Research Council of Canada is thanked for financial support.

1. W. E. Dascent. Non-existent compounds. Marcel Dekker, New York. 1965. p. 162.
2. J. Passmore, P. Taylor, T. K. Whidden, and P. S. White. J. Chem. Soc. Chem. Commun. 689 (1976).
3. J. Passmore, G. Sutherland, and P. S. White. J. Chem. Soc. Chem. Commun. 901 (1979).
4. J. Passmore, G. Sutherland, T. Whidden, and P. S. White. J. Chem. Soc. Chem. Commun. 289 (1980).
5. J. Passmore, G. Sutherland, and P. S. White. J. Chem. Soc. Chem. Commun. 330 (1980).
6. V. G. Vahl and R. Minkwitz. Z. Anorg. Allg. Chem. **217**, 443 (1978).
7. G. Krummel and R. Minkwitz. Inorg. Nucl. Chem. Lett. **13**, 213 (1977).
8. L. Field and J. E. White. Proc. Nat. Acad. Sci. **70**, 328 (1973).
9. D. L. Nosco, M. J. Heeg, M. D. Glick, R. C. Elder, and E. Deutsch. J. Am. Chem. Soc. **102**, 7784 (1980) and references therein.
10. J. Passmore and P. Taylor. J. Chem. Soc. Dalton Trans. 804 (1976).
11. J. Passmore, G. Sutherland, and P. S. White. Can. J. Chem. **59**, 2876 (1981).
12. T. Birchall and R. D. Myers. J. Chem. Soc. Dalton Trans. 1060 (1980).
13. M. J. Potasek. Phys. Lett. **45**A, 489 (1973).
14. K. Ruebenbauer and T. Birchall. Hyperfine Interact. **7**, 125 (1979).
15. G. Perlow and M. R. Perlow. J. Chem. Phys. **45**, 2193 (1966).
16. T. P. Das and E. L. Hahn. Nuclear quadrupole resonance spectroscopy. *Edited by* F. Seitz and D. Turnbull. Academic Press, New York. 1958.
17. M. S. Lazarus and T. D. Thomas. J. Chem. Phys. **60**, 4682 (1974).
18. H. de Waard and F. L. Spanhoff. Unpublished work.
19. C. H. W. Jones and J. L. Warren. J. Chem. Phys. **53**, 1740 (1970).
20. H. Sakai. J. Sci. Hiroshima Univ. Ser. A, **36**, 47 (1972).
21. J. Trotter. Z. Kristallogr. **121**, 81 (1965).
22. J. Trotter and T. Zobel. Z. Kristallogr. **123**, 67 (1966).
23. T. Okuda, K. Yamada, Y. Furukawa, and H. Negita. Bull. Chem. Soc. Jpn. **48**, 3480 (1975).
24. C. H. W. Jones and M. Mauguin. J. Chem. Phys. **68**, 3067 (1978).
25. V. Paulat and B. Krebs. Angew. Chem. Int. Ed. **15**, 39 (1976).
26. J. Passmore, W. A. S. Nandana, C. M. Wong, and P. S. White. Private communication.

# Dihydropyridines in synthesis and biosynthesis. IV.[1] Dehydrosecodine, in vitro precursor of indole alkaloids

JAMES P. KUTNEY, YISHAI KARTON, NORIAKI KAWAMURA, AND BRIAN R. WORTH

*Department of Chemistry, University of British Columbia, 2036 Main Mall, Vancouver, B.C., Canada V6T 1Y6*

Received November 6, 1981

JAMES P. KUTNEY, YISHAI KARTON, NORIAKI KAWAMURA, and BRIAN R. WORTH. Can. J. Chem. **60**, 1269 (1982).

The synthesis of the two isomeric dehydrosecodines is described. Stabilization of these systems is achieved by chromium carbonyl complexation of the dihydropyridine unit in these molecules. Reaction of the complexes with pyridine, or preferably ethylenediamine, allows *in situ* generation of the dehydrosecodines. A study of their chemistry and conversion to alkaloid systems is presented.

JAMES P. KUTNEY, YISHAI KARTON, NORIAKI KAWAMURA et BRIAN R. WORTH. Can. J. Chem. **60**, 1269 (1982).

On décrit la synthèse de deux déhydrosécodines isomères. On a stabilisé ces systèmes en complexant l'unité dihydropyridine de ces molécules à l'aide de chromecarbonyle. La réaction de ces complexes avec la pyridine, ou de préférence avec l'éthylènediamine, permet de former *in situ* les déhydrosécodines. On présente une étude de la chimie de ces composés et de leur transformation en des systèmes d'alcaloïdes.

[Traduit par le journal]

The possible role of dihydropyridines as late-stage intermediates in indole alkaloid biosynthesis has been discussed for some time. Wenkert (2) first provided a postulate involving such systems and others subsequently speculated on the utilization of such intermediates during their various investigations on the later stages of indole alkaloid biosynthesis (3, 4). Scheme 1 illustrates the proposed possible biosynthetic pathway from stemmadenine **1** (a member of the Strychnos family) to catharanthine **2** (Iboga) and vindoline **3** (Aspidosperma). Direct evidence for an intermediate of type "A" (Scheme 1) has been provided via a series of experiments conducted in these laboratories (4–6) and summarized in Scheme 2. Thus, variously labelled forms of secodine **4** were incorporated intact into the alkaloids catharanthine **2**, vindoline **3**, vincamine **5**, and apparicine **6**. Significantly, 50–60% of the tritium in the piperideine unit of **4** was consistently lost during incorporation, suggesting a higher oxidized form of **4** as a better representation of the key, late-stage, biointermediate. Efforts were therefore directed toward the study of the dehydrosecodines **7** and **8**. The unstable nature of **4**, **7**, and **8** has been discussed earlier (6) and the indole protected derivatives **9** and **10**

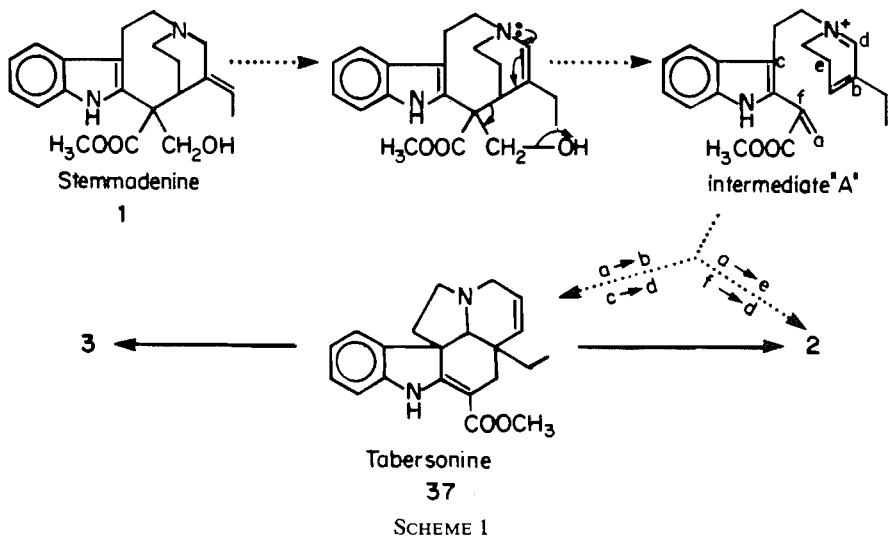


SCHEME 1

[1]For part III see ref. 1.

0008-4042/82/111269-10$01.00/0

©1982 National Research Council of Canada/Conseil national de recherches du Canada

Can. J. Chem. Downloaded from www.nrcresearchpress.com by 210.87.254.6 on 09/06/12
For personal use only.

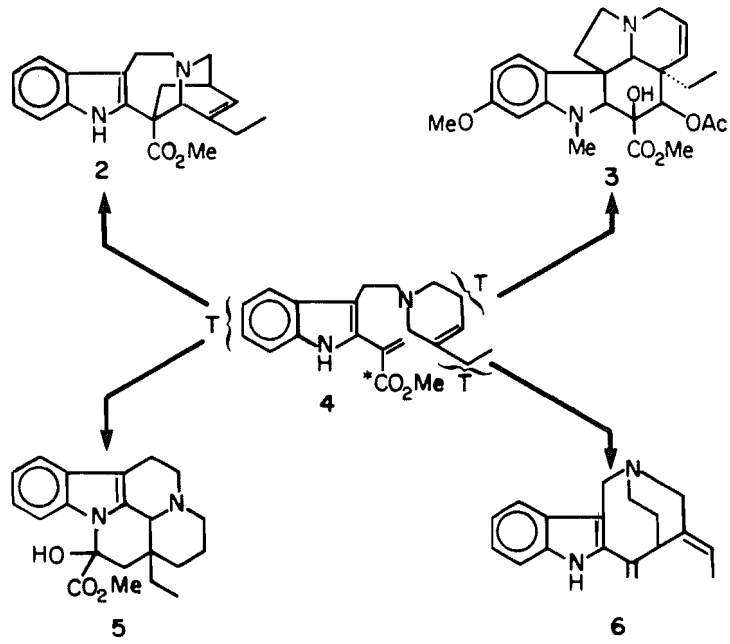


SCHEME 2

were chosen as substrates for a true biomimetic investigation of the latter stages of indole alkaloid formation.

The expected in vitro behaviour of the dehydrosecodines **9** and **10** is outlined in Schemes 3 and 4.

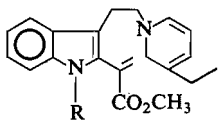

**7** R = H
**9** R = $CH_2C_6H_5$

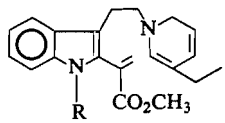

**8** R = H
**10** R = $CH_2C_6H_5$

For the 1,2-dihydropyridine isomer, **9**, enamine behaviour, via β-alkylation, should lead to the *N*-benzylcleavamine derivative **11** or by transannular cyclization to the pseudo-vincadifformine **12** (7, 8). Alternatively, the dehydrovincadine **13** would arise via δ-alkylation (Scheme 3).

On the other hand, for the 1,6-isomer **10**, β-alkylation would give **13**, or, via transannular cyclization, the tabersonine derivative **14**. Alternatively, δ-alkylation would be expected to yield either **11** or *N*-benzylcatharanthine **15**. Diels–Alder cyclization might also yield **15** (Scheme 4).

In earlier work (9) it was shown that the model compound, *N*-methyl-3-ethyl-1,2-dihydropyridine **16**, derived via controlled borohydride reduction of the pyridinium salt or from the corresponding tricarbonylchromium(0) complex **17**, suffered β-alkylation with benzyl bromide to give the 3,5-disubstituted piperideine **18** (Scheme 5). Recently we have shown that the analogous benzylation of *N*-methyl-3-ethyl-1,6-dihydropyridine **19** (derived from **20**) also gave **18**, indicating preference for δ-alkylation in the 1,6-isomer (Scheme 5). With this information base, it was expected that the 1,2-isomer **9** would undergo β-alkylation to give the cleavamine **11** and the pseudo-vincadifformine **12**, while the 1,6-isomer **10** would suffer δ-alkylation to **11** and *N*-benzylcatharanthine **15**. The tabersonine and quebrachamine derivatives, **14** and **13** respectively, were not expected to arise.

Kuehne *et al.* (10) converted the spiroammonium salt **21** to vincadifformine **22**, and proposed intermediacy of secodine **4**, arising via a Hoffmann elimination, in the transformation. Alternatively, thermolysis of **23** gave **22** again, presumably via **4** (11). Indeed separate syntheses of secodine **4** have been described (5, 12).

To date, no successful synthesis of dehydrosecodines has been reported. Our objective was to synthesize the tricarbonylchromium complexes **24** and **25** by controlled reduction of the salt **26** and to subsequently elaborate to **27** and **28** before removal of the $Cr(CO)_3$ group to generate the dehydrosecodines **9** and **10**.

Initially, Fisher indole synthesis with phenylhydrazine and levulinic acid gave the ester **29** (13) which was reduced with lithium aluminum hydride to yield 2-methyltryptophol (**30**) (14). Condensation with benzyl chloride gave the dibenzyl deriva-

Can. J. Chem. Downloaded from www.nrcresearchpress.com by 210.87.254.6 on 09/06/12
For personal use only.

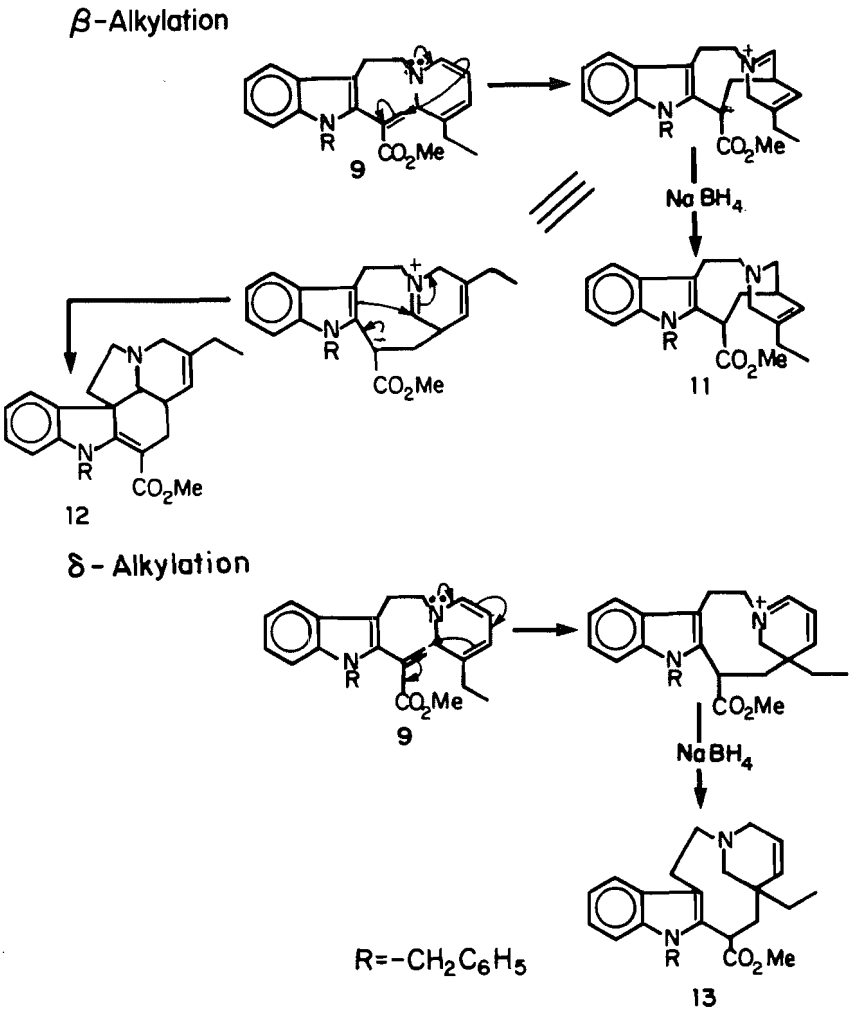


SCHEME 3

tive **31**. Reaction with *N*-bromosuccinimide in pyridine followed by displacement with cyanide gave nitrile **33** and, after methanolysis, the bromo ester **34**. Alkylation of 3-ethylpyridine gave the required salt **26** (in 10% overall yield from phenylhydrazine (Scheme 7)) analogous to the iodide and chloride salts prepared earlier (5, 6).

Controlled reduction of **26** and complexation using trisacetonitriletricarbonylchromium(0) gave a 54% yield of the two complexes **24** and **25** (6) in the ratio 9:1. The mixture of complexes was treated with KH and Eschenmoser's salt to give the labile amines which were subsequently decomposed ($K_2CO_3$) to give the dehydrosecodine complexes (35%) **27** and **28** in the ratio 4:1. In order to obtain a higher yield of **28**, the mixture of **24** and **25** was equilibrated in refluxing *n*-octane. Subsequent elaboration, as before, gave an approximately equimolar mixture of **27** and **28**.

With the protected dehydrosecodines now in hand, samples of the possible products of in vitro decomplexation and cyclization (viz: **11–15**) were prepared.

Reaction of catharanthine (**2**) with sodium borohydride in acetic acid readily furnished 18β-carbomethoxycleavamine (**35**) (15) which was oxidized and cyclized, with mercuric acetate, to dehydropseudovincadifformine (**36**) (7) and subsequently benzylated (KH, $C_6H_5CH_2Cl$) to **12**. Direct *N*-benzylation of **35** was not possible since *C*-benzylation involving the ester-bearing carbon atom was a competing reaction. However, cleavage of **12** with sodium borohydride in acetic acid gave *N*-benzyl-18β-carbomethoxycleavamine (**11**) (Scheme 8).

*N*-Benzylcatharanthine (**15**) was prepared by direct benzylation of **2**. Similarly, tabersonine (**37**) gave **14** which on reductive cleavage with sodium

Can. J. Chem. Downloaded from www.nrcresearchpress.com by 210.87.254.6 on 09/06/12
For personal use only.

Can. J. Chem. Downloaded from www.nrcresearchpress.com by 210.87.254.6 on 09/06/12
For personal use only.

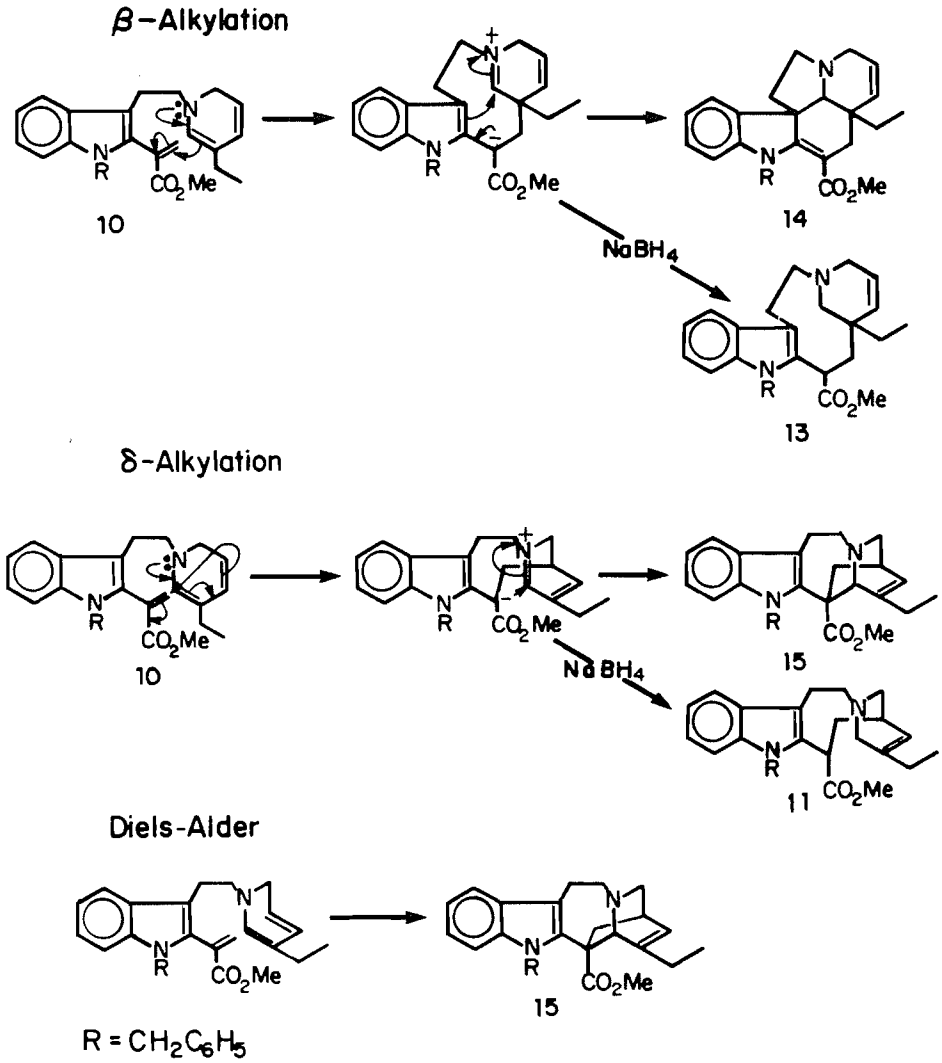


SCHEME 4

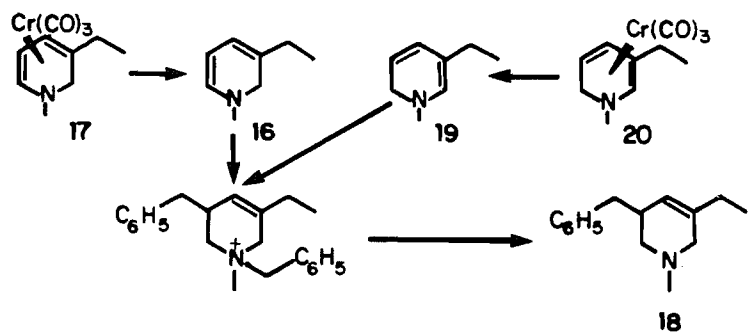


SCHEME 5

Can. J. Chem. Downloaded from www.nrcresearchpress.com by 210.87.254.6 on 09/06/12
For personal use only.

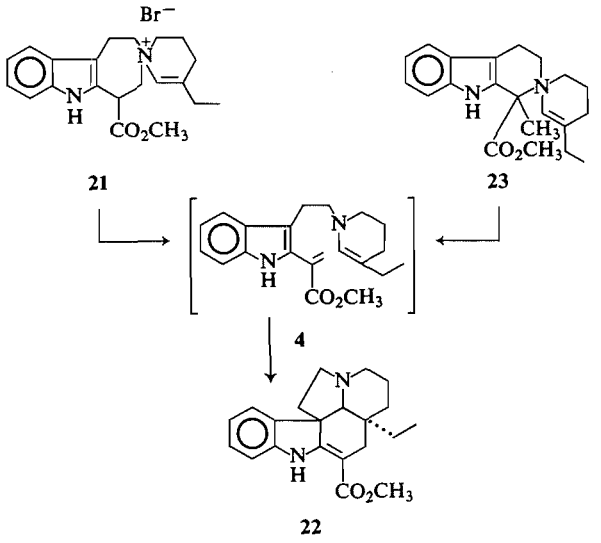


borohydride in acetic acid gave *N*-benzyldehydrovincadine (**13**). Thus all five possible cyclization products were available for analysis (hplc) of reaction product mixtures.

The 1,2-dihydropyridine complex **27** was investigated first. Here, treatment with pyridine at ambient temperature in the usual manner (9) did not give any observable change. At 55°C, however, the red colour of the complex quickly dissipated but the major product after sodium borohydride reduction was **38** arising from simple reduction of **9**. At higher temperature (110°C), the carbazole derivative **39** was isolated (79%). Scott and Cherry (16) had observed the same type of product from the thermolysis of catharanthine or tabersonine and suggest the intermediacy of dehydrosecodine **7** in this reaction.

Ethylenediamine (EDA) was found to be much more effective in removing the tricarbonylchromium group. Table 1 summarizes the large number of experiments carried out to determine optimum conditions for the formation of **11** and **12** from **27**.

Initially, only the *N*-benzylcleavamine derivative **11** was obtained when the 1,2-dihydropyridine complex **27** was treated with EDA followed by sodium borohydride reduction. The transannular cyclization product **12** was not observed under these conditions. However, addition of acetic acid after removal of the tricarbonylchromium group by EDA resulted in the formation of **12**. Compound **11** was also obtained in these reactions even before reduction with sodium borohydride, probably due to the reducing character of the dihydropyridine moiety. As expected from model compound studies (9), no δ-alkylation product was detected in all these experiments with the 1,2-dihydropyridine complex **27**.

Table 2 summarizes the in vitro reactions of the 1,6-dihydropyridine **10** derived from the complex **28**. The latter behaved similarly to the 1,2-isomer when treated with pyridine/$NaBH_4$. The major product obtained was either **38** or **39**. Replacing pyridine with $CH_3CN$ again provided **38** as the major product by simple reduction of **10**. Here again EDA was found to be the most effective reagent for removal of the tricarbonylchromium group. Thus, when **28** was treated with EDA at

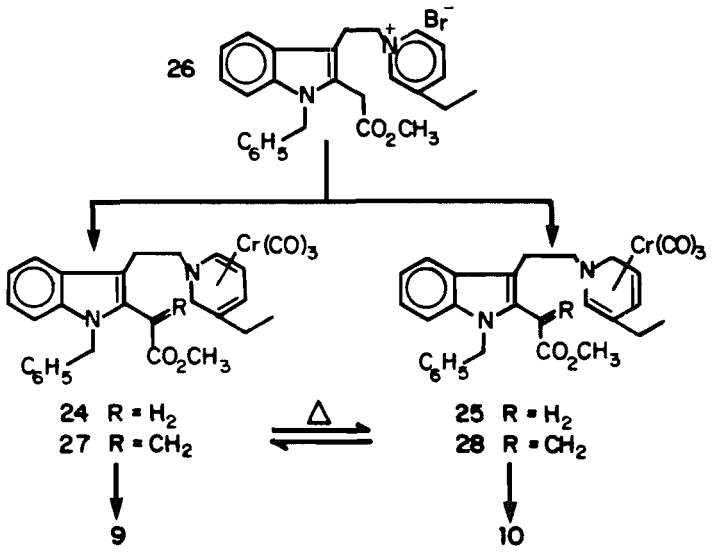


SCHEME 6

Can. J. Chem. Downloaded from www.nrcresearchpress.com by 210.87.254.6 on 09/06/12
For personal use only.

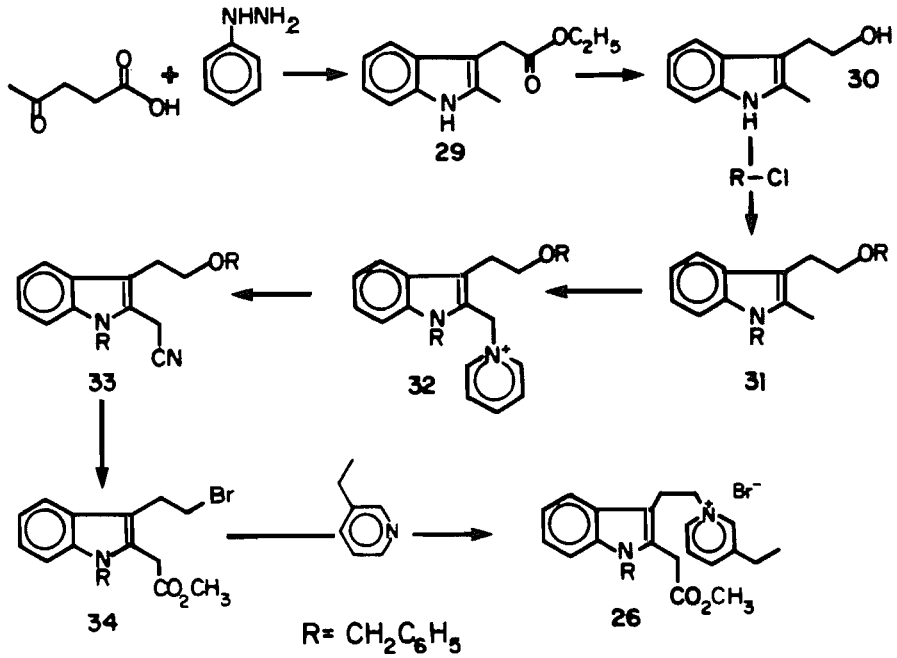


SCHEME 7

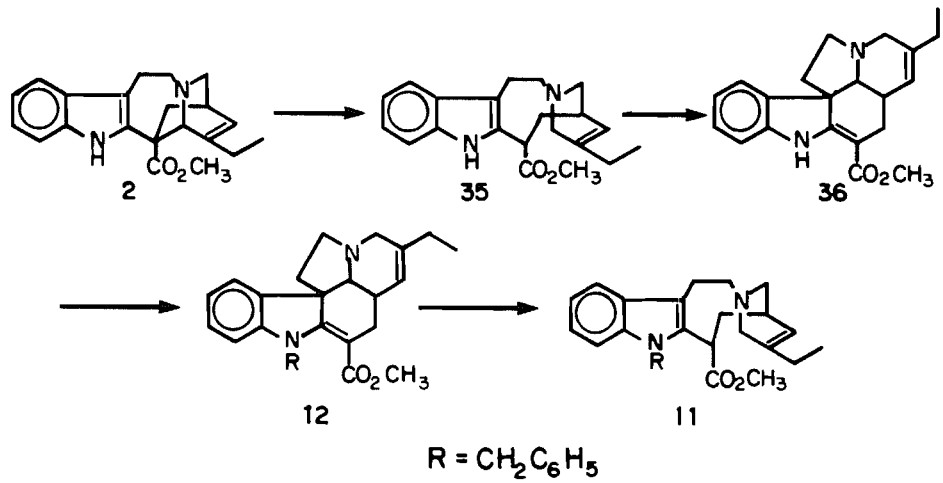


SCHEME 8

ambient temperature followed by sodium borohydride reduction, compounds **11** and **15** were obtained in 11% and 1.5% yield respectively. Both **11** and **15** are products which arose from an intramolecular δ-alkylation of the 1,6-dihydropyridine **10**. This is in good agreement with the result described earlier in model compound studies that alkylation occurred preferentially at the δ position for the 1,6-isomer.

We have thus demonstrated for the first time the

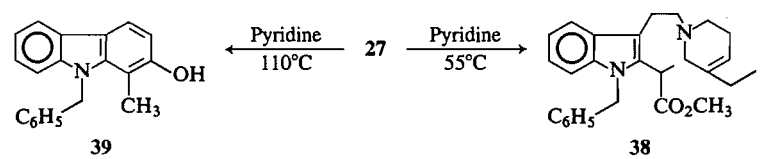

Can. J. Chem. Downloaded from www.nrcresearchpress.com by 210.87.254.6 on 09/06/12
For personal use only.

TABLE 1. In vitro reactions of **9** from the complex **27**

| | Solvent | Time (h) | Temperature (°C) | Products | Yield (%) |
|---|---|---|---|---|---|
| 1 | (i) Pyridine<br>(ii) $NaBH_4$ | 7–17 | 55 | **38** | 60–70 |
| 2 | (i) Pyridine<br>(ii) $NaBH_4$ | 4–24 | 110 | **39**<br>**38** | 70–80<br>10–15 |
| 3 | (i) 5% EDA*/MeOH<br>(ii) $NaBH_4$ | 10–23 | 25 | **38** | 60–70 |
| 4 | 3% EDA/Xylene | 17 | 140 | **39** | 70 |
| 5 | (i) 10% EDA/MeOH<br>(ii) $NaBH_4$ | 24–120 | 25 | **38** | 60–70 |
| 6 | (i) EDA<br>(ii) $NaBH_4$ | 5<br>17<br>96 | 25<br>25<br>25 | **38**, **11**<br>**38**, **11**<br>**11** | **38**, 50; **11**, 7<br>**38**, 3; **11**, 37<br>30 |
| 7 | (i) EDA<br>(ii) $NaBH_4$ | ½<br>5<br>24 | 55<br>55<br>55 | **11**<br>**11**<br>**11** | Trace<br>20<br>15 |
| 8 | (i) EDA 1 mL<br>(ii) HOAc 5 mL<br>(iii) $NaBH_4$ | 17<br>2 | 25<br>25<br>25 | **11**, **12** | **11**, 33; **12**, 3 |
| 9 | as for 8 | | 50 | **11**, **12** | **11**, 32; **12**, 2.5 |
| 10 | (i) EDA 1 mL<br>(ii) HOAc 5 mL<br>(iii) $NaBH_4$ | 17<br>2 | 25<br>25<br>25 | **11**, **12**<br>**11** | **11**, 30; **12**, 3.5<br>Trace |
| 11 | EDA | 17 | 25 | **11** | 30 |
| 12 | (i) EDA 1 mL<br>(ii) AcOH 5 mL<br>(iii) $NaBH_4$ | 1<br>17 | 25<br>25 | **11**<br>**11**, **38** | Trace<br>**11**, 15; **38**, 30 |
| 13 | (i) EDA 1 mL<br>(ii) HOAc 5 mL<br>(iii) $NaBH_4$ | 5½<br>2 | 25<br>25 | **11**<br>**11**, **38** | Trace<br>**11**, 25; **38**, 12 |
| 14 | (i) EDA 1 mL<br>(ii) HOAc 5 mL | 12½<br>2 | 25<br>25 | **11**, **12** | **11**, 17; **12**, 10 |
| 15 | (i) EDA 1 mL<br>(ii) HOAc 0.5 mL | ½<br>17 | 25<br>25 | **11**, **12** | **11**, 25; **12**, 12 |
| 16 | (i) EDA 1 mL<br>(ii) HOAc 0.25 mL | ½<br>17 | 25<br>25 | **11**, **12** | **11**, 12; **12**, 22 |

*EDA = Ethylenediamine.

formation of *Aspidosperma* and *Iboga* type alkaloids by in vitro reactions of the dehydrosecodines **9** and **10**.

## Experimental

Melting points were determined on a Kofler block and are uncorrected. Ultraviolet (uv) spectra were recorded on a Cary 15 spectrophotometer in methanol solution. The wavelengths of absorption maxima are reported in nanometers (nm) with log ε values in parentheses. Infrared (ir) spectra were measured on a Perkin Elmer model 710 or 457 spectrophotometer in chloroform solution. The absorption maxima are reported in wavenumbers ($cm^{-1}$), calibrated with respect to the absorption band of polystyrene at 1601 $cm^{-1}$. Proton magnetic resonance ($^1Hmr$) spectra were measured in deuteriochloroform ($CDCl_3$) solution at ambient temperature on a Varian XL-100, Nicolet-Oxford H-270, or Bruker WH-400 spectrometer. Chemical shift values are given in the δ (ppm) scale relative to tetramethylsilane (TMS) used as internal standard. The integrated peak areas, signal multiplicities, and proton assignments are given in parentheses. Low resolution mass spectra (ms) were determined on an AEI-MS-902 or Atlas CH-4B spectrometer. High resolution mass spectra were measured on an AEI-MS-902 instrument. Microanalyses were carried out by Mr. P. Borda of the Microanalytical Laboratory, University of British Columbia.

Column chromatography utilized Merck silica gel 60 (70–230 mesh). Preparative high pressure liquid chromatography (hplc) utilized Waters Associates Prep-LC/system 500 Liquid chromatogram. Analytical hplc instruments consisted of two Waters Associates Model 6000 A solvent delivery systems, 730 data module, 740 system controller, RCM-100 with $C_{18}$-radial pak-A column, and 440 uv detector (254 and 280 nm). A solvent system of $MeOH/H_2O$ (4:1), each containing 0.1% $Et_3N$, was used at a flow rate of 2 mL/min.

*N-Methyl-3-ethyl-5-benzyl-1,2,5,6-tetrahydropyridine* ***18***

*N*-Methyl-3-ethyl-1,6-dihydropyridine tricarbonylchromium-

Can. J. Chem. Downloaded from www.nrcresearchpress.com by 210.87.254.6 on 09/06/12
For personal use only.

TABLE 2. In vitro reactions of **10** from the complex **28**

| | Solvent | Time (h) | Temperature (°C) | Major product(s) | Yield (%) |
|---|---|---|---|---|---|
| 1 | (i) Pyridine<br>(ii) $NaBH_4$ | 7–19 | 55 | **38** | 50–60 |
| 2 | (i) Pyridine<br>(ii) $NaBH_4$ | 2–60 | 110 | **39**<br>**38** | 70–80<br>Trace |
| 3 | (i) $CH_3CN$<br>(ii) $NaBH_4$ | 4 | 60 | **38** | 55 |
| 4 | (i) 5% EDA/$CH_3OH$<br>(ii) $NaBH_4$ | 1–6 | 65 | **38** | 50–60 |
| 5 | (i) EDA<br>(ii) $NaBH_4$ | ½–4½ | 55 | **38** | 20–30 |
| 6 | (i) EDA<br>(ii) $NaBH_4$ | 4–46 | 25 | **11**<br>**15** | 5–11<br>1–1.5 |
| 7 | (i) EDA/HOAc (4:1)<br>(ii) $NaBH_4$ | 24 | 25 | **11**<br>**15** | 6<br>Trace |

(0) complex **20** (240 mg) was dissolved in ethylenediamine (1 mL) and the mixture was stirred at ambient temperature for 15 min under a nitrogen atmosphere. The mixture was poured into ice and 2 *N* NaOH and extracted with ether. The ether solution was added to the mixture of 2 *N* NaOH (2.6 mL), methanol (2.6 mL), sodium borohydride (68 mg), potassium iodide (140 mg), and benzyl bromide (1.5 mL) and stirred at ambient temperature for 15 h. The solution was acidified with 2 *N* HCl, washed with ether, and evaporated. The yellow residue (200 mg), lithium hydride (80 mg), and *n*-propyl mercaptan (0.5 mL) were stirred in HMPA (3 mL) at ambient temperature for 18 h under a nitrogen atmosphere. The mixture was cooled, acidified with 2 *N* HCl, and washed with ether. The aqueous layer was basified with 2 *N* NaOH and extracted with ether. The organic extract was dried ($Na_2SO_4$) and evaporated. Chromatography on silica gel afforded **18** (41 mg, 20% yield). The physical data were identical with those of the compound prepared from *N*-methyl-3-ethyl-1,2-dihydropyridinetricarbonylchromium(0) (7).

N,O-*Dibenzyl-2-methyltryptophol* ***31***

A solution of 2-methyltryptophol (**30**) (11, 12) (35 g) in dry ether (100 mL) was added slowly to a suspension of potassium hydride (80 g, 23% suspension) and benzylchloride (45 mL) in dry ether (400 mL) and HMPA (100 mL) at 0°C. The mixture was stirred at ambient temperature for 2.5 h. The mixture was cooled to 0°C and methanol and water were added to destroy the excess hydride. The mixture was extracted with ether. The extract was washed with water, dried ($Na_2SO_4$), and concentrated *in vacuo*. Recrystallization of the residue gave **31** (70 g, 99%); mp 55–57°C; uv $\lambda_{max}$: 293 (3.77), 284 (3.81), 276 (3.78), 225 (4.21); ir $\nu_{max}$: 1500, 1475, 1460; $^1$Hmr (100 MHz) δ: 2.22 (3H, s, —$CH_3$), 3.04 (2H, t, $J$ = 6 Hz, —$CH_2$$CH_2$—O—), 3.64 (2H, t, $J$ = 6 Hz, —$CH_2$$CH_2$—O—), 4.48 (2H, s, —O$CH_2$$C_6H_5$), 5.20 (—N$CH_2$-$C_6H_5$) 6.9–7.8 (14H, m, aromatic H); ms *m/e*: 355 ($M^+$), 234, 91 (100%), 65. High resolution molecular weight determination calcd. for $C_{25}H_{25}NO$: 355.1937; found: 355.1938.

*The dibenzylpyridinium salt* ***32***

*N*-Bromosuccinimide (5.5 g) was added to a solution of **31** (10 g) in benzene (50 mL) and pyridine (0.5 mL) at 0°C. The mixture was stirred at 0°C for 1 h. The precipitate was removed by filtration. The filtrate was stirred with pyridine (30 mL) at 0°C for 1 h. The precipitate was collected by filtration and washed with cold tetrachloromethane to give **32** (13.2 g, 91%) as a yellow powder; mp 105–107°C; uv $\lambda_{max}$: 300 (3.53), 285 (3.73), 273 (3.78), 220 (4.52); ir $\nu_{max}$: 2950, 1485, 1460; $^1$Hmr (400 MHz) δ: 3.26 (2H, t, $J$ = 6 Hz, —$CH_2$$CH_2$—), 4.08 (2H, t, $J$ = 6 Hz, —$CH_2$O—), 4.42 (2H, s, —O$CH_2$$C_6H_5$), 5.77 (2H, s, —N$CH_2$-$C_6H_5$), 6.57 (2H, s, —$CH_2$—$N^+$), 6.6–7.4 (14H, m, aromatic H), 7.55 (1H, t, $J$ = 8 Hz), 7.73 (1H, d, $J$ = 8 Hz), 9.44 (2H, d, $J$ = 8 Hz); ms *m/e*: 435 ($M^+$ − pyridine), 433, 354, 262, 248, 232, 91 (100%). *Anal.* calcd. for $C_{30}H_{31}N_2O_2Br \cdot H_2O$: C 67.80, H 5.90, N 5.27, Br 15.03; found: C 68.07, H 5.87, N 5.40, Br 15.20.

*The nitrile* ***33***

The pyridinium salt **32** (12.6 g) and potassium cyanide (10 g) were heated in refluxing methanol (200 mL) for 24 h. The mixture was cooled and methanol was evaporated. The residue was dissolved in benzene and filtered. The filtrate was evaporated and the residue was chromatographed on silica gel to yield **33** (3.1 g, 33%); uv $\lambda_{max}$: 293 (3.92), 282 (3.99), 275 (3.97); ir $\nu_{max}$: 2260; $^1$Hmr (100 MHz) δ: 3.09 (2H, t, $J$ = 6.5 Hz, —$CH_2$—$CH_2$—), 3.73 (2H, t, $J$ = 6.5 Hz, —$CH_2$O—), 3.75 (2H, s, —$CH_2$CN), 4.51 (2H, s, —O$CH_2$$C_6H_5$), 5.47 (2H, s, —N$CH_2$-$C_6H_5$), 6.9–7.7 (14H, m, aromatic H); ms *m/e*: 380 ($M^+$), 290, 259, 91 (100%). These spectral data of **33** were identical with those of the nitrile prepared previously (2).

*The pyridinium salt* ***26***

The nitrile **33** (16.5 g) was treated with methanol (50 mL) and acetylbromide (20 mL) at 0°C for 1 h. The mixture was heated at 55°C for 72 h. The mixture was cooled and concentrated *in vacuo*. The residue was partitioned between water and dichloromethane. The organic layer was washed with 5% sodium carbonate solution and water, dried ($Na_2SO_4$), and evaporated. Chromatography on silica gel afforded the bromoester **34**. The crude bromoester **34** was heated at 50°C in 3-ethylpyridine (100 mL) for 18 h. Excess 3-ethylpyridine was removed and recrystallization of the residue from acetone afforded **26** (7.9 g, 37% from **33**); mp 119–121°C; uv $\lambda_{max}$: 292 (3.95), 284 (4.00), 265 (4.15), 220 (4.45); ir $\nu_{max}$: 2930, 1740, 1230; $^1$Hmr (400 MHz) δ: 0.94 (3H, t, $J$ = 8 Hz, —$CH_2$$CH_3$), 2.55 (2H, q, $J$ = 8 Hz, —$CH_2$$CH_3$), 3.57 (3H, s, —$OCH_3$), 3.58 (2H, t, $J$ = 6 Hz, —$CH_2$$CH_2$), 3.86 (2H, s, —$CH_2$CO), 5.25 (2H, t, $J$ = 6 Hz, —$CH_2N^+$), 5.31 (2H, s, —N$CH_2$$C_6H_5$), 6.8–7.3 (9H, m, aromatic H), 7.70 (1H, dd, $J$ = 6, 8 Hz, C(5')-H), 7.98 (1H, d, $J$ = 8 Hz, C(4')-H), 8.80 (1H, s, C(2')-H), 9.37 (1H, d, $J$ = 6 Hz, C(6')-H); ms *m/e*: 413 ($M^+$ − Br), 354, 352, 121, 107, 93, 91 (100%). *Anal.* calcd. for $C_{27}H_{29}N_2O_2$-Br: C 65.72, H 5.92, N 5.67, Br 16.19; found: C 65.50, H 6.09, N 5.55, Br 16.00.

Can. J. Chem. Downloaded from www.nrcresearchpress.com by 210.87.254.6 on 09/06/12
For personal use only.

*The tricarbonylchromium(0) complexes **24** and **25***

A solution of **26** (1.02 g) in methanol (12.5 mL) was added to a vigorously stirred mixture of 0.2 *M* sodium carbonate solution (12.5 mL), ether (50 mL), and sodium borohydride (117 mg) at 0°C under a nitrogen atmosphere. The two-phase system was stirred at 0°C for 45 min. The ether layer was separated and washed with 0.2 *M* potassium carbonate solution (10 mL), dried ($Na_2SO_4$), and then added to trisacetonitriletricarbonylchromium(0) (1.5 equiv.) at 0°C under nitrogen. The mixture was stirred at 0°C for 2.5 h and then warmed to ambient temperature for 30 min. The solvent was removed *in vacuo* and the red residue was chromatographed on previously degassed silica gel with degassed benzene under a nitrogen atmosphere to afford a mixture of **24** and **25** (614 mg, 54%).

The mixture of **24** and **25** (318 mg; ratio 9:1 by $^1$Hmr) was stirred in refluxing *n*-octane (57 mL) for 65 min under a nitrogen atmosphere. The mixture was cooled and concentrated *in vacuo*. Preparative hplc separation with chloroform – petroleum ether (1:1.1) gave **24** (148 mg) and **25** (143 mg).

*The complex **24***, uv $\lambda_{max}$: 400 (3.59), 295 (4.05), 279 (4.12), 275 (4.15); ir $\nu_{max}$: 1940, 1870, 1830, 1735; $^1$Hmr (270 MHz) δ: 0.95 (3H, t, $J$ = 7.5 Hz, —$CH_2CH_3$), 2.12 (2H, q, $J$ = 7.5 Hz, —$CH_2CH_3$), 2.7–2.95 (4H, m, —$CH_2CH_2N$), 3.33 (2H, s, C(2′)-H), 3.48 (3H, s, —OMe), 3.59 (2H, s, —$CH_2CO$), 4.93 (1H, d, $J$ = 5.5 Hz, C(4′)-H), 5.30 (2H, s, —$NCH_2C_6H_5$), 5.42 (1H, d, $J$ = 4 Hz, C(6′)-H), 5.51 (1H, dd, $J$ = 4, 5.5 Hz, C(5′)-H), 6.9–7.6 (9H, m, aromatic H); ms *m/e*: 550 ($M^+$), 466, 434, 341, 306, 262, 234, 135, 122, 91 (100%). High resolution molecular weight determination calcd. for $C_{30}H_{30}N_2O_5Cr$: 550.1560; found: 550.1553.

*The complex **25***, uv $\lambda_{max}$: 396, 284, 275; ir $\nu_{max}$: 1940, 1870, 1830, 1730; $^1$Hmr (270 MHz) δ: 1.17 (3H, t, $J$ = 6 Hz, —$CH_2CH_3$), 2.35–2.9 (6H, m, —$CH_2CH_2N$, —$CH_2CH_3$), 3.30 (2H, m, C(6′)-H), 3.54 (3H, s, —$OCH_3$), 3.62 (2H, s, —$CH_2CO$), 5.15–5.3 (2H, m, C(4′), (5′)-H), 5.33 (2H, s, —$NCH_2C_6H_5$), 5.36 (1H, s, C(2′)-H), 6.8–7.5 (9H, m, aromatic H); ms *m/e*: 550 ($M^+$), 466, 434, 341, 306, 135, 122, 91 (100%). High resolution molecular weight determination calcd. for $C_{30}H_{30}N_2O_5Cr$: 550.1560; found: 550.1551.

*The dehydrosecodine complexes **27** and **28***

A solution of **24** and **25** (224 mg; 9:1 ratio) in dry tetrahydrofuran (5 mL) was added to a suspension of potassium hydride in dry tetrahydrofuran (10 mL) at −23°C under a nitrogen atmosphere. The mixture was stirred for 15 min at −23°C and for 15 min at 0°C, and gradually allowed to warm to ambient temperature for 17 min. The mixture was cooled to −23°C again and dimethyl (methylene) ammonium iodide (500 mg) was added. The mixture was stirred at −23°C for 5 min and stirring continued for 1 h at ambient temperature. Saturated potassium carbonate solution was added to the red solution at 0°C and the solution was stirred at ambient temperature for 30 min. Ether and water were added and the mixture was extracted with ether. The ether solution was dried and concentrated. Chromatography on silica gel under a nitrogen atmosphere afforded a crude mixture of **27** and **28**; hplc separation with ether – petroleum ether (1:4.1) gave **27** (63 mg, 27%) and **28** (19 mg, 8%).

*The complexes **27** and **28** after isomerization*

Using the procedure described above, the isomerized mixture of **24** and **25** (1:1) (250 mg) gave **27** (51 mg, 20%) and **28** (57 mg, 22%).

*The complex **27***, uv $\lambda_{max}$: 398 (3.6), 291 (4.1), 280 (4.2), 265 (4.2); ir $\nu_{max}$: 1945, 1870, 1840, 1730; $^1$Hmr (400 MHz) δ: 1.00 (3H, t, $J$ = 6 Hz, —$CH_2CH_3$), 2.17 (2H, dq, $J$ = 6, 20 Hz, —$CH_2CH_3$), 2.7–2.95 (4H, m, —$CH_2CH_2N$), 3.30 (2H, s, C(2′)-H), 3.61 (3H, s, —$OCH_3$), 4.99 (1H, d, $J$ = 6 Hz, C(4′)-H), 5.20 (2H, s, —$NCH_2C_6H_5$), 5.37 (1H, d, $J$ = 4.5 Hz, C(6′)-H), 5.57 (1H, dd, $J$ = 4.5, 6 Hz, C(5′)-H), 5.84 (1H, d, $J$ = 1.5 Hz, olefinic H), 6.77 (1H, d, $J$ = 1.5 Hz, olefinic H), 6.9–7.6 (9H, m, aromatic H); ms *m/e*: 562 ($M^+$), 478, 450, 260, 135, 122, 121, 107 (100%), 91. High resolution molecular weight determination calcd. for $C_{31}H_{30}N_2O_5Cr$: 562.1560; found: 562.1593.

*The complex **28***, uv $\lambda_{max}$: 395 (3.3); ir $\nu_{max}$: 1955, 1865, 1840, 1725; $^1$Hmr (400 MHz) δ: 1.15 (3H, t, $J$ = 6 Hz, —$CH_2CH_3$), 2.4–2.8 (6H, m, —$CH_2CH_3$, —$CH_2CH_2N$), 3.33 (2H, m, C(6′)-H), 3.51 (3H, s, —$CH_3$), 5.13 (2H, s, —$NCH_2C_6H_5$), 5.15 (2H, m, C(4′), C(5′)-H), 5.24 (1H, s, C(2′)-H), 5.90 (1H, d, $J$ = 2 Hz, olefinic H), 6.82 (1H, d, $J$ = 2 Hz, olefinic H), 7.0–7.4 (9H, m, aromatic H); ms *m/e*: 562 ($M^+$), 478, 450, 135, 121, 107, 92, 91 (100%). High resolution molecular weight determination calcd. for $C_{31}H_{30}N_2O_5Cr$: 562.1560; found: 562.1566.

N-*Benzyldehydropseudovincadifformine **12***

Dehydropseudovincadifformine **36** was prepared by mercuric acetate oxidation of 18β-carbomethoxycleavamine **35** (5) which was obtained from catharanthine **2** (13). A solution of **36** (328 mg) in dry tetrahydrofuran (10 mL) was added to a suspension of potassium hydride (0.5 g, 23% in oil) in dry tetrahydrofuran (15 mL) at −23°C. The mixture was stirred at −23°C for 5 min and at ambient temperature for 15 min. The mixture was cooled to −23°C again when benzyl chloride (1 mL) was added. The mixture was stirred at ambient temperature for 30 min, and at 50°C for 3.5 h. Excess potassium hydride was destroyed by additions of methanol and water at −23°C. The mixture was extracted with dichloromethane. The organic layer was washed with water, dried ($Na_2SO_4$), and evaporated; hplc separation of the residue gave **12** (315 mg, 76%); uv $\lambda_{max}$: 331 (4.1), 299 (4.0); ir $\nu_{max}$: 1680, 1600; $^1$Hmr (400 MHz) δ: 1.05 (3H, t, —$CH_2CH_3$), 2.04 (2H, m, —$CH_2CH_3$), 3.37 (3H, s, —$OCH_3$), 5.10 (2H, s, —$NCH_2C_6H_5$), 5.52 (1H, d, $J$ = 6 Hz, olefinic H), 6.7–7.4 (9H, m, aromatic H); ms *m/e*: 426 ($M^+$), 395, 335, 318, 260, 135 (100%), 91. High resolution molecular weight determination calcd. for $C_{28}H_{30}N_2O_2$: 426.2307; found: 426.2311.

N-*Benzyl-18β-carbomethoxycleavamine **11***

A solution of **12** (219 mg) in glacial acetic acid (15 mL) was heated to 90°C. Sodium borohydride (1 g) was added at intervals to keep the solution gently refluxed. The mixture was stirred at 90°C for 1 h, cooled, poured into the ice-cooled aqueous ammonia solution, and extracted with dichloromethane. The organic layer was washed with water, dried ($Na_2SO_4$), and evaporated; hplc separation of the residue gave **11** (107 mg, 49%); uv $\lambda_{max}$: 288 (3.94), 285 (4.00), 273 (3.98); ir $\nu_{max}$: 1720; $^1$Hmr ($C_6D_6$, 400 MHz) δ: 0.98 (3H, t, $J$ = 6 Hz, —$CH_2CH_3$), 1.91 (2H, q, $J$ = 6 Hz, —$CH_2CH_3$), 3.84 (3H, s, —$OCH_3$), 5.30 (2H, q, $J_{AB}$ = 18 Hz, —$NCH_2C_6H_5$), 5.38 (1H, d, $J$ = 6 Hz, olefinic H), 6.06 (1H, d, $J$ = 8 Hz, —$CHCO$—): 6.7–7.8 (9H, m, aromatic H); ms *m/e*: 428 ($M^+$), 413, 305, 279, 149 (100%), 112, 91. High resolution molecular weight determination calcd. for $C_{28}H_{32}N_2O_2$: 428.2463; found: 428.2469.

N-*Benzylcatharanthine **15***

Potassium hydride (0.5 g, 23% in oil) and benzyl chloride (0.7 mL) were added to a solution of catharanthine hydrochloride (320 mg) in dry tetrahydrofuran (12 mL) and HMPA (3 mL) at −23°C. The mixture was heated at 70°C for 5 h, cooled, diluted with water, and extracted with dichloromethane. The organic extract was washed with water, dried ($Na_2SO_4$), and evaporated; hplc separation of the residue gave **15** (212 mg, 57%); uv $\lambda_{max}$: 294 (4.06), 286 (4.10), 225 (4.56); ir $\nu_{max}$: 1730; $^1$Hmr (400 MHz) δ: 1.05 (3H, t, $J$ = 6 Hz, —$CH_2CH_3$), 1.90 (2H, q, $J$ = 6 Hz, —$CH_2CH_3$), 3.03 (3H, s, —$OCH_3$), 5.24 (2H, q, $J_{AB}$ = 18 Hz, —$NCH_2C_6H_5$), 6.13 (1H, d, $J$ = 5 Hz, olefinic H), 6.8–7.7 (9H, m, aromatic H).

N-*Benzyltabersonine **14***

Potassium hydride (2 g, 23% in oil) and benzyl chloride (1.2

Can. J. Chem. Downloaded from www.nrcresearchpress.com by 210.87.254.6 on 09/06/12
For personal use only.

mL) were added to a solution of tabersonine hydrochloride (1 g) in dry tetrahydrofuran (16 mL) and HMPA (4 mL) at −23°C. The mixture was heated at 65°C for 4.5 h, cooled, diluted with water, and extracted with dichloromethane. The extract was washed with water, dried ($Na_2SO_4$), and evaporated. Chromatography on silica gel gave **14** (800 mg, 70%); uv $\lambda_{max}$: 333 (4.12), 303 (3.96); ir $\nu_{max}$: 1675, 1595; $^1$Hmr (400 MHz) δ: 0.55 (3H, t, $J$ = 6 Hz, $-CH_2CH_3$), 0.90 (2H, q, $J$ = 6 Hz, $-CH_2CH_3$), 3.42 (3H, s, $-OCH_3$), 5.16 (2H, q, $J_{AB}$ = 18 Hz, $-NCH_2C_6H_5$), 5.70 (1H, d, $J$ = 8 Hz, olefinic H), 5.80 (1H, dd, $J$ = 8 Hz, 4 Hz, olefinic H), 6.8–7.35 (9H, m, aromatic H); ms *m/e*: 426 ($M^+$), 411, 395, 335, 318, 234, 204, 167, 154, 135 (100%), 122, 91. High resolution molecular weight determination calcd. for $C_{28}H_{30}N_2O_2$: 426.2307; found: 426.2317.

N-*Benzyldehydrovincadine* ***13***

A solution of **14** (105 mg) in glacial acetic acid (10 mL) was heated to 90°C. Excess sodium borohydride was added at intervals to keep the solution gently refluxed. The mixture was stirred at 90°C for 10 min, cooled, and poured into ice-cooled aqueous ammonia solution. The mixture was extracted with dichloromethane. The extract was washed with water, dried ($Na_2SO_4$), and evaporated; hplc separation gave **13** (65 mg, 62%); uv $\lambda_{max}$: 292 (3.78), 285 (3.83), 226 (4.43); ir $\nu_{max}$: 1730; $^1$Hmr (400 MHz) δ: 0.64 (3H, t, $J$ = 7 Hz, $-CH_2CH_3$), 1.06 (2H, q, $J$ = 7 Hz, $-CH_2CH_3$), 3.15 (3H, s, $-OCH_3$), 5.30 (2H, q, $J_{AB}$ = 18 Hz, $-NCH_2C_6H_5$), 5.85 (1H, m, olefinic H), 5.95 (1H, d, $J$ = 7 Hz, olefinic H), 6.8–7.6 (9H, m, aromatic H); ms *m/e*: 428 ($M^+$), 413, 399, 305 (100%), 124, 122, 91. High resolution molecular weight determination calcd. for $C_{28}H_{32}N_2O_2$: 428.2463; found: 428.2469.

*In vitro reactions of* ***9*** *from the complex* ***27*** *(see Table 1)*

*The carbazol* ***39*** *and the reduced product* ***38***

A solution of **27** (34.4 mg) in pyridine (3 mL) was added to refluxing pyridine (10 mL) under a nitrogen atmosphere. The solution was heated at 110°C for 3 h, cooled, diluted with methanol, and acidified with acetic acid. The mixture was treated with excess sodium borohydride at ambient temperature for 1 h, basified with aqueous ammonia solution, and extracted with dichloromethane. The extract was washed with water, dried ($Na_2SO_4$), and evaporated. Preparative hplc afforded the following.

*The carbazol* **39** (13.9 mg, 79%); uv $\lambda_{max}$: 330 (3.44), 318 (3.79), 300 (4.15); ir $\nu_{max}$: 3400; $^1$Hmr (270 MHz) δ: 2.49 (3H, s, $-CH_3$), 5.76 (2H, s, $-NCH_2C_6H_5$), 6.78 (1H, d, $J$ = 8 Hz, aromatic H), 7.0–7.4 (8H, m, aromatic H), 7.84 (1H, d, $J$ = 8 Hz, aromatic H), 8.03 (1H, m, aromatic H); ms *m/e*: 287 ($M^+$), 196, 91 (100%). High resolution molecular weight determination calcd. for $C_{20}H_{17}NO$: 287.1309: found: 287.1309.

*The reduced product* **39** (2.6 mg, 10%); uv $\lambda_{max}$: 293 (4.2), 284 (4.8), 275 (4.2); ir $\nu_{max}$: 1715; $^1$Hmr (100 MHz) δ: 1.03 (3H, t, $J$ = 7 Hz, $-CH_2CH_3$), 1.44 (3H, d, $J$ = 7 Hz, $-CH_3$), 3.45 (3H, s, $-OCH_3$), 5.38 (2h, s, $-NCH_2C_6H_5$), 5.56 (1H, m, olefinic H), 6.8–7.8 (9H, m, aromatic H); ms *m/e*: 430 ($M^+$), 415, 306, 124 (100%), 91. High resolution molecular weight determination calcd. for 430.2619; found: 430.2594.

*Compound* ***11*** *from the complex* ***27***

A solution of **27** (27.5 mg) in ethylenediamine (3 mL) was stirred at ambient temperature for 20 h under a nitrogen atmosphere. The mixture was cooled to 0°C, diluted with methanol, acidified with acetic acid, and then treated with excess sodium borohydride at ambient temperature for 1.5 h. The mixture was basified with the aqueous ammonia solution and extracted with dichloromethane. The extract was washed with water, dried ($Na_2SO_4$), and evaporated. Chromatography on silica gel afforded **11** (7.8 mg, 37%). The physical data of **11** were identical with those of *N*-benzyl-18β-carbomethoxycleavamine reported above.

*Compounds* ***11*** *and* ***12*** *from the complex* ***27***

A solution of **27** (28.3 mg) in ethylenediamine (4 mL) was stirred at ambient temperature for 30 min under a nitrogen atmosphere. The solution was cooled to 0°C and glacial acetic acid (1 mL) was added dropwise. The mixture was stirred at ambient temperature for 17 h under a nitrogen atmosphere and then extracted with dichloromethane. The extract was washed with water, dried ($Na_2SO_4$), and evaporated. Chromatography on silica gel afforded **11** (2.5 mg, 11.6%) together with **12** (4.8 mg, 22.4%). The latter was found to be identical with *N*-benzyldehydropseudovincadifformine **12**.

*In vitro reactions of* ***10*** *from the complex* ***28*** *(see Table 2)*

*Compounds* ***11*** *and* ***15***

A solution of **28** (50 mg) in ethylenediamine (4 mL) was stirred at ambient temperature for 24 h under a nitrogen atmosphere. Excess sodium borohydride was added and the mixture stirred at ambient temperature for an additional 1 h. Ice-water was added and the mixture extracted with dichloromethane. The extract was washed with water, dried ($Na_2SO_4$), and evaporated. Chromatography on silica gel afforded **11** (4.3 mg, 11%) and **15** (0.55 mg, 1.5%). These products **11** and **15** were found to be identical with authentic samples of *N*-benzyl-18β-carbomethoxycleavamine and *N*-benzylcatharanthine, respectively.

## Acknowledgements

Financial aid from the National Sciences and Engineering Research Council of Canada is gratefully acknowledged. One of us (Y.K.) also wishes to thank the Killam Foundation for the tenure of a postdoctoral fellowship during this research.

1. J. P. KUTNEY, L. KACZMAREK, D. MOSTOWICZ, and B. R. WORTH. Can. J. Chem. **60**, 323 (1982).
2. E. WENKERT. J. Am. Chem. Soc. **84**, 98 (1962).
3. A. I. SCOTT. Acc. Chem. Res. **3**, 151 (1970).
4. J. P. KUTNEY. Heterocycles, **7**, 593 (1977).
5. J. P. KUTNEY, R. A. BADGER, J. F. BECK, H. BOSSHARDT, F. S. MATOUGH, V. E. RIDAURA-SANZ, Y. H. SO, R. S. SOOD, and B. R. WORTH. Can. J. Chem. **57**, 289 (1979).
6. J. P. KUTNEY, R. A. BADGER, W. R. CULLEN, R. GREENHOUSE, M. NODA, V. E. RIDAURA-SANZ, Y. H. SO, A. ZANAROTTI, and B. R. WORTH. Can. J. Chem. **57**, 300 (1979).
7. J. P. KUTNEY, R. T. BROWN, E. PIERS, and J. R. HADFIELD. J. Am. Chem. Soc. **92**, 1708 (1970).
8. M. ZECHES, M. M. DEBRAY, G. LEDOUBLE, L. LE MEN-OLIVIER, and J. LE MEN. Phytochemistry, **14**, 1122 (1975).
9. J. P. KUTNEY, R. GREENHOUSE, and V. E. RIDAURA. J. Am. Chem. Soc. **96**, 7364 (1974).
10. M. E. KUEHNE, D. M. ROLAND, and R. HAFTER. J. Org. Chem. **43**, 3705 (1978).
11. M. E. KUEHNE, J. A. HUEBNER, and T. H. MATSKO. J. Org. Chem. **44**, 2477 (1979).
12. S. RAUCHER, J. E. MACDONALD, and R. F. LAWRENCE. J. Am. Chem. Soc. **103**, 2419 (1981).
13. M. W. BULLOCK and S. W. FOX. J. Am. Chem. Soc. **73**, 5155 (1951).
14. M. NAKAZAKI. Bull. Chem. Soc. Jpn. **32**, 588 (1959).
15. J. P. KUTNEY, W. J. CRETNEY, J. R. HADFIELD, E. S. HALL, and V. R. NELSON. J. Am. Chem. Soc. **92**, 1704 (1970).
16. A. I. SCOTT and P. C. CHERRY. J. Am. Chem. Soc. **91**, 5872 (1969).

# Trichlorosilyl and dichloromethylsilyl derivatives of ruthenium carbonyl

R. K. POMEROY AND XIANG HU[1]

*Department of Chemistry, Simon Fraser University, Burnaby, B.C., Canada V5A 1S6*

Received November 3, 1981

R. K. POMEROY and XIANG HU. Can. J. Chem. **60**, 1279 (1982).

The preparation of a number of derivatives of the type $Ru(CO)_3(L)(SiRCl_2)(X)$ and $[Ru(CO)_3(SiRCl_2)(X)]_2$ (L = CO, phosphorus donor ligand; R = $CH_3$, Cl; X = H, Cl, Br, I; not all possibilities) is described. The syntheses of $M(CO)_4(SiMeCl_2)_2$ (M = Ru, Os) and *mer*-$M(CO)_3(PPh_3)(SiMeCl_2)_2$ are also reported. The pattern of substitution in the tetracarbonyl molecules is consistent with the $SiRCl_2$ ligand as having a large *trans*-effect in these compounds. From a qualitative study of the rates of substitution, it appears the *trans*-effect of the $SiMeCl_2$ ligand is at least comparable to that of $SiCl_3$.

R. K. POMEROY et XIANG HU. Can. J. Chem. **60**, 1279 (1982).

On décrit la préparation d'une série de dérivés du type $Ru(CO)_3(L)(SiRCl_2)(X)$ et $[Ru(CO)_3(SiRCl_2)(X)]_2$ (L = CO, ligand donneur de phosphore; R = $CH_3$, Cl; X = H, Cl, Br, I; pas toutes les possibilités). On rapporte également les synthèses du $M(CO)_4(SiMeCl_2)_2$ (M = Ru, Os) et du *mer*-$M(CO)_3(PPh_3)(SiMeCl_2)_2$. D'après le schéma des substitutions dans les molécules tétracarbonylées, on en déduit que le ligand $SiRCl_2$ a un large effet *trans* dans ces composés. En se basant sur une étude quantitative des vitesses de substitution, il semble que l'effet-*trans* du ligand $SiMeCl_2$ est au moins comparable à celui du $SiCl_3$.

[Traduit par le journal]

## Introduction

The most common pathway by which transition metal carbonyl compounds undergo substitution reactions is the initial loss of a CO ligand in the rate determining step. For most substituted metal carbonyl complexes the *cis*-effect of the non-carbonyl substituent appears to be a major factor in determining the lability of the carbonyl groups (1).

The compound *cis*-$Ru(CO)_4(SiCl_3)_2$ is, therefore, interesting in that the CO substituents *trans* to the $SiCl_3$ are labile: they undergo stereospecific exchange with $^{13}CO$ when solutions of the complex are stirred at room temperature under 1 atm of $^{13}CO$ (2). Not surprisingly, derivatives of the type $Ru(CO)_{4-n}(L)_n(SiCl_3)_2$ (L = two electron donor ligand; $n$ = 1, 2) may be readily prepared from *cis*-$Ru(CO)_4(SiCl_3)_2$ (3). This is in contrast to the iron and osmium analogues which required much more forcing conditions to bring about substitution of the equatorial carbonyls (3).

In this study we report the preparation of a number of complexes which contain a Ru—$SiRCl_2$ (R = $CH_3$, Cl) linkage. In those compounds which contain a CO group *trans* to the silyl ligand, facile substitution of that carbonyl by phosphines is once again observed.

The preparation and reaction with $PPh_3$ of *cis*-$Ru(CO)_4(SiCl_3)(H)$ has been briefly described in a preliminary communication (4).

[1]Permanent address: Department of Chemistry, Inner-Mongolian University, Huhehot, Inner-Mongolian Autonomous Region, China.

## Results and discussion

### *$M(CO)_4(SiMeCl_2)_2$ complexes*

The $M(CO)_4(SiMeCl_2)_2$ (M = Ru, Os) complexes were prepared by the method previously employed in the synthesis of the trichlorosilyl analogues (3). This involved the ultraviolet irradiation of a solution of $M_3(CO)_{12}$ in the presence of excess $HSiMeCl_2$ under 2 atm of carbon monoxide. The yield was almost quantitative.

These compounds have been previously synthesized by the reaction of $M_3(CO)_{12}$ and the silane at 180°C under a high pressure of carbon monoxide (5). For the osmium case this gave a mixture of *cis* and *trans* isomers, whereas the present method yields exclusively the *cis* form. This is probably because the *trans* isomer rearranges to a *cis* geometry on ultraviolet irradiation. It has been established that uv irradiation of *trans*-$Ru(CO)_4(SiCl_3)_2$ causes complete isomerization to the *cis* form and that this occurs via CO dissociation (2).

The observation of five CO stretches in the infrared spectrum of $Ru(CO)_4(SiMeCl_2)_2$ indicates the presence of some *trans* isomer since a maximum of four bands is expected for the *cis* molecule. The presence of approximately 12% of the *trans* isomer has been established by $^{13}C$ nmr spectroscopy (6). It is probable that the *cis* isomer is initially formed in the reaction and, on removal from the uv light, it undergoes a non-dissociative isomerization to give an equilibrium mixture. It has been found that for compounds of the type $M(CO)_4(SiMe_xCl_{3-x})_2$ (M = Fe, Os; $x$ = 1–3), there is a non-dissociative equilibrium between the *cis* and *trans*

0008-4042/82/111279-07$01.00/0

©1982 National Research Council of Canada/Conseil national de recherches du Canada

Can. J. Chem. Downloaded from www.nrcresearchpress.com by 210.87.254.42 on 09/06/12
For personal use only.

Can. J. Chem. Downloaded from www.nrcresearchpress.com by 210.87.254.42 on 09/06/12
For personal use only.

forms which in some cases is rapid on the nmr time-scale at room temperature. It was also found that the barrier to rearrangement increases with increasing chlorine substitution at silicon (6). Since it is known (7) that $Ru(CO)_4(SiCl_3)_2$ isomerizes at a measurable rate above 70°C, it is reasonable that $Ru(CO)_4(SiMeCl_2)_2$ undergoes isomerization at room temperature, at a rate which prevents separation of the two isomers.

It might be argued that the extra CO stretching band observed in the infrared spectrum of $Ru(CO)_4(SiMeCl_2)_2$ arises because of the presence of different forms of the *cis* molecule due to different orientations of the $SiMeCl_2$ ligands about the Ru—Si bond. Such a phenomenon gives rise to a doubling of the CO stretching frequencies in $(C_5H_5)Fe(CO)_2(SiMeCl_2)$ (8). However, it has been observed before (9), and in this study, that in the infrared spectra of the present type of compounds with a M—$SiMeCl_2$ linkage there is only a broadening of the CO stretching absorptions, rather than a splitting, compared to those observed in the $SiCl_3$ analogues.

The reaction of *cis*-$Ru(CO)_4(SiMeCl_2)_2$ with $PPh_3$ to give *mer*-$Ru(CO)_3(PPh_3)(SiMeCl_2)_2$ proceeded at a convenient rate at room temperature. This is in contrast to $Os(CO)_4(SiMeCl_2)_2$ where a temperature of 110°C was required to bring about a comparable rate of reaction with $PPh_3$. A similar pattern was observed for the $SiCl_3$ analogues (3). However, unlike *cis*-$Ru(CO)_4(SiCl_3)_2$ the exchange of $Ru(CO)_4(SiMeCl_2)_2$ with $^{13}CO$ is non-stereospecific.[2] This is presumably due to *cis–trans* isomerization.

It was also noted that the rate of reaction of *cis*-$Ru(CO)_4(SiMeCl_2)_2$ with $PPh_3$ was very similar to that of *cis*-$Ru(CO)_4(SiCl_3)_2$ with the same ligand. Indeed, in a preliminary study, an exact measurement of the rate of substitution of the remaining equatorial carbonyl group in *mer*-$Ru(CO)_3(PPh_3)(SiRCl_2)_2$ by $P(OMe)_3$ showed that the rate of substitution was slightly faster in the $SiMeCl_2$ compound than in the $SiCl_3$ derivative.[3] These results are consistent with the $SiMeCl_2$ ligand as having a *trans*-effect in these molecules at least comparable to the $SiCl_3$ ligand. This pattern was also observed in the $Ru(CO)_4(SiRCl_2)(H)$ molecules. It is a surprising result. The CO stretching frequencies of *cis*-$Ru(CO)_4(SiMeCl_2)_2$ (Table 2) are lower than those of *cis*-$Ru(CO)_4(SiCl_3)_2$ (2150, 2103, 2094, and 2084 $cm^{-1}$). Such a lowering is usually taken to indicate that there is more overlap between the filled metal *d*-orbitals and the $\pi^*$-orbitals on the CO ligands. This would be expected to strengthen the M—C bond and, hence, raise the activation energy for CO dissociation. However, as previously observed (3), there appears to be no correlation between the carbonyl stretching frequencies in these molecules and the ease at which substitution occurs. This is interpreted in that it is the ease of formation of the five-coordinate intermediate which dictates the lability of a particular carbonyl group.

The $^1H$ nmr spectrum of $Ru(CO)_3(PPh_3)(SiMeCl_2)_2$ in the methyl region consists (Table 1) of two doublets. One pair is barely resolved (a difference between the two signals of 0.35 Hz), the other has a larger separation (0.9 Hz). This is consistent with the $PPh_3$ in an equatorial position; i.e., *cis* to one $SiMeCl_2$ group ($J_{P-H}$ 0.35 Hz) but *trans* to the other ($J_{P-H}$ 0.9 Hz). This is shown in **1**.

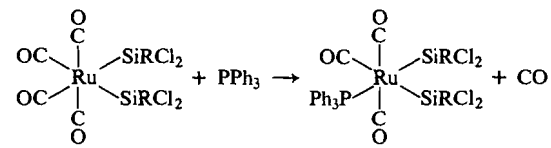


**1**

The osmium compound is similar.

*Ru(CO)$_4$(SiRCl$_2$)(H) complexes*

The *cis*-$Ru(CO)_4(SiRCl_2)(H)$ (R = Cl, $CH_3$) complexes were isolated in approximately 30% yield, by the ultraviolet irradiation of $Ru_3(CO)_{12}$ and excess $HSiRCl_2$ in pentane under carbon monoxide. The time period of 5–10 h was much shorter than that used in the preparation of the $Ru(CO)_4(SiRCl_2)_2$ compounds. The hydrides were separated from the other products, $[Ru(CO)_4(SiRCl_2)]_2$ and $Ru(CO)_4(SiRCl_2)_2$, by vacuum sublimation (or distillation) at room temperature.

Both the *cis*-$Ru(CO)_4(SiRCl_2)(H)$ compounds are low-melting solids which are extremely air-sensitive. They exhibit four carbonyl stretching bands in the infrared spectrum, expected for a *cis* arrangement of the non-carbonyl ligands. They also show the high field $^1H$ nmr resonance, typical of the metal–hydride linkage. In the mass spectrum of $Ru(CO)_4(SiCl_3)(H)$ the peaks of highest mass corresponded to $[P - CO]^+$. This is consistent with the chemical evidence, reported below, which indicates the carbonyl group *trans* to the $SiCl_3$ is particularly labile. Because of its extreme air-sensitivity, mass spectral and analytical data were not obtained for *cis*-$Ru(CO)_4(SiMeCl_2)(H)$.

The osmium compound *cis*-$Os(CO)_4(SiCl_3)(H)$ was not detected in the preparation of *cis*-

[2]R. K. Pomeroy. Unpublished results.

[3]K. L. Chalk and R. K. Pomeroy. Unpublished results.

Can. J. Chem. Downloaded from www.nrcresearchpress.com by 210.87.254.42 on 09/06/12
For personal use only.

TABLE 1. Spectroscopic data

| Compound | Mass spectrum[a] | ν(CO) cm$^{-1}$[b] | | | $^1$H nmr, ppm[d] | |
|---|---|---|---|---|---|---|
| $Ru(CO)_4(SiMeCl_2)_2$ | (P) | 2137m | 2090m | 2083m | 1.29 | 1.28[h] |
| | | 2066s | 2061vs | | | |
| *cis*-$Os(CO)_4(SiMeCl_2)_2$ | (P) | 2140w | 2083m | 2068m | 1.33 | |
| | | 2059s | | | | |
| $Ru(CO)_3(PPh_3)(SiMeCl_2)_2$ | (P − Cl − CO) | 2098w | 2056m | 2027s[c] | 1.33 (0.9) | 1.07 (0.35) |
| $Os(CO)_3(PPh_3)(SiMeCl_2)_2$ | (P − $SiMeCl_2$) | 2097w | 2045m | 2020s | 1.38 (0.75) | 1.10 (0.2) |
| $Ru(CO)_4(SiCl_3)(H)$ | (P − CO) | 2147w | 2089m | 2074sh | | |
| | | 2071s | | | −7.35[e] | |
| $Ru(CO)_4(SiMeCl_2)(H)$ | nm | 2138w | 2082m | 2069s | 1.16 (0.45[i]) | −7.45 (0.45[i])[f] |
| | | 2058s | | | | |
| $Ru(CO)_3(PPh_3)(SiCl_3)(H)$ | nm | 2105w | 2048m | 2033s | −6.35 (14.5)[e] | |
| $Ru(CO)_3(P(OPh)_3)(SiCl_3)(H)$ | (P − 2CO − Cl) | 2118w | 2065m | 2051s | nm | |
| $Ru(CO)_3(ETPB)(SiCl_3)(H)$ | (P) (w) (P − CO) | 2124w | 2068m | 2056s | −7.12 (18.3)[g] | |
| $Ru(CO)_3(PPh_3)(SiMeCl_2)(H)$ | (P − $SiMeCl_2$) | 2096w | 2042m | 2022s | 1.18 (0.9, 0.5[i]) | −7.04 (14.5, 0.5[i])[g] |
| $Ru(CO)_3(ETPB)(SiMeCl_2)(H)$[j] | (P − $SiMeCl_2$) | 2114w | 2060m | 2041s | 1.24 (1.4, 0.5[i]) | −7.42 (18.8, 0.5[i])[g] |
| $[Ru(CO)_3(SiCl_3)(Cl)]_2$ | (P − $SiCl_3$ − Cl − 2CO) | 2146w | 2092vs | 2056s | — | |
| $[Ru(CO)_3(SiCl_3)(Br)]_2$ | (P − $SiCl_3$ − Br − 2CO) | 2140w | 2088vs | 2056s | — | |
| $[Ru(CO)_3(SiCl_3)(I)]_2$ | P (w) | 2132w | 2082vs | 2058s | — | |
| $[Ru(CO)_3(SiMeCl_2)(Cl)]_2$ | (P − $SiMeCl_2$ − Cl − 2CO) | 2138w | 2079s | 2045s | 1.15 | |
| $[Ru(CO)_3(SiMeCl_2)(Br)]_2$ | (P − $SiMeCl_2$ − Br − 2CO) | 2134w | 2077s | 2046m | 1.15 | |
| $[Ru(CO)_3(SiMeCl_2)(I)]_2$ | (P) (w) | 2124w | 2069s | 2046m | 1.20 | |
| *trans*-$Ru(CO)_4(SiCl_3)(Br)$ | (P) | | 2098vs | | — | |
| *trans*-$Ru(CO)_4(SiMeCl_2)(Br)$ | (P) | | 2085s | | 1.27 | |
| *trans*-$Ru(CO)_4(SiMeCl_2)(I)$ | (P) | | 2081s | | 1.29 | |
| $Ru(CO)_3(PPh_3)(SiCl_3)(Cl)$ | nm | 2134w | 2071s | 2041m[c] | — | |
| $Ru(CO)_3(PPh_3)(SiCl_3)(Br)$ | (nv) | 2137w | 2069s | 2041m[c] | — | |
| $Ru(CO)_3[P(OMe)_3](SiCl_3)(Cl)$ | nm | 2133w | 2072s | 2051m | nm | |
| $Ru(CO)_3[P(OMe)_3](SiCl_3)(Br)$ | (P − $SiCl_3$ − Br] | 2132w | 2071s | 2053m | nm | |
| $Ru(CO)_3(PPh_3)(SiMeCl_2)(Cl)$ | (P − $SiMeCl_2$ − Cl − CO) | 2122w | 2058s | 2030m[c] | 1.30 (0.75) | |
| $Ru(CO)_3(PPh_3)(SiMeCl_2)(Br)$ | (P − Br − 2CO) | 2120w | 2056s | 2032m[c] | 1.39 (0.7) | |
| $Ru(CO)_3(PPh_3)(SiMeCl_2)(I)$ | (P − $SiMeCl_2$ − I) | 2115w | 2051s | 2031m[c] | 1.53 (0.7) | |
| $[Ru(CO)_4(SiCl_3)]_2$ | (P) | 2086w | 2059vs | | — | |
| Lit. (ref. 12) | (P) | 2086w | 2056s | 2050w | — | |
| $[Ru(CO)_4(SiMeCl_2)]_2$ | (P) | 2073w | 2045s | | 1.37 | |
| Lit. (ref. 12) | (P) | 2073w | 2044s | 2035w | — | |

[a]Highest mass peak given, P = parent ion, nv = not sufficiently volatile.
[b]Hexane solution, except those marked *c*.
[c]$CH_2Cl_2$ solution.
[d]Chemical shift (δ), P—H coupling given in parentheses, $CDCl_3$ solution, except those marked *e*, *f*, and *g*; signals due to phosphorus–donor ligands are not reported.
[e]Benzene solution.
[f]$CD_2Cl_2$ solution.
[g]Toluene-$d_8$ solution.
[h]Due to the *trans* isomer.
[i]H–H coupling; nm: not measured; w: weak; m: medium; s: strong.
[j]ETPB = $P(OCH_2)_3CC_2H_5$.

$Os(CO)_4(SiCl_3)_2$ by the uv irradiation of a solution of $Os_3(CO)_{12}$ and $HSiCl_3$ (3). However, *cis*-$Os(CO)_4(SiCl_3)(H)$ and the dichloromethylsilyl analogue have been prepared by the action of carbon monoxide on the appropriate $Os_3H_3(CO)_9(SiRCl_2)_3$ compound. On pyrolysis at 140°C, under vacuum, the *cis*-$Os(CO)_4(SiRCl_2)(H)$ complexes gave mainly $[Os(CO)_4(SiRCl_2)]_2$ (10). In this study, it was found that heating a solution of $Ru(CO)_4(SiRCl_2)(H)$ under vacuum similarly gave $[Ru(CO)_4(SiRCl_2)]_2$. The preparation of the dinuclear compounds, which contain a linear SiRuRuSi backbone, has been reported in the literature (11). A variation of the literature method which gives an improved yield is reported in the Experimental section.

The most interesting property of the $Ru(CO)_4(SiRCl_2)(H)$ molecules is that they also readily undergo substitution by phosphorus donor ligands:

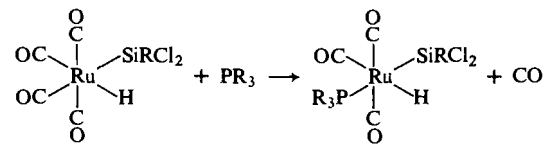


**2**

The geometry (**2**) of the $SiMeCl_2$ derivatives may be unambiguously assigned by $^1$H nmr spectroscopy. For example, the hydride signal in the $^1$H nmr spectrum of $Ru(CO)_3[P(OCH_2)_3CC_2H_5](SiMeCl_2)(H)$ consists of a doublet of quartets (Fig. 1) due to coupling to phosphorus ($J_{P-H}$ 18.8 Hz) and to the silyl methyl protons ($J_{H-H}$ 0.5 Hz). The size of the

Can. J. Chem. Downloaded from www.nrcresearchpress.com by 210.87.254.42 on 09/06/12
For personal use only.

phosphorus coupling is indicative of a *cis* arrangement of the phosphorus–donor ligand and the hydride group (12). The silyl methyl signal (Fig. 1) is a doublet of doublets. The proton–proton coupling to the hydride signal allows the smaller coupling to the methyl signal to be attributed to $J_{H-H}$. The larger coupling may therefore be assigned to $J_{P-H(CH_3)}$. The value of this parameter (1.4 Hz) indicates a *trans* arrangement of the $SiMeCl_2$ and $P(OCH_2)_3CC_2H_5$ ligands (cf. the $^1H$ nmr spectrum of $Ru(CO)_3(PPh_3)(SiMeCl_2)_2$). This is sufficient to establish the geometry as that shown as **2**. It should be also noted that $J_{H-H(CH_3)}$ (0.5 Hz) is consistent with a *cis* arrangement of the H and $SiMeCl_2$ substituents (cf. *cis*-$Ru(CO)_4(SiMeCl_2)(H)$), and that the pattern of absorptions observed in the carbonyl region of the infrared spectrum is typical of a *mer* arrangement of noncarbonyl ligands (as in the $Ru(CO)_3(L)(SiCl_3)_2$ derivatives (3)).

That substitution has occurred *trans* to the $SiRCl_2$ ligand implies that in these molecules the silyl ligand has a greater *trans*-effect than either the carbon monoxide or hydride substituents, both of which are known to exhibit a large *trans*-effect in square-planar complexes (13). It is also interesting that the substitution of CO by $PPh_3$ in $Ru(CO)_4(SiRCl_2)(H)$ proceeds at a faster rate than in $Ru(CO)_4(SiRCl_2)_2$. This could be taken to indicate that the *cis*-effect of hydrogen is greater than the $SiRCl_2$ ligand in these compounds.

Derivatives of the type $Ru(CO)_3(L)(SiRCl_2)(H)$ are reasonably air-stable, white crystalline solids and are easily characterized. As with other compounds with chlorosilyl groups (3), the air-sensitivity appears, in most cases, to be related to the presence of labile carbonyl groups and not to the sensitivity of the Si—Cl bonds to atmospheric moisture.

### *$[Ru(CO)_3(SiRCl_2)(X)]_2$ and* trans-*$Ru(CO)_4(SiRCl_2)(X)$ complexes*

Treatment of the hydrides *cis*-$Ru(CO)_4(SiRCl_2)(H)$ with $CCl_4$ resulted in the rapid formation of the dimeric product $[Ru(CO)_3(SiRCl_2)(Cl)]_2$. A similar reaction with $CBr_4$, in place of $CCl_4$, gave not only $[Ru(CO)_3(SiRCl_2)(Br)]_2$, but also *trans*-$Ru(CO)_4(SiRCl_2)(Br)$.[4] Similar products were obtained when the Ru—Ru bond in $[Ru(CO)_4(SiRCl_2)]_2$ was cleaved with $Br_2$:

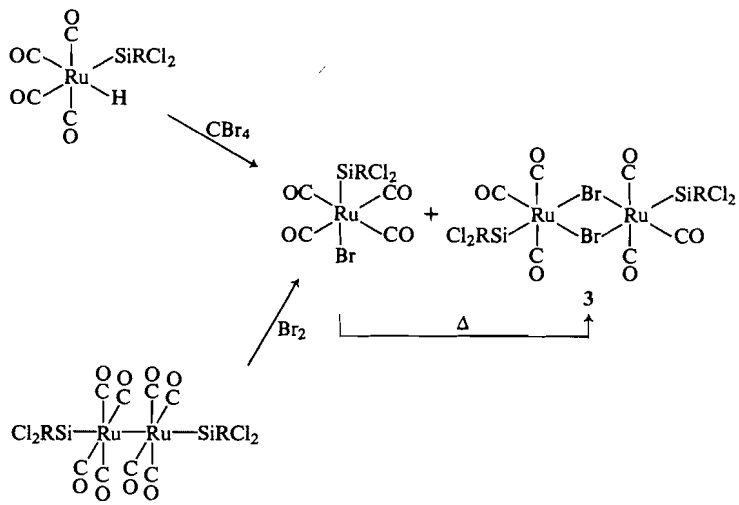


In the corresponding reaction of $[Ru(CO)_4(SiRCl_2)]_2$ with $I_2$, to give analogous products, the *trans*-$Ru(CO)_4(SiRCl_2)(I)$ was thermally unstable, with respect to $[Ru(CO)_3(SiRCl_2)(I)]_2$, and could not be completely characterized.

The formation of the dimeric product, $[Ru(CO)_3(SiRCl_2)(X)]_2$, probably results from dimerization of *cis*-$Ru(CO)_4(SiRCl_2)(X)$ (X = Cl, Br, I) which may be formed directly in the reaction, or result from isomerization of *trans*-$Ru(CO)_4(SiRCl_2)(X)$. The mode of the exchange of coordinated CO in $Mn(CO)_5Br$ with free $^{13}CO$, which takes place under mild conditions, is consistent with the bromide ligand as having a *cis*-labilizing effect (14). Similarly, the exchange (which is also facile) in *cis*-$Fe(CO)_4I_2$ (15) and *cis*-$Ru(CO)_4I_2$ (16) is, within the limitations of the experimental method, ran-

[4]The stereochemistry of this compound was indicated by the single carbonyl stretch it exhibited in the infrared spectrum (Table 2).

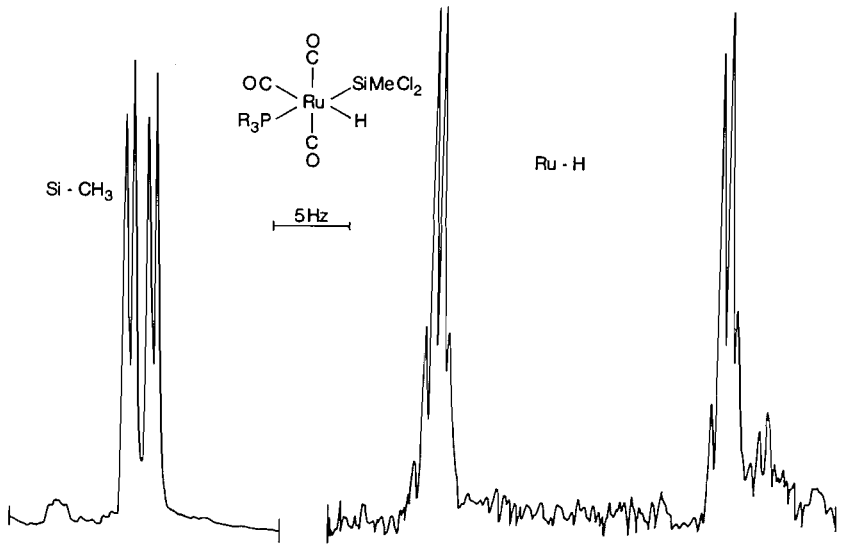


FIG. 1. The silyl methyl and hydride resonances of the 100 MHz $^1$H nmr spectrum of $Ru(CO)_3[P(OCH_2)_3CC_2H_5](SiMeCl_2)(H)$ in toluene-$d_8$.

dom. This is also consistent with the halogen substituents in these molecules having a *cis*-labilizing effect (both the axial and equatorial carbonyls are *cis* to at least one iodine atom). It is therefore reasonable that in *cis*-$Ru(CO)_4(SiRCl_2)(X)$, the CO ligand which is both *trans* to the $SiRCl_2$ group and *cis* to X is particularly labile. This suggests that dimerization would readily take place and *cis*-$Ru(CO)_4(SiRCl_2)(X)$ would not be detected in the reaction.

The preparation of the trimethylsilyl derivatives, $[Ru(CO)_3(SiMe_3)(X)]_2$, has been reported (17). These compounds were found to exist as a mixture of isomers. One form was thought to have a structure analogous to that proposed for the present dimeric derivatives (i.e., **3**), the other with the $SiMe_3$ ligands in axial positions as shown in **4**.

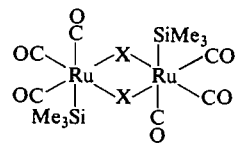

**4**

The reason why the trimethylsilyl compounds exist in two isomeric forms, but the chlorosilyl derivatives do not, is not clear. It is not inconceivable that the molecules with $SiMe_3$ groups are nonrigid (not necessarily on the nmr time-scale). As previously mentioned, in the monomeric derivatives $M(CO)_4(SiMe_xCl_{3-x})_2$ (M = Fe, Ru, Os; $x$ = 0–3) the barrier to *cis*–*trans* isomerization is lowest for the trimethylsilyl derivatives (6).

The compounds $[Ru(CO)_3(SiRCl_2)(X)]_2$ rapidly react in solution with phosphorus donor ligands (L) to give $Ru(CO)_3(L)(SiRCl_2)(X)$. The structure of these derivatives is believed to be analogous to the corresponding hydrides: a *mer* arrangement of the non-carbonyl ligands with L *trans* to the $SiRCl_2$ group. This is based primarily on the observation of a P—H coupling of ~ 0.7 Hz for the methyl signal in the $^1$H nmr of $Ru(CO)_3(PPh_3)(SiMeCl_2)(X)$. It is also the geometry one would predict from the *cis*-effect of X and the *trans*-effect of the $SiRCl_2$ group. The pattern of the CO stretching frequencies in the infrared spectra of the $Ru(CO)_3(L)(SiRCl_2)(X)$ (X = Cl, Br, I) compounds is different from the corresponding hydrides (X = H) which might be taken to indicate a different geometry. However, the patterns for *cis*-$Fe(CO)_4(EX_3)(X)$ (E = Ge, Sn; X = Cl, Br, I) (18) and *cis*-$M(CO)_4I_2$ (M = Ru, Os) (16, 19) are different to those of *cis*-$Ru(CO)_4(SiCl_3)(X)$ (X = $SiCl_3$ (2), H). For the latter compounds the most intense absorption has the lowest frequency which is not the case for the halogen derivatives. This difference parallels that observed in the molecules presently under discussion.

It should be pointed out that the geometry favored for the $Ru(CO)_3(L)(SiRCl_2)(X)$ compounds in this study differs from that suggested for the analogous $SiMe_3$ derivatives (17). In that work a P—H($SiMe_3$) coupling of 1–2 Hz, observed in the $^1$H nmr spectra of the complexes, was taken to indicate a *cis* arrangement of the $PPh_3$ and $SiMe_3$ ligands. However, it is apparent from this work that such a coupling signifies a *trans* configuration.

Can. J. Chem. Downloaded from www.nrcresearchpress.com by 210.87.254.42 on 09/06/12
For personal use only.

Can. J. Chem. Downloaded from www.nrcresearchpress.com by 210.87.254.42 on 09/06/12
For personal use only.

## Conclusion

This study has shown that the $SiRCl_2$ (R = $CH_3$, Cl) ligand exhibits a large *trans*-effect in a number of octahedral, carbonyl–ruthenium complexes. It has also indicated the *trans*-effect of the $SiMeCl_2$ group is at least comparable to that of $SiCl_3$ in these molecules.

## Experimental

The general experimental procedures used in the preparation of the new compounds have been described elsewhere (3). The method of preparation of $M(CO)_4(SiMeCl_2)_2$ and *mer*-$M(CO)_3(PPh_3)(SiMeCl_2)_2$ (M = Ru, Os) was essentially that used to prepare the trichlorosilyl analogues (3). The yields were excellent in all cases. Spectroscopic data for the new compounds are reported in Table 1. Analytical data (Table 2) have been placed in the Depository.[5]

*Preparation of* cis-*Ru(CO)$_4$(SiCl$_3$)(H)*

A quartz tube with $Ru_3(CO)_{12}$ (0.64 g, 1.0 mmol) and $Cl_3SiH$ (3 mL, 30 mmol) in pentane (25 mL) was evacuated at −196°C and the solution degassed with two freeze–thaw cycles. It was allowed to warm to room temperature and then pressurized with carbon monoxide (2 atm). The solution was subjected to uv irradiation for 10 h. The resulting, almost colorless, solution was transferred to a Schlenk flask and the pentane and excess $Cl_3SiH$ were removed on the vacuum line at 0°C. A second Schlenk flask was connected to the first and both were evacuated to $< 5 \times 10^{-3}$ mm. The second flask was cooled to −196°C to which, over 4 h, *cis*-$Ru(CO)_4(SiCl_3)(H)$ (ca. 0.36 g, 35%) distilled. The compound is extremely air-sensitive, turning yellow almost immediately on exposure to air. The melting point was determined by placing a Schlenk flask with the compound in an ice-water bath, allowing the bath to warm slowly, and recording the temperature at which the compound melted.

The products remaining, after removal of *cis*-$Ru(CO)_4(SiCl_3)(H)$, were *cis*-$Ru(CO)_4(SiCl_3)_2$ and $[Ru(CO)_4(SiCl_3)]_2$. The former compound may be separated from the dimer by sublimation at 30°C and $< 5 \times 10^{-3}$ mm to a probe of −78°C (see ref. 3). The dimer, $[Ru(CO)_4(SiCl_3)]_2$, may then be purified by recrystallization from hexane.

The hydride, *cis*-$Ru(CO)_4(SiMeCl_2)(H)$, (mp 2–3°C) was prepared, in similar yield, by the same method. With an irradiation period of 5 h and with use of a glass tube, no $Ru(CO)_4(SiMeCl_2)_2$ formed and $[Ru(CO)_4(SiMeCl_2)]_2$ was the only other product. The dimer could thus be obtained by recrystallization, from hexane, after removal of the hydride.

*Preparation of [Ru(CO)$_4$(SiCl$_3$)]$_2$*

A glass tube with $Ru_3(CO)_{12}$ (0.40 g, 0.63 mmol) and $HSiCl_3$ (0.26 g, 1.92 mmol) in hexane (15 mL) was evacuated, and the solution degassed, as before. The tube was pressurized with carbon monoxide (2 atm) and then heated at 80°C for 2.5 h. An infrared spectrum of the solution at this stage (after removal of the $HSiCl_3$) indicated only $[Ru(CO)_4(SiCl_3)]_2$ with perhaps a trace of $Ru_3(CO)_{12}$. The hexane and the excess $HSiCl_3$ were removed on the vacuum line. The material remaining was recrystallized from hexane to give pure $[Ru(CO)_4(SiCl_3)]_2$ as pale-yellow crystals.

*Pyrolysis of* cis-*Ru(CO)$_4$(SiMeCl$_2$)(H)*

An evacuated round-bottom flask with *cis*-$Ru(CO)_4(SiMeCl_2)(H)$ (0.20 g, 0.61 mmol) in hexane (15 mL) was heated at 50–60°C for 4.5 h. An infrared spectrum of the solution at this point indicated complete conversion to $[Ru(CO)_4(SiMeCl_2)]_2$. The solution was reduced in volume to about 5 mL and placed in the refrigerator to afford crystals of the dimer.

The pyrolysis of $Ru(CO)_4(SiCl_3)(H)$ was similar. It did appear to require a longer period to bring about the conversion, since an infrared spectrum taken of the reaction solution after 7 h indicated a trace of starting material remained.

*Preparation of Ru(CO)$_3$(PPh$_3$)(SiCl$_3$)(H) and related derivatives*

To a solution of *cis*-$Ru(CO)_4(SiCl_3)(H)$ (0.20 g, 0.57 mmol) in pentane (15 mL) was added $PPh_3$ (0.15 g, 0.57 mmol). The solution was stirred for 2 h during which time a white crystalline precipitate formed. After the 2 h period, the solution was placed in the refrigerator at −15°C for several hours to complete the precipitation. The supernatant solution was then removed from the product which was washed with hexane (2 × 5 mL) and dried on the vacuum line. The product, *mer*-$Ru(CO)_3(PPh_3)(SiCl_3)(H)$ (0.31 g, 93%), was thus isolated as a white crystalline solid which appeared reasonably air-stable. The analytical sample was obtained by recrystallization from benzene–hexane.

Other derivatives of the type *mer*-$Ru(CO)_3(L)(SiRCl_2)(H)$ (R = Cl, Me) were prepared in essentially the same manner. The ETPB derivatives were somewhat air-sensitive. Attempts to prepare the $P(OMe)_3$ analogues gave oils, the elemental analyses of which were not quite satisfactory.

*Preparation of [Ru(CO)$_3$(SiCl$_3$)(Cl)]$_2$*

To $Ru(CO)_4(SiCl_3)(H)$ (0.15 g, 0.43 mmol) in hexane (15 mL) was added $CCl_4$ (0.40 mL, 0.64 g, 4.1 mmol) and the solution stirred for 10 min during which time needle-shaped crystals formed. After the solution had stood in the refrigerator for several hours to complete the crystallization, the solvent was removed from the crystals of $[Ru(CO)_3(SiCl_3)(Cl)]_2$, which were washed with hexane (2 × 5 mL) and dried on the vacuum line. There was no spectroscopic evidence for *trans*-$Ru(CO)_4(SiCl_3)(Cl)$ in the reaction.

The preparation of $[Ru(CO)_3(SiMeCl_2)(Cl)]_2$ was similar.

*Preparation of [Ru(CO)$_3$(SiMeCl$_2$)(Br)]$_2$ and* trans-*Ru(CO)$_4$(SiMeCl$_2$)(Br)*

Method 1: to a solution of *cis*-$Ru(CO)_4(SiMeCl_2)(H)$ (ca. 0.30 g, 0.91 mmol) in hexane (12 mL) was added $CBr_4$ (0.25 g, 0.75 mmol). The solution was stirred for 15 min; an infrared spectrum revealed only *trans*-$Ru(CO)_4(SiMeCl_2)(Br)$ and $[Ru(CO)_3(SiMeCl_2)(Br)]_2$. The hexane was removed on the vacuum line and from the residue *trans*-$Ru(CO)_4(SiMeCl_2)(Br)$ obtained by sublimation ($< 5 \times 10^{-3}$ mm) at room temperature to a probe maintained at −78°C. The first fraction which sublimed to the probe was discarded since it may have contained starting materials. The solid remaining after the removal of *trans*-$Ru(CO)_4(SiMeCl_2)(Br)$ was recrystallized from hexane to give pure $[Ru(CO)_3(SiMeCl_2)(Br)]_2$ as yellow crystals.

The trichlorosilyl analogues, $[Ru(CO)_3(SiCl_3)(Br)]_2$ and *trans*-$Ru(CO)_4(SiCl_3)(Br)$, were prepared in the same manner.

Method 2: to $[Ru(CO)_4(SiMeCl_2)]_2$ (0.55 g, 0.84 mmol) in hexane (25 mL) was added bromine (0.30 g, 1.9 mmol) and the solution stirred for 10 min at room temperature. The hexane and excess bromine were removed on the vacuum line to give a mixture which, by infrared spectroscopy, consisted mainly of *trans*-$Ru(CO)_4(SiMeCl_2)(Br)$ and a small fraction of $[Ru(CO)_3(SiMeCl_2)(Br)]_2$. The products were isolated pure as in Method 1.

The iodo analogues were prepared by Method 2. However, *trans*-$Ru(CO)_4(SiMeCl_2)(I)$ was thermally unstable with respect to the dimer even at room temperature. For this reason it was not analyzed. An improved preparation of the dimeric compound is given below.

[5]Complete set of data may be obtained, at a nominal charge, from the Depository of Unpublished Data, CISTI, National Research Council of Canada, Ottawa, Ont., Canada K1A 0S2.

*Preparation of* $[Ru(CO)_3(SiMeCl_2)(I)]_2$

A glass Carius tube with $[Ru(CO)_4(SiMeCl_2)]_2$ (0.25 g, 0.38 mmol) and iodine (0.10 g, 0.39 mmol) in hexane (15 mL) was evacuated (at −196°C) and the solution degassed. The solution was then heated to 50–60°C for 10 h (the tube was reevacuated three times during this period). An infrared spectrum of the solution at this stage indicated complete conversion of *trans*-$Ru(CO)_4(SiMeCl_2)(I)$ to $[Ru(CO)_3(SiMeCl_2)(I)]_2$. After the 10 h period, the tube was cooled and the solution transferred to a Schlenk tube, concentrated to ~ 5 mL on the vacuum line, and then allowed to stand in the refrigerator at −15°C, whereupon $[Ru(CO)_3(SiMeCl_2)(I)]_2$ was obtained as yellow needles. The crystals are soluble in hexane; they are also somewhat air-sensitive.

Although not confirmed, it is probable that other compounds of the type $[Ru(CO)_3(SiRCl_2)(X)]_2$ (R = Me, Cl; X = Br, I) could be prepared in this manner.

*Preparation of* mer-$Ru(CO)_3(PPh_3)(SiCl_3)(Cl)$ *and related derivatives*

Method 1: a solution of *mer*-$Ru(CO)_3(PPh_3)(SiCl_3)(H)$ (0.37 g, 0.63 mmol) and $CCl_4$ (0.50 mL, 0.79 g, 5.2 mmol) in benzene (10 mL) was placed in a glass Carius tube which was evacuated, and the solution degassed, as before. The tube was then pressurized with carbon monoxide (2 atm) and the bottom half heated in an oil-bath at 100°C for 4.5 h. The tube was then allowed to cool, the solution transferred to a Schlenk flask where the solvent (and the excess $CCl_4$) was removed on the vacuum line. The residue was recrystallized from benzene–hexane to give *mer*-$Ru(CO)_3(PPh_3)(SiCl_3)(Cl)$ as air-stable, plate-shaped crystals. (*Anal.* calcd.: C 40.86, H 2.45; found: C 40.44, H 2.52.)

Method 2: to a solution of $[Ru(CO)_3(SiCl_3)(Cl)]_2$ (0.15 g, 0.21 mmol) in hexane (15 mL) was added $PPh_3$ (0.10 g, 0.38 mmol). The solution was stirred for 15 min during which time crystals formed. The solution was placed in the refrigerator at −15°C to complete the crystallization of the product. The solvent was then removed from the white crystals, which were washed with hexane (2 × 5 mL) and dried on the vacuum line. The yield of *mer*-$Ru(CO)_3(PPh_3)(SiCl_3)(Cl)$ was judged to be almost quantitative.

Related derivatives were prepared according to Method 2.

## Acknowledgements

We thank the Natural Sciences and Engineering Research Council of Canada and the Science Council of British Columbia for financial support. We would also like to thank the government of the People's Republic of China for leave of absence, from the Inner-Mongolian University, for Xiang Hu.

1. J. D. Atwood and T. L. Brown. J. Am. Chem. Soc. **98**, 3160 (1976).
2. R. K. Pomeroy, R. S. Gay, G. O. Evans, and W. A. G. Graham. J. Am. Chem. Soc. **94**, 272 (1972).
3. R. K. Pomeroy and K. S. Wijesekera. Inorg. Chem. **19**, 3729 (1980).
4. R. K. Pomeroy. J. Organomet. Chem. **177**, C37 (1979).
5. R. K. Pomeroy. Ph.D. Thesis, University of Alberta, Edmonton, Alta. 1972.
6. L. Vancea, R. K. Pomeroy, and W. A. G. Graham. J. Am. Chem. Soc. **98**, 1407 (1976).
7. R. K. Pomeroy and W. A. G. Graham. J. Am. Chem. Soc. **94**, 274 (1972).
8. W. Jetz and W. A. G. Graham. J. Am. Chem. Soc. **89**, 2773 (1967).
9. G. N. van Buuren, A. C. Willis, F. W. B. Einstein, L. K. Peterson, R. K. Pomeroy, and D. Sutton. Inorg. Chem. **20**, 4361 (1981).
10. R. K. Pomeroy. J. Organomet. Chem. **221**, 323 (1981).
11. S. A. R. Knox and F. G. A. Stone. J. Chem. Soc. A, 2560 (1969).
12. E. L. Muetterties (*Editor*). Transition metal hydrides. Marcel Dekker, New York. 1971. p. 119.
13. F. A. Cotton and G. Wilkinson. Advanced inorganic chemistry. 4th Ed. John Wiley, New York. 1980. p. 1200.
14. J. D. Atwood and T. L. Brown. J. Am. Chem. Soc. **97**, 3380 (1975).
15. I. S. Butler and H. K. Spendjian. J. Organomet. Chem. 18, 145 (1969); B. F. G. Johnson, J. Lewis, P. W. Robinson, and J. R. Miller. J. Chem. Soc. A, 1043 (1968).
16. R. S. Gay. Ph.D. Thesis, University of Alberta, Edmonton, Alta. 1970.
17. M. J. Ash, A. Brookes, S. A. R. Knox, and F. G. A. Stone. J. Chem. Soc. A, 458 (1971).
18. R. Kummer and W. A. G. Graham. Inorg. Chem. 7, 1208 (1968).
19. L. Vancea and W. A. G. Graham. J. Organomet. Chem. **134**, 219 (1977) and references therein.

Can. J. Chem. Downloaded from www.nrcresearchpress.com by 210.87.254.42 on 09/06/12
For personal use only.

# Measurement of self-association and ion-pair dissociation constants by solvent extraction using a membrane phase separator

MURRAY CARMICHAEL AND FREDERICK F. CANTWELL[1]

*Department of Chemistry, University of Alberta, Edmonton, Alta., Canada T6G 2G2*

Received November 25, 1981

MURRAY CARMICHAEL and FREDERICK F. CANTWELL. Can. J. Chem. **60**, 1286 (1982).

The "filter-probe" membrane phase separator is used with a gravimetric buret to obtain the following constants at 25°C by measuring solvent-extraction isotherms: dimerization constant of benzoic acid in chloroform (log $K_{2,HBz} = 2.12 \pm 0.01$); "self-ion-pair extraction" constant of Naloxone into chloroform ($K_{I,H_2A.A} < 10^7$); and ion-pair dissociation constant of tetraethylammonium picrate in methylene chloride (log $K_{diss} = -4.52 \pm 0.09$).

MURRAY CARMICHAEL et FREDERICK F. CANTWELL. Can. J. Chem. **60**, 1286 (1982).

On a utilisé la "sonde filtre" d'une phase membraneuse séparatrice avec une burette gravimétrique pour obtenir les constantes suivantes à 25°C en mesurant les isothermes d'extractions à l'aide de solvants: la constante de dimérisation de l'acide benzoique dans le chloroforme (log $K_{2,HBz} = 2{,}12 \pm 0{,}01$); la constante d'extraction de la paire "auto-ionisée" de Naloxone dans le chloroforme ($K_{I,H_2A.A} < 10^7$); et la constante de dissociation de la paire d'ions du picrate de tétraéthylammonium dans le chlorure de méthylène (log $K_{diss} = -4{,}52 \pm 0{,}09$).

[Traduit par le journal]

Association and dissociation reactions occurring in either the aqueous or the organic solvent phase during liquid–liquid extraction can profoundly influence the distribution ratio of the component being extracted. Reversible reactions such as dimerization in one or both phases and dissociation of ion-pairs in the organic phase may be encountered, depending on the nature of the sample and solvent involved (1–3). Such "side-reactions" often lead to a non-linear distribution isotherm over the concentration range where significant fractions of both the associated and dissociated species are present. It is therefore important to have an estimate of the magnitude of their equilibrium constants when designing a solvent extraction separation scheme.

Association/dissociation equilibria can be studied by a variety of techniques including spectroscopy (4), electrical conductivity (5, 6), two-phase potentiometric titrations (7–9), and measurement of liquid–liquid distribution ratios as a function of sample concentration (1, 10). When the equilibrium constants are used to predict solvent extraction behavior, regardless of the technique used, they should be measured in solutions that are saturated with the second liquid phase. This is particularly true when equilibria in the organic phase are under study, since low concentrations of dissolved water can profoundly influence them (3, 11).

A recently described "filter-probe" membrane phase separator has been shown to greatly facilitate the measurement of liquid–liquid distribution equilibria, especially in situations where it is desired to incrementally alter the composition of the system, such as in two-phase titrations and distribution isotherm measurements (12–17). This characteristic makes the "filter-probe" an obvious device to use in solvent extraction studies designed to evaluate association/dissociation equilibria, because such studies are necessarily done as a function of changing sample concentration. In the present investigation we have examined three equilibria using the "filter-probe": dimerization of benzoic acid in chloroform; "self-ion-pair extraction" of Naloxone from water into chloroform, and dissociation of the ion-pair tetraethylammonium picrate in methylene chloride.

## Experimental

*Apparatus*

Measurement of the absorbance of the aqueous phase was made continuously at 25 ± 0.1°C on an apparatus based on the two-phase titration device previously described (12). A three-layer paper membrane was employed. The Mini-Micro 2/6 pump used in the original design was replaced with a variable speed Minipuls-2 peristaltic pump (Gilson France S.A., Villiers-le-Bel, France) and the short Acidflex pump tube was replaced with an 18-cm long, 1.14 mm i.d. tube (Technicon Corp., Tarrytown, NY). Instead of the original micrometer buret, either of two types of gravimetric buret was used. One was simply a gas-tight syringe (2 or 5 mL, Hamilton Co., Reno, Nev.). This was weighed, after deliveries of increments of sample stock solution, on a Mettler PL 200 electronic top-loading balance (18). The second type of gravimetric buret employed a solvent reservoir and remotely activated Teflon valve. It has already been described (15, 19). The weight of sample stock solution added from the buret was converted to volume via its density and incremented to $V_o$ in eqs. [7], [13], or [18], as appropriate.

Necessary pH measurements were made with a glass and

[1]To whom all correspondence should be addressed.

0008-4042/82/111286-05$01.00/0

©1982 National Research Council of Canada/Conseil national de recherches du Canada

Can. J. Chem. Downloaded from www.nrcresearchpress.com by 210.87.254.5 on 09/06/12
For personal use only.

Can. J. Chem. Downloaded from www.nrcresearchpress.com by 210.87.254.5 on 09/06/12
For personal use only.

calomel electrode pair using an Accumet Model 520 pH meter (Fisher Scientific Co.).

Wavelengths used were 273 nm for benzoic acid, 281 nm for Naloxone, and 400 nm for picrate, the wavelengths of maximum absorbance.

*Reagents*

Water used throughout was demineralized, distilled, and finally distilled from alkaline permanganate. Reagent grade chloroform was washed four times with equal volumes of water to remove ethanol preservative and then filtered through dry Whatman No. 2 filter paper to remove entrained water. Reagent grade methylene chloride, benzoic acid (HBz) (Fisher Scientific Co.), $Na_2HPO_4 \cdot 7H_2O$, picric acid (Matheson, Coleman and Bell), tetraethylammonium chloride (Eastman #3022), hydrochloric acid, perchloric acid, ammonium chloride, and ammonia water were used without further purification. Naloxone base (1-*N*-allyl-7,8-dihydro-14-hydroxynormorphinone) (Endo Laboratories Inc., Garden City, NY) was used as 100%.

The tetraethylammonium picrate (TEA·P) stock solution in methylene chloride was prepared as follows: 55 mL of an aqueous pH 6.7 phosphate buffer solution containing approximately 0.5 mmol each of picric acid and tetraethylammonium chloride was multiply-extracted with small volumes of methylene chloride to yield a final volume of about 100 mL. Concentration of TEA·P in the final solution was accurately determined by evaporating 1 g of it to dryness, diluting to 50.0 mL with 0.1 *M* NaOH, and measuring the picrate concentration of the resulting solution spectrophotometrically at 400 nm.

*Measurement procedure*

After combining the initial quantities of the two phases specified below in the titration beaker, the Teflon lid containing the filter-probe, the return line, the spoiler, and (when the valve-controlled weight buret was used) the buret tip was clamped in place. The stirrer and pump were started and the 100%T set on the spectrophotometer with the aqueous phase circulating through the flow cell. Increments of sample stock solution were added from the gravimetric buret to the stirred two-phase mixture and, between each increment, the equilibrium absorbance value was recorded as previously described (12). Stock solutions of the three compounds studied and maximum weights of solution added were as follows: 0.1371 mmol/g of HBz in water-washed chloroform, up to 4.0 g added; $0.212_6$ mmol/g of Naloxone in water-washed chloroform, up to 2.3 g added; and $4.62 \times 10^{-3}$ mmol/g of TEA·P in methylene chloride, whose preparation is described above, up to 3.2 g added.

Initially present in the titration beaker in each of the three studies were the following: *HBz study*, 80.0 mL of 0.10 *M* perchloric acid previously equilibrated with chloroform and $20.0_0$ mL of washed chloroform previously equilibrated with 0.1 *M* $HClO_4$. *Naloxone study*, 85.0 mL of 0.14 *M* $NH_3/NH_4Cl$ buffer pH = $8.6_8$ and $20.0_0$ mL of washed chloroform; *TEA·P study*, 70.0 mL of 0.11 *M* phosphate buffer pH = 6.7 and 30.0 mL of methylene chloride.

In the three systems under investigation the association/dissociation reaction takes place in the organic phase. It is, therefore, important to measure the absorbance of the aqueous phase rather than that of the organic since there are no side reactions taking place in the aqueous phase which would cause a change in molar absorptivity with changing sample concentration. For this reason a paper membrane is used in the filter probe. In the experiments the aqueous phase concentration of [HBz], [NAL], or [$P^-$] is calculated from the absorbance and the appropriate molar absorptivity, determined in a separate one-phase experiment. The equilibrium volumes of aqueous ($V$) and organic ($V_o$) phases in the TEA·P study were corrected for the slight mutual solubilities of methylene chloride and water (20), since neither phase was pre-equilibrated in this case. A similar correction was made for the solubility of chloroform in water in the Naloxone study since the aqueous phase was not pre-equilibrated.

## Results and discussion

*Dimerization of HBz*

In a chloroform–water system benzoic acid HBz is involved in the following equilibria:

$$[1] \quad HBz \overset{K_{HBz}}{\rightleftharpoons} (HBz)_o$$

$$[2] \quad 2(HBz)_o \overset{K_{2,HBz}}{\rightleftharpoons} (HBz)_{2,o}$$

where the subscript "o" indicates species in the organic phase, and species without subscript are in the aqueous phase. It is assumed that the aqueous phase is acidified so that ionization of HBz, which has a $pK_a$ value of 4.05 at 0.1 ionic strength (21), can be neglected. The distribution coefficient of monomeric benzoic acid is defined as:

$$[3] \quad K_{HBz} = [HBz]_o/[HBz]$$

and the dimerization constant of HBz in chloroform is,

$$[4] \quad K_{2,HBz} = [HBz]_{2,o}/[HBz]_o^2$$

The species-independent distribution ratio of benzoic acid is given by,

$$[5] \quad D_{HBz} = ([HBz]_o + 2[HBz]_{2,o})/[HBz]$$

Combining eqs. [3]–[5] gives:

$$[6] \quad D_{HBz} = K_{HBz} + 2K_{2,HBz}K_{HBz}^2[HBz]$$

which shows that a plot of $D_{HBz}$ versus [HBz] allows the determination of $K_{HBz}$ from the intercept and $K_{2,HBz}$ from the slope.

In chloroform-saturated 0.10 *M* aqueous perchloric acid the molar absorptivity is $9.51 \times 10^2$, as measured from the linear Beer's Law plot of absorbance vs. [HBz] in a one-phase system. The linearity of this plot supports the view (21–24) that no dimerization of HBz occurs in the aqueous phase.

The following, derived using the mass balance of benzoic acid, allows $D_{HBz}$ to be calculated from [HBz]:

$$[7] \quad D_{HBz} = (T_{HBz} - [HBz]V)/[HBz]V_o$$

where $V$ is the volume of the aqueous phase and is constant throughout the experiment; $V_o$ is the volume of organic phase including both the initial volume and the incremental additions of the chloro-

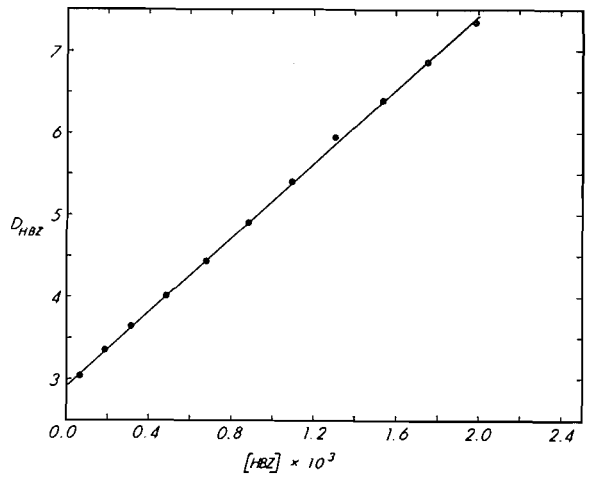


FIG. 1. Distribution ratio of benzoic acid versus concentration of benzoic acid in the aqueous phase, according to eq. [6].

form solution of benzoic acid; and $T_{HBz}$ is the total number of moles of benzoic acid added at any time. Three minutes are required per data point so that triplicate runs of ten points each are performed in under 2 h.

Figure 1 shows a typical plot of the data. Linear least-squares treatment of three such plots yields a slope of 2250 ± 24 sd and intercept of 2.90 ± 0.04 sd. From eq. [6] the constants $K_{HBz} = 2.90 \pm 0.04$ sd and $K_{2,HBz} = 133 \pm 3$ sd are calculated. Corresponding log values are log $K_{HBz} = 0.463 \pm 0.006$ sd and log $K_{2,HBz} = 2.12 \pm 0.01$ sd which may be compared with previously reported log values obtained by batch extraction between chloroform and aqueous phases: 0.50 and 2.09 using 0.1 *M* HCl at 25°C (22); 0.68 and 1.90 using water at 25°C (23); 0.55 and 1.92 using water at 15°C (24); 0.62 and 2.51 using water at 45°C (24). They may also be compared with log values of 0.54 and 1.99 obtained at 25°C by a two-phase potentiometric titration technique using 0.1 *M* NaCl as aqueous phase (21).

Van Duyne *et al.* (25) have shown that benzoic acid extracted into "wet" benzene not only dimerizes but also forms hydrates and, furthermore, that the dimer forms a hydrate. The type and extent of hydrate formation depends strongly on the water content of the organic solvent. Though benzoic acid hydrate formation has not been studied in chloroform, it is likely that similar phenomena occur in this solvent. The values of $K_{HBz}$ and $K_{2,HBz}$ measured by liquid–liquid partition, as in the present study and in the quoted literature studies, does not distinguish between hydrated and unhydrated species and, consequently, the measured constants will vary with the water content of the chloroform phase. It may be that this is, in part, responsible for the rather large range of values of log $K_{HBz}$ and log $K_{2,HBz}$ observed when aqueous phases are used that contain different types and concentrations of electrolyte, since these factors would be expected to influence the water content of the organic phase (3, 26). Differences in type and concentration of electrolyte may also produce differences in salting-out of HBz (3). Considering such possible small differences arising from the above processes, the values of 0.46 and 2.12 obtained using 0.1 *M* $HClO_4$ in the present study are in good agreement with the values of 0.50 and 2.09 obtained using 0.1 *M* HCl (22).

*"Self-ion-pair extraction"*

The synthetic phenanthrene alkaloid Naloxone is an important narcotic antagonist. It is an aminophenol compound whose protonated form is a diprotic acid of charge type $H_2A^+$. In aqueous solution the two acid-dissociation steps are:

[8] $H_2A^+ + H_2O \rightleftharpoons HA + H_3O^+$

[9] $HA + H_2O \rightleftharpoons A^- + H_3O^+$

with $K_{a,H_2A} = 7.53 \times 10^{-9}$ and $K_{a,HA} = 5.87 \times 10^{-10}$.

In a recent paper it was shown that titration of $H_2A^+$ with strong base in a chloroform–water two-phase medium yields a sharp pH-break at the first equivalence point, even when $K_{a,H_2A}$ and $K_{a,HA}$ are close (27). It was possible also to quantitatively predict the shape of the titration curve by inserting all of the independently measured equilibrium constants into the derived titration equation. Measurement of all of the relevant species-distribution coefficients was performed by batch distribution experiments. In those studies a value of 433 was obtained for the distribution coefficient of the species HA. However, because $K_{a,H_2A}$ and $K_{a,HA}$ are close to one another in value, significant concentrations of both $H_2A^+$ and $A^-$ are also present in the aqueous solution near the isoelectric point, and it is therefore possible that the organic cation $H_2A^+$ and organic anion $A^-$ might form a chloroform-extractable ion-pair viz:

[10] $H_2A^+ + A^- \rightleftharpoons (H_2A \cdot A)_o$

[11] $K_{I,H_2A \cdot A} = [H_2A \cdot A]_o/[H_2A^+][A]$

If this reaction occurs, then not only is the value quoted above for the distribution coefficient of HA in error, but also the apparent constant will change with sample concentration.

In order to determine whether the "self-ion-pair extraction" can be neglected the distribution ratio of Naloxone ($D_{NAL}$) has been studied as a function of Naloxone concentration in the aqueous phase at

Can. J. Chem. Downloaded from www.nrcresearchpress.com by 210.87.254.5 on 09/06/12
For personal use only.

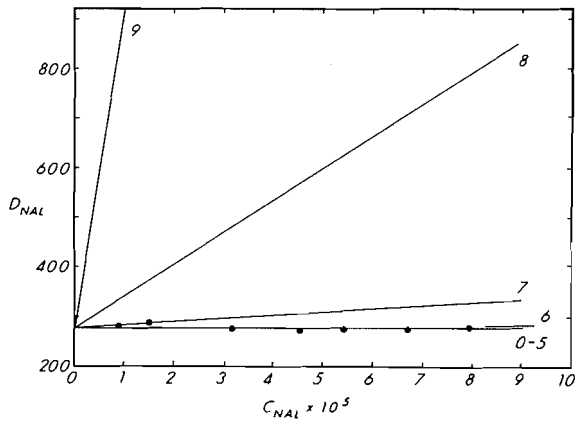


FIG. 2. Distribution ratio of Naloxone versus concentration of Naloxone in the aqueous phase, according to eq. [12]. Points are experimental. Lines are theoretical, assuming values of log $K_{I,H_2A\cdot A}$ from 0 to 9, as shown.

a pH buffered near the isoelectric point. An expression for the distribution ratio has already been derived (27).[2] Since the constants $K_{I,H_2AX}$ and $K_{I,MA}$ in that expression have values of 0.0 and 0.14 ± 0.32 they can be neglected. After inserting the known values of the other constants, the expression takes the following form at pH $8.6_8$:

$$[12] \quad D_{NAL} = k + 0.0642K_{I,H_2A\cdot A}C_{NAL}$$

where $k$ is a constant and $C_{NAL}$ is the formal (analytical) concentration of Naloxone in the aqueous phase. The slope of a plot of $D_{NAL}$ vs. $C_{NAL}$ yields the desired constant $K_{I,H_2A\cdot A}$.

$C_{NAL}$ is calculated from the measured absorbance and the molar absorptivity obtained at pH $8.6_8$ ($\varepsilon_{NAL} = 1.38 \times 10^3$). $D_{NAL}$ is calculated from $C_{NAL}$ as follows:

$$[13] \quad D_{NAL} = \frac{T_{NAL} - C_{NAL}V}{C_{NAL}V_o}$$

in which the symbols are defined as in eq. [7] above.

A plot is shown in Fig. 2. The points fall on a line (not shown) with slope $-1.3 \times 10^5 \pm 1.2 \times 10^5$ sd, which is equal to zero within experimental error. In order to identify the maximum value of $K_{I,H_2A\cdot A}$ which is consistent with the experimental data, plots are made in Fig. 2 of the curves which would be expected for values of $K_{I,H_2A\cdot A}$ of 0 through $10^9$. By comparing the experimental points with these curves it is concluded that $K_{I,H_2A\cdot A}$ is less than $10^7$. (It may, of course, be much less.) Values lower than $10^7$ are too small to produce any perceptible effect on the two-phase potentiometric titration curve of Naloxone hydrochloride (27).

[2]The factor 2 was inadvertently omitted in eq. [10] of ref. 27.

It should be noted that in this experiment the absorbance of the aqueous phase varied between zero and an upper value of 0.12. The membrane so completely excludes the organic solvent phase that the background noise in the absorbance is low enough to permit even these low absorbances to be measured with high precision.

*Ion-pair dissociation*

Dissociation of ion-pairs in the organic phase is often negligible (1, 12–15). However, the tendency toward dissociation is greater when the ions involved are less hydrophobic and when the solvent is more polar (1, 2). The dissociation of the ion-pair tetraethylammonium picrate (TEA·P) in methylene chloride is represented as follows:

$$[14] \quad (TEA\cdot P)_o \rightleftharpoons (TEA^+)_o + (P^-)_o$$

$$[15] \quad K_{diss} = [TEA^+]_o[P^-]_o/[TEA\cdot P]_o$$

The ion-pair extraction constant for TEA·P is given by:

$$[16] \quad K_I = [TEA\cdot P]_o/[TEA^+][P^-]$$

and the distribution ratio of picrate is

$$[17] \quad D_p = ([TEA\cdot P]_o + [P^-]_o)/[P^-]$$

The quantity $D_p$ can be calculated from absorbance measurements of picrate concentration in the aqueous phase using the expression:

$$[18] \quad D_p = (T_{TEA\cdot P} - [P^-]V)/[P^-]V_o$$

where the symbols are defined in eq. [7]. During the course of the experiment incremental additions are made of a methylene chloride stock solution of TEA·P. Extraction of ion-pairs such as TEA·$H_2PO_4$ or Na·P, involving components of the buffer, are expected to be negligible (1, 13), and at pH = 6.7 no picric acid extracts (15). Consequently, mass balance considerations require that $[TEA^+] = [P^-]$ and $[TEA^+]_o = [P^-]_o$. Combining these equalities with eqs. [15] through [17] gives the following expression:

$$[19] \quad D_p = (K_IK_{diss})^{1/2} + K_I[P^-]$$

which suggests that $K_I$ can be obtained from the slope and $K_{diss}$ from the intercept of a plot of $D_p$ vs. $[P^-]$.

Figure 3 shows a typical plot of eq. [19]. From linear least-squares treatment of such data $\log K_I = 2.54 \pm 0.02$ sd and $\log K_{diss} = -4.52 \pm 0.09$ sd. These values, obtained at 25°C using a pH 6.7 aqueous phase of ionic strength 0.18, may be compared with earlier reported values of 2.34 and −4.26 obtained using a pH 7.5 aqueous phase at the lower ionic strength of 0.1 and the lower tempera-

Can. J. Chem. Downloaded from www.nrcresearchpress.com by 210.87.254.5 on 09/06/12
For personal use only.

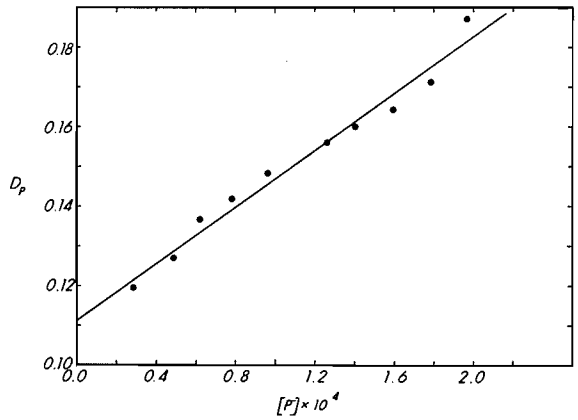


FIG. 3. Distribution ratio of picrate versus concentration of picrate in the aqueous phase, according to eq. [19].

ture of 20°C (28). The fraction of TEA·P extracted is small under all conditions in this experiment. For example, a $D_p$ of 0.15 corresponds to less than 6% of the TEA·P extracted into the organic phase. The rather large scatter in the data points in Fig. 3 is typical for this type of measurement of ion-pair dissociation constants of compounds which extract only slightly into the organic phase (see Fig. 4 in ref. 28). Its origin lies in the fact that the value of $[P^-]V$ is only slightly less than $T_{TEA\cdot P}$. The uncertainty in the numerator of eq. [18] is therefore large, since the numerator is the difference between two similar quantities.

## Conclusion

Use of the filter-probe membrane phase separator combined with a gravimetric buret provides a particularly convenient and rapid technique for measuring liquid–liquid distribution isotherms, by which a variety of association/dissociation equilibria can be studied. In this technique, calculation of distribution coefficients relies on concentration measurements made in one phase combined with the mass balance expression for the sample, as in eqs. [7], [13], and [18]. Therefore, it is important to demonstrate that interfacial adsorption of the sample is negligible, as previously described (14, 16). With especially large or surface-active organic ions adsorption may present a problem. For example, attempts to quantify dimerization of the ionic indicator Calmagite ($A^-$) by studying the distribution isotherm for the extraction of its tetraethylammonium ion-pair (TME·A) were fraught with adsorption problems. However, most of the compounds studied thus far show negligible adsorption, and the filter-probe technique may be considered to be of broad utility in solvent extraction studies.

## Acknowledgements

The authors thank Robert Evans for performing preliminary experiments and James Nolan for assistance in setting up the gravimetric buret. Naloxone free-base was kindly provided by Endo Laboratories Inc., Garden City, NY. Research support by the Natural Sciences and Engineering Research Council of Canada and the University of Alberta is also gratefully acknowledged.

1. G. SCHILL. *In* Ion exchange and solvent extraction. Vol. 6. *Edited by* J. A. Marinsky and Y. Marcus. Marcel Dekker, New York. 1974. Chapt. 1.
2. K. BEHRENDS. Z. Anal. Chem. **250**, 161 (1970).
3. T. SEKINE and Y. HASEGAWA. Solvent extraction chemistry. Marcel Dekker, New York. 1977. Chapts. 4 and 6.
4. G. ALLEN, J. G. WATKINSON, and K. H. WEBB. Spectrochim. Acta, **22**, 807 (1966).
5. Y. MARCUS and A. S. KERTES. Ion exchange and solvent extraction of metal complexes. Wiley-Interscience, Toronto. 1969. Chapts. 2, 8, and 10.
6. Y. YAMAMATO, E. SIMIMURA, K. MIYOSHI, and T. TOMINAGA. Anal. Chim. Acta, **64**, 225 (1973).
7. M. A. LODHI and E. HÖGFELDT. *In* Solvent extraction chemistry. *Edited by* D. Dyrssen, J. O. Liljenzin, and J. Rydberg. North-Holland, Amsterdam. 1967. p. 421.
8. P.-A. JOHANSSON and K. GUSTAVII. Acta Pharm. Suec. **14**, 1 (1977).
9. I. M. KORENMAN and I. A. GUREV. J. Anal. Chem. U.S.S.R. Engl. Transl., **30**, 1601 (1975).
10. C. K. SHIM, R. NISHIGAKI, T. IGA, and M. HANANO. Int. J. Pharm. **8**, 143 (1981).
11. A. LEO, C. HANSCH, and D. ELKINS. Chem. Rev. **71**, 525 (1971).
12. F. F. CANTWELL and H. Y. MOHAMMED. Anal. Chem. **51**, 218 (1979).
13. H. Y. MOHAMMED and F. F. CANTWELL. Anal. Chem. **51**, 1006 (1979).
14. H. Y. MOHAMMED and F. F. CANTWELL. Anal. Chem. **52**, 553 (1980).
15. F. F. CANTWELL and M. CARMICHAEL. Anal. Chem. In press.
16. B. KRATOCHVIL, J. NOLAN, and F. F. CANTWELL. Can. J. Chem. **59**, 2539 (1981).
17. J. F. M. KINKEL, E. TOMLINSON, and P. SMIT. Int. J. Pharm. In press.
18. W. E. HARRIS and B. KRATOCHVIL. An introduction to chemical analysis. Saunders, Phila. p. 144.
19. J. NOLAN and B. KRATOCHVIL. Private communication.
20. J. A. RIDDICK and W. B. BUNGER. Organic solvents: physical properties and methods of purification. 3rd ed. Wiley-Interscience, Toronto. 1970. pp. 348–351.
21. P.-A. JOHANSSON and K. GUSTAVII. Acta Pharm. Suec. **13**, 407 (1976).
22. R. MODIN and A. TILLY. Acta Pharm. Suec. **5**, 311 (1968).
23. H. W. SMITH and T. A. WHITE. J. Phys. Chem. **33**, 1953 (1929).
24. D. GRIFFITHS and M. DAVIES. J. Chem. Soc. 132 (1955).
25. R. VAN DUYNE, S. A. TAYLOR, S. D. CHRISTIAN, and H. E. AFFSPRUNG. J. Chem. Phys. **71**, 3427 (1967).
26. Y. MARCUS and A. S. KERTES. Ion exchange and solvent extraction of metal complexes. Wiley-Interscience, Toronto. 1969. Chapt. 9.
27. R. A. HUX, S. PUON, and F. F. CANTWELL. Anal. Chem. **52**, 2388 (1980).
28. K. GUSTAVII and G. SCHILL. Acta Pharm. Suec. **3**, 241 (1966).

Can. J. Chem. Downloaded from www.nrcresearchpress.com by 210.87.254.5 on 09/06/12
For personal use only.

# Theoretical studies of $S_N2$ transition states. Substituent effects

SAUL WOLFE AND DAVID JOHN MITCHELL
*Department of Chemistry, Queen's University, Kingston, Ont., Canada K7L 3N6*
AND
H. BERNHARD SCHLEGEL[1]
*Department of Chemistry, Wayne State University, Detroit, MI 48202, U.S.A.*

Received October 14, 1981

SAUL WOLFE, DAVID JOHN MITCHELL, and H. BERNHARD SCHLEGEL. Can. J. Chem. **60**, 1291 (1982).

Similar substituent and angular constraint effects are noted for pyramidal inversion at tricoordinate nitrogen and inversion at a carbon centre undergoing an $S_N2$ displacement reaction. The former process has been analyzed successfully by a quantitative PMO analysis which focuses on the frontier orbital interactions between X and $NH_2$ in the planar and pyramidal structures of X—$NH_2$ molecules having X = F, $CH_3$, CHO. Based on total energy calculations at the 6-311G*//4-31G level, the effects of X upon the rates of the gas phase $S_N2$ reactions $F^- + XCH_2F \rightarrow XCH_2F + F^-$ are found to be CHO ≫ H > F > $CH_3$ > OH. Taking the treatment of nitrogen inversion as a precedent, the origin of this trend has been examined by a quantitative PMO analysis which focuses on the frontier orbital interactions between X and $CH_2F_2^-$ in the transition states, and between X and $CH_2F$ in the reactants. This has revealed that the rate enhancement associated with an α-carbonyl substituent in these $S_N2$ reactions can be related to the presence of a stabilizing orbital interaction of a new type in the transition state, coupled to an exceptionally low destabilizing orbital interaction.

SAUL WOLFE, DAVID JOHN MITCHELL et H. BERNHARD SCHLEGEL. Can. J. Chem. **60**, 1291 (1982).

On note des effets de substitutants et des effets de contrainte angulaire similaire dans le cas de l'inversion pyramidale au niveau de l'azote tricoordonné et dans le cas de l'inversion au niveau du centre carboné subissant la réaction de déplacement $S_N2$. On a analysé avec succès le premier processus en faisant appel à l'analyse quantitative des OMP qui porte sur les interactions d'orbitales frontières entre X et $NH_2$ dans les structures planes et pyramidales des molécules de X—$NH_2$ où X = F, $CH_3$, CHO. En se basant sur les calculs d'énergie totale au niveau 6-311G*//4-31G, on a trouvé que les effets de X, sur les vitesses des réactions $S_N2$ en phase gaseuze, sont dans l'ordre suivant: CHO ≫ H > F > $CH_3$ > OH. En considérant le traitement de l'azote comme un précédent, on a étudié l'origine de cette tendance par l'analyse quantitative de OMP qui porte sur les interactions d'orbitales frontières entre X et $CH_2F_2^-$ dans les états de transition et entre X et $CH_2F$ dans les réactifs. Cette étude révèle que le taux d'augmentation, associée au substituant en position α du carbonyle dans ces réactions $S_N2$, peut être relié à la présence d'interactions d'orbitales stabilisantes d'un nouveau type dans l'état de transition, qui s'ajoutent à une interaction d'orbitale déstabilisante exceptionnellement faible.
[Traduit par le journal]

The deformation of a carbon atom from tetrahedral to trigonal–bipyramidal geometry makes a significant contribution to the energy barrier associated with an $S_N2$ displacement reaction (1). There is some analogy between such geometrical effects at an initially tetracoordinate centre and the geometrical changes associated with pyramidal inversion at a tricoordinate centre. It is, therefore, not surprising that the two seemingly different processes exhibit rather similar substituent and angular constraint effects. For example, α-halogen or α-alkyl substituents cause an increase in the barrier to pyramidal inversion at nitrogen (2), and a decrease in $S_N2$ reactivity at carbon (3, 4). Conversely, an α-carbonyl substituent causes a substantial decrease in the pyramidal inversion barrier (5), and a substantial increase in $S_N2$ reactivity (4, 6).

Table 1 compares $\Delta G^{\neq}$ for pyramidal inversion at nitrogen in a series of cyclic amines (2) with the $S_N2$ reactivities of the corresponding series of bromocycloalkanes upon reaction with lithium iodide in acetone solvent (4). The same trends with ring size (i.e., angular constraint) are observed in both cases.

TABLE 1. Effect of ring size upon pyramidal inversion at nitrogen in cyclic amines and upon $S_N2$ reactivities of bromocycloalkanes

| Ring size | Nitrogen inversion[a] | $S_N2$ reactivity[c] |
|---|---|---|
| 3 | 23.8[b] | <0.0001[d] |
| 4 | 13.4 | 0.0075 |
| 5 | 10.3 | 1.6 |
| 6 | 13.7 | 0.010 |
| 7 | 9.0 | 0.98 |

[a]Data from ref. 2.
[b]Refers to $\Delta G^{\neq}$ in kcal/mol.
[c]Data from ref. 4.
[d]Relative rates for reaction with lithium iodide in acetone at 25°C ($Me_2CHBr$ = 1.00).

These observations suggested that the effects of substituents upon $S_N2$ displacement reactions might be rationalized by an appeal to interpretations that have been proposed (7) to account for substituent effects upon pyramidal inversion barriers. One such interpretation is based on the perturbational molecular orbital (PMO) approach, and focuses (8)

[1]Fellow of the Alfred P. Sloan Foundation, 1981–1983.

0008-4042/82/111291-04$01.00/0
©1982 National Research Council of Canada/Conseil national de recherches du Canada

Can. J. Chem. Downloaded from www.nrcresearchpress.com by 210.87.254.105 on 09/06/12
For personal use only.

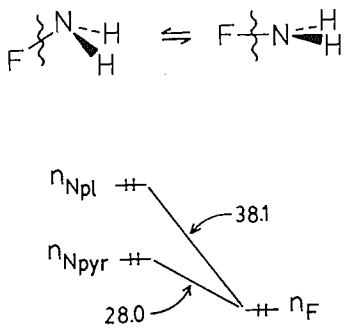


FIG. 1. Frontier orbital interaction between $n_F$, a fluorine lone pair and $n_{N_{pyr}}$ or $n_{N_{pl}}$, the nitrogen lone pairs of the pyramidal and planar forms, respectively, of F—$NH_2$. The numbers shown refer to the magnitude of this interaction in kcal/mol based on 4-31G level computations on the fully optimized pyramidal and planar structures. See ref. 9, eq. [64], and ref. 10.

on the frontier orbital interactions both in the pyramidal ground state and in the planar transition state for the inversion process. The application of this procedure to pyramidal inversion in fluoramine is illustrated in Fig. 1. Replacement of one hydrogen of ammonia by fluorine introduces a two-orbital, four-electron destabilizing interaction between the nitrogen lone pair and a fluorine lone pair. The geometrical change affects principally the orbital energy and overlap associated with the nitrogen lone pair, and leads to a 10.1 kcal/mol difference between the destabilizing interactions in the two structures. This difference compares favorably with the 9.4 kcal/mol difference between the computed pyramidal inversion barriers of ammonia (0.4 kcal/mol) and fluoramine (9.8 kcal/mol).

Although the 4-31G basis set employed to obtain these data is known (11) to be deficient for the quantitative calculation of specific inversion barriers, it should be adequate for the determination of trends associated with substituents. Table 2 summarizes the total energy changes and PMO interaction energy changes associated with $NH_2$ bending in fluoramine, methylamine, and formamide, and appears to validate a frontier orbital analysis of substituent effects upon pyramidal inversion barriers.

For the $S_N2$ displacement reaction $F^- + XCH_2F \rightleftarrows XCH_2F + F^-$, the corresponding frontier orbital analysis refers to the fragmentation $X\cdots CH_2F$ in the reactant, and $X\cdots CH_2F_2^-$ in the transition state. For several reasons the problem is simplified considerably by restriction to a thermoneutral or degenerate process: (*i*) the rates of gas phase $S_N2$ reactions and the geometries of the transition states depend upon the heat of reaction (12, 13); (*ii*) for a degenerate reaction, trends in substituent effects are revealed by a comparison between the energies

TABLE 2. Calculated total energy differences[a] ($\Delta E_T$) and PMO interaction energies[a] ($\Delta E_{PMO}$) associated with $NH_2$ bending in $NH_2X$ molecules

| X | PMO interaction energy[b] | | | $\Delta E_{PMO}$ | $\Delta E_T$[c] |
|---|---|---|---|---|---|
| F | Pyramidal | $n_N-n_F$ | 28.0 | | |
| | | | | 10.1 | 9.4 |
| | Planar | $n_N-n_F$ | 38.1 | | |
| $CH_3$ | Pyramidal | $n_N-\pi_{CH_3}$ | 39.4 | | |
| | | $n_N-\pi_{CH_3}^*$ | −1.8 | | |
| | | | | 4.7 | 1.1 |
| | Planar | $n_N-\pi_{CH_3}$ | 44.4 | | |
| | | $n_N-\pi_{CH_3}^*$ | −2.1 | | |
| CHO | Pyramidal[d] | $n_N-\pi_{CO}$ | 37.8 | | |
| | | $n_N-\pi_{CO}^*$ | −23.1 | | |
| | | | | −1.6 | −4.0 |
| | Planar | $n_N-\pi_{CO}$ | 38.9 | | |
| | | $n_N-\pi_{CO}^*$ | −25.8 | | |

[a]In kcal/mol.
[b]Calculated by the procedure of refs. 9 and 10.
[c]At the fully optimized 4-31G geometries.
[d]The $NH_2$ group was constrained to the geometry of pyramidal $CH_3NH_2$. All other parameters retained the values found for planar formamide.

TABLE 3. Calculated energy difference between $F^-$ + $XCH_2F$ and $XCH_2F_2^-$ transition structures (6-311G*//4-31G)

| X | $\Delta E_{F,F}$[a,b] |
|---|---|
| H | −3.3[c] |
| F | −2.1[c] |
| OH | +1.0[d] |
| $CH_3$ | −1.9[c] |
| CHO | −17.4[c,e] |

[a]In kcal/mol.
[b]See Fig. 1 of ref. 13.
[c]The transition state lies below the reactants.
[d]The transition state lies above the reactants.
[e]The 6-311G* computation of $HCOCH_2F_2^-$ was performed by J. M. Lefour, Orsay, France, whose assistance is gratefully acknowledged.

of the separated reactants and the transition state (13); (*iii*) the principal effect of a transfer of gas phase data to solution is associated with the different heats of solvation of the entering and leaving groups (14). Restriction to a thermoneutral process should, therefore, allow comparison between the calculated trends and experimental data in solution (4). Unfortunately, direct comparison with experimental gas phase results is not possible, because the latter are complicated by competing reaction channels.[2]

Figure 2 shows the C—F bond lengths (Å) and FCX bond angles (deg) in the series of transition states $XCH_2F_2^-$, in which X = H, F, OH, $CH_3$,

[2]Personal communications from Professors J. I. Brauman and W. E. Farneth.

Can. J. Chem. Downloaded from www.nrcresearchpress.com by 210.87.254.105 on 09/06/12
For personal use only.

Can. J. Chem. Downloaded from www.nrcresearchpress.com by 210.87.254.105 on 09/06/12
For personal use only.

TABLE 4. PMO analyses of $X\cdots CH_2F_2^-$ and $X\cdots CH_2F$ (9, 10)

| System | X | Interacting orbital on X | Interaction energy[a,b] A | B | C | Total |
|---|---|---|---|---|---|---|
| $XCH_2F_2^-$ | F | $n_F$ | 17.0 | −7.1 | 3.6 | 13.5 |
| | OH | $n_O$ | 23.4 | −11.0 | 3.5 | 15.9 |
| | $CH_3$ | $\pi_{CH_3}$ | 13.3 | −0.4 | 5.7 | 18.1 |
| | | $\pi_{CH_3}^*$ | −0.5 | | −0.0 | |
| | CHO | $\pi_{CO}$ | 8.4 | −0.0 | 6.3 | 5.4 |
| | | $\pi_{CO}^*$ | −1.8 | | −7.5 | |

| System | X | Interacting orbital on X | Interaction energy $\sigma_{CF}$ | $\sigma_{CF}^*$ | $n_F$ | Total |
|---|---|---|---|---|---|---|
| $XCH_2F$[c] | F | $n_F$ | 14.6 | −5.0 | 0.0 | 9.6 |
| | OH | $n_O$ | 20.9 | −6.1 | 0.0 | 14.8 |
| | $CH_3$ | $\pi_{CH_3}$ | 11.2 | −0.5 | 0.1 | 10.4 |
| | | $\pi_{CH_3}^*$ | −0.3 | | −0.1 | |
| | CHO | $\pi_{CO}$ | 7.8 | −0.0 | 0.1 | 6.3 |
| | | $\pi_{CO}^*$ | −1.3 | | −0.3 | |

[a]In kcal/mol.
[b]4-31G computations.
[c]At the conformation in which the interacting orbital of X lies in the symmetry plane of $CH_2F$.

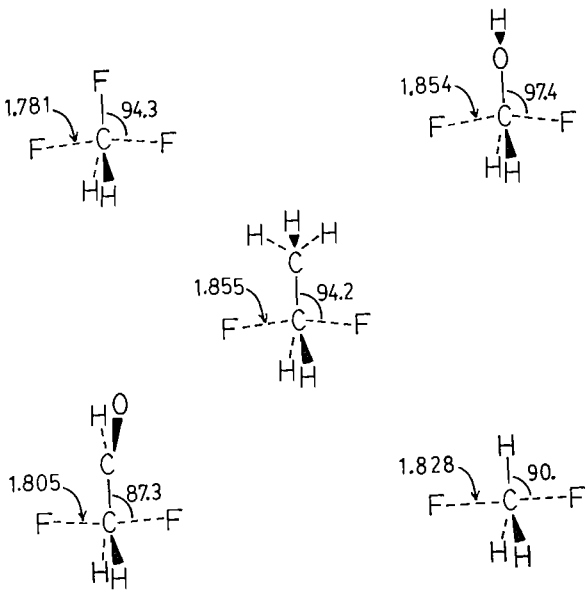


FIG. 2. The C—F bond lengths (Å) and FCX bond angles (deg) in the series of transition states $XCH_2F_2^-$ in which X = H, F, OH, $CH_3$, and CHO. These data are taken from the fully optimized structures at 4-31G.

CHO, from the fully optimized 4-31G level wavefunctions. The total energy data summarized in Table 3 were obtained at the 6-311G* level (15) using the 4-31G geometries of the reactants and transition states. Based on these data, the effects of these substituents on $S_N2$ reactivity at carbon are CHO ≫ H > F > $CH_3$ > OH. The position of the α-oxygen substituent in this sequence strongly suggests that the rate enhancement observed for this substituent in solution (4) is associated with an $S_N1$ process (16). The rate-enhancing effect of an α-carbonyl substituent and rate-retarding effects of α-fluoro and α-methyl substituents are reproduced by the calculations.

For the fragmentation $X\cdots CH_2F_2^-$ in the transition states, the orbital interactions forming the HOMOs were found to be **A**, **B**, and **C**; interactions possibly corresponding to **A** or **B** have often been proposed in the literature (4, 17) to account for the α-carbonyl rate enhancement, but without specification of their stabilizing or destabilizing nature. Interaction **C** has not been considered previously.

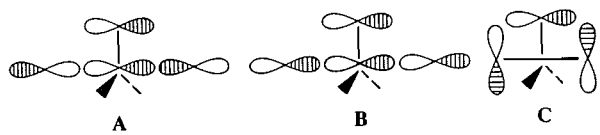


Table 4 summarizes the PMO results and allows the following *qualitative* interpretation of the trends in substituent effects: (*1*) with X = F or OH, interactions **A** and **C** are entirely destabilizing and **B** is stabilizing; (*2*) the availability of acceptor orbitals on $CH_3$ and CHO introduces a stabilizing contribution to **A** and **C**; (*3*) the difference between CHO and F, OH, or $CH_3$ is the result of a small destabilizing interaction of type **A** coupled with a large stabilizing interaction of type **C**; (*4*) correction of the transition state PMOs for the $X\cdots CH_2F$ orbital interactions in the reactants places α-carbonyl more reactive than α-hydrogen, as observed in the total energy calculations.

## Acknowledgements

This research has been supported by grants from the Natural Sciences and Engineering Research Council of Canada and the Petroleum Research Fund, administered by the American Chemical Society. The authors gratefully thank the Advisory Research Committee of Queen's University and Wayne State University for generous allocation of computing funds.

1. S. NAGASE and K. MOROKUMA. J. Am. Chem. Soc. **100**, 1666 (1978).
2. J. B. LAMBERT. Top. Stereochem. **6**, 19 (1971).
3. J. HINE, C. H. THOMAS, and S. J. EHRENSON. J. Am. Chem. Soc. **77**, 3886 (1955).
4. A. STREITWIESER, JR. Chem. Rev. **56**, 571 (1956).
5. N. R. CARLSEN, L. RADOM, N. V. RIGGS, and W. R. RODWELL. J. Am. Chem. Soc. **101**, 2233 (1979).
6. (*a*) J. B. CONANT, W. R. KIRNER, and R. E. HUSSEY. J. Am. Chem. Soc. **47**, 488 (1925); (*b*) F. G. BORDWELL and W. T. BRANNEN, JR. J. Am. Chem. Soc. **86**, 4645 (1964), and references therein; (*c*) J. W. THORPE and J. WARKENTIN. Can. J. Chem. **51**, 927 (1973); (*d*) A. HALVORSEN and J. SONGSTAD. J. Chem. Soc. Chem. Commun. 327 (1978).
7. C. C. LEVIN. J. Am. Chem. Soc. **97**, 5649 (1975); W. CHERRY and N. D. EPIOTIS. J. Am. Chem. Soc. **98**, 1135 (1976).
8. A. H. COWLEY, D. J. MITCHELL, M.-H. WHANGBO, and S. WOLFE. J. Am. Chem. Soc. **101**, 5224 (1979).
9. M.-H. WHANGBO, H. B. SCHLEGEL, and S. WOLFE. J. Am. Chem. Soc. **99**, 1296 (1977).
10. D. KOST, H. B. SCHLEGEL, D. J. MITCHELL, and S. WOLFE. Can. J. Chem. **57**, 729 (1979).
11. W. A. LATHAN, W. J. HEHRE, L. A. CURTISS, and J. A. POPLE. J. Am. Chem. Soc. **93**, 6377 (1971); J. P. COLPA, H. B. SCHLEGEL, and S. WOLFE. Can. J. Chem. **54**, 526 (1976).
12. S. WOLFE, D. J. MITCHELL, and H. B. SCHLEGEL. J. Am. Chem. Soc. **103**, 7692 (1981).
13. S. WOLFE, D. J. MITCHELL, and H. B. SCHLEGEL. J. Am. Chem. Soc. **103**, 7694 (1981).
14. D. K. BOHME and G. I. MACKAY. J. Am. Chem. Soc. **103**, 978 (1981), and references therein.
15. R. KRISHNAN, J. S. BINKLEY, R. SEEGER, and J. A. POPLE. J. Chem. Phys. **72**, 650 (1980).
16. J. HINE and R. J. ROSSUP. J. Am. Chem. Soc. **82**, 6115 (1960).
17. T. H. LOWRY and K. S. RICHARDSON. *In* Mechanism and theory in organic chemistry. 2nd ed. Harper and Row, New York. 1981. p. 347.

Can. J. Chem. Downloaded from www.nrcresearchpress.com by 210.87.254.105 on 09/06/12
For personal use only.

# Interprétation par la méthode CNDO/S des spectres ultra-violets d'hétérocycles azotes et soufres comportant une double liaison

DANIELLE BOUIN-ROUBAUD, JACKY KISTER, THIERRY AVIGNON ET LUC BOUSCASSE

*Laboratoire de Chimie Organique A, Faculté des Sciences et Techniques de Saint-Jérome, Rue Henri Poincaré, 13397 Marseille, Cedex 13, France*

Reçu le 25 novembre 1981

DANIELLE BOUIN-ROUBAUD, JACKY KISTER, THIERRY AVIGNON et LUC BOUSCASSE. Can. J. Chem. **60**, 1295 (1982).

La détermination des spectres ultra-violets par la méthode CNDO/S a permis l'attribution des transitions électroniques expérimentales. Les transitions caractéristiques sont de type $\pi \rightarrow \pi^*$ pour toutes les molécules de type **1**, **2**, **3** et **4** étudiées.

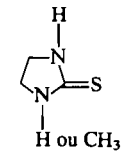


**1 ou 1'**

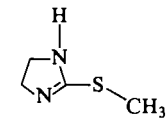


**2**

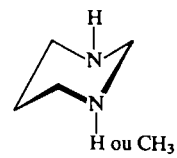


**3 ou 3'**

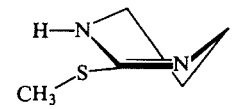


**4**

DANIELLE BOUIN-ROUBAUD, JACKY KISTER, THIERRY AVIGNON, and LUC BOUSCASSE. Can. J. Chem. **60**, 1295 (1982).

The use of CNDO/S calculations for the determination of ultra-violet spectra allowed the attribution of the experimental $\pi \rightarrow \pi^*$ transitions for the systems **1**, **2**, **3**, and **4**.

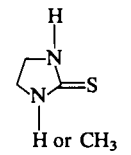


**1 or 1'**

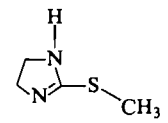


**2**

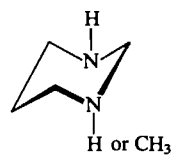


**3 or 3'**

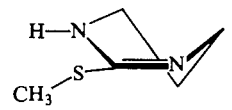


**4**

## Introduction

Le but de cette note est d'interpréter par un calcul théorique les spectres de l'imidazolidinethione-2, de l'héxahydropyrimidinethione-2 et de leurs dérivés *N*-méthylés (molécules **1**, **3**, **1'** et **3'**) ainsi que de la méthylthio-2 Δ-2 imidazoline et de la méthylthio-2 Δ-2 tétrahydropyrimidine (molécules **2** et **4**).

Le calcul des spectres a été fait par la méthode CNDO/S (1, 2) en introduisant des orbitales *d* du soufre qui sont traitées selon le procédé de Schulte et Schweig (3) dans les conditions identiques à celles employées pour les molécules conjuguées que nous avons étudiées précédemment (4, 5).

La géométrie des molécules est celle adoptée dans un travail précédent (6). Elle est donnée en annexe. Les cycles à 5 chainons sont plans, les cycles à 6 chainons ont une forme dérivée du

0008-4042/82/111295-03$01.00/0

©1982 National Research Council of Canada/Conseil national de recherches du Canada

Can. J. Chem. Downloaded from www.nrcresearchpress.com by 210.87.254.6 on 09/06/12
For personal use only.

Can. J. Chem. Downloaded from www.nrcresearchpress.com by 210.87.254.6 on 09/06/12
For personal use only.



cyclohexane pour la molécule **3** et du cyclohexène pour la molécule **4**. Les atomes en α des doubles liaisons sont tous maintenus dans le même plan.

## Discussion des résultats

Les résultats sont donnés dans le tableau 1. Ils peuvent y être comparés aux valeurs des transitions expérimentales obtenues précédemment (7, 8) dans l'éthanol. Ils montrent que la seule transition qui a pu être observée expérimentalement est de type $\pi \rightarrow \pi^*$.

Pour les thiones le schéma 1 montre que la configuration intervenant principalement dans cette transition correspond à une orbitale virtuelle fortement localisée sur la double liaison C=S. Ce résultat est identique à celui observé pour la Δ-4 imidazolinethione-2 (4), molécule différant de la molécule **1** par une double liaison supplémentaire entre les deux carbones. Par contre l'orbitale moléculaire occupée correspondante se trouve plus délocalisée dans la Δ-4 imidazolinethione-2 que dans les thiones étudiées ici. Cette orbitale correspond donc à une énergie plus élevée pour ces dernières molécules et cela se traduit par un effet hypsochrome quand l'insaturation diminue. Le calcul CNDO/S rend compte de cet effet en le surestimant, la valeur calculée passant de 270,5 nm pour la Δ-4 imidazolinethione-2 (4) à 234,6 pour **1** alors qu'expérimentalement elle passe dans l'éthanol de 259 à 240 nm. Ceci s'observe pour les thiols correspondants avec une surestimation négligeable, le calcul théorique donnant 252,9 nm pour le méthylthio-2 imidazole (4) et 223,6 nm pour la molécule **2**. Expérimentalement on passe de 250,5 nm à 224 nm dans l'éthanol.

Toutefois on observe dans le cas de la plus insaturée de ces deux molécules que le carré des coefficients de la configuration principale intervenant dans le calcul de la transition est de 0,60 et que les orbitales définissant cette configuration

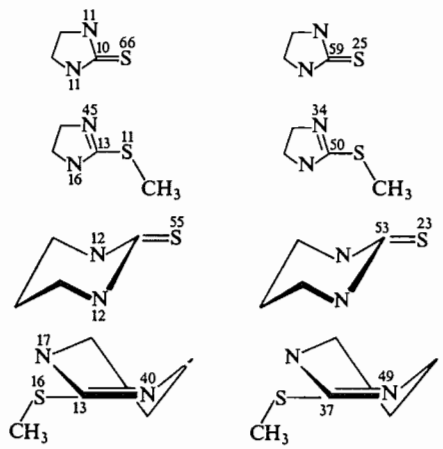

SCHÉMA 1

TABLEAU 1

| Nature de la transition | Molécule **1** | | Molécule **1'** | | Molécule **2** | | Molécule **3** | | Molécule **3'** | | Molécule **4** | |
|---|---|---|---|---|---|---|---|---|---|---|---|---|
| | Théor. | Exp. | Théor. | Exp. | Théor. | Exp. | Théor. | Exp. | Théor. | Exp. | Théor. | Exp. |
| $n \rightarrow \pi^*$ | 476,7[a] | | 481,6 | | 291,4 | | 490,9 | | 514,0 | | 301,3 | |
| | 0,0000 | | 0,0000 | | 0,0000 | | 0,0000 | | 0,0000 | | 0,00504 | |
| $\pi \rightarrow \pi^*$ | 234,6 | 240 | 236,4 | 240 | 223,6 | 224 | 242,5 | 244,5 | 244,9 | 244,8 | 200,0 | 225 |
| | 0,5199 | 4,215 | 0,5145 | 4,230 | 0,4621 | 3,734 | 0,4169 | 4,032 | 0,3997 | 4,125 | 0,3511 | 3,748 |
| $n \rightarrow \sigma^*$ | 201,2 | | 202,5 | | | | | | | | | |
| | 0,0000 | | 0,0030 | | | | | | | | | |
| $\pi \rightarrow \pi^*$ | 195,0 | | 201,8 | | 195,0 | | 201,8 | | 204,9 | | 190,4 | |
| | 0,1354 | | 0,1541 | | 0,0837 | | 0,0162 | | 0,0966 | | 0,0727 | |

[a]Le premier nombre correspond à la longueur d'onde de transition en nanomètres, le second à la force oscillatrice pour la valeur théorique et à log ε pour la valeur expérimentale obtenue en utilisant l'éthanol comme solvant.

sont toutes deux très délocalisées (4). Par contre pour la molécule **2** le carré du coefficient de la configuration principale est de 0,92, les orbitales étant plus localisées, surtout l'orbitale virtuelle comme le montre le schéma 1.

L'agrandissement du cycle correspond pour les thiones à un effet bathochrome expérimental de 4,5 nm surestimé de 3,4 nm par le calcul comme on peut le voir en comparant dans le tableau 1 les valeurs relatives aux molécules **1** et **3**.

Entre les molécules **2** et **4** le très léger effet bathochrome observé n'est pas traduit par le calcul.

L'effet hypsochrome observé expérimentalement entre les molécules **1**′ et **2** d'une part et **3**′ et **4** d'autre part, c'est à dire quand on passe d'une forme thione à une forme thiol, est traduit correctement par le calcul, qui donne les valeurs respectives de 240 et 224 nm pour **1**′ et **2** et de 244,8 et 225 nm pour **3**′ et **4**. On peut remarquer que cela s'observait pour les molécules plus insaturées (4).

De même le schéma 1 permet d'expliquer l'effet bathochrome observé (7, 8) quand on passe de l'éthanol au chlorure de méthylène, c'est à dire d'un solvant protique à un solvant aprotique, le site de protonation étant plus chargé négativement à l'état fondamental qu'à l'état excité.


1. J. Del Bene et H. H. Jaffe. J. Chem. Phys. **48**, 1807 (1968).
2. M. Rajzmann et P. Francois. QCPE no 382 (1979).
3. Y. W. Schulte et A. Schweig. Theor. Chim. Acta, **33**, 19 (1974).
4. D. Bouin-Roubaud, J. Kister, M. Rajzmann et L. Bouscasse. Can. J. Chem. **59**, 2883 (1981).
5. D. Bouin-Roubaud, J. Kister, L. Bouscasse et J. Metzger. Spectrosc. Lett. **14**, 431 (1981).
6. D. Bouin-Roubaud. Thèse Sciences, Marseille (1980).
7. G. Assef, D. Bouin-Roubaud, J. Kister et J. Metzger. C. R. Acad. Sci. Ser. C, **282**, 485 (1976).
8. D. Bouin-Roubaud, J. Kister, G. Assef et J. Metzger. C. R. Acad. Sci. Ser. C, **286**, 521 (1978).


## Annexe

Géométrie des molécules **1**, **2**, **3** et **4**

| Nature de la transition | Carré du coefficient de la configuration principale | Orbitale moléculaire occupée | Orbitale moléculaire virtuelle |
|---|---|---|---|
| $\pi \rightarrow \pi^*$ 234,6 nm | 0,88 | 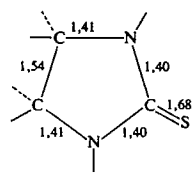 | 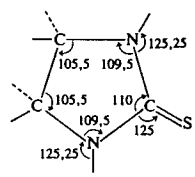 |
| | | | **1** |
| $\pi \rightarrow \pi^*$ 223,6 nm | 0,92 | 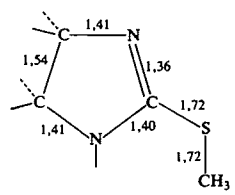 | 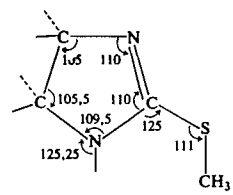 |
| | | | **2** |
| $\pi \rightarrow \pi^*$ 242,5 nm | 0,85 | 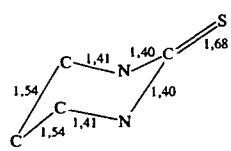 | 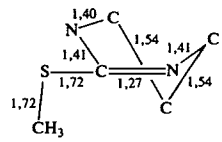 |
| $\pi \rightarrow \pi^*$ 200 nm | 0,88 | 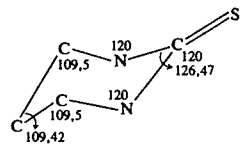 | 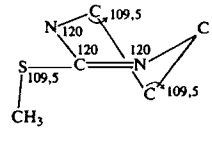 |
| | | **3** | **4** |

Les nombres attenant aux schémas des molécules sont les carrés des coefficients des orbitales atomiques intervenant dans l'orbitale moléculaire multipliés par $10^2$

Can. J. Chem. Downloaded from www.nrcresearchpress.com by 210.87.254.6 on 09/06/12
For personal use only.

# Hydrolysis of the thorium(IV) ion in sodium nitrate medium

NIKOLA B. MILIĆ[1]

*Faculty of Science, Svetozar Marković University, 34000 Kragujevac, Yugoslavia*

AND

TEREZIJA M. ŠURANJI

*Faculty of Science, The University, 21000 Novi Sad, Yugoslavia*

Received June 30, 1981

NIKOLA B. MILIĆ and TEREZIJA M. ŠURANJI. Can. J. Chem. **60**, 1298 (1982).

The hydrolysis of the thorium(IV) ion in sodium nitrate medium was studied by the emf method at 25°C. The data show that the extent of the thorium hydrolysis depends both on the concentration of thorium and the sodium nitrate medium. Thus, at a definite pH, the extent of the hydrolysis of thorium increases with increasing its concentration, but decreases with increasing concentration and the hydration energy of the medium ions. The stability constants of complexes $Th_2(OH)_2^{6+}$, $Th_3(OH)_5^{7+}$, and $Th_6(OH)_{15}^{9+}$ also slightly differ going from one concentration of sodium nitrate to another. The observed effect of the medium is in agreement with the linear free energy relationship proposed for the metal ion hydrolysis.

NIKOLA B. MILIĆ et TEREZIJA M. ŠURANJI. Can. J. Chem. **60**, 1298 (1982).

Utilisant la méthode de la fem à 25°C, on a étudié l'hydrolyse de l'ion thorium(IV) dans un milieu de nitrate de sodium. Les données révèlent que le taux d'hydrolyse du thorium dépend à la fois de la concentration en thorium et de la concentration en nitrate de sodium. Ainsi, à un pH défini le taux d'hydrolyse du thorium augmente avec sa concentration; toutefois il diminue lorsqu'on augmente la concentration et l'énergie d'hydratation des ions du milieu. Les constantes de stabilité des complexes du type $Th_2(OH)_2^{6+}$, $Th_3(OH)_5^{7+}$ et $Th_6(OH)_{15}^{9+}$ diffèrent légerement d'une concentration en nitrate de sodium à une autre. L'effet observé pour le mileu est en accord avec la relation linéaire d'énergie libre proposée pour l'hydrolyse de l'ion métallique.

[Traduit par le journal]

## Introduction

Hydrolysis of the thorium(IV) ion has been studied in various ionic media (1). The data indicate that the principal hydrolytic complex of thorium is $Th_2(OH)_2^{6+}$. The composition of the other complexes differs slightly in dependence on the concentration of thorium, the pH range, and the ionic medium. Values of the stability constants of the same complexes formed in various ionic media are also different, indicating the effect of the medium. In our previous work (2, 3), it was observed that this effect depends on concentration, $c$, the hydration energy, $E_h$, and charge, $z$, of the ions of the medium. Correlating these parameters and the hydrolysis extent, the medium factor, $F_{(m)}$,

$$[1] \quad F_{(m)} = c_{(a)}E_{h(a)}z_{(a)} + c_{(c)}E_{h(c)}/z_{(c)}$$

and the linear free energy relationship

$$[2] \quad \log K_{M(w)} - \log K_{M(m)} = nF_{(m)}$$

have been established. In eq. [1] the subscripts (c) and (a) denote cations and anions of the medium. In eq. [2] $K_{M(w)}$ and $K_{M(m)}$ denote equilibrium constants of the metal-ion hydrolysis in pure water and in an ionic medium, respectively. The medium factor, $F_{(m)}$, is characteristic of the medium concerning interaction of its ions with water molecules, whereas constant $n$ is determined by the reaction of the metal ions with anions of the medium. Since there are no available hydrolysis data for diluted media, a possible deviation from linearity in this range might require introduction of some correction of the parameters in the expression for the medium factor. In spite of that, this kind of quantitative examination should lead to evaluation of the contribution of each parameter of the medium to the total medium effect, and consequently to a better understanding of the complicated interactions in water solutions.

In order to get some information on the particular contribution of concentration and the hydration energy of the cations of the nitrate medium to the total medium effect, as well as to check the established relationship, in this work hydrolysis of the thorium(IV) ion has been studied in various concentrations of the sodium nitrate medium.

## Experimental

*Reagents and analysis*

All chemicals were of reagent grade. In addition, thorium and sodium nitrate were purified by double recrystallization. To prevent initial hydrolysis of the thorium(IV) ion in the stock solution, a small amount of nitric acid was added. Its free concentration was determined potentiometrically using a Gran plot (4). The thorium content was determined by precipitation with oxalic acid and ammonia. The precipitates were ignited at 1000°C, and weighted as $ThO_2$. Both methods gave the same results to within ±0.18%.

[1]To whom all correspondence should be addressed.

0008-4042/82/111298-06$01.00/0

©1982 National Research Council of Canada/Conseil national de recherches du Canada

Can. J. Chem. Downloaded from www.nrcresearchpress.com by 210.87.254.6 on 09/06/12
For personal use only.

Can. J. Chem. Downloaded from www.nrcresearchpress.com by 210.87.254.6 on 09/06/12
For personal use only.

The sodium nitrate content was determined by evaporating a known volume of solution to dryness at 150°C (5), as well as transforming nitrate to chloride, which was then heated at 600°C to constant weight (6). Both methods gave the same results to within ±0.26%.

Sodium hydroxide, nitric acid, and sodium hydrogen carbonate solutions were standardized by a procedure described elsewhere (7). At these standardizations the equivalence point was determined potentiometrically using a Gran plot. Purification of nitrogen gas for stirring and providing an inert atmosphere was also described in ref. 7.

*Apparatus and procedure*

All emf measurements were carried out as potentiometric titrations with a glass electrode and Ag,AgCl electrode at 25.0 ± 0.2°C (7). Titrations of various concentrations of thorium (2.5, 5.0, 10, 25, 50, and 100 m*M* $Th^{4+}$) in a constant concentration of the sodium nitrate medium (3.0 *M* $(Na)NO_3$),[2] as well as titrations of the constant concentration of the thorium(IV) ion (10 m*M* $Th^{4+}$) in various concentrations of the medium (0.5, 1.0, 1.5, 2.0, 2.5, and 3.0 *M* $(Na)NO_3$) were carried out by adding the sodium hydrogen carbonate solution from one buret and the thorium solution of a twice higher concentration in the same portions from the other buret. All solutions were prepared in corresponding concentrations of sodium nitrate. In this way, the total concentration of thorium (*B*) and the total concentration of nitrate ions were kept constant, while the analytical excess of $H^+$ (denoted as *H*) was decreased, so that it became negative during the course of the titration. The concentration of the free $H^+$ (denoted as *h*) at each point was calculated by the Nernst formula

$$[3] \quad E = E_0 + E_j + 59.16 \log h$$

where *E* is the measured potential, $E_0$ a constant which includes the standard potential of the glass electrode, and $E_j$ the liquid junction potential. The potential was measured after each new addition of the solution from burets, until a constant value was reached. Determination of $E_0$ and $E_j$ has already been described (7). The emf was measured with a Beckman Digital pH meter, Model 4500, or Radiometer pH meter, M-52 b.

## Results and discussion

The emf data of the hydrolysis of 2.5, 5.0, 10, 25, 50, and 100 m*M* $Th^{4+}$ in 3.0 *M* $(Na)NO_3$ medium are represented in Fig. 1, as the dependence of the hydroxide number of thorium on the concentration of the free hydrogen ions, *h*. The hydroxide number of thorium, $Z_{Th}$ (the average number of $OH^-$ ions bonded per thorium), was calculated from the analytical excess of hydrogen ions, *H*, the measured concentration of the free hydrogen ions, *h*, and the total concentration of the thorium(IV) ions, *B*, according to the expression $Z_{Th} = (h - H)/B$. The data obtained show that the thorium(IV) ion hydrolyzes between pH 1.5 and 3.5 depending upon its concentration. Thus, as the thorium concentration increases the beginning of the hydrolysis is shifted to lower pH values. In order to check the reversibility of the hydrolytic process in some experiments (Fig. 1, full symbols) after a certain value of hydroxide number was reached ($Z_{Th}$ = 0.35–0.40), the direction of titration was changed by adding nitric acid instead of sodium hydrogen carbonate, to a solution with negative value of *H*. Good agreement between forward and back titrations indicates reversibility of the hydrolytic reaction under the conditions studied.[3]

The emf data of the hydrolysis of 10 m*M* $Th^{4+}$ in 0.5, 1.0, 1.5, 2.0, 2.5, and 3.0 *M* $(Na)NO_3$ media are represented in Fig. 2, also as a dependence of the hydroxide number of thorium on concentration of the free hydrogen ions. The data show that the hydroxide number of thorium, at definite pH, decreases with increasing concentration of the medium ions.

Representation of the values of the hydroxide number of thorium obtained in 3.0 *M* $(K)NO_3$ (7), 3.0 *M* $(Na)NO_3$ (this work), and 3.0 *M* $(Li)NO_3$ (7) on dependence of the hydration energy of potassium, sodium, and lithium (9) shows that the hydrolysis extent decreases with increasing the hydration energy of the medium cations. Comparison of a decrease of the extent of hydrolysis obtained at the similar enhancement of the concentration of the medium cations and their hydration energies indicates that contribution of the hydration energy of the cation to the total medium effect is higher than contribution of its concentration.

Since it is difficult to obtain reliable values for the equilibrium constants of the hydrolytic reactions, stability constants for the particular complexes, $\beta_{pq}$, or the experimental values of the hydroxide number could be used in consideration of the medium effect. At using the hydroxide number, some deviations from the linearity of the function

$$[4] \quad \log Z_{M(m)} = f(F_{(m)})$$

might appear, because $Z_M$ is not exactly proportional to $\beta_{pq}$ (eq. [8]). The hydroxide number approaches proportionality with $\beta_{pq}$ only if one hydrolysis species predominates or if the $Z_M$ values are chosen in the pH range where only the main complex exists. In spite of these limitations, the linear free energy approach with the experimental values of the hydroxide number might give useful information on the effect of the ionic medium. Therefore, the data obtained in various concentrations of sodium nitrate medium are represented in Fig. 3, as dependence of the hydroxide number on

[2]Notation is in accordance with ref. 8.

[3]Complete set of the potentiometric titration data and results showing the calculation of *Z* may be obtained, at a nominal charge, from the Depository of Unpublished Data, CISTI, National Research Council of Canada, Ottawa, Ont., Canada K1A 0S2.

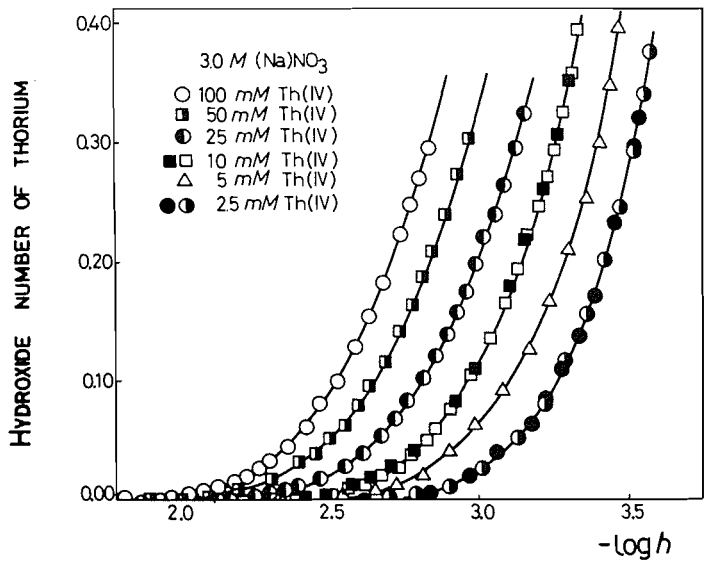


FIG. 1. Hydrolysis of the thorium(IV) ion in 3.0 *M* $(Na)NO_3$ medium (full symbols denote back titrations).

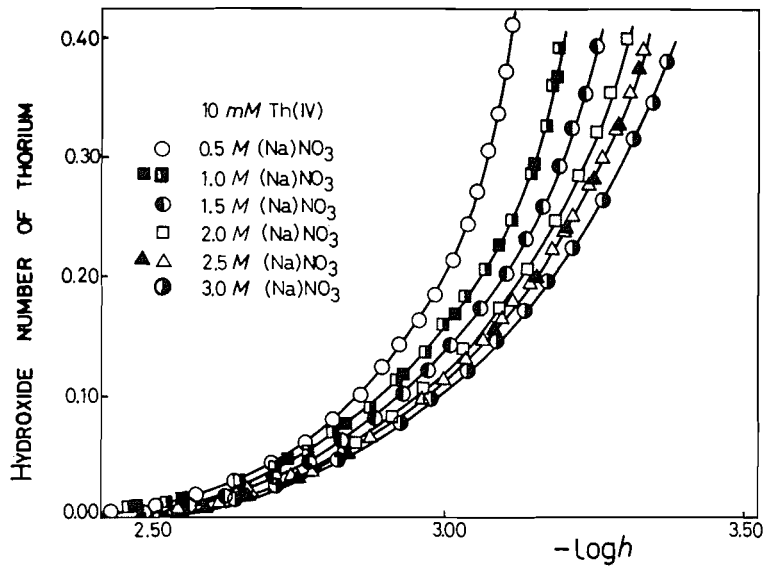


FIG. 2. Hydrolysis of 10 m*M* Th(IV) ion in various concentrations of sodium nitrate medium (full symbols denote back titrations).

the medium factor. The linearity obtained supports the proposed correlation between the extent of hydrolysis and the properties of the medium, enabling the prediction of the thorium hydrolysis in the similar media.

Supposing that the thorium(IV) ion, on interaction with water molecules, forms one or more hydrolytic complexes of general formula $Th_q(OH)_p^{(4q-p)+}$, formation constants $\beta_{pq}$ for each $(p,q)$ species can be defined as the equilibrium constant of the reaction [5]

$$[5] \quad pH_2O + qTh^{4+} \rightleftharpoons Th_q(OH)_p^{(4q-p)+} + pH^+$$

Although the hydrolytic complexes contain a certain number of nitrate ions and water molecules, in reaction [5] the hydration of the individual ions and complex-formation of thorium with nitrate ions are omitted. There are two reasons for this: (*a*) the concentration of both nitrate ions and water molecules is much higher than the concentration of thorium, therefore, there are great difficulties in determining the changes in concentration of nitrate

Can. J. Chem. Downloaded from www.nrcresearchpress.com by 210.87.254.6 on 09/06/12
For personal use only.

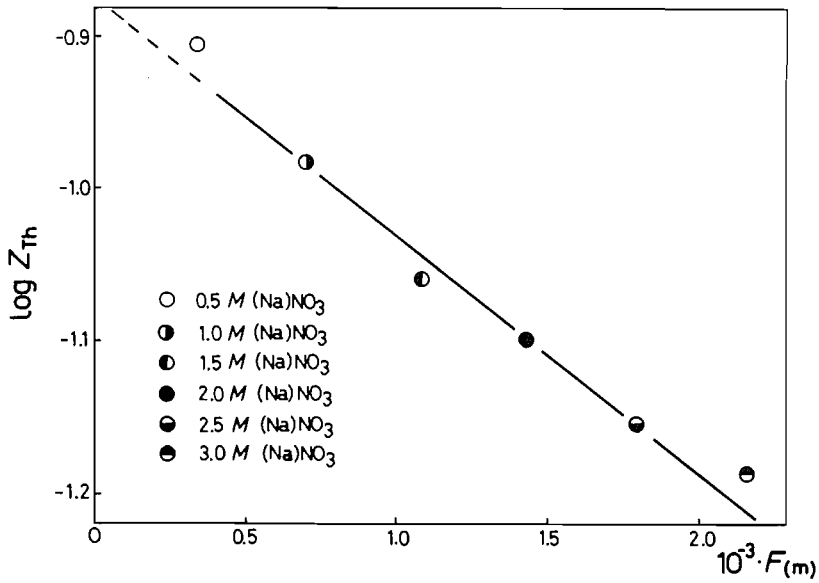


FIG. 3. Dependence of the logarithmic values of the hydroxide number of thorium (obtained in various concentrations of sodium nitrate medium at pH = 2.9) on the medium factor.

TABLE 1. Stability constants, log ($\beta_{pq} \pm 3\sigma$) of the hydrolytic complexes of the $Th^{4+}$ ion obtained in sodium nitrate medium, and corresponding values of the medium factor, $F_{(m)}$*

| Medium $(Na)NO_3$ ($M$) | $F_{(m)}$ | log ($\beta_{pq} \pm 3\sigma$) | | |
|---|---|---|---|---|
| | | $Th_2(OH)_2^{6+}$ | $Th_3(OH)_5^{7+}$ | $Th_6(OH)_{15}^{9+}$ |
| 0.5 | 345 | −5.06±0.07 | −12.59±0.12 | −38.06±0.23 |
| 1.0 | 707 | −5.08±0.06 | −13.04±0.15 | −39.56< −39.41 |
| 1.5 | 1080 | −5.14±0.05 | −13.30±0.16 | −40.47< −40.13 |
| 2.0 | 1430 | −5.16±0.04 | −13.61±0.16 | −41.10< −40.83 |
| 2.5 | 1791 | −5.18±0.03 | −13.79±0.15 | −41.77< −41.42 |
| 3.0 | 2153 | −5.19±0.02 | −14.23±0.17 | −42.32±0.23 |

*In the calculation of the medium factor, $F_{(m)}$, concentrations of the ions of the medium are expressed in mol/dm³, the hydration energies in kJ/mol (ref. 9), while $z$ is the corresponding charge.

ions and water molecules, and ($b$) concentration of nitrate ions was kept constant during each titration, thus the complex-formation appears as a constant effect.

Denoting by $b$ and $h$ the concentrations of the free thorium and hydrogen ions respectively, the concentration of the ($p$,$q$) complexes is given by eq. [6]

$$[6] \quad c_{pq} = \beta_{pq} h^{-p} b^q$$

If the total concentration of thorium ions, $B$ (free and in complexes) is

$$[7] \quad B = b + \Sigma q c_{pq} = b + \Sigma q \beta_{pq} h^{-p} b^q$$

then the hydroxide number of thorium or the amount (in mol/dm³) of $OH^-$ bond to $B$ or, in equivalent, the amount of $H^+$ ions set free by reaction [5], can be represented by expression [8]

$$[8] \quad Z = \Sigma p c_{pq}/B = (\Sigma p \beta_{pq} h^{-p} b^q)/(b + \Sigma q \beta_{pq} h^{-p} b^q)$$

The composition of the hydrolytic complexes and their stability constants has been determined by minimization of the error square sum $U = \Sigma(Z_{cal} - Z_{exp})^2$ using the generalized least-squares program Letagrop (10) and the procedure described in ref. 7.

The hydrolysis data of 2.5–100 m$M$ $Th^{4+}$ in 3.0 $M$ $(Na)NO_3$ medium indicate formation of the polynuclear complexes $Th_2(OH)_2^{6+}$, $Th_3(OH)_5^{7+}$, and $Th_6(OH)_{15}^{9+}$ with stability constants log $\beta_{2,2} = -5.25 \pm 0.02$, log $\beta_{5,3} = -13.76 \pm 0.06$, and log $\beta_{15,6} = -42.35 \pm 0.20$. The same complexes were obtained as a result of the calculation of the hydrolysis data of 10 m$M$ $Th^{4+}$ in 0.5–3.0 $M$ $(Na)NO_3$ media. However, in this case the complex (15,6) is not certain enough, perhaps due to the low

Can. J. Chem. Downloaded from www.nrcresearchpress.com by 210.87.254.6 on 09/06/12
For personal use only.

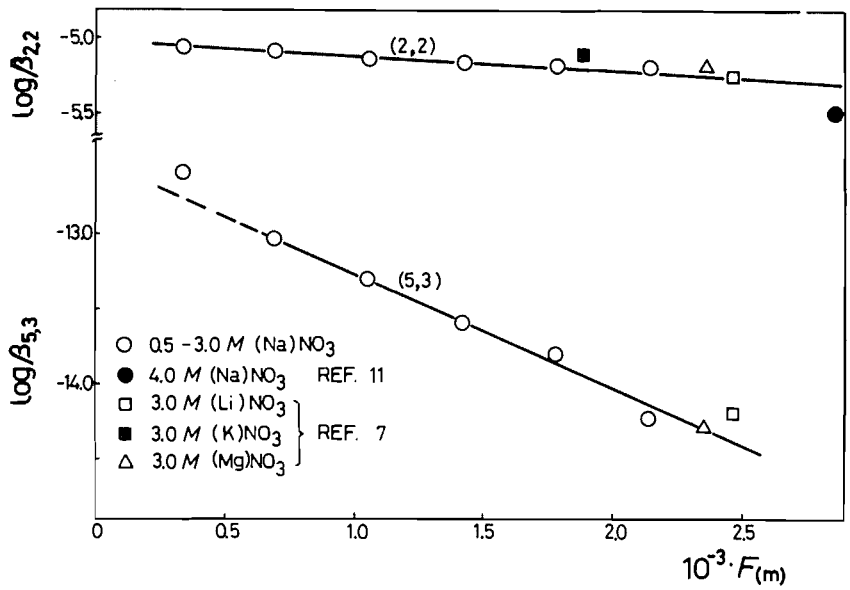


FIG. 4. Dependence of the logarithmic values of the stability constants of the thorium complexes (formed in various nitrate media) on the medium factor.

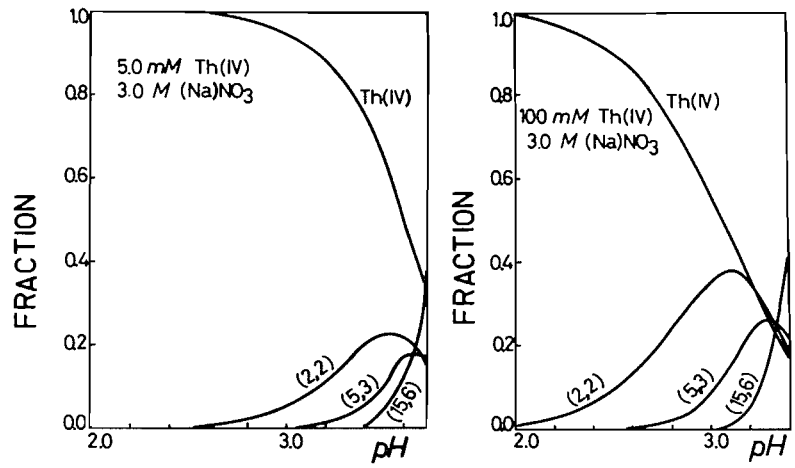


FIG. 5. Distribution of the hydrolytic complexes of thorium formed in 3.0 $M$ $(Na)NO_3$ medium.

concentration of thorium. As the water activity and the activity coefficient of the thorium(IV) ion are different going from one concentration of sodium nitrate to another, calculation of these data was done separately for each concentration of the medium. Table 1 shows that the obtained values of the stability constants, given as $\log(\beta \pm 3\sigma)$, follow changes of the medium factor. Graphical representation of these values, as well as the values obtained in 3.0 $M$ lithium, potassium, magnesium (7), and 4 $M$ sodium nitrate media (11) as a function $\log \beta_{p,q(m)} = f(F_{(m)})$ (Fig. 4) shows a linear dependence confirming the correlation between the free energy changes of the system and the medium factor.

Determination of the distribution of complexes (2,2), (5,3), and (15,6) using the Haltafall program (12) shows that $Th_2(OH)_2^{6+}$ is the principal complex (Fig. 5). Its concentration follows the extent of hydrolysis. Thus, at definite pH, the concentration of complex (2,2) increases with increasing concentration of thorium, but slightly decreases with increasing concentration of the medium. Complexes (5,3) and (15,6) are formed at higher pH, indicating the enhancement of the polynuclearity with increasing pH.

Can. J. Chem. Downloaded from www.nrcresearchpress.com by 210.87.254.6 on 09/06/12
For personal use only.

1. C. F. BAES, JR. and R. E. MESMER. The hydrolysis of cations. Wiley, Toronto. 1976.
2. N. B. MILIĆ. J. Chem. Soc. Dalton Trans. 229, 1973.
3. N. B. MILIĆ. J. Chem. Soc. Dalton Trans. 1445, 1981.
4. G. GRAN. Analyst, **77**, 661 (1952).
5. F. H. VAN CAUWELAERT and H. J. BOSMANS. Rev. Chim. **6**, 611 (1969).
6. L. ERDEY. Gravimetric analysis. Pergamon Press, Oxford. 1965.
7. N. B. MILIĆ. Acta Chem. Scand. **25**, 2487 (1971).
8. L. G. SILLÉN and A. E. MARTELL. Stability constants of metal-ion complexes. Special Publ. The Chemical Society. London, No. 17, 1964; No. 25, 1971.
9. D. W. SMITH. J. Chem. Educ. **54**, 541 (1977).
10. P. BRAUNER, L. G. SILLÉN, and R. WHITEKER. Ark. Kemi, **31**, 365 (1968).
11. P. R. DANESI, M. MAGINI, S. MARGHERITA, and G. D'ALESSANDRO. Energ. Nucl. **15**, 335 (1968).
12. N. INGRI, W. KAKOLOWICZ, L. G. SILLÉN, and B. WARNQUIST. Talanta, **14**, 1261 (1967).

Can. J. Chem. Downloaded from www.nrcresearchpress.com by 210.87.254.6 on 09/06/12
For personal use only.

# Nuclear magnetic resonance studies on the anions $[M(SnCl_3)_5Cl]^{4-}$ (M = Ru, Os) and $[Ru(SnCl_3)_5(MeCN)]^{3-}$: the X-ray crystal structure of $[N(C_2H_5)_4]_4[Ru(SnCl_3)_5Cl]$

LOUIS J. FARRUGIA AND BRIAN R. JAMES[1]

*Department of Chemistry, University of British Columbia, Vancouver, B.C., Canada V6T 1Y6*

AND

CLAUDE R. LASSIGNE AND EDWARD J. WELLS

*Department of Chemistry, Simon Fraser University, Burnaby, B.C., Canada V5A 1S6*

Received November 4, 1981

LOUIS J. FARRUGIA, BRIAN R. JAMES, CLAUDE R. LASSIGNE, and EDWARD J. WELLS. Can. J. Chem. **60**, 1304 (1982).

The octahedral anions $[M(SnCl_3)_5Cl]^{4-}$ (M = Ru, Os) have been fully characterized by $^{119}Sn$ FT nmr spectroscopy. For M = Ru, $^{117}Sn$ and $^{115}Sn$ nmr spectra were also recorded, and an X-ray crystallographic study was carried out on the tetraethylammonium salt, isolated as a disolvate from acetonitrile. The Ru—Sn bond lengths indicate some degree of $d_\pi$–$d_\pi$ interactions. The slight distortions from octahedral geometry are discussed in connection with the packing of the chlorine atoms. The Sn nmr spectra reveal the first observed coupling to a $^{99}Ru$ nucleus ($I = 5/2$, 12.7% natural abundance), very large $^2J(^{119}Sn—^{117}Sn)$ coupling constants, and the first observed second-order effects on a heteronuclear system. The octahedral anion $[Ru(SnCl_3)_5(MeCN)]^{3-}$ was also synthesized as the tetraethylammonium salt and characterized spectroscopically.

LOUIS J. FARRUGIA, BRIAN R. JAMES, CLAUDE R. LASSIGNE et EDWARD J. WELLS. Can. J. Chem. **60**, 1304 (1982).

Faisant appel à la spectroscopie de rmn du $^{119}Sn$ par TF, on a caractérisé complètement les anions octaédriques du type $[M(SnCl_3)_5Cl]^{4-}$ (M = Ru, Os). On a également enregistré les spectres de rmn des anions où M = Ru, $^{117}Sn$ et $^{115}Sn$ et on a fait une étude par cristallographie des rayons X sur le sel de triéthylammonium que l'on a isolé d'une solution dans l'acétonitrile. Les longueurs de liaison Ru—Sn indiquent un certain degré d'interactions $d_\pi$–$d_\pi$. On discute des légères distorsions par rapport à la géométrie octaédrique en les reliant à l'entassement des atomes de chlore. Les spectres de rmn du Sn ont permis d'observer pour la première fois un couplage impliquant un noyau de $^{99}Ru$ ($I = 5/2$, abondance nat. 12,7%), des constantes de couplage très grandes $^2J(^{119}Sn—^{117}Sn)$ et les premiers effets d'ordre deux observés dans un système hétéronucléaire. On a également synthétisé l'anion octaédrique $[Ru(SnCl_3)_5(MeCN)]^{3-}$ sous forme de sel de triéthylammonium et on l'a caractérisé par spectroscopie.

[Traduit par le journal]

## Introduction

Although the reaction of tin(II) chloride with platinum metal halides to give coloured solutions has been known for a long time (1), the exact nature of some of the species present has been ascertained only recently (2–5). Notwithstanding, however, there have been numerous reports on the catalytic activity of such systems for several reactions, including hydrogenation (6), hydroformylation (7), isomerization of olefins (8), dehydrogenation of alcohols (9), and the Water Gas Shift reaction (10, 11). The reaction of $SnCl_2$ with $RuCl_3$ has been reported by several workers. Initially, Young *et al.* (1) formulated the anionic product as $[Ru(SnCl_3)_2Cl_2]^{2-}$ but, on the basis of elemental analysis, later workers (12, 13) preferred the octahedral formulation $[Ru(SnCl_3)_5Cl]^{4-}$. From our studies concerning the potential catalytic activity of the ruthenium system, we report here the full characterization of the $[Ru(SnCl_3)_5Cl]^{4-}$ anion by X-ray crystallography and Sn FT nmr spectroscopy. Brief accounts of some of the work described here have been published previously (14, 15).

[1]To whom all correspondence should be addressed.

## Experimental

*Starting materials*

The $RuCl_3 \cdot 3H_2O$ and $(NH_4)_2OsCl_6$ compounds were used as supplied by Johnson Matthey Ltd.; $SnCl_2 \cdot 2H_2O$ was of reagent grade ACS. The preparative reactions were carried out under argon, although subsequent work-up was performed in air. Acetonitrile was dried over $P_2O_5$, and distilled under $N_2$.

*Preparation of $[NEt_4^+]_4[Ru(SnCl_3)_5Cl]^{4-}$ (I)*

A solution of $RuCl_3 \cdot 3H_2O$ (0.5 g, 41.8% Ru) and $SnCl_2 \cdot 2H_2O$ (3.0 g, 13.3 mmol) in 90 mL 3 *M* HCl was heated on a water-bath until the solution became bright orange (~0.5 h). After cooling the solution to room temperature, $NEt_4^+Cl^-$ (20% in water) was added dropwise until no further orange precipitate formed. The supernatant was pale pink at this stage. On shaking the orange flocculent precipitate over a period of several minutes it crystallized as platelets. These were filtered and washed with 0.1 *M* HCl (*not* water, which caused extensive hydrolysis), methanol, and finally diethyl ether, and dried *in vacuo* to give 3.0 g (81%) of the analytically pure, bright orange salt, **I**. Crystals suitable for X-ray work were obtained as a disolvate by recrystallization from dry acetonitrile.

*Preparation of $[NEt_4^+]_4[Os(SnCl_3)_5Cl]^{4-}$ (II)*

Following the literature method (13), $(NH_4)_2OsCl_6$ (0.30 g, 0.68 mmol) and $SnCl_2 \cdot 2H_2O$ (1.0 g, 4.44 mmol) in 40 mL 3 *M* HCl gave 1.05 g (82%) of straw-yellow platelets of **II**.

*Preparation of $[NEt_4^+]_3[Ru(SnCl_3)_5(MeCN)]^{3-}$ (III)*

A solution of **I** (1.07 g, 0.6 mmol) and $Ag^+SbF_6^-$ (0.24 g, 0.69 mmol) in 40 mL acetonitrile was stirred for 12 h. The

0008-4042/82/111304-13$01.00/0

©1982 National Research Council of Canada/Conseil national de recherches du Canada

Can. J. Chem. Downloaded from www.nrcresearchpress.com by 210.87.254.40 on 09/06/12
For personal use only.

Can. J. Chem. Downloaded from www.nrcresearchpress.com by 210.87.254.40 on 09/06/12
For personal use only.

precipitated AgCl was removed and the bright yellow filtrate reduced in volume to 15 mL under vacuum. Addition of diethyl ether (15 mL) gave a canary-yellow precipitate, which was filtered, washed with acetone (2 × 3 mL), and dried *in vacuo* to give a bright yellow powder of analytically pure **III** (0.82 g, 82%). *Anal.* calcd. for $C_{26}H_{66}Cl_{15}N_4RuSn_5$: C 18.76, H 3.97, N 3.36; found C 18.77, H 3.86, N 3.34.

*X-ray crystallographic analysis*

A crystal of complex **I** of approximate dimensions 0.25 × 0.35 × 0.40 mm was mounted along the $a^*$ axis and coated with acrylic glue to prevent loss of solvent. Precession photography revealed orthorhombic symmetry, as well as the absences $h0l$, $l \neq 2n$, and $0kl$, $k \neq 2n$, allowing the space groups $Pmca$ or $P2_1ca$. The crystal was then transferred, in a general orientation, to an Enraf-Nonius CAD4-F diffractometer. Unit cell parameters were refined by least squares on 2 sin θ/λ values for 25 reflections measured on the diffractometer with MoK radiation (λ = 0.71069 Å). Crystal data (at 22°C) were:

$C_{32}H_{80}Cl_{16}N_4RuSn_5 \cdot C_4H_6N_2$ fw = 1864.9

Orthorhombic, $a$ = 19.796(5), $b$ = 13.882(2), $c$ = 24.772(2) Å; $V$ = 6807.5(9) Å$^3$, $Z$ = 4, $D_c$ = 1.833 g cm$^{-3}$, $D_M$ = 1.835 g cm$^{-3}$, $F(000)$ = 3640, μ(MoKα$_1$) = 27.4 cm$^{-1}$. Space group $P2_1ca$ (non-standard setting of $Pca2_1$, $C_{2v}^5$ No. 29) from structure analysis.

Intensities were measured with graphite-monochromatized MoKα radiation. An ω–2θ scan at 2.01–10.06° min$^{-1}$ was employed over a range of (0.60 + 0.35 tan θ) degrees in ω (extended by 25% on both sides for background measurements). Data were collected to 2θ = 50°. Three reflections (5 $\bar{2}$ $\bar{15}$), (2 0 $\bar{12}$), and (5 $\bar{4}$ 8) were used as intensity checks and measured every 3600 s, whilst the orientation of the crystal was rechecked every 100 measurements using the reflections (5 $\bar{2}$ $\bar{15}$), (5 $\bar{5}$ $\bar{11}$), and (5 $\bar{4}$ 8), with a maximum allowable deviation of any scattering vector of 0.05°.

After data reduction, an analysis of the intensity control reflections revealed a decay of ca. 18% following an X-ray exposure time of 42 h. An isotropic decay correction was applied. A total of 6587 independent reflections were measured with 4098 (62%) having intensities greater than 3σ($I$) above background ($\sigma^2(I) = S + 2B + [0.04(S - B)]^2$ with $S$ = scan count and $B$ = background count). An absorption correction using the analytical method was applied with transmission factors ranging from 0.450 to 0.541 (16).

Analysis was initiated in the centrosymmetric space group $Pmca$, on the basis of $E$-statistics and crystal density, but a three-dimensional Patterson function strongly indicated the non-centrosymmetric $Pca2_1$. The positions of six heavy metal atoms were then obtained from an $E$-map using phases generated by MULTAN (17) for 150 reflections with $E > 1.5$. The identities of the heavy metal atoms Ru ($Z$ = 44) and Sn ($Z$ = 50) were determined from chemical sense, and refinement of their thermal parameters. Subsequent least-squares refinements and difference Fourier syntheses revealed the locations of the remaining non-hydrogen atoms.

The refinement of atomic parameters was carried out using full-matrix least-squares techniques on $F$, minimizing the function $\Sigma\omega(|F_o| - |F_c|)^2$ where $|F_o|$ and $|F_c|$ are the observed and calculated structure factor amplitudes, respectively. The weighting scheme, $\omega = 1/\sigma^2(F)$ gave uniform average values of $\omega(|F_o| - |F_c|)^2$ over ranges of $|F_o|$, and was used in all stages of refinement. The scattering factors used were those of Cromer and Mann (18) for the neutral atoms except hydrogen (19). A correction for the real and imaginary components of anomalous dispersion was applied to metal and chlorine atoms (20). A least-squares refinement of all non-hydrogen atoms, with anisotropic thermal parameters for the metal and chlorine atoms and isotropic ones for the carbon and nitrogen atoms, gave $R$ = 0.041. A difference Fourier synthesis calculated at this stage failed to reveal unequivocally the hydrogen atoms, and these were subsequently included at calculated positions (assuming staggered geometry) for the four tetraethylammonium cations only (C—H = 0.98 Å). The hydrogen atoms were assigned isotropic thermal parameters 1.5 times greater than the carbon atoms to which they were attached. The parameters for the hydrogen atoms were not refined but their contributions were included in the structure factor calculations. A final three cycles of refinement, with all non-hydrogen atoms allowed anisotropic thermal parameters, resulted in convergency at $R$ = 0.035, $R'$ = 0.043 for 4098 reflections with $I \geq 3\sigma(I)$. The $R$ values are of the usual form:

$$R = \Sigma(||F_o| - |F_c||)/\Sigma F_o$$

$$R' = \{\Sigma\omega(|F_o| - |F_c|)^2/\Sigma\omega(F_o)^2\}^{1/2}$$

The mean and maximum parameter shifts corresponded to 0.03 and 0.28σ, respectively, whilst the mean error in an observation of unit weight was 1.149. A final difference Fourier synthesis revealed no residuals greater than +0.36 or less than −0.55 e Å$^{-3}$.

The final positional parameters for the non-hydrogen atoms are given in Table 1, whilst their thermal parameters appear in Table 2.[2] The calculated hydrogen atom positional and isotropic thermal parameters are given in Table 3.[2] Table 4 gives selected bond lengths and angles, and Table 5[2] the least-squares mean plane parameters of the octahedral axes. Measured and calculated structure factors have been placed in the Depository of Unpublished Data.[2]

*Nuclear magnetic resonance instrumentation and techniques*

Spectra for $^{119}$Sn at 37.3 MHz, $^{117}$Sn at 35.6 MHz, and $^{115}$Sn at 32.7 MHz for $[Ru(SnCl_3)_5Cl]^{4-}$ were obtained on natural abundance samples ($^{119}$Sn (8.58%), $^{117}$Sn (7.61%), $^{115}$Sn (0.35%)) on a modified XL-100 nmr spectrometer using a home-built (21) 22 mm probe. Other $^{119}$Sn spectra at 37.3 MHz for $[Os(SnCl_3)_5Cl]^{4-}$ and $[Ru(SnCl_3)_5(MeCN)]^{3-}$ were obtained in 12 mm tubes again on natural abundance samples using the XL-100 nmr spectrometer in the Fourier Transform mode. The $^{13}$C nmr spectrum of the acetonitrile complex was also obtained on the XL-100 using the 22 mm probe operating at 25.2 MHz.

The $^{119}$Sn nmr spectra at 15.02 MHz were obtained on natural abundance samples in 12 mm tubes (not spun) using a modified Specialities spectrometer with a home-built crossed-coil, external water-lock probe (22). Fourier Transform of the FID was accomplished using a Nicolet 1082 FT system.

Both 5 kHz and 25 kHz spectra were acquired in order to measure all coupling constants of the species studied. The numbers of scans for $^{119}$Sn at 15.02 MHz was usually 500–600 K. For the $^{119,117}$Sn spectra measured using the 22 mm probe, this number was usually 5 K, whilst for the $^{115}$Sn spectra 116 K were required because of the very small natural abundance (0.35%).

At 15.02 MHz the digital resolution was 1.25 and 6.25 Hz, respectively, for the 5 kHz and 25 kHz sweep-widths, whilst at 37.3 MHz the corresponding resolutions were 0.63 and 3.13 Hz. Chemical shifts were all measured relative to external tetramethyltin, and are quoted as positive to high frequency.

[2]The structure factor table and Tables 2, 3, and 5 are available, at a nominal charge, from the Depository of Unpublished Data, CISTI, National Research Council of Canada, Ottawa, Ont., Canada K1A 0S2.

Can. J. Chem. Downloaded from www.nrcresearchpress.com by 210.87.254.40 on 09/06/12
For personal use only.

*Infrared spectra*

Infrared spectra were recorded on a Perkin-Elmer 598 infrared spectrophotometer using KBr discs.

## Results and discussion

It was evident from the reproducible complexity of the $^{119}Sn$ nmr spectrum (*vide infra*) that the orange salt obtained from the reaction of $RuCl_3$ and $SnCl_2$, in a 1:6 molar ratio, could not be $[Ru(SnCl_3)_2Cl_2]^{2-}$ as formulated by Young *et al.*, at least not in solution. Such an anion should show in the $^{119}Sn$ nmr spectra one singlet, together with one set of satellites due to spin–spin coupling to $^{117}Sn$. We were prompted to study complex **I** by X-ray crystallography in the hope that knowledge of the solid state structure would be of use in understanding the solution chemistry.

*X-ray crystallographic analysis*

The asymmetric unit in the crystal structure of complex **I**, $[NEt_4^+]_4[Ru(SnCl_3)_5Cl]^{4-}\cdot 2MeCN$, consists of a discrete anion, associated with four tetraethylammonium cations and two solvent molecules of acetonitrile, all separated by normal Van der Waals distances. A stereoview of the anion (Fig. 1) shows the near idealized $C_s$ symmetry, and the crystallographic numbering system. The Ru—Sn bond lengths (Table 4) range from 2.553(2) to 2.586(1) Å, the shortest distance being associated with the tin atom *trans* to the chloride ligand. Important factors are likely to be the π-acidity and strong *trans* influence of the $SnCl_3^-$ group (23–25). In a number of structural studies of transition metal complexes containing ligated $SnCl_3^-$, a significantly shortened metal–tin bond has been noted (5, 24, 26–29) and attributed to multiplicity of the bond due to metal–tin $d_\pi$–$d_\pi$ interactions. In complex **I** the average Ru—Sn distance of 2.574 Å is considerably shorter than the values derived from the sum of the atomic radii in the respective metals 2.84 Å (30), or of their covalent radii 2.67 Å. The corresponding distances in the complexes $[Ru_2Cl_3(SnCl_3)(CO)_5]$ (24) and $[RuCl(SnCl_3)(CO)(Me_2CO)(PPh_3)_2]$ (29) are 2.565(4) and 2.5935(9) Å, respectively. The competition for the ruthenium $d_\pi$ electrons in complex **I** is more severe for the mutually *trans*-$SnCl_3$ ligands, resulting in a lengthening of these Ru—Sn bonds compared to the Ru—Sn(2) bond *trans* to chlorine.

During the course of this work, a preliminary report on the crystal structure of the analogous osmium anion $[Os(SnCl_3)_5Cl]^{4-}$ appeared (31). The average Os—Sn distance was 2.57 Å, with the shortest distance (2.53 Å) again being associated with the tin atom *trans* to chlorine. The osmium and ruthenium complexes appear to have similar molecular structures, though the lack of detailed

TABLE 1. Final positional parameters (fractional × $10^4$, Ru and Sn × $10^5$) with estimated standard deviations in parentheses[a]

| Atom | *x* | *y* | *z* |
|---|---|---|---|
| Ru | 32000 | 22586( 7) | 41462( 4) |
| Sn(1) | 31190( 9) | 12225( 6) | 50080( 4) |
| Sn(2) | 19123( 8) | 23557( 7) | 41260( 4) |
| Sn(3) | 32607( 9) | 7410( 6) | 35581( 4) |
| Sn(4) | 32611( 9) | 32856( 6) | 32765( 4) |
| Sn(5) | 34329( 8) | 37843( 7) | 47156( 4) |
| Cl(1) | 4445( 2) | 2164( 3) | 4175( 2) |
| Cl(11) | 2603( 3) | −337( 3) | 5039( 2) |
| Cl(12) | 2469( 3) | 1849( 3) | 5742( 2) |
| Cl(13) | 4072( 3) | 685( 4) | 5520( 2) |
| Cl(21) | 1264( 3) | 3450( 4) | 4643( 2) |
| Cl(22) | 1353( 3) | 2680( 4) | 3304( 2) |
| Cl(23) | 1244( 2) | 1004( 3) | 4373( 2) |
| Cl(31) | 3978( 3) | 782( 4) | 2778( 2) |
| Cl(32) | 2317( 3) | 26( 4) | 3128( 2) |
| Cl(33) | 3752( 3) | −731( 3) | 3873( 2) |
| Cl(41) | 2823( 2) | 2810( 3) | 2415( 2) |
| Cl(42) | 4311( 3) | 3837( 4) | 2903( 2) |
| Cl(43) | 2699( 3) | 4803( 3) | 3297( 2) |
| Cl(51) | 2683( 3) | 4997( 3) | 5043( 2) |
| Cl(52) | 4025( 3) | 3614( 4) | 5557( 2) |
| Cl(53) | 4206( 3) | 4952( 4) | 4355( 2) |
| N(1) | 4158( 7) | 2668(10) | 903( 5) |
| C(11) | 3509(10) | 2118(12) | 901( 8) |
| C(12) | 2883(10) | 2585(11) | 738( 9) |
| C(13) | 4744(11) | 2091(14) | 1047( 8) |
| C(14) | 4717(11) | 1611(20) | 1578(10) |
| C(15) | 4068(12) | 3507(17) | 1292( 9) |
| C(16) | 4689(11) | 4161(18) | 1391(10) |
| C(17) | 4286(11) | 3119(13) | 372( 7) |
| C(18) | 4298(15) | 2429(17) | −90( 9) |
| N(2) | 1417( 7) | 5250( 9) | 1502( 5) |
| C(21) | 1470(10) | 6117(13) | 1145( 8) |
| C(22) | 798(13) | 6670(17) | 1051(11) |
| C(23) | 2090(10) | 4758(12) | 1528( 8) |
| C(24) | 2670(11) | 5362(15) | 1753( 8) |
| C(25) | 1215(10) | 5547(11) | 2064( 7) |
| C(26) | 1116(10) | 4804(15) | 2453( 8) |
| C(27) | 905(11) | 4535(13) | 1281( 8) |
| C(28) | 994(12) | 4183(16) | 704( 9) |
| N(3) | 1076( 7) | 188( 9) | 1616( 5) |
| C(31) | 1716(11) | 389(13) | 1311( 8) |
| C(32) | 2349(11) | 477(15) | 1663(10) |
| C(33) | 495(10) | 251(13) | 1213( 7) |
| C(34) | 523(13) | −462(14) | 757( 9) |
| C(35) | 1142(11) | −772(12) | 1865( 8) |
| C(36) | 449(13) | −1198(16) | 2080( 8) |
| C(37) | 959(11) | 895(16) | 2078( 7) |
| C(38) | 913(13) | 1967(13) | 1894( 8) |
| N(4) | 1254( 8) | 2482( 9) | −915( 5) |
| C(41) | 769(13) | 2428(20) | −448(10) |
| C(42) | 836(14) | 1625(15) | −61( 9) |
| C(43) | 1953(15) | 2683(19) | −629(10) |
| C(44) | 2538(15) | 2784(17) | −1083(15) |
| C(45) | 1316(18) | 1616(23) | −1238(11) |
| C(46) | 637(18) | 1248(24) | −1443(10) |
| C(47) | 1112(15) | 3317(20) | −1275(11) |
| C(48) | 1068(14) | 4289(14) | −1008( 9) |
| C(1) | 3499(20) | 1639(23) | −3032(16) |
| C(2) | 2907(21) | 2022(21) | −2802(15) |
| N(5) | 2394(17) | 2325(18) | −2649(13) |
| N(6) | 4812(13) | 3414(18) | −2695(10) |
| C(4) | 4433(14) | 3430(17) | −2327(12) |
| C(3) | 3976(15) | 3370(21) | −1846(12) |

[a]Equivalent positions: $(x, y, z; x, -y, \frac{1}{2}+z; \frac{1}{2}+x, -y, -z; \frac{1}{2}+x, y, \frac{1}{2}-z)$.

TABLE 4. Selected bond lengths (Å) and angles (deg) with estimated standard deviations in parentheses

| Bond | Length | Bond | Length |
|---|---|---|---|
| Ru—Sn(1) | 2.579(1) | Sn(1)—Cl(11) | 2.395(4) |
| Ru—Sn(2) | 2.553(2) | Sn(1)—Cl(12) | 2.392(5) |
| Ru—Sn(3) | 2.564(1) | Sn(1)—Cl(13) | 2.392(5) |
| Ru—Sn(4) | 2.586(1) | | |
| Ru—Sn(5) | 2.586(1) | Sn(2)—Cl(21) | 2.365(5) |
| Ru—Cl(1) | 2.468(4) | Sn(2)—Cl(22) | 2.361(4) |
| | | Sn(2)—Cl(23) | 2.376(4) |
| Sn(3)—Cl(31) | 2.400(5) | Sn(4)—Cl(41) | 2.398(4) |
| Sn(3)—Cl(32) | 2.368(5) | Sn(4)—Cl(42) | 2.401(5) |
| Sn(3)—Cl(33) | 2.393(4) | Sn(4)—Cl(43) | 2.383(4) |
| Sn(5)—Cl(51) | 2.386(4) | | |
| Sn(5)—Cl(52) | 2.404(6) | | |
| Sn(5)—Cl(53) | 2.402(5) | | |
| For the $NEt_4^+$ cation | | For the solvent molecules | |
| C—C | ave. 1.51(2) | (*i*) C(1)—C(2) | 1.41(4) |
| | | C(2)—N(5) | 1.16(4) |
| C—N | ave. 1.52(3) | (*ii*) C(3)—C(4) | 1.50(4) |
| | | C(4)—N(6) | 1.18(3) |

| Bonds | Angle | Bonds | Angle |
|---|---|---|---|
| Cl(1)—Ru—Sn(2) | 179.5(1) | Sn(2)—Ru—Sn(5) | 98.36(5) |
| Cl(1)—Ru—Sn(3) | 85.7(1) | Sn(3)—Ru—Sn(1) | 98.86(4) |
| Cl(1)—Ru—Sn(1) | 90.5(1) | Sn(3)—Ru—Sn(4) | 88.71(4) |
| Cl(1)—Ru—Sn(4) | 90.4(1) | Sn(3)—Ru—Sn(5) | 167.01(7) |
| Cl(1)—Ru—Sn(5) | 81.4(1) | Sn(1)—Ru—Sn(4) | 179.00(6) |
| Sn(2)—Ru—Sn(3) | 94.53(5) | Sn(1)—Ru—Sn(5) | 90.93(4) |
| Sn(2)—Ru—Sn(1) | 89.05(5) | Sn(4)—Ru—Sn(5) | 89.69(4) |
| Sn(2)—Ru—Sn(4) | 90.07(5) | | |
| Ru—Sn(1)—Cl(11) | 123.8(1) | Ru—Sn(4)—Cl(41) | 125.0(1) |
| Ru—Sn(1)—Cl(12) | 117.4(1) | Ru—Sn(4)—Cl(42) | 122.5(1) |
| Ru—Sn(1)—Cl(13) | 124.3(1) | Ru—Sn(4)—Cl(43) | 116.6(1) |
| Cl(11)—Sn(1)—Cl(12) | 94.3(2) | Cl(41)—Sn(4)—Cl(42) | 93.3(2) |
| Cl(11)—Sn(1)—Cl(13) | 92.1(2) | Cl(41)—Sn(4)—Cl(43) | 95.4(2) |
| Cl(12)—Sn(1)—Cl(13) | 97.7(2) | Cl(42)—Sn(4)—Cl(43) | 97.5(2) |
| Ru—Sn(2)—Cl(21) | 124.3(1) | Ru—Sn(5)—Cl(51) | 130.7(1) |
| Ru—Sn(2)—Cl(22) | 119.7(1) | Ru—Sn(5)—Cl(52) | 118.7(1) |
| Ru—Sn(2)—Cl(23) | 120.6(1) | Ru—Sn(5)—Cl(53) | 117.6(1) |
| Cl(21)—Sn(2)—Cl(22) | 95.1(2) | Cl(51)—Sn(5)—Cl(52) | 94.5(2) |
| Cl(21)—Sn(2)—Cl(23) | 93.8(2) | Cl(51)—Sn(5)—Cl(53) | 92.7(2) |
| Cl(22)—Sn(2)—Cl(23) | 96.4(2) | Cl(52)—Sn(5)—Cl(53) | 94.5(2) |
| Ru—Sn(3)—Cl(31) | 117.8(1) | | |
| Ru—Sn(3)—Cl(32) | 124.3(1) | | |
| Ru—Sn(3)—Cl(33) | 122.4(1) | | |
| Cl(31)—Sn(3)—Cl(32) | 96.6(2) | | |
| Cl(31)—Sn(3)—Cl(33) | 92.4(2) | | |
| Cl(32)—Sn(3)—Cl(33) | 96.3(2) | | |

information on the osmium compound precludes a meaningful comparison.

Apart from a distortion along one axis, ∠Sn(5)—Ru—Sn(3) = 167.01(7)°, the coordination about the ruthenium atom is very close to octahedral (Tables 4, 5).[2] The atoms Sn(3) and Sn(5) are bent towards the chlorine atom Cl(1), in the plane defined by Ru, Sn(2), Sn(3), Sn(5), and Cl(1) (Table 5).[2] There is no similar distortion along the Sn(1)—Ru—Sn(4) axis, presumably due to steric repulsions between Cl(1) and Cl(42), and Cl(1) and Cl(13). The respective non-bonded contact distances are 3.922(6) and 3.983(7) Å, whilst in the structure as a whole, non-bonded Cl—Cl close contacts range within the $SnCl_3$ groups from 3.447(7) to 3.603(8) Å, and between groups from 3.671(7) to 4.794(7) Å.

The overall symmetrical configuration of the $SnCl_3$ groups is presumably adopted so as to

Can. J. Chem. Downloaded from www.nrcresearchpress.com by 210.87.254.40 on 09/06/12
For personal use only.

Can. J. Chem. Downloaded from www.nrcresearchpress.com by 210.87.254.40 on 09/06/12
For personal use only.

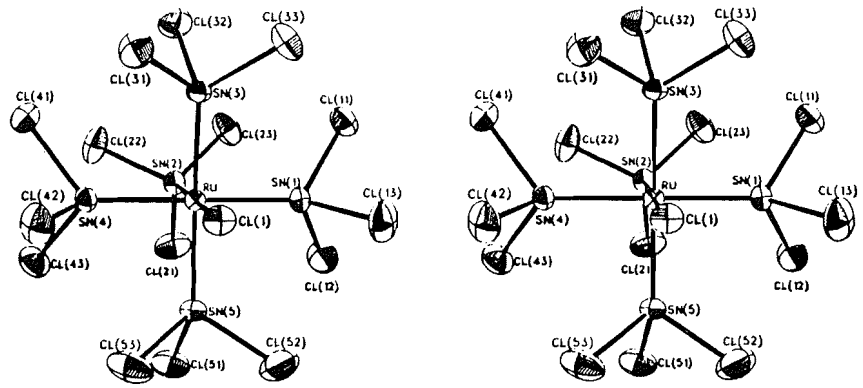


FIG. 1. A stereoview of the $[Ru(SnCl_3)_5Cl]^{4-}$ anion, drawn with 50% probability ellipsoids.

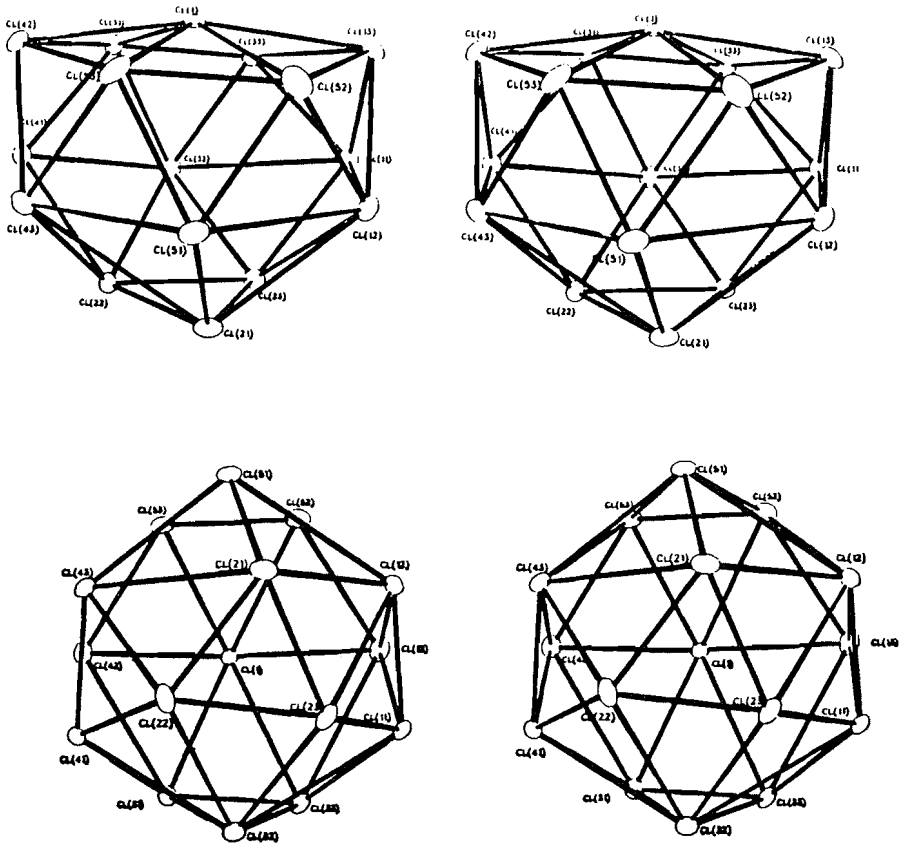

FIG. 2. Two stereoviews of the polyhedral cage of chlorine atoms (see text).

minimize non-bonded interactions between chlorine atoms. From this point of view, it is of interest to examine their arrangement in more detail. Figure 2 presents two stereoviews of the polyhedron formed by the chlorine atoms, showing only nearest neighbour non-bonded contacts. Benfield and Johnson recently reported (32) a study on the configurations of the carbonyl ligands within polynuclear carbonyl clusters. If the $[Ru(SnCl_3)_5Cl]^{4-}$ anion is viewed as a "cluster", the arrangement of the chlorine atoms (Fig. 2) is similar to that of two polyhedra discussed by these workers; Fig. 3*a* represents the most favourable way of packing sixteen identical ligands, while Fig. 3*b* shows the slightly less favourable tetracapped truncated tetrahedron. Since one of the chlorine atoms, Cl(1), in

Can. J. Chem. Downloaded from www.nrcresearchpress.com by 210.87.254.40 on 09/06/12
For personal use only.

Fig. 2 is directly bonded to the ruthenium atom in the centre of the polyhedron, there is a distortion from ideality at this vertex, but otherwise the similarity to the polyhedra of Fig. 3 is very close, suggesting that the ideas of Benfield and Johnson may be extended to systems other than carbonyl clusters. The chlorine atom polyhedron is also similar to that described by Casey *et al.* (33) as [$T_d$-($1v^6633v^63$)-$\Delta^{28}$-*closo*] in their classification of polyboron polyhedra.

The geometry about the tin atoms shows the distortions from idealized tetrahedral symmetry in accordance with Bent's rules (34) and observed previously in related structures (28, 31); the M—Sn—Cl angles are ~10° greater than, and the Cl—Sn—Cl angles ~10° less than 109.5°. The Sn—Cl distances, which range from 2.361(4) to 2.404(6) Å, are longer than in $SnCl_4$, 2.31(2) Å (35), and may be compared with the reported values in $[Os(SnCl_3)_5Cl]^{4-}$ 2.31–2.41, ave. 2.37 Å (31). The Sn—Cl distances in uncoordinated $SnCl_3^-$ are longer still, e.g. 2.425(8)–2.447(2) Å in $[Co(diphos)_2Cl]^+[SnCl_3]^-$ (36), 2.50–2.52 Å in $Cs^+SnCl_3^-$ (37), and 2.54(3)–2.63(3) Å in $KCl\cdot KSnCl_3\cdot H_2O$ (38). We note that in **I** the shortest Sn—Cl distances are associated with Sn(2), which has the shortest Sn—Ru separation.

The Ru—Cl(1) separation of 2.468(4) Å is greater than the range of observed Ru—Cl distances with mutually *trans*-chloride ligands, 2.391–2.446 Å (39), and is presumably due to the *trans* influence of the $SnCl_3^-$ ligand, which is probably similar to that of CO (39). The complex $[RuCl(SnCl_3)(CO)(Me_2CO)(PPh_3)_2]$ with chloride *trans* to $SnCl_3^-$ has a Ru—Cl distance of 2.405(2) Å (29).

The four tetraethylammonium cations in complex **I** are all ordered, and show the expected geometry, with C—C separations ranging from 1.46(3)–1.62(4), ave. 1.51 Å, and C—N distances of 1.45(3)–1.58(3), ave. 1.52 Å. The two crystallographically independent molecules of acetonitrile exhibit large esd's for the positional and thermal parameters, as commonly found for solvate molecules. Their internuclear separations are reasonable, however, and both molecules are approximately linear.

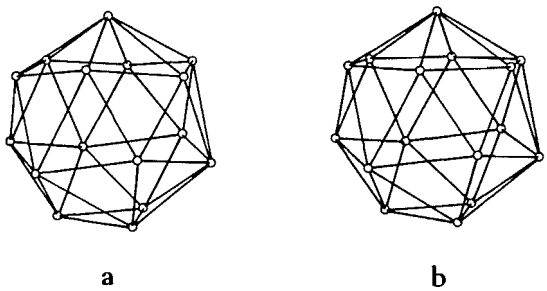


FIG. 3. Two sixteen vertex polyhedra (see text): (*a*), the most energetically favourable polyhedron; (*b*), a tetracapped truncated tetrahedron.

*Infrared spectroscopy*

Infrared spectroscopy proved to be of little use for characterization of the trichlorostannate complexes mainly due to difficulties in bond assignments, particularly in distinguishing M—Cl and Sn—Cl stretching modes (40). The coordinated nitrile in complex **III** was not observed in the expected region (~2300 $cm^{-1}$), but nmr data show the acetonitrile unambiguously (*vide infra*).

*Assignments of the tin nmr resonances*

Figures 4–6 show the $^{119}Sn$ spectra of the $[M(SnCl_3)_5Cl]^{4-}$ anions (M = Ru, Os) recorded at both 15.02 and 37.3 MHz. A knowledge of the structure of complex **I** allows for an unambiguous assignment of all the resonances. The four equivalent equatorial tin nuclei and the unique axial tin nucleus each have distinct chemical shifts (Tables 6, 7), and both resonances are flanked by satellites due to coupling to other tin nuclei. Within the set of four equatorial tin nuclei only $^{119}Sn$—$^{117}Sn$ spin–spin couplings are observable, the *trans* $^{119}Sn$—$^{117}Sn$ couplings being an order of magnitude greater than the corresponding *cis* couplings. Also observable are the couplings of $^{119}Sn_{eq}$ to both $^{119}Sn_{ax}$ and $^{117}Sn_{ax}$. Because of proximity of the chemical shifts, species containing two $^{119}Sn$ nuclei (one in the axial and the other in an equatorial position) give rise to an AB pair. The weaker outer pairs were usually not observed due to noise, but for $[Os(SnCl_3)_5Cl]^{4-}$ recorded at 37.3 MHz (Fig. 6), one of these outer pairs is clearly visible. Calculations were carried out on the AB patterns for all species and at both operating frequencies, assuming the assigned resonances for $^{119}Sn_{ax}$ and $^{119}Sn_{eq}$ and values of $J(^{119}Sn_{eq}—^{119}Sn_{ax})$ calculated from the observed $J(^{119}Sn_{eq}—^{117}Sn_{ax})$. The calculations were all in excellent agreement with the observed line separations and intensities. The resonance due to the unique axial tin is flanked by only one set of satellites due to the $^{119}Sn_{ax}—^{117}Sn_{eq}$(*cis*) coupling.

Also visible in Fig. 4 are lines due to coupling to the $^{99}Ru$ nucleus ($I$ = 5/2, 12.72% natural abundance). Of the expected six lines, four are seen in the 15.02 MHz spectrum and three in the 37.3 MHz spectrum, the missing lines being obscured by other couplings. The line separations were constant at the two observing frequencies, as expected. Figures 5 and 6 also show coupling to $^{187}Os$ ($I$ = ½,

Can. J. Chem. Downloaded from www.nrcresearchpress.com by 210.87.254.40 on 09/06/12
For personal use only.

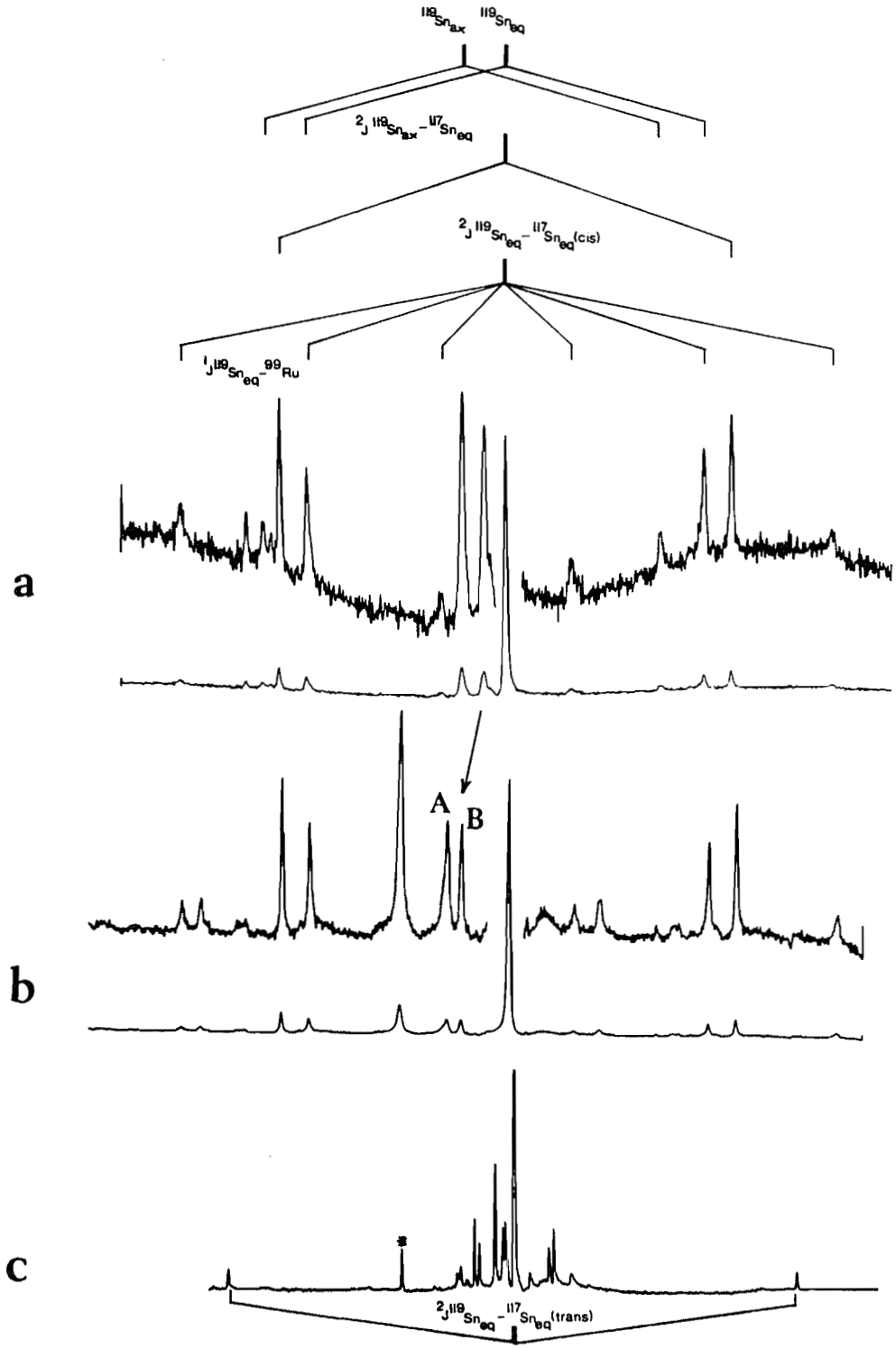


FIG. 4. $^{119}Sn$ nmr spectra of $(NEt_4)_4[Ru(SnCl_3)_5Cl]$ in nitromethane: (*a*) 15.02 MHz, 5 kHz sweepwidth; (*b*) 37.3 MHz, 5 kHz sweepwidth; (*c*) 37.3 MHz, 25 kHz sweepwidth; *impurity. A and B are the central resonances of an AB quartet (see text).

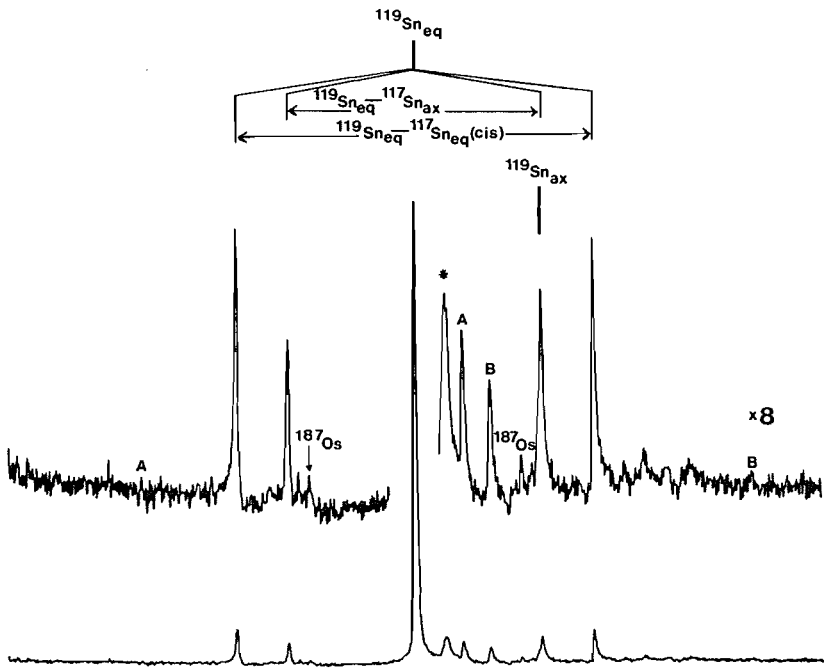


FIG. 5. $^{119}Sn$ nmr spectrum of $(NEt_4)_4[Os(SnCl_3)_5Cl]$ in nitromethane at 15.02 MHz and 5 kHz sweepwidth. AB quartet designated AABB (outer two are from calculations); *impurity.

1.64% natural abundance), but otherwise the spectra of the ruthenium and osmium complexes are essentially the same.

The acetonitrile derivative $[Ru(SnCl_3)_5(MeCN)]^{3-}$, prepared by halide abstraction from complex **I** in acetonitrile, shows very similar splitting patterns to the parent complex, except that some of the couplings are less well resolved (Fig. 7). This strongly indicates a geometry analogous to that of complex **I**, and although there was no ir evidence for a C≡N stretch, $^{13}C$ and $^{1}H$ nmr data (*vide infra*) and the microanalysis reveal the presence of coordinated acetonitrile.

Finally, the spectra in the case of $[Ru(SnCl_3)_5Cl]^{4-}$ had such a high S/N ratio that resonances were observed due to extremely minor amounts of species of the type:

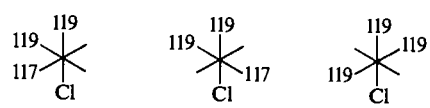


Calculations carried out on the assumed axial and equatorial shifts and relevant coupling constants were in excellent agreement with observed line positions, further confirming the correct assignment of these parameters.

*Chemical shifts*

The chemical shifts of the axial and equatorial tin atoms in complex **I** are very similar (Table 6), quite possibly due to the nearly perfect octahedral symmetry of the electric field gradient at the ruthenium nucleus. The corresponding $^{119}Sn$ shifts for the osmium analogue (Table 8) are towards increased shielding. This effect has been observed for a number of compounds involving third-row transition metals (41) and may arise from a decrease in the $d_\pi$–$d_\pi$ overlap between the tin and transition metal, leading to an increase in the average electronic excitation ($\Delta E$) which in turn leads to a decrease in the paramagnetic term. For the heavier third-row metal this $\pi$-interaction and/or the higher polarizability of the larger atom could lead to the low frequency shifts.

Replacement of the chloride in **I** by the less electronegative MeCN produces more shielding and the effect is felt more by the adjacent equatorial tins (97 ppm upfield) than the axial tin (45 ppm upfield), Table 8.

*Spin–spin coupling constants*

*(a) $[Ru(SnCl_3)_5Cl]^{4-}$, I*

The $^{119}Sn$ nmr spectrum reveals resonances due to a number of isotopic species, containing one to

Can. J. Chem. Downloaded from www.nrcresearchpress.com by 210.87.254.40 on 09/06/12
For personal use only.

Can. J. Chem. Downloaded from www.nrcresearchpress.com by 210.87.254.40 on 09/06/12
For personal use only.

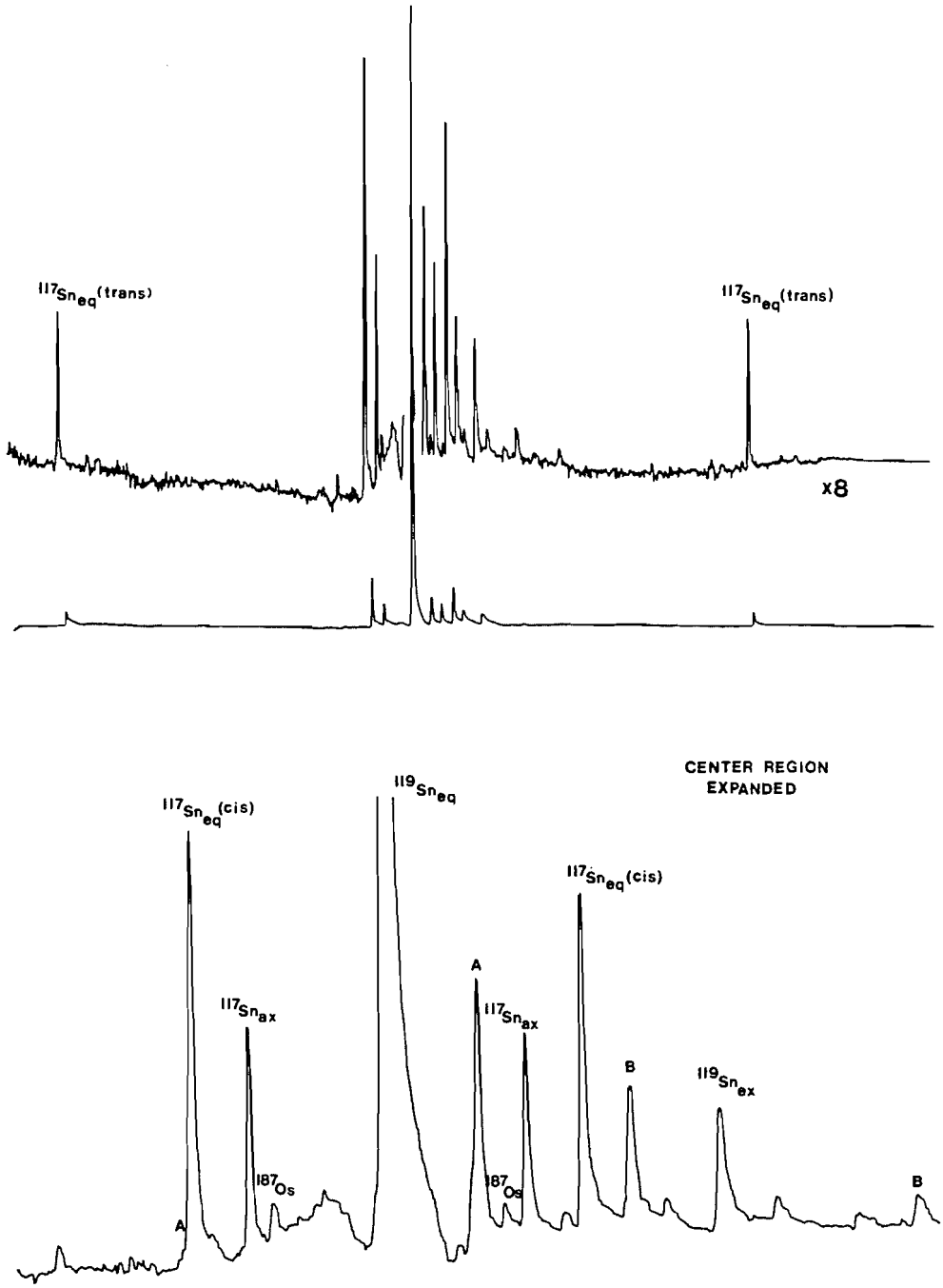


FIG. 6. $^{119}Sn$ nmr spectrum of $(NEt_4)_4[Os(SnCl_3)_5Cl]$ in nitromethane at 37.3 MHz and 25 kHz sweepwidth. AB quartet designated AABB (weak member of A set hidden under the $^{117}Sn_{eq}$(*cis*) signal).

three spin-active tin nuclei ($^{115}Sn$, $^{117}Sn$, and $^{119}Sn$ all have $I = \frac{1}{2}$). Populations of species with more than three spin-active tin nuclei were far too low to be observable. The intensities of the signals due to four equatorial and unique axial tin nuclei are not in the ratio 4:1, since other species also contribute intensity, and the observed ratio of 5.3:1 is very close to that calculated for up to three spin-active tin nuclei, possible differences in $T_1$ relaxation times not being taken into account.

The equatorial $^{119}Sn$ nuclei show three couplings which appear as doublets with $J$ values of 2580,

TABLE 6. Tin nmr data for the $[Ru(SnCl_3)_5Cl]^{4-}$ anion[a,b]

$\delta^{119}Sn_{eq} = -167.9$ ppm[c]; $-167.7$ ppm[d]
$\delta^{119}Sn_{ax} = -149.2$ ppm[c]; $-148.9$ ppm[d]

| Coupling constant (Hz) | $^{119}Sn—^{117}Sn$[c] | $^{119}Sn—^{117}Sn$[d] | $^{117}Sn—^{119}Sn$[e] | $^{115}Sn—^{119}Sn$[f] | $^{115}Sn—^{117}Sn$[f] |
|---|---|---|---|---|---|
| $^2J(Sn_{eq}—Sn_{eq})$*trans* | 21254(6) | 21236(12) | 21243(6) | 19485(6) | 18624(6) |
| $^2J(Sn_{eq}—Sn_{eq})$*cis* | 2938(2) | 2930(2) | 2935(2) | 2694(2) | 2568(2) |
| $^2J(Sn_{eq}—Sn_{ax})$*cis* | 2581(2) | 2583(2) | 2578(2) | 2361(2) | 2266(2) |
| | 2582(2) | 2578(2) | 2577(2) | | |
| $^1J(Sn_{eq}—^{99}Ru)$[g] | 846(2) | 848(2) | 810(2) | | |

[a]Chemical shifts downfield relative to $Sn(CH_3)_4$ as external standard.
[b]Estimated errors in parentheses.
[c]From $^{119}Sn$ spectrum at 37.3 MHz.
[d]From $^{119}Sn$ spectrum at 15.02 MHz.
[e]From $^{117}Sn$ spectrum at 35.6 MHz.
[f]From $^{115}Sn$ spectrum at 32.7 MHz.
[g]$Sn_{eq}$ refers to observed tin nucleus ($^{119}Sn$ and $^{117}Sn$; $^{115}Sn$ too weak).

TABLE 7. Tin nmr data for the $[Os(SnCl_3)_5Cl]^{4-}$ anion[a,b]

$\delta^{119}Sn_{eq} = -531.8$ ppm[c]; $-531.7$ ppm[d]
$\delta^{119}Sn_{ax} = -581.8$ ppm[c]; $-581.9$ ppm[d]

| Coupling constant (Hz) | $^{119}Sn—^{117}Sn$[c] | $^{119}Sn—^{117}Sn$[d] |
|---|---|---|
| $^2J(Sn_{eq}—Sn_{eq})$*trans* | 18600(6) | 18600(6) |
| $^2J(Sn_{eq}—Sn_{eq})$*cis* | 2169(2) | 2167(2) |
| $^2J(Sn_{eq}—Sn_{ax})$*cis* | 1542(2) | 1538(2) |
| $^1J(^{119}Sn_{eq}—^{187}Os)$ | 1290(2) | 1289(2) |

[a–d]Footnotes as for Table 6.

2934, and 21 245 Hz, that are due to the $^{119}Sn_{eq}—^{117}Sn_{ax}$, $^{119}Sn_{eq}—^{117}Sn_{eq}$(*cis*), and $^{119}Sn_{eq}—^{117}Sn_{eq}$(*trans*) interactions, respectively (Table 6). The extremely large value of $^2J(^{119}Sn_{eq}—^{117}Sn_{eq})$ *trans* is reminiscent of those observed in platinum(II)–$SnCl_3$ complexes (42). The intensity ratios of the three sets of satellites were the expected 1:2:1. The $^{119}Sn_{eq}—^{117}Sn_{ax}$ coupling of 2580 Hz is also observable as a doublet flanking the $^{119}Sn_{ax}$ resonance, i.e., as ($^{119}Sn_{ax}—^{117}Sn_{eq}$), the coupling constant being the same within experimental error. As mentioned above, the $^{119}Sn_{ax}—^{119}Sn_{eq}$ coupling is observed as an AB set at 37.3 MHz ($J(^{119}Sn_{ax}—^{119}Sn_{eq})$ = 2702 Hz, $\delta(^{119}Sn_{ax}—^{119}Sn_{eq})$ = 700 Hz).

The $^{115}Sn$ nmr spectra (Fig. 8) revealed all satellites as doublets due to coupling to both $^{119}Sn$ and $^{117}Sn$. The values of the coupling constants agree in all cases with those calculated from the gyromagnetic ratios, while the $^{115}Sn$ shifts agree quite well with those obtained from the $^{119}Sn$ and $^{117}Sn$ nmr spectra and show no sign of any isotope effect.

During analysis of the $^{119}Sn$ nmr spectrum at 15.02 MHz, it was observed (15) that the doublet caused by coupling of an equatorial $^{119}Sn$ to a $^{117}Sn$ in the *trans* position was asymmetric about the main $^{119}Sn_{eq}$ resonance, which itself results from molecules having only one $^{119}Sn$ in the equatorial position; at 37.3 MHz there was a decrease in this asymmetry. The $^{115}Sn$ nmr spectrum also showed the doublets resulting from $^2J(^{115}Sn—^{119}Sn)$*trans* and $^2J(^{115}Sn—^{117}Sn)$*trans* couplings to be asymmetric about the main resonance, the latter being more asymmetric than the former. We attribute these asymmetries to second-order effects in the heteronuclear systems. The unusually large $^2J(^{119}Sn—^{117}Sn)$*trans* coupling constant (21 248 Hz), together with $\Delta\delta(^{119}Sn—^{117}Sn)$ being 0.668 MHz for $^{119}Sn$ at 15.02 MHz, makes the supposedly "pure" AX pattern begin to show the characteristics of a second-order AB spectrum. In the $^{115}Sn$ nmr spectrum the second-order effect becomes much smaller because $\Delta\delta(^{119}Sn—^{115}Sn)$ = 4.6 MHz and $\Delta\delta(^{117}Sn—^{115}Sn)$ = 2.9 MHz at 2.35T. Calculations have been carried out for the $^{119}Sn$ and $^{115}Sn$ spectra at 2.35T, and the $^{119}Sn$ spectrum at 0.95T, to show this effect (Table 9). Following our first report of these novel second-order effects in $^{119}Sn$ nmr (15), Pregosin and Rüegger independently discovered the same phenomenon in some platinum(II) complexes (43).

The spectrum shown in Fig. 4 also reveals spin–spin coupling between $^{119}Sn$ and $^{99}Ru$ ($I$ = 5/2). The values of $^1J(^{119}Sn—^{99}Ru)$ = 846 Hz, $^1J(^{117}Sn—^{99}Ru)$ = 810 Hz, represent the first reported couplings to the quadrupolar $^{99}Ru$ nucleus. The high symmetry of the anion and the relatively low quadrupole moment, $+0.076 \times 10^{-28}$ m$^2$ (44), minimize the electric field gradient at the $^{99}Ru$ nucleus, thus reducing the quadrupolar relaxation rate and allowing observation of the spin–spin coupling constant, $^1J(^{99}Ru—^{119,117}Sn)$ ($\Delta\nu_{1/2} \simeq 60$ Hz). Coupling to $^{101}Ru$ ($I$ = 5/2; 17.07% natural abundance) with a larger quadrupole moment $+0.45 \times 10^{-28}$ m$^2$ (44) was not observed presumably because of line broadening. (The quadrupole moment ratio of ~6 implies that line-widths for $^{101}Ru$ would be about 2000 Hz.)

*(b) $[Os(SnCl_3)_5Cl]^{4-}$, II*

All three $^{119}Sn—^{117}Sn$ couplings are smaller than

Can. J. Chem. Downloaded from www.nrcresearchpress.com by 210.87.254.40 on 09/06/12
For personal use only.

Can. J. Chem. Downloaded from www.nrcresearchpress.com by 210.87.254.40 on 09/06/12
For personal use only.

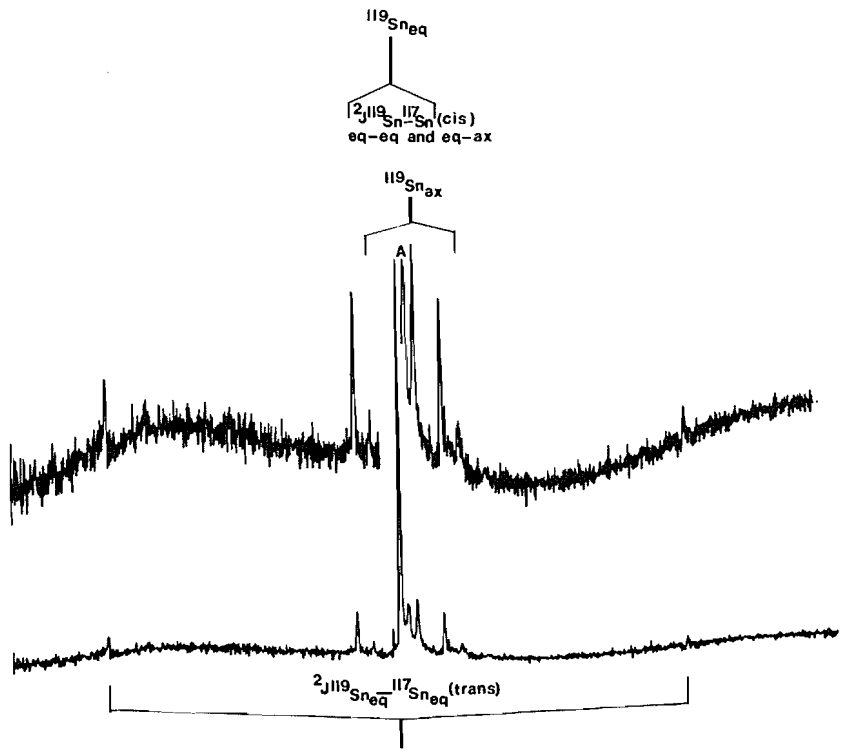


FIG. 7. $^{119}$Sn nmr spectrum of $(NEt_4)_3[Ru(SnCl_3)_5(MeCN)]$ in nitromethane at 15.02 MHz and 25 kHz sweepwidth. Resonance A due to collapsed pair of inner two members of AB pattern.

for the ruthenium analogue (Tables 6, 7), presumably due to the increase in size of the central atom. However, the same relative pattern exists, with the *trans* $^{119}Sn_{eq}$—$^{117}Sn_{eq}$ coupling being an order of magnitude larger than the corresponding *cis* coupling constants.

The large *trans* coupling again shows the second-order asymmetry effects about the main resonance, the calculated asymmetries 258 Hz (at 15.02 MHz) and 104 Hz (at 37.3 MHz) being in excellent agreement with observed values of 264 and 104 Hz, respectively.

Osmium possesses two magnetic isotopes $^{187}$Os ($I = \frac{1}{2}$, 1.64% natural abundance) and $^{189}$Os ($I =$ 3/2, 16.1% natural abundance). Careful observation (Figs. 5, 6) revealed the $^{119}Sn_{eq}$—$^{187}$Os spin–spin coupling at 15.02 and 37.3 MHz (1289 and 1290 Hz, respectively). Splitting due to $^{189}$Os is not observed presumably due to quadrupolar line broadening, $Q = 0.8 \times 10^{-28}$ m$^2$ (44).

*(c) $[Ru(SnCl_3)_5(MeCN)]^{3-}$, III*

The $^{119}$Sn nmr spectrum (Fig. 7, Table 8) reveals the same splitting patterns shown by **I** and **II**, but the couplings are less well resolved due to increased linewidths. No coupling to $^{99}$Ru is observed, whilst compared to **I** the *trans* $^{119}Sn_{eq}$—$^{117}Sn_{ax}$ coupling is reduced to 17 483 Hz. The two other couplings are almost equal (Table 8), and are only resolvable at the higher operating frequency. Heteronuclear second-order coupling effects were again observed for the large *trans* coupling, and calculated and observed asymmetries were in excellent agreement.

TABLE 8. Tin nmr data for the $[Ru(SnCl_3)_5(MeCN)]^{3-}$ anion[a,b]

| $\delta^{119}Sn_{eq} = -70.6$ ppm[c]; $-70.3$ ppm[d]<br>$\delta^{119}Sn_{ax} = -103.9$ ppm[c]; $-103.4$ ppm[d] | | |
|---|---|---|
| Coupling constant (Hz) | $^{119}$Sn—$^{117}$Sn[c] | $^{119}$Sn—$^{117}$Sn[d] |
| $^2J(Sn_{eq}—Sn_{eq})$*trans* | Not done | 17483(12) |
| $^2J(Sn_{eq}—Sn_{eq})$*cis* | 2650[e] | 2637(6) |
| $^2J(Sn_{eq}—Sn_{ax})$*cis* | 2650[e] | 2692(6) |

[a–d]Footnotes as in Table 6. Sharper resonances were observed for *d* which used a different sample to the *c* spectrum.
[e]Each resonance could not be resolved because $\Delta\nu_{1/2} \approx 80$ Hz.

A $^{13}$C nmr spectrum in $CD_3NO_2$ showed resonances due to the nitrile carbon (131.1δ) and the methyl carbon (3.8δ) of the coordinated acetonitrile, as well as those due to the $NEt_4^+$ cation (7.0 and 62.7δ). The nitrile carbon resonance was flanked by satellites, $^3J(^{119,117}Sn_{eq}—^{13}C) = 15.4$ Hz, but no such satellites were visible on the methyl

Can. J. Chem. Downloaded from www.nrcresearchpress.com by 210.87.254.40 on 09/06/12
For personal use only.

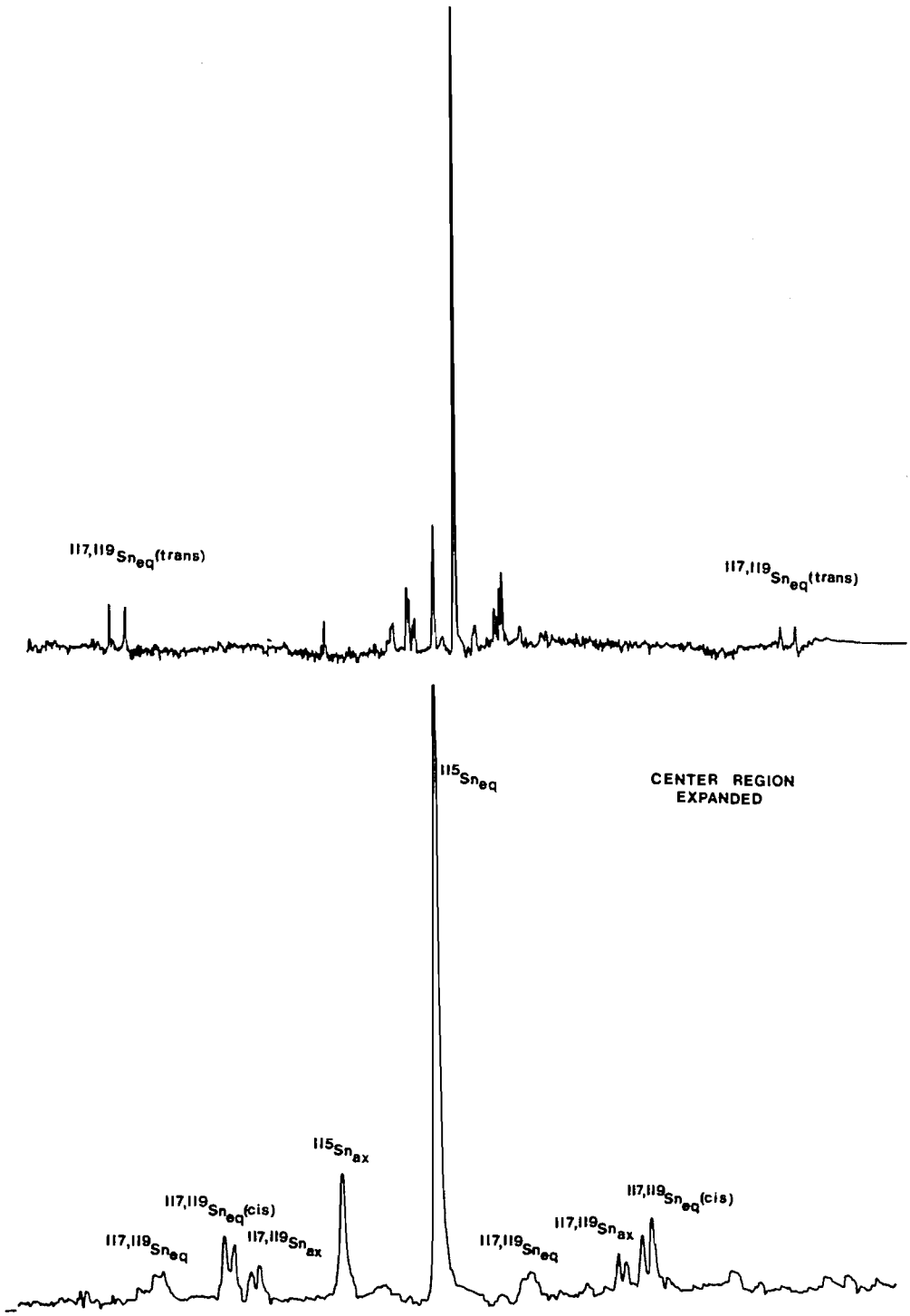


FIG. 8. $^{115}$Sn nmr spectrum of $(NEt_4)_4[Ru(SnCl_3)_5Cl]$ in nitromethane at 32.7 MHz and 25 kHz sweepwidth.

carbon resonance. A $^1$H nmr spectrum in $(CD_3)_2SO$ revealed a broad resonance at 3.30δ with satellites, $^4J(^{119,117}Sn—^1H) = 12$ Hz; this resonance was not apparent in $CD_3CN$ solution, and is thus attributed to the methyl protons of the coordinated acetonitrile.

TABLE 9. Calculated and observed resonance frequencies for $^{119}Sn$ and $^{115}Sn$, showing second-order coupling effects in $[Ru(SnCl_3)_5Cl]^{4-}$

| Tin system | Resonance frequency | | |
|---|---|---|---|
| | Observed | | Calculated |
| $^{119}Sn$ at 37.3 MHz[a] | 10699 | $J = 21254$ Hz | 10695.5 |
| | 10555 | | 10558.5 |
| | $\Delta = 144$ | | $\Delta = 137.0$ |
| $^{115}Sn$ at 32.7 MHz[b] | 9759 | $J = 19485$ Hz | 9763.3 |
| | 9726 | | 9721.7 |
| | $\Delta = 33$ | | $\Delta = 41.6$ |
| $^{115}Sn$ at 32.7 MHz[a] | 9341 | $J = 18624$ Hz | 9341.7 |
| | 9283 | | 9282.3 |
| | $\Delta = 58$ | | $\Delta = 59.4$ |

[a]From $^{117}Sn$ *trans* coupling.
[b]From $^{119}Sn$ *trans* coupling.

## Concluding remarks

Our initial studies aimed at the potential catalytic activity of ruthenium(II)–trichlorostannate(II) systems forced us into using the techniques of X-ray crystallography and tin nmr spectroscopy for characterization of the ruthenium(II) complexes. Although straightforward, the studies have revealed for the first time coupling to a $^{99}Ru$ nucleus ($I = 5/2$), very large two-bond coupling between $^{119}Sn$ and $^{117}Sn$, and the first observed second-order effects in seemingly "simple AX" systems. Studies on the solution chemistry of the ruthenium(II) complexes, particularly their interaction with carbon monoxide and hydrogen, will be reported later.

## Acknowledgements

We thank A. Brook and P. Morris for their efforts in obtaining the tin nmr spectra, Johnson Matthey Ltd. for the loan of ruthenium, and the Natural Sciences and Engineering Research Council of Canada for financial support.

1. J. F. YOUNG, R. D. GILLARD, and G. WILKINSON. J. Chem. Soc. A, 5176 (1964), and references therein.
2. P. G. ANTONOV, Y. N. KUKUSHKIN, V. I. ANUFRIEV, L. N. VASIL'EV, and L. V. KONOVALOV. Russ. J. Inorg. Chem. **24**, 231 (1979).
3. H. MORIYAMA, T. AOKI, S. SHINODA, and Y. SAITO. J. Chem. Soc. Dalton Trans. 639 (1981).
4. J. H. NELSON, V. COOPER, and R. W. RUDOLPH. Inorg. Nucl. Chem. Lett. **16**, 263 (1980).
5. J. H. NELSON and N. W. ALCOCK. Inorg. Chem. **20**, (1981).
6. B. R. JAMES. Homogeneous hydrogenation. Wiley, New York. 1973.
7. Y. KAWABATA, T. HAYASHI, and I. OGATA. J. Chem. Soc. Chem. Commun. 462 (1979).
8. G. C. BOND and M. HELLIER. J. Catal. **7**, 217 (1967).
9. S. SHINODA, H. MORIYAMA, Y. KISE, and Y. SAITO. J. Chem. Soc. Chem. Commun. 348 (1978).
10. C-H. CHENG and R. EISENBERG. J. Am. Chem. Soc. **100**, 5968 (1978).
11. B. R. JAMES, D. C. THACKRAY, and D. K. W. WANG. 63rd Can. Inst. Chem. Conf., Ottawa, Abstract ENER-32 (1980).
12. H. OKUNO, T. ISHIMORI, K. MIZUMACHI, and H. IHOCHI. Bull. Chem. Soc. Jpn. **44**, 415 (1971).
13. P. G. ANTONOV, Y. N. KUKUSHKIN, and V. I. KONNOV. Koord. Khim. (Eng.), **3**, 589 (1977).
14. L. J. FARRUGIA, B. R. JAMES, C. R. LASSIGNE, and E. J. WELLS. Inorg. Chim. Acta Lett. **53**, L261 (1981).
15. C. R. LASSIGNE, E. J. WELLS, L. J. FARRUGIA, and B. R. JAMES. J. Magn. Reson. **42**, 488 (1981).
16. J. DE MEULENAER and H. TOMPA. Acta Crystallogr. **19**, 1014 (1965).
17. G. GERMAIN, P. MAIN, and M. M. WOLFSON. Acta Crystallogr. B**26**, 274 (1970).
18. D. T. CROMER and J. B. MANN. Acta Crystallogr. A**24**, 321 (1968).
19. R. F. STEWART, E. R. DAVIDSON, and W. T. SIMPSON. J. Chem. Phys. **42**, 3175 (1965).
20. D. T. CROMER and D. LIBERMAN. J. Chem. Phys. **53**, 1891 (1970).
21. A. P. ZENS and D. M. GRANT. J. Magn. Reson. **30**, 85 (1978).
22. T. P. HIGGS, A. BROOKE, and E. J. WELLS. Unpublished results.
23. R. V. LINDSEY, JR., G. W. PARSHALL, and V. G. STOLBERG. J. Am. Chem. Soc. **87**, 658 (1965).
24. M. ELDER and D. HALL. J. Chem. Soc. A, 245 (1970).
25. S. F. WATKINS. J. Chem. Soc. A, 1552 (1969).
26. R. MASON and P. O. WHIMP. J. Chem. Soc. A, 2709 (1969).
27. P. PORTA, H. M. POWELL, R. J. MAWBY, and L. M. VENANZI. J. Chem. Soc. A, 455 (1967).
28. M. R. CHURCHILL and K. G. LIN. J. Am. Chem. Soc. **96**, 76 (1974).
29. R. O. GOULD, W. J. SIME, and T. A. STEPHENSON. J. Chem. Soc. Dalton Trans. 76 (1978).
30. International tables for X-ray crystallography. Vol. III. Kynoch Press. 1974.
31. E. N. YURCHENKO, E. T. DEVYATKINA, T. S. KHODASHOVU, M. A. PORAI-KOSHITS, V. I. KONNOV, V. A. VARNEK, P. G. ANTONOV, and YU. N. KUKUSHKIN. Koord. Khim. **5**, 552 (1979).
32. R. E. BENFIELD and B. F. G. JOHNSON. J. Chem. Soc. Dalton Trans. 1743 (1980).
33. J. B. CASEY, W. J. EVANS, and W. H. POWELL. Inorg. Chem. **20**, 1333 (1981).
34. H. A. BENT. Chem. Rev. **61**, 275 (1961).
35. R. L. LIVINGSTONE and C. N. R. RAO. J. Chem. Phys. **30**, 339 (1959).
36. J. K. STALICK, P. W. R. CORFIELD, and D. W. MEEK. Inorg. Chem. **12**, 1668 (1973).
37. F. R. POULSEN and S. E. RASMUSSEN. Acta Chem. Scand. **24**, 150 (1970).
38. B. KAMENAR and D. GRDENIC. J. Inorg. Nucl. Chem. **24**, 1039 (1962).
39. L. D. BROWN, C. F. J. BARNARD, J. A. DANIELS, R. J. MAWBY, and J. A. IBERS. Inorg. Chem. **17**, 2932 (1978).
40. E. N. YURCHENKO, V. A. VARNEK, G. L. ELIZAROVA, L. G. MATVIENKO, and M. S. IOFFE. Soviet J. Coord. Chem. **10**, 1178 (1979).
41. D. H. HARRIS, M. F. LAPPERT, J. S. POLAND, and N. MCFARLANE. J. Chem. Soc. Dalton Trans. 311 (1975).
42. K. A. OSTOJA STARZEWSKI and P. S. PREGOSIN. Adv. Chem. Ser. **196**, 23 (1982).
43. P. S. PREGOSIN and H. RÜEGGER. J. Magn. Reson. In press.
44. S. BOTTGENBACH, M. HERSCHEL, G. HERSEL, E. SCHRÖDL, N. WHITTLE, and W. J. CHILDS. Z. Phys. **269**, 189 (1974).

Can. J. Chem. Downloaded from www.nrcresearchpress.com by 210.87.254.40 on 09/06/12
For personal use only.

# A surface tension approach to the salting-out of nonpolar nonelectrolytes

ROBERT AVEYARD
*Department of Chemistry, The University, Hull, HU6 7RX England*
Received June 23, 1981

ROBERT AVEYARD. Can. J. Chem. **60**, 1317 (1982).

A simple approach is developed for the salting-out of nonpolar molecules by strongly solvated salts. The standard free energy of transfer of solute from pure solvent to salt solution, and hence the salting coefficient, $k$, is calculated in terms of the surface tension increment caused by the addition of salt to the solvent. In its simplest form the method gives $k$ in terms of the molar volumes of solvent and solute, and the osmotic coefficient of the salt solution. It is more successful in the prediction of $k$ than the McDevit and Long theory, and it also has advantages over the more complex scaled particle theory of salt effects. In addition to a range of nonpolar solutes, the salt effects on some alcohols are also considered but application to polar solutes generally requires a knowledge of experimentally determined surface tension increments which are not widely available. The correct order of magnitude for the temperature coefficient of $k$ at room temperature for some alkanes and $H_2$ in water is given, although minima in $k$ as a function of temperature, which have sometimes been observed, are not reproduced.

ROBERT AVEYARD. Can. J. Chem. **60**, 1317 (1982).

On a mis au point une méthode simple de relargage des molécules non polaires par les sels fortement solvatés. On a calculé l'énergie libre standard de transfert du soluté à partir du solvant pur jusqu'à une solution saline, et par conséquent le coefficient de salinité, $k$, en fonction de l'incrément de la tension de surface provoqué par l'addition de sel au solvant. Dans sa forme la plus simple, la méthode permet d'obtenir $k$ en fonction des volumes molaires de solvant et de soluté et du coefficient d'osmose de la solution saline. Elle a plus de succès dans la prévision de $k$ que la théorie de McDevit et Long et elle a certains avantages sur la théorie plus complexe de la particule à l'échelle des effets de sel. En plus d'une variété de solutés non polaires, on a également considéré les effets de sel sur certains alcools; toutefois son application à des solutés polaires requiert généralement une connaissance des incréments de la tension de surface déterminés expérimentalement et ces incréments ne sont généralement pas disponibles. On donne l'ordre de grandeur réel du coefficient de température de $k$ à la température ambiante pour quelques alcanes et l'hydrogène dans l'eau bien que les minima observés quelque fois pour $k$ en fonction de la température ne soient pas reproduits.

[Traduit par le journal]

## Introduction

The effects which salts have on the activity coefficients of nonelectrolytes in solution (usually in water) have long been of interest. A large body of experimental data exists concerning these "salt effects" and much is known empirically about the way in which different salts and nonelectrolytes behave when together in aqueous solution (1, 2). The situation with regard to the theoretical treatment of the effects, however, is not entirely satisfactory (3). In general, electrostatic theories have proved unsatisfactory, and until recently a thermodynamic approach of McDevit and Long (4) has had the most success in describing experimental results. In 1969 Shoor and Gubbins (5) applied scaled particle theory to the problem, and this has, relative to the McDevit–Long formulation (MLT), had a fair measure of success (6–12). The limitations of all these approaches have been summarised by Cross (3).

In 1975, Aveyard and Heselden (13) advanced an empirical approach to salting-out based on the effect of the salt on the surface tension of the solvent. At that time, however, a knowledge of the experimentally determined surface tension increment was required for the calculation of the free energy change accompanying salting-out. Subsequent work (14, 15) has led to a clearer understanding of salt desorption from liquid surfaces and allowed the fuller and more satisfactory treatment of the surface tension approach to salting-out which is described here. The method is tested on a wide variety of systems for which experimental data already exist.

## Theory

There are various possible contributions to salt effects depending on the kind of systems involved. The present approach is for nonpolar solutes in the presence of strongly solvated salts. It will not be expected to apply in its simple form to weakly solvated salts or to polar nonelectrolytes for reasons that will be apparent.

We consider the transfer, at a given concentration in ideal dilute solution, of 1 mol of nonpolar nonelectrolyte (component 3), from pure solvent (component 1) to 1 molar salt solution. The change in standard chemical potential, $\Delta\mu^{\ominus}$, of the nonelectrolyte for this transfer was previously given as (13)

$$[1] \quad \Delta\mu^{\ominus} = N_A\Omega(\gamma - \gamma_0) = 2.3RT\log f_3 = 2.3RTk$$

0008-4042/82/111317-10$01.00/0
©1982 National Research Council of Canada/Conseil national de recherches du Canada

Can. J. Chem. Downloaded from www.nrcresearchpress.com by 210.87.254.6 on 09/06/12
For personal use only.

Can. J. Chem. Downloaded from www.nrcresearchpress.com by 210.87.254.6 on 09/06/12
For personal use only.

where $\Omega$ is the effective surface area of the cavity required to contain a dissolved nonelectrolyte molecule, and $\gamma$ and $\gamma_0$ are the surface tensions of salt solution and pure solvent, respectively. The quantity $k$ ($= \log f_3$) is the salting-out constant in terms of which most experimental data are expressed, and $f_3$ is the activity coefficient of nonelectrolyte in the salt solution, relative to that (unity) in pure solvent. The other symbols have their usual significance. In the case of slightly soluble nonelectrolytes $k$ is usually determined as the initial slope of the plot of log solubility against electrolyte molality, although in practice such plots are almost always linear within the experimental errors, at least up to 1 molal electrolyte.

In writing eq. [1] it has been assumed that (*a*) the "surface tension" of a cavity of molecular dimensions can be taken as the macroscopic value, and (*b*) the solvent–solute interactions are the same in pure solvent and in salt solution. The former assumption is discussed later. With regard to the solvent–solute interactions it is known that strongly solvated salts are desorbed from macroscopic liquid–vapour surfaces (14, 15), and the basis of the present approach is that such salts are similarly repelled from the vicinity of nonpolar molecules in solution. This is equivalent to saying that the nonelectrolyte molecules cannot replace solvent molecules in the primary solvation sheath of an ion. Under these circumstances a solute molecule in salt solution is surrounded in its immediate vicinity by solvent molecules only, and so the predominant "solvent"–solute interactions involve only solvent molecules and not ions. For this reason solvent–solute interactions are supposed not to contribute significantly to salting-out.

The extent of the desorption of several strongly solvated 1,1-electrolytes (component 2) from a macroscopic interface between solvent and a second phase of low relative permittivity (e.g. air or alkane) can be accounted for by assuming the presence of an ion-free layer, thickness $\delta$, at the interface. On this basis it can be shown that (14)

$$[2] \quad d\gamma = c_2\delta\, d\mu_2 = -c_1\delta\, d\mu_1$$

where $\mu$ is chemical potential and $c$ is concentration (mol volume$^{-1}$). The molal osmotic coefficient, $\phi$, of salt solution, molality $m_2$, is defined by (16)

$$[3] \quad \ln a_1 = -\nu m_2 M_1 \phi$$

where $a_1$ is the molal activity of the solvent, $\nu$ the number of mol of ions per mol of salt, and $M_1$ is the molar mass (kg mol$^{-1}$) of solvent. Combination of eqs. [2] and [3] leads to

$$[4] \quad d\gamma = \nu c_1 \delta M_1 RT\, d(m_2\phi)$$

For a linear variation of $\gamma$ with $m_2\phi$, which is frequently observed (14, 15),

$$[5] \quad \Delta\gamma = \gamma - \gamma_0 = \nu c_1 \delta M_1 R T m_2 \phi$$

For $c_2 = 1$ mol dm$^{-3}$, from eq. [1], we have

$$[6] \quad k = N_A \Omega \Delta\gamma_{(c_2=1)}/2.3RT$$

so that, from eqs. [5] and [6]

$$[7] \quad k = \nu N_A \Omega \delta \phi_{(c_2=1)} (c_1 M_1 m_2)_{(c_2=1)}/2.3$$

Since $c_1 M_1 m_2 = c_2 = 1$ mol dm$^{-3}$

$$[8] \quad k = \nu N_A \Omega \delta \phi_{(c_2=1)}/2.3$$

The application of eq. [8] requires methods for the estimation of $\Omega$ and $\delta$. If we make the approximation that the solute (molar volume $V_3$) consists of close-packed spherical molecules in its pure state and assume the cavity area is equal to the surface area of the solute molecule (see Discussion), then

$$[9] \quad \Omega = \pi^{1/3}(4.44V_3/N_A)^{2/3}$$

It has been shown elsewhere (15) that $\delta$ is often approximately equal to $(r_H^+ - r_X^+)$ where $r_H^+$ is the effective radius of the solvated cation (17) and $r_X^+$ is the cation crystallographic radius. In this case

$$[10] \quad k = (\pi N_A)^{1/3}(4.44V_3)^{2/3}\nu(r_H^+ - r_X^+) \times \phi_{(c_2=1)}/2.3$$

Alternatively $\delta$ may be assumed equal to the molecular diameter $d_1$ of the solvent (15). On the assumption that the solvent (molar volume $V_1$) consists of close-packed spherical molecules in its pure state

$$[11] \quad \delta = d_1 = (4.44V_1/\pi N_A)^{1/3}$$

and combination of eqs. [8], [9], and [11] yields for a 1,1-electrolyte the very simple expression

$$[12] \quad k = 3.86 V_1^{1/3} V_3^{2/3} \phi_{(c_2=1)}$$

where the $V$ and $k$ are in m$^3$ mol$^{-1}$.

The quantities $r_H^+$ and $r_X^+$ are available for a variety of ions in water (17). Also $\phi$ values are readily available for many aqueous salt solutions (16), and we now proceed to investigate the applicability of eqs. [10] and [12], or their equivalents, to a range of systems for which experimental $k$ values have been reported.

## Comparison with experimental results

### *(a) Nonpolar solutes in water*

The experimental data referred to subsequently are taken from refs. 4, 7, 8, 13, and 18 to 22. Results for the salting-out from water of nonpolar solutes, from methane to dibenzyl, by LiCl, NaCl, and KCl

Can. J. Chem. Downloaded from www.nrcresearchpress.com by 210.87.254.6 on 09/06/12
For personal use only.

are plotted according to eq. [12] in Figs. 1 and 2. The lines are theoretical, and the agreement for NaCl and KCl is excellent for all the solutes. For LiCl the agreement is good, with the theoretical values of $k$ being about 20% higher than experiment in most cases. It should be mentioned that MLT predicts values of $k$ which are normally high by a factor of between 2 and 3 for the kind of systems of present interest (4). Further results for 1,1-electrolytes are shown in Tables 1 and 2. The values of $\Omega$ for the gases represented in Table 1 were calculated using the equilibrium diameters, $d_{min}$, quoted by de Boer (23), and $k$ was calculated using the equation equivalent to eq. [12].

$$[13] \quad k = 0.715\nu(\pi N_A)^{2/3} d_{min}^2 V_1^{1/3} \phi_{(c_2=1)}$$

For NaCl the agreement is reasonable, the theoretical values (except for He) being low, by up to 50% in the case of Kr. The correct value is given for $H_2$. The predicted $k$ values for both He and Kr with a range of salts are also in good agreement with experiment.

In cases where $\delta$ is known from surface tension measurements $k$ may be calculated using eq. [8] and so for the gases in Table 1 we have

$$[14] \quad k = \nu N_A \pi d_{min}^2 \delta \phi_{(c_2=1)}/2.3$$

Reassuringly this procedure gives values of $k$ very similar to those from eq. [13], as shown in Table 1. The $k$ values obtained from eq. [10], or its equivalent in terms of $d_{min}$, are in some cases lower than $k$ (eq. [14]) and hence in poorer agreement with experiment.

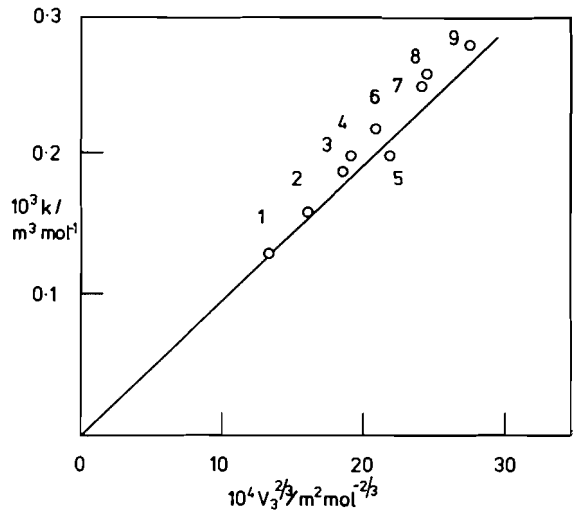


FIG. 1. Salting constants $k$ for nonpolar solutes in aqueous NaCl at 298 K. Full line according to eq. [12]; points are experimental values for *1*, methane; *2*, ethane; *3*, propane; *4*, benzene; *5*, toluene; *6*, butane; *7*, ethyl benzene; *8*, naphthalene; *9*, diphenyl. Molar volumes of methane to *n*-butane (as liquids) obtained by linear extrapolation of molar volumes of liquid alkanes pentane and upwards.

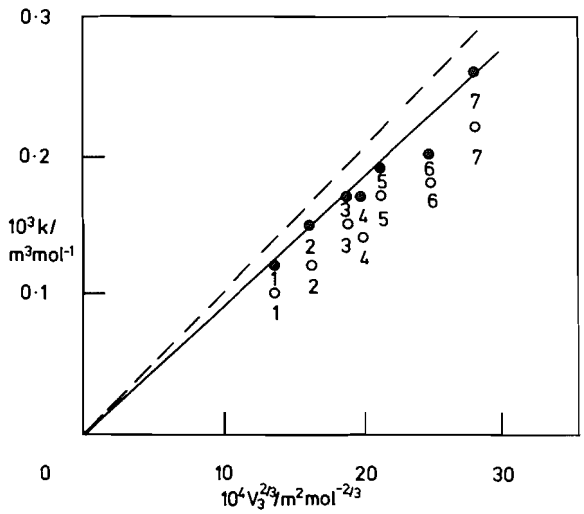


FIG. 2. Salting constants $k$ for nonpolar solutes in aqueous KCl and LiCl at 298 K. Full line and dashed line according to eq. [12] for KCl and LiCl respectively. Points (○ for LiCl and ● for KCl) are experimental values for *1*, methane; *2*, ethane; *3*, propane; *4*, benzene; *5*, butane; *6*, naphthalene; *7*, diphenyl. Molar volumes of alkanes obtained as in legend to Fig. 1.

Results for the salting-out of benzene by alkali halides are shown in Table 2. The $k$ values from eq. [12] are in most cases in very reasonable accord with experiment, the poorest agreement being for CsCl and NaI where $k$ (eq. [12]) is high by a factor of about 2. This is perhaps not surprising since NaI is not strongly repelled from the air–water surface (24), and the same is probably true for CsCl, so that it is likely that solute–ion interactions become important in these instances. Equation [10] also predicts reasonable values for $k$ relative to those given by MLT, which are also shown for comparison in Table 2.

For systems containing salts other than simple strongly solvated 1,1-electrolytes it would be optimistic to expect the simple model on which eq. [12] is based to be very successful; eq. [10] might be thought to offer a better hope. Apparently reliable data exist for the salting-out of hydrocarbons from aqueous solution by $Na_2SO_4$, $Al_2(SO_4)_3$, $NaNO_3$, $NaClO_4$, $BaCl_2$, and $LaCl_3$, and these results are now considered. Results are compared for salts other than $Na_2SO_4$ in Table 3; comparisons for systems containing $Na_2SO_4$ are given in Table 4. With reference to Table 3, eq. [10] gives remarkably good agreement with experiment. Values of $k$ obtained using $\delta$ rather than $(r_H^+ - r_X^+)$ where available, are in even better agreement except for butane with $LaCl_3$ where in any case the experimental value for $k$ at 298 K is in some doubt (19).

Can. J. Chem. Downloaded from www.nrcresearchpress.com by 210.87.254.6 on 09/06/12
For personal use only.

TABLE 1. Values of $10^3\,k/m^3\,mol^{-1}$ at 298 K for various gases with alkali halides and $BaCl_2$

(*a*) NaCl with various gases ($\delta = 0.38$ nm)

| | Value for gas = | | | | | | |
|---|---|---|---|---|---|---|---|
| Parameter | He | Ne | A | Kr | Xe | $H_2$ | $N_2$ |
| $k$ (expt) | 0.08 | 0.10 | 0.13 | 0.15 | 0.15 | 0.09 | 0.13 |
| $d_{min}$/nm | 0.425 | 0.340 | 0.405 | 0.422 | 0.465 | 0.407 | 0.423 |
| $k$ (eq. [13]) | 0.10 | 0.06 | 0.09 | 0.10 | 0.12 | 0.09 | 0.10 |
| $k$ (eq. [14]) | 0.11 | 0.07 | 0.10 | 0.10 | 0.13 | 0.10 | 0.10 |

(*b*) Helium with various salts ($d_{min} = 0.425$ nm)

| | Value for salt = | | | | |
|---|---|---|---|---|---|
| Parameter | LiCl | KCl | KI | NaBr | $BaCl_2$ |
| $k$ (expt) | 0.06 | 0.07 | 0.08 | 0.09 | 0.17 |
| $k$ (eq. [13]) | 0.11 | 0.09 | 0.10 | 0.10 | 0.15 |
| $\delta$/nm | 0.32 | 0.35 | 0.27 | 0.30[a] | |
| $k$ (eq. [14]) | 0.10 | 0.09 | 0.07 | 0.09 | |

(*c*) Krypton with various salts ($d_{min} = 0.422$ nm)

| | Value for salt = | | | | |
|---|---|---|---|---|---|
| Parameter | LiCl | KCl | KI | KBr | $BaCl_2$ |
| $k$ (expt) | 0.12 | 0.12 | 0.12 | 0.12 | 0.30 |
| $k$ (eq. [13]) | 0.10 | 0.09 | 0.09 | 0.09 | 0.14 |
| $\delta$/nm | 0.32 | 0.35 | 0.27 | 0.30 | |
| $k$ (eq. [14]) | 0.10 | 0.09 | 0.07 | 0.08 | |

[a] Value for NaBr not available; that shown is for KBr. All values of $\delta$ taken from ref. 14.

TABLE 2. Values of $10^3\,k/m^3\,mol^{-1}$ at 298 K for the salting-out of benzene by alkali halides

| | Value for salt = | | | | | | |
|---|---|---|---|---|---|---|---|
| Parameter | LiCl | NaCl | KCl | RbCl | CsCl | NaBr | NaI |
| $k$ (expt) | 0.14 | 0.20 | 0.17 | 0.14 | 0.09 | 0.16 | 0.10 |
| $k$ (eq. [12]) | 0.21 | 0.19 | 0.18 | 0.18 | 0.17 | 0.19 | 0.20 |
| $k$ (eq. [10]) | 0.19 | 0.14 | 0.10 | 0.09 | 0.08 | 0.15 | 0.15 |
| $k$ (MLT) | 0.31 | 0.42 | 0.34 | 0.31 | 0.26 | 0.35 | 0.27 |

TABLE 3. Values of $10^3\,k/m^3\,mol^{-1}$ for the salting-out of hydrocarbons at 298 K by salts other than alkali halides

| | Value for system = | | | |
|---|---|---|---|---|
| Parameter | Benzene/ $BaCl_2$ | Benzene/ $Al_2(SO_4)_3$ | Benzene/ $NaNO_3$ | Benzene/ $NaClO_4$ |
| $k$ (expt) | 0.33 | 1.2 | 0.12 | 0.11 |
| $k$ (eq. [10]) | 0.22 | 0.57 | 0.13 | 0.14 |
| $k$ ($\delta$)[a] | 0.34 | 0.86 | — | — |

| | Value for system = | | | |
|---|---|---|---|---|
| Parameter | Ethylene/ $LaCl_3$[b] | Butane/ $LaCl_3$[b] | Naphthalene/ $NaClO_4$ | Diphenyl/ $NaClO_4$ |
| $k$ (expt) | 0.28 | ~0.5 | 0.10 | 0.11 |
| $k$ (eq. [10]) | 0.38 | 0.49 | 0.18 | 0.21 |
| $k$ ($\delta$) | 0.33 | 0.42 | — | — |

[a] $\delta$ values taken from ref. 50.
[b] $V$(butane) obtained by extrapolation from liquid alkanes and $V$(ethylene) has been taken as that for ethane, obtained in the same way.

The poorest agreement in Table 3 is for benzene with $Al_2(SO_4)_3$; that for systems containing $Na_2SO_4$ (Table 4) is even less satisfactory. It is tempting to suggest that the discrepancies arise in some way from the surface chemical properties of the $SO_4^{2-}$ ion. The values of $(r_H^+ - r_X^+)$ for $Al^{3+}$ and $Na^+$ are 0.425 nm and 0.263 nm respectively and yet the $\delta$ values for the plane surfaces of aqueous solutions of $Al_2(SO_4)_3$ and $Na_2SO_4$ are 0.64 nm and 0.56 nm respectively. It is obvious then that these salts are repelled from the macroscopic air–water surface to a greater extent than would be indicated by the thickness of the cation solvation sheaths. The reasons for this are not known, and indeed judging from the experimental $k$ values it may be that the $\delta$ value around a microscopic cavity is even larger. It is instructive to note that the average separation between ions in a solution of a concen-

TABLE 4. Values of $10^3 k/m^3\,mol^{-1}$ for the salting-out of hydrocarbons by $Na_2SO_4$ at 298 K

| Parameter | Value for solute = | | | | | |
|---|---|---|---|---|---|---|
| | Benzene | Naphthalene | THN[a] | Diphenyl | DPM[b] | DPMP[c] |
| $k$ (expt) | 0.54 | 0.72 | 0.74 | 0.84 | 0.88 | 1.05 |
| $k$ (eq. [10]) | 0.14 | 0.19 | 0.20 | 0.22 | 0.23 | 0.29 |
| $k$ ($\delta = 0.56$ nm) | 0.30 | 0.40 | 0.43 | 0.47 | 0.49 | 0.62 |
| $k$ ($\delta = 1.00$ nm) | 0.54 | 0.71 | 0.77 | 0.84 | 0.88 | 1.11 |

[a] 1,2,3,4-Tetrahydronaphthalene.
[b] Diphenylmethane.
[c] 2,4-Diphenyl-2-methyl-2-pentene.

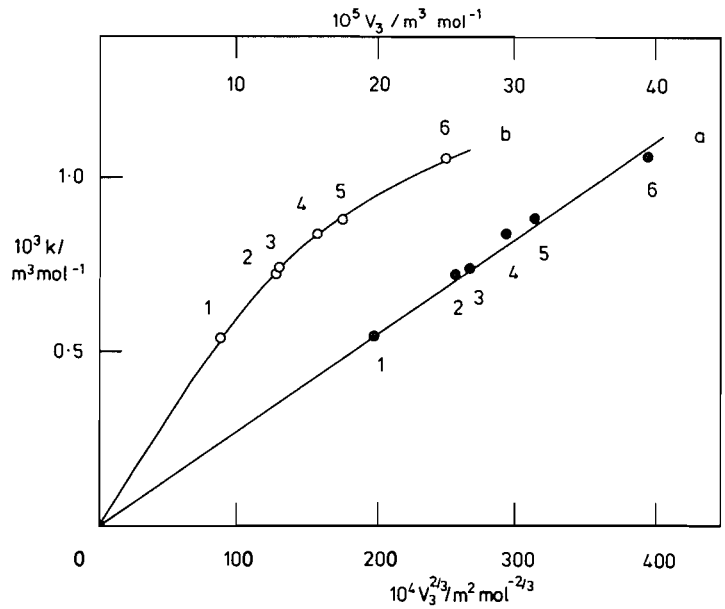


FIG. 3. Relationship between $k$ and solute molar volumes in aqueous $Na_2SO_4$. (*a*) $k$ versus $V_3^{2/3}$; (*b*) $k$ versus $V_3$. Points for *1*, benzene; *2*, naphthalene; *3*, 1,2,3,4-tetrahydronaphthalene; *4*, diphenyl; *5*, diphenylmethane; *6*, 2,4-diphenyl-2-pentene.

tration of 1 mol dm$^{-3}$ is only about 0.8 nm for a 1,2-electrolyte (16). If solvated anion, cation, or both are large it is not difficult to imagine that this, coupled with the requirement for electroneutrality in the "surface" region surrounding a small cavity could mean the desorption here is very different from that at a macroscopic surface. In any event it is interesting that if a $\delta$ value of 1.0 nm is assumed for $Na_2SO_4$ around a cavity excellent agreement between $k(\delta)$ and $k$(expt) is obtained in all cases for the wide range of solutes represented in Table 4.

Finally in this context we note that MLT predicts a linear dependence of $k$ on $\bar{V}_3$ for a given salt and solvent, and the partial molar volume $\bar{V}_3$ can usually, without large error, be equated to $V_3$. In contrast, eq. [12] gives $k \propto V_3^{2/3}$. It can be seen in Fig. 3 that the experimental $k$ values plotted against $V_3^{2/3}$ for the systems in Table 4 lie on a straight line passing through the origin, whereas the plot involving $V_3$ has marked curvature.

*(b) Alcohols in water*

The present approach, based as it is on the desorption of ions from the interface with a region of low dielectric constant, is clearly inappropriate for application to polar regions of nonelectrolyte molecules. However, if $\Delta\gamma$ for the salt desorption (or adsorption) at an interface between the solvent and an appropriate second polar phase is known, the salt effect on the polar group can be estimated and hence $k$ for the whole molecule obtained.

It is assumed that $k$ can be considered to be made up of additive group contributions (7). Then for the salt effect on, say, an alcohol

[15] $k = k_c + k_h$

Can. J. Chem. Downloaded from www.nrcresearchpress.com by 210.87.254.6 on 09/06/12
For personal use only.

TABLE 5. Values of $10^3\,k/m^3\,mol^{-1}$ for the salting-out of *n*-alkanols and ethylene glycol at 298 K[a]

(*a*) Sodium chloride

| | Value for solute = | | | | | | |
|---|---|---|---|---|---|---|---|
| Parameter | Methanol | Ethanol | Propanol | Butanol | Pentanol | Hexanol | Ethylene glycol |
| *k* (expt) | 0.07 | 0.12 | 0.17 | 0.19 | 0.21 | 0.23 | 0.04 |
| *k* (eq. [16]) | 0.08 | 0.11 | 0.15 | 0.18 | 0.22 | 0.25 | 0.10 |

(*b*) Sodium bromide

| | Value for solute = | | | |
|---|---|---|---|---|
| Parameter | Methanol | Ethanol | Propanol | Ethylene glycol |
| *k* (expt) | 0.06 | 0.10 | 0.13 | 0.03 |
| *k* (eq. [16]) | 0.05 | 0.07 | 0.10 | 0.06 |

(*c*) Sodium iodide

| | Value for solute = | | | |
|---|---|---|---|---|
| Parameter | Methanol | Ethanol | Propanol | Ethylene glycol |
| *k* (expt) | 0.04 | 0.08 | 0.10 | 0.01 |
| *k* (eq. [16]) | −0.02 | −0.02 | −0.03 | −0.03 |

[a]Experimental results for methanol, ethanol, propanol, and ethylene glycol are from ref. 7 and are for 25°C. For butanol, pentanol, and hexanol data from ref. 13 for 20°C are given. Small adjustments for temperature and concentration scale differences have not been made since they are insignificant in the present context. $\Delta\gamma(c_2 = 1)$ for NaCl at the decanol/water interface = 0.75 mN m$^{-1}$ (25). Corresponding values for NaBr and NaI are unknown but have been assumed equal to those for KBr and KI (0.40 and −0.55 mN m$^{-1}$ respectively) since $\Delta\gamma(c_2 = 1)$ for NaCl is equal to that for KCl. $\Delta\gamma(c_2 = 1)$ for the hydrocarbon/water interfaces are taken from ref. 14 and are 1.41 and 0.95 mN m$^{-1}$ for NaCl and NaBr respectively. The value for NaI has been taken to be equal to that, −0.07 mN m$^{-1}$, for KI.

where subscript c refers to the hydrocarbon moiety and h to the hydroxyl region. Combination of eqs. [6] and [15] gives

$$[16]\quad k = (N_A/2.3RT)(\Omega_c\Delta\gamma_c + \Omega_h\Delta\gamma_h)$$

where $\Delta\gamma$ refers to $c_2 = 1\,mol\,dm^{-3}$.

For the systems considered we have estimated $\Omega$ as follows. On the assumption of spherical close-packed molecules in the pure liquid state the molecular surface areas of methanol and ethylene glycol are 0.67 nm$^2$ and 0.81 nm$^2$ respectively. It is supposed that in each of these molecules the hydroxyl groups contribute half the surface area and the hydrocarbon the other half. In the case of the *n*-alkanols the dissolved alkyl chain has been supposed to be a square prism giving $\Omega$ per methylene group of 0.24 nm$^2$. The appropriate $\Delta\gamma$ values have been taken from desorption studies of salts from hydrocarbon–water and decanol–water interfaces (14, 25). Theoretical values of *k* calculated on this basis are compared with experiment in Table 5, where it is seen that agreement for systems containing NaCl and NaBr is remarkably good. Both $\Delta\gamma$ values (eq. [16]) for NaI are negative so the predicted *k* values are also negative, but small, whereas experimental values are small and positive.

Although this method is fairly successful it is unlikely to be of great use at present since experimental $\Delta\gamma$ are required and these are not generally available.

## Discussion

Previous workers (26–29) have used values of surface or interfacial tension to calculate the free energy of cavity formation in connection with solubilities in various kinds of system. Two obvious difficulties which arise with the application of such methods concern the possible variation of the free energy of cavity formation with curvature of the cavity surface, and the suitable choice of the effective surface of the cavity. Sinanoglu (30) has developed a theory for the estimation of the free energy of formation, $G_c$, of microscopic cavities with highly curved surfaces. The expression for $G_c$ may be written

$$[17]\quad G_c(J\,mol^{-1}) = 29.127K_1^{e}v_2^{2/3}\gamma \times \left\{1 - \left(1 - \frac{K_1^{s}}{K_1^{e}}\right)\left(\frac{\partial \ln\gamma}{\partial \ln T} + \frac{2\alpha T}{3}\right)\right\}$$

where $K_1^e$ and $K_1^s$ are quantities which modify the surface energy and entropy of planar surfaces to allow for curvature, and $\alpha$ is the coefficient of

Can. J. Chem. Downloaded from www.nrcresearchpress.com by 210.87.254.6 on 09/06/12
For personal use only.

Can. J. Chem. Downloaded from www.nrcresearchpress.com by 210.87.254.6 on 09/06/12
For personal use only.

thermal expansion of the solvent. In eq. [17], $\gamma$, the solvent surface tension, is in mN m$^{-1}$ and $v_2$, the solute molecular volume, is in Å$^3$. The values for $G_c$ given by eq. [17], however, does not differ greatly from the value of $N_A\Omega\gamma$. For example, the introduction of spherical cavities of diameter 6 Å into water at 25°C using values of $K_1^s$ and $K_1^e$ calculated as described in ref. 30 with the molecular diameter of water taken as 2.75 Å, results in $G_c$ = 51.9 kJ mol$^{-1}$, whereas for the same process $N_A\Omega\gamma$ is 49.0 kJ mol$^{-1}$.

More generally it has been widely supposed that, for liquid droplets and vapour bubbles in liquids, surface tension should vary with curvature (31, 32). Thus for a spherical bubble of radius $r$ in a liquid, the equation

$$[18] \quad \gamma(\infty)/(r) = [1 - (d_1/r)]^{-1}$$

has been advanced, where $\infty$ refers to the plane surface. Equation [18] is based on thermodynamic arguments which may not be expected to hold for very small $r$, where the equation obviously breaks down. It has been suggested that the equivalent of eq. [18] for small droplets considerably overestimates the change in surface tension with curvature (33) and it is interesting that experiments on critical condensation nuclei (with radii between about 1.0 and 1.5 nm) tend to confirm this view (34). Recent work (35) involving the formation of capillary condensed liquids between crossed mica cylinders has also led to the claim that the equations of macroscopic thermodynamics are valid, and macroscopic surface tensions pertain, for highly curved surfaces, in some cases with radii as small as 5 Å.

To calculate the free energy of cavity formation it is necessary to choose the appropriate value of $\Omega$, which is obviously an ill-defined quantity for a molecular cavity. In a discussion of hydrophobic bonding Reynolds *et al.* (36) and Hermann (37) took the surface of hydrocarbon groups in contact with water as being through the centres of water molecules in contact with hydrocarbon. This choice was made because the interest was in the number of water molecules at the "interface"; it has the disadvantage that the area is not zero for a point solute molecule. Israelachvili *et al.* (38), in the calculation of the transfer free energy of hydrocarbon chains from water to hydrocarbon, on the other hand, claim that $\Omega$ should be calculated on the assumption that the surface passes through the van der Waals boundary of the methylene groups. However, the free energy change for the transfer of the —$CH_2$— group from hydrocarbon to water calculated on this basis is high, for any reasonable choice of $\Omega(CH_2)$, by a factor of about 2 (29). Clearly then, there are conceptual and practical ambiguities in the application of ideas appropriate for macroscopic systems to microscopic systems, and the present approach to salting-out must, for the time being, be regarded as semi-empirical at best. It is worth noting, however, that the method only requires that *changes* in free energy of cavity formation on salt addition be correctly given by $\Omega\Delta\gamma$. It is, of course, possible that both $\Omega$ and $\Delta\gamma$ are incorrectly chosen but that their product is correct as a result of the fortuitous cancellation of errors.

An alternative method for the calculation of the free energy of cavity formation is to use the scaled particle theory (SPT) (39). Pierotti has employed SPT to calculate the thermodynamic parameters of solution of nonpolar gases in nonpolar solvents (40) and in water (41), although some aspects of this procedure have been questioned (42, 43). Subsequently Shoor and Gubbins (5) advanced a theory of salt effects on nonpolar nonelectrolytes using SPT, which was developed further by Masteron and Lee (6). Since then several sets of workers have used the approach for both polar and nonpolar solutes and for systems containing tetraalkylammonium ions (7–13).

In the application of SPT to salt effects it is supposed that ions and solvent molecules are randomly distributed around dissolved nonelectrolyte molecules and so changes in solvent–solute interactions accompanying solute transfer must be allowed for. This gives rise to a contribution, $k_i$, to $k$; the contribution from cavity transfer is denoted $k_{cav}$. In the surface tension method $k_i = 0$ so that clearly the two approaches are based on different assumptions.

For NaCl, SPT is successful for small nonpolar solutes but less so for larger molecues such as benzene, the disagreement between experiment and theory being supposed to arise from the magnitude of the calculated ion–solute interactions (6, 8). The present method, on the other hand, is very successful for NaCl with both large and small solute molecules (see Fig. 1). It is interesting that even for small solute molecules such as methane, $k_i$ makes a substantial contribution to $k$ in SPT so that although both approaches give agreement with experiment, the cavity terms are substantially different (see Table 6).

An alternative statistical mechanical approach to salt effects has been advanced by Friedman and co-workers (44, 45). Experimental values of $k$ can

TABLE 6. Comparison of SPT and surface tension approach

| | $k_i$ (SPT) | $k$ (SPT) | $k$ (eq. [12]) | $k$ (expt) |
|---|---|---|---|---|
| $CH_4$/NaCl | −0.08 | 0.13 | 0.13 | 0.13 |

Can. J. Chem. Downloaded from www.nrcresearchpress.com by 210.87.254.6 on 09/06/12
For personal use only.

be considered to be made up of additive contributions from ions of the electrolyte (1), and this feature is brought out by Friedman's theory. We cannot say if the surface tension approach reflects this however, since it is not clear from the available data if $d\gamma/dm_2$ is ion additive or not. Further, ion additivity in $k$ suggests that $Li^+$ salts out a given nonelectrolyte less strongly than $Na^+$ and sometimes less than $K^+$. Values of $k$ calculated from the present approach do not reflect this (Table 2) even though eq. [10] (but not eq. [12]) might have been expected to be successful in this respect.

An interesting but tentative conclusion arising from Friedman's work is that it appears possible from the generally negative signs of the ion–nonelectrolyte Gurney parameters (i.e. the free energy change per mol of solvent displaced from the solute cospheres due to overlap) that the nonelectrolyte molecules may penetrate the ion cospheres. In contrast the basis of the surface tension approach is that nonelectrolyte and ions are always separated by the ion solvation sheath, for the kind of systems considered.

A final point from Friedman's work which is relevant in the present context is the way in which $k$ varies with the nonelectrolyte molar volume for a given electrolyte. For 1,1-electrolytes the statistical mechanical approach gives $k$, in the limit of low concentration of salt and nonelectrolyte, as the sum of the osmotic virial coefficients B (volume per mol) for interactions between nonelectrolyte and each of the ion species. The surface tension approach suggests that $k$ is linearly related to the surface area of the nonelectrolyte molecule and hence to $V_3^{2/3}$ (eq. [12]; Figs. 1–3). There appears to be no theoretical basis for supposing that, for a given salt with a series of nonelectrolyte molecules, the sum of the ion–molecule virial coefficients should vary linearly with the molecular surface area, although in practice such an approximate relationship could exist.

The prediction of the temperature variation of $k$ is a much more stringent test of theory than the prediction of $k$ at a single temperature. Enthalpies of transfer of various solutes from water to aqueous solutions of tetraalkylammonium bromides have been calculated by Lucas and Feillolay using SPT with qualitative, and in some cases quantitative success (11, 12), while Desrosiers and Desnoyers have obtained enthalpies of transfer of $Bu_4N^+$ ions from water to mixed aqueous solvents (9). Aveyard and Heselden (13) calculated enthalpies for the salting-out of some alkanols by NaCl obtaining reasonable agreement between experiment and theory. More recently Cross and McTigue (46) have calculated the temperature variation of $k_c$ using SPT but the interaction parameters for various alkyl acetates and (mainly) alkali halides were then obtained by subtraction of the cavity contributions from experimentally determined values. The SPT does not, however, appear to have been used to calculate the temperature dependence of $k$ for the simple kind of systems which are the main concern of this paper.

On the basis of the surface tension approach we have from eq. [1]

$$[19]\quad \frac{\partial k}{\partial T} = -\frac{N_A \Delta\gamma \Omega}{2.3RT^2} + \frac{N_A}{2.3RT} \times \left\{\Omega\left(\frac{\partial \Delta\gamma}{\partial T}\right) + \Delta\gamma\left(\frac{\partial \Omega}{\partial T}\right)\right\}$$

Also from standard thermodynamics

$$[20]\quad \frac{\partial k}{\partial T} = -\frac{\Delta h^\ominus}{2.3RT^2}$$

so that from eqs. [1], [19], and [20]

$$[21]\quad \Delta s^\ominus = -N_A\left\{\Omega\left(\frac{\partial \Delta\gamma}{\partial T}\right) + \Delta\gamma\left(\frac{\partial \Omega}{\partial T}\right)\right\}$$

where $\Delta h^\ominus$ and $\Delta s^\ominus$ are respectively the standard enthalpy and entropy of solute transfer. The quantity $(\partial\Delta\gamma/\partial T)$ is not known for many systems but for NaCl in water it is effectively zero at around room temperature (24). The coefficient $(\partial\Omega/\partial T)$ cannot be calculated with certainty; for methane in water, solute partial molar volumes have been obtained by dilatometry (see ref. 47) at 0 and 50°C, and from these data $(\partial\Omega/\partial T) \simeq 5 \times 10^{-4}\ \mathrm{nm^2\ K^{-1}}$. The contribution to $(\partial k/\partial T)$ from this source is therefore about $+1 \times 10^{-4}\ \mathrm{dm^3\ mol^{-1}\ K^{-1}}$. For the same system the term $-(N_A\Delta\gamma\Omega/2.3RT^2)$ at 298 K is about $-5 \times 10^{-4}\ \mathrm{dm^3\ mol^{-1}\ K^{-1}}$. In this case, and we believe for the other systems (at 298 K) mentioned below, we may therefore write the approximation

$$[22]\quad \frac{\partial k}{\partial T} \simeq -\frac{N_A \Delta\gamma \Omega}{2.3RT^2}$$

In writing eq. [22] we are thus assuming $\Delta s^\ominus$ is negligible. It is interesting that the entropy of cavity transfer from water to aqueous NaCl as calculated by SPT (46) is also about zero.

In Fig. 4 some $k$ values, experimentally determined over a range of temperature, are compared with those calculated from eq. [1] assuming $\Omega$ and $\Delta\gamma$ to be constant. The agreement is moderately good but the calculated $(\partial k/\partial T)$ (eq. [22]) are

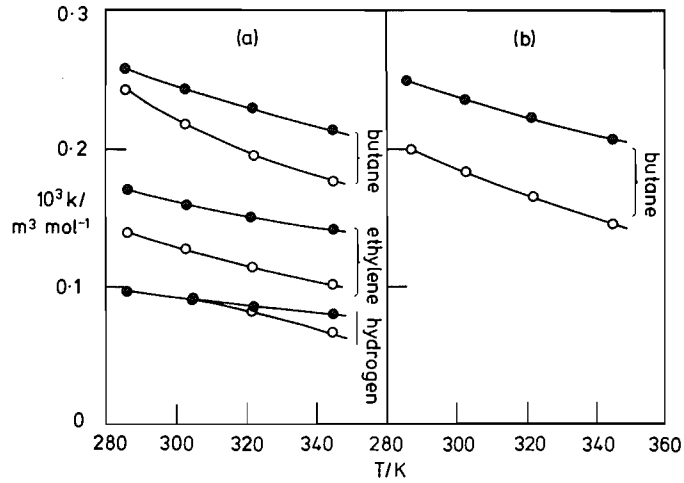


FIG. 4. Salting constants as a function of $T$. (*a*) NaCl, (*b*) KCl. ●, from eq. [1], ○, experimental.

smaller in all instance than the experimental temperature coefficients. Clearly, eq. [1] will not reproduce minima in $k$ versus $T$ plots which have been observed in some cases (48), but it may be that the inclusion of correct values of the terms in $(\partial\Delta\gamma/\partial T)$ and $(\partial\Omega/\partial T)$ in eq. [19] would lead to a prediction of the minima.

## Conclusions

(*1*) The present approach is expected to apply to nonpolar solutes and strongly solvated salts in any solvent, including water.

(*2*) For such systems the method is generally considerably more successful in the prediction of $k$ than the theory of McDevit and Long.

(*3*) The proposed model differs from that assumed in the scaled particle treatment; in particular in the former, ions are supposed to be absent from the immediate surroundings of a solute molecule and so solute–solvent interactions do not contribute to the calculated $k$. The surface tension approach is at least as successful as SPT for appropriate systems and appears to be superior for large solutes.

(*4*) The SPT, though elegant, is not easy to apply unambiguously since the required parameters are not always known with sufficient accuracy. In particular the selection of reliable Lennard–Jones parameters ($\varepsilon$ and $\sigma$) for the solute can be troublesome, and calculated $k$ values are very sensitive to the choice of ion diameters. In contrast, in its simplest form, the surface tension method requires only a knowledge of solvent and solute molar volumes, and of osmotic coefficients.

(*5*) The correct sign and order of magnitude are given for the temperature coefficient of $k$ although eqs. [1] and [22] do not predict minima in $k$ as a function of $T$. It is possible that the full form (eq. [19]) would be successful in this respect.

The simplicity and apparent success of the present approach bring to mind Rothschild's Law (49): "To any problem, no matter how difficult, there is a simple solution if you will only search for it. This solution will turn out to be wrong."

## Acknowledgment

The author wishes to thank one of the referees for drawing his attention to the work of Friedman and co-workers, and for pointing out some of the salient features of this work.

1. F. A. LONG and W. F. MCDEVIT. Chem. Rev. **51**, 119 (1952).
2. V. F. SERGEEVA. Russ. Chem. Rev. **34**, 309 (1965).
3. R. F. CROSS. J. Phys. Chem. **79**, 1822 (1975).
4. W. F. MCDEVIT and F. A. LONG. J. Am. Chem. Soc. **74**, 1773 (1952).
5. S. K. SHOOR and K. E. GUBBINS. J. Phys. Chem. **73**, 498 (1969).
6. W. L. MASTERTON and T. P. LEE. J. Phys. Chem. **74**, 1776 (1970).
7. F. L. WILCOX and E. E. SCHRIER. J. Phys. Chem. **75**, 3757 (1971).
8. Y. T. CHANG, M. Y. SCHRIER, and E. E. SCHRIER. J. Phys. Chem. **78**, 165 (1974).
9. N. DESROSIERS and J. E. DESNOYERS. Can. J. Chem. **54**, 3800 (1976).
10. M. LUCAS and A. TROBRIAND. J. Phys. Chem. **75**, 1803 (1971).
11. M. LUCAS and A. FEILLOLAY. J. Phys. Chem. **75**, 2330 (1971).
12. M. LUCAS and A. FEILLOLAY. J. Phys. Chem. **76**, 3068 (1972).
13. R. AVEYARD and R. HESELDEN. J. Chem. Soc. Faraday I **71**, 312 (1975).
14. R. AVEYARD and S. M. SALEEM. J. Chem. Soc. Faraday I **72**, 1609 (1976).

Can. J. Chem. Downloaded from www.nrcresearchpress.com by 210.87.254.6 on 09/06/12
For personal use only.

15. R. AVEYARD and Y. THOMPSON. Can. J. Chem. **57**, 856 (1979).
16. R. A. ROBINSON and R. H. STOKES. Electrolyte solutions. Butterworth, London. 1955.
17. E. R. NIGHTINGALE. J. Phys. Chem. **63**, 1381 (1959).
18. W. L. MASTERSON, D. BOLOCOFSKY, and T. P. LEE. J. Phys. Chem. **75**, 2809 (1971).
19. T. J. MORRISON and F. BILLETT. J. Chem. Soc. 3819 (1952).
20. T. J. MORRISON and N. B. B. JOHNSTONE. J. Chem. Soc. 3655 (1955).
21. M. A. PAUL. J. Am. Chem. Soc. **74**, 5274 (1952).
22. N. C. DENO and C. H. SPINK. J. Phys. Chem. **67**, 1347 (1963).
23. J. H. DEBOER. The dynamical character of adsorption. Oxford. 1953.
24. K. JOHANSSON and J. C. ERIKSSON. J. Colloid Interface Sci. **49**, 469 (1974).
25. R. AVEYARD and S. M. SALEEM. J. Chem. Soc. Faraday I **73**, 84 (1977).
26. H. H. UHLIG. J. Phys. Chem. **41**, 1215 (1937).
27. M. BLANDER, W. R. GRIMES, N. V. SMITH, and G. M. WATSON. J. Phys. Chem. **63**, 1164 (1959).
28. P. SCHATZBERG. J. Phys. Chem. **67**, 776 (1963).
29. R. AVEYARD and R. W. MITCHELL. Trans. Faraday Soc. **64**, 1757 (1968).
30. O. SINANOGLU. Solvent effects on molecular association. *In* Proc. Internat. Conf. Molec. Assoc. Biol. *Edited by* B. Pullman. Academic Press, New York. 1968.
31. R. C. TOLMAN. J. Chem. Phys. **17**, 333 (1949).
32. R. DEFAY, I. PRIGOGINE, A. BELLEMANS, and D. H. EVERETT. Surface tension and adsorption. Longmans, London. 1966.
33. F. F. ABRAHAM. Adv. Theoret. Chem. *Edited by* H. Eyring. Supplement 1. Homogeneous nucleation theory. Academic Press. 1974. Chapt. 2.
34. M. P. ANISIMOV, V. G. KOSTROVSKII, and M. S. SHTEIN. Colloid J. USSR, **40**, 257 (1978).
35. L. R. FISHER and J. N. ISRAELACHVILI. Nature, **227**, 548 (1979); J. N. ISRAELACHVILI. Private communication.
36. J. A. REYNOLDS, D. B. GILBERT, and C. TANFORD. Proc. Nat. Acad. Sci. USA, **71**, 2925 (1974).
37. R. B. HERMANN. J. Phys. Chem. **76**, 2754 (1972).
38. J. N. ISRAELACHVILI, D. J. MITCHELL, and B. W. NINHAM. J. Chem. Soc. Faraday Trans. II **72**, 1525 (1976).
39. H. REISS. Adv. Chem. Phys. *Edited by* I. Prigogine. Vol. IX, P. 1. Interscience, London. 1965.
40. R. A. PIEROTTI. J. Phys. Chem. **67**, 1840 (1963).
41. R. A. PIEROTTI. J. Phys. Chem. **69**, 281 (1965).
42. A. BEN-NAIM and H. L. FRIEDMAN. J. Phys. Chem. **71**, 448 (1967).
43. R. A. PIEROTTI. J. Phys. Chem. **71**, 2366 (1967).
44. C. V. KRISHNAN and H. L. FRIEDMAN. J. Solution Chem. **3**, 727 (1974).
45. H. L. FRIEDMAN, C. V. KRISHNAN, and C. JOLICOEUR. Ann. N.Y. Acad. Sci. **204**, 79 (1973).
46. R. F. CROSS and P. T. MCTIGUE. Aust. J. Chem. **30**, 2597 (1977).
47. D. N. GLEW. J. Phys. Chem. **66**, 605 (1962).
48. H. L. CLEVER and C. J. HOLLAND. J. Chem. Eng. Data, **13**, 411 (1968).
49. M. J. PITT. Chem. Tech. 392 (1978).
50. J. E. RANDLES. Adv. Electrochem. Electrochem. Eng. *Edited by* P. Delahay and D. V. Tobias. Interscience. 1963.

Can. J. Chem. Downloaded from www.nrcresearchpress.com by 210.87.254.6 on 09/06/12
For personal use only.

# New cyclohexane- and cyclohexene-1,3-diones from tetraacetylethylene

ANGELA M. CELLI AND LUCIA R. LAMPARIELLO
*Istituto di Chimica Organica, Piano dei Mantellini, 44, Siena, Italy*
AND
STEFANO CHIMICHI, RODOLFO NESI, AND MIRELLA SCOTTON[1]
*Centro di studio del C.N.R. sulla Chimica e la struttura dei composti eterociclici, c/o Istituto di Chimica Organica, Via G. Capponi, 9, Firenze, Italy*

Received August 20, 1981[2]

ANGELA M. CELLI, LUCIA R. LAMPARIELLO, STEFANO CHIMICHI, RODOLFO NESI, and MIRELLA SCOTTON. Can. J. Chem. **60**, 1327 (1982).

The new substituted cyclohexane- and cyclohexene-1,3-diones **3–6** and **9**, **10**, respectively, have been synthesized from tetraacetylethylene **1**, through a ring expansion of the cyclopentenone **2**. The structures of these products, as well as some features of their tautomeric behavior, were established on the basis of chemical properties and spectroscopic data.

ANGELA M. CELLI, LUCIA R. LAMPARIELLO, STEFANO CHIMICHI, RODOLFO NESI et MIRELLA SCOTTON. Can. J. Chem. **60**, 1327 (1982).

On a synthétisé les nouvelles cyclohexane- et cyclohexènediones-1,3 (**3–6** et **9** et **10**), à partir du tétraacétyl-éthylène **1** en faisant appel à une extension du cycle de la cyclopenténone **2**. On a établi la structure de ces composés, aussi bien que quelques caractéristiques de leur comportement tautomère, en s'appuyant sur leurs propriétés chimiques et de données spectroscopiques.
[Traduit par le journal]

Tetraacetylethylene (TAE) **1** has proven to be a quite versatile intermediate for different heterocyclic systems such as furans, pyrans, furo[2,3-*b*]-furans, cyclopenta[*b*]pyrans, pyridazino[4,5-*d*]-, and furo[3,4-*d*]-pyridazines (1–4). In order to ascertain the possibility of employing the same product for the synthesis of carbocyclic derivatives, we carried out some experiments the results of which we report here.

Treatment of TAE in aprotic solvents with a catalytic amount of a base such as 1,5-diazabicyclo[4.3.0]non-5-ene (DBN) or sodium acetate, formed a high yield of cyclopentenone **2** together with a small amount of a dimer, from which the former was separated by column chromatography. The structure of compound **2** followed from analytical and spectral evidence (see Experimental and Table 1).

The possibility of obtaining substituted cyclopentenones seemed very attractive in view of the considerable effort devoted in recent years to the synthesis of these products, potential intermediates for several biologically active compounds (5).

Treatment of **2** with aqueous sodium hydroxide afforded, after acidification, a high yield of a mixture of isomers ($C_{10}H_{14}O_5$) in a ratio 4:1 (mp 108–110°C and 124–126°C respectively). These were formulated as epimeric 2-acetyl-4,5-dihydroxy-4,5-dimethylcyclohexane-1,3-diones **3** and **4** on the basis of their spectroscopic and chemical behavior. The same mixture was also obtained through compound **2** (easily identified by $^1$H nmr monitoring of the reaction) under the same conditions with TAE as starting material. The ir spectra of these products, for which the tautomeric structures **3***a–e* and **4***a–e* are possible in principle, exhibit, besides bands at ca. 3460 and 3440 cm$^{-1}$ (2 × OH) and 1670 cm$^{-1}$ (CO), a very broad diffuse absorption between 3600 and 2400 cm$^{-1}$ and a broad band at about 1570 cm$^{-1}$ which were assigned to a conju-

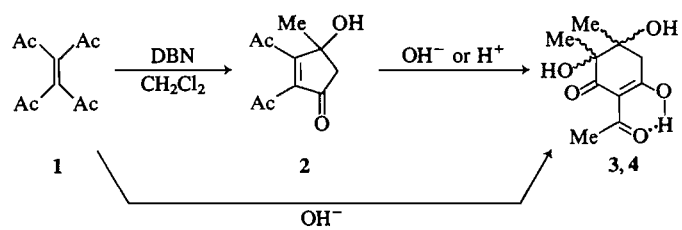


SCHEME 1

[1]Author to whom correspondence may be addressed.
[2]Revision received February 5, 1982.

0008-4042/82/111327-06$01.00/0
©1982 National Research Council of Canada/Conseil national de recherches du Canada

Can. J. Chem. Downloaded from www.nrcresearchpress.com by 210.87.254.5 on 09/06/12
For personal use only.

Can. J. Chem. Downloaded from www.nrcresearchpress.com by 210.87.254.5 on 09/06/12
For personal use only.



TABLE 1. $^1$H nmr data[a]

| Compound | $CH_3$ | $CH_2$ | CH | Ac | OH[b] | Other H |
|---|---|---|---|---|---|---|
| 2 | 1.61 | 2.78 (AB, *J* 16) | | 2.44, 2.48 | | 3.78 b (OH) |
| 3 | 1.26, 1.36 | 2.80 (AB, *J* 18) | | 2.58 | 18.0 | 2.80 b (OH), 4.25 (OH) |
| 4 | 1.25, 1.38 | 2.80 (AB, *J* 18) | | 2.59 | 18.0 | 2.80 b (OH), 4.10 (OH) |
| 5 | 1.29, 1.58 | 2.93 (AB, *J* 18) | | 2.70 | 18.1 | 4.38 (OH) |
| 6 | 1.31, 1.60 | 2.73 b | | 2.60 | 17.9 | 4.24 (OH) |
| 9 | 1.44, 2.14 (d, $J_{CH_3,4}$ 1.7) | | 6.01 (q, $J_{4,CH_3}$ 1.7) | 2.57 | 17.9 | 3.81 (OH) |
| 10 | 1.62, 2.10 (d, $J_{CH_3,4}$ 1.0) | 3.62 (AB, *J* 18) | 6.04 (q, $J_{4,CH_3}$ 1.0) | | | 3.62 b (OH) |
| 11 | 1.39, 2.02 (d, $J_{CH_3,4}$ 1.2)[c] | | 5.38 (d, $J_{2,4}$ 2.6), 5.78 m[d] | | | 3.60 b (OH), 3.74 ($OCH_3$) |
| 12 | 1.50, 2.04 (d, $J_{CH_3,4}$ 1.2)[c] | | 5.38 (d, $J_{2,4}$ 2.0), 5.86 m[d] | | | 3.70 b (OH), 3.74 ($OCH_3$) |
| 13 | 2.04, 2.20 | | 6.14 | 2.70 | 12.06 | 7.05 (OH) |
| 14 | 2.12, 2.26 | | | 2.61, 2.70 | 14.42, 14.60 | |
| 16 | 1.45, 1.94 (d, $J_{CH_3,4}$ 1.3) | | 6.07 (q, $J_{4,CH_3}$ 1.3) | 2.55 | 18.5 | 2.1 (OAc) |

[a]Chemical shifts are reported in ppm downfield from internal $Si(CH_3)_4$ and coupling constants in Hz. Unless otherwise stated, the signals are singlets.
[b]Chelated OH.
[c]The doublets collapsed to singlets by irradiation at δ 5.78 and 5.86, respectively.
[d]The multiplets collapsed to doublets ($J_{2,4}$ 2.6 and 2.0) by irradiation at δ 2.02 and 2.04, respectively.

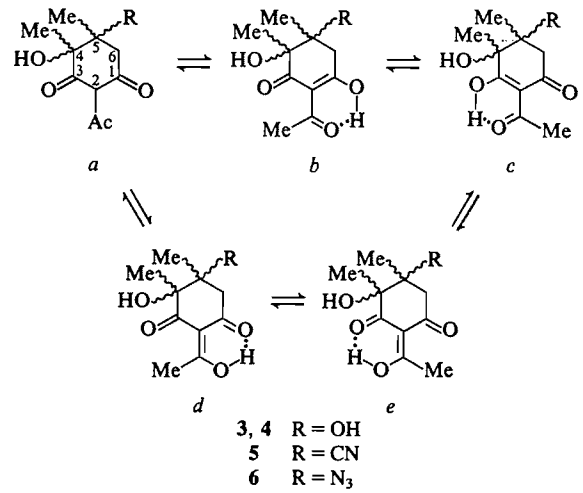


**3, 4** R = OH
**5** R = CN
**6** R = $N_3$

SCHEME 2

gated chelate OH---CO system (6). An AB system is present in their $^1$H nmr spectra (Table 1) at δ 2.80 for the methylene group together with a singlet at δ 18.0, attributable to hydrogen-bonded enolic protons; the latter shows a remarkable downfield shift characteristic of a six-membered cyclic β-diketone (7). Furthermore, no signal was detectable for CH groups in the $^1$H and $^{13}$C nmr spectra (Tables 1 and 2). These data excluded the dioxo forms **3***a* and **4***a* in the solid state and in chloroform solution.

Attempts to assign the stereochemistry of the epimers based on shifts of the hydroxyl absorption bands in dilute $CCl_4$ solution were not fruitful. Under these conditions, one OH group of compounds **3** and **4** showed an observable shift (from 3460 to 3570 $cm^{-1}$), whereas the other OH group remained substantially unchanged (ca. 3440 $cm^{-1}$). This behavior clearly indicated that, in addition to a strong chelate system (forms *b*–*e*), another intramolecular hydrogen bond was present, but it did not distinguish between the *cis* and *trans* epimers.

The conversion of the cyclopentenone **2** into **3** and **4**, which was carried out both with alkali and acids, could be rationalized on the basis of the reaction scheme illustrated above. The mechanism presumably involves first an attack of the nucleophilic agent ($H_2O$ or $OH^-$) at the position 3 of the starting material, leading either to the cyclopentanones **7** and **8** (route b) or to the corresponding anions (route a), which were formerly regarded as the final products of the reaction (8). However, it is reasonable to assume that these intermediates would react further under the reaction conditions, and would undergo ring expansion into cyclohexane-1,3-diones, through an acyloin rearrangement (9).

TABLE 2. $^{13}C$ nmr data[a]

| Compound | C-1 | C-2 | C-3 | C-4 | C-5 | C-6 | C=O | Other C |
|---|---|---|---|---|---|---|---|---|
| 3 | 195.2[b] | 109.4 | 198.1[b] | 78.0[c] | 72.9[c] | 43.3 | 202.4[b] | 22.8 (4- and 5-$CH_3$), 27.8 ($CH_3CO$) |
| 4 | 195.7[b] | 109.2 | 198.1[b] | 79.4[c] | 72.55[c] | 44.9 | 202.9[b] | 21.3 ($CH_3$), 23.45 ($CH_3$), 27.9 ($CH_3CO$) |
| 9 | 199.35[b] | 106.7 | 186.2 | 118.5 | 165.4 | 76.5 | 201.0[b] | 18.25 (6-$CH_3$), 26.7 (5-$CH_3$), 30.2 ($CH_3CO$) |
| 10 | 204.7 | 50.2 | 191.3 | 125.8 | 164.7 | 76.6 | | 17.1 (6-$CH_3$), 27.1 (5-$CH_3$) |
| 11 | 204.7 | 94.2 | 171.9 | 116.8 | 156.4 | 76.5 | | 17.4 (6-$CH_3$), 29.7 (5-$CH_3$), 55.8 (O-$CH_3$) |
| 12 | 186.7 | 99.5 | 176.7 | 70.4 | 157.6 | 124.8 | | 18.9 (4-$CH_3$), 26.5 (5-$CH_3$), 55.9 (O-$CH_3$) |
| 13 | 108.0 | 160.8[b] | 115.0 | 146.0 | 108.1 | 156.5[b] | 204.8 | 10.5 ($CH_3$), 20.6 ($CH_3$), 33.1 ($CH_3CO$) |

[a]Chemical shifts are reported in ppm downfield from $Si(CH_3)_4$ as secondary reference standard.
[b,c]These numbers can be interchanged within the same row.

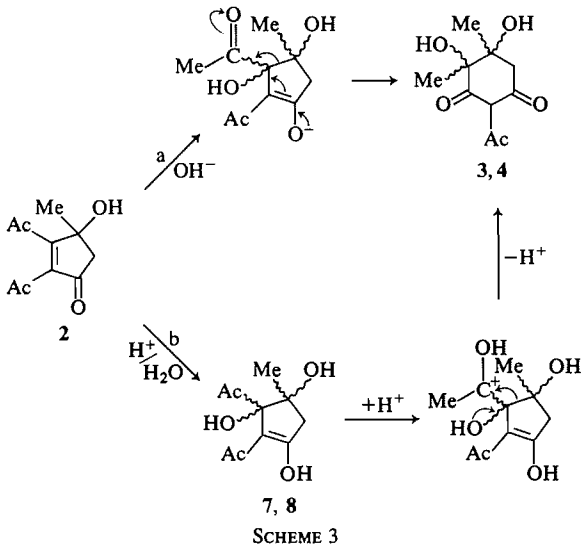


SCHEME 3

Heating either of the cyclohexane derivatives **3** and **4** with acids under mild conditions produced the cyclohexene-1,3-dione **9**, which reacted with base at room temperature to give compound **10**; the latter could also be obtained from **3** and **4** in lower yield under similar conditions, and it was converted into a mixture of the methyl derivatives **11** and **12** by treatment with ethereal diazomethane.

Significantly, both isomers **3** and **4**, as well as compound **9**, were converted into 2,6-dihydroxy-3,4-dimethylacetophenone **13** by treatment with zinc in aqueous acetic acid at 60–70°C; this behavior, characterized by a reductive elimination of a tertiary hydroxyl group, closely resembled that of some steroid ketols (10).

Compound **13**, for which conflicting data were previously reported in the literature (11, 12) was unambiguously synthesized together with **14** by Fries rearrangement of 1,3-diacetoxy-4,5-dimethylbenzene **15**.

Conjugate addition of nucleophiles to compound **9** was shown to represent a useful synthetic route for functionalized cyclohexane-1,3-diones. When the former was treated with an excess of KCN or $NaN_3$, the derivatives **5** and **6** respectively were obtained in excellent yields; in both cases the reaction was also highly stereoselective as often reported for the hydrocyanation of conjugated cyclohexenones (13, 14), although the stereochemistry of the products could not readily be determined.

All the structures of the new products reported in Schemes 2 and 4 were consistent with their spectroscopic properties (Experimental, Tables 1 and 2).

The 2,4- and 2,5-dienones **11** and **12** were distinguished on the basis of the uv maxima (230 sh and 308 nm vs. 237 and 283 nm) and by comparison of the $^{13}C$ nmr CO resonances, which exhibit a diagnostic difference for C-1 (204.7 vs. 186.7 ppm) in full agreement with the values reported for similar compounds (192–205 and 178–187 ppm respectively, refs. 15 and 16).

As in the case of the cyclohexane-diones **3–6**, the ir and $^1H$ nmr spectra of **9** were characterized respectively by broad absorptions (3400–2000 and 1570–1490 $cm^{-1}$) and by a signal at very low field ($\delta$ = 17.9 ppm), attributable to a chelate OH---CO system. This behavior, as well as the absence of resonances for saturated CH groups in the $^1H$ and $^{13}C$ nmr spectra ruled out the form **9***a*. On the other hand, the $^{13}C$ nmr values for the CO groups (Table 2) and the uv pattern in $CHCl_3$ ($\lambda_{max}$ = 258 and 310 nm), led us to discard also the 2,5-dienonic structure **9***c* and to prefer the enolized chelate form **9***b* to the external tautomers **9***d* and **9***e*.

As regards the tautomeric behavior of **10**, the uv absorption in $CHCl_3$ ($\lambda_{max}$ < 240 nm) and the presence of resonances for the $CH_2$ group in the $^1H$ and $^{13}C$ nmr spectra (Tables 1 and 2) indicate that it exists almost exclusively in the dioxo form **10***a* in this solvent. In contrast, comparison of the uv spectrum in MeOH with those of compounds **11** and **12** (Experimental) led us to conclude that the product under investigation gives rise to a mixture of the enolic forms **10***b* and **10***c* in methanol solution.

Can. J. Chem. Downloaded from www.nrcresearchpress.com by 210.87.254.5 on 09/06/12
For personal use only.

Can. J. Chem. Downloaded from www.nrcresearchpress.com by 210.87.254.5 on 09/06/12
For personal use only.

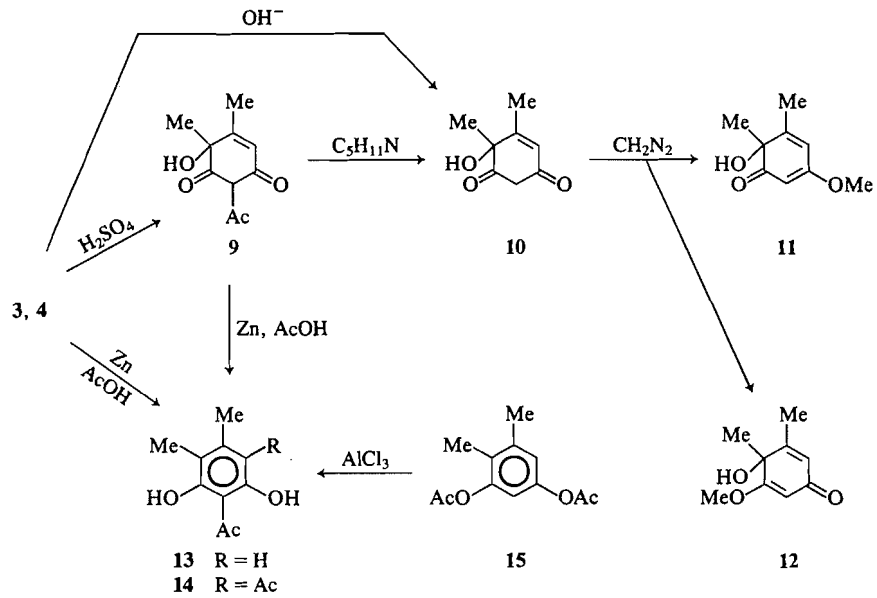


SCHEME 4

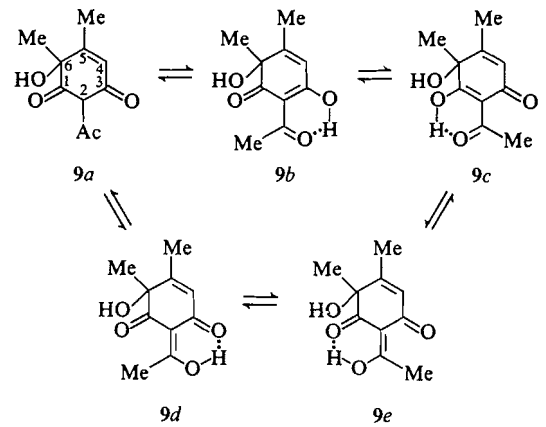


SCHEME 5

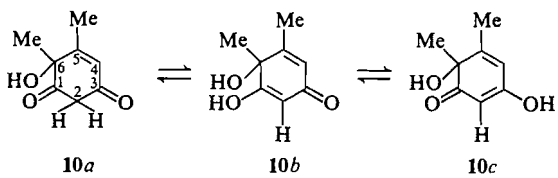


SCHEME 6

## Experimental

Melting points were determined with a Kofler apparatus and are uncorrected. Unless otherwise stated, the spectroscopic measurements were carried out under the following conditions: ir and uv spectra were determined for dispersions in potassium bromide with a Perkin–Elmer 457 spectrometer and for solutions in methanol with a Cary 14 spectrophotometer respectively; $^1H$ nmr spectra were recorded in $CDCl_3$ with a Perkin–Elmer R32 instrument, whereas $^{13}C$ nmr spectra were obtained in the same solvent by the Fourier-transform technique with a Varian FT-80 A spectrometer. Silica gel plates (Merck $F_{254}$) and silica gel 60 (Merck; 70–230 mesh) were used for analytical and preparative tlc and for column chromatography respectively. Petroleum ether refers to the fraction of bp 30–50°C.

*Tetraacetylethylene (TAE) (1)*

The procedure used for the synthesis of TAE is essentially that already reported (1) but, in order to obtain a good yield, it is necessary to follow strictly the conditions described below.

To a boiling solution of thrice sublimed tetraacetylethane (9 g) in dry toluene (100 mL) was added a solution of thallium(I) ethoxide (Aldrich) (27 g) in the same solvent (80 mL), previously filtered through a sintered disc of porosity 3. The yellow dithallium(I) salt of tetraacetylethane which precipitated was separated by filtration and washed with chloroform to eliminate the unreacted starting material; after a further washing with petroleum ether, it was dried in a desiccator over solid paraffin to give a solid (25.5 g, 93%), which darkened above 145°C; ir $\nu_{max}$: 3500–3050, 1570, 1550, 1450, 1366, 1330 $cm^{-1}$. *Anal.* calcd. for $C_{10}H_{12}O_4Tl_2$: C 19.84, H 1.98; found: C 19.65, H 2.02. A solution of iodine (Merck Suprapur) (4.9 g) in anhydrous ether (80 mL) was added slowly (ca. 3 h), with stirring, at 12–14°C to a suspension of the dithallium salt (12 g) in anhydrous ether (200 mL), and the mixture was stirred for a further 30 min. The solid (TlI and TAE) was filtered and extracted exhaustively with methylene chloride at room temperature; removal of the solvent at the same temperature afforded TAE (1) (3.15 g, 81%), mp 139–140°C (from benzene).

*2,3-Diacetyl-4-hydroxy-4-methylcyclopent-2-en-1-one (2)*

1,5-Diazabicyclo[4.3.0]non-5-ene (0.02 mL) was added to a solution of TAE (0.5 g) in methylene chloride (5 mL) at room temperature and the mixture was stirred for 30 min. Removal of the solvent left a residue which was resolved into two components by column chromatography with ether – petroleum ether (3:1 v/v) as eluent. The faster eluting band afforded a small amount (0.015 g) of a dimer of **2**, mp 219–221°C (from benzene). *Anal.* calcd. for $C_{20}H_{24}O_8$: C 61.22, H 6.16, *Mol. Wt.* 392.4; found: C 60.92, H 6.16, *Mol. Wt.* 390.

The second fraction gave compound **2** as colorless thick oil

Can. J. Chem. Downloaded from www.nrcresearchpress.com by 210.87.254.5 on 09/06/12
For personal use only.

(0.43 g, 86%), which crystallized on standing, mp 53–55°C (from petroleum ether); uv $\lambda_{max}$ (log ε): 227 (3.87) and 285 sh (2.95) nm; ir $\nu_{max}$: 3450 (OH), 1725 (CO), 1690 (CO), 1610 (C=C) $cm^{-1}$. *Anal.* calcd. for $C_{10}H_{12}O_4$: C 61.22, H 6.16; found: C 60.88, H 6.24.

*2-Acetyl-4,5-dihydroxy-4,5-dimethylcyclohexane-1,3-diones (3) and (4)*

(a) The cyclopentenone **2** (1 g) was added to an aqueous solution of 1 *N* NaOH (10 mL) and stirred until the whole solid was dissolved (ca. 1 h). Acidification with concentrated HCl (pH 1) precipitated the isomer **3** as colorless crystals (0.5 g), mp 108–110°C (from cyclohexane); uv $\lambda_{max}$ (log ε): 233 (3.98) and 274 (4.04) nm; ir $\nu_{max}$: 3460 (OH), 3440 (OH), 3600–2400 (chelated OH), 1660 (CO), 1600–1530 (chelated CO) $cm^{-1}$. *Anal.* calcd. for $C_{10}H_{14}O_5$: C 56.07, H 6.59; found: C 56.37, H 6.71.

The acid solution was exhaustively extracted in a liquid–liquid extractor with ether. Evaporation of the extracts yielded a residue (0.5 g) which was resolved into two components by preparative layer chromatography with benzene–ether (3:2 v/v) as developer. The first band afforded a second crop of compound **3** (0.3 g), whereas the other gave the isomer **4** (0.2 g), mp 124–126°C (from cyclohexane); uv $\lambda_{max}$ (log ε): 234 (3.99) and 274 (4.05) nm; ir $\nu_{max}$: 3450 (OH), 3430 (OH), 3600–2000 (chelated OH), 1665 (CO), 1610–1530 (chelated CO). *Anal.* calcd. for $C_{10}H_{14}O_5$: C 56.07, H 6.59; found: C 55.82, H 6.62.

(b) Reaction of TAE with NaOH, followed by the same work-up as above, gave the same mixture of the isomers **3** and **4** identical (mp, ir and $^1H$ nmr spectra) with the foregoing products.

(c) A solution of compound **2** (0.3 g) in 30% $H_2SO_4$ (4 mL) was stirred for 6 h at room temperature. Filtration of the reaction mixture yielded the isomer **4** (0.02 g). The solution was extracted with ether and the extracts were evaporated to dryness to give a mixture of **3** (0.05 g) and **4** (0.06 g), identical (mp, ir and $^1H$ nmr spectra) with the materials prepared above.

*2-Acetyl-6-hydroxy-5,6-dimethylcyclohex-4-ene-1,3-dione (9)*

A solution of the isomer **3** (or **4**) (1 g) in 60% $H_2SO_4$ (10 mL) was heated at 50°C for 6 h; filtration of the cooled reaction mixture yielded compound **9** (0.65 g), mp 83–84°C (from cyclohexane). The solution was then exhaustively extracted with ether in a liquid–liquid extractor to give another crop (0.22 g) of the same product (total yield 0.87 g, 95%); uv $\lambda_{max}$ (log ε): 233 (4.11), 260 (3.72), and 312 (3.81) nm; $\lambda_{max}$ (log ε) ($CHCl_3$): 258 (3.79) and 310 (3.83) nm; ir $\nu_{max}$: 3460 (OH), 3400–2000 (chelated OH), 1655 (CO), 1570–1490 (chelated CO) $cm^{-1}$. *Anal.* calcd. for $C_{10}H_{12}O_4$: C 61.22, H 6.16; found: C 61.41, H 6.30.

*Acetyl-derivative 16*

Treatment of compound **9** with acetyl chloride at room temperature afforded **16** in 85% yield, mp 75–77°C (from petroleum ether); ir $\nu_{max}$: 3400–2300 (chelated OH), 1740 (OAc), 1670 (CO), 1570–1490 (chelated CO) $cm^{-1}$. *Anal.* calcd. for $C_{12}H_{14}O_5$: C 60.50, H 5.92; found: C 60.55, H 5.98.

*5-Cyano-2-acetyl-4-hydroxy-4,5-dimethylcyclohexane-1,3-dione (5)*

Sodium cyanide (0.16 g) was added portionwise with stirring to a solution of compound **9** (0.6 g) in DMSO (3 mL) and the mixture was heated at 50°C for 30 min. After cooling and neutralization with 25% HCl (ca. 7 mL), the solution was concentrated (4 mL) and acidified with concentrated HCl (pH 1) to give the nitrile **5** which separated as colorless needles (0.5 g), mp 134–135°C (from cyclohexane). Another crop of the same product (0.12 g, total yield 91%) was obtained by extraction of the acid mother liquors with ether; uv $\lambda_{max}$ (log ε): 234 (3.99) and 273 (4.03) nm; ir $\nu_{max}$: 3475 (OH), 3100–2000 (chelated OH), 2240 (CN), 1660 (CO), 1580–1510 (chelated CO) $cm^{-1}$. *Anal.* calcd. for $C_{11}H_{13}NO_4$: C 59.19, H 5.87, N 6.27; found: C 59.54, H 5.78, N 6.12.

*5-Azido-2-acetyl-4-hydroxy-4,5-dimethylcyclohexane-1,3-dione (6)*

Reaction of compound **9** (0.3 g) with sodium azide (0.2 g) in DMSO (2 mL), carried out essentially as above, afforded the derivative **6** (0.29 g, 79%), mp 89–90°C (from ethanol); ir $\nu_{max}$: 3520 (OH), 3200–2000 (chelated OH), 2140 ($N_3$), 1660 (CO), 1580–1520 (chelated CO) $cm^{-1}$. *Anal.* calcd. for $C_{10}H_{13}N_3O_4$: C 50.21, H 5.48, N 17.56; found: C 49.90, H 5.54, N 17.77.

*6-Hydroxy-5,6-dimethylcyclohex-4-ene-1,3-dione (10)*

(a) Piperidine (0.6 mL) was added to a solution of compound **9** (0.5 g) in $CHCl_3$ (10 mL) and the mixture was stirred at room temperature for 3 h. Removal of the solvent left a residue which was dissolved in water (5 mL); the solution was acidified and extracted with ether (3 × 10 mL). Evaporation of the extracts yielded compound **10** (0.31 g, 79%), mp 133–135°C (from toluene); uv $\lambda_{max}$ (log ε): 236 (3.98), 296 (3.60), and 335 sh (3.31) nm; ir $\nu_{max}$: 3485 (OH), 3200–2100 (chelated OH), 1650 (CO), 1580–1490 $cm^{-1}$. *Anal.* calcd. for $C_8H_{10}O_8$: C 62.33, H 6.54; found: C 62.63, H 6.54.

(b) A solution of compound **9** (1 g) in 1 *N* NaOH (15 mL) was heated at 60°C for 24 h; the cooled solution was acidified with concentrated HCl and extracted with ether (3 × 20 mL). Evaporation of the extracts afforded compound **10** (0.4 g, 51%), identical (mp, ir and $^1H$ nmr spectra) with material prepared by method (a).

*Methylation of compound 10 with diazomethane*

A solution of **10** (1 g) in ether (50 mL) was treated with ethereal diazomethane (0.4 g) and set aside overnight. Removal of the solvent left a residue which was resolved into two components by column chromatography using ether as eluent. The first was identified as 3-methoxy-6-hydroxy-5,6-dimethylcyclohexa-2,4-dien-1-one (**11**) which crystallized from petroleum ether as pale yellow needles, mp 64–65°C (0.45 g, 41%); uv $\lambda_{max}$ (log ε): 230 sh (3.57) and 308 (3.70) nm; ir $\nu_{max}$: 3400 (OH), 1665, 1640, 1570 (conjugated CO) $cm^{-1}$. *Anal.* calcd. for $C_9H_{12}O_3$: C 64.27, H 7.19; found: C 64.27, H 7.15.

The second was identified as 3-methoxy-4-hydroxy-4,5-dimethylcyclohexa-2,5-dien-1-one (**12**), which sublimed at 60°C/0.04 Torr as colorless crystals, mp 82–84°C (0.35 g, 32%); uv $\lambda_{max}$ (log ε): 237 (4.15) and 283 (3.69) nm; ir $\nu_{max}$: 3270 (OH), 1665, 1600 (conjugated CO) $cm^{-1}$. *Anal.* calcd. for $C_9H_{12}O_3$: C 64.27, H 7.19; found: C 64.42, H 7.27.

*2,6-Dihydroxy-3,4-dimethylacetophenone (13)*

(a) A mixture of **3** (1 g) and zinc dust (0.6 g) in 50% AcOH (15 mL) was heated at 65°C for 10 h. The yellow needles which separated on cooling were filtered off, washed with water, and dried to give compound **13** (0.55 g), mp 125–127°C (after crystallization from cyclohexane and sublimation at 70°C/0.03 Torr) (lit. (11) mp 82–83°C and (12) mp 122–124°C). Another crop (0.06 g, total yield 71%) precipitated from the mother liquors after dilution with water; uv $\lambda_{max}$ (log ε): 222 (4.03), 276 (4.16), and 350 (3.39) nm; ir $\nu_{max}$: 3270 (OH), 3100–1750 (chelated OH), 1625 b (chelated CO) $cm^{-1}$. *Anal.* calcd. for $C_{10}H_{12}O_3$: C 66.65, H 6.71; found: C 66.61, H 6.63.

(b) Under the same conditions, **9** gave the title compound **13** (82%), identical (ir and $^1H$ nmr spectra) with material prepared with method (a).

*Fries rearrangement of 1,3-diacetoxy-4,5-dimethylbenzene (15)*

Anhydrous aluminium chloride (2 g) was added portionwise to the title compound **15** (17) (1.3 g) in a beaker suspended in an oil bath maintained at 115–120°C. After the initial reaction had begun (3–4 min), the mixture was stirred vigorously with a glass

rod. Heating with periodic stirring was then continued for 30 min, after which time the cooled reaction mixture was ground in a mortar and then added, with stirring, to a mixture of crushed ice (20 mL) and concentrated HCl (1 mL). Decantation of the acid solution left a viscous solid, which was treated with the minimum amount of cold methanol to yield 1,3-diacetyl-2,4-dihydroxy-5,6-dimethylbenzene (**14**) (0.65 g) as pale yellow crystals, mp 78–80°C (from methanol); uv $\lambda_{max}$ (log ε): 257 (4.28), 272 (4.20), and 354 (3.78) nm; ir $\nu_{max}$: 3200–2000 (chelated OH), 1620 b (chelated CO) $cm^{-1}$. *Anal.* calcd. for $C_{12}H_{14}O_4$: C 64.85, H 6.35; found: C 64.88, H 6.27.

A preparative thin layer chromatography of the methanolic solution with ether – petroleum ether (2:1, v/v) as eluent gave in order of mobility another crop of **14** (0.05 g, total yield 54%) and compound **13** (0.1 g), identical (mp, ir and $^1H$ nmr spectra) with material obtained above.

## Acknowledgements

This work was financially supported by the "Progetto Finalizzato Chimica Fine e Secondaria" C. N. R. Rome. We thank Mr. S. Papaleo for the analytical data, and Dr. E. Belgodere for the determination of the uv absorption spectra.

1. G. ADEMBRI, F. DE SIO, R. NESI, and M. SCOTTON. J. Chem. Soc. C, 1536 (1970).
2. G. ADEMBRI, R. NESI, and M. SCOTTON. Tetrahedron Lett. 3961 (1977).
3. G. ADEMBRI, R. CINI, P. L. ORIOLI, R. NESI, and M. SCOTTON. J. Chem. Soc. Perkin Trans. II, 903 (1979).
4. G. ADEMBRI, D. DONATI, R. CINI, R. NESI, and M. SCOTTON. Can. J. Chem. **58**, 1645 (1980).
5. R. A. ELLISON. Synthesis, 397 (1973).
6. E. GREENS, A. GRINWALD, and J. STRADINS. Spectrochim. Acta, Part A, **31**, 555 (1975).
7. S. FORSÉN, F. MERÉNYI, and M. NILSSON. Acta Chem. Scand. **18**, 1208 (1964).
8. G. ADEMBRI, R. NESI, and M. SCOTTON. Chim. Ind. Milan, **57**, 782 (1975).
9. N. L. WENDLER. *In* Molecular rearrangements. *Edited by* P. De Mayo. Wiley–Interscience, New York. 1964. p. 1114.
10. R. S. ROSENFELD. J. Am. Chem. Soc. **79**, 5540 (1957).
11. D. J. CRAM and F. W. CRANZ. J. Am. Chem. Soc. **72**, 595 (1950).
12. M. MATSUI, K. YAMASHITA, and I. SUGIMURA. Japan Pat. No. 6.905.214. Chem. Abstr. **71**, P 3257r (1969).
13. W. NAGATA and M. YOSHIOKA. Org. React. **25**, 255 (1977).
14. C. AGAMI, M. FADLALLAH, and J. LEVISALLES. Tetrahedron, **37**, 909 (1981).
15. A. RIEKER and S. BERGER. Org. Magn. Reson. **4**, 857 (1972).
16. R. HOLLESTEIN and W. VON PHILIPSBORN. Helv. Chim. Acta, **55**, 2030 (1972).
17. M. S. KABLAOUI. J. Org. Chem. **39**, 3696 (1974).

Can. J. Chem. Downloaded from www.nrcresearchpress.com by 210.87.254.5 on 09/06/12
For personal use only.

# Confacial bioctahedral complexes of tungsten(IV) containing tungsten-to-tungsten bonds: X-ray crystal structures of di-μ-ethanethiolato-μ-sulfidobis[dichloro(dimethyl sulfide)-tungsten(IV) (W—W)] and tetraphenylphosphonium di-μ-ethane thiolato-μ-sulfido-bis[trichlorotungstate(IV) (W—W)][1]

P. MICHAEL BOORMAN,[2] PENELOPE W. CODDING, K. ANN KERR, KELLY J. MOYNIHAN, AND VIKRAM D. PATEL

*Department of Chemistry, University of Calgary, Calgary, Alta, Canada T2N 1N4*

Received August 25, 1981

P. MICHAEL BOORMAN, PENELOPE W. CODDING, K. ANN KERR, KELLY J. MOYNIHAN, and VIKRAM D. PATEL. Can. J. Chem. **60**, 1333 (1982).

The complex $(Me_2S)Cl_2W(\mu\text{-}S)(\mu\text{-}SEt)_2WCl_2(Me_2S)$, **1**, has been prepared by reaction of $[WCl_4(Me_2S)_2]$ with 1 mol-equiv. of $SiMe_3(SEt)$ in $CH_2Cl_2$ solution. A single-crystal X-ray diffraction study shows that the molecule has a confacial bioctahedral structure with a W—W bond length of 2.526(2) Å. The structure was solved by heavy atom methods and refined to $R = 0.061$ and $R_w = 0.061$ for 2715 reflections with $I \geq 3\sigma(I)$. Crystals of **1** are triclinic, space group $P\bar{1}$, with $a = 9.661(1)$, $b = 10.695(1)$, $c = 13.253(4)$ Å, $\alpha = 61.84(2)$, $\beta = 66.98(2)$, and $\gamma = 66.44(1)°$, $Z = 2$.

Reaction of **1** with 2 mol-equiv. of $Ph_4PCl$ in $CH_2Cl_2$ solution yields $(Ph_4P)_2[Cl_3W(\mu\text{-}S)(\mu\text{-}SEt)_2WCl_3]$, **2**. Crystals of **2** are triclinic, space group $P\bar{1}$, with $a = 10.153(1)$, $b = 13.043(1)$, $c = 21.876(3)$ Å, $\alpha = 95.16(1)$, $\beta = 96.48(2)$, and $\gamma = 108.90(1)°$, $Z = 2$. The structure was refined to $R = 0.041$, $R_w = 0.048$ for 2384 reflections with $I \geq 3\sigma(I)$; **2** also has a confacial bioctahedral structure with a W—W bond length of 2.522(1) Å.

P. MICHAEL BOORMAN, PENELOPE W. CODDING, K. ANN KERR, KELLY J. MOYNIHAN et VIKRAM D. PATEL. Can. J. Chem. **60**, 1333 (1982).

On a préparé le complexe $(Me_2S)Cl_2W(\mu\text{-}S)(\mu\text{-}SEt)_2WCl_2(Me_2S)$ (**1**) en faisant réagir le $[WCl_4(Me_2S)_2]$ avec un équivalent molaire de $SiMe_3(SEt)$ en solution dans le $CH_2Cl_2$. Une étude par diffraction de rayons X sur un monocristal montre que cette molécule a une structure bioctaédrique concafaciale avec une longueur de liaison de 2,52(2) Å. On a résolu la structure par la méthode des atomes lourds et on l'a affiné jusqu'à des valeurs de $R = 0{,}061$ et de $R_w = 0{,}061$ pour 2715 réflexions avec $I \geq 3\sigma(I)$. Les cristaux du composé de **1** sont tricliniques et appartiennent au groupe d'espace P, avec $a = 9{,}661(1)$, $b = 10{,}695(1)$, $c = 13{,}253(4)$Å, $\alpha = 61{,}84(2)$, $\beta = 66{,}98(2)$ et $\gamma = 66{,}44(1)°$, $Z = 2$.

Le composé **1** réagit avec 2 équivalents molaires de $Ph_4PCl$ en solution dans le $CH_2Cl_2$ pour donner le $(Ph_4P)_2[Cl_3W(\mu S)(\mu\text{-}SEt)_2WCl_3]$, **2**. Les cristaux du composé **2** sont tricliniques et appartiennent au groupe d'espace $P\bar{1}$, avec $a = 10{,}153(1)$, $b = 13{,}043(1)$, $c = 21{,}876(3)$Å, $\alpha = 95{,}16(1)$, $\beta = 96{,}48(2)$ et $\gamma = 108{,}90(1)°$, $Z = 2$. On a affiné la structure jusqu'à des valeurs de $R = 0{,}041$ et de $R_w = 0{,}048$ pour 2384 réflexions avec $I \geq 3\sigma(I)$, le composé **2** a une structure bioctaédrique concafaciale avec une longueur de liaison W—W de 2,522(1) Å.

[Traduit par le journal]

Examples of tungsten(IV) complexes with well-established metal–metal bonded dimeric structures are rare (1, 2). We recently reported the structure of $(C_4H_8S)Cl_2W(\mu\text{-}S)(\mu\text{-}SEt)_2WCl_2(C_4H_8S)$ which possesses a confacial bioctahedral framework with a W—W bond length of 2.524(1) Å. A number of interesting structural features in this molecule prompted us to extend the study to analogous complexes. We report here the X-ray structures of $(Me_2S)Cl_2W(\mu\text{-}S)(\mu\text{-}SEt)_2WCl_2(Me_2S)$, **1**, and of the anionic derivative $(Ph_4P)_2[Cl_3W(\mu\text{-}S)(\mu\text{-}SEt)_2WCl_3]$, **2**.

## Experimental

Synthesis of **1** was carried out by a route analogous to what we reported for the compound $[(C_4H_8S)Cl_2W(\mu\text{-}S)(\mu\text{-}SEt)_2WCl_2(C_4H_8S)]$, **3** (2). The starting material, $WCl_4(Me_2S)_2$, was synthesised as previously described (3). Reaction with 1 mol-equiv. of $SiMe_3(SEt)$ in $CH_2Cl_2$ solution yielded the compound **1** after working up the solution as reported in ref. 2. *Anal.* calcd. for $W_2Cl_4(SEt)_2S(SMe_2)_2$: W 46.70, Cl 18.00, C 12.19, H 2.79; found: W 48.7, Cl 18.9, C 12.6, H 2.85. Crystals suitable for an X-ray study were grown from $CH_2Cl_2$/hexane solutions cooled to ~ −20°C for 5 days.

**2** was prepared by adding $Ph_4PCl$ (0.57 g, 1.54 mmol) to a solution of **1** (0.54 g, 0.69 mmol) in $CH_2Cl_2$ (30 mL). After stirring for 6 h the solution was pumped to dryness. The microcrystalline sample of **2** was recrystallized from MeCN/$Et_2O$ at −10°C. *Anal.* calcd. for $(Ph_4P)_2[W_2Cl_6(SEt)_2S]$: Cl 15.06, C 44.18, H 3.50, S 6.79, P 4.38; found: Cl; 16.1, C 44.7, H 4.20, S 6.80, P 4.60. The spectroscopic properties of these and related compounds will be described elsewhere (4).

### *X-ray structure of $(Me_2S)Cl_2W(\mu\text{-}S)(\mu\text{-}SEt)_2WCl_2(Me_2S)$, 1*

*Collection and reduction of the X-ray data*

A crystal ca. 0.12 × 0.16 × 0.16 mm in size was mounted in epoxy resin on a glass fibre in a general orientation. A coating of the resin was also applied to protect the crystal from aerial degradation and/or loss of $Me_2S$ during the data collection.

[1] Taken in part from the Ph.D. thesis of V.D.P., University of Calgary, Calgary, Alta, 1981.

[2] To whom all correspondence should be addressed.

0008-4042/82/111333-06$01.00/0

©1982 National Research Council of Canada/Conseil national de recherches du Canada

Can. J. Chem. Downloaded from www.nrcresearchpress.com by 210.87.254.105 on 09/06/12
For personal use only.

Can. J. Chem. Downloaded from www.nrcresearchpress.com by 210.87.254.105 on 09/06/12
For personal use only.

Preliminary photographic study of the compound indicated a triclinic space group. The data crystal was then mounted on an Enraf-Nonius CAD4 Automatic Diffractometer. Cell parameters and an orientation matrix were determined from a least-squares fit using 25 accurately centred reflections. Crystal data at 21°C are:

$C_8H_{22}W_2Cl_4S_5$ fw = 787.8
Triclinic, $a$ = 9.661(1), $b$ = 10.695(1), $c$ = 13.253(4) Å, $\alpha$ = 61.84(2), $\beta$ = 66.98(2), $\gamma$ = 66.44(1)°, $V$ = 1071.2 Å; $Z$ = 2, $\rho_{calcd}$ = 2.44; $\rho_{obsd}$ = 2.42 g cm$^{-3}$ (by flotation in $CHBr_3/CCl_4$), $F_{000}$ = 732; $\mu(MoK_\alpha)$ = 121.7 cm$^{-1}$; space group $P\bar{1}$.

The centrosymmetric space group $P\bar{1}$ was confirmed later by use of $E$ statistics and successful refinement in this space group.

Intensities were measured with graphite-monochromatized $MoK_\alpha$ radiation in the $\omega/2\theta$ scan mode, using a scan width of $\Delta\omega = 1.5(0.6 + 0.35 \tan\theta)°$, and a scan speed ranging from (20/3) to (20/40)° min$^{-1}$ in the range $3.0° \leq \theta \leq 27°$. Of the 4660 unique reflections measured, 2715 had $I > 3\sigma(I)$, where $\sigma(I) = (P + 4B)^{1/2}$, $P$ is the sum of the counts accumulated in the central 64 steps of the scan, and $B$ is the sum of the counts in the 16 steps at either end of the scan. Three standard reflections were measured every 3000 s of exposure, and their intensities remained constant to within ±2%. Standard Lorentz and polarization corrections were applied. Data were corrected for absorption using the program CADABS (5).[3] The minimum and maximum values of the correction were 2.805 and 4.655, respectively.

*Solution and refinement*

The structure was solved by the heavy atom technique and refined by a full-matrix least-squares procedure based on $F$. The scattering factors were taken from ref. 6 and anomalous dispersion corrections from ref. 7. All heavy atoms were refined anisotropically. Hydrogen atoms could not be located in the final difference map, and were not included in the model. Secondary extinction was included in the final refinement cycles ($g$ = 0.19(8) × 10$^{-3}$). The maximum shift-to-error in the final cycle was 0.08, with the average value 0.01. The final $R$ values are $R = \Sigma(|F_o| - |F_c|)/\Sigma|F_o| = 0.061$ and $R_w = [\Sigma w(|F_o| - |F_c|)^2/\Sigma w|F_o|^2]^{1/2} = 0.061$ for 2715 observed reflections. The weighting scheme used was $w = [\sigma^2(F) + 0.0003F^2]^{-1}$ where $\sigma(F)$ was derived from counting statistics. The standard deviation of an observation of unit weight was 1.08. No peaks of chemical significance could be located in the final difference map which showed maximum fluctuations of ±0.3 e Å$^{-3}$. The final positional and thermal parameters appear in Tables 1 and 2 respectively. The measured and calculated structure factors, and $\sigma(F)$ values have been placed in the Depository of Unpublished Data,[4] as also has Table 2.

*Crystal structure of $(Ph_4P)_2[Cl_3W(\mu\text{-}S)(\mu\text{-}SEt)_2WCl_3]$, 2*

Procedures for data collection followed closely those described for compound **1**. The essential data (21°C) are summarized below:

$C_{52}H_{50}W_2Cl_6S_3P_2$ fw = 1412.2
Triclinic, $a$ = 10.153(1), $b$ = 13.043(1), $c$ = 21.876(3) Å, $\alpha$ = 95.16(1), $\beta$ = 96.48(2), $\gamma$ = 108.90(1)°, $Z$ = 2; $\rho_{calcd}$ = 1.73, $\rho_{obsd}$ = 1.78 g cm$^{-3}$ (flotation in $CHBr_3/CCl_4$), $F_{000}$ = 1380, $\mu(MoK_\alpha)$ = 48.7 cm$^{-1}$, space group $P\bar{1}$.

[3]CADABS: a local modification of a program by Coppens *et al.* to calculate absorption factors by numerical gaussian integration.

[4]The structure factor table and other deposited tables are available, at a nominal charge, from the Depository of Unpublished Data, CISTI, National Research Council of Canada, Ottawa, Ont., Canada K1A 0S2.

TABLE 1. Fractional coordinates for the non-hydrogen atoms in $(Me_2S)Cl_2W(\mu\text{-}S)(\mu\text{-}SEt)_2WCl_2(SMe_2)$

| Atom | $x/a$ | $y/b$ | $z/c$ |
|---|---|---|---|
| W(1) | 0.1698(1) | 0.03943(9) | 0.22410(7) |
| W(2) | 0.2574(1) | 0.22078(9) | 0.24057(7) |
| S(1) | 0.1512(6) | 0.2916(5) | 0.0729(4) |
| S(2) | 0.4176(6) | −0.0254(6) | 0.2629(5) |
| S(3) | 1.0091(6) | 0.1885(6) | 0.3300(5) |
| S(4) | 0.1224(7) | 0.4935(6) | 0.2187(5) |
| S(5) | −0.0661(8) | 0.0342(7) | 0.1823(5) |
| Cl(1) | 0.4672(6) | 0.3158(6) | 0.1001(5) |
| Cl(2) | 0.3196(7) | 0.1962(6) | 0.4056(5) |
| Cl(3) | 0.1240(8) | −0.1836(6) | 0.3762(5) |
| Cl(4) | 0.2936(7) | 0.9533(6) | 0.0675(5) |
| C(1) | 0.698(3) | 0.706(2) | 0.067(2) |
| C(2) | 0.414(3) | 0.859(3) | 0.421(2) |
| C(3) | 0.898(3) | 0.174(3) | 0.046(2) |
| C(4) | 0.704(3) | 0.544(3) | 0.147(2) |
| C(5) | −0.012(3) | 0.500(3) | 0.356(2) |
| C(6) | 0.258(3) | 0.572(3) | 0.218(2) |
| C(7) | 0.754(3) | 0.083(3) | 0.292(2) |
| C(8) | 0.510(4) | 0.705(3) | 0.430(3) |

TABLE 3. Fractional coordinates for the non-hydrogen atoms in the anion $[Cl_3W(\mu\text{-}S)(\mu\text{-}SEt)_2WCl_3]^{2-}$ with estimated standard deviations in parentheses

| Atom | $x/a$ | $y/b$ | $z/c$ |
|---|---|---|---|
| W(1) | 0.1688(1) | 0.39422(8) | 0.26751(5) |
| W(2) | 0.3335(1) | 0.55168(8) | 0.22476(5) |
| S(1) | 0.1606(7) | 0.5775(5) | 0.2868(3) |
| S(2) | 0.4206(7) | 0.4379(5) | 0.2882(3) |
| S(3) | 0.1752(8) | 0.3999(5) | 0.1626(3) |
| Cl(1) | 0.1690(7) | 0.3829(5) | 0.3774(3) |
| Cl(2) | 0.9141(7) | 0.3286(5) | 0.2554(3) |
| Cl(3) | 0.1495(8) | 0.2029(5) | 0.2532(3) |
| Cl(4) | 0.5077(6) | 0.7075(5) | 0.2908(3) |
| Cl(5) | 0.5155(7) | 0.5554(5) | 0.1609(3) |
| Cl(6) | 0.2745(7) | 0.6771(5) | 0.1597(3) |
| C(1) | 1.004(3) | 0.590(2) | 0.238(1) |
| C(2) | 0.003(3) | 0.708(2) | 0.248(1) |
| C(3) | 0.476(3) | 0.347(2) | 0.235(1) |
| C(4) | 0.547(3) | 0.282(2) | 0.276(1) |

Crystal size 0.22 × 0.16 × 0.09 mm; data collected on an Enraf-Nonius CAD4 diffractometer using $MoK_\alpha$ radiation with a graphite monochromator, $\omega$–$2\theta$ scan mode, variable scan speed, scan width $\Delta\omega = 1.5(0.20 + 0.35 \tan\theta)°$, $2° \leq \theta \leq 25°$; three standard reflections checked every 1200 s of exposure with no significant decrease in intensity; 9465 unique reflections of which 2384 have $I > 3\sigma(I)$; minimum and maximum values of absorption corrections are 1.139 and 1.309 respectively.

*Solution and refinement*

The structure was solved by heavy atom methods and refined on $F$. All the atoms were refined anisotropically, except the carbon atoms. The phenyl rings were refined as rigid bodies, while the ethyl carbon atoms were refined isotropically. Phenyl hydrogen atoms were placed in calculated positions but were not refined. Convergence was reached at $R = \Sigma(|F_o| - |F_c|)/\Sigma|F_o| = 0.041$ for 2384 observed reflections and $R_w = [\Sigma w(|F_o| - |F_c|)^2/\Sigma w|F_o|^2]^{1/2} = 0.048$. The weighting scheme used was $w = [\sigma^2(F) + 0.001F^2]^{-1}$ where $\sigma(F)$ was based on

Can. J. Chem. Downloaded from www.nrcresearchpress.com by 210.87.254.105 on 09/06/12
For personal use only.

counting statistics. The refined value of the secondary extinction parameter is $g = 4.4(4) \times 10^{-3}$. A final electron-density difference map revealed no peaks higher than $\pm 0.2\,e\,Å^{-3}$. The standard deviation of an observation of unit weight was 1.0 and the average shift-to-error in the final cycle was 0.01. Final positions of the non-hydrogen atoms in the $[Cl_3W(\mu\text{-}S)(\mu\text{-}SEt)_2WCl_3]^{2-}$ anion are given in Table 3. The thermal parameters of the anion (Table 4), the positions and thermal parameters for the two $Ph_4P^+$ cations (Tables 5, 6, and 7), and a listing of observed and calculated structure factors and $\sigma(F)$ values have been placed in the Depository of Unpublished Data.

Programs used: the XRAY-76 programs (8) were used for all calculations with the exception of absorption corrections for which CADABS (5) was used.

## Results and discussion

The structures of **1** and the anion of **2** are shown in Figs. 1 and 2, respectively. Bond lengths for the two binuclear tungsten complexes are given in Tables 8 and 9 while pertinent bond angle information for **1** and **2** is presented in Tables 10 and 11. In Table 12 certain comparisons are drawn between these complexes and the related complex **3**.

The three complexes all possess the same bridging groups in a confacial bioctahedral ditungsten species. The W—W bond lengths show a remarkable consistency, all being within experimental error, 2.523 Å. The implication of this observation is that the interaction is indeed due to a direct metal–metal double bond, as was previously suggested (2). The distance is almost identical to that reported by Cotton and co-workers (2.530(2) Å) for the benchmark compound $[W_2S_2(S_2CNEt_2)_4]$ (1). The acute angles subtended at the μ-S atoms are also consistent with a confacial bioctahedral structure severely distorted by a strong metal–metal interaction.

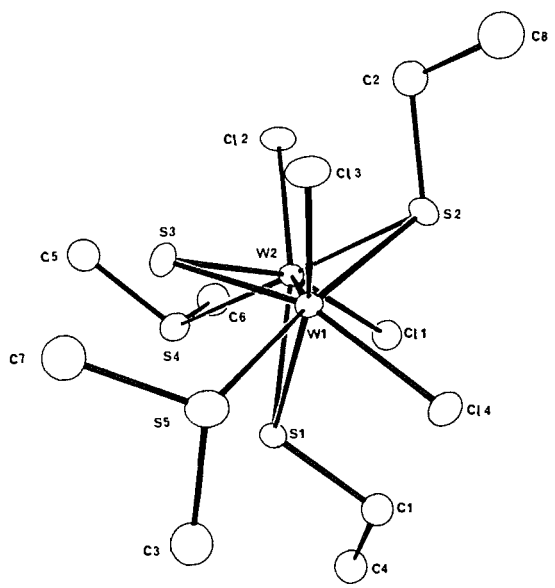


FIG. 1. ORTEP view of the structure of $(Me_2S)Cl_2W(\mu\text{-}S)(\mu\text{-}SEt)_2WCl_2(Me_2S)$, **1**. The envelopes enclose 20% probability thermal ellipsoids.

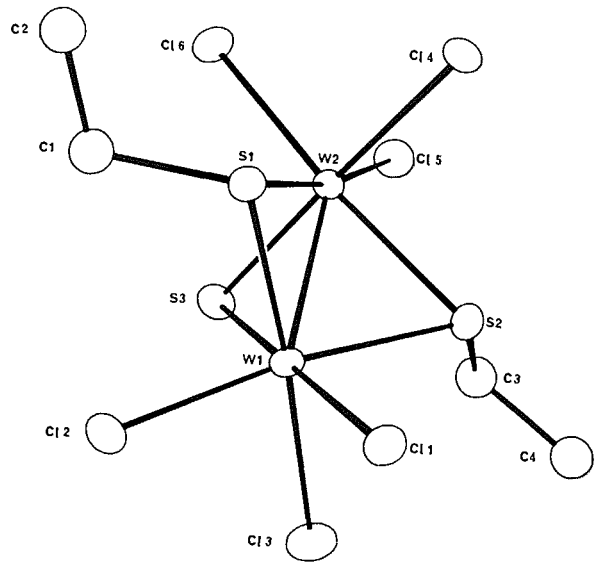


FIG. 2. ORTEP view of the anion $[Cl_3W(\mu\text{-}S)(\mu\text{-}SEt)_2WCl_3]^{2-}$ in complex **2**. (20% probability thermal ellipsoids shown.)

There are two differences, however, in the geometry of the three $W(\mu\text{-}S)(\mu\text{-}SEt)_2W$ moieties. First, the presence of a terminal thioether with a long W—S bond allows the W—S bond *trans* to it to be significantly shorter than the analogous bonds *trans* to chlorine. The surprising feature of the structures of **1** and **3** is that in both cases the thioether is *trans* to a thiolate rather than to the sulfide ligand. This reduces the symmetry of the molecules from the $C_{2v}$ point group potentially available, to $C_s$ in **3**, and $C_1$ in **1**. The relatively short sulfide–tungsten bonds might be expected to be *trans* to the thioether. Since the stereochemistry of the two starting complexes $WCl_4(Me_2S)_2$ and $WCl_4(C_4H_8S)_2$ is believed to be different (9), the products must be thermodynamically stable in their observed geometries, rather than being the result of a kinetically controlled process.

The second feature in which the complexes **1** and **2** differ is in the configurations adopted by the two thiolato sulfur atoms. The anion of **2** possesses the *ee* configuration (following the nomenclature used by Bor and co-workers (10)), but the dimethyl sulfide complex **1** possesses an *ae* configuration. On steric grounds the *ee* isomer would be expected to be the more stable. It may be noted that the —SEt group *trans* to the thioether, which has the shorter W—S bonds, is in the equatorial configuration while the axial configuration is adopted by the

Can. J. Chem. Downloaded from www.nrcresearchpress.com by 210.87.254.105 on 09/06/12
For personal use only.

TABLE 8. Bond lengths and non-bonded contacts (Å) in $(Me_2S)Cl_2W(\mu\text{-}S)(\mu\text{-}SEt)_2WCl_2(Me_2S)$ with estimated standard deviations in parentheses

(*i*) Bonding interactions

| Bond | Length (Å) | Bond | Length |
|---|---|---|---|
| W(1)—W(2) | 2.526(2) | | |
| W(1)—Cl(3) | 2.357(5) | W(2)—Cl(1) | 2.348(5) |
| W(1)—Cl(4) | 2.359(7) | W(2)—Cl(2) | 2.361(8) |
| W(1)—S(1) | 2.473(4) | W(2)—S(1) | 2.477(7) |
| W(1)—S(2) | 2.403(7) | W(2)—S(2) | 2.404(5) |
| W(1)—S(3) | 2.313(6) | W(2)—S(3) | 2.309(6) |
| W(1)—S(5) | 2.574(9) | W(2)—S(4) | 2.598(6) |
| S(1)—C(1) | 1.85(2) | S(5)—C(3) | 1.77(2) |
| S(2)—C(2) | 1.86(2) | S(5)—C(7) | 1.85(3) |
| S(4)—C(5) | 1.79(2) | C(1)—C(4) | 1.54(3) |
| S(4)—C(6) | 1.82(4) | C(2)—C(8) | 1.50(4) |

(*ii*) Non-bonded contacts

| Atoms | Distance | Atoms | Distance |
|---|---|---|---|
| S(1)···S(2) | 3.807(7) | S(2)···Cl(2) | 3.335(11) |
| S(1)···S(3) | 2.952(7) | S(2)···Cl(3) | 3.357(10) |
| S(2)···S(3) | 3.682(7) | S(2)···Cl(1) | 3.370(8) |
| | | S(2)···Cl(4) | 3.375(12) |
| S(1)···S(4) | 3.393(11) | | |
| S(1)···S(5) | 3.544(11) | S(3)···S(4) | 3.327(10) |
| S(1)···Cl(1) | 3.330(10) | S(3)···S(5) | 3.493(13) |
| S(1)···Cl(4) | 3.343(9) | S(3)···Cl(2) | 3.555(11) |
| | | S(3)···Cl(3) | 3.486(9) |
| Cl(2)···S(4) | 3.360(7) | | |
| Cl(2)···Cl(1) | 3.481(7) | Cl(3)···S(5) | 3.166(9) |
| Cl(1)···S(4) | 3.293(7) | Cl(3)···Cl(4) | 3.548(7) |
| | | Cl(4)···S(5) | 3.138(8) |
| C(3)···C(7) | 2.83(4) | | |
| | | C(5)···C(6) | 2.70(4) |
| S(2)···C(8) | 2.73(3) | | |
| | | S(1)···C(4) | 2.74(2) |

TABLE 9. Bond lengths and non-bonded contacts (Å) in the $[Cl_3W(\mu\text{-}S)(\mu\text{-}SEt)_2WCl_3]^{2-}$ anion with estimated standard deviations in parentheses

(*i*) Bonding interactions

| Bond | Length | Bond | Length |
|---|---|---|---|
| W(1)—W(2) | 2.522(1) | | |
| W(1)—Cl(1) | 2.422(6) | W(2)—Cl(4) | 2.432(5) |
| W(1)—Cl(2) | 2.421(6) | W(2)—Cl(6) | 2.433(7) |
| W(1)—Cl(3) | 2.427(7) | W(2)—Cl(5) | 2.431(7) |
| W(1)—S(1) | 2.420(7) | W(2)—S(1) | 2.424(7) |
| W(1)—S(2) | 2.411(7) | W(2)—S(2) | 2.420(7) |
| W(1)—S(3) | 2.311(7) | W(2)—S(3) | 2.305(5) |
| S(1)—C(1) | 1.87(3) | S(2)—C(3) | 1.84(3) |
| C(1)—C(2) | 1.53(4) | C(3)—C(4) | 1.56(5) |

(*ii*) Non-bonded contacts

| Atoms | Distance | Atoms | Distance |
|---|---|---|---|
| S(1)···S(3) | 3.457(9) | S(3)···Cl(2) | 3.461(10) |
| S(1)···S(2) | 3.659(11) | S(3)···Cl(6) | 3.433(9) |
| S(2)···S(3) | 3.379(9) | S(3)···Cl(3) | 3.347(10) |
| | | S(3)···Cl(5) | 3.400(9) |
| S(1)···Cl(6) | 3.341(9) | | |
| S(1)···Cl(2) | 3.351(7) | S(2)···Cl(5) | 3.384(10) |
| S(1)···Cl(4) | 3.366(9) | S(2)···Cl(3) | 3.346(8) |
| S(1)···Cl(1) | 3.375(9) | S(2)···Cl(4) | 3.331(9) |
| | | S(2)···Cl(1) | 3.323(10) |
| Cl(6)···Cl(4) | 3.412(9) | | |
| Cl(6)···Cl(5) | 3.320(12) | Cl(2)···Cl(1) | 3.352(9) |
| Cl(4)···Cl(5) | 3.342(9) | Cl(2)···Cl(3) | 3.310(11) |
| | | Cl(1)···Cl(3) | 3.372(9) |
| S(1)···C(2) | 2.80(3) | | |
| | | S(2)···C(4) | 2.75(4) |

SEt group *trans* to a Cl atom. These observations imply that during the reaction of **1** with $Cl^-$ to produce **2**, inversion occurs at one of the sulfur atoms. The possible interconversion of *ee* to *ae* isomers of complexes of this type in solution has been studied by nmr spectroscopy and will be described elsewhere (4).

The presence of the thioether ligands in terminal positions in complexes **1** and **3** seems to be related to another potentially important aspect of the structure. In both these complexes there is a short S···SEt contact (Table 12) whereas in the chloro-anion of **2** this effect is not pronounced. Similar effects have been observed by other workers, who have advanced a variety of explanations. For example, Stiefel and co-workers (11) suggested that partial bond formation between adjacent sulfurs could arise through a redox process. In another case McCarley and co-workers ascribed a close contact between two bridging Br atoms to the electrostatic repulsion caused by the electrons in a metal–metal bond (12). The phenomenon has also been discussed by Fackler (13), and by Dance, Wedd, and Boyd (14). The simplest explanation in the present case would seem to be a steric repulsion caused by the terminal thioethers. Examination of Fig. 1 does not support this suggestion, since the two sulfur atoms which form the close contact are in fact closest to these ligands, and would more probably be displaced in the opposite direction. There is no systematic trend in the sums of the angles subtended at the sulfur atoms of the μ-SEt groups (Table 12), which might be expected from a steric effect. It may be significant that the closest contact is formed by the sulfur with an axial alkyl group (complex **1**).

We therefore conclude that the most likely

Can. J. Chem. Downloaded from www.nrcresearchpress.com by 210.87.254.105 on 09/06/12
For personal use only.

TABLE 10. Bond angles (deg) in $(Me_2S)Cl_2W(\mu\text{-}S)(\mu\text{-}SEt)_2WCl_2(Me_2S)$

| Bonds | Angle | Bonds | Angle |
|---|---|---|---|
| | W—bridge—W angles | | |
| W(1)—S(1)—W(2) | 61.4(1) | W(1)—S(3)—W(2) | 66.2(1) |
| W(1)—S(2)—W(2) | 63.4(2) | | |
| | Bridge—W—bridge angles | | |
| S(1)—W(1)—S(2) | 102.6(2) | S(1)—W(2)—S(2) | 102.5(2) |
| S(1)—W(1)—S(3) | 76.1(2) | S(1)—W(2)—S(3) | 76.1(2) |
| S(2)—W(1)—S(3) | 102.6(2) | S(2)—W(2)—S(3) | 102.7(2) |
| | Terminal—W—terminal angles | | |
| Cl(3)—W(1)—Cl(4) | 97.5(2) | Cl(1)—W(2)—Cl(2) | 95.3(2) |
| Cl(3)—W(1)—S(5) | 79.8(2) | Cl(1)—W(2)—S(4) | 83.3(2) |
| Cl(4)—W(1)—S(5) | 78.9(2) | Cl(2)—W(2)—S(4) | 85.2(2) |
| | Bridge—W—terminal angles | | |
| S(1)—W(1)—Cl(3) | 166.7(2) | S(1)—W(2)—Cl(2) | 168.4(2) |
| S(1)—W(1)—Cl(4) | 87.5(2) | S(1)—W(2)—Cl(1) | 87.2(2) |
| S(1)—W(1)—S(5) | 89.2(2) | S(1)—W(2)—S(4) | 83.9(2) |
| S(2)—W(1)—Cl(3) | 89.7(2) | S(2)—W(2)—Cl(2) | 88.8(2) |
| S(2)—W(1)—Cl(4) | 90.2(2) | S(2)—W(2)—Cl(1) | 90.3(2) |
| S(2)—W(1)—S(5) | 163.6(2) | S(2)—W(2)—S(4) | 170.8(3) |
| S(3)—W(1)—Cl(3) | 96.5(2) | S(3)—W(2)—Cl(2) | 99.1(2) |
| S(3)—W(1)—Cl(4) | 160.9(2) | S(3)—W(2)—Cl(1) | 160.6(2) |
| S(3)—W(1)—S(5) | 91.1(2) | S(3)—W(2)—S(4) | 85.1(2) |
| | Carbon—sulfur—metal angles | | |
| C(1)—S(1)—W(1) | 111.8(7) | C(2)—S(2)—W(1) | 111.7(9) |
| C(1)—S(1)—W(2) | 113.9(10) | C(2)—S(2)—W(2) | 110.8(8) |

TABLE 11. Bond angles (deg) in the $[Cl_3W(\mu\text{-}S)(\mu\text{-}SEt)_2WCl_3]^{2-}$ anion

| Bonds | Angle | Bonds | Angle |
|---|---|---|---|
| | W—bridge—W angles | | |
| W(1)—S(1)—W(2) | 62.8(2) | W(1)—S(3)—W(2) | 62.2(2) |
| W(1)—S(2)—W(2) | 62.9(2) | | |
| | Bridge—W—bridge angles | | |
| S(1)—W(1)—S(2) | 98.5(2) | S(1)—W(2)—S(2) | 98.1(2) |
| S(1)—W(1)—S(3) | 93.9(2) | S(1)—W(2)—S(3) | 93.9(2) |
| S(2)—W(1)—S(3) | 91.3(2) | S(2)—W(2)—S(3) | 91.3(2) |
| | Terminal—W—terminal angles | | |
| Cl(1)—W(1)—Cl(2) | 87.6(2) | Cl(4)—W(2)—Cl(6) | 89.0(2) |
| Cl(1)—W(1)—Cl(3) | 88.1(2) | Cl(4)—W(2)—Cl(5) | 86.8(2) |
| Cl(2)—W(1)—Cl(3) | 86.1(2) | Cl(6)—W(2)—Cl(5) | 86.1(2) |
| | Bridge—W—terminal angles | | |
| S(1)—W(1)—Cl(1) | 88.4(2) | S(1)—W(2)—Cl(4) | 87.8(2) |
| S(1)—W(1)—Cl(2) | 87.6(2) | S(1)—W(2)—Cl(6) | 86.9(2) |
| S(1)—W(1)—Cl(3) | 172.9(2) | S(1)—W(2)—Cl(5) | 171.2(2) |
| S(2)—W(1)—Cl(1) | 86.9(2) | S(2)—W(2)—Cl(4) | 86.7(2) |
| S(2)—W(1)—Cl(2) | 171.7(2) | S(2)—W(2)—Cl(6) | 173.3(2) |
| S(2)—W(1)—Cl(3) | 87.5(2) | S(2)—W(2)—Cl(5) | 88.5(2) |
| S(3)—W(1)—Cl(1) | 177.3(3) | S(3)—W(2)—Cl(4) | 177.5(3) |
| S(3)—W(1)—Cl(2) | 94.0(2) | S(3)—W(2)—Cl(6) | 92.8(2) |
| S(3)—W(1)—Cl(3) | 89.8(2) | S(3)—W(2)—Cl(5) | 91.7(2) |
| | Carbon—sulfur—metal angles | | |
| C(1)—S(1)—W(1) | 110.6(8) | C(3)—S(2)—W(1) | 110.2(9) |
| C(1)—S(1)—W(2) | 112.1(9) | C(3)—S(2)—W(2) | 106.6(10) |

TABLE 12. Comparison of the structures of the confacial bioctahedral complexes $(Me_2S)Cl_2W(\mu\text{-}S)(\mu\text{-}SEt)_2WCl_2(Me_2S)$, **1**; $[Cl_3W(\mu\text{-}S)(\mu\text{-}SEt)_2WCl_3]^{2-}$, **2**; and $(C_4H_8S)Cl_2W(\mu\text{-}S)(\mu\text{-}SEt)_2WCl_2(C_4H_8S)$, **3**

| Property | Value | | |
|---|---|---|---|
| | **1** | **2** | **3** |
| W—W (Å) | 2.526(2) | 2.522(1) | 2.524(1) |
| Configuration of μ-SEt groups | *ae* | *ee* | *ee* |
| Shortest S···SEt contact (Å) | 2.952(7) | 3.379(9) | 3.162(4) |
| Sum of angles subtended at μ-S(Et) atoms | | | |
| (*a*)* | 285.9° | 285.5° | 289.6° |
| (*b*)† | 287.1° | 279.7° | 284.7° |

*For S with no short S···SEt contact.
†For S with a short S···SEt contact.

explanation is that there is an attractive interaction between the two sulfurs, which is influenced by the presence of the terminal thioether ligands. We are continuing our study of thiolato-bridged metal clusters to try to shed further light on this problem.

## Acknowledgements

We thank the Natural Sciences and Engineering Research Council of Canada for financial support and the University of Calgary for a contribution towards computing costs.

1. A. BINO, F. A. COTTON, Z. DORI, and J. C. SEKUTOWSKI. Inorg. Chem. **17**, 2946 (1978).
2. P. M. BOORMAN, K. A. KERR, and V. D. PATEL. J. Chem. Soc. Dalton Trans. 506 (1981).
3. P. M. BOORMAN, T. CHIVERS, and K. N. MAHADEV. Can. J. Chem. **53**, 383 (1975).
4. V. D. PATEL and P. M. BOORMAN. Can. J. Chem. This issue.
5. P. COPPENS *et al.* Acta Crystallogr. **18**, 1035 (1965).
6. D. T. CROMER and J. B. MANN. Acta Crystallogr. Sect. A, **24**, 321 (1968).
7. International tables for crystallography. Kynock Press, Birmingham, England. 1974.
8. J. M. STEWART (*Editor*). Technical Report TR-446. Computer Science Center, University of Maryland.
9. M. A. SCHAEFER-KING and R. E. MCCARLEY. Inorg. Chem. **12**, 1972 (1973).
10. G. NATILE, L. MARESCA, and G. BOR. Inorg. Chim. Acta, **23**, 37 (1977).
11. E. I. STIEFEL, K. F. MILLER, A. E. BRUCE, J. L. CORBIN, J. M. BERG, and K. O. HODGSON. J. Am. Chem. Soc. **102**, 3624 (1980).
12. J. L. TEMPLETON, W. C. DORMAN, J. C. CLARDY, and R. E. MCCARLEY. Inorg. Chem. **17**, 1263 (1978).
13. J. P. FACKLER, JR. Prog. Inorg. Chem. **21**, 55 (1976).
14. I. G. DANCE, A. G. WEDD, and I. W. BOYD. Aust. J. Chem. **31**, 519 (1978).

Can. J. Chem. Downloaded from www.nrcresearchpress.com by 210.87.254.105 on 09/06/12
For personal use only.

# Studies of confacial bioctahedral tungsten complexes containing metal-to-metal bonds: synthesis, reactions, and nuclear magnetic resonance studies of $W_2Cl_4(\mu\text{-}SR)_2(\mu\text{-}S)L_2$ (R = alkyl; L = monodentate ligand)[1]

VIKRAM D. PATEL AND P. MICHAEL BOORMAN[2]

*Department of Chemistry, University of Calgary, Calgary, Alta., Canada T2N 1N4*

Received August 27, 1981

VIKRAM D. PATEL and P. MICHAEL BOORMAN. Can. J. Chem. **60**, 1339 (1982).

A series of new binuclear tungsten(IV) complexes, $W_2Cl_4(\mu\text{-}SR)_2(\mu\text{-}S)L_2$ (R = Me, Et, $^i$Bu, $CH_2Ph$; L = $Me_2S$ or THT), is readily synthesized from the metathetical reaction of $WCl_4L_2$ with 1 mol-equiv. of alkylthiotrimethylsilane ($Me_3Si(SR)$). These complexes react with stronger nucleophiles ($Ph_3P$, MeCN, $C_5H_5N$, $Cl^-$) under ambient conditions to yield simple disubstituted products. Reaction of $W_2Cl_4(\mu\text{-}SEt)_2(\mu\text{-}S)(SMe_2)_2$ with $PhCH_2X$ (X = Cl, Br) yields $[Me_2SCH_2Ph]_2[W_2Cl_4(\mu\text{-}SEt)_2(\mu\text{-}S)X_2]$, whilst with stronger alkylating agents, $MeSO_3F$ or $Et_3OBF_4$, intractable residues result.

The series of homologous complexes has been studied by $^1H$ and $^{13}C$ nmr spectroscopy. When R = Me, two stable configurational isomers are present in solution, whilst only a single isomer exists for more bulky R groups. Trends in the $^1H$ nmr chemical shifts of the methylene and methyl protons of the SEt groups in the complexes $W_2Cl_4(\mu\text{-}SEt)_2(\mu\text{-}S)L_2$ allow absolute assignment of the resonances to two magnetically inequivalent thiolato groups.

VIKRAM D. PATEL et P. MICHAEL BOORMAN. Can. J. Chem. **60**, 1339 (1982).

On a préparé facilement une série de nouveaux complexes binucléaires du tungstène (IV), $W_2Cl_4(\mu\text{-}SR)_2(\mu\text{-}S)L_2$ (R = Me, Et, Bu$^i$, $CH_2Ph$; L = $Me_2S$ ou THT) à partir de la réaction de double décomposition du $WCl_4L_2$ avec un équivalent molaire d'alkylthiotriméthylsilane ($Me_3Si(SR)$). Ces complexes réagissent avec des nucléophiles plus forts ($Ph_3P$, MeCN, $C_5H_5N$, $Cl^-$) à la température ambiante pour donner de simples produits bisubstitués. Le composé $W_2Cl_4(\mu\text{-}SEt)_2(\mu\text{-}S)(SMe_2)_2$ réagit avec $PhCH_2X$ (X = Cl, Br) pour donner le composé $[Me_2SCH_2Ph]_2[W_2Cl_4(\mu\text{-}SEt)_2(\mu\text{-}S)X_2]$ tandis qu'avec des agents alkylants plus forts, du type $MeSO_3F$ ou $Et_3OBF_4$, on obtient des résidus qu'on ne peut isoler.

On a étudié la série des complexes homologues par la spectroscopie de rmn du $^1H$ et du $^{13}C$. En solution, on obtient deux isomères de configurations stables lorsque R = Me tandis qu'il n'existe qu'un seul isomère avec les groupes R plus encombrés. La tendance dans les déplacements chimiques en rmn du $^1H$ des protons du méthylène et du méthyle des groupes SEt des complexes $W_2Cl_4(\mu\text{-}SEt)_2(\mu\text{-}S)L_2$ permet une identification absolue des résonances des deux groupes thiolato magnétiquement inéquivalents.

[Traduit par le journal]

## Introduction

We have recently reported (1, 2) the syntheses and crystal structures of two types of tungsten thiolate dimers possessing a confacial bioctahedral framework (Fig. 1). Complexes of type *a* (Fig. 1) (1) have several features of unusual interest. First, it is worthy of note that they possess three types of divalent sulfur ligands ($S^{2-}$, $RS^-$, and $R_2S$), coordinated to a relatively high oxidation state metal centre (W(IV)), and thus should allow assessment of the electrophilic and/or nucleophilic reactivity of these ligands. Second, these complexes are isostructural and isoelectronic with the complexes $M_2Br_6(THT)_3$ (M = Nb, Ta; THT = tetrahydrothiophene) (3). The tantalum complex has been shown to undergo some unusual reactions with nitriles and acetylenes under mild conditions (4). The availability of complexes of type *a* with a variety of R and L substituents has allowed us to study the reactivity of this type of complex, and to compare the chemistry with their niobium and tantalum homologues. Herein we report the reactions of these complexes with electrophiles and nucleophiles, and their solution behaviour as studied by $^1H$ and $^{13}C$ nmr spectroscopy.

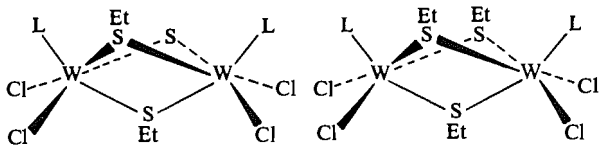


FIG. 1. Structures and solid state geometry of tungsten thiolato complexes.

## Experimental

*General procedures*

All manipulations were carried out in a dry nitrogen-filled glovebox or on a standard double manifold. Analytical grade solvents were dried ($P_2O_5$ or $CaH_2$) and distilled under nitrogen before use. Alkyl sulfides (Aldrich Chemicals) were dried over calcium hydride and distilled under nitrogen prior to use. Tungsten carbonyl was purchased from Alfa Inorganics, as was

[1]Taken in part from the Ph.D. Thesis of V.D.P., University of Calgary, Calgary, Alta., 1981.

[2]To whom all correspondence should be addressed.

0008-4042/82/111339-08$01.00/0

©1982 National Research Council of Canada/Conseil national de recherches du Canada

Can. J. Chem. Downloaded from www.nrcresearchpress.com by 210.87.254.105 on 09/06/12
For personal use only.

Can. J. Chem. Downloaded from www.nrcresearchpress.com by 210.87.254.105 on 09/06/12
For personal use only.

tungsten hexachloride. The latter compound was twice resublimed before use. Tungsten tetrachloride was synthesized by the method of McCarley and Schaefer-King (5). Chlorotrimethylsilane was purchased from Aldrich Chemicals as were thiols. (Alkylthio)trimethylsilanes ($Me_3SiSR$; R = Me, Et, $^t$Bu, $CH_2Ph$) were synthesized via the lead salt of RSH by the published procedure (6). The adducts $WCl_4(SMe_2)_2$ and $WCl_4(THT)_2$ were prepared as previously described (5, 7). Tungsten was analyzed by ignition to the oxide ($WO_3$). Other analyses were obtained commercially (Galbraith Laboratories Inc., Knoxville, TN, U.S.A.). Routine ir spectra were recorded as Nujol mulls between CsI plates using a Perkin-Elmer 467 spectrophotometer. Electronic spectra were recorded as solutions in matched quartz cells using a Beckman DB-G spectrophotometer. $^1$H nmr spectra of the complexes were obtained using either a Hitachi Perkin-Elmer R-24B spectrometer (60 MHz), a Bruker WH90 FT spectrometer (90 MHz) or a Varian XL200 FT spectrometer (200 MHz). Proton decoupled $^{13}$C nmr spectra were recorded at room temperature on a Bruker WH90 spectrometer operating at 22.63 MHz.

*Synthesis of $W_2Cl_4(\mu\text{-}SR)_2(\mu\text{-}S)L_2$ (L = THT, $Me_2S$): 1*a, *1*b *(R = Me); 2*a, *2*b *(R = Et); 3 (R = $^t$Bu); 4 ($R = CH_2Ph$)*

The general reaction employed in the syntheses of the above complexes is represented by reactions [1] and [2].

$$[1]\quad [WCl_4L_2] + Me_3SiSR \xrightarrow{CH_2Cl_2} [WCl_3(SR)L_2] + Me_3SiCl$$

L = $Me_2S$ or THT

$$[2]\quad [WCl_3(SR)L_2] \rightarrow \text{products}$$

In a typical reaction, the compound $WCl_4L_2$ (ca. 2.0 g) was dissolved in $CH_2Cl_2$ (35 mL) and to this stirred solution was added the exact, calculated 1 mol-equiv. of $Me_2SiSR$ dissolved in $CH_2Cl_2$. $^1$H nmr studies (8) showed immediate conversion of $Me_3SiSR$ to $Me_3SiCl$ and there was also an instantaneous colour change of the solution from orange–red to a darker red. A light brown precipitate was observed within 2 h, and after stirring overnight at room temperature the solution was filtered to remove this precipitate. Analytical and various spectroscopic data confirmed that this precipitate was a sulfonium salt of the $WCl_6^{2-}$ anion, as shown previously (8, 9). The dark-red-coloured filtrate was diluted to 100 mL with $CH_2Cl_2$, and hexane (40–50 mL) was added to deposit an intractable brown oil. Filtration, followed by slow evaporation of the filtrate solvent *in vacuo*, yielded the desired complex as a red microcrystalline powder, which was collected on a medium frit, washed with hexane, and dried under vacuum (yield ca. 50%). Crystals of the complexes are obtained on allowing the mother liquor (after removal of sulfonium salt and the oily residue) to stand undisturbed at −20°C for 48–72 h. The formulation of these complexes is not evident from the available analytical data (9) (Table S1), but was confirmed by single crystal X-ray analyses of the complexes **2***a* and **2***b* [1]. The difficulty in obtaining reliable analytical data probably results from several causes. The tendency of these complexes to lose thioether ligands upon standing not only leads to erroneous analytical results, but it also precluded recrystallization as a means of purification in many instances. Furthermore, we have found it difficult to obtain reliable commercial analyses for sulfur and chlorine, in particular, on this type of complex. Characterization has therefore been based not only on analytical data, but also on comparisons between the spectroscopic properties of new compounds and those of compounds with crystallographically determined structures. The complexes **2***a* and **2***b* exhibit analogous spectroscopic (ir, uv-visible, and $^1$H and $^{13}$C nmr) properties to the other compounds in this series. Infrared spectra for all the complexes contain an identical broad band centered at 315 cm$^{-1}$, which can be assigned to ν(W—Cl), together with characteristic vibrations due to the hydrocarbon parts of the thiolate and thioether ligands. However, the spectra are devoid of any peak assignable to the bridging W—S—W moiety. The complexes exhibit three strong absorptions in their visible spectra at ~365 (ε = 4000), ~525 (ε ~ 1500), and 780 nm [ε ~ 2000) respectively.

*$(Et_4N)_2[W_2Cl_6(\mu\text{-}SMe)_2(\mu\text{-}S)]$ (1*c*)*

Tetraethylammonium chloride (0.23 g; 1.39 mmol) was added to a solution of **1***a* (0.48 g; 0.57 mmol) in dichloromethane (30 mL). The solution was stirred at ambient temperature for 14 h and to the solution hexane (50 mL) was slowly added. The red microcrystalline precipitate was filtered, washed with hexane, and dried under vacuum. *Anal.* calcd. for $W_2Cl_6S_3C_{18}H_{46}N_2$: C 22.35, H 4.76, S 9.94, N 2.89; found: C 22.40, H 5.0, S 9.70, N 2.80. The same product was obtained from **1***b* under similar reaction conditions.

*$(Et_4N)_2[W_2Cl_6(\mu\text{-}SEt)_2(\mu\text{-}S)]$ (2*f*)*

The complex **2***f* was synthesized from **2***b* and tetraethylammonium chloride by a procedure identical to that used for **1***c*. *Anal.* calcd. for $W_2Cl_6S_3C_{20}H_{50}N_2$: Cl 21.38, C 24.14, H 5.03, S 9.65, N 2.82; found: Cl 21.40, C 24.30, H 4.80, S 9.40, N 2.80.

*$W_2Cl_4(\mu\text{-}SEt)_2(\mu\text{-}S)(NCMe)_2$ (2*c*)*

Acetonitrile (0.7 mL; 13.3 mmol) was added to a solution of **2***b* (0.68 g; 0.86 mmol) in dichloromethane (30 mL). The solution was stirred at ambient temperature for 15 h and then the solvent was removed under vacuum. The residue was redissolved in $CH_2Cl_2$ (50 mL) and hexane (30 mL) was slowly added. Reduction in volume of the solution (to ca. 40 mL) afforded **2***c* as a red microcrystalline precipitate which was filtered off, washed with hexanes, and dried under vacuum (yield 0.5 g; 70%). ir: ν(C≡N) at 2310 and 2295 cm$^{-1}$ which are assigned to coordinated acetonitrile (10). Variable amounts of occluded acetonitrile is present in the solid as indicated by its $^1$H nmr spectra (δ 2.02). The displacement of dimethylsulfide by acetonitrile is less facile than in the case of **2***d* and **2***f* as indicated by the recovery of small amounts of **2***b* from the mother liquor.

*$W_2Cl_4(\mu\text{-}SEt)_2(\mu\text{-}S)(PPh_3)_2$ (2*d*)*

A solution of **2***b* (0.85 g; 1.08 mmol) and triphenylphosphine (1.41 g; 5.37 mmol) in dichloromethane (50 mL) was gently refluxed for 4 h. After being allowed to cool to room temperature, the mixture was filtered, and hexane (100 mL) was slowly added to the filtrate. Reduction in volume of the solution (to ca. 50 mL) resulted in the precipitation of **2***d* as a red microcrystalline powder. The same complex results (under identical reaction and workup conditions outlined above) from the use of a two molar equivalent of triphenylphosphine.

*$W_2Cl_4(\mu\text{-}SEt)_2(\mu\text{-}S)(Py)_2\cdot Py$ (2*e*)*

Excess pyridine (Py) (2.5 mL; 31.2 mmol) was added to a solution of **2***a* (0.50 g; 0.5 mmol) in dichloromethane (20 mL). The resultant dark red solution was stirred at ambient temperature for 2 h before slowly adding hexane (20 mL). Reduction in volume of the solution (to ca. 20 mL) resulted in the precipitation of **2***e*, which was collected by filtration, washed with hexane, and dried under vacuum. *Anal.* calcd. for $W_2Cl_4S_3C_{19}H_{25}N_3$: C 25.71, H 2.82, N 4.73; found: C 25.50, H 3.0, N 4.60.

The ir spectrum of **2***e* contains bands due to both free and coordinated pyridine (Py) as indicated by the presence of the characteristic in-plane ring vibrations at 1578 and 604 cm$^{-1}$ and out-of-plane ring vibration at 405 cm$^{-1}$ of free Py, which are shifted to 1620, 675 cm$^{-1}$ and 445 cm$^{-1}$, respectively, on coordination (11).

Can. J. Chem. Downloaded from www.nrcresearchpress.com by 210.87.254.105 on 09/06/12
For personal use only.

*$[Me_2SCH_2Ph]_2[W_2Cl_4(\mu\text{-}SEt)_2(\mu\text{-}S)Br_2]$ (2g)*

Benzyl bromide (1.0 mL; 8.4 mmol) was added to a solution of **2***b* (0.65 g; 0.83 mmol) in benzene (25 mL). The solution began to take on a dark-black–green tinge after 3 h, and a greenish precipitate formed. The solution was stirred for a further 12 h and the precipitate collected by filtration, washed with hexane, and dried under vacuum (yield 0.40 g; 43.0%). *Anal.* calcd. for $W_2Cl_4S_5Br_2C_{22}H_{38}$: C 23.33, H 3.40, Cl 12.53; found: C 21.30, H 2.90, Cl 13.40.

*$[Me_2SCH_2Ph]_2[W_2Cl_6(\mu\text{-}SEt)_2(\mu\text{-}S)]$* (2h)

Benzyl chloride (1.0 mL; 8.69 mmol) was added to a solution of **2***b* (0.46 g; 0.58 mmol) in $CH_2Cl_2$ (25 mL). The solution was stirred at ambient temperature for 14 h. The red–black precipitate was collected by filtration, washed with hexane, and dried under vacuum (yield 0.35 g; 55%). $^1$H nmr data ($CD_3CN$) δ: 1.00 (t, 6); 2.75 (s, 12); 3.0 (q, 4); 4.55 (s, 4); 7.3–7.5 (m, 10).

*$[(Ph_4P)_2][W_2Cl_6(\mu\text{-}SEt)_2(\mu\text{-}S)]$* (2i)

Tetraphenylphosphonium chloride (0.57 g; 1.54 mmol) was added to a solution of **2***b* (0.54 g; 0.68 mmol) in $CH_2Cl_2$ (30 mL). The solution was stirred at ambient temperature for 6 h, before removing the solvent under vacuum. The dark red residue was redissolved in $CH_3CN$ (35 mL). Slow addition of anhydrous $Et_2O$ (~60 mL) resulted in the precipitation of the title complex, as dark red needles, which were collected by filtration and washed with hexanes. A further crop of crystals was obtained on allowing the mother liquor to stand undisturbed at −10°C for 48 h. $^1$H nmr data ($CD_2Cl_2$) δ: 1.38 (t, 6); 2.91 (q, 4); 7.5–7.9 (m, 40).

*Attempted reaction of $[Ph_4P]_2[W_2Cl_6(\mu\text{-}SEt)_2(\mu\text{-}S)]$ with EtI and MeI*

Ethyl iodide (0.2 mL; 2.46 mmol) was added to a solution of **2***i* (0.20 g; 0.14 mmol) in $CH_2Cl_2$ (20 mL). The solution was refluxed for 3 h and stirred for an additional 14 h at room temperature. The solvent was removed *in vacuo* and the residue washed with hexanes. The $^1$H nmr spectrum indicated the residue to be unreacted starting materials. Similar results were obtained from the attempted reaction with MeI.

*Attempted reaction of **3** with $PhC{\equiv}CPh$*

A solution of diphenylacetylene (0.035 g; 0.2 mmol) and complex **3** (0.16 g; 0.19 mmol) in $CH_2Cl_2$ (15 mL) was stirred at room temperature for 14 h. No noticeable colour change occurred. The solvent was removed *in vacuo*. The $^1$H nmr spectrum of the residue ($CDCl_3$) showed characteristic resonances attributable to unreacted starting materials.

## Results and discussion

*Synthesis and reactions of $W_2Cl_4(\mu\text{-}SR)_2(\mu\text{-}S)L_2$ ($L = Me_2S$ or THT; R = Me, Et, $^i$Bu, $CH_2Ph$) complexes*

Previously (9, 12), we demonstrated that it was possible to introduce the $SR^-$ ligand into the coordination sphere of tungsten in lieu of $Cl^-$ by utilizing alkyl(aryl)thiotrimethylsilane ($Me_3Si(SR)$) reagents (reaction [1]). The reaction in [1] was found to be sensitive to the stoichiometry of the reactants and the nature of the R groups used (9, 12). Thus, reaction of $WCl_4L_2$ (L = $Me_2S$ or THT) with 2 mol-equiv. of $Me_3SiSEt$ in $CH_2Cl_2$ proceeds smoothly to yield the dimeric mixed oxidation state (W(III, IV)) complex $W_2Cl_4(\mu\text{-}SEt)_3L_2$ (2) (Fig. 1*b*). In contrast to this, under analogous reaction conditions, the use of 1 mol-equiv. of the silyl reagent allows isolation of the red diamagnetic W(IV) complexes, $W_2Cl_4(\mu\text{-}SR)_2(\mu\text{-}S)L_2$ (L = $Me_2S$ or THT) (Fig. 1*a*) in high yields, for R groups possessing protons on the α carbon atom (9). Their formation in the above reaction is the result of a series of complex intermediate reactions (1). Although these W(IV) thiolato complexes are air-, moisture-, and heat-sensitive, they are easily prepared, and well characterized with the structural studies of the complexes for R = Et; L = THT and $Me_2S$ (1). They are also stable and soluble in most common organic solvents ($CH_2Cl_2$, $C_6H_6$, $CHCl_3$, etc.). Hence these complexes are particularly well suited for the exploration of their chemistry.

The chemistry is summarized in Scheme 1. Substitution of the thioether ligands in complexes **2***a*, *b* (and their homologues) by a variety of stronger donor ligands ($Cl^-$, $Ph_3P$, Py, MeCN) proceeds rapidly and cleanly in $CH_2Cl_2$ (Scheme 1). The quaternary salts of the hexachlorotungstate dimers **1***c*, **2***f*, **2***i* are red microcrystalline solids which are air-stable for short periods of time in the solid state but are rapidly air-oxidized in solution. The $Et_4N^+$ salts (**1***c*, **2***f*) are only sparingly soluble in dichloromethane but exhibit increased solubility in acetonitrile. However, the $Ph_4P^+$ salt, **2***i*, is more soluble in $CH_2Cl_2$ as compared to **2***f*. The ir spectra of these hexachloroditungstate anions show a characteristic strong absorption at ~265 $cm^{-1}$ with shoulders at 305 and 250 $cm^{-1}$, which are assigned to ν(W—Cl) and which appear at a frequency ~40 $cm^{-1}$ lower than found in the neutral complexes. In addition to reacting with quaternary salts, the thioether complexes react with acetonitrile, pyridine, and triphenylphosphine in a single type of reaction, namely, simple substitution of the terminal thioether ligands. The complexes, **2***c–e*, are dark red or brown, slightly air-sensitive solids. The facile and quantitative conversion of the neutral thioether dimers to the corresponding substituted products under mild conditions reflects on the relative nucleophilicities and donor strengths of the various ligands at the W(IV) centres.

The most striking feature of the chemistry of these new thioether complexes is their stability towards gross structural disruption. The simple substitution of the thioether by acetonitrile to give **2***c* contrasts directly with the behaviour exhibited by the isostructural and isoelectronic $Ta_2Cl_6(THT)_3$ complex. This latter complex, under analogous reaction conditions, reacts with a variety of nitriles (RCN, R = Me, Et, etc.) to give tantalum complexes possessing reductively coupled nitrile ligands (4*a*).

Can. J. Chem. Downloaded from www.nrcresearchpress.com by 210.87.254.105 on 09/06/12
For personal use only.

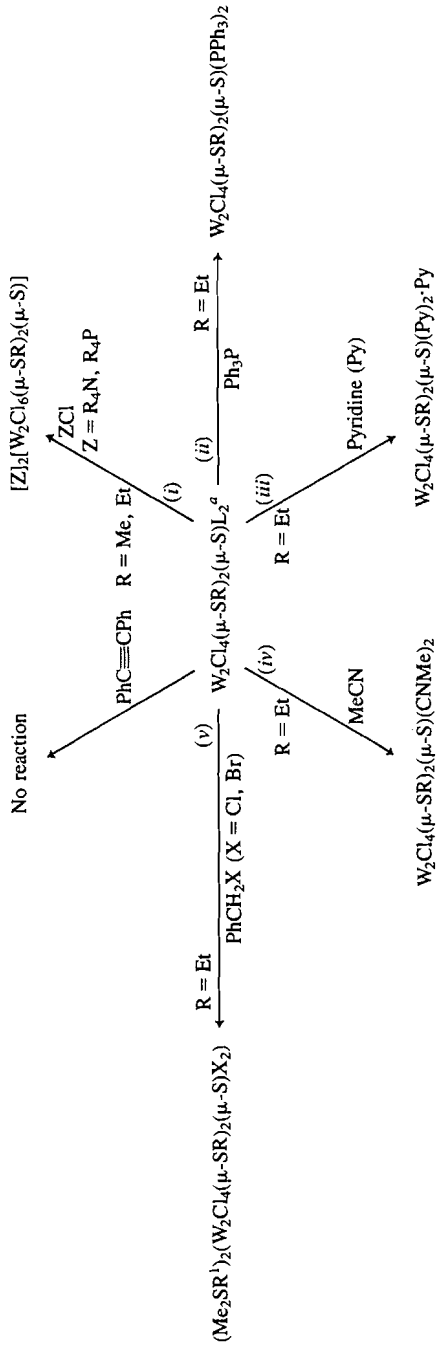


SCHEME 1. Substitution reactions of $W_2Cl_4(\mu\text{-}SR)_2(\mu\text{-}S)L_2$; [a]L = $Me_2S$ or THT (see Experimental for details); all reactions carried out in $CH_2Cl_2$ at 25°C.

In this context it is noteworthy that the complex **2***i* can be crystallized from an acetonitrile solution. Further differences in the behaviour of the two types of complexes becomes evident from the lack of reactivity exhibited by complex **3** towards tolane, PhC≡CPh, whereas the tantalum(III) dimer undergoes facile reactions with a variety of acetylenes (RC≡CR′) to produce mononuclear and binuclear tantalum acetylides (4).

In view of the structural similarities between complexes of type *a* and *b* (Fig. 1), the alkylation of the μ-sulfido ligand in *a* seemed to be an attractive route to the synthesis of compounds of type *b*, which are oxidized by one electron. *S*-Alkylation of sulfur atoms has previously been accomplished by using alkyl halides (12*a*, 13–15), phenylsulfonyl chloride (13), and a variety of other alkylating agents (13–15).

The reaction of excess $PhCH_2X$ (X = Cl, Br) with **2***b* under ambient conditions results in the *S*-alkylation of the thioether ligand to give the corresponding halide-substituted ionic species, **2***g* and **2***h*. These complexes are sparingly soluble in $CH_2Cl_2$, but have increased solubility in acetonitrile. Attempted alkylation of the μ-sulfido ligand by using stronger alkylating agents such as $MeSO_3F$ and $Et_3OBF_4$ resulted only in the formation of intractable residues. The ready *S*-alkylation of the terminal thioether ligand is likely metal-mediated by a mechanism analogous to that proposed for the alkylation of some Ni, Pd, and Pt thiolates by alkyl halides (16). This is further aided by the labile nature of the thioether ligand and the non-coordinating ability of the sulfonium cation at the high oxidation state W(IV) centre.[3] Attempted alkylation of the μ-sulfido ligand of the chloroanions **1***c* and **2***f* with alkyl iodides (MeI or EtI) under ambient and under reflux conditions were unsuccessful and resulted in the recovery of the starting tungsten species.

*Nuclear magnetic resonance studies*

Binuclear complexes possessing two bridging mercaptide ($SR^-$) ligands can exist as configurational isomers, as shown in Fig. 2, depending upon the orientation of the R groups and lone pairs on the bridging sulfur atoms. For cases in which all three terminal ligands are the same (A = B, Fig. 2),

[3]Examples where a sulfonium cation acts as a formal two electron donor have recently been reported, but only for complexes in which the metal is in a low oxidation state; e.g. $[(C_5H_5)Mn(CO)_2(SMe_3)]^+$ (17) and $[Ru(NH_3)_5(SMe_3)]^{2+}$ (18). In these species, the large positive charge on the sulfur can be neutralized by π back-donation to sulfur from the metal centre.

Can. J. Chem. Downloaded from www.nrcresearchpress.com by 210.87.254.105 on 09/06/12
For personal use only.

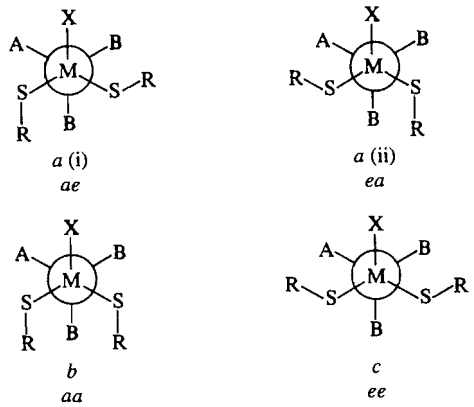


FIG. 2. The possible configurational isomers for the complexes $M_2Cl_4(\mu\text{-}SR)_2(\mu\text{-}S)L_2$, as viewed down the M···M axis.

only three isomers can occur, since the *ae* and *ea* isomers are identical.

In the solid state the molecular configurations of the complexes $W_2Cl_4(\mu\text{-}SEt)_2(\mu\text{-}S)(THT)_2$ (**2***a*) (1*a*) and $[Ph_4P]_2[W_2Cl_6(\mu\text{-}SEt)_2(\mu\text{-}S)]$ (**2***i*) (1*b*) correspond to the *ee* type in Fig. 2, whereas $W_2Cl_4(\mu\text{-}SEt)_2(\mu\text{-}S)(SMe_2)_2$ (**2***b*) (1*b*) exhibits the *ae* configuration of Fig. 2. Steric considerations in analogous complexes showed that the *aa* isomer (Fig. 2*b*) is energetically the least favourable (19, 20). The observation of the *ae* and *ee* structures in the solid state suggested that the homologous complexes would be capable of existence as mixtures of these two configurational isomers in solution. Conversion of the *ee* isomer to the *ae* or *ea* isomers would require inversion at one sulfur atom. Inversion barriers about coordinated sulfur atoms have been estimated at 50–80 kJ mol$^{-1}$ (19, 21), but this will presumably be dependent upon the stereochemistry and substituent of the sulfur atom (*vide infra*).

In the interpretation of spectra below, it is assumed that the symmetric isomers observed will be *ee*, rather than *aa*, and that the *ae* geometry observed in the crystal structure of **2***b* (1*b*) will be the more likely of the *ae* and *ea* isomers to exist in solution. However, the possible existence of the other isomers cannot be rigorously excluded.

The $^1H$ and $^{13}C$ chemical shift data for $W_2Cl_4(\mu\text{-}SR)_2(\mu\text{-}S)L_2$ complexes, obtained at 25°C, are reported in Tables 1 and 2 respectively. $^1H$ nmr spectra of the complexes show that whereas only one environment occurs for the ligands L in the neutral complexes **2***a–e*, **3**, and **4**, two sets of resonances occur for the SR ligands, when R is other than Me (the SMe complexes **1***a–c* behave differently and are discussed below). The two sets

TABLE 1. $^1H$ nmr spectral data for the complexes $W_2Cl_4(\mu\text{-}SR)_2(\mu\text{-}S)L_2$ (25°C)

| Complex | | Chemical shift ($\delta$)[b] | |
|---|---|---|---|
| | | R | L |
| $W_2Cl_4(\mu\text{-}SMe)_2(\mu\text{-}S)(THT)_2$ | (1*a*)[a,d] | 2.70 (s); 2.80 (s); 3.60 (s) | 2.20 (m); 3.70 (m) |
| $W_2Cl_4(\mu\text{-}SMe)_2(\mu\text{-}S)(SMe_2)_2$ | (1*b*)[b,d] | 2.70 (s); 2.75 (s); 3.60 (s) | 2.90 (s) |
| $[Et_4N]_2[W_2Cl_6(\mu\text{-}SMe)_2(\mu\text{-}S)]$ | (1*c*)[c,d,e] | 2.90 (s); 3.12 (s); 3.15 (s) | — |
| $W_2Cl_4(\mu\text{-}SEt)_2(\mu\text{-}S)(THT)_2$ | (2*a*)[b] | 0.95 (t, 3); 1.75 (t, 3); 3.00 (q, 2); 3.85 (q, 2) | 2.20 (m, 8); 3.80 (m, 8) |
| $W_2Cl_4(\mu\text{-}SEt)_2(\mu\text{-}S)(SMe_2)_2$ | (2*b*)[b] | 0.95 (t, 3); 1.75 (t, 3); 3.00 (q, 2); 3.95 (q, 2) | 2.90 (s, 12) |
| $W_2Cl_4(\mu\text{-}SEt)_2(\mu\text{-}S)(NCMe)_2$ | (2*c*)[b,d] | 1.00 (t, 3); 1.73 (t, 3); 3.40 (q, 2); 3.90 (q, 2) | 2.84 (s, 6) |
| $W_2Cl_4(\mu\text{-}SEt)_2(\mu\text{-}S)(PPh_3)_2$ | (2*d*)[b] | −0.20 (t, 3); 1.73 (t, 3); 2.20 (q, 2); 4.10 (q, 2) | 7.67–7.23 (m, 30) |
| $W_2Cl_4(\mu\text{-}SEt)_2(\mu\text{-}S)(Py)_2\cdot Py$ | (2*e*)[a] | 0.95 (t, 3); 1.75 (t, 3); 3.40 (q, 2); 4.15 (q, 2) | 8.0 (m, 6); 8.85 (m, 6); 9.55 (m, 3) |
| $[Et_4N]_2[W_2Cl_6(\mu\text{-}SEt)_2(\mu\text{-}S)]$ | (2*f*)[c,e] | 1.38 (t, 6); 2.91 (q, 4) | — |
| $[Me_2SCH_2Ph]_2[W_2Cl_4(\mu\text{-}SEt)_2(\mu\text{-}S)Br_2]$ | (2*g*)[c,f] | 1.05 (t, 3); 1.60 (t, 3); 3.60 (q, 2); 4.0 (q, 2) | — |
| $W_2Cl_4(\mu\text{-}S^tBu)_2(\mu\text{-}S)(SMe_2)_2$ | (3)[a] | 0.93 (d, 6); 1.15 (d, 6); 3.10 (d, 2); 3.90 (d, 2) | 2.90 (s, 12) |
| $W_2Cl_4(\mu\text{-}SCH_2Ph)_2(\mu\text{-}S)(THT)_2$ | (4)[a] | 4.30 (s, 2); 5.25 (s, 2); 7.35 (m, 10) | 2.25 (m, 8); 3.65 (m, 8) |

[a] Chemical shift measured with reference to internal solvent resonance ($CDCl_3$) set at 7.29 $\delta$ vs. $Me_4Si$.
[b] Chemical shift measured with reference to internal solvent resonance ($CD_2Cl_2$) set at 5.29 $\delta$ vs. $Me_4Si$.
[c] Chemical shift measured with reference to internal solvent resonance ($CD_3CN$) set at 2.05 $\delta$ vs. $Me_4Si$.
[d] Two configurational isomers (*ee*,*ae*) present in solution. Ratio of *ee*:*ae*; 1*a* = 2:1; 1*b* ≈ 1:1; 1*c* ≈ 2:1 (see text): 2[e] ($CDCl_3$) ≈ 1:1 (δ $CH_3CN$: 2.88, 2.90); ethanethiolate resonances are not resolved.
[e] $\delta$ $Et_4N^+$: 1.36 (t, 24); 3.66 (q, 16).
[f] $\delta$ $Me_2SCH_2Ph$: 2.80 (s, 12); 4.5 (s, 4); 7.3–7.5 (m, 10).
[g] s = singlet, d = doublet, t = triplet, q = quartet, m = multiplet; THT = tetrahydrothiophene ($C_4H_8S$).

TABLE 2. $^{13}C$ {$^1H$} nmr spectral data for selected $W_2Cl_4(\mu\text{-}SR)_2(\mu\text{-}S)L_2$ complexes (25°C)

| Complex | $^{13}C$ chemical shift (singlets, δ) and assignments[a] |
|---|---|
| **1***a*[b] | 29.90 ($SCH_3$); 30.22 ($SCH_3$); 30.55 (β*C*, THT); 37.95 ($SCH_3$); 38.86 ($SCH_3$); 39.97 (α*C*, THT) |
| **1***b*[b] | 22.41 ($SCH_3$); 24.04 ($S(CH_3)_2$); 26.76 ($SCH_3$); 36.63 ($SCH_3$); 37.77 ($SCH_3$) |
| **2***a* | 15.99 ($CH_2CH_3$); 16.18 ($CH_2CH_3$); 30.55 (βC, THT); 39.77 (αC, THT); 43.48 ($CH_2CH_3$); 49.59 ($CH_2CH_3$) |
| **2***b* | 15.92 ($SCH_2CH_3$); 16.12 ($SCH_2CH_3$); 24.18 ($S(CH_3)_2$); 42.89 ($SCH_2CH_3$); 49.07 ($SCH_2CH_3$) |
| **3** | 21.77 ($SCH_2CH(CH_3)_2$); 22.88 ($SCH_2CH(CH_3)_2$); 24.18 ($S(CH_3)_2$); 30.16 ($SCH_2CH(CH_3)_2$); 30.55 ($SCH_2CH(CH_3)_2$); 55.76 ($SCH_2CH(CH_3)_2$); 60.50 ($SCH_2CH(CH_3)_2$) |

[a]In $CDCl_3$; $Me_4Si$ as internal standard.
[b]Two configurational isomers (*ee*, *ae*) present.

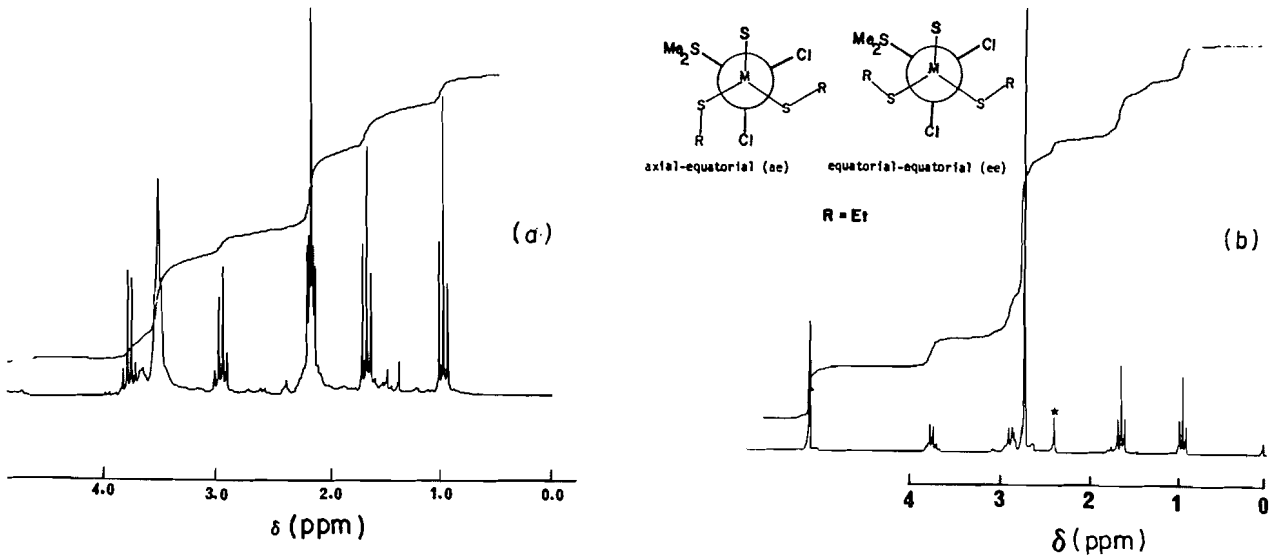


FIG. 3. (*a*) 200-MHz $^1H$ nmr spectrum of complex **2***a* in $CD_2Cl_2$ at 25°C. (*b*) 200-MHz $^1H$ nmr spectrum of complex **2***b* in $CD_2Cl_2$ at 25°C; resonance marked with an asterisk is an impurity in the solvent.

of resonances due to bridging thiolate ligands, which are usually separated by ~1.0 δ for protons on the α-carbon atom, are of equal intensity and, in total, represent a 1:1 intensity ratio with the ligands L (Fig. 3). The two distinct sets of $^1H$ (and $^{13}C$ for complexes **2***a*, **2***b*, and **3**) nmr signals are in accord with the solid state structures of complexes **2***a* (**1***a*) and **2***b* (**1***b*). The low molecular symmetry, in which the two μ-SEt groups are *trans* to different terminal ligands, causes the R groups to be magnetically inequivalent, irrespective of the configuration of the SR groups. The SR groups which are *trans* to thioether ligands have significantly shorter W—S bonds than those *trans* to $Cl^-$ in the structures of **2***a* and **2***b* (**1***a*, **1***b*). A consistent interpretation of the spectra can be made if it is assumed that the more strongly bound SR ligands (*trans* to the weakly bound thioether) are more deshielded than those *trans* to $Cl^-$, and that their $^1H$ and $^{13}C$ resonances therefore occur at lower field. Thus, although for these complexes the existence of a single configurational isomer in solution is evident,[4] the identity of this isomer cannot be established.

The complexes $W_2Cl_4(\mu\text{-}SMe)_2(\mu\text{-}S)L_2$ (**1***a*–*c*) show evidence for the existence of at least two isomers in solution, with the possibility of small quantities of others. $^1H$ nmr spectra (25°C) of complexes **1***a* and **1***b* show three strong resonances of unequal intensity for the SMe groups (Table 1, Fig. 4). Interpretation of these spectra requires the presence of two isomers, for which one pair of resonances at 3.60 δ are accidentally degenerate. It is likely that this low field signal is due to the SMe group *trans* to thioether, and that the configuration

[4]The $^1H$ nmr spectrum of **2***b* shows sharp resonances for the bridging thiolate ligand over the temperature range −90 to +25°C ($CD_2Cl_2$). However, the $Me_2S$ resonance is temperature dependent, being a singlet at 25°C, which splits into two resonances at −60°C. The temperature dependence of the $Me_2S$ signal is attributed to the onset of rapid inversion at sulfur in the high temperature limit, with it being slow on the nmr time scale at −60°C (22, 23).

Can. J. Chem. Downloaded from www.nrcresearchpress.com by 210.87.254.105 on 09/06/12
For personal use only.

Can. J. Chem. Downloaded from www.nrcresearchpress.com by 210.87.254.105 on 09/06/12
For personal use only.

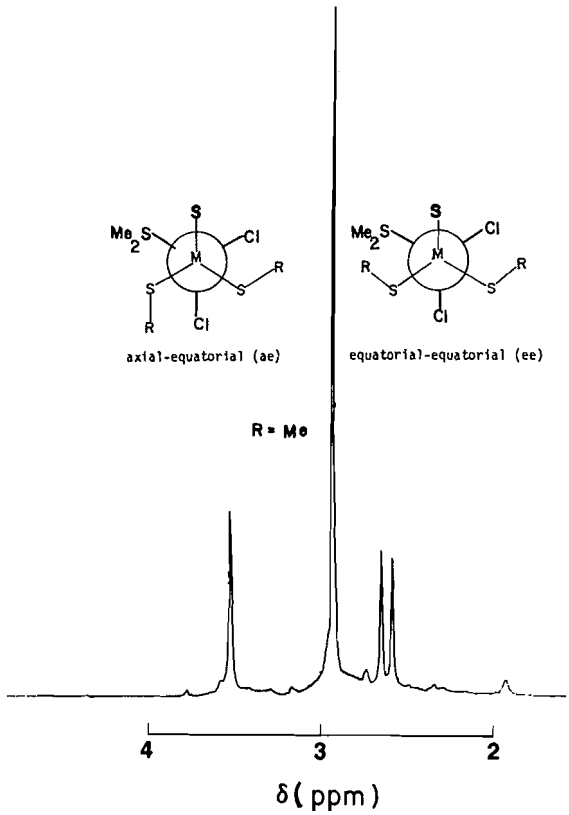


FIG. 4. 200 MHz $^1$H nmr spectrum of **1***b* in $CD_2Cl_2$ at 25°C.

in each case is the same (probably *e*). The assignment is confirmed by the $^{13}$C spectra in which the downfield resonances are resolved (Table 2). It is not possible to assign unequivocally the four SMe $^{13}$C resonances to their respective isomers (i.e., which low field resonance is associated with which high field resonance). If the low field resonances are assigned to the SMe groups *trans* to the thioether ligands in **1***a* and **1***b*, and in the two isomers the configurations are the same, then the other SMe group *trans* to Cl would be the one to exhibit *a* or *e* stereochemistry, thus generating the *ae* and *ee* isomers discussed earlier. The alternative interpretation would necessitate assigning the isomers as *aa* and *ea*. The weak, unassigned resonances found in certain spectra may be associated with these isomers. However, the assumption that the *ae* and *ee* isomers found in the solid state are also the important isomers in solution seems to be most reasonable.

Further information was obtained by the synthesis of the complex $[Et_4N]_2[W_2Cl_6(\mu\text{-}SMe)_2(\mu\text{-}S)]$ (**1***c*) from **1***a* and **1***b*. The higher symmetry of **1***c* allows the SMe groups to be magnetically equivalent in the *ee* isomer. The $^1$H spectrum exhibits three resonances of which the strong resonance at 3.15 δ is due to a symmetric isomer, presumably the *ee* (*vide supra*). The shift to higher field from the **1***a* and **1***b* spectra is consistent with the replacement of thioether by $Cl^-$ *trans* to one bridging SMe group. The two resonances of equal intensity (3.12, 2.90 δ) are assigned to the *ae* isomer (ratio of *ee*:*ae* ≈ 2:1). Attempts to study the interconversion of these isomers of **1***c* in $C_2D_2Cl_4$ at various temperatures were unsuccessful due to overlapping of the $-CH_2$ resonances of the $Et_4N^+$ cation with the methyl resonance of the anion.

The $[W_2Cl_6(\mu\text{-}SEt)_2(\mu\text{-}S)]^{2-}$ anion of the complex **2***f*, derived from either **2***a* or **2***b*, shows only one set of resonances for the SEt groups (Table 1), in the temperature range examined (−90°C to +25°C; $CD_2Cl_2$). We conclude that one of the following conditions exists: (*i*) the barrier to isomerization is very low; (*ii*) the chemical shift differences between the isomers are too small to detect; (*iii*) only one isomer exists in solution.

For **2***f* the acute angles subtended at the bridging thiolate sulfur atoms (~62.5°), which result from the strong metal–metal interaction (1*b*) are likely to increase the inversion barrier[5] about the coordinated sulfur from the normal 50–80 kJ mol$^{-1}$ (19, 21–25). Furthermore, it is unlikely that the chemical shifts will be totally insensitive to stereochemistry (cf. complex **1***c*) and hence we conclude that the solution contains predominantly a single symmetric isomer, namely, the *ee* isomer which was found in the solid state structure (16).

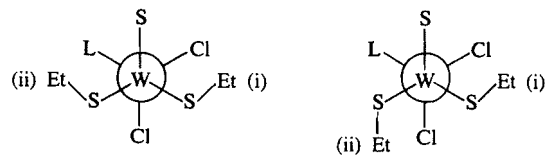


The complex $W_2Cl_4(\mu\text{-}SEt)_2(\mu\text{-}S)(PPh_3)_2$ (**2***d*) appears at first to have an anomalous $^1$H nmr spectrum. However, it can be rationalized in a way which corroborates the above assignments. One of the SEt groups shows a large upfield shift. The methylene resonance at 2.20 δ for **2***d* is ~1 ppm upfield from the corresponding resonances in complexes **2***a*–*c*, **2***e*, and **2***g* (~3.50 δ). Similarly the $CH_3$ resonance is found at −0.2 δ for **2***d* compared with 1.0 δ found for the other complexes. In

[5]Whilst only a single isomer exists for complex **3**, the isostructural anion in the complex $[Ph_4As][W_2O_2Cl_4(\mu\text{-}S^iBu)_2(\mu\text{-}Cl)]$ (angle subtended at $\mu$-S$^i$Bu is ≃ 70.5°) exists as two isomers (*ee* and *ae*) in solution, with a barrier to inversion of ≃ 75 kJ mol$^{-1}$ (27).

contrast, the low field resonances due to the SEt ligand at ~4.0 δ and ~1.75 δ show no marked effect with change of L (Table 1).

Since a *through bond* type of shielding of the ethanethiolate ligand (SEt(i)) *trans* to L is unlikely to cause such a large upfield shift in the case of **2***d*, a *through space* interaction between the hydrogens of the proximal ethanethiolate ligand (SEt(ii)) and an adjacent phenyl ring appears to be the most likely cause of this shift. A similar argument was advanced by Roundhill and co-workers (26) to explain an anomalous chemical shift of the methyl protons in the complex $RuCl_2(\sigma\text{-}MeSC_6H_4PPh_2)_2$. This assignment for **2***d* would necessitate assigning the lower field resonances (1.73, 4.10 δ) in the $^1H$ nmr spectrum to the SEt(i), which is *trans* to the phosphine. This would be consistent with the argument presented earlier.

**Acknowledgements**

The financial support of Natural Sciences and Engineering Research Council of Canada is gratefully acknowledged. The authors wish to thank Dr. R. Yamdagni for assistance in obtaining the nmr spectra, K. J. Moynihan and K. B. Burgess for experimental assistance, and Drs. E. A. Dixon and R. T. Oakley for valuable discussion.

1. (*a*) P. M. Boorman, K. A. Kerr, and V. D. Patel. J. Chem. Soc. Dalton, 506 (1981); (*b*) P. M. Boorman, P. W. Codding, K. A. Kerr, K. J. Moynihan, and V. D. Patel. Can. J. Chem. **60**, 1333 (1982).
2. P. M. Boorman, V. D. Patel, K. A. Kerr, P. W. Codding, and P. Van Roey. Inorg. Chem. **19**, 3508 (1980).
3. (*a*) E. T. Maas, Jr. and R. E. McCarley. Inorg. Chem. **12**, 1096 (1973); (*b*) J. L. Templeton, W. C. Dorman, J. C. Clardy, and R. E. McCarley. Inorg. Chem. **17**, 1263 (1978); (*c*) J. L. Templeton and R. E. McCarley. Inorg. Chem. **17**, 2293 (1978).
4. (*a*) F. A. Cotton and W. T. Hall. J. Am. Chem. Soc. **101**, 5094 (1979); (*b*) F. A. Cotton and W. T. Hall. Inorg. Chem. **19**, 2352 (1980); (*c*) F. A. Cotton and W. T. Hall. Inorg. Chem. **19**, 2354 (1980).
5. (*a*) M. A. Schaefer-King and R. E. McCarley. Inorg. Chem. **12**, 1972 (1973); (*b*) M. A. Schaefer-King. Ph.D. Dissertation, Iowa State University, Ames, IA. 1971.
6. E. W. Abel. J. Chem. Soc. 4406 (1960).
7. P. M. Boorman, T. Chivers, and K. N. Mahadev. Can. J. Chem. **53**, 383 (1975).
8. V. D. Patel. Ph.D. Dissertation, University of Calgary, Calgary, Alta., Canada. 1981.
9. P. M. Boorman and V. D. Patel. Inorg. Chim. Acta, **44**, L85 (1980).
10. D. L. Kepert and R. S. Nyholm. J. Chem. Soc. 2871 (1965).
11. (*a*) R. J. H. Clark and C. S. Williams. Inorg. Chem. **4**, 350 (1965); (*b*) M. Goldstein, E. F. Mooney, A. Anderso, and H. A. Gebbie. Spectrochim. Acta, **21**, 105 (1965).
12. (*a*) P. M. Boorman and B. D. O'Dell. J. Chem. Soc. Dalton, 257 (1980); (*b*) P. M. Boorman, T. Chivers, K. N. Mahadev, and B. D. O'Dell. Inorg. Chim. Acta, **19**, L35 (1976).
13. R. G. W. Gingerlich and R. J. Angelici. J. Am. Chem. Soc. **101**, 5604 (1979).
14. M. H. Quick and R. J. Angelici. Inorg. Chem. **20**, 1123 (1980).
15. R. B. McCormick and R. J. Angelici. Inorg. Chem. **20**, 1118 (1980).
16. (*a*) D. P. N. Satchell. Chem. Soc. Rev. **6**, 345 (1977); (*b*) T. B. Rauchfuss and D. M. Roundhill. J. Am. Chem. Soc. **97**, 3386 (1975); (*c*) S. E. Livingstone. Q. Rev. **19**, 387 (1965).
17. R. D. Adams and D. F. Chodosh. J. Organomet. Chem. **120**, C39 (1976).
18. C. A. Stein and H. Taube. J. Am. Chem. Soc. **100**, 336 (1978).
19. S. D. Killops and S. A. R. Knox. J. Chem. Soc. Dalton, 1260 (1978).
20. L. F. Dahl and C. Wei. Inorg. Chem. **2**, 328 (1963).
21. G. Natile, L. Maresca, and G. Bor. Inorg. Chim. Acta, **23**, 37 (1977).
22. E. W. Abel, M. Booth, and K. G. Orrell. J. Chem. Soc. Dalton, 1994 (1979).
23. P. Haake and P. C. Turley. J. Am. Chem. Soc. **89**, 4611 (1967).
24. I. B. Benson, S. A. R. Knox, P. J. Naish, and A. J. Welch. J. Chem. Soc. Chem. Commun. 878 (1978).
25. A. Rauk, L. C. Allen, and K. Mislow. Angew. Chem. Int. Ed. **9**, 400 (1970).
26. D. M. Roundhill, S. G. N. Roundhill, W. B. Beaulieu, and U. Bagchi. Inorg. Chem. **19**, 3365 (1980).
27. V. D. Patel, P. M. Boorman, K. A. Kerr, and K. J. Moynihan. Inorg. Chem. In press.

Can. J. Chem. Downloaded from www.nrcresearchpress.com by 210.87.254.105 on 09/06/12
For personal use only.

# Charge distributions and chemical effects. XXIX. On the vibrational energies of chair and boat cyclohexane

J. P. HUVENNE, G. VERGOTEN, AND G. FLEURY

*Laboratoire de Physique, Faculté de Pharmacie, 3, rue du Professeur Laguesse, 59045 Lille, France et Centre de Technologie Biomédicale, INSERM 13 à 17, rue Camille Guérin, 59800 Lille, France*

AND

S. ODIOT[1] AND S. FLISZÁR

*Department of Chemistry, University of Montreal, Montreal, P.Q., Canada H3C 3V1*

Received December 18, 1981

J. P. HUVENNE, G. VERGOTEN, G. FLEURY, S. ODIOT, and S. FLISZÁR. Can. J. Chem. **60**, 1347 (1982).

Local symmetry force field calculations are presented for the chair and boat forms of cyclohexane and the assignments of frequencies are given. The calculated zero-point and thermal vibrational energies indicate a near invariance of total vibrational energy with respect to chair–boat conformational changes of the cyclohexane ring, thus confirming results of similar nature derived from earlier theoretical thermochemical analyses.

J. P. HUVENNE, G. VERGOTEN, G. FLEURY, S. ODIOT et S. FLISZÁR. Can. J. Chem. **60**, 1347 (1982).

Les calculs en champ de forces de symétrie locale sont présentés pour les formes chaise et bateau du cyclohexane, ainsi que l'attribution des fréquences. Les énergies au point zéro et thermiques indiquent que l'énergie vibrationnelle totale est virtuellement insensible au changement conformationnel du cycle cyclohexanique, en confirmant ainsi des résultats antérieurs de nature similaire, déduits d'analyses thermochimiques théoriques.

[Traduit par le journal]

## Introduction

Molecular energies are determined by a blend of terms referring (*i*) to molecules in their hypothetical vibrationless state at 0 K and (*ii*) of vibrational energies. The latter play an important role in the evaluation of molecular energies at the level of actual experimental conditions, while the energy of atomization

$$\Delta E_a^* = \sum_k \langle \psi_k{}^{at} | H_k{}^{at} | \psi_k{}^{at} \rangle - \langle \psi^{mol} | H^{mol} | \psi^{mol} \rangle$$

only contains the information pertaining to the nuclear-electronic stability of an isolated molecule at equilibrium, which is not an information describing the situation at, say, 25°C. This state of affairs is described by eq. [1]

$$[1] \quad \Delta E_a^* = \sum_i n_i [\Delta H_f^0(A_i) - 5RT/2] - \Delta H_f^0 + \text{ZPE} + H_T - H_0$$

in which $\Delta H_f^0(A_i)$ is the enthalpy of formation of the gaseous atom $A_i$ and $\Delta H_f^0$ that of the molecule consisting of $n_i$ atoms $A_i$ at 298.15 K. ZPE is the zero-point energy, $H_T - H_0 = E_{vibr} + 4RT$ is the change in enthalpy between $T = 0$ and $T = T$ of a nonlinear molecule and $E_{vibr}$ the corresponding increase in vibrational energy.

The atomization energy of the vibrationless molecule at 0 K, $\Delta E_a^*$, can be expressed as a sum of energy terms associated with the individual chemical bonds, plus a very small contribution arising from Coulomb-type interactions between nonbonded atoms, and its calculation is one involving the atomic charges of the individual atoms forming the molecule (1). Theoretical $\Delta E_a^*$ energies deduced along these lines were shown to agree within 0.16 kcal/mol (average deviation) with their experimental counterparts derived from eq. [1], namely, for normal and branched paraffins, cyclohexane, and polycyclic compounds containing chair and/or boat cyclohexane rings (1–3) and for a series of oxygen-containing compounds (4). Conversely, the use of theoretical $\Delta E_a^*$'s in eq. [1], combined with the appropriate enthalpies of formation, leads to rapid and accurate evaluations of ZPE $+ H_T - H_0$ energies (2). This type of calculation is greatly facilitated by the use of carefully established charge–nmr shift correlations for $^{13}C$ and $^{17}O$ nuclei (5), the H charges being determined from charge normalization so that, ultimately, the vibrational results are simply deduced from the appropriate nmr and enthalpy data.

In this manner it was deduced from a study (2, 3) of hydrocarbons containing chair and/or boat cyclohexane rings that the ZPE $+ H_T - H_0$ energy is

[1]Visiting Scientist, on temporary leave from the "Service de Spectroscopie Moléculaire en Milieu Condensé, Laboratoire de Recherches Physiques Associé au CNRS, Université Pierre et Marie Curie", Paris. We thank the authorities of the "France–Québec Exchange Program" who made this cooperation possible.

0008-4042/82/111347-05$01.00/0

©1982 National Research Council of Canada/Conseil national de recherches du Canada

Can. J. Chem. Downloaded from www.nrcresearchpress.com by 210.87.254.40 on 09/06/12
For personal use only.

Can. J. Chem. Downloaded from www.nrcresearchpress.com by 210.87.254.40 on 09/06/12
For personal use only.

virtually invariant upon a chair–boat structural change. Typical examples are offered by bicyclo-[2.2.2]octane, the comparison between the *trans-anti-trans* and *trans-syn-trans* forms of perhydroanthracene and that of twistane with adamantane. The energy difference between the chair and boat forms of cyclohexane itself is traced back to non-vibrational energy contributions, as a consequence of an electron enrichment at the carbon atoms in the chair form, at the expense of the electron populations at the hydrogen atoms, resulting in a destabilization (0.88 kcal/mol) of the CH bonds and a gain in stability of the carbon skeleton (6.27 kcal/mol) for a total difference of 5.39 kcal/mol favoring the chair form (1).

Because of the exceptional importance of the cyclohexane ring in conformational chemistry, we examine here the problem of total vibrational energies in chair and boat cyclohexane. Indeed, although many papers have dealt with the vibrational properties of nonplanar six-membered ring molecules of the cyclohexane type, none has considered specifically this aspect of structure-related energy contributions. Presently, the only available information about total vibrational energies, featuring explicitly the effects related to the chair–boat structural changes, is that derived from thermodynamic energy analyses involving eq. [1] (2). Here we approach the question via detailed calculations of the fundamental vibrational frequencies of both forms, which give access to the respective ZPE + $H_T - H_0$ energies.

## Outline of calculations

Important studies on cyclohexane were presented by Takahashi *et al.* (6) and by Snyder and Schachtschneider (7). More recently, Wiberg and Shrake (8) have investigated the appropriate selection of an independent subset of valence force constants from a dependent or redundant set when redundant internal coordinates are included. In the earlier studies (6, 7), the cyclohexane geometry was taken in its chair form, in a strictly tetrahedral arrangement, with torsion angles along the CC bonds of 60°. In ref. 6, a Urey–Bradley force field was used and the description of modes was obtained through potential energy distributions. Snyder and Schachtschneider (7), however, used a general valence force field for the study of 17 hydrocarbons, including cyclohexane and adamantane. None of these model force fields was applied for predicting the vibrational frequencies of the boat form of cyclohexane.

On the other hand, it was shown that the "local symmetry force field" (LSFF) (9–11) is the only one based on bond properties which can take advantage of any type of model force field, namely, the general valence or the Urey–Bradley force fields. Here we take full advantage of the LSFF approach which is unique in that it permits the transferability of local symmetry force fields, deduced and refined for the chair form of cyclohexane, to the theoretical study of the boat form. Of course, the main difficulty in the local symmetry approach is to take the local and the cyclic redundancies into proper account.

The normal coordinate treatment was carried out as follows. Firstly, the chair form of cyclohexane was chosen as in ref. 6, with $r_{CC} = 1.54$ and $r_{CH} = 1.09$ Å. Secondly, the symmetry point group being $D_{3d}$, a total of 60 internal coordinates was defined, namely, 18 for the ring part alone (i.e., 6 CC bonds, 6 CCC angle bends, and 6 CCCC torsions) and 42 coordinates involving the hydrogen atoms (i.e., 12 CH bonds, 24 CCH angle bends, and 6 HCH angle bends). This leads to 12 redundant symmetry coordinates of which 6 are the "tree redundant" type (taking coordinates like the bending, scissoring, wagging, rocking, and the twisting of a $CC_2H_2$ group into account), while 6 are cyclic redundant symmetry coordinates determined among the 18 ring internal coordinates (10, 11). In this way, we define a $3n - 6$ dimentional reduced symmetry space.

In order to permit the prediction of the fundamental vibrations of the boat form (symmetry $C_{2v}$) we chose to treat the chair form (symmetry $D_{3d}$) as belonging to the $C_s$ symmetry subgroup of both the $D_{3d}$ and $C_{2v}$ groups. The correlation between these groups is as follows.

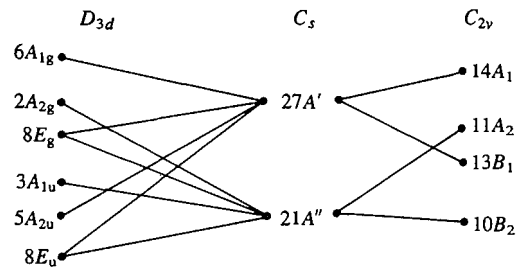


With these premises, the local symmetry force field (LSFF) described in local symmetry coordinate space (9) was appropriately expressed in the reduced symmetry space. The original LSFF force constants were obtained from the MVIB library (11, 12). We added some interaction parameters (which are not required for the acyclic hydrocarbons) in order to take the ring structure into proper account (11), i.e., for interaction terms involving neighboring atoms, $CH_2$ sst/$CH_2$ sst = −0.0592, $CH_2$ ast/$CH_2$ ast = −0.0057, $CH_2$ scis/$CH_2$ scis = −0.0081, CC tors/CC tors = 0.0196,

TABLE 1. Observed and calculated wavenumbers ($cm^{-1}$) for the chair form of cyclohexane

| $D_{3d}$ symm. specy | Wavenumbers ($cm^{-1}$) Observed | Calculated $A'$ | Calculated $A''$ | Potential energy distribution (%) |
|---|---|---|---|---|
| $A_{1g}$ | 2939 | 2944 | | 98 $CH_2$ ast |
| | 2856 | 2851 | | 99 $CH_2$ sst |
| | 1465 | 1465 | | 94 scis |
| | 1159 | 1154 | | 64 rock + 21 bend–tors |
| | 801 | 798 | | 78 stret + 17 rock |
| | 384 | 386 | | 80 bend–stret + 18 rock |
| $A_{2g}$ | ia | | 1353 | 96 wag |
| | ia | | 1136 | 96 twis |
| $E_g$ | 2923 | 2928 | 2928 | 99 $CH_2$ ast |
| | 2898 | 2898 | 2898 | 99 $CH_2$ sst |
| | 1445 | 1446 | 1446 | 98 scis |
| | 1349 | 1352 | 1352 | 70 wag + 29 twis |
| | 1267 | 1269 | 1269 | 60 twis + 39 wag |
| | 1029 | 1016 | 1016 | 83 rock + 13 stret |
| | 787 | 788 | 788 | 90 stret + 9 rock |
| | 427 | 426 | 426 | 87 bend–tors + 10 stret |
| $A_{1u}$ | ia | | 1321 | 60 twis + 40 wag |
| | ia | | 1288 | 63 wag + 34 twis |
| | ia | | 667 | 82 stret–bend + 17 wag |
| $A_{2u}$ | 2930 | 2928 | | 87 $CH_2$ ast + 11 $CH_2$ sst |
| | 2916 | 2914 | | 87 $CH_2$ sst + 11 $CH_2$ ast |
| | 1450 | 1447 | | 100 scis |
| | 1108 | 1114 | | 86 rock + 13 bend |
| | 537 | 536 | | 88 bend + 11 rock |
| $E_u$ | 2943 | 2934 | 2934 | 99 $CH_2$ ast |
| | 2858 | 2865 | 2865 | 99 $CH_2$ sst |
| | 1460 | 1462 | 1462 | 85 scis + 9 wag |
| | 1353 | 1349 | 1349 | 92 wag + 8 scis |
| | 1258 | 1256 | 1256 | 76 twis + 8 wag |
| | 903 | 913 | 913 | 87 rock + 10 twis |
| | 862 | 866 | 866 | 80 stret–bend–tors + 13 rock |
| | 248 | 248 | 248 | 100 bend–tors |

$CH_2$ rock/CC tors = −0.1835, and $CH_2$ scis/$CH_2$ wag = −0.0124. The units are mdyn $Å^{-1}$ for stretching/stretching interactions and mdyn Å for deformation/deformation and deformation–torsion/torsion interactions. We also recorded the far infrared and the classical infrared spectra, as well as the full Raman spectra, of both $C_6H_{12}$ and $C_6D_{12}$ in the liquid phase and completed the normal coordinate analysis of the free molecule using the LSFF parameters adapted to the chair form. The results are as below.

## Results

Table 1 reports the observed and the calculated fundamental frequencies of chair cyclohexane, as well as the potential energy distribution. The abbreviations are: $CH_2$ sst = symmetrical stretching of a $CH_2$ group, $CH_2$ ast = antisymmetrical stretching coordinate of a $CH_2$ group; scis = scissoring deformation coordinate; wag = wagging deformation coordinate; rock = rocking deformation coordinate; twis = twisting deformation coordinate. The following coordinates concern only the ring part: stret = CC stretching; bend = CCC bending, and tors = CCCC torsion coordinate.

These results suggest the following comments. (*i*) The chair form of cyclohexane belongs to the $D_{3d}$ group, in which the $A_{2g}$ and $A_{1u}$ vibrations are inactive, meaning that a total of 5 frequencies cannot be observed. In the correlation $D_{3d} \leftrightarrow C_s$ which allows us to use the same LSFF constants for the chair and the boat forms, this implies that 5 fundamentals of the $A''$ class have no experimental counterparts. Moreover (*ii*), in the same $D_{3d} \leftrightarrow C_s$ correlation, the degenerate vibration $E_g$ and $E_u$ of the chair form split as follows

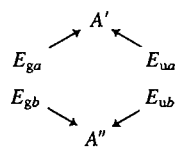


Can. J. Chem. Downloaded from www.nrcresearchpress.com by 210.87.254.40 on 09/06/12
For personal use only.

Can. J. Chem. Downloaded from www.nrcresearchpress.com by 210.87.254.40 on 09/06/12
For personal use only.

thus preventing us from gaining additional experimental information as regards the $A''$ class. Finally (*iii*), as a direct consequence of (*i*) and (*ii*), it is not possible to obtain any additional experimental evidence for the $A''$ class, which would be useful in refinements of the force field, because the only contributions to this class are the inactive modes (case *i*) or the degenerate components of modes included in class $A'$ (case *ii*).

These observations should be born in mind when comparing to one another the results calculated for the chair and boat forms of cyclohexane (Table 2). Indeed, it appears that the sum of the vibrational frequencies belonging to the $A'$ class is remarkably constant when going from one form to the other (i.e., 42 553 $cm^{-1}$ for the chair form and 42 555 $cm^{-1}$ for the boat cyclohexane), whereas a less good agreement is observed for the $A''$ class (29 781 $cm^{-1}$ for the chair vs. 29 718 $cm^{-1}$ for the boat form). While it is difficult to assess how much of this difference is real, and no additional theoretical argument can be presently invoked in this matter, it remains that the sums of vibrational frequencies appear to be nearly the same, 72 334 $cm^{-1}$ for the chair and 72 273 $cm^{-1}$ for the boat cyclohexane.

The individual zero-point (ZPE) and thermal vibrational energies ($E_{vibr}$) can be estimated in the harmonic oscillator approximation form eqs. [2] and [3], i.e.,

$$[2] \quad \text{ZPE} = N_{av} \sum_i h\nu_i/2$$

$$[3] \quad E_{vibr} = N_{av} \sum_i h\nu_i \exp(-h\nu_i/kT) \div [1 - \exp(-h\nu_i/kT)]$$

Using the calculated frequencies indicated in Table 2, we obtain (in kcal/mol at 298.15 K) ZPE = 103.41 and $E_{vibr}$ = 1.85, giving a total of 105.26 in vibrational energy for the chair form. Similarly, using the experimental results of Table 1 plus the 5 calculated values for the nonobserved vibrations, we find ZPE = 103.40, $E_{vibr}$ = 1.86 and a total of 105.26 kcal/mol. On the other hand, considering now boat cyclohexane (Table 2), the values are ZPE = 103.32 and $E_{vibr}$ = 1.92, for a total of 105.24 kcal/mol in vibrational energy. Finally, using the Snyder and Schachtschneider results (7), we obtain ZPE = 103.30, $E_{vibr}$ = 1.87 and a total of 105.17 kcal/mol. We may conclude from this analysis that the chair and boat cyclohexanes do not differ from one another in their vibrational energy content, at least not to any significant extent.

It is also instructive to consider selected ZPE + $E_{vibr}$ results derived from eq. [1]. These were deduced from $\Delta E_a^*$ energies calculated from charge distributions (1–3), experimental enthalpies of formation, $\Delta H_f^0$(298.15 K, gas), and the appropriate enthalpies $\Delta H_f^0$(C) = 170.89 and $\Delta H_f^0$(H) = 52.09 kcal/mol (13). The results are indicated in Table 3.

TABLE 2. Calculated wavenumbers ($cm^{-1}$) for the chair and boat forms of cyclohexane

| Chair | | Boat | |
|---|---|---|---|
| $A'$ | $A''$ | $A'$ | $A''$ |
| 2944 | | 2944 | |
| 2934 | 2934 | 2935 | 2935 |
| 2928 | | 2931 | |
| 2928 | 2928 | 2924 | 2926 |
| 2914 | | 2915 | |
| 2898 | 2898 | 2898 | 2898 |
| 2865 | 2865 | 2865 | 2865 |
| 2851 | | 2850 | |
| 1465 | | 1472 | 1468 |
| 1462 | 1462 | 1461 | |
| 1447 | | 1447 | |
| 1446 | 1446 | 1441 | 1438 |
| | 1353 | | |
| 1352 | 1352 | 1367 | 1361 |
| 1349 | 1349 | | 1358 |
| | 1321 | | 1331 |
| | 1288 | 1319 | 1317 |
| 1269 | 1269 | 1306 | 1297 |
| 1256 | 1256 | | 1282 |
| 1154 | | 1251 | 1240 |
| | 1136 | 1132 | 1146 |
| 1114 | | 1063 | |
| 1016 | 1016 | 1020 | |
| 913 | 913 | 936 | 943 |
| 866 | 866 | | 939 |
| 798 | | 860 | 859 |
| 788 | 788 | 822 | 844 |
| | 667 | 784 | |
| 536 | | | 668 |
| 426 | 426 | 584 | |
| 386 | | | 441 |
| 248 | 248 | 415 | |
| | | 310 | |
| | | 303 | |
| | | | 162 |

We note, to begin with, that the ZPE + $E_{vibr}$ results derived from eq. [1] are in good agreement with their spectroscopic counterparts, namely, for cyclohexane. This sort of agreement is, indeed, verified for a total of ~80 molecules (1–4): their enthalpies of formation were deduced from calculated $\Delta E_a^*$ energies and the appropriate ZPE + $E_{vibr}$ data (eq. [1]), with an average deviation (< 0.2 kcal/mol) which is well within experimental uncertainties. Next, we observe that the *trans-anti-trans* and the *trans-syn-trans* perhydroanthracenes, which differ only because of the center boat in the former compound, have virtually the same ZPE + $E_{vibr}$ energy. Finally the results indicate that adamantane and its (all twist–boat) structural isomer

TABLE 3. Calculation of ZPE + $E_{vibr}$ from eq. [1] (kcal/mol)

| Molecule[a] | $\Delta E_a^{*b}$ | $\Delta H_f^0$ | ZPE + $E_{vibr}$ from Eq. [1] | ZPE + $E_{vibr}$ from Eqs. [2], [3] |
|---|---|---|---|---|
| Cyclohexane | 1760.81 | −29.50 | 105.18 | 105.2 |
| Bicyclo[2.2.2]octane | 2218.53 | −23.75 | 128.61 | 128.46 |
| *trans*-Decalin | 2815.57 | −43.52 | 164.63 | 164.53 |
| *trans-syn-trans*-PHA | 3870.15 | −58.13 | 223.31 | |
| *trans-anti-trans*-PHA | 3865.08 | −52.74 | 223.63 | |
| Adamantane | 2688.01 | −30.65 | 151.16 | 151.17 |
| Twistane | 2979.0 | −21.6 | 151.2 | |

[a]PHA = Perhydroanthracene.
[b]The $\Delta E_a^*$ values are extracted from refs. 1–4. The $\Delta H_f^0$ values are from ref. 14 (cyclohexane, PHA, and *trans*-decalin), ref. 15 (bicyclo[2.2.2]octane and adamantane), and ref. 3 (twistane). The ZPE + $E_{vibr}$ results are taken from refs. 2 and 15 (for bicyclo[2.2.2]octane).

twistane also have the same total vibrational energy. This type of analysis, which was carried further in an earlier work (2), indicates a near invariance of vibrational energies with respect to chair–boat conformational changes of the cyclohexane ring. These results are now supported by the present vibrational analyses of isolated cyclohexane in its chair and boat forms.

## Acknowledgements

The financial aid given by the "Institut National de la Santé et de la Recherche Médicale" INSERM/SCN4, Lille (years 1979–1980) and by the National Research Council of Canada is gratefully acknowledged.

1. S. FLISZÁR. J. Am. Chem. Soc. **102**, 6946 (1980).
2. S. FLISZÁR and J.-L. CANTARA. Can. J. Chem. **59**, 1381 (1981).
3. J. K. CHOI, M. J. JONCICH, Y. LAMBERT, P. DESLONGCHAMPS, and S. FLISZÁR. Theochem. In press.
4. S. FLISZÁR and M.-T. BÉRALDIN. Can. J. Chem. **60**, 792 (1982).
5. M.-T. BÉRALDIN, E. VAUTHIER, and S. FLISZÁR. Can. J. Chem. **60**, 160 (1982); S. FLISZÁR. Can. J. Chem. **54**, 2839 (1976); G. KEAN, D. GRAVEL, and S. FLISZÁR. J. Am. Chem. Soc. **98**, 4749 (1976); S. FLISZÁR, A. GOURSOT, and H. DUGAS. J. Am. Chem. Soc. **96**, 4358 (1974).
6. H. TAKAHASHI, T. SHIMANOUCHI, F. FUKUSHIMA, and T. MIYAZANA. J. Mol. Spectrosc. **13**, 43 (1964).
7. R. G. SNYDER and J. H. SCHACHTSCHNEIDER. Spectrochim. Acta, A**21**, 169 (1965).
8. K. B. WIBERG and A. SHRAKE. Spectrochim. Acta, A**29**, 583 (1973).
9. T. SHIMANOUCHI. Physical chemistry. Vol. 4. Molecular properties. *Edited by* D. Henderson. Academic Press, New York, NY. 1970. p. 233.
10. J. P. HUVENNE. Ph.D. Thesis. Université des Sciences et Techniques, Lille France; J. P. HUVENNE, G. VERGOTEN, P. LEGRAND, and G. FLEURY. To be published.
11. T. SHIMANOUCHI, H. MATSUHURA, Y. OGAWA, and I. HARADA. J. Phys. Chem. Ref. Data, **7**, 1323 (1978).
12. H. MATSUHURA. VIIth International Conference on Raman Spectroscopy. Ottawa, Canada, August 1980.
13. D. R. STULL and G. C. SINKE. Adv. Chem. Ser. No. 18 (1956).
14. J. D. COX and G. PILCHER. Thermochemistry of organic and organometallic compounds. Academic Press, New York, NY. 1970.
15. R. H. BOYD, S. N. SANWAL, S. CHARY-TEHRANY, and D. MCNALLY. J. Phys. Chem. **75**, 1264 (1971).

Can. J. Chem. Downloaded from www.nrcresearchpress.com by 210.87.254.40 on 09/06/12
For personal use only.

# Simulation of edge-effects in electroanalytical experiments by orthogonal collocation. Part 1. Two-dimensional collocation and theory for chronoamperometry

BERND SPEISER AND STANLEY PONS
*Department of Chemistry, University of Alberta, Edmonton, Alta., Canada T6G 2G2*
Received November 26, 1981

BERND SPEISER and STANLEY PONS. Can. J. Chem. **60**, 1352 (1982).

A two-dimensional model to describe edge-effects at planar circular disc electrodes has been developed. Two-dimensional orthogonal collocation is used to discretize the corresponding partial differential equations. The equations for the simulation of a chronoamperometric experiment are derived.

BERND SPEISER et STANLEY PONS. Can. J. Chem. **60**, 1352 (1982).

On a mis au point une méthode bidimensionnelle pour décrire les effets d'arète au niveau des électrodes à disques circulaires plans. On a utilisé une disposition orthogonale pour les équations différentielles partielles correspondantes. On a dérivé les équations de la simulation d'une expérience de chronoampérométrie.

[Traduit par le journal]

Can. J. Chem. Downloaded from www.nrcresearchpress.com by 210.87.254.40 on 09/06/12
For personal use only.

## Introduction

One common simplification in the theoretical treatment of electrode processes of planar disc electrodes is the assumption of semi-infinite linear diffusion. This results in the reduction of the three-dimensional system to a one-dimensional model, where the distance $x$ from the electrode surface is the only coordinate to be considered. Consequently, the three-dimensional form of Fick's second law

$$[1] \qquad \frac{\partial c}{\partial t} = D\left[\frac{\partial^2 c}{\partial x^2} + \frac{\partial^2 c}{\partial y^2} + \frac{\partial^2 c}{\partial z^2}\right]$$

reduces to the simpler differential equation

$$[2] \qquad \frac{\partial c}{\partial t} = D\frac{\partial^2 c}{\partial x^2}$$

and the mathematical and computational efforts decrease considerably. The assumption of linear diffusion to a planar electrode might imply an infinite disc without edges. For real systems, however, this of course is not possible.

Thus, measurements at finite disc electrodes should deviate from the simple one-dimensional theory. In fact, it has been shown for different electroanalytical techniques such as chronoamperometry and chronopotentiometry (1) that the diffusion current is higher than expected from the theoretical calculations based on eq. [2], i.e. the Cottrell equation (2) for chronoamperometry. For cyclic voltammograms (3) the peak separation is larger than the theoretical values given by Nicholson and Shain (4). A number of papers have accounted for these deviations as being due to additional diffusion from directions other than perpendicular to the disc electrode (see e.g. refs. 5, 6). In a system with several coupled charge transfer and chemical reactions dramatic changes of the overall voltammogram have been attributed to edge effects (7).

Several attempts have been made to calculate the effects of edge diffusion and to simulate model systems without assuming one-dimensional diffusion (5, 6). Recently, Heinze published a two-dimensional model based on the finite difference method (8, 9), while Oldham (10) and Aoki and Osteryoung (11) developed analytical solutions for the simple reversible mechanism.

These calculations showed, in agreement with experiments, that edge diffusion rates increase with increasing time and decreasing radius of the disc electrode. The deviation from pure Cottrell behavior is claimed to be between 9 and 10% for typical conditions: diffusion coefficient = $10^{-5}$ cm$^2$/s, electrode radius 0.1 cm, electrolysis time 2.65 s (5, 9–11). All methods presented thus far, however, demonstrate results for only the simplest mechanisms (e.g. reversible electron transfer case). Extensions apparently require extensive computational effort.

Orthogonal collocation has been shown to provide a powerful method to simulate responses of several electroanalytical techniques to a variety of mechanisms (12–18). Up to now all these calculations have been performed using one-dimensional diffusion models. We want to report the construction of a two-dimensional model for the diffusion to and from a planar disc electrode and the discretization of the resulting second order partial differential equations to give a set of simultaneous first order ordinary differential equations.

The comparison of the results of this new model with those already presented is the subject of a

0008-4042/82/111352-11$01.00/0
©1982 National Research Council of Canada/Conseil national de recherches du Canada

Can. J. Chem. Downloaded from www.nrcresearchpress.com by 210.87.254.40 on 09/06/12
For personal use only.

separate report now in preparation. Extensions to other mechanisms and electroanalytical experiments will also be considered.

### The two-dimensional model

Consider a planar, circular disc of conducting material imbedded into an insulator (Fig. 1). The radius of the disc is $r_0$. The radius $r_0'$, of the insulator may go to infinity. From the symmetry of the problem, it follows that we may use two coordinates $x$ (perpendicular to the disc) and $r$ (along the radius vector of the disc). We are required to calculate the concentration $c$ of all species as a function of $x$, $r$ and the time $t$, where $c$ is given by second order partial differential equations of the type (9)

$$[3] \qquad \frac{\partial c}{\partial t} = D\left[\frac{\partial^2 c}{\partial x^2} + \frac{1}{r}\frac{\partial c}{\partial r} + \frac{\partial^2 c}{\partial r^2}\right] - f(c)$$

and $f(c)$ is determined by the kinetics of the system investigated. $D$ is the diffusion coefficient.

Let us consider an EC-mechanism (4). There the differential equations describing the concentration of species A, B, and C are given by [5]–[7].

$$[4] \qquad A \underset{+e^-}{\overset{-e^-}{\rightleftharpoons}} B \xrightarrow{k} C$$

$$[5] \qquad \frac{\partial c_A}{\partial t} = D_A\left[\frac{\partial c_A}{\partial x^2} + \frac{1}{r}\frac{\partial c_A}{\partial r} + \frac{\partial^2 c_A}{\partial r^2}\right]$$

$$[6] \qquad \frac{\partial c_B}{\partial t} = D_B\left[\frac{\partial^2 c_B}{\partial x^2} + \frac{1}{r}\frac{\partial c_B}{\partial r} + \frac{\partial^2 c_B}{\partial r^2}\right] - kc_B$$

$$[7] \qquad \frac{\partial c_C}{\partial t} = D_C\left[\frac{\partial^2 c_C}{\partial x^2} + \frac{1}{r}\frac{\partial c_C}{\partial r} + \frac{\partial^2 c_C}{\partial r^2}\right] + kc_B$$

For $k = 0$ we deal with a simple reversible electron transfer. The electrode reaction in eq. [4] is drawn as an oxidation but the extension to reductions is immediate. For simplification we may assume that the diffusion coefficients are equal:

$$[8] \qquad D_A = D_B = D_C$$

This, however, is not necessary for orthogonal collocation simulations.

Depending on the electroanalytical method we wish to simulate for the mechanism chosen, certain initial and boundary conditions are imposed upon the solution of eq. [3]. Let us consider a chronoamperometric experiment, where species A, the substrate, is present at a homogeneous concentration $c_A^0$ at the beginning of the experiment. The product species B and C may not be present at $t = 0$ (initial conditions [9], [10]).

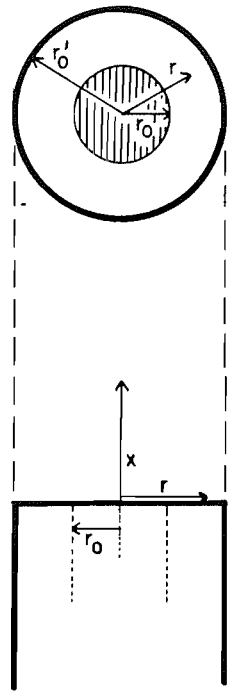


FIG. 1. Geometry of the two-dimensional model.

$t = 0,\ x \geq 0,\ r \geq 0$

$$[9] \qquad c_A(x, r, 0) = c_A^0$$

$$[10] \qquad c_B(x, r, 0) = c_C(x, r, 0) = 0$$

At the boundary $x \to \infty$, i.e. at a distance $x$ far from the electrode where the concentrations are not changed during the experiment:

$t > 0,\ x \to \infty,\ r \geq 0$

$$[11] \qquad c_A(\infty, r, t) = c_A^0$$

$$[12] \qquad c_B(\infty, r, t) = c_C(\infty, r, t) = 0$$

The same condition may hold for a distance $r$ far from the electrode radially:

$t > 0,\ x \geq 0,\ r \to \infty$

$$[13] \qquad c_A(x, \infty, t) = c_A^0$$

$$[14] \qquad c_B(x, \infty, t) = c_C(x, \infty, t) = 0$$

At the electrode surface the Nernst equation has to be fulfilled for $c_A$ and $c_B$ (eq. [14*a*]). If we step to a potential $E$ at least 200 mV past the formal potential $E_{A/B}^0$ the concentration of the substrate A at the electrode is immediately forced to zero and [14*a*] may be replaced by [14*b*]. Additional conditions at

Can. J. Chem. Downloaded from www.nrcresearchpress.com by 210.87.254.40 on 09/06/12
For personal use only.

the electrode surface are given by the flux equations [15] and [16].

$t > 0,\ x = 0,\ 0 \leq r \leq r_0$

$$[14a] \quad \frac{c_A(0, r, t)}{c_B(0, r, t)} = \exp\left[\frac{nF}{RT}(E^0 - E)\right]$$

$$[14b] \quad c_A(0, r, t) = 0$$

$$[15] \quad \left(\frac{\partial c_A}{\partial x}\right)_{x=0} = -\left(\frac{\partial c_B}{\partial x}\right)_{x=0}$$

$$[16] \quad \left(\frac{\partial c_C}{\partial x}\right)_{x=0} = 0$$

At $x = 0$, but outside the electroactive area ($r > r_0$), no species may undergo electron transfer and we have boundary condition [17].

$t > 0,\ x = 0,\ r_0 \leq r \rightarrow \infty$

$$[17] \quad \left(\frac{\partial c_A}{\partial x}\right)_{x=0} = \left(\frac{\partial c_B}{\partial x}\right)_{x=0} = \left(\frac{\partial c_C}{\partial x}\right)_{x=0} = 0$$

Because of the symmetry of the problem there may be no net flux of any species across the $x$-axis at the center of the electrode ($r = 0$).

$t > 0,\ x \geq 0,\ r = 0$

$$[18] \quad \left(\frac{\partial c_A}{\partial r}\right)_{r=0} = \left(\frac{\partial c_B}{\partial r}\right)_{r=0} = \left(\frac{\partial c_C}{\partial r}\right)_{r=0} = 0$$

Equations [4]–[18] describe the two-dimensional model system for an EC-mechanism under chronoamperometric conditions.

Since there are different boundary conditions for $x = 0$ inside ($r \leq r_0$) and outside ($r > r_0$) the electrode, it is convenient to describe the whole system by two concentration functions $c_1$ and $c_2$ which are defined for $0 \leq r \leq r_0$ and $r_0 < r$ respectively. To avoid discontinuities at $r = r_0$ we have to apply some additional "boundary" conditions for all species:

$$[19] \quad c_1(x, r_0, t) = c_2(x, r_0, t)$$

The second derivative of $c$ with respect to $r$ is only defined if the first derivative with respect to $r$ has no discontinuity at $r = r_0$ and this gives the further conditions

$$[20] \quad \left(\frac{\partial c_1}{\partial r}\right)_{r_0} = \left(\frac{\partial c_2}{\partial r}\right)_{r_0}$$

for all species.

It has been pointed out (12) that orthogonal collocation may be applied only to dimensionless systems which have been converted from semi-infinite models to models in the range 0 to 1.

In order to meet these requirements we use the following transformation equations:

$$[21] \quad X = x/L$$

$$[22] \quad c^* = c/c_A^0$$

$$[23a] \quad R = r/r_0$$

$$[23b] \quad R' = (r - r_0)/(M - r_0)$$

$$[24] \quad \alpha = k \cdot r_0^2/D$$

$$[25] \quad T' = Dt/r_0^2$$

where $X$ is the dimensionless distance from the electrode, $L$ is the distance from the electrode in the $x$ direction defined so that at $X = L$ no changes in concentration take place during the time of the experiment, $c^*$ is the dimensionless concentration, $R$ and $R'$ are the dimensionless distances in the $r$ direction inside and outside the electrode disc respectively, $M$ is the distance in the $r$ direction defined in the same manner as $L$, and $T'$ is the dimensionless simulation time.

Application of eqs. [21]–[25] and the subdivision into inner and outer functions $c_1$ and $c_2$ of eqs. [4]–[18] yield the dimensionless model [26]–[33]

$$[26] \quad \frac{\partial c_{A1}^*}{\partial T'} = \beta \frac{\partial^2 c_{A1}^*}{\partial X^2} + \frac{1}{R}\frac{\partial c_{A1}^*}{\partial R} + \frac{\partial^2 c_{A1}^*}{\partial R^2}$$

$$[27] \quad \frac{\partial c_{B1}^*}{\partial T'} = \beta \frac{\partial^2 c_{B1}^*}{\partial X^2} + \frac{1}{R}\frac{\partial c_{B1}^*}{\partial R} + \frac{\partial^2 c_{B1}^*}{\partial R^2} - \alpha c_{B1}^*$$

$$[28] \quad \frac{\partial c_{C1}^*}{\partial T'} = \beta \frac{\partial^2 c_{C1}^*}{\partial X^2} + \frac{1}{R}\frac{\partial c_{C1}^*}{\partial R} + \frac{\partial^2 c_{C1}^*}{\partial R^2} + \alpha c_{B1}^*$$

where

$$[29] \quad \beta = r_0^2/L^2$$

and

$$[30] \quad \frac{\partial c_{A2}^*}{\partial T'} = \beta \frac{\partial^2 c_{A2}^*}{\partial X^2} + \frac{\beta'}{R' + \sqrt{\beta'}}\frac{\partial c_{A2}^*}{\partial R'} + \beta' \frac{\partial^2 c_{A2}^*}{\partial R'^2}$$

$$[31] \quad \frac{\partial c_{B2}^*}{\partial T'} = \beta \frac{\partial^2 c_{B2}^*}{\partial X^2} + \frac{\beta'}{R' + \sqrt{\beta'}}\frac{\partial c_{B2}^*}{\partial R'} + \beta' \frac{\partial^2 c_{B2}^*}{\partial R'^2} - \alpha c_{B2}^*$$

$$[32] \quad \frac{\partial c_{C2}^*}{\partial T'} = \beta \frac{\partial^2 c_{C2}^*}{\partial X^2} + \frac{\beta'}{R' + \sqrt{\beta'}}\frac{\partial c_{C2}^*}{\partial R'} + \beta' \frac{\partial^2 c_{C2}^*}{\partial R'^2} + \alpha c_{B2}^*$$

Can. J. Chem. Downloaded from www.nrcresearchpress.com by 210.87.254.40 on 09/06/12
For personal use only.

where

[33] $\beta' = r_0^2/(M - r_0)^2$

with the initial conditions

$T' = 0,\ 0 \le X \le 1,\ 0 \le R \le 1,\ 0 \le R' \le 1$

[34] $c^*_{A1}(X, R, 0) = c^*_{A2}(X, R', 0) = 1$

[35] $c^*_{B1}(X, R, 0) = c^*_{C1}(X, R, 0) = c^*_{B2}(X, R', 0) = c^*_{C2}(X, R', 0) = 0$

and boundary conditions

$T' > 0,\ X = 1,\ 0 \le R \le 1$

[36] $c^*_{A1}(1, R, T') = 1$

[37] $c^*_{B1}(1, R, T') = c^*_{C1}(1, R, T') = 0$

$T' > 0,\ X = 1,\ 0 \le R' \le 1$

[38] $c^*_{A2}(1, R', T') = 1$

[39] $c^*_{B2}(1, R', T') = c^*_{C2}(1, R', T') = 0$

$T' > 0,\ 0 \le X \le 1,\ R' = 1$

[40] $c^*_{A2}(X, 1, T') = 1$

[41] $c^*_{B2}(X, 1, T') = c^*_{C2}(X, 1, T') = 0$

$T' > 0,\ X = 0,\ 0 \le R \le 1$

[42a] $\dfrac{c^*_{A1}(0, R, T')}{c^*_{B1}(0, R, T')} = \exp\left[\dfrac{nF}{RT}(E^0 - E)\right]$

[42b] $c^*_{A1}(0, R, T') = 0$

[43] $\left(\dfrac{\partial c^*_{A1}}{\partial X}\right)_{X=0} = -\left(\dfrac{\partial c^*_{B1}}{\partial X}\right)_{X=0}$

[44] $\left(\dfrac{\partial c^*_{C1}}{\partial X}\right)_{X=0} = 0$

$T' > 0,\ X = 0,\ 0 < R' \le 1$

[45] $\left(\dfrac{\partial c^*_{A2}}{\partial X}\right)_{X=0} = \left(\dfrac{\partial c^*_{B2}}{\partial X}\right)_{X=0} = \left(\dfrac{\partial c^*_{C2}}{\partial X}\right)_{X=0} = 0$

$T' > 0,\ 0 \le X \le 1,\ R = 0$

[46] $\left(\dfrac{\partial c^*_{A1}}{\partial R}\right)_{R=0} = \left(\dfrac{\partial c^*_{B1}}{\partial R}\right)_{R=0} = \left(\dfrac{\partial c^*_{C1}}{\partial R}\right)_{R=0} = 0$

$T' > 0,\ 0 \le X \le 1,\ R = 1\ (R' = 0)$

[47] $c^*_{A1}(X, 1, T') = c^*_{A2}(X, 0, T')$

[48] $c^*_{B1}(X, 1, T') = c^*_{B2}(X, 0, T')$

[49] $c^*_{C1}(X, 1, T') = c^*_{C2}(X, 0, T')$

[50] $\left(\dfrac{\partial c^*_{A1}}{\partial R}\right)_{R=1} = \sqrt{\beta'}\left(\dfrac{\partial c^*_{A2}}{\partial R'}\right)_{R'=0}$

[51] $\left(\dfrac{\partial c^*_{B1}}{\partial R}\right)_{R=1} = \sqrt{\beta'}\left(\dfrac{\partial c^*_{B2}}{\partial R'}\right)_{R'=0}$

[52] $\left(\dfrac{\partial c^*_{C1}}{\partial R}\right)_{R=1} = \sqrt{\beta'}\left(\dfrac{\partial c^*_{C2}}{\partial R'}\right)_{R'=0}$

We have to calculate the inner and outer concentrations of species A, B, and C respectively as a function of $X$, $R(R')$, and $T'$.

### Two-dimensional collocation

Orthogonal collocation uses a mathematically suitable trial function to describe the solution of a differential equation at certain points. If one uses a set of weighted orthogonal polynomials as the trial function, the differential equation is satisfied at the zeroes of the polynomial of highest order used (19, 20) for a set of coefficients which depend on time.

To perform orthogonal collocation in two-dimensions, $x$ and $r$, we use a trial function depending on $x$ and $r$

[53] $$c(x, r, t) = \lambda_{1,1}x^0r^0 + \lambda_{2,1}x^1r^0 + \ldots + \lambda_{N_x+2,1}x^{N_x+2-1}r^0 + \lambda_{1,2}x^0r^1 + \lambda_{2,2}x^1r^1 + \ldots + \lambda_{N_x+2,2}x^{N_x+2-1}r^1 + \ldots + \lambda_{1,N_r+2}x^0r^{N_r+2-1} + \lambda_{2,N_r+2}x^1r^{N_r+2-1} + \ldots + \lambda_{N_x+2,N_r+2}x^{N_x+2-1}r^{N_r+2-1}$$

or

[54] $$c(x, r, t) = \sum_{l=1}^{N_r+2}\sum_{j=1}^{N_x+2}\lambda_{j,l}x^{j-1}r^{l-1}$$

i.e. we represent the concentration by a polynomial in $x$ and $r$ whose time-dependent coefficients are the $\lambda_{j,l}$. The polynomial is of order $N_x + 2$ and $N_r + 2$ with respect to $x$ and $r$, respectively. The dummy variables $j$ and $l$ perform the summations over the powers of $x$ and $r$ respectively.

The coefficients are determined thus, that at all collocation points $(x_i, r_k)$, i.e. $N_x + 2$ and $N_r + 2$

Can. J. Chem. Downloaded from www.nrcresearchpress.com by 210.87.254.40 on 09/06/12
For personal use only.

points in the $x$ and $r$ directions, respectively

$$[55] \quad c(x_i, r_k, t) = \sum_{l=1}^{N_r+2} \sum_{j=1}^{N_x+2} \lambda_{j,l} x_i^{j-1} r_k^{l-1}$$

The concentrations at the collocation points may be the elements of a concentration matrix $\Gamma_{i,k}$

$$[56] \quad \Gamma_{i,k} = \mathbf{X}_{i,j} \cdot \Lambda_{j,l} \mathbf{R}^{\mathrm{T}}_{k,l}$$

which is calculated by multiplication of a matrix $\mathbf{X}_{i,j}$, containing the $x_i^{j-1}$ as elements, a matrix $\Lambda_{j,l}$, containing the elements $\lambda_{j,l}$, and a matrix $\mathbf{R}^{\mathrm{T}}_{k,l}$, containing the elements $r_k^{l-1}$. The superscript T denotes a transposed matrix.

Now we can calculate the first and second derivatives of the concentration at the collocation points with respect to $x$ and $r$ respectively:

$$[57] \quad \Gamma^{x}_{i,k} = \mathbf{X}^{x}_{i,j} \cdot \Lambda_{j,l} \cdot \mathbf{R}^{\mathrm{T}}_{k,l}$$

$$[58] \quad \Gamma^{xx}_{i,k} = \mathbf{X}^{xx}_{i,j} \cdot \Lambda_{j,l} \cdot \mathbf{R}^{\mathrm{T}}_{k,l}$$

$$[59] \quad \Gamma^{r}_{i,k} = \mathbf{X}_{i,j} \cdot \Lambda_{j,l} \cdot \mathbf{R}^{r\mathrm{T}}_{k,l}$$

$$[60] \quad \Gamma^{rr}_{i,k} = \mathbf{X}_{i,j} \cdot \Lambda_{j,l} \cdot \mathbf{R}^{rr\mathrm{T}}_{k,l}$$

where the superscript $x(r)$ denotes the first and accordingly $xx(rr)$ characterises the second derivative with respect to $x(r)$.

From eq. [56] it follows that

$$[61] \quad \Lambda_{j,l} = \mathbf{X}^{-1}_{i,j} \cdot \Gamma_{i,k} \cdot (\mathbf{R}^{\mathrm{T}}_{k,l})^{-1}$$

After inserting [61] into [57] we arrive at

$$[62] \quad \Gamma^{x}_{i,k} = \mathbf{X}^{x}_{i,j} \cdot \mathbf{X}^{-1}_{i,j} \cdot \Gamma_{i,k} = \mathbf{A}_{i,j} \cdot \Gamma_{i,k}$$

where the first derivative of the concentration with respect to $x$ is expressed as a function of the concentration itself. In analogy eqs. [61] and [58] give

$$[63] \quad \Gamma^{xx}_{i,k} = \mathbf{X}^{xx}_{i,j} \cdot \mathbf{X}^{-1}_{i,j} \cdot \Gamma_{i,k} = \mathbf{B}_{i,j} \cdot \Gamma_{i,k}$$

From [61] and [59] we get

$$[64] \quad \Gamma^{r}_{i,k} = \Gamma_{i,k} \cdot (\mathbf{R}^{\mathrm{T}}_{k,l})^{-1} \cdot \mathbf{R}^{r\mathrm{T}}_{k,l} = \Gamma_{i,k} \cdot (\mathbf{R}^{-1}_{k,l})^{\mathrm{T}} \cdot \mathbf{R}^{r\mathrm{T}}_{k,l} = \Gamma_{i,k} \cdot (\mathbf{R}^{r}_{l,k} \cdot \mathbf{R}^{-1}_{l,k})^{\mathrm{T}}$$

or

$$[65] \quad \Gamma^{r}_{i,k} = \Gamma_{i,k} \cdot \mathbf{C}_{l,k}$$

Analogous from [61] and [60]

$$[66] \quad \Gamma^{rr}_{i,k} = \Gamma_{i,k} \cdot (\mathbf{R}^{rr}_{l,k} \cdot \mathbf{R}^{-1}_{l,k})^{\mathrm{T}} = \Gamma_{i,k} \cdot \mathbf{D}_{l,k}$$

We may calculate the matrices containing the derivatives of the concentration at the collocation points from the concentration matrix once the matrices $\mathbf{A}_{i,j}$, $\mathbf{B}_{i,j}$, $\mathbf{C}_{l,k}$, and $\mathbf{D}_{l,k}$ have been determined. Returning to summation expressions we can write

$$[67] \quad \left(\frac{\partial c}{\partial x}\right)_{x_i, r_k} = \sum_{j=1}^{N_x+2} A_{i,j} c(x_j, r_k, t)$$

$$[68] \quad \left(\frac{\partial^2 c}{\partial x^2}\right)_{x_i, r_k} = \sum_{j=1}^{N_x+2} B_{i,j} c(x_j, r_k, t)$$

$$[69] \quad \left(\frac{\partial c}{\partial r}\right)_{x_i, r_k} = \sum_{l=1}^{N_r+2} C_{l,k} c(x_i, r_l, t)$$

and

$$[70] \quad \left(\frac{\partial^2 c}{\partial r^2}\right)_{x_i, r_k} = \sum_{l=1}^{N_r+2} D_{l,k} c(x_i, r_l, t)$$

As has been pointed out by Whiting and Carr (12) for the one-dimensional case, the matrices $\mathbf{A}_{i,j}$, $\mathbf{B}_{i,j}$, $\mathbf{C}_{l,k}$, and $\mathbf{D}_{l,k}$ depend solely on the type of polynomial used as trial function and may be calculated from the zeroes of this polynomial. This has to be done only once. Using the values of the elements of those matrices we are able to express the differential quotients of $c$ with respect to $x$ and $r$ at all collocation points.

For linear diffusion problems it has been shown that Legendre polynomials are most suitable (12). Pons (18) used Chebysheff polynomials for diffusion under spherical geometry. It may be noted, however, that the choice of the trial function does not have a large effect on the accuracy of the solutions for higher order approximations. In general, the best trial function is determined by the symmetry of the problem.

In this work, Legendre polynomials have been used for discretization along the $x$-coordinate. The collocation in the direction of the $r$-coordinate has been performed using different types of functions including Legendre, Chebysheff, and polynomials constructed from even powers of $r$, which is suggested by the symmetry of the problem around $r = 0$ (19).

### Discretization of the equations for chronoamperometry

We can substitute the summation expressions [67]–[70] for the partial differential quotients in eqs. [26]–[28] and [30]–[32]. This yields expressions for the time derivative of the concentration of species A, B, and C at all the collocation points as a function of the concentrations at the collocation points. If we substitute the boundary conditions [36]–[41], [42*b*] (i.e. we assume a step to a potential far behind $E^0$) and [47]–[49], we arrive at

Can. J. Chem. Downloaded from www.nrcresearchpress.com by 210.87.254.40 on 09/06/12
For personal use only.

$$[71]\quad \left.\frac{dc^*_{A1}}{dT'}\right|_{X_i,R_k} = \beta\cdot\left\{B_{i,N_x+2} + \sum_{j=2}^{N_x+1} B_{i,j}c^*_{A1}(X_j, R_k, T')\right\} + \left\{E_{1,k}c^*_{A1}(X_i, 0, T') + E_{N_R+2,k}c^*_{A1}(X_i, 1, T') + \sum_{l=2}^{N_R+1} E_{l,k}c^*_{A1}(X_i, R_l, T')\right\}$$

$$[72]\quad \left.\frac{dc^*_{B1}}{dT'}\right|_{X_i,R_k} = \beta\cdot\left\{B_{i,1}c^*_{B1}(0, R_k, T') + \sum_{j=2}^{N_x+1} B_{i,j}c^*_{B1}(X_j, R_k, T')\right\} + \left\{E_{1,k}c^*_{B1}(X_i, 0, T') + E_{N_R+2,k}c^*_{B1}(X_i, 1, T') + \sum_{l=2}^{N_R+1} E_{l,k}c^*_{B1}(X_i, R_l, T')\right\} - \alpha c^*_{B1}$$

$$[73]\quad \left.\frac{dc^*_{C1}}{dT'}\right|_{X_i,R_k} = \beta\left\{B_{i,1}c^*_{C1}(0, R_k, T') + \sum_{j=2}^{N_x+1} B_{i,j}c^*_{C1}(X_j, R_k, T')\right\} + \left\{E_{1,k}c^*_{C1}(X_i, 0, T') + E_{N_R+2,k}c^*_{C1}(X_i, 1, T') + \sum_{l=2}^{N_R+1} E_{l,k}c^*_{C1}(X_i, R_l, T')\right\} + \alpha c^*_{B1}$$

$$[74]\quad \left.\frac{dc^*_{A2}}{dT'}\right|_{X_i,R_{k'}} = \beta\left\{B_{i,1}c^*_{A2}(0, R'_k, T') + B_{i,N_x+2} + \sum_{j=2}^{N_x+1} B_{i,j}c^*_{A2}(X_j, R'_k, T')\right\} + \beta'\left\{F'_{1,k}c^*_{A2}(X_i, 0, T') + F'_{N_{R'}+2,k} + \sum_{l=2}^{N_{R'}+1} F'_{l,k}c^*_{A2}(X_i, R'_l, T')\right\}$$

$$[75]\quad \left.\frac{dc^*_{B2}}{dT'}\right|_{X_i,R_{k'}} = \beta\left\{B_{i,1}c^*_{B2}(0, R'_k, T') + \sum_{j=2}^{N_x+1} B_{i,j}c^*_{B2}(X_j, R'_k, T')\right\} + \beta'\left\{F'_{1,k}c^*_{B2}(X_i, 0, T') + \sum_{l=2}^{N_{R'}+1} F'_{l,k}c^*_{B2}(X_i, R'_l, T')\right\} - \alpha c^*_{B2}$$

$$[76]\quad \left.\frac{dc^*_{C2}}{dT'}\right|_{X_i,R_{k'}} = \beta\left\{B_{i,1}c^*_{C2}(0, R'_k, T') + \sum_{j=2}^{N_x+1} B_{i,j}c^*_{C2}(X_j, R'_k, T')\right\} + \beta'\left\{F'_{1,k}c^*_{C2}(X_i, 0, T') + \sum_{l=2}^{N_{R'}+1} F'_{l,k}c^*_{C2}(X_i, R'_l, T')\right\} + \alpha c^*_{B2}$$

where

$$[77]\quad E_{l,k} = \frac{C_{l,k} + R_k D_{l,k}}{R_k}$$

and

$$[78]\quad F'_{l,k} = \frac{C'_{l,k}}{\sqrt{\beta'} + R'_k} + D'_{l,k}$$

The primed terms, except $T'$ and $\beta'$, correspond to the outer functions. Equations [71]–[76] contain $9N_x + 2N_R + 3N_{R'}$ unknowns, i.e. $c^*_{A1}(X_i, 0, T')$, $c^*_{A1}(X_i, 1, T')$, $c^*_{B1}(X_i, 0, T')$, $c^*_{B1}(X_i, 1, T')$, $c^*_{C1}(X_i, 0, T')$, $c^*_{C1}(X_i, 1, T')$, $c^*_{A2}(X_i, 0, T')$, $c^*_{B2}(X_i, 0, T')$, $c^*_{C2}(X_i, 0, T')$ for all $X_i$; $c^*_{B1}(0, R_k, T')$ and $c^*_{C1}(0, R_k, T')$ for all $R_k$; $c^*_{A2}(0, R'_k, T')$, $c^*_{B2}(0, R'_k, T')$, $c^*_{C2}(0, R'_k, T')$ for all $R'_k$ which may be computed from the boundary conditions as is shown below.

Condition [43] yields

$$[79]\quad \sum_{j=1}^{N_x+2} A_{1,j}c^*_{A1}(X_j, R_k, T') = -\sum_{j=1}^{N_x+2} A_{1,j}c^*_{B1}(X_j, R_k, T')$$

Expanding the sums, introducing [36], [37], and [42*b*], and solving for the concentration of species B at the electrode surface ($X_1 = 0$) gives:

[80] $$c^*_{B1}(0, R_k, T') = -\frac{1}{A_{1,1}}\left\{A_{1,N_x+2} + \sum_{j=2}^{N_x+1} A_{1,j}[c^*_{A1}(X_j, R_k, T') + c^*_{B1}(X_j, R_k, T')]\right\}$$

Condition [44] is changed to

$$\sum_{j=1}^{N_x+2} A_{1,j} c^*_{C1}(X_j, R_k, T') = 0$$

which gives, after introduction of [37],

[81] $$c^*_{C1}(0, R_k, T') = -\frac{1}{A_{1,1}} \sum_{j=2}^{N_x+1} A_{1,j} c^*_{C1}(X_j, R_k, T')$$

In analogy it may be derived from [45] and [40] or [41]

[82] $$c^*_{A2}(0, R'_k, T') = -\frac{1}{A_{1,1}}\left\{A_{1,N_x+2} + \sum_{j=2}^{N_x+1} A_{1,j} c^*_{A2}(X_j, R'_k, T')\right\}$$

[83] $$c^*_{B2}(0, R'_k, T') = -\frac{1}{A_{1,1}} \sum_{j=2}^{N_x+1} A_{1,j} c^*_{B2}(X_j, R'_k, T')$$

and

[84] $$c^*_{C2}(0, R'_k, T') = -\frac{1}{A_{1,1}} \sum_{j=2}^{N_x+1} A_{1,j} c^*_{C2}(X_j, R'_k, T')$$

The condition [46] gives, for species A, B, and C

[85] $$c^*_{A1}(X_i, 0, T') = -\frac{1}{C_{1,1}}\left\{C_{N_R+2,1} c^*_{A1}(X_i, 1, T') + \sum_{l=2}^{N_R+1} C_{l,1} c^*_{A1}(X_i, R_l, T')\right\}$$

[86] $$c^*_{B1}(X_i, 0, T') = -\frac{1}{C_{1,1}}\left\{C_{N_R+2,1} c^*_{B1}(X_i, 1, T') + \sum_{l=2}^{N_R+1} C_{l,1} c^*_{B1}(X_i, R_l, T')\right\}$$

and

[87] $$c^*_{C1}(X_i, 0, T') = -\frac{1}{C_{1,1}}\left\{C_{N_R+2,1} c^*_{C1}(X_i, 1, T') + \sum_{l=2}^{N_R+1} C_{l,1} c^*_{C1}(X_i, R_l, T')\right\}$$

Condition [50] yields

[88] $$\sum_{l=1}^{N_R+2} C_{l,N_R+2} c^*_{A1}(X_i, R_l, T') = \sum_{l=1}^{N_R+2} \sqrt{\beta'}\, C'_{l,1} c^*_{A2}(X_i, R'_l, T')$$

which may be expanded and transformed using [40] and [47]

[89] $$[c_{N_R+2,N_R+2} - \sqrt{\beta'}\, C'_{1,1}] \cdot c^*_{A1}(X_i, 1, T') + C_{1,N_R+2} c^*_{A1}(X_i, 0, T') = -\sum_{l=2}^{N_R+1} C_{l,N_R+2} c^*_{A1}(X_i, R_l, T') + \sum_{l=2}^{N_{R'}+1} \sqrt{\beta'}\, C'_{l,1} c^*_{A2}(X_i, R'_l, T') + \sqrt{\beta'}\, C'_{N_{R'}+2,1}$$

From [85] and [89] it follows that

[90] $$c^*_{A1}(X_i, 1, T') = c^*_{A2}(X_i, 0, T') = \frac{1}{G_1}\left\{\sum_{l=2}^{N_R+1} H_l c^*_{A1}(X_i, R_l, T') + \sum_{l=2}^{N_{R'}+1} C_{1,1}\sqrt{\beta'}\, C'_{l,1} c^*_{A2}(X_i, R'_l, T') + C_{1,1}\sqrt{\beta'}\, C'_{N_{R'}+2,1}\right\}$$

where

[91] $$G_l = [C_{N_R+2,N_R+2} - \sqrt{\beta'}\, C'_{1,1}] C_{l,1} - C_{l,N_R+2} C_{N_R+2,1}$$

Can. J. Chem. Downloaded from www.nrcresearchpress.com by 210.87.254.40 on 09/06/12
For personal use only.

Can. J. Chem. Downloaded from www.nrcresearchpress.com by 210.87.254.40 on 09/06/12
For personal use only.

and

[92] $H_l = C_{1,N_R+2}C_{l,1} - C_{1,1}C_{l,N_R+2}$

Conditions [46] and [51] ([46] and [52]) are treated similarly using the corresponding boundary expressions. Thus,

[93] $$c^*_{B1}(X_i, 1, T') = c^*_{B2}(X_i, 0, T') = \frac{1}{G_1}\left\{\sum_{l=2}^{N_R+1} H_l c^*_{B1}(X_i, R_l, T') + \sum_{l=2}^{N_{R'}+1} C_{1,1}\sqrt{\beta'}\, C'_{l,1} c^*_{B2}(X_i, R'_l, T')\right\}$$

and

[94] $$c^*_{C1}(X_i, 1, T') = c^*_{C2}(X_i, 0, T') = \frac{1}{G_1}\left\{\sum_{l=2}^{N_R+1} H_l c^*_{C1}(X_i, R_l, T') + \sum_{l=2}^{N_{R'}+1} C_{1,1}\sqrt{\beta'}\, C_{l,1} c^*_{C2}(X_i, R'_l, T')\right\}$$

Finally, the concentrations of species A at $R = 0$ and all $X_i$ may be calculated by introducing [90] into [85]:

[95] $$c^*_{A1}(X_i, 0, T') = -\frac{1}{G_1}\left\{\sum_{l=2}^{N_R+1} G_l c^*_{A1}(X_i, R_l, T') + \sum_{l=2}^{N_{R'}+1} C_{N_R+2,1}\sqrt{\beta'}\, C'_{l,1} c^*_{A2}(X_i, R'_l, T') + C_{N_R+2,1}\sqrt{\beta'}\, C'_{N_{R'}+2,1}\right\}$$

while it holds from [93] and [86] ([94] and [87]), that

[96] $$c^*_{B1}(X_i, 0, T') = -\frac{1}{G_1}\left\{\sum_{l=2}^{N_R+1} G_l c^*_{B1}(X_i, R_l, T') + \sum_{l=2}^{N_{R'}+1} C_{N_R+2,1}\sqrt{\beta'}\, C'_{l,1} c^*_{B2}(X_i, R'_l, T')\right\}$$

and that

[97] $$c^*_{C1}(X_i, 0, T') = -\frac{1}{G_1}\left\{\sum_{l=2}^{N_R+1} G_l c^*_{C1}(X_i, R_l, T') + \sum_{l=2}^{N_{R'}+1} C_{N_R+2,1}\sqrt{\beta'}\, C'_{l,1} c^*_{C2}(X_i, R'_l, T')\right\}$$

Now we may substitute the unknown terms in eqs. [71]–[76]. From [71], using [90] and [95] it follows

[98] $$\left.\frac{dc^*_{A1}}{dT'}\right|_{X_i,R_k} = \beta\left\{B_{i,N_x+2} + \sum_{j=2}^{N_x+1} B_{i,j} c^*_{A1}(X_j, R_k, T')\right\} + \frac{1}{G_1}\left\{I_{1,k}\sqrt{\beta'}\, C'_{N_{R'}+2,1} + \sum_{l=2}^{N_R+1}\left[J_{l,k}(\sqrt{\beta'}\, C'_{1,1} - C_{N_R+2,N_R+2}) - I_{1,k}C_{l,N_R+2} + I_{l,k}C_{1,N_R+2}\right]\cdot c^*_{A1}(X_i, R_l, T') + \sum_{l=2}^{N_{R'}+1} I_{1,k}\sqrt{\beta'}\, C_{l,1} c^*_{A2}(X_i, R'_l, T')\right\}$$

where

[99] $I_{l,k} = E_{N_R+2,k}C_{l,1} - E_{l,k}C_{N_R+2,1}$

and

[100] $J_{l,k} = E_{1,k}C_{l,1} - E_{l,k}C_{1,1}$

Combination of [72] with [80], [93], and [96] gives

[101] $$\left.\frac{dc^*_{B1}}{dT'}\right|_{X_i,R_k} = \frac{\beta}{A_{1,1}}\left\{\sum_{j=2}^{N_x+1} K_{i,j} c^*_{B1}(X_j, R_k, T') - B_{i,1}\left[A_{1,N_x+2} + \sum_{j=2}^{N_x+1} A_{1,j} c^*_{A1}(X_j, R_k, T')\right]\right\} + \frac{1}{G_1}\left\{\sum_{l=2}^{N_R+1}\left[J_{l,k}(\sqrt{\beta'}\, C'_{1,1} - C_{N_R+2,N_R+2}) - I_{1,k}C_{l,N_R+2} + I_{l,k}C_{1,N_R+2}\right]c^*_{B1}(X_i, R_l, T') + \sum_{l=2}^{N_{R'}+1} I_{1,k}\sqrt{\beta'}\, C_{l,1} c^*_{B2}(X_i, R'_l, T')\right\} - \alpha c^*_{B1}$$

Can. J. Chem. Downloaded from www.nrcresearchpress.com by 210.87.254.40 on 09/06/12
For personal use only.

where

[102] $K_{i,j} = B_{i,j}A_{1,1} - B_{i,1}A_{1,j}$

For the inner function describing the concentration of species C it holds from [73] with [81], [94] and [97]

$$[103]\quad \left.\frac{dc^*_{C1}}{dT'}\right|_{X_i,R_k} = \frac{\beta}{A_{1,1}}\left\{\sum_{j=2}^{N_x+1} K_{i,j}c^*_{C1}(X_j, R_k, T')\right\} + \frac{1}{G_1}\left\{\sum_{l=2}^{N_R+1}[J_{l,k}(\sqrt{\beta'}\,C'_{1,1} - C_{N_R+2,N_R+2}) - I_{1,k}C_{l,N_R+2} + I_{l,k}C_{1,N_R+2}]c^*_{C1}(X_i, R_l, T') + \sum_{l=2}^{N_{R'}+1} I_{1,k}\sqrt{\beta'}\,C'_{l,1}c^*_{C2}(X_i, R'_l, T')\right\} + \alpha c^*_{B1}$$

The outer functions for all three species are derived following the same scheme. The time derivative of $c^*_A$ in the outer domain is found from [74], [82], and [90], and in analogy the corresponding equations for species B or C may be calculated from [75], [83], and [93] or [76], [84], and [94].

$$[104]\quad \left.\frac{dc^*_{A2}}{dT'}\right|_{X_i,R_{k'}} = \frac{\beta}{A_{1,1}}\left\{K_{i,N_x+2} + \sum_{j=2}^{N_x+1} K_{i,j}c^*_{A2}(X_j, R'_k, T')\right\} + \frac{\beta'}{G_1}\left\{L'_{N_R+2,k} + \sum_{l=2}^{N_R+1} F'_{1,k}H_l c^*_{A1}(X_i, R_l, T') + \sum_{l=2}^{N_{R'}+1} L'_{l,k}c^*_{A2}(X_i, R'_l, T')\right\}$$

with

[105] $L'_{l,k} = F'_{l,k}G_1 + C_{1,1}\sqrt{\beta'}\,C_{l,1}F'_{1,k}$

$$[106]\quad \left.\frac{dc^*_{B2}}{dT'}\right|_{X_i,R_{k'}} = \frac{\beta}{A_{1,1}}\left\{\sum_{j=2}^{N_x+1} K_{i,j}c^*_{B2}(X_j, R'_k, T')\right\} + \frac{\beta'}{G_1}\left\{\sum_{l=2}^{N_R+1} F'_{1,k}H_l c^*_{B1}(X_i, R_l, T') + \sum_{l=2}^{N_{R'}+1} L'_{l,k}c^*_{B2}(X_i, R'_l, T')\right\} - \alpha c^*_{B2}$$

$$[107]\quad \left.\frac{dc^*_{C2}}{dT'}\right|_{X_i,R_{k'}} = \frac{\beta}{A_{1,1}}\left\{\sum_{j=2}^{N_x+1} K_{i,j}c^*_{C2}(X_j, R'_k, T')\right\} + \frac{\beta'}{G_1}\left\{\sum_{l=2}^{N_R+1} F'_{1,k}H_l c^*_{C1}(X_i, R_l, T') + \sum_{l=2}^{N_{R'}+1} L'_{l,k}c^*_{C2}(X_i, R'_l, T')\right\} + \alpha c^*_{B2}$$

Now the set of six second order partial differential equations [26]–[28] and [30]–[32] has been transformed into a set of $3N_x(N_R + N_{R'})$ simultaneous ordinary differential equations [98], [101], [103], [104], [106], and [107]. Such systems may be easily integrated by computer programs to give the time dependence of the concentrations of species A, B, and C at the collocation points $(X_i, R_k)$ and $(X_i, R'_k)$. We describe the concentration profiles which develop in front of the electrode by the concentrations at the collocation points.

We note the structural similarity of the formulae describing the time derivatives of the concentrations. This is one of the advantages of the orthogonal collocation method, for if the theory has been derived once it is very easy to express it in a computer language. Furthermore, if more complicated mechanisms are to be simulated, only minor changes in the formulae have to be performed. Also, the extension of the theory to other experimental techniques, i.e. other boundary conditions, is easy. This will be shown in another paper of this series.

We also note that the implementation of the expressions describing species C is not essential to calculate the concentration profiles of A and B, for C is not electroactive and does not react to or with an electroactive intermediate (16). However, if one

Can. J. Chem. Downloaded from www.nrcresearchpress.com by 210.87.254.40 on 09/06/12
For personal use only.

desires, for example, to calculate the spectroelectrochemical response (14) of species C one is interested in the concentration profiles of C as well.

### Calculation of the current

In the one-dimensional diffusion model the current $i$ is simply calculated from the flux of the substrate at the electrode surface:

$$[108] \quad i = nFAD\left(\frac{\partial c_A}{\partial x}\right)_{x=0}$$

where $A$ is the electroactive area of the electrode. This implies that the flux of the substrate is uniform over $A$.

This is clearly not true in the case of a two-dimensional model considering edge effects. Instead, the current is given by

$$[109] \quad i = nFD\int_0^{r_0} 2\pi r\left(\frac{\partial c_A}{\partial x}\right)_{x=0} dr$$

where the $r$-dependent flux through an infinitesimally small part $2\pi r dr$ of the electrode is integrated over the electroactive section $0$–$r_0$ of the $r$-coordinate.

Using the transformation equations [21]–[23], [25], and the definition of β (eq. [29]), eq. [109] yields

$$[110] \quad i = \frac{nFD2\pi r_0^2 c_A^0}{L}\int_0^1 R\left(\frac{\partial c_{A1}^*}{\partial X}\right)_{X=0} dR$$

$$= 2uFAc_A^0\frac{\sqrt{D}}{\sqrt{t}}\sqrt{\beta T'}\int_0^1 R\left(\frac{\partial c_{A1}^*}{\partial X}\right)_{X=0} dR$$

The chronoamperometric "constant" $i\sqrt{t}$ is given by

$$[111] \quad i\sqrt{t} = 2uFAc_A^0\sqrt{D}\sqrt{\beta T'} \times \int_0^1 R\left(\frac{\partial c_{A1}^*}{\partial X}\right)_{X=0} dR$$

Alternatively, we may express this product in terms of the "Cottrell constant" (2)

$$[112] \quad (i\sqrt{t})_C = \frac{uFAc_A^0\sqrt{D}}{\sqrt{\pi}}$$

as

$$[113] \quad \frac{i\sqrt{t}}{(i\sqrt{t})_C} = 2\sqrt{\beta\pi T'}\int_0^1 R\left(\frac{\partial c_{A1}^*}{\partial X}\right)_{X=0} dR$$

Since the differential quotients $(\partial c_A^*/\partial X)$ are given at the collocation points we may calculate the integral exactly by a quadrature formula of the type (ref. 20, p. 134)

$$[114] \quad \int_0^1 y(r)w_k(r)\,dr = \sum_{l=1}^{N_r+2} Q_l y_l$$

where the $Q_l$ are elements of a vector depending on the trial function chosen.

Thus, from [67]

$$[115] \quad \int_0^1 R\left(\frac{\partial c_{A1}^*}{\partial X}\right)_{X=0} dR = \sum_{l=1}^{N_R+2} Q_l\left[R_l\sum_{j=1}^{N_x+2} A_{1,j}c_{A1}^*(X_j, R_l, T')\right]$$

Expanding the sum over $j$ and introducing the boundary conditions [36] and [42$b$], [115] changes to

$$[116] \quad \int_0^1 R\left(\frac{\partial c_{A1}^*}{\partial X}\right)_{X=0} dR = \sum_{l=1}^{N_R+2} Q_l \times\left[R_l A_{1,N_x+2} + R_l\sum_{j=2}^{N_x+1} A_{1,j}c_{A1}^*(X_j, R_l, T')\right]$$

The Gaussian weights $Q_l$ for $l = 1$ and $l = N_R + 2$ are equal to zero, thus [116] reduces to

$$[117] \quad \int_0^1 R\left(\frac{\partial c_{A1}^*}{\partial X}\right)_{X=0} dR = \sum_{l=2}^{N_R+1} Q_l \times\left[R_l A_{1,N_x+2} + R_l\sum_{j=2}^{N_x+1} A_{1,j}c_{A1}^*(X_j, R_l, T')\right]$$

which is a convenient form for computation of the integral.

### Acknowledgement

We thank the Office of Naval Research, Washington, D.C., for support of part of this work.

1. P. J. LINGANE. Anal. Chem. **36**, 1723 (1964).
2. D. D. MCDONALD. Transient techniques in electrochemistry. Plenum Press, New York and London. 1977. p. 72.
3. R. LINES and V. D. PARKER. Acta Chem. Scand. **31**, 369 (1977).
4. R. S. NICHOLSON and I. SHAIN. Anal. Chem. **36**, 706 (1964).
5. Z. G. SOOS and P. J. LINGANE. J. Phys. Chem. **68**, 3821 (1964).
6. J. B. FLANAGAN and L. MARCOUX. J. Phys. Chem. **77**, 1051 (1973).
7. B. SPEISER and A. RIEKER. Electrochim. Acta, **23**, 983 (1978).
8. J. HEINZE. Ber. Bunsenges. Phys. Chem. **84**, 785 (1980).
9. J. HEINZE. J. Electroanal. Chem. **124**, 73 (1981).

10. K. B. OLDHAM. J. Electroanal. Chem. **122**, 1 (1981).
11. K. AOKI and J. OSTERYOUNG. J. Electroanal. Chem. **122**, 19 (1981).
12. L. F. WHITING and P. W. CARR. J. Electroanal. Chem. **81**, 1 (1977).
13. A. BEWICK, J. MELLOR, and S. PONS. Electrochim. Acta, **23**, 77 (1978).
14. A. BEWICK, J. MELLOR, and S. PONS. Electrochim. Acta, **25**, 931 (1980).
15. S. PONS and P. P. SCHMIDT. Electrochim. Acta, **25**, 987 (1980).
16. B. SPEISER and A. RIEKER. J. Electroanal. Chem. **102**, 1 (1979).
17. B. SPEISER. J. Electroanal. Chem. **110**, 69 (1980).
18. S. PONS. Can. J. Chem. **59**, 1538 (1981).
19. B. A. FINLAYSON. *In* Mathematics in science and engineering. Vol. 87. *Edited by* R. Bellman. Academic Press, New York and London. 1972. p. 102.
20. J. VILLADSEN and M. L. MICHELSEN. Solution of differential equation models by polynomial approximation. Prentice Hall, Englewood Cliffs. 1978.

Can. J. Chem. Downloaded from www.nrcresearchpress.com by 210.87.254.40 on 09/06/12
For personal use only.

# Correlation of the hydrogenation catalytic activity of dinuclear complexes of rhodium(I) with the formation of carbonyl-bridged complexes

ALAN R. SANGER

*Alberta Research Council, 11315-87 Avenue, Edmonton, Alta., Canada T6G 2C2*

Received May 8, 1981[1]

ALAN R. SANGER. Can. J. Chem. **60**, 1363 (1982).

Methanolic solutions of the dinuclear cationic complexes of rhodium(I), $[Rh_2(\mu\text{-}X)(CO)_2(Ph_2ECH_2EPh_2)_2]^+$ (X = Cl, Br; E = P, As) and iridium(I), $[Ir_2Cl(CO)_3(Ph_2PCH_2PPh_2)_2]$, are each active catalysts for the hydrogenation of alkynes to alkenes, and alkenes to alkanes. Neutral complexes with pseudohalide ligands have also been investigated but only the cyano-complex $[Rh_2(CN)_2(CO)_2(Ph_2PCH_2PPh_2)_2]$, and the arsine analog, are of significant catalytic activity. Only those complexes which reversibly form bridged complexes with ligands such as CO are also catalytically active.

Similar complexes with dithioether ligands are not efficient catalysts under the conditions tested.

ALAN R. SANGER. Can. J. Chem. **60**, 1363 (1982).

Les complexes cationiques binucléaires de rhodium(I), $[Rh_2(\mu\text{-}X)(CO)_2(Ph_2ECH_2EPh_2)_2]^+$ (X = Cl, Br; E = P, As), et d'iridium(I), $[Ir_2Cl(CO)_3(Ph_2PCH_2PPh_2)_2]^+$, en solutions dans le méthanol, sont des catalyseurs actifs d'hydrogénation des alcynes en alcènes et d'alcènes en alcanes. On a également étudié les complexes neutres ayant des ligands pseudohalogénés, mais seuls les complexes du type cyano $[Rh_2(CN)_2(CO)_2(Ph_2PCH_2PPh_2)_2]$ et leurs analogues du type arsine ont une activité catalytique significative. Seuls les complexes qui forment de manière réversible des complexes liés par un pont avec des ligands, tels le CO, sont également des catalyseurs actifs.

Les complexes semblables avec les ligands dithioéthers ne sont pas des catalyseurs efficaces dans les conditions utilisées.

[Traduit par le journal]

## Introduction

The first dinuclear rhodium complex of the geometry designated "A-frame" (**1**) $[Rh_2(\mu\text{-}S)(CO)_2(dpm)_2]$ (dpm is $Ph_2PCH_2PPh_2$ and dam is $Ph_2AsCH_2AsPh_2$) was described in 1977 (1). The synthesis and structure of related complexes of rhodium or iridium has since received much attention (2–16). For complexes of rhodium(I), several instances of co-ordination of two-electron donor ligands (L; e.g. CO, $SO_2$) at the site bridging the metal centers (**2**) have been reported (2, 3, 6, 9, 12–16). The complex cation, $[Rh_2(\mu\text{-}Cl)(CO)_2(dpm)_2]^+$, forms a 1:1 labile, symmetrical (ir, $^{31}P$ nmr) complex with diphenylacetylene (6),[2] and similar neutral complexes have also recently been described (11). Co-ordination of an alkyne at the bridging site (**2**; L = alkyne) is accompanied by lengthening of the carbon–carbon bond such that the product is accurately described as a *cis*-dimetallated alkenyl complex (11). No complex in which an alkene is co-ordinated at either a bridging or terminal site of an A-frame complex has yet been described.

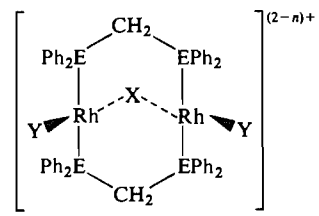


**1** (E = P or As; X is an anionic ligand of formal charge $n-$; Y is a neutral two-electron donor ligand, usually CO)

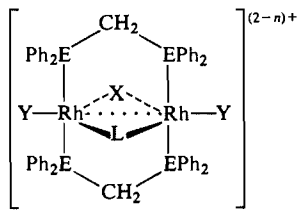


**2**

The A-frame structure, with the proximity of the two metal centres, has strong potential for dinuclear activation of unsaturated substrates. However, the complex $[Rh_2(\mu\text{-}S)(CO)_2(dpm)_2]$ has been shown to have low activity for the hydrogenation of ethylene (13). Herein I report that those cationic or neutral complexes of rhodium (or iridium) which form carbonyl-bridged complexes (**2**, L = CO) are also effective for the hydrogenation of alkynes and

[1]Revision received February 12, 1982.

[2]This system has been reinvestigated elsewhere (M. Cowie, private communication) and in this laboratory. The differences in spectroscopic parameters between solutions of the cation alone and with diphenylacetylene are now considered to be due to differences in conditions. A cationic complex containing bridging $CH_3OCOCCCO_2CH_3$ has been well characterized (18).

0008-4042/82/111363-05$01.00/0

©1982 National Research Council of Canada/Conseil national de recherches du Canada

Can. J. Chem. Downloaded from www.nrcresearchpress.com by 210.87.254.6 on 09/06/12
For personal use only.

Can. J. Chem. Downloaded from www.nrcresearchpress.com by 210.87.254.6 on 09/06/12
For personal use only.

alkenes. One system has also been found to be active for the water–gas shift reaction (12).

## Experimental

Complexes tested for hydrogenation activity were prepared as described in refs. 6 and 15. Catalyst solutions were prepared by stirring (30 min) a solution or suspension (cyanato or thiocyanato complexes) of the complex to be tested (0.02 mmol) in methanol (50 $cm^3$) at 25 ± 1°C under an atmosphere of oxygen-free hydrogen at a total pressure of 1 atm. Subsequently, the substrate (0.100–0.500 $cm^3$) was injected into the catalyst mixture. The stability of successful catalysts was such that injection of successive aliquots of substrate was possible. The composition of the reaction mixture was monitored at frequent intervals (10–30 min), and samples were analyzed by gas chromatography: Hewlett-Packard model 5830A, 10′ × 0.125″ od column packed with Carbowax 20M (25%) on Chromosorb W (60–80 mesh, acid-washed), injection port temperature 250°C. At regular intervals standard solutions were injected to calibrate, and to confirm that no catalysis occurred within the injection port or on the column.

## Results

At low to intermediate concentrations the catalytic activity of a methanol solution of $[Rh_2Cl(CO)_2(dpm)_2]BPh_4$ is similar to that of the $[RhCl_2(CO)_2]^-$ salt, as is appropriate for a fully dissociated complex of which the cation is the catalytically active species. Interactions of the cation with $BPh_4^-$ (17) may therefore be not considered. The structures of complexes in solutions of intermediate concentration have been confirmed by ir and (E = P) $^{31}P$ nmr spectroscopy (6, 15). At higher concentrations the activity of solutions varies in a non-linear manner. The reasons for this phenomenon are not yet known.

The complexes examined were more soluble in acetone than in methanol, but solutions in acetone were less active. Attempts to recover starting materials gave complexes in which acetone was strongly retained (6, 15). These results suggest that acetone is strongly co-ordinated to rhodium, thereby reducing the ability of the complex to co-ordinate and activate an alkene or alkyne.

For the above reasons methanol solutions of intermediate concentration (ca. $0.4 \times 10^{-3}$ *M*) of the various complexes have been tested. The rates of hydrogenation of either phenylacetylene to styrene, or of 1-hexene to hexane, using various complexes as catalysts, are listed in Table 1. Styrene is subsequently hydrogenated to ethylbenzene (Figs. 1, 2), and a variety of other alkynes and alkenes have also been successfully hydrogenated using $[Rh_2Cl(CO)_2(dpm)_2]^+$ or the arsine analogue as catalyst (Table 2). In each case multiple successive aliquots of 1-hexene or phenylacetylene were successfully hydrogenated (see Fig. 1).

Hydrogenation of an alkyne catalyzed by $[Rh_2X(CO)_2(dpm)_2]^+$ (X = Cl or Br) yields successively the corresponding *cis*-alkene and alkane (Fig. 1). This indicates that, while alkyne is present in solution, displacement of the product alkene from the co-ordination sphere of the catalyst by alkyne is more rapid than hydrogenation of the alkene. Hydrogenation of phenylacetylene or 1-phenylpropyne, catalyzed by the arsine complexes, $[Rh_2X(CO)_2(dam)_2]^+$, is also rapid, but subsequent hydrogenation of product styrene or *cis*-1-

TABLE 1. Hydrogenation catalytic activity of A-frame complexes

| Catalyst[a] | Concentration (× $10^{-3}$ *M*) | Rate[b] |
|---|---|---|
| *For 1-hexene → n-hexane* | | |
| $[Rh_2Cl(CO)_2(dpm)_2]^+$ | 0.40 | 2.3 |
| $[Rh_2Cl(CO)_2(dam)_2]^+$ | 0.40 | 3.4 |
| $[Rh_2Br(CO)_2(dpm)_2]^+$ | 0.40 | 1.1 |
| $[Rh_2Br(CO)_2(dam)_2]^+$ | 0.40 | 0.17 |
| *For phenylacetylene → styrene* | | |
| $[Rh_2Cl(CO)_2(dpm)_2]^+$ | 0.39 | 0.31 |
| $[Rh_2Cl(CO)_2(dam)_2]^+$ | 0.40 | 0.20 |
| $[Rh_2Br(CO)_2(dpm)_2]^+$ | 0.40 | 0.23 |
| $[Rh_2Br(CO)_2(dam)_2]^+$ | 0.42 | 0.45 |
| $[Rh_2(CN)_2(CO)_4(dpm)_2]$ | 0.40 | 3.0 |
| $[Rh_2(CN)_2(CO)_4(dam)_2]$ | 0.40 | 0.31 |
| $[Rh_2(NCO)_2(CO)_2(dpm)_2]$ | 0.40 | 0.03 |
| $[Rh_2(NCO)_2(CO)_2(dam)_2]$ | 0.41 | 0.0001 |
| $[Rh_2(NCS)_2(CO)_4(dpm)_2]$ | 0.38 | 0.002 |
| $[Rh_2(NCS)_2(CO)_4(dam)_2]$ | 0.39 | 0 |
| $[Rh_2Cl(N_3)(CO)_2(dpm)_2]$ | 0.42 | 0.12 |

[a]The formulation of the catalytically active species may differ from that of the "catalyst" originally dissolved in methanol under an atmosphere of dihydrogen.
[b]Moles of substrate hydrogenated per minute per mole of catalyst, at 25°C (steady state). In some cases an induction period was observed on injection of the first aliquot of the substrate to be hydrogenated.

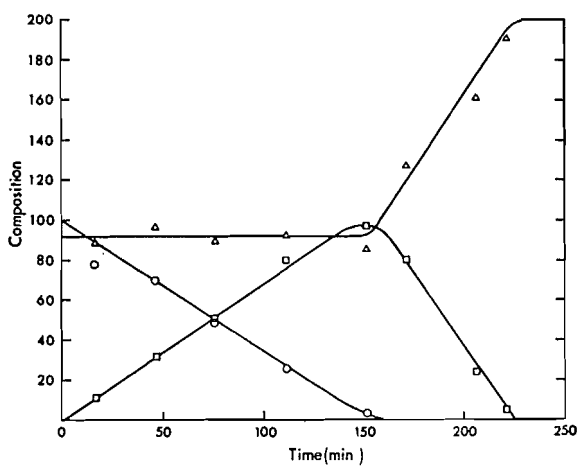


FIG. 1. Hydrogenation of the second aliquot of phenylacetylene catalyzed by a solution of $[Rh_2Br(CO)_3(dpm)_2]BPh_4$ ($0.70 \times 10^{-3}$ *M*) in methanol. The ethylbenzene present at time = 0 is the product from hydrogenation of the first aliquot of phenylacetylene (⊙ = phenylacetylene, ⊡ = styrene, △ = ethylbenzene).

Can. J. Chem. Downloaded from www.nrcresearchpress.com by 210.87.254.6 on 09/06/12
For personal use only.

TABLE 2. Alkenes and alkynes hydrogenated[a]

| Reagent | Initial product | Subsequent products |
|---|---|---|
| 1-Pentene | *n*-Pentane | |
| 1-Hexene | *n*-Hexane | |
| 2-Hexene | *n*-Hexane | |
| *c*-Hexene | *c*-Hexane | |
| Vinyl cyclohexane | Ethylcyclohexane | |
| Styrene | Ethylbenzene | |
| *cis*-Stilbene | 1,2-Diphenylethane | |
| *trans*-Stilbene | 1,2-Diphenylethane | |
| Phenylacetylene | Styrene | Ethylbenzene |
| 1-Phenylpropyne | *cis*-1-Phenylpropene | 1-Phenylpropane |
| 1-Phenylpropyne[b,c] | *cis*-1-Phenylpropene | *trans*-1-Phenylpropene, 1-phenylpropane |
| Diphenylacetylene | *cis*-Stilbene | 1,2-Diphenylethane |

[a]Catalyst: $[Rh(\mu\text{-}Cl)(CO)_2(dpm)_2]^+$ ($2.0 \times 10^{-3} M$) in methanol (50 cm³), at 22°C and 1 atm total pressure.
[b]Reference 18.
[c]Catalyst: $[Rh_2(\mu\text{-}Cl)(CO)_2(dam)_2]^+$; for this catalyst hydrogenation of the alkene was very slow, and concurrent *cis* to *trans* isomerization occurred.

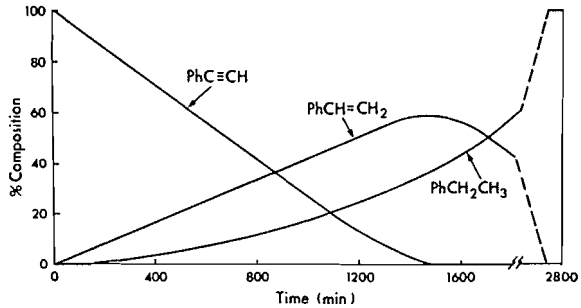


FIG. 2. Hydrogenation of phenylacetylene catalyzed by a solution of $[Ir_2Cl(CO)_4(dpm)_2][IrCl_2(CO)_2]$ ($0.27 \times 10^{-3} M$) in methanol.

phenylpropene is slow. Hydrogenation of *cis*-1-phenylpropene is so slow that, in this case, isomerization to the *trans* isomer occurs concurrently at a comparable rate (18).

Styrene and ethylbenzene are formed concurrently during hydrogenation of phenylacetylene catalysed by $[Ir_2Cl(CO)_2(dpm)_2]^+$ (6), as shown in Fig. 2. No hydrido-complex of the rhodium complex (1) has been isolated or detected by ir or nmr spectroscopy (6). However, $^{31}P$ nmr spectra of solutions of the iridium complex $[Ir_2Cl(CO)_2(dpm)_2][IrCl_2(CO)_2]$ under an atmosphere of hydrogen indicate formation of a novel, unidentified complex.

## Discussion

The mechanism of addition of CO to the cationic A-frame complex $[Rh_2(\mu\text{-}Cl)(CO)_2(dpm)_2]^+$ (1) has been shown to occur initially by attack at a terminal site, followed by rearrangement to form a carbonyl-bridged A-frame complex, (2) (reaction [1]) (6).

[1]

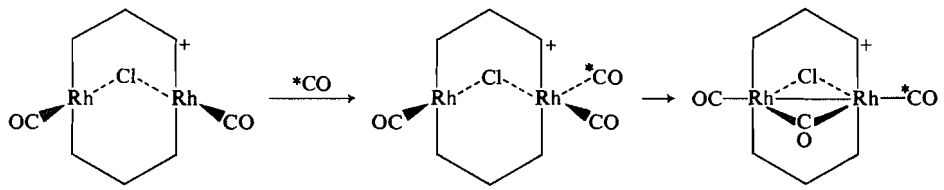


1 2

The cyano complex, $[Rh_2(CN)_2(CO)_4(dpm)_2]$, reversibly dissociates two carbonyl ligands to form successively a carbonyl-bridged and a dicarbonyl complex (reaction [2]) (15*a*).

[2]

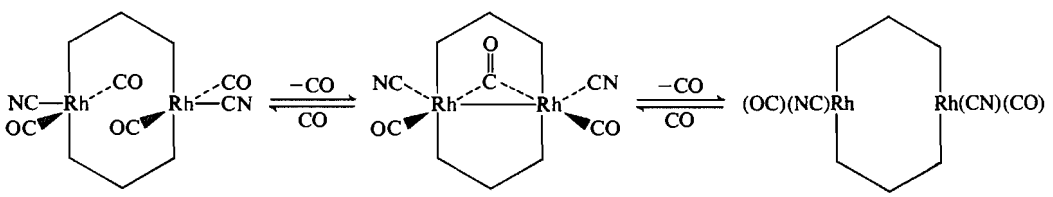


3 4 5

TABLE 3. Formation of carbon monoxide bridged complexes (ref. 15*a*)

| Complex | Product |
|---|---|
| *(i) Association of carbon monoxide* | |
| $[Rh_2(\mu\text{-}Cl)(CO)_2(dpm)_2]^+$ | $[Rh_2(\mu\text{-}Cl)(CO)_2(\mu\text{-}CO)(dpm)_2]^+$ |
| $[Rh_2(\mu\text{-}Cl)(CO)_2(dam)_2]^+$ | $[Rh_2(\mu\text{-}Cl)(CO)_2(\mu\text{-}CO)(dam)_2]^+$ |
| $[Rh_2(\mu\text{-}Br)(CO)_2(dpm)_2]^+$ | $[Rh_2(\mu\text{-}Br)(CO)_2(\mu\text{-}CO)(dpm)_2]^+$ |
| $[Rh_2(\mu\text{-}Br)(CO)_2(dpm)_2]^+$ | $[Rh_2(\mu\text{-}Br)(CO)_2(\mu\text{-}CO)(dam)_2]^+$ |
| $[Rh_2(CN)_2(CO)_2(dpm)_2]$ | $[Rh_2(CN)_2(CO)_2(\mu\text{-}CO)(dpm)_2]$ |
| $[Rh_2(CN)_2(CO)_2(dam)_2]$ | $[Rh_2(CN)_2(CO)_2(\mu\text{-}CO)(dam)_2]$ |
| $[Rh_2(NCO)_2(CO)_2(dpm)_2]$ | None detected |
| $[Rh_2(NCO)_2(CO)_2(dam)_2]$ | None detected |
| $[Rh_2Cl(N_3)(CO)_2(dpm)_2]$ | $[Rh_2(\mu\text{-}N_3)(CO)_2(\mu\text{-}CO)(dpm)_2]^+$[a] |
| *(ii) Dissociation of carbon monoxide* | |
| $[Rh_2(CN)_2(CO)_4(dpm)_2]$ | $[Rh_2(CN)_2(CO)_2(\mu\text{-}CO)(dpm)_2]$ |
| $[Rh_2(CN)_2(CO)_4(dam)_2]$ | $[Rh_2(CN)_2(CO)_2(\mu\text{-}CO)(dam)_2]$ |
| $[Rh_2(NCS)_2(CO)_4(dpm)_2]$ | None detected |
| $[Rh_2(NCS)_2(CO)_4(dam)_2]$ | None detected |

[a]This product is present in low equilibrium amounts in solution; the solid product has not yet been isolated.

A series of reversible reactions of dinuclear complexes with CO is shown in Table 3. Similar bridged complexes are obtained by reaction of $SO_2$ or other two-electron donor ligands (2, 3, 12–16), but it should be noted that attack by $SO_2$ occurs directly at the bridging site (9). Neutral dicarbonyl complexes have structure **5**, and tetracarbonyl complexes have structure **3** (15*a*). It is noteworthy that structure **4** is obtained only when the anionic ligand is cyanide (15*a*).

In solution under an atmosphere of CO the neutral complex $[Rh_2Cl(N_3)(CO)_2(dpm)_2]$ is in equilibrium with lesser amounts of the cationic complex $[Rh_2(\mu\text{-}N_3)(CO)_2(\mu\text{-}CO)(dpm)_2]Cl$ (15*a*). The only complexes which reversibly associate or dissociate CO to form carbonyl-bridged complexes are therefore the chloro-, bromo-, cyano-, and, weakly, azido-complexes (Table 3), and it is precisely these complexes which are highly active for the hydrogenation of alkynes or alkenes (Table 1).

In contrast to these observations, and in a direct parallel to the behaviour of the cyanato or thiocyanato complexes, $[Rh_2(\mu\text{-}S)(CO)_2(dpm)_2]$ does not readily associate CO at the bridging site (1), and is also a poor catalyst for the hydrogenation of ethylene (13). The analogous iridium complex reacts with CO and is also an effective hydrogenation catalyst (14). The correlation of the catalytic activity of A-frame complexes with the ability to form carbonyl-bridged complexes suggests that the catalytic intermediate may also be a carbonyl-bridged complex, formed by attack of the substrate at a terminal site. However, elucidation of the precise mechanism of hydrogenation catalyzed by the above complexes awaits further kinetic studies. Formation of a carbonyl-bridged complex would explain why complexes with dpm or dam ligands are so active, but related diphosphine-bridged complexes of ligands $Ph_2P(CH_2)_nPPh_2$ ($n \geq 3$) (19), which cannot form CO-bridged metal–metal bonded complexes, are less active. The reasons why the systems with terminal $NCO^-$ or $NCS^-$, or bridging sulphide ligands do not readily form carbonyl-bridged complexes are not yet understood.

A similar system to the above is that of the complexes of rhodium(I) with dithioethers $PhS(CH_2)_mSPh$ ($m$ = 1–6), especially $[Rh_2Cl_2(\mu\text{-}CO)(PhSCH_2SPh)_2]$ (20). However, they are not efficient catalysts for the following reasons. The activity of the systems is moderate compared to that of phosphine systems, the complexes are not as air- or water-stable as the phosphine or arsine complexes, and they are readily reduced to rhodium(0) under hydrogenation conditions (20).

**Acknowledgements**

I wish to thank L. R. Schallig for assistance with this project, Drs. M. Cowie (University of Alberta), X. Guo (Dalian Institute of Chemical Physics, Peoples' Republic of China), and A. T. Blades of this laboratory for helpful comments, and Dr. J. T. Mague (Tulane University) for communication of results prior to publication (18).

1. C. P. KUBIAK and R. EISENBERG. J. Am. Chem. Soc. **99**, 6129 (1977).
2. M. COWIE, J. T. MAGUE, and A. R. SANGER. J. Am. Chem. Soc. **100**, 3628 (1978).
3. M. COWIE, S. K. DWIGHT, and A. R. SANGER. Inorg. Chim. Acta, **31**, L407 (1978).
4. L. S. BENNER and A. L. BALCH. J. Am. Chem. Soc. **100**, 6099 (1978).

Can. J. Chem. Downloaded from www.nrcresearchpress.com by 210.87.254.6 on 09/06/12
For personal use only.

5. A. D. RATTRAY and D. SUTTON. Inorg. Chim. Acta, **27**, L85 (1978).
6. J. T. MAGUE and A. R. SANGER. Inorg. Chem. **18**, 2060 (1979).
7. M. COWIE and S. K. DWIGHT. Inorg. Chem. **18**, 2700 (1979).
8. A. L. BALCH, L. S. BENNER, and M. M. OLMSTEAD. Inorg. Chem. **18**, 2996 (1979).
9. M. COWIE and S. K. DWIGHT. Inorg. Chem. **19**, 209 (1980).
10. M. COWIE and S. K. DWIGHT. Inorg. Chem. **19**, 2500 (1980); **19**, 2508 (1980).
11. M. COWIE and T. G. SOUTHERN. J. Organomet. Chem. **193**, C46 (1980).
12. C. P. KUBIAK and R. EISENBERG. J. Am. Chem. Soc. **102**, 3637 (1980).
13. C. P. KUBIAK and R. EISENBERG. Inorg. Chem. **19**, 2726 (1980).
14. C. P. KUBIAK, C. WOODCOCK, and R. EISENBERG. Inorg. Chem. **19**, 2733 (1980).
15. (*a*) A. R. SANGER. J. Chem. Soc. Dalton 228 (1981); (*b*) A. R. Sanger. Unpublished results.
16. M. M. OLMSTEAD, C. H. LINDSAY, L. S. BENNER and A. L. BALCH. J. Organomet. Chem. **179**, 289 (1979).
17. P. ALBANO, M. ARESTA, and M. MANASERRO. Inorg. Chem. **19**, 1069 (1980).
18. J. T. MAGUE. Private communication.
19. A. R. SANGER. J. Chem. Soc. Dalton 120 (1977).
20. A. R. SANGER, C. G. LOBE, and J. R. WEINER-FEDORAK. Inorg. Chim. Acta, **53**, L123 (1981).

Can. J. Chem. Downloaded from www.nrcresearchpress.com by 210.87.254.6 on 09/06/12
For personal use only.

# Nouveaux hétéropolyanions mixtes contenant le plomb(II)

ANNA SCHOUTEN ET BERNARD CROS

*Laboratoire de Chimie des Matériaux, École Normale Supérieure, Takaddoum, B.P. 5118, Rabat, Maroc*

Reçu le 2 décembre 1981

ANNA SCHOUTEN et BERNARD CROS. Can. J. Chem. **60**, 1368 (1982).

Des hétéropolyanions mixtes nouveaux de formules $XPb(II)W_{11}O_{39}^{m-}$ (X = Si, Ge, B, Ga), $XPb(II)W_{11}O_{40}^{7-}$ (X = As(V), P(V)) et $X_2'Pb(II)W_{17}O_{61}^{8-}$ (X' = As(V), P(V)) sont préparés. Les résultats des études conductimétriques, polarographiques, spectrophotométriques et cristallographiques sont rapportés. La structure particulière de ces hétéropolyanions mixtes, liée au rayon important du plomb(II) est discutée. La formation de nouveaux types de polyanions de formule symbolique $Pb(XW_{11})_2$ a été observée avec X = Si et Ge.

ANNA SCHOUTEN and BERNARD CROS. Can. J. Chem. **60**, 1368 (1982).

New mixed heteropolyanions with formulae $XPb(II)W_{11}O_{39}^{m-}$ (X = Si, Ge, B, Ga), $XPb(II)W_{11}O_{40}^{7-}$ (X = As(V), P(V)) and $X_2'Pb(II)W_{17}O_{61}^{8-}$ (X' = As(V), P(V)) were prepared. The results of conductimetric, polarographic, spectrophotometric, and crystallographic studies are reported. The peculiar structure of these mixed heteropolyanions due to the large radius of Pb(II) is discussed. The formation of new types of polyanions with the symbolic formula $Pb(XW_{11})_2$ has been noted with X = Si and Ge.

## Introduction

Dans le cadre de l'étude de la complexation des cations d'éléments contenant des électrons *p* dans la couche de valence par les hétéropolyanions[1] tungstiques lacunaires, nous avons décrit (1) la formation d'hpa mixtes de formules $XZW_{11}O_{39}(OH)^{m-}$ (X = Si, Ge, B, As(V), Ga, Co(II), Zn; Z = Ge(IV), Sn(IV)) et $X_2'ZW_{17}O_{61}(OH)^{7-}$ (X' = As(V), P(V); Z = Ge(IV), Sn(IV)). Dans cette étude, le plomb(II) se singularise par son rayon trés important, à priori incompatible avec la dimension du site offert dans la structure lacunaire des hpa $XW_{11}$ ou $X_2'W_{17}$[2] et en tout cas nettement supérieur au rayon du tungstène(VI) occupant les sites homologues. Si le germanium(IV) et l'étain(IV) avaient déjà été utilisés pour la préparation d'hpa mixtes, essentiellement pour permettre de greffer des coordinats organiques (2–4), en revanche l'étude systématique de la complexation du plomb par les hpa lacunaires constitue un travail nouveau.

Nous rapportons ici la préparation d'hpa mixtes $XPbW_{11}$ et $X_2'PbW_{17}$.

## Préparations et analyses

*Produits de départ*

Les hpa lacunaires $XW_{11}$ et $X_2'W_{17}$ sur lesquels Pb(II) est ajouté sont préparés selon les méthodes décrites par Zonnevijlle (5).

*Méthode générale de préparation*

La quantité calculée de nitrate de plomb en solution est ajoutée à une suspension du sel de potassium d'hpa $XW_{11}$ ou $X_2'W_{17}$ (de concentration de l'ordre de 0,1 *M*) préalablement chauffée à 60°C (40°C pour $BW_{11}$). Le sel en suspension se dissout rapidement dès l'addition de la moitié de la solution de plomb. Le pH final dépend du produit préparé: il est de 6,5 à 6,7 pour $GaPbW_{11}$, de 6 à 6,5 pour $SiPbW_{11}$, $GePbW_{11}$, $P_2PbW_{17}$ et $As_2PbW_{17}$, de 5,5 à 6 pour $BPbW_{11}$ et voisin de 5 pour $PPbW_{11}$ et $AsPbW_{11}$. Les hpa mixtes cristallisent à la température ambiante sous forme d'aiguilles incolores. L'addition de nitrate de potassium ou d'une solution d'acétate de potassium dans le méthanol permet d'atteindre un rendement de 90%.

L'hpa d'arsenic $AsPbW_{11}$ est préparé à partir d'une solution sodique de l'hpa lacunaire et le sel de potassium est précipité par addition d'une solution d'acétate de potassium dans le méthanol.

Tous les produits obtenus sont incolores et assez solubles dans l'eau. Comme les autres hpa mixtes contenant un élément Z(II), les hpa contenant le plomb ne sont stables que dans un étroit domaine de pH et les acides correspondants n'existent pas.

La formation du composé de stoechiométrie $Z/XW_{11}$ (ou $Z/X_2'W_{17}$) = 1/1 est mise en évidence par l'évolution de la conductivité de la solution au cours de la réaction d'addition (Fig. 1).

*Analyses chimiques*

Les éléments K, W, Ga sont dosés par les méthodes classiques (gravimétrie à la 8-hydroxyquinoléine pour W et Ga; gravimétrie au tétraphénylborate de sodium pour K). Le pourcentage en eau de cristallisation est déterminé par calcination à 600°C. Le plomb est dosé par volumétrie à l'EDTA en milieu basique (à pH 10, dosage en retour d'un excès d'EDTA par une solution de chlorure de zinc); la présence d'un autre élément métallique (gallium) nécessite la séparation préalable du plomb par fixation sur résine acide fort (Amberlite IR-120).

*Autres méthodes d'analyse*

L'appareillage utilisé pour les mesures spectrophotométriques, potentiométriques, conductimétriques, polarographiques et cristallographiques (sur poudre et sur monocristal) a été décrit par ailleurs (6).

## Résultats

### *Résultats des analyses et formulations*

Les analyses chimiques conduisent aux formules

[1]Par la suite l'abréviation "hpa" est utilisée pour hétéropolyanion.

[2]Dans la rédaction, la formule de composition symbolique simplifiée est souvent utilisée; par exemple $SiW_{11}$ et $P_2W_{17}$ pour $SiW_{11}O_{39}^{8-}$ et $P_2W_{17}O_{61}^{10-}$ respectivement.

0008-4042/82/111368-06$01.00/0

©1982 National Research Council of Canada/Conseil national de recherches du Canada

Can. J. Chem. Downloaded from www.nrcresearchpress.com by 210.87.254.105 on 09/06/12
For personal use only.

TABLEAU 1. Résultats des analyses

| | % K | | % W | | % Pb | | $H_2O$ |
|---|---|---|---|---|---|---|---|
| | calc. | exp. | calc. | exp. | calc. | exp. | total |
| $K_6SiPbW_{11}O_{39}$ | 7,16 | 7,26 | 61,69 | 61,30 | 6,32 | 6,12 | 9 |
| $K_6GePbW_{11}O_{39}$ | 7,02 | 7,00 | 60,53 | 60,23 | 6,20 | 6,03 | 10 |
| $K_8P_2PbW_{17}O_{61}$ | 6,20 | 6,47 | 61,98 | 62,37 | 4,11 | 3,97 | 20 |
| $K_8As_2PbW_{17}O_{61}$ | 6,10 | 6,48 | 60,91 | 61,19 | 4,04 | 3,92 | 20 |
| $K_7AsPbW_{11}O_{40}$ | 7,85 | 7,70 | 57,98 | 58,52 | 5,94 | 6,20 | 15 |
| $K_7PPbW_{11}O_{40}$ | 8,02 | 8,09 | 59,25 | 58,95 | 6,07 | 5,95 | 13 |
| $K_7BPbW_{11}O_{39}$ | 8,17 | 8,13 | 60,33 | 60,15 | 6,18 | 6,12 | 12 |
| $K_7GaPbW_{11}O_{39}$ | 7,85 | 7,60 | 58,03 | 57,80 | 5,95 | 6,06 | 16 |
| | (% Ga calc. 2,00; exp. 2,00) | | | | | | |

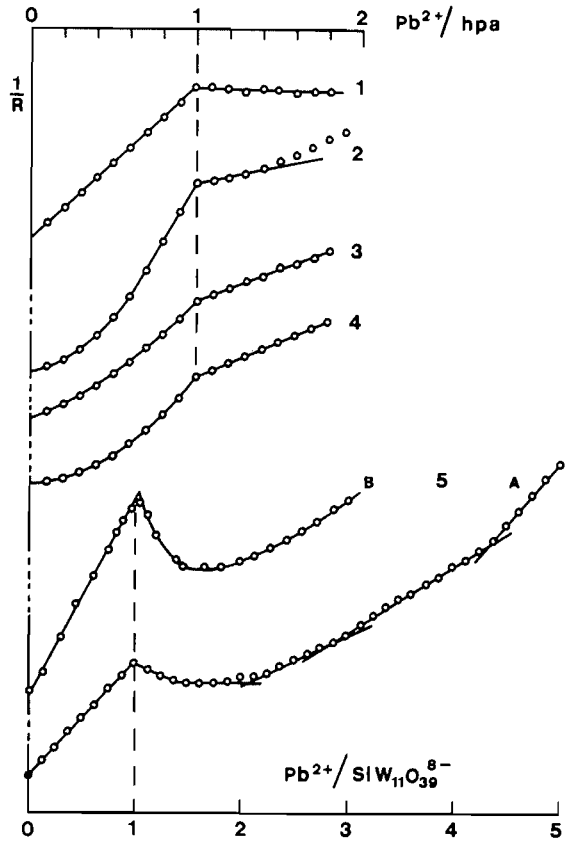


FIG. 1. Evolution de la conductivité des solutions en fonction du rapport des concentrations Pb(II)/$XW_{11}$ (ou Pb(II)/$X_2'W_{17}$): 1, $Pb/GeW_{11}O_{39}^{8-}$; 2, $Pb/P_2W_{17}O_{61}^{10-}$; 3, $Pb/As_2W_{17}O_{61}^{10-}$; 4, $Pb/PW_{11}O_{39}^{7-}$; 5, $Pb/SiW_{11}O_{39}^{8-}$ (A pour $c = 2{,}8 \times 10^{-3}$ *M*; B pour $c = 11{,}7 \times 10^{-3}$ *M*). Les valeurs de $1/R$ sont portées dans une échelle arbitraire.

rassemblées dans le tableau 1. L'hétéroélément n'a été dosé que dans le complexe $GaPbW_{11}$. La formulation proposée pour les sels potassiques des hpa contenant le plomb est différente de celle des sels d'hpa connus contenant d'autres éléments Z(II) pour lesquels la formule fait apparaître une molécule d'eau qui complète la coordination octaédrique de l'élément bivalent substitué. La discussion justifiera ces formules qui excluent une coordination octaèdrique du plomb. Les sels des hpa $AsPbW_{11}$ et $PPbW_{11}$ font exception, la charge déterminée pour les anions conduisant à une formule compatible avec un environnement octaédrique d'atomes d'oxygène pour le plomb.

*Étude conductimétrique*

La réaction en solution du plomb(II) avec les différents hpa lacunaires a été suivie par conductimétrie et les résultats sont reportés sur la figure 1. Dans tous les cas un changement de pente fait apparaître nettement l'existence d'une espèce complexe pour le rapport [Pb(II)]/[hpa] = 1. Les courbes 5A et 5B représentent de façon plus complète les mesures de conductivité pour la réaction d'une solution de nitrate de plomb sur une solution sodique de $SiW_{11}$ à deux concentrations différentes. Dans les deux cas apparaît pour un rapport molaire voisin de 2 un trouble qui se transforme rapidement en précipité. La courbe B se limite à cette région, le précipité formé, très volumineux, gênant les mesures de conductivité. Il semble qu'au delà du rapport 1/1 la formation d'une association soit possible, telle que le nombre et la mobilité des espèces chargées diminue. Au delà du rapport 2, des portions rectilignes de la courbe de conductivité, correspondant à des valeurs croissantes, se coupent pour un rapport 3 et un peu au delà de 4 (courbe A). Si on admet que le complexe 1/1 se forme selon la réaction $SiW_{11}O_{39}^{8-} + Pb^{2+} \rightarrow SiPbW_{11}O_{39}^{6-}$, l'addition des trois autres ions $Pb^{2+}$ pourrait correspondre à la précipitation du sel de plomb de l'hpa $SiPbW_{11}O_{39}^{6-}$. Ces mesures n'excluent cependant pas la formation d'un polyanion contenant plus d'un atome de plomb. Les mesures polarographiques permettent de lever cette incertitude.

Can. J. Chem. Downloaded from www.nrcresearchpress.com by 210.87.254.105 on 09/06/12
For personal use only.

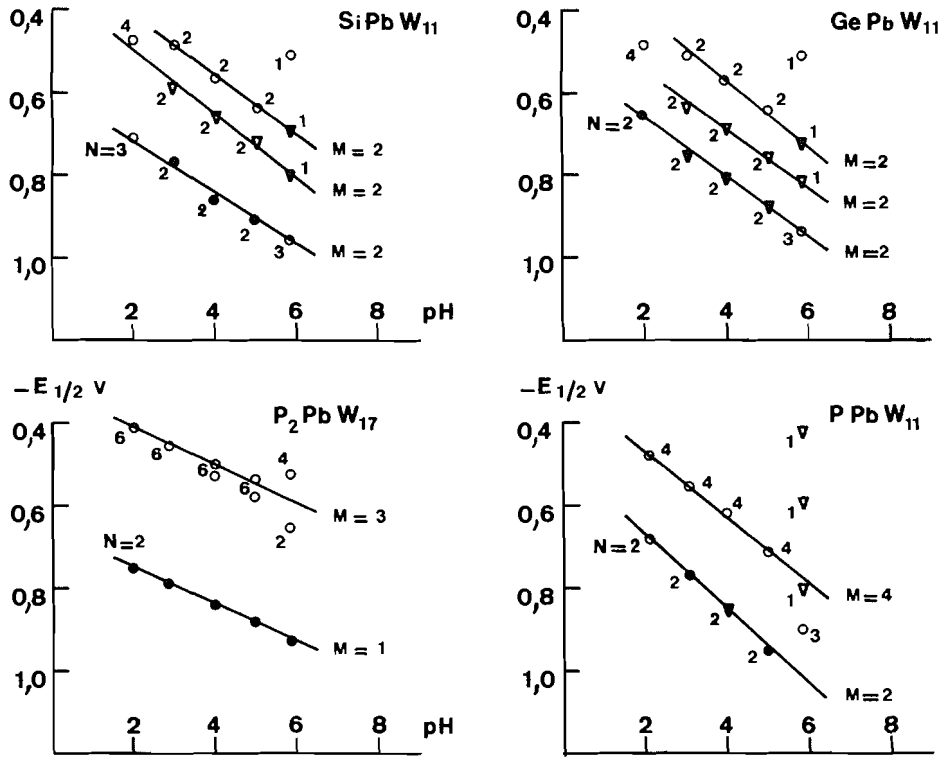


FIG. 2. Potentiel de demi-vague en fonction du pH des solutions d'hpa mixtes contenant le plomb(II). $c_{hpa} = 10^{-3}$ *M*; $c_{tampon} = 0{,}5$ *M*; $c_{NaNO_3} = 0{,}5$ *M*. *N* représente le nombre d'électrons intervenant dans la réaction de réduction; *M* représente le nombre de protons qui participent à la réaction de réduction. Les symboles indiquent: ▽ une réaction réversible; ▼ une réaction assez réversible; ● une réaction peu réversible; ○ une réaction irréversible.

*Étude polarographique*

L'étude est faite par polarographie sur cathode de mercure dans le domaine des potentiels négatifs (Fig. 2). Par rapport aux hpa lacunaires, il apparaît pour tous les polyanions substitués $XPbW_{11}$ et $X_2'PbW_{17}$ une vague de réduction supplémentaire à deux électrons pour un potentiel légèrement moins négatif. On trouve ensuite deux autres vagues, chacune à deux électrons, qui correspondent sensiblement à celles des hpa lacunaires $XW_{11}$ ou $X_2'W_{17}$. Toutes ces vagues sont dépendantes du pH et correspondent à un rapport *M* (nombre de protons fixés)/*N* (nombre d'électrons) égal à 1. Quel que soit le pH, cette première vague supplémentaire, liée à la présence du plomb, est extrêmement voisine de celle qui la suit. Dans certains cas elle est bien détectée à l'aide de la courbe dérivée (ainsi avec $SiPbW_{11}$), mais il est parfois impossible de la distinguer (avec $PPbW_{11}$ ou $P_2PbW_{11}$).

Une étude plus complète est menée avec des solutions de $SiW_{11}$ additionnées de quantités croissantes de Pb(II). La figure 3 présente les résultats obtenus pour des solutions tamponnées à pH 4,12. On a préalablement noté la position de la vague de réduction $Pb^{2+} \rightarrow Pb$ à ce pH ($E_{1/2} = -0{,}42$ V). Pour tous les rapports $[Pb(II)]/[SiW_{11}] < 1$, la vague du plomb cationique libre n'apparaît pas, ce qui confirme la formation de complexes. Par contre, pour un potentiel $E_{1/2} = -0{,}63$ V, apparaît une première vague dont la hauteur est proportionnelle à la quantité de plomb(II) ajouté et dont le potentiel de demi-vague reste inchangé lorsque les rapports varient de 0 à 1. Dès que la valeur de $[Pb(II)]/[SiW_{11}]$ devient supérieure à 1, la vague correspondant au plomb(II) libre ($E_{1/2} = -0{,}42$ V) réapparait, la suite du polarogramme ètant identique à celui de $SiPbW_{11}$. La première vague décelée dans le polarogramme de $SiPbW_{11}$ (vague supplémentaire par rapport aux hpa lacunaires) correspond à la réduction du plomb(II) dans le complexe, soit sa mise en liberté avec protonation de l'anion lacunaire: $SiPbW_{11}O_{39}^{6-} + 2e^- + 2H^+ \rightarrow Pb + H_2SiW_{11}O_{39}^{6-}$. La complexation du plomb entraîne une diminution du potentiel de demi-vague de la réaction de réduction du plomb(II).

*Existence d'autres hpa mixtes*

Les complexes $XPbW_{11}$ et $X_2'PbW_{17}$ correspondant au rapport [Pb(II)]/[hpa] = 1 sont nette-

Can. J. Chem. Downloaded from www.nrcresearchpress.com by 210.87.254.105 on 09/06/12
For personal use only.

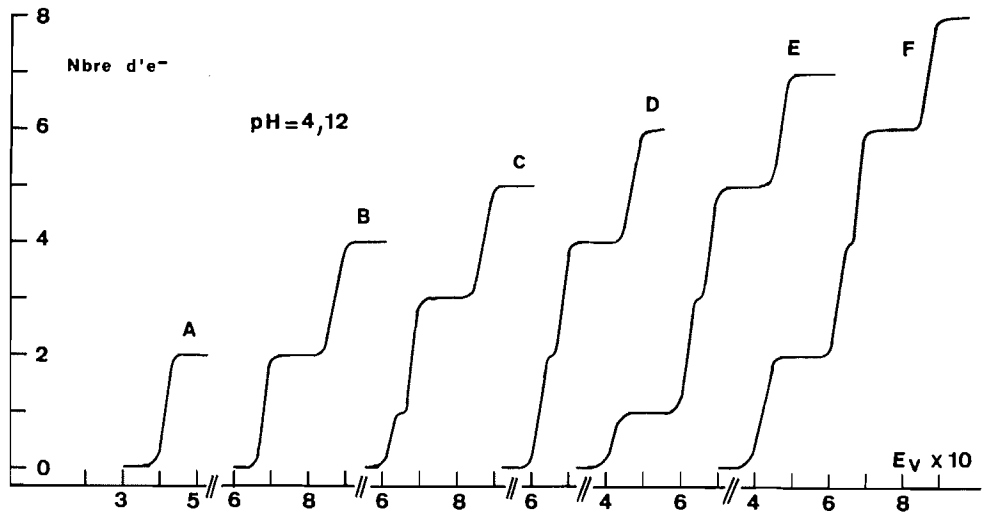


FIG. 3. Mise en évidence de la formation du complexe $SiPbW_{11}$ par étude polarographique de mélanges différents de solutions d'hpa $SiW_{11}$ et de plomb(II) ($c_{hpa} = 10^{-3}$ *M*). A, $Pb^{2+}$; B, $SiW_{11}$; C, $SiW_{11}$ + 0,5 $Pb^{2+}$; D, $SiW_{11}$ + $Pb^{2+}$; E, $SiW_{11}$ + 1,5 $Pb^{2+}$; F, $SiW_{11}$ + 2 $Pb^{2+}$.

ment mis en évidence, mais l'allure particulière des courbes de conductivité des solutions d'hpa lacunaires en présence de proportions différentes de plomb(II) amène à considérer l'éventualité de la formation de complexes pour d'autres rapports.

L'étude par diffraction des rayons X des phases en présence dans les produits de cristallisation de mélanges de différentes concentrations de nitrate de plomb et du sel de potassium de $SiW_{11}$ montre la formation d'une nouvelle phase, isolée pour le rapport [Pb]/[hpa] = 1/2, alors que l'étude conductimétrique ne l'avait pas mise en évidence. L'existence de ce nouveau type de complexe de plomb, observée avec X = Si et Ge, a été confirmée par le passage de sa solution sur résine échangeuse de cations (Amberlite IR-120) sous forme $K^+$. L'analyse de l'éluat montre que le plomb(II) n'est pas retenu sur l'échangeur.

La difficulté de l'étude de cette phase tient à sa très grande solubilité en milieu aqueux et à la fragilité des cristaux mis au contact de l'air. Ce complexe n'est pas mis en évidence par l'étude polarographique en raison de la faible concentration des solutions et du pH relativement bas. Lorsqu'on opère à pH plus élevé, la première vague à 1 $e^-/SiW_{11}$ se détache nettement des vagues tungstiques, ce qui est compatible avec l'existence de $Pb(SiW_{11})_2$.

Au cours de l'étude polarographique (Fig. 3), on n'observe, au delà de la valeur 1 du rapport [Pb(II)]/[$SiW_{11}$], l'apparition d'aucun autre complexe contrairement à ce que l'étude conductimétrique laissait supposer. Le précipité dont l'apparition correspondait à un changement de pente de la courbe enregistrant l'évolution de la conductivité est un sel de plomb (ou mixte de plomb et de potassium) de l'hpa $SiPbW_{11}$. Les cassures successives correspondent à la formation de sels de l'hpa $SiPbW_{11}$ qui diffèrent par le nombre de plombs cationiques par molécule. La faible solubilité des sels de plomb des hpa $XPbW_{11}$ nécessite des précautions pour la cristallisation des complexes mixtes contenant le plomb, habituellement isolés sous forme de sels de potassium. En effet les analyses montrent que, même pour la fraction qui cristallise la première, le sel obtenu est excédentaire en plomb et déficitaire en potassium par rapport à la composition théorique. La recristallisation après passage de la solution sur échangeur d'ions sous forme $K^+$ constitue une méthode de purification. La précipitation des hpa mixtes contenant le plomb sous forme de sels de cations de bases organiques fortes (guanidinium, ammonium tétrasubstitué) évite généralement les anomalies de composition rencontrées avec les sels de cations alcalins.

*Étude spectrophotométrique*

La figure 4 montre les spectres électroniques d'hpa mixtes contenant le plomb. Les bandes d'absorption sont entièrement dans l'uv. Ces spectres diffèrent très peu de ceux des hpa homologues lacunaires. Cette particularité des hpa mixtes contenant le plomb laisse prévoir que cet élément s'incorpore peu à la grappe polytungstique, son addition ne modifiant ainsi pas très sensiblement le système de bandes des hpa lacunaires. Ces résultats sont en accord avec la taille très importante du plomb(II) et la formulation qui attribue un environnement inhabituel à l'élément substitué.

Can. J. Chem. Downloaded from www.nrcresearchpress.com by 210.87.254.105 on 09/06/12
For personal use only.

Can. J. Chem. Downloaded from www.nrcresearchpress.com by 210.87.254.105 on 09/06/12
For personal use only.

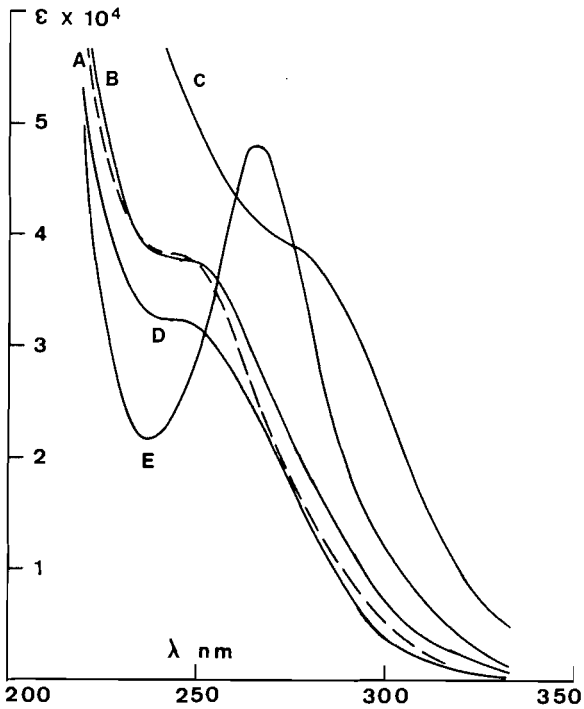


FIG. 4. Spectres d'absorption uv des sels potassiques des hpa mixtes contenant le plomb(II): A, $SiPbW_{11}O_{39}^{6-}$; B, $GePbW_{11}O_{39}^{6-}$; C, $P_2PbW_{17}O_{61}^{8-}$ à comparer à ceux de D, $SiW_{11}O_{39}^{8-}$; E, $SiW_{12}O_{40}^{4-}$.

Ils conduisent à l'étude cristallographique des sels d'hpa mixtes contenant le plomb.

*Étude cristallographique*

Les diagrammes de diffraction X des sels des hpa mixtes contenant le plomb ne correspondent pas aux systèmes cristallins attendus d'après le nombre de cations par polyanion et la nature des cations (7). Ainsi les sels potassiques n'appartiennent à aucun des types structuraux connus des sels alcalins des complexes $XZW_{11}$ et $X_2'ZW_{17}$. Les sels $K_6SiPbW_{11}O_{39},9H_2O$, $K_6GePbW_{11}O_{39},10H_2O$ et $K_7GaPbW_{11}O_{39},16H_2O$ cristallisent dans le système orthorhombique (groupe d'espace $P2_122$ ou $P2_12_12$ pour les deux premiers et *Pnma* pour le troisième). L'étude radiocristallographique d'un monocristal de $K_7GaPbW_{11}O_{39},16H_2O$ a permis de mettre en évidence les particularités structurales des hpa mixtes contenant le plomb. La description de la résolution structurale est reportée par ailleurs (8). Elle confirme l'originalité de l'environnement du plomb et l'absence de coordination octaédrique. L'atome de plomb n'est lié fortement qu'aux quatre atomes d'oxygène du site dans lequel il a été substitué, formant avec ceux-ci un arrangement

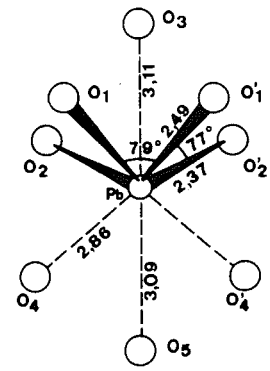


FIG. 5. Proche environnement de l'atome de plomb (les notations $O_n$ et $O_n'$ indiquent des atomes symétriques par rapport au plan dans lequel se situent les atomes Pb, $O_3$ et $O_5$; les atomes $O_4$ et $O_5$ appartiennent à un polyanion voisin).

pyramidal qui le déplace vers l'extérieur de la grappe polytungstique. Cette disposition du proche environnement du plomb est comparable à celle que l'on trouve dans l'oxyde PbO; les distances Pb—O sont du même ordre, 2,37 et 2,49 Å (Fig. 5). Une liaison avec le cinquième oxygène de la lacune parait exclue étant donné la distance de 3,11 Å. En revanche deux atomes d'oxygène d'un anion voisin sont distants de 2,86 Å. Les six atomes d'oxygène formant ainsi le proche environnement de l'atome de plomb constituent un arrangement comparable au polyèdre de coordination de Pb(II) dans $Pb_2O_3$ (9). En solution la coordination du plomb est à quatre atomes d'oxygène et la formulation $XPbW_{11}O_{39}^{p-}$ est justifiée.

## Discussion

Le plomb(II) se distingue dans les réactions de complexation avec les hpa lacunaires par une coordination inhabituelle pour un élément bivalent. Les éléments de taille plus petite (Co(II), Zn, etc.) substitués au tungstène dans les hpa sont entourés octaédriquement par 5 atomes d'oxygène, dont un fait partie de l'environnement tétraédrique de l'hétéroélément central X, et par une molécule d'eau (10). Cette coordination est interdite au plomb par sa taille et par l'effet stérique de la paire électronique libre: il est lié aux 4 atomes d'oxygène qui dans l'hpa lacunaire forment le site vacant, mais reste éloigné de l'oxygène appartenant au tétraèdre central. En phase solide il donne également des liaisons avec 2 atomes d'oxygène d'un hpa voisin, ce type d'hexacoordination se retrouvant dans $Pb_2O_3$. Il est probable qu'en solution des molécules d'eau prennent la place de l'hpa voisin dans le solide.

La phase cristalline trés soluble mise en évidence

pour le rapport $SiW_{11}/Pb = 2$ pourrait correspondre à un composé dans lequel le plomb serait lié à 2 hpa par les atomes d'oxygène formant le site lacunaire. De tels polyanions sont obtenus avec des éléments de grande taille comme les lanthanides et les actinides (11). Dans ces complexes l'hétéroélément substitué a une coordination de 8 par formation de liaisons avec les 4 atomes d'oxygène constituant la lacune des 2 hpa.

Au cours des réactions de complexation par les hpa lacunaires, le plomb joue donc un rôle intermédiaire entre, d'une part les éléments de taille inférieure, et d'autre part les lanthanides et actinides.

1. A. SCHOUTEN et B. CROS. Polyhedron. 1982. Sous presse.
2. W. H. KNOTH. J. Am. Chem. Soc. **101**, 759 (1979).
3. W. H. KNOTH. J. Am. Chem. Soc. **101**, 2211 (1979).
4. F. ZONNEVIJLLE et M. T. POPE. J. Am. Chem. Soc. **101**, 2731 (1979).
5. F. ZONNEVIJLLE. Thèse, Montpellier. 1976.
6. A. SCHOUTEN. Thèse, Montpellier. 1980.
7. C. TOURNE. C.R. Acad. Sci. Ser. C, **266**, 1363 (1968).
8. G. TOURNE, C. TOURNE et A. SCHOUTEN. Acta Crystallogr. Sous presse.
9. J. BOUVAIST et D. WEIGEL. Acta Crystallogr. Sect. A, **26**, 501 (1970).
10. V. E. SIMMONS et L. C. W. BAKER. J. Am. Chem. Soc. **81**, 4744 (1959).
11. G. TOURNE, C. TOURNE et M. C. BRIANSO. Acta Crystallogr. Sect. B, **36**, 2012 (1980)

Can. J. Chem. Downloaded from www.nrcresearchpress.com by 210.87.254.105 on 09/06/12
For personal use only.

Can. J. Chem. Downloaded from www.nrcresearchpress.com by 210.87.254.42 on 09/06/12
For personal use only.

COMMUNICATION

# Isolation and structure of combretastatin[1]

GEORGE R. PETTIT[2], GORDON M. CRAGG, DELBERT L. HERALD, JEAN M. SCHMIDT, AND PRASERT LOHAVANIJAYA

*Cancer Research Institute and Department of Chemistry, Arizona State University, Tempe, AZ 85287, U.S.A.*

Received February 15, 1982

GEORGE R. PETTIT, GORDON M. CRAGG, DELBERT L. HERALD, JEAN M. SCHMIDT, and PRASERT LOHAVANIJAYA. Can. J. Chem. **60**, 1374 (1982).

The South African tree *Combretum caffrum* has been shown to contain a constituent capable of significantly reversing astrocyte formation employing the National Cancer Institute's 9ASK system. The constituent responsible for astrocyte reversal was isolated and designated combretastatin (**1**). Structural elucidation was initiated employing spectral methods and completed by X-ray crystallographic analysis. By this means combretastatin was assigned structure **1**. Further biological evaluation and a total synthesis are now in progress.

GEORGE R. PETTIT, GORDON M. CRAGG, DELBERT L. HERALD, JEAN M. SCHMIDT et PRASERT LOHAVANIJAYA. Can. J. Chem. **60**, 1374 (1982).

On montre que l'arbre Sud Africain *Combretum caffrum* contient un constituant capable d'inverser de façon significative la formation de l'astrocyte lorsqu'on l'utilise dans le système 9ASK de l'Institut National du Cancer. On a isolé le constituant responsable de l'inversion de l'astrocyte et on l'a appelé la combrétastatine (**1**). On a entrepris des études structurales en utilisant des méthodes spectrales et l'analyse par cristallographie de rayons X. Sur cette base, on a attribué la structure **1** à la combrétastatine. On travaille actuellement à son évaluation biologique et sa synthèse totale.

[Traduit par le journal]

Malignant gliomas such as anaplastic and malignant astrocytomas and glioblastoma multiforme constitute some 43% of malignant brain tumors. The prognosis for such patients is very grave with a median survival time of six months (2). The need for effective and indeed curative cancer chemotherapeutic drugs for such neoplastic diseases is quite urgent (3). As one approach to this problem, the National Cancer Institute has instituted a biological evaluation system based on the change of immature AC cells (from a rat glioma) to mature differentiated astrocytes (for details of the experimental technique, see ref. 4). We are pleased to report the first isolation of a plant constituent (**1**) based on bioassay techniques using the new astrocyte reversal (9ASK) system. A summary of the isolation and structural elucidation of alcohol **1**, designated combretastatin, now follows.

Root bark of the South African tree *Combretum caffrum* (Eckl. Zeyh.) Kuntze[3] is used as a Zulu charm (5) for harming an enemy and some eight species of this family (Combretaceae) have found application in primitive treatment of cancer (6). We have found *C. caffrum* to afford a methylene chloride – methanol extract that caused astrocyte reversal in the 9ASK system. The methylene chloride – methanol extract obtained from 55 kg of branches, leaves, and fruit was diluted with water and the methylene chloride phase was partitioned employing the sequence 9:1 → 4:1 → 3:2 methanol–water with ligroin → carbon tetrachloride → methylene chloride. The methylene chloride fraction (159 g) was separated by a series of chromatographic steps utilizing Sephadex LH-20 → silica gel. Separation was guided by results of the 9ASK evaluation and led to 0.45 g of combretastatin (**1**) that caused substantial astrocyte reversal[4] and inhibition ($ED_{50}$ 0.011 μg/mL) of the murine P388 lymphocytic leukemia cell line (7).

A pure specimen of combretastatin recrystallized from acetone–hexane as needles melting at 130–131°C: $[\alpha]_D^{26}$ − 8.51°C (*c* 1.41, chloroform); $\lambda_{max}$

[1]Antineoplastic agents. 84. For contribution 83, see ref. 1.

[2]Author to whom correspondence may be addressed.

[3]Also known as *combretum salicifolium* E., yielded an extract significantly active against the P388 lymphocytic leukemia in the National Cancer Institute's collaborative program with the U.S. Department of Agriculture directed by Drs. John D. Douros, Matthew I. Suffness, and James A. Duke.

[4]The percent astrocyte reversal observed was 71–90% at dose levels of 100 to 1 μg/mL and 51–70% at 0.1 μg/mL with only 0–5% cytotoxicity being exhibited. According to NCI procedure a sample showing 51–90% astrocyte reversal with cytotoxicity not exceeding 50% is considered as active.

0008-4042/82/111374-03$01.00/0

©1982 National Research Council of Canada/Conseil national de recherches du Canada

Can. J. Chem. Downloaded from www.nrcresearchpress.com by 210.87.254.42 on 09/06/12
For personal use only.

($CH_3OH$) (log ε):212 (4.33), 228 (sh, 4.11), 279 (3.47), and 287 (sh, 3.36) nm; ir (KBr) $\nu_{max}$:3500, 3420, 1600, 1515, 1465, 1423, 1350, 1330, 1282, 1238, 1121, 1053, 1010, 978, 852, 824, 790, 768, 705, and 653 $cm^{-1}$; $^1H$ nmr (100 MHz, $CDCl_3$), δ: 2.12 (1H, br s, C-10—OH), 2.91 (2H, distorted AB system 9-H's), 3.90 (12H, s, 4 × $OCH_3$), 4.83 (1H, dd, $J$ = 9 and 5 Hz, 10-H), 5.72 (1H, br s, C-5—OH), 6.64 (2H, s, 1 and 4a-H's), 6.74–6.93 (3H, 7, 8 and 8b-H's) ppm; and $^{13}C$ nmr (22.63 MHz, $CDCl_3$), δ: 153.28 (2C, C-2, and C-4), 145.77, 145.54 (C-5 and C-6), 139.70, 137.42, 131.28 (C-3, C-4b, and C-8a), 121.04, 115.62, 110.81 (C-7, C-8, and C-8b), 103.01 (2C, C-1, and C-4a), 75.45 (C-10), 60.86 (C-3—$OCH_3$), 56.18 (2C, C-2-, and C-4—$OCH_3$), 56.05 (C-6—$OCH_3$), 45.59 (C-9) ppm; EI mass spectrum *m/e*: 334 ($M^+$ for $C_{18}H_{22}O_6$), 198 (base peak), and 138.

The two prominent peaks at *m/e* 138 and 198 in the mass spectrum of combretastatin were assigned to the products arising from cleavage of the C-9—C-10 bond, namely $(C_8H_9O_2 + H)^+$ and $(C_{10}H_{13}O_4 + H)^+$. Signals in the $^1H$ nmr spectrum that appeared as a three peak multiplet at 2.91 ppm were assigned to a distorted AB pattern typical of a methylene group adjacent to a chiral center whose methinyl proton resonated as a double doublet at 4.83 ppm. The aromatic protons at positions 1 and 4a appeared as a singlet at 6.64 and the three proton multiplet at 6.74–6.93 ppm was assigned to the 7, 8, and 8b protons. An off-resonance decoupled $^{13}C$ nmr spectrum displayed signals at 45.59 (triplet) and 75.45 (doublet) that substantiated the presence of the C-9—C-10 ethyl alcohol system. Assignment of structure **1** to combretastatin and determination of the absolute configuration at C-10 was completed by X-ray crystal structure determination.

A single crystal (from acetone–hexane) of combretastatin was subjected to analysis employing a computer-controlled Enraf Nonius CAD-4 diffractometer and SDP (Structure Determination Package) soft-ware system. Combretastatin (**1**) displayed 222 point group symmetry and accurate lattice constants determined by a least-squares fitting of the orientation matrix components for 25 automatically collected reflections, providing values of $a$ = 5.2046 (0.0029), $b$ = 14.1130 (0.0062), and $c$ = 22.4234 (0.0078) Å. A crystal density of 1.33 g/cc, the known chirality, and systematic extinctions were consistent with the orthorhombic space group $P2_12_12_1$ with one molecule of $C_{18}H_{22}O_6$ per asymmetric unit. By means of graphite-monochromated CuKα radiation (λ 1.54178 Å) and ω/2θ scan technique, one octant comprising a total of 1930 reflections was recorded. After removal of standard reflections and correction for Lorentz polarization and background effects, 1891 reflections were utilized, of which 1787 (94.5%) were greater than 1.0 standard deviation and 1656 (87.5%) greater than 3.0 standard deviations of their intensities. The phasing model was obtained using a multisolution weighted tangent formula (MULTAN 80) (ref. 8) approach coupled with successive difference Fourier analyses. Refinement and visualization was provided with the following major crystallographic programs: ORFFE (9*a*), ORTEP (9*b*), and LSBD (9*c*). The resulting *E*-synthesis and tangent formula recycling procedure revealed all twenty-four non-hydrogen atoms. Hydrogen atoms were located on a difference electron density synthesis following partial refinement. Full matrix least-squares refinements with anisotropic non-H atoms and isotropic hydrogen were carried out to crystallographic unweighted and weighted residuals of 4.36% and 6.12%, respectively, corresponding to structure **1**. Unfortunately, the opposite enantiomorph also refined to $R$ and $wR$ values of 4.38 and 6.12, respectively. The correct enantiomorph will eventually be determined by suitable preparation of a heavy atom derivative.

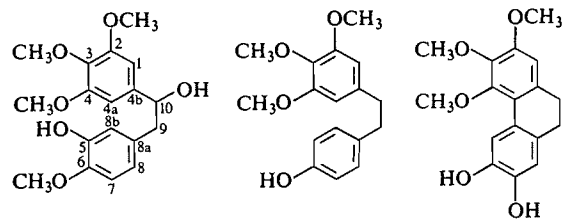


**1** **2** **3**

Combretaceae species have received very little prior chemical investigation. The principal past effort directed at the genus *Combretum* has uncovered a number of bibenzyl derivatives (e.g. **2** (10)) and a series of related 9,10-dihydrophenanthrenes such as phenol D′ (**3**) (11). Possibly combretastatin is a biosynthetic precursor of such substances and eventually the 9,10-dihydrophenanthrene corresponding to phenol **1** may be located. Presently combretastatin is most interesting from the viewpoint of central nervous system antineoplastic activity and is being evaluated against several of the National Cancer Institute's key evaluation systems. At the same time we are completing assignment of the absolute configuration and a total synthesis of combretastatin.

**Acknowledgements**

Very necessary financial assistance was provided by Contract NO1-CM-97297 with the Division of Cancer Treatment, NCI, National Institutes of Health, DHW, Grant No. CA-16049-06 and 07 awarded by the National Cancer Institute, DHW, Mrs. Mary Dell Pritzlaff, the Olin Foundation (Spencer T. and Ann W.), the Fannie E. Rippel Foundation, Mrs. Eleanor W. Libby, the Donald Ware Waddell Foundation, Mrs. Pearl Spear, Mr. Robert B. Dalton, and Mr. Jack W. Whiteman. We are also pleased to thank Drs. M. I. Suffness, G. G. Weigend, H. B. Hunnicutt, C. M. Woolf, J. J. Einck, and J. A. Duke for other helpful assistance.

1. G. R. PETTIT, Y. KAMANO, P. BROWN, D. GUST, M. INOUE, and C. L. HERALD. J. Am. Chem. Soc. Submitted.
2. M. D. WALKER, S. B. GREEN, D. P. BYAR, E. ALEXANDER, JR., U. BATZDORF, W. H. BROOKS, W. E. HUNT, C. S. MACCARTY, M. S. MAHALEY, JR., J. MEALEY, JR., G. OWENS, J. RANSOHOFF II, J. T. ROBERTSON, W. R. SHAPIRO, K. R. SMITH, JR., C. B. WILSON, and T. A. STRIKE. New England J. Med. **303**, 1323 (1980).
3. M. S. EDWARDS, V. A. LEVIN, and C. B. WILSON. Cancer Treatment Rep. **64**, 1179 (1980); T. TOMITA and A. J. RAIMONDI. J. Am. Med. Assoc. **246**, 53 (1981); V. A. LEVIN, M. S. EDWARDS, D. C. WRIGHT, M. L. SEAGER, T. P. SCHIMBERG, J. TOWNSEND, and C. B. WILSON. Cancer Treatment Rep. **64**, 237 (1980); D. L. SWEET, F. J. HENDLER, K. HANLON, J. HEKMATPANAH, M. L. GRIEM, E. E. DUDA, B. MULLIGAN, and R. L. WOLLMAN. Cancer Treatment Rep. **63**, 1707 (1979); A. KESSINGER, H. M. LEMON, and J. F. FOLEY. Cancer Treatment Rep. **63**, 511 (1979); F. H. HOCHBERG, R. LINGGOOD, L. WOLFSON, W. H. BAKER, and P. KORNBLITH. J. Am. Med. Assoc. **241**, 1016 (1979).
4. D. G. BADEN, T. J. MENDE, W. LICHTER, and L. WELLHAM. Toxicon, **19**, 455 (1981); K. IGARASHI, S. IKEYAMA, M. TAKEUCHI, and Y. SUGINO. Cell Struct. Funct. **3**, 103 (1978).
5. J. M. WATT and M. G. BREYER-BRANDWIJK. The medicinal and poisonous plants of southern and eastern Africa. E. and S. Livingstone, Ltd., London. 1962. p. 194.
6. J. L. HARTWELL. Lloydia, **31**, 71 (1968).
7. J. M. SCHMIDT and G. R. PETTIT. Experientia, **34**, 659 (1978).
8. (*a*) G. GERMAIN, P. MAIN, and M. M. WOOLFSON. Acta Crystallogr. Sect. B, **26**, 274 (1970); (*b*) Acta Crystallogr. Sect. A, **27**, 368 (1971).
9. (*a*) W. A. BUSING and H. A. LEVY. Oak Ridge National Laboratory Publication ORNL-59-12-3; (*b*) C. K. JOHNSON. Oak Ridge National Laboratory Report ORNL-TM-3794; (*c*) Ames Laboratory, Least Squares Block Diagonal Program, small computer adaption, Frenz, Bert., 505 University East, Suite 502, College Station, Texas 77840.
10. R. M. LETCHER and L. R. M. NHAMO. J. Chem. Soc. Perkin Trans. I, 2941 (1972).
11. R. M. LETCHER, L. R. M. NHAMO, and I. T. GUMIRO. J. Chem. Soc. Perkin Trans. I, 206 (1972); 1179 (1973).

Can. J. Chem. Downloaded from www.nrcresearchpress.com by 210.87.254.42 on 09/06/12
For personal use only.

# Radical reactions in aqueous solution: use of the *aci*-anion of nitromethane as a spin trap

BRUCE C. GILBERT AND RICHARD O. C. NORMAN
*Department of Chemistry, University of York, Heslington, York YO1 5DD, U.K.*

Received July 15, 1981

BRUCE C. GILBERT and RICHARD O. C. NORMAN. Can. J. Chem. **60**, 1379 (1982).

The type of radical detected by esr when first-formed short-lived radicals are generated by photolytic, radiolytic, or flow techniques in the presence of nitromethane is shown to depend upon the nature and structure of the transient radical and on the pH. Thus electron-donating radicals may react with $CH_3NO_2$ itself under certain conditions to give rise to $CH_3NO_2^{-\cdot}$ and the alkoxy nitroxides $CH_3N(OR)O\cdot$. At higher pH, a wide variety of radicals (X) react very readily with the *aci*-anion $CH_2{:}NO_2^-$ to give adducts $XCH_2NO_2^{-\cdot}$ (and, from radicals capable of one-electron transfer, $O_2NCH_2CH_2NO_2^{-\cdot}$). Structural characteristics of adducts $XCH_2NO_2^{-\cdot}$ are described and it is shown how radicals which are normally undetectable in fluid solution can be trapped and recognized in this way. Mechanistic pathways diagnosed with this trap (involving, e.g. alkoxyl radicals, aroyloxyl radicals, aromatic carboxylate cation-radicals) are exemplified.

BRUCE C. GILBERT et RICHARD O. C. NORMAN. Can. J. Chem. **60**, 1379 (1982).

Lorsqu'on produit des radicaux par écoulement, par radiolyse ou par photolyse en présence de nitrométhane, le type de radical détecté par rpe, lorsqu'apparaissent les premiers radicaux de courte vie, dépend de la nature et de la structure du radical intermédiaire et du pH. Ainsi les radicaux électrodonneurs peuvent réagir avec le $CH_3NO_2$ lui-même dans certaines conditions pour donner le $CH_3NO_2$ et les alkoxynitroxydes du type $CH_3N(OR)O$. A des pH plus élevés, une grande variété de radicaux (X) réagit très facilement avec l'anion *aci* $CH_2{:}NO_2^{-\cdot}$ en donnant des adduits $XCH_2NO_2^{-\cdot}$ (et le radical $O_2NCH_2CH_2NO_2^{-\cdot}$ à partir des radicaux pouvant subir un transfert d'un électron). On décrit les caractéristiques structurales des adduits $XCH_2NO_2^{-\cdot}$ et on montre comment les radicaux non détectables normalement en solution fluide peuvent être piégés et identifiés de cette façon. On propose un mécanisme relatif à ce piégeage (qui fait intervenir par exemple les radicaux alkoxy, les radicaux aryloxy et les radicaux cationiques du type carboxylate aromatique) et on l'illustre par des exemples.

[Traduit par le journal]

## Introduction

The increase in our understanding of the radical chemistry of nitro compounds has largely gone hand-in-hand with the development of esr spectroscopy as a physical–organic tool for probing the structures and mechanisms of reaction of free radicals.

Thus both electrochemical techniques, with aromatic (1) and aliphatic (2) substrates, and alkali-metal reduction (3) methods were developed to study relatively stable nitro radical-anions; mechanistic information often resulted, as in the reductive dehalogenation of some aromatic examples (4), electron-transfer reactions involving carbanions and *p*-nitrobenzyl halides (5), and the formation of nitroxides during alkali-metal reduction of nitroalkanes (6). Nitro compounds also provided early examples of the correlation of esr parameters with the results of molecular orbital calculations (1*b*), the occurrence of restricted rotation (for *p*-nitrobenzaldehyde$^{-\cdot}$ (1*a*)), steric inhibition of resonance when bulky substituents are present in the *ortho* positions (1*b*), buttressing effects (7), and many instances of alternating line-width phenomena (8) and solvent effects (2, 9). More recent examples include investigations of substituent effects for $ArNO_2^{-\cdot}$ (10) (and a correlation between angles of twist and rates of electron-transfer from $\cdot CMe_2OH$), $pK_a$ values and hydrogen-bonding effects in aromatic radical-anions (11) and more sophisticated MO calculations (12).

A further important area, to be described here, is the use of esr to study the reactions of nitroalkanes in the presence of short-lived radicals in aqueous solution, and, in particular, the development of "spin-trapping" methods employing both $CH_3NO_2$ and its *aci*-anion $CH_2{:}NO_2^-$.

## Experimental method

Most of the reactions to be described have been studied using an esr spectrometer in conjunction with simple two- or three-way flow systems in which separate solutions are mixed ca. 70 ms before passage of the combined solution through the cavity of the spectrometer; although in the earlier experiments gravity feed was normally employed, it is customary now to maintain the flow with a peristaltic pump. Full experimental details of the flow systems, spectrometers, measurement and calibration of spectra, reagent concentrations, and control and measurement of pH have been given previously (ref. 13 and references therein) and will not be repeated here.

## Results and discussion

### *Radical reactions of nitromethane in aqueous solution*

A variety of redox reactions, normally employing titanium(III) as reductant, have been utilized to generate "primary" radicals (see, e.g. reactions [1]–[4] (13, 14)) whose further reactions have been studied. It should be noted that when a reactive first-formed radical (e.g. $\cdot OH$) is scavenged in the

0008-4042/82/121379-13$01.00/0
©1982 National Research Council of Canada/Conseil national de recherches du Canada

Can. J. Chem. Downloaded from www.nrcresearchpress.com by 210.87.254.105 on 09/06/12
For personal use only.

Can. J. Chem. Downloaded from www.nrcresearchpress.com by 210.87.254.105 on 09/06/12
For personal use only.

flow system by reaction solely with an excess of an added substrate (RH), then if the resulting radical R· is short-lived (i.e. $2k_t$ ca. $10^9$ dm$^3$ mol$^{-1}$ s$^{-1}$), a pseudo-steady state condition for the formation and destruction of R· is achieved and kinetic analysis of the reaction system is possible (15); applications will be described later. We shall also describe results, analogous to those obtained using flow systems, from investigations in which ·OH is generated by *in situ* radiolysis (16).

[1] $Ti^{III} + H_2O_2 \rightarrow Ti^{IV} + \cdot OH + OH^-$

[2] $Ti^{III} + S_2O_8^{2-} \rightarrow Ti^{IV} + SO_4^{-\cdot} + SO_4^{2-}$

[3] $Ti^{III} + NH_3OH^+ \rightarrow Ti^{IV} + NH_3^{+\cdot} + OH^-$

[4] $Ti^{III} + RO_2H \rightarrow Ti^{IV} + RO\cdot + OH^-$

*(a) Electron transfer and addition to $CH_3NO_2$.* When ·OH is generated in the presence of ethanol (0.6 mol dm$^{-3}$) and nitromethane (0.03 mol dm$^{-3}$) at pH ca. 8, the strong esr signal detected has $a$(N) 2.57, $a$(3H) 1.20 mT, with $g$ 2.0051 (17); this is assigned to the nitromethane radical-anion $MeNO_2^{-\cdot}$ (1), whose structure will be described later. This radical also results under similar circumstances in the presence of other alcohols with an α-hydrogen atom, and it is concluded that the α-hydroxyalkyl radicals formed by reaction of the electrophilic hydroxyl radical with added alcohols react via an overall one-electron transfer reaction (facilitated by the +M effect of the oxygen substituent). In contrast, a variety of different radicals with parameters somewhat similar to this is detected from the reactions of the same alcohols at low pH (ca. 2) and from the corresponding ether-derived species at both pH 2 and 8. For example, the radical formed from ·CHMeOH and $MeNO_2$ at pH 2 has $a$(N) 2.79, $a$(3H) 1.02 mT, $g$ 2.0052; that from ·CHMeOEt and $MeNO_2$ (at both pH 2 and 8) has $a$(N) 2.74, $a$(3H) 0.86 mT, with $g$ 2.0052. These signals are assigned to the alkoxynitroxide radical-adducts $CH_3N(O\cdot)OCHMeOH$ (**2**) and $CH_3N(O\cdot)OCHMeOEt$ (**3**), formed in reactions which are again facilitated by the +M effect of the oxygen substituents as indicated in Scheme 1 (for an alcohol-derived radical) and Scheme 2 (for an ether-derived example); in the former the base-catalysed route to the radical-anion is also indicated. The reactions of other aliphatic nitrocompounds, the formation of aromatic analogues of the adducts (with splittings from protons in the alkoxy moiety), and the production of nitroxides from $RNO_2H$ (formed in acid solution) have also been described (17). It should be stressed that reactions as shown in Schemes 1 and 2 are typical of radicals with a *reducing* capacity, and are not shown by, for example, Me· (see below).

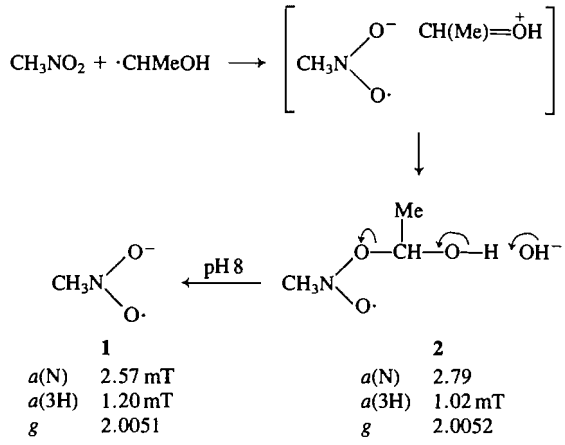


**1**

| | |
|---|---|
| $a$(N) | 2.57 mT |
| $a$(3H) | 1.20 mT |
| $g$ | 2.0051 |

**2**

| | |
|---|---|
| $a$(N) | 2.79 |
| $a$(3H) | 1.02 mT |
| $g$ | 2.0052 |

SCHEME 1

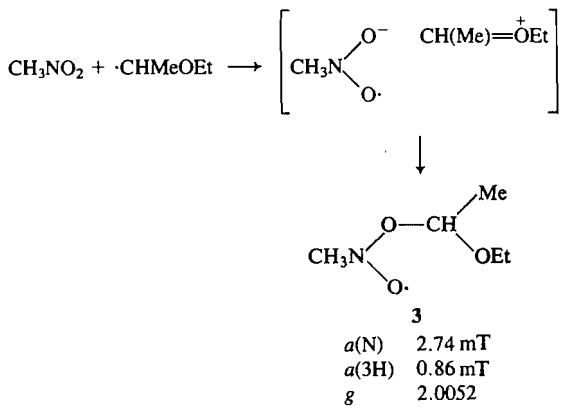


**3**

| | |
|---|---|
| $a$(N) | 2.74 mT |
| $a$(3H) | 0.86 mT |
| $g$ | 2.0052 |

SCHEME 2

*(b) Reactions of $CH_2$:$NO_2^-$: addition and oxidative electron-transfer.* The attractions of $MeNO_2$ as a spin-probe for radicals in aqueous solution include not only its ready availability and its solubility in water but also the relative stability of its *aci*-anion $CH_2$:$NO_2^-$ ($CH_3NO_2$ has p$K_a$ 10.2 (18)); at pH values ≥ ca. 8.5 (which can be readily achieved in flow system experiments) a significant — and adjustable — concentration of the *aci*-anion can be achieved and its high reactivity exploited.

For example, when ·OH is generated either by the redox reaction [1] in a flow system (19) or by *in situ* γ-irradiation (16) in the presence of $N_2O$ (to convert $e^-$ into ·OH), its resultant reaction with $CH_2$:$NO_2^-$ leads to the detection of the adduct (**4**), with $a$(N) 2.49, $a$(2H) 0.89 mT, $g$ 2.0051 (reaction [5]). Several points are important here; firstly, the very rapid rate of *trapping* of ·OH is notable ($k_5$ has been estimated as $9 \times 10^9$ dm$^3$ mol$^{-1}$ s$^{-1}$ from a pulse radiolysis study (20); in contrast, the electrophilic ·OH radical is relatively unreactive towards $CH_3NO_2$ (21)); secondly, the fact that whereas ·OH itself is undetectable in fluid solution (22),

strong signals from the adduct (**4**) are readily obtained (it has been shown (21) that the related radical-ion $CH_3NO_2^{-\cdot}$, and to a less marked extent $CH_3N(O\cdot)OH$, are significantly longer-lived than simple short-lived organic radicals in solution); and thirdly, that the parameters for the radical detected characterize its structure (see later).

[5] $HO\cdot + CH_2{:}NO_2^- \xrightarrow{k_5} HOCH_2NO_2^{-\cdot}$
**4**

Reaction of ·OH with dimethyl sulphoxide in the presence of $CH_2{:}NO_2^-$ leads to the formation and trapping of Me· (reactions [6] and [7]) to give the easily recognized esr signal of the nitro*ethane* radical-anion (**5**) (Fig. 1) (23, 24); this spectrum (with $a$(N) 2.60, $a$(2H) 0.97, $a$(3H) 0.05 mT, $g$ 2.0050) illustrates the narrow line-widths (and hence good resolution) obtained with this type of trap, which, as in this case, often reveals the presence of a characteristic γ-proton coupling. From the point of view of structural verification it is helpful that independent routes to the spin-adducts are often available (e.g. in this case, the electron-transfer reaction of ·CHMeOH and nitroethane at pH ca. 8; *cf.* Scheme 1). We might also note here that relatively electron-rich radicals, e.g. ·CHMeOH, can also be trapped (24) via addition to $CH_2{:}NO_2^-$ at pH ca. 9 (reaction [8]); the parameters of **6**, and the general usefulness of this spin-trapping reaction, will be discussed subsequently.

[6] $HO\cdot + Me_2S{=}O \rightarrow Me\cdot + MeSO_2H$

[7] $Me\cdot + CH_2{:}NO_2^- \rightarrow MeCH_2NO_2^{-\cdot}$
**5**

[8] $\cdot CHMeOH + CH_2{:}NO_2^- \rightarrow HOCHMeCH_2NO_2^{-\cdot}$
**6**

The spectrum detected (25) during the oxidation of nitromethane in a flow system at pH ca. 9 with $SO_4^{-\cdot}$ is identical to that observed (26) in the one-electron reduction of 1,2-dinitroethane with $\cdot CO_2^-$ and is accordingly assigned to the radical-anion (**7**) (with $a$(N) 2.54, $a$(2H) 1.12, $a$(2H) 0.04 mT, $g$ 2.0050); evidently the sulphate radical-anion effects overall one-electron oxidation of the *aci*-anion to $\cdot CH_2NO_2$, which is subsequently trapped (reactions [9] and [10]). The spectrum of the *adduct* $^-O_3SOCH_2NO_2^{-\cdot}$ is also detected as a minor component in both flow and photolytic experiments. The oxidative reaction sequence illustrated in reactions [9] and [10] is also brought about by the anion-radical $Br_2^{-\cdot}$ (from $Br^-$ and ·OH) and some related species (16).

[9] $CH_2{:}NO_2^- + SO_4^{-\cdot} \rightarrow \cdot CH_2NO_2 + SO_4^{2-}$

[10] $\cdot CH_2NO_2 + CH_2{:}NO_2^- \rightarrow O_2NCH_2CH_2NO_2^{-\cdot}$
**7**

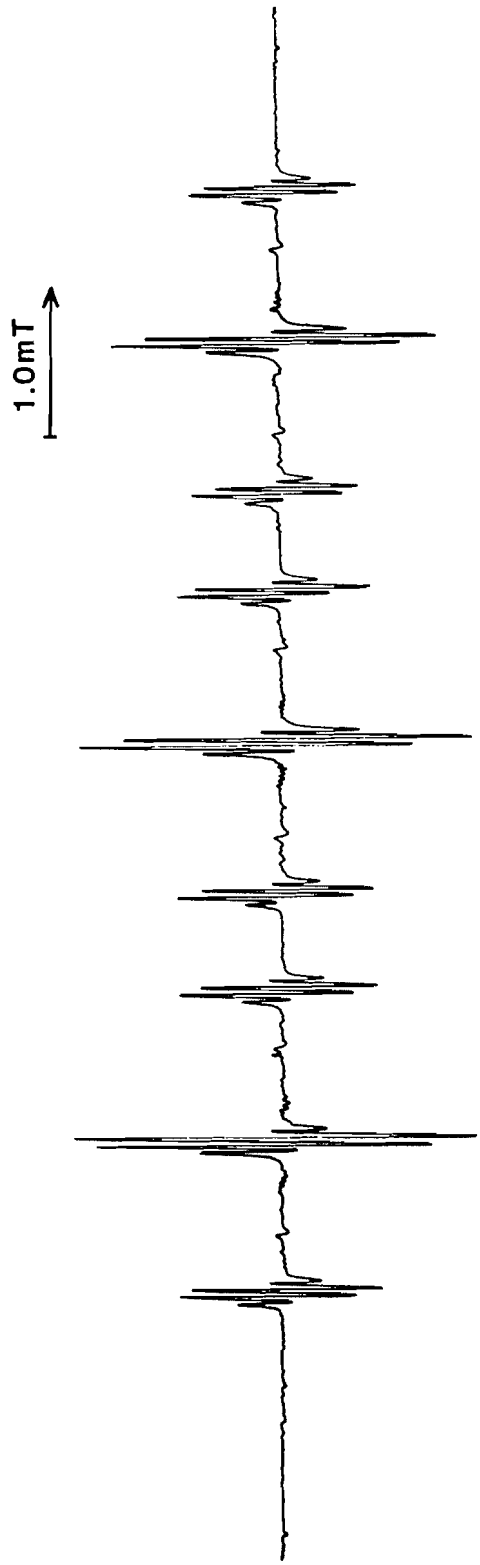


FIG. 1. Electron spin resonance spectrum of $MeCH_2NO_2^{-\cdot}$, formed from the reaction of Me· (from ·OH and $Me_2SO$) and $CH_2NO_2^-$ at pH ca. 9.

Can. J. Chem. Downloaded from www.nrcresearchpress.com by 210.87.254.105 on 09/06/12
For personal use only.

Can. J. Chem. Downloaded from www.nrcresearchpress.com by 210.87.254.105 on 09/06/12
For personal use only.

*(c) Hydrogen-atom abstraction from $CH_3NO_2$.* Evidence has been adduced that the radical $\cdot CH_2NO_2$ is also obtained by reaction of the parent nitroalkane with ·Me under appropriate conditions (23). This follows from the detection in the $Ti^{III}$–$H_2O_2$–$Me_2SO$–$MeNO_2$ system of, at pH ca. 6, the radical-anion $EtNO_2^{-\cdot}$ and, at pH ca. 2, the conjugate acid EtN(O·)OH (with $a$(N) 2.81, $a$(2H) 0.91, $a$(1H) 0.32 (23), $g$ 2.0049 (26)): under these conditions the concentration of $CH_2{:}NO_2^-$ formed by ionization of nitromethane is too low (even at pH 6) to serve effectively as a trap and another route to its generation is required. It is proposed that both $CH_2{:}NO_2^-$ and, at lower pH, the conjugate acid $CH_2{:}NO_2H$ are formed by one-electron reduction by $Ti^{III}$ of $\cdot CH_2NO_2$ generated in the initial hydrogen-abstraction reaction (see Scheme 3) and that they can then serve as effective spin

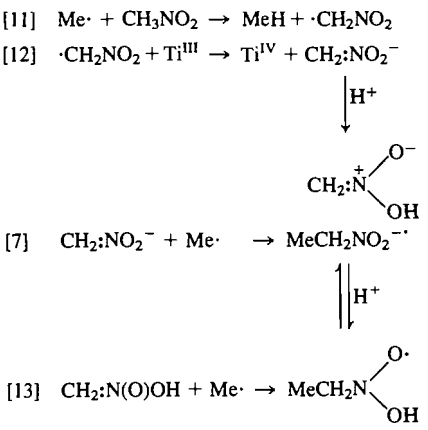


SCHEME 3

traps. It is suggested that $k_{11}$ is ca. $10^3$ dm$^3$ mol$^{-1}$ s$^{-1}$ under these conditions and that both trapping reactions [7] and [13] are very rapid. Electron spin resonance experiments of this sort also enable p$K_a$ to be determined for the nitro radical-anion protonation equilibria (e.g. a value for p$K_a$ of 4.4 was obtained (23) for $Pr^iNO_2H \rightleftharpoons Pr^iNO_2^{-\cdot} + H^+$, these radicals being generated from Me· and CHMe:$NO_2H$ and CHMe:$NO_2^-$ in experiments with nitroethane). A broadly similar mechanism, involving loss of bromide ion from a first-formed radical-anion and subsequent reduction of the α-nitro radical is thought to explain the formation of $O_2NCH_2CH_2NO_2^{-\cdot}$ in the reaction of $Ti^{III}$ with $BrCH_2NO_2$ (see Scheme 4) (28).

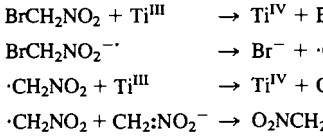


SCHEME 4

*Structural properties of $XCH_2NO_2^{-\cdot}$*

In assessing the usefulness of the *aci*-anion $CH_2{:}NO_2^-$ as a spin trap it is helpful to discuss briefly what is known about the structures of the radical-anions $RCH_2NO_2^{-\cdot}$ and to examine the sensitivity of the esr parameters ($a$(N), $a$(β-H), long-range couplings, line-widths, and $g$-values) to variations in the nature of the addend X.

It has been suggested (12*a*) that the enhanced nitrogen splitting of ca. 2.5 mT observed for aliphatic nitro radical-anions and the corresponding alkoxynitroxides, in comparison with typical values of $a$(N) of ca. 1.5 mT for dialkyl nitroxides, is a result of the non-planarity of the bonds at the radical centre; in contrast, most nitroxides are deduced to be essentially planar at the nitrogen atom (29). This conclusion is supported by the results (12*a*) from INDO calculations on $MeNO_2^{-\cdot}$ and $EtNO_2^{-\cdot}$ (for which an angle for out-of-plane bending at the N—O bonds of ca. 6° is suggested) and by the estimate from anisotropic spectra of a $2p{:}2s$ ratio of ca. 11.5 for the orbital of the unpaired electron in nitroalkane radical-anions and related alkoxynitroxides (30). Despite the lack of planarity at the radical centre, it nevertheless appears (12*a*) that the angular dependence of the β-proton splitting in $RNO_2^{-\cdot}$ (R = Me, Et) essentially follows the $B\cos^2\theta$-type expected for hyperconjugative interaction in planar π-radicals (for $MeNO_2^{-\cdot}$ the calculated (INDO) variation of $a$(β-H) with θ is

$$a(\beta\text{-H}) = 0.023 + 0.359\cos\theta + 2.114\cos^2\theta \text{ mT}$$

i.e. with the last term dominant). Variations in $a$(N) and $a(CH_2)$ with structure can generally be interpreted in terms of alterations to the geometry of the radical centre as well as to conformational changes, as will subsequently be explained.

*(a) Carbon-centred radicals.* Table 1 contains details of the esr parameters of some nitro radical-anions formed by trapping carbon-centred radicals (generated in a variety of reactions) with $CH_2{:}NO_2^-$ (24). Although most of these can actually be directly detected under certain circumstances, several others (e.g. Ph·, ·COMe) are generally undetectable by esr under these conditions.

Radicals of the type $RCH_2NO_2^{-\cdot}$ are normally characterized by a nitrogen splitting in the range 2.53–2.60 mT and a β-proton triplet splitting of ca. 1.0 mT; in addition, long-range coupling to γ-$CH_2$ protons and, sometimes, to δ-protons can be observed. This provided crucial diagnostic evidence for the formation of certain radicals, e.g. $\cdot CH_2CHO$ in the base-catalysed rearrangement of $\cdot CH(OH)CH_2OH$ from glycol.

Two other trends are noticeable, and their recognition assists radical diagnosis and hence mech-

TABLE 1. Electron spin resonance parameters for adducts $RCH_2NO_2^{-\cdot}$ formed from carbon-centred radicals[a,b]

| Radical | Reaction employed | Hyperfine splitting/mT | | |
|---|---|---|---|---|
| | | $a$(N) | $a$($CH_2$) | $a$(γ,δ-H) |
| Me· | HO·/$Me_2SO$<br>HO·/MeCHO/$H_2O_2$ | 2.60 | 0.97 | 0.05 (3H) |
| Et· | $SO_4^{-\cdot}$/$EtCO_2^-$ | 2.54 | 1.01 | 0.06 (2H)<br>0.03 (3H) |
| ·$CH_2OH$ | ·OH/MeOH | 2.55 | 1.07 | 0.04 (2H) |
| ·$CH_2CO_2^-$ | ·OH/$MeCO_2^-$ | 2.60 | 1.00 | 0.07 (2H) |
| ·$CH_2CH_2CO_2^-$ | ·OH/$EtCO_2^-$<br>$SO_4^{-\cdot}$/$^-O_2CCH_2CH_2CO_2^-$ | 2.55 | 1.02 | 0.06 (2H) |
| ·$CH_2COCH_3$ | ·OH/$Me_2C{=}O$ | 2.60 | 1.07 | 0.06 (2H) |
| ·$CH_2CHO$ | ·OH/$HOCH_2CH_2OH$,$OH^-$ | 2.60 | 1.05 | 0.06 (2H)<br>0.05 (1H) |
| ·$CMe_2OH$ | ·OH/$Me_2CHOH$ | 2.43[c] | 1.01[c] | |
| ·$CMe_3$ | HO·/$HC(O)OBu^t$<br>$SO_4^{-\cdot}$/$Me_3CCO_2^-$ | 2.37 | 0.87 | |
| Ph· | $SO_4^{-\cdot}$/$PhCO_2^-$ | 2.59 | 0.95 | |
| ·COMe | HO·/MeCHO | 2.43 | 0.77 | |
| ·$CO_2Et$ | HO·/$HCO_2Et$ | 2.50 | 0.78 | |
| ·$CCl_3$ | HO·/$CCl_4$, $CHCl_3$ | 2.21[d] | 0.77[d] | |

[a]Data taken from ref. 24.
[b]$g$ = 2.0050 except where stated otherwise.
[c]Line broadening: see text.
[d]$g$ = 2.0052.

anistic deductions (though mechanistic features will not be elaborated here). The first is the small but significant decrease in $a$(N) associated with bulky β-substituents (cf. in particular, values of $a$(N) of 2.37 and 2.21 mT for adducts with ·$Bu^t$ and ·$CCl_3$ respectively (the enhanced $g$-value for the latter is also notable)); this we attribute to a tendency towards *flattening* of the pyramidal nitro-group induced by the increased size of R. The second is the reduction in $a$(β-H) for such substituents (cf. 0.77 mT for R = $CCl_3$); this we attribute to increased conformational preference for the eclipsed structures **8***a* and **8***b*. The line-width alternation of the 1:2:1 pattern from the β-protons in, e.g. $HOCMe_2CH_2NO_2^{-\cdot}$, and related radicals (25), presumably reflects restricted rotation about either the C—N or the $C_\beta$—$C_\gamma$ bonds or both.

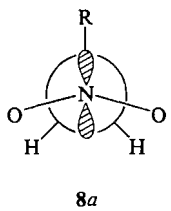


**8***a*

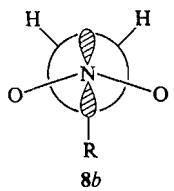


**8***b*

*(b) Spin-adducts from oxygen-centred and nitrogen-centred radicals*. Table 2 contains details of spin-adducts formed from $CH_2{:}NO_2^-$ and some short-lived oxygen- and nitrogen-centred radicals in aqueous solution. The adducts of the oxygen-centred radicals (which themselves are not directly detectable in aqueous solution) are characterized by rather low $a$(N) and $a$(β-H) values (see above) which suggests that the β C—O bond tends to eclipse the orbital of the unpaired electon (and probably lowers $a$(N) by favouring (flattened) structures of type **9**; cf. ·$CH(OH)CH_2OH$ and other radicals with an inductively electron-withdrawing β-substituent and a +M substituent at the radical centre (34)). Further evidence for some assignments derives from changes in the relative concentrations of different adducts with the concentration of the trap; for example, in the oxidation (32) of benzoate with $SO_4^{-\cdot}$ the assignments of adducts **10** (see Table 2) and **11** (see Table 1) are consistent with the increase in concentration of the former, with respect to the latter, as [$CH_2{:}NO_2^-$] is increased so that addition of $PhCO_2$· to trap competes more effectively with fragmentation (see e.g. Fig. 2). Kinetic applications of this type of study will be described later, but it may be noted that simple acyloxy radicals ($RCO_2$·) fragment too rapidly for trapping in this way (35).

The formation of amino radicals and alkylamino radicals in the one-electron reduction (33) of hydroxylamine and *N*-alkylhydroxylamines, respectively, is confirmed by the detection of spin-adducts with $CH_2{:}NO_2^-$ (see Table 2); these possess β-nitrogen couplings as well as long-range splittings from N—H and *N*-alkyl protons. The first-formed radicals in these systems (e.g. ·NHMe) are not detected directly under our conditions, evidently due to the occurrence of very rapid reactions including rearrangement (to α-amino-

Can. J. Chem. Downloaded from www.nrcresearchpress.com by 210.87.254.105 on 09/06/12
For personal use only.

Can. J. Chem. Downloaded from www.nrcresearchpress.com by 210.87.254.105 on 09/06/12
For personal use only.

TABLE 2. Electron spin resonance spectra of spin adducts $RCH_2NO_2^{-\cdot}$ formed from oxygen- and nitrogen-centred radicals

| Radical | Method of generation | Hyperfine splitting/mT $a$(N) | $a$(2H) | $a$(other) | $g$ |
|---|---|---|---|---|---|
| ·OH | $Ti^{III}/H_2O_2$[a] | 2.45 | 0.89 | | 2.0051 |
| | $e^-/H_2O$[b] | 2.523 | 0.904 | | 2.00502 |
| ·OPr | $Ti^{III}$/PrOOH[c] | 2.38 | 0.85 | | 2.0050 |
| ·OPr$^i$ | $Ti^{III}$/Pr$^i$OOH[d] | 2.39 | 0.85 | | 2.0050 |
| $PhCO_2$· | $SO_4^{-\cdot}/PhCO_2^-$[e] | 2.40 | 0.74 | | 2.0050 |
| ·$NH_2$ | $Ti^{III}/NH_2OH$[a] | 2.55 | 0.89 | 0.11 (1N)<br>0.05 (2H) | 2.0051 |
| ·NHMe | $Ti^{III}$/NHMeOH[f] | 2.48 | 0.915 | 0.15 (N)<br>0.02 (NH)<br>0.01 (NMe) | 2.0051 |
| ·$N_3$ | ·OH/$N_3^-$[b] | 2.474 | 0.546 | 0.273 (γ-N)<br>0.027 (2N) | 2.00513 |

[a]Reference 19.
[b]Reference 16.
[c]Reference 14.
[d]Reference 31.
[e]Reference 32.
[f]Reference 33.

alkyl radicals), hydrogen abstraction from parent hydroxylamine, and, possibly, one-electron reduction. Trapping of the azido radical $N_3$· (from azide ion and ·OH, generated radiolytically) leads to the formation of an adduct with long-range coupling from all the nitrogen atoms (see Table 2) (16); a structure with a linear arrangement of the azido nitrogen atoms, $\bar{N}=\overset{+}{N}=NCH_2NO_2^{-\cdot}$ is preferred.

*(c) The trapping of sulphur- and phosphorus-centred radicals*. Table 3 illustrates the potential of this spin-trapping method in characterizing a variety of first-formed radicals, and hence in providing useful mechanistic information, in both radiolysis (16) and flow (36–40) studies. This is nowhere more important than in probing the mechanisms of oxidation of sulphur-containing compounds, especially as most sulphur-centred radicals (e.g. thiyl radicals, RS·) are not directly detectable yet play a key rôle in oxidation pathways. The most notable features of these trapped adducts are the particularly low nitrogen and β-proton splittings, which indicate that there is strong preference for the eclipsed conformation (**12**) (cf. also radicals of the type $\cdot CH_2CH_2SR$ (41)), as well as, in most cases, enhanced $g$-values suggestive of spin-transfer from the radical centre. Recognition of these features leads to the proposal for **13** as the structure of the adduct formed from the reaction of ·OH with $S_2O_3^{2-}$ in the presence of $CH_2{:}NO_2^-$ (16, 36). Further useful information comes from long-range coupling "across sulphur" in the adducts with ·SCN (**14**), $(Pr^iO)_2P(S)S\cdot$ (**15**) (the parent radical's esr spectrum can be detected (42) in fluid media at low temperature but the line-width increases with temperature to render it undetectable under ambient conditions), and in thioalkyl adducts $RCH_2$-$SCH_2NO_2^{-\cdot}$ (**16**) (see Fig. 3). Phosphorus-centred radicals are trapped to give species with large (3–4 mT) β-phosphorus splittings, and, in one case, detectable interaction with a P—H proton (**17**).

*(d) Magnetic inequivalence due to chirality*. A further aid to correct structural identification of adducts is the recognition that for radicals XYZ-$CCH_2NO_2^{-\cdot}$ in which three different groups are

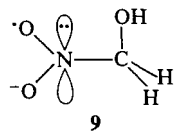

**9**

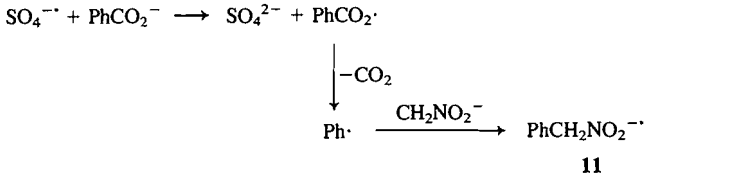

**10**

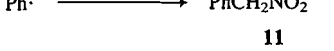

**11**

Can. J. Chem. Downloaded from www.nrcresearchpress.com by 210.87.254.105 on 09/06/12
For personal use only.

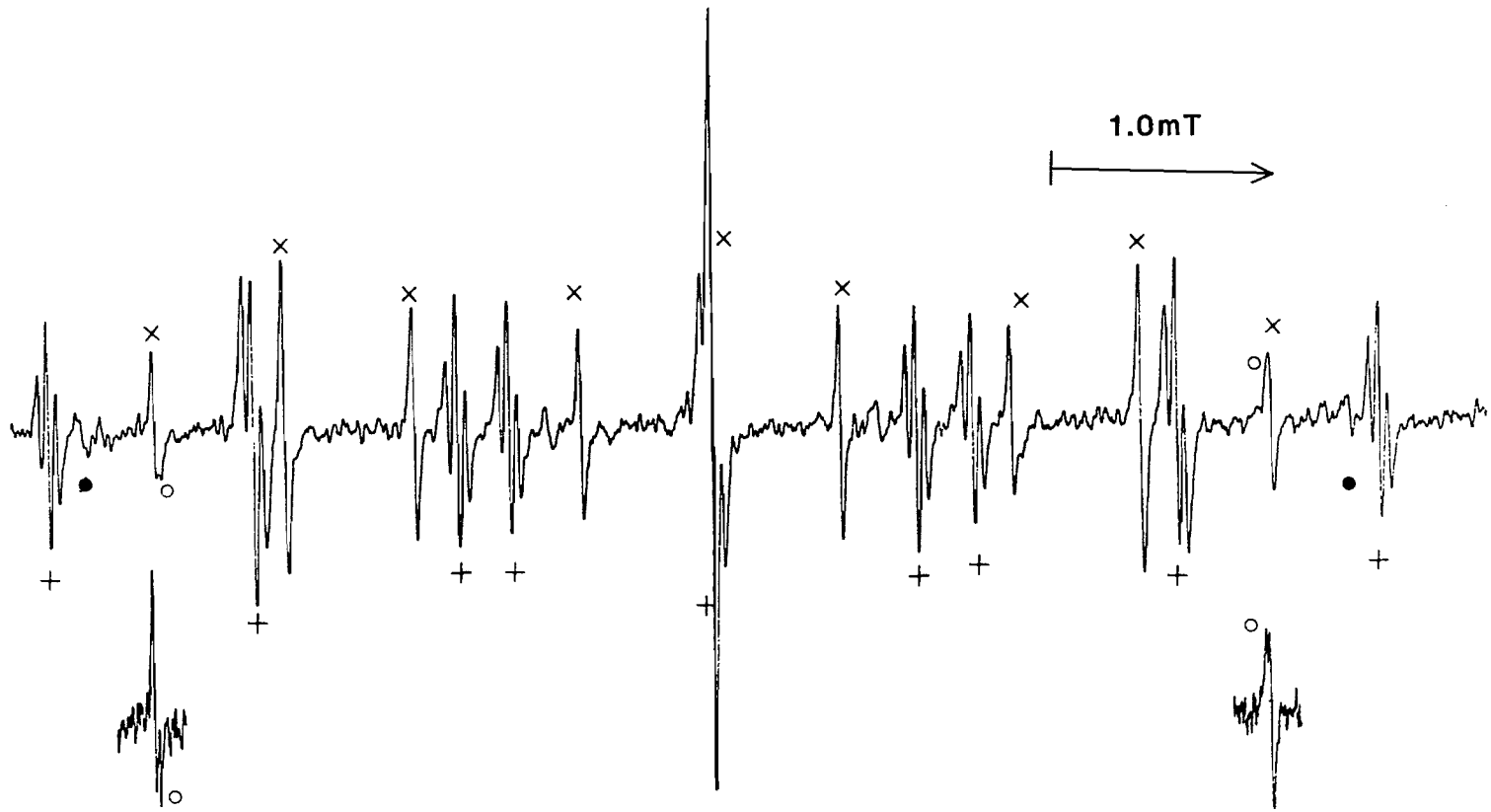


FIG. 2. Electron spin resonance spectra of radical-anions detected during the reaction of $SO_4^{-\cdot}$ and $ArCO_2^-$ (Ar = 3-chlorophenyl) in the presence of a relatively high concentration of $CH_2NO_2^-$ (0.015 mol $dm^{-3}$). The most intense signals are from $O_2NCH_2CH_2NO_2^{-\cdot}$ (+) and $ArCO_2CH_2NO_2^{-\cdot}$ (×); traces of signals from $^-O_3SOCH_2NO_2^{-\cdot}$ (○) and $ArCH_2NO_2^{-\cdot}$ (●) may also be discerned.

Can. J. Chem. Downloaded from www.nrcresearchpress.com by 210.87.254.105 on 09/06/12
For personal use only.

TABLE 3. Electron spin resonance spectra of spin-adducts $RCH_2NO_2^{-\cdot}$ formed from sulphur- and phosphorus-centred radicals

| Substrate (reaction with ·OH) | Radical | Hyperfine splitting/mT $a$(N) | $a$(β-H) | $a$(other) | $g$ | Footnote |
|---|---|---|---|---|---|---|
| $S^{2-}$ | $\cdot S^-$ | 2.436 | 0.664 | | 2.00584 | *a*,*b* |
| $SO_3^{2-}$ | $\cdot SO_3^-$ | 2.219 | 0.750 | | 2.00498 | *a*,*b* |
| $S_2O_3^{2-}$ | $\cdot S_2O_3^-$ | 2.394 | 0.600 | | 2.00551 | *a*,*b* |
| $SCN^-$ | ·SCN | 2.169 | 0.339 | 0.031(N) | 2.00616 | *a* |
| $S(CH_2CMe_2OH)_2$ | $\cdot SCH_2CMe_2OH$ | 2.42 | 0.580 | 0.080(2H) | 2.0056 | *c* |
| $(Pr^iO)_2P(S)S^-$ | $\cdot S(S)P(OPr^i)_2$ | 2.325 | 0.538 | 0.100(P) | 2.0055 | *d* |
| $HPO_3^{2-}$ | $\cdot PO_3^{2-}$ | 2.49 | 1.07 | 3.14(P) | 2.0050 | *e*,*f* |
| $H_2PO_2^-$ | $HPO_2^{-\cdot}$ | 2.51 | 1.01 | 2.92(P)<br>0.15(P—H) | 2.0050 | *e*,*f* |
| $PhP(H)O_2^-$ | $PhPO_2^{-\cdot}$ | 2.45 | 1.01 | 3.34(P) | 2.0050 | |
| $(EtO)_2P(O)H$ | $(EtO)_2P(O)\cdot$ | 2.470 | 0.980 | 3.773(P) | 2.0050 | *d* |

[a]Data from ref. 16; ·OH generated photolytically.
[b]See also ref. 34.
[c]Reference 37.
[d]Reference 38.
[e]Reference 39.
[f]See also refs. 16, 40.

FIG. 3. Electron spin resonance spectrum of the adduct (**16**) of $\cdot SCH_2CH_2OH$ (from ·OH and 2-mercaptoethanol) and $CH_2NO_2^-$.

attached to the γ-carbon, the adjacent methylene protons are rendered non-equivalent (diastereotopic) by the chirality at $C_\gamma$, and two non-equivalent splittings result (with consequently a 1:1:1:1 pattern for the β-protons). Examples are given in Table 4 and in Figs. 4 and 5. It should be stressed that this phenomenon occurs *even in the absence of restricted rotation*; where restricted rotation also occurs the inner two lines of the β-protons' 1:1:1:1 pattern are broadened compared with the outer lines (see e.g. the spectrum of $^-O_2CCH_2CH(CO_2^-)CH_2NO_2^{-\cdot}$ in Fig. 4); the crucial observation in this and related examples is that, as the temperature is raised, the inner two lines simply sharpen but do not coalesce, as would have been expected had restricted rotation alone been the cause of inequivalence.

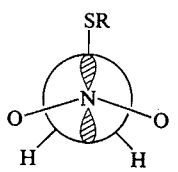


**12**

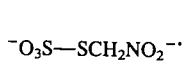


**13**

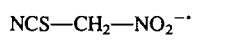


0.031(N) 0.339(2H) 2.169(N) mT

**14**

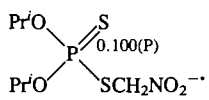


2.325(N) mT
0.538(2H)

**15**

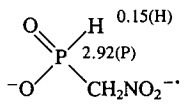


2.51(N) mT
1.01(2H)

**17**

TABLE 4. Magnetic non-equivalence of β-protons in radicals of the type $XYZCCH_2NO_2^{-\cdot}$[a]

| | | | Hyperfine splittings/mT | | | | ΔH/mT | |
|---|---|---|---|---|---|---|---|---|
| X | Y | Z | a(N) | a(β-H) | a(β-H') | a(γ-H) | (inner) | (outer) |
| H | Me | OH | 2.51 | 1.12 | 0.97 | 0.06 | 0.04 | 0.025 |
| H | Me | OEt | 2.50 | 1.21 | 0.86 | 0.06 | 0.04 | 0.025 |
| H | Me | OAc | 2.47 | 1.27 | 0.68 | 0.06 | 0.04 | 0.03 |
| H | Me | $CO_2^-$ | 2.51 | 1.44 | 0.68 | 0.06 | 0.03 | 0.02 |
| H | $CH_2CO_2^-$ | $CO_2^-$ | 2.51 | 1.22 | 0.94 | 0.06 | 0.055 | 0.02 |
| H | Me | $CO_2^-$ | 2.47 | 1.34 | 0.66 | 0.06 | 0.04 | 0.025 |
| H | $CO_2^-$ | Cl | 2.49 | 1.64 | 0.41 | 0.08 | 0.035 | 0.015 |

[a]Taken from ref. 24; $g = 2.0050$.

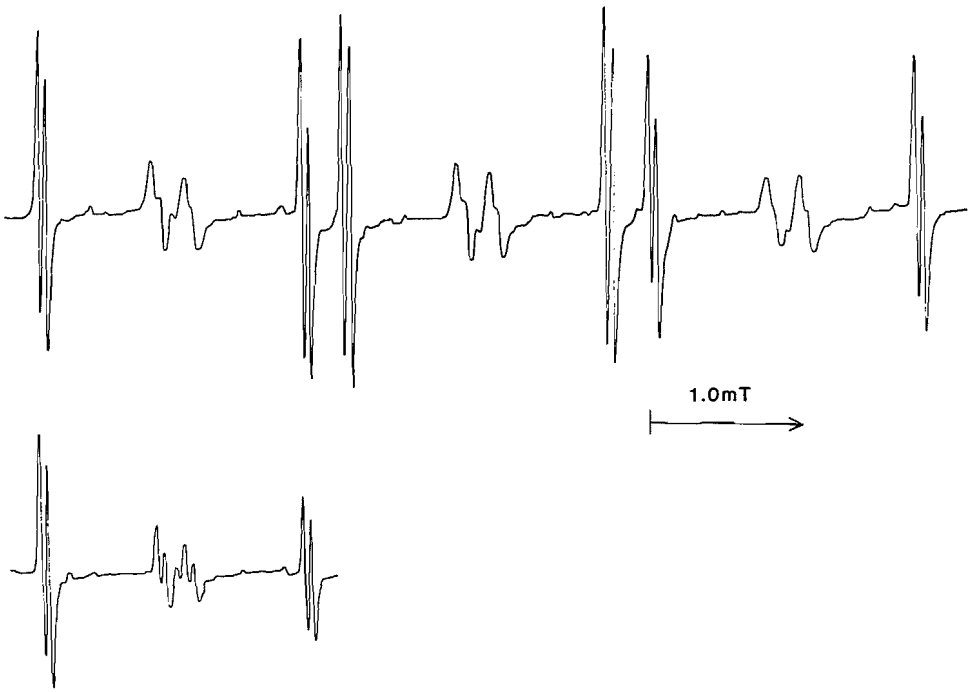


FIG. 4. An example of an adduct $XYZCCH_2NO_2^{-\cdot}$ with non-equivalent splittings from diastereotopic β-protons: $^-O_2CCH_2CH(CO_2^-)CH_2NO_2^{-\cdot}$ (from $SO_4^{-\cdot}$ and succinate) at 20°C, showing the marked line-broadening of the inner lines of the proton hyperfine pattern. The peaks inset are from the low-field components at 40°C.

These phenomena have been discussed in some detail elsewhere (24, 43) and the arguments will not be rehearsed here; however, it might simply be noted now that for these adducts and related nitroxides (43) (e.g. $XYZCCH_2N(Bu^t)O\cdot$) both the differences between the two non-equivalent splittings *and* the extent of differential line-broadening increase with the bulk of the γ-substituents (being particularly marked for carboxylate, chlorine and bromine substituents, see e.g. **18** (24)). This observation can in itself serve a useful diagnostic purpose, as in the characterization of $\cdot CHBrCO_2^-$ (not directly detectable) in the reaction of ·OH with bromoethanoate (see Fig. 5).

*Kinetic and mechanistic studies of radical reactions*

Finally, we illustrate with several examples how the knowledge of the structures of adducts $XCH_2NO_2^{-\cdot}$, as revealed by $a$(N), $a$(H), $g$ etc., can prove helpful in mechanistic and kinetic studies; particular emphasis will be placed upon examples where

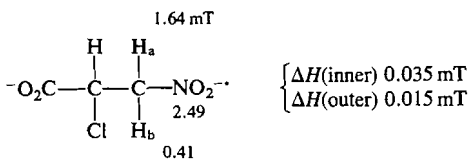


**18**

Can. J. Chem. Downloaded from www.nrcresearchpress.com by 210.87.254.105 on 09/06/12
For personal use only.

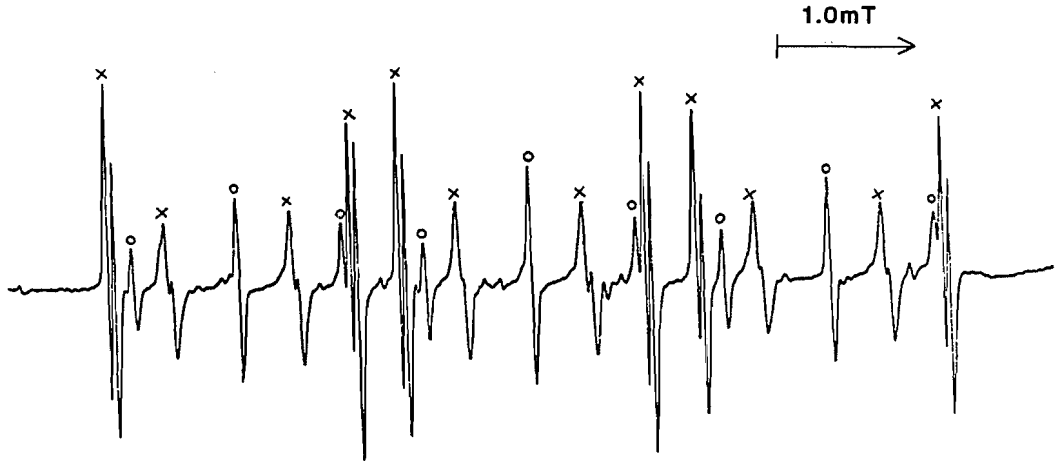


FIG. 5. Electron spin resonance spectrum of $BrCH(CO_2^-)CH_2NO_2^{-\cdot}$ (×) (with $a$(β-H) 1.60, 0.50 mT) formed in the reaction of ·OH with bromoethanoate in the presence of $CH_2{:}NO_2^-$; peaks marked O are from $HOCH_2NO_2^{-\cdot}$.

TABLE 5. Electron spin resonance spectra of radicals generated from alkoxy radicals in the presence of $CH_2NO_2^-$[a]

| Alkoxy radical | $RCH_2NO_2^{-\cdot}$ R = | Hyperfine splitting/mT | | |
|---|---|---|---|---|
| | | $a$(N) | $a$(β-H) | $a$(other) |
| Bu'O· | Bu'O— | 2.53 | 1.01(2H) | |
| | Me— | 2.60 | 0.97(2H) | 0.05(3H) |
| PrO· | PrO— | 2.38 | 0.85(2H) | |
| | EtCH(OH)— | 2.52 | 1.15(1H), 0.93(1H) | 0.06(1H) |
| BuO· | BuO— | 2.38 | 0.85(2H) | |
| | PrCH(OH)— | 2.48 | 1.22(1H), 0.96(1H) | 0.05(1H) |
| | $HOCH_2CH_2CH_2$— | 2.51 | 1.03(2H) | 0.05(2H) |
| $CH_2{=}CHCH_2CH_2CH_2O$· |  | 2.55 | 1.06(1H), 0.94(1H) | 0.06(2H) |
| $MeCH_2CH_2CH_2CMe_2O$· | $Me_2C(OH)CH_2CH_2CHMe$— | 2.46 | 1.01(1H), 0.93(1H) | 0.06(2H) |
| | $MeCH_2CH_2CH_2$— | 2.46 | 1.00(2H) | 0.06(2H) |

[a] $g$ = 2.0050.

the intermediate radicals themselves are not directly detectable in solution by esr (e.g. RO·, $RCO_2$·) or where the radicals show particularly high reactivity, and hence a low, often undetectable, signal-to-noise ratio.

*(a) Decomposition of alkyl hydroperoxides*. It is found (14, 31) that when various alkyl hydroperoxides are reduced by $Ti^{III}$ in a flow system in the presence of $CH_2{:}NO_2^-$, adducts formed from the appropriate alkoxyl radicals (RO·) can be detected (reactions [4] and [14]). Alkoxyl radicals are also formed in the reaction between HO· and dialkyl sulphites (reaction [15]), and they have been characterized similarly (44).[1]

[4] $ROOH + Ti^{III} \rightarrow RO\cdot + OH^- + Ti^{IV}$

[14] $RO\cdot + CH_2NO_2^- \rightarrow ROCH_2NO_2^{-\cdot}$

[15] $HO\cdot + (RO)_2S{=}O \rightarrow RO\cdot + ROSO_2H$

[16] $RO\cdot \xrightarrow{-O-} R'\cdot$

[17] $R'\cdot + CH_2NO_2^- \rightarrow R'CH_2NO_2^{-\cdot}$

In these reactions, the concentration of the spin trap employed is crucial; thus although at high concentrations of spin trap the corresponding alkoxyl radical can in many cases be intercepted, to give $ROCH_2NO_2^{-\cdot}$, other reactions of the alkoxyl radical (fragmentation, rearrangement) can compete effectively with the addition at lower values of $[CH_2NO_2^-]$, and secondary radicals (·R′) can be characterized (reactions [16] and [17]); parameters of the appropriate radicals are given in Table 5.

[1] Confirmation that alkoxy adducts have been correctly identified derives from the independent generation of the radical assigned the structure $EtOCHMeNO_2^{-\cdot}$ (from EtO· and $CHMe{:}NO_2^-$) from the reaction between ·CHMeOEt (from ·OH and diethyl ether) and $NO_2^-$ (45).

Can. J. Chem. Downloaded from www.nrcresearchpress.com by 210.87.254.105 on 09/06/12
For personal use only.

Can. J. Chem. Downloaded from www.nrcresearchpress.com by 210.87.254.105 on 09/06/12
For personal use only.

For example, in experiments with $Bu^tO_2H$ and $Ti^{III}$, the methyl radical (see reactions [18] and [19]) is directly detectable (45). When the experiment is carried out in the presence of $CH_2{:}NO_2^-$, the spectrum of $MeCH_2NO_2^{-\cdot}$ becomes detectable; at pH 9.5, with $[CH_2{:}NO_2^-]$ ca. $10^{-3}$ mol $dm^{-3}$ the methyl radical is completely scavenged in this way (reaction [7]). Knowledge of the steady-state concentration of Me· in the absence of nitromethane (ca. $10^{-6}$ mol $dm^3$) and the rate constant for self-termination of ·Me (ca. $5 \times 10^9$ $dm^{-3}$ $mol^{-1}$ $s^{-1}$ (46)) leads to the conclusion that to scavenge Me· in this way the rate constant for the addition reaction [7] must be $>10^7$ $dm^3$ $mol^{-1}$ $s^{-1}$. When $[CH_2{:}NO_2^-]$ is raised, the signal from $MeCH_2NO_2^{-\cdot}$ is joined by that attributed to $Bu^tOCH_2NO_2^{-\cdot}$ (with a 1:1 ratio of the Me· and $Bu^tO$· adducts for $[CH_2{:}NO_2^-]$ ca. 0.005 mol $dm^{-3}$): we conclude that addition now competes with fragmentation and also, employing steady-state analysis of the kind described in ref. (14), that $k_{20}/k_{19}$ is ca. $2 \times 10^2$ $dm^3$ $mol^{-1}$.

[18] $Bu^tO_2H + Ti^{III} \rightarrow Ti^{IV} + OH^- + Bu^tO\cdot$

[19] $Bu^tO\cdot \rightarrow Me_2C{=}O + Me\cdot$

[7] $Me\cdot + CH_2{:}NO_2^- \rightarrow MeCH_2NO_2^{-\cdot}$

[20] $Bu^tO\cdot + CH_2{:}NO_2^- \rightarrow Bu^tOCH_2NO_2^{-\cdot}$

Other reactions which can be demonstrated (14) in this way include the 1,2-shift typical of primary alkoxy radicals in aqueous solution (reactions [21] and [22]) and the competing 1,5-shift in [23] (with $k_{22} \simeq k_{23}$); from experiments in which the 1,2-shift is in competition with intermolecular hydrogen-atom abstraction (e.g. the formation of $\cdot CH_2OH$ from PrO· and $CH_3OH$) it is suggested that the pseudo first-order rate constant $k_{21}$ is ca. $10^7$ $s^{-1}$ ($k_{22}$ and $k_{23}$ are presumably also of this magnitude), and the lower limit for addition of propoxyl to $CH_2{:}NO_2^-$ is estimated as $10^8$ $dm^3$ $mol^{-1}$ $s^{-1}$. It is likely that $k_{20}$ is $>10^8$ $dm^3$ $mol^{-1}$ $s^{-1}$ (it may be as high as $10^9$ $dm^3$ $mol^{-1}$ $s^{-1}$) and that $k_{19}$ is in the range $10^6$–$10^7$ $s^{-1}$ (much faster than the fragmentation rate in non-aqueous solution, cf. ref. 47). Particularly rapid reactions ($>10^8$ $s^{-1}$) are the cyclisation (reaction [24]) and the fragmentation and intramolecular abstraction reactions [25] and [26], in which no intermediate alkoxyl radicals could be intercepted.

*(b) Generation and reaction of aroyloxyl and acyloxyl radicals.* As mentioned earlier, oxidation of benzoate ion with $SO_4^{-\cdot}$ in the presence of $CH_2{:}NO_2^-$ at pH 9 led to the detection of signals assigned to $PhCO_2CH_2NO_2^{-\cdot}$ and $PhCH_2NO_2^{-\cdot}$ (evidently formed as in reactions [9] and [10]), as

[21] $CH_3CH_2CH_2{-}O\cdot \xrightarrow{(H_2O)} CH_3CH_2\dot{C}HOH$

[22] $CH_3CH_2CH_2CH_2{-}O\cdot \rightarrow CH_3CH_2CH_2\dot{C}HOH$

[23] $CH_3CH_2CH_2CH_2{-}O\cdot \rightarrow \cdot CH_2CH_2CH_2CH_2OH$

[24]

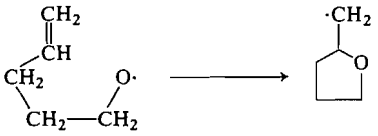

[25]

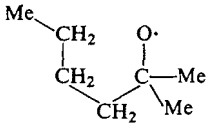

$\rightarrow MeCHCH_2CH_2CMe_2OH$

[26] $\rightarrow MeCH_2CH_2\dot{C}H_2 + Me_2CO$

well as to those of $O_2NCH_2CH_2NO_2^{-\cdot}$ and $^-O_3OSCH_2NO_2^{-\cdot}$ formed by direct reaction between $SO_4^{-\cdot}$ and the trap (32). The assignment $PhCO_2CH_2NO_2^{-\cdot}$ has been challenged (27, 48) on the grounds that an (unassigned) spectrum with these parameters is also detected from the reaction between photolytically generated $SO_4^{-\cdot}$ and $CH_2{:}NO_2^-$ in the absence of benzoate (48). However, important structural evidence (which also provides interesting mechanistic insight) that the assignments to $PhCO_2CH_2NO_2^{-\cdot}$ (**10**) and $PhCH_2NO_2^{-\cdot}$ (**11**) are correct stems from the observation that these same two signals are detected (32) when peroxybenzoic acid is reduced by $Ti^{III}$ under identical conditions. As expected if reactions [27]–[30] are involved, the intensity of the signal assigned to **10** increased at the expense of **11** as $[CH_2{:}NO_2^-]$ was increased (precisely as found for the $PhCO_2^-/SO_4^{-\cdot}$ oxidation). An upper limit for the decarboxylation of benzoyloxyl of ca. $2.5 \times 10^5$ $s^{-1}$ is calculated from the concentration of nitromethane needed to capture $PhCO_2\cdot$ (35).

[27] $PhCO_2OH + Ti^{III} \rightarrow PhCO_2\cdot + OH^- + Ti^{IV}$

[28] $PhCO_2\cdot + CH_2{:}NO_2^- \rightarrow PhC(=O)OCH_2NO_2^{-\cdot}$

**10**

[29] $PhCO_2\cdot \rightarrow Ph\cdot + CO_2$

[30] $Ph\cdot + CH_2{:}NO_2^- \rightarrow PhCH_2NO_2^{-\cdot}$

**11**

For some substituted aromatic derivatives, however, oxidation of $ArCO_2^-$ by $SO_4^{-\cdot}$ and reduction of the corresponding peroxyacid by $Ti^{III}$ led to contrasting esr observations. For example, *p*-peroxytoluic acid and $Ti^{III}$ gave not only the adducts attributed the structures **19** and **20** but also a weak signal of the adduct **21**; in the oxidation of *p*-toluate with $SO_4^{-\cdot}$, however, only **19** and **21**

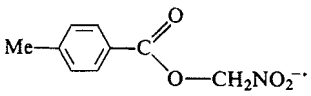

**19**

| | |
|---|---|
| *a*(N) | 2.39 mT |
| *a*(2H) | 0.74 mT |
| *g* | 2.0050 |

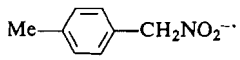

**20**

| | |
|---|---|
| *a*(N) | 2.565 mT |
| *a*(2H) | 0.95 mT |
| *g* | 2.0050 |

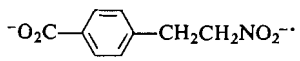

**21**

| | |
|---|---|
| *a*(N) | 2.55 mT |
| *a*(2H) | 0.945 mT |
| *a*(2H) | 0.076 mT |
| *g* | 2.0050 |

could be detected, with no trace of **20**. Increase of $CH_2{:}NO_2^-$ in the former system led to an increase of [**19**] at the expense of [**20**] and [**21**], whereas in the latter experiment the ratio of [**19**] to [**21**] remained constant.

These results cannot be rationalized on the basis of a scheme in which a common intermediate ($MeC_6H_4CO_2\cdot$) is formed *directly* from both $ArCO_2^-$ and $ArCO_3H$ in the two systems. Our findings can, however, be rationalized by the mechanism outlined in Scheme 5; we envisage that in the peroxyacid reduction, the aroyloxyl radical (**22**), once formed, can undergo competing reactions involving fragmentation (to give the aryl radical, which is then trapped), addition to $CH_2{:}NO_2^-$, and intermolecular hydrogen abstraction from *p*-toluate formed *in situ* to give, ultimately **21** (the benzyl radical itself can be directly detected in the absence of trap; its signal is intensified when *p*-toluate is added to the system). In contrast, in the oxidation of *p*-toluate with $SO_4^{-\cdot}$ the relatively low concentration of aroyloxyl radical trapped and the much stronger signal from **21** — and the invariance of their ratio with $[CH_2NO_2^-]$ — implies that a first-formed intermediate (evidently the radical-cation **23**, *cf.* also ref. 49) is partitioned between loss of a proton, to give the benzyl radical, and conversion into the aroyloxyl radical *before* trapping with $CH_2{:}NO_2^-$. Our finding thus emphasizes the fact that **22** and **23** are not representations (canonical forms) of a single species but that the two are distinct chemical entities; these results are in accord with the suggestion (50) that **22** is a σ-radical (*cf.* **24**), with the unpaired electron in an in-plane σ-orbital, in contrast with the structure of the π-type zwitterion **23** (*cf.* **25**) (examples of this type of radical have been characterized by esr (49)).

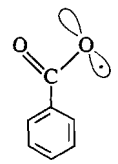

**24**

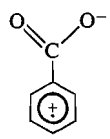

**25**

Similar observations were made for the reactions of *o*-toluate and *o*-peroxytoluic acid with the notable difference that in the reduction of the peracid in the presence of the trap a much greater concentration of the benzyl-type adduct was obtained; this is consistent with the occurrence of very rapid intramolecular hydrogen-atom transfer in the aroyloxyl radical (reaction [31]).

[31] 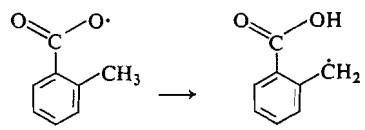

Decomposition with $Ti^{III}$ of a variety of peroxoacids (formed in the perhydrolysis of esters and anhydrides with $HO_2^-$ at ca. pH 9) is also thought to proceed via the corresponding aroyloxyl and acyloxyl radicals as precursors of decarboxylated radicals (Ar·, R·) (35). Although the acetoxyl radical was not itself trapped, some aliphatic acyloxy radicals $RCO_2\cdot$ (R = cyclopropyl, $CH_2{=}CH$) live

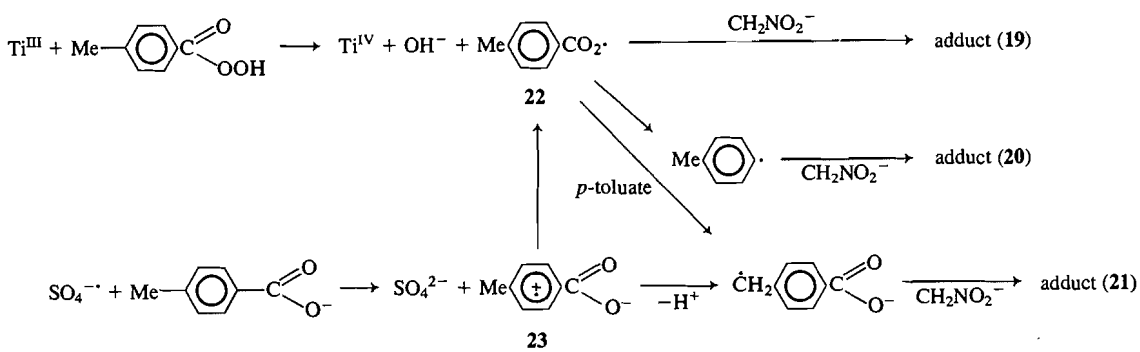

**22**

**23**

SCHEME 5

Can. J. Chem. Downloaded from www.nrcresearchpress.com by 210.87.254.105 on 09/06/12
For personal use only.

long enough to be detected via their adducts with the nitromethane *aci*-anion: the rate constants of their decarboxylation are thought to be in the range $10^5$–$10^7$ $s^{-1}$.


## Acknowledgements

We thank the S.R.C. for financial assistance for this work and the Royal Society of Chemistry for providing travel assistance (Career Award) for B.C.G.



1. (*a*) A. H. Maki and D. H. Geske. J. Am. Chem. Soc. **83**, 1852 (1961); (*b*) D. H. Geske, J. L. Ragle, M. A. Bambenek, and A. L. Balch. J. Am. Chem. Soc. **86**, 987 (1964).
2. P. Ludwig, T. Layloff, and R. N. Adams. J. Am. Chem. Soc. **86**, 4568 (1964).
3. R. L. Ward. J. Chem. Phys. **30**, 852 (1959); J. Am. Chem. Soc. **83**, 1296 (1961).
4. T. Fujinaga, Y. Deguchi, and K. Umemoto. Bull. Chem. Soc. Jpn. **37**, 822 (1964).
5. (*a*) G. A. Russell, E. G. Janzen, and E. T. Ström. J. Am. Chem. Soc. **86**, 1807 (1964); (*b*) R. C. Kerber, G. W. Urry, and N. Kornblum. J. Am. Chem. Soc. **87**, 4520 (1965).
6. A. K. Hofmann, A. M. Feldman, E. Gelblum, and W. G. Hodgson. J. Am. Chem. Soc. **86**, 639 (1964).
7. T. M. McKinney and D. H. Geske. J. Chem. Phys. **44**, 2277 (1966).
8. J. H. Freed and G. K. Fraenkel. J. Chem. Phys. **40**, 1815 (1964); **41**, 699 (1964).
9. W. M. Gulick, Jr. and D. H. Geske. J. Am. Chem. Soc. **87**, 4049 (1965); J. Gendell, J. H. Freed, and G. K. Fraenkel. J. Chem. Phys. **37**, 2832 (1962).
10. P. Neta and D. Meisel. J. Phys. Chem. **80**, 819 (1976).
11. P. B. Ayscough, A. J. Elliott, and G. A. Salmon. J. Chem. Soc. Faraday Trans. I, **74**, 511 (1978).
12. (*a*) B. C. Gilbert and M. Trenwith. J. Chem. Soc. Perkin Trans. II, 2010 (1973); (*b*) J. Spanget-Larsen. Theor. Chim. Acta, **51**, 65 (1979).
13. B. C. Gilbert, R. O. C. Norman, and P. S. Williams. J. Chem. Soc. Perkin Trans. II, 207 (1981).
14. B. C. Gilbert, R. G. G. Holmes, H. A. H. Laue, and R. O. C. Norman. J. Chem. Soc. Perkin Trans. II, 1047 (1976).
15. G. Czapski. J. Phys. Chem. **75**, 2957 (1971); B. C. Gilbert, R. O. C. Norman, and R. C. Sealy. J. Chem. Soc. Perkin Trans. II, 2174 (1973).
16. D. Behar and R. W. Fessenden. J. Phys. Chem. **76**, 1710 (1972).
17. M. McMillan and R. O. C. Norman. J. Chem. Soc. B, 590 (1968).
18. A. Albert and E. P. Serjeant. Ionization constants of acids and bases. Methuen, London. 1962.
19. D. J. Edge and R. O. C. Norman. J. Chem. Soc. B, 182 (1969).
20. K.-D. Asmus and I. A. Taub. J. Phys. Chem. **72**, 3382 (1968).
21. K.-D. Asmus, A. Henglein, and G. Beck. Ber. Busenges. Phys. Chem. **70**, 459 (1966).
22. M. C. R. Symons. J. Am. Chem. Soc. **91**, 5924 (1969).
23. B. C. Gilbert, R. O. C. Norman, G. Placucci, and R. C. Sealy. J. Chem. Soc. Perkin Trans. II, 885 (1975).
24. B. C. Gilbert, J. P. Larkin, and R. O. C. Norman. J. Chem. Soc. Perkin Trans. II, 1272 (1972).
25. D. J. Edge, R. O. C. Norman, and P. M. Storey. J. Chem. Soc. B, 1096 (1970).
26. D. J. Edge and R. O. C. Norman. J. Chem. Soc. B, 1083 (1970).
27. H. Zemel and R. W. Fessenden. J. Phys. Chem. **79**, 1419 (1975).
28. N. H. Anderson, M. McMillan, and R. O. C. Norman. J. Chem. Soc. B, 1075 (1970).
29. E. G. Janzen. Top. Stereochem. **6**, 177 (1971).
30. M. C. R. Symons and J. H. Sharp. Nature, **224**, 1297 (1969); C. Chachaty. C. R. Hebd. Seances Acad. Sci. **262**, 680 (1966); C. Chachaty and C. Rosilio. J. Chim. Phys. Phys. Chim. Biol. **64**, 777 (1967).
31. B. C. Gilbert, R. G. G. Holmes, and R. O. C. Norman. J. Chem. Res. (M) 0101, (S) 1 (1977).
32. B. Ashworth, B. C. Gilbert, R. G. G. Holmes, and R. O. C. Norman. J. Chem. Soc. Perkin Trans. II, 951 (1978).
33. N. H. Anderson and R. O. C. Norman. J. Chem. Soc. B, 993 (1971).
34. A. J. Dobbs, B. C. Gilbert, and R. O. C. Norman. J. Chem. Soc. Perkin Trans. II, 786 (1972).
35. B. C. Gilbert, R. G. G. Holmes, P. D. R. Marshall, and R. O. C. Norman. J. Chem. Res. (S) 172, (M) 1949 (1977).
36. R. O. C. Norman and P. M. Storey. J. Chem. Soc. B, 1009 (1971).
37. B. C. Gilbert, J. P. Larkin, and R. O. C. Norman. J. Chem. Soc. Perkin Trans. II, 272 (1973).
38. G. Brunton, B. C. Gilbert, and R. J. Mawby. J. Chem. Soc. Perkin Trans. II, 650 (1976).
39. B. C. Gilbert, J. P. Larkin, R. O. C. Norman, and P. M. Storey. J. Chem. Soc. Perkin Trans. II, 1508 (1972).
40. A. L. J. Beckwith. Aust. J. Chem. **25**, 1887 (1972).
41. P. J. Krusic and J. K. Kochi. J. Am. Chem. Soc. **93**, 846 (1971).
42. J. A. Howard, Y. Ohkatsu, J. H. B. Chenier, and K. U. Ingold. Can. J. Chem. **51**, 1543 (1973).
43. B. C. Gilbert and M. Trenwith. J. Chem. Soc. Perkin Trans. II, 1834 (1973).
44. B. C. Gilbert, H. A. H. Laue, R. O. C. Norman, and R. C. Sealy. J. Chem. Soc. Perkin Trans. II, 1040 (1976).
45. M. F. R. Mulcahy, J. R. Steven, and J. C. Ward. Aust. J. Chem. **18**, 1177 (1965).
46. B. C. Gilbert, R. O. C. Norman, and R. C. Sealy. J. Chem. Soc. Perkin Trans. II, 303 (1975).
47. D. J. Carlsson and K. U. Ingold. J. Am. Chem. Soc. **89**, 4891 (1967).
48. H. Zemel and R. W. Fessenden. J. Phys. Chem. **82**, 2670 (1978).
49. S. Steenken, P. O'Neill, and D. Schulte-Frohlinde. J. Phys. Chem. **81**, 26 (1977).
50. M. B. Yim, O. Kikuchi, and D. E. Wood. J. Am. Chem. Soc. **100**, 1869 (1978); J. M. McBride and R. A. Merrill. J. Am. Chem. Soc. **102**, 1723 (1980).


Can. J. Chem. Downloaded from www.nrcresearchpress.com by 210.87.254.105 on 09/06/12
For personal use only.

# Metal-nitroxyl interactions. 25. Exchange interactions via saturated linkages in spin-labeled porphyrins

KUNDALIKA M. MORE AND GARETH R. EATON[1]
*Department of Chemistry, University of Denver, Denver, CO 80208 U.S.A.*
AND
SANDRA S. EATON[1]
*Department of Chemistry, University of Colorado at Denver, Denver, CO 80202 U.S.A.*

Received July 15, 1981

KUNDALIKA M. MORE, GARETH R. EATON, and SANDRA S. EATON. Can. J. Chem. **60**, 1392 (1982).

A series of spin-labeled copper porphyrins has been prepared in which nitroxyl radicals are attached to a porphyrin pyrrole ring by propionamide and propionate ester linkages. The solution epr spectra at room temperature indicate that the values of the electron spin – electron spin coupling constant, $J$, for these compounds are in the range 4 to 18 G, depending on the solvent and the size of the nitroxyl ring. Below −45°C two isomers with different values of $J$ were observed in the epr spectra of two of the compounds. Variable temperature epr spectra were also analyzed for analogous spin-labeled copper porphyrins which have *cis* and *trans* acrylic ester and acrylamide linkages between the porphyrin and the nitroxyl ring. Comparison of the values of $J$ for the complexes with saturated and unsaturated linkages suggests that σ-bonding pathways dominate the copper–nitroxyl interaction in these compounds.

KUNDALIKA M. MORE, GARETH R. EATON et SANDRA S. EATON. Can. J. Chem. **60**, 1392 (1982).

On a préparé une série de phorphyrines de cuivre, contenant un marqueur de spin, dans lesquelles les radicaux nitroxyles sont attachés à la portion porphyrine du cycle pyrrole par des amides et des esters propioniques. Les spectres de rpe, en solution et à la température ambiante, indique que les constantes de couplage spin électron – spin électron dans ces composés varient de 4 à 18 G selon le solvant et la taille du cycle nitroxyle. A des températures inférieures à −45°C, on a observé, dans les spectres de rpe de deux de ces composés, la présence de deux isomères ayant des valeurs différentes de $J$. On a également analysé les spectres de rpe à température variable des porphyrines de cuivre analogues contenant un marqueur de spin dans lesquelles on a intercalé entre le cycle nitroxyle et la portion porphyrine, des amides ou des esters acryliques avec des isomères *cis* et *trans*. La comparaison des valeurs de $J$ de ces complexes avec celles des produits saturés indique que l'interaction cuivre–nitroxyle induite dans ces composés se transmet principalement par les liaisons σ.

[Traduit par le journal]

## Introduction

Interactions between unpaired electrons may be observed via a variety of physical measurements. Of particular interest in biological systems are the interactions observable by electron paramagnetic resonance (epr) among various pairs or clusters of paramagnetic transition metals and/or organic free radicals (1). These paramagnetic centers may be a natural component of the biological system or they may be species purposely added as probes or labels (2). Interactions between these centers may affect the epr spectra enough to invalidate the usual interpretations. For example, a spin-labeled biomolecule may yield an epr spectrum which is not validly interpreted in terms of the motion of the label if a paramagnetic metal is present. If, however, the effect of the metal on the nitroxyl epr spectrum were understood in detail, additional information could be obtained from the epr spectrum. For example, an assessment was made several years ago of the effect of dipolar interactions between a metal and a nitroxyl radical on the epr lineshape of the nitroxyl in a rigid matrix (3). This approach has been used by many investigators to obtain metrical information on spin-labeled biomolecules (1). Others have studied the closely related problem of metal – organic radical interactions in vitamin $B_{12}$-dependent enzyme reactions also seeking metrical information (4, 5).

There is promise of achieving considerable insight into the metric and dynamic features of complicated systems, such as enzymes and membranes, by theoretical analysis and experimental calibration of the impact on their epr spectra and relaxation properties of interaction between unpaired electrons. Substantial confusion can result, however, if proper attention is not given to relevant features of the interaction regime. For example, one must consider relative motion of the two species, whether this motion is correlated or not, the nature of the interaction pathway, environment effects such as specific solvation, and potential nonstatistical effects such as specific ion pair or acid/base interactions. Consideration must also be given to relative values of the various characteristic times of the system, such as tumbling or collisional

[1]To whom all correspondence should be addressed.

0008-4042/82/121392-10$01.00/0
©1982 National Research Council of Canada/Conseil national de recherches du Canada

Can. J. Chem. Downloaded from www.nrcresearchpress.com by 210.87.254.105 on 09/06/12
For personal use only.

Can. J. Chem. Downloaded from www.nrcresearchpress.com by 210.87.254.105 on 09/06/12
For personal use only.

correlation times, electron spin relaxation times, nuclear spin relaxation times, reciprocal of the microwave frequency, and modulation frequency, etc. In some cases the electron–electron interaction can be observed in the lineshape of the normal continuous wave (CW) epr spectrum, and in other cases the interaction is observed only via a non-linear technique (such as CW saturation studies) or time domain (pulsed) epr.

Most work on interacting spin systems has been conducted either in low viscosity fluid solutions or in essentially rigid matrices such as frozen solutions or very slowly tumbling biomolecules. Still to be explored are intermediate tumbling regimes, liquid crystals, phase boundaries (e.g., membrane surfaces), and single crystals.

In this paper we briefly survey the range of phenomena which have been observed in low viscosity fluid solutions of paramagnetic transition metal complexes containing nitroxyl radicals, and mention some preliminary results from work in progress. Detailed description is given of a series of copper(II) porphyrin complexes **I–IX** in which a nitroxyl is observed to exhibit exchange interaction with the copper through a variety of metal–nitroxyl linkages, including a saturated $-CH_2-CH_2-$ chain.

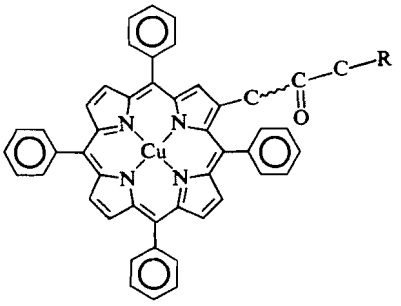

| R | C~C linkage | | |
|---|---|---|---|
| | *cis* C=C | *trans* C=C | saturated $-CH_2-CH_2-$ |
| 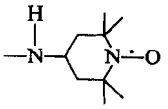 | I | IV | VII |
| 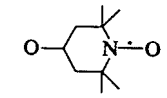 | II | V | VIII |
| 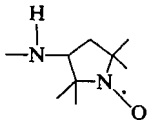 | III | VI | IX |

## Experimental section

Infrared spectra were obtained in Nujol mulls on a Perkin-Elmer 337 grating spectrometer. Electronic spectra were obtained in chloroform solution on a Beckman Acta V spectrometer. Data are given below with wavelengths in nm and log ε in parentheses. X-band epr spectra were obtained on a Varian E-9 spectrometer as previously described (6). Electron paramagnetic resonance spectra were run on degassed samples in dried purified solvents with concentrations about $10^{-3}$ *M*. All spectra were obtained with power levels well below saturation. *g*-Values were measured relative to DPPH ($g = 2.0036$). Electron paramagnetic resonance spectra are shown in the figures with the magnetic field increasing to the right. All coupling constants are given in G. High resolution mass spectra were obtained at the Midwest Center for Mass Spectrometry. Elemental analyses were performed by Spang Microanalytical Laboratory.

Can. J. Chem. Downloaded from www.nrcresearchpress.com by 210.87.254.105 on 09/06/12
For personal use only.

*Preparation of compounds*

Spin-labeled copper pophyrins **I–VI** were prepared as previously reported (7). *meso*-Tetraphenyl-1-[2-ethoxycarbonylethyl]porphyrin, **X**, was prepared by the method of Momenteau *et al.* (8). The presence of the propionate ester was confirmed by a high resolution mass spectrum. $M^+/e$ observed: 714.3051 ± 0.0126. Calcd. for $C_{49}H_{38}N_4O_2$: 714.2995.

*Copper(II)* meso-*tetraphenyl-1-[2-ethoxycarbonylethyl]-porphyrin,* ***XI***

Cupric chloride (0.2 g, 1.2 mmol) was refluxed with porphyrin **X** (0.72 g, 1 mmol) in DMF (100 mL) until the visible spectra indicated complete conversion to the metalloporphyrin. Water (100 mL) was added to the cooled reaction mixture and the precipitate was collected by filtration. The product was chromatographed on silica gel in $CHCl_3$ solution and the first red band was collected. The product was recrystallized from $CHCl_3$/heptane. Yield: 90%, ir: $\nu_{CO}$ 1720 $cm^{-1}$; vis: 570 (sh, 3.50), 539 (4.29), 416 (5.66).

*Copper(II)* meso-*tetraphenyl-1-[3-propionic acid]porphyrin,* ***XII***

KOH methanol in (7.5 mL, 2 *N*) was added to 100 mg of **XI** in 30 mL of pyridine. The solution was stirred for 24 h at room temperature. The solvent was removed and the residue was neutralized with aqueous HCl. The product was extracted into $CHCl_3$ and the solution was dried over $Na_2SO_4$. The volume of the solution was reduced to 30 mL before putting it on a silica gel column. Unreacted **XI** was eluted with $CHCl_3$. The product was eluted with 2% ethanol in $CHCl_3$ and recrystallized from $CHCl_3$/heptane. The acid appears to decompose when heated for prolonged periods in vacuum. Yield: 67%; ir: $\nu_{CO}$ 1685 $cm^{-1}$; vis: 570 (sh, 3.62), 539 (4.42), 416 (5.81).

*Copper(II)* meso-*tetraphenyl-1-[3-(N-(2,2,6,6-tetramethyl-piperidinyl-1-oxy))propionamido]porphyrin,* ***VII***

Oxalyl chloride (1.1 g, 10 mmol) was added to a solution of **XII** (0.15 g, 0.2 mmol) in 50 mL of dry benzene. The solution was stirred for 2 h at room temperature. The solvent was removed in vacuum and the residue was kept under vacuum for 2 h before dissolving it in 75 mL dry THF and 1 mL dry pyridine. 4-Amino-2,2,6,6-tetramethylpiperidinyl-1-oxy (0.034 g, 0.2 mmol) in 2 mL dry THF was added dropwise under nitrogen. After refluxing the solution for 6 h, the solvent was removed in vacuum and the residue was chromatographed on silica gel in $CHCl_3$ solution. The first red band was collected. The product was recrystallized from $CHCl_3$/heptane. Yield: 61%; ir: $\nu_{CO}$ 1655 $cm^{-1}$, $\nu_{NH}$ 3300 $cm^{-1}$; vis: 570 (sh, 3.65), 539 (4.48), 416 (5.86). *Anal.* calcd. for $C_{56}H_{49}CuN_6O_2$: C 74.60, H 5.48, N 9.32; found: C 74.81, H 5.59; N 9.47.

*Copper(II)* meso-*tetraphenyl-1-[3-(O-(2,2,6,6-tetramethyl-piperidinyl-1-oxy))propionic ester]porphyrin,* ***VIII***

The ester was prepared from copper porphyrin **XII** and 4-hydroxy-2,2,6,6-tetramethyl-piperidinyl-1-oxy by the same procedure as described for **VII**. Yield: 55%. ir: $\nu_{CO}$ 1725 $cm^{-1}$; vis: 570 (sh, 3.64), 539 (4.51), 416 (5.89). *Anal.* calcd. for $C_{56}H_{48}CuN_5O_3$: C 74.52, H 5.36, N 7.76; found: C 74.24, H 5.23, N 7.57.

*Copper(II)* meso-*tetraphenyl-1-[3-(N-(2,2,5,5-tetramethyl-pyrrolidinyl-1-oxy))propionamido]porphyrin,* ***IX***

The amide was prepared from copper porphyrin **XII** and 3-amino-2,2,5,5-tetramethylpyrrolidinyl-1-oxy by the same procedure as described for **VII**. Yield: 67%; ir: $\nu_{C=O}$ 1650 $cm^{-1}$, $\nu_{NH}$ 3320 $cm^{-1}$; vis: 570 (sh, 3.47), 539 (4.28), 416 (5.66). *Anal.* calcd. for $C_{55}H_{47}CuN_6O_2$: C 74.43, H 5.34, N 9.47; found: C 74.27, H 5.21, N 9.28.

## Computer simulations

The interaction between two spins can be expressed in terms of dipolar and exchange components. The main distinguishing feature of dipolar interactions relative to exchange interactions is the angular and distance dependence of the dipolar interactions. It can be shown that expansion of the exchange and dipolar parts of the spin–spin interaction both lead to linear combinations of the same set of nine components of the interaction dyadic (5). The exchange and dipolar components differ only in the scalar coefficients of the dyads (which are bilinear in the spin operators). An epr experiment can yield the values of the coefficients, but their interpretation in terms of exchange and/or dipolar contribution is not unambiguous without additional information such as the geometry of the interaction. The exchange interaction can be written as the sum of three matrices: isotropic exchange, antisymmetric exchange, and symmetric anisotropic exchange. The symmetric anisotropic exchange matrix has precisely the same formal structure as the dipole–dipole interaction matrix, i.e., it is anisotropic but symmetrical about the main diagonal. In rigid media all of these terms have to be considered. However, in rapidly tumbling molecules with the normally encountered $g$-values and distances, it can be estimated that terms other than isotropic exchange average to nearly zero, i.e., less than the linewidths due to other effects. In this case, to which we shall restrict our attention in the rest of the discussion, the isotropic exchange can be treated as a scalar $J$.

It has sometimes been assumed that spin–spin exchange interactions are negligible for distances greater than about 6 Å (9, 10). However, proton–proton spin–spin coupling attributable to exchange interactions has been observed through five bonds in saturated systems and through nine bonds in conjugated hydrocarbons (11). Coupling to distant protons has also been observed in ENDOR spectra (12). Since the electron magnetic moment is much larger than the proton magnetic moment, it is reasonable to expect even longer range spin–spin interactions between two electrons than between two protons or between a proton and an electron. Orbital interactions through six bonds have also been found to be sufficiently large to alter chemical reactivity (13).

A few years ago we reported the first examples of high resolution electron spin – electron spin splitting in epr spectra (14, 15). These spectra can be interpreted in terms of the Hamiltonian [1].

Can. J. Chem. Downloaded from www.nrcresearchpress.com by 210.87.254.105 on 09/06/12
For personal use only.

$$[1]\quad \mathcal{H} = g_1\beta H\hat{S}_{1Z} + g_2\beta H\hat{S}_{2Z} + hJ\hat{S}_{1Z}\hat{S}_{2Z} + \frac{hJ}{2}(\hat{S}_{1+}\hat{S}_{2-} + \hat{S}_{1-}\hat{S}_{2+}) + hA_M\hat{S}_{1Z}\hat{I}_{1Z} + hA_N\hat{S}_{1Z}\hat{I}_{2Z} + hA_{N'}\hat{S}_{2Z}\hat{I}_{3Z} + \frac{hA_M}{2} \times (\hat{S}_{1+}\hat{I}_{1-} + \hat{S}_{1-}\hat{I}_{1+}) - g_M\beta_N H\hat{I}_{1Z} - g_N\beta_N H\hat{I}_{2Z} - g_{N'}\beta_N H\hat{I}_{3Z}$$

where $g_1$ and $g_2$ are the $g$ values of the metal and nitroxyl electrons; $\hat{S}_1$ and $\hat{S}_2$ refer to the metal and nitoxyl electron spins, respectively; $J$ is the electron–electron coupling constant in Hertz; $I_1$, $I_2$, and $I_3$ refer to the metal nuclear spin, the nuclear spin of the coordinated nitrogens, and the nuclear spin of the nitroxyl nitrogen, respectively; $A_M$ is the metal electron – metal nuclear coupling constant in Hertz; $A_N$ is the coupling constant in Hertz between the metal electron and the nuclear spins of the coordinated nitrogens; $A_{N'}$ is the coupling constant in Hertz between the nitroxyl electron and the nuclear spin of the nitroxyl nitrogen; and all other symbols are defined as in ref. 16. The first seven terms in the Hamiltonian were treated exactly and the last four were treated as a perturbation to second order for the transition energies and to first order for the transition probabilities. To facilitate visual comparison with the field-swept experimental spectra the values of $J$, $A_M$, $A_N$, and $A_{N'}$ are discussed below in units of G with the conversion between Hertz and Gauss given by eqs. [2]–[4]. The conversion factor for $A_N$ is the same as for $A_M$. Only the absolute value of $J$ can be determined from these calculations.

$$[2]\quad J(\mathrm{G}) = J(\mathrm{Hz}) \cdot \frac{h}{2\beta}\left(\frac{1}{g_1} + \frac{1}{g_2}\right)$$

$$[3]\quad A_M(\mathrm{G}) = A_M(\mathrm{Hz}) \cdot \frac{h}{g_1\beta}$$

$$[4]\quad A_{N'}(\mathrm{G}) = A_{N'}(\mathrm{Hz}) \cdot \frac{h}{g_2\beta}$$

The simulation of epr spectra using Hamiltonian [1] has been reported in detail (16). The computer program CUNO described in ref. 16 has been extended to handle any nuclear spin and to allow more flexibility in simulating linewidths. The essential feature of the calculation can be seen with a simple "stick" diagram (Fig. 1). Each copper transition interacts with each nitroxyl transition producing an "AB quartet" of four lines, analogous to the well-known AB patterns of $^1$H nmr. The

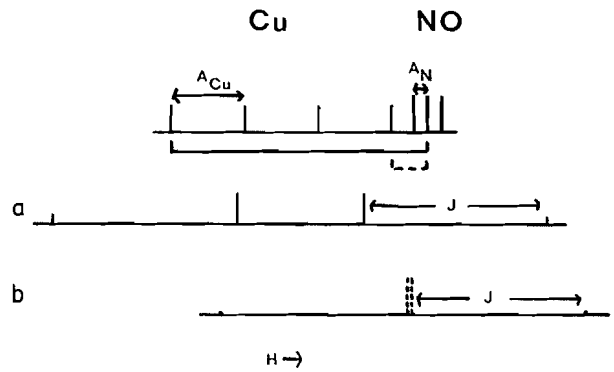


FIG. 1. Schematic representation of two of the AB patterns resulting from interaction of a copper electron ($A_{Cu}$ = 86 G) with a nitroxyl electron ($A_N$ = 15 G) for a value of $J$ of 200 G. The stick spectrum labeled *a* arises from coupling between the $m_I$ = 3/2 copper line (lowest field copper line) and the $m_I$ = 0 nitroxyl line. The stick spectrum labeled *b* arises from coupling between the $m_I$ = −3/2 copper line (highest field copper line) and the $m_I$ = 0 nitroxyl line.

lines in the spectra are referred to as copper or nitroxyl depending on the nature of the transition as $J$ approaches zero. The intensities of the inner and outer lines of the quartet are dependent on the magnetic field separation between the original copper and nitroxyl lines that are interacting and the magnitude of $J$. Figure 1 illustrates this for two different cases. The $m_I$ = +3/2 Cu line and the $m_I$ = 0 line of the nitroxyl are sufficiently far apart that with a $J$ of 200 G, a clear four-line pattern is produced in which the outer lines have significant intensity (Fig. 1, stick spectrum *a*). The Cu −3/2 line and the nitroxyl 0 line are so close together, though, that with a $J$ of 200 G the inner copper and nitroxyl lines are almost superimposed, and the outer lines have little intensity and may in practice not be observable if the linewidths are large (Fig. 1, stick spectrum *b*). Thus, even within a single compound a wide range of ratios of $J$ to the metal-nitroxyl energy separations may occur.

Figure 2 shows observed and calculated room temperature epr spectra for spin-labeled copper porphyrins **VIII**, **XIII** (15, 17), and **XIV** (18). When $J$ is small, as in Fig. 2*A*, the nitroxyl region of the spectrum is an overlapping doublet of triplets and the copper lines only appear to be broadened. In Fig. 2*B* the value of $J$ (78 G) is close to the copper nuclear hyperfine coupling (86 G) so the copper signal is an apparent five-line pattern partially obscured by the sharper nitroxyl lines. The nitroxyl lines are a clearly resolved doublet of triplets. When $J$ is 800 G, as in Fig. 2*C*, the copper and nitroxyl inner lines are nearly coincident, the

Can. J. Chem. Downloaded from www.nrcresearchpress.com by 210.87.254.105 on 09/06/12
For personal use only.

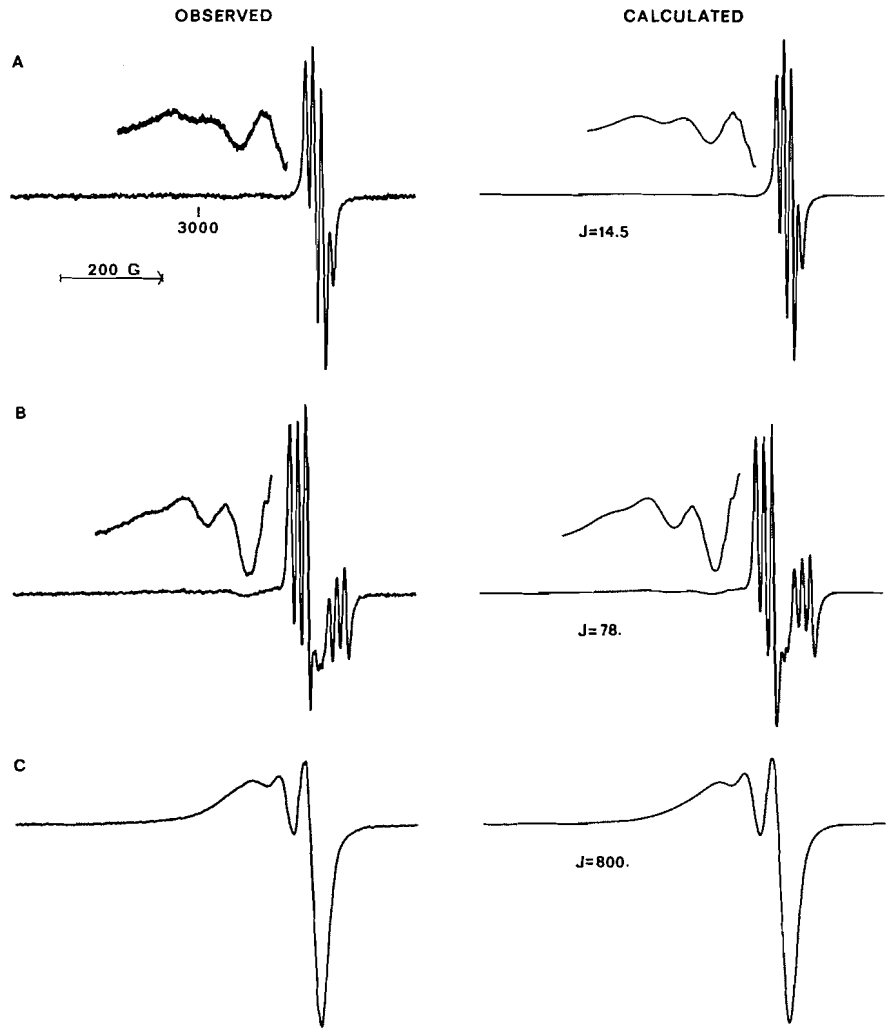


FIG. 2. X-band epr spectra of three spin-labeled copper porphyrins at room temperature and computer simulations to demonstrate the effect of the value of $J$ on the appearance of the spectra. The three spectra are 800 G scans centered at 3025 G. *A*, The spectrum of **VIII** in toluene solution was obtained with 0.63 G modulation amplitude and 4.0 mW power. The computer simulated spectrum was obtained with $J$ = 14.5 G. *B*, The spectrum of **XIII** in $CHCl_3$ solution was obtained with 0.8 G modulation amplitude and 20 mW power. The value of $J$ in the simulated spectrum is 78 G. *C*, The spectrum of **XIV** in toluene solution was obtained with 2 G modulation amplitude and 15 mW power. The value of $J$ in the simulated spectrum is 800 G.

apparent copper hyperfine splitting is one-half $A_{Cu}$ (1/2 × 86 G) and the outer lines of the AB pattern are not observed. Overall there is good agreement between the observed and calculated spectra. There is, however, some discrepancy for the lowest field copper lines due to incomplete motional averaging of $g$- and $A$-anisotropy which is not included in the computer simulations.

## Results and discussion

Details are given in the Experimental section for the preparation and characterization of the nitroxyl spin labeled copper porphyrin complexes **VII–IX**. In this section we describe the epr spectra of these compounds and compare them with the spectra of the closely related compounds **I–VI** for which the room temperature epr spectra have previously been reported (7). This series of compounds was designed to compare spin–spin interaction through saturated and unsaturated C—C linkages, keeping everything else as similar as is possible in a series of different compounds.

In a variety of solvents at room temperature the value of $J$ for spin-labeled copper porphyrin **VII**

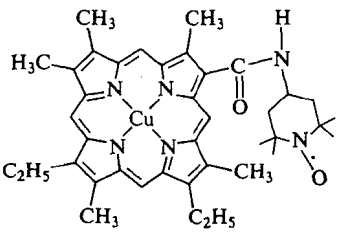

XIII

ranged from 9 to 17 G (cf. Table 1). Similar values of $J$ were observed for **VIII** which contains an ester linkage instead of an amide linkage. The epr spectra of **VIII** in $CHCl_3$ solution (Fig. 2*A*) are typical of the spectra observed for both **VII** and **VIII** at room temperature. The values of $J$ for **VII** and **VIII** are smaller than those previously observed for **IV** and **V** (19–26 G, cf. Table 1) which have a *trans* olefinic linkage between the porphyrin and the nitroxyl (7). For the analogous *cis* isomers **I–III** in noncoordinating solvents the values of $J$ are strongly dependent on solvent and temperature which was attributed to an interaction between the carbonyl oxygen and the porphyrin $\pi$-system or the copper (7). This interaction is blocked by pyridine coordination, so all comparisons in this paper involving the *cis* isomers will be based on spectra taken in the presence of coordinating solvents. Under these conditions the values of $J$ for **I** and **II** are smaller than for **VII** and **VIII**, indicating that exchange interactions through the C—C linkages at room temperature increase in the order

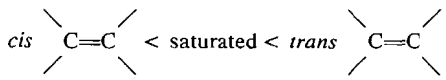


The values of $J$ for **III**, **VI**, and **IX** which contain the pyrrolidine nitroxyl are so small for all three linkages that trends are difficult to ascertain.

We had previously observed that at room temperature in $CHCl_3$ solution two species were observed in the epr spectrum of **V** (7) with values of $J$ of 15.5 and 26.0 G. When the solution is cooled, the lines in the spectrum sharpen and at −40°C the values of $J$ are 13 and 38 G. At room temperature in 2:1 toluene: pyridine solution and in other solvents tested, a single value of $J$ is observed for **V**. However, when a solution of **V** in 2:1 toluene: pyridine is cooled, two species are observed in the epr spectra at 10°C and below (cf. Fig. 3). The values of $J$ for the two isomers at −60°C are 11 and 38 G. We previously reported that nmr studies indicated a specific interaction between halogenated solvents and spin-labeled copper porphyrin **V** (7). It appears that this interaction raises the barrier

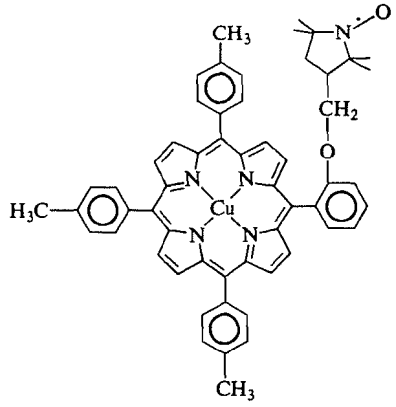

XIV

to interconversion of the two isomers such that two species are observable at room temperature in halogenated solvents but reduced temperatures are required to observe separate signals for the two

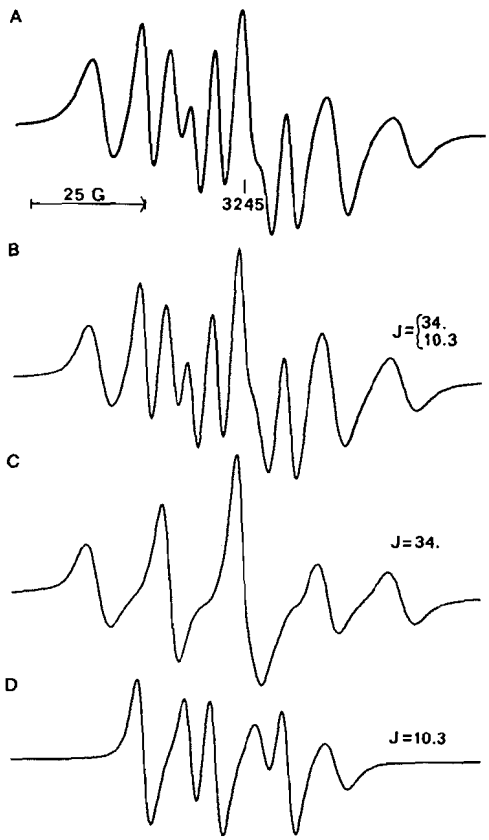


FIG. 3. *A*, 100 G scan of the nitroxyl region of the X-band epr spectrum of **V** at −29°C in 2:1 toluene:pyridine solution obtained with 0.4 G modulation amplitude and 20 mW power. *B*, Computer simulated spectrum with two isomers, $J$ = 34 G (60%) and $J$ = 10.3 (40%). *C*, Contribution to the simulated spectrum from isomer with $J$ = 34 G. *D*, Contribution to the simulated spectrum from isomer with $J$ = 10.3 G.

Can. J. Chem. Downloaded from www.nrcresearchpress.com by 210.87.254.105 on 09/06/12
For personal use only.

Can. J. Chem. Downloaded from www.nrcresearchpress.com by 210.87.254.105 on 09/06/12
For personal use only.

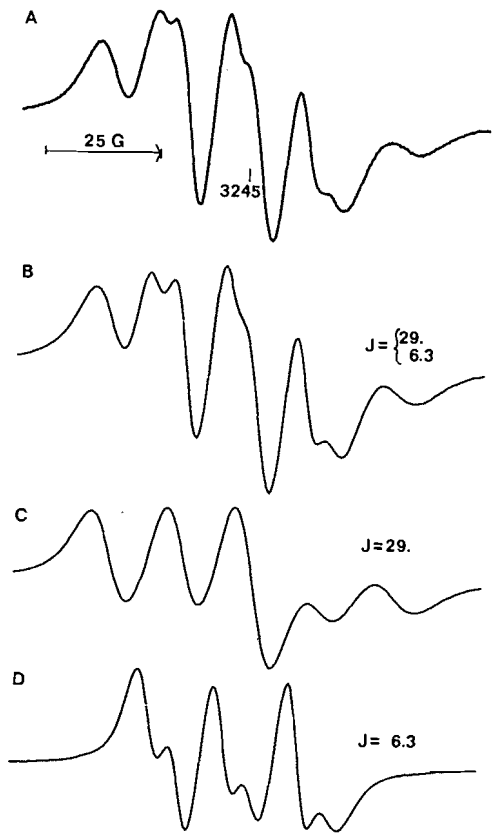


FIG. 4. *A*, 100 G scan of the nitroxyl region of the X-band epr spectrum of **VIII** at −59°C in 1:1 toluene:$CH_2Cl_2$ solution obtained with 0.4 G modulation amplitude and 10 mW power. *B*, Computer simulated spectrum with two isomers $J = 29$ G (65%), and $J = 6.3$ G (35%). *C*, Contribution to the simulated spectrum from isomer with $J = 29$ G. *D*, Contribution to the simulated spectrum from isomer with $J = 6.3$ G.

isomers in other solvents. Only a single isomer was observed in the epr spectra of the amides with *trans* olefin linkages, **IV** and **VI**.

When solutions of **VIII** in 1:1 toluene:$CH_2Cl_2$ or 2:1 toluene:pyridine were cooled, two isomers were observed in the epr spectra at temperatures below −45°C. As shown in Fig. 4 the spectra in 1:1 toluene:$CH_2Cl_2$ at −59°C could be simulated with $J = 6$ and 30 G. Similarly at temperatures below −45°C two isomers were observed in the epr spectra of **VII**. At −60°C in 1:1 toluene:$CH_2Cl_2$ the values of $J$ are 4 and 25 G. Low temperature spectra of **I–III** and **IX** were also examined, but the values of $J$ are sufficiently small and the low temperature linewidths sufficiently broad that it is difficult to determine whether more than one isomer is present.

*Conformational equilibria*

Wojcik and Witanowski have studied halogenated acrylamides and concluded that for the *trans* olefin there is a single conformer **XV** (X = Cl, Br, I) (19) with a *Z* conformation (20) around the $C_a$—$C_b$ bond. The barrier to rotation about the amide C—N bond in acrylamides has been observed to be 12–16 kcal/mol, depending on the substituents on the olefin (21) so the rotation about the C—N bond in **IV** would be expected to be slow on the epr time scale at room temperature. By analogy with polypeptide amide linkages it would be expected that the piperidine ring would be oriented *cis* to the carbonyl group (22). These analogies suggest that **XVI** (Y = NH) is the conformation of **IV**, that other

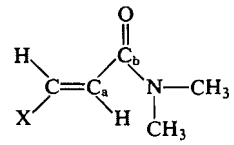


**XV**

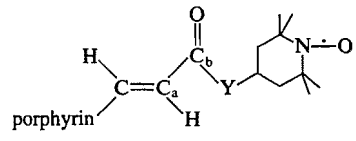


**XVI**

isomers are unlikely, and that the structure is rigid on the epr time scale. The observation of a single isomer of **IV** with relatively narrow lines over a wide temperature range is consistent with the prediction of structural rigidity. Conformation **XVI** (Y = NH) gives a zig-zag or "extended W plan" orientation of the bonds between the porphyrin and nitroxyl ring. This bond geometry has frequently been observed to give rise to large long-range couplings in σ-bonded systems in both nmr and epr studies (11, 23).

For the two isomers of the *trans* ester **V** at low temperature the values of $J$ are 11–13 G and 38 G. The similarity of the larger value of $J$ to that observed for amide **IV** suggests that the isomer with the larger value of $J$ has conformation **XVI** (Y = O). The smaller value of $J$ could then be due to an isomer which does not exhibit a zig-zag conformation. Most carboxylic esters have been observed to adopt conformation **XVII** (24, 25). Oki and Nakashi observed that formate esters exist exclusively in conformation **XVII** (R′ = H)

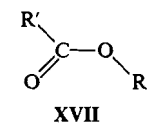


**XVII**

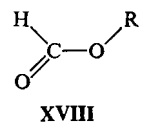


**XVIII**

unless R is sterically demanding (26). When R is *t*-butyl or 3-ethylpentyl 7–9% of the ester exists in conformation **XVIII** at temperatures below −100°C (26). Since the two isomers of **V** have approximately equal populations and the piperidine ring is less sterically demanding than a *t*-butyl group, it appears that rotation around the C—O bond is not the source of the isomerism in **V**. Wennerbeck and

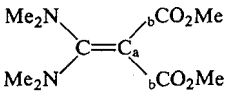

XIX

Sandstrom have observed that the barrier to rotation about the $C_a$—$C_b$ bond in **XIX** is 8.1 kcal/mol (27). In this "push–pull" ethylene the formal C=C bond is weaker than a usual C—C double bond and the $C_a$—$C_b$ bond stronger than in a typical acrylic ester (27). Thus 8.1 kcal/mol should be substantially greater than the barrier to rotation around the analogous bond in **V**. Based on a coalescence temperature of 293 K and an energy separation of 20 G the $\Delta G^{\ddagger}$ for interconversion of the two isomers of **V** is 6.3 kcal/mol (28). This would appear to be a reasonable barrier for rotation about the olefin to carbonyl bond in **V** and suggests that the *Z* and *E* conformers about this bond, **XVI** (Y=O) and **XX**, are the two isomers which are observable below room temperature.

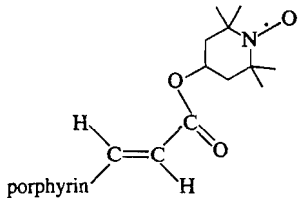

XX

In the spin-labeled complexes with $CH_2$ linkages between the porphyrin and the amide or ester linkage, **VII** and **VIII**, two isomers were observed in the epr spectra at temperatures below −45°C. With a coalescence temperature of about 228 K and an energy separation of 25 G (cf. Table 1) the $\Delta G^{\ddagger}$ for interconversion of the isomers is about 5 kcal/mol. This barrier to rotation is sufficiently low that it is difficult to determine which bonds are involved. However, the larger of the two values of *J* observed for both **VII** and **VIII**, 25 and 30 G, respectively, is sufficiently similar to that observed for conformation **XVI** of **IV** and **V** to suggest that a zig-zag conformation may also occur for **VII** and **VIII**. In the *cis* isomers **I** and **II** the conformation around the olefin linkage precludes a zig-zag conformation consistent with the observation that *J* is small at all temperatures for **I** and **II**. The order *cis* < saturated < *trans* observed at room temperature is consistent with rapid rotation in the complexes with saturated linkages between zig-zag conformers like those of the *trans* isomers in which *J* can be relatively large and conformers like those of the *cis* isomers in which *J* is small. It appears that variations in the values of *J* for **I**, **II**, **IV**, **V**, **VII**, and **VIII** are consistent with explanations in terms of the stereochemistry around the bonds in the linkage between the porphyrin and nitroxyl rings. Although solvent effects shift the equilibria and the observed activation energies the similarity of behavior in a variety of solvents suggests that the differences in *J* are not due primarily to solvation effects. The similarity in the values of *J* for the saturated and unsaturated linkages indicates that in these compounds the metal–nitroxyl interaction is likely dominated by σ-bonding interactions.

*Comparison with other results*

In the perspective of the epr background available at the time these studies were initiated, the observation of high resolution electron spin – electron spin coupling over a distance of about 12 Å, including a saturated carbon pathway, could be considered surprising. However, such an observation is not out of line with nuclear spin coupling data when the differences between nuclear and electron properties are considered. Over the past five years our studies have shown that AB patterns in epr spectra can be observed due to interaction of a nitroxyl unpaired electron with Cu(II), Ag(II) (29), and vanadyl (30) unpaired electrons. Since the electron–electron interaction is so sensitive to the orbital overlaps in the intervening bonds, it is proving to be a useful technique for detection of isomers which cannot readily be studied by other physical methods (17, 30–34). It is also not surprising that in some cases the values of *J* have been found to be strongly dependent on both solvent and temperature (6, 17, 18).

The present study emphasizes the importance of σ-bonding pathways for metal–nitroxyl interactions. In a study of spin-labeled pyridine adducts of $Cu(hfac)_2$, $VO(tfac)_2$, and $VO(hfac)_2$ it was observed that spin-delocalization into the pyridine orbitals was dominated by σ-bonding pathways for Cu(II) but π-bonding pathways were also important for the vanadyl complexes (30). In the same series of compounds it was also observed that interactions through ester, amide, and Schiff base linkages between the pyridine and nitroxyl rings appeared to correlate with the extent of π bonding (27). In a series of spin-labeled metalloporphyrins the magnitude of the metal–nitroxyl exchange interaction increases in the order VO(IV) < Cu(II) < Ag(II), which parallels other indications of the extent of delocalization of the metal unpaired electron into the porphyrin orbitals (29). It can be anticipated that long range exchange interactions through σ as well as π pathways may be a general feature affecting nitroxyl epr spectra. Unless the possibility of exchange interactions affecting the

Can. J. Chem. Downloaded from www.nrcresearchpress.com by 210.87.254.105 on 09/06/12
For personal use only.

TABLE 1. Values of the spin–spin coupling constant, $J$, for spin-labeled copper porphyrins I–IX[a]

| R | Solvent | Linkage: *trans*[b] C=C | Linkage: Saturated $-CH_2-CH_2-$ | Linkage: *cis*[b] C=C |
|---|---|---|---|---|
| | | **IV** | **VII** | **I** |
| 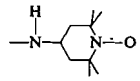 | $CHCl_3$ | 19.9 | 9.3 | ~0 |
| | Toluene | | 17.5 | |
| | 1:1 Toluene:$CH_2Cl_2$ | | 4<br>25 (−60°C) | |
| | 2:1 Toluene:pyridine | 25.6 | 14.0 | 3.5 |
| | 2:1 Toluene:pyridine | 32 (−60°C) | 3<br>22 (−60°C) | 6 (−60°C) |
| | Pyridine | 25.6 | 13.5 | 3.5 |
| | | **V** | **VIII** | **II** |
| 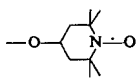 | $CHCl_3$ | 15.5<br>26.0 | 15.5 | ~0 |
| | $CHCl_3$ | 13<br>38 (−40°C) | | |
| | Toluene | 23.5 | 14.5 | |
| | 1:1 Toluene:$CH_2Cl_2$ | | 6<br>30 (−60°C) | |
| | 2:1 Toluene:pyridine | 20 | 13 | ~4 |
| | 2:1 Toluene:pyridine | 11<br>38 (−60°C) | 6<br>26 (−55°C) | 4 (−50°C) |
| | Pyridine | 20.5 | 14 | |
| | | **VI** | **IX** | **III** |
| 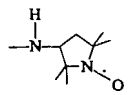 | $CHCl_3$ | 3 | 5 | 550[c] |
| | Toluene | | 4.5 | |
| | 2:1 Toluene:pyridine | 5 | 5.5 | ~8 |
| | 2:1 Toluene:pyridine | 5 (−60°C) | 4 (−50°C) | 10 (−50°C) |
| | Pyridine | 5.2 | 6.6 | 5.9 |

[a]The designations R and linkage refer to the structural diagram for I–IX. Values of $J$ are in G for solutions at room temperature (20–22°C) unless a different temperature is noted in parentheses after the value of $J$.
[b]Some of the room temperature values in this column were taken from ref. 7.
[c]The large value of $J$ for III in noncoordinating solvents is discussed in ref. 7.

results is somehow excluded, caution should be exercised in applying calculations which assume only dipolar interactions.

The observation of metal–nitroxyl interactions is not limited to lineshape changes of "normal" epr spectra. The interaction also changes the nitroxyl relaxation times. For an accurate measure of this change in relaxation time, time domain (pulsed) epr spectroscopy is needed. However, significant relative measurements can be made using non-linear CW epr, such as a power saturation curve (signal amplitude vs. square root of power) and simulation of saturated spectra. In all of the AB spectra we have obtained, the relaxation times of the nitroxyl signals are substantially altered, such that it is often impossible to saturate the nitroxyl signals at room temperature whereas free nitroxyl spectra generally show effects of saturation above 1–5 mW at the same concentration. In work not yet complete we have also observed nitroxyl relaxation time changes in spin-labeled complexes of Ni(II), Mn(II), Mn(III), and Fe(III). In some cases the unsaturated epr spectrum is almost indistinguishable from a spectrum of the same nitroxyl in the absence of metal, but the power saturation curves clearly reveal the metal–nitroxyl interaction. In these studies it is critically important to distinguish between inter- and intra-molecular interactions.

Beyond the answers these studies are providing to the interpretation of epr in biological systems, and to fundamental magnetic interactions, they also are of importance as measures of the electronic structure and stereochemistry of molecules.

## Acknowledgments

This work was supported in part by the National

Can. J. Chem. Downloaded from www.nrcresearchpress.com by 210.87.254.105 on 09/06/12
For personal use only.

Institutes of Health (GM21156). Microanalyses were performed by Spang Microanalytical Laboratory. We appreciate the use of the JEOL FX-90Q spectrometer at the Solar Energy Research Institute, Golden, CO, to obtain Fourier Transform $^1H$ nmr spectra. The mass spectrometry results were obtained at the Midwest Center for Mass Spectrometry at the University of Nebraska, supported under the National Science Foundation Regional Instrumentation Facilities Program.

1. S. S. EATON and G. R. EATON. Coord. Chem. Rev. **26**, 207 (1978).
2. J. S. HYDE, H. M. SWARTZ, and W. E. ANTHOLINE. *In* Spin labeling II: theory and applications. *Edited by* L. J. Berliner. Academic Press, New York. 1979. p. 71.
3. J. S. LEIGH, JR. J. Chem. Phys. **50**, 2608 (1970).
4. J. F. BOAS, P. R. HICKS, J. R. PILBROW, and T. D. SMITH. J. Chem. Soc. Faraday II, **74**, 417 (1978).
5. G. R. BUETTNER and R. E. COFFMAN. Biochim. Biophys. Acta, **480**, 495 (1977).
6. K. M. MORE, G. R. EATON, and S. S. EATON. Inorg. Chem. **18**, 2492 (1979).
7. K. M. MORE, S. S. EATON, and G. R. EATON. Inorg. Chem. **20**, 2641 (1981).
8. M. MOMENTEAU, B. LOOCK, E. BISAGNI, and M. ROUGEE. Can. J. Chem. **57**, 1804 (1979).
9. V. T. WEE, B. K. SINHA, P. W. TAYLOR, and C. F. CHIGNELL. Mol. Pharm. **12**, 667 (1976).
10. H. H. RUF and W. NASTAINCZYK. Eur. J. Biochem. **66**, 139 (1976).
11. M. BARFIELD and B. CHAKRABARTI. Chem. Rev. **69**, 759 (1969).
12. L. KEVAN and L. D. KISPERT. Electron spin double resonance spectroscopy. Wiley-Interscience, New York. 1976. Chapt. 3.
13. M. N. PADDON-ROW and R. HARTCHER. J. Am. Chem. Soc. **102**, 671 (1980).
14. P. M. BOYMEL, J. R. CHANG, D. L. DUBOIS, D. J. GREENSLADE, G. R. EATON, and S. S. EATON. J. Am. Chem. Soc. **99**, 5500 (1977).
15. G. A. BRADEN, K. T. TREVOR, J. M. NERI, D. J. GREENSLADE, G. R. EATON, and S. S. EATON. J. Am. Chem. Soc. **99**, 4854 (1977).
16. S. S. EATON, D. L. DUBOIS, and G. R. EATON. J. Magn. Reson. **32**, 251 (1978).
17. B. M. SAWANT, G. A. BRADEN, R. E. SMITH, G. R. EATON, and S. S. EATON. Inorg. Chem. **20**, 3349 (1981).
18. K. M. MORE, B. M. SAWANT, G. R. EATON, and S. S. EATON. Inorg. Chem. **20**, 3354 (1981).
19. J. WOJCIK and M. WITANOWSKI. J. Mol. Struct. **49**, 249 (1978).
20. J. MARCH. Advanced organic chemistry. 2nd ed. McGraw-Hill, New York. 1977, p. 113.
21. R. F. HOBSON and L. W. REEVES. J. Mag. Res. **10**, 243 (1973).
22. R. H. HASCHEMEYER and A. E. V. HASCHEMEYER. Proteins: a guide to study by physical and chemical methods. Wiley, New York. 1973. p. 333.
23. F. W. KING. Chem. Rev. **76**, 157 (1976).
24. G. I. L. JONES and N. L. OWEN. J. Mol. Struct. **18**, 1 (1973).
25. A. D. LOPATA and R. L. KUCZKOWSKI. J. Am. Chem. Soc. **103**, 3304 (1981) and references therein.
26. M. OKI and H. NAKASHI. Bull. Chem. Soc. Jpn. **43**, 2558 (1970).
27. I. WENNERBECK and J. SANDSTROM. Org. Mag. Res. **4**, 783 (1972).
28. F. A. L. ANET and R. ANET. *In* Dynamic nuclear magnetic resonance spectroscopy. *Edited by* L. M. Jackman and F. A. Cotton. Academic Press, New York. 1975. pp. 543–619.
29. K. M. MORE, S. S. EATON, and G. R. EATON. J. Am. Chem. Soc. **103**, 1087 (1981).
30. B. M. SAWANT, A. L. W. SHROYER, G. R. EATON, and S. S. EATON. Inorg. Chem. In press.
31. D. L. DUBOIS, G. R. EATON, and S. S. EATON. J. Am. Chem. Soc. **101**, 2624 (1979).
32. D. L. DUBOIS, G. R. EATON, and S. S. EATON. Inorg. Chem. **18**, 75 (1979).
33. S. S. EATON, K. M. MORE, D. L. DUBOIS, P. M. BOYMEL, and G. R. EATON. J. Mag. Res. **41**, 150 (1980).
34. P. M. BOYMEL, G. R. EATON, and S. S. EATON. Inorg. Chem. **19**, 727 (1980); **19**, 735 (1980).

Can. J. Chem. Downloaded from www.nrcresearchpress.com by 210.87.254.105 on 09/06/12
For personal use only.

# Utilisation des pièges à radicaux en vue de mettre en évidence des intermédiaires dans la photolyse de complexes contenant une liaison $Co^{III}$—C

PHILIPPE MAILLARD ET CHARLES GIANNOTTI

*Institut de Chimie des Substances Naturelles, C.N.R.S., 91190 Gif-sur-Yvette, France*

Reçu le 3 août 1981

Can. J. Chem. Downloaded from www.nrcresearchpress.com by 210.87.254.40 on 09/06/12
For personal use only.

PHILIPPE MAILLARD et CHARLES GIANNOTTI. Can. J. Chem. **60**, 1402 (1982).

En utilisant divers pièges à radicaux comme la diméthyl-5,5′ pyrroline-*N* oxyde (DMPO), le phényl *N-tert*-butylnitrone (PBN), le nitrosodurène (ND) et l'α-pyridyl-4 oxyde-1 *tert*-butyl-2 nitrone (4-POBN) et leur mélange, nous avons pu détecter deux types de radicaux provenant des adduits formés soit avec un atome d'hydrogène, soit avec le radical alkyle libre des alkylcobaloximes, alkylsalen et alkylcobalamines.

En effectuant des deuterations sélectives et en préparant le benzyl bis(diphenylglyoximato)-pyridinato cobaloxime, nous avons montré que l'atome d'hydrogène piégé provient probablement de l'hydrogène chelaté de l'anion diméthylglyoximato du ligand équatorial du complexe du $Co^{III}$. En utilisant un mélange formé de deux pièges à radicaux nous obtenons un spectre rpe contenant, en même temps, les adduits formés par un atome d'hydrogène et un radical alkyle libre.

Pour expliquer l'efficacité du piégeage, alors que les réactions d'homolyse sont en compétition avec des réactions de β-élimination, il faut postuler que la photolyse de ces composés s'effectue dans une cage de solvant. Cette hypothèse explique la forte influence de la nature des solvants utilisés sur la nature des radicaux piégés. Aussi le piège à radicaux peut diffuser dans la cage de solvant et est ainsi capable de piéger, d'une manière très efficace, tout radical libre formé dans la cage de solvant. Le complexe du $Co^{III}$ à l'état excité et le piège à radicaux dans la cage de solvant se comportent comme un exciplex, ce qui pourrait expliquer le piégeage d'atomes d'hydrogène.

PHILIPPE MAILLARD and CHARLES GIANNOTTI. Can. J. Chem. **60**, 1402 (1982).

Using the spin trapping technique with 5,5′-dimethyl 1-pyrroline *N*-oxide (DMPO), phenyl-*N-tert*-butyl nitrone (PBN), nitrosodurene (ND), and α-4-pyridyl 1-oxide *N-tert*-butyl nitrone (4-POBN), or their mixtures, we have been able to detect two types of radicals, one is a hydrogen atom spin adduct and the other is the corresponding alkyl of the alkylcobaloximes, salens or cobalamines.

By the use of selective deuteration and the preparation of the benzyl bis(diphenylglyoximato)-pyridinato cobaloxime, we have shown that the spin trapped hydrogen atom comes from the chelated hydrogen of the dimethylglyoximato anion of the equatorial ligand of $Co^{III}$ complexes. Using a mixture of two spin traps gives rise to an esr spectrum containing, at the same time, the hydrogen atom and alkyl spin adducts.

To explain such an efficient spin trapping reaction while the homolysis is in competition with a β-elimination process, it should be postulated that the photolysis of such compounds proceeds through a solvent cage environment. This hypothesis explains the strong influence of solvents on the nature of the free radicals trapped. Also the spin trap diffuses in the solvent cage, and is able to trap in a very efficient manner any free radicals occurring in the solvent cage. The excited $Co^{III}$ complexes and the spin trap in the solvent cage behave like an exciplex, which could explain the spin trapping of the hydrogen atom.

Ce travail fait le point, avec l'aide de quelques expériences nouvelles, sur le piègeage d'atome d'hydrogène et de radicaux alkyles, apparaissant au cours de la photolyse d'alkylcobaloximes et de quelques composés voisins.

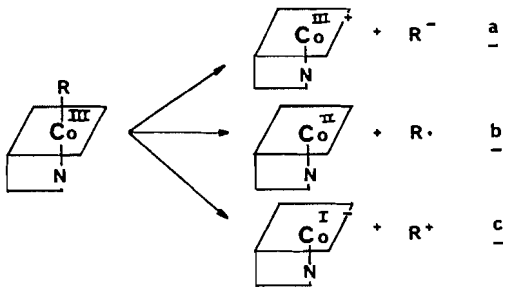


La rupture de la liaison $Co^{III}$—C dans les complexes du $Co^{III}$ peut s'effectuer de trois manières différentes: une voie radicalaire donne un radical alkyle libre et un complexe du $Co^{II}$ (b); deux voies ioniques possibles qui se décomposent en formation d'un anion alkyle et d'un complexe du $Co^{III}$ (a), ou coupure en un cation alkyle et un complexe du $Co^{I}$ (c).

La photolyse des alkylcobaloximes et des alkyl cobalamines en absence d'oxygène conduit à la rupture plus ou moins rapide de la liaison $Co^{III}$—C et à la formation de produits pratiquement identiques à ceux obtenus par thermolyse anaérobique.

A partir des résultats théoriques (1), un mécanisme expliquant la réaction de photolyse de la liaison $Co^{III}$—C des cobaloximes et des cobalamines a été proposé:

0008-4042/82/121402-12$01.00/0

©1982 National Research Council of Canada/Conseil national de recherches du Canada

Can. J. Chem. Downloaded from www.nrcresearchpress.com by 210.87.254.40 on 09/06/12
For personal use only.

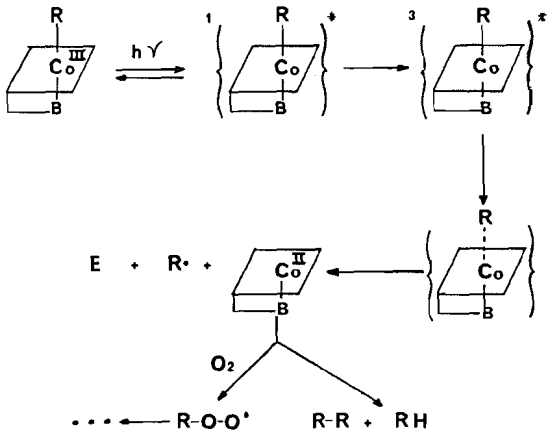

La similitude des produits de dégradation obtenus, soit après photolyse, soit après thermolyse des cobalamines et des cobaloximes à pH = 7, montre que ces deux types de réactions se déroulent selon des mécanismes très proches. La mise en évidence de l'hydrure de cobaloxime (2–4), permet d'envisager un mécanisme concerté de β-élimination.

Par contre la mise en évidence de complexe du $Co^{II}$ et de radicaux alkyles libres au cours de la photolyse des cobalamines (5–8), des cobaloximes (9–12) et des complexes salen du $Co^{III}$ (13, 14) montre que la rupture homolytique de la liaison $Co^{III}$—C est possible. En outre, il a été montré (15–17) qu'il existe un autre mécanisme conduisant à la formation photochimique d'un atome d'hydrogène provenant probablement du ligand équatorial des cobaloximes.

De plus, récemment il a été proposé un mécanisme dans lequel le radical R· formé par thermolyse peut perdre un atome d'hydrogène pour conduire à l'hydrure de cobalt et à l'éthylénique issu de R· (18*a*).

On peut résumer les différents résultats de la littérature en écrivant le mécanisme global suivant:

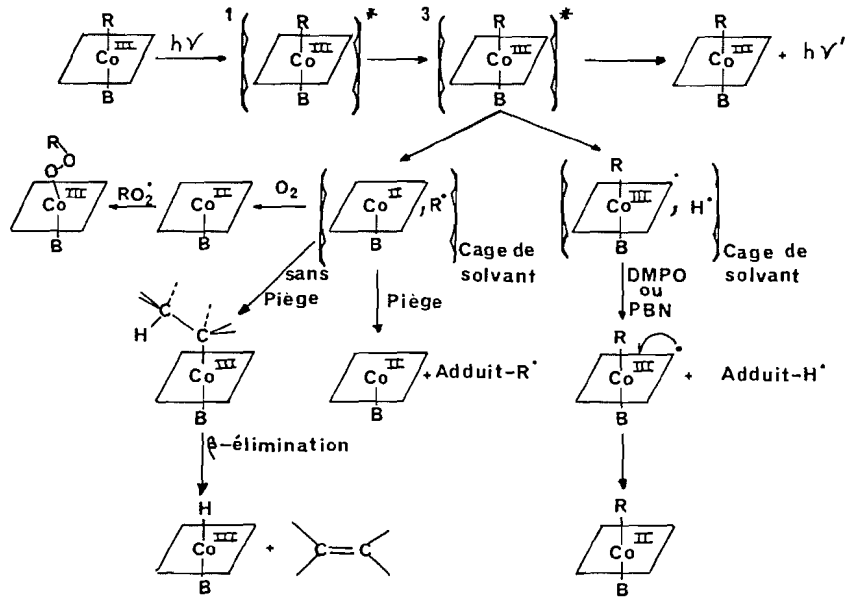

Dans tous ces mécanismes, les points suivants restent obscurs.

L'hydrogène photolabile des alkylcobaloximes, récemment mis en évidence (15–18*a*), provient-il réellement du méthyle ou de l'hydroxyle du ligand équatorial?

La rupture homolytique de la liaison $Co^{III}$—C des cobaloximes est-elle générale en présence de composés capables de piéger les radicaux?

Existe-t-il une influence du solvant en présence de pièges à radicaux?

Nous allons essayer de répondre à certaines de ces questions.

### 1. Photolyse des alkylcobaloximes (1) dans les solvants aprotiques

Au cours de la photolyse anaérobique des alkylcobaloximes en présence de DMPO, il a été observé qu'un atome d'hydrogène est piégé (15–17). Dans le but d'essayer de déterminer l'origine exacte de cet atome d'hydrogène, nous avons synthétisé et étudié la pureté isotopique de la

diméthylglyoxime deutérée et de diverses cobaloximes deutérées.

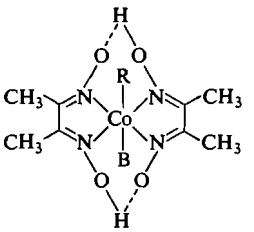


R = alkyle
B = Base aromatique

1

*Synthèse et détermination de la pureté isotopique de la diméthylglyoxime (DMG-$d_8$) et de quelques cobaloximes deutérées*

La diméthylglyoxime (DMG) est deutérée par échange hydrogène, deutérium en milieu acide (11); on obtient la perdeutéro diméthylglyoxime (DMG-$d_8$) ainsi que tous les composés contenant de 1 à 8 atomes de deutérium.

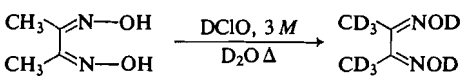


2

La pureté isotopique moyenne en deutérium de la DMG-$d_8$ **2**, calculée à partir des spectres de rmn $^1H$ de deux solutions titrées de DMG et de DMG-$d_8$, dans l'acétone deutérée, est supérieure à 95% pour la fonction N—OD et d'environ 42% pour les groupements méthyles.

Les cobaloximes deutérées sont préparées à partir de la DMG-$d_8$ **2**, selon la méthode décrite par Schrauzer *et al.* (1).

Les différentes cobaloximes marquées au deutérium **3**–**6** sont purifiées par dissolution dans un mélange MeOD/$CDCl_3$ et précipitées par $D_2O$.

La comparaison des spectres rmn $^1H$ du composé **3**, partiellement deutéré, et de son homologue **7**, non deutéré, confirme l'incorporation de deux molécules de DMG-$d_8$ dans le composé **3**. La pureté isotopique des $CD_3$ des ligands équatoriaux de ce dernier, déterminée par rmn $^1H$, est de 40 à 45%. Il n'est pas possible de mesurer la pureté isotopique des fonctions oximes des cobaloximes deutérées par rmn $^1H$, le pic rmn correspondant aux atomes d'hydrogène de ces groupements étant trop large.

L'analyse du spectre infrarouge d'une solution, dans le chloroforme fraîchement désséché, de perdeutéro isopropylcobaloxime **6**, enregistré à des temps réguliers, *permet de constater que la bande d'absorption de la fonction N—OD (2670 $cm^{-1}$) diminue alors que la bande d'absorption de la fonction N—OH (3660 $cm^{-1}$) augmente. Ce phénomène est la conséquence de l'échange rapide (total en moins d'une heure) du deutérium du groupement hydroxyle des oximes de la cobaloxime* **6** *par un atome d'hydrogène provenant du milieu réactionnel.* Par contre, on ne note aucune modification des bandes comprises entre 2000 et 2500 $cm^{-1}$ correspondant aux diverses liaisons C—D. L'absence des bandes à 3080, 2915 et 2850 $cm^{-1}$ correspondant aux liaisons C—H de la pyridine et du groupement isopropyle hydrogéné, montre que ces derniers sont deutérés à plus de 90%. Ces résultats ont été développés précédemment (17).

L'étude des spectres infrarouge et rmn $^1H$ des cobaloximes deutérés **3** à **6** montre que: (*a*) les ligands axiaux sont deutérés à plus de 80% et ne sont le siège d'aucun échange isotopique; (*b*) les méthyles des deux diméthylglyoximes équatoriales sont deutérés à 40% et n'échangent pas leurs atomes de deutérium avec le milieu réactionnel; (*c*) par contre, les deutériums des groupements hydroxyles des fonctions oximes s'échangent rapidement avec des hydrogènes du milieu extérieur.

*Étude par rpe de la photolyse des alkylcobaloximes perdeutérées*

Nous avons utilisé les pièges à radicaux suivants:

Diméthyl-5,5′ pyrroline-*N*-oxyde (DMPO)

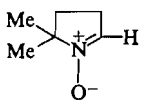


Nitrosodurène

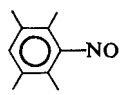


(ND)

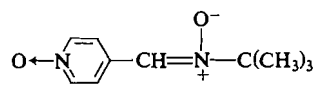


α-Pyridyl-4 oxyde-1 *tert*-butyl-2 nitrone (4-POBN)

Phényl *N-tert*-butyl nitrone (PBN)

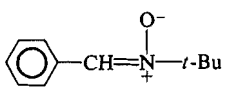


En étudiant les spectres rpe obtenus après photolyse anaérobique des cobaloximes deutérées **4**, **5** et **6**, dissoutes dans les solvants aprotiques appropriés ($CHCl_3$, $CDCl_3$, $C_6H_6$, $C_6D_6$, $CH_3C_6H_5$ et $CD_3C_6D_5$), contenant un excès de DMPO, nous n'avons mis en évidence que la formation d'un seul adduit correspondant au piègeage d'un atome d'hydrogène (15).

Le fait que le DMPO ne piège aucun atome de deutérium au cours de la photolyse des cobaloximes deutérées **4**, **5** et **6** nous ayant paru surprenant, nous avons vérifié que le DMPO était capable de former un adduit stable avec les atomes de deutérium.

Can. J. Chem. Downloaded from www.nrcresearchpress.com by 210.87.254.40 on 09/06/12
For personal use only.

Can. J. Chem. Downloaded from www.nrcresearchpress.com by 210.87.254.40 on 09/06/12
For personal use only.

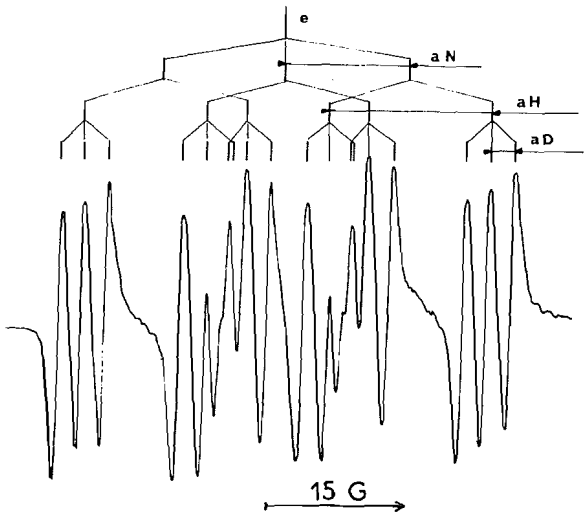


FIG. 1. Spectre rpe obtenu à 100 KHz et à 25°C, de $(C_4H_9)_3SnD$ en solution dans le toluène, en présence de DMPO. Signal gain $6{,}3 \times 10^5$, radiofréquence 9516 MHz, puissance de détection 25 mW.

Pour cela, nous avons irradié, dans le toluène contenant du DMPO, une solution de $(C_4H_9)_3SnD$, ce composé étant connu pour libérer facilement des atomes de deutérium sous l'action de la lumière (18*b*).

Le spectre de l'adduit obtenu (fig. 1) est caractéristique du couplage hyperfin d'un atome d'azote ($a_N$ = 14,33 G), et des couplages hyper-hyperfins d'un atome d'hydrogène ($a_H$ = 18,99 G) et de deutérium ($a_D$ = 2,83 G) avec l'électron célibataire du centre radicalaire. Le rapport $a_H/a_D$ = 6,7, calculé à partir des constantes de couplage mesurées est proche du quotient des rapports gyromagnétiques des atomes H et D $a_H/a_D$ = 6,51 (19).

L'irradiation d'un mélange équimoléculaire de $(C_4H_9)_3SnH$ et $(C_4H_9)_3SnD$ conduit à la mise en évidence par rpe, d'une quantité sensiblement égale d'adduit DMPO–H et DMPO–D (fig. 2). Ceci montre qu'aucun effet isotopique notable ne vient perturber la vitesse de formation de l'adduit DMPO–D, celle-ci étant pratiquement égale à celle de l'adduit DMPO–H.

Bien que capable de piéger des atomes de deutérium, le DMPO ne conduit cependant, lors de la photolyse anaérobique des alkylcobaloximes deutérées **4**, **5** et **6**, qu'à la formation d'un adduit DMPO–H aussi bien après une photolyse courte (18 s à 1 min) qu'après une photolyse longue (plusieurs minutes à 1 h).

Ceci permet d'exclure l'hypothèse d'un effet isotopique ralentissant la libération d'un atome de deutérium par rapport à celle d'atome d'hydrogène.

Afin de confirmer que les groupements méthyles

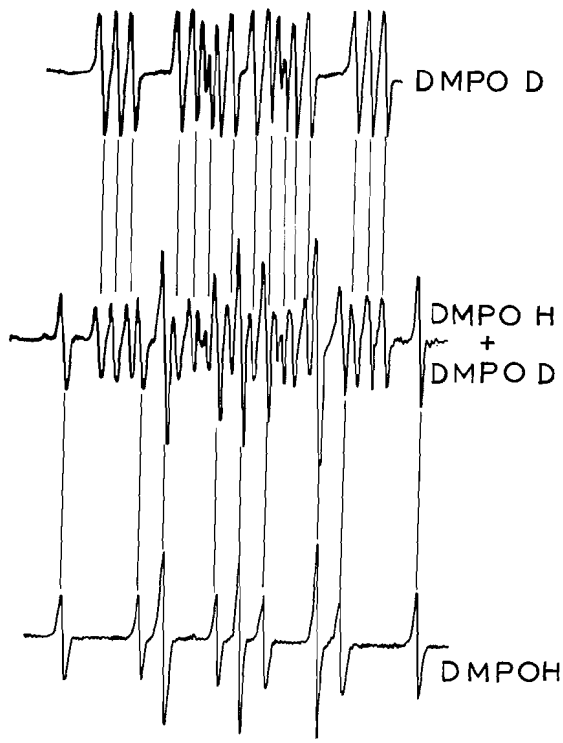


FIG. 2. Spectre rpe obtenu à 100 kHz et à 25°C après photolyse d'un mélange équimoléculaire de $(C_4H_9)_3SnH$ et $(C_4H_9)_3SnD$ dans le toluène en présence de DMPO. Signal gain $5 \times 10^5$, radiofréquence 9517 MHz, puissance de détection 31 mW.

des diméthylglyoximes des cobaloximes ne sont pas la source des atomes d'hydrogène piégé par le DMPO pendant la photolyse (11), nous avons irradié, dans le visible, une solution dégazée de benzyl bis(diphénylglyoximato)-pyridinato cobalt (19) et de DMPO dans le toluène, cette expérience n'a pas été rapportée précédemment.

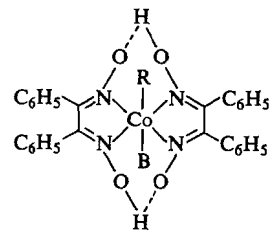


**9**

R = $CH_2C_6H_5$
B = Py

Sous ces conditions expérimentales, le complexe **9** conduit à la mise en évidence, par rpe, de l'adduit DMPO–H.

Les groupements phényles (étant de mauvais donneurs d'atome d'hydrogène) ne peuvent pas être la source des atomes d'hydrogène photolabiles des alkylcobaloximes.

Ainsi, l'étude de la photolyse des cobaloximes

deutérés **4**, **5** et **6** et du complexe **9** pourrait suggérer qu'une majorité des atomes d'hydrogène photolabile des cobaloximes pourrait provenir des OH des fonctions oximes des ligands équatoriaux de ces composés.

*Étude de la photolyse des cobaloximes non deutérées en présence de DMPO*

Tous les composés deutérés ou non deutérés **3** à **22**, dissous dans des solvants aprotiques dégazés et photolysés dans le visible ($\nu > 420$ nm), donnent un atome d'hydrogène piégé par le DMPO.

Par contre, la photolyse de l'adamantyl-1 cobaloxime **23** (20) dans le toluène, en présence de DMPO, conduit à la formation simultanée de deux adduits dont l'un est caractéristique de l'adduit DMPO–H et l'autre du radical adamantyle-1 libre avec le DMPO (17, 21).

La présence de radical adamantyle-1 et d'atome d'hydrogène, piégés par le DMPO au cours de la photolyse anaérobique du composé **23** dans les solvants aprotiques, montre que la rupture homolytique de la liaison Co—C, et le piégeage d'un atome d'hydrogène du ligand équatorial sont deux réactions en compétition.

Par contre, le fait que, dans des conditions analogues, la photolyse des composés **3**–**22** ne conduise pas à la formation d'adduits DMPO–alkyles, ne permet pas de confirmer la rupture homolytique de la liaison Co—C pour ceux-ci.

Le fait que toutes les cobaloximes étudiées conduisent, sous photolyse anaérobique, à la formation de l'adduit DMPO–H, ne permet pas de préciser si le piègeage des atomes d'hydrogène est la réaction principale prépondérante. Seul le dosage de l'adduit DMPO–H peut permettre de préciser ce point.

TABLEAU 1. Dosage de la concentration de l'adduit DMPO–H effectué entre la 1ère et la 4ème min d'irradiation*

| Composé | $\% = \frac{[\text{DMPO–H}]}{[\text{R(Co)B initiale}]}$ | % Moyen |
|---|---|---|
| Me(Co)Py | 0,75<br>0,20<br>0,57 | 0,5±0,1 |
| $C_6H_5CH_2$(Co)Py | 0,17<br>0,38<br>0,49 | 0,34±0,1 |

*Solvant: toluène; température 300 K; DMPO: $5 \times 10^{-2}$ *M*/L; R(Co)Py: $10^{-3}$ *M*/L. Solution de référence: diphényl-1,1 picryl-hydrazyle $10^{-4}$ *M*/L.

L'adduit DMPO–H n'a une durée de vie que de quelques secondes (15); seul un dosage effectué à l'état stationnaire peut donner un ordre de grandeur de la quantité d'adduit formé. Les résultats obtenus pour la méthyle et la benzylcobaloxime **7** et **8** sont donnés dans le tableau 1. Ces résultats n'ont pas été publiés précédemment.

Ces pourcentages montrent qu'à l'état stationnaire la quantité d'adduit DMPO–H présent dans la solution est très faible, mais ne permettent pas de déduire la quantité totale d'adduit formé.

Une étude complémentaire de la photolyse anaérobique de ces cobaloximes, dans les solvants aprotiques, est nécessaire pour vérifier la rupture homolytique de la liaison $Co^{III}$—C.

Nous avons alors étudié la photolyse des composés **3**–**23** en présence de nouveaux pièges à

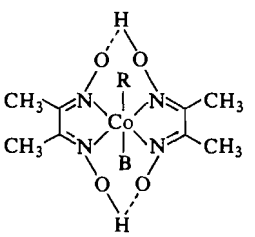

| R | B | | R | B | |
|---|---|---|---|---|---|
| $C_6H_5CH_2$ (DMG-$d_7$)$_2$ | Py | **3** | $C_6H_5CH_2$ | $H_2O$ | **14** |
| $CD_3$ (DMG-$d_7$)$_2$ | Py-$d_5$ | **4** | $C_6H_5CH_2$ | Morpholine | **15** |
| $C_2D_5$ (DMG-$d_7$)$_2$ | Py-$d_5$ | **5** | *p*-$BrC_6H_4CH_2$ | Py | **16** |
| *iso*-$C_3D_7$ (DMG-$d_7$)$_2$ | Py-$d_5$ | **6** | *p*-$CNC_6H_4CH_2$ | Py | **17** |
| $C_6H_5CH_2$ | Py | **7** | *p*-$NO_2C_6H_4CH_2$ | Py | **18** |
| $CH_3$ | Py | **8** | $C_{10}H_{21}$ | Py | **19** |
| $C_2H_5$ | Py | **10** | $C_{12}H_{25}$ | Py | **20** |
| *iso*-$C_3H_7$ | Py | **11** | $C_{12}H_{25}$ | $H_2O$ | **21** |
| $CNCH_2$ | Py | **12** | $C_{16}H_{33}$ | Py | **22** |
| $HOCH_2CH_2$ | Py | **13** | Adamantyl-1 | Py | **23** |

Can. J. Chem. Downloaded from www.nrcresearchpress.com by 210.87.254.40 on 09/06/12
For personal use only.

Can. J. Chem. Downloaded from www.nrcresearchpress.com by 210.87.254.40 on 09/06/12
For personal use only.

radicaux, le nitrosodurène (ND) (22, 23) et le phényl *tert*-butyl nitrone (PBN) (24, 25).

*Photolyse des alkylcobaloximes en présence de nitrosodurène et de PBN*

La photolyse anaérobique, dans le benzène ou le toluène de tous les composés **3** à **23**, en présence de nitrosodurène, conduit à des adduits du type nitrosodurène–alkyle (17).

Le nitrosodurène semble donc incapable de piéger les atomes d'hydrogène mis en évidence par le DMPO, pendant la photolyse des cobaloximes.

Nous avons vérifié, en irradiant une solution de $(C_4H_9)_3SnH$ ou de $(C_4H_9)_3SnD$, dans le toluène contenant un excès de nitrosodurène, que ce dernier était bien incapable de former un adduit stable avec les atomes d'hydrogène ou de deutérium.

On peut supposer que l'adduit **24**, formé entre le nitrosodurène et un atome d'hydrogène ou un atome de deutérium, a une durée de vie très courte et qu'il réagit rapidement avec un second atome d'hydrogène ou de deutérium pour former une hydroxylamine diamagnétique **25**, non détectable par rpe, selon le schéma suivant:

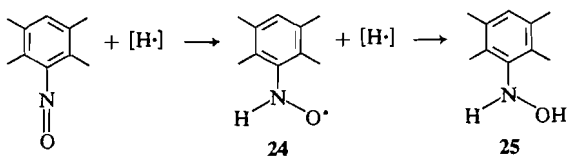


**24** **25**

En effet, après photolyse continue d'un mélange équimoléculaire de nitrosodurène et d'alkylcobaloxime ou de nitrosodurène et de $(C_4H_9)_3SnH$, une hydroxylamine aromatique et des composés minoritaires non identifiés sont détectés et isolés.

Les spectres infrarouge et rmn $^1H$ du produit majoritaire montrent la présence d'une fonction hydroxylamine aromatique dans ce composé (ir ν NOH 3540 $cm^{-1}$, ν NO 1540 $cm^{-1}$ dans $CHCl_3$; rmn $^1H$ multiplet à 5,2 ppm et 5.5 ppm).

Le fait que la formation d'adduit nitrosodurène alkyle soit générale, au cours de la photolyse anaérobique des cobaloximes, ne permet pas de savoir si la rupture homolytique de la liaison cobalt–carbone est la réaction prépondérante.

Les résultats non publiés des dosages de l'adduit nitrosodurène–alkyle effectués par rpe, pendant la photolyse de la méthyl cobaloxime **8** et de la benzylcobaloxime **7** dans le toluène sont rassemblés dans le tableau 2.

Il est impossible par la technique que nous avons employée, de connaître la quantité totale d'adduit nitrosodurène–alkyle qui est formée au cours de la photolyse anaérobique des deux cobaloximes que nous avons étudiées, car l'adduit est photosensible et se détruit lentement au cours de la photolyse.

TABLEAU 2. Dosage de la concentration de l'adduit ND–R effectué entre la 1ère et la 4ème min d'irradiation*

| Composé | $\% = \frac{[ND-R]}{[R(Co)Py\ initiale]}$ | % Moyen |
|---|---|---|
| Me(Co)Py | 3,5<br>3,7 | 3,6±0,1 |
| $C_6H_5CH_2(Co)Py$ | 1,4<br>1,4 | 1,4±0,1 |

*Solvant: toluène: température 300 K; nitrosodurène: 5 × $10^{-3}$ *M*/L; R(Co)Py: $10^{-3}$ *M*/L. Solution de référence: diphényl-1,1 picryl-hydrazyle $10^{-4}$ *M*/L.

Nous ne pouvons atteindre, par cette technique, que la concentration en adduit nitrosodurène-alkyle à l'état stationnaire.

L'étude par rpe, de la photolyse anaérobique des alkylcobaloximes **3**–**23** dans les solvants aprotiques, en présence de DMPO, de nitrosodurène ou de PBN comme pièges à radicaux, suggère aussi le départ d'un atome d'hydrogène du ligand équatorial et montre que la rupture homolytique simultanée de la liaison $Co^{III}$—C a bien lieu.

Dans le but de vérifier ces résultats, nous avons étudié la photolyse anaérobique de deux cobaloximes **7** et **8**, en présence d'un mélange équimoléculaire de DMPO et de nitrosodurène ainsi que de DMPO et de PBN (17). Les différents spectres rpe montrent simultanément des signaux caractéristiques, des adduits DMPO–H, ND–R et DMPO–H, PBN–H et PBN–alkyle (17).

Ces deux expériences confirment la rupture homolytique de la liaison axiale $Co^{III}$—C et le départ simultané par piégeage d'un atome d'hydrogène des alkylcobaloximes.

Bien que le DMPO soit capable de piéger des radicaux alkyles (21, 26), il ne permet pas de les mettre en évidence dans les expériences de photolyse des cobaloximes **3**, **22**. Seule l'irradiation de l'adamantyl-1 cobaloxime **23** donne les deux adduits, DMPO–alkyle et DMPO–H, attendus.

Le piègeage du radical alkyle par le DMPO est en compétition avec la formation très rapide de l'adduit DMPO–H (27) et avec la réaction de recombinaison de la liaison $Co^{III}$—C (6, 11, 12). Ainsi, la concentration de l'adduit DMPO–alkyle dans le milieu réactionnel est trop faible pour permettre l'enregistrement de son spectre rpe. Dans le cas de l'adamantyl-1 cobaloxime **23**, le radical adamantyle-1, suffisamment stable pour être détecté directement par rpe dans certaines conditions (28, 29), ne subit pas facilement de réactions secondaires (recombinaison de la liaison $Co^{III}$—C par exemple).

Can. J. Chem. Downloaded from www.nrcresearchpress.com by 210.87.254.40 on 09/06/12
For personal use only.

Il peut donc former avec le DMPO un adduit en quantité suffisante pour être détecté. Par contre, le PBN, réagissant plus lentement que le DMPO avec les atomes d'hydrogène (28), piège suffisamment de radicaux alkyles pour que le spectre rpe de leurs adduits avec le PBN soit enregistrable.

*Étude de la photolyse de complexes du cobalt III proches des alkylcobaloximes: alkylnioxime et alkylsalen*

La structure des différents composés étudiés est donnée ci-dessous:

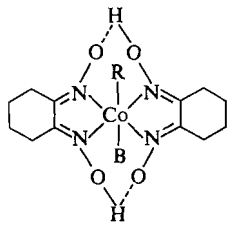

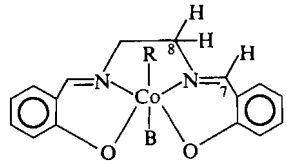

| R | B | | R | B | |
|---|---|---|---|---|---|
| $CH_3$ | Py | **26** | $CH_3$ | Py | **32** |
| $(CH_3)_2CH$ | Py | **27** | $CH_3$ | $H_2O$ | **33** |
| $C_6H_5CH_2$ | Py | **28** | $CH_3$ | *p*-CNPy | **34** |
| $C_{10}H_{21}$ | Py | **29** | | | |
| $C_{12}H_{25}$ | Py | **30** | | | |
| $C_{16}H_{33}$ | Py | **31** | | | |

L'étude de la photolyse des composés **26–31**, dans des conditions analogues à celles des cobaloximes **3–23**, montre que ces types de complexes du $Co^{III}$ se comportent de manière identique.

Par contre, les complexes **32–34** irradiés dans le toluène désoxygéné en présence de DMPO, conduisent à la formation de deux espèces radicalaires: un atome d'hydrogène et un radical méthyle (17).

Il a été montré, par rmn $^1H$, que les hydrogènes situés sur les carbones 7 et 8 des complexes salen du $Co^{III}$ sont labiles (30). Il est donc raisonnable de penser que ces hydrogènes C7 et C8 et plus probablement les hydrogènes C8 pourraient être expulsé facilement par photolyse, bien qu'aucune expérience de marquage isotopique de ces positions n'ait pu être réalisée pour confirmer cette hypothèse.

### 2. Photolyse dans les solvants protiques

Les composés **8** et **11** étant pratiquemment insolubles dans l'eau, nous avons dû synthétiser la cobaloxime **13** rendue soluble dans l'eau grâce à un ligand $CH_2CH_2OH$ axial (31). Aucune trace d'atome d'hydrogène piégé par le PBN n'est détectée lors de la photolyse des composés **8**, **11**, **13** et **33** dans le méthanol. Par contre, la photolyse anaérobique de ces mêmes composés **8**, **11**, **13**, **33**, en présence de DMPO, conduit à la formation unique de l'adduit DMPO–H aussi bien dans $CH_3OH$ que dans $CD_3OD$. La photolyse anaérobique du complexe salen **34**, dans le méthanol ou $CD_3OD$ contenant du DMPO, conduit à la formation de deux radicaux: l'adduit DMPO–méthyle ($a_N$ = 15,35 ± 0,01 G et $g_{iso}$ = 2,0064 ± 0,0003) et l'adduit DMPO–hydrogène ($a_N$:15,58 ± 0,01 G, $a_H$ = 20,66 ± 0,01 G et $g_{iso}$ = 2,0072 ± 0,0003). Ces résultats confirment que l'atome d'hydrogène piégé par le DMPO ne provient ni du solvant ni d'un hydrogène facilement échangeable avec les deutérium du méthanol.

La concentration de l'adduit DMPO–H est environ deux fois supérieure à celle de l'adduit DMPO–méthyle. La photolyse du composé **33** dans le MeOH, en présence de PBN, conduit à la formation immédiate d'un adduit PBN–méthyle. Lorsque la photolyse est arrêtée le spectre rpe de *l'adduit PBN–hydrogène apparaît lentement*. Cet atome d'hydrogène pourrait provenir probablement de la positions 7 ou 8 du complexe salen.

On peut donc dire qu'en présence de pièges à radicaux, la photolyse anaérobique des composés **8**, **11**, **13** et **33**, dans les solvants aprotiques et dans le méthanol, conduit à la formation d'un adduit entre le PBN et un atome d'hydrogène provenant du ligand équatorial et d'un adduit entre le PBN et un radical alkyle provenant de l'homolyse de la liaison $Co^{III}$—C. Ces deux processus photochimiques se produisent sur des molécules différentes et sont en compétition.

*Photolyse des composés 13, 33 dans l'eau*

L'étude rpe de la photolyse anaérobique des complexes **13** et **33**, en milieu aqueux à pH = 7 et en présence de DMPO, ne montre la formation d'aucun adduit.

Par contre, en présence de 4-POBN, on observe la formation instantanée d'adduits formés à partir de radicaux alkyles (fig. 3). Les caractéristiques rpe des deux adduits formés sont les suivantes.

4-POBN – $CH_2CH_2OH$: $g_{iso}$ = 2,0044 ± 0,0003; $a_N$ = 15,75 ± 0,01 G; $a_{\beta H}$ = 2,75 ± 0,01 G.

4-POBN – $CH_3$: $g_{iso}$ = 2,0059 ± 0,0003; $a_N$ = 15,83 ± 0,01 G; $a_{\beta H}$ = 2,16 ± 0,01 G.

Les cobaloximes **8** et **11** sont totalement insolubles dans l'eau et n'ont donc pas pu être étudiées dans ces conditions de photolyse.

Les complexes **13** et **33** photolysés dans l'eau à pH = 7 ne subissent qu'une rupture homolytique de la liaison $Co^{III}$—C.

Golding *et al.* (11) ont montré que, durant la photolyse de solution aqueuse de cobaloximes à pH = 7, la rupture homolytique de la liaison $Co^{III}$—C est un processus très efficace (éq. [1]). Ce résultat est sans doute dû au fait que les molécules

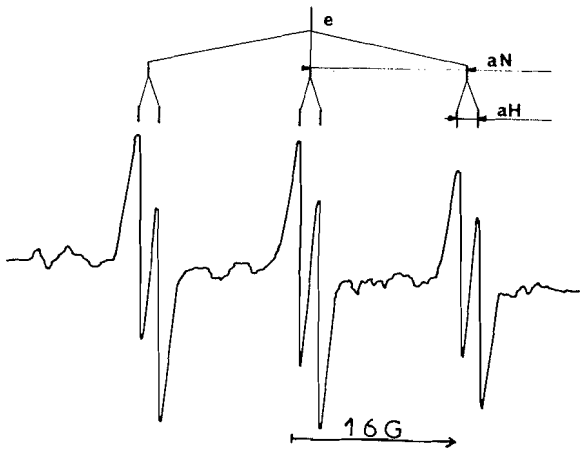


FIG. 3. Spectre rpe obtenu à 100 kHz et à 25°C après photolyse de l'isopropyl pyridinato cobaloxime dans l'eau et en présence de 4-POBN. Signal gain 4 × $10^5$, radiofréquence 9517 MHz, puissance de détection 25 mW.

d'eau qui solvatent le complexe $Co^{II}$ (éq. [3]) formé après rupture de la liaison $Co^{III}$—C peuvent bloquer la réaction inverse de recombinaison $Co^{II} + {}^{\cdot}R \rightarrow Co—R$ (éq. [2]) et ainsi favoriser la formation des radicaux alkyles libres plutôt que celle d'atomes d'hydrogène. Le méthanol, solvant moins polaire que l'eau solvate moins le complexe $Co^{II}$ et rend ainsi le départ de l'atome d'hydrogène plus aisé.

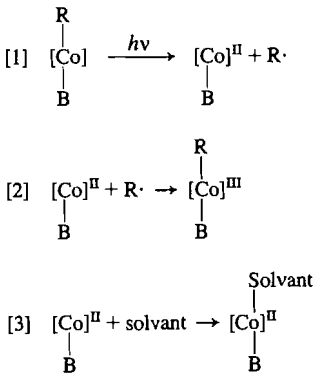


### 3. Photolyse de quelques cobalamines en présence de pièges à radicaux

Les trois cobalamines, dont la photochimie nous a plus particulièrement intéressés, sont: le coenzyme $B_{12}$ **35**, la cyanocobalamine **36** et la méthylcobalamine **37**.

L'étude rpe de la photolyse anaérobique de la cyano et de la méthylcobalamine **36** et **37**, dans le méthanol contenant du DMPO ou du PBN, révèle la formation de radicaux $CH_3{}^{\cdot}$ ou $CN^{\cdot}$ (32).

Par contre, la photolyse anaérobique du coenzyme **35** dans le méthanol conduit à la formation des adduits correspondant à l'addition d'un atome d'hydrogène et du radical déoxy-5′-adénosyle libre sur le DMPO et seulement du radical déoxy-5′-adénosyle libre quand on utilise le PBN comme piège (31).

La mise en évidence grâce aux DMPO et PBN de radicaux déoxyadénosyles lors de la photolyse du coenzyme $B_{12}$ **35** dans le méthanol confirme les résultats obtenus par Joblin *et al.* (8). Ces auteurs ont montré que le coenzyme $B_{12}$ ou l'éthylcobalamine subissent sous irradiation anaérobique, une homolyse de la liaison Co–carbone dans l'eau neutre, le DMSO ou un mélange 1:1 de phénol et de chloroforme.

Les traces d'oxygène présentes dans le méthanol modifient de façon notable le cours de la photolyse de la méthylcobalamine **37**. En effet, dans ces conditions, le DMPO piège un radical méthyle et un atome d'hydrogène.

Lorsque la photolyse des cobalamines **35**, **36** et **37** est effectuée dans l'eau ou $D_2O$, à pH = 7, contenant un excès de DMPO, on met en évidence la formation de deux adduits: l'un correspond au radical $R^{\cdot}$ et l'autre au piègeage d'un atome d'hydrogène. Par contre, le 4-POBN ne piège, dans ces conditions, que le radical $R^{\cdot}$.

La structure des radicaux formés au cours de la photolyse des trois cobalamines ne peut être déterminée uniquement grâce aux caractéristiques (structure et couplages hyperfins) des spectres rpe de leur adduit avec le DMPO, le PBN ou le 4-POBN.

Les structures hyperfines dues à ces adduits ne donnent aucun renseignement sur la nature des atomes des radicaux initiaux, situés sur le centre radicalaire ou en position β. Seule l'utilisation de piège à radicaux du type nitroso permet de connaître la nature de ces atomes. Le nitrosodurène n'étant pas soluble dans l'eau ou le méthanol, nous avons étudié la photolyse des cobalamines **35**, **36** et **37** dans le DMSO (31).

### Discussion et conclusion

L'étude de la photolyse, dans divers solvants, d'alkylcobaloximes, de quelques complexes salen du $Co^{III}$, du coenzyme $B_{12}$ et de deux cobalamines, par résonance paramagnétique électronique (rpe) couplée à la technique des pièges à radicaux, nous a permis de préciser les mécanismes gouvernant la photochimie de ces composés.

Cependant, malgré toutes ces expériences, nous n'avons pas pu obtenir d'évidence directe de la provenance exacte de l'atome d'hydrogène, mais par un processus d'élimination, nous suggérons, jusqu'à preuve du contraire, que l'atome d'hydro-

Can. J. Chem. Downloaded from www.nrcresearchpress.com by 210.87.254.40 on 09/06/12
For personal use only.

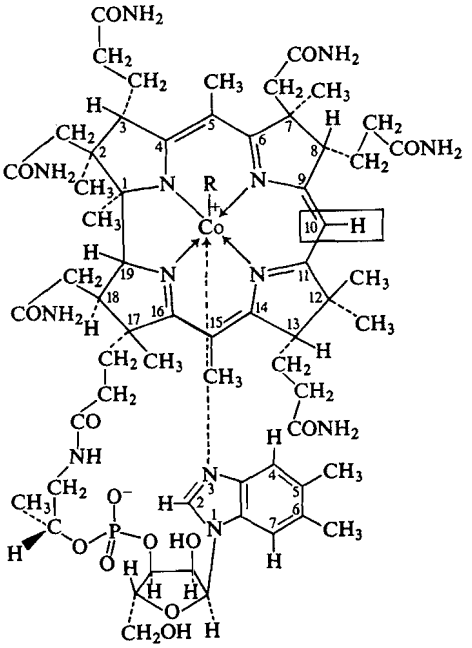

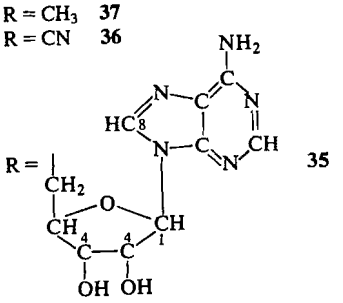


gène piégé lors de la photolyse anaérobique des alkylcobaloximes et des complexes salen, en solution dans les solvants pourrait avoir sa source dans le ligand équatorial de ces composés. L'étude de la photolyse de la benzyl bis(diphénylglyoximato)-pyridinato cobaloxime **9** suggère que l'atome d'hydrogène photolabile ne provient pas des méthyles du ligand équatorial. Il pourrait provenir des hydroxyles des fonctions oximes chélatantes, dans le cas des cobaloximes, et probablement de la position C7 ou C8 du ligand équatorial, dans le cas des complexes salen **32–34**.

Une autre possibilité pourrait être la réduction du DMPO en hydroxylamine diamagnétique par les complexes du $Co^{III}$.[1] Mais ces composés ne sont pas réducteur par eux-mêmes la formation d'un hydrure de cobalt, réducteur puissant, sous photolyse n'est possible qu'avec les composés ayant un atome d'hydrogène en position β par rapport à la liaison $Co^{III}$—C et non avec les autres. De plus la photolyse de l'hydroxylamine, n'absorbant pas la lumière, ne peux se faire que dans l'ultraviolet et dans toutes nos expériences nous avons utilisé une lumière visible ($\nu > 420$ nm).

L'emploi de divers pièges à radicaux utilisés pour étudier les réactions de photolyse de trois cobalamines **35–37**, dans différents solvants, a permis de mettre en évidence d'un part, la rupture homolytique de la liaison Co—C et d'autre part, le départ d'un atome d'hydrogène piègeable suivant le solvant.

[1]Suggestion du referee.

L'atome d'hydrogène piègeable au cours de la photolyse pourrait probablement provenir du ligand corrine équatorial dans le cas de la méthyle ou de la cyanocobalamine, et du ligand équatorial ou du groupement déoxy-5′ adénosyle dans le cas du coenzyme.

A partir de ces résultats, nous pouvons postuler le mécanisme suivant lié à la présence de piège à radicaux (schéma 1).

Le complexe de cobalt solvaté, donc en cage de solvant,

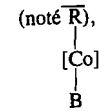


en présence d'un grand excès de piège à radicaux, donne une nouvelle espèce en cage où le piège et le complexe de cobalt sont associés à l'état fondamental (A).

Cette espèce (A) irradiée conduit à la formation d'un exciplexe à l'état singulet qui, par conversion intersystème, évolue vers un exciplexe composé du complexe de cobalt à l'état triplet et du piège dans une même cage de solvant (B).

Cet exciplexe (B) à l'état triplet peut évoluer soit vers la formation d'une paire de radicaux: alkyle, complexe du $Co^{II}$ soit vers la formation d'une paire de radicaux: hydrogène, complexe du $Co^{III}$ (D). Ces deux types de paires de radicaux sont dans une cage de solvant contenant toujours le piège à radicaux.

Le fait que le piège soit à l'intérieur de la cage de

Can. J. Chem. Downloaded from www.nrcresearchpress.com by 210.87.254.40 on 09/06/12
For personal use only.

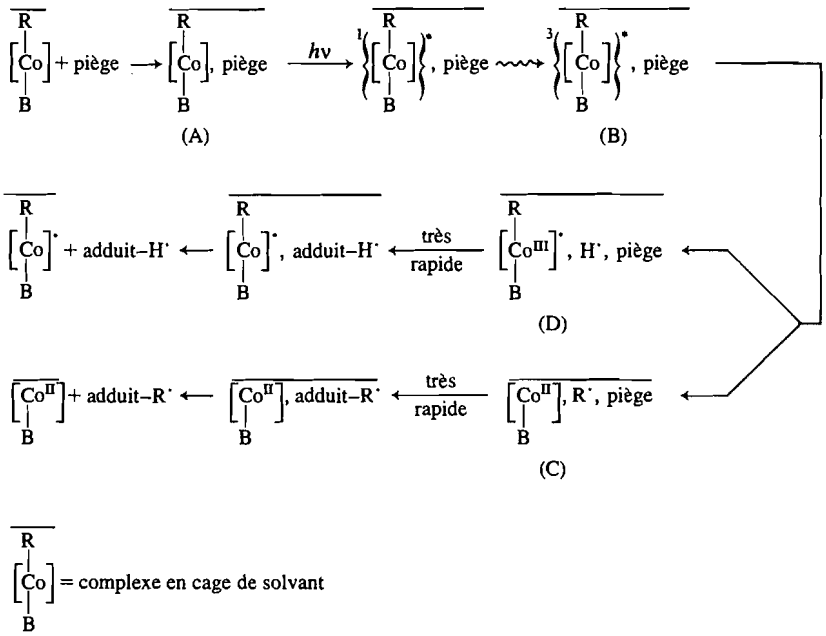


SCHÉMA 1

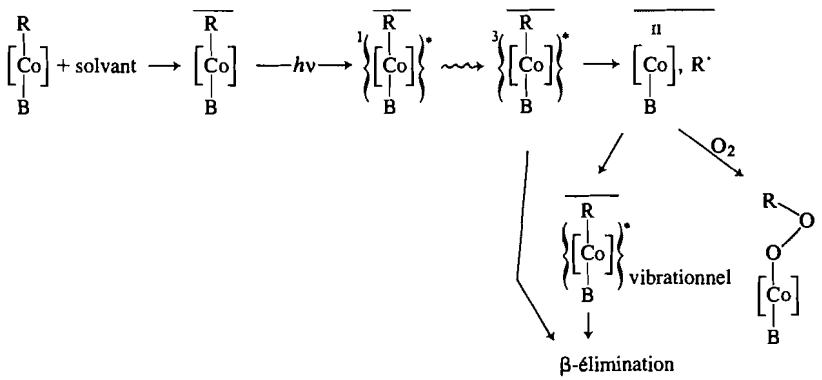


SCHÉMA 2

solvant, donc très proche des radicaux R· ou H·, lui permet de piéger ces espèces avant la recombinaison des paires de radicaux et de diffuser dans la solution.

Il a été montré que la réaction de recombinaison de la liaison $Co^{III}$—C des cobaloximes est fortement ralentie par la présence d'un piège à radicaux (12). Ceci est compatible avec un effet de séparation du radical R· et de l'espèce $Co^{II}$, induit par le piège.

Un effet de cage semblable a été décrit par Ghanekar et Coffman (33) pour expliquer les spectres rpe observés lors de la photolyse de complexes $C_6H_5Co^{III}BAE$. De plus, Endicott et Netzel (7) ont montré que la vitesse de recombinaison $Co^{II}$ + R· → $Co^{III}$ R des cobaloximes est indépendante de la nature du radical R· en absence de pièges à radicaux.

De tels mécanismes en cage de solvant ont déjà été proposés par Roewer *et al.* (13) pour la photolyse des complexes salen du $Co^{II}$ et par Grate et Schrauzer (34) dans le cas d'alkylcobalamines secondaires.

En absence de piège à radicaux, le complexe de cobalt en cage de solvant évolue, sous irradiation, vers son état singulet puis, par conversion intersystème, vers son état triplet. Cette espèce peut subir, soit l'homolyse de la liaison $Co^{III}$—C et par recombinaison de la liaison $Co^{III}$—C évoluer vers une espèce excitée vibrationnelle se désactivant par le processus de β-élimination décrit par différents auteurs (2–4, 13, 34) soit évoluer par le

Can. J. Chem. Downloaded from www.nrcresearchpress.com by 210.87.254.40 on 09/06/12
For personal use only.

processus de β-élimination, directement à partir de l'espèce dans son état triplet. Ce processus de β-élimination n'est possible que si le groupement axial R contient un hydrogène en position β par rapport à la liaison $Co^{III}$—C.

Ainsi, nous avons montré que le solvant joue un rôle fondamental dans la réactivité photochimique des complexes organométalliques du cobalt. La structure de la cage de solvant liée au complexe du cobalt peut modifier la réactivité de ceux-ci.

De plus, le fait que les pièges à radicaux utilisés pour étudier le mécanisme homolytique de photolyse des complexes du cobalt diffusent à l'intérieur de la cage de solvant contenant le complexe, défavorise le processus de recombinaison et facilite la détection des espèces radicalaires (12). Le processus de β-élimination étant considérablement ralenti, le fait que les pièges à radicaux pénètrent différemment dans les cages de solvant peut expliquer des cinétiques différentes de celles observées (35).

## Partie expérimentale

Les méthodes expérimentales ont été décrites précédemment (9, 10, 15, 16, 31).

Les diverses cobaloximes connues sont synthétisées selon les méthodes décrites par Schrauzer et coll. (1, 36). Les caractéristiques physiques (rmn, infrarouge et uv–visible) sont comparées à celles décrites dans la littérature (1, 36).

*Préparation des pièges à radicaux*

Les différents pièges à radicaux sont préparés suivant les méthodes indiquées dans la littérature: DMPO (37–39), ND (40), PBN (41, 42), 4-POBN (43). Des points de fusion et des microanalyses satisfaisantes ont été obtenus pour l'ensemble des composés.

Tous les pièges à radicaux photolysés, en lumière visible (ν > (ν C—D), 2140 (ν CD$\langle^{CD_3}_{CD_3}$), 2110 (ν CD$\langle^{CD_3}_{CD_3}$). 420 nm) dans les solvants utilisés, ne donnent pas de signaux.

*Synthèse des cobaloximes deutérées*

La diméthylglyoxime perdeutérée a été obtenue en suivant la méthode précédemment décrite (11).

*Isopropyl pyridinato cobaloxime perdeutérée*

Chlorure de cobalt (0,950 g) et 0,950 g de diméthylglyoxime perdeutérée sont dissous dans 5 mL de MeOD déoxygéné, sous azote, contenant 1 $cm^3$ de NaOD 8 *M* et 0,37 mL de pyridine-$d_5$. La solution est agitée, sous azote, 20 min, puis est purgée cinq fois avec du deutérium. On ajoute, sous deutérium, 2 mL de bromure d'isopropyle deutéré. On agite jusqu'à ce que le deutérium ne soit plus absorbé. On purge l'appareil à l'azote, puis on neutralise la solution avec DCl. La solution est diluée dans $D_2O$ et est filtrée. Les cristaux sont lavés avec $D_2O$, à l'éther de pétrole, puis avec l'éther. Les cristaux sont dissous dans un mélange $CDCl_3$/MeOD et précipités par $D_2O$, puis séchés. On récupère 1,4 g de cristaux purs (Rdt 86%); ir ($CHCl_3$) $cm^{-1}$: 2670 (ν OD), 2235 (ν C—D), 2190 (ν C—D), 2160 (ν C—D), 2140 (ν CD$\langle^{CD_3}_{CD_3}$), 2110 (ν CD$\langle^{CD_3}_{CD_3}$).

*Benzyl bis(diphénylglyoximato)-pyridinato cobalt*

Chloro bis(diphénylglyoximato)-pyridinato cobalt (0,554 g), préparé selon la méthode Schrauzer (44), est dégazé sous vide dans un tricol. Quinze millilitres d'un mélange 1:1 d'éthanol et d'eau déoxygénés par barbotage d'argon sont introduits à travers un septum dans le tricol, la suspension obtenue est agitée et refroidie à −10°C, 1,265 g de chlorure de benzyle désoxygéné par barbotage d'argon sont ajoutés à la suspension au travers du septum, puis 180 mg d'acide borique dissous dans le minimum d'eau déoxygénée sont ajoutés à la suspension. Borohydrure de sodium (100 mg), dissous dans le minimum d'eau déoxygénée, est ajouté lentement à l'aide d'une seringue. La solution obtenue est agitée une nuit. L'huile brune surnageante est extraite au chlorure de méthylène et lavée à l'eau. La phase organique est séchée sur sulfate de sodium, et évaporée sous vide. Les cristaux bruns sont dissous dans un minimum de méthanol chaud, puis sont reprécipités par addition d'eau. On obtient 0,230 g de cristaux jaunes (Rdt 38%); ir ($CHCl_3$) $cm^{-1}$: 3050 (ν C—H aromatique), 2975 (ν CH), 1600, 1575 (ν C=C), 1440–1420 (ν CH), 1060–890 (ν CH); rmn ($CDCl_3$), δ: 3,38 (2H, s, $CH_2\phi$), 6.92 (5H, m, $CH_2\phi$), 7,33 (20H, s, *H* DPG), 7,77 (3H, m) et 8,80 (2H, d) (*H* pyridine), 17,33 (2H, s, NO*H*). *Anal.* calc. pour $C_{40}H_{34}N_5O_4Co \cdot 1/2H_2O$ (715,93): C 67,04; H 4,88; N 9,47; tr.: C 66,76; H 4,78; N 9,81.

L'adamantyl-1 pyridinato cobaloxime a été préparée en suivant le processus indiqué précédemment (20). Des analyses centesimales correctes ont été obtenues pour l'ensemble des composés.

## Remerciements

Les auteurs remercient A. Gaudemer, K. N. V. Duong et M. Weber pour de fructueuses discussions.

1. G. N. Schrauzer, L. P. Lee et J. W. Sibert. J. Am. Chem. Soc. **92**, 2997 (1970).
2. K. Nguyen-Van-Duong. Thèse d'Etat, No A07749, Orsay, France. 1974.
3. M. Naumberg, K. Nguyen-Van-Duong et A. Gaudemer. J. Organometal. Chem. **25**, 231 (1970).
4. K. Nguyen-Van-Duong, A. Ahond, C. Merienne et A. Gaudemer. J. Organometal. Chem. **55**, 375 (1973).
5. J. M. Pratt. J. Chem. Soc. A, 252 (1971).
6. J. F. Endicott et C. J. Ferraudi. J. Am. Chem. Soc. **99**, 243 (1977).
7. J. F. Endicott et T. L. Netzel. J. Am. Chem. Soc. **101**, 4000 (1979).
8. K. H. Joblin, A. W. Johnson, M. F. Lappert et B. K. Nicholson. J. Chem. Soc. Chem. Commun. 441 (1975).
9. C. Giannotti et J. R. Bolton. J. Organometal. Chem. **80**, 379 (1974).
10. C. Giannotti, G. Merle et J. R. Bolton. J. Organometal. Chem. **99**, 145 (1975).
11. B. T. Golding, T. J. Kemp, P. J. Sellers et E. Nocchi. J. Chem. Soc. Dalton Trans. A, 1266 (1977).
12. D. Lerner, R. Bonneau et C. Giannotti. J. Photochem. **11**, 73 (1979).
13. G. Roewer, G. A. Shagisultanova et I. W. Wojakin. J. Prakt. Chem. **6**, 1031 (1977).
14. G. Roewer et D. Rehorek. J. Prakt. Chem. **4**, 566 (1978).
15. C. Giannotti, G. Merle, C. Fontaine et J. R. Bolton. J. Organometal. Chem. **91**, 357 (1975).
16. C. Giannotti et J. R. Bolton. J. Organometal. Chem. **110**, 383 (1976).
17. P. Maillard, J. C. Massot et C. Giannotti. J. Organometal. Chem. **159**, 219 (1978).

Can. J. Chem. Downloaded from www.nrcresearchpress.com by 210.87.254.40 on 09/06/12
For personal use only.

18. (*a*) J. HALPERN, F. T. T. NG et G. L. REMPEL. J. Am. Chem. Soc. **101**, 7124 (1979); (*b*) H. KUIVILA et O. F. BEUMEL, JR. J. Am. Chem. Soc. **83**, 1246 (1961).
19. J. R. HARBOUR, V. CHOW et J. R. BOLTON. Can. J. Chem. **52**, 3549 (1974).
20. H. ECKERT, D. LENOIR et I. UGI. J. Organometal. Chem. **141**, C23 (1977).
21. E. G. JANZEN et J. I. PING LUU. J. Magn. Reson. **9**, 510 (1973).
22. S. TERABE, K. KURUMA et R. KONAKA. J. Chem. Soc. Perkin Trans. II, 1252 (1973).
23. L. J. SMITH et F. L. TAYLOR. J. Am. Chem. Soc. **57**, 2370 (1975).
24. W. D. EMMONS. J. Am. Chem. Soc. **79**, 5739 (1957).
25. E. G. JANZEN et B. J. BLACKBURN. J. Am. Chem. Soc. **91**, 4481 (1969).
26. E. G. JANZEN, C. A. EVANS et J. I. PING LUU. J. Magn. Reson. **9**, 593 (1973).
27. C. A. EVANS. Aldrichimica Acta, **12**, 23 (1979).
28. J. KRUSIC, T. A. RETTIG et P. V. R. SCHLEYER. J. Am. Chem. Soc. **94**, 927 (1972).
29. H. FISHER. *Dans* Free radicals. Vol. II. *Edité par* J. K. Kocchi. J. Wiley, New York. 1973. p. 435.
30. C. SRIVANAVIT et D. G. BROWN. J. Am. Chem. Soc. **100**, 5777 (1978).
31. P. MAILLARD et C. GIANNOTTI. J. Organometal. Chem. **182**, 225 (1979).
32. J. M. PRATT. The inorganic chemistry of vitamin $B_{12}$. Academic Press, New York. 1972.
33. V. D. GHANEKAR et R. E. COFFMAN. J. Organometal. Chem. **198**, C15 (1980).
34. J. H. GRATE et G. H. SCHRAUZER. J. Am. Chem. Soc. **101**, 4601 (1979).
35. P. SCHIMID et K. U. INGOLD. J. Am. Chem. Soc. **100**, 2493 (1978).
36. G. N. SCHRAUZER et R. J. WINDGASSEN. J. Am. Chem. Soc. **89**, 143 (1967).
37. D. T. WARNER et D. A. MOE. J. Am. Chem. Soc. **74**, 1064 (1952).
38. H. SCHECHTER, D. E. LEY et L. ZELDIN. J. Am. Chem. Soc. **74**, 3664 (1952).
39. R. BONNETT, V. M. CLARK, A. GIDDEYAND et SIR A. TODD. J. Chem. Soc. 2087 (1959).
40. L. I. SMITH et F. L. TAYLOR. J. Am. Chem. Soc. **57**, 2370 (1935).
41. K. N. CAMPBELL, A. H. SOMMERS et R. K. CAMPBELL. J. Am. Chem. Soc. **66**, 82 (1944).
42. W. D. EMMONS. J. Am. Chem. Soc. **79**, 5739 (1957).
43. E. G. JANZEN, Y. Y. LANG et R. V. SHETTY. J. Am. Chem. Soc. **100**, 2923 (1978).
44. G. N. SCHRAUZER. Inorg. Synth. **11**, 61 (1968).

Can. J. Chem. Downloaded from www.nrcresearchpress.com by 210.87.254.40 on 09/06/12
For personal use only.

# Nitroxides as reaction intermediates

HANS GÜNTER AURICH

*Fachbereich Chemie of the University Marburg, Hans-Meerwein-Straße, D-3350-Marburg, Federal Republic Germany*

Received August 10, 1981

HANS GÜNTER AURICH. Can. J. Chem. **60**, 1414 (1982).

Vinyl nitroxides **4** are obtained by oxidation of the nitrones **3**, as was shown by esr studies and by identification of the reaction products. The formation of **4***d–f* is even observed in oxidation of the hydroxylamines **1***d–f*, nitroxides **2***d–f* and nitrones **3***d–f* being the intermediates. The high reactivity of the vinyl nitroxides **4** at their β-position is illustrated by the reactions of **4***a* with various compounds affording the nitroxides **7–10**, respectively. Compound **4***c* reacts with its precursor **3***c* to give **11**, **12**, or **13**, depending on the reaction conditions. From oxidation of **3***a*, *c*, and *e* the dimerization products **5***a*, *c*, and *e*, respectively, could be isolated. Whereas further oxidation of **5***d* yields **6***d*, the acyl nitroxides **14***a* and *c* are formed in the oxidation of **5***a* and *c*, respectively.

The formation of quinone **23** in the reaction of 2-methyl-2-nitrosopropane with potassium *tert*-butoxide in isopropyl alcohol in the presence of oxygen is discussed. The nitroxide **20** has been detected in the reaction mixture. Imines **24** react with nitrosobenzene giving nitroxides **26**. These are further oxidized by nitrosobenzene to afford nitrones **27**. Whereas **27***a* and *b* could be isolated, **27***c* and *d* undergo further reaction yielding the diimines **30***c* and *d* along with dinitrone **29**.

The formation and reactions of imino nitroxides **31** and of the nitronyl nitroxide **41** are discussed. Electron spin resonance studies revealed the high reactivity of the imidazolyl-1,3-dioxides **46** and the imidazolyl-1-oxides **50**, which easily form radicals **47–49** and **51**, respectively, which are derived from secondary reactions.

---

HANS GÜNTER AURICH. Can. J. Chem. **60**, 1414 (1982).

On obtient les vinylnitroxydes **4** par oxydation des nitrones **3** comme le révèlent les études de rpe et l'identification des produits de la réaction. On observe aussi la formation des composés **4***d–f* lors de l'oxydation des hydroxylamines **1***d–f* qui procède par l'intermédiaire des nitroxydes **2***d–f* et des nitrones **3***d–f*. On illustre la grande réactivité de la position β des vinylnitroxydes **4** par les réactions du composé **4***a* avec divers composés qui conduisent respectivement aux nitroxydes des **7–10**. Le composé **4***c* réagit avec son précurseur **3***c* en donnant, en suivant les conditions de la réaction, les composés **11**, **12** ou **13**. L'oxydation des composés **3***a*, *c* et *e*, permet d'isoler respectivement les produits de dimérisation **5***a*, *c* et *e*. Alors qu'une oxydation plus poussée du composé **5***d* conduit au composé **6***d*, l'oxydation des composés **5***a* et *c* conduit respectivment aux acylnitroxydes **14***a* et **14***c*.

On discute de la formation de la quinone **23** lors de la réaction du méthyl-2 nitroso-2 propane avec le *tert*-butoxyde de potassium dans l'alcool isopropylique, en présence d'oxygène. On décelé la présence du nitroxyde **20** dans le mélange réactionnel. Les imines **24** réagissent avec le nitrosobenzène en donnant les nitroxydes **26**. Ces derniers sont de plus oxydés par le nitrosobenzène en donnant les nitrones **27**. Alors qu'on peut isoler les composés **27***a* et *b*, les composés **27***c* et *d* subissent une réaction supplémentaire en donnant les diimines **30***c* et *d* ainsi que la dinitrone **29**.

On discute de la formation et des réactions des iminonitroxydes **31** et du nitronyl nitroxyde **41**. Les études de rpe révèlent la grande réactivité des imidazolyldioxydes-1,3 **46** et des imidazolyloxydes-1 **50** qui forment facilement les radicuax **47–49** et **51** respectivement qui proviennent de réactions secondaires.

[Traduit par le journal]

Nitroxides are stabilized by delocalization of the unpaired electron between oxygen and nitrogen (structures A and B), the delocalization energy being of the order of 30 kcal/mol for dialkyl nitroxides (1). A consequence of this inherent stabilization of the nitroxide group is the easy formation of nitroxides by oxidation of hydroxylamines, as is indicated by the low bond dissociation energy for the OH bond of these compounds (2).

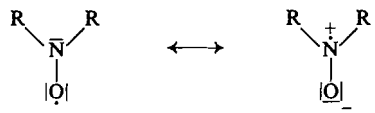

A B

Among the many other reaction routes affording nitroxides, spin trapping by nitrones or nitroso compounds appears to be the most important (3). The facile formation of nitroxides by spin trapping is reflected by the low activation energies for these reactions (4).

Contrary to di-*tert*-alkylnitroxides, which are very persistent radicals, nitroxides with at least one hydrogen atom at the α-carbon atom usually disproportionate to give hydroxylamines and nitrones (5). Because of the facile dehydrogenation of such nitroxides, the oxidation of appropriate hydroxylamines via intermediate nitroxides to give nitrones should be a common reaction. However, complications can arise by reaction of the nitrone with the intermediate nitroxide (6).

Furthermore, oxidation of nitrones with a hydrogen atom at the β-position should afford vinyl nitroxides, which are expected to be additionally stabilized by delocalization of the unpaired electron into the vinyl group (7).

Whereas di-*tert*-alkyl substituted nitroxides are usually extremely persistent, phenyl substituted

0008-4042/82/121414-07$01.00/0

©1982 National Research Council of Canada/Conseil national de recherches du Canada

Can. J. Chem. Downloaded from www.nrcresearchpress.com by 210.87.254.6 on 09/06/12
For personal use only.

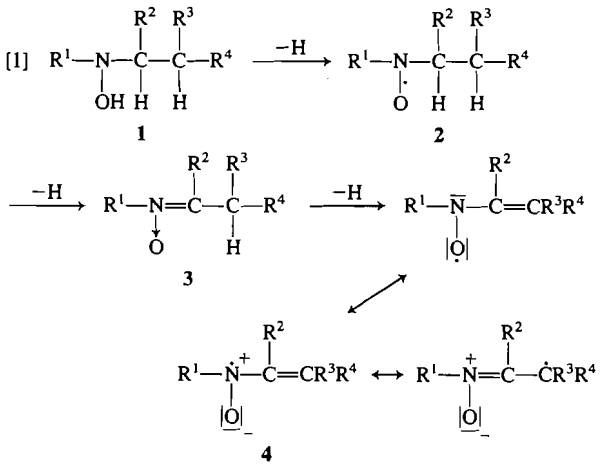

nitroxides are not. The reason is that the extended delocalization of the unpaired electron into the phenyl ring makes dimerization by attack at the *para* position possible, thus giving rise to further decomposition (8*a*). This behavior illustrates nicely the difference between stabilization and persistence of radicals (8*b*).

The delocalization of the unpaired electron into the vinyl group of vinyl nitroxides should cause an even more enhanced reactivity of these radicals compared to phenyl nitroxides. Therefore we decided to study the formation of vinyl nitroxides by esr spectroscopy as well as their reaction pathways by product analysis. More generally, we have been interested in the question of how the nitroxide group affects the reactivity at neighbouring positions in cooperation with other functional groups.

## Results and discussion

### A. *Formation and reactions of vinyl nitroxides*

Oxidation of the nitrones **3** (9)[1] or their corresponding tautomers (10) by lead dioxide or nickel peroxide gave the vinyl nitroxides **4**. The lifetime of radicals **4***a*, *b*, *e*, and *f* is sufficient for them to be detected by esr. Their coupling constants are summarized in Table 1. Radicals **4***c* and *d* could not be observed directly, since they react immediately with their precursor nitrones **3***c* and *d*, respectively, to yield derived radicals. However spin trap reactions as well as product formation indicate that they are real intermediates.

In the oxidation of hydroxylamines **1***d*–*f* (10, 11) the esr signals of the nitroxides **2***d*–*f* can be observed initially but after some time they disappear and, instead, that of the radical derived from a secondary reaction of **4***d*, and those of **4***e* and **4***f*, respectively, arise.[1] To the best of our knowledge this is the first time that the formation of a vinyl nitroxide **4** from hydroxylamine via the intermediates **2** and **3** has been observed.

TABLE 1. Coupling constants of the vinylnitroxides **4** in Gauss[a]

| Compound | $a^N$ | $a^H_\alpha$ | $a^H_\beta$ | $a^H_{other}$ |
|---|---|---|---|---|
| **3***a*[b] (7) | 8.6 | — | 6.5 | 0.45 (3H) $R^2$ or $R^3$ |
| **3***b*[c] | 8.4 | 4.8 | — | 1.45 (3H), 0.93 (3H) $R^3$ and $R^4$ |
| **3***e*[d] | 8.1 | 2.55 | — | 1.85 (3H), 0.65 (2H), 1.35 (3H), 0.65 (2H) $R^1$ and $R^4$ |
| **3***f*[e] | 8.8 | 2.85 | — | 1.7 (3H), 0.65 (2H) $R^4$ |

[a] See footnote 1.
[b] In Et—O—Et.
[c] In $CCl_4$.
[d] In $CHCl_3$.
[e] In $CH_2Cl_2$.

The fate of the vinylnitroxides **4** can be derived from oxidation reactions of **3** on a preparative scale.[1] By performing the oxidation reactions of **3***a*–*e* with lead dioxide or nickel peroxide on a preparative scale we isolated the dimers **5***a*, *c*, and *e* in 81, 85, and 63% yield, respectively; **5***d* could not be isolated but was directly oxidized further to give **6***d*. Only in the case of the oxidation of **3***b* a variety of unidentified products was formed in low yield. Likewise the products **6***d* and **5***e* were isolated in comparable yields by oxidation of the hydroxylamines **1***d* and **1***e*, respectively. These results indicate that *dimerization by formation of a carbon–carbon bond at the β-position of the vinyl group is the major reaction pathway of the intermediate vinyl nitroxides*.

Electron spin resonance studies revealed further that reactions of the vinylnitroxides **4** with other compounds usually also occur at the β-position. The reactions of **4***a* with nitroso compounds,

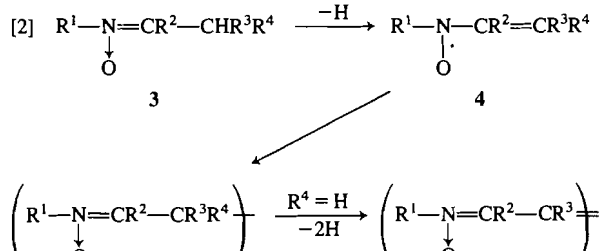

| | $R^1$ | $R^2$ | $R^3$ | $R^4$ |
|---|---|---|---|---|
| *a* | *t*-Bu | COOMe | COOMe | H |
| *b* | *t*-Bu | H | 3,5-*t*-$Bu_2C_6H_3$ | 3,5-*t*-$Bu_2C_6H_3$ |
| *c* | *t*-Bu | H | Ph | H |
| *d* | Ph | H | Ph—CO | H |
| *e* | Ph | H | Ph—CO | Ph |
| *f* | *t*-Bu | H | Ph—CO | Ph |

[1] H. G. Aurich and M. Schmidt, unpublished results; M. Schmidt, Dissertation, Marburg, in preparation.

Can. J. Chem. Downloaded from www.nrcresearchpress.com by 210.87.254.6 on 09/06/12
For personal use only.

TABLE 2. Coupling constants of the nitroxides **2** in Gauss[a]

| Compound | $R^1$ | $R^2$ | $R^3$ | $R^4$ | $a^N$ | $a_\alpha^H$ | $a_\beta^H$ | $a_{R'}^H$ |
|---|---|---|---|---|---|---|---|---|
| **2***d*[b] | Ph | H | PhCO | H | 11.15 | 10.0 (2H) | 0.45 (2H) | 2.9 (3H), 0.95 (2H) |
| **2***e*[b] | Ph | H | PhCO | Ph | 11.8 | 12.75 (1H), 10.4 (1H) | 0.45 (1H) | 3.0 (3H), 1.0 (2H) |
| **2***f*[c] | *t*-Bu | H | PhCO | Ph | 15.25 | 12.75 (2H) | — | — |

[a]See footnote 1.
[b]In $CHCl_3$.
[c]In Et—O—Et.

*N*-benzylidene-aniline-*N*-oxide, 2,4,6-trimethoxybenzonitrile-*N*-oxide, and 2,3-dimethylbuta-1,3-diene, which afford the nitroxides **7–10**, are representative examples (7). Whereas the reactions with the nitroso compounds are simple spin-trapping processes, the formation of **8–10** occurs by cyclizations which are formally 1,3-dipolar cycloadditions. However, it seems more likely that they are

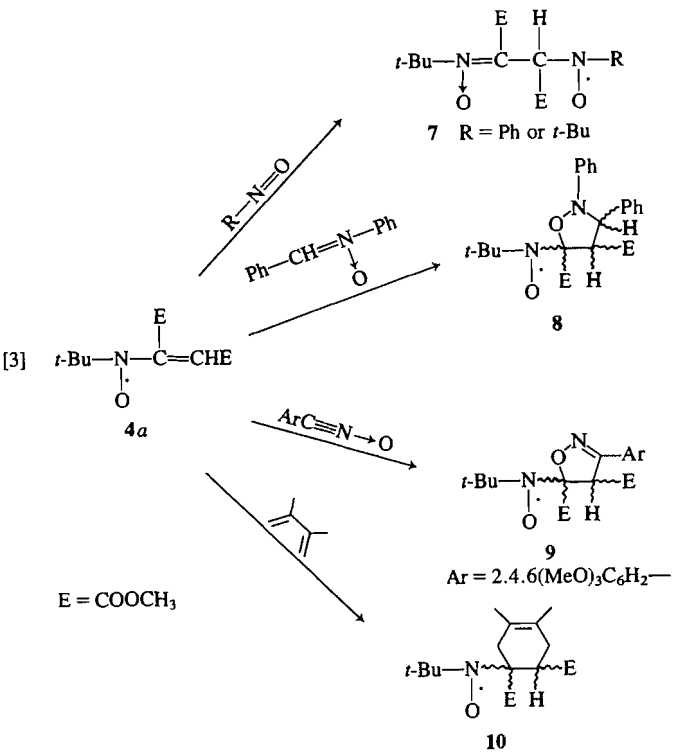


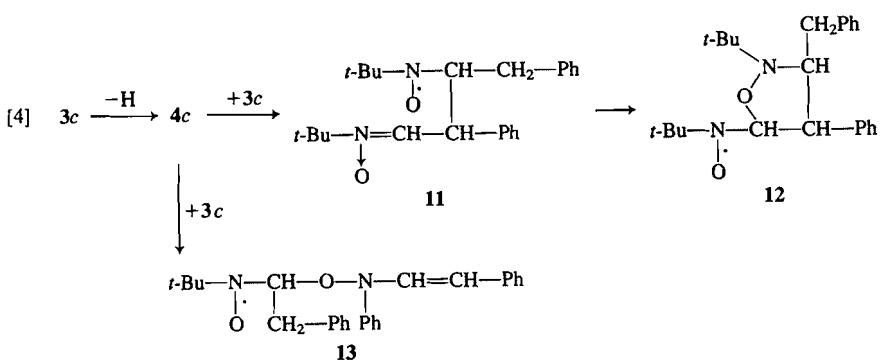


Can. J. Chem. Downloaded from www.nrcresearchpress.com by 210.87.254.6 on 09/06/12
For personal use only.

Can. J. Chem. Downloaded from www.nrcresearchpress.com by 210.87.254.6 on 09/06/12
For personal use only.

two-step reactions. In this case the formation of **8** and **9** must be considered as a twofold spin-trapping process.

Depending on the reaction conditions, three different radicals, obviously formed by secondary reactions of the rather reactive vinylnitroxide **4***c* with its precursor, have been detected in the oxidation of nitrone **3***c*. The coupling constants of these radicals are: $a^N = 15.45$, $a^H = 2.5$ G (1H) in chloroform; $a^N = 13.5$, $a^H = 5.8$ G (1H) in benzene; and $a^N = 13.9$ G, no proton splitting in benzene.[1] The structures **11**–**13** appear to be most probable for these radicals, but at present unambiguous assignment is not possible.

Whereas the intermediate dinitrone **5***d*, which probably exists in its tautomeric *N*-hydroxyenamine form (10), is easily oxidized to afford product **6***d*, the isolated dinitrones **5***a* and **5***c* surprisingly yield the acylnitroxides **14***a* and **14***c* (12) on oxidation with nickel peroxide. After prolonged oxidation of **5***c*, 2,3-diphenylpropen-2-al was isolated,[2] which is obviously formed by hydrolysis of the corresponding *N*-*tert*-butylimine **17**. Thus it appears that the oxidation of **5***c* initially gives the nitroxide **15***c* which then undergoes an intramolecular spin-trap reaction to yield the nitroxide **16**. The formylnitroxide **14***c* and the imine **17** can then arise by a retro-Diels–Alder reaction of **16**.

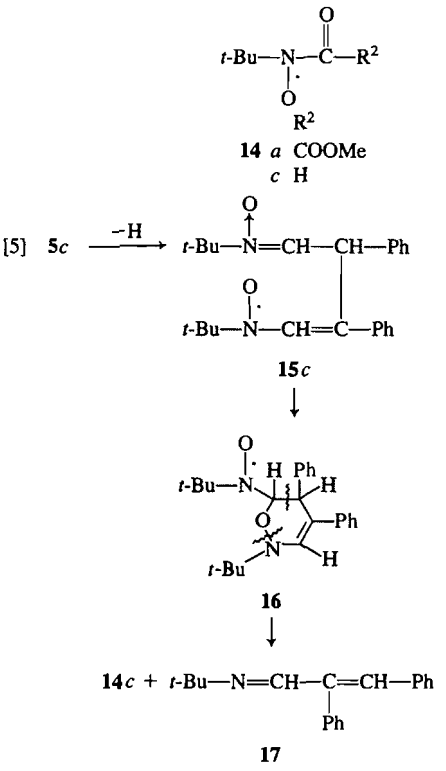


B. *Nitroxides as intermediates in other oxidation reactions*

The formation of 2,5-bis-(*tert*-butylamino)-1,4-benzoquinone **23**[3] in 31% yield from the reaction of 2-methyl-2-nitroso propane with potassium *tert*-butoxide in isopropyl alcohol in the presence of oxygen is a rather obscure reaction (14*a*). Electron spin resonance studies indicated that the nitroxide **20** ($a^N = 15.2$ G, $a^H = 10.4$ G (2H), $a^H = 0.65$ G (1H)) is involved. The same radical was obtained by Lagercrantz and Setaka (14*b*) in the reaction of hydroxy radicals with isopropyl alcohol in the presence of 2-methyl-2-nitrosopropane: $a^N = 16.3$ G, $a^H = 13.3$ G (1H), $a^H = 8.9$ G (1H), $a^H = 0.74$ G (1H) in $H_2O$. The larger values for the coupling constants are due to the more polar solvent. In contrast to our findings, Lagercrantz observed two different coupling constants for the methylene protons, but this may be due to the different reaction conditions. Nevertheless, exactly the same ratio $a^N/a^H_{CH_2}$ is obtained in the two cases, if one uses the mean values of the proton couplings.

It must be assumed that the reaction is induced by the formation of the nitroso anion radical **18** on treatment of the nitroso compound with *tert*-butylate (15). Anion radical **18** reacts readily with oxygen and, as is known from reaction in various solvents, hydrogen abstraction from the solvent occurs under these conditions (15). Radical **19** formed from isopropyl alcohol (eq. [6]) is then trapped by the nitroso compound to give the nitroxide **20**. One would expect hydrogen abstraction from isopropyl alcohol to occur exclusively at its central position, as was also pointed out by a referee. But under the very different conditions, applied by Lagercrantz (14*b*) and us, radical **20** could be detected unambiguously, whereas no evidence for the trapping of the radical $CH_3—\dot{C}(OH)CH_3$ was found. Under the oxidative reaction conditions a successive dehydrogenation of **20** to afford the acylnitrone **22** via the intermediate vinyl nitroxide **21** is reasonable. Since it was found that nitrone **22**,[4] which was synthesized independently,

[2]Melting point 94°C (lit. (13*a*) mp 94°C, see also p. 281, ref. 13*a*); ir (KBr): 1660 and 1620 $cm^{-1}$; $^1H$ nmr ($CDCl_3$): 9.65 (1H, s), 7.4–7.1 (11H, m) ppm; ms: $M^+$ 208.

[3]Structural proof by comparison with a sample prepared in an independent way (13*b*).

[4]Nitrone **22** was obtained by reaction of *tert*-butylhydroxylamine with 2-oxo-propanal;[1] $^1H$ nmr ($CDCl_3$): 7.0 (1H, s), 2.35 (3H, s), 1.45 (9H, S) ppm.

Can. J. Chem. Downloaded from www.nrcresearchpress.com by 210.87.254.6 on 09/06/12
For personal use only.

[6] $t\text{-Bu—}\dot{N}\text{—}\overline{O}|^{-} + O_2 + CH_3\text{—}CH(OH)\text{—}CH_3 \longrightarrow$

**18**

$t\text{-BuNO}_2 + OH^- + \cdot CH_2\text{—}CH(OH)\text{—}CH_3$

**19**

[7] $t\text{-Bu—N=O} + \cdot CH_2\text{—}CH(OH)\text{—}CH_3 \longrightarrow$

$t\text{-Bu—N(O}\cdot\text{)—}CH_2\text{—}CH(OH)\text{—}CH_3 \xrightarrow{-2H}$

**20**

$t\text{-Bu—N(O}\cdot\text{)—CH=CH(OH)—CH}_3 \xrightarrow{-H} t\text{-Bu—N(O)=CH—C(=O)—CH}_3$

**21** **22**

$\xrightarrow{\text{base}}$ 4-(*t*-Bu—NH)-4-(NH—Bu-*t*)-cyclohexa-2,5-dien-1-one

**23**

is converted into the quinone **23** on treatment with various bases, the reaction seems to be rationalized best by the proposed reaction sequence (eq. [7]).

As was found some years ago by Layer (16), imines react in their tautomeric enamine form with nitrosobenzene to give hydroxylamines which are oxidized by further nitrosobenzene to afford the corresponding nitroxides. We performed this reaction with less substituted imines **24** having at least two hydrogen atoms at the β-position (17). The nitroxides **26** could be detected by esr, as expected, but there was no evidence for the existence of the tautomeric β-amino substituted vinylnitroxides **28**. Oxidation of the nitroxides **26** by nitrosobenzene afforded the rather unstable imino nitrones **27** which could be isolated only when substituted as in **27***a* and **27***b*.

In the reactions with imines **24***c* and **24***d*, however, the diimines **30***c* and **30***d* were formed along with the dinitrone **29** (eq. [9]) (18). Since the existence of small amounts of vinylnitroxides **28***c* and **28***d* in equilibrium with **26***c* and **26***d*, respectively, could not be excluded, a dimerization of **28***c* and **28***d* by bond formation at the β-position may be considered to be the first step in a reaction sequence yielding **30***c* and **30***d* along with **29**. But this possibility was refuted by the labelling experiments. The distribution of the carbon-13 label agrees only with a dimerization at the oxidation level of the nitrone **27** in the indicated way.

## C. *Imino and nitronyl nitroxides*

Contrary to the vinyl nitroxides **4**, imino nitroxides **31** do not dimerize, since the gain in energy for the formation of a nitrogen–nitrogen bond does not compensate the loss of delocalization energy for the two nitroxide molecules (ref. 19, see also p. 91).

As in the case of hydroxylamines **1***e* and **1***f*, amino-substituted hydroxylamines such as **33**, which exist in equilibrium with their educts, can be oxidized by lead dioxide to yield imino nitroxides via the corresponding intermediates (20). Starting with nitrone **32** and methylamine, nitroxide **34** was first detected, which was slowly converted to the imino nitroxide **36**. Surprisingly, the oxidation process did not stop at this level. The methyl group was destroyed by further oxidation, the imino nitroxide **37** being the final radical product in the reaction sequence [10]. Compound **35** could be isolated from the reaction mixture as the lead complex in 31% yield.

Similarly, oxidation of **38** (21) proceeds via **39** and **40** to afford the nitronyl nitroxide **41** (eq. [11]). But after some hours the esr signal of **41** disappears, and the imino nitroxide **42** is observed instead. The *N*-hydroxy formhydroxamic acid **43**

[8] $Ph\text{—N=O} + R'\text{—}CH_2\text{—CH=N—R} \longrightarrow$

**24**

$Ph\text{—N(OH)—CH(R')—CH=N—R} \xrightarrow[(PhNO)]{-H} Ph\text{—N(O}\cdot\text{)—CH(R')—CH=N—R}$

**25** **26**

$\xrightarrow{-H} Ph\text{—N(O)=C(R')—CH=NR}$ $\qquad$ $Ph\text{—N(O}\cdot\text{)—C(R')=CH—NH—R}$

**27** **28**

[9] $Ph\text{—N=O} + CH_3\text{—}{}^{*}\text{CH=N—R} \longrightarrow$ **25***c*,*d* $\longrightarrow$ **26***c*,*d* $\longrightarrow$

$Ph\text{—N(O)=CH—}{}^{*}\text{CH=N—R} \longrightarrow Ph\text{—N(O)=CH—}{}^{*}\text{CH=N—R}$

**27**

$\longrightarrow Ph\text{—N=CH—}{}^{*}\text{CH=N—Ph} + R\text{—N=CH—}{}^{*}\text{CH=N—R}$

**29** **30**

* $^{13}$C-labelled

| | R′ | R |
|---|---|---|
| *a* | *i*-Pr | *t*-Bu |
| *b* | Ph | *t*-Bu |
| *c* | H | *t*-Bu |
| *d* | H | *c*-$C_6H_{11}$ |

Can. J. Chem. Downloaded from www.nrcresearchpress.com by 210.87.254.6 on 09/06/12
For personal use only.

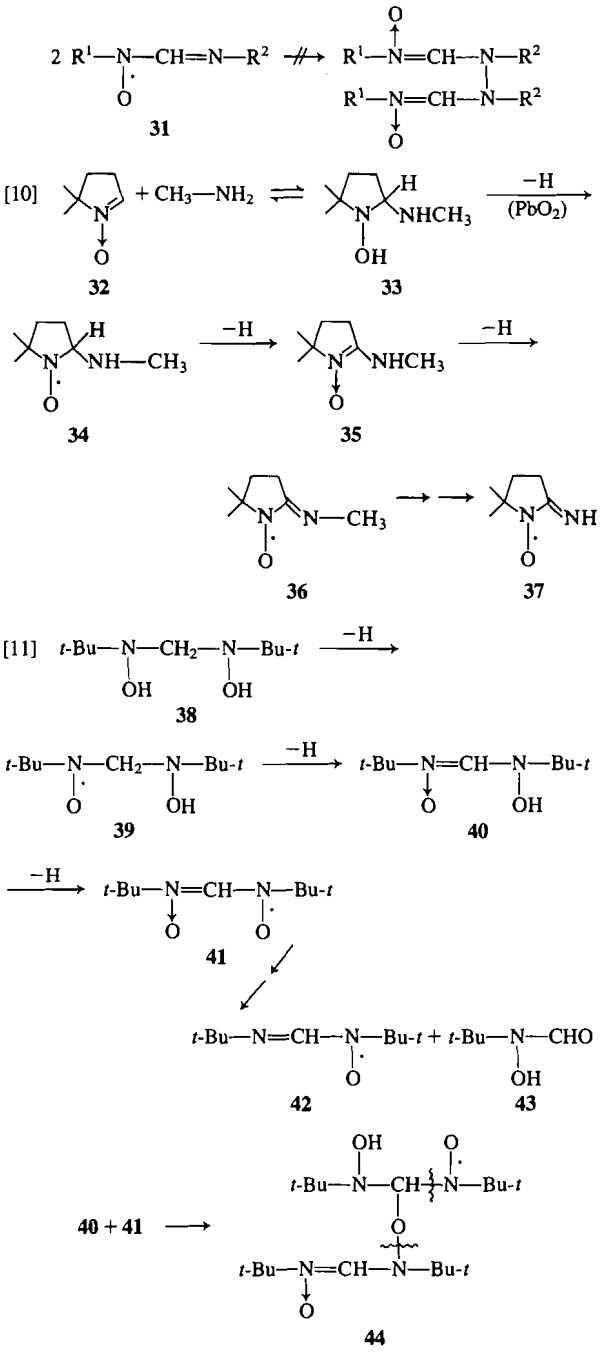

was isolated as the lead complex in 5% yield from the reaction mixture (20). The formation of **42** and **43** can be rationalized if one assumes that **41** is trapped by its precursor **40** to give the adduct **44**, which is then split as indicated.

D. *Imidazolyl-1,3-dioxides and imidazolyl-1-oxides*

In imidazolyl-1,3-dioxides the vinyl group and the nitronyl group are both conjugated with the nitroxide moiety. Whereas the 4,5-diaryl substituted imidazolyl-1,3-dioxides (22) as well as the benzimidazolyl-1,3-dioxides (23) are relatively persistent, this is not true for the 4,5-dimethyl substituted radicals **46**. Thus, the radical to which structure **46***a* has been assigned (22) is in fact a radical derived from a secondary reaction.[5]

When we oxidized the 4,5-dimethyl-3-hydroxyimidazole-1-oxides **45***a* (22) and **45***b* to afford **46***a* and **46***b*, we found that the lifetime of these radicals is markedly influenced by the substituent at the 2-position. Although **46***a* was studied at low temperatures its esr spectrum changes so rapidly that it never could be recorded without superposition of the spectrum of the radical derived from a secondary reaction. On the other hand, radical **46***b* has a lifetime of more than five minutes at room temperature. Whereas **46***a* is converted into a cyclic nitronyl nitroxide **47** (24) with slightly different coupling constants for the two nitrogen atoms, indicating an unsymmetric substitution, **46***b* is converted into the oximino nitroxide **48** (eq. [12]). The structure of **48** was assigned by comparison with the coupling constants of related radicals (23*b*). Finally **48** is converted to give the nitronyl nitroxide **49**, which is presumably symmetrically substituted.

Obviously, the easy conversion of **46***a* and **46***b* reveals the particular reactivity of the vinyl group which is conjugated with a nitroxide group. The difference in the reactivity of **46***a* and **46***b* suggests that an attack at the 2-position of **46** or its precursor **45** is involved in the reaction sequence forming the derived radicals.

From this it seems possible that the conversion begins with bond formation between the vinylic carbon atom of **46** and the 2-position of the precursor molecule **45** to afford again a vinyl nitroxide moiety which then undergoes further intramolecular reactions, e.g. spin trapping.

TABLE 3. Coupling constants of the radicals **46**–**51** in Gauss[a]

| Radical | $a_1^N$ | $a_3^N$ | $a_2^H$ | $a_{4,5}^H$ | *g*-value |
|---|---|---|---|---|---|
| **46***a* | 4.0 | 4.0 | 0.8 (3H) | 1.7 (6H) | |
| **46***b* | 4.0 | 4.0 | — | 1.65 (6H) | |
| **47** | 7.1 | 6.8 | 3.2 (3H) | — | 2.0065 |
| **49** | 6.85 | 6.85 | — | — | 2.0065 |
| **48** | 8.2 | 4.8 | — | — | 2.0062 |
| **50***b* | 4.3 | 2.0 | — | 7.6 (3H); 2.0 (3H) | |
| **51***a* | 8.15 | 3.6 | 1.76 (3H) | — | |
| **51***b* | 8.7 | 3.8 | 0.53 (3H) | 0.33 (3H) | |

[a]See footnote 5. In $CHCl_3$.

[5]H. G. Aurich and J. Schmock, unpublished results.

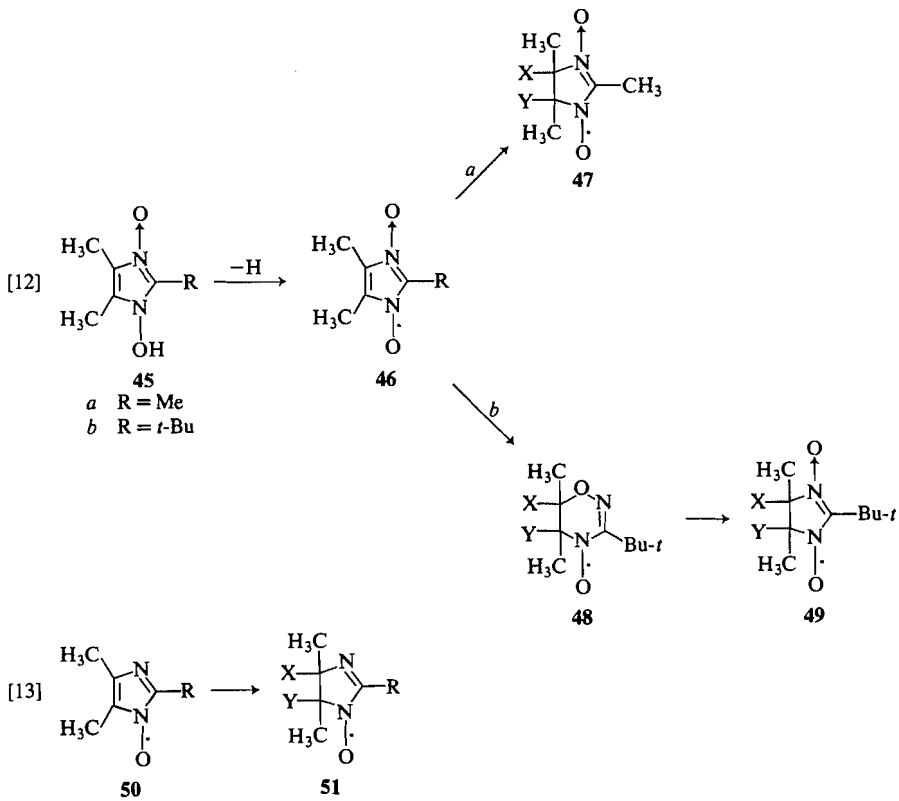


The conversion of the imidazolyl-1-oxides **50** into the imidazolinyl-1-oxides **51** is thought to occur in a similar way. Since the esr spectrum of **50***a*, in contrast to that of **50***b*, could never be observed, it must be concluded that this radical is even more reactive than the corresponding radical **46***a*.


## Acknowledgements

I would like to thank my co-workers for their cooperation. This work was supported by the Fonds der Chemischen Industrie.



1. E. G. Rozantsev. Free nitroxyl radicals. Plenum Press, New York, London. 1970. p. 125.
2. L. R. Mahoney, G. D. Mendenhall, and K. U. Ingold. J. Am. Chem. Soc. **95**, 8611 (1973).
3. (*a*) E. G. Janzen. Acc. Chem. Res. **4**, 31 (1971); (*b*) M. J. Perkins. Essays on free radical chemistry. *Edited by* R. O. C. Norman. Chem. Soc. Spec. Publication No. 24, 1970. p. 97.
4. P. Schmid and K. U. Ingold. J. Am. Chem. Soc. **100**, 2493 (1978).
5. D. F. Bowman, T. Gillan, and K. U. Ingold. J. Am. Chem. Soc. **93**, 6555 (1971).
6. R. Briere and A. Rassat. Tetrahedron, **32**, 2891 (1976).
7. H. G. Aurich, K. Hahn, and K. Stork. Chem. Ber. **112**, 2776 (1979).
8. (*a*) A. R. Forrester and R. H. Thomson. Nature, **203**, 74 (1964); (*b*) K. U. Ingold. Acc. Chem. Res. **9**, 13 (1976).
9. H. G. Aurich and K. Hahn. Chem. Ber. **112**, 2769 (1979).
10. F. De Sarlo and G. Renzi. J. Chem. Soc. Perkin Trans. I, 1113 (1978).
11. J. Thesing, A. Müller, and G. Michel. Chem. Ber. **88**, 1027 (1955).
12. H. G. Aurich and J. Trösken. Chem. Ber. **106**, 3483 (1973).
13. (*a*) H. Meerwein. J. Prakt. Chem. [2], **97**, 225 (1918); (*b*) J. L. Huntington and D. G. Davis. J. Magn. Reson. **3**, 456 (1970).
14. (*a*) W. Dersch. Diss. Univ. Marburg, 1974; (*b*) C. Lagercrantz and M. Setaka. Acta Chem. Scand. B, **28**, 619 (1974).
15. H. G. Aurich and W. Dersch. Z. Naturforsch. Teil B, **28**, 525 (1973).
16. R. W. Layer. Tetrahedron Lett. 4413 (1970).
17. H. G. Aurich, J.-M. Heinrich, and G. Waßmuth. J. Chem. Res. (S), 222 (1980); (M), 3046 (1980).
18. H. G. Aurich, J.-M. Heinrich, and G. Waßmuth. J. Chem. Res. (S), 224 (1980); (M), 3062 (1980).
19. H. G. Aurich and W. Weiss. Top. Curr. Chem. **59**, 65 (1975).
20. H. G. Aurich, S. K. Duggal, P. Höhlein, H.-G. Klingelhöfer, and W. Weiss. Chem. Ber. **114**, 2440 (1981).
21. G. Zinner and U. Dybowski. Arch. Pharm. Weinheim, **304**, 877 (1971).
22. K. Volkamer and H. W. Zimmermann. Chem. Ber. **102**, 4177 (1969).
23. (*a*) H. G. Aurich and W. Weiss. Chem. Ber. **106**, 2408 (1973); (*b*) H. G. Aurich and K. Stork. Chem. Ber. **108**, 2764 (1975).
24. D. G. B. Boocock, R. Darcy, and E. F. Ullman. J. Am. Chem. Soc. **90**, 5945 (1968).


Can. J. Chem. Downloaded from www.nrcresearchpress.com by 210.87.254.6 on 09/06/12
For personal use only.

# Spin labelling ribosomes: an overview

HERMANN DUGAS AND ANGEL RODRIGUEZ

*Department of Chemistry, Université de Montréal, Montreal (Qué.), Canada H3C 3V1*

Received August 10, 1981

HERMANN DUGAS and ANGEL RODRIGUEZ. Can. J. Chem. **60**, 1421 (1982).

This paper reviews the spin label approach to the problem of structure and function of the bacterial ribosomes from *Escherichia coli*. The work of different research groups towards selective spin labelling of 70S ribosomes is presented and results are compared. Information obtained by binding these derivatized ribosomes with magnesium ions, tRNA, and antibiotics are analyzed. The interaction of selectively spin-labeled $tRNA^{Phe}$ and spin-labeled kanamycin and puromycin with the ribosomes is also discussed.

HERMANN DUGAS et ANGEL RODRIGUEZ. Can. J. Chem. **60**, 1421 (1982).

Cet article fait une revue de l'étude de la structure et de la fonction des ribosomes bactériens de *Escherichia coli* par la méthode du marqueur de spin. Les travaux de différents groupes de chercheurs dans le but de marquer sélectivement les ribosomes 70S sont présentés et comparés. On analyse l'information obtenue lors de la fixation d'ions magnésium, de tRNA et d'antibiotiques sur les ribosomes marqués. On discute aussi les résultats de l'interaction des ribosomes avec du $tRNA^{Phe}$ sélectivement marqué ainsi qu'avec des marqueurs de spin de kanamycine et de puromycine.

## Introduction

In all organisms, the biosynthesis of proteins occurs on a complex "molecular machinery" called the ribosome. The best-characterized ribosome is from the bacterium *Escherichia coli* and consists of three different RNA molecules and 53 to 55 different proteins. The ribosomal particle has a sedimentation value of 70S and is composed of two nonidentical subunits, the 30S and 50S subparticles. The specific nucleic acid protein interactions involved in the assemblage of the ribosome subparticles have interested not only biochemists but also chemists and biophysicists in the last decade, and many aspects of the ribosome's structure and function have been reviewed recently (1–3).

For the ribosome to be active in protein synthesis, many molecules, factors, and ions must interact with its structural components. Of particular interest is the perturbation that can be created by the binding of antibiotics and transfer RNA (tRNA) molecules on the ribosome structure. In this regard, different techniques such as tritium exchange (4) and iodination (5) of ribosomal proteins, fluorescence labelling (6, 7), and the spin-label method (8–14) have been applied to elucidate any structural change taking place on the ribosome. The objective of the present paper is to review the spin-label approach. Contributions from our laboratory (8–11) as well as from others (12–14) will be presented and compared.

## Results and discussion

A simplified representation of the composition of *Escherichia coli* ribosomes is pictured in Fig. 1. How does one go about selectively spin labelling such an organelle? Obviously, an important condition for the application of the spin-label method is the implantation of covalent labels on specific protein groups. In this respect, the reactivity of protein SH groups for alkylating agents such as NEM[1] has been examined in detail. In particular,

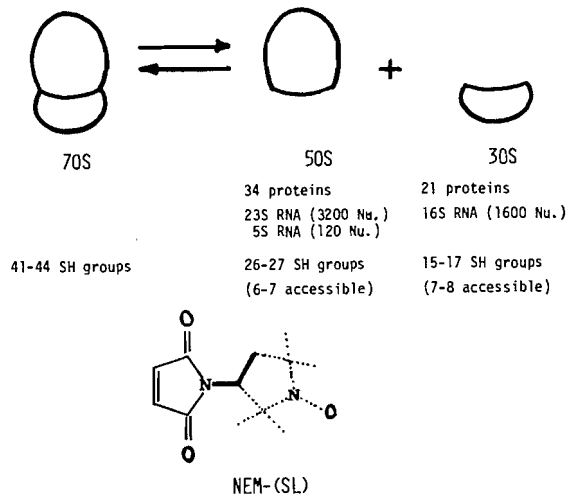


FIG. 1. Representation of the 70S ribosome from *E. coli*. The composition of each subunit and the number of available SH groups are indicated. The structure below emphasizes the similarity between NEM and its spin-label analogue (spin label I).

[1]*Abbreviations*: epr, electron paramagnetic resonance; SL, spin label; ribo, ribosome; NEM, *N*-ethylmaleimide; Cbz, carbobenzyloxy; Sm, streptomycin; Nm, neomycin B; Km, kanamycin A; Pm, puromycin; BSL, 3-(2-bromoacetamido)-2,2,5,5-tetramethyl pyrrolidine-1-oxyl, (bromo-SL); CSL, 1-(*N*-methyl-2-morpholinoethyl)-3-(2,2,6,6-tetramethyl piperidine)-1-oxyl, (carbodiimide-SL); HSL, *N*-hydroxysuccinimide ester of 3-carboxy-2,2,5,5-tetramethyl pyrrolidine-1-oxyl, (hydroxysuccinimide-SL); AMSL, 4-amino-2,2,6,6-tetramethyl piperidine-1-oxyl, (amino-SL); ADPSL, adenosine 5'-diphosphate-4-(2,2,6,6-tetramethyl-piperidine)-1-oxyl; FWR, factors washable from ribosomes.

0008-4042/82/121421-11$01.00/0

©1982 National Research Council of Canada/Conseil national de recherches du Canada

Can. J. Chem. Downloaded from www.nrcresearchpress.com by 210.87.254.5 on 09/06/12
For personal use only.

Can. J. Chem. Downloaded from www.nrcresearchpress.com by 210.87.254.5 on 09/06/12
For personal use only.

Bakardjieva and Crichton (15) have done an extensive study on the accessibility of SH groups from ribosomal proteins towards radioactive NEM. Fortunately, spin-labeled analogues of NEM are available. We have thus chosen for our studies the 5-membered ring analogue (spin label I) which bears a close spatial resemblance with NEM as illustrated in Fig. 1 and therefore should not appreciably perturb the ribosome structure beyond the perturbation caused by the presence of NEM itself. Other groups have worked with the nitroxyl 6-membered ring analogue.

*Selective spin labelling of ribosomes*

In the complex structure of the 70S ribosome each SH group of the ribosomal proteins should have a microenvironment unique to itself and the motion of the spin label bound to them should be a characteristic of this environment. Furthermore, the epr signal should also be sensitive to structural modifications of the ribosome during its multiple functions. In order to study a local region of the ribosome without ambiguity, it is essential to label that region as specifically as possible. To achieve a selective spin labelling, the differences in reactivity of the SH groups have been exploited in several laboratories and are summarized in Table 1. Selective spin labelling is indeed possible but only if the labelling is carried out for short periods of time and preferably when the ratio of spin label to ribosome is not too high. It is well established that labelling the 70S ribosome with NEM can perturb some of its functions (16–18) and even affect its conformation (19). Further, dissociation and degradation of the ribosome occur under conditions of intensive labelling (12). For the same reasons, prolonged treatment of the ribosome above room temperature should also be avoided. The utilisation of NEM analogues as probes has thus necessitated a control of the activity and the integrity of the ribosome structure.

It is important to realize that during the assignment of the spin-labeled proteins we have observed that we cannot assume a complete analogy between the reactivity of [$^{14}$C]NEM and the spin-labeled analogues. For instance, L2 and S13 are both reactive proteins towards NEM, but neither is alkylated by the spin label I (9). Furthermore, we have found that proteins L6, L11, and L17 have a reactivity for NEM which is superior to the number of SH groups present on the proteins and suggests that other NEM-sensitive groups (possibly ε-amino groups from lysine residues) are present. Extreme care should thus be exercised during spin-label work if reactivity of analogous probes are compared.

The location on the ribosome of the spin-labeled proteins from our work (9) is depicted in Fig. 2. Cross-linking experiments with bifunctional reagents have suggested physical proximity for these proteins (2). Although some of these proteins (S18, S21) are elongated and can span across the 30S subunit, it is now accepted that proteins S1, S18, S21, and 3′-end of 16S RNA are all localized in the head portion of the 30S subunit and constitute the domain of codon–anticodon interactions (1, 2, 20). It has also been established that the SH groups of proteins S1, S18, and S21 (all one SH per protein) are part of the head portion of the 30S, close to the anticodon region (2, 21). Furthermore, S12 (a neighbor of S21) is implicated in the process of recognition of mRNA and the binding of initiator-tRNA (fMet-tRNA) at the ribosomal P site (20). As for protein L27, it is known to be part of the P site in the 50S subunit in proximity to the 3′-end of tRNA (22). Interestingly, it is the only labeled protein from the 50S subunit and its location is directly facing the other spin-labeled proteins on the 30S subunit when both subunits are associated. This specific region is thus particularly sensitive to alkylating agents. We can thus infer that under our conditions of labelling with spin label I, the labels

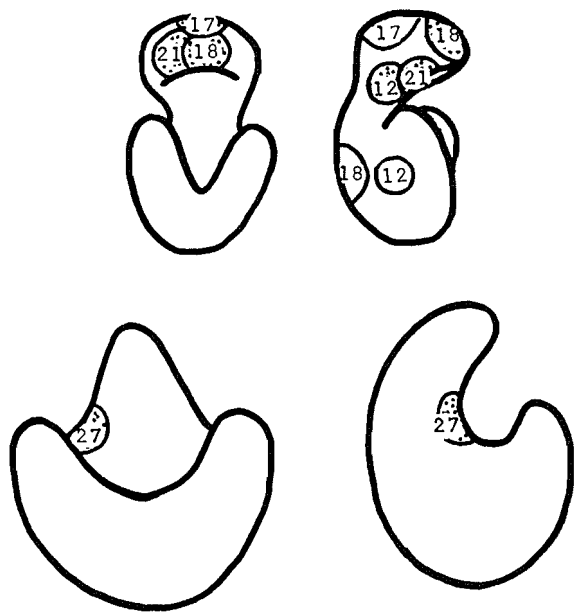


FIG. 2. Location of the spin-labeled proteins on the individual 30S and 50S subunits (9). The two views presented are obtained by rotation through an angle of 90° (2). Spin-labeled regions are represented by dotted zones.

Can. J. Chem. Downloaded from www.nrcresearchpress.com by 210.87.254.5 on 09/06/12
For personal use only.





TABLE 1. Summary of the results obtained with spin-labeled ribosomes

| Spin label used | Conditions of labelling | Proteins spin-labeled | Remarks on selectivity | Activity of SL-ribosomes* | Effect of $Mg^{2+}$ ions | Binding of antibiotics | Addition of tRNA |
|---|---|---|---|---|---|---|---|
| 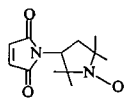 Dugas *et al.* (9) | 2 min 22°C SL/ribo ratio of 40 | S18 > S21, L27 > S17, S12 | 1.5 SL/ribo, 80% on 30S, 48% of S18 labeled | 90% active | SL not affected by changes in $Mg^{2+}$ concentration | Loosening of ribosome structure upon binding Sm (8) | Loosening of ribosome structure on the 30S subunit (11) |
| 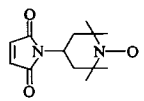 Brakier-Gingras *et al.* (12, 13) | 1.5 min 37°C SL/ribo ratio of 125 | S18 > S1 > L 17, L10 | About 1 SL/ribo, 70% on 30S, 57% of S18 labeled | Not determined | | Binding of Sm does not affect reactivity of SH groups. Loosening of ribosome structure upon binding of Sm (Nm had no effect) | |
| | Same conditions but S18 blocked first with NEM | S1, L10 > L17 > S21 | About 1 SL/ribo, 45% on 30S, 30% on S1 | Not determined | | Loosening of ribosome structure upon binding of Nm (Sm had no effect) | |
| 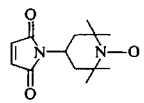 Tritton (14) | 16h, 4°C SL/ribo ratio about 250 | About 20 (not determined) | Not selective but either subunit could be separated and reassociated with non-SL-subunits | Inactive | SL more mobile when SL-subunits associated with non-SL-partners | Loosening of structure upon binding Sm but only when SL are in the 50S subunits | |
| 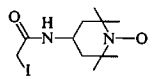 (14) | Labeled fraction L7/L12 and reconstituted the ribosome | Complex L7/L12 selectively labeled | 0.5 to 1 SL/ribo, only on 50S subunit | Fully active | | | |

*Activity towards poly(U)-directed poly-Phe synthesis.

Can. J. Chem. Downloaded from www.nrcresearchpress.com by 210.87.254.5 on 09/06/12
For personal use only.

are in a well-localized domain to allow an adequate monitoring of ribosome–mRNA–tRNA interactions. Furthermore, the head part of the 30S subunit is in the region of binding of the tRNA molecule where local perturbation could be followed (*vide infra*).

Representative epr spectra of the selectively spin-labeled ribosomes are presented in Fig. 3. For spin label I, the spectrum is fairly immobilized and suggests that the environment of the SH groups is rather hydrophobic in nature with an hyperfine splitting ($a_N$) of only 15.9 G. Similar spectra were obtained with the 6-membered ring analogue of NEM (12). Using a series of homologous spin labels, the average depth of the cavity occupied by the spin label has been estimated to around 6 Å (9).

We have performed a series of simulations of the epr spectra[2] of the 70S ribosome, labeled with spin label I (1.5 SL/ribosome). The resemblance between experimental and simulated spectra indicated that 30% of the epr signal corresponds to a $\tau_c$ of 0.5 to 3.0 ns and that the remaining 70% corresponds to a motion of the spin labels characteristic of a $\tau_c$ value between 10 and 80 ns. Free diffusion of 70S ribosome in an aqueous medium corresponds to 2.5 μs (25). Consequently, spectral analysis by simulation showed that a major fraction of the signal corresponds to spin labels strongly immobilized.

Using a different approach, Tritton selectively spin labeled the isolated proteinaceous complex L7/L12 (no SH group present) with an iodoacetamide spin label and reconstituted active ribosomal 70S particles (14). The corresponding epr spectra were indicative of mobile probes, even after reconstitution. This result seems to show that at least a portion of the L7/L12 domain maintains a good deal of flexibility when localized in the ribosome (14). The author suggested that such flexibility in this region of the ribosome structure may be related to its activity. This kind of selective labelling should be very useful for the eventual study of binding of initiation and elongation factors IF-2, EF-Tu, and EF-G (2).

*Selective spin labelling of 16S RNA*

Figure 4 summarized how we have attempted to label specifically the 3′-end of 16S RNA present in the 30S subunits. First, we have used the intact 70S ribosomes and labeled them under conditions similar to those used to label the 3′-end of tRNA molecules (26). The labelling was directed towards the terminal ribose residue by reductive acylation in the presence of amino-SL (AMSL) and $NaBH_4$, using material pretreated with $NaIO_4$. The corresponding epr spectrum has a $\tau_c$ value of 0.09 ns and the incorporation of spin label was 0.28 SL/ribosome. Since AMSL alone could in principle react with certain ribosomal proteins, labelling was also carried out in absence of $NaIO_4$ as a control. Without $NaIO_4$ we obtained an incorporation of 0.11 SL/ribosome ($\tau_c$ = 0.22 ns).

Therefore, the 3′-end of 16S RNA does not seem to be hindered but our labelling is not selective enough; some 23S RNA and some protein residues might also be modified (27). In order to obtain a completely selective labelling, the 16S RNA would have to be isolated from the 30S subunits, labeled, and the 70S ribosomes reconstituted in the presence of spin-labeled 16S RNA.

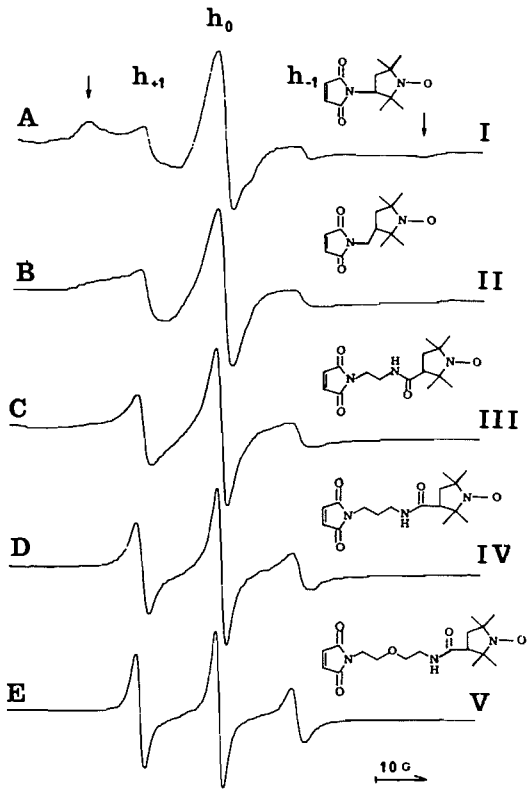


FIG. 3. The epr spectra of selectively spin-labeled 70S ribosomes from *E. coli* at 21°C in 20 m*M* Tris-HCl, 10 m*M* $Mg(OAc)_2$, 0.1 *M* $NH_4Cl$, pH 7.4. The concentration of spin-labeled ribosomes used is $6 \times 10^{-6}$ *M* and the number of spin labels per ribosome was estimated to be 1.5 (9). The distance from the center of each ring for spin labels I to V are, respectively, 4.4, 5.7, 9.3, 10.5, and 12.9 Å. This corresponds to an approximation for the distance between the nitroxide group and the site of attachment on the ribosomal proteins. The spectra were recorded on a Bruker 414S spectrometer.

[2]We have considered an isotropic motion and an axial symmetry of the nitroxide group. The spectra were obtained from a linear combination of four simulated components with the following $\tau_c$ values and relative populations: 0.5 ns (1.5%), 3.0 ns (28%), 10 ns (24.5%), and 80 ns (46%) (23, 24).

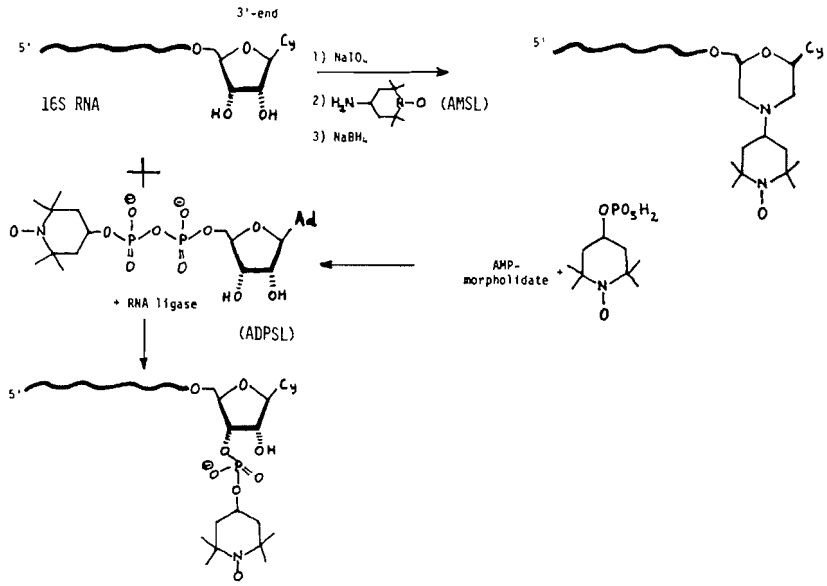


FIG. 4. Approaches to spin labelling the 3'-end of 16S RNA.

In a different approach, we have attempted an enzymatic labelling of the 3'-end of 16S RNA in the presence of RNA ligase (28). As substrate we used a spin-labeled ADP analogue (ADPSL), prepared by the method used by Weiner (29). Unfortunately, using a mixture of 16S and 23S RNA the efficiency of labelling was only 3%. With isolated 30S subunits, the yield of labelling was even lower. Nonetheless, in both cases the spectra showed a very mobile component ($\tau_c = 0.1$ ns), characteristic of a rather exposed 3'-end for the 16S RNA.

*Effect of magnesium ions*

The presence of $Mg^{2+}$ ions is essential for the ribosome to be active and to function normally at 37°C. Since lowering the $Mg^{2+}$ concentration could result in many modifications of the ribosome structural integrity (17), it became interesting to see if such structural perturbations could be detected and followed spectroscopically with spin-labeled ribosomes.

Contrary to previous expectation (17), no epr-detectable changes in the ribosome structure seemed to take place with ribosomes labeled with spin label I, upon dissociation of the 70S particles into subunits by lowering the $Mg^{2+}$ concentration from 20 m*M* to 0.5 m*M* (9). This observation agrees with results obtained by other techniques, especially electron microscopy (30). However, when the ribosomes were spin labeled in their dissociated state, new SH groups became alkylated at the subunit interfaces and the epr spectrum was indicative of more mobile probes. Glick and Brubacher (31) had already shown that, indeed, additional NEM-reactive groups are available upon dissociation of 70S ribosomes.

On the other hand, Tritton (14), using his multi-spin-labeled ribosomes, observed an increase in the motion of the labels when 30S or 50S spin-labeled subunits were associated with non-spin-labeled partners to form 70S particles. The author proposed that such relaxation of structure in both subparticles when they are joined together to form a 70S ribosome may be functionally important for the procession of the organelle through the various steps of protein synthesis (14). In contrast, Favaudon and Pochon (32), with stopped-flow technique using either 30S or 50S subparticles and a fluorescent probe, have observed that only the 30S subunit exhibits a $Mg^{2+}$-dependent conformational change. This divergence thus remains to be clarified by further studies.

*Binding of antibiotics*

Structurally related aminoglycoside antibiotics such as streptomycin (Sm), neomycin B (Nm), and kanamycin A (Km) bind to the ribosomes and interfere with several steps in protein synthesis in bacteria (33). Their structures are shown in Fig. 5. For instance, they can either induce inhibition of protein synthesis by altering the initiation step or, at different degrees, cause misreading of the genetic code. They can also affect the stability of the ribosomal particles. These antibiotics bind to the 30S subunit, on nonidentical but possibly closely related sites (34, 35). Although their mode of action

Can. J. Chem. Downloaded from www.nrcresearchpress.com by 210.87.254.5 on 09/06/12
For personal use only.

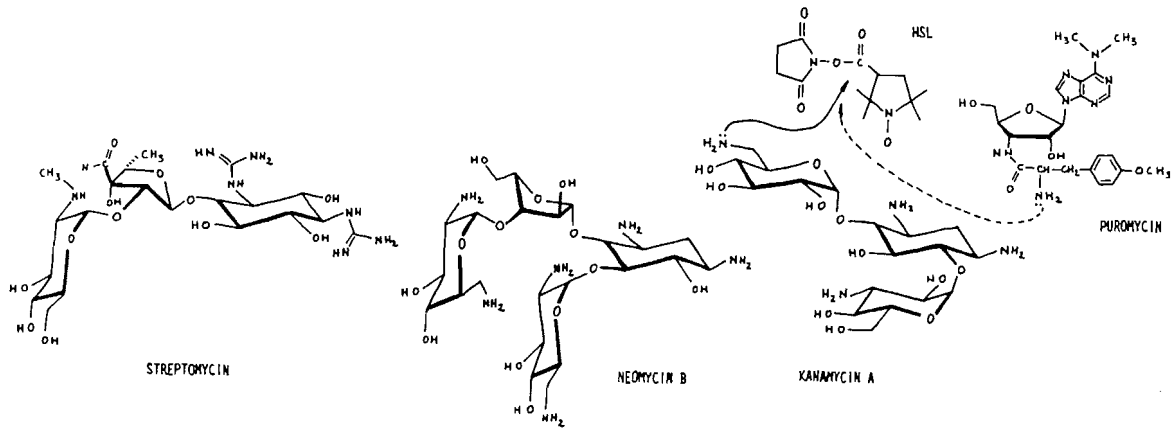


FIG. 5. Structures of the antibiotics discussed in the text. As shown, SL-Km and SL-Pm were prepared by reaction with HSL (see Experimental).

has been studied in some detail, particularly for Sm, the exact location of their binding sites on the ribosome and the extent of perturbation caused on the ribosome structure are still not very well understood. Some workers have argued that the 3′-end of 16S RNA could be involved in the binding of Sm (36), while others have suggested that proteins S1, S12, and S18 are among the proteins implicated in the binding (37). This last hypothesis makes the spin-labeled ribosomes excellent candidates to study the binding of these antibiotics with ribosomes.

Preliminary studies, in which many ribosomal proteins were spin labeled with either spin label I or the 6-membered analogue, suggested already that the binding of Sm seems to loosen the structure of the ribosome (8). A more elaborate work on the interaction of Sm and Nm was carried out by Brakier-Gingras and co-workers (12, 13) using selectively spin-labeled ribosomes (see Table 1). First of all they were able to show that the presence of Sm neither protects the SH groups from reaction with NEM nor induces structural changes so as to expose new SH groups (12). Secondly, they confirmed that indeed the presence of Sm loosens the structure of spin-labeled ribosomes and suggested that this loosening is probably located in a restricted area of the ribosome, since it was observed only when a limited number of ribosomal sites were labeled, especially S1 and S18.

To follow the binding of the antibiotics, they relied on the fluctuation of the relative intensities of the two low field maxima of the spectra. Such exercise must be practiced with much caution because it corresponds to a gross oversimplification of the exact proportion of strongly and weakly immobilized components present in the spectra. Nevertheless, qualitative information can be compared.

More interesting was the finding that Nm had no effect on the epr spectra of ribosomes spin labeled mainly on protein S18. On the other hand, if this protein is first blocked by NEM and then the ribosomes spin labeled, proteins S1 and L10 are the main proteins containing the paramagnetic probe (13). With these new derivatized ribosomes a local loosening was still observed, but only upon binding of Nm; this time Sm had no effect. Proteins S1 and S18 are neighbors and protein L10 is located close to the complex L7/L12 in the 50S subunit (2). These data thus provide evidence that Sm and Nm distort the conformation of the ribosome at different sites, and this could be a consequence of the difference in their mode of action (13). For instance, Nm induces more misreading than Sm.

Tritton (14) has also studied the effect of Sm on reassociated spin-labeled 70S ribosomes. Again a loosening of the ribosome structure was observed but only when the spin labels were in the 50S subunits.

*Spin-labeled antibiotics*

To gain more information on the location of the binding site of antibiotics, spin-labeled kanamycin (SL-Km) and spin-labeled puromycin (SL-Pm) were synthesized by coupling with HSL (see Fig. 5). The objective was to study their interaction with ribosomes and spin-labeled ribosomes. Such an approach could allow the determination of distances between the site of labelling on the ribosome and the site of binding of the spin-labeled antibiotics. Km is an aminoglycoside which binds to the 30S subunit whereas Pm is an antibiotic that binds to the aminoacyl-site (A site) of the ribosome. It can

Can. J. Chem. Downloaded from www.nrcresearchpress.com by 210.87.254.5 on 09/06/12
For personal use only.

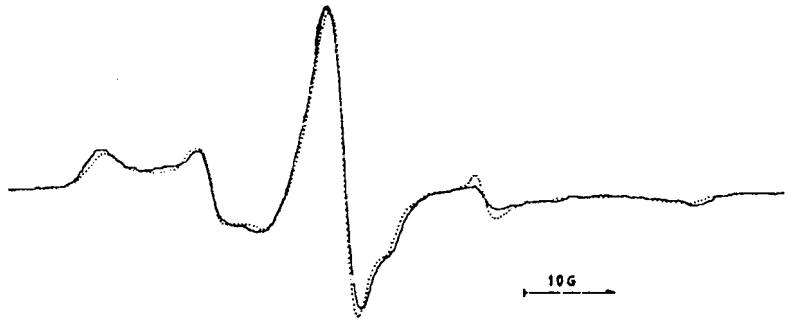


FIG. 6. The epr spectra of spin-labeled 70S ribosomes from *E. coli* in 50 m*M* Tris-HCl, 20 m*M* $Mg(OAc)_2$, 0.14 *M* $NH_4Cl$, pH 7.4 at room temperature. Spectra were normalized in such a way that the central lines have the same amplitude, 6 scans using a Nicolet 1180 computer, total time 20 min; (———), spin-labeled ribosomes containing 1.5 mol of spin label I per mole of ribosome; (---), spin-labeled ribosomes in the presence of poly(U) and $tRNA^{Phe}$ (11).

mimic the 3′-end of aminoacyl-tRNA molecules and its mode of action involves the formation of a peptide bond with the growing peptide chain in the peptidyl-site (P site). This results in a premature termination of polypeptide (protein) synthesis (38).

It should be recalled that the distances from the center of each ring for spin labels III and V are respectively 9.3 and 12.9 Å (see Fig. 3). Unfortunately, upon binding SL-Km or SL-Pm to SL(III)-ribosomes, no sign of nitroxide–nitroxide interactions could be detected. In fact, the only modification detectable in the epr spectra came from a slight increase in the mobility of the epr signal when SL-Pm binds to ribosomes spin labeled with SL(III) or SL(V). On the other hand, binding of SL-Km to ribosomes spin labeled with SL(III) or SL(V) resulted in a slight immobilization of the epr signal. Km binds to the 30S subunit and possibly close enough to protein S18 so as to immobilize the spin-label motion. Therefore, our efforts in this "molecular stick" approach, although preliminary, were rather disappointing. This could result from the fact that the binding capacity ($EC_{50}$) of the spin-labeled antibiotics was found to be much too weak.[3] Since these SL-antibiotics do not bind efficiently with the ribosome, and very large quantities of ribosomes are needed in these experiments, the experiments were not pursued any further.

*Binding of transfer RNA (tRNA)*

As mentioned earlier, some of the spin-labeled proteins, in particular S18 and S21, are believed to be directly implicated in the region of binding of tRNA to the ribosome (21, 39). Our selectively spin-labeled ribosomes (9) are thus properly suited for that type of monitoring. It was found that binding of spin-labeled ribosomes with $tRNA^{Phe}$ or poly(U) alone did not appreciably modify the epr spectra, but when both are present an increase in the mobility of the spin labels was readily detected. This is presented in Fig. 6 and the same effect was observed with an aminoacyl-tRNA molecule, Cbz-Phe-$tRNA^{Phe}$ (11). This spectral change corresponds to a perturbation of the ribosome structure in the environment of the labeled SH groups upon formation of the tertiary complex. Such a subtle fluctuation of the ribosome may be required during the process of protein synthesis. A similar conformational change was previously detected by fluorescence spectroscopy (7) but the spin label contribution indicates that it corresponds to a loosening in the ribosome structure. It is very likely that this perturbation is in the neighborhood of proteins S18 and S21 since the accessibility of their SH groups has been shown to be affected (reduced) by the presence of poly(U) or tRNA molecules (7). However, the technique of iodination of ribosomal proteins has also been used to identify a set of 30S ribosomal proteins involved in the poly(U)-directed nonenzymatic binding of the $tRNA^{Phe}$ (40). The proteins identified were S1, S2, S3, S14, and S19. Since none of these proteins contain a spin label, it is likely that other perturbations away from the site of labelling be involved, yet undetectable by epr spectroscopy.

A comparison of the rate of reduction by ascorbic acid of the nitroxide groups present on spin-labeled ribosomes alone and on spin-labeled ribosomes having tRNA and poly(U) bound to their surface clearly showed that the labels are more accessible in the tertiary complex (11). This finding not only confirms that a structural change has taken

[3]The $EC_{50}$ is the amount of SL-antibiotic necessary to displace 50% of non-spin-labeled antibiotic. It was determined for both SL-antibiotics by N. Moreau, Thiais, France. For SL-Pm a value of $14 \times 10^{-4}$ *M* was obtained and for SL-Km the value was $1.25 \times 10^{-4}$ *M*. Typical values for good binding affinity should be in the $10^{-6}$ *M* range.

Can. J. Chem. Downloaded from www.nrcresearchpress.com by 210.87.254.5 on 09/06/12
For personal use only.

Can. J. Chem. Downloaded from www.nrcresearchpress.com by 210.87.254.5 on 09/06/12
For personal use only.

place on the ribosome upon binding of the tRNA molecule but also that the labels are more exposed. This is expected if the ribosome structure is more open after binding tRNA and poly(U).

Addition of poly(U) and tRNA to 70S ribosome labeled with SL(V) reduced the motion of the nitroxide group, suggesting that at least the binding of tRNA is at a distance less than 13Å from the labeled SH groups.

In conclusion, the binding of tRNA to spin-labeled ribosomes at the P site (*vide infra*) loosens the ribosomal structure (11) but similar experiments where the tRNA binds predominantly to the A site showed no modification of the epr signal. Therefore, the A site is structurally and conformationally different from the P site with respect to tRNA binding, at least as monitored by epr spectroscopy.

*Binding of spin-labeled tRNA to 70S ribosomes*

An approach complementary to the one described above is to use selectively spin-labeled tRNA molecules and study their interaction with intact ribosomes. This way conformational changes on the tRNA molecules can be monitored. Among the numerous spin-labeled tRNA derivatives known (26, 41), two of them, BSL-Cbz-Phe-tRNA$^{Phe}$, labeled at position $s^4U_8$, and CSL-Cbz-Phe-tRNA$^{Phe}$, labeled at position $U_{33}$ in the anticodon region, were used to study the dynamics of tRNA–ribosome interaction in the presence of poly(U) and factors washable from ribosomes (FWR) (10).[4]

As expected, the spin label CSL in the anticodon loop could follow perturbations in this region. On the other hand, the spin label BSL in the center of the molecule at position $s^4U_8$, because of its unique location in the sequence, could witness structural changes either in the tertiary interactions between dihydrouridine and TψCG loops or in the aminoacceptor arm (3′-CCA arm). Figure 7 shows that indeed the binding of these two selectively spin-labeled aminoacyl-tRNA molecules to the ribosomes could be followed readily by monitoring the variation in the correlation time ($\tau_c$). This was manifested principally by a substantial increase in the amplitude of motion of the spin label BSL at position $s^4U_8$, but it is clear that the environment of both spin labels is affected. The spectroscopic evidence indicates that the tRNA molecules had undergone a conformational change in tertiary structure when bound to the ribosomes.

[4]FWR are obtained during the purification of ribosomes and are rich in initiation factors which bind to tRNA during protein biosynthesis. Experiments in the presence of FWR are referred to as enzymatic binding of tRNA to ribosomes.

Interestingly, BSL-tRNA$^{Phe}$ which was not aminoacylated showed no change in the epr spectra when bound to the ribosome. Therefore, nonspecific binding was unlikely because it should have been observed with uncharged tRNA. As compared to Phe-tRNA$^{Phe}$, the binding capacity of Cbz-Phe-tRNA$^{Phe}$ was, however, reduced to about 68% and the presence of a spin label reduced this value again, but only slightly. Therefore, the presence of the Cbz group seems to be the main factor responsible for lowering the association constant of these tRNA molecules (10).

Experiments in the presence of the antibiotic puromycin, which binds exclusively to the A site, clearly showed that spin-labeled Cbz-Phe-tRNA$^{Phe}$ molecules were bound preferentially to the ribosomal P site (up to 70%) and the effect was more pronounced (83%) in the presence of FWR. It was also found that the presence of poly(U) did not appreciably modify the epr signals of the spin-labeled tRNA's. The main contribution to the variation in the $\tau_c$ values observed then must come from binding to the P site and suggests that specific codon–anticodon recognition cannot be the prime factor responsible for the structural change taking place on the aminoacyl-tRNA molecule upon binding to the ribosome (42). Furthermore, a recent $^1$H nmr study (43) showed that no conformational changes in the $T_{54}$ region of the tRNA could be detected upon formation of the tight complex via complementary anticodon–anticodon interaction between *E. coli* tRNA$^{Glu}$ and yeast tRNA$^{Phe}$. If such a tRNA$^{Phe}$–tRNA$^{Glu}$ duplex can be used as a model of codon–anticodon interaction, it becomes rather unlikely that codon–anticodon recognition may trigger an unfolding of the tertiary structure of tRNA and induce accessibility of the TψCG region. Along the same lines of thought, Vlassov and Mamayev (44) arrived at the conclusion that codon binding does not change the conformation of the tRNA from a chemical modification study of the interaction of tRNA$^{Phe}$ with $(pU)_4$.

By tritium exchange and fluorescence measurement, Farber and Cantor (4) have also found that tRNA$^{Phe}$ interacts with the ribosome similarly in the presence and absence of poly(U). In this direction, Kurland *et al.* (45) have already suggested a "conformational selection mechanism" for tRNA recognition whereby a perturbation away from the anticodon could allow a better codon–anticodon recognition process and at the same time would be responsible for the selection of the right aminoacyl-tRNA. Therefore, the conformational change of tRNA$^{Phe}$ when bound to poly(U)-programmed ribosomes is induced by ribosomes and not by poly(U) or messenger RNA (mRNA) (4, 10).

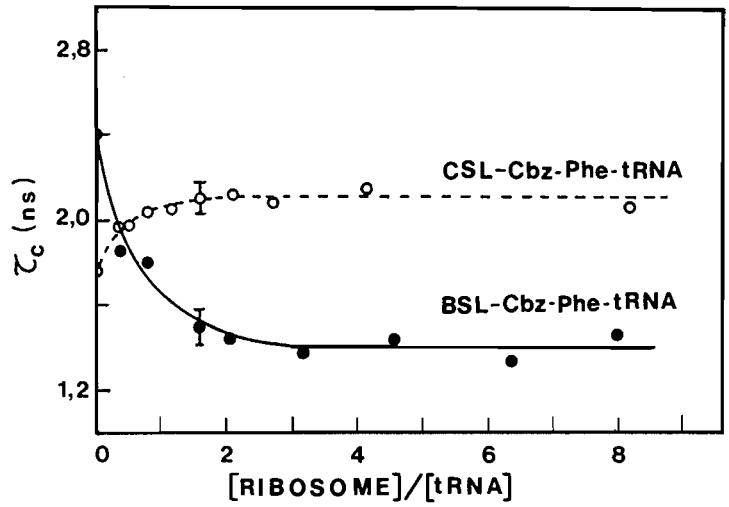


FIG. 7. Variation in the correlation times ($\tau_c$) of spin-labeled Cbz-Phe-tRNA$^{Phe}$ bound to 70S ribosomes in the presence of poly(U), at different ribosome to spin-labeled tRNA ratios. BSL is at position $s^4U_8$ while CSL is in the anticodon region at position $U_{33}$ (10).

In addition, structural changes on the tRNA, at a region remote from the anticodon, could have an important impact on its role in the fidelity of translation of the genetic message.

It is believed that this structural change could be mediated by the binding of tRNA to 5S RNA on the ribosome. For this to happen, some of the intramolecular tertiary hydrogen bonds present between the dihydrouridine and TψCG loops must be broken to allow new intermolecular hydrogen bonds between the TψCG sequence on the tRNA and a complementary Watson–Crick base pair sequence on the 5S RNA. Most of the evidence from the literature suggests that this segment of 5S RNA is located in, or close to, the ribosomal A site (46). This is illustrated in Fig. 8. However, it has been clearly demonstrated that N-blocked aminoacyl-tRNA molecules (spin-labeled derivatives as well) bind primarily to the ribosomal P site (10). Thus the structural loosening in the environment of the $s^4U_8$ residue which has been detected by epr must correspond to a perturbation of the tRNA structure of another kind, different from the one used to bind to 5S RNA.

Different but converging results in this direction came also from the recent work of Farber and Cantor (47). They studied the accessibility of ribosomal 5S RNA within the ribosome by monitoring the slow tritium exchange rates of specific sites with those rates in the free 5S RNA. Most interesting was the finding that the presence of deacylated tRNA$^{Phe}$ bound tightly to the P site of poly(U)-programmed ribosomes did not modify significantly the exchange pattern of 5S RNA.

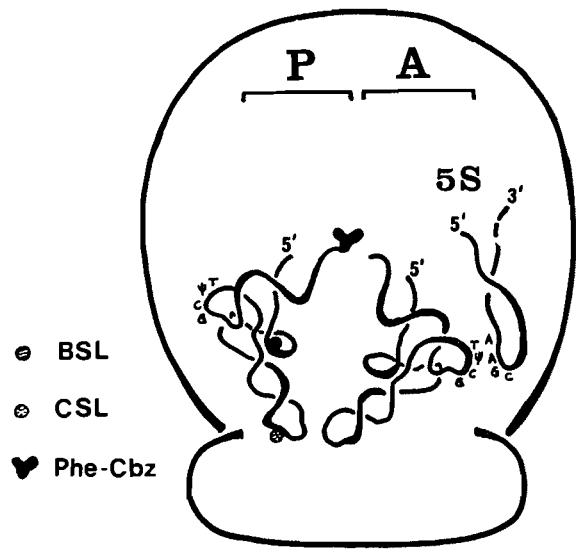


FIG. 8. Hypothetical representation of the binding of two tRNA molecules on the ribosome. Spin-labeled aminoacyl-tRNA$^{Phe}$ is in the peptidyl site (P) and tRNA$^{Phe}$ (or Phe-tRNA$^{Phe}$) is in the aminoacyl site (A). The 3'-end and anticodon regions of each tRNA should be facing each other (22). Part of the ribosomal 5S RNA is also shown in the vicinity of the A site where the fragment CGAA can hydrogen bond to the TψCG loop of the tRNA. The circles on the tRNA structure represent the position of either BSL or CSL.

Consequently, the presence of tRNA in the P site does not seem to induce any ribosomal conformation change to expose the complementary sequence CGAA of 5S RNA in the A site.

Since the epr spectra of uncharged tRNA are not modified by the presence of ribosomes and poly-(U), Rodriguez *et al.* (10) argued that the structural

Can. J. Chem. Downloaded from www.nrcresearchpress.com by 210.87.254.5 on 09/06/12
For personal use only.

Can. J. Chem. Downloaded from www.nrcresearchpress.com by 210.87.254.5 on 09/06/12
For personal use only.

rearrangement on the tRNA could be mediated by the presence of the amino acid at the 3′-end. In other words, the presence of the amino acid (or the peptidyl group) would facilitate tRNA-ribosome interactions at the P site and such recognition would induce a structural change on the tRNA molecule to maximize these interactions. Earlier findings also converged towards such a rationale where a stereochemically favored disposition of the aminoacyl residue has been shown to increase the affinity of the 3′-end for the ribosome (48, 49). The spin-label method has thus brought another element of proof for this hypothesis.

Probably this modification of the tRNA molecule is due to an interaction between its 3′-end and the 50S subunit since the interaction of BSL-CBz-Phe-tRNA$^{Phe}$ with isolated 30S subunits does not result in an increase in the mobility of the spin label (we have not verified, however, if the 30S subunits were still active).

## Conclusion

Work with spin-labeled ribosomes and spin-labeled tRNA molecules has shown at least one consistency. The binding of tRNA to ribosomes results in a molecular fluctuation in the structure of both molecules. This alteration corresponds, in both cases, to a loosening or opening of their structure. Such a conformational difference in three-dimensional structure between free and bound biological molecules could be a universal consequence of their role, which is molecular adaptation for more efficient function.

## Experimental

The preparation of ribosomes, spin-labeled ribosomes, spin-labeled tRNA, and the binding studies with magnesium ions and antibiotics have been adequately described before (9–14) and will not be repeated here.

*Spin labelling 16S RNA with AMSL*

To 5 μ*M* of 70S ribosomes in 1 mL of buffer C (Tris-HCl 20 m*M*, $Mg(OAc)_2$ 10 m*M*, $NH_4Cl$ 100 m*M*, pH 7.4) was added 1 mL of $NaIO_4$ (2 m*M*) in acetate buffer pH 5.0. After 2 h at 21°C in the dark, the solution was neutralized with sodium acetate 4 *M*, concentrated on a membrane, and washed with carbonate buffer 0.2 *M*, pH 9.5, to eliminate excess $NaIO_4$. Following this, 100 μL of AMSL (120 μ*M*) in carbonate – 10% DMSO buffer was added and the mixture kept at 4°C for 90 min. Then 7.5 μL of $NaBH_4$ (200 m*M*) in carbonate – 10% DMSO buffer was added and after 30 min at 4°C, the reaction mixture was chromatographed on a Sephadex G-25 column (0.6 × 18 cm) equilibrated with buffer C. This chromatography allows the separation of spin-labeled ribosomes from free AMSL.

*Enzymatic spin labelling of 30S subunits*

30S subunits were prepared by differential ultracentrifugation according to Traub *et al.* (50). ADPSL was prepared by the method of Weiner (29) from AMP-morpholidate (Sigma). The labelling via the RNA ligase (P.L. Biochemicals Inc.) was carried out according to England *et al.* (28). The reaction mixture contained 30S subunits (9 μ*M*), ADPSL (136 μ*M*), serumalbumine (10 μg/mL), glycerol 8.3%, $Mg^{2+}$ (20 m*M*), and RNA ligase (200 units/mL). The total volume was 250 μL in Tris-HCl buffer 20 m*M*, pH 7.4, containing $NH_4Cl$ 0.1 *M*, $Mg(OA_c)_2$ 20 m*M*, and β-mercaptoethanol 10 m*M*. After 1 h at 37°C the mixture was chromatographed on a Sephadex G-25 (fine) column (0.7 × 20 cm).

*Preparation of spin-labeled kanamycin*

Kanamycin A sulfate (gift from Bristol Canada) (590 mg) was converted to the free base by chromatography on an anion exchange resin AG 1-X8 ($OH^-$ form) with water and lyophilized. The product was dissolved in $H_2O$–MeOH (1:1), cooled to −5°C, and HSL (35 mg) dissolved in a minimal amount of MeOH was added dropwise. The reaction mixture was kept at 0°C for 6 h, left at room temperature overnight, then lyophilized. The products of the reaction were dissolved in a mixture of $CHCl_3$–MeOH–$NH_4OH$ (2:2:1) containing a few drops of water and chromatographed on a silica gel column (1 × 20 cm). The fractions containing the spin-labeled kanamycin (followed by tlc and detected with Zindzadze reagent) were combined, lyophilized, and passed through a cation exchange resin AG W50-X8 ($NH_4^+$ form) column. After lyophilization 30 mg of crystalline spin-labeled kanamycin was obtained (mp 215°C dec.). A fraction (5 mg) of the product was N,O-permethylated for mass spectrum characterization. The spectral pattern ($M^+$ 848, a *m/e* 169 for the loss of SL and other characteristic *m/e* at 232, 371, 386, 403, 446, 542, 557, 600) is in agreement with the 6′-$NH_2$ position selectively derivatized (51). Spin-labeled kanamycin gave the characteristic 3 lines epr spectrum (Bruker Co.), $a_N$ = 17 G ($H_2O$), $\tau_c$ = 0.29 ns. A spin-concentration determination indicated 0.95 mol of spin label per molecule of kanamycin. The compound was judged adequate for the subsequent binding studies.

*Preparation of spin-labeled puromycin*

A procedure was used similar to that employed for kanamycin. Puromycin $2Cl^-$ (Sigma) was converted to the free base by passage on an anion exchange resin. HSL was dissolved in dioxane and added to a 0.4 *M* $NaHCO_3$–MeOH 20% (pH 8) solution of puromycin. After a few hours at room temperature, the mixture was purified by preparative tlc on silica gel (Merck) using MeOH–$CHCl_3$ (1:9) as eluant to give a crystalline product (mp 230°C); $a_N$ = 17 G ($H_2O$), $\tau_c$ = 0.08 ns. A spin-concentration estimation showed the presence of 0.4 spin label per puromycin molecule. No further purification was needed since only a qualitative epr study with ribosomes was carried out.

## Acknowledgments

The authors would like to express their sincere appreciation to the following diligent co-workers: N. Brisson, G. Tougas, and M. Janssens. We also thank Dr. B. Nayar for the analysis of the mass spectra of the spin-labeled antibiotics. Financial support from the Natural Sciences and Engineering Research Council of Canada and the J. March Foundation (Spain) is acknowledged.

1. C. G. KURLAND. *In* Molecular mechanisms of proteins biosynthesis. *Edited by* H. Weissbach and S. Pestka. Academic Press, Inc., New York, NY. 1977. pp. 81–116.
2. G. STOFFLER and H. G. WITTMANN. *In* Molecular mechanisms of proteins biosynthesis. *Edited by* H. Weissbach and S. Pestka. Academic Press, Inc., New York, NY. 1977. pp. 117–202.

Can. J. Chem. Downloaded from www.nrcresearchpress.com by 210.87.254.5 on 09/06/12
For personal use only.

3. H. G. WITTMANN. *In* Chemical recognition in biology. *Edited by* F. Chapeville and A. L. Haenni. Springer-Verlag, Berlin. 1980. pp. 376–397.
4. N. FARBER and C. R. CANTOR. Proc. Natl. Acad. Sci. U.S.A. **77**, 5135 (1980).
5. D. J. LITMAN, C. C. LEE, and C. R. CANTOR. FEBS Lett. **47**, 268 (1974).
6. R. H. FAIRCLOUGH, C. R. CANTOR, W. WINTERMEYER, and H. G. ZACHAU. J. Mol. Biol. **132**, 557 (1979).
7. M. PERRIN and F. POCHON. Eur. J. Biochem. **57**, 319 (1975).
8. L. BRAKIER-GINGRAS, L. PROVOST, and H. DUGAS. Biochem. Biophys. Res. Commun. **60**, 1238 (1974).
9. H. DUGAS, A. RODRIGUEZ, and N. BRISSON. Can. J. Biochem. **57**, 1407 (1979).
10. A. RODRIGUEZ, G. TOUGAS, N. BRISSON, and H. DUGAS. J. Biol. Chem. **255**, 8116 (1980).
11. A. RODRIGUEZ and H. DUGAS. Can. J. Biochem. **59**, 311 (1981).
12. L. BRAKIER-GINGRAS, G. BOILEAU, S. GLORIEUX, and N. BRISSON. Biochim. Biophys. Acta, **521**, 413 (1978).
13. J. NOREAU, L. GRISÉ-MIRON, and L. BRAKIER-GINGRAS. Biochim. Biophys. Acta, **608**, 72 (1980).
14. T. R. TRITTON. Biochemistry, **17**, 3959 (1978).
15. A. BAKARDJIEVA and R. R. CRICHTON. Biochem. J. **143**, 599 (1974).
16. P. B. MOORE. J. Mol. Biol. **60**, 169 (1971).
17. I. GINZBURG and A. ZAMIR. J. Mol. Biol. **93**, 465 (1975).
18. A. KOLB, J. M. HERMOSO, J. O. THOMAS, and N. SZER. Proc. Natl. Acad. Sci. U.S.A. **74**, 2379 (1977).
19. T. LEE and R. L. HEINTZ. Eur. J. Biochem. **66**, 105 (1976).
20. J. C. LELONG, R. MASCHLER, M. CREPIN, C. JEANTET, G. W. TISCHENDORF, and F. GROS. Biochim. **61**, 881 (1979).
21. T. G. FANNING, M. CANTRELL, C. Y. TING SHIH, and G. R. CRAVEN. Nucleic Acid Res. **5**, 933 (1978).
22. O. PONGS. *In* Transfer RNA. *Edited by* S. Altman. The MIT Press, Cambridge, MA. 1978. p. 99.
23. P. COFFEY, B. H. ROBINSON, and L. R. DALTON. Mol. Phys. **31**, 1703 (1976).
24. P. COFFEY, B. H. ROBINSON, and L. R. DALTON. Chem. Phys. Lett. **35**, 360 (1975).
25. B. AMAND, F. POCHON, and D. LAVALETTE. Biochim. **59**, 779 (1977).
26. M. CARON and H. DUGAS. Nucleic Acid Res. **3**, 19 (1976).
27. J. P. SCHREIBER, N. H. SIUNG, and C. R. CANTOR. Nucleic Acid Res. **6**, 181 (1979).
28. T. E. ENGLAND, R. I. GUMPORT, and O. C. UHLENBECK. Proc. Natl. Acad. Sci. U.S.A. **74**, 4839 (1977).
29. H. WEINER. Biochemistry, **8**, 526 (1969).
30. J. A. LAKE. J. Mol. Biol. **105**, 131 (1976).
31. B. R. GLICK and L. J. BRUBACHER. J. Mol. Biol. **93**, 319 (1975).
32. V. FAVAUDON and F. POCHON. Biochemistry, **15**, 3903 (1976).
33. O. SCHLESSINGER and G. MEDOFF. *In* Antibiotics. III. Mechanism of action of antimicrobial and antitumor agents. *Edited by* J. W. Corcoran and F. E. Hahn. Springer-Verlag, New York, NY. 1975. pp. 535–550.
34. F. N. CHANG and J. G. FLAKS. Antimicrob. Agents Chemother. **2**, 294 (1972).
35. K. MASUDA and T. YAMADA. Biochim. Biophys. Acta, **435**, 333 (1976).
36. R. T. GARVIN, D. K. BISWAS, and L. GORINI. Proc. Natl. Acad. Sci. U.S.A. **71**, 3814 (1974).
37. J. C. LELONG, D. GROS, F. GROS, A. BOLLEN, R. MASCHLER, and G. STOFFLER. Proc. Natl. Acad. Sci. U.S.A. **71**, 248 (974).
38. R. TRAUT and R. MONRO. J. Mol. Biol. **10**, 63 (1964).
39. M. USTAV, M. SAARMA, A. LIND, and R. VILLEMS. FEBS Lett. **87**, 315 (1978).
40. M. SHIMIZU and G. R. CRAVEN. Eur. J. Biochem. **61**, 307 (1976).
41. H. DUGAS. Acc. Chem. Res. **10**, 47 (1977).
42. A. MÖLLER, U. WILD, D. RIESNER, and M. G. GASSEN. Proc. Natl. Acad. Sci. U.S.A. **76**, 3266 (1979).
43. P. DAVANLOO, M. SPRINZL, and F. CRAMER. Biochemistry, **18**, 3189 (1979).
44. V. V. VLASSOV and S. V. MAMAYEV. FEBS Lett. **113**, 65 (1980).
45. C. G. KURLAND, R. RIGLER, M. EHRENBERG, and C. BLOMBERG. Proc. Natl. Acad. Sci. U.S.A. **92**, 4248 (1975).
46. C. BLOMBERG. J. Theor. Biol. **66**, 307 (1977).
47. N. M. FARBER and C. R. CANTOR. J. Mol. Biol. **146**, 241 (1981).
48. G. CHINALI, M. SPRINZL, A. PARMEGGIANI, and F. CRAMER. Biochemistry, **13**, 3001 (1974).
49. T. HISHIZAWA, J. L. LESSARD, and S. PESTKA. Proc. Natl. Acad. Sci. U.S.A. **66**, 523 (1970).
50. P. TRAUB, S. MIZUSHIMA, C. V. LOWRY, and M. NOMURA. Methods Enzymol. **20**, 391 (1971).
51. D. C. DEJONGH, E. B. HILLS, J. D. HRIBAR, S. HANESSIAN, and T. CHANG. Tetrahedron, **29**, 2707 (1973).

# Methods for preparation of heterobifunctional nitroxides: α,β-unsaturated ketones, β-ketoesters, cyano-nitro-derivatives

H. Olga Hankovszky, Kálmán Hideg, László Lex, Gyula Kulcsár, and H. Anna Halász

*Central Laboratory, Chemistry, University of Pécs, H-7643 Pécs, Hungary*

Received August 10, 1981

H. Olga Hankovszky, Kálmán Hideg, László Lex, Gyula Kulcsár, and H. Anna Halász. Can. J. Chem. **60**, 1432 (1982).

The reactions of 1-oxyl-2,2,5,5-tetramethyl-3-pyrroline-3-carboxaldehyde (**1**), 1-oxyl-2,2,5,5-tetramethyl-3-cyano-3-pyrroline (**2**), ethyl 1-oxyl-2,2,5,5-tetramethyl-3-pyrroline-3-carbonyl carbonate (**3**), and *N*-(1-oxyl-2,2,5,5-tetramethyl-3-pyrroline-3-carbonyl)imidazolide (**4**) are investigated with several nucleophiles (dialkylcadmium, diethyl sodio-malonate, magnesium enolate of ethyl hydrogen malonate, nitromethane-anion) to obtain α,β-unsaturated ketones, β-ketoesters, or conjugated reaction products. Aldehyde **1** is reacted with several methyl ketones (acetylmethylene-triphenylphosphorane, acetophenone, 2-acetylpyridine, 4-phenyl-3-butyn-2-one) to give spin labeled polyenones. The reaction of 4-(1-oxyl-2,2,5,5-tetramethyl-3-pyrroline-3-yl)-2-buten-2-one (**24***a*) with ethylenediamine gives 7,14-bis-(1-oxyl-2,2,5,5-tetramethyl-3-pyrroline-3-yl)-5,12-dimethyl-1,4,8,11-tetraazatetradeca-7,14-diene biradical (**25**).

H. Olga Hankovszky, Kálmán Hideg, László Lex, Gyula Kulcsár et H. Anna Halász. Can. J. Chem. **60**, 1432 (1982).

On a étudié les réactions de l'oxyl-1 tétraméthyl-2,2,5,5 pyrroline-3 carboxaldéhyde-3 (**1**), de l'oxyl-1 tétraméthyl-2,2,5,5 cyano-3 pyrroline-3 (**2**), de l'oxyl-1 tétraméthyl-2,2,5,5 pyrroline-3 carbonyl-3 carbonate d'éthyle (**3**) et de la *N*-(oxyl-1 tétraméthyl-2,2,5,5 pyrroline-3 carbonyl-3) imidazolide (**4**) avec plusieurs nucleophiles (dialkylcadmium sodio malonate de diéthyle, énolate magnesien du malonate double d'éthyle et d'hydrogène et anion du nitrométhane) en vue d'obtenir des cétones α,β non saturées, des β-cétoesters ou des produits de réactions conjuguées. L'aldéhyde **1** réagit avec plusieurs méthyl cétones (acétylméthylène-triphénylphosphorane, acétophénone, acétyl-2 pyridine, phényl-4 butyne-3 one-2) pour donner des polyénones avec des spins marqués. La réaction de la (oxyl-1 tétraméthyl-2,2,5,5 pyrroline-3 yl-3)-4 butène-2 one-2 (**24***a*) avec l'éthylènediamine donne le biradical, bis-(oxyl-1 tétraméthyl-2,2,5,5 pyrroline-3 yl-3)-7,14 diméthyl-5,12 tétraaza-1,4,8,11 tétradecadiène-7,14 (**25**).

[Traduit par le journal]

## Introduction

There is a continuing interest in research of novel nitroxide free radicals having reactive functional groups by which they can be coupled to biologically important macromolecules for the study of the internal properties of the spin-labeled biomolecules by esr spectroscopy (1–3). We have published in the previous papers in this series the synthesis and reactions of 1-oxyl-2,2,6,6-tetramethylpiperidine-4-sulfonates with nucleophiles (4), synthesis and reactions of reactive derivatives of 1-oxyl-2,2,5,5-tetramethylpyrroline-3-carboxylic acid (5), nitroxide acylated aminoacids and peptides (6), synthesis of spin-label azidoformate (7), spin-labeled local anesthetics (8), synthesis and reactions with 1-oxyl-2,2,5,5-tetramethyl-3-pyrroline-3-carboxaldehyde (9), preparation and reaction of a highly reactive allylic sulfonate (or halide) nitroxide (10), and synthesis and reaction of spin-label phosphinimines (11). Very recently as a part of the collaboration between J. F. W. Keana's and our laboratory a joint paper was prepared about the reactions of 3-substituted 1-oxyl-2,2,5,5-tetramethyl-3-pyrroline derivatives, carboxaldehyde, acid, and nitrile, with methyllithium (12). A characteristic of all of these reactions with methyllithium was that the diamagnetic *N*-methoxy derivative was also formed beside the *N*-hydroxy derivative which spontaneously oxidized in air to the corresponding paramagnetic nitroxide derivative.

In the present study we wish to report our attempts to prepare novel spin label nitroxides having two possible reaction centres for biomolecules.

## Results and discussion

For starting compounds the 3-substituted derivatives of 1-oxyl-2,2,5,5-tetramethyl-3-pyrroline were chosen: the aldehyde (**1**), nitrile (**2**), acyl carbonate (**3**), and acyl imidazole (**4**).

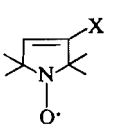

**1** X = CHO
**2** X = CN
**3** X = COOCOOEt
**4** X = CO—N

The reactions of aldehyde **1** with alkyllithium to prepare the nitroxide secondary alcohol were accompanied by the formation of *N*-alkoxy alcohol (12). The reaction of aldehyde **1** with methylmagnesium iodide or ethylmagnesium bromide has resulted in essentially the same mixture of secondary alcohols which was oxidized to diamagnetic and paramagnetic ketones (**5**, **6** and **7**, **8**). The reaction

0008-4042/82/121432-07$01.00/0

©1982 National Research Council of Canada/Conseil national de recherches du Canada

Can. J. Chem. Downloaded from www.nrcresearchpress.com by 210.87.254.105 on 09/06/12
For personal use only.

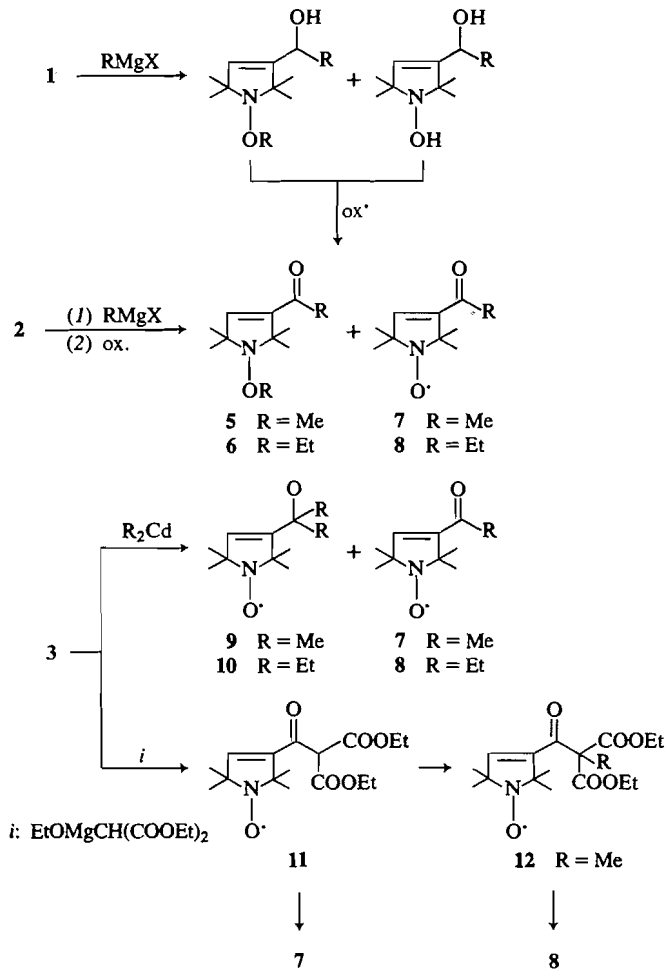


SCHEME 1

of nitrile **2** with ethylmagnesium iodide was even less promising because the dominating product after the oxidations was the diamagnetic ketone (**6**), while the paramagnetic ketone (**8**) was the minor product. Therefore it was necessary to find a reactive derivative of carboxylic acid which exhibits suitable reactivity toward milder organometallic reagents which are inert toward the nitroxide radical. The synthesis of the ketone directly from the reaction of acyl carbonate **3** with methylmagnesium iodide could not be carried out in a reasonable yield. However, the reaction of acyl carbonate **3** with *in situ* formed dialkylcadmium (dimethylcadmium or diethylcadmium) has resulted in a fair yield of the desired ketone (**7** or **8**) without any loss of the radical. In this reaction, as a minor product, the tertiary alcohol (**9** or **10**) was also formed, which could be separated by column chromatography.

Another approach was also successful in obtaining the ketones by an alternative route. The diethyl ethoxymagnesium malonate (13), either with acyl carbonate **3** or acyl imidazole **4**, could be converted in a good yield to the acyl malonate (**11**). The **11** could be alkylated with methyl iodide to **12**. The diethyl acyl malonates (**11** or **12**) could be hydrolysed with dilute acid via the *N*-hydroxy derivative to the corresponding ketone (**7** or **8**).

The reaction of the magnesium enolate of ethyl hydrogen malonate (14) either with acyl carbonate **3** or acyl imidazole **4** with concomitant decarboxylation gave the β-ketoester (**13**) in good yield. Utilization of the well-known reactivity of the β-ketoesters (15) may make this spin-label β-ketoester a very versatile building block in further synthesis starting from β-ketoesters. As an example of this type of reaction **13** was alkylated with dodecyl bromide to α-dodecyl-β-ketoester (**14**). The ester group could be eliminated by hydrolysis

Can. J. Chem. Downloaded from www.nrcresearchpress.com by 210.87.254.105 on 09/06/12
For personal use only.

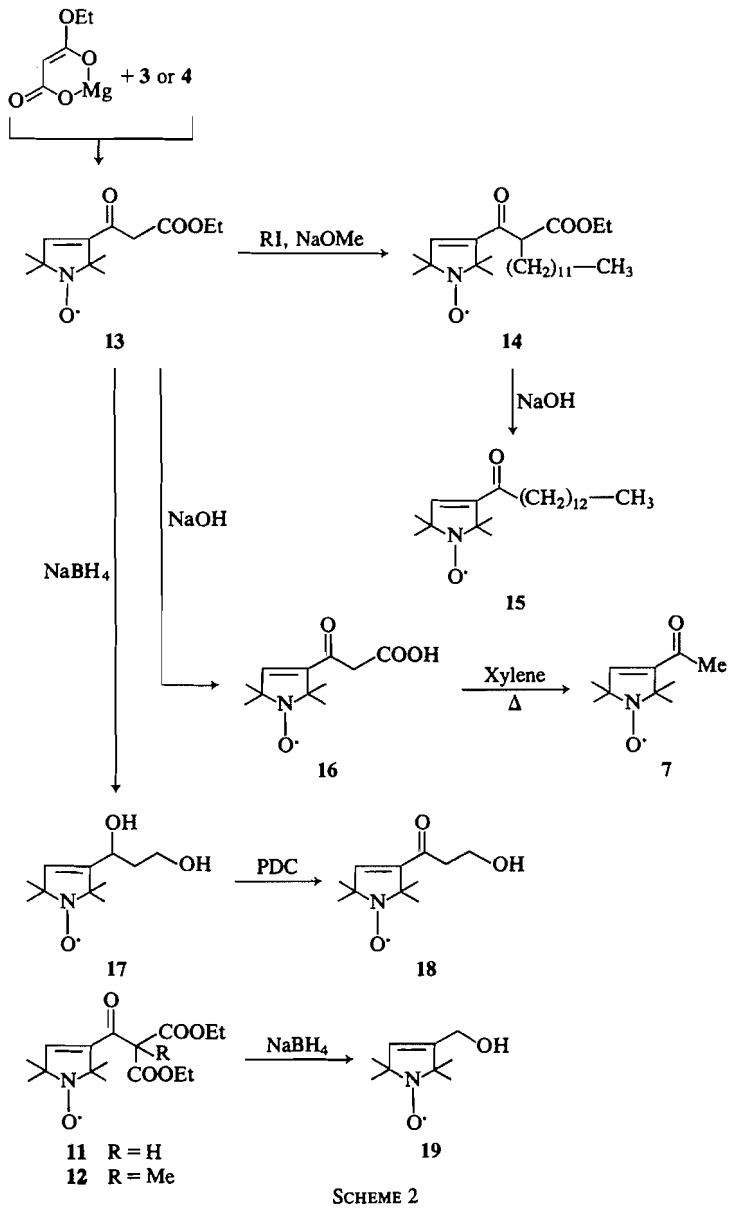


SCHEME 2

with dilute sodium hydroxide to get a long chain alkyl α,β-unsaturated ketone (**15**). However, the preparation of α-unsubstituted β-ketoacid (**16**) was also possible when **13** was hydrolysed with dilute sodium hydroxide. The ketoacid (**16**) could be decarboxylated to **7** when refluxed in xylene. By the reduction of the β-ketoester (**13**) with sodium borohydride the dihydroxy compound **17** could be obtained in a fair yield. Diol **17** could be selectively oxidized at the allylic hydroxy group to a β′-hydroxy-α,β-unsaturated ketone (**18**). It is interesting to note that, in contrast, the reduction of another type of β-ketoester, the diethyl acyl malonates (**11**, **12**), has resulted in the elimination of the malonate and gives the hydroxymethylpyrroline derivative (**19**). By analogy to the recently described reaction of addition of ethyl monomagnesium enolate to the α,β-unsaturated ketones (16), the aldehyde **1** was reacted with ethyl monomagnesium enolate affording the conjugate adduct (**20**) in moderate yield. The 1,2-condensation reaction product diene ester (**21**), which can be separated by column chromatography, was also obtained from the reaction.

A conjugate addition reaction could be carried out on unsaturated nitrile (**2**) with diethyl malonate or with nitromethane (in the presence of base

Can. J. Chem. Downloaded from www.nrcresearchpress.com by 210.87.254.105 on 09/06/12
For personal use only.

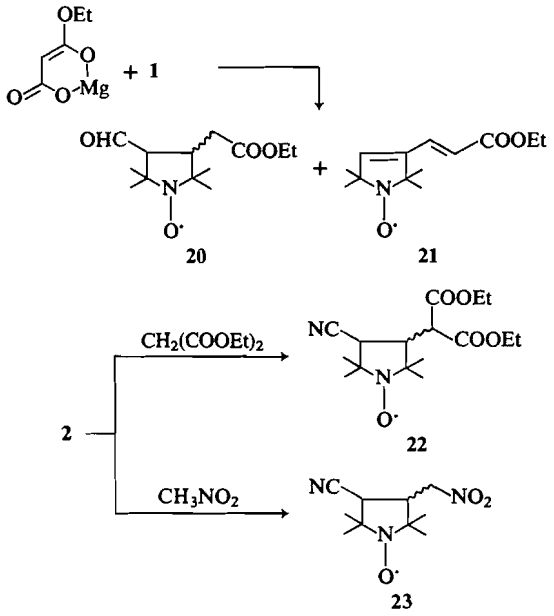


SCHEME 3

catalysts sodium ethoxide or Triton B) to obtain cyanoalkylated diethyl malonate (**22**) and cyanoalkylated nitro spin label (**23**). These molecules may be very versatile synthons in further synthesis.

We also wished to prepare potentially more reactive, novel dienones suitable for nucleophilic addition of thiol or amino groups. While in the aldol type of condensation of unsaturated aldehyde **1** with various methyl ketones (acetophenone, 2-acetylpyridine, or acetylphenylacetylene) polyenones (**24***b–e*) could be obtained in reasonable yield, the methyl dienone (**24***a*) could be obtained only by a Wittig reaction with acetylmethylene-triphenylphosphorane. Utilizing the method for preparation of a 14-membered macrocyclic ligand (17, 18), a 14-membered macrocycle (**25**) can be prepared from **24***a* with ethylenediamine. By the reduction of the azomethine groups with sodium borohydride, the more stable saturated macrocycle (**26**) could be prepared, which may be a useful spin-labeled tetradentate ligand in complex formation reaction.

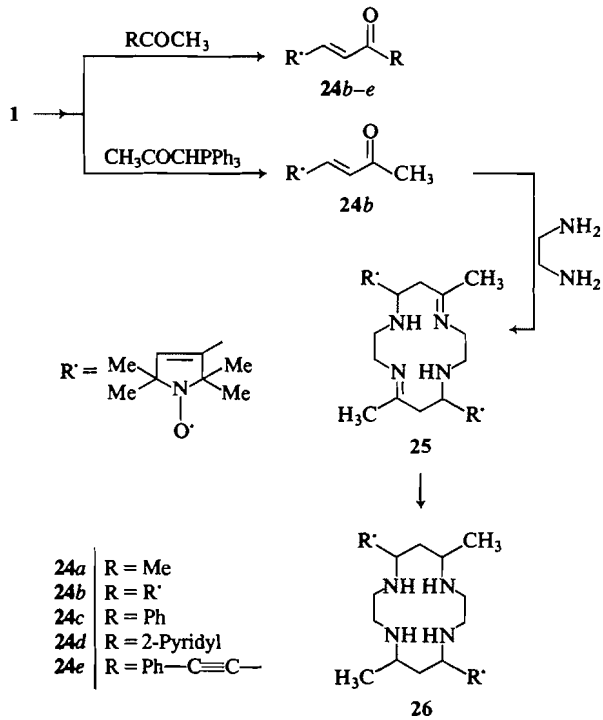


SCHEME 4

## Experimental

Melting points were measured using a Boetius micro mp-determining instrument and were not corrected. The ir spectra were measured as a neat oil or in Nujol suspensions with a Zeiss Specord 75 type of instrument. The esr spectra were obtained from a $10^{-3}$ *M* solution using a Zeiss ER9 spectrometer. All the monoradicals exhibited three equidistant lines and the biradical showed five equidistant lines with $n_N$ = 14.8–15.0 G. The $^1H$ nmr spectra were recorded on a Perkin–Elmer R12 instrument in $CDCl_3$, using tetramethylsilane as internal standard. The nmr spectra of radicals were taken in a 10% solution of diphenylhydrazine in $CDCl_3$ ($CDCl_3$–DPH). The mass spectra were taken in a Varian-MAT-SM-1 instrument. Solvents were reagent grade and dried prior to use. All organic extracts obtained during the work-up of the reaction mixture were dried over anhydrous magnesium sulfate and distilled off *in vacuo*. For column chromatography silica gel 60, for preparative tlc silica gel F(254 Merck-60 or Whatman PK6F), were used.

*Reactions with organometallic reagents*

(a). *Reaction of aldehyde 1 with alkylmagnesium iodides. Synthesis of 1-oxyl-2,2,5,5-tetramethyl-3-acetyl-3-pyrroline (7) and 1-oxyl-2,2,5,5-tetramethyl-3-ethanoyl-3-pyrroline (8)*

To a stirred solution of the Grignard reagent (prepared from magnesium turnings (0.36 g, 0.15 mol) and methyl iodide (2.1 g, 15 mmol) in dry ether (20 mL)) a solution of unsaturated aldehyde **1** (9) (1.68 g, 10 mmol) in dry ether (20 mL) was added at 0°C under nitrogen and stirred for 3 h. The reaction was quenched with saturated aqueous $NH_4Cl$ (25 mL). The ether phase was separated, dried, and evaporated to dryness. A mixture of manganese(IV) dioxide (15 g) and lead(IV) dioxide (5 g) was added to the stirred solution of remaining pale yellow oil in carbon tetrachloride (50 mL) and refluxed for 6 h. The filtrate was subjected to column chromatography with carbon tetrachloride/ethyl acetate (10:1); two fractions were separated.

The first colorless fraction was the *N*-methoxy derivative **5**: 0.40 g (20%) as a colorless oil. The product was identical with the authentic (12) sample of **5**. The second yellow fraction was the main product **7** (from hexane), 1.01 g (55%), mp 71–72°C (lit. (12) mp 71–72°C).

The ethyl ketone **8** was prepared in the same way from aldehyde **1** (10 mmol) and ethylmagnesium bromide (15 mmol) to give the *N*-ethoxy derivative **6**, 0.70 g (31%) as a colorless oil. Infrared $\nu_{max}$: 1670, 1620 $cm^{-1}$; $^1H$ nmr ($CDCl_3$) δ: 0.9–1.5 (m, 18H), 2.61 (q, 2H), 3.83 (q, 2H), 6.32 (s, 1H). *Anal.* calcd. for $C_{13}H_{23}NO_2$ (mol. wt. 225.3): C 69.30, H 10.29, N 6.22; found: C 69.33, H 10.35, N 6.18.

Can. J. Chem. Downloaded from www.nrcresearchpress.com by 210.87.254.105 on 09/06/12
For personal use only.

Can. J. Chem. Downloaded from www.nrcresearchpress.com by 210.87.254.105 on 09/06/12
For personal use only.

The second yellow band was the paramagnetic ethyl ketone **8**, yield 0.82 g (41%), mp 65–66°C; ir $\nu_{max}$: 1670, 1620 $cm^{-1}$. *Anal.* calcd. for $C_{11}H_{18}NO_2$ (mol. wt. 196.3): C 67.32, H 9.24, N 7.14; found: C 67.45, H 8.93, N 7.16.

(b). *Reaction of nitrile (2) with ethylmagnesium bromide*

A solution of nitrile **2** (19) (1.65 g, 10 mmol) in dry ether was added to a freshly prepared solution of ethylmagnesium bromide (20 mmol) in ether under nitrogen at 0°C and stirred for 3 h, then the reaction was quenched with a saturated solution of ammonium chloride (5 mL) and the ether phase separated, dried, and evaporated to dryness. The pale oil was taken up in 5 *M* hydrochloric acid (20 mL) and refluxed for 2 h, then basified (to pH 10) and extracted with ether (3 × 10 mL). The ether solution was stirred with lead(IV) dioxide (3 g) for 3 h, then filtered. The filtrate was evaporated to dryness to give **6**, yield 1.58 g (70%), which was contaminated with only a minimal amount (less than 8%) of paramagnetic ketone **8**.

(c). *Reaction of acyl carbonate with dimethylcadmium: synthesis of 1-oxyl-2,2,5,5-tetramethyl-3-acetyl-3-pyrroline (7) and 2-(1-oxyl-2,2,5,5-tetramethyl-3-pyrrolin-3-yl)-propan-2-ol (9)*

The dimethylcadmium (20) was freshly prepared as follows. Anhydrous cadmium chloride (3.6 g, 20 mmol) was added to a freshly prepared solution of Grignard reagent (magnesium turnings (0.96 g, 40 mmol) with methyl iodide (6.25 g, 44 mmol) in dry ether (40 mL)) under nitrogen. A solution of acyl carbonate **3** (5, 21) (5.12 g, 20 mmol) in dry ether (25 mL) was added to the stirred suspension of dimethylcadmium and the mixture was stirred overnight. The reaction was quenched with a saturated solution of $NH_4Cl$, the organic phase was dried and evaporated to dryness. The residual yellow oil was column chromatographed with carbon tetrachloride/ethyl acetate (1:1).

The first yellow band was the ketone (**7**), yield 2.21 g (60%), mp 71–72°C (from hexane). The ketone **7** was identical with an authentic sample of **7** obtained above or as it has been described earlier (12). The second yellow band was the tertiary alcohol **9**, yield 0.32 g, (8%), mp 127–129°C (from chloroform/hexane); ir $\nu_{max}$: 3400–3200 $cm^{-1}$. *Anal.* calcd. for $C_{11}H_{20}NO_2$ (mol. wt. 198.3): C 66.63, H 10.17, N 7.06; found: C 66.79, N 9.98, N 6.96.

(d) *Reaction of acyl carbonate 3 with diethylcadmium: synthesis of 1-oxyl-2,2,5,5-tetramethyl-3-ethanoyl-3-pyrroline (8) and 3-(1-oxyl-2,2,5,5-tetramethyl-3-pyrrolin-3-yl)pentan-3-ol (10)*

A solution of acyl carbonate **3** (2.56 g, 10 mmol) in dry ether (10 mL) was added to a solution of diethylcadmium (20) (10 mmol) (prepared from a solution of ethyl magnesium bromide (20 mmol) and dry cadmium chloride (20 mmol) in ether (20 mL)), reacted, and worked up as above for methylketone **7**. The first yellow band obtained from the silica gel column was ethyl ketone **8**, yield 1.00 g (51%), mp 65–66°C (from hexane); it was identical with **8** obtained from the Grignard method above. The second minor yellow band was the tertiary alcohol **10**, yield 0.30 g (13%), mp 117–119°C (from ether/hexane); ir $\nu_{max}$: 3400–3200 $cm^{-1}$. *Anal.* calcd. for $C_{13}N_{24}NO_2$ (mol. wt. 226.3): C 68.98, H 10.69, H 6.19; found: C 69.04, H 10.76, H 6.26.

*Diethyl (1-oxyl-2,2,5,5-tetramethyl-3-pyrroline-3-carbonyl-malonate (11)*

A solution of acyl carbonate **3** (2.56 g, 10.0 mmol) in dry ether was added slowly to a stirred solution of freshly prepared diethyl ethoxy magnesium malonate (13) (2.28 g, 10.0 mmol) in dry ether (30 mL) under nitrogen. The reaction mixture was kept at room temperature overnight, then saturated $NH_4Cl$ solution (10 mL) was added. The ether phase was separated and washed with dilute (5%) sulphuric acid (20 mL), saturated $NaHCO_3$, water, dried, and evaporated to dryness. The remaining thick yellow oil was practically pure product **11**, yield 2.86 g (87.6%); ir $\nu_{max}$: 1745, 1685, 1620 $cm^{-1}$; $^1H$ nmr ($CDCl_3$–DPH) δ: 1.1–1.5 (m, 18H), 4.2 (q, 4H), 4.90 (s, 1H), 6.36 (s, 1H). *Anal.* calcd. for $C_{16}H_{24}NO_6$ (mol. wt. 326.4): C 58.89, H 7.41, N 4.29; found: C 59.05, H 7.39, N 4.22.

*1-Oxyl-2,2,5,5-tetramethyl-3-acetyl-3-pyrroline (7)*

The acyl malonate (**11**) (3.26 g, 10.0 mmol) was dissolved in a mixture of acetic acid (6 mL), concentrated sulphuric acid (1 mL), and water (4 mL) and refluxed for 4 h. The cooled solution was extracted with ether (3 × 20 mL). The ether phase was worked up as above to give the pure ketone (**7**), yield 1.02 g (55%), mp 71–72°C. The product was identical with an authentic sample of **7**.

*Reaction of 12 to ethyl ketone (8)*

The reaction of alkylated acyl malonate (**12**) with acids under the same condition as above gave **8**, mp 65–66°C, yield 30%.

*Diethyl 2-methyl-2-(1-oxyl-2,2,5,5-tetramethyl-3-pyrroline-3-carbonyl)malonate (12)*

A solution of sodium ethoxide (1 *M*) (10 mL) in ethanol was added under nitrogen to a stirred solution of acyl malonate **11** (3.26 g, 10.0 mmol) in dry ether (15 mL), followed by a solution of methyl iodide (2.13 g, 15.0 mmol) in dry THF (15 mL), and refluxed for 4 h. To the cooled solution saturated NaCl was added and the organic phase was separated, dried, and evaporated to dryness. The remaining yellow oil was purified on a silica gel column (solvent: hexane/ethyl acetate, 3:1). The first band was the unreacted **11** (0.90 g, 27%), the second band was **12** (1.03 g, 30%), mp 72–73°C (from hexane); ir $\nu_{max}$: 1770, 1730, 1680, 1620 $cm^{-1}$. $^1H$ nmr ($CDCl_3$–DPH) δ: 1.0–1.5 (m, 18H), 1.7 (s, 3H), 4.2 (q, 4H), 6.3 (s, 1H). *Anal.* calcd. for $C_{17}H_{26}NO_6$ (mol. wt. 340.4): C 59.98, H 7.70, N 4.12; found: C 60.05, H 7.72, N 4.22.

*Ethyl 2(1-oxyl-2,2,5,5-tetramethyl-3-pyrrolin-3-yl)-2-oxopropionate (13)*

To a freshly prepared and well stirred solution of magnesium monoethyl malonate (14) (2.20 g, 14 mmol) in dry tetrahydrofuran (20 mL) was added dropwise a solution of acyl carbonate **3** (2.56 g, 10.0 mmol) in dry tetrahydrofuran (20 mL) under nitrogen at room temperature and kept overnight. Saturated ammonium chloride solution was added to the reaction mixture and the organic phase separated and washed with dilute (5%) sulphuric acid, saturated sodium chloride, dried, and evaporated to dryness. The residue was a yellow oil contaminated with ethyl 1-oxyl-2,2,5,5-tetramethyl-3-pyrroline-3-carboxylic acid, therefore it was column chromatographed with carbon tetrachloride. The fast moving band was the contaminating ester (identified by an authentic sample). The second band was the β-ketoester as a thick yellow oil after evaporating from the solvent. Yield 1.28 g (50%); ir $\nu_{max}$: 1720, 1660, 1600 $cm^{-1}$. $^1H$ nmr ($CDCl_3$–DPH) δ: 1.0–1.5 (m, 15H), 3.5 (s, 2H), 4.1 (q, 2H), 6.4 (s, 1H). *Anal.* calcd. for $C_{13}H_{20}NO_4$ (mol. wt. 254.3): C 61.40, H 7.93, N 5.51; found: C 61.35, H 8.02, N 5.62. The ketoester **13** was prepared as above but acylimidazole (**4**) (22, 23), (2.34 g, 10.0 mmol) was used instead of **3**. Yield 1.85 g (73%).

*Ethyl 2-(1-oxyl-2,2,5,5-tetramethyl-3-pyrroline-3-carbonyl)tridecanoic acid (14)*

Sodium methoxide (0.108 g, 2.00 mmol) was added under nitrogen to a solution of **13** (0.508 g, 2.00 mmol) and dodecylbromide (0.498 g, 2.0 mmol) in dry ethanol (10 mL) and refluxed for 8 h. The reaction mixture was diluted with water (20 mL) and extracted with ether (3 × 20 mL). The ether phase was dried and evaporated to dryness. The remaining yellow oil was purified from the unreacted starting compounds on preparative tlc (silica gel Whatman PK6F) with hexane/ethyl acetate (3:1) to give the

Can. J. Chem. Downloaded from www.nrcresearchpress.com by 210.87.254.105 on 09/06/12
For personal use only.

pure **14** as a thick yellow oil, yield 0.690 g (81%); ir $\nu_{max}$: 1735, 1670, 1615 $cm^{-1}$. *Anal.* calcd. for $C_{25}H_{44}NO_4$ (mol. wt. 422.7): C 71.05, H 10.49, N 3.31; found: C 71.12, H 10.53, N 3.36.

*Hydrolysis of **14** to 1-oxyl-2,2,5,5-tetramethyl-3-*n*-tridecyl-3-pyrroline (**15**)*

Sodium hydroxide (10%) (3 mL) was added to a solution of **14** (211.3 mg, 0.5 mmol) in ethanol (3 mL) and allowed to stay at room temperature for two days. The reaction mixture was acidified (to pH 3) with sulfuric acid (5%) and extracted with chloroform (3 × 10 mL). The chloroform phase was evaporated to dryness. The crude oil was purified on preparative tlc with ethyl acetate/hexane (1:1) to give the pure ketone, 132 mg (75%); ir $\nu_{max}$: 1675, 1610 $cm^{-1}$. *Anal.* calcd. for $C_{22}H_{40}NO_2$ (mol. wt. 350.6): C 75.37, H 11.50, N 4.00; found: C 75.31, H 11.43, N 4.12.

*2-(1-Oxyl-2,2,5,5-tetramethyl-3-pyrrolin-3-yl)-2-oxopropanoic acid (**16**)*

A solution of **13** (0.254 g, 1.00 mmol) in 2.5 *M* sodium hydroxide (2 mL) was kept at room temperature for 2 h, then extracted with chloroform (3 × 2 mL). The aqueous phase was acidified (pH 3) with dilute sulphuric acid (5%), saturated sodium chloride (10 mL) was added to the solution, and it was extracted again with chloroform (3 × 5 mL). The chloroform solution was dried and evaporated to dryness. The remaining solid was **16**, yield 183 mg (80%). The analytical sample was crystallized from ether/hexane, mp 107–108°C; ir $\nu_{max}$: 1735, 1665, 1615 $cm^{-1}$. *Anal.* calcd. for $C_{11}H_{16}NO_4$ (mol. wt. 226.3): C 58.40, H 7.13, N 6.19; found: C 58.46, H 7.27, N 6.23.

*Decarboxylation of **16** to **7***

A solution of **16** (113 mg, 0.5 mmol) in xylene (5 mL) was boiled for 4 h and evaporated to dryness. The residue was the ketone **7**, yield 47 mg (51%), which was identical with an authentic sample of 7 obtained by an alternative method.

*Reduction of **13** to 1(1-oxyl-2,2,5,5-tetramethyl-3-pyrrolin-3-yl)-1,3-dihydroxypropane (**17**)*

Sodium borohydride (756 mg, 20.0 mmol) was added to a solution of **13** (508 mg, 2.0 mmol) in dry ethanol (10 mL) and refluxed for 2 h. The reaction mixture was diluted with saturated sodium chloride solution and extracted with ether (3 × 10 mL). The ether phase was dried and evaporated to dryness. The residue was a thick oil, yield 342 mg (80%), and showed one spot on tlc; ir $\nu_{max}$: 3600–3100 $cm^{-1}$, and no ester bond was present; $^1H$ nmr, δ: 1.0–1.3 (m, 12H) 1.5–2.0 (m, 2H), 3.2–3.6 (m, 2H, 2HO), 3.6–3.9 (m, 2H), 4.0–4.4 (m, 1H, CH); ms, *m/e*: $M^+$ 214 (56), 151 (29), 139 (72), 135 (100).

*Oxidation of diol **17** with pyridinium dichromate (ref. 24) to β-hydroxyketone (**18**)*

The diol (**17**) (428 mg, 2 mmol) was dissolved in methylene chloride (15 mL) and pyridinium dichromate (PDC) (2.78 g, 7.4 mmol) was added to the solution and stirred for 2 h. Then ether (20 mL) was added to the black suspension, which was stirred for one further hour and filtered. The filtrate was evaporated to dryness. The residue was subjected to preparative tlc (Whatman PK6F) with hexane/ethyl acetate (1:3); the intensive yellow band was the β-hydroxy ketone **18**, 300 mg (70%), mp 96–98°C; ir $\nu_{max}$: 3600–3300, 1660, 1610 $cm^{-1}$; ms, *m/e*: $M^+$ 212 (50), 182 (100), 167 (45), 138 (55). *Anal.* calcd. for $C_{11}H_{18}NO_3$ (mol. wt. 212.3): C 62.24, H 8.55, N 6.60; found: C 62.12, H 8.40, N 6.49.

*Reduction of diethyl acyl malonates (**11** or **12**) with sodium borohydride to 1-oxyl-2,2,5,5-tetramethyl-3-hydroxymethyl-3-pyrroline (**19**)*

Sodium borohydride (378.3 mg, 10.0 mmol) was added to a solution of **11** (326.4 mg, 1.0 mmol) in dry ethanol (20 mL) and refluxed for 3 h. The reaction mixture was concentrated *in vacuo*, then the residue was taken up with saturated sodium chloride solution (10 mL) and extracted with chloroform (3 × 10 mL). The chloroform phase was dried and evaporated to dryness. The solid yellow residue was recrystallized from chloroform/hexane to give **19**, yield 140 mg (82%), mp 75–77°C. The **19** was also prepared from **12** (340.4 mg, 1.0 mmol) under the same condition as above, yield 133 mg (78%), mp 75–77°C; ir $\nu_{max}$: 3500–3100 $cm^{-1}$. The above samples of **19** were identical with the authentic sample of **19** (9).

*Ethyl (1-oxyl-4-formyl-2,2,5,5-tetramethylpyrrolidin-3-yl)-acetate (**20**)*

A freshly prepared solution of magnesium monoethyl malonate (14) (2.20 g, 14 mmol) in dry DMF (10 mL) was added under a nitrogen atmosphere to a stirred solution of 1-oxyl-2,2,6,6-tetramethyl-3-pyrroline-3-carboxaldehyde (**1**) (1.68 g, 10 mmol). The reaction mixture was kept at 40°C for three days, then acetic acid (1.6 mL) was added and kept at 80°C for two further days to achieve the decarboxylation. The solution was diluted with water (about 50 mL) and extracted with ether (3 × 20 mL). The ether phase was washed with saturated sodium hydrogen carbonate, saturated sodium chloride, dried, and evaporated to dryness. The remaining yellow oil (1 g) showed 3 spots on tlc (hexane/ethyl acetate (1:1)). The crude oil was subjected to column chromatography with carbon tetrachloride/ether (10:1). The second band proved to be **20**, yield 0.80 g (31%) (yellow oil); ir $\nu_{max}$: 1730, 1680 $cm^{-1}$; ms, *m/e*: $M^+$ 256 (100), $M^+ + 1$ 257(20), 226(27), 211(25), 143(91), 140(28), 111(32), 110(63). *Anal.* calcd. for $C_{13}H_{22}NO_4$ (mol. wt. 256.3): C 60.91, H 8.65, N 5.47; found: C 60.83, H 8.54, N 5.59. The first band was proved to be the unreacted **1** by ir. The third band isolated as yellow crystals was the diene ester, ethyl 3-(1-oxyl-2,2,5,5-tetramethyl-3-pyrrolin-3-yl)-2-propenoate (**21**), yield 0.90 g (38%), mp 80–81°C (from hexane), identical with the authentic sample.

*Preparation of authentic **21** by Wittig reaction*

A solution of **1** (168 mg, 1.00 mmol) and (ethoxycarbonyl methylene)triphenylphosphorane (348 mg, 1 mmol) in dry THF was refluxed for 3 h, then evaporated to dryness. The solid residue was dissolved in hot petroleum ether (bp 40–70°C) (3 × 10 mL), then evaporated to a minimal volume and cooled. The yellow crystals were filtered off to give **21**, yield 210 mg (88%), mp 80–81°C (from hexane); ir $\nu_{max}$: 1685, 1620, 1590 $cm^{-1}$. *Anal.* calcd. for $C_{13}H_{20}NO_3$ (mol. wt. 238.3): C 65.52, H 8.46, N 5.88; found: C 65.46, H 8.46, N 5.99.

*Diethyl 2(1-oxyl-4-cyano-2,2,5,5-tetramethylpyrrolidin-3-yl)-malonate (**22**)*

A solution of unsaturated nitrile (**2**) (1.65 g, 10.0 mmol) was added to a solution of diethyl malonate (2.40 g, 15.0 mmol) and sodium ethoxide (1 *M*) (3 mL, 3 mmol) in dry ethanol (10 mL) and refluxed for 16 h. The reaction mixture was diluted with a solution of saturated sodium chloride (20 mL) and extracted with ether (3 × 10 mL). The organic phase was dried and evaporated to dryness. The residual yellow oil (3 g) was subjected to column chromatography on silica gel with chloroform/petroleum ether (bp 40–70°C) (9:11). The first yellow band was the unreacted nitrile (**2**), 0.50 g (30%). The second wide band was a mixture of the two stereoisomers of **22**, yield 1.64 g (50%), mp 86–88°C (from hexane); ir $\nu_{max}$: 2235, 1750, 1710 $cm^{-1}$; $^1H$ nmr δ: 0.5–1.5 (m, 18H), 2.3–2.5 (m, 2H), 3.3–3.5 (m, 1H), 3.9–4.4 (m, 4H). *Anal.* calcd. for $C_{16}H_{25}N_2O_5$ (mol. wt. 325.4): C 59.06, H 7.74, N 8.61; found: C 58.95, H 7.73, N 8.77.

*(1-Oxyl-2,2,5,5-tetramethyl-4-cyanopyrrolidin-3-yl) nitromethane (**23**)*

A solution of unsaturated nitrile (**2**) (1.65 g, 10 mmol) and nitromethane (0.91 g, 15 mmol) in dry THF (20 mL) was refluxed

Can. J. Chem. Downloaded from www.nrcresearchpress.com by 210.87.254.105 on 09/06/12
For personal use only.

in the presence of Triton B catalyst (0.2 mL) for 3 days, then worked up as above for the reaction of **22**. The products were separated on a silica gel column; the first band was unreacted nitrile (**2**) (0.70 g, 42%) and the second one the two nonseparated stereoisomers of **23** (0.70 g, 31%). The stereoisomers were separated on a second column with carbon tetrachloride/ether (6:4); $R_f$ I: 0.50, $R_f$ II: 0.65. Isomer I: 0.50 g (17.6%), mp 69–70°C; ir $\nu_{max}$: 2230, 1550 $cm^{-1}$. *Anal.* calcd. for $C_{10}H_{16}N_3O_3$ (mol. wt. 226.3): C 53.08, H 7.13, N 18.57; found: C 52.98, H 6.96, N 18.43. Isomer II: 0.30 g (13.4%), mp 55–56°C; ir $\nu_{max}$: 2230, 1540 $cm^{-1}$. *Anal.* calcd. for $C_{10}H_{16}N_3O_3$ (mol. wt. 226.3): C 53.08, H 7.13, N 18.57; found: C 53.17, H 7.20, N 18.40.

*4-(1-Oxyl-2,2,5,5-tetramethyl-3-pyrrolin-3-yl)-3-buten-2-on (24a)*

A solution of (acetylmethylene)triphenylphosphorane (3.18 g, 10.0 mmol) and unsaturated aldehyde **1** (1.68 g, 10.0 mmol) in dry tetrahydrofuran (30 mL) was refluxed for 16 h, then evaporated to dryness. The remaining semisolid was dissolved in light petroleum ether (bp 40–70°C) (50 mL), then evaporated again. The orange oil was subjected to column chromatography with chloroform/ether (1:1) to give an orange oil, yield 1.31 g (63%); ir $\nu_{max}$: 1670, 1620, 1590 $cm^{-1}$; $^1H$ nmr ($CDCl_3$–DPH) δ: 1.28 (s, 6H), 1.38 (s, 6H) 2.24 (s, 3H), 5.95 (s, 1H), 6.32 (d, 1H, HC=C, $J$ = 16.8 Hz). *Anal.* calcd. for $C_{12}H_{18}NO_2$ (mol. wt. 208.3): C 69.20, H 8.71, N 6.73; found: C 69.19, H 8.69, N 6.71.

*General procedure for Claisen condensation of 1 with methyl ketones*

The equivalent amount (0.5 mmol) of **1** and a methyl ketone were dissolved in aqueous methanol (50%) (5 mL) and sodium hydroxide (3 drops of 10% solution) was added to the reaction mixture and kept at room temperature overnight, then diluted with water (5 × 10 mL) to make the crystallization more complete. The crystals were filtered and the analytical samples were crystallized from ether/hexane.

Compound **24b**: yield 75%, mp 170–171°C; ir $\nu_{max}$: 1650, 1595, 1578 $cm^{-1}$. *Anal.* calcd. for $C_{19}H_{28}N_2O_3$ (mol. wt. 332.4): C 68.65, H 8.49, N 8.43; found: C 68.74, H 8.42, N 8.37.

Compound **24c**: yield 68%, mp 106–107°C; ir $\nu_{max}$: 1660, 1620, 1590 $cm^{-1}$. *Anal.* calcd. for $C_{17}H_{20}NO_2$ (mol. wt. 270.4): C 75.53, H 7.46, N 5.18; found: C 75.44, H 7.36, N 5.10.

Compound **24d**: this derivative was isolated after extraction of the reaction mixture with ether, then chromatographed on preparative tlc with ethyl acetate/hexane (1:1). Yield: 50%, mp 100–101°C; ir $\nu_{max}$: 1660, 1595, 1570 $cm^{-1}$. *Anal.* calcd. for $C_{16}H_{19}N_2O_2$ (mol. wt. 271.3): C 70.83, H 7.06, N 10.32; found: C 70.82, H 6.98, N 10.46.

Compound **24e**: yield 74%, mp 111–112°C; ir $\nu_{max}$: 2205, 1610, 1575 $cm^{-1}$. *Anal.* calcd. for $C_{19}H_{20}NO_2$ (mol. wt. 294.4): C 77.52, H 6.85, N 4.76; found: C 77.44, H 7.00, N 4.96.

*7,14-Bis-(1-oxyl-2,2,5,5-tetramethyl-3-pyrrolin-3-yl)-5,12-dimethyl-1,4,8,11-tetraazatetradeca-7,11-diene (25)*

Ethylene diamine (0.72 g, 12.0 mmol) and anhydrous $K_2CO_3$ (1 g) were added to a solution of dienone (**24a**) (2.08 g, 10.0 mmol) in cyclohexane/ether (2:1) (30 mL) and refluxed for 6 h then filtered. The filtrate was evaporated to dryness at 0°C *in vacuo*. The residue was crystallized from ether to give macrocyclic diene **25**, yield 3.75 g (75%), mp 139–140°C; ir $\nu_{max}$: 3270, 1660, 1570 $cm^{-1}$. *Anal.* calcd. for $C_{28}H_{48}N_6O_2$ (mol. wt. 500.7): C 67.16, H 9.67, N 16.78; found: C 67.08, H 9.76, N 16.80.

*7,14-Bis-(1-oxyl-2,2,5,5-tetramethyl-3-pyrrolin-3-yl)-5,12-dimethyl-1,4,8,11-tetraazatetradecane (26)*

The diene (**25**) (500 mg, 1 mmol) was added to a suspension of sodium borohydride (76 mg, 2.0 mmol) in dry ethanol (5 mL) and refluxed for 2 h, then diluted with water and extracted with chloroform (3 × 10 mL). The chloroform phase was dried and evaporated to dryness. The solid residue was recrystallized from chloroform/hexane to give **26**, yield 362 mg (72%), mp 200°C; ir $\nu_{max}$: 3240 $cm^{-1}$. *Anal.* calcd. for $C_{28}H_{52}N_6O_2$ (mol. wt. 504.8): C 66.63, H 10.38, N 16.65; found: C 66.70, H 10.22, N 16.55.

## Acknowledgements

This work was supported in part by the Hungarian Academy of Sciences, Grant No 134/79/II and by the Scientific Research Council, Ministry of Health, Hungary. The authors are indebted to Dr. J. Belágyi for the esr spectra and for the mass spectra to Dr. J. Jerkovich, Institute for Drug Research, Budapest, to Mrs. M. Ott for the microanalyses, to Mrs. L. Lovas and Mrs. B. Csukás for preparation of intermediates.

1. H. M. McConnell and B. McFarland-Gafney. Q. Rev. Biophys. **3**, 91 (1970), and references therein.
2. L. J. Berliner (*Editor*). Spin labeling, theory and application. Vols. I. and II. Academic Press, New York. 1976 and 1979.
3. G. I. Likhtenshtein. Method spinovykh metok v. molekularnoi biologii. Nauka, Moscow. 1973 (in Russian); translation: G. I. Likhtenshtein. Spin labeling methods in molecular biology. Wiley–Interscience, New York. 1976.
4. K. Hideg, H. O. Hankovszky, and J. Tigyi. Acta Chim. Acad. Sci. Hung. **92**, 85 (1977).
5. H. O. Hankovszky, K. Hideg, and J. Tigyi. Acta Chim. Acad. Sci. Hung. **98**, 339 (1978).
6. K. Hideg, L. Lex, H. O. Hankovszky, and J. Tigyi. Synthesis, 914 (1978).
7. H. O. Hankovszky, K. Hideg, L. Lex, and J. Tigyi. Synthesis, 530 (1979).
8. K. Hideg, L. Lex, H. O. Hankovszky, and J. Tigyi. Synth. Commun. **9**, 781 (1979).
9. K. Hideg, H. O. Hankovszky, L. Lex, and Gy. Kulcsár. Synthesis, 911 (1980).
10. H. O. Hankovszky, K. Hideg, and L. Lex. Synthesis, 914 (1980).
11. H. O. Hankovszky, K. Hideg, and L. Lex. Synthesis 147 (1981).
12. J. F. W. Keana, K. Hideg, G. B. Birrell, and H. O. Hankovszky. Can. J. Chem. **60**, 1439 (1982).
13. H. Muxfeldt, W. Rogalski, and G. Klauenberg. Chem. Ber. **98**, 3040 (1965).
14. G. Bram and M. Wilkas. Bull. Soc. Chim. Fr. 945 (1964).
15. C. R. Hauser and B. E. Hudson. Org. React. **1**, 266 (1942).
16. J. E. McMurry, W. A. Andrus, and J. H. Musser. Synth. Commun. **8**, 53 (1978).
17. K. Hideg and D. Lloyd. Chem. Commun. 929 (1970); J. Chem. Soc. C, 3441 (1971).
18. G. Ferguson, P. J. Roberts, D. Lloyd, K. Hideg, R. W. Hay, and D. P. Piplani. J. Chem. Res. (S), 314 (1978), and references therein.
19. E. G. Rosantsev. Free nitroxyl radicals. Plenum Press, New York. 1970. p. 207.
20. H. Gilman and J. F. Nelson. Recl. Trav. Chim. Pays-Bas, **55**, 518 (1936).
21. O. H. Griffith, J. F. W. Keana, L. D. Noall, and J. L. Ivey. Biochim. Biophys. Acta, **148**, 583 (1967).
22. P. Ferruti, D. Gill, M. P. Klein, H. H. Wang, G. Entine, and M. Calvin. J. Am. Chem. Soc. **92**, 3704 (1970).
23. M. D. Barratt, G. H. Dodd, and D. Chapman. Biochim. Biophys. Acta, **194**, 600 (1969).
24. E. J. Corey and G. Schmidt. Tetrahedron Lett. 399 (1979).

# New mono- and difunctionalized 2,2,5,5-tetramethylpyrrolidine- and $\Delta^3$-pyrroline-1-oxyl nitroxide spin labels

JOHN F. W. KEANA, KÁLMÁN HIDEG,[1] AND G. BRUCE BIRRELL
*Department of Chemistry, University of Oregon, Eugene, OR 97403, U.S.A.*

OLGA H. HANKOVSZKY
*Central Laboratory, Chemistry, University of Pécs, P.O. Box 99, 7643 Pécs, Hungary*

AND

GEORGE FERGUSON AND MASOOD PARVEZ
*Department of Chemistry, University of Guelph, Guelph, Ont., Canada N1G 2W1*

Received September 1, 1981

JOHN F. W. KEANA, KÁLMÁN HIDEG, G. BRUCE BIRRELL, OLGA H. HANKOVSZKY, GEORGE FERGUSON, and MASOOD PARVEZ. Can. J. Chem. **60**, 1439 (1982).

Several new nitroxide spin labels have been prepared. Nitroxide mesylate **5** and *p*-hydroxyacetophenone gave **6** which was selectively brominated with cupric bromide to give the alkylating agent **7**. The more water soluble phenacyl bromide analogue **17** was prepared either via the route **8** → **11** → **17** or else via the route **15** → **16** → **11** → **17**. Preliminary results indicate that toward aconitase, nitroxide alkylating agent **17** behaves similarly to phenacyl bromide. Several new difunctional nitroxides were prepared with an eye toward application as saturation transfer esr spin labels. Conjugate addition of HCN to **11** gave **18**, condensation of which with *p*-azidobenzaldehyde gave photolabile **19**. Azide **20** could similarly be prepared directly from **11**. Aldehyde **15** underwent condensation with *p*-azidoacetophenone to give azide **21**. This substance was allowed to react with hemoglobin. Upon photolysis the esr spectral mobile component was substantially reduced, suggesting covalent attachment at more than one site. Conjugate addition of HCN to **23** gave a mixture of *cis*, *trans* isomers **24** and **25**; the structure of **25** was established by X-ray crystallographic analysis to be the *trans* isomer. Conjugate addition of ethyl thioglycolate to **15** led to heterocycles **29–34**.

JOHN F. W. KEANA, KÁLMÁN HIDEG, G. BRUCE BIRRELL, OLGA H. HANKOVSZKY, GEORGE FERGUSON et MASOOD PARVEZ. Can. J. Chem. **60**, 1439 (1982).

On a préparé plusieurs nouveaux marqueurs de spin de type nitroxyde. Le mésylate nitroxyde (**5**) et la *p*-hydroxyacétophénone donnent le composé **6** que l'on brome sélectivement avec le bromure cuivrique pour accéder à l'agent alkylant **7**. On prépare le bromure de phénacycle **17** analogue, plus soluble dans l'eau, soit selon la voie **8** → **11** → **17** ou selon la voie **15** → **16** → **11** → **17**. Des études préliminaires indiquent que l'agent alkylant nitroxyde **17** se comporte vis à vis de l'aconitase de façon analogue au bromure de phénacyle. On a préparé plusieurs nouveaux nitroxydes bifonctionnels dans le but de les utiliser comme transfert de saturation dans la rpe des marqueurs de spin. L'addition conjuguée du HCN sur le composé **11** conduit au composé **18** dont la condensation sur le *p*-azidobenzaldéhyde donne le composé photolabile **19**. On peut préparer de la même façon l'acide **20** en partant directement du composé **11**. L'aldéhyde **15**, par condensation sur le *p*-azidoacétophénone, conduit à l'azoture **21**. On a fait réagir ce dernier avec l'hémoglobine. Lors de la photolyse, le spectre rpe du composant mobile est réduit de façon significative, suggérant ainsi une liaison covalente en plusieurs endroits. L'addition conjuguée de HCN sur le composé **23** donne un mélange des isomères *cis* et *trans*, **24** et **25**; on a établi par cristallographie de rayons-X que le composé **25** est l'isomère *trans*. L'addition conjuguée du thioglycolate d'éthyle sur le composé **15** conduit aux hétérocycles **29** à **34**.

[Traduit par le journal]

The nitroxide spin labeling method constitutes a productive approach to the study of biological and other macromolecular systems by electron spin resonance (esr) spectroscopy (1). Central to this method is the availability of an array of functionalized stable nitroxide molecules which may be selectively attached to reactive sites on the molecule to be spin labeled (2). In connection with an ongoing collaborative investigation involving the non-heme iron–sulfur enzyme aconitase (EC 4.2.1.3), we required a series of nitroxide alkylating agents which were similar in reactivity to that of phenacyl bromide (**1**). Phenacyl bromide is known to react stoichiometrically with a single SH group near the active site of aconitase, leading to a loss of enzymatic activity (3). The first objective of this paper is to report the synthesis and some preliminary results with two new nitroxide alkylating agents modeled after phenacyl bromide.

The second objective of this paper is the development of several new hetero- and homodifunctionalized nitroxide spin labels. Difunctional spin

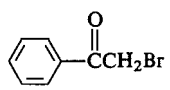


**1**

[1]Visiting Professor, on leave from the Central Laboratory, Chemistry, University of Pécs, Pécs, Hungary.

0008-4042/82/121439-09$01.00/0
©1982 National Research Council of Canada/Conseil national de recherches du Canada

Can. J. Chem. Downloaded from www.nrcresearchpress.com by 210.87.254.40 on 09/06/12
For personal use only.

Can. J. Chem. Downloaded from www.nrcresearchpress.com by 210.87.254.40 on 09/06/12
For personal use only.

labels have the possibility of becoming rigidly attached to a macromolecule through simultaneous or sequential covalent bonding at more than one site. By essentially confining the motion experienced by such a label to that of the macromolecule itself, molecular motion of the macromolecule in the correlation time range $10^{-7} < \tau < 10^{-3}$ s may be conveniently studied using the relatively new saturation transfer electron paramagnetic resonance (STEPR) method (4, 5). Studies of protein motion in this time range are of considerable current interest owing to its possible functional significance (5, 6). Those relevant difunctional nitroxides already described are relatively few and include nitroxides **2** (7), **3** (8), and **4** (9).

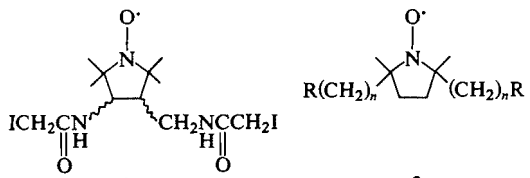

**2**



**3**

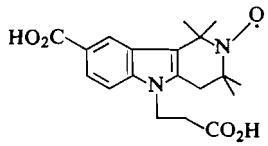

**4**

## Results and discussion

Our first objective was to prepare several representative spin labeled phenacyl bromide analogues for subsequent studies with aconitase. Thus, nitroxide mesylate **5** (10) was allowed to react with *p*-hydroxyacetophenone in the presence of sodium hydroxide to give ketone **6** (52%), mp 101–102°C. Selective bromination of **6** was effected with cupric bromide (11), affording nitroxide phenacyl bromide **7** (14%), mp 73–74°C. The low yield of **7** resulted at least partially because of the difficulty in separating (by preparative tlc) the bromo derivative from the starting ketone.

Preliminary experiments with **7** and aconitase[2] were not promising owing to the low aqueous solubility of **7**, even in the presence of tolerable levels of organic cosolvents. For an alternative approach we prepared amide **9** (86%), mp 165–166°C, by reaction of the acid chloride of nitroxide acid **8** with *p*-aminoacetophenone. Unfortunately, initial attempts to prepare bromo derivative **10** led to intractable mixtures of many products.

Success was achieved through the synthesis of nitroxide bromoketone **17**. It was anticipated that the overall shape, solubility, polarity, and chemical reactivity of **17** might better approximate that of phenacyl bromide as compared with **7**. The precursor of **17**, nitroxide ketone **11**, was prepared in two ways. Firstly, nitroxide acid **8** was allowed to react with excess methyllithium (12), affording after air oxidation a readily separable mixture of ketone **11**, mp 71–72°C (18%) and *N*-methoxy derivative **13** (19%) as a colorless oil.

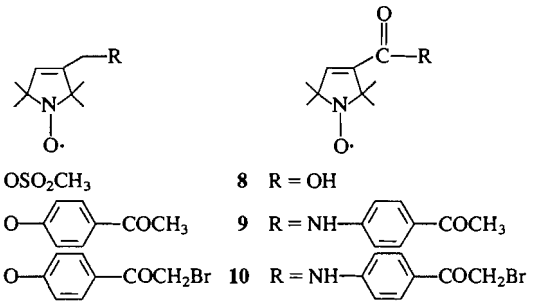

**5** R = $OSO_2CH_3$ **8** R = OH

**6** R = O—$COCH_3$ **9** R = NH—$COCH_3$

**7** R = O—$COCH_2Br$ **10** R = NH—$COCH_2Br$

The successful reaction of a nitroxide carboxylic acid with methyllithium to produce (after reoxidation) a nitroxide methyl ketone is of special interest in view of the known rapid reaction of butyllithium with the nitroxide moiety of 2,2,6,6-tetramethylpiperidine-1-oxyl to give the corresponding N—H, N—OH, and N—OBu derivatives (13). Our results with **8** demonstrate that even though reaction at the nitroxide moiety of **8** does occur with methyllithium, nevertheless through use of excess reagent,

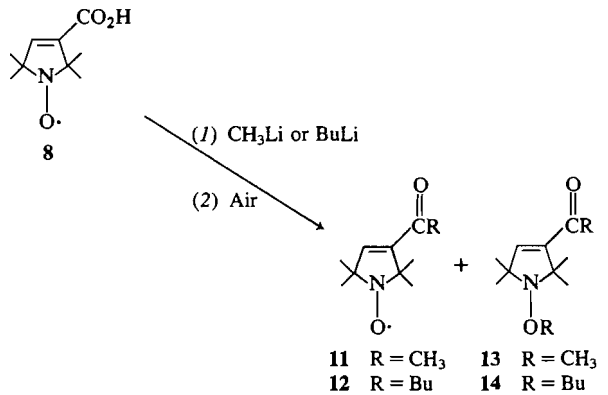

**11** R = $CH_3$ **13** R = $CH_3$

**12** R = Bu **14** R = Bu

the carboxyl group reacts in the expected manner to give the methyl ketone. In order to check the generality of this procedure, acid **8** was allowed to react with excess butyllithium. Useful amounts of the analogous product, nitroxide ketone **12** (oil, 24%), and *N*-butoxy derivative **14** (oil, 23%) were produced after air oxidation of the reaction mixture.

The versatile (see below) intermediate ketone **11** was also prepared by a second method. Reaction of

[2]Prof. H. Beinert, University of Wisconsin, Madison, WI, private communication.

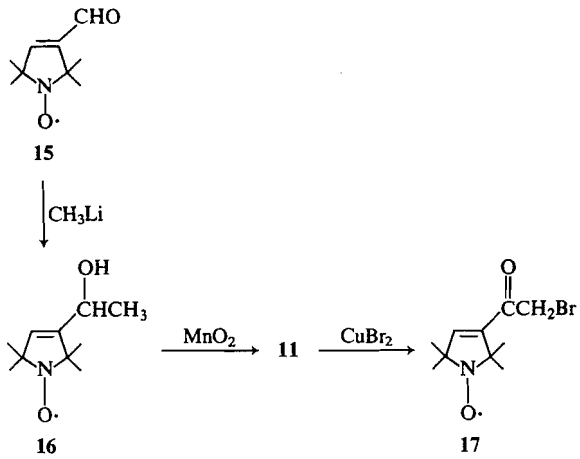


methyllithium with aldehyde **15** (14, 15) gave alcohol **16**, mp 80–81°C (45%). Oxidation of **16** with activated manganese dioxide afforded **11** in 83% yield.

Selective bromination of **11** with cupric bromide proceeded somewhat better than in the case of **6**, affording nitroxide bromoketone **17**, mp 67–69°C, in 25% yield (adjusted for recovered **11**). Preliminary experiments[2] demonstrate that treatment of aconitase with **17** under conditions similar to those employed with phenacyl bromide (3) likewise results in inactivation of the enzyme. These results and associated biophysical studies will be reported in detail later.

We next turned to the synthesis of several difunctional nitroxides while at the same time exploring some of the chemistry of ketone **11**, nitrile **23**, and aldehyde **15** (14, 15). The initial plan was to introduce one of the functions by way of a 1,4-conjugate addition reaction. The reaction of cyanide ion with **11** and **23** was first investigated with the ultimate aim of converting the cyano group into either an activated carbonyl group or else an imidate, for example. Thus, treatment of ketone **11** with potassium cyanide – ammonium chloride – DMF readily afforded the adduct **18** (29%), mp 104–107°C, likely as a mixture of stereoisomers. The adduct smoothly underwent a base-catalyzed condensation reaction with *p*-azidobenzaldehyde, giving phenylazidocyanonitroxide **19**, mp 110–114°C (41%). Alternatively, ketone **11** could be condensed directly with the azidoaldehyde, affording nitroxide **20**, mp 138–141°C (dec.) (47%). Also, aldehyde **15** underwent condensation with *p*-azidoacetophenone to give the α,β,γ,δ-unsaturated ketone **21**, mp 135–136°C (77%).

Nitroxides **19**, **20**, and **21** constitute a potentially versatile series of difunctional spin labels. Each is capable of reacting with a protein SH or $NH_2$ group in a 1,4-conjugate addition reaction analogous to the reaction of maleimide spin label **22** (16) with proteins. While only a single point of covalent attachment to the protein is possible with label **22**, a second point of attachment may be introduced by photolysis of protein adducts of **19**, **20**, and **21**. The reactive phenylnitrene intermediate so generated

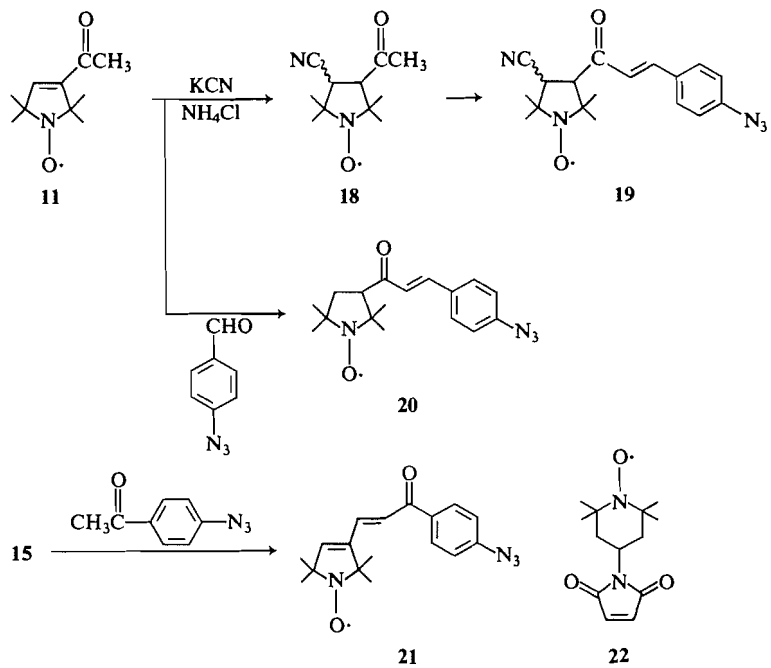


Can. J. Chem. Downloaded from www.nrcresearchpress.com by 210.87.254.40 on 09/06/12
For personal use only.

Can. J. Chem. Downloaded from www.nrcresearchpress.com by 210.87.254.40 on 09/06/12
For personal use only.

should be capable of forming a covalent bond with an adjacent protein residue (or the solvent (17)).

In order to test this approach nitroxide **21** and maleimide label **22** were attached covalently to hemoglobin under identical conditions. The top spectrum in Fig. 1 is a conventional esr spectrum of **21** bound to hemoglobin. The spectrum is dominated by a large bound component, but a small amount of mobile component (indicated by the arrows) is also evident. After photolysis (bottom spectrum of Fig. 1) the mobile component was reduced substantially. The amount of mobile component in the maleimide nitroxide **22**-labeled preparation was comparable to that of **21**-labeled hemoglobin before photolysis. After photolysis, however, the esr spectrum of maleimide **22**-labeled hemoglobin was unchanged.

It is useful to compare the splitting between the low field maximum and the high field minimum ($2A_{max}$) for hemoglobin labeled with the maleimide label **22** and difunctional nitroxide **21** (after photolysis). At 25°C $2A_{max}$ for maleimide-labeled hemoglobin is 66.3 gauss while for hemoglobin labeled with nitroxide **21**, $2A_{max}$ is 69.9 gauss. This difference could result from either polarity differences (a more polar environment would cause $2A_{max}$ to be larger) or from the maleimide label undergoing a small amount of molecular motion independent of that of the protein. By obtaining esr spectra at −196°C where molecular motion is negligible, any differences in $2A_{max}$ should be due to polarity effects alone. The esr spectra recorded at −196°C of hemoglobin labeled with the two spin labels are essentially the same, indicating that differences in polarity are not significant. We conclude, therefore, that differences in $2A_{max}$ in the room temperature esr spectra of these labels covalently bound to hemoglobin are due to nitroxide **21** being more motion-restricted than the maleimide label.

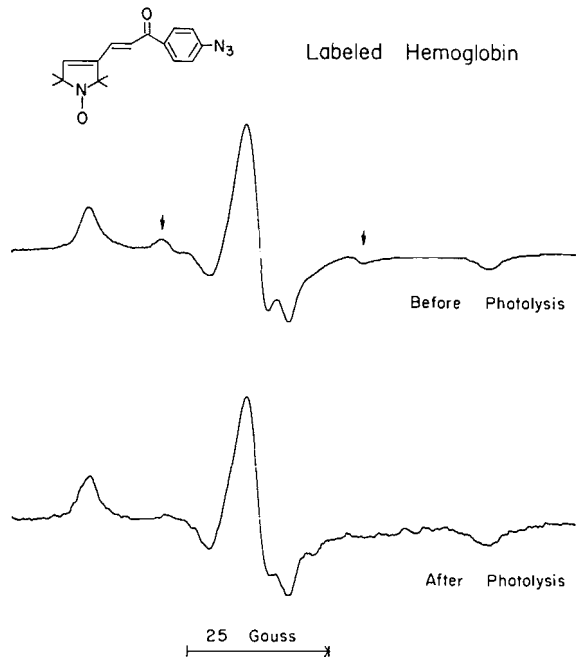


FIG. 1. The 25°C esr spectra of hemoglobin covalently labeled with nitroxide **21** before and after photolysis. The arrows in the top spectrum indicate the mobile component, the relative amount of which is reduced when the preparation is exposed to visible light.

With the 1,4-addition of potassium cyanide to ketone **11** in hand, we next investigated the corresponding reaction with unsaturated nitrile **23**. A separable mixture of *cis* dinitrile **24**, mp 85°C (21%) and *trans* dinitrile **25**, mp 146–147°C (18%) was produced. Vigorous hydrolysis of **24** and **25** with aqueous sodium hydroxide gave acids **26**, mp >250°C, and **27**, mp 220°C, respectively.

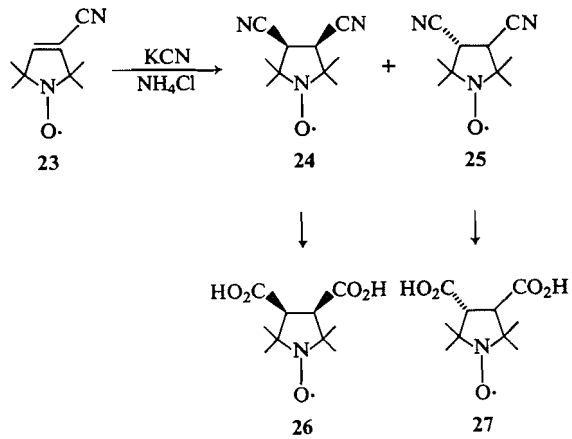


Initially, we had planned to establish the stereochemistry of **24** and **25** through formation of the cyclic anhydride from the *cis* acid **26**. Preliminary attempts to form a cyclic anhydride from either isomer using for example, heat, hot acetic anhydride, or dicyclohexylcarbodiimide were not promising. Eventually, we turned to an X-ray crystallographic analysis of the higher melting dinitrile isomer **25** which unambiguously establishes that it has the *trans* configuration (Fig. 2). The crystal structure (Fig. 3) contains discrete molecules separated by normal van der Waals distances. Molecular dimensions are in Table 1. The N—O distance, 1.269(4) Å, is within the usual range for unconjugated radicals (18) and other distances (N—C$sp^3$ 1.476 and 1.484(4), C$sp^3$—C$sp^3$ 1.503–1.555(4), C$sp^3$—C(N) 1.468 and 1.488(5), C≡N 1.104 and 1.109(4) Å) are unexceptional. The five membered ring adopts a slightly distorted envelope conforma-

Can. J. Chem. Downloaded from www.nrcresearchpress.com by 210.87.254.40 on 09/06/12
For personal use only.

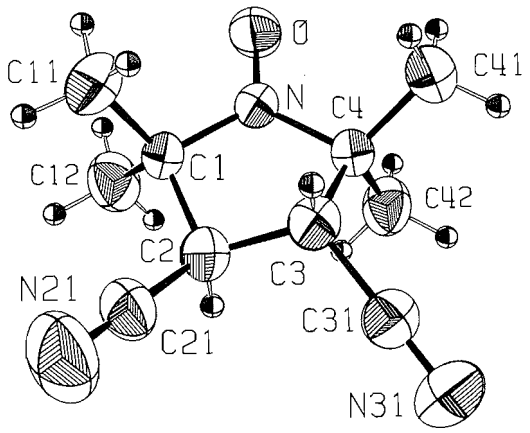


FIG. 2. View of molecule **25** showing the *trans*-configuration of the nitrile groups.

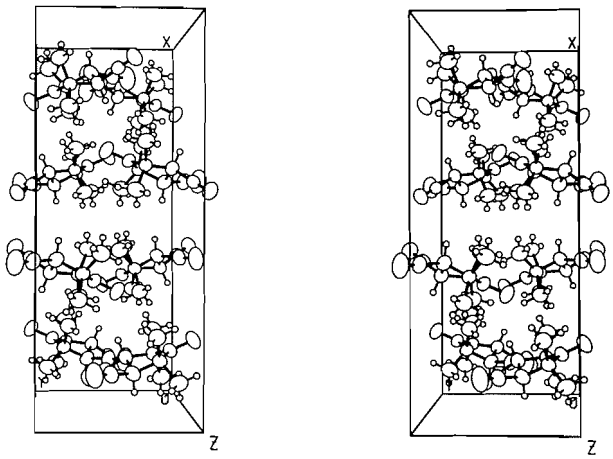


FIG. 3. Stereoview of the crystal structure of **25**.

tion with C(3) (see Fig. 2 for crystallographic numbering scheme) at the flap.

The 1,4-conjugate addition of sulfur reagents to nitroxide acceptors was particularly interesting owing to the generally excellent nucleophilicity of sulfur and also the presence of free reactive sulfhydryl groups on many proteins. Preliminary model experiments involving the addition of sodium phenylsulfinate to aldehyde **15** were not encouraging. Reaction of **15** with ethyl thioglycolate, however, led to the sulfur heterocycle **29**, mp 86–88°C (49%) (mixture of stereoisomers), likely through the intermediacy of adduct **28**. Preparative tlc of **29** followed by two recrystallizations of one of the bands gave a single pure isomer, mp 138–139°C.

Several other heterocycles were prepared from the stereoisomeric mixture **29**. Acetylation of **29** gave acetate **31**, mp 126–127°C (82%), while hydrogen peroxide oxidation of **29** gave sulfone **32**, mp

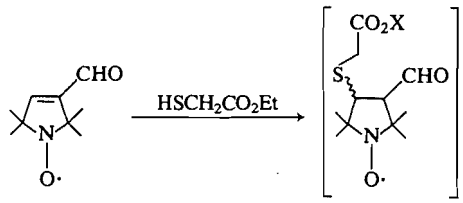


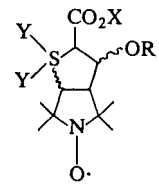


**29** R = H; X = Et; Y = :
**30** R = H; X = Me; Y = :
**31** R = Ac; X = Et; Y = :
**32** R = H; X = Et; Y = O
**33** R = X = H; Y = :

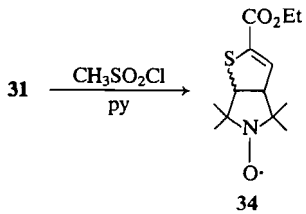


156–157°C (63%). Reaction of **29** with methanesulfonyl chloride in pyridine gave olefin **34**, mp 113–116°C, (74%) as the major product, confirming the β-hydroxyester formulation for **29**. Reaction of **15** with methyl thioglycolate gave ester **30**, mp 136–137°C (44%), hydrolysis of which led to the acid **33**, mp 212–213°C (81%).

## Experimental

Infrared spectra were recorded with either a Beckman IR-5 or IR-7 spectrometer. The nmr spectra were recorded on a Varian XL-100 high resolution spectrometer in $CDCl_3$ and only the characteristic peaks are reported. Chemical shifts are reported in parts per million (δ) downfield from internal $Me_4Si$; mass spectra (70 eV) (*m/e*) were determined on a CEC 110-2B double-focusing mass spectrometer equipped with a direct inlet. Elemental analyses were performed at the University of Oregon by Dr. R. Wielesek. Ultraviolet spectra were determined on a Cary 15 uv spectrometer. Silica gel column chromatography was done with Baker 60-200 mesh silica gel. Preparative thin layer chromatography (tlc) was done on either Analtech 1000 μ silica gel GF 254 or Whatman PKF6 plates. Melting points were recorded on a Thomas–Hoover apparatus. Solvents were routinely distilled.

*1-Oxyl-2,2,5,5-tetramethyl-3-(4-acetylphenoxymethyl)pyrroline (6)*

To a stirred solution of 4-hydroxyacetophenone (150 mg, 1.10 mmol) and nitroxide mesylate **5** (10) (248 mg, 1.00 mmol) in MeOH (5 mL) was added a solution of $Na_2CO_3$ (100 mg) in water

Can. J. Chem. Downloaded from www.nrcresearchpress.com by 210.87.254.40 on 09/06/12
For personal use only.

TABLE 1. Interatomic distances and angles

| Bond | Distance (Å) | Bond | Angle (°) |
|---|---|---|---|
| O—N | 1.269(4) | O—N—C(1) | 121.7(3) |
| N—C(1) | 1.476(4) | O—N—C(4) | 121.2(3) |
| N—C(4) | 1.484(4) | C(1)—N—C(4) | 117.0(2) |
| C(1)—C(2) | 1.538(4) | N—C(1)—C(2) | 99.8(2) |
| C(1)—C(11) | 1.514(4) | N—C(1)—C(11) | 109.7(3) |
| C(1)—C(12) | 1.503(4) | N—C(1)—C(12) | 110.0(3) |
| C(2)—C(3) | 1.514(5) | C(2)—C(1)—C(11) | 115.5(3) |
| C(2)—C(21) | 1.468(5) | C(2)—C(1)—C(12) | 110.3(3) |
| C(3)—C(4) | 1.555(5) | C(11)—C(1)—C(12) | 110.9(3) |
| C(3)—C(31) | 1.488(5) | C(1)—C(2)—C(3) | 105.0(3) |
| C(4)—C(41) | 1.504(4) | C(1)—C(2)—C(21) | 113.5(3) |
| C(4)—C(42) | 1.512(4) | C(3)—C(2)—C(21) | 114.1(3) |
| N(21)—C(21) | 1.104(4) | C(2)—C(3)—C(4) | 104.1(3) |
| N(31)—C(31) | 1.109(4) | C(2)—C(3)—C(31) | 114.6(3) |
| | | C(4)—C(3)—C(31) | 113.3(3) |
| Ring torsion angles (°) | | N—C(4)—C(3) | 97.4(2) |
| | | N—C(4)—C(41) | 111.1(3) |
| C(4)—N—C(1)—C(2) | −3.2 | N—C(4)—C(42) | 109.7(3) |
| N—C(1)—C(2)—O—C(3) | 27.0 | C(3)—C(4)—C(41) | 111.2(3) |
| C(1)—C(2)—C(3)—C(4) | −41.4 | C(3)—C(4)—C(42) | 115.7(3) |
| C(2)—C(3)—C(4)—N | 36.3 | C(41)—C(4)—C(42) | 111.0(3) |
| C(3)—C(4)—N—C(1) | −20.7 | N(21)—C(21)—C(2) | 179.3(4) |
| | | N(31)—C(31)—C(3) | 177.6 (4) |

(3 mL). After a 3 h stir at 25°C, the precipitated product was collected and washed with water, affording 150 mg (52%) of nitroxide **6** as long yellow needles. Recrystallization from MeOH/water afforded the analytical specimen, mp 101–102°C; esr ($CHCl_3$) 3 lines ($a_n$ = 15.0 G); ir (Nujol): 1690 and 1610 $cm^{-1}$. *Anal.* calcd. for $C_{17}H_{22}NO_3$: C 70.80, H 7.69, N 4.86; found: C 70.91, H 7.76, N 4.84.

*1-Oxyl-2,2,5,5-tetramethyl-3-(4-bromoacetylphenoxymethyl)-pyrroline (7)*

To a well stirred solution of ketone **6** (86 mg, 0.30 mmol) in ethyl acetate/$CHCl_3$ (dry) (1:1) (20 mL) was added $CuBr_2$ (134 mg, 0.600 mmol). The mixture was refluxed for 5 h and then filtered. The filtrate was treated briefly with activated charcoal, filtered, and evaporated to dryness. Preparative tlc (Whatman) (ethyl acetate/hexanes (1:1)) gave two major bands which were eluted with ethyl acetate: $R_f$ 0.56 amounted to 45 mg (52%) of unreacted ketone **2**: $R_f$ 0.65 amounted to 15 mg (14%) of desired crystalline **7**. Recrystallization from ether/hexanes gave the analytical specimen, mp 73–74°C; esr ($CHCl_3$) 3 lines ($a_n$ = 15.0 G); ms *m/e*: 368 (8), 366.070 (10) (calcd. for $C_{17}H_{21}NO_3Br$, 366.071), 288 (14), 168 (32), 149 (55), 138 (90), 123 (100), 122 (40), 107 (40).

*1-Oxyl-2,2,5,5-tetramethylpyrroline-3-(N′-p-acetylphenyl)-carboxamide (9)*

To a stirred solution of 1-oxyl-2,2,5,5-tetramethyl-3-carboxypyrroline (**8**) (3.68 g, 20.0 mmol) in benzene (20 mL) and dry pyridine (5 mL) at 0°C was added dropwise a solution of thionyl chloride 3.0 g (0.025 mmol) in benzene (10 mL). After 30 min a solution of 4-aminoacetophenone (2.7 g, 20 mmol) in benzene (50 mL) was added dropwise and the resulting solution was refluxed for 1 h. The cooled reaction mixture was extracted with 1 *N* HCl followed by 10% aqueous $K_2CO_3$ and water. Concentration of the dried ($Na_2SO_4$) benzene layer gave a yellow oil which was triturated in ether. The resulting solid was filtered, affording 5.2 g (86%) of crude **9** suitable for further reactions. Recrystallization of a portion from $CHCl_3$/hexanes afforded the analytical specimen, mp 165–166°C; ir (Nujol): 3125, 1670, and 1590 $cm^{-1}$. *Anal.* calcd. for $C_{17}H_{21}N_2O_3$: C 67.75, H 7.02, N 9.30; found: C 67.54, H 7.27, N 9.28.

*1-Oxyl-2,2,5,5-tetramethyl-3-acetylpyrroline (11) and 1-methoxy-2,2,5,5-tetramethyl-3-acetylpyrroline (13)*

To a stirred suspension ($N_2$) of acid **8** (552 mg, 3.00 mmol) in ether (10 mL) was added dropwise 5.0 mL (7.5 mmol) of a 1.5 *M* solution of MeLi in ether at a rate such that a gentle reflux was maintained. After addition was complete, the mixture was quenched by dropwise addition of saturated aqueous $NH_4Cl$. The mixture was diluted with brine and extracted with ether. The almost colorless ether phase was dried ($Na_2SO_4$) and concentrated, affording a pale yellow oil. In order to facilitate the oxidation of the *N*-hydroxy intermediate, the oil was dissolved in $CHCl_3$ (15 mL) and vigorously stirred under air for 12 h. Evaporation of the solvent gave 310 mg of a viscous yellow oil which was subjected to preparative tlc (Analtech) (ethyl acetate/hexanes (1:1)). The band at $R_f$ 0.93 was *N*-methoxy ketone **13**, obtained as a colorless oil; 110 mg (19%); ir (film): 1675 and 1622 $cm^{-1}$; nmr δ: 1.30 (s, 6), 1.38 (s, 6), 2.30 (s, 3), 3.72 (s, 3), 6.42 (s, 1); ms *m/e*: 197.142 (11) (calcd. for $C_{11}H_{19}NO_2$, 197.142), 196 (19), 182 (72), 136 (100), 105 (20).

The band at $R_f$ 0.75 afforded nitroxide **11** as yellow needles (98 mg, 18%) from hexanes, mp 71–72°C; esr ($CHCl_3$) 3 lines ($a_n$ = 14.8 G); ir (Nujol): 1675 and 1620 $cm^{-1}$; ms *m/e*: 183 (6), 182.118 (28) (calcd. for $C_{10}H_{16}NO_2$, 182.118), 152 (53), 138 (11), 137 (100), 126 (16), 110 (16), 109 (53). *Anal.* calcd. for $C_{10}H_{16}NO_2$: C 65.90, H 8.85, N 7.69; found: C 65.82, H 8.90, N 7.73.

*1-Oxyl-2,2,5,5-tetramethyl-3-butanoylpyrroline (12) and 1-butoxy-2,2,5,5-tetramethyl-3-butanoylpyrroline (14)*

Preparation of **12** and **14** was similar to that of **11** and **13**. From acid **8** (184 mg, 1.00 mmol) and 3.0 mL (4.8 mmol) of 1.6 *M* butyllithium in hexane, there was obtained after preparative tlc 65 mg (23%) of oily *N*-butoxy ketone **14** ($R_f$ 0.95; ir (film): 1675 and 1623 $cm^{-1}$; nmr δ: 2.63 (t, 2), 3.86 (t, 2), 6.20 (s, 1); ms *m/e*: 282 (10), 281.237 (36) (calcd. for $C_{17}H_{31}NO_2$, 281.235), 267 (28), 266 (100), 210 (30), 182 (57), 126 (15), 109 (12)) and 53 mg (24%) of yellow oily nitroxide **12** ($R_f$ 0.73; esr ($CHCl_3$) 3 lines ($a_n$ = 14.8

Can. J. Chem. Downloaded from www.nrcresearchpress.com by 210.87.254.40 on 09/06/12
For personal use only.

G); ir (film): 1675 and 1620 $cm^{-1}$; ms *m/e*: 226 (25), 225 (29), 224.165 (59) (calcd. for $C_{13}H_{22}NO_2$, 224.165), 210 (61), 194 (59), 179 (25), 137 (100), 126 (32), 110 (33), 109 (79)). The pale yellow aqueous phase from the original work-up of this reaction was acidified (pH 3) and extracted with $CHCl_3$. From the extract there was obtained 25 mg (14%) of the starting acid **8**.

*1-Oxyl-2,2,5,5-tetramethyl-3-(1-hydroxyethyl)pyrroline (16)*

To a stirred solution of nitroxide aldehyde **15** (14, 15) (505 mg, 3.00 mmol) in dry ether (15 mL) at 25°C was added dropwise 4.0 mL (3.9 mmol) of a 1.3 *M* solution of MeLi in ether. After 30 min the reaction was quenched by addition of saturated aqueous $NH_4Cl$ (1 mL) followed by brine (20 mL). The mixture was extracted with ether. The extract was dried ($Na_2SO_4$) and concentrated. The pale yellow residue was dissolved in $CHCl_3$ (20 mL) and stirred under air for 12 h (solution now deep yellow). The solvent was evaporated and the residue was crystallized from ether–hexane (0°C), affording 250 mg (45%) of crystalline **16**, suitable for further reactions. Recrystallization from $CHCl_3$/hexanes afforded the analytical specimen, mp 80–81°C; ir (Nujol): 3400 $cm^{-1}$. *Anal.* calcd. for $C_{10}H_{18}NO_2$: C 65.18, H 9.85, N 7.60; found: C 64.70, H 9.80, N 7.68.

The mother liquors were combined, evaporated, and the residue was dissolved in $CHCl_3$ (30 mL). Active $MnO_2$ (3 g) was added to the stirred solution and the mixture was refluxed for 3 h and then filtered. The filtrate was concentrated and then subjected to preparative tlc (Analtech) (ethyl acetate/hexanes, 1:1). There was obtained 120 mg (20%) of *N*-methoxy ketone **13** and 30 mg (6%) of nitroxide ketone **11**.

Alternatively, pure nitroxide alcohol **16** (46 mg, 0.25 mmol) was dissolved in $CHCl_3$ (10 mL) and treated with active $MnO_2$ (0.5 g). The mixture was stirred under reflux for 3 h (monitored by tlc) and filtered. The filtrate was subjected to preparative tlc, affording 38 mg (83%) of ketone **11**, mp 71–72°C.

*1-Oxyl-2,2,5,5-tetramethyl-3-(bromoacetyl)pyrroline (18)*

To a stirred solution of ketone **11** (91 mg, 0.50 mmol) in ethyl acetate/$CHCl_3$ (20 mL) (1:1) was added powdered $CuBr_2$ (223 mg, 1.00 mmol). The mixture was refluxed for 7 h after which period the black $CuBr_2$ was nearly completely replaced by a white precipitate of CuBr. The green supernatant was treated with activated charcoal and filtered. The filtrate was evaporated to dryness and the residue was subjected to preparative tlc (Whatman), giving two major bands which were eluted with ethyl acetate: $R_f$ 0.43 amounted to 35 mg (38%) of unreacted ketone **11**. $R_f$ 0.55 amounted to 20 mg (15%) of desired bromo ketone **17**, mp 67–69°C; esr ($CHCl_3$) 3 lines, $a_n$ = 14.7 G; ms *m/e*: 262 (32), 260.029 (32) (calcd. for $C_{10}H_{15}BrNO_2$, 260.029), 152 (24), 151 (100), 137 (38), 110 (24), 109 (67).

*1-Oxyl-2,2,5,5-tetramethyl-3-acetyl-4-cyanopyrroline (18)*

A mixture of ketone **11** (91 mg, 0.50 mmol) KCN (65 mg, 1.0 mmol), and $NH_4Cl$ (59 mg, 1.1 mmol) was dissolved in water–ethanol (10 mL, 8:2) and refluxed for 2 days. Brine (20 mL) was added and the mixture was extracted with ether. The extract was dried ($Na_2SO_4$), evaporated, and the residue was subjected to preparative tlc (Analtech) ($CHCl_3$/ether, 1:1). Starting ketone **11** (15 mg, 16%) was recovered from the upper band. The lower band afforded 30 mg (29%) of adduct **18**, likely as a mixture of stereoisomers, mp 104–107°C; ir ($CHCl_3$): 2230 and 1720 $cm^{-1}$; ms *m/e*: 210 (7), 209.128 (26) (calcd. for $C_{11}H_{17}N_2O_2$, 209.129), 195 (16), 179 (45), 135 (22), 110 (100). *Anal.* calcd. for $C_{11}H_{17}N_2O_2$: C 63.13, H 8.19, N 13.39; found: C 62.51, H 8.64, N 13.15.

*1-Oxyl-2,2,5,5-tetramethyl-3-(4-azidocinnamoyl)pyrroline (20)*

To a stirred solution of ketone **11** (109 mg, 0.600 mmol) in MeOH (3 mL) (protected from light) was added aqueous NaOH (0.3 mL, 1 *N*), followed by a solution of 4-azidobenzaldehyde (97 mg, 0.66 mmol) in MeOH (1 mL). During the addition the color became deep orange. Afte 2 h the precipitated yellow crystals were collected, washed with MeOH–water, and dried in the dark, affording 87 mg (47%) of azide **20**, mp 138–141°C (dec.); ir (Nujol): 2100 and 1655 $cm^{-1}$; ms *m/e*: 312 (46), 311.150 (100) (calcd. for $C_{17}H_{19}N_4O_2$, 311.151), 297 (62), 253 (56), 238 (50), 210 (27), 146 (62), 144 (81), 125 (56), 116 (100), 109 (42), 108 (30), 106 (42).

*1-Oxyl-2,2,5,5-tetramethyl-3-(4-azidocinnamoyl)-4-cyanopyrroline (19)*

The above procedure was followed. From cyano ketone **18** (52 mg, 0.25 mmol) and 4-azidobenzaldehyde (37 mg, 0.25 mmol) there was obtained 35 mg (41%) of yellow crystalline **19**, mp 110–114°C (dec.); ir (Nujol): 2245, 2210, 1685, 1655, and 1595 $cm^{-1}$; ms *m/e*: 339 (11), 338.161 (19) (calcd. for $C_{18}H_{20}N_5O_2$, 338.162), 172 (26), 146 (35), 145 (21), 144 (100), 116 (58), 110 (22).

*1-Oxyl-2,2,5,5-tetramethyl-3-(2-(4-azidobenzoyl)ethenyl)-pyrroline (21)*

To a stirred solution of aldehyde **15** (16.8 mg, 0.100 mmol) in MeOH (1.0 mL) (protected from light) was added a solution of 4-azidoacetophenone (16.1 mg, 0.100 mmol) in MeOH (3.0 mL) followed by 1.0 *N* NaOH (0.1 mL). After a 3 h stirring period at 25°C the precipitated yellow crystalline plates were collected and washed with aqueous MeOH, affording 24 mg (77%) of crystalline ketone **21**, mp 125–129°C. Recrystallization from aqueous MeOH afforded the analytical specimen: mp 135–136°C; esr ($CHCl_3$) 3 lines ($a_n$ = 14.7 G); ir (Nujol): 2120, 1665, and 1610 $cm^{-1}$; ms *m/e*: 312 (36), 311.151 (100) (calcd. for $C_{17}H_{19}N_4O_2$, 311.151), 297 (23), 283 (14), 269 (22), 253 (26), 238 (43), 225 (48), 212 (40), 210 (28), 182 (14), 135 (20), 120 (41), 105 (18). *Anal.* calcd. for $C_{17}H_{18}N_4O_2$: C 65.57, H 6.15, N 18.00; found: C 65.62, H 6.23, N 17.98.

*1-Oxyl-2,2,5,5-tetramethyl-3,4-dicyanopyrrolidine* cis, trans *isomers (24 and 25)*

A mixture of nitrile **23** (165 mg, 1.00 mmol), KCN (130 mg, 2.00 mmol), and $NH_4Cl$ (107 mg, 2.00 mmol) was dissolved in DMF (3 mL)/water (30 mL), heated at 70°C for 3 h, and then set aside at 25°C for 48 h. Brine (15 mL) was added and the mixture was extracted with ether. The extract was dried ($Na_2SO_4$) and evaporated to dryness. Preparative tlc (Analtech) of the residue gave three major bands ($CHCl_3$/ether, 1:1): $R_f$ 0.80 amounted to 43 mg (26%) of starting **23**. $R_f$ 0.63 amounted to 35 mg (18%) of yellow crystalline *trans* dinitrile isomer **25**, mp 146–147°C ($CHCl_3$/hexane); ir (Nujol): 2220 $cm^{-1}$; ms *m/e*: 193 (11), 192.113 (59) (calcd. for $C_{10}H_{14}N_3O$, 192.114), 179 (4), 178 (35), 177 (31), 163 (6), 162 (46), 83 (11), 82 (100), 81 (73). *Anal.* calcd. for $C_{10}H_{14}N_3O$: C 62.48, H 7.34, N 21.86; found: C 61.82, H 7.37, N 21.36. $R_f$ 0.37 amounted to 40 mg (21%) of the *cis* isomer **24** which slowly crystallized, mp 85°C; ir (film): 2220 $cm^{-1}$; ms *m/e*: 193 (3), 192.113 (15) (calcd. for $C_{10}H_{14}N_3O$, 192.114), 178 (18), 162 (16), 85 (28), 83 (100), 82 (19). *Anal.* found: C 62.1, H 6.9, N 21.0.

*X-ray analysis of 25*

Crystal data:

$C_{10}H_{14}N_3O$ f.w. = 192.1

Orthorhombic, $a$ = 19.155(2), $b$ = 7.634(1), $c$ = 15.059(3) Å, $U$ = 2202.1 Å$^3$, $Z$ = 8, $D_c$ = 1.16, $F(000)$ = 824, $MoK_\alpha(\lambda = 0.71069$ Å), $\mu$ = 0.5 $cm^{-1}$, space group $Pbcn$ ($D_{2h}^{14}$) from the systematic absences $hk0$, $k = 2n + 1$; $h0l$, $h + l = 2n + 1$.

A small crystal of dimensions 0.40 × 0.33 × 0.13 mm was used in the analysis. Unit cell contstants and intensity data were determined using an Enraf–Nonius computer-controlled CAD-4 diffractometer. For the cell dimension determination, the setting angles of 25 reflexions with θ near 15° were used in a

Can. J. Chem. Downloaded from www.nrcresearchpress.com by 210.87.254.40 on 09/06/12
For personal use only.

least-squares refinement. During data collection three well separated reflections were monitored at regular intervals and showed no reduction in intensity. The intensities of 1930 reflections with $2 < \theta < 25°$ were measured by the $\theta/2\theta$ scan technique. The 1068 reflections with $I > 3\sigma(I)$ were labelled "observed" and used, after correction for Lorentz and polarization factors, in the determination and refinement of the structure.

The structure was determined by direct methods using the SHELX program (19). The first $E$-map calculated with $E$'s > 1.2 revealed all 14 non-hydrogen atoms. Four cycles of full-matrix isotropic refinement reduced $R$ to 0.14 and a subsequent difference map revealed positions for all 14 protons. These were then allowed for in idealized positions (C—H 0.95 Å) and only an overall isotropic temperature factor was refined for protons in subsequent refinement. After six further rounds of full-matrix calculations, with the non-hydrogen atoms allowed anisotropic motion, the refinement was completely converged with $R = 0.058$ and $R' = \Sigma w\Delta^2/\Sigma wF_0^2 = 0.074$. In the refinement cycles, weights were derived from the counting statistics, $w = 1/(\sigma^2 F + 0.005F^2)$, and scattering factors were taken from refs. 20 and 21. A final difference map was free of any significant features. Final atomic coordinates are given in Table 2. The measured and calculated structure factors and thermal parameters have been placed in the Depository of Unpublished Data.[3]

trans-*1-Oxyl-2,2,5,5-tetramethyl-3,4-dicarboxypyrrolidine (27)*

A solution of **25** (10 mg, 0.52 mmol) and 2 *N* aqueous NaOH (0.62 mL, 1.2 mmol) was heated at 90°C until evolution of $NH_3$ (22) ceased (34 h). The solution was cooled, carefully neutralized to pH 4 by addition of 6 *N* HCl, and extracted with ether. Evaporation of the extract afforded 2.8 mg of crude partially hydrolyzed nitroxide which still contained cyano absorption in the ir spectrum. The original aqueous phase was further acidified to pH 2 and again extracted with ether. The extract was dried ($Na_2SO_4$) and evaporated. The residue was recrystallized from ether–hexane, affording 7.3 mg (61%) of **27**, mp 220°C; ms *m/e*: 230.102 (70) (calcd. for $C_{10}H_{16}NO_5$, 230.103), 216 (23), 197 (20), 170 (18), 169 (30), 154 (25), 110 (22), 109 (25), 101 (95), 100 (65), 83 (100), 82 (60).

*cis-1-Oxyl-2,2,5,5-tetramethyl-3,4-dicarboxypyrrolidine (26)*

The *cis* dinitrile isomer **24** (27 mg) was hydrolyzed as in the previous experiment, affording 18 mg (56%) of diacid **26** as a yellow powder, mp >250°C; ms *m/e*: 231 (15), 230.104 (50) (calcd. for $C_{10}H_{16}NO_5$, 230.103), 216 (45), 197 (14), 170 (30), 169 (23), 154 (21), 110 (24), 109 (21), 101 (79), 100 (49), 83 (100), 82 (57).

*2-Carboethoxy-3-hydroxy-4,4,6,6-tetramethyl-2,3,3a,4,6,6a-hexahydrothieno[2,3-c]pyrrole-5-oxyl (29)*

Ethyl thioglycolate (120 mg, 1.00 mmol) was added to a solution of aldehyde **15** (168 mg, 1.00 mmol) in MeOH (5 mL) containing diethylamine (14.6 mg, 0.200 mmol). After a 24 h reflux period, the solution was concentrated and subjected to preparative tlc (Analtech) (ethyl acetate/hexanes, 1:1). The $R_f$ 0.64 band amounted to 35 mg (21%) of starting aldehyde **15**. Two very close lower bands, $R_f$ 0.54, were collected together, affording 140 mg (49%) of the title compound, likely as a mixture of stereoisomers, mp 86–88°C; ir (Nujol): 3550–3250 and 1740 $cm^{-1}$; ms *m/e*: 290 (2), 289 (8), 288.128 (31) (calcd. for $C_{13}H_{22}NO_4S$, 288.127), 215 (16), 174 (59), 143 (4), 142 (13), 141 (100), 110 (75), 101 (52). *Anal.* calcd. for $C_{13}H_{22}NO_4S$: C 54.14, H 7.69, N 4.85; found: C 53.94, H 7.56, N 5.35. Repeated preparative tlc followed by two crystallizations from ether–hexane gave one pure isomer of **29**, mp 138–139°C.[3]

[3]The tables are available, at nominal charge, from the Depository of Unpublished Data, CISTI, National Research Council of Canada, Ottawa, Ont., Canada, K1A 0S2.

TABLE 2. Final fractional coordinates (× $10^4$) with standard deviations in parentheses

| Atom | *x* | *y* | *z* |
|---|---|---|---|
| O | 1861(1) | 313(3) | 577(2) |
| N | 1591(1) | −1203(4) | 610(2) |
| N(21) | 1084(3) | −3742(5) | −2784(3) |
| N(31) | 761(2) | −6374(5) | −749(2) |
| C(1) | 1384(1) | −2013(4) | 1460(2) |
| C(2) | 1035(2) | −6308(5) | −3889(2) |
| C(3) | 1385(2) | −4052(4) | 229(2) |
| C(4) | 1447(1) | −2216(4) | −211(2) |
| C(11) | 2023(2) | −2290(5) | 2035(2) |
| C(12) | 857(2) | −879(5) | 1924(3) |
| C(21) | 1066(2) | −4840(5) | −3260(2) |
| C(31) | 1019(2) | −5358(5) | −337(3) |
| C(41) | 2057(2) | −2141(6) | −838(2) |
| C(42) | 791(2) | −1532(6) | −649(2) |
| H(21) | 546 | −6452 | −3965 |
| H(31) | 1830 | −4576 | 314 |
| H(111) | 1897 | −2809 | 2586 |
| H(112) | 2238 | −1188 | 2141 |
| H(113) | 2340 | −3035 | 1732 |
| H(121) | 719 | −1409 | 2467 |
| H(122) | 460 | −738 | 1553 |
| H(123) | 1058 | 234 | 2041 |
| H(411) | 1958 | −2794 | −1360 |
| H(412) | 2453 | −2629 | −550 |
| H(413) | 2152 | −959 | −994 |
| H(421) | 694 | −2186 | −1171 |
| H(422) | 851 | −333 | −799 |
| H(423) | 413 | −1645 | −245 |

*2-Carbomethoxy-3-hydroxy-4,4,6,6-tetramethyl-2,3,3a,4,6,6a-hexahydrothieno[2,3-c]pyrrole-5-oxyl (30)*

The above procedure was followed. From methyl thioglycolate (106 mg, 1.00 mmol) and aldehyde **15** (168 mg, 1.00 mmol) there was obtained 40 mg (24%) of recovered aldehyde and 120 mg (44%) of ester **30**, mp 136–137°C (ether/hexane); ms *m/e*: 275 (36), 274.111 (91) (calcd. for $C_{12}H_{20}NO_4S$, 274.111), 260 (56), 244 (31), 160 (100), 127 (87), 110 (69), 101 (44), 99 (80).

*2-Carboethoxy-3-acetoxy-4,4,6,6-trimethyl-2,3,3a,4,6,6a-hexahydrothieno[2,3-c]pyrrole-5-oxyl (31)*

Acetic anhydride (20.4 mg, 0.200 mmol) was added to alcohol **29** (28.8 mg, 0.100 mmol) in pyridine (1.0 mL) and the solution was allowed to stand at 25°C for 3 h. The usual work-up afforded a yellow solid which crystallized from ether/hexane to give 27 mg (82%) of acetate **31**, mp 126–127°C; ms *m/e*: 332 (6), 331 (25), 330.136 (69) (calcd. for $C_{15}H_{24}NO_5S$, 330.137), 242 (11), 241 (16), 240 (82), 216 (34), 174 (100), 167 (40), 141 (41), 99 (72).

*2-Carboethoxy-3-hydroxy-4,4,6,6-tetramethyl-2,3,3a,4,6,6a-hexahydrothieno[2,3-c]pyrrole-5-oxyl-1,1-dioxide (32)*

Hydrogen peroxide (30%) (1.0 mL) was added to a solution of alcohol **29** (28.8 mg) in MeOH (2.0 mL). Sodium tungstate (3 mg) was then added and the solution was allowed to stand for 3 h at 25°C. The solution was diluted with brine (10 mL) and extracted with $CHCl_3$. The extract was dried ($Na_2SO_4$) and evaporated to dryness, affording a solid residue which was triturated with ether. Filtration afforded 20 mg (63%) of crystalline sulfone **32**, mp 156–157°C; ms *m/e*: 320.118 (10) (calcd. for $C_{13}H_{22}NO_6S$, 320.117), 164 (20), 139 (3), 111 (35), 110 (100), 109 (13), 95 (29).

*2-Carboxy-3-hydroxy-4,4,6,6-tetramethyl-2,3,3a,4,6,6a-hexahydro[2,3-c]pyrrole-5-oxyl (**33**)*

A solution of methyl ester **30** (144 mg, 0.500 mmol) and 1.0 mL (1.0 mmol) of 1 *N* NaOH in MeOH (3.0 mL) was allowed to stand at 25°C for 3 h. The solution was diluted with brine, acidified, and extracted with ether. Evaporation of the dried ($Na_2SO_4$) extract gave 105 mg (81%) of crystalline acid **33**. Recrystallization from $CHCl_3$/ether/hexenes gave the analytical specimen, mp 212–213°C; ms *m/e*: 260.096 (5) (calcd. for $C_{11}H_{18}NO_4S$, 260.096), 169 (29), 154 (95), 138 (67), 126 (100), 123 (38), 110 (86), 109 (33), 108 (29), 95 (52), 92 (71).

*2-Carboethoxy-4,4,6,6-tetramethyl-3a,4,6,6a-tetrahydrothieno[2,3-c]pyrrole-5-oxyl (**34**)*

Methanesulfonyl chloride (22.9 mg, 0.200 mmol) was added to a solution of alcohol **29** (28.9 mg, 0.100 mmol) in pyridine (1.0 mL) and the solution was allowed to stand at 25°C for 6 h. The mixture was diluted with brine, acidified to pH 4 with 6% hydrochloric acid, and extracted with ether. The dried ($Na_2SO_4$) extract was evaporated and the residue was subjected to preparative tlc (Analtech) (ethyl acetate/hexanes, 1:1). The major band, $R_f$ 0.74, afforded 20 mg (74%) of crystalline **34**. Recrystallization from ether/hexanes gave the analytical specimen, mp 113–116°C; ir (Nujol): 1720 and 1560 $cm^{-1}$; ms *m/e*: 272 (5), 271 (14), 270.116 (54) (calcd. for $C_{13}H_{20}NO_3S$, 270.116), 241 (11), 240 (63), 226 (16), 225 (100), 198 (16), 197 (87), 184 (14), 183 (89), 181 (16), 169 (53), 167 (84), 155 (37), 153 (42), 151 (47), 133 (33), 125 (73), 113 (94), 111 (65).

*Spin labeled hemoglobin*

Stock solutions (5 mg/mL) of 3-maleimido-2,2,5,5-tetramethyl-1-pyrrolidinyloxyl (**22**) (Syva Co.) and nitroxide **21** were prepared in ethanol. Hemoglobin (20 mg, Sigma, Type I, bovine) was dissolved in 30 m*M* Tris pH 8.0 buffer (0.5 mL) in subdued light. The spin label stock solution (6 μL) was added and the resulting solution was stirred 2 h at 25°C. After removal of unreacted spin label by dialysis, the sample was concentrated to 50 μL using a collodion bag apparatus (Schleicher & Schuell, MW cutoff 25 000) before esr spectra were recorded. Samples to be photolyzed were diluted to 0.5 mL with the Tris buffer and then illuminated 5 min at 0°C with filtered (1 *M* $KNO_2$) radiation from a 1000 W quartz–halogen lamp. After the photolysis, the samples were concentrated to 50 μL and esr spectra (Varian E-Line spectrometer) were again recorded.

## Acknowledgments

This research was supported in part by Public Health Service Research Grant GM 24951 to J.F.W.K.; K.H. and O.H.H. thank the Hungarian Academy of Sciences Grant No. 134/79/II for financial support. G.F. thanks NSERC Canada for the award of an operating grant.

1. L. J. Berliner (*Editor*). Spin labeling: theory and applications. Vols. I and II. Academic Press, New York. (1976) and (1979).
2. J. F. W. Keana. Chem. Rev. **78**, 37 (1978).
3. P. G. Johnson, A. Waheed, L. Jones, A. J. Glaid, and O. Gawron. Biochem. Biophys. Res. Commun. **74**, 384 (1977).
4. J. S. Hyde and L. R. Dalton. *In* Spin labeling: theory and applications. Vol. II. *Edited by* L. J. Berliner. Academic Press, New York. 1979. Chapt. 1.
5. R. T. Cherry. Biochim. Biophys. Acta, **559**, 289 (1979).
6. F. R. N. Gurd and T. M. Rothgeb. Adv. Protein Chem. **33**, 74 (1979).
7. H. R. Wenzel, G. Becker, and E. von Goldammer. Chem. Ber. **111**, 2453 (1978).
8. M. W. Tse-Tang, B. J. Gaffney, and R. E. Kelly. Heterocycles, **15**, 965 (1981).
9. E. G. Rozantsev. Free nitroxyl radicals. Plenum Press, New York. 1970. pp. 220 and 235–236.
10. H. O. Hankovszky, K. Hideg, and L. Lex. Synthesis, 914 (1980).
11. L. C. King and G. K. Ostrum. J. Org. Chem. **29**, 3459 (1964).
12. M. J. Jorgenson. Org. React. **18**, 1 (1970).
13. G. M. Whitesides and T. L. Newirth. J. Org. Chem. **40**, 3448 (1975).
14. K. Hideg, H. O. Hankovszky, L. Lex, and Gy. Kulcsár. Synthesis, 911 (1980).
15. T. R. Koch, L. C. Kuo, E. G. Douglas, S. Jaffer, and M. W. Makiner. J. Biol. Chem. **254**, 12 310 (1980).
16. B. J. Gaffney. *In* Spin labeling: theory and applications. Vol. I. *Edited by* L. J. Berliner. Academic Press, New York. 1976. Chapt. 5.
17. Ann. N.Y. Acad. Sci. **346**, 1–502 (1980) (entire issue).
18. F. J. Lalor, F. L. Scott, G. Ferguson, and W. C. Marsh. J. Chem. Soc. Perkin Trans. I, 789 (1978).
19. G. M. Sheldrick. SHELX, a program for crystal structure determination. University Chemical Laboratories, Cambridge, England.
20. D. Cromer and J. B. Mann. Acta Crystallogr. Sect. A, **24**, 321 (1968).
21. R. F. Stewart, E. R. Davidson, and W. T. Simpson. J. Chem. Phys. **42**, 3178 (1965).
22. R. F. Milton and W. A. Waters. Methods of quantitative micro-analysis. 2nd ed. Arnold, Inc., London. 1955. p. 318.

Can. J. Chem. Downloaded from www.nrcresearchpress.com by 210.87.254.40 on 09/06/12
For personal use only.

# Nitroxides. IX.[1] Synthesis of nitroxide free radical α-amino acids

LÁSZLÓ LEX, KÁLMÁN HIDEG,[2] AND H. OLGA HANKOVSZKY
*Central Laboratory, Chemistry, University of Pécs, H-7643 Pécs, Hungary*

Received September 12, 1981

LÁSZLÓ LEX, KÁLMÁN HIDEG, and H. OLGA HANKOVSZKY. Can. J. Chem. **60**, 1448 (1982).

Three methods are described for preparation of a new stable nitroxide free radical amino acid, 2-amino-3-(1-oxyl-2,2,5,5-tetramethyl-3-pyrrolin-3-yl) propionic acid and its derivates. This amino acid may be used as a paramagnetic amino acid synthon in studies of peptides.

LÁSZLÓ LEX, KÁLMÁN HIDEG et H. OLGA HANKOVSZKY. Can. J. Chem. **60**, 1448 (1982).

On décrit trois méthodes de préparation d'un nouveau radical libre nitroxyde stable d'un acide aminé: l'acide amino-2 (oxyl-1 tétraméthyl-2,2,5,5 pyrroline-3 yl-3)-3 propionique et ses dérivés. On utilise cet acide aminé comme synthon paramagnétique dans des études de peptides.

[Traduit par le journal]

## Introduction

Reactive functional groups containing nitroxides have often been used for acylating or alkylating peptides and proteins at reactive functional groups such as amino, thiol, or carboxyl groups (2–5).

It is essential to carry out the labeling with as minimal perturbance of the biomolecule as possible to fulfill the requirements for an ideal reporter-group. That is of course not possible, because the modification of any essential function (e.g. acylating an amino group, alkylating a thiol group, or acylating a carbonyl group) may result in the loss of biological activity.

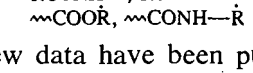

Relatively few data have been published on the synthesis of nitroxide free radical analogues of amino acids (6–8):

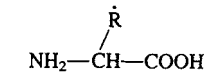

We wish to report methods generally applicable for synthesis of nitroxide α-amino acids, which can be used as synthons due to their structural resemblance to natural aralkyl amino acids like histidine or tryptophane:

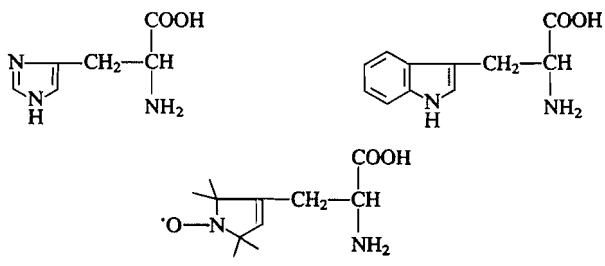

As starting compounds, nitroxide derivatives are needed which are reactive enough and do not have a chiral centre. These requirements are fulfilled excellently by either the 1-oxyl-2,2,5,5-tetramethyl-3-bromomethyl-3-pyrroline (**1***a*) or the 1-oxyl-2,2,5,5-tetramethyl-3-methanesulfonyloxymethyl-3-pyrroline (**1***b*) (9).

## Results and discussion

Three esters of α-functionalized carboxylic acids are acylated on their active methylene or methine group with **1***a* or **1***b* in alkaline media. In the first route (Method A) the dimethyl 2-acetamino malonate (**2**) is alkylated with **1***a* to **3** in the presence of sodium ethoxide. After partial hydrolysis of **3** the monomethyl ester of dicarboxylic acid (**4**) is formed. The acetamino nitroxide amino acid (**6**) can be obtained via decarboxylation of **4** and the hydrolysis of **5**. The compound **6** is suitable for reactions of its free carboxylic group with amino acids or peptides because its amino terminal is protected by an acetyl group.

The second method (Method B) utilizes a synthetic route by which the Schiff's base **7** (formed from benzophenone and glycine ester) can be alkylated with alkyl halides in a two-phase system using tetrabutylammonium hydrogen sulfate as a phase transfer catalyst (10). Following this, **7** can be alkylated with **1***a* to **8**. After acidic hydrolysis of **8** with aqueous citric acid (11) the ethyl ester of the nitroxide amino acid (**9**) is obtained. This route leads to a free α-amino group containing ester which can be acylated on its amino terminal. For longer storage the more stable tosylate salt of **9** is prepared with toluenesulfonic acid in dry acetone. On acetylation of **9** with 1-acetylimidazole, **10** is formed, which can be hydrolyzed to **6** obtained at the end of Method A.

[1]For Part VIII, see ref. 1.

[2]Author to whom correspondence may be addressed.

0008-4042/82/121448-04$01.00/0

©1982 National Research Council of Canada/Conseil national de recherches du Canada

Can. J. Chem. Downloaded from www.nrcresearchpress.com by 210.87.254.40 on 09/06/12
For personal use only.

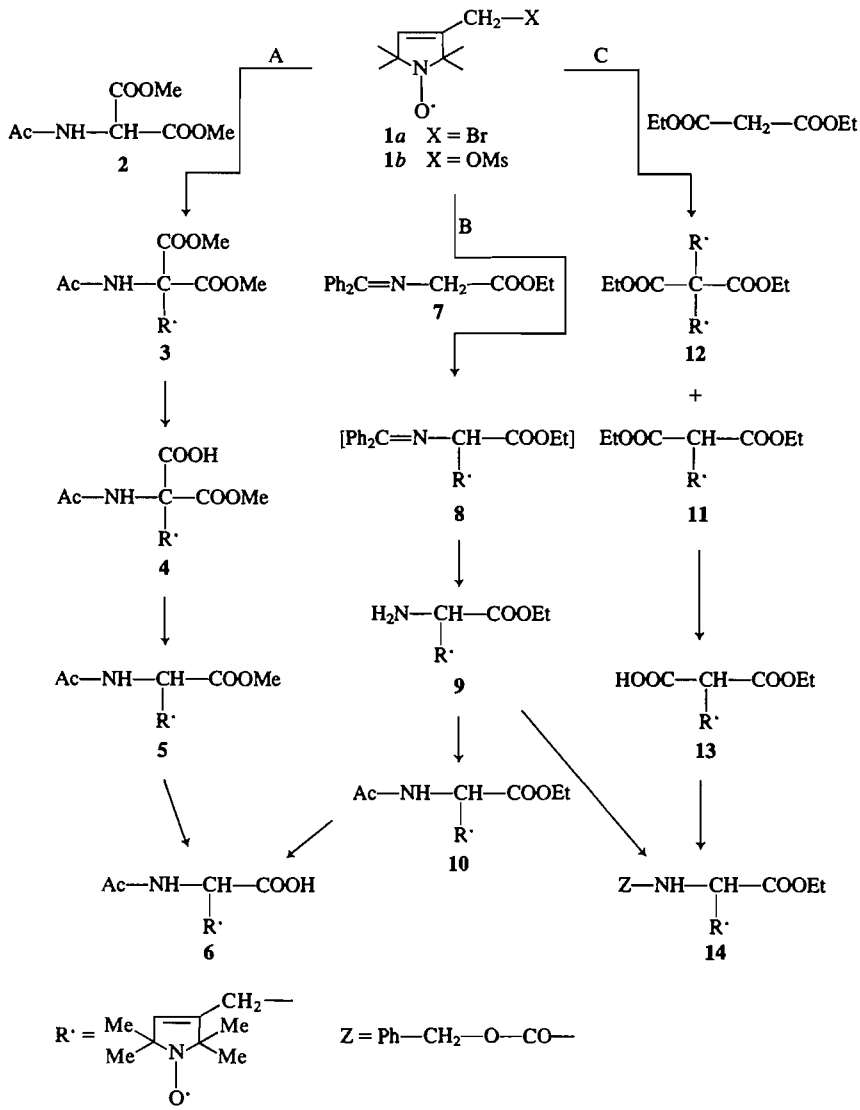


SCHEME 1

In the third route (Method C) the sodium diethyl malonate is alkylated with **1***b* (9) to **11** with formation of some bis-alkylated compound (**12**) as well. The biradical compound exhibits a 5-line esr spectrum characteristic of nitroxide biradicals.

In a partial hydrolysis of diester **11** the acid monoethyl ester (**13**) is formed. Utilizing the carbonyl-azide formation reaction with diphenyl phosphorylazide (DPPA) (12) **13** is allowed to react with DPPA and then with benzyl alcohol to obtain the desired ethylester of nitroxide amino acid (**14**) which is protected on its amino terminal by a carbobenzyloxy group (Z). This derivative can also be obtained when **9** is reacted with benzyl chloroformate in the presence of triethylamine.

These methods are equally useful for preparing derivates of nitroxide amino acids protected either on amino or carboxyl terminal groups. All of these amino acids are racemates; the experiments for resolution are in progress.

## Experimental

Melting points were measured using a Boetius micro mp-determining instrument and are not corrected. The ir spectra were measured as a neat oil or in Nujol suspensions with a Zeiss Specord 75 type of instrument. The esr spectra were obtained

Can. J. Chem. Downloaded from www.nrcresearchpress.com by 210.87.254.40 on 09/06/12
For personal use only.

Can. J. Chem. Downloaded from www.nrcresearchpress.com by 210.87.254.40 on 09/06/12
For personal use only.

from $10^{-3}$ *M* solution using a Zeiss ER9 spectrometer. All the monoradicals exhibited three equidistant lines and the biradical showed five equidistant lines with $a_N$ = 14.8–15.0 G. The mass spectra were taken using a Varian-MAT-SM-1 instrument. Solvents were reagent grade and dried prior to use. All organic extracts obtained during the work-up of the reaction mixture were dried over anhydrous magnesium sulfate and distilled off *in vacuo*. For column chromatography silica gel 60 was used.

*Dimethyl 2-acetamino-2-[(1-oxyl-2,2,5,5-tetramethyl-3-pyrrolin-3-yl)methyl] malonate (3)*

To a stirred solution of **2** (0.95 g, 5.0 mmol) in dry ethanol (15 mL) with sodium ethoxide (1 *M*, 5 mL, 5.0 mmol) a solution of **1***a* (1.17 g, 5.0 mmol) in dry ethanol (10 mL) was added, refluxed for 5 h, and then evaporated *in vacuo* to dryness. The residue was taken up in water (10 mL) and extracted with chloroform (3 × 10 mL). The organic phase was separated, dried, and evaporated. The solid residual was subjected to column chromatography on silica gel with tetrachloromethane/ethyl acetate (2:1). The first yellow band was unreacted **1***a*, 0.3 g (25%); the second one was compound **3**, yield: 0.9 g (53%), mp 97–98°C; ir $\nu_{max}$: 3345 (NH), 1725 (CO), 1665 (CONH) $cm^{-1}$. *Anal.* calcd. for $C_{16}H_{25}N_2O_6$ (Mol. Wt. 341.4): C 56.30, H 7.38, N 8.21; found: C 56.42, H 7.37, N 8.35.

*Monomethyl ester of 2-acetamino-2-[(1-oxyl-2,2,5,5-tetramethyl-3-pyrrolin-3-yl)methyl] malonic acid (4)*

Sodium hydroxide solution (1 *M*, 2 mL, 2.0 mmol) was added to a solution of **3** (0.341 g, 1.0 mmol) in methanol (2 mL) and allowed to stay at room temperature overnight, then diluted with water (10 mL), acidified with dilute sulfuric acid (5%), and extracted with chloroform (3 × 10 mL). The organic phase was dried and evaporated to dryness. The solid residue was crystallized from chloroform/hexane to give **4**, yield: 0.27 g (82%), mp 120–121°C; ir $\nu_{max}$: 3500–3200 (OH), 3365 (NH), 1730 (CO), 1640 (CONH) $cm^{-1}$. *Anal.* calcd. for $C_{15}H_{23}N_2O_6$ (Mol. Wt. 327.4): C 55.04, H 7.08, N 8.56; found: C 55.20, H 7.09, N 8.54.

*Methyl 2-acetamino-3-(1-oxyl-2,2,5,5-tetramethyl-3-pyrrolin-3-yl)propionate (5)*

A suspension of the monomethyl ester (**4**) (0.327 g, 1.0 mmol) in water (10 mL) was refluxed for 3 h, then extracted with chloroform (3 × 10 mL). The organic phase was dried, evaporated, and crystallized from ether/hexane to give the pure **5**, yield: 0.22 g (78%), mp 87–88°C; ir $\nu_{max}$: 3250 (NH), 1740 (CO), 1635 (CONH) $cm^{-1}$. *Anal.* calcd. for $C_{14}H_{23}N_2O_4$ (Mol. Wt. 283.4): C 59.35, H 8.18, N 9.89; found: C 59.41, H 8.08, N 9.92.

*2-Acetamino-3-(1-oxyl-2,2,5,5-tetramethyl-3-pyrrolin-3-yl) propionic acid (6)*

A solution of sodium hydroxide (2 *N*, 5 mL, 10.0 mmol) was added to a solution of **5** or **10** (5.0 mmol) in ethanol (15 mL) and left at room temperature overnight, then diluted with water (20 mL) and extracted with chloroform (3 × 10 mL). The aqueous phase was acidified with 1 *N* hydrochloric acid to pH 3, saturated with sodium chloride, and extracted with chloroform (3 × 10 mL), dried, evaporated to dryness, and crystallized from chlorform/methanol/ether to give **6**, yield: 0.99 g (74%) from **5**, and 0.96 g (72%) from **10**; mp in both cases 174–176°C; ir $\nu_{max}$: 3330 (NH), 1700 (CO), 1620 (CONH) $cm^{-1}$. *Anal.* calcd. for $C_{13}H_{21}N_2O_4$ (Mol. Wt. 269.3): C 57.98, H 7.86, N 10.40; found: C 57.81, H 7.66, N 10.65.

*Ethyl 2-amino-3-(1-oxyl-2,2,5,5-tetramethyl-3-pyrrolin-3-yl)-propionate (9) and its tosylate salt*

A solution of sodium hydroxide (2 *N*, 18 mL, 36.0 mmol) was added to a methylene chloride solution (15 mL) of **7** (4.0 g, 15.0 mmol), tetrabutylammonium hydrogen sulfate (TBAH) (6.1 g, 18.0 mmol), and **1***a* (4.2 g, 18.0 mmol) and stirred at room temperature for 2 days. The organic layer was separated, washed with water, dried, and evaporated to dryness to remove the residue quaternary bromide. The residue was taken up in ether and filtered. The filtrate was evaporated to dryness. The aqueous citric acid (10%, 30 mL) was added to the tetrahydrofuran (20 mL) solution of the Schiff's base **8** and stirred overnight. The reaction mixture was diluted with water (30 mL) and extracted with chloroform (2 × 25 mL) to remove the benzophenone. The aqueous phase was basified with 2 *N* sodium hydroxide solution to pH 8, extracted with chloroform (3 × 20 mL), dried, and evaporated to dryness to give **9** as a red oil, yield: 2.9 g (75%); ir $\nu_{max}$: 3400–3200 ($NH_2$), 1730 (CO) $cm^{-1}$. *Anal.* calcd. for $C_{13}H_{23}N_2O_3$ (Mol. Wt. 255.4): C 61.15, H 9.08, N 10.97; found: C 61.05, H 9.10, N 11.16.

*The tosylate salt of 9*

A solution of *p*-toluenesulfonic acid monohydrate (0.95 g, 5.0 mmol) was added to the solution of **9** (1.27 g, 5.0 mmol) in dry acetone (10 mL) and diluted with ether until the crystallization started. The crude product was recrystallized from chloroform/ether/hexane to give the pure salt of **9**, yield: 1.8 g (84%), mp 145–146°C; ir $\nu_{max}$: 1750 (CO) $cm^{-1}$. *Anal.* calcd. for $C_{20}H_{31}N_2O_6S$ (Mol. Wt. 427.5): C 56.19, H 7.31, N 6.55; found: C 56.07, H 7.02, N 6.44.

*Ethyl 2-acetamino-3-(1-oxyl-2,2,5,5-tetramethyl-3-pyrrolin-3-yl)propionate (10)*

To a stirred solution of **9** (1.27 g, 5.0 mmol) in dry tetrahydrofuran (15 mL) a solution of 1-acetylimidazole (0.55 g, 5.0 mmol) was added in dry tetrahydrofuran (10 mL). The reaction mixture was allowed to stay for 2 h, then evaporated to dryness, and taken up in ethyl acetate. The ethyl acetate solution was extracted with 1 *N* hydrochloric acid solution, the organic phase was washed with saturated sodium hydrogen carbonate solution (5%), dried, evaporated to dryness, and the solid residue was crystallized from ether/hexane to give **10**, yield: 1.2 g (80%); mp 87–88°C; ir $\nu_{max}$: 3240 (NH), 1745 (CO), 1640 (CONH) $cm^{-1}$. *Anal.* calcd. for $C_{15}H_{25}N_2O_4$ (Mol. Wt. 297.4): C 60.59, H 8.47, N 9.42; found: C 60.54, H 7.99, N 9.61.

*Diethyl 2-[(1-oxyl-2,2,5,5-tetramethyl-3-pyrrolin-3-yl)methyl]-malonate (11) and diethyl bis-2-[(1-oxyl-2,2,5,5-tetramethyl-3-pyrrolin-3-yl)methyl]malonate (12)*

A solution of diethyl malonate (1.6 g, 10.0 mmol) in dry ethanol (10 mL) was added to a freshly prepared solution of sodium ethoxide (1 *M*, 10 mL, 10.0 mmol) and stirred for 30 min. Then a solution of **1***b* (2.48 g, 10.0 mmol) in dry ethanol (25 mL) was added to the reaction mixture and heated at 60°C for 2 h. The reaction mixture was diluted with water (30 mL) and extracted with chloroform (3 × 30 mL). The chloroform extract was washed with water, dried, and evaporated to dryness to give a red oil. The oil was suspended in ether (10 mL) and the precipitated crystals were filtered to give as a by-product the bis-alkylated malonate (**12**), yield: 0.9 g (19%), mp 189–190°C; ir $\nu_{max}$: 1720 (CO) $cm^{-1}$; esr ($CHCl_3$): 5 lines, $a_N$ = 14.9 G. *Anal.* calcd. for $C_{25}H_{40}N_2O_6$ (Mol. Wt. 464.6): C 64.63, H 8.68, N 6.03; found: C 64.79, H 8.41, N 6.07.

The filtrate was evaporated and subjected to column chromatography on silica gel with tetrachloromethane/ethyl acetate (10:1) to give the monoalkylated product (**11**) as a red oil, yield: 1.6 g (51%); ir $\nu_{max}$: 1735 (CO) $cm^{-1}$. *Anal.* calcd. for $C_{16}H_{26}NO_5$ (Mol. Wt. 312.4): C 61.52, H 8.39, N 4.48; found: C 61.25, H 8.15, N 4.89.

*Monoethyl ester of 2-[(1-oxyl-2,2,5,5-tetramethyl-3-pyrrolin-3-yl)methyl] malonic acid (13)*

A solution of potassium hydroxide (0.56 g, 10.0 mmol) was

added in ethanol (10 mL) to a stirred solution of **11** (3.12 g, 10.0 mmol) in absolute ethanol (20 mL) and refluxed for 2 h. The reaction mixture was evaporated *in vacuo* to dryness and dissolved in water (30 mL). The aqueous solution was extracted with chloroform (2 × 20 mL). The aqueous phase was acidified with 1 *N* hydrochloric acid to pH 3 and extracted again with chloroform (3 × 10 mL), dried, and evaporated to dryness. The solid residue was crystallized from ether/hexane to give the pure **13**, yield: 2.2 g (77%), mp 110–111°C; ir $\nu_{max}$: 3200–2600 (OH), 1730 (CO) $cm^{-1}$. *Anal.* calcd. for $C_{14}H_{22}NO_5$ (Mol. Wt. 284.4): C 59.14, H 7.80, N 4.93; found: C 59.32, H 7.46, N 5.02.

*Ethyl 2-benzyloxycarbonylamino-3-(1-oxyl-2,2,5,5-tetramethyl-3-pyrrolin-3-yl)propionate (**14**)*

Triethylamine (0.5 g, 5.0 mmol) and diphenylphosphoryl azide (1.38 g, 5.0 mmol) were added to a solution of **13** (1.42 g, 5.0 mmol) in dry benzene (30 mL) and refluxed for 1 h, then benzyl alcohol (0.7 g, 7.0 mmol) was added to the reaction mixture and refluxed for 2 days. The reaction mixture was evaporated to dryness *in vacuo* and chromatographed on a silica gel column with benzene/tetrahydrofuran (10:1) to give **14**, yield: 1.0 g (51%), mp 61–62°C; ir $\nu_{max}$: 3310 (NH), 1740 (CO), 1690 (CONH) $cm^{-1}$; ms, *m/e*: $M^+$ 389(31), $M^+ + 1$ 390(8), 316(27), 224(14), 223(20), 135(19), 123(12), 91(100). *Anal.* calcd. for $C_{21}H_{29}N_2O_5$ (Mol. Wt. 389.5): C 64.76, H 7.51, N 7.14; found: C 64.74, H 7.41, N 7.48.

*Preparation of **14** from **9***

Triethylamine (0.1 g, 1.0 mmol) and benzylchloroformate (0.170 g, 1.0 mmol) were added to the solution of **9** (0.255 g, 1.0 mmol) in dry tetrahydrofuran (10 mL) and stirred at room temperature for 1 h. The reaction mixture was diluted with water (20 mL) and extracted with ethyl acetate (3 × 10 mL). The ethyl acetate phase was washed with 1 *N* hydrochloric acid, saturated sodium bicarbonate, saturated sodium chloride, dried, and evaporated to dryness *in vacuo*. The residue was crystallized from chloroform/hexane to give **14**, yield: 0.3 g (77%), mp 61–62°C.

## Acknowledgements

This work was supported in part by the Hungarian Academy of Sciences, Grant No 134/79/II. The authors are indebted to Dr. J. Belágyi for the esr spectra and for the mass spectra to Dr. J. Jerkovich, Institute for Drug Research, Budapest, and to Mrs. M. Ott for the microanalyses.

1. H. O. Hankovszky, K. Hideg, and L. Lex. Synthesis, 147 (1981).
2. G. I. Likhtenshtein. Method Spinovykh Metok v. Molekularnoi Biologii. Nauka, Moscow. 1973 (In Russian). Translation: G. I. Likhtenshtein. Spin labeling methods in molecular biology. Wiley–Interscience, New York. 1976.
3. L. J. Berliner (*Editor*). Spin labeling, theory and application. Vols. I and II. Academic Press, New York. 1976 and 1979.
4. K. Hideg, L. Lex, H. O. Hankovszky, and J. Tigyi, Synthesis, 914 (1978).
5. H. O. Hankovszky, K. Hideg, L. Lex, and J. Tigyi. Synthesis, 530 (1979).
6. A. Rassat and P. Rey. Bull. Soc. Chim. Fr. 815 (1967).
7. R. J. Weinkam and E. C. Jorgensen. J. Am. Chem. Soc. **93**, 7028 (1971).
8. J. D. Morrisett. *In* Spin labeling, theory and application. Vol. I. *Edited by* L. J. Berliner. Academic Press, New York. 1976. Chapt. 8. p. 331.
9. H. O. Hankovszky, K. Hideg, and L. Lex. Synthesis, 914 (1980).
10. M. J. O'Donnell, J. M. Boniece, and S. E. Earp. Tetrahedron Lett. 2641 (1978).
11. S. Yamada, T. Oguri, and T. Shioiri. Chem. Commun. 136 (1976).
12. S. Yamada, K. Ninomiya, and T. Shioiri. Tetrahedron Lett. 2343 (1973).

Can. J. Chem. Downloaded from www.nrcresearchpress.com by 210.87.254.40 on 09/06/12
For personal use only.

# Nitroxide destruction and flavin-photosensitized damage in inner mitochondrial membranes

ROLF JOACHIM MEHLHORN AND LESTER PACKER

*Membrane Bioenergetics Group, Lawrence Berkeley Laboratory and Department of Physiology–Anatomy, University of California, Berkeley, CA 94720, U.S.A.*

Received August 10, 1981

ROLF JOACHIM MEHLHORN and LESTER PACKER. Can. J. Chem. **60**, 1452 (1982).

Nitroxide free radicals lost their paramagnetic absorption spectrum when they were illuminated with visible light in aged but not freshly isolated inner mitochondrial membranes (SMP's). The action spectrum of spin loss rates coincided with a flavin absorption spectrum. Spin loss consisted of one-electron reduction and "destruction", the latter being defined as spin loss that cannot be reversed by ferricyanide oxidation. By placing SMP's in gas permeable tubing and illuminating alternately under nitrogen and air, it was possible to discriminate qualitatively between spin reduction and destruction. Aerobic spin loss consisted entirely of destruction. When aged SMP's were centrifuged, spin loss was observed in supernatants but not pellets. Flavin fluorescence was observed in the supernatants, suggesting that free flavins catalyzed spin loss. However, addition of exogenous flavins to fresh SMP's did not cause spin loss; hence some other factor was required to cause nitroxide destruction. This factor accumulates during either aerobic or anaerobic aging of SMP's and may be present in mitochondria. Supernatants of aged SMP's, when added to freshly isolated SMP's, induced rapid nitroxide destruction, slightly accelerated photodamage to succinate oxidase, and considerably increased photo-induced lipid peroxidation.

ROLF JOACHIM MEHLHORN et LESTER PACKER. Can. J. Chem. **60**, 1452 (1982).

Les spectres d'absorbtion paramagnétique des radicaux libres du type nitroxyde disparaissent lorsqu'on les illumine avec de la lumière visible dans des membranes mitochondriales internes (SMP) qui ont veilli; ce n'est pas le cas avec des membranes fraîchement isolées. Le taux de disparition des spin concide avec le spectre d'absorption d'une flavine. La perte de spin correspond à une réduction par un électron et une "destruction"; on définit la "destruction" comme une perte de spin qui ne peut être renversée par une oxydation au ferrocyanure. Si on place des SMP dans un tube perméable aux gaz et si on les illumine alternativement sous azote et à l'air, il est possible de distinguer qualitativement entre une réduction de spin et une "destruction". La perte de spin aérobique est uniquement une destruction. Lorsqu'on soumet des SMP qui ont vieilli à la centrifugation, on observe une perte de spin avec le liquide qui surnageant mais pas avec le précipité. Dans le liquide qui surnage, on observe la fluorescence de la flavine, ceci suggère que les flavines libres exogènes à des SMP fraîchement isolées ne provoque aucune perte de spin; on doit donc faire appel à d'autres facteurs pour expliquer la destruction du nitroxyde. Ces facteurs s'accumulent pendant le vieillissement aérobique ou anaérobique des SMP et peuvent être présents dans la mitochondrie. L'addition de liquide surnageant des SMP vieillies, à des SMP fraîchemenet isolées, induit une destruction rapide du nitroxyde, accélère légèrement le dommage photochimique à l'oxydase du succinate et augmente considérablement la peroxydation photo-induite des lipides.

(Traduit par le journal)

## Introduction

The destructive effect of visible light on tissues, cells, and organelles has been studied extensively (1). Blue light is particularly damaging in many cases, suggesting flavin involvement. Previously, this laboratory reported on visible light effects in mitochondria (2, 3). Progressive functional inactivation was observed, beginning with the loss of ATP synthesis, and followed by inactivation of dehydrogenase flavoenzymes. Functional damage was accompanied by loss of flavins, sulfhydryl groups, and lipid peroxidation. Although light damage was enhanced by exogenous flavins, covalently bound flavins were destroyed at rates comparable to those for dissociable flavins. Furthermore, the inactivation required oxygen but it was unclear whether this requirement was merely to maintain the flavins in their light absorbing oxidized form or whether active oxygen species were directly responsible for damage. Failure to achieve protection with SOD, singlet oxygen scavengers, hydroxyl radical quenchers, and antioxidants, suggested a minor role if any for these potentially destructive species except perhaps at the active sites of flavoenzymes (2).[1]

Two aspects of the damage process interested us particularly because of the possibility of further studies using nitroxide spin probes. These were (*i*) the possibility that damage was mediated by free radicals that might have been generated by the excited flavins and (*ii*) the role of bound vs. free flavins. Nitroxides are potentially useful to study oxygen involvement in free radical reactions because they are themselves free radicals, N—O•, which resemble ground state oxygen, •O—O•, and

[1]Abbreviations: SMP, submitochondrial preparations; EDTA, ethylene diamine tetraacetic acid; TBA, thiobarbituric acid; TEMPOL, 2,2,6,6-tetramethyl-4-piperidinol-1-oxyl (see Materials and Methods for other nitroxide structures); DMPO, 5,5-dimethyl-1-pyrroline-*N*-oxide; POBN, 2-(4-pyridyl 1-oxide)-*N*-*tert*-butylnitrone; PRETOL, 2,2,6,6-tetramethyl-4-piperidinol; SOD, superoxide dismutase.

0008-4042/82/121452-11$01.00/0

©1982 National Research Council of Canada/Conseil national de recherches du Canada

Can. J. Chem. Downloaded from www.nrcresearchpress.com by 210.87.254.40 on 09/06/12
For personal use only.

Can. J. Chem. Downloaded from www.nrcresearchpress.com by 210.87.254.40 on 09/06/12
For personal use only.

which may thus compete with oxygen in free radical addition reactions. However, $O_2$ adducts are reactive peroxy radicals which may participate in chain reactions, whereas nitroxide spin pairing products are expected to be relatively unreactive. A number of stable nitroxide adducts have been described (4, 5). Nitroxides also have the potential to serve as free radical detectors in another sense, since they should readily undergo one-electron or hydrogen transfer reactions with other free radical molecules. One-electron transfer reactions of nitroxides have been demonstrated with reduced flavins (6), and with electron transport components of mitochondria (7). However, since reduction of nitroxides can occur by two-electron reductants like ascorbate, loss of nitroxide paramagnetism as assayed by electron spin resonance is not sufficient to establish free radical involvement in an interaction per se, and additional analyses are required to establish such involvement.

In other detection schemes, nitroxide precursors and derivatives have been used to detect active oxygen species, including superoxide radicals (8, 9) and singlet oxygen (10). These detection schemes exploit oxidation of the nitroxide derivatives to elicit a paramagnetic signal.

Mechanisms and biological effects of photosensitized oxidation were recently reviewed (11). The photooxidation of amino acids by flavins in particular has been studied extensively (e.g., 12, 13). Analysis of the photoinactivation of a flavoenzyme, porcine D-amino acid oxidase, provided evidence of localized destruction of amino acid residues at the flavin binding site (14). The light mediated reduction of many flavoproteins appears to be catalyzed by traces of free flavins, i.e., aqueous photoreductants generally do not appear to have direct access to enzyme-bound flavins (15).

In this report, the effect of illumination on nitroxides in mitochondrial membrane suspensions is described and correlated with photodamage to succinate oxidase of the respiratory chain and with light induced lipid peroxidation.

## Materials and methods

*Preparations*

Rat liver mitochondria were isolated and suspended in 200 m*M* mannitol, 70 m*M* sucrose, and 1 m*M* Tris, pH 7.4. They were washed twice in the same medium and finally resuspended in 30 m*M* potassium phosphate, pH 7.4. Submitochondrial preparations (SMP's) were prepared by intermittent sonication of the mitochondria with a Branson 350 cell disruptor at a power setting of 5 for a cumulative time of 2 minutes. Undisrupted mitochondria were removed by centrifugation at 8,500 × g for 10 min and the SMP's collected by centrifugation at 100 000 × g for 30 min. They were resuspended in 30 m*M* potassium phosphate, pH 7.4, at protein concentrations indicated in the figures.

*Aging procedure*

SMP's were placed in 25 mL Erlenmeyer flasks, and the flasks were sheathed with aluminum foil and closed with a rubber stopper to prevent evaporation. In one experiment, flasks were flushed for 30 min with argon on an ice bath before being stoppered. The flasks were then placed on a shaking water bath at 37°C for the time periods indicated in the figures.

Nitroxides, some reduced derivatives and a precursor are shown below:

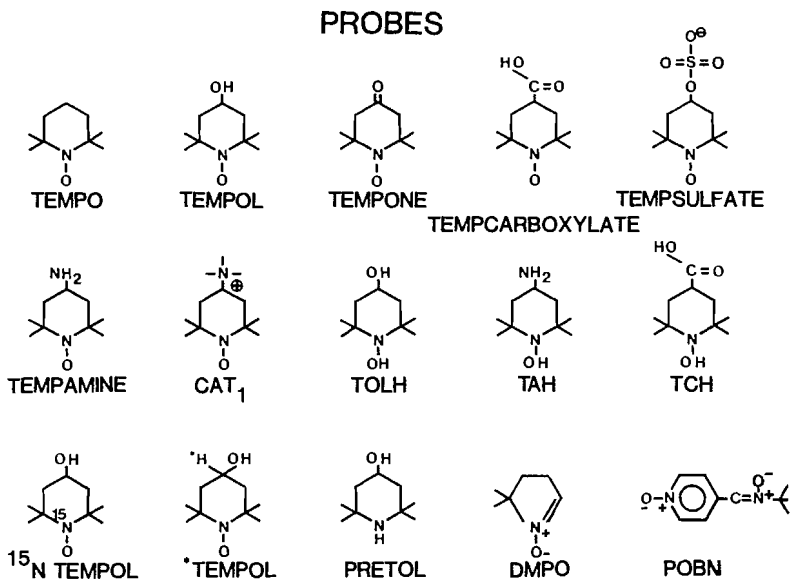

Can. J. Chem. Downloaded from www.nrcresearchpress.com by 210.87.254.40 on 09/06/12
For personal use only.

The designation, TEMPR, refers to the structure 4-*R*-2,2,6,6-tetramethyl piperidine-1-oxyl (except for TEMPO).

TEMPOL, TEMPONE, TEMPAMINE, PRETOL, DMPO, and POBN were purchased from Aldrich Chemical Co. TEMPCARBOXYLATE (16) and $CAT_1$ (17) were synthesized. TEMPO, TEMPOL, and $^{15}N$ TEMPONE were generous gifts from A. D. Keith. $^{15}N$ TEMPOL was prepared by reducing $^{15}N$ TEMPONE with sodium borohydride and extracting the product into diethyl ether.

The reduced nitroxides TOLH, TAH, and TCH were prepared by treating TEMPOL, TEMPAMINE, and TEMPCARBOXYLATE, respectively, with ten equivalents of sodium ascorbate at pH 7, adjusting the pH to 7, 11, and 3, respectively, and extracting the products into diethyl ether. The ether extracts were washed once with phosphate buffer solutions at pH 7, 11, and 3 as above, dried over $Na_2SO_4$, and the solvent was removed under reduced pressure.

TEMPSULFATE was prepared as follows: 3 g of TEMPOL and 4.45 g of *N*,*N*-diisopropyl-ethylamine were taken up in 100 mL of acetone. The solution was stirred rapidly on an ice bath and 1.76 g of chlorosulfonic acid were added over a period of 10 min. The reaction mixture was removed from the ice bath, allowed to stand at room temperature for 2 hours, treated with 1.4 g of NaOH in 20 mL of water, and then the amine and unreacted TEMPOL were extracted exhaustively with diethyl ether. The water fraction was dried under an air stream and used without further purification.

*Electron spin resonance experiments*

Stock solutions of the probes in water were adjusted to pH 7.0 with HCl or NaOH. In a 0.6 mL test tube, 35 microliters of SMP's were mixed with 0.35 microliter of probe. Mixing was effected with hand agitation. Except for the action spectrum experiment, labeled samples were transferred to gas-permeable tubing (18) with a 100 microliter syringe, and then the flexible tubing was bent in the middle and inserted in a thin-walled quartz tube open at both ends. The pressure of the tubing on the walls of the quartz housing tube was sufficient to immobilize the sample within the esr cavity even in the presence of a nitrogen stream. The action spectrum was obtained with samples in 50 μL glass capillaries sealed at one end with a propane torch. The esr experiments were conducted in a Varian E109E spectrometer at a power setting of 10 mW and a modulation amplitude of 1.25 gauss at a frequency of 100 kHz. A typical gain setting for a kinetic scan was $3.2 \times 10^4$.

*Illumination*

Samples were illuminated within the microwave cavity of the esr instrument with a 100 W projector and a glass heat filter. The light intensity at the sample was 150 mW/cm². The intensity was determined outside the esr instrument with a Hewlett–Packard 8330A radiant flux meter and a 8334A detector and subsequently determined within the instrument by comparing FMN-mediated oxidation rates of TOLH inside and outside the cavity under nonsaturating conditions. The action spectrum of spin loss rates was determined using Oriel interference filters of 10 nm band width (G-522-11) and normalizing spin loss rates with respect to light intensities transmitted by the filters as measured with the radiant flux meter. Except where white light is indicated in the figure legends, all sample illumination in the esr instrument was conducted with an Oriel broadband interference filter with a peak position at 450 nm and a 50 nm bandwidth. With this filter, FMN-mediated TOLH oxidation occurred at 1/3 the rate observed with white light. For the ferricyanide-reoxidation experiment, SMP's in an Erlenmeyer flask at room temperature were illuminated with the same light source but the light was passed through a Corning glass #3389 400 nm cutoff filter. The photodamage experiment was conducted at 10°C in an apparatus that was described previously (3), providing an intensity of 300 mW/cm² with the Corning #3389 filter.

TBA reactive materials, a measure of lipid peroxidation, were assayed according to published methods, with the inclusion of 0.01% butylated hydroxytoluene (BHT) in the reaction mixture prior to heating (19). Total flavins were identified and quantitated fluorometrically with a Perkin Elmer MPF 44A spectrofluorometer at an excitation wavelength of 375 nm and bandwidth of 5 nm. Emission spectra were recorded from 390 nm to 620 nm and flavins were identified by comparison with fluorescence spectra of defined flavins in buffer. No attempt was made to discriminate between different flavin nucleotides or their hydrolysis products.

Succinate oxidation by the mitochondrial respiratory chain was assayed in a Rank oxygen electrode (Rank Brothers, Bottisham, Cambridge, England). Typically protein concentrations of 3 mg/mL were used in a reaction medium of 30 m*M* potassium phosphate, pH 7.4, with 10 m*M* sodium succinate.

## Results

*Description of the spin loss phenomenon*

A spectrum of TEMPOL in a suspension of SMP's is shown in the inset of Fig. 1. The effect of visible light on this spectrum is to cause a decrease of the intensity of the spectrum, but only if the membranes have been allowed to incubate prior to illumination. As shown in Fig. 1, the onset of spin loss with illumination as well as its cessation in the dark are virtually instantaneous.

*Action spectrum*

Spin loss rates at different wavelengths of light are shown in Fig. 2. Because of the narrow bandwidths of the interference filters used for these experiments, effective light intensities were low and about 15 min of illumination were required to obtain measurable spin loss rates at some wavelengths. An absorption spectrum of flavin mononucleotide (FMN) is shown for comparison.

*Direct interactions between flavins and nitroxides*

The action spectrum of spin loss rates implicated flavins in the spin loss process observed in aged SMP's. Therefore, several flavins, i.e., riboflavin, FMN, and FAD, were tested to study direct interactions of flavins with nitroxides in the light, if any. There was no interaction between flavins and TEMPOL in aerobic solution as assayed by esr. In anaerobic solution, TEMPOL signal loss was observed, but at a considerably slower rate than that observed for aerobic, aged SMP's. There was no effect of TEMPOL on FMN fluorescence at TEMPOL concentrations that were tested (< 1 m*M*). Flavins photooxidize the reduced nitroxides TOLH and TAH. The photooxidation of TCH was also observed, but at a ten-fold lower rate than that of TOLH. To study the interaction between flavin radicals and nitroxides, FMN, 30 μ*M* $^{14}N$ TOLH as an electron donor, and 30 μ*M* $^{15}N$ TEMPOL, as

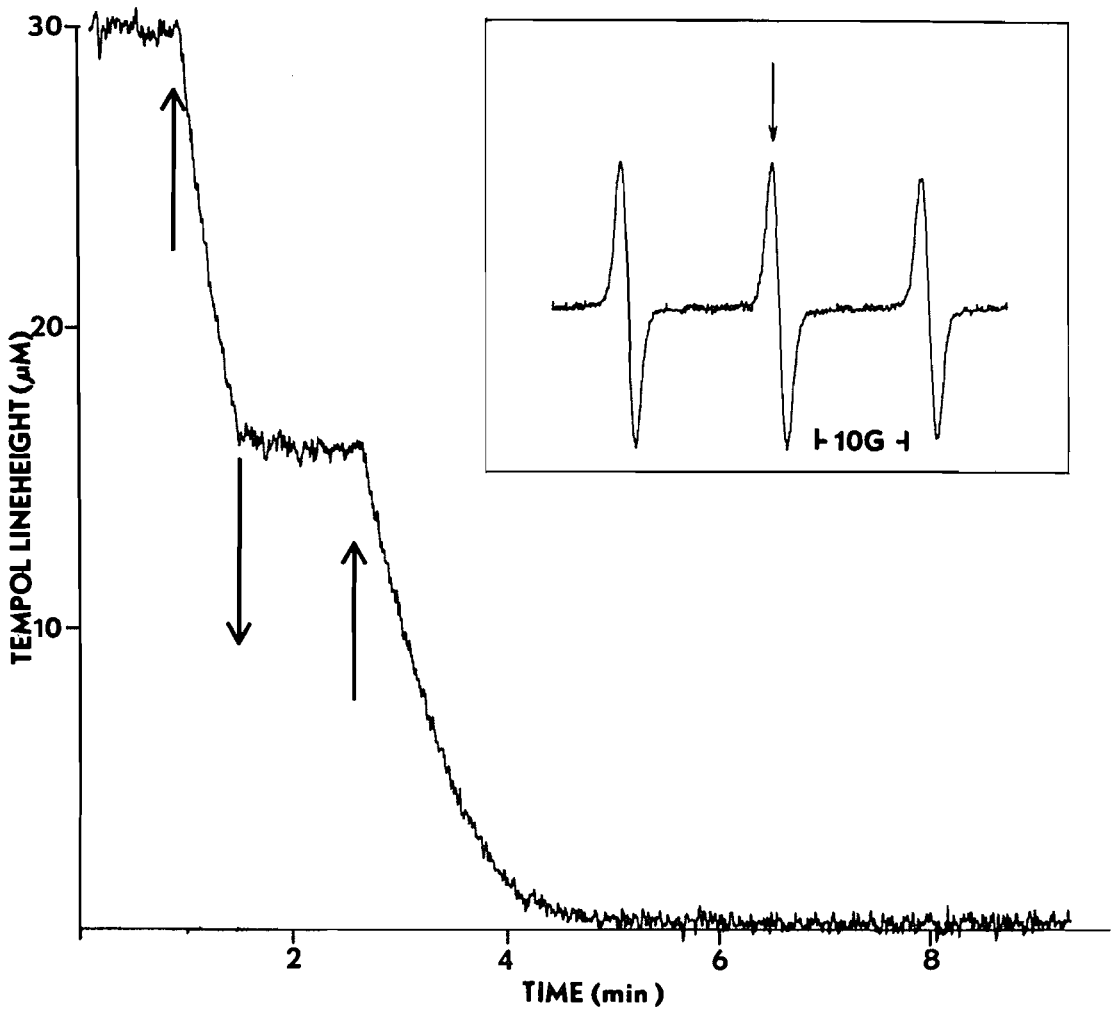


FIG. 1. The line height of TEMPOL expressed in terms of known TEMPOL concentration in buffer as a function of illumination. Inset, esr spectrum of TEMPOL in SMP; arrow points to the field position where the line height was monitored. Upward arrows denote light on, downward light off. Protein concentration 12 mg/mL. SMP incubated for three hours at 36°C prior to white light illumination.

an electron acceptor, were illuminated anaerobically. The nitroxides having $^{14}N$ and $^{15}N$ paramagnetic centers give rise to distinct spectral lines; hence, reduction and oxidation rates can be monitored simultaneously. Upon illumination, there was a decrease in the $^{15}N$ TEMPOL signal and a simultaneous increase in the $^{14}N$ TEMPOL signal at the same rates. Upon admitting air to the sample under continuous illumination, both spectra increased to the original line height seen for 30 μ*M* $^{15}N$ TEMPOL.

*Comparison of TEMPOL reduction and other processes of spin loss*

One-electron reduction of TEMPOL yields the nonparamagnetic hydroxylamine TOLH. Reoxidation of TOLH to TEMPOL is rapidly effected by ferricyanide. Thus, when 30 μmol of TOLH is treated with 2 m*M* potassium ferricyanide at pH 7.4, a spin signal rapidly appears, increasing to a maximum within two minutes at 25°C. The final line height corresponds to 30μmol of a fresh TEMPOL solution in the presence of 2 m*M* ferricyanide. Accordingly, ferricyanide oxidation was used in SMP's after illumination with TEMPOL to determine the fraction of spin loss due to reduction. The remaining fraction of spin loss is operationally defined as nitroxide "destruction." If ferricyanide is added to SMP's during illumination, it effectively inhibits light-driven spin loss, i.e. spin loss rates progressively decrease with increasing ferricyanide concentrations such that in the presence of 7

Can. J. Chem. Downloaded from www.nrcresearchpress.com by 210.87.254.40 on 09/06/12
For personal use only.

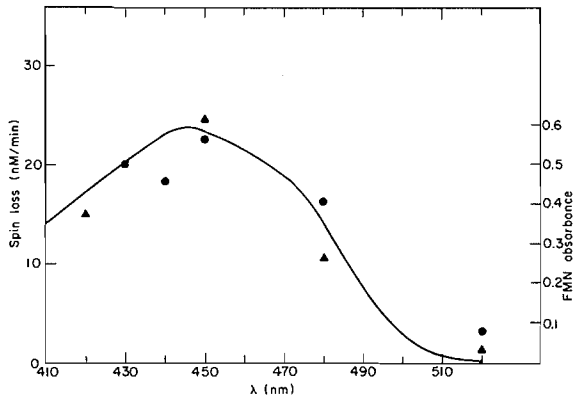


FIG. 2. Action spectrum of spin loss rates. SMP at 29 mg/mL protein, were incubated for 1.5 h at 37°C prior to illumination. Two experiments are denoted by ● and ▲. The solid line shows an absorption spectrum of 40 μ*M* FMN, the absorbance units are arbitrary.

μ*M* ferricyanide, the spin loss rate is half of what is observed in the absence of ferricyanide. Therefore, reoxidation of any TOLH produced during illumination was carried out in post-illumination experiments.

To compare reduction and destruction rates, illumination of 30μ*M* TEMPOL and SMP's containing 10 mg/mL protein was conducted in an aerobic flask. At one-minute time intervals, 70 μL samples were withdrawn for esr analysis of TEMPOL line heights; 35 μL were examined directly and the remaining 35 μL were treated with 2 m*M* ferricyanide. The signal heights were identical for the two sets of samples. A similar experiment was conducted with 100 μmol TOLH and SMP's. In this case, there was a light-driven appearance of TEMPOL line heights in the samples. The ferricyanide treated samples showed that no spin destruction occurred initially. Spin destruction became apparent only after TOLH had been converted to TEMPOL during the illumination. When the TEMPOL concentration had reached 30 μ*M*, the destruction rate was comparable to what was observed for the sample containing only TEMPOL initially.

To study the effect of oxygen on spin loss, experiments were conducted in gas permeable tubing surrounded by air or nitrogen. Figure 3 shows that aerobic illumination of TEMPOL and SMP's causes less rapid spin loss than is observed under nitrogen. Upon admitting air into the anaerobic sample, a partial recovery of the spin signal is seen which gives way to complete signal loss upon prolonged illumination. This result is similar to aerobic illumination of TOLH, where transient and partial oxidation is observed under illumination. No oxidation of TOLH is seen under nitrogen. A comparison of initial rates seen for aerobic TEMPOL destruction and TOLH oxidation shows that destruction occurs at a rate comparable to oxidation.

Iron had a marked effect upon spin loss rates. As indicated earlier, ferricyanide was inhibitory at low concentrations. On the other hand, ferric chloride accelerated spin loss about two-fold at a concentration of 10 μ*M*. Considerable variability was seen in spin loss rates among different membrane preparations that were studied, possibly due to fluctuations in the concentrations and binding states of traces of iron among the different preparations.

*The role of membranes in spin loss*

To define the source of light-induced spin loss, SMP's that had been incubated in the dark for three hours at 37°C were centrifuged and spin destruction rates, i.e., aerobic rates of spin loss, were measured in the pellet, supernatant, and in pellets that had been resuspended in their supernatants. The maximum spin loss rate was observed in the supernatant, the intermediate rate in the resuspended membranes, and the minimum rate in the pellet. Washed pellets had no spin loss activity.

The effect of charged groups on the nitroxides is shown in Table 1. The positively charged nitroxides exhibit significantly lower rates of spin loss and the positively charged hydroxylamine, TAH, a significantly higher photooxidation rate than the other nitroxides. The most hydrophobic nitroxide, TEMPO, exhibits the most rapid spin loss rate. The rates of photooxidation of the reduced nitroxides, i.e., TAH > TOLH > TCH, are the same as observed for the direct interaction between flavins and reduced nitroxides. However, whereas TCH is photooxidized by FMN or riboflavin, only spin loss of a trace of TEMPCARBOXYLATE in the sample is observed with SMP's.

*Flavin fluorescence and spin loss rates*

Figure 4 shows the aerobic spin loss rates and the appearance of flavin fluorescence in the supernatants of centrifuged SMP's as a function of time of incubation of the SMP's at 37°C in the dark. At two temperatures the two parameters increase in parallel with time up to about three hours of incubation. Longer incubation does not substantially increase flavin fluorescence or spin loss rates.

*The effect of exogenous flavins on spin loss rates*

SMP's that had been incubated in the dark at 37°C for various time periods were treated with FMN to study the effect of exogenous flavins on spin loss. As shown in Fig. 5, freshly isolated

Can. J. Chem. Downloaded from www.nrcresearchpress.com by 210.87.254.40 on 09/06/12
For personal use only.

Can. J. Chem. Downloaded from www.nrcresearchpress.com by 210.87.254.40 on 09/06/12
For personal use only.

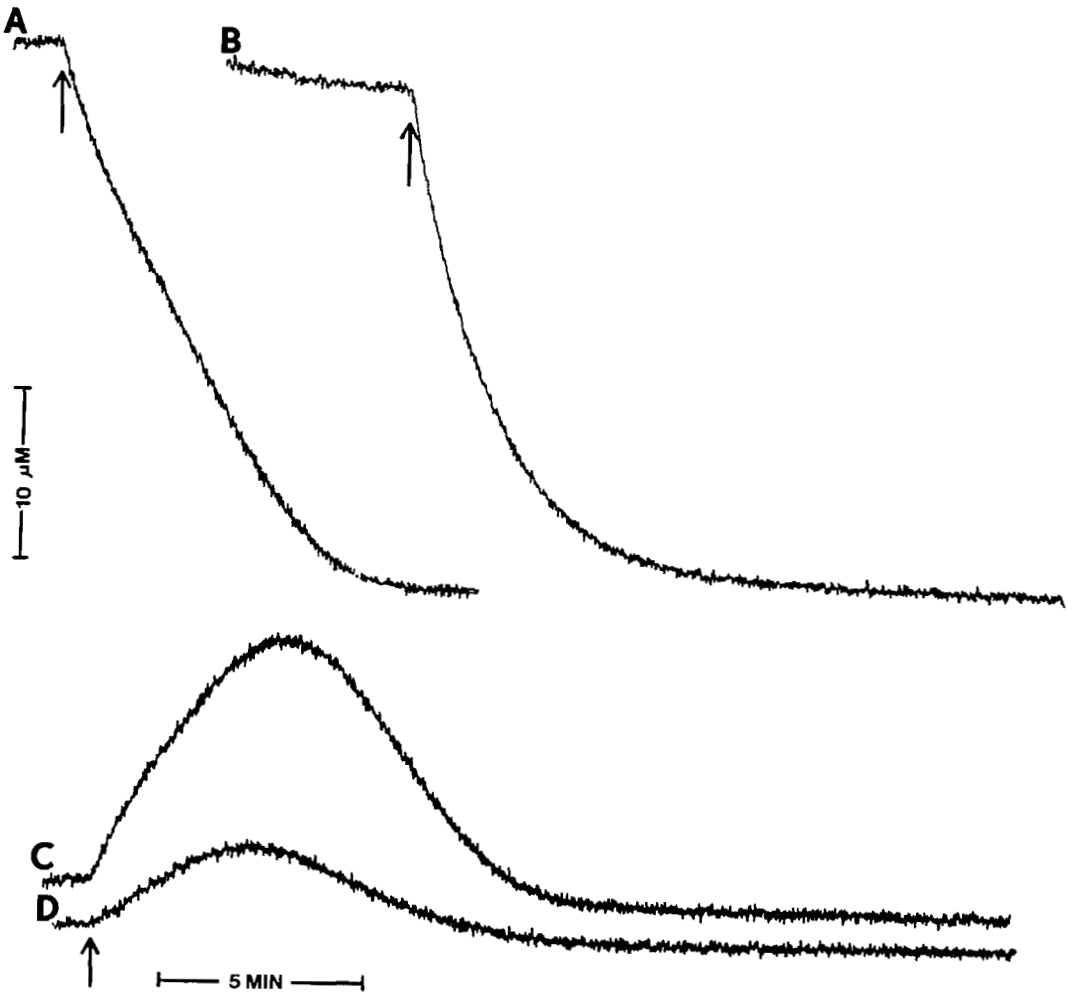


FIG. 3. Aerobic and anaerobic esr line height changes of TEMPOL in illuminated SMP's. Conditions as in Fig. 1. A, 30 μ*M* TEMPOL in air; B, 30 μ*M* TEMPOL under $N_2$; C, 30 μ*M* TOLH in air; D, same sample as B, but now in air.

TABLE 1. Light-dependent aerobic spin loss and oxidation rates for different nitroxides and hydroxylamines*

| Nitroxide | Initial rate of spin loss (μmol/min) | Hydroxylamine | Initial rate of oxidation (μmol/min) |
|---|---|---|---|
| TEMPO | 32 | TOLH | 3.1 |
| TEMPOL | 16 | TAH | 12.7 |
| TEMPAMINE | 5.5 | TCH | −2.8 |
| $CAT_1$ | 3.8 | | |
| TEMPCARBOXYLATE | 11.5 | | |
| TEMPSULFATE | 9.5 | | |

*Protein, 10 mg/mL; SMP's preincubated 2 h at 37°C in the dark.

SMP's do not cause spin loss of nitroxides in the light even in the presence of added FMN. The presentation of data in this figure takes into account flavin release during dark incubation by referring to the results in Fig. 4. It is assumed that the flavins observed in the supernatant of centrifuged SMP's behave photochemically like free FMN and hence can be pooled with exogenous flavins as "free flavins." Figure 5 shows that at a fixed concentration of free flavin, there is an increase in aerobic

Can. J. Chem. Downloaded from www.nrcresearchpress.com by 210.87.254.40 on 09/06/12
For personal use only.

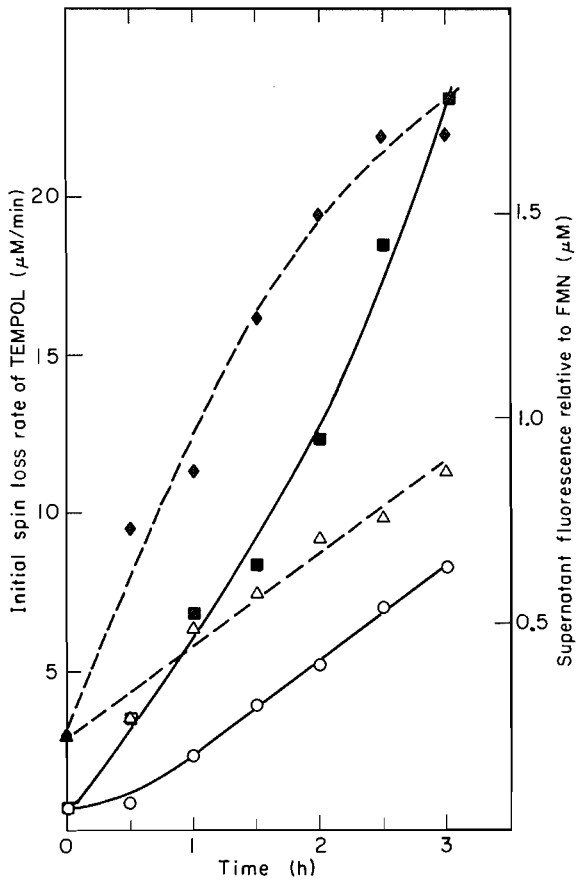


FIG. 4. SMP supernatant flavin fluorescence and aerobic TEMPOL spin loss rates as a function of incubation time in the dark. SMP protein was 7.9 mg/mL. △: supernatant flavin fluorescence at 31°C; ○: spin loss rate at 31°C; ■: supernatant flavin fluorescence at 37°C; ◆: spin loss rate at 37°C. Flavin fluorescence is expressed as FMN equivalents.

spin loss rates with increasing time of dark incubation. Similar data were obtained for SMP's that had been incubated in the dark under argon.

*Partial characterization of "destroyed" TEMPOL*

Radioactively labeled *TEMPOL was illuminated in the presence of SMP's for a sufficient period of time to completely destroy the spin. The suspension was centrifuged and essentially all of the radioactivity was found in the supernatant. Another preparation of destroyed TEMPOL was extracted into ether at alkaline pH and the ether extract was oxidized with the strong oxidant *m*-chloroperoxybenzoic acid. The product of this procedure was concentrated and taken up in phosphate buffer at pH 7.4. An esr spectrum of this sample was observed and was similar to a spectrum obtained when PRETOL was subjected to the same oxidation procedure.

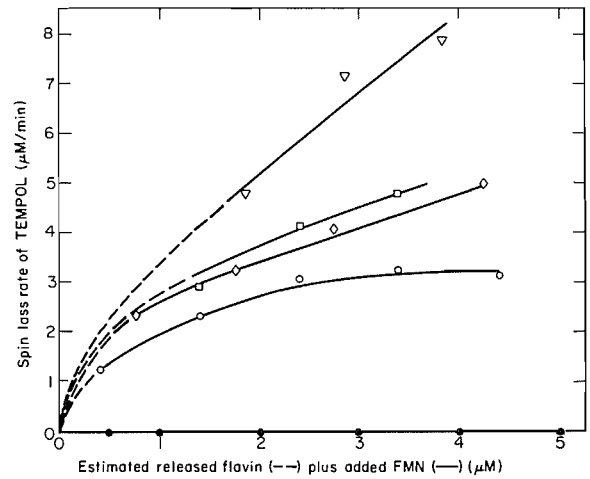


FIG. 5. Effect of dark incubation time and exogenous FMN on aerobic TEMPOL spin loss rates. SMP protein was 10 mg/mL. Dashed lines indicate that the free flavin concentration for that region of the curve was estimated from the flavin supernatant fluorescence data in Fig. 4.

*Spin trapping experiments with nitrones*

In the presence of 100 m*M* DMPO, the rate of light-induced TEMPOL destruction with SMP's decreased by a factor of two, while 100 m*M* POBN completely inhibited TEMPOL destruction. An esr spectrum was observed with DMPO both in the presence and absence of TEMPOL. This spectrum was identical to a spectrum obtained with DMPO and FMN in buffer (Fig. 6). No esr spectrum was observed for POBN and SMP's with the broadband interference filter. With white light a spectrum appeared very slowly, i.e., 30 min of illumination were required to obtain measureable coupling constants ($A_N = 15.8$ G, $A_H = 2.0$ G).

*Relation of spin loss to photodamage*

Since freshly isolated SMP's exhibited little or no spin destruction with or without exogenous flavins and since aging of SMP's caused the appearance of the spin loss phenomenon in the aqueous environment of membranes, these diverse conditions were compared in terms of photodamage to the respiratory chain and to membrane lipids. Figure 7 shows that succinate oxidase activity is progressively lost under illumination and that conditions which induce spin loss, i.e., addition of supernatant from aged SMP's, only slightly acelerate photodamage of these components of the respiratory chain. However, there is a marked correlation between lipid peroxidation and spin destruction. The supernatant treated SMP's yield considerably more TBA-reactive material during illumination than either freshly isolated control

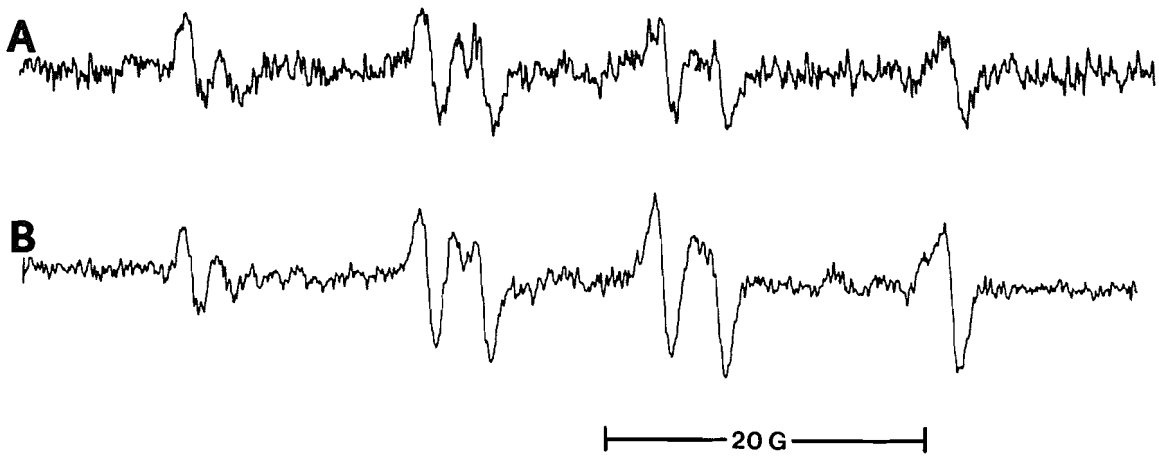


FIG. 6. A, Spectrum of DMPO adducts in SMP's. SMP protein was 10.8 mg/mL. B, Spectrum formed within two minutes of illumination of 100 m*M* DMPO and 10 μ*M* FMN in the cavity of the esr instrument.

SMP's or SMP's containing exogenous FMN at a concentration equal to "released" flavin in the supernatant. Some aging of the freshly isolated SMP's is reflected in the small spin loss rates seen in the two preparations without added supernatant.

*Photochemical model systems*

EDTA is a well-known photoreductant for flavins. Figure 8 shows that a TEMPOL signal was reduced on illuminating a mixture of FMN and EDTA. Spin loss was rapid under nitrogen and could be largely reversed when air was admitted to the sample. A sample that was illuminated aerobically suffered relatively little spin loss.

## Discussion

*Characterization of nitroxide esr signal changes*

We were interested in using nitroxides as spin traps to elucidate photodamage mechanisms in mitochondria. Intact mitochondria were not suitable for study because their electron transport activity causes one-electron reduction of nitroxides in the dark (20). Therefore, our studies were conducted with isolated inner mitochondrial membranes (SMP's) where substrates for electron transport have been removed from the membranes. Since nitroxides are quite stable in the presence of SMP's in the dark, these preparations were deemed suitable for studies of photodamage with nitroxides.

Aerobic aged SMP's illuminated with visible light cause nitroxides to lose their paramagnetism and subsequent treatment of these SMP's with the oxidant ferricyanide does not cause a reappearance of the esr signal; hence the phenomenon is not one-electron photoreduction of the nitroxides. It was also observed that the reduced nitroxides TOLH and TAH are photooxidized by aged SMP's and by flavins. By illuminating anaerobic SMP's and subsequently allowing them to become aerobic, a partial recovery of the nitroxide esr signal was observed. Hence, under anaerobic conditions, some of the nitroxides are photoreduced to hydroxylamines under illumination. The use of gas permeable tubing permits a comparison of the effects of anaerobic and aerobic illumination in the same sample and thus represents a convenient tool for discriminating qualitatively between one-electron photoreduction and other mechanisms of spin loss. When this technique was applied to a simple photochemical system, FMN and EDTA, spin loss was seen to be comprised primarily of one-electron photoreduction. This is to be expected since FMN becomes photoreduced by EDTA anaerobically (21) and since it is known that reduced flavins reduce nitroxides (6).

The action spectrum of spin loss implicated flavins as the sensitizers for nitroxide spin loss. However, studies with simple model systems showed the oxidized flavins had no effect on nitroxide spectra. Reduced flavins, $FlH_2$, and flavin radicals, $FlH^{\bullet}$, reduce nitroxides (6). The experiment with $^{14}N$ TOLH and $^{15}N$ TEMPOL showed that neither the flavin radical $FlH^{\bullet}$, which is necessarily produced during photooxidation of TOLH, nor its oxidation product with molecular oxygen cause spin destruction. Hence it is concluded that flavins are not directly responsible for the observed aerobic spin loss of nitroxides.

The association of spin loss activity with supernatants but not pellets of centrifuged SMP's implies that "released" flavins are necessary for the spin loss. "Released" flavins is an operational term

Can. J. Chem. Downloaded from www.nrcresearchpress.com by 210.87.254.40 on 09/06/12
For personal use only.

Can. J. Chem. Downloaded from www.nrcresearchpress.com by 210.87.254.40 on 09/06/12
For personal use only.

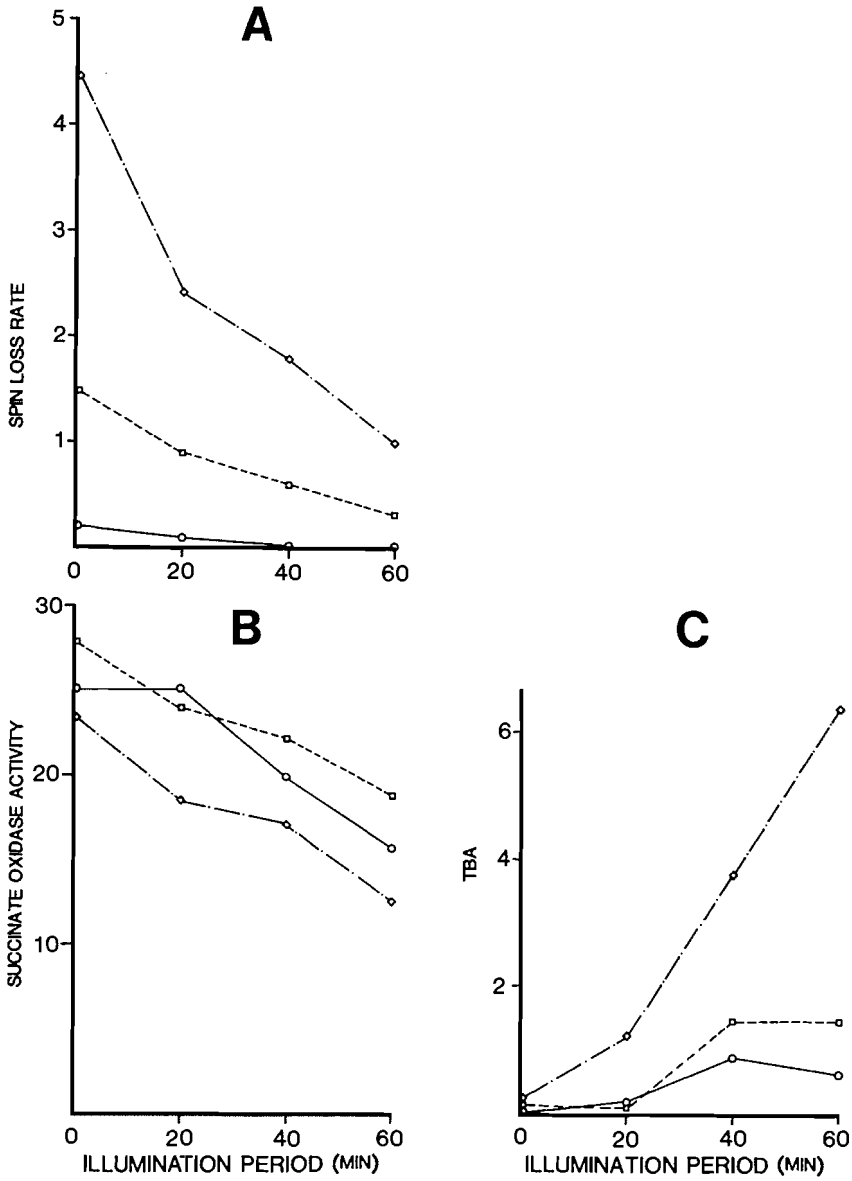


FIG. 7. Effect of addition of FMN or supernatant from aged SMP's on spin loss rates μmol/min, SMP's at 6.32 mg/mL protein (A); light dependent succinate oxidase inactivation μmol $O_2$/min, SMP's at 0.31 mg/mL protein (B); formation of TBA-reactive materials mmol/mg (C). (——) control; (----) 2.7 μ*M* FMN; (-·-·) supernatant containing 2.7 μmol "released" flavin as estimated from fluorescence.

since centrifugation speeds were insufficient to pellet individual proteins or membrane fragments. The most likely source of released flavin is NADH dehydrogenase, which contains noncovalently bound FMN. The steep temperature dependence of flavin release suggests that only low concentrations of free flavins exist in SMP's illuminated at 10°C, where photoinactivation of respiratory activities is nevertheless observed (3).

Since certain amino acids are photoreductants for flavins (12, 13), it seemed possible that anaerobic SMP's would cause nitroxide reduction under illumination. However, freshly isolated anaerobic SMP's exhibit no significant light-dependent spin reduction, even in the presence of 5 μ*M* exogenous FMN or riboflavin (data not shown). Hence, mitochondrial membranes are poor photoreductants and direct oxidation of membranes, e.g., hydrogen abstraction from amino acid residues by free flavins, is not likely to play an important role in photo-

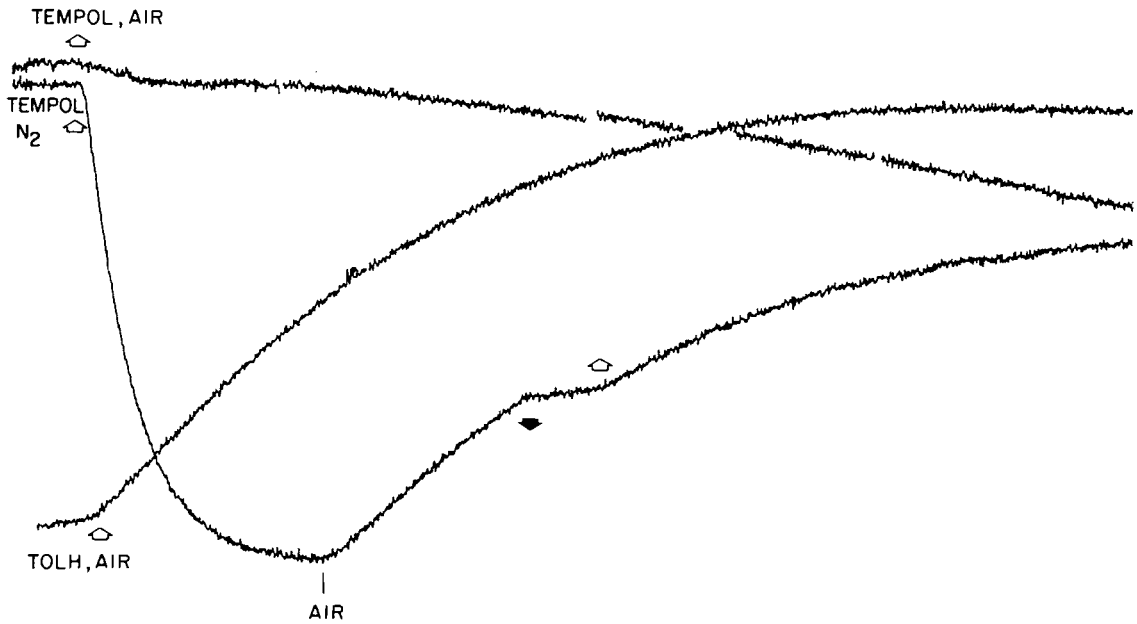


FIG. 8. Aerobic and anaerobic esr line height changes of TEMPOL and TOLH in a photochemical model system. The model system contained 10 μ*M* FMN, 10 m*M* EDTA, and 30 m*M* potassium phosphate, pH 7.4. Aerobic illumination, and alternately anaerobic and aerobic illumination as indicated.

damage. The aerobic experiment with exogenous flavins (Fig. 5) showed that at a given concentration of free flavins there is an acceleration of nitroxide spin loss with aging of the membranes. Hence, some phenomenon other than flavin release occurs during the aging process which together with free flavins causes spin loss. Taken together with the occurrence of spin loss in supernatants of centrifuged SMP's, it is inferred that some other factor(s) in addition to flavins are released from the SMP's into their aqueous environment during dark incubation. These factors react with excited flavins to bring about nitroxide spin loss. Since 30 μmol TEMPOL are destroyed by less than 2 μmol flavin, as estimated from supernatant fluorescence, it is clear the flavins act catalytically in the nitroxide destruction process, strengthening the conclusion that neither flavins nor their degradation products cause spin destruction.

*Inference that free radicals probably cause nitroxide destruction*

Destruction of nitroxides could occur by several mechanisms. One is the direct coupling of nitroxides with other radicals. Known examples of radicals which form stable products with nitroxides include several alkyl radicals (4, 5). Also, it has been shown in pulse radiolysis experiments that nitroxides react with hydroxyl radicals (22). However, the products of the latter reaction seem to decompose rapidly since model systems, e.g., uv photolysis of $H_2O_2$ and Fenton reagents, did not destroy the paramagnetic signal of TEMPOL. Another example of spin pairing is the reaction of nitroxides with thiyl radicals, a process which ultimately leads to the formation of tetramethyl piperidines, e.g., PRETOL (23). Studies of reactions between nitroxides and free radicals derived from ethylbenzene suggest that peroxy radicals, R′OO·, do not react with nitroxides (24). Oxidation of nitroxides with a powerful oxidant would yield ammonium ions which would immediately decompose in aqueous solution to nitroxides and hydroxyl radicals (5). Under strongly reducing conditions, TEMPOL can be reduced to PRETOL. This mechanism is unlikely to explain the spin loss observed in SMP's, however, since over-reduction would probably proceed via the TOLH intermediate (5) and since TEMPOL destruction is much more rapid than TOLH destruction. Thus, the mechanism of spin destruction appears to be radical pairing of nitroxides with other radicals, excluding oxygen-centered radicals, like hydroxyl or peroxy radicals.

Nitrone spin traps like DMPO and POBN have been used extensively to demonstrate the existence of free radicals (25). Since the esr spectrum arising from DMPO with illuminated SMP's is identical to the spectrum seen with only DMPO and FMN,

Can. J. Chem. Downloaded from www.nrcresearchpress.com by 210.87.254.40 on 09/06/12
For personal use only.

there appears to be no correlation between nitroxide spin destruction and DMPO spin formation. It was suggested previously that nitroxides could arise from DMPO and light-excited flavins by a nonradical mechanism (26). The spin adduct seen with POBN with white light is difficult to interpret owing to its rather low rate of appearance and the failure to observe an adduct with the broad-band interference filter. In summary, these nitrone traps do not appear to trap radicals observable by esr in illuminated SMP's even under conditions of rapid TEMPOL destruction. This does not rule out the interpretation that TEMPOL destruction is caused by radicals; rather it suggests that these nitrones with illuminated SMP's do not form radicals sufficiently stable to be observed by esr spectrometry.

*Relationship to membrane damage*

It was of interest to determine whether the species causing nitroxide destruction played a role in the mechanism of flavin-sensitized photodamage. In freshly isolated SMP's without exogenous FMN, there is appreciable photodamage to succinate oxidase even though no TEMPOL destruction was detected under these conditions. Thus, it is inferred that bound flavin exerts its destructive effects in close proximity to its binding site, and that there is no propagation of damage to distant sites as seen in the lack of lipid peroxidation and spin destruction. Exogenous FMN increases photodamage only slightly, suggesting that singlet oxygen generated by free flavin is not a major damaging species in SMP photodamage.

The addition of supernatant from aged SMP's greatly increases lipid peroxidation and slightly increases inactivation of succinate oxidase. Since the supernatant contains factor(s) that interact with light-excited flavins to destroy nitroxides, it is seen that these factors have destructive potential. Once initiated exogenously, damage propagation seems to occur in the SMP membranes since the most hydrophobic nitroxide, TEMPO, is destroyed appreciably more rapidly than the other probes. The relevance of these observations to photodamage in vivo is not clear. The factors we describe in aged SMP's could also be present in vivo. Since they are water soluble, they would be removed from the SMP's during membrane isolation procedures, and hence freshly centrifuged SMP's would not exhibit light-dependent nitroxide destruction. Given the potential of these factors for causing damage to lipids and enzymes, their further characterization is warranted.

**Acknowledgments**

We gratefully acknowledge the participation of B. Aggarwal in the initial phases of this work and thank A. G. Lewis for expert technical assistance. This work was supported by research grant GM 24273 from NIH and by the Assistant Secretary for Environment, Office of Health and Environmental Research, Life Sciences Division of the U.S. Department of Energy under Contract No. W-7405-ENG-48.

1. B. L. Epel. Photophysiology, **8**, 209 (1973).
2. B. B. Aggarwal. Ph.D. Thesis, University of California, Berkeley; Lawrence Berkeley Laboratory Report LBL-6848, 1973.
3. B. B. Aggarwal, A. T. Quintanilha, R. Cammack, and L. Packer. Biochim. Biophys. Acta, **502**, 367 (1978).
4. J. F. W. Keana, R. J. Dinerstein, and F. Baitis. J. Org. Chem. **36**, 209 (1971).
5. E. G. Rozantzev. Free nitroxyl radicals. Plenum Press, New York, London. 1970.
6. T. W. Chan and T. C. Bruice. J. Am. Chem. Soc. **99**, 7287, (1977).
7. A. T. Quintanilha and L. Packer. Proc. Natl. Acad. Sci. U.S.A. **74**, 570 (1977).
8. E. J. Rauckman, G. M. Rosen, and B. B. Kitchell. Mol. Pharmacol. **15**, 131 (1978).
9. A. Rigo, E. Argese, R. Stevanato, E. F. Orsega, and P. Viglino. Inorg. Chim. Acta, **24**, L71 (1977).
10. Y. Lion, M. Delmelle, and A. Van de Vorst. Nature, **263**, 442 (1976).
11. C. S. Foote. *In* Free radicals in biology. Vol. II. *Edited by* W. A. Pryor. Academic Press, New York. 1976. p. 85.
12. G. R. Penzer, and G. K. Radda. Biochem. J. **109**, 259 (1968).
13. G. R. Penzer. Biochem. J. **116**, 733 (1970).
14. S.-C. Tu and D. B. McCormick. J. Biol. Chem. **18**, 6339 (1973).
15. V. Massey, M. Stankovich, and P. Hemmerich. Biochemistry, **17**, 1 (1978).
16. E. J. Rauckman, G. M. Rosen, and M. B. Abou-Donia. J. Org. Chem. **41**, 564 (1976).
17. R. J. Mehlhorn and L. Packer. Biochim. Biophys. Acta, **423**, 382 (1976).
18. W. Z. Plachy and D. A. Windrem. J. Magn. Reson. **27**, 237 (1977).
19. J. A. Buege and S. D. Aust. *In* Methods in enzymology. Vol. III. *Edited by* S. Fleischer and L. Packer. Academic Press, New York. pp. 302–310.
20. A. T. Quintanilha and L. Packer. Proc. Natl. Acad. Sci. U.S.A. **74**, 570 (1977).
21. L. P. Vernon. Biochim. Biophys. Acta, **36**, 177 (1959).
22. K.-D. Asmus, S. Nigam, and R. L. Willson. Int. J. Radiat. Biol. **29**, 211 (1976).
23. K. Murayama and T. Yoshioka. Bull. Chem. Soc. Jpn. **42**, 1942 (1969).
24. M. B. Neiman and E. G. Rozantzev. Izv. Akad. Nauk SSR Ser. Khim. **1966**, 571 (1966).
25. E. G. Janzen. *In* Free radical in biology. Vol. IV. *Edited by* W. A. Pryor. Academic Press, New York. 1980. p. 115.
26. E. Finkelstein, G. M. Rosen, and E. J. Rauckman. J. Am. Chem. Soc. **102**, 4994 (1980).

Can. J. Chem. Downloaded from www.nrcresearchpress.com by 210.87.254.40 on 09/06/12
For personal use only.

# Use of spin traps to elucidate radical mechanisms of oxidations by hydroperoxides catalyzed by hemeproteins

BRENDA WALKER GRIFFIN[1]

*Department of Biochemistry, The University of Texas Health Science Center at Dallas, 5323 Harry Hines Blvd., Dallas, TX 75235, U.S.A.*

Received August 10, 1981

BRENDA WALKER GRIFFIN. Can. J. Chem. **60**, 1463 (1982).

The use of the spin traps nitrosobenzene and 2-methyl-2-nitrosopropane has established that metmyoglobin and liver microsomal cytochrome P-450 initiate a radical decomposition of cumene hydroperoxide. With metmyoglobin and the alkyl nitroso compound, the only radical product of cumene hydroperoxide trapped was the methyl radical formed by β scission of the cumyloxy radical. With both hemeprotein initiators, nitrosobenzene trapped only the cumyl radical, considered to be a decomposition product of the unstable spin adduct phenylcumyloxynitroxide. Support for this proposal includes: (1) previous spin trapping studies of the chemical decomposition of cumene hydroperoxide; and (2) significant inhibition by nitrosobenzene of the one-electron oxidation of aminopyrine and the autoxidation of unsaturated membrane lipids resulting from addition of the hydroperoxide to liver microsomes. Aminopyrine altered the epr signal amplitudes of the spin adducts produced with both nitroso compounds, indicative of oxidation of aminopyrine by the methyl radical and reduction of cumene hydroperoxide by the aminopyrine radical. The participation of hydroperoxide-derived radicals in the low peroxidatic activities of certain hemeproteins is quite distinct from the catalytic function of the true hemeprotein peroxidases, which bring about an efficient two-electron reduction of specific hydroperoxides.

BRENDA WALKER GRIFFIN. Can. J. Chem. **60**, 1463 (1982).

L'utilisation du nitrosobenzène et du méthyl-2 nitroso-2 propane comme capteurs de spin a permis de démontrer que la métmyoglobine et le cytochrome microsomique P-450 provoquent la décomposition radicalaire de l'hydroperoxyde de cumène. Avec la métmyoglobine et le composé nitrosoalkyle, le radical méthyle, formé par la scission β du radical cumylpéroxy, est le seul produit radicalaire piégé de l'hydroperoxyde de cumène. Avec les deux initiateurs du type hèmeprotéine, le nitrosobenzène piège seulement le radical cumyle qui serait un produit de décomposition du phenylcumyloxynitroxyde, un adduit de spin instable. Cette proposition est basée sur: (1) les études antérieures de piégeage de spin lors de la décomposition chimique de l'hydroperoxyde de cumène; (2) le fait que le nitrosobenzène inhibe de façon significative l'oxydation, par un électron, de l'aminopyrine et l'autoxydation des lipides de la membrane insaturées résultant de l'addition de l'hydroperoxyde aux microsomes du foie. L'aminopyrine modifie les amplitudes du signal de rpe des adduits de spin provenant des deux composés nitrosés indiquant ainsi une oxydation de l'aminopyrine par le radical méthyle et une réduction de l'hydroperoxyde de cumène par le radical aminopyrine. La participation des radicaux provenant de l'hydroperoxyde dans des activités peroxydantes faibles de certaines hèmeprotéines est tout à fait distincte de la fonction catalytique des vraies peroxydases de l'hèmeprotéines qui provoquent une réduction efficace par deux électrons d'hydroperoxydes spécifiques.

[Traduit par le journal]

## Introduction

Hemeprotein peroxidases are among the most efficient and best studied protein catalysts. These enzymes utilize $H_2O_2$, and in certain cases, a limited number of organic hydroperoxides and peroxy acids, to oxidize various electron donors (1). A class of peroxidase isozymes isolated from horseradish root exhibits rather low specificity for the reducing substrate, which includes aromatic amines, phenols, and many other compounds (1). However, catalases from mammalian and other sources exhibit their largest activities with $H_2O_2$ as the reducing substrate, thereby effecting a rapid decomposition of $H_2O_2$ to $O_2$ and $H_2O$ (2). It has been clearly established that the mechanism of catalysis by horseradish peroxidase (HRP) involves the following sequence of reactions (1):

[1*a*] HRP ($Fe^{3+}$) + $H_2O_2$ → Compound I

[1*b*] Compound I + AH → Compound II + A·

[1*c*] Compound II + AH → HRP ($Fe^{3+}$) + A·

[1*d*] A· + A· → A–A

Reaction of the ferric hemeprotein with $H_2O_2$ produces the spectroscopically distinct enzyme species designated as Compound I (1); this species retains both oxidizing equivalents of the peroxide, as evidenced by regeneration of the ferric enzyme (via another hemeprotein species compound II), upon the sequential transfer of two electrons from two molecules of the reducing substrate AH (1). Some of the more stable radical species (A·) formed in this catalytic cycle have been detected directly by epr (1); the final oxidation products of AH result from non-enzymatic reactions of the A· radicals; dimerization, disproportionation, or other reactions are possible, depending on the chemical reactivity of the particular radical and the experimental conditions (1).

[1]Present address: Alcon Laboratories, Inc., 6201 S. Freeway, P.O. Box 1959, Fort Worth, TX 76101, U.S.A.

0008-4042/82/121463-11$01.00/0

©1982 National Research Council of Canada/Conseil national de recherches du Canada

Can. J. Chem. Downloaded from www.nrcresearchpress.com by 210.87.254.42 on 09/06/12
For personal use only.

Can. J. Chem. Downloaded from www.nrcresearchpress.com by 210.87.254.42 on 09/06/12
For personal use only.

The catalysis of $H_2O_2$ decomposition by catalase also involves the formation of a species very similar to Compound I of horseradish peroxidase (2); however, reduction of this enzyme species by $H_2O_2$ appears to be a concerted two-electron transfer reaction, without the involvement of a Compound II-like enzyme intermediate (2). The electronic structure of Compound I is considered to be that of a porphyrin $\pi$ cation radical associated with Fe(IV) (3); the single oxidizing equivalent of Compound II of horseradish peroxidase remains as Fe(IV) (3). It is very significant that, although the catalysis of $H_2O_2$-supported oxidations by free and complexed metal ions often produces radical species from the peroxide ($HO_2\cdot$ and $OH\cdot$) (4), these species play no role in the formal catalytic cycle of hemeprotein peroxidases given by reaction [1]. However, low levels of peroxy radicals and superoxide radical anion may be produced during the peroxidase-catalyzed oxidation of certain electron donors; these species arise from non-enzymatic reactions of the substrate radicals $A\cdot$ with molecular $O_2$ present in the reaction system (5).

The studies described herein were initiated after several reports of the "peroxidatic" activities of cytochrome P-450 appeared (6). This hemeprotein is found in many mammalian and non-mammalian organisms, where it catalyzes the oxidation by molecular $O_2$ of compounds, such as hydrocarbons and steroids, having relatively unactivated C—H bonds (7). These reactions are designated as monooxygenations because one atom of the $O_2$ molecule is incorporated into the organic substrate and the other is reduced to $H_2O$ by two electrons originating in reduced pyridine nucleotides (NADH or NADPH), the electron-transfer agents in biological systems (7):

$$[2] \quad NADPH + H^+ + O_2 + BH \rightarrow NADP^+ + H_2O + BOH$$

The mechanism by which cytochrome P-450 "activates" molecular $O_2$ for specific insertion into an organic compound is of considerable interest. The reports that organic hydroperoxides could function as the oxidant in certain cytochrome P-450-catalyzed oxidations led to the proposal that these reactions were altogether similar to those of other hemeprotein peroxidases, involving the formation of a Compound I-like species of cytochrome P-450 (8). This species was presumed to function as the oxygen-transfer agent in both the peroxidatic and monooxygenase reactions catalyzed by this hemeprotein (8). However, several features of the cytochrome P-450-catalyzed reactions with hydroperoxides were inconsistent with the well-known chemistry of peroxidase catalytic function: the catalytic activities were extremely low, yet substantial destruction of the heme group occurred (8); also, $H_2O_2$ was much less effective as the oxidant than were organic hydroperoxides, such as cumene hydroperoxide (6, 8) which is a very poor oxidizing substrate for horseradish peroxidase (1, 8). On the other hand, these properties and others were compatible with cytochrome P-450 initiation of a radical decomposition of cumene hydroperoxide, as occurs with various metal ions (9). We have tested this hypothesis by using epr and other techniques to characterize the decomposition of cumene hydroperoxide by well-defined model systems and by cytochrome P-450.

## Experimental

Metmyoglobin was a highly purified preparation isolated from beef heart (10); other purified hemeproteins and hemin were purchased from commercial sources. Microsomal fractions were prepared from the livers of phenobarbital-treated male rats, as described in (11). Aminopyrine, 4-aminoantipyrine, nitrosobenzene, 2-methyl-2-nitrosopropane (MNP), and metyrapone were purchased from Aldrich; acetone-$d_6$ was a product of Merck, Sharp and Dohme.[2] The sodium salt of cumene hydroperoxide was prepared (12) from a technical grade product supplied by Matheson, Coleman, and Bell; the purity of the salt was confirmed by high-performance liquid chromatography and iodometric titration. All other reagents were the highest quality commercially available. The experimental techniques employed for the epr experiments, which made use of a Varian E-4 spectrometer interfaced to a Digital Equipment Corporation PDP 11/05 computer, have been described in detail elsewhere (13, 14). Details of the high-performance liquid chromatographic analysis of the products of decomposition of cumene hydroperoxide have been published (14).

## Results and discussion

### *Model system studies*

Aminopyrine (Fig. 1) has served in this study as a convenient spectroscopic probe for monitoring the formation of one-electron oxidants in enzymatic reactions. The *N*-demethylation of this drug has been commonly used to assay the monooxygenase activity of liver microsomal cytochrome P-450, a membrane-associated hemeprotein (7). The electrochemical oxidation of aminopyrine was reported by Sayo and Masui (15) to produce a relatively stable, violet radical species of this compound. In

[2]The common chemical names and abbreviations used are: aminopyrine, 4-dimethylamino-2,3-dimethyl-1-phenyl-3-pyrazolin-5-one; 4-aminoantipyrine, 4-amino-2,3-dimethyl-1-phenyl-3-pyrazolin-5-one; MNP, 2-methyl-2-nitrosopropane; metyrapone, 2-methyl-1,2-di-3-pyridyl-1-propanone; cumene hydroperoxide, $\alpha,\alpha$-dimethylbenzyl hydroperoxide; Tris, tris-(hydroxymethyl)aminomethane; Hepes, *N*-2-hydroxyethylpiperazine-*N'*-2-ethanesulfonic acid; NAD, NADP, nicotinamide adenine dinucleotide, nicotinamide adenine dinucleotide phosphate; DMPO, 5,5-dimethyl-1-pyrroline-1-oxide.

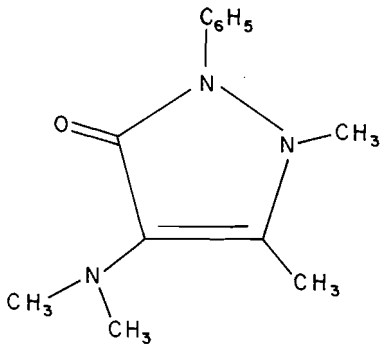

Aminopyrine

FIG. 1. Structure of aminopyrine.

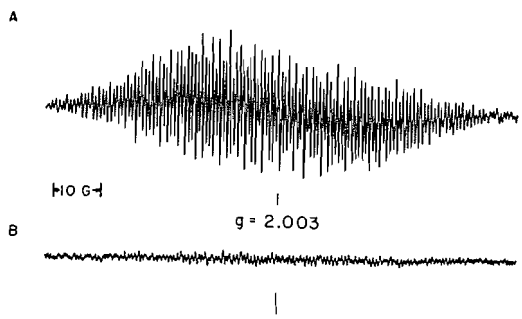


FIG. 2. Electron paramagnetic resonance spectrum of the aminopyrine free radical produced with cumene hydroperoxide and metmyoglobin. (*A*) The reaction mixture contained 20 m*M* aminopyrine, 30 m*M* cumene hydroperoxide, and 40 μ*M* metmyoglobin in 0.1 *M* potassium phosphate buffer, pH 5.0 (*B*) Control experiment: identical to *A*, except for omission of metmyoglobin. Microwave power, 10 mW; modulation amplitude, 0.25 G; temperature, 22°C.

our laboratory, it was shown that the horseradish peroxidase-catalyzed oxidation of aminopyrine with $H_2O_2$ produced the same radical species, which was proposed to be an intermediate in the *N*-demethylation of aminopyrine by this enzymatic system (13):

$$[3]\quad R_2N{-}CH_3 \xrightarrow{-e^-} R_2N{-}CH_3{}^{\cdot+} \xrightarrow{-H\cdot} R_2N^+{=}CH_2 \xrightarrow{H_2O} R_2NH_2^+ + H_2C{=}O$$

This reaction sequence is consistent with: (*1*) the mechanism of peroxidase-catalyzed generation of radical species from many reducing substrates (1); (*2*) non-enzymatic *N*-demethylation reactions effected by various chemical oxidants (16); and (*3*) the chemical structure of aminopyrine, which is closely related to the well-studied violenes, such as *N*,*N*,*N*′,*N*′-tetramethyl-*p*-phenylenediamine (17). The unusual stability of the aminopyrine radical, coupled with its rather intense absorbance in the visible region (with a maximum near 565 nm in aqueous solution (18)), is an obvious advantage for studying oxidizing systems with low catalytic activities, a characteristic property of cytochromes P-450 (6–8).

In model-system studies of the oxidation of aminopyrine by cumene hydroperoxide catalyzed by metmyoglobin, the epr signal of the aminopyrine radical was readily detected in aqueous buffered solutions at room temperature, as shown in Fig. 2. Metmyoglobin was selected for these studies because it not only exhibits peroxidatic activities with cumene hydroperoxide comparable to those reported for cytochrome P-450 (6, 8, 19), but it also has somewhat larger peroxidatic activities with $H_2O_2$ as oxidant (13, 20). Indeed, the reaction of metmyoglobin with a two-fold excess of $H_2O_2$ has been shown to produce an enzyme species with the spectral properties of Compound II of horseradish peroxidase, which also retains a single oxidizing equivalent of the oxidant (20). Both the rate of formation of this so-called higher oxidation state of the heme iron and its subsequent reduction by electron donors are considerably slower than for horseradish peroxidase (13, 20), consistent with large differences in their catalytic activities toward common electron donors. Our efforts to demonstrate that a discrete higher oxidation state of metmyoglobin comparable to Fe(IV) is formed by reaction of the hemeprotein with cumene hydroperoxide were unsuccessful; a large excess of the hydroperoxide was required to perturb appreciably the absorbance spectrum of the hemeprotein, and the observed changes could be correlated with irreversible destruction of the heme group (18).

The chemistry of the induced radical decomposition of cumene hydroperoxide has been shown to be complex (9), and the radical species produced in this reaction (alkoxy, peroxy, and alkyl) are not particularly persistent (21). As expected, no epr signals were detected at room temperature when metmyoglobin was mixed with cumene hydroperoxide in aqueous buffered solutions. However, when 2-methyl-2-nitrosopropane (MNP) was present, the reaction produced an epr signal, Fig. 3, which contained two nitroxide radicals, assigned to spin adducts of MNP with a methyl radical and a butyl radical (14). The latter nitroxide has been shown to arise from light-induced decomposition of the spin trap (22), and was, accordingly, observed in all control experiments. However, the epr signal of the spin adduct of MNP and the methyl radical was detected only when both metmyoglobin and cumene hydroperoxide were present with the spin trap. Among the large number of control experi-

Can. J. Chem. Downloaded from www.nrcresearchpress.com by 210.87.254.42 on 09/06/12
For personal use only.

Can. J. Chem. Downloaded from www.nrcresearchpress.com by 210.87.254.42 on 09/06/12
For personal use only.

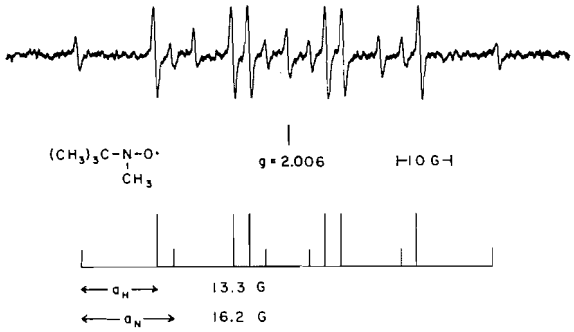


FIG. 3. Electron paramagnetic resonance signals detected in a solution of metmyoglobin, cumene hydroperoxide and MNP. The reaction mixture contained 24 $\mu M$ metmyoglobin, 30 m$M$ cumene hydroperoxide, 50 m$M$ MNP, and 10% acetone-$d_6$ in 0.1 $M$ Tris–HCl buffer, pH 9.0. Microwave power, 20 mW; modulation amplitude, 0.82 G; temperature, 22°C. (Reprinted from ref. 14 with permission.)

ments performed were variation of the pH and the solvent, which was required at low levels to increase the solubility of the spin trap in these aqueous solutions; because alcohols were oxidized to radicals which were trapped by MNP, deuterated acetone proved to be the most suitable solvent. At the level (10%) employed in these epr experiments, acetone did not have any significant effect on the measured aminopyrine $N$-demethylase activity of metmyoglobin with cumene hydroperoxide.

Addition of aminopyrine to the reaction mixture containing metmyoglobin, cumene hydroperoxide, and MNP caused the amplitude of the epr signal of the MNP-trapped methyl radical to decrease dramatically, as shown in Fig. 4. One possible explanation of this effect, namely a direct reaction of aminopyrine with the spin adduct, was eliminated by appropriate control experiments, also shown in Fig. 4. Product assays showed that the metmyoglobin-initiated decomposition of cumene hydroperoxide produced significant amounts of acetophenone, in addition to cumenol (14). Acetophenone formation was clearly incompatible with the usual mechanism of peroxidase catalysis, which would be expected to yield cumenol as the sole product of reduction of cumene hydroperoxide. In the presence of aminopyrine, under experimental conditions comparable to those of the epr experiments, the total yield of both acetophenone and cumenol was increased, but their ratio was not significantly affected, Table 1. These experimental results are consistent with the known chemistry of the radical decomposition of cumene hydroperoxide: formation of the cumyloxy radical, which undergoes a one-electron reduction to cumenol or

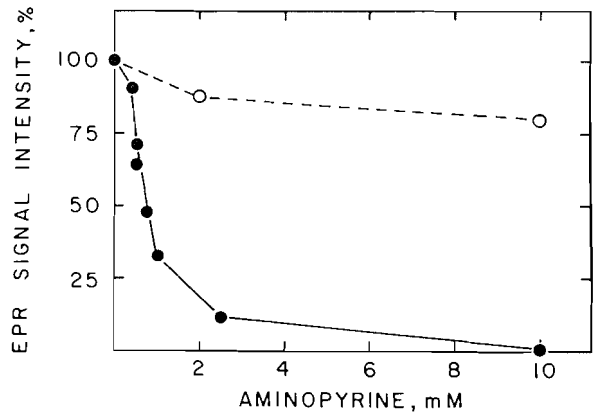


FIG. 4. Effect of aminopyrine on the relative EPR signal amplitude of the MNP-trapped methyl radical produced by the reaction of cumene hydroperoxide with metmyoglobin. The reaction mixture (●) was identical to that described in Fig. 3, except that the cumene hydroperoxide concentration was 20 m$M$ and aminopyrine was present at the indicated concentration. For the control experiment (○), the epr signal amplitude of the spin adduct of MNP and the $t$-butyl radical (decomposition product of MNP) was measured in the presence of cumene hydroperoxide alone, or metmyoglobin and $H_2O_2$, in 0.1 $M$ Tris–HCl buffer, pH 9.0. (Reprinted from ref. 14 with permission.)

β-scission to yield acetophenone and the methyl radical (9).

[4] 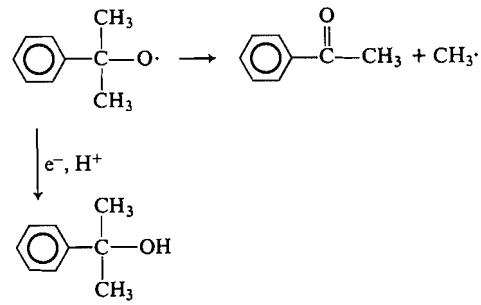


The finding that aminopyrine stimulated acetophenone formation, but inhibited trapping of the methyl radical, formed in equimolar amounts with

TABLE 1. Effect of aminopyrine on the products of cumene hydroperoxide decomposition stimulated by metmyoglobin[a]

| pH | Aminopyrine added, m$M$ | Cumenol formed, m$M$ | Acetophenone formed, m$M$ |
|---|---|---|---|
| 7.0 | 0 | 0.71 | 0.38 |
| | 0.44 | 1.42 | 0.82 |
| 9.0 | 0 | 0.68 | 0.44 |
| | 0.44 | 1.04 | 0.58 |

[a]The reaction mixtures contained 22 $\mu M$ metmyoglobin, 20 m$M$ cumene hydroperoxide, and stated concentration of aminopyrine in 0.1 $M$ buffer (Tris–HCl, pH 9.0, or potassium phosphate, pH 7.0) at 22°C. Reaction products were assayed as described in the Experimental section 5 min after the reaction was initiated.

Can. J. Chem. Downloaded from www.nrcresearchpress.com by 210.87.254.42 on 09/06/12
For personal use only.

acetophenone, suggested that aminopyrine reacted predominantly with the more reactive radical species ($CH_3$·) arising from cumene hydroperoxide. According to the simple scheme above, one-electron reduction of the cumyloxy radical by aminopyrine would be expected to decrease significantly the ratio of acetophenone to cumenol produced. Later experiments suggested that the aminopyrine radical can function as an electron donor to cumene hydroperoxide, thereby promoting the radical chain decomposition of the oxidant.

We next investigated nitrosobenzene as a potential trap of the cumyloxy radical produced in the metmyoglobin – cumene hydroperoxide system (23). In these experiments an unusually stable nitroxide was detected (Fig. 5), which exhibited no hyperfine splitting from nuclei of the trapped moiety. This splitting pattern is that expected for a trapped *tertiary* alkyl or *tertiary* alkoxy radical, and is quite distinct from that previously reported for the methyl radical trapped by nitrosobenzene (24). Indeed, when both nitrosobenzene and MNP were present, the wings of the broader epr signal of the MNP-trapped methyl radical were not detected, and the epr signal of the nitrosobenzene spin adduct was unchanged. These results suggested that $CH_3$· was not formed in the presence of this concentration of nitrosobenzene, consistent with efficient trapping of the cumyloxy radical by the spin trap. The effect of aminopyrine on the epr signal amplitude of the spin adduct was stimulation, as shown in Fig. 6, which was observed only

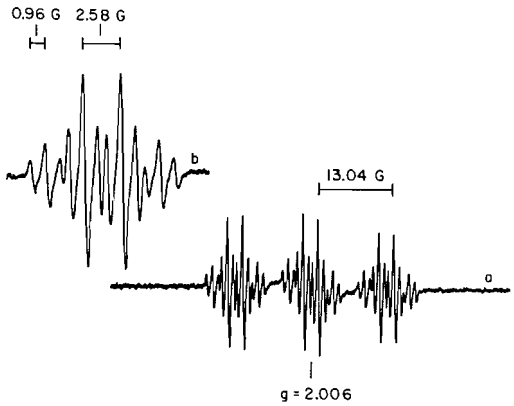


FIG. 5. Electron paramagnetic resonance signal produced in a solution of metmyoglobin, cumene hydroperoxide, and nitrosobenzene. The reaction mixture contained 27.5 μ*M* metmyoglobin, 30 m*M* cumene hydroperoxide, 25 m*M* nitrosobenzene, and 5% acetone-$d_6$ in 0.1 *M* Tris–HCl buffer, pH 9.0. (*a*) Complete signal; (*b*) low-field portion of the signal on an expanded magnetic field scale. Microwave power, 20 mW; modulation amplitude, 0.4 G; temperature, 22°C. (Reprinted from ref. 23 with permission.)

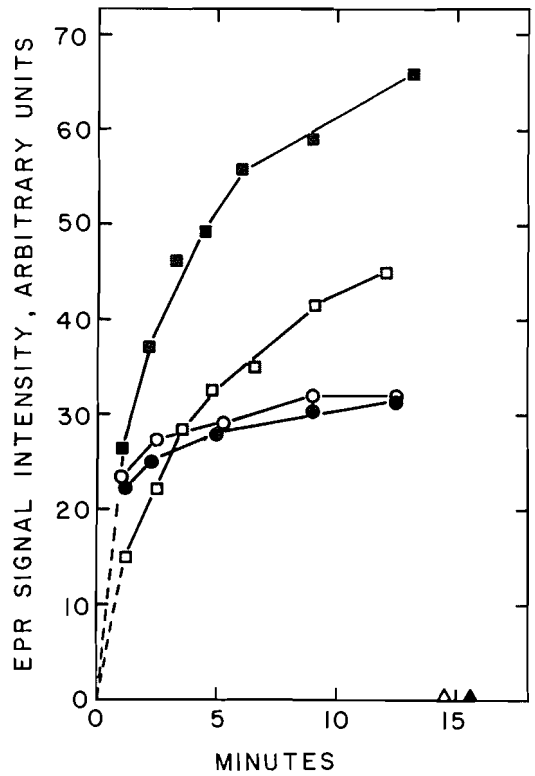


FIG. 6. Effect of aminopyrine on the epr signal amplitude of the nitrosobenzene spin adduct produced by the reaction of cumene hydroperoxide with metmyoglobin. The reaction mixtures contained 27.3 μ*M* metmyoglobin, either no aminopyrine (open symbols) or 40 m*M* aminopyrine (closed symbols), and additional components, as described, in 0.1 *M* Tris–HCl buffer, pH 9.0 with 5% acetone-$d_6$: (□, ■), 7.5 m*M* nitrosobenzene and 10 m*M* cumene hydroperoxide; (○, ●), 25 m*M* nitrosobenzene and 30 m*M* cumene hydroperoxide. Control experiments (△, ▲): metmyoglobin was omitted. Other conditions as given in Fig. 5 legend. For clarity of presentation, the instrument gain was 1.67 times larger for the open and filled square symbols. (Reprinted from ref. 23 with permission.)

when the concentration of aminopyrine was much larger than that of nitrosobenzene. This experiment was possible because the aminopyrine radical (Fig. 2) was not detected at the alkaline pH which was optimal for formation of the spin adduct of nitrosobenzene (23). Also, addition of aminopyrine to the reaction after the epr signal had attained its maximal intensity produced no effect, indicating that aminopyrine does not react directly with the nitroxide.

The reaction scheme shown in Fig. 7 provides a consistent explanation of the experimental results obtained by the use of two nitroso spin traps as probes of the reaction of metmyoglobin with cumene hydroperoxide. With nitrosobenzene, the initially-formed spin adduct is considered to be the unstable

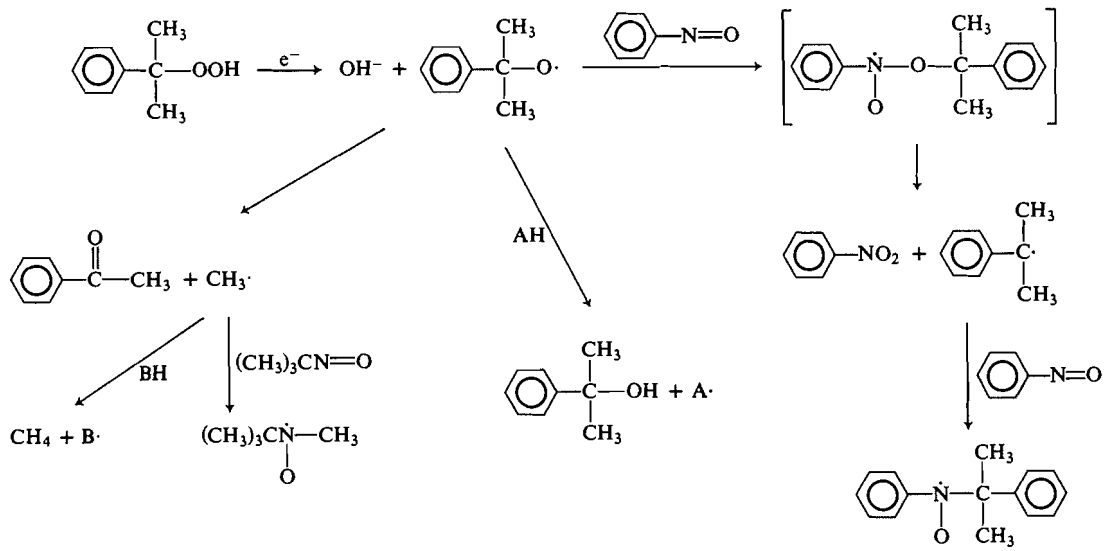


FIG. 7. Proposed mechanism for the metmyoglobin-initiated radical decomposition of cumene hydroperoxide, including the trapping reactions of MNP and nitrosobenzene. AH and BH are electron donors.

phenylcumyloxynitroxide, which decomposes to nitrobenzene and the cumyl radical; subsequent trapping of the cumyl radical by nitrosobenzene produces the stable nitroxide detected by epr. Evidence for the identity of this trapped species as the cumyl radical was previously published by Terabe and Konaka (25), who studied the trapping reactions of a series of aromatic nitroso compounds in purely chemical systems. They reported the hyperfine splitting constants of an epr signal which developed when a solution of cumene hydroperoxide and nitrosobenzene in benzene was heated (25). We observed that benzene extraction of the nitroxide produced in aqueous solutions of metmyoglobin, cumene hydroperoxide, and nitrosobenzene decreased the hyperfine splitting constants to those observed under Terabe and Konaka's experimental conditions (23, 25), Table 2. Those workers based their identification upon a number of control experiments with cumene, which gave identically the same epr signal (25). The same nitroxide has been generated by photochemical means, which established the structure rather conclusively as phenylcumylnitroxide (26). A comparison of the hyperfine splitting constants of this nitroxide with those reported for phenylbutylnitroxide (27) and phenylbutoxynitroxide (28), shown in Table 2, supports the assignment of a trapped cumyl radical. Finally, the failure to detect the methyl radical trapped by nitrosobenzene or by MNP in the presence of nitrosobenzene can be attributed to very efficient trapping of the cumyloxy radical by nitrosobenzene, Fig. 7.

The stimulatory effect of aminopyrine on the nitroxide radical produced in the presence of nitrosobenzene can also be explained by this scheme, Fig. 7: the requirement for a large excess of aminopyrine relative to nitrosobenzene is consistent with efficient trapping of the cumyloxy radical by the nitroso compound. Those cumyloxy radicals which escape trapping at low concentrations of the trap will lead to one-electron oxidation of aminopyrine, either directly or by the methyl radical product of β scission of the cumyloxy radical (9). The additional phenylcumylnitroxide formed in the presence of aminopyrine is attributed to one-electron reduction of cumene hydroperoxide by the aminopyrine radical (cf. reaction [3]), which sustains the radical chain reaction. The stimulation of the $Fe^{2+}$-induced decomposition of cumene hydroperoxide by hydroquinone (9) has been proposed to involve the semiquinone radical in a similar role. Control experiments showed that aminopyrine, even at high concentrations, could not initiate formation of phenylcumylnitroxide in the absence of metmyoglobin. However, aqueous solutions of cumene hydroperoxide and nitrosobenzene, in the absence of the hemeprotein, slowly developed the same epr signal which formed rapidly in the presence of the enzyme (Fig. 6).

Although the experimental observations support the proposed origin of the cumyl radical, i.e., as a decomposition product of phenylcumyloxynitroxide, other possible sources of the cumyl radical were considered and eliminated. Cumene present as a contaminant in the hydroperoxide could be

Can. J. Chem. Downloaded from www.nrcresearchpress.com by 210.87.254.42 on 09/06/12
For personal use only.

TABLE 2. Hyperfine splitting constants reported for *t*-alkyl-and *t*-alkoxyphenyl-nitroxides:

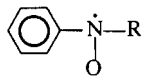

| R | $A_i$, G i = N | i = $H_{o,p}$ | i = $H_m$ | Solvent | Reference |
|---|---|---|---|---|---|
| — | 13.04 | 2.58 | 0.96 | $H_2O$ | This work |
| $-C(C_6H_5)(CH_3)_2$ | 11.53 | 2.45 | 0.9 | Benzene | 25 |
| | 11.21 | 2.46 | 0.88 | Cumene | 26 |
| $-OC(CH_3)_3$ | 14.9 | 3.1 | 1.0 | $CFCl_3$ | 27 |
| $-C(CH_3)_3$ | 13.35 | 1.7 | 0.85 | $CH_2Cl_2$ | 28 |

oxidized to the cumyl radical. However, the hydroperoxide was highly purified, with no detectable cumene. Moreover, addition of low levels of cumene to the metmyoglobin – cumene hydroperoxide system containing nitrosobenzene produced no significant effect on the amplitude of the epr signal. Another potential source of the cumyl radical is reversible dissociation of $O_2$ from the cumylperoxy radical (29). While we obtained no direct evidence for formation of the cumylperoxy radical in these reactions, it should arise by transfer of a hydrogen atom from the hydroperoxide to the cumyloxy and methyl radicals in the absence of any other electron donors (28). However, in the presence of a good electron donor like aminopyrine, the cumylperoxy radical is not expected to be formed; even if it were formed, it should play no significant role in the oxidation of aminopyrine because of the characteristically low reactivity of peroxy radicals in hydrogen atom abstraction (29). This has been clearly demonstrated by the recent publication (30) of absolute rate constants for hydrogen atom abstraction from a carbon α to a nitrogen (quite analogous to the oxidation of aminopyrine, reaction [3]) effected by *t*-butoxy and *t*-butylperoxy radicals; the alkoxy radical was more reactive by a factor of $10^5$ to $10^6$ (30).

Rosen and Rauckman detected in a system containing hematin, cumene hydroperoxide, and DMPO a nitroxide assigned to the cumylperoxy adduct of the nitrone (31). However, this species was detected only weakly at pH 3.0, where nitrones readily undergo acid-promoted hydrolysis. There is other experimental evidence (40) that alkylperoxy spin adducts of nitrones are highly unstable, particularly at temperatures greater than 0°C. We must conclude that the identity of the nitroxide reported by Rosen and Rauckman (31) is uncertain, and that the proposed role of the cumylperoxy radical is not supported by their data. Available data indicate that in aqueous solutions the common nitroso and nitrone spin traps are not suitable for positive identification of oxygen-centered organic radicals. However, the use of nitrones appears to be subject to more oxidation artefacts, i.e., 5,5-dimethylpyrrolidone-(2)-oxyl-(1) (31, 40), than is the use of nitroso spin traps.

*Studies with liver microsomes*

For spin trapping experiments with cumene hydroperoxide and liver microsomal fractions containing the membrane-associated hemeprotein cytochrome P-450, nitrosobenzene was chosen because of the stability of the spin adduct and the greater detection sensitivity for this radical. As shown in Fig. 8, the epr signal detected in this system clearly contained the sharp resonances of phenylcumylnitroxide and another broad component, considered to be the membrane-associated fraction of the same nitroxide (32); the broadening is attributed to slower rotational motion of the nitroxide in the membrane and measurable paramagnetic exchange interaction with $O_2$, present at a higher concentration in the lipid phase of this system. It was observed that: (*1*) this epr signal was considerably less stable in microsomes than in the model system, and (*2*) all control experiments except one were negative: microsomes containing only nitrosobenzene gave a very weak epr signal quite distinct from that detected with both cumene hydroperoxide and nitrosobenzene present. This epr signal was consistent with that reported for the phenylhydronitroxide radical (33), suggesting that it arises from reduction of nitrosobenzene by substances in the microsomes. This epr signal was destroyed by oxidants such as *t*-butyl hydroperoxide, and also was not detected in the presence of cumene hydroperoxide. Significantly, metyrapone, a bipyridyl compound which is a specific inhibitor of cytochrome P-450, produced measurable inhibition (46%) of the epr signal detected with liver microsomes, cumene hydroperoxide, and nitro-

Can. J. Chem. Downloaded from www.nrcresearchpress.com by 210.87.254.42 on 09/06/12
For personal use only.

Can. J. Chem. Downloaded from www.nrcresearchpress.com by 210.87.254.42 on 09/06/12
For personal use only.

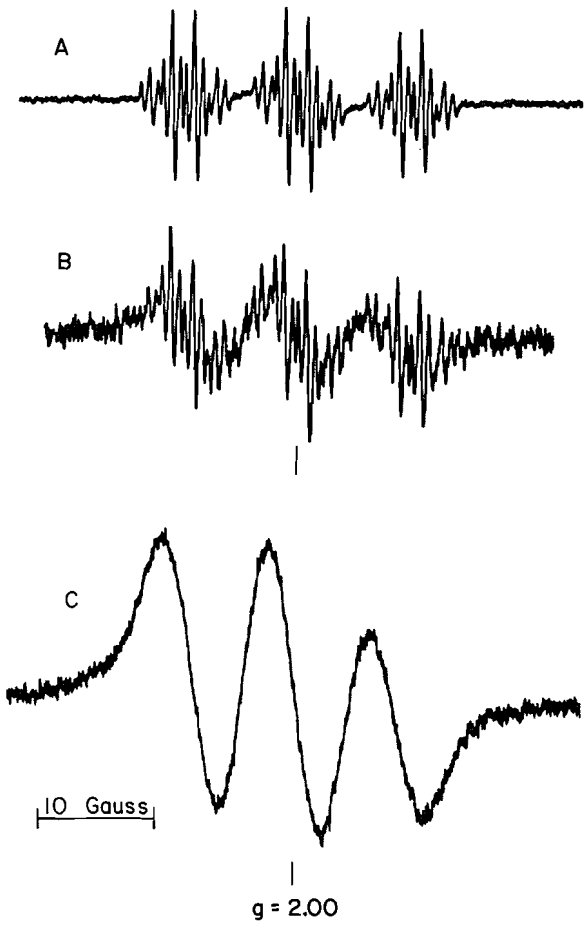


FIG. 8. Comparison of epr signals resulting from addition of metmyoglobin or rat liver microsomes to cumene hydroperoxide in the presence of nitrosobenzene. The reaction with metmyoglobin (*A*) was that described in the Fig. 5 legend. The reaction mixtures for *B* and *C* contained 18.8 μ*M* liver microsomal cytochrome P-450, 30 m*M* cumene hydroperoxide, 12.5 m*M* nitrosobenzene, and 2.5% acetone-$d_6$ in 0.1 *M* Hepes–Tris buffer, pH 6.5. Microwave power, 20 mW; modulation amplitude, 0.4 G (*A*, *B*) or 5.0 G (*C*); gain, $8 \times 10^2$ (*A*); $5 \times 10^3$ (*B*); $1.5 \times 10^3$ (*C*).

sobenzene, but had no effect on metmyoglobin-dependent generation of this nitroxide (32). Also, the metmyoglobin system was much more sensitive to inhibition by cyanide than was the microsomal system (32), consistent with the relative affinities of the two hemeproteins for this ligand. These results strongly implicated cytochrome P-450 as the initiator of cumene hydroperoxide decomposition in these liver microsomal fractions.

The possibility that inorganic iron, a likely contaminant of microsomes, could be responsible for the results obtained with microsomes was eliminated by control experiments. The addition of ferrous (but not ferric) ion to aqueous solutions of cumene hydroperoxide and nitrosobenzene (pH ~ 4.0) produced the phenylcumylnitroxide and also detectable levels of the less stable spin adduct of nitrosobenzene and the methyl radical. The $Fe^{2+}$-dependent reaction was also distinguished from that initiated by the hemeproteins by: (*1*) the requirement for $Fe^{2+}$ concentrations approximately 20-fold larger than the hemeprotein concentrations employed; and (*2*) complete inhibition of the epr signal by 10 m*M* EDTA. Neither hemeprotein–cumene hydroperoxide system displayed any sensitivity to EDTA. Moreover, the addition of 200 μ*M* $Fe^{2+}$ to microsomes had no effect on the epr signal detected in the absence of this metal ion.

The epr experiments indicated that nitrosobenzene trapped efficiently the initial radical arising from cumene hydroperoxide in the presence of hemeproteins or $Fe^{2+}$; but the failure to detect the spin adduct of the cumyloxy radical made independent confirmation of these results important, especially for the microsomal system. Spectral changes observed during the microsomal oxidation of aminopyrine by cumene hydroperoxide demonstrated the rapid formation of the violet aminopyrine radical, Fig. 9; however, the absorbance con-

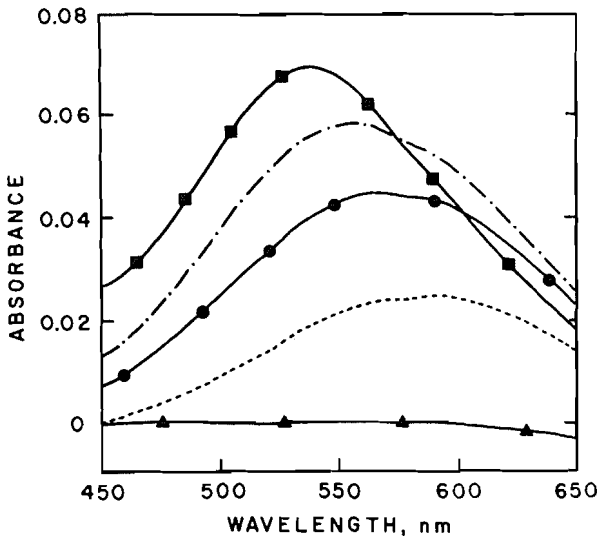


FIG. 9. Spectral changes observed during the microsomal oxidation of aminopyrine by cumene hydroperoxide. A solution containing 1 mg total microsomal protein/mL in 50 m*M* Hepes–Tris buffer, pH 6.5, with 0.15 *M* KCl, 10 m*M* $MgCl_2$, and 30 m*M* aminopyrine was added to both sample and reference cuvets, and the baseline was recorded (▲). The spectrum was scanned at the indicated times after addition of 0.25 m*M* cumene hydroperoxide to the sample cuvet: 15 s (---), 1 min (●), 3 min (—·—·), and 5 min (■), which corresponded to the maximal absorbance increase. The spectrum recorded at 1 min is nearly identical to that of the aminopyrine radical produced in other enzymatic oxidizing systems (18). (Reprinted from ref. 34 with permission.)

Can. J. Chem. Downloaded from www.nrcresearchpress.com by 210.87.254.42 on 09/06/12
For personal use only.

tinued to increase with a concomitant shift in the absorbance maximum from 560 nm to 535 nm, followed by a slower decay and a further shift of the absorbance maximum to 527 nm (34). It was shown that oxidation of 4-aminoantipyrine by microsomes and cumene hydroperoxide, or other oxidizing systems, produced a 525 nm-absorbing chromophore; this species had been identified from earlier studies of the chemistry of 4-aminoantipyrine as antipyrine red, a coupling product of two molecules of the parent compound (35). We note that 4-aminoantipyrine is the product of oxidative cleavage of two *N*-methyl groups from the amino group of aminopyrine (cf. Fig. 1) and is oxidized much more easily than aminopyrine (13). Thus, the spectral changes of Fig. 9 are considered to represent initial formation of the aminopyrine radical, followed by rapid loss of two *N*-methyl groups from the radical, and subsequent oxidation of the product, 4-aminoantipyrine, to antipyrine red. This reaction sequence apparently occurs even though the aminopyrine concentration is considerably larger than the concentration of both cumene hydroperoxide and 4-aminoantipyrine which is formed; the localization of these reactions in the microsomal membrane, which has a limited capacity for the very water-soluble aminopyrine, is probably responsible for this phenomenon. The important point for this study, however, is that nitrosobenzene very effectively inhibited the absorbance changes which occurred during the microsomal oxidation of aminopyrine by cumene hydroperoxide (Fig. 10), or the oxidation of 4-aminoantipyrine by this system (34). The sensitivity of spectrophotometric detection of the aminopyrine radical (15, 18) and the adequate solubility of nitrosobenzene in $H_2O$ made the use of organic solvents unnecessary in these experiments.

Nitrosobenzene also inhibited another reaction – the consumption of molecular $O_2$ — which occurs when cumene hydroperoxide is added to liver microsomes (34); the concentrations of nitrosobenzene which produced significant inhibition of this reaction (Fig. 11) and the microsomal oxidation of aminopyrine by cumene hydroperoxide (Fig. 10) were very similar. Both phenomena dependent on cumene hydroperoxide — aminopyrine oxidation and $O_2$ consumption — were similarly inhibited by metyrapone and known substrates of liver microsomal cytochrome P-450. The $O_2$ consumption was attributed to autoxidation (peroxidation) of unsaturated membrane lipids initiated by one or more of the radical species derived from cumene hydroperoxide. This proposal was tested by control experiments with a model system in which metmyoglobin

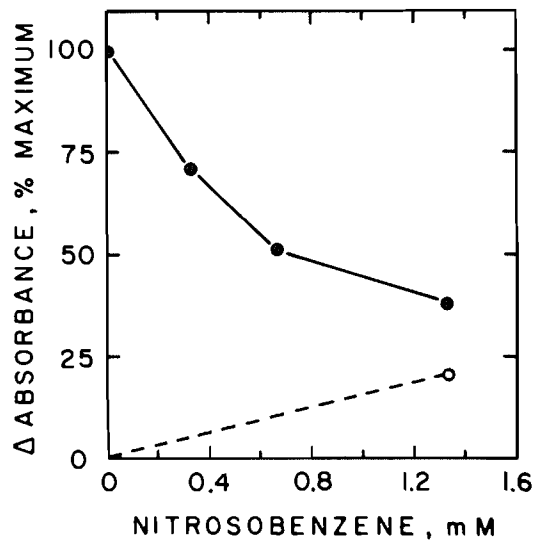


FIG. 10. Effect of nitrosobenzene on the maximal absorbance measured during the microsomal oxidation of aminopyrine by cumene hydroperoxide. Experimental conditions were identical to those described in the Fig. 9 legend, with nitrosobenzene added at the indicated concentrations (●). The maximal absorbance increase which developed near 535 nm was measured. The control experiment (○), in which aminopyrine was omitted, developed a measurable, but featureless, absorbance in the visible region. (Reprinted from ref. 34 with permission).

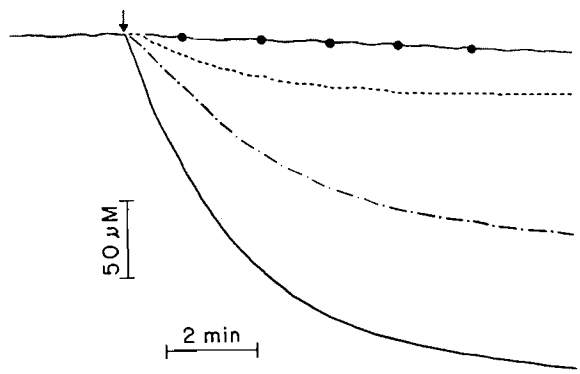


FIG. 11. Effect of nitrosobenzene on $O_2$ consumption resulting from addition of cumene hydroperoxide to rat liver microsomes. Experimental conditions were identical to those described in the Fig. 9 legend, except that aminopyrine was omitted and nitrosobenzene was added at the stated concentrations: —, 0; ----, 0.33 m*M*; ---, 0.67 m*M*; ●, 1.33 m*M*. The reaction was initiated by adding 0.25 m*M* cumene hydroperoxide at the point indicated by the arrow. The $O_2$ concentration was monitored continuously by a Clark-type electrode in stirred solutions within a cell which was closed to the atmosphere and maintained at 25°C. (Reprinted from ref. 34 with permission.)

and arachidonic acid were substituted for cytochrome P-450 and for the unsaturated membrane lipids of the microsomes. In the absence of arachidonic acid, no measurable $O_2$ uptake occurred in aqueous solutions of metmyoglobin and cumene

Can. J. Chem. Downloaded from www.nrcresearchpress.com by 210.87.254.42 on 09/06/12
For personal use only.

hydroperoxide under the experimental conditions of Fig. 11. With 0.3 m*M* arachidonic acid also present, the rate of $O_2$ consumption dependent on cumene hydroperoxide was somewhat lower than the control rate observed for the microsomal system (Fig. 11). At relatively higher concentrations of arachidonic acid, low levels of contaminating hydroperoxides formed by air oxidation of this compound were sufficient to sustain $O_2$ consumption with metmyoglobin without any requirement for cumene hydroperoxide. Significantly, both the cumene hydroperoxide-dependent and -independent $O_2$ uptake in the metmyoglobin/arachidonic acid system were inhibited by levels of nitrosobenzene which were effective in the analogous microsomal reaction (Fig. 11). Finally, it was shown that cyanide, but not metyrapone, could inhibit metmyoglobin-initiated autoxidation of arachidonic acid. The inhibitory effect of nitrosobenzene on hemeprotein-initiated autoxidation of unsaturated lipids is also consistent with the trapping of a carbon-centered radical produced by hydrogen atom abstraction from the lipid molecule. Enzymatic oxygenation reactions of polyunsaturated fatty acids have been probed by 2-methyl-2-nitrosopropanol (36), MNP (37), and nitrosobenzene (38); in each case, a secondary carbon-centered radical adduct of the nitroso compound was identified by its epr spectrum (36–38). However, epr data obtained with the lipid-free model system in our study have provided the best evidence for the point of nitrosobenzene inhibition of the radical decomposition of cumene hydroperoxide initiated by hemeproteins. Based on various kinds of experimental data obtained with two spin traps, as well as numerous similarities between the model system containing metmyoglobin and the microsomal system containing cytochrome P-450, we conclude that the reaction sequence of Fig. 7 accounts for the major reactions that occur in the hemeprotein-initiated decomposition of cumene hydroperoxide, in the absence or presence of nitroso spin traps.

These experimental results indicate that reactive one-electron oxidants produced by the addition of cumene hydroperoxide to liver microsomes are responsible for both aminopyrine oxidation and initiation of autoxidation of unsaturated lipids. The findings that rather low levels of nitrosobenzene significantly inhibited both reactions, taken with the epr spin trapping data, strongly implicate the cumyloxy and/or methyl radicals as the oxidizing species. The reactions initiated by adding cumene hydroperoxide to liver microsomes clearly required cytochrome P-450, since metyrapone, a specific and high-affinity ligand of this hemeprotein, was an excellent inhibitor of these reactions. The results obtained with metmyoglobin and cumene hydroperoxide were analogous, with this system, however, showing sensitivity to inhibition by cyanide, a known ligand of metmyoglobin. The ability of $H_2O_2$ (and certain organic hydroperoxides and peroxy acids) to oxidize ferric hemeprotein peroxidases to species containing Fe(IV) (1–3) suggests that those hemeproteins which react with cumene hydroperoxide may transfer a single electron to this oxidant. The products of this reaction would presumably be the cumyloxy radical and an Fe(IV) heme species of unknown structure. It also seems likely that the heme group in this or other oxidation state of the enzyme is attacked by one or both of the hydroperoxide-derived radicals which are responsible for oxidation of other electron donors. Indeed, we have observed that destruction of the heme group of metmyoglobin by cumene hydroperoxide can be inhibited by aminopyrine or nitrosobenzene. Also, recent evidence was published for the reaction of methyl radicals with ferric, ferrous, and iron-free deuteroporphyrin (39). The low selectivity of the organic free radical oxidants derived from cumene hydroperoxide in the presence of hemeproteins can, thus, account for all of the phenomena which have been observed in these systems.

These experiments are now being extended to other hemeproteins, as well as other organic hydroperoxides. With hemin and catalase, the same cumene hydroperoxide-derived radicals trapped by MNP and nitrosobenzene have been detected; both heme compounds also exhibit low peroxidatic activities with this hydroperoxide. However, horseradish peroxidase shows no reactivity with cumene hydroperoxide by any of the techniques employed in this study. These results suggest that, while the high catalytic activities of hemeprotein peroxidases with $H_2O_2$ and a limited number of other peroxidic agents derive from the characteristic reactivity of iron and its chelated forms with peroxides, evolutionary development of the protein structures of peroxidases has modified this reactivity to prevent the formation of reactive oxidizing radicals from the oxidant. The advantage to these enzymes of such altered reactivity would appear to be self-preservation, so that "the show (efficient catalysis) may go on". Those hemeproteins with biological functions not directly related to efficient catalytic reduction of hydroperoxides have retained to varying degrees the ability to effect one-electron reduction of hydroperoxides, which accounts for their low peroxidatic activities. Finally, it seems appropriate to emphasize what

others (40) have cautioned about spin trapping applications, especially in biological systems: a critical approach is essential. In addition to using several spin traps to investigate a given system, and other experimental techniques in conjunction with epr, it is necessary to perform all possible control experiments. Only then can one draw definitive conclusions about the formation and possible significance of free radicals in the system under study.

**Acknowledgment**

This research was funded by NIH Grant No. AM 19027 and Robert A. Welch Foundation Grant No. I-601.

1. M. MORRISON and G. SCHONBAUM. Ann. Rev. Biochem. **45**, 861 (1976).
2. G. SCHONBAUM and B. CHANCE. Enzymes. **13C**, 363 (1976).
3. J. E. ROBERTS, B. M. HOFFMAN, R. RUTTER, and L. P. HAGER. J. Biol. Chem. **256**, 2118 (1981).
4. C. WALLING. Acc. Chem. Res. **8**, 125 (1975).
5. I. YAMAZAKI. *In* Molecular mechanisms of oxygen activation. *Edited by* O. Hayaishi. Academic Press, New York. 1974. pp. 535–558.
6. A. D. RAHIMTULA and P. J. O'BRIEN. Biochem. Biophys. Res. Commun. **60**, 440 (1974).
7. B. W. GRIFFIN, J. A. PETERSON, and R. W. ESTABROOK. *In* The porphyrins. Vol. VII. *Edited by* D. Dolphin. Academic Press, New York. 1969. pp. 333–375.
8. G. D. NORDBLOM, R. E. WHITE, and M. J. COON. Arch. Biochem. Biophys. **175**, 524 (1976).
9. M. S. KHARASCH, A. FONO, and W. NUDENBERG. J. Org. Chem. **15**, 763 (1950).
10. T. GOTOH and K. SHIKAMA. Arch. Biochem. Biophys. **163**, 476 (1974).
11. J. WERRINGLOER and R. W. ESTABROOK. Arch. Biochem. Biophys. **167**, 270 (1975).
12. R. D. MAIR and R. T. HALL. *In* Organic peroxides. Vol. 2. *Edited by* D. Swern. Wiley-Interscience, New York. 1971. pp. 535–635.
13. B. W. GRIFFIN and P. L. TING. Biochemistry, **17**, 2206 (1978).
14. B. W. GRIFFIN and P. L. TING. FEBS Lett. **89**, 196 (1978).
15. H. SAYO and M. MASUI. J. Chem. Soc. Perkin Trans. II, 1640 (1973).
16. D. H. ROSENBLATT, L. A. HULL, D. C. DELUCA, G. T. DAVIS, R. C. WEGLEIN, and K. K. R. WILLIAMS. J. Am. Chem. Soc. **89**, 1158 (1967).
17. J. M. FRITSCH, H. WEINGARTEN, and J. D. WILSON. J. Am. Chem. Soc. **92**, 4038 (1970).
18. B. W. GRIFFIN, C. MARTH, Y. YASUKOCHI, and B. S. S. MASTERS. Arch. Biochem. Biophys. **205**, 543 (1980).
19. B. W. GRIFFIN. *In* Fundamental research in homogeneous catalysis. Vol. 3. *Edited by* M. Tsutsui. Plenum Press, New York. 1979. pp. 773–791.
20. T. YONETANI and H. SCHLEYER. J. Biol. Chem. **242**, 1974 (1967).
21. K. U. INGOLD. *In* Free radicals. Vol. 1. *Edited by* J. K. Kochi. Wiley-Interscience, New York. 1973. pp. 37–112.
22. E. G. JANZEN. Acc. Chem. Res. **4**, 31 (1971).
23. B. W. GRIFFIN and D. RAMIREZ. Bioorg. Chem. **10**, 177 (1981).
24. M. J. PERKINS and P. WARD. J. Chem. Soc. Sect. B, 395 (1970).
25. S. TERABE and R. KONAKA. J. Chem. Soc. Perkin Trans. II, 2163 (1972).
26. V. MALATESTA and K. U. INGOLD. Tetrahedron Lett. 3307 (1973).
27. G. CHAPELET-LETOURNEUX, H. LEMAIRE, and A. RASSAT. Bull. Soc. Chim. Fr. 3283 (1965).
28. A. MACKOR, TH. A. J. W. WAJER, TH. J. DE BAER, and J. D. W. VAN VOORST. Tetrahedron Lett. 385 (1967).
29. B. C. GILBERT and A. J. DOBBS. *In* Organic peroxides. Vol. 3. *Edited by* D. Swern. Wiley-Interscience, New York. 1972. p. 284.
30. D. GRILLER, J. A. HOWARD, P. R. MARRIOTT, and J. C. SCAIANO. J. Am. Chem. Soc. **103**, 619 (1981).
31. G. M. ROSEN and E. J. RAUCKMAN. Mol. Pharmacol. **17**, 233 (1980).
32. B. W. GRIFFIN. *In* Microsomes, drug oxidations and chemical carcinogenesis. Vol. 1. *Edited by* M. J. Coon, A. H. Conney, R. W. Estabrook, H. V. Gelboin, J. R. Gillette, and P. J. O'BRIEN. Academic Press, New York. 1980. pp. 319–322.
33. H. LEMAIRE, A. RASSAT, and J-P. RAVET. Tetrahedron Lett. **47**, 3507 (1964).
34. P. L. ASHLEY and B. W. GRIFFIN. Mol. Pharmacol. **19**, 146 (1981).
35. E. EISENSTAEDT. J. Org. Chem. **3**, 153 (1939).
36. J. J. M. C. DEGROOT, G. J. GARSSEN, J. F. G. VLIEGENTHART, and J. BOLDINGH. Biochim. Biophys. Acta, **326**, 279 (1973).
37. R. P. MASON, B. KALYANARAMAN, B. E. TAINER, and T. E. ELING. J. Biol. Chem. **255**, 5019 (1980).
38. H. AOSHIMA, T. KAJIWARA, A. HATANAKA, and H. HATANO. J. Biochem. Tokyo, **82**, 1559 (1977).
39. D. BRAULT and P. NETA. J. Am. Chem. Soc. **103**, 2705 (1981).
40. E. G. JANZEN. *In* Free radicals in Biology. Vol. 4. *Edited by* W. A. Pryor. Academic Press, New York. 1980. pp. 115–154.

Can. J. Chem. Downloaded from www.nrcresearchpress.com by 210.87.254.42 on 09/06/12
For personal use only.

# Photochemistry of protein and nucleic acid constituents: electron spin resonance and spin-trapping with 2-methyl-2-nitrosopropane

PETER RIESZ AND IONEL ROSENTHAL[1]

*Laboratory of Pathophysiology, National Cancer Institute, National Institutes of Health, Bethesda, MD 20205, U.S.A.*

Received August 10, 1981

PETER RIESZ and IONEL ROSENTHAL. Can. J. Chem. **60**, 1474 (1982).

Our recent studies of the direct uv-photolysis of aliphatic and aromatic peptides, DNA constituents, and their 5-haloderivatives in aqueous solution and the photo-induced reactions of benzoylperoxide with amino acids, peptides, fatty acids, and pyrimidines in dimethylsulfoxide-containing solutions are reviewed.

2-Methyl-2-nitrosopropane was used for spin-trapping and characterization of free radicals generated photochemically with light in the wavelength range of 220–313 nm in aqueous or aprotic solvents. Direct photolysis of aliphatic dipeptides and of phenylalanine peptides produced mostly decarboxylation radicals, while for tyrosine peptides both decarboxylation and deamination radicals were spin-trapped; for tryptophan di- and tripeptides, deamination radicals were predominantly produced, while for long chain polypeptides, main-chain scission was observed.

When pyrimidine bases were photolysed, radicals consistent with the addition of an H-atom or an OH-radical at the C(5) position of the 5,6-double bond could be detected. The general reaction pattern in the photolyses of 5-chloro, bromo, or iodouracil was the homolytic cleavage of the carbon–halogen bond, while for 5-fluorouracil, the α-fluoro radical was spin-trapped.

Dibenzoylperoxide was found to photoinduce the free radical generation in amino acids, peptides, and fatty acids exposed to ultraviolet light, which is not absorbed by these compounds, that is, $\lambda = 313 \pm 10$ nm. The most predominant reaction is the decarboxylation of the terminal acid moiety. This process is explained by an electron transfer from the acid to the photoexcited peroxide or its fragmentation products. Pyrimidine bases, such as cytosine and thymine, can be oxidized under these conditions to generate C(5) centered radicals.

PETER RIESZ et IONEL ROSENTHAL. Can. J. Chem. **60**, 1474 (1982).

On passe en revue nos récentes études sur la photolyse direct uv des peptides aromatiques et aliphatiques, des constituants de l'ADN et de leurs dérivés halogénés en solution aqueuse ainsi que les réactions photo-induites du peroxyde de benzoyle avec les acides aminés, les peptides, les acides gras et les pyrimidines dans des solutions contenant du diméthylsulfoxyde.

Nous avons utilisé le méthyl-2 nitroso-2 propane comme capteur de spin et pour caractériser les radicaux libres produits photochimiquement avec une lumière dont la longueur d'onde varie de 220 à 313 nm dans des solvants aqueux ou aprotiques. La photolyse directe des dipeptides aliphatiques et des peptides contenant de la phénylalanine produit surtout des radicaux de décarboxylation, tandis que dans les cas des peptides contenant la tyrosine, on a capté des radicaux de décarboxylation et de désamination. Dans le cas des di- et des tripeptides du tryptophane, on obtient surtout des radicaux de désamination tandis que l'on observe une scission de la chaîne principale dans le cas des longues chaînes de polypeptides.

Quant on photolyse les bases du type pyrimidine, on détecte des radicaux qui correspondent à l'addition d'un atome d'hydrogène ou d'un radical OH sur le carbone en position 5 de la double liaison en position 5,6. Le schéma général des photolyses du chloro-5, bromo-5 ou iodo-5 uracile est le clivage homolytique de la liaison carbone–halogène tandis que dans le cas du fluoro-5 uracile il y a piégeage de spin du radical α fluoro.

On a trouvé que le peroxyde de dibenzoyle induit photochimiquement la formaton de radicaux libres dans les acides aminés, dans les peptides et les acides gras exposés à lumière ultraviolette que ces composés n'absorbent pas soit à $\lambda = 313 \pm 10$ nm. La décarboxylation de l'unité acide terminale constitue la réaction la plus courante. On explique cette réaction par un transfert d'électron de l'acide au peroxyde excité photochimiquement ou à ses produits de fragmentation. Les bases du type pyrimidine telles la cytosine et la thymine peuvent être oxydées dans ces conditions en produisant des radicaux centrés en C(5).

[Traduit par le journal]

## Introduction

The damaging effects of ultraviolet light on biological systems have been extensively described in the literature. Correlations have been made between survival of uv-irradiated cells and the production of certain types of photochemical damage in their DNA. Vital proteins and enzymes are denatured and inactivated due to changes which could be traced to particular amino acid residues. Finally, DNA and protein could be photochemically cross-linked in cells (1, 2).

The understanding of these effects requires basic knowledge of the primary chemical events which followed the light absorption. In this respect, esr provides the experimental tool for detecting the initial transients generated in response to the specific energy input in a certain chromophore moiety of a complex biological polymer.

With the advent of the spin-trapping method (3, 4), it is now possible to gain information about free radicals generated at physiological temperatures without suppressing thermally activated processes

[1]On sabbatical leave from the Department of Technology, Agricultural Research Organization, Volcani Center, Bet-Dagan, Israel.

0008-4042/82/121474-06$01.00/0

©1982 National Research Council of Canada/Conseil national de recherches du Canada

Can. J. Chem. Downloaded from www.nrcresearchpress.com by 210.87.254.42 on 09/06/12
For personal use only.

Can. J. Chem. Downloaded from www.nrcresearchpress.com by 210.87.254.42 on 09/06/12
For personal use only.

and hydration interaction with the solvent. We have extensively used 2-methyl-2-nitrosopropane (MNP) for trapping and characterization of free radicals generated in protein and nucleic acid constituents over a wide range of wavelengths of (220–313 nm) by direct or sensitized photolyses.

## Experimental

Aqueous solutions of MNP (1.5 mg/mL) were prepared by stirring overnight at room temperature. Dimethylsulfoxide solutions were prepared by stirring MNP (15 mg) and dibenzoylperoxide (50 mg) in 10 mL of solvent for 15 min. The photolyses were performed *in situ* at room temperature in aerated solutions, in a standard aqueous quartz cell placed in the esr cavity, using a Schoeffel 1000 W high pressure Hg–Xe lamp coupled with a grating monochromator. The irradiation times varied between 10 s up to 45 min. A Varian E-9, X-band spectrometer was used for esr measurements. The spectra from spin-trapped radicals were recorded at room temperature as first derivatives. The magnetic field modulation frequency was 100 kHz, and 10 mW of microwave power were used.

In many cases a large di-*tert*-butyl nitroxide (DTBN) signal prevented the identification of the underlying spectrum due to other radical species. Two methods were used to remove the DTBN signal: one was to adjust the pH to about 4 and allow the DTBN signal to decay, since it generally decayed faster than the other spin-adducts; the other was to extract the DTBN formed after irradiation with petroleum ether (boiling range 37–55°C). Except in some instances, where the spin-adduct was also soluble in the organic phase, good results were generally obtained. The procedure was the following: after irradiation of the esr cell outside the cavity, which was often carried out three or four times to expose the entire flat part of the cell to the uv beam, the solution contained in the cell was transferred to a small test tube and extracted three times with an equal volume of petroleum ether. The aqueous phase was then transferred back into the cell and the spectrum recorded. The spectrum before extraction was usually also recorded in order to check for possible loss of signals other than DTBN.

## Results and discussion

### A. *Direct photolyses in aqueous solutions*

#### I. *MNP*

Since MNP became a part of the system investigated, knowledge of its photochemical properties is required.

In aqueous solution, MNP exists in a monomer–dimer equilibrium (eq. [1]) (5).

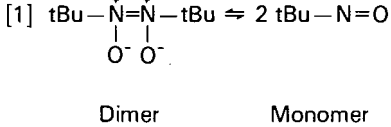

[1] $tBu-\overset{+}{N}(O^-)=\overset{+}{N}(O^-)-tBu \rightleftharpoons 2\ tBu-N=O$

Dimer Monomer

After 12 h at 30°C the monomer concentration reaches its maximum value (ca. 60%). The aqueous MNP exhibits a light absorption at 662 nm due to the monomer, and more intense absorptions at 287 and 224 nm attributed mainly to the dimer. The photochemistry of MNP in water has not been studied, but the following reactions (eqs. [2], [3]) are known to occur in organic solvents (6, 7):

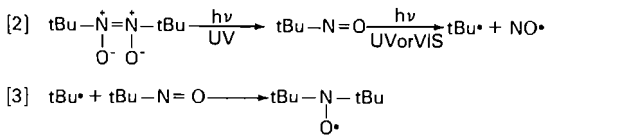

[2] $tBu-\overset{+}{N}(O^-)=\overset{+}{N}(O^-)-tBu \xrightarrow[UV]{h\nu} tBu-N=O \xrightarrow[UVorVIS]{h\nu} tBu^{\bullet} + NO^{\bullet}$



[3] $tBu^{\bullet} + tBu-N=O \longrightarrow tBu-\underset{O^{\bullet}}{N}-tBu$

We assume that the generation of this undesired di-*tert*-butyl nitroxide radical was the reason for the lack of enthusiasm in using MNP for spin-trapping in photochemical reactions (8). However, we found that frequently the formation of di-*tert*-butyl nitroxide can be entirely avoided by choosing the right experimental conditions such as reactant concentration and irradiation time. Even when produced, its very simple and characteristic esr expression (a sharp triplet of hyperfine splitting constant which is solvent dependent) has a minimal interference with the spin-adduct and can be easily subtracted. When, however, the concentration of the spin-adduct of interest is very low compared to di-*tert*-butyl nitroxide, two methods could be used to remove this undesired signal: one is to adjust the pH to about 4 and allow it to decay, since it generally decays faster than the other spin adducts; the second is to extract it with petroleum ether after photolysis. Except in instances when the spin-adduct is also soluble in the organic phase, useful results can be obtained. We note, however, that occasionally the excessive formation of di-*tert*-butyl nitroxide is symptomatic of a different process. Thus, during an attempt to detect free radicals following the photoexcitation ($\lambda_{exc}$ = 365 nm) of psoralens (5-hydroxy psoralen, trioxsalen, and 8-methoxypsoralen) in a dimethylsulfoxide solution, di-*tert*-butyl nitroxide was generated exclusively in amounts much larger than in control experiments performed under identical conditions but in the absence of psoralens. We suggest that psoralens photosensitize the homolytic breakdown of MNP (unpublished results from this laboratory).

#### II. *Protein constituents*

The absorption spectrum for peptide bonds shows a peak in the region of 180–190 nm which decreases essentially to zero by about 240 nm (9). It was found that the direct photolyses of aliphatic dipeptides of the types X-Gly, Gly-X, X-Ala, and Ala-X in aqueous solution with 220 ± 10 nm light, generated free radicals as a result of decarboxylation (eq. [4]) (10).

In these dipeptides no scission between the two amino acids residues was observed. The reaction was found to occur over a wide pH range from 2 to

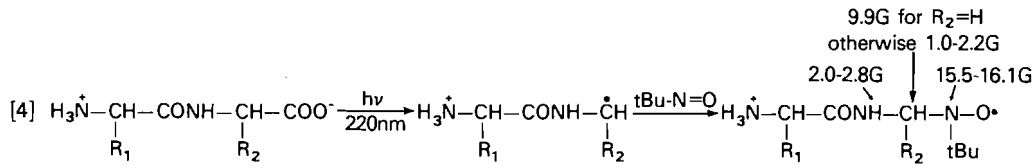


11.5; however, the yield of decarboxylation radicals rises steeply in acid solution below pH = 3.5, suggesting an increase with the concentration of the nonionized form of the carboxyl group.

In strongly alkaline solutions (9 *M* NaOH) this reaction does not occur and only secondary deamination radicals were detected (eq. [5]).

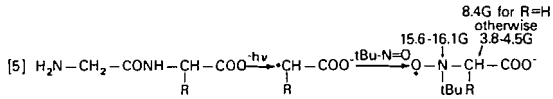


The photolyses of several polypeptides of the type $(Ala)_n$ where $n = 3-90$ was investigated in aqueous solution in order to ascertain whether the decarboxylation radical of the C-terminal residue was the only radical product or whether main-chain scission would occur. The experiments were carried out with solutions containing 10 mg/mL of the polypeptide, and all other conditions of the experiment (spin-trap concentration, pH, duration of photolysis) were kept constant. Under these conditions the concentration of peptide bonds is kept constant while that of the C-terminal carboxyl group decreases with increasing chain length. If the radical products arise only from the C-terminal carboxyl residue, the yield of the decarboxylation radical would be expected to decrease when the number of alanine residues increases from 2 to 90. However, the results indicate that main-chain scission must occur since the radical yield does not decrease appreciably when the average number of alanine residues in the polypeptide is 90.

As a model compound for proteins, poly (Gly-LAla-LPro)$_{12}$ was photolysed. This amino acid sequence frequently occurs in collagen which is the major component of the cornea of the eye. The major radical formed with this compound is the same as the one observed from polyalanine. This indicates that the chain scission occurs predominantly between the alanine and proline residues.

Photodecarboxylation is not limited to aliphatic peptides. It was also found to occur in phenylalanine-containing peptides (11). In this case, the reaction can also be induced by uv light of longer wave-length, that is 260 nm which is absorbed by the aromatic chromophore (eqs. [6], [7]).

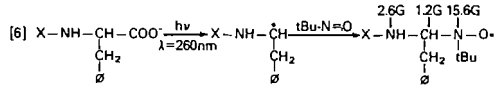


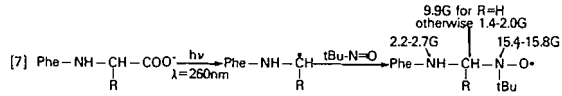


However, when the aromatic chromophore is excited the yield of decarboxylation is not sensitive to pH, and is independent of the state of ionization of the carboxyl group.

In Phe-X type dipeptides the primary deamination radicals were also detected (eq. [8a]).

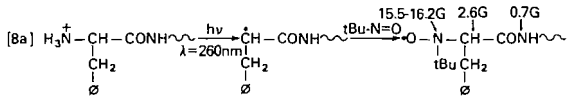


Occasionally the spectrum of spin-trapped benzyl radical generated by photo-dissociation of the Phe residue overlapped the main signal (eq. [8b]).

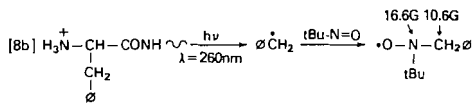


When phenylalanine was embedded in a larger peptide such as ribonuclease-*S*-peptide, following photolyses, chain scission occurred to give a small fragment attached to the decarboxylation radical of the phenylalanine.

In tyrosine-containing peptides several reaction patterns could also be detected (12). While the direct excitation of the peptide bond with $\lambda = 220$ nm consistently generated the decarboxylation radicals, excitation of the aromatic chromophore with $\lambda = 265$ nm in neutral solution yielded a spin adduct formed by trapping of the fragment resulting from the scission between the $\alpha$ carbon atom and the methylene group attached to the aromatic ring (eq. [9]).

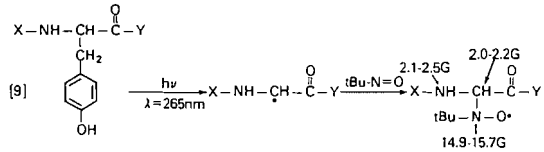


Can. J. Chem. Downloaded from www.nrcresearchpress.com by 210.87.254.42 on 09/06/12
For personal use only.

Can. J. Chem. Downloaded from www.nrcresearchpress.com by 210.87.254.42 on 09/06/12
For personal use only.

In addition, deamination radicals could also be detected. The relative yield of deamination adducts was found to be pH dependent, increasing with the increase in pH. As a model for longer proteins, the oxidized insulin A chain was uv-photolysed. This compound was chosen because it is a relatively short polypeptide (21 amino acids) and contains only two tyrosine residues at positions 14 and 19. In this case the only fragment which could be identified was tentatively attributed to the photoscission of the side chain of the tyrosine moiety. In alkaline medium an additional type of deamination spin adduct was observed which could be a deamination radical from any residue of the chain.

Finally, the photolyses of tryptophan-containing dipeptides ($\lambda = 280 \pm 10$ nm) was investigated (13). Consistently, these compounds generated the deamination radical of the N-terminal amino acid. These results were explained in terms of hydrated electrons photoejected from the tryptophan residue (14) reacting with the carbonyl group followed by deamination of the N-terminus. This mechanism was proved by a sensitization experiment using tryptophan as a sensitizer and glycine as substrate. The ultraviolet irradiation of a mixture of these two amino acids, with light of 280 nm absorbed exclusively by tryptophan, generated the deamination radical spin-adduct of glycine which has very characteristic hyperfine coupling constants (two equivalent β-protons, $a_H^\beta = 9.9$ G).

III. *Nucleic acid constituents*

The photochemical reactions of nucleic acids and their constituents have been the subject of extensive investigations in recent years in attempts to clarify, at the molecular level, the ultraviolet induced damage of living systems. Thus, major photochemical products of pyrimidines such as cyclobutane-type dimers and photohydrates have been correlated to biological effects (15).

We found that direct photolyses of several pyrimidine bases (uracil and substituted derivatives) in aqueous solution ($D_2O$), at room temperature generated free radicals which could be trapped by MNP and characterized (16).

The general reaction pattern is exemplified for uracil in eq. [10] and is consistent with the addition of an unidentified radical (D or OD) at the C(5) position of the uracil ring.

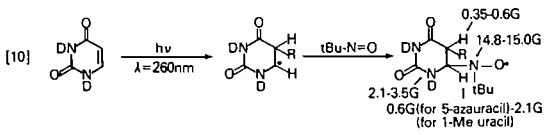


The added radical was unambiguously identified as H when 5-azauracil was photolysed in $H_2O$.

Orotic and isoorotic acid behaved differently. Both these compounds afforded identical 3 × 3 lines spectra suggestive of a radical localized at N(3).

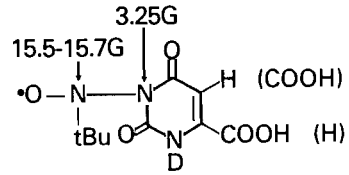


It is, however, noted that in the nucleosides tested, uridine and 2-deoxyuridine, the addition of the D-atom took place at C(6) to yield a paramagnetic center localized at C(5).

All these results indicate that the photochemical excitation of pyrimidine bases yields free radicals as a general phenomenon. While these species cannot lead to the formation of the major photoproducts in irradiated nucleic acids, such as cyclobutane-type dimers and photohydrates, they may precede the formation of dihydropyrimidines and other pyrimidine bimolecular photoproducts.

It is well known that the incorporation of 5-halogenated derivates of uracil in DNA causes an increased sensitivity to the lethal effect of uv-irradiation (17). In order to obtain information concerning the mechanism of photosensitization, the free radicals produced in 5-halopyrimidines by direct uv photolyses in aqueous solution were studied (18).

The general reaction pattern in photolyses of 5-chloro, bromo, iodo uracil was the homolytic cleavage of the carbon–halogen bond (eq. [11]).

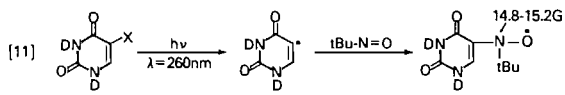


5-Fluorouracil reacted in a different manner; this was the addition of an unidentified radical (H· or OH) to the C(6) position (eq. [12]).

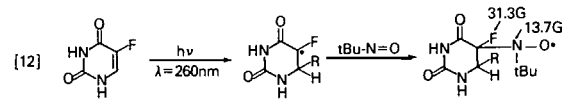


The same basic reactions could be detected when the corresponding nucleosides were photolysed. However, in these cases additional free radicals could be detected, which were tentatively attributed to the abstraction from the C(5′) position of the sugar moiety.

Can. J. Chem. Downloaded from www.nrcresearchpress.com by 210.87.254.42 on 09/06/12
For personal use only.

Finally, we investigated the photolyses of 5,6-dihydropyrimidines (19). The chromophoric group in these compounds is the amido moiety

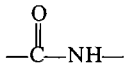

and consequently their photolysis was expected to be induced by light of 220 nm which was required in the photolysis of aliphatic dipeptides. When 5,6-dihydroorotic acid was photolysed under these conditions, decarboxylation occurred at C(6), entirely analogous to the reaction of peptides (eq. [13]).

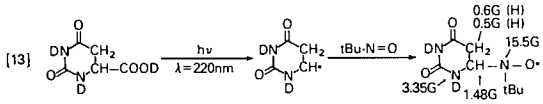

The same type of C(6) centered radical was detected when several alkyl derivatives of 5,6-dihydrouracils, dihydrothymines, and dihydrocytosines were photolysed. The reaction is exemplified for 5,6-dihydrouracil in eq. [14].

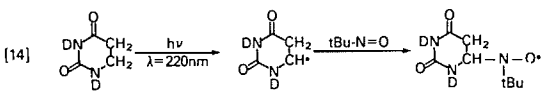

It was noted that the same radicals were trapped when polycrystalline samples of the parent compounds were γ-irradiated and subsequently dissolved in the spin-trap solution.

B. *Photolyses in organic solvents*

I. *Dibenzoylperoxide photo-induced reactions*

Dibenzoylperoxide can photoinitiate the free radical generation in amino acids and peptides by uv-light which is not absorbed by these compounds, that is $\lambda = 313$ nm. The most predominant reaction is the decarboxylation of the amino acids or of the carboxyl-terminal residue in peptides (eq. [15]) (20).

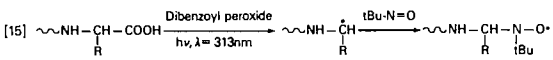

These reactions were performed in dimethylsulfoxide solutions without any interference from the solvent. Over 50 amino acids and dipeptides were tested and followed this reaction pattern. The hyperfine splittings varied between 14.55–15.00 G for nitroxide nitrogen, 2.5–3.0 G for the peptide nitrogen, and 1.0–1.8 G for the β nitrogen. When the glycine residue was terminal and consequently decarboxylated, the two equivalent β-hydrogens had the characteristic large splitting of 7.3 G.

Two mechanistic schemes could explain these results. Both are initiated by the light absorption by dibenzoylperoxide (eq. [16]). Dibenzoylperoxide has a broad adsorption band at $\lambda_{max} = 275$ nm (21) whose end absorption extends beyond 300 nm under our experimental conditions, thus acting as the exclusive light absorption system in the reaction mixture. Subsequently the nucleophilic attack of the carboxyl group cleaves the excited molecule (eq. [17]). Alternatively, the excited dibenzoylperoxide homolyses to benzoyloxy radicals (eq. [18]) which, by one-electron oxidation of the amino acid carboxyl group, generate the corresponding neutral radical (eq. [19]). This species dissociates spontaneously to $CO_2$ and to the trapped decarboxylation radical (eq. [20]).

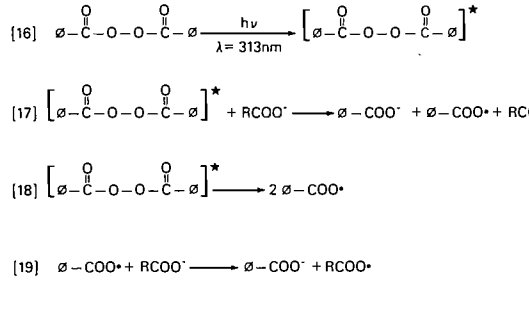

This reaction is not limited to amino acids. Carboxylic acids of different chain-lengths, from formic to linolenic, were tested and found to be decarboxylated by the photoexcited dibenzoylperoxide (22) (eq. [21]).

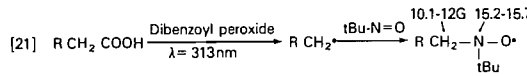

Even pyrimidine bases such as cytosine and thymine can be oxidized by a one-electron transfer under these reaction conditions to generate C(5) centered radicals (eq. [22]).

These results are of interest since dibenzoyl peroxide is extensively used as a topical medication for the treatment of facial acne (23) and was recently discovered to be a potent promoter of carcinogenesis (24).

The present review indicates that MNP is a useful spin-trap for identifying intermediate radical species in the photochemistry of protein and nucleic acid constituents. Since radicals produced in the photolysis of high molecular weight polypeptides (10–12) can be spin-trapped with MNP, it is reasonable to expect that in the future enzymatic hydrolysis followed by high performance liquid chromatography, which allows the separation of nitroxide radicals, will lead to the identification of

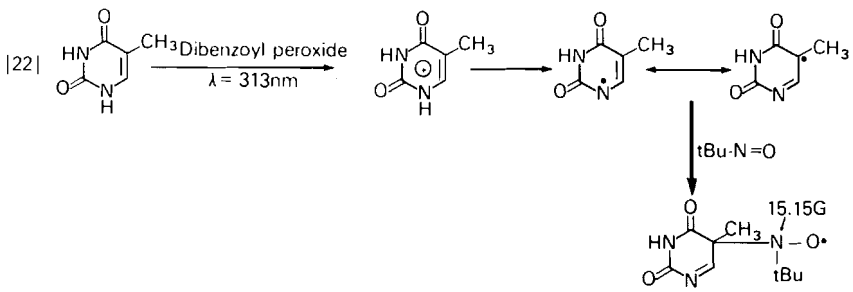


radicals in the photolysis of proteins and nucleic acids.


## Acknowledgements

We acknowledge the invaluable contributions of Drs. M. Kuwabara, Y. Lion, and M. M. Mossoba to the research which is reviewed in the present work.



1. K. C. Smith (*Editor*). Aging, carcinogenesis, and radiation biology. Plenum Press, New York. 1976.
2. K. C. Smith. *In* The science of photobiology. *Edited by* K. C. Smith. Plenum Press, New York. 1977. p. 113.
3. C. Lagercrantz. J. Phys. Chem. **75**, 3466 (1971).
4. E. G. Janzen. *In* Free radicals in biology. Vol. IV. *Edited by* W. A. Pryor. Academic Press, New York. 1980. p. 116.
5. A. Joshi, H. Moss, and P. Riesz. Int. J. Radiat. Biol. **34**, 165 (1978).
6. J. A. Maassen, H. Hittenhausen, and T. J. DeBoer. Tetrahedron Lett. 3213 (1971).
7. T. Doba, T. Ichikawa, and H. Yoshida. Bull. Chem. Soc. Jpn. **50**, 3158 (1977).
8. C. A. Evans. Aldrichimica Acta, **12**, 23 (1979).
9. K. C. Smith and P. C. Hanawalt. Molecular photobiology. Academic Press, New York. 1969. p. 86.
10. Y. F. Lion, M. Kuwabara, and P. Riesz. J. Phys. Chem. **84**, 3378 (1980).
11. Y. F. Lion, M. Kuwabara, and P. Riesz. Photochem. Photobiol. **34**, 297 (1981).
12. Y. F. Lion, M. Kuwabara, and P. Riesz. Photochem. Photobiol. **35**, 43 (1982).
13. Y. F. Lion, M. Kuwabara, and P. Riesz. Photochem. Photobiol. **35**, 53 (1982).
14. E. Amouyal, A. Bernas, and D. Grand. Photochem. Photobiol. **29**, 1071 (1979).
15. S. Y. Wang (*Editor*). Photochemistry and photobiology of nucleic acids. Academic Press, New York. 1976.
16. I. Rosenthal, M. M. Mossoba, and P. Riesz. Int. J. Rad. Biol. **40**, 385 (1981).
17. F. Hutchinson and W. Kohnlein. *In* Progress in molecular and subcellular biology. Vol. 7. Springer-Verlag, Berlin. 1981. p. 1.
18. M. Kuwabara, Y. Lion, and P. Riesz. Int. J. Rad. Biol. **39**, 491 (1981).
19. M. M. Mossoba, I. Rosenthal, and P. Riesz. Int. J. Rad. Biol. **40**, 541 (1981).
20. I. Rosenthal, M. M. Mossoba, and P. Riesz. J. Phys. Chem. **85**, 2398 (1981).
21. L. Lebourgeois, R. Arnaud, and J. Lemaire. J. Chim. Phys. Phys.-Chim. Biol. **69**, 1633 (1972).
22. I. Rosenthal, M. M. Mossoba, and P. Riesz. J. Magn. Reson. **47**, 200 (1982).
23. A. B. Fitzpatrick, A. Z. Eisen, K. Wolff, I. M. Freedberg, and K. F. Austen. Dermatology in general medicine. 2nd ed. McGraw–Hill, New York. 1979. p. 448.
24. T. J. Slaga, A. J. P. Klein-Szanto, L. L. Triplett, L. P. Yotti, and J. E. Trosko. Science, **213**, 1023 (1981).


Can. J. Chem. Downloaded from www.nrcresearchpress.com by 210.87.254.42 on 09/06/12
For personal use only.

# Electron spin resonance of spin trapped radicals in γ-irradiated polycrystalline dipeptides. Chromatographic separation of radicals

KEISUKE MAKINO AND PETER RIESZ

*Laboratory of Pathophysiology, National Cancer Institutes, National Institute of Health, Bethesda, MD 20205, U.S.A.*

Received August 13, 1981

KEISUKE MAKINO and PETER RIESZ. Can. J. Chem. **60**, 1480 (1982).

Polycrystalline dipeptides (glycyl-glycine, glycyl-L-valine, glycyl-L-leucine, L-alanyl-glycine, and L-prolyl-L-alanine) were γ-irradiated at room temperature in the absence of air. Subsequently they were dissolved in aqueous solutions containing 2-methyl-2-nitrosopropane as the spin trap. From the esr spectra of the nitroxide radicals separated by high-performance liquid chromatography, structural assignments of the radicals were made. For glycyl peptides, H-abstraction from the α-carbon atoms of the carboxyl terminal residues and from the side-chains were observed. For L-alanyl-glycine, H-abstraction from the glycyl residue and the formation of the deamination radical could be shown to occur. For L-prolyl-L-alanine, the ring opening (deamination) reaction, decarboxylation and H-abstraction from the C-terminal α-carbon were seen.

KEISUKE MAKINO et PETER RIESZ. Can. J. Chem. **60**, 1480 (1982).

On a irradié aux rayons γ, à la température ambiante et en l'absence d'air, les dipeptides polycristallins suivants: (glycyl-glycine, glycyl-L-valine, glycyl-L-leucine, L-alanyl-glycine et L-prolyl-L-alanine). On les a ensuite dissous dans des solutions aqueuses contenant le capteur de spin, méthyl-2 nitroso-2 propane. A partir des spectres de rpe des radicaux nitroxydes, séparés par chromatographie en phase liquide à haute performance, on a pu déterminer les structures des radicaux. On a observé, dans le cas des peptides glycidiques, l'élimination d'un hydrogène à partir des atomes de carbone en α du residue terminal carbxyle et à partir des chaînes latérales. Dans le cas du L-alanyl-glycine, on peut montrer qu'il se produit une élimination d'hydrogène à partir du résidu glycyle et la formation d'un radical de désamination. Dans le cas du L-prolyl-L-alanine, on a observé une réaction d'ouverture de cycle (désamination), de décarboxylation et d'élimination d'un atome d'hydrogène à partir du carbone terminal en position 2.

[Traduit par le journal]

## Introduction

Among spin trapping studies, 2-methyl-2-nitrosopropane (MNP) has been utilized as one of the most informative spin traps (1–5). However, it is known that when the method of spin trapping with MNP is applied to γ-radiolysis in aqueous solutions, esr spectra obtained are often too complicated to be analyzed accurately. Recently this problem has been overcome by the combination of high-performance liquid chromatography and esr spectroscopy (6–12). By this method, each spin adduct present in the sample is separated and shows its individual esr spectrum.

It has been demonstrated previously that spin trapping with MNP can be applied to the study of the effect of ionizing radiation on polycrystalline solids (13–16). The solids are γ-irradiated and subsequently dissolved in aqueous MNP solutions. By this method, free radicals produced by γ-irradiation of polycrystalline amino acids, *N*-acetyl amino acids, and dipeptides have been analyzed (14). However, when the esr spectra overlap, only major components in the spectra obtained by spin trapping have been analyzed. Since single crystal esr studies of room temperature free radicals produced in such compounds are difficult, particularly when several different radicals are present, the spin trapping method appears to be helpful. For γ-irradiated dipeptides, only glycyl-glycine has been studied by single crystal esr (17) and nine dipeptides have recently been studied by ENDOR and ELDOR of the polycrystalline powder X-irradiated at 77 K and subsequently warmed to room temperature (18).

In the present work, the method of chromatographic separation of nitroxide spin adducts was applied to polycrystalline dipeptides irradiated at room temperature in the absence of air. It should be noted that the validity of this method depends on the stability of the nitroxide spin adduct on the column during the separation.

## Experimental

MNP was purchased from Aldrich Chemical Company and kept under $N_2$ at 5°C in the dark. Dipeptides were obtained from Sigma Chemical Company and Vega Fox Biochemicals.

Aqueous MNP solutions (5 mg/mL) were prepared by stirring in the dark for 1.5 h at 45°C (7).

Polycrystalline dipeptides samples were evacuated at $10^{-4}$ Torr for at least 24 h so that oxygen and moisture could not affect the production of free radicals. The evacuated samples were irradiated with $^{60}$Co γ-rays at a dose rate of $6.0 \times 10^5$ rad/h to a total dose of ca. 20 Mrad at room temperature and subsequently dissolved in the aqueous MNP solutions. The range of dipeptide concentrations was 10–100 mg/mL.

The sample solution (2.0 mL) was loaded on an IEX-210SC column (Toyo Soda, 3/8 in. id × 60 cm) which was attached to the chromatograph (Waters, Model 6000A). A Pyrex flow cell, which was fixed in the esr sample cavity, was connected to the exit of the column with ca. 0.25 mm id Teflon tubing. In order to obtain higher resolution, gradient elution was adopted. Eluents

0008-4042/82/121480-06$01.00/0

©1982 National Research Council of Canada/Conseil national de recherches du Canada

Can. J. Chem. Downloaded from www.nrcresearchpress.com by 210.87.254.40 on 09/06/12
For personal use only.

Can. J. Chem. Downloaded from www.nrcresearchpress.com by 210.87.254.40 on 09/06/12
For personal use only.

were: 0.3 *M* phosphate buffer (pH 6.8) and 0.3 *M* NaOH–$Na_2HPO_4$ buffer (pH 10.8). Other chromatographic conditions were: pressure, ca. 200 psi; flow rate, 0.3 mL/min; temperature, ca. 25°C. The eluate was collected in a fraction collector after passing through the flow cell. During the separation, the magnetic field was fixed at one position and a high amplitude of 10 G modulation was applied to cover a wide range of signal. The collected fractions which showed the chromatographic radical peaks were measured by esr (Varian, E-9, X-band) in the standard aqueous flat cell.

## Results and discussion

In Figs. 1, 2 and 3, the esr spectra obtained from γ-irradiated polycrystalline glycyl dipeptides (glycyl-glycine (Gly-Gly), glycyl-L-valine (Gly-L-Val), and glycyl-L-leucine (Gly-L-Leu)) are shown. Figure 1 displays the original esr spectrum of γ-irradiated Gly-Gly, which was dissolved in an aqueous MNP solution. When this sample solution was loaded on the column, only one peak appeared in the chromatogram. From the fraction which gave the peak, the same spectrum as the original one was obtained. The spectrum changed with pH in acidic solution as shown in the same figure whereas it was not altered in alkaline solution. This suggests that

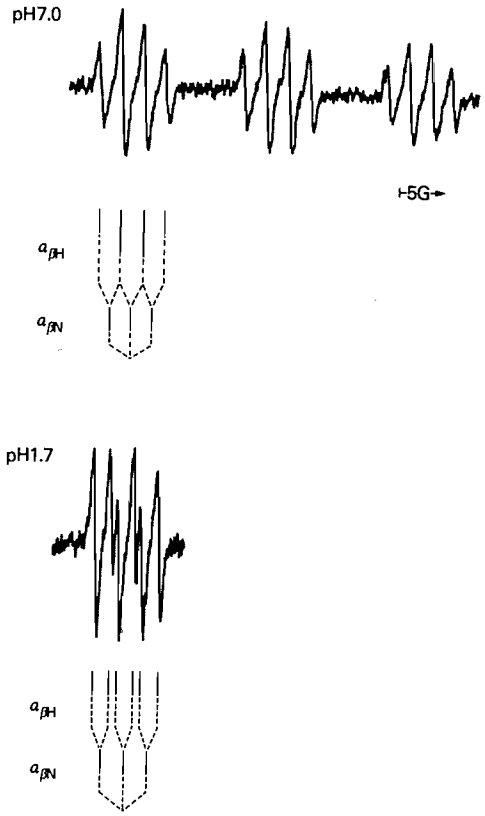


FIG. 1. Electron spin resonance spectra and stick diagram of polycrystalline Gly-Gly γ-irradiated at room temperature and subsequently dissolved in aqueous MNP solutions.

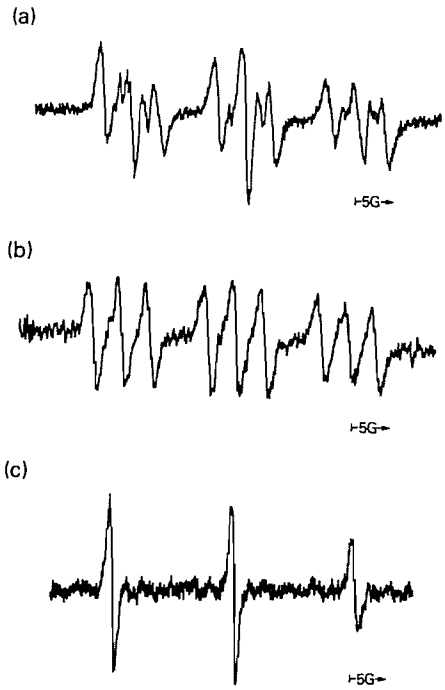


FIG. 2. (*a*) Electron spin resonance spectrum of polycrystalline Gly-L-Val γ-irradiated at room temperature and subsequently dissolved in aqueous MNP solutions. (*b*), (*c*), Electron spin resonance spectra obtained from the same sample by chromatographic separation. The spin adduct whose esr spectrum is shown in (*b*) was eluted faster than the other.

the nitroxide group is close to the carboxyl group. The stick diagram in the same figure shows that the spin adduct has a β-H and a β-N. Consequently the spectrum is assigned to structure **I**

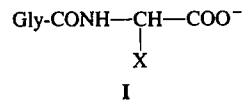


**I**

where X = $^t$Bu—N(O•)— The parent radical of the spin adduct is formed by H-abstraction from the C-terminal carbon. The hyperfine coupling constants (hfcc) measured in the spectrum are listed in Table 1. This spin adduct has been previously identified (12, 17) and the parent radical of **I** has been found in the single crystal studies of Gly-Gly (19).

In Fig. 2(*a*), the original esr spectrum of γ-irradiated Gly-L-Val which was dissolved in the spin trap aqueous solution is shown. Overlapping lines are observed in the spectrum. By chromatographic separation, two different esr spectra were obtained as shown in Fig. 2 (*b*) and (*c*), respectively. The spectrum in Fig. 2 (*b*) consists of triplet split into a further triplet with a 1:1:1 intensity ratio. The

Can. J. Chem. Downloaded from www.nrcresearchpress.com by 210.87.254.40 on 09/06/12
For personal use only.

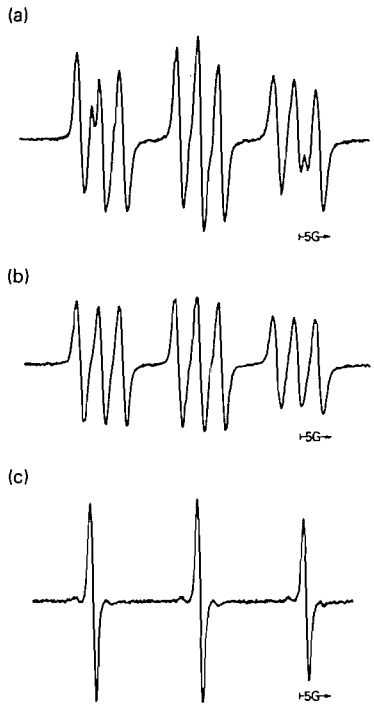


FIG. 3. (*a*), Electron spin resonance spectrum of polycrystalline Gly-L-Leu γ-irradiated at room temperature and subsequently dissolved in aqueous MNP solutions. (*b*), (*c*), Electron spin resonance spectra obtained from the same sample by chromatographic separation. The spin adduct whose esr spectrum is shown in (*b*) was eluted faster than the other.

TABLE 1. Hyperfine coupling constants of the separated spin adducts*

| | Hyperfine coupling constants (G) | | | | |
|---|---|---|---|---|---|
| Spin adduct | N | β-H | β-N | γ-H | γ-N |
| **I** | 15.5 | 2.2 | 2.4 | | |
| **II** | 15.4 | | 3.8 | | |
| **III** | 16.5 | | | | |
| **IV** | 15.5 | | 3.4 | | |
| **V** | 16.7 | | | | |
| **VI** | 15.7 | 2.6 | 2.6 | 0.5 | 0.5 |
| **VII** | 15.4 | 2.4 | 2.4 | | |
| **VIII** | 15.8 | 2.0 | 2.3 | | |
| **IX** | 15.3 | | 3.3 | | |
| **X** | 15.4 | 3.6 | | 0.6 | 0.6 |

*All the values were obtained in neutral solutions.

primary splitting is due to a N nucleus in the nitroxide group and the secondary splitting is attributed to the β-N in the peptide group. The unusually broad lines imply that the spin adduct might contain γ-nuclei with different characteristics. Consequently the spectrum is assigned to the spin adduct formed by H-abstraction from the C-terminal α-carbon (**II**). The spectrum was unchanged with pH in alkaline solutions. The other spectrum shown in Fig. 2 (*c*) has only three lines, implying that the spin adduct does not have any β-nuclei. The only possible structure is

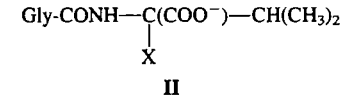


**II**

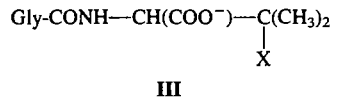


**III**

The untrapped free radical of **III** is produced by H-abstraction from the side-chain carbon of the C-terminal carbon. The hfcc of spin adduct **II** and **III** are shown in Table 1. The spin adduct **III** could not be found in a previous work (14).

Similar to the results obtained with Gly-L-Val, in the analogous experiment with Gly-L-Leu, a triple–triplet and a simple triplet were detected as shown in Fig. 3 (*b*) and (*c*), respectively. According to the assignment made for the spectrum in Fig. 2 (*b*), the spectrum in Fig. 3 (*b*) is assigned to structure **IV**. The parent radical of the spin adduct **IV** is formed by H-abstraction from the C-terminal α-carbon. The spectrum was unchanged with pH in alkaline

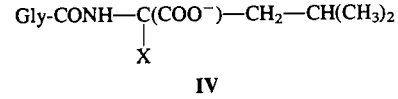


**IV**

solutions. The triplet in Fig. 3 (*c*) is also consistent with structure **V**. The hfcc of the spin adducts **IV** and **V** are summarized in Table 1.

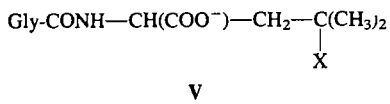


**V**

Considering the results obtained in the γ-radiolysis and subsequent spin trapping of three glycyl dipeptides, the following facts were revealed: (*1*), The deamination radicals which are usually observed in the analogous experiments with amino acids are not detected. (*2*), The decarboxylation radical is not observed. (*3*), The major products are the spin adducts whose parent radicals are generated by H-abstraction from the C-terminal α-carbon and the carbon of the side-chain on the C-terminal residue. In previous papers (20, 21), it has been demonstrated that the deamination radicals, which are produced by the reaction of the hydrated electron with these three dipeptides and the decarboxylation radicals, which are generated by the

Can. J. Chem. Downloaded from www.nrcresearchpress.com by 210.87.254.40 on 09/06/12
For personal use only.

reaction of $SO_4^{\cdot -}$ can be efficiently spin trapped with MNP.

From γ-irradiated polycrystalline L-Ala-Gly which was dissolved in an aqueous MNP solution, two kinds of esr spectra were detected by the method of chromatographic separation, as shown in Fig. 4 (*b*) and (*c*), respectively. The spin adduct giving the spectrum in Fig. 4 (*b*) was eluted very fast compared to the other one. As exhibited by the expanded spectrum of the $M_I = 0$ component of Fig. 4 (*b*) and by the stick diagram in the same figure, the primary N triplet is split into doublets due to a β-H which are further split into sextets with an intensity ratio of 1:4:7:7:4:1 by three equivalent γ-hydrogens and a γ-N. Consequently the spectrum can be assigned to the spin adduct which is produced by deamination, **VI**.

$$\begin{array}{l} CH_3—CH—CONH\text{-}Gly \\ \quad\quad\ | \\ \quad\quad\ X \end{array}$$

**VI**

The other spectrum shown in Fig. 4 (*c*) consists of a triplet which is further split into four lines due to a β-H and a β-N. The structure of the spin adduct is

$$L\text{-}Ala\text{-}CONH—CH(COO^-)—X$$

**VII**

The hfcc are listed in Table 1. Both the spin adduct **VI** and **VII** have been detected previously (14). In the same paper (14), the spin adduct produced by decarboxylation has been found.

Figure 5 (*a*) shows the original esr spectrum of γ-irradiated polycrystalline L-Pro-L-Ala dissolved in an aqueous MNP solution. The major component in the spectrum consists of a triplet further split into four lines. This has been analyzed previously (14) as the decarboxylation radical, **VIII**.

$$L\text{-}Pro\text{-}CONH—CH(CH_3)—X$$

**VIII**

Using chromatographic separation, two other spectra could be obtained from the same sample solution, as shown in Fig. 5 (*b*) and (*c*), respectively. The triple triplet in Fig. 5 (*b*) is attributed to a N nucleus in the nitroxide group and to a β-N nucleus

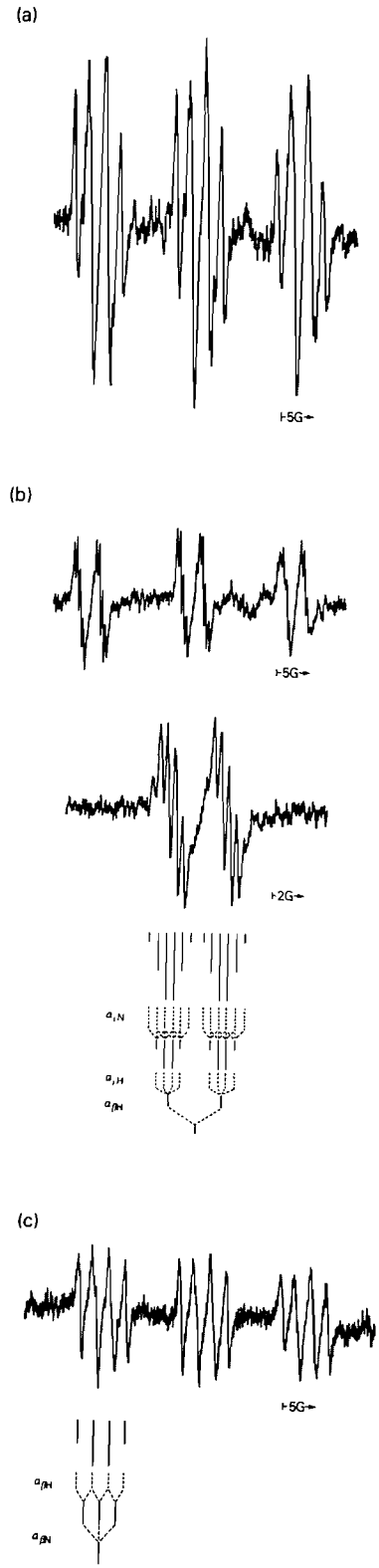


FIG. 4. (*a*), Electron spin resonance spectrum of polycrystalline L-Ala-Gly γ-irradiated at room temperature and subsequently dissolved in aqueous MNP solutions. (*b*) Electron spin resonance spectrum of the separated spin adduct and the expansion of the $M_I = 0$ component with the stick diagram. (*c*) Electron spin resonance spectrum of the separated spin adduct, which was eluted more slowly than that whose esr spectrum is shown in (*b*).

Can. J. Chem. Downloaded from www.nrcresearchpress.com by 210.87.254.40 on 09/06/12
For personal use only.

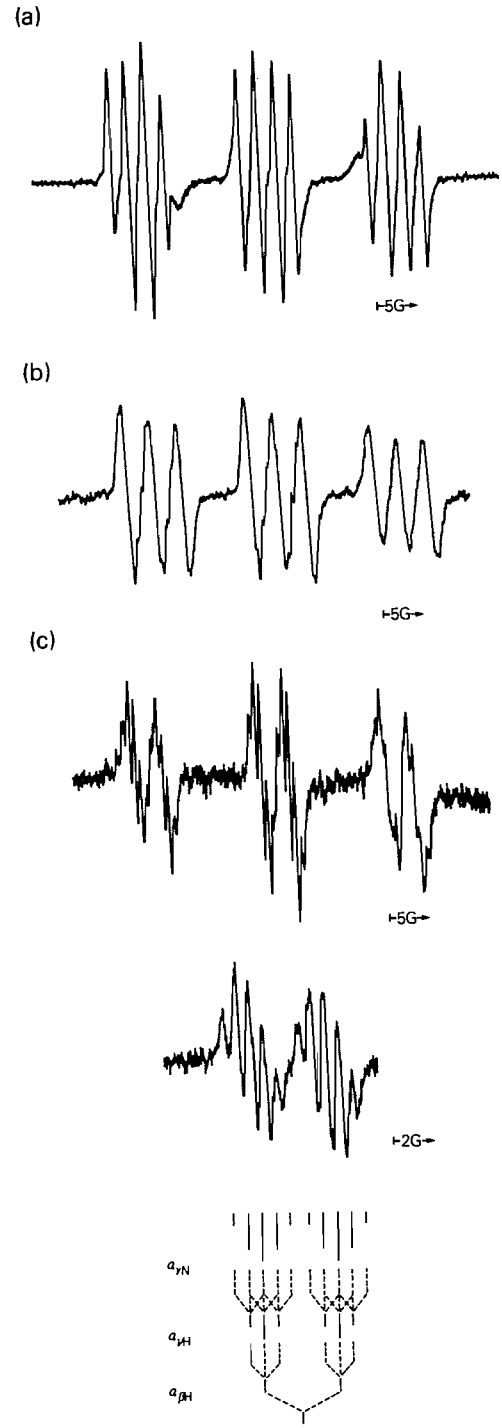


FIG. 5. (*a*) Electron spin resonance spectrum of polycrystalline L-Pro-L-Ala γ-irradiated and subsequently dissolved in aqueous MNP solutions. (*b*) Electron spin resonance spectrum of the separated spin adduct, which was eluted faster than the other. (*c*) Electron spin resonance spectrum of the separated spin adduct and the expansion of the $M_I = 0$ component with the stick diagram.

in the peptide group. The structure of the spin adduct is

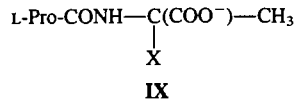


**IX**

This spin adduct has not been found previously. The fine structure due to γ-hydrogens could not be observed even when a low modulation amplitude was used. In Fig. 5 (*c*), the other spectrum is shown with the expansion of the $M_I = 0$ component and its stick diagram. The triple doublet is split into five lines with an intensity ratio of 1:3:4:3:1. This spectrum is due to the ring opening (deamination) radical which has been identified (14);

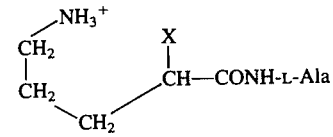


**X**

The hfccs of spin adducts **VIII**, **IX**, and **X** are listed in Table 1.

In experiments with γ-irradiated polycrystalline L-Ala-Gly and L-Pro-L-Ala, the deamination radicals and the decarboxylation radical could be detected in addition to the spin adducts produced by H-abstruction. These results are quite different from those obtained in the experiments of γ-irradiated polycrystalline glycyl dipeptides (Gly-Gly, Gly-L-Val, and Gly-L-Leu).

The present work indicates that spin trapping combined with high-performance liquid chromatography is a useful method, apart from single crystal esr, for studying the room-temperature free radicals in γ-irradiated polycrystalline peptides. Further work remains to be done to establish quantitative methods for determining free radical distributions in γ-irradiated solids.

1. C. LAGERCRANTZ. J. Am. Chem. Soc. **95**, 220 (1973).
2. S. RUSTGI, A. JOSHI, H. MOSS, and P. RIESZ. Int. J. Radiat. Biol. **31**, 415 (1977).
3. S. RUSTGI, A. JOSHI, P. RIESZ, and F. FRIEDBERG. Int. J. Radiat. Biol. **32**, 533 (1977).
4. H. TANIGUCHI and H. HATANO. Chem. Lett. 531 (1974).
5. H. TANIGUCHI and H. HATANO. Chem. Lett. 9 (1975).
6. K. MAKINO. J. Phys. Chem. **83**, 2520 (1979).
7. K. MAKINO. J. Phys. Chem. **84**, 1012 (1980).
8. K. MAKINO. J. Phys. Chem. **84**, 1016 (1980).
9. K. MAKINO. J. Phys. Chem. **84**, 1968 (1980).
10. F. MORIYA, K. MAKINO, N. SUZUKI, S. ROKUSHIKA, and H. HATANO. J. Phys. Chem. **84**, 3085 (1980).
11. N. SUZUKI, K. MAKINO, F. MORIYA, S. ROKUSHIKA, and H. HATANO. J. Phys. Chem. **85**, 263 (1981).
12. F. MORIYA, K. MAKINO, N. SUZUKI, S. ROKUSHIKA, and H. HATANO. J. Phys. Chem. **84**, 3614 (1980).

13. C. LAGERCRANTZ and S. FORSHULT. Nature, London, **218**, 1247 (1968).
14. A. MINEGISHI, R. BERGENE, and P. RIESZ. Int. J. Radiat. Biol. **38**, 627 (1980).
15. M. KUWABARA, Y. LION, and P. RIESZ. Int. J. Radiat. Biol. **39**, 451 (1981).
16. M. MOSSOBA, I. ROSENTHAL, and P. RIESZ. Int. J. Radiat. Biol. **40**, 397 (1981).
17. A. JOSHI, S. RUSTGI, H. MOSS, and P. RIESZ. Int. J. Radiat. Biol. **33**, 205 (1978).
18. T. HENRIKSEN, T. B. MELO, and G. SAXEBØL. Free radicals in biology. Vol. 2. *Edited by* W. A. Pryor. New York. Academic Press, Inc. p. 213.
19. J. S. HWANG, A. C. DICKINSON, and L. D. KISPERT. J. Phys. Chem. **83**, 3381 (1979).
20. S. RUSTGI and P. RIESZ. Int. J. Radiat. Biol. **34**, 127 (1978).
21. S. N. RUSTGI and P. RIESZ. Int. J. Radiat. Biol. **34**, 301 (1978).

Can. J. Chem. Downloaded from www.nrcresearchpress.com by 210.87.254.40 on 09/06/12
For personal use only.

# Spin-trapping with 2-methyl-2-nitrosopropane: photochemistry of carbonyl-containing compounds. Methyl radical formation from dimethyl sulfoxide

IONEL ROSENTHAL,[1] MAGDI M. MOSSOBA, AND PETER RIESZ

*Laboratory of Pathophysiology, National Cancer Institute, National Institutes of Health, Bethesda, MD 20205, U.S.A.*

Received September 1, 1981

IONEL ROSENTHAL, MAGDI M. MOSSOBA, and PETER RIESZ. Can. J. Chem. **60**, 1486 (1982).

The photochemical reactions of several carbonyl-containing compounds investigated by spin-trapping with 2-methyl-2-nitrosopropane revealed different modes of scission depending on the structure of the initial compound. Thus, in photo-Fries rearrangements, the acyl radical was detected. 1,3-Diphenyl-2-propanone decarbonylated to yield the benzyl radical. Finally, valerophenone yielded the radicals expected by γ-hydrogen abstraction. In a dark reaction, dimethyl sulfoxide reacts with NaOH to generate methyl radicals. The latter result suggests the need for caution in the use of dimethyl sulfoxide with 2-methyl-2-nitrosopropane for the detection of hydroxyl radicals.

IONEL ROSENTHAL, MAGDI M. MOSSOBA et PETER RIESZ. Can. J. Chem. **60**, 1486 (1982).

Les réactions photochimiques de plusieurs composés contenant un carbonyle, étudiés par captage de spin avec le méthyl-2 nitroso-2 propane, révèlent des modes différents de scission selon la structure du composé de départ. Ainsi dans les réarrangements photochimiques de Fries, on a décelé le radical acyle. La diphényl-1,3 propanone-2 par décarbonylation conduit au radical benzyle. Finalement, la valérophénone donne les radicaux attendus par élimination γ d'hydrogène. A l'abri de la lumière, le diméthylsulfoxyde réagit avec la NaOH en générant des radicaux méthyles. Ce dernier résultat suggère d'utiliser avec précaution le diméthylsulfoxyde avec le méthyl-2 nitroso-2 propane lors de la détection des radicaux hydroxyles.

[Traduit par le journal]

## Introduction

The advent of the spin-trapping method in esr spectroscopy (1, 2) has facilitated the identification of the free radicals produced at room temperature in fluid solutions. Consequently, it is feasible to use spin-trapping to provide direct support for conceivable reaction pathways, otherwise indirectly implied, in various chemical processes, or to reveal the basic chemical reactions.

In this note we report the results of studying several chemical reactions by spin-trapping with 2-methyl-2-nitrosopropane (MNP).

## Experimental

Spin-trap solutions were prepared by dissolving about 1–1.5 mg of MNP per mL of organic solvent at room temperature in the dark for 20 min. Aqueous solutions of MNP were prepared by stirring 1.5 mg of MNP per mL of $H_2O$ (or $D_2O$) at room temperature in the dark overnight. MNP, phenyl acetate, phenyl benzoate, acetanilide, 1,3-diphenyl-2-propanone, valerophenone, dibenzoyl peroxide, and hexadecyltrimethylammonium chloride were purchased from Aldrich Chemical Co. 1,8-Diaminooctane was obtained from Sigma Chemical Co. Hydrogen peroxide (30%) was acquired from Fisher Scientific Co. Deuterium oxide (99.8%) was purchased from Bio-Rad Laboratories.

The photolyses were performed *in situ* at room temperature, in aerated solutions, in the standard aqueous quartz cell (60 × 10 × 0.25 mm) placed in the esr cavity, using a Schoeffel 1000 W high pressure Hg–Xe lamp coupled with a grating monochromator. The irradiation time was about 5 minutes.

A Varian E-9, X-band Spectrometer was used for esr measurements. The magnetic field modulation frequency was 100 kHz. The scans were traced with a modulation amplitude equal to, or lower than 0.2 G, and the microwave power level was maintained at 10 mW to avoid saturation. An NMR Gauss Meter was used to calibrate the magnetic field. The hyperfine couplings are accurate to ± 0.05 G. All esr measurements were carried out at room temperature.

[1] On sabbatical leave from Department of Technology, Agricultural Research Organization, Volcani Center, Bet-Dagan, Israel.

## Results and discussion

The short-lived radicals generated by uv photolysis which react with MNP to produce stable nitroxide radicals exhibit a primary triplet hyperfine coupling from the $^{14}N$ of the nitroxyl group. The primary triplet is split into secondary lines which generally arise from the interaction of the free electron with the magnetic nuclei of the trapped radical. The α, β, and γ positions of the nuclei on the spin adduct are defined with respect to the nitroxyl nitrogen as illustrated below:

$$(CH_3)_3CN(\dot{O})C^{\alpha}H_2^{\beta}—C^{\beta}H_2^{\gamma}—$$

### I. *Study of the photo-Fries rearrangement*

The photo-Fries rearrangement has attracted intensive attention (3) (eq. [1])

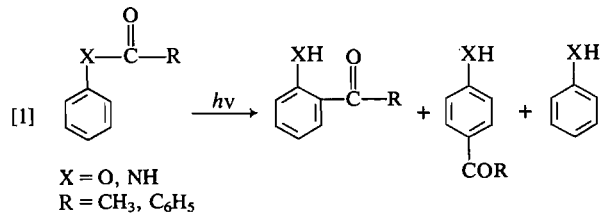


X = O, NH
R = $CH_3$, $C_6H_5$

Flash photolyses (4) and CIDNAP studies (5) indicated the homolytic cleavage of the O-acyl

0008-4042/82/121486-07$01.00/0

©1982 National Research Council of Canada/Conseil national de recherches du Canada

Can. J. Chem. Downloaded from www.nrcresearchpress.com by 210.87.254.40 on 09/06/12
For personal use only.

TABLE 1. Hyperfine coupling constants $a_{N(nitroxyl)}$ (G) of the spin-trapped radicals in the photo-Fries rearrangement at 260 ± 10 nm

| Substrate | Radical | $a_{N(nitroxyl)}$ | | | |
|---|---|---|---|---|---|
| | | $CH_3OH$ | $CH_3CN$ | $C_6H_6$ | Dioxan |
| Phenyl acetate | $CH_3CO\cdot$ | 7.8 | 7.9 | 7.8 | 8.0 |
| Phenyl benzoate | $C_6H_5CO\cdot$ | 8.1 | 8.1 | 8.0 | 8.0 |
| Acetanilide | $CH_3CO\cdot$ | 7.8 | 7.9 | 7.8 | 8.0 |

bond, as the first step in the rearrangement of aryl esters.

We attempted the direct detection of the free radicals involved in the photo-Fries rearrangements of phenyl acetate, phenyl benzoate, and acetanilide by spin-trapping with MNP. Thus, MNP solutions containing the substrates (50 μL/mL) in different solvents were irradiated with light of λ = 260 ± 10 nm.

In all cases, a spectrum composed of a sharp triplet was recorded, and it was assigned to acyl radicals in view of the characteristically small hyperfine splittings of the nitrogen of the nitroxyl group (6). The results of these experiments are summarized in Table 1. The aromatic radical counterpart of the acyl radical could not be spin-trapped. Occasionally, di-*tert*-butylnitroxide radical (DTBN) was also detected and the lines due to DTBN are labelled (S) in the figures. The $^{14}N$ hyperfine coupling constants of the nitrogen of the nitroxyl group were 16.03 G (methanol) and 15.15 G (benzene or acetonitrile).

Parenthetically, we noted that an unusual spin adduct was recorded when the photolysis of phenyl acetate in acetonitrile was induced with light of λ = 313 ± 10 nm. This spin adduct (Fig. 1a) could be analyzed in terms of 3 × 3 × 3 lines and was initially attributed tentatively to the hydrogen atom abstraction from acetonitrile (I) ($a_N$ = 15.3 G, $a_H$ = 10.9 G (2H), and $a_N$ = 2.0 G).

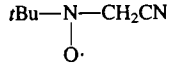

I

Spin adduct I was not reported previously in the literature, acetonitrile being considered to be fairly inert to radical attack.[2] However, by reaction of acetonitrile with OH· generated photochemically from $H_2O_2$ (100 μL of 30% $H_2O_2$ per mL of $CH_3CN$ containing MNP (1 mg/mL) irradiated with λ = 260 nm for 20 s) we successfully generated I and recorded it as a simple triplet of triplets (Fig. 1b) of $a_{N(nitroxyl)}$ = 15.5 G and $^{\beta}a_H$ = 9.0 G (2H). Furthermore, the 313 nm photolyses of phenyl acetate in solvents other than $CH_3CN$, such as benzene, also generated a similar 3 × 3 × 3 line spectrum ($a_{N(nitroxyl)}$ = 14.8 G, $^{\beta}a_H$ = 10.9 G (2H) and $^{\beta}a_N$ = 2.0 G) which under these circumstances can be attributed only to radical II, whose complete structure could not be ascertained from the present data, in which the nitrogen originates from the spin trap.

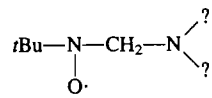

II

II. *Photodecarbonylation of 1,3-diphenyl-2-propanone*

1,3-Diphenyl-2-propanone is one of the few non-cyclic ketones which loses carbon monoxide nearly quantitatively and with high quantum yield when irradiated (7–10) (eq. [2]).

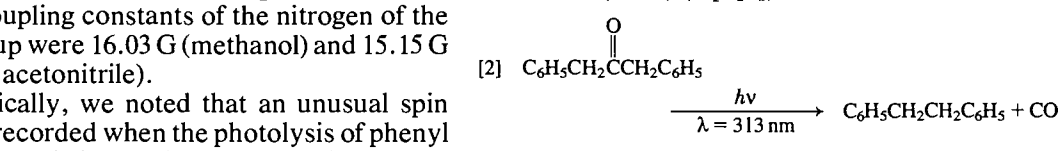

[2]

A free radical mechanism which involves decarbonylation and radical recombination was suggested on the basis of the analyses of the chemical products (7–9) and CIDNAP studies (11). The question of whether the mechanism is concerted, or stepwise, involving the formation of phenylacetyl radical and benzyl radical, has been decided in favor of the latter (10) by experiments of radical recombination of these two radicals with the nitroxide 2,2,6,6-tetramethylpiperidine-1-oxyl.

We found that the uv irradiation (λ = 313 nm) of 1,3-diphenyl-2-propanone ($5 \times 10^{-4}$ *M*) in different solvents at room temperature generated benzyl radical which could be detected as its spin adduct with MNP (III) (Fig. 2). DTNB was found in addition to radical III when dilute solutions of 1,3-diphenyl-2-propanone were photolyzed in

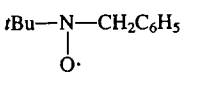

III

[2] Y. Y. Wang and L. T. Williams, unpublished results cited in ref. 2, p. 134.

Can. J. Chem. Downloaded from www.nrcresearchpress.com by 210.87.254.40 on 09/06/12
For personal use only.

Can. J. Chem. Downloaded from www.nrcresearchpress.com by 210.87.254.40 on 09/06/12
For personal use only.

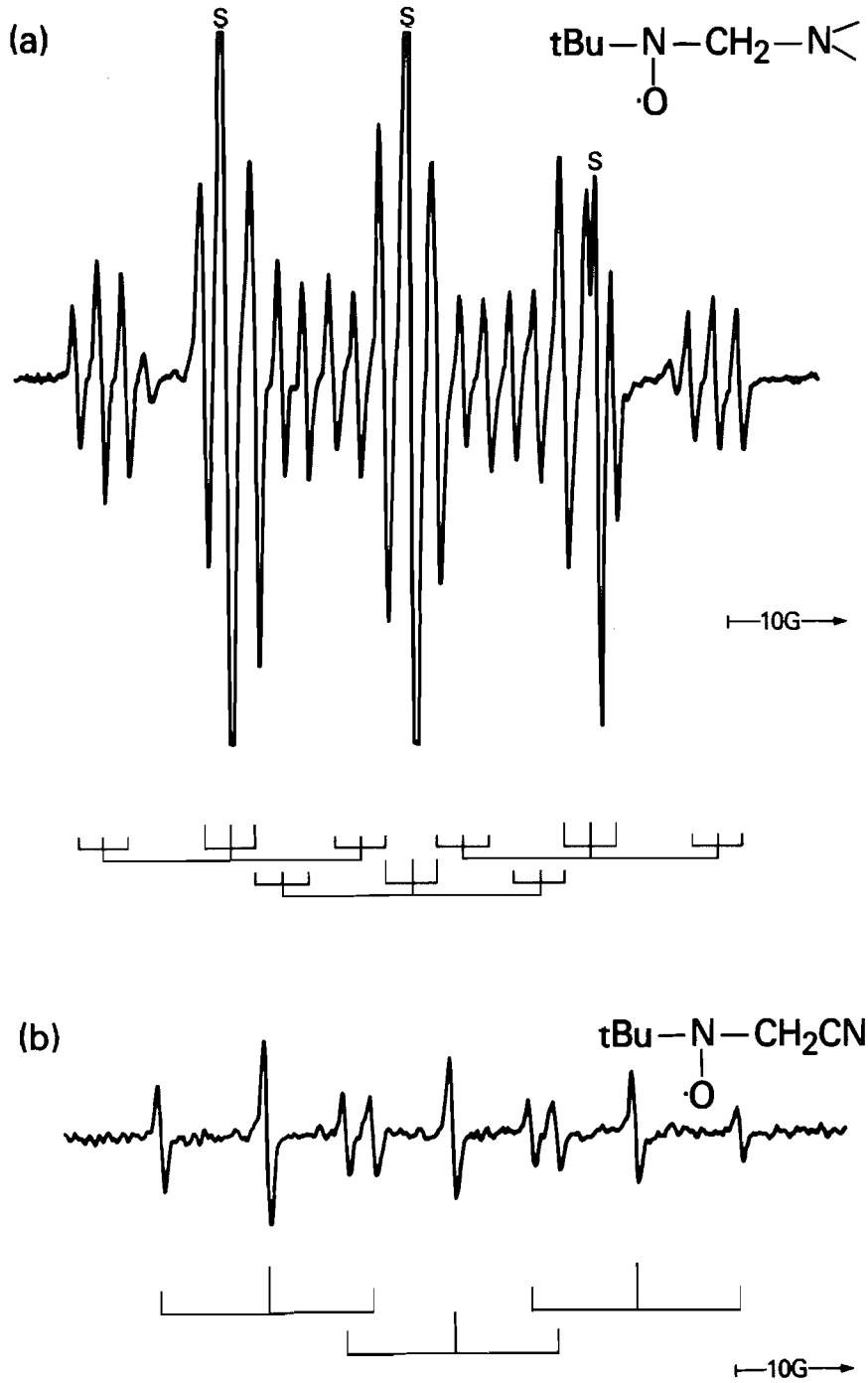


FIG. 1. The esr spectrum of the spin-trapped radical from (a) 313 nm photolysis of phenyl acetate in $CH_3CN$ in the presence of MNP; (b) 260 nm photolysis of $CH_3CN$ containing MNP and $H_2O_2$. The lines labelled (S) are due to DTBN.

aqueous solutions in which this ketone is only slightly soluble. The hyperfine coupling constants of radical III are summarized in Table 2.

Since no acyl radicals could be detected in our reaction conditions, we assume that the rate of decarbonylation of the phenylacetyl radical is much faster than its addition to MNP. The failure to trap the phenyl acetyl radical with MNP has been reported previously in benzene at 40°C (12).

The recombination of benzyl radicals generated

Can. J. Chem. Downloaded from www.nrcresearchpress.com by 210.87.254.40 on 09/06/12
For personal use only.

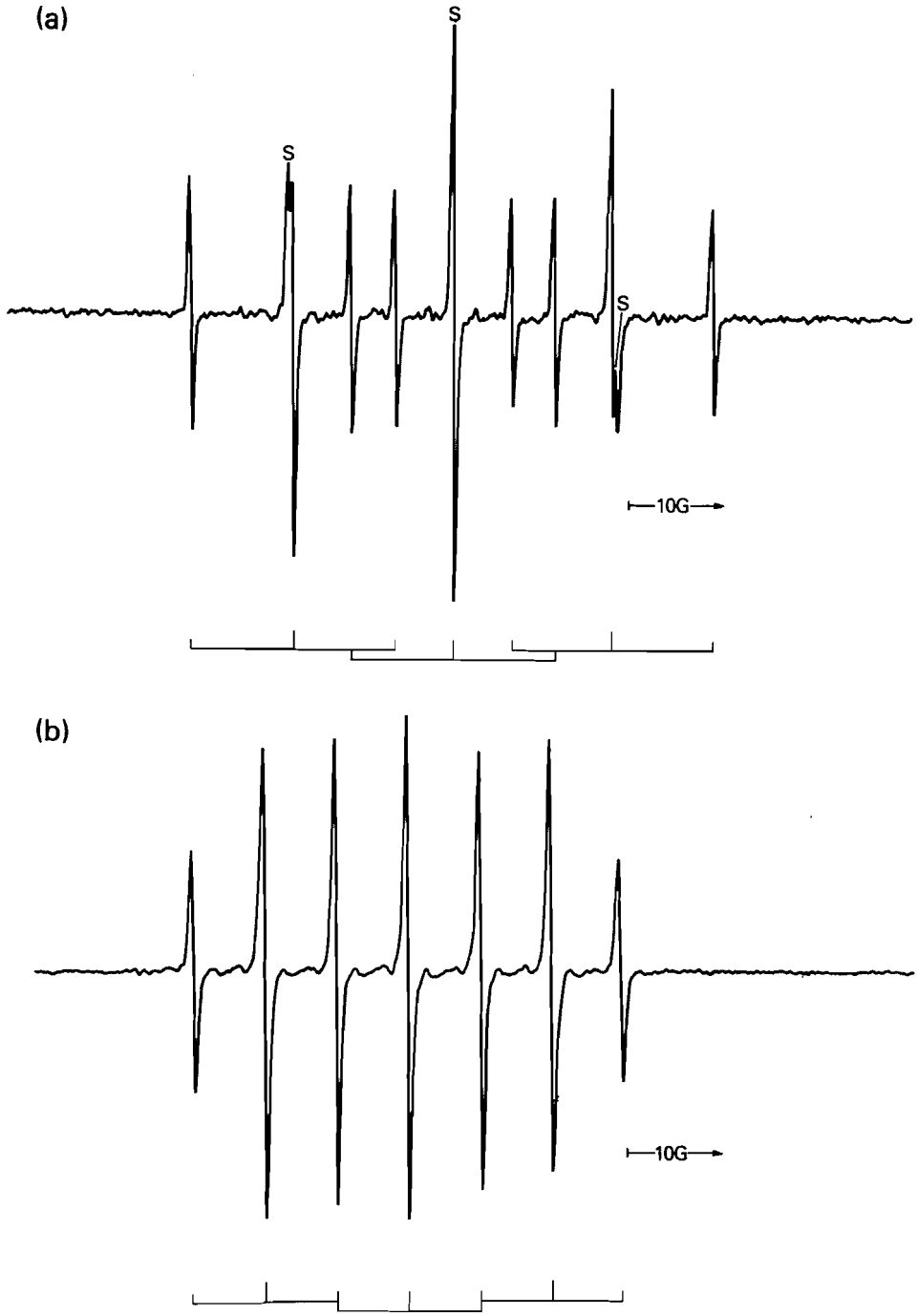


FIG. 2. The esr spectrum of the spin-trapped benzyl radical from 313 nm photolysis of 1,3-diphenyl-2-propanone in the presence of MNP in (a) water and (b) benzene. The lines labelled (S) are due to DTBN.

by photodecarbonylation of dibenzyl ketones has been shown to be predetermined in micellar solution (13, 14). We attempted to trap the benzyl radical under these conditions ($5 \times 10^{-2}$ *M* hexadecyltrimethylammonium chloride in water which is above the critical micelle concentration) at concentrations of 1,3-diphenyl-2-propanone ($5 \times 10^{-4}$ *M*) employed for its detection in other solvents. However, the exclusive paramagnetic species detected was di-*tert*-butylnitroxide ($a_N$ = 16.6 G). Since in micellar solution at the concentration ratio employed, the benzyl radical generation is confined to

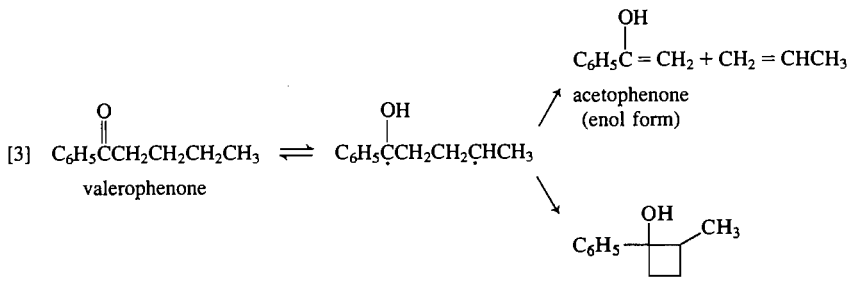


the small hydrophobic portion of the micelle with very little diffusion out (13), radical recombination is highly favored, leaving no chance for competitive trapping by MNP. When, however, the same experiment was repeated at a much higher ketone concentration ($5 \times 10^{-3}$ *M*) so that the ketone is forced into the aqueous phase, the photolysis occurs as in a homogeneous solution and the benzyl spin adduct could be detected.

III. *Photolyses of valerophenone*

The photoinduced intramolecular γ-hydrogen abstraction by the triplet state of phenyl alkyl ketones has been well documented (15–17) (eq. [3]).

The irradiation of valerophenone at 313 ± 10 nm in the presence of MNP generated a mixture of two radicals (Fig. 3). The predominant one, which was stable in the dark after initial photogeneration (radical A), showed a triplet of doublets attributed to intramolecular γ-hydrogen abstraction (IV). The

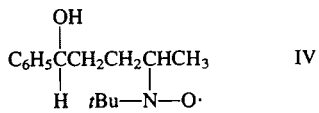


IV

minor signal which could be detected only during uv-irradiation (radical B) could be analyzed in terms of 3 × 3 lines, and it was attributed to radical (V). The H-atom could be abstracted from acetophenone by photoexcited valerophenone or acetophenone, in an intermolecular reaction subsequent to the cleavage of valerophenone (18). Thus, the identity of radical (V) was confirmed by irradiating solutions of acetophenone in benzene and acetonitrile in the presence of MNP. The results are summarized in Table 3.

TABLE 2. Hyperfine coupling constants (G) of benzyl radical spin adducts obtained by uv photolysis of 1,3-diphenyl-3-propanone at 313 ± 10 nm

| Solvent | $a_{N(nitroxyl)}$ | $^{\beta}a_H$ |
|---|---|---|
| $H_2O$ | 16.63 | 10.56 |
| $D_2O$ | 16.63 | 10.56 |
| Benzene | 15.00 | 7.50 |
| Methanol | 15.80 | 8.50 |
| Acetonitrile | 15.23 | 8.53 |

The photolysis of valerophenone was suggested

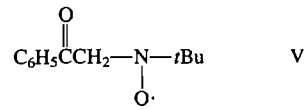


V

as a device to probe solute location in micelles (19). When valerophenone (0.01 *M*) was irradiated in an aqueous solution of MNP (1.5 mg/mL) containing hexadecyltrimethyl ammonium chloride ($5 \times 10^{-2}$ *M*), two overlapping spectra were recorded. Again, the major and the stable one, composed of a triplet of doublets, is explained by the attachment of a —CH— radical to the spin trap ($a_{N(nitroxyl)}$ = 15.56 G, $^{\beta}a_H$ = 1.9 G). This radical could originate from the intramolecular γ-hydrogen abstraction in valerophenone or intermolecular H-abstraction from the alkyl chain of the surfactant by valerophenone. The less prominent signal of 3 × 2 lines of equal intensity was light-dependent and was attributed to the H-adduct (VI).

FIG. 3. The esr spectrum of the spin-trapped radical from photolysis of valerophenone in the presence of MNP at 313 nm.

Can. J. Chem. Downloaded from www.nrcresearchpress.com by 210.87.254.40 on 09/06/12
For personal use only.

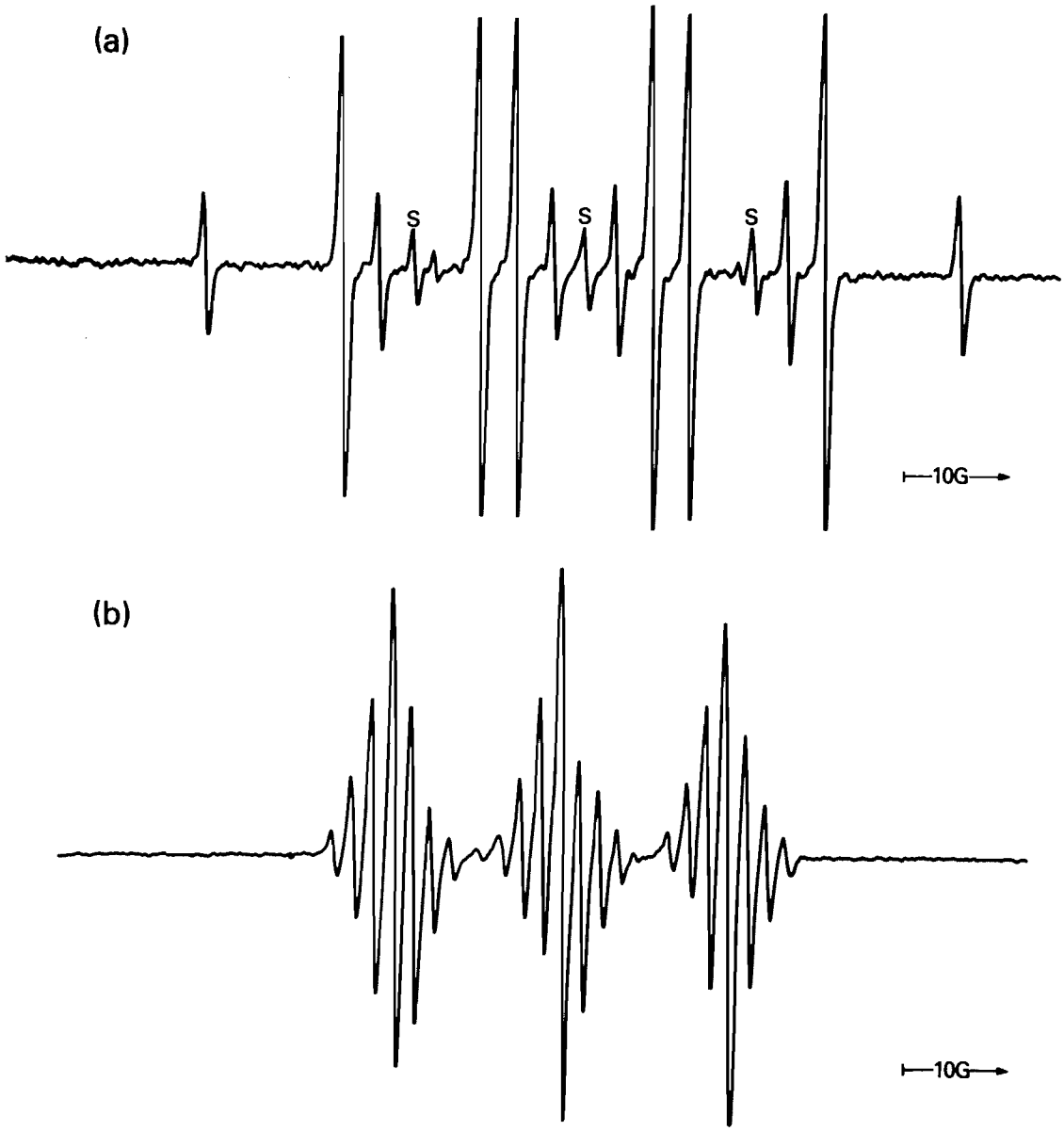


FIG. 4. The esr spectrum of the spin-trapped (a) $CH_3$-radical and (b) $CD_3$-radical, generated in the dark reactions between dimethyl sulfoxide and NaOH in the presence of MNP. The lines labelled (S) are due to DTBN.

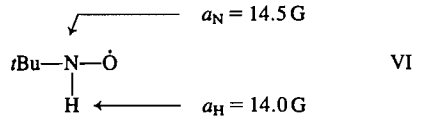


VI

The formation of the H-adduct can be easily explained by the reaction of an unstable phenylbutylhydroxyl radical with MNP (20–23) (eq. [4]).

## IV. *On the generation of methyl radical from dimethyl sulfoxide*

The photochemically generated OH-radicals react with dimethyl sulfoxide to generate methyl radicals which are trapped by MNP to yield a very persistent and characteristic spin adduct (24). This reaction has been used in biological systems to detect OH radicals (25).

We found, however, that dimethyl sulfoxide can

[4] $C_6H_5\dot{C}(OH)(CH_2)_3CH_3 + tBu{-}N{=}O \rightarrow C_6H_5C(=O)(CH_2)_3CH_3 + tBu{-}N(H){-}\dot{O}$

Can. J. Chem. Downloaded from www.nrcresearchpress.com by 210.87.254.40 on 09/06/12
For personal use only.

TABLE 3. Hyperfine coupling constants (G) of spin-trapped radicals generated by uv photolysis of valerophenone at 313 ± 10 nm

| Solvent | Radical IV | | Radical V | |
|---|---|---|---|---|
| | $a_{N(nitroxyl)}$ | $^{\beta}a_H$ | $a_{N(nitroxyl)}$ | $^{\beta}a_H$ |
| Neat | 14.63 | 1.75 (H) | | |
| Benzene | 14.75 | 1.65 (H) | 14.25 | 7.75 (2H) |
| Methanol | 15.38 | 1.75 (H) + unidentified radical | | |
| Acetonitrile | 15.00 | 1.73 (H) | 14.50 | 8.06 (2H) |

generate the MNP–methyl spin adduct under reaction conditions which do not involve hydroxyl radical, such as the chemical reaction with a base. Thus, after mixing in the dark, at ambient temperature, a solution of MNP in dimethyl sulfoxide (1.5 mg/mL) with a solution of NaOH in water (2%) in the ratio 1:1, the $CH_3$ spin adduct can be easily detected ($a_{N(nitroxyl)} = 16.4$ G, $^{\beta}a_H = 12.5$ G (3H)). When the reaction is performed in dimethyl sulfoxide-$d_6$, the corresponding $CD_3$-adduct is recorded ($a_{N(nitroxyl)} = 15.9$ G, $^{\beta}a_D = 1.9$ G (3D)) (Fig. 4). Since the reaction proceeds relatively slowly at room temperature, a continuous increase in the intensity of the spin adduct can be observed with time. A possible reaction mechanism is depicted in eq. [5].

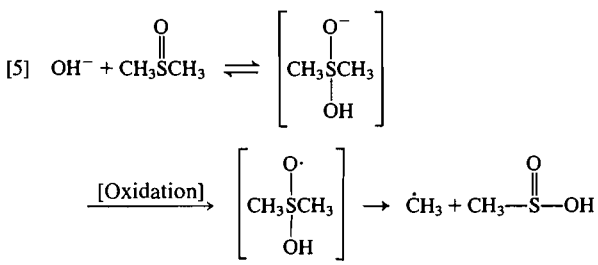

This suggested mechanism is supported by the observation that dimethyl sulfoxide undergoes oxygen exchange with NaOH (26).

Accidentally, we also detected the methyl spin adduct in an entirely anhydrous medium. Thus, in the course of an investigation of free radicals derived from polyamines (27) it was found that when a dimethyl sulfoxide solution of MNP (1.5 mg/mL) and dibenzoyl peroxide (5 mg/mL) was saturated with 1,8-diaminooctane in the dark, at room temperature, the methyl spin adduct spectrum was exclusively observed. Control experiments indicated that all of these components were necessary for the formation of the methyl adduct. The mechanism of this particular process is unknown at the present time.

We feel that these observations should serve as a cautionary mark for the nondiscriminatory conclusion that the detection of methyl spin adduct from dimethyl sulfoxide is an indisputable proof for hydroxyl radical generation in complex chemical systems.


1. C. LAGERCRANTZ. J. Phys. Chem. **75**, 3466 (1971).
2. E. G. JANZEN. *In* Free radicals in biology. Vol. IV. *Edited by* W. A. Pryor. Academic Press, New York. 1980. p. 116.
3. D. BELLUS. Adv. Photochem. **8**, 109 (1971).
4. C. E. KALMUS and D. M. HERCULES. J. Am. Chem. Soc. **96**, 449 (1974).
5. W. ADAM, J. A. DESANABIA, and H. FISHER. J. Org. Chem. **38**, 2571 (1973).
6. A. MACKOR, T. A. J. W. WAJER, and T. J. DEBOER. Tetrahedron, 1623 (1968).
7. G. QUINKERT, K. OPITZ, W. W. WIERSDORF, and J. WEINLICH, Tetrahedron Lett. 1863 (1963).
8. P. S. ENGEL. J. Am. Chem. Soc. **92**, 6074 (1970).
9. W. K. ROBBINS and R. EASTMAN. J. Am. Chem. Soc. **92**, 6076 (1970).
10. W. K. ROBBINS and R. EASTMAN. J. Am. Chem. Soc. **92**, 6077 (1970).
11. B. BLANK, A. HENNE, G. P. LAROFF, and H. FISHER. Pure Appl. Chem. **41**, 475 (1975).
12. M. J. PERKINS and B. P. ROBERTS. J. Chem. Soc. Perkin Trans. II, 297 (1974).
13. N. J. TURRO and W. R. CHERRY. J. Am. Chem. Soc. **100**, 7431 (1978).
14. R. S. HUTTON, H. D. ROTH, B. KRAEUTLER, W. R. CHERRY, and N. J. TURRO. J. Am. Chem. Soc. **101**, 2227 (1978).
15. P. J. WAGNER and A. E. KEMPPAINEN. J. Am. Chem. Soc. **94**, 7495 (1972).
16. P. J. WAGNER, P. A. KELSO, A. E. KEMPPAINEN, and R. G. ZEPP. J. Am. Chem. Soc. **94**, 7500 (1972).
17. P. J. WAGNER, P. A. KELSO, A. E. KEMPPAINEN, J. M. MCGRATH, N. N. SCOTT, and R. G. ZEPP. J. Am. Chem. Soc. **94**, 7506 (1972).
18. K. TORSSEL. Tetrahedron, **26**, 2759 (1970).
19. N. J. TURRO, K. C. LIU, and M. F. CHOW. Photochem. Photobiol. **26**, 413 (1977).
20. I. H. LEAVER and G. C. RAMSAY. Tetrahedron, **25**, 5669 (1969).
21. M. J. PERKINS, P. WARD, and A. HORSFIELD. J. Chem. Soc. B, 395 (1970).
22. E. G. JANZEN. Acc. Chem. Res. **4**, 32 (1971).
23. I. ROSENTHAL, M. M. MOSSOBA, and P. RIESZ. J. Magn. Reson. In press.
24. C. LAGERCRANTZ and S. FORSHULT. Acta Chem. Scand. **23**, 811 (1969).
25. M. J. PERKINS. Adv. Phys. Org. Chem. **17**, 1 (1980).
26. S. OAE, M. KISE, N. FURUKAWA, and Y. A. KHIM. Tetrahedron Lett. 1415 (1967).
27. M. M. MOSSOBA, I. ROSENTHAL, and P. RIESZ. Can. J. Chem. **60**, 1493 (1982).


Can. J. Chem. Downloaded from www.nrcresearchpress.com by 210.87.254.40 on 09/06/12
For personal use only.

# Electron spin resonance of spin-trapped radicals of amines and polyamines. Hydroxyl radical reactions in aqueous solutions and γ-radiolysis in the solid state

MAGDI M. MOSSOBA, IONEL ROSENTHAL,[1] AND PETER RIESZ

*Laboratory of Pathophysiology, National Cancer Institute, National Institutes of Health, Bethesda, MD 20205, U.S.A.*

Received September 4, 1981

MAGDI M. MOSSOBA, IONEL ROSENTHAL, and PETER RIESZ. Can. J. Chem. **60**, 1493 (1982).

The reactions of hydroxyl radicals with methylamine, dimethylamine, trimethylamine, diethylamine, *sec*-butylamine, ethylenediamine, 1,3-diaminopropane, putrescine, cadaverine, 1,7-diaminoheptane, ornithine, spermidine, spermine, agmatine, and arcaine in aqueous solutions have been investigated by spin-trapping and esr. Hydroxyl radicals were generated by the uv photolysis of $H_2O_2$ and 2-methyl-2-nitrosopropane (MNP) was used as the spin-trap. The effects of ionizing radiation on the same polyamines in the polycrystalline state were also investigated. The free radicals produced by γ-radiolysis of these solids at room temperature in the absence of air were identified by dissolution in aqueous solutions of MNP. The predominant reaction of ȮH with amines and polyamines below pH 7 was the abstraction of hydrogen atoms from a carbon that is not adjacent to the protonated amino group. For agmatine and arcaine which contain guanidinium groups abstraction occurred from the α-CH. Dimethylamine was oxidized to the dimethylnitroxyl radical by $H_2O_2$ in the dark. γ-Radiolysis of polyamines in the polycrystalline state generated radicals due to H-abstraction from either the α-CH or from a carbon atom in the middle of the alkyl chain. The deamination radical was obtained from ornithine.

MAGDI M. MOSSOBA, IONEL ROSENTHAL et PETER RIESZ. Can. J. Chem. **60**, 1493 (1982).

Faisant appel à la rpe et à l'utilisation de piegeurs de spin, on a étudié la réaction des radicaux hydroxyles avec des solutions aqueuses des amines suivantes: méthylamine, diméthylamine, triméthylamine, diéthylamine, *sec*-butylamine, éthylènediamine, diamino-1,3 propane, putrescine, cadavérine, diamino-1,7 heptane, ornithine, spermidine, spermine, agmatine et arcaine. Les radicaux hydroxyles furent produits par la photolyse uv de $H_2O_2$ et on a utilisé le méthyl-2 nitroso-2 propane (MNP) comme piégeur de spin. On a également étudié les effets des radiations ionisantes sur les mêmes polyamines à l'état polycristallin. On a identifié les radicaux libres produits par radiolyse-γ de ces solides à la température ordinaire en l'absence de l'air en les dissolvant dans des solutions aqueuses de MNP. L'élimination d'atomes d'hydrogène de l'atome de carbone non adjacent au groupe amino protoné est la réaction principale du radical ȮH avec les amines et les polyamines à un pH inférieur à 7. Dans le cas de l'agmatine et de l'arcaine, qui contiennent des groupes guanidiniums, l'élimination se produit au niveau du CH en α. On a oxydé la diméthylamine en radical diméthylnitroxyde par $H_2O_2$ à l'obscurité. La radiolyse γ des polyamines à l'état polycristallin produit des radicaux par suite de l'élimination d'hydrogène soit du CH en α ou de l'atome de carbone qui se trouve au centre de la chaîne alkylée. À partir de l'ornithine, on a obtenu le radical de désamination.

[Traduit par le journal]

## Introduction

Polyamines, which consist of hydrocarbon chains with multiple amine groups, are intimately involved in the control of normal and malignant growth processes (1, 2). Polyamines are especially useful as biochemical markers of cancer patient response to radiation, surgery, immunotherapy, and chemotherapy (2). They are found in elevated concentrations in physiological fluids of patients and appear to be markers of pathology related to overproliferation and cell death (2).

In this work, we have investigated the effects of γ-radiolysis in the solid state and the reactions of OH radicals in aqueous solutions with a number of biologically significant polyamines such as putrescine (1,4-diaminobutane), cadaverine (1,5-diaminopentane), spermidine ($H_3\overset{+}{N}—(CH_2)_3—\overset{+}{N}H_2—(CH_2)_4—NH_3^+$), spermine ($H_3\overset{+}{N}—(CH_2)_3—\overset{+}{N}H_2—(CH_2)_4—\overset{+}{N}H_2—(CH_2)_3—\overset{+}{N}H_3$), etc., as well as several primary, secondary, and tertiary amines.

Free radical formation from aliphatic amines has been investigated previously by a number of methods. For studies of the solid state, electron spin resonance was used to observe radical species produced by X-rays (3) and γ-radiolysis (4–6) in single crystals or by uv photolysis (7, 8) in frozen glasses. Optical absorption was used to follow the radicals produced by pulse radiolysis (9–12) in aqueous solutions that were saturated with $N_2O$ to convert $e^-_{aq.}$ to ȮH. The radicals generated by ȮH (or Ḣ) attack formed by steady-state radiolysis of aqueous solutions (13, 14) or by the $Ti^{3+}$–$H_2O_2$ flow system (15–17) were detected by direct, *in situ* esr observation. The flow method is limited by the requirement of considerable amounts of substrate to be investigated.

In the single crystal studies, H-abstraction from carbon as in $\cdot CH_2\overset{+}{N}H_3$ (5) and from nitrogen (e.g., $Me_3\dot{N}^+$ (6)) was produced by ionizing radiation.

[1]On leave of absence from the Department of Technology, Agricultural Research Organization, Volcani Center, Bet-Dagan, Israel.

0008-4042/82/121493-08$01.00/0

©1982 National Research Council of Canada/Conseil national de recherches du Canada

Can. J. Chem. Downloaded from www.nrcresearchpress.com by 210.87.254.6 on 09/06/12
For personal use only.

Can. J. Chem. Downloaded from www.nrcresearchpress.com by 210.87.254.6 on 09/06/12
For personal use only.

*N*-centered radicals were also formed by ultraviolet irradiation of glassy samples of mono-, di-, and trialkyl amines at low temperatures (7, 8). However, in the reaction of OH radicals with aliphatic amines in aqueous solution (9–14, 17), H-abstraction from the nitrogen as well as from the carbon adjacent to it occurred in alkaline medium. In acid solution, abstraction was observed to take place only from those carbons which were not adjacent to the $-\overset{+}{N}H_3$ group.

In this work electron spin resonance and spin-trapping (18–21) were used to identify the free radicals. The reactions of $\dot{O}H$ radicals were investigated by uv photolysis of aqueous solutions containing hydrogen peroxide and the amine or polyamine. The direct effects of ionizing radiation on the polyamines in the solid state were investigated by γ-radiolysis of the polycrystalline solids followed by dissolution in a solution containing the spin-trap (22, 23).

In principle, a spin-trap, such as 2-methyl-2-nitrosopropane (MNP), $Me_3CN{=}O$, reacts with short-lived radicals, $R^{\bullet}$, to produce longer-lived spin-adducts, $Me_3CN(R)\dot{O}$, whose structures can conveniently be identified by esr. The α, β, and γ positions are defined with respect to the nitrogen of the nitroxyl group as illustrated for the spin-adduct of methylamine:

[1] $O{=}N{-}CMe_3 + {\cdot}CH_2\overset{+}{N}H_3 \rightarrow O^-{-}\dot{N}^+(CMe_3){-}C^{\alpha}H_2{-}C^{\beta}H_2{-}\overset{+}{N}H_3^{\gamma}$

## Experimental

Polyamines as well as primary, secondary, and tertiary amines were purchased from Sigma Chemical Company. 2-Methyl-2-nitrosopropane (MNP) was obtained from Aldrich Chemical Company and $D_2O$ (99.8%) was acquired from Bio-Rad Laboratories.

Aqueous solutions of the MNP were prepared in water by adding 50 mg of the spin-trap to 10 mL of $D_2O$ and stirring in the dark at 45°C for 2 hours (24).

*In the γ-radiolysis experiments, solid samples of polyamines* were irradiated in a $^{60}Co$ γ-source to a dose of 120 kGy in the absence of air at room temperature. The irradiated samples were subsequently dissolved in the spin-trap solution.

For the study of OH radical reactions in aqueous solution, the amines and polyamines were dissolved in the spin-trap solutions to which 25 μL of 30% $H_2O_2$ per mL were added just prior to uv illumination. The radicals were generated by photolysis *in situ* at room temperature in the standard aqueous quartz cell (60 × 10 × 0.25 mm) placed in the esr cavity, using a Schoeffel 1000 W high-pressure Hg–Xe lamp coupled with a grating monochromator. The excitation light had a maximum centered at 260 ± 10 nm and the irradiation time ranged from 5 to 30 seconds.

The esr measurements were made on a Varian E-9, X-band (9.4 GHz) spectrometer. The esr spectra from spin-trapped radicals were recorded at room temperature as first derivatives. The esr scans were traced with a 100 kHz modulation of 0.05 or 0.1 G amplitude and the microwave power level was maintained at 10 mW to avoid saturation of the esr signals. Thermal decay studies of the spin-adducts were performed at room temperature and proved helpful in analyzing overlapping spectra due to the presence of more than a single radical species. The magnetic field was calibrated with an nmr Gauss Meter.

## Results and discussion

In spin-adducts the free-electron spin density is mostly localized on the nitrogen and oxygen atoms of the nitroxyl group and the interaction of the unpaired electron with $^{14}N$ ($I = 1$) of the nitroxyl group generates a primary triplet. Some of the electron spin is also delocalized on the atoms of the trapped radicals and produces hyperfine structures, referred to as secondary splittings, which are most useful in identifying the structure of the spin-adducts. The primary and secondary hyperfine splitting constants of the spin-trapped radicals of the polyamines and amines investigated are listed in Table 1. The esr spectra of photolyzed aqueous solutions of MNP usually show a 17.2 G triplet from the di-*tert*-butylnitroxyl radical. This spectrum is marked S in the figures.

Initially, the simple amines were studied as models for more complex polyamines. Aqueous solutions of several primary, secondary, and tertiary amines were uv-photolyzed in the presence of MNP and $H_2O_2$ at room temperature. The esr spectrum produced by the spin-trapped radicals of diethylamine showed detailed hyperfine structure. Figure 1(a) displays the observed spectrum which has a primary nitrogen hyperfine coupling constant of 16.2 G and a secondary structure consisting of a 1:2:1 triplet of 13.6 G which is further split into another 1:2:1 triplet of 0.4 G. Only radical **1** is

$${\cdot}CH_2{-}CH_2{-}\overset{+}{N}H_2{-}CH_2{-}CH_3$$
**1**

consistent with this observation and is formed by H-abstraction from a terminal carbon. Radical **1** has been previously detected by esr in the reaction of $\dot{O}H$ with diethylamine using a $Ti^{3+}$–$H_2O_2$ flow method (17).

Figure 1(b) shows the spectrum obtained from the spin-adducts of *sec*-butylamine which is due to the presence of two radial species. Radical **2** is due

$${\cdot}CH_2{-}CH_2{-}CH(\overset{+}{N}H_3){-}CH_3$$
**2**

to H-abstraction, as in diethylamine, from a terminal carbon except that the middle lines of the 11.5 G secondary triplet overlap with the more intense 2.0 G secondary doublet arising from the spin-adduct of radical **3**. This doublet is clearly observed

Can. J. Chem. Downloaded from www.nrcresearchpress.com by 210.87.254.6 on 09/06/12
For personal use only.

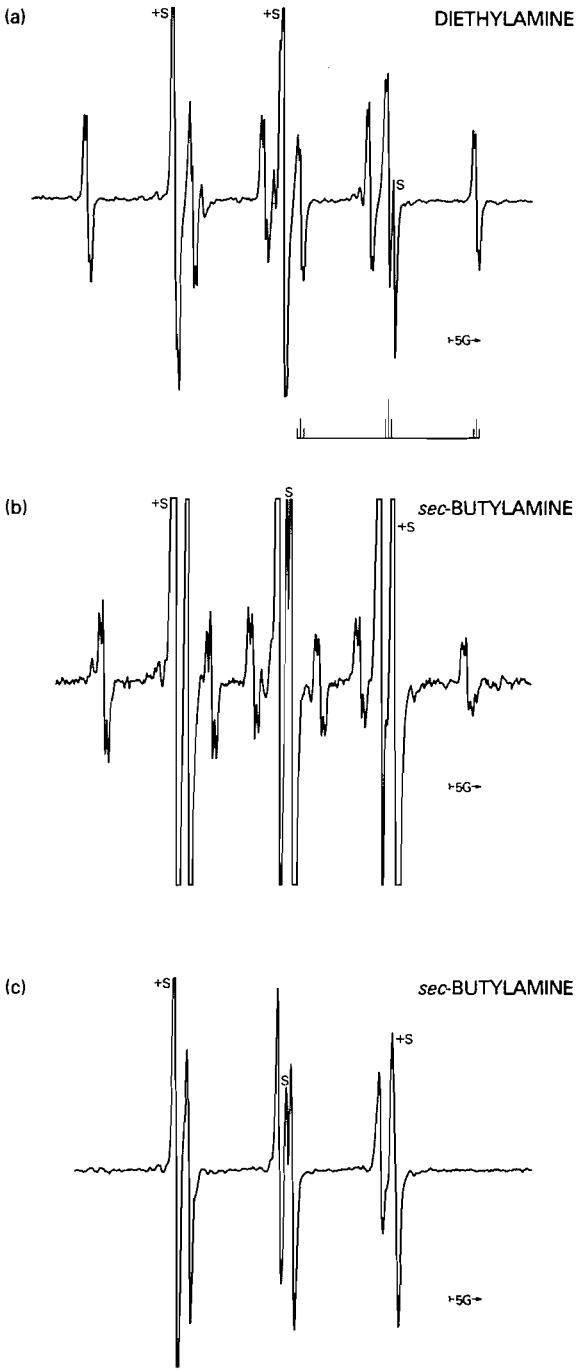


FIG. 1. The esr spectrum from uv-photolyzed aqueous solutions containing MNP, $H_2O_2$, and (a) diethylamine, (b) *sec*-butylamine, (c) *sec*-butylamine after decay.

in Fig. 1(c) since the spin-adduct of radical **2** decayed in about 10 min at room temperature.

The spectrum of the spin-trapped radicals of trimethylamine obtained by ȮH attack is shown in

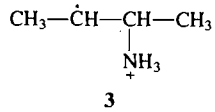

**3**

Fig. 2(a) and arises from the spin-adduct of radical **4** since it consists of a 1:2:1 triplet of 8.3 G, due to two equivalent hydrogen atoms, which is further split into a 1:1:1 triplet of 3.0 G due to the nitrogen atom.

Radical **4** has been previously observed in alka-

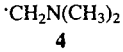

**4**

line medium (9, 13). During radiolysis of acid solutions of trimethylamine, a minor product, the aminium radical $Me_3\dot{N}^+$ was detected by esr at pH 1 and 3 (14). This radical has also been observed in γ-irradiated single crystals of tetramethylammonium chloride (6). However, the aminium radical could not be detected by spin-trapping under our experimental conditions.

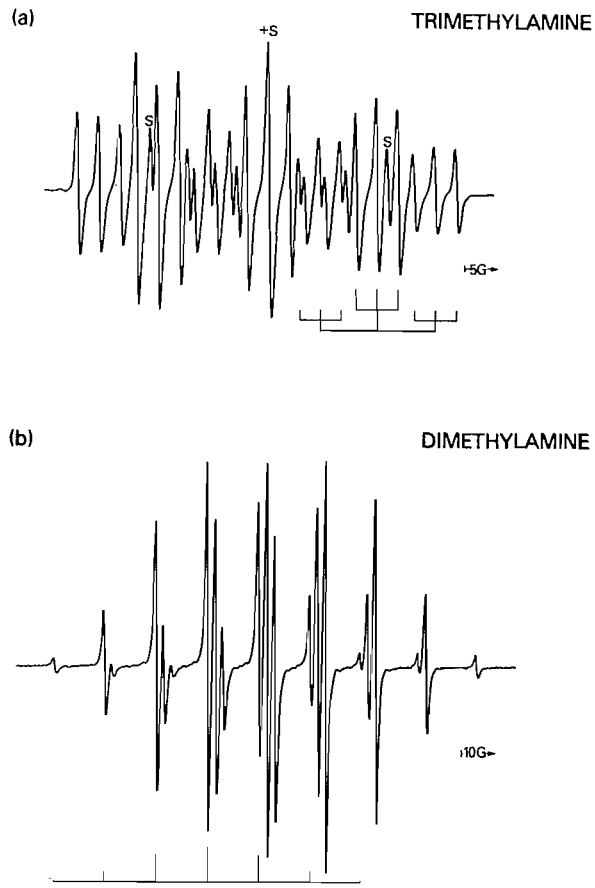


FIG. 2. (a) The esr spectrum from uv-photolyzed aqueous solutions containing MNP, $H_2O_2$, and trimethylamine; (b) esr spectrum from aqueous solutions containing $H_2O_2$ and dimethylamine in the dark.

Can. J. Chem. Downloaded from www.nrcresearchpress.com by 210.87.254.6 on 09/06/12
For personal use only.



TABLE 1. Hyperfine coupling constants[a] of the spin-trapped polyamines and amines radicals

| Compound | pD value[b] | Primary $^{14}N$ splitting (G) | Secondary splittings (G) β | Secondary splittings (G) γ | Method | Radical | |
|---|---|---|---|---|---|---|---|
| Diethylamine | 6 | 16.2 | 13.6 (2H) | 0.4 (2H) | ·OH | $^{\cdot}CH_2—CH_2—\overset{+}{N}H_2—CH_2—CH_3$ | 1 |
| *sec*-Butylamine | 5.2 | 16.5 | 11.5 (2H) | 0.6 (2H) | ·OH | $^{\cdot}CH_2—CH_2—\underset{\overset{+}{N}H_3}{CH}—CH_3$ | 2 |
| | | 15.8 | 2.0 (H) | | ·OH | $CH_3—\dot{C}H—\underset{\overset{+}{N}H_3}{CH}—CH_3$ | 3 |
| Trimethylamine | 11 | 15.7 | 8.3 (2H) 3.0 (N) | | ·OH | $^{\cdot}CH_2—N(CH_3)_2$ | 4 |
| Methylamine | 5.3 | 15.2 | 11.7 (2H) 2.2 (N) | | ·OH | $^{\cdot}CH_2—\overset{+}{N}H_3$ | 5 |
| Dimethylamine | 12 | 17.0 | 14.6 (6H) | | $H_2O_2$ | $^{\cdot}ON(CH_3)_2$ | 6 |
| Ethylenediamine | 3.5 | 13.7 | 3.0 (N) 1.3 (H) | | γ, ȮH | $H_3\overset{+}{N}—\dot{C}H—CH_2—\overset{+}{N}H_3$ | 7 |
| 1,3-Diaminopropane | 6.4 | 16.0 | 1.3 (N) 1.3 (H) | | γ, ȮH | $H_3\overset{+}{N}—\dot{C}H—(CH_2)_2—\overset{+}{N}H_3$ | 8 |
| | | 15.4 | 1.8 (H) | | ȮH | $H_3\overset{+}{N}—CH_2—\dot{C}H—CH_2—\overset{+}{N}H_3$ | 9 |
| L-Ornithine $H_3\overset{+}{N}—(CH_2)_3—\underset{COO^-}{CH}—\overset{+}{N}H_3$ | 5 | 15.6 | 4.5 (H) | 0.5 (2H) | γ | $H_3\overset{+}{N}—(CH_2)_3—\dot{C}H—COO^-$ | 10 |
| 1,4-Diaminobutane (Putrescine) | 5.1 | 15.2 | 2.0 (H) | | γ, ȮH | $H_3\overset{+}{N}—CH_2—\dot{C}H—(CH_2)_2—\overset{+}{N}H_3$ | 11 |
| | | 14.2 | 2.8 (N) 1.4 (H) | | ȮH | $H_3\overset{+}{N}—\dot{C}H—(CH_2)_3—\overset{+}{N}H_3$ | 12 |
| | | 15.7 | 8.8 (2H) | | ȮH | $^{\cdot}CH_2—CH_2—\overset{+}{N}H_3$ | 13 |
| 1,5-Diaminopentane (Cadaverine) | 4.6 | 15.5 | 2.0 (H) | | γ, ȮH | $\sim\!\!\sim—CH_2—\dot{C}H—CH_2—\sim\!\!\sim$ | 14 |
| | | 14.3 | 2.7 (N) 1.5 (H) | | ȮH | $H_3\overset{+}{N}—\dot{C}H—(CH_2)_4—\overset{+}{N}H_3$ | 15 |
| | | 15.7 | 8.8 (2H) | | ȮH | $^{\cdot}CH_2—CH_2—\overset{+}{N}H_3$ | 16 |
| 1,7-Diaminoheptane | 4.5 | 15.8 | 2.0 (H) | | ȮH | $\sim\!\!\sim—CH_2—\dot{C}H—CH_2—\sim\!\!\sim$ | 17 |
| 1,8-Diaminooctane | 12.1 | 16.1 | 2.5 (N) 1.5 (H) | | γ | $H_2N—\dot{C}H—(CH_2)_7—NH_2$ | 18 |
| Spermidine | 5.4 | 15.9 | 1.4 (N) 1.4 (H) | | γ | $\sim\!\!\sim N—\dot{C}H—CH_2—\sim\!\!\sim$ | 19 |
| $H_3\overset{+}{N}—(CH_2)_3—\overset{+}{N}H_2—(CH_2)_4—\overset{+}{N}H_3$ | | 15.2 | 2.0 (H) | | ȮH | $\sim\!\!\sim—CH_2—\dot{C}H—CH_2—\sim\!\!\sim$ | 20 |
| | | 15.7 | 8.8 (2H) | | ȮH | $^{\cdot}CH_2—CH_2—\overset{+}{N}H_3$ | 21 |

Can. J. Chem. Downloaded from www.nrcresearchpress.com by 210.87.254.6 on 09/06/12
For personal use only.



TABLE 1. (*Concluded*)

| Compound | pD value[b] | Primary $^{14}N$ splitting (G) | Secondary splittings (G) β | Secondary splittings (G) γ | Method | Radical | |
|---|---|---|---|---|---|---|---|
| Spermine | 5.6 | 15.9 | 1.4 (N)<br>1.4 (H) | | γ | ~~N—ĊH—CH$_2$—~~ | 22 |
| $H_3\overset{+}{N}$—(CH$_2$)$_3$—$\overset{+}{N}H_2$—(CH$_2$)$_4$—$\overset{+}{N}H_2$—(CH$_2$)$_3$—$\overset{+}{N}H_3$ | | 15.5 | 2.0 (H) | | ȮH | ~~—CH$_2$—ĊH—CH$_2$—~~ | 23 |
| Agmatine | 4.8 | 15.5 | 2.8 (N)<br>2.0 (H) | | γ, ȮH | ~~N—ĊH—CH$_2$—~~ | 24 |
| $H_2N$—C(=$\overset{+}{N}H_2$)—NH—(CH$_2$)$_4$—$\overset{+}{N}H_3$ | | 15.5 | 2.0 (H) | | ȮH | ~~—CH$_2$—ĊH—CH$_2$—~~ | 25 |
| Arcaine | 5.1 | 15.5 | 2.8 (N)<br>1.9 (H) | | γ, ȮH | $H_2N$—C(=$\overset{+}{N}H_2$)—NH—ĊH—(CH$_2$)$_3$—NH—C(=$\overset{+}{N}H_2$)—$NH_2$ | 26 |

[a]Accurate to ± 0.1 G.
[b]pD = observed pH + 0.4 (31).

When ȮH radicals reacted with methylamine a spectrum similar to the one obtained for trimethylamine was observed and the untrapped radical from methylamine has structure **5**. The spin-adducts of both radicals **4** and **5** decayed after about 4 min at room temperature.

$$\cdot CH_2\overset{+}{N}H_3$$
**5**

Radical **5** has been previously observed by esr in a single-crystal study of methylammonium alum (5). In acid solutions, **5** was detected by pulse radiolysis (9) but not by esr (13, 17) due to line broadening caused by chemical exchange of the ammonium protons (13). Only in the pH range 7–13.5 the conjugate base of **5**, $\cdot CH_2NH_2$, was observed by esr in γ-irradiated aqueous solution of methylamine (13).

Dimethylamine was found to react with $H_2O_2$ in the dark in the absence of MNP. The observed spectrum (Fig. 2(b)) is characteristic of a 17.0 G 1:1:1 triplet which was further split into a 14.6 G septet with a relative intensity of 1:6:15:20:15:6:1 due to six equivalent hydrogen atoms. This evidence is consistent with the formation of the nitroxyl radical **6**.


**6**

$H_2O_2$-oxidation of dimethylamine has previously been obtained in a 1 *N* NaOH solution (25). The oxidation product **6** has also been produced in a titanous ion – hydrogen peroxide flow system (15, 16).

After ethylenediamine dihydrochloride was γ-irradiated in the solid state to a dose of 120 kGy, it was dissolved in an aqueous solution of MNP. The observed esr spectrum of the spin-adduct consisted of a secondary 1:1:1 triplet (3.0 G) which was further split into a doublet (1.3 G). This observation is consistent with the formation of radical **7**. The

$$H_3\overset{+}{N}—\dot{C}H—CH_2—\overset{+}{N}H_3$$
**7**

same radical species was also found when an aqueous solution of ethylenediamine containing MNP and $H_2O_2$ was photolyzed for 5 seconds at 260 nm as shown in Fig. 3(a).

Solid-state radiolysis of 1,3-diaminopropane dihydrochloride yielded radical **8**. The esr spectrum, shown in Fig. 3(b), indicates the equivalence of the β-nitrogen and the β-hydrogen of the spin-adduct

Can. J. Chem. Downloaded from www.nrcresearchpress.com by 210.87.254.6 on 09/06/12
For personal use only.

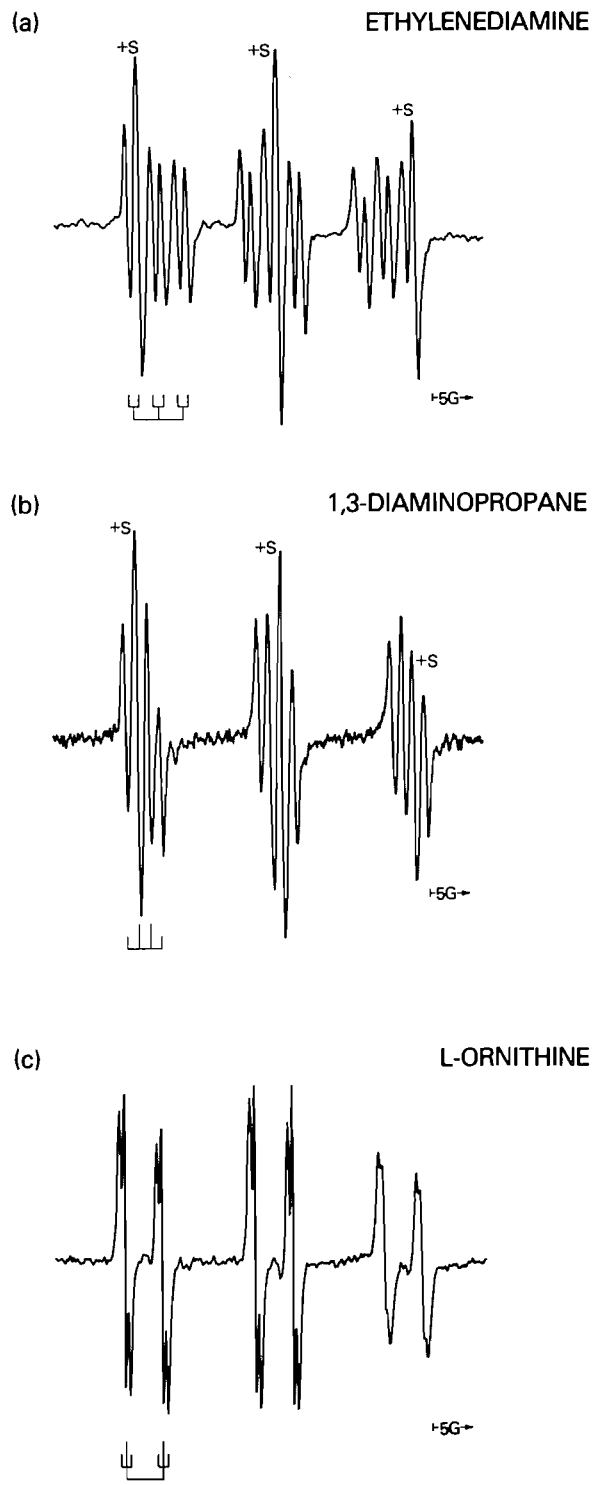


FIG. 3. (a) The esr spectrum from uv-photolyzed aqueous solutions containing MNP, $H_2O_2$, and ethylenediamine; (b, c) esr spectra of spin-trapped radicals from polycrystalline (b) 1,3-diaminopropane, (c) L-ornithine γ-irradiated at room temperature and subsequently dissolved in an MNP solution.

$H_3\overset{+}{N}—\dot{C}H—CH_2—CH_2—\overset{+}{N}H_3$

**8**

of radical **8**. In the $H_2O_2$-photolysis experiment a mixture consisting of radical **8** as well as the one (structure **9**) generated by H-abstraction from the C(2) carbon was obtained.

$H_3\overset{+}{N}—CH_2—\dot{C}H—CH_2—\overset{+}{N}H_3$

**9**

The esr spectrum of the spin-adduct generated from γ-radiolysis of polycrystalline L-ornithine hydrochloride and spin-trapping in aqueous solution exhibited a 4.5 G doublet which was further resolved into a 0.5 G triplet (1:2:1). This spectrum is due to the formation of the deamination radical **10**. This result is similar to that obtained for

$H_3\overset{+}{N}—(CH_2)_3—\dot{C}H—COO^-$

**10**

γ-irradiated polycrystalline α-amino acids (23). The interaction of OH radicals with L-ornithine did not generate radical **10**, but gave rise to an unresolved mixture of H-abstraction radicals.

Similar esr spectra were recorded for 1,4-diaminobutane and 1,5-diaminopentane. Hydrogen abstraction from the middle of the chain was observed by both $H_2O_2$-photolysis and γ-radiolysis. The spin adduct of radical **11** shows an esr spectrum (Fig. 4(a) and (b)) that consists of a 2.0 G secondary doublet. At higher gain, the esr spectrum (Fig. 4(c)) observed in the photolysis experiment also shows two other sets of lines. The lines labelled A arise from radical **12**, while the ones

$H_3\overset{+}{N}—CH_2—\dot{C}H—(CH_2)_2—\overset{+}{N}H_3$

**11**

$H_3\overset{+}{N}—\dot{C}H—(CH_2)_3—\overset{+}{N}H_3$

**12**

labelled with numbers are tentatively attributed to a $\cdot CH_2$-type radical which could be obtained from **12** by a β-scission mechanism (26) giving radical **13**:

[2] $H_3\overset{+}{N}—\dot{C}H—CH_2—CH_2—CH_2—\overset{+}{N}H_3$

**12**

$\xrightarrow{\beta\text{-scission}}$ $H_3\overset{+}{N}—CH{=}CH_2 + \cdot CH_2—CH_2—\overset{+}{N}H_3$

**13**

This type of radical was also observed for spermidine (radical **21** in Table 1). The esr spectrum obtained by $H_2O_2$-photolysis of 1,7-diaminoheptane only showed the radical generated by

Can. J. Chem. Downloaded from www.nrcresearchpress.com by 210.87.254.6 on 09/06/12
For personal use only.

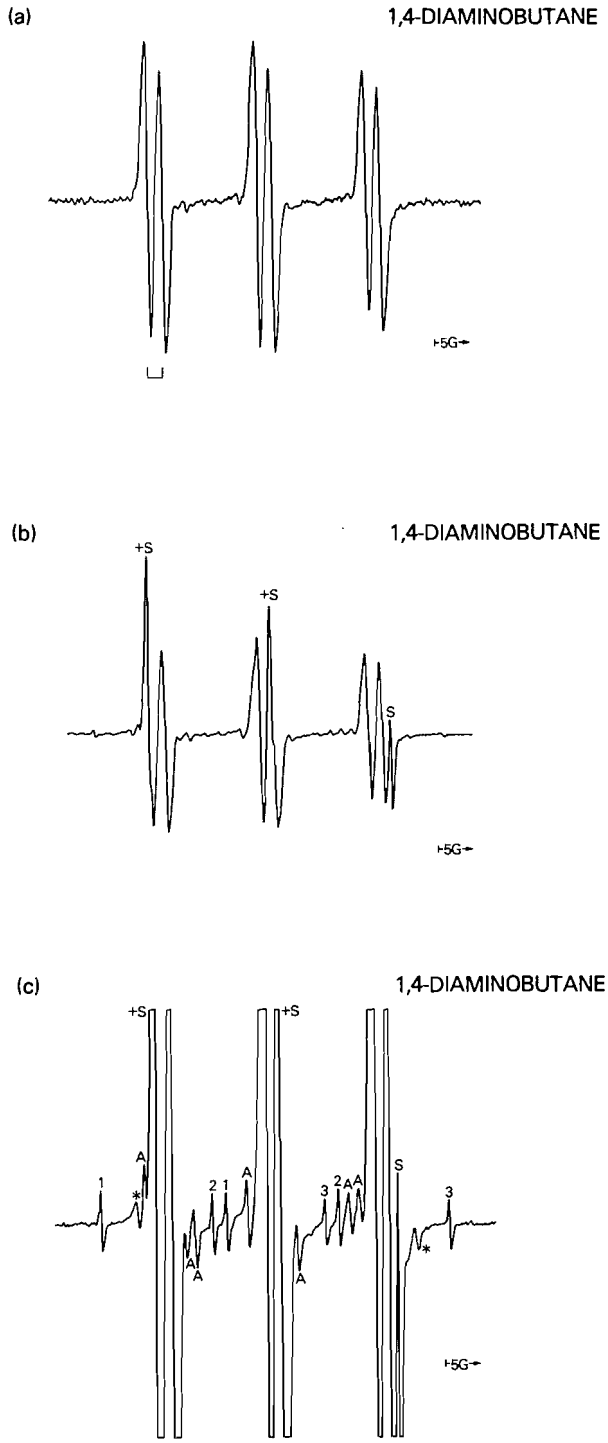


FIG. 4. (a) The esr spectrum of spin-trapped radicals from polycrystalline 1,4-diaminobutane γ-irradiated at room temperature and subsequently dissolved in an MNP solution; (b) esr spectrum from uv-photolyzed aqueous solutions containing MNP, $H_2O_2$, and 1,4-diaminobutane; (c) like (b) with higher gain (× 5); (*) are the $^{13}C$ satellites of di-*tert*-butylnitroxyl radical (marked S).

H-abstraction from the middle of the hydrocarbon chain.

γ-Radiolysis of the free base 1,8-diaminooctane yielded radical **18**. This type of radical was also

$$H_2N—\dot{C}H—(CH_2)_7—NH_2$$

**18**

found in the γ-irradiation of spermidine and spermine in which the β-nitrogen and β-hydrogen were found to be equivalent since their esr spectra exhibited a secondary 1:2:2:1 pattern. Abstraction of ȮH from a middle carbon was, however, observed for spermidine and spermine. The radicals obtained from agmatine and arcaine, by γ-radiolysis or $H_2O_2$-photolysis, exhibited esr spectra with a 6-line secondary pattern due to the nonequivalence of the β-N and β-H and are due to abstraction from a carbon adjacent to a nitrogen. For agmatine a second radical was also observed during photolysis, due to abstraction from the middle of the carbon chain. Radical **26** was generated from the $H_2O_2$-photolysis of arcaine.

$$H_2N—\underset{\underset{\overset{+}{N}H_2}{\|}}{C}—NH—\dot{C}H—(CH_2)_3—NH—\underset{\underset{\overset{+}{N}H_2}{\|}}{C}—NH_2$$

**26**

Previous work has shown that the nature of the radicals produced from the reaction of ȮH radicals with amines is strongly pH dependent (9–12, 27–29). The rate of reactions of ȮH with amines in their basic form, $RNH_2$, is close to being diffusion controlled and it is one to two orders of magnitude larger than that with $R\overset{+}{N}H_3$ (9, 27). In alkaline solutions, at pH values where the amines are deprotonated, $R—\underset{\underset{H}{|}}{\overset{H}{\overset{|}{C}}}—NH_2$, ȮH radicals abstract H atoms mainly from —$NH_2$ and α-CH (9). On the other hand, the strong inductive effect of a protonated amino group leads to the transmission of negative charge from the H atoms in the α-position through the carbon atom to the —$\overset{+}{N}H_3$ group. Hence an electrophilic attack of ȮH on hydrogen atoms in the position adjacent to the —$\overset{+}{N}H_3$ group becomes less favorable and abstraction is more likely to occur from positions further away from the ammonium group (9).

In the present study, the observed products in the reaction of ȮH radicals with amines and polyamines in their protonated form are consistent with the pathways described above. The predominant site of ȮH attack is not on the carbon attached

to the ammonium group. This is clearly illustrated in the cases of diethylamine, *sec*-butylamine, 1,4-diaminobutane, or spermine. For agmatine and arcaine, which contain one and two guanidinium groups respectively, H-abstraction occurred at a carbon adjacent to a nitrogen, possibly because the proton is shared between the three nitrogen atoms of the guanidinium moiety and the inductive force of $-\overset{+}{N}H_3$ is no longer present.

The observed radicals from polyamines generated by ionizing radiation in the polycrystalline state were not the same as those obtained by ȮH radicals. It can be seen from Table 1 that radicals due to H-abstraction from either the α-CH or from a carbon atom in the middle of the alkyl chain were produced. A deamination radical was only formed in the γ-radiolysis of ornithine. This result is in agreement with the conclusion of previous studies (30) that deamination requires the presence of a carboxyl group separated by one $-CH_2-$ from the amino group.


1. R. AIGNER-HELD and G. D. DANES, JR. Physiol. Chem. Phys. **12**, 389 (1980).
2. D. H. RUSSELL and B. G. M. DURIE. Prog. Cancer. Res. Ther. **8**, 1 (1978).
3. T. COLE. J. Chem. Phys. **35**, 1169 (1961).
4. P. B. AYSCOUGH and A. K. ROY. Trans. Faraday Soc. **64**, 582 (1968).
5. R. P. KOHIN and P. G. NADEAU. J. Chem. Phys. **44**, 691 (1966).
6. A. J. TENCH. J. Chem. Phys. **38**, 593 (1963).
7. S. G. HADLEY and D. H. VOLMAN. J. Am. Chem. Soc. **89**, 1053 (1967).
8. W. C. DANEN and T. T. KENSLER. J. Am. Chem. Soc. **92**, 5235 (1970).
9. M. SIMIĆ, P. NETA, and E. HAYON. Int. J. Radiat. Phys. Chem. **3**, 309 (1971).
10. N. GETOFF and F. SCHWÖRER. Int. J. Radiat. Phys. Chem. **3**, 429 (1971).
11. A. WIGGER, W. GRÜNBEIN, A. HENGLEIN, and E. J. LAND. Z. Naturforsch. B, **24**, 1262 (1969).
12. N. GETOFF and F. SCHWÖRER. Int. J. Radiat. Phys. Chem. **2**, 81 (1970).
13. P. NETA and R. W. FESSENDEN. J. Phys. Chem. **75**, 738 (1971).
14. R. W. FESSENDEN and P. NETA. J. Phys. Chem. **76**, 2857 (1972).
15. R. POUPKO, A. LOEWENSTEIN, and B. L. SILVER. J. Am. Chem. Soc. **93**, 580 (1971).
16. R. E. FLORIN, F. SICILIO, and L. A. WALL. J. Res. Natl. Bur. Stand. Sect. A, **72**, 49 (1968).
17. H. TANIGUCHI, K. FUKUI, S. OHNISHI, H. HATANO, H. HASEGAWA, and T. MARUYAMA. J. Phys. Chem. **72**, 1926 (1968).
18. C. LAGERCRANTZ. J. Phys. Chem. **75**, 3466 (1971).
19. E. G. JANZEN. Acc. Chem. Res. **4**, 31 (1971).
20. P. RIESZ and S. RUSTGI. Radiat. Phys. Chem. **13**, 21 (1979).
21. M. J. PERKINS. Adv. Phys. Org. Chem. **17**, 1 (1980).
22. C. LAGERCRANTZ and S. FORSHULT. Nature, **218**, 1247 (1968).
23. A. MINEGISHI, R. BERGENE, and P. RIESZ. Int. J. Radiat. Biol. **38**, 627 (1980).
24. K. MAKINO, N. SUZUKI, F. MORIYA, S. ROKUSHIKA, and H. HATANO. Radiat. Res. **86**, 294 (1981).
25. A. HUDSON and H. A. HUSSAIN. J. Chem. Soc. B, 1299 (1977).
26. W. A. PRYOR. Free radicals. McGraw-Hill, New York. 1966. pp. 280–284.
27. M. ANBAR, D. MEYERSTEIN, and P. NETA. J. Chem. Soc. B, 742 (1966).
28. K. M. BANSAL, A. HENGLEIN, and R. M. SELLERS. Ber. Bunsenges. Phys. Chem. **78**, 569 (1974).
29. A. J. SWALLOW. Prog. React. Kinet. **9**, 271 (1978).
30. Y. TAL and M. FARAGGI. Radiat. Res. **62**, 337 (1975).
31. R. G. BATES. Determination of pH. Wiley, New York. 1973. p. 375.


Can. J. Chem. Downloaded from www.nrcresearchpress.com by 210.87.254.6 on 09/06/12
For personal use only.

# Do spin-adducts of 5,5-dimethylpyrroline-*N*-oxide dimerize?[1]

A. L. CASTELHANO,[2] D. GRILLER, AND K. U. INGOLD
*Division of Chemistry, National Research Council of Canada, Ottawa, Ont., Canada K1A 0R6*

Received September 1, 1981

A. L. CASTELHANO, D. GRILLER, and K. U. INGOLD. Can. J. Chem. **60**, 1501 (1982).

The conclusion by Bullock *et al.* that aminoxyls formed by radical addition to 5,5-dimethylpyrroline-*N*-oxide are extensively dimerized in aqueous solution is shown to be incorrect. Aminoxyl dimerization is not a serious limitation to the use of this spin trap in quantitative studies of radical production.

A. L. CASTELHANO, D. GRILLER et K. U. INGOLD. Can. J. Chem. **60**, 1501 (1982).

On montre que la conclusion de Bullock et de ses collaborateurs, relative au fait que les aminoxydes formés par additions radicalaires sur le *N*-oxyde de diméthyl-5,5 pyrroline sont très fortement dimérisés en solution aqueuse, est incorrecte. La dimérisation de l'aminoxyle ne constitue par une limitation sérieuse à l'utilisation de ce capteur de spin lors des études quantitatives de production de radicaux.

[Traduit par le journal]

In a recent note entitled "5,5-Dimethylpyrroline-*N*-oxide: a trap for the unwary", Bullock, Gavin, and Ingram (1) claimed that the "nitroxides (**2**) formed by radical addition to the spin trap 5,5-dimethylpyrroline-*N*-oxide (**1**) are extensively dimerized in aqueous solution and this constitutes a serious limitation to the use of the trap in quantitative studies of radical production," viz.

[1] 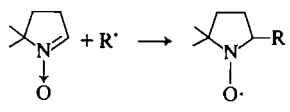

**1** **2** (**2***a*, R = H)

[2] 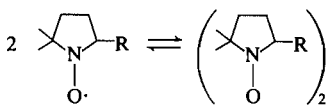

We wish to present evidence that the so-called "trap for the unwary" has nothing to do with the dimerization of **2**. Instead it appears to have been due to excessive consumption of **1** combined with back-oxidation of the hydroxylamine **3** which was presumably formed mainly by the well-known bimolecular self-reaction of primary and secondary dialkyl aminoxyls (2–4), viz.:

[3] 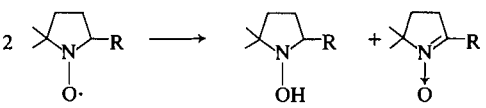

**2** **3** (**3***a*, R = H)

[4] 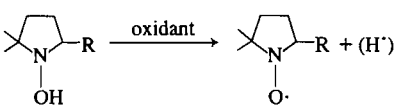

[1]NRCC No. 20077.
[2]NRCC Research Associate 1980–1981.

Bullock *et al.*'s (1) experimental evidence for the equilibrium [2] was that the strength of epr signal for **2** having R = H (**2***a*) or HO (these radicals having been generated by glow-discharge electrolysis in the presence of **1**) could be increased and decreased in an "almost completely reversible" manner (not more than four heating and cooling cycles) on raising and lowering the temperature in the range 5 to 24°C. A value of 50 ± 7 kJ mol$^{-1}$ was estimated for $\Delta H_2$, though if all the data given had been used to calculate $\Delta H_2$, a value nearer to 65–71 kJ mol$^{-1}$ would have been obtained. However, it should be noted that a plot of log [**2**] vs. $1/T$, using Bullock *et al.*'s data is curved in the *opposite* sense from that to be expected for a radical–dimer equilibrium (5).

It is well known that sterically unhindered dialkylaminoxyls can dimerize reversibly *at low temperatures in non-polar solvents* (3, 4, 6). However, at ambient temperatures the equilibrium very strongly favors the monomeric radical over its dimer (6). For example, for the process

[5] $2(CH_3CD_2)_2NO\cdot \underset{-5}{\overset{5}{\rightleftharpoons}} ((CH_3CD_2)_2NO)_2$

the equilibrium constant, $K = k_{-5}/k_5$, has a value of 0.63 *M* at 25°C in isopentane and $\Delta H_5 = 32$ kJ mol$^{-1}$ (4). Equilibrium constants of comparable magnitude have been found for other sterically unhindered dialkylaminoxyls (6). Equilibrium constants in water are expected to favor the radical even more strongly (7).

In view of the growing importance of **1** in quantitative studies of spin trapping we felt it was essential to check on whether **2** really did behave in the unprecedented manner suggested by Bullock *et al.* (1), i.e., do **2** exist in equilibrium with their dimer in water at the concentrations ($< 10^{-4}$ *M*)

0008-4042/82/121501-03$01.00/0
©1982 National Research Council of Canada/Conseil national de recherches du Canada

Can. J. Chem. Downloaded from www.nrcresearchpress.com by 210.87.254.6 on 09/06/12
For personal use only.

Can. J. Chem. Downloaded from www.nrcresearchpress.com by 210.87.254.6 on 09/06/12
For personal use only.

encountered in spin trapping?[3] For study we chose **2***a* since Bullock *et al.* (1) did most of their work with this aminoxyl and we investigated its behavior by epr spectroscopy.

## Results

The "cleanest" method known to us for producing aminoxyl radicals in solution is the direct uv photolysis of the parent hydroxylamine (3).

$$[6] \quad R_1R_2NOH \xrightarrow{h\nu} R_1R_2NO^{\cdot} + H^{\cdot}$$

$$[7] \quad H^{\cdot} + R_1R_2NOH \longrightarrow R_1R_2NO^{\cdot} + H_2$$

Though not a very efficient process it is quite satisfactory for most aminoxyls because of their relative persistence.

Carefully purified **3***a* dissolved ($[\mathbf{3}a] = 0.5–1.0\,M$) in deionized water or in benzene that had been *rigorously* deoxygenated showed, at most, a very weak epr signal due to **2***a* ($[\mathbf{2}a] < 10^{-7}\,M$). A strong signal of **2***a* ($[\mathbf{2}a] = 10^{-4}–10^{-5}\,M$) could be obtained by continuous uv photolysis of the solution. On shuttering the light **2***a* decayed with the expected (3, 4) second order kinetics with $2k_3 = 7.5 \times 10$ and $2.4 \times 10^3\,M^{-1}\,s^{-1}$ in water and benzene, respectively, at 25°C. With such *relatively* slow radical decays it was possible to undertake heating and cooling experiments on the "residual" aminoxyl signal remaining after decay had proceeded for a few half-lives. At $[\mathbf{2}a] = 10^{-5}–10^{-6}\,M$ the increase in the concentration of **2***a* caused by an increase in temperature from 5 to 25°C was negligible, varying from 0% to 20% in different experiments.[4,5] In contrast, Bullock *et al.* (1) observed a nearly 300% increase in $[\mathbf{2}a]$ on raising the temperature from 5 to 24°C with a similar concentration of **2***a* (8).

An alternative procedure that has been used to demonstrate the occurrence of a reversible dimerization of free radicals is to generate the radical in a series of light flashes (9). When there is an equilibrium this step-wise approach leads to higher concentrations of radical (and dimer) after each light flash. When **2***a* was generated from **3***a* in deoxygenated water or benzene using a series of well-spaced light pulses of equal intensity and duration the decay traces were superimposable and there was no net accumulation of aminoxyl. Therefore, **2***a* is not in equilibrium with its dimer at ambient temperatures and the experimental observations reported by Bullock *et al.* must clearly have an alternative explanation.

One possibility is that the samples used by Bullock *et al.* were contaminated by atmospheric oxygen. We have previously shown that diethyl hydroxylamine reacts with atmospheric oxygen to give diethyl nitroxide (3). The reaction has a substantial activation energy so that the steady-state radical concentration observed becomes larger as the temperature increases (3). The concentration of the nitroxide can be repeatedly increased and decreased by raising and lowering the temperature (3). However, the nitroxide is not in reversible equilibrium with the dimer since its epr signal ultimately disappeared when all of the oxygen was consumed (3). These characteristics are essentially the same as those observed by Bullock.

As confirmation of these and similar (10) observations we found that a relatively strong signal of **2***a* was obtained when **3***a* was dissolved in water or benzene which had not been deoxygenated, or if air were let into a carefully degassed sample. Under such conditions the concentration of **2***a* increased by more than 100% on raising the temperature from ca. 5 to 25°C, and decreased again on lowering the temperature. The whole process was almost reversible, except that the radical concentration (at one temperature) decreased with time in systems in which the oxygen could become depleted.

$$[8] \quad \mathbf{3}a + O_2 \rightarrow \mathbf{2}a + HOO^{\cdot} \text{ (or } H^+ + O_2^{-\cdot})$$

A second potential oxidant in Bullock *et al.*'s experiments is hydrogen peroxide, it being well known that both organic hydroperoxides (2) and hydrogen peroxide (11) oxidize hydroxylamines to the corresponding aminoxyls. Addition of a 10% mole equivalent of a 3% $H_2O_2$ solution to a degassed aqueous solution of **3***a* gave a very strong signal of **2***a*. Again the intensity of the signal could be increased by more than 100% on raising the temperature from ca. 5 to 25°C. The effect of temperature was reversible, but only for limited periods of time, the length of time depending on the temperature program and the amount of hydrogen peroxide added. Once all the $H_2O_2$ had been consumed the concentration of **2***a* decreased rapidly.

$$[9] \quad \mathbf{3}a + H_2O_2 \rightarrow \mathbf{2}a + H_2O + (^{\cdot}OH)$$

[3]If **2** did exist in equilibrium with their dimers under spin-trapping conditions the work reported in refs. 10 and 19 would be wrong!

[4]The signal did, however, increase appreciably on further raising the temperature to 65°C, an effect we attribute either to an increased rate of reaction of **3***a* with residual oxygen (*vide infra*), or to the thermal instability of the hydroxylamine.

[5]Similarly, the OH spin adduct of **1**, i.e., **2** (R = OH), prepared at a steady concentration of $2 \times 10^{-5}\,M$ by making up a $1.2\,M$ solution of **1** in 1% $H_2O_2$, showed no change in concentration on changing the temperature between 5 and 25°C, whereas Bullock *et al.* (1) found a change similar to what they found for **2***a*. In this system the spin adduct is probably formed mainly by photolysis of the $H_2O_2$ by the normal laboratory lighting since the signal was barely detectable in the dark, under which conditions it is presumably formed by hydrolysis of the nitrone followed by oxidation (11).

Can. J. Chem. Downloaded from www.nrcresearchpress.com by 210.87.254.6 on 09/06/12
For personal use only.

By analogy with the known formation of mono-alkyl and mono-arylaminoxyls by reaction of their parent hydroxylamine with their parent nitroso compound (12) and of iminoxyl radicals by reaction of oximes with nitrile oxides (13) the possibility that the nitrone **1** might also oxidize **3***a* to **2***a* could not be ignored. However, when prepared under as nearly oxygen-free conditions as possible, a solution 1.0 *M* in **1** and 1.0 *M* in **3***a* in benzene or in water gave an epr signal due to **2***a* which was of virtually the same strength ($< 10^{-7}$ *M*) as a 1.0 *M* solution of **3***a* prepared under the same conditions. This result was obtained at both 25 and at 65°C. Reaction [3] is therefore irreversible at normal temperatures.

## Discussion

Our results prove that the aminoxyl **2***a* is not in equilibrium with a dimer at ambient temperature and at radical concentrations $\leq$ca. $10^{-4}$ *M*. The cause of the observation that led to Bullock *et al.*'s proposed "trap for the unwary" is most probably excessive consumption of **1**, with the consequence that **3** is formed via reaction [3], combined with oxidation of **3** by adventitious oxygen and/or $H_2O_2$ formed by glow-discharge electrolysis (14).[6]

Our present results serve to reemphasize earlier studies (3, 4) which implied that spin-trapping experiments should not be permitted to proceed to the point where hydroxylamine is formed by aminoxyl disproportionation if the reaction medium contains oxygen or some other oxidizing agent. Since the technique of spin trapping is now used extensively in free radical chemistry (15), particularly in biological systems (16), we hope that this work will lead to an increased awareness of the potential problems due to inadvertant hydroxylamine oxidation.

## Experimental

The hydroxylamine **3***a* was synthesized by $LiAlH_4$ reduction of **1** (Aldrich) by the method of Morgan and Beckett (17). In dry conditions under $N_2$, 1.0 g **1** was dissolved in 50 mL dry ether and was then added dropwise to a stirred suspension of 1 g $LiAlH_4$ in 100 mL dry ether. After 3½ h a minimum amount (4 mL) of water was added dropwise to decompose excess hydride. A white residue formed and upon addition of 2 g celite the solution was filtered. The filtrate was dried over $MgSO_4$ and concentrated under reduced pressure (30 Torr) to yield a light yellow oil. Double bulb-to-bulb distillations gave the colorless hydroxylamine in 60% yield. Since this is sensitive to oxygen (*vide supra*) and light it was kept under $N_2$ in the dark. Attempted analytical gas chromatography was frustrated by thermal decomposition. The hydroxylamine readily reduced aqueous alkaline triphenyltetrazolium chloride to the red formazan (18). **1** $^1$H nmr: $\delta(CDCl_3)$, 1.12 (s, 6H, $C_5CH_3$), 1.6 (m, 4H, $C_3$—H, $C_4$—H), 3.0 (m, 2H, $C_2$—H), 8.0–8.5 ppm (broad, 1H, OH); $^{13}$C nmr: $\delta(C_6D_6)$, 19.2 (t, C-3), 23.3 (broad at room temperature; 18.9, 26.6 at −11°C, two quartets, $C_5$—$CH_3$), 35.2 (t, C-4), 54.6 (t, C-2), 64.2 ppm (s, C-5).

[6]The concentration of $H_2O_2$ in the glow discharge electrolysis experiments was $\leq 4 \times 10^{-3}$ *M* (8). Conventional electrolysis, i.e., cathodic reduction of **1**, gave **2***a* and the signal showed the same large variation with temperature as that of **2***a* formed by glow-discharge electrolysis (8). In the conventional electrolysis $H_2O_2$ should be absent (8); the most likely oxidant is therefore $O_2$.

## Acknowledgements

We are extremely grateful to Miss Ann Sneddon and to Mrs. L. Planinic for preliminary studies of the **1** + **3***a* system.

1. A. T. Bullock, D. L. Gavin, and M. D. Ingram. J. Chem. Soc. Chem. Commun. 327 (1980).
2. H. E. De La Mare and G. M. Coppinger. J. Org. Chem. **28**, 1068 (1963).
3. K. Adamic, D. F. Bowman, T. Gillan, and K. U. Ingold. J. Am. Chem. Soc. **93**, 902 (1971).
4. D. F. Bowman, T. Gillan, and K. U. Ingold. J. Am. Chem. Soc. **93**, 6555 (1971).
5. K. Adamic, J. A. Howard, and K. U. Ingold. Can. J. Chem. **47**, 3803 (1969).
6. G. D. Mendenhall and K. U. Ingold. J. Am. Chem. Soc. **95**, 6390 (1973).
7. P. R. Marriott and K. U. Ingold. J. Phys. Chem. **84**, 937 (1980).
8. A. T. Bullock. Private communication.
9. J. C. Scaiano and K. U. Ingold. J. Am. Chem. Soc. **99**, 2079 (1977).
10. J. W. Lown and H.-H. Chen. Can. J. Chem. **59**, 390 (1981).
11. E. G. Janzen, Y. Y. Wang, and R. V. Shetty. J. Am. Chem. Soc. **100**, 2923 (1978).
12. D. F. Bowman, J. L. Brokenshire, T. Gillan, and K. U. Ingold. J. Am. Chem. Soc. **93**, 6551 (1971).
13. J. L. Brokenshire, J. R. Roberts, and K. U. Ingold. J. Am. Chem. Soc. **94**, 7040 (1972).
14. A. T. Bullock, G. L. Gavin, and M. D. Ingram. J. Chem. Soc., Faraday Trans. I, **76**, 648 (1980).
15. M. J. Perkins. Adv. Phys. Org. Chem. **17**, 1 (1980).
16. E. G. Janzen. Free Radicals Biol. **4**, 115 (1980).
17. P. H. Morgan and A. H. Beckett. Tetrahedron, **31**, 2595 (1975).
18. G. A. Snow. J. Chem. Soc. 2588 (1954).
19. E. Finkelstein, G. M. Rosen, and E. J. Rauckman. J. Am. Chem. Soc. **102**, 4994 (1980); P. R. Marriott, M. J. Perkins, and D. Griller. Can. J. Chem. **58**, 803 (1980).

# Some physical and chemical aspects of spin trapping of organometallic radicals by quinones: optically active radical complexes

KATHERINE A. M. CREBER, TONG-ING HO, M. CATHERINE DEPEW, DOUGLAS WEIR, AND JEFFREY K. S. WAN

*Department of Chemistry, Queen's University, Kingston, Ont., Canada K7L 3N6*

Received September 1, 1981

KATHERINE A. M. CREBER, TONG-ING HO, M. CATHERINE DEPEW, DOUGLAS WEIR, and JEFFREY K. S. WAN. Can. J. Chem. **60**, 1504 (1982).

A brief account is presented on the use of substituted quinones as spin traps for organometallic radicals and on the applications of CIDEP and esr–HPLC techniques to the study of quinone – organometallic radical complexes. Many of these radical adducts are thermally very stable and can be isolated by the HPLC technique for detailed spectroscopic and chemical studies. This in turn allows us to present a different approach to the "spin trapping" chemistry of unstable organometallic radicals by generating initially a stable quinone – metal carbonyl radical complex, separating the parent radicals by esr–HPLC and using them to react with other organometals via ligand exchange between the CO group(s) and the organometals. It then follows that if the entering organometal ligand is optically active, the substituted radical complex would also be chiral. This simple concept has led to the isolation of the first pure optically active radical complex with well-defined physical properties, including optical rotation.

KATHERINE A. M. CREBER, TONG-ING HO, M. CATHERINE DEPEW, DOUGLAS WEIR et JEFFREY K. S. WAN. Can. J. Chem. **60**, 1504 (1982).

On présente un bref compte rendu sur l'utilisation des quinones substituées comme capteurs de spin pour les radicaux organo-métalliques et sur les applications des techniques de PEDIC et de rpe–CLHP à l'étude des complexes de quinone – radical-organométallique. Plusieurs de ces adduits radicalaires sont très stables thermiquement et peuvent être séparés par la technique de CLHP en vue d'études spectroscopiques et chimiques approfondies. Ceci nous permet ainsi de présenter une approche différente de la chimie de "captage de spin" des radicaux organométalliques instables en générant initialement un complexe de quinone – radical métal carbonyle stable et en séparant les radicaux apparentés par la rpe–CLHP et en les faisant réagir par la suite avec d'autres produits organométalliques par l'intermédiaire d'un échange de ligand entre le groupe CO et l'organométallique. Il s'en suit que si le ligand organométallique de l'ion introduit est optiquement actif, le complexe radicalaire substitué sera également chiral. Ce concept simple a conduit à la séparation du premier complexe radicalaire optiquement actif à l'état pur ayant des propriétés physiques bien définies y compris le pouvoir rotatoire.

[Traduit par le journal]

For many years the popular nitroxide spin trapping technique has provided evidence for numerous transient metal centered radicals (1). The ability of quinones to form radical complexes and spin adducts with a variety of organometals was recently emphasized (2, 3) and added another dimension to the spin trapping chemistry. The quinone – metal radical complexes are interesting generally because both the metal centre and the quinone ligands can be redox active. Since the first major study on quinone–metal complexes was carried out by Eaton (4), many other interesting complexes have been synthesized directly by the reactions of metal carbonyls with quinones (5, 6). The use of quinones in spin trapping photochemistry has yet another advantage. There is a large pool of information available for the photochemical and photophysical properties of carbonyl compounds but the quenching of the excited states of carbonyl compounds by various electron donors, including some of the organometals, has continued to attract attention (7). In this laboratory, the photoreduction of quinones by alcohols and phenols (8, 9) and by vitamins such as C and $K_1$ (10) have been extensively used as model systems for chemically induced magnetic polarization studies. They in turn provide some valuable information about the relative efficiencies of the triplet quenching reaction, the mechanisms of the secondary radical reactions, and the dynamics of the intersystem crossing processes which are responsible for the difference in the spin populations of the triplet sub-levels. The CIDEP technique was further applied to study the quenching of quinone triplets by organometals (11) and the results indicate the nature of electron transfer between the organotin compounds and the triplet quinone in the photochemical primary process. Unequivocal evidence of the electron transfer mechanism was subsequently obtained by the direct esr characterization of the triplet state of the primary radical ion pair formed and trapped during the photolysis of a solid solution containing the quinone and the organotin at 77 K (12).

When the metal – quinone radical complexes exhibit time-resolved CIDEP, their spin–lattice relaxation times $T_1$ can be estimated at low micro-

0008-4042/82/121504-08$01.00/0

©1982 National Research Council of Canada/Conseil national de recherches du Canada

Can. J. Chem. Downloaded from www.nrcresearchpress.com by 210.87.254.42 on 09/06/12
For personal use only.

Can. J. Chem. Downloaded from www.nrcresearchpress.com by 210.87.254.42 on 09/06/12
For personal use only.

wave power levels (13). These experimental $T_1$'s provide interesting data for studies of the structural and dynamic properties of these novel radical complexes such as the uranyl–phenanthroquinone radical ion (14). However, we were a little surprised when we found that the $T_1$'s for the quinone – tin radical adducts are essentially the same as the parent semiquinone radicals (11). Subsequently, with the collaboration of Professor D. A. Hutchinson we have successfully interpreted the $T_1$ data by approximate calculations on the odd electron in the $\pi$ system (15), in which the state of the odd electron is described by the Hückel method and the contributions to $T_1$ of **G** tensor modulation and spin rotation coupling are treated. The results show that $T_1$ is just as sensitive to the number of rings as it is to the actual size of the radical. The addition of the organotin moiety does not contribute significantly to the $\pi$ system and thus has little effect on the magnitude of the $T_1$ in the radical adduct.

In recent years we have extended out quinone–metal complex studies to include other metal carbonyls, such as Re, Mn, W, Cr, and Mo. For the series of radical complexes containing rhenium carbonyl and the substituted analogs, the trapping using *ortho*-quinones has produced some extremely stable species. These radical complexes have been successfully isolated by an integral esr–HPLC (high performance liquid chromatography) technique (16). The ability of preparing and isolating these radical complexes in *pure* form has opened up many possibilities for detailed spectroscopic studies, including the emission/fluorecence of these radical complexes (16).

Another interesting aspect of the quinone spin trapping chemistry is the facility of ligand exchange in these radical complexes. We have reported earlier (17) the general exchange reactions between alkali radical ion pairs and triple ions of dicarbonyl compounds and group IVB organometals. Using *ortho*-quinone radical complexes, other exchange reactions observed include the uranyl ion (14), the organomercury (18), the group IVB organometals (19), the group VIB (3, 20) and group VIIB metal carbonyls (21). The application of these ligand exchange techniques provides another approach to the art of spin trapping of some elusive radicals. For example, substituted rhenium carbonyl radicals such as $\dot{R}e(CO)_4PPh_3$ and $\dot{R}e(CO)_3(PPh_3)_2$ have been proposed (22) in chemical reactions but not yet detected or trapped by nitroxides. In our approach (20) we began by preparing the stable quinone – rhenium carbonyl radical complex as the "trap" which is then further allowed to exchange its labile carbonyl ligand with phosphine in a thermal process. In the direct photolysis, the trapping of the elusive rhenium carbonyl – phosphine radicals is also possible by *ortho*-quinones and 1,2-dicarbonyl compounds. Further exploration of the chemistry of these stable quinone – organometal radical complexes has led to the formation of numerous hetero-binuclear and trinuclear metal organic radical complexes as well as the use of other bidentate organic ligands such as bipyridines. Some of these systems will be described here for the first time.

The key development and combination of the esr–HPLC with the radical ligand exchange technique have further excited our imagination. It follows that when the organometal ligand under exchange is optically active, the daughter radical complex would exhibit chirality. Moreover, if these chiral radical complexes can be separated by esr–HPLC, a pure optically active radical would be obtained. Such an extremely simple idea has been made into a fact in our current studies. To the best of our knowledge, *isolation* and direct identification of a pure optically active radical has not been heretofore achieved. A few of the previous studies have involved optically active radical intermediates (23–26) by inferring from product analysis or by observing different optical rotation values for the solution containing both the presumed chiral radical and the parent optically active reactant.

The implications of stable optically active radicals have yet to be fully understood. Our current efforts directed towards both the physical and chemical characterizations, including CIDEP of chiral radicals, hopefully will shed some light on this novel area of optically active radicals. This paper is dedicated to the present and former students of this laboratory and much of the experimental detail can be found in previous publications (11, 16, 17).

We shall now proceed to describe some of the current results.

## I. Spin trapping of rhenium carbonyl fragment by *ortho*-quinones, 1,2-diketones, and some nitrogen donor ligands

Formation of the $\dot{R}e(CO)_5$ fragment is accomplished by irradiation of the $\sigma \rightarrow \sigma^*$ band at 310 nm of $Re_2(CO)_{10}$ (27). In the presence of a spin trap such as *d,l*-camphorquinone (CQ) the reaction proceeds as shown below:

$$[1]\quad Re_2(CO)_{10} \xrightarrow[\text{benzene}]{h\nu,\ 310\,\text{nm}} 2\dot{R}e(CO)_5$$

Can. J. Chem. Downloaded from www.nrcresearchpress.com by 210.87.254.42 on 09/06/12
For personal use only.

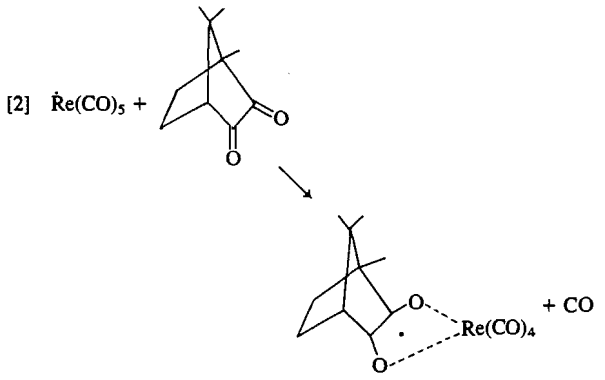


1

The esr spectrum of the complex **1** is shown in Fig. 1. In an earlier study we have shown, using 3,5-di-*tert*-butyl-0-benzoquinone (DTBQ) as the spin trap in an analogous reaction, that the resulting radical complex displays octahedral symmetry about the Re centre (3). The use of CQ in the current experiments is obvious, since there are asymmetric centres in CQ. However, reaction [2] does not lead to any observable optical resolution, as expected. Partial enantioselective complexation is possible in reaction [2], when the rhenium centered radical contains an optically active ligand.[1]

Table 1 lists the esr parameters of a number of rhenium carbonyl radical complexes with quinones and 1,2-diketones. All radical complexes studied in this series are relatively stable thermally and many of them have been isolated by the esr–HPLC technique using a Partisil-5 or Partisil-10 column. For example, under identical conditions and a flow rate of 1.44 mL/min, the retention times for the series of quinone – rhenium carbonyl radical complexes are 138 s for the DTBQ–$\dot{}$–$Re(CO)_4$, 161 s for the NQ–$\dot{}$–$Re(CO)_4$, and 145 s for the PQ–$\dot{}$–$Re(CO)_4$. Generally, the quinone complexes are more stable than the diketone complexes.

Table 2 shows the esr parameters of the radical complexes between the rhenium carbonyl and the organic spin traps with various nitrogen-donor ligands, instead of quinones. The esr spectra of these complexes were found to be more resolved at room temperatures, in contrast to the quinone-type spin traps. However, these complexes were not nearly as stable as the quinone-type complexes and no attempts were made to isolate any of these complexes by HPLC. For the phenanthroline – rhenium carbonyl radical complex, the well-resolved esr spectrum shown in Fig. 2 clearly identifies the structure of the radical species as a coplanar complex. The resolved hyperfine couplings due to four equivalent nitrogen atoms indicate that two phenanthroline molecules are co-ordinated to the rhenium centre.

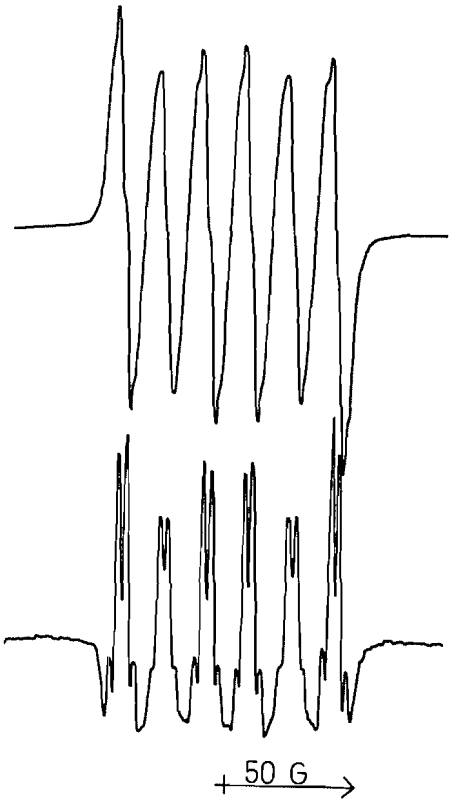


FIG. 1. The first derivative (upper) and second derivative (lower) esr spectra of CQ–$\dot{}$–$Re(CO)_4$ in toluene at 50°C.

The benzofuroxan – rhenium carbonyl radical complex is very interesting, as the splittings due to two equivalent nitrogen atoms are readily observed in the spectrum. If the rhenium is co-ordinated via the two oxygen atoms in the benzofuroxan molecule, then inequivalent nitrogen splittings would be expected. One possible structure of the radical complex is the following:

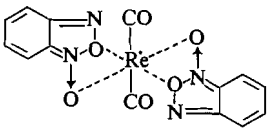


The fact that these radical complexes involving donor nitrogen ligands are less stable than the

[1]Preliminary experiments using a shift reagent Eu(III)-tris-[3-(heptafluoropropylhydroxymethylene)d-camphorato] in the pmr analysis of the unreacted camphoroquinone showed a definite excess of one enantiomer but the quantitative separation and yield have not yet been obtained. We wish to thank Professor M. J. Perkins for suggesting the use of the shift reagent.

Can. J. Chem. Downloaded from www.nrcresearchpress.com by 210.87.254.42 on 09/06/12
For personal use only.

TABLE 1. Electron spin resonance parameters of radical complexes X–$\dot{}$–Re(CO)$_4$ in toluene at 50°C; the organic moiety X is either a quinone or a diketone

| Organic moiety | $g$-Factor | $a_{Re}$ (G) | $a_H$'s (G) | $a_{Other}$ (G) |
|---|---|---|---|---|
| 3,5-DTBQ | 2.0032±0.0005 | 28.2 | $a_H^4 = 3.5$ | |
| Tetrachloro-*o*-quinone | 2.0014 | 35.4 | | — |
| Tetrabromo-*o*-quinone | 2.0070 | 35.3 | | — |
| Acenapthroquinone | 2.0048 | 17.4 | — | |
| 1,2-Napthoquinone | 2.0030 | 24.2 | $a_H^2 = 3.4$ | |
| Phenanthroquinone | 2.0019 | 21.5 | — | |
| Camphorquinone | 2.0048 | 16.5 | $a_H^1 = a_H^2 = a_H^3 = 3.0$ | |
|  | 2.0051 | 21.3 | $a_H = 8.0$ (6H) | |
| Benzil | 2.0058 | 22.6 | — | |
| Furil | 2.0049 | 20.0 | $a_H^1 = a_H^3 = 1.9$ (4H) | |
| Di-*t*-butylazodicarboxylate | 2.0077 | 39.2 | — | $a_N^1 = 9.4$<br>$a_N^2 = 4.7$ |
| 2,2′-Pyridil | 2.0046 | 20.0 | — | — |

TABLE 2. Electron spin resonance parameters of radical complexes X–$\dot{}$–Re(CO)$_n$ in toluene at 25°C

| Radical complex | $g$-Factor | $a_{Re}$ (G) | $a_N$ (G) |
|---|---|---|---|
| (Phenanthroline)$_2$–$\dot{}$–Re(CO)$_2$ | 2.0100 | 20.7 | 3.4 (4N) |
| (2,2′-Bipyridine)–$\dot{}$–Re(CO)$_4$ | 2.0042 | 20.6 | Unresolved |
| (Benzofuroxan)$_2$–$\dot{}$–Re(CO)$_2$ | 2.0206 | 21.6 | 2.7 (2N) |
| (2,4,6-tri-(2-pyridyl)-*s*-triazine)–$\dot{}$–Re(CO)$_4$ | 2.0009 | 17.9 | Unresolved |

analogous oxygen donors suggests that in a molecule such as benzofuroxan containing both the nitrogen and the oxygen donors, the more stable structure would be obtained by using the oxygen donors for co-ordination.

## II. Spin trapping of group VIB metal carbonyl fragments by phenanthroquinone

Few systematic studies of spin trapping of group VIB metal carbonyl fragments have been carried out with quinones. Earlier, trapping of Mo(Cp)(CO)$_3$ fragment by nitrosodurene was reported by Hudson and co-workers (28) while the Russian workers have used other nitroso spin traps to co-ordinate Cr(CO)$_4$Cl species (29). We have examined (21) systematically the photochemical reactions of group VIB metal hexacarbonyls (including Mo, W, and Cr hexacarbonyls) in toluene and in the presence of phenanthroquinone as a spin trap. In all three cases stable metal carbonyl – quinone radical complexes were observed by esr during irradiation.

The structure of these metal carbonyl – quinone radical complexes is of great interest, since the diamagnetic group VIB metal–PQ complexes in the form of M(PQ)$_3$ are well known (3). Furthermore, data from the electrochemical redox reactions of the diamagnetic neutral quinone complexes of group VIB metals are available in the literature (30, 31). It is, therefore, noteworthy that the photochemical reactions of these metal hexacarbonyls with PQ lead to the formation of stable radical complexes involving only one quinone ligand.

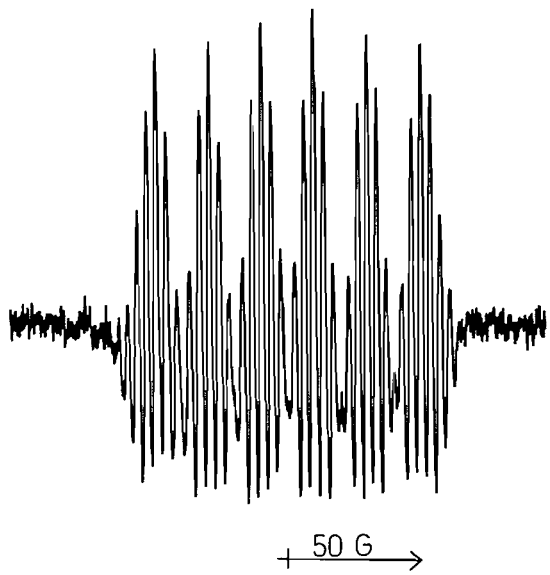


FIG. 2. The second derivative esr spectrum of the [phenanthroline]$_2$–$\dot{}$–Re(CO)$_2$ radical complex in toluene at 25°C.

On the other hand, current studies have further indicated the presence of another series of radical complexes in which *two* PQ molecules are involved in each metal radical complex. The $g$-factors for the $\dot{M}(CO)_2(PQ)_2$ are significantly lower than the corresponding $\dot{M}(CO)_4PQ$ complexes (Table 3). For Mo and W carbonyl systems, $\dot{Mo}(CO)_2(PQ)_2$ and $\dot{W}(CO)_2(PQ)_2$ radical complexes were observed after about 15 min of continuous degassing, without irradiation. The esr intensity of these complexes indicates that they are formed only as a

TABLE 3. The $g$-factors of the two series of radical complexes, $M(CO)_4$–PQ and $M(CO)_2$–$(PQ)_2$ in toluene at 25°C*

| Metal | $g$-Factor | |
|---|---|---|
| | $M(CO)_4$–PQ | $M(CO)_2$–$(PQ)_2$ |
| W | 2.0056 (with resolved proton hyperfine) | 1.9707 (proton hyperfine not resolved) |
| Mo | 2.0045 (with proton hyperfine resolved) | 1.9702 (proton hyperfine not resolved) |
| Cr | 2.0038 | 1.9692 (with Cr hyperfine resolved) |

*PQ = Phenanthroquinone.

minor intermediate. Upon irradiation, they quickly disappeared with the simultaneous formation of the major $\dot{M}(CO)_4PQ$ complexes. In the Cr hexacarbonyl system, the results are different. Here the $\dot{C}r(CO)_2(PQ)_2$ was the major radical complex either in the dark or under irradiation. The minor radical species was the $\dot{C}r(CO)_4PQ$ complex which was produced only by photolysis.

### III. Radical ligand exchange reactions between quinone – metal carbonyl complexes and group VA organometals

It is well known that 17-electron species are very labile towards CO substitution (32). Thus, our series of stable metal carbonyl – quinone radical complexes offered excellent possibilities for ligand exchange study. Normally, the parent metal carbonyl – quinone complexes, $M(CO)_4$–Q, were first prepared and characterized by esr. Appropriate organometal ligands were then added to the solution and the substitution reactions were monitored either by esr or uv/visible spectrophotometry. Table 4 gives the esr parameters of some representative substituted heterobinuclear and trinuclear radical complexes formed via these simple ligand exchange reactions. In the DTBQ–rhenium carbonyl series, substitution by group VA ligands proceeded quite readily, with the ease of reaction under similar concentration range and other experimental conditions decreasing in the order: N > P > As > Sb. In the majority of cases, only one CO could be replaced readily by an organometal ligand. However, when the entering ligand was a phosphite two CO groups could be replaced in a consecutive manner. Preliminary studies also indicate that the ligand substitution is an equilibrium process in which the exchange can be retarded by saturating the solution of added carbon monoxide under high pressure.

TABLE 4. Electron spin resonance parameters of some group VA organometal substituted DTBQ–$Re(CO)_xM_y$ radical complexes in benzene at 25°C

| Ligand substitution | $g$-Factor | $a_{Re}$ (G) | $a_M$ (G) |
|---|---|---|---|
| $PPh_3$[a] | 2.0012 | 38.0 | $a_P = 24.7$ |
| $AsPh_3$[a] | 2.0017 | 36.0 | $a_{As} = 36$ |
| $SbPh_3$[a] | 2.0024 | 36.0 | $a_{^{121}Sb} = 93$<br>$a_{^{123}Sb} = 50$ |
| $P(OCH_3)_3$[a] | 2.0020 | 35.1 | $a_P = 29.2$ |
| $(P(OCH_3)_3)_2$: disubstitution | 2.0009 | 49.9 | $a_P = 30.8$ (2P) |
| $Ph_2P(CH_2)_2PPh_2$ | 2.0023 | 37.5 | $a_P = 25.4$ |
| $Ph_2P(CH_2)_2AsPh_2$[a] | 2.0016 | 37.5 | $a_P = 25.1$ |
| 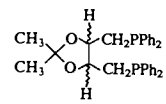 | 2.0010 | 37.9 | $a_P = 26.5$ |

[a]Taken from ref. 20.

It is interesting to examine the trends in the esr parameters on going from the parent DTBQ–$Re(CO)_4$ complex to the monosubstituted followed by the disubstituted complex where $P(OCH_3)_3$ is the entering ligand. Heat was necessary for disubstitution. As ligands are added, $a_H$ decreases, $a_{Re}$ increases, $a_P$ increases, and the $g$-factor decreases. These trends indicate that the electron density is being withdrawn from the quinone moiety towards the phosphite ligands. The increase in the $a_{Re}$ and the lower $g$-factor are consistent with the increased participation of the rhenium in the co-ordination through the phosphite ligands. When bidentate phosphorous ligands were used, in no case could both P atoms be forced to co-ordinate the rhenium atom.

Kinetic studies of these radical ligand exchange reactions are underway in an effort to elucidate the mechanism of the substitution, as the current views differ on whether an associative (33) or a dissociate (34) mechanism prevails. Our preliminary results tend to favour the dissociative mechanism, as rates for the substitution by $PPh_3$, $AsPh_3$, and $SbPh_3$ in the DIBQ–$Re(CO)_4$ complex are very close, while addition of CO apparently retards the rate significantly.

It appears rather unusual at first that although nitrogen donor ligands generally reacted faster than other ligands, neither $NPh_3$ nor $NHPh_2$ would replace a CO group on the DTBQ–$Re(CO)_4$. In an effort to explain this, we looked at a number of nitrogen–donor ligands, shown in Table 5. It became clear that the complexes fell into two distinct classes: those with high $g$-factors and low $a_{Re}$, which were very stable and those with much lower $g$-factors and higher $a_{Re}$ values, which were not at all stable. From these observations we concluded that in order to form stable substituted complexes,

Can. J. Chem. Downloaded from www.nrcresearchpress.com by 210.87.254.42 on 09/06/12
For personal use only.

Can. J. Chem. Downloaded from www.nrcresearchpress.com by 210.87.254.42 on 09/06/12
For personal use only.

TABLE 5. Electron spin resonance parameters of some nitrogen donor ligand substituted DTBQ·—$Re(CO)_3N$ radical complexes in benzene at 25°C

| Ligand | $g$-Factor | $a_{Re}$ (G) |
|---|---|---|
| Aniline | 2.0027 | 22.8 |
| Pyridine | 2.0029 | 20.1 |
| 3,5-Diethoxycarbonyl-1,4-dihydropyridine | 2.0024 | 19.5 |
| 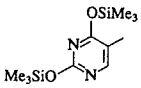 | 2.0032 | 21.8 |
| Pyrrolidine | 2.0013 | 26.4 |
| | 2.0010 | 24.2 |
| Morpholine | 2.0024 | 25.1 |
| 1,1-Carbonyldiimidazole | 2.0028 | 23.3 |
| Quinidine | 2.0029 | 18.7 |
| Methylbenzylamine | 2.0027 | 22.3 |
| Triethylamine | 2.0022 | 24.6 |
| Bicyclohexylamine | 2.0017 | 24.9 |
| Tetrahydropyridine | 2.0013 | 26.4 |

the incoming ligand must not be sterically hindered at the donor atom centre (as were $NPh_3$ and $NHPh_2$). They must also possess some way to delocalize the excess electron density such as aromatic $\pi$ system (as in $PhNH_2$), a heteroatom as in morpholine, or empty $d$-orbitals as in the phosphine ligands.

Other quinone·—$Re(CO)_4$ complexes will also undergo substitution reactions with a variety of ligands. A representative group of different quinones involved is shown in Table 6. Several interesting effects due to the choice of quinone can be seen from the esr parameters. Napthoquinone has an extensive $\pi$ system, hence delocalizes electron density very efficiently, resulting in lower $g$-factors and smaller metal hyperfine coupling constants. Camphorquinone, on the other hand, has no aromatic character and in the case of a substituted phosphite ligand $a_P$ becomes much greater than $a_{Re}$.

Similar ligand substitution reactions also occur with the group VIB metal carbonyl – PQ radical complexes. The noted difference is that for the $Mo(CO)_4$·—PQ complex, both equatorial CO groups can be replaced by two $PPh_3$ ligands (21). On the other hand, substitution reactions involving $Cr(CO)_2$·—$PQ^2$ complex were much more difficult. With $PPh_3$, the reaction took a few hours to complete and only one of the two axial CO groups was replaced. Attempt to replace the CO group with other group VA organometals was not successful.

These results represent a comprehensive and systematic study of the radical ligand exchange reactions in metal carbonyl complexes. The information is extremely valuable as we move further towards the novel radical complex systems which contain exchanged ligands exhibiting optical activity.

## IV. The stable optically active organometallic radical adducts

Many of the substituted metal carbonyl—quinone radical complexes studied above are thermally stable and have been separated by the esr–HPLC method. A simple idea was then developed to prepare the first pure optically active radical complex by combining our experience in esr–HPLC and in radical ligand exchange technique. When the entering ligand is optically active, the stable daughter radical complex will also be chiral. We have recently succeeded in making and *isolating* the first two pure optically active radical complexes by the following reactions:

[3] DTBQ·—$Re(CO)_4$ + 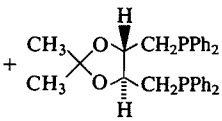

(+)DIOP

↓

DTBQ·—$Re(CO)_3$—(+)DIOP + CO

**2**

[4] DTBQ·—$Re(CO)_4$ + 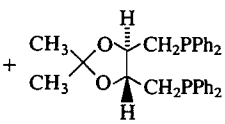

(−)DIOP

↓

DTBQ—$Re(CO)_3$—(−)DIOP + CO

**3**

Electron spin resonance–HPLC was then used to separate the optically active radical complexes **2** and **3** in respective systems from the parent radical as well as the unreacted optically active phosphine. At a typical flow rate of chloroform at 2.0 mL/min through a Partisil-10 column, the retention times were 115 s for the parent radical, 490 s for the optically active radical complexes **2** or **3**, and 150 s for DIOP. Obviously, the different optically active configurations are not separated by HPLC, and therefore pure (+) or pure (−)DIOP ligands must be used to produce the corresponding optically active daughter radicals.

Can. J. Chem. Downloaded from www.nrcresearchpress.com by 210.87.254.42 on 09/06/12
For personal use only.

TABLE 6. Electron spin resonance parameters of organometal substituted radical complexes for TTBQ–$\dot{}$–$Re(CO)_3M$,* NQ–$\dot{}$–$Re(CO)_3M$, and CQ–$\dot{}$–$Re(CO)_3M$ in benzene at 25°C

| Ligand substituted | g-Factor | | |
|---|---|---|---|
| | NQ–$\dot{}$–$Re(CO)_3M$ | TTBQ–$\dot{}$–$Re(CO)_3M$ | CQ–$\dot{}$–$Re(CO)_3M$ |
| $PPh_3$ | $g = 2.0013$<br>$a_{Re} = 33.0$ G<br>$a_p = 20.3$<br>$a_H = 3.9$ | $g = 2.0054$<br>$a_{Re} = 59.6$<br>$a_p = 29.1$ | $g = 2.0035$<br>$a_{Re} = 17.5$<br>$a_p = 11.4$ |
| $AsPh_3$ | $g = 2.0026$<br>$a_{Re} = 30.8$<br>$a_{As} = 25.8$<br>$a_H = 4.9$ | $g = 2.0029$<br>$a_{Re} = 55.5$<br>$a_{As} = 35.5$ | No observable substitution |
| $SbPh_3$ | No observable substitution | $g = 2.0081$<br>$a_{Re} = 59.4$<br>$a_{^{121}Sb} = 97.9$, $a_{^{123}Sb} = 52.5$ | No observable substitution |
| Triethylamine | $g = 2.0034$<br>$a_{Re} = 13.0$<br>$a_H = 4.3$ | Only TTBQ radical anion was observed | $g = 2.0039$<br>$a_{Re} = 16.2$<br>$a_H = 3.0$ (3H) |
| Pyridine | $g = 2.0033$<br>$a_{Re} = 16.2$<br>$a_H = 4.1$ | $g = 2.0071$<br>$a_{Re} = 27.3$ | $g = 2.0041$<br>$a_{Re} = 14.4$<br>$a_H = 3.5$ (3H) |
| $PhNH_2$ | $g = 2.0030$<br>$a_{Re} = 19.0$ | $g = 2.0069$<br>$a_{Re} = 26.6$ | No observable substitution |
| $P(O—Ph)_3$ | $g = 2.0018$<br>$a_{Re} = 28.6$<br>$a_p = 28.6$ | $g = 2.0065$<br>$a_{Re} = 48.0$<br>$a_p = 31.0$ | $g = 2.0030$<br>$a_{Re} = 17.4$<br>$a_p = 34.7$ |

*TTBQ = Tetrabromo-*o*-quinone.

TABLE 7. Optical rotation measurements for (±)DIOP ligands, and for the DTBQ–$\dot{}$–$Re(CO)_3$(±)DIOP radical complexes in benzene at room temperature with light at 436 nm

| System | c, mg/mL | α, deg | $[\alpha]^{22°}_{436\ nm}$, deg |
|---|---|---|---|
| (+)DIOP | 12.2±0.5 | 0.022±0.002 | 18.0±1.0 |
| (−)DIOP | 13.7±0.5 | −0.025±0.002 | −18.0±1.0* |
| DTBQ–$\dot{}$–$Re(CO)_3$(+)DIOP | 1.40±0.10 | 0.010±0.002 | 7.0±1.0 |
| DTBQ–$\dot{}$–$Re(CO)_3$(−)DIOP | 0.86±0.10 | −0.006±0.002 | −7.0±1.0 |

*Compared with the literature value of $[\alpha]^{22°}_{D} = -12.3$ (c, 4.57).

Optical rotation, esr, and uv/visible spectroscopy were used to characterize these two pure optically active radical complexes. The measurement of the optical rotation was carried out at 436 nm, since the radicals absorbed strongly in the 589 nm (sodium line) region. The optical rotation of the pure DIOP ligand was therefore also checked at 436 nm and compared with the value of the daughter radicals (Table 7).

In another exploratory investigation of the photolysis of $Re_2(CO)_{10}$ in the presence of optically pure DIOP ligand and with a racemic mixture of camphorquinone as a spin trap, an optically active radical complex containing the camphorquinone–$\dot{}$–$Re(CO)_3$DIOP was obtained and isolated. The remaining unreacted camphorquinone, however, exhibited optical activity, indicating a partial optical resolution during the spin trapping process. The results also suggest that a $Re(CO)_3$(+)DIOP fragment would selectively complex with the (+) camphorquinone while a $Re(CO)_3$(−)DIOP would similarly select the (−) camphorquinone for complexation. The results are extremely important and have far-reaching implications. To answer a few questions, we have also prepared, using established procedures, the pure optically active camphorquinones and studied their chemical reactions as spin traps in the Re carbonyl reactions. Furthermore, we have looked into the CIDEP of the optically active camphorquinone reactions with organotin compounds. For example, we have established that the reactions of camphorquinone with amines or phenols do not lead to CIDEP observation and concluded that the intersystem

crossing to the camphorquinone triplet sublevels produced no primary electron polarization. However, in the presence of organotin compound, a charge-transfer triplet state involving both the tin and the camphorquinone may result in a different set of spin dynamics leading to CIDEP of the camphorquinone – tin radical adducts, as observed experimentally. A detailed account of the chemistry of optically active organometallic radical complexes and adducts will be published in the near future.

As we progress from the early spin trapping experiments with quinones to the exciting development of optically active spin traps, we have the feeling that this is not the time to reflect or summarize past results; this is the time to expand and search for the new horizons in the world of free radicals and spin traps.

### Acknowledgments

The expert assistance of Susan Allen, a summer undergraduate student, and Mike Bishop, a fourth year chemistry student, was essential in many of the experimental work. Financial support by the Natural Sciences and Engineering Research Council of Canada is gratefully acknowledged.

1. D. REHOREK and H. HENNIG. Can. J. Chem. **60**, 000 (1982).
2. K. MOCHIDA, J. K. KOCHI, K. S. CHEN, and J. K. S. WAN. J. Am. Chem. Soc. **100**, 2927 (1978); T. FOSTER, K. S. CHEN, and J. K. S. WAN. J. Organomet. Chem. **184**, 113 (1980).
3. A. ALBERTI and C. M. CAMAGGI. J. Organomet. Chem. **181**, 355 (1979).
4. D. R. EATON. Inorg. Chem. **3**, 1268 (1964).
5. C. G. PIERPONT, H. H. DOWNS, and T. G. RUKAVINA. J. Am. Chem. Soc. **96**, 5573 (1974); C. G. PIERPONT and R. M. BUCHANAN. J. Am. Chem. Soc. **97**, 6450 (1975); M. W. LYNCH, R. M. BUCHANAN, C. G. PIERPONT, and D. H. HENDRICKSON. Inorg. Chem. **20**, 1038 (1981).
6. Y. S. SOHN and A. L. BALCH. J. Am. Chem. Soc. **94**, 1144 (1972); A. M. BOND, R. COLTON, and J. J. JACKOWSKI. Inorg. Chem. **14**, 2526 (1975); W. E. ANTHOLINE, J. M. KNIGHT, and D. H. PETERING. Inorg. Chem. **16**, 569 (1977).
7. M. GORDON and W. R. WARE (*Editors*). The exciplex. Academic Press, New York. 1975.
8. J. K. S. WAN and A. J. ELLIOT. Acc. Chem. Res. **10**, 161 (1977).
9. J. K. S. WAN. Adv. Photochem. **12**, 283 (1980) and references therein.
10. M. C. DEPEW, B. B. ADELEKE, and J. K. S. WAN. Can. J. Chem. In press.
11. K. S. CHEN, J. K. S. WAN, and J. K. KOCHI, J. Phys. Chem. **85**, 1726 (1981).
12. S. EMORI, D. WEIR, and J. K. S. WAN. Chem. Phys. Lett. In press.
13. J. W. DEBOER, T. Y. C. CHUNG, and J. K. S. WAN. Can. J. Chem. **57**, 2971 (1979) and references therein.
14. J. W. M. DEBOER, K. S. CHEN, Y. C. CHUNG, and J. K. S. WAN. J. Am. Chem. Soc. **101**, 5425 (1979); D. A. HUTCHINSON, K. S. CHEN, J. RUSSELL, and J. K. S. WAN. J. Chem. Phys. **73**, 1862 (1980).
15. D. A. HUTCHINSON, J. RUSSELL, J. W. M. DEBOER, and J. K. S. WAN. Chem. Phys. **53**, 149 (1980).
16. K. A. M. CREBER and J. K. S. WAN. J. Am. Chem. Soc. **103**, 2101 (1981).
17. K. S. CHEN and J. K. S. WAN. J. Am. Chem. Soc. **100**, 6051 (1978).
18. K. S. CHEN, R. T. SMITH, and J. K. S. WAN. Can. J. Chem. **56**, 2503 (1978).
19. K. S. CHEN, T. FOSTER, and J. K. S. WAN. J. Phys. Chem. **84**, 2473 (1980) and references therein.
20. K. A. M. CREBER and J. K. S. WAN. Chem. Phys. Lett. **81**, 453 (1981).
21. D. WEIR and J. K. S. WAN. J. Organomet. Chem. In press.
22. D. J. COX and R. DAVIS. J. Organomet. Chem. **186**, 339 (1980); **186**, 347 (1980).
23. C. BERTI and M. J. PERKINS. Angew. Chem. Int. Ed. Engl. **18**, 864 (1979).
24. C. E. BROWN and W. E. ANTHOLINE. J. Phys. Chem. **83**, 3314 (1979).
25. T. KOENIG and J. M. OVENS. J. Am. Chem. Soc. **95**, 8484 (1973); **96**, 4052 (1974); H. M. WALBORSKY and J. C. CHEN. J. Am. Chem. Soc. **93**, 671 (1971).
26. J. M. J. TRONCHET, J. OJHA-PONCET, E. WINTER-MIHALY, B. KOHLER, and M. GEOFFROY. Helv. Chim. Acta, **60**, 888 (1977).
27. M. S. WRIGTON and D. S. GINLEY. J. Am. Chem. Soc. **97**, 2065 (1975).
28. A. HUDSON, M. F. LAPPERT, and B. K. NICHOLSON. J. Chem. Soc. Dalton, 551 (1977).
29. R. G. GASONOV and R. Kh. FREIDLINA. Dokl. Akad. Nauk SSSR, **254**, 113 (1980).
30. C. J. PICKETT and D. PLETCHER. J. Chem. Soc. Dalton, 636 (1976).
31. H. H. DOWNS, R. M. BUCHANAN, and C. G. PIERPONT. Inorg. Chem. **18**, 1736 (1979).
32. T. L. BROWN. Ann. NY Acad. Sci. **333**, 80 (1979).
33. J. P. FAWCETT, R. A. JACKSON, and A. POE. Chem. Commun. 733 (1975).
34. D. R. KIDD, C. P. CHEUNG, and T. L. BROWN. J. Am. Chem. Soc. **100**, 4103 (1978).

Can. J. Chem. Downloaded from www.nrcresearchpress.com by 210.87.254.42 on 09/06/12
For personal use only.

# Synthesis of new radical-cations with 2,2,6,6-tetramethylpiperidine-*N*-oxyl and pyridinium moieties

ILEANA DRAGUTZAN

*Center of Organic Chemistry, 202 B Splaiul Independenţei, 78100 Bucharest, Romania*

AND

ALEXANDRU T. BALABAN

*Department of Organic Chemistry, The Polytechnic, Bucharest, Romania*

Received September 1, 1981

ILEANA DRAGUTZAN and ALEXANDRU T. BALABAN. Can. J. Chem. **60**, 1512 (1982).

Two new radical-cations (as crystalline perchlorates) **1** and **2** were synthesized from the respective amines **3** and **4**, and 2,4,6-trimethylpyrylium perchlorate **5**. The properties and spectra of the new radical-cation perchlorates (which may be recrystallized from ethanol or from water) are described.

ILEANA DRAGUTZAN et ALEXANDRU T. BALABAN. Can. J. Chem. **60**, 1512 (1982).

Deux nouveaux radicaux-cations **1** et **2** ont été synthétisés (sous la forme de perchlorates cristallisés) à partir des amines **3**, respectivement **4**, et du perchlorate de 2,4,6-triméthylpyrylium **5**. On décrit les propriétés et les spectres des perchlorates **1** et **2** qui peuvent être recristallisés en utilisant de l'eau ou de l'éthanol.

Spin labels (1–6) have become widely used in biochemistry (7, 8) or in polymer chemistry (9, 10). So far, cationic nitroxides have only been known as quaternary ammonium salts with 2,2,6,6-tetramethylpiperidine-*N*-oxyl (11, 12) or phosphonium salts with pyrrolidine-*N*-oxyl moieties (13). Since pyridinium rings can be easily formed from pyrylium salts and primary amino groups (14–16), and since both pyrylium salts (17, 18) and nitroxides with primary amino groups are readily available, we now report the preparation of spin labels possessing pyridinium rings, namely **1** and **2**.

The primary amines **3** and **4** were prepared with suitable modifications following the general pathways described in refs. 19–21 and 22–24, respectively.

Unlike the usual spin labels which are lipophilic and water insoluble, the new spin labels **1** and **2** are soluble in ethanol and may be recrystallized from water. The delocalization of the positive charge over the pyridinium ring makes these new cation-radicals **1** and **2** different from ammonium or phosphonium radical-cations described earlier (11–13), because the latter compounds have a more

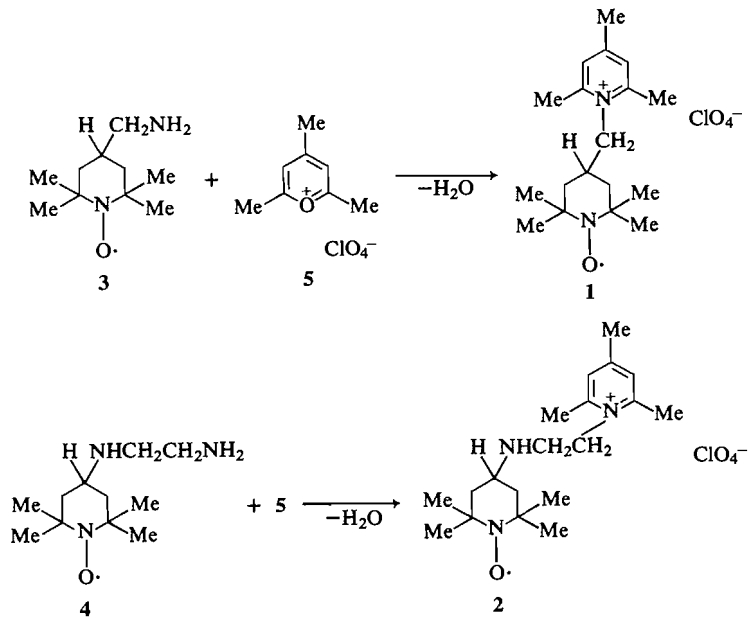


0008-4042/82/121512-02$01.00/0

©1982 National Research Council of Canada/Conseil national de recherches du Canada

Can. J. Chem. Downloaded from www.nrcresearchpress.com by 210.87.254.6 on 09/06/12
For personal use only.

Can. J. Chem. Downloaded from www.nrcresearchpress.com by 210.87.254.6 on 09/06/12
For personal use only.

localized positive charge. The spacing between the nitroxide group and the pyridinium ring is larger in **2** than in **1**, assuming a stretched conformation of the molecule.

The properties of the new spin labels **1** and **2** related to their use in studying biological systems by esr are being checked by R. J. Mehlhorn and L. Packer and they will be reported in a future paper.

## Experimental

*2,4,6-Trimethyl-*N*-(4'-methylene-2',2',6',6'-tetramethyl-piperidine-*N*'-oxyl)-pyridinium perchlorate (1)*

Reaction of **3** (bp 123–124°C/3 Torr, mp 52°C, lit. (19) mp 56.5°C; ir ($CH_2Cl_2$) $\nu_{NH}$: 3385 and 3650 $cm^{-1}$; esr triplet in benzene indicates $a_N = 1.673$ mT, $g = 2.0059$) (0.4 g, 2.16 mmol) in 5 mL dry ethanol with 0.35 g (1.57 mmol) 2,4,6-trimethylpyrylium perchlorate (17) at room temperature for 15 min, followed by addition of 0.1 mL acetic acid and stirring for another 15 min, yielded a red solution. Gaseous ammonia was bubbled to convert any unreacted pyrylium salt into liquid 2,4,6-collidine, then the orange-coloured precipitate was filtered off (0.29 g, mp 212°C). On dilution with ethyl ether the filtrate deposits a second crop of crystals, mp 195°C (0.165 g), total yield 54%. The combined product **1** was purified by recrystallization from ethanol–ether yielding yellow crystals, mp 217–219°C. In the ir spectrum (KBr pellet) the $ClO_4$ anion presents bands at 622 and 1090 $cm^{-1}$ and the pyridinium ring gives rise to a band at 1635 $cm^{-1}$. The esr spectrum (in benzene) presents a triplet indicating $a_N = 1.673$ mT, $g = 2.0059$. *Anal.* calcd. for $C_{18}H_{30}N_2O^+ClO_4^-$: C 55.46, H 7.70, N 7.19%; found: C 55.26, H 7.83, N 7.08%.

*2,4,6-Trimethyl-*N*-(2',2',6',6'-tetramethylpiperidine-*N*'-oxyl-4'-aminoethyl)-pyridinium perchlorate (2)*

2,4,6-Trimethylpyrylium perchlorate (17) (0.7 g, 3.15 mmol) and 0.8 g (3.75 mmol) **4** (ir spectrum ($CCl_4$) has a broad massif with maxima at 3310 and 3400 $cm^{-1}$, and bands at 1470 and 1630 $cm^{-1}$; lit. (24) ir (neat): 3350, 3300, 1590 $cm^{-1}$) were stirred at room temperature in 10 mL dry ethanol. After work-up as in the preceding analogous reaction, 1.1 g orange-coloured product (70% yield) was obtained, with mp 153–155°C (from ethanol–ether). Infrared spectrum (KBr pellet): $ClO_4^-$ anion with bands at 625 and 1095 $cm^{-1}$, 1643 (ring stretch), and 3313 $cm^{-1}$ ($\nu_{NH}$); esr triplet in ethanol indicates $a_N = 1.64$ mT. *Anal.* calcd. for $C_{19}H_{33}N_3O^+ClO_4^-$: C 54.49, H 7.89, N 10.04%; found: C 54.79, H 8.26, N 9.73%.


1. L. J. Berliner (*Editor*). Spin labeling. Theory and applications. Academic Press, New York. 1976; Spin labeling. II. Academic Press, New York. 1979.
2. E. G. Rozantsev. Free nitroxyl radicals. Plenum Press, New York. 1970.
3. R. Brière, H. Lemaire, and A. Rassat. Bull. Soc. Chim. Fr. 3273 (1965).
4. J. F. W. Keana. Chem. Rev. **78**, 37 (1978); J. F. W. Keana, S. B. Keana, and D. Beetham. J. Am. Chem. Soc. **89**, 3055 (1967).
5. E. G. Janzen. Acc. Chem. Res. **4**, 31 (1971).
6. A. L. Buchachenko and A. M. Vasserman. Stabilnye radikaly. Khimia, Moscow. 1970.
7. B. J. Gaffney and C. M. McNamee. Methods Enzymol. **32**, 161 (1974).
8. G. I. Likhtenshtein. Metod spinovykh metok v molekulyarnoi biologii. Nauka, Moscow. 1974; A. N. Kuznetsov. Metod spinogo zonda (osnovy i primenenie). Nauka, Moscow. 1976; I. C. P. Smith. *In* Biological applications of esr. *Edited by* H. Schwartz, J. R. Bolton, and D. Borg. Wiley–Interscience, New York. 1972.
9. L. J. Berliner. *In* Molecular motion in polymers by esr. *Edited by* R. F. Boyer and S. E. Keinath. Harwood Academic Publishers, Chur–London–New York. 1980.
10. A. T. Bullock and G. G. Cameron. Structural study of macromolecular spectroscopic methods (Meeting, 1974). *Edited by* K. J. Ivin. Wiley, Chichester, England. 1976. p. 273.
11. B. K. Sinha and C. F. Chignell. J. Med. Chem. **18**, 669 (1975); E. J. Rauckman, G. M. Rosen, and M. B. Abou-Donia. Org. Prep. Proced. Int. **8**, 159 (1976).
12. R. J. Mehlhorn and L. Packer. Biochim. Biophys. Acta, **423**, 382 (1976); J. C. Williams, R. J. Mehlhorn, and A. D. Keith. Chem. Phys. Lipids, **7**, 207 (1971).
13. D. Cafiso and W. L. Hubbell. Biochemistry, **17**, 187 (1978); R. J. Mehlhorn and L. Packer. Proc. 5th Internat. Photosynthesis Congress. Halkidiki, Greece. Nov. 28, 1980.
14. A. T. Balaban. *In* New trends in heterocyclic chemistry. *Edited by* R. M. Mitra *et al.* Studies in Organic Chemistry No. 3, Elsevier, Amsterdam. 1979.
15. K. Dimroth and K. H. Wolf. *In* Newer methods of preparative organic chemistry. Vol. 3. *Edited by* W. Foerst. Academic Press, New York. 1974. p. 357.
16. A. T. Balaban, W. Schroth, and G. Fischer. Adv. Heterocycl. Chem. **10**, 241 (1969); A. T. Balaban, A. Dinculescu, G. N. Dorofeenko, G. W. Fischer, A. V. Koblik, V. V. Mezheritski, and W. Schroth. Adv. Heterocycl. Chem. Suppl. 2. In press.
17. A. T. Balaban and C. D. Nenitzescu. Org. Synth. Coll. Vol. 5, 1106 (1973).
18. A. T. Balaban and A. J. Boulton. Org. Synth. Coll. Vol. 5, 1112 (1973); 1114 (1973).
19. A. B. Shapiro, L. S. Bogach, V. M. Chumakov, A. A. Kropacheva, V. I. Suskina, and E. G. Rozantsev. Izv. Akad. Nauk SSSR Ser. Khim. 2077 (1975).
20. V. S. Usovskaya, I. M. Sharapov, E. S. Nikitskaya, E. I. Levkoeva, M. D. Mashkovskii, and L. N. Yakhontov. French Pat. Appl. 2043474 (Mar. 26, 1971); Chem. Abstr. **76**, 14364 c (1972); E. S. Nikitskaya, E. I. Levkoeva, V. S. Usovskaya, L. N. Yakhontov, I. M. Sharapov and M. D. Mashkovskii. USSR Pat. 267633 (Apr. 18, 1973); Chem. Abstr. **79**, 66199 j (1973); E. S. Nikitskaya, I. M. Sharapov, E. I. Levkoeva, V. S. Usovskaya, A. S. Vlasov, T. E. Kukushkina, L. N. Yakhontov, and M. V. Rubtsov. Khim.-Farm. Zh. **4**, 58 (1970).
21. R. I. Zhdanov, Z. L. Gordon, and E. G. Rozantsev. Dokl. Akad. Nauk, **224**, 593 (1975).
22. C. Harries. Chem. Ber. **29**, 523 (1896).
23. E. G. Rozantsev and I. V. Kokhanov. Izv. Akad. Nauk SSSR Ser. Khim. 1477 (1966).
24. B. K. Sinha, M. G. Cox, C. F. Chignell, and R. L. Cysyk. J. Med. Chem. **22**, 1051 (1979).

# Synthesis and spin trapping kinetics of new alkyl substituted cyclic nitrones

D. L. HAIRE AND EDWARD G. JANZEN

*Department of Chemistry, Guelph–Waterloo Centre for Graduate Work in Chemistry, University of Guelph, Guelph, Ont., Canada N1G 2W1*

Received September 1, 1981

D. L. HAIRE and EDWARD G. JANZEN. Can. J. Chem. **60**, 1514 (1982).

Three new nitrones, 5-*n*-propyl-5-methyl-1-pyrroline-*N*-oxide (PMPO), 5-*n*-hexyl-5-methyl-1-pyrroline-*N*-oxide (HMPO), and 5-*n*-decyl-5-methyl-1-pyrroline-*N*-oxide (DeMPO), amphiphilic versions of the spin trap 5,5-dimethyl-1-pyrroline-*N*-oxide (DMPO), have been synthesized. A comparative study of the absolute rate constants for formation and decay of the *tert*-butoxyl spin adducts to these cyclic nitrones as well as 3,3,5,5-tetramethyl-1-pyrroline-*N*-oxide ($M_4PO$) has been undertaken using esr kinetic techniques.

D. L. HAIRE et EDWARD G. JANZEN. Can. J. Chem. **60**, 1514 (1982).

On a synthétisé trois nouvelles nitrones: le *N*-oxyde de *n*-propyl-5 méthyl-5 pyrroline-1 (OPMP), le *N*-oxyde de *n*-hexyl-5 méthyl-5 pyrroline-1 (OHMP) et le *N*-oxyde de *n*-décyl-5 méthyl-5 pyrroline-1 (ODeMP) qui sont des versions amphiphiles du capteur de spin *N*-oxyde de diméthyl-5,5 pyrroline-1 (ODMP). Faisant appel aux techniques cinétique de rpe, on a entrepris des études comparatives des constantes absolues de vitesse de formation et de désintégration des adduits de spin *tert*-butoxyle de ces nitrones cycliques ainsi que du *N*-oxyde de la tétraméthyl-3,3,5,5 pyrroline-1 ($OM_4P$).

[Traduit par le journal]

Can. J. Chem. Downloaded from www.nrcresearchpress.com by 210.87.254.42 on 09/06/12
For personal use only.

## Introduction

Heightened attention has been drawn lately to the intermediacy of free radical species in biological systems. The increased activity has been due in part to the considerable success of spin trapping (see refs. 1 (for biochemical applications) and 2 (for a general review)) with cyclic nitrones (3). The detection and identification of transient bio-radicals includes ·OH (4) and $\cdot O_2^-$ (5) which are difficult to study by other methods. It was realized (6) that effective examination of free radical phenomena in biphasic media such as biological membranes or models thereof required the development of "tailored" spin trapping agents of hydrophilic and/or lipophilic design. A number of these new nitrone (7) and nitroso (8) spin traps have become available. However, 5,5-dimethyl-1-pyrroline-*N*-oxide (DMPO) counterparts have not yet been reported. The present research was directed towards the synthesis of spin traps wherein hydrocarbon chains of systematically increasing length (*n*-propyl, *n*-hexyl, *n*-decyl) were connected to C-5 of the pyrroline ring to impart increased lipophilic character to the DMPO nucleus.

The general procedures employed in synthesis of the cyclic nitrone spin traps (I, II, III) are outlined in Scheme 1.

Several years ago (9) it was demonstrated that spin trapping could serve as a quantitative probe for certain free radical reactions in solution. However, only recently has there emerged an increased awareness of the importance of kinetic spin trapping data. Maeda and Ingold (10*a*) have suggested that spin trapping will not fully evolve until rate constants for all ·R's and spin traps become available.

The viability of a given spin trap is dependent to a large extent upon the rates of formation of spin adducts ($k_f$) and their subsequent decay ($k_d$). An objective of the present study was to apply kinetic esr spectroscopic techniques to ascertain the effect, if any, of alkyl chains of differing lengths (*n*-propyl, *n*-hexyl, *n*-decyl) at C-5 of the pyrroline ring on the spin trapping and spin adduct decay rate constants relative to those for DMPO.

## Results and discussion

### *Diastereomeric cyclic aminoxyl radicals*[1]

The capture of a free radical by DMPO creates an enantiomeric mixture of spin adducts with an asymmetric center located at position 2 of the pyrrolidine ring. Only one esr spectrum is anticipated and this indeed is observed (3*c*), see Fig. 1 (a). When the group that was the radical possesses an element of chirality, however, diastereomeric aminoxyls are produced (eq. [1]). Differences in the hyperfine patterns are expected and may be observed (11).

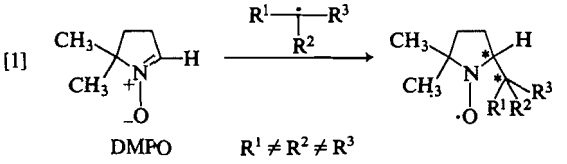


[1]Note, the term "aminoxyl" was introduced during the spin trapping conference and was deemed more appropriate than "nitroxyl".

0008-4042/82/121514-09$01.00/0

©1982 National Research Council of Canada/Conseil national de recherches du Canada

Can. J. Chem. Downloaded from www.nrcresearchpress.com by 210.87.254.42 on 09/06/12
For personal use only.

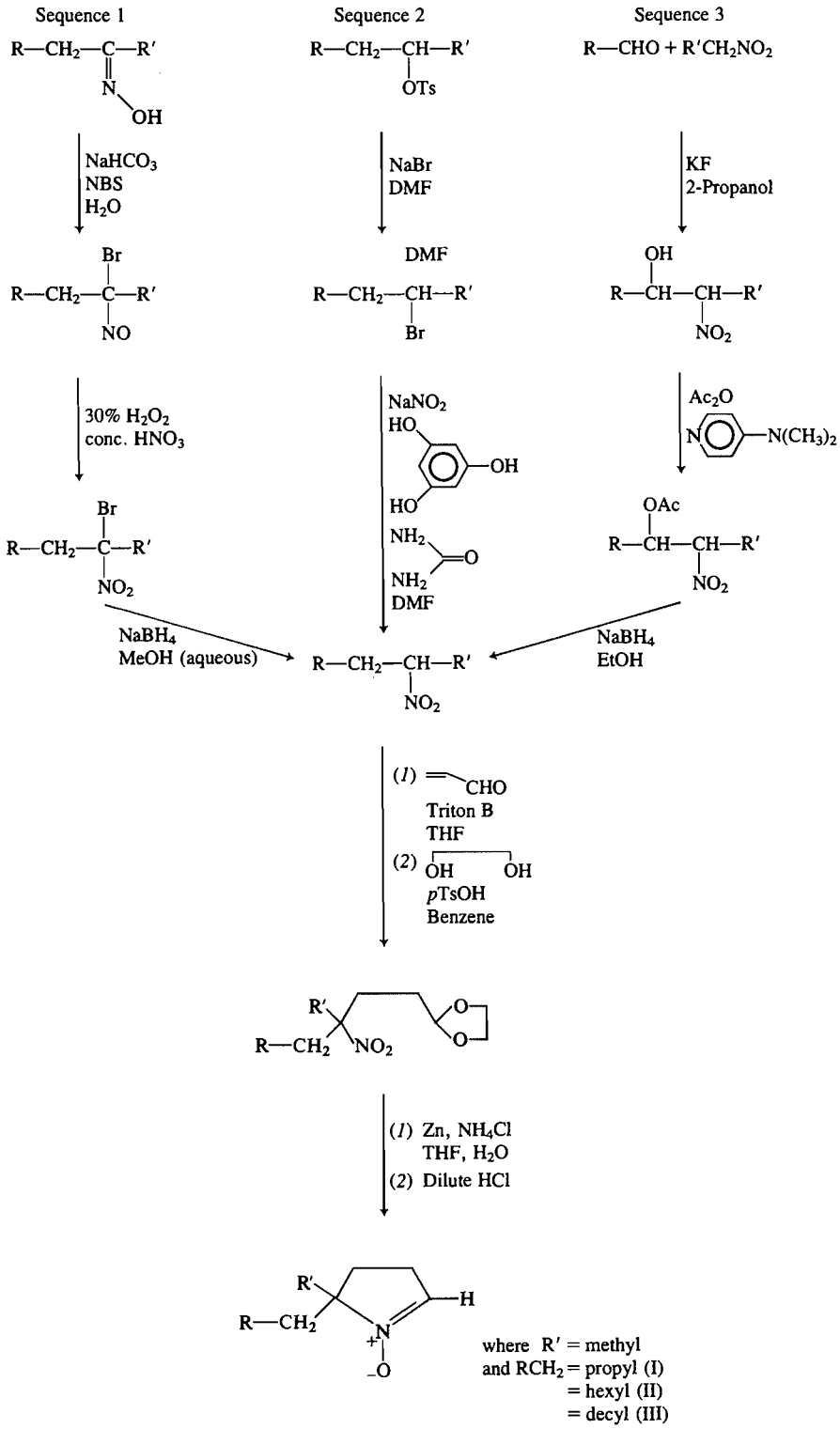


SCHEME 1

Can. J. Chem. Downloaded from www.nrcresearchpress.com by 210.87.254.42 on 09/06/12
For personal use only.

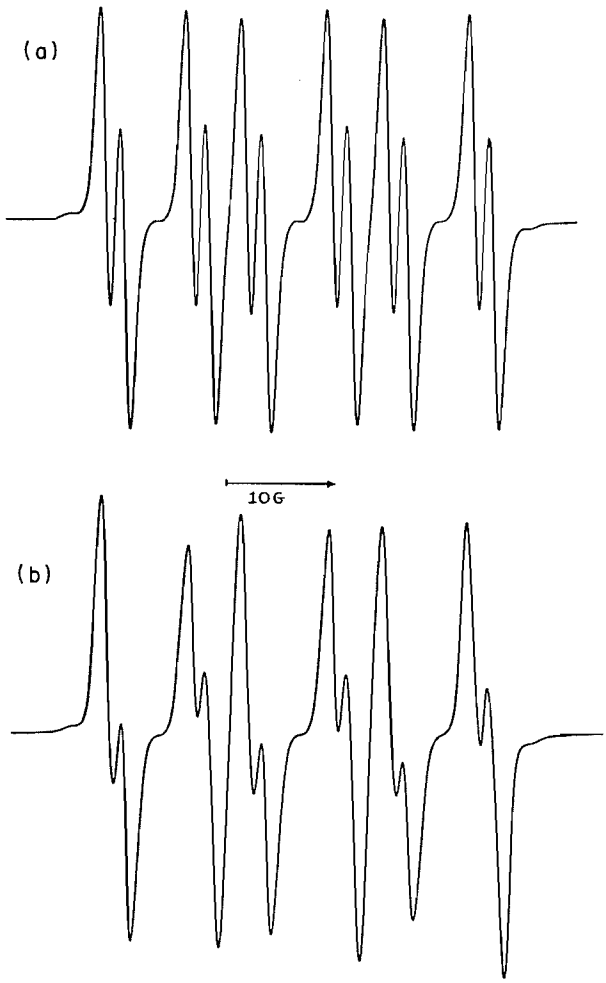


FIG. 1. (*a*) Spectrum from 0.05 *M* DMPO and 0.01 *M* DBPO in benzene (25°C). (*b*) Spectrum from 0.10 *M* HMPO and 0.05 *M* DBPO in benzene (25°C).

The *tert*-butoxyl adduct derived from an RMPO spin trap is diastereomeric. This is due to the presence of the two chiral sites which are incorporated in this case within the pyrrolidine framework at C-2 and C-5 (eq. [2]).

[2] 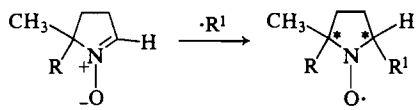

RMPO

R = (*n*-propyl, *n*-hexyl, *n*-decyl), $R^1 \neq H$

Linewidths ranging from 0.12 to 0.13 G were observed with all *tert*-butoxyl adducts of DMPO and RMPO. Existence of the relatively wide lines decreases the chances of detecting a distinct esr spectrum for each diastereomer. For this reason the spectra of RMPO BO· adducts might be expected to exhibit dissymmetry when the spectra of diastereomers superimpose, i.e. the typical asymmetric spectral appearance of RMPO *tert*-butoxyl adducts, Fig. 1 (b) may be indicative of diastereomeric cyclic aminoxyls.

The question of asymmetric spectra arising from impurity radicals rather than diastereomeric spin adducts appears unlikely. *tert*-Butoxyl radicals are known (12*a*) to fragment to acetone and methyl radicals. Asymmetry is definitely not due to spin trapping of methyl or other *C*-centered radicals because the spectra of these adducts are character-

[3] 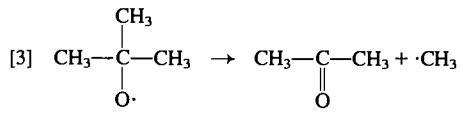

ized by sharp lines and sizably different in their hfsc's; e.g. for the methyl adduct of DMPO in benzene, $a_N = 14.31$ and $a_\beta^H = 20.52$ G (3*d*). The hfsc's for the cyclic nitrone BO· spin adducts are listed in Table 1.

*Formation kinetics*

The absolute rate constant of *tert*-butoxyl trapping by PBN was determined by correlation with the well established rate constant of hydrogen abstraction from cyclohexane by BO· radicals (12*b*). Rate constants for spin trapping *tert*-butoxyl radicals with cyclic nitrones were obtained by competitive *in situ* scavenging experiments with PBN. *tert*-Butoxyl radicals generated in reaction [4] are trapped by the cyclic nitrone and PBN in reactions [5] and [6] respectively.

[4] 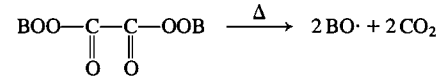

[5] 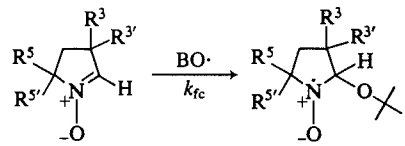

[6] 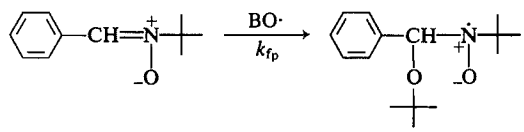

Due to marked differences in their hfsc's, Table 1, initial formation rate constants of the two adducts may be quantitated by monitoring as a function of time the peaks indicated in Fig. 2. The formation rate constants of the BO· adducts of the cyclic nitrone and PBN are represented by expressions [7] and [8] respectively.

Can. J. Chem. Downloaded from www.nrcresearchpress.com by 210.87.254.42 on 09/06/12
For personal use only.

TABLE 1. Hyperfine splitting constants for *tert*-butoxyl spin adducts[a]

| Nitrone | $a_N$ | $a_\beta^H$ | $a_\gamma^H$ |
|---|---|---|---|
| DMPO | 13.19[b] | 8.16 | 1.82 (1H) |
| | (13.01)[c] | (6.63) | (2.04) |
| PMPO | 13.24 | 8.17 | 1.94 (1H) |
| | (12.92) | (6.91) | (1.98) |
| HMPO | 13.03 | 7.99 | 1.87 (1H) |
| | (12.88) | (6.87) | (1.65) |
| DeMPO | 13.08 | 7.97 | 1.77 (1H) |
| | (12.95) | (6.92) | (2.17) |
| $M_4$PO | 13.39[d] | 5.88 | |
| | (13.16) | (4.90) | |
| PBN | 14.29[e] | 1.84 | |

[a] All spectra were recorded at 25°C in benzene from 0.05 *M* nitrone and 0.01 *M* di-*tert*-butylperoxalate, all hfsc's are in Gauss.
[b] Compare with $a_N$ = 13.11, $a_\beta^H$ = 7.93, $a_\gamma^H$ = 1.97 (1H) G, ref. 3*c*.
[c] Bracketed values indicate spectra recorded in di-*tert*-butylperoxide.
[d] Compare with $a_N$ = 13.31, $a_\beta^H$ = 5.81 G, ref. 3*e*.
[e] Compare with $a_N$ = 14.22, $a_\beta^H$ = 1.95 G, ref. 9*b*.

[7] $$\frac{d[\text{cyclic adduct}]_0}{dt} = k_{fc}[\text{cyclic nitrone}]_0[BO\cdot]_0$$

[8] $$\frac{d[\text{PBN adduct}]_0}{dt} = k_{fp}[\text{PBN}]_0[BO\cdot]_0$$

Since $k_{fp}$, $[PBN]_0$, $[\text{cyclic nitrone}]_0$ are known, $k_{fc}$, the spin trapping rate constant for the cyclic nitrone may be determined by measuring the initial rates of growth of the two spin adducts.

[9] $$\frac{d[\text{cyclic adduct}]_0/dt}{d[\text{PBN adduct}]_0/dt} = \frac{k_{fc}[\text{cyclic nitrone}]_0}{k_{fp}[\text{PBN}]_0}$$

Plots of esr growth for cyclic nitrone and PBN BO·

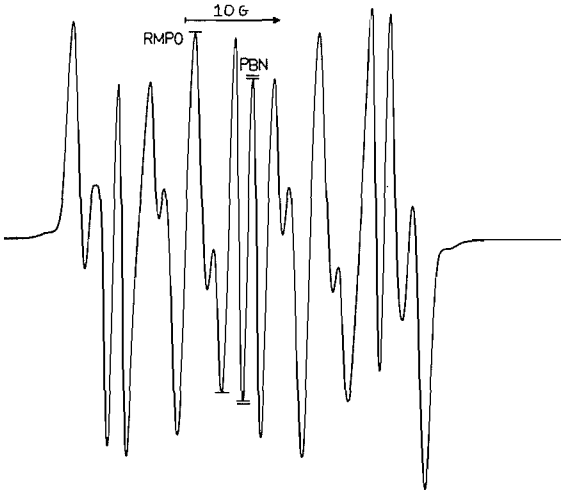


FIG. 2. Spectrum from 0.01 *M* HMPO, 0.30 *M* PBN, and 0.005 *M* DBPO in benzene (25°C).

adducts were characteristically linear (all corr. >0.999) over a 1500 s timescale. A representative plot, i.e. the PMPO adduct, is provided in Fig. 3. Cyclic nitrone adduct growth gradually slowed thereafter causing curvature in the plots due to the onset of spin adduct decay. When the cyclic nitrone concentration was increased from 0.001 to 0.10 *M* nonlinearity effects occurred earlier (~200 s) and were considerably more pronounced. This observation might suggest that spin adduct disappearance was due in some degree to spin adduct reaction with the spin trap. A similar rate constant of *tert*-butoxyl adduct production (within experimental error), $5.2 \times 10^8$ vs. $4.1 \times 10^8$ $M^{-1}$ $s^{-1}$ (Table 2) was, nevertheless, obtained with 0.10 *M* PMPO. This adds further support (9*b*) to the argument that all BO· radicals generated in this system are scavenged by spin trapping.

Spin trapping rate constants for *tert*-butoxyl are reported in Table 2. Reproducibility of the results, as judged by duplicate runs, was ±10%. The rate constant of *tert*-butoxyl trapping by DMPO was $7.3 \times 10^8$ $M^{-1}$ $s^{-1}$. This is slightly greater than the value of $5.0 \times 10^8$ $M^{-1}$ $s^{-1}$ previously reported (9*b*). Rate constants for RMPO (R = *n*-propyl, *n*-hexyl,

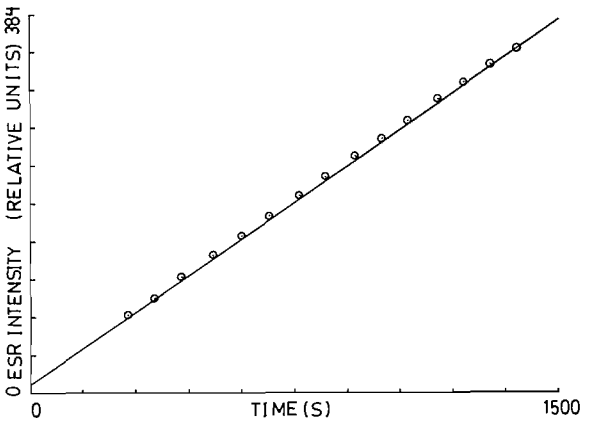


FIG. 3. Plot of the esr signal intensity for the *tert*-butoxyl spin adduct of PMPO versus time in benzene.

TABLE 2. Absolute *tert*-butoxyl spin trapping rate constants of various cyclic nitrones[a]

| Spin trap | Spin trapping rate constant $k_{fc} \times 10^{-8}$, $M^{-1}$ $s^{-1}$ |
|---|---|
| DMPO | 7.3[b] |
| PMPO | 4.1 |
| HMPO | 3.8 |
| DeMPO | 3.3 |
| $M_4$PO | 0.086[c] |

[a] All rate constants were determined at 25°C in benzene.
[b] Compare with $5.0 \times 10^8$ $M^{-1}s^{-1}$, ref. 9*b*.
[c] Compare with $0.16 \times 10^8$ $M^{-1}$ $s^{-1}$, ref. 3*e*.

Can. J. Chem. Downloaded from www.nrcresearchpress.com by 210.87.254.42 on 09/06/12
For personal use only.

*n*-decyl) BO· trapping of 4.1, 3.8, and 3.3 × $10^8\ M^{-1}\ s^{-1}$ respectively are marginally lower than the DMPO value. Examination of molecular models indicates that the rate constant decrease relative to DMPO might rest in a steric effect wherein a propyl or longer alkyl substituent at C-5 of the pyrroline ring is required to interfere with radical addition at C-2. *tert*-Butoxyl addition to $M_4PO$, $0.086\ M^{-1}\ s^{-1}$ (compare $0.16 \times 10^8\ M^{-1}\ s^{-1}$ (3*e*)), was decreased 85× with respect to DMPO obviously due to steric interactions caused by the two additional methyl groups located "β" to the nitrone functionality.

*Decay kinetics*

Rate constants for the decay of the *tert*-butoxyl adducts of the various nitrones are listed in Table 3. Duplicate experiments indicated a reproducibility of ±20%. Ultraviolet photolysis of di-*tert*-butylperoxide (BOOB) over approximately five minutes produced $\sim 1.5 \times 10^{-6}\ M$ steady-state *tert*-butoxyl adduct concentrations according to reactions [5] and [10].

[10] $\text{BOOB} \xrightarrow{\hbar\nu} 2\,\text{BO}\cdot$

Solubilization of each of the cyclic nitrones (except $M_4PO$) at 25°C in di-*tert*-butylperoxide produced an exceedingly weak yet persistent triplet ($a_N$ = 15.29). The anomalous signal situated midway between doublets 1 & 2, 3 & 4, 5 & 6 (Figs. 1 (a) and (b)), presumably of a di-*tert*-alkyl aminoxyl, was completely unaffected by photolysis and remained unchanged even days later. This aminoxyl does not appear to interfere with the spin trapping system chemically or spectrally (i.e. the triplet does not overlap the BO· adduct peaks). Hence the kinetic data reported here should remain valid.

Simple dialkyl aminoxyls bearing at least one β-H substituent, such as diethylaminoxyl, are known to decay via disproportionation to the respective hydroxylamine and nitrone.[2]

[11] 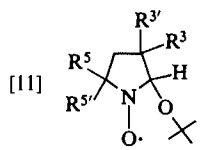 $\xrightarrow{k_d}$ nonradical products

[2]For the mechanism of diethylaminoxyl decay,

$$(CH_3CH_2)_2NO\cdot \xrightarrow{k_d} (CH_3CH_2)_2NOH + CH_3CH{=}\overset{+}{N}(-O)CH_2CH_3$$

see ref. 10*b*. Further examples exhibiting the second order decay of dialkylaminoxyls are presented in ref. 10*c*.

TABLE 3. Absolute rate constants for the second order decay of the various cyclic *tert*-butoxyl adducts[a]

| Spin trap[b] | Initial radical concentration ($M$) | Decay rate constant $k_d \times 10^{-2}$, $M^{-1}\ s^{-1}$ |
|---|---|---|
| DMPO | $1.8 \times 10^{-6}$ | 5.1 |
| PMPO | $1.8 \times 10^{-6}$ | 3.9 |
| HMPO | $1.3 \times 10^{-6}$ | 5.5 |
| DeMPO | $1.2 \times 10^{-6}$ | 4.1 |
| $M_4PO$ | $1.5 \times 10^{-6}$ | 0.65 |

[a]All rate constants were determined at 25°C in di-*tert*-butylperoxide.
[b]All nitrones were 0.20 *M*.

Best fits were obtained with second order plots (all corr. >0.99). The decay of the DeMPO *tert*-butoxyl adduct is representative (Fig. 4). A degree of first order character may also be present because these plots were also reasonably linear (all corr. 0.90–0.95).

The decay rate constants of the RMPO *tert*-butoxyl adducts are effectively equal within experimental error. This suggests that despite the increased number of methylene hydrogens (due to the longer alkyl substituents in the RMPO adducts) their persistence remains essentially the same as DMPO adducts. The rate constant of decay for the BO· adduct of $M_4PO$, $0.65 \times 10^2\ M^{-1}\ s^{-1}$, is 8× slower than that of DMPO. Decay rate constants for all the cyclic nitrone adducts are of comparable magnitude though slightly smaller than that reported for a *C*-radical spin adduct of related structure, i.e. the $\cdot CH_2OH$ adduct of DMPO decayed at $184\ M^{-1}\ s^{-1}$ (4*c*).

*Summary*

In this study the viability of five cyclic nitrone spin traps (DMPO, PMPO, HMPO, DeMPO, and $M_4PO$) as scavengers of BO· radicals has been

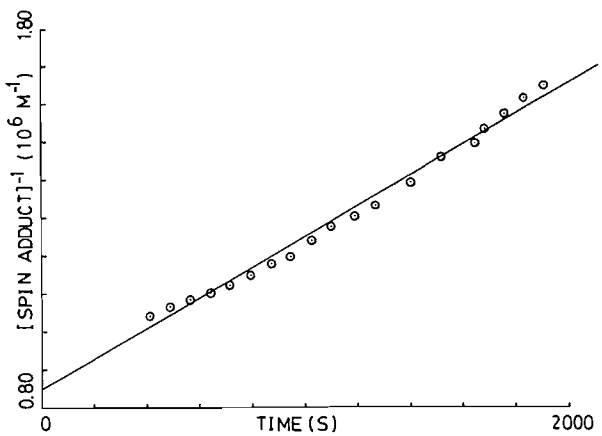


FIG. 4. Plot showing decay of the *tert*-butoxyl adduct of DeMPO is second order at 25°C in di-*tert*-butylperoxide.

Can. J. Chem. Downloaded from www.nrcresearchpress.com by 210.87.254.42 on 09/06/12
For personal use only.

evaluated. We find that the RMPO spin traps offer the following advantages in spin trapping.

(a) There is potential for preferentially probing radical reactions in lipid-like regions of mixed phase media.

(b) The spin trapping rate constants for radicals are fast, Table 2, e.g. *tert*-butoxyl ($\sim 3.7 \times 10^8\ M^{-1}\ s^{-1}$).

(c) The spin adducts, e.g. *tert*-butoxyl, are persistent, Table 3, ($\sim 4.5 \times 10^2\ M^{-1}\ s^{-1}$).

(d) Isotropic esr spectra are obtained which are (in addition) sensitive to the nature (polar versus nonpolar) of the radical trapped, Fig. 1 (b) (also refs. 3*c*, 3*d*).

Interpretation of esr spectra of RMPO adducts thus far has not been hampered by the existence of diastereomers because differences in hfsc's have been less than the linewidths. Detailed examination of RMPO adducts by ENDOR spectroscopy is planned. Preliminary experiments with the RMPO spin adducts in model membrane systems are currently in progress.

*Synthetic methodology*

Synthesis involved essentially the conversion of secondary aliphatic nitroalkanes to nitrones via a procedure developed by Todd and co-workers (13). Several variations in experimental conditions for these reactions were required. Details are given in the Experimental.

Three distinct Sequences (1, 2, 3), Scheme 1, to 2-nitroalkanes were examined. A recent Corey modification (14) is evidence that the oxidation of oximes through intermediate halonitroso compounds is still an important route to nitro compounds. The route, however, seems to be limited to the preparation of cyclic and short chain (< 6 carbons) 2-nitroalkanes. Sequence 1 utilized a modified version of the original procedure (15). A major inconvenience inherent in Sequence 2 is the high yield (> 30%) of the side product 2-alcohols. Removal of these impurities from long chain (> 12 carbons) 2-nitroalkanes proved exceedingly difficult. Described in Sequence 3 is the successful extension of a recently developed primary nitroalkane procedure (16) to the synthesis of long chain secondary nitroalkanes.

## Experimental

The nmr spectra were recorded on a Varian (T60 or EM 360L) spectrometer and only the characteristic peaks are reported. Chemical shifts were reported in $CDCl_3$ as a solvent in parts per million (δ) downfield from internal tetramethylsilane. The ir spectra were obtained from a Beckman Acculab 6 spectrophotometer. Elemental analyses were performed by Guelph Chemical Laboratories, Guelph, Ontario. References to the original literature accompany all known compounds.

*Synthesis of nitrones and precursors*

I. *Secondary nitroalkanes*

*Sequence 1*

*2-Bromo-2-nitrosopentane*

Freshly distilled 2-pentoxime (24.0 g; 237.1 mmol) (94% from 2-pentanone (17)) was added gradually to a vigorously stirred suspension of 63.3 g (355.7 mmol) *N*-bromosuccinimide and 39.8 g (474.2 mmol) sodium bicarbonate in 400 mL of 5°C water. After the reaction subsided, the ice/$H_2O$ bath was removed and stirring was continued for 3 h. The thermally labile bromonitrosoalkane was extracted with pentane (3 × 150 mL), dried over sodium sulfate, and filtered. Approximately 80% of the solvent was removed at atmospheric pressure giving a dark blue oil, (not distillable, lit. (15)), which was used directly in the next step.

*2-Bromo-2-nitropentane*

30% Aqueous hydrogen peroxide (120 mL) and 50 mL of concentrated nitric acid were added in succession to the crude bromonitrosoalkane. The mixture was heated at 50°C for 4 h, cooled, extracted with 3 × 200 mL pentane, washed with 2 × 120 mL 2% NaOH, dried over sodium sulfate, filtered, and solvent removed under reduced pressure. 2-Bromo-2-nitropentane (27.9 g; 142.3 mmol) was isolated in 60% yield (from the oxime) as a clear colorless oil, bp 72°C/12 Torr (lit. (15) 3-isomer, 3-bromo-3-nitropentane, bp 70°C/10 Torr); $^1$H nmr ($CDCl_3$) δ: 2.20–2.60 (s, 3H, Br ($NO_2$)—C—$CH_3$), 2.20–2.60 (t, 2H, Br ($NO_2$)—C—$CH_2$).

*2-Nitropentane*

2-Bromo-2-nitropentane (27.9 g; 142.3 mmol) was gradually added to a mechanically stirred solution (0°C) of 20.0 g (528.7 mmol) of sodium borohydride in 270 : 90 (mL) methanol–water. Stirring was continued for 12 h after which the mixture was filtered through sintered glass, methanol was evaporated under reduced pressure, and the resulting aqueous phase acidified by dropwise addition of 15% aqueous hydroxylamine hydrochloride solution. After stirring for 2 h the aqueous mixture was extracted with 3 × 200 mL pentane, dried ($Na_2SO_4$), and filtered. The solvent was evaporated under reduced pressure (25°C) and the residue fractionated to provide 10.0 g (85.4 mmol), 60% yield, of colorless 2-nitropentane, bp 152°C/ 750 Torr (lit. (18) bp 149°C/760 Torr); $^1$H nmr ($CDCl_3$) δ: 1.52 (d, 3H, $NO_2$—C—$CH_3$), 4.62 (sextet, 1H, $NO_2$—C—H).

*Sequence 2*

*2-Bromooctane*

2-Octyl-*p*-toluenesulphonate (19) was obtained as a thermally labile faint yellow oil in 72% yield by reaction of 56.5 g (433.8 mmol) of dried, freshly distilled 2-octanol with 90.9 g (476.8 mmol) of purified *p*-toluenesulphonyl chloride in 350 mL (4.33 mol) of dry pyridine for 4 h at −5°C. 2-Octyl-*p*-toluenesulphonate (88.7 g; 312.3 mmol) and 32.3 g (313.9 mmol) of anhydrous sodium bromide in 500 mL of dry *N*,*N*-dimethylformamide were stirred for 3.5 days at 25°C. To the mixture were added 200 : 200 (mL) pentane–water. The aqueous DMF portion was extracted with 3 × 150 mL pentane. The combined organic layers were washed with 3 × 150 mL of water, dried over sodium sulfate, filtered, and solvent evaporated under reduced pressure. 2-Bromooctane (57.9 g; 299.8 mmol) (96% yield) was collected as a colorless oil, bp 69°C/12 Torr (lit. (19) bp 87°C/20 Torr); $^1$H nmr ($CDCl_3$) δ: 1.70 (d, 3H, Br—C—$CH_3$), 4.01 (m, 1H, Br—C—H).

*2-Nitrooctane*

2-Bromooctane (57.9 g; 299.8 mmol), dry sodium nitrite (36.0 g; 521.7 mmol), dry phloroglucinol (37.8 g; 299.7 mmol), and dry urea (39.9 g; 664.6 mmol) were stirred in the dark for 45 h at 25°C in 600 mL of dry DMF. Pentane (300 mL) and 300 mL of water

Can. J. Chem. Downloaded from www.nrcresearchpress.com by 210.87.254.42 on 09/06/12
For personal use only.

were added to the mixture. The aqueous DMF layer was extracted with 3 × 150 mL pentane. The combined organic phases were washed with 3 × 150 mL of water, dried over sodium sulfate, filtered, and solvent evaporated under reduced pressure. The crude product was fractionated through a 1 × 20 cm Vigreux column, and 22.9 g (143.9 mmol) of 2-nitrooctane (48% yield) were collected as a colorless oil, bp 70°C/3 Torr (lit. (20) bp 67°C/3 Torr); $^1$H nmr ($CDCl_3$) δ: 1.52 (d, 3H, $NO_2$—C—$CH_3$), 4.60 (sextet, 1H, $NO_2$—C—H).

*Sequence 3*

*3-Hydroxy-2-nitrododecane*

To 58.1 g (371.6 mmol) of freshly distilled decanal and 1.75 g (18.59 mmol) finely ground potassium fluoride dihydrate in 400 mL of 2-propanol at 25°C were added 55.8 g (743.2 mmol) nitroethane. The mixture was stirred for 48 h, dried over magnesium sulfate, filtered, and solvent evaporated under reduced pressure. 3-Hydroxy-2-nitrododecane was obtained in 85% yield as a pale yellow oil; ir (film): 3380–3600 (O—H), 1560, 1390 ($NO_2$) cm$^{-1}$; $^1$H nmr ($CDCl_3$) δ: 1.64 (d, 3H, $NO_2$—C—$CH_3$), 3.58 (s, 1H, C—OH, $D_2O$ exch.), 4.00 (m, 1H, O—C—H), 4.55 (m, 1H, $NO_2$—C—H).

*3-Acetoxy-2-nitrododecane*

3-Hydroxy-2-nitrododecane (73.1 g; 315.9 mmol) was dissolved in 600 mL of anhydrous ether. To this solution was added a mixture of 47.4 g (464.3 mmol) acetic anhydride and 2.27 g (18.59 mmol) 4-dimethylaminopyridine. The mixture was stirred at 25°C for 18 h, dried over magnesium sulfate, and solvent evaporated under reduced pressure at 25°C. Note evaporation under reduced pressure at 45°C caused formation of the highly reactive nitroalkene 2-nitro-2-dodecene identified by ir (film): 1660 (C=C), 1510, 1330 ($NO_2$) cm$^{-1}$ and $^1$H nmr ($CDCl_3$) δ: 1.90–2.32 (s and m, 5H, $NO_2$—C—$CH_3$ and $NO_2$—C=C—$CH_2$), 7.08 (t, 1H, $NO_2$—C=C—H). 3-Acetoxy-2-nitrododecane was obtained in 85% yield as a light yellow oil; ir (film): 1750 (C=O), 1550, 1375 ($NO_2$) cm$^{-1}$; $^1$H nmr ($CDCl_3$) δ: 2.1 (s, 3H, O=C—$CH_3$), 4.71 (m, 1H, $NO_2$—C—H), 5.34 (m, 1H, O=C—O—C—H).

*2-Nitrododecane*

To an ice cooled/mechanically stirred solution of 73.4 g (268.5 mmol) 3-acetoxy-2-nitrododecane in 500 mL of absolute ethanol were added gradually ($T < 30$°C) 28.1 g (742.2 mmol) of sodium borohydride. Stirring was continued for 12 h at 25°C. Acidification was effected by dropwise addition of 10% hydrochloric acid. The mixture was extracted with pentane, dried over sodium sulfate, and solvent evaporated under reduced pressure. The crude product was triply distilled through a 1 × 15 cm Vigreux column affording 34.7 g (161.1 mol) of 2-nitrododecane as a colorless oil, bp 120°C/1.4 Torr (lit. (21) 1-isomer, 1-nitrododecane, bp 128°C/2.0 Torr); ir (film): 1580, 1365 ($NO_2$) cm$^{-1}$; $^1$H nmr ($CDCl_3$) δ: 1.53 (d, 3H, $NO_2$—C—$CH_3$), 4.55 (sextet, 1H, $NO_2$—C—H).

II. *Michael addition (4-nitroaldehydes)*

*4-Methyl-4-nitroheptanal*

2-Nitropentane (10.0 g; 85.4 mmol) and 0.57 mL (1.37 mmol) of Triton B (40% hydroxide in methanol) were dissolved in 75 mL of dry THF. Dropwise addition ($T < 0$°C) of 4.21 g (75.08 mmol) of freshly distilled acrolein in 25 mL of dry THF caused the initially colorless solution to turn brown-green. After stirring for 4 h at 0°C the reaction was quenched with 4.72 mL of 10% aqueous HCl. The mixture was shaken thoroughly with 300 mL of methylene chloride, washed with 3 × 100 mL of saturated NaCl, dried over sodium sulfate, filtered, and solvent evaporated under reduced pressure (25°C). The viscous brown-orange residue was immediately fractionated by distillation; 7.6 g (58% yield) of 4-methyl-4-nitroheptanal were obtained as a faint yellow oil, bp 57°C/ 0.010 Torr; $^1$H nmr ($CDCl_3$) δ: 1.54 (s, 3H, $NO_2$—C—$CH_3$), 9.96 (s, 1H, O=C—H).

*Precaution*! Thermally unstable residues may form. The product must be distilled over quickly, though preferably with an oil bath temperature < 150°C. Distillation must be halted immediately when black residues appear.

*4-Methyl-4-nitrodecanal*

Similarly 22.90 g (143.9 mmol) of 2-nitrooctane and 0.96 mL (2.30 mmol) Triton B in 127 mL THF were reacted with 7.09 g (126.5 mmol) acrolein in 50 mL THF. 4-Methyl-4-nitrodecanal (14.71 g; 68.33 mmol) was collected as a faint yellow oil (54% yield), bp 127°C/0.060 Torr; $^1$H nmr ($CDCl_3$) δ: 1.52 (s, 3H, $NO_2$—C—$CH_3$), 9.98 (s, 1H, O=C—H).

*4-Methyl-4-nitrotetradecanal*

Similarly 34.7 g (161.1 mmol) of 2-nitrododecane and 1.08 mL (2.57 mmol) of Triton B in 150 mL THF were reacted with 7.94 g (141.6 mmol) acrolein in 100 mL THF. 4-Methyl-4-nitrotetradecanal (17.93 g; 66.07 mmol) was isolated as a pale yellow oil (47% yield), bp 145°C/0.050 Torr; $^1$H nmr ($CDCl_3$) δ: 1.53 (s, 3H, $NO_2$—C—$CH_3$), 10.00 (s, 1H, O=C—H).

Note: a heating mantle ($T > 150$°C) was required to distil the product.

III. *4-Nitroacetals*[3]

*4-Methyl-4-nitroheptanal (ethylene acetal)*

4-Methyl-4-nitroheptanal (7.60 g; 43.88 mmol), 3.23 g (52.04 mmol) of ethylene glycol, and 0.0938 g (0.493 mmol) of *p*-toluenesulphonic acid monohydrate were refluxed in 75 mL benzene (25°C) utilizing a Dean–Stark separator. The cooled mixture was added to 200 mL pentane, washed with 3 × 75 mL of 10% aqueous sodium bicarbonate, dried over sodium sulfate, filtered, and solvent evaporated under reduced pressure. The residue was distilled providing 6.86 g of the nitroacetal (72% yield, 31.59 mmol), bp 90°C/0.10 Torr; $^1$H nmr ($CDCl_3$) δ: 1.57 (s, 3H, $NO_2$—C—$CH_3$), 3.90 (m, 4H, $OCH_2CH_2O$), 4.85 (t, 1H, $(CH_2O)_2C$—H).

*4-Methyl-4-nitrodecanal (ethylene acetal)*

4-Methyl-4-nitrodecanal (14.71 g; 68.33 mmol), 5.03 g (80.88 mmol) of ethylene glycol, and 0.1460 g (0.767 mmol) of *p*-toluenesulphonic acid monohydrate were refluxed under similar conditions in 125 mL of benzene to give (70% yield) 12.40 g (47.83 mmol) of nitroacetal, bp 140°C/0.05 Torr; $^1$H nmr ($CDCl_3$) δ: 1.56 (s, 3H, $NO_2$—C—$CH_3$), 3.87 (m, 4H, $OCH_2CH_2O$), 4.83 (t, 1H, $(CH_2O)_2C$—H).

*4-Methyl-4-nitrotetradecanal (ethylene acetal)*

Similarly, 17.93 (66.07 mmol) of 4-methyl-4-nitrotetradecanal, 4.86 g (78.30 mmol) of ethylene glycol, and 0.1412 g (0.742 mmol) *p*-toluenesulphonic acid monohydrate in 125 mL benzene gave 13.88 g (44.00 mmol) nitroacetal in 67% yield; $^1$H nmr ($CDCl_3$) δ: 1.54 (s, 3H, $NO_2$—C—$CH_3$), 3.88 (m, 4H, $OCH_2$—$CH_2O$), 4.85 (t, 1H, $(CH_2O)_2C$—H).

IV. *1-Pyrroline-*N*-oxides and acetal-*N*-hydroxy intermediates*[3]

*5-Propyl-5-methyl-1-pyrroline-*N*-oxide*[4] *(PMPO) (I)*

To a mechanically stirred mixture of 7.10 g (32.67 mmol) of 4-methyl-4-nitroheptanal (ethylene acetal) and 1.86 g (34.77 mmol) ammonium chloride in 12:24 (mL) THF–$H_2O$ were added 8.66 g (119.1 mmol) 90% zinc dust keeping $T < 5$°C. Stirring was continued for approximately 4 h at 25°C. The reduction was monitored by analysis of a 0.25 mL aliquot which was filtered, extracted (pentane), dried ($Na_2SO_4$), filtered, and

[3]The nitroacetals and hydroxylaminoacetals in the text have been named as ethylene acetal derivatives rather than nitrodioxolans and hydroxylaminodioxolans respectively.

[4]5-Methyl-5-propyl-1-pyrroline-*N*-oxide may strictly be the more appropriate nomenclature.

Can. J. Chem. Downloaded from www.nrcresearchpress.com by 210.87.254.42 on 09/06/12
For personal use only.

solvent evaporated under reduced pressure. 4-Methyl-4-hydroxylaminoheptanal (ethylene acetal) was detected by $^1$H nmr ($CDCl_3$) δ: 3.87 (m, 4H, $OCH_2CH_2O$), 4.83 (t, 1H, $(CH_2O)_2$—C—H), 5.46 (s, 2H, C—NHOH, $D_2O$ exch.). The mixture was vacuum filtered, the filtercake washed with 3 × 40 mL hot (50°C) THF. The filtrate was evaporated under reduced pressure ($T$ < 30°C); 4.9 : 60 (mL) of concentrated HCl – $H_2O$ were added and the mixture stirred for 2 h (70°C). The mixture was cooled (25°C), neutralized with $NaHCO_3$, stirred for 1 h, filtered through sintered glass, extracted with 3 × 75 mL pentane, washed with 3 × 75 mL saturated NaCl, dried ($Na_2SO_4$), and solvent evaporated under reduced pressure. The residue was distilled, bp 56°C/0.070 Torr. Successive elution on a silica gel column with pentane, benzene, and finally methylene chloride provided 3.0 g (21.24 mmol) of the nitrone (65% yield) as a colorless hygroscopic oil; ir (film): 1560 (C=N), 1242 (N—O) cm$^{-1}$; $^1$H nmr ($CDCl_3$) δ: 1.39 (s, 3H, O—N—C—$CH_3$), 2.15 (m, 2H, $CH_2$), 2.55 (m, 2H, $CH_2$), 6.82 (t, 1H, O—N=C—H). The nitrone afforded a complex (1:1) with 2,4,6-trinitrophenol, mp 82°C (from absolute ethanol). *Anal.* calcd. for $C_{14}H_{18}N_4O_8$: C 45.41, H 4.90, N 15.13; found: C 45.98, H 5.00, N 14.93.

*5-Hexyl-5-methyl-1-pyrroline-*N*-oxide (HMPO) (II)*

Similarly, stirring of 12.40 g (47.83 mmol) of 4-methyl-4-nitrodecanal (ethylene acetal), 2.72 g (50.85 mmol) ammonium chloride, and 12.68 g (174.5 mmol) of 90% zinc dust gave 4-methyl-4-hydroxylaminodecanal (ethylene acetal) identified by $^1$H nmr ($CDCl_3$) δ: 3.85 (m, 4H, $OCH_2CH_2O$), 4.81 (t, 1H, $(CH_2O)_2C$—H), 5.49 (s, 2H, C—NHOH, $D_2O$ exch.). Acidification followed by distillation, bp 110°C/0.30 Torr, and silica gel chromatography (methylene chloride) provided the nitrone (57%), 5.0 g (27.26 mmol) as a pale yellow oil;[5] ir (film): 1567 (C=N), 1241 (N—O) cm$^{-1}$; $^1$H nmr ($CDCl_3$) δ: 1.39 (s, 3H, O—N—C—$CH_3$), 2.16 (m, 2H, $CH_2$), 2.61 (m, 2H, $CH_2$), 6.76 (t, 1H, O—N=C—H).

*5-Decyl-5-methyl-1-pyrroline-*N*-oxide (DeMPO) (III)*

Similarly, reaction of 13.88 g (44.00 mmol) of 4-methyl-4-nitrotetradecanal (ethylene acetal), 2.51 (46.92 mmol) of ammonium chloride, and 11.66 g (160.4 mmol) of 90% zinc dust produced 4-methyl-4-hydroxylaminotetradecanal (ethylene acetal) detected by $^1$H nmr ($CDCl_3$) δ: 3.88 (m, 4H, $OCH_2CH_2O$), 4.82 (t, 1H, $(CH_2O)_2$—C—H), 5.44 (s, 2H, C—NHOH, $D_2O$ exch.). Acidification gave the crude nitrone which decomposed upon attempted distillation (110°C/0.05 Torr). The nitrone was purified instead by filtration through Celite and silica gel chromatography (methylene chloride). The isolated yield (53%) was 5.6 g (23.39 mmol) as a pale yellow oil.[5] ir (film): 1564 (C=N), 1244 (N—O) cm$^{-1}$; $^1$H nmr ($CDCl_3$) δ: 1.38 (s, 3H, O—N—C—$CH_3$), 2.16 (m, 2H, $CH_2$), 2.60 (m, 2H, $CH_2$), 6.72 (t, 1H, O—N=C—H).

*Electron spin resonance (kinetic esr procedure)*

The esr spectra were observed with a Varian E-104 spectrometer and were calibrated by comparison with Fremy's salt (22) ($a_N$ = 13.09 G, $g$ = 2.0055). The quartz esr cell was equipped with two adjoining compartments to house separately the radical source and spin trap(s). This arrangement has been amply described previously (23).

*Thermally generated* tert-*butoxyl radicals*

Di-*tert*-butylperoxalate (DBPO) prepared by Bartlett's method (24) was freshly recrystallized (hexane, −40°C) before kinetic runs. One compartment of the esr cell arrangement was cooled by liquid $N_2$. Into this sidearm was placed approximately 2.5 mg of DBPO. A 2.0 mL benzene solution (25°C) containing both nitrones, typically (0.01 *M*) in RMPO and (0.30 *M*) in PBN, except $M_4$PO which was equimolar (0.05 *M*) with PBN, was placed into the other compartment. Deoxygenation was accomplished by purging the esr cell and sidearms simultaneously with dry $N_2$ gas for 5–10 min. The contents were mixed vigorously and esr spectra recorded immediately thereafter as a function of time. DBPO decomposes at 25°C in benzene according to reaction [4].

Four lines (2 independent doublets) in the middle of the 18-line spectrum due to the cyclic nitrone and PBN adducts were scanned repeatedly at 70 s intervals for 20–25 min. The specific peaks that were evaluated kinetically are depicted in the esr spectrum derived from (PBN/HMPO/DBPO) in benzene, Fig. 2.

*Photochemically generated* tert-*butoxyl radicals*

Di-*tert*-butylperoxide (Lucidol–Penwalt) was routinely eluted through a silica gel column to remove possible traces of hydroperoxide. Photolysis of BOOB, reaction [10], was accomplished by irradiating the quartz cell with a medium pressure Hg arc equipped with a Pyrex filter.

A 0.20 *M* solution of cyclic spin trap in di-*tert*-butylperoxide scavenged the BO· radicals thus formed. The second doublet in the 12-line pattern was scanned repeatedly at 70 s intervals for 25–30 min. It was important that all decay rates be obtained under as similar experimental conditions as possible since these were direct kinetic measurements. This involved utilization of identical reaction temperatures, esr spectrometer settings, esr cells, and uv lamp intensities for every experiment.

*Spin adduct concentrations*

Concentrations (or ratios of concentrations) of spin adducts were determined by double integration of nonoverlapping lines (of known degeneracy) in the esr spectra. Area units were calibrated by the use of the stable aminoxyl spin label, 2,2,5,5-tetramethyl-3-carbamidopyrrolidine-1-oxyl (Aldrich). The general procedure has been described elsewhere (9*c*).

[5]Alicyclic nitrones are typically thermally labile hygroscopic oils. Elemental analysis is thus usually restricted to their solid derivatives (13). Unfortunately, HMPO and DeMPO did not form crystalline 2,4,6-trinitrophenol complexes or methiodides; ir, $^1$H nmr, and tlc (silica gel – acetone, HMPO ($R_f$ 0.6); DeMPO ($R_f$ 0.5)) indicated the nitrones' purity at 99+%.

## Acknowledgements

This work is being supported by the Natural Sciences and Engineering Research Council of Canada. Grateful acknowledgement is hereby made.

1. E. G. Janzen; P. B. McCay, T. Noguchi, K. L. Fong, E. K. Lai, and J. L. Pryor. *In* Free radicals in biology. Vol. IV. Academic Press, New York. *Edited by* W. A. Pryor. 1980. Chapts. 4; and 5, respectively.
2. M. J. Perkins. Advances in physical organic chemistry. Vol. 17. 1980. p. 1.
3. (*a*) M. Iwamura and N. Inamoto. Bull. Chem. Soc. Jpn. **40**, 703 (1967); (*b*) Bull. Chem. Soc. Jpn. **43**, 860 (1970); (*c*) E. G. Janzen and J. I.-P. Liu. J. Magn. Reson. **9**, 510 (1973); (*d*) E. G. Janzen, C. A. Evans, and J. I.-P. Liu. J. Magn. Reson. **9**, 513 (1973); (*e*) E. G. Janzen, R. V. Shetty, and S. M. Kunanek. Can. J. Chem. **59**, 756 (1981).
4. (*a*) J. R. Harbour, V. Chow, and J. R. Bolton. Can. J. Chem. **52**, 3549 (1974); (*b*) E. G. Janzen, D. E. Nutter, E. R. Davis, R. J. Blackburn, J. Lee Poyer, and P. B. McCay. Can. J. Chem. **56**, 2237 (1978); (*c*) P. R. Marriott, M. J. Perkins, and D. Griller. Can. J. Chem. **58**, 803 (1980).
5. J. R. Harbour and L. M. Hair. J. Phys. Chem. **82**, 1397

(1978); E. FINKELSTEIN, G. M. ROSEN, and E. J. RAUCKMAN. J. Am. Chem. Soc. **102**, 4994 (1980).
6. E. G. JANZEN, R. L. DUDLEY, and R. V. SHETTY. J. Am. Chem. Soc. **101**, 243 (1979).
7. E. G. JANZEN, Y. Y. WANG, and R. V. SHETTY. J. Am. Chem. Soc. **100**, 2923 (1978); E. G. JANZEN and R. C. ZAWALSKI. J. Org. Chem. **43**, 1900 (1978); E. G. JANZEN and R. V. SHETTY. Tetrahedron Lett. 3229 (1979).
8. H. KAUR, K. H. W. LEUNG, and M. J. PERKINS. Chem. Commun. 142 (1981).
9. (*a*) L. LUNAZZI, G. PLACUCCI, M. TIECO, and G. ARTELLI. J. Chem. Soc. Perkin Trans. II, 2215 (1972); (*b*) E. G. JANZEN and C. A. EVANS. J. Am. Chem. Soc. **95**, 8205 (1973); (*c*) E. G. JANZEN, C. A. EVANS, and Y. NISHI. J. Am. Chem. Soc. **94**, 8236 (1972).
10. (*a*) Y. MAEDA and K. U. INGOLD. J. Am. Chem. Soc. **101**, 4975 (1979); (*b*) P. R. MARRIOT and K. U. INGOLD. J. Phys. Chem. **84**, 937 (1980); (*c*) K. U. INGOLD. *In* Free radicals. Vol. 1. *Edited by* J. K. Kochi. John Wiley & Sons, New York. 1973. p. 38.
11. Y. KOTAKE, K. KUWATA, and E. G. JANZEN. J. Phys. Chem. **83**, 3024 (1979).
12. (*a*) C. WALLING and P. J. WAGNER. J. Am. Chem. Soc. **86**, 3368 (1964); (*b*) C. WALLING and V. P. KURKOV. J. Am. Chem. Soc. **89**, 4895 (1967); D. J. CARLSSON and K. U. INGOLD. J. Am. Chem. Soc. **89**, 4885 (1967).
13. R. BONNETT, R. F. C. BROWN, V. M. CLARK, I. O. SUTHERLAND, and A. TODD. J. Chem. Soc. 2094 (1959).
14. E. J. COREY and H. ESTREICHER. Tetrahedron Lett. 117 (1981).
15. D. C. IFFLAND and C. X. CRINER. J. Am. Chem. Soc. **75**, 4083 (1953).
16. R. H. WOLLENBURG and S. J. MILLER. Tetrahedron Lett. 3219 (1978).
17. E. W. BOUSQUET. Org. Synth. Coll. Vol. **II**, 313 (1943).
18. G. D. BUCKLEY and E. ELLERY. J. Chem. Soc. 1497 (1947).
19. J. CASON and J. S. CORREIRA. J. Org. Chem. **26**, 3645 (1961).
20. K. KORNBLUM, H. O. LARSON, R. K. BLACKWOOD, D. D. MOOBERRY, E. P. OLIVETO, and G. E. GRAHAM. J. Am. Chem. Soc. **78**, 1497 (1956).
21. C. KIMURA, K. KASHIWAYA, and T. ASAHARA. Chemical Abstr. **53**, 1849 (1959).
22. R. J. FABER and G. K. FRAENKEL. J. Chem. Phys. **47**, 2462 (1967).
23. G. A. RUSSELL, E. G. JANZEN, and E. T. STROM. J. Am. Chem. Soc. **86**, 1807 (1964).
24. P. D. BARTLETT, E. P. BENZING, and R. E. PINCOCK. J. Am. Chem. Soc. **82**, 1762 (1960).

Can. J. Chem. Downloaded from www.nrcresearchpress.com by 210.87.254.42 on 09/06/12
For personal use only.

# The utilization of nitrone spin traps in a study of the photochemistry of pigment dispersions

JOHN R. HARBOUR, MICHAEL L. HAIR, AND SANDRA L. ISSLER
*Xerox Research Centre of Canada, 2480 Dunwin Drive, Mississauga, Ont., Canada L5L 1J9*

Received September 1, 1981

JOHN R. HARBOUR, MICHAEL L. HAIR, and SANDRA L. ISSLER. Can. J. Chem. **60**, 1523 (1982).

Examples of the use of nitrone spin traps for the elucidation of reaction mechanisms during the illumination of pigment dispersions are presented. Detection of superoxide and hydroxyl radicals with CdS, phthalocyanine, and ZnO is discussed. Singlet oxygen is also detectable with spin traps by following the $O_2$ consumption in these dispersions as a function of illumination. These results are discussed in relation to the applications of pigment dispersions in both novel imaging systems and solar energy utilization systems.

JOHN R. HARBOUR, MICHAEL L. HAIR et SANDRA L. ISSLER. Can. J. Chem. **60**, 1523 (1982).

On présente des exemples d'utilisation des capteurs de spin du type nitrone pour établir les mécanismes de réaction lors de l'irradiation des dispersions de pigments. On discute de la détection des radicaux superoxyde par CdS, la phthalocyanine et le ZnO. On peut également détecter l'oxygène singulet avec les capteurs de spin, en suivant la consommation du $O_2$ dans ces dispersions en fonction de l'irradiation. On discute de ces résultats en rapport avec des applications des dispersions de pigments à la fois dans le nouveau système d'image et dans les systèmes qui utilisent l'énergie solaire.

[Traduit par le journal]

## Introduction

Pigments are highly insoluble materials which are usually obtained commercially as fine powders. Particle size can vary significantly but most pigments have an average particle size of less than 1 micron. These pigments can be dispersed in a liquid phase, sometimes with the aid of a surfactant or polymer dispersant creating opaque suspensions. In most applications, pigments are used for their absorbing or reflecting nature as in paints or inks. In these cases, it is desired that the pigments are photostable. This, however, is not always the case, as, for example, in the phenomenon of chalking in the paint industry where the polymer binder is destroyed by a photosensitized reaction involving the pigment (1).

There are, however, applications of pigment photochemistry where the photoactivity of semiconducting pigments is exploited. Two examples of this will be given. They are: (*1*) Photoactive Pigment Electrophotography (PAPE) Imaging systems (2) and (*2*) Solar Energy Utilization (SEU) systems (3).

In PAPE systems (2), the photoactive pigment must be capable of a photoinduced interfacial charge transfer with the surroundings, thereby reversing the polarity of the charged particle. This is shown in Fig. 1, for a system referred to as Photoelectrophoresis (PEP) (4). The particles which (for example) are negatively charged adhere to the top positively biased transparent electrode. The pigment absorbs the incident imaging light and subsequently undergoes electron loss to create a positively charged particle which is electrophoretically driven through the insulating solvent to the negatively charged counterelectrode.

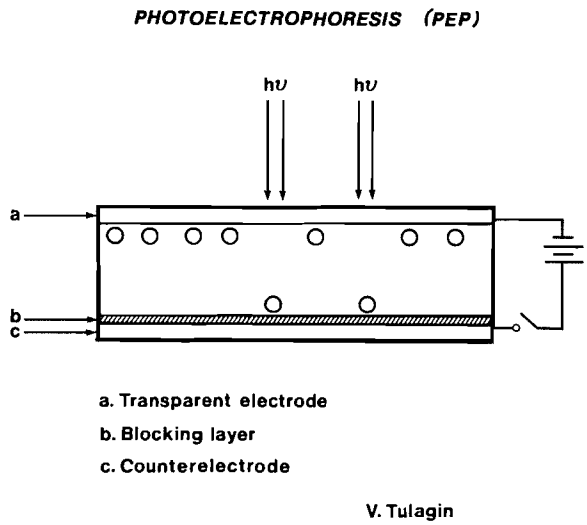


FIG. 1. The general concept of PEP imaging. Particles are electrophoretically driven to the top electrode, *a*, in the dark. Imaging light causes a reversal of particle charge driving the particle to the opposite electrode, *c*, which is covered with a blocking layer, *b*, to prevent additional charge exchange.

A second example is shown in Fig. 2 of a system referred to as PEP Stimulated Imaging (PEPSI) (5). In this system photosensitive particles are mixed with an inert pigment and sandwiched between two electrodes overcoated with a blocking layer. In the exposed region, light induces a charge transfer ultimately from the photosensitive to the inert

0008-4042/82/121523-05$01.00/0
©1982 National Research Council of Canada/Conseil national de recherches du Canada

Can. J. Chem. Downloaded from www.nrcresearchpress.com by 210.87.254.105 on 09/06/12
For personal use only.

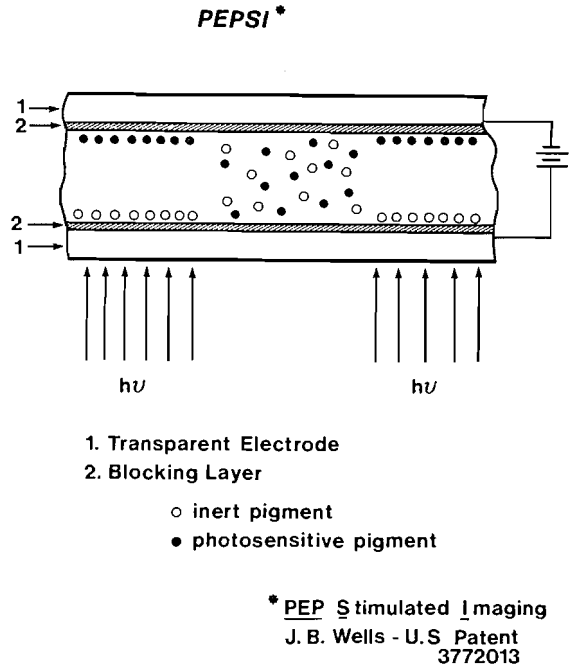


FIG. 2. In this imaging system, called PEPSI, an inert pigment (○) is mixed with a photosensitive pigment (●) in low dielectric solvent. Imaging light causes a charge exchange between the inert and photosensitive pigment and they are driven by the electric field to opposite transparent electrodes (1) which are overcoated with a blocking layer.

pigment. This charges the particles oppositely in the insulating organic fluid and they are again driven electrophoretically to opposite electrodes. In this case, the blocking electrode prevents a direct involvement of the electrode itself and suggests that the charge transfer occurs in dispersion. The molecular mechanism for these processes is not well understood and spin trapping (6) offers an excellent means whereby radical intermediates can be detected and identified in these imaging systems.

The photoactivity of semiconducting pigments can also be used for solar energy utilization (3). Most photoelectrochemical systems use single crystals of materials as electrodes but a recent article has demonstrated that pigments with a polymer binder are also effective as photoelectrodes (7). Pigment dispersions can also be employed as a means of utilizing solar irradiation for photocatalysis or photosynthesis (8). This was first suggested by Rubin *et al.* in 1953 (9) in the photogeneration of $H_2O_2$ in aqueous ZnO dispersions. The present authors have shown that CdS was capable of reducing methyl viologen at the expense of EDTA. It was stated and later proved that $H_2$ evolution was indeed possible from this system. Frank and Bard (11) suggested photocatalysis with $TiO_2$ as a means of removal of $CN^-$ and $SO_2$ in waste streams. Reiche *et al.* (12) extended these ideas to the removal of Cu by photodeposition onto $TiO_2$ or $WO_3$. The metallization of pigments offered new alternatives for production of fuels using these systems and platinization (of $TiO_2$) was particularly useful in this regard (13). We have synthesized platinized CdS (14) which is capable of $H_2$ production upon illumination, using EDTA as a sacrificial donor. This was carried further by Gratzel (15) who codeposited $RuO_2$ and was able to generate both $H_2$ and $O_2$ upon excitation of the CdS.

Many of the reactions which occur in these systems are thought to involve radical intermediates and spin trapping offers a unique way of experimentally determining this. This paper will review several examples of the way in which this has been accomplished. In addition, the ability of nitrone spin traps to react with $^1O_2$ in aqueous medium is discussed. This reaction can be monitored by $O_2$ uptake with an oxygen electrode (16). Therefore, with nitrone spin traps (17) using both esr spectroscopy and $O_2$ uptake, it is possible to detect both radical intermediates and $^1O_2$ produced during the photolysis of pigment dispersions.

## Results and discussion

An electron photochemically promoted to the conduction band has an energy determined by the particular semiconductor being used (18). It is convenient to express this band edge energy in terms of standard redox potentials, $E^{0\prime}$ (vs. $H_2$ electrode, pH = 7) by eq. [1] (19). For ZnO, which has a CB edge energy

$$[1] \quad E^{0\prime} = -4.5 - E_F^{0\prime}\,(\text{eV})$$

of −4.0 eV (20), the standard redox potential would be, $E_{CB}^{0\prime} = -0.5$ V. (Many semiconductors including $TiO_2$ and CdS have $E_{CB}^{0\prime}$ values less than or equal to −0.5 V (20)). Molecular oxygen is a good oxidizer and consequently is easily reduced ($E^{0\prime} = -0.15$ V) (21). Since $O_2$ is present in most technical applications it seems likely that formation of superoxide ($O_2^-$) at the solid/liquid interface will occur to a significant extent. It had in fact been postulated as an intermediate during the photolysis of pigment dispersions (8) but its detection was not accomplished due to its short lifetime. However, in 1974, Harbour *et al.* (22), used the technique of spin trapping with nitrones to successfully detect $O_2^-$ in solution. Thus spin trapping appeared to be an ideal technique for application to the study of short-lived radical intermediates generated during the photolysis of pigment dispersions.

Historically, the first system studied was an aqueous suspension of CdS (10). The sub-micron

Can. J. Chem. Downloaded from www.nrcresearchpress.com by 210.87.254.105 on 09/06/12
For personal use only.

Can. J. Chem. Downloaded from www.nrcresearchpress.com by 210.87.254.105 on 09/06/12
For personal use only.

sized CdS particles were dispersed in water using ultrasonic irradiation. The nitrone spin trap, DMPO, was then added and the dispersion transferred to an aqueous esr cell. In situ irradiation with light of wavelength less than 510 nm resulted in the generation of the $O_2^-$ adduct of DMPO ($a^N = 14.1$ G, $a^H = 11.2$ G, $a^H = 1.2$ G, $g = 2.0061$) (22). This adduct only appeared when dissolved $O_2$ was present. The addition of a good electron donor, ethylene diamine tetraacetic acid, significantly enhanced the amount of $O_2^-$ adduct produced. This enhancement is understandable in terms of maintaining electrical neutrality and will be discussed in more detail in the case of ZnO dispersions. In the absence of EDTA, the photogenerated hole can oxidize CdS itself creating $Cd^{2+}$ in solution and elemental sulfur.

Spin trapping gives indirect evidence for the generation of short-lived radicals. It is therefore important to parallel the trapping results with a directly detected radical intermediate. In the CdS case this was accomplished by incorporating methyl viologen ($MV^{2+}$) into a $N_2$-purged dispersion. $MV^{2+}$ has a redox potential of $-0.44$ V and is reduced to a stable cation radical, $MV^+$. Thus, this photoreduction is thermodynamically allowed. Experimentally this is confirmed by the light-induced formation of $MV^+$, which is evidenced by both its readily identifiable esr spectrum as well as its blue optical absorption (23). Addition of EDTA again enhanced this photoreduction exactly paralleling the indirect spin trapping results. Hence the direct detection results give strong support to the interpretation of the spin trapping experiments.

The use of spin trapping techniques has since been extended to non-aqueous dispersions, particularly those of CdS and the organic pigment x-phthalocyanine ($H_2Pc$) (24). A variety of solvents were used and these demonstrated the general mechanism of photoinduced reduction of $O_2$ to superoxide. Clearly, the hyperfine splittings of the DMPO adducts are a function of solvent polarity. These have been determined and application to most solvent systems is now possible.

The understanding of the primary steps which occur when these semiconducting pigments are irradiated, particularly in low dielectric solvents, is of direct consequence to our understanding of the PAPE imaging process mentioned in the introduction. Molecular oxygen is an ever present "impurity" in the imaging fluids and can clearly act as an electron trap for photoproduced electrons. In the absence of electron donors it is clear that the particle must become positively charged and that photoelectrophoretic imaging can then occur.

Up to this point we have mainly been discussing the fate of electrons in the conduction band. The holes which were created during illumination are also reactive intermediates which can oxidize species in solution. The application of spin trapping to the study of the photochemical events occurring in ZnO aqueous dispersions provides perhaps the best example of the use of this technique in elucidating the oxidative reactions of photogenerated holes (25).

It has long been known that $H_2O_2$ is produced when aqueous ZnO dispersions are irradiated (9) and that the formation of $H_2O_2$ is enhanced when a suitable donor is added to the system. When DMPO was added to an aqueous ZnO suspension containing no added donors and irradiated ($\lambda <$ 380 nm), large quantities of $^{\cdot}OH$ radical adducts were produced. It was determined that the number of $^{\cdot}OH$ radicals produced was dependent upon the amount of dissolved $O_2$ in the system. $O_2$ uptake studies revealed that oxygen was consumed during photolysis and that $H_2O_2$ was generated. Yet no superoxide adduct could be detected by spin trapping. When a donor such as formate or oxalate was added to this system significant changes were observed. Hydroxyl adducts were no longer observed but large quantities of the $^{\cdot}CO_2^-$ adduct were detected. The results for the oxidation are summarized below.

*Oxidation*

[2] $OH^- + \oplus \rightarrow {}^{\cdot}OH$

or

[3] $Zn\text{—}OH + \oplus \rightarrow Zn^{2+} + {}^{\cdot}OH$

*With additives*

[4] $HCO_2^- + {}^{\cdot}OH \rightarrow H_2O + {}^{\cdot}CO_2^-$

and

[5] $HCO_2^- + \oplus \rightarrow H^+ + {}^{\cdot}CO_2^-$

The oxidation of $H_2O$ ($OH^-$) is thermodynamically allowed since the redox level of the $\oplus$ approaches $E_{\oplus}^{0\prime} = +2.6$ V (20) while $E^{0\prime}$ for the oxidation of $H_2O$ is $+0.8$ V. However, the oxidation of ZnO ($E^{0\prime} = 0.7$ V) (20) is also allowed and therefore both eqs. [2] and [3] are possible and lead to the same intermediate, the hydroxyl radical. Which of the two reactions will predominate is determined by the kinetics of the reactions. Similarly two reactions can occur in the presence of formate (eqs. [4] and [5]) and both account for $^{\cdot}CO_2^-$ production. In one case (eq. [4]), the formate anion acts as an hydroxyl radical scavenger whereas in (eq. [5]), a direct oxidation of $HCO_2^-$ by the hole is occurring. The rate of $O_2$ uptake is increased when a donor is added reflecting that both the oxidation of $H_2O$ and ZnO itself are sluggish kinetically compared to formate oxida-

Can. J. Chem. Downloaded from www.nrcresearchpress.com by 210.87.254.105 on 09/06/12
For personal use only.

tion. Hence, in the case where formate is excluded, the hole has a greater opportunity to back react with an $e_{CB}^-$ reducing the overall quantum efficiency. This in fact is observed.

The reduction mechanism deduced from both $O_2$ uptake studies and spin trapping is shown in eqs. [6]–[10] where the subscript "s" refers to a surface species.

[6] $(O_2)_s + e^- \rightarrow (O_2^-)_s$

[7] $(O_2^-)_s + H^+ \rightarrow (HO_2^{\cdot})_s$

[8] $(HO_2^{\cdot})_s + e^- \rightarrow (HO_2^-)_s$

[9] $(HO_2^-)_s + H^+ \rightarrow (H_2O_2)_s \leftrightarrows H_2O_2$

or

[10] $2(HO_2^{\cdot})_s \rightarrow H_2O_2 + O_2$

Quantitative studies revealed that the quantum efficiency for the production of spin adducts was 0.04 compared to a value of 0.14 from the $O_2$ uptake measurements for the formate case. Several reasons make the $\Phi = 0.04$ a minimum value for the esr measurement and therefore it was demonstrated that the radical production was reflecting the major photochemical reactions in this system rather than a side reaction. Hence spin trapping allows for a determination of the mechanisms occurring during the photolysis of pigment dispersions.

Recently there has been an evolving interest in the use of metallized semiconductor particles for solar energy conversion and hydrogen production (3). Nitrone spin traps can play an important role in determining the short-lived radical intermediates formed in these systems. Thus, Jaeger and Bard (26) describe a recent application of the spin trapping technique to the photolysis of platinized $TiO_2$ dispersions. One interesting result was that they were unable to observed an $H^{\cdot}$ adduct despite the fact that hydrogen gas is produced in these dispersions. The present authors (14) have used DMPO to study aqueous Pt/CdS dispersions but found no spin adducts upon illumination.

While all previous studies indicate that nitrone spin traps can be exceedingly useful in studying the initial photochemistry in pigment dispersions, the results must be treated with some caution: Nitrone spin traps also react with singlet oxygen in aqueous media (16). The rate constants for the quenching of $^1O_2$ by several nitrone spin traps have been recorded. The rates vary from 14 to $1.8 \times 10^7\ M^{-1}\ s^{-1}$ for PBN and DMPO respectively. It is noted that this is a chemical quenching which results in consumption of oxygen. Clearly, if $^1O_2$ is also being produced when the semiconducting pigment dispersions are irradiated, then an oxygen depletion could occur to the extent that the normal radical reaction may be inhibited. Since the rate constant for quenching by DMPO is approximately one order of magnitude less than with PBN and other nitrones it would be the better choice for spin trapping in systems where the presence of $^1O_2$ is suspected. The rate of quenching of the singlet oxygen by nitrones can be monitored by incorporating an oxygen membrane electrode into the closed photochemical cell. This technique conveniently measures dissolved oxygen concentration and can be applied to both solutions and dispersions. It thus provides a useful method for allowing the kinetics of the oxygen uptake. Thus addition of a nitrone to an illuminated dispersion should cause an observable increase in the rate of oxygen uptake if $^1O_2$ is being photochemically generated.

Pappas and Fischer (1) have presented data using a different experimental technique which suggests that both $TiO_2$ and ZnO can generate singlet oxygen in methanol. Conversely, Spikes (27) has presented data suggesting that singlet oxygen is not generated when aqueous suspensions of CdS are irradiated. By monitoring the rate of oxygen uptake as a function of PBN concentration, we have been able to confirm that indeed CdS does not generate singlet oxygen in aqueous media. However, aqueous ZnO suspensions appear to produce singlet oxygen. With $TiO_2$ only a marginal increase in the rate of oxygen consumption is noted when PBN is added to the system. Clearly the mechanism by which singlet oxygen is generated in these dispersions is an interesting but complex subject and this will be the subject of a separate paper (28).

In this paper we have shown that the short-lived intermediates formed when particulate suspensions of semiconducting pigments are irradiated can be crucial to the understanding of photoelectrophoresis (PAPE). In particular, the use of nitrone spin traps in the detection of superoxide and hydroxyl radicals is emphasized. The chemical interaction of $^1O_2$ with the nitrones is a complication, but the introduction of oxygen uptake measurements adds a new dimension to the studies and enables the observation of both radical and singlet oxygen formation in these photoactive dispersions.

1. S. P. PAPPAS and R. M. FISHER. J. Paint Tech. **46**, 65 (1974).
2. J. W. WEIGL. Angew. Chem. Int. Ed. Engl. **16**, 374 (1977).
3. A. J. BARD. J. Photochem. **10**, 59 (1979).
4. V. TULAGIN. J. Opt. Soc. Am. **59**, 328 (1969).
5. J. B. WELLS. U.S. Pat. 3772013, 1973.
6. E. G. JANZEN. Acc. Chem. Res. **4**, 31 (1971).
7. L. R. WEISBERG, C. F. GRAIN, and R. R. ADDISS, JR. Appl. Phys. Lett. **4**, 31 (1975).
8. T. FREUND and W. P. GOMES. Catal. Rev. **3**, 1 (1969).
9. T. R. RUBIN, J. G. CALVERT, G. T. RANKIN, and W. MACNEVIN. J. Am. Chem. Soc. **75**, 2850 (1953).

10. J. R. HARBOUR and M. L. HAIR. J. Phys. Chem. **81**, 1791 (1977).
11. S. N. FRANK and A. J. BARD. J. Phys. Chem. **81**, 1484 (1977).
12. H. REICHE, W. W. DUNN, and A. J. BARD. J. Phys. Chem. **83**, 2248 (1979).
13. B. KRAEUTLER and A. J. BARD. J. Am. Chem. Soc. **100**, 4318 (1978).
14. J. R. HARBOUR, R. WOLKOW, and M. L. HAIR. J. Phys. Chem. **85**, 4026 (1981).
15. K. KALYANASUNDARAM, E. BORGARELLO, D. DUONG-HONG, and M. GRATZEL. Angew. Chem. Int. Ed. In press.
16. J. R. HARBOUR, S. L. ISSLER, and M. L. HAIR. J. Am. Chem. Soc. **102**, 7778 (1980).
17. E. G. JANZEN and J. I. LIU. J. Magn. Reson. **9**, 510 (1973).
18. H. GERISCHER. J. Electroanal. Chem. Interfacial Electrochem. **58**, 263 (1975).
19. A. HENGLEIN and M. GRATZEL. *In* Solar power and fuels. *Edited by* J. R. Bolton. Academic Press, New York. 1977.
20. H. GERISCHER. *In* Solar power and fuels. *Edited by* J. R. Bolton. Academic Press, New York. 1977.
21. D. MEISEL. Chem. Phys. Lett. **34**, 263 (1975).
22. J. R. HARBOUR, V. CHOW, and J. R. BOLTON. Can. J. Chem. **52**, 3549 (1974).
23. F. D. SAEVA, G. R. OLIN, and J. R. HARBOUR. J. Chem. Soc. Chem. Commun. 401 (1980).
24. J. R. HARBOUR and M. L. HAIR. J. Phys. Chem. **82**, 1397 (1978).
25. J. R. HARBOUR and M. L. HAIR. J. Phys. Chem. **83**, 652 (1979).
26. C. D. JAEGER and J. A. BARD. J. Phys. Chem. **83**, 3146 (1979).
27. J. SPIKES. Photochem. Photobiol. **34**, 549 (1981).
28. J. R. HARBOUR and S. L. ISSLER. Unpublished data.

Can. J. Chem. Downloaded from www.nrcresearchpress.com by 210.87.254.105 on 09/06/12
For personal use only.

# Free radical production during phenylhydrazine-induced hemolysis

H. A. O. Hill and P. J. Thornalley

*Inorganic Chemistry Laboratory, University of Oxford, South Parks Road, Oxford, England OX1 3QR*

Received September 1, 1981

H. A. O. Hill and P. J. Thornalley. Can. J. Chem. **60**, 1528 (1982).

The production of phenyl radicals during phenylhydrazine-induced hemolysis has been demonstrated by the use of the spin traps, DMPO, $M_4PO$, and LINPyBN. The phenyl spin adducts of DMPO and $M_4PO$ were produced in moderate yield by an oxygenated 1% erythrocyte suspension. With the lipid soluble spin trap LINPyBN, a dramatic increase (400%) in the yield of phenyl spin adduct was observed despite little increase in the rate of phenyl radical trapping. The production of phenyl spin adducts was decreased when phenylhydrazine-4-sulphonic acid or carbonmonoxyhemoglobin-containing erythrocytes were used. These results suggest that the reaction of phenylhydrazine with oxyhemoglobin leads to the formation of phenyl radicals that are preferentially trapped in the erythrocyte membrane.

H. A. O. Hill et P. J. Thornalley. Can. J. Chem. **60**, 1528 (1982).

Faisant appel aux capteurs de spin du type DMPO, $M_4PO$ et LINPyBN, on a démontré qu'il y a production de radicaux phényles lors de l'hemolyse induite par la phénylhydrazine. A l'aide d'une suspension à 1% d'érythrocytes oxygénés, on a produit avec un rendement modéré les adduits de spin phényle du DMPO et du $M_4PO$. Dans le cas du capteur de spin LINPyBN soluble dans les lipides, on observe une augmentation considérable (400%) du rendement en adduit de spin du type phényle en dépit d'une faible augmentation de la vitesse de piégeage du radical phényle. La production des adduits de spin du type phényle diminue lorsqu'on utilise de l'acide phénylhydrazinesulfonique-4 ou des érythrocytes contenant de la carbonemonoxyhémoglobine. Ces résultats suggèrent que la réaction de la phénylhydrazine avec l'oxyhémoglobine conduit à la formation des radicaux phényles qui sont piégés préférentiellement dans la membrane de l'érythrocyte.

[Traduit par le journal]

## Introduction

The factors that affect the useful life of erythrocytes have been much studied (1). Certain drugs have been demonstrated to show a remarkable specificity to oxidise cellular components and cause lysis in erythrocytes (2). Phenylhydrazine is one such drug (3, 4). It has found clinical use in lowering the red cell count in polycythemia vera (5), and experimentally is used to produce hemolytic anaemias (6). Phenylhydrazine is known to increase the level of hydrogen peroxide in erythrocytes, exceeding the levels with which glutathione peroxidase and catalase can cope. This is a contributory factor to the overall toxicity of phenylhydrazine towards erythrocytes, particularly where inherited defects or aging give diminished activity of glucose-6-phosphate dehydrogenase (7). The reactive intermediates which cause hemoglobin breakdown, membrane oxidation, and cell lysis, have yet to be identified. An explanation of the specificity (8) of phenylhydrazine for erythrocytes is lacking. Hemolysis is (9) commonly intravascular. A method of measuring the active hemolytic agent *in vitro* would be of value in the screening of drugs for possible hemolytic acitivity (9).

The involvement of superoxide (10), hydroxyl (11) and phenyl radicals (12) in phenylhydrazine-induced hemolysis has been proposed. We have used three spin traps (Fig. 1) to study the hemolytic reaction: (*i*) 5,5-dimethyl-1-pyrroline-1-oxide (DMPO) — this was used initially (12) because of its high reactivity and water solubility; (*ii*) 5,5,3,3-tetramethyl-1-pyrroline-1-oxide ($M_4PO$) — this has a similar reactivity to DMPO but forms more stable adducts; (*iii*) α,4-(*N'*-linoleylpyridinium chloride)-*N*-*t*-butyl nitrone (LINPyBN) — a lipid soluble spin trap which we presume is preferentially located in the erythrocyte membrane.

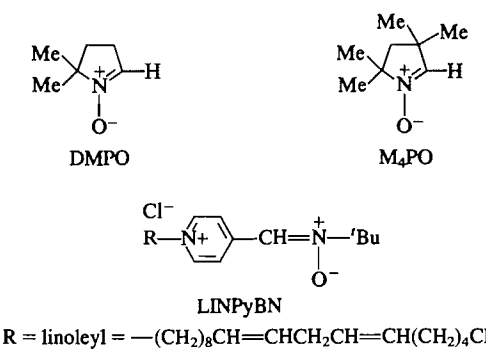


FIG. 1. Spin traps used.

## Experimental

*Preparation of erythrocytes*

Erythrocytes were prepared from blood drawn from normal human subjects by venous puncture, as described in ref. 12. Carbonmonoxyhemoglobin-containing erythrocytes were prepared by the method of Goldberg and Stern (13).

*Spin traps*

The spin traps DMPO and $M_4PO$ were prepared by the

0008-4042/82/121528-04$01.00/0

©1982 National Research Council of Canada/Conseil national de recherches du Canada

Can. J. Chem. Downloaded from www.nrcresearchpress.com by 210.87.254.6 on 09/06/12
For personal use only.

Can. J. Chem. Downloaded from www.nrcresearchpress.com by 210.87.254.6 on 09/06/12
For personal use only.

method of Bonnet *et al.* (14). LINPyBN was prepared by the method of Emmons (15) from *t*-butylhydroxylamine and *N*-linoleyl-4-carboxaldehydopyridinium chloride. The latter was prepared from the reaction of the tosylate of linoleyl alcohol (Sigma Chemical Company Ltd, Poole, Dorset, U.K.) with excess pyridine-4-carboxaldehyde (Aldrich Chemical Company Ltd, Gillingham, Dorset, U.K.), followed by ion exchange chromatography of the tosylate for chloride using a Dowex-1 column. The nitrone product was characterised by mass spectral data (molecular ion $m/e = 462.5$), $^1$H nmr (linoleyl residue — methylene protons 0, divinyl methylene protons 11.6, and vinyl protons 14.0 ppm; nitrone residue — *t*-butyl protons 1.6, vinyl proton 8.4, and aromatic protons 8.8–9.1 ppm), CHN analysis (calcd. C 72.6, H 10.2, N 6.1; found: C 71.2, H 10.8, N 7.0). A chloroform solution (0.5 *M*) did not give an esr spectrum.

*Other reagents*

The complexing ligand, diethylenetriaminepentaacetic acid (DETAPAC), was obtained from Aldrich. All other reagents were of standard analytical grade except phenylhydrazine (Fisons laboratory reagent) and phenylhydrazine-4-sulphonic acid (Fluka, Basle, Switzerland) which were both recrystallised twice (mp 20°C and 286°C, respectively) before use and subsequently stored at 0–4°C in the dark.

*Electron spin resonance*

Electron spin resonance spectra were recorded on a Varian E104 ESR spectrometer fitted with an E935 data acquisition system. The reaction time course of spin adduct production was followed by measuring the amplitude of the signal at an appropriate constant value of the applied field. Spin adduct concentrations were determined from a calibrated second integral.

## Results

The initial results (12) from a phenylhydrazine-treated erythrocyte suspension in the presence of DMPO provided evidence for the production of a phenyl radical spin adduct, Fig. 2 (**1***a*). Using phenylhydrazine-4-sulphonate, however, very little phenyl-4-sulphonate spin adduct was observed, despite little change in trapping rates. This effect was ascribed to poor transport of the sulphonate derivative across the erythrocyte membrane.

A similar yield of phenyl spin adduct was obtained using an identical system but with $M_4PO$ at the same concentration as DMPO, Fig. 2 (**2***a* and **2***b*), though the stability of the spin adduct was slightly greater. Using LINPyBN, a dramatic increase in yield of the phenyl spin adduct was observed, Fig. 2 (**3***a* and **3***b*). (The additional discontinuity in the center of the spectrum in Fig. 2 (**3***a*, **3***b*) is probably due to a decomposition product of LINPyBN, viz., di-*t*-butylnitroxide). DMPO, $M_4PO$, and LINPyBN have similar trapping rates for phenyl radicals. The ratio of the phenyl radical trapping rates for DMPO:$M_4PO$ (aq., pH 7):LINPyBN (hexane) is 1:0.6:0.9, as determined by competition experiments using uv photolysis of phenylhydrazine as a source of phenyl radicals. The phenyl radical

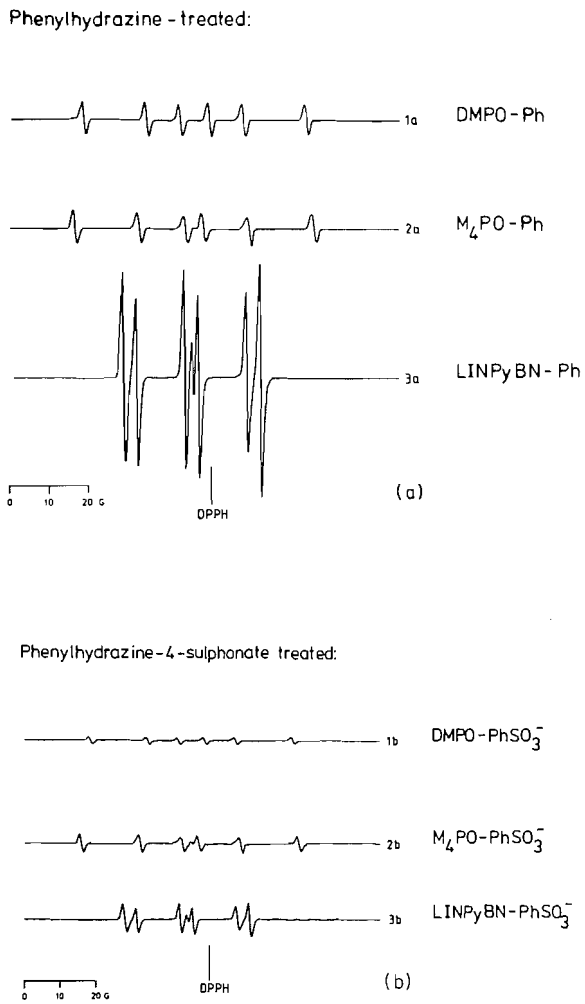


FIG. 2. Phenyl radical spin adducts generated during phenylhydrazine-induced hemolysis. The reaction mixtures contain: 1% suspension of human erythrocytes, 2 m*M* phenylhydrazine (*a*) or 2 m*M* phenylhydrazine-4-sulphonate (*b*), 1 m*M* DETAPAC, 20 m*M* spin trap using (1) DMPO, (2) $M_4PO$, and (3) LINPyBN in isotonic phosphate buffer, pH 7.4. The instrumental details were: field set 3385 G, field scan 100 G, mod. freq. 100 kHz, mod. amp. 1.0 G, receiver gain $2 \times 10^3$, time constant 0.128 s, scan time 120 s, microwave frequency 9.478 GHz, microwave power 10 mW.

LINPyBN spin adduct also has an increased stability as is indicated by Fig. 3, which shows the time course of the reaction for all the spin traps used. It also illustrates in Fig. 3 (**2***c*) the very low yield of $M_4PO$—Ph obtained using erythrocytes in which the hemoglobin was in the carbonmonoxy form. This is consistent with the observation that such erythrocytes are known (13) to be resistant to phenylhydrazine attack.

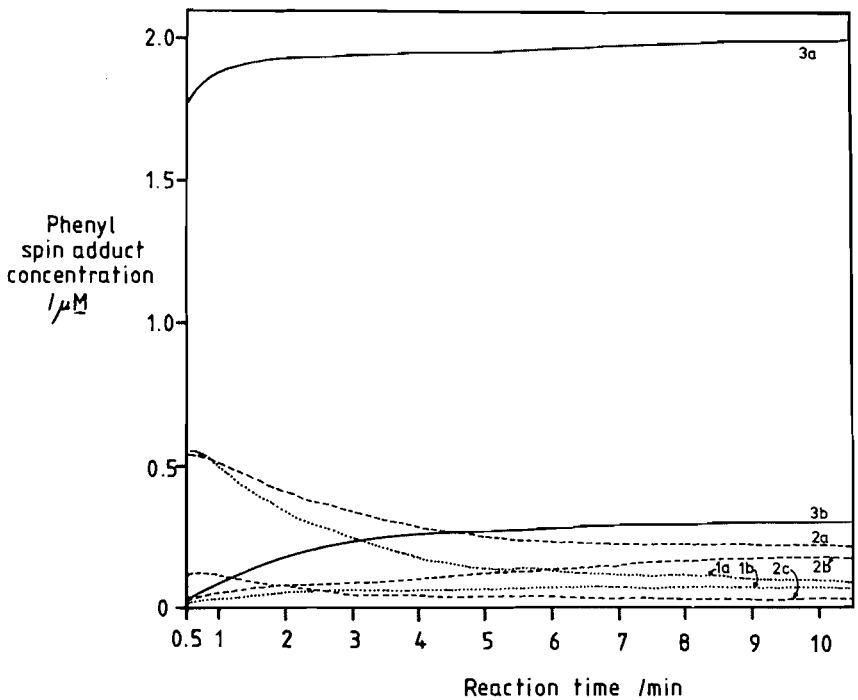


FIG. 3. The reaction time course studied with the field held constant at a value of the lowest field resonance in the esr spectrum; receiver gain $5 \times 10^3$, time constant 4.0 s, remaining settings as for the spectra. The curves are labelled as in Fig. 2 except that (2*c*) is the time course of a reaction carried out using the erythrocytes in the carbonmonoxy form.

TABLE 1. Hyperfine splitting constants; phenyl spin adducts formed in 1% erythrocyte suspension in isotonic phosphate buffer at pH 7.4

| | $a_N$/G | $a^H$/G |
|---|---|---|
| DMPO—Ph | 15.8 | 24.4 |
| $M_4$PO—Ph | 16.2 | 27.2 |
| LINPyBN—Ph | 15.8 | 3.7 |

## Discussion

*The autoxidation of phenylhydrazine*

Misra and Fridovich (16) showed phenylhydrazine to be stable in acid solutions but autoxidised in neutral and alkaline buffers. The oxidation was catalysed by traces of metal ion complexes, of which oxyhemoglobin was the most effective. The scheme they proposed to account for the observations is shown below. Phenyldiazene rapidly decays (17), giving traces of benzene and biphenyl. A kinetic analysis emphasised (16) the role of superoxide. Following initiation, there are two possible routes to phenyldiazene: (*a*) a superoxide-dependent propagation producing hydrogen peroxide; (*b*) a superoxide-independent autocatalysis via a benzadiazonium cation intermediate. Therefore, after an initial lag phase, the autoxidation of phenylhydrazine to phenyldiazene may not be effectively inhibited by superoxide dismutase (SOD), and may indeed be stimulated by SOD (16).

Initiation:

[*a*] $PhNHNH_2 + \underset{\text{OxyHb}}{HbFe^{3+}—O_2^-} + H^+ \rightarrow PhNH\dot{N}H + \underset{\text{MetHb}}{HbFe^{3+}} + H_2O_2$

Superoxide-dependent propagation:

[*b*] $PhNH\dot{N}H + O_2 \rightarrow H^+ + O_2^- + PhN{=}NH$

[*c*] $O_2^- + H^+ + PhNHNH_2 \rightarrow H_2O_2 + PhNH\dot{N}H$

Superoxide-independent autocatalysis:

[*d*] $PhN{=}NH + (1/2)O_2 \rightarrow PhN{\equiv}N^+ + H_2O$

[*e*] $PhN{\equiv}N^+ + PhNHNH_2 \rightarrow 2PhN{=}NH + H^+$

Phenyldiazene decay:

[*f*] $PhN{=}NH + (1/2)O_2 \rightarrow [PhN{=}\dot{N}] + O_2^- + H^+$

$[PhN{=}\dot{N}] \xrightarrow{\text{v. fast}} Ph^\cdot + N_2$

[*g*] $Ph^\cdot + subH \rightarrow PhH + sub^\cdot$

Termination:

[*h*] $2PhNH\dot{N}H \rightarrow PhNHNH_2 + PhN{=}NH$

[*i*] $2O_2^- + 2H^+ \xrightarrow{SOD} H_2O_2$

Can. J. Chem. Downloaded from www.nrcresearchpress.com by 210.87.254.6 on 09/06/12
For personal use only.

Can. J. Chem. Downloaded from www.nrcresearchpress.com by 210.87.254.6 on 09/06/12
For personal use only.

SCHEME 1. Mechanism for the autoxidation of phenylhydrazine catalysed by oxyhemoglobin

*Spin trapping of the products of autoxidation of phenylhydrazine*

It has long been suspected (18) that phenyl radicals are produced in the oxidation of phenylhydrazine. Consequently the formation of phenyl spin adducts in the spin trapping of phenylhydrazine-induced hemolysis is not surprising. The lack of other spin adducts, however, is. Why, for example, is superoxide not trapped? It is generated in the oxidation of phenylhydrazine — reactions [*b*] and [*f*], but it is consumed in reactions [*c*] and [*i*]. The spin trap is competing for the superoxide with SOD, which is present in the erythrocyte, phenylhydrazine, and possibly the benzadiazonium cation. Given the low rate (19) of reaction of superoxide with the spin traps at pH 7, it is understandable that no superoxide spin adduct is detected. The decay of phenyldiazene in aerobic media is so rapid that the lifetime of phenyldiazenyl radicals may be too short to form a phenyldiazenyl spin adduct. The phenylhydrazyl radical is generated and consumed in the propagation steps — reactions [*b*] and [*c*]. Phenylhydrazyl may also dismute — reaction [*h*]. The lack of detection of a phenylhydrazyl spin adduct during phenylhydrazine autoxidation may be due to the inability of the spin traps to compete successfully with $O_2$ and dismutation reactions for the phenylhydrazyl radicals.

*A mechanism for phenylhydrazine-induced hemolysis*

The autoxidation of phenylhydrazine is catalysed by oxyhemoglobin within the erythrocytes, producing high levels of hydrogen peroxide (20) and phenyl radicals (12). The use of a membrane-solvated spin trap, LINPyBN, which we assume to be preferentially located in the erythrocyte membrane, suggests that either the phenyl radicals are produced in the membrane or they diffuse to the membrane where they are trapped. We note that the esr spectrum of the LINPyBN phenyl spin adduct is not that of an immobilised nitroxide. It is known (21) that simple lipid soluble nitroxides may orient themselves parallel to the membrane but within the membrane, to give isotropic nitroxide esr spectra. It is possible that the cytotoxic activity (13) of phenylhydrazine is due to the attack of phenyl radicals on the membrane thus initiating the oxidation of unsaturated fatty acid residues in phospholipids (22) and aggregation of membrane proteins (23). Indeed, high levels of lipid peroxidation products and spectrin polymers have been observed in the reticulocyte membranes prepared from phenylhydrazine-treated animals (23). It was suggested that the polymerisation of spectrin may lead to the loss of integrity of the erythrocyte membrane.

Phenylhydrazine-induced hemolysis may be mediated by phenyl radicals through an intravascular route, the hydrogen peroxide-dependent extravascular route playing an increasingly important role as the detoxification mechanisms for reduced oxygen species are overcome. However, it is unlikely that either route occurs in isolation.

## Acknowledgements

P.J.T. thanks the Science and Engineering Research Council (U.K.) for a studentship. H.A.O.H. thanks the British Heart Foundation for support for the purchase of the esr spectrometer. This is a contribution from the Oxford Enzyme Group.

1. J. DACIE. J. R. Soc. Med. London, **72**, 447 (1979).
2. E. BEUTLER. Pharm. Rev. **21**, 73 (1969).
3. R. M. LEMBURG and J. W. LEGGE. Aust. J. Exp. Med. Sci. **20**, 65 (1942).
4. G. H. BEAVEN and J. C. WHITE. Nature, **173**, 389 (1954).
5. H. Z. GIFFEN and E. V. ALLEN. Am. J. Med. Sci. **185**, 1 (1933).
6. W. TELO. J. Clin. Med. **30**, 113 (1949).
7. P. HOCHSTEIN. Exp. Eye Res. **11**, 389 (1971).
8. W. F. VON OTTINGEN. U.S. Public Health Service Bull. **271**, 158 (1941).
9. L. LUZZATTO and U. TESTA. *In* Current topics in hematology. Vol. 1. *Edited by* S. Piomelli and S. Yachin. A. R. Liss, NY. 1978. p. 29.
10. B. GOLDBERG and A. STERN. J. Biol. Chem. **251**, 3045 (1976).
11. H. MISRA and I. FRIDOVICH. J. Biol. Chem. **147**, 3170 (1972).
12. H. A. O. HILL and P. J. THORNALLEY. FEBS Lett. **125**, 235 (1981).
13. B. GOLDBERG and A. STERN. Mol. Pharmacol. **13**, 832 (1977).
14. R. BONNET, R. F. C. BROWN, I. O. SUTHERLAND, and A. TODD. J. Chem. Soc. 2094 (1959).
15. W. D. EMMONS. J. Am. Chem. Soc. **79**, 6522 (1957).
16. H. MISRA and I. FRIDOVICH. Biochemistry, **15**, 681 (1976).
17. P. C. HUANG and E. M. KOSOWER. J. Am. Chem. Soc. **89**, 2367 (1968).
18. J. NICHOLSON and S. G. COHEN. J. Am. Chem. Soc. **88**, 2247 (1966).
19. E. FINKELSTEIN, G. M. ROSEN, and E. J. RAUCKMAN. J. Am. Chem. Soc. **102**, 4994 (1980).
20. G. COHEN and P. HOCHSTEIN. Biochemistry, **3**, 895 (1964).
21. B. J. GAFFNEY. *In* Methods in membrane biology. *Edited by* E. D. Korn. Vol. 8. Plenum Press. 1977. p. 291.
22. H. W. GARDNER. J. Agric. Food Chem. **27**, 220 (1979).
23. P. HOCHSTEIN and S. K. JAIN. Fed. Proc. **40**, 183 (1981).

# Spin trapping by use of nitrosodurene and its derivatives

RYUSEI KONAKA,[1] SHIGERU TERABE,[2] TAIICHI MIZUTA, AND SHIGERU SAKATA
*Shionogi Research Laboratories, Shionogi & Co., Ltd., Fukushima-ku, Osaka 553, Japan*
Received September 1, 1981

RYUSEI KONAKA, SHIGERU TERABE, TAIICHI MIZUTA, and SHIGERU SAKATA. Can. J. Chem. **60**, 1532 (1982).

In spin trapping the *N*-methyl-*N*-phenylaminomethyl radical with nitrosodurene, an esr spectrum exhibiting line width alternation was observed despite the normal spectral pattern found with the use of nitroso-*tert*-butane.

Nitrosodurene derivatives, *N*-duryl nitrone and methyl *N*-duryl nitrone, have been revealed to be other excellent spin traps for the *N*-, *O*-, and *S*-centered radicals. Spin adducts of these radicals, which can be independently prepared by spin trapping with nitrosodurene, are stable and can be easily discriminated by large differences in β-hydrogen splittings or characteristic patterns.

Methyl *N*-duryl nitrone reacted with *tert*-butyl hydroperoxide to give a spin adduct which could be clearly distinguished in the esr spectra from the *tert*-butoxy adducts prepared independently from other sources. Accordingly, it seems to be the *tert*-butylperoxy adduct. Similarly, hydrogen peroxide gave a different spectrum from the hydroxy adducts.

Alkyl hydroperoxides caused molecule-induced homolysis with the nitroso compounds to produce alkoxy adducts of the respective nitroso compounds. Some phenyl and duryl alkoxy nitroxides undergo decomposition to give alkyl radicals which were trapped by the nitroso compounds.

RYUSEI KONAKA, SHIGERU TERABE, TAIICHI MIZUTA et SHIGERU SAKATA. Can. J. Chem. **60**, 1532 (1982).

Lors du piégeage du radical *N*-méthyl *N*-phénylamino méthyle avec le nitrosodurène, le spectre de rpe présente une alternance de largeur de ligne en dépit de l'allure de spectre normal trouvé lors de l'utilisation du nitroso-*tert*-butane.

Les dérivés du nitrosodurène, la *N*-durylnitrone et la méthyl *N*-durylnitrone, se sont révélés d'excellents capteurs de spin pour les radicaux ayant en leur centre le N, le O ou le S. Les adduits de spin de ces radicaux, qui peuvent être préparés indépendemment par captage de spin avec le nitrosodurène, sont stables et peuvent être facilement différenciés par des grandes différences dans le dédoublement de l'hydrogène en β ou par des traits caractéristiques. La méthyl *N*-duryl nitrone réagit avec l'hydroperoxyde de *tert*-butyle pour donner un adduit de spin que l'on peut clairement distinguer, par la rpe, des adduits *tert*-butoxy préparés indépendemment à partir d'autres sources. En conséquence, il ressemble à un adduit *tert*-butylperoxy. De la même façon, le peroxyde d'hydrogène donne un spectre différent de celui des adduits hydroxy.

Les hydroperoxydes d'alkyles, provoquent une hémolyse induite des composés nitrosés conduisant à la formation d'adduits alkoxy des composés nitroso respectifs. Quelques phényl et duryl alkoxynitroxydes donnent, par décomposition, des radicaux alkyles qui sont captés par les composés nitroso.

[Traduit par le journal]

## Introduction

In 1968, Konaka and Terabe applied the spin trapping technique using nitrosobenzene (NB) to oxidation reactions with nickel peroxide (NiPO) and were able to identify the free radicals involved as reaction intermediates (1, 2). Although NB is a useful spin trap whose spin adducts show characteristic finger-print spectra, the assignment of esr spectra of the spin adducts is very tedious because of their complexity.

Among alternative spin traps, nitrosodurene (ND) has proved to be a particularly interesting compound because of the following advantages (3).

(*1*) The nitroxides formed have simple esr spectra: In general, no resolvable splitting due to the aromatic ring of the spin adducts of ND is observed. This suggests that the nitroxyl group twists along the ring-carbon–nitrogen bond from the plane of the aromatic ring.

(*2*) ND does not undergo photolysis to produce detectable paramagnetic species: A benzene solution of ND irradiated with light from a 1 kW high-pressure mercury lamp did not show any esr signal. Accordingly, ND can be used as a spin trap in photochemistry.

(*3*) Wide scattering of β-hydrogen splitting constants leads to ready discrimination of the radicals trapped: The most characteristic feature in esr spectra of alkyl duryl nitroxides is the wide variation of the β-hydrogen splitting constants depending on the structure of the radical trapped. As an example, β-hydrogen splitting constants of the secondary alkyl radical adducts produced by trapping with nitroso-*tert*-butane (NtB), NB, or ND can be compared in Table 1. In the case of ND, the steric requirements owing to the *ortho* methyl groups emphasized by the buttressing effects of the *meta* methyl groups of the duryl nitroxide seem to cause significant differences.

(*4*) Highly efficient trapping occurs in spite of the fact that a large portion of the dimeric form exists in solution: Recently, Maeda and Ingold determined

[1]To whom all correspondence should be addressed.
[2]Present address: Department of Industrial Chemistry, Faculty of Engineering, Kyoto University, Yoshida, Sakyo-ku, Kyoto 606, Japan.

0008-4042/82/121532-10$01.00/0
©1982 National Research Council of Canada/Conseil national de recherches du Canada

TABLE 1. Comparison of β-hydrogen coupling constants[a]

| | —CH(Me)ϕ | —CH(Et)ϕ | —CHϕ$_2$ | 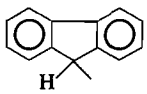 | 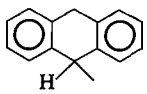 | 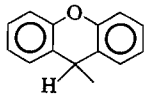 | 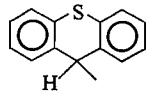 |
|---|---|---|---|---|---|---|---|
| 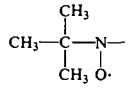 | 3.41[b] | 3.21[b] | 2.08[b] | 1.07 | 0.86 | | |
| 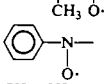 | 5.31 | 4.00 | 3.59 | 0.91 | 0.98 | 0.95 | 1.08 |
| 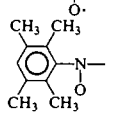 | 3.77 | 7.60 | 1.48 | 15.01 | 5.23 | 6.98 | 8.99 |

[a]In G in benzene at room temperature.
[b]Reference 4.

the rate constants for spin trapping alkyl radicals using a variety of spin traps in benzene at 40°C (5), and also Yoshida and Doba measured the trapping rate constants of the *tert*-butyl radical using various spin traps in benzene at 26°C (6). From these results, ND proved to give the largest rate constants among the spin traps examined. Even though ND is mostly in the dimeric form in benzene ($K$ = [dimer]/[monomer]$^2$, $K = 303\,M^{-1}$ at 40°C (5)), it is highly efficient for trapping alkyl radicals.

This paper describes an interesting example of spin trapping carbon-centered radicals with an adjacent nitrogen atom using ND.

Generally, nitrones such as phenyl *tert*-butyl nitrone (PBN) (7), 5,5-dimethylpyrroline-*N*-oxide (DMPO) (8), and 3,3,5,5-tetramethylpyrroline-*N*-oxide ($M_4$PO) (9) have been used extensively as spin traps other than nitroso compounds so far. This paper also reports the usefulness of *N*-duryl nitrone (DN) and methyl *N*-duryl nitrone (MDN), which are related to ND. In addition, esr spectroscopy of the peroxy adducts of MDN or DN, which appears to be an attractive problem in radical chemistry, is described.

Finally, molecule-induced homolysis of hydroperoxides with *C*-nitroso compounds was investigated by applying the spin trapping technique, and the behavior of the alkoxy nitroxides is discussed.

## Spin trapping carbon-centered radicals with an adjacent nitrogen atom

Although an enormous amount of spectral data is available for nitroxide radicals, not much has appeared on spin trapping of carbon-centered radicals adjacent to the nitrogen atom (10–14). This section compares the trapping of aminoalkyl radicals using ND ($d_{12}$) and NtB.

On mixing *N*,*N*-dimethylaniline with NiPO in benzene or fluorobenzene in the presence of NtB at room temperature, a spectrum consisting of 27 lines was observed. Analysis of this spectrum showed that two equivalent β-hydrogen couplings exist, and this spectrum was assigned to *N*-methyl-*N*-phenylaminomethyl *tert*-butyl nitroxide. Even at −20°C in fluorobenzene, the same spectrum as that at room temperature was obtained. On oxidation of *N*-methyl-*N*-phenylaniline with NiPO in the presence of NtB, almost the same spectrum was observed.

When the radical generated photochemically from *N*,*N*-dimethylaniline in benzene or fluorobenzene was trapped with ND ($d_{12}$) at room temperature, an unusual spectrum was observed. The photolysis of 1,4-dimethyl-1,4-diphenyl-2-tetrazene in benzene in the presence of DN, which is described later, gave the same spectrum.

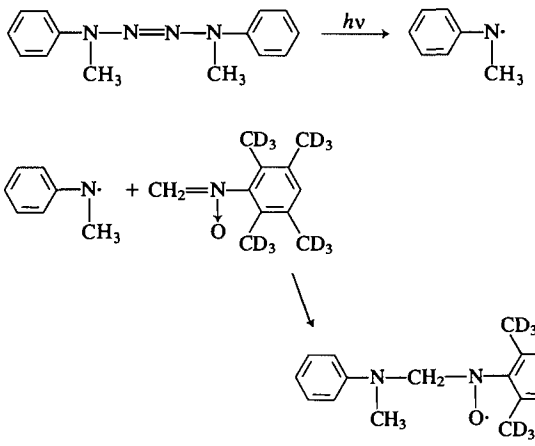

To discover the reason for this phenomenon, the spectra were followed with variation of tempera-

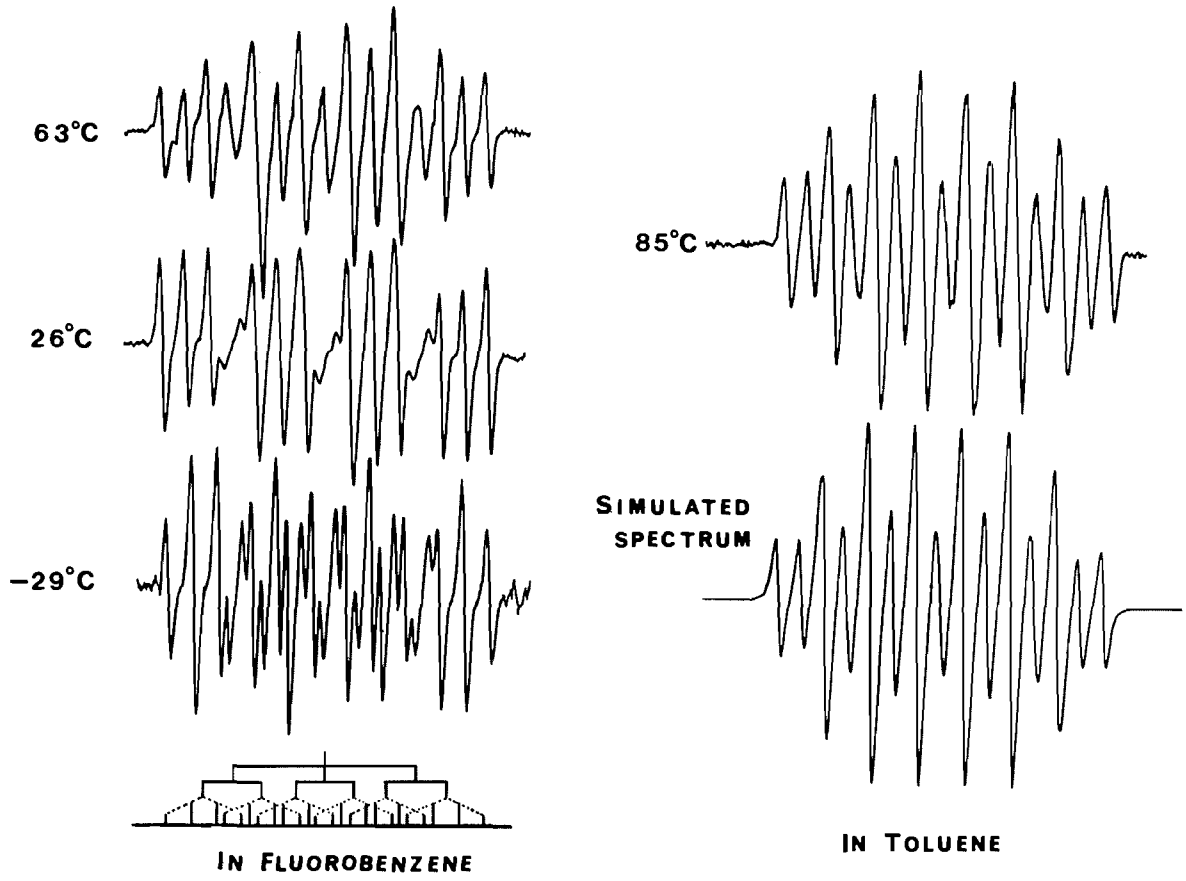


FIG. 1. Electron spin resonance of the *N*-methyl-*N*-phenylaminomethyl spin adduct of nitrosodurene ($d_{12}$) obtained by photolysis of *N*,*N*-dimethylaniline in the presence of di-*tert*-butyl peroxide at various temperatures.

ture (Fig. 1). At −29°C in fluorobenzene, the spectrum showed non-equivalent β-hydrogen splitting constants. Increase in temperature made the spectral lines broader, and at 63°C in fluorobenzene, the shoulder peaks disappeared and other new lines appeared. This behavior is a typical line width alternation (LWA) which takes place for a slow interconversion process between two conformers. The exchange rate constant at about 30°C was calculated to be $3.1 \times 10^7\ s^{-1}$.

However, the spectrum of the duryl nitroxide produced by trapping the radical generated photochemically from *N*-methyl-*N*-phenylaniline using ND ($d_{12}$) at room temperature showed a usual spectrum which is similar to that of the *tert*-butyl nitroxide. Even at −40°C in fluorobenzene, the spectrum, in which two β-hydrogen splittings are equivalent, did not change.

These spectral parameters are summarized in Table 2. Only the case of trapping the *N*-methyl-*N*-phenylaminomethyl radical with ND ($d_{12}$) showed a quite different behavior from the other cases. Other examples of the duryl adducts of the aminomethyl radicals which exhibit LWA are shown in Table 3. Although in LWA in a sterically hindered nitroxide the importance of solvent interaction is emphasized (15), this type of nitroxide seems to be subject to LWA owing to an internal factor based on comparison with the behavior of the *t*-butyl nitroxides under the same circumstances. The reason for this phenomenon arising from the use of ND is not clear, but is probably associated with the bulkiness of the duryl group.

From the esr parameters in Table 2, the conformation of *N*-methyl-*N*-phenylaminomethyl duryl nitroxide was estimated as follows. Assuming planar geometry around the nitroxide nitrogen atom, the approximation eq. [1] of the Heller–McConnell relation (16) was applied.

$$[1] \quad a_{\beta\text{-H}} = B_H \cos^2 \theta_\beta \rho_N$$

where $\rho_N$ is spin density on nitrogen, $B_H$ is a constant, and $\theta_\beta$ is the dihedral angle between the C—$H_\beta$ bond and the $p_z$ orbital containing an odd

TABLE 2. Hyperfine splitting constants of aminomethyl adducts of NtB and ND in fluorobenzene (G)

| Compound | R | Source | $a_N$ | $a_{\beta\text{-H}}$ | $a_{\beta\text{-N}}$ | $T$ |
|---|---|---|---|---|---|---|
| Bu$^t$—N(—R)—O· | —CH$_2$—N(Ph)(Ph) | RH + NiPO | 14.57 | 9.40 | 2.66 | rt[a] |
| | —CH$_2$—N(Ph)(CH$_3$) | RH + NiPO | 14.78 | 8.43 | 2.83 | rt |
| | | | 14.73 | 8.46 | 2.84 | −20°C |
| | —CH$_2$—N(Ph)(Ph) | RH + Ph$_2$CO ($h\nu$) | 13.19 | 7.89 | 3.17 | rt[a] |
| | | | 13.18 | 7.96 | 3.13 | −40°C |
| | | | 13.47 | 6.24 | 3.36 | 63°C |
| | —CH$_2$—N(Ph)(CH$_3$) | RH + DTBP ($h\nu$) | 13.31 | 8.33, 4.34 | 3.36 | 26°C |
| | | | 13.31 | 8.49, 3.52 | 3.61 | −29°C |

[a] In benzene.

TABLE 3. Hyperfine splitting constants of aminomethyl adducts of ND in fluorobenzene

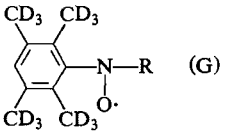

(G)

| R | Source | $a_N$ | $a_{\beta\text{-H}}$ | $a_{\beta\text{-N}}$ | $T$ |
|---|---|---|---|---|---|
| —CH$_2$—N(Ph)(C$_2$H$_5$) | RH + Ph$_2$CO ($h\nu$) | 13.28 | 8.92, 3.61 | 3.61 | rt |
| —CH$_2$—N(Ph)(CH$_2$Ph) | RH + Ph$_2$CO ($h\nu$) | 13.11 | 8.65, 3.58 | 3.58 | −35°C |
| —CH$_2$—N(—NO$_2$)(CH$_3$) | RH + DTBP ($h\nu$) | 13.05 | 7.22, 4.98 | 3.59 | rt |
| —CH$_2$—N(—N)(CH$_3$) | RH + Ph$_2$CO ($h\nu$) | 13.03 | 7.65, 3.86 | 3.86 | −40°C |
| | | 13.13 | 12.55($H_A$ + $H_B$) | 3.57 | +20°C |
| | | 13.02 | 6.35(2H) | 3.52 | +50°C |

electron. In the methyl adduct of ND, the β-hydrogen splitting constant is reported to be 12.17 G (3). Based on the free rotation of the methyl group around the N—C bond, the averaged dihedral angle can be considered to be 45°. Hence eq. [2] was obtained.

$$[2] \quad B_H = 24.34/\rho_N$$

Using the β-hydrogen splitting constants at −29°C in Table 2 and eq. [2], eqs. [3] and [4] were obtained.

$$[3] \quad 8.49 = \frac{24.34}{\rho_N} \times \cos^2\theta_\beta \times \rho_N'$$

$$[4] \quad 3.52 = \frac{24.34}{\rho_N} \times \cos^2(120 - \theta_\beta) \times \rho_N'$$

The nitrogen splitting constant of the methyl adduct is approximately equal to that of this nitroxide. Thus, $\rho_N$ approximately equals $\rho_N'$. From eqs. [3] and [4], $\theta_\beta$ = 53.8° and 52.4° were obtained, respectively; the two values agreed well with each other. Using the average value, $\theta_\beta$ = 53°, the dihedral angle of the $C_\alpha$—$N_\beta$ bond was estimated to be 7°, so that this bond seems to be almost eclipsed by the $p_z$ orbital of the nitrogen atom of the nitroxide.

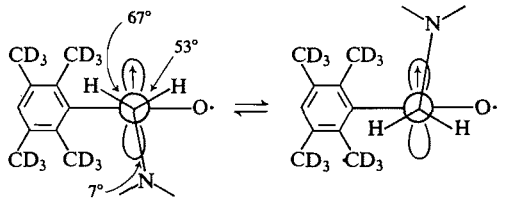

### Spin trapping by use of duryl nitrones

The typical nitrone used as a spin trap, PBN, unfortunately has the property of narrow scattering of the β-hydrogen splitting constants. 5,5-Dimethylpyrroline-*N*-oxide (DMPO) developed by Janzen (8) has the nature of wide scattering of the β-hydrogen splitting constants.

As mentioned previously, the β-hydrogen splitting constants of duryl nitroxides vary markedly with the nature of the radical trapped, and moreover, duryl nitroxides can be obtained in two ways.

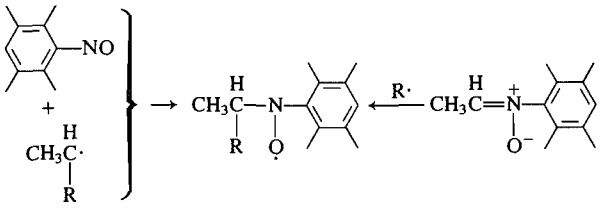

Accordingly, duryl nitrones can be expected to be a useful nitrone type spin trap other than PBN and DMPO.

Duryl nitrones were prepared from nitrosodurene by use of diazomethane or diazoethane (17); methyl *N*-duryl nitrone (MDN, mp 87.5–89°C) is more stable than *N*-duryl nitrone (DN, mp 89–91°C). DN was able to trap the hydroxymethyl or α-hydroxyethyl radicals generated photochemically by use of di-*tert*-butyl peroxide in methanol or ethanol solutions, respectively. However, in general it is not so ready to trap the carbon-centered radicals using DN or MDN. The trapping rate is probably very slow. On the other hand, duryl nitrones could readily trap heteroatom-centered radicals. The spectrum of the MDN adduct of the *n*-propylthiyl radical produced by photolysis of the corresponding disulfide in benzene is shown in Fig. 2. The thiyl adducts of MDN are considerably more stable than the thiyl adducts of DN. The spectrum of the carbazolyl adduct of MDN is shown in Fig. 3.

The results obtained in spin trapping the heteroatom-centered radicals using MDN are summarized in Table 4. In the thiyl radical adducts, the variation of the β-hydrogen splittings is not very large, but small splittings probably arising from γ-hydrogen are available for identifying a spectrum. In the amino radical adducts, the β-hydrogen splittings varied remarkably, demonstrating the characteristic feature of duryl nitroxide. Among these radicals, the assignment of ethylthiyl, carbazolyl, and *tert*-butoxy adducts was also confirmed using ND. As shown in Table 4, MDN can be used in photochemistry but is less stable to ultraviolet light than ND.

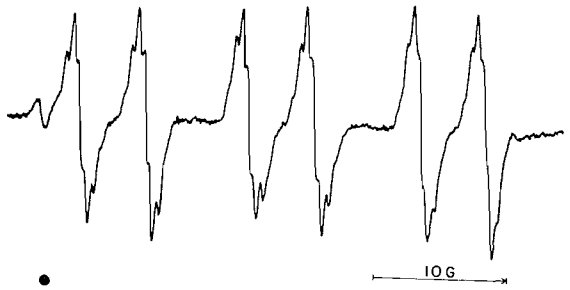


FIG. 2. Electron spin resonance spectrum of the *n*-propylthiyl spin adduct of methyl *N*-duryl ($d_{12}$) nitrone obtained by photolysis of *n*-propyl disulfide in benzene at room temperature.

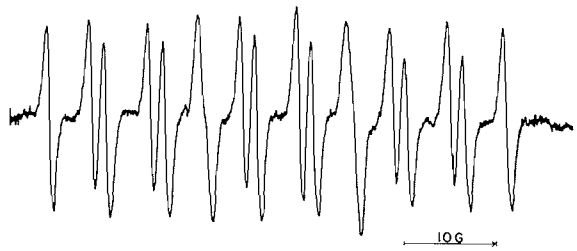


FIG. 3. Electron spin resonance spectrum of the carbazolyl spin adduct of methyl *N*-duryl ($d_{12}$) nitrone obtained by oxidation of carbazole with nickel peroxide in benzene at room temperature.

### Molecule-induced homolysis of hydroperoxides with nitrones

It is well known that a variety of reagents cause 1,3-dipolar addition to nitrones (18). However, there has been no report about the reaction of hydroperoxides and hydrogen peroxide with nitrones.

Mixing *tert*-butyl hydroperoxide with PBN in benzene–*tert*-butanol at room temperature produced an esr spectrum of a nitroxide. In order to identify this radical, the *tert*-butoxy adduct of PBN was prepared in the following two ways: by trapping the *tert*-butoxy radical generated from di-*tert*-butyl peroxyoxalate using PBN and by trapping the radical generated from benzyl *tert*-butyl ether with di-*tert*-butyl peroxyoxalate using NtB. From the results shown in Table 5 and the data summarized from the literatures in Table 6, the radical under consideration was identified as the *tert*-butoxy adduct of PBN. Table 6 shows that the nitrogen and β-hydrogen splittings of the *tert*-butylperoxy adduct are somewhat different from those of the *tert*-butoxy adduct.

The reaction of *tert*-butyl hydroperoxide with nitrones was re-examined using MDN and DN. Similarly, on mixing *tert*-butyl hydroperoxide with

TABLE 4. Hyperfine splitting constants of MDN spin adducts (G)

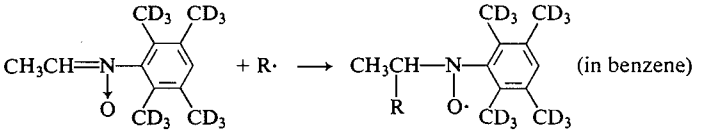


| R | Method[a] | $a_N$ | $a_{\beta\text{-H}}$ | $a$ (other) |
|---|---|---|---|---|
| PhS· | *A* | 12.61 | 5.36 | 0.45(4H) |
| $CH_3S$· | *A* | 12.67 | 4.44 | 0.90(3H), 0.45(4H) |
| $CH_3CH_2S$· | *A* | 12.78 | 4.80 | 0.57(6H) |
| $CH_3CH_2CH_2S$· | *A* | 12.79 | 4.91 | 0.56(6H) |
| 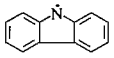 | *B* | 13.00 | 3.72 | 4.96(1N) |
| | *B* | 12.80 | 2.19 | 3.88(1N) |
| 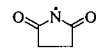 | *C* | 13.93 | 16.90 | 1.19(1N) |
| Bu'O· | *D* | 13.13 | 7.91 | |

[a] *A*: R'SSR' + $h\nu \rightarrow$ R'S·; *B*: RH + NiPO $\rightarrow$ R·; *C*: RX + $h\nu \rightarrow$ R·; *D*: Bu'OOBu' + $h\nu \rightarrow$ Bu'O·.

TABLE 5. Electron spin resonance parameters for *t*-butoxy adducts of PBN (hyperfine splittings in G)

| Nitroxide | System | *g*-Value | $a_N$ | $a_{\beta\text{-H}}$ |
|---|---|---|---|---|
| 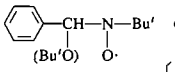 | 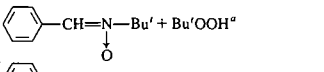 | 2.0058 | 14.6 | 2.0 |
| 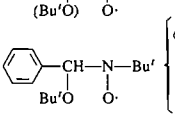 | 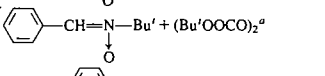 | 2.0060 | 14.61 | 1.99 |
| | 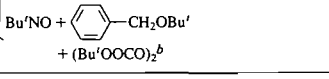 | 2.0062 | 14.64 | 1.81 |

[a] ϕH—Bu'OH.
[b] ϕH—ϕ$CH_2$OBu'.

TABLE 6. Spin trapping *t*-butylperoxy or *t*-butoxy radicals with PBN

| | Source[a] | *T* | $a_N$ | $a_{\beta\text{-H}}$ | Solvent | Reference |
|---|---|---|---|---|---|---|
| Bu'OO· | Bu'OOH + DBPO | rt | 13.40 | 1.57 | ϕH | 19 |
| | Bu'OOH + $Pb(OAc)_4$ | −80°C | 13.39 | 1.19 | $CH_2Cl_2$ | 20 |
| | $(Bu^t)_2C{=}O + O_2$ ($h\nu$) | −20°C | 13.42 | 0.95 | ϕ$CH_3$ | 21 |
| Bu'O· | DBPO | rt | 14.22 | 1.95 | ϕH | 22 |
| | DBPO | rt | 14.21 | 1.83 | ϕH | 19 |
| | DBPO | rt | 14.61 | 1.99 | ϕH—Bu'OH | This work |

[a] DBPO: di-*t*-butyl peroxyoxalate.

MDN, a nitroxide spectrum was observed. However, this spectrum was quite different from that of the *tert*-butoxy adduct prepared from di-*tert*-butyl peroxyoxalate (Fig. 4). A spectrum similar to the latter was observed in trapping the radical generated from *tert*-butyl ethyl ether in the presence of di-*tert*-butyl peroxyoxalate by use of ND.

In a similar manner, two types of the spin adduct were observed by employing DN instead of MDN. Furthermore, trapping the radical produced from *tert*-butyl methyl peroxide in the presence of di-*tert*-butyl peroxyoxalate with ND gave a spectrum which could be assigned to the *tert*-butylperoxy adduct of DN, although another signal was mixed in the spectrum.

From these spectral data, summarized in Table 7, the nitroxides observed in the reaction of *tert*-butyl hydroperoxide with MDN or DN seem to be α-*tert*-butylperoxyethyl or *tert*-butylperoxymethyl duryl nitroxides, respectively.

TABLE 7. Electron spin resonance parameters for *t*-butoxy and *t*-butylperoxy adducts (hyperfine splittings in G)

| Nitroxide | System[a] | *g*-Value | $a_N$ | $a_{\beta\text{-H}}$ |
|---|---|---|---|---|
| 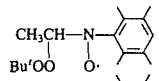 | **III** + Bu$^t$OOH | 2.0059 | 12.82 | 4.76 |
| 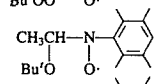 | **III** + $(Bu^tOOCO)_2$ | 2.0059 | 13.45 | 8.40 |
| | **I** + Bu$^t$OEt + $(Bu^tOOCO)_2$ | 2.0059 | 13.26 | 8.47 |
| 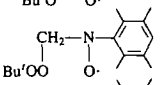 | **II** + Bu$^t$OOH | 2.0060 | 12.53 | 6.24 |
| | **I** + $CH_3OOBu^t$ + $(Bu^tOOCO)_2$ | — | 12.56 | 6.28 |
| 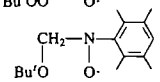 | **II** + $(Bu^tOOCO)_2$ | 2.0059 | 12.98 | 6.00 |
| | **I** + Bu$^t$OMe + $(Bu^tOOCO)_2$ | 2.0059 | 12.75 | 5.59 |

[a]I: ND; II: DN; III: MDN (solvent: ϕH—Bu$^t$OH).

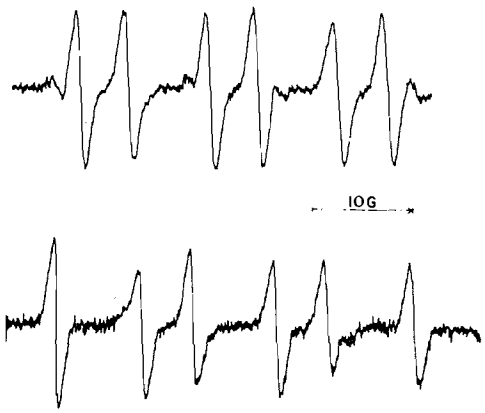


FIG. 4. Top: esr spectrum obtained from the reaction of *tert*-butyl hydroperoxide with methyl *N*-duryl nitrone in benzene/*tert*-butanol (2:1) at room temperature. Bottom: esr spectrum obtained from the reaction of di-*tert*-butyl peroxyoxalate with methyl *N*-duryl nitrone in benzene/*tert*-butanol (2:1) at room temperature.

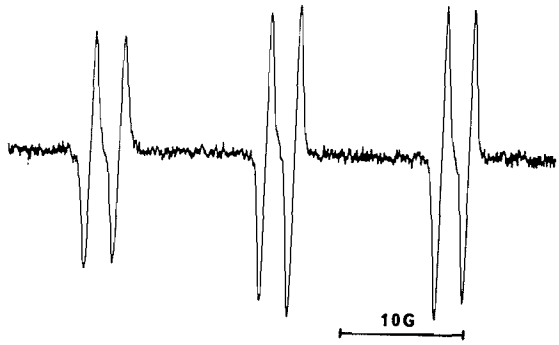


FIG. 5. Electron spin resonance spectrum obtained from the reaction of hydrogen peroxide (90% grade) with phenyl *tert*-butyl nitrone in benzene/*tert*-butanol (2:1) at room temperature.

In the experiment of the reaction of MDN with 90% hydrogen peroxide instead of *tert*-butyl hydroperoxide, a spectrum having the esr parameters shown in Table 8 was observed. Since these parameters are different from those of α-hydroxyethyl duryl nitroxide, which was obtained in trapping by use of ND (Table 8), the former appears to be α-hydroperoxyethyl duryl nitroxide. From the results of the experiments using DN instead of MDN and trapping the hydroxymethyl radical by ND (Table 8), it seems that the spectrum of hydroperoxymethyl duryl nitroxide was similarly obtained in the reaction of hydrogen peroxide with ND.

In addition, when 90% hydrogen peroxide was added into the benzene–*tert*-butanol (2:1) solution of PBN, the spectrum shown in Fig. 5 was obtained ($a_N$ = 14.13, $a_{\beta\text{-H}}$ = 2.26 G). According to the plot of the nitrogen and β-hydrogen splitting constants proposed by Janzen *et al.* (23), this nitroxide is presumed to be the hydroperoxy adduct.

Based on the results mentioned above, these phenomena can be explained by the following scheme.

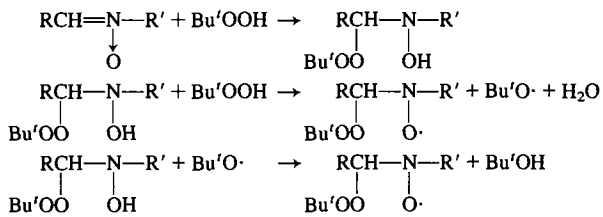


Hydroxylamines are known to react with hydroperoxides to produce radicals by molecule-induced homolysis (24–26). The reaction of *N*-*tert*-butyl-*N*-benzyl hydroxylamine with *tert*-butyl hydroperoxide produced a spectrum of the corresponding nitroxide.

### Molecule-induced homolysis of hydroperoxides with nitroso compounds and the behavior of alkoxy nitroxides

On mixing *tert*-butyl hydroperoxide with *m*-

TABLE 8. Electron spin resonance parameters for hydroxy and hydroperoxy adducts (hyperfine splittings in G)

| Nitroxide | System[f] | g-Value | $a_N$ | $a_{\beta\text{-H}}$ |
|---|---|---|---|---|
| 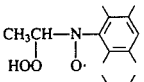 | III + $H_2O_2$[a] | 2.0059 | 13.12 | 4.67 |
| 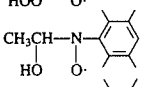 | I + EtOH + Bu$^t$OOH[b] | 2.0060 | 13.89 | 6.61 |
| | I + EtOH + (Bu$^t$OOCO)$_2$[c] | 2.0057 | 13.62 | 6.41 |
| 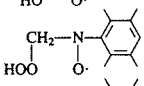 | II + $H_2O_2$[a] | 2.0059 | 12.95 | 6.59 |
| 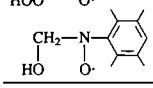 | I + $CH_3OH$ + Bu$^t$OOH[d] | 2.0060 | 13.65 | 7.65 |
| | I + $CH_3OH$ + (Bu$^t$OOCO)$_2$[e] | 2.0059 | 13.79 | 7.41 |

[a] ϕH–Bu$^t$OH.
[b] ϕH–EtOH.
[c] ϕH–Bu$^t$OH–EtOH.
[d] ϕH–MeOH.
[e] ϕH–Bu$^t$OH–MeOH.
[f] I: ND, II: DN, III: MDN.

deuterated nitrosobenzene ($d_2$), an esr spectrum was obtained, which was assigned to *tert*-butoxy phenyl nitroxide ($d_2$) based on the parameters reported by de Boer *et al.* (27). When the solution was allowed to stand for 4 h at room temperature, an additional signal appeared in the spectrum. After 24 h, only the second signal was observed, which was assigned to *tert*-butyl phenyl nitroxide ($d_2$) based on the literature by de Boer *et al.* (28). Figure 6 shows the change of spectra with time. Even in the dark, the same spectrum was obtained. The concentration of the former radical was much higher than that predicted from the spontaneous decomposition rate of *tert*-butyl hydroperoxide reported by Hiatt *et al.* (29). Thus, this reaction is considered to be one of molecule-induced homolysis.

A considerable amount of nitrobenzene was found by gas phase chromatography in this reaction. A further interesting fact is that even when *tert*-butyl peroxyoxalate was used as a peroxide, nitrobenzene was produced.

In addition, spin trapping using ND on the photolysis of dicumyl peroxide at −80°C gave the spectrum shown in Fig. 7 assigned to the cumyloxy adduct. However, at room temperature, two kinds

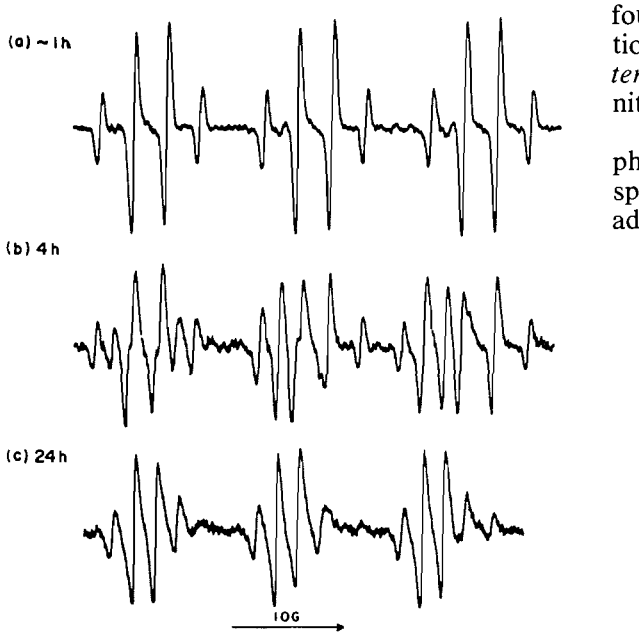


FIG. 6. Electron spin resonance spectra of the spin adducts obtained on mixing *m*-dideuterionitrosobenzene and *tert*-butyl hydroperoxide in benzene at room temperature at various times. Top spectrum: $a_N$ = 14.68 G, $a_{o,p\text{-H}}$ = 2.89 G (*tert*-butoxy adduct). Bottom spectrum: $a_N$ = 12.59 G, $a_{o,p\text{-H}}$ = 1.87 G (*tert*-butyl adduct). Middle spectrum: mixture of the top and bottom spectra.

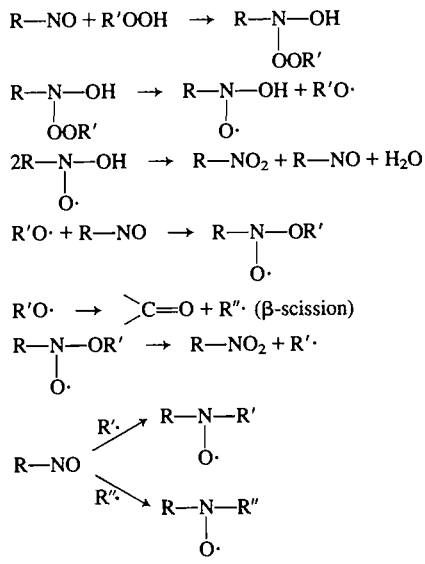

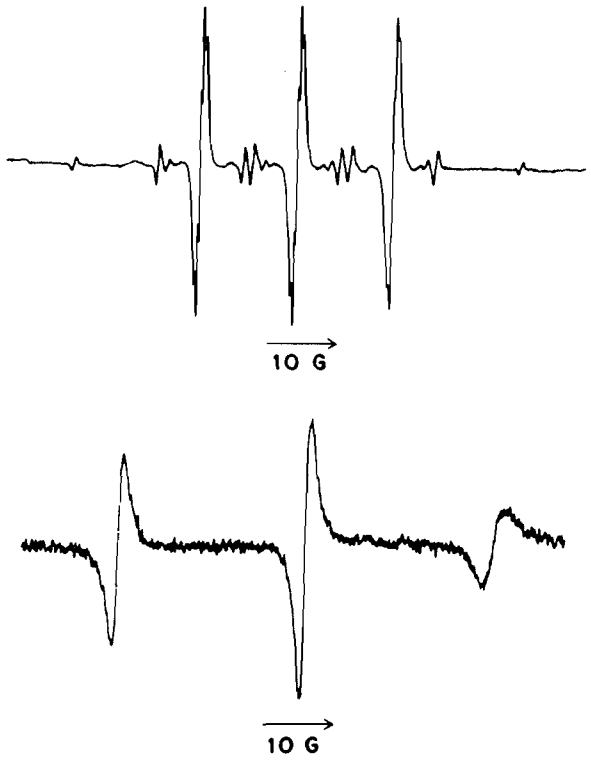


FIG. 7. Electron spin resonance spectra of the spin adducts obtained by photolysis of dicumyl peroxide in the presence of nitrosodurene ($d_{12}$). Top spectrum: in benzene at room temperature; $a_N$ = 13.69 G, $a_{\gamma\text{-H}}$ = 0.41 G (6H) (cumyl adduct); $a_N$ = 13.61 G, $a_{\beta\text{-H}}$ = 12.18 G (3H) (methyl adduct). Bottom spectrum: in dichloromethane at −80°C; $a_N$ = 26.21 G (cumyloxy adduct).

of signals were observed which were assignable to the cumyl and methyl adducts.

Based on these results, the following mechanism of molecule-induced homolysis of hydroperoxides with nitroso compounds is proposed.

In 1978, Pfab attempted to trap peroxy radicals by using *C*-nitroso compounds. However, this method did not permit discrimination between the alkylperoxy and alkoxy radicals, since ready fission of the O—O bond of the alkylperoxy adduct occurs and produces the alkoxy radicals (30).

In general, the formation and decomposition pathways of alkoxy nitroxides can be summarized as follows.

$$\mathrm{RNO + R'O\cdot} \underset{b}{\overset{a}{\rightleftharpoons}} \mathrm{RNOR'} \underset{d}{\overset{c}{\rightleftharpoons}} \mathrm{RNO_2 + R'\cdot}$$

$$\mathrm{RNOR'} \quad (\mathrm{O\cdot}) \qquad e \Updownarrow f$$

$$\mathrm{R\cdot + R'ONO}$$

The process ($d \rightarrow b$) was confirmed by Inamoto and Shimamura (31), Waters *et al.* (32), and Sutcliff *et al.* (33). The pathway ($a \rightarrow e$) was established by de Boer *et al.* (34) and Ingold *et al.* (35). The process ($f \rightarrow b$) is presumed by the papers of Kharasch *et al.* (36), Gray *et al.* (37), and Jest *et al.* (38). In addition to these pathways, the present study confirmed the existence of the process ($a \rightarrow c$). Which process predominates may depend on the stability of the R or R′ radicals.

A similar phenomenon has been reported by Kochi *et al.* (39) in regard to bond fission of phosphoranyl radicals.

## Acknowledgment

The authors are grateful to Professor E. G. Janzen for his helpful discussions.

1. R. KONAKA and S. TERABE. The VIIth ESR Symposium (Japan). Sapporo, Sept. 1968, Abstracts, p. 44.
2. S. TERABE and R. KONAKA. J. Am. Chem. Soc. **91**, 5655 (1969).
3. S. TERABE, K. KURUMA, and R. KONAKA. J. Chem. Soc. Perkin II, 1252 (1973).
4. E. G. JANZEN and B. J. BLACKBURN. J. Am. Chem. Soc. **91**, 4481 (1969).
5. Y. MAEDA and K. U. INGOLD. J. Am. Chem. Soc. **101**, 4975 (1979).
6. H. YOSHIDA and T. DOBA. Bull. Fac. Eng. Hokkaido Univ. **91**, 161 (1978); T. DOBA, S. NODA, and H. YOSHIDA. Bull. Chem. Soc. Jpn. **52**, 21 (1979).
7. E. G. JANZEN. Acc. Chem. Res. **4**, 31 (1971).
8. E. G. JANZEN and J. I.-P. LIU. J. Magn. Reson. **9**, 510 (1973).
9. E. G. JANZEN, R. V. SHETTY, and S. M. KUNANEC. Can. J. Chem. **59**, 756 (1981).
10. I. H. LEAVER and G. C. RAMSEY. Tetrahedron, **25**, 5669 (1969).
11. G. R. CHALFONT, M. J. PERKINS, and A. HORSFIELD. J. Chem. Soc. B, 401 (1970).
12. C. LAGERCRANTZ. J. Am. Chem. Soc. **95**, 220 (1973); C. LAGERCRANTZ and M. SETAKA. Acta Chem. Scand. B**28**, 619 (1974).
13. E. G. JANZEN, C. A. EVANS, and J. I.-P. LIU. J. Magn. Reson. **9**, 513 (1973).
14. H. G. AURICH and F. BAER. Chem. Ber. **101**, 1770 (1968); H. G. AURICH and K. KABS. Angew. Chem. Int. Ed. **9**, 636 (1970).
15. L. JONKMAN and J. KOMMANDEUR. Chem. Phys. Lett. **5**, 579 (1970).
16. C. HELLER and H. M. MCCONNEL. J. Chem. Phys. **32**, 1535 (1960).
17. J. E. BALDWIN, A. K. QURESHI, and B. SKLARZ. J. Chem. Soc. C, 1073 (1969).
18. J. HAMER and A. MACALUSO. Chem. Rev. **64**, 473 (1964).
19. N. OHTO, E. NIKI, and Y. KAMIYA. J. Chem. Soc. Perkin II, 1770 (1977).
20. K. V. MERRITT and R. A. JOHNSON. J. Am. Chem. Soc. **99**, 3713 (1977).
21. J. A. HOWARD and J. C. TAIT. Can. J. Chem. **56**, 176 (1978).
22. E. G. JANZEN and C. A. EVANS. J. Am. Chem. Soc. **95**, 8205 (1973).
23. E. G. JANZEN, D. E. NUTTER, JR., E. R. DAVIS, B. J. BLACKBURN, J. L. POYER, and P. B. MCCAY. Can. J. Chem. **56**, 2237 (1978).
24. J. T. WEIL and J. J. WINDLE. Nature, **217**, 842 (1968).

25. K. MARUYAMA, T. OTSUKI, and T. IWAO. J. Org. Chem. **32**, 82 (1967).
26. H. SAYO, S. OZAKI, and M. MASUI. Chem. Pharm. Bull. **20**, 1012 (1972).
27. A. MACKOR, TH. A. J. W. WAJER, TH. J. DE BOER, and J. D. W. VAN VOORST. Tetrahedron Lett. 385 (1967).
28. TH. A. J. W. WAJER, A. MACKOR, TH. J. DE BOER, and J. D. W. VAN VOORST. Tetrahedron, **23**, 4021 (1967).
29. R. R. HIATT and W. M. J. STRACHAN. J. Org. Chem. **28**, 1893 (1963).
30. J. PFAB. Tetrahedron Lett. 843 (1978).
31. N. INAMOTO and O. SHIMAMURA. J. Org. Chem. **23**, 408 (1958).
32. R. A. JACKSON, W. A. WATERS, and D. H. WATSON. Chem. Ind. 47 (1959).
33. D. J. COWLEY and L. H. SUTCLIFFE. J. Chem. Soc. B, 569 (1970).
34. A. MACKOR, TH. A. J. W. WAJER, and TH. J. DE BOER. Tetrahedron, **24**, 1623 (1968).
35. D. F. BOWMAN, J. L. BROKENSHIRE, T. GILLAN, and K. U. INGOLD. J. Am. Chem. Soc. **93**, 6551 (1971).
36. M. S. KHARASCH, T. H. MELTZER, and W. NUDENBERG. J. Org. Chem. **22**, 37 (1957).
37. P. GRAY and P. RATHBONE. Proc. Chem. Soc. 316 (1960).
38. B. JEST and L. PHILLIPS. Proc. Chem. Soc. 73 (1960).
39. J. K. KOCHI and P. J. KRUSIC. J. Am. Chem. Soc. **91**, 3944 (1969).

# Simulation of isotropic electron spin resonance spectra: a transportable basic program

UWE M. OEHLER AND EDWARD G. JANZEN

*Guelph-Waterloo Centre for Graduate Work in Chemistry, Department of Chemistry, University of Guelph, Guelph, Ont., Canada N1G 2W1*

Received September 1, 1981

UWE M. OEHLER and EDWARD G. JANZEN. Can. J. Chem. **60**, 1542 (1982).

A computer program written in BASIC is presented for the simulation of isotropic esr spectra using a microprocessor. Since BASIC is the most common microprocessor language, this program can easily be adapted to most microprocessors. Through the use of more efficient methods the capabilities of much larger FORTRAN programs, run on mainframe computers, are retained in the more restricted environment of the microprocessor. As a result, most spin trapping results can be dealt with easily. A number of sample simulations illustrate the program's features.

UWE M. OEHLER et EDWARD G. JANZEN. Can. J. Chem. **60**, 1542 (1982).

On présente un programme pour ordinateur écrit dans le langage BASIC pour la simulation des spectres de rpe isotropes à l'aide d'un micropresseur. Puisque le langage BASIC est le plus courant des langages des microprocesseurs, on peut facilement adapter ce programme à la plupart des microprocesseurs. En faisant appel à des méthodes plus efficaces, on a retenu, dans l'environnement plus restreint du microprocesseur, les possibilités qu'offrent les programmes FORTRAN plus étendus utilisés de concert avec des ordinateurs centraux. Par conséquent, la plupart des expériences de captage de spin peuvent être traités facilement. Un certain nombre de simulations d'échantillons illustre les caractéristiques du programme.

[Traduit par le journal]

## Introduction

Electron spin resonance spectra can be very complicated and often it is only through spectral simulation that an analysis can be verified. Comparison of calculated and experimental spectra usually leads to better estimates of the parameters involved.

Simulations have normally been implemented on large, centralized, mainframe computers which offer high speed operation and large memory capacities. These computers can, however, be unavailable or inconvenient at times. Through the use of more efficient programs inexpensive microprocessors can perform these simulations as well, albeit more slowly. A recent review (1) has surveyed the use of computers in esr over the last 10 years. Of the references offering simulation programs to the reader, most deal with simulation of anisotropic spectra. None of the references offer a general, microprocessor compatible simulation program for isotropic esr spectra (2).[1]

When surrounded by abundant memory and fast calculation speeds more emphasis is commonly placed on programming ease than on program efficiency. The resulting code is more straightforward but usually longer and less space efficient. Not surprisingly, these programs seldom translate well directly into the relatively restricted memory of a microprocessor. More efficient algorithms can produce programs which are better suited to these constraints.

A further consideration when using microprocessors is that BASIC is the "universal" language and that to maintain transportability it must be used. Unfortunately, "interpreter" as opposed to "compiled" BASIC is most common and is slow in execution. There is, therefore, an urge to use machine language programs which execute much more rapidly. This restricts programs to computers having a common machine language and similar memory layouts, reducing their applicability. Our own purpose has been to provide a simulation program which can easily be used by anyone with a microprocessor and this has dictated the use of BASIC. This program should prove useful to any spin trappers who want to implement a simulation program on a microprocessor based system. We are currently using a 2 MHz, 6502 based Ohio Scientific Challenger 8P computer with 48K RAM (random access memory) and a Hewlett Packard 7202A graphics plotter. The computer is equipped with Microsoft BASIC.

## Method

There are many different ways in which an isotropic esr spectrum can be simulated. We have used a modified Stone–Maki (3) program successfully on the main university computer. When a microprocessor is used and the Stone–Maki program is translated into BASIC the result is too

[1]In ref. 2 the authors report an esr data aquisition system using an APPLE II PLUS computer. A BASIC simulation program is included but will work only on the specified computer since several features peculiar to the internal architecture of the APPLE were used.

0008-4042/82/121542-07$01.00/0

©1982 National Research Council of Canada/Conseil national de recherches du Canada

Can. J. Chem. Downloaded from www.nrcresearchpress.com by 210.87.254.105 on 09/06/12
For personal use only.

Can. J. Chem. Downloaded from www.nrcresearchpress.com by 210.87.254.105 on 09/06/12
For personal use only.

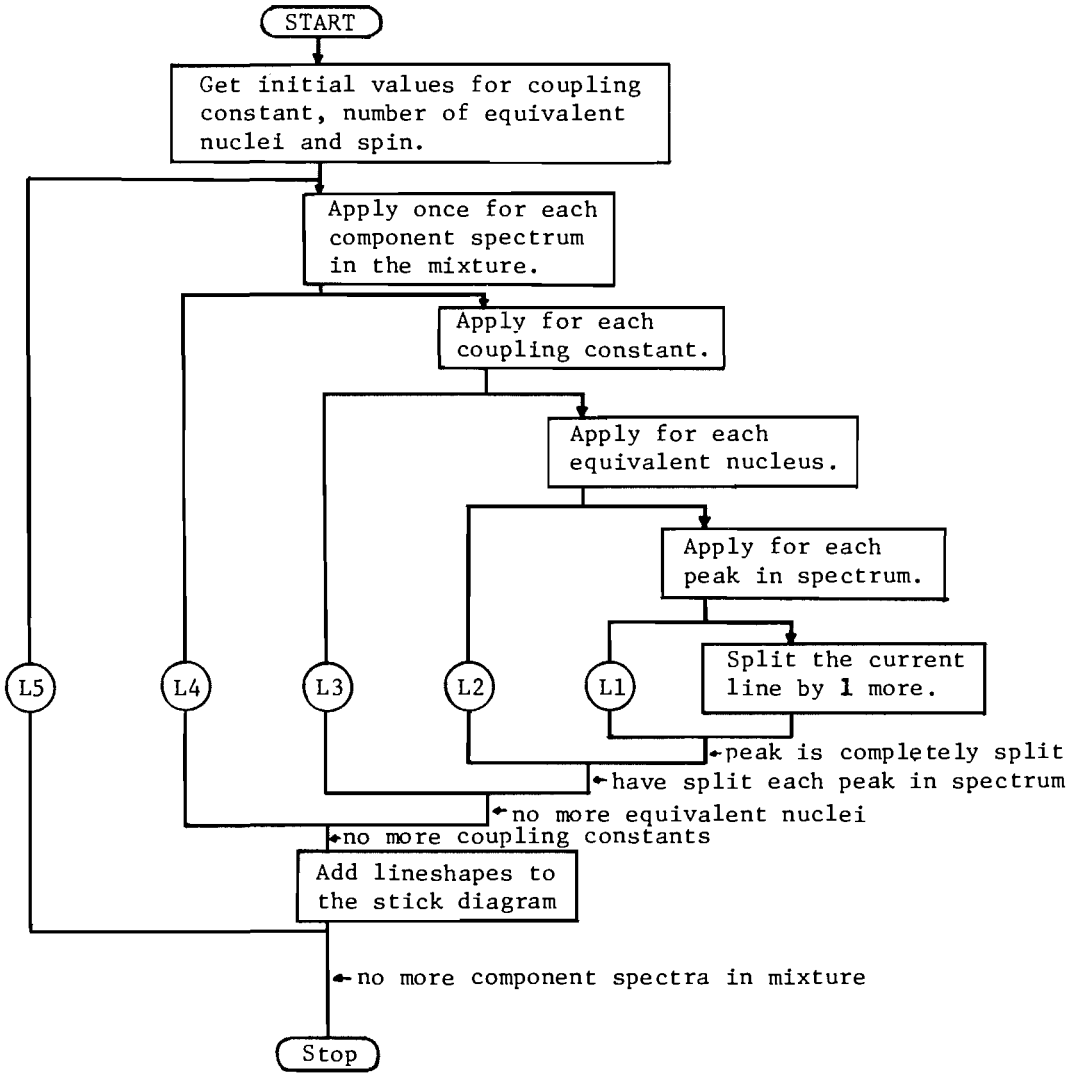


FIG. 1. A simplified flow chart of the program logic.

wasteful of memory space. Very promising programs have been based on fast fourier transforms (FFT) (4, 5) but to use these on a microprocessor requires that the transform routine be written in machine language. This is precluded by our desire for portability. The program presented here represents a compromise which retains the capabilities of larger programs while using less space and retains portability through the use of BASIC.

The spectrum is simulated through the use of two arrays. One is used to generate a stick diagram which represents the location and intensity of each peak. A single lineshape is then calculated and, using the stick diagram as a map, is copied into the second array to build the final spectrum. By clearing the stick diagram and building another in its place it is possible to overlay several spectra into the second array allowing mixtures to be simulated.

The generation of the stick diagram is handled in a highly general manner and as a result any spin or number of equivalent nuclei can be simulated. The algorithm used is highly repetitive and consists of five nested loops as seen in Fig. 1.

The innermost loop, L1, is used to generate the splitting of one peak due to the presence of a single nucleus of spin $S$. The loop is executed $2S$ times and during each repetition, it places one new stick to the right of the parent stick, maintaining spacings of one coupling constant between all the added lines and the parent. The next loop, L2, searches

Can. J. Chem. Downloaded from www.nrcresearchpress.com by 210.87.254.105 on 09/06/12
For personal use only.

```
-----All statements preceded by ----- can be removed.
-----They are not needed for operation.
  20 DIM SP(3000),MK(3000),LN(100),NU(20),CC(20),SN(20)
  25 MT=1
  30 PRINT"ESR SIMULATION PROGRAM"
  40 PRINT
  50 PRINT"BY  UWE OEHLER"
  60 PRINT"GUELPH-WATERLOO CENTRE FOR GRADUATE WORK"
  70 PRINT"UNIVERSITY OF GUELPH, GUELPH, ONTARIO"
  80 PRINT
-----Enter information required for the simulation.
  90 PRINT"NUMBER OF SPECTRA,  X INCREMENT,  PHASE"
 100 INPUT TS,XC,PH
 110 PRINT
-----Start L5.  Repeat for each component in the mixture.
 150 FOR I1=1 TO TS
 160 IF I1=1 GOTO 200
 170 FOR J=1 TO 3000
 180 MK(J)=0
 190 NEXT J
 200 PRINT"NUMBER OF COUPLING CONSTANTS"
 210 INPUT NC
 220 PRINT
 230 PRINT"LINE WIDTH,  MAXIMUM Y,  DELTA G,  FRACTION LORENTZIAN"
 240 PRINT"FRACTION LORENTZIAN IS COMMONLY 0.3 - 0.5"
 250 INPUT LW,YM,DG,LR
 260 PRINT
-----Convert LR from height contribution to area contribution.
-----Now LR=0.5 means 50 % of the area is due to Lorentzian shape.
 270 LR=.275664*LR/(.275664*LR+.967883*(1-LR))
 280 DG=DG/XC
 290 LW=LW/XC
 300 PRINT"NUMBER OF NUCLEI,  COUPLING CONSTANT,  SPIN( 0.5, 1.0, 1.5 ETC)"
 310 FOR J=1 TO NC
 320 PRINT J;
 330 INPUT NU(J),CC(J),SN(J)
 340 CC(J)=CC(J)/XC
 360 NEXT J
-----Calculate STICK diagram.
 400 N=1
 405 MK(1)=1
-----Start L4.  Repeat once for each DIFFERENT coupling constant.
 410 FOR I2=1 TO NC
-----Start L3.  Repeat once for each equivalent nucleus.
 420 FOR I3=1 TO NU(I2)
-----Start L2.  Repeat until all peaks in spectrum have been located.
 440 I4=N
 450 IF MK(I4)=0 THEN I4=I4-1:GOTO 450
-----Start L1.  Repeat 2*S times where S=spin of the nucleus.
 460 FOR I5=1 TO 2*SN(I2)
 470 T1=I4+INT(I5*CC(I2))
 480 MK(T1)=MK(T1)+MK(I4)
-----Add up number of unit lineshapes used in simulation.
-----This times the area of the lineshape is the total area.
 485 MT=MT+1
 490 IF MA<MK(T1) THEN MA=MK(T1)
-----End L1.  Done splitting one peak for one nucleus.
 500 NEXT I5
 510 IF T1>N THEN N=T1
 515 I4=I4-1
-----End L2.  Done splitting each peak in the stick diagram.
 520 IF I4>1 GOTO 450
-----End L3.  No more equivalent nuclei.
 530 NEXT I3
-----End L4.  No more different coupling constants.
```

Electron spin resonance simulation program listing

```
 540 NEXT I2
-----Center stick diagram w.r.t. first spectrum.  Include G shift.
 541 IF I1=1 THEN FI=N+2*INT(8*LW): GOTO 550
 542 T6=INT((FI-N-2*INT(8*LW))/2+DG)
 543 IF T6=0 GOTO 550
 544 FOR J=N TO 1 STEP -1
 545 MK(J+T6)=MK(J)
 546 MK(J)=0
 547 NEXT J
 548 N=N+T6
 550 IF TL<N+INT(16*LW) THEN TL=N+INT(16*LW)
 560 SR=-INT(8*LW)
 570 ST=SR+99
 580 IF ST>0 THEN ST=0
 590 T4=1
-----Calculate 100 points of LINESHAPE from SR(start) to ST(stop).
 600 FOR I6=SR TO ST
 610 T1=-PH*YM/MA*(1-LR)
 620 T2=LR*16*YM/MA*-PH
 630 T3=I6*2/LW
 640 LN(T4)=T3*T1*EXP(-.5*(T3^2-1))
 650 LN(T4)=LN(T4)+T3*T2/((3+T3^2)^2)
 680 T4=T4+1
 690 NEXT I6
-----Locate each stick in stick diagram.
 700 FOR I7=1 TO N
 710 IF MK(I7)=0 GOTO 770
 720 T4=1
-----Copy LINESHAPE*INTENSITY into SP() at location of stick.
 730 FOR I8=SR+INT(8*LW) TO ST+INT(8*LW)
 740 SP(I7+I8)=SP(I7+I8)+LN(T4)*MK(I7)
 750 SP(I7+2*INT(8*LW)-I8)=SP(I7+2*INT(8*LW)-I8)+LN(T4)*-MK(I7)
 755 T4=T4+1
 760 NEXT I8
 770 NEXT I7
-----If LINESHAPE calculation is incomplete go back and
-----calculate up to 100 more points.
 780 IF ST<>0 THEN SR=SR+100:GOTO 570
-----Calculate AREA from line width, height, % Lorentzian,
-----number of unit lineshapes and relative height of largest peak.
 783 AR(I1)=LR*2*3.14159/(3^.5)*(YM*(LW^2))
 784 AR(I1)=AR(I1)+(1-LR)*(2*3.14159*EXP(1))^.5*(.5*LW)^2*YM
 785 AR(I1)=AR(I1)*MT/MA
 787 MT=1:MA=0
-----End L5.  No more component spectra in mixture.
 790 NEXT I1
-----Find minimum and maximum values in SP() for scaling.
 800 FOR J=1 TO TL
 810 IF MN>SP(J) THEN MN=SP(J):GOTO 830
 820 IF MX<SP(J) THEN MX=SP(J)
 830 NEXT J
-----Sum total area of all components in mixture.
 880 FOR J=1 TO TS
 890 TA=TA+AR(J)
 900 NEXT J
 910 PRINT:PRINT:PRINT
 920 PRINT"AREAS OF COMPONENT SPECTRA"
 930 PRINT
-----Print component spectra areas as percentages of the total area.
 940 FOR J=1 TO TS
 950 PRINT"AREA OF COMPONENT ";J;" IS ";AR(J)/TA*100
 960 NEXT J
-----At this point the spectrum can be plotted.  The points are
-----contained in the array SP().  The variable TL contains the number
-----of points in SP() to be plotted. MX has the value of the largest
-----number in SP() and MN has the value of the smallest.
```

Electron spin resonance simulation program listing (*Concluded*)

Can. J. Chem. Downloaded from www.nrcresearchpress.com by 210.87.254.105 on 09/06/12
For personal use only.

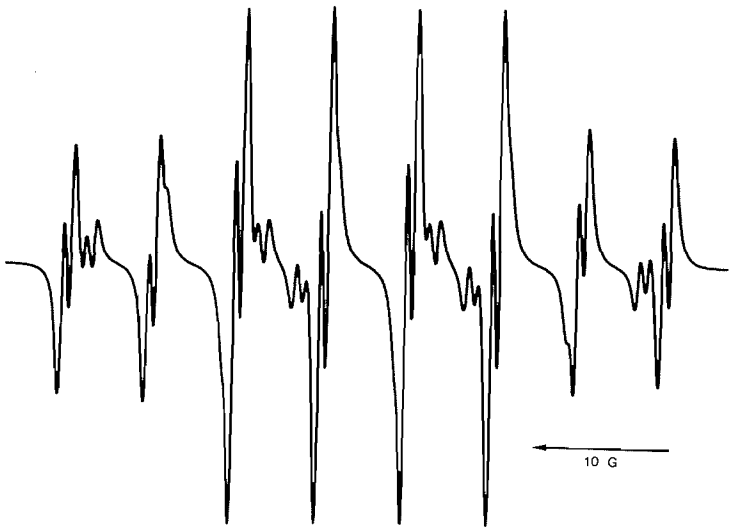


FIG. 2. Simulation of the spectrum due to the chlorine adduct to PBN. $A_N = 12.33$ G, $A_H = 0.70$ G, $A_{^{35}Cl} = 6.15$ G, $A_{^{37}Cl} = 5.04$ G, linewidth = 0.50 G, 3.5 min required to calculate for an $x$ increment of 0.05 G.

the spectrum from right to left and applies L1 to each peak that it locates thereby introducing the splitting, due to one nucleus, into the entire spectrum. Loop 3, L3, applies both L1 and L2 once for each equivalent nucleus and loop 4, L4, applies all of the inner loops once for each different coupling constant generating the final stick diagram. The outermost loop, L5, is used in the case of mixtures and repeats the entire process for each component spectrum. Before this is done, however, the stick diagram must serve as a map to locate the individual first derivative lineshapes in the spectrum.

The calculated lineshape contains contributions from both Lorentzian and Gaussian lineshapes. The ratio used can be varied for the best fit with the experimental lineshape. Since the lineshape is symmetrical about a point of inversion only half is actually calculated. When the lineshape is copied into the final spectrum the missing portion is supplied by reflecting and inverting the calculated half.

Further, since the number of points required to represent one half the lineshape will vary widely with both the line width and the $x$ axis increment it was decided to calculate the lineshape in 100 point portions. This means that the memory required to hold the lineshape at any given time will never exceed the equivalent of 100 points although in its entirety the lineshape might actually require much more. By doing this the amount of space available for the final spectrum remains constant irrespective of the lineshape.

## Results

To illustrate the operation of the program several sample simulations are shown. The calculation times do not include plotting since this is highly dependent on the plotter used.

It is important to realize the potential weaknesses of the method of simulation presented in this paper. When these are kept in mind, few problems occur. Problems can arise from the fact that we are approximating a continuous function, the esr spectrum, as a set of points. The result is that peaks can only be placed at specific locations in the spectrum and these may not correspond perfectly to their actual locations. The error in the peak location can be as large as plus or minus one half the $x$ axis step size. To solve this we must choose an $x$ increment which results in an error smaller than that in the actual measurement from the experimental spectrum. When this is done, however, the number of points calculated increases. For a spectral width of 30 G the $x$ increment cannot be below 0.01 G and still yield less than 3000 points. Further, the time required to calculate 3000 points becomes excessive for routine work. Fortunately a compromise can be struck for many spectra by using an $x$ increment of about 0.05 G and calculating about 1000–1500 points. This is because the pen width itself is often greater than 0.05 G on a 100 G scan and also because typical linewidths of about 0.5 G mask such small positional errors. It is in cases of extremely narrow lines combined with small coupling constants that care must be taken.

Can. J. Chem. Downloaded from www.nrcresearchpress.com by 210.87.254.105 on 09/06/12
For personal use only.

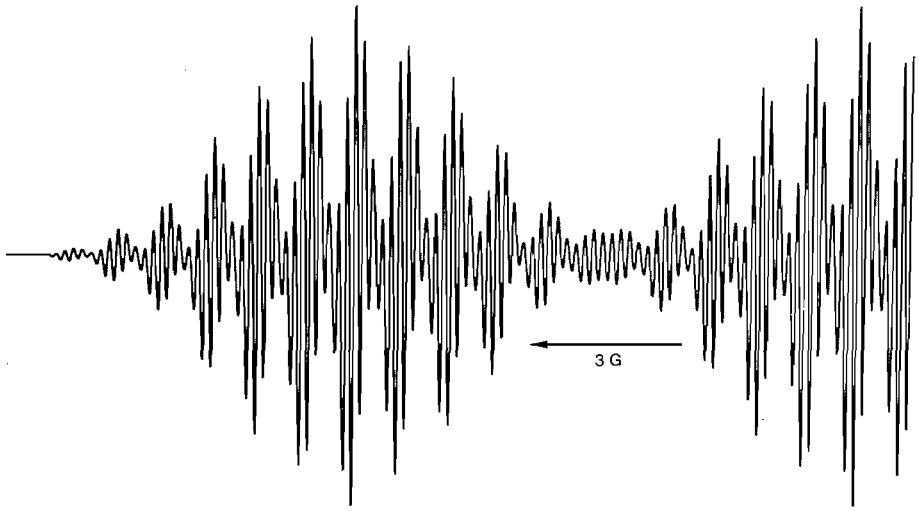


FIG. 3. Simulation of the spectrum due to di-*p*-anisylnitroxide. $A_N = 10\,G, A_{H(ortho)} = 1.92\,G, A_{H(meta)} = 0.90\,G, A_{H(methoxy)} = 0.18\,G$, linewidth = 0.10 G, 27 min required to calculate for an $x$ increment of 0.012 G.

Figure 2 shows a simulation of the spectrum due to the chlorine adduct of PBN (phenyl-*N*-*tert*-butylnitrone) (6). In this case the spectrum is actually a mixture since there are two isotopes of chlorine. The calculation time is the sum of the times required for the individual components. An important point to note is that the same error which can occur in peak placement can occur as well in the location of the center of the spectrum. The result of this is that a small but unintentional $g$ shift can be introduced into a mixture. In the case of the chlorine adduct each isotope of chlorine has a different coupling constant. As a result, the widths of the component spectra are different and the numbers of points required to represent them differ. The components of this simulation contain 877 and 810 points respectively between the two outermost sticks of their stick diagrams. Since one contains an odd number of points and the other an even number their respective centers must be offset by one half the $x$ increment. In this case the offset is only 0.025 G. While the offset is small it must be considered in critical cases. In the simulation shown the shift is not visible.

The simulation in Fig. 3 is that for the spectrum of di-*p*-anisylnitroxide (7). This spectrum is more challenging (525 peaks, 27 min calculation time). However, the 3000 point resolution of this program is sufficient to introduce negligible error. The coupling constants are measured to two decimal places implying a minimum error of +/−0.005 G. by using an $x$ increment of 0.012 G we introduce a maximum error in peak position of 0.006 G which is similar to the experimental accuracy.

In the course of our testing we also simulated the spectrum for the *N*,*N*,*N*′,*N*′-tetramethylbenzenediamine radical cation (Wurster's blue) (8). This spectrum is unusual in that it has a width of about 117 G as compared to 30–40 G for most common spectra in spin trapping. As a result the $x$ increment cannot be much smaller than 0.042 G. This introduces an error which is about 4 times the experimental error of 0.005 G. This spectrum represents a practical limit beyond which another program, capable of finer resolution, would be needed to further refine the coupling constants. These sorts of situations typically arise when sharp lines with widths approaching the $x$ increment in size are combined with small line separations also nearing this increment size.

As shown, this program can perform routine simulations in about 2–5 min when 1000–1500 points are calculated. The small positional errors in peak and center locations introduced by this method have also been shown to be minimal, generally being less than the experimental error. Only in extreme cases is the 3000 point resolution insufficient for the job. Even very complicated spectra can be simulated if attention is payed to the $x$ increment size and patience is practiced.

1. H. L. VANCAMP and A. H. HEISS. Magn. Reson. Rev. **7**, 1 (1981).
2. R. A. HOWIE, C. J. HUNTER, C. REGAN, and D. B. SMITH. Chemistry and Industry. 7, Nov. (1981).

Can. J. Chem. Downloaded from www.nrcresearchpress.com by 210.87.254.105 on 09/06/12
For personal use only.

3. E. W. STONE and A. H. MAKI. J. Chem. Phys. **38**, 1999 (1963).
4. J. C. EVANS, P. H. MORGAN, and R. H. RENAUD. Anal. Chim. Acta, **103**, 175 (1978).
5. S. BRUMBY. J. Magn. Reson. **40**, 397 (1980).
6. E. G. JANZEN, B. R. KNAUER, L. T. WILLIAMS, and W. B. HARRISON. J. Phys. Chem. **74**, 3025 (1970).
7. A. L. BUCHACHENKO. *In* Stable radicals. Consultants Bureau Ent. Inc. New York, NY. 1965.
8. J. R. BOLTON, A. CARRINGTON, and J. DOS SANTOS-VEIGA. Mol. Phys. **5**, 615 (1962).

## Appendix

This program is written in Microsoft BASIC and requires about 33 K of free RAM to operate. The memory requirements can be reduced by lowering the maximum number of points that can be calculated. This is done by changing the numbers 3000 in lines 20 and 170 to the new maximum.

Since not all versions of BASIC are exactly identical, those features which might cause some confusion are explained below.

(*1*) all variables are automatically assigned the value of zero when the program is executed;

(*2*) variable names may consist of one or two letters or a letter followed by a single digit;

(*3*) the symbol ^ means "raised to the power";

(*4*) the symbol : is the end of a line;

(*5*) the symbol $\langle\ \rangle$ means "not equal to";

(*6*) in IF THEN statements, all instructions occurring on the same line after the THEN are executed only if the condition is true.

The input required by the program follows.

(*1*) *number of spectra*: this is the number of components in a mixture;

(*2*) x *increment*: the step size in G, along the $x$ axis, between calculated points;

(*3*) *phase*: if 1, the first derivative lineshape goes positive and then negative. If $-1$, the reverse occurs.

The following information must be supplied for each component spectrum in a mixture:

(*4*) *number of coupling constants*: the number of different coupling constants required to simulate the $n$th component;

(*5*) *line width*: the $x$ axis distance between the positive and negative peaks of the first derivative lineshape;

(*6*) *maximum* Y: relative height of the largest stick in the $n$th component's spectrum as compared to the largest stick in that of component one;

(*7*) *delta* G: the shift, in G, between the center of the $n$th component's spectrum and the first components spectrum. The delta $G$ for the first radical must be 0;

(*8*) *fraction lorentzian*: the fractional contribution to the area of the lineshape by a lorentzian lineshape. The remainder is gaussian.

The following information must be supplied for each different coupling constant:

(*9*) *number of nuclei*: the number of nuclei having the same coupling constant and value of spin;

(*10*) *coupling constant*: the coupling constant in G;

(*11*) *spin*: the spin of the nuclei. May be any integral multiple of 0.5 other than 0.

One important point to note is that when a mixture is being simulated the component spectrum which extends the furthest downfield (to the left) must be entered as the first component. Each spectrum extends eight linewidths past the location of the last peak.

Can. J. Chem. Downloaded from www.nrcresearchpress.com by 210.87.254.105 on 09/06/12
For personal use only.

# Lyoluminescence and spin trapping

KAMIL V. ETTINGER, ALEXANDER R. FORRESTER, AND CHARLES H. HUNTER

*Department of Biomedical Physics and Bioengineering, and Department of Chemistry, University of Aberdeen, Aberdeen, Scotland, U.K.*

Received September 12, 1981

KAMIL V. ETTINGER, ALEXANDER R. FORRESTER, and CHARLES H. HUNTER. Can. J. Chem. **60**, 1549 (1982).

The chemical origin of lyoluminescence has been probed using spin trapping techniques. Radicals derived from amino acids and saccharides by γ-irradiation in the solid state have been identified after trapping with aliphatic and aromatic nitroso compounds. Most of the radicals trapped were secondary alkyl radicals. Reaction of peroxyl radicals derived therefrom are thought to produce the emitting species (excited carbonyl compound and/or singlet oxygen). The effect which thermal annealing of the solids after γ-irradiation has on (*a*) the concentration of radicals in the solid, (*b*) the concentration of trapped radicals, and (*c*) the light yield has been investigated. One new water-soluble spin trap has been prepared.

KAMIL V. ETTINGER, ALEXANDER R. FORRESTER et CHARLES H. HUNTER. Can. J. Chem. **60**, 1549 (1982).

On a prouvé l'origine chimique de la lyoluminescence en utilisant les techniques de captage de spin. On a identifié les radicaux provenant des acides aminés et des saccharides en les irradiant aux rayons γ dans l'état solide après les avoir captés avec des composés nitroso aliphatiques et aromatiques. La plupart des radicaux piégés sont des radicaux alkyles secondaires. On pense que la réaction des radicaux peroxydes qui en découlent produit les espèces émétrices (composé carbonylé excité et/ou oxygène singulet). On a étudié l'effet d'annellation thermique des solides après l'irradiation aux rayons γ sur: (*a*) la concentration des radicaux dans le solide, (*b*) la concentration des radicaux piégés et (*c*) le faible rendement. On a préparé un nouveau capteur de spin soluble dans l'eau.

[Traduit par le journal]

Can. J. Chem. Downloaded from www.nrcresearchpress.com by 210.87.254.42 on 09/06/12
For personal use only.

Lyoluminescence is the term used to describe the phenomenon by which light is emitted on dissolution of a previously γ-irradiated solid. Although discovered (1) at the end of the nineteenth century it was not until the pioneering work of Ahnström and Ehrenstein (2) and Westermark and Grapengiesser (3) at about 1960 that interest in the subject was awakened. For several organic compounds, the "light yield" is proportional to dose over a wide range, hence lyoluminescence provides the basis of a dosimetric method (4, 5) suitable for measuring therapeutic doses and, because it is so sensitive, accidental doses of irradiation. The light yield is obtained by integrating the area under the glow curve, a typical example of which is shown in Fig. 1. Lyoluminescence has been observed for virtually all organic compounds but by far the most useful at this stage appear to be amino acids and sugars (Figs. 2 and 3) (4, 5). These are also said to have "tissue equivalence" and hence work on such substrates has relevance to radiation damage in biological systems.

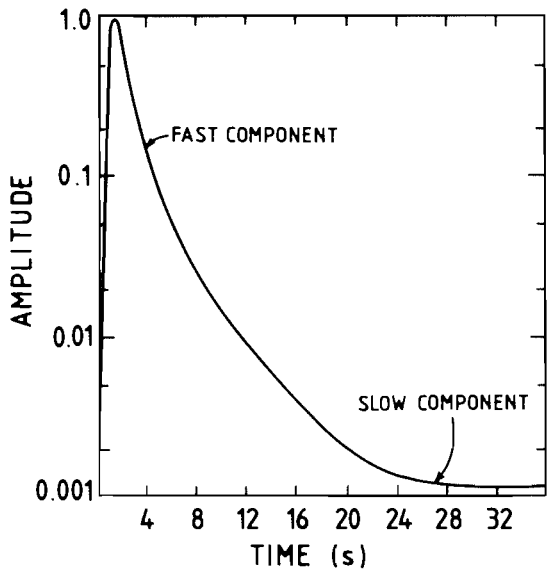


FIG. 1. Glow curve for a saccharide dissolved in water.

The ideal lyoluminescent material (phosphor) would (*a*) give a high light yield; (*b*) have a linear dose – light yield relationship over a wide dose range; (*c*) give reproducible light yields after storage under a variety of conditions (humidity, temperature, aerobic and anaerobic atmospheres). Design of such a phosphor clearly requires an understanding of the fundamental chemical reactions leading to the emission process. There is very strong circumstantial evidence from a variety of sources (2, 4–6) that free radicals are implicated. Of the several reaction sequences which have been postulated to account for the emission, by far the most attractive in our view is that described by the Russell–Vassilev scheme, Scheme 1 (7). In this scheme, primary and/or secondary alkyl radicals generated during γ-irradiation react with oxygen to give the corresponding peroxyl radicals which

0008-4042/82/121549-11$01.00/0

©1982 National Research Council of Canada/Conseil national de recherches du Canada

Can. J. Chem. Downloaded from www.nrcresearchpress.com by 210.87.254.42 on 09/06/12
For personal use only.

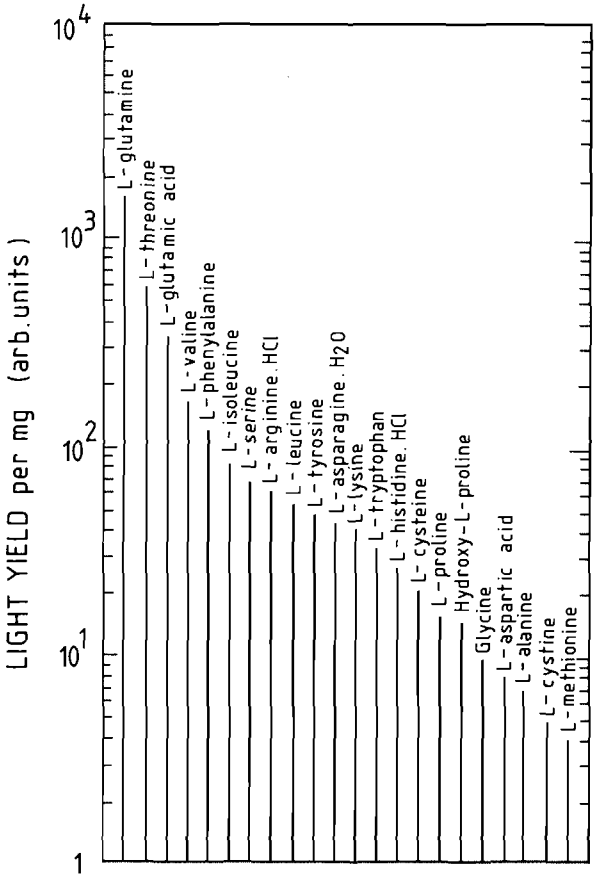


FIG. 2. Relative light yields from amino acids.

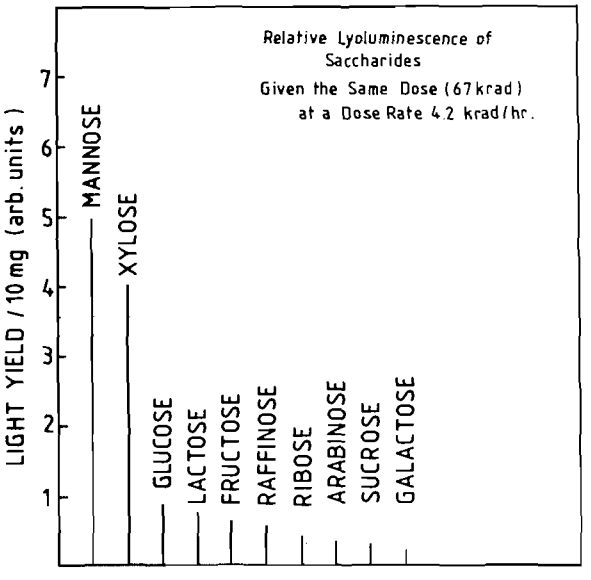


FIG. 3. Relative light yields from saccharides.

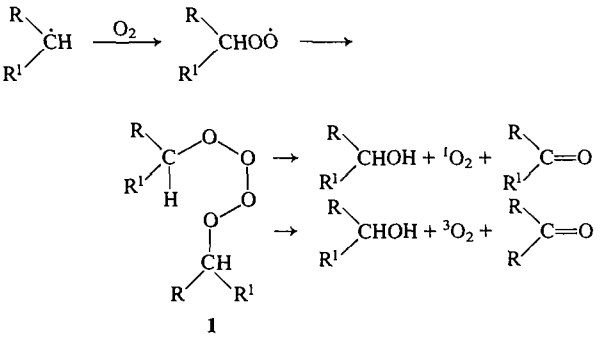

1

SCHEME 1. The Russell–Vassilev mechanism

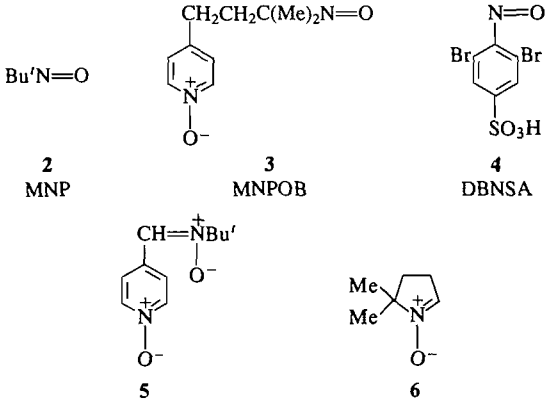


2 MNP 3 MNPOB 4 DBNSA




5 6

disproportionate via a tetroxide, **1** (7). The Wigner conservation rule requires that either (*a*) the oxygen is generated in the singlet state with ground state singlet carbonyl or (*b*) the carbonyl is generated in the triplet state with ground state triplet oxygen. The overall reaction is highly exothermic (115–120 K cal $mol^{-1}$) and, according to Kellog (8), the exothermicity is concentrated in the carbonyl function, de-excitation of the carbonyl compound being the origin of the observed chemiluminescence. Excited carbonyls emit (9) in the range 397–510 nm and the spectra observed from amino acids usually show a maximum in this region. For example, glutamine and threonine emit at 460 ± 10 nm and glutamic acid at about 480 nm with a low intensity continuum towards longer wavelengths (Fig. 4). Spectra of saccharides (Fig. 5), unlike those of aminoacids, vary with pH. For many at pH 6, there is a maximum between 600–700 nm tailing off to ca. 400 nm (9). In alkaline solution, pH 11, there is a hypsochromic shift to about 450 nm. However, it must be stressed that there is a much greater variety of shape in the spectra of saccharides.

If singlet oxygen is formed then emission at 1270 nm corresponding to $^1\Delta_g \rightarrow {}^3\Sigma_g^-$ and/or 760 nm corresponding to $^1\Sigma_g^+ \rightarrow {}^3\Sigma_g^-$ should be detectable.

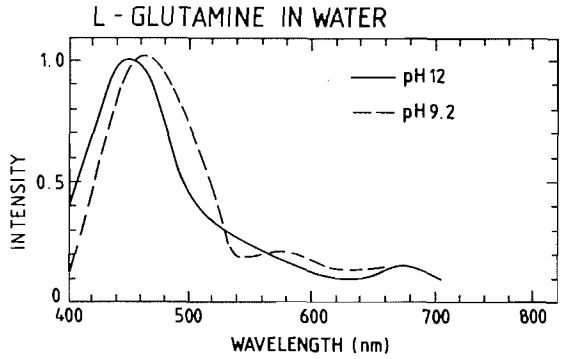


FIG. 4. LL spectra of L-glutamine.

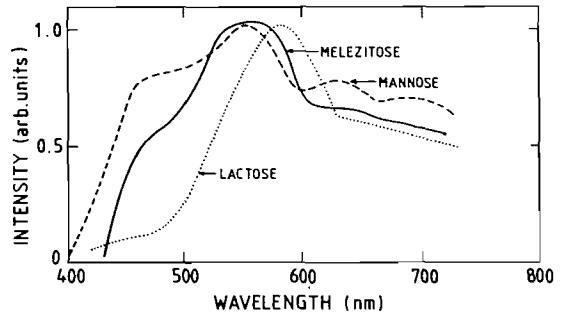


FIG. 5. LL spectra of saccharides.

Emission at 1270 nm has been observed after dissolution of heavily irradiated glutamine and some saccharides (melezitose) (5). Collisional pairs of singlet oxygen molecules could give rise to emission at 380, 480, 520, 635, and 703 nm (10) but with the lifetime of singlet oxygen in water being so short (2 μs for $^1\Delta_g$ and 10 ps for $^1\Sigma_g^+$) these would have to form in gas bubbles (in gas phase $^1\Delta_g$ has a lifetime of 64 min and $^1\Sigma_g^+$ 10 s). Significantly, the singlet oxygen quencher β-carotene reduced the LL emission from mannose by about 20% (11). Further replacement of water by deuterium oxide (in which the lifetime of singlet oxygen is increased about ten-fold) gave only a 13% increase in the LL yield of mannose and no change for glutamine at 635 nm but a significant increase at 1270 nm (5).

We conclude that the LL emissions observed from amino acids and saccharides in alkaline solution are more easily understood if a triplet carbonyl is the main emitter but with saccharides in neutral solution collisional pairs of singlet oxygen are also likely to play a part. Better understanding of the LL process requires more precise knowledge of the concentration, structure, and reactivity of the radicals present in the solid and in the solution at the moment of dissolution. With this aim we undertook a spin-trapping study of γ-irradiated amino acids and saccharides.

## Spin trapping[1]

For our purposes water-soluble spin traps were required. Also, nitroso traps were generally preferred over nitrone traps since the spin adducts from the former usually give more structural information about the radical trapped. It is also important to use more than one trap in view of the wide variation in reactivity of traps to different types of radical. This is a general point about spin trapping which has yet to be fully recognised. The following were the traps used.

*(a) 2-Methyl-2-nitrosopropane (MNP), 2 (13)*

This is not very soluble in water (1 mg/mL) and is light- and heat-sensitive but there is a very large body of data available on the esr parameters of *t*-butyl nitroxides which often helps the interpretation of observed spectra.

*(b) 2-Methyl-2-nitroso-4(4'-pyridyl-1'-oxide)-butane (MNPOB), 3*

This is a new water-soluble trap which was synthesised according to Scheme 2. It exists in the solid state as the colourless dimer. Variable temperature nmr measurements indicate that at room temperature in deuterium oxide it is dissociated to 22% and at 80°C to 79%. However, the dimer ⇌ monomer equilibration rate is relatively slow, hence solutions of the trap were warmed before use. Its trapping reactivity appears to be similar to that of MNP but much higher concentrations of trap can be used and hence stronger spectra are observed. The spin adduct spectra usually have slightly larger linewidths than those from MNP. In other respects (heat and light sensitivity), it resembles MNP.

*(c) 3,5-Dibromo-4-nitrosobenzenesulphonic acid (DBNSA), 4 (14)*

The sodium salt of this acid was recently reported. We shortened its preparation by using *p*-nitroperoxybenzoic acid rather than hydrogen peroxide to oxidise the amine in the final stage. Nuclear magnetic resonance measurements indicated that the dimer was 94% dissociated at room temperature. This trap has the advantage that it is much less sensitive to light than the corresponding alkyl nitroso compounds and it does not give the corresponding diaryl nitroxide on exposure of its aqueous solutions to daylight. Unfortunately, it gives spin adduct spectra with relatively broad lines; in the worst circumstances 2 G wide. When L-glutamine (8 Mrad dose) was added to a series of solutions

[1]See ref. 12.

Can. J. Chem. Downloaded from www.nrcresearchpress.com by 210.87.254.42 on 09/06/12
For personal use only.

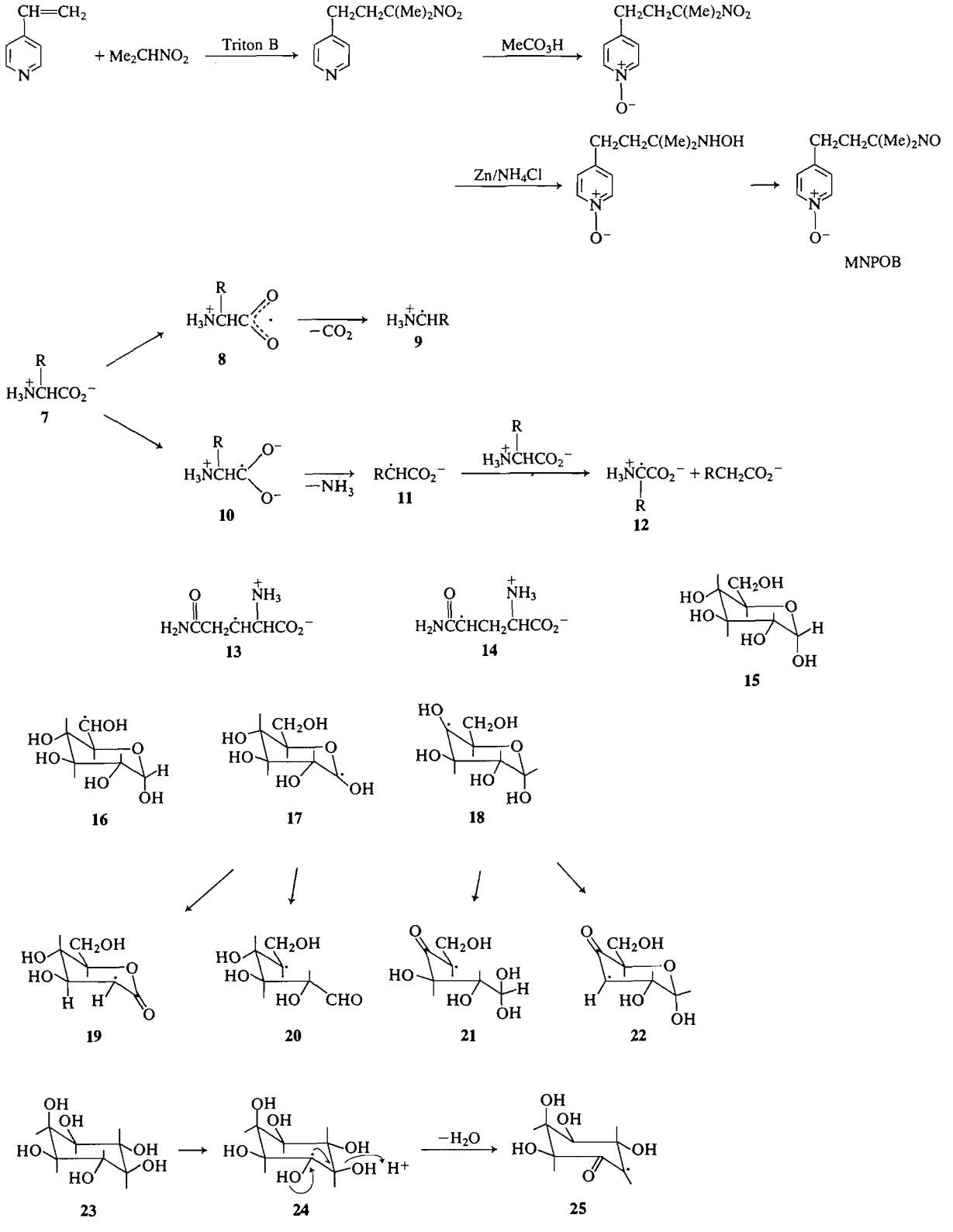


SCHEME 2

Can. J. Chem. Downloaded from www.nrcresearchpress.com by 210.87.254.42 on 09/06/12
For personal use only.

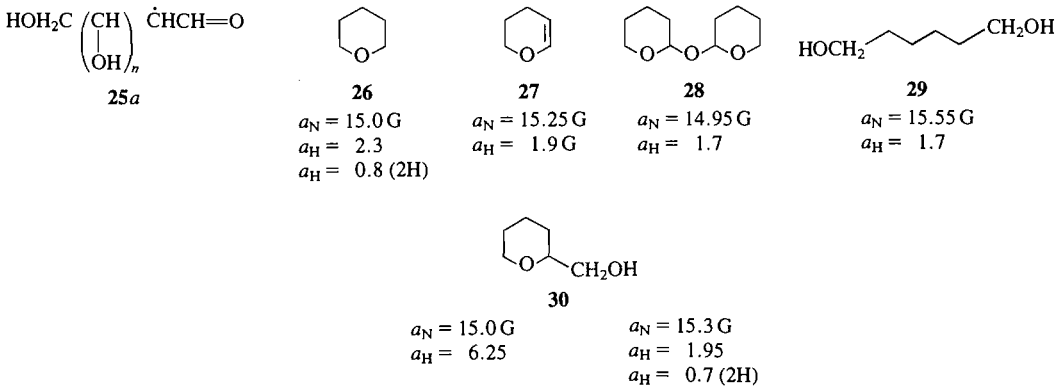


SCHEME 2. (*Concluded*)

0.004–0.2 *M* of this trap, the maximum concentration of spin adduct was achieved with solutions >0.02 *M*.

*(d)* N-t-*Butyl*-C-*(4'-pyridyl-1'-oxide)nitrone (POBN) 5 (15)*

This water-soluble nitrone has approximately the same trapping efficiency as DMPO. When irradiated, L-threonine (8 Mrad) was dissolved in an aqueous solution 0.1 *M* with respect to DMPO and POBN the two spin adduct spectra observed were of approximately equal intensity.

*(e) 5,5-Dimethylpyrrol-1-ine-1-oxide (DMPO), 6 (16)*

On storage, DMPO turns yellow and its solutions then display esr spectra with $a_N = 14.4$ G. To avoid this the trap was distilled before use and stored in the cold. Preliminary trapping experiments with this trap using irradiated amino acids confirmed that the trapped radicals were carbon-centred (Table 1). However, the $a_H$ values were not sufficiently different for these spectra to be used for structural identification of the trapped radicals.

## Relationship between dose, radical concentration, and light yield

For several organic compounds the LL light yield is proportional to (5) (*a*) the dose over a fairly wide range (Fig. 6) and (*b*) the radical concentration in the solid (Fig. 7). Another important relationship to establish is that between the LL light yield and the concentration of radicals in solution since it is these radicals which are thought to be responsible for the emission process. This has now been done (Fig. 8) using both a nitrone (POBN) and nitroso (DBNSA) trap and L-glutamine samples dosed to 100–600 krad. We have also shown that for L-glutamine there is a linear relationship between trapped radical concentration and solid state radical concentration (Fig. 9). Significantly this plot does not pass through the origin, hence not all of the radicals in the solid state are trapped. However, these radicals which are trapped must be responsible for the light emission since there was a sharp

TABLE 1. Coupling constants (G) of radicals trapped by DMPO

| | DMPO spin adduct | |
|---|---|---|
| Irradiated substrate | $a_N$ | $a_H$ |
| L-Threonine | 15.6 | 23.0 |
| Glycine | 15.75 | 22.6 |
| L-ArginineHCl | 15.3 | 21.5 |
| β-Alanine | 15.6 | 23.6 |

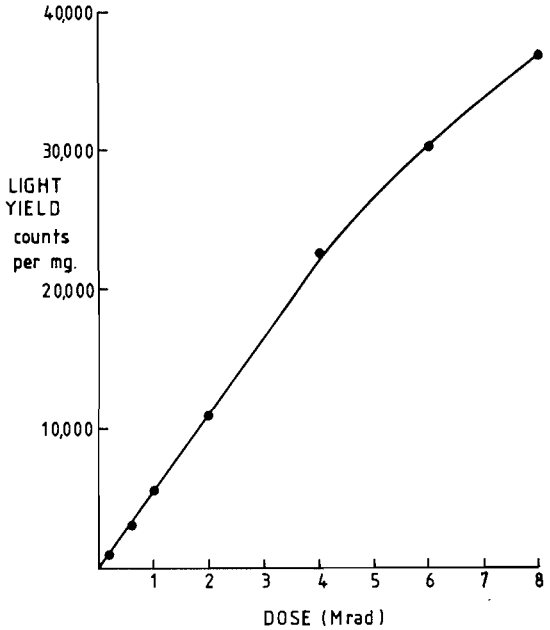


FIG. 6. Dose – light yield relationship for L-glutamine.

Can. J. Chem. Downloaded from www.nrcresearchpress.com by 210.87.254.42 on 09/06/12
For personal use only.

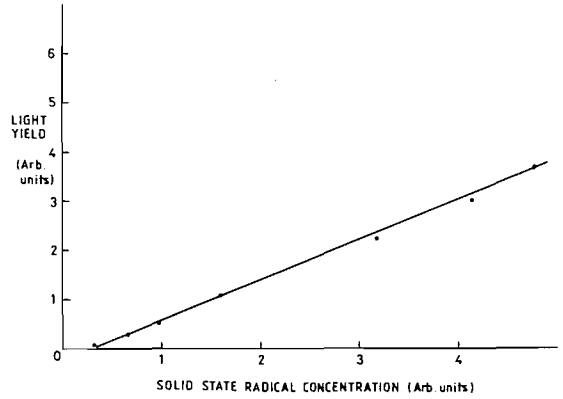


FIG. 7. Radical concentration (solid state) – light yield relationship for L-glutamine.

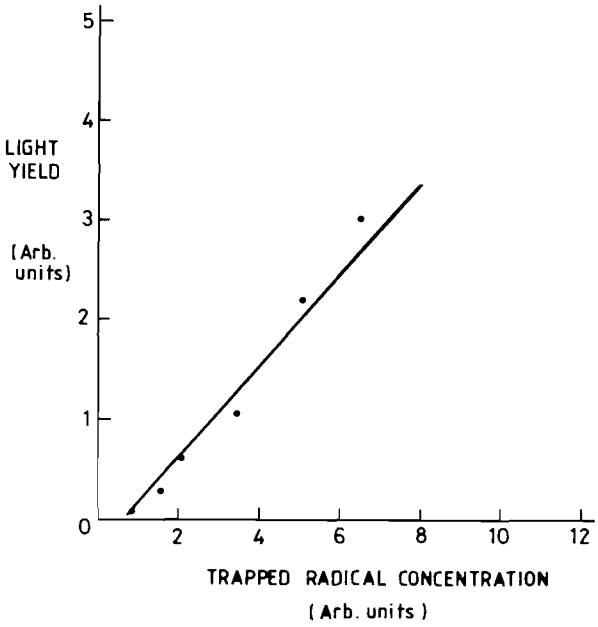


FIG. 8. Light yields – trapped radical concentration (DBNSA) relationship for L-glutamine.

decrease in the light yield when a solution of the trap DBNSA was used instead of water in the LL measurements with L-glutamine (8 Mrad). Further, the minimum concentration of trap (0.01 *M*) required to suppress the LL light emission corresponded almost exactly to the minimum concentration of trap required to give maximum yield of spin adduct.

## Annealing

When a series of irradiated samples of L-glutamine was heated to 110°C for 5 h the average concentration of radicals in the solids decreased by 32%. This was not unexpected. The increased temperature of

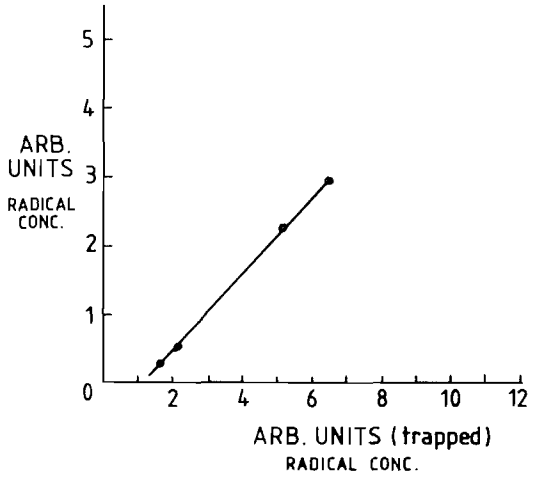


FIG. 9. Radical concentration (solid) – radical concentration (trapped) relationship for L-glutamine.

the crystals presumably allowed greater reaction between proximate radical centres. Surprisingly, however, the average LL light yield from the annealed samples increased by 50% which corresponded approximately to the increased concentration of trapped radicals using DBNSA (42% increase), and POBN (25% increase). We rationalise these observations as follows. Selective destruction of radical sites in the solid by heating increases the probability of reaction of the remaining radicals with oxygen or a trap on dissolution. Increase in the concentration of peroxyl radicals leads to an increase in light yield.

## Structure of radicals trapped

*(a) Amino acids*

γ-Irradiation of α-amino acids **7** leads primarily to oxidised **8** and/or reduced **10** species by electron loss or gain, respectively. These decay by decarboxylation (**8** → **9**) or deamination (**10** → **11**) to radicals which may react further. Most commonly, they abstract hydrogen from the parent amino acid to give what will be referred to hereafter as "hydrogen abstraction" radicals, **12**. Evidence for these reaction sequences has been adduced from direct esr and ENDOR measurements of single crystals, and product studies. The primarily formed species are only detected at low temperatures (4 and 77 K). At room temperature "deaminated" and "hydrogen abstraction" radicals are the most frequently encountered (17).

Thirteen amino acids were investigated using the nitroso traps MNP, MNPOB, and DBNSA. The radicals trapped with the corresponding coupling constants are given in Table 2. In general, the radicals trapped were "deaminated" and "hydro-

Can. J. Chem. Downloaded from www.nrcresearchpress.com by 210.87.254.42 on 09/06/12
For personal use only.

Can. J. Chem. Downloaded from www.nrcresearchpress.com by 210.87.254.42 on 09/06/12
For personal use only.

gen abstraction'' radicals in accord with the esr work reported for the solid state. The results are similar to those recently and independently obtained by Riesz and co-workers (18) who used only MNP as trap. However, there are significant differences.

The rate constants for reaction of radicals with spin traps are a function, *inter alia*, of the structure of the radical and of the trap. The relative ease with which primary, secondary, and tertiary alkyl radicals are trapped by several nitrones and nitroso compounds has been quantified (19). Hence, it is important to use more than one trap if all of the radicals in the system are to be detected. Even then the relative concentrations of the spin adducts do not necessarily reflect the concentration of radicals present in the solid. For example, with glycine the ''hydrogen abstraction'' radical was the main radical trapped with MNP but with DBNSA only the ''deaminated'' radical was trapped. Our results with glutamine are of special interest in view of its high light yield and hence potential utility. Computer simulation gives the best fit when there is weak equal coupling (0.6 G) with one nitrogen and *three* protons. This corresponds better to the spin adduct from the ''hydrogen abstraction'' radical **13** rather than that from radical **14** although the latter would seem the more likely on chemical grounds. It is clear from Table 2 that the type of radical most frequently trapped in this work was secondary alkyl, thus providing circumstantial evidence for the Russell–Vassilev mechanism.

*(b) Sugars*

Spectra from the sugars were invariably much weaker than those from the amino acids and best results were obtained when the spectra were accumulated (~30 scans). Spectra obtained after trapping with DBNSA were stronger than those obtained with the alkyl nitroso compounds but the lines were broader. Results are given in Tables 3 and 4. Splittings from β-protons do not usually exceed 1 G in aliphatic nitroxides and hence it is clear from the tables that many of the radicals trapped are secondary alkyl radicals, some with and others without β-hydrogen atoms. The task of assigning these spectra to particular radical structures is not a trivial one with such multifunctional substrates and it is constructive at this stage to consider some of the possibilities.

Carbon–hydrogen bond breaking is one of the most frequently encountered processes in studies of γ-irradiation of solid carbohydrates (33). Of the six possible radicals formed by hydrogen removal from a monosaccharide such as glucose **15**, only one, **16**, is a secondary alkyl radical. What then is the fate of the *t*-oxyalkyl radicals such as **17** and **18** which should be the predominant radical species initially formed? Significantly, it is only with DBNSA that *t*-alkyl spin adducts are usually detected. Hence, the *t*-oxyalkyl radicals must be converted into other radicals before they can be trapped or react with the *t*-alkyl nitroso compounds in some other way. Apparent in all of the spectra of the spin adducts with MNP and MNPOB is the spectrum of

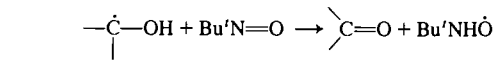


the corresponding monoalkyl nitroxide (*t*-RNHȮ). The intensity of this spectrum increased with increasing concentration of MNPOB. Hence, we believe that the *t*-oxyalkyl radicals reduce the nitroso compound as shown. With the amino acids, significant quantities of monoalkyl nitroxide were only detected with hydroxyproline and threonine, both of which are hydroxy acids.

Consumption of oxyalkyl radicals in this way cannot be total, otherwise no radicals would be trapped. Production of secondary alkyl radicals from tertiary oxyalkyl radicals could occur in a number of ways but a likely route is that described by Norman and Pritchett (34) (reaction [1]). This

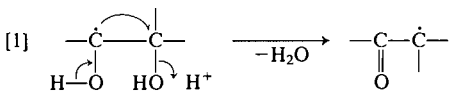


reaction is acid- and base-catalysed in solution but there is evidence that it can occur in stored solid samples of γ-irradiated sugars such as trehalose (35). A further possibility is that ring-opening (fragmentation) (reaction [2]) of the initial oxyalkyl

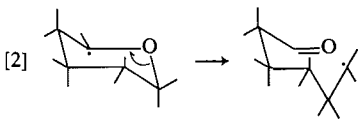


radicals occurs to give a secondary alkyl or other radical (36). Thus, glucose **15** could give initially five tertiary and one secondary oxyalkyl radicals (e.g. **16**, **17**, and **18**), all of which have been detected by esr after reaction of glucose with hydroxyl radicals in a flow system (37). Rearrangement of these according to reaction [1] could lead to six possible cyclic secondary α-acylalkyls (e.g. **19** and **22**), four ring-opened secondary alkyls (e.g. **20** and **21**), and fragmentation to two further radicals.

Support for the rearrangement step at least is provided by spin trapping studies of *meso*-inositol **23**. When a neutral solution of *meso*-inositol, hydrogen peroxide, and MNP or MNPOB in water

TABLE 2. Spin trapping of radicals from γ-irradiated amino acids

| Substrate | Radical trapped | Hyperfine splittings[a] (G) of spin adducts MNP | MNPOB | DBNSA |
|---|---|---|---|---|
| Glycine[a] | $\dot{C}H_2CO_2^-$ | $a_N = 16.1$<br>$a_H = 8.42$ (2H) | —<br>— | $a_N = 13.05$<br>$a_H = 9.9$ (2H) |
| | $H_3\overset{+}{N}\dot{C}HCO_2^-$ | $a_N = 14.3$<br>$a_H = 2.5$ (1H)<br>$a_N^{+NH_3} = 2.15$<br>$a_H = 0.4$ (3H) | | |
| L-α-Alanine[b] | $CH_3\dot{C}HCO_2^-$ | $a_N = 16.1$<br>$a_H = 5.05$ (1H)<br>$a_H = 0.4$ (3H) | $a_N = 15.6$<br>$a_H = 5.05$ (1H) | $a_N = 13.5$<br>$a_H = 6.4$ (1H) |
| β-Alanine[c] | $H_3\overset{+}{N}CH_2\dot{C}HCO_2^-$ | $a_N = 15.35$<br>$a_H = 4.90$ (1H) | $a_N = 15.1$<br>$a_H = 4.75$ (1H) | $a_N = 13.25$<br>$a_H = 6.85$ (1H) |
| L-Valine[d] | $Me_2CH\dot{C}HCO_2^-$ | $a_N = 15.7$<br>$a_H = 3.7$ (1H) | $a_N = 15.5$<br>$a_H = 3.9$ | $a_N = 13.55$<br>$a_H = 6.7$ (1H) |
| | $Me_2\dot{C}CH(\overset{+}{N}H_3)CO_2^-$ | $a_N = 16.35$ | | $a_N = 13.75$<br>$a_H = 0.5$ (many H) |
| L-Threonine[e] | $MeCH(OH)\dot{C}HCO_2^-$ | $a_N = 15.5$<br>$a_H = 4.15$ (1H) | $a_N = 15.25$<br>$a_H = 4.2$ (1H) | $a_N = 13.3$<br>$a_H = 6.4$ (1H) |
| L-Glutamine[f] | $H_2N\overset{O}{\overset{\|}{C}}CH_2\dot{C}HCH(\overset{+}{N}H_3)CO_2^-$ | $a_N = 15.2$<br>$a_H = 4.0$ (1H)<br>$a_N^{NH_3} = 0.6$<br>$a_H = 0.6$ (3H) | $a_N = 15.0$<br>$a_H = 4.4$ | $a_N = 13.4$<br>$a_H = 5.85$ (1H) |
| L-Glutamic acid[g] | $HO_2C\dot{C}HCH_2CH(\overset{+}{N}H_3)CO_2^-$ | $a_N = 15.4$<br>$a_H = 3.95$ (1H)<br>$a_H = 0.6$ (2H) | $a_N = 15.15$<br>$a_H = 4.4$ (1H) | $a_N = 13.35$<br>$a_H = 5.95$ |
| L-Arginine hydrochloride[h] | $H_2\overset{+}{N}=C(NH_2)NH\dot{C}H(CH_2)_2\overset{\overset{+}{N}H_3}{\overset{\|}{C}}HCO_2^-$ | $a_N = 15.3$<br>$a_N^{NH} = 2.9$<br>$a_H = 1.75$ (1H) | $a_N = 15.0$<br>$a_N^{NH} = 2.9$<br>$a_H = 1.9$ (1H) | |
| | $H_2\overset{+}{N}=C(NH_2)NH(CH_2)_3\dot{C}HCO_2^-$ | | $a_N = 15.25$<br>$a_H = 4.55$<br>$a_H = 0.65$ (2H) | $a_N = 13.35$<br>$a_H = 6.10$ (2H) |

is photolysed the spin adduct of a tertiary alkyl radical **24** is detected. At pH 1 only a secondary alkyl spin adduct ($a_N$ = 15.0 and $a_H$ = 1.75 G), presumably that of **25**, is formed. When γ-irradiated *meso*-inositol is dissolved in neutral aqueous solutions of MNP or MNPOB the spectrum of only the spin adduct of the secondary alkyl radical is detected. Similar changes with pH have been reported for radicals generated from *meso*-inositol by reaction with hydroxyl radicals in a flow system and detected directly by esr (38).

To aid the interpretation of the spectra, details of which are given in Tables 3 and 4, and hence identify or at least classify the saccharide-derived radicals, we have adopted the following approaches. (*a*) Examined γ-irradiated model compounds. (*b*) Generated radicals from the saccharides and their models in other ways and tried to characterise their spin adducts. In this respect saccharide-derived radicals whose structures have been confirmed by direct esr measurement are the most attractive. (*c*) Relate the differences in the spectra of the spin adducts to structural differences in the saccharides.

*(a) Model compounds*. Several γ-irradiated polyols including mannitol, sorbitol, ribitol, and dulcitol were first examined. There are lyoluminescent phophors in their own right but results with the three traps were disappointing. The same secondary alkyl radicals were trapped at pH 1 and pH 7 (for MNP and MNPOB, $a_N$ = 15.53, $a_H$ = 1.4–2.3 G) and hence rearrangement must have occurred before dissolution of the trap. Under these circumstances, it is difficult to be certain of the structures of the radicals trapped but they are probably of the general structure **25***a*.

Can. J. Chem. Downloaded from www.nrcresearchpress.com by 210.87.254.42 on 09/06/12
For personal use only.

TABLE 2. (*concluded*)

| Substrate | Radical trapped | Hyperfine splittings[a] (G) of spin adducts | | |
|---|---|---|---|---|
| | | MNP | MNPOB | DBNSA |
| L-Asparagine monohydrate[i] | $H_2NCO\dot{C}H(\overset{+}{N}H_3)CO_2^-$ | $a_N = 15.0$<br>$a_H = 3.8$ (1H)<br>$a_H = 0.55$ (1H)<br>$a_N = 0.55$ (2N) | $a_N = 15.1$<br>$a_H = 4.2$ (1H) | $a_N = 13.25$<br>$a_H = 5.05$ (1H) |
| L-Proline[j] | $H_3\overset{+}{N}(CH_2)_3\dot{C}HCO_2^-$ 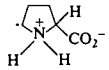 | $a_N = 15.55$<br>$a_H = 4.85$ (1H)<br>$a_H = 0.55$ (2H) | | |
| | | | | $a_N = 13.0$<br>$a_H = 3.65$ (1H)<br>$a_H = 0.75$ (2H)<br>$a_N = 0.75$ |
| L-Lysine hydrochloride[k] | $H_3\overset{+}{N}(CH_2)_4\dot{C}HCO_2^-$ | $a_N = 15.65$<br>$a_H = 4.65$ (1H)<br>$a_H = 0.55$ (2H) | $a_N = 15.3$<br>$a_H = 5.0$<br>$a_H = 0.5$ (2H) | $a_N = 13.4$<br>$a_H = 6.4$ |
| L-Histidine[l] | $^-O_2C\dot{C}HCH_2$ | $a_N = 15.35$<br>$a_H = 3.83$ (1H)<br>$a_H = 0.5$ (2H) | | $a_N = 15.35$<br>$a_H = 3.85$<br>$a_H = 0.5$ (2H) |
| L-Hydroxyproline[m] | $H_3\overset{+}{N}CH_2CH(OH)CH_2\dot{C}HCO_2^-$ | $a_N = 15.75$<br>$a_H = 4.5$ (1H) | | |
| | 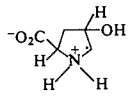 | | | $a_N = 13.2$<br>$a_N = 0.7$<br>$a_H = 3.35$ (1H)<br>$a_H = 0.7$ (2H) |

[a] Both radicals trapped have been detected in the solid at room temperature (20): the "hydrogen abstraction" radical has been trapped by MNP after reaction of the hydroxyl radical with glycine and the "deaminated" radical after reaction of glycine with the hydrated electron (21, 22).
[b] "Deaminated radical" detected in the solid state at room temperature (23): "hydrogen abstraction" radical trapped after reaction of L-α-alanine with the hydrated electron (22).
[c] "Hydrogen abstraction" radical detected among others in the solid state (24).
[d] "Hydrogen abstraction" radicals detected in the solid state (25): "deaminated radical" previously trapped by MNP after reaction of amino acid with the hydrated electron (22).
[e] "Deaminated" and "hydrogen abstraction" radical detected in the solid state (26).
[f] "Hydrogen abstraction" radicals trapped with MNP after reaction of glutamine with hydroxyl radicals (21).
[g] "Hydrogen abstraction" radical detected in solid state at room temperature (27): the "deaminated radical" has been trapped after reaction of L-glutamic acid with the hydrated electron and the "hydrogen abstraction" radical after reaction with hydroxyl radicals (21, 22).
[h] "Hydrogen abstraction" radical detected in the solid state and trapped with MNP after reaction of L-arginine with the hydroxyl radical or hydrated electron (28): the "deaminated radical" has also been trapped (21, 22).
[i] "Hydrogen abstraction" and "deaminated" radicals detected in the solid state (29): the deaminated radical has been trapped with MNP after reaction of asparagine with the hydrated electron and with hydroxyl radicals (21, 22).
[j] "Hydrogen abstraction" and "deaminated" radicals previously trapped by MNP (21, 22).
[k] "Deaminated" radical detected in the solid state at low temperature and trapped by MNP after γ-irradiation of aqueous solutions of lysine (22, 30).
[l] "Deaminated" radical detected in the solid state and trapped by MNP after reaction of histidine with the hydrated electron (22, 31).
[m] "Hydrogen abstraction" and "deaminated" radicals detected in the solid state (32): deaminated radical trapped by MNP after reaction with the hydrated electron (22).
[n] In some cases γ-H and/or β-N splittings were not resolved because of the linewidth.

*(b) Model reactions*. Reaction of saccharides with hydroxyl radicals produces all possible C—H abstraction radicals which rearrange with change in pH (37). When MNP and MNPOB were included in these reaction mixtures, complex mixed spectra of spin adducts were detected whose full interpretation has still to be achieved. However, the saccharide models **26–30** with MNP gave spectra with the coupling constants shown. From these we draw the general conclusions: (*a*) Spin adducts of pyran-2-yl radicals with MNP have $a_{\alpha\text{-H}} = 2$ G and $a_{\beta\text{-H}} < 1$ G. (*b*) Spin adducts of aliphatic hydroxyalkyl radicals have $a_{\alpha\text{-H}} = 2$ G. (*c*) Spin adducts of pyran-2-ylhydroxymethyl radicals have a $a_{\alpha\text{-H}} = 6$ G.

With this information it is now possible to make some assignment at least of radical type, of some of the radicals trapped on dissolution of the sugars. With glucose, mannose, and galactose radicals of type **16** ($a_H = 5$–6 G) and of type **19** or **20** are being trapped (39). Because of the similarity in the α-proton splittings the spin adducts of pyran-2-yl and aliphatic secondary hydroxyalkyl radicals (both 1.5 to 2.5 G), it is not possible at this stage to confidently distinguish between the adducts from **19** and **22** and those from **20** and **21**. These and other fine distinctions will only be made after a series of specifically deuterated or substituted saccharides have been examined. Only with gluconolactone and arabinose was there evidence of trapping *t*-oxyalkyl radicals with MNP. However, with DBNSA, *t*-oxyalkyl radicals were often the major type of radical trapped at pH 7. Spin adducts of rearranged radicals predominated at low pH. A continuing aim of the work is to establish better criteria for distinguishing between the spin adducts of saccharide derived radicals. However, even at this stage it is

Can. J. Chem. Downloaded from www.nrcresearchpress.com by 210.87.254.42 on 09/06/12
For personal use only.

Can. J. Chem. Downloaded from www.nrcresearchpress.com by 210.87.254.42 on 09/06/12
For personal use only.

TABLE 3. Spin trapping of radicals from γ-irradiated (5 Mrad) saccharides with MNP at pH 7

| Saccharide | Coupling constants (G) of trapped radicals (MNP) | |
|---|---|---|
| D-Glucose | $a_N = 15.0, a_H = 6.0$<br>$a_N = 14.5, a_H = 1.9, a_H = 0.75$ | |
| D-Mannose | $a_N = 15.05, a_H = 5.8$<br>$a_N = 14.7, a_H = 2.0, a_H = 0.7$ | |
| D-Galactose | $a_N = 15.0, a_H = 5.0$<br>$a_N = 15.4, a_H = 1.8$<br>$a_N = 15.0$ | |
| 1,5-Gluconolactone | $a_N = 15.0, a_H = 1.5$<br>$a_N = 15.0$ | |
| D-Rhamnose | $a_N = 14.5, a_H = 6.35$<br>$a_N = 14.5, a_H = 2.25, a_H = 0.9$ | |
| D-Glucuronic acid | $a_N = 15.25, a_H = 2.25$ | |
| D-Fructose | $a_N = 14.5, a_H = 1.45$ (br) | |
| D-Arabinose | $a_N = 14.3, a_H = 2.0$<br>$a_N = 14.0$ | |
| D-Ribose | $a_N = 14.25, a_H = 2.0$ (weak) | |
| D-Xylose | $a_N = 14.25, a_H = 2.0$ | |
| Mesoinositol | $a_N = 14.95, a_H = 1.75$<br>$a_N = 15.1, a_H = 1.85$ | pH 7<br>pH 1 |

clear that secondary alkyl radicals are commonly present in solution when γ-irradiated saccharides are dissolved, lending further support to the Russell–Vassilev mechanism.

## Experimental

*2-Methyl-2-nitro-4-(4'-pyridyl-1-oxide)butane*

2-Methyl-2-nitro-4-(4'-pyridyl)butane (40) (5 g, 2.6 mmol) in glacial acetic acid (12 mL) and 30% aqueous hydrogen peroxide (5 mL) was heated under reflux for 6 h and left at room temperature overnight. After removal of solvent *in vacuo* the resulting yellow oil was dissolved in chloroform and the solution was extracted with aqueous bicarbonate solution until evolution of carbon dioxide ceased, washed with water, and finally dried. Removal of solvent gave the *product* (5.14 g, 94%) as a yellow oil, bp 190–240°C/0.15 mm Hg (which was used without further purification. $\nu_{max}$ 1535, 1350, and 1245 $cm^{-1}$; δ 1.66 (6H, s, 2Me), δ 2.20 (2H, m, $CH_2$), 2.59 (2H, m, $CH_2$), 7.12 (2H, d, *J* 5.9 Hz, ArH), and 8.16 (2H, d, *J* 5.9 Hz, ArH).

*2-Hydroxylamino-2-methyl-4-(4'-pyridyl-1-oxide)butane*

The above nitro compound (43.5 g, 0.21 mol) in methanol (435 mL) was treated with a solution of ammonium chloride (6.51 g, 0.12 mol) in water (50 mL) and heated to boiling under reflux. Zinc dust (104 g, 116 mol) was added in small portions with vigorous stirring and the reaction mixture was heated and stirred for a further 2 h. The zinc residues were collected and washed with methanol. The filtrate and washings were evaporated, giving a brown oil which partially solidified on standing. Recrystallisation from chloroform–petrol gave the product (17.5 g, 43%), mp 146–150°C. (*Anal.* calcd. for $C_{10}H_{16}N_2O_2$: C 61.2, H 8.2, N 14.2, *M*, 196.1211; found: C 61.3, H 8.1, N 14.4, $M^+$, 196.1211.) $\nu_{max}$ 3222, 3180, δ 1.14 (6H, s, 2Me), 1.75 (2H, m, $CH_2$), 2.64 (2H, m, $CH_2$), 7.15 (2H, d, *J* 6.4 Hz, ArH), 8.15 (2H, d, *J* 6.4 Hz, ArH).

*2-Methyl-2-nitroso-4-(4'-pyridyl-1'-oxide)butane (MNPOB)*

The above hydroxylamine (2 g, 10 mmol) in water (100 mL) was treated with five portions of a solution of sodium metaperiodate (each 0.4 g, 0.18 mmol) in water (5 mL). After each addition the reaction mixture was extracted with chloroform (25 mL). The combined chloroform extracts were washed with water, dried, and the solvent was removed to give the product (1.19 g, 61%) as a blue oil which slowly solidified to a pale green solid, mp 87–90°C (from chloroform–petrol) (*Anal.* calcd. for $C_{10}H_{14}N_2O_2 \cdot H_2O$: C 61.9, H 7.2, $M^+ - NO$ 164.1073; found: C 60.0, H 7.4. *Anal.* calcd. for $C_{10}H_{14}NO$: *M* 164.1075). $\nu_{max}$ 3200, 1270, 1235, 850 $cm^{-1}$; δ 1.20 and 1.66 (2H, s, 2Me), 2.39 (4H, m, $2CH_2$), 7.12 (2H, d, ArH), and 8.15 (2H, d, ArH).

*3,5-Dibromo-4-nitrosobenzenesulphonic acid (DBNSA)*

4-Amino-3,5-dibromobenzenesulphonic acid (41) (3.31 g, 10 mmol) in water (100 mL) was treated with 4-nitroperoxybenzoic

TABLE 4. Spin trapping of radicals from γ-irradiated (5 Mrad) saccharides with DBNSA at pH 7

| Saccharide | Coupling constants of radicals trapped DBNSA | |
|---|---|---|
| D-Glucose | $a_N = 13.5$<br>$a_N = 12.75, a_H = 4.0$ | |
| D-Mannose | $a_N = 13.5$<br>$a_N = 12.75, a_H = 6.4$ | |
| D-Galactose | $a_N = 13.5$<br>$a_N = 13.25, a_H = 4.0$ | |
| 1,5-Gluconolactone | $a_N = 13.0$<br>$a_N = 13.25, a_H = 4.3$ | not seen at pH 1 |
| D-Rhamnose | — | |
| D-Glucuronic acid | $a_N = 13.0$<br>$a_N = 13.25, a_H = 5.25$ | not seen at pH 1 |
| D-Fructose | — | |
| D-Arabinose | $a_N = 14.35$ | |
| D-Ribose | — | |
| D-Xylose | $a_N = 13.4$ | |

Can. J. Chem. Downloaded from www.nrcresearchpress.com by 210.87.254.42 on 09/06/12
For personal use only.

acid (6.46 g, 30 mmol of 85% purity) and stirred at room temperature for 48 h. The reaction mixture was extracted twice with ether (2 × 100 mL) and then the aqueous phase was evaporated to drynes to yield a brown waxy solid. Trituration of the residue with benzene followed by evaporation of the benzene extracts to dryness gave the *product* (3.16 g, 92%), mp 200°C (decomp.) which was used for spin trapping studies without further purification. (*Anal.* calcd. for $C_6H_3Br_2NO_4S$: *M* 342.8149; found:[2] $M^+$ 342.8150.) $\nu_{max}$ 3400, 1555, 1370, 1285, 1215, 1140, and 1040 $cm^{-1}$; $\delta(D_2O)$ 8.22 (2H, s, 2ArH).

*γ-Irradiation*

Amino acids were purchased from BDH or Sigma Chemicals and were used without further purification. The materials were irradiated at the Scottish Universities Research and Reactor Centre, East Kilbride in a Cobalt 60 rig. The dose rate was approximately 0.2 Mrad per hour at room temperature. Doses were calculated using the "Red Perspex" method (42) and are accurate to about 5%.

*Spin trapping with MNP*

An aqueous solution of MNP was prepared by warming a mixture of the trap (5 mg) and water (2 mL) in the dark until the blue colour of the monomer was apparent. The irradiated material (200 mg) was then added with rapid stirring and the resulting solution transferred to a flat esr cell. A similar procedure was used with MNPOB.

*Spin trapping*

To a solution of the trap in water (1–2 mL) the irradiated material (200 mg) was added with stirring or shaking. The pH of the solution was varied when required by addition of sulphuric acid, sodium hydroxide solution, or a buffer powder.

## Acknowledgements

We thank the National Radiological Protection Board and the Science Research Council for grants.

1. E. WIEDEMANN and G. C. SCHMIDT. Ann. Phys. Chem. **54**, 604 (1895).
2. G. AHNSTRÖM and G. V. EHRENSTEIN. Acta Chem. Scand. **13**, 855 (1959); G. AHNSTRÖM, Acta Chem. Scand. **15**, 463 (1961); G. AHNSTRÖM. Acta Chem. Scand. **19**, 300 (1965).
3. T. WESTERMARK and B. GRAPENGIESSER. Nature, **188**, 395 (1960).
4. K. J. PUITE and K. V. ETTINGER. *In* Modern trends in radiation dosimetry. Special Issue of Journal of Applied Radiation and Isotopes. *Edited by* W. L. McLaughlin. Pergammon, London. 1982. In press.
5. K. V. ETTINGER and K. J. PUITE. *In* Modern trends in radiation dosimetry. Special Issue of Journal of Applied Radiation and Isotopes. *Edited by* W. L. McLaughlin. Pergammon, London. 1982. In press.
6. I. I. SAPEZHINSKII, YU. V. SILAEV, and N. M. EMANUEL. Dokl. Akad. Nauk. SSSR, **151**, 584 (1963).
7. G. A. RUSSELL. J. Am. Chem. Soc. **79**, 3871 (1957); R. F. VASSILEV. Prog. Reaction Kinet. **4**, 305 (1967).
8. R. R. KELLOG. J. Am. Chem. Soc. **91**, 5433 (1969).
9. P. J. WAGNER and G. S. HAMMOND. *In* Adv. Photochem. **5**, 21 (1968).
10. A. U. KHAN and M. KASHA. J. Am. Chem. Soc. **92**, 3294 (1970); **88**, 1574 (1966).
11. P. J. BAUGH and P. LAFLIN. Radiat. Phys. Chem. **16**, 51 (1980).
12. M. J. PERKINS. Adv. Phys. Org. Chem. **17**, 1 (1980) and references therein.
13. A. CALDER, A. R. FORRESTER, and S. P. HEPBURN. Org. Synth. **52**, 77 (1972).
14. H. K. KAUR, K. H. W. LEUNG, and M. J. PERKINS. J. Chem. Soc. Chem. Commun. 142 (1981).
15. E. G. JANZEN, Y. Y. WANG, and R. V. SHETTY. J. Am. Chem. Soc. **100**, 2923 (1978).
16. E. G. JANZEN and J. I-P. LIU. J. Magn. Reson. **9**, 510 (1973).
17. H. C. BOX. Radiation effects: ESR and ENDOR analyses. Academic Press, New York. 1971.
18. A. MINEGISHI, R. BERGENE, and P. RIESZ. Int. J. Radiat. Biol. **38**, 627 (1980).
19. Y. MAEDA and K. U. INGOLD. J. Am. Chem. Soc. **101**, 4975 (1979); P. SCHMID and K. U. INGOLD. J. Am. Chem. Soc. **100**, 2493 (1978).
20. J. SINCLAIR. J. Chem. Phys. **55**, 245 (1971).
21. S. RUSTGI, A. JOSHI, H. MOSS, and P. RIESZ. Int. J. Radiat. Biol. **31**, 415 (1977); S. N. RUSTGI and P. RIESZ. Int. J. Radiat. Biol. **34**, 301 (1978).
22. S. RUSTGI, A. JOSHI, P. RIESZ, and F. FREIDBERG. Int. J. Radiat. Biol. **32**, 533 (1977).
23. A. MESHITSUKA, K. SHINDO, A. MINEGISHI, H. SUGORO, and Y. SHINOZAKI. Bull. Chem. Soc. Jpn. **37**, 928 (1964); A. MINEGISHI. J. Phys. Chem. **81**, 1688 (1977).
24. D. M. CLOSE, G. W. FOUSSE, and W. A. BERNHARD. J. Chem. Phys. **70**, 2130 (1970).
25. M. D. SEVILLA. J. Phys. Chem. **74**, 2096 (1970).
26. D. M. CLOSE and R. S. ANDERSON. J. Chem. Phys. **60**, 2828 (1973).
27. D. J. WHELAN. J. Chem. Phys. **49**, 4734 (1968); I. G. BIKCHANTAEV and A. I. RIRKIND. Teor. Eksop. Khim. **11**, 132 (1975).
28. A. JOSHI and R. H. JOHNSEN. J. Phys. Chem. **80**, 46 (1976).
29. D. M. CLOSE, G. W. FOUSSE, and W. A. BERNHARD. J. Chem. Phys. **66**, 1534 (1977).
30. M. FUJIMOTO, W. A. SEDDON, and D. R. SMITH. J. Chem. Phys. **48**, 3345 (1968).
31. F. Q. NGO, E. E. BUDZINSKI, and H. C. BOX. J. Chem. Phys. **28**, 151 (1974); E. WESTHOFF, W. FLOSSMANN, and A. MÜLLER. Mol. Phys. **28**, 151 (1974).
32. C. L. KO and H. C. BOX. J. Chem. Phys. **68**, 5357 (1978).
33. N. K. KOTCHETKOV, L. I. KUDRJGASHOV, and M. A. CHELNOV. Radiation chemistry of carbohydrates. Pergammon, Oxford. 1979.
34. R. O. C. NORMAN and R. J. PRITCHETT. J. Chem. Soc. B, 1329 (1967).
35. A. GRÄSLUND and G. LOFROTH. Acta Chem. Scand. B**29**, 475 (1975).
36. C. VON SONNTAG. Adv. Carbohydr. Chem. Biochem. **37**, 7 (1980).
37. B. C. GILBERT, D. M. KING, and C. B. THOMAS. J. Chem. Soc. Perkin Trans. **2**, 1186 (1981).
38. B. C. GILBERT, D. M. KING, and C. B. THOMAS. J. Chem. Soc. Perkin Trans. **2**, 1821 (1980).
39. M. KUWABARA, Y. LION, and P. RIESZ. Int. J. Radiat. Biol. **39**, 451 (1981).
40. E. PROFFT. Chem. Tech. Leipzig, **8**, 705 (1956); Chem. Abstr. **53**, 3219 (1963).
41. J. J. SUDBOROUGH and J. V. LUKUMATANI. J. Chem. Soc. **111**, 45 (1917).
42. B. WHITTAKER. *In* Manual on radiation dosimetry. *Edited by* N. W. Hohn and R. J. Berry. Marcel Dekker, New York. 1970. p. 363.

[2]Analysis results for monohydrate varied with time and temperature of drying.

# Substituent effects in the kinetic analysis of free radical reactions with nitrone spin traps[1]

C. L. GREENSTOCK AND R. H. WIEBE

*Medical Biophysics Branch, Whiteshell Nuclear Research Establishment, Atomic Energy of Canada Limited, Pinawa, Man., Canada R0E 1L0*

Received September 12, 1981

C. L. GREENSTOCK and R. H. WIEBE. Can. J. Chem. **60**, 1560 (1982).

The kinetics of reactions of the water radiolysis species with substituted phenyl-N-*tert*-butyl nitrones (PBN), have been studied directly, *in situ*, using a pulsed Van de Graaff accelerator and kinetic spectrophotometry. The spin trapping of other secondary radiation-induced electrophilic and nucleophilic free radical species was also studied. The mechanistic aspects of these reactions are discussed in terms of the kinetic data. The effect of structure and substituents on the rate of spin trapping was tested for five *para*-substituted PBN's. It was found that electron-withdrawing groups increase the rate of nucleophilic reactions involving hydrated electrons, formyl anions, and α-hydroxyalkyl radicals with substitued PBN. Electron-donating substituents produce the opposite effect.

These studies confirm that nitrones are effective spin traps because of their high reactivity towards radiation-induced free radicals. Caution must be observed, however, in view of their lack of specificity, in interpreting spin-trapping data in complex steady-state systems involving more than one primary or secondary radical species, or where unstable spin-adducts are formed.

C. L. GREENSTOCK et R. H. WIEBE. Can. J. Chem. **60**, 1560 (1982).

En utilisant un accélérateur de Van de Graaff à impulsions et la spectrophotométrie cinétique, on a étudié directement *in situ* la cinétique des réactions de phényl N-*tert* butyl nitrones (PBN) substituées avec les espèces provenant de la radiolyse de l'eau. On a également étudié le piégeage de spin d'autres espèces secondaires de radicaux libres électrophile et nucléophile induits par radiation. On discute du mécanisme de ces réactions en fonction des données cinétiques. On a vérifié l'effet de la structure et des substituants sur la vitesse de piégeage de spin, dans le cas des PBN substituées en position para. On a trouvé que les groupes électroattracteurs augmentent la vitesse des réactions nucléophiles impliquant des électrons hydratés, des anions du type formyle et des radicaux α-hydroxyalkyles, avec les PBN substituées. Les substituants électrodonneurs produisent l'effet inverse.

Ces études confirment le fait que les nitrones sont des capteurs de spin efficaces par suite de leur grande réactivité vis-à-vis des radicaux libres induits par radiation. En raison de leur manque de spécifité, on doit faire attention en interprétant les données de piégeage de spin dans des systèmes complexes à l'état stationnaire impliquant plus d'une espèce radicalaire primaire ou secondaire ou lorsqu'il se forme des adduits de spin instables.

[*Traduit par le journal*]

## Introduction

Free radicals are implicated in a variety of normal biological processes (1), as well as in certain diseases and pathological or xenobiotic processes (2). The harmful effects of physical and chemical carcinogens may be attributed to free radicals (3–6). It has long been recognized that free radicals, particularly the activated oxygen species, are involved in radiation damage (3, 4, 7, 8). Unfortunately, because of the ubiquitous and transient nature of such free radical species, their indiscriminate reactivity, and their proclivity to take part in interconversion or chain reactions (9), their unambiguous identification and mechanistic characterization in any chemical, biochemical, or biological system are often difficult. This situation was helped by the development of spin traps (10, 11) which react with free radicals to produce relatively stable or persistent paramagnetic spin-adducts with characteristic properties allowing, ideally, identification of the trapped radicals by esr techniques. Recently, a number of nitrones (RNO) have been developed (12) that appear to be well suited to the spectroscopic study of simple free radicals such as those generated by water radiolysis, but there is a dearth of kinetic information on such spin trapping reactions. We have used the radiation chemistry of aqueous solutions in the presence of different free radical scavengers to generate specific free radicals. The technique of pulse radiolysis (13) is used to observe, directly, these simple radiation-induced free radicals including the hydrated electron ($e_{aq}^-$), hydroxyl radical ($^\cdot OH$), superoxide ($O_2^{-\cdot}$), formyl ($CO_2^{-\cdot}$), and hydroxymethyl ($CH_2O^{-\cdot}$) radical anions and α-hydroxyalkyl radicals, and to measure the rates of spin trapping of these radicals with substituted 4-phenyl-N-*tert*-butyl nitrones:

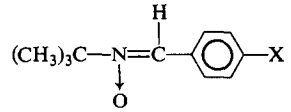

where X = $CH_3$, $CH_3O$, H, CN, $NO_2$.

The effect of *para*-substitution of PBN on the rate constants for electrophilic and nucleophilic free radical reactions is discussed in terms of the

[1]AECL No. 7396.

0008-4042/82/121560-05$01.00/0

©1982 National Research Council of Canada/Conseil national de recherches du Canada

Can. J. Chem. Downloaded from www.nrcresearchpress.com by 210.87.254.6 on 09/06/12
For personal use only.

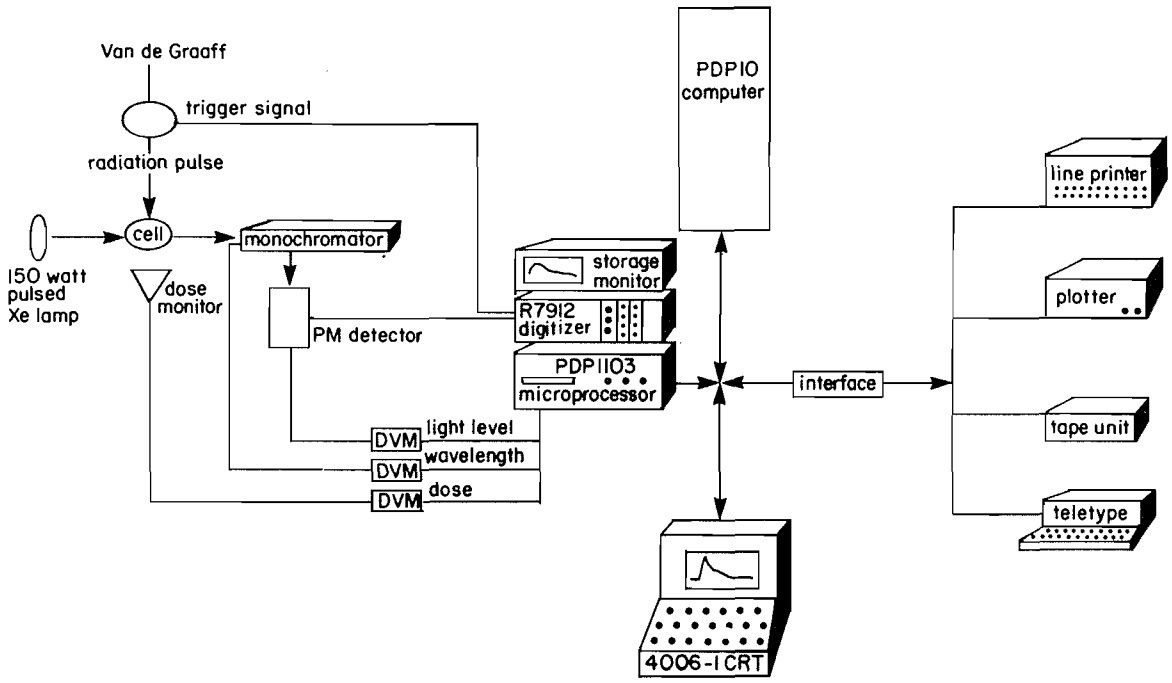


FIG. 1. Schematic diagram of the equipment for automatic data analysis in computerized pulse radiolysis.

kinetic design and interpretation of spin-trapping experiments.

## Experimental

The nanosecond pulse radiolysis system is similar to that described previously (13). The present optical detection system employs a Tektronix R 7912 transient digitizer in place of a conventional oscilloscope to monitor light output from a six-stage RCA C 7912 E or modified IP 28 photomultiplier tube. Automatic analysis of the kinetic spectrophotometric data from the digitizer is achieved on-line, by means of a PDP 10 computer interacting with a PDP 1103 microprocessor via a Tektronix 4006-1 video terminal (Fig. 1). The errors associated with measuring rate constants by directly monitoring the kinetics of the reactive species (i.e. hydrated electrons, see Table 1) are estimated to be ±5%. In the case of competition kinetics the errors associated with measuring the rate data are ±10%. In the special case of competition between a fast and a slow reaction, such as the competing reactions of $O_2^{\cdot-}$ with *p*-benzoquinone and spin traps, the errors are larger.

TABLE 1. Absolute bimolecular rate constants for the reaction of hydrated electrons with nitrone spin traps (RNO)

$$RNO + e_{aq}^- \xrightarrow{H_2O} R(H)NO\cdot + OH^-$$

| Spin trap | $k$ ($10^{10}$ L mol$^{-1}$ s$^{-1}$) |
|---|---|
| $CH_3$–PBN | $1.0_5$ |
| $CH_3O$–PBN | $1.5_5$ |
| PBN | 1.0 |
| CN–PBN | 1.0 |
| $NO_2$–PBN | $1.2_5$ |

A High Voltage Engineering KS-4000 Van de Graaff accelerator delivers single 50 ns pulses of 4 MeV electrons. The dose per pulse is typically 1–2 krad (10–20 Gy), producing 3–6 μmol L$^{-1}$ of radicals. In aqueous aerated solution, pulse radiolysis generates $e_{aq}^-$, H·, ·OH, and $O_2^{\cdot-}$ and their molecular products, $H_2$ and $H_2O_2$. In the presence of scavengers such as nitrous oxide ($N_2O$), formate ($HCO_2^-$), *t*-butanol ($(CH_3)_3COH$) or other additives, a principal reactive species can be generated for individual study (13).

[1] $H_2O \rightsquigarrow e_{aq}^-, H\cdot, \cdot OH, H_2, H_2O_2$

[2] $e_{aq}^- + N_2O \xrightarrow{H_2O} N_2 + OH^- + \cdot OH$

[3] $e_{aq}^- + O_2 \rightarrow O_2^{\cdot-}$

[4] $\cdot OH(H\cdot) + HCO_2^- \rightarrow CO_2^{\cdot-} + H_2O(H_2)$

[5] $CO_2^{\cdot-} + O_2 \rightarrow CO_2 + O_2^{\cdot-}$

[6] $\cdot OH(H\cdot) + (CH_3)_3COH \rightarrow \cdot CH_2(CH_3)_2COH + H_2O(H_2)$

[7] $\cdot OH(H\cdot) + HROH \rightarrow \cdot ROH + H_2O(H_2)$

[8] $\cdot ROH \xrightarrow{OH^-} RO^{\cdot-}$

The *para*-substituted PBN's were a gift from Professor E. G. Janzen. Solutions of spin traps were prepared with triply distilled water.

## Results and discussion

The reactivity of PBN's with $e_{aq}^-$ was studied in neutral deaerated solution containing *t*-butanol, which scavenges ·OH and H· (reaction [6]). The rate constants for these reactions were determined directly by monitoring the rate ($k'$(s$^{-1}$)) of decay of

Can. J. Chem. Downloaded from www.nrcresearchpress.com by 210.87.254.6 on 09/06/12
For personal use only.

Can. J. Chem. Downloaded from www.nrcresearchpress.com by 210.87.254.6 on 09/06/12
For personal use only.

the $e_{aq}^-$ absorbance at 650 nm as a function of PBN concentration. The pseudo-first order bimolecular rate constants, $k(=k'[\text{PBN}]\,\text{L mol}^{-1}\,\text{s}^{-1})$ for the reaction of $e_{aq}^-$ with the substituted PBN spin traps are given in Table 1. These reactions, which, in neutral or acidic solutions, presumably yield a paramagnetic H-spin adduct capable of being detected by esr spectroscopy, are close to diffusion-controlled, and show little or no effect of *p*-substitution of PBN.

In nitrous oxide saturated aqueous solutions, $e_{aq}^-$ is converted to ·OH (reaction [2]). Since neither ·OH nor the ·OH-spin adduct could be observed directly using our kinetic spectrophotometric detection system, the rate constants for the reaction of ·OH with PBN's were determined by competition kinetics (reactions [9] and [10]) using thiocyanate ion ($CNS^-$) as the competitive solute (14):

[9] $\cdot OH + CNS^- \xrightarrow{CNS^-} (CNS)_2^{-\cdot}$

[10] $\cdot OH$ + spin trap → spin-adduct

Rate constants are obtained from competitive plots showing the change in absorbance of $(CNS)_2^{-\cdot}$ at 490 nm with ($A$) and without ($A_0$) increasing the concentration of the spin trap, in accordance with eq. [11]:

$$[11]\quad k_{10} = 1.1\times 10^{10}(A_0/A - 1)\,[CNS^-]/[\text{spin trap}]$$

This equation assumes that the absorbance of the spin-adduct does not interfere with that of $(CNS)_2^{-\cdot}$, and this has been confirmed experimentally. Rate constants obtained in this manner (15) are listed in Table 2. These rate constants, like those for $e_{aq}^-$, are also very fast, and show no significant effects of PBN substitution. The rate constants obtained by the pulse radiolysis technique (16) agree well with those obtained by other less direct methods (17).

In oxygen-saturated aqueous solutions containing formate or *t*-butanol (reactions [3]–[6]), $O_2^{-\cdot}$ is the principal reactive species. Attempts to observe, directly, a reaction between $O_2^{-\cdot}$ and PBN were unsuccessful. A kinetic competition method using *p*-benzoquinone (*p*-BQ) as the competitive solute (18) provided only an upper limit of $\lesssim 0.6\times 10^7\,\text{L mol}^{-1}\,\text{s}^{-1}$ for the reactions (Table 3):

[12] $O_2^{-\cdot} + p\text{-BQ} \rightarrow O_2 + p\text{-BQ}^{-\cdot}$

[13] $O_2^{-\cdot}$ + spin trap → non-absorbing product

The rate constant, $k_{13}$, is estimated by monitoring the change in the $p\text{-BQ}^{-\cdot}$ absorbance at 420 in the absence ($A_0$) and presence ($A$) of increasing concentrations of the spin trap according to eq. [14]:

$$[14]\quad k_{13} = 1.0\times 10^9\,(A_0/A - 1)\,[p\text{-BQ}]/[\text{spin trap}]$$

Equation [14] assumes that the absorbance of the product of reaction [13] does not interfere with that of $p\text{-BQ}^{-\cdot}$, and this has been confirmed experimentally. This is a much slower reaction than that of $e_{aq}^-$ or ·OH. The results in Table 3 are only upper limits but may indicate the apparently weak nucleophilic nature of the species. Preliminary studies indicate a differential reactivity of $O_2^{-\cdot}$ and its protonated form $HO_2\cdot$ towards PBN, the latter being more reactive. More experiments are necessary to confirm this and to investigate the effects of *para*-substitution. Finkelstein *et al.* (17), using an indirect steady-state method, have reported rate constants $\sim 10\,\text{L mol}^{-1}\,\text{s}^{-1}$ for the reaction of $O_2^{-\cdot}$ with α-4-pyridyl-1-oxide-*N*-*tert*-butylnitrone.

A study of the reactivity of the radical anions $e_{aq}^-$, $CO_2^{-\cdot}$, $CH_2O^{-\cdot}$, and $O_2^{-\cdot}$ with unsubstituted PBN yielded the results shown in Table 4. In these experiments, there is a clear correlation between the rate constant for the reactions and the standard reduction potential $E^0$ (V) of the radiolytic species, indicating a strong nucleophilic reaction with the nitrone group. It appears from these results that the reduction potential of the unsubstituted nitrone moiety is between −1.25 and −2.87 V, i.e. between the reduction potentials of $CO_2^{-\cdot}$ and $e_{aq}^-$.

In a further attempt to clarify the role of *p*-substituents in modifying the free radical reactivity of PBN's, the reactivity of α-hydroxyalkyl radicals

TABLE 2. Rate constants for the reaction of hydroxyl radicals with nitrone spin traps (RNO)

$$RNO + \cdot OH \rightarrow R(OH)NO\cdot$$

| Spin trap | $k$ ($10^9\,\text{L mol}^{-1}\,\text{s}^{-1}$) |
|---|---|
| $CH_3$–PBN | 4.7 |
| $CH_3O$–PBN | 6.4 |
| PBN | 8.5 |
| CN–PBN | 6.5 |
| $NO_2$–PBN | 7.4 |

TABLE 3. Rate constants for the reaction of superoxide radical anions with nitrone spin traps (RNO)

$$RNO + O_2^{-\cdot} \xrightarrow{H_2O} R(OOH)NO\cdot + OH^-$$

| Spin trap | $k$ ($10^7\,\text{L mol}^{-1}\,\text{s}^{-1}$) |
|---|---|
| $CH_3$–PBN | <0.1 |
| $CH_3O$–PBN | <0.1 |
| PBN | <0.5 |
| CN–PBN | <0.6 |
| $NO_2$–PBN | <0.3 |

Can. J. Chem. Downloaded from www.nrcresearchpress.com by 210.87.254.6 on 09/06/12
For personal use only.

TABLE 4. Rate constants for the reaction of radical anions ($r^{-\cdot}$) with 4-phenyl-*N*-*tert*-butylnitrone (RNO), as a function of their standard redox potentials ($E^0$ (V))

$$RNO + r^{-\cdot} \xrightarrow{H_2O} R(r)NO\cdot + OH^-$$

| Radical anion | $k$ ($10^7$ L mol$^{-1}$ s$^{-1}$) | $E^0$ (V) |
|---|---|---|
| $e_{aq}^-$ | 1000 | −2.87 |
| $CO_2^{-\cdot}$ | 1.5 | −1.25 |
| $CH_2O^{-\cdot}$ | 1.2 | −0.73 |
| $O_2^{-\cdot}$ | <0.5 | −0.33 |

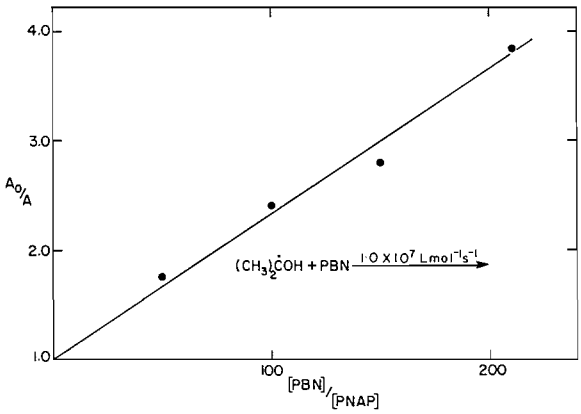


FIG. 2. Kinetic competition between PBN and *p*-nitroacetophenone (PNAP) for isopropyl alcohol radicals. Nitrous oxide saturated solutions containing 10 μmol L$^{-1}$ PNAP and 50 μm mol L$^{-1}$ isopropanol are irradiated with single doses ~1–2 krad (10–20 Gy). The yields of the *p*-nitroacetophenone radical anion in the presence ($A$) and absence ($A_0$) of PBN were determined, 100 μs after the pulse, by kinetic spectrophotometric methods.

(·ROH) derived from the OH-induced hydrogen abstraction of primary and secondary alcohols (reaction [7]) was studied, using *p*-nitroacetophenone (PNAP) as a competitive solute (19):

[15] $\cdot R'OH + PNAP \rightarrow PNAP^- + R'OH^+$

[16] $\cdot R'OH$ + spin trap → non-absorbing product

$$[17] \quad k_{16} = k_{15}(A_0/A - 1)[PNAP]/[\text{spin trap}]$$

A typical competition plot is shown in Fig. 2. Rate constants (eq. [17]) derived from such plots are shown in Table 5 for various *p*-substituted PBN's reacting with α-hydroxyalkyl radicals derived from methanol, ethanol, *n*- and isopropanol. The results clearly show that, in all cases, electron withdrawing substituents on PBN increase the reactivity of α-hydroxyalkyl radicals, as expected on the basis of their nucleophilic nature. In addition, a progressively greater α-hydroxyalkyl radical reactivity is observed in going from long chain to short chain alcohols, reflecting the inductive, ionic, and possible steric influence of the alkyl group.

TABLE 5. Rate constants for the reaction of various α-hydroxyalkyl radicals with nitrone spin traps (RNO)

$$RNO + \cdot R'OH \xrightarrow{H_2O} \begin{cases} \rightarrow R(R'OH)NO\cdot \\ \rightarrow R(H)NO\cdot + R'OH^+ + OH^- \end{cases}$$

| | $k$ ($10^7$ L mol$^{-1}$ s$^{-1}$) | | | |
|---|---|---|---|---|
| Spin trap | ·MeOH | ·EtOH | ·*n*-ProOH | ·*iso*-ProOH |
| $CH_3$–PBN | 2.5 | 0.1 | 0.35 | 0.1 |
| $CH_3O$–PBN | 2.9 | 0.9 | 0.1 | 0.15 |
| PBN | 4.3 | 1.6 | 1.3 | 1.0 |
| CN–PBN | 75 | 2.0 | 1.7 | — |
| $NO_2$–PBN | 120 | 3.5 | 0.65 | — |

Although spin traps are proving to be important spectroscopic probes of transient free radical species, caution must be used in the interpretation of results obtained under steady-state conditions. It must be remembered that the esr spin-trapping technique is only applicable to the study of persistent, paramagnetic spin-adducts. It will not detect redox reactions such as that shown in reaction [16] (see Table 5), or other reactions not yielding a paramagnetic product; neither will it detect many unstable spin-adducts. In complex systems, esr spin-trapping experiments may not detect either unreactive or highly reactive free radicals, and may not necessarily reflect the principal transient species or the main reaction sequence.

It is clear that nitrones react very rapidly with simply reducing ($e_{aq}^-$) and oxidizing (·OH) species, whereas the reaction with other nucleophiles ($O_2^{-\cdot}$, $CO_2^{-\cdot}$), and α-hydroxyalkyl radicals) is much slower. Consequently, care must be taken in studies of free radical interconversion or in complex mixtures of radicals to ensure that the reactions of reactive species do not obscure the more specific or selective spin trapping of a less reactive, but perhaps more important, reactant. The use of appropriate free radical scavengers, selected on the basis of kinetic considerations, may help to clarify future studies of the application of spin traps in free radical chemistry.

1. M. S. BLOIS, JR., H. W. BROWN, R. M. LEMMON, R. D. LONDBLOM, and M. WEISSBLUTH. (*Editors*). Free radicals in biological systems. Academic Press, New York. 1961.
2. T. F. SLATER. Free radical mechanisms in tissue injury. Pion Press, London. 1972.
3. D. E. LEA. Actions of radiation on living cells. Cambridge University Press, London. 1946.
4. Z. M. BACQ and P. ALEXANDER. Fundamentals of radiobiology. Butterworths, London. 1956.
5. J. A. MILLER and E. C. MILLER. Adv. Cancer Res. **1**, 339 (1953).
6. P. O. P. Ts'o and J. A. DIPAOLO. (*Editors*). Chemical carcinogenesis. Marcel Dekker, New York. 1974.
7. J. F. WARD. Adv. Radiat. Biol. **5**, 181 (1975).

8. C. L. GREENSTOCK. Radiat. Res. **86**, 196 (1981).
9. C. L. GREENSTOCK and R. H. WIEBE. *In* Oxygen and oxy-radicals. *Edited by* M. A. J. Rodgers and E. L. Powers. Academic Press, New York. 1981.
10. E. G. JANZEN. Acc. Chem. Res. **4**, 31 (1971).
11. E. G. JANZEN. Free radicals in biology. Vol. IV. *Edited by* W. A. Pryor. Academic Press, New York. 1980.
12. E. G. JANZEN, C. A. EVANS, and E. R. DAVIS. *In* Organic free radicals. *Edited by* W. A. Pryor. American Chemical Society Symposium Series. 1978. p. 433.
13. J. W. HUNT, C. L. GREENSTOCK, and M. J. BRONSKILL. Int. J. Radiat. Phys. Chem. **4**, 87 (1972).
14. G. E. ADAMS, J. W. BOAG, J. CURRANT, and B. D. MICHAEL. *In* Pulse radiolysis. *Edited by* M. Ebert, J. P. Keene, A. J. Swallow, and J. H. Baxendale. Academic Press, New York. 1965. p. 131.
15. R. L. WILLSON, C. L. GREENSTOCK, G. E. ADAMS, R. WAGEMAN, and L. M. DORFMAN. Int. J. Radiat. Phys. Chem. **3**, 211 (1971).
16. (*a*) S. SRIDHAR. Private communication; C. L. Greenstock, R. H. Wiebe, and E. M. Gardy. 61st Canadian Chemical Congress, abstr. OR-5, 1978. p. 65; (*b*) P. NETA, S. STEENKEN, E. G. JANZEN, and R. V. SHETTY. J. Phys. Chem. **84**, 532 (1980).
17. E. FINKELSTEIN, G. M. ROSEN, and E. L. RAUCKMAN. J. Am. Chem. Soc. **102**, 4994 (1980).
18. C. L. GREENSTOCK and G. W. RUDDOCK. Int. J. Radiat. Phys. Chem. **8**, 367 (1976).
19. C. L. GREENSTOCK and I. DUNLOP. J. Am. Chem. Soc. **95**, 6917 (1973).

Can. J. Chem. Downloaded from www.nrcresearchpress.com by 210.87.254.6 on 09/06/12
For personal use only.

# Spin trapping in photochemistry of coordination compounds

DETLEF REHOREK AND HORST HENNIG

*Sektion Chemie, Karl-Marx-Universität Leipzig, DDR-7010 Leipzig, German Democratic Republic*

Received September 12, 1981

Can. J. Chem. Downloaded from www.nrcresearchpress.com by 210.87.254.42 on 09/06/12
For personal use only.

DETLEF REHOREK and HORST HENNIG. Can. J. Chem. **60**, 1565 (1982).

The application of spin-trapping technique to detect short-lived paramagnetic species formed during photochemical reactions of coordination compounds is reviewed. Interference of radical recombinations by scavenging action of spin traps has been pointed out to be important at high spin-trap concentrations only. Due to only a limited extent of side reactions, nitrosodurene and phenyl N-*tert*-butyl nitrone were found to be excellent spin traps for the study of photoreactions of metal complexes in nonpolar solutions, whereas 5,5-dimethyl pyrroline-1-oxide is recommended for aqueous solutions. Using these spin traps, both organic and inorganic radicals, e.g. H, Cl, $N_3$, CN, OH, $O_2^-$, as well as solvated electrons and metal-centered free radicals have been detected during the photolysis of coordination compounds. The detection of singlet oxygen by reaction with 2,2,6,6-tetramethyl piperidine is briefly discussed.

DETLEF REHOREK et HORST HENNIG. Can. J. Chem. **60**, 1565 (1982).

On examine de nouveau l'application de la technique de captage de spin à la détermination des espèces paramagnétiques de courte vie qui se forment lors de réactions photochimiques de composés de coordination. ON a mis en évidence le fait que l'influence des recombinaisons de radicaux sous l'action protectrice des capteurs de spin, devient importance uniquement pour des fortes concentration en capteurs de spin. En raison de l'existence de très peu de réactions secondaires, on a trouvé que le nitrosodurène et la phènyl N-*tert*-butyle nitrone sont d'excellents capteurs de spin pour l'étude des réactions photochimiques des complexes métalliques dans des solutions non polaires, tandis que la diméthyl-5,5 pyroline-oxyde-1 convient pour les solutions aqueueses. L'utilisation de ces capteurs de spin a permis, lors de la photolyse des composés de coordination, de détecter les radicaux organiques et inorganiques tels que; H, Cl, $N_3$, CN, OH, $O_2^-$ aussi bien que les électrons solvatés et les radicaux libres centrés sur des métaux. On discute brièvement de la détection de l'oxygène singulet par la réaction avec le tétraméthyl-2,2,6,6, pipéridine.

[Traduit par le journal]

## 1. Introduction

The use of radical addition reactions to detect short-lived radicals was first proposed by Janzen (1) in 1965. Since then this technique for which Janzen and Blackburn (2) coined the name "spin trapping" has been extensively developed. Now it has become a powerful method widely used for the detection of short-lived paramagnetic intermediates in thermally, photochemically, and radiation-induced reactions as described in several review articles (3).

Although some early papers by Janzen and Blackburn (2) and Lagercrantz *et al.* (4) have pointed out the possible application of spin trapping in photochemistry of coordination compounds, its wider use has been reported only relatively recently. There are many reasons behind this: some are subjective (as for a long time nitroxyl radical chemistry did not find any interest among inorganic chemists) but the peculiarities of metal complexes complicating the application of the spin-trapping technique may have played a significant role.

In this paper we would first like to discuss some general problems connected with the application of the spin-trapping technique (exclusively based on the nitroxyl method) to the photochemistry of metal complexes, we then turn to some reactions in detail. Other questions will be considered at the end of the paper.

## 2. General modes of interactions of metal complexes with spin traps and spin adducts

Quantum yields for the production of short-lived paramagnetic species from typical photoactive coordination compounds are often less than 0.1. Due to further reactions with either the solvent or the metal complex the stationary concentration of the paramagnetic intermediate is normally extremely low. As a result there is only a very limited number of publications on direct electron spin resonance detection of short-lived paramagnetic species during the photolysis of coordination compounds in liquid solution.

The spin-trapping technique, which normally leads to very persistent radicals exhibiting well-resolved esr spectra, therefore, would be a recommendable method for the detection of these species. One of the conditions to be met by the spin traps is that they do not interfere with the photochemical reaction of the metal complex. However, this condition is seldom fulfilled. Since radicals photogenerated from coordination compounds often undergo secondary reactions with the metal complex, at least the total quantum yield of metal reduction and/or oxidation is influenced by the

0008-4042/82/121565-09$01.00/0

©1982 National Research Council of Canada/Conseil national de recherches du Canada

Can. J. Chem. Downloaded from www.nrcresearchpress.com by 210.87.254.42 on 09/06/12
For personal use only.

presence of the spin trap. It is, however, by far more important that in many cases the metal complex reacts with the spin trap or with the nitroxides to form other radicals or to lead to the disappearance of radical signals.

From our experience, difficulties in the application of the spin-trapping technique to the photochemistry of coordination compounds do arise from the interaction of the nitroxide spin adducts with the metal complex rather than from the interactions of the spin trap with the complex.

Despite the low complexing ability of nitroso compounds and nitrones, however, there are some known examples of nitroso compounds which react with metal complexes by substitution (6). Due to the low $\pi$-acceptor ability of nitroso compounds such reactions are expected only for electron-rich complexes, i.e. metal complexes in a low oxidation state such as organometallic compounds. Typical Werner-type complexes such as Co(III), Cu(II), and Fe(III) normally do not interact with nitroso compounds and nitrones by substitution. Furthermore, Blount *et al.* (7) have shown that nitrones and also nitroso compounds exhibit a large electroinactive window, i.e. a potential range where they can be neither oxidized nor reduced. In accordance with these investigations we have preference for the spin traps nitrosodurene (ND) and C-phenyl N-*tert*-butyl nitrone (PBN), which are found to be stable even toward oxidation by Ce(IV), at least in neutral solution. However, in acidic or alkaline solutions redox reactions have to be considered. Thus, during the reaction of $UO_2(NO_3)_2 \cdot 6H_2O$ with ND in the presence of $CF_3COOH$ or $CCl_3$-COOH, the spectrum of a radical showing large $^{14}N$-hyperfine splitting ($a_N = 3.36$ mT, $a_H^1 = 0.195$ mT (3H), $a_H^2 = 0.056$ mT (4H)) could be observed (8). It has to be noted that such a signal assigned to the nitrosodurene cation radical ($ND^{+\cdot}$) is detectable only in strongly acidic media. Weaker acids such as acetic acid and propionic acid do not stabilize $ND^{+\cdot}$. On the other hand, nitrosodurene anion radical ($ND^{-\cdot}$) is considerably more stable. It could be detected during many different photoreactions, e.g. $[Cr(CN)_5NO]^{3-}$ in alkaline methanol, $NO_2^-$ and $NO_2$ in alcohols, and $UO_2^{2+}$ in $CH_2Cl_2$/alcohol (9). Surprisingly, $ND^{-\cdot}$ was also observed during the photolysis of Ce(IV) in alcohols (10). However, it could be shown that $ND^{-\cdot}$ stems from secondary photoreaction of $NO_2^-$ which is a byproduct of the photoreduction of $(NH_4)_2[Ce(NO_3)_6]$ with polychromatic light.

The $^{14}N$ hyperfine splitting of $ND^{-\cdot}$ varies from about 1.2 to 1.4 mT depending on the solvent and the metal complex. Obviously, there are coordinative interactions of $ND^{-\cdot}$ with metal ions and metal complexes. However, in those cases where the metal ion has no nuclear spin, it is not easy to make a clear distinction between free nitrosodurene anion radicals and coordinated ones. Probably, the triplets observed by Giannotti *et al.* (11) and Gasanov and Freidlina (12), originally assigned to U(IV) or U(III) and $Cr(CO)_5Cl$ spin adducts, respectively, correspond to the nitrosodurene anion radical.

In comparison with nitroso compounds and nitrones, nitroxides normally interact more strongly with metal complexes. It is well known that nitroxides behave as Lewis bases which may coordinate to metal centers (13).

[1] $\dot{N}(+)—\bar{O}|^- + M \rightleftharpoons \dot{N}(+)—\bar{O}|^- \longrightarrow M$

This effect is often indicated only by an increased line-width. However, under certain circumstances drastic changes in hyperfine splitting patterns are observed. Thus, for 1-hydroxyalkyl duryl nitroxides significantly increased $\beta$-hydrogen hyperfine splittings were found in the presence of uranyl ions indicating the formation nitroxide complexes with $UO_2^{2+}$, **I** (14).

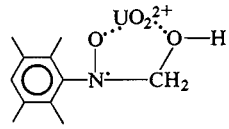


**I**

It should be noted that the two $\beta$-protons still remain equivalent, probably due to twisting vibrations of the chelate ring. A more pronounced interference to the spin-trapping method is caused by redox reactions of metal complexes with nitroxides. Since this effect is a kinetically-controlled reaction, the stability of sterically more shielded nitrosodurene spin adducts is greater than the spin adducts of, e.g., 2-methyl-2-nitroso propane (MNP). Therefore, nitrosodurene appears to be a more reliable spin trap for reactions of metal complexes than aliphatic nitroso compounds. However, in most cases the lifetime of spin adducts is so short that they can be detected only *in situ*. In some cases, the spin-trapping technique breaks down completely. For example, we have studied the photoreaction of dithiolato nickel(II) complexes in halocarbon solvents (15). During the photolysis of Ni(II) chelates, **II** and **III**, the esr signal of Ni(III) $(MNT)_2^-$ ($g = 2.063$ (16)) was readily detectable. Furthermore, from scavenging experiments with

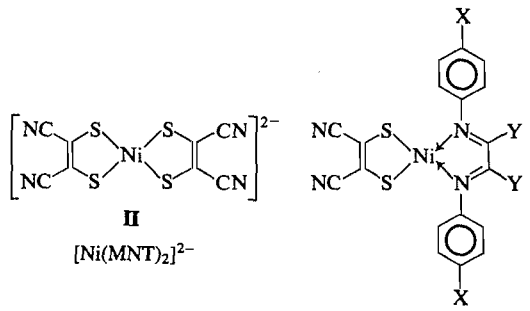

II
$[Ni(MNT)_2]^{2-}$

III
X = Cl, $CH_3$, $OCH_3$
Y = H, $CH_3$

acrylamide in $CCl_4$ this process was clearly shown to be radical in nature (reaction [2]).

[2] $Ni(II) + RX \xrightarrow{h\nu} Ni(III) + R^{\cdot} + X^{-}$

However, no spin adducts could be observed in the presence of spin traps such as nitrosodurene, 2-methyl-2-nitroso propane, and phenyl *N-tert*-butyl nitrone. Mixing of independently prepared nitroxides with $Ni(MNT)_2^{2-}$ immediately led to the formation of a Ni(III) complex, indicating that nitroxides are readily reduced by Ni(II).

On the other hand, the oxidizing properties of many coordination compounds exclude the application of spin traps such as that proposed by Pacifici and Browning (17), since aroxyl radicals may be formed thermally, reaction [3].

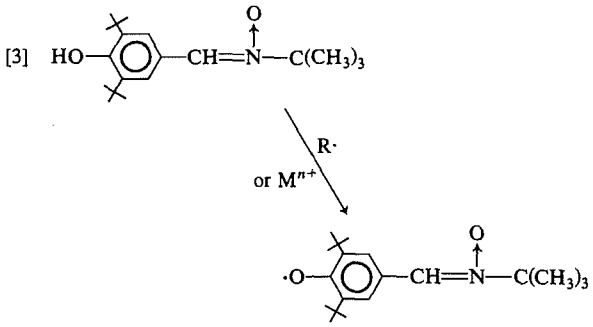

Further problems do arise from the photochemical behaviour of spin traps and spin adducts.

Nitroso compounds exhibit weak absorption bands in the visible spectral region (n,π* transitions of monomeric form) and strong bands in the uv region (π,π*), whereas nitrones have absorptions only in the uv region (18). These absorption bands can act as internal filters, thus leading to complications in quantitative photochemical studies. However, it is by far more important that irradiation into these bands can lead to formation of nitroxide radicals as it was shown for both aliphatic nitroso compounds (19) and nitrones (3*a*, 20). The main advantage of aromatic nitroso compounds is in their greater photochemical stability, albeit a slight photosensitivity has been reported even for the sterically-hindered aromatic nitroso compounds (21).

Furthermore, the resulting nitroxides are known to be very efficient quenchers for both excited singlet and triplet states (22). However, since lifetime of excited states of metal complexes normally is very short ($\ll 10^{-6}$ s), substantial quenching is expected for extremely high concentrations of nitroxides, i.e., after long irradiation time, only.

A further possibility of interference by spin traps is related to radical recombination processes which may be suppressed by spin traps.

If there is a photochemical process with geminate radical pairs formed, which underlies a very efficient recombination process, the quantum yield normally will be close to zero (Scheme 1).

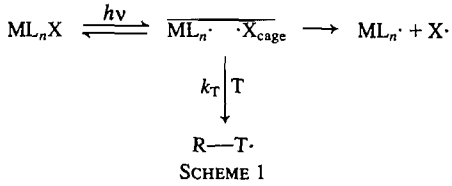

SCHEME 1

The fraction of radicals which escapes the cage in the presence of a scavenger T, but otherwise would undergo secondary recombination, has been derived by Noyes (23) as to be given by eq. [4].

[4] $P = 2a(2\pi k_T c_T)^{1/2}$

where $a = 10^{-6}$ s$^{1/2}$ (23).

It is important to know that spin traps can serve as such scavengers. The photoreactions of alkyl cobaloximes and alkyl cobalamines studied by Giannotti *et al.* (24) and Roewer *et al.* (25), respectively, are well known examples for such a type of interference.

It is quite interesting that neglecting the possibility of such interaction may lead to qualitatively different results as it was shown in the case of copper(II) chelates with sterically-hindered 1,2-diimine ligands such as dmp (dmp = 2,9-dimethyl-1,10-phenanthroline) (26).

From scavenger experiments Sundararajan and Wehry (27) deduced the radical nature of the photoreaction in alcoholic solutions. However, no evidence for free radicals was found by low temperature esr experiments or by spin-trapping studies with low spin trap concentrations. Flash photolysis demonstrates that the reaction may be described by Scheme 2 (26).

Can. J. Chem. Downloaded from www.nrcresearchpress.com by 210.87.254.42 on 09/06/12
For personal use only.

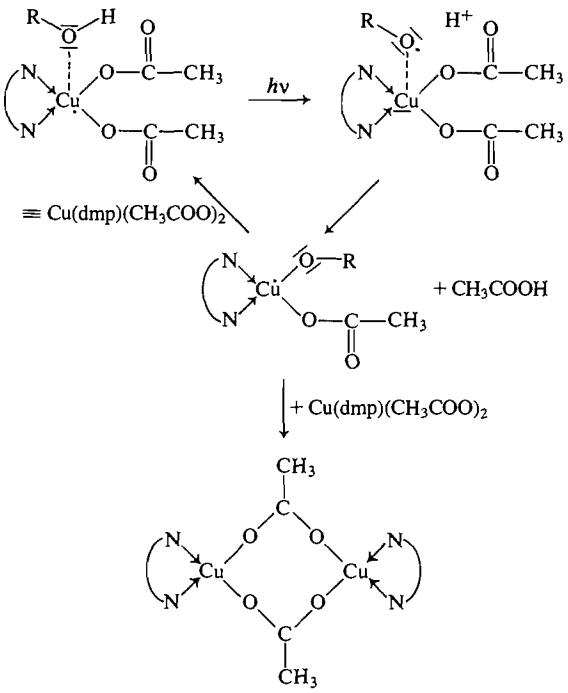


SCHEME 2

Using very high concentrations of spin traps, esr signals of alkoxy spin adduct could be detected in the case of 2-methyl propane-1-ol. The signal intensity was found to be linearly dependent on the square root of spin trap (PBN) concentration as one would expect from Noyes' theory (23).

However, flash experiments show that it is quite understandable for spin traps to interact with the primarily formed Cu(I)–alkoxyl pair and that the reaction in alcohols is, unlike in nonpolar solvents (28), indeed a non-radical one.

The interaction of spin traps with caged radicals seem to be a general problem in photochemistry of metal complexes. In this case the study of concentration dependency does offer an opportunity to distinguish between free and caged radicals.

### 3. Application of the spin-trapping technique to photochemistry of coordination compounds

#### *3.1. Spin trapping of organic free radicals formed in photoreactions of coordination compounds*

Already in the early stages of spin-trapping studies (2, 4, 5), the photolytic scission of organometallic complexes, e.g. $Et_4Pb$, $Bu_4Sn$, $Bu_3SnCl$, $Pb(CH_3COO)_4$, $Tl(CH_3COO)_3$ etc., has been reported. However, the aim of investigations of such compounds was directed to well-defined radical sources rather than to the study of unknown photoreactions. The first interesting results (with respect to photochemistry) came from the investigations by Ledwith *et al.* (29) who showed that uranyl nitrate, which so far was known to react with alcohols exclusively by α-hydrogen abstraction, reaction [5], can also react by electron transfer, reaction [6].

[5] $*UO_2^{2+} + R'RCHOH \rightarrow UO_2H^{2+} + R'\dot{R}COH$

[6] $*UO_2^{2+} + R'RCHOH \searrow UO_2^{+} + R'RCH\dot{O}H^{+}$ $(R'RCHO\cdot + H^{+})$

These investigations have also been extended to other alcohols (9) and other metal ions such as Ce(IV) (10), Cr(VI) (30), Fe(III) (31), and V(V) compounds (32). It should be noted that the alkoxyl radicals, although easily detectable by spin trapping, hitherto have not been detected in photoreactions of coordination compounds by other spectroscopic methods.

Alkoxyl radicals have also been trapped during the aerobic photolysis of alkyl cobalt(III) complexes (24, 25). However, up till now it is not clear whether these radicals are really free radicals produced by the cleavage of cobalt peroxyl complexes, reaction [7], or if they are produced by the decay of the peroxyl spin adducts (33).

[7] $\left[\begin{matrix}OOR\\|\\Co\end{matrix}\right] \xrightarrow[\text{or } kT]{h\nu} \left[\begin{matrix}O\cdot\\|\\Co\end{matrix}\right] + RO\cdot$

Since it is known (34–36) that the alkyl peroxyl spin adducts of PBN are sufficiently stable to be detected at lower temperatures, reexamination of the aerobic photolytic decomposition of alkyl cobalt(III) complexes at low temperature should provide more information concerning the primary photochemical processes.

The high sensitivity of the spin-trapping method does permit the study of the outer-sphere redox reactions which proceed only with low quantum yields. Thus, organic free radicals formed during the photoreaction of Co(III) and Cu(II) ion pairs with tetraphenylborate were readily detected by spin trapping (37, 38). In this context, it is quite interesting that during the photolysis of tetraphenylborates, phenyl radicals are observed exclusively, unlike the photolytic decomposition of tetraphenylborates of aryl diazonium salts (39) and diaryl iodonium salts which lead to both phenyl radicals and diphenyl(phenylcyclohexadienyl)borane radicals. The latter may be trapped by nitrosodurene ($a_N = 1.38$ mT, $a_H = 1.44$ mT).

In contrast to these results, no radicals have been detected with PBN during the electrochemical

Can. J. Chem. Downloaded from www.nrcresearchpress.com by 210.87.254.42 on 09/06/12
For personal use only.

Can. J. Chem. Downloaded from www.nrcresearchpress.com by 210.87.254.42 on 09/06/12
For personal use only.

oxidation of $BPh_4^-$ (40). Probably metal ions can catalyze the formation of phenyl radicals from diphenyl(phenylcyclohexadienyl)borane.

*3.2. Trapping of atoms and inorganic radicals*

Upon photolysis many coordination compounds yield short-lived paramagnetic species such as atoms or small reactive radicals, e.g. $\cdot N_3$, $\cdot NO_3$, $\cdot CN$, $\cdot SO_4^-$, $\cdot OH$, $\cdot O_2^-$ etc., which are often named inorganic radicals. The possibility of spin trapping of hydrogen atoms has been known for a long time (see ref. 3*a* and references therein). Its formation during the photolysis of alkyl cobaloximes has been shown by Giannotti and Bolton (24*a*) using PBN and 5,5-dimethyl pyrroline-1-oxide (DMPO) as spin traps, respectively. These authors found that hydrogen atoms stem from the equatorial oxime ligand, whereas the corresponding alkyl cobalamines give hydrogen atoms only when the axial alkyl ligand has active β-hydrogen atoms (25*b*). However, it has been pointed out that the formation of hydrogen spin adduct is very likely due to the thermal reaction of PBN with intermediate Co(III) hydride complex.

Although fluorine atoms were shown to form stable spin adducts with PBN (3*a*), hitherto no examples are known for the formation of F· atoms from photoexcited coordination compounds.

Very recently we were able to detect chlorine atoms during the photolysis of $(Bu_4N)_3[Co(C_2O_4)_2Cl_2]$ ($C_2O_4^{2-}$ = oxalate anion) in $CH_2Cl_2$ using PBN as a spin trap ($a_N$ = 1.21 mT, $a_H$ = 0.072 mT, $a_{^{35}Cl}$ = 0.61 mT, $a_{^{37}Cl}$ = 0.49 mT). On the other hand, all attempts to detect Cl· atoms during the photolysis of chlorocuprates(II) and $[Cu(dmp)_2Cl]Cl$ hitherto did not succeed.

It has been expected that photolysis of $[Cu(dmp)_2Br]Br$ and $[Co(phen)_2Br_2]Br$ yields bromine atoms. However, only in the presence of PBN could the benzoyl *tert*-butyl nitroxide ($a_N$ = 0.79 mT) be observed. Interestingly, Gasanov and Freidlina (41) have detected a spin adduct ($a_N$ = 1.48 mT, $a_H$ = 0.62 mT) showing no bromine hyperfine splitting which they have assigned to the Br· adduct to PBN.

In benzene we obtained the spin adduct of a 4-substituted phenyl radical ($a_N$ = 0.95 mT, $a_H$ = 0.27 mT (2H)) with nitrosodurene as a spin trap. This spin adduct may be attributed to the 4-bromo phenyl adduct (42). Its formation may be explained by Scheme 3.

$[Cu(dmp)_2NO_3]NO_3$ was found to react in a similar way. However, since no hyperfine splitting due to substituents in the 4-position has been resolved, these experiments are not of much use as diagnostic probes except in decision-making as to whether or not a reaction proceeds via free radicals.

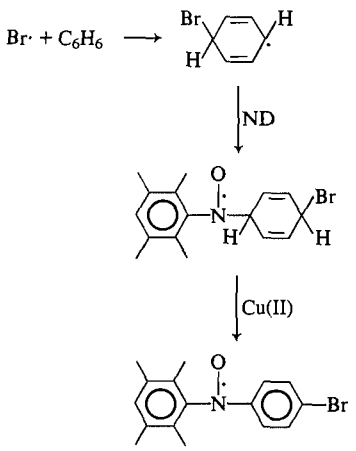


SCHEME 3

Spin trapping of pseudohalide radicals is possible too. It was shown that azidyl radicals, $\cdot N_3$, produced by the photolysis of $[Co(NH_3)_5N_3]^{2+}$ and $[Co(CN)_5N_3]^{3-}$, respectively, are readily trapped by both PBN and nitrosodurene (43). It is interesting that $\cdot N_3$ radicals normally are not detectable by other methods such as flash photolysis. Recently Janzen *et al.* (44) and Kremers and Singh (45) confirmed the possibility of spin trapping of $\cdot N_3$ radicals by nitrones. Furthermore, the latter could show that DMPO is a very efficient spin trap for both $\cdot N_3$ and $(N_3)_2^{-\cdot}$ radicals.

Surprisingly, spin adducts of $\cdot N_3$ radicals with nitrosodurene are very persistent too (43*b*). The esr spectrum exhibits a 1:2:3:2:1 quintet of triplets which has been assigned to structure **IV**.

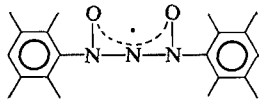


**IV**

Although it has been proved that this spin adduct really originates from $\cdot N_3$ radicals (or ·N atoms!), the mechanism of its formation remains unclear. Based on the recently published paper by Suehiro *et al.* (46), who showed that nitrosodurene can act as spin trap in its dimeric form, the mechanism in Scheme 4 seems to be very likely.

This suggestion is further supported by the fact that the intensity of the esr signal correlates well with the concentration of dimeric nitrosodurene rather than with the monomer concentration. The possibility of spin trapping of other pseudohalide radicals such as ·CN and ·OCN has been demonstrated by Janzen *et al.* (44). In this context it should be noted that during the photolysis of

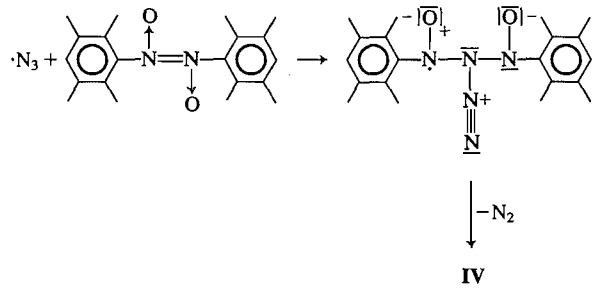

IV

SCHEME 4

$Mo(CN)_8^{3-}$ in methanol at −80°C we were able to detect a weak esr signal of a spin adduct to PBN ($a_N^1$ = 1.46 mT, $a_N^2$ = 0.16 mT, $a_H$ = 0.46 mT). Based on the data given by Mao and Kevan (49), this spin adduct was originally attributed to ·CN radical (48). However, it was shown by Janzen *et al.* (44) that this assignment is obviously not correct. Thus the assignment of the spin adduct reported by Mao and Kevan and by ourselves still remains unclear. It is quite interesting that in $CH_2Cl_2$ instead of methanol, the ·CN spin adduct to PBN ($a_N$ = 1.49 mT, $a_H$ = 0.20 mT) can be readily observed during the photolysis of $Mo(CN)_8^{3-}$. In methanol, $\cdot OCH_3$ radicals are the major oxidation product (48). Other important intermediates during the photolysis of metal complexes are known to be hydroxyl, ·OH, and superoxide, $\cdot O_2^-$, radicals, respectively. Both Harbour, Chow, and Bolton (50) and Janzen *et al.* (51) have shown that these radicals add readily to nitrones to give quite persistent spin adducts. However, the stability of superoxide spin adduct was found to be strongly dependent on pH (52).

Recently Giannotti *et al.* (53) and Harbour and Hair (54) have studied the formation of superoxide radicals during the photolysis of porphyrins and phthalocyanines, both in its free and metal-complexed form. The spin-trapping technique was found to be a reliable method for the elucidation of rather complicated photochemical mechanisms.

Hydroxyl radicals were formed during the photolysis of $Mo(CN)_8^{3-}$ and $W(CN)_8^{3-}$ in aqueous solution, whereas irradiation ($\lambda > 320$ nm) of the corresponding Mo(IV) and W(IV) complexes, respectively, did not give rise to any free radicals. In these experiments, DMPO could be used as spin trap without any detectable interference.

With regard to the experiments made with Mo(IV) and W(IV), it was very surprising for us to find signals of ·OH spin adducts to DMPO when solutions containing $Mo(CN)_8^{4-}$ and $Cu^{2+}$ were irradiated with light of $\lambda > 320$ nm. Since neither of these compounds alone cause the formation of hydroxyl radicals, a sequential two-photon process is assumed (55), see Scheme 5.

It has to be stressed that the lifetime of the Cu(I), Mo(V) couple, formed by irradiation into the intervalence charge transfer band, is less than $10^{-6}$ s, as confirmed by flash experiments. The formation of hydroxyl radicals during the irradiation of $Cu^{2+}/Mo(CN)_8^{4-}$ solutions is further confirmed by the bleaching of 4-*N*,*N*-dimethylaminonitrosobenzene which is known to be a very efficient ·OH scavenger (56). In principle, it is also possible to detect solvated electrons by the spin-trapping technique. Since solvated electrons are common intermediates in many photooxidation reactions of low-valent coordination compounds, e.g., $Mo(CN)_8^{4-}$, $W(CN)_8^{4-}$, $Fe(CN)_6^{4-}$, and $Ru(CN)_6^{4-}$ (57), such a simple method for the detection of solvated electrons would be of great importance to inorganic photochemists. Indeed, it was found that nitroso compounds are able to trap solvated electrons forming anion radicals (8*c*, 58), but this reaction is not a very efficient one. On the other hand, if there are additional typical electron scavengers such as carbon halides and thio-compounds, formation of alkyl spin adducts may be used as a diagnostic probe for solvated electrons provided other strongly reducing species are absent.

$$Cu^{2+} + [Mo(CN)_8]^{4-} \rightleftharpoons Cu^{2+}, [Mo(CN)_8]^{4-}$$

$$\downarrow h\nu_1 \ (\lambda = 500\ \text{nm})$$

$$Cu^{+}, [Mo(CN)_8]^{3-}$$

$$\downarrow h\nu_2, H_2O \ (\lambda = 385\ \text{nm})$$

$$Cu^{+} + [Mo(CN)_8]^{4-} + \cdot OH$$

SCHEME 5

### 3.3. *Spin trapping of metal-centered free radicals*

The photolysis of coordination compounds often leads to both free organic or inorganic radicals, ·X, and unstable coordinatively unsaturated metal fragments, $\cdot ML_n$, reaction [8].

$$[8] \quad ML_nX \xrightarrow{h\nu} ML_n\cdot + \cdot X$$

In some cases the metal fragment, which is sometimes named metallo radical, may also be trapped by the usual spin traps. The first examples were reported by Waters *et al.* (59), who demonstrated the trapping of $Co(CN)_5^{3-}$ by both aromatic and aliphatic nitroso compounds. However, first reference to photochemistry was made by Hudson *et al.* (60) who showed that carbonyl complex fragments

Can. J. Chem. Downloaded from www.nrcresearchpress.com by 210.87.254.42 on 09/06/12
For personal use only.

TABLE 1. Electron spin resonance parameters of spin adducts with metal-centered radicals[a]

| Radical | Spin trap[b] | $a_N$ | $a_M$ | $a_L$ | $a_H$ | $g$ | Reference |
|---|---|---|---|---|---|---|---|
| $Co(CN)_5^{3-}$ | NB | 1.38 | 1.06 ($^{59}$Co) | | 0.32 ($a_H^{o,p}$) | 2.0051 | 59*a* |
| $Co(CN)_5^{3-}$ | MNP | 1.87 | 1.11 ($^{59}$Co) | | 0.11 ($a_H^m$) | 2.0054 | 59*b* |
| $Co(dmg)_2$[c] | NB | 1.30 | 1.30 ($^{59}$Co) | | | | 59*a* |
| $Mo(CN)_7^{2-}$ | ND | 0.38 | 3.56 ($^{95,97}$Mo) | | | 1.9823 | 48 |
| $Fe(CO)_4Cl$ | MNP | 1.58 | | 0.09 (Cl) | | 2.0049 | 41 |
| $UCp_3$ | ND | 1.306 | | | | 2.0076 | 11 |
| $Mn(CO)_5$ | ND | 1.59 | 0.88 ($^{55}$Mn) | | | 2.006 | 60*b* |
| $Mn(CO)_5$ | MNP | 1.66 | 0.69 ($^{55}$Mn) | | | 2.006 | 60*b* |
| $Mn(CO)_5$ | BNB | 1.325 | 0.715 ($^{55}$Mn) | | 0.168 | | 65 |
| $Mn(CO)_5$[d] | BNB | 1.13 | 0.325 ($^{55}$Mn) | | 0.17 | | 65 |
| $Re(CO)_5$ | BNB | 1.175 | 0.183 ($^{185,187}$Re) | | 0.165 | | 65 |
| $Re(CO)_5$ | ND | 1.47 | 0.409 ($^{185,187}$Re) | | | 2.01 | 60*b* |
| $C(O)Mn(CO)_4$ | BNB | 0.900 | 2.15 ($^{55}$Mn) | | 0.19 | | 65 |
| $Co(CO)_3P(OEt)_3$ | ND | 1.79 | 1.39 ($^{59}$Co) | 0.45 (P) | | 2.007 | 60*b* |
| $Fe(Cp)(CO)_2$ | ND | 1.75 | | | | 2.005 | 60*b* |
| $Mo(Cp)(CO)_3$ | ND | 1.45 | 0.40 ($^{95,97}$Mo) | | | 2.005 | 60*b* |
| $Mn(CO)_4P(OPh)_3$ | ND | 1.59 | 0.89 ($^{55}$Mn) | 1.44 (P) | | 2.006 | 60*b* |
| $Mn(CO)_4PMePh_2$ | ND | 1.59 | 0.82 ($^{55}$Mn) | 1.29 (P) | | 2.006 | 60*b* |
| $Mn(CO)_4PMe_2Ph$ | ND | 1.59 | 0.84 ($^{55}$Mn) | 1.31 (P) | | 2.006 | 60*b* |
| $Mn(CO)_4PBu_3$ | ND | 1.59 | 0.86 ($^{55}$Mn) | 0.93 (P) | | 2.006 | 60*b* |
| $Mn(CO)_4P(C_6H_{11})_3$ | ND | 1.59 | 0.87 ($^{55}$Mn) | 0.92 (P) | | 2.006 | 60*b* |
| $Mn(CO)_4Mn(CO)_5$ | ND | 1.67 | 0.99 ($^{55}$Mn) | 0.33 ($^{55}$Mn) | | | 60*b* |
| $Mn(CO)_4PPh_3$ | MNP | 1.944 | 1.133 ($^{55}$Mn) | 0.386 (P) | | | 66 |
| $Mn(CO)_4py$ | MNP | 1.792 | 1.169 ($^{55}$Mn) | 0.058 (N) | | | 66 |
| $Mn(CO)_4PEt_3$ | MNP | 1.880 | 1.090 ($^{55}$Mn) | 0.462 (P) | | | 66 |
| $Mn(CO)_4PPh_2Me$ | MNP | 1.916 | 1.107 ($^{55}$Mn) | 0.544 (P) | | | 66 |
| $Mn(CO)_4P(4\text{-}CH_3C_6H_4)_3$ | MNP | 1.937 | 1.130 ($^{55}$Mn) | 0.395 (P) | | | 66 |
| $Mn(CO)_4P(3\text{-}CH_3C_6H_4)_3$ | MNP | 1.953 | 1.139 ($^{55}$Mn) | 0.386 (P) | | | 66 |
| $Mn(CO)_4PPh(OMe)_2$ | MNP | 1.924 | 1.077 ($^{55}$Mn) | 0.609 (P) | | | 66 |
| $Mn(CO)_4P(OEt)_3$ | MNP | 1.917 | 1.097 ($^{55}$Mn) | 0.697 (P) | | | 66 |
| $Mn(CO)_4PEt_2Ph$ | MNP | 1.917 | 1.111 ($^{55}$Mn) | 0.558 (P) | | | 66 |
| $Cr(CO)_5Cl$ | MNP | 0.73 | 1.86 ($^{53}$Cr) | | | 1.9993 | 12 |
| $Cr(CO)_4Cl$ | MNP | 0.83 | 1.86 ($^{53}$Cr) | | | 1.9983 | 12 |
| $Cr(CO)_4Cl$ | BNB | 0.80 | | | 0.17 | 2.0043 | 12 |

[a]Hyperfine coupling constants in mT; interacting nucleus in parentheses.
[b]NB = nitrosobenzene; ND = nitrosodurene; MNP = 2-methyl-2-nitroso propane; BNB = 2,4,6-tri-*tert*-butyl nitrosobenzene.
[c]*dmg = diacetyldioxime.*
[d]Anilino radical.

of transition metals such as Mn, Re, Mo, Co, and Fe may be trapped by nitrosodurene. Later, the list of possible spin adducts with metallo radicals has been extended to further examples, see Table 1. It should be noted that these spin adducts are often photochemically unstable and decompose as in reaction [9].

$$[9]\quad R{-}\overset{\displaystyle O}{\overset{|}{N}}{\cdot}{-}ML_n \xrightarrow{h\nu} RNO^{-\cdot} + ML_n^{+}$$

Probably for that reason, only nitrosomesitylene anion radicals have been observed during the photolysis of $[Co(CN)_5N_3]^{3-}$. Interestingly, $Mo(CN)_7^{2-}$ forms rather stable spin adducts with both nitrosodurene and nitrosomesitylene even during irradiation (48). As shown by Alberti and Camaggi (61), nitro compounds may serve as efficient spin traps for manganese-centered radicals too.

Metallo radicals formed by photolysis of Group IVB organometallic compounds are not trapped by nitroso compounds (62). Instead, they add to nitro derivatives affording the corresponding relatively stable oxynitroxides (63). (For spin trapping with aromatic and aliphatic ketones, which will not be considered here, see ref. 64 and references therein.)

It is interesting that the same entire spectrum obtained by Davies and Hawari (63*c*) in the reaction of $Bu_3Sn\cdot$ with 2-nitro-2-methyl-propane was found during the photolysis of tributyl stannyl chromate(VI) in the presence of MNP (67). Thus it is assumed that the formation of tributylstannoxyl radicals, $Bu_3SnO\cdot$, is by cleavage of the Cr—O bond.

$$[10]\quad Bu_3Sn{-}O{-}Cr(O)_2OSnBu_3 \xrightarrow{h\nu} Bu_3SnO\cdot + \cdot Cr(O)_2OSnBu_3$$

$$[11]\quad Bu_3SnO\cdot + O{=}N{-}C(CH_3)_3 \rightarrow Bu_3Sn{-}O{-}\overset{\displaystyle O}{\overset{|}{N}}{\cdot}{-}C(CH_3)_3$$

$Bu_3SnO\cdot$ radicals may be trapped by PBN too ($a_N$ = 1.41 mT, $a_H$ = 0.21 mT, Sn hyperfine splitting not clearly resolved). It should also be noted that

Can. J. Chem. Downloaded from www.nrcresearchpress.com by 210.87.254.42 on 09/06/12
For personal use only.

germanium-centered radicals may be trapped by PBN (68).

*3.4. Detection of singlet oxygen*

The Detection of singlet oxygen ($^1\Delta_g$) by a spin-trapping-like reaction of 2,2,6,6-tetramethyl piperidine with $^1O_2$ to form stable piperidineoxyl radical was first demonstrated by Lion, Delmelle, and Van de Vorst (69). This is no doubt one of the most remarkable results in application of spin-trapping technique to photochemical problems.

Recently it was shown by several authors (53*a*, 70) that $^1O_2$ may also be detected by this method during photoreactions of metal complexes. However, the possibility of formation of piperidineoxyl radicals by other reactions, e.g. by reaction with peroxyl radicals (71) or with oxidizing metal complexes, has to be taken into account before one turns to wider applications, of this attractive method. No systematic studies of formation of piperidineoxyl radicals by reactions other than $^1O_2$ have been published up till now.

## 4. Concluding remarks

The spin-trapping technique provides a useful method for the detection of short-lived paramagnetic species formed in the photoreaction of coordination compounds. If one considers possible side reactions (redox reactions, substitution), usually there is no special problem in the spin trapping of organic free radicals in the presence of metal complexes. However, spin trapping of typical inorganic radicals is by far less well understood, thus, spin trapping of a series of important inorganic radicals, e.g. $NO_3$, $NH_2$, SCN, Br, I, still remains an open problem. The detection of coordinatively unsaturated paramagnetic metal complexes is limited to organometallic species and to some cyano complexes. The interactions of nitroso compounds with complex fragments, which contain more than one unpaired electron, have not been studied systematically up till now.

Most of the spin-trapping studies concerning the photoreactions of coordination compounds hitherto published were made in non-aqueous solutions. Considerable progress is expected by using water-soluble spin traps such as DMPO (72) and recently described substituted C-aryl nitrones (73). However, till now no soluble nitroso compounds are known to be suitable for the study of photoreactions in aqueous solution.

The main disadvantage of any spin trap based on the formation of stable nitroxides may be attributed to its limitation only to neutral or weakly acidic media. No spin trapping is possible with nitroso compounds and nitrones in strongly acidic solutions.


1. E. G. JANZEN. Chem. Eng. News, **43**, 50 (1965).
2. E. G. JANZEN and B. J. BLACKBURN. J. Am. Chem. Soc. **91**, 4481 (1969).
3. (*a*) E. G. JANZEN. Acc. Chem. Res. **4**, 31 (1971); (*b*) M. J. PERKINS. Essays on free-radical chemistry, Spec. Publ. No. 24, The Chemical Society, Burlington House, London 1970. Chapt. 5, p. 97; (*c*) C. LAGERCRANTZ. J. Phys. Chem. **75**, 3466 (1971); (*d*) E. G. JANZEN. Creat. Detect. Excited State, **4**, 83 (1976); (*e*) R. KH. FREIDLINA, I. I. KANDROR, and R. G. GASANOV. Usp. Khim. **47**, 508 (1978); (*f*) V. E. ZUBAREV, V. N. BELEVSKIJ, and L. T. BUGAENKO. Usp. Khim. **48**, 1361 (1979); (*g*) V. N. BELEVSKIJ. Khim. Vys. Energ. **15**, 3 (1981); (*h*) D. REHOREK. Z. Chem. **20**, 325 (1980); (*i*) K. TORSSELL. Tetrahedron, **26**, 2759 (1970); (*j*) M. L. HAIR and J. R. HARBOUR. Adv. Chem. Ser. **184**, 173 (1980).
4. E. G. JANZEN and J. L. GERLOCK. Nature, **222**, 867 (1967).
5. S. FORSHULT, C. LAGERCRANTZ, and K. TORSSELL. Acta Chem. Scand. **23**, 522 (1969).
6. E. DINJUS, D. WALTHER, R. KIRMSE, and J. STACH. J. Organomet. Chem. **198**, 215 (1980).
7. G. L. MCINTIRE, H. N. BLOUNT, H. J. STRONKS, R. V. SHETTY, and E. G. JANZEN. J. Phys. Chem. **84**, 916 (1980).
8. (*a*) D. REHOREK. Z. Chem. **19**, 227 (1979); (*b*) E. G. DEROUANE, J. N. BRAHAN, and R. HUBIN. J. Catal. **35**, 196 (1974); (*c*) S. MURABAYASHI, M. SHIOTAMI, and J. SOHMA. J. Phys. Chem. **83**, 844 (1979).
9. D. REHOREK. Z. anorg. allg. Chem. **443**, 255 (1978).
10. D. REHOREK. Acta Chim. Budapest, **101**, 395 (1979).
11. E. KLÄHNE, C. GIANNOTTI, H. MARQUET-ELLIS, G. FOLCHER, and R. D. FISCHER. J. Organomet. Chem. **201**, 399 (1980).
12. R. G. GASANOV and R. KH. FREIDLINA. Dokl. Akad. Nauk SSSR, **254**, 113 (1980).
13. S. S. EATON and G. R. EATON. Coord. Chem. Rev. **26**, 207 (1978) and references therein.
14. D. REHOREK. Radiochem. Radioanalyt. Lett. **33**, 195 (1978).
15. D. REHOREK. Z. Chem. In press.
16. A. DAVISON, N. EDELSTEIN, R. H. HOLM, and A. H. MAKI. J. Am. Chem. Soc. **85**, 2029 (1963).
17. J. G. PACIFICI and H. L. BROWNING. J. Am. Chem. Soc. **92**, 5231 (1970).
18. (*a*) H. YOSHIDA and T. DOBA. Bull. Fac. Eng., Hokkaido Univ. **91**, 161 (1976); (*b*) T. DOBA, T. ICHIKAWA, and H. YOSHIDA. Bull. Chem. Soc. Jpn. **50**, 3158 (1977); (*c*) Y. MAEDA and K. U. INGOLD. J. Am. Chem. Soc. **101**, 4975 (1979).
19. (*a*) A. MACKOR, TH. A. J. W. WAJER, TH. J. DE BOER, and J. D. W. VAN VOORST. Tetrahedron Lett. 2115 (1966); (*b*) TH. A. J. W. WAJER, A. MACKOR, TH. J. DE BOER, and J. D. W. VAN VOORST. Tetrahedron, **23**, 4021 (1967); (*c*) J. A. MAASSEN and TH. J. DE BOER. Recl. Trav. Chim. Pays-Bas Belg. **92**, 185 (1973).
20. E. FINKELSTEIN, G. M. ROSEN, and E. J. RAUCKMAN. J. Am. Chem. Soc. **102**, 4994 (1980)
21. L. R. C. BARCLAY, D. L. CARSON, J. A. GRAY, M. GROSSMAN, P. G. KHAZANIE, J. R. MILTON, and C. E. SCOTT. Can. J. Chem. **56**, 2665 (1978).
22. D. R. ANDERSON and T. H. KOCH. Tetrahedron Lett. 3015 (1977).
23. R. M. NOYES. J. Am. Chem. Soc. (*a*) **77**, 2042 (1955); (*b*) **78**, 5486 (1956).
24. (*a*) C. GIANNOTTI and J. R. BOLTON. J. Organomet. Chem.


Can. J. Chem. Downloaded from www.nrcresearchpress.com by 210.87.254.42 on 09/06/12
For personal use only.

Can. J. Chem. Downloaded from www.nrcresearchpress.com by 210.87.254.42 on 09/06/12
For personal use only.

**110**, 383 (1976); (*b*) PH. MAILLARD, J. G. MASSOT, and C. GIANNOTTI. J. Organomet. Chem. **159**, 219 (1978); (*c*) C. GIANNOTTI, G. MERLE, C. FONTAINE, and J. R. BOLTON. J. Organomet. Chem. **91**, 357 (1975); (*d*) D. A. LERNER, F. RICCHIERO, and C. GIANNOTTI. J. Phys. Chem. **84**, 3007 (1980).

25. (*a*) G. ROEWER, G. A. SHAGISULTANOVA, and I. W. WOJAKIN. J. Prakt. Chem. **319**, 1031 (1977); (*b*) G. ROEWER and D. REHOREK. J. Prakt. Chem. **320**, 566 (1978).
26. D. REHOREK, T. JARZYNOWSKI, and Z. STASICKA. J. Prakt. Chem. **322**, 411 (1980).
27. (*a*) S. SUNDARARAJAN and E. L. WEHRY. J. Inorg. Nucl. Chem. **34**, 3699 (1972); (*b*) S. SUNDARARAJAN and E. L. WEHRY. J. Phys. Chem. **76**, 1528 (1972).
28. D. REHOREK. (*a*) J. Signal AM, **6**, 221 (1978); (*b*) Tetrahedron Lett. 2611 (1977); (*c*) Z. Chem. **18**, 194 (1978).
29. A. LEDWITH, P. J. RUSSELL, and L. H. SUTCLIFFE. Proc. R. Soc. London A, **332**, 151 (1973).
30. D. REHOREK and R. WAGENER. (*a*) J. Prakt. Chem. **321**, 466 (1979); (*b*) Inorg. Chim. Acta, **33**, L 129 (1979).
31. D. REHOREK. (*a*) Z. Chem. **19**, 262 (1979); (*b*) **20**, 312 (1980).
32. S. M. ALIWI and C. H. BAMFORD. J. Chem. Soc. Faraday Trans. I, (*a*) **71**, 1733 (1975) (*b*) **73**, 776 (1977).
33. J. PFAB. Tetrahedron Lett. 843 (1978).
34. E. G. JANZEN, D. E. NUTTER, E. R. DAVIS, B. J. BLACKBURN, J. L. POYER, and P. B. MCCAY. Can. J. Chem. **56**, 2237 (1978).
35. J. A. HOWARD and J. C. TAIT. Can. J. Chem. **56**, 176 (1978).
36. M. V. MERRITT and R. A. JOHNSON. J. Am. Chem. Soc. **99**, 3713 (1977).
37. D. REHOREK, D. SCHMIDT, and H. HENNIG. Z. Chem. **20**, 223 (1980).
38. D. REHOREK, M. ACKERMANN, H. HENNIG, and P. THOMAS. Z. Chem. **19**, 149 (1979).
39. D. REHOREK and J. MARX. J. Prakt. Chem. **322**, 872 (1980).
40. E. E. BANCROFT, H. M. BLOUNT, and E. G. JANZEN. J. Am. Chem. Soc. **101**, 3692 (1979).
41. R. G. GASANOV and R. KH. FREIDLINA. Dokl. Akad. Nauk SSSR, **235**, 1309 (1977).
42. T. SUEHIRO, M. KAMIMORI, K. TOKUMARU, and M. YOSHIDA. Chem. Lett. 531 (1976).
43. (*a*) D. REHOREK, P. THOMAS, and H. HENNIG. Inorg. Chim. Acta, **32**, L1 (1979); (*b*) D. REHOREK and H. HENNIG. Z. Chem. **19**, 263 (1979).
44. E. G. JANZEN, H. J. STRONKS, D. E. NUTTER, E. R. DAVIS, H. N. BLOUNT, J. L. POYER, and P. B. MCCAY. Can. J. Chem. **58**, 1596 (1980).
45. N. KREMERS and A. SINGH. Can. J. Chem. **58**, 1592 (1980).
46. T. SUEHIRO, S. MASUDA, and N. MOTOYAMA. Chem. Lett. 53 (1980).
47. H. KARLSSON and C. LAGERCRANTZ. Acta Chem. Scand. **24**, 3411 (1970).
48. D. REHOREK, J. SALVETTER, A. HANTSCHMANN, H. HENNIG, Z. STASICKA, and A. CHODKOWSKA. Inorg. Chim. Acta, **37**, L471 (1979).
49. S. W. MAO and L. KEVAN. J. Phys. Chem. **80**, 2330 (1976).
50. J. R. HARBOUR, V. CHOW, and J. R. BOLTON. Can. J. Chem. **52**, 3549 (1974).
51. E. G. JANZEN, D. E. NUTTER, E. R. DAVIS, B. J. BLACKBURN, J. L. POYER, and P. B. MCCAY. Can. J. Chem. **56**, 2237 (1978).
52. G. R. BUETTNER and L. W. OBERLEY. Biochem. Biophys. Res. Commun. **83**, 69 (1978).
53. (*a*) P. MAILLARD, P. KRAUSZ, C. GIANNOTTI, and S. GASPARD. J. Organomet. Chem. **197**, 285 (1980); (*b*) G. S. COX, D. G. WHITTEN, and C. GIANNOTTI. Chem. Phys. Lett. **67**, 511 (1979).
54. J. R. HARBOUR and M. L. HAIR. J. Phys. Chem. **84**, 1500 (1980).
55. D. REHOREK, A. REHOREK, P. THOMAS, and H. HENNIG. Inorg. Chim. Acta. In press.
56. M. HATADA, I. KRALJIC, A. EL SAMALY, and C. N. FRUMBORE. J. Phys. Chem. **78**, 888 (1974).
57. W. L. WALTZ and A. W. ADAMSON. J. Phys. Chem. **73**, 4250 (1969).
58. D. REHOREK. Z. Chem. **20**, 30 (1980).
59. (*a*) M. G. SWANWICK and W. A. WATERS. J. Chem. Soc. B, 1059 (1971); (*b*) D. MULVEY and W. A. WATERS. J. Chem. Soc. Perkin Trans. II, 666 (1974).
60. (*a*) A. HUDSON, M. F. LAPPERT, P. W. LEDNOR, and B. K. NICHOLSON. J. Chem. Soc. Chem. Commun. 966 (1974); (*b*) A. HUDSON, M. F. LAPPERT, and B. K. NICHOLSON. J. Chem. Soc. Dalton Trans. 551 (1977).
61. A. ALBERTI and C. M. CAMAGGI. J. Organomet. Chem. **194**, 343 (1980).
62. C. M. CAMAGGI, M. CASER, M. GUERRA, and G. PLACUCCI. J. Chem. Soc. Perkin Trans. II, 1675 (1979).
63. (*a*) C. M. CAMAGGI, R. LEARDINI, and G. PLACUCCI. J. Chem. Soc. Perkin Trans. II, 1195 (1974); (*b*) A. ALBERTI, G. MARTELLI, and G. F. PEDULLI. J. Chem. Soc. Perkin Trans. II, 1252 (1977); (*c*) A. G. DAVIES and J. A. A. HAWARI. J. Organomet. Chem. **201**, 221 (1980).
64. (*a*) K. S. CHEN, T. FOSTER, and J. K. S. WAN. J. Chem. Soc. Perkin Trans. II, 1288 (1979); (*b*) B. B. ADELEKE and J. K. S. WAN. J. Chem. Soc. Perkin Trans. II, 225 (1980); (*c*) A. ALBERTI, A. HUDSON, C. F. PEDULLI, and P. ZANIRATO. J. Organomet. Chem. **198**, 145 (1980).
65. A. S. HUFFADINE, B. M. PEAKE, B. H. ROBINSON, J. SIMPSON, and P. A. DAWSON. J. Organomet. Chem. **121**, 391 (1976).
66. L. S. BENNER and A. L. BALCH. J. Organomet. Chem. **134**, 121 (1977).
67. D. REHOREK, W. WINKLER, R. WAGENER, and H. HENNIG. Inorg. Chim. Acta. **64**, L7 (1981).
68. P. RIVIERE, S. RICHELME, M. RIVIERE-BAUDET, J. SATGE, M. J. S. CYNANE, and M. F. LAPPERT. J. Chem. Res. M, 2801 (1978).
69. Y. LION, M. DELMELLE, and A. VAN DE VORST. Nature, **263**, 442 (1976).
70. A. VOGLER and H. KUNKELY. J. Am. Chem. Soc. **103**, 6222 (1981).
71. N. S. ALLEN. Makromol. Chem. **181**, 2413 (1980) and references therein.
72. E. G. JANZEN and J. I-P. LIU. J. Mag. Reson. **9**, 510 (1973); **9**, 513 (1973).
73. (*a*) E. G. JANZEN, R. L. DUDLEY, and R. V. SHETTY. J. Am. Chem. Soc. **101**, 243 (1979); (*b*) E. G. JANZEN and R. V. SHETTY. Tetrahedron Lett. 3229 (1979); (*c*) E. G. JANZEN, Y. Y. WANG, and R. V.SHETTY. J. Am. Chem. Soc. **100**, 2923 (1978).

# An electron paramagnetic resonance study of the reaction of nitrosobenzene with cholesterol

RAJAGOPALAN SRIDHAR AND ROBERT A. FLOYD

*Biomembrane Research Laboratory, Oklahoma Medical Research Foundation, Oklahoma City, OK 73104, U.S.A.*

Received September 12, 1981

RAJAGOPALAN SRIDHAR and ROBERT A. FLOYD. Can. J. Chem. **60**, 1574 (1982).

The reaction of nitrosobenzene with cholesterol ($\Delta^5$-cholesten-3β-ol) produces a fairly stable aminoxyl (nitroxyl) derivative. This steroidal aminoxyl is presumed to be the oxidation product of the hydroxylamine formed by Alder-ene addition of nitrosobenzene to cholesterol. Evidence is presented to show that, in this ene reaction, the double bond in the $\Delta^5$ position of the steroid shifts to the $\Delta^4$ rather than the $\Delta^6$ position.

RAJAGOPALAN SRIDHAR et ROBERT A. FLOYD. Can. J. Chem. **60**, 1574 (1982).

La réaction du nitrosobenzène avec le cholestérol ($\Delta^5$-cholestérol-3β) produit un dérivé aminoxyle (nitroxyle) moyennement stable. On pense que cet aminoxyle stéroïdal est le produit d'oxydation de l'hydroxylamine formée par une addition ène-Alder du nitrosobenzène sur le cholestérol. On prouve que, dans cette réaction du type ène, le double liaison en position $\Delta^5$ du stéroïde glisse en position $\Delta^4$ de préférence à la position $\Delta^6$.

[Traduit par le journal]

## Introduction

Many carcinogens and pharmaceutical agents are derivatives of arylamines and aromatic nitro compounds. The formation of nitroso intermediates during the metabolism of arylamines and nitroaromatics has been known or suspected for some time. In view of the biological activity of these compounds, it would be of interest to study the reactions of nitroso compounds with biologically important molecules. In this paper, we describe the reaction of nitrosobenzene (**1**) with cholesterol (**2**).

## Experimental

*Chemicals*

All solvents were of reagent grade and obtained from commercial suppliers. Nitrosobenzene, nitrobenzene-$d_5$, 99 at.% D, cholesterol, mesityl oxide, and phorone were purchased from Aldrich Chemical Company. Nitrobenzene-$d_5$ was converted into *N*-hydroxylaminobenzene-$d_5$ by reduction with a mixture of zinc dust and ammonium chloride in aqueous ethanol. Oxidation of the hydroxylamine with potassium ferricyanide yielded pentadeuterated nitrosobenzene.

*Electron paramagnetic resonance spectra*

The epr spectra were run at room temperature using a Varian E-9 x-band spectrometer. This instrument operates in the $TE_{104}$ mode and incorporates a 9-inch electromagnet with 100 kc/s in addition to low frequency (29 to 400 cps) field modulation. The instrument is also equipped with a Varian variable temperature control unit which maintains a constant temperature (± 1°C) while the spectrum is recorded.

## Results and discussion

A stable aminoxyl free radical (the terms nitroxyl and nitroxide have been used instead of aminoxyl in earlier literature), detectable by room temperature electron paramagnetic resonance spectroscopy, is produced when cholesterol and nitrosobenzene are mixed together in an organic solvent such as methanol or ethyl acetate at room temperature (Fig. 1). The epr spectral characteristics are unaffected when cholesteryl acetate is substituted for cholesterol in this reaction. This indicates that the 3β-OH group of the steroid is not involved in the reaction leading to the free radical product. Further, the spectral features are preserved irrespective of whether the steroid or the nitroso compound is employed in a molar excess. The reaction mixtures usually contained the free radical product along with unreacted starting materials. The instability of the free radical to long term chromatographic procedures hampered the isolation of the aminoxyl in a pure crystalline form.

Sullivan (1) has shown that nitrosobenzene can participate in an ene reaction with 2,3-dimethylbut-2-ene to yield a hydroxylamine which undergoes subsequent oxidation to yield an aminoxyl derivative. Since other examples of ene reactions involv-

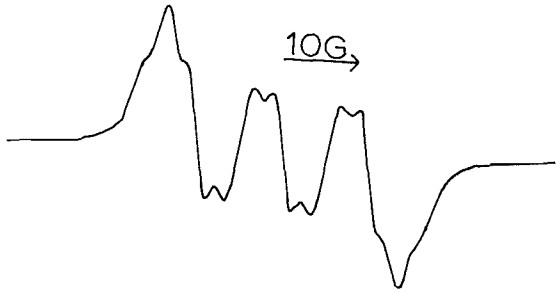


FIG. 1. The epr spectrum of the aminoxyl produced by the reaction of nitrosobenzene (11 mg) with cholesterol (20 mg) in ethyl acetate (1 mL) after 15 h at room temperature.

0008-4042/82/121574-03$01.00/0

©1982 National Research Council of Canada/Conseil national de recherches du Canada

Can. J. Chem. Downloaded from www.nrcresearchpress.com by 210.87.254.42 on 09/06/12
For personal use only.

Can. J. Chem. Downloaded from www.nrcresearchpress.com by 210.87.254.42 on 09/06/12
For personal use only.

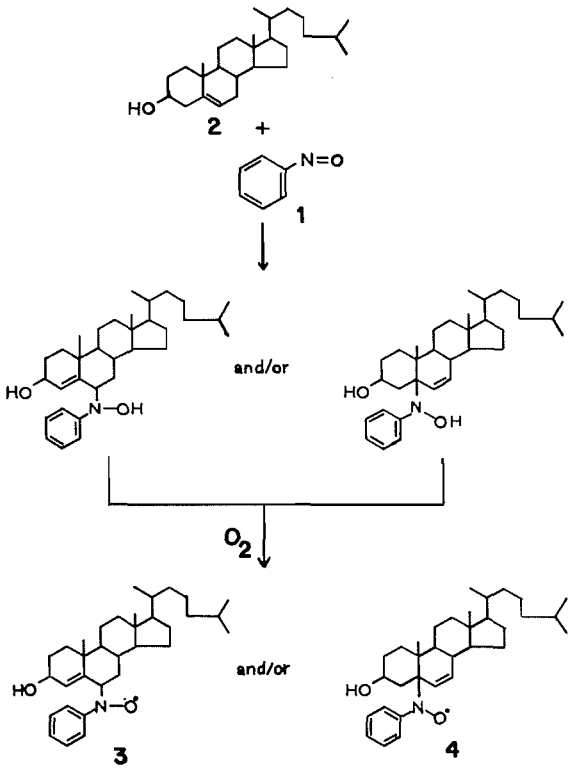


FIG. 2. Reaction scheme illustrating the pathway to aminoxyls via Alder-ene addition of nitrosobenzene to cholesterol.

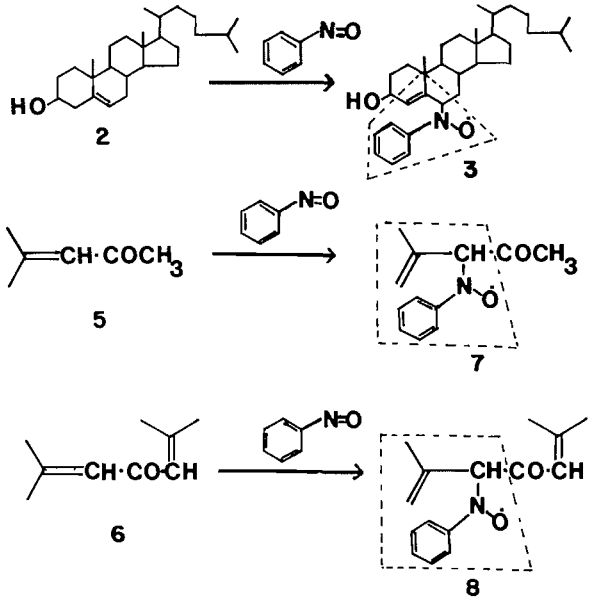


FIG. 3. Reaction of nitrosobenzene with mesityl oxide (5) and phorone (6) respectively, leading to the model aminoxyls (7) and (8) that bear a structural resemblance to the aminoxyl (3) derived from cholesterol.

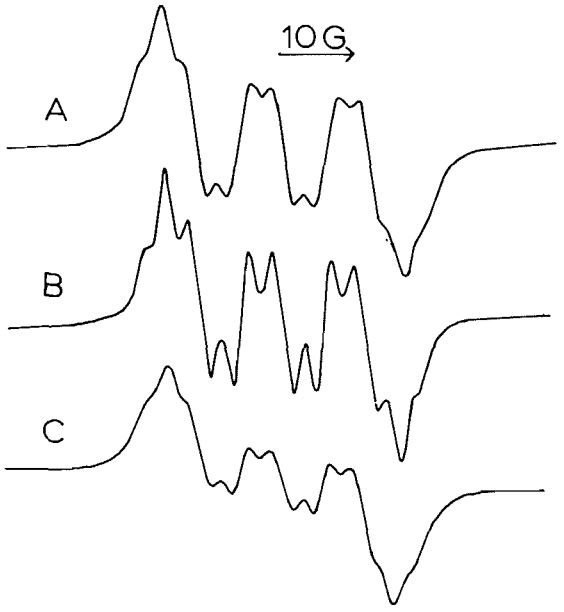


FIG. 4. The epr spectra of the aminoxyls **3**, **7**, and **8**. Spectrum A: the aminoxyl **3** from cholesterol; Spectrum B: the aminoxyl **7** from mesityl oxide; and Spectrum C: the aminoxyl **8** from phorone. The reaction conditions were as follows. Nitrosobenzene (11 mg) was dissolved in ethyl acetate (1 mL) and mixed with (*i*) cholesterol (20 mg) for spectrum A; (*ii*) mesityl oxide (40 μL) for spectrum B; and (*iii*) phorone (40 μL) for spectrum C. The reaction mixtures were contained in glass pasteur pipettes whose narrow end had been sealed off in order to serve as esr sample cells. Spectra were run after the mixtures had stood at room temperature for 15 h.

ing aromatic nitroso compounds and olefins are also known (2–4), we believe that nitrosobenzene adds to the steroid in an Alder-ene manner to yield a hydroxylamine which is easily oxidized to the corresponding aminoxyl (Fig. 2).

The ene reaction of nitrosobenzene (**1**) with cholesterol (**2**) can lead to two different aminoxyls (**3** and **4**) depending on whether the double bond in the $\Delta^5$ position of the steroid shifts to the $\Delta^4$ or the $\Delta^6$ position. The aminoxyl **3**, formed as a result of the shift of the double bond to the $\Delta^4$ position, would be characterized by its epr spectrum which should reflect the presence of a hydrogen β to the aminoxyl. Such a β hydrogen is not present in the aminoxyl **4**.

The experimentally obtained spectrum shown in Fig. 1 seems very similar to a computer simulated spectrum[1] generated by assuming the following

[1]The authors are grateful to Dr. Robert Clarkson and Dr. John Paxton of the Varian Associates for computer simulation of the spectrum.

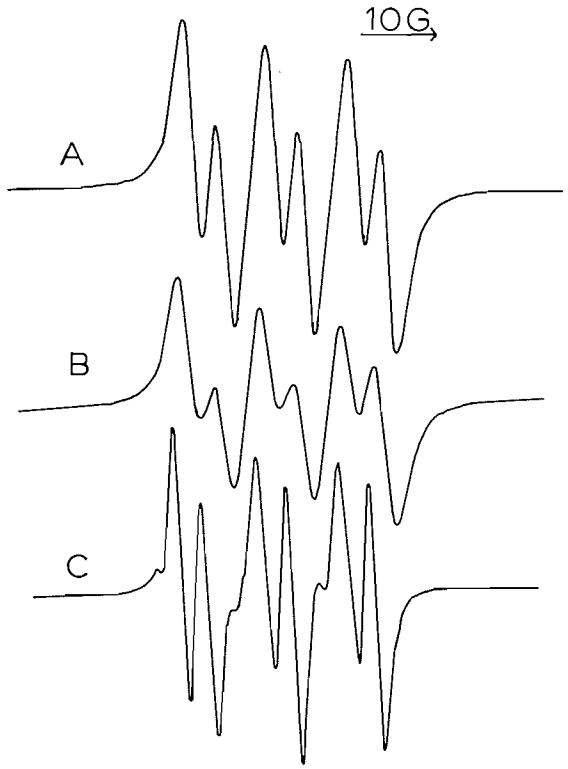


FIG. 5. The epr spectra of the aminoxyls produced by the reaction of nitrosobenzene-$d_5$. Spectrum A: the aminoxyl from cholesterol (**3**-$d_5$); Spectrum B: the aminoxyl from mesityl oxide (**7**-$d_5$); and Spectrum C: the aminoxyl from phorone (**8**-$d_5$). Reaction conditions were similar to those for Fig. 4.

parameters: line width 1.5 G; $a_N = 11.0$ G; $a^H_{ortho} = a^H_{para} = 3.1$ G; $a^H_{meta} = 0.75$ G; and $a^H_\beta = 3.05$ G.

In order to determine whether **3** or **4** was formed in the reaction, model aminoxyl compounds possessing the essential structural features of **3** were prepared so that their epr spectra could be compared with that of the steroidal aminoxyl. The reaction of nitrosobenzene with (*i*) mesityl oxide and (*ii*) an excess of phorone gave the required aminoxyls with defined structures, since ene-type addition could occur in an unambiguous way in these reactions. The structural similarity of the aminoxyl **3** and the model aminoxyl compounds prepared from mesityl oxide and phorone are indicated by the portion enclosed within the dotted boundaries (Fig. 3).

The spectra of these model aminoxyls are quite similar to that of the steroidal aminoxyl, indicating that **3** and not **4** is produced in the reaction of cholesterol with nitrosobenzene (Fig. 4). Substituting pentadeuterated nitrosobenzene for nitrosobenzene in the reactions with mesityl oxide, phorone, and cholesterol simplified the epr spectra and the prominent splitting due to the hydrogen atom β to the aminoxyl was seen in all three cases (Fig. 5). The reaction of pentadeuterated nitrosobenzene with 2,3-dimethylbut-2-ene leads to an aminoxyl which contains no β hydrogens. As expected, the epr spectrum does not show the splitting due to β-H (spectrum not shown).

**Acknowledgements**

We wish to thank Ms. Ellie Miser for her help in the preparation of this manuscript.

1. A. B. SULLIVAN. J. Org. Chem. **31**, 2811 (1966).
2. G. T. KNIGHT. Chem. Commun. 1016 (1970).
3. R. A. FLOYD, L. M. SOONG, M. A. STUART, and D. L. REIGH. Arch. Biochem. Biophys. **185**, 450 (1978).
4. R. SRIDHAR, M. J. HAMPTON, J. E. STEWARD, and R. A. FLOYD. Appl. Spectrosc. **34**, 289 (1980).

Can. J. Chem. Downloaded from www.nrcresearchpress.com by 210.87.254.42 on 09/06/12
For personal use only.

# Observations on nitroxyl free radicals in arylamine carcinogenesis and on spin-trapping hydroxyl free radicals

ROBERT A. FLOYD

*Biomembrane Research Laboratory, Oklahoma Medical Research Foundation, Oklahoma City, OK 73104, U.S.A.*

Received October 10, 1981

ROBERT A. FLOYD. Can. J. Chem. **60**, 1577 (1982).

The work presented illustrates the valuable ways that spin-trapping and nitoxyl free radical chemistry has helped us in gaining a better view of the nature of certain biological processes and thus, hopefully, will help to disentangle the principles governing the causes of certain diseases.

ROBERT A. FLOYD. Can. J. Chem. **60**, 1577 (1982).

Le présent travail illustre les moyens intéressants qu'offre la chimie des capteurs de spin et des radicaux libres du type nitroxyle en vue de nous aider à mieux comprendre la nature de certains processus biologiques et éventuellement, nous aider, on l'espère, à éclaircir les principes régissant les causes de certaines maladies.

[Traduit par le journal]

## Introduction

The techniques of spin-trapping and spin-labeling, as well as nitroxyl free radical chemistry in general, have contributed significantly to a better understanding of free radical aspects of biologically important reactions and have provided a more comprehensive view of the organization of biological systems. This has resulted in contributions to the solution of certain medically important problems. This report is a summary of the work of my own laboratory over the last several years.

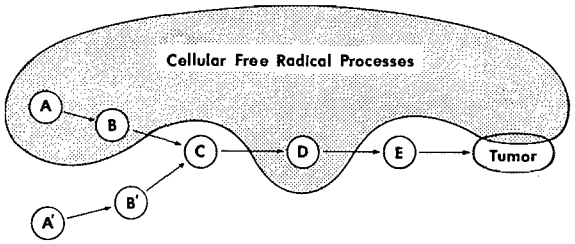


FIG. 1. Schematic representation of sequential development of tumor leading through the domain of cellular free radical processes (3).

## Free radicals in arylamine carcinogenesis

Free radicals have been considered as being closely linked with cancer for a long time. Apparently the notion originated with the demonstration of cancer induction by ionizing irradiation (1). The pace of work in this area has increased rapidly in recent years, apparently spurred on by demonstrations showing that, in general, antioxidants slowed down cancer development (2). It appears likely now that chemical carcinogen induction of tumor in many cases may progress through steps involving free radicals as illustrated in highly schematic form in Fig. 1 (3). If specific free radical steps are rate limiting, then modification of the rate of these steps would be expected to influence the overall rate of cancer development.

### 1. *Activation of 2-acetylaminofluorene*

The arylamine carcinogens consist of a large class of chemicals shown to induce tumors in laboratory animals and considered to be human carcinogens on the basis of epidemiological studies. The most widely studied member of this class of carcinogens is 2-acetylaminofluorene (AAF). It has been known for over 40 years that AAF will induce tumors in rats. In fact, when AAF is fed at about 0.02% in the diet, it induces liver tumor in male and mammary gland tumor in female rats. The single most important advancement in terms of understanding the mechanism of action of this chemical carcinogen occurred in 1960 when Cramer *et al.* (4) demonstrated that *N*-hydroxylation of AAF was a necessary first step in the metabolic activation of this chemical by liver enzymes; that is,

### 2. *Peroxidase activation of* N-*hydroxy-2-acetylaminofluorene*

It should be pointed out that the *N*-hydroxylated product, *N*-hydroxy-2-acetylaminofluorene (N-OH-AAF) itself is not the ultimate reactive chemical species of this carcinogen but must be further activated to yet another chemical species, the identity of which is not resolved at the present time (1).

As far as our approach to this problem, a key observation was made in 1970 by Forrester *et al.* (5) and Bartsch and Hecker (6). Bartsch and Hecker (6) demonstrated that N-OH-AAF was activated to 2-nitrosofluorene (NOF) and *N*-acetoxy-2-acetylaminofluorene (N-OAc-AAF) in a system containing horseradish peroxidase (HRP) and $H_2O_2$. The

0008-4042/82/121577-10$01.00/0

©1982 National Research Council of Canada/Conseil national de recherches du Canada

Can. J. Chem. Downloaded from www.nrcresearchpress.com by 210.87.254.105 on 09/06/12
For personal use only.

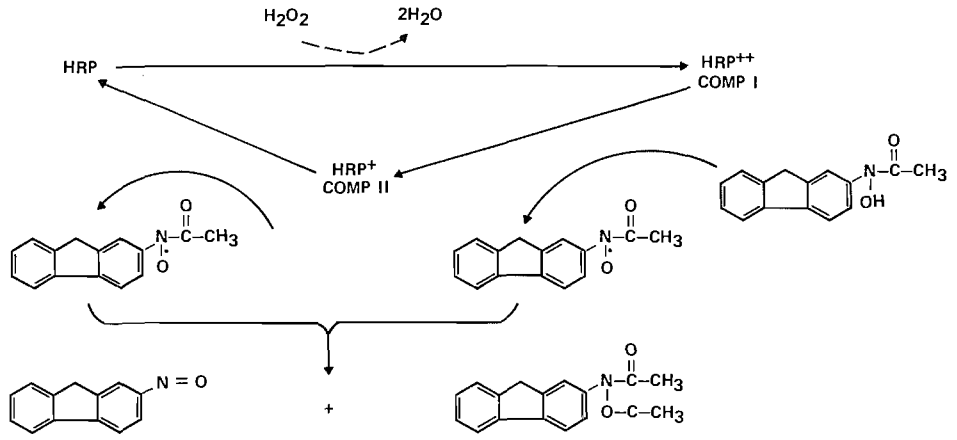


FIG. 2. Schematic representation of the nitroxyl free radical route of the activation of *N*-hydroxy-2-acetylaminofluorene (6). HRP refers to horseradish peroxidase and $HRP^{+++}$ (Comp I) and $HRP^{+}$ (Comp II) refer to compound one and compound two of HRP, respectively.

scheme they proposed to explain their results is shown in Fig. 2. In this scheme, N-OH-AAF acts as a one-electron donor to facilitate HRP cycling through three oxidation states. The nitroxyl free radical of N-OH-AAF is formed in this process, and this free radical dismutates to form NOF and N-OAc-AAF. This system has been investigated much more extensively (7); it has been shown to activate N-OH-AAF readily and, in addition, very interestingly is inhibited by antioxidants such as ascorbate (7).

### 3. *Membrane lipid peroxides as substrate for peroxidase activation of N-OH-AAF*

Membrane lipid peroxidation apparently involves oxygen free radical events and yields lipid hydroperoxides. We therefore reasoned that it was desirable to determine if lipid hydroperoxides act as a substrate to activate N-OH-AAF in a manner similar to the peroxidase route. It was shown that linoleic acid hydroperoxide in the presence of hematin activated N-OH-AAF to NOF and N-OAc-AAF stoichiometrically (8) as shown in Fig. 3. The nitroxyl free radical of N-OH-AAF is shown as an obligatory intermediate in this reaction, but to prove that this was the actual case required much more extensive work including a careful study (9) of two parameters, (A) the rate of oxidation of N-OH-AAF, and (B) the amount of N-OH-AAF nitroxyl free radical as the reaction proceeded. The rate of oxidation of N-OH-AAF and the amount of nitroxyl free radical became zero at the same time after the initiation of the reaction (9). If oxidation of N-OH-AAF is proceeding through a nitroxyl free radical step, then the equations shown below are true (9).

$$(a)\quad \text{N-OH-AAF} \underset{k_{-1}}{\overset{k_1}{\rightleftharpoons}} \text{N-}\dot{\text{O}}\text{-AAF}$$

$$(b)\quad \text{N-}\dot{\text{O}}\text{-AAF} + \text{N-}\dot{\text{O}}\text{-AAF} \xrightarrow{k_2} \text{NOF} + \text{N-OAc-AAF}$$

$$(c)\quad \frac{d(\text{N-OH-AAF})}{dt} + -k_1(\text{N-OH-AAF}) + k_{-1}(\text{N-}\dot{\text{O}}\text{-AAF})$$

$$(d)\quad \frac{d(\text{N-}\dot{\text{O}}\text{-AAF})}{dt} = -k_2(\text{N-}\dot{\text{O}}\text{-AAF})^2 + k_1(\text{N-OH-AAF}) - k_{-1}(\text{N-}\dot{\text{O}}\text{-AAF})$$

$$(e)\quad -\frac{d(\text{N-OH-AAF})}{dt} = \frac{d(\text{N-}\dot{\text{O}}\text{-AAF})}{dt} + k_2(\text{N-}\dot{\text{O}}\text{-AAF})^2$$

The bottom equation states that the rate of N-OH-AAF oxidation can be expressed in terms of the nitroxyl free radical of N-OH-AAF. Therefore, if the reaction is proceeding via an obligatory nitroxyl free radical step, then it should be possible, using the bottom equation, to calculate one parameter, say the rate of N-OH-AAF oxidation utilizing the other parameter, the amount of nitroxyl free radical at any time during the reaction. This indeed was the case (9). In addition, utilizing the bottom equation, it was possible to calculate the N-OH-AAF nitroxyl free radical dismutation constant, $k_2$. This calculated value is $2.7 \times 10^5\ M^{-1}\ s^{-1}$ (9) which indicates that the nitroxyl free radical of N-OH-AAF dismutates in a physiological buffer solution more slowly than, for instance, the ascorbyl free radical (10).

### 4. *$P_{450}$ activation of N-OH-AAF via peroxidase route*

It was necessary to test whether the heme protein $P_{450}$ was capable of activating N-OH-AAF

Can. J. Chem. Downloaded from www.nrcresearchpress.com by 210.87.254.105 on 09/06/12
For personal use only.

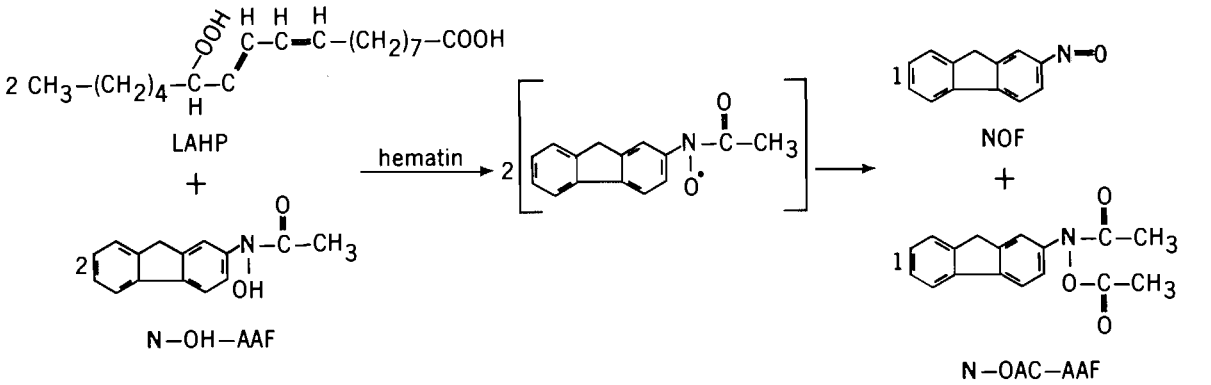


FIG. 3. The stoichiometry of the activation of *N*-hydroxy-2-acetylaminofluorene by hematin with linoleic acid hydroperoxide (LAHP) acting as a substrate (8).

in a peroxidase pathway. Utilizing rat liver "$P_{450}$ particles" which are liver microsomes treated such as to enrich them with respect to $P_{450}$, we showed that $P_{450}$ per se was relatively inactive in the peroxidase type oxidation of N-OH-AAF (11). However, conversion of $P_{450}$ to the high spin $P_{420}$ form caused a significant increase in oxidation of N-OH-AAF whereas the low spin $P_{420}$ form was almost completely inactive in this regard (11). To further substantiate this observation, we utilized purified $P_{450}$ $LM_2$, a gift of Dr. M. Coon (Univ. of Michigan). In this case as well, the high spin $P_{420}$ form was quite active whereas the low spin $P_{420}$ form as well as $P_{450}$ itself was relatively inactive (11). The effectiveness with which the various hydroperoxides act as a substrate in combination with low spin $P_{420}$ to oxidize N-OH-AAF was investigated. Linoleic acid hydroperoxide was found to be much more effective than cumene hydroperoxide or hydrogen peroxide (11). In this regard, we previously have shown that with the hematin – linoleic acid hydroperoxide system, N-OH-AAF-oxidation to the nitroxyl free radical was detected with as little as 1.8 μM of the hydroperoxide [8].

### 5. *Peroxidase activation of N-OH-AAF in mammary gland*

The relevance of the peroxidase route of N-OH-AAF activation to the true mechanism of AAF carcinogenesis remains to be completely elucidated. However, on the basis of our recent findings, it appears that the peroxidase route may be very important in the AAF-induced development of tumor in female rat mammary gland. First evidence to support this came when we showed that rat mammary gland homogenate contained an active peroxidase capable of activating N-OH-AAF to NOF and N-OAc-AAF (12). Linoleic acid hydroperoxide proved to be a very effective substrate for this peroxidase and it was found that N-OH-AAF activation was inhibited by the antioxidants propyl gallate and ascorbate (12).

Much more definitive observations demonstrating the importance of the peroxidase route have come about recently as a result of the use of high pressure liquid chromatography (hplc) to study the metabolism of N-OH-AAF in isolated rat mammary gland parenchymal cells, a target tissue for AAF. Our results (13) can be summarized as follows: (A) Utilizing hplc, we have demonstrated that N-OH-AAF is metabolized in rat mammary gland parenchymal cells to NOF and N-OAc-AAF; (B) The metabolism of N-OH-AAF in these cells is inhibited by the antioxidants ascorbate and *p*-aminophenol, which implicates a peroxidase route, but is not inhibited by paraoxon, an inhibitor of the deacetylase route of NOF formation from N-OH-AAF; (C) exogenously added arachidonic acid enhances N-OH-AAF activation and the inhibitor 5,8,11,14-eicosatetraynoic acid (ETYA) considerably decreased N-OH-AAF activation, whereas indomethacin or aspirin were ineffective as inhibitors; (D) the lipid hydroperoxide 12L-hydroperoxy-5,8,10,14-eicosatetraenoic acid (12-HPETE) is an effective substrate for activation of N-OH-AAF; (E) rat blood platelets which are a rich source of the lipoxygenase pathway activated N-OH-AAF

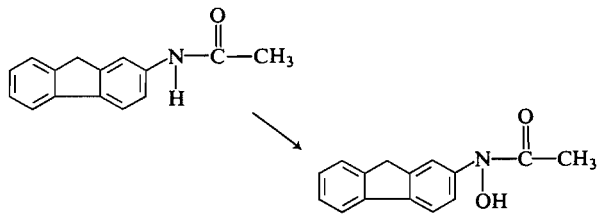

Can. J. Chem. Downloaded from www.nrcresearchpress.com by 210.87.254.105 on 09/06/12
For personal use only.

Can. J. Chem. Downloaded from www.nrcresearchpress.com by 210.87.254.105 on 09/06/12
For personal use only.

when exogenous arachidonate was added; and, (F) ram seminal vesicle microsomes, a source rich in the prostaglandin synthetase pathway, activated N-OH-AAF when exogenous arachidonate was added.

6. *Prostaglandin synthetase activation of N-OH-AAF*

The scheme presented in Fig. 4 will help to understand the mechanism of the peroxidative activation of N-OH-AAF by the prostaglandin synthetase system as well as the lipoxygenase system. The reaction which starts the cascade of reactions involves phospholipase $A_2$ cleavage of arachidonic acid from the membrane phospholipid. Arachidonate can then be oxidized by the prostaglandin cyclooxygenase to produce prostaglandin $G_2$ ($PGG_2$). Alternatively, arachidonate can be oxidized by a lipoxygenase to yield several hydroperoxides including 12-HPETE. Ram seminal vesicle microsomes have a high activity of the prostaglandin synthetase system but the lipoxygenase activity is very low or absent. We demonstrated N-OH-AAF activation by ram seminal vesicle microsomes in a peroxidative manner (13). Our postulate as to how this occurs is that the peroxidase, an enzymatic activity intimately associated with (most likely the same enzyme as) the cyclooxygenase (14), activates N-OH-AAF utilizing $PGG_2$ as a substrate. Our postulate is partially based upon demonstrations by Zenser *et al.* (15), Marnett *et al.* [16], Eling and co-workers [17], and Egan *et al.* [18] of similar type cooxidative reactions with other drugs or carcinogens. In the mammary gland, our results lead us to the conclusion that an active lipoxygenase forms a lipid hydroperoxide which acts as a substrate for a peroxidase, which most likely is not the same peroxidase associated with prostaglandin cyclooxygenase, to oxidatively activate N-OH-AAF. These results are exciting since they provide a way of explaining the mechanism as to why AAF induces tumor of the mammary gland, because other than the peroxidase route, other known routes of N-OH-AAF activation such as the sulfotransferase are either absent (19) or the acyltransferase, although apparently present, is lower in activity than liver (20), a somewhat resistant tissue in female rats.

7. *Covalent binding of 2-nitrosofluorene to membrane lipids*

Very surprisingly, I found that when 2-nitrosofluorene (NOF) was added to a solution containing oleic acid, a nitroxyl free radical type esr spectrum was formed (21). In addition, we found that not only oelic acid, but linoleic acid and squalene, as well as several other membrane lipid components, yielded nitroxyl free radicals when NOF was added to the solution in which any one of these compounds was present. Further study demonstrated that the presence of carbon–carbon double bonds in the lipid component was necessary for nitroxyl free radical formation (21). We subsequently demonstrated that when NOF was added to natural membranes, an esr signal resembling a nitroxyl exhibiting hindered rotation was formed quite rapidly (22). The addition of NOF to liposomes formed from the total lipids extracted from rat liver microsomes yielded a similar type esr spectrum as was seen with the natural membranes (22). This result illustrated that the membrane proteins did not contribute to the reaction of NOF with membrane lipids to form the nitroxyl free radical. The nitroxyl free radical which formed upon addition of NOF to rat liver microsomes was subject to reduction–oxidation control. NADPH reduced the nitroxyl; subsequent oxidation could be obtained by ferricyanide addition (22). After much work on this problem, we conclude that NOF adds to natural membranes in a manner as illustrated in Fig. 5. This scheme follows the scheme outlined by Sullivan to explain his observations of nitrosobenzene addition to 2,3-dimethylbutene to form a nitroxyl free radical adduct (23). All the work we have conducted on these systems over the last 5 years can be explained by the scheme presented in Fig. 5. Thus, these results, in effect for the first time, demonstrate that a carcinogen adds covalently to membrane lipids.

8. *Metabolism of* N*-hydroxylated aromatic amine carcinogens to form NOF–Lipid adducts*

Formation of NOF from N-OH-AAF may occur by mechanisms other than via the nitroxyl free radical route. One possible route, shown in the equation below, is by deacetylation of N-OH-AAF to form *N*-hydroxy-2-aminofluorene which undergoes rapid oxidation to NOF which then may covalently bind to membrane lipids. Paroxon, a powerful esterase inhibitor, has been shown to inhibit the deacetylation reaction (24). We have tested microsomes from male rat liver, a target

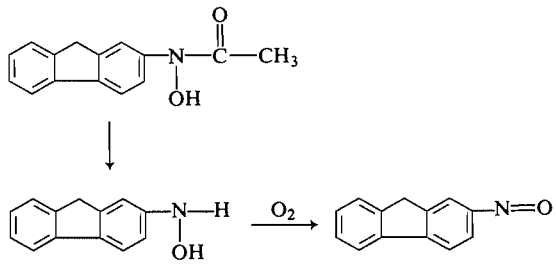

Can. J. Chem. Downloaded from www.nrcresearchpress.com by 210.87.254.105 on 09/06/12
For personal use only.



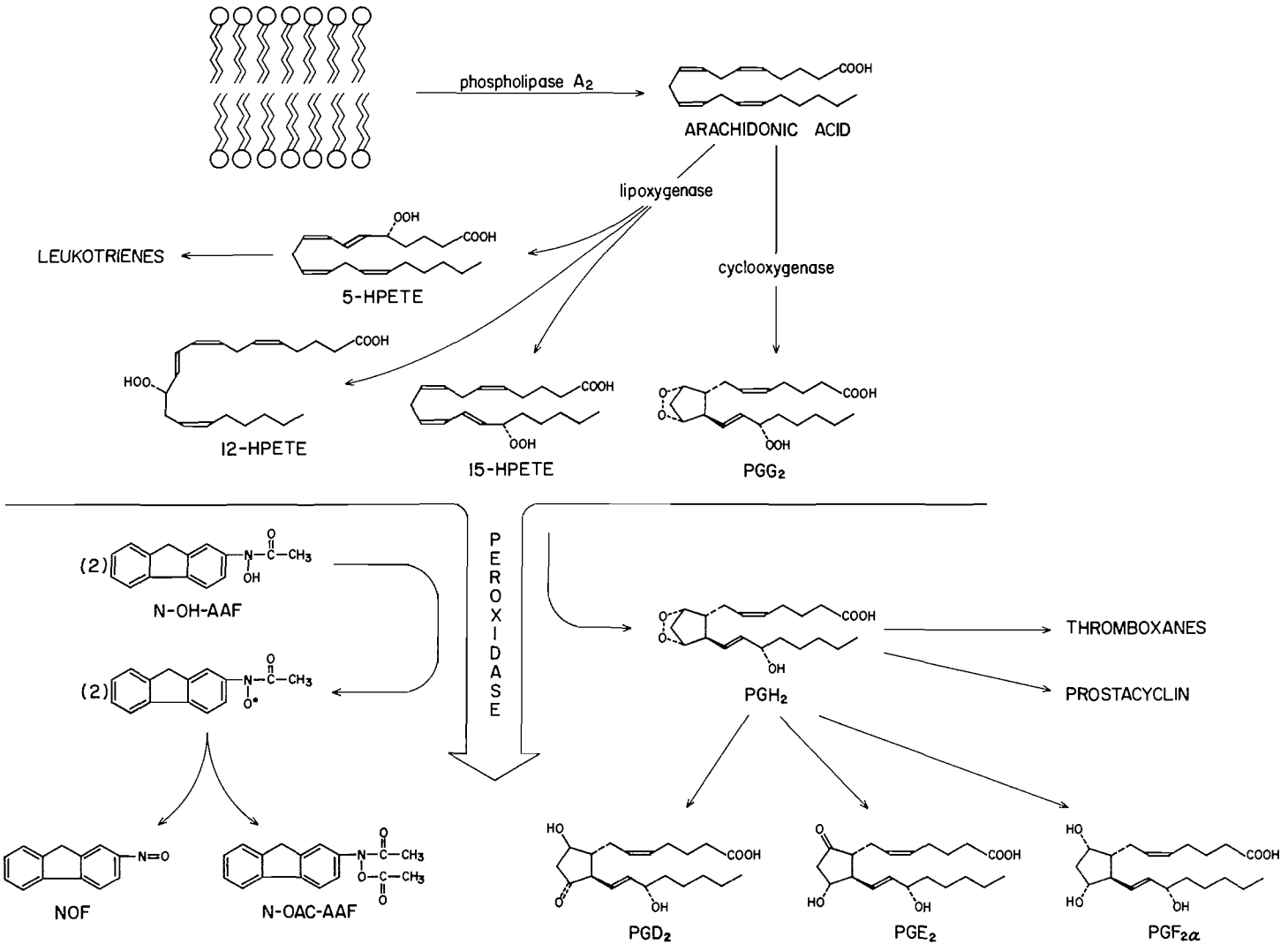


FIG. 4. Schematic representation of the activation of *N*-hydroxy-2-acetylaminofluorene via the prostaglandin synthetase system or via lipoxygenase *plus* peroxidase pathway which appears to be the route of activation of this carcinogen in female rat mammary gland (13).

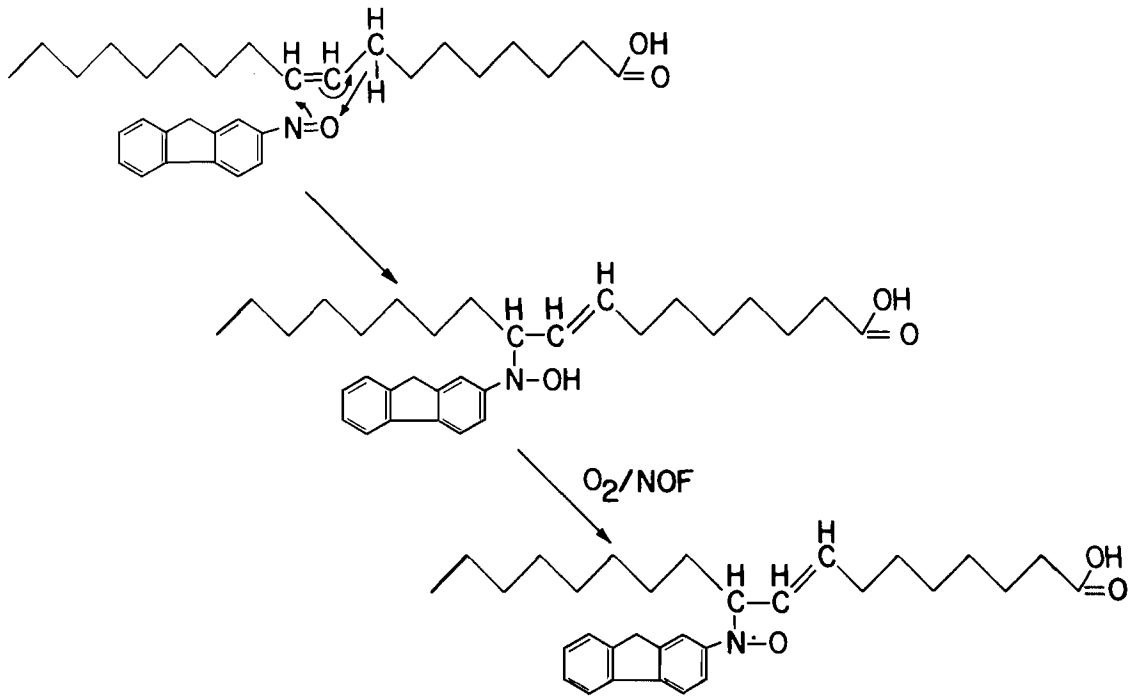


FIG. 5. The Alder-ene addition scheme to explain 2-nitrosofluorene addition to carbon–carbon double bonds in membrane lipids (22).

tissue, to determine if deacetylation of N-OH-AAF occurs. Optical as well as esr experiments demonstrated that this was the case (25). If TME (2,3-dimethylbutene), which acts as a ready substrate for NOF-adduct formation, was added to microsomes then a larger amount of adduct was apparent (1). Heated microsomes were ineffective in carrying out the deacetylation reaction, and paroxon at $5 \times 10^{-6}$ *M* level prevented deacetylation of N-OH-AAF (25).

Deacetylation of other *N*-hydroxylated aromatic amine carcinogens occurs, resulting in formation of the membrane lipid adducts. Thus, *N*-hydroxy-4-acetyl aminobiphenyl is a bladder carcinogen and its deacetylation to eventually form the *C*-nitroso membrane lipid adduct is readily apparent in rat liver microsomes (1).

We have found that the NOF-lipid adduct is formed when N-OH-AAF is given to the whole animal (1). N-OH-AAF dissolved in corn oil was given interperitoneally to a rat. After 1.5 hours, the animals were killed, the liver removed, homogenized, and extracted with ethyl acetate. The esr spectrum of the concentrated ethyl acetate extract from an animal receiving corn oil only illustrated the absence of nitroxyl free radical, whereas in the concentrated ethylacetate extract from an animal receiving N-OH-AAF, the presence of a nitroxyl free radical was obvious (1). The coupling constant of the nitroxyl free radical was similar to that of the NOF-lipid adducts observed previously (21, 22).

9. *Formation of 2-nitrosofluorene – cholesterol adduct*

We have found that NOF adds covalently to cholesterol to form a nitroxyl free radical adduct (1). There are two possible NOF–cholesterol adducts, as is shown in Fig. 6. Work where specific hydrogens on cholesterol are replaced by deuterium, as well as the reaction of NOF with model compounds, has proven that the carbon-5 adduct of cholesterol is the predominant species formed in this reaction.

10. *Relevance of 2-nitrosofluorene – lipid adducts to carcinogens*

It is not possible to know the relevance of the formation of the NOF–lipid adducts to the carcinogenesis of either AAF or NOF at the present time. It is possible, however, to point out some interesting relationships and observations that may have bearing upon this problem. First of all, the attachment of a lipid component to NOF would most likely change the carcinogenic properties of NOF. Possibly a relevant observation is the one made by Bartsch *et al.* (26) who showed that if the acetyl group of N-OH-AAF is replaced by the myristate,

Can. J. Chem. Downloaded from www.nrcresearchpress.com by 210.87.254.105 on 09/06/12
For personal use only.

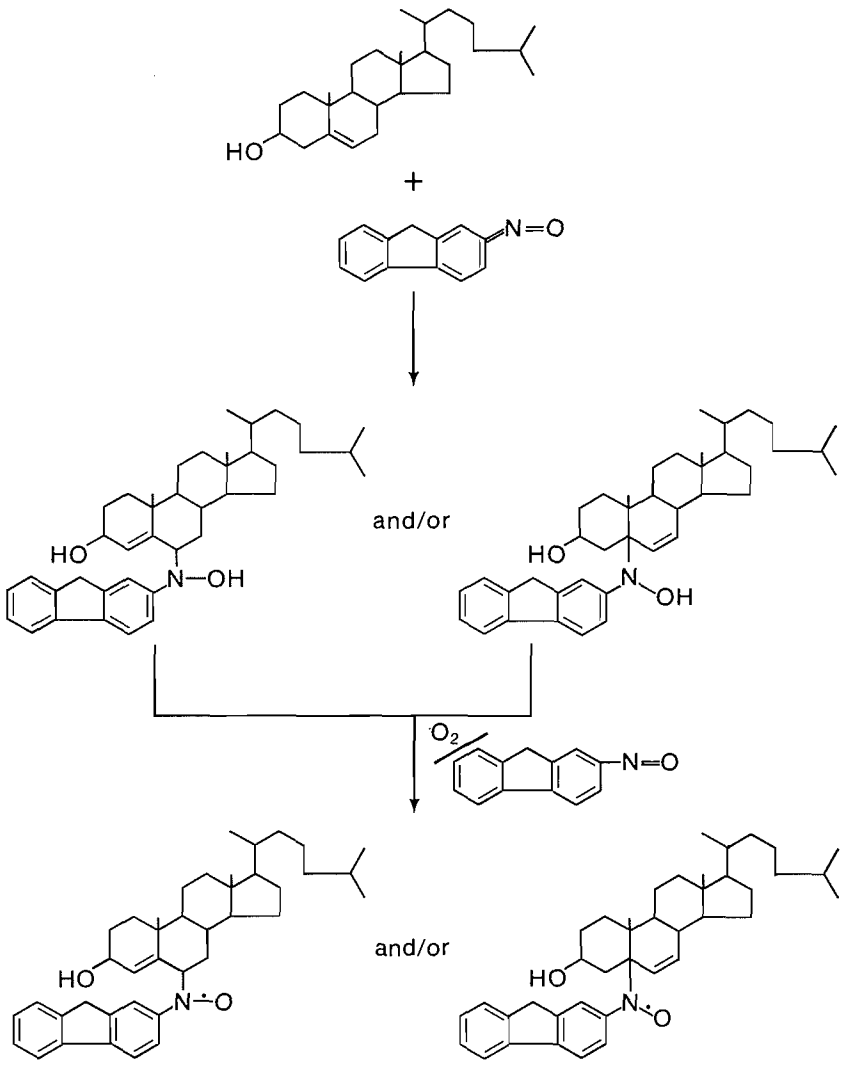


FIG. 6. The Alder-ene addition of 2-nitrosofluorene to cholesterol. Two pathways are possible. The one on the left is the one found to occur.

i.e. becoming N-OH-MyAF, or if the acetoxy group of N-OAc-AAF is replaced by the myristate ester, i.e. becoming N-OMy-AAF, then the compounds possessing the long lipophilic moieties were much more carcinogenic than the compounds having the acetyl or acetoxy groups. They attributed the increased carcinogenicity to enhanced retention of the more lipophilic compounds at the site of injection. Based upon Bartsch's work, it is tempting to speculate that the attachment of NOF to a lipophilic component may enhance its carcinogenicity. This remains to be proven, but we have conducted a study of the carcinogenicity of the NOF – oleic acid methyl ester adduct and the NOF–cholesterol adduct in the newborn mouse model utilized by Miller *et al.* (27). We found in our preliminary study that the NOF–cholesterol adduct was more carcinogenic than NOF per se, but the NOF – oleic acid methyl ester adduct was less carcinogenic than NOF. This study was preliminary and is complicated by the fact that, as we discovered later, more than one product was present in the adducts injected into the animals. This study needs to be repeated with highly purified NOF adducts.

Another observation that may have some relevance concerns our work on the mutagenicity of NOF as influenced by the number of carbon–carbon double bonds in the membrane lipids of the Ames tester strain bacteria TA98. In general, we found that as the membrane unsaturation increased (28) in the 37°C and 27°C grown bacteria which

Can. J. Chem. Downloaded from www.nrcresearchpress.com by 210.87.254.105 on 09/06/12
For personal use only.

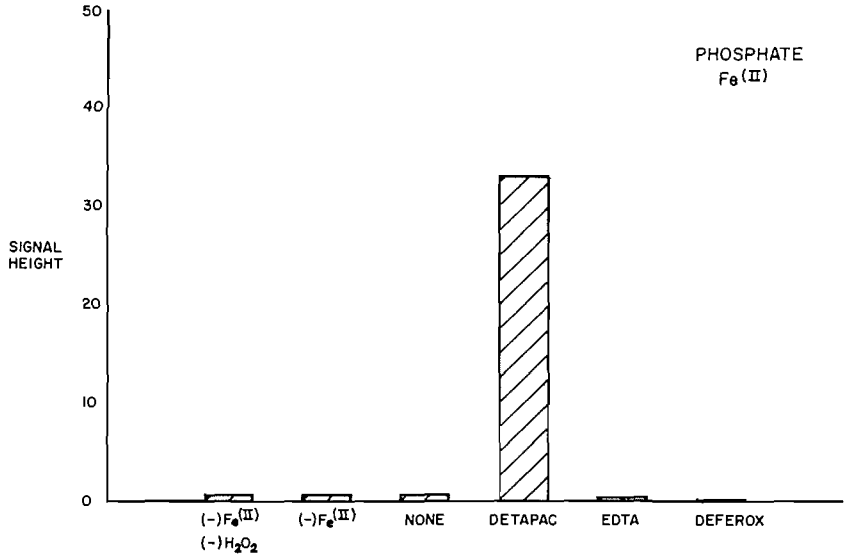


FIG. 7. The amount of ȮH spin-trapped by DMPO in the Fenton system using phosphate buffer, pH 7.4.

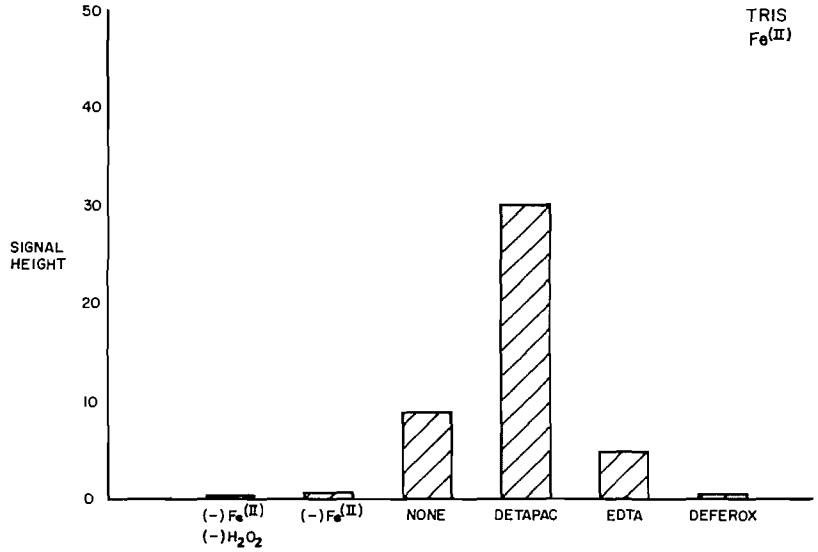


FIG. 8. The amount of ȮH spin-trapped by DMPO in the Fenton system using Tris (trihydroxylaminomethane) buffer, pH 7.4.

were the best comparisons, then mutagenicity of NOF increased (29). It should be noted that the NOF – oleic acid methyl ester is only slightly mutagenic as compared to NOF (30); however, the mutagenicity may not correlate with the carcinogenicity of the compounds (see, for instance, Bartsch *et al.* (26)).

## Oxygen free radicals

Oxygen free radicals is a subject that has been given more and more attention lately. A large amount of this recent interest in oxygen free radicals is due to the discovery of superoxide and the demonstration of its relevance to biological processes largely due to the work of Fridovich and co-workers (31). It is becoming quite apparent that oxygen free radicals have a major role in the etiology of many disease states.

## Spin-trapping hydroxyl free radicals in a Fenton-type reaction

Since oxygen free radicals are implicated in so many damaging biological processes, it appears necessary to know more about their properties and

Can. J. Chem. Downloaded from www.nrcresearchpress.com by 210.87.254.105 on 09/06/12
For personal use only.

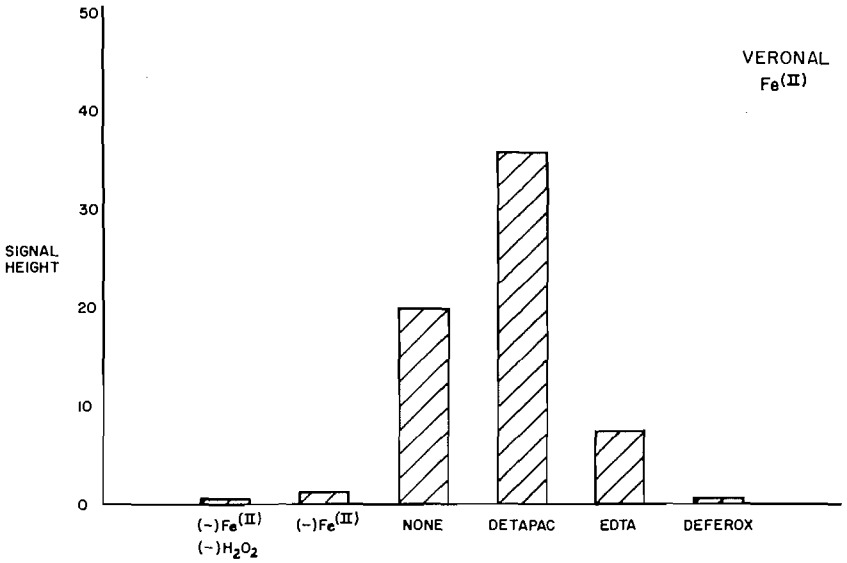


FIG. 9. The amount of ȮH spin-trapped by DMPO in the Fenton system using veronal buffer, pH 7.4.

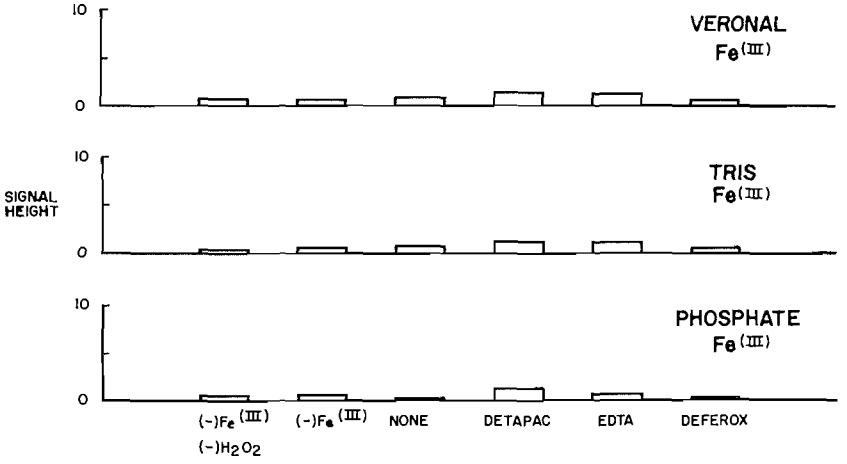


FIG. 10. The amount of ȮH spin-trapped in a Fenton system using Fe(III) with various buffers and various chelators.

the conditions under which they manifest their action. In particular, we have concentrated upon examining the conditions affecting hydroxyl free radical formation from a Fenton-type reaction. We have utilized spin-trapping in this regard because of the difficulty of observing hydroxyl free radicals directly, and also because ȮH reacts with the spin-trap 5,5-dimethylpyrolidine-*N*-oxide (DMPO) at nearly a diffusion limited rate ($3.4 \times 10^9\ M^{-1}\ s^{-1}$) (32). The DMPO–hydroxy free radical spin-adduct formed has a unique esr spectrum with a 1:2:2:1 pattern where $A_N = A_\beta{}^H = 14.9$.

Our first attempts at characterizing the conditions for hydroxyl free radical formation from $H_2O_2$ as catalyzed by chelated iron illustrated the magnitude of our misconception of the complexity of the problem. That is, we found that there was on the order of a 50-fold difference in the amount of hydroxyl free radical spin trapped depending upon the order of addition of reagents. The order of additions between the two experiments are shown below. The top sequence corresponds to a 50-fold increased amount of spin-trapped ȮH versus that for the bottom sequence of reagent addition.

$$\text{Buffer, DMPO, DETAPAC, Fe(II)} \xrightarrow[37°C]{30\ s} + H_2O_2$$

$$\text{Buffer, DMPO, Fe(II), DETAPAC} \xrightarrow[37°C]{30\ s} + H_2O_2$$

Thus, a reversal in the order of addition of the

Can. J. Chem. Downloaded from www.nrcresearchpress.com by 210.87.254.105 on 09/06/12
For personal use only.

Can. J. Chem. Downloaded from www.nrcresearchpress.com by 210.87.254.105 on 09/06/12
For personal use only.

chelator DETAPAC (diethylene triamine pentaacetic acid) and iron as Fe(II) made the difference between the two results.

The amount of ȮH spin-trapped was sensitive to several other variables including the type of buffer, the type of metal ion chelator, the oxidation state of the metal ion, and the time interval after addition of the metal ion (33). Figure 7 demonstrates that for potassium phosphate buffer pH 7.4, the amount of ȮH spin-trapped was vastly different depending upon the chelator used. The experiments were carried out by the protocol illustrated by the top sequence above, only the chelator was changed. Thus, Fe(II) with DETAPAC, as compared to EDTA (ethylenediaminetetraacetic acid) or deferoxamine, was quite effective in producing ȮH from the added $H_2O_2$. The amount of Fe(II) added was about 25 μmol; the other components DMPO (200 mmol), chelator (100 μmol), and $H_2O_2$ (400 μmol) were in excess. The amount of radical trapped was about 15 μmol in the case of DETAPAC in the phosphate buffer. Therefore, since the following equation describes the reaction

$$Fe(II) + H_2O_2 \rightarrow Fe(III) + OH^- + \dot{O}H$$

and if Fe(II) is limiting and DMPO is in large excess, then it follows, since the rate of the Fenton reaction is slower than the spin-trapping reaction, that Fe(II) is either not at 25 μmol or the reaction as written is wrong. It turns out, based upon the work of Cohen and Sinet (34), that Fe(II) is rapidly becoming oxidized and that the difference between the chelators is due to the effectiveness of each in preventing the rapid oxidation of Fe(II). Therefore, since we are spin-trapping about 15 μmol ȮH with DETAPAC as the chelator, then about 40% of the added Fe(II) has become oxidized in 30 s at 37°C. With buffers other than phosphate, similar but slightly different amounts of ȮH were spin-trapped as is shown in Fig. 8 for Tris (trihydroxylaminomethane) or veronal buffer (Fig. 9).

The importance of the oxidation state of iron is illustrated by the data presented in Fig. 10 demonstrating that irrespective of buffer or chelator, Fe(III) was quite ineffective in catalyzing ȮH formation from $H_2O_2$.

## Acknowledgments

The work presented was supported in part by National Institutes of Health grants CA18591 and CA21542. I thank Ms. E. Miser for typing of the manuscript.

1. R. A. FLOYD. Radiat. Res. **86**, 243 (1981).
2. R. A. FLOYD. *In* Free radicals in biology. Vol. IV. *Edited by* W. A. Pryor. Academic Press, New York. 1980. Chapt. 6. pp. 187–208.
3. R. A. FLOYD. *In* Free radicals and cancer. *Edited by* R. A. Floyd. Marcel Dekker, New York. 1981. In press.
4. J. W. CRAMER, J. A. MILLER, and E. C. MILLER. J. Biol. Chem. **235**, 885 (1960).
5. A. R. FORRESTER, M. M. OGILVY, and R. H. THOMSON. J. Chem. Soc. Sec. C, 1081 (1970).
6. H. BARTSCH and E. HECKER. Biochim. Biophys. Acta, **237**, 567 (1971).
7. R. A. FLOYD, L. M. SOONG, and P. L. CULVER. Cancer Res. **36**, 1510 (1976).
8. R. A. FLOYD, L. M. SOONG, R. N. WALKER, and M. STUART. Cancer Res. **36**, 2761 (1976).
9. R. A. FLOYD and L. M. SOONG. Biochim. Biophys. Acta, **498**, 244 (1977).
10. I. YAMAZAKI, H. S. MASON, and L. PIETTE. J. Biol. Chem. **235**, 2444 (1960).
11. D. L. REIGH, and R. A. FLOYD. Cancer Biochem. Biophys. **5**, 213 (1981).
12. D. L. REIGH, M. STUART, and R. A. FLOYD. Experientia, 34, 107 (1978).
13. P. K. WONG, M. J. HAMPTON, and R. A. FLOYD. Prostaglandins and cancer. Alan R. Liss, Publisher, New York. 1981. In press.
14. T. MIYAMOTO, N. OGINO, S. YAMAMOTO, and O. HAYAISHI. J. Biol. Chem. **251**, 2629 (1976).
15. T. V. ZENSER, M. B. MATTAMMAL, H. J. ARMBRECHT, and B. B. DAVIS. Cancer Res. **40**, 2839 (1980).
16. L. J. MARNETT, P. WLODAWER, and B. SAMUELSSON. J. Biol. Chem. **250**, 8510 (1975).
17. K. SIVARAJAH, J. M. LASKER, and T. E. ELING. Cancer Res. **41**, 1834 (1981).
18. R. W. EGAN, P. H. GALE, W. J. A. VANDELHEUVEL, E. M. BAPTISTIA, and F. A. KUEHL, JR. J. Biol. Chem. **255**, 323 (1980).
19. C. C. IRVING, D. H. JANSS, and L. T. RUSSELL. Cancer Res. **31**, 387 (1971).
20. C. M. KING, N. R. TRAUB, Z. M. LARTZ, and M. R. THISSEN. Cancer Res. **39**, 3369 (1979).
21. R. A. FLOYD. Experientia, **33**, 197 (1977).
22. R. A. FLOYD, L. M. SOONG, M. A. STUART, and D. L. REIGH. Arch. Biochem. Biophys. **185**, 450 (1978).
23. A. B. SULLIVAN. J. Org. Chem. **31**, 2811 (1966).
24. H. A. J. SCHUT, P. J. WIRTH, and S. S. THORGIERSSON. Molec. Pharmacol. **14**, 682 (1978).
25. J. E. STEWARD, and R. A. FLOYD. Cancer Biochem. Biophys. **5**, 47 (1980).
26. H. BARTSCH, C. MALAVEILLE, H. F. STICH, E. C. MILLER, and J. A. MILLER. Cancer Res. **37**, 1461 (1977).
27. E. C. MILLER, F. F. KADLUBAR, J. A. MILLER, H. C. PITOT, and N. R. DRINKWATER. Cancer Res. **39**, 3411 (1979).
28. M. J. HAMPTON, R. A. FLOYD, J. B. CLARK, and J. H. LANCASTER. Chem. Phys. Lipids, **27**, 177 (1980).
29. M. J. HAMPTON, R. A. FLOYD, J. B. CLARK, and J. H. LANCASTER. Mutation Res. **69**, 231 (1980).
30. R. SRIDHAR, M. J. HAMPTON, J. E. STEWARD, and R. A. FLOYD. Appl. Spectrosc. **34**, 289 (1980).
31. I. FRIDOVICH. Science, **201**, 876 (1978).
32. E. FINKELSTEIN, G. M. ROSEN, and E. J. RAUCKMAN. J. Am. Chem. Soc. **102**, 4994 (1980).
33. R. A. FLOYD. Fed. Proc. **40**, 1672 (1981).
34. G. COHEN and P. M. SINET. *In* Chemical and biological aspects of superoxide and superoxide dismutase (Developments in Biochemistry, Vol. IIA). *Edited by* J. V. Bannister and H. A. O. Hill. Elsevier/North Holland, New York. 1980. pp. 27–37.

# From early spin-trapping experiments to acyl nitroxide chemistry: synthesis of and spin trapping with a water-soluble nitrosopyrazole derivative

HARPARKASH KAUR AND M. JOHN PERKINS[1]

*Department of Chemistry, Chelsea College, Manresa Road, London SW3 6LX, England*

Received September 19, 1981

HARPARKASH KAUR and M. JOHN PERKINS. Can. J. Chem. **60**, 1587 (1982).

A personal view of early experiments which led to the use of *C*-nitroso-compounds as spin traps is presented, and it is shown how these experiments resulted in the first isolation, and subsequent investigation, of acyl nitroxide radicals: the use of 1-methyl-4-nitroso-3,5-diphenylpyrazole as a spin trap, and the preparation and preliminary investigation of its water-soluble analogue (**1**) are described.

HARPARKASH KAUR et M. JOHN PERKINS. Can. J. Chem. **60**, 1587 (1982).

*On présente une façon personnelle de concenvoir les premières expériences qui ont conduit à l'utilisation des composés C*-nitrosés comme capteurs de spin. On montre comment ces expériences ont conduit à la première séparation et à l'étude des radicaux acylnitroxydes. On décrit l'utilisation du méthyl-1 nitroso-4 diphényl-3,5 pyrazole comme capteur de spin ainsi que la préparation et les études préliminaires de son analogue (**1**) soluble dans l'eau.

[Traduit par le journal]

Can. J. Chem. Downloaded from www.nrcresearchpress.com by 210.87.254.40 on 09/06/12
For personal use only.

This article is sub-divided into two sections. In the first, we summarise the work which was the basis of the review paper presented at the Guelph symposium; in the second we give a more detailed account of the evolution of the new water-soluble spin trap, **1**.

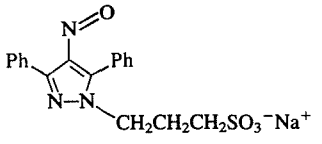

**1**

## 1. Review section

Our interest in nitroxide chemistry began with investigations of free-radical arylation in D. H. Hey's laboratory at King's College in London. It was known at that time (ca. 1960), that whilst thermolyses of benzoyl peroxide in benzene gave poor yields of organic products (ca. 40%, but see ref. 1) according to the simple stoichiometry of reaction [1] (Ar = Ph), similar reactions with

$$[1]\quad (ArCO_2)_2 + PhH \xrightarrow[N_2]{80^\circ C} ArCO_2H + ArPh + CO_2$$

nitrobenzene as solvent (or with equimolar mixtures of benzene and nitrobenzene employed in "competition" experiments) gave surprisingly good yields. It was also known that nitrobenzoyl peroxides, on thermolysis in benzene, gave high yields of the appropriate nitro-substituted products.

The natural extension of these observations was to examine the products of reaction of benzoyl peroxide in benzene containing a "catalytic" quantity (ca. 1%) of added nitrobenzene. The yields of biphenyl and benzoic acid rose dramatically to around 90%.

The explanation (2) of the effect of added nitro-compound was eventually traced to the reduction of a small fraction of the nitrobenzene to nitroso-benzene, and formation from that of diphenyl nitroxide and related species which then take part in a hydrogen transfer redox process wherein the key cyclohexadienyl intermediate **2** is oxidised before it can proceed to products of self-reaction (dimerisation or disproportionation). The essential features of the process are summarised in Scheme 1.

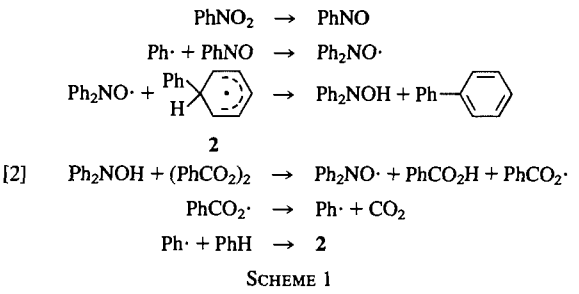

**2**

SCHEME 1

The molecule-induced homolysis of benzoyl peroxide (reaction [2]) by diphenylhydroxylamine was established in separate experiments (3).[2]

The most puzzling aryl precursors had for a long time been the nitrosoacylarylamines (e.g. *N*-

[1]To whom all correspondence should be addressed.

[2]We do not believe that our kinetic data in this work (3) can be reinterpreted in terms of "homosolvolysis" by nitroxide as has been suggested recently. (4).

0008-4042/82/121587-07$01.00/0

©1982 National Research Council of Canada/Conseil national de recherches du Canada

Can. J. Chem. Downloaded from www.nrcresearchpress.com by 210.87.254.40 on 09/06/12
For personal use only.

nitrosoacetanilide). It was shown by Rüchardt and co-workers that the apparent anomalies reported for this system could all be accounted for if a relatively persistent radical were to mediate in the reaction (5); one role for this was again the oxidation of cyclohexadienyl intermediates. Rüchardt also succeeded in demonstrating (6) the presence of such an intermediate using esr techniques. However, the species detected did *not* have the diazotate structure (PhN:NO·) originally assigned, although that radical is still believed to play an important role in nitrosoacetanilide decomposition (7). By analogy with our earlier work with nitrocompounds in the benzoyl peroxide reaction, we suggested an alternative structure for the species detected, namely that of the nitroxide (**3**) formed by addition of phenyl radicals to the nitrosoamide (reaction [3]). This formulation was quickly corroborated by a reaction ([4]) (8) which proved for us

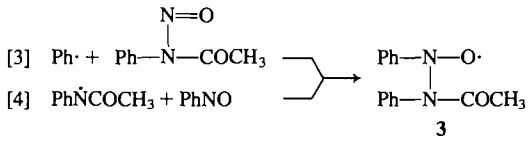


**3**

to be the fore-runner of the technique named "spin trapping" by Professor Janzen (9).

The ready detection of nitroxides in systems containing radical precursors and a trace of *C*-nitroso-compound led to a more general examination of this procedure for the study of free-radical reactions. In view of the interception of amidyl radicals (reaction [4]), it was natural that we should examine the succinimidyl radical problem.[3] However, because of the complexity of spectra of nitroxides derived from nitrosobenzene, we turned our attention to 2-methyl-2-nitrosopropane (MNP, **4**) as a radical trap. This had been shown by De Boer and his colleagues to give nitroxides by radical addition, and most of the adducts displayed exceedingly simple esr spectra which were readily interpreted in terms of the structure of the radical trapped.

In photochemical experiments with *N*-bromosuccinimide, MNP gave the succinimidyl adduct **5** (11), reported also by Lagercrantz and Forshult (12). In contrast, when the succinimidyl source was the perester **6**, the nitroxide **7** was unexpectedly formed. The explanation of this, involving the methylene nitrone intermediate **8**, has been detailed elsewhere (11). The nitrone (**8**) can be synthesised, and was indeed mentioned as an alternative radical trap in our first paper advocating the use of

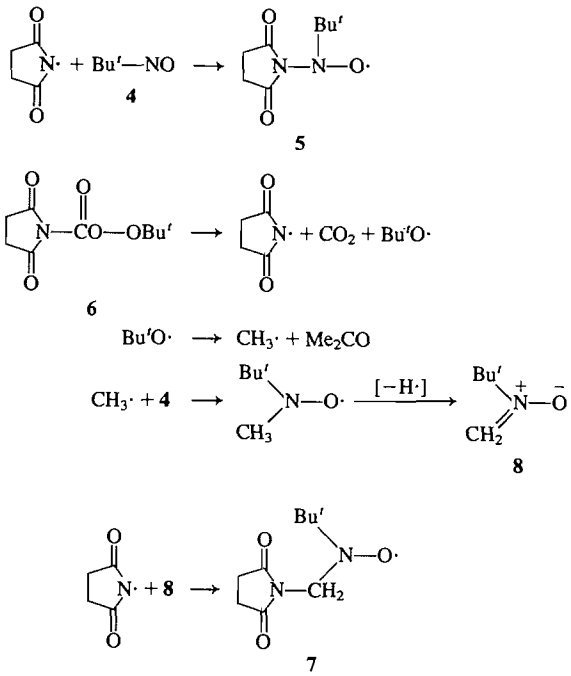


nitroso-compounds to investigate radical reactions (13). More recently it has found wider application, and is a particularly reactive radical scavenger which can be used in aqueous as well as non-aqueous systems.

Much of the early work from our group was summarised in a short review (14) and will not be re-examined here.[4] One of the more fruitful observations recorded in that early review was the trapping by MNP of trichloromethyl radicals. Under normal experimental conditions, the trichloromethyl nitroxide adduct is converted into the chlorocarbonyl nitroxide **9**, which is readily transformed by alcohols or amines into alkoxycarbonyl or aminocarbonyl nitroxides respectively (Scheme 2) (16). These proved to be exceptionally persistent at very high concentrations, which prompted us to attempt to isolate them.

Initial experiments involving ethoxycarbonyl chloride and *N*-*t*-butylhydroxylamine gave both *N*- and *O*-acylated products, of which the former could be oxidised to the desired ethoxycarbonyl *t*-butyl nitroxide (a blue oil) in good yield by nickel peroxide. Although the product was not particularly stable, a range of acyl *t*-butyl nitroxides, including several biradicals, have now been isolated (17), and crystal structures have been determined for two of these (18).

Equilibration of the hydroxamic acid precursors

[3]For a recent evaluation, see ref. 10.

[4]A more recent review of the spin-trapping technique and its varied applications will be found in ref. 15.

Can. J. Chem. Downloaded from www.nrcresearchpress.com by 210.87.254.40 on 09/06/12
For personal use only.

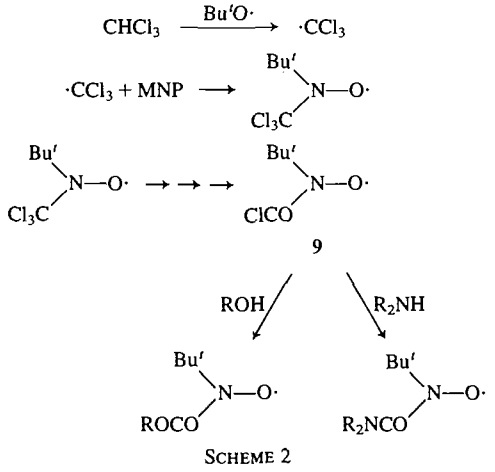


SCHEME 2

**10** for these acyl nitroxides with 2,2,6,6-tetramethylpiperid-4-one-*N*-oxyl, and measurement of the equilibrium constant, allows the strengths of the OH-bonds in the hydroxamic acids to be estimated (19), since the strength of the OH-bond in the hydroxylamine **11** is known. The results indi-

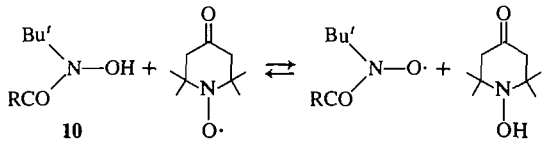


cate that the acyl nitroxides should be appreciably more reactive in radical reactions than are hindered dialkyl nitroxides, and this has been verified in a wide variety of oxidation experiments (20). Two examples are the efficient oxidation of Vitamin A alcohol to retinal by an alkanoyl nitroxide (reaction [5]) (21), and the enantioselective oxidation of benzoin to benzil by the chiral pinane derivative **12** (22).

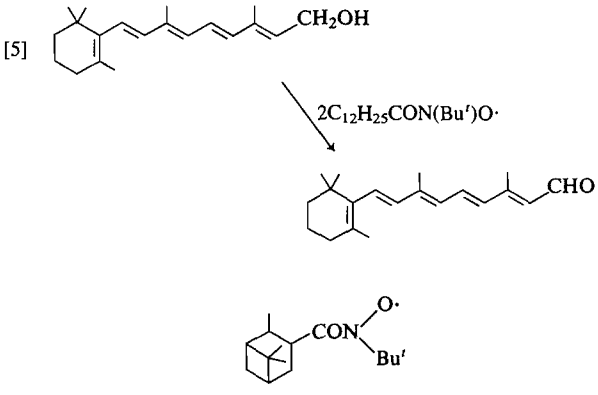


(12)

More recently our attention has been focused on intramolecular reactions, among which is the finding that intramolecular benzylic hydrogen transfer in **13** is faster than that in **14**. This can be accounted for in terms of the relatively planar carbonyl nitroxide "template", the structure of which is supported by the crystallographic results. This relatively rigid $\pi$-electron system is easily spanned by the four-methylene chain in **13** (see structure **13***a*), but much less readily by the two-methylene unit in **14** (23).

In an unpublished work (24), this type of behaviour is being investigated for intra-complex reactions, and we have obtained preliminary kinetic evidence consistent with intra-complex oxidation of the alcohol **15** by nitroxide **16**. Work is now in hand to further quantify this result, and to overcome the disadvantage of the present system wherein the preferred orientation in the complex is

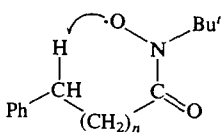


**13**: $n = 3$
**14**: $n = 1$

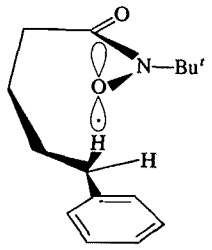


**13***a*

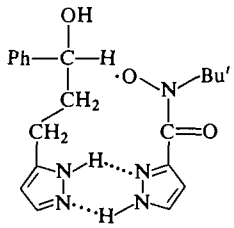


**15** **16**

undoubtedly that in which oxidation of the benzylic centre is impossible!

### 2. A water-soluble nitrosopyrazole spin trap

Whilst our primary efforts in nitroxide chemistry have now shifted away from spin trapping to the acyl nitroxides, we have retained an interest in the former topic (15). In the course of their work on nitrone traps, Janzen and his colleagues have synthesised several compounds having water solubility (25), as well as others which are amphiphilic (26). 2-Methyl-2-nitrosopropan-1-ol was the first nitroso spin trap which was studied specifically to take advantage of its water solubility (27). However, this compound shares with MNP the disadvantage of high sensitivity to visible light (in which photo-reactions di-*t*-alkyl nitroxides are produced (28)). The hindered nitrosobenzenes developed by Konaka *et al.*, for example nitrosodurene, have proved to be especially useful spin traps (29). It

Can. J. Chem. Downloaded from www.nrcresearchpress.com by 210.87.254.40 on 09/06/12
For personal use only.

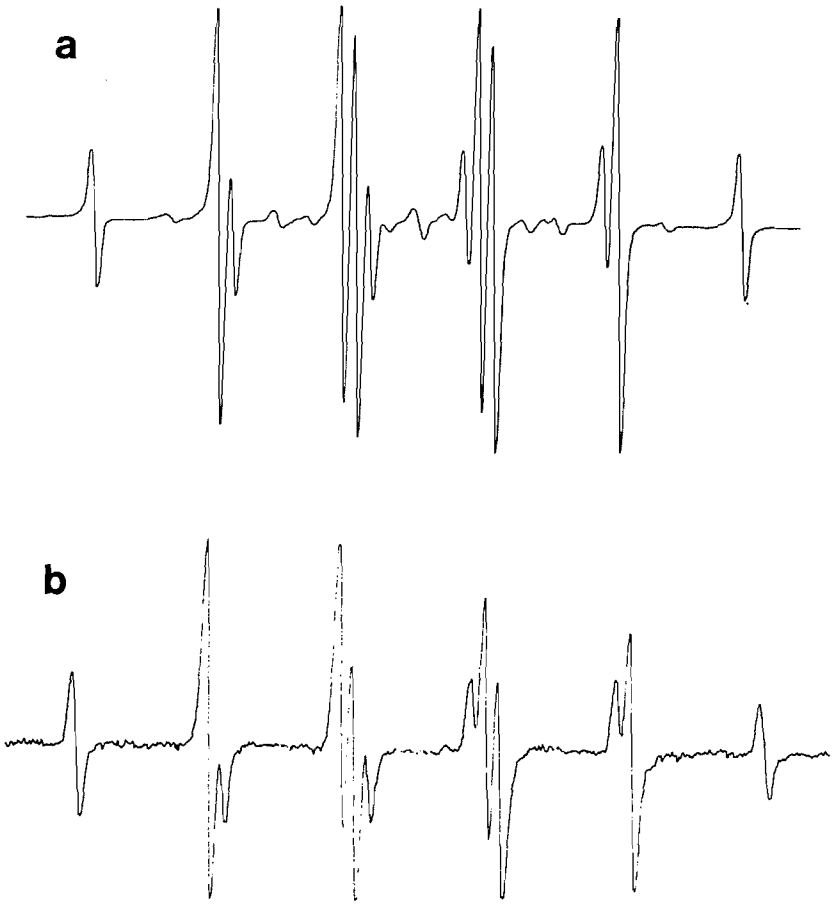


FIG. 1. Electron spin resonance spectra of methyl spin adducts (*a*) from nitrosopyrazole **18** in benzene, and (*b*) from nitrosopyrazole **1** in glacial acetic acid.

seemed of interest to develop a water-soluble analogue of these compounds, and we recently reported the first examples, namely the nitrosobenzenesulphonate **17***a*, and its dideutero-derivative **17***b* (30). Spectra of spin adducts of **17***b* are uncomplicated by small splittings from the two *meta* protons present in **17***a*.

A trap which is closely related to the hindered nitrosobenzenes, and which is introduced for the first time here, is the nitrosopyrazole **18**. In organic solvents this scavenges reactive radicals to give nitroxides whose esr spectra are readily interpreted, since they have no resolvable splittings from magnetic nuclei in the pyrazole unit, and they display quite sharp lines. The spectrum of the methyl adduct is traced in Fig. 1, and splitting constants for a representative range of spin adducts are summarised in Table 1. In addition to the simplicity of spectra of nitroxides derived from **18**, this trap has the advantage of being completely monomeric over a wide range of concentrations in solution, and, as judged by its green colour, is at least partially monomeric as a solid.

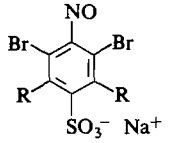


**17** a: R = H
b: R = D

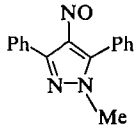


**18**

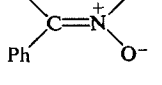


**19**

Simple kinetic experiments have been carried out to compare the reactivity of **18** with that of "phenyl *t*-butyl nitrone" (PBN, **19**) towards primary alkyl radicals produced by thermolysis of lauryl peroxide in benzene at 40°C. Under these conditions, a rate constant of $1.5 (\pm 1) \times 10^7$ L mol$^{-1}$ s$^{-1}$ has been estimated for scavenging of undecyl radicals by **18**, based on a value of $1.3 \times 10^5$ L mol$^{-1}$ s$^{-1}$ for PBN (31). Close scrutiny of the figures in the experimental section of this and the accompanying

Can. J. Chem. Downloaded from www.nrcresearchpress.com by 210.87.254.40 on 09/06/12
For personal use only.

TABLE 1. Hyperfine splitting constants obtained for spin adducts of the nitrosopyrazole traps **18** and **1**

| Radical R· trapped | Trap | Radical source and solvent* | $a_N$ | $a_{other}$ |
|---|---|---|---|---|
| $CH_3$· | **18** | $(RCO_2)_2$/PhH | 12.8 | 11.5 (3H) |
| $CH_3$· | **1** | $(RCO_2)_2$/AcOH | 13.5 | 13.0 (3H) |
| $CH_3$· | **1** | $H_2O_2$/DMSO/*hν*/$H_2O$ | $13.9_5$ | 13.0 (3H) |
| $CH_3(CH_2)_{10}$· | **18** | $(RCO_2)_2$/PhH | 12.8 | 9.4 (2H) |
| $CH_3(CH_2)_{10}$· | **1** | $(RCO_2)_2$/AcOH | 13.5 | 10.0 (2H) |
| $(CH_3)_2CH$· | **18** | $(RCO_2)_2$/PhH | 13.2 | 5.9 (1H) |
| Cyclohexyl | **18** | DTBPO/$C_6H_{12}$ | 12.9 | 6.0 (1H) |
| $(CH_3)_3C$· | **18** | $(CH_3)_3CNO$/*hν*/PhH | 13.4 | |
| $(CH_3)_3C$· | **1** | $(CH_3)_3CNO$/*hν*/AcOH | 14.5 | |
| $PhCH_2$· | **18** | DTBPO/$PhCH_3$ | 13.0 | 7.7 (2H) |
| $Cl_3C$· | **18** | DTBPO/$CHCl_3$ | 11.3 | 1.4 (3Cl) |
| Ph· | **18** | $(RCO_2)_2$/PhH | 9.8 | $2.6_5$ (3H) |
| | | | | 0.8 (2H) |
| Ph· | **1** | $(RCO_2)_2$/AcOH | 10.4 | $2.8_5$ (3H) |
| | | | | 1.0 (2H) |
| $HOCH_2$· | **1** | $H_2O/H_2O_2$/*hν*/MeOH | 13.3 | 6.7 (2H) |
| $HO\dot{C}HCH_3$ | **1** | $H_2O/H_2O_2$/*hν*/EtOH | 13.5 | 4.6 (1H) |
| $Bu^tO$· | **18** | $(Bu^tO)_2$/*hν* | $29.9_5$ | |

*$(RCO_2)_2$ = appropriate diacyl peroxide; DMSO = dimethyl sulphoxide; AcOH = glacial acetic acid; DTBPO = di-*t*-butyl peroxyoxalate.

paper indicates that the nitrosopyrazole was marginally *more* reactive than the nitrosotriptycene, yet we have preferred values (with large error limits) indicating the opposite to be true. Direct comparison of the two nitrosocompounds towards attack by undecyl radicals showed the nitrosotriptycene to be more reactive than **18** by a factor of 2. We are unable to offer an explanation for this discrepancy. The results, however, are considered valuable in view of the convenience of the traps described and the "factor of two" error limits estimated for other spin-trapping rate constants (15).

Exposure of solutions of **18** to visible light apparently does not give detectable concentrations of nitroxides under the normal conditions of spin-trapping experiments. In view of this, of the simplicity of the spectra of spin adducts of **18**, and of the fact that, unlike **18**, most of the hindered nitrosobenzene traps (including **17**) are highly associated (as nitroso-dimers) in solution, we have investigated the synthesis of water-soluble analogues of **18**.

The synthesis of **18** is achieved by condensation of the isonitroso-derivative (**20**) of dibenzoylmethane with methylhydrazine (32). Initial attempts to reproduce this chemistry with a hydrazine derivative incorporating a sulphonate salt employed hydrazine analogues of aldehyde bisulphite addition complexes, e.g. **21** (33). These, however, were degraded during attempted condensation, and the only pyrazole which could be isolated was unsubstituted at nitrogen (**22**).

An alternative approach utilised the hydrazine **24**

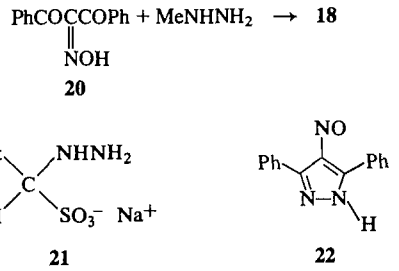


obtained by hydrazinolysis of the sultone **23** (34). In this case we were successful in isolating **1** as a green solid, readily soluble in water to give green solutions. The spectrum of the methyl spin adduct of **1**, obtained by thermolysis of acetyl peroxide in glacial acetic acid in the presence of **1** is also traced in Fig. 1, and hyperfine splittings of other spin adducts are collected in Table 1. As with **17**, we were unable to characterise either a hydrogen spin adduct or a hydroxyl adduct of **1**.

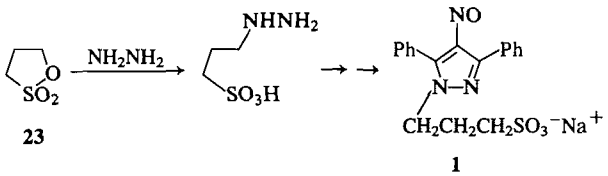

Can. J. Chem. Downloaded from www.nrcresearchpress.com by 210.87.254.40 on 09/06/12
For personal use only.

A final, and rather curious feature, of importance in connection with foreign-compound metabolism studies, is our failure to detect trichloromethyl adducts to either **1** or **17**, despite the fact that such adducts are easily formed from nitrosodurene or from **18** in organic solvents, and are characterised by well resolved chlorine hyperfine splittings in their esr spectra.

## Experimental

*1-Methyl-4-nitroso-3,5-diphenylpyrazole (18)*

This compound was obtained as a green solid, mp 117–118°C by the method of Boyd and Norris (32). It has been our experience that the product needs careful purification, which may account for the lower melting point (96–97°C) given in the earlier work. We have not, however, encountered any significant differences in behaviour as a spin trap between the initial product and that which has been purified by chromatography and repeated crystallisation. The visible absorbtion of **18** at 738 nm (benzene) had an extinction coefficient of 92, independent of concentration up to at least 0.03 *M*.

*Sodium 3-(4-nitroso-3,5-diphenyl-1-pyrazolyl)propane-1-sulphonate (1)*

An aqueous solution of 3-hydrazinopropane-4-sulphonic acid (2.6 g in 60 mL), prepared from propane sultone by the method of Schindler and Pietrzok (34), was added with stirring to a solution of isonitrosodibenzoylmethane (4.2 g) in methanol (120 mL). The mixture was boiled under reflux for 7 h, after which most of the solvent was removed under reduced pressure. The residual green aqueous solution was washed twice with ether and then dissolved in 3 *M* $H_2SO_4$ (150 mL) and subjected to continuous extraction with ether. Removal of solvent from the dried ether extract gave a brown crystalline solid considered to be the pyrazolylpropanesulphonic acid corresponding to **1**. ($\lambda_{max}$(ethanol) 715 (ε 71)] (2.3 g, 38%, softens 73°C, mp, 100–104°C). This acid (1 g) in water (10 mL) was treated with sodium bicarbonate (0.24 g) at room temperature. After 30 min the green microcrystalline solid which had separated was removed by filtration. Its proton nmr ($D_2O$) showed peaks at δ 2.0–2.45, 2H, broad m; 2.55–2.95, 2H, broad t; 3.95–4.20, 2H, broad t; 7.3–7.8, 10H, m. Found: C 54.2, H 4.0, N 10.1. $C_{18}H_{16}N_3O_4SNa$ requires C 55.0, H 4.1, N 10.7.

*Spin trapping*

Experiments were carried out in solutions deoxygenated by nitrogen bubbling or by vacuum out-gassing. Spectra were recorded using a Varian E4 spectrometer, and were calibrated by comparison with those of di-*t*-butyl nitroxide.

Competition experiments using the nitrosopyrazole **18** and phenyl *t*-butyl nitrone were carried out by preparing solutions of lauryl peroxide and measured quantities of the two traps in benzene at ca. 10°C, and, after degassing, rapidly warming the solutions to 40°C in the cavity of the spectrometer. The initial growth of the two spin adducts was then monitored using spectral lines which showed little or no overlap. Double integration of these permitted relative concentrations to be estimated. The ratios of concentrations remained constant during the initial stages of each reaction, and from these ratios and the known ratios of concentrations of the traps, the relative reactivities of the two traps were deduced. The relative reactivities were found to be independent of the ratios of spin-trap concentrations when these were changed nearly thirty-fold. Results of individual experiments were as follows (in each case the first figure is the ratio [PBN]/[**18**], the second is the estimated reactivity ratio); 193, 0.006; 49.8, 0.009; 24.9, 0.006; 6.7, 0.006. Taking 0.006 as the mean value, and using $1.3 \times 10^5$ L $mol^{-1}$ $s^{-1}$ for the rate of reaction of primary alkyl radicals with PBN in benzene at 40°C (31), we deduce a value of ca. $1.5 (\pm 1) \times 10^7$ L $mol^{-1}$ $s^{-1}$ for the reaction with **18** under these conditions. This conclusion depends on the assumption that trapping of undecyl radicals will occur at a rate similar to that of hexyl and hex-5-enyl radicals used in the earlier work (31).

## Acknowledgements

We thank the Science Research Council for support of this work, André Scheffer for preliminary experiments with compound **18**, and Roger Tye for technical assistance.

1. D. H. Hey, M. J. Perkins, and G. H. Williams. J. Chem. Soc. 3412 (1964).
2. G. R. Chalfont, D. H. Hey, K. S. Y. Liang, and M. J. Perkins. J. Chem. Soc. B, 233 (1971).
3. G. R. Chalfont and M. J. Perkins. J. Chem. Soc. B, 245 (1971).
4. A. C. Scott, J. M. Tedder, J. C. Walton, and S. Mhatre. J. Chem. Soc. Perkin II, 260 (1980).
5. C. Rüchardt and B. Freudenberg. Tetrahedron Lett. 3623 (1964).
6. G. Binsch and C. Rüchardt. J. Am. Chem. Soc. **88**, 173 (1966).
7. J. I. G. Cadogan. Acc. Chem. Res. **4**, 186 (1971).
8. G. R. Chalfont and M. J. Perkins. J. Am. Chem. Soc. **89**, 3054 (1967).
9. E. G. Janzen. Acc. Chem. Res. **4**, 31 (1971); E. G. Janzen and B. J. Blackburn. J. Am. Chem. Soc. **90**, 5909 (1968).
10. P. S. Skell and J. C. Day. Acc. Chem. Res. **11**, 381 (1978).
11. G. R. Chalfont, A. Horsfield, and M. J. Perkins. J. Chem. Soc. B, 401 (1970).
12. C. Lagercrantz and S. Forshult. Acta Chem. Scand. **23**, 708 (1969).
13. G. R. Chalfont, M. J. Perkins, and A. Horsfield. J. Am. Chem. Soc. **90**, 7141 (1968).
14. M. J. Perkins. Chemical Society Special Publication No. 24. 1970. Chapt. 5.
15. M. J. Perkins. Adv. Phys. Org. Chem. **17**, 1 (1980).
16. C. M. Camaggi, R. J. Holman, and M. J. Perkins. J. Chem. Soc. Perkin II, 501 (1972).
17. P. F. Alewood, S. A. Hussain, T. C. Jenkins, M. J. Perkins, A. H. Sharma, N. P. Y. Siew, and P. Ward. J. Chem. Soc. Perkin I, 1066 (1978).
18. S. A. Hussain, T. J. King, M. J. Perkins, and A. H. Sharma. Unpublished results.
19. T. C. Jenkins, M. J. Perkins, and N. P. Y. Siew. J. Chem. Soc. Chem.Commun. 880 (1975).
20. S. A. Hussain, T. C. Jenkins, M. J. Perkins, and N. P. Y. Siew. J. Chem. Soc. Perkin I, 2805 (1979); S. A. Hussain, T. C. Jenkins, and M. J. Perkins. J. Chem. Soc. Perkin I, 2809 (1979).
21. M. J. Perkins and A. H. Sharma. Unpublished results.
22. C. Berti and M. J. Perkins. Angew. Chem. Int. Ed. **18**, 864 (1979).
23. C. Berti and M. J. Perkins. J. Chem. Soc. Chem. Commun. 1167 (1979).
24. M. J. Perkins and E. S. Turner. Unpublished results.
25. E. G. Janzen, Y. Y. Wang, and R. V. Shetty. J. Am. Chem. Soc. **100**, 2923 (1978); E. G. Janzen and R. C.

ZAWALSKI. J. Org. Chem. **43**, 1900 (1978); E. G. JANZEN and R. V. SHETTY. Tetrahedron Lett. 3229 (1979).
26. E. G. JANZEN, R. L. DUDLEY, and R. V. SHETTY. J. Am. Chem. Soc. **101**, 243 (1979).
27. J. J. M. C. DE GROOT, G. J. GARSSEN, J. F. G. VLIEGENTHART, and J. BOLDINGH. Biochim. Biophys. Acta, **326**, 279 (1973).
28. A. MACKOR, TH. A. J. W. WAJER, TH. J. DE BOER, and J. D. W. VAN VOORST. Tetrahedron Lett. 2115 (1966).
29. S. TERABE, K. KURUMA, and R. KONAKA. J. Chem. Soc. Perkin II, 1252 (1973).
30. H. KAUR, K. H. W. LEUNG, and M. J. PERKINS. J. Chem. Soc. Chem. Commun. 142 (1981).
31. P. SCHMID and K. U. INGOLD. J. Am. Chem. Soc. **100**, 2493 (1978).
32. G. V. BOYD and T. NORRIS. J. Chem. Soc. Perkin I. 1028 (1974).
33. K. MIYATAKE and T. YOSKIKAWA. Japan Pat. 6734, Aug. 1956 (Chem. Abstr. **52**, 8207 (1956)).
34. W. SCHINDLER and H. PIETRZOK. E. Ger. Pat. 44067, Dec. 1965 (Chem. Abstr. **64**, 17426 (1965)).

Can. J. Chem. Downloaded from www.nrcresearchpress.com by 210.87.254.40 on 09/06/12
For personal use only.

# Spin trapping with 9-nitrosotriptycene

HARPARKASH KAUR, M. JOHN PERKINS,[1] ANDRÉ SCHEFFER, AND DAVID C. VENNOR-MORRIS
*Department of Chemistry, Chelsea College, Manresa Road, London SW3 6LX, England*

Received September 26, 1981

HARPARKASH KAUR, M. JOHN PERKINS, ANDRÉ SCHEFFER, and DAVID C. VENNOR-MORRIS. Can. J. Chem. **60**, 1594 (1982).

Nitrosotriptycene is found to be a potentially useful spin trap when used in organic solvents; the esr spectra of its spin adducts are simple, but they may show marked temperature dependence due to restricted rotation. Nitrosotriptycene traps primary alkyl radicals with a rate constant of ca. $2 \times 10^7$ L mol$^{-1}$ s$^{-1}$ at 40°C in benzene.

HARPARKASH KAUR, M. JOHN PERKINS, ANDRÉ SCHEFFER et DAVID C. VENNOR-MORRIS. Can. J. Chem. *60*, 1594 (1982).

On a trouvé que le nitrosotriptycène est un capteur de spin potentiel utile lorsqu'on l'utilise dans des solvants organiques. Les spectres de rpe des adduits de spin sont simples mais ils montrent une influence marquée de la température en raison d'une rotation limitée. Le nitrosotriptycène capte les radicaux alkyles primaires avec une constante de vitesse d'environ $2 \times 10^7$ L mol$^{-1}$ s$^{-1}$ dans le benzène à 40°C.

[Traduit par le journal]

For a *C*-nitroso-compound, RNO, to be a good spin trap (1), it should be largely or entirely monomeric in solution, and be reasonably stable to heat, and stable to visible light. Furthermore, in its spin adducts (RR'NO·) there should be minimal interaction between the unpaired electron and magnetic nuclei in the R group derived from the nitroso-compound, so that esr spectra of these adducts are simple and show easily identified hyperfine splittings from nuclei in the radicals that are trapped. Amongst the most commonly used nitroso-traps, nitrosodurene (ND; **1**) is quite strongly associated in solution as the nitroso-dimer (2), and 2-methyl-2-nitrosopropane (MNP; **2**) is well known to be sensitive to red light, rapidly giving di-*t*-butyl nitroxide on photolysis. The spectra of adducts of these two traps also suffer from line-broadening due to unresolved splitting by the protons in the duryl and *t*-butyl groups respectively, though in both cases narrower spectral lines (and improved resolution) have been achieved by deuteration (3, 4).

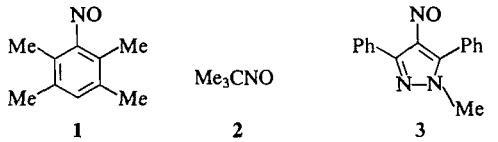


**1**

$Me_3CNO$

**2**




**3**

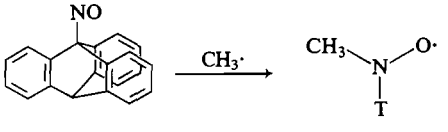


**4** = TNO **5**

A useful and readily accessible alternative nitroso-trap, the nitrosopyrazole **3**, as well as a water-soluble analogue, has been introduced in the accompanying paper, and we now outline results which suggest that 9-nitrosotriptycene, **4** (TNO), whilst less readily available, may also be a useful spin trap for investigations using organic solvents.

Compound **4** (5) was obtained as a pale blue solid which gives blue solutions in organic solvents. We have detected no evidence for association up to a concentration of 0.1 *M* in benzene at room temperature. Unlike those of MNP, its solutions do not give esr signals on exposure to visible light. Presumably, since the trivalent carbon in the 9-triptycyl radical cannot become planar, and the unpaired electron is in an orbital orthogonal to the $\pi$-electrons of the benzene rings, the triptycyl–nitrogen bond in **4** is much stronger than that in MNP and a quantum of red light absorbed by the molecule carries insufficient energy to cause dissociation. We have made no attempt to study the ultraviolet photochemistry of **4**, except in the esr spectrometer, where signals believed to be due to ditriptycyl nitroxide are observed. This is discussed briefly at the end of this paper.

Figure 1 shows the spectrum of the methyl spin adduct **5** of **4**. Although in this example it is at once clear that there is no resolvable hyperfine structure in the spectrum other than that from nitrogen and from the methyl protons, in some spin-adduct spectra there was evidence for weak interaction with three equivalent protons from the triptycene nucleus (the "*peri*" protons?). Table 1 lists splitting parameters found for spectra of representative nitrosotriptycene spin adducts.

The spectrum of the butoxymethyl spin adduct **7** was first observed in experiments in which substan-

[1]To whom all correspondence should be addressed.

0008-4042/82/121594-03$01.00/0
©1982 National Research Council of Canada/Conseil national de recherches du Canada

Can. J. Chem. Downloaded from www.nrcresearchpress.com by 210.87.254.42 on 09/06/12
For personal use only.

TABLE 1. Hyperfine splittings obtained for spin adducts of nitrosotriptycene

| Radical trapped | Source* | Solvent | $a_N$ | $a_{other}$ |
|---|---|---|---|---|
| $CH_3^{\cdot}$ | a | PhH | 15.2 | 11.0 (3H) |
| $C_2H_5^{\cdot}$ | a | PhH | 15.2 | 9.3 (2H) |
| $CH_3(CH_2)_{10}^{\cdot}$ | a | PhH | 15.2 | 9.1 (2H) |
| $Me_2CH^{\cdot}$ | a | PhH | 13.7$_5$ | 2.3 (1H) |
| Cyclohexyl | a | $C_6H_{12}$ | 13.5 | 2.4 (1H) |
| $Me_3C^{\cdot}$ | b | PhH | 14.5 | |
| Triptycyl† | a | PhH | 12.5 | |
| $Ph^{\cdot}$ | a | PhH | 11.1 | 2.2 (3H) |
| | | | | 0.9 (2H) |
| $PhCH_2^{\cdot}$ | c | $PhCH_3$ | 15.0 | 7.4 (2H) |
| $Cl_3C^{\cdot}$ | c | $CHCl_3$ | 11.5$_5$ | 1.4 (3Cl) |
| $Bu^tOCH_2^{\cdot}$ | c | $Bu^tOCH_3$ (50°C) | 14.2 | 4.2 (2H) |
| $Bu^tOCH_2^{\cdot}$ | c | $Bu^tOCH_3$ (−57°C) | 14.1 | 5.6 (1H) |
| | | | | 2.8 (1H) |
| $Bu^tO^{\cdot}$ | d | PhH | 27.7$_5$ | 0.4$_5$ (3H)‡ |

*Radical sources: a = $RCO_2OCOR \rightarrow R^{\cdot}$; b = $Bu^tNO$ + red light; c = $Bu^tOCOCOOBu^t + RH \rightarrow R^{\cdot}$; d = $Bu^tOCOCOOBu^t$.
†g-value = 2.0062.
‡Poorly resolved quartet splitting, probably from three triptycyl hydrogens.

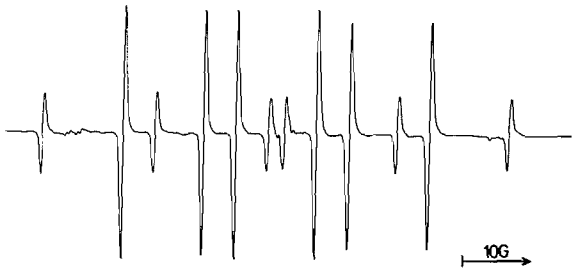


FIG. 1. Electron spin resonance spectrum of the methyl spin adduct of 9-nitrosotriptycene in benzene.

tial quantities of di-*t*-butyl peroxyoxalate had decomposed in benzene solutions of **4**. Its appearance in that system may be attributed to the formation of the methyl spin adduct and its subsequent oxidation *in situ* to the methylene nitrone **6**. Trapping of butoxy radicals by **6** then gives **7**, the identity of which was confirmed by an experiment in which butoxymethyl radicals were generated by

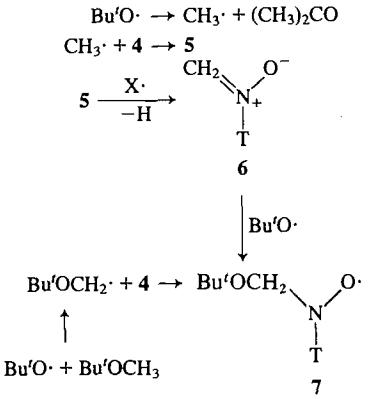


hydrogen abstraction from *t*-butyl methyl ether in the presence of **4**. The temperature dependence of the spectrum of **7** (Fig. 2) is of interest, since it may be interpreted in terms of a rocking of the butoxymethyl group; possibly the methylene hydrogens may be meshing with the triptycene cogwheel (structures *7a* ⇌ *7b*). In any case, it is important to recognise that *free* rotation of the butoxymethyl group is not required for the methylene protons to become equivalent. We estimate a free energy barrier of ca. 6.5 kcal $mol^{-1}$ at 17°C for the conformational change responsible for the observed change in spectrum.

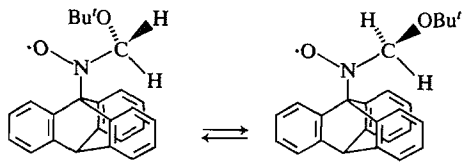


*7a* *7b*

There has been interest recently in the meshing of two triptycene residues attached to a common atom (6). Although we obtained a spectrum attributed to ditriptycyl nitroxide both by photolysis (see above) and by thermolysis of bis-9-triptoyl peroxide in benzene in the presence of **4**, this showed only nitrogen splitting and the question of triptycyl rotation could not be investigated. The nitrogen splitting in this nitroxide is relatively small, but the *g*-value of 2.0062 is in the range expected for a dialkyl nitroxide, so that the alternative alkoxyaminyl structure, TONT, seems unlikely for the radical responsible for this spectrum. It may be noted that $a_N$ for the relatively hindered isopropyl and

Can. J. Chem. Downloaded from www.nrcresearchpress.com by 210.87.254.42 on 09/06/12
For personal use only.

Can. J. Chem. Downloaded from www.nrcresearchpress.com by 210.87.254.42 on 09/06/12
For personal use only.

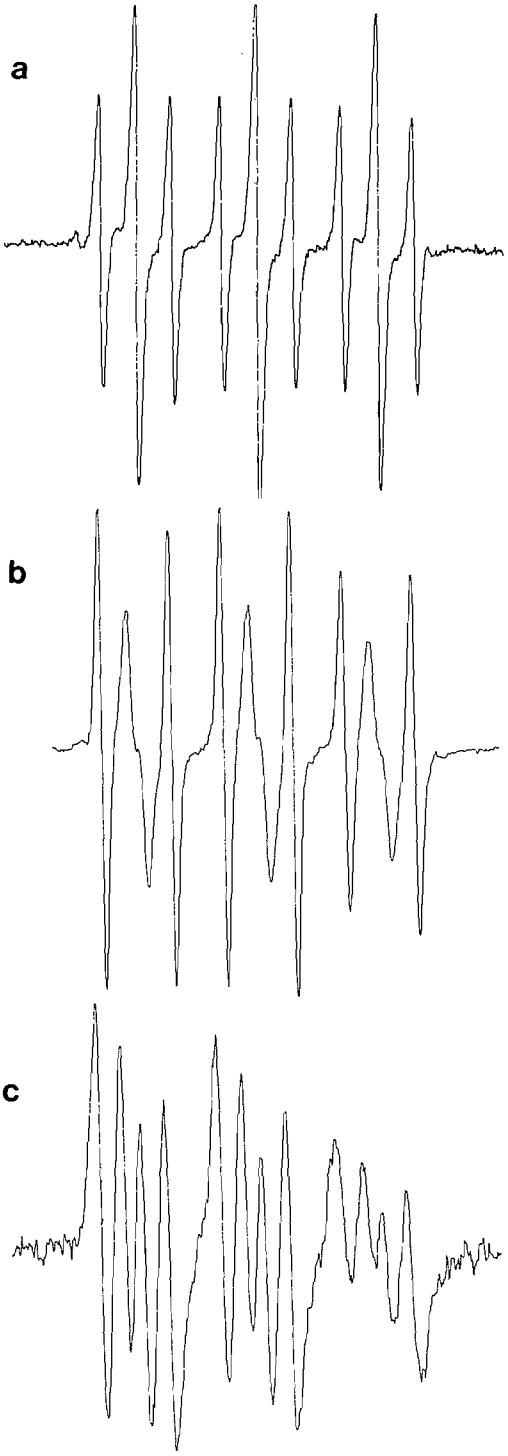


FIG. 2. Electron spin resonance spectra of the $Bu^tOCH_2^{\bullet}$ spin adduct of 9-nitrosotriptycene in *t*-butyl methyl ether (*a*) at 50°C; (*b*) at −18°C; (*c*) at −57°C.

cyclohexyl spin adducts are also small. In view of this, the rather larger value of $a_N$ found for the *t*-butyl adduct, formed by photolysis of MNP in the presence of excess **4**, may seem surprising. However a similar spectrum was obtained in an experiment in which ditriptoyl peroxide was allowed to decompose in the presence of MNP. A further point of interest is that the spectrum of the cyclohexyl adduct of **4** does not show long-range splittings similar to those observed in the spectrum of MNP–cyclohexyl spin adduct.

Finally, the reactivity of **4** towards primary alkyl radicals was estimated by allowing it to compete with PBN for undecyl radicals formed by thermolysis of lauryl peroxide in benzene. At 40°C, a value of $2(\pm 1) \times 10^7$ L mol$^{-1}$ s$^{-1}$ was estimated. The large error limits reflect the current level of precision of these measurements (2).

## Experimental

*Materials*

9-Nitrotriptycene was prepared from 9-nitroanthracene by the method of Bowden *et al.* (7) and converted into 9-nitrosotriptycene by the method of Theilacker and Beyer (5). Di-9-triptoyl peroxide was derived from triptoic acid by the method of Bartlett and Greene (8).

*Spin trapping*

Experiments followed the same general procedure as indicated in the accompanying paper. In the competition study using PBN and nitrosotriptycene in benzene at 40°C, the ratio of concentrations of traps in individual experiments ([PBN]/[**4**]) and calculated relative reactivities were as follows: 273, 0.007; 193, 0.007; 50, 0.006; 25, 0.007. From these, the mean reactivity ratio was taken to be 0.007, whence the rate constant of $2(\pm 1) \times 10^7$ L mol$^{-1}$ s$^{-1}$ is estimated for trapping of undecyl radicals by nitrosotriptycene in benzene at 40°C. This is based on a value of $1.3 \times 10^5$ L mol$^{-1}$ s$^{-1}$ for PBN under these conditions (9) and depends on the assumption that there is negligible difference between the rates of trapping of undecyl and those of hexyl and hexenyl radicals (9).

## Acknowledgements

We thank the Science Research Council for support of this work and Roger Tye for technical assistance.

1. M. J. PERKINS. Adv. Phys. Org. Chem. **7**, 1 (1980) and references therein.
2. Y. MAEDA and K. U. INGOLD. J. Am. Chem. Soc. **101**, 4975 (1979).
3. S. TERABE, K. KURUMA, and R. KONAKA. J. Chem. Soc. Perkin II, 1252 (1973).
4. H. J. JAKOBSEN and K. TORSSELL. Tetrahedron Lett. 5003 (1970); R. J. HOLMAN and M. J. PERKINS. J. Chem. Soc. C, 2324 (1971).
5. W. THEILACKER and K.-H. BEYER. Chem. Ber. **94**, 2968 (1961).
6. Y. KAWADA and H. KURUMA. J. Org. Chem. **45**, 2547 (1980).
7. K. BOWDEN, J. G. IRVING, and M. J. PRICE. Can. J. Chem. **46**, 3903 (1968).
8. P. D. BARTLETT and F. D. GREENE. J. Am. Chem. Soc. **76**, 1088, (1954).
9. P. SCHMID and K. U. INGOLD. J. Am. Chem. Soc. **100**, 2493 (1978).

# Spin trapping of the azide radical with nitroso compounds[1]

WALTER KREMERS, GRANT W. KOROLL, AND AJIT SINGH[2]

*Medical Biophysics Branch, Whiteshell Nuclear Research Establishment, Atomic Energy of Canada Research Company, Pinawa, Man., Canada R0E 1L0*

Received September 19, 1981

WALTER KREMERS, GRANT W. KOROLL, and AJIT SINGH. Can. J. Chem. **60**, 1597 (1982).

Azide radicals ($N_3^{\cdot}$) are formed in aqueous solutions by the reaction of hydroxyl radicals ($^{\cdot}OH$) with azide anions ($N_{3aq}^{-}$). Azide radicals have been spin trapped with three nitroso spin traps: nitrosodurene (ND), 2,6-dideutero-3,5-dibromo-4-nitrosobenzene sulfonate (DDNBS), and 2-methyl-2-nitrosopropane (MNP). The electron spin resonance (esr) spectra show the presence of two molecules of the spin traps in the spin-trapped species.

WALTER KREMERS, GRANT W. KOROLL et AJIT SINGH. Can. J. Chem. **60**, 1597 (1982).

On obtient les radicaux azotures ($N_3^{\cdot}$) en solution aqueuses en faisant réagir les radicaux hydroxyles ($^{\cdot}OH$) avec les anions azotures ($N_3^{-}{}_{aq}$). On a capté les radicaux azotures avec trois capteurs de spin du type nitroso: le nitrosodurène (ND), le sulfonate de dideutéro-2,6 dibromo-3,5 nitroso-4 benzène (DDNNB) et le méthyl-2 nitroso-2 propane (MNP). Les spectres de rpe montrent la présence de deux molécules de capteurs de spin dans les espèces piégées.

[Traduit par le journal]

## Introduction

The azide radical ($N_3^{\cdot}$) has been trapped by several spin traps (1–6). The spectra of nitrone adducts are straightforward and show contributions of one nitrogen from the trap and one additional nitrogen from the azide radical (1–6). The nitrosodurene (ND) adduct, however, indicates the presence of two equivalent nitrogens and one nonequivalent one (hfs: $a_N^{1,2} = 0.73$ mT, $a_N^3 = 0.23$ mT) (4, 5). Rehorek and Hennig (5) have suggested that, with ND, the adduct dissociates to produce $N_2$ and the residual radical adds onto another molecule of the spin trap. We have, therefore, undertaken further work with nitroso spin traps to try to resolve the identity of the adduct.

Azide radicals were generated by uv photolysis of a 1% solution of $H_2O_2$ in the presence of $NaN_3$ (1).

$N_3^{\cdot}$ was trapped with 2,6-dideutero-3,5-dibromo-4-nitrosobenzene sulphonate (DDNBS) (hfs: $a_N^{1,2} = 0.71$ mT, $a_N^3 = 0.27$ mT) and the well-known trap methylnitrosopropane (MNP) (hfs: $a_N^{1,2} = 0.11$ mT, $a_N^3 = 1.29$ mT). Both spectra show the presence of two equivalent nitrogens and one nonequivalent one. We further trapped azide radicals generated from 100% $^{15}N$-labelled $NaN_3$ with ND. The quintet of triplets collapsed into a quintet of doublets (hfs: $a_N^{1,2} = 0.77$ mT, $a_N^3 = 0.33$ mT). These results show that the two equivalent nitrogens originate from ND and only one from the azide radical, i.e. the adduct contains two ND molecules and one azide radical.

## Acknowledgements

We are grateful to Dr. M. J. Perkins for sending us samples of ND and DDNBS. We gratefully acknowledge helpful suggestions from Dr. D. Rehorek, along with comments on our previous paper (1).

1. W. KREMERS and A. SINGH. Can. J. Chem. **58**, 1592 (1980).
2. M. SETAKA, T. OZAWA, and T. KWAN. Chem. Pharm. Bull. **20**, 1063 (1972).
3. D. BEHAR and R. W. FESSENDEN. J. Phys. Chem. **76**, 1710 (1972).
4. D. REHOREK, P. THOMAS, and H. HENNIG. Inorg. Chim. Acta, **32**, L1 (1979).
5. D. REHOREK and H. HENNIG. Z. Chem. 263 (1979).
6. E. G. JANZEN, H. J. STRONKS, D. E. NUTTER, JR., E. R. DAVIS, H. N. BLOUNT, J. L. POYER, and P. B. MCCAY. Can. J. Chem. **58**, 1596 (1980).

[1]AECL No. 7364.

[2]Author to whom correspondence should be addressed.

0008-4042/82/121597-01$01.00/0

©1982 National Research Council of Canada/Conseil national de recherches du Canada

Can. J. Chem. Downloaded from www.nrcresearchpress.com by 210.87.254.40 on 09/06/12
For personal use only.

# Electron spin resonance studies of the reactions of sorbate with nitrite in the presence of a spin trap

AVINASH JOSHI, DENNIS M. HINTON, AND GEORGE C. YANG[1]

*Food and Drug Administration, Washington D.C. 20204, U.S.A.*

Received October 8, 1981

AVINASH JOSHI, DENNIS M. HINTON, and GEORGE C. YANG. Can. J. Chem. **60**, 1598 (1982).

An esr spectrum was generated when a spin trap, *t*-nitroso butane (*t*NB), was added to potassium sorbate solution at pH of 6.4. This spectrum can be explained by the abstraction of allylic hydrogen by $NO_2$, generated by the decomposition of *t*NB, followed by spin trapping of the radical product. With increasing concentration of $NO_2$, which was accomplished by either the addition of sodium nitrite or by lowering the pH to cause rapid decomposition of *t*NB, a different esr spectrum was observed. This spectrum can be accounted for by a radical formed by addition of $NO_2$ to the 4,5 double bond of the sorbate and subsequent trapping by *t*NB.

AVINASH JOSHI, DENNIS M. HINTON et GEORGE C. YANG. Can. J. Chem. **60**, 1598 (1982).

On a enregistré le spectre de rpe du capteur de spin, nitroso *tert*-butane (*t*NB), dans une solution de sorbate de potassium à un pH de 6,4. On peut expliquer le spectre par l'élimination de l'hydrogène allylique par le $NO_2$, provenant de la décomposition du tNB, suivie de la capture du produit radicalaire. On observe un spectre de rpe différent en augmentant la concentration $NO_2$ soit par l'addition de nitrite de sodium soit par une diminution du pH provoquant une décomposition rapide du *t*NB. On peut attribuer ce spectre à un radical provenant de l'addition de $NO_2$ sur la double liaison en positions 4,5 du sorbate suivie du piègeage par le *t*NB.

[Traduit par le journal]

## Introduction

The implication of nitrites as precursors in the formation of certain carcinogenic nitrosamines has led to studies of the use of other food preservatives. Since potassium sorbate exhibits both fungicidal and bacteriostatic activity, reduction of nitrite concentration combined with relatively high concentrations of sorbate has been tested experimentally as a substitute for nitrite alone (1). Several reports have appeared which address the potential toxicity of the combination of sorbate and nitrite (2, 3).

At low pH, 2 to 5, sorbic acid, **I**, has been shown to react with sodium nitrite (4–6). Recently Osawa *et al.* (7) isolated and identified three new compounds, a furoxan derivative, **II**, and its two precursors, **III** and **IV**, in the reaction of sorbate with sodium nitrite. They further proposed that sorbate can be easily transformed to compounds **II** and **III** by the addition of nitro and nitroso groups to its 4,5 double bond. In a previous study, we also investigated the conditions under which sorbate and nitrite react (8). In the present study, we have attempted to spin trap the transient free radicals generated in this reaction in order to gain additional information on the reactive intermediates which led to the formation of the final product.

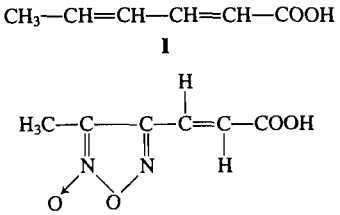

**I**



**II**

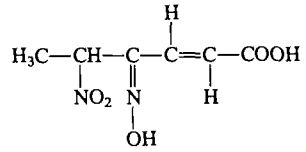

(*syn* and *anti*)

**III, IV**

## Experimental

Potassium sorbate was obtained from Monsanto Chemical Co. Sodium nitrite was Fisher Certified ACS Grade. Tertiary nitrosobutane (*t*NB) was obtained from Aldrich Chemical Co. Inc. All chemicals were used without further purification. Hydrochloric acid was used to attain pH 3.5 to 4.0. To improve solubility, sorbate was dissolved in 50% ethanol in the case of low pH. Electron spin resonance spectra were obtained on a Varian E-9 Spectrometer. Chromatographic separations were done using a Perkin Elmer 601 HPLC in conjunction with a Perkin Elmer LC55 UV detector at 235 nm. A reverse phase PXS 5/25 ODS Whatman column was used at 50°C. The composition of the elution solvent was 60% water, 25% acetonitrile, and 15% methanol.

*pH 6.4*

When 0.0125 *M* *t*NB was present in a solution of 0.5 *M* sorbate, 0.05 *M* phosphate buffer, and 25% methanol at a final pH of 6.4, the esr spectrum shown in Fig. 1 was observed. This spectrum consists of a triplet (N) and its $^{13}C$ satellite lines arising from di-*t*-butyl nitroxide radical, and also contained another triplet with $A_N = 15.3$ G, further split into a triplet of intensity ratio 1:2:1 with $A_H = 5.8$ G. Sargent and Gardy (9) have observed a similar spectrum from the addition of $^{\bullet}CH_2OH$ to

[1]To whom all correspondence should be addressed.

Can. J. Chem. Downloaded from www.nrcresearchpress.com by 210.87.254.6 on 09/06/12
For personal use only.

Can. J. Chem. Downloaded from www.nrcresearchpress.com by 210.87.254.6 on 09/06/12
For personal use only.

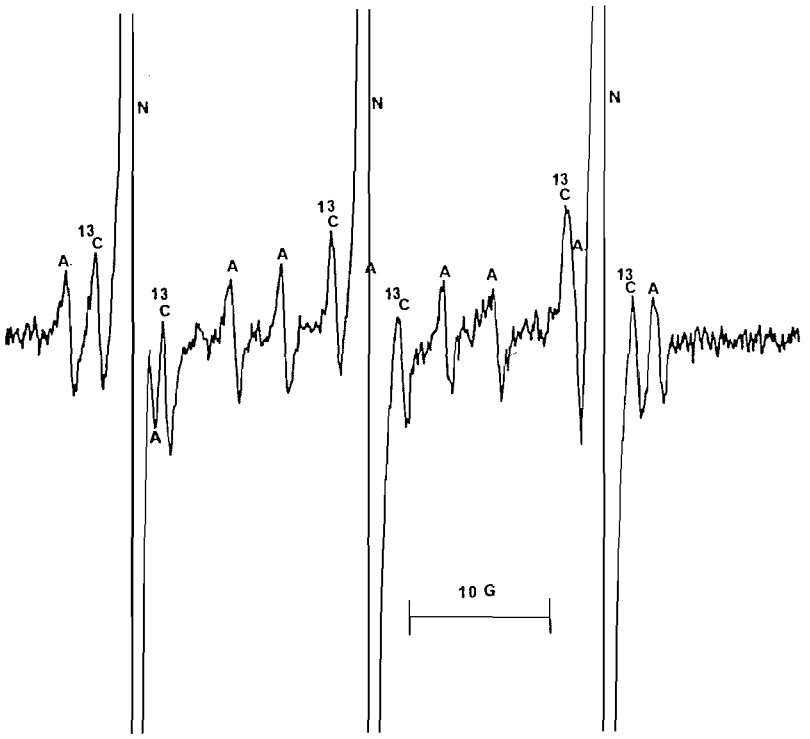


FIG. 1. Electron spin resonance spectrum observed in the mixture of 0.0125 *M* *t*NB, 0.5 *M* potassium sorbate, 0.05 *M* phosphate buffer in 25% MeOH at pH 6.4. N = di-*t*-butyl nitroxide; $^{13}C{=}^{13}C$ lines of the di-*t*-butyl nitroxide; A = reaction product.

*t*NB with $A_N = 14.5$ G and $A_H = 4.5$ G. In our experiments, *t*NB was dissolved in both methanol and methanol-$d_4$ and no spectral differences were observed. This indicated that the reaction of *t*NB with methanol was not responsible for the observed spectrum.

Pryor and Lightsey (10) proposed that at low concentration of nitrogen dioxide, nitrogen dioxide reacts with cyclohexene almost exclusively by abstraction of allylic hydrogen.

$$NO_2 + \text{—CH=CH—CH}_2 \rightarrow HONO + \text{—}\bar{C}\text{H—}\dot{C}\text{H—}\bar{C}\text{H—}$$

Based on this mechanism, as well as the observed esr spectrum, the following is proposed for the reaction between *t*NB spin trap and sorbate.

Radical **V**, which contains one nitrogen and two equivalent protons, is consistent with the observed spectrum.

$$2(CH_3)_3C\text{—}N{=}O \rightarrow (CH_3)_3C\text{—}\underset{\displaystyle C(CH_3)_3}{\underset{|}{N}}\text{—}O\cdot + NO$$

$$NO + O_2 \rightarrow NO_2$$

$$NO_2 + CH_3\text{—}CH{=}CH\text{—}CH{=}CH\text{—}COOH \rightarrow$$

$$HNO_2 + \bar{C}\bar{H}_2\text{—}\dot{C}\bar{H}\text{—}\bar{C}\bar{H}\text{—}CH{=}CH\text{—}COOH \xrightarrow{(CH_3)_3CN{=}O}$$

$$(CH_3)_3C\text{—}\underset{\displaystyle O\cdot}{\underset{|}{N}}\text{—}CH_2\text{—}CH{=}CH\text{—}CH{=}CH\text{—}COOH$$

**V**

When 0.25 *M* sodium nitrite was present in the reaction mixture of sorbate and *t*NB, as described above, and again pH measured to be 6.4, an esr spectrum shown in Fig. 2 was obtained. This spectrum contains a triplet of $A_N = 17.0$ G due to di-*t*-butyl nitroxide and another triplet with $A_N = 15.9$ G, further split into doublets with $A_H = 3.5$ G.

In acidic medium nitrite decomposes into nitric oxide which is easily oxidized to nitrogen dioxide. It has been demonstrated that $NO_2$ adds to the double bonds of the unsaturated fatty acids (11, 12).

$$NO_2 + \text{—C=C—} \rightleftarrows O_2N\text{—}\dot{C}\text{—C—}$$

Pryor and Lightsey (10) also demonstrated this reaction mechanism when the concentration of $NO_2$ is relatively high. Based on this assumption and the esr spectrum, we propose the following reaction in the mixture of sorbate, nitrite, and *t*NB.

$$\text{Sorbate} + NO_2 \rightarrow CH_3\text{—}\underbrace{\dot{C}H\text{—}\dot{C}H}_{NO_2}\text{—}CH{=}CH\text{—}COOH$$

$$\xrightarrow{(CH_3)_3C\text{—}NO} CH_3\text{—}\underbrace{CH\text{—}CH}_{NO_2,\ N\text{—}O\cdot}\text{—}CH{=}CH\text{—}COOH$$

$$\text{(}C(CH_3)_3\text{ on N)}$$

**VI**

Although not considered in this paper, the presence of NO in this mixture and its possible involvement in this reaction should not be ruled out.

*pH 3–4*

When 0.0125 *M* or 0.145 *M* *t*NB was present with 0.5 *M* or

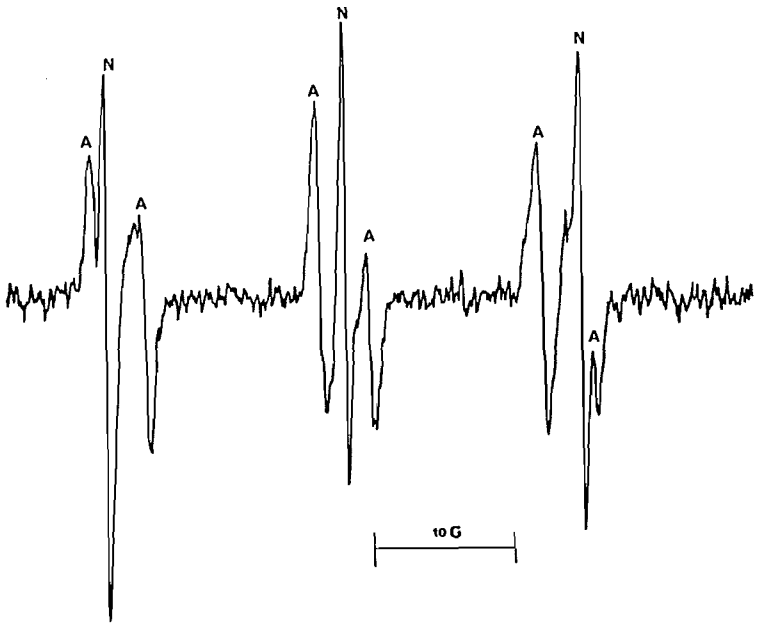


FIG. 2. Electron spin resonance spectrum observed in the mixture as in Fig. 1, with the presence of 0.25 *M* $NaNO_2$. N = di-*t*-butyl nitroxide; A = reaction product.

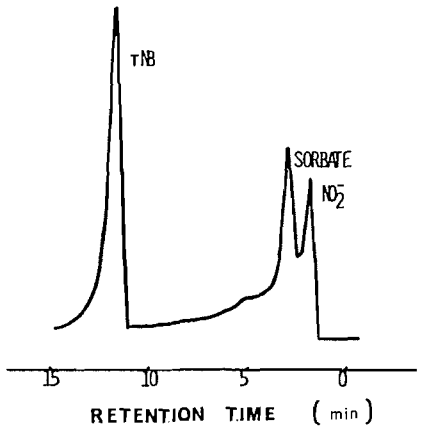


FIG. 3. HPLC chromatograph showing the retention times for $NO_2^-$, *t*NB, and sorbate.

0.225 *M* potassium sorbate respectively, in 50% ethanol and the pH was adjusted to 3.5, using HCl or HBr, an esr spectrum identical to that in Fig. 2, rather than to Fig. 1, was observed. In acidic medium, *t*NB decomposes much more readily, resulting in high $NO_2$ concentration. The addition of $NO_2$ to the 4,5 double bond of sorbate now becomes more favorable as compared to H· abstraction. This mechanism is the same as in the mixture of *t*NB, sorbate, and nitrite at pH 6.4, yielding radical **VI** whose esr spectrum is presented in Fig. 2.

When *t*NB and sorbate were mixed at pH 3.5, an additional peak in the HPLC chromatogram, as shown in Fig. 3, indicated the presence of nitrite, on the basis of the known retention time. Thus, with *t*NB in acidic medium or with nitrites in pH 6.4 solution, nitrite ions are evidently involved in the reaction. This accounts for the observation of identical esr spectra for *t*NB with sorbate in low pH or nitrite plus *t*NB with sorbate at pH 6.4. The same esr spectrum was obtained when nitrite was also present in the reaction mixture at low pH, which favors the formation of $HNO_2$.

## Conclusions

Depending upon the pH range and the presence or absence of nitrite, two distinct esr spectra were observed when nitroso spin trap (tNB) is added to sorbate solution. At pH of 6.4, spectrum whose hyperfine parameters corresponding to that of the addition of $^{\cdot}CH_2$— to *t*NB was observed. We attribute the formation of this radical to the abstraction of the allylic hydrogen of the sorbate by $NO_2$ and the subsequent trapping by *t*NB. Since the source for $NO_2$ primarily depends on the degradation of *t*NB, $NO_2$ concentration remains fairly low. However, if one substantially increases the $NO_2$ concentration by either the addition of nitrite or by lowering the pH to hasten *t*NB degradation, a different esr spectrum appears. The spin trapping of the radical created by the $NO_2$ addition to the 4,5 double bond of sorbate by *t*NB has hyperfine parameters consistent with the observed spectrum.

The reaction mechanisms for nitrogen dioxide are in complete agreement with the recent finding of Pryor and Lightsey (10). At high $NO_2$ concentrations, they demonstrated that $NO_2$ adds to the double bonds of the unsaturated fatty acids while at low concentrations of $NO_2$, abstraction of allylic hydrogen dominates.

We are currently isolating reaction products,

Can. J. Chem. Downloaded from www.nrcresearchpress.com by 210.87.254.6 on 09/06/12
For personal use only.

including those formed at the higher pH range, in order to further understand the chemistry of the interactions of sorbate and nitroso compounds.

**Acknowledgements**

Critical review and suggestions made by Drs. A. E. Pohland and S. Page are greatly appreciated.

1. Food Safety and Quality Service, USDA, Wash., D.C. 20250. Four plant study to investigate the use of 40 ppm sodium nitrite and 0.26 percent potassium sorbate in bacon. July 23, 1979.
2. H. HAYATSU, K. C. CHUNG, T. KADA, and T. NAKAJINA. Mutat. Res. **30**, 417 (1975).
3. D. M. HINTON, E. A. BROWER, F. C. VOCCI, and D. I. RUGGLES. Office of Toxicological Sciences – Report of FDA pilot studies on toxicological testing of USDA experimental bacon containing varying levels of sodium nitrite and potassium sorbate. FDA, Washington D.C. 20204, Nov. 1980; J. Food Cosmetic Toxicology. To be published.
4. D. M. HINTON, A. JOSHI, and G. YANG. Spectral and chemical properties of sorbate and nitrite reactivity. To be published.
5. M. NAMIKI and T. KADA. Agri. Biol. Chem. **6**, 1335 (1975).
6. Y. KITO and M. NAMIKI. Tetrahedron, **34**, 585 (1978).
7. T. OSAWA, Y. KITO, M. NAMIKI, and K. TSUJI. Tetrahedron Lett. **45**, 4399 (1979).
8. D. M. HINTON, E. A. BROWER, F. VOCCI, JR., A. JOSHI, G. YANG, and D. I. RUGGLES. Pilot studies of the membrane toxicity and chemical reactivity of sorbates and nitrite in a processed food. 65th Annual Society of Federation of American Society for Experimental Biology, April 1981.
9. E. R. SARGENT and E. M. GARDY. Can. J. Chem. **52**, 3645 (1974).
10. W. A. PRYOR and J. W. LIGHTSEY. Science, **214**, 435 (1981).
11. G. A. BONETTI, C. B. DESAVIGNY, C. MICHALSKI, and R. ROSENTHAL. Am. Chem. Soc. Div. Pet. Chem. Prepr. **10**, 135 (1965).
12. G. SOSNOVSKY. Free radical reactions in preparative organic chemistry. Macmillan, New York. 1964. pp. 255–269.

Can. J. Chem. Downloaded from www.nrcresearchpress.com by 210.87.254.6 on 09/06/12
For personal use only.

# Spin-trapping in early and some recent nitroso chemistry

TH. J. DE BOER

*Laboratory for Organic Chemistry, University of Amsterdam, Nieuwe Achtergracht 129, 1018 WS Amsterdam, The Netherlands*

Received October 10, 1981

TH. J. DE BOER. Can. J. Chem. **60**, 1602 (1982).

The radical scavenging properties of nitroso compounds were discovered accidentally during investigations of photochemical nitrosation of hydrocarbons with alkyl nitrites. Depending on the nature of substrates and nitrosating agent, various nitroxides can be generated. Identification of these nitroxides by their esr spectra has triggered the development of the spin-trapping technique which has been useful in the elucidation of many organic radical reaction mechanisms. Recent studies have shown that the behavior of nitrosocyclopropanes and α-chloro-nitroso alkanes is unorthodox upon irradiation. Dark reactions of α-chloro-nitroso alkanes with Grignard reagents lead to nitrones by a polar mechanism and to oximes by electron transfer. In the latter case high yields of hydrocarbon dimers are sometimes obtained from the Grignard and other organometallic reagents, despite the presence of nitroso compounds. In the postulated reaction mechanism dimers and higher associates from the organometallic reagent play an essential role.

TH. J. DE BOER. Can. J. Chem. **60**, 1602 (1982).

On a découvert accidentellement les propriétés de pièges à radicaux des composés nitroso en étudiant la nitrosation photochimique des hydrocarbures par les nitrites d'alkyles. En fonction de la nature des substrats et de l'agent nitrosant, on peut produire divers nitroxydes. L'identfication de ces nirtoxydes, d'après leurs spectres de rpe, a permis le développement de la technique de captage de spin qui est très utile pour clarifier plusieurs mécanismes de réactions radicalaires organiques. Des étudés récentes ont montré que le comportement des nitroso-cyclopropanes et des α-chloro-nitroso alcanes est inhabituel lors de l'irradiation. La réaction des α-chloro-nitroso alcanes avec les réactifs de Grignard à l'obscurité conduit aux nitrones selon un mécanisme polaire et aux oximes par transfert d'électron. Dans ce dernier cas, on obtient quelquefois d'excellents rendements d'hydrocarbures dimères à partir du réactif de Grignard ou d'autres réactifs organométalliques, en dépit de la présence des compos és nitroso. Dans le mécanisme de réaction proposé, les molécules dimères et celles possédent un plus haut degré d'association à partir du réactif organométallique jouent un rôle essentiel.

[Traduit par le journal]

## Introduction

Photochemical nitrosation of hydrocarbons was developed for industrial purposes in the sixties, especially in Japan, and also studied in Germany along closely related routes. In the Toray process (1) the nitrosating agent is nitrosyl chloride while in the so-called Tubingen method (2) it consists of a mixture of NO and $Cl_2$. A quantum yield below 1.0 is in accordance with the following scheme for NOCl.

$$\text{NOCl} \xrightarrow{h\nu} \text{NO}^{\cdot} + \text{Cl}^{\cdot}$$
$$\text{RH} + \text{Cl}^{\cdot} \longrightarrow \text{R}^{\cdot} + \text{HCl}$$
$$\text{R}^{\cdot} + \text{NO}^{\cdot} \longrightarrow \text{RNO}$$

Chlorine atoms are generated photochemically and these abstract hydrogen from the hydrocarbon RH, leaving a radical R· which combines with NO. There is no selectivity problem for hydrogen abstraction from cyclohexane and this is one reason why this abundant petrochemical has found wide application. The product nitrosocyclohexane is easily isomerized to the oxime, which in turn can undergo Beckmann rearrangement to caprolactam, the monomer for the production of nylon-6. In the Japanese as well as in the German process, the presence of acid makes sure that the isomerization of nitrosocyclohexane to the oxime is fast and far more rapid than dimerization, which normally takes place in neutral medium.

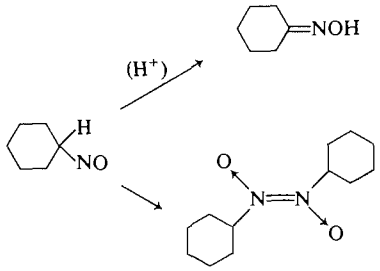


*Photochemical nitrosation with* tert-*butylnitrite*

When we tested *tert*-butylnitrite as an alternative less corrosive nonhalogen-containing nitrosating agent for cyclohexane, dimeric nitrosocyclohexane could be isolated in 80% yield (3). Under the reaction conditions there is little oxime formation, because the liberated *tert*-butanol is a much poorer catalyst for the isomerizations of the nitroso compound (at room temperature) than mineral acid and consequently dimerization prevails. At elevated

$$t\text{-BuONO} \xrightarrow{h\nu} t\text{-BuO}^{\cdot} + \text{NO}^{\cdot}$$
$$t\text{-BuO}^{\cdot} + \text{RH} \longrightarrow \text{R}^{\cdot} + t\text{-BuOH}$$
$$\text{R}^{\cdot} + \text{NO}^{\cdot} \longrightarrow \text{RNO} \rightarrow \text{dimer}$$

0008-4042/82/121602-08$01.00/0

©1982 National Research Council of Canada/Conseil national de recherches du Canada

Can. J. Chem. Downloaded from www.nrcresearchpress.com by 210.87.254.105 on 09/06/12
For personal use only.

Can. J. Chem. Downloaded from www.nrcresearchpress.com by 210.87.254.105 on 09/06/12
For personal use only.

temperatures the dimer dissociates and the monomer isomerizes to oxime, as outlined in the relevant patent (3). Yet it is inadvisable to carry out the photochemical nitrosation above room temperature, because this has a detrimental effect on combined product yields of nitroso-dimer and oxime. It will be shown that a shift in the nitrosoalkane dimer/monomer equilibrium is responsible for this effect.

Poor yields are also obtained at low temperatures. For instance at −60°C the photochemically produced monomer dimerizes so slowly that it becomes subject to side-reactions other than isomerization to the oxime. Electron spin resonance studies are helpful in explaining the nature of side-reactions.

*Mechanism of nitroxide formation*

At the time it was known that nitroso compounds can give rise to radical reactions, but in the mid-sixties German and American investigators postulated that nitroso compounds "which exist only as monomers do not give disubstituted nitroxides on irradiation" (4). It was therefore thought that the dimer is an essential precursor for nitroxide formation.

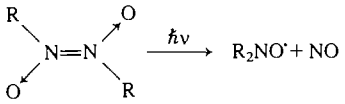


A study of the combined influence of temperature and wavelength of incident light on nitroxide formation provided a more realistic mechanistic picture. Irradiation of solutions of nitrosocyclohexane with red light ($\lambda > 660$ nm) gave no esr signals, but when the temperature was raised above room temperature (40°C) the esr spectrum of dicyclohexylnitroxide appeared (5). The red light cannot be absorbed by the dimer simply because it lacks an absorption band in this spectral region. But at elevated temperatures the dimer dissociates partly and the monomer thus formed can absorb visible light which triggers homolytic rupture of the weak R—NO bond. It should be noted that the dimer can also dissociate under the influence of uv light.

Radicals R generated by R—NO homolysis add to the (monomeric) nitroso compound with nitroxide formation, providing the key step in what later has aptly been described by Janzen and Blackburn as spin-trapping (6). The technique involves capture of a short-living radical by a suitable scavenger (nitroso compound or nitrone) and conversion into a more persistent (nitroxide) radical (7). The nitroso dimer/monomer equilibrium in solution lies far more to the monomer side for tertiary nitroso alkanes than for primary and secondary nitroso compounds. Consequently nitroxide formation at low temperatures (−100°C) is possible by irradiation of *tertiary* nitroso compounds with red light.

As to the behaviour of aromatic nitroso compounds, the main difference from their aliphatic counterpart lies in a stronger C—NO bond and a somewhat longer wavelength absorption ($\lambda_{max}$ = 750 nm). The $n-\pi^*$ excitation energy in (monomeric) nitrosobenzene turns out to be insufficient for C—NO homolysis and therefore nitrosobenzene gives no nitroxide upon irradiation with red light. This property can be exploited for the generation of mixed alkyl-aryl nitroxides from a monomeric aliphatic nitroso compound in the presence of an excess of an aromatic nitroso compound (5).

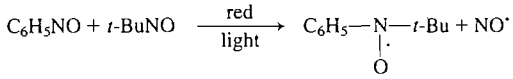


At increasing concentrations of *t*-BuNO the formation of the symmetrical di-*tert*-butylnitroxide becomes more and more important. The symmetrical diphenylnitroxide is only formed with actinic light. It so happens that alkyl nitrites have their absorption maximum round 380 nm which is just in between the absorption maxima of dimeric and monomeric nitroso compounds (approx. 300 and 700 nm respectively). In the photochemical nitrosation of cyclohexane with *tert*-butyl nitrite, optimum yields of (dimeric) nitrosocyclohexane were obtained by irradiation at wavelengths around 400 nm (3).

Mechanistic aspects of nitroxide formation continue to attract attention, and "spontaneous" radical formation can be due to inadvertent homolysis (27).

*Photochemical and thermal generation of alkoxynitroxides*

In photochemical nitrosation of toluene, ethylbenzene, and cumene with *tert*-butyl nitrite at −40°C (a temperature where the monomeric nitroso compound is not immediately removed by dimerization), esr studies indicated that beside nitroxides with an $a_N$ value of 15 Gauss, typical for dialkyl nitroxides, there were also signals pointing to the presence of nitroxides with the much higher $a_N$ value of 28 Gauss (8). These were identified as *tert*-butoxy-aralkyl nitroxides, the simplest esr spectrum arising from cumene because of the

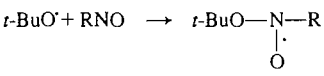

absence of β-hydrogens in the nitroxide. Each line in the nitroxide obtained similarly from ethylbenzene (R = $C_6H_5CHCH_3$) appeared as a doublet, and from toluene (R = $C_6H_5CH_2$) as a triplet, in accordance with the increasing number of β-hydrogens responsible for further splitting in the nitroxide.

The same type of nitroxides with a similarly high $a_N$ value could be obtained from an unambiguous nonphotochemical source for *tert*-butoxy radicals, i.e. di-*tert*-butyl peroxalate. When this decomposes slowly at 20°C in the presence of *t*-BuNO, the esr spectrum of *tert*-butoxy-*tert*-butyl nitroxide with $a_N$ = 28.3 Gauss appears. It was noticed that the original spectrum of *tert*-butoxy-*tert*-butyl nitroxides ($a_N$ = 28.1) is gradually replaced by that of di-*tert*-butyl nitroxide ($a_N$ = 15.4 Gauss), presumably because the nitroxide can undergo a β-fission in two ways, each producing a *tert*-butyl radical. Some of the latter nitroxide may arise by trivial thermal dissociation of *t*-BuNO.

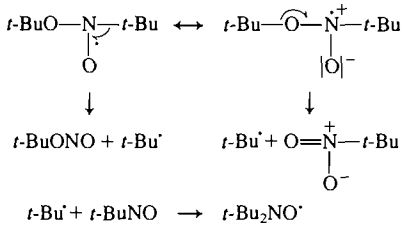


*Photochemical and thermal generation of acyl-nitroxides*

In all previous experiments on photochemical nitrosation, the nitrosating agent was *tert*-butyl nitrite. When this is replaced by *s*-butyl or by *n*-butyl nitrite in the photochemical nitrosation of cumene, esr spectra of reaction mixtures alter distinctly. The most conspicuous change is the appearance of signals pointing to the presence of a new nitroxide with $a_N$ around 8 Gauss. We have attributed this to an acylnitroxide (9), formed by addition of acyl radicals to the nitrosation product 2-nitroso-2-phenyl-propane ("nitrosocumene"). Acyl radicals arise in turn by β-fission of *s*-butoxy and *n*-butoxy radicals generated in nitrite-photolysis.

The strongest signals are obtained with *n*-butyl-nitrite, presumably because the intermediary *n*-butoxy radical can form an aldehyde easily by β—C—H fission, e.g. by disproportionation. *s*-Butoxy radicals must undergo a more difficult β—C—C fission in order to form an aldehyde, while *tert*-butoxy radicals only produce ketones by β-fission. Aldehydes being the essential precursors for acyl radicals, it is clear that acylnitroxides are

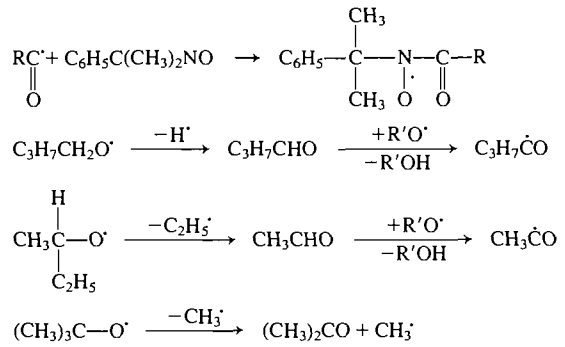


only formed during photolysis of hydrocarbons with *n*-butyl and *s*-butyl nitrites, and never with *tert*-butyl nitrites. In principle methyl radicals can be generated in the latter case but these have never been captured as spin adducts, possibly because rapid disproportionation of methyl *tert*-butyl nitroxide prevents detection. Acylnitroxides can also be formed by photolysis of *t*-BuNO in the presence of aldehydes. The esr signals become stronger by supplying some *tert*-butyl peroxalate as a convenient source of *tert*-butoxy radicals. These abstract aldehydic hydrogen more efficiently than the radical generated by photolysis of *t*-BuNO.

The preceding sections illustrate how monomeric nitroso compounds can function as radical traps. As such, 2-methyl-2-nitrosopropane ("*tert*-nitrosobutane") has found wide application, despite the precautions that must be taken to avoid unwanted photochemical or thermal formation of symmetrical di-*tert*-butylnitroxide.

On the other hand, the nitroso compound has the advantage that in its spin adducts the scavenged radical is directly attached to the nitroxide nitrogen and will therefore exert a relatively large influence on $a_N$. Furthermore, the esr spectrum of the spin adduct is likely to reveal splittings from magnetic nuclei in the trapped radical, which will greatly facilitate its identification. For a comparison with alternative spin traps we refer to Perkin's recent review (10).

*Reactivity of nitrosocyclopropanes*

As part of our interest in small ring chemistry we were prompted to investigate the properties of nitroxides with a cyclopropyl group. In their polar structure, nitroxides have an electron deficiency on nitrogen and the question is whether this can induce opening of a neighbouring small ring, as it does for instance in related cyclopropylmethyl (11) and cyclopropyloxy radicals (12).

Applying the preparation of a nitroxide from a nitro compound and a Grignard reagent (13) we found that nitrocyclopropane reacts with *t*-BuMgBr

Can. J. Chem. Downloaded from www.nrcresearchpress.com by 210.87.254.105 on 09/06/12
For personal use only.

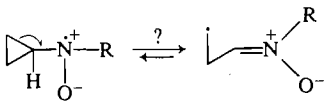

to give a nitroxide with $a_N = 16.0$ Gauss (in $CFCl_3$ at 20°C) and a doublet splitting $a_H = 3.3$ Gauss due to one β-hydrogen, suggesting the presence of a cyclopropyl-*tert*-butylnitroxide. The same nitroxide was obtained by oxidation of *tert*-butylcyclopropylamine with *p*-nitroperbenzoic acid (14). The nitroxide has a persistence comparable with ordinary dialkylnitroxides as judged from its esr spectrum.

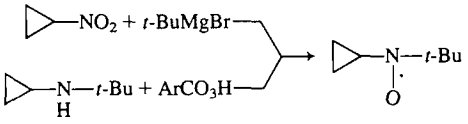

The straightforward approach employing nitrosocyclopropane is somewhat hampered because this spin trap is not easily accessible (see ref. 14 and, for an earlier approach with $F_2O$ as the oxidant, ref. 15). Recently we found that nitrosocyclopropane can be prepared in 30% yield from cyclopropylamine by oxidation with sodium tungstate and $H_2O_2$ in a two-phase system ($CFCl_3/H_2O$) (16). Unlike other nitroso compounds possessing α-hydrogen, nitrosocyclopropane has no tendency to isomerize to the corresponding oxime. Apparently the energy barrier for formation of the exocyclic double bond in cyclopropanone oxime is so large, that the reaction simply does not take place.

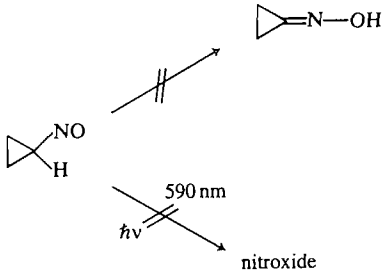


Nitrosocyclopropane differs also from aliphatic nitroso compounds in that it gives no nitroxide upon irradiation with red light, presumably because of the relatively strong C—N bond due to its high *s*-character. As a spin trap, nitrosocyclopropane functions normally with alkyl and acyl radicals, nitroxides being obtained with $a_N = 15.3$–$16.0$ Gauss and $a_H = 3$–$4$ Gauss. The fact that nitrosocyclopropane forms no nitroxide upon irradiation does not mean that nitrosocyclopropanes are photochemically inert. For instance when α-methylnitrosopropane is irradiated with red light, it undergoes decomposition and the main products are an isoxazoline (40%), a furoxan (10%), and ethylene, first identified by its singlet in nmr at $\delta = 5.3$ (17).

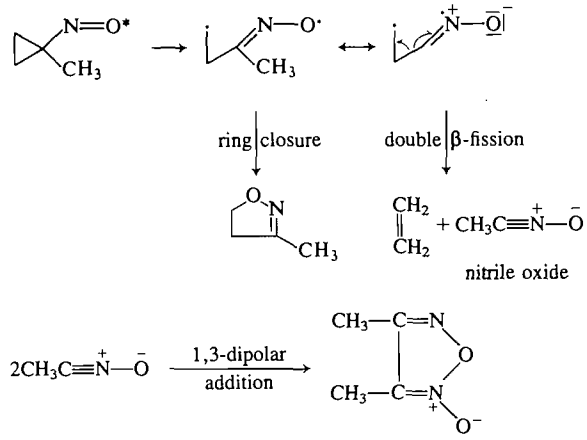


All these products follow logically from ring opening of the excited nitroso compound to a biradical (not observed in esr). This has, on the one hand, the properties of an alkyl radical and, on the other, of an oximino radical. Ring closure to a five-membered ring leads to an oxazoline. When the oximino moiety is written in its polar canonical structure it becomes formally a 1,4-diradical. Such radicals can undergo a double β-fission with greater ease than cyclization to a four-membered ring. The double β-fission produces ethylene and a nitrile oxide, the latter undergoing dimerization to a furoxan.

The striking difference in photochemical behaviour between nitrosocyclopropane and its α-methyl derivative is caused by the totally different properties of acetonitrile oxide and its lower homologue HCNO (fulminic acid), obtainable in an analogous process from unsubstituted nitrosocyclopropane. Because of its labile proton, fulminic acid can tautomerize and form polymeric products with complicated structures (18). The tremendous influence of an α-substituent on the photochemistry of nitrosocyclopropanes is also obvious in α-

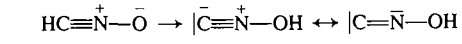

phenylcyclopropane. Upon irradiation with red light it gives an "ordinary" nitroxide because C—N homolysis in the excited state is now facilitated by the radical stabilizing effect of the phenyl group in the α-phenylcyclopropyl radical.

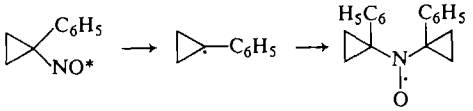

Can. J. Chem. Downloaded from www.nrcresearchpress.com by 210.87.254.105 on 09/06/12
For personal use only.

Can. J. Chem. Downloaded from www.nrcresearchpress.com by 210.87.254.105 on 09/06/12
For personal use only.

Finally it should be noticed that quantum yields for disappearance of α-methyl-nitrosocyclopropane ($\phi \approx 0.2$) are concentration independent and distinctly lower than the concentration dependent quantum yields for the α-phenyl derivative or for *t*-BuNO ($\phi = 0.9$–$1.3$). In the latter case the nitroso compound is not only removed by photolysis but also in dark reactions (e.g. nitroxide formation) in contrast with α-methyl-nitrosocyclopropane which reacts in an entirely different way as illustrated above.

*α-Chloro-nitrosoalkanes*

It was noted already in the early days of nitroxide esr spectroscopy, that α-chloro-nitroso compounds, largely present as monomers in solution, do not seem to form nitroxides by photolysis under standard conditions. The apparent resistance to form di(α-haloalkyl) nitroxides is somewhat surprising if one considers that *mono*(α-haloalkyl) nitroxides can be generated without special precautions along various routes, as summarized in the following scheme (19). Although the nitroxides generated in

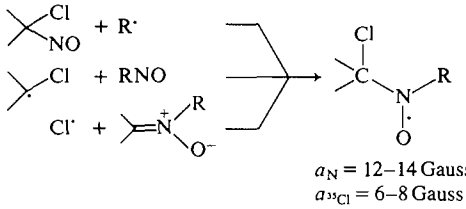


one of these ways are not particularly persistent, their esr spectra can be recorded without difficulty. Spectra are somewhat complicated because of the two chlorine isotopes each with a spin quantum number $I = 3/2$. They can be considerably simplified, when tributyltinhydride is added (20).

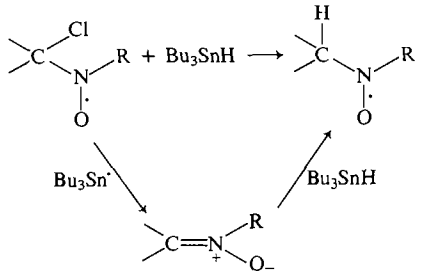


As in ordinary aliphatic chlorides, the halogen atom is replaced by hydrogen, and the same happens in our halogenated nitroxides, presumably by a mechanism involving $Bu_3Sn^{\cdot}$ radicals and a nitrone which is known to react with $Bu_3SnH$. When $Bu_3SnH$ is added to solutions of α-chloro-nitroso compounds, replacement of chlorine by hydrogen is slow and only after prolonged reaction times can the reduction product oxime (the tautomer of the halogen-free nitroso compound) be isolated. However, when reaction mixtures are irradiated with red light, rapid nitroxide formation takes place. Judging from esr spectra, these nitroxides do not contain halogen. Presumably a di(α-chloroalkyl)-nitroxide is formed in the early stages of the reaction, but this reacts rapidly with $Bu_3SnH$ much like a nitroxide containing only one α-chloroalkyl group.

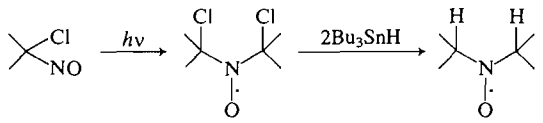


During photolysis of α-chloro-nitroso compounds in the absence of BuSnH, we assume that it is the NO and the α-chloroalkyl radical (instead of $Bu_3Sn^{\cdot}$) which is responsible for removing chlorine from the di(α-alkyl)-nitroxide. In the case of α-chloro-nitrosoadamantane, the *gem* dichloride has been isolated in 44% yield from photolyses in benzene (21). Some of it may also be formed by combination of α-chloroadamantyl radicals with $Cl^{\cdot}$, arising from photolysis of NOCl. Because the nitrone formed in the last two reactions is also a radical scavenger, reaction mixtures become complicated. In alco-

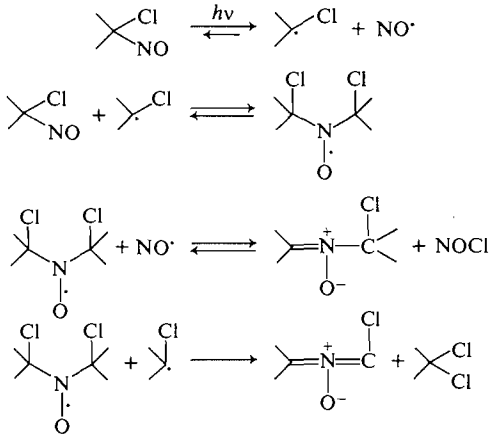


holic solvents the product distribution changes drastically. The main products, ketone, oxime, and nitrite, arise by solvolysis of the nitrone and of NOCl, thus supporting the suggested mechanism (22).

The foregoing illustrates that α-chloroalkyl nitroxides contain labile chlorine which can easily be

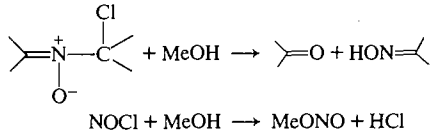

Can. J. Chem. Downloaded from www.nrcresearchpress.com by 210.87.254.105 on 09/06/12
For personal use only.

removed by a variety of radicals. The lability of chlorine plays also an essential role in the reactions to be described in the final section.

*Reaction of α-chloro-nitroso compounds with Grignard reagents*

Reaction of aliphatic and aromatic nitroso compounds leads in the first instance to hydroxylamines, much as ketones give alcohols. Because hyroxylamines and nitroso compounds can couple, complicated product mixtures are often obtained.

When the (aliphatic) nitroso compound contains an α-chloro substituent the reaction with a Grignard reagent is remarkably simplified, because the substituted hydroxylamine can lose halogen and a nitrone can be isolated in many cases (23). In principle, nitrones can also react with Grignard reagents, and therefore addition of an excess must be avoided. In practice this means that the Grignard reagent must be added slowly to the α-chloro-

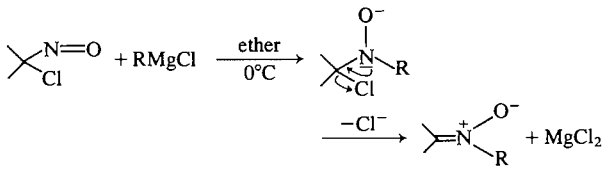


nitroso compound until its blue colour has disappeared. In this way nitrone yields of up to 90% have been reached. The stoichiometry of the nitrone formation is such that discoloration of the nitroso compound requires an equimolar amount of Grignard reagent.

In actual fact we find that in some cases almost twice as much of the Grignard reagent is necessary, particularly when access to the nitroso group is sterically hindered, as for instance in 1-chloro-1-nitroso-2,2,6,6-tetramethylcyclohexane. The high consumption of Grignard reagent is not due to its further attack on an intermediary nitrone. In fact nitrone formation is hardly or not at all involved. Instead of a sterically hindered polar reaction, a more facile electron transfer from the Grignard reagent to the nitroso compound takes preference. The resulting radical anion loses a halide ion and leaves an oximino radical. This radical can pick up another electron from the Grignard reagent to form an oxime anion (24*a*; for a recent review on Grignard reagents as electron donors, see ref. 24*b*). This scheme is not meant to imply free radicals or free (solvated) electrons but merely illustrates that in this stoichiometry, discoloration of the nitroso compound requires two equivalents of Grignard reagent and leaves formally two radicals R·.

In the reaction of benzylmagnesiumchloride with the earlier mentioned sterically hindered chloronitroso compound, dibenzyl can be isolated in 80% yield. Even with phenylmagnesium bromide the yield of diphenyl amounts to 45%. It is immediately clear that such yields cannot be caused by the dimerization of free benzyl or phenyl radicals in the presence of the nitroso spin trap. The absence of

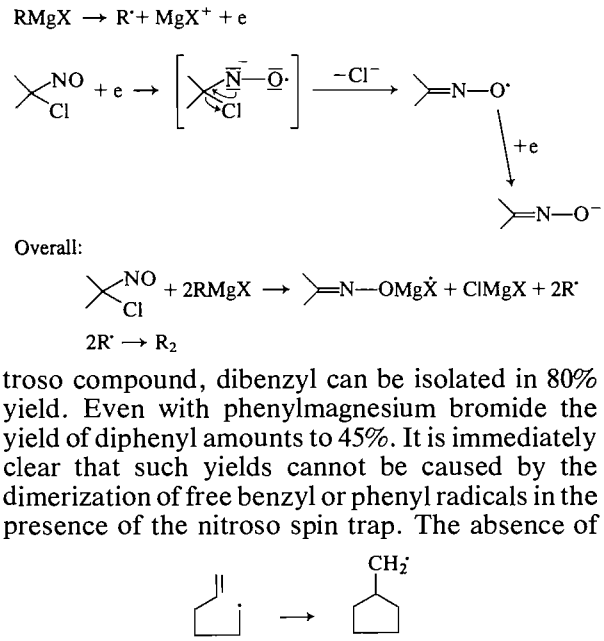





*free* radicals is also obvious from an experiment with 5-hexenylmagnesium bromide. It is known that the hexenyl radical can undergo ring closure very rapidly (25). The cyclization is so fast that it often serves as a sensitive test for radical-type processes. In the reaction of 5-hexenylmagnesium bromide with chloronitroso compounds, the formation of cyclopentyl derivatives is negligible and this again illustrates that free radicals cannot very well be involved.

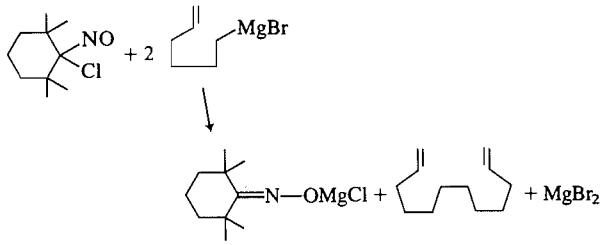


In order to rationalize the efficient production of dimers RR it should be realized that Grignard reagents RMgX are normally present as dimers in ethereal solution. We postulate that, in such a dimeric complex, one of the two ether molecules is displaced by the nitroso compound. Transfer of two electrons, one from each RMgX moiety, to the oxygen of the nitroso compound in rapid succession, combined with coupling of the two R fragments which remain in close proximity within the complex, leads to the dimer RR and the oxime salt.

The presence of the organometallic compound as a complex in solution is essential in this explanation. It is supported by the finding that an aromatic

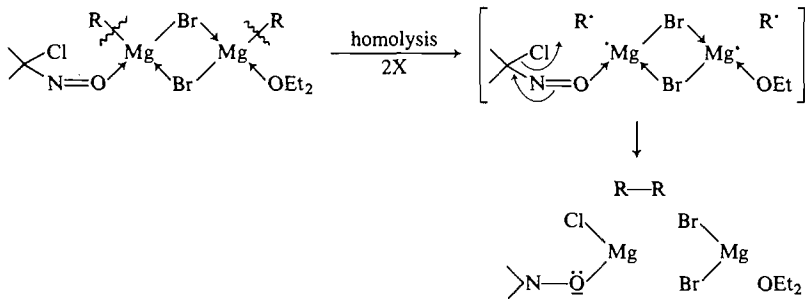


copper complex of known tetrameric structure (26) can react with an α-chloro-nitroso compound to form diaryl quantitatively.

At high dilution the Grignard reagent is (partly) present in solution in its monomeric form, and consequently formation of the dimer RR is made more difficult. For instance when benzylmagnesium bromide reacts in high dilution with a sterically hindered α-chloro-nitroso compound, only one

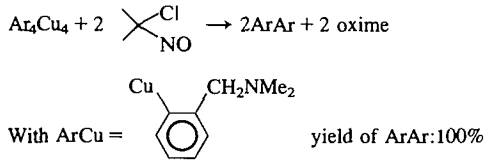


(not two) electron(s) can be transferred to the nitroso group within the complex. After loss of halide anion, this leaves formally an oximino radical and a benzyl radical. Radical combination leads to the benzyl ether of the oxime, isolated in 10–20% yield. That this by-product is not simply formed by polar attack of the Grignard reagent on the oxygen atom of the sterically hindered nitroso group finds support in the nature of reaction products obtained with other Grignard reagents at high dilution such as methyl- or phenyl-magnesium bromide. Instead of the methyl- or phenyl-ether of the oxime we now find the hydrocarbons methane and benzene while the oximino radical has coupled with a radical derived from the solvent diethylether. Apparently the (formal) methyl and phenyl radicals are in such a position within the complex that it is easier to abstract a hydrogen atom from a

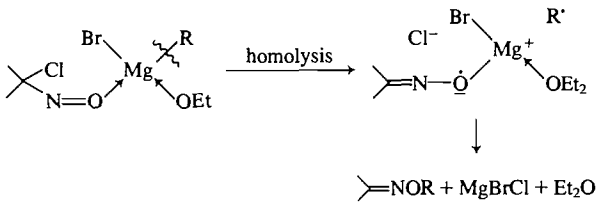


nearby diethylether molecule, than to combine with the oximino radical. Methane was detected mass spectrometrically and $CH_3D$ was analysed unambiguously, when diethylether was replaced by fully deuterated tetrahydrofuran $(CD_2)_4O$ as the solvent. This supports the suggested reaction scheme. It is also in accordance with the observation that in the reaction with phenylmagnesium bromide equimolar amounts of benzene and solvent-derived oxime ether are found.

We have seen that with benzyl radicals, direct combination with the oximino radical is the preferred route, presumably because benzyl radicals are incapable of abstracting an α-hydrogen atom from an ether molecule. That α-hydrogen abstraction from the ether by $CH_3$ or phenyl radicals takes place within the complex, is supported by the observation that the addition of cumene or the even better hydrogen donor 1,4-diisopropylbenzene has no influence, i.e. the labile side-chain hydrogen does not take part in the reaction, presumably because these aromatic compounds are not associated with the metalorganic complex.

All the above reactions require that the Grignard reagent is (partly) present in its monomeric form. This prompted us to test organic aluminium compounds such as trimethylaluminium which are known to be present in ethereal solution in their monomeric form (complexed with one molecule of ether). In the absence of steric hindrance we find that the polar nitrone reaction prevails, as illustrated with α-chloro-nitrosoadamantane.

On the other hand, when the chloro-nitroso compound is sterically hindered, solvent participation (up to 85%) is observed, thus clearly illustrating the tremendous influence on the reaction course exerted by association of the organometallic complex (or the lack thereof). This is particularly true when sterically hindered chloro-nitroso compounds are involved and electron transfer becomes easier than polar attack by the organometallic reagent.

In the above reactions it has been shown that the oximino radical can undergo a variety of coupling reactions with other radicals. However, when there is a nearby efficient electron donor (as in higher organometallic complexes) it will rapidly accept an electron. This is in full agreement with the polarographic behaviour of α-chloro-nitroso compounds. After acceptance of the first electron,

Can. J. Chem. Downloaded from www.nrcresearchpress.com by 210.87.254.105 on 09/06/12
For personal use only.

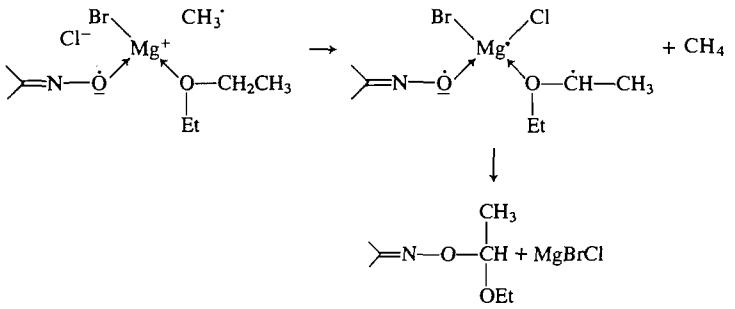

chloride ion is rapidly and irreversibly eliminated. The uptake of a second electron by the resulting

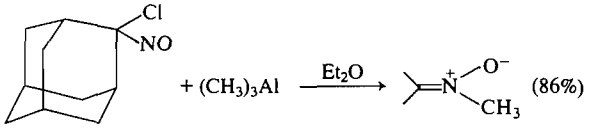

oximino radical is found to be even easier than the first, i.e. α-chloro-nitroso compounds act as two-electron oxidants. Considering that they are prepared from oxime and chlorine, their use as oxidants in the conversion of Grignard reagents RMgX

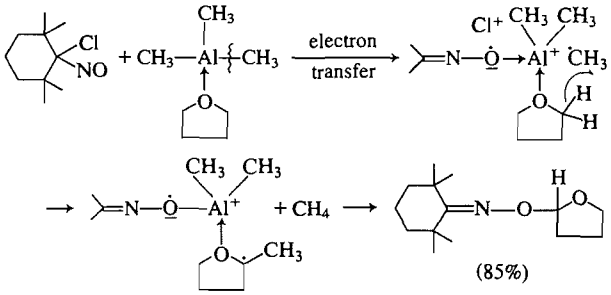

into dimers RR (with the regeneration of oxime), is therefore essentially an overall oxidation with chlorine.

**Acknowledgement**

The author wishes to express his gratitude to all past and present co-workers whose names are mentioned in the references. Their experimental and intellectual contributions have been invaluable.

1. C. MATASA. Chim. Ind. **91**, 57 (1964); M. PAPE. Fortschr. Chem. Forsch. 7, 559 (1967).
2. E. MULLER *et al.* Angew. Chem. **71**, 229 (1959). E. MULLER, H. G. PADEKEN, M. SALAMON, and G. FIEDLER. Chem. Ber. **98**, 1893 (1965).
3. A. MACKOR, J. U. VEENLAND, and TH. J. DE BOER. Recl. Trav. Chim. Pays-Bas, **88**, 1249 (1969); A. MACKOR and TH. J. DE BOER. Recl. Trav. Chim. Pays-Bas, **89**, 151 (1970); **89**, 159 (1970); U.S. Patent No. 3,544,438 (1970).
4. W. THEILACKER, A. KNOP, and H. UFFMANN. Angew. Chem. **77**, 717 (1965); E. TH. STROM and A. L. BLUHM. Chem. Commun. 115 (1966).
5. A. MACKOR, TH. A. J. W. WAJER, J. D. W. VAN VOORST, and TH. J. DE BOER. Tetrahedron Lett. 2115 (1966); TH. A. J. W. WAJER, A. MACKOR, TH. J. DE BOER, and J. D. W. VAN VOORST. Tetrahedron, **23**, 4021 (1967).
6. E. G. JANZEN and B. J. BLACKBURN. J. Am. Chem. Soc. **90**, 5909 (1968).
7. E. G. JANZEN. Acc. Chem. Res. **4**, 31 (1971).
8. A. MACKOR, TH. A. J. W. WAJER, TH. J. DE BOER, and J. D. W. VAN VOORST. Tetrahedron Lett. 385 (1967).
9. A. MACKOR, TH. A. J. W. WAJER, and TH. J. DE BOER. Tetrahedron, **24**, 1623 (1968).
10. M. J. PERKINS. *In* Advances in physical organic chemistry. Vol. 17. *Edited by* V. Gold and D. Bethell. Academic Press, London. 1980. p. 12.
11. J. K. KOCHI, P. J. KRUSIC, and D. R. EATON. J. Am. Chem. Soc. **91**, 1877 (1969).
12. S. E. SCHAAFSMA, H. STEINBERG, and TH. J. DE BOER. Recl. Trav. Chim. Pays-Bas, **85**, 70 (1966).
13. H. LEMAIRE, Y. MARECHAL, R. RAMASSEUL, and A. RASSAT. Bull. Soc. Chim. Fr. 1980 (1963).
14. R. STAMMER, J. B. F. N. ENGBERTS, and TH. J. DE BOER. Recl. Trav. Chim. Pays-Bas, **89**, 169 (1970).
15. R. F. MERRITT and J. K. RUFF. J. Am. Chem. Soc. **86**, 1392 (1964).
16. K. DE BOER. Thesis, University of Amsterdam. In preparation.
17. K. DE BOER and TH. J. DE BOER. International Symposium on Organic Free Radicals. Freiburg i. Br. Contribution T 14. 1981.
18. CH. GRUNDMANN and P. GRÜNANGER. The nitrile oxides. Springer-Verlag, Berlin. 1971. p. 72.
19. A. H. M. KAYEN, TH. A. B. M. BOLSMAN, and TH. J. DE BOER. Recl. Trav. Chim. Pays-Bas, **95**, 14 (1976).
20. A. H. M. KAYEN, K. DE BOER, and TH. J. DE BOER. Recl. Trav. Chim. Pays-Bas, **96**, 1 (1977); E. G. JANZEN, T. KASAI, and K. KUWATA. Bull. Chem. Soc. Jpn. **46**, 2061 (1973).
21. A. H. M. KAYEN, L. R. SUBRAMANIAN, and TH. J. DE BOER. Recl. Trav. Chim. Pays-Bas, **90**, 866 (1971).
22. A. H. M. KAYEN and TH. J. DE BOER. Recl. Trav. Chim. Pays-Bas, **96**, 237 (1977); B. G. GOWENLOCK, G. KRESZE, and J. PFAB. Tetrahedron Lett. 593 (1972); B. G. GOWENLOCK, J. PFAB, and G. KRESZE. J. Chem. Soc. Perkin Trans. II, 511 (1974).
23. C. SCHENK, M. L. BEEKES, and TH. J. DE BOER. Recl. Trav. Chim. Pays-Bas, **99**, 246 (1980); C. SCHENK, M. L. BEEKES, J. A. M. VAN DER DRIFT, and TH. J. DE BOER. Recl. Trav. Chim. Pays-Bas, **99**, 278 (1980).
24. (*a*) M. L. BEEKES. Thesis, University of Amsterdam, 1981; (*b*) E. G. ASHBY. Pure Appl. Chem. **52**, 545 (1980).
25. P. SCHMID and K. U. INGOLD. J. Am. Chem. Soc. **100**, 2493 (1978); Y. MEADA and K. U. INGOLD. J. Am. Chem. Soc. **101**, 4975 (1979).
26. G. VAN KOTEN and J. G. NOLTES. J. Organomet. Chem. **84**, 129 (1975).
27. C. CHATGILIALOGLU and K. U. INGOLD. J. Am. Chem. Soc. **103**, 4833 (1981).

Can. J. Chem. Downloaded from www.nrcresearchpress.com by 210.87.254.105 on 09/06/12
For personal use only.

# Electron spin resonance and electron nuclear double resonance study of diastereomeric nitroxyl radicals produced by spin trapping

YASHIGE KOTAKE AND KEIJI KUWATA

*Department of Chemistry, Faculty of Science, Osaka University, Toyonaka, Osaka, 560 Japan*

Received September 1, 1981

YASHIGE KOTAKE and KEIJI KUWATA. Can. J. Chem. **60**, 1610 (1982).

Electron spin resonance and electron nuclear double resonance spectra of nitroxyl radicals having two asymmetric carbons on one side of the nitroxyl function were observed. The radicals were produced by the abstraction of hydrogen by photoexcited benzophenone from amines, ethers, and alcohols followed by spin trapping with phenyl-*N*-*t*-butylnitrone. The difference in esr parameters of diastereomers depends on the functional group attached to the asymmetric carbon. The nature of the intramolecular interaction which brings about this difference is discussed in detail.

YASHIGE KOTAKE et KEIJI KUWATA. Can. J. Chem. **60**, 1610 (1982).

On a observé les spectres de rpe et de résonance nucléaire double de l'électron des radicaux nitroxydes ayant deux carbones asymétriques sur un côté de la fonction nitroxyle. On produit les radicaux par l'élimination d'un hydrogène des amines, des éthers et des alcools par de la benzophénone photoexcitée, suivie du captage de spin par le phényl-*N*-*tert*-butylnitrone. La différence des paramètres des rpe des diastérioisomères dépend de la nature des groupes fonctionnels attachés au carbone asymétrique. On discute en détail de la nature des interactions intramoléculaires qui sont responsables de ces différences.

[Traduit par le journal]

## Introduction

It is evident that the differences in chemical and physical properties of diastereomers arise from the differences in the interactions between substituents. However, detailed investigation into the factors influencing the magnitude of the spectroscopic separation of diastereomers is not always an easy task.

Recently it was reported that the spin trapping technique is capable of systematically producing various diastereomeric nitroxyl radicals (1, 2). The presence of diastereomers has been detected by characteristic esr spectra due to the slight differences in the hyperfine splittings (hfs) of the β-hydrogen and nitroxyl nitrogen, and the *g*-values of the two radicals. The small difference in β-H hfs which was not resolved by esr spectroscopy was also detected by making use of electron nuclear double resonance (ENDOR) spectroscopy.

In the present study the modes of separation of diastereomers in the three different kinds of spin adducts from alkylamines, ethers, and alcohols are compared. Since small differences in the β-H hfs of diastereomers in aminoalkyl adducts were detected by ENDOR experiments, it is possible to discuss the origin of the differing esr parameters.

All of the formed diastereomeric radicals have two asymmetric carbons on one side of the nitroxyl group. The magnitude of the hfs of the β-H reflects the conformation of the side chain. On the other hand, the nitrogen hfs and *g*-value reflect changes in the electronic structure of the nitroxyl group as a result of the differences of the steric configurations assumed by the substituents on the two asymmetric carbon atoms. Therefore the analysis of the separation of the diastereomeric spectra clarifies the intramolecular interaction which gives them different chemical and physical properties.

## Experimental

Nitroxyl radicals having two asymmetric carbons on one side of the nitroxyl group were produced by photosensitized hydrogen abstraction followed by spin trapping with phenyl-*N*-*t*-butylnitrone (PBN) (3, 4). The neat solution of the radical precursor (amines, ethers, and alcohols) which contains $10^{-3}$ mol $dm^{-3}$ PBN and $10^{-3}$ mol $dm^{-3}$ benzophenone was photolyzed by a 1 kw mercury arc for 10 min under vacuum. The reaction schemes of the trapping of the radicals from amines, ethers, and alcohols are shown as follows:

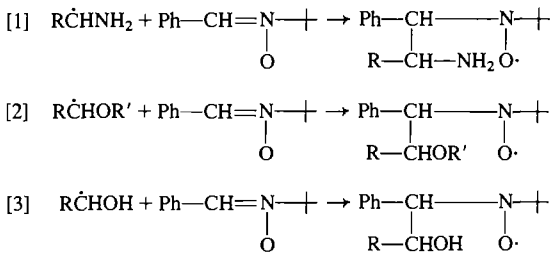


Materials used were purified by the method described elsewhere (1, 2). Electron spin resonance spectra were measured by a home-made spectrometer equipped with 15 kHz field modulation. Electron nuclear double resonance spectra were measured by combining a home-built rf unit with the esr spectrometer. The rf unit operates with a 150 W frequency-modulated radiofrequency. The modulation frequency is 7 to 10 kHz. Field modulation was not applied. The external magnetic field was fixed at one of the central doublet lines of the esr spectrum. The temperature of the sample was controlled by the flow of chilled nitrogen so as to obtain the best ENDOR signal.

0008-4042/82/121610-04$01.00/0

©1982 National Research Council of Canada/Conseil national de recherches du Canada

Can. J. Chem. Downloaded from www.nrcresearchpress.com by 210.87.254.6 on 09/06/12
For personal use only.

Can. J. Chem. Downloaded from www.nrcresearchpress.com by 210.87.254.6 on 09/06/12
For personal use only.

## Results

*Aminoalkyl adducts*

Electron spin resonance spectra of aminoalkyl adducts of PBN have been observed with the parent amine as the solvent. The spectrum parameters (hfs and $g$-value) determined by spectral simulation have been listed elsewhere (2). In most aminoalkyl adducts the presence of diastereomers was not confirmed by esr due to the small differences in the spectrum parameters.

The ENDOR spectrum of the adduct from di-*n*-butylamine was observed in di-*n*-butylamine. Figure 1 shows the ENDOR spectrum with its esr spectrum. An important feature of the ENDOR spectrum is the doublet peak at around 17.3 MHz, which is assigned to the β-hydrogens of each diastereomer. Two pairs of peaks around the free proton frequency were assigned to the γ- and δ-protons. The results of the analysis are listed in Table 1. Splitting of the peaks of the γ- and δ-protons was not observed. Although the diastereomeric radicals have slightly different β-H hfs constants, the esr spectrum is symmetrical (Fig. 1*B*). This fact shows that the difference in $g$-values is negligible. Di-*n*-butylamine is the only amine for which ENDOR spectra were obtained. The observation of ENDOR spectra of other adducts was unsuccessful because of the low concentration of the adduct or the lack of suitable solvents.

*Alkoxyalkyl adducts*

Diastereomers of several alkoxyalkyl adducts have been observed by esr. The analysis based upon spectral simulation has been given elsewhere (2). The differences in the hfs constants and $g$-values were large enough for esr identification in most cases.

TABLE 1. Hyperfine-splitting constants of diastereomeric nitroxyl radicals determined by ENDOR

| Parent chemicals of adducts | $A_{\beta\text{-H}}$/mT | $A_{\gamma\text{-H}}$/mT | $A_{\delta\text{-H}}$/mT |
|---|---|---|---|
| Di-*n*-butylamine* | 0.263 | 0.068 | 0.021 |
| | 0.236 | 0.068 | 0.021 |
| Tetrahydrofuran† | 0.268 | 0.054 | 0.020 |
| | 0.171 | 0.054 | 0.020 |

*The structure of the adduct is shown in Fig. 1.
†The structure of the adduct is shown in Fig. 2.

The only ENDOR spectrum observed for an alkoxyalkyl adduct is that of the tetrahydrofuranyl adduct. The ENDOR spectrum is shown in Fig. 2 with its esr spectrum. Toluene was chosen as the solvent for the ENDOR measurement (5). Two separated peaks were detected at 16.2 MHz and 17.6 MHz, and assigned to the β-hydrogens of the diastereomers. Small splittings due to the γ- and δ-protons were also observed. The results of the analysis are given in Table 1. Since the low and high field doublets are not symmetric the diastereomers must have different hfs constants and $g$-values.

In spite of the expectation that the diastereomeric radicals have the same concentration, the inten-

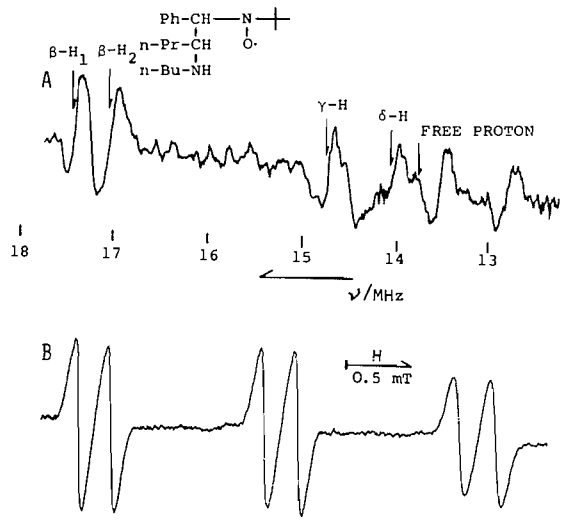


FIG. 1. Electron nuclear double resonance and esr spectra of spin adducts formed from di-*n*-butylamine and PBN. *A*: ENDOR spectrum in di-*n*-butylamine at −47°C. *B*: esr spectrum in di-*n*-butylamine at room temperature.

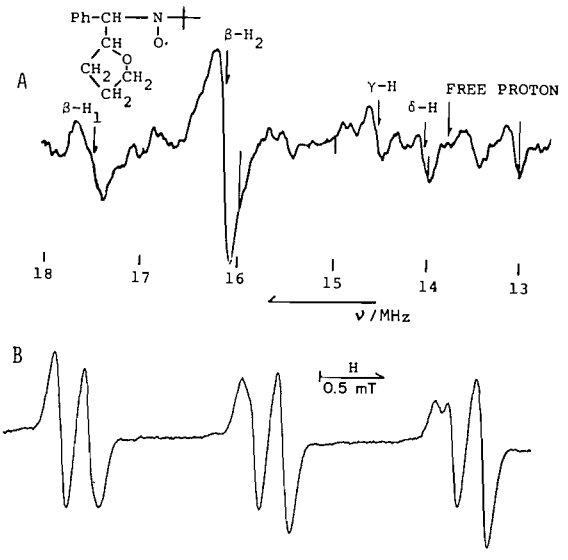


FIG. 2. Electron nuclear double resonance and esr spectra of spin adducts formed from tetrahydrofuran and PBN. *A*: ENDOR spectrum in toluene at −78°C. *B*: esr spectrum in tetrahydrofuran at room temperature.

Can. J. Chem. Downloaded from www.nrcresearchpress.com by 210.87.254.6 on 09/06/12
For personal use only.

sities of the two ENDOR peaks were not the same. Because of the slight difference in $g$-value in isomer it is very difficult to choose the fixed position of the external field, where the contribution from both radical to the esr intensities are the same (6, 7). In this work internal field lock was employed to fix the external field at the one of the zero crossing points of the central doublet. The relative ENDOR intensities of the two β-hydrogens were observed to change considerably by changing the fixed position of the field. It is also noted that the esr lines of isomer have different linewidths. This may be attributed either to the different relaxation time or to the difference in the hfs of protons beyond γ-position. This can also be a probable cause of the unequal ENDOR intensity for the isomer.

ENDOR spectra of other alkoxyalkyl adducts were not observed mainly because of the low concentrations of the radicals.

*Hydroxyalkyl adducts*

The presence of diastereomers has been confirmed by changing the solvent from the parent alcohol to an aprotic solvent such as toluene (1). Typical esr spectra in both solvents are shown in Fig. 3 for the hydroxybutyl adduct. Such a drastic solvent effect has been attributed to the formation of an intramolecular hydrogen bond. The spectrum parameters for several hydroxyalkyl adducts have been published elsewhere (1).

Electron nuclear double resonance spectra have not been observed although it is not difficult to get high concentrations of the radical. Perhaps the dynamics of hydrogen bond formation affects the electron and nuclear spin relaxation processes resulting in the inability to find optimum conditions for obtaining an ENDOR signal (8).

## Discussion

It is noted that the diastereomers formed from the hydrogen-abstracted radicals of amines, ethers, and alcohols have different spectral parameters as detected by esr and ENDOR. Judging from the esr spectra each of the pairs of diastereomeric spin adducts show different modes of separation: aminoalkyl adducts only show differences in the hfs of the β-H while alkoxyalkyl adducts show differences in both the hfs and $g$-value. Hydroxyalkyl adducts have different hfs constants and $g$-values only when they are dissolved in aprotic solvents. It is proposed that intramolecular interactions are responsible for such modes of separation.

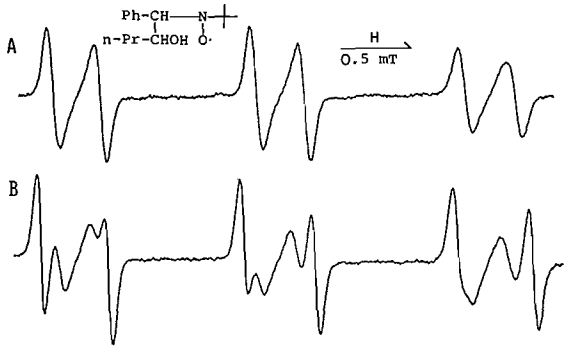


FIG. 3. Electron spin resonance spectra of spin adducts formed from butanol and PBN. *A*: in butanol at room temperature. *B*: in toluene at room temperature.

The reason for the spectroscopic separation of diastereomers may be due to the differences in the interactions of the substituents on the two asymmetric carbons $C_\alpha$ and $C_\beta$. The differences in the hfs and $g$-value are the indirect result of the interactions of substituents on $C_\alpha$ and $C_\beta$. Thus it has been proposed that in the stable conformers for these diastereomers the hydrogens on $C_\alpha$ and $C_\beta$ are *trans* to each other (9). The Newman projections of these isomers are shown in Fig. 4. The functional group X can interact with the nitroxyl group only in structure **A** of Fig. 4.

*Steric repulsion*

If the steric repulsion among bulky groups on the α and β carbons is predominant, the structure shown in Fig. 4 is realistic. When one expresses the interaction between R and R′ as (R, R′) then the dominant interactions are (R, Ph) and (X, NO) for Fig. 4*A* and (X, Ph) and (R, NO) for Fig. 4*B*. This results in differences in the overall conformation of the N—$C_\alpha$—$C_\beta$ chain and thus affects the dihedral angle between the β-H and the orbital containing the unpaired electron (10). This leads to slight differences in the β-H hfs constants for the isomers, which are resolved only by ENDOR. This is the case for the aminoalkyl adducts.

*Intramolecular solvation*

If the functional group X contains an electronegative atom such as oxygen, the nitroxyl radical having the structure **A** of Fig. 4 tends to favor the polar resonance structure.

[4]


The hfs of the nitrogen increases when compared to that in structure **B**. The usual solvent effect shifts

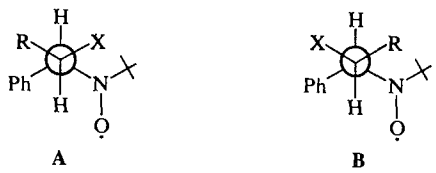


FIG. 4. Stereochemical diagram of diastereomeric nitroxyl radicals.

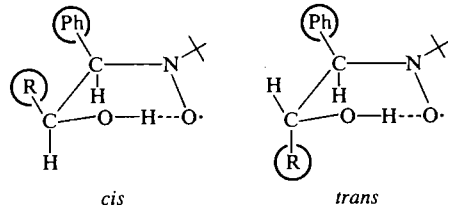


FIG. 5. Stereochemical diagram of hydrogen bonded chelate rings from diastereomers.

the $g$-value to a higher value, as well (11). This proximity effect of the functional group to the nitroxyl group explains the case of the alkoxyalkyl adduct well.

*Intramolecular hydrogen bonding*

If the functional group X in Fig. 4 is a hydroxy group then the intramolecular hydrogen bond between the OH and nitroxyl groups is possibly stronger than the steric repulsion (12). In such a case the radical is forced to take the conformations shown in Fig. 5. The conformation of R and Ph becomes *cis* or *trans* depending on the configuration of substituents on the two asymmetric carbons. The steric repulsion between R and Ph in the *cis* structure causes a distorted chelate ring changing the dihedral angle of the β-H with the unpaired electron orbital. In addition to the change in the hfs of the β-H the hydrogen bond also favors the polarized structure in reaction [4]. Changes in the strength of the hydrogen bond cause small differences in the hfs of the nitrogen and the $g$-value. This occurs in the case of the hydroxyalkyl adduct. The separation of the isomers was seen most clearly in aprotic solvents, which provides additional support for the presence of a hydrogen bond.

**Acknowledgement**

The authors express their sincere thanks to Professor E. G. Janzen for the helpful discussions and the critical reading of the manuscript.

1. Y. KOTAKE, K. KUWATA, and E. G. JANZEN. J. Phys. Chem. **83**, 3024 (1979).
2. Y. KOTAKE and K. KUWATA. Bull. Chem. Soc. Jpn. **54**, 394 (1981).
3. E. G. JANZEN. Acc. Chem. Res. **4**, 31 (1971).
4. E. G. JANZEN and J. I.-P. LIU. J. Magn. Reson. **9**, 510 (1973).
5. Y. KOTAKE, M. OKAZAKI, and K. KUWATA. J. Am. Chem. Soc. **99**, 5198 (1977).
6. N. M. ATHERTON and A. J. BLACKHURST. J. Chem. Soc. Faraday II, 470 (1972).
7. Y. KOTAKE and K. KUWATA. Bull. Chem. Soc. Jpn. **45**, 2663 (1972).
8. Y. KOTAKE and K. KUWATA. Bull. Chem. Soc. Jpn. **47**, 45 (1974).
9. E. L. ELIEL. Stereochemistry of carbon compounds. McGraw-Hill, New York, NY. 1962.
10. E. G. JANZEN. Top. Stereochem. **6**, 177 (1971).
11. T. KAWAMURA, S. MATSUNAMI, and T. YONEZAWA. Bull. Chem. Soc. Jpn. **38**, 1935 (1965).
12. M. D. JOESTEN and L. J. SCHAAD. Hydrogen bonding. Marcell Decker, New York, NY. 1974. pp. 253–290.

Can. J. Chem. Downloaded from www.nrcresearchpress.com by 210.87.254.6 on 09/06/12
For personal use only.

# Involvement of nitroxide radicals in cocaine-induced hepatotoxicity

ELMER J. RAUCKMAN, MICHELLE W. KLOSS, AND GERALD M. ROSEN
*Departments of Surgery and Pharmacology, Duke University Medical Center, Durham, NC 27710, U.S.A.*

Received September 12, 1981

ELMER J. RAUCKMAN, MICHELLE W. KLOSS, and GERALD M. ROSEN. Can. J. Chem. **60**, 1614 (1982).

Cocaine administration can produce hepatotoxicity in non-induced mice of at least one strain, DBA/2Ha and hepatotoxicity in induced mice of several strains. Metabolic studies and the administration of metabolites indicate that the minor metabolic pathway, cocaine → norcocaine → *N*-hydroxynorcocaine → norcocaine nitroxide, is responsible for the observed cocaine-induced hepatotoxicity. *In vitro* experiments show that cytochrome P-450 can oxidize *N*-hydroxynorcocaine to norcocaine nitroxide. Norcocaine nitroxide is unreactive towards cellular proteins or glutathione but does react directly with reduced pyridine nucleotides and is rapidly reduced enzymatically by the microsomal flavoproteins, NADPH-cytochrome P-450 reductase and FAD-containing monooxygenase. These reactions constitute a futile cycle in which NADPH is consumed and superoxide and hydrogen peroxide are generated. We postulate that the destruction of hydrogen peroxide by glutathione peroxidase results in the accumulation of excess oxidized glutathione which is actively excreted by the cell, since insufficient NADPH is available for glutathione reductase to maintain the GSH/GSSG ratio at an acceptable level. As reduced glutathione levels diminish, the cell can no longer protect itself against toxic lipid hydroperoxides which accumulate as a result of stimulation of lipid peroxidation (caused by the one electron cycling reaction, *N*-hydroxynorcocaine to norcocaine nitroxide cycle). Finally, as glutathione is depleted below a certain level, the cell loses the ability to maintain the GSH/GSSG ratio in a range consistent with homeostasis resulting in loss of cellular function. Ultimately, necrosis results. This mechanism is consistent with all the information available concerning cocaine-induced hepatotoxicity.

ELMER J. RAUCKMAN, MICHELLE W. KLOSS et GERALD M. ROSEN. Can. J. Chem. **60**, 1614 (1982).

L'administration de cocaine peut produire de l'hépatotoxicité chez les souris non-induites de la souche DBA/ZHA ainsi que de l'hépatotoxicité chez plusieurs souches de souris induites. Des études métaboliques et l'administration des métabolites indiquent que la séquence métabolique mineure: cocaine → norcocaine → *N*-hydroxynorcocaine → nitroxyde de cocaine est responsable de l'hépatotoxicité induite par la cocaine que l'on a observée. Des expériences *in vitro* montrent que le cytochrome P-450 peut oxyder la *N*-hydroxynorcocaine en nitroxyde de cocaine. Le nitroxyde de cocaïne n'a aucun effet sur les protéines cellulaires ou sur le glutathion mais il réagit directement avec la pyridine réduite des nucléotides et elle est rapidement réduite enzymatiquement par les flavoprotéines microsomiques: la réductase du NADPH-cytochrome P-450 et la mono-oxygénase contenant le ADF. Ces réactions constituent un cycle non efficace au cours duquel le NADPH est consommé et où un superoxyde et le peroxyde d'hydrogène se forment. Nous pensons que la destruction du peroxyde d'hydrogène par la peroxydase du glutathion provient de l'accumulation d'un excès de glutathion oxydé qui est activement secrété par la cellule, puisqu'une insuffisance de NADPH est nécessaire à la peroxydase du glutathion pour maintenir le rapport GSH/GSSG à un niveau acceptable. Lorsque le niveau du glutathion réduit baisse, la cellule ne peut plus se protéger contre la toxicité des hydroperoxydes des lipides (provoqué par une réaction cyclique à un électron de la *N*-hydroxynorcocaine en cycle de nitroxyde de norcocaine). Finalement quand le glutathion baisse en dessous d'un certain niveau, la cellule perd sa capacité de maintenir le rapport GSH/GSSG dans un intervalle qui serait favorable à l'homéostasie qui provient d'une perte de fonction cellulaire. En dernier ressort, il se forme des nécroses. Ce mécanisme est en accord avec toute l'information disponible relative à l'hépatotoxicité induite par la cocaine.

[Traduit par le journal]

## Introduction

The illicit use of cocaine as a recreational drug has steadily increased during the past decade. Although this drug of abuse has been extensively investigated psychopharmacologically, it has only recently been discovered that cocaine administration results in hepatic injury in mice (1). In this review article, we will examine some of the current investigations into the mechanism of cocaine-mediated hepatotoxicity.

## Discussion

### *Chemistry and metabolism of cocaine*

Relatively little is known about the metabolism of cocaine, despite its history of widespread use. Chemically, cocaine is a benzoylmethylecgonine, an ester of benzoic acid and a nitrogen-containing base, methylecgonine. In the body, cocaine rapidly achieves high concentrations in plasma after intravenous and intraperitoneal injections and a major part of cocaine is hydrolyzed by serum and liver esterases to produce benzoylecgonine, ecgonine methyl ester, and ecgonine (2–4). The work of Misra *et al.* (5) provides evidence that cocaine (**I**) is also *N*-demethylated to norcocaine (**II**) via microsomal oxidation in the rat. Additional studies have demonstrated that norcocaine is further metabolized *in vivo* by the liver to *N*-hydroxynorcocaine (**III**) (6–8). The subsequent fate of *N*-hydroxynorcocaine *in vivo* is somewhat controversial; suggestions of the formation of an epoxide derivative and a reactive nitroxide (**IV**) (9–11) both appear in the literature. It is important to note that all hepatic metabolites subsequent to norcocaine have been demonstrated to be pharmacologically inert.

0008-4042/82/121614-07$01.00/0
©1982 National Research Council of Canada/Conseil national de recherches du Canada

Can. J. Chem. Downloaded from www.nrcresearchpress.com by 210.87.254.42 on 09/06/12
For personal use only.

Can. J. Chem. Downloaded from www.nrcresearchpress.com by 210.87.254.42 on 09/06/12
For personal use only.

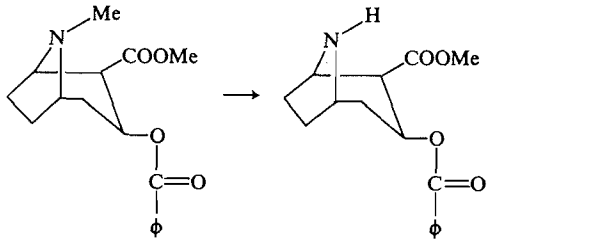


I




II

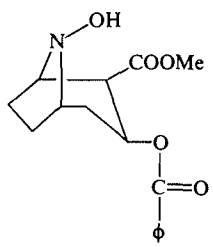


III

*Animal models and the role of oxidative enzymes in cocaine hepatotoxicity*

The reports of Evans *et al.* (12) and Shuster *et al.* (13) clearly implicate cocaine as a potent hepatotoxin in mice when given by intraperitoneal injection to this species induced with phenobarbital or housed on pine shaving bedding. Recent work by Freeman and Harbison (14) also demonstrated that chronic intraperitoneal injection of cocaine produced hepatotoxicity in non-induced mice but not in rats. This hepatotoxicity is manifested by fatty infiltration, midzonal and periportal necrosis, and marked elevation of serum glutamic-oxaloacetic transaminase (SGOT) levels. Similarly, hepatic dysfunction, as measured by elevated SGOT levels, has also been described in human heroin and cocaine addicts (14).

The work of Evans and Harbison (1) and Evans *et al.* (12) first suggested that a metabolite of cocaine, rather than cocaine itself, was responsible for the observed hepatotoxicity, based on data obtained when known cytochrome P-450 inducing agents were used. These investigations suggested that the active metabolite might be an *N*-oxide intermediate that was formed during the initial dealkylation of cocaine to norcocaine. Subsequent data later indicated, however, that the actual hepatotoxin was a further metabolite of norcocaine oxidation (15).

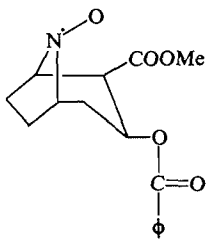


IV

More recent work by Thompson *et al.* (8) suggests that the bioactivation of cocaine to a more hepatotoxic metabolite is carried out by the cytochrome P-450 monooxygenase system and confirms data implicating a norcocaine metabolite as the reactive species. When tested for their ability to elevate SGOT levels, hydrolytic metabolites of cocaine were found not to be hepatotoxic; both norcocaine and *N*-hydroxynorcocaine, however, were shown to produce marked hepatotoxicity. Furthermore, cytochrome P-450 inhibitors such as SKF-525A blocked this liver damage, while inducing agents greatly enhanced the hepatotoxicity from cocaine, norcocaine, and *N*-hydroxynorcocaine administration. Thus, it was concluded that the cytochrome P-450 system was responsible for all metabolic conversions of the three compounds. Unfortunately, this study chose to measure drug metabolism only in terms of hepatotoxic manifestations, as opposed to the actual isolation of metabolites. It might therefore have been misleading to conclude that only one oxidative enzyme system participates in the bioactivation of cocaine based merely on data derived from the end result of complete metabolism. For example, the FAD-containing monooxygenase system, and not the cytochrome P-450 system, may be operative in the oxidation of norcocaine to *N*-hydroxynorcocaine, since this enzyme is known to catalyze the *N*-oxidation of many secondary amines (16, 17). What may be inferred from the current data is that a further metabolite of *N*-hydroxynorcocaine is responsible for the observed hepatotoxicity and that the cytochrome P-450 system participates in at least one metabolic conversion of the multi-step bioactivation of cocaine.

To date, all published investigations had failed to demonstrate cocaine-induced hepatic injury in mice without induction of cytochrome P-450. We have, however, recently developed an animal model, the DBA/2Ha male mouse, in which a cocaine dose of as little as 30 mg/kg, i.p., produces pronounced hepatic injury without the administration of cytochrome P-450 inducing agents. This hepatic injury was assessed by histopathology, depression of various hepatic enzyme activities, and elevation of

Can. J. Chem. Downloaded from www.nrcresearchpress.com by 210.87.254.42 on 09/06/12
For personal use only.

TABLE 1. Effect of single dose of cocaine on SGOT and selected hepatic enzymes in DBA/2Ha mice

| Cocaine dose mg/kg | Cyt P-450 content | FAD-M activity | Isocit. D.H. | SGOT | SOD |
|---|---|---|---|---|---|
| 10 | N/S | N/S | N/S | N/S | N/S |
| 20 | ↓ 26%* | N/S | N/S | ↑ 26%* | N/S |
| 30 | ↓ 48%* | ↓ 21%* | ↓ 21%* | ↑ 447%* | ↓ 24%* |
| 40 | ↓ 45%* | ↓ 34%* | ↓ 19%* | ↑ 718%* | ↓ 29%* |
| 60 | ↓ 60%* | ↓ 41%* | ↓ 24%* | ↑ 826%* | ↓ 30%* |

*$p < 0.05$ or better, FAD-M = FAD-containing monooxygenase; Isocit. D.H. = isocitric dehydrogenase; Cyt P-450 = cytochrome P-450; SOD = superoxide dismutase; SGOT = serum glutamic – oxaloacetic transaminase.

serium glutamic-pyruvic transaminase levels (Table 1). The use of phenobarbital as an inducing agent in this strain of mouse enhances the hepatotoxicity that results from cocaine exposure. Furthermore, a preliminary experiment designed to determine the time course and rate of recovery from cocaine-induced hepatotoxicity (and, hence, the severity of hepatic impairment) was conducted using adult male DBA/2Ha mice (Table 2). These data clearly demonstrate that hepatic cellular damage occurs within the first 24 h after cocaine administration; recovery, however, is not yet complete 3 days after cocaine exposure. Thus, an animal model for cocaine-induced hepatotoxicity which does not require induction of cytochrome P-450 is available in which the hepatotoxic effects of cocaine affect a wide variety of hepatic enzymes.

It is clear from the current literature that microsomal metabolism of cocaine is a prerequisite for the resulting hepatotoxicity; however, the enzymes responsible for the various steps in the bioactivation of cocaine to its nitroxide have not been established. As discussed earlier, it has been inferred that the cytochrome P-450 system is involved in the activation of cocaine based on a series of induction and inhibition studies using cocaine (9, 18), norcocaine (8), or *N*-hydroxynorcocaine (8). In principle, however, only the final step, activation of *N*-hydroxynorcocaine to the toxic intermediate, need be mediated by this hemoprotein to account for all the findings. Evans and Harbison (9) have found evidence of increased *N*-demethylation of cocaine after pretreatment with phenobarbital; even with this reaction, however, cytochrome P-450 could be of secondary importance to FAD-containing monooxygenase, since *N*-demethylation is known to be catalyzed by this enzyme acting in concert with cytochrome P-450 (19, 20).

TABLE 2. Effect of a single dose (60 mg/kg) of cocaine on SGPT and selected hepatic enzymes in DBA/2Ha mice as a function of time

| Post-injection time (h) | Cyt P-450 content | FAD-M activity | SGPT |
|---|---|---|---|
| 24 | ↓ 69%* | ↓ 40%* | ↑ 1676%* |
| 48 | ↓ 64%* | ↓ 30%* | ↑ 171%* |
| 72 | ↓ 42%* | ↓ 19%* | N/S |

*$p < 0.05$ or better; Cyt P-450 = cytochrome P-450; FAD-M = FAD-containing monooxygenase; SGPT = serum glutamic-pyruvic transaminase.

The hydroxylation of basic amines, such as norcocaine, is now generally considered to be mediated by the FAD-containing monooxygenase (21, 22). In fact, it is known that enhancement of FAD-containing monooxygenase activity occurs by castration of male mice (23) and we have observed that castration enhances the hepatotoxicity induced by norcocaine administration (unpublished observations). Furthermore, we have found that purified porcine liver FAD-containing monooxygenase will oxidize norcocaine to *N*-hydroxynorcocaine (unpublished results).

*Role of norcocaine nitroxide in cocaine hepatotoxicity*

Nayak *et al.* (6) first suggested that a nitroxide radical formed subsequent to norcocaine could be the species responsible for cocaine-induced hepatic injury. Later, Thompson *et al.* (8) proposed that this radical might either bind covalently to proteins or serve to initiate lipid peroxidation as a mechanism to account for the hepatotoxicity induced by cocaine. More recently, Evans (10) and Evans and Johnson (11) have presented evidence for the formation of norcocaine nitroxide from *N*-hydroxynorcocaine by phenobarbital-induced mouse microsomes and have attempted to correlate this formation with the covalent binding of radiolabeled cocaine to cellular proteins. To support their argument that norcocaine nitroxide is the ultimate toxic intermediate, these investigators cited their inability to detect the production of this nitroxide in rat and hamster microsomes, both of which are species that do not exhibit cocaine-induced hepatotoxicity *in vivo*. We have, however, found that the addition of *N*-hydroxynorcocaine to microsomes from non-induced mice, rats, or hamsters (in the presence of a NADPH-generating system)

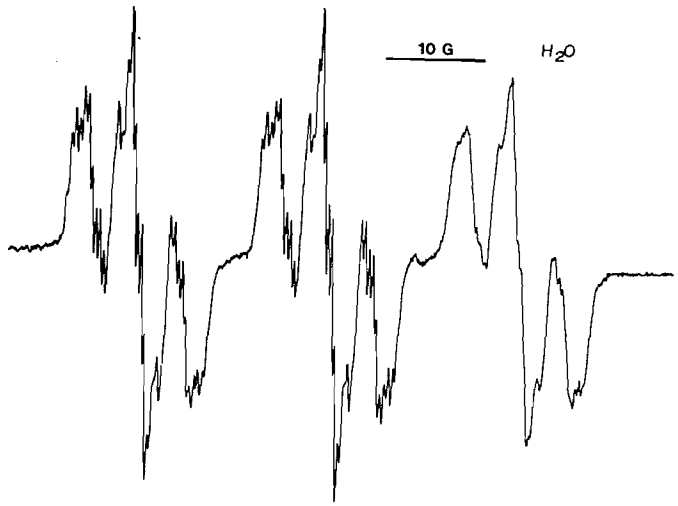


FIG. 1. The electron paramagnetic resonance spectrum of norcocaine nitroxide in water at ambient temperature. This spectrum was recorded on a Varian Associates model E-9 spectrometer, gain = $4 \times 10^3$; microwave power = 10 mW; modulation amplitude = 0.32 G; time constant = 0.3 s; scan time = 12.5 G/min.

results in the formation of norcocaine nitroxide (24). The formation of this nitroxide in the reaction mixture was determined by observation of its electron paramagnetic resonance (epr) spectrum which was identical to that of norcocaine nitroxide synthesized by the oxidation of norcocaine with *m*-chloroperbenzoic acid (Fig. 1). This nitroxide exhibited the characteristic hyperfine splitting pattern for a nitroxide with two β-hydrogens (25), and appeared immediately after the reaction was initiated by the addition of *N*-hydroxynorcocaine to microsomes in the presence of a NADPH generating system. The epr signal intensity reached maximum after 2 to 10 min (depending on the microsomal concentration) after admixture of the reactants, at which point, the signal decreased steadily. Norcocaine nitroxide, itself, however, was found to be relatively stable, decomposing at about 1% per hour in aqueous solution. This observation suggests that norcocaine nitroxide reacts with some constituent of the microsomal mixture and that the level of norcocaine nitroxide observed in the incubation mixture is controlled by its rate of formation and subsequent rate of reaction. Phenobarbital-induced animals (mice, rats, or hamsters) were found to produce maximal levels of norcocaine nitroxide, which were about five times greater than was observed using non-induced animals (24). These observations suggest that a specific subpopulation of cytochrome P-450 preferentially oxidizes *N*-hydroxynorcocaine to its corresponding nitroxide and that the ability of a hepatic microsomal system to convert *N*-hydroxynorcocaine to norcocaine nitroxide is not the only factor to be considered in cocaine-induced hepatotoxicity, since rats and hamsters are not known to exhibit hepatic necrosis after exposure to cocaine (10).

The mechanism of this microsomal one electron oxidation of *N*-hydroxynorcocaine to norcocaine nitroxide appears to be unusual. We have previously reported that the microsomal one electron oxidation of hydroxylamines to nitroxides is a result of microsomal superoxide production rather than a direct enzymatic conversion (26). The oxidation of *N*-hydroxynorcocaine to its corresponding nitroxide, however, appears to be an exception to this generalization. All data compiled to date indicate that cytochrome P-450 directly mediates this oxidation. Phenobarbital induction enhances the microsomal oxidation of *N*-hydroxynorcocaine to norcocaine nitroxide, metyrapone and SKF-525A inhibit the conversion, and a type I binding spectrum for *N*-hydroxynorcocaine is observable. Compounds which produce type I binding spectra are almost invariably substrates for cytochrome P-450 (27). Thus, *N*-hydroxynorcocaine meets at least three of the four criteria commonly used to establish the involvement of cytochrome P-450 in the oxidation of a substrate (28). The reaction of *N*-hydroxynorcocaine with cytochrome P-450 to produce norcocaine nitroxide is not, then, a mixed function oxidation reaction, but rather a form of "substrate activation" by cytochrome P-450. It is possible that in the tertiary cytochrome P-450-substrate – oxygen complex, a hydrogen atom is abstracted from the substrate (29). In this situation, the substrate becomes a donor of the reducing equivalents. It has been suggested that hydrogen

Can. J. Chem. Downloaded from www.nrcresearchpress.com by 210.87.254.42 on 09/06/12
For personal use only.

Can. J. Chem. Downloaded from www.nrcresearchpress.com by 210.87.254.42 on 09/06/12
For personal use only.

TABLE 3. Reduction of norcocaine nitroxide and TEMPO by non-induced rat hepatic microsomes

| Mixture | Rate of substrate reduction* | |
|---|---|---|
| | TEMPO† | Norcocaine nitroxide |
| NADPH | 0 | 2.2 |
| NADPH + microsomes | 2.9 | 17.0 |
| NADPH + microsomes + metyrapone | 0.99 | 16.8 |
| NADH | 0 | 1.2 |
| NADH + microsomes | 0.7 | 8.9 |
| NADH + microsomes + metyrapone | 0.4 | 8.8 |

*Rates were determined by following the loss of epr signal intensity with time and are expressed in μmol substrate reduced per minute per mg protein. The NADPH and NADH rates have been divided through by the protein values so they are comparable directly to the enzymatic rates.
†TEMPO = 2,2,6,6-tetramethylpiperidinoxyl.

peroxide is formed as a consequence of this "substrate activation" reaction (30). A likely mechanism for this reaction is depicted in Fig. 2.

*Reactivity of norcocaine nitroxide*

Nitroxide radicals are known to be relatively unreactive chemically. In fact, a wide variety of chemical reactions may be performed on other parts of a molecule containing a nitroxide moiety without affecting the nitroxide (31). Purified synthetic norcocaine nitroxide was found to be unreactive with proteins in the form of either washed hepatic microsomes or dialized hepatic cytosol (24). This observation eliminates the possibility that covalent binding of cocaine to microsomal proteins occurs by simple reaction of the nitroxide moiety with proteins.

The direct reaction of nitroxides with sulfhydryl groups is often mentioned in the literature (31); however, we have found that this reaction is generally an artifact produced by heavy metal contamination (unpublished observations). In the case of cocaine-mediated hepatotoxicity, it is tempting to ascribe the observed depletion of hepatic glutathione to direct reaction of reduced glutathione with norcocaine nitroxide. Unfortunately, purified norcocaine nitroxide was determined not to react with either reduced glutathione or cysteine (24). Norcocaine nitroxide was, however, found to react rapidly with dithiothreitol or β-mercaptoethanol (24).

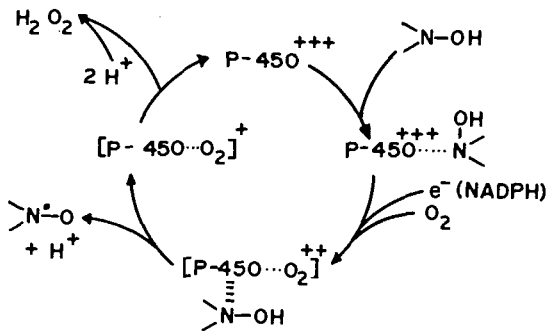


FIG. 2. Proposed mechanism for the oxidation of *N*-hydroxynorcocaine to norcocaine nitroxide by cytochrome P-450.

Norcocaine nitroxide was demonstrated to oxidize directly the pyridine nucleotides NADH and NADPH resulting in the reduction of the nitroxide free radical (Table 3) (24). Furthermore, it was determined that microsomal enzymes rapidly reduce norcocaine nitroxide in the presence of NADPH or NADH (Table 3). It had previously been shown that microsomal reduction of simple nitroxides, such as 2,2,6,6-tetramethylpiperidinoxyl (TEMPO), was mediated by cytochrome P-450 (32). In the case of norcocaine nitroxide, however, free radical reduction was not inhibited by metyrapone (Table 3), suggesting that cytochrome P-450 was not responsible for this reduction. Experiments with purified enzymes indicated that the flavoproteins NADPH-cytochrome P-450 reductase and FAD-containing monooxygenase reduce norcocaine nitroxide (Table 4) (24). The fact that these reductions of norcocaine nitroxide are one electron reactions implies that the reductant (pyridine nucleotide or flavoprotein) is oxidized to a free radical species. In the presence of oxygen, one reaction which is known to occur with these species is an electron transfer producing superoxide and the oxidized pyridine nucleotide (33) or flavoprotein. This was shown to be the case for NADH, NADPH, and FAD-containing monooxygenase, but not for NADPH-cytochrome P-450 reductase as illustrated in Table 4. Norcocaine nitroxide was demonstrated to inhibit the normal superoxide production by purified NADPH-cytochrome P-450 reductase.

In vitro *stimulation of lipid peroxidation by norcocaine nitroxide*

The reaction of norcocaine nitroxide with reduced pyridine nucleotide and flavoproteins to

TABLE 4. Reaction of norcocaine nitroxide with NADPH, NADH, and purified enzymes*

| Mixture | NCN reduction† (n*M*/min) | Superoxide production‡ (n*M*/min) |
|---|---|---|
| NADPH + NCN | 580 | 160 |
| NADH + NCN | 640 | 158 |
| NADPH + FADM | — | 26 |
| NADPH + FADM + NCN | 940 | 391 |
| NADH + FADM | — | 12 |
| NADH + FADM + NCN | 900 | 400 |
| NADPH + RED | — | 618 |
| NADPH + RED + NCN | 4320 | 395 |
| NADH + RED + NCN | 1000 | — |

*FADM = FAD-containing monooxygenase; RED = cytochrome P-450 reductase; NCN = norcocaine nitroxide.
†Norcocaine nitroxide reduction was measured by loss of epr signal intensity. NCN, 3 μ*M*; NAD(P)H, 55 μ*M*; FADM, 170 n*M*; RED, 44 n*M*; in pH 8.3 tricine buffer containing 1 m*M* DETAPAC.
‡Superoxide production was measured as the superoxide dismutase (SOD) (10 μg/mL) inhibitable cytochrome c reduction (39). The cytochrome P-450 reductase superoxide production was measured using succinylated cytochrome c. Conditions were the same as in † except norcocaine nitroxide used was 30 μ*M*.

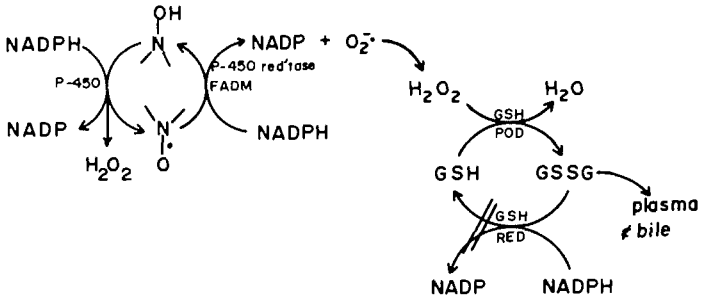


FIG. 3. Proposed mechanism for cocaine induced hepatotoxicity mediated by the cocaine metabolite, norcocaine nitroxide.

produce radical species suggested that lipid peroxidation may be stimulated *in vitro*. It was demonstrated that the addition of the spin trap α-(4-pyridyl-1-oxide)-*N*-*tert*-butylnitrone (4-POBN) to a microsomal-NADPH – norcocaine nitroxide mixture resulted in the spin trapping of higher levels of free radicals than were trapped in the absence of norcocaine nitroxide (24). The spin-trapped radical species were identified as lipid peroxyl radicals (24, 34), indicating that stimulation of lipid peroxidation by norcocaine nitroxide had occurred *in vitro*. The mechanism of this *in vitro* stimulation of lipid peroxidation was not investigated.

*Mechanism of cocaine-induced hepatotoxicity*

The studies demonstrating cytochrome P-450's oxidation of *N*-hydroxynorcocaine to norcocaine nitroxide and the investigation of the reactivity of norcocaine nitroxide with biomolecules allows us to speculate how norcocaine nitroxide participates in cocaine-induced hepatotoxicity.

We favor a complex mechanism where a futile redox cycle is set up between oxidation of *N*-hydroxynorcocaine to norcocaine nitroxide and reduction of norcocaine nitroxide to *N*-hydroxynorcocaine, both at the expense of NADPH. This cycle (note Fig. 3) results in the loss of NADPH and the production of hydrogen peroxide (from the cytochrome P-450 oxidation reaction and from dismutation of superoxide produced as a result of the reductive reaction). The hydrogen peroxide is destroyed by glutathione peroxidase concomitantly converting reduced glutathione to oxidized glutathione. Reduction of oxidized glutathione, we postulate, is partially blocked because levels of NADPH are reduced by the futile redox cycle. This results in the buildup of oxidized glutathione which is actively excreted by the cell in order to maintain its GSH/GSSG ratio in a "normal" range (35, 36). This active excretion of GSSG accounts for the observed cocaine-induced glutathione depletion. Toxic lipid hydroperoxides, produced by norcocaine-induced stimulation of lipid peroxidation, would also accumulate if sufficient glutathione were not available as a co-factor for glutathione peroxidase to reduce organic hydroperoxides to alcohols. As reduced glutathione continues to be oxidized, the cell can no longer excrete oxidized glutathione to maintain a physiologic GSH/GSSG ratio. Because of the resulting imbal-

Can. J. Chem. Downloaded from www.nrcresearchpress.com by 210.87.254.42 on 09/06/12
For personal use only.

ance, various enzymatic activities which depend upon a "normal" GSH/GSSG ratio being maintained are lost (36). With lipid peroxidation damaging cellular membranes and with GSH/GSSG ratios at a level incompatible with homeostatis, cellular death is inevitable.

This hypothetical mechanism is consistent with what is known about cocaine-induced hepatotoxicity and accounts for the observed loss of glutathione (8, 9). The known protection afforded by glutathione against cocaine-induced hepatotoxicity (8) and the known reactivity of norcocaine nitroxide (24) are also supported by this model. This mechanism is also consistent with the established relationship of exogenous hydroperoxide administration to oxidized glutathione efflux. Sies *et al.* (37) have demonstrated that GSSG is released from isolated perfused liver in the presence of exogenous hydroperoxide administration with a concomitant decrease in the NADPH/$NADP^+$ ratio as observed by surface fluorescence. Sies *et al.* (38) have proposed that when levels of NADPH are diminished past a critical level, the cell's ability to reduce GSSG to GSH via glutathione reductase is compromised.

Can. J. Chem. Downloaded from www.nrcresearchpress.com by 210.87.254.42 on 09/06/12
For personal use only.

## Acknowledgments

The authors wish to thank for partial support: the National Institutes of Health, grant numbers GM 25188 and GM 25753, and the Department of Defense, DAAG 29-80-K-0075. M.W.K. is a recipient of a National Research Service Award Number GM 07184 from the National Institutes of Health.

1. M. A. Evans and R. D. Harbison. Pharmacologist, **18**, 142 (1976).
2. T. Inaba, D. J. Stewart, and W. Kalow. Clin. Pharm. Ther. **23**, 547 (1979).
3. W. Kalow. J. Pharmacol. Exp. Ther. **104**, 122 (1954).
4. F. Montesinos. Bull. Narcot. **17**, 11 (1965).
5. A. L. Misra, P. K. Nayak, M. N. Patel, N. L. Vadlamani, and S. J. Mule. Experientia, **69**, 1312 (1974).
6. P. K. Nayak, A. L. Misra, and S. J. Mule. J. Pharmacol. Exp. Ther. **196**, 556 (1976).
7. A. L. Misra, R. B. Pontani, and N. L. Vadlamani. Xenobiotica, **9**, 189 (1979).
8. M. L. Thompson, L. Shuster, and K. Shaw. Biochem. Pharmacol. **28**, 2389 (1979).
9. M. A. Evans and R. D. Harbison. Toxicol. Appl. Pharmacol. **45**, 739 (1978).
10. M. A. Evans. Toxicologist, **1**, 1 (1981).
11. M. A. Evans and M. E. Johnson. Fed. Proc. **40**, 638 (1981).
12. M. A. Evans, C. Dwivedi, and R. D. Harbison. *In* Cocaine and other stimulants. *Edited by* E. H. Ellinwood, Jr. and M. Marlyne Kilbey. Plenum Press, New York. 1977. p. 253.
13. L. Shuster, F. Quimby, A. Bates, and M. L. Thompson. Life Sci. **20**, 1035 (1977).
14. V. Marks and P. A. L. Chapple. Br. J. Addict. **62**, 189 (1967).
15. M. A. Evans. Pharmacologist, **20**, 182 (1978).
16. B. S. S. Masters and D. M. Ziegler. Arch. Biochem. Biophys. **145**, 358 (1971).
17. D. M. Ziegler and C. H. Mitchell. Arch. Biochem. Biophys. **150**, 116 (1972).
18. A. C. Smith, R. W. Freemand, and R. D. Harbison. Biochem. Pharmacol. **30**, 453 (1981).
19. M. S. Gold and D. M. Ziegler. Xenobiotica, **3**, 179 (1973).
20. M. L. Das and D. M. Ziegler. Arch. Biochem. Biophys. **140**, 300 (1970).
21. J. W. Gorrod. Chem.-Biol. Interactions, 7, 289 (1973).
22. J. D. George, G. M. Rosen, E. J. Rauckman, and D. M. Ziegler. *In* Autoxidation in food and biological systems. *Edited by* M. G. Simic and M. Karel. Plenum Press, New York. 1980. p. 541.
23. M. W. Duffel, J. M. Graham, and D. M. Ziegler. Mol. Pharmacol. **19**, 134 (1981).
24. E. J. Rauckman and G. M. Rosen. *In* Microsomes and drug oxidations. *Edited by* R. Sato. Japan Scientific Societies Press, Tokyo. 1982. In press.
25. P. F. Knowles, D. Marsh, and H. W. E. Rattle. *In* Magnetic resonance of biomolecules. John Wiley and Sons, London. 1976. p. 168.
26. E. J. Rauckman, G. M. Rosen, and B. B. Kitchell. Mol. Pharmacol. **15**, 131 (1979).
27. C. R. Jefcoate. Method Enzymol. **52**, 258 (1978).
28. P. G. Wislocki, G. T. Mina, and A. Y. H. Lu. *In* Enzymatic bases of detoxification. *Edited by* W. B. Jakoby. Academic Press, New York. 1980. p. 135.
29. I. Bjorkhem. Eur. J. Biochem. **18**, 299 (1971).
30. A. G. Hildebrandt, G. Heinmeyer, S. Nigam, and I. Roots. *In* Microsomes, drug oxidations and chemical carcinogenesis. *Edited by* M. J. Coon, A. H. Conney, R. W. Estabrook, H. V. Gelboin, J. R. Gillette, and P. J. O'Brien. Vol. 1. Academic Press, New York. 1980. p. 335.
31. B. J. Gaffney. *In* Spin labeling theory and application. *Edited by* L. J. Berliner. Academic Press, New York. 1976. p. 184.
32. G. M. Rosen and E. J. Rauckman. Biochem. Pharmacol. **26**, 675 (1977).
33. E. J. Land and A. J. Swallow. Biochim. Biophys. Acta, **234**, 34 (1971).
34. G. M. Rosen and E. J. Rauckman. Proc. Natl. Acad. Sci. USA. In press.
35. G. M. Bartoli and H. Sies. FEBS Lett. **86**, 89 (1978).
36. N. S. Kosower and E. M. Kosower. Int. Rev. Cytol. **54**, 109 (1978).
37. H. Sies, H. Noack, and K. H. Halder. Eur. J. Biochem. **38**, 247 (1973).
38. H. Sies, C. Gerstnecker, H. Menzel, and L. Flohe. FEBS Lett. **27**, 171 (1972).
39. J. M. McCord and I. Fridovich. J. Biol. Chem. **243**, 5753 (1968).

# Spin trapping in heterogeneous electron transfer processes

THOMAS H. WALTER, ERIC E. BANCROFT, GREGORY L. MCINTIRE,[1] EDWARD R. DAVIS, LILA M. GIERASCH,[2] AND HENRY N. BLOUNT[2]

*Center for Catalytic Science and Technology and Brown Chemical Laboratory, The University of Delaware, Newark, DE 19711, U.S.A.*

AND

HENRY J. STRONKS AND EDWARD G. JANZEN

*Guelph–Waterloo Centre for Graduate Work in Chemistry, Department of Chemistry, The University of Guelph, Guelph, Ont., Canada N1G 2W1*

Received September 1, 1981

THOMAS H. WALTER, ERIC E. BANCROFT, GREGORY L. MCINTIRE, EDWARD R. DAVIS, LILA M. GIERASCH, HENRY N. BLOUNT, HENRY J. STRONKS, and EDWARD G. JANZEN. Can. J. Chem. **60**, 1621 (1982).

An overview of applications of spin trapping to electrochemical investigations is presented. Cited studies include characterizations of primary electrode reaction products (e.g., electrooxidations of halide and pseudohalide species, electroreduction of *N*-methylpyridinium ion) as well as the identification of transient intermediates arising from homogeneous reactions which are electroinitiated. The validity of spatially resolved spin trapping as a probe in the investigation of interfacial processes is demonstrated with examples drawn both from the previously reported covalent attachment of nitrone derived spin traps to silaceous surfaces and from recent studies of spin trapping in micelle and vesicle systems. Amphiphilic nitrone spin traps have been shown to coassemble with both micelles and vesicles such that the nitrone functionality resides in the interfacial region of the ordered system. The ability of these interfacially localized nitrones to trap transient radicals generated both in the hydrophobic domain of the micelle or vesicle and in the aqueous exterior domain is demonstrated.

THOMAS H. WALTER, ERIC E. BANCROFT, GREGORY L. MCINTIRE, EDWARD R. DAVIS, LILA M. GIERASCH, HENRY N. BLOUNT, HENRY J. STRONKS et EDWARD G. JANZEN. Can. J. Chem. **60**, 1621 (1982).

Une revue des applications des pièges à spins dans les études électrochimiques est presentée. Les travaux décrits comprennent la caractérisation des produits primaires des réactions sur les électrodes (par example, les électrooxydations des halides et des pseudohalides, et l'électroréduction du *N*-méthylpyridinium) ainsi que l'identification des intermédiaires transitoires qui sont produits dans des réactions homogènes électroinitiées. La validité d'une méthode utilisant des pièges à spins situés à un endroit précis pour l'étude des procédés interfaciaux est montrée. Deux exemples sont donnés: les études déjà rapportées des pièges à spins derivés du nitrone liés aux surfaces silacieuses, et les études récentes des pièges à spins dans les micelles et dans les vésicules. Il a été montré que les pièges à spins sont des nitrones amphiphiliques qui se sont rassemblés avec les micelles et les vésicules de sorte que le nitrone se situe dans la région interfaciale du système organisé. La capacité de ces nitrones, situés à l'inferface, de pièger les radicaux transitoires créés dans la région hydrophobique du micelle ou de la vésicule et dans la phase aqueuse extérieure est montrée.

[Traduit par le journal]

## Introduction

The detection and characterization of transient radical intermediates produced in reactions which are initiated by heterogeneous electron transfer processes are essential to the mechanistic definition of those processes. The necessity of such mechanistic understanding is becoming increasingly pronounced in areas of energy conversion and storage, electrosynthesis, heterogeneous catalysis, and biological electron transfer. Spin trapping (1, 2) with various nitroso and nitrone derived moieties has proven to be a fruitful approach to the detection and characterization of transient radical intermediates ensuing from electrooxidations (3–6), photoassisted oxidations (7–9), and electroreductions (4, 10–12) of various substrates in solution. The viability of spin trapping as an investigative tool in electron transfer processes requires that (*i*) the spin trap reagent be electroinactive at potentials required to discharge the substrate, (*ii*) the rate of reaction of radical intermediates with the spin trap be favorable relative to those of other radical-consuming reactions, and (*iii*) the product of the radical/spin trap reaction (the *spin adduct*) also be electroinactive at potentials which are employed to oxidize or to reduce the substrate. Several studies (3, 4, 6–8, 10, 12, 13) have provided insight into the electroactivities of spin traps and spin adducts. Also, the kinetics of spin trapping reactions have recently been reviewed (14).

In addition to the three general requirements for spin trapping in electron transfer processes, a fourth constraint may have to be met for mechanistic definition of *interfacial* electron transfer reac-

[1]Present address: Research Laboratories, Eastman Kodak Company, Rochester, NY 14650, U.S.A.

[2]Authors to whom correspondence should be directed.

0008-4042/82/121621-16$01.00/0

©1982 National Research Council of Canada/Conseil national de recherches du Canada

Can. J. Chem. Downloaded from www.nrcresearchpress.com by 210.87.254.40 on 09/06/12
For personal use only.

Can. J. Chem. Downloaded from www.nrcresearchpress.com by 210.87.254.40 on 09/06/12
For personal use only.

tions of interest. In heterogeneous electron transfer systems, the spin trapping reaction should be spatially resolved, i.e., the spin trap reagent should be localized in the vicinity of the interface where the primary redox process takes place. Recently, strategies have been developed which permit spin traps to be attached to solid surfaces (15, 16). These approaches hold promise for productive spin trapping investigations of mechanisms of electrocatalytic processes (16). In addition, protocols for localization of spin traps at the interfaces between micelles and aqueous solutions, and between vesicles and aqueous solutions, have been developed (17). These findings suggest the use of spin trapping as a viable mechanistic probe for reactions which are initiated by heterogeneous electron transfer reactions which take place at membrane/solution interfaces.

This report provides an overview of spin trapping in electrochemical studies conducted in these laboratories and also details recent developments in spin trapping in micellar and vesicular media.

## Experimental

*Materials*

Sources of and purification procedures for acetonitrile (AN), tetraethylammonium perchlorate (TEAP), tetra-*n*-butylammonium perchlorate (TBAP), and lithium perchlorate have already been reported (18–20). Tetraethylammonium (TEA) and tetra-*n*-butylammonium (TBA) salts of cyanide (TEACN), cyanate (TEAOCN), thiocyanate (TBASCN), chloride (TBACl), azide ($TBAN_3$), and tetra-*n*-butylboride ($TBABBu_4$) were either commercially available or were prepared by standard methods (21). The synthesis and purification of α-(4-dodecyloxyphenyl)-*N*-*tert*-butylnitrone (DOPBN) is described elsewhere (22). The preparations, purification procedures, and characterizations of all other nitrone and nitroso spin trap reagents used in this work have been previously summarized (13). The preparation of *N*-methylpyridinium ($NMP^+$) salts has also been described (12). Sources of controlled pore glass beads (CPG) and cyanuric chloride (CC), and synthetic protocols for the immobilization of HOPBN (Table 1) to CPG have been previously detailed (15). Sodium dodecylsulfate (SDS, Aldrich) was purified as reported elsewhere (23). Dioctadecyldimethylammonium chloride (DODAC) was prepared from the bromide salt (Eastman) by ion exchange after the manner of Lim and Fendler (24). Lecithin was obtained from fresh egg yolks by the method of Singleton *et al.* (25). DODAC/DOPBN vesicles (10:1 mol ratio, 60 mg DODAC/mL) were prepared by ultrasound irradiation (Sonicor ultrasonic cleaner) of an aqueous mixture of the two components for 30 min at 50°C. Lecithin/DOPBN vesicles (20:1 w/w, 10 mg lecithin/mL) were prepared by ultrasonication under nitrogen of a mixture of these two components in 0.10 *M* NaCl for 100 min at 25°C. Phenylazotriphenylmethane (PAT, Eastman) was used as received. Phenyldiazonium tetrafluoroborate (PDT) was synthesized by conventional methods (26). All other materials were reagent grade or equivalent.

*Apparatus*

Electron spin resonance (esr) spectra were recorded at room temperature on Varian E-104 or Varian E-109E spectrometers which were periodically calibrated with Fremy's salt. *In situ* electrolyses were performed at controlled potentials in the esr cavity using a Varian E-256 electrolytic sample cell configured with either a Pt gauze or a Hg pool working electrode. Electrochemical instrumentation and cells have already been described (13). All potentials are reported relative to the aqueous saturated calomel electrode (SCE). Measurements of hyperfine splitting constants (hfsc's) were verified by spectral simulation.

## Results and discussion

The structures, designations, and electrochemical properties of eighteen of the most well-characterized spin traps are summarized in Table 1. The effects of molecular structure on the electrochemical behavior of these spin traps have been described, as have the homogeneous chemical reactions which follow the oxidation and reduction of these species (13). All of the spin traps shown in Table 1 exhibit broad "potential windows" (ranges of electrode potentials over which the entities in question are electroinactive) which render them suitable for use in a wide variety of electrochemical investigations.

*Spin trapping of primary electrode reaction products*

Spin trapping investigations of the oxidative electrochemistry of pseudohalide and halide species provide examples of systems in which the *primary* electrode reaction product can be detected and characterized. The general reaction scheme which describes the oxidative discharge of pseudohalide and halide species ($X^-$) can be represented by

$$[1]\quad X^- \rightleftharpoons X^{\cdot} + e^-$$

$$[2]\quad 2X^{\cdot} \rightarrow X_2$$

$$[3]\quad X_2 + X^- \rightleftharpoons X_3^-$$

where the primary electrode reaction product, $X^{\cdot}$, is most often adsorbed onto the electrode surface. While the perpseudohalide or perhalide is the ultimate reaction product in many pseudohalide and halide electrooxidations, there are exceptions as noted below. Radical dimerization (eq. [2]) is quite fast in these systems and is the process with which the spin trapping reaction must compete.

Cyanide can be selectively oxidized in the presence of PBN (Tables 1 and 2). *In situ* electrooxidation of TEACN in TEAP/AN containing PBN gives rise to the cyanyl spin adduct of PBN which affords the esr spectrum shown in Fig. 1A. That this spin adduct is only observable at PBN/TEACN ratios ≥ 3000 attests to the velocity of the radical dimerization process (eq. [2]). The triplet of doublets seen in Fig. 1A suggests a spin adduct of structure **1** resulting from a carbon-centered cyanyl radical as

Can. J. Chem. Downloaded from www.nrcresearchpress.com by 210.87.254.40 on 09/06/12
For personal use only.

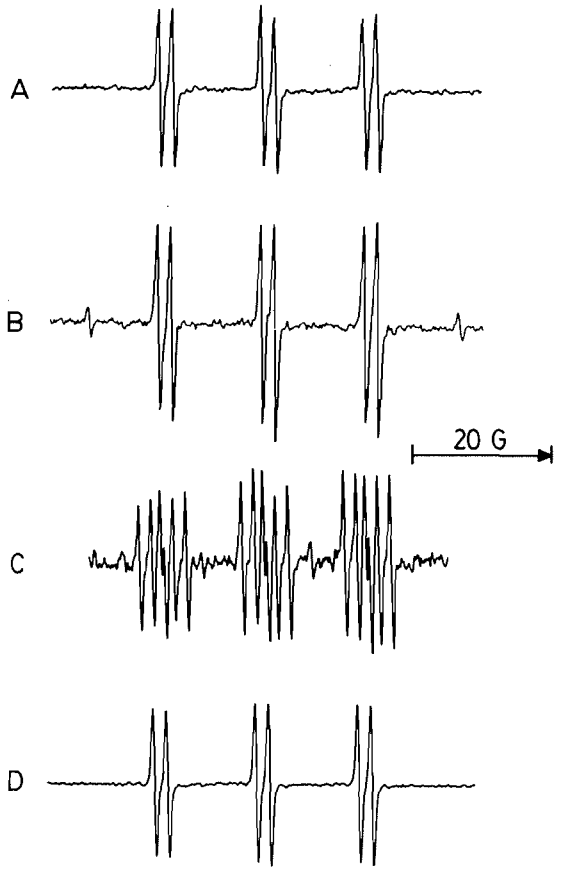


FIG. 1. The esr spectra of spin adducts produced by (A) *in situ* electrooxidation of TEACN in the presence of PBN in TEAP/AN; (B) reaction of *t*-BuO· with benzyl cyanide in the presence of N*t*B; (C) *in situ* electrooxidation of TEAOCN in the presence of PBN in TEAP/AN; (D) *in situ* electrooxidation of TBASCN in the presence of PBN in TEAP/AN.

reported by Forrester and Hepburn (27) and Mao and Kevan (28). Verification of the assignment of the spectrum shown in Fig. 1A to **1** has been provided through an alternate preparation and esr characterization of **1**. Thermal decomposition of

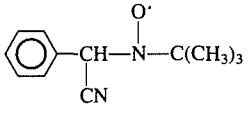

**1**

di-*tert*-butylperoxyoxalate (DBPO) produces *t*-BuO· (eq. [4]) which abstracts an α-hydrogen atom from benzyl cyanide (eq. [5]). The resulting α-cyanobenzyl radical is trapped by N*t*B (eq. [6]) and gives rise to the esr spectrum shown in Fig. 1B. The agreement between the hyperfine splitting constants (hfsc's) of this spin adduct ($a_N = 15.04$, $a_\beta^H = 1.98$ G) and those of the spin adduct derived from electrooxidation of TEACN (Table 2) confirms the

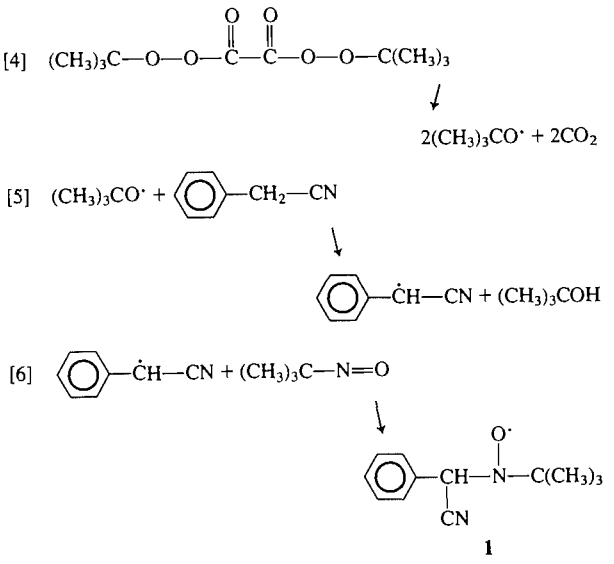


**1**

assignment of the spectrum shown in Fig. 1A to the carbon-centered cyanyl spin adduct of PBN (**1**).

The electrooxidation of cyanate (as TEAOCN) in the presence of PBN in TEAP/AN gives rise to the spin adduct **2** whose esr spectrum is shown in Fig. 1C. This result is consistent with the findings of Cauquis and Pierre (29, 30) that the electrooxidation of cyanate initially gives rise to the cyanatyl radical which dimerizes and subsequently decomposes to cyanogen and oxygen. Like the cyanyl case, the cyanatyl radical adds to PBN via the "softer" atom (31). Additionally, the assignment of the esr spectrum in Fig. 1C to structure **2** is consistent with the spin trapping of cyanatyl radicals produced both by persulfate oxidation of cyanate in the presence of PBN and by the photolysis of aqueous solutions of cyanate containing PBN (6).

On the basis of the spin trapping behavior of cyanyl and cyanatyl radicals which add to PBN

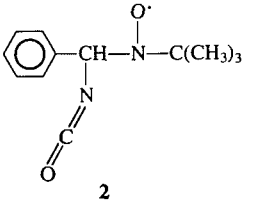

**2**

through the "softer" atom, thiocyanatyl radical could be expected to add to PBN to give the spin adduct **3**. *In situ* electrooxidation of thiocyanate (as TBASCN) in TEAP/AN containing PBN gives rise to a spin adduct whose esr spectrum is shown in Fig. 1D. Whereas **3** is predicted to give rise to such a triplet of doublets, the $a_N$ and $a_\beta^H$ values of the observed spin adduct are identical to those noted

Can. J. Chem. Downloaded from www.nrcresearchpress.com by 210.87.254.40 on 09/06/12
For personal use only.

TABLE 1. Electrochemical properties of spin traps

| Spin trap | Notation | Nonaqueous medium[a] $E_{p(a)}$[c] | $n$[d] | $E_{p(c)}$[e] | $n$[d] | Aqueous medium[b] $E_{p(a)}$ | $E_{p(c)}$[g] | $n$[d] |
|---|---|---|---|---|---|---|---|---|
| 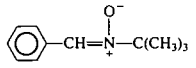 | PBN | 1.47 | 1[h] | −2.40 | — | [f] | −1.88 | 2–4[r] |
| 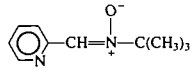 | 2PyBN | 1.82<br>2.45 | 1[h]<br>1[h] | −2.02[m] | 2[h] | [f] | −1.20 | 2–4[r] |
| 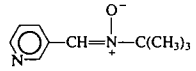 | 3PyBN | 1.67 | — | −2.10 | 2 | [f] | −1.62 | — |
| 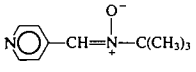 | 4PyBN | 1.93 | 1 | −1.85[m] | 2[h] | [f] | −1.17 | 2–4[r] |
| 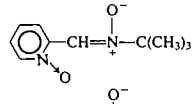 | 2PyOBN | 1.63<br>2.20 | 1<br>2 | −1.67[n] | 2[h] | [f] | −1.22 | 2–4[r] |
| 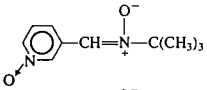 | 3PyOBN | 1.84 | — | −1.78 | 2 | [f] | −1.89 | — |
| 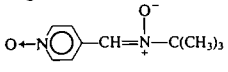 | 4PyOBN | 1.37<br>2.29 | 1[h]<br>2[h] | −1.77[n] | 2[h] | [f] | −1.20 | 2–4[r] |
| 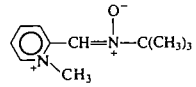 | 2MePyBN[i] | 2.35 | 2 | −0.88[n]<br>−1.77 | 1[h] | [f] | −0.88<br>−1.55 | 2–4[h,r] |
| 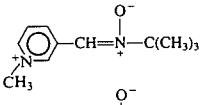 | 3MePyBN[i] | 2.10 | — | −1.12 | — | [f] | −1.17 | — |
| 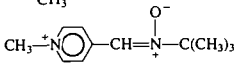 | 4MePyBN[i] | 2.32 | 2 | −0.87[n]<br>−1.67 | 1[h] | [f] | −0.92<br>−1.53 | 2–4[h,r] |
| 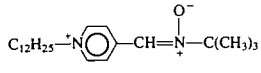 | 4LPyBN[j] | 2.37 | 2 | −0.87[n]<br>−1.67 | 1 | [f] | −1.65 | 2–4[r] |

for the cyanyl adduct of PBN (Table 2). Although initially disturbing, the observation that the cyanyl spin adduct of PBN ensues from the electrooxida-

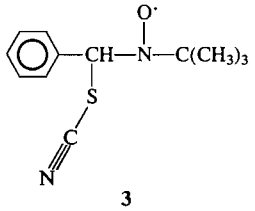

3

tion of thiocyanate is consistent with the conclusions of Pereiro *et al.* (32), that upon electrooxidation, the thiocyanatyl radical is strongly adsorbed onto the platinum electrode:

[7] $SCN^- \underset{}{\overset{\text{Pt electrode}}{\rightleftharpoons}} Pt(SCN)^{\cdot}_{surf} + e^-$

Decomposition of the Pt(SCN)$^{\cdot}$ surface species to the extremely stable PtS (33) with concomitant loss of the cyanyl radical is a tenable mechanism for formation of **1** in this system:

[8] $Pt(SCN)^{\cdot}_{surf} \rightarrow PtS_{surf} + {}^{\cdot}CN$

[9] ${}^{\cdot}CN + PBN \rightarrow \mathbf{1}$

Alternatively, **1** may be formed by the heterogeneous reaction of PBN with the Pt(SCN)$^{\cdot}$ surface species:

[10] $Pt(SCN)^{\cdot}_{surf} + PBN \rightarrow PtS_{surf} + \mathbf{1}$

The spin trapping results do not permit distinction

TABLE 1. (*Concluded*)

| Spin trap | Notation | Nonaqueous medium[a] $E_{p(a)}$[c] | $n$[d] | $E_{p(c)}$[e] | $n$[d] | Aqueous medium[b] $E_{p(a)}$ | $E_{p(c)}$[g] | $n$[d] |
|---|---|---|---|---|---|---|---|---|
| 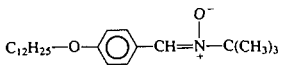 | DOPBN | 1.40 | 1 | −2.60 | — | [s] | [s] | — |
| 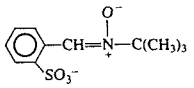 | 2SPBN[k] | 1.34 | 1 | −1.75 | — | [f] | −1.78 | 2–4[r] |
| 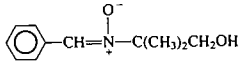 | HOPBN | 1.53 | 1 | −2.21 | — | [f] | −1.82 | 2–4[h,r] |
| 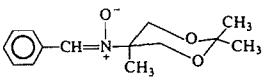 | DMPDN | 1.60 | 1 | −2.26 | — | [f] | −1.79 | 2–4[r] |
| 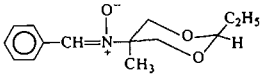 | EPDN | 1.61 | 1 | −2.22 | — | [f] | −1.78 | 2–4[r] |
| | DMPO | 1.63 | — | −2.35 | — | [f] | −1.92 | — |
| | NtB | 1.45[p] 1.82[q] 2.40[p] | | −1.77[q] | — | [f] | −1.77[q] | — |

[a] AN containing 0.10 *M* TEAP.
[b] Aqueous 0.10 *M* $LiClO_4$.
[c] Peak anodic potential (V vs. SCE) at Pt, sweep rate = 150 mV/s.
[d] From voltammetric peak height unless otherwise noted.
[e] Peak cathodic potential (V vs. SCE) at Pt, sweep rate = 150 mV/s.
[f] No oxidation noted at Pt prior to onset of solvent oxidation at +1.2 V vs. SCE.
[g] Peak cathodic potential (V vs. SCE) at Hg, sweep rate = 150 mV/s.
[h] Based on controlled potential electrolysis.
[i] Methyl sulfate counterion.
[j] Dodecyl sulfate counterion.
[k] Sodium counterion.
[m] Reversible ($i_{p_a} = i_{p_c}$) and $n \approx 1$ at sweep rate ≥ 500 mV/s.
[n] Reversible ($i_{p_a} = i_{p_c}$) at sweep rate = 100 mV/s.
[p] Dimer.
[q] Monomer.
[r] Scan rate dependent; see ref. 13.
[s] Insoluble in water.

Reprinted with permission from J. Phys. Chem. **84**, 916 (1980), copyright 1980 American Chemical Society.

to be made between these two possible modes of formation of **1**.

The observed solution-resident reaction product, parathiocyanogen (32), may be formed via two suggested mechanisms (34) which do not require ·SCN to be present in solution where it would presumably be trapped. The first of these mechanisms involves dimerization of adsorbed, *mobile* ·SCN species:

[11] $2Pt(SCN)^{\cdot}_{surf} \rightarrow 2Pt + (SCN)_2$

The second mechanism reflects the oxidative dimerization of adsorbed, *nonmobile* ·SCN species:

[12] $Pt(SCN)^{\cdot}_{surf} + SCN^- \rightarrow Pt + (SCN)_2 + e^-$

There are three observations which, in concert, afford evidence for the existence of the Pt(SCN)· surface species and subsequent formation of PtS. Firstly, ·SCN is not detected in solution; secondly, ·CN is trapped by solution-resident PBN; and thirdly, the growth in intensity of the spectrum of the cyanyl spin adduct of PBN (**1**) is seen to cease shortly after onset of *in situ* steady state electrolysis of $SCN^-$. This last observation suggests that the electrode surface is altered during the initial stages of the electrolysis process, probably through formation of PtS (eq. [8] or eq. [10]).

Spin trapping of the product of the electrooxidation of chloride with PBN is another case in which spin adduct formation may proceed via a heterogeneous reaction between PBN and an adsorbed radical species (35, 36). *In situ* electrooxidation of $Cl^-$ (as TBACl in TEAP/AN) in the presence of PBN gives rise to the spin adduct **4** whose esr spectrum is shown in Fig. 2A. This spectrum is characteristic of the two isotopes of chlorine (37) which have different nuclear magnetic moments that result in spin adducts (Table 2) of different

Can. J. Chem. Downloaded from www.nrcresearchpress.com by 210.87.254.40 on 09/06/12
For personal use only.

TABLE 2. Electrochemical properties of pseudohalide and halide substrates and hyperfine splitting constants of the spin adducts of their oxidation products[a]

| Substrate[b] | $E_{p(a)}$[c] | Radical trapped | Spin trap | Experimental conditions | $a_N$ | $a_\beta^H$ | $a_\beta^X$ |
|---|---|---|---|---|---|---|---|
| $CN^-$ | +1.65[d] | ·CN | PBN | 1 m*M* TEACN, 3.6 *M* PBN, 0.10 *M* TEAP, AN, +0.85 V | 15.04 | 1.98 | — |
| $OCN^-$ | +1.60[e] | ·NCO | PBN | 5 m*M* TEAOCN, 50 m*M* PBN, 0.10 *M* TEAP, AN, +0.90 V | 15.09 | 3.15 | 1.84 (X = N) |
| $SCN^-$ | +0.70 | ·CN | PBN | 4 m*M* TBASCN, 50 m*M* PBN, 0.10 *M* TEAP, AN, +0.85 V | 15.04 | 1.98 | — |
| $Cl^-$ | +1.04 | ·Cl | PBN | 2 m*M* TBACl, 80 m*M* PBN, 0.10 *M* TEAP, AN, +0.95 V | 12.70<br>12.70 | 0.82<br>0.82 | 6.20 (X = $^{35}$Cl)<br>5.12 (X = $^{37}$Cl) |
| $Cl^-$ | +1.04 | ·Cl | 4MePyBN | 3 m*M* TBACl, 60 m*M* 4MePyBN, 0.10 *M* TEAP, AN, +0.90 V | 12.27<br>12.27 | 0.82<br>0.82 | 6.20 (X = $^{35}$Cl)<br>5.12 (X = $^{37}$Cl) |
| $N_3^-$ | +0.70 | $\cdot N_3$ | PBN | 4 m*M* $TBAN_3$, 50 m*M* PBN, 0.10 *M* TEAP, AN, +0.80 V | 14.06 | 1.89 | 1.89 (X = N) |
| $N_3^-$ | +0.70 | $\cdot N_3$ | 4PyOBN | 4 m*M* $TBAN_3$, 50 m*M* 4PyOBN, 0.10 *M* TEAP, AN, +0.80 V | 13.87 | 1.43 | 2.09 (X = N) |
| $N_3^-$ | +0.70 | $\cdot N_3$ | 2PyOBN | 4 m*M* $TBAN_3$, 50 m*M* 2PyOBN, 0.10 *M* TEAP, AN, +0.85 V | 13.93 | 1.68 | 2.50 (X = N) |
| $N_3^-$ | +0.70 | $\cdot N_3$ | 2SPBN | 6 m*M* $TBAN_3$, 30 m*M* 2SPBN, 0.10 *M* TEAP, AN, +0.80 V | 14.36 | 2.97 | 2.17 (X = N) |

[a]Experimental results obtained at room temperature; hfsc values in G; all potentials in volts vs. SCE.
[b]Introduced as the quarternary alkylammonium salt.
[c]Anodic peak potential (Pt electrode) determined at a sweep rate of 150 mV/s.
[d]Irreversible electrode process; reversible $E^{0\prime} \simeq +0.6$ V.
[e]Irreversible electrode process; reversible $E^{0\prime} \simeq +0.8$ V.

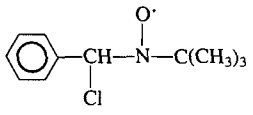

4

*g*-values. The intense triplet ($a_N \simeq 8$ G) in the center of this spectrum is due to the nitroxone **5** which likely arises from oxidation of PBN by $Cl_2$.

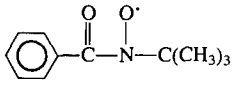

5

When 4MePyBN is used as the trapping reagent in these electrooxidation experiments, the spin adduct spectrum shown in Fig. 2C is obtained. The diminished nitroxone component in this spectrum may reflect the fact that 4MePyBN is more difficult to oxidize than PBN (Table 1). Alternatively, the $Cl^\cdot$ electrode reaction product may undergo far more rapid addition to 4MePyBN than to PBN, in which case the competitive formation of $Cl_2$, the expected oxidant in nitroxone production, is diminished.

Electrooxidation of azide to produce the azidyl radical ($N_3^\cdot$) and subsequent trapping with PBN, 4PyOBN, 2PyOBN, and 2SPBN provides an example of the importance of choice of spin trap reagent on the spin adduct spectrum observed. Electrooxidation of azide (as $TBAN_3$ in TEAP/AN) in the presence of PBN gives rise to the spin adduct **6** whose esr spectrum is shown in Fig. 3A. The assignment of this spectrum to the spin adduct

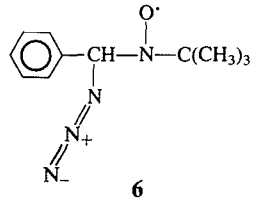

6

of structure **6** is consistent with PBN spin trapping of $N_3^\cdot$ produced by photolysis of aqueous solutions of sodium azide (6), photolysis of aqueous and methanolic solutions of $K_3[Co(CN)_5N_3]$ and $[Co(NH_3)_5N_3]Cl_2$ (38, 39), oxidation of sodium azide by Fenton's reagent in aqueous solution (6), and persulfate oxidation of aqueous solutions of sodium azide (6). It is noteworthy that far more well resolved spin adduct spectra are obtained from electrooxidations than from these other routes to the spin adduct. The triplet of 1:2:2:1 quartets seen in Fig. 3A arises from equality of β-nitrogen and β-hydrogen hfsc's in **6** (Table 2). Information regarding the radical which has been trapped may be obscured by the linewidth of the spectrum. As seen in Fig. 3C, the equality of β-N and β-H hfsc's

Can. J. Chem. Downloaded from www.nrcresearchpress.com by 210.87.254.40 on 09/06/12
For personal use only.

Can. J. Chem. Downloaded from www.nrcresearchpress.com by 210.87.254.40 on 09/06/12
For personal use only.

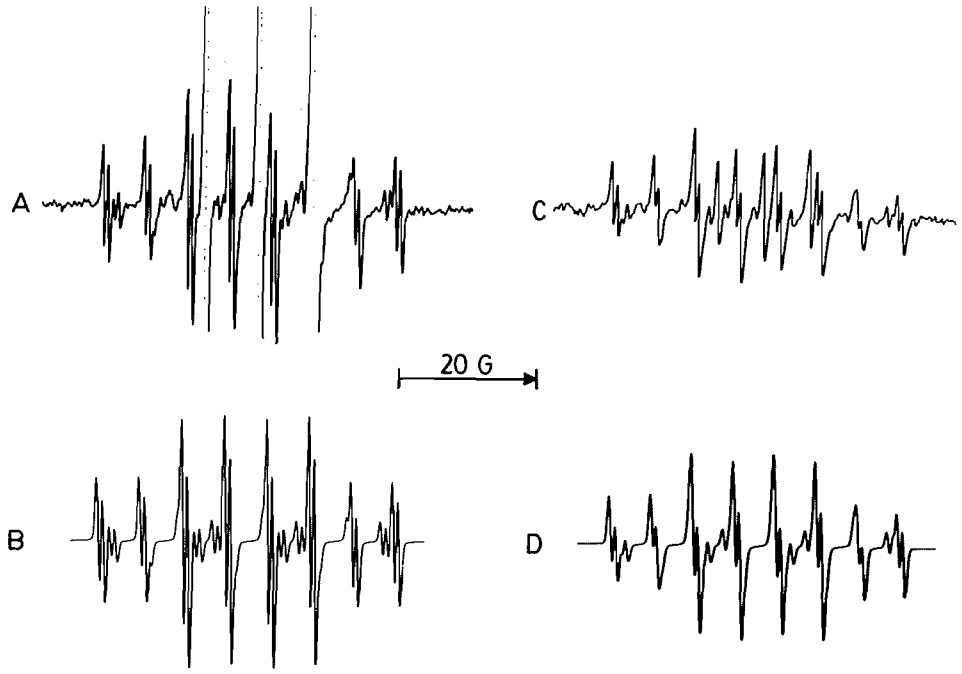


FIG. 2. The esr spectra of spin adducts formed upon *in situ* electrooxidation of TBACl in TEAP/AN in the presence of (A) PBN; (B) computer simulation of A; (C) 4MePyBN; (D) computer simulation of C. Parameters for computer simulations are given in Table 2.

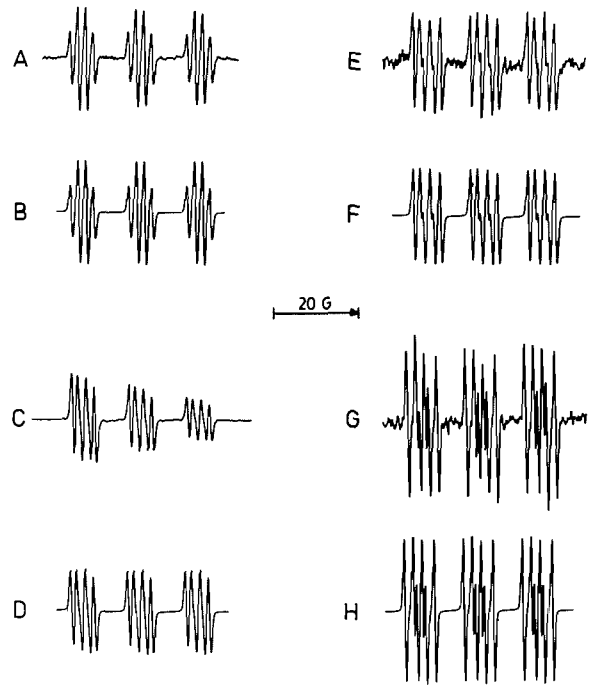


FIG. 3. The esr spectra of spin adducts derived from *in situ* electrooxidation of $TBAN_3$ in TEAP/AN in the presence of (A) PBN; (B) computer simulation of A; (C) 4PyOBN; (D) computer simulation of C; (E) 2PyOBN; (F) computer simulation of E; (G) 2SPBN; (H) computer simulation of G. Parameters for computer simulations are given in Table 2.

is removed when 4PyOBN, rather than PBN, is used as the trapping agent. Here, the 1:2:2:1 pattern observed with PBN (Fig. 3A) has been altered to a 1:1, 1:1, 1:1 pattern. Although a difference in $a_\beta^N$ and $a_\beta^H$ is observed (Table 2), resolution of the two additional lines in each multiplet is incomplete, and they appear as shoulders in Fig. 3C. Further improvement in resolution of the azidyl spin adduct spectrum is achieved when 2PyOBN is employed as the spin trap (Fig. 3E). The increased difference in $a_\beta^N$ and $a_\beta^H$ (Table 2) derives from sterically induced alteration of the time-averaged dihedral angle between the β-hydrogen, α-carbon, nitrone nitrogen plane, and the plane defined by the α-carbon, nitrone nitrogen, and its *p*-orbital (1). In the case of trapping electrogenerated azidyl radical with 2SPBN (Fig. 3G, Table 2), all eighteen lines of the spectrum are well resolved. The spin adduct spectra shown in Fig. 3 clearly demonstrate the impact of spin trap selection on the ease of unambiguous spectral analysis.

Spin trapping of primary electrode reaction products has recently been utilized in an investigation of the mechanism of the electroreduction of *N*-alkylpyridinium ions (12). Reduction of *N*-methylpyridinium ion ($NMP^+$) in aqueous solution has long been believed to be a monoelectronic process resulting in a transient radical which subsequently dimerizes:

Can. J. Chem. Downloaded from www.nrcresearchpress.com by 210.87.254.40 on 09/06/12
For personal use only.

[13] $CH_3-N^+(\bigcirc) + e^- \rightleftharpoons CH_3-N(H)(\cdot)$ (7)

[14] $2\,CH_3-N(H)(\cdot) \longrightarrow CH_3-N(H)-C_6H_4-N-CH_3$ (H)

Although the 1-methyl-1,4-dihydro-4-pyridinyl radical (**7**) has been widely proposed (40–43), its existence has not been established.

*In situ* electroreduction of $NMP^+$ at a mercury pool cathode in aqueous media saturated with PBN gives rise to an esr spectrum consisting of a triplet of doublets (Table 3) which has been tentatively assigned to the spin adduct **8** formed by addition of

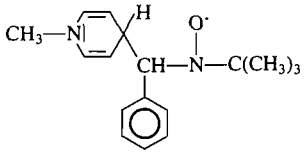

**8**

**7** to PBN (12). Verification of this assignment by independent preparation of authentic **8** has not been possible as no successful synthetic route has been found. Assignment of the observed esr spectrum to **8** is based on the observations that $a_\beta^H$ is indicative of an adducted radical having steric properties characteristic of a pseudoplanar six-membered ring (48) and that the linewidth reflects unresolved γ-H hyperfine splitting. Considerations of other radicals which might likely form during reduction of $NMP^+$ have discounted $H^\cdot$, $HO^\cdot$, $CH_3^\cdot$, $CH_3O^\cdot$, and $CH_3-N^+(\bigcirc)\cdot$ spin adducts of PBN by comparison of accepted hfsc values for these nitroxyl radicals with those observed for **8** (Table 3).

Alternate spin trapping experiments performed with spin traps which typically afford more informative spin adduct spectra (e.g., N*t*B or DMPO) have not been successful. Whether the absence of detectable spin adducts when these traps are used is a consequence of **7** not being trapped or is due to the electroactivity of the resulting spin adduct is not known.

### *Spin trapping of intermediates in coupled chemical reactions*

The identification of intermediates in reactions which are initiated by heterogeneous electron transfer is essential to an understanding of the mechanisms of those processes (49, 50). A clear illustration of the utility of spin trapping in assessing the influence of solution conditions on the intermediates produced in an electrochemically initiated reaction is provided by the electrooxidation of tetra-*n*-butylboride anion ($BBu_4^-$) at a platinum electrode in AN containing 0.10 *M* TBAP (3). Selective oxidation of $BBu_4^-$ (as $TBABBu_4$) in rigorously deoxygenated TBAP/AN containing PBN affords the spin adduct spectrum shown in Fig. 4A. Electrooxidation without deoxygenation of $BBu_4^-$ in TBAP/AN containing PBN gives rise to a mixture of two spin adducts (Fig. 4B), one of which is spectrally identical to that obtained in the absence of oxygen (Fig. 4A). Electrooxidation of $BBu_4^-$ in oxygen-saturated TBAP/AN containing PBN affords a single spin adduct whose esr spectrum, recorded after removal of oxygen, is shown in Fig. 4C. This spectrum is identical with the

TABLE 3. Electron spin resonance spectral parameters of spin adducts of radicals related to $NMP^+$ reduction[a]

| Radical | Spin trap | Solvent system | $a_N$ | $a_\beta^H$ | Linewidth | Reference |
|---|---|---|---|---|---|---|
| $CH_3-N^+(\bigcirc)\cdot$ | PBN | 0.10 *M* $LiClO_4$, $H_2O$ | 15.76 | 2.58 | 1.00 | 12 |
| $C_6H_5^\cdot$[b] | 4MePyBN | 0.10 *M* $LiClO_4$, $H_2O$ | 15.20 | 2.88 | 0.50 | 12 |
| $H^\cdot$ | PBN | 0.10 *M* $KClO_4$, $H_2O$ | 16.7 | 10.6 | — | 4,5 |
| $HO^\cdot$ | PBN | $H_2O$ | 15.76 | 3.17[c] | — | 44 |
| $CH_3^\cdot$ | PBN | $C_6H_6$ | 14.94 | 3.54 | 1.24 | 45 |
| $CH_3^\cdot$ | DMPDN | $H_2O$ | 15.67 | 3.87 | — | 46 |
| $CH_3O^\cdot$ | PBN | $CH_3OH$ | 14.38 | 2.91 | — | 47 |

[a] Values reported in G.
[b] The spin adduct resulting from phenyl radical addition to 4MePyBN is also that which would be observed for the addition of $CH_3-N(H)(\cdot)$ to PBN.
$C_6H_5^\cdot$[b]
$H^\cdot$
$HO^\cdot$
$CH_3^\cdot$
$CH_3^\cdot$
$CH_3O^\cdot$
[c] Expected value based on $a_N$ = 15.76 G and the relationship between $a_\beta^H$ and $a_N$ given in ref. 44.

Can. J. Chem. Downloaded from www.nrcresearchpress.com by 210.87.254.40 on 09/06/12
For personal use only.

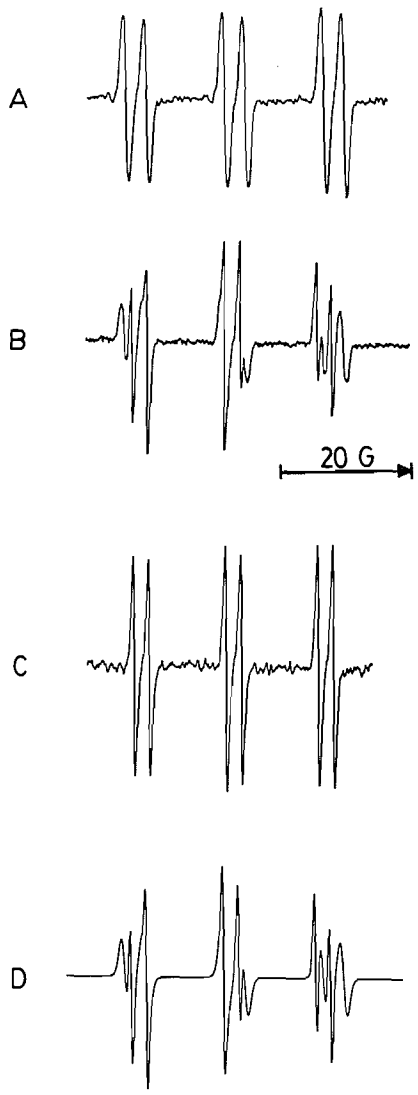


FIG. 4. The esr spectra of spin adducts formed upon electrooxidation of $TBABBu_4$ in TBAP/AN under various conditions: (A) rigorous exclusion of oxygen during electrolysis; (B) no exclusion of oxygen during electrolysis; (C) saturation with oxygen during electrolysis; (D) computer simulation of a mixture of 68% A and 32% C (cf. spectrum B). Reprinted with permission from J. Am. Chem. Soc. **101**, 3692 (1979), copyright 1979 American Chemical Society.

second component of the mixture spectrum shown in Fig. 4B. Using the hfsc's from the spectra in Figs. 4A and 4C (Table 4), the spectrum shown in Fig. 4D was computer simulated for a mixture of 68% 4A and 32% 4C.

The spectrum in Fig. 4A was assigned to **9** in that authentic **9**, produced by the photolysis of tri-*n*-butylplumbyl acetate (*n*-$Bu_3PbOAc$) in TBAP/AN containing PBN gave rise to a spin adduct that

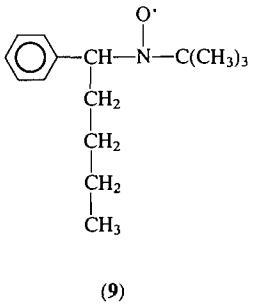

(**9**)

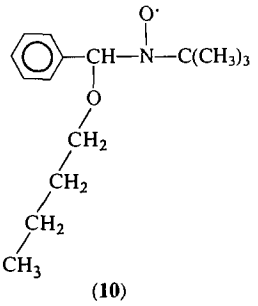

(**10**)

exhibited hfsc's which were identical (Table 4) to those in Fig. 4A (3). The spectrum in Fig. 4C was assigned to **10** (3) on the basis of known reactions of alkyl radicals with $O_2$ (51, 52), the spectral linewidth (1, 48), the *g*-value (1), and the sameness of the hfsc's of this spectrum and those of the *n*-pentyloxy spin adduct of PBN (51). The use of other spin traps was also diagnostic in this study in that the presence of $R—CH_2—CH_2^{\cdot}$ in **9** was established through spin trapping with N*t*B (3).

*Spatially resolved spin trapping in heterogeneous systems*

In cases where spin trapping techniques are to be employed to characterize primary reaction products in heterogeneous electron transfer processes, localization of the spin trap reagent in the interfacial region is desirable. This is true in conventional electrochemical processes involving solid or liquid electrodes, in photoelectrochemical reactions, and in electron transfer processes occurring at membrane/solution interfaces. To this end, methods for localizing spin trap reagents in these interfacial regions have been pursued. Not only must the spin trap be constrained near the interface, but once there, it must retain its facility for trapping radical species and also give rise to well resolved spin adduct spectra.

Progress toward the goal of constraining spin traps at solid/solution interfaces is reflected in the recently reported covalent attachment of HOPBN to silaceous surfaces (15). In that work, cyanuric chloride (CC) was attached to the surface of controlled pore glass beads (eq. [15]):

[15] 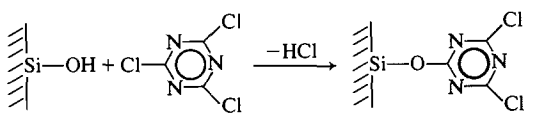

The CC derivatized beads were then reacted with HOPBN to produce the covalently attached nitrone **11**:

TABLE 4. Electron spin resonance hyperfine splitting constants of spin adducts related to $BBu_4^-$ oxidation

| Radical source and experimental conditions[a] | Spin trap[b] | $a_N$ | $a_\beta^H$ | Radical assignment |
|---|---|---|---|---|
| External CPE[c] of $TABABu_4$ (rigorous deoxygenation)[d] | PBN | 14.88 (±0.02)[e] | 3.06 (±0.02)[e] | *n*-Bu· |
| *In situ* CPE of $TABABu_4$ (rigorous deoxygenation)[d] | PBN | 14.88 (±0.02) | 3.05 (±0.02) | *n*-Bu· |
| External CPE of $TABABu_4$ (no deoxygenation)[d] | PBN | 14.88 | 3.05 | *n*-Bu· (68%)[f] |
| | | 13.80 | 2.27 | *n*-BuO· (32%)[f] |
| External CPE of $TABABu_4$ (oxygen saturated)[d] | PBN | 13.80 (±0.02) | 2.27 (±0.02) | *n*-BuO· |
| *In situ* photolysis of $n$-$Bu_3PbOAc$ (rigorous deoxygenation)[g] | PBN | 14.89 (±0.02) | 3.05 (±0.02) | *n*-Bu· |
| *In situ* CPE of $TABABu_4$ (rigorous deoxygenation)[d] | NtB | 15.44 (±0.03) | 10.30 (±0.03)[h] | *n*-Bu· |
| Reaction of 1-bromopropane with $KO_2$ in AN containing 25 m*M* dicyclohexyl-18-crown-6[i] | PBN[j] | 13.83 (±0.01) | 2.27 (±0.01) | *n*-pentyloxy |

[a] In 0.10 *M* TBAP/AN unless otherwise noted; room temperature.
[b] 0.10 *M* unless otherwise noted.
[c] Controlled potential electrolysis.
[d] At platinum electrode poised at +0.40 V vs. SCE.
[e] The hfsc values in G; parentheses contain one standard deviation.
[f] Composition assigned from simulation.
[g] Reference 48.
[h] $a_\gamma^H$ = 0.54 (±0.01) G (2H).
[i] Reference 51.
[j] 50 m*M*.

Reprinted with permission from J. Am. Chem. Soc. **101**, 3692 (1979), copyright 1979 American Chemical Society.

[16]

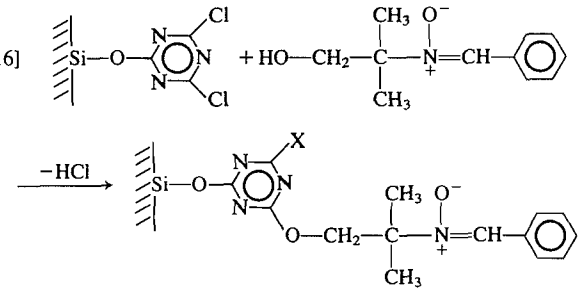


**11**

That **11** functions as a spin trap was demonstrated by its exposure to phenyl radicals arising from the thermal decomposition of phenylazotriphenylmethane (PAT). A dispersion of **11** in deoxygenated benzene containing millimolar PAT afforded the esr spectrum shown in Fig. 5A. This spectrum, recorded after 21 h, increased in intensity over a period of 48 h. Assignment of this spectrum to the spin adduct **12** was made on the basis of agreement

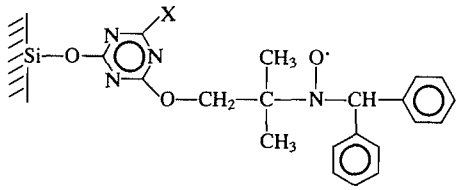


**12**

between the hfsc's measured from Fig. 5A ($a_N$ = 14.56, $a_\beta^H$ = 2.36 G) and those determined from the spectrum of the spin adduct formed by reaction of phenyl radicals (from PAT) with HOPBN in isotropic benzene solution ($a_N$ = 14.54, $a_\beta^H$ = 2.40 G). The absence of a detectable esr signal in the supernatant solution indicated that the spectrum in Fig. 5A was indeed derived from attached nitroxyls only.

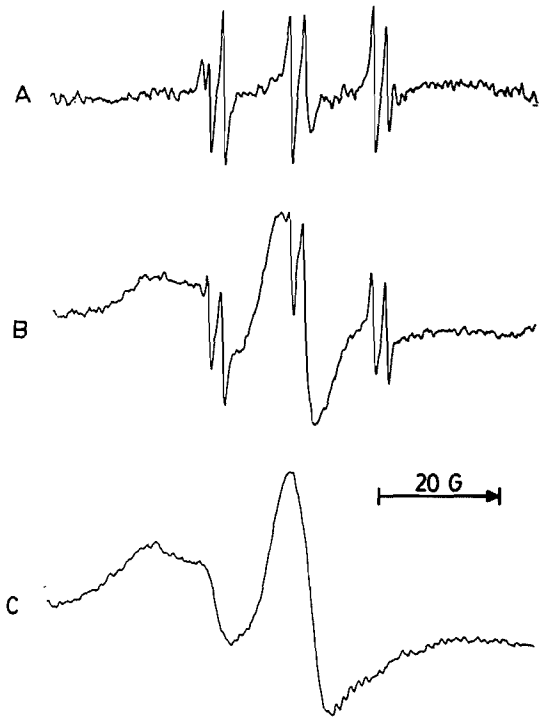


FIG. 5. The esr spectra obtained by contacting benzene solutions of a phenyl radical source (PAT) with HOPBN which had been covalently linked through cyanuric chloride (CC) to glass beads. (A) 5% CC – 5% HOPBN loading exposed to 1 m*M* PAT for 21 h; (B) 5% CC – 5% HOPBN loading exposed to 6 m*M* PAT for 20 h; (C) 30% CC – 30% HOPBN loading exposed to 6 m*M* PAT for 8.5 h. See text for details of glass bead loading. *Reprinted with permission from J. Phys. Chem.* **84**, 557 (1980), copyright 1980 American Chemical Society.

Prolonged exposure (48 h) of the derivatized

Can. J. Chem. Downloaded from www.nrcresearchpress.com by 210.87.254.40 on 09/06/12
For personal use only.

Can. J. Chem. Downloaded from www.nrcresearchpress.com by 210.87.254.40 on 09/06/12
For personal use only.

beads to this millimolar solution of phenyl radical source resulted in the observation of an additional weak, broad resonance. This resonance is the dominant spectral feature observed upon exposure of **11** to higher concentrations of phenyl radical precursor (Fig. 5B). In cases of higher surface loading of **11** and higher PAT concentrations, the sharp spectral features seen in Fig. 5A are lost and only a spectrum which is indicative of a "highly immobilized" nitroxyl species (53) is observed (Fig. 5C). It is significant that under conditions of low surface loading of **11**, where dipolar broadening is minimal (54), immobilized spin traps can give rise to relatively sharp-lined spin adduct spectra which indicate freedom of rotation of the nitroxyl radical about an axis perpendicular to a plane containing the nitroxyl $z$-axis (15, 53).

In addition to the development of a protocol for the localization of spin traps at solid/solution interfaces, recent work in these laboratories has been directed toward the design and evaluation of a spin trap system with which the interfacial regions of membranes and membrane models can be probed. The detection and characterization of radical intermediates arising from heterogeneous electron transfer reactions taking place at membrane/solution interfaces is essential to mechanistic delineation of many physiological processes (55). Inasmuch as the well controlled characterization of membrane/solution interfacial processes involving intact, naturally occurring systems is an experimentally complex problem, several membrane-mimetic systems have been devised for such studies. Principal among these are micelles and vesicles (56, 57). The order imparted to the reaction environment by these membrane models can significantly affect the observed redox properties of substrates resident within the respective microstructures. For example, when 10-methylphenothiazine (MPTH), an analogue of several common membrane-active neuroleptic agents (58), is incorporated into anionic sodium dodecylsulfate (SDS) micelles, its oxidation potential is observed to be 80 mV less anodic than that noted in isotropic aqueous media (59). These results indicate that the product of the electrooxidation, the cation radical ($MPTH^{+\cdot}$), is stabilized by the local microenvironment. Electron spin resonance spectroscopy confirms the interactions between $MPTH^{+\cdot}$ and SDS micelles. In the absence of SDS, the esr spectrum of $MPTH^{+\cdot}$ exhibits the 254 lines shown in Fig. 6A. At SDS concentrations above the critical micelle concentration (CMC), the esr spectrum of $MPTH^{+\cdot}$ is strikingly broadened (Fig. 6B), reflecting the slow tumbling of the $MPTH^{+\cdot}$/micelle aggregate.

Recent work in these laboratories has been

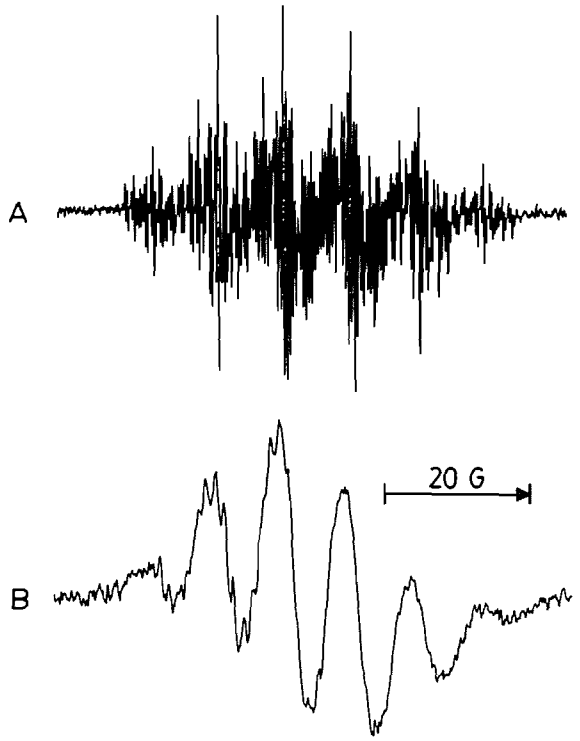


FIG. 6. The esr spectra of $MPTH^{+\cdot}$ in (A) 50 m$M$ $LiClO_4$; (B) 50 m$M$ $LiClO_4$ containing 20 m$M$ SDS.

directed toward the design of spin trapping systems with which transient radical species arising from heterogeneous electron transfer processes at membrane/solution interfaces may be perceived. Radical species produced in such reactions may be generated either on the hydrophobic side of the interface or on the hydrophilic (aqueous) side external to the membrane. Consequently, the ability of the spin trapping apparatus to react efficiently with radicals produced on either side of the interface must be evaluated. To address this question, a nitrone derived spin trap has been synthesized (22) and incorporated into micellar and vesicular systems. The ability of these assemblies to trap radical species produced on either side of the interface has been assessed through the use of the same radical (phenyl) derived from precursors which are resident in either the hydrophobic or in the hydrophilic regions of the ordered systems (17).

The nitrone spin trap which has been designed to be intimately associated with the microstructure of micellar and vesicular systems is the water-insoluble 4-dodecyloxy derivative of PBN, DOPBN (**13**). DOPBN has been found to coassemble with SDS up to a maximum mole ratio of 1:5 DOPBN to SDS. At ratios in excess of 2:5, liquid crystalline phases become evident at room temperature. The SDS/

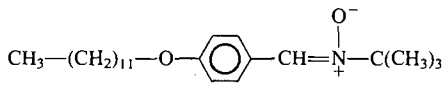

13

DOPBN micelles are quite stable (>1 week) and afford no detectable esr signals. Based on the literature value of the aggregation number of SDS (56), an average micelle consists of approximately 60 SDS and 12 DOPBN entities. The uv absorption maxima of DOPBN indicate that the nitrone functionality resides in a region of the micelle having a micropolarity comparable to that of ethanol ($\lambda_{max}$ (DOPBN/SDS) = 224 nm, $\lambda_{max}$ (DOPBN/pentane) = 210 nm, $\lambda_{max}$ (DOPBN/EtOH) = 223 nm). This is consistent with residence of the nitrone function in the Stern layer (interfacial region) of the micelle (56).

The ability of the interfacially resident nitrone to trap radicals generated within the micelle has been tested by using phenyl radicals produced by the thermal decomposition of PAT. The pronounced hydrophobicity of this molecule together with its micelle-dependent solubilization by SDS in aqueous solution points to its residence in the hydrocarbon region of the SDS/DOPBN aggregate. Phenyl radicals generated from this precursor are indeed trapped by the coassembled DOPBN and give rise to markedly broadened spin adduct spectra typified by that shown in Fig. 7A. Upon addition of an equal volume of AN to this solution, the system order is destroyed and the resulting isotropic solution affords the well resolved spin adduct spectrum shown in Fig. 7B. Generation of the phenyl adduct of DOPBN in an *isotropic* solution of AN/$H_2O$ (50 vol.%) containing SDS, DOPBN, and PAT gives rise to hfsc values (Tables 5) which are equal to those observed in the disrupted micelle solution. Additionally, the authentic phenyl adduct of DOPBN was synthesized by reaction of equimolar amounts of phenyllithium and DOPBN in diethyl ether, followed by air oxidation of the resulting anion to the nitroxyl radical and subsequent solvent exchange (48). Electron spin resonance examination of this radical in AN/$H_2O$ (50% v/v) also affords hfsc values (Table 5) which are in excellent agreement with those noted above. This finding permits assignment of the spectra shown in Fig. 7 to the phenyl adduct of DOPBN.

Addition of a *water-soluble* phenyl radical source to a solution of SDS/DOPBN micelles provides a test for the ability of the interfacially resident nitrone to trap radicals generated external to the micelle. Whereas phenyldiazonium tetrafluoroborate (PDT) is stable in nonaqueous media (60), it has been shown to rapidly decompose in aqueous solution to afford a convenient source of phenyl radicals (12). Addition of PDT to a solution containing SDS/DOPBN micelles gives rise to the esr spectrum shown in Fig. 8A. Again, destruction of the system order through addition of an equal volume of AN affords an isotropic solution whose esr spectrum is shown in Fig. 8B. Identical hfsc values are observed for the spin adduct in this disrupted micelle solution and for the phenyl adduct of DOPBN generated in an *isotropic* solution of PDT, DOPBN, and SDS in 50% aqueous AN (Table 5). These values are also in agreement with those noted for the authentic phenyl adduct of DOPBN prepared by the phenyllithium reaction (*vide supra*). Hence, the spectra shown in Fig. 8 are also assigned to the phenyl adduct of DOPBN.

These results indicate that micelle-resident DOPBN traps phenyl radicals generated both within the micelle and external to that structure. This trapping of radicals produced on either side of the

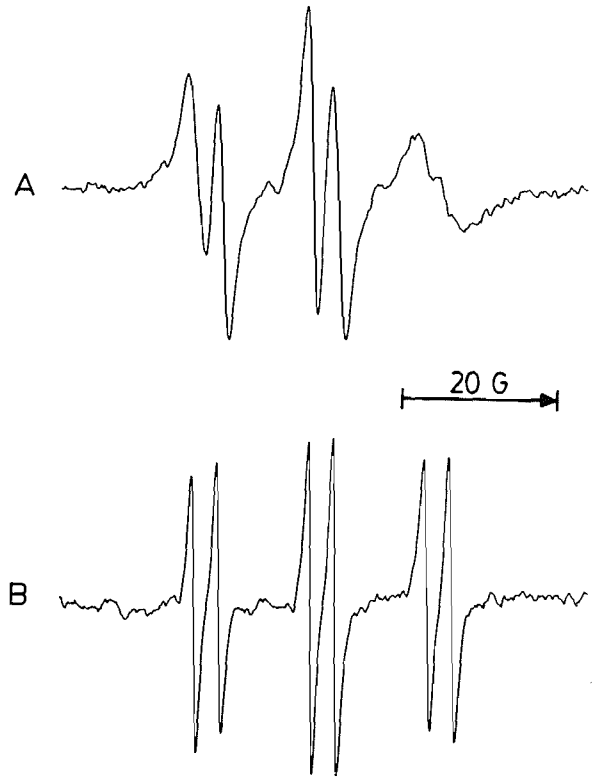


FIG. 7. The esr spectra of phenyl adduct of DOPBN arising from the room temperature thermal decomposition of PAT solubilized within SDS/DOPBN micelles. (A) spectrum observed in a solution of intact SDS/DOPBN micelles; (B) spectrum observed upon disruption of micelles by addition of AN. Reprinted with permission from Biochem. Biophys. Res. Commun. **102**, 1350 (1981), copyright 1981 Academic Press, Inc.

Can. J. Chem. Downloaded from www.nrcresearchpress.com by 210.87.254.40 on 09/06/12
For personal use only.

TABLE 5. Hyperfine splitting constants of phenyl radical adduct of DOPBN formed in micellar and isotropic solutions[a]

| Conditions for spin adduct formation | $a_N$ | $a_\beta^H$ |
|---|---|---|
| SDS/DOPBN micelles,[b] 0.3 m*M* PAT[c] | 15.05 (±0.06)[d] | 3.19 (±0.04)[d] |
| SDS/DOPBN micelles,[b] 1 m*M* PDT[c] | 15.02 (±0.14) | 3.22 (±0.08) |
| 50 m*M* SDS, 10 mM DOPBN, 1 m*M* PAT in 50 vol.% aqueous AN[e] | 15.05 (±0.11) | 3.21 (±0.03) |
| 50 m*M* SDS, 10 mM DOPBN, 1 m*M* PDT in 50 vol.% aqueous AN[e] | 15.06 (±0.05) | 3.23 (±0.05) |
| Reaction of phenyllithium with DOPBN,[f] 50 vol.% aqueous AN | 15.08 (±0.09) | 3.19 (±0.02) |

[a]At room temperature.
[b]Micelles formed from 50 m*M* SDS, 10 m*M* DOPBN, see text.
[c]Radical precursor added to intact micelles; equal volume of AN added after spin adduct formation but before recording of spectrum.
[d]The hfsc values in G; parentheses contain one standard deviation.
[e]Radical precursor added to isotropic solution.
[f]Reaction in diethyl ether followed by air oxidation and solvent exchange (48).

micelle/solution interface further supports residence of the nitrone functionality at that interface. Recent reports, however, suggest that the micelle structure is relatively "open" (61, 62) and consequently the interior of the micelle may be accessible to water-resident species. Additionally, micelle dynamics are rapid (56, 63) and provide ample opportunity for the micelle solubilized trap to interact with both solution-resident and micelle-resident radical species. Given the dynamic nature of micelle aggregates and the possible penetration of aqueous species into their interiors, micelles may be of limited utility as models for the study of interfacial spin trapping processes.

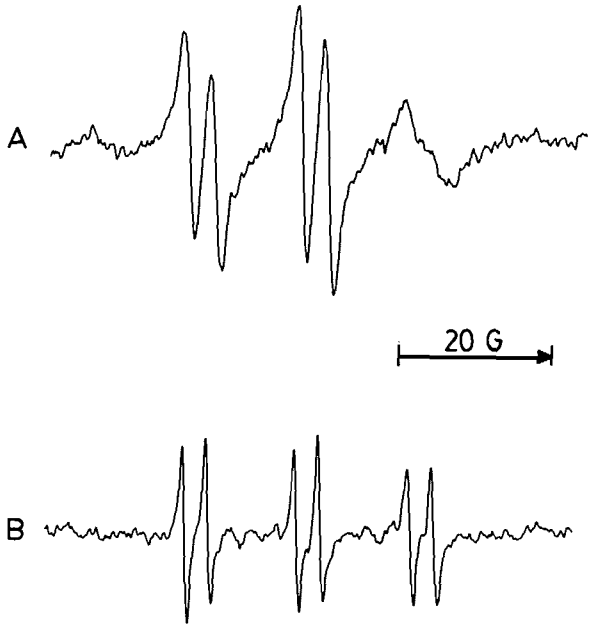


FIG. 8. The esr spectra of phenyl adduct of DOPBN produced by decomposition of PDT in the presence of SDS/DOPBN micelles. (A) spectrum observed in a solution of intact SDS/DOPBN micelles; (B) spectrum observed upon disruption of micelles by the addition of AN.

Vesicles, on the other hand, are ordered systems which are characterized by profoundly longer monomer residence times (hours vs. microseconds) (57) and a more well-defined interface which is less penetrable by aqueous species. DOPBN has been assembled into vesicle structures with dioctadecyldimethylammonium chloride (DODAC) and with lecithin in order to again test the interfacial residency of the nitrone and its bilateral trapping ability in these model membranes.

Water-insoluble PAT is solubilized by DODAC/DOPBN and lecithin/DOPBN vesicles. Thermal decomposition of this phenyl radical precursor in DODAC/DOPBN vesicles gives rise to the extremely broadened esr spectrum shown in Fig. 9A. Addition of an equal volume of $CHCl_3$ results in disruption of the vesicles and extraction of the spin adduct into the $CHCl_3$ phase. Figure 9B shows the esr spectrum of the extracted spin adduct. The authentic phenyl adduct of DOPBN, prepared by the phenyllithium reaction, was examined by esr in $CHCl_3$. The hfsc's of this species, together with those from the spectrum shown in Fig. 9B, are summarized in Table 6. The sameness of these parameters and those derived from the spectrum shown in Fig. 9B permits the assignment of the spin adduct spectra in Fig. 9 to the phenyl adduct of DOPBN. Parallel spin trapping experiments with lecithin/DOPBN vesicles afforded similar results. The hfsc values observed for the $CHCl_3$ extract of the spin adduct formed in lecithin/DOPBN vesicles are given in Table 6. In this case as well, the spin adduct formed from the decomposition of PAT in

Can. J. Chem. Downloaded from www.nrcresearchpress.com by 210.87.254.40 on 09/06/12
For personal use only.

TABLE 6. Hyperfine splitting constants of phenyl radical adduct of DOPBN formed in vesicular and isotropic media[a]

| Conditions for spin adduct formation | $a_N$ | $a^H_\beta$ |
|---|---|---|
| DODAC/DOPBN vesicles,[b] 0.3 m*M* PAT[c] | 14.73 (±0.11)[d] | 2.81 (±0.11)[d] |
| DODAC/DOPBN vesicles,[b] 1 m*M* PDT[c] | 14.77 (±0.11) | 2.70 (±0.07) |
| Lecithin/DOPBN vesicles,[e] 0.3 m*M* PAT[c] | 14.76 (±0.10) | 2.75 (±0.08) |
| Lecithin/DOPBN vesicles,[e] 1 m*M* PDT[c] | 14.77 (±0.10) | 2.75 (±0.03) |
| Reaction of phenyllithium with DOPBN,[f] $CHCl_3$ | 14.70 (±0.05) | 2.73 (±0.05) |

[a]At room temperature.
[b]Vesicles formed from 10 m*M* DODAC, 1 m*M* DOPBN.
[c]Radical precursor added to intact vesicles; extraction with equal volume of $CHCl_3$ after spin adduct formation but before recording of spectrum.
[d]The hfsc values in G; parentheses contain one standard deviation.
[e]Vesicles formed from 10 mg/mL lecithin, 1 m*M* DOPBN, 0.10 *M* NaCl.
[f]Reaction in diethyl ether followed by air oxidation and solvent exchange (48).

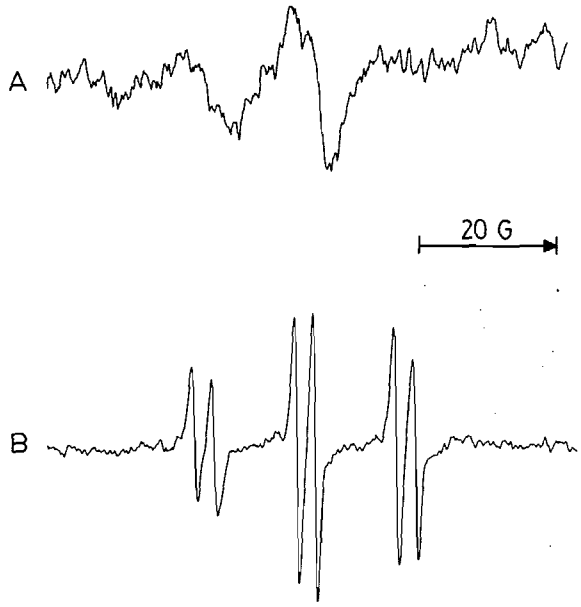


FIG. 9. The esr spectra of phenyl adduct of DOPBN formed by the room temperature thermal decomposition of PAT solubilized within DODAC/DOPBN vesicles. (A) spectrum observed in a solution of intact DODAC/DOPBN vesicles; (B) spectrum of $CHCl_3$ extract of A. Reprinted with permission from Biochem. Biophys. Res. Commun. **102**, 1350 (1981), copyright 1981 Academic Press, Inc.

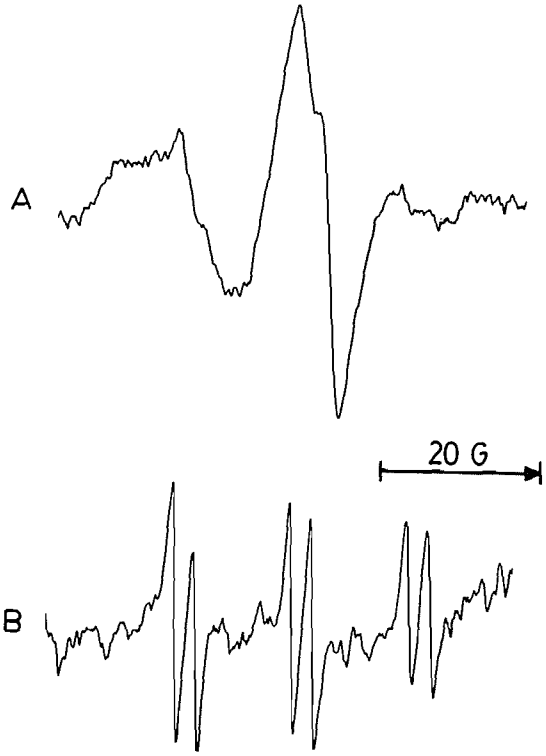


FIG. 10. The esr spectra of phenyl adduct of DOPBN arising from the decomposition of PDT in the presence of DODAC/DOPBN vesicles. (A) spectrum observed in a solution of intact DODAC/DOPBN vesicles; (B) spectrum of $CHCl_3$ extract of A.

the hydrophobic region of the bilayer is the phenyl adduct of DOPBN.

The addition of water-soluble PDT to DODAC/DOPBN vesicle preparations affords broad esr spectra typified by that shown in Fig. 10A. Extraction of the spin adduct/vesicle solution with an equal volume of $CHCl_3$ and subsequent esr examination of the $CHCl_3$ solution gives rise to the spectrum shown in Fig. 10B. The hfsc values derived from this spectrum are identical to those of the authentically prepared phenyl adduct of DOPBN described above (Table 6) and permit assignment of the spectra in Fig. 10 to the phenyl adduct of DOPBN. The same sequence of experiments carried out in lecithin/DOPBN vesicles gives rise to analogous results. Once again, the esr spectrum of the $CHCl_3$ extract of the spin adduct formed from reaction of the lecithin/DOPBN vesicles with phenyl radicals derived from the non-vesicle resident PDT indicates formation of the phenyl adduct of DOPBN.

The results obtained in DODAC/DOPBN and lecithin/DOPBN vesicles show that DOPBN traps phenyl radicals which have been generated on either side of the membrane/solution interface.

Can. J. Chem. Downloaded from www.nrcresearchpress.com by 210.87.254.40 on 09/06/12
For personal use only.

This bilateral trapping ability of DOPBN in these systems where monomer exchange rates and interfacial penetration by the aqeuous solution are minimal is consistent with residence of the nitrone functionality at the membrane/solution interface. Moreover, the results obtained in these vesicle systems lend credence to the validity of the interfacial description of the spin trapping processes observed in micelles (*vide supra*). In sum, these experimental findings in micelle and vesicle systems suggest that spatially resolved spin trapping can be profitably employed for the detection and characterization of radical species arising from heterogeneous electron transfer processes at membrane/solution interfaces.

## Acknowledgments

This work was supported in part by the University of Delaware Research Foundation, the University of Delaware Institute of Neuroscience (NIH Biomedical VII), the National Science Foundation (CHE-7803312), and the Natural Sciences and Engineering Research Council of Canada (AM-08397).

1. E. G. JANZEN. Acc. Chem. Res. **4**, 31 (1971).
2. C. LAGERCRANTZ. J. Phys. Chem. **75**, 3466 (1971).
3. E. E. BANCROFT, H. N. BLOUNT, and E. G. JANZEN. J. Am. Chem. Soc. **101**, 3692 (1979).
4. P. H. KASAI and D. MCLEOD. J. Phys. Chem. **82**, 619 (1978).
5. E. G. JANZEN, R. L. DUDLEY, E. R. DAVIS, and C. A. EVANS. J. Phys. Chem. **82**, 2445 (1978).
6. E. G. JANZEN, H. J. STRONKS, D. E. NUTTER, JR., E. R. DAVIS, H. N. BLOUNT, J. L. POYER, and P. B. MCCAY. Can. J. Chem. **58**, 1596 (1980).
7. B. KRAEUTLER, C. D. JAEGER, and A. J. BARD. J. Am. Chem. Soc. **100**, 4903 (1978).
8. C. D. JAEGER and A. J. BARD. J. Phys. Chem. **83**, 3146 (1979).
9. M. L. HAIR and J. R. HARBOUR. Adv. Chem. Ser. **184**, 173 (1980).
10. A. J. BARD, J. C. GILBERT, and R. D. GOODIN. J. Am. Chem. Soc. **96**, 620 (1974).
11. G. J. GORES, C. E. KOEPPE, and D. E. BARTAK. J. Org. Chem. **44**, 380 (1979).
12. J. F. GAUDIELLO, D. LARKIN, J. D. FAWN, J. J. SOSNOWSKI, E. E. BANCROFT, and H. N. BLOUNT. J. Electroanal. Chem. **131**, 203 (1982).
13. G. L. MCINTIRE, H. N. BLOUNT, H. J. STRONKS, R. V. SHETTY, and E. G. JANZEN. J. Phys. Chem. **84**, 916 (1980).
14. C. A. EVANS. Aldrichimica Acta, **12**, 23 (1979).
15. E. E. BANCROFT, H. N. BLOUNT, and E. G. JANZEN. J. Phys. Chem. **84**, 557 (1980).
16. G. L. MCINTIRE and H. N. BLOUNT. To be published.
17. T. H. WALTER, G. L. MCINTIRE, E. E. BANCROFT, E. R. DAVIS, L. M. GIERASCH, and H. N. BLOUNT. Biochem. Biophys. Res. Commun. **102**, 1350 (1981).
18. J. F. EVANS and H. N. BLOUNT. Anal. Lett. **7**, 445 (1974).
19. D. T. SHANG and H. N. BLOUNT. J. Electroanal. Chem. **54**, 305 (1974).
20. J. F. EVANS and H. N. BLOUNT. J. Org. Chem. **41**, 516 (1976).
21. J. F. EVANS. Ph.D. Dissertation, The University of Delaware. 1977.
22. E. G. JANZEN, R. V. SHETTY, and G. L. COULTER. To be published.
23. G. L. MCINTIRE and H. N. BLOUNT. *In* Solution behavior of surfactants: theoretical and applied aspects. *Edited by* K. L. Mittal and E. J. Fendler. Plenum Press, New York. 1982.
24. Y. Y. LIM and J. H. FENDLER. J. Am. Chem. Soc. **101**, 4023 (1979).
25. W. S. SINGLETON, M. S. GRAY, M. L. BROWN, and J. L. WHITE. J. Am. Oil Chem. Soc. **42**, 53 (1965).
26. E. B. STARKEY. Org. Synth. Coll. Vol. II. Wiley, New York. 1943. p. 225.
27. A. R. FORRESTER and S. P. HEPBURN. J. Chem. Soc. C, 701 (1971).
28. S. W. MAO and L. KEVAN. J. Phys. Chem. **80**, 2330 (1976).
29. G. CAUQUIS and G. PIERRE. Bull. Soc. Chim. Fr. 997 (1975).
30. G. CAUQUIS and G. PIERRE. Bull. Soc. Chim. Fr. 736 (1976).
31. R. G. PEARSON (*Editor*). Hard and soft acids and bases. Dowden, Hutchinson, and Ross, Inc., Stroudsburg, PA. 1973.
32. R. PEREIRO, A. J. ARVIA, and A. J. CALANDRA. Electrochim. Acta, **17**, 1723 (1972).
33. J. F. EVANS and H. N. BLOUNT. J. Phys. Chem. **80**, 1011 (1976).
34. H. J. STRONKS. M.Sc. Thesis, The University of Guelph. 1980.
35. L. SERENO, V. A. MACAGNO, and M. C. GIORDANO. Electrochim. Acta, **17**, 561 (1972).
36. A. FRUMKIN and G. TEDORADSE. Z. Elektrochem. **62**, 251 (1957).
37. E. G. JANZEN, B. R. KNAUER, L. T. WILLIAMS, and W. B. HARRISON. J. Phys. Chem. **74**, 3025 (1970).
38. D. REHOREK, P. THOMAS, and H. HENNIG. Inorg. Chim. Acta, **32**, L1 (1979).
39. D. REHOREK and H. HENNIG. Z. Chem. **19**, 263 (1979).
40. S. G. MAIRANOVSKII. Dokl. Akad. Nauk S.S.S.R. **110**, 593 (1956).
41. S. G. MAIRANOVSKII. Dokl. Akad. Nauk S.S.S.R. **114**, 1272 (1957).
42. J. KOUTECKY and V. HANUS. Collect. Czech. Chem. Commun. **20**, 124 (1955).
43. K. YASUKOUCHI, I. TANIGUCHI, H. YAMAGUCHI, and M. SHIRAISHI. J. Electroanal. Chem. **105**, 403 (1979).
44. E. G. JANZEN, D. E. NUTTER, JR., E. R. DAVIS, B. J. BLACKBURN, J. L. POYER, and P. B. MCCAY. Can. J. Chem. **56**, 2237 (1978).
45. C. A. EVANS. Ph.D. Dissertation, The University of Georgia. 1974.
46. E. G. JANZEN, R. L. DUDLEY, and R. V. SHETTY. J. Am. Chem. Soc. **101**, 243 (1979).
47. D. E. NUTTER, JR. Ph.D. Dissertation, The University of Georgia. 1974.
48. E. G. JANZEN and B. J. BLACKBURN. J. Am. Chem. Soc. **91**, 4481 (1969).
49. M. M. BAIZER (*Editor*). Organic electrochemistry. Marcel Dekker, Inc., New York. 1973.
50. A. J. BARD and L. R. FAULKNER. Electrochemical methods. John Wiley and Sons, New York. 1980.
51. M. V. MERRITT and R. A. JOHNSON. J. Am. Chem. Soc. **99**, 3713 (1977).
52. J. A. HOWARD and J. C. TAIT. Can. J. Chem. **56**, 176 (1978).

Can. J. Chem. Downloaded from www.nrcresearchpress.com by 210.87.254.40 on 09/06/12
For personal use only.

53. O. H. GRIFFITH and P. C. JOST. *In* Spin labeling. *Edited by* L. G. Berliner. Academic Press, New York. 1976. p. 453.
54. L. D. HALL and J. C. WATERTON. J. Am. Chem. Soc. **101**, 3697 (1979).
55. W. A. PRYOR. *In* Free radicals in biology. Vol. I. *Edited by* W. A. Pryor. Academic Press, New York. 1976. p. 1.
56. J. H. FENDLER and E. J. FENDLER. Catalysis in micellar and macromolecular systems. Academic Press, New York. 1975.
57. J. H. FENDLER. Acc. Chem. Res. **13**, 7 (1980).
58. E. USDIN and I. S. FORREST (*Editors*). Psychotherapeutic drugs, Part II. Marcel Dekker, Inc., New York. 1977. Chapts. 1–3.
59. G. L. MCINTIRE and H. N. BLOUNT. J. Am. Chem. Soc. **101**, 7720 (1979).
60. R. D. GOODIN. Ph.D. Dissertation, The University of Texas at Austin. 1975.
61. F. M. MENGER. Acc. Chem. Res. **12**, 111 (1979).
62. J. C. RUSSELL and D. G. WHITTEN. J. Am. Chem. Soc. **103**, 3219 (1981).
63. H. HOFFMANN. Ber. Bunsenges. Phys. Chem. **82**, 988 (1978).

Can. J. Chem. Downloaded from www.nrcresearchpress.com by 210.87.254.40 on 09/06/12
For personal use only.

REVIEW/SYNTHÈSE

# Biosynthetic studies using $^{18}O$ isotope shifts in $^{13}C$ nuclear magnetic resonance[1,2]

JOHN C. VEDERAS

*Department of Chemistry, University of Alberta, Edmonton, Alta., Canada T6G 2G2*

Received January 8, 1982

JOHN C. VEDERAS. Can. J. Chem. **60**, 1637 (1982).

Isotopic substitution with oxygen-18 induces an observable upfield shift in the $^{13}C$ nmr positions of directly-attached carbons, and in some cases, β-carbons. The magnitudes of these shifts range from about 0.05 ppm to 0.01 ppm, and are dependent on structure in an empirically predictable fashion. Incorporation of doubly labeled ($^{13}C$, $^{18}O$) precursors into polyketides followed by $^{13}C$ nmr analysis can identify carbon–oxygen bonds remaining intact during microbial biosynthesis. This technique has been applied to studies on antibiotics such as brefeldin A, cytochalasin B, granaticin, and lasalocid A, as well as aflatoxin precursors such as averufin, versicolorin A, and sterigmatocystin.

JOHN C. VEDERAS. Can. J. Chem. **60**, 1637 (1982).

La substitution isotopique par de l'oxygène-18 induit, en rmn du $^{13}C$, un déplacement chimique observable vers les hauts champs des positions des atomes de carbone qui leur sont directement liés et, dans certains cas, des déplacements des atomes de carbone en position β. L'ordre de grandeur de ces déplacements varie de 0,05 ppm à 0,01 ppm et ils dépendent d'une façon empirique de la structure. L'incorporation de précurseurs doublement marqués ($^{13}C$, $^{18}O$) dans les polycétides suivie d'une analyse par rmn du $^{13}C$ permet d'identifier les liaisons carbone–oxygène qui demeurent intactes durant la synthèse microbienne. On a utilisé cette technique pour étudier les antibiotiques tels la brefeldine A, la cytochalasine B, la granaticine et la lasalocide A de même que des précurseurs d'aflatoxine tels que l'avérufine, la versicolorine A et la stérigmatocystine.

[Traduit par le journal]

During the last decade the development of $^{13}C$ nmr techniques in biosynthesis has elucidated the arrangement of precursor units in carbon skeletons of most classes of secondary metabolites (1). However, the mechanisms and sequence by which these units are linked remain largely speculative, partly because of lack of methods to follow changes in intermediate oxidation states. In response there is a growing interest in determination of the biosynthetic fate of precursor hydrogens using $^{2}H$ nmr (2) and of oxygens using mass spectrometry (3, 4). The latter technique can detect both commonly-employed stable isotopes of oxygen, $^{17}O$ and $^{18}O$, but ascertaining the exact structure of the mass spectrometric fragments in partially-labeled polyoxygenated molecules is often difficult. Frequently preliminary specific labeling experiments or chemical degradations are necessary (4). Unlike $^{16}O$ and $^{18}O$, oxygen-17 has a nuclear spin (5/2) and can be observed directly by nmr. Unfortunately its use in biological studies (5, 6) has been limited by low natural abundance (0.037%) and consequent expense, as well as by broadness of nmr signals due to its quadrupole and spin–spin coupling.

Recently, investigations by Boyer and co-workers (7), Risley and Van Etten (8), Darensbourg *et al.* (9), and our group (10) have confirmed the theoretical prediction (11) that the more abundant oxygen-18 (0.204%) can be indirectly detected by changes induced in the $^{13}C$ nmr chemical shifts of directly-attached carbon atoms. For example, propyl cyclohexane carboxylate **1** labelled with $^{18}O$ in the ether oxygen exerts moderate isotope shifts at both adjacent carbons (Fig. 1) and a much smaller one (0.005 ppm) at the β-carbon of the propyl group (10). The magnitudes of these shifts are governed by structure in an empirically predictable way and display almost no solvent dependence except for [$^{18}O$] alcohols (8, 10). Generally, single-bonded oxygens show smaller effects (approx. 0.035 to 0.010 ppm) than doubly bonded oxygens (approx. 0.055 to 0.030 ppm). For carbonyl compounds the shifts decrease in the order: ketones ≥ aldehydes ≥ esters ≥ amides, while for alcohols the order is: tertiary ≥ secondary ≥ primary ≥ phenols (8, 10). Other noticeable trends include direct additivity of shift magnitudes at both α and β carbons upon multiple $^{18}O$ substitution, and reduction of the effect due to conjugation or electron donation through a π system. Since this technique can directly determine the location and extent of $^{18}O$ labeling in organic molecules, it has already seen interesting applications in study of

[1]Dedicated to Professor George H. Büchi (Massachusetts Institute of Technology).

[2]Presented at the 28th Congress of the International Union of Pure and Applied Chemistry, Vancouver, British Columbia, August 1981.

0008-4042/82/131637-06$01.00/0

©1982 National Research Council of Canada/Conseil national de recherches du Canada

Can. J. Chem. Downloaded from www.nrcresearchpress.com by 210.87.254.40 on 09/06/12
For personal use only.

Can. J. Chem. Downloaded from www.nrcresearchpress.com by 210.87.254.40 on 09/06/12
For personal use only.

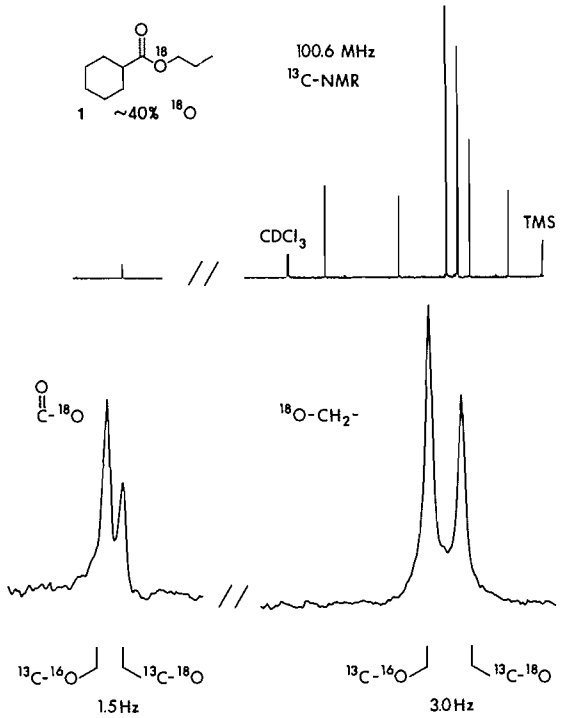


FIG. 1. 100.6 MHZ $^{13}C$ nmr spectra of propyl [$^{18}O$]cyclohexane carboxylate **1** (isotopic purity: 40% $^{18}O$; natural abundance $^{13}C$) with expansions of signals for carbons attached to oxygen (1.0 Hz=0.01 ppm) (10).

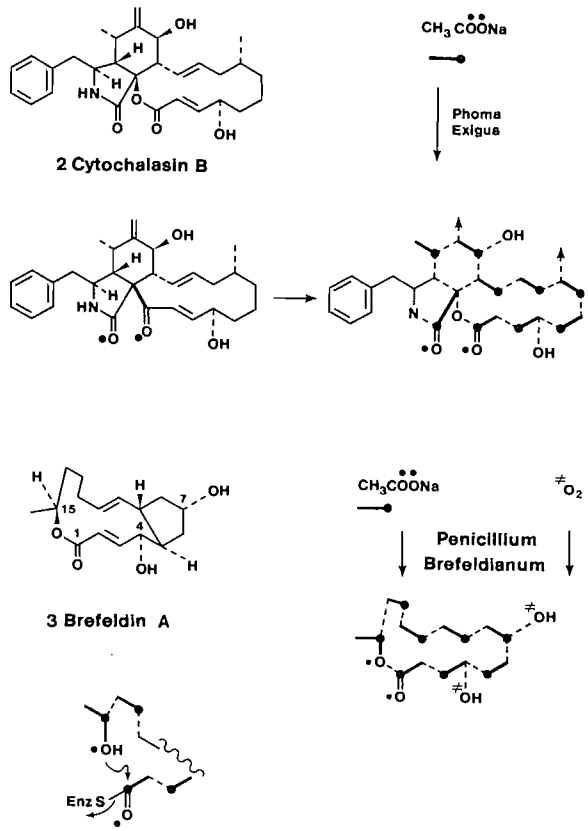


FIG. 2. Incorporation of sodium [1-$^{13}C$, $^{18}O_2$]acetate into cytochalasin B **2** and brefeldin A **3**.

chemical mechanism (9, 12). Obviously the methodology also promises to be a valuable tool for probing a variety of biological mechanisms, including those of polyketide biosynthesis.

Among the fungal secondary metabolites we examined in our early work were cytochalasin B **2**, an important tool in cell biology (13), and the structurally-related antibiotic brefeldin A **3** (14).[3] The highly functionalized macrocyclic rings of both of these compounds originate by head to tail coupling of acetate units (Fig. 2) (13, 15, 16). In considering possible biogenetic intermediates, a key question is whether the functionality is introduced by aerobic oxidation of a saturated precursor resulting from normal fatty acid biosynthesis, or whether it arises from incomplete reduction during assembly of the acetate chain.

Earlier mass spectrometric studies on several metabolites had already demonstrated that $^{18}O$ labeling could provide the answer if the location and extent of isotopic oxygen could be determined (4, 17). However, this type of analysis has often required extensive work to identify the mass spectral fragments. Incorporation[3] of doubly labeled sodium [1-$^{13}C$, $^{18}O_2$]acetate into brefeldin A **3** by *Penicillium brefeldianum* followed by $^{13}C$ nmr analysis confirmed Hutchinson's previous results (4) that only the two lactone oxygens were labeled. The observation of a single $^{18}O$ isotope shift at C-1 for the doubly-bonded oxygen as well as a shift at C-15 due to the bridging oxygen shows that these two carbon–oxygen bonds originate from acetate during biosynthesis, and that lactone formation involves attack by the oxygen at C-15 on the carbonyl (C-1). Since the natural abundance of $^{13}C$ is low (1.1%) and the likelihood that two neighboring acetate units will both be labeled within the same molecule is small in a typical incorporation experiment, doubly-labeled [$^{13}C$, $^{18}O$] precursors allow detection of intact carbon–oxygen bonds. This is true even in cases like brefeldin A **3** where the labeled oxygen bridges via a newly-formed bond to a carbon which is likely to be $^{13}C$-labeled in another molecule. Analogous incorporation of sodium [1-$^{13}C$, $^{18}O_2$]acetate into cytochalasin B **2** and $^{13}C$ nmr spectral examination demonstrated that only the two doubly-bonded oxygens were labelled (18). The lack of label in the singly-bonded lactone

[3]Brefeldin A was studied in collaboration with Prof. C. R. Hutchinson, School of Pharmacy, University of Wisconsin.

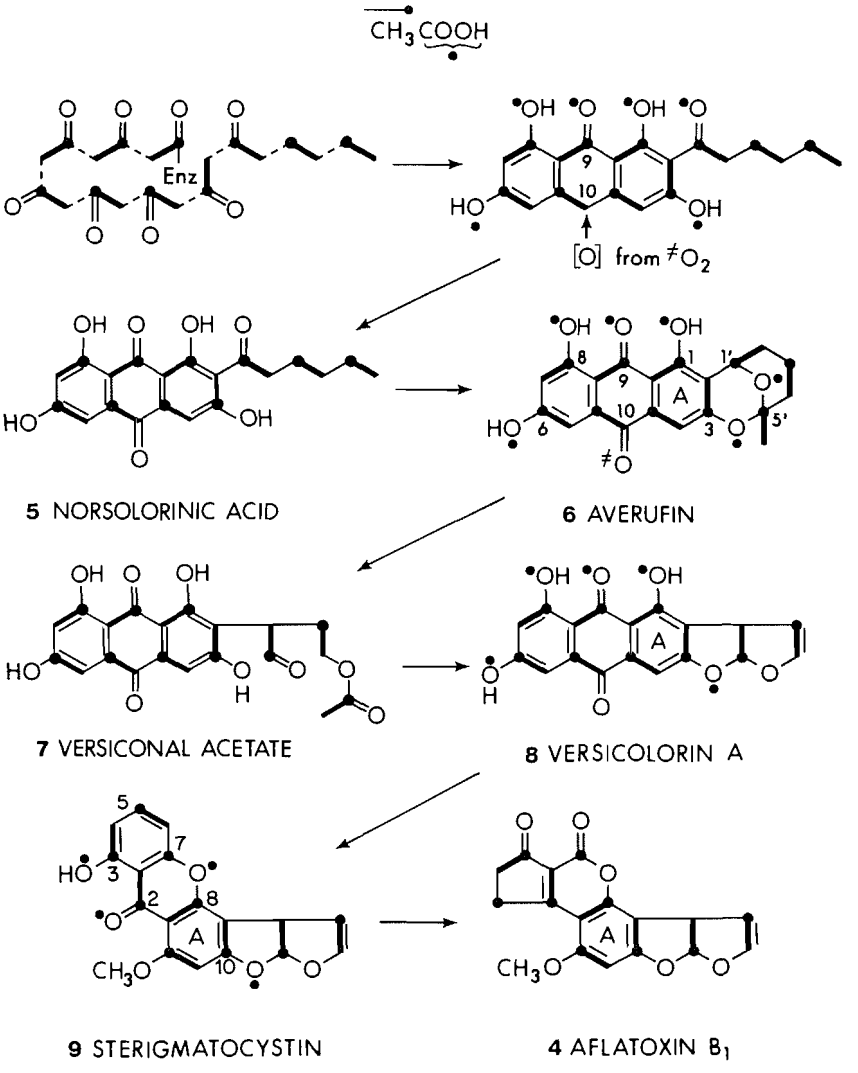


FIG. 3. Biosynthetic sequence to aflatoxin $B_1$ 4.

oxygen agrees with earlier work (19) indicating that, in contrast to brefeldin A **3**, this macrolide ring originates via a biological Baeyer–Villiger oxidation (20) of a ketonic precursor.

Aflatoxin $B_1$ **4** and related compounds which possess a bis-dihydrofuran moiety fused onto an aromatic ring are toxic hepatocarcinogens produced by fungi (usually *Aspergillus*) which frequently contaminate food products (21). Extensive investigation by various research groups has elucidated the arrangement of acetate carbons in most of these compounds and has suggested a fascinating biosynthetic pathway: acetate → norsolorinic acid **5** → averufin **6** → versiconal acetate **7** → versicolorin A **8** → sterigmatocystin **9** → aflatoxin $B_1$ **4** (Fig. 3) (21). Recent pulse labeling experiments indicate that an alternative route to aflatoxin may also be present which does not have sterigmatocystin **9** as an obligatory precursor (22). Since oxygen labeling patterns in such highly oxidized metabolites are not easily analyzed by mass spectrometry, the $^{13}C$ nmr isotope shift method seemed especially useful for obtaining mechanistic insights.

In our first study (23) a mutant of *Aspergillus parasiticus* blocked in aflatoxin formation was used to incorporate sodium [1-$^{13}C$, $^{18}O_2$]acetate into averufin **6**. All of the anthraquinone carbons bearing oxygen showed isotope shifts except the carbonyl at C-10. A separate fermentation with [$^{18}O$] oxygen gas and an unlabeled carbon source produced averufin **6** containing isotopic oxygen only at that carbonyl. Our findings support the hypothesis that intramolecular aldol reactions in the polyketonic chain are followed by enolizatons to gener-

Can. J. Chem. Downloaded from www.nrcresearchpress.com by 210.87.254.40 on 09/06/12
For personal use only.

Can. J. Chem. Downloaded from www.nrcresearchpress.com by 210.87.254.40 on 09/06/12
For personal use only.

ate an anthrone which is then aerobically oxidized to an anthraquinone. The acetal carbon at C-5′ had a very low intensity isotope-shifted peak in the acetate feeding experiment due to the small proportion of molecules which were intramolecularly dilabeled at C-5′ ($^{13}C$ only) as well as at C-3 or C-1′ ($^{13}C$ and $^{18}O$). Although these experiments cannot determine the source of oxygen presumably present at C-5′ prior to acetal formation, the apparent intermediacy of norsolorinic acid **5** and averantin (22, 24) implies complete reduction of the first two carbonyls during assembly of the polyketide chain and subsequent aerobic oxidation at C-5′ just before averufin **6** formation.

Preliminary results on the relatively insoluble pigment versicolorin A **8** produced by another blocked mutant of *A. parasiticus* indicate that the anthraquinone oxygens are labeled as would be predicted by biosynthesis from averufin **6** (Fig. 3). The oxygen in the terminal dihydrofuran ring probably originates from the aqueous medium since no $^{18}O$ could be detected by $^{13}C$ nmr examination of the adjacent carbon after incorporation of [$^{18}O$] acetate or [$^{18}O$] oxygen gas. This is not unexpected in view of the intermediacy of versiconal acetate 7 (21, 25) which can easily exchange the aldehyde oxygen.

In order to determine the source of oxygens in sterigmatocystin **9**, sodium [1-$^{13}C$, $^{18}O_2$]acetate was fed to *A. versicolor*, a species which produces many of the same aflatoxin precursors as *A. parasiticus* (21, 22). However, the normal proton decoupled $^{13}C$ nmr spectra of this toxin gave signals which were complex patterns due to long range carbon–carbon couplings resulting from multiple intramolecular precursor incorporation. Although these complex patterns initially obscured the small $^{18}O$ isotope shifts, we have recently been able to resolve the uncoupled singlets from the superimposed doublets using spin echo Fourier transform techniques (26).[4] Presence of [$^{18}O$] acetate-derived oxygens could be detected by isotope shifts at C-1, C-3, C-8, and C-10 of sterigmatocystin **9**. Xanthone ring formation must therefore proceed by attack of the oxygen at C-8 on the C-7 position, probably via an addition–elimination process (27) on an unsymmetrical intermediate since the carbon labeling pattern in the phenolic ring is unscrambled (21, 28). Lack of $^{18}O$ label at C-12 is in accord with probable aerobic cleavage of the anthraquinone ring of a versicolorin A type precursor, but the absence of any oxygen functionality at C-5 of sterigmatocystin **9** remains unexpected.

[4]Descriptions of spin echo resolution of $^{18}O$ isotope shifts in $^{13}C$ nmr have been published (36, 37).

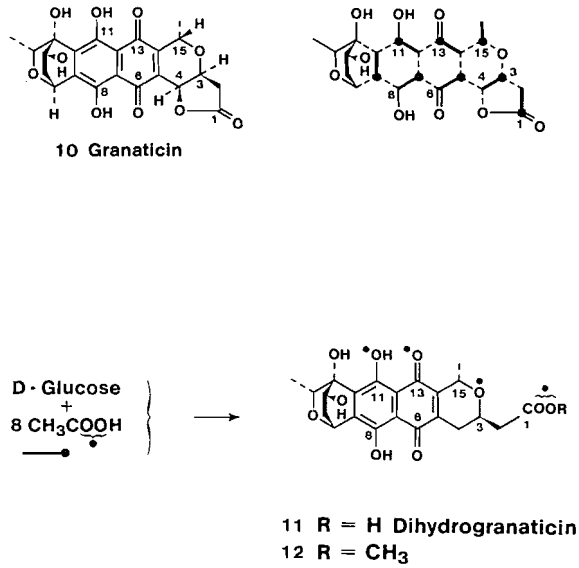


FIG. 4. Biosynthesis of granaticin **10** and dihydrogranaticin **11** from sodium [1-$^{13}C$, $^{18}O_2$]acetate.

A separate study[5] centers on granaticin **10**, an antitumor antibiotic from *Streptomyces violaceoruber*. Its carbon skeleton originates from acetate and glucose, and it often occurs with dihydrogranaticin **11** which can be converted to it by cell free extracts of the producing organism (Fig. 4) (29). Incorporation of sodium [1-$^{13}C$, $^{18}O_2$]acetate into **10** was followed by chemical conversion to dihydrogranaticin methyl ester **12** and $^{13}C$ nmr analysis. Preliminary results indicate that acetate-derived oxygens are retained at C-1, C-3, C-11, and probably C-13. Observation of an isotope shift at C-3 but not at C-15 demonstrates that the C-3 carbon–oxygen bond is preserved during closure of the dihydropyran ring. Additional work is in progress to also determine the mechanism of lactone formation in granaticin **10**.

Since the construction of macrolide and polyether antibiotics is thought to be similar to that of fatty acids and polyaromatics (30), we[6] investigated the biosynthesis of lasalocid A **13** (Fig. 5) (31). Lasalocid A **13** (also known as X537A) is an ionophoric antibiotic (32) from *Streptomyces lasaliensis* which is effective against certain poultry infections (33). The carbon skeleton had already been shown to be assembled from acetate, propionate, and butyrate units (34). Three plausible biosynthetic mechanisms could account for the oxygen substituents and the overall stereochem-

[5]Granaticin is being studied in collaboration with Prof. H. G. Floss, School of Pharmacy, Purdue University.

[6]Lasalocid A was investigated in collaboration with Prof. C. R. Hutchinson, University of Wisconsin.

Can. J. Chem. Downloaded from www.nrcresearchpress.com by 210.87.254.40 on 09/06/12
For personal use only.

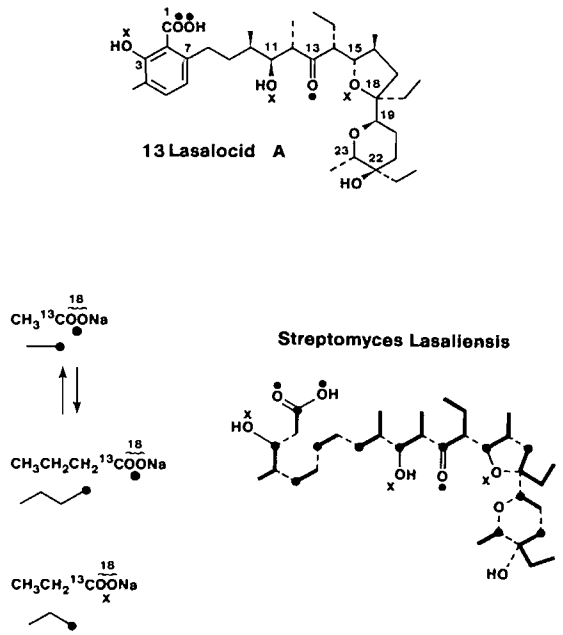


FIG. 5. Incorporation of sodium [1-$^{13}$C, $^{18}O_2$]propionate and [1-$^{13}$C, $^{18}O_2$]butyrate into lasalocid A **13**.

istry: divergent stereospecific fatty-acid type condensations and partial reductions of the growing chain to produce the observed functionality; condensation–reduction followed by dehydration and stereospecific rehydration of the resulting enones; or multistep reduction to a deoxygenated chain followed by stereospecific aerobic oxidation. In principle each of the fatty acid units could be transformed to the appropriate oxidation state and stereochemistry by one of these three sequences. Separate incorporations of sodium [1-$^{13}$C, $^{18}O_2$]-propionate and [1-$^{13}$C, $^{18}O_2$]butyrate (which is biologically also converted to [1-$^{13}$C, $^{18}O_2$]acetate) produced labeled lasalocid A **13** samples. Direct $^{13}$C nmr analysis proved fruitless because of peak broadening, probably due to intramolecular hydrogen bonding (10), but chemical derivatization of the hydroxyls permitted resolution of the isotope shifts. Propionate-derived oxygen was found attached to C-3, C-11, and C-15, while butyrate (and acetate) oxygen was detected at C-1 and C-13. The results clearly exclude the latter two of the three mechanisms proposed for oxygen origin and stereochemistry for the C-1 to C-15 portion of the lasalocid A chain. Absence of oxygen labeling in the rest of the chain supports the biosynthetic proposal by Westley *et al.* (34) shown in Fig. 6.

Elegant biosynthetic applications of the $^{18}$O isotope shift in $^{13}$C nmr have recently been reported by Cane *et al.* on monensin and erythromycins A and B (35) and by Sankawa *et al.* on

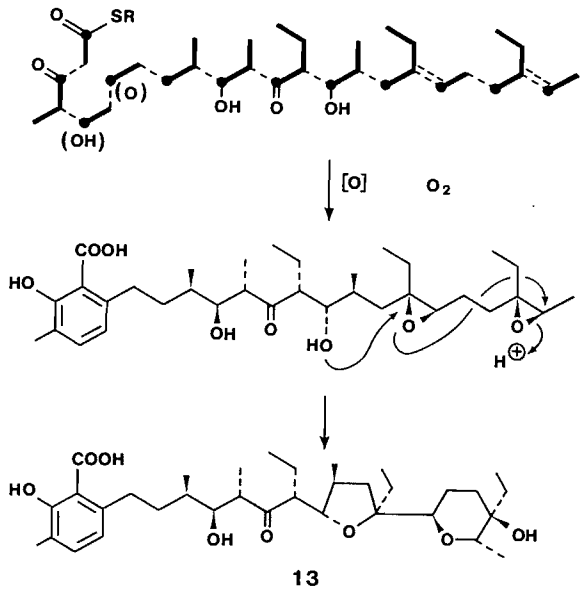


FIG. 6. Proposed biosynthetic sequence to lasalocid A **13** (34).

citrinin (6). It is not unlikely that further uses of this technique with more advanced [$^{18}$O] precursors will aid in understanding the detailed chemistry of complex biological transformations (36).

## Acknowledgements

The author gratefully acknowledges the research of his collaborators and co-workers whose names appear in the footnotes and references. Reference samples and fungal strains for mycotoxin work were donated by Dr. P. S. Steyn (Council for Scientific and Industrial Research, Pretoria, South Africa), Dr. C. A. Townsend (Chemistry Department, Johns Hopkins University), and Dr. D. T. Wicklow (Northern Regional Research Laboratory, U. S. Department of Agriculture). The Stable Isotopes Resource of Los Alamos National Laboratory sent generous gifts of [$^{18}$O] water and oxygen gas, and the Natural Sciences and Engineering Research Council of Canada provided financial support.

1. F. W. WEHRLI and T. NISHIDA. Prog. Chem. Org. Nat. Prod. **36**, 1 (1979).
2. M. J. GARSON and J. STAUNTON. Chem. Soc. Rev. 539 (1979).
3. E. R. KLEIN and P. D. KLEIN. Biomed. Mass Spectrom. **5**, 425 (1978).
4. C. T. MABUNI, L. GARLASCHELLI, R. A. ELLISON, and C. R. HUTCHINSON. J. Am. Chem. Soc. **101**, 707 (1979); I. BJORKHEM AND A. LEWENHAUPT. J. Biol. Chem. **254**, 5252 (1979).
5. K. D. ROSE and R. G. BRYANT. J. Am. Chem. Soc. **102**, 21 (1980).
6. U. SANKAWA, Y. EBIZUKA, H. NOGUCHI, Y. ISHIKAWA, S. KITGAWA, and T. KOBAYASHI. Heterocycles, **16**, 1115 (1981).

7. D. D. HACKNEY, J. A. SLEEP, G. ROSEN, R. L. HUTTON, and P. D. BOYER. NMR and biochemistry. A symposium honoring Mildred Cohn. *Edited by* S. J. Opella and P. Lu. Marcel Dekker, New York. 1979. pp. 299–300.
8. J. M. RISLEY and R. L. VAN ETTEN. J. Am. Chem. Soc. **101**, 252 (1979); **102**, 4609 (1980); **102**, 6699 (1980).
9. D. J. DARENSBOURG, J. Organomet. Chem. **174**, C70 (1979); D. J. DARENSBOURG AND B. J. BALDWIN. J. Am. Chem. Soc. **101**, 6447 (1979); D. J. DARENSBOURG, B. J. BALDWIN, and J. A. FROELICH, J. Am. Chem. Soc. **102**, 4688 (1980).
10. J. C. VEDERAS. J. Am. Chem. Soc. **102**, 374 (1980); J. DIAKUR, T. T. NAKASHIMA, and J. C. VEDERAS. Can. J. Chem. **58**, 1311 (1980); R. N. MOORE, J. DIAKUR, T. T. NAKASHIMA, S. L. MCLAREN, and J. C. VEDERAS. J. Chem. Soc. Chem. Commun. 501 (1981).
11. C. J. JAMESON. J. Chem. Phys. **66**, 4983 (1977).
12. S. BRANDÄNGE, O. DAHLMAN, and L. MÖRCH. J. Chem. Soc. Chem. Commun. 555 (1980); S. A. BENNER, J. E. MAGGIO, and H. E. SIMMONS III. J. Am. Chem. Soc. **103**, 1581 (1981); J. M. RISLEY and R. L. VAN ETTEN. J. Am. Chem. Soc. **103**, 4389 (1981).
13. S. W. TANENBAUM (*Editor*). Cytochalasins, biochemical and cell biological aspects. Elsevier/North Holland Press, Amsterdam. 1978; R. WYSS, CH. TAMM, and J. C. VEDERAS. Helv. Chim. Acta, **63**, 1538 (1980), and references therein.
14. C. R. HUTCHINSON, I. KUROBANE, D. E. CANE, H. HASLER, and A. G. MCINNES. J. Am. Chem. Soc. **103**, 2477 (1981), and references therein.
15. W. GRAF, J. L. ROBERT, J. C. VEDERAS, CH. TAMM, P. H. SOLOMON, I. MIURA, and K. NAKANISHI. Helv. Chim. Acta, **57**, 1801 (1974).
16. U. HANDSCHIN, H. P. SIGG, and CH. TAMM. Helv. Chim. Acta, **51**, 1943 (1968); R. G. COOMBE, P. S. FOSS, J. J. JACOBS, and T. R. WATSON. Aust. J. Chem. **22**, 1943 (1969).
17. S. GATENBECK and K. MOSBACH. Acta Chem. Scand. **13**, 1561 (1959); B. SAMUELSSON, J. Am. Chem. Soc. **87**, 3011 (1965); A. I. SCOTT and K. J. WIESNER. J. Chem. Soc. Chem. Commun. 1075 (1972).
18. J. C. VEDERAS, T. T. NAKASHIMA, and J. DIAKUR. Planta Med. **39**, 201 (1980).
19. J. L. ROBERT and CH. TAMM. Helv. Chim. Acta, **58**, 2501 (1975).
20. J. M. SCHWAB. J. Am. Chem. Soc. **103**, 1876 (1981).
21. P. S. STEYN, R. VLEGGAAR, and P. L. WESSELS. The biosynthesis of mycotoxins. *Edited by* P. S. Steyn. Academic Press, New York, 1980. pp. 105–155, and references therein; A. E. DE JESUS, C. P. GORST-ALLMAN, P. S. STEYN, R. VLEGGAAR, P. L. WESSELS, C. C. WAN, and D. P. H. HSIEH. J. Chem. Soc. Chem. Commun. 389 (1980).
22. L. O. ZAMIR and K. D. HUFFORD. Appl. Environ. Microbiol. **42**, 168 (1981).
23. J. C. VEDERAS and T. T. NAKASHIMA. J. Chem. Soc. Chem. Commun. 183 (1980).
24. J. W. BENNETT, L. S. LEE, S. M. SHOSS, and G. H. BOUDREAUX. Appl. Environ. Microbiol. **39**, 835 (1980).
25. N. C. WAN and D. P. H. HSIEH. Appl. Environ. Microbiol. **39**, 109 (1980).
26. D. L. RABENSTEIN and T. T. NAKASHIMA. Anal. Chem. **51**, 1465A (1979), and references therein; D. W. BROWN, T. T. NAKASHIMA, and D. L. RABENSTEIN. J. Magn. Reson. **45**, 302 (1981).
27. R. M. SANDIFER, A. K. BHATTACHARYA, and T. M. HARRIS. J. Org. Chem. **46**, 2260 (1981).
28. K. G. R. PACHLER, P. S. STEYN, R. VLEGGAAR, P. L. WESSELS, and D. B. SCOTT. J. Chem. Soc. Perkin Trans. I, 1182 (1976).
29. C. E. SNIPES, C. J. CHANG, and H. G. FLOSS. J. Am. Chem. Soc. **101**, 701 (1979); J. Nat. Prod. **42**, 627 (1979).
30. S. MASAMUNE, G. S. BATES, and J. W. CORCORAN. Angew. Chem. Int. Ed. Engl. **16**, 585 (1977); S. OMURA and A. NAKAGAWA. J. Antibiot. **28**, 401 (1975); S. W. QUEENER, O. K. SEBEK, and C. VEZINA. Annu. Rev. Microbiol. **32**, 593(1978).
31. C. R. HUTCHINSON, M. M. SHERMAN, J. C. VEDERAS, and T. T. NAKASHIMA. J. Am. Chem. Soc. **103**, 5953 (1981), and references therein; C. R. HUTCHINSON, M. M. SHERMAN, A. G. MCINNES, J. A. WALTER, and J. C. VEDERAS. J. Am. Chem. Soc. **103**, 5956 (1981).
32. G. D. SMITH, W. L. DUAX, and S. FORTIER. J. Am. Chem. Soc. **100**, 6725 (1978).
33. J. W. WESTLEY, E. P. OLIVETO, J. BERGER, R. H. EVANS, R. GLASS, A. STEMPAC, V. TOOME, and T. WILLIAMS. J. Med. Chem. **16**, 397 (1973).
34. J. W. WESTLEY, R. H. EVANS, G. HARVEY, R. G. PITCHER, D. L. PREUSS, A. STEMPEL, and J. BERGER. J. Antibiot. **27**, 288 (1974); J. W. WESTLEY, J. F. BLOUNT, R. H. EVANS, A. STEMPEL, and J. BERGER. J. Antibiot. **27**, 597 (1974); J. W. WESTLEY, W. BENZ, J. DONAHUE, R. H. EVANS, C. G. SCOTT, A. STEMPEL, and J. BERGER. J. Antibiot. **27**, 744 (1974).
35. D. E. CANE, H. HASLER, and T. C. LIANG. J. Am. Chem. Soc. **103**, 5960 (1981); D. E. CANE, T. C. LIANG, and H. HASLER, J. Am. Chem. Soc. **103**, 5962 (1981).
36. M. P. LANE, T. T. NAKASHIMA, and J. C. VEDERAS. J. Am. Chem. Soc. **104**, 913 (1982); T. T. NAKASHIMA and J. C. VEDERAS. J. Chem. Soc. Chem. Commun. 206 (1982); J. G. HILL, T. T. NAKASHIMA, and J. C. VEDERAS. J. Am. Chem. Soc. **104**, 1745 (1982).
37. T. T. NAKASHIMA and D. L. RABENSTEIN. J. Magn. Reson. **47**, 339 (1982).


Can. J. Chem. Downloaded from www.nrcresearchpress.com by 210.87.254.40 on 09/06/12
For personal use only.

# Specific adsorption of sulfamate ions at the mercury/solution interface

ERNESTO R. GONZALEZ[1]

*Instituto de Fisica e Quimica de São Carlos, USP, C.P. 369, 135650 São Carlos, SP, Brazil*

Received April 23, 1981

ERNESTO R. GONZALEZ. Can. J. Chem. **60**, 1643 (1982).

The adsorption of sulfamate ions on mercury electrodes has been studied by measuring the double layer capacity in constant ionic strength solutions of composition $xM$ $NH_4SO_3NH_2$ + $(1 - x)M$ $NH_4F$. It was found that sulfamate ions are weakly adsorbed on mercury, the amount adsorbed being significant only for $x > 0.1$ at positive charges on the electrode. Because of this, the properties of the inner layer were found to be strongly dependent on the adsorbed water molecules and the structure of the diffuse layer. It was determined that the adsorption of sulfamate ions can be described by an isotherm based on the electrostatic model of the double layer. The possible effects of the activity coefficient variation with solution composition are discussed.

ERNESTO R. GONZALEZ. Can. J. Chem. **60**, 1643 (1982).

On a étudié l'adsorption des ions sulfamates sur des électrodes de mercure en mesurant la capacité de la couche double, à force ionique constante, des solutions de composition $xM$ $NH_4SO_3NH_2$ + $(1 - x)M$ $NH_4F$. On a trouvé que les ions sulfamates sont faiblement adsorbés sur le mercure, la quantité adsorbée étant significative seulement pour $x > 0,1$ aux charges positives sur l'électrode. Pour cette raison, on a trouvé que les propriétés de la couche interne dépendent fortement des molécules d'eau adsorbées et de la structure de la couche diffuse. On a déterminé que l'adsorption des ions sulfamates peut être discuté par un isotherme en s'appuyant sur le modèle électrostatique de la couche double. On discute des effets possibles de la variation du coefficient d'activité avec la composition de la solution.

[Traduit par le journal]

## Introduction

The study of the influence of the electrical double layer on the kinetics and mechanisms of electrode processes is of primary importance in electrochemistry. In the absence of specific adsorption of ions of the supporting electrolyte, the well-known Frumkin's theory accounts reasonably well for the observed effect. On the other hand, when specific adsorption is present, the situation is much more complicated, and it is only recently that quantitative treatments have been attempted with some degree of success. Specific adsorption of supporting electrolyte ions is also a complicating factor in the studies of adsorption of neutral molecules on electrodes. Within this context, the importance of having electrolytes that present negligible or low specific adsorption becomes evident.

Capacity–potential curves for the system mercury – aqueous solutions of sulfamic acid, recorded over a restricted concentration range (1), showed that the sulfamate ion may present a low specific adsorption on mercury. This observation prompted the present study aimed to a quantitative determination of the adsorbed charge and to an evaluation of the properties of the double layer. The system was studied by recording capacity–potential curves for mercury electrodes in aqueous solutions of $NH_4SO_3NH_2$ + $NH_4F$ at constant ionic strength. The possible change of activity coefficients with solution composition was not considered in the calculation because of the lack of data on activity coefficients for sulfamate solutions and the difficulties involved in the experimental determination. However, the effect that this change might have on the present results is discussed.

## Experimental

Ammonium sulfamate (Carlo Erba, RPE) and ammonium fluoride (Carlo Erba, RPE) were used without further purification. Water and mercury were purified as described previously (2). The differential capacity ($C$) was measured using equipment, cells, and electrodes already described (2). Potentials of zero charge ($E_z$) were measured using the streaming electrode technique (3). Twelve solutions of composition $xM$ $NH_4SO_3NH_2$ + $(1 - x)M$ $NH_4F$, where $x$ had the values 0, 0.01, 0.015, 0.025, 0.05, 0.075, 0.1, 0.15, 0.25, 0.5, 0.75, and 1.0 were used. In all experiments, the temperature was maintained at 25.0 ± 0.1°C. All potentials were measured against a commercial saturated calomel electrode (Coleman 3-712). Attempts at preparing a $Hg/Hg_2(SO_3NH_2)_2$ electrode to measure activity coefficients in sulfamate solutions were unsuccessful because of the instability of the mercurous salt.

## Results

Figure 1 shows the capacity–potential plots for the system $NH_4SO_3NH_2$ + $NH_4F$. No difference was found between the curve for $1M$ $NH_4F$ and curves for the mixed system for which $x < 0.01$. By comparison with the behavior of most other systems, this fact alone is indicative of the weak adsorption of the sulfamate ion. A maximum in the capacity curves develops at potentials positive of $E_z$. However, this maximum is not very pro-

[1]Presently a Guest Scientist at the Los Alamos National Laboratory, P.O. Box 1663, MS 429, Los Alamos, NM 87545.

0008-4042/82/131643-05$01.00/0

©1982 National Research Council of Canada/Conseil national de recherches du Canada

Can. J. Chem. Downloaded from www.nrcresearchpress.com by 210.87.254.105 on 09/06/12
For personal use only.

Can. J. Chem. Downloaded from www.nrcresearchpress.com by 210.87.254.105 on 09/06/12
For personal use only.

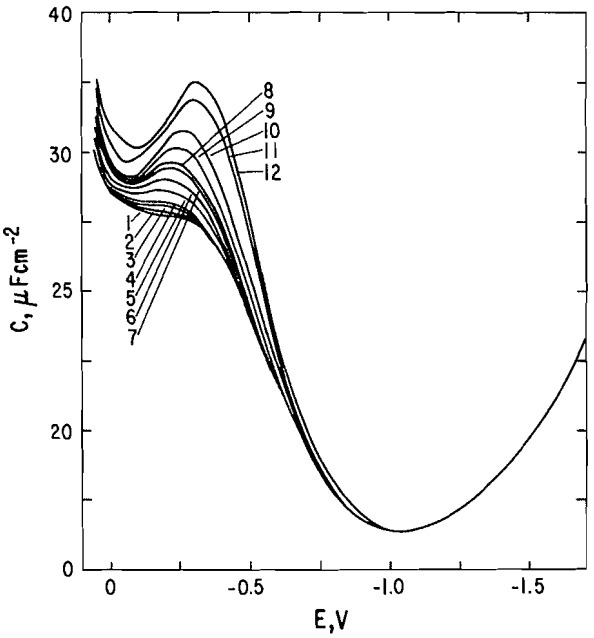


FIG. 1. Differential capacity of the electrical double layer for a mercury electrode in aqueous $xM$ $NH_4SO_3NH_2$ + $(1 - x)M$ $NH_4F$ at 25°C. $x$ = (*1*) 0, (*2*) 0.01, (*3*) 0.015, (*4*) 0.025, (*5*) 0.05, (*6*) 0.075, (*7*) 0.1, (*8*) 0.15, (*9*) 0.25, (*10*) 0.5, (*11*) 0.75, (*12*) 1.0.

nounced. It increases slightly with sulfamate concentration and, at the same time, shifts toward more negative potentials. Another feature of these curves is the fact that they seem to converge at the most positive potentials. However, an extension of the potential range examined would be required to draw more definite conclusions.

Using the experimental values of $E_z$ presented in Table 1, the capacity–potential curves were integrated to obtain the electrode charge density ($q$). A second integration was performed to obtain the surface tension ($\gamma$) as a function of potential. The necessary integration constants (Table 1) were obtained from the value 425.7 mN $m^{-1}$ for $\gamma$ at $E_z$ for the pure fluoride solution (4) and noting that all the capacity curves coincide for potentials more negative than −1.00 V. The magnitudes of $\gamma$ and $q$ were combined to obtain Parsons' function, $\xi_+ = \gamma + qE_+$ (in the present case $E_+$ is taken as being equal to $E$) from which the values of the specifically adsorbed charge density ($q_-'$) due to sulfamate ions were obtained in the usual way (2). The calculation described here was performed using suitable computer programs. Differentiation of the function $\xi$ vs. $\log x$ was done by fitting a quadratic equation to a five-point moving segment using a least-squares procedure. The quadratic was normally differentiated at the central point, although results in both extremes of the concentration range were also

TABLE 1. Coordinates of the point of zero charge for mercury electrodes in aqueous $xM$ $NH_4SO_3NH_2$ + $(1 - x)M$ $NH_4F$ at 25°C

| $x$ | $E_z$ (V) | $C_z$ mNm$^{-1}$ | $C_z$ LF cm$^{-2}$ |
|---|---|---|---|
| 0 | −0.4286 | 425.7 | 25.67 |
| 0.01 | −0.4286 | 425.7 | 25.67 |
| 0.015 | −0.4286 | 425.7 | 25.73 |
| 0.025 | −0.4295 | 425.7 | 25.92 |
| 0.05 | −0.4300 | 425.7 | 26.11 |
| 0.075 | −0.4309 | 425.7 | 26.33 |
| 0.1 | −0.4321 | 425.6 | 26.45 |
| 0.15 | −0.4346 | 425.6 | 26.98 |
| 0.25 | −0.4391 | 425.4 | 27.57 |
| 0.5 | −0.4436 | 425.3 | 28.48 |
| 0.75 | −0.4509 | 425.0 | 28.76 |
| 1.0 | −0.4540 | 424.8 | 29.44 |

obtained. With this method, and taking into account that five points per decade were used in the concentration range, the error in $q_-'$ is expected to be no greater than 0.5 μC $cm^{-2}$ (5). On the other hand, the values of $q_-'$, particularly for high values of $x$ and $q$, may be affected by an error for not having considered the variation of activity coefficients with solution composition (6). This point is discussed below.

Figure 2 shows the specifically adsorbed charge as a function of ln $x$ for different values of $q$. Considering that values of $q_-' < 5$ μC $cm^{-2}$ are probably without much relevance, it is seen that the adsorption of sulfamate ions on mercury becomes significant only for $x > 0.1$ and at fairly positive values of $q$. From the same figure, it is apparent that for most of the concentration interval $q_-' < q$. On the basis of the electrostatic model of the double layer, this means that the values of $q_-'$ are probably lower than those that would be obtained in solutions of single sulfamate salts, where the compensating effect of the diffuse layer is smaller. However, the difference is not expected to be large.

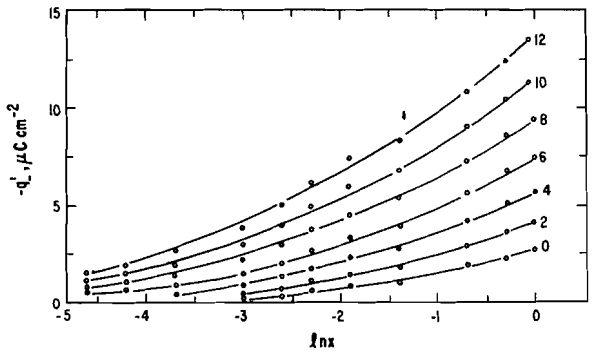


FIG. 2. Adsorbed charge density due to $SO_3NH_2^-$ ions against the logarithm of $SO_3NH_2^-$ concentration in the bulk. Figures on the curves indicate charge density on the electrode in μC $cm^{-2}$.

Can. J. Chem. Downloaded from www.nrcresearchpress.com by 210.87.254.105 on 09/06/12
For personal use only.

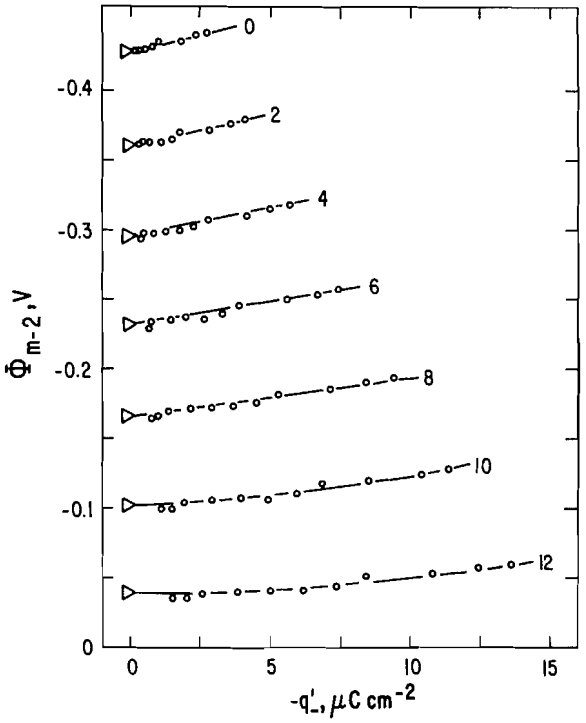


FIG. 3. Potential drop across the inner layer as a function of specifically adsorbed charge at constant charge on the electrode (indicated by the figures on the lines in μC cm$^{-2}$).

Figure 3 shows plots of potential drop across the inner layer, $\phi_{m-2}$, against the adsorbed charge density at constant $q$. $\phi_{m-2}$ was obtained by subtracting the potential $\phi_2$ of the outer Helmholtz plane (o.H.p.), calculated from the diffuse layer theory, from the electrode potential. The figure also includes the values corresponding to the base solution. For $q < 10$ μC cm$^{-2}$, the plots are fairly linear, extrapolating through the base solution points. An important fact to be noted is that the slope of the lines is not constant, decreasing with increasing values of $q$. Furthermore, for the most positive values of $q$, an extrapolation through the points corresponding to the base solution means that a certain degree of curvature has to be admitted.

Adsorption studies in single salt and constant ionic strength solutions have indicated the adequacy of the isotherm based on electrostatic models of the double layer (see, for example, refs. 2 and 7). This isotherm can be derived from detailed electrostatic models of ionic adsorption (8) or from more simple approaches (7, 9, 10). It has even been used as a working hypothesis to discuss the entrance of counter-ions in the inner layer (11). Disregarding the volume differences between the adsorbed ions and the displaced water molecules, and considering that the values of the adsorbed charge are small, the isotherm can be written (8, 12) as follows:

$$[1] \quad \ln(-q_-') = \ln x + \Phi + \frac{F}{RT}\phi_2 + aq_-' + bq$$

where as a first approximation, $\Phi$ can be considered a constant and $a$ and $b$ are functions of the inner layer parameters. Equation [1] was tested by plotting $q_-'$ vs. $(RT/F)\ln(-q_-'/x) - \phi_2$. It was found that the dispersion of the points was too large. According to diffuse layer theory and for the type of solution under consideration

$$[2] \quad \phi_2 = \frac{2RT}{F}\sinh^{-1}\left(\frac{q+q'}{2A}\right)$$

where $A = 5.86I^{1/2}$ in water at 298 K, $I$ being the ionic strength of the solution. As in a previous case (13), the values of $q + q_-'$ are small, so minor errors in $q_-'$ produce large variations in $\phi_2$, which explains the dispersion found in the plot of eq. [1]. On the other hand, small values of $q + q_-'$ mean that eq. [2] can be approximated to

$$[3] \quad \phi_2 \simeq \frac{RT}{F}\frac{(q+q_-')}{A}$$

For most of the experimental range in this work $\phi_2 < 25$ mV, so the difference between eq. [2] and eq. [3] is $< 1$ mV. In extreme cases $\phi_2 \simeq 40$ mV, for which the difference is ~3 mV.

Introducing eq. [3] into eq. [1]

$$[4] \quad \ln(-q_-'/x) = \Phi + \left(a + \frac{1}{A}\right)q_-' + \left(b + \frac{1}{A}\right)q$$

This expression can be tested by plotting $q_-'$ vs. $(RT/F)\ln(-q_-'/x)$, and the results are shown in Fig. 4. In spite of some dispersion, reasonable straight lines are obtained. A least-squares analysis of the lines shows that the slope varies from 106 μC cm$^{-2}$ at $q = 0$ to 170 μC cm$^{-2}$ at $q = 10$ μC m$^{-2}$, indicating that $a$ is dependent on $q$. It may then be concluded that the approximation for $\phi_2$ (eq. [3]) partly solves the problem created by the explicit introduction of $\phi_2$ in the isotherm.

## Discussion

*Effects of activity coefficient variation*

The variation of activity coefficients with solution composition may be one of the sources of error in the determination of the adsorbed charge. The effect is twofold: on the one hand, the assumption that potential variations measured against a fixed

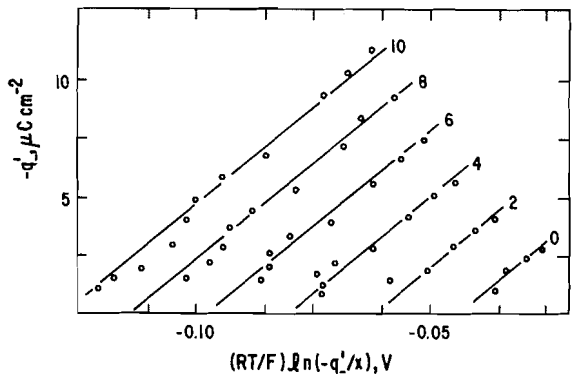


FIG. 4. Plots of adsorption data for $SO_3NH_2^-$ ions according to the isotherm (eq. [4]), at constant charge on the electrode (indicated by the figures on the lines in $\mu C\ cm^{-2}$).

reference electrode are equal to those measured on a thermodynamic scale may not be valid (6). However, this effect is expected to be small and will not be further considered. On the other hand, when activity coefficient variations are introduced in the thermodynamics of the double layer, the relationship between the differential of $\xi$ and $q_-'$ takes the form (6)

$$[5]\quad \frac{F}{RT}\left(\frac{1}{1+\beta x}\right)\left(\frac{\partial \xi}{\partial \ln x}\right)_q = q_-' + \left(\frac{\beta x}{1+\beta x}\right) q_-^{\,d}$$

where $q_-^{\,d}$ is the anionic charge in the diffuse layer. In this case $\beta$ is defined as

$$\beta = (\beta_{NH_4SO_3NH_2} - \beta_{NH_4F})I$$

where $\beta_{MA}$ is the interaction coefficient between the cation M and the anion A. $\beta$ can be determined experimentally (6), evaluated from available data (13), or estimated from the values of the activity coefficients of the pure salts (14). In the present case, $\beta$ could not be determined because, to the author's knowledge, no published data on activity coefficients for sulfamate solutions are available and attempts at an experimental determination of $\beta$ using a $Hg/Hg_2(SO_3NH_2)_2$ electrode were unsuccessful. However, in order to have an indication of the error introduced, eq. [5] was written in the form

$$[6]\quad \frac{F}{RT}\left(\frac{\partial \xi_+}{\partial \ln x}\right)_q = q_-' - \beta x(q + q_+^{\,d})$$

where $q_+^{\,d}$ is the cationic charge in the diffuse layer. If a difference as large as 15% exists between the activity coefficients of $NH_4F$ and $NH_4SO_3NH_2$ at $1\,M$ concentration, $\beta$ can be estimated as being $\sim$0.3. After obtaining $q_+^{\,d}$ from the diffuse layer theory (here the already determined values of $q_-'$ are used so the procedure is not exact), it is easy to estimate that for $x = 1$ and $q > 3\ \mu C\ cm^{-2}$ the error introduced in $q_-'$ is larger than the experimental one. The same situation applies to $x = 0.75$ and $q > 4$ and to $x = 0.5$ and $q > 6$. For lower values of $x$ the correction can be neglected. As a consequence, application of the least-squares procedures to the lines of Figs. 3 and 4 did not consider the points falling in those ranges. However, the same general conclusion would be obtained by taking them into account, which means that in the above considerations the error in $q_-'$ was probably overestimated.

*The inner layer*

According to a simplified electrostatic model (9), the potential drop in the inner layer can be divided into a component dependent on the electrode charge and a component dependent on the adsorbed charge. Thus, $\phi_{m-2}$ can be written in the form:

$$[7]\quad \phi_{m-2} = \frac{q}{{}_qK^i} + \frac{q_-'}{{}_{q'}K^i}$$

where ${}_qK^i$ and ${}_{q'}K^i$ are the integral capacities of the inner layer at constant amount adsorbed and at constant charge on the electrode, respectively.

The integral capacity ${}_qK^i$ is related to the inverse of the vertical separation of the curves presented in Fig. 3. Thus, it is apparent that ${}_qK^i$ decreases with increasing $q_-'$. As in previous studies (2, 13), this can be attributed to changes in the thickness of the double layer. For low values of $q_-'$, the electroneutrality of the interface is brought about by an excess of $F^-$ ions in the diffuse layer. As $q_-'$ increases and $q_-' + q$ becomes negative, $F^-$ ions are replaced by $NH_4^+$ ions in the diffuse layer. So it is reasonable to assume that in this process the thickness of the double layer will increase due to the fact that cations are more strongly solvated than anions.

According to eq. [7], the integral capacity ${}_{q'}K^i$ is related to the inverse of the slopes of the curves in Fig. 3. Up to $q = 8\ \mu C\ cm^{-2}$, the plots may be considered linear, which means that ${}_{q'}K^i$ does not depend on $q_-'$. On the other hand, ${}_{q'}K^i$ increases with $q$, as shown by the decreasing slope of the Christie plots. This is probably because of the fact that the amount of specifically adsorbed sulfamate ions is quite low, the electrode charge influences the adsorbed water molecules so as to make ${}_{q'}K^i$ increase with $q$. This effect will still be more pronounced if the interaction between adsorbed sulfamate ions and water molecules is weak as is observed with the $ClO_4^-$ ions (15).

These arguments could also explain the onset of curvature on the plots for $q > 8\ \mu C\ cm^{-2}$ in Fig. 3. At low values of $q_-'$, the properties of the interface

Can. J. Chem. Downloaded from www.nrcresearchpress.com by 210.87.254.105 on 09/06/12
For personal use only.

Can. J. Chem. Downloaded from www.nrcresearchpress.com by 210.87.254.105 on 09/06/12
For personal use only.

are dominated by the effect of $q$ on the adsorbed water molecules. As the amount of adsorbed sulfamate ions increases, the effect is less marked and ${}_{q'}K^{i}$ increases. At the same time, this transition is enhanced by the already discussed change from negative to positive diffuse layer charge.

In the region $3 < q < 7\ \mu C\ cm^{-2}$, average values of ${}_{q}K^{i}$ and ${}_{q'}K^{i}$ can be used (9) to give an indication of the relationship between the distances from the metal to the inner Helmholtz plane (i.H.p., $x_1$) and from the metal to the o.H.p. ($x_2$). For the present system $x_1/x_2 \simeq 0.9$, which means that the i.H.p. is very near the o.H.p. This point is further discussed below. Thus, the nature of the ion defining the diffuse layer charge is expected to have a marked influence on the dielectric properties of the i.H.p. Christie plots could also be distorted by the entrance of counter-ions into the inner layer (16) but this phenomenon can be ruled out in the present system due to the low values of the adsorbed charge.

*The adsorption isotherm*

The coefficients $a$ and $b$ in the isotherm (eq. [1]) have been obtained by using the cutoff-disc model of ionic adsorption (8). The expression for $a$ is

$$[8]\quad a = \frac{F}{RTK_2}\left(1 - g\,\frac{K}{K_1}\right)$$

where $K$ is the integral capacity of the inner layer, $K_1$ that between the metal and the i.H.p., and $K_2$ that between the i.H.p. and the o.H.p. The parameter $g$ expresses the self-atmosphere potential of the adsorbed ion. The coefficient $b$ is given by

$$[9]\quad b = \frac{F}{RTK_2}$$

The integral capacity $K$ can be identified with ${}_{q}K^{i}$ in eq. [7]. Also, if the adsorbed ions are confined to the i.H.p. $K_2 = {}_{q'}K^{i}$. From the plots in Fig. 3 it is evident that the parameters of the isotherm depend on both $q$ and $q_-'$ so a quantitative analysis is difficult to make. However, in the range $3 < q < 7\ \mu C\ cm^{-2}$, the slope of the lines in Figs. 3 and 4 have the smallest variation, so it will be assumed that $a$, and also $b$, are constant in that region. From Fig. 3 $K_2 = 286\ \mu F\ cm^{-2}$ and $K = 26.0\ \mu F\ cm^{-2}$, so $K = 28.6\ \mu F\ cm^{-2}$. From Fig. 4, $(RT/F)a = -2.3 \times 10^{-3}$ V cm$^2$ $\mu C^{-1}$, so that from eq. [8], $g = 1.8$.

The parameter $g$ has been evaluated for two different models of dielectric constant variation in the inner layer (17, 18). In both cases, $g$ is strongly dependent on the relative positions of the i.H.p. and the o.H.p., the value obtained here indicating again that the i.H.p. is near the o.H.p. The situation is similar to that found for nitrate (13) in the sense that for contact adsorption and according to the structure of the sulfamate ion (19), the i.H.p. should be at about 2 Å from the metal surface while the o.H.p. would be at more than twice that distance. Thus it is possible that the sulfamate ion is separated from the surface by a layer of water molecules as it was postulated for $ClO_4^-$ (20). The model on which this discussion is based will not hold if the cations enter the inner layer (11) but, as stated before, this is highly improbable due to the low values of the adsorbed charge. In spite of the limited relevancy of this discussion based on the slope of the lines in Fig. 4, the characteristics of those plots do not seem to justify an analysis of the other parameters of the isotherm.

**Acknowledgments**

The author thanks the Conselho Nacional de Desenvolvimento Cientifico e Tecnologico (CNPq), Brazil, for financial support, and Mr. R. C. Rocha Filho of UFSCar for helping with the computer work.

1. E. R. Gonzalez and R. Parsons. Unpublished work.
2. E. R. Gonzalez. J. Electroanal. Chem. **90**, 431 (1978).
3. D. C. Grahame, R. P. Larsen, and M. A. Poth. J. Am. Chem. Soc. **71**, 2978 (1949).
4. A. W. M. Verkroost, M. Sluyters-Rebach, and J. H. Sluyters. J. Electroanal. Chem. **24**, 1 (1970).
5. W. R. Fawcett and J. E. Kent. Can. J. Chem. **48**, 47 (1970).
6. W. R. Fawcett and T. A. McCarrick. J. Electrochem. Soc. **123**, 1325 (1976).
7. C. V. D'Alkaine, E. R. Gonzalez, and R. Parsons. J. Electroanal. Chem. **32**, 57 (1971).
8. S. Levine. J. Colloid Interface Sci. **37**, 619 (1971).
9. J. M. Parry and R. Parsons. Trans. Faraday Soc. **59**, 241 (1963).
10. R. de Levie. J. Electrochem. Soc. **118**, 185C (1971).
11. B. Damaskin, L. Kuznetsova, U. Palm, M. Väärtnõu, and M. Salve. J. Electroanal. Chem. **100**, 365 (1979).
12. W. R. Fawcett. J. Electroanal. Chem. **84**, 303 (1977).
13. W. R. Fawcett and J. B. Sellan. Can. J. Chem. **55**, 3871 (1977).
14. D. R. Rosseinsky and R. J. Hill. J. Electroanal. Chem. **30**, App 7, (1971).
15. R. Parsons and R. Payne. Z. Phys. Chem. **98**, 9 (1975).
16. U. Palm, M. Väärtnõu, and M. Salve. J. Electroanal. Chem. **86**, 35 (1978).
17. S. Levine and K. Robinson. J. Electroanal. Chem. **41**, 159 (1973).
18. K. Robinson and S. Levine. J. Electroanal. Chem. **47**, 395 (1973).
19. B. E. Cain and F. A. Kanda. Z. Kristallogr. Kristallgeom. Kristallphys. Kristallchem. **135**, 253 (1972).
20. B. B. Damaskin, A. N. Frumkin, V. F. Ivanov, N. I. Melekhova, and V. F. Khonina. Elektrokhimiya, **4**, 1336 (1968).

# Orientations of hydroxyl groups. Conformational studies on 2,3:5,6-di-*O*-isopropylidene-α-D-mannofuranose by nuclear magnetic resonance spectroscopy

PHOTIS DAIS AND ARTHUR S. PERLIN

*Department of Chemistry, McGill University, Montreal, P.Q., Canada H3C 3G1*

Received September 21, 1981

Can. J. Chem. Downloaded from www.nrcresearchpress.com by 210.87.254.40 on 09/06/12
For personal use only.

PHOTIS DAIS and ARTHUR S. PERLIN. Can. J. Chem. **60**, 1648 (1982).

Various nmr spectroscopic techniques have been used to determine the orientation of the anomeric hydroxyl group of 2,3:5,6-di-*O*-isopropylidene-α-D-mannofuranose (**1**) in dimethylsulfoxide solution, as well as other conformational features of the molecule. $^{13}C$ and $^{1}H$ coupling constants indicate that in its most probable orientation the O—H bond is *anti* with respect to carbon-2, and forms an angle of ~40° with the C-1—H-1 bond. Spin-lattice relaxation rates ($R_1$) and nuclear Overhauser enhancements (nOe) have been measured for the pertinent protons and used, in conjunction with $^{13}C$ relaxation times, as additional criteria for characterizing the geometry of the anomeric alcohol group of **1**. These results are in good agreement with the coupling constant data. The conformations of the mannofuranose ring, the 2,3-*O*-isopropylidene ring, and the C-4 to C-6 region of the molecule are also described.

PHOTIS DAIS et ARTHUR S. PERLIN. Can. J. Chem. **60**, 1648 (1982).

On a utilisé diverses techniques de spectroscopie de rmn pour déterminer l'orientation du groupe hydroxyle anomère du di-*O*-isopropylidène-2,3:5,6 α-D-mannofurannose (**1**) dans une solution de diméthylsulfoxyde, ainsi que d'autres caractéristiques conformationnelles de la molécule. Les constantes de couplage du $^{13}C$ et du $^{1}H$ indiquent, que dans son orientation la plus probable, la liaison O—H est *anti* par rapport au carbone en position-2 et forme un angle d'environ 40° avec la liaison C-1—H-1. On a mesuré les vitesses de relaxation spin-réseau ($R_1$) et l'augmentation des effets Overhauser nucléaires (eOn) pour les protons concernés et on les a utilisés, en relation avec les temps de relaxation du $^{13}C$, comme critère additionnel pour caractériser la géométrie du groupe alcool anomère du composé **1**. Ces résultats sont en bon accord avec les données de constante de couplage. On décrit également les conformations du cycle mannofurannose, du cycle *O*-isopropylidène-2,3 et les régions de la molécule allant de C-4 à C-6.

[Traduit par le journal]

## Introduction

Although a great deal is known (1, 2) from X-ray crystallographic data about the disposition of hydroxyl groups of carbohydrate molecules in the solid state, little is available as to their stereochemistry in solution. An indication of favorable orientations in solution is given (3–6) by the magnitude of spin–spin coupling between a hydroxyl proton and a vicinal $^{1}H$ or $^{13}C$ nucleus. However, a more definitive description of rotamers of hydroxyl groups should be afforded by augmenting coupling data with spatial parameters derived from spin-lattice relaxation rates and nuclear Overhauser effect measurements. This approach is examined in the present study, which deals with a sugar derivative containing a single hydroxyl group, namely 2,3:5,6-di-*O*-isopropylidene-α-D-mannofuranose (**1**). To ensure slow exchange (7) of the hydroxyl proton, as well as to preserve the compound exclusively in the α-anomeric form (8), dimethyl sulfoxide was used as the solvent.

It was apparent that measurements dealing with the geometry of the anomeric centre of **1** had to take account of a larger segment of the molecule. Indeed, in this particular instance, there was the added incentive of simultaneously examining the conformations of the furanose and *O*-isopropylidene rings by the same overall approach. Consequently, in the discussion to follow, a detailed analysis of nmr spectra of **1** is presented together with the results of relaxation rate and nOe measurements on various protons, so that several structural features of the molecule are treated qualitatively, in addition to a quantitative treatment of the C-1 alcohol moiety.

## Results and discussion

### A. *$^{1}H$ and $^{13}C$ nmr chemical shifts*

At 200 MHz, the $^{1}H$ nmr spectrum of **1** was almost fully resolved and first order (Fig. 1*a*), although the H-4 and H-6 resonances overlapped, even at 400 MHz. The assignments listed for the proton resonances in Table 1 were straightforward, especially with the aid of homo decoupling. Also given in Table 1 are the $^{13}C$ chemical shifts for **1**, the assignments made having been confirmed by off-resonance and selective decoupling. Being diastereotopic, the four *C*-methyl groups produce separate signals in both the $^{1}H$ and $^{13}C$ nmr spectra (Table 1).

### B. *$^{1}H$ and $^{13}C$ coupling constants*

A first approximation for determining the shape of **1** is afforded by various coupling constants (Table 1), which reflect (9) not only the geometries of the coupling pathways, but also the influences of

0008-4042/82/131648-09$01.00/0

©1982 National Research Council of Canada/Conseil national de recherches du Canada

Can. J. Chem. Downloaded from www.nrcresearchpress.com by 210.87.254.40 on 09/06/12
For personal use only.

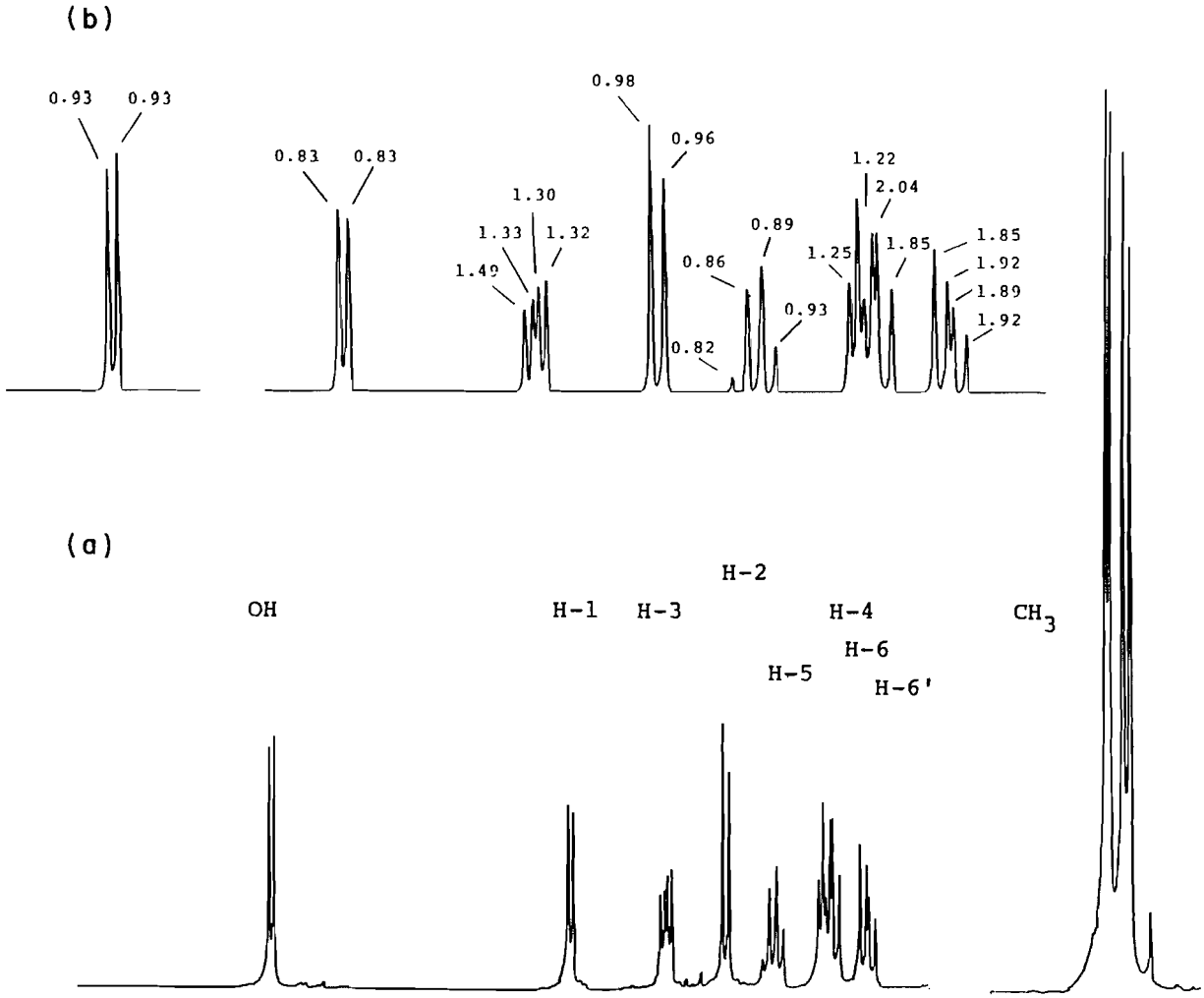


FIG. 1. (a) 200 MHz $^1$H nmr spectrum of 2,3:5,6-di-*O*-isopropylidene-α-D-mannofuranose (**1**) in dimethyl sulfoxide-$^2H_6$ (0.1 *M*; 20°C). (b) Relaxation rates ($R_1$, $s^{-1}$) associated with individual components of signals in the 200 MHz $^1$H nmr spectrum of **1** in dimethyl sulfoxide-$^2H_6$ (0.1 *M*; 20°C).

TABLE 1. $^1$H and $^{13}$C chemical shifts (δ) and coupling constants (Hz) for 2,3:5,6-di-*O*-isopropylidene-α-D-mannofuranose

| Proton | δ$^1$H | Carbon | δ$^{13}$C | $J_{H,H}$ | | $J_{C,H}$ | |
|---|---|---|---|---|---|---|---|
| OH | 6.45 | C-I$_p$[a] | 111.55 | $^3J_{H\text{-}1,OH}$ = 4.34 | $^1J_{C\text{-}1,H\text{-}1}$ = 171.50 | $^2J_{C\text{-}1,H\text{-}2}$ = 1.81 | $^3J_{C\text{-}1,H\text{-}4}$ = 3.34 |
| H-1 | 5.13 | C-I$_p$[a] | 108.08 | $^3J_{H\text{-}1,H\text{-}2}$ = < 0.1 | $^1J_{C\text{-}2,H\text{-}2}$ = 158.53 | | $^3J_{C\text{-}2,OH}$ = 7.65 |
| H-2 | 4.44 | C-1 | 100.63 | $^3J_{H\text{-}2,H\text{-}3}$ = 5.88 | $^1J_{C\text{-}3,H\text{-}3}$ = 144.18[b] | | |
| H-3 | 4.71 | C-2 | 85.70 | $^3J_{H\text{-}3,H\text{-}4}$ = 3.66 | $^1J_{C\text{-}4,H\text{-}4}$ = 159.56[b] | | $^3J_{C\text{-}5,H\text{-}3}$ = 4.30 |
| H-4 | 4.00 | C-3[b] | 79.38 | $^3J_{H\text{-}4,H\text{-}5}$ = 6.41 | $^1J_{C\text{-}5,H\text{-}5}$ = 150.17 | | |
| H-5 | 4.24 | C-4[b] | 79.57 | $^3J_{H\text{-}5,H\text{-}6}$ = 6.38 | $^1J_{C\text{-}6,H\text{-}6}$ = 149.50 | | $^3J_{C\text{-}6,H\text{-}4}$ = 3.31 |
| H-6 | 3.97 | C-5 | 73.05 | $^3J_{H\text{-}5,H\text{-}6'}$ = 5.82 | $^1J_{C\text{-}6,H\text{-}6'}$ = 150.79 | $^2J_{C\text{-}6,H\text{-}5}$ = < 0.5 | |
| H-6′ | 3.81 | C-6 | 66.09 | $^2J_{H\text{-}6,H\text{-}6'}$ = 8.34 | | | |
| CH$_3$ | 1.34 | | 26.77 | | | $^2J_{C\text{-}Me}$ = 4.83 | |
| | 1.32 | | 25.91 | | | | |
| | 1.23 | | 24.49 | | | | |
| | 1.26 | | 25.41 | | | | |

[a]Quaternary carbon of *O*-isopropylidene groups.
[b]Assignments may be interchanged.

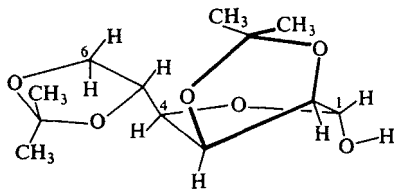

FIG. 2. Representation of the $^2T_3$ conformation of 2,3:5,6-di-*O*-isopropylidene-α-D-mannofuranose (**1**).

such structural parameters as carbon hybridization, electronegative substituents, etc.

Protons 1 and 2 may be positioned on a molecular frame at an angle of ~ 90° with respect to each other, because they exhibit no coupling, as has been found (10) also with structurally-related compounds, α-D-mannofuranose 2,3-carbonate and 2,3-*O*-isopropylidene-α-L-rhamnofuranose. Similarly, as the vicinal couplings between H-2 and H-3, and H-3 and H-4, are less than that expected (11, 12) for pairs of eclipsed hydrogens, the overall data are consistent with a twist conformation ($^2T_3$) in which C-2 and C-3 lie, respectively, above and below the plane formed by ring atoms C-4, O-4, and C-1 (Fig. 2). Additional support for this proposal comes from the value of 4.3 Hz for coupling between $^{13}$C-5 and H-3, which is commensurate (13) with a dihedral angle of about 140° relating these two nuclei in the depicted projection along the C-3,C-4 bond (*a*). By way of contrast, the furanose ring of methyl-α-D-mannofuranoside appears (14, 15) to favor a $^3T_4$ conformation, illustrating the strongly distorting impact of the fused 2,3-*O*-isopropylidene moiety.

Implicit in the representation of the α-D-mannofuranose ring in Fig. 2, is a nonplanar conformation for the fused 2,3-*O*-isopropylidene ring as well, in accord with earlier findings (12) on various *O*-isopropylidene derivatives. The projected dihedral angle between H-2 and H-3 is ~35°, based on the value of 5.88 Hz for $^3J_{H\text{-}2,H\text{-}3}$.

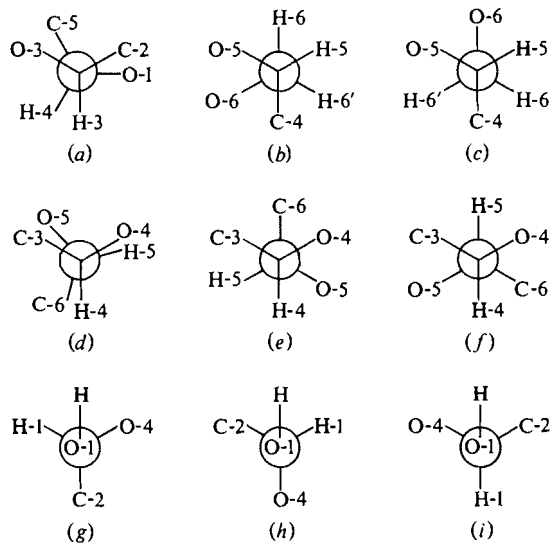


Projection formulas *b* and *c* represent the extreme limits of puckering by the 5,6-*O*-isopropylidene ring. Because spin–spin coupling of H-5 with H-6 and H-6′ (6.38 and 5.82 Hz, respectively) is intermediate in value, contributions from both *gauche* and *anti* interactions are implied. However, as there was no observable two-bond coupling between $^{13}$C-6 and H-5, an *anti* orientation of O-6 with respect to H-5 (as in *b*) should be a prominent characteristic (13, 16).

Stereochemical models indicate that rotation about the C-4,C-5 bond is restricted by nonbonded interactions, mainly involving the methyl groups, to a librational motion having an angular amplitude of ~ 180°: *d* and *e* represent the two extremes of the rotamer population, and *f* an intermediate array. According to coupling data, both of the energetically more favored rotamers, *e* and *f*, appear to be represented. That is, the value of 6.41 Hz for $^3J_{H\text{-}4,H\text{-}5}$ is intermediate between that expected for the *gauche* relationship of H-4 and H-5 in *e* and the value for their *anti* relationship in *f*, whereas the coupling of 3.3 Hz between $^{13}$C-6 and H-4 is smaller than should be anticipated for *e*, and slightly large for *f*. It is noteworthy that in the absence of analogous substitutions at the 5,6-positions, as in α-D-mannofuranose 2,3-carbonate, the rotamer corresponding to *f* is strongly favored, as shown (10) by the value of 9.0 Hz for $^3J_{H\text{-}4,H\text{-}5}$.

Turning to the anomeric hydroxyl group of **1**, there are two experimentally-determined coupling constants (Table 1) that reflect its orientation, i.e., a value of 4.34 Hz for $^3J_{H\text{-}1,OH}$, and of 7.65 Hz for $^3J_{C\text{-}2,OH}$. By applying eq. [1], derived (4) from a

$$[1] \quad J_{HCOH} = 10.4\cos^2\phi - 1.5\cos\phi + 0.2$$

least-squares fit of various values of $^3J_{H,OH}$, angle φ is estimated to be 39° or 142°. Because of the strong coupling between C-2 and the hydroxyl proton, rotamer *g*, in which these two nuclei are *antiperiplanar*, must be a major contributor as compared with rotamers *h* and *i*. Consequently, the vicinal coupling between H-1 and OH-1 is most prominently represented by the *gauche* orientation of these nuclei in *g* and, hence, the time-average value of φ is much closer to 30° than to 142°. As noted earlier (5), for a solution of **1** in $CDCl_3$ the corresponding values of $^3J_{H\text{-}1,OH}$ and $^3J_{C\text{-}2,OH}$ are 2.6 Hz and 9.2 Hz, respectively, which are both consistent with an even greater preponderance of rotamer *g*, assuming that the magnitude of these $^3J$ values is not appreciably solvent-dependent.

Can. J. Chem. Downloaded from www.nrcresearchpress.com by 210.87.254.40 on 09/06/12
For personal use only.

Can. J. Chem. Downloaded from www.nrcresearchpress.com by 210.87.254.40 on 09/06/12
For personal use only.

TABLE 2. $^1$H nmr nonselective spin-lattice relaxation rates ($s^{-1}$) of protio (OH) and deutero (OD) 2,3:5,6-di-*O*-isopropylidene-α-D-mannofuranose[a]

| Proton | $R_1$(OH)[b] | $R_1$(OD)[b] |
|---|---|---|
| OH | 0.94±0.01 | — |
| H-1 | 0.83±0.01 | 0.37±0.01 |
| H-2 | 0.97±0.01 | 0.93±0.01 |
| H-3 | 1.32±0.01 | 1.37±0.01 |
| H-4 | 1.25±0.02 | 1.25±0.01 |
| H-5 | 0.87±0.02 | 0.91±0.01 |
| H-6 | 1.92±0.00 | 1.92±0.01 |
| H-6′ | 1.92±0.01 | 1.92±0.01 |
| $CH_3$(1) | 1.78±0.01 | 1.79±0.01 |
| $CH_3$(2) | 1.64±0.02 | 1.65±0.01 |
| $CH_3$(3) | 1.87±0.02 | 1.87±0.01 |
| $CH_3$(4) | 2.36±0.01 | 2.31±0.01 |

[a]0.1 *M* solution in DMSO-$^2H_6$.
[b]Values with standard deviations of the linear two parameter fit.

To summarize, conformational characteristics of molecule **1** pertaining to the anomeric hydroxyl group, the furanose ring, the C-4,C-5 bond, and the two *O*-isopropylidene rings have been described in terms of the coupling observed between protons and other protons or $^{13}$C-nuclei. In the sections to follow, these characteristics are assessed independently on the basis of relaxation and nOe measurements.

### C. *$^1$H relaxation rates*

The proton relaxation rates ($R_1$) listed in Table 2 furnish a complementary source of information about the molecular architecture of **1**. This stems from the fact (17–19) that, under normal experimental circumstances, proton relaxation occurs preponderantly by the intramolecular dipole–dipole mechanism,[1] which is strongly distance-dependent. Provided that a molecule undergoes a rapid reorientation, so that the extreme narrowing condition is met, the nonselective relaxation rate ($R_1$) of any proton, or set of equivalent protons, is represented by the specific relaxation contributions between the receptor nucleus and the donor nuclei, and by the molecular correlation time $\tau_c^0$, characterizing the overall molecular motion.[2] Consequently, as the relaxation rate is dependent on the inverse sixth power of the distance separating the nuclei, the value of $R_1$ is determined largely by the proximity of its immediate neighbours, as well as their number. Furthermore, because of its relationship to $\tau_c^0$, the $R_1$ value can provide information about the reorientational motion of a molecule as a whole, and of the internal motion of flexible molecular segments.

Di-*O*-isopropylidene derivative **1** was shown to be characterized by an isotropic overall motion. That is, the $^{13}$C spin-lattice relaxation times of the mannose ring carbons, each of which bears a single proton, were found to be essentially the same.[3] Consequently, the relaxation rates of the various protons (Table 2) should primarily be a reflection of intramolecular contributions from other protons in the immediate vicinity, although they could be influenced significantly by cross-relaxation and cross-correlation effects (19–22). However, this latter possibility was found to be negligible for the protons of **1**. An experimental criterion (23) of contributions by cross-correlation effects *plus* possible nonexponential relaxation, is a difference in $R_1$ values for individual components of a multiplet, whereas the appropriate data for **1** (Fig. 1b) show that differences within multiplets do not exceed 10–15%. Furthermore, as additional means for effectively cancelling out these effects, the sums of the intensities for all components of each proton were taken as the basis for measuring total magnetization recoveries, and the initial-slope method (23–25) was used in determining relaxation rates. Overall, then, circumstances appeared to ensure that direct dipole–dipole interactions were preeminent in the acquisition of these rates (Table 2).

Comparing the $R_1$ values for protons of the mannose ring, it is found that H-3 and H-4 relax faster than the other two, whereas the rate for H-2 is about 15% faster than that of H-1. These differences accord with evidence (23) from studies on monosaccharides indicating that a *gauche* $^1$H–$^1$H orientation is much more effective in promoting relaxation than is a *trans*-diaxial one. Hence H-3, which possesses the highest rate, is *quasi-gauche* to both H-2 and H-4. Presumably, these latter two interact similarly with H-3, and as H-4 has a faster rate than H-2, it is evidently provided with additional relaxation pathways by H-5, and possibly protons at C-6. Of the two staggered rotamers consistent with spin-coupling data, *e* is more favored on the basis of the relaxation measurements because of the *gauche* relationship of H-4 with H-5, in contrast to their *anti* disposition in *f*. Proton 2 can receive no comparable contribution from vicinal proton H-1, because these two protons are *trans* in α-anomer **1**. Analogously, H-1 has the slowest rate

[1]Although intermolecular dipole–dipole mechanisms may contribute significantly to proton-relaxation, the use of a highly dilute solution minimized their importance in the present study.

[2]See eqs. [5*a*] and [5*b*].

[3]The $T_1$ values, measured for a 1.0 *M* solution of **1** in dimethyl sulfoxide-$^2H_6$ at 20°C were: C-1, 0.65; C-2, 0.67; C-3, 0.69; C-4, 0.70 s (±5%). All of these carbons relaxed by dipole–dipole interactions, as evidenced by 100% $^{13}$C-[$^1$H] nuclear Overhauser enhancements.

Can. J. Chem. Downloaded from www.nrcresearchpress.com by 210.87.254.40 on 09/06/12
For personal use only.

among the ring protons, consistent with its relative isolation from the influence of H-2, as well as of H-3,H-4 and the *endo*-$CH_3$ group of the 1,2-*O*-isopropylidene ring; stereomodels indicate that H-1 is 4.25, 4.16, and 4.32 Å, respectively, from these latter protons (the value for $CH_3$ being an average distance). As shown later, the hydroxyl proton furnishes the main relaxation pathway for H-1.

The geminal disposition of the 6,6′-protons ensures a mutually efficient relaxation for them, and characteristically fast relaxation rates (Table 2). Contributions of these two protons towards the relaxation of H-5 through *gauche*,*gauche* interactions in rotamer *b*, as well as the *gauche* orientation of H-5 with respect to H-4 in rotamer *e*, presumably account for the fact that although H-5 is in a relatively mobile environment, its relaxation rate is comparable to those of ring protons 1 and 2.

Values of $R_1$ for the methyl groups of the *O*-isopropylidene rings range from 1.64 to 2.36 $s^{-1}$ (Table 2). Evidently, these variations reflect the sensitivity of relaxation rates to changes in the rates of anisotropic modes of reorientation. Although, overall, the molecular tumbling of **1** appears to be isotropic, additional degrees of freedom expressed as internal methyl rotation, librational and puckering motions of the flexible *O*-isopropylidene rings can affect the motional correlation times ($\tau_c$) of individual interproton vectors, and hence their relaxation efficiencies. These factors, and such questions as potential barriers to methyl rotation, are to be considered in some detail in a forthcoming publication.

D. *Relaxation characteristics of OH-1*

Earlier, it was surmised that OH-1 makes the major contribution to the rate of relaxation of H-1. A direct measure of this contribution may be obtained by comparing the effect of exchanging the hydroxyl proton by deuterium. Equation [2] relates the nonselective relaxation rates for H-1 (A-*i*) in the normal molecule [$R_1^{A\text{-}i}(ns, H\text{-}j)$] and in its deuterated analog [$R_1^{A\text{-}i}(ns, D\text{-}j)$], assuming that the protons relax exclusively by the dipole–dipole mechanism and that molecular tumbling is in the extreme narrowing range:

$$[2] \quad \rho_{A\text{-}i,H\text{-}j} = 0.6959\,[R_1^{A\text{-}i}(ns, H\text{-}j) - R_1^{A\text{-}i}(ns, D\text{-}j)]$$

Equation [2] not only gives the relative importance of atom H-*j* to the relaxation of atom A-*i* but also, in conjunction with eq. [5*b*], can be used to predict their relationship in various models of conformational dynamics, given a value of $\tau_c^0$ and a reasonable estimate of the geometry of the molecule.

TABLE 3. Interatomic distances (Å) for the α-D-mannofuranose ring[a]

| $\phi$[b] | $r_{H\text{-}1,OH}$ | $r_{H\text{-}2,OH}$ | $r_{H\text{-}3,OH}$ | $r_{H\text{-}4,OH}$ | |
|---|---|---|---|---|---|
| 0 | 2.00 | 3.02 | 4.50 | 4.52 | $r_{H\text{-}1,H\text{-}2} = 2.65$ |
| 30 | 2.07 | 3.28 | 4.54 | 4.38 | |
| 60 | 2.23 | 3.41 | 4.36 | 3.98 | $r_{H\text{-}1,H\text{-}3} = 4.12$ |
| 90 | 2.43 | 3.39 | 4.00 | 3.50 | |
| 120 | 2.61 | 3.23 | 3.76 | 3.36 | $r_{H\text{-}1,H\text{-}4} = 4.04$ |
| 150 | 2.74 | 2.93 | 3.38 | 3.16 | |
| 180 | 2.79 | 2.57 | 3.16 | 3.24 | $r_{H\text{-}2,H\text{-}3} = 2.32$[c] |
| 210 | 2.74 | 2.23 | 3.10 | 3.56 | |
| 240 | 2.61 | 2.01 | 3.38 | 3.88 | $r_{H\text{-}2,H\text{-}4} = 3.82$ |
| 270 | 2.43 | 2.05 | 3.74 | 4.32 | |
| 300 | 2.23 | 2.30 | 4.16 | 4.56 | $r_{H\text{-}3,H\text{-}4} = 2.28$[c] |
| 330 | 2.07 | 2.67 | 4.34 | 4.62 | |
| 360 | 2.00 | 3.02 | 4.50 | 4.52 | |

[a] The $^2T_3$ skew conformation was considered.
[b] The H-1—C-1—O—H dihedral angle.
[c] The dihedral angles relating H-2,H-3 and H-3,H-4 were taken to be 30°.

Hence, it is possible to compare the distance of the hydroxyl-proton in various rotamers from the other protons, based on the geometry expected for **1**, with average values of $\langle r_{H_i\text{—}OH} \rangle$ where $i$ = H-1, -2, etc.) obtained from the $^1$H-relaxation data, before and after deuteration of the hydroxyl group. Because of internal motion by the hydroxyl group, vector $r_{H_i\text{—}OH}$ is a time dependent quantity representing an "effective", or average, distance.

Although no crystallographic data were found for **1**, information from X-ray studies (26) on several, related, *O*-isopropylidene aldofuranose derivatives provided an appropriate basis for a quantitative description of its geometry in the $^2T_3$ conformation (Fig. 2). Atomic coordinates and interatomic distances were generated by employing the Z-matrix method of a Gaussian-79 program (27). Interproton distances as a function of the H-1—C-1—O—H dihedral angle ($\phi$) are listed in Table 3.

Relaxation rates for the various protons of **1** following deuteration of the hydroxyl group are presented in Table 2, for comparison with the data for the protio compound.[4] It is evident that the effect of introducing the deuterium atom was confined almost exclusively to H-1.

By utilizing eqs. [2] and [5*b*], and the value of $\tau_c^0 = (69.3 \pm 0.2) \times 10^{-12}$ s obtained from the $^{13}$C relaxation measurements, interatomic distances were calculated for the H-1,OH and H-2,OH pairs of protons. These distances were 2.23 ± 0.03 and

[4] To avoid exchange between the —OD group and traces of water in the solvent, a drop of deuterium oxide was introduced. As $R_1$ values for protons far removed from the hydroxyl group are closely similar in both sets of measurements (Table 2), changes in viscosity and polarity due to deuterium oxide were negligible.

TABLE 4. $^1$H nuclear Overhauser enhancement for 2,3:5,6-di-*O*-isopropylidene-α-D-mannofuranose

| Proton irradiated | Proton observed[a] | | | | |
|---|---|---|---|---|---|
| | OH | H-1 | H-2 | H-3 | H-4 |
| OH | — | 0.252 (±0.002) | 0.041 (±0.003) | — | 0.032 (±0.003) |
| H-1 | 0.127 (±0.006) | — | 0.051 (±0.002) | — | — |
| H-2 | −0.367 (±0.006) | 0.167 (±0.006) | — | 0.055 (±0.006) | — |
| H-3 | −0.228 (±0.004) | — | 0.10 (±0.002) | — | 0.085 (±0.003) |
| H-4 | −0.101 (±0.004) | — | −0.020 (±0.005) | 0.150 (±0.005) | — |

[a] Values in parentheses are standard deviations.

3.32 ± 0.27 Å, respectively, the error in these calculations being based on the errors in the $T_1$ measurements for $^1$H and $^{13}$C. When compared with the interproton distances given in Table 3, these values indicate that in its preferred orientation, the O—H bond forms a dihedral angle (ϕ) of about 60° with the H-1—C-1 bond. Hence, of such rotamers as *g*, *h*, and *i* that may be depicted for the C-1 alcohol moiety, the rotamer that occurs with the greatest frequency must be confined to the first quadrant (60° ± 30°) of the circular motion of the OH group. In agreement with the spin-coupling data already considered, rotamer *g* is representative of this most highly populated region.

E. *$^1$H nOe experiments*

Steady-state nOe data for the hydroxyl proton and ring protons of **1** (Table 4) show that although the hydroxyl proton exhibited a positive nOe upon irradiation of H-1, negative nOe effects were produced when H-2, -3, or -4 was irradiated.[5] In the present instance, the negative nOe's were not spurious but, rather, characteristic of the molecule, and strongly dependent on the orientation of the hydroxyl group. This was first verified qualitatively by an analysis of 3-spin systems according to the method of Noggle and Shirmer (19). As represented by Fig. 3, the geometry of a group of three spins can be specified by angle θ and interproton distances α and λα, parameter α being constant whereas θ and λ are time-dependent variables. Analysis of this system showed that negative enhancements are associated with values of θ greater than 90°. Consequently, in evaluating various orientations of the hydroxyl group with respect to 3-spin systems formed by H-2,H-1,OH, by H-3,H-2,OH, and by H-4,H-1,OH, only those orientations conforming to the condition 90° ≤ θ ≤ 180° were regarded as consistent with the experimental data of Table 4.

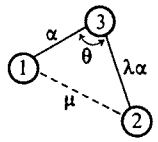


FIG. 3. Representation of the geometry of a group of three spins, according to Noggle and Shirmer (19).

Stereomodels indicate that OH rotamers incorporating angles of that magnitude are confined mainly to the first quadrant of circular motion by the OH group, that is, a finding in accord with the relaxation rate measurements. More satisfactorily, however, a quantitative determination of most probable interproton distances in **1**, and hence of most probable conformations, was effected by combining the results of the nOe measurements with those on $^1$H and $^{13}$C spin-lattice relaxation rates.

For loosely coupled spin 1/2 systems, the fractional nOe of a spin *k* when spin *l* is irradiated, $f_k(l)$, under conditions such that intramolecular dipole–dipole interactions dominate relaxation and cross-correlation effects may be neglected, is expressed as

$$[3] \quad R_k f_k(l) = 0.5\rho_{kl} - 0.5 \sum_{\eta \neq k,l} \rho_{k\eta} f_\eta(l)$$

where

$$[4] \quad f_k(l) = \frac{\langle I_{zk} \rangle - I_{ok}}{I_{ok}}$$

[5] Negative intramolecular nOe effects observed in a number of studies have been accounted for either on conformational grounds (19), or by the contribution of relatively low-frequency components to the motion of large molecular systems (28).

Can. J. Chem. Downloaded from www.nrcresearchpress.com by 210.87.254.40 on 09/06/12
For personal use only.

Can. J. Chem. Downloaded from www.nrcresearchpress.com by 210.87.254.40 on 09/06/12
For personal use only.

$$[5a] \quad R_i = \sum_{j \neq i} \rho_{ij} + \rho_i^*$$

and

$$[5b] \quad \rho_{ij} = \frac{\gamma_i^2 \cdot \gamma_j^2 \hbar^2}{r_{ij}^6} \tau(ij)$$

$\rho_i^*$ is the relaxation rate of spin $i$ due to other relaxation paths (e.g. intermolecular interactions, spin-rotation, etc.), $\tau(ij)$ is the correlation time of vector $r_{ij}$ between spins $i$ and $j$, $\langle I_{zk} \rangle$ is the magnetization of the observed nucleus $k$ when nucleus $l$ is irradiated, and $I_{ok}$ is the equilibrium magnetization in the absence of irradiation.

For the 5-spin system, x, a, b, c, d (where x = OH, a = H-1, b = H-2, c = H-3, and d = H-4), eq. [3] becomes

$$\begin{aligned}
R_x f_x(a) &= 0.5\rho_{ax} - 0.5\rho_{bx} f_b(a) \\
&\quad - 0.5\rho_{cx} f_c(a) - 0.5\rho_{dx} f_d(a) \\
R_x f_x(b) &= -0.5\rho_{ax} f_a(b) + 0.5\rho_{bx} \\
&\quad - 0.5\rho_{cx} f_c(b) - 0.5\rho_{dx} f_d(b) \\
R_x f_x(c) &= -0.5\rho_{ax} f_a(c) - 0.5\rho_{bx} f_b(c) \\
&\quad + 0.5\rho_{cx} - 0.5\rho_{dx} f_d(c) \\
R_x f_x(d) &= -0.5\rho_{ax} f_x(d) - 0.5\rho_{bx} f_b(d) \\
&\quad - 0.5\rho_{cx} f_c(d) + 0.5\rho_{dx}
\end{aligned} \quad [6a]$$

plus four additional, analogous, expansions of eq. [3] where, according to eq. [5a],

$$\begin{aligned}
[7] \quad R_x &= \rho_{ax} + \rho_{bx} + \rho_{cx} + \rho_{dx} + \rho_x^* \\
R_a &= \rho_{ax} + \rho_{ab} + \rho_{ac} + \rho_{ad} + \rho_a^* \\
&\text{etc.}
\end{aligned}$$

The five expansions of eq. [3] can be solved to determine either the ratio of $\rho_{ij}$'s or the individual $\rho_{ij}$'s, for instance,

$$[8] \quad \rho_{ab} = 2R_b \begin{vmatrix} 1 & f_b(x) & -f_c(x) & -f_d(x) \\ -f_x(a) & f_b(a) & -f_c(a) & -f_d(a) \\ -f_x(c) & f_b(c) & 1 & -f_d(c) \\ -f_x(d) & f_b(d) & -f_c(d) & 1 \end{vmatrix} \Big/ \begin{vmatrix} 1 & -f_a(x) & -f_c(x) & -f_d(x) \\ -f_x(a) & 1 & -f_c(a) & -f_d(a) \\ -f_x(c) & -f_a(c) & 1 & -f_d(c) \\ -f_x(d) & -f_a(d) & -f_c(d) & 1 \end{vmatrix}$$

As mentioned earlier, the relaxation of any given spin is complex. Therefore, the relaxation rates ($R_i$) appearing in the various equations above may contain contributions from cross-relaxation and cross-correlation effects. However, one can always define an initial relaxation rate, $R_i^0$, which will describe the relaxation before cross-relaxation causes significant nonexponential behaviour. To the extent that

$$\rho_i^* \ll \sum_{j \neq i} \rho_{ij}$$

the nonselective relaxation rates for the protio compound listed in Table 2 can be identified with the initial relaxation rates, $R_i^0$, and as they were calculated by the initial-slope method, cross-relaxation effects may be neglected. By substituting values for $R_i$ and nOe into the 16 equations taking the form of eq. [8], all of the corresponding values for $\rho_{ij}$ were obtained (two determinations for $\rho_{ij}$, $ij \neq$ x, one determination for $\rho_{ij}$, $i$ or $j$ = x). The values are listed in Table 5. Using these, and the correlation time ($\tau_c^0$) of (69.3 ± 0.2) × $10^{-12}$ s (for a 0.1 *M* solution of **1** in dimethyl sulfoxide-$^2H_6$), already cited, the set of interproton distances ($r_{ij}$) listed in Table 5 was determined (again, two determinations for $r_{ij}$, $ij \neq$ x, and one for $r_{ij}$, $i$ or $j$ = x). The error limits cited for the values of $\rho_{ij}$ and $r_{ij}$ reflect how accurately the errors in the various experimental quantities are known.

For internuclear distances between the ring protons of **1**, the data of Table 5 and the values expected from the molecular model (Table 3) are in good agreement. This is true especially when the distances are relatively small. Hence, experimentally, $r_{H\text{-}1,H\text{-}2}$ is 2.61 ± 0.14 Å, whereas the expected distance is 2.65 Å, and the comparable data for $r_{H\text{-}3,H\text{-}4}$ are 2.22 ± 0.10 Å and 2.28 Å, respectively. This high level of concurrence suggests that the assumptions involved in the measurements of relaxation and nOe were reasonable. Nevertheless, as there is poorer agreement when internuclear distances are longer (≥3.5 Å) and, accordingly,

TABLE 5. Relaxation rates ($\rho_{ij}$, $s^{-1}$) and interproton distances (Å) for 2,3:5,6-di-*O*-isopropylidene-α-D-mannofuranose

| (*ij*) | $\rho_{ij} \times 10^2$ | $r_{ij}$ (exptl.) | $r_{ij}$ (calcd.) |
|---|---|---|---|
| $\rho_{H\text{-}1,H\text{-}2}$ | 12.49±3.02 | 2.61±0.14 | 2.65 |
| | 10.20±3.16 | 2.70±0.17 | |
| $\rho_{H\text{-}1,H\text{-}3}$ | [a] | — | 4.12 |
| $\rho_{H\text{-}1,H\text{-}4}$ | [a] | — | 4.04 |
| | 0.90 | 4.05 | |
| $\rho_{H\text{-}2,H\text{-}3}$ | 18.77±3.86 | 2.44±0.12 | 2.35 |
| | 14.45±5.05 | 2.55±0.17 | |
| $\rho_{H\text{-}2,H\text{-}4}$ | [a] | — | 3.82 |
| $\rho_{H\text{-}3,H\text{-}4}$ | 39.24±6.52 | 2.16±0.09 | 2.28 |
| | 32.91±5.64 | 2.22±0.10 | |
| $\rho_{H\text{-}1,OH}$ | 41.07±4.17 | 2.14±0.08 | 2.00–2.43[b] |
| $\rho_{H\text{-}2,OH}$ | 2.55±2.49 | 3.40±0.56 | 3.02–3.39[b] |
| $\rho_{H\text{-}3,OH}$ | [a] | — | 4.50–4.00[b] |
| $\rho_{H\text{-}4,OH}$ | 7.50±3.55 | 2.84±0.25 | 4.52–3.50[b] |

[a] Negative values not shown.
[b] Range of distances in the first quadrant of circular motion for the OH group (see Table 3 and text).

Can. J. Chem. Downloaded from www.nrcresearchpress.com by 210.87.254.40 on 09/06/12
For personal use only.

interproton relaxation less effective, the neglect of contributions from such remote sources as the $CH_3$ groups may not be justified. Perhaps, for example, this accounts for the negative $\rho_{ij}$ values in Table 5. The largest errors might be associated with H-4, because its relaxation receives contributions from H-5,H-6 and -6′ in a variety of orientations.

Distances of various protons from the hydroxyl proton, given in Table 5, reflect the most probable orientation attained by the hydroxyl group during its rotation about the C-1—O-1 bond. The close agreement between the experimental values and the calculated values of $r_{H\text{-}1,OH}$ and $r_{H\text{-}2,OH}$ is commensurate with a dihedral angle of 60° ± 30° for the H-1—C-1—O—H array, and hence with a conformation of **1** in which rotamer *g* for the anomeric alcohol group is the most heavily populated. Consequently, these findings are in complete agreement with the 3-spin system analysis already described, as well as with the relaxation rate and spin–spin coupling data presented earlier. Finally, it is worth noting that the conformational angle ($\theta$) for O-4—C-1$^{\theta}$—O—H in favored rotamer *g* is 60°, whereas calculations on methoxymethanol predict (29) that the most favored value of $\theta$ for the hemiacetal moiety of an aldose is ~65°.

## Experimental

All $^1H$ and $^{13}C$ nmr experiments were conducted with a Varian XL-200 spectrometer, operating at 200 and 50.3 MHz for $^1H$ and $^{13}C$ nuclei, respectively. The probe temperature was 20°C. The solutions of 2,3:5,6-di-*O*-isopropylidene-α-D-mannofuranose (**1**) in dimethyl sulfoxide-$^2H_6$ were 0.1 *M* for all of the $^1H$ and $^{13}C$ nmr measurements. Each sample was carefully degassed by using at least 4 "freeze–pump–thaw" cycles, and then sealed.

*Measurement of* $R_1$

Proton spin-lattice relaxation rates were measured by the $(180°\text{–}\tau\text{–}90°\text{–}t)_x$ inversion recovery sequence (30), with an average of 16 free induction decays (fid). The delay between sequences was at least 5× the estimated value of the longest $T_1$ and, in all, three sets of experiments were performed. The optimal 180° pulse length, determined by producing a null in the amplitude of the fid, was 14 s. Typically, about 25 values of $\tau$ were "arrayed" in each run by utilizing the XL-200 $T_1$ programme, an appropriate range of $\tau$ values having been selected in preliminary experiments. Intensities of the components of each resonance were obtained from the computer printout; for multiplet resonances, they were summed. The total magnetization intensity for each resonance (except those of the overlapping H-4 and H-6 multiplets, only two of the four resonance components of each being summed) was then processed by a two-parameter linear regression analysis, to give an $R_1$ value. In all determinations, the initial-slope method (23–25) was used to ensure that cross-relaxation effects would be negligible. $R_1$ values are listed in Table 2; the error limits given are standard deviations of the fit.

$^{13}C$ spin-lattice relaxation measurements were made under conditions of full $^1H$ noise decoupling, by the two-pulse inversion recovery technique. The pulse duration for a 180° flip angle, checked as mentioned previously, was 24 μs, whereas the acquisition and waiting times were 1.023 and 6 s, respectively. A spectral window of 4000 Hz was used, and 100 scans were accumulated for each spectrum, while arraying 15–20 values of $\tau$. To minimize systematic errors, and factor out time as a variable in long experiments, the interleaving procedure available with the XL-200 spectrometer was used. Values of $T_1$ were determined by a two-parameter linear fit, using an equilibrium magnetization value ($M_0$) that was the average of at least 4 separate determinations.

*Measurement of nOe*

Steady-state proton nOe values were obtained from the intensities of the observed peaks in the "enhanced" spectrum, obtained with the irradiating field on, as compared with the intensities in the normal spectrum. At least 10 experiments were performed for each nOe value. In order to protect the receiver from overload, and to eliminate distortion of the spectrum by spin-decoupling, the irradiating field was gated off during acquisition of the fid. Delays of more than 10× the longest $T_1$ were used between the 90° pulses, and the irradiating power was the minimum required for effective saturation of the irradiated nucleus. The nOe values listed in Table 4, together with standard deviations, were calculated from eq. [8] by using integrated intensities.

## Acknowledgments

The authors express sincere thanks to McGill University for the granting (to P.D.) of the Harold Hibbert Memorial Fellowship, and to the Natural Sciences and Engineering Research Council of Canada for generous support.

1. G. A. JEFFREY and M. SUNDARALINGAM. Adv. Carbohydr. Chem. Biochem. **38**, 417 (1981), and earlier volumes.
2. R. H. MARCHESSAULT and S. PEREZ. Biopolymers, **18**, 2369 (1979).
3. N. L. BAULD and Y. S. RIM. J. Org. Chem. **33**, 1303 (1968).
4. R. R. FRASER, M. KAUFMAN, P. MORAND, and G. GOVIL. Can. J. Chem. **47**, 403 (1969).
5. A. S. PERLIN, N. CYR, R. G. S. RITCHIE, and A. PARFONDRY. Carbohydr. Res. **37**, C-1 (1974).
6. A. S. PERLIN. MTP Intern. Rev. Sci. Org. Chem. Ser. 2. Vol. 7. Butterworth. 1976. p. 1.
7. O. L. CHAPMAN and R. W. KING. J. Am. Chem. Soc. **86**, 1256 (1964).
8. M. MACKIE and A. S. PERLIN. Can. J. Chem. **44**, 2039 (1966).
9. M. KARPLUS. J. Am. Chem. Soc. **84**, 2458 (1962).
10. A. S. PERLIN. Can. J. Chem. **42**, 1365 (1964).
11. F. A. L. ANET. Can. J. Chem. **39**, 789 (1961).
12. R. J. ABRAHAM, L. D. HALL, L. HOUGH, and K. A. MACLAUCHLAN. J. Chem. Soc. 3699 (1962).
13. J. A. SCHWARZ and A. S. PERLIN. Can. J. Chem. **50**, 3667 (1972).
14. N. CYR and A. S. PERLIN. Can. J. Chem. **57**, 2504 (1979).
15. S. J. ANGYAL. Carbohydr. Res. **77**, 37 (1979).
16. (*a*) J. A. SCHWARCZ, N. CYR, and A. S. PERLIN. Can. J. Chem. **53**, 1872 (1975); (*b*) N. CYR, G. K. HAMER, and A. S. PERLIN. Can. J. Chem. **56**, 297 (1978).
17. I. SOLOMON. Phys. Rev. **99**, 559 (1955).
18. A. ABRAGAM. The principles of nuclear magnetism. Oxford Univ. Press. 1961.
19. J. H. NOGGLE and R. E. SHIRMER. The nuclear Overhauser effect. Academic Press, New York. 1971.

20. P. S. HUBBARD. J. Chem. Phys. **52**, 563 (1970).
21. L. D. HALL and H. D. W. HILL. J. Am. Chem. Soc. **98**, 1269 (1975).
22. E. HASLINGER and W. ROBEIN. J. Am. Chem. Soc. **102**, 1237 (1980), and references therein.
23. C. H. PRESTON and L. D. HALL. Carbohydr. Res. **37**, 267 (1974).
24. R. FREEMAN, S. WITTENBOEK, and R. R. ERNST. J. Chem. Phys. **52**, 1529 (1970).
25. L. D. COLEBROOK and L. D. HALL. Can. J. Chem. **58**, 2016 (1980).
26. (*a*) H. OGURA, K. FURUHATA, H. TAKAHASHI, and V. JITAKA. Chem. Pharm. Bull. **26**, 2782 (1978); (*b*) J. C. A. BOEYENS, E. B. RATHBONE, and G. R. WOOLARD. Carbohydr. Res. **62**, 39 (1978); (*c*) C. RICHE and C. PASCARD-BILLY. Acta Crystallogr. Sect. 3, **31**, 2565 (1975); (*d*) S. TAKAGI, R. SHIONO, and R. D. ROSENSTEIN. Acta Crystallogr. **29**, 1177 (1973); (*e*) A. AUBRY, J. PROTAS, P. DUCHAUSSOY, P. DI CESARE, and B. GROSS. Acta Crystallogr. **36**, 187 (1980); (*f*) J. C. A. BOEYENS, H. J. NOLTE, and G. R. WOOLARD. Carbohydr. Res. **70**, 103 (1979); (*g*) S. J. RETTIG and J. TROTTER. Can. J. Chem. **55**, 1454 (1977); (*h*) J. S. BRIMACOMBE, P. A. GENT, and T. A. HAMOR. J. Chem. Soc. B, 1566 (1968); (*k*) H. OHRUI, G. H. JONES, J. G. MOFFAT, M. L. MADDOX, A. T. CHRISTENSEN, and S. K. BYRAM. J. Am. Chem. Soc. **97**, 4602 (1975).
27. M. R. PETERSON and R. A. POIRIER. Monstergauss 79, loosely-based on Gaussian 76, Chem. Dept., Univ. Toronto.
28. D. H. WILLIAMS and J. R. KALMAN. J. Am. Chem. Soc. **99**, 2768 (1976).
29. G. A. JEFFREY, J. A. POPLE, and L. RADOM. Carbohydr. Res. **38**, 81 (1974).
30. R. FREEMAN and H. D. W. HILL. J. Chem. Phys. **53**, 4103 (1970).

Can. J. Chem. Downloaded from www.nrcresearchpress.com by 210.87.254.40 on 09/06/12
For personal use only.

# Photorearrangement of 2-cyanobicyclo[2.2.1]hept-2-ene. Observation of 1,2- and 1,3-sigmatropic shifts

IKBAL A. AKHTAR, JOHN J. MCCULLOUGH,[1] AND SUSAN VAITEKUNAS
*Department of Chemistry, McMaster University, Hamilton, Ont., Canada L8S 4M1*
AND
ROMOLO FAGGIANI AND COLIN J. L. LOCK
*Department of Chemistry and Institute for Materials Research, McMaster University, Hamilton, Ont., Canada L8S 4M1*

Received September 29, 1981

IKBAL A. AKHTAR, JOHN J. MCCULLOUGH, SUSAN VAITEKUNAS, ROMOLO FAGGIANI, and COLIN J. L. LOCK. Can. J. Chem. **60**, 1657 (1982).

Irradiation of 2-cyanobicyclo[2.2.1]hept-2-ene (2-cyanonorbornene, **4**) in hexane, with the full arc of a mercury vapour lamp, gives the rearrangement products 1-cyanobicyclo[4.1.0]hept-2-ene **5** and 7-cyanotricyclo[4.1.0.$0^{3,7}$]heptane **6** in the ratio 20:1. These products were separated by preparative vpc. The structure of the major product **5** was determined by single crystal X-ray analysis. Reduction of **5** with lithium aluminum hydride gave the corresponding primary amine, which was converted to the *p*-bromobenzenesulfonamide **9**, mp 150–151°C, which gave single crystals from ethanol–water. The crystal and molecular structures are described. The minor product **6** was hydrogenated to give 7-cyanobicyclo[2.2.1]heptane. Formation of **5** and **6** may involve concerted $\sigma_{2s} + \pi_{2s}$ and $\sigma_{2a} + \pi_{2a}$ processes respectively, which are photochemically allowed.

IKBAL A. AKHTAR, JOHN J. MCCULLOUGH, SUSAN VAITEKUNAS, ROMOLO FAGGIANI et COLIN J. L. LOCK. Can. J. Chem. **60**, 1657 (1982).

L'irradiation du cyano-2 bicyclo[2.2.1] heptène-2 (cyano-2 norbornène, **4**) dans l'hexane avec l'arc complet d'une lampe à vapeur de mercure conduit aux produits de transposition suivants: cyano-1 bicyclo[4.1.0] heptène-2 (**5**) et cyano-7 tricyclo [4.1.0.$0^{3,7}$] heptane (**6**) dans un rapport de 20:1. On a isolé ces produits par cpg préparative. On a déterminé la structure du produit majoritaire **5** par analyse aux rayons-X d'un mono-cristal. La réduction du composé *1* par l'alanate de lithium conduit à l'amine primaire correspondante. On transforme cette dernière en *p*-bromobenzènesulfonamide (**9**), pf 150–151°C, qui donne des monocristaux dans l'éthanol–eau. On décrit la structure du cristal et la structure moléculaire. Le produit secondaire **6**, par hydrogénation, conduit au cyano-7 bicyclo [2.2.1] heptane. La formation des composés **5** et **6** peut impliquer respectivement des processus concertés $\alpha_{2s} + \pi_{2s}$ et $\sigma_{2a} + \pi_{2a}$ qui sont permis photochimiquement.

[Traduit par le journal]

## Introduction

We have described (1) the rearrangement of 1-cyanocyclohexene **1**, which on direct irradiation in hexane gives the bicyclohexane derivatives **2** and **3**. Formation of these products must involve rearrangement of the σ-bonded group, and although these kinds of rearrangements are known in the photochemistry of neutral molecules, they are not numerous (some examples are enone "type A" rearrangements (2*a*), methyl migration (2*b*), and Wagner–Meerwein shifts (2*c*)). To determine the generality of the above rearrangement, and to study the effect of structure on the reaction, we have investigated the photochemistry of 2-cyanobicyclo[2.2.1]hept-2-ene **4**. This bicyclic nitrile also rearranges on irradiation, and the structure

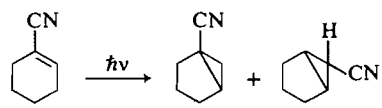


**1** **2** **3**

work on the products is described. The bicyclic system might be used later for labelling experiments to determine reaction stereochemistry.

## Results

The required nitrile **4** was prepared by reaction of 2-chloronorbornene with cuprous cyanide in *N*-methylpyrrolidinone (1). The 2-chloronorbornene was prepared via 2,2-dichloronorborane, which was obtained by reaction of norcamphor with phosphorus pentachloride. Details are given in the experimental section.

Irradiation of 2-cyanonorbornene **4** in hexane with unfiltered light from a Hanovia 450 W lamp gave two products, identified as 1-cyanobicyclo[4.1.0]hept-2-ene, **5**, and 7-cyanotricyclo-[4.1.0.$0^{3,7}$]heptane, **6**, in the ratio 20:1. The reaction is shown in Scheme 1.

The products were separated by preparative vpc and the gross structural features determined from their spectra. Product **5** had ir: 2240 $cm^{-1}$ (CN stretch); $^1H$ nmr, δ: 6.02 (1h, doublet, $J$ = 10.0 Hz, vinylic), 5.66 (1H, multiplet, vinylic), 1.1–2.1 (7H,

[1]Author to whom correspondence may be addressed.

0008-4042/82/131657-07$01.00/0
©1982 National Research Council of Canada/Conseil national de recherches du Canada

Can. J. Chem. Downloaded from www.nrcresearchpress.com by 210.87.254.5 on 09/06/12
For personal use only.

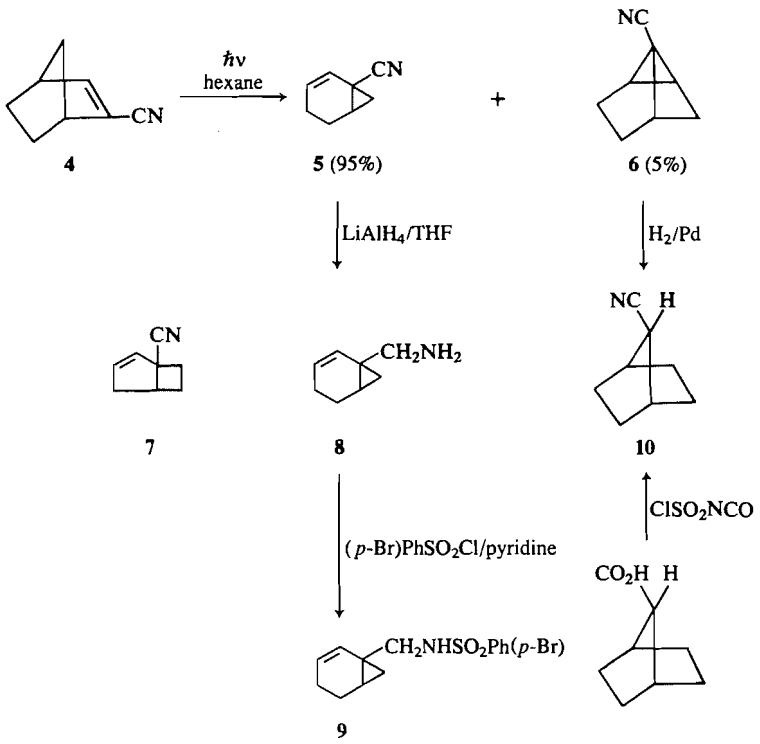


SCHEME 1

envelope of aliphatic protons); mass spectrum, *m/e*: 119 ($M^+$, $C_8H_9N$).

Although $J_{vinyl\text{-}vinyl}$ of 10.0 Hz is in the range for a cyclohexene derivative (3), we attempted to distinguish between structure **5** and the isomer **7** by synthesizing the latter (4).[2] None of the synthetic approaches proved successful, and X-ray crystal structure analysis was used. Reduction of **5** with $LiAlH_4$ gave the amine **8**, which readily formed a *p*-bromobenzenesulphonyl chloride in pyridine (Scheme 1). This gave crystals suitable for X-ray work, which is described below and in the experimental section. The structure **9** is shown[3] in Fig. 1.

The minor product **6** had the following spectral data: infrared, bands at 2215 $cm^{-1}$ (CN) and 3050 $cm^{-1}$ (cyclopropyl CH); $^1H$ nmr, envelope from δ: 1.0–3.0; mass spectrum, *m/e*: 119 ($M^+$). Catalytic hydrogenation gave 7-cyanobicyclo[2.2.1]heptane **10**, and structure 7-cyanotricyclo[4.1.0.$0^{3,7}$] heptane is assigned (Scheme 1).

*Description of crystal and molecular structure*

The molecule is illustrated in Fig. 1 and selected bond lengths and angles are given in Table 1. There is excellent agreement between the bond lengths in

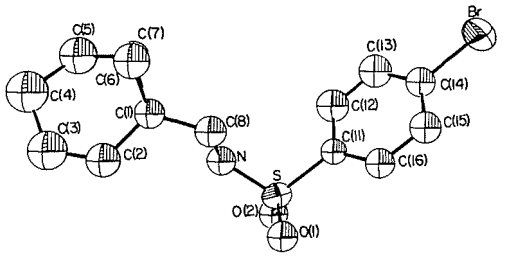


FIG. 1. The molecule bicyclo[4.1.0]hept-2-en-1-ylmethanamine *p*-bromobenzenesulphonamide (**9**), showing the atom numbering. Hydrogen atoms have been omitted for simplicity.

the cyclohexene moiety and values found previously (5–8). Internal angles at the olefin agree well with previous values, but angles adjacent to the cyclopropane ring (C(2)—C(1)—C(6), 115.2(6)°, C(1)—C(6)—C(5), 117.1(8)°) and possibly (C(4)—C(5)—C(6) 114.3(9)°) are larger than normal values of 111°. Presumably this increase is caused by steric requirements of the cyclopropane ring. Further distortions are observed by comparing distances of atoms from the C(1)C(2)C(3)C(4) plane or torsional angles within the cyclohexene ring with previous results (6, 8). Thus C(5) is 0.768(9) Å out of the plane compared with 0.340(7) Å for C(6), both in the same direction, whereas a value of ~0.38 Å on opposite sides of the plane is more normal (5, 7). Alternately the torsional angles differ significantly

[2]While this work was in progress, structure **7** (*cis*-fused) was described (4). The vinyl–vinyl coupling is 5.6 Hz.

[3]The three-membered ring can be seen more clearly in Fig. 2.

Can. J. Chem. Downloaded from www.nrcresearchpress.com by 210.87.254.5 on 09/06/12
For personal use only.

Can. J. Chem. Downloaded from www.nrcresearchpress.com by 210.87.254.5 on 09/06/12
For personal use only.

TABLE 1. Selected interatomic distances (Å) and angles (deg)

| Bond | Length | Bond | Length | Bond | Length |
|---|---|---|---|---|---|
| C(1)—C(2) | 1.50(1) | C(2)—C(3) | 1.33(2) | C(3)—C(4) | 1.51(2) |
| C(4)—C(5) | 1.53(1) | C(5)—C(6) | 1.52(2) | C(6)—C(1) | 1.52(1) |
| C(1)—C(7) | 1.51(1) | C(6)—C(7) | 1.48(1) | C(1)—C(8) | 1.47(1) |
| C(8)—N | 1.48(1) | N—S | 1.606(1) | S—O(1) | 1.423(6) |
| S—O(2) | 1.438(6) | S—C(11) | 1.741(8) | C(11)—C(12) | 1.39(1) |
| C(12)—C(13) | 1.37(1) | C(13)—C(14) | 1.36(1) | C(14)—C(15) | 1.36(1) |
| C(15)—C(16) | 1.40(1) | C(16)—C(11) | 1.37(1) | C(14)—Br | 1.895(9) |

| Bonds | Angle | Bonds | Angle | Bonds | Angle |
|---|---|---|---|---|---|
| C(6)—C(1)—C(2) | 115.2(6) | C(1)—C(2)—C(3) | 124.0(9) | C(2)—C(3)—C(4) | 122(1) |
| C(3)—C(4)—C(5) | 111.7(9) | C(4)—C(5)—C(6) | 114.3(9) | C(5)—C(6)—C(1) | 117.1(8) |
| C(7)—C(1)—C(6) | 58.5(6) | C(1)—C(6)—C(7) | 60.6(6) | C(6)—C(7)—C(1) | 60.9(6) |
| C(2)—C(1)—C(8) | 116.9(7) | C(7)—C(1)—C(8) | 118.4(8) | C(7)—C(1)—C(2) | 115.5(6) |
| C(6)—C(1)—C(8) | 119.6(6) | C(1)—C(8)—N | 109.6(7) | C(8)—N—S | 119.5(3) |
| N—S—O(1) | 108.5(3) | N—S—O(2) | 105.4(4) | N—S—C(11) | 108.4(3) |
| O(1)—S—O(2) | 119.4(3) | O(1)—S—C(11) | 107.4(4) | O(2)—S—C(11) | 107.3(3) |
| S—C(11)—C(12) | 119.5(6) | S—C(11)—C(16) | 121.5(6) | C(16)—C(11)—C(12) | 119.0(8) |
| C(11)—C(12)—C(13) | 121.2(9) | C(12)—C(13)—C(14) | 118.4(9) | C(13)—C(14)—C(15) | 122.6(8) |
| C(14)—C(15)—C(16) | 118.6(9) | C(15)—C(16)—C(11) | 120.2(8) | C(13)—C(14)—Br | 118.4(3) |
| C(15)—C(14)—Br | 118.9(4) | | | | |

TABLE 2. Best planes, and dihedral and torsional angles (deg)

| Plane | Distance of atoms from the plane (Å) |
|---|---|
| 1. C(1)C(2)C(3)C(4) | C(1) −0.001(7); C(2) 0.004(9); C(3) −0.005(9); C(4) 0.002(9); C(5) 0.768(9); C(6) 0.340(7); C(7) −1.065(9); C(8) 0.382(7). |
| 2. C(1)C(6)C(7) | |
| 3. C(11)C(12)C(13)C(14)C(15)C(16) | C(11) −0.009(7); C(12) 0.010(9); C(13) 0.004(9); C(14) −0.010(8); C(15) 0.008(9); C(16) 0.004(8); S 0.020(2); Br −0.020(1). |

Dihedral angles (deg)

Plant 1 – Plane 2 81.2(9) Plane 1 – Plane 3 30.0(9) Plane 2 – Plane 3 74.5(9)

Torsional angles (deg)

| | | | | | |
|---|---|---|---|---|---|
| C(1)C(2)C(3)C(4) | 1.2(9) | C(2)C(3)C(4)C(5) | 31.2(9) | C(3)C(4)C(5)C(6) | −48.7(9) |
| C(4)C(5)C(6)C(1) | 36.5(9) | C(5)C(6)C(1)C(2) | −5.4(8) | C(6)C(1)C(2)C(3) | −15.2(8) |
| C(3)C(2)C(1)C(8) | −163.5(7) | C(3)C(2)C(1)C(7) | 50.3(7) | C(5)C(6)C(1)C(7) | −111.0(9) |
| C(5)C(6)C(1)C(8) | 142.0(8) | C(2)C(1)C(8)N | 59.3(8) | C(6)C(1)C(8)N | −87.6(8) |
| C(7)C(1)C(8)N | −155.5(8) | C(8)NSC(11) | −63.5(6) | C(8)NSO(1) | 52.9(6) |
| C(8)NSO(2) | −178.1(6) | NSC(11)C(12) | −51.4(6) | NSC(11)C(16) | 131.3(6) |
| O(1)SC(11)C(16) | 14.2(6) | O(1)SC(11)C(12) | −168.6(6) | O(2)SC(11)C(16) | 61.9(6) |
| O(2)SC(11)C(12) | −115 (6) | | | | |

from those in $\Delta^{1,11}$-dicyclohexenyl ketone (6). The resulting form is a modified "boat" and corresponds neither to the $C_2$ "half-chair" form, observed in other structures (5–9) or the "1–2 diplanaire", calculated by Bucourt to be the next most stable form (10). Clearly the abnormal structure observed here arises from the interaction (one bond separation) of the constraints of the olefin and the cyclopropane ring, both of which will tend to make torsional angles about their C—C bonds as close to 0° as possible.

Bond lengths and angles within the *p*-bromosulfonamide portion of the molecule agree very well with those observed previously (11). The torsional angles (Table 2) show that the backbone of the molecule is arranged to minimize nonbonded interactions, except that between C(11)—H(16) and O(1) (O(1)SC(11)—C(16) = 14.2°). Apparently the

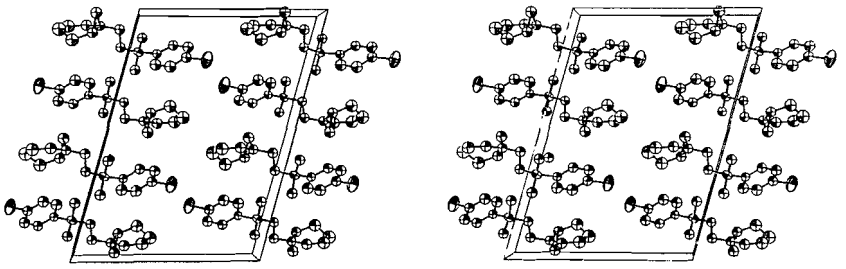

FIG. 2. The packing of *p*-bromobenzenesulphonamide (**9**), within the unit cell; *a* and *c** are parallel to the bottom and sides of the page and the view is down *b* (hydrogen atoms omitted).

steric requirements of the $-NH_2$ group are more important in determining the orientation of the aromatic ring.

Bond lengths and angles in the cyclopropane unit are normal and the dihedral angle of 108.1(2)° between C(1)C(6)C(7) and C(5)C(6)C(1)C(2) is similar to values observed previously by others (12) (Range 104.2° to 110.1°) and ourselves (105.7(2)°) (13).

The packing of the molecules is shown in Fig. 2. The overall shape of the molecule resembles a shallow V (see Fig. 1) and the molecules are arranged in layers centred on the 100 faces so that the apices of the V's lie roughly in the face. The V is symmetric about the face and the angle of the V is roughly parallel to the 001 face. Within these layers adjacent molecules related by the $2_1$ axes at $x = 0, z = 1/4, 3/4$ are hydrogen bonded together through N···O(2)′ (2.92(1) Å) to form a spiral chain parallel to *b*. Adjacent chains in the layer have the apices of the V's pointing in opposite directions along *b* and contact between the chains involves hydrocarbon fragments and van der Waals interactions. Between layers, in the *a* direction, contacts at $x = 1/2$ are hydrocarbon–hydrocarbon, bromine–bromine, and bromine–hydrocarbon.

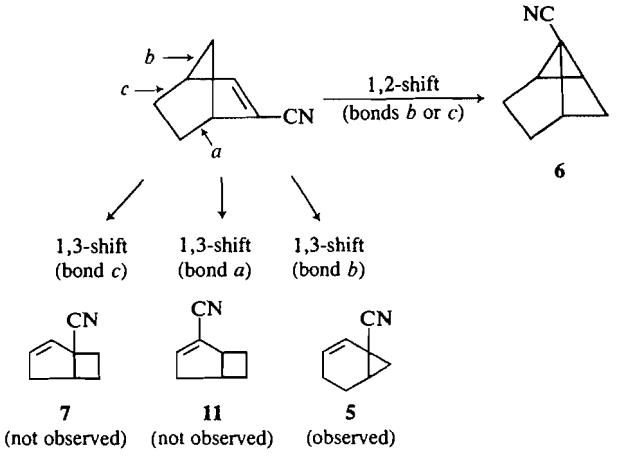


SCHEME 2

## Discussion

The tricyclic product **6** is the product of the 1,2-shift of a σ-bond, in the same fashion as reported previously (1). The tricyclo[4.1.0.$0^{3,7}$]-heptane ring system is well-known, and is formed in solvolysis reactions (14, 24), in photochemistry of unsaturated ketones (15), and in the photorearrangement of benzonorbornadiene (16). Note that 1,2-migration of either bond "*b*" or "*c*" (Scheme 2) would give product **6**, and labelling studies will be needed to distinguish which bond is involved.

Formation of the major product **5** involves 1,3-migration of a σ-bond, and although this process is known in photochemical (17) and thermal reactions (18), it was not observed in the photochemistry of 1-cyanocyclohexene (1). Formation of **5** requires 1,3-migration of bond "*b*" (Scheme 2); in contrast, migration of bonds of the ethano-bridge ("*c*" or "*a*") would give the bicyclo[3.2.0]heptane system, e.g. **7** or **11** respectively.

Thus, formation of **6** and **5** involves competing 1,2- and 1,3-sigmatropic shifts. Both processes are

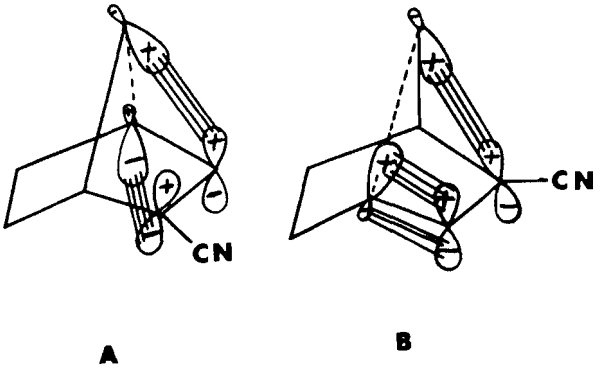


FIG. 3. Possible transition states for the photochemical symmetry allowed 1,2-(A) and 1,3-(B) sigmatropic shifts. A is $\sigma_{2a} + \pi_{2a}$ and B is $\sigma_{2s} + \pi_{2s}$.

Can. J. Chem. Downloaded from www.nrcresearchpress.com by 210.87.254.5 on 09/06/12
For personal use only.

Can. J. Chem. Downloaded from www.nrcresearchpress.com by 210.87.254.5 on 09/06/12
For personal use only.

symmetry allowed (19, 20) in the excited state ($\sigma_{2a} + \pi_{2a}$ and $\sigma_{2s} + \pi_{2s}$ respectively). The orbitals involved are shown in Fig. 3. We are not sure at present that the reaction is concerted, and plan further work on the mechanism, stereochemistry, and generality of the rearrangement.

## Experimental

*Materials*

The norcamphor, chlorosulphonyl isocyanate, and other organic reagents were obtained from the Aldrich Chemical Company. Hexane for the photolysis was "Spectrograde", or was purified using fuming sulphuric acid (1). Tetrahydrofuran was distilled from LAH immediately before use. Pyridine was distilled and kept over KOH pellets. 2,2-Dichloronorbornane was prepared as described by Bixler and Niemann (21).

*Instruments*

Irradiations were carried out using a Hanovia 450 W lamp and a quartz water-cooled immersion well. The solution was purged with argon. Ultraviolet spectra were run on a Carey 14 spectrometer, infrared spectra on a Perkin–Elmer 283, and nmr spectra on a Varian EM-390 or a Bruker WH-90 spectrometer. Mass spectra were obtained with a VG Micromass 7601 instrument.

Gas chromatography was performed on a Varian Aerograph 202 instrument with thermal conductivity detectors (preparative) or on a Tracor 560 with flame ionization detectors (analytical). Carrier gas was helium, and columns used are given below. Elemental analyses were by Galbraith Laboratories, Knoxville, Tenn., and Guelph Chemical Laboratories, Guelph, Ontario.

*2-Chlorobicyclo[2.2.1]heptene*

This compound was prepared from 2,2-dichlorobicyclo-[2.2.1]heptane (21) by dehydrochlorination using potassium *tert*-butoxide (22*b*). It has bp 29–30°/12 Torr, and infrared and $^1$H nmr spectra in good agreement with the literature (22).

*2-Cyanobicyclo[2.2.1]hept-2-ene*

The above vinyl chloride (8.0 g, 0.062 mol) and $Cu_2(CN)_2$ (11.1 g, 0.062 mol) were heated under reflux in 50 mL of 1-methyl-2-pyrrolidinone for 3 h. After cooling the mixture was poured into 300 mL of water containing 12.9 g of NaCN. Benzene (300 mL) was added, and the mixture was filtered through Celite. The layers were separated, and the aqueous phase was extracted with 2 × 50 mL benzene. The benzene extracts were washed with 200 mL of 10% aqueous NaCN, 200 mL of water, and dried ($Na_2SO_4$). The benzene was evaporated and the residue distilled to yield crude 2-cyanobicyclo[2.2.1]hept-2-ene, bp 67–69°C/12 Torr, 2.35 g (35%). The ir showed that 1-methyl-2-pyrrolidinone was present (band at 1700 cm$^{-1}$). The product was dissolved in 25 mL ether, and washed with 3 × 50 mL water. After distillation, infrared showed the band at 1700 cm$^{-1}$ was absent; ir (neat): 2210, 1570 cm$^{-1}$; $^1$H nmr ($CCl_4$), δ: 6.90 (1H, d, $J$ = 4 Hz, vinylic proton), 3.0–3.2 (2H, m, bridgehead proton), 1.0–1.9 (6H, M, other ring protons). $J_{(vinyl-bridgehead)}$ of 4 Hz is reported (23). *Anal.* calcd. for $C_8H_9N$: C 80.63, H 7.60, N 11.75%; found: C 80.14, H 7.60, N 11.95%.

*Irradiation of 2-cyanobicyclo[2.2.1]*heptene

The unsaturated nitrile **4** (550 mg, 4.5 mmol) in hexane (400 mL) was irradiated under argon for 3 h, using the Hanovia 450 W lamp. Vapor phase chromatographic analysis (6 ft × ¼ in. of 3% OV-1, glass column, at 80°C) showed two products, ratio 20:1 with retention times 350 and 455 s respectively. The solution was filtered through Celite, and the hexane distilled (1 atm) through a column of glass helices. The residue was distilled in a Kugelrohr apparatus (100°C/15 Torr) to yield 320 mg of the mixed photoproducts. These were separated by vpc (5 ft × ¼ in. of 7% QF-1 on Chromosorb W at 125°C, with the flow rate of 30 mL/min). The minor product (retention time 19 min) had $m/e$ = 119 ($M^+$); ir (neat): 3055, 2215 cm$^{-1}$; $^1$H nmr ($CDCl_3$), δ: 1.2–2.9 (envelope); $^{13}$C nmr ($CDCl_3$); 42.6 ppm (d), 37.7 (t), 33.7 (d), 27.2 (d), 25.1 (t), 22.6 (t) ppm. The structure **6** is assigned from the hydrogenation to 7-cyanonorbornane, described below. The major product (retention time 14 min) also had $m/e$ = 119 ($M^+$); ir (neat): 1648, 2240 cm$^{-1}$; $^1$H nmr ($CDCl_3$)δ: 6.02 (1H, d, $J$ = 10.0 Hz) and 5.66 (1H, m, vinylic protons), 1.2–2.2 (7H, m); $^{13}$C nmr ($CDCl_3$): 125.3, 123.7, 24.3, 20.2, 19.4, 17.0 ppm. *Anal.* calcd. for $C_8H_9N$: C 80.63, H 7.61, N 11.76; found: C 80.61, H 7.61, N 11.90%. The structure 1-cyanobicyclo[4.10]hept-2-ene **5** is assigned from the X-ray work described below.

*Hydrogenation of minor product **6** from photolysis*

The tricyclic nitrile **6** (81 mg, 5.6 × 10$^{-3}$ mol) (83% pure by vpc) in ethyl acetate (7.0 mL) was hydrogenated over 10% Pd-on-carbon catalyst at 1 atm. Nine milliliters of $H_2$ were absorbed (4 × 10$^{-3}$ mol), and vpc analysis (6 ft × ¼ in. of 3% OV-1 at 100°C) showed the reaction was essentially complete. The catalyst was filtered, the solvent was evaporated, and the residue distilled (Kugelrohr, 100°/12 Torr) to give 64.3 mg, which was purified by vpc (6 ft. × ¼ in. of 7% QF-1 on WP 80/100, at 90°C). This afforded 7-cyanobicyclo[2.2.1]heptane, mp 61–64°C (lit. (24) mp 65–67°).

*Preparation of 7-cyanobicyclo[2.2.1]heptane from bicyclo-[2.2.1]heptane-7-carboxylic acid*

The method of Lohaus (25) was used. Bicyclo[2.2.1]heptane-7-carboxylic acid[4], mp 75–78°C (5 mg, 3.6 × 10$^{-5}$ mol) in pentane (10 mL) was treated with several drops (~100 mg) of chlorosulphonyl isocyanate at 40°C, under argon. After 4 h the mixture was cooled to 20°C, and dimethylformamide was added until gas evolution ceased. After 30 min crushed ice was added, aqueous and pentane layers were separated, and the aqueous layer was extracted with 2 × 10 mL pentane. The pentane layers were combined, dried, and concentrated; vpc analysis (6 ft × ¼ in. 3% OV-1 at 100°C) showed a product with the same retention time (192 s) as the above hydrogenation product. The structure 7-cyanotricyclo[4.1.0.0$^{3,7}$]heptane **6** is assigned to the minor photoproduct.

*Preparation of derivative of **5** for X-ray work. Reduction of 1-cyanobicyclo[4.1.0]hept-2-ene with lithium aluminum hydride*

The major photoproduct **5** (100 mg, 8.4 mmol) in hexane (~1.0 mL) was added to $LiAlH_4$ in tetrahydrofuran (5.0 mL). The mixture was stirred and heated under reflux for 24 h. Excess $LiAlH_4$ was decomposed with wet THF, and the mixture was filtered through Celite. Water and ether were added, and the ether layer was separated and dried ($Na_2SO_4$). The ether was evaporated and the residue distilled (Kugelrohr) to yield bicyclo[4.1.0]hept-2-en-1-ylmethanamine, 70 mg (68%); ir (neat): 3700–3100 cm$^{-1}$, no CN band.

*Preparation of p-bromobenzensulphonamide of bicyclo[4.1.0]-hept-2-en-1-ylmethanamine **8***

The products from the above reduction (70 mg) and *p*-bromobenzenesulphonyl chloride (118 mg) were dissolved in pyridine and kept in the refrigerator for 24 h. The mixture was poured into ice-cold 6*N* HCl, and extracted with 3 × 25 mL of ether. The extracts were dried and evaporated to afford the crude

[4]We thank Dr. J. Warkentin for this sample.

Can. J. Chem. Downloaded from www.nrcresearchpress.com by 210.87.254.5 on 09/06/12
For personal use only.

TABLE 3. Crystal data

| | |
|---|---|
| Compound | $C_{14}H_{16}BrNO_2S$ |
| Formula weight | 342.26 |
| Crystal size (mm) | cylinder, $r = 0.10$, $l = 0.40$ |
| Systematic absences | $hol$, $l \neq 2n + 1$, $oko$, $k \neq 2n + 1$ |
| Space group | $P2_1/c$ |
| Unit cell (Å and deg) | $a = 13.551(5)$, $b = 5.993(2)$, $c = 18.832(4)$ $\beta = 105.44(2)$ |
| Volume (Å$^3$) | 1474.2(5) |
| $Z$ | 4 |
| $\rho_{calc}$[g cm$^{-3}$] | 1.54 |
| $\rho_{obs}$[g cm$^{-3}$] | 1.50(2) |
| Linear absorption coefficient (cm$^{-1}$) | 30.89 |
| Max 2θ, reflections collected | 55°, $h, k, \pm l$ |
| Standard reflections (esd, %) | 6 1 −5 (1.53), 7 0 2 (1.53) |
| Temperature (°C) | 22 |
| No. of independent reflections | 3410 |
| No. with $I > 3\sigma(I)$ | 1004 |
| No. with $3\sigma(I) > I > \sigma(I)$, $F_c < F_o$ | 1089[a] |
| No. with $I < \sigma(I)$, rejected | 872[a] |
| Final $R_1$,[b] $R_2$[b] | 0.0809, 0.0694 |
| Final shift/error, max(ave) (non-H) | 0.0014, 0.0001 |
| max(ave) (all parameters) | 4.19, 0.84 |
| g(secondary extinction) | $6.64 \times 10^{-8}$ |
| No. of variables | 156 |
| Final difference map | |
| Highest peak (e/Å$^3$); location | 0.56; 0.10, 0.35, 0.25 |
| Lowest valley (e/Å$^3$); location | −0.46; 0.05, 0.40, 0.15 |
| Weighting | $w = (\sigma^2 + (0.03F_o)^2)^{-1}$ |
| Error in an observation of unit weight | 1.265 |

[a]Most unobserved reflections occurred above 2θ = 30°.
[b]$R_1 = \Sigma||F_o| - |F_c||/\Sigma|F_o|$; $R_2 = \{\Sigma w(|F_o| - |F_c|)^2/\Sigma wF_o^2\}^{1/2}$

derivative, mp 124–140°C. Two cyrstallizations from ethanol–water gave an analytical sample, mp 150–151°C. *Anal.* calcd. for $C_{15}H_{16}NSO_2Br$: C 49.13, H 4.71, N, 4.09; found: C 49.22, H 4.79, N 3.92%. A crystal suitable for the following X-ray work was obtained by slow crystallization from ethanol–water.

*Collection of the X-ray data*

An acicular crystal of the above *p*-bromosulphonamide, selected after examination under a polarizing microscope for homogeneity, was ground to a cylinder and sealed to a glass fibre for X-ray examination. Precession photographs showed the crystal was monoclinic and unit cell parameters were obtained from a least squares fit of χ, φ, and 2θ for 15 reflections in the range 17.7° < 2θ < 25.1° recorded on a Syntex $P2_1$ diffractometer using graphite-monochromated MoKα radiation (λ 0.70926 Å). Crystal data and other numbers related to data collection are summarized in Table 3. The density was obtained by flotation in an aqueous zinc bromide solution to which a few drops of liquid detergent had been added in order to wet the crystal. Intensities were also recorded on the Syntex $P2_1$ diffractometer using a coupled θ(crystal) – 2θ(counter) scan. The methods of selection of scan rates and initial data treatment have been described (26, 27). Corrections were made for Lorentz polarization effects, but not for absorption. This will make a maximum error in $F_o$ of < 1.0%.

*Solution of the structure*

The bromine atom was found from a three dimensional Patterson synthesis, and a series of full-matrix least-squares refinements and electron density difference syntheses revealed all the atoms. At this stage the temperature factors of the bromine and sulphur atoms were made sequentially isotropic.

TABLE 4. Atomic positional parameters (× 10$^4$) and temperature factors (Å) (× 10$^3$)

| Atom | $x$ | $y$ | $z$ | $U$ |
|---|---|---|---|---|
| Br | −4292.4(8) | −524(2) | 7972.7(7) | |
| S | −544(2) | 6225(3) | 8407(1) | |
| C(1) | 1874(6) | 2792(13) | 9419(4) | 50(2) |
| C(2) | 2652(7) | 4613(15) | 9496(5) | 63(3) |
| C(3) | 3605(8) | 4295(18) | 9448(5) | 84(3) |
| C(4) | 3970(8) | 2046(19) | 9269(6) | 96(4) |
| C(5) | 3088(8) | 630(17) | 8809(5) | 82(3) |
| C(6) | 2133(6) | 635(15) | 9087(4) | 57(2) |
| C(7) | 2227(7) | 743(15) | 9888(5) | 67(3) |
| C(8) | 800(6) | 3479(14) | 9281(4) | 55(2) |
| C(11) | −1570(5) | 4397(12) | 8308(4) | 41(2) |
| C(12) | −1660(7) | 2582(16) | 7835(5) | 68(3) |
| C(13) | −2463(7) | 1123(16) | 7736(5) | 70(3) |
| C(14) | −3182(6) | 1498(14) | 8109(4) | 55(2) |
| C(15) | −3144(7) | 3281(15) | 8561(5) | 61(2) |
| C(16) | −2317(6) | 4755(14) | 8663(4) | 53(2) |
| N | 495(4) | 4792(10) | 8589(3) | 50(2) |
| O(1) | −526(4) | 7628(9) | 9020(3) | 54(2) |
| O(2) | −627(4) | 7212(9) | 7698(3) | 57(2) |

Anisotropic temperature factors $V_{ij}$ are given by the expression $\exp[-2\pi^2(h^2a^{*2}U_{11} + \ldots + 2hka^*b^*U_{12} + \ldots)]$. For Br, $U_{11} = 0.0639(8)$, $U_{22} = 0.0675(8)$, $U_{33} = 0.158(1)$, $U_{12} = -0.0127(6)$, $U_{13} = 0.0146(7)$, $U_{23} = -0.0012(8)$; for S, $U_{11} = 0.059(1)$, $U_{22} = 0.041(1)$, $U_{33} = 0.041(1)$, $U_{12} = 0.004(1)$, $U_{13} = 0.022(1)$, $U_{23} = 0.003(1)$.

# Selection of ternary fused chlorides for the electrowinning of aluminum based on calculated thermodynamic properties

A. D. PELTON

*Département de génie métallurgique, Ecole Polytechnique (Campus de l'Université de Montréal), C.P. 6079, Montréal (Qué.), Canada H3C 3A7*

J. M. SKEAFF

*Pyrometallurgy Section, Extractive Metallurgy Laboratory, Mineral Sciences Laboratories, CANMET, Dept. of Energy, Mines and Resources, Ottawa, Ont., Canada K1A 0G1*

AND

C. W. BAL AND P. L. LIN

*Pyrometallurgy Section, Extractive Metallurgy Laboratory, Mineral Sciences Laboratories, CANMET, Dept. of Energy, Mines and Resources, Ottawa, Ont., Canada K1A 0G1*

Received October 9, 1981

A. D. PELTON, J. M. SKEAFF, C. W. BALE, and P. L. LIN. Can. J. Chem. **60**, 1664 (1982).

Phase diagrams and total vapour pressures in the reciprocal ternary systems LiCl–NaCl–$LiAlCl_4$–$NaAlCl_4$, LiCl–KCl–$LiAlCl_4$–$KAlCl_4$, and NaCl–KCl–$NaAlCl_4$–$KAlCl_4$ have been calculated by means of computerized optimization and interpolation techniques based on an analysis of the constituent binary systems.

The system LiCl–NaCl–$LiAlCl_4$–$NaAlCl_4$ exhibits an extensive composition region of one-phase liquid solution whereas the LiCl–KCl–$LiAlCl_4$–$KAlCl_4$ system has a miscibility gap which covers ~ 50% of the composition region. Comparison of the calculated phase diagram with measured data for NaCl–KCl–$NaAlCl_4$–$KAlCl_4$ was made and the agreement between the two was found to be satisfactory.

Temperatures and compositions of chloride electrolytes suitable for the electrowinning of aluminum have been proposed from the isothermal sections of the phase diagrams and total vapour pressure curves. In all of the systems, the total vapour pressure is greater than the minimum for non-volatilization.

A. D. PELTON, J. M. SKEAFF, C. W. BALE et P. L. LIN. Can. J. Chem. **60**, 1664 (1982).

Faisant appel à une maximisation calculée et à des techniques d'interpolation basées sur une analyse de constituants des systèmes binaires, on a calculé les diagrammes de phase et les pressions totales de vapeurs des systèmes linéaires réciproques de LiCl–NaCl–$LiAlCl_4$–$NaAlCl_4$, LiCl–KCl–$LiAlCl_4$– $KAlCl_4$ et de NaCl–KCl–$NALCl_4$–$KAlCl_4$.

Le système LiCl–NaCl–$LiAlCl_4$–$NaAlCl_4$ montre une région de composition extensive d'une solution en phase liquide tandis que le système LiCl–KCl–$LiAlCl_4$–$KAlCl_4$ a une intervalle de miscibilité qui couvre environ 50% de la composition de la région. On a comparé les diagrammes de phase calculés avec les données mesurées dans le cas du système NaCl–KCl–$NaAlCl_4$–$KAlCl_4$ et on a trouvé que les résultats s'accordent bien. A partir des sections isothermes des diagrammes de phase et des courbes de pression totales de vapeur, on a proposé les températures et les composition des électrolytes contenant des chlorures qui conviennent parfaitement à l'électro-gain de l'aluminium. Dans tous les systèmes, la pression totale de vapeur est supérieure au minimum de non volatilisation.

[Traduit par le journal]

## Introduction

The problems of high energy consumption as well as the production of CO, $CO_2$, and fluoride emissions associated with conventional Hall-Heroult process aluminum smelters (1) have prompted investigation into new processes which would reduce or eliminate these difficulties. One such process is the electrowinning of aluminum from fused chloride salts, which has been reviewed elsewhere (1, 2).

Major considerations in the fused salt electrowinning of liquid metals from chloride media are: (*1*) that the electrolyte be a one-phase liquid; (*2*) that the electrolyte losses due to volatilization be minimized; (*3*) that the metal chloride decomposition potential be determined; (*4*) that the difference in density between the electrolyte and the electrowon liquid metal be sufficient to cause their rapid gravity separation; (*5*) that the electrolyte have a low viscosity; and (*6*) that the electrolyte have a high ionic conductivity. It is thus necessary to have data on phase diagrams, vapour pressures, decomposition potentials, densities, viscosities, and electrical conductivities of possible electrolytes in order to determine temperatures and compositions suitable for electrowinning or electrorefining.

While aluminum electrowinning experiments have been conducted to determine current densities, current efficiencies, and energy consumptions, usually with binary fused chloride systems as the electrolyte, the literature indicates that ternary fused chloride systems which have been employed or may be suitable for the electrowinning of alumi-

0008-4042/82/131664-17$01.00/0

©1982 National Research Council of Canada/Conseil national de recherches du Canada

Can. J. Chem. Downloaded from www.nrcresearchpress.com by 210.87.254.40 on 09/06/12
For personal use only.

Can. J. Chem. Downloaded from www.nrcresearchpress.com by 210.87.254.40 on 09/06/12
For personal use only.

num have not been thermodynamically well characterized. Most notably, published data are lacking on the phase diagrams and vapour pressures of ternary chloride systems involving aluminum chloride with the alkali chlorides.

In a previous publication (3), the authors presented the results of the calculation of the phase diagrams and vapour pressures of the ternary fused chloride systems LiCl–KCl–$PbCl_2$, LiCl–KCl–$ZnCl_2$, NaCl–KCl–$PbCl_2$, and NaCl–KCl–$ZnCl_2$ from the known properties of the constituent binary systems. Temperatures and compositions in these electrolytes suitable for the electrowinning of lead and zinc were then proposed from isothermal sections of the phase diagrams and from iso-vapour pressure curves of $PbCl_2$ and $ZnCl_2$.

In the present publication, we extend this method of calculating phase diagrams and vapour pressures to the systems LiCl–NaCl–$AlCl_3$, LiCl–KCl–$AlCl_3$, and NaCl–KCl–$AlCl_3$. The method, which has been described in detail previously (3–7), consists of a computer-assisted critical analysis of the available phase diagrams and thermodynamic data for the binary subsystems in order to obtain mathematical expressions for the thermodynamic properties of all known phases. At the same time, this critical analysis serves to help resolve discrepancies in the literature and to help set error limits on all data and calculations. The thermodynamic properties of the ternary systems are estimated from these binary data, and the ternary phase diagrams and vapour pressures are then calculated.

Based on the results of these calculations, we then discuss electrolyte temperatures and compositions for aluminum electrowinning from the view point of (*1*) maintaining a one-phase liquid solution, and (*2*) minimizing the total vapour pressures to reduce volatilization losses.

Because of very high vapour pressures which have been calculated (8) to occur in these systems for $X_{AlCl_3} > 0.5$, and therefore render $AlCl_3$-rich compositions of limited practical interest for electrowinning, in this paper we will be concerned only with compositions for which $X_{AlCl_3} \leq 0.5$.

## One-component chlorides

There are three alkali metal chlorides and one light metal chloride listed in Table 1, which are to be considered in the present study. For the phase diagram calculations, the free energies of fusion of the alkali chlorides are required. Values from the literature (9) are listed in Table 2.

TABLE 1. Systems investigated in the present study

| |
|---|
| *One-component chlorides* |
| LiCl |
| NaCl |
| KCl |
| $AlCl_3$ |
| *Binary systems* |
| LiCl–NaCl |
| NaCl–KCl |
| LiCl–KCl |
| LiCl–$LiAlCl_4$ |
| NaCl–$NaAlCl_4$ |
| KCl–$KAlCl_4$ |
| $LiAlCl_4$–$NaAlCl_4$ |
| $LiAlCl_4$–$KAlCl_4$ |
| $NaAlCl_4$–$KAlCl_4$ |
| *Reciprocal ternary systems* |
| LiCl–NaCl–$LiAlCl_4$–$NaAlCl_4$ |
| LiCl–KCl–$LiAlCl_4$–$KAlCl_4$ |
| NaCl–KCl–$NaAlCl_4$–$KAlCl_4$ |

## Binary systems

The binary systems which must be analyzed in order to calculate the ternary phase diagrams are also listed in Table 1. Note that for the $AlCl_3$ – alkali chloride systems we are concerned only with the sub-systems ACl–$AAlCl_4$ (where A = Li, Na, or K). Furthermore, three quasi-binary systems, e.g., $NaAlCl_4$–$KAlCl_4$, etc., have been included. This treatment is discussed later.

A thorough literature search of all available phase diagram and thermodynamic data for these systems was performed by R. J. C. MacDonald, Information Officer of CANMET, Dept. of Energy, Mines and Resources, Canada, using the following computerized data bases: Chemical Abstracts, Engineering Index, Inspec, SSIE, Conference Papers, CDI and NTIS.

The method described and employed previously (3–7) was used to analyse the binary systems listed in Table 1. Briefly, a least-squares optimization technique is used to obtain the coefficients $h_{ij}$ and $s_{ij}$ of polynomial expansions for the molar enthalpies and excess entropies of each solution phase in the following form:

$$[1] \quad \Delta H = \sum_{i,j} h_{ij} X_A^i X_B^j$$

$$[2] \quad S^E = \sum_{i,j} s_{ij} X_A^i X_B^j$$

where $X_A$ and $X_B$ are the mole fractions of the components. The optimization analysis is also used to obtain the Henrian activity coefficients of dilute solid solutions and the free energies of formation of intermediate stoichiometric solid phases.

Can. J. Chem. Downloaded from www.nrcresearchpress.com by 210.87.254.40 on 09/06/12
For personal use only.

TABLE 2. Free energies of fusion and melting points of pure chlorides (9)
$\Delta G^0_{fusion}$ (cal/mol) = $a + bT + cT^2 + dT \ln T + eT^{-1}$

| Chloride | $T^0_{fusion}$ (K) | $a$ | $b$ | $c \times 10^3$ | $d$ | $e \times 10^{-5}$ |
|---|---|---|---|---|---|---|
| KCl | 1044 | 1136.6 | 51.481 | 3.0435 | −8.026 | 0.436 |
| LiCl | 883 | 1056.5 | 47.16 | 3.928 | −7.64 | |
| NaCl | 1074 | 1848.6 | 48.3 | 2.85 | −7.606 | |

The details of the critical analyses for each binary system are discussed below and error limits are given. The computer-calculated phase diagrams for each binary system are given in Figs. 1–7, and the coefficients $h_{ij}$ and $s_{ij}$ are listed in Table 3.

*LiCl–NaCl (Fig. 1)*

$\Delta H$ for the liquid is as reported by Hersh and Kleppa (10). It is reasonable to suppose that $S^E = 0$ for the liquid. There are several measured phase

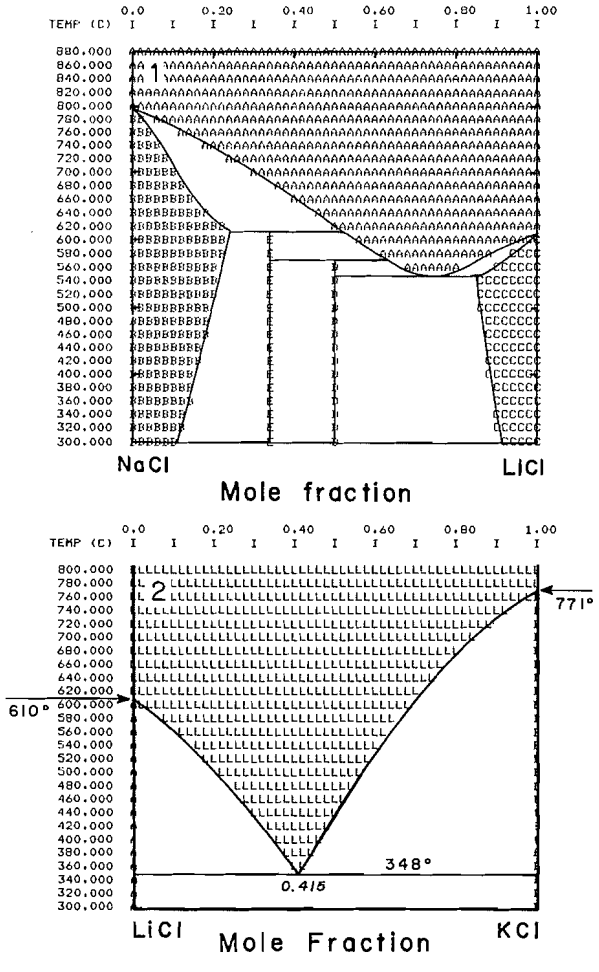


FIGS. 1, 2. Computer-generated phase diagram for LiCl–NaCl (*1*) and KCl–LiCl (*2*).

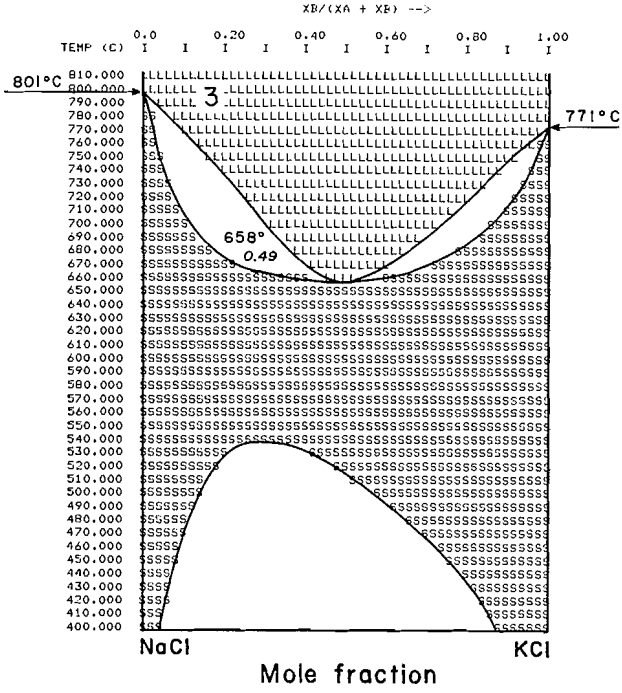


FIG. 3. Computer-generated phase diagram for KCl–NaCl.

diagrams for this system. All are in reasonable agreement as regards the liquidus curves. However, the diagrams of Plyushchev *et al.* (11*a*) and of Smits *et al.* (11*a*) show complete solid solution, while the most recent diagram of Akopov and Bergman (11*b*) shows no solid solubility at all and in addition shows two intermediate compounds. These intermediate compounds also appear in the measured ternary phase diagram of the LiCl–NaCl–KCl system which the present authors have also calculated obtaining good agreement between measured and calculated diagrams. This supports the existence of these two compounds. If no solid solubility is assumed, then the calculated liquidus curves do not agree with the measured. On the other hand, fitting the diagram with the assumption of complete solid solubility requires the thermodynamic functions of the solid solution to be highly asymmetric and rather unlikely functions of composition. As a compromise, it was assumed that limited solid solutions exist and that these are

Can. J. Chem. Downloaded from www.nrcresearchpress.com by 210.87.254.40 on 09/06/12
For personal use only.

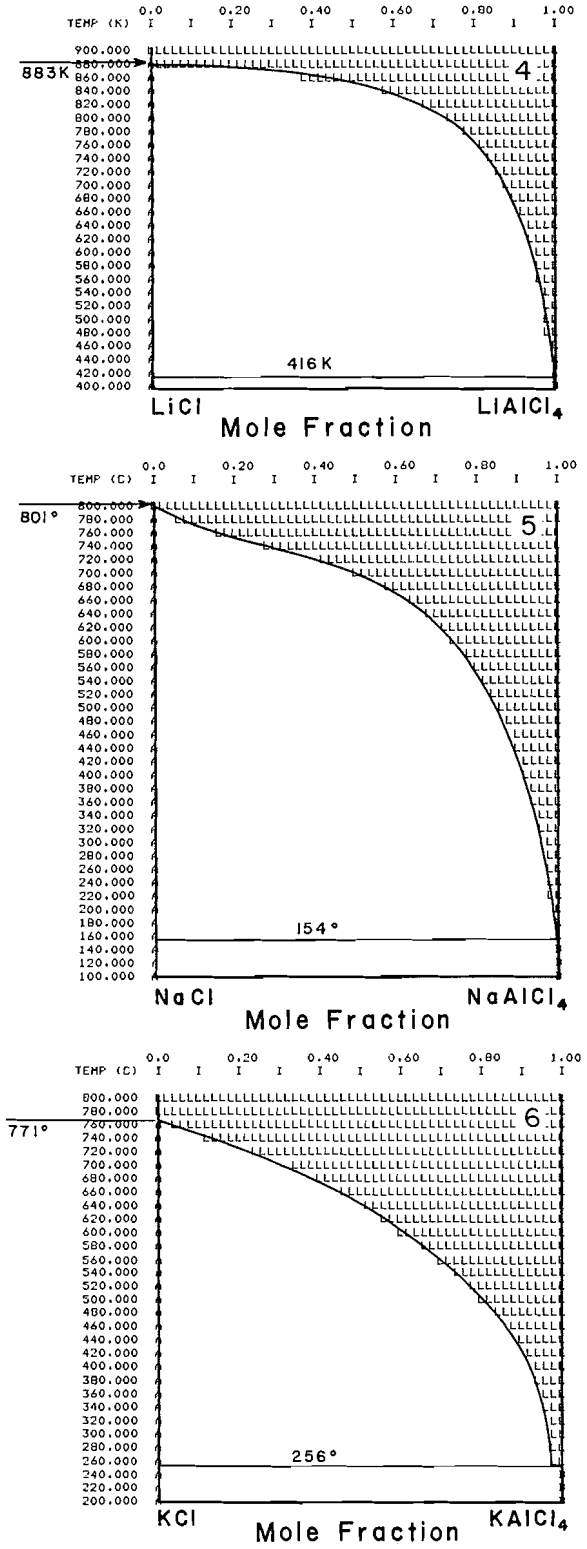


FIGS. 4–6. Computer-generated phase diagram for LiCl–$LiAlCl_4$ (*4*); NaCl–$NaAlCl_4$ (*5*); and KCl–$KAlCl_4$ (*6*).

Henrian solutions. The calculated and measured liquidus curves are then in agreement to within 2 mol% everywhere except near pure NaCl where the diagram of Akopov and Bergman (11*b*) does not agree with the other diagrams. However, in this region the two other diagrams agree with each other and with the calculated diagram. The Henrian activity coefficients of the solid phases were obtained as:

$$RT \ln \gamma_{LiCl} = 1200 \text{ cal}$$

$$RT \ln \gamma_{NaCl} = 1700 \text{ cal}$$

The free energies of formation from pure liquid LiCl and NaCl of the two intermediate compounds were also obtained by the phase diagram analysis as:

$$\Delta G^0 (LiCl)_{1/2} (NaCl)_{1/2} = -7894 + 7.526T \text{ cal/mol}$$

$$\Delta G^0 (LiCl)_{1/3} (NaCl)_{2/3} = -6701 + 5.86T \text{ cal/mol}$$

Probable maximum error of calculated liquidus: ±10°.

*KCl–LiCl (Fig. 2)*

$\Delta H$ was fitted to the measured values of Hersh and Kleppa (10). $S^E$ was determined by fitting the measured phase diagram. Limiting slopes of liquidus curves indicate negligible solid solubility. The two measured diagrams agree with each other within 5°. The more recent eutectic temperature of 348°C (11*b*) is more consistent with smooth thermodynamic functions for the liquid phase than is the older value of 354°C (11*a*).

Probable maximum error of calculated diagram: ±5°.

*KCl–NaCl (Fig. 3)*

The measured enthalpies of Hersh and Kleppa (10) were used to obtain the expression for $\Delta H_{liquid}$. The most recently measured liquidus (12) and solidus (11*c*) were then analysed in order to obtain the coefficients for $S_{liq}^E$, $\Delta H_{solid}$, and $S_{solid}^E$ given in Table 3. The measured (11*c*, 12) and calculated liquidus and solidus agree within less than 2° and less than 5° respectively. The calculated consolute point agrees with the measured (11*a*) within 50° in temperature, and in composition within the limits of experimental error. All parts of the calculated diagram thus agree with the experimental within the error limits of the latter.

Probable maximum error of calculated diagram: ±2° for liquidus and ±5° for solidus.

Can. J. Chem. Downloaded from www.nrcresearchpress.com by 210.87.254.40 on 09/06/12
For personal use only.

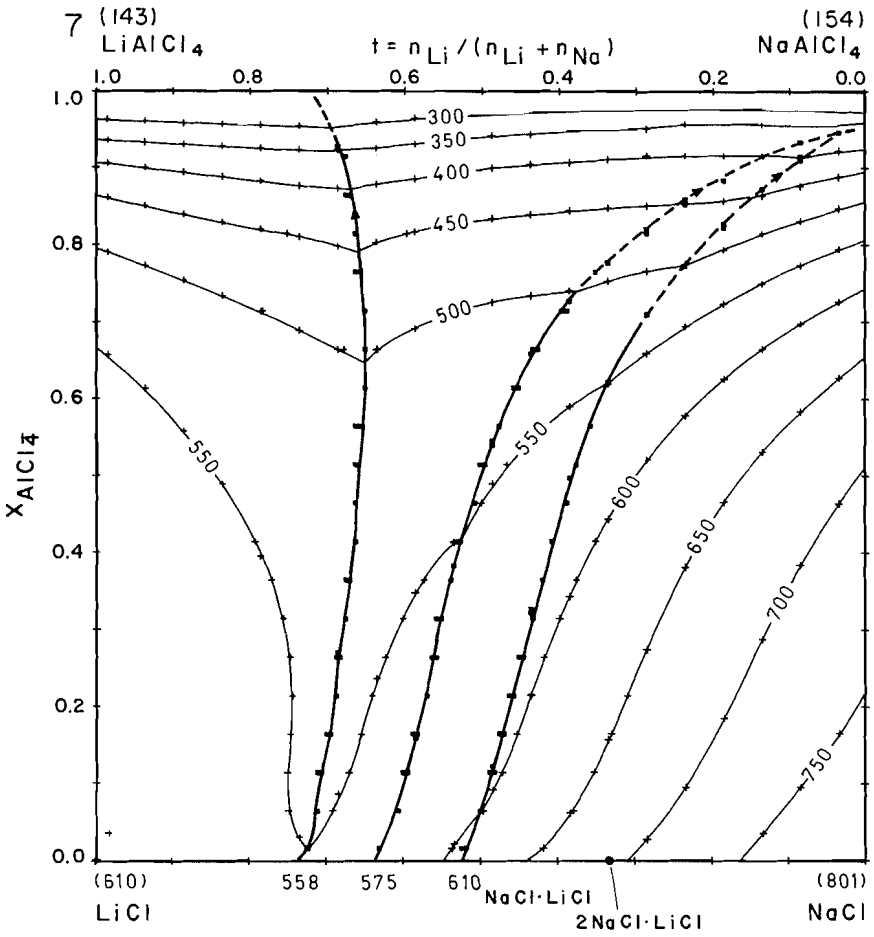


FIG. 7. Calculated phase diagram for LiCl–NaCl–$LiAlCl_4$–$NaAlCl_4$. Temperatures are in °C.

*$LiCl$–$LiAlCl_4$ (Fig. 4)*

The system $AlCl_3$–LiCl has been divided into two sub-systems: LiCl–$LiAlCl_4$, and $LiAlCl_4$–$AlCl_3$. This is consistent with the strong evidence provided by the vapour pressure measurements to be discussed later in this paper that the melts contain very stable $AlCl_4^-$ complex anions. As noted previously, we are concerned only with compositions for which $X_{AlCl_3} \leq 0.5$, i.e., the LiCl–$LiAlCl_4$ sub-system. The measured phase diagram of this sub-system can be fitted by assuming ideal entropy for the sub-system and only small well-behaved deviations from ideality in the enthalpy. That is, the general shape of the measured phase diagram also strongly supports the splitting into two sub-systems.

With $S^E$ taken to be zero in the sub-system, the recent phase diagram of Sato and Ejima (13) was fitted to obtain the expression for $\Delta H$. Agreement between measured and calculated diagrams is of the order of 10°. The entropy of fusion of the compound $LiAlCl_4$ was taken to be 8.0 cal/mol K, which is approximately that of similar compounds. The enthalpy of fusion was then determined from this entropy and the reported melting point. (Most recent evidence indicates that this is a congruently melting compound.) The fit is consistent with the vapour pressure measurements which will be mentioned later in this report.

Probable maximum error in calculated diagram: ±5 to 10°.

*$NaCl$–$NaAlCl_4$ (Fig. 5)*

Exactly the same comments as given above for the LiCl–$LiAlCl_4$ system also apply to this system. Data for the measured phase diagram were taken from ref. 11*a*.

*$KCl$–$KAlCl_4$ (Fig. 6)*

Exactly the same comments as given above for the NaCl–$NaAlCl_4$ system also apply for this system.

TABLE 3. Summary of optimized thermodynamic parameters of eqs. [1], [2] for the enthalpy and excess entropy of binary liquid phases

| Binary system (liquid phase unless otherwise stated) | | | | | |
|---|---|---|---|---|---|
| A | B | $i$ | $j$ | Enthalpy coefficient $h_{ij}$ (cal) | Excess entropy coefficient $s_{ij}$ (cal $K^{-1}$) |
| KCl | LiCl | 1 | 1 | −4290 | −0.6211 |
| | | 2 | 1 | 90 | −0.6047 |
| NaCl | KCl | 1 | 1 | −555 | −0.4 |
| | | 1 | 2 | 65 | |
| NaCl | KCl (solid phase) | 1 | 1 | 6690 | 3.0 |
| | | 1 | 2 | −2880 | |
| | | 1 | 3 | 1900 | |
| LiCl | NaCl | 1 | 1 | −1120 | |
| LiCl | $LiAlCl_4$ | 1 | 1 | 5464 | |
| | | 1 | 2 | −10687 | |
| | | 1 | 3 | 19276 | |
| | | 1 | 4 | −17786 | |
| | | 1 | 5 | 6049 | |
| NaCl | $NaAlCl_4$ | 1 | 1 | 2933 | |
| | | 1 | 2 | −1754 | |
| KCl | $KAlCl_4$ | 1 | 1 | 2936 | |
| | | 1 | 2 | −4083 | |
| | | 1 | 3 | 3213 | |
| $LiAlCl_4$–$NaAlCl_4$ | | | Ideal | | |
| $NaAlCl_4$–$KAlCl_4$ | | | Ideal | | |
| $LiAlCl_4$–$KAlCl_4$ | | | Ideal | | |

*$KAlCl_4$–$NaAlCl_4$*

The entropies of fusion were taken to be 8.0 cal/mol K, which is approximately that of similar compounds. The enthalpies of fusion were then determined from this entropy and the measured melting points. Under the assumption that the liquid is an ideal solution and that there is no solid solubility, the system was calculated to exhibit a simple eutectic at 125 ± 1°C and mole fraction 0.74 ± 0.03 $NaAlCl_4$, which is within the error limits of the diagram measured by Chikanov (11*b*).

Probable maximum error of calculated diagram: ±10°.

*$KAlCl_4$–$LiAlCl_4$ and $LiAlCl_4$–$NaAlCl_4$*

No data are available for these two quasi-binary systems. In light of the above findings for the $KAlCl_4$–$NaAlCl_4$ system, it is assumed that the liquid phases are ideal and that there is no solid solubility.

## Calculation of ternary systems containing $AlCl_3$ from binary systems

Once all the binary systems have been analysed, the thermodynamic properties of the ternary systems can be estimated by means of standard interpolation procedures which have been applied elsewhere (3–7) with success to many other ionic systems.

As discussed previously, the binary systems $ACl$–$AlCl_3$ (A = Li, Na, K) were each divided into two sub-systems, $ACl$–$AAlCl_4$ and $AAlCl_4$–$AlCl_3$. By extension, the composition triangle of each of the three ternary systems $ACl$–$BCl$–$AlCl_3$ (A, B = Li, Na, K) can be considered to be divided into two regions by a line joining the two compounds $AAlCl_4$ and $BAlCl_4$. The upper region becomes the ternary system $ACl_3$–$AAlCl_4$–$BAlCl_4$, and the lower region becomes the "reciprocal ternary system" $ACl$–$BCl$–$AAlCl_4$–$BAlCl_4$. As noted previously, we are concerned only with the reciprocal ternary systems, i.e., those composition regions for which $X_{AlCl_3} \leq 0.5$.

*Reciprocal systems $ACl$–$BCl$–$AAlCl_4$–$BAlCl_4$ (A, B = Li, Na, K)*

*Calculation of phase diagrams*

The calculated phase diagrams for the subsystems LiCl–NaCl–$LiAlCl_4$–$NaAlCl_4$, LiCl–KCl–$LiAlCl_4$–$KAlCl_4$, and NaCl–KCl–$NaAlCl_4$–$KAlCl_4$ are presented in Figs. 7, 8, and 9 respectively. Each of these "reciprocal systems" contains two cations, $A^+$ and $B^+$, and two anions, $Cl^-$ and $AlCl_4^-$. The horizontal axes of these diagrams

Can. J. Chem. Downloaded from www.nrcresearchpress.com by 210.87.254.40 on 09/06/12
For personal use only.

Can. J. Chem. Downloaded from www.nrcresearchpress.com by 210.87.254.40 on 09/06/12
For personal use only.

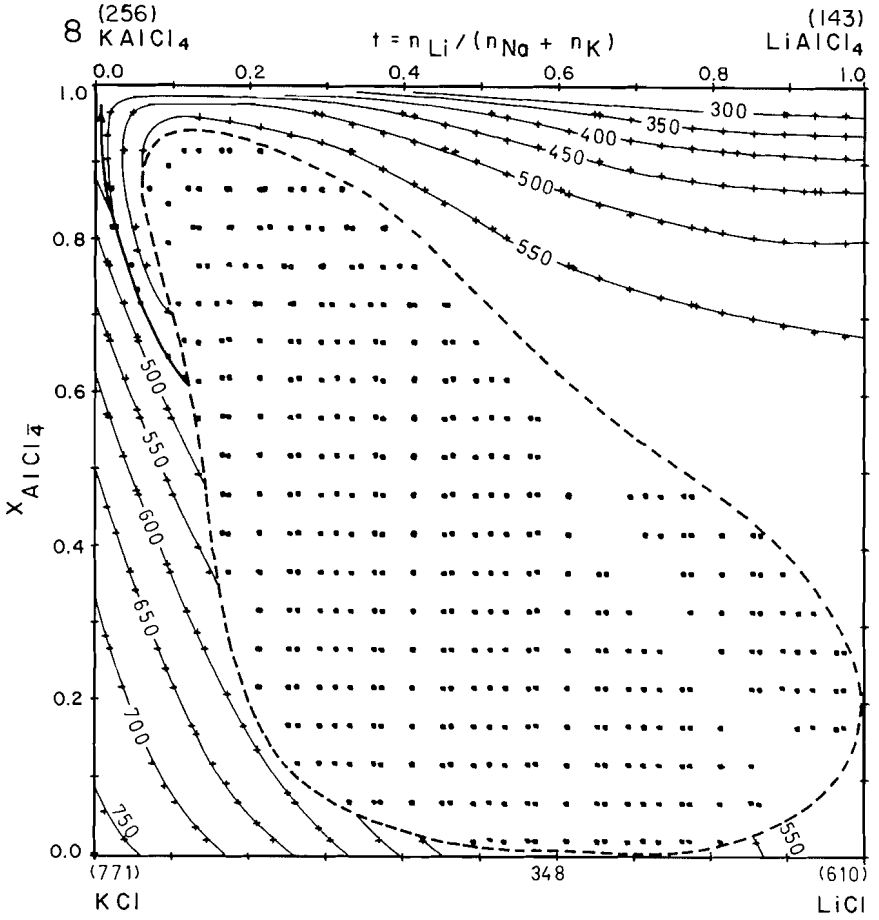


FIG. 8. Calculated phase diagram for LiCl–KCl–$LiAlCl_4$–$KAlCl_4$. Temperatures are in °C.

are the cationic fractions $t = n_{B^+}/(n_{A^+} + n_{B^+})$ and the vertical axes are the anionic fractions $X_{AlCl_4^-} = n_{AlCl_4^-}/(n_{Cl^-} + n_{AlCl_4^-})$[1] (where $n_i$ = moles of ion $i$). The dashed lines on the diagram for the LiCl–KCl–$LiAlCl_4$–$KAlCl_4$ systems are the loci of intersection of a liquid immiscibility gap with the liquidus. These phase diagrams were calculated by interpolation from the four binary systems which form the edges of the composition diagrams. The Conformal Ionic Solution (CIS) theory (14) for reciprocal salts was employed for the calculations. Details of the interpolation formulae are given in ref. 14. It has been shown in several studies (14–19) that good approximations to reciprocal salt phase diagrams can be obtained by this approach.

A factor which is of prime importance in the calculation of a reciprocal salt phase diagram via the CIS theory is $\Delta G^{EX}$, the free energy change of the "exchange reaction":

[A] $ACl + BAlCl_4 \rightleftharpoons BCl + AAlCl_4$

[1] $X_{AlCl_3} = X_{AlCl_4^-}/(1 + X_{AlCl_4^-})$ and $X_{AlCl_4^-} = X_{AlCl_3}/(1 - X_{AlCl_3})$.

$\Delta G^{EX}$ cannot be obtained solely from the four binary sub-systems, but rather, it must be obtained independently. for the three exchange reactions in the present case, $\Delta G^{EX}$ was determined from analysis of vapour pressure and other thermodynamic data (9, 20). Values are given in Table 4.

If $\Delta G^{EX} < 0$ for reaction [A], then BCl and $AAlCl_4$ are called the "stable pair" while ACl and $BAlCl_4$ are the "unstable pair".

If $\Delta G^{EX} < 0$, then it is energetically favorable to have $B^+$ ions next to $Cl^-$ and $A^+$ ions next to $AlCl_4^-$ ions. If we mix pure BCl with pure $AAlCl_4$, we force some $B^+$ ions to be situated next to $AlCl_4^-$ ions and force some $A^+$ ions to be next to $Cl^-$ ions. This is energetically unfavourable. On the other hand, mixing of the pure members of the unstable pair is energetically favourable. The result is that strong positive deviations from ideality (manifested by a flat liquidus with widely spaced isotherms) are observed along the diagonal of the phase diagram which joins the stable pair (the "stable diagonal"), while strong negative deviations from ideality (steep liquidus, closely spaced isotherms) are ob-

Can. J. Chem. Downloaded from www.nrcresearchpress.com by 210.87.254.40 on 09/06/12
For personal use only.

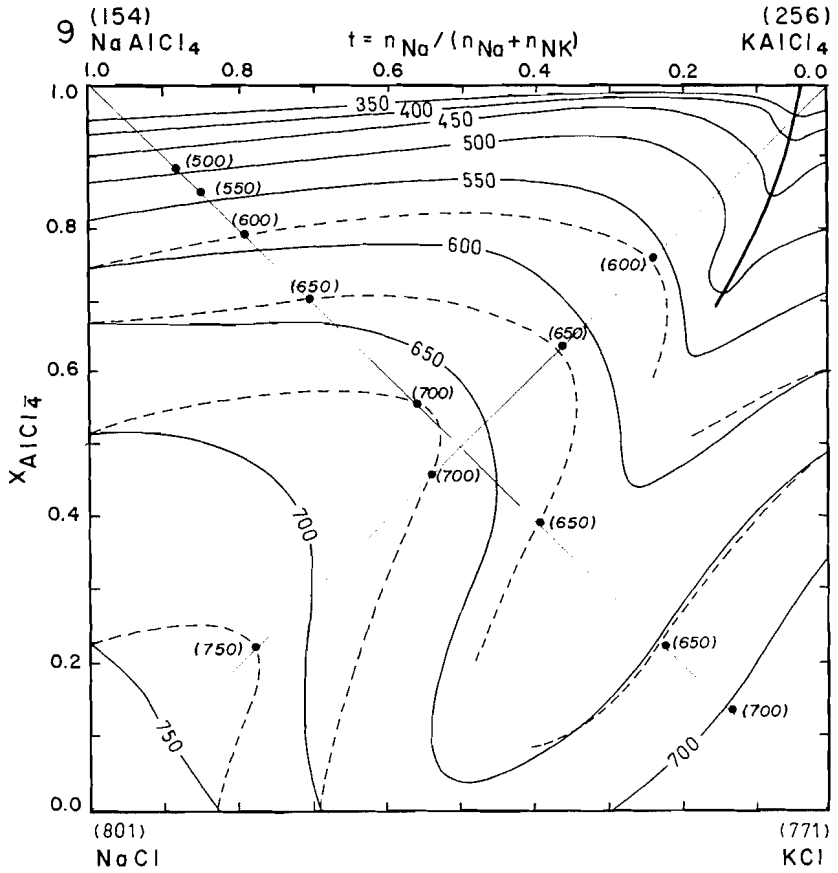


FIG. 9. Calculated phase diagram for NaCl–KCl–$NaAlCl_4$–$KAlCl_4$ plus experimental points (21) and estimated experimental isotherms (---). Temperatures are in °C.

served along the "unstable diagonal". This can clearly be seen in the three calculated phase diagrams. As $\Delta G^{EX}$ becomes more and more negative, these deviations are accentuated until, as in the case of the LiCl–KCl–$LiAlCl_4$–$KAlCl_4$ system, a miscibility gap appears with tie lines lying approximately parallel to the stable diagonal.

The NaCl–KCl–$NaAlCl_4$–$KAlCl_4$ phase diagram has been determined experimentally along the two composition diagonals by Fischer and Simon (21). Points from their experimental phase diagram are also shown in Fig. 9 along with some experimental isotherms estimated from the curves measured by Fischer and Simon (21). These isotherms are shown terminating at points from the calculated binary phase diagrams from the present study because these points agree closely with the most recently measured binary phase diagrams, whereas the binary phase diagrams of Fischer and Simon are not in good agreement with the latter. The difference between the measured and calculated diagrams is greatest in the central portion of the figure. The apparent disagreement between the measured and calculated diagrams is accentuated by the very flat liquidus in this region which causes a small difference in temperature to be accompanied by a large difference in composition. For lower concentrations of $AlCl_3$, which are of most interest in electrowinning, the discrepancy is less. The difference between the measured and calculated diagrams is most likely caused by errors in the literature value of $\Delta G^{EX}$ for this system. Nonetheless, the calculated diagram maintains all the qualitative features of the measured diagram, and the agreement is not unsatisfactory. Clearly the CIS model gives a reasonable estimate of the thermodynamic properties of the ternary liquids.

The isothermal boundaries of the miscibility gap in the system LiCl–KCl–$LiAlCl_4$–$KAlCl_4$ have been measured at several temperatures by Moore (22). In the present work only the intersection of the gap with the liquidus surface was calculated, so

TABLE 4. Thermodynamic data (9, 20) for $AlCl_3$-containing systems

(*a*) Exchange free energies

| Reaction | $\Delta G^{EX}$ |
|---|---|
| $NaCl_{(l)} + LiAlCl_{4(l)} \rightarrow LiCl_{(l)} + NaAlCl_{4(l)}$ | $-3370 - 1.56T$ cal/mol |
| $KCl_{(l)} + LiAlCl_{4(l)} \rightarrow LiCl_{(l)} + KAlCl_{4(l)}$ | $-8170 - 0.96T$ cal/mol |
| $KCl_{(l)} + NaAlCl_{4(l)} \rightarrow NaCl_{(l)} + KAlCl_{4(l)}$ | $-4800 + 0.60T$ cal/mol |

(*b*) Free energies of vaporization

| Process | $\Delta G_V^0$ |
|---|---|
| $LiAlCl_{4(l)} \rightarrow LiAlCl_{4(g)}$ | $24070 - 21.89T$ cal/mol |
| $NaAlCl_{4(l)} \rightarrow NaAlCl_{4(g)}$ | $28060 - 22.99T$ cal/mol |
| $KAlCl_{4(l)} \rightarrow KAlCl_{4(g)}$ | $27105 - 20.72T$ cal/mol |
| $AlCl_{3(l)} \rightarrow AlCl_{3(g)}$ | $12760 - 19.12T$ cal/mol |

(*c*) Dissociation energies for $AAlCl_{4(l)} \rightarrow ACl_{(l)} + AlCl_{3(l)}$

| A | $\Delta G^0$ |
|---|---|
| Li | $16970 - 7.82T$ cal/mol |
| Na | $20340 - 6.26T$ cal/mol |
| K | $25140 - 6.86T$ cal/mol |

(*d*) Dimerization free energy for $2AlCl_{3(g)} \rightarrow Al_2Cl_{6(g)}$

$$\Delta G^0 = -RT \ln K = -31057 + 62.768T + 2.4 \times 10^{-5} T^2 - 4.066T \ln T + 7050T^{-1} \text{ cal/mol}$$

a direct comparison is difficult. However, the overall extent and shape of the calculated and measured miscibility gaps appear to be in good agreement.

*Calculation of vapour pressures*

The total vapour pressures above melts in the binary systems $LiCl–LiAlCl_4$, $NaCl–NaAlCl_4$, and $KCl–KAlCl_4$ have been measured recently by Linga *et al.* (20) at several temperatures. This experimental work appears to be very reliable. Experimental vapour pressure curves for the three binary systems at selected temperatures are shown in Figs. 10–12. By a sophisticated and convincing thermodynamic analysis involving their data as well as literature data, Linga *et al.* (20) managed to separate their measured total vapour pressures into partial vapour pressures of the various gaseous species. As can be seen from Figs. 10–12, the major contribution comes from the partial pressures of the gaseous species $LiAlCl_{4(g)}$, $NaAlCl_{4(g)}$, and $KAlCl_{4(g)}$. $AlCl_{3(g)}$ plays lesser role and $Al_2Cl_{6(g)}$ plays a negligible role except at high concentrations of $AlCl_3$. A summary of the thermodynamic data involving the gaseous species in these systems as obtained from the analysis of Linga *et al.* (20) as well as from the literature (9) is presented in Table 4.

The analysis of Linga *et al.* (20) also yielded values for the excess free energies in the liquid $ACl–AAlCl_4$ systems (A = Li, Na, K). For the sodium and potassium systems these values agree very well with those obtained by the present phase diagram analysis as presented in Table 3. Phase diagrams calculated from the partial excess free energy ($G^E$) values of Linga *et al.* reproduce the measured phase diagrams of $NaCl–NaAlCl_4$ and $KCl–KAlCl_4$ to within about 5°. From the values in Table 4 and from the thermodynamic properties of the liquid phases in Table 3 determined from the phase diagram analyses discussed previously, the partial vapour pressures as well as the total vapour pressures of the binary systems with sodium and potassium were calculated. Agreement with the experimental values of $P_{tot}$ is excellent as can be seen from Figs. 11 and 12. At other temperatures, agreement is just as good.

For the $LiCl–LiAlCl_4$ system, however, the $G^E$ values obtained by Linga *et al.* yield a binary diagram differing by up to 60° from the measured (13). Conversely, if the values in Table 4 are used along with the thermodynamic properties of the liquid phase in Table 3 obtained from the phase diagram analysis discussed previously, then the calculated $P_{tot}$ does not agree with the measured at higher concentrations of $AlCl_3$.

An attempt was made to alter the values for the free energies of vapourization and of dissociation of $LiAlCl_{4(l)}$ in Table 4 within reasonable limits, in

Can. J. Chem. Downloaded from www.nrcresearchpress.com by 210.87.254.40 on 09/06/12
For personal use only.

Can. J. Chem. Downloaded from www.nrcresearchpress.com by 210.87.254.40 on 09/06/12
For personal use only.

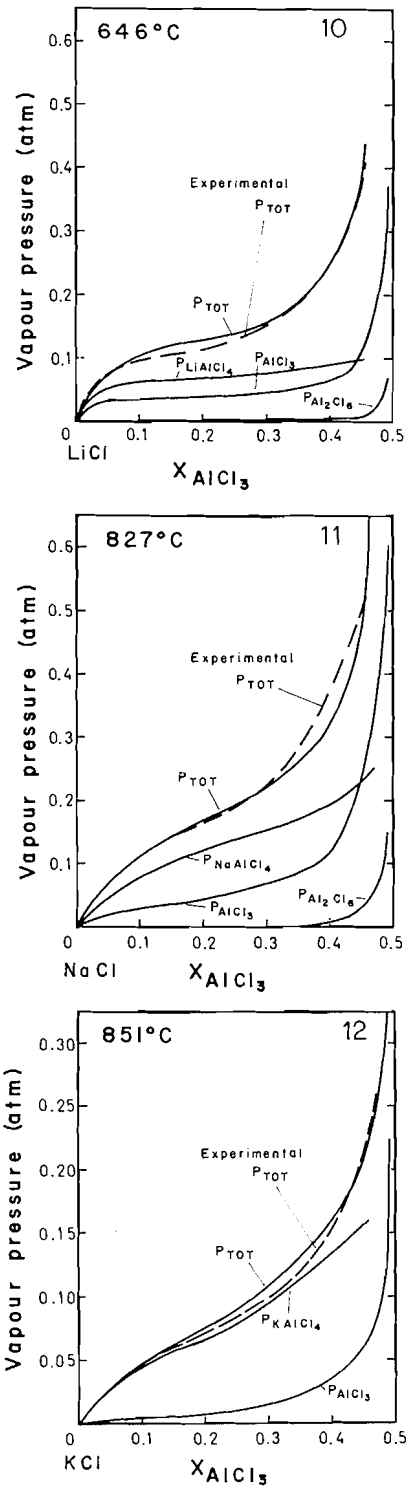


FIGS. 10–12. Calculated partial and total vapour pressures, and experimental (20) total vapour pressures in the system $LiCl–AlCl_3$ at 646°C (*10*); $NaCl–AlCl_3$ at 827°C (*11*); and $KCl–AlCl_3$ at 851°C (*12*).

order to reproduce the measured $P_{tot}$ curves while still retaining $G^E$ for the liquid obtained from the phase diagram analysis. This proved unsuccessful. Hence, it would seem impossible to reconcile all the available data. Fortunately, the problem affects only those reciprocal ternary compositions near the $LiAlCl_4$ composition and this composition region is not of great practical importance due to anticipated high vapour pressures and hydroscopicity.

In order to calculate the vapour pressures in the $LiCl–LiAlCl_4$ system, the values of $G^E$ for the liquid phase obtained by the analysis of Linga *et al.* were fitted to the following power series expansion:

$$[3]\quad G^E = X_{LiCl}X_{LiAlCl_4}(3709 - 5234X_{LiAlCl_4} + 2891X^2_{LiAlCl_4})\ \text{cal/mol}$$

The excess entropy was assumed to be zero by Linga *et al.* From the values of Table 4 and from eq. [3], the partial and total vapour pressures of the binary system were calculated. Agreement with the experimental $P_{tot}$ at 646°C was excellent, as can be seen from Fig. 10. At other temperatures the agreement was as good.

From the data of Table 4 and the reciprocal ternary thermodynamic properties calculated from the CIS theory, partial vapour pressures of all species were calculated at 675, 700, 725, and 775°C for all three reciprocal ternary systems (8) (eq. [3] was used for the $LiCl–LiAlCl_4$ system in these calculations).

## Temperatures and compositions for aluminum electrowinning

The calculated total vapour pressures, $P_{tot}$, in atm for the one-phase liquid solution regions of the three reciprocal ternary systems at 675, 700, and 775°C are given in Figs. 13 to 21. Data for 725°C, although omitted from the figures for the sake of brevity, will be discussed in the text and are available from the authors. In the (*a*) series of these diagrams, isobars of total vapour pressure, in atm, have been combined with isothermal sections of the calculated reciprocal phase diagrams, or in the case of $NaCl–KCl–NaAlCl_4–KAlCl_4$, with isothermal sections derived from the measured reciprocal diagonals and the calculated binaries. Cross-hatched areas of these diagrams indicate compositions where the liquid is in equilibrium with a solid phase. As with the phase diagrams, the dashed lines in the series (*a*) figures for $LiCl–KCl–LiAlCl_4–KAlCl_4$ represent the loci of intersection of a liquid miscibility gap with the liquidus surface.

In order to show on a more enlarged scale the variation of total vapour pressure in composition

Can. J. Chem. Downloaded from www.nrcresearchpress.com by 210.87.254.40 on 09/06/12
For personal use only.

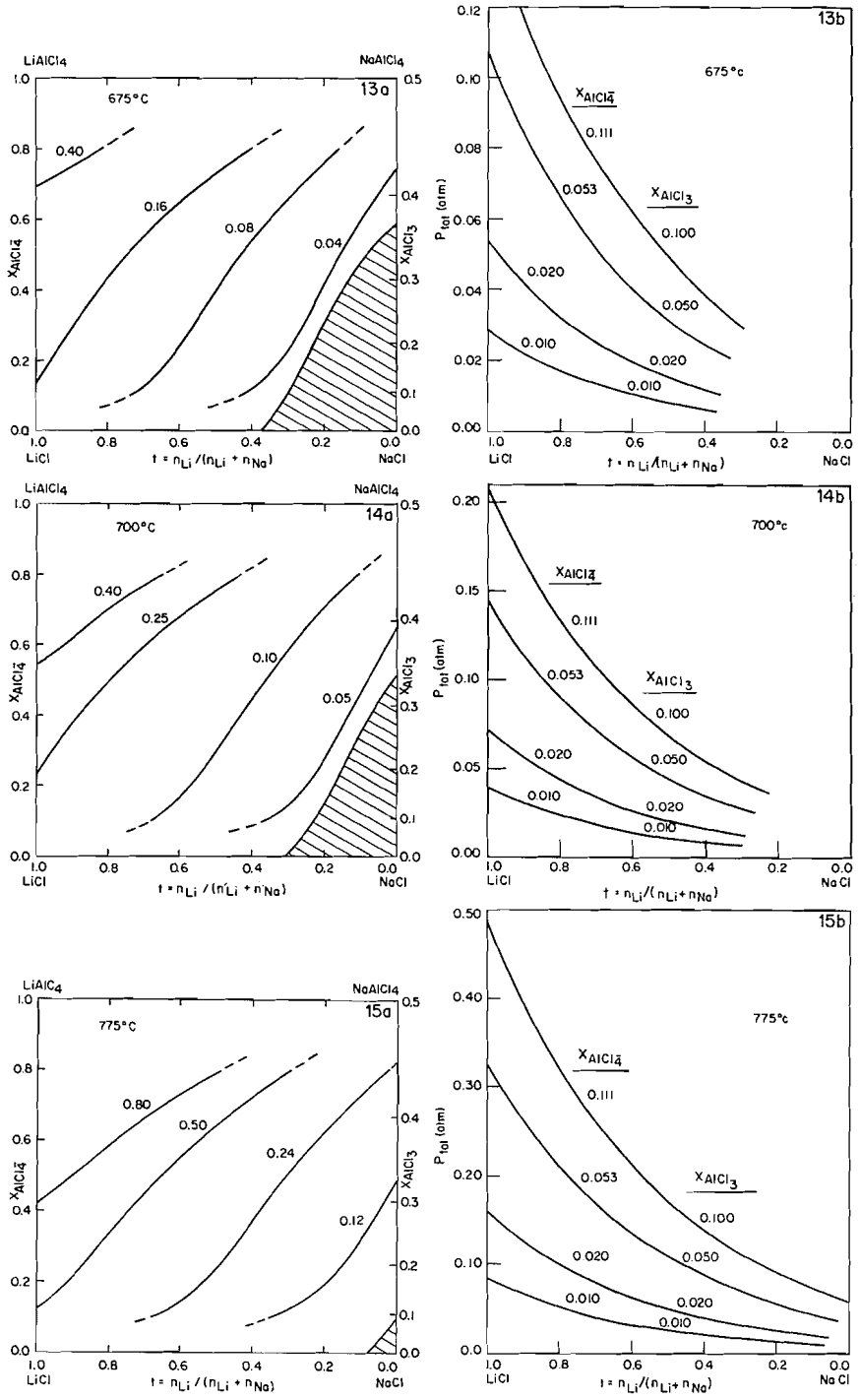


FIGS. 13–15. Calculated total vapour pressure lines in atm for one-phase liquid solution regions of LiCl–NaCl–$LiAlCl_4$–$NaAlCl_4$ at 675°C (*13*a), 700°C (*14*a), and 775°C (*15*a). Calculated total vapour pressures vs. $t$ for $X_{AlCl_3} < 0.10$ in one-phase liquid solution regions of LiCl–NaCl–$LiAlCl_4$–$NaAlCl_4$ at 675°C (*13*b), 700°C (*14*b), and 775°C (*15*b); $t = n_{Li}/(n_{Li} + n_{Na})$.

Can. J. Chem. Downloaded from www.nrcresearchpress.com by 210.87.254.40 on 09/06/12
For personal use only.

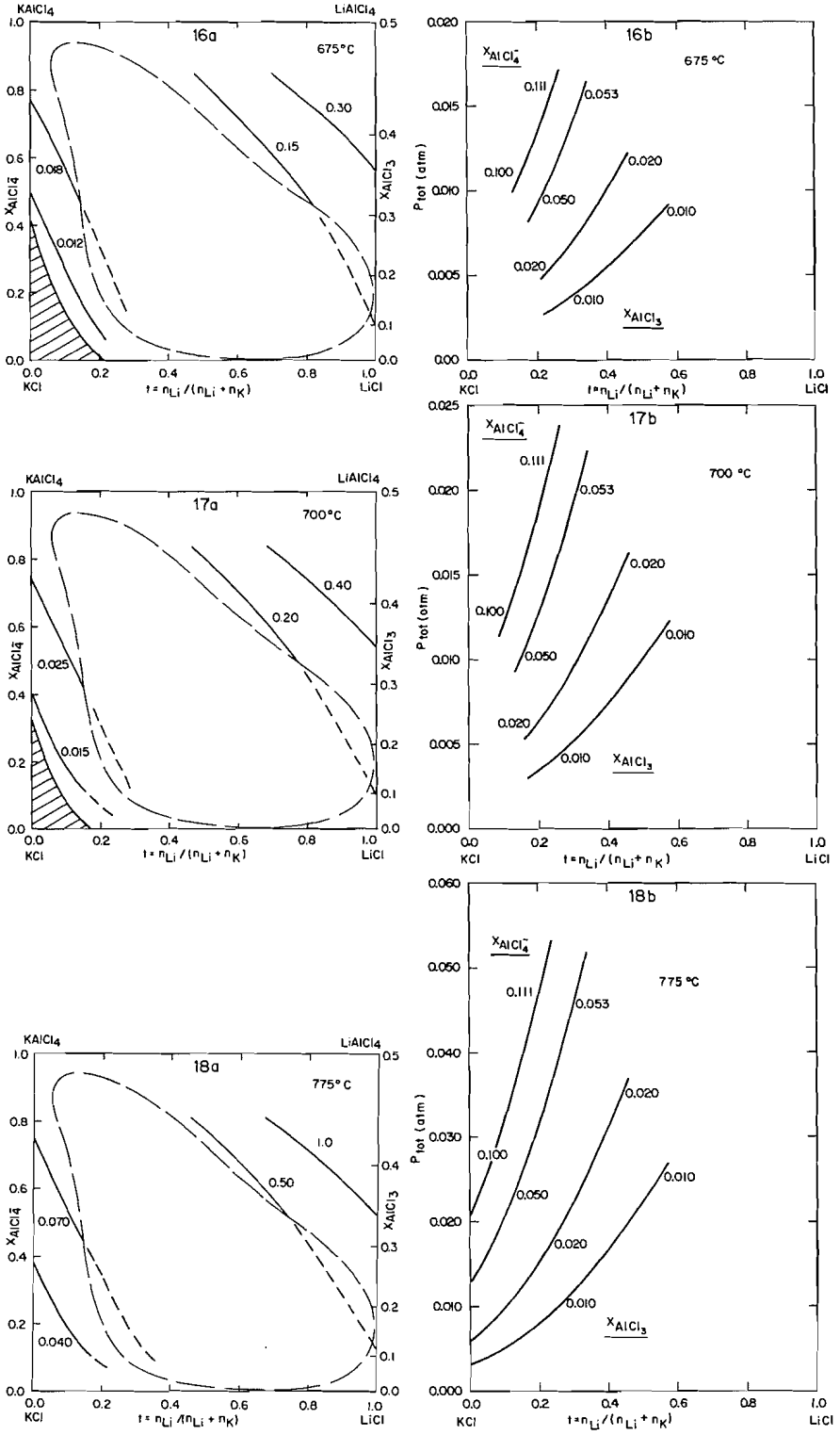


FIGS. 16–18. Calculated total vapour pressure lines in atm for one-phase liquid solution regions of LiCl–KCl–$LiAlCl_4$–$KAlCl_4$ at 675°C (16*a*), 700°C (17*a*), and 775°C (18*a*). Calculated total vapour pressures vs. $t$ for $X_{AlCl_3} < 0.10$ in one-phase liquid solution regions of LiCl–KCl–$LiAlCl_4$–$KAlCl_4$ at 675°C (16*b*), 700°C (17*b*), and 775°C (18*b*). $t = n_{Li}/(n_{Li} + n_K)$.

Can. J. Chem. Downloaded from www.nrcresearchpress.com by 210.87.254.40 on 09/06/12
For personal use only.

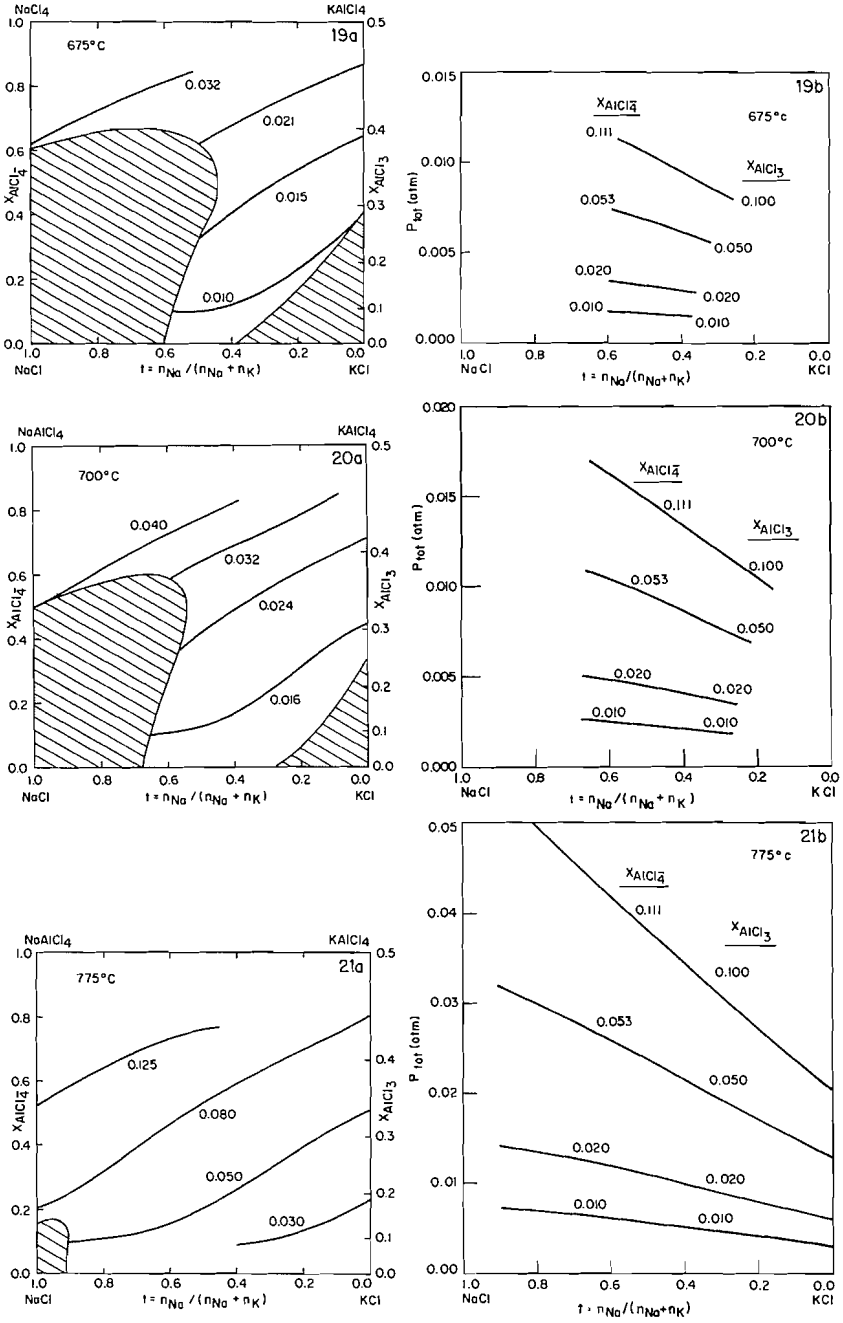


FIGS. 19–21. Calculated total vapour pressure lines in atm for one-phase liquid solution regions of NaCl–KCl–$NaAlCl_4$–$KAlCl_4$ at 675°C (19*a*), 700°C (20*a*), and 775°C (21*a*). Calculated total vapour pressures vs. $t$ for $X_{AlCl_3} < 0.10$ in one-phase liquid solution regions of NaCl–KCl–$NaAlCl_4$–$KAlCl_4$ at 675°C (19*b*), 700°C (20*b*), and 775°C (21*b*). $t = n_{Na}/(n_{Na} + n_K)$.

regions which are of practical interest in aluminum electrowinning, the (*b*) series of Figs. 13–21 gives the total vapour pressures, in atm, for the one-phase liquid solution regions of each system at 675, 700, and 775°C as a function of the cationic fraction, $t$, for values of $X_{AlCl_3} = 0.01$, 0.02, 0.05, and 0.10.

According to Good *et al.* (23), electrowinning of aluminum from a NaCl–KCl 1:1 mole ratio electrolyte containing less than 2 wt% $AlCl_3$ (~1 mol% $AlCl_3$) causes the formation and burning of sodium. Hence, to avoid proposing electrolytes which decompose producing an alkali metal, the minimum

Can. J. Chem. Downloaded from www.nrcresearchpress.com by 210.87.254.40 on 09/06/12
For personal use only.

attainable vapour pressures in each system will be taken as those which occur at $X_{AlCl_3} = 0.02$ (2 mol% $AlCl_3$) and at a value of $t$, $t_{min}$, which is a minimum when the mole fraction of the larger alkali cation is a maximum in a one-phase liquid solution. We seek to minimize $t$ because, for a given value of $X_{AlCl_3}$, introducing more of the larger cation into solution will reduce $P_{tot}$.

Although the vapour loss of a component of a fused salt solution depends on its vapour pressure, the geometry of the enclosure, and the turbulence of the surrounding or imposed atmosphere, volatilization of the fused salt chlorides is not expected to lead to significant electrolyte losses if the total vapour pressure is less than $1.32 \times 10^{-4}$ atm (0.1 Torr).

The compositions suitable for electrowinning at various temperatures have been determined within areas of one-phase liquid solution to ensure that no solid phases precipitate in the electrolytes, and by taking into account the maximum probable errors associated with each calculated system. These compositions are based on thermodynamic considerations only and may in fact be unsuitable with respect to electrolyte viscosity, conductivity (particularly for high concentrations of KCl), stability in the presence of air, kinetic considerations, and electrode stability (e.g., the presence of $K^+$ in the melt may cause swelling of graphite electrodes).

The discussions which follow apply to the systems at constant temperature. Temperature gradients within the molten salts could cause the formation of solid phases and interfere with electrolysis.

*LiCl–NaCl–LiAlCl$_4$–NaAlCl$_4$*

In this system, Figs. 13(*a*) to 15(*a*), there exists a wide range of compositions between 675 and 775°C which exhibit a one-phase liquid solution. Only a minor part of the NaCl-rich corner at the lower temperature has a solid phase in equilibrium with the liquid.

The highest total vapour pressures are to be found, as expected, in the LiCl- and $AlCl_3$-rich composition regions where, as an example, for $X_{AlCl_4^-} = 0.67$ and $t = 0.8$, $P_{tot}$ has values of ~0.26, 0.37, 0.52, and 0.99 atm at 675, 700, 725, and 775°C respectively. These high LiCl and $AlCl_3$ compositions would probably be unsuitable for aluminum electrowinning since their high vapour pressures would lead to significant melt losses by volatilization. The vapour consists of gaseous $LiAlCl_4$, $NaAlCl_4$, $AlCl_3$, and $Al_2Cl_6$, the quantities of which are approximately 56, 3.6, 40, and 1.3 mol% respectively at 725°C (8). These percentages do not change significantly between 675 and 775°C (8).

Of more practical importance, since the vapour pressures are lower, are composition regions containing low concentrations of aluminum chloride, i.e., $X_{AlCl_3} \sim 0.05$. For example, one electrolyte mentioned in the ALCOA process for aluminum electrowinning has a composition in mol% of 47.5 NaCl, 49.4 LiCl, 2.0 $AlCl_3$, 0.5 $CaCl_2$, 0.3 $MgCl_2$, and 0.4 KCl maintained at 700°C (24). Neglecting the small reduction in $P_{tot}$ due to the presence of the alkaline earth chlorides and KCl, we can see from Fig. 14(*b*) that $P_{tot} = 0.021$ atm for $X_{AlCl_3} = 0.02$ and $t = 0.50$. At 700°C, the components of the vapour in equilibrium with this solution are calculated (8) to consist of 33 mol% $LiAlCl_4$, 43 mol% $NaAlCl_4$, and 24 mol% $AlCl_3$. The alkali–aluminum chlorides and $AlCl_3$ are thus calculated to comprise ~81 wt% and ~19 wt% of this vapour respectively. This is in reasonable agreement with the values of 72 wt% and 28 wt% for the alkali–aluminum chlorides and $AlCl_3$ which are obtained by a suitable interpretation of the somewhat ambiguous ALCOA patent on fume recovery (25).

The minimum total vapour pressures in this system are calculated to vary between 0.010 and 0.018 atm for 675 and 775°C; these data are given in Table 5 and are several orders of magnitude greater than the minimum vapour pressure for non-volatilization.

*LiCl–KCl–LiAlCl$_4$–KAlCl$_4$*

Since the shape of the miscibility gap in LiCl–KCl– $LiAlCl_4$–$KAlCl_4$ is not known as a function of temperature, the non-isothermal intersection, which varies in temperature between 450 and 600°C, of the miscibility gap with the liquidus surface is shown in Figs. 16(*a*)–18(*a*) in order to give an indication of compositions in which

TABLE 5. Minimum calculated vapour pressures in the reciprocal systems ACl–BCl–$AAlCl_4$–$BAlCl_4$ for $X_{AlCl_3} = 0.02$ (A, B = Li, Na, K)

| Alkali cations | | | | |
|---|---|---|---|---|
| *A* | *B* | *T* (°C) | $t_{min}$[a] | $P_{tot}$ (atm) |
| Li | Na | 675 | 0.35 | 0.010 |
| | | 700 | 0.29 | 0.012 |
| | | 725 | 0.22 | 0.014 |
| | | 775 | 0.06 | 0.018 |
| Li | K | 675 | 0.21 | 0.0048 |
| | | 700 | 0.16 | 0.0053 |
| | | 725 | 0.08 | 0.0050 |
| | | 775 | 0.00 | 0.0060 |
| Na | K | 675 | 0.36 | 0.0029 |
| | | 700 | 0.26 | 0.0034 |
| | | 725 | 0.16 | 0.0042 |
| | | 775 | 0.00 | 0.0060 |

[a] $t_{min}$ = mol% ACl/(mol% ACl + mol% BCl) = minimum value of $t$ for a one-phase liquid solution.

Can. J. Chem. Downloaded from www.nrcresearchpress.com by 210.87.254.40 on 09/06/12
For personal use only.

two liquids exist. However, this composition region will diminish in area with increasing temperature so that the composition regions of one-phase liquid solution at 675, 700, 725, and 775°C are likely to be significantly larger than indicated.

On the $AlCl_3$-rich side of the $LiCl–KAlCl_4$ pseudo-binary, one-phase liquid solutions do exist which have total vapour pressures greater than 0.1 atm. For instance, for $X_{AlCl_4^-} = 0.67$ and $t = 0.8$, the total vapour pressures are 0.23, 0.33, 0.46, and 0.87 atm at 675, 700, 725, and 775°C, respectively. As with the corresponding composition in the $LiCl–NaCl–LiAlCl_4–NaAlCl_4$ system, compositions in this region would undoubtedly be unsuitable as electrolytes due to the probability of high volatilization losses. At 725°C and this composition, the vapour consists of gaseous $LiAlCl_4$, $KAlCl_4$, $AlCl_3$, and $Al_2Cl_6$, the quantities of which are 50, 3.1, 38, and 1.1 mol% respectively. As with the previous system, these quantities do not change significantly between 675 and 775°C (8).

For $X_{AlCl_4^-} > 0.1$, relatively lower vapour pressures are calculated to exist for low values of $t$ in the narrow composition band of the one-phase liquid solution occurring between the miscibility gap and either the line of solid–liquid equilibrium or $t = 0.0$. These calculated vapour pressures also have a significant dependence on $t$ and are in the approximate ranges:

| $T$ (°C) | Vapour pressure (atm) |
|---|---|
| 675 | 0.012–0.018 |
| 700 | 0.015–0.025 |
| 725 | 0.020–0.035 |
| 775 | 0.040–0.070 |

Total vapour pressures for $X_{AlCl_3} \leq 0.10$ in this system are given in Figs. 16(*b*) to 18(*b*). While the composition region of one-phase liquid solution is severely restricted, it would likely be possible to employ an electrolyte of composition $t = 0.2$ and $X_{AlCl_3} = 0.02$, for which $P_{tot}$ has values of 0.0048, 0.0064, 0.0086, and 0.015 atm at 675, 700, 725, and 775°C, respectively. An increase in $X_{AlCl_3}$ to 0.05 will double the respective total vapour pressures. The gaseous species in equilibrium with these solutions are calculated (8) to contain approximately 88–92 mol% $KAlCl_4$, 10–6 mol% $AlCl_3$, and 2 mol% $LiAlCl_4$.

The minimum vapour pressures for this system, as given in Table 5, are calculated to be in the order of 0.005 atm, which is somewhat lower than in $LiCl–NaCl–LiAlCl_4–NaAlCl_4$, but not low enough to prevent significant volatilization.

It would be of interest to calculate or experimentally determine the quantities of NaCl to be added to this system to transform the miscibility gap to a one-phase liquid solution.

### *$NaCl–KCl–NaAlCl_4–KAlCl_4$*

For this system, the lines of solid–liquid equilibrium estimated from experimental data as discussed previously have been combined with the calculated total vapour pressures in Figs. 19(*a*) to 21(*a*). At 675°C, sub-liquidus compositions occupy approximately 50% of the isothermal section, and this significantly restricts the composition region suitable for electrowinning, particularly in the sodium-rich corner. However, there is a corridor of one-phase liquid solution in the KCl-rich side for $0.0 < X_{AlCl_4^-} < 0.55$ in which $P_{tot} < 0.015$ atm. Because $T$ vs. $X_{AlCl_3}$ is shallow for $X_{AlCl_4^-} < 0.55$, the region of one-phase liquid solution widens rapidly as the temperature is increased, Figs. 20(*a*) and 21(*a*), until the isothermal section at 775°C exhibits no significant area of sub-liquidus composition.

For $X_{AlCl_4^-} = 0.67$ and $t = 0.8$, the total vapour pressures are 0.029, 0.044, 0.064, and 0.13 atm at 675, 700, 725, and 775°C, respectively. At 725°C, the vapour consists of gaseous $NaAlCl_4$, $KAlCl_4$, and $AlCl_3$, which are calculated (8) to comprise 58, 14, and 27 mol% of the vapour respectively at 725°C. As with the other systems, these mole percentages do not vary significantly with temperature (8).

The total vapour pressures for $X_{AlCl_3} < 0.10$ are given in Figs. 19(*b*) to 21(*b*). For $X_{AlCl_3} = 0.02$ and $t = 0.50$, the total vapour pressures are 0.0032, 0.0045, 0.0061, and 0.011 atm at 675, 700, 725, and 775°C, respectively. Increasing $X_{AlCl_3}$ to 0.05 has the effect of increasing the total vapour pressures by factors between 2.11 and 2.17.

As reviewed elsewhere (2), several investigators (23, 26, 27) have studied the deposition of liquid aluminum from fused $NaCl–KCl–AlCl_3$ electrolytes containing NaCl and KCl in a 1:1 mole ratio and concentrations of $AlCl_3$ between 2.7 wt% and 30 wt% ($0.014 < X_{AlCl_3} < 0.176$) at temperatures between 685 and 750°C. Since the calculated total vapour pressures associated with these compositions are between 0.0025 atm for 2.7 wt% $AlCl_3$ and 0.0364 atm for 30 wt% $AlCl_3$, the electrolytes used by these investigators probably became significantly depleted in $AlCl_3$-bearing species due to volatilization of aluminum-bearing gases.

The minimum total vapour pressures in this

Can. J. Chem. Downloaded from www.nrcresearchpress.com by 210.87.254.40 on 09/06/12
For personal use only.

system, as given in Table 5, are calculated to vary between 0.0028 and 0.0060 atm for 675 to 775°C, i.e. not substantially different from those of the previous system and not low enough to prevent significant volatilization.

## Conclusions

Phase diagrams and total vapour pressure curves at 675, 700, 725, and 775°C in the reciprocal ternary fused salt systems LiCl–NaCl–$LiAlCl_4$–$NaAlCl_4$, LiCl–KCl–$LiAlCl_4$–$KAlCl_4$, and NaCl–KCl–$NaAlCl_4$–$KAlCl_4$ have been calculated via the Conformal Ionic Solution Theory from the known thermodynamic properties of the appropriate binary systems by means of computer-assisted analytical techniques. Among the three ternary systems, only the latter's phase diagram has been reported in any detail in the literature. Agreement in this latter case between the experimental and calculated phase diagrams was acceptable.

A miscibility gap which occupies more than 50% of the composition region was calculated to occur in the system LiCl–KCl–$LiAlCl_4$–$KAlCl_4$.

Compositions suitable for electrowinning of aluminum from the viewpoint of maintaining a one-phase liquid solution were proposed. These are severely restricted in LiCl–KCl–$LiAlCl_4$–$KAlCl_4$ because of the miscibility gap and only somewhat less so at lower temperatures in NaCl–KCl–$NaAlCl_4$–$KAlCl_4$ because of the solid–liquid equilibrium. The system LiCl–NaCl–$LiNaCl_4$–$NaAlCl_4$ exhibits the widest range of one-phase liquid solutions.

Minimum total vapour pressures in systems involving potassium were calculated to be 20–40 times the maximum vapour pressure for non-volatilization. The minimum vapour pressures in LiCl–NaCl–$LiAlCl_4$–$NaAlCl_4$ were calculated to be 75–140 times this value. It can thus be expected that the use of these systems as electrolytes in the electrowinning of aluminum will necessitate extensive fume recovery systems regardless of the compositions employed.

With each region of one-phase liquid solution, extensive variations of density, viscosity, and electrical conductivity can be expected to occur. The experimental measurement of these properties, combined with the thermodynamic properties given in this report, will enable a determination of the optimum temperature and composition for each of the three ternary systems. Hence, future investigation into these systems could involve the measurement of the density, viscosity, and conductivity of their regions of one-phase liquid solution as well as the experimental verification of some of the calculated total vapour pressures and of the two ternary phase diagrams involving lithium.

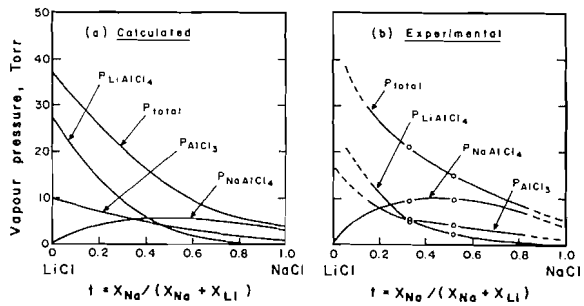


FIG. 22. Calculated and experimental (28) total and partial vapour pressures over LiCl–NaCl–$AlCl_3$ melts versus the molar ratio of NaCl to LiCl at 700°C at 4 wt. % $AlCl_3$.

NOTE ADDED IN PROOF:

In an article which appeared after the present article was submitted, Knapstad *et al.* (28) report vapour pressure measurements over LiCl–NaCl–$AlCl_3$ ternary melts dilute in $AlCl_3$ (over the range 2 to 10 wt. % $AlCl_3$). In addition, they report vapour composition measurements which permit them to calculate partial pressures under the assumption that $LiAlCl_4$, $NaAlCl_4$, and $AlCl_3$ are the major vapour species. Some results showing total and partial pressures versus the NaCl to LiCl ratio at 700°C over melts containing 4 wt. % $AlCl_3$ are compared with calculated values in Fig. 22. Measurements were reported by Knapstad *et al.* at $t = X_{Na}/(X_{Na} + X_{Li}) = 0.33$ and at $t = 0.52$. Dashed lines in Fig. 22 indicate that results for pure LiCl and NaCl were extrapolated by the authors from previous (20) measurements at higher $AlCl_3$ contents.

It can be seen that the calculations reproduce well the observed negative deviations from linearity in the $P_{total}$ curve. In addition, the observation that $NaAlCl_4$ is the major vapour species over most of the composition range even though $P_{total}$ for LiCl–$AlCl_3$ is much higher than $P_{total}$ for NaCl–$AlCl_3$ is reproduced by the calculations. The maximum deviation between measured and calculated values of $P_{total}$ in Fig. 22 is about 20%. Deviations at other reported compositions in the range 2 to 10 wt. % $AlCl_3$ were all less than ±20%.

1. K. GRJOTHEIM, C. KROHN, and H. ØYE. Aluminum, **51** (supple. in English), 6 (1975).
2. J. M. SKEAFF. Trans. IMM, **89**, C71 (1980).
3. J. M. SKEAFF, C. W. BALE, A. D. PELTON, and W. T. THOMPSON. Selection of ternary fused chlorides for the electrowinning of lead and zinc based on calculated thermodynamic properties. CANMET Report 79–23, Depart-

ment of Energy, Mines and Resources, Ottawa, Canada K1A 0G1. 1980.
4. P.-L. LIN, A. D. PELTON, and C. W. BALE. J. Am. Ceram. Soc. **62**, 414 (1979).
5. M. L. SABOUNGI, P.-L. LIN, P. CERISIER, and A. D. PELTON. Met. Trans. **11B**, 493 (1980).
6. W. W. LIANG, P.-L. LIN, and A. D. PELTON. High Temp. Sci. **12**, 41 (1980).
7. A. D. PELTON and C. W. BALE. CALPHAD J. **1**, 253 (1977).
8. A. D. PELTON, C. W. BALE, and W. T. THOMPSON. Calculation of liquidus surfaces, vapour pressures and decomposition potentials in certain ternary and quaternary fused salt systems. Report on Contract No. 23440-8-9076. Department of Energy, Mines and Resources, Ottawa, Canada. 1979.
9. I. BARIN and O. KNACKE. Thermochemical properties of inorganic substances. Springer-Verlag, New York. 1973 and supplement, with O. Kubaschewski (1977).
10. L. S. HERSH and O. J. KLEPPA. J. Chem. Phys. **42**, 1309 (1965).
11. (*a*) E. M. LEVIN, C. R. ROBBINS, and H. F. MCMURDIE. Phase diagrams for ceramists. The American Ceramic Society, Columbus, Ohio, U.S.A. (1964); (*b*) E. M. LEVIN, C. R. ROBBINS and H. F. MCMURDIE. *ibid*. 1969 Supplement (1969); (*c*) E. M. LEVIN and H. F. MCMURDIE. *ibid*. 1975 Supplement (1975).
12. A. GABRIEL. Master's Dissertation. Ecole Polytechnique de Montréal, Montréal. 1980.
13. Y. SATO and T. EJIMA. J. Jpn. Inst. Met. **42**, 905 (1978).
14. M. L. SABOUNGI and M. BLANDER. J. Am. Ceram. Soc. **58**, 1 (1975).
15. M. BLANDER and E. TOPOL. Inorg. Chem. **5**, 1641 (1966).
16. M. L. SABOUNGI and M. BLANDER. High Temp. Sci. **6**, 37 (1974).
17. M. L. SABOUNGI, H. SCHNYDERS, M. S. FOSTER, and M. BLANDER. J. Phys. Chem. **78**, 1091 (1974).
18. P.-L. LIN, C. W. BALE, and A. D. PELTON. Calculation of phase diagrams and thermochemistry of alloy phases. *Edited by* Y. A. Chang and J. F. Smith. Proc. AIME Symposium, Milwaukee, Met. Soc. of AIME Conference Proceedings (1979).
19. A. D. PELTON, C. W. BALE, and P.-L. LIN. Calculation of thermodynamic equilibria in the carbonate fuel cell. U.S. Dept. of Energy Report, Contract No. DE-AC02-79ET/15416. 1981.
20. H. LINGA, K. MOTZFELDT, and H. A. ØYE. Ber. Bunsenges. Phys. Chem. **82**, 568 (1978).
21. W. FISCHER and A.-L. SIMON. Z. anorg. allg. Chem. **306**(1–2), 1 (1960).
22. R. H. MOORE. J. Chem. Eng. Data, **8**, 164 (1963).
23. P. C. GOOD, M. O. BUTLER, and L. A. YERKES. U.S.B.M. Rep. Invest. 6785 (1966).
24. W. E. HAUPIN. U.S. Patent 3,755,099 (to ALCOA) (1973).
25. S. C. JACOBS and R. C. SCHOENER. U.S. Patent 3,904,494 (to ALCOA) (1975).
26. E. L. SINGLETON, D. E. KIRBY, and T. A. SULLIVAN. U.S.B.M. Rep. Invest. 7212 (1968).
27. D. E. KIRBY, E. L. SINGLETON, and T. A. SULLIVAN. U.S.B.M. Rep. Invest. 7353 (1970).
28. B. KNAPSTAD, H. LINGA, and H. A. ØYE. Ber. Bunsenges. Phys. Chem. **85**(12), 1132 (1981).

Can. J. Chem. Downloaded from www.nrcresearchpress.com by 210.87.254.40 on 09/06/12
For personal use only.

# Kinetics and mechanism of ion exchange sorption of some detergents on zinc ferrocyanide

SURESH K. SRIVASTAVA, CHAKRESH K. JAIN, CHANDER K. OBEROI, AND ASHOK K. SHARMA

*Department of Chemistry, University of Roorkee, Roorkee-247667, India*

Received October 9, 1981

SURESH K. SRIVASTAVA, CHAKRESH K. JAIN, CHANDER K. OBEROI, and ASHOK K. SHARMA. Can. J. Chem. **60**, 1681 (1982).

Studies have been made on the kinetics and mechanism of exchange sorption of detergents on zinc ferrocyanide using a modified limited bath technique. The effects of concentration, particle size of the sorbent material, and temperature on the sorption rate have been investigated. In the case of cationic detergents (cetyl pyridinium bromide and cetyl trimethylammonium bromide), equilibrium is attained in a period of 2–3 h while 12–16 h are required for anionic detergents, viz., sodium dodecyl sulphate and sodium dodecyl benzene sulphonate. The slowest step governing the sorption rate is found to be the diffusion within the exchanger particles at higher concentrations. The effective diffusion coefficients have been evaluated at four different temperatures and found to be comprised of mainly two components. The energy barriers against the diffusion of exchanging ions have been assessed from the Arrhenius equation. Entropies of activation for various sorption systems have also been calculated. The results are discussed in terms of the size and geometry of the detergents, pore-widths in the sorbent material, and the electric potential gradient along the diffusion path. No change in the internal structure of zinc ferrocyanide is inferred due to the sorption of detergent ions.

SURESH K. SRIVASTAVA, CHAKRESH K. JAIN, CHANDER K. OBEROI et ASHOK K. SHARMA. Can. J. Chem. **60**, 1681 (1982).

Faisant appel à la technique modifiée du bain limité, on a étudié la cinétique et le mécanisme de la sorption d'échange des détergents sur le ferrocyanure de zinc. On a étudié les effets de la concentration, de la dimension de la particule du matériel adsorbant et de la température sur la vitesse de sorption. Dans le cas des détergents cationiques (bromure de cétyl pyridinium et bromure de cétyl triméthylammonium), on atteint l'équilibre sur une période de 2–3 h tandis que dans le cas des détergents anioniques (dodécylsulfate de sodium et dodécylbenzènesulfonate de sodium), il faut 12–16 h. On a trouvé que la vitesse de diffusion, à l'intérieur des particules échangées à des concentrations plus élevées, est l'étape déterminante de la vitesse de sorption. On a évalué les coefficients de diffusion effective à quatre températures différentes et on a trouvé qu'ils sont constitués principalement de deux composantes. On a évalué les barrières d'énergie de la diffusion des ions échangés à partir des équations d'Arrhénius. On a également calculé les entropies d'activation de systèmes de sorption différents. On discute des résultats en fonction de la dimension et de la géométrie des détergents, de la largeur des pores du matériel adsorbant et du gradient de potentiel électrique près de la cellule de diffusion. Aucun changement de la structure interne du ferrocyanure de zinc n'est attribué à sorption des ions du détergent.

[Traduit par le journal]

## Introduction

A survey of the literature shows that inorganic gels exhibiting good sorption properties so far have not been explored for waste treatment. Recently, we have reported the use of chromium ferrocyanide gel for the removal of heavy metal ions (*1*). Preliminary studies with zinc ferrocyanide (ZFC), which is found to possess both cation and anion exchange properties (*2*), reveal the utility of this compound as a good scavenger for detergents (*3*). It is quite well known that detergents, even in low concentrations, pollute water and affect the sorption characteristics of the soil. As the rate factor in sorption processes is of great significance for the exploitation of sorbent materials on an industrial scale, extensive studies have been reported in this article on the kinetics and thermodynamics of ion-exchange sorption of some cationic and anionic detergents on ZFC. Cationic and anionic detergents, cetyl pyridinium bromide (CPB), cetyl trimethylammonium bromide (CTAB), sodium dodecyl sulphate (SDS), and sodium dodecyl benzene sulphonate (SDBS), which are non-biodegradable in nature, have been chosen for these investigations. Some parameters, viz., effective diffusion coefficient, entropy of activation, and energy of activation, have been evaluated and utilized to interpret the mechanism of sorption and interaction between ZFC and detergent ions.

## Experimental

Detergents were obtained from B.D.H. All other chemicals used were of analytical grade. Doubly distilled water was used for preparing solutions.

pH measurements were made with a pH-meter, model pH 821, E.C.I., India. The Bausch and Lomb Spectronic-20 and the Unicam-500 were used for spectrophotometric work. Infrared spectra of the samples were recorded on a Beckmann IR-20 spectrophotometer in a potassium bromide medium.

*Preparation and characterization of zinc ferrocyanide*

Zinc ferrocyanide was prepared according to the method of Kourim *et al.* (*2*) by the reaction of 0.1 *M* sodium ferrocyanide with 0.1 *M* zinc nitrate. The reaction mixture was heated on a boiling water bath (1–2 h). It was then cooled, filtered, and washed with water. After thorough draining, it was heated slowly for 4 h. Maximum temperature after 1 h of drying was ~110°C. A faint green coloured material, obtained after drying, was quite stable in water, concentrated salt solutions, and acids (4 *M*).

Analysis of the product was carried out by first drying the material over $P_2O_5$ under vacuum and then dissolving in a

0008-4042/82/131681-06$01.00/0

©1982 National Research Council of Canada/Conseil national de recherches du Canada

Can. J. Chem. Downloaded from www.nrcresearchpress.com by 210.87.254.40 on 09/06/12
For personal use only.

Can. J. Chem. Downloaded from www.nrcresearchpress.com by 210.87.254.40 on 09/06/12
For personal use only.

mixture of aqua regia and sulphuric acid. The estimations of iron and zinc were made by classical methods (4).

Iron and zinc contents in ZFC were found to be 15.0 and 32.9% respectively, corresponding to a molar ratio of Zn/Fe ≈ 2:1. The water content determined by thermogravimetric analysis was about 12%. The content of cyanide group was calculated by subtraction to be 40.1%. The formula assigned (4) to the product is $Zn_2[Fe(CN)_6]2.5H_2O$.

Infrared spectra of the compound showed all the characteristic absorption frequencies reported in the literature for metal ferrocyanides. A broad band at 3700 $cm^{-1}$ was due to interstitial water molecules and OH groups (5), while the characteristic HOH bending (5) appeared at 1600 $cm^{-1}$. The sharp bands, one at 2080 $cm^{-1}$ and other at 580 $cm^{-1}$, were assigned to cyanide stretching and Fe—C stretching frequencies (6). Another sharp band at 500 $cm^{-1}$ was attributed to the Zn—N stretching mode, thus indicating a certain degree of polymerization in the product (7, 8).

Zinc ferrocyanide was treated with 1 *M* HCl to convert it into homoionic form ($H^+$, $Cl^-$) and used as such for subsequent investigations. Cation and anion exchange capacities of ZFC, determined by standard methods (9–11), were found to be 4.65 mequiv. $g^{-1}$ and 0.14 mequiv. $g^{-1}$, respectively.

*Estimation of detergents*

The method of Few and Ottewill (12) was used for the estimation of cationic detergents. The solutions were treated with an anionic dye (Orange II) and the complex formed between the detergent and dye was extracted into chloroform. Estimations of the colour intensity in the organic phase were made spectrophotometrically at 485 nm.

The modified methylene blue method of Wang (13) was used for estimating the concentrations of SDBS and SDS in solutions. The sample to be analysed was treated with an excess of methylene blue reagent at pH 10. The methylene blue – detergent complex thus formed was extracted in the chloroform layer and the concentrations were measured spectrophotometrically at 650 nm.

*Particle size*

Dried ZFC was ground and sieved to collect the fractions of (50–100), (100–170), and (170–200) B.S.S. mesh-size. Average particle radius of each fraction was determined (14) with the help of a projector, Agfa Diamator m (Germany). No significant change in the mean particle radius was observed when the samples were kept in water or detergent solutions for 48 h.

*Kinetic measurements*

For kinetic measurements, the modified limited bath technique (batch technique) was employed (14–16) because of its relative simplicity over the column and shallow-bed arrangement.

Known volumes (10 mL) of the detergent solutions were placed in a number of stoppered Pyrex glass tubes and subjected to continuous mechanical shaking in a thermostat at the desired temperature. Weighed amounts of ZFC (0.1 g for anionic and 0.05 g for cationic detergents) were then introduced into each tube. The tubes were taken out from the thermostat at appropriate time intervals and the sorption process was checked by immediate filtration. To observe the effect of concentration on the rate of sorption, experiments were performed for different concentrations of CPB, CTAB, SDBS, and SDS ($10^{-4}$–$10^{-5}$ *M*). The investigations were also carried out with different particle sizes of ZFC and at four different temperatures (30, 35, 40, 45 ± 0.1°C).

*Rate expression and evaluation of kinetic and thermodynamic parameters*

The fractional attainment of equilibrium $F$ at time $t$ has been determined as:

$$[1]\quad F = \frac{Q_t}{Q_\infty} = \frac{\text{Amount of exchange sorption at time } t}{\text{Amount of exchange sorption at infinite time or at equilibrium}}$$

The equations developed by Boyd *et al.* (17) and later improved by Reichenberg (18) have been applied for particle-diffusion-controlled rate processes. According to these expressions, if the rate of exchange sorption is governed by particle diffusion, i.e. the diffusion of exchanging ions through the exchanger is slowest, $F$ is related to $t$ and the particle radius $r$ as:

$$[2]\quad F = 1 - \frac{6}{\pi^2}\sum_{n=1}^{\infty}\frac{\exp(-n^2Bt)}{n^2}$$

where $n$ is the number of exchanger particles and $B$, the time co-ordinate, is expressed as:

$$[3]\quad B = \frac{\pi^2}{r^2}D_i$$

where $D_i$ stands for the effective diffusion coefficient of ingoing ions.

Obviously, plots of $Bt$ vs. $t$ must be straight lines passing through the origin. In the present studies, for every observed value of $F$, the corresponding $Bt$ value has been obtained from Reichenberg's table (18). The experimental conditions were set for the particle-diffusion mechanism to evaluate the thermodynamic parameters of the sorption processes. The energy of activation $E_a$ has been determined by applying the Arrhenius type expression (14, 16):

$$[4]\quad D_i = D_0 \exp(-E_a/RT)$$

The pre-exponential constant $D_0$ gives the entropy of activation $\Delta S^*$ as (14, 16, 19):

$$[5]\quad D_0 = 2.72d^2\frac{kT}{h}\exp\left(\frac{\Delta S^*}{R}\right)$$

where $k$, $h$, and $R$ are the Boltzmann, Planck, and gas constants, respectively, $d$ is the average distance between the successive exchange sites and is taken as 5 Å (14, 16). $T$ (=273 K) is the temperature on the Kelvin scale.

All linear plots have been drawn according to the method of least-squares. The standard deviations on all reported values are less than 5%.

## Results and discussion

The effects of detergent concentration, particle size, and temperature on the rate of exchange sorption are depicted for some typical systems in Figs. 1, 2, and 3, respectively. The representative log $(1 - F)$ vs. $t$ plots (McKay plots (20)) are shown in Fig. 4. Figure 5 indicates the relationship between the logarithm of the effective diffusion coefficient and the reciprocal temperature ($K^{-1}$) for the sorption of cationic and anionic detergents on ZFC. Tables 1 and 2 record the kinetic and

Can. J. Chem. Downloaded from www.nrcresearchpress.com by 210.87.254.40 on 09/06/12
For personal use only.

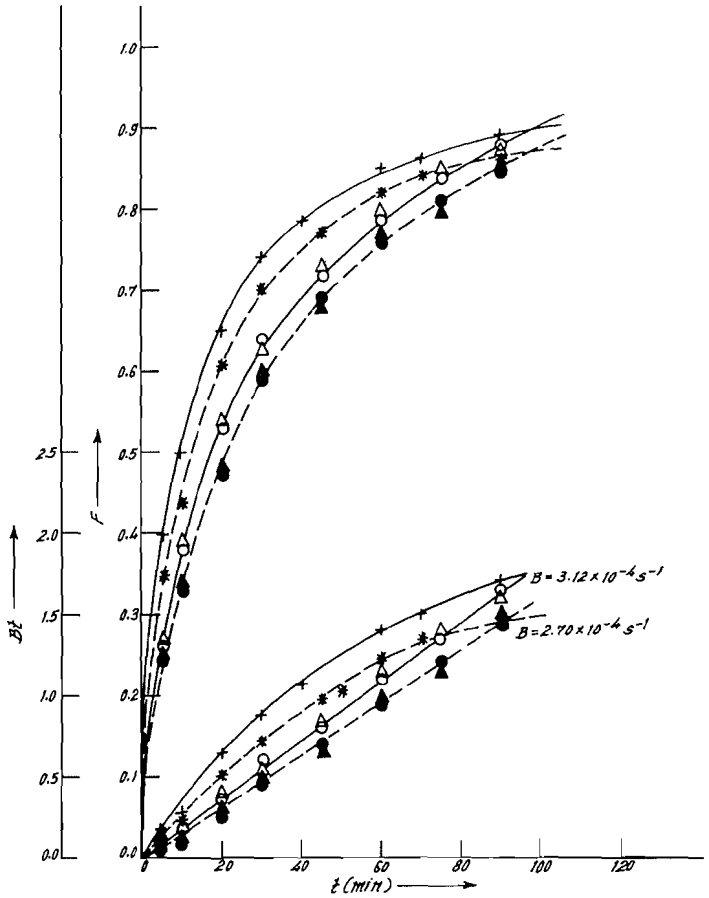


FIG. 1. Plots of $F$ vs. $t$ and $Bt$ vs. $t$ for CPB, solid lines, and CTAB, broken lines, using different solution concentrations at 30°C on ZFC ($r = 12.05 \times 10^{-3}$ cm): (△, ▲) $1.0 \times 10^{-4}$ $M$; (○, ●) $7.5 \times 10^{-5}$ $M$; (□, ■) $4.0 \times 10^{-5}$ $M$.

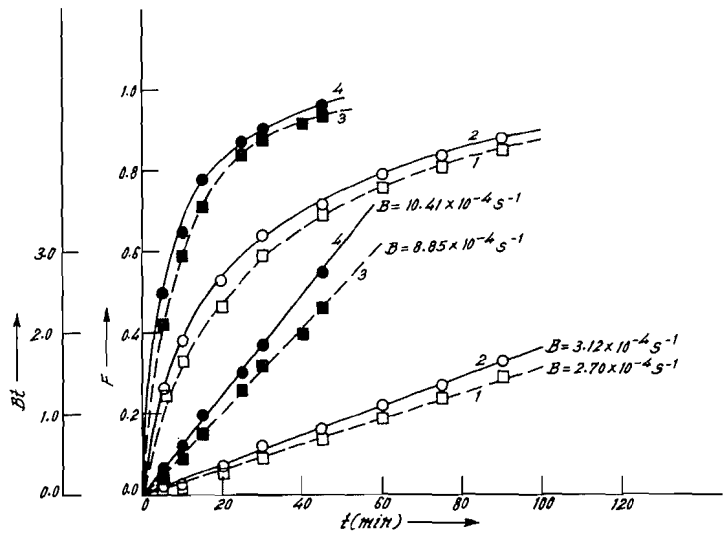


FIG. 2. Plots of $F$ vs. $t$ and $Bt$ vs. $t$ for CPB, solid lines, and CTAB, broken lines, using different particle sizes of ZFC at 30°C and solution concentration $7.5 \times 10^{-5}$ $M$; (*1*,*2*) $r = 12.05 \times 10^{-3}$ cm; (*3*,*4*) $r = 6.57 \times 10^{-3}$ cm.

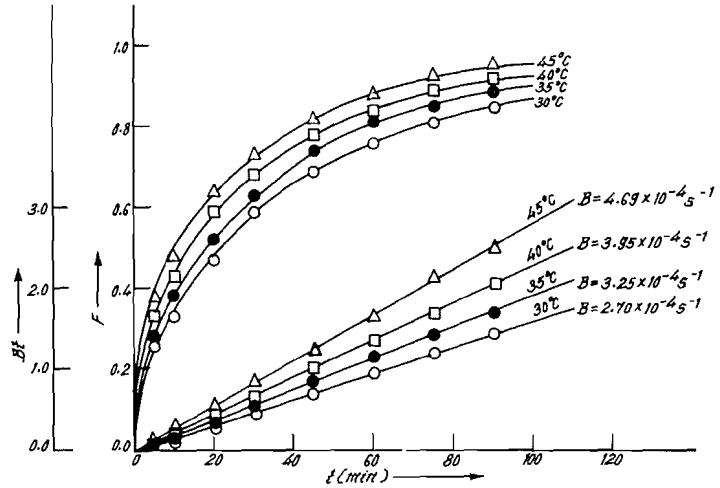


FIG. 3. Plots of $F$ vs. $t$ and $Bt$ vs. $t$ for CTAB at different temperatures using ZFC ($r$ = 12.05 × $10^{-3}$ cm) and a solution concentration 7.5 × $10^{-5}$ $M$.

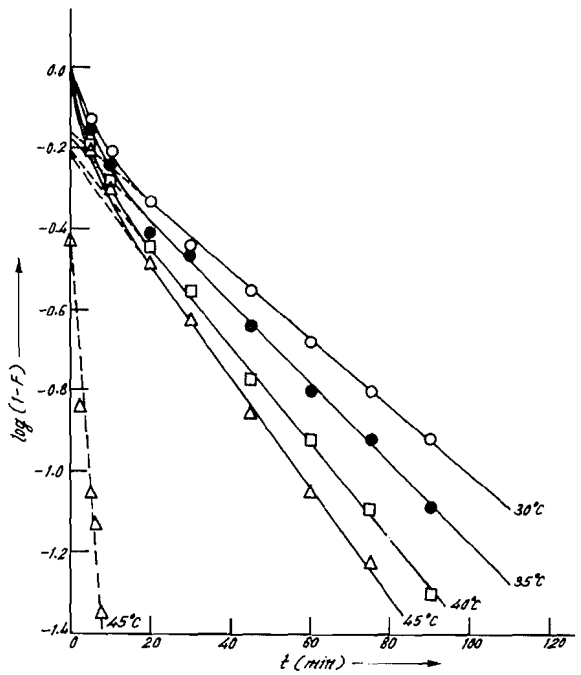


FIG. 4. McKay plots for the sorption of CPB on zinc ferrocyanide.

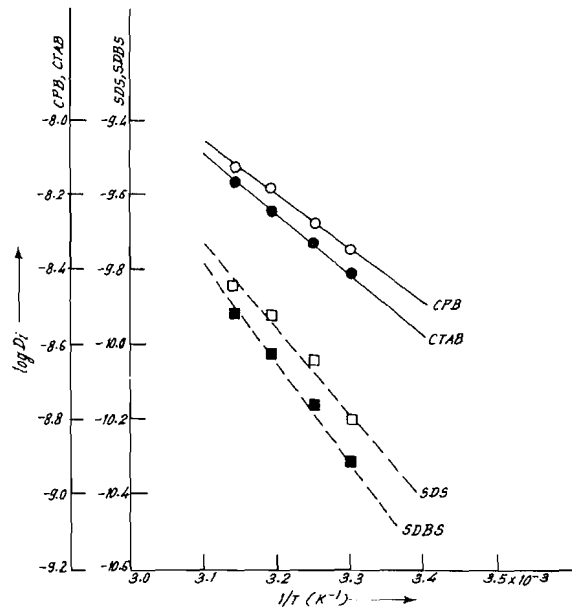


FIG. 5. Plots of log $D_i$ vs. $1/T$; ○ for CPB, ● for CTAB, □ for SDS, and ■ for SDBS.

thermodynamic parameters for all the systems reported herein.

The sorption of cationic detergents has been found to be faster than that of anionic detergents. The equilibrium is reached in a period of 2–3 h for $CP^+$ and $CTA^+$, while in the case of $DS^-$ and $DBS^-$ 12–16 h are required. Also, the capacities of $CP^+$ and $CTA^+$ (2.97 and 2.12 mequiv. $g^{-1}$, respectively) are much greater than those of $DS^-$ and $DBS^-$ (0.05 and 0.04 mequiv. $g^{-1}$, respectively) on ZFC. The higher uptake and relatively faster sorption rate of cationic detergents may be attributed to a higher cation exchange, viz., 4.65 mequiv. $g^{-1}$, as compared to anion-exchange value viz., 0.14 mequiv. $g^{-1}$, of the sorbent material.

It is evident from Fig. 1 that plots of $Bt$ vs. $t$ for the sorption of cationic detergents on ZFC are linear and independent of initial solution concentration at and above 7.5 × $10^{-5}$ $M$. However, at 4.0 × $10^{-5}$ $M$, the plots deviate from linear behaviour.

Can. J. Chem. Downloaded from www.nrcresearchpress.com by 210.87.254.40 on 09/06/12
For personal use only.

TABLE 1. Effective diffusion coefficients ($D_i$) for ionic detergents at different temperatures

| Detergent | $D_i$ (cm$^2$ s$^{-1}$) 30°C | 35°C | 40°C | 45°C |
|---|---|---|---|---|
| CPB | $5.0 \times 10^{-9}$ | $5.4 \times 10^{-9}$ | $6.7 \times 10^{-9}$ | $7.6 \times 10^{-9}$ |
| CTAB | $4.0 \times 10^{-9}$ | $4.8 \times 10^{-9}$ | $5.8 \times 10^{-9}$ | $6.9 \times 10^{-9}$ |
| SDS | $62.9 \times 10^{-12}$ | $90.9 \times 10^{-12}$ | $121.0 \times 10^{-12}$ | $142.4 \times 10^{-12}$ |
| SDBS | $49.0 \times 10^{-12}$ | $69.6 \times 10^{-12}$ | $94.8 \times 10^{-12}$ | $117.9 \times 10^{-12}$ |

TABLE 2. $D_0$ values and thermodynamic parameters for the exchange sorption of ionic detergents

| Detergent | $D_0$ (cm$^2$ s$^{-1}$) | $E_a$ (kcal mol$^{-1}$) | $\Delta S^*$ (cal deg$^{-1}$ mol$^{-1}$) |
|---|---|---|---|
| CPB | $2.6 \times 10^{-4}$ | 6.6 | −10.0 |
| CTAB | $8.0 \times 10^{-4}$ | 7.4 | −7.7 |
| SDS | $2.5 \times 10^{-3}$ | 10.5 | −5.5 |
| SDBS | $3.2 \times 10^{-2}$ | 12.2 | −0.40 |

This shows that the sorption rate of $CTA^+$ and $CP^+$ is particle-diffusion controlled at and above $7.5 \times 10^{-5}$ $M$, while at lower solution concentration ($4.0 \times 10^{-5}$ $M$), film-diffusion also affects the process (14–18). Similar behaviour has also been observed for the exchange sorption of $DS^-$ and $DBS^-$ on ZFC, where plots of $Bt$ vs. $t$ are concentration independent and linear at and above $4.0 \times 10^{-6}$ $M$. The increases in sorption rate with decrease in particle size of sorbent material (Fig. 2) and also with increase in temperature (Fig. 3) further support a particle-diffusion mechanism as the rate-controlling process (14–18). The non-linear behaviour of plots of log $(1 - F)$ vs. $t$ (Fig. 4) drawn for only one system, $CP^+/H^+$, is also evidence in favour of a particle-diffusion mechanism as the rate-controlling step in the sorption of detergent ions on zinc ferrocyanide (15, 16).

It is interesting to note that the concentrations of anionic detergents required for the particle-diffusion mechanism are lower compared to those of cationic detergents for the exchange on the same sorbent material ZFC. Such behaviour may be due to the relatively more rapid uptake for cationic than for anionic detergents (16, 17). Obviously, in systems with fast sorption rates, a significant concentration gradient exists in the liquid film surrounding the sorbent particles, and if mechanical agitation is kept unchanged, a higher concentration of sorbate is required to level out the concentration gradient so that film-diffusion does not remain dominant (17).

The observed concentrations of detergents for the particle-diffusion mechanism are considerably less than those reported for the exchange sorption of some simple as well as complex cations on various sorbents (14–16, 21–28). It is well known that the rate of uptake and mobility of ions in solution effectively determine the characteristics of the liquid film surrounding the sorbent particle. In the present case, the bigger size of $CTA^+$, $CP^+$, $DS^-$, and $DBS^-$ ions and their relatively slow rate of sorption, as compared to simple metal ions, reduce the possibility of the existence of a concentration gradient at the solid–liquid interface (14, 17), and hence even at such lower concentrations ($10^{-5}$–$10^{-6}$ $M$), the rate is governed by the particle-diffusion mechanism.

The shapes of the McKay plots (Fig. 4) for the sorption of $CP^+$ on ZFC are similar to those obtained for independently decaying radioactivities (29). Also for other systems under study (McKay plots not shown here), the same behaviour has been observed. The resolution (29) of these plots has been depicted for one temperature only. It can be inferred that in the sorption of detergent ions two interdiffusion processes contribute to the overall rate of exchange. As the system tends towards equilibrium, the faster of these becomes less significant and the slower one dominates. This behaviour is also evident from the shape of $F$ vs. $t$ plots (Figs. 1–3) where the rate of uptake is initially rapid and decreases with time.

The values of $D_i$, $D_0$, $E_a$, and $\Delta S^*$ have been calculated using eqs. [3], [4], and [5] for all the sorption systems. It is clear from Table 1 that the values of effective diffusion coefficients are higher for $CP^+$ and $DS^-$ as compared to those for $CTA^+$ and $DBS^-$, respectively. This may be due to the larger sizes of $CTA^+$ and $DBS^-$ compared to those of $CP^+$ and $DS^-$, thus are hindered in their mobility within the pores of the sorbent material. It may further be argued that effective diffusion coefficients ($D_i$) are mainly comprised of two components, which are due to the diffusion of the ingoing detergent ions through pores of different widths, and different electric fields along the diffusion path. The diffusion within the wider pores and weaker electrostatic retarding forces (particularly at the surface of the sorbent) accounts for the faster, and that within the narrower pores and

Can. J. Chem. Downloaded from www.nrcresearchpress.com by 210.87.254.40 on 09/06/12
For personal use only.

Can. J. Chem. Downloaded from www.nrcresearchpress.com by 210.87.254.40 on 09/06/12
For personal use only.

stronger retarding forces accounts for the slower, component of $D_i$. With increase of temperature the contribution of the faster component to $D_i$ also increases, due to the increasing mobility of the ions and this to some extent overcomes the influence of retarding forces. Helfferich *et al.* (30–33) have observed a similar behaviour and explained the variable interdiffusion coefficients on the basis of electric field gradient along the diffusion path.

It is worthwhile to note (Tables 1, 2) that the order in the values of pre-exponential constants ($D_0$), viz., $DBS^- > DS^- > CTA^+ > CP^+$, is the reverse of that of $D_i$ values. This may be attributed to the higher activation energy values associated with higher values of $D_0$ (Table 2, eq. [4]). These observations are analogous to those observed in this laboratory for the exchange sorption of complex cations on chromium ferrocyanide gel (14) and for ion-exchange in felspathoids by Barrer *et al.* (34).

It is found (Table 2) that the energies of activation for the sorption systems under study are in the order: $CP^+ > CTA^+ > DS^- > DBS^-$. This sequence in $E_a$ values can also be understood on the basis of higher affinity of ZFC towards cations as compared to anions, and the fact that $CTA^+$ and $DBS^-$ are larger than $CP^+$ and $DS^-$, respectively.

The entropies of activation are negative for all the sorption systems. Negative values of $\Delta S^*$ have also been observed for the exchange sorption of heavy alkali metal ions on chromium ferrocyanide gel (16), and other workers have reported analogous results for various sorption systems (24–28, 35, 36). In the case of diffusion of alkaline earth metal ions in zeolites, the negative values of $\Delta S^*$ have been taken as indicative of a comparatively higher degree of mobility and the lack of an orientational effect which the ingoing ion influences upon its water environment (37). It can also be inferred from the negative values of entropies of activation that there is no significant change in the internal structure of the sorbent material (16, 26, 27) as a result of sorption of cationic and anionic detergents.

**Acknowledgements**

Three of the authors (C.K.J., C.K.O., and A.K.S.) are grateful to the Council of Scientific and Industrial Research for providing research fellowship.

1. S. K. Srivastava, G. Bhattacharjee, A. K. Sharma, and C. K. Oberoi. Water Res. **14**, 113 (1980).
2. V. Kourim, J. Rais, and B. Million. J. Inorg. Nucl. Chem. **26**, 1111 (1964).
3. C. K. Oberoi. Ph.D. Thesis, Roorkee University, India. 1980.
4. M. T. Ganzerli-Valentini, S. Meloni, and V. Maxia. J. Inorg. Nucl. Chem. **34**, 1427 (1972).
5. P. J. Lucchesi and W. A. Glasson. J. Am. Chem. Soc. **78**, 1347 (1956).
6. K. Nakamoto. Infrared spectra of inorganic and coordination compounds. John Wiley, New York. 1963. pp. 166–171.
7. P. Ratnasamy and A. J. Leonard. J. Phys. Chem. **76**, 1838 (1976).
8. K. Nakamoto, J. Fujita, and H. Murata. J. Am. Chem. Soc. **80**, 4817 (1958).
9. O. Samuelson. Ion exchange separations. John Wiley, New York. 1965.
10. F. Helfferich. Ion exchange. McGraw Hill, New York. 1962.
11. C. B. Amphlett. Inorganic ion exchangers. Elsevier, Amsterdam. 1964.
12. A. V. Few and R. H. Ottewill. J. Colloid Sci. **11**, 34 (1958).
13. L. K. Wang. J. Am. Water Works Assoc. **67**, 19 (1975).
14. I. P. Saraswat, S. K. Srivastava, and A. K. Sharma. Can. J. Chem. **57**, 1214 (1979).
15. C. Heitner-Wirguin and G. Markovits. J. Phys. Chem. **67**, 2263 (1963).
16. I. P. Saraswat, S. K. Srivastava, and A. K. Sharma. J. Inorg. Nucl. Chem. **43**, 1653 (1981).
17. G. E. Boyd, A. W. Adamson, and L. S. Myers, Jr. J. Am. Chem. Soc. **69**, 2836 (1947).
18. D. Reichenberg. J. Am. Chem. Soc. **75**, 589 (1953).
19. A. Dyer and J. M. Fawcett. J. Inorg. Nucl. Chem. **28**, 615 (1966).
20. H. McKay. Nature (London), **142**, 997 (1938).
21. C. B. Amphlett, L. A. McDonald, and M. J. Redman. J. Inorg. Nucl. Chem. **6**, 220 (1958).
22. C. B. Amphlett, L. A. McDonald, and M. J. Redman. J. Inorg. Nucl. Chem. **6**, 236 (1958).
23. G. H. Nancollas and R. Paterson. J. Inorg. Nucl. Chem. **22**, 259 (1961).
24. J. P. Rawat and P. S. Thind. J. Phys. Chem. **80**, 1384 (1976).
25. J. P. Rawat and D. K. Singh. J. Inorg. Nucl. Chem. **40**, 897 (1978).
26. J. Mathew and S. N. Tandon. Can. J. Chem. **55**, 3857 (1977).
27. J. Mathew, N. J. Singh, C. B. Gupta, and S. N. Tandon. Indian J. Chem. **16A**, 524 (1978).
28. A. K. Jain, R. P. Singh, and S. Agrawal. Bull. Chem. Soc. Jpn. **54**, 599 (1981).
29. G. Friedlander and J. W. Kennedy. Nuclear and radiochemistry. Wiley, New York. 1956. pp. 128–129.
30. R. Schlogl and F. Helfferich. J. Chem. Phys. **26**, 5 (1957).
31. F. Helfferich and M. S. Plesset. J. Chem. Phys. **28**, 418 (1958).
32. M. S. Plesset, F. Helfferich, and J. N. Franklin. J. Chem. Phys. **29**, 1064 (1958).
33. F. Helfferich. J. Phys. Chem. **66**, 39 (1962).
34. R. M. Barrer and J. D. Falconer. Proc. R. Soc. London. A**236**, 227 (1956).
35. D. C. Freeman, Jr. and D. N. Stamires. J. Chem. Phys. **35**, 799 (1961).
36. A. Dyer and J. M. Fawcett. J. Inorg. Nucl. Chem. **28**, 615 (1966).
37. V. Pekarek and V. Vesely. Talanta Rev. **19**, 1266 (1972).

# Electrochemical oxidation of trifluoroacetic acid anion. V. Formation of bis(trifluoromethyl) alicyclic compounds from activated dienes[1]

ROGER N. RENAUD,[2] CAMPBELL J. STEPHENS, AND DENIS BÉRUBÉ
*Division of Chemistry, National Research Council of Canada, Ottawa, Ont., Canada K1A 0R6*

Received November 16, 1981

ROGER N. RENAUD, CAMPBELL J. STEPHENS, and DENIS BÉRUBÉ. Can. J. Chem. **60**, 1687 (1982).

The electrochemical oxidation of trifluoroacetate anion in the presence of activated dienes, ROOCCH=CH(CH$_2$)$_n$CH=CHCOOR, gave bis(trifluoromethyl) alicyclic products. The ring size of the products was determined by comparing the fluorine nuclear magnetic resonance spectra of the protonated with the corresponding α,α′-dideuterated compounds. The results can be explained by an intramolecular radical addition and by an intramolecular coupling of a biradical intermediate.

ROGER N. RENAUD, CAMPBELL J. STEPHENS et DENIS BÉRUBÉ. Can. J. Chem. **60**, 1687 (1982).

L'oxydation électrochimique de l'anion trifluoroacétate en présence de dioléfines activées, ROOCCH=CH(CH$_2$)$_n$CH=CHCOOR, donne des produits cycliques bis(trifluorométhylés). La dimension des cycles fut déterminée en comparant les spectres de la résonance magnétique nucléaire du fluor du composé protoné avec celui du composé α,α′-dideutérié correspondant. Les résultats peuvent être expliqués par une addition radicalaire intramoléculaire et par un couplage intramoléculaire d'un biradical.

Can. J. Chem. Downloaded from www.nrcresearchpress.com by 210.87.254.6 on 09/06/12
For personal use only.

The addition of electrochemically generated trifluoromethyl radicals to olefinic double bonds has been the subject of previous studies (1–3).

$$CF_3COO^- \xrightarrow[-CO_2]{-e^-} CF_3\cdot \xrightarrow{>C=C<} \text{Products}$$

It has been shown that, in the case of an activated olefin **1** (Scheme 1), the first $CF_3$ radical always adds to the β-carbon of the electron-withdrawing substituent to give **2**. This was based on the observation that only the head-to-head dimeric product **3** was obtained and never the head-to-tail or the tail-to-tail analogues. Under a low concentration of the olefin **1** acceptable yields of the monomer **4** were obtained with only small amounts of dimer **3**. When the concentration of the olefin **1** was increased, the yield of dimer **3** increased accordingly.[3] Chkir and Lelandais (4) similarly observed the formation of the head-to-head dimer (as **3**) in high yields by the electrochemical oxidation of acetate anion in the presence of activated olefins.

To our knowledge, dimer **6** was never detected but telomer **7** has been isolated (3). Assuming that **6** and **7** are formed through the common radical **5**, it is difficult to explain the formation of **7** without the formation of **6**.

The objective of the present investigation was to study the formation of cyclic molecules by a radical alkylation of a series of substrates having two activated double bonds. Therefore the trifluoromethylation of activated diethylenic compounds **8** (Scheme 2) was done under experimental conditions favouring the formation of monomeric ring products (high current density and low olefin concentration). This should also permit us to observe the formation of an intramolecular analogue of **6**.

## Results and discussion

Trifluoromethylation of diolefinic dicarboxylate esters via the electrolysis of trifluoroacetate anion gives bis(trifluoromethyl) alicyclic compounds in acceptable yields (Scheme 2 and Table 1). The actual proof for the formation of a cyclic system is based on the observation that infrared and proton nuclear magnetic resonance spectra show no CH=CH group and the elemental and the mass spectrometric analyses agree for monomeric bis(trifluoromethyl) alicyclic products. The ring size of the products obtained was determined by the comparison of the fluorine nuclear magnetic resonance spectra of the protonated with the corresponding α,α′-dideuterated products (Scheme 2). The number of doublets[4] is the same for **10** and **10**-*d* while the doublets due to the $CF_3$ group on the α-carbon in **9** become singlets[5] for **9**-$d_2$ (Table 1). The results show that both rings **9** and **10** are formed in a ratio depending on the number of carbons *n* involved in the process.

The analytical glc of the volatile fraction ob-

[1]NRCC No. 20120.
[2]Author to whom correspondence should be addressed.
[3]Unpublished work.
[4]The number of doublets depends on the nature of the stereoisomers formed.
[5]The singlets are actually narrow multiplets.

0008-4042/82/131687-05$01.00/0
©1982 National Research Council of Canada/Conseil national de recherches du Canada

Can. J. Chem. Downloaded from www.nrcresearchpress.com by 210.87.254.6 on 09/06/12
For personal use only.

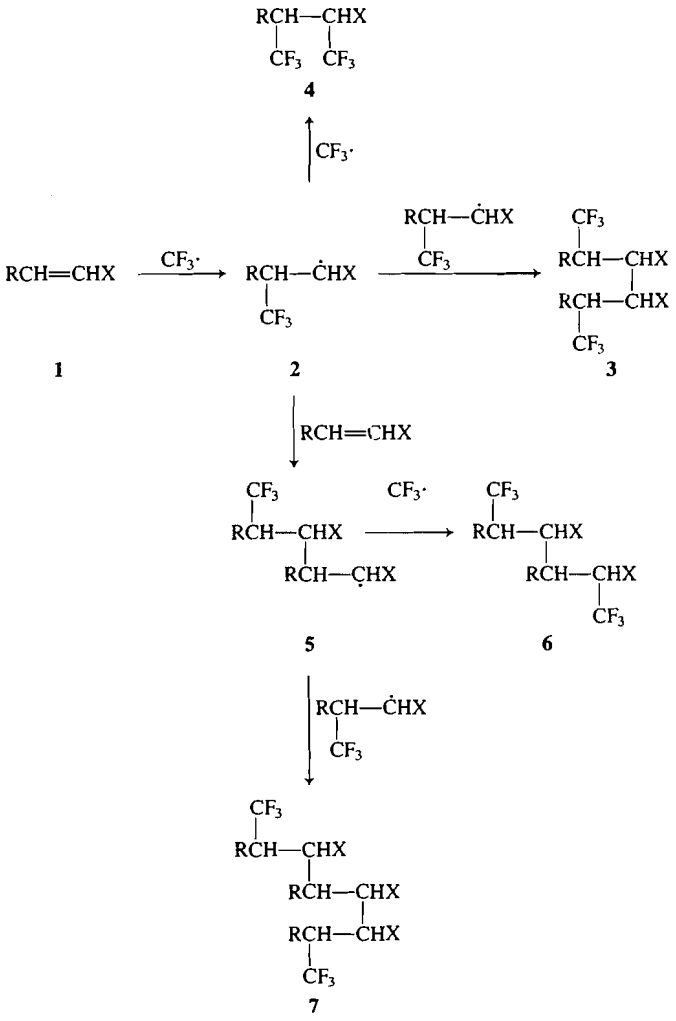


X = electron-withdrawing group
R = alkyl group

SCHEME 1

tained from $n = 0$, 1, and 2, when distilled under reduced pressure at 20°C, showed two major peaks and a number of minor peaks. The two major peaks obtained from the protonated and the dideuterated analogues analyzed as either structural isomers ($n = 0$) or stereoisomers[6] ($n = 1$ and 2) by elemental analysis, mass spectrometry, and $^{19}F$ nmr spectroscopy. The reaction is more complex with $n = 3$. The high vapor pressure fraction gave three important peaks in the analytical glc. The elemental analysis of the mixture of the three peaks and the gc–ms analysis showed only monomeric bis-(trifluoromethylated) products. However, the $^{19}F$ nmr spectrum of the mixture gave twelve doublets while the corresponding dideuterated mixture showed two doublets and ten singlets. Two of the three peaks were separated by preparative glc and analyzed as six-membered ring stereoisomers (**9***d*).[6] The remaining peak was shown by glc analysis to be a mixture of at least two compounds. The $^{19}F$ nmr spectrum gave only doublets while the corresponding $\alpha,\alpha'$-dideuterated products showed only singlets with $\delta < 70$ ppm. Unfortunately, these compounds could not be obtained pure enough for identification. Nevertheless, they do not analyze for the seven-membered ring **10***d*.

Different pathways describing the formation of

[6]The stereochemistry of the products could not be determined because the 60 Mz $^1H$ nmr spectra were far too complex. A systematic spectroscopic study is necessary before any conclusion can be given on the stereochemistry of this new class of compounds.

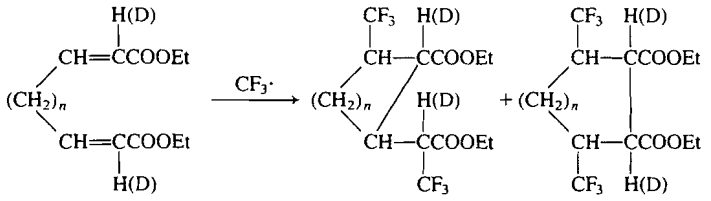

*a*, $n = 0$; *b*, $n = 1$; *c*, $n = 2$; *d*, $n = 3$

SCHEME 2

the products **9** and **10** are presented in Scheme 3. The postulation that the attack of the first $CF_3$ radical on **8** gives the radical **11** is well founded since never as yet, from similar reactions (1–3), was a product obtained from the attack of the first $CF_3$ radical on the carbon adjacent to the carbethoxy group. Therefore, the radical **11** was considered to be the first intermediate in the reaction.

In order to explain the formation of **9** and **10** from the radical **11**, four important factors have to be considered. (*i*) Baldwin's rules and Beckwith's guidelines: Baldwin (5*a*) has demonstrated that, in an intramolecular radical addition to a double bond, the 3 to 7-*exo*-trig ring closures are all favoured processes while the 3 to 5-*endo*-trig are disfavoured and the 6 to 7-*endo*-trig are favoured. However, according to Beckwith *et al.* (5*b*), the 3 to 7-*exo*-trig processes are all favoured while the 3 to 7-*endo*-trig processes are all disfavoured. (*ii*) The stability of the radical intermediates. (*iii*) The strain of the ring system involved. (*iv*) The rate of addition of a second $CF_3$ radical compared with the rate of an intramolecular radical addition.

The formation of the intermediate **12** can be explained by the favoured *exo*-trig ring closure according to Baldwin's rules (*i*). Moreover, the carbethoxy group should exert a stabilizing effect on the adjacent radical center (*ii*). Thus, considering these two factors, the involvement of the intermediate **13** (*endo*-trig closure) can be ruled out. The exclusive formation of **9***c* and **9***d*, corresponding to a 5 and 6-*exo*-trig ring closure respectively, is in accord with these factors. The product **9***a* (3-*exo*-trig process) was also observed but in a very small amount. In fact, it is known that cyclopropylmethyl radicals have very short lifetimes and the reversed reaction to the open chain radicals is very fast (6). The small quantity of **9***a* detected may be attributed to a trapping of the radical **12***a* by a $CF_3$ radical. Note that the concen-

TABLE 1. Electrochemical formation of bis(trifluoromethyl) alicyclic compounds

| Substrate | Product | Yield %[a] | Apparent ratio of isomers[c] | $^{19}F$ nmr spectra[d] |
|---|---|---|---|---|
| **8***a* | **9***a* | 4 | 1 | −71.64<br>−66.75(s) |
| | **10***a* | 33 | 9 | −71.35 |
| **8***b* | **10***b* | 37[b] | 5 | −74.50<br>−71.39 |
| | | | 1 | −72.49<br>−69.49 |
| **8***c* | **9***c* | 42[b] | 2 | −74.48<br>−68.46(s) |
| | | | 1 | −74.75<br>−69.80(s) |
| **8***d* | **9***d* | 26[b] | 1 | −74.69<br>−69.50(s) |
| | | | 1 | −74.43<br>−64.14(s) |

[a]Yields determined by glc.
[b]Total yield of stereoisomers.
[c]The ratio of isomers was determined by analytical glc and $^{19}F$ nmr spectroscopy.
[d]All the peaks observed for the protonated products are doublets. The letter s in parentheses corresponds to a singlet for the corresponding α,α'-dideuterated compound.

Can. J. Chem. Downloaded from www.nrcresearchpress.com by 210.87.254.6 on 09/06/12
For personal use only.

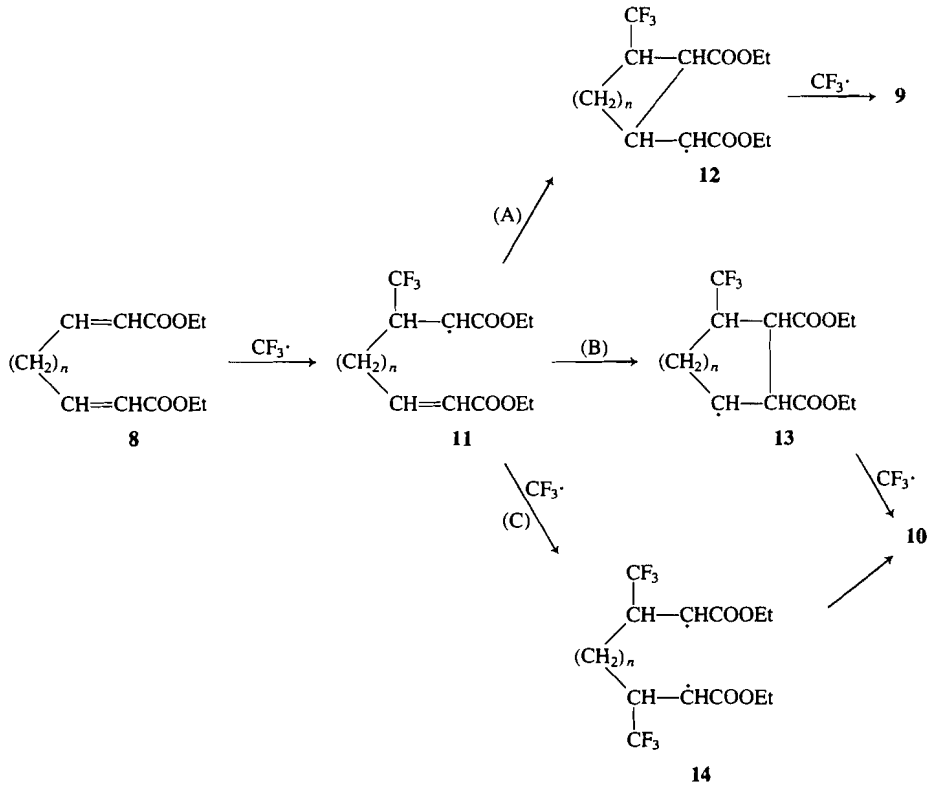


*a*, $n = 0$; *b*, $n = 1$; *c*, $n = 2$; *d*, $n = 3$

SCHEME 3

tration of $CF_3$ radicals at the electrode surface would be large since a high current density was used in our study. Thus it seems that, in the case of the three-membered ring **12***a*, the reversed process to **11***a* is preferred, probably because the release in strain (*iii*) becomes the predominant factor. This process should allow the radical **11***a* to proceed to other possible reaction products. The same type of argument can be applied to the four-membered ring intermediate **12***b* and explains, at least in part, the lack of **9***b*.

The exact mechanism for the formation of **10***a* and **10***b* is not straightforward because at least two pathways are possible: pathway B to form **13** and pathway C to give **14**. The radical intermediate **13** from **11** is somewhat disfavoured as outlined before by Baldwin's rules (*i*) and the loss of some energy of stabilization (*ii*). This is particularly true in the case of **10***a* for which the intermediate **13***a* corresponds to a 4-*endo*-trig closure. This type of closure appears to be disfavoured kinetically and thermodynamically. Moreover, the product **9***b* resulting from the more favoured 4-*exo*-trig closure was not observed. Thus it appears that the intramolecular addition is much slower than the addition of a second $CF_3$ radical to form the biradicals **14***a* and **14***b* respectively. Such a biradical intermediate is also involved in the formation of cyclic acyloins from esters of aliphatic dibasic acids (7). So the formation of the biradical **14** (pathway C) by the fast addition of two $CF_3$ radicals before cyclization seems to be the most plausible mechanism whenever the intramolecular addition gives a strain ring.

## Experimental

The starting diolefinic compounds **8** and **8**-*d* were prepared according to methods described in the literature (8, 9). The acetonitrile (from Aldrich) was used without further purification. The cell used in this study was described before (10). Gas–liquid chromatographic analyses and separations were performed respectively on a Fisher/Victoreen Series 4400 and an Aerograph Autoprep model A-700 using a 20 ft × 3/8 in. column, 30% SE30 on 45/60 Chromosorb P. The $^1H$ nmr spectra were taken in $CDCl_3$ on a Varian Associates spectrometer model EM 360 and the chemical shifts are reported on the δ scale. The $^{19}F$ nmr spectra were obtained in $CHCl_3$ on a Varian Associates XL100A FT accessory and are reported in ppm using $CFCl_3$ as reference. The mass spectra were obtained from a Finnigan 400 gc–ms spectrometer.

*Electrolysis of sodium trifluoroacetate in the presence of the diolefinic substrate 8*

Trifluoroacetic acid (45 mL) was added to a cold solution of

Can. J. Chem. Downloaded from www.nrcresearchpress.com by 210.87.254.6 on 09/06/12
For personal use only.

Can. J. Chem. Downloaded from www.nrcresearchpress.com by 210.87.254.6 on 09/06/12
For personal use only.

sodium hydroxide (6 g) in water (60 mL). This solution was added to the anodic compartment containing acetonitrile (150 mL). The cathodic compartment was charged with a 1.0 *M* solution of NaOH in water. A current of 1.8 A was passed through the solution for a period of 15 min. The temperature of the solution was maintained at 22°C using a cold ethanol bath. Then the substrate **8** (5 mmol; 0.02 *M*) was added and the electrolysis was continued for 7 h at a current of 1.8 A (0.15 A/cm$^2$).

The organic solution was concentrated on a rotary evaporator and the residue was poured into water (400 mL). The resulting mixture was extracted with four 75 mL portions of $CH_2Cl_2$. The organic solution was successively washed with an aqueous solution of $NaHCO_3$, dried over $MgSO_4$, and concentrated on a rotary evaporator to leave an oil. The high vapor pressure fraction was separated by a bulb-to-bulb distillation under a pressure of $10^{-2}$ Torr.

*Purification and physical properties of the products*

A. *From diethyl 2,4-hexadienedioate (8a)*

The oil obtained from the bulb-to-bulb distillation at 45°C amounted to 0.62 g (37%); ir and $^1$H nmr: no CH=CH. Analytical glc: two important peaks in a ratio of 9:1 and a few very small peaks. Mass spectrum *m/e*: (major peak) 336 $(M)^+$, 291 $(M - OC_2H_5)^+$, 263 $(M - CO_2C_2H_5)^+$; (minor peak) 291 $(M - OC_2H_5)^+$, 263 $(M - CO_2C_2H_5)^+$. *Anal.* calcd. for $C_{12}H_{14}F_6O_4$: C 42.86, H 4.17; found (mixture of the two important peaks purified by preparative glc): C 42.86, H 4.10. The two peaks were fractionated by preparative glc. Major peak: ir (film): 2960, 1745, 1230, 1125; $^1$H nmr:[7] 1.30 (6H, t), 1.82–2.90 (2H, m), 3.50–4.00 (2H, m), 4.20 (4H, q); $^{19}$F nmr: the spectrum corresponded to the four-membered ring **10***a* (Table 1). The minor peak was overlapping with the major peak and could not be obtained pure. However, the $^{19}$F nmr of the enriched protonated and $\alpha,\alpha'$-dideuterated products agreed with the three-membered ring **9***a* (Table 1). Unfortunately, the $^1$H nmr data were not conclusive.

B. *From diethyl 2,5-heptadienedioate (8b)*

The anodic solution gave, after a bulb-to-bulb distillation at 65°C, 0.65 g (37%) of a slightly yellow oil; ir and $^1$H nmr: no CH=CH. The analytical glc of this oil showed two important peaks in a ratio of 5:1 and a few other small peaks. Mass spectrum *m/e*: (major peak) 350 $(M)^+$, 330 $(M - HF)^+$, 310 $(M - 2HF)^+$, 305 $(M - OC_2H_5)^+$; (minor peak) 350 $(M)^+$, 305 $(M - OC_2H_5)^+$. *Anal.* calcd. for $C_{13}H_{16}F_6O_4$: C 44.57, H 4.57; found (the mixture of the two main peaks purified by preparative glc): C 44.41, H 4.61. The two peaks were separated by preparative glc. Major peak: ir (film): 2996, 1752, 1260, 1175, 1125; $^1$H nmr:[7] 1.28 (6H, 2t), 2.35–4.00 (6H, complex m), 4.17 (4H, 2q); $^{19}$F nmr: Table 1. Minor peak: $^1$H nmr: 1.27 (6H, t), 1.8–3.5 (complex m), 4.18 (4H, 2q); $^{19}$F nmr: Table 1. The $^{19}$F nmr data suggested two stereoisomers of the five-membered ring **10***b*.

C. *From diethyl 2,6-octadienedioate (8c)*

The diolefinic compound **8***c* gave 0.75 g (42%) of a yellow oil from the bulb-to-bulb fractionation at 65°C; ir and $^1$H nmr: no CH=CH. Analytical glc: two important peaks in a ratio of 2:1 and other small peaks. Mass spectrum *m/e*: (major and minor peaks) 364 $(M)^+$, 319 $(M - OC_2H_5)^+$, 291 $(M - CO_2C_2H_5)^+$. *Anal.* calcd. for $C_{14}H_{18}F_6O_4$: C 46.15, H 4.95; found (the mixture of the two main peaks purified by preparative glc): C 46.08, H 4.74. The two peaks were separated by preparative glc. Major peak: ir (film): 2998, 1752, 1745; $^1$H nmr: 1.28 (6H, 2t), 1.50–2.35 (4H, m), 2.55–3.40 (4H, m), 4.20 (4H, 2q); $^{19}$F nmr: Table 1. Minor peak: ir (film): 2996, 1750; $^1$H nmr: 1.30 (6H, 2t), 1.50–2.20 (4H, m), 2.55–3.90 (4H, m), 4.20 (4H, 2q); $^{19}$F nmr: Table 1. The $^{19}$F nmr data showed that the two products were stereoisomers of **9***c*.

D. *From diethyl 2,7-nonadienedioate (8d)*

The bulb-to-bulb distillation at 65°C gave 0.80 g (42%) of distillate; ir and $^1$H nmr: no CH=CH. Analytical glc: three important equivalent peaks and a number of less important peaks. Mass spectrum: all the peaks have a *m/e* 378 $(M)^+$, 333 $(M - OC_2H_5)^+$, 291 $(M - CO_2C_2H_5)^+$. *Anal.* calcd. for $C_{15}H_{20}F_6O_4$: C 47.62, H 5.29; found (the mixture of the three peaks after purification by preparative glc): C 47.90, H 5.39. The three peaks were separated by preparative glc. The first peak analyzed as a mixture of two compounds by analytical glc. These compounds could not be separated by conventional methods of purification. Second and third peaks: ir (film): 2995, 1735, 1265, 1190; $^1$H nmr: 1.28 (6H, t) 1.40–3.70 (10H, m), 4.21 (4H, q). The $^{19}$F nmr data showed the presence of two stereoisomers (**9***d*) (Table 1).

[7] A small multiplet was always appearing at δ 5.82–6.08. It may be due to an impurity or to the presence of a minor isomer.

## Acknowledgements

We wish to acknowledge the assistance of Mr. H. Séguin for elemental analyses, Dr. S. Brownstein and Mr. J. Bornais for fluorine nmr spectra, and Mr. M. E. Bednas for the mass spectral determinations.

1. R. N. Renaud and P. J. Champagne. Can. J. Chem. **53**, 529 (1975).
2. R. N. Renaud, P. J. Champagne, and M. Savard. Can. J. Chem. **57**, 2617 (1979).
3. C. J. Brookes, P. L. Coe, D. M. Owen, A. E. Peddler, and J. C. Tatlow. J. Chem. Soc. Chem. Commun. 323 (1974); C. J. Brookes, P. L. Coe, A. E. Peddler, and J. C. Tatlow. J. Chem. Soc. Perkin Trans. I, 202 (1978).
4. M. Chkir and D. Lelandais. J. Chem. Soc. Chem. Commun. 1369 (1971).
5. (*a*) J. E. Baldwin. J. Chem. Soc. Chem. Commun. 734 (1976); (*b*) A. L. J. Beckwith, C. J. Easton, and A. K. Seleris. J. Chem. Soc. Chem. Commun. 482 (1980).
6. J. K. Kochi, P. J. Krusic, and D. R. Eaton. J. Am. Chem. Soc. **91**, 1877 (1969).
7. S. M. McElvain. Org. React. **4**, 256 (1948).
8. J. D. Anderson, M. M. Baizer, and J. P. Petrovich. J. Org. Chem. **31**, 3890 (1966).
9. J. G. Atkinson, J. J. Csakvary, G. T. Herbert, and R. S. Stuart. J. Am. Chem. Soc. **90**, 498 (1968).
10. R. N. Renaud and P. J. Champagne. Can. J. Chem. **57**, 990 (1979).

# The kinetics of proton and deuteron transfer from 1-(4-nitrophenyl)-1-nitroethane to 1,8-diazabicyclo[5.4.0]undec-7-ene in aprotic solvents

KENNETH T. LEFFEK AND PRZEMYSLAW PRUSZYNSKI[1]

*Department of Chemistry, Dalhousie University, Halifax, N.S., Canada B3H 4H6*

Received December 14, 1981

KENNETH T. LEFFEK and PRZEMYSLAW PRUSZYNSKI. Can. J. Chem. **60**, 1692 (1982).

1-(4-Nitrophenyl)-1-nitroethane reacts with the base 1,8-diazabicyclo[5.4.0]undec-7-ene (DBU) in both acetonitrile and toluene solvents in a normal second-order proton-transfer reaction, in contrast to its behaviour with the base 2,7-dimethoxy-1,8-bis(dimethylamino)naphthalene in acetonitrile.

The primary isotope effect, $k_H/k_D$ = 12.0 at 25° in toluene is very similar to that observed by other workers for the reaction of 4-nitrophenylnitromethane with DBU under the same conditions. In acetonitrile solvent a $k_H/k_D$ ratio of 7.8 was found at 25°C. The isotope effects on the activation parameters for the reaction in both solvents indicate that tunnelling of the proton through the potential energy barrier makes a significant contribution to the reaction rate.

KENNETH T. LEFFEK et PRZEMYSLAW PRUSZYNSKI. Can. J. Chem. **60**, 1692 (1982).

Contrairement à son comportement vis-à-vis de la base diméthoxy-2,7 bis(diméthylamino)-1,8 naphtalène dans l'acétonitrile, le (nitro-4 phényl)-1 nitro-1 éthane réagit avec la base diaza-1,8 bicyclo[5.4.0] undécène-7 (DBU) dans l'acétonitrile et le toluène selon une réaction normale de transfert de proton d'ordre deux.

L'effet isotopique primaire $k_H/k_D$ = 12,0 à 25°C dans le toluène est très voisin de celui observé par d'autres chercheurs dans le cas de la réaction du nitro-4 phényl nitrométhane avec le DBU dans les mêmes conditions. On a trouvé un rapport de $k_H/k_D$ = 7,8 dans l'acétonitrile à 25°C. L'effet isotopique, sur les paramètres d'activation dans les deux solvants, indique que l'effet tunnel du proton à travers la barrière d'énergie potentielle apporte une contribution significative à la vitesse de réaction.

[Traduit par le journal]

## Introduction

In a recent study of the proton transfer reaction from 1-(4-nitrophenyl)-1-nitroethane **1** to 2,7-dimethoxy-1,8-bis(dimethylamino)naphthalene in acetonitrile solvent (1), the reaction was found to follow first-order kinetics with respect to the substrate with no dependence on the base concentration. This behaviour was in marked contrast to the reaction of the same base with 4-nitrophenylnitromethane **2**, which showed the normal second-order kinetics. It is of interest, therefore, to investigate the generality of the phenomenon by studying the reaction of the ethane **1** with other bases.

Caldin and Rogne (2) reported the kinetic isotope effects for the proton transfer reaction of the methane **2** with 1,8-diazabicyclo[5.4.0]undec-7-ene (DBU) in toluene solvent. This reaction gave very good first-order kinetics, with the base concentration in large excess over that of the acid, both with the normal and deuterated acid, and gave a primary deuterium isotope effect $k_H/k_D = 13.3 \pm 1.2$ at 25°C.

The study of the reaction [1] of the ethane **1** with DBU in acetonitrile solvent allows a comparison of the kinetics with those of the reaction of the 2,7-dimethoxy-1,8-bis(dimethylamino)naphthalene, and in toluene solvent allows a comparison of the isotope effect with that determined by Caldin and Rogne (2). The ethane **1**, having only one acid hydrogen, gives a primary isotope effect undistorted by a secondary effect, as in the case of the methane **2**.

[1] 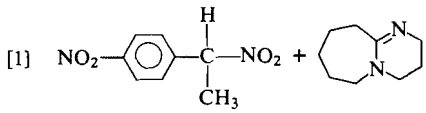


**1** DBU

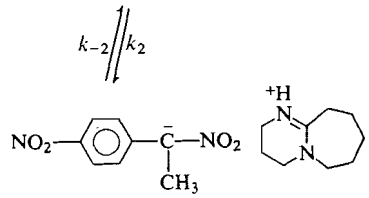


## Results and discussion

The reaction [1] gives a coloured product consisting of a single absorption peak, $\lambda_{max}$ = 445 nm in toluene and 505 nm in acetonitrile solvent. The optical density variation with base concentration was fitted to eq. [2] which is derived from eq. [1] assuming that the product is an ion-pair; [A] and [B] are the initial concentrations

[2] $[A]/OD = 1/K\varepsilon[B] + 1/\varepsilon$

of **1** and DBU respectively, OD is the optical density, $\varepsilon$ the molar absorptivity, and $K$ the equilib-

[1]Postdoctoral Fellow 1979–1980.

0008-4042/82/131692-04$01.00/0

©1982 National Research Council of Canada/Conseil national de recherches du Canada

Can. J. Chem. Downloaded from www.nrcresearchpress.com by 210.87.254.6 on 09/06/12
For personal use only.

TABLE 1. Pseudo-first-order and second-order rate constants for the proton and deuteron transfer reaction between 1-(4-nitrophenyl)-1-nitroethane and 1,8-diazabicyclo[5.4.0]-undec-7-ene

| Temperature (°C) | $10^2$[DBU] ($M$) | $k_{1H}$ ($s^{-1}$) | $k_{1D}$ ($s^{-1}$) | $k_{2H}$ (L $mol^{-1}$ $s^{-1}$) | $k_{2D}$ (L $mol^{-1}$ $s^{-1}$) |
|---|---|---|---|---|---|
| (a) Solvent toluene | | | | | |
| 15.0 | 1.03 | 2.05 | 0.132 | | |
| | 2.05 | 3.66 | 0.252 | | |
| | 3.08 | 5.20 | 0.365 | 157±3 | 11.7±0.2 |
| | 4.10 | 6.65 | 0.500 | | |
| | 5.13 | 8.63 | 0.610 | | |
| 20.0 | 1.03 | 2.27 | 0.157 | | |
| | 2.05 | 4.19 | 0.296 | | |
| | 3.08 | 6.00 | 0.432 | 184±4 | 13.5±0.2 |
| | 4.10 | 8.03 | 0.564 | | |
| | 5.13 | 9.83 | 0.715 | | |
| 25.0 | 1.03 | 2.63 | 0.191 | | |
| | 2.05 | 4.67 | 0.363 | | |
| | 3.08 | 6.99 | 0.545 | 215±3 | 17.9±±0.2 |
| | 4.10 | 9.40 | 0.731 | | |
| | 5.13 | 11.3 | 0.924 | | |
| 30.0 | 1.03 | 2.97 | 0.242 | | |
| | 2.05 | 5.61 | 0.441 | | |
| | 3.08 | 8.20 | 0.681 | 263±4 | 21.6±0.3 |
| | 4.10 | 11.1 | 0.918 | | |
| | 5.13 | 13.7 | 1.11 | | |
| 35.0 | 1.03 | 3.31 | 0.286 | | |
| | 2.05 | 6.27 | 0.568 | | |
| | 3.08 | 9.69 | 0.890 | 306±4 | 28.7±0.5 |
| | 4.10 | 12.9 | 1.20 | | |
| | 5.13 | 15.7 | 1.44 | | |
| (b) Solvent acetonitrile | | | | | |
| 15.0 | 1.05 | 3.12 | 0.321 | | |
| | 2.10 | 6.98 | 0.651 | | |
| | 3.15 | 10.4 | 1.08 | 363±7 | 40.6±1.0 |
| | 4.20 | 13.8 | 1.61 | | |
| | 5.25 | 18.7 | 1.98 | | |
| 20.0 | 1.05 | 4.79 | 0.575 | | |
| | 2.10 | 9.31 | 1.15 | | |
| | 3.15 | 13.8 | 1.67 | 441±6 | 51.2±3.0 |
| | 4.20 | 18.3 | 2.18 | | |
| | 5.25 | 23.6 | 2.75 | | |
| 25.0 | 1.05 | 6.22 | 0.738 | | |
| | 2.10 | 11.8 | 1.45 | | |
| | 3.15 | 17.4 | 2.15 | 510±6 | 65.5±0.5 |
| | 4.20 | 22.4 | 2.79 | | |
| | 5.25 | 27.8 | 3.51 | | |
| 30.0 | 1.05 | 8.21 | 1.02 | | |
| | 2.10 | 13.8 | 1.87 | | |
| | 3.15 | 21.6 | 2.75 | 653±12 | 80.7±0.5 |
| | 4.20 | 28.2 | 3.55 | | |
| | 5.25 | 35.4 | 4.43 | | |
| 35.0 | 1.05 | 10.4 | 1.25 | | |
| | 2.10 | 18.4 | 2.37 | | |
| | 3.15 | 26.3 | 3.45 | 746±5 | 104±1 |
| | 4.20 | 34.2 | 4.55 | | |
| | 5.25 | 41.7 | 5.62 | | |

Can. J. Chem. Downloaded from www.nrcresearchpress.com by 210.87.254.6 on 09/06/12
For personal use only.

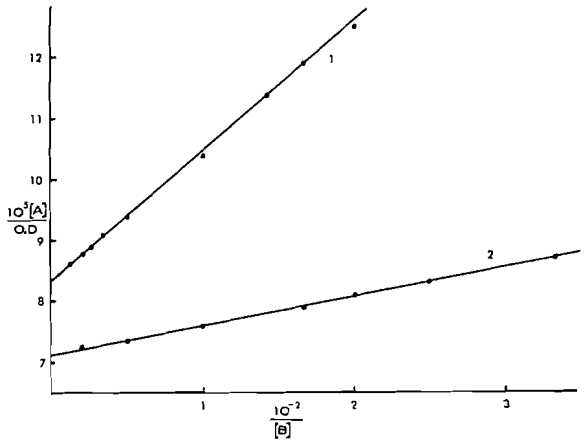


FIG. 1. Plots of [A]/OD vs. 1/[B] for the reaction of 1-(4)-nitrophenyl)-1-nitroethane with 1,8-diazabicyclo[5.4.0]undec-7-ene at 20°C in (1) toluene and (2) acetonitrile.

rium constant. The plots of [A]/OD vs. 1/[B] are shown in Fig. 1 and yield $K = 390\,dm^3\ mol^{-1}$ (20°C), $\varepsilon = 12\,000\,dm^3\ mol^{-1}\ cm^{-1}$ in toluene, and $K = 1400\,dm^3\ mol^{-1}$ (20°C), $\varepsilon = 14\,000$ in acetonitrile.

The positions of the absorption maxima are very similar to those previously reported; for the methane **2** and DBU Caldin and Rogne (2) found $\lambda_{max} = 440$ nm in toluene and for **1** and 2,7-dimethoxy-1,8-bis(dimethylamino)naphthalene in acetonitrile $\lambda_{max} = 520$ nm (1). It is clear that the product is the ion-pair containing the anion of **1**.

The equilibrium constant in toluene is much smaller than that of $2.9 \times 10^4\ dm^3\ mol^{-1}$ observed (2) for the methane **2**, as expected, since **1** is a weaker acid. Thus, the reaction is more symmetrical for the ethane substrate than for the methane, so at least as much proton tunnelling should occur in this reaction as in the methane reaction provided that the barrier dimensions are the same.

For the reaction of **1** and deuterated **1** pseudo-first-order rate constants were determined at a number of different base concentrations with the base always in large excess, for a series of temperatures. The second-order rate constants are the calculated slopes of plots of $k_1$ vs. [DBU]. All of these rate constants are shown in Table 1. The isotope effects are given in Table 2 and the activation parameters are collated in Table 3. The errors quoted in these tables are the standard deviations.

The first-order rate constants are directly proportional to the base concentration, indicating a second-order proton transfer similar to that observed by Caldin and Rogne (2), in contrast to the first-order reaction found with the base 2,7-dimethoxy-1,8-bis(dimethylamino)naphthalene(2,7-DMDAN) in acetonitrile solvent (1). The first-order rate constant with DBU at 25°C is about 150 times greater than that with 2,7-DMDAN. Thus, it appears that the absence of steric hindrance in the DBU reaction, compared to that in the 2,7-DMDAN reaction, allows the direct bimolecular proton transfer to take place, whereas the 2,7-DMDAN is sufficiently hindered that a two-step reaction is observed involving an initial slow ionization of the carbon acid (1).

The second-order rate constant for the reaction of ethane **1** with DBU in toluene is about 1000 times smaller at 25°C than the corresponding constant for methane **2** determined by Caldin and Rogne (2), as would be expected, since the ethane is a much weaker acid than the methane. This rate difference is entirely due to a difference in enthalpy of activation, which at 6.2 kcal $mol^{-1}$ for the ethane is 4.2 kcal $mol^{-1}$ greater than that for the methane. This is consistent with the idea that the difference in reactivity of the two acids is due to electronic and steric effects.

The isotopic rate ratio at 25°C for ethane **1** and DBU in toluene is 12.0, very similar to the 13.3 reported by Caldin and Rogne (2) for methane **2**. If the secondary isotope effect contained in the latter result is assumed to be 15% (3–5), the primary effect for the methane is a ratio of 11.6. The ethane might be expected to have a larger isotope effect because of the greater steric hindrance to the reaction and because of the more symmetrical transition state, but the two measurements are the same within experimental error. Similarly, the differences between the isotope effects on $\Delta H^{\neq}$ and $\Delta S^{\neq}$ for ethane **2** and methane **1** are the same within the reliability of the experiments.

The enthalpy of activation isotopic differences of 2.0 and 1.7 kcal $mol^{-1}$ for toluene and acetonitrile solvent, respectively, indicate that tunnelling of the proton through the potential energy barrier probably makes a significant contribution to this reaction, as proposed by Caldin and Rogne for the

TABLE 2. Isotope effects for the reaction of 1-(4-nitrophenyl)-1-nitroethane and DBU

| | $k_H/k_D$ | |
|---|---|---|
| Temperature | Toluene | Acetonitrile |
| 15.0 | 13.4±0.3 | 8.9±0.3 |
| 20.0 | 13.6±0.4 | 8.7±0.5 |
| 25.0 | 12.0±0.2 | 7.8±0.1 |
| 30.0 | 12.2±0.2 | 8.1±0.2 |
| 35.0 | 10.7±0.2 | 7.2±0.1 |

Can. J. Chem. Downloaded from www.nrcresearchpress.com by 210.87.254.6 on 09/06/12
For personal use only.

TABLE 3. Activation parameters for the reaction of 1-(4)-nitrophenyl)-1-nitroethane and 1,8-diazabicyclo[5.4.0]undec-7-ene

| | Toluene | | Acetonitrile | |
|---|---|---|---|---|
| Parameter | Proton transfer | Deuteron transfer | Proton transfer | Deuteron transfer |
| $\Delta H^{\ddagger}$ (kcal mol$^{-1}$) | 6.2±0.2 | 8.2±0.2 | 5.9±0.4 | 7.6±0.1 |
| $\Delta S^{\ddagger}$ (cal mol$^{-1}$ del$^{-1}$) | −27.2±0.7 | −25.2±0.7 | −26.4±1.3 | −24.7±0.5 |
| $\Delta H_D^{\ddagger} - \Delta H_H^{\ddagger}$ (kcal mol$^{-1}$) | 2.0±0.4 | | 1.7±0.6 | |
| $\Delta S_D^{\ddagger} - \Delta S_H^{\ddagger}$ (cal mol$^{-1}$ deg$^{-1}$) | 2.0±1.4 | | 1.7±1.6 | |

TABLE 4. Tunnelling and barrier parameters for the reaction of 1-(4-nitrophenyl)-1-nitroethane and DBU

| Parameter | Toluene | Acetonitrile |
|---|---|---|
| $E_{H\ obs}$ (kcal mol$^{-1}$) | 6.8 | 6.5 |
| $E_{D\ obs}$ (kcal mol$^{-1}$) | 8.8 | 8.2 |
| $E_{H\ calc}$ (kcal mol$^{-1}$) | 7.8 | 7.1 |
| $E_{D\ calc}$ (kcal mol$^{-1}$) | 8.8 | 8.2 |
| Barrier width $2b$(Å) | 0.80 | 0.90 |
| $E_{H\ obs}/E_{H\ calc}$ | 0.87 | 0.92 |
| $E_{D\ obs}/E_{D\ calc}$ | 1.0 | 1.0 |

methane **2** reaction (2). The actual barrier heights in the absence of tunnelling and the barrier width, assuming a parabolic barrier, may be computed using Bell's equation (6–8) and the trial and error technique of Caldin and Mateo (9). The results, shown in Table 4, give tunnelling corrections to the activation energy of 1.0 kcal mol$^{-1}$ and 0.6 kcal mol$^{-1}$ for the reaction in toluene and acetonitrile solvent, respectively. These values and the calculated barrier widths, $2b$, are in general agreement with those of Caldin and Mateo (9) for other proton transfer reactions. Thus, the kinetic measurements are consistent with some contribution from proton tunnelling.

Thus, we have found that, although the ethane **1** is more sterically hindered than the methane **2**, the effect is not large enough to interfere with the normal bimolecular proton transfer to the base DBU. The similarity of the isotope effects for the reaction of the two acids with DBU in toluene serves to confirm the work of Caldin and Rogne (2) and leads to the conclusion that the width of the energy barrier is very similar for the two reactions.

## Experimental

*Materials*

1-(*p*-Nitrophenyl)-1-nitroethane and its α-deuterated analogue were prepared as described previously (1). The deuterated material showed no nmr peak for the α-hydrogen and was, therefore, at least 98% deuterated.

1,8-Diazabicyclo[5.4.0]undec-7-ene (Aldrich) was dried with potassium hydroxide and fractionally distilled under reduced pressure.

Toluene was dried with sodium and fractionally distilled. Acetonitrile was purified by the method of O'Donnell *et al.* (10) and fractionally distilled from $P_2O_5$.

*Equilibrium constant measurements*

The absorbance at equilibrium was measured for a series of reactions with acid concentration of $5 \times 10^{-5}$ *M* and nine different base concentrations ranging between $1 \times 10^{-3}$ and $8 \times 10^{-2}$ *M*. The values of the equilibrium constants obtained from the slopes of the graphs in Fig. 1 agreed with those derived from the kinetic measurements to within 10%, well within the precision of the two methods.

*Kinetic measurements*

The reaction rates were measured with a Durrum stopped-flow spectrophotometer using the standard technique previously described (11). Acid concentrations of $1 \times 10^{-5}$ to $4 \times 10^{-5}$ *M* were used with the base concentrations shown in Table 1, which gave an excess of base over acid never less than 250. The reaction traces fitted the first-order kinetic equation very well.

## Acknowledgement

The authors are grateful for financial support by the Natural Sciences and Engineering Research Council of Canada.

1. K. T. LEFFEK and P. PRUSZYNSKI. Can. J. Chem. **59**, 3034 (1981).
2. E. F. CALDIN and O. ROGNE. J. Chem. Soc. Faraday Trans. I, 2065 (1978).
3. R. P. BELL and D. M. GOODALL. Proc. R. Soc. London Ser. A, **294**, 273 (1966).
4. W. J. BOYLE, JR. Ph.D. Thesis, Northwestern Univ. 1971; Diss. Abstr. B, **324**, 32 (1971).
5. K. T. LEFFEK. *In* Isotopes in organic chemistry. Vol. 2. *Edited by* E. Buncel and C. C. Lee. Elsevier Pub. Co., Amsterdam. 1976. Chapt. 3. p. 112.
6. R. P. BELL. Trans. Faraday Soc. **55**, 1 (1959).
7. R. P. BELL, W. H. SACHS, and R. L. TRAINER. Trans. Faraday Soc. **67**, 1995 (1971).
8. R. P. BELL. *In* The proton in chemistry. 2nd ed. Chapman and Hall, London. 1973. p. 275.
9. E. F. CALDIN and S. MATEO. J. Chem. Soc. Faraday Trans. I, 1876 (1975).
10. J. F. O'DONNELL, J. T. AYERS, and C. K. MANN. Anal. Chem. **37**, 1161 (1965).
11. A. JARCZEWSKI and K. T. LEFFEK. Can. J. Chem. **50**, 24 (1972).

Can. J. Chem. Downloaded from www.nrcresearchpress.com by 210.87.254.6 on 09/06/12
For personal use only.

# The reinvestigation of the kinetics of the reactions of fluorodi(4-nitrophenyl)ethanes with sodium methoxide in methanol

KENNETH T. LEFFEK AND GRZEGORZ SCHROEDER[1]

*Department of Chemistry, Dalhousie University, Halifax, N.S., Canada B3H 4H6*

Received December 14, 1981

KENNETH T. LEFFEK and GRZEGORZ SCHROEDER. Can. J. Chem. **60**, 1696 (1982).

The procedure previously described for the preparation of 1-fluoro-2,2,-di(4-nitrophenyl)ethane actually yields 1,1,2-tri-(4-nitrophenyl)ethane. 1-Fluoro-2,2-di(4-nitrophenyl)ethane has been prepared and rate constants, isotope effects, and activation parameters for the β-elimination reaction with methoxide ion in methanol are reported. These parameters indicate a concerted E2 mechanism, with a fairly symmetrical transition state. The subsequent dimerization reaction of the olefin product to yield 1,1,3,3-tetra(4-nitrophenyl)butene-1 is described.

The reaction of 1,1,1-trifluoro-2,2-di(4-nitrophenyl)ethane with methoxide ion in methanol has been reinvestigated and the reaction of the first product 1,1-difluoro-2,2-di(4-nitrophenyl)ethylene with excess methoxide, to give di(4-nitrophenyl)ketene dimethylacetal in a multistep reaction, is reported.

KENNETH T. LEFFEK et GRZEGORZ SCHROEDER. Can. J. Chem. **60**, 1696 (1982).

La méthode proposée antérieurement pour la préparation du fluoru-1 bis(nitro-4 phényl)-2,2 éthane donne en fait du tris(nitro-4 phényl)-1,1,2 éthane. On a préparé le fluoro-1 bis(nitro-4 phényl)-2,2 éthane et on rapporte les constantes de la réaction d'élimination β avec l'ion méthanolate dans le méthanol. Ces paramètres indiquent un mécanisme concerté E2 impliquant un état de transition moyennement symétrique. On décrit la réaction ultérieure de dimérisation du produit oléfinique qui conduit au tétra kis(nitro-4 phényl)-1,1,3,3 butène-1.

On a de nouveau étudié la réaction du trifluoro-1,1,1 bis(nitro-4 phényl)-2,2 éthane avec l'ion méthanolate dans le méthanol et on rapporte la réaction du premier produit, le difluoro-1,1 bis(nitrophényl-4)-2,2 éthane, avec un excès de méthanolate qui en plusieurs étapes conduit au diméthylacétal du bis(nitro-4 phényl) cétène.

[Traduit par le journal]

## Introduction

In an earlier study (1), it was reported that 1-fluoro-2,2-di(4-nitrophenyl)ethane underwent a β-elimination reaction with sodium methoxide in methanol to give the olefin product, di(4-nitrophenyl)ethylene, which had an absorption maximum at 380 nm. Rates of reaction, activation parameters, and primary deuterium isotope effects were also reported.

Subsequently, attempts to prepare this substrate again, by the methods of Kaluszyner *et al.* (2) and Bergmann and Kalmus (3) which we had used in the earlier study, were unsuccessful. The first step of the preparation, the conversion of ethyl monofluoroacetate to the fluorodiphenylcarbinol by reaction with phenylmagnesium bromide was reported (4–6) to give, at low temperature, ω-fluoroacetophenone as the main product and 1-fluoro-2,2-diphenylethanol as the minor product. Under the reaction conditions the ω-fluoroacetophenone could react further with phenylmagnesium bromide to form ω-phenylacetophenone (7), which would then yield 1,1,2-triphenylethane. This led to the suspicion that our earlier work was not based on an authentic sample of the fluoroethane, so a reinvestigation has been carried out.

[1]Postdoctoral Fellow 1980–1981.

## Results and discussion

When ethyl monofluoroacetate was reacted with phenylmagnesium bromide and the product reduced with red phosphorus in hydriodic and glacial acetic acids according to the conditions used in our earlier work (1), the nmr and ir spectra of the purified product matched almost exactly with the standard literature spectra (8, 9) of 1,1,2-triphenylethane. Thus, the product of this reaction was not, as we previously reported, 1-fluoro-2,2-diphenylethane, but 1,1,2-triphenylethane.

The rate constants and isotope effects published as those for the reaction of 1-fluoro-2,2-di-(4-nitrophenyl)ethane and sodium methoxide in methanol (1) actually refer to the reaction of 1,1,2-tri(4-nitrophenyl)ethane with sodium methoxide in methanol. A sample of the latter substrate was prepared by nitration of 1,1,2-triphenylethane with a mixture of nitric and sulfuric acids and the purified product was reacted with sodium methoxide in methanol at 30.0°C. The second-order rate constant for the appearance of the absorption peak at 380 nm was determined by the same technique used in the earlier study (1) and found to be 0.070 L $mol^{-1}$ $s^{-1}$, in good agreement with the value of 0.073 L $mol^{-1}$ $s^{-1}$ reported previously (1).

Thus, the absorption peak at 380 nm is due, since the reaction shows a significant primary deuterium isotope effect (1), to the product of a proton

0008-4042/82/131696-06$01.00/0

©1982 National Research Council of Canada/Conseil national de recherches du Canada

Can. J. Chem. Downloaded from www.nrcresearchpress.com by 210.87.254.42 on 09/06/12
For personal use only.

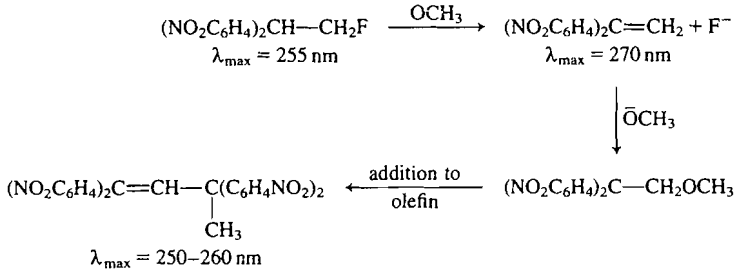


SCHEME 1

abstraction from the substrate. This product must be the carbanion of 1,1,2-tri(4-nitrophenyl)ethane. This absorption peak is at rather short wavelength compared to the carbanion of di(4-nitrophenyl)methane at over 500 nm, which caused it to be mistaken for an olefin absorption in our earlier work (1). This might indicate some double bond character between the two aliphatic carbon atoms, resulting from a 4-nitrophenyl bridged structure in the carbanion.

*The 1-fluoro-2,2-di(4-nitrophenyl)ethane reaction*

The material was prepared from sodium monofluoroacetate via fluoroacetyl chloride, ω-fluoroacetophenone, 1-fluoro-2-phenylethanol, and 1-fluoro-2,2-diphenylethane. The substrate was characterized by its nmr spectrum and fluorine analysis.

The reaction of 1-fluoro-2,2-di(4-nitrophenyl)ethane with sodium methoxide is complex. The substrate has a uv absorption maximum at 255 nm, which disappears after about 15 minutes and is replaced by a broad absorption at higher wavelength. When isolated, the product of this reaction gives a uv absorption at 270 nm. Comparison of the uv and nmr spectra with an authentic sample of 1,1-di(4-nitrophenyl)ethylene established this as the first product of the reaction.

When the reaction is allowed to proceed to completion the product is 1,1,3,3-tetra(4-nitrophenyl)butene-1 with a broad absorption peak at $\lambda_{max}$ 250–260 nm, characterized by its nmr spectrum. The reaction sequence is shown in Scheme 1. The butene-1 is formed by a nucleophilic addition of methoxide ion to the ethylene to give the carbanion shown. When the reaction was stopped by addition of HCl before completion, the mass spectrum of the product showed a molecular ion of 302 corresponding to the ether derived from the carbanion. The final product is formed by nucleophilic addition of the carbanion to the ethylene. This reaction probably proceeds via a cyclodimerization reaction (10). The preparation of 1,1,3,3-tetraphenylbutene-1 from 1,1-diphenylethylene by this mechanism has been described (11).

The kinetics of the reaction were measured spectrophotometrically by recording the increase in absorbance with time at 330 nm, using two different time scales. At this wavelength the consecutive reactions to yield first the ethylene and then the butene-1 did not interfere with each other, since the rates of the two reactions were sufficiently different to allow their separate measurement.

The first-order rate constants were measured, using varying methoxide ion concentrations always in large excess, at a series of different temperatures. The second-order rate constant at each temperature was calculated from the slope of the plot of $k_1$ vs. $[\bar{O}CH_3]$. The measurements were repeated for the deuterated substrate, but no isotope effect was found ($k_H/k_D$ was unity within experimental error at all temperatures) for the appearance of the butene-1. The results are shown in Tables 1 and 2.

The primary isotope effect of $k_H/k_D = 4.7$ at 30°C for the appearance of the ethylene indicates a concerted E2 mechanism for this reaction. Although the second-order rate constant of 0.64 L mol$^{-1}$ s$^{-1}$ at 30°C is about the same as that for the trifluoro compound (1), this rate constant is 64 times greater than the value of 0.01 L mol$^{-1}$ s$^{-1}$ predicted by the results of McLennan and Wong (12) for the irreversible ElcB mechanism (1). Therefore, the monofluoro compound reacts 64 times faster than it is predicted to form carbanions. Thus, the monofluoro compound reacts by the E2 mechanism and, from the magnitude of the isotope effect, the transition state must be fairly symmetrical with respect to the breaking of the C—H bond.

The activation parameters, calculated from Table 1, are $\Delta H_H^{\ddagger} = 9.9 \pm 0.7$ kcal mol$^{-1}$, $\Delta S_H^{\ddagger} = -26.6 \pm 3.3$ cal mol$^{-1}$ deg$^{-1}$, $\Delta H_D^{\ddagger} = 10.6 \pm 0.8$ kcal mol$^{-1}$, $\Delta S_D^{\ddagger} = -27.6 \pm 2.7$ cal mol$^{-1}$ deg$^{-1}$. The enthalpies of activation are considerably lower than those for the β-elimination reactions of the trifluoro and trichloro compounds and the entro-

Can. J. Chem. Downloaded from www.nrcresearchpress.com by 210.87.254.42 on 09/06/12
For personal use only.

Can. J. Chem. Downloaded from www.nrcresearchpress.com by 210.87.254.42 on 09/06/12
For personal use only.

TABLE 1. Rate constants and isotopic rate ratios for the appearance of 1,1-di(4-nitrophenyl)ethylene in the reaction of $CH_2FCH(4\text{-}NO_2C_6H_4)_2$* ($k_H$) and $CH_2FCD(4\text{-}NO_2C_6H_4)_2$* ($k_D$) with sodium methoxide in methanol

| Temperature (°C) | $10^3[\bar{O}CH_3]$ ($M$) | $10^4k_H$ ($s^{-1}$) | $10^4k_D$ ($s^{-1}$) | $k_{2H}$ (L $mol^{-1}$ $s^{-1}$) | $k_{2D}$ (L $mol^{-1}$ $s^{-1}$) | $k_{2H/k_{2D}}$ |
|---|---|---|---|---|---|---|
| 15.0 | 0.5 | 7.3 | | | | |
| | 1.0 | 8.6 | | | | |
| | 1.5 | 10.2 | | $0.27_4$ | | |
| | 2.5 | 12.8 | | | | |
| | 5.0 | 19.6 | | | | |
| 20.0 | 0.5 | 10.0 | | | | |
| | 1.0 | 12.0 | | | | |
| | 1.5 | 14.0 | | $0.39_4$ | | |
| | 2.5 | 17.5 | | | | |
| | 5.0 | 27.8 | | | | |
| 25.0 | 0.5 | 12.8 | 1.01 | | | |
| | 1.0 | 13.5 | 1.54 | | | |
| | 1.5 | 17.0 | 2.00 | $0.48_3$ | 0.099 | $4.8_8$ |
| | 2.5 | 22.0 | 3.09 | | | |
| | 5.0 | 33.8 | 5.50 | | | |
| 30.0 | 0.5 | 13.8 | 1.74 | | | |
| | 1.0 | 17.2 | 2.33 | | | |
| | 1.5 | 20.4 | 3.09 | $0.64_2$ | $0.13_6$ | $4.7_2$ |
| | 2.5 | 26.8 | 4.45 | | | |
| | 5.0 | 42.9 | 7.77 | | | |
| 35.0 | 0.5 | 15.1 | 2.15 | | | |
| | 1.0 | 20.5 | 3.01 | | | |
| | 1.5 | 25.1 | 4.04 | $0.95_4$ | $0.21_0$ | $4.5_4$ |
| | 2.5 | 35.1 | 6.32 | | | |
| | 5.0 | 58.4 | 11.5 | | | |
| 40.0 | 0.5 | | 2.43 | | | |
| | 1.0 | | 3.66 | | | |
| | 1.5 | | 4.80 | | $0.24_5$ | |
| | 2.5 | | 7.30 | | | |
| | 5.0 | | 13.4 | | | |
| 45.0 | 0.5 | | 4.63 | | | |
| | 1.0 | | 6.30 | | | |
| | 1.5 | | 7.87 | | $0.32_4$ | |
| | 2.5 | | 11.2 | | | |
| | 5.0 | | 19.2 | | | |

*Initial concentration of substrates $5 \times 10^{-5}$ $M$.

pies of activation are much more negative (1). This is in accord with the assignment of the E2 mechanism for the monofluoro compound and the $(ElcB)_R$ mechanism for the trifluoro compound (1). It has been noted (13) that E2 dehydrohalogenations have more negative entropies of activation by 20–30 cal $mol^{-1}$ $deg^{-1}$ than ElcB dehydrohalogenations by alkoxide ions in alcohols (14–16).

The second-order rate constants for the dimerization reaction of the ethylene, given in Table 2, are about 13 times slower than those for the β-elimination reaction (Table 1) and give $\Delta H^{\ddagger} = 15.9 \pm 0.8$ kcal $mol^{-1}$ and $\Delta S^{\ddagger} = -11.92 \pm 2.5$ cal $mol^{-1}$ $deg^{-1}$. This dimerization reaction is multistage, consisting of two nucleophilic additions to the ethylene double bond and possibly the formation of a cyclic addition product (10, 11). However, if the latter is formed it would rapidly decompose to give the butene-1 product. Thus, the rate-determining step of the reaction is either the addition of $\bar{O}CH_3$ to the ethylene or the addition of the carbanion thus formed, shown in Scheme 1, to the ethylene. Since the ether derived from the latter carbanion could be detected by mass spectroscopy of the reaction product when the reaction was stopped before completion, it is concluded that the nucleophilic addition of the carbanion to the ethylene must be at least partly rate determining. However, the kinetics follow a first-order rate law with respect to the ethylene when the base is in large excess, as shown in Table 2. For a consecutive reaction scheme of this type, eqs. [1] and [2], in

Can. J. Chem. Downloaded from www.nrcresearchpress.com by 210.87.254.42 on 09/06/12
For personal use only.

TABLE 2. Rate constants for the appearance of 1,1,3,3-tetra(4-nitrophenyl)butene-1 in the reaction of $CH_2FCH(4\text{-}NO_2C_6H_4)_2$* with sodium methoxide in methanol

| Temperature (°C) | $10^3[\bar{O}CH_3]$ ($M$) | $10^4k$ ($s^{-1}$) | $k_2$ ($L\,mol^{-1}\,s^{-1}$) |
|---|---|---|---|
| 25.0 | 0.5 | 1.09 | |
| | 1.0 | 1.27 | |
| | 1.5 | 1.55 | 0.035 |
| | 2.5 | 1.80 | |
| | 5.0 | 2.69 | |
| 30.0 | 0.5 | 1.26 | |
| | 1.0 | 1.50 | |
| | 1.5 | 1.75 | 0.049 |
| | 2.5 | 2.30 | |
| | 5.0 | 3.46 | |
| 35.0 | 0.5 | 1.34 | |
| | 1.0 | 2.06 | |
| | 1.5 | 2.24 | 0.084 |
| | 2.5 | 3.28 | |
| | 5.0 | 5.22 | |
| 40.0 | 0.5 | 1.75 | |
| | 1.0 | 2.22 | |
| | 1.5 | 3.09 | 0.135 |
| | 2.5 | 4.43 | |
| | 5.0 | 7.77 | |
| 45.0 | 0.5 | 1.88 | |
| | 1.0 | 2.83 | |
| | 1.5 | 3.70 | 0.189 |
| | 2.5 | 5.67 | |
| | 5.0 | 10.4 | |

*Initial concentration of substrate $5 \times 10^{-5}$ $M$.

which the ethylene (E) reacts with base (B) to form the carbanion (C) which then reacts with

$$[1]\quad E + B \xrightarrow{k_1} C$$

$$[2]\quad C + E \xrightarrow{k_2} P$$

another molecule of ethylene to yield the product (P), the rate of appearance of the carbanion and of the product are given by eqs. [3] and [4].

$$[3]\quad \frac{d[C]}{dt} = k_1[E][B] - k_2[E][C]$$

$$[4]\quad \frac{d[P]}{dt} = k_2[E][C] = k_1[E][B] - \frac{d[C]}{dt}$$

Although it is not valid to assume the steady state approximation with respect to the carbanion, under the conditions used to follow the rate of appearance of the product, $d[C]/dt$ may be small compared to $k_1[E][B]$ giving rise to the observed kinetics. The rate constants and activation parameters are, therefore, approximately identified with the addition of methoxide to the ethylene.

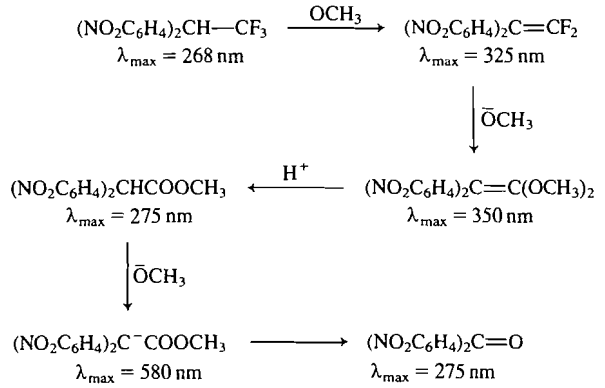


SCHEME 2

*The 1,1,1-trifluoro-2,2-di(4-nitrophenyl)ethane reaction*

In the previous study (1), the kinetics of the olefin-forming β-elimination reaction, initiated by methoxide ion, were reported and the mechanism deduced. A subsequent study (17) of the same substrate with *tert*-butoxide ion in *tert*-butyl alcohol showed that the olefin product reacts further with the excess *tert*-butoxide. The changes in the uv spectrum of the substrate with methoxide in methanol clearly indicate a set of consecutive reactions (Scheme 2). The first product of the reaction is 1,1-difluoro-2,2-di(4-nitrophenyl)ethylene with an absorption peak at 325 nm, for which the kinetics and primary isotope effects have been reported (1).

The reaction of the olefin to the second product is slow. This has an absorption maximum at 350 nm and is stable only in a water-free solvent. The substance contains no fluorine and was shown to be di(4-nitrophenyl)ketene dimethylacetal by ms and nmr analysis. When treated with HCl in methanol, conversion to methyl di(4-nitrophenyl)acetate took place. The acetate, with an excess of methoxide in methanol, gave a product with an absorption at 580 nm and this product decomposed to the final product 4,4′-dinitrobenzophenone. The complete reaction is shown in Scheme 2. A similar reaction to that of the last two steps was found for ethyl di(4-nitrophenyl)acetate with tetramethylguanidine in a mixture of methanol and tetrahydrofuran solvents (18).

The conversion of the difluoroethylene to the dimethylacetal must proceed via two steps of nucleophilic addition of methoxide ion to the double bond and two steps of elimination of fluoride ion. A similar reaction has been described by Mechoulam *et al.* (19).

Fluoro olefins are well known for their susceptibility to nucleophilic addition (20). The adducts

Can. J. Chem. Downloaded from www.nrcresearchpress.com by 210.87.254.42 on 09/06/12
For personal use only.

decompose to give products, either by addition of $H^+$ or, as in the present case, by the elimination of $F^-$ to yield another olefin. Evidence exists (20) that the rate determining step is the addition of the nucleophile rather than the elimination of $F^-$. In the present reaction, however, there are two nucleophilic additions, the first to a difluoro olefin and the second to a monofluoro olefin. The fluorine atoms strongly stabilize the carbanion formed by the nucleophilic addition and are assumed to lower the activation energy of the reaction (20). Of the two nucleophilic additions, therefore, the second addition to the monofluoro olefin would be expected to be slower, with a higher activation energy than the first. This second nucleophilic addition would, therefore, be the rate-determining step for that part of Scheme 2 in which the difluoroethylene is converted to di(4-nitrophenyl)ketene dimethylacetal.

Rate constants for the appearance of ketene product are given in Table 3 from which the second-order constants yield activation parameters, $\Delta H^{\ddagger} = 9.0 \pm 0.9$ kcal mol$^{-1}$ and $\Delta S^{\ddagger} = -35.0 \pm 3.0$ cal mol$^{-1}$ deg$^{-1}$.

If the theory of Chambers (20), quoted above, is correct, the activation energy of the nucleophilic addition in the reaction of the trifluoroethane should be lower than that measured in the monofluoroethane reaction, since in the latter the addition is to an olefin containing no fluorine. This is indeed the case, the difference in enthalpies of activation being almost 7 kcal mol$^{-1}$. However, the difference in the entropies of activation cancels a large proportion of this so that the second-order rate constant for the ketene product step is about the same as that for the dimerization step in the reaction of the monofluoroethane.

TABLE 3. Rate constants for the appearance of di-(4-nitrophenyl)ketene dimethylacetal in the reaction of $CF_3CH(4\text{-}NO_2C_6H_4)_2$* with sodium methoxide in methanol

| Temperature (°C) | $10^3[\bar{O}CH_3]$ ($M$) | $10^4k$ ($s^{-1}$) | $k_2$ (L mol$^{-1}$ s$^{-1}$) |
|---|---|---|---|
| 20.0 | 0.5 | 0.47 | |
| | 1.0 | 0.61 | |
| | 1.5 | 0.76 | 0.029 |
| | 2.5 | 1.05 | |
| | 5.0 | 1.78 | |
| 25.0 | 0.5 | 0.70 | |
| | 1.0 | 0.90 | |
| | 1.5 | 1.15 | 0.041 |
| | 2.5 | 1.53 | |
| | 5.0 | 2.54 | |
| 30.0 | 0.5 | 0.84 | |
| | 1.0 | 1.08 | |
| | 1.5 | 1.32 | 0.048 |
| | 2.5 | 1.79 | |
| | 5.0 | 3.01 | |
| 35.0 | 0.5 | 0.93 | |
| | 1.0 | 1.27 | |
| | 1.5 | 1.60 | 0.067 |
| | 2.5 | 2.27 | |
| | 5.0 | 3.95 | |

*Initial concentration $5 \times 10^{-5}$ $M$.

## Experimental

*Preparation of 1,1,2-tri(4-nitrophenyl)ethane*

Ethyl fluoroacetate (0.1 mol) was added dropwise to phenylmagnesium bromide (0.3 mol) in ether at 0°C during 15 min. The reaction mixture was hydrolyzed immediately by the slow addition of ammonium chloride in ice-water. The carbinol product was recovered by extraction with ether, dried, and distilled under vacuum. The carbinol was reduced with red phosphorus in a mixture of hydriodic and glacial acetic acids by refluxing for 10 days. The product was purified by recrystallization from methanol. The nmr spectrum ($CDCl_3$) δ: 3.30 (2H,d,$J$ = 8.0 Hz), 4.20 (1H,t,$J$ = 7.5 Hz), 6.9–7.5 (15H) agrees very closely with the literature spectrum (8). The peaks in the ir spectrum (Nujol) also matched very closely with the literature melt spectrum (9). The ethane was nitrated by a mixture of nitric and sulfuric acids and the product was crystallized several times from methanol.

*Preparation of 1-fluoro-2-2-di(4-nitrophenyl)ethane*

Sodium monofluoroacetate (0.23 mol) was mixed with $PCl_5$ (0.25 mol) and crude fluoroacetyl chloride was distilled off. This was fractionally distilled, 0.16 mol dissolved in methylene chloride (30 mL), and added to aluminum chloride (0.19 mol) in methylene chloride (100 mL) (3). The reaction mixture was stirred for 30 min, then the solution was decanted from the solid residue and cooled to 0°C. Benzene (0.1 mol) in methylene chloride (16 mL) was added dropwise during 15 min with stirring and the stirring was continued for a further 20 min. The mixture was poured onto ice and HCl, and the product ω-fluoroacetophenone was separated, dried, and distilled under vacuum (3).

The ω-fluoroacetophenone was reduced by $AlLiH_4$ ($AlLiD_4$ for the deuterium analogue) on a 0.015 mol scale by the procedure of Bergmann and Kalmus (3) to yield the carbinol, which was dissolved in a 4-fold molar excess of benzene, then cooled to 0°C. A 5:1 mixture of concentrated $H_2SO_4$/oleum was added dropwise with constant stirring and 1-fluoro-2,2-diphenylethane was isolated, nmr spectrum ($CDCl_3$) δ: 4.76(2H,d, $J$ = 48 Hz), 4.25(1H,t,$J$ = 4.0 Hz), 7.15(10H).

Finally, the fluoroethane was nitrated with a mixture of nitric and sulfuric acids. The product was crystallized several times from methanol, mp 87–92°C (dec.); nmr ($CDCl_3$) δ: 5.12 (2H,d,$J$ = 48 Hz), 5.45(1H,t,$J$ = 4.0 Hz), 7.50–8.50 (8H). Fluorine, found: 6% (neutron activation); calcd.: 6.5%.

The tertiary hydrogen nmr signals were completely absent in the deuterated compound, indicating at least 98% deuteration in that position.

*Reaction of 1-fluoro-2,2,di(4-nitrophenyl)ethane with methoxide ion*

The first product was isolated by neutralizing the reaction mixture with HCl after about 15 min. Removal of the solvent and repeated extraction with diethyl ether, then with chloroform, gave the product in about 60% yield with an nmr spectrum ($CDCl_3$) δ: 5.65(2H,s), 7.40–8.40 (8H). A sample of di(4-nitrophenyl)ethylene, prepared from acetophenone by standard methods, confirmed the above nmr spectrum.

When the reaction was allowed to proceed for four hours before the work-up of the products, the nmr spectrum was

Can. J. Chem. Downloaded from www.nrcresearchpress.com by 210.87.254.42 on 09/06/12
For personal use only.

TABLE 4 (*i*). Kinetic run: temperature 25.0°C; initial concentration $CH_2FCH(4\text{-}NO_2C_6H_4)_2 = 5 \times 10^{-5}$; initial concentration $CH_3\bar{O}Na^+ = 5 \times 10^{-3}$ *M*

| Time(s) | $x_1$ (absorbance) | $x_2$ (absorbance) |
|---|---|---|
| 0 | 0.098 | 0.186 |
| 56.4 | 0.119 | 0.192 |
| 112.8 | 0.144 | 0.196 |
| 169.2 | 0.160 | 0.200 |
| 225.6 | 0.166 | 0.202 |
| 228.0 | 0.176 | 0.204 |
| 338.4 | 0.180 | 0.206 |
| 394.8 | 0.186 | 0.208 |
| 451.2 | 0.192 | 0.210 |

Guggenheim analysis yields $k_H = 33.8 \times 10^{-4}$ s$^{-1}$

TABLE 4 (*ii*). Kinetic run: temperature 25.0°C; initial concentration $CH_2FCH(4\text{-}NO_2C_6H_4) = 5 \times 10^{-5}$; initial concentration $CH_3\bar{O}Na^+ = 5 \times 10^{-3}$ *M*

| Time (min) | $x_1$ (absorbance) | $x_2$ (absorbance) |
|---|---|---|
| 0 | 0.280 | 0.444 |
| 12 | 0.315 | 0.450 |
| 24 | 0.343 | 0.453 |
| 36 | 0.365 | 0.456 |
| 48 | 0.385 | 0.460 |
| 60 | 0.407 | 0.468 |
| 72 | 0.421 | 0.471 |
| 84 | 0.433 | 0.474 |
| 96 | 0.444 | 0.478 |
| 108 | 0.450 | 0.479 |

Guggenheim analysis yields $k_H = 2.69 \times 10^{-4}$ s$^{-1}$

δ: 1.15(3H,s), 7.15(1H,s), 7.40–8.40(16H). The same material was obtained when the synthetic di(4-nitrophenyl)ethylene was treated with sodium methoxide in methanol. The spectrum is characteristic of 1,1,3,3-tetra(4-nitrophenyl)butene-1.

*Preparation of 1,1,1-trifluoro-2,2-di(4-nitrophenyl)ethane*

This material was prepared as previously described (1).

*Reaction of 1,1,1-trifluoro-2,2-di(4-nitrophenyl)ethane with methoxide ion*

The first olefin product ($\lambda_{max}$ 325 nm) of this reaction was isolated as reported earlier (1).

When the reaction was allowed to proceed for two hours the peak at 325 nm was replaced by one at 350 nm. This second product was isolated by evaporation of the solvent under reduced pressure and repeated extraction with anhydrous ether. The material contained no fluorine (neutron activation analysis) and decolourized bromine solution. The ms showed a molecular ion of 330 awu and the nmr spectrum ($CDCl_3$) showed δ: 5.2 (6H,s), 7.2–8.4 (8H). This product is, therefore, di(4-nitrophenyl)ketene dimethylacetal.

The acetal is stable only in the absence of water and decomposes slowly with adventitious water. The addition of HCl (0.02 mol) to the acetal (0.002 mol) in methanol solution yielded a product, mp 138°C, after recrystallization from methanol. The ms gave a molecular ion of 316 awu and the nmr ($CDCl_3$) δ: 4.4(3H,s), 5.4 (1H,s), 7.6–8.6 (8H), indicating that the product is methyl di(4-nitrophenyl)acetate. A corresponding reaction was also described by Mechoulam *et al.*(16).

A mixture of methyl di(4-nitrophenyl)acetate and sodium methoxide in methanol gave a coloured solution ($\lambda_{max}$ 580 nm), which slowly decomposed during 10 h to a product with $\lambda_{max}$ 275 nm, identified as 4,4′-dinitrobenzophenone, mp 186–188°C (lit. (21) mp 188–189°C).

*Kinetic measurements*

The reaction rates were measured spectrophotometrically using a technique previously described (1). Two sample runs are given in Table 4.

## Acknowledgment

The authors are grateful for financial support by the Natural Sciences and Engineering Research Council of Canada.

1. J. KURZAWA and K. T. LEFFEK. Can. J. Chem. **55**, 1696 (1977).
2. A. KALUSZYNER, S. REUTER, and E. D. BERGMANN. J. Am. Chem. Soc. **77**, 4164 (1955).
3. F. BERGMANN and A. KALMUS. J. Am. Chem. Soc. **76**, 4137 (1954).
4. M. HUDLICKY. Chemistry of organic fluorine compounds. John Wiley, New York. 1976. p. 359.
5. E. ELKIK and H. ASSADI-FAR. C. R. Acad. Sci. Ser. C, **267**, 333 (1968).
6. E. ELKIK and H. ASSADI-FAR. Bull. Soc. Chim. Fr. 991 (1970).
7. E. D. BERGMANN, S. COHEN, E. HOFFMAN, and Z. RAND-MEIR. J. Chem. Soc. 3452 (1961).
8. SADTLER Standard Spectra, Sadtler Research Labs. Philadelphia. 1972. NMR Vol. 22. #14234.
9. SADTLER Standard Spectra, Sadtler Research Labs. Philadelphia. 1972. Infrared Vol. 42. #42398.
10. S. PATAI. The chemistry of the alkenes. Vol. 1. Interscience, New York. 1964. p. 472.
11. C. S. SCHOEPFLE and J. D. RYAN. J. Am. Chem. Soc. **52**, 4021 (1930).
12. D. J. MCLENNAN and R. J. WONG. J. Chem. Soc. Perkin Trans. II, 1373 (1974).
13. W. H. SAUNDERS, JR. and A. F. COCKERILL. Mechanisms of elimination reactions. Wiley-Interscience, New York. 1973. p. 26.
14. W. H. SAUNDERS, JR. and D. H. EDISON. J. Am. Chem. Soc. **82**, 138 (1960).
15. C. H. DEPUY and C. A. BISHOP. J. Am. Chem. Soc. **82**, 2532 (1960).
16. J. HINE, R. WIESBOECK, and O. B. RAMSAY. J. Am. Chem. Soc. **83**, 1222 (1961).
17. A. JARCZEWSKI and K. T. LEFFEK. Can. J. Chem. **58**, 1979 (1980).
18. K. T. LEFFEK and A. E. MATINOPOULOS-SCORDOU. J. Chem. Soc. Perkin Trans. II, 1099 (1979).
19. R. MECHOULAM, S. COHEN, and A. KALUSZYNER. J. Org. Chem. **21**, 801 (1956).
20. R. C. CHAMBERS. Fluorine in organic chemistry. John Wiley. New York. 1973. p. 148.
21. W. LORENZ. Chem. Ber. **81**, 422 (1948).

# $^1$H nuclear magnetic resonance study of tunnelling in molecules with multiple methyl groups trapped in hydrates[1]

J. A. RIPMEESTER

*Division of Chemistry, National Research Council, Ottawa, Ont., Canada K1A 0R9*

Received June 11, 1981[2]

Can. J. Chem. Downloaded from www.nrcresearchpress.com by 210.87.254.105 on 09/06/12
For personal use only.

J. A. RIPMEESTER. Can. J. Chem. **60**, 1702 (1982).

Methyl group tunnelling frequencies were derived from low-temperature $^1$H lineshapes for isobutane-$d_1$, *tert*-butyl fluoride, and trimethylamine trapped in heavy water hydrates and for *tert*-butyl chloride, *tert*-butyl alcohol, and neopentane enclathrated in the heavy water double hydrates with $D_2S$. Methyl group rotational barriers derived from the tunnelling frequencies are generally not very different from values found for the pure solids and gases and are much larger than barriers to overall reorientation of the guest molecules in the hydrate cages. Disorder in the orientation of the water molecules which make up the hydrate cages led to a distribution in barrier heights.

---

J. A. RIPMEESTER. Can. J. Chem. **60**, 1702 (1982).

A partir des formes des raies en rmn du $^1$H, on a déduit les fréquences de l'effet tunnel des groupes méthyles de l'isobutane-$d_1$, du fluorure de *tert*-butyle et de la triméthylamine piégés avec des hydrates d'eau lourde ainsi que celles des groupes méthyles du chlorure de *tert*-butyle, de l'alcool *tert*-butylique et du néopentane sous formes de clathrate dans des hydrates doubles d'eau lourde et de $D_2S$. Les barrières à la rotation du groupe méthyle, déduites des fréquences de l'effet tunnel, ne sont pas généralement très différentes des valeurs trouvées dans le cas des solides purs et des gaz et elles sont beaucoup plus élevées que les barrières de la réorientation globale des molécules hôtes dans les cages de l'hydrate. Le désordre dans l'orientation des molécules d'eau qui façonne les cages de l'hydrate conduit à une distribution des hauteurs de la barrière.

[Traduit par le journal]

In a previous publication (1) we have illustrated the use of methyl group tunnelling frequencies to derive information on methyl group rotational barriers of molecules bearing a single methyl group enclathrated in heavy water clathrates. There was found to be a contribution to methyl group barriers from guest–host interactions, the magnitude of which depended on the relative size of the guest molecule and the free diameter of the hydrate cage. In addition, it was found that the guest–host barrier contribution was distributed about a mean value presumably because of disorder in the orientation of the water molecules and the possibility of off-centre sites of the guest molecules in the hydrate cages.

In this contribution $^1$H nmr lineshapes for molecules containing 3 or 4 methyl groups are examined and tunnelling frequencies and barrier heights are derived.

## Experimental

Heavy water clathrates of ideal composition $M.17D_2O$ of isobutane-$d_1$ (Merck, Sharp and Dohme) and *tert*-butyl fluoride (PCR Inc.) were prepared as described in ref. 2, method B. The preparation of heavy water double hydrates of $D_2S$ with *tert*-butyl chloride, *tert*-butyl alcohol-OD, and neopentane of ideal composition $M.2D_2S.17D_2O$ has also been described (1). The hydrate of trimethylamine resulted on freezing an aqueous solution of composition $NMe_3.10\ 1/4D_2O$ (4).

Other experimental details have been given previously (1).

## Results and discussion

The $^1$H nmr lineshape derivatives of the enclathrated molecules were essentially independent of temperature below ~10 K, and are shown in Figs. 1–6. The lineshapes differ considerably from those expected for either rigidly held or rapidly rotating methyl groups (3). Hence the dipolar split Zeeman levels for the methyl groups must be perturbed by

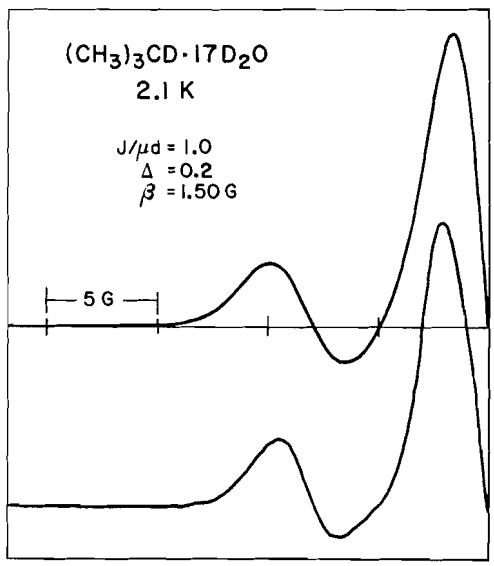


FIG. 1. Experimental and calculated $^1$H nmr lineshape derivative for $(CH_3)_3CD.17D_2O$.

[1]Issued as NRCC No. 20188.

[2]Revision received March 31, 1982.

0008-4042/82/131702-04$01.00/0

©1982 National Research Council of Canada/Conseil national de recherches du Canada

Can. J. Chem. Downloaded from www.nrcresearchpress.com by 210.87.254.105 on 09/06/12
For personal use only.

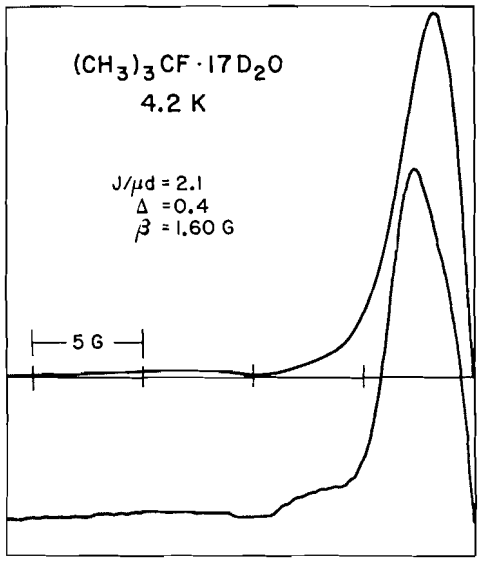


FIG. 2. Experimental and calculated $^1$H nmr lineshape derivative for $(CH_3)_3CF.17D_2O$.

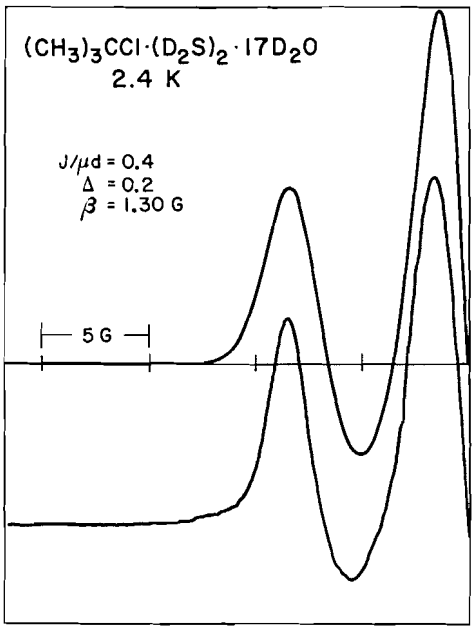


FIG. 3. Experimental and calculated $^1$H nmr lineshape derivative for $(CH_3)_3CCl.2D_2S.17D_2O$.

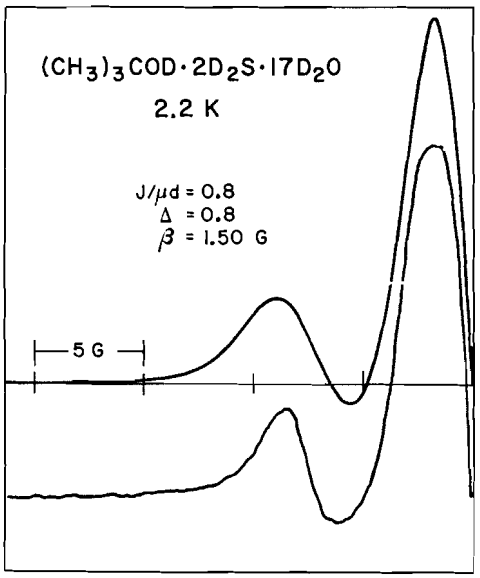


FIG. 4. Experimental and calculated $^1$H nmr lineshape derivative for $(CH_3)_3COD.2D_2S.17D_2O$.

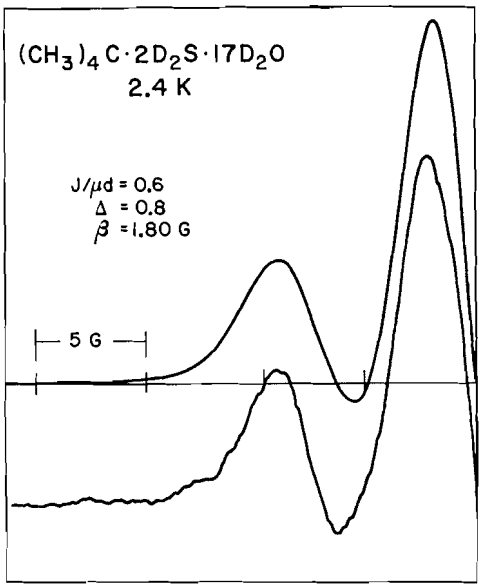


FIG. 5. Experimental and calculated $^1$H nmr lineshape derivative for $(CH_3)_4C.2D_2S.17D_2O$.

methyl group tunnelling at frequencies of some tens of kHz (5).

At the low temperatures employed, the methyl groups should be in their torsional ground states so that the equations of Apaydin and Clough (6) are applicable to the lineshape calculation. It must also be assumed that there is no coupling between methyl groups and that all intermethyl group dipolar interactions can be included in the isotropic Gaussian broadening parameter.

However, as found previously (1), a good fit of calculated lineshapes with experimental results could not be obtained unless a distribution in methyl group tunnelling frequencies was assumed.

For convenience a log-Gaussian distribution in

Can. J. Chem. Downloaded from www.nrcresearchpress.com by 210.87.254.105 on 09/06/12
For personal use only.

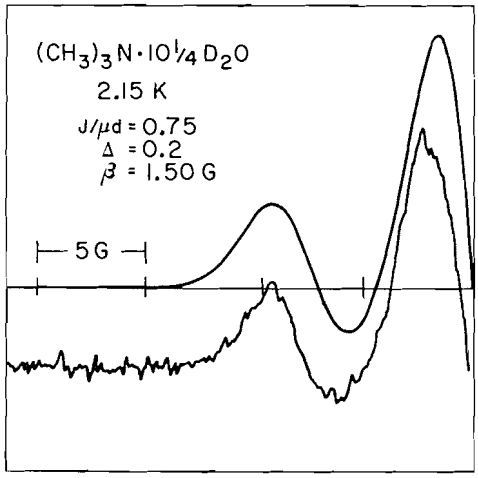


FIG. 6. Experimental and calculated $^1$H nmr lineshape derivative for $NMe_3$.10 1/4$D_2O$.

tunnelling frequencies, which leads approximately to a Gaussian distribution in barrier heights, was assumed. The parameters in the lineshape calculation then are: $J_0/\mu d$ where $3J_0/h$ is the mean tunnelling frequency, $\mu d/h$ the dipolar coupling frequency with $\mu = \gamma h/2$, $d = 3/2\ \mu/R^3$, $\gamma$ the proton gyromagnetic ratio, $R$ the methyl group interproton distance; $\beta$ is the Gaussian broadening parameter, $\Delta$ is the width parameter of the distribution in tunnelling frequencies, and $\delta V$ is the corresponding width of the barrier height distribution.

The lineshape intensity at $\omega_i$ for any tunnelling frequency $J_j$, $f(\omega_i,J_j)$, can be calculated using the equations of Apaydin and Clough. The total lineshape intensity at $\omega_i$ is then given by

$$F(\omega_i) \propto \sum_j f(\omega_i,J_j)\, g(Z_j)$$

where

$$g(Z_j) = \frac{1}{\Delta\sqrt{2\pi}} \exp(-Z_j^2/2\Delta^2)$$

and

$$Z_j = \ln J_j/J_0$$

Typically $j$ was equal to 30–50 for adequate definition of the lineshape. The splitting of the tunnelling side band away from the centre is governed by the mean tunnelling frequency, $J$, the amplitude of the tunnelling side band by distribution width $\Delta$, and the broadening parameter $\beta$. The uncertainty estimates, given in Table 1 along with the parameters, reflect the points at which the fit deteriorates noticeably. Calculated lineshape derivatives are given in Figs. 1–6. It should be emphasized that the exact nature of the distribution function is not critical, only that a distribution exists.

TABLE 1. Lineshape parameters and tunnelling frequencies

| Guest molecule | Mean $J/\mu d$ | $\Delta$ | $\beta$(gauss) | $3J_0/h$ (kHz) |
|---|---|---|---|---|
| $(CH_3)_3CD$ | 1.0±0.1 | 0.2±0.1 | 1.5±0.1 | 23.5 |
| $(CH_3)_3CF$ | 2.1±0.2 | 0.4±0.2 | 1.6±0.1 | 49.3 |
| $(CH_3)_3CCl$ | 0.4±0.1 | 0.2±0.1 | 1.3±0.1 | 9.4 |
| $(CH_3)_3COD$ | 0.8±0.2 | 0.8±0.2 | 1.5±0.1 | 18.8 |
| $(CH_3)_4C$ | 0.6±0.1 | 0.8±0.2 | 1.8±0.1 | 14.1 |
| $(CH_3)_3N$ | 0.75±0.05 | 0.2±0.1 | 1.5±0.1 | 17.6 |

The relationship derived by Hecht and Dennison (7) was used to obtain mean barrier heights, as well as barrier height distributions (Table 2). Also shown are barrier heights derived by other techniques both for the solid and gaseous materials.

Barriers to overall molecular reorientation of the guest molecules in the hydrate cages may be estimated from the second moment vs. temperature behaviour. The relationship used in a modified form (8) of the Waugh and Fedin estimate (9) and is expressed as

$$V = 32.4\, T_{1/2}$$

where $T_{1/2}$ is the temperature at which the second moment has fallen to half the rigid lattice value.

The barriers to overall reorientation of the guest molecules can be seen to be much lower than the methyl internal rotation barriers. This is consistent with the weak nature of guest–host interactions in clathrate hydrates.

The low barrier to overall reorientation of neopentane, 0.78 kcal/mol as opposed to 1.2–1.7 kcal/mol for the other molecules of similar shape and size, points to a fundamental difference in the motional averaging process for octahedral or tetrahedral molecules on the one hand, and molecules of lower symmetry on the other (14). For a molecule of tetrahedral symmetry with a rotational symmetry number of 12, any motion which causes exchange between the 12 indistinguishable sites at sufficiently rapid rate is enough to cause complete averaging of all intramolecular nuclear dipolar fields. For molecules of lower symmetry, however, complete averaging of the dipolar fields can take place only if the molecule can occupy distinguishable and hence potentially inequivalent sites in the hydrate cage.

For the partially deuterated ethyl halides enclathrated in the hydrate cages, the methyl group barrier height could be written as $V = V_{gas} + V_{cage}$, where $V_{gas}$ is the barrier for a molecule in the gas phase, and $V_{cage}$ is a contribution to the methyl group barrier from interactions with the hydrate cage. There was a clear trend of $V_{cage}$ with molecu-

TABLE 2. Summary of barrier height data

| Guest molecule | Mean barrier to guest reorientation (kcal/mol) | Mean methyl tunnelling barrier (kcal/mol) | Width of barrier distribution $\delta V$ (kcal/mol) | Barriers of solid(s) and gas (g) phases (kcal/mol) |
|---|---|---|---|---|
| $(CH_3)_3CD$ | 1.20 | 4.06 | 0.09 | 4.36(s)[a] 3.94(s)[b] 3.39(g)[b] |
| $(CH_3)_3CF$ | — | 3.74 | 0.22 | 4.41(s)[a] 4.34(g) |
| $(CH_3)_3CCl$ | 1.68 | 4.42 | 0.10 | 4.98(s)[a] 4.51(s)[b] |
| $(CH_3)_3COD$ | 1.39 | 4.15 | 0.38 | 4.13(s)[d] |
| $(CH_3)_4C$ | 0.78 | 4.26 | 0.38 | 4.40(s)[a] 4.34(s)[c] |
| $(CH_3)_3N$ | — | 4.17 | 0.10 | 4.35(s)[b] 3.63(g)[a] |

[a] From inelastic neutron scattering, ref. 10.
[b] From far ir, ref. 11.
[c] From far ir, ref. 12.
[d] From far ir, ref. 13.

lar size with $V_{cage} = 0$, 0.5, 1.0 kcal/lmol for $CH_3CD_2X$, X = Cl, Br, I.

For the structure II hydrates considered here, such a clear trend is not evident. The guest molecules are all relatively large compared to the structure II large cage, the $(CH_3)_3CCl$, $(CH_3)_3COD$, and $(CH_3)_4C$ requiring the presence of a help gas in the small structure II cage for hydrate stability. The methyl group rotational barriers for the enclathrated molecules considered here are generally slightly smaller than the barrier found for these molecules in the solid phase, and somewhat larger than those found for the gas phase. This is in keeping with the barrier being largely intramolecular in origin.

An interesting trend evident in Table 2 concerns the methyl group rotation barriers $V_X$ for $(CH_3)_3CX$, X = D, F, Cl. Clearly for the enclathrated molecules $V_F < V_D < V_{Cl}$. For the pure solids $V_F \sim V_D < V_{Cl} < V_{Br}$ (10), and for other solids of the type $CH_3CX_3$, $(CH_3)_2CX_2$, $V_F < V_H < V_{Cl} < V_{Br}$ (10). Evidently a simple argument involving steric repulsion and van der Waal's radii is inadequate in explaining such trends.


1. J. A. RIPMEESTER. J. Chem. Phys. **68**, 7835 (1978).
2. J. A. RIPMEESTER and D. W. DAVIDSON. Mol. Cryst. Liq. Cryst. **43**, 189 (1977).
3. E. R. ANDREW and R. BERSOHN. J. Chem. Phys. **18**, 159 (1950).
4. D. PANKE. J. Chem. Phys. **48**, 2990 (1968).
5. P. S. ALLEN. J. Chem. Phys. **48**, 3031 (1968).
6. F. APAYDIN and S. CLOUGH. J. Phys. C, **1**, 932 (1968).
7. K. T. HECHT and D. M. DENNISON. J. Chem. Phys. **26**, 31 (1957).
8. D. W. DAVIDSON, S. K. GARG, S. R. GOUGH, R. E. HAWKINS, and J. A. RIPMEESTER. Can. J. Chem. **55**, 3641 (1977).
9. J. S. WAUGH and E. I. FEDIN. Fiz. Tverd. Tela Leningrad, **4**, 2233 (1962).
10. C. I. RATCLIFFE and T. C. WADDINGTON. J. Chem. Soc. Faraday Trans. II, 1821 (1976).
11. J. R. DURIG, S. M. CRAVEN, and J. BRAGIN. J. Chem. Phys. **53**, 58 (1970).
12. J. R. DURIG and C. W. HAWLEY. J. Chem. Phys. **58**, 237 (1973).
13. J. R. DURIG, S. M. CRAVEN, J. H. MULLIGAN, C. W. HAWLEY, and J. BRAGIN. J. Chem. Phys. **58**, 1281 (1973).
14. D. W. DAVIDSON and J. A. RIPMEESTER. J. Glaciol. **21**, 33 (1978).


Can. J. Chem. Downloaded from www.nrcresearchpress.com by 210.87.254.105 on 09/06/12
For personal use only.

# Étude des bases de Schiff derivées de la salicylaldehyde et de la 2-aminopyridine. Propriétés et capacité de complexation

L. F. CAPITÁN-VALLVEY, F. SALINAS, C. JIMÉNEZ ET L. CUADROS

*Département de Chimie Analytique de la Faculté des Sciences de l'Université de Granada et Département de Recherches Chimiques du C.S.I.C., Granada, Espagne*

Reçu le 25 septembre 1981

L. F. CAPITÁN-VALLVEY, F. SALINAS, C. JIMÉNEZ et L. CUADROS. Can. J. Chem. **60**, 1706 (1982).

Les propriétés spectroscopiques (ir, uv, rmn et spectre de masse) et thermiques des azométhines (*N*-(4-méthyl-2-pyridyl)benzaldimine, *N*-(6-méthyl-2-pyridyl)benzaldimine, *N*-(4-méthyl-2-pyridyl)salicylaldimine, et *N*-(6-méthyl-2-pyridyl)salicylaldimine) ont été étudiées. La valeur de leurs constantes d'acidité est discutée en fonction de la stéréochimie de ces molécules. Enfin la réaction avec des sels métalliques a été étudiée qualitativement.

L. F. CAPITÁN-VALLVEY, F. SALINAS, C. JIMÉNEZ, and L. CUADROS. Can. J. Chem. **60**, 1706 (1982).

The spectroscopic (ir, uv, nmr, and ms) and thermal properties of *N*-(4-methyl-2-pyridyl)benzaldimine, *N*-(6-methyl-2-pyridyl)benzaldimine, *N*-(4-methyl-2-pyridyl)salicylaldimine and *N*-(6-methyl-2-pyridyl)salicylaldimine have been studied. Their acidity constants are discussed in relationship to their stereochemistry. Finally, reaction of these compounds with metal salts has been studied in a qualitative manner.

[Journal translation]

## Introduction

Dans des travaux précédents (1–4) nous avons fait connaître les résultats obtenus sur l'étude des propriétés, de la capacité complexante et des applications analytiques des bases de Schiff hétérocycliques, et plus spécialement l'influence qu'exerce l'introduction de différents groupes fonctionnels en position *ortho* par rapport au groupe azométhinique sur la molécule (formules **1–4**).

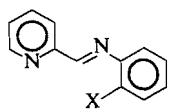

**1** X = H
**2** X = OH
**3** X = SH
**4** X = COOH

En suivant toujours la même ligne de travail, nous avons étudié la capacité de complexation de ces bases de Schiff. D'une part, nous avons inverti la position du groupe azométhinique dans la molécule par rapport aux précédents, et d'autre part, nous avons introduit des groupes méthyles dans diverses positions de l'anneau pyridinique.

L'objectif est double: d'un côté, augmenter la sélectivité de ces composés dans leurs réactions en presence d'ions inorganiques et d'un autre côté, diminuer la solubilité des complexes qui ont pu se former.

Les azométhines que nous avons étudiés sont: *N*-(4-méthyl-2-pyridyl)benzaldimine (4-MPBI) (**5**), *N*-(6-méthyl-2-pyridyl)benzaldimine (6-MPBI) (**6**), *N*-(4-méthyl-2-pyridyl)salicylaldimine (4-MPSI) (**7**)

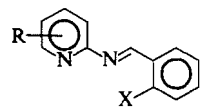

**5** R = 4-$CH_3$; X = H (4-MPBI)
**6** R = 6-$CH_3$; X = H (6-MPBI)
**7** R = 4-$CH_3$; X = OH (4-MPSI)
**8** R = 6-$CH_3$; X = OH (6-MPSI)

et *N*-(6-méthyl-2-pyridyl)salicylaldimine (6-MPSI) (**8**).

Malgré une intense recherche bibliographique, nous n'avons réussi à trouver aucun travail traitant des bases de Schiff 4-MPBI et 6-MPBI. Au sujet de 4-MPSI et 6-MPSI nous avons trouvé une référence dans un travail de Császár et Balog (5) dans lequel ils étudient l'influence qu'exerce, sur la capacité complexante, l'introduction de groupes méthyles dans des positions différentes de l'anneau pyridinique et le type de liaisons de ces potentiels ligands tridentés.

Bien qu'on ne trouve plus d'information au sujet de nos azométhines, il y en a cependant quelques-unes qui se rapportent fondamentalement au *N*-(2-pyridyl)salicylaldimine dans les travaux de Pitea *et al.* (6), Geary *et al.* (7), Garnovskii *et al.* (8) et Holzbecher et Van Trung (9).

## Expérimental

*Produits*

Les produits employés sont de qualité réactive (Merck ou BDH) ou purifiés par nous.

*Synthèse—4-MPBI et 6-MPBI*

On condense des quantités équimoléculaires d'aldéhyde et d'amine dans l'éthanol. L'huile jaunâtre résultant de l'élimination du solvant à vide est insolubilisée avec du cyclohexane, on

0008-4042/82/131706-07$01.00/0
©1982 National Research Council of Canada/Conseil national de recherches du Canada

Can. J. Chem. Downloaded from www.nrcresearchpress.com by 210.87.254.5 on 09/06/12
For personal use only.

TABLEAU 1. Fréquences charactéristiques ($cm^{-1}$) des réactifs

| Assignation | 4-MPBI | 6-MPBI | 4-MPSI | 6-MPSI |
|---|---|---|---|---|
| ν (OH) phénolique | — | — | 2300–3800b | 2500–3500b |
| ν (C=N) azométhinique | 1608s | 1595s | 1614s | 1608s |
| ν (C=N) pyridinique | * | 1572s | 1595s | 1586s |
| δ ($CH_3$) as. | 1472s | 1451s | 1451s | 1450s |
| δ (C—O) phénolique | — | — | 1143s | 1142s |
| δ (O—H) phénolique | — | — | 1275s | 1282s |

*Inclue dans la ν (C=N) azométhinique.

lave plusieurs fois la poudre blanche cristalline obtenue avec du cyclohexane chaud. Puis on la recristallise dans l'éthanol; 4-MPBI: 72% de rendement; pf 86–87°C. *Anal.* calc. pour $C_{13}H_{11}N_2$: C 79,56; H 6,60; N 14,27; trouvée: C 79,18; H 6,32; N 14,54. 6-MPBI: 65% de rendement; pf 80–81°C. *Anal.* trouvée: C 79,57; H 6,12; N 14,21.

*4-MPSI et 6-MPSI*

On condense des quantités équimoléculaires d'aldéhyde et d'amine dans l'éthanol. Le solvant et l'excès d'aldéhyde s'éliminent à vide. L'huile obtenue est dissoute dans l'éthanol chaud qui permet la cristallisation. On recristallise dans l'éthanol. 4-MPSI: cristaux jaunes; 90% de rendement; pf 98°C (litt. (5) pf 99,4°C). *Anal.* calc. pour $C_{13}H_{12}N_2O$: C 73,57; H 5,71; N 13,20; trouvée: C 73,20; H 5,67; N 13,06. 6-MPSI: cristaux aciculaires jaunes; 85% de rendement; pf 68°C (litt. (5) pf 65,8°C). *Anal.* trouvée: C 73,77; H 5,73; N 13,49.

*Appareil et mesures*

Spectrophotomètre ir Beckman 4240; thermoanalyseur Setaram GDTD-10, muni d'une électrobalance B-70 avec thermopaires Pt/Pt-Rh; spectrographe de masses Hewlett Packard 5930 A (70 eV) à 110°C de température de sonde; potentiomètre Methrom Herisau E-536 muni d'une burette automatique et d'électrodes en verre et calomel; spectrophotomètre uv–vis Beckman ACTA III; spectrofluorimètre Aminco–Bowman SPF.

Pour l'analyse thermique on a employé 10 mg d'échantillon dans un creuset en Pt de 5 mm de diamètre, en opérant dans une atmosphère statique d'air à la vitesse de 5°C/min. On a employé de l'alumine calcinée comme matériel de référence pour ATD, avec une particule du même ordre que celle de l'échantillon (> 63 nm).

On a étudié la stabilité des dissolutions spectrophotomètriquement, en régistrant la variation d'absorption avec le temps à la longueur d'onde du maximum de la bande K dans des dissolutions préparées récemment d'azométhine en milieu dioxane–eau 50% v/v; on a étudié également spectrofluorimétriquement en éthanol–eau 5% v/v en régistrant le spectre d'émission à des temps différents en excitant à 290 nm. Le maximum d'émission se trouve à 367 nm.

On a calculé les constantes de dissociation acide par l'application de la méthode directe, vu que des expériences précédentes ont démontré qu'entre $pK_1$ et $pK_2$ il existe une différence suffisante pour considérer les deux équilibres séparément. De cette façon on a calculé $pK_2$ de 4-MPBI et 6-MPBI et $pK_1$ de 4-MPSI et 6-MPSI, à partir des courbes de neutralisation obtenues en valorant l'acide conjugué de la base de Schiff présente. La valeur de $pK_2$ et $pK_3$ de ces dernières a été calculée par l'application de la méthode de Irving et Rossotti (10). On a opéré dans du dioxane–eau au 50% v/v de force ionique 0,1 *M* ($KNO_3$) et à 25, 0 ± 0,1°C.

L'étude de la réactivité qualitative en présence d'ions inorganiques a été effectuée dans des concentrations de 1 g/L. L'observation a été réalisée au moyen d'illumination avec lumière visible et uv (de 360 et 245 nm). Les réactions ont été étudiées dans toute la gamme de pH.

## Résultats et discussion

*Étude des propriétes des réactifs*

Les bandes ir assignées (comprimé de KBr) ont été réunies au tableau 1, où les fréquences caractéristiques des azométhines apparaissent. Nous remarquons la large bande entre 2500 et 3500 $cm^{-1}$ pour 4-MPSI et 6-MPSI, ce qui nous indique l'existence de forte association par liaison d'hydrogène. Les données obtenues ne concordent pas totalement avec les données bibliographiques (5), ainsi pour la ν (C=N) azométhinique que nous assignons à 1614 $cm^{-1}$ pour 4-MPSI et 1608 $cm^{-1}$ pour 6-MPSI, dans la bibliographie on l'indique à 1603 et 1619 $cm^{-1}$ respectivement.

Les principaux caractéristiques du spectre de rmn ($Cl_3CD$) sont enregistrées au tableau 2. Les données trouvées dans la bibliographie sont relativement en concordance (5) avec celles que nous avons trouvées excepté pour le signal du proton phénolique qu'ils assignent entre 12,16 et 13,69 ppm et nous entre les signaux aromatiques.

Seulement nous remarquons le fait que le proton azométhinique de la 4-MPSI et la 6-MPSI apparaît dans un champ plus bas que celui de deux autres. Phénomène qui appuie l'existence des liaisons d'hydrogène entre l'OH phénolique et le N iminique, le H azométhinique restant moins blindagé pour cette même raison. L'intégration nous donne dans tous les cas la relation 1:8:3 qui est correcte.

L'ensemble des données qu'offre le spectre de masses des quatre composés obéit au schéma fondamental de fragmentation de bases de Schiff

TABLEAU 2. Signaux fondamentaux du spectre de rmn des réactifs dans $Cl_3CD$

| Assignation | 4-MPBI | 6-MPBI | 4-MPSI | 6-MPSI |
|---|---|---|---|---|
| H azométhinique | 9,02 | 9,40 | 9,18 | 9,35 |
| H méthyliques | 2,58 | 2,57 | 2,45 | 2,45 |
| H aromatiques | 6,85–7,71 | 6,77–7,75 | 6,7–8,4 | 6,7–8,4 |

Can. J. Chem. Downloaded from www.nrcresearchpress.com by 210.87.254.5 on 09/06/12
For personal use only.

TABLEAU 3. Spectre de masses. Fragments majoritaires

| Base de Schiff | *M* | *a* | *b* | *c* | Pique base |
|---|---|---|---|---|---|
| 4-MPBI | 196(13)* | 195(3) | 119(6) | 92(19) | 93 |
| 6-MPBI | 196(16) | 195(2) | 119(2) | 92(20) | 93 |
| 4-MPSI | 212(20) | 211(4) | 119(3) | 92(18) | 93 |
| 6-MPSI | 212(22) | 211(2) | 119(1) | 92(13) | 93 |

*Dans la parenthèse % abondance.

hétérocycliques étudié par Barnes *et al.* (11) (Schéma 1).

Les ions les plus grands que nous avons trouvés sont réunis au tableau 3. Les bases de Schiff que nous étudions nous montrent un spectre de masses en accord avec le spectre de la *N*-(2-pyridyl)benzaldimine (11). Le pic base est le *m/e* 93 qui correspond à la picoline protonée, lequel se trouve à *m/e* 93 et non à 92 dû à ce que l'hydrogène du carbone azométhinique se transfère a l'anneau pyridinique, la charge restant positive sur l'azote.

Le spectre ultraviolet réalisé à partir de dissolutions éthanoliques montre les bandes recueillies au tableau 4. De cette façon la bande $E_1$ a des longueurs d'onde inférieures à 220 nm et que l'on attribue à des transitions localisées dans le noyau pyridinique. La bande $E_2$ entre 260–270 nm que l'on assigne à la transition d'électrons que comprennent l'anneau benzolique et la double liaison azométhinique et enfin la bande K, bande de conjugaison. Dans 4-MPSI et 6-MPSI apparaît en plus une bande sur 350 nm qui appartient aux bandes de conjugaison (29).

L'analyse thermique des composés (Fig. 1) montre un comportement différent de 4-MPBI et 6-MPBI par rapport à ses hydroxy derivés (4-MPSI et 6-MPSI). Dans les deux premières on aperçoit un processus de volatilisation totale sur les 200°C (de manière analogue à ce que nous avons trouvé pour la 2-pyrilidenaniline (1)), tandis que dans la 4-MPSI et 6-MPSI, nous voyons un processus pyrolitique qui a deux étapes, dans la première une perte de l'anneau pyridinique (perte de poids expérimental: 4-MPSI 43,0%, 6-MPSI 43,3%; calculée 43,8%) et après une combustion du reste.

Les constantes de dissociation des réactifs que nous étudions ont été déterminées potentiométri-

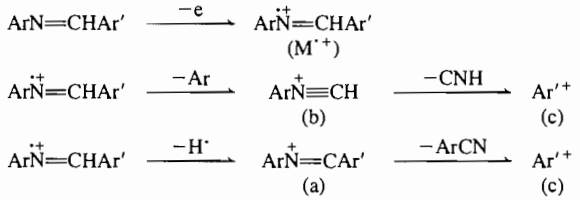


SCHÉMA I

TABLEAU 4. Bandes uv des réactifs en éthanol

| Base de Schiff | Bande $E_1$ | Bande $E_2$ | Bande K | |
|---|---|---|---|---|
| 4-MPBI | 213(4,53)* | 262(4,13) | 290(4,20) | — |
| 6-MPBI | 219(4,16) | 260(4,11) | 295(4,16) | — |
| 4-MPSI | 213(4,13) | 267(4,17) | 301(4,22) | 348(4,17) |
| 6-MPSI | 218(4,23) | 270(4,09) | 310(4,14) | 350(4,14) |

*Dans la parenthèse log ε.

quement, en milieu dioxane–eau au 50% v/v dans lequel ils sont solubles et relativement stables. Les temps de semidécomposition déterminés spectrophotométriquement, dans ces conditions, sont presque de deux heures pour 4-MPSI et 6-MPSI (d'accord avec ceux obtenus par Geary *et al.* (7)) et d'une heure pour 4-MPBI et 6-MPBI, et ils sont relativement élevés par rapport aux cinq minutes employées pour la valoration.

Etant donné le faible caractère basique des azotes, on a déterminé les constantes de dissociation des acides conjugués de ces bases. Les valeurs de p*K* obtenues sont indiquées au tableau 5. Le $pK_1$ de 4-MPBI et 6-MPBI n'est pas indiqué puisque quand on opère en milieu aussi acide, l'hydrolyse de ces deux composés est exaltée sans obtenir des valeurs reproductibles malgré que son ordre de grandeur soit près de 2.

Les constantes obtenues correspondent aux équilibres indiqués ensuite (7, 9, 12) (Schéma 2).

Les valeurs de $pK_2$ et $pK_3$ concordent avec celles des composés avec des fonctions semblables. Ainsi pour le salicylaldéhyde, Jones *et al.* trouvent une valeur de $pK_{OH}$ de 9,50 (13) tandis que nous trouvons pour 4-MPSI et 6-MPSI les valeurs de 9,18 et de 9,15 respectivement. On pourrait attribuer ces petites variations à ce que dans le premier cas est la liaison d'hydrogène avec un oxygène et dans notre cas avec l'azote azométhinique, le premier étant un peu plus fort que le second.

TABLEAU 5. Valeurs de p*K* des bases de Schiff

| Base de Schiff | $pK_1$ | $pK_2$ | $pK_3$ |
|---|---|---|---|
| 4-MPBI | — | 6,6±0,1 | — |
| 6-MPBI | — | 6,7±0,1 | — |
| 4-MPSI | 1,64±0,03 | 6,82±0,06 | 9,18±0,06 |
| 6-MPSI | 1,72±0,03 | 6,70±0,06 | 9,15±0,06 |

Can. J. Chem. Downloaded from www.nrcresearchpress.com by 210.87.254.5 on 09/06/12
For personal use only.

Can. J. Chem. Downloaded from www.nrcresearchpress.com by 210.87.254.5 on 09/06/12
For personal use only.

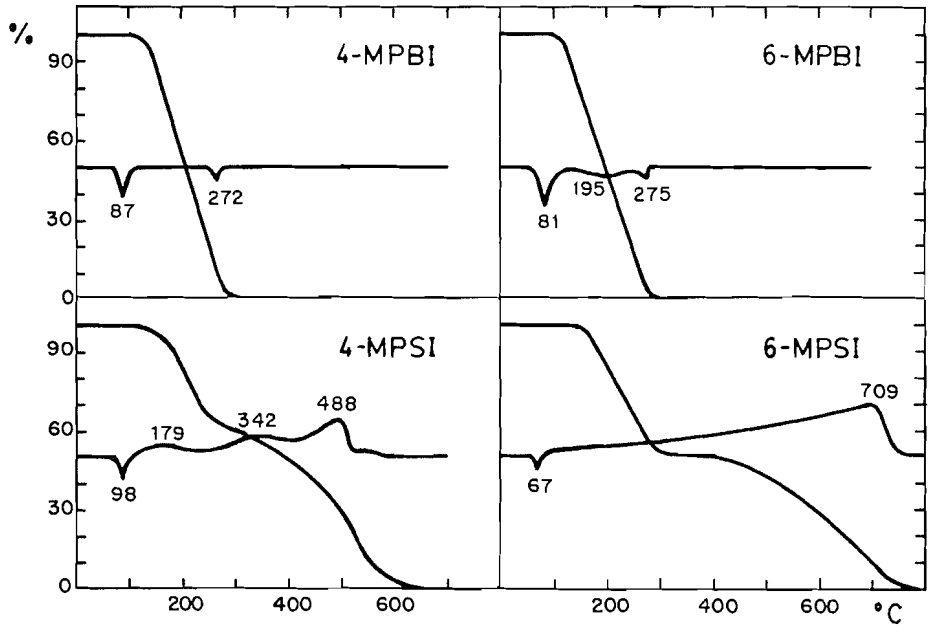


FIG. 1. Analyse thermique des azométhines.

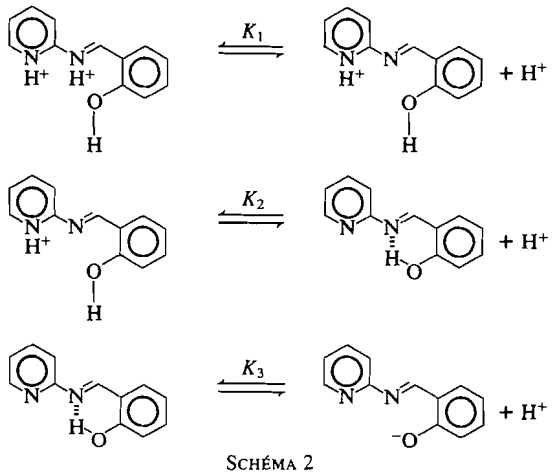


SCHÉMA 2

Pour la constante de dissociation de l'acide conjugué de l'aminopyridine, Maley et Mellor (14) ont donné la valeur 6,71. Les valeurs de $pK_2$ que nous avons trouvées pour les quatre bases de Schiff étudiées oscillent entre 6,6 et 6,82.

Par contre pour $pK_1$ de 4-MPSI et 6-MPSI nous trouvons des valeurs très basses malgré qu'en principe les azotes pyridiniques et azométhiniques montrent assez de similitude structurale.

Ce dernier fait a été observé dans les données bibliographiques et aussi dans les valeurs déterminées par nous pour d'autres bases de Schiff *N*-aromatiques. Cependant la valeur de p*K* azométhinique est du même ordre que le pyridinique quand il s'agit de bases de Schiff *N*-alkyldérivées. Dans le tableau 6 nous avons recueilli les valeurs de constantes qui démontrent l'affirmation précédente.

À notre avis, il faut chercher la raison de ce comportement, qui suppose que la paire électronique du nitrogène azométhinique n'est pas aussi capable que le pyridinique de former la liaison avec le proton, dans des considérations structurelles des bases de Schiff en général. On pourrait penser à priori que les bases de Schiff aromatiques (type bencylidenaniline) présentent une structure plane. Cependant il existe une série de faits expérimentaux, résumés par Pitea *et al.* (6), qui sont en contradiction avec la même. Cela est dû à l'existence d'une interaction estérique entre l'hydrogène azométhinique et l'hydrogène du carbone en *ortho* par rapport à l'azote iminique (**9**).

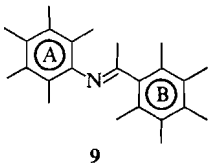


**9**

Dans le but de justifier les données expérimentaux en contradiction avec la structure plane on a proposé différentes hypothèses structurelles. La première indique que le nitrogène azométhinique passe d'un état d'hybridation $sp^2$ à un état $sp$, de cette façon l'angle Ar—N=C est de 180° et non de 120° et la molécule reste plane (23). Une deuxième hypothèse suppose que l'anneau B tourne par rapport au reste de la molécule d'un angle de 90° et

TABLEAU 6. Donnés bibliographiques de $pK_a$ de bases de Schiff aliphatiques et aromatiques

| Base de Schiff | $pK_1$* | $pK_2$ | $pK_3$ | Milieu | Méthode | Référence |
|---|---|---|---|---|---|---|
| $(C_6H_5)_2C{=}NH$ | 7,0 | — | — | a | S | 15 |
| $(C_6H_5)_2C{=}NCH_3$ | 7,2 | — | — | a | S | 15 |
| $C_6H_5C{=}NC(CH_3)_3$ | 6,7 | — | — | a | S | 16 |
| $p$—$NO_2C_6H_4C{=}NC(CH_3)_3$ | 5,4 | — | — | a | S | 16 |
| $C_6H_5(p$—$ClC_6H_4)C{=}NCH_3$ | 6,55 | — | — | a | S | 15 |
| $p$—$OCH_3C_6H_4C{=}NC(CH_3)_3$ | 7,7 | — | — | a | S | 16 |
| $p$—$ClC_6H_4CH{=}NC_6H_5$ | 2,75 | — | — | b | S | 17 |
| $p$—$(CH_3)_3NC_6H_4CH{=}N$—$p$—$OHC_6H_4$ | 2,11 | — | 9,10 | a | S | 19 |
| $C_5H_4NCH{=}NC_6H_5$ | 2,7 | 4,33 | — | a | P | 1 |
| $C_5H_4NCH{=}N$—$o$—$OHC_6H_4$ | 3,05 | 4,45 | 11,8 | e | P | 20 |
| $C_5H_4NCH{=}N$—$o$—$OHC_6H_4$ | 3,65 | 4,60 | 11,53 | c | P | 9 |
| $C_5H_4NCH{=}N$—$o$—$OHC_6H_4$ | 3,69 | 4,30 | 9,99 | e | P | 12 |
| $C_5H_4NCH{=}N$—$p$—Cl—$o$—$OHC_6H_3$ | 3,43 | 4,08 | 9,52 | a | P | 12 |
| $C_5H_4NCH{=}N$—$o$—$COOHC_6H_4$ | 2,1 | 3,1 | 6,39 | e | P | 4 |
| $C_5H_4NCH{=}NC_{10}H_7$ | 3,05 | 4,45 | — | e | P | 21 |
| $C_5H_4NCH{=}N$—$o$—$OHC_{10}H_6$ | 2,95 | 4,17 | 11,40 | e | P | 22 |
| $C_5H_4NN{=}CH$—$o$—$OHC_6H_4$ | — | 6,37 | 9,77 | e | P | 20 |
| $C_5H_4NN{=}CH$—$o$—$OHC_6H_4$ | 3,91 | 7,0 | 9,35 | e | P | 9 |
| $C_5H_4CH{=}NC_5H_4N$ | 3,50 | 6,66 | 7,33 | d | P | 9 |
| $o$—$OHC_6H_4CH{=}NC_6H_5$ | 4,16 | — | 9,11 | c | P | 18 |

*$pK_1$: correspond au N azométhinique; $pK_2$ au N pyridinique; $pK_3$ au OH phénolique excepté pour 14 et 19. a: eau; b: eau–méthanol; c: eau–éthanol 5%; d: eau–éthanol 10%; e: dioxane–eau 50%. S: spectrophotométrie. P: potentiométrie.

pour cela tous les deux résultent orthogonaux, et de cette façon l'hybridation du nitrogène azométhinique est $sp^2$ (24). De cette façon il y a une conjugaison compétitive de la paire électronique du nitrogène entre la conjugaison qui rend la molécule plane et la conjugaison de la paire d'électrons avec les électrons de l'anneau B. Pour la troisième hypothèse il faut qu'il y ait rotation d'un anneau par rapport à l'autre, ainsi qu'un changement dans l'hybridation du nitrogène de $sp^2$ à $sp$, avec cela la paire libre du nitrogène azométhinique reste dans l'orbitale atomique $p$ et vient faire partie de la conjugaison de l'anneau B. Cela suppose l'existence de deux systèmes conjugués orthogonaux à l'intérieur de la molécule (25).

L'acceptation de la deuxième comme de la troisième hypothèse justifierait la basse basicité du nitrogène azométhinique par rapport au pyridinique, puisque cela suppose une dislocalisation effective de la paire électronique du nitrogène azométhinique. Cependant il faut tenir compte qu'étant donné que la plus grande interaction estérique est celle qui a lieu entre l'hydrogène azométhinique et l'hydrogène en *ortho* par rapport au pont iminique, il y aura une diminution de l'empêchement estérique par azosubstitution du carbone en *ortho* par rapport au nitrogène azométhinique, comme cela se produit précisément dans les bases de Schiff dérivées de la 2-aminopyridine. Sa conformation sera d'autant plus proche à la plane comme le démontrent Pitea *et al.* (6). Pour les bases de Schiff étudiées par nous, dérivées de la 2-amino-X-méthylpyridine, on peut penser à une structure conformationnelle analogue, c'est-à-dire proche de la plane. Cependant nous avons trouvé très peu de basicité, ce qui n'est pas en accord avec une structure proche à la plane pour des bases de Schiff dérivées de la 2-aminopyridine.

On pourrait justifier ceci si nous tenons compte du schéma de protonation, que nous avons déjà proposé, dans lequel le premier nitrogène qui se protone est le pyridinique, de cette façon nous arrivons à une structure similaire à celle de la benzylidénaniline, en obligeant à un changement de conformation vers une autre forme plus tournée et donc a une plus grande conjugaison de la paire du nitrogène avec l'anneau pyridinique et de cette façon la basicité diminuera beaucoup (**10**).

Un dernier fait à commenter, c'est que les valeurs de $pK_1$ trouvées par nous sont plus petites que celles que nous avons trouvées pour des azométhines analogues, tandis que les valeurs de $pK_2$ sont notamment plus grandes. On pourrait justifier ceci en considérant que la 2-aminopyridine

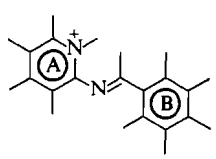


**10**

présente une structure de résonance entre les deux nitrogènes, comme cela a été démontré par Angyal et Angyal (26), et à la suite de quoi le proton s'unira de préférence au N pyridinique et ce sera une base plus forte que la pyridine ($pK_a$ pyridine: 5,23 (27);

Can. J. Chem. Downloaded from www.nrcresearchpress.com by 210.87.254.5 on 09/06/12
For personal use only.

TABLEAU 7. Reactivité qualitative des bases de Schiff

| Cation | 4-MPBI | 6-MPBI | 4-MPSI | 6-MPSI |
|---|---|---|---|---|
| Fe(III) | orange (4,3)* | orange (4,5) | violet (5,3) | violet (5,3) |
| Fe(II) | bleu (4,7) | bleu (4,8) | rouge (5,3) | rouge (5,3) |
| $MoO_4^{2-}$ | p. blanc (4,8)† | p. blanc (4,8) | p. blanc (4,8) | p. blanc (4,8) |
| $Fe(CN)_6^{4-}$ | p. jaune (5,5) | p. jaune (5,3) | p. jaune (5,5) | p. jaune (5,3) |
| Cu(II) | — | — | jaune (4,3) | jaune (5,5) |
| Co(II) | — | — | p. orange (4,3) | p. orange (5,5) |
| Ni(II) | — | — | p. jaune (5,7) | p. jaune (5,5) |
| $UO_2$(II) | — | — | p. orange (5,0) | p. orange (4,7) |
| Ag(I) | — | — | p. orange (4,0) | — |

*Dans la parenthèse on indique la sensibilité comme cologarithme de la concentration limite (p$D$).
†p = précipité.

p$K_a$ 2-aminopyridine 6,71 (14); 2-amino-6-méthylpyridine: 7,41 (28)). On peut suggérer une résonance similaire pour les bases de Schiff étudiées, ce qui justifierait les valeurs basses de p$K_1$ du N azométhinique et les hautes valeurs de p$K_2$ du N pyridinique de la même façon que Geary *et al.* (7), qui a justifié le fait que la *N*-(2-pyridyl)salicylaldimine ajoute un proton comme base à cette hypothèse. Cependant en opérant dans les conditions adéquates on peut déterminer le p$K_1$ qui, comme on peut s'y attendre, est exceptionnellement bas.

*Réaction avec des ions métalliques*

Les résultats dans la réactivité qualitative en présence d'ions inorganiques sont montrés au tableau 7, où nous pouvons apprécier qu'elle est peu abondante pour les quatre azométhines, bien qu'elle soit plus grande pour les *o*-hydroxydérivées.

Dans la comparaison des résultats obtenus quand nous étudions la réactivité de la 4-MPBI et de la 6-MPBI avec celle qui correspond à la 2-pyrilideneaniline (**1**) nous pouvons voir que les deux premières ont une réactivité plus petite, les réactions de cette dernière étant plus sensibles. Ainsi, par exemple, pour la réaction avec Fe(II), la sensibilité pour les deux premières est du p$D$ = 4,8, tandis que pour le 2-pyrilideneaniline elle est de 6,3.

On peut attribuer cette différente réactivité au fait que la 4-MPBI, comme la 6-MPBI, à la groupe azométhinique inverti par rapport à la 2-pyrilideneaniline et de cette façon les complexes de deux premières formeraient des anneaux de cinq membres (**11** et **12**).

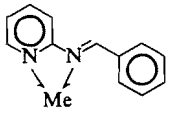


**11**

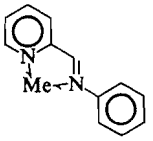


**12**

La comparaison de réactivité entre la 4-MPSI et la 6-MPSI avec la 2-pyrilidene-*o*-hydroxyaniline, nous amène à une conclusion similaire. La 6-MPSI réagit avec 8 ions et la 4-MPSI avec 9 parmi tous ceux que nous avons essayés, tandis que la 2-pyrilidene-*o*-hydroxyaniline réagit avec 45 ions. La plus grande sensibilité trouvée pour les trois réactifs correspond à la réaction avec le Ni(II) dont les p$D$ sont 5,5 (6-MPSI), 5,7 (4-MPSI) et 7,2 (2-pyrilidene-*o*-hydroxyaniline). Ce comportement différent dans les composés qui possèdent les mêmes groupes chelants est dû, comme dans le cas précédent, à la différente position que ceux-ci occupent dans la molécule.

La 2-pyrilidene-*o*-hydroxyaniline agit comme tridenté en formant deux métallocycles de cinq membres, tandis que les deux autres le font comme tridentés en formant un métallocycle de six et un autre de quatre, ou comme bidenté en formant un métallocycle de six membres.

Quelques-uns des complexes formés, ceux de Fe(II), Ni(II), $UO_2$(II), Co(II) et Cu(II), sont partiellement extractibles en $CHCl_3$ et donnent une couleur jaune à la couche organique, excepté avec celui de Fe(II) qui donne une couleur rouge. La sensibilité trouvée est basse dans tous les cas (p$D$ = 5,7).

Quand nous étudions la réactivité de ces composés avec Al(III), Be(II) et Zn(II) on obtient des produits fluorescents, fluorescence engendrée par hydrolyse des bases de Schiff, catalysée par ces ions métalliques. Dans le cas du Be(II) la fluorescence est particulièrement intense (p$D$ = 7,2) et selon Holzbecher et Van Trung (9) elle est due à la formation d'un composé avec salicylaldéhyde.

Les dissolutions de 6-MPSI et 4-MPSI présentent une fluorescence jaune en milieu basique en l'absence d'ions métalliques. Dans ce milieu apparaît lentement et dans le milieu acide plus rapidement une fluorescence violette qui est due, selon ce que nous avons prouvé, aux amines obtenues par hydrolyse des réactifs. On observe que, quand nous diminuons le pH, la vitesse d'hydrolyse augmente en accord avec les résultats de Cordes et

Can. J. Chem. Downloaded from www.nrcresearchpress.com by 210.87.254.5 on 09/06/12
For personal use only.

Jencks (16) et Koehler *et al.* (15) dans l'étude des bases de Schiff aromatiques, qui indique qu'il existe une catalyse acide–base du processus d'hydrolyse.

**Remerciement**

Ce travail a été traduit par le Prof. J. J. Arnedo.

1. F. Capitán, F. Salinas et L. F. Capitán-Vallvey. An. Quim. **73**, 1308 (1977).
2. F. Capitán, F. Salinas et L. F. Capitán-Vallvey. Bol. Soc. Quim. Perú, **69**, XLIII (1977).
3. F. Capitán, F. Salinas et L. F. Capitán-Vallvey. Bull. Soc. Chim. Fr. I-35 (1979).
4. F. Capitán, L. F. Capitán-Vallvey et J. L. Vilchez. J. Inorg. Nucl. Chem. **43**, 683 (1981).
5. J. Császar et J. Balog. Acta Chim. Acad. Sci. Hung. **87**, 321 (1975).
6. D. Pitea, G. Favini et D. Grasso. Gazz. Chim. Ital. **100**, 301 (1970).
7. W. J. Geary, G. Nickless et F. H. Pollard. Anal. Chim. Acta, **26**, 575 (1968).
8. A. D. Garnovskii, V. I. Minkin, O. A. Osipov, V. T. Panyushkin, L. K. Isaeva et M. I. Khyazhanskii. Zh. Neorg. Khim. **12**, 2443 (1967).
9. Z. Holzbecher et H. Van Trung. Collect. Czech. Chem. Commun. **41**, 1506 (1976).
10. H. Irving et H. S. Rossotti. J. Chem. Soc. 2904 (1954).
11. C. S. Barnes, E. J. Halbert, R. J. Goldsack et J. G. Wilson. Aust. J. Chem. **26**, 1031 (1973).
12. M. Otomo et K. Kodama. Bull. Chem. Soc. Jpn. **46**, 2421 (1973).
13. J. G. Jones, J. B. Poole, J. C. Tomkinson et R. J. P. Williams. J. Chem. Soc. 2001 (1958).
14. L. E. Maley et D. P. Mellor. Nature, **370**, 159 (1947).
15. K. Koehler, W. Sandstrom et E. H. Cordes. J. Am. Chem. Soc. **86**, 2413 (1964).
16. E. H. Cordes et W. P. Jencks. J. Am. Chem. Soc. **85**, 2843 (1963).
17. E. H. Cordes et W. P. Jencks. J. Am. Chem. Soc. **84**, 832 (1962).
18. N. Shori, B. S. Garg, Y. Dutt et R. P. Singh. Indian J. Chem. **9**, 161 (1971).
19. R. L. Reeves. J. Am. Chem. Soc. **84**, 3332 (1962).
20. W. J. Geary, G. Nickless et F. H. Pollard. Anal. Chim. Acta, **27**, 71 (1962).
21. M. Jiménez. Tesis Doctoral, Université de Granada, 1976.
22. M. Otomo, K. Fukui et K. Kodama. Bull. Soc. Chim. Jpn. **47**, 455 (1974).
23. C. Wergand et E. Merkel. Justus Liebigs Ann. Chem. **550**, 175 (1942).
24. V. A. Ismailski et E. A. Smirnov. J. Gen. Chem. USSR, **26**, 3389 (1956).
25. N. Ebara. Bull. Chem. Soc. Jpn. **33**, 534 (1960); **34**, 1151 (1961).
26. S. J. Angyal et C. L. Angyal. J. Chem. Soc. 292 (1938).
27. A. Albert, R. Goldacre et J. N. Phillips. J. Chem. Soc. 2240 (1948).
28. F. Fastier. Aust. J. Exp. Biol. **36**, 491 (1958).
29. O. H. Wheeler et P. H. Gore. J. Chem. Soc. 3298 (1961).

Can. J. Chem. Downloaded from www.nrcresearchpress.com by 210.87.254.5 on 09/06/12
For personal use only.

# Complexes de Cu(II), Co(II), Ni(II) et $UO_2$(II) avec les bases de Schiff *N*-(4-méthyl-2-pyridyl)salicylaldimine et *N*-(6-méthyl-2-pyridyl)salicylaldimine

L. F. Capitán-Vallvey, C. Jiménez et L. Cuadros

*Département de Chimie Analytique de la Faculté des Sciences de l'Université de Granada et Département de Recherches Chimiques du C.S.I.C., Granada, Espagne*

Reçu le 25 septembre 1981

L. F. Capitán-Vallvey, C. Jiménez et L. Cuadros. Can. J. Chem. **60**, 1713 (1982).

On isole les complexes des bases de Schiff *N*-(4-méthyl-2-pyridyl)salicylaldimine et *N*-(6-méthyl-2-pyridyl)salicylaldimine avec Co(II), Ni(II), Cu(II) et $UO_2$(II) aussi bien en milieu hydroalcoolique qu'en milieu éthanolique absolu. On remarque une forme différente d'agir en tant que ligands de ces bases de Schiff suivant le milieu. D'ailleurs, les complexes déjà nommés en milieu hydroalcoolique ont une capacité remarquable de réaction face à des substances présentes en solution. On propose deux nouvelles méthodes gravimétriques pour le dosage du Ni(II) et $UO_2$(II).

L. F. Capitán-Vallvey, C. Jiménez, and L. Cuadros. Can. J. Chem. **60**, 1713 (1982).

We have isolated the complexes of the Schiff bases *N*-(4-methyl-2-pyridyl)salicylaldimine and *N*-(6-methyl-2-pyridyl)salicylaldimine with Co(II), Ni(II), Cu(II), and $UO_2$(II) in both aqueous alcoholic and absolute alcoholic solutions. We note different modes of action of these Schiff bases according to the medium used. However, in aqueous alcoholic solution the complexes mentioned have a remarkable capacity for reaction with the substances in solution. We propose two new gravimetric methods for Ni(II) and $UO_2$(II).

[Journal translation]

## Introduction

Dans une publication précédente (1), nous avons commencé l'étude des bases de Schiff *N*-(4-méthyl-2-pyridyl)benzaldimine (4-MPBI) et *N*-(6-méthyl-2-pyridyl)benzaldimine (6-MPBI), de même que celle de leurs *o*-hydroxydérivés: *N*-(4-méthyl-2-pyridyl)salicylaldimine et *N*-(6-méthyl-2-pyridyl)salicylaldimine (4-MPSI et 6-MPSI respectivement). Après avoir synthétisé ces composés, nous en étudions diverses propriétés et, parmi d'autres, leur réactivité en face d'ions inorganiques. Dans ce travail nous essayons d'élargir la connaissance des chélates métalliques qui forment les composés 4-MPSI et 6-MPSI en étudiant les complexes de Co(II), Ni(II), Cu(II) et $UO_2$(II).

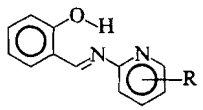

**1** R = H
4-MPSI R = 4-$CH_3$
6-MPSI R = 6-$CH_3$

Dans la bibliographie consultée il existe un nombre réduit de données sur la capacité complexante des bases de Schiff dérivées de la 2-aminopyridine. Les seules données existantes sur 4-MPSI et 6-MPSI sont dues à Császár et Balog (2) qui étudient les complexes de Ni(II) en milieu chloroformique et acétonique et leur attribuent les formules $(4\text{-MPSI})_2Ni\cdot 2H_2O$ et $(6\text{-MPSI})_2Ni$, en agissant 4-MPSI comme ligand bidenté et 6-MPSI comme tridenté.

Au sujet de la *N*-(2-pyridyl)salicylaldimine (**1**) composé très lié aux ligands à l'étude, et qui doit se conduire de façon similaire à ceux-ci, Geary *et al.* (3) remarquent que celui-là agit comme ligand bidenté en dissolution (dioxane–eau 50%), où ils ont établi potentiométriquement l'existence d'un complexe de Cu(II) 2:1 (L:Cu) et la libération pendant la complexation d'un proton par molécule de ligand. Ils indiquent de même la possibilité pour le ligand d'agir comme tridenté, en se basant sur le fait qu'ils ont isolé le complexe **1**-CuCl en milieu éthanolique.

Garnovskii *et al.* (4), de leur côté, informent sur l'obtention du complexe $TiCl_4$-**1** en benzène, et ils supposent que la complexation a lieu à travers des nitrogènes azométhinique et pyridinique, sans l'intervention du groupe OH dans la chélation. Verkhovodova et coll. (5) obtiennent, d'après eux, dans du méthanol le complexe $Cu(\mathbf{1})_2$, où les atomes coordonnants sont le N azométhinique et le O phénolique avec la perte du proton correspondant.

Holzbecher et Van Trung (6), de leur côté, étudient les complexes de **1** avec Zn(II) et Be(II), et remarquent la formation de composés de stoechiométrie 1:1 et 2:1 respectivement, bien qu'ils ne les isolent pas en tant que solides.

Enfin Mahmoud et El-Haty (7) isolent les complexes solides de **1** avec Co(II), Ni(II), Cu(II), $UO_2$(II) et Th(IV), en opérant en éthanol absolu, et ce sont les bases de Schiff non déprotonnées qui agissent comme des ligands bidentés. L'enchaîne-

0008-4042/82/131713-07$01.00/0
©1982 National Research Council of Canada/Conseil national de recherches du Canada

TABLEAU 1. Complexes synthétisés et analyse élémentaire

| Complexe[a] | Formule brute | Milieu[b] | Couleur | % N calc. | % N tr. | % Me calc. | % Me tr. |
|---|---|---|---|---|---|---|---|
| $L_1$-Co(II) | $Co(C_{13}H_{11}N_2O)_2$ | 1 | Orange | 11,58 | 11,36 | 12,37 | 12,24 |
| $L_2$-Co(II) | $Co(C_{13}H_{11}N_2O)_2$ | 1 | Orange | 11,58 | 11,43 | 12,37 | 12,10 |
| $L_3$-Co(II) | $Co(C_7H_5O_2)_2(H_2O)_2$ | 1 | Orange | — | — | 17,48 | 17,24 |
| $L_1$-Ni(II) | $Ni(C_{13}H_{11}N_2O)_2$ | 1 | Jaune | 11,59 | 11,43 | 12,33 | 12,72 |
| $L_2$-Ni(II) | $Ni(C_{13}H_{11}N_2O)_2$ | 1 | Jaune | 11,59 | 11,19 | 12,33 | 12,03 |
| $L_3$-Ni(II) | $Ni(C_7H_5O_2)_2(H_2O)_2$ | 1 | Vert | — | — | 17,42 | 17,38 |
| $L_1$-Cu(II) | $Cu(C_{13}H_{11}N_2O)_2$ | 1 | Vert foncé | 11,47 | 11,35 | 13,07 | 12,98 |
| $L_2$-Cu(II) | $Cu(C_{13}H_{11}N_2O)_2$ | 1 | Marron | 11,47 | 10,84 | 13,07 | 13,28 |
| $L_3$-Cu(II) | $Cu(C_7H_5O_2)_2$ | 1 | Vert foncé | — | — | 20,78 | 20,55 |
| $L_1$-$UO_2$(II) | $UO_2(C_{13}H_{11}N_2O)_2$ | 1,2 | Orange | 8,06 | 7,96 | 34,39 | 34,33 |
| $L_2$-$UO_2$(II) | $UO_2(C_{13}H_{11}N_2O)_2$ | 1,2 | Orange | 8,06 | 7,87 | 34,39 | 34,21 |
| $L_4$-Ni(II) | $Ni(C_7H_6NO)_2$ | 1 | Orange brillant | 9,36 | 9,39 | 19,65 | 19,44 |
| $L_4$-Cu(II) | $Cu(C_7H_6NO)_2$ | 1 | Vert brillant | 9,31 | 9,50 | 20,91 | 20,68 |
| $L_2$-Cu(II)$Cl_2$ | $Cu(C_{13}H_{12}N_2O)Cl_2$ | 2 | Vert | 8,08 | 8,24 | 18,32 | 18,54 |
| $L_1$-$UO_2$(II)Ac | $UO_2(C_{13}H_{11}N_2O)CH_3$—COO | 2 | Rouge | 5,18 | 5,33 | 44,05 | 43,87 |

[a] $L_1$ = 4-MPSI; $L_2$ = 6-MPSI; $L_3$ = salicylaldéhyde; $L_4$ = salicylaldimine.
[b] 1 = EtOH–$H_2O$ 50%; 2 = EtOH.

ment a lieu à travers du N azométhinique et du groupe OH phénolique.

## Partie expérimentale

*Produits employés*

*N*-(4-méthyl-2-pyridyl)salicylaldimine et *N*-(6-méthyl-2-pyridyl)salicylaldimine synthétisés par le procédé indiqué dans une publication précédente (1). Dissolutions de Co(II), Ni(II) et Cu(II) (à partir de nitrates et de chlorures) et de $UO_2$(II) (à partir de nitrates et d'acétates) $10^{-2}$ *M* en éthanol absolu et éthanol–eau 1:1. Cela a été étalonné comme d'habitude. Ces mêmes sels sont employés pour la synthèse de complexes solides.

*Synthèse des complexes métalliques*

1. *Synthèse en milieu hydroalcoolique*

Les complexes ont été obtenus en ajoutant à la solution aqueuse du sel métallique une solution éthanolique de la correspondante base de Schiff en proportion molaire 1:2. Les produits obtenus, comme nous commenterons plus tard, sont différents selon le milieu – neutre, ammoniacal ou basique fort – où ils sont obtenus. De même leur constitution diffère également si après avoir été précipité le complexe est filtré immédiatement ou par contre est soumis à digestion. Le temps de digestion a été, dans ce cas, de deux heures à 60°C. Les produits obtenus, après avoir été filtrés, ont été lavés avec de l'éthanol chaud et désséchés à vide sur $CaCl_2$ et $H_2SO_4$.

2. *Synthèse en milieu éthanolique absolu*

Au sel métallique dissous en éthanol absolu on ajoute dissolution éthanolique des bases de Schiff en relation molaire 1:2 et l'on maintient à reflux pendant une heure. Et on continue l'obtention dans la forme ci-dessus indiquée. Au tableau 1 on indique les complexes obtenus à partir de 4-MPSI, 6-MPSI, salicylaldéhyde et salicylaldimine, leur couleur, le milieu utilisé et les résultats de l'analyse de nitrogène et métal déterminés par des méthodes conventionnelles.

*Mesures physiques*

On a utilisé un spectrophotomètre uv–vis Beckman ACTA III muni de cuvettes de quartz d'un centimètre et un spectrophotomètre ir Beckman mod. 4240. Les mesures de conductivité sur des dissolutions éthanoliques $10^{-4}$ – $10^{-5}$ *M* en complexe, ainsi que les données précises pour la détermination du produit de solubilité ont été obtenues avec un conductimètre Radiometer mod. CDM2e. La diffraction de rayons X a été réalisée dans un appareil Philips PW 1060, le TG-ATD dans un équipement SETARAM GDTD-10, muni d'une électrobalance B-70 dans les conditions spécifiées dans une publication précédente (1). Pour les titrages conductimétriques on a utilisé un équipement Metrohm–Herisau comportant un conductoscope E 365B, une burette automatique E 536 et une cellule de conductivité EAG08. Toutes les courbes de titrage obtenues, en ajoutant à la dissolution éthanolique du cation celle du réactif au même milieu, ont été corrigées compte tenu de la dilution. De celles qui ont été réalisées en milieu hydroalcoolique on a tenu compte de l'effet de la dilution et de la variation de la constante diélectrique du milieu lorsqu'on ajoute du réactif dans l'éthanol.

## Résultats et discussions

L'étude a été réalisée en essayant d'obtenir les chélates en milieu éthanol–eau ou en éthanol absolu et en changeant le pH des dissolutions.

1. *Milieu hydroalcoolique (1:1)*

En ce milieu on n'a observé qu'un réaction en solution neutre et basique, et l'on a vérifié que les produits de réaction dépendent aussi bien de la base utilisée que des conditions opératoires.

(a) En milieu neutre, Co(II), Ni(II) et Cu(II) provoquent avec 6-MPSI et 4-MPSI l'apparition de précipités dont la couleur évolue par digestion. Après avoir isolé les différentes phases solides et les avoir étudié dans la forme que l'on indique ensuite, on arrive à la conclusion que bien que les deux bases de Schiff forment d'abord des complexes de stoechiométrie 2:1 (L:Me), après, pendant le processus de digestion à 60°C, elles se transforment en bissalicylaldéhydo-complexes, d'après l'équation [1].

En effet, les solides isolés immédiatement après leur formation sont des complexes des bases de

[1] 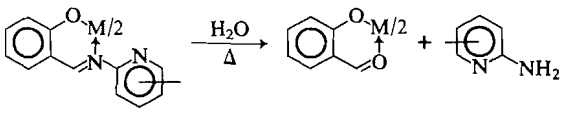

Schiff avec Co(II), Ni(II) et Cu(II) tel que le démontre l'analyse élémentaire (Tableau 1). Les données de conductivité (Tableau 2) indiquent qu'ils ne sont pas des electrolytes, ce qui suppose, en principe, que le groupe phénolique des réactifs se déprotonne préalablement à la formation du complexe. Le spectre ir (Tableau 3) corrobore ces extrêmes car il n'apparaît dans les complexes ni la vibration ν (OH) (ca. 3400 $cm^{-1}$), ni la δ (OH) (ca. 1280 $cm^{-1}$) qui apparaissent dans les réactifs. D'autre part, les vibrations de ν (C=N) azométhinique et pyridinique apparaissent dans des fréquences légèrement inférieures dans les complexes plutôt que dans les réactifs (sur 10 $cm^{-1}$ pour les complexes de 4-MPSI et de 2 $cm^{-1}$ pour ceux de 6-MPSI dans la vibration ν (C=N) azométhinique). Ce fait pourrait être en rapport avec un accroissement dans l'ordre de liaison du groupe azométhinique, tel que Teyssie et Charette (8) l'indiquent, dû à l'existence d'une conjugaison croisée du métallocycle formé par rapport au reste de la molécule.

Les donnés du spectre uv–vis de ces complexes sont montrées au tableau 2. Dans les deux réactifs apparaissent deux bandes, la première d'une plus grande longueur d'onde (350 nm) (9, 10) et qui par complexation se déplace vers de plus grandes longueurs d'onde (400–440 nm) grâce au fait que la présence de l'atome métallique facilite le transfert de charge; la deuxième d'une moindre longueur d'onde (300 nm), née de transitions $\pi \rightarrow \pi^*$ qui embrassent toute la molécule et qui se modifie légèrement par complexation (305–325 nm).

Comme nous avons déjà indiqué, la digestion de ces complexes provoque la formation de salicylaldéhydo-complexes, lesquels ont été identifiés au moyen d'une analyse élémentaire (Tableau 1) et du spectre ir (Tableau 3). La donnée plus expressive du spectre est l'apparition de la ν (C=O) à 1645 $cm^{-1}$. Il y a lieu d'attribuer le processus de transformation en premier lieu à la tendance hydrolytique de ces bases de Schiff, déjà mise en évidence dans une publication précedente (1) et remarquée par Geary *et al.* (3), et en deuxième lieu, peut-être, à la plus grande stabilité des salicylaldéhydo-complexes.

TABLEAU 2. Bandes des spectres uv–vis des complexes et coefficient d'extinction molaire dans éthanol. Valeurs de conductance des complexes dans DMF

| Composé | $\lambda_1$ nm | $\varepsilon_1 \times 10^3$ | $\lambda_2$ nm | $\varepsilon_2 \times 10^3$ | Λμs |
|---|---|---|---|---|---|
| $L_1$ | 348 | 14,76 | 301 | 16,70 | |
| $L_2$ | 350 | 14,76 | 310 | 13,80 | |
| $L_1$-Co(II) | 392 | 7,28 | 305 | 15,54 | 14,5 |
| $L_2$-Co(II) | 402 | 8,97 | 310 | 17,62 | 4,3 |
| $L_1$-Ni(II) | 402 | 5,36 | 294 | 13,52 | 11,8 |
| $L_2$-Ni(II) | 415 | 6,86 | 307 | 14,78 | 7,7 |
| $L_1$-Cu(II) | 400 | 4,96 | 293 | 15,60 | 10,6 |
| $L_2$-Cu(II) | 403 | 5,05 | 298 | 18,75 | 9,8 |
| $L_1$-$UO_2$(II) | 432 | 3,08 | 312 | 14,88 | 19,8 |
| $L_2$-$UO_2$(II) | 436 | 3,28 | 324 | 14,14 | 19,7 |
| $L_2$-Cu(II)$Cl_2$ | 410 | 4,32 | 302 | 11,21 | 31,1 |
| $L_1$-$UO_2$(II)Ac | 438 | 3,53 | 310 | 16,05 | 26,7 |

(b) En milieu ammoniacal se forment des composés solides. Nous avons vérifié que ces phases solides sont, sauf celle de Co(II), salicylaldimine-complexes formées par réaction de l'ammoniac sur les complexes des bases de Schiff. Ces complexes ont été caractérisés par analyse élémentaire (Tableau 1) et spectroscopie ir (Tableau 3) où apparaît la bande caractéristique ν (NH) environ 3300 $cm^{-1}$.

Bien que nous n'ayons pas étudié le mécanisme de cette réaction de substitution d'amine il y aurait lieu de penser, suivant Nuñez et Eichhorn (11) que la réaction passe à travers d'une attaque nucléophilique de l'ammoniac sur le carbone azométhinique de la base de Schiff complexée avec l'ion métallique, alors la réaction a lieu grâce, d'une part, au fait que le $NH_3$ possède un caractère basique très supérieur à celui des 2-aminométhylpyridines (12, 13), et, d'autre part, à l'insolubilité des salicylaldimine complexes formés (équation [2]).

[2] 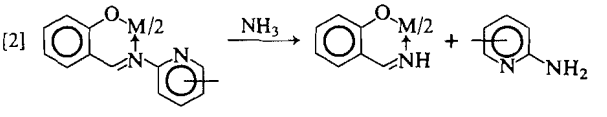

Dans le cas du cobalt la transformation ne se produit pas due, nous croyons, à la facile oxydation de celui-ci à cobaltiammines stables dont la présence a été détectée en essayant de synthétiser le complexe. Seul dans le cas où l'on ajoute une très petite quantité de $NH_3$ on obtient les complexes de Co(II) avec les bases de Schiff ci-dessus commentées, des complexes qui se dissolvent à nouveau dans un excès de $NH_3$.

(c) En milieu basique de NaOH on a obtenu des complexes avec les bases de Schiff à l'étude, avec des propriétés et stoechiométrie identiques aux isolés en milieu neutre. Ces complexes des bases de Schiff doivent être isolés très rapidement, car si on les laisse en digestion à 60°C, ils se transforment dans les correspondants oxydes métalliques comme il a été démontré en enregistrant le spectre ir qui a montré toute une absence de bandes dues au ligand, ainsi que la présence des bandes correspondantes aux oxydes. Pour NiO: 651m et 460m (litt. (14) 650m et 465s); CuO: 611m, 490s et 412m (litt.

TABLEAU 3. Assignations de bandes ir des complexes

| Composé | ν (OH) | ν (NH) | ν (C=O) | ν (C=N)$_{az}$ | ν (C=N)$_{py}$ | δ (OH) | δ (C—O) |
|---|---|---|---|---|---|---|---|
| $L_1$ | | | | 1614 s | 1595 s | 1275 s | 1143 m |
| $L_2$ | | | | 1608 s | 1586 s | 1282 s | 1142 m |
| $L_3$ | | | 1660 s | | 1623 s | 1275 s | 1147 m |
| $L_4$ | | 3238 s | | | | 1273 s | 1145 m |
| $L_1$-Co(II) | | | | 1602 s | 1590 s | — | 1140 s |
| $L_2$-Co(II) | | | | 1607 s | 1588 s | — | 1142 s |
| $L_3$-Co(II) | 3340 b | | 1645 s | | | — | 1152 s |
| $L_1$-Ni(II) | | | | 1603 s | [a] | — | 1145 s |
| $L_2$-Ni(II) | | | | 1606 s | 1592 s | — | 1145 s |
| $L_3$-Ni(II) | 3340 b | | 1645 s | | | — | 1152 s |
| $L_1$-Cu(II) | | | | 1607 s | 1588 s | — | 1148 s |
| $L_2$-Cu(II) | | | | 1606 s | 1585 s | — | 1142 s |
| $L_3$-Cu(II) | 3342 b | | 1647 s | | | — | 1154 s |
| $L_1$-$UO_2$(II) | | | | 1622 s | 1607 s | — | 1143 s |
| $L_2$-$UO_2$(II) | | | | 1610 s | 1598 s | — | 1143 s |
| $L_4$-Ni(II) | | 3295 s | | | 1625 s | — | 1142 s |
| $L_4$-Cu(II) | | 3305 s | | | 1621 s | — | 1142 s |
| $L_2$-Cu(II)$Cl_2$ | 3460 b | | | 1628 s | 1602 s | 1318 m | 1138 s |
| $L_1$-$UO_2$(II)Ac | | | | 1622 s | 1604 s | — | 1143 s |

[a]Celle-lá est comprise dans la bande large ν (C=N)$_{az}$.

610m, 500s et 410m); CoO: 650m, 570s, 465b (litt. 655s, 562s et 460b). En outre, l'analyse élémentaire a été réalissée; calculée: CuO 79,88, NiO 78,58, CoO 78,65; trouvée: CuO 79,41, NiO 78,06, CoO 78,47.

On n'obtient pas dans ce cas les salicylaldéhydocomplexes qui proviendraient de l'attaque nucléophilique du $OH^-$ au carbone azométhinique, puisqu'on a vérifié que ces complexes sont instables en dit milieu basique en se dissolvant et en précipitant les cations métalliques tels des oxydes (équation [3]).

[3] 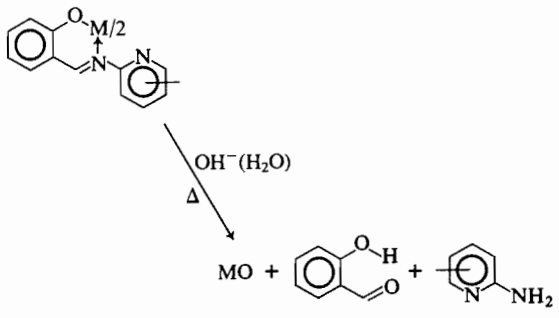


Il faut remarquer d'une manière spéciale (cela a été déjà fait dans la publication précédente (1)) la réaction avec $UO_2$(II) car elle revêt des caractéristiques spéciales. Elle provoque avec les deux réactifs en milieu neutre des phases solides couleur orange. Nous avons montré que tels solides sont les complexes (4-MPSI)$_2UO_2$ et (6-MPSI)$_2UO_2$, lesquels diffèrent remarquablement dans leur solubilité, car tandis que le dérivé de la 4-MPSI est insoluble, celui de la 6-MPSI est relativement soluble. On a déterminé la constante du produit de solubilité de (4-MPSI)$_2UO_2$, par des mesures conductimétriques dans l'eau (conductance molaire à dilution infinie de l'anion de 4-MPSI 80,4 $ohm^{-1}$ $cm^2$ $mol^{-1}$) qui résulte de $1,3 \pm 0,1 \times 10^{-15}$. Si l'on tient compte du fait que la solubilité molaire du complexe est insignifiante, la solubilité ionique présente une valeur de $7 \times 10^{-6}$ mol $L^{-1}$.

D'ailleurs, le spectre ir des uranylcomplexes, de même que les autres complexes, ne montre pas les bandes ν (OH) et δ (OH). D'autre part, les ν (C=N) pyridinique et azométhinique se déplacent, dans ce cas, en sens inverse, bien qu'avec une magnitude pareille à celle des autres complexes étudiés, où ν (C=N) azométhinique varie davantage que la ν (C=N) pyridinique. Tel qu'il a été indiqué par quelques auteurs (15, 16) ce fait peut se rapporter à une diminution de l'ordre de liaison du groupe C=N, dû à la haute électronégativité des oxygènes du $UO_2$(II). Il y a lieu de penser aussi que cette diminution de l'ordre de liaison est compensée par une stabilisation des cycles formés par le $UO_2$(II) avec la base de Schiff, ce qui est d'accord avec les données fournies par Geary *et al.* (3), lesquelles prouvent que la constante de stabilité du complexe $UO_2$(II) – 2-pyridylsalicylaldimine est plus grande que celle des complexes de Cu(II), Co(II), et Ni(II) ($\log K_1 = 8,1$ face à 7,3, 5,3 et 4,9 respectivement).

Il est à remarquer, par ailleurs, que tandis que le composé (4-MPSI)$_2UO_2$ ne s'altère pas par digestion, le dérivé de la 6-MPSI se transforme en un autre solide jaune qui, d'après les données suivantes, est $UO_3 \cdot 2H_2O$ (% U calculé: 73,91; trouvé: 73,52). L'analyse thermique indique la présence de

deux molécules d'éau (% $H_2O$ calculé: 11,19; trouvé: 10,97). Le spectre ir ne présente pas les bandes correspondants au ligand organique, tandis qu'il présente les bandes correspondantes à $UO_3$ ($\nu_1 = 840\,cm^{-1}$ et $\nu_3 = 935\,cm^{-1}$ (14)). La diffraction de rayons X montre un diagramme dont les lignes fondamentales apparaissent à 7,25 (*I/I* 100), 3,21 (50) et 3,35 (40), ce qui s'accorde avec ce qui a été indiqué par Debets et Loopstra (17) pour le $UO_3 \cdot 2H_2O$ dans sa forme β (orthorhombique).

Cette réaction de démolition du complexe pourrait être représentée par la équation [4].

[4] 2 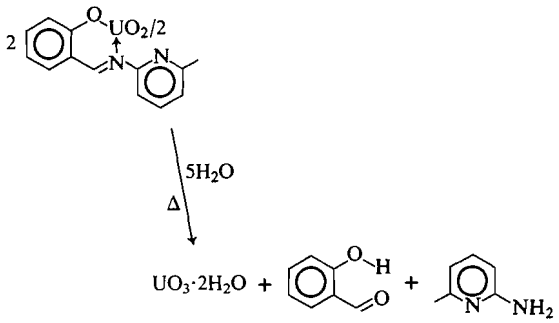


2. *Milieu éthanolique*

En ce milieu on a obtenu le complexe (6-MPSI)-$CuCl_2$, composé non électrolyte et dont le spectre ir montre, en outre des bandes déjà commentées, une à 3460 $cm^{-1}$ due à ν (OH) et une autre à 1318 $cm^{-1}$ de δ (OH), ce qui indique que le groupe phénolique se coordonne, dans ce cas, sans perdre son proton.

On a synthétisé les complexes de $UO_2$(II) à partir de $UO_2(NO_3)_2$, et prouvé qu'ils ne sont pas des électrolytes avec stoechiométrie 2:1 et spectre ir identiques à ceux obtenus en milieu hydroalcoolique. Le complexe de $UO_2$(II) obtenu à partir du $UO_2(CH_3—COO)_2$ répond à la formule (6-MPSI)-$UO_2(CH_3—COO)$, il n'est pas un électrolyte et ne présente pas la bande ν (OH) ni δ (OH).

## Discussion

En milieu hydroalcoolique il y a lieu de déduire que 4-MPSI et 6-MPSI agissent comme des ligands bidentés s'enchaînant à travers du nitrogène azométhinique et l'oxygène phénolique, après avoir fait une déprotonnation des réactifs. Cela prouve, à notre avis, la disparition des fréquences ν (OH) et δ (OH) du réactif dans le spectre ir des complexes, ainsi que la légère variation de la ν (C=N) pyridinique par complexation, excepté les complexes de $UO_2$(II) où l'on observe une plus grande variation, laquelle est du même ordre que celle que l'on remarque pour la ν (C=N) azométhinique. Cependant nous ne pensons pas que le ligand agisse comme tridenté face au $UO_2$(II), puisque la variation de la ν (C=N) pyridinique malgré tout est petite (12 $cm^{-1}$) en comparaison avec les 50 $cm^{-1}$ de variation trouvés par Garnovsky *et al.* (4) pour le complexe Ti(2-pyridylsalicylaldimine)$Cl_4$.

Les résultats obtenus des titrages conductométriques en ce milieu s'accordent avec les stoechiométries attribuées aux complexes solides (2:1) et l'on trouve en plus ceux de stoechiométrie 1:1 (Fig. 1).

Dans de l'éthanol absolu le groupe OH agit comme coordonnant, c'est-à-dire sans se déprotoner préalablement. Voilà ce qui est déduit des données citées avant et qui s'accorde avec les données trouvées par Mahmoud et El-Haty (7) dans leur étude des complexes de la 2-pyridylsalicylaldimine avec plusieurs ions métalliques. Les complexes de $UO_2$(II) obtenus en ce milieu, où l'on remarque que la groupe phénolique subit toujours une déprotonation, sont un cas à part.

Il y a une influence du sel de $UO_2$(II) dès le debut sur le complexe obtenu. Si l'on part de $UO_2(NO_3)_2$ le complexe est de stoechiométrie 2:1. Par contre l'emploi de $UO_2(CH_3—COO)_2$ en provoque un de stoechiométrie 1:1. Ces stoechiométries ont été

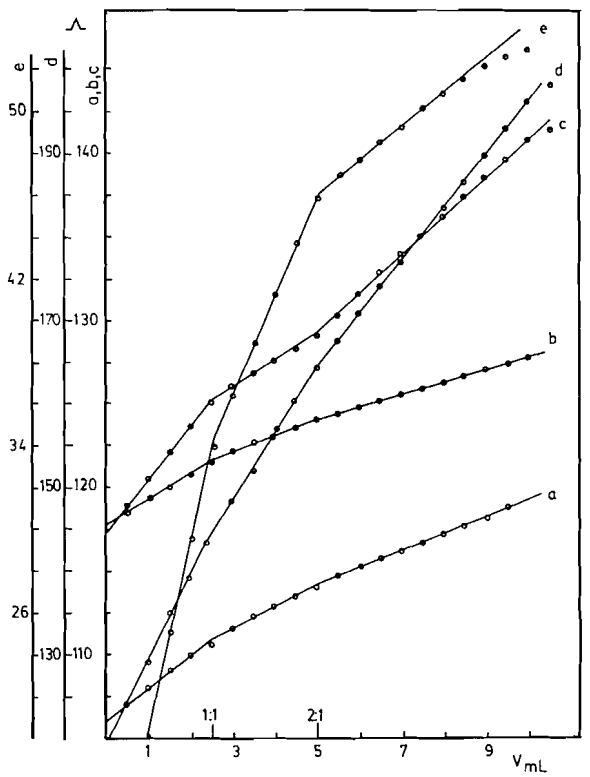


FIG. 1. Titrages conductimétriques en milieu hydroalcoolique 50%. [Me] = $10^{-3}$ *M*; [L] = $10^{-2}$ *M*; T = 25°C ± 0,1. a: Ni(II), b: Co(II), c: $UO_2$(II) ($NO_3^-$), d: Cu(II), e: $UO_2$(II) ($CH_3—COO^-$).

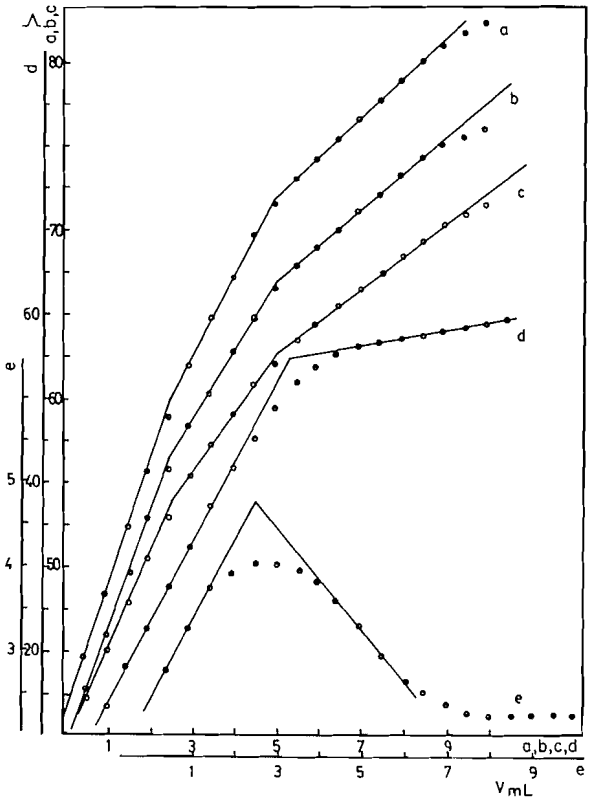


FIG. 2. Titrages conductimétriques en milieu éthanolique. [Me] = $10^{-3}M$; [L] = $10^{-2}M$; T = 25°C ± 0,1. a: Cu(II), b: Ni(II), c: Co(II), d: $UO_2$(II) ($NO_3^-$), e: $UO_2$(II) ($CH_3$—$COO^-$).

conformées au moyen d'une titration conductimétrique (Fig. 2). La structure de ce dernier complexe ne peut s'expliquer qu'en acceptant que le ligand agisse comme tridenté, hypothèse peu vraisemblable car cela supposerait une structure octaédrique avec une tension remarquable ou bien que l'acétate agisse comme ligand bidenté. À l'appui de cette dernière hypothèse nous trouvons que la ν (C═O) de la groupe acétate apparaît à 1527 $cm^{-1}$ et la ν (C—O) à 1436 $cm^{-1}$, c'est un déplacement à des fréquences plus petites que la première (1560 $cm^{-1}$ en acétate libre) et à des fréquences plus grandes que la deuxième (1416 $cm^{-1}$), ce qui suppose une différence entre les deux fréquences dans le complexe de 91 $cm^{-1}$, ce qui s'accorde avec les données présentées par Itoh et Berstein (18), qui trouvent une différence entre les deux fréquences de l'ordre de 80 $cm^{-1}$ dans la façon d'agir comme ligand bidenté de l'acétate et de l'ordre de 250 $cm^{-1}$ lorsqu'il agit comme monodenté.

Ces données contredisent les résultats obtenus par Mahmoud et El-Haty (7) pour le complexe de $UO_2$(II) avec 2-pyridylsalicylaldimine, puisqu'ils indiquent que la groupe se coordonne sans le perte de $H^+$.

On n'a observé qu'une influence de la différente position de la groupe méthyl avec la solubilité des complexes, les complexes de 4-MPSI étant dans tous les cas plus insolubles. Ces différences de solubilité ont été également observées dans les bases de Schiff et amines dès le commencement.

*Applications analytiques*

On propose l'emploi de ces réactifs pour l'analyse gravimétrique de $UO_2$(II) et Ni(II).

1. La détermination de $UO_2$(II) se réalise moyennant 4-MPSI (entre 0,07 et 0,2 g de U) en agissant à pH 3–5 ajusté avec $HNO_3$ et précipitant et pesant comme $(4\text{-MPSI})_2UO_2$ après avoir séché à 105–110°C (facteur gravimétrique 0,3437). L'erreur relative de la détermination est 0,1% et le nombre d'interférences petit, et celle de Fe(III) et Pd(II) se remarquent.

2. La détermination de Ni(II) (entre 0,015 et 0,075 g de Ni) se réalise moyennant 6-MPSI en milieu ammoniacal, ce qui suppose une précipitation homogène (par synthèse *in situ* de la salicylaldimine qui est le réactif de précipitation), en pesant à l'état de bissalicylaldiminate de Ni(II) (facteur gravimétrique 0,1905). L'erreur relative de la détermination est 0,14% et réduit le nombre d'interférents dont nous remarquons Co(II), Cu(II) et $UO_2$(II).

## Conclusions

1. On observe une influence remarquable du milieu dans la façon d'agir des bases de Schiff 4-MPSI et 6-MPSI. En milieu hydroalcoolique les ligands se coordonnent comme des anions avec les ions métalliques étudiés à travers du N azométhinique et le O phénolique après avoir perdu le proton. En milieu éthanolique ils s'enchaînent à travers du N azométhinique et le OH phénolique sans déprotonation préalable, excepté dans le cas du $UO_2$(II) où la coordination a lieu comme en milieu hydroalcoolique.

2. Les complexes tendent à réagir avec des substances présentes au milieu hydroalcoolique en provoquant des composés plus stables.

3. Le complexe de 4-MPSI avec $UO_2$(II) et le produit de réaction de Ni(II) avec 6-MPSI peuvent être utilisés comme des méthodes analytiques pour la détermination gravimétrique de ces ions.

## Remerciement

Ce travail a été traduit par le Prof. J. J. Arnedo.

1. L. F. CAPITÁN-VALLVEY, F. SALINAS, L. CUADROS et C. JIMÉNEZ. Can. J. Chem. **60**, 000 (1982).
2. J. CSÁSZÁR et J. BALOG. Acta Chim. Acad. Sci. Hung. **87**, 321 (1975).
3. W. J. GEARY, G. NICKLESS et F. H. POLLARD. Anal. Chim. Acta, **27**, 71 (1962).

4. A. D. GARNOVSKII, V. I. MINKIN, O. A. OSIPOV, V. T. PANYUSHKIN, L. K. ISAEVA et M. I. KHYAZHANSKII. Zh. Neorg. Khim. **12**, 2443 (1967).
5. D. SH. VERKHOVODOVA et M. I. KHYAZHANSKII, Zh. Neorg. Khim., **12**, 1549 (1967).
6. Z. HOLZBECHER et H. VAN TRUNG. Collect. Czech. Chem. Commun. **41**, 1506 (1976).
7. M. R. MAHMOUD et M. EL-HATY. J. Inorg. Nucl. Chem. **42**, 349 (1980).
8. P. TEYSSIE et J. J. CHARETTE. Spectrochim. Acta, **19**, 1407 (1963).
9. O. H. WHEELER et P. H. GORE. J. Chem. Soc. 3298 (1961).
10. S. S. LIAPINA et coll. Dokl. Acad. Nauk SSSR, **190**, 3 (1970).
11. L. J. NUÑES et G. L. EICHHORN. J. Chem. Soc. **78**, 1137 (1963).
12. H. S. VERTER et A. E. FROST. J. Am. Chem. Soc. **82**, 85 (1960).
13. E. L. OLSZEWSKI et D. F. MARTIN. J. Inorg. Nucl. Chem. **27**, 345 (1965).
14. J. R. FERRARO. Low frequency vibration of inorganic and coordination compounds. Plenum Press. New York. 1971.
15. D. H. BUSCH et S. C. BAILAR, JR. J. Am. Chem. Soc. **78**, 1137 (1956).
16. V. A. KOGAN, O. A. OSIPOV, V. I. MINKIN et V. P. SOKALOV. Zhur. Neorg. Khim. **15**, 678 (1970).
17. P. C. DEBETS et B. O. LOOPSTRA. J. Inorg. Nucl. Chem. **25**, 945 (1963).
18. K. ITOH et H. J. BERNSTEIN. Can. J. Chem. **34**, 170 (1956).

# An infrared study of the photoisomerization of *N*-benzylideneaniline

J. W. LEWIS AND C. SANDORFY

*Département de Chimie, Université de Montréal, Montréal (Qué.), Canada H3C 3V1*

Received August 25, 1981

J. W. LEWIS and C. SANDORFY. Can. J. Chem. **60**, 1720 (1982).

The infrared spectra of Nujol solutions and thin polycrystalline films of *N*-benzylideneaniline have been investigated. The 313 nm irradiation of ambient temperature samples produces no observable changes in the infrared spectra, however, similar irradiation of samples maintained at 77 K results in spectral changes that are thermally and photochemically reversible. The infrared spectra of low temperature irradiated samples are interpreted in terms of *trans* → *cis* photoisomerization.

J. W. LEWIS et C. SANDORFY. Can. J. Chem. **60**, 1720 (1982).

Les spectres infrarouges de l'*N*-benzylideneaniline en solution dans le Nujol ont été examinés. L'irradiation à 313 nm à la température ambiante ne produit aucun changement observable dans le spectre ir; cependant à 77 K cette irradiation provoque des changements qui sont réversibles thermiquent aussi bien que photochimiquement. Ce dernier spectre est interprété en termes d'une photoisomérisation *trans* → *cis*.

## Introduction

Despite some early doubts (1) as to the existence of more than one stable geometric form of anils or of other compounds that contain the carbon–nitrogen double bond, the experimental evidence is now overwhelmingly supportive of at least two stable geometric isomers. Kuhn and Weitz (2) proposed that a *syn* ⇌ *anti* photoisomerization about a carbon–nitrogen double bond was reponsible for reversible color changes which result from the irradiation of triphenylformazan. Fisher and Frei (3) have demonstrated beyond any doubt that reversible ultraviolet spectral changes result from the irrradition of low temperature solutions of *N*-benzylideneaniline and *N*-(1-naphthylidene)-1-naphthylamine. These authors proposed that the observed, reversible spectral changes were due to a *trans* → *cis* photoisomerization with respect to the C=N bond. Following this pioneering work, there have been several studies (4–7) of the phenomenon by means of ultraviolet absorption and nuclear magnetic resonance techniques. Other groups (8, 9) have studied the thermal *trans–cis* isomerization and have reported activation energies of 61.0 to 78.6 kilojoules per mole.

In addition to the above studies of the *trans–cis* isomerization, there have been others (10–17, and references therein), both theoretical and experi the structure and conformation of Schiff bases. the structure and confrontation of Schiff bases. There has been some controversy regarding the planarity of *N*-benzylideneaniline, but it now appears certain that the aniline nucleus is twisted with respect to the plane of the remainder of the molecule. X-ray analysis (18) indicates that the angle of twist, $\theta_n$, is near 55.1° for *N*-benzylideneaniline. By

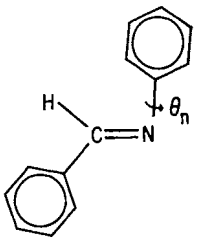


means of photoelectron spectroscopy, Bally *et al.* (19) estimate $\theta_n$ as 36° and, by means of gas phase electron diffraction, Traetteburg *et al.* (20) have determined that $\theta_n$ equals 52°. Akaba *et al.* (12, 13) estimate a solution phase $\theta_n$ of 30–35° and a gas phase $\theta_n$ of 48–55°.

The thermally stable form of *N*-benzylideneaniline is reported to be the *trans* form (18–21). As outlined above, a wealth of ultraviolet spectral changes regarding the *trans* → *cis* photoisomerization is available in the literature. More recently, Maeda *et al.* (5) have observed nuclear magnetic resonance spectral changes following the irradiation of suitably cooled solutions of substituted *N*-benzylideneanilines. These authors reported that the *cis*-isomer of the parent compound was unstable at the temperature of the experiments, −70°C. It was, however, found to be stable at −100°C in agreement with the results of Fischer and Frei (3).

In the present work, the vibrational spectral changes which result from the photoisomerization of *N*-benzylideneaniline will be considered. The interpretation of the new infrared spectrum provides additional insight towards the actual geometric changes that result from photoisomerization and complements that provided by other physical

0008-4042/82/131720-07$01.00/0

©1982 National Research Council of Canada/Conseil national de recherches du Canada

Can. J. Chem. Downloaded from www.nrcresearchpress.com by 210.87.254.42 on 09/06/12
For personal use only.

Can. J. Chem. Downloaded from www.nrcresearchpress.com by 210.87.254.42 on 09/06/12
For personal use only.

methods. In addition, spectral evidence that *N*-benzylideneaniline crystallizes from melts in both the *trans*- and *cis*-conformations is presented. The *trans* is the dominant isomer in melt derived crystals and is even more dominant in low temperature Nujol solutions.

## Experimental

*N*-Benzylideneaniline was prepared by mixing anhydrous ethanol solutions containing equimolar quantities of benzaldehyde and aniline. The anil was then purified by recrystallization in anhydrous ethanol and by careful fractional sublimation.

The source used for the irradiation of the anils was an Oriel Model 7340 equipped with a 200 W medium pressure mercury arc. The irradiation wavelengths were isolated by means of an Oriel Model 7240 monochromator. The bandwidths of the excitation lines were approximately 20 nm, according to the manufacturer's specifications.

The low temperature infrared cell was constructed after the pattern described by Wagner and Hornig (22). The infrared spectra were recorded by means of a Perkin Elmer 621 Spectrometer. The spectra were recorded from samples in the form of thin polycrystalline films and of Nujol solutions. In both cases the samples were held between sodium chloride plates. The frequency scales of the spectra are calibrated to that of a thin polystyrene film.

It should also be pointed out that the reported Nujol solutions are true solutions, not mulls. Despite the polar nature of this compound, a solution, 0.35 molar in *N*-benzylideneaniline, in Nujol was easily attained at room temperature. A thin film of this solution, when cooled to 77 K, showed no signs of crystallization.

## Results and discussion

The 1750 to 1550 $cm^{-1}$ region of the infrared spectrum of a Nujol solution of *N*-benzylideneaniline is reproduced in Fig. 1 (for reference purposes, a listing of previously assigned vibrational bands in the infrared spectra of *N*-benzylideneaniline and related compounds is provided in Table 1). Quite clearly, irradiation of the low temperature solution produces substantial changes in this region of the spectrum. The spectral changes produced by irradiation at 313 nm are reversible by re-irradiation at longer wavelengths. The amount of the second form present at the photostationary state depends on the wavelength of irradiation and a definite photostationary state is reached at each wavelength (3). Maeda *et al.* (5) indicate that 85% of the *cis*-isomer of *N*-benzylideneaniline is present at the photostationary state (methylcyclohexane solution, −100°C and irradiation at 313 nm). Therefore, if the sample temperature is maintained at or below −100°C and if irradiation is begun, then a certain percentage of each isomer is always present. The amount of each isomer present at the photostationary state is dependent solely on the ratio of the molar absorptivities of the *trans*- and *cis*-isomers at the wavelength of excitation, provided, of course, that other experimental conditions are equal. Apparently there is not a wavelength at which one isomer absorbs exclusively. The phenomena are illustrated by the curves reproduced in Fig. 1. The shoulder at the high frequency side of the C=N stretching band of the nonirradiated sample indicates that some of the *cis*-isomer may be present in Nujol solutions at liquid nitrogen temperature.

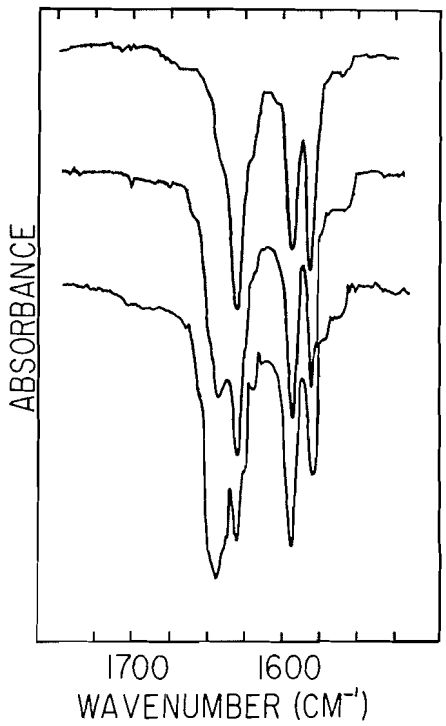


FIG. 1. The 1700–1500 $cm^{-1}$ region of the infrared spectra of a 0.35 *M* solution of *N*-benzylideneaniline in Nujol maintained at 77 K. Upper, nonirradiated solution; middle, after an intermediate period of irradiation (2–3 hours); and lower, after a long period of irradiation (5 hours).

The new infrared band at 1642 $cm^{-1}$ which appears upon irradiation of the sample is assigned as the C=N stretching of the *cis*-isomer of *N*-benzylideneaniline. The fact that the C=N stretching of the *cis*-isomer occurs at higher frequency than does the *trans*-isomer is perhaps surprising. For the central C=C stretching of stilbene and other substituted ethylenes, the opposite effect is found. Freeman (28) lists frequencies of 1629 $cm^{-1}$ for *cis*-stilbene and 1648 $cm^{-1}$ for *trans*-stilbene. On the contrary, the carbonyl stretching of 3-penten-2-one shows an effect similar to that of *N*-benzylideneaniline. The *trans*-isomer has the lower fre-

Can. J. Chem. Downloaded from www.nrcresearchpress.com by 210.87.254.42 on 09/06/12
For personal use only.

TABLE 1. Assigned vibrations of *N*-benzylideneanilines

| Vibration | Frequency ($cm^{-1}$) | Reference |
|---|---|---|
| νC=N | 1631 | 23 |
| νC=N | 1631 | 24 |
| νC—H (azomethine) | 2890 (2865 sh) | 24 |
| δC—H (out-of-plane, azomethine) | 872 | 24 |
| ν ring* | 1612–1605 | 24 |
| νAr—N | 1191 | 25 |
| δC—N (in-plane, azomethine) | 976 | 25 |
| C—H (out-of-plane, azomethine) | 873 | 25 |
| νC=N | 1625 | 26 |
| ν ring | 1591 | 26 |
| ν ring + C=N | 1578 | 26 |
| ν C=N † | 1625–1576 | 27 |
| νAr—N† | Two bands in 1375–1475 $cm^{-1}$ range | 27 |
| C=N—C† | Two bands (891–919) and (830–877 $cm^{-}$) | 27 |

*This band was found to increase in relative intensity with increasing basicity of the nitrogen, whereas the C=N band at 1631 $cm^{-1}$ was found to decrease in intensity with increasing basicity.
†These assignments are for a related compound, *N*-(2-hydroxybenzylidene)-4′-toluidine and the assignments are based on the results of $^{15}N$-labelling experiments.

quency, 1674 $cm^{-1}$, as compared to 1693 $cm^{-1}$ for the *cis*-isomer (29, 30).

In Fig. 1 it should also be noted that the lower frequency "aromatic" band at 1579 $cm^{-1}$ is the more intense of the two bands in the nonirradiated, low temperature solution spectrum. This band dramatically decreases in intensity as the intensity of the 1642 $cm^{-1}$ band increases. In some of our experiments this band has been observed to decrease to less than one-seventh its original intensity, indicating that there is perhaps greater than 80% conversion to the *cis*-isomer.

Percy and Thornton (27), in their $^{15}N$-labelling study, have associated the lower frequency of the two "aromatic" bands with the C=N stretching of *N*-(2-hydroxybenzylidene)aniline since it appeared to be more vibrationally pure than did a band at 1625$cm^{-1}$, ($\Delta\nu = -8\,cm^{-1}$ compared to $\Delta\nu = -5\,cm^{-1}$). In the present work, the 1579 $cm^{-1}$ band of *N*-benzylideneaniline is to be associated with the 1576 $cm^{-1}$ of *N*-(2-hydroxybenzylidene)aniline discussed by Percy and Thornton. This seems reasonable since the two molecules are structurally very similar.

The relative intensities and positions of the three bands in the 1700–1500 $cm^{-1}$ region need some elaboration. For the *trans* form the bands are at 1628, 1595, and 1579 $cm^{-1}$. The first one is naturally assigned to the C=N stretching vibration, the two others to the well-known phenyl ring vibrations. Under the given conditions these vibrations cannot be "pure" group frequencies. Indeed in previous studies (26, 27) of anils, as well as in the present study, there is substantial evidence for coupling of the C=N and a phenyl group vibration. A consequence of this coupling is likely to be a shift to higher frequency of the C=N band. Furthermore, since the C=N group is a part of an extended conjugated system its force constant is lowered by interaction with the π systems of the two phenyl rings. Conjugation would perhaps put the C=N stretching frequency as low as 1615 $cm^{-1}$ but mechanical coupling makes it appear at 1628 $cm^{-1}$. After *trans* → *cis* photoisomerization the aniline ring will tilt out of the plane of the benzaldehyde moiety (see below). This must greatly diminish the extent of conjugation as well as mechanical coupling. The first effect should raise the C=N frequency while the second one would lower it. The result, 1642 $cm^{-1}$, observed for the *cis*-isomer is surprisingly high and makes one think that mechanical coupling is less important than has been presumed. (In examples of mechanical coupling it is usually assumed that one of the vibrations is raised to higher frequency and the other is lowered; so the higher frequency must come down if coupling is suppressed.)

In this respect it should be remembered that the phenyl bands near 1600 $cm^{-1}$ constitute a well-known case of Fermi resonance (see Herzberg (31), p. 364). In benzene itself, in the vapor state, the Raman active $\nu_{16}$ fundamental ($e_{2g}$) is at 1584.8 $cm^{-1}$ while the $\nu_2 + \nu_{18}$ ($E_{2g}$) combination band is 1606.4$cm^{-1}$ ($\nu_2$: 991.6 $cm^{-1}$ ($a_{1g}$); $\nu_{18}$: 605.6 $cm^{-1}$ ($e_{2g}$)). The anharmonic (Fermi) resonance of the fundamental and the combination, both of $e_{2g}$ symmetry, is inherited by most benzene derivatives. In *N*-benzylideneaniline the relative intensities of the bands at 1595 and 1579 $cm^{-1}$ are probably greatly influenced by this Fermi resonance. (One might try to assign one of these bands to the aniline ring and the other to the benzaldehyde ring but in

Can. J. Chem. Downloaded from www.nrcresearchpress.com by 210.87.254.42 on 09/06/12
For personal use only.

view of the above this would be probably naive. The degree of contribution of the two rings to the intensities of the bands is probably different, however.) Furthermore, in view of the mechanical (harmonic) coupling of the C=N and phenyl motions there is likely to be a significant amount of anharmonic coupling between the C=N and phenyl fundamentals in this part of the spectrum giving rise to Fermi resonance involving the three bands. Finally, the relative intensities of the three bands will depend on (a) the extent of conjugation and coplanarity; (b) mechanical coupling; and (c) Fermi resonance.

Now, it is hard to see how the spectacular decrease in the intensity of the 1579 $cm^{-1}$ band upon *trans* → *cis* photoisomerization together with the 1628 → 1642 $cm^{-1}$ increase can be explained on the basis of mechanical coupling only. In itself it would *lower* the C=N frequency; the loss of coplanarity and conjugation might go some way in raising the frequency of the 1628 $cm^{-1}$ band and decreasing the intensity of the 1579 $cm^{-1}$ band; the raising of the frequency to 1642 $cm^{-1}$ could spoil conditions for Fermi resonance making the 1579 $cm^{-1}$ band lose much of its intensity borrowed from the C=N band.

In Fig. 2 the partial spectra (1250–650 $cm^{-1}$) of irradiated and nonirradiated low temperture Nujol solutions of *N*-benzylideneaniline are reproduced. The spectral changes observed here parallel those shown in Fig. 1. They are also reversible in that they may be erased by re-irradiating the sample at longer wavelengths. In both regions the spectral changes may then safely be identified with the *trans* → *cis* photoisomerization product and not with one or more photochemical degradation products. Samples that have been cycled as many as twenty times show no spectral evidence of irreversible photochemical decomposition. These observed spectral changes may also be erased by allowing the sample temperature to rise to the neighbourhood of −78°C.

In Fig. 2, it is interesting to note that the Ar—N stretching band of *trans*-*N*-benzylideneaniline at 1191 $cm^{-1}$ moves to higher frequency in the spectrum of the *cis*-isomer (1206 $cm^{-1}$). The +15 $cm^{-1}$ shift is very similar to that observed for the C=N vibration. On the other hand, the C—H deformation bands of the azomethine group are shifted to lower frequency in the spectra of the *cis*-isomer. The in-plane deformation band shifts from 976 to 956 $cm^{-1}$ and the out-of-plane deformation band shifts from 873 to 845 $cm^{-1}$. The latter assignment is somewhat tentative since there is also a band that develops at slightly higher frequency than that of

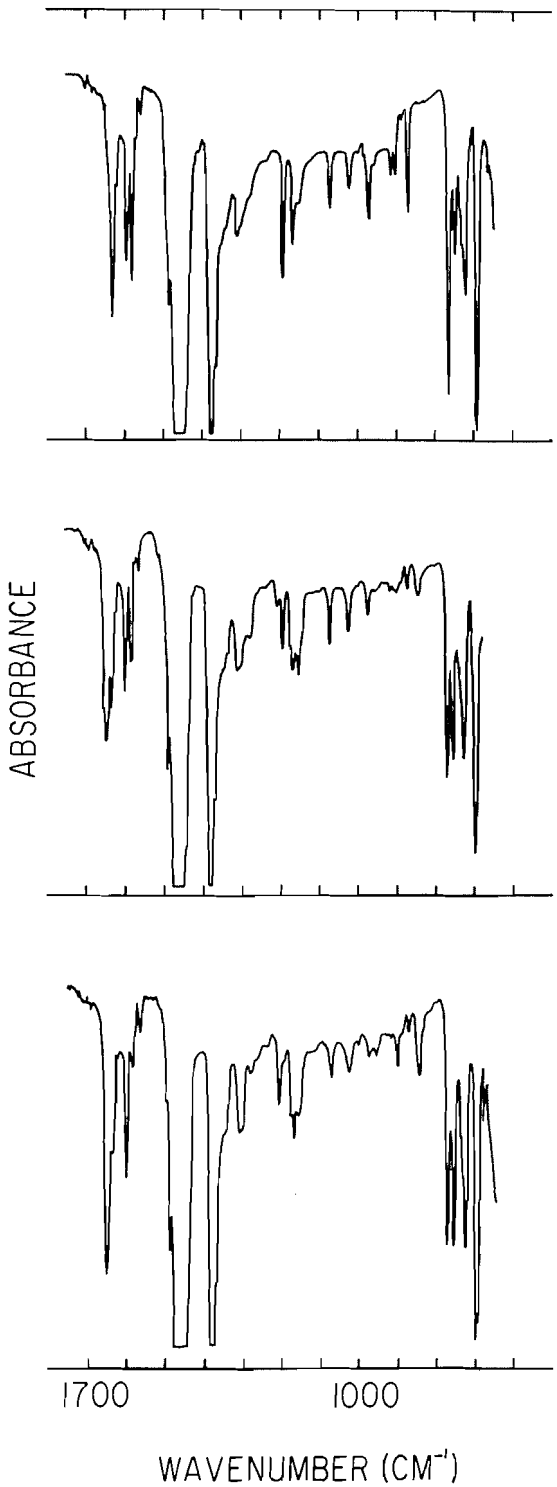


FIG. 2. The 1700–650 $cm^{-1}$ region of the infrared spectra of a 0.35 *M* solution of *N*-benzylideneaniline in Nujol maintained at 77 K. Upper, nonirradiated solution; middle, after a long period of irradiation (5 hours); and lower, photostationary state.

Can. J. Chem. Downloaded from www.nrcresearchpress.com by 210.87.254.42 on 09/06/12
For personal use only.

the out-of-plane deformation band of the *trans*-isomer.

The spectral changes that are observed in Fig. 2 are also explicable in terms of a *trans* → *cis* isomerization. It has been argued that when the *N*-benzylideneaniline molecule assumes the *cis*-conformation the aniline ring is further out of the plane of the remainder of the molecule. As the angle of twist increases, the conjugation of the aniline ring and the C=N group is lost. This results in a shortening of the C=N bond. The stretching frequency of the C=N is thereby increased to the point that Fermi resonance is no longer possible. (The arguments regarding the angle of twist, θ, are not meant to imply that the increase in non-coplanarity is achieved by means of a rotation about the C=N single bond. Various authors (7, 9) have successfully demonstrated that the *cis*-isomer is produced by means of an inversion at the nitrogen.)

The increase in non-coplanarity of the aniline ring also provides for more effective participation of the nitrogen lone pair (9). This participation increases the Ar—N bond order, as is indicated by the shift of the infrared absorption band to higher frequency. The increased participation of the nitrogen lone pair of the *cis*-isomer should result in decreased basicity, as has been proposed (9). It

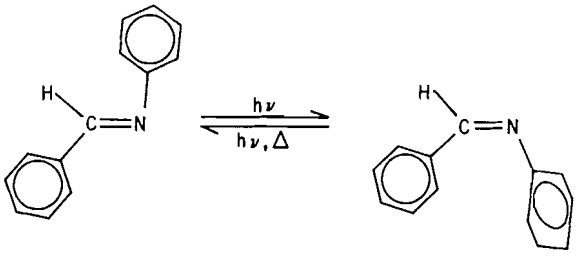


also results in a change in the direction and magnitude of the dipole moment (8, 9, 32).

It has been noted that the azomethine C—H deformation frequencies are lower for the *cis*-isomer. The C—H stretching frequency is not affected by *trans* → *cis* isomerization; hence it seems reasonable that the lowering of the deformation frequencies of the azomethine C—H is due to the removal of steric repulsions (5) between the azomethine hydrogen and the *ortho* hydrogen of the aniline ring. This further substantiates the argument that the aniline ring of the *cis*-isomer is further out of the molecular plane than it is in the *trans*-isomer.

In a study of a related compound, *p*-chlorobenzophenone methylimine, Curtin and Hausser

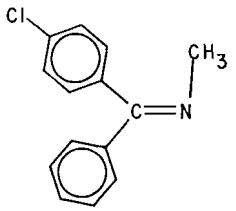


(33) have found some interesting results. This compound crystallizes as the *cis*-isomer (*cis* refers to the relative positions of the methyl group and the *p*-chlorophenyl group). If the crystals are held at 125°C for 15 min or if cyclohexane solutions of the compound are allowed to stand at room temperature for two weeks, the corresponding infrared spectra indicate a mixture of the *cis*- and *trans*-isomers. The C=N stretching band at 1620 $cm^{-1}$ did not change upon isomerization but two other infrared bands showed a definite shift. A sharp band at 693 $cm^{-1}$, which is assigned as a vibration of a monosubstituted phenyl group (34), decreased in intensity upon standing of the solution and another band developed at 701 $cm^{-1}$. A second sharp band located at 827 $cm^{-1}$, which is assigned as the C—H deformation of the *p*-chlorophenyl ring (34), decreased in intensity upon standing of the solution and another band developed at at 837 $cm^{-1}$.

Although the vibrational assignments in the 800–650 $cm^{-1}$ region of the spectrum of *N*-benzylideneaniline have not been made, it is of interest to compare the results of the present experiments to those of Curtin and Hausser. In Fig. 2 it is noted that a very strong band is located at 695 $cm^{-1}$. There is some indication that the intensity of this band varies with 313 nm irradiation of these solutions, but the changes are within the limits of error of these experiments. At somewhat higher frequencies two bands are apparent. In the spectrum of nonirradiated Nujol solutions the higher frequency band at 768 $cm^{-1}$ is the most intense. This 768 $cm^{-1}$ band decreases in intensity and the band at 749 $cm^{-1}$ increases with the irradiation of the samples. In keeping with previous assignments in this study, the higher frequency band is assigned as an absorption of the *trans*-isomer and the lower frequency band is assigned as a vibration of the *cis*-isomer.

Changes in the aromatic C—H deformation frequency of the aniline portion of the molecule are entirely expected. It has been argued that the conformation of the *cis*-isomer leads to favorable interaction of the nitrogen lone pair with the aniline ring and to a lessening of steric repulsions. It is

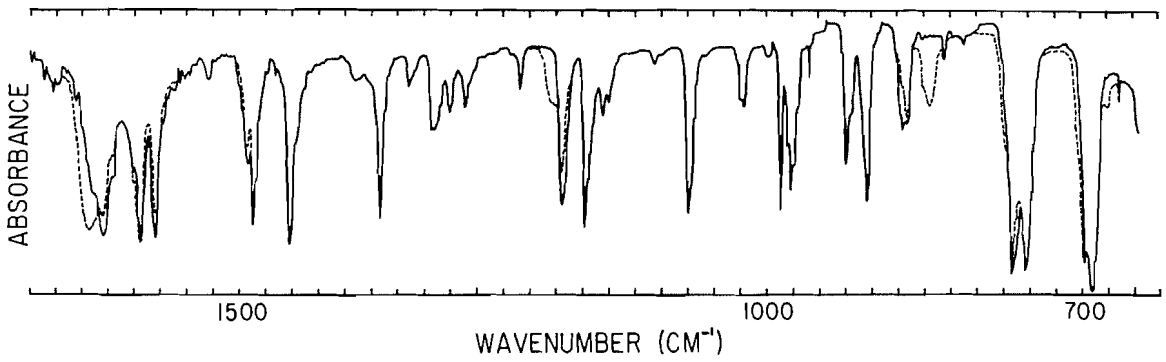


FIG. 3. The 1700–650 $cm^{-1}$ region of the infrared spectra of a thin polycrystalline film of *N*-benzylideneaniline maintained at 77 K. The solid line indicates absorption prior to irradiation and the broken line indicates changes in absorption after 5 hours of irradiation at 313 nm.

believed that these interactions result in a net lowering of the aniline C—H deformation frequency. In this respect the present interpretation is in line with that of Curtin and Hausser. These authors expected to observe a lower frequency for the *cis*-isomer of *p*-chlorobenzophenone methylimine but, when the opposite effect was observed, they concluded that there were no favorable lone pair – ring interactions.

All the effects of *trans* → *cis* photoisomerization on the infrared spectrum of Nujol solutions of *N*-benzylideneaniline are also observed in the spectrum of thin polycrystalline films maintained at low temperature. These spectra are reproduced in Fig. 3. As might be expected, these changes are less well defined than are those in the solution spectra. This depends, among others, on *cis–trans* ratios. Apparently the quantum yield of photoisomerization is lower in the solid state so that prolonged irradiation times would be necessary in order to achieve the same *cis–trans* ratio that is observed in the solution spectra.

In Fig. 3 it is evident that some spectral changes occur in the 1550–1350 $cm^{-1}$ region that is obscured in the Nujol solution spectra. The greatest changes occur in a pair of bands which appear at 1490 and 1485 $cm^{-1}$. This region is expected to be dominated by vibrations of a phenyl group, so it might be that these changes reflect electron redistributions in the aniline nucleus.

## Conclusions

It has been shown that major infrared spectral changes result from the 313 nm iradiation of low temperture Nujol solutions and polycrystalline films of *N*-benzylideneaniline. These changes reflect those which are expected to result from a *trans* → *cis* photoisomerization. The changes also indicate that as a result of isomerization there is an increase of the non-coplanarity of the aniline ring with the remainder of the molecule.

In order to interpret frequency and intensity variations in the 1628 and 1579 bands, changes in coplanarity and Fermi resonance had to be invoked.

## Acknowledgements

Financial assistance from the Natural Sciences and Engineering Research Council of Canada, the Ministère de l'Education du Québec, and the Canada Council through the grant of the Killam memorial scholarship to C. Sandorfy is gratefully acknowledged.

1. G. M. WYMAN. Chem. Rev. **55**, 625 (1955).
2. R. KUHN and H. M. WEITZ. Chem. Ber. **86**, 1199 (1953).
3. E. FISCHER and Y. FREI. J. Chem. Phys. **27**, 808 (1957).
4. K. GEIBEL, B. STAUDINGER, K. H. GRELLMANN, and K. WENDT. J. Photochem. **3**, 241 (1974).
5. K. MAEDA, K. A. MUSZKAT, and S. SHARIF-OZERI. J. Chem. Soc. Perkin Trans. II, 1292 (1980).
6. M. KOBAYASHI, M. YOSHIDA, and H. MINATO. Chem. Lett. 185 (1976).
7. M. KOBAYASHI, M. YOSHIDA, and H. MINATO. J. Org. Chem. **41**, 3322 (1976).
8. VON W. GAJEWSKI, H. WENDT, and R. WOLFBAUER. Ber. Bunsenges. Phys. Chem. **76**, 450 (1972).
9. K. GEIBEL, B. STAUDINGER, K. H. GRELLMANN, and H. WENDT. Ber. Bunsenges. Phys. Chem. **76**, 1246 (1972).
10. M. A. EL-BAYOUMI, M. EL-AASSER, and F. ABEL-HALIM. J. Am. Chem. Soc. **93**, 586 (1971).
11. C. H. WARREN, G. WETTERMARK, and K. WEISS. J. Am. Chem. Soc. **93**, 4658 (1971).
12. R. AKABA, K. TOKUMARU, and T. KOBAYASHI. Bull. Chem. Soc. Jpn. **53**, 1993 (1980).
13. R. AKABA, K. TOKUMARU, and T. KOBAYASHI. Bull. Chem. Soc. Jpn. **53**, 2001 (1980).
14. J. A. HOULDEN and I. G. CSIZMADIA. Tetrahedron, **25**, 1137 (1969).
15. V. I. MINKIN, YU. A. ZHADNOV, E. A. MEDYANTZEVA, and YU. A. OSTROUMOV. Tetrahedron, **23**, 3651 (1967).
16. P. SKRABAL, J. STEIGER, and H. ZOLLINGER. Helv. Chim. Acta, **58**, 800 (1975).

Can. J. Chem. Downloaded from www.nrcresearchpress.com by 210.87.254.42 on 09/06/12
For personal use only.

17. K. MAEDA and E. FISCHER. Mol. Photochem. **9**, 309 (1979).
18. H. B. BÜRGI and J. D. DUNITZ. Helv. Chim. Acta, **53**, 1747 (1970).
19. T. BALLY, E. HASELBACH, J. LANYIOVA, F. MARSCHNER, and M. ROSSI. Helv. Chim. Acta, **59**, 486 (1976).
20. N. TRAETTEBERG, I. HILMO, R. J. ABRAHAM, and S. LJUNGGREN. J. Mol. Struct. **48**, 395 (1978).
21. G. WETTERMARK, J. WEINSTEIN, J. SOUSA, and L. DOGLIOTTI. J. Phys. Chem. **69**, 1584 (1965).
22. E. L. WAGNER and D. F. HORNIG. J. Chem. Phys. **18**, 296 (1950).
23. L. E. CLOUGHERTY, J. SOUSA, and G. M. WYMAN. J. Org. Chem. **22**, 462 (1957).
24. J. D. MARGERUM and J. A. SOUSA. Appl. Spectrosc. **19**, 91 (1965).
25. K. TABEI and E. SAITOU. Bull. Chem. Soc. Jpn. **42**, 2693 (1969).
26. J. W. LEDBETTER, JR. J. Phys. Chem. **81**, 54 (1977).
27. G. C. PERCY and D. A. THORNTON. J. Inorg. Nucl. Chem. **34**, 3357 (1972).
28. S. K. FREEMAN. Applications of laser spectroscopy. John Wiley & Sons, New York. 1974. p. 115.
29. K. NOACK and R. N. JONES. Can. J. Chem. **39**, 2225 (1961).
30. M. AVRAM and GH. D. MATEESCU. Infrared spectroscopy. *Translated by* L. Birladeanu Wiley–Interscience, New York. 1972. p. 352.
31. G. HERZBERG. Molecular structure and molecular spectra. Vol. II. D. Van Nostrand, New York. 1945.
32. F. FEICHTMAYR and F. WÜRSTLIN. Festschrift Carl Wurster. 1960. p. 177.
33. D. Y. CURTIN and J. W. HAUSSER. J. Am. Chem. Soc. **83**, 3474 (1961).
34. L. J. BELLAMY. The infrared spectra of complex molecules. Methuen and Company, London. 1958.

Can. J. Chem. Downloaded from www.nrcresearchpress.com by 210.87.254.42 on 09/06/12
For personal use only.

# A spectroscopic study of the solvent dependent processes of the anils of benzaldehyde and salicylaldehyde

JERRY W. LEWIS AND CAMILLE SANDORFY
*Département de Chimie, Université de Montréal, Montréal (Qué.), Canada H3C 3V1*
Received August 25, 1981

JERRY W. LEWIS and CAMILLE SANDORFY. Can. J. Chem. **60**, 1727 (1982).

The ultraviolet–visible, infrared, and Raman spectral characteristics of some anils of benzaldehyde and salicylaldehyde in several solvents have been investigated. The ultraviolet–visible absorption data indicate that in solvents with a proton donating ability less than or equal to trifluoroethanol a single equilibrium exists in solutions of *N*-(2-hydroxybenzylidene)aniline, whereas in solvents with a proton donating ability equal to or greater than hexafluoroisopropanol more than one equilibrium occurs. The infrared spectra of this compound dissolved in trifluoroethanol do not show new absorption bands in the 1700–1500 $cm^{-1}$ region; however, new absorption bands in this region do appear when hexafluoroisopropanol is employed as solvent. From these data it is inferred that the first equilibrium involves the breaking of the chelate hydrogen bond and the second equilibrium involves actual protonation of *N*-(2-hydroxybenzylidene)aniline in the electronic ground state. A comparison of the infrared and Raman spectra of the title compounds is also made and alternate assignments for several observed bands in the 1700–1500 $cm^{-1}$ region are proposed.

JERRY W. LEWIS et CAMILLE SANDORFY. Can. J. Chem. **60**, 1727 (1982).

Les spectres ultraviolet–visible, infrarouge et Raman d'un certain nombre d'anils de la benzaldéhyde et de l'aldéhyde salicylique ont été déterminés. Les spectres d'absorption électroniques montrent qu'il y a un équilibre entre deux espèces dans les solutions de la *N*-(2-hydroxybenzylidene)aniline dans des solvants qui sont des donneurs de protons moins bons ou aussi bons que le trifluoroethanol. Par contre dans les solvants ayant un pouvoir de donneur de proton égal ou supérieur à celui de l'hexafluoroisopropanol un équilibre entre un plus grand nombre d'espèces existe. Les spectres infrarouges de ce composé dissout dans l'trifluoroethanol ne présentent aucune bande nouvelle entre 1700 et 1500 $cm^{-1}$. Par contre des bandes nouvelles apparaissent dans hexafluoroisopropanol. On peut déduire de ces spectres que le premier équilibre implique la rupture de la liaison hydrogène du chélate alors que le second implique la protonation de *N*-(2-hydroxybenzylidene)aniline dans son état fondamental. La comparaison entre les spectres ir et Raman de ces composés conduit à des attributions nouvelles pour certaines bandes dans la région spectrale de 1700 à 1500 $cm^{-1}$.

## Introduction

The ultraviolet–visible absorption spectra of aromatic anils of salicylaldehyde have long been observed to undergo dramatic changes when the solvent is changed from a nonpolar to a polar hydrogen-bonding one. In the polar hydrogen-bonding solvents, a new absorption band develops in the spectral region near 440 nm. Charette *et al.* (1), in a study of a series of *N*-salicylidene alkylimines, attributed a long wavelength absorption band to an enol form which had the intramolecular hydrogen bond replaced by an intermolecular hydrogen bond to the solvent molecules. It was suggested that there was stronger solvent stabilization of the excited state than of the ground state; hence the absorption band shifted to longer wavelengths.

Cohen and Flavian (2) have criticized the Charette explanation on several grounds, including the fact that the expected variation of band position with solvents of varying polarity was not observed. These authors concluded that the absorption band was due to a transition of the *cis-ortho*-quinone form. This conclusion was reached in apparent contradiction to a preceding paper (3) in which Cohen and Flavian described the behavior of anils according to Scheme 1. In this particular case, the authors based their conclusions on the very large Stokes shift of the observed fluorescence from the normal absorption, the reasonable overlap between the observed fluorescence and the long wavelength band, and the identity of the fluorescences excited by irradiation into the normal and the long wavelength absorption bands.

Richey and Becker (4) and Barbara *et al.* (5) state that there are subtle but real differences in the fluorescence spectra, depending upon whether the excitation wavelength lies within the normal absorption band or within the long wavelength absorption band.

To date, no conclusive vibrational data which support the existence of the *ortho*-quinone or the "ion-pair" have been presented. Despite this lack of data, the ground state equilibrium proposed by Charette *et al.* (1) and excited state acid–base reactions of the type first discussed by Förster (6) and greatly expanded by Weller (7), and modifications thereof, have now been abandoned in favor of the enol → keto equilibrium and the *ortho*-quinone form (2, 4, 5, 8, 9, 15, and 16).

In the present study a comparison of the ultraviolet–visible, infrared, and Raman spectra of *N*-

0008-4042/82/131727-11$01.00/0
©1982 National Research Council of Canada/Conseil national de recherches du Canada

Can. J. Chem. Downloaded from www.nrcresearchpress.com by 210.87.254.6 on 09/06/12
For personal use only.

Can. J. Chem. Downloaded from www.nrcresearchpress.com by 210.87.254.6 on 09/06/12
For personal use only.

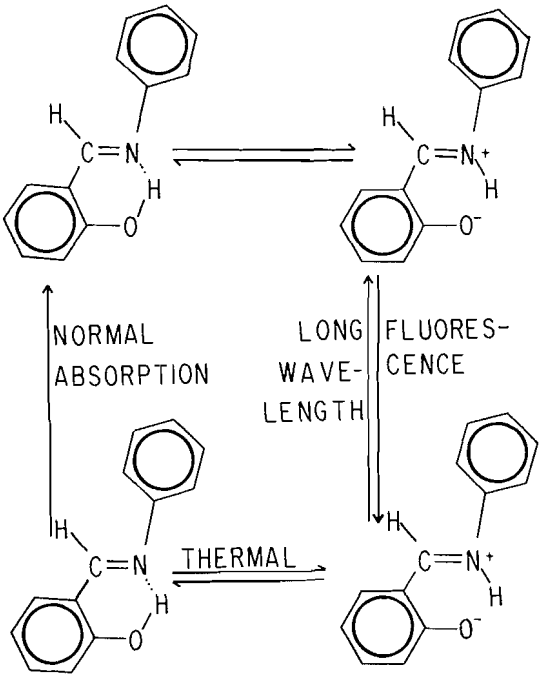


SCHEME 1

benzylideneaniline (BA), *N*-(2-hydroxybenzylidene)aniline (HBA), and other aromatic anils will be made. It is found that there is indeed a significant shift of the long wavelength visible absorption band of HBA as the solvent becomes increasingly acidic. The shift is, however, in the opposite direction to that expected purely on the basis of solvent stabilization of the excited state. It is further noted that there are no changes in the carbon–nitrogen double bond stretching frequency when this compound is dissolved in a solvent of sufficient acidity to cause the ultraviolet–visible absorption spectrum to be dominated by the long wavelength band. These results lead to the conclusion that neither the enol–keto nor the enol – "ion-pair" ground state equilibrium is supported by these vibrational spectroscopic experiments. These results are such that no single equilibrium mechanism is capable of explaining them.

## Experimental

The anils used in this study were prepared and purified by means of the methods described for the preparation and purification of BA in the preceding paper.

The Raman spectra were recorded by means of a Spex Ramalog 6 spectrometer. This instrument was equipped with a Coherent Radiation CR 6 argon-ion laser or a Coherent Radiation Model 590 dye laser. The reported Raman frequencies were calibrated to known frequencies of carbon tetrachloride.

It should be noted that solutions of the hydrochlorides of the anils are particularly unstable in the presence of moisture. The hydrochlorides are also relatively insoluble in dry, ethanol-free chloroform. Suitable spectra, free of contributions by hydrolysis products, were obtained from anhydrous chloroform solutions which contained 0.1 to 0.2% by volume of anhydrous ethanol.

## Results and discussion

### A. *Ultraviolet–visible absorption studies*

In order to demonstrate the anomalous ultraviolet–visible absorption characteristics of aromatic anils, several of these spectra are presented in Figs. 1 and 2. Several observations can be made from these spectra.

1. In the polar hydrogen-bonding solvents a new band develops in the absorption spectrum of HBA.

2. The normal absorption bands of HBA and BA undergo hypsochromic shifts when the solvent is changed from a nonpolar to a polar hydrogen-bonding one.

3. The new band in the spectrum of HBA intensifies and undergoes a hypsochromic shift as the solvent becomes more acidic. On the other hand, in a mixed solvent system, an increase in the concentration of the acidic component causes an intensification of the band but does not greatly affect the band position.

4. The longest wavelength absorption bands of the fully protonated forms of HBA and BA are bathochromically shifted with respect to the corresponding normal absorptions of the neutral species. The new solvent-dependent absorption band in the spectrum of HBA appears to converge to the lowest energy absorption band of the hydrochloride.

Clearly these observations are consistent with the idea of a ground state equilibrium or equilibria. As was noted in the introduction, three different equilibria have been proposed in the literature in order to account for the presence of the long wavelength absorption band of anils. However, it has not been clearly demonstrated whether or not more than one equilibrium is involved in a particular solvent or whether or not the same equilibrium is implicated in the different solvents. For example, for any monomolecular reaction, $A \rightleftharpoons B$, where A and B are characterized by at least one noncommon absorption band, it is a well-known fact that the absorption spectra of solutions containing varying concentrations of A and B will exhibit well-defined isosbestic points. Deviation from this strict requirement normally indicates that more than one reaction is involved (a deviation from this requirement could also mean that one of the components does not follow the Beer–Lambert law in its absorption spectral characteristics). Thus, while many have described the solvent-dependent absorption spectra of HBA and its derivatives in

Can. J. Chem. Downloaded from www.nrcresearchpress.com by 210.87.254.6 on 09/06/12
For personal use only.

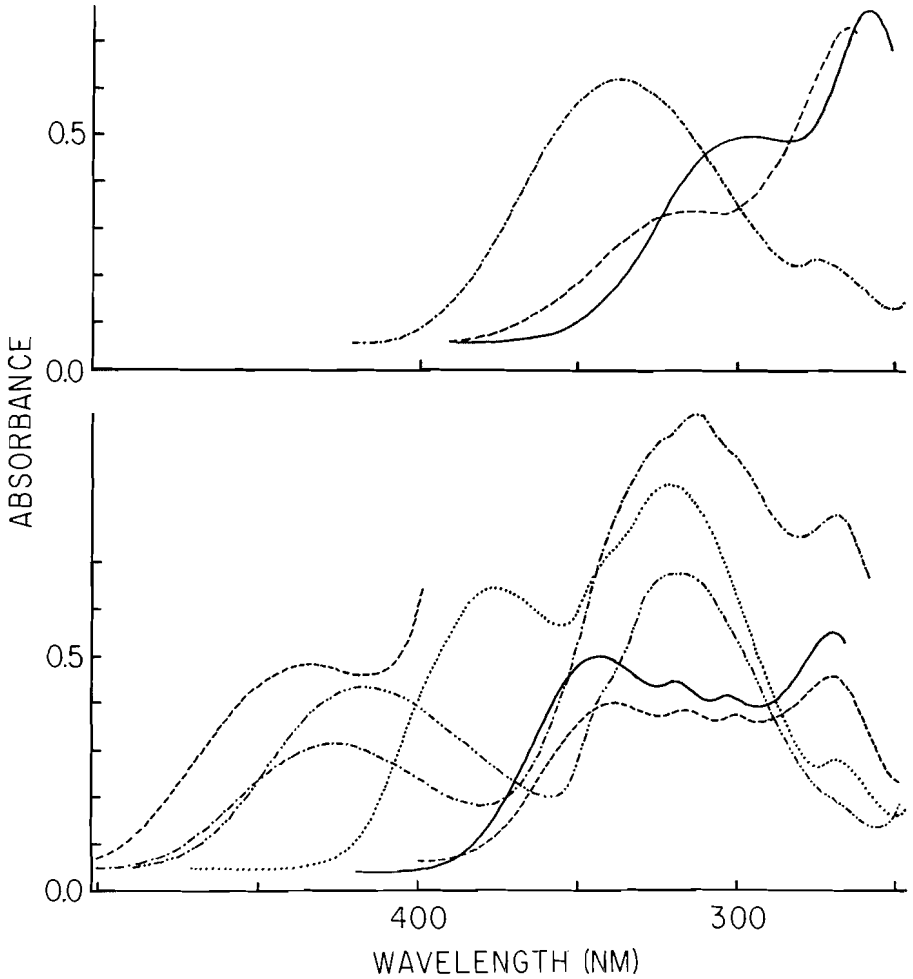


FIG. 1. Upper curves: absorption spectra of *N*-benzylideneaniline; - · - $3.53 \times 10^{-4}$ *M* in trifluoroacetic acid; — $4.23 \times 10^{-5}$ *M* in TFE, - - - - $3.57 \times 10^{-5}$ *M* in $CCl_4$. Lower curves: absorption spectra of *N*-(2-hydroxybenzylidene)aniline; — $4.40 \times 10^{-5}$ *M* in $CCl_4$, - - - - $2.25 \times 10^{-3}$, $2.25 \times 10^{-5}$ *M* in MeOH, - · - · $7.28 \times 10^{-5}$ *M* in TFE, - · - · - · $3.95 \times 10^{-5}$ *M* in HFIPr, · · · · · · · $4.5 \times 10^{-5}$ *M* in TFE saturated with HCl gas.

terms of a single monomolecular reaction, only a single author (8) actually provides spectra of something other than the new long wavelength absorption band. In order to explore this variable, a study was made and the results are summarized in Figs. 3 and 4. It is found that in solutions containing a simple alcohol such as ethanol or a more acidic alcohol such as 1,1,1-trifluoroethanol (TFE), the strict requirement of an A → B reaction is met. However, in a more acidic solvent such as that containing hexafluoroisopropanol (HFIPr), the requirement is not met. In solutions containing difluoroacetic acid, it is observed that the A → B reaction requirement is not met and that the long wavelength absorption band shifts over a wide range of wavelength, depending on the concentration of difluoroacetic acid. Therefore, it must be concluded that once a certain solvent acidity, namely that of HFIPr, is by-passed, a single monomolecular reaction is incapable of explaining the experimental facts.

The principal argument in favour of the enol ⇌ keto tautomerization of HBA seems to reside in the fact that a new absorption band does not appear in the spectrum of BA when the solvent is changed from a nonpolar to a polar hydrogen-bonding one. For example, compare the spectra of HBA and BA shown in Fig. 2. It is noted that no new band appears in the spectrum of BA even in strongly hydrogen-bonding solvents and that the new band is clearly observable in the spectrum of HBA in methanol solution.

Ottolenghi and McClure (9) have also discussed the possibility of an intra ⇌ intermolecular hydro-

Can. J. Chem. Downloaded from www.nrcresearchpress.com by 210.87.254.6 on 09/06/12
For personal use only.

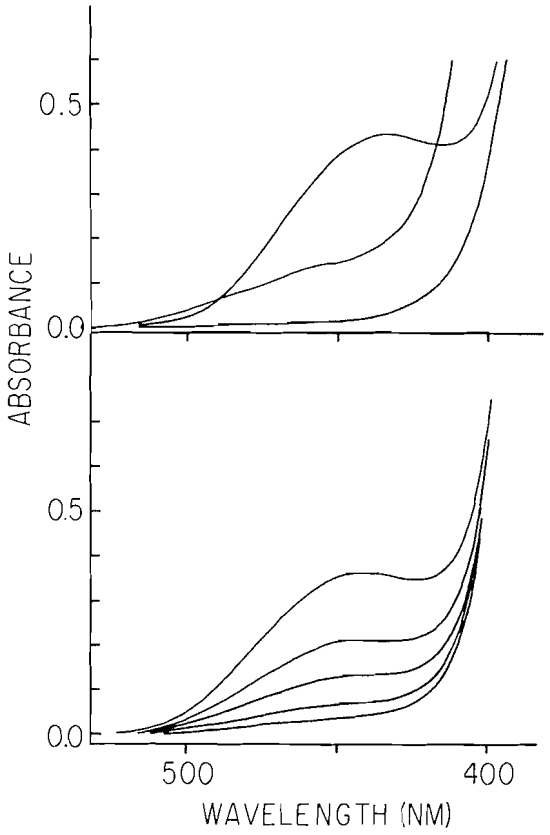


FIG. 2. Upper curves: absorption spectra of *N*-(2-hydroxybenzylidene)aniline methanol solution; liquid film, crystalline film. Lower curves: absorption spectra of *N*-(2-hydroxybenzylidene)-4′-chloroaniline $1.29 \times 10^{-3}$ *M* in $CHCl_3$ containing, top to bottom, 9, 5, 2, 1, 0% TFE.

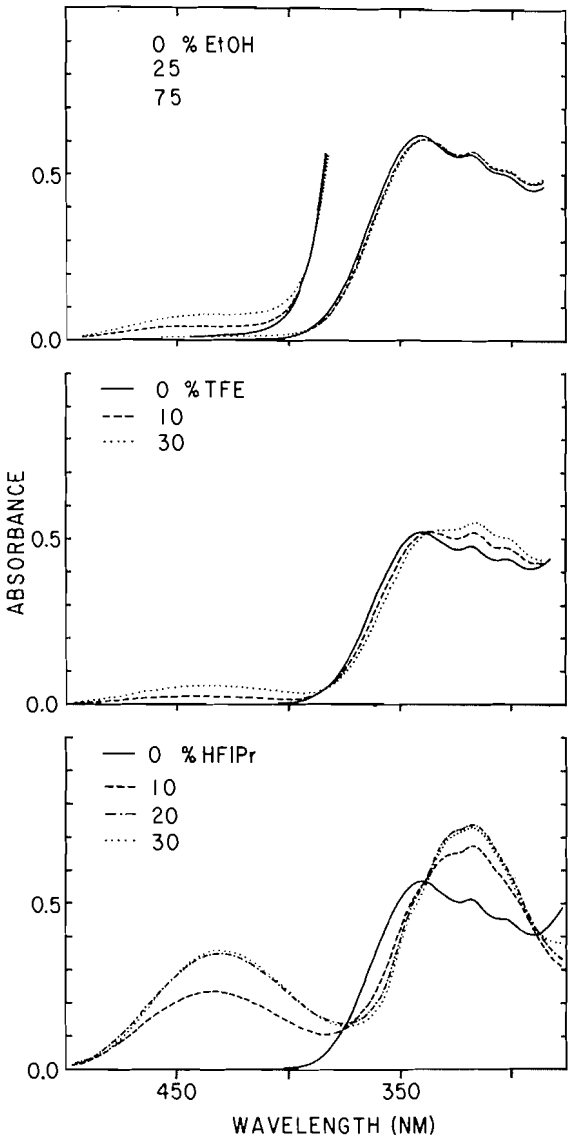


FIG. 3. Absorption spectra of *N*-(2-hydroxybenzylidene)aniline $4.62 \times 10^{-5}$ *M* in $CHCl_3$ containing the indicated amounts of ethanol, TFE, and HFIPr.

gen bond equilibrium. To account for the long wavelength band of HBA, these authors proposed that it could be rationalized on the grounds that the transition probabilities of the hydrogen bridged species are different in the case of the unbridged species. Since BA does not contain the intramolecular chelate ring, there is no a priori reason to suspect that its absorption spectrum would be greatly affected by solvent.

As noted earlier, the normal absorption bands of HBA and BA undergo blue shifts when the solvent is changed from a nonpolar to a polar one. As expected, the shift of the HBA absorption bands in methanol solution is much smaller than the shift of the BA absorption bands in TFE solution (it is not possible to compare the shift of the normal absorption bands of HBA in TFE since in this solvent the spectrum is dominated by the long wavelength band). It might be argued that this observation is proof that the excited state of HBA cannot be stabilized more than is the ground state, contrary to what was argued by Charette *et al.* It must be recalled, however, that in these solutions an equilibrium exists. For example, in methanol solution the majority of HBA molecules remain intramolecularly hydrogen bonded and the weaker bond with the solution is an additional stabilizing force on their ground state.

The blue shift of the normal absorption band of HBA and its derivatives has been observed previously (9). Allen and Roberts (10) have examined in detail the effects of hydrogen bonding and protonation on the nitrogen-15 chemical shifts of

Can. J. Chem. Downloaded from www.nrcresearchpress.com by 210.87.254.6 on 09/06/12
For personal use only.

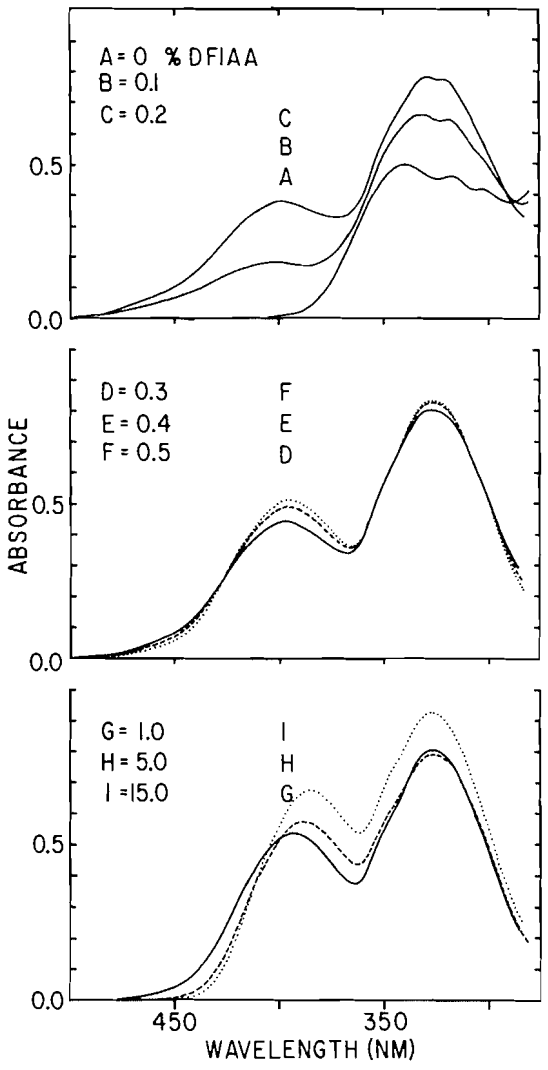


FIG. 4. Absorption spectra of *N*-(2-hydroxybenzylidene)aniline $4.62 \times 10^{-5}$ *M* in $CHCl_3$ containing the indicated amounts of difluoroacetic acid (DFIAA).

several compounds that contain the C=N group. They concluded that in TFE solution BA and several of its derivatives are hydrogen bonded to the solvent, whereas in a more acidic solvent, trifluoroacetic acid (TFAA), the same derivatives are fully protonated. (Unfortunately, this study did not include any 2-hydroxy derivatives wherein a combination of hydrogen bonds could exist.) If, in Fig. 2, the wavelengths of 315 and 297 nm are chosen as the reference maxima of the BA absorption bands in carbon tetrachloride and TFE solution, respectively, then the observed shift represents an energy difference of about 23 kilojoules per mole. This value for the energy of the H-bond is quite normal. Furthermore, this is the energy shift expected for an $\pi^* \leftarrow n$ transition (11). Jaffé *et al.* (12) have proposed that the $\pi^* \leftarrow$ n is the lowest energy transition of BA, but this has not been confirmed experimentally and even if the $\pi^* \leftarrow n$ were the lowest energy transition this would not explain the large blue shift of both absorption bands of BA.

In terms of the normal explanation, the effect of hydrogen bonding on an $\pi^* \leftarrow n$ transition is to stabilize the *n* orbital by an amount approximately equal to the energy of the hydrogen bond (13). During the process of excitation an *n* electron is promoted to a $\pi^*$ orbital and the remaining *n* electron is unable to maintain the hydrogen bond. The hydrogen bond is thus broken in the excited state and the polar hydrogen-bonding solvent should not significantly affect the energy of the excited state (14). It should be pointed out, however, that the examples used to arrive at these conclusions involve molecules with well defined $\pi^* \leftarrow n$ transitions. This is the equivalent of not allowing for any $n$–$\pi$ mixing in the ground and/or excited states. For the examples of BA, HBA, and related compounds, $\pi^* \leftarrow n$ transitions have not been located in the absorption spectra. On the other hand, both the absorption bands of BA and, perhaps to a lesser extent, three bands of HBA behave as though they contained *n*-character, since the observed solvent shift is in the opposite direction and is much larger than any solvent shift expected for a $\pi^* \leftarrow \pi$ transition.

It has been noted that the long wavelength absorption band of HBA intensifies and undergoes a blue shift as one acidic solvent is exchanged for another and that this band appears to converge to that of the protonated species. It is believed that these data and those presented in Figs. 3 and 4 imply the existence of more than one equilibrium. It is difficult to imagine how the *ortho*-quinone structure could fit into such a scheme. The apparent smooth convergence of the long wavelength band with the absorption band of the protonated species implies that, at some point, solvent-dependent ionic species are involved. In order to retain the *ortho*-quinone idea, it is necessary to assume that such a structure is solvent favored up to a point, and that beyond this point the enol and protonated enol are once again favored.

Some supporting evidence for the existence of more than one equilibrium is found in the literature. Smith *et al.* (15), in an optical rotatory dispersion (ord) study of optically active amines, examined the absorption spectra and ord curve of (*S*)-(+)-*N*-salicylidene-α-phenylethyl amine in hexane, dioxane, and 95% ethanol solutions. Two positive

Can. J. Chem. Downloaded from www.nrcresearchpress.com by 210.87.254.6 on 09/06/12
For personal use only.

Cotton effects centered near 410 and 315 nm were observed in the 95% ethanol solution (the corresponding absorption maxima occur at 403 and 315 nm). In hexane and dioxane solution only one Cotton effect, that at 315 nm, was observed. In spite of this fact, the 410 nm absorption band is of significant intensity in the dioxane solution spectrum, but is absent in the hexane solution spectrum. These authors concluded that a simple shift in a tautomeric equilibrium did not adequately explain the presence of the 410 nm band in the dioxane solution spectrum.

B. *Infrared and Raman studies*

In order to study the effects of solvents on the carbon–nitrogen double bond stretching frequency and thus better identify the implicated equilibrium or equilibria, the infrared and Raman spectra of HBA and BA in several solvents were obtained. If the proposed ground state enol–keto or enol – "ion pair" equilibrium occurs in hydrogen-bonding solvents, substantial changes in the infrared and Raman spectra are expected, barring an identity of the spectra of the enol and the *ortho*-quinone or of the enol and the ion-pair. If either of these equilibria occurred, then infrared and/or Raman spectral changes which could be correlated with the 440 nm visible absorption band would be expected. A number of spectra are presented in Figs. 5–9.

Particular attention should be paid to the infrared spectra of BA in chloroform solution and in the 50% chloroform – 50% TFE solution. It will be noted in Fig. 5 that the C=N stretching band of BA at 1625 $cm^{-1}$ is unchanged with respect to position in the solvent of greater acidity. Since, according to general experience as well as Allen and Roberts' (10) observation of the $^{15}N$ nmr spectrum, a hydrogen bond must be formed between BA and TFE, this is somewhat surprising. The insensitivity of the C=N stretching frequency can perhaps be connected with the relative weakness of the hydrogen bond; also, since the proton acceptor is likely to be the nitrogen lone pair its participation in the H-bond may not affect significantly the C=N force constant. Freedman (17) has noted that, while the strength of the intramolecular H-bond of *N*-salicylidene-anilines is comparable to that of carboxylic acid dimers or enolized β-diketones, the chelate ring has little effect on the carbon–nitrogen double bond stretching frequency; this can be taken for another sign of the insensitivity of C=N to H-bonding. Furthermore, since, as it has been suggested, the C=N frequency is influenced by Fermi resonance, the downward H-bond shift could be compensated for by slightly increased

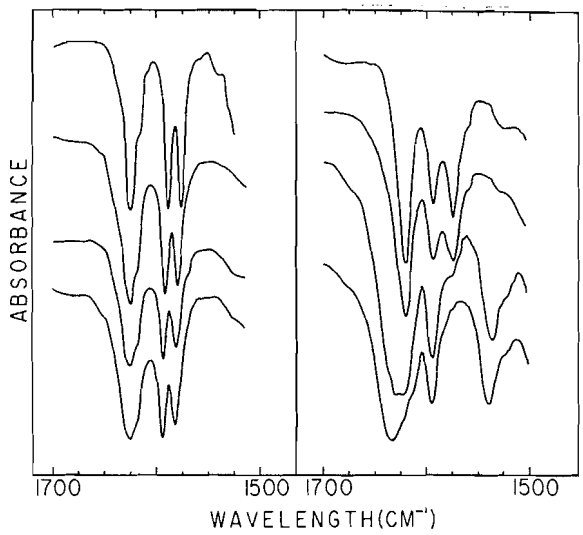


FIG. 5. Infrared absorption spectra of *N*-(2-hydroxybenzylidene)aniline and *N*-benzylideneaniline. Right side, HBA, top to bottom: 0.28 *M* in $CHCl_3$, 0.30 *M* in $CHCl_3$ · TFE, 0.36 *M* in $CHCl_3$ · HFIPr, 0.34 *M* in HFIPr. Left side, BA,top to bottom: 0.20 *M* in $CHCl_3$, 0.29 *M* in $CHCl_3$ · TFE, 0.39 *M* in $CHCl_3$ · HFIPr, 0.34 *M* in HFIPr.

Fermi resonance. The lack of a frequency shift cannot be taken for a proof of the absence of H-bonding.

A similar situation is encountered when the infrared spectra of HBA in chloroform and in a one-to-one mixture of chloroform and TFE are compared (Fig. 5). The three bands in the 1700–1500 $cm^{-1}$ region are slightly broadened in the mixed solvent spectrum, as are those of BA, but there is essentially no shift in position. (The broadening in itself may be considered as an indication of H-bonding.) More importantly, no new bands which might be attributed to the stretching motions of $C{=}NH^+$ or C=O have appeared. These findings are in complete agreement with the results of Ledbetter's study (16). He also obtained the infrared spectrum of HBA in pure TFE and found no new absorption bands in the 1700–1500 $cm^{-1}$ region. Since no new bands are observed in this region of the infrared spectra of HBA dissolved in TFE or in a mixture of TFE and chloroform, it is concluded that neither the enol–keto tautomerization nor ion-pair formation occurs in the ground state. The similarity of the infrared spectra of HBA and BA in this region strongly suggests that in TFE-chloroform solution both compounds undergo the same transformation; namely, both compounds are H-bonded to the solvent. It could be argued that the expected "new" C=O or $C{=}NH^+$ bands are simply too weak to appear in the infrared

Can. J. Chem. Downloaded from www.nrcresearchpress.com by 210.87.254.6 on 09/06/12
For personal use only.

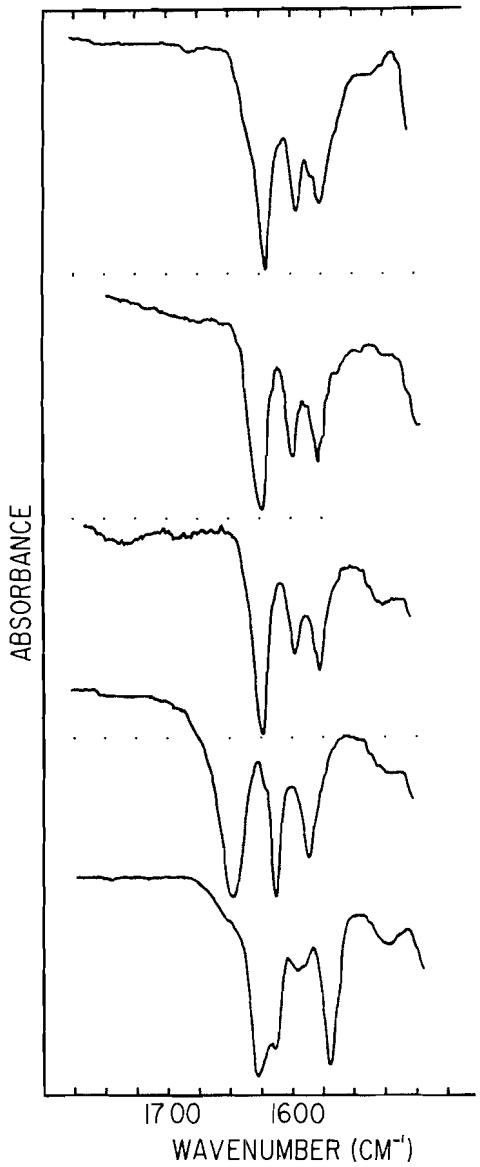


FIG. 6. Infrared absorption spectra of *N*-(2-hydroxybenzylidene)aniline. Top to bottom: solid film, 0.21 *M* in Nujol, 0.18 *M* in $CHCl_3$, 0.18 *M* in $CHCl_3$ saturated with HCl, 0.18 *M* in $CHCl_3$ saturated with DCl.

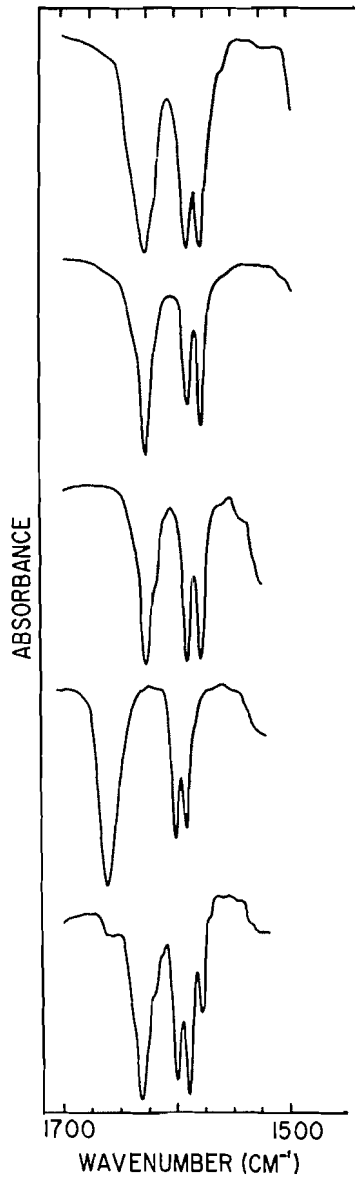


FIG. 7. Infrared absorption spectra of *N*-benzylideneaniline. Top to bottom: solid film, 0.35 *M* in Nujol, 0.20 *M* in $CHCl_3$, 0.26 *M* in $CHCl_3$ saturated with HCl, 0.26 *M* in $CHCl_3$ saturated with DCl.

spectrum. This could be so if only a slight amount of the keto tautomer or ion-pair was present, perhaps up to 2 or 3%, but this is not the issue. The amounts that have been claimed are much larger, and, since the C=O or $C{=}NH^+$ bands are by no means weaker than a C=N band they would be seen if the related species was present in the solutions.

The surprising fact is that a relatively weak H-bond is capable of causing the appearance of the 440 nm band in the visible. No other alternative seems to be possible, however.

We now have to describe the spectra of HBA and BA in the more acidic solvents: in a one-to-one mixture of chloroform and HFIPr and in neat HFIPr (Fig. 5). Ledbetter (16) previously obtained the spectra of HBA and BA in pure HFIPr. In the present study no new bands are found in the spectrum of BA in either the mixed solvent or in pure HFIPr. The C=N stretching is not affected

Can. J. Chem. Downloaded from www.nrcresearchpress.com by 210.87.254.6 on 09/06/12
For personal use only.

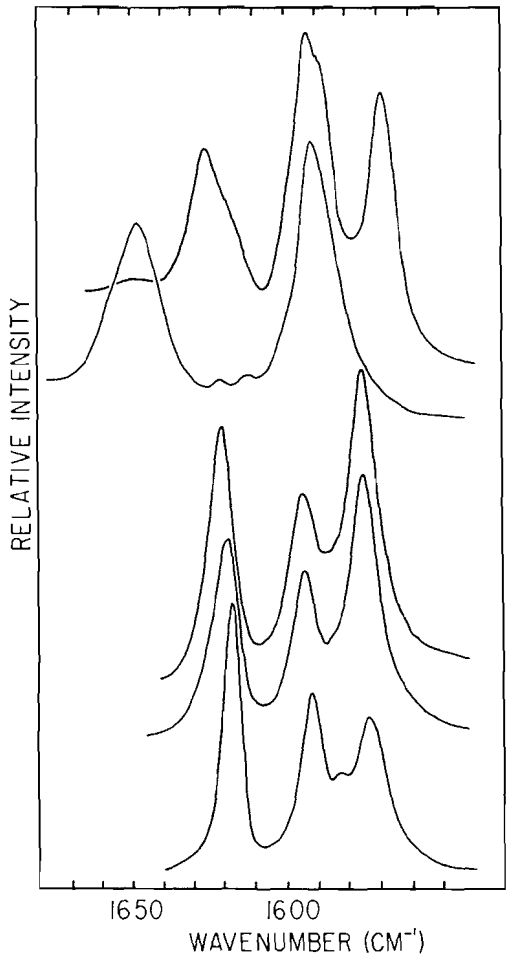


FIG. 8. Raman Spectra of *N*-(2-hydroxybenzylidene)aniline. Bottom to top: solid, 0.21 *M* in Nujol, 0.12 *M* in $CHCl_3$, 0.23 *M* in $CHCl_3$ saturated with HCl, 0.20 *M* in $CHCl_3$ saturated with DCl.

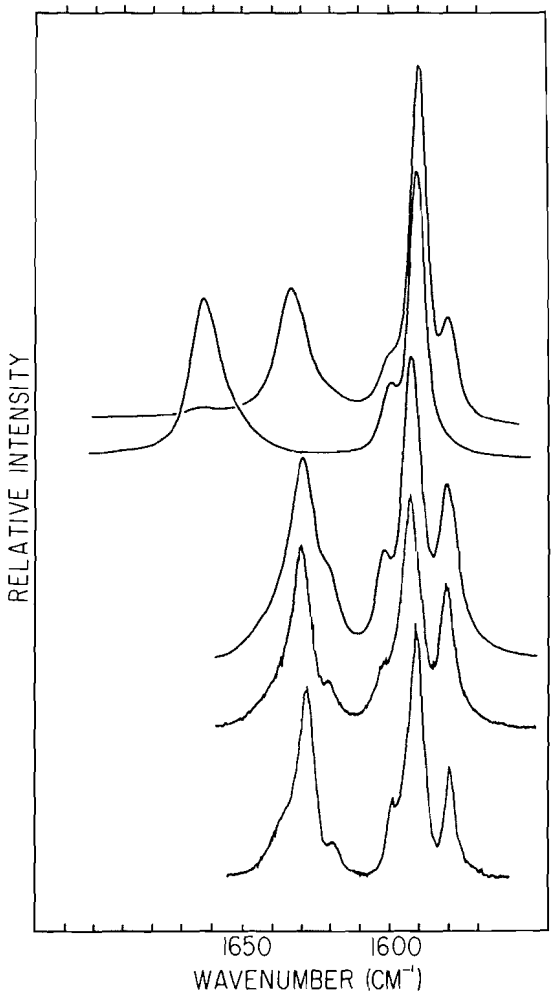


FIG. 9. Raman spectra of *N*-benzylideneaniline. Bottom to top: solid, 0.35 *M* in Nujol, 0.29 *M* in $CHCl_3$, 0.31 *M* in $CHCl_3$ saturated with HCl, 0.29 *M* in $CHCl_3$ saturated with DCl.

by these solvents, except for a slight broadening of the bands. For HBA, the situation is somewhat different. In the mixed solvent spectrum the high frequency band is still broader and appears to be composed of two overlapping bands at 1630 and 1622 $cm^{-1}$ and a shoulder at perhaps 1635 $cm^{-1}$. This is likely to correspond to conditions in which a fraction of HBA remains nonprotonated and is simply H-bonded to the solvent and another fraction is protonated and probably also H-bonded to the solvent in various ways. The higher frequency constituent of the broad band would then correspond the $C{=}NH^+$ absorption. In pure HFIPr the fraction of the protonated species is larger, but complete protonation apparently does not occur. Favrot *et al.* (18) have reported that other simpler imines are H-bonded in TFE and are fully protonated in perfluoro-*tert*-butanol, whereas in HFIPr these simpler imines exist as a mixture of hydrogen bonded and protonated species. Whether protonation is due to the proton transfer in the original intramolecular H-bond or if the latter opens in favor of direct protonation by a solvent molecule cannot be ascertained at this stage. It should be pointed out that if any significant amount of the quinoid form were present, a much more intense (carbonyl) band would be present at the high frequency side but this is not the case.

In the spectrum of HBA in HFIPr and in the mixed solvent it will be noticed that the band near 1574 $cm^{-1}$, in the chloroform solution spectrum, decreases in intensity and that a new band appears near 1540 $cm^{-1}$. It is at 1536 $cm^{-1}$ in the mixed solvent spectrum. The disappearance of the band at 1574 $cm^{-1}$ and the appearance of another band in the 1550–1500 $cm^{-1}$ region has first been pointed out by Ledbetter (16). The 1550–1500 $cm^{-1}$ band in

Can. J. Chem. Downloaded from www.nrcresearchpress.com by 210.87.254.6 on 09/06/12
For personal use only.

the spectrum of HBA in HFIPr solution was assigned by this author as due to a stretching vibration of the vinyl C=C bond of the quinoid form. He asserted that for the quinoid structure the band occurs near 1545 $cm^{-1}$, that for the protonated imine the band occurs near 1525 $cm^{-1}$, and that in both cases the band might shift to slightly higher or lower frequency depending on the amount of double-bond character in the bond. The appearance of such a band in the spectrum of the proposed quinoid might easily be rationalized in these terms. However, if it is supposed that the external C=C bond acquires more "double-bond" character, then it must also be granted that the C=N bond has less "double-bond" character. This is not substantiated by experiment. As to the protonated imine which has no external double bond the assignment is even more difficult to accept. The $C{=}NH^+$ frequency of HBA (for the hydrochloride) occurs at 1643 $cm^{-1}$ while the C=N frequency occurs at 1619 $cm^{-1}$.

Thus, in order to properly evaluate the solution equilibrium or equilibria of *ortho*-hydroxy Schiff bases, it is critical to firmly establish the identity of the infrared and Raman bands that are found in the 1700–1500 $cm^{-1}$ region. The difficulties in making such assignments have previously been discussed (18).

As pointed out by Aton *et al.* (19) it seems reasonable to expect that the $C{=}NH^+$ stretching should occur at lower frequency than that of C=N (i.e., protonation should lower the C=N force constant and increase the effective mass of the nitrogen, and both these effects should tend to lower the stretching frequency). Experience, on the other hand, often dictates that this is not the case. To explain this apparent anomaly, Aton *et al.* propose that upon protonation the $C{=}NH^+$ stretching and the $C{=}N^+{-}H$ deformation are coupled. Therefore the observed $C{=}NH^+$ stretching occurs much higher in frequency than would otherwise be expected.

For the examples of the aromatic anils under consideration here, this is an especially interesting observation. Several infrared spectra of HBA are presented in Fig. 6. Note that there are some relative intensity changes in the three 1700–1500 $cm^{-1}$ bands as the spectra of the solid, the Nujol solution, and the chloroform solution are compared. It appears that protonation causes an upward shift of 24 $cm^{-1}$ in the C=N stretching frequency and that a subsequent deuterium exchange lowers the $C{=}NH^+$ stretching frequency by 16 $cm^{-1}$.

An identical series of infrared spectra of BA is presented in Fig. 7. It should be observed that, with one notable exception, these spectra reflect changes identical to those seen in the spectra of HBA. The infrared spectrum of the deuterochloride of BA exhibits four principal bands, whereas all the other spectra of BA and of HBA exhibit only three principal bands.

Identical series of Raman spectra of HBA and BA are presented in Figs. 8 and 9, and the vibrational data are summarized in Tables 1 and 2. The Raman spectra of the solid, the Nujol solution, and the chloroform solution of each compound are essentially identical to the corresponding infrared spectra except that the relative intensity changes are more pronounced. For example, the lowest frequency band in the spectrum of HBA is the weakest band in the infrared and Raman spectra of the solid sample; but in the chloroform solution spectra this band is the strongest band in the Raman and it has also gained considerable intensity in the infrared spectrum.

The Raman spectra of the hydrochlorides and deuterochlorides of HBA and BA are, however, different from the corresponding infrared spectra. Each of these Raman spectra consist of one fewer bands than the infrared spectra. The lowest frequency infrared bands, located at 1574 and 1579 $cm^{-1}$, respectively, in the chloroform solution spectra of HBA and BA, are absent in the Raman spectra of the hydrochlorides. It may further be observed that all the Raman spectra of HBA and

TABLE 1. Infrared and Raman assignments for *N*-benzylideneaniline

| Solvent | ν C=N ($cm^{-1}$) | ν Phenyl ($cm^{-1}$) | ν $C{=}NH^+ + N^+ - H$ ($cm^{-1}$) | ν $C{=}ND^+$ ($cm^{-1}$) |
|---|---|---|---|---|
| Infrared | | | | |
| None (solid) | 1625<br>1578 | 1590 | | |
| Nujol | 1625<br>1577 | 1589 | | |
| $CHCl_3$ | 1626<br>1579 | 1592 | | |
| $CHCl_3$ + HCl | | 1590<br>1600 | 1660<br>(1600) | |
| $CHCl_3$ + DCl | | 1589<br>1600 | | 1630<br>1578 |
| Raman | | | | |
| None (solid) | 1628<br>1580 | 1591 | | |
| Nujol | 1631<br>1582 | 1594 | | |
| $CHCl_3$ | 1630<br>1582 | 1594 | | |
| $CHCl_3$ + HCl | | 1591 | 1663 | |
| $CHCl_3$ + DCl | | 1590 | | 1634<br>1580 |

Can. J. Chem. Downloaded from www.nrcresearchpress.com by 210.87.254.6 on 09/06/12
For personal use only.

TABLE 2. Infrared and Raman assignments for *N*-(2-hydroxybenzylidene)aniline

| Solvent | ν C=N ($cm^{-1}$) | ν Phenyl ($cm^{-1}$) | ν C=$NH^+$ + $N^+$ − H ($cm^{-1}$) | ν C=$ND^+$ ($cm^{-1}$) |
|---|---|---|---|---|
| Infrared | | | | |
| None (solid) | 1615<br>1571 | 1590<br>(1578) | | |
| Nujol | 1618<br>1573 | 1593 | | |
| $CHCl_3$ | 1619<br>1574 | 1593 | | |
| $CHCl_3$ + HCl | | 1610 | 1643<br>1583 | |
| $CHCl_3$ + DCl | | 1609<br>(1587) | | 1627<br>1565 |
| Raman | | | | |
| None (Solid) | 1617<br>1573 | 1592 | | |
| Nujol | 1621<br>1576 | 1595 | | |
| $CHCl_3$ | 1621<br>1576 | 1595 | | |
| $CHCl_3$ + HCl | | 1592 | 1648 | |
| $CHCl_3$ + DCl | | 1593 | | 1627<br>1569 |

BA exhibit a phenyl band in the 1595–1589 $cm^{-1}$ region. A similar band is found in all the infrared spectra of BA and in all the infrared spectra of HBA except those of the hydrochloride and the deuterochloride. (A weak band in the 1590–1585 $cm^{-1}$ region of the infrared spectrum of the deuterochloride of HBA is observed; however, its origin is questionable. It could be the result of incomplete deuteration.)

Now, since the $N^+$—H deformation is expected to be very weak in the Raman, the lowest frequency band at 1583 $cm^{-1}$ in the infrared spectrum of the hydrochloride of HBA is most probably the $N^+$—H deformation which is coupled with the C=$NH^+$ stretching motion. Note that the band is absent in the Raman spectrum. The reappearance of a low frequency band in the Raman spectrum of the deuterochloride would, at first, appear to refute this assignment; but, this Raman band at 1569 $cm^{-1}$ is likely to be of different origin than that of the infrared band at 1583 $cm^{-1}$. Note that upon deuterium substitution the C=$ND^+$ stretching occurs very near the frequency of the neutral C=N group. Since protonation of the imine nitrogen is not expected to greatly perturb the combinations and overtones of the aromatic nuclei, Fermi resonance of the C=$ND^+$ stretching mode may occur once again. Thus the lowest frequency band in the Raman spectrum of the deuterochloride of HBA is of the same origin as the lowest frequency bands in the Raman spectra of the neutral molecule.

The ultimate location of the infrared spectral band which might be attributed to the $N^+$—H deformation is dependent on the extent of coupling of the C=$NH^+$ stretching mode and the $N^+$—H deformation, and on the strength of the $N^+$—H bond (or N...H in the case of hydrogen bonding). Therefore, it is clear that this vibration might be found to occur over a relatively wide frequency range. For example, the band in the spectrum of a hexafluoroisopropanol solution of HBA is located at 1540 $cm^{-1}$, and at 1537 $cm^{-1}$ in the spectrum recorded from a one-to-one mixture of hexafluoroisopropanol and chloroform. The band occurs at 1583 $cm^{-1}$ in the spectrum of the fully protonated hydrochloride. In the case of the deuterochloride the coupling is much less extensive since the frequencies of the two vibrations are widely separated. The $N^+$—D deformation occurs outside the spectral region shown in the present spectra.

The next major difference between the infrared and Raman spectra of the hydrochloride of HBA is that observed in the 1595 and 1610 $cm^{-1}$ regions. All the Raman spectra exhibit a strong band in the 1595–1592 $cm^{-1}$ region but do not exhibit a band of significant intensity near 1610 $cm^{-1}$. On the other hand, the infrared spectra of the neutral forms of HBA exhibit a band in the 1593–1590 $cm^{-1}$ region that is not present (or is very weak) in the spectra of the hydrochloride and the deuterochloride. These latter spectra do, however, contain a strong band near 1610 $cm^{-1}$. There is general agreement that the band near 1595 $cm^{-1}$ may be attributed to an aromatic C=C stretching motion. Since there exists the possibility of two quadrant stretching vibrations in the 1620–1585 and 1590–1565 $cm^{-1}$ region (20), it is felt that both these bands may be assigned as vibrations of the aromatic nuclei. The reasons for widely different intensities of the 1595 $cm^{-1}$ band in the infrared and of the 1610 $cm^{-1}$ band in the Raman spectra of the hydrochloride and deuterochloride are not clear.

The infrared and Raman spectra of BA may be explained in the same terms as were the spectra of HBA. The spectra of the neutral molecule are almost identical to the corresponding spectra of HBA and thus deserve no further comment than to add that these Raman spectra exhibit a fairly intense band or shoulder in the 1605–1600 $cm^{-1}$ region. The spectra of the hydrochloride and deuterochloride do, however, require more explanation. It is observed that all the spectra of BA contain a strong band in the 1594–1589 $cm^{-1}$ region, whereas the similar band in the infrared

Can. J. Chem. Downloaded from www.nrcresearchpress.com by 210.87.254.6 on 09/06/12
For personal use only.

spectra of the hydrochloride and deuterochloride of HBA was missing. It can also be seen that the infrared spectra of the hydrochloride and deuterochloride of BA exhibit a strong band at 1600 $cm^{-1}$. It seems reasonable to believe that this band is of similar origin as the 1610 $cm^{-1}$ band in the corresponding spectra of HBA, and is of the same origin as the 1605–1600 $cm^{-1}$ band in the Raman spectra of BA.

It is also observed that a band which might be attributed to the $N^+$—H deformation mode of the hydrochloride of BA is not to be found in the spectrum. Since there are relative intensity differences in the 1600 $cm^{-1}$ band of the hydrochloride and deuterochloride it is probable that the $N^+$—H deformation is located in this region.

A comparison of the infrared and Raman spectra of protonated and neutral forms of HBA and BA thus leads to alternate assignments for several observed bands. It is believed that these assignments, which are summarized in Tables 1 and 2, provide a consistent set for the 1700–1500 $cm^{-1}$ region of the spectra of these compounds. The key point seems to be the recognition of the role played by mixing with the $N^+$—H bending mode in determining the frequencies of the C=N stretching and phenyl ring vibrations. These assignments also provide an alternate explanation of the "1550–1500" infrared band described by Ledbetter and, this, together with the absence of a carbonyl stretching band, suggests that substantial amounts of an *ortho*-quinone tautomer do not exist in solution.

## Conclusion

The ultraviolet–visible, infrared, and Raman data presented herein offer no proof for the presence of substantial amounts of enol–keto or enol–"ion-pair" tautomers in the ground state. New infrared bands which might be correlated with the "440 nm" optical absorption band of HBA are not found. As a result of this evidence, it is proposed that in solvents less acidic than hexafluoroisopropanol the C=N bond of HBA is intact and thus no tautomerization or ionization has occurred. This evidence also indicates that in solvents with acidities somewhat greater than or equal to that of hexafluoroisopropanol more than one equilibrium must be taken into account in order to explain the spectral characteristics. The apparent convergence of the "440 nm" absorption band to that of the protonated species strongly suggests that the second equilibrium involves ionic species. It appears therefore that the origin of the 440 nm visible absorption band is still open for future research.

## Acknowledgements

Financial assistance from the Natural Sciences and Engineering Research Council of Canada, the Ministère de l'Education du Québec, and the Canada Council through the grant of the Killam Memorial scholarship to C. Sandorfy is gratefully acknowledged.

1. J. Charette, G. Faithansl, and Ph. Teyssie. Spectrochim. Acta, **20**, 597(1964).
2. M. D. Cohen and S. Flavian. J. Chem. Soc. B, 321(1967).
3. M. D. Cohen and S. Flavian. J. Chem. Soc. B, 317(1967).
4. W. F. Richey and R. S. Becker. J. Chem. Phys. **49**, 2092(1968).
5. P. F. Barbara, P. M. Rentzepis, and L. E. Brus. J. Am. Chem. Soc. **102**, 2786(1980).
6. T. Förster. Z. Elektrochem. **54**, 42(1955).
7. A. Weller. Z. Elektrochem. **56**, 662(1957).
8. J. W. Ledbetter, Jr. J. Phys. Chem. **70**, 2245(1966); **71**, 2351(1967).
9. M. Ottolenghi and D. S. McClure. J. Chem. Phys. **46**, 4620(1967).
10. M. Allen and J. D. Roberts. J. Org. Chem. **45**, 130(1980).
11. H. H. Jaffé and M. Orchin. Theory and applications of ultraviolet spectroscopy. John Wiley and Sons Inc., New York. 1962. p. 187.
12. H. H. Jaffé, S.-J. Yeh, and R. W. Gardner. J. Mol. Spectrosc. **2**, 120(1958).
13. G. J. Brealy and M. Kasha. J. Am. Chem. Soc. **77**, 4462(1955).
14. V. G. Krishna and L. Goodman. J. Am. Chem. Soc. **83**, 2042(1961).
15. H. E. Smith, S. L. Cook, and M. E. Warren, Jr. J. Org. Chem. **29**, 2265(1964).
16. J. W. Ledbetter Jr. J. Phys. Chem. **81**, 54(1977).
17. H. H. Freedman. J. Am. Chem. Soc. **83**, 2900(1961).
18. J. Favrot, J. M. Leclercq, R. Roberge, C. Sandorfy, and D. Vocelle. Photochem. Photobiol. **29**, 99(1979).
19. B. Aton, A. G. Doukas, D. Narva, R. H. Callender, U. Dinur, and B. Honig. Biophys. J. **29**, 79(1980).
20. N. B. Colthup, L. H. Daly, and S. E. Wiberley. Introduction to infrared and Raman spectroscopy. 2nd ed. Academic Press, New York. 1975. p. 260.

# A spectroscopic study of proton transfer and photochromism in *N*-(2-hydroxybenzylidene)aniline

J. W. LEWIS AND C. SANDORFY

*Département de Chimie, Université de Montréal, Montréal (Qué.), Canada H3C 3V1*

Received 25 August 1981[1]

J. W. LEWIS and C. SANDORFY. Can. J. Chem. **60**, 1738 (1982).

The infrared spectral characteristics of *N*-(2-hydroxybenzylidene)aniline, its deuterium substituted analogue, *N*-(2-hydroxybenzylidene)-*m*-toluidine, and their photoproducts have been investigated. The infrared spectrum of a low temperature polycrystalline film of *N*-(2-hydroxybenzylidene)aniline exhibits new absorption bands at 3380, 1646, 1537, 1502, 1319, and 1310 $cm^{-1}$ upon irradiation at 365 nm. Likewise, the spectrum of the *m*-toluidine derivative exhibits new absorption bands at 3320, 1650, 1535, 1503, 1321, 1310, and 995 $cm^{-1}$ upon irradiation at 365 nm. These new data, in conjunction with the newly acquired data on the hydrochloride and deuterochloride of the title compound, indicate that the photoproduct is a zwitterion, not an *ortho*-quinone. It is also inferrred that the photoproduct exists in a conformation which is *cis* about the central carbon–nitrogen double bond.

J. W. LEWIS et C. SANDORFY. Can. J. Chem. **60**, 1738 (1982).

Les spectres infrarouges de l'*N*-(2-hydroxybenzylidène)aniline (HBA), de son analogue deutérié, de l'*N*-(2-hydroxybenzylidène)-*m*-toluidine et ceux de leurs produits obtenus par irradiation ont été examinés. Dans le spectre infrarouge de l'HBA de nouvelles bandes apparaissent à 3380, 1646, 1537, 1502, 1319 et 1310 $cm^{-1}$ après irradiation à 365 nm. D'une manière analogue le spectre du dérivé *m*-toluidinique présente des bandes nouvelles à 3320, 1650, 1535, 1503, 1321, 1310 et 995 $cm^{-1}$ après irradiation à 365 nm. Ces données nouvelles ajoutées à celles obtenues pour l'hydrochlorure et le deutérochlorure du HBA indiquent que le produit de l'irradiation est un zwitterion et non pas une *ortho*-quinone. En outre, on peut conclure que le produit d'irradiation a une configuration *cis* par rapport à la liaison centrale C=N.

## Introduction

In recent years, there has been much interest in the thermochromic and photochromic activities of salicylaldehyde anils. Many publications on various aspects of these phenomena have appeared. For example, Cohen *et al.* (1–10) have reported that some crystalline anils are photochromic while others are thermochromic, but none of the anils was found to exhibit both properties. Insofar as different crystalline modifications of an anil are concerned, however, one modification might be thermochromic while another is photochromic. These studies also provided proof that the 2-hydroxy group of the salicylaldehyde portion of the anil is a necessary, but insufficient, condition for the observation of the photochromic or the thermochromic phenomenon in the solid state. The sufficient condition was established to be related to the molecular packing in the crystal. A "loose" packing which permits movement of parts of the molecule upon absorption of ultraviolet light was found to be necessary for the observation of photochromism. In a similar manner, a "tight" packing in the crystal was related to the thermochromic behavior of some solid anils. These investigators also demonstrated that in rigid glassy matrices all anils derived from salicylaldehyde and substituted salicylaldehydes are photochromic, independently of whether or not they are so in crystalline form.

In 1962, Cohen and Schmidt (3) proposed mechanisms for the two phenomena. These mechanisms involve the existence of the three tautomers shown in Scheme 1.

In these formulae the labels *cis* and *trans* refer only to the relative positions of the oxygen atom and the hydrogen atom that is covalently bound to the nitrogen atom, and not to any specific conformation of the molecule. The thermochromic process thus involves a simple proton transfer that is made possible by means of certain unspecified intermolecular interactions. The photochromic process involves a proton transfer and a geometric rearrangement (an isomerization about the ring carbon – azomethine carbon bond).

A number of publications on the subject of photochromic anils have appeared since 1962 (4–10, 11–26). With few exceptions, these papers

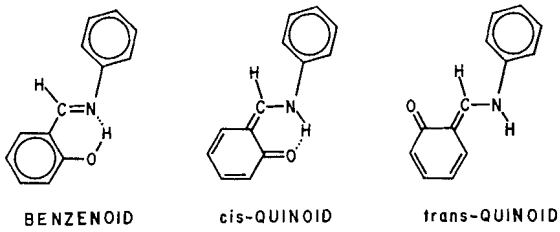


SCHEME 1

[1]Revision received March 1, 1982.

0008-4042/82/131738-09$01.00/0

©1982 National Research Council of Canada/Conseil national de recherches du Canada

Can. J. Chem. Downloaded from www.nrcresearchpress.com by 210.87.254.105 on 09/06/12
For personal use only.

Can. J. Chem. Downloaded from www.nrcresearchpress.com by 210.87.254.105 on 09/06/12
For personal use only.

would appear to confirm the basic proposals of Cohen and Schmidt. That is, the *cis*-quinoid should be identified with the species produced in the thermochromic process as well as the second species found in solutions of anils in hydrogen-bonding solvents, and the *trans*-quinoid should be identified with the species produced photochemically. The exceptions include those of Cohen and Flavian (7, 8), Richey and Becker (14), Rosenfeld *et al.* (18), Wettermark and Dogliotti (15), and Anderson and Wettermark (16).

In their investigation of the luminescence properties of the anils, Cohen and Flavian proposed that ionic species are involved in the long wavelength absorption and emission. Richey and Becker suggested that the final photocolored product is a nonequilibrium form of the true *cis*-quinoid tautomer. Rosenfeld and co-workers, on the basis of theoretical calculations and experimental results, suggested that more than one photocolored species is produced in the forward photochemical reaction. Wettermark and Dogliotti, as well as Anderson and Wettermark, proposed that there are two equilibria in the photochemical reaction. One equilibrium involves proton transfer and tautomerization and the other involves a *trans* → *cis* isomerization about the central carbon–nitrogen double bond. Other authors (5, 6, 22) have also suggested that more than three molecular species may be involved in these processes.

Hadjoudis *et al.* (26) have studied the thermochromic and photochromic properties of a series of Schiff bases derived from 2-hydroxybenzaldehydes and 2-aminopyridines. It was found that none of these compounds, in the form of crystalline films, was photochromic. The crystalline films did show thermochromic effects and, in solution, the compounds were photochromic. These authors concluded that in the crystalline state the compounds are essentially planar and thermochromic, whereas in solution the molecules are able to assume various geometries and are photochromic.

Despite this apparent wealth of spectroscopic data, very little direct structural information concerning the forward (photochemical) and the reverse (photochemical or thermochemical) reaction products of the anils is to be found in the literature. The lack of infrared spectral changes, upon the irradiation of these compounds with ultraviolet light, has been attributed to the unfavorably small quantity of the photoproduct that is attainable by means of ordinary laboratory techniques.

Due to the structural and electronic similarity of these compounds to *N*-benzylideneaniline, it is convincing to argue that the photochemistry should also be somewhat similar. The spectral properties are, however, further complicated by internal hydrogen bonding and by proton transfer in the excited state. In this paper, the nature of the stable photoproduct of *N*-(2-hydroxybenzylidene)aniline will be discussed. On the basis of this investigation it is concluded that it is not necessary to invoke the presence of *ortho*-quinone tautomers to explain the spectral changes that are observed to occur.

## Experimental

*N*-(2-Hydroxybenzylidene)aniline (HBA) and *N*-(2-hydroxybenzylidene)-*m*-toluidine were prepared and purified by the methods described in the preceding papers. The deuterium substituted anil was prepared by refluxing the parent anil in a one-to-three mixture of $D_2O$ and methanol-$d_1$. The process was repeated twice and the final product contained > 90%—OD. The thin polycrystalline films of the anils were produced from a melt between either quartz or sodium chloride plates. Ultra thin films were produced by means of the technique described by Cohen *et al.* (9).

The light source used for the irradiation of the compounds was an Oriel Model 7340 equipped with a 200 W medium pressure mercury arc. The excitation wavelengths were isolated by means of an Oriel Model 7240 monochromator. The bandwidths of the excitation lines were approximately 20 nm, according to the manufacturer's specifications.

The low temperature infrared cell was constructed after the pattern described by Wagner and Hornig (27). The ultraviolet–visible absorption spectra were recorded by means of a Cary 17 spectrometer and the infrared spectra were recorded by means of a Perkin–Elmer 621 spectrometer. The reported infrared frequencies were calibrated to the known bands of polystyrene.

## Results and discussion

### A. *Ultraviolet–visible measurements*

Several absorption spectra of thin polycrystalline films of *N*-(2-hydroxybenzylidene)aniline (HBA) are reproduced in Fig. 1. The visible absorption spectra of the irradiated films exhibit a broad new absorption band with maximum absorbance near 480 nm. In contrast to the featureless absorption band near 440 nm that is observed in the spectra of anils in hydrogen-bonding solvents, the photochemically produced band of this anil has some structure. The spectrum shows shoulders at about 550, 510, and 460 nm in addition to the maximum at 478 nm. The absorption band observed in these spectra has been assigned to a $\pi^* \leftarrow \pi$ transition of the *trans*-quinoid tautomer (3).

The new absorption band reproduced in Fig. 1 is observable only after the irradiation of the anil. (In this work the irradiation was normally carried out at 365 nm since this is the most intense line in the ultraviolet portion of the medium pressure mercury arc spectrum.) The new absorption band is erased or bleached by irradiation at any wavelength which

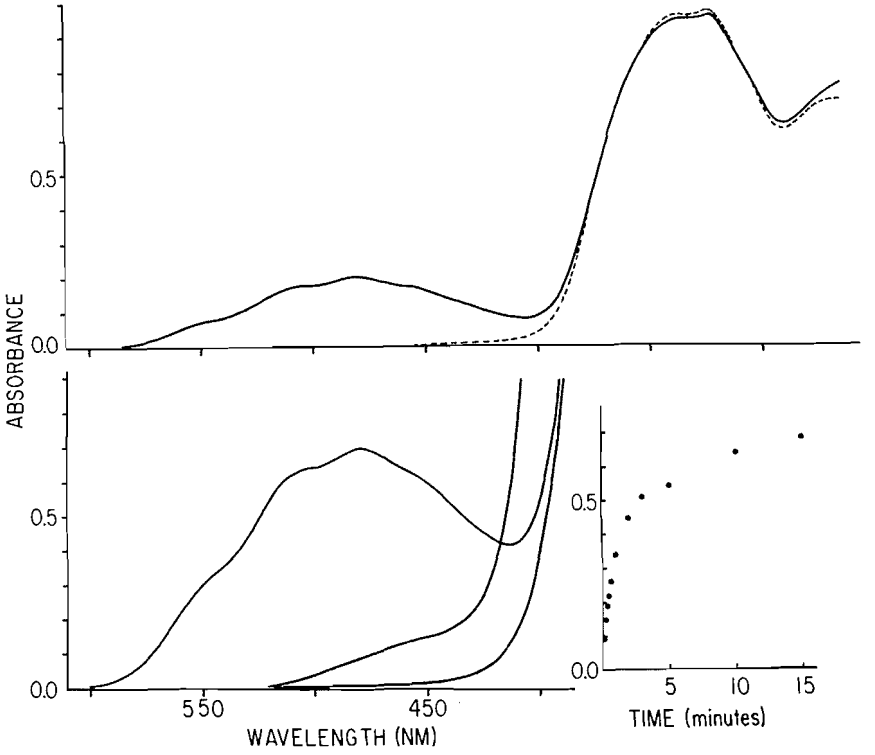


FIG. 1. Absorption spectra of *N*-(2-hydroxybenzylidene)aniline; upper curves: ultra-thin polycrystalline film, ----- before irradiation, — after irradiation at 365 nm; lower curves: thin polycrystalline film; lower right: absorbance at 478 nm as a function of time of irradiation.

lies within this band. It is then obvious that once a sufficient, and small, quantity of the photoproduct has accumulated, the photoproduct begins to absorb the 365 nm radiation and the bleaching commences. In this manner, a limiting concentration of the photoproduct is quickly attained. The development of absorbance at 478 nm as a function of time of irradiation is shown in the bottom right of Fig. 1. In addition to the screening effect or inner filter effect, thermal bleaching is also a contributor to the observed nonlinearity. In these room temperature experiments there is considerable deviation from linearity even after only two minutes of irradiation, although there continues to be an increase in 478 nm absorbance throughout at least fifteen minutes of irradiation.

The thermal bleaching is effectively eliminated by lowering the sample temperature to 77 K, where the photocolor is stable for long periods of time. The inner filter effect is not eliminated, however, by lowering the temperature. Both the forward and the reverse photochemical transformations of crystalline HBA occur at 77 K, but the quantum yields of both are greatly reduced as compared with the room temperature yields. Therefore, some advantage in the form of slightly higher concentration of photoproduct and the elimination of thermal bleaching is gained by lowering the sample temperature to 77 K, but only at the expense of greatly lengthened irradiation times.

It should also be mentioned that the recorded absorption spectra are not corrected for thermal bleaching nor for the photochemical bleaching caused by the measurement process. It is estimated that these errors amount to less than about 8%. (This estimate was made by scanning the entire spectrum, then rapidly returning to various wavelengths within the absorption band and measuring the decrease in absorbance.) The overall shape of the absorption spectra should not, therefore, be greatly affected.

In an attempt to reduce the inner filter effect, irradiation of low temperature thin films of polycrystalline HBA was carried out at 340, 330, 313, and 303 nm. In each case there was no significant change in the amount of photoproduct attained. This could mean that the photoproduct also absorbs at these wavelengths or simply that, due to the diminished intensity of the source at these wavelengths, a much longer period of irradiation is necessary.

At this point, it is perhaps of interest to make

Can. J. Chem. Downloaded from www.nrcresearchpress.com by 210.87.254.105 on 09/06/12
For personal use only.

Can. J. Chem. Downloaded from www.nrcresearchpress.com by 210.87.254.105 on 09/06/12
For personal use only.

some comments relative to the apparent molar absorption coefficient of the photoproduct. The spectra of an irradiated and a nonirradiated ultra thin film are also shown in Fig. 1. Clearly the increase in absorbance at 478 nm is at least ten times greater than the decrease in absorbance at 340 nm. If it is assumed that absorbance at 340 nm is linear with concentration of the enol, then it must be concluded that the coefficient of the photoproduct is ten times that at the solid enol. It is, of course, a distinct possibility that enol absorbance at 340 nm is not linear with concentration despite the fact that the total absorbance is less than 1.0. Cohen *et al.* (5, 6) report the spectra of irradiated and nonirradiated low temperature solutions of several *N*-salicylideneanilines and in all cases it appears that the increase in absorbance at the visible wavelength is greater than the decrease in absorbance at the near ultraviolet wavelength. In no case, however, is the ratio so large as in the case of the ultrathin polycrystalline film reported here. Some of the photoproduct spectra reported by Cohen and coworkers may also indicate an additional new absorption band in the region of the lowest energy band of the enol. The spectra reported in this present work do not give such an indication. While no conclusions may be made, it appears that the absorption coefficient of the photoproduct exceeds that of the enol. In any case, it is a matter which requires further investigation.

On the basis of similar electronic structure, it might be assumed that the photochemistry of HBA and *N*-benzylideneaniline (BA) are also closely related. The scheme shown (Scheme 2) might be proposed for overall photoproduct formation. Like BA, the initial enol of HBA exists in a conformation which is *trans* about the C=N bond and the aniline ring is somewhat twisted out of the molecular plane. (Note that *trans* and *cis*, as used here, describe the conformation about the C=N bond and not the relative positions of the hydrogen and oxygen atoms as was the case in Scheme 1.) The absorption of a photon causes an ultrafast proton transfer (24) which might be followed by a slower inversion at the nitrogen. The inversion results in a conformation which is *cis* about the C=N bond. This model differs considerably from that proposed by other investigators. It has been argued that the *trans*-quinoid (see Scheme 1) is produced by means of a rotation about the ring carbon – imine carbon bond (13), but there is no valid reason to suspect that the photochemistry of HBA and BA should be so different.

It is well known that protonation of the imine nitrogen actually stabilizes the *cis*-conformation of

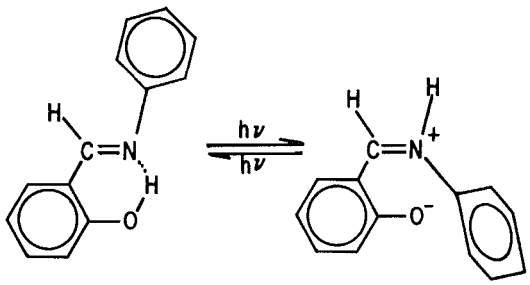


SCHEME 2

BA (28). For example, the irradiation of room temperature solutions of BA produces no stable photoisomers, although the *cis*-conformer may be observed by means of flash techniques (29). The irradiation of room temperature solutions of BA in 96% sulfuric acid, on the other hand, results in the formation of the thermally stable *cis*-*N*-benzylideneanilinium cation (28). In this solvent system BA is protonated in the ground state, hence the protonated imine nitrogen inhibits the return to the *trans*-conformation. It would be of interest to know whether a similar phenomenon occurs in solvent systems wherein BA is not protonated in the electronic ground state but in which protonation could occur in the excited state.

The ultraviolet–visible absorption spectrum of irradiated solutions of thin polycrystalline films of HBA may then contain contributions from three species. These are the original intramolecularly hydrogen bonded enol, an enol that is not internally hydrogen bonded, and the *cis* "ion-pair". The spectrum is dominated by the absorption of the original hydrogen bonded enol because inner filter effects (reverse, *cis* → *trans* photoisomerization) limit the concentration of the *cis* "ion-pair".

B. *Infrared measurements*

According to the arguments presented in the previous sections, the infrared spectrum of an irradiated thin polycrystalline film of HBA should reflect changes similar to those of an irradiated film of BA. In addition to the spectral changes that result from the *trans* → *cis* isomerization, changes indicating the transferred proton and changes involving the phenolate anion are to be expected. It should be added that perhaps very little change in the Ar—N stretching frequency is expected since there can be little favorable nitrogen lone pair – aniline ring interactions (see Scheme 2).

The 3500–2500 and 1700–1500 $cm^{-1}$ regions of the spectra of irradiated and nonirradiated thin films of HBA are shown in Fig. 2. As was expected, the new photoproduct bands are weak but assignments are entirely possible. The three new bands at

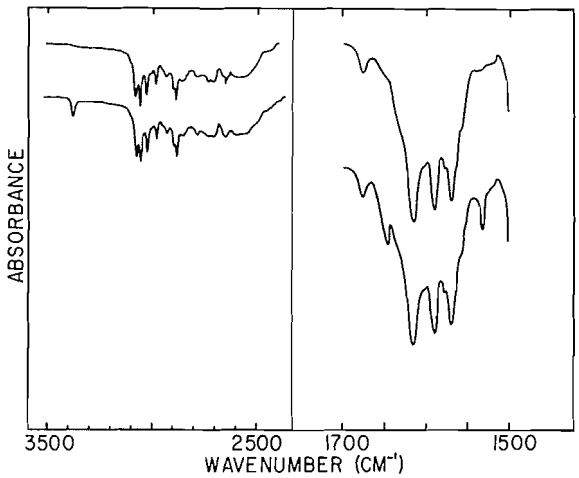


FIG. 2. Infrared absorption spectra of *N*-(2-hydroxybenzylidene)aniline; upper curve: thin polycrystalline film before irradiation, 77 K; lower curve: thin polycrystalline film after irradiation at 365 nm, 77 K.

3380, 1646, and 1537 $cm^{-1}$ are directly associated with the development of the 478 nm optical absorption band. These bands may be bleached by re-irradiating the sample at 547 nm, for example, or by allowing the sample to warm. The irradiation and re-irradiation of the sample may be repeated at will without any sign of fatigue or photodecomposition. The new bands in the spectrum of the irradiated sample shown in Fig. 2 result from six hours of continuous irradiation at 365 nm of a film maintained at 77 K. A similar intensity of the 1646 $cm^{-1}$ band may be developed by only 30 min of irradiation at 365 nm of a room temperature sample; however, in the infrared beam of the spectrometer, the photocolor fades very rapidly as attempts to record a spectrum are made. For example, during the time required for the normal recording of the spectrum from 1700 to 1500 $cm^{-1}$, the 1537 $cm^{-1}$ band will have decreased in intensity by more than one-half. It is thus not surprising that ordinary infrared spectra of the photoproduct have not previously been published.

Nakagaki *et al.* (23) have obtained a difference spectrum, by means of Fourier transform infrared techniques (FTIR), of *N*-(2-hydroxybenzylidene)-*m*-toluidine. These authors' results are summarized in Table 1. In view of our observations, it seems to be necessary to modify some of these assignments.

(a) It is rather unusual that the C=N stretching frequency of a deuterium substituted Schiff base should be higher than that of the hydrogen derivative. It is true that intramolecular hydrogen bonding does not produce the magnitude of spectral

TABLE 1. Infrared bands of *N*-(2-hydroxybenzylidene)-*m*-toluidine after Nakagaki *et al.* (23)[a]

| Assignment | Frequency ($cm^{-1}$)(—OH) | Frequency ($cm^{-1}$)(—OD) |
|---|---|---|
| C=N | 1616 | 1620 |
| Ring skeletal stretching | 1597 | 1597 |
| | 1570 | 1570 |
| C=O | 1651 | 1644 |
| Amide vinylog and ring skeletal stretching | 1539 | 1529 |
| | 1510 | 1505 |
| | 1487 | 1487 |
| C—N | 1319 | 1319 |

[a]The recorded data were obtained from an FTIR difference spectrum of a KBr disc at room temperature.

shifts that might be expected on reasonable theoretical grounds and intermolecular hydrogen bonding has essentially no effect at all, but the shifts, when observed, are generally in the proper direction.

(b) The band assigned by Nakagaki and co-workers as due to a C=O stretching and two of the three bands assigned to modes of a "quinoid ring and the amide vinylog, HN—C=C—C=O", of the photoproduct exhibit deuterium isotope shifts of 7, 10, and 5 $cm^{-1}$, respectively. On the other hand, the C—N (single bond) stretching mode, which is subject to a greater isotope effect since this bond is nearer to the site of deuterium exchange, shows no isotope effect at all. The proposed structure of the photoproduct, a *trans*-quinoid (see Scheme 1), is not capable of exhibiting hydrogen (deuterium) bonding, hence the reported isotope shifts must be due to a mass effect. The mass effect must be transmitted along the DN—C=C—C=O chain and, as a result, the lack of an effect on the adjacent C—N bond is hard to understand.

(c) One of the 1579, 1510, and 1487 $cm^{-1}$ bands must be the so-called amide II band. Amide II bands are normally ascribed to an interaction between the N—H bending and the C—N stretching modes (30–32). The resultant two bands, amide II and amide III, are sensitive to isotope effects. Deuterium shifts are smaller than expected but still amount to about 6% (32) or approximately 100 $cm^{-1}$ in the case of the amide II band. The small deuterium frequency shifts observed by Nakagaki and co-workers are then not easily reconcilable with an amide II band assignment.

In the present work, experiments have also been carried out with HBA-$d_1$, and the spectra are reproduced in Fig. 3. Before further discussion of the photoproduct spectral bands, it is of interest and indeed necessary to examine the spectrum of a polycrystalline film of nonirradiated HBA-$d_1$. It is observed that this spectrum exhibits bands at 1614,

Can. J. Chem. Downloaded from www.nrcresearchpress.com by 210.87.254.105 on 09/06/12
For personal use only.

Can. J. Chem. Downloaded from www.nrcresearchpress.com by 210.87.254.105 on 09/06/12
For personal use only.

FIG. 3. Infrared absorption spectra of *N*-(2-hydroxybenzylidene)aniline-$d_1$; upper curve: thin polycrystalline film before irradiation; lower curve: thin polycrystalline film after irradiation at 365 nm.

1589, 1578 (shoulder), and 1558 $cm^{-1}$. The corresponding spectrum of HBA shows bands at 1615, 1590, 1578 (shoulder), and 1571 $cm^{-1}$. It is quite obvious that the shift of the 1571 $cm^{-1}$ band to 1558 $cm^{-1}$, upon deuterium exchange, cannot be explained if its assignment as a pure ring skeletal vibration is retained. In the preceding article it was shown that the band at 1571 $cm^{-1}$ in the spectrum of polycrystalline HBA is influenced by Fermi resonance with the 1615 $cm^{-1}$ C=N stretching mode. For HBA-$d_1$ the same arguments are applicable if the changed conditions for Fermi resonance are taken into account. The expected downward deuterium shift of the C=N stretching band is not accurately represented by the negligible 1 $cm^{-1}$ shift of the 1615 $cm^{-1}$ component. Deuterium substitution leads to increased repulsion between the two states and leads to the apparent lack of a shift of the 1615 $cm^{-1}$ band and the observed shift of the 1571 $cm^{-1}$ band to 1558 $cm^{-1}$. The extent of the deuterium shift on the C=N stretching frequency is, therefore, not known since the true position of the C=N stretching frequency is in question.

Percy and Thornton (33), in a study of 28 *N*-(2-hydroxybenzylidene)anilines, assign a pair of bands in each infrared spectrum as due to the C=N stretching mode. In these examples the high frequency band occurs in the range from 1629 to 1613 $cm^{-1}$ and the low frequency band occurs in the range from 1582 to 1568 $cm^{-1}$. Further, these authors discuss the infrared spectra of 38 Co(II), Ni(II), Cu(II), and Zn(II) chelates derived from these Schiff bases. A pair of bands attributable to the C=N stretching mode were found in 37 of the 38 infrared spectra. In these examples the high frequency bands were found in the 1618 to 1602 $cm^{-1}$ range and the low frequency bands were found in the 1597 to 1574 $cm^{-1}$ range. They also invoked Fermi resonance in order to interpret their spectra.

A comparison of Figs. 2 and 3 reveals that the photoproduct bands of HBA at 1646 and 1537 $cm^{-1}$ are apparently shifted to 1642 and 1529 $cm^{-1}$, respectively, in the spectrum of the deuterium substituted photoproduct, HBA-$d_1$. It will also be noted that the ordinary infrared spectra of the HBA and HBA-$d_1$ photoproducts exhibit only one band in the 1550–1510 $cm^{-1}$ range, whereas Nakagaki and co-workers report two bands in this region of the FTIR difference spectra of the *N*-(2-hydroxybenzylidene)-*m*-toluidine photoproduct and its deuterium substituted photoproduct. Obviously, the comments made earlier with respect to the assignments of Nakagaki and co-workers are also applicable here in the case of HBA and HBA-$d_1$. The small apparent isotope effects that are observed are not consistent with the assignment of these bands to the C=O stretching and the C=C or H—N (D—N) + C—N (amide II) stretching modes. On the one hand, a large (100 $cm^{-1}$) deuterium shift is expected for an amide II band and the observed shift is only 8 $cm^{-1}$, and, on the other hand, only a negligible deuterium shift is expected for a C=O stretching vibration and a 4 $cm^{-1}$ shift is observed. It is quite possible, however, that the 1537 $cm^{-1}$ band observed in the spectrum of the HBA photoproduct is of different origin than the 1529 $cm^{-1}$ band of the HBA-$d_1$ photoproduct.

The band at 3380 $cm^{-1}$ in the spectrum of the HBA photoproduct is attributed to the $N^+$—H stretching vibration. This spectrum provides the first recorded experimental evidence related to the disposition of the phototransferred proton. Clearly the sharpness of this band and its relatively high frequency (34, 35) eliminate the possibility of hydrogen bonding to the phenolate oxygen or to neighboring molecules. Unfortunately, an $N^+$—D stretching band was not located in the spectrum of the HBA-$d_1$ photoproduct. It is likely, however, that the $N^+$—D stretching band is much weaker than the already weak $N^+$—H stretching band.

It is proposed, therefore, that the 1646 and 1537 $cm^{-1}$ bands in the spectrum of the HBA photoproduct are attributable to the C=$NH^+$

Can. J. Chem. Downloaded from www.nrcresearchpress.com by 210.87.254.105 on 09/06/12
For personal use only.

stretching and the N—H deformation modes. These modes are not completely independent. It was shown previously that these modes of the HBA hydrochloride are strongly coupled, so there is every reason to suspect that they would also be coupled in this case. The differences between the frequencies of the photoproduct bands and those of the hydrochloride may be rationalized in terms of changes in the degree of coupling. For example, the photoproduct is necessarily a zwitterion, which is probably in a *cis*-conformation about the C=N bond, while the hydrochloride is a true salt. In addition, the spectrum of the hydrochloride was obtained from a solution while that of the photoproduct was obtained from a polycrystalline film. These environmental perturbations could exaggerate the frequency differences.

The stretching frequency of a $C{=}NH^+$ group is expected to decrease some 25–35 $cm^{-1}$ (36) when the hydrogen is replaced by a deuterium atom. The observed frequency shift in the spectrum of the HBD-$d_1$ photoproduct is only 4 $cm^{-1}$. Meanwhile the HBA photoproduct band at 1537 $cm^{-1}$ apparently shifts to 1529 $cm^{-1}$ in the spectrum of the HBA-$d_1$ photoproduct. These small isotope shifts would appear to invalidate the above assignments for the photoproduct of HBA, but it must be recalled that the lower frequency infrared bands in the spectra of the hydrochloride and deuterochloride of HBA were interpretable only (paper II) when different degrees of Fermi resonance, by which the bands are affected, are considered. There are small differences between the corresponding band positions of the photoproduct and the deuterochloride, but these may be satisfactorily accounted for by differences in the structure of the two species and by changes in the amount of resonance.

The infrared spectra of a polycrystalline film of *N*-(2-hydroxybenzylidene)-*m*-toluidine, recorded before and after irradiation at 365 nm, are presented in Fig. 4. These spectra are severely distorted in the range from 1650 to 1550 $cm^{-1}$, as may be ascertained by a comparison with the accompanying spectrum which was obtained from a chloroform solution of the compound. Numerous attempts to obtain a better quality film were not successful and KBr discs, even after repeated grindings, failed to yield a quality spectrum in the 1650–1550 $cm^{-1}$ region. In order not to complicate the spectra only those regions wherein major spectral changes occur are reproduced in Fig. 4. Despite the quality of the spectra, new photoproduct bands are observable at near 3320, (1650), 1535, 1503, 1321, 1310, and 995 $cm^{-1}$. Note that the band

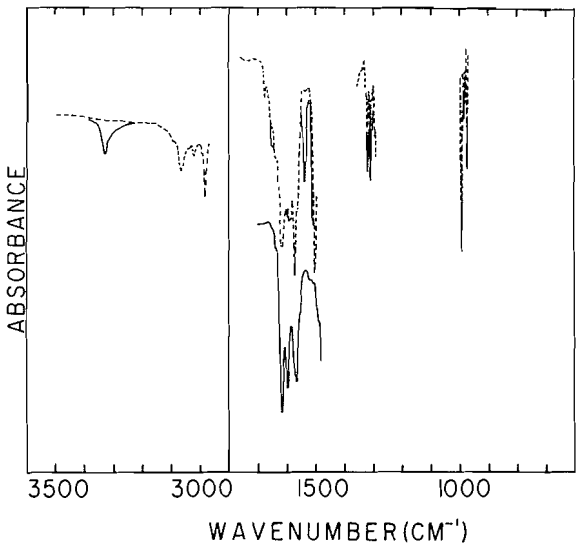


FIG. 4. Infrared absorption spectra of *N*-(2-hydroxybenzylidene)-*m*-toluidine; upper curves: ----- thin polycrystalline film before irradiation, — thin polycrystalline film after irradiation at 365 nm, 77 K; lower curve: chloroform solution.

located near 1650 $cm^{-1}$ appears only as a slight broadening.

For the reasons outlined earlier the 3320 $cm^{-1}$ band is attributable to the $N^+$—H stretching mode and the pair of bands at (1650) and 1535 $cm^{-1}$ are attributable to the coupled $C{=}NH^+$ stretching and $N^+$—H deformation modes. It is probable that the band located near 1503 $cm^{-1}$ reflects a slight shift of an aromatic skeletal stretching motion, which is produced by the geometric rearrangement. This assignment is made since a similar band is observed in the spectrum of irradiated *N*-benzylideneaniline, which is not capable of undergoing any structural change except *trans* → *cis* isomerization. The two bands at 1321 and 1310 $cm^{-1}$ may be related to the phenolate anion; however, it should be mentioned that a pair of bands occurs at these frequencies in the spectrum of the nonirradiated compound. It is likely therefore that these spectral changes represent intensifications of existing bands and do not represent new vibrational modes such as the C—N stretching as proposed by Nakagaki *et al.* (23). The weak band located near 995 $cm^{-1}$ is of undetermined origin but may reflect a vibration of the aromatic phenolate nucleus.

The 1500–700 $cm^{-1}$ region of the infrared spectra of nonirradiated and irradiated films of HBA is not presented since these spectra are very similar to those of *N*-(2-hydroxybenzylidene)-*m*-toluidine. New but weaker photoproduct bands are observed near 1502, 1319, and 1310 $cm^{-1}$ and these bands

Can. J. Chem. Downloaded from www.nrcresearchpress.com by 210.87.254.105 on 09/06/12
For personal use only.

show no deuterium isotope effects. No new photoproduct band was observed near 1000 $cm^{-1}$, but an intensification of a band near 863 $cm^{-1}$ is noted.

The infrared study of the photochromic properties of other Schiff bases was also attempted. Films of Schiff bases derived from salicylaldehyde and *p*-methoxy-, *p*-bromo-, *p*-chloro, *p*-iodo-, and 2,5-dimethylaniline and *p*-aminoacetophenone were formed and tested. Only the film formed from *N*-(2-hydroxybenzylidene)-*p*-aminoacetophenone proved to be slightly photochromic, although no useful infrared bands of the photoproduct could be found in the spectrum. This latter compound proved, however, to be most interesting. The solid compound, as obtained by crystallization from ordinary solvents, is highly photochromic, perhaps even more so than any of the compounds studied. Crystals that are derived from a melt, on the other hand, were very weakly photochromic. The 3500–3000 and 1800–1500 $cm^{-1}$ regions of the infrared spectra of a perchloroethylene solution and a crystalline film (derived from a melt) are shown in Fig. 5. The solid state spectrum is greatly distorted in the 1800–1500 $cm^{-1}$ region and the carbonyl C=O stretching is split into two bands. Apparently this is due to intermolecular hydrogen bonding between the phenolic O—H and the C=O of the acetyl group. There is also evidence (the sharp band at 3400 $cm^{-1}$) that at least some of the molecules exhibit free phenolic O—H groups. Thus several different species exist in the melt-derived crystals. The solution spectrum shows no evidence of free O—H groups nor of intermolecular hydrogen bonding. It is therefore highly probable that for this particular compound the photochromic character is strictly dependent on the internal chelate ring involving the O—H...N hydrogen bond. Apparently intermolecularly hydrogen bonded and non-hydrogen bonded molecules do not exhibit photochromism.

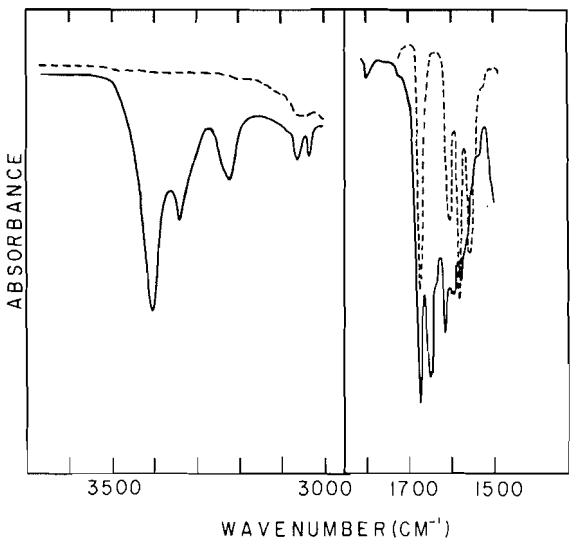


FIG. 5. Infrared absorption spectra of *N*-(2-hydroxybenzylidene)-*p*-aminoacetophenone, ----- perchloroethylene solution, — thin polycrystalline film.

## Conclusion

The infrared spectra of *N*-(2-hydroxybenzylidene)aniline, its deuterium substituted counterpart, *N*-(2-hydroxybenzylidene)-*m*-toluidine, and their photoproducts have been presented. These new data, in conjunction with the information gained in the studies of *N*-benzylideneaniline and its photoproduct and of the solvent dependent processes of these compounds, permit well founded assignments of the observed bands in the infrared spectra of the photoproducts. The photoproduct is thus determined to be a zwitterion, not an *ortho*-quinone. It is further noted that the *cis*-conformation about the C=N bond is required since hydrogen bonding between the $C—O^-$ and $N^+—H$ groups does not exist.

## Acknowledgements

Financial assistance from the Natural Sciences and Engineering Research Council of Canada, the Ministère de l'Education du Québec, and the Canada Council through the grant of the Killam Memorial scholarship to C. Sandorfy is gratefully acknowledged.

1. M. D. COHEN, Y. HIRSHBERG, and G. M. T. SCHMIDT. *In* Hydrogen bonding. *Edited by* D. Hadzi. Pergamon Press, London. 1959. p. 293.
2. M. D. COHEN and G. M. T. SCHMIDT. *In* Reactivity of solids. *Edited by* J. H. de Boer. Elsevier, Amsterdam. 1961. p. 556.
3. M. D. COHEN and G. M. T. SCHMIDT. J. Phys. Chem. **66**, 2442 (1962).
4. M. D. COHEN, G. M. T. SCHMIDT, and S. FLAVIAN. J. Chem. Soc. 2041 (1964).
5. M. D. COHEN, Y. HIRSHBERG, and G. M. T. SCHMIDT. J. Chem. Soc. 2051 (1964).
6. M. D. COHEN, Y. HIRSHBERG, and G. M. T. SCHMIDT. J. Chem. Soc. 2060 (1964).
7. M. D. COHEN and S. FLAVIAN. J. Chem. Soc. B, 317 (1967).
8. M. D. COHEN and S. FLAVIAN. J. Chem. Soc. B, 321 (1967).
9. M. D. COHEN, S. FLAVIAN, and L. LEISEROWITZ. J. Chem. Soc. B, 329 (1962).
10. M. D. COHEN and S. FLAVIAN. J. Chem. Soc. B, 334 (1967).
11. M. OTTOLENGHI and D. S. MCCLURE. J. Chem. Phys. **46**, 4613 (1967).
12. M. OTTOLENGHI and D. S. MCCLURE. J. Chem. Phys. **46**, 4620 (1967).
13. R. S. BECKER and W. F. RICHEY. J. Am. Chem. Soc. **89**, 1298 (1967).

14. W. F. RICHEY and R. S. BECKER. J. Chem. Phys. **49**, 2092 (1968).
15. G. WETTERMARK and L. DOGLIOTTI. J. Chem. Phys. **40**, 1486 (1964).
16. D. G. ANDERSON and G. WETTERMARK. J. Am. Chem. Soc. **87**, 1433 (1965).
17. R. POTASHNIK and M. OTTOLENGHI. J. Chem. Phys. **51**, 3671 (1969).
18. T. ROSENFELD, M. OTTOLENGHI, and A. Y. MEYER. Mol. Photochem. **5**, 39 (1973).
19. C. PASTERNAK, M. A. SLIFKIN, and M. SHINITZKY. J. Chem. Phys. **68**, 2669 (1978).
20. J. W. LEDBETTER, JR. J. Phys. Chem. **70**, 2245 (1966).
21. J. W. LEDBETTER, JR. J. Phys. Chem. **81**, 54 (1977).
22. E. HADJOUDIS, F. MILIA, J. SELIGER, A. BLINC, and V. ZAGAR. Chem. Phys. **47**, 105 (1980).
23. R. NAKAGAKI, T. KOBAYASHI, J. NAKAMURA, and S. NAGAKURA. Bull. Chem. Soc. Jpn. **50**, 1909 (1977).
24. P. F. BARBARA, P. M. RENTZEPIS, and L. E. BRUS. J. Am. Chem. Soc. **91**, 102 (1980).
25. J. P. BIDEGARAY and R. VIOVY. C.R. Acad. Sci. **270**, 1337 (1970).
26. E. HADJOUDIS, L. MOSTAKALI-MAVRIDIS, and J. XEXAKIS. Israel J. Chem. **18**, 202 (1979).
27. E. L. WAGNER and D. F. HORNIG. J. Chem. Phys. **18**, 296 (1950).
28. K. GEIBEL, B. STAUDINGER, K. H. GRELLMAN, and H. WENDT. J. Photochem. **69**, 1584 (1965).
29. G. WETTERMARK, J. WEINSTEIN, J. SOUSA, and L. DOGLIOTTI. J. Phys. Chem. **69**, 1584 (1965).
30. J. MIYAZAWA, T. SHIMANOUCHI, and S. I. MIZUSHIMA. J. Chem. Phys. **29**, 611 (1958).
31. R. M. SILVERSTEIN and G. C. BASSLER. Spectrometric identification of organic compounds. 2nd ed. John Wiley and Sons Inc., New York. 1967. p. 95.
32. L. J. BELLAMY. The infrared spectra of complex molecules. Vol. 1. 3rd ed. Chapman and Hall, London. 1975. p. 244.
33. G. C. PERCY and D. A. THORNTON. J. Inorg. Nucl. Chem. **34**, 3357 (1972).
34. W. KYNASTON, B. E. LARCOME, and H. S. TURNER. J. Chem. Soc. 1772 (1960).
35. P. CHEVALIER and C. SANDORFY. Can. J. Chem. **38**, 2524 (1960).
36. B. ATON, A. G. DOUKAS, D. NARVA, R. H. CALLENDER, U. DINUR, and B. HONIG. Biophys. J. **29**, 79 (1980).

Can. J. Chem. Downloaded from www.nrcresearchpress.com by 210.87.254.105 on 09/06/12
For personal use only.

FOR ERRATA SEE
v.62 #6 1984 p. 1227



# Existence and characterization of double salts in indium trihalide – potassium halide – water systems at 21°C (halide = Cl, Br)

J. P. WIGNACOURT, G. MAIRESSE, AND P. BARBIER

*Laboratoire de Cristallochimie et de Physicochimie du Solide, Université des Sciences et Techniques de Lille, 59655 Villeneuve d'Ascq, France*

AND

A. LORRIAUX-RUBBENS[1] AND F. WALLART

*Laboratoire de Spectrochimie Infrarouge et Raman, CNRS, Université des Sciences et Techniques de Lille, Bât. C.5, 59655 Villeneuve d'Ascq, France*

Received September 25, 1981

J. P. WIGNACOURT, G. MAIRESSE, P. BARBIER, A. LORRIAUX-RUBBENS, and F. WALLART. Can. J. Chem. **60**, 1747 (1982).

The degree of hydration of stable hydrates is discussed on the basis of early literature results and our determination of the phase diagrams for the systems $InCl_3$–KCl–$H_2O$ and $InBr_3$–KBr–$H_2O$ at 21°C. The existing double salts are formulated: $3KCl \cdot InCl_3 \cdot H_2O$ and $2KCl \cdot InCl_3 \cdot H_2O$ in the chloride system, and $3KBr \cdot InBr_3 \cdot 1.5H_2O$, $2KBr \cdot InBr_3 \cdot H_2O$, $KBr \cdot InBr_3 \cdot 2H_2O$, and $3KBr \cdot 2InBr_3$ in the bromide system. All of them are incongruently saturating at 21°C. A summary of their crystallographic and Raman spectroscopic data is given.

J. P. WIGNACOURT, G. MAIRESSE, P. BARBIER, A. LORRIAUX-RUBBENS et F. WALLART. Can. J. Chem. **60**, 1747 (1982).

A partir de la détermination des diagrammes de phase à 21°C: $InCl_3$–KCl–$H_2O$ et $InBr_3$–KBr–$H_2O$, la composition exacte des hydrates stables à cette température est discutée par rapport aux données bibliographiques antérieures. Les sels doubles existants sont formulés: $3KCl \cdot InCl_3 \cdot H_2O$ et $2KCl \cdot InCl_3 \cdot H_2O$ dans le système des chlorures; $3KBr \cdot InBr_3 \cdot 1.5H_2O$, $2KBr \cdot InBr_3 \cdot H_2O$, $KBr \cdot InBr_3 \cdot 2H_2O$ et $3KBr \cdot 2InBr_3$ dans le système des bromures. Ceux-ci sont tous à solubilité non congruente à 21°C. Un résumé de leurs caractéristiques cristallographiques et spectroscopiques (Diffusion Raman) est donné.

## Introduction

Although the hydrated double salts between indium trihalides and potassium halides (general formula $K_3InX_6 \cdot nH_2O$) were reported in early literature, their degree of hydration is still a much debated question. The $K_3InCl_6 \cdot 1.5H_2O$ complex was first proposed by Meyer (1) in 1869. Early in the present century, Wallace (2) identified compounds with the $K_3InX_6 \cdot 2H_2O$ (X = Cl, Br) formulation. In 1974, we established the $InCl_3$–KCl–$H_2O$ solubility diagram at 21°C (3) which characterises the existence of the $K_3InCl_6 \cdot H_2O$ and $K_2InCl_5 \cdot H_2O$ incongruently saturating compounds, as well as the salt $InCl_3 \cdot 4H_2O$. The formulation $K_3InCl_6 \cdot 2H_2O$ was given more recently in a study by Kartzmark of the same system at 25°C (4).

Arguing from the results of X-ray and Raman structural investigations, we discuss the formulation of the existing double salts at 21°C in the $InCl_3$–KCl–$H_2O$ system, as well as in the corresponding one $InBr_3$–KBr–$H_2O$.

## Experimental

The starting materials were $InCl_3$ and $InBr_3$ synthesised in this laboratory and reagent grade potassium halides. The systems studied were stirred at 21°C in a water bath thermostated at 20 ± 0.2°C.

The solubility diagrams were established using the "global point" and the "wet residue" methods. We chose the starting mixture composition (global point) so that the whole diagram is covered with a minimum set of experiments. Indium trihalide is introduced in the solubility reactor and weighed in a dry box, and the corresponding quantities of potassium halide and water are then calculated and added (the total mass being about 5 g). Equilibrium is considered to be reached when the solution density, measured by means of a double capillary (Cornec-Cottet) pipette, remains constant. About 2 or 3 days are required for equilibrium in the bromide system and most of the chloride one. For the highly viscous indium halide-rich solutions, crystallisation of the solid phase requires thermal treatment (5) to transform the vitreous metastable state into a thermodynamic equilibrium between the solid phase and its saturated solution.

In all cases, the solution is sampled by means of the densimetric pipette and submitted to chemical analysis. Then, the solid phase is separated from the remaining solution through sintered glass, and identified by X-ray diffraction, Raman scattering, and chemical analysis.

Chloride and bromide are analysed by mercurimetry, the reactive indicator being nitroprusside. Indium is determined by precipitation of the $In(C_9H_6NO)_3$ oxinate, and the potassium ion is determined with a Perkin-Elmer atomic absorption apparatus. Both are reproducible to within 1%.

The results of the analyses, plotted on the diagrams of Figs. 1 and 3, are consistent when a straight line joins the solution, the global and the solid points, respectively. The composition of the stable compounds and the invariant solutions are obtained from the intersection points of sets of these lines. As numerous double salts have been identified in both systems, the right-triangle representation (6) was adopted, resulting in better separation of existence areas than is obtained with the usual equilateral triangle.

X-ray diffraction patterns are obtained from dried polycrys-

[1]To whom all correspondence should be addressed.

0008-4042/82/131747-04$01.00/0

©1982 National Research Council of Canada/Conseil national de recherches du Canada

Can. J. Chem. Downloaded from www.nrcresearchpress.com by 210.87.254.6 on 09/06/12
For personal use only.

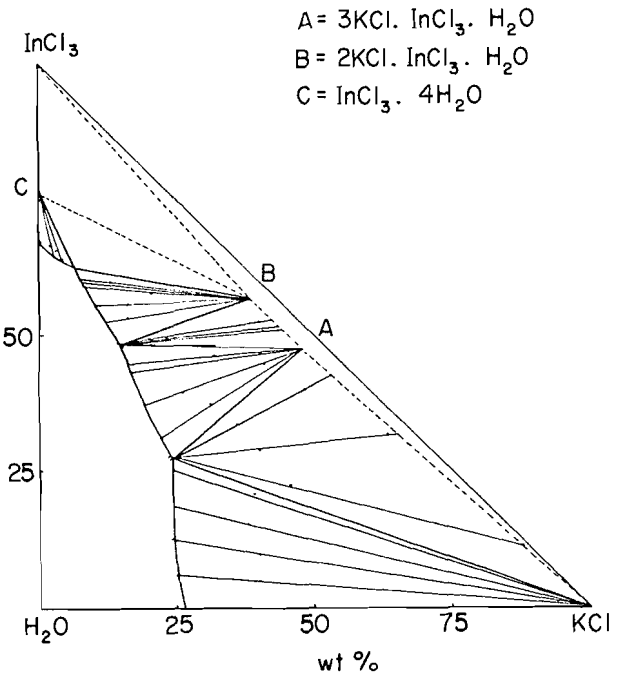


FIG. 1. $InCl_3$–KCl–$H_2O$ system at 21°C.

talline samples. The unit cell dimensions have been determined from single crystals studied on the Philips PW 1100 four circle automated diffractometer of the University of Lille.

The Raman spectra were obtained with a triple monochromator spectrometer using the 514.5 nm exciting line of a Spectra Physics $Ar^+$ laser. Polycrystalline samples were studied directly in the reactor, whereas single crystals were sealed in glass tubes.

## Results and discussion

### *$InCl_3$–KCl–$H_2O$ system*

The experimental data are plotted in Fig. 1 and the compositions of the invariant solutions given in Table 1. The identification of the compounds was made using Raman spectroscopy and X-ray diffraction. The low-frequency Raman spectra, which are shown in Fig. 2, are very specific; thus identification is possible from the analysis of the spectra in the 270–300 $cm^{-1}$ frequency range, which includes the $\nu_s$(In—Cl) stretching vibration (Fig. 2). The band shapes are quite different, as well as their frequencies: 274 and 288 $cm^{-1}$ for $K_3InCl_6 \cdot H_2O$ (7); 286 $cm^{-1}$ for $K_2InCl_5(H_2O)$ (8), and 296 $cm^{-1}$ in $InCl_3 \cdot 4H_2O$ (9).

The $K_3InCl_6 \cdot nH_2O$ molar masses, with $n = 1$, 1.5, or 2 are not very different, being 463.1, 472.1, and 481.1 respectively. Thus the precise determination of $n$ is difficult.

From this study we propose three arguments in favour of the monohydrate $K_3InCl_6 \cdot H_2O$: (*1*) The determination of $n$ from the diagram is unambiguous, as the composition results from the convergence of a set of lines displayed on such a wide area of concentration, that the value obtained is sufficiently precise. (*2*) The chemical analyses of large crystals (5 × 4 × 4 mm), carefully dried from the mother liquor, lead to a value of $n = 1$ (Table 2). (*3*) The thermal dehydration beginning at 50°C shows a mass loss corresponding to one water molecule per salt molecule.

Furthermore a recent crystal structure determination (10) confirms the $K_3InCl_6 \cdot H_2O$ formulation.

The room-temperature stable hydrate of indium trichloride was given as the tetrahydrate $InCl_3 \cdot 4H_2O$ by Ensslin *et al.* (11) in 1942. We have proven its existence at 21°C by the controlled hydrolysis of $InCl_3$ (3): when submitted to a constant vapor

TABLE 1. Composition of the invariant solutions at 21°C in the $InCl_3$–KCl–$H_2O$ system

| $InCl_3$ g/100 g of solution | KCl g/100 g of solution | Nature of solid phase |
|---|---|---|
| | 26.10 | KCl |
| 27.85 | 24.25 | $KCl + K_3InCl_6 \cdot H_2O$ |
| 48.90 | 14.80 | $K_3InCl_6 \cdot H_2O + K_2(InCl_5 \cdot H_2O)$ |
| 62.95 | 6.45 | $K_2(InCl_5 \cdot H_2O) + InCl_3 \cdot 4H_2O$ |
| 67.60 | | $InCl_3 \cdot 4H_2O$ |

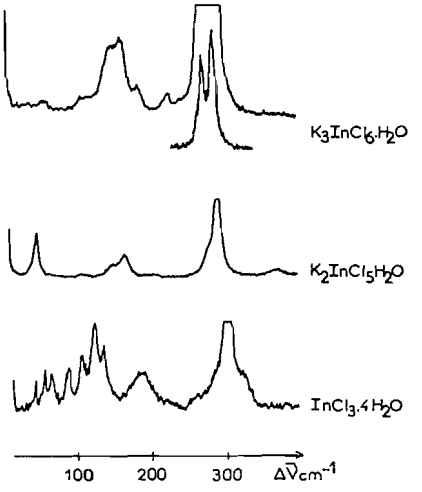


FIG. 2. Raman spectra of the stable solid phases in the chloride system.

TABLE 2. Chemical analysis results for $K_3InCl_6 \cdot H_2O$ sample weight transformed into $1 \times 10^{-3}$ $K_3InCl_6 \cdot H_2O$; $M = 463.1$ mg

| K | In | Cl | $H_2O$ calcd |
|---|---|---|---|
| 3.05 | 0.99 | 5.94 | 1.06 |
| 3.06 | 0.98 | 5.95 | 1.13 |
| 2.98 | 1.00 | 6.04 | 0.92 |

Can. J. Chem. Downloaded from www.nrcresearchpress.com by 210.87.254.6 on 09/06/12
For personal use only.

Can. J. Chem. Downloaded from www.nrcresearchpress.com by 210.87.254.6 on 09/06/12
For personal use only.

pressure, the sample mass first goes up, and then stabilizes at a level corresponding to a $4H_2O/1InCl_3$ mass ratio. Furthermore, the resulting compound shows an X-ray pattern and a Raman spectrum identical to those obtained on the basis of the solubility diagram.

In several recent papers (12, 13) concerning the diagrams of the systems $InCl_3$–pyridine–$H_2O$, $InCl_3$–NaCl–$H_2O$, $InCl_3$–$CaCl_2$–$H_2O$, and $InCl_3$–dioxane–$H_2O$ at 25°C, Kartzmark indicated the existence of $InCl_3 \cdot 3H_2O$. The author proposed this formulation as the one given on the label from the commercial supplier. The knowledge of our results (3) made her reexamine her formulation, and in a recent paper (4) the tetrahydrate was reported as the stable salt at 25°C in the systems $InCl_3$–$In_2(SO_4)_3$–$H_2O$ and $InCl_3$–$M^ICl$–$H_2O$ ($M^I$ = Li, K, Rb, Cs, $NH_4$).

The selective preparation of the incongruently saturating double salts $K_2InCl_5 \cdot H_2O$ and $K_3InCl_6 \cdot H_2O$ on the basis of the ternary diagram has enabled their complete structural investigation by X-ray and Raman scattering (7, 8, 10), the results being widely discussed and compared with the literature. The crystallographic data are summarized in Table 3.

*$InBr_3$–KBr–$H_2O$*

Data which were obtained from the analyses of 36 solubility tubes are plotted on Fig. 3. They indicate the existence at 21°C of the dihydrate $InBr_3$–$2H_2O$, and of four incongruently saturating double salts: $K_3InBr_6 \cdot 1.5H_2O$; $K_2(InBr_5,H_2O)$; $KInBr_4(H_2O)_2$ and $K_3In_2Br_9$. The composition of invariant solutions are given in Table 4.

The two salts $K_3InBr_6 \cdot 1.5H_2O$ and $K_2(InBr_5, H_2O)$ are isomorphous with the corresponding chlorinated compounds, as shown by the crystallographic data (9) given in Table 3.

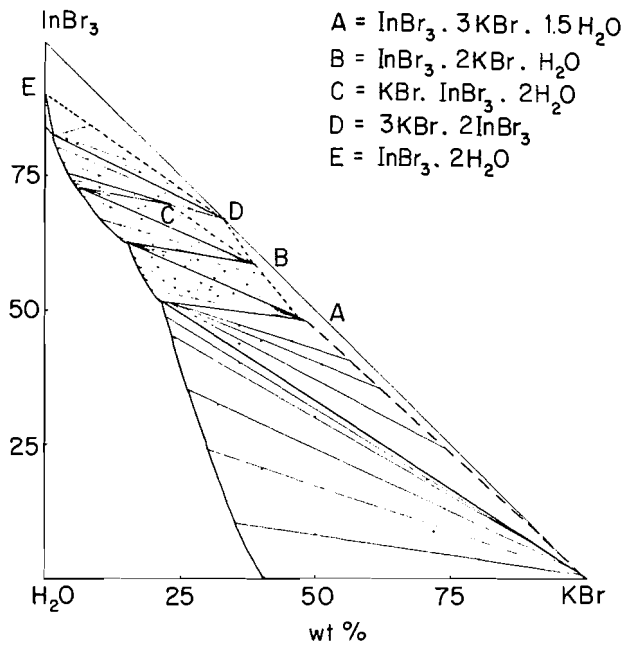


FIG. 3. $InBr_3$–KBr–$H_2O$ system at 21°C.

At 21°C, the area of existence of $KInBr_4(H_2O)_2$ is narrow; experiments at higher temperatures (25–30°C) show enlargement to the detriment of the area for $K_2InBr_5 \cdot H_2O$. In this part of the diagram, we used Raman identification of the solid phases, as X-ray diffraction is less reliable on highly hygroscopic polycrystalline samples. Nevertheless, a single crystal X-ray study led to a characterisa-

TABLE 3. Crystallographic data for the solid phases

| Chemical formula | Space group | $Z$ | Lattice parameters (Å) |
|---|---|---|---|
| $K_3InCl_6 \cdot H_2O$ | *I4mm* | 14 | $a = 15.723(9)$; $c = 18.069(18)$ |
| $K_3InBr_6 \cdot 1.5H_2O$ | | | $a = 16.563(7)$; $c = 18.936(6)$ |
| $K_2(InCl_5 \cdot H_2O)$ | *Pnma* | 4 | $a = 13.905(8)$; $b = 9.952(5)$; $c = 7.185(5)$ |
| $K_2(InBr_5 \cdot H_2O)$ | | | $a = 14.509(6)$; $b = 10.369(7)$ $c = 7.590(3)$ |
| $K(InBr_4(H_2O)_2)$ | $P2_1/c$ | 2 | $a = 6.852(15)$; $b = 11.984(8)$; $c = 6.966(6)$; $\beta = 113.38(5)°$ |
| $K_3In_2Br_9$ | $P4_2/nnm$ | 2 | $a = 10.395(5)$; $c = 7.931(15)$ |
| $InCl_3 \cdot 4H_2O$ | *Pnma* | 4 | $a = 12.053(13)$; $b = 10.601(19)$; $c = 6.463(11)$ |
| $InBr_3 \cdot 2H_2O$ | *Pmcm* *Pmc2₁* *P2cm* | | $a = 33.11$; $b = 6.49$; $c = 5.90$ |

Can. J. Chem. Downloaded from www.nrcresearchpress.com by 210.87.254.6 on 09/06/12
For personal use only.

TABLE 4. Composition of the invariant solutions at 21°C in the $InBr_3$–KBr–$H_2O$ system

| $InBr_3$ g/100 g of solution | KBr g/100 g of solution | Nature of solid phase |
|---|---|---|
| 0 | 41 | KBr |
| 51.80 | 21.55 | $KBr + K_3InBr_6 \cdot 1.5H_2O$ |
| 62.15 | 15.45 | $K_3InBr_6 \cdot 1.5H_2O + K_2(InBr_5 \cdot H_2O)$ |
| 72.90 | 5.75 | $K_2(InBr_5 \cdot H_2O) + K(InBr_4(H_2O)_2)$ |
| 75 | 4.65 | $K(InBr_4(H_2O)_2) + K_3In_2Br_9$ |
| 82.60 | 1.25 | $K_3In_2Br_9 + InBr_3 \cdot 2H_2O$ |
| 85 | 0 | $InBr_3 \cdot 2H_2O$ |

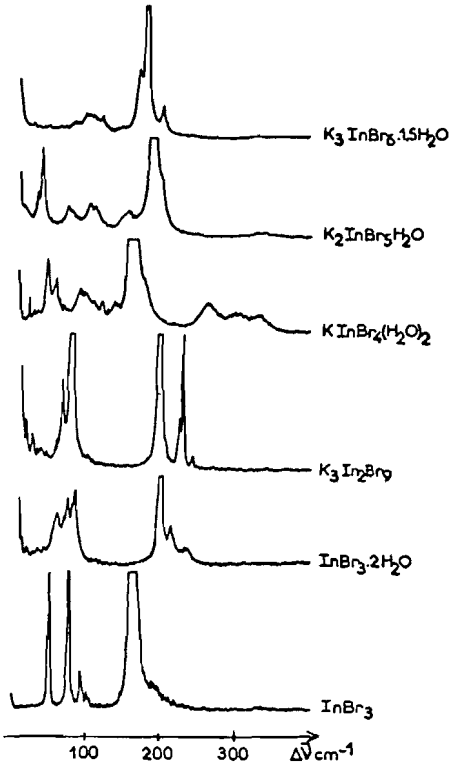


FIG. 4. Raman spectra of the stable solid phases in the bromide system.

tion of the $(InBr_4(H_2O)_2)^-$ centrosymmetric ion, in which the water molecules are *trans*-located (14).

The fact that $K_3In_2Br_9$ was obtained from an aqueous bromide mixture is rather surprising because the $InBr_3$–KBr binary system (15) does not show the existence of such a double salt. An analogous phenomenon has been observed in the $TlCl_3$–CsCl–$H_2O$ system (16) with the formation of $Cs_3Tl_2Cl_9$.

In the $InBr_3$–$H_2O$ binary system, Ensslin *et al.* (11) have shown the existence of $InBr_3 \cdot 2H_2O$ over the temperature range 21 to 33°C. The hydrate existing under 21°C was $InBr_3 \cdot 5H_2O$ and the anhydrous salt was obtained above 33°C. In this work, we found that the hydrate stable at 21°C is $InBr_3 \cdot 2H_2O$. It should be pointed out, however, that some experiments carried out at 20.7°C have yielded $InBr_3 \cdot 5H_2O$. Curiously, in a study of the $InBr_3$–NaBr–$H_2O$ system (17) at 25°C, Kartzmark found $InBr_3$ as the stable solid phase.

The different compounds are identified by their low-frequency Raman spectra (Fig. 4), in which the 150–250 $cm^{-1}$ region is characteristic. The $\nu_s$(In—Br) band shape and position are different for each compound, the frequency values being: 169 $cm^{-1}$ in $InBr_3$; 195 $cm^{-1}$ for $InBr_3 \cdot 2H_2O$; 197 $cm^{-1}$ for $K_3In_2Br_9$; 162 $cm^{-1}$ in $KInBr_4(H_2O)_2$; 185 $cm^{-1}$ for $K_2(InBr_5, H_2O)$ and 175 $cm^{-1}$ in $K_3InBr_6 \cdot 1.5H_2O$.

## Conclusion

The preparation of incongruently saturating double salts from aqueous solution can only be reliably carried out with a knowledge of the appropriate ternary phase diagram. In this work the double salts between $InX_3$ and KX (X = Cl, Br) were prepared at 21°C by this method. In such an investigation Raman spectroscopy serves as a powerful solid phase identification tool.

A summary gives the crystallographic data and the frequencies $\nu_s$(In—X) of the indium–halogen symmetric stretching vibration for each stable solid phase.

1. R. E. MEYER. Lieb. Am. **150**, 152 (1869).
2. R. C. WALLACE. Z. Krystallogr. **49**, 424 (1911).
3. J. P. WIGNACOURT. Thèse 3ème Cycle, University of Lille. 1974.
4. E. M. KARTZMARK. Can. J. Chem. **55**, 2792 (1977).
5. J. J. KESSIS. Bull. Soc. Chim. 2063 (1960).
6. B. HOCHEID and PH. POUPEAU. Techniques de l'Ingénieur, M.76. 1978.
7. A. LORRIAUX-RUBBENS, F. WALLART, J. P. WIGNACOURT, P. BARBIER, and G. MAIRESSE. Spectrochim. Acta, **37A**, 1021 (1981).
8. J. P. WIGNACOURT, A. LORRIAUX-RUBBENS, P. BARBIER, G. MAIRESSE, and F. WALLART. Spectrochim. Acta, **36A**, 403 (1979).
9. J. P. WIGNACOURT. Thèse d'Etat, University of Lille. 1981.
10. J. P. WIGNACOURT, G. NOWOGROCKI, G. MAIRESSE, and P. BARBIER. Rev. Inorg. Chem. **2**, 207 (1980).
11. F. ENSSLIN, B. ZIEMECK, and L. DE SCHAEPDRYVER. Z. Anorg. Chem. **254**, 305 (1947).
12. E. M. KARTZMARK. Can. J. Chem. **52**, 3459 (1974).
13. E. M. KARTZMARK. Can. J. Chem. **53**, 2995 (1975).
14. J. P. WIGNACOURT, G. MAIRESSE, and P. BARBIER. Acta Crystallogr. **36B**, 669 (1980).
15. P. I. FEDOROV and N. I. IL'INA. Zh. Neorg. Khim. **9**, 1207 (1964).
16. G. MALQUORI. Gaz. Chim. Ital. **56**, 37 (1926).
17. E. M. KARTZMARK. Can. J. Chem. **54**, 1884 (1976).

# Observation de la résonance paramagnétique électronique dans les composés organométalliques de l'uranium (III)

E. J. SOULIÉ, G. FOLCHER ET H. MARQUET-ELLIS

*Département de Physico-Chimie, Centre d'Etudes Nucléaires de Saclay, 91191 Gif-sur-Yvette Cedex, France*

Reçu le 25 septembre 1981[1]

E. J. SOULIÉ, G. FOLCHER et H. MARQUET-ELLIS. Can. J. Chem. **60**, 1751 (1982).

L'état de valence III de l'uranium peut être facilement mis en évidence en solution gelée par RPE. Un signal de résonance large, observé à température très basse (7 K) à $g = 3.5$ est caractéristique de l'état trivalent de l'uranium dans $UZrF_7$(poudre), $U(C_5H_5)_3$·tétrahydrofurane et $U(C_5H_5)_3{\cdot}CH_3^-$ (solution gelées).

E. J. SOULIÉ, G. FOLCHER, and H. MARQUET-ELLIS. Can. J. Chem. **60**, 1751 (1982).

The trivalency of uranium can be easily established in frozen solution by epr. The broad resonance signal observed at low temperature (7 K) with $g = 3.5$ appears as characteristic of the trivalent state in $UZrF_7$(powder), $U(C_5H_5)_3$· tétrahydrofuran, and $U(C_5H_5)_3{\cdot}CH_3^-$ (frozen solutions).

Le degré d'oxydation III de l'uranium est relativement instable en solution aqueuse où le potentiel du couple $U^{III}/U^{IV}$ est de −0,620 V/ENH. Par contre il apparaît que l'$U^{III}$ est stabilisé par les ligands de type $C_5H_5$ (noté Cp). C'est ainsi que l'adduit $UCp_3$·THF où THF désigne le tétrahydrofurane est obtenu facilement par plusieurs méthodes à partir de $UCp_3Cl$ ou $UCp_3$-alkyl (1–4). De même un trimère $[(Me_5C_5)_2U\text{-}Cl]_3$ a été isolé par Marks et coll. (5).

Mais alors que dans le cas des métaux de transition et des lanthanides le degré d'oxydation de l'ion métallique est clairement caractérisé par son spectre électronique, la situation, en ce qui concerne les dérivés organométalliques de l'uranium, est plus confuse. D'une part les transitions de transfert de charge oblitèrent assez largement la région des bandes $f$–$f$; d'autre part la champ cristallin loin d'être une perturbation de la répulsion coulombienne et du couplage spin-orbite mélange les multiplets et rend le spectre des transitions $f$–$f$ trop compliqué, et de ce fait insuffisamment caractéristique du degré d'oxydation pour nous renseigner de manière définitive à son sujet.

L'identification de composés d'uranium III devra donc se faire par d'autres méthodes. L'analyse chimique du composé, s'il peut être isolé et purifié, ne laisse en général aucun doute mais la purification est toujours délicate. Une technique indirecte consiste à utiliser le pouvoir réducteur de l'uranium III.

L'électrochimie ne peut généralement pas être employée sur des composés non isolés.

Il nous a semblé intéressant d'utiliser la résonance paramagnétique électronique (RPE): l'uranium III de structure électronique $5f^3$ est un ion à nombre impair d'électrons dont le niveau fondamental est dégénéré d'après le théorème de Kramers en l'absence de champ magnétique appliqué; contrairement au cas de l'uranium (IV) (6), il doit donc avoir un spectre RPE, sauf cas particulier. (La probabilité de transition entre les deux états issus du doublet de Kramers du niveau fondamental est nulle lorsque ces états n'ont pas de composante $Jz = \pm \frac{1}{2}$. C'est par exemple le cas en symétrie $C_{3v}$ pour un niveau fondamental de représentation irréductible $\Gamma_{5T} + \Gamma_{6T}$.)

Une telle méthode présente l'avantage de pouvoir être mise en oeuvre sur des solutions gelées, elle devrait être sensible si le signal n'est pas trop élargi et surtout sélective dans la mesure ou $U^{IV}$ ne donne aucun signal (6) et $U^V$ apparaît avec un facteur $g$ nettement inférieur à 2 (7) tandis que les radicaux organiques résonnent en donnant des raies fines, parfois nombreuses, s'écartant très peu de $g = 2$. Nous allons voir comment cette méthode a pu être appliquée à l'identification du degré d'oxydation d'un composé d'uranium en solution.

## Résultats et discussion

Aucun spectre d'$U^{III}$ dans un composé pur n'a jamais été rapporté mais l'on connaît le spectre de cristaux où $U^{III}$ intervient comme dopant $LaCl_3$ (8) et $CaF_2$ (9).

Nous disposons d'un composé d'$U^{III}$ parfaitement stable à savoir $UZrF_7$ (10). Ce composé sous forme de poudre a le spectre RPE présenté dans la figure 1. L'allure du spectre résulte de l'élargissement consécutif aux interactions qui sont absentes des composés en matrice.

[1]Revision reçue le 15 mars 1982.

0008-4042/82/131751-03$01.00/0

©1982 National Research Council of Canada/Conseil national de recherches du Canada

Can. J. Chem. Downloaded from www.nrcresearchpress.com by 210.87.254.5 on 09/06/12
For personal use only.

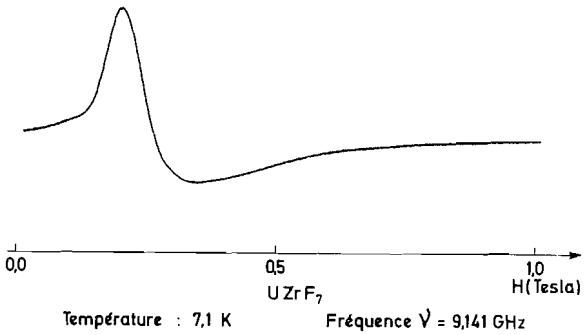


FIG. 1. Spectre RPE de $UZrF_7$ en bande X.

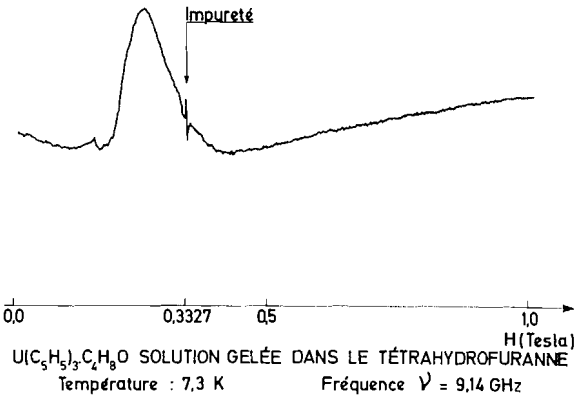


FIG. 2. Spectre RPE de l'adduit de $U(C_5H_5)_3$ et des tétrahydrofurane.

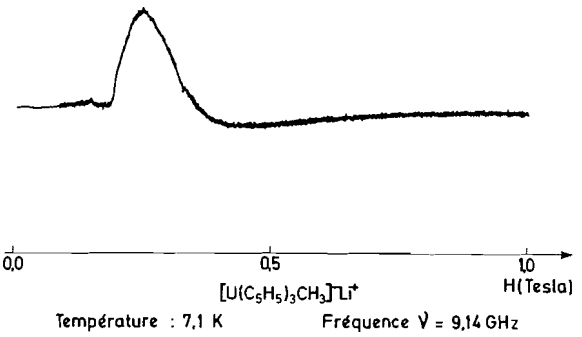


FIG. 3. Spectre RPE de $[U(C_5H_5)_3CH_3]^-Li^+$ en solution gelée dans le tétrahydrofurane en bande.

La forme du signal observé est caractéristique d'un tenseur $g$ axial et présentant une très forte anisotropie.[2] L'intersection de la courbe dérivée d'absorption avec la ligne de base donne approximativement la valeur du facteur $g$ perpendiculaire $g_\perp \sim 2{,}56$ (à 0,1 près). Aucun autre signal n'apparaissant sur le spectre, on en déduit que le champ de résonance correspondant à $g$ parallèle est supérieur au champ maximum atteint soit 1 Tesla; par conséquent $g$ parallèle est inférieur à la valeur de $g$ correspondant à ce champ: $g_{\|} < 0{,}65$. On ne pouvait guère attendre que la structure hyperfine due à l'uranium 235 (8) fût observable dans un composé en poudre où cet isotope est en abondance naturelle (0,7%).

La figure 2 présente le spectre de $UCp_3 \cdot THF$. Ce spectre est très voisin du précédent du point de vue de la dissymétrie et des valeurs de $g$. Ce composé préparé par photolyse de $Cp_3UMe$ ou par réduction de $Cp_3UCl$ par LiH (11) ou $LiAlH_4$ (2) est facilement identifié par son spectre RMN (2) et son spectre électronique publié par Kanellakopulos *et al.* (1).

L'intensité du signal observé d'une part, l'analogie morphologique avec celui de $UZrF_7$, et les arguments exposés plus haut en ce qui concerne les degrés d'oxydation (IV) et (V) de l'uranium permettent d'attribuer ce signal à l'uranium (III).

Cette conclusion s'est trouvée confirmée par l'expérience suivante. Dans un "bitube" scellé, on a mis d'un côté $LiAlH_4 \cdot THF$ et de l'autre $UCl_4 \cdot THF$. Les deux tubes ont été successivement placés dans la cavité de résonance paramagnétique en étant refroidis à 5 K environ. Aucun spectre n'a été observé dans le cas de $LiAlH_4 \cdot THF$, mais on a observé pour $UCl_4 \cdot THF$ un sextuplet caractéristique d'une impureté de manganèse.

Puis après réchauffement des deux branches du bitube, on fait passer $LiAlH_4 \cdot THF$ d'une branche vers l'autre. On refroidit alors le tube où se trouve le mélange vers 5 K. Un spectre entièrement nouveau apparaît, qui ressemble à ceux des figures 1 et 2, et est beaucoup plus intense que celui de l'impureté de manganèse. Ces observations ne peuvent s'interpréter que par la réduction de l'uranium (IV) en uranium (III) lors du mélange, et démontrent que le signal de résonance électronique de l'uranium (III) est observable à basse température dans la solution gelée.

Nous considérons maintenant le produit préparé en réduisant $Cp_3UCH_3$ par $LiCH_3$. Les détails de la préparation seront publiés par ailleurs (12).

La RMN permettait de proposer une formule de la forme $UCp_3 \cdot CH_3^- \cdot Li^+$ mais il n'était pas possible d'isoler le composé. Le degré d'oxydation de l'uranium ne peut pas être déduit du spectre optique qui comporte de multiples transitions dans les régions du spectre occupées par les transitions $f$–$f$.

L'analogie de ce signal RPE (Fig. 3) dont la bande de résonance est à $g = 2{,}56$ avec ceux des deux composés présentes (Figs. 1 et 2) confirme le degré d'oxydation III de l'uranium dans ce nouveau composé.

[2]E. Soulié. Calculs de simulation de spectres, non publié.

Can. J. Chem. Downloaded from www.nrcresearchpress.com by 210.87.254.5 on 09/06/12
For personal use only.

Cet exemple montre l'intérêt et la simplicité de la méthode. Il faut cependant signaler que l'hélium liquide est indispensable, les spectres disparaissant entre 10 et 20 K.

En conclusion, ce travail a permis de montrer qu'un signal de résonance paramagnétique de l'uranium (III) est effectivement observable à basse température dans des composé organométalliques. Et la RPE a été utilisée pour mettre en évidence la valance III de l'uranium dans un composé organométallique difficile à caractériser par ailleurs.

1. B. KANNELLAKOPULOS, E. DORNBERGER et F. BAUMGARTNER. J. Organometal. Chem. **24**, 507 (1970).
2. G. FOLCHER et H. MARQUET-ELLIS. J. Organometal. Chem. **31**, 251 (1977).
3. E. KLAHNE, C. GIANNOTTI, H. MARQUET-ELLIS, G. FOLCHER et R. D. FISCHER. J. Organometal Chem. **201**, 399 (1980).
4. D. G. KARRAKER et J. A. STONE. Inorgan. Chem. **11**, 1742 (1972).
5. J. M. MANRIQUEZ, P. J. FAGAN et T. J. MARKS. J. Am. Chem. Soc. **101**, 5075 (1979).
6. E. SOULIÉ, G. FOLCHER et B. KANNELLAKOPOULOS. Can. J. Chem. **58**, 2377 (1980).
7. L. A. BOATNER et M. M. ABRAHAM. Rep. Prog. Phys. **41**, 87 (1978).
8. C. A. HUTCHINSON, P. M. LLEWELLYN, E. WONG et P. O. DORAIN. Phys. Rev. **102**, 292 (1956).
9. B. BLEANEY, P. M. LLEWELLYN et D. A. JONES. Proc. Phys. Soc. London, Sect. B, **69**, 858 (1956).
10. G. FONTENEAU et J. LUCAS. J. Inorg. Nucl. Chem. **36**, 1515 (1974).
11. D. C. MOODY et J. D. ODOM. J. Inorg. Nucl. Chem. **41**, 533 (1979).
12. L. ARNAUDET, G. FOLCHER, H. MARQUET-ELLIS, E. KLAHNE et R. D. FISCHER. À paraître.

Can. J. Chem. Downloaded from www.nrcresearchpress.com by 210.87.254.5 on 09/06/12
For personal use only.

# Osmotic and activity coefficients of sodium sulphate in water from 150 to 250°C

OM N. BHATNAGAR AND A. N. CAMPBELL

*Department of Chemistry, University of Manitoba, Winnipeg, Man., Canada R3T 2N2*

Received October 22, 1981

OM N. BHATNAGAR and A. N. CAMPBELL. Can. J. Chem. **60**, 1754 (1982).

Osmotic and activity coefficients of sodium sulphate in aqueous solution have been determined at temperatures up to 250°C, at solute concentration from 0.3 *m* to saturation, by measurements of vapour pressure using a newly designed high pressure cell. A precision pressure transducer is used in this cell for pressure measurement. Certain thermodynamic quantities have been calculated from the activity coefficients.

OM N. BHATNAGAR et A. N. CAMPBELL. Can. J. Chem. **60**, 1754 (1982).

Opérant à des températures allant jusqu'à 250°C et à des concentrations allant de 0,3 *m* à la saturation, on a déterminé les coefficients de pression osmétique et d'activité du sulfate de sodium en solution aqueuse, en mesurant la pression de vapeur à l'aide d'une nouvelle cellule à haute pression de conception récente. On a utilisé un transducteur de pression de précision dans cette cellule pour mesurer la pression. On a calculé certaines quantités thermodynamiques à partir des coefficients d'activité.

[Traduit par le journal]

## Introduction

The problems of corrosion and scale formation in steam generators are widespread and are of great concern to industry (1, 2). Knowledge and understanding of thermodynamic properties of aqueous electrolyte solutions at elevated temperatures are helpful in attempts to solve these problems. Moreover, the thermodynamic data are of interest to the oil industry for understanding the problem of secondary recovery in oil wells. Some work on the thermodynamic properties of electrolyte solutions at elevated temperatures has been reported in the last few years (3–13, 22). In a previous paper (4) we reported the osmotic and activity coefficients of sodium sulphate from 50 to 150°C. Recently, Rogers and Pitzer (23) have reported heat capacities of aqueous sodium sulphate solutions from 30 to 200°C. They have used their data to calculate a number of thermodynamic properties, such as osmotic and activity coefficients. In this paper, we report the osmotic and activity coefficients of sodium sulphate in water from 150 to 250°C, and at concentrations from 0.3 *m* to saturation using a newly designed vapour pressure cell.

## Experimental

Our method consists in the determination of vapour pressure. In order to extend our work beyond 150°C it was necessary to design a vapour pressure cell that could withstand high pressure and in which the pressure could be measured without visual observation.

The design of the cell is shown in Fig. 1. The cell is made from 316 stainless steel, machined from a solid 9 cm diameter rod. The inside of the cell, which is a cavity of 2.5 cm diameter and 10 cm deep, was plated with gold to protect it from corrosion. The pressure is measured using a pressure transducer, specially made for high temperature work by Kaman Science Corporation (P.O. Box 7463, Colorado Springs, CO 80933, U.S.A.).

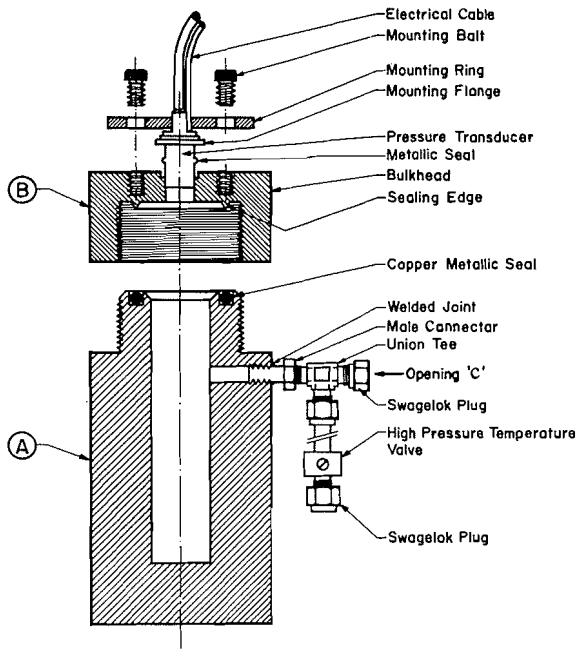


FIG. 1. High temperature vapour pressure cell.

The pressure transducer is mounted on the Cap (B) as shown in Fig. 1. A pressure-tight seal is made by using a silver metallic seal between transducer and the cap. The cap is screwed on to the lower part of the cell (A). The sealing edge inside the cap presses on to the copper metallic seal, providing a pressure-tight seal. The Swagelok connections and high-temperature high-pressure valve serve to introduce and degas the solutions. Before performing an experiment, the cell is assembled as shown in Fig. 1. It is attached to a helium leak detector through the high-pressure high-temperature valve, and the system is checked for any leaks. A sample of liquid is then introduced into the cell through the opening "C", and the end is sealed with a

0008-4042/82/131754-05$01.00/0

©1982 National Research Council of Canada/Conseil national de recherches du Canada

Can. J. Chem. Downloaded from www.nrcresearchpress.com by 210.87.254.6 on 09/06/12
For personal use only.

Can. J. Chem. Downloaded from www.nrcresearchpress.com by 210.87.254.6 on 09/06/12
For personal use only.

Swagelok plug. The sample is degassed several times after freezing in an acetone and solid $CO_2$ mixture, through the high-temperature high-pressure valve. After degassing, the cell is placed in the constant temperature oil bath. The pressure readings are measured as millivolt output from the transducer. By using a calibration curve provided by the manufacturer, the pressure at each temperature can be obtained readily. The system was tested using triply distilled water and 1 *m* NaCl solution; our values of osmotic coefficients of NaCl were within 1% of the literature values (8). By knowing the vapour pressures of water and those of the solutions, the values of $\Delta P$, the vapour pressure lowerings, were evaluated for each concentration, in the temperature range of 150 to 250°C. Analytical grade sodium sulphate was used to make the solutions. The concentrations of solutions were determined after each experiment by gravimetric analysis of the sample as barium sulphate (14). The temperature of the bath was measured by a platinum resistance thermometer. The saturation concentration values were taken from the literature (20).

## Results and discussion

The osmotic coefficients were calculated using the following equation (8):

$$[1]\quad \phi = \frac{1000}{\nu m M_1 RT}\left[RT\ln(P^0/P) - \int_P^{P^0}\xi\,dP - \bar{V}_1{}^0(l)\Delta P\right]$$

where $\phi$ is the osmotic coefficient, $R$ the gas constant, $T$ the absolute temperature, $\nu$ the number of ions resulting from the ionization of one molecule, $m$ the molality, $M_1$ the molecular weight of water, and $P^0$ and $P$ the vapour pressures of pure water and solution respectively. The first term in the brackets gives the osmotic coefficient at low pressures, the second term gives the correction for deviations of the vapour from the perfect gas law, while the third term is a reasonable approximation for the isothermal compression of the solution from its own vapour pressure to that of liquid water. The term $\xi$ was calculated from the equations of Smith, Keyes and Gerry (15). The molar volume of pure water, $V_1{}^0(l)$ and $P^0$ were calculated using the equations in ref. 15. In our calculations $\bar{V}_1{}^0(l)$ is used instead of $\bar{V}_1(l)$ for the partial molal volume of water because under these conditions the difference is negligible. The osmotic coefficients calculated from eq. [1] were fitted to the recently developed equations of Pitzer (16). These equations are semiempirical but they are quite successful in predicting the thermodynamic properties of electrolyte solutions up to 6 *M* (17–19) and can be applied to any valence type compounds. Pitzer's equations for osmotic and activity coefficients are given below:

$$[2]\quad \phi - 1 = -|Z_M Z_X| A\phi\,\frac{I^{1/2}}{1+bI^{1/2}} + \frac{m 2\nu_M\nu_X}{\nu}\left[\beta_{MX}{}^{(0)} + \beta_{MX}{}^{(1)}\exp(-\alpha I^{1/2})\right] + \frac{m^2 2(\nu_M\nu_X)^{3/2}}{\nu}\,C_{MX}{}^{\phi}$$

$$[3]\quad \ln\gamma_{\pm} = -|Z_M Z_X| A\phi\left[\frac{I^{1/2}}{1+bI^{1/2}} + \frac{2}{b}\ln(1+bI^{1/2})\right] + \frac{2m\nu_M\nu_X}{\nu} \times \left[2\beta_{MX}{}^{(0)} + \frac{2\beta_{MX}{}^{(1)}}{\alpha^2 I}\left\{1-\left(1+\alpha I^{1/2}-\frac{\alpha^2 I}{2}\right)\exp(-\alpha I^{1/2})\right\}\right] + \frac{3m^2 2(\nu_M\nu_X)^{3/2} C_{MX}{}^{\phi}}{2\nu}$$

where $Z_M$ and $Z_X$ are the positive and negative ionic charges in electronic units. $I$ is the ionic strength, $A\phi$ is the Debye–Hückel coefficient for osmotic functions, $\nu_M$ and $\nu_X$ are the numbers of ions of each type in the formulae, and $\nu = \nu_M + \nu_X$. $\beta_{MX}{}^{(0)}$ and $\beta_{MX}{}^{(1)}$ account for various short range interactions between M and X and for cosphere overlap effect, $C_{MX}{}^{\phi}$ accounts for triple ion interaction and is of importance at high concentration. The parameters $\alpha$ and $b$ are given values of 2 and 1.2 respectively for the present calculations and are treated as temperature independent (17). The Debye–Hückel coefficient $A\phi$ is given by

$$[4]\quad A\phi = 1/3\left(\frac{2\pi N_0\rho_\omega}{1000}\right)^{1/2}\left(\frac{e^2}{DkT}\right)^{3/2}$$

where $N_0$ is the Avogadro number, $\rho_\omega$ is the density of water at temperature $T$, $D$ is the static dielectric constant of water, $k$ is the Boltzmann's constant, and $e$ is the electronic charge. The experimental values of $\phi$ and $m$ were used to evaluate $\beta_{MX}{}^{(0)}$, $\beta_{MX}{}^{(1)}$, and $C_{MX}{}^{\phi}$ which, in turn, were used to calculate mean ionic activity coefficients, $\gamma_{\pm}$, using eq. [3]. As reported earlier (4) the possibility of $HSO_4^-$ ion formation was considered but it was

Can. J. Chem. Downloaded from www.nrcresearchpress.com by 210.87.254.6 on 09/06/12
For personal use only.

TABLE 1. Osmotic and activity coefficients of sodium sulphate in water

| Temp. (°C) | $m$ (mol/kg) | $\Delta P$ (Torr) | $\phi$ | $\gamma_\pm$ |
|---|---|---|---|---|
| 150 | 0.2885 | 37.22 | 0.641 | 0.250 |
| 150 | 0.3800 | 48.76 | 0.639 | 0.223 |
| 150 | 0.5720 | 69.92 | 0.611 | 0.187 |
| 150 | 0.8875 | 103.16 | 0.584 | 0.153 |
| 150 | 1.7530 | 208.37 | 0.606 | 0.119 |
| 150 | 2.9700 | 433.21 | 0.771 | 0.117 |
| 175 | 0.2885 | 64.64 | 0.579 | 0.163 |
| 175 | 0.3800 | 86.70 | 0.590 | 0.141 |
| 175 | 0.5720 | 122.42 | 0.555 | 0.114 |
| 175 | 0.8875 | 183.46 | 0.539 | 0.091 |
| 175 | 1.7530 | 356.20 | 0.538 | 0.067 |
| 175 | 3.0410 | 624.51 | 0.556 | 0.054 |
| 200 | 0.2885 | 93.26 | 0.462 | 0.123 |
| 200 | 0.3800 | 119.98 | 0.452 | 0.103 |
| 200 | 0.5720 | 174.84 | 0.439 | 0.080 |
| 200 | 0.8875 | 260.93 | 0.424 | 0.061 |
| 200 | 1.7530 | 515.16 | 0.430 | 0.042 |
| 200 | 3.1040 | 969.62 | 0.467 | 0.031 |
| 225 | 0.2885 | 128.82 | 0.371 | 0.109 |
| 225 | 0.3800 | 165.48 | 0.362 | 0.091 |
| 225 | 0.5720 | 241.69 | 0.353 | 0.069 |
| 225 | 0.8875 | 356.10 | 0.336 | 0.051 |
| 225 | 1.7530 | 683.66 | 0.330 | 0.033 |
| 225 | 3.1820 | 1454.88 | 0.397 | 0.024 |
| 250 | 0.2885 | 283.39 | 0.493 | 0.118 |
| 250 | 0.3800 | 365.52 | 0.483 | 0.099 |
| 250 | 0.5720 | 527.64 | 0.465 | 0.076 |
| 250 | 0.8875 | 774.58 | 0.443 | 0.057 |
| 250 | 1.7530 | 1327.57 | 0.389 | 0.038 |
| 250 | 3.0970 | 2798.35 | 0.480 | 0.029 |

TABLE 2. Parameters for eqs. [2] and [3]

| Temp. (°C) | $\beta_{MX}^{(0)}$ | $\beta_{MX}^{(1)}$ | $C_{MX}^{\phi}$ |
|---|---|---|---|
| 150 | 0.0708 | 1.9066 | 0.0098 |
| 175 | 0.1243 | 0.1732 | −0.0113 |
| 200 | 0.1149 | −0.4343 | −0.0115 |
| 225 | 0.1029 | +0.0840 | −0.0065 |
| 250 | 0.1413 | +1.7282 | −0.0077 |

found to be insufficient to cause any change in the final results. The values of $m$, $\Delta P$, $\phi$, and $\gamma_\pm$ are given in Table 1. The values of $\beta_{MX}^{(0)}$, $\beta_{MX}^{(1)}$, and $C_{MX}^{\phi}$ for various temperatures are given in Table 2. The smoothed values of $m$, $\phi$, and $\gamma_\pm$ are given in Table 3. The values of osmotic coefficients, determined from present and previous work (4), at 150°C, are compared in Fig. 2. The activity coefficients at 150°C obtained from this work are compared with our previous results (4) and with those reported by Rogers and Pitzer (23). In general the agreement is good. Since the activity coefficients have been calculated up to saturation concentrations at each temperature the standard

TABLE 3. Smoothed values of osmotic and activity coefficients

| Temp. (°C) | Molality | $\phi$ | $\gamma_\pm$ |
|---|---|---|---|
| 150 | 0.250 | 0.666 | 0.265 |
| 150 | 0.500 | 0.612 | 0.200 |
| 150 | 0.750 | 0.592 | 0.167 |
| 150 | 1.000 | 0.584 | 0.147 |
| 150 | 1.500 | 0.591 | 0.125 |
| 150 | 2.000 | 0.626 | 0.116 |
| 150 | 2.500 | 0.687 | 0.113 |
| 175 | 0.250 | 0.607 | 0.176 |
| 175 | 0.500 | 0.560 | 0.122 |
| 175 | 0.750 | 0.545 | 0.099 |
| 175 | 1.000 | 0.539 | 0.086 |
| 175 | 1.500 | 0.536 | 0.071 |
| 175 | 2.000 | 0.539 | 0.063 |
| 175 | 2.500 | 0.545 | 0.057 |
| 200 | 0.250 | 0.476 | 0.132 |
| 200 | 0.500 | 0.439 | 0.086 |
| 200 | 0.750 | 0.428 | 0.067 |
| 200 | 1.000 | 0.424 | 0.056 |
| 200 | 1.500 | 0.425 | 0.045 |
| 200 | 2.000 | 0.433 | 0.038 |
| 200 | 2.500 | 0.445 | 0.033 |
| 225 | 0.250 | 0.377 | 0.117 |
| 225 | 0.500 | 0.354 | 0.073 |
| 225 | 0.750 | 0.341 | 0.056 |
| 225 | 1.000 | 0.333 | 0.046 |
| 225 | 1.500 | 0.328 | 0.036 |
| 225 | 2.000 | 0.334 | 0.030 |
| 225 | 2.500 | 0.352 | 0.026 |
| 250 | 0.250 | 0.484 | 0.122 |
| 250 | 0.500 | 0.477 | 0.079 |
| 250 | 0.750 | 0.452 | 0.061 |
| 250 | 1.000 | 0.429 | 0.051 |
| 250 | 1.500 | 0.396 | 0.040 |
| 250 | 2.000 | 0.389 | 0.033 |
| 250 | 2.500 | 0.411 | 0.029 |

free energy change, $\Delta G^0$, can be calculated from the following equations:

[5] $$\Delta G^0 = -RT \ln K$$

for $Na_2SO_4$

[6] $$\Delta G^0 = -RT \ln K_{sp} = -RT \ln [2m_+\gamma_\pm]^2[m_-\gamma_\pm]$$

where $K_{sp}$ is the solubility product constant and $m_+$ and $m_-$ refer to analytical molalities of $Na^+$ and $SO_4^{2-}$ respectively.

The values of $\log K_{sp}$ calculated from eq. [6] were fitted to a polynomial equation of the following form

[7] $$\log K_{sp} = A + A_1\left(\frac{1}{T}\right) + A_2\left(\frac{1}{T}\right)^2$$

Using a least-squares programme for polynomial

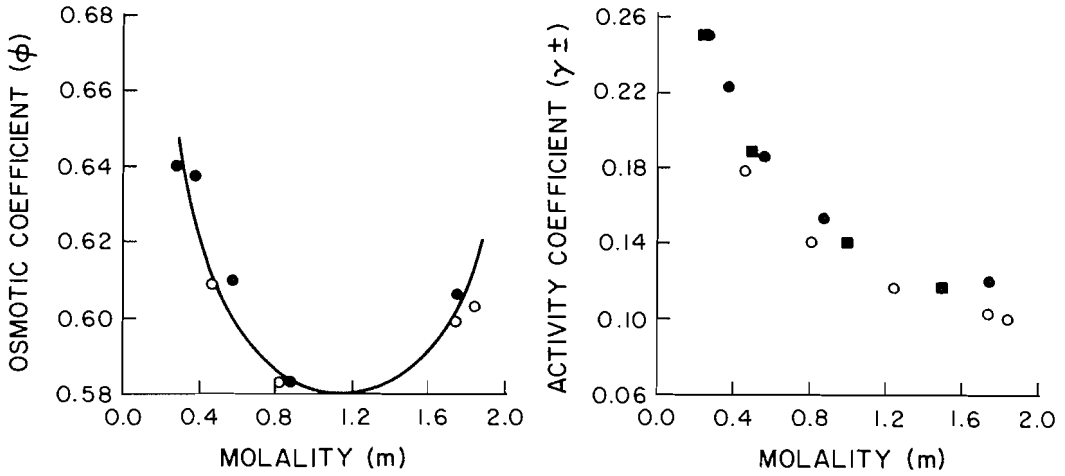


FIG. 2. Osmotic and activity coefficients of sodium sulphate in water at 150°C. ○ data from ref. 4; ■ data from ref. 23; ● data from present work.

TABLE 4. Parameters for eq. [7]

| Parameter | Value |
|---|---|
| $A$ | $4.4110 \times 10$ |
| $A_1$ | $-4.7513 \times 10^4$ |
| $A_2$ | $1.2068 \times 10^7$ |

curve fitting, values of $A$, $A_1$, and $A_2$ were evaluated and these are given in Table 4. The Van't Hoff equation can be written as

$$[8] \quad \left(\frac{\partial \log K_{sp}}{\partial\left(\frac{1}{T}\right)}\right)_p = -\frac{\Delta H^0}{2.303R}$$

Differentiations of eq. [7] with respect to $1/T$ and subsequent substitution in eq. [8] give the values of $\Delta H^0$, the standard change in enthalpy at a given temperature. From the values of $\Delta G^0$ and $\Delta H^0$ the values of $\Delta S^0$ were evaluated. The values of $K_{sp}$, $\Delta G^0$, $\Delta H^0$, and $\Delta S^0$ are given in Table 5. The values of $\gamma_\pm$ can also be used to calculate relative partial molal heat capacity, $\bar{J}_2$.

The osmotic and activity coefficients decrease with increasing temperature and reach a minimum at approximately 225°C; beyond this temperature they increase again. For each temperature, the osmotic coefficients decrease with increasing concentration and pass through a minimum at about 1 molal. Marshall (21) has reported the thermodynamic data on the $Na_2SO_4$–$H_2O$ system from 300 to 350°C, but our results cannot be compared with those of Marshall because anhydrous sodium sulphate undergoes an allotropic change, from rhombic to monoclinic, at 241°C. Marshall's work throughout is in a temperature range where sodium sulphate is in the monoclinic form.

Our $\beta_{MX}^{(0)}$ values are in good agreement with those reported by Rogers and Pitzer (23), considering that their values refer to a different concentration range from ours. Our $C_{MX}^{\phi}$ values show a similar trend, with respect to change in temperature, to those of Rogers and Pitzer (23) but the numerical values are different. The variation with temperature of the $\beta_{MX}^{(1)}$ values reported by us show a minimum at 200°C, but Rogers and Pitzer (23) report no such minimum and we find this quite puzzling. Recently, Homes and Mesmer (24) have reported $\beta_{MX}^{(0)}$, $\beta_{MX}^{(1)}$, and $C_{MX}^{\phi}$, for $SrCl_2$ and

TABLE 5. The values of $K_{sp}$ and other thermodynamic functions of $Na_2SO_4$ in water

| Temp. (°C) | $K_{sp}$ | $\Delta G^0$ kcal mol$^{-1}$ | $\Delta H^0$ kcal mol$^{-1}$ | $\Delta S^0$ cal mol$^{-1}$ deg$^{-1}$ |
|---|---|---|---|---|
| 150 | $1.670 \times 10^{-1}$ | 1.500 | −43.576 | −106.5 |
| 175 | $1.73 \times 10^{-2}$ | 3.612 | −29.024 | −72.8 |
| 200 | $3.53 \times 10^{-3}$ | 5.309 | −15.998 | −45.0 |
| 225 | $1.83 \times 10^{-3}$ | 6.242 | −4.288 | −21.1 |
| 250 | $2.99 \times 10^{-3}$ | 6.043 | +6.305 | +0.5 |

Can. J. Chem. Downloaded from www.nrcresearchpress.com by 210.87.254.6 on 09/06/12
For personal use only.

$BaCl_2$, from isopiestic measurements. They have found a minimum in $\beta_{MX}{}^1$ values of $SrCl_2$ and $BaCl_2$ below 100°C.

**Acknowledgements**

We want to thank Atomic Energy of Canada Ltd., Chalk River, Ontario, for the financial support of this project.

1. P. V. BALAKRISHNAN. 41st International Water Conference. Pittsburgh, PA. October 20–22, 1980.
2. R. C. MURRAY and J. W. COBBLE. 41st International Water Conference. Pittsburgh, PA. October 20–22, 1980.
3. H. F. HOLMES and R. E. MESMER. J. Chem. Thermodyn. **13**, 131 (1981).
4. O. N. BHATNAGAR and A. N. CAMPBELL. Can. J. Chem. **59**, 123 (1981).
5. A. N. CAMPBELL and O. N. BHATNAGAR. Can. J. Chem. **57**, 2542 (1979).
6. H. F. HOLMES, C. F. BAES, and R. E. MESMER. J. Chem. Thermodyn. **10**, 983 (1978).
7. C. LIU and W. T. LINDSAY, JR. J. Solution Chem. **1**, 45 (1972).
8. C. LIU and W. T. LINDSAY, JR. J. Phys. Chem. **74**, 341 (1970).
9. E. R. GARDNER. Trans. Faraday Soc. **65**, 91 (1969).
10. E. R. GARDNER, P. J. JONES, and H. J. DENORDWALL. Trans. Faraday Soc. **59**, 1994 (1963).
11. H. F. HOLMES, C. F. BAES, and R. E. MESMER. J. Chem. Thermodyn. **11**, 1035 (1979).
12. B. A. SOLDANO and P. B. BIEN. J. Chem. Soc. A, 1825 (1966).
13. C. M. CRISS and J. W. COBBLE. J. Am. Chem. Soc. **86**, 5385 (1964).
14. J. M. KOLTHOFF, E. B. SANDELL, E. J. MECHAN, and S. BRUCKENSTEIN. Qualitative chemical analysis. 4th ed. The MacMillan Company, New York, NY. 1969.
15. L. B. SMITH, F. G. KEYES, and H. T. GERRY. Proc. Am. Acad. Arts Sci. **69**, 137 (1934).
16. K. S. PITZER. J. Phys. Chem. **77**, 268 (1973).
17. K. S. PITZER and G. MAYORGA. J. Phys. Chem. **77**, 2309 (1973).
18. K. S. PITZER and G. MAYORGA. J. Solution Chem. **3**, 539 (1974).
19. L. F. SILVESTER and K. S. PITZER. J. Phys. Chem. **81**, 1822 (1977).
20. W. C. SCHROEDER, A. GABRIEL, and E. P. PARTRIDGE. J. Am. Chem. Soc. **57**, 1539 (1935).
21. W. L. MARSHALL. J. Inorg. Nucl. Chem. **37**, 2155 (1975).
22. S. LIKKE and L. A. BROMLEY. J. Chem. Eng. Data, **18**, 189 (1973).
23. P. S. G. ROGERS and K. S. PITZER. J. Phys. Chem. **85**, 2886 (1981).
24. H. F. HOLMES and R. E. MESMER. J. Chem. Thermodyn. **13**, 1025 (1981).

Can. J. Chem. Downloaded from www.nrcresearchpress.com by 210.87.254.6 on 09/06/12
For personal use only.

# Calculated uranium solubility in groundwater: implications for nuclear fuel waste disposal[1]

BRUCE GOODWIN

*Environmental and Safety Assessment Branch, Whiteshell Nuclear Research Establishment, Pinawa, Man., Canada R0E 1L0*

Received October 22, 1981

BRUCE GOODWIN. Can. J. Chem. **60**, 1759 (1982).

Uranium solubilities of the order of $10^{-10}$ *M* have been calculated for a range of conditions which are considered to be representative of those expected in a Canadian nuclear fuel waste disposal vault. Factors taken into consideration include the pH and Eh range expected for deep groundwaters, the projected temperature range near a nuclear fuel waste disposal vault, the effect of the composition of two representative groundwaters, the effect of non-ideality, and the effect of the stability of several uranium solids.

The model used in these calculations is based on the assumption of chemical equilibrium. Calculations show that the most important factors influencing uranium solubility under the postulated conditions are pH and Eh.

These results applied to an assessment of the nuclear fuel waste disposal program suggest that uranium concentrations will be very low in the disposal vault, and that the irradiated $UO_2$ fuel matrix will remain relatively intact for long periods of time.

BRUCE GOODWIN. Can. J. Chem. **60**, 1759 (1982).

On a calculé des solubilités de l'uranium de l'ordre de $10^{-10}$ *M* dans un intervalle de conditions que l'on considère représentatif de celles attendues dans une voute d'entreposage de déchets de combustibles nucléaires canadiens. Les facteurs considérés comprennent les domaines de pH et de Eh auxquels on peut s'attendre pour les eaux souterraines profondes, le domaine de température prévue près d'une voute de déchets de combustibles nucléaires, l'effet de la composition de deux eaux souterraines représentatives, l'effet de non-idéalité et l'effet de stabilité de plusieurs solides contenant de l'uranium.

Le modèle utilisé dans ces calculs repose sur l'hypothèse d'un équilibre chimique. Les calculs révèlent que la plupart des facteurs importants qui influencent la solubilité de l'uranium dans les conditions choisies sont le pH et le Eh.

Ces calculs, appliqués à une évaluation du programme d'entreposage des déchets de combustible nucléaire, suggèrent que les concentrations en uranium seront très faibles dans les voutes d'entreposage et que la matrice de combustible $UO_2$ irradié restera relativement intacte pendant un temps assez long.

[Traduit par le journal]

## Introduction

The solubility of uranium in natural groundwater is of interest from two viewpoints. For some time, this subject has been studied in relation to the formation and dissolution of uranium ores (1), often in oxidizing environments. More recently the subject has become of interest in relation to the nuclear fuel waste disposal program. This report is oriented towards the latter aspect.

Nuclear fuel waste disposal is the final stage of the nuclear energy cycle, and is intended to safeguard man and the environment for the hazardous lifetime of the wastes. The proposed Canadian approach to this problem involves isolating the irradiated fuel or reprocessing waste in a deep underground vault in a crystalline pluton in the Precambrian Shield, and includes "engineered barriers" such as metal containers and a low-permeability backfill material (2–4). The isolation of the wastes and the integrity of the vault are expected to be such that the only feasible mechanism for escape of radioactive material would be transport in groundwater. This scenario requires that groundwater penetrates the vault, corrodes the metal container, and eventually leaches the contained radioactive waste for transport to the surface.

One of the parameters critical to these studies is the degree to which radioactive waste dissolves in natural groundwater. In particular, the solubility of uranium oxide is very important since the irradiated fuel from a CANDU[2] reactor consists of approximately 98% by weight $UO_2$, and less than 2% by weight of the more hazardous fission product and actinide isotopes (5). Knowledge of uranium solubilities can lead to estimates of (*i*), the time required to dissolve the uranium in irradiated fuel, and (*ii*), the rate of release of radionuclides which are trapped in the $UO_2$ fuel matrix, and which are released as uranium dissolves. Other information required for these estimates includes the availability of groundwater and the mechanism of fuel dissolution.

In addition, knowledge of the parameters affecting uranium solubility can be used in a feedback process to influence the criteria used in the design of engineered barriers and in the selection of a suitable vault site. By way of example, data presented in this report indicate that the environment

[1]AECL-7138.

[2]*CA*Nada *D*euterium *U*ranium.

0008-4042/82/131759-08$01.00/0

©1982 National Research Council of Canada/Conseil national de recherches du Canada

Can. J. Chem. Downloaded from www.nrcresearchpress.com by 210.87.254.105 on 09/06/12
For personal use only.

Can. J. Chem. Downloaded from www.nrcresearchpress.com by 210.87.254.105 on 09/06/12
For personal use only.

of an ideal vault would include a groundwater which is slightly acid to neutral and which is buffered at a reducing Eh.

Details of the calculated results are presented, as is a brief description of the chemical model used to produce these results.

### Description of the chemical model

The model used in these calculations is based on the assumption of chemical equilibrium, using relationships which derive from the laws of thermodynamics. One approach to calculation of an equilibrium assemblage is based on solution of the non-linear equations deriving from the law of mass action (6–8).

A non-linear equation may be written for each of the possible chemical reactions, and an auxiliary set of (linear) mass balance equations is also required so that the number of equations equals the number of unknowns.

This system of linear and non-linear equations is easily solved only for simple chemical systems. Many problems of interest involve large numbers of competing reactions, and the requirement to analyze such systems has led to the development of a variety of computer programs (6–8). The results reported here were computed using a modified version of the program SOLMNEQ — a geochemical solution–mineral equilibrium program (9).

Modifications to SOLMNEQ included the introduction of the uranium aqueous species and solids listed in Table 1. Calculation of uranium speciation parallels existing logic in SOLMNEQ; for example, starting from the mass balance equation for uranium:

$$[1] \quad [U]_{total} = [U^{3+}] + [U^{4+}] + [UO_2^{+}] + [UO_2^{2+}] + [U(SO_4)_2^{0}] + \ldots.$$

one develops a single non-linear equation in $[U^{4+}]$ and the anionic species by substituting for all uranium species from their corresponding mass action equation. Typical substitutions might be

$$[2a] \quad [U(SO_4)_2^{0}] = [U^{4+}]\,[SO_4^{2-}]^2/K$$

where $K$ is the equilibrium constant for the reaction

$$[2b] \quad U(SO_4)_2^{0} \rightleftarrows U^{4+} + 2SO_4^{2-}$$

Other substitutions invoke the Nersnt equation to account for redox reactions between U(IV) and U(III), U(V), or U(VI) species. It was also necessary to modify the logic of SOLMNEQ to evaluate these equations in log units, because of the wide range in speciation constants that are encountered for uranium species.

TABLE 1. Aqueous and solid uranium species included in the calculations*

| | Aqueous species | Solids |
|---|---|---|
| U(III): | $U^{3+}$ | — |
| U(IV): | $U^{4+}$ | $UO_2$ |
| | $U(OH)^{3+}$ to $U(OH)_5^{-}$ | $UF_4$ |
| | $UCl^{3+}$ | $UF_4 \cdot \frac{5}{2}H_2O$ |
| | $UF^{3+}$ to $UF_6^{2-}$ | |
| | $U(HPO_4)^{2+}$ to $U(HPO_4)_4^{4-}$ | |
| | $U(SO_4)^{2+}$ to $U(SO_4)_2^{0}$ | |
| U(V): | $UO_2^{+}$ | $NaUO_3$ |
| U(VI): | $UO_2^{2+}$ | $\gamma$-$UO_3$ |
| | $UO_2(OH)^{+}$ to $UO_2(OH)_2^{0}$ | $UO_2CO_3$ |
| | $(UO_2)_3(OH)_5^{+}$ | $(UO_2)_3(PO_4)_2$ |
| | $(UO_2)_3(OH)_7^{-}$ | $(UO_2)_2(HPO_4)_2$ |
| | $UO_2(CO_3)^{0}$ to $UO_2(CO_3)_3^{4-}$ | $\beta$-$UO_2(OH)_2$ |
| | $UO_2F^{+}$ to $UO_2F_4^{2-}$ | $UO_3 \cdot 2H_2O$ |
| | $UO_2Cl^{+}$ | $Na_2U_2O_7$ |
| | $UO_2(HPO_4)^{0}$ to $UO_2(HPO_4)_2^{2-}$ | $\alpha$-$Na_2UO_4$ |
| | $UO_2(H_2PO_4)^{+}$ to $UO_2(H_2PO_4)_3^{-}$ | |
| | $UO_2(SO_4)^{0}$ | |
| U(IV) – U(VI): | — | $U_3O_8$ |
| | | $U_4O_9$ |

*The corresponding thermodynamic data were taken from ref. 13.

Equation [1] may now be solved iteratively, taking an initial guess for the free ionic species and $[U]_{total}$ from the reported chemical analysis. When all feasible competing reactions are taken into account (for example $Ca^{2+}$ will compete with $U^{4+}$ for $SO_4^{2-}$, etc.), a new guess of the free ionic species is computed, and the entire process is repeated until the calculated sums of *free* anionic species (e.g., $SO_4^{2-}$) and *complexed* ionic species (e.g., $U(SO_4)^{2+}$, $U(SO_4)_2^{0}$, $CaSO_4^{0}$) converge to the reported anion concentration. Convergence tests are performed for carbon, chlorine, sulphur, phosphorous, and fluorine aqueous anionic species.

These computations result in the calculated concentration of various charged and neutral species in solution. SOLMNEQ also computes activity products and compares them with solubility products to indicate the state of saturation of various minerals and solids. For uranium solids, a new option added to SOLMNEQ searches for the maximum uranium in solution which is in equilibrium with the most stable (least soluble) uranium solid under specified conditions of Eh, pH, groundwater composition, and temperature. This is achieved by backward substitution of a new estimate for $[U]_{total}$ based on the uranium solid which is most supersaturated (or nearest saturation). In most cases convergence is obtained within three iterations.

Other features of SOLMNEQ are described in

TABLE 2. Groundwater compositions (molar) at 25°C assumed for the nuclear fuel waste vault

| Components | Granite groundwater | Brine groundwater* |
|---|---|---|
| Ca | $3.24\times10^{-4}$ | 0.396 |
| Mg | $1.60\times10^{-4}$ | $8.71\times10^{-3}$ |
| Na | $3.61\times10^{-4}$ | 0.232 |
| K | $8.95\times10^{-5}$ | $1.35\times10^{-3}$ |
| Cl | $1.41\times10^{-4}$ | 1.02 |
| $SO_4$ | $8.95\times10^{-5}$ | $8.71\times10^{-3}$ |
| $HCO_3$ | $1.01\times10^{-3}$ | $1.74\times10^{-4}$ |
| $SiO_2$ | — | $8.81\times10^{-4}$ |
| Sr | — | $2.42\times10^{-4}$ |
| F | $1.00\times10^{-5}$ | — |
| $NO_3$ | $1.00\times10^{-5}$ | $8.45\times10^{-4}$ |
| pH | 7.00 | 7.00 |
| Total dissolved solids (g/L) | 0.105 | 55.5 |
| Ionic strength | 0.00184 | 1.43 |

*SOLMNEQ predicts that this brine is supersaturated at 25°C in several minerals, including tremolite, talc, gypsum, anhydrite, and quartz. Tremolite and talc are considerably supersaturated, but since they have not been detected experimentally (16), we conclude that their formation must be kinetically hindered. Gypsum, anhydrite, and quartz are also not observed, but these minerals are only slightly supersaturated, and the disparity is more likely due to the inaccuracy in calculation of activity coefficients at the very high ionic strength of the brine.

detail elsewhere (9) and include: (*i*), provision to handle over 230 inorganic aqueous species (including over 70 uranium and plutonium species added to the modifications described above); (*ii*), calculation of aqueous speciation in the temperature range 0–350°C; (*iii*) calculation of non-ideality effects on the activity coefficients by means of a modified Debye–Hückel equation for charged species and by analogy with the activity coefficient of $CO_2$ for neutral species (10); and (*iv*) calculation of changes in pH as a function of temperature, using an extra mass balance constraint for species containing $H^+$ and $OH^-$ and taking into account the variation with temperature of the equilibrium constants for the ionization of water and other reactions (11). This latter calculation assumes pH is known at some reference temperature.

The database required by SOLMNEQ and used in these calculations is largely from the original SOLMNEQ database (9), with a few minor corrections. Equilibrium constants for uranium species were generated by the program COTDET (12) using the free energy and heat capacity data contained in a recent review by Lemire and Tremaine (13). Parameters required for the Debye–Hückel equation for uranium species were chosen using guidelines in the report by Kielland (14).

Copies of this version of SOLMNEQ and its database are available on request from the author.

## Results and discussion

In order to estimate uranium solubilities in the proposed nuclear fuel waste disposal vault, we have chosen a range of environments which are expected to be representative of the geochemical conditions in a crystalline pluton. The environments are characterized by several important parameters which describe the chemistry of the groundwater permeating the vault, including the groundwater composition, the electrochemical potential (Eh), pH, and temperature. We have not taken into consideration the effect of the vault backfill, which may contain additives to reinforce the expected conditions for pH and Eh.

### *Groundwater composition*

Two extremes of groundwater types have been chosen for this study. These are a synthetic granite groundwater used for experimental studies of sorption (15), and a synthetic brine groundwater used for experimental leaching studies (16). The latter has been included since saline waters have been found in the Canadian Precambrian Shield (17).

Analytical compositions of both groundwaters are presented in Table 2. Although there are obvious differences between real and synthetic groundwaters, results given below, and in other compositional sensitivity studies, suggest that water composition does not constitute an important variable for maximum uranium solubilities near the Eh and pH regimes of interest, and hence the differences are not expected to be important. In particular, neither groundwater includes the presence of phosphate anions, but results presented

Can. J. Chem. Downloaded from www.nrcresearchpress.com by 210.87.254.105 on 09/06/12
For personal use only.

TABLE 3. Calculated reference groundwater pH and Eh (V) at elevated temperatures

| Temperature (°C) | Granite groundwater | | | Brine groundwater | | |
|---|---|---|---|---|---|---|
| | pH* | Eh-low† | Eh-high‡ | pH* | Eh-low† | Eh-high‡ |
| 25 | 7.00 | −0.200 | −0.011 | 7.00 | −0.200 | −0.011 |
| 50 | 6.93 | −0.239 | −0.080 | 6.70 | −0.225 | −0.066 |
| 75 | 6.94 | −0.269 | −0.137 | 6.42 | −0.233 | −0.101 |
| 100 | 6.97 | −0.314 | −0.218 | 6.14 | −0.253 | −0.157 |
| 125 | 7.02 | −0.355 | −0.283 | 5.85 | −0.263 | −0.190 |
| 150 | 7.06 | −0.396 | −0.347 | 5.58 | −0.271 | −0.222 |
| 175 | 7.11 | −0.437 | −0.425 | 5.34 | −0.280 | −0.267 |

*pH is assumed to be 7.00 at 25°C, and is calculated by SOLMNEQ for the other temperatures.
†Calculated assuming the Eh is buffered by the equilibrium between magnetite and hematite, and using eq. [4] with $\Delta G^0$ from ref. 21 ($\Delta G_{175}^0$ was interpolated).
‡As above, but assuming the Eh buffer is the siderite–goethite reaction with $p_{CO_2}$ fixed at $10^{-3.5}$ atm.

elsewhere (18) suggest that uranium–phosphate complexes are not important for the particular cases described in this report.

*pH*

Both groundwaters have an assumed pH of 7.00 at 25°C, which is within the expected range of 6–10 for natural groundwaters (19). In some plots reproduced below, calculated curves are over a wider pH range to show the effect of its variation.

For temperatures other than 25°C, the pH of the groundwaters can be expected to vary due to temperature-dependent change in the dissociation constants for water and aqueous species, and due to temperature-dependent water–mineral reactions. If the latter reactions are not important for water near the $UO_2$ fuel, SOLMNEQ can be used to estimate a "reference" vault pH at elevated temperatures for both groundwaters. Some results are shown in Table 3, and it may be noted that, relative to neutral water, the pH of the brine groundwater remains near neutral at 150°C, whereas the granite groundwater is somewhat more basic. These differences in calculated pH can be attributed to the complex temperature-dependent behaviour of a variety of complexes, such as $Ca(HCO_3)^+$, $Mg(OH)^+$, etc.

*Eh*

There is little experimental data for the electrochemical potential or Eh of deep groundwaters, although it has been postulated that the Eh of these waters tends to approach the relatively reducing potential of the magnetite–hematite pair (19, 20). Since these minerals are common in the Precambrian Shield, a reasonable assumption is that the magnetite–hematite reaction:

$$[3a] \quad \underset{\text{magnetite}}{Fe_3O_4(c)} + \tfrac{1}{2}H_2O \rightleftarrows \tfrac{3}{2}\underset{\text{hematite}}{Fe_2O_3(c)} + H^+ + e^-$$

is *representative* of the lower Eh limit which can be expected near the proposed waste disposal vault. We have also assumed that the siderite–goethite reaction:

$$[3b] \quad \underset{\text{siderite}}{FeCO_3(c)} + 2H_2O \rightleftarrows \underset{\text{goethite}}{Fe(OH)_3(c)} + H^+ + CO_2 + e^-$$

can be taken to be *representative* of an upper limit of the Eh near the vault (20). For both reactions, Eh is a function of pH given by the Nernst equation:

$$[4] \quad Eh = -\frac{\Delta G^0}{nF} - \frac{2.3RT}{nF}\,pH$$

where $\Delta G^0$ is the Gibbs energy for the reaction, $n$ is the number of electrons involved in the reaction, $F$ is the Faraday constant (the activity of water is set to unity), $R$ is the gas constant, and $T$ is the temperature in Kelvin. For reaction [3*b*], we have included in $\Delta G^0$ a term which involves the partial pressure of $CO_2$ ($p_{CO_2}$). For our calculations $p_{CO_2}$ was fixed at $10^{-3.5}$ atm, which is $p_{CO_2}$ in the atmosphere and which is a reasonable value for groundwaters near the water table (20). Higher values of $p_{CO_2}$ might be expected for deep groundwaters, resulting in higher carbonate concentrations and a more oxidizing Eh, but these changes do not have a large effect on the results presented here.

Equation [4] was used with data from ref. 21 to evaluate the low and high Eh values listed in Table 3. At temperatures other than 25°C, pH was chosen to be that calculated by SOLMNEQ, so that the upper and lower Eh limits effectively correspond to the equilibrium Eh–pH boundaries between magnetite–hematite and siderite–goethite, respectively.

*Temperature*

The last parameter used to define vault geochemistry is the temperature. The ambient temperature of a pluton in the Precambrian Shield at 1000 m is approximately 20 to 25°C, and heat transport

Can. J. Chem. Downloaded from www.nrcresearchpress.com by 210.87.254.105 on 09/06/12
For personal use only.

Can. J. Chem. Downloaded from www.nrcresearchpress.com by 210.87.254.105 on 09/06/12
For personal use only.

studies have suggested that the vault temperature will rise to approximately 100°C due to the imposed heat loading of the radioactive wastes (22). Results reproduced here are at 25 and 100°C.

*Calculated solubilities*

Figures 1 and 2 display the calculated uranium solubilities in the synthetic granite and brine groundwaters as a function of pH. Note that although the abscissa is labelled pH, the Eh is also varied according to eq. [4] for both Eh buffers at the two temperatures. Except for some exceptions noted below, the stable uranium solid was predicted to be $UO_2$. Other uranium solids, such as coffinite, etc. (23), were not included in these calculations due to a lack of high-temperature data, but some scoping calculations suggest that these other minerals are not likely to be more stable than $UO_2$ under the reference conditions of pH, Eh, and groundwater compositions considered here.

These results show that expected uranium solubilities in the waste vault are very low — of the order of $10^{-10}$ *M* or 0.02 parts per billion. This value is in agreement with uranium concentrations found in naturally occurring groundwaters in reducing environments (23–25), and with recent experimental results under similar conditions (26).

A comparison of Figs. 1 and 2, and other sensitivity studies, reveal that uranium solubility is not greatly affected by groundwater composition over the pH range 6–9 at the low Eh boundary. This

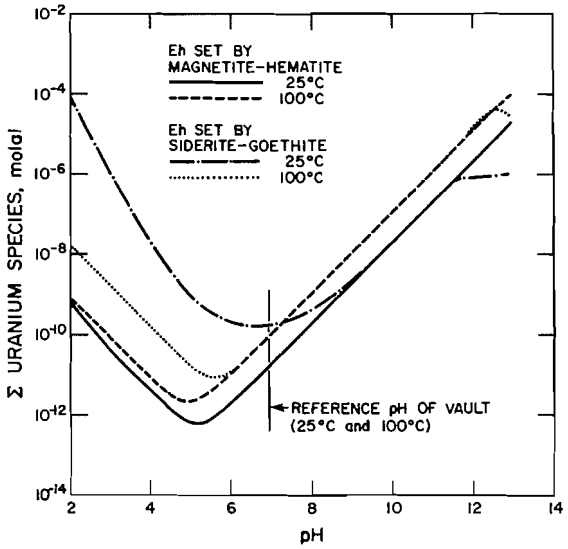


FIG. 1. Calculated uranium solubilities in granite groundwater. The Eh also varies with pH, and was calculated from eq. [4] for the equilibrium reactions [3*a*] for magnetite–hematite and [3*b*] for siderite–goethite (see text). The "reference" vault pH at each temperature is denoted by the arrows.

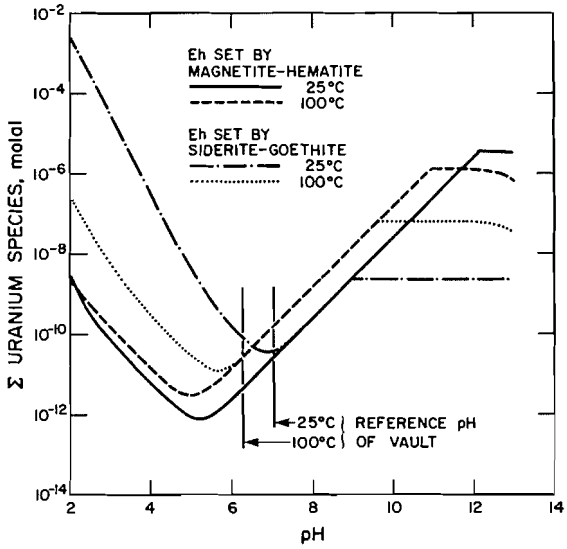


FIG. 2. Calculated uranium solubilities in brine groundwater. Other details as in Fig. 1.

is because the major uranium species is $U(OH)_5^-$, whose abundance is largely determined by pH. At the high Eh boundary of siderite–goethite, similar conclusions follow, except that the 25°C curves vary up to about pH 8 due to varying abundances of other species such as $UO_2(CO_3)_2^{2-}$.

These features are clearer in Figs. 3 and 4, which are distribution of species diagrams along the Eh–pH boundary of the magnetite–hematite and siderite–goethite reactions, respectively. Figure 3 shows that the species $U(OH)_5^-$ accounts for almost all the uranium in solution above pH 6 in granite groundwater. A similar diagram may be obtained for brine groundwater. Figure 4 shows a much more complicated pattern, with uranium carbonate species being important up to about pH 8. A similar diagram results for brine groundwater at the siderite–goethite boundary.

On the high pH side of Figs. 1 and 2, the abrupt changes in slope are due to the change in type of uranium solid which is in equilibrium with the aqueous solution. Below about pH 10, the most stable solid is $UO_2$, whereas $Na_2U_2O_7$ or $NaUO_3$ become more stable above pH 10. The slope change is most obvious in the brine groundwater, largely because of its much higher $Na^+$ concentration. Also shown at high pH for brine groundwater is the unusual result that uranium is less soluble at the higher oxidizing siderite–goethite boundary than at the magnetite–hematite boundary. This is due to the shape of the stability field for $NaUO_3$ (18). Along the siderite–goethite boundary, the stability field of $NaUO_3$ is reached near pH 9.5 and

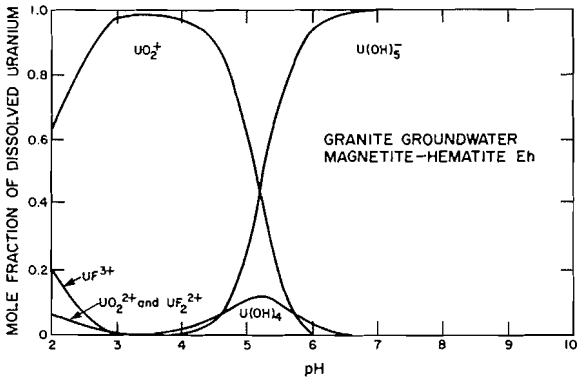


FIG. 3. Calculated distribution of uranium species in granite groundwater at 25°C. The Eh used corresponds to the equilibrium boundary for the magnetite–hematite reaction. Species with ionic fractions less than 0.01 are not shown.

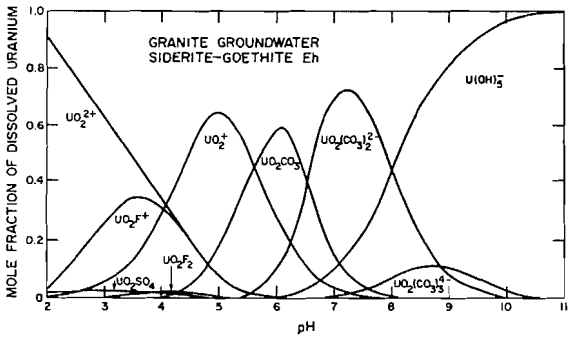


FIG. 4. Calculated distribution of uranium species in granite groundwater at 25°C along the siderite–goethite equilibrium boundary (with $p_{CO_2}$ fixed at $10^{-3.5}$ atm). Other details are as described in Fig. 3.

$[U]_{total} \simeq 10^{-8} M$, whereas along the lower magnetite–hematite boundary the stability field of $NaUO_3$ is not reached until pH ~ 12 and $[U]_{total} \sim 10^{-5} M$.

Figures 1 and 2 also reveal that the effect of temperature on uranium solubility is small. In fact, uranium solubility shows a "reverse" or weak temperature dependence, as indicated in Fig. 5, which was computed using Eh and pH data of Table 3. Although the exact shape of these curves may be questionable due to the uncertainty in the thermodynamic data (13), it is more certain that uranium solubility is only slightly dependent on temperature at reducing and near neutral conditions.

The above discussion and other data not reproduced here can also be used to study the sensitivity of uranium solubility under conditions expected in deep groundwaters. It follows that uranium solubilities are mostly dependent on pH, with decreasing dependence on the parameters Eh, temperature,

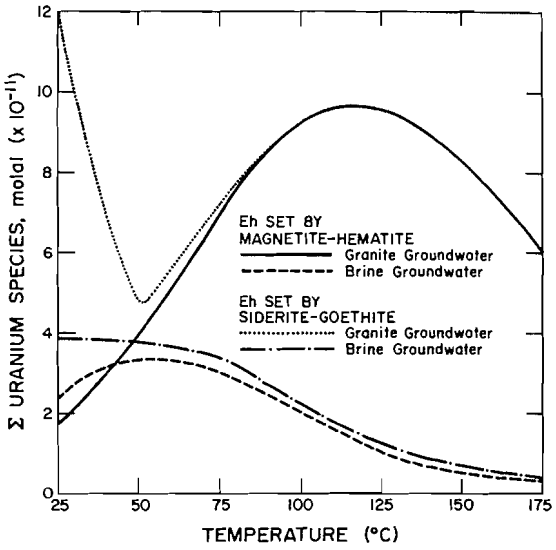


FIG. 5. Calculated uranium solubilities as a function of temperature. The four curves are for granite and brine groundwater along the siderite–goethite and magnetite–hematite equilibrium boundaries (see text).

and groundwater composition. This conclusion is also reflected in the following reaction, which describes most of the uranium "chemistry" expected to occur in deep groundwaters:

[5] $UO_2 + 3H_2O \rightleftarrows U(OH)_5^- + H^+$

For the siderite–goethite Eh boundary, other uranium reactions (involving uranium(VI) carbonates) are also important at lower pH. In all cases, however, it appears that uranium solubilities are very low, ranging from approximately $10^{-8}$ to $10^{-12} M$ in the pH range 6–10, and with a value near $10^{-10}$ under the conditions expected in a nuclear fuel waste vault. It also appears that the most stable uranium solid is likely to be $UO_2$, except in the brine groundwaters at high pH (other uranium minerals, such as coffinite (23), may also be important in groundwaters containing higher concentrations of dissolved silica than were considered here).

### Limitations of the model

Due to the complex nature of these calculations, it is probably as important to be aware of the inherent qualifications and limitations as it is to be knowledgeable of the final results. Some limitations are mentioned below, and although it is not possible to provide a quantitative estimate of their effects, it is expected that they will not influence the results by more than one or perhaps two orders of magnitude.

A major limitation of equilibrium models is that

Can. J. Chem. Downloaded from www.nrcresearchpress.com by 210.87.254.105 on 09/06/12
For personal use only.

Can. J. Chem. Downloaded from www.nrcresearchpress.com by 210.87.254.105 on 09/06/12
For personal use only.

they cannot describe non-equilibrium effects such as chemical kinetics or the formation of colloids. By way of example, it has already been mentioned in the footnote to Table 2 that the brine groundwater does not correspond to a stable system since it is supersaturated with respect to some minerals. These objections may be unimportant, however, if we take into account the extremely low water velocity expected for deep groundwaters (of the order of 0.3 m/year (22)), which increases the time allowed for the system to equilibrate. Another important non-equilibrium process not considered here is the effect of radiolysis, which might give rise to local variations in Eh and pH near the irradiated fuel containers.

Other important limitations follow from uncertainties in the database, or missing data. In the calculations described here, for example, a number of uranium minerals, such as coffinite and tyuyamunite (23), are missing, as are data (possibly) for aqueous U(IV) carbonates. Missing solids result in an over-estimation of uranium solubilities, if they are more stable than $UO_2$, whereas the reverse is true of missing aqueous species.

Other simplifications in the equilibrium model used here will also affect the results; for example, pressure effects were not studied, and it is well known that the modified semi-empirical Debye–Hückel equation is inaccurate at the high ionic strength of the brine groundwater under consideration. The effect of solid solutions such as $UO_{2+x}$, $0 \leq x \leq 0.6$ (27) were also not considered. These effects and the others mentioned above suggest areas requiring further experimental research.

## Implications and conclusions

Maximum uranium concentrations of the order of $10^{-10}$ *M* have been calculated for a range of conditions which bracket the conditions expected in a deep underground nuclear fuel waste vault in crystalline rock. Parameters studied included pH, Eh, temperature, and groundwater composition.

Given the low solubility of $UO_2$, and because irradiated CANDU fuel is largely $UO_2$, we can expect that the irradiated fuel matrix will also be characterized by a very low solubility. We can also expect that the original fuel matrix will persist for a long time in the postulated vault environment, since $UO_2$ is likely the stable thermodynamic solid and since groundwater flows are expected to be very small. Recent analysis (28, 29) of the leaching behaviour of irradiated fuel also suggests that the fission products (except iodine and cesium, which apparently are preferentially leached during the initial stages) and the actinides will be released in very low concentrations, because they appear to be released congruently as the $UO_2$ fuel matrix dissolves. We can also find geological evidence supporting these conclusions; in particular, observations made on the natural reactor discovered at Oklo suggest that irradiated uraninite grains have remained intact for over a billion years (30).

The calculated results also suggest that the environment of the ideal nuclear fuel waste vault would include a groundwater which is buffered at a slightly acid to near neutral pH and at a moderately reducing Eh. This environment may be reinforced by the addition of suitable materials to the low permeability backfill surrounding the irradiated fuel containers.

## Acknowledgements

I am indebted to R. J. Lemire and P. R. Tremaine for a preliminary copy of their review on uranium equilibria. R. J. Lemire, J. Paquette, and D. Langmuir also provided some very useful suggestions and comments.

1. R. M. Garrels and C. L. Christ. Solutions, minerals and equilibria. Freeman, Cooper and Company, San Francisco. 1965.
2. J. Boulton (*Editor*). Management of radioactive fuel wastes: the Canadian disposal program. Atomic Energy of Canada Limited Report, AECL-6314. 1978.
3. Acres Consulting Services Ltd., RE/SPEC Inc., Dilworth, Secord and Meagher and Associates Ltd., and Hagconsult AB. Atomic Energy of Canada Limited Report, AECL-6188-1, -2, and -3. 1978.
4. Acres Consulting Services Limited. A disposal centre for irradiated nuclear fuel: conceptual design study; and A disposal centre for immobilized nuclear waste: conceptual design study. Atomic Energy of Canada Limited Reports, AECL-6415 and AECL-6416. 1980.
5. L. J. Clegg and J. R. Coady. Radioactive decay properties of CANDU fuel. Vol. 1. The natural uranium fuel cycle. Atomic Energy of Canada Limited Report, AECL-4436/1. 1977.
6. F. van Zeggeren and S. H. Storey. The computation of chemical equilibria. Cambridge University Press. 1970.
7. F. J. Zeleznik and S. Gordon. Ind. Eng. Chem. **60**(6), 27 (1968).
8. W. R. Smith. Ind. Eng. Chem. Fundam. **19**, 1 (1980).
9. Y. K. Kharaka and I. Barnes. SOLMNEQ — solution mineral equilibrium computations. U.S. Geol. Surv. Comp. Contr. PB-215-899. 1973.
10. H. C. Helgeson. Am. J. Sci. **267**, 729 (1969).
11. Y. K. Kharaka. Private communication.
12. R. J. Lemire. COTDET — calculation of thermodynamic data at elevated temperatures.
13. R. J. Lemire and P. R. Tremaine. J. Chem. Eng. Data, **25**, 361 (1980).
14. J. Kielland. J. Am. Chem. Soc. **59**, 1675 (1937).
15. T. T. Vandergraaf. Unpublished results.
16. L. H. Johnson. Unpublished results.
17. Initial groundwater sample from the Lac du Bonnet Batholith. Atomic Energy of Canada Limited Technical Record, TR-21. 1979.

18. J. PAQUETTE and R. J. LEMIRE. Nuc. Sci. Tech. **79**, 26 (1981).
19. L. G. M. BAAS BECKING, I. R. KAPLAN, and D. MOOR. J. Geol. **68**, 243 (1960).
20. M. SATO. Econ. Geol. **55**, 928 (1960).
21. H. E. BARNER and R. V. SCHEUERMAN. Handbook of thermochemical data for compounds and aqueous species. J. Wiley and Sons, New York. 1978.
22. S. A. MAYMAN. Private communication.
23. D. LANGMUIR. Geochim. Cosmochim. Acta, **42**, 547 (1978).
24. T. F. KRAEMER. Private communication.
25. International Atomic Energy Agency. Proceedings of a Symposium on the Oklo Phenomenon, IAEA, Vienna, 1975 (STI/PUB/405); Proceedings of a Meeting of the Technical Committee on Natural Fission Reactors, IAEA, Vienna, 1978 (STI/PUB/475).
26. P. R. TREMAINE, J. D. CHEN, G. J. WALLACE, and W. A. BOIVIN. J. Solution Chem. In press.
27. E. J. BROOKER and E. W. NUFFIELD. Am. Mineral. **37**, 363 (1952).
28. L. H. JOHNSON, D. W. SHOESMITH, G. E. LANANSKY, M. G. BAILEY, and P. R. TREMAINE. Proceedings of the Second Annual Workshop on Comparative Leaching Behaviour of Radioactive Waste Forms, Argonne National Laboratory, Sept. 3–4, 1980.
29. B. W. GOODWIN, L. H. JOHNSON, and D. M. WUSCHKE. Radionuclide Source Terms for Irradiated $UO_2$ Fuel. Presented at the Workshop on Near Field Phenomena, Seattle, Aug. 31–Sept. 3, 1981; to be published in the NEA proceedings.
30. G. A. COWAN. Migration paths for OKLO reactor products and application to the problem of geological storage of nuclear wastes. IAEA-TC-119. p. 693. 1978.

Can. J. Chem. Downloaded from www.nrcresearchpress.com by 210.87.254.105 on 09/06/12
For personal use only.

# Quenching of the singlet and triplet state of benzene by halogenated alkanes in the vapor phase

H. A. KHWAJA, G. P. SEMELUK, AND I. UNGER

*Department of Chemistry, University of New Brunswick, Fredericton, N.B., Canada E3B 5A3*

Received September 16, 1981

H. A. KHWAJA, G. P. SEMELUK, and I. UNGER. Can. J. Chem. **60**, 1767 (1982).

The second order rate constants ($k_q$) for the quenching of the singlet state of benzene by several halogenated alkanes (viz. $CH_2Br_2$, $CCl_4$, $CH_3CCl_3$, $CHCl_3$, $CHF_3$, $CH_3Cl$, $CH_3F$, $CH_2F_2$, $CH_2Cl_2$, $CFCl_3$, $CF_2Cl_2$, $CF_3Cl$, $CF_4$) in the vapor phase have been measured. For $CCl_4$, $CHCl_3$, $CH_2Cl_2$, and $CH_3Cl$, which were previously studied by Das Gupta and Phillips, there is satisfactory agreement between the $k_q$ values obtained in the separate investigations. The linear dependence of the electron affinity of quencher with the corresponding quenching rate constants supports an exciplex mechanism in accordance with Klein's model. Charge transfer occurs from benzene to halogenated alkane and is greater for the chloro alkanes than for mixed fluoro–chloro alkanes. In the case of the triplet state of benzene, whose behaviour was monitored using the sensitized emission of biacetyl technique, quenching effects were at best one order of magnitude smaller and probably involve more than one bimolecular process.

H. A. KHWAJA, G. P. SEMELUK et I. UNGER. Can. J. Chem. **60**, 1767 (1982).

On a mesuré les constantes de vitesse de second ordre ($k_q$) du piégeage en phase vapeur de l'état singulet du benzène par divers alcanes halogénés (tels: $CH_2Br_2$, $CCl_4$, $CH_3CCl_3$, $CHCl_3$, $CHF_3$, $CH_3Cl$, $CH_3F$, $CH_2F_2$, $CH_2Cl_2$, $CFCl_3$, $CF_2Cl_2$, $CF_3Cl$, $CF_4$). Dans le cas des alcanes suivants, $CCl_4$, $CHCl_3$, $CH_2Cl_2$ et $CH_3Cl$ que Das Gupta et Phillips ont étudié antérieurement, il y a un accord satisfaisant entre les valeurs de $k_q$ obtenues par études différentes. Le fait que l'affinité électronique du piège dépende linéairement des constantes de vitesse de piégeage correspondant, constitue une preuve de mécanisme par exciplex prévu par le modèle de Klein. Le transfert de charge a lieu du benzène vers l'alcane halogéné et il est plus grand dans le cas des chloroalcanes que dans celui des fluoro–chloroalcanes mixtes. Dans le cas de l'état triplet du benzène dont on a enregistré le comportement en utilisant la technique d'émission sensibilisée de biacétyle, les effets de piégeage sont au plus d'un ordre de grandeur plus faible et impliquent probablement plus qu'un processus bimoléculaire.

[Traduit par le journal]

## Introduction

The quenching of electronically excited states of aromatics can occur by at least four mechanisms: (*1*) electronic energy transfer, which requires acceptors possessing energy states lower than those of the aromatic donor molecules, (*2*) enhancement of non-radiative decay, (*3*) chemical reaction, and (*4*) exciplex formation.

Exciplexes are excited state complexes between donor and acceptor having definite stoichiometry but which are dissociative in the ground state. These may be formed by charge transfer from the excited aromatic to the additive or vice versa depending upon the relative ionization potentials and electron affinities of the aromatic molecule and the quencher. Considerable evidence supporting the intermediacy of exciplex formation in the quenching of aromatic singlet excited states by a variety of additives has been provided in recent years (1–5). Most of these investigations have been carried out in dilute solutions (1, 2, 4, 5). Only a limited amount of work in the vapor phase has been reported so far (3).

The quenching of the excited singlet states of aromatic hydrocarbons and their derivatives by halogenated alkanes (1–4), dienes (6), and amines (7) is generally believed to proceed via an intermediate contact exciplex of charge-transfer character. The rate of formation of these exciplexes is considered to be the rate determining step in these quenching processes. According to Klein's model (1), which is based on the absolute rate theory of Eyring, the charge-transfer nature of such exciplexes can be expressed as a linear correlation between the overall second order quenching rate constant ($k_q$) and the exponential of some measure of the free energy change associated with the excited state complex formation:

$$[1] \quad k_q \propto \exp[-(IP_D - EA_A - C - P - h\nu_s)]/kT$$

In eq. [1] $IP_D$ represents the ionization potential of the donor; $EA_A$, the electron affinity of the acceptor; $C$, the coulomb stabilization energy of the complex; $P$, the polarization energy of the separated charges; and $h\nu_s$ the excitation energy of the first excited state.

The purpose of this study of the quenching of singlet and triplet states of a common aromatic donor molecule (benzene) by a variety of electron-deficient quenchers (halogenated alkanes) was: (*a*) to establish whether or not an exciplex is formed in the vapor phase and to test the validity of Klein's

0008-4042/82/131767-08$01.00/0

©1982 National Research Council of Canada/Conseil national de recherches du Canada

Can. J. Chem. Downloaded from www.nrcresearchpress.com by 210.87.254.40 on 09/06/12
For personal use only.

Can. J. Chem. Downloaded from www.nrcresearchpress.com by 210.87.254.40 on 09/06/12
For personal use only.

model (1) for these systems; (*b*) to determine the mechanism which is operative in benzene – halogenated alkanes system; and (*c*) to examine the possibility of any increase in quenching efficiency due to a heavy-atom effect.

Because the surrounding matrix in solutions plays an important role in determining the stability of these excited complexes and other factors such as media polarity and/or polarizability also may contribute to excited-state complexation, our study was undertaken in the vapor phase, where such complications would be reduced.

## Experimental

*Chemicals*

Benzene was obtained from Fisher Scientific Company as a Spectrograde product having a stated purity of 99.9%. It was used without further purification.

The biacetyl used was from Aldrich Chemical Company and was purified by bulb-to-bulb distillation "in vacuo" and stored in a blackened bulb on a vacuum line. All the halogenated alkanes were purified by gas–liquid chromatography using an HP Model 7620A chromatograph attached to a 5797A collecting unit, with He as the carrier gas; detection was by flame ionization. This chromatographic procedure gave a purity of >99.9% for each of the materials.

*Apparatus and measurements*

Most details of the apparatus and data collection and processing used in this study have been provided elsewhere (9). The apparatus consisted of a steel vacuum line equipped with Hoke packless diaphragm valves, a flow system incorporating a quartz cuvette and U-tube in series with an all-glass circulating pump, and a modified Aminco-Bowman spectrophotofluorometer (SPF). The principal modification is an optical-electronic system for obtaining spectra corrected for photomultiplier and phototube spectral response, which also compensates for variations in lamp intensity, and an accurate transmittance measuring-recording circuit. For 20 Torr benzene in a 1 cm path, more than 300 determinations over a five-month period yielded a transmittance value of 0.9355, with a standard deviation of 0.0041 (0.43%). The accuracy of the compensating analog electronics was ~0.2%, while the stability over a 12-h period, as determined with the help of precision test equipment, was ~0.02%. For a 1-h period, typical of the time to do a "run", the stability was better than 0.01%. The intensity of the lamp, whose "flicker" (period ≥0.008 s) was minimized by a magnetic arc stabilizer, typically decreased during a 12-h period by less than 1%. The compensating electronic system was able to maintain an output constant to <0.1% for a variation of 30% in lamp intensity in the form of either a 120 Hz sine or square wave (actual fluctuations seldom exceed 1%). The 935 phototubes used to monitor lamp intensity and transmitted intensity were both operated at photocurrents less than 33 nA in order to avoid the fatigue effects noted by Yip and Dickinson (10).

The vacuum line was evacuated to better than $5 \times 10^{-6}$ Torr. Pressures of samples were measured with an MKS Baratron type 170 M capacitance gauge. Inside dimensions of the quartz cuvette were 1 cm × 1 cm × 4.5 cm. Samples were admitted to the working manifold from sample reservoirs attached to the vacuum line and were degassed prior to use by three to four freeze–pump–thaw cycles to remove dissolved gases. All experiments were carried out at room temperature (297.6 ± 0.5 K).

A relative method was adopted to convert measured photocurrents and emission intensities into quantum yields. The standard compound for this purpose was benzene with a known vapor phase fluorescence quantum yield of 0.183 (11). In the singlet-state quenching experiments, 20 Torr of benzene was introduced into the cell and frozen down in the U-tube. A known pressure (5 to 80 Torr) of halogenated alkane was then admitted into the U-tube containing the frozen material. Mixing was accomplished in the U-tube by several flash vaporizations, followed by circulating the vapors with the help of a glass circulating pump. The gaseous mixture was excited using a wavelength of 254 nm (see below) and the benzene fluorescence was recorded. Using the standard fluorescence yield value for benzene alone, a separate calibration constant was calculated for each individual additive pressure, and the quantum yield in the presence of the additive could then be determined by using this constant (12).

The sensitized emission of biacetyl technique (13) was used to investigate the quenching of the triplet state of benzene by halogenated alkanes. The quantum yield of the triplet state of benzene (20 Torr) and biacetyl (0.1 to 0.3 Torr) mixture excited at 253.7 nm has been reported to be 0.63 (14). Varying amounts (5 to 80 Torr) of halogenated alkanes were added to a mixture of benzene (20 Torr) and biacetyl (0.1 to 0.2 Torr). Mixing was carried out in a way similar to that of the singlet-state experiments. The mixture was irradiated to 254 nm and the sensitized emission of biacetyl was recorded from 200–650 nm. In order to eliminate the "pump effect" (15), the pump was turned off immediately prior to recording the emission spectrum. Triplet yields could then be calculated using a calibration constant obtained from the experiment involving benzene and biacetyl alone, for each individual pressure of additive.

Emission intensities were in all cases determined by measuring the areas recorded in the spectral scan. This area measurement was carried out by a computer program using input from a Summagraphics tablet digitizer having a resolution of 0.1 mm, interfaced to a PDP-11/10 computer. Calibration against known areas indicated a precision of ~0.5% for the areas involved in the singlet quenching experiments, and ~1% for the areas involved in the triplet quenching experiments.

The slit arrangements used in the excitation monochromator produced a band width at half intensity of 3 nm at the mercury resonance line. The monochromator output actually observed at a setting of 254 nm (using a Xenon-Mercury Compact Arc lamp) was asymmetric, with the low wave length side dominant and the maximum at 253 nm.

## Results and discussion

### *A. Singlet-state quenching*

The quenching of the excited singlet state of benzene by $CH_2Br_2$, $CCl_4$, $CH_3CCl_3$, $CHCl_3$, $CHF_3$, $CH_3Cl$, $CH_3F$, $CH_2F_2$, $CH_2Cl_2$, $CFCl_3$, $CH_2Cl_2$, $CF_3Cl$, and $CF_4$ has been measured. In all the systems examined, the fluorescence quantum yield of benzene ($\phi_f$) in the presence of halogenated alkanes shows a steady decrease with increasing pressure of quencher. The most effective quencher was $CH_2Br_2$ while the least effective was $CF_4$, whose quenching effect was smaller by four orders of magnitude. In general, quenching efficiency increased with increasing number of chlorine atoms; the mixed fluoro–chloro alkanes were far less effective in quenching than the corresponding

Can. J. Chem. Downloaded from www.nrcresearchpress.com by 210.87.254.40 on 09/06/12
For personal use only.

hydro–chloro alkanes. For fluorescent yields >0.10 the uncertainty in $\phi_f$ is calculated to be no larger than 10%, while for lower values it is ~15%. The absorption spectra of benzene in vapor phase in the presence of the highest pressures of quenchers employed in the emission experiments did not show any sign of ground-state complex formation.

Figures 1 and 2 depict the Stern–Volmer plots of $\phi_f^0/\phi_f$ (the fluorescence yield of benzene in the absence of quencher divided by the fluorescence yield at a given amount of quencher) against the pressure of quencher. Each calculated ratio involves recording and measuring two areas at constant incident intensity, and is therefore calculated to have a precision of better than 4%. The least-squares fit of the data to a straight line were obtained in all cases by omitting the co-ordinate (0,1) from the calculation as a more stringent test of how closely the best fit line extrapolates to an intercept of 1. It is evident that these data fit the Stern–Volmer relation satisfactorily, with the possible exception of $CH_2Br_2$, whose intercept is somewhat greater than 1 (see Table 1). Non-linear Stern–Volmer plots may be due to a variety of reasons (16) and for benzene may show upward or downward curvature (17). It should also be noted that $CH_2Br_2$ has a continuous unstructured absorption spectrum in the spectral region of this investigation, and that the extinction coefficient is of the same order as that of benzene. The absorbance of the mixture of benzene and $CH_2Br_2$ was the sum of the individual absorbances at the applicable partial pressures, and no reaction was detectable during the time of a complete measurement, as evidenced by the constant transmittance of the mixture (if photolysis of $CH_2Br_2$ was significant the expected

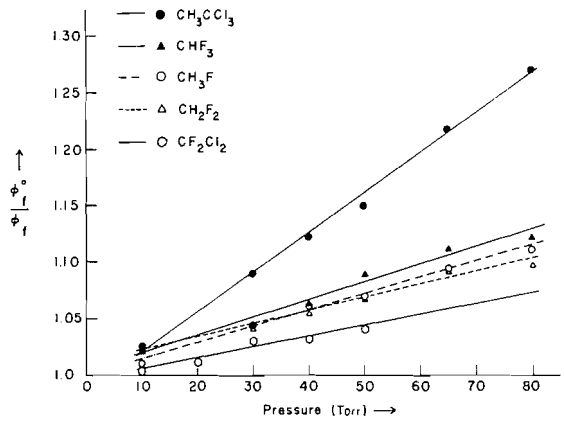


FIG. 1. Plot of $\phi_f^0/\phi_f$ for the benzene (20 Torr) singlet-state quenching by varying amounts of halogenated alkanes ($CH_3CCl_3$, $CHF_3$, $CH_3F$, $CH_2F_2$, $CF_2Cl_2$). $\lambda_{ex} = 254$ nm, $T = 297.6 \pm 0.5$ K.

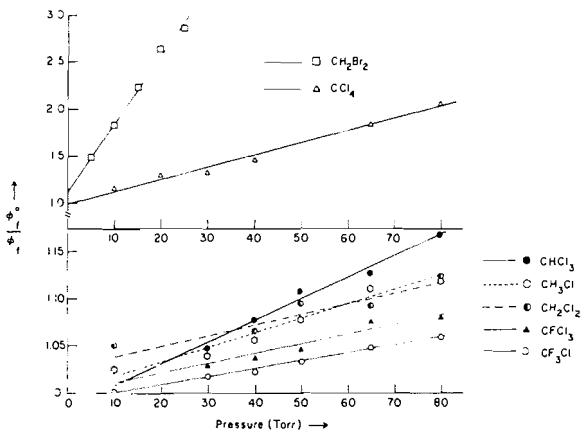


FIG. 2. Plot of $\phi_f^0/\phi_f$ for the benzene (20 Torr) singlet-state quenching by varying amounts of halogenated alkanes ($CH_2Br_2$, $CCl_4$, $CHCl_3$, $CH_3Cl$, $CH_2Cl_2$, $CFCl_3$, $CF_3Cl$). $\lambda_{ex} = 254$ nm, $T = 297.6 \pm 0.5$ K.

products would include bromobenzene which has an $\varepsilon$ approximately ten times that for benzene and $CH_2Br_2$).

The slopes of the least-square fits of the data give the product $k_q\tau$, where $k_q$ is the observed second order quenching rate constant and $\tau$ is the observed lifetime of benzene in the absence of quencher. Several workers (18–22), using three different techniques, have determined the fluorescence lifetime ($\tau$) of benzene vapor to be 75 ± 10 ns for conditions similar to those used in this experiment. A comparable value has been obtained recently for solid benzene (23). Using this value of $\tau$, $k_q$ values were then evaluated. Table 1 provides a summary of the data obtained from our experiments, additional information from other sources, and a summary of the data obtained by Das Gupta and Phillips for the compounds common to the two investigations. Because the latter workers used a different value of $\tau$ in their calculations, we have recalculated and listed their observed slopes for a more appropriate comparison of the derived data. Also given in Table 1 are the standard deviations for the intercepts and slopes obtained from the least-squares analysis.

The agreement between the two investigations on the molecules in common is satisfactory considering the differences in such experimental details as lamps, bandwidths, cells, and method of emission measurement. A major source of uncertainty is the low absorbance of benzene. Our choice of individual pair experiments, i.e., benzene alone followed immediately by introduction of a known pressure of quencher with discarding of this mixture as soon as measurements were complete, was designed to

Can. J. Chem. Downloaded from www.nrcresearchpress.com by 210.87.254.40 on 09/06/12
For personal use only.





TABLE 1. Vapor-phase singlet state quenching of benzene by halogenated alkanes. ($\tau = 75$ ns, $\lambda_{ex} = 254$ nm, $T = 297.6 \pm 0.5$ K). Ionization potential of benzene = 9.25 eV[a]

| Quencher | Intercept[b] std. dev. | Slope[b] std. dev. | $k_q \times 10^{-8}$ (L mol$^{-1}$ s$^{-1}$) | ln $k_q$ | Das Gupta and Phillips[j] Slope | Das Gupta and Phillips[j] $k_q \times 10^{-8}$ (L mol$^{-1}$ s$^{-1}$) | IP[a] (eV) | EA[c] (eV) | $\sigma \times 10^{16}$[d] (cm$^2$ molecule$^{-1}$) | $\xi$[e] (cm$^{-1}$) | $\Sigma\xi$[f] (cm$^{-1}$) |
|---|---|---|---|---|---|---|---|---|---|---|---|
| $CH_2Br_2$ | 1.135<br>0.062 | 1315.9<br>69.1 | 175.5 | 23.59 | — | — | 10.80 | — | 2.71 | 2460 | 4920 |
| $CCl_4$ | 0.995<br>0.036 | 238.87<br>13.86 | 31.9 | 21.88 | 297.2 | 38.6 | 11.47 | 2.12 | 0.483 | 587 | 2348 |
| $CH_3{\cdot}C{\cdot}Cl_3$ | 0.987<br>0.006 | 64.90<br>2.33 | 8.65 | 20.58 | — | — | — | 1.88[g] | 0.128 | 587 | 1761 |
| $CHCl_3$ | 0.988<br>0.005 | 41.69<br>1.94 | 5.56 | 20.14 | 18.5 | 2.4 | 11.42 | 1.75 | 0.080 | 587 | 1761 |
| $CHF_3$ | 1.006<br>0.006 | 28.59<br>2.25 | 3.81 | 19.76 | 18.5 | 2.4 | — | — | 0.049 | 272 | 816 |
| $CH_3Cl$ | 1.004<br>0.007 | 28.17<br>2.70 | 3.76 | 19.74 | 35.4 | 4.6 | 11.28 | — | 0.044 | 587 | 587 |
| $CH_3F$ | 1.000<br>0.004 | 26.58<br>1.52 | 3.54 | 19.69 | — | — | 12.85 | — | 0.036 | 272 | 272 |
| $CH_2F_2$ | 1.013<br>0.009 | 21.01<br>2.97 | 2.80 | 19.45 | — | — | — | — | 0.033 | 272 | 544 |
| $CH_2Cl_2$ | 1.029<br>0.011 | 20.30<br>4.05 | 2.71 | 19.42 | 18.5 | 2.4 | 11.40 | 1.36 | 0.036 | 587 | 1174 |
| $CFCl_3$ | 1.002<br>0.005 | 18.43<br>1.99 | 2.46 | 19.32 | — | — | — | 1.10[h] | 0.037 | | 2033 |
| $CF_2Cl_2$ | 0.997<br>0.004 | 17.48<br>2.39 | 2.33 | 19.27 | — | — | 11.80 | 0.40[h] | 0.034 | | 1718 |
| $CF_3Cl$ | 0.993<br>0.002 | 15.60<br>0.67 | 2.08 | 19.15 | — | — | 12.92 | −0.40[i] | 0.029 | | 1403 |
| $CF_4$ | 0.999<br>0.013 | < 0.12 | < 0.016 | < 14.3 | — | — | 17.80 | −0.70[i] | — | 272 | 1088 |

[a] Reference 28.
[b] Determined from least-squares analysis; the point $\phi_f^0/\phi_f = 1$ at 0 pressure was omitted from the analysis.
[c] Reference 4.
[d] Cross-section calculated from equation $\sigma^2 = k_q(8\pi RT/\mu)^{-1/2}$.
[e] Spin–orbit coupling constants adopted from ref. 29.
[f] Sum of spin–orbit coupling constant of substituent heavy atoms.
[g] EA value was interpolated from the relationship of electron affinity with thermal electron attachment rate for gaseous chloromethanes.
[h] Reference 30.
[i] Reference 31.
[j] Reference 3.

avoid the problem of product accumulation which manifests itself as a change in transmittance if the alternate procedure of adding increments of quencher to a single charge of benzene is adopted. An experimental check of the influence of refractive index changes caused by changing gas pressures on a nonparallel beam showed this to be negligible at the transmittances of our experiments.

The competitive process following benzene excitation to its first singlet state in the presence of halogenated alkanes may be initially represented by a general scheme which includes reactions previously established or postulated between benzene and other additives. A reasonable set of such reactions to which reference can be made, and with which our results are consistent, is

| | | |
|---|---|---|
| [2] | $D + h\nu(254\,nm) \xrightarrow{I_a} {}^1D^*$ | photoexcitation |
| [3] | ${}^1D^* \xrightarrow{k_f} D + h\nu_f$ | fluorescence |
| [4] | ${}^1D^* \xrightarrow{k_\Delta} D + \Delta$ | internal conversion |
| [5] | ${}^1D^* \xrightarrow{k_{isc}} {}^3D^*$ | intersystem crossing |
| [6] | ${}^1D^* \xrightarrow{k_4}$ isomeric D | isomer formation |
| [7] | ${}^1D^* + A \xrightarrow{k_a} {}^1(D\text{—}A)^*$ | complex formation |
| [8] | ${}^1(D\text{—}A)^* \xrightarrow{k_d'} {}^1D^* + A$ | complex dissociation |
| [9] | ${}^1(D\text{—}A)^* \xrightarrow{k_{ic}'} D + A$ or products | internal conversion or chemical reaction |
| [10] | ${}^1(D\text{—}A)^* \xrightarrow{k_f'} D + A + h\nu_f'$ | complex emission |
| [11] | ${}^1(D\text{—}A)^* \xrightarrow{k_{et}'} D + {}^1A^*$ | electronic energy transfer |
| [12] | ${}^1(D\text{—}A)^* \xrightarrow{k_{isc}'} {}^3(D\text{—}A)^*$ | complex intersystem crossing |

where D and A refer to ground-state benzene and ground-state halogenated alkane, respectively. An asterisk denotes an electronically excited state while the prefixes give the multiplicity of the electronic states. $I_a$ represents the rate of absorption of light by the benzene molecule.

Janda *et al.* (24) have shown in the benzene–acetone system that vibrational relaxation can influence the quenching efficiency of the added molecule. At the pressures and excitation wavelength of our experiments, it is reasonable to assume that benzene vibrational deactivation is complete prior to the occurrence of both unimolecular and bimolecular processes.

Some of the processes given above may be neglected for various reasons: (*i*) The extent of isomer formation process [6] is not appreciable under the experimental conditions used here and may be neglected in comparison to the much more rapid processes of intersystem crossover and fluorescence (13). (*ii*) None of the benzene – halogenated alkane systems examined exhibited any emission other than the fluorescence of benzene molecule. Moreover, the fluorescence spectra of benzene does not reveal any basic structural change upon the addition of the quenchers used in this study. On the basis of the above, the complex emission process [10] is excluded from the scheme. (*iii*) It has been shown that the extent of overlap of the fluorescence emission spectrum of the donor with that of the absorption spectrum of the acceptor provides a measure of the probability for radiationless intermolecular energy transfer. There is no overlap between the absorption spectrum of the halogenated alkanes used in this study and the fluorescence spectrum of benzene. Therefore, the possibility of singlet-state quenching by energy transfer, step [11], may be omitted.

Application of the steady state approximation to the above mechanism yields:

$$[13]\quad \frac{\phi_f^0}{\phi_f} = 1 + \frac{(k_{ic}' + k_{isc}')k_a[A]}{(k_f + k_\Delta + k_{isc})(k_d' + k_{ic}' + k_{isc}')} = 1 + k_q\tau[A]$$

where

$$\tau = (k_f + k_\Delta + k_{isc})^{-1}$$

Can. J. Chem. Downloaded from www.nrcresearchpress.com by 210.87.254.40 on 09/06/12
For personal use only.

Can. J. Chem. Downloaded from www.nrcresearchpress.com by 210.87.254.40 on 09/06/12
For personal use only.

expresses the fluorescence lifetime of benzene in the absence of quencher, and

$$[14] \quad k_q = \frac{(k_{ic}' + k_{isc}')k_a}{(k_d' + k_{ic}' + k_{isc}')}$$

is the expected second order rate constant for singlet-state quenching. According to eq. [13], plots of $\phi_f^0/\phi_f$ as a function of halogenated alkane pressure should be linear. This is found to be the case in all systems examined (see Figs. 1 and 2).

According to eq. [14] $k_q$ should be dependent upon several factors including the binding energy of the complex and it may be influenced by heavy-atom quenchers. A detailed quantitative discussion of the quenching mechanism can be made only if each component rate constant for a particular aromatic/quencher pair is available. $k_q$, other than for $CH_2Br_2$, was determined to be some two orders of magnitude smaller than what would be expected on the basis of ground-state collision cross sections (Table 1). Thus, either benzene and the halogenated alkane must approach each other closely before interaction occurs, or both $k_a$, the association constant, and $k_d'$ the dissociation constant of the complex, must be large.

The ionization potentials of the halogenated alkanes are much higher than that of $C_6H_6$. This, coupled with the fact that quenching efficiency increases with increasing electron affinity of the quencher, suggests that quenching is due to a charge transfer complex, of the type described by Klein *et al.* (1), and that the charge transfer is from $C_6H_6$ to chlorinated alkane.

The electron affinities (EA) of seven of the compounds are known and these were plotted against ln $k_q$ as a check of eq. [1] (see Fig. 3). Inspection of Fig. 3 shows that the model proposed by Klein *et al.* (1) is indeed appropriate for the halogenated alkanes; further, two distinct apparently linear relationships exist, one for the chlorinated alkanes and another for the mixed fluoro–chloro alkanes. Since the slope of the line in plots of ln $k_q$ vs. EA is considered a measure of the amount of charge transfer, it is obvious that benzene transfers a greater amount of charge to hydro–chloro (8%) than to fluoro–chloro alkanes (0.3%). It must be noted that the Klein equation does not take into account heavy atom effect. Thus departure from linearity is to be expected as $\xi$ values of quencher increase.

*B. Triplet-state quenching*

The triplet state of benzene does not exhibit emission in the vapor phase, although a considerable body of evidence demonstrates its existence in various phases (13, 25) including the gas phase. An indirect technique is therefore necessary to monitor this species. The sensitized emission of biacetyl technique (13) was employed to determine the rate constants for the quenching of the triplet state of benzene by the same molecules described in part A. The following additional steps describe the behavior of the triplet state of benzene in the presence of biacetyl.

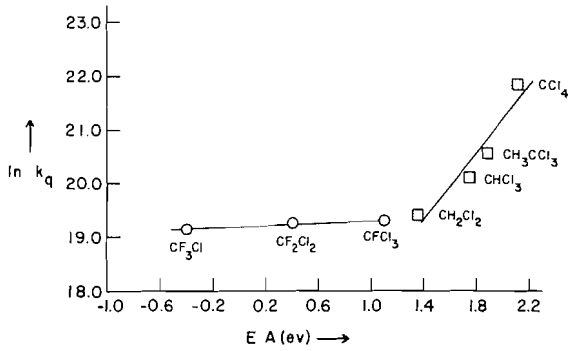


FIG. 3. Dependence of the observed quenching rate constant ($k_q$) of benzene fluorescence on the electron affinity of the halogenated alkane quenchers.

$$[15] \quad {}^3D^* \xrightarrow{k_{isc}'} D$$

$$[16] \quad {}^3D^* + A \xrightarrow{k_d'} \text{Quenching}$$

$$[17] \quad {}^3D^* + BiA \xrightarrow{k_{et}'} D + {}^3BiA^*$$

$$[18] \quad {}^3BiA^* \xrightarrow{k_p'} BiA + h\nu_p$$

$$[19] \quad {}^3BiA^* \xrightarrow{k_{isc}''} BiA$$

BiA refers to a ground-state biacetyl molecule and all the other symbols have the same meaning as above. Under the experimental conditions employed, reaction [16] is much less important than reaction [18]. Thus the above mechanism leads to expression [20] for quantum yield of phosphorescence of biacetyl sensitized by the benzene in the presence of quenchers ($\phi_t$):

$$[20] \quad \phi_t = \frac{k_{isc}}{(k_f + k_\Delta + k_{isc} + k_q[A])} \times \frac{k_{et}'[BiA]}{(k_q'[A] + k_{et}'[BiA]} \times \frac{k_p'}{(k_p' + k_{isc}'')}$$

The expression for fluorescence efficiency of benzene in the presence of quencher is:

$$[21] \quad \phi_f = \frac{k_f}{k_f + k_\Delta + k_{isc} + k_q[A]}$$

Combination of eqs. [20] and [21] gives:

Can. J. Chem. Downloaded from www.nrcresearchpress.com by 210.87.254.40 on 09/06/12
For personal use only.

$$[22] \quad \frac{\phi_f}{\phi_t} = \frac{k_f}{k_{isc}} \times \frac{(k_p' + k_{isc}'')}{k_p'} \times \frac{k_{et}'[BiA] + k_q'[A]}{k_{et}'[BiA]}$$

A ratio form of this equation which is particularly convenient for test purposes in our case is obtained by dividing eq. [22] for the general case of any quencher concentration [A] by the reference value obtained when [22] is evaluated for zero quencher concentration. This results in:

$$[23] \quad \frac{R_q}{R_0} \equiv \frac{(\phi_f/\phi_t)_q}{(\phi_f/\phi_t)_0} = 1 + \frac{k_q'[A]}{k_{et}'[BiA]}$$

Since [BiA] is constant and known, and $k_{et}' = 3.43 \times 10^{10}$ L mol$^{-1}$ s$^{-1}$ (27), then assuming [23] holds, a plot of $R_q/R_0$ vs. quencher concentration will yield a straight line whose slope (L mol$^{-1}$ s$^{-1}$) = ($k_q'/2.80 \times 10^5$). The determination of this ratio involves recording and measuring four areas at constant incident intensity. Under these relatively favourable conditions the calculated uncertainty is a maximum of 5% and is almost entirely due to uncertainty in the areas. The results for five of the compounds are summarized in Table 2.

Values of $k_q'$ calculated from [23] (see Table 2), except for $CH_3F$, show a large relative standard deviation (0.18, 0.3, 0.3, for $CH_3Cl$, $CCl_4$, and $CF_3Cl$ respectively, and 0.07 for $CH_3F$) suggesting that the linear relationship [23] may not be applicable. This is illustrated best by $CH_2Br_2$ (Fig. 4), for which $k_q'$ calculated from [23] is negative. The quenchers $CHCl_3$ and $CH_3CCl_3$ also show small negative values, $\sim -10^5$ to $-10^6$, for $k_q'$. For the remaining molecules the calculated $k_q'$ values are $< 5 \times 10^6$ L mol$^{-1}$ s$^{-1}$, and have very large relative standard deviations. The experimental observations indicate that three of the molecules, $CF_3Cl$, $CH_3Cl$, and $CCl_4$, exhibit a small but significant increase in $\phi_f/\phi_t$ with increasing quencher pressure

TABLE 2. Variation of $R_q/R_0$ for various quenchers as a function of quenchers pressure[a]

| Pressure (Torr) | Relative ratio singlet/triplet yields $R_q/R_0$ (uncertainty ~5%) | | | | |
|---|---|---|---|---|---|
| | $CH_2Br_2$ | $CH_3Cl$ | $CCl_4$ | $CF_3Cl$ | $CH_3F$ |
| 5.0 | 1.28 | — | — | — | — |
| 10.0 | 1.07 | 1.01 | 0.95 | 1.00 | — |
| 15.0 | 0.81 | — | — | — | — |
| 20.0 | 0.70 | 1.03 | 1.02 | 1.01 | 1.01 |
| 40.0 | — | 1.08 | 1.08 | 1.10 | 1.03 |
| 60.0 | — | 1.16 | 1.05 | 1.06 | 1.05 |
| 80.0 | — | 1.15 | 1.16 | 1.13 | 1.06 |
| $k_q \times 10^{-7}$[b] (L mol$^{-1}$ s$^{-1}$) | | 1.15[b] | 1.07[b] | 0.86[b] | 0.48[b] |

[a] $R_q/R_0 \equiv (\phi_f/\phi_t)_q/(\phi_f/\phi_t)_0$, where q stands for quencher.
[b] See text for discussion of significance.

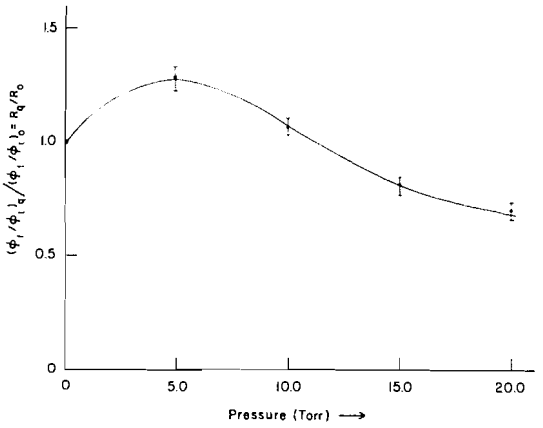


FIG. 4. Quenching of benzene triplet by $CH_2Br_2$.

indicating the occurrence of some quenching of the triplet state of benzene by these molecules. This phenomenon has been shown to occur (27) with molecules having high $\zeta$ values. $CH_2Br_2$, on the other hand, exhibits an overall decrease in $\phi_f/\phi_t$ with increasing quencher pressure, i.e., the singlet is depleted much more rapidly than the triplet state. This suggests that quenching of the benzene singlet by $CH_2Br_2$ probably occurs via two steps, reaction [7] discussed earlier and in addition

$$[24] \quad {}^1D^* + CH_2Br_2 \rightarrow {}^3D^* + CH_2Br_2$$

This is to be expected since $CH_2Br_2$ should exhibit a much greater heavy atom effect than any other of the molecules studied. For the remaining molecules $\phi_f/\phi_t$ is much less sensitive to quencher pressure.

**Acknowledgement**

The authors are grateful to the Natural Sciences and Engineering Research Council for financial support of this work.

1. J. KLEIN, V. PLAZANET, and G. LAUSTRIAT. J. Chim. Phys. Physicochim. Biol. **67**, 302 (1970).
2. W. R. WARE and C. LEWIS. J. Chem. Phys. **57**, 3546 (1972).
3. G. DAS GUPTA and D. PHILLIPS. J. Chem. Soc. Faraday II, **68**, 2003 (1972).
4. D. SAPERSTEIN and E. LEVIN. J. Chem. Phys. **62**, 3560 (1975).
5. M. E. R. MARCONDES, V. G. TOSCANO, and R. G. WEISS. J. Photochem. **10**, 315 (1979).
6. D. A. LABIANCA, G. N. TAYLOR, and G. S. HAMMOND. J. Am. Chem. Soc. **94**, 3679 (1972).
7. (*a*) D. REHM and A. WELLER. Isr. J. Chem. **8**, 259 (1970); (*b*) A. WELLER and H. BEENS. *In* Organic molecular photophysics. Vol. 2. *Edited by* J. B. Birks. Wiley, New York. 1975. p. 158.
8. R. S. DAVIDSON, A. LEWIS, and T. D. WHELAN. J. Chem. Soc. Chem. Commun. 204 (1975).

9. J. B. ADDISON, G. P. SEMELUK, and I. UNGER. J. Luminescence, **15**, 323 (1977).
10. R. W. YIP and D. R. DICKINSON. J. Scient. Inst. **43**, 758 (1966).
11. W. A. NOYES, JR., W. A. MULAC, and D. A. HARTER. J. Chem. Phys. **44**, 2100 (1966).
12. J. L. DURHAM, G. P. SEMELUK, and I. UNGER. Can. J. Chem. **46**, 3177 (1968).
13. H. ISHIKAWA and W. A. NOYES, JR. J. Chem. Phys. **37**, 583 (1962).
14. W. A. NOYES, JR. and D. A. HARTER. J. Chem. Phys. **46**, 674 (1967).
15. M. E. MACBEATH and I. UNGER. Can. J. Chem. **48**, 1607 (1970).
16. R. J. CAMPBELL, E. W. SCHLAG, and B. W. RISTOW. J. Am. Chem. Soc. **89**, 5098 (1967).
17. E. M. ANDERSON and G. B. KISTIAKOWSKY. J. Chem. Phys. **51**, 182 (1969).
18. T. CHEN and E. W. SCHLAG. Molecular luminescence. *Edited by* E. C. Lim. W. A. Benjamin, New York. NY. 1969. p. 381.
19. G. M. BREWER and E. K. C. LEE. J. Chem. Phys. **51**, 3130 (1969).
20. M. NISHIKAWA and P. K. LUDWIG. J. Chem. Phys. **52**, 107 (1970).
21. B. K. SELINGER and W. R. WARE. J. Chem. Phys. **53**, 3160 (1970); **52**, 5482 (1970).
22. C. S. BURTON and H. E. HUNZIKER. J. Chem. Phys. **52**, 3302 (1970).
23. A. O. AL-CHALOBI. Chem. Phys. Lett. **70**, 371 (1980).
24. K. C. JANDA, J. M. KOERT, and F. S. WETTACK. J. Photochem. **1**, 345 (1972/73).
25. R. B. CUNDALL and J. R. VOSS. Chem. Commun. 902 (1968).
26. C. S. PARMENTER and B. L. RING. J. Chem. Phys. **46**, 1998 (1967).
27. A. COOK, G. P. SEMELUK, and I. UNGER. Can. J. Chem. **47**, 4527 (1969).
28. V. I. VEDENEYEV, L. V. GURVICH, V. N. KONDRAT'YER, V. A. MEDVEDEV, and YE L. FRANKEVICH. Bond energies, ionization potential, and electron affinities. Edward Arnold Publishers Ltd. 1966.
29. D. S. MCCLURE. J. Chem. Phys. **17**, 905 (1949).
30. H. DISPERT and K. LACMANN. Int. J. Mass Spectrom. Ion Phys. 49 (1978).
31. H. J. T. PRESTON and J. J. KAUFMAN. Chem. Phys. Lett. **50**(1), 157 (1977).

Can. J. Chem. Downloaded from www.nrcresearchpress.com by 210.87.254.40 on 09/06/12
For personal use only.

# Synthesis and spectroscopic study of aminals derived from 8-aminoquinoline

JUANA BELLANATO
*Instituto de Optica, C.S.I.C. Serrano, 121. Madrid-6. Spain*
ENRIQUE GALVEZ
*Department of Organic and Pharmaceutical Chemistry, School of Pharmacy, Universidad Complutense, Madrid-3, Spain*
AND
ROSARIO ESCOBAR AND JOSE MANUEL CANO-PAVON
*Department of Analytical Chemistry, Faculty of Chemistry, The University, Sevilla-4, Spain*
Received August 28, 1981

JUANA BELLANATO, ENRIQUE GALVEZ, ROSARIO ESCOBAR and JOSE MANUEL CANO-PAVON. Can. J. Chem. **60**, 1775 (1982).

Treating 8-aminoquinoline with di-2-pyridyl ketone, pyridine-2-carboxaldehyde, or 6-methylpyridine-2-carboxaldehyde leads to the formation of the corresponding aminal instead of the expected Schiff base. The ir, $^1$H nmr, and mass spectra of these compounds are described and discussed.

Infrared and $^1$H nmr analyses indicate that these aminals enjoy intramolecular hydrogen bonding. This effect is considered to contribute significantly to their unusual stability.

JUANA BELLANATO, ENRIQUE GALVEZ, ROSARIO ESCOBAR et JOSE MANUEL CANO-PAVON. Can. J. Chem. **60**, 1775 (1982).

L'amino-8 quinoléine réagit avec la di-pyridyl-2 cétone, la pyridinecarboxaldéhyde-2 ou la méthyl-6 pyridinecarboxaldéhyde-2 en donnant les composés aminés correspondants au lieu des bases de Schiff attendues. On décrit les spectres de rmn, les spectres de masse et les spectres ir de ces composés et on en discute. L'analyse des spectres ir et de rmn indique que ces composés aminés possèdent des liaisons hydrogènes intramoléculaires. On pense que cet effet contribue grandement à leur stabilité inusitée.

[Traduit par le journal]

## Introduction

There are few data in the literature concerning formation of aminals from the reaction of primary amines with aldehydes (1–4). Lions *et al.* reported that 8-aminoquinoline (**1**) reacts readily with pyridine-2-carboxaldehyde (5, 6) and 6-methylpyridine-2-carboxaldehyde (7) to give the Schiff bases. However, under the working conditions described in the present paper, the corresponding aminals were obtained instead of the Schiff bases.

In a previous paper (8) we described the synthesis and some analytical properties of the compound di(2-pyridyl)-*N*,*N*-di((8-quinolyl)amino)methane (DPQAM, **2**), which was obtained by reaction of **1** with di-2-pyridyl ketone. We describe here the preparation and spectroscopic features of the aminals formed by condensation of **1** with pyridine-2-carboxaldehyde (PQAM, **3**) and 6-methylpyridine-2-carboxaldehyde (6M-PQAM, **4**). The structures of **2**–**4** are also discussed.

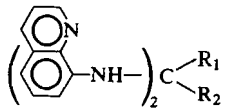

2, $R_1 = R_2 =$

3, $R_1 = H$, $R_2 =$ 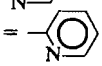

4, $R_1 = H$, $R_2 =$ 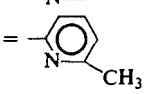

## Experimental

*Synthesis*

*DPQAM (2)*

Compound **2** was prepared as previously described (8).

*PQAM (3)*

Pyridine-2-carboxaldehyde (0.56 g) was added to a solution of 8-aminoquinoline (1.5 g) in absolute ethanol (1.2 mL) and the mixture was warmed at 40°C for 5 min. After cooling to room temperature, ether (50 mL) was added, and the collected product (yellow needles) was recrystallized from ethanol (mp 109–112°C, yield 25%). A change in the reactant ratio did not affect the yield. *Anal.* calcd. for $C_{24}H_{19}N_5$: C 76.37, H 5.07, N 18.56; found: C 76.70, H 4.79, N 18.90.

*6M-PQAM (4)*

6-Methylpyridine-2-carboxaldehyde (0.66 g) was added to a solution of 8-aminoquinoline (1.5 g) in absolute ethanol (1.5 mL) and the mixture was heated at 60°C for 10 min and then cooled to room temperature. After addition of ether, the yellow-brownish needles were collected and recrystallized from ethanol (mp 119–121°C, yield 30%). As in the case of **2** and **3**, modification of the reactant ratio did not affect the yield. *Anal.* calcd. for $C_{25}H_{21}N_5$: C 76.70, H 5.40, N 17.88; found: C 76.69, H 5.33, N 17.65.

*Methods*

Infrared spectra were recorded on a Perkin-Elmer 457 spectrophotometer. Indene and polystyrene were used for instrument calibration. All compounds were compressed into KBr pellets. Spectra in deuterated chloroform and carbon tetrachloride solutions at different dilutions were also recorded.

0008-4042/82/131775-05$01.00/0
©1982 National Research Council of Canada/Conseil national de recherches du Canada

Can. J. Chem. Downloaded from www.nrcresearchpress.com by 210.87.254.105 on 09/06/12
For personal use only.

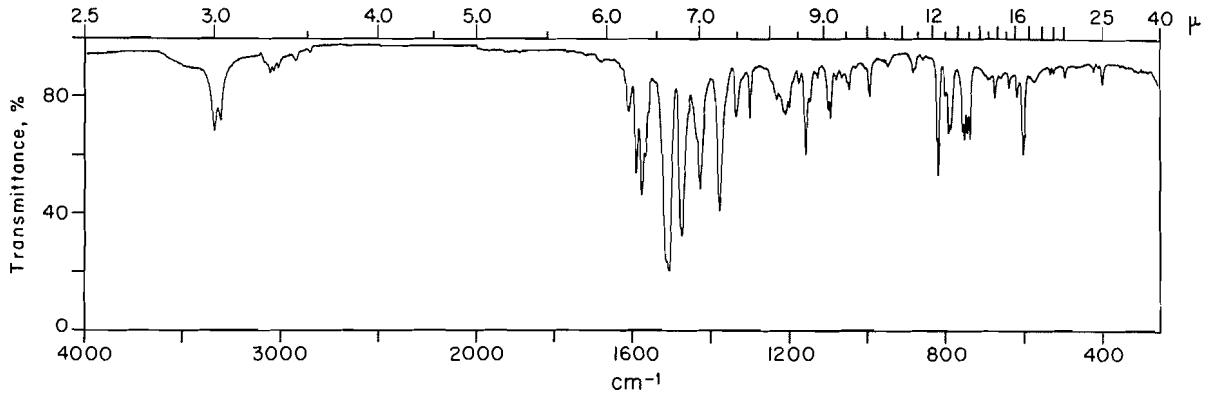


FIG. 1. Infrared spectrum of **2** in the solid state (KBr).

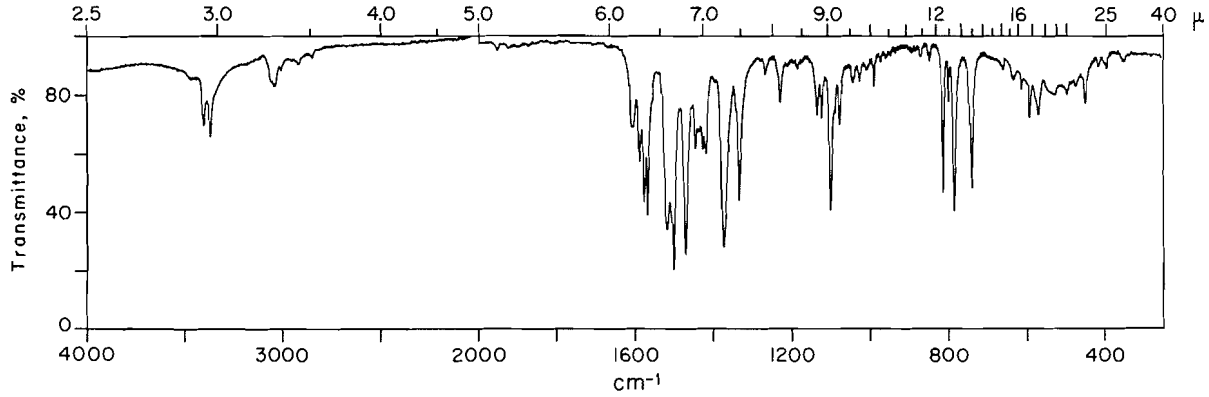


FIG. 2. Infrared spectrum of **3** in the solid state (KBr).

$^1$H nmr spectra were obtained in DMSO-$d_6$ or deuterated chloroform at 90 MHz with a Varian EM 390 spectrometer using tetramethylsilane as internal reference.

The $^{13}$C nmr spectrum of **2** was recorded at 20 MHz with a Varian FT-80A spectrometer in the Fourier transform mode; the spectrum was obtained under moderate heating; DMSO-$d_6$ (39.6 downfield relative to tetramethylsilane) was used as reference.

The mass spectra were measured at 70 eV on an AEI Model MS-30 instrument. Spectra of solid samples were obtained by direct injection into the source at 250°C with the probe at a temperature 20°C below the melting points.

## Results and discussion

*Infrared spectra*

The KBr-infrared spectra of compounds **2–4** are given in Figs. 1–3, and the N—H stretching frequencies determined from their solid and solution spectra, including data for **1** in Table 1.

Some infrared characteristics of 8-aminoquinoline have been discussed by Jensen and Nielsen (9).

It can be expected that in the molecule of 8-aminoquinoline one of the hydrogen atoms of the amino group takes part in intramolecular hydrogen bonding with the heterocyclic nitrogen, and consequently the two infrared bands at 3450 and 3350 cm$^{-1}$ in the spectrum of the solid are assigned to the "free" and bonded N—H, respectively. In $CDCl_3$ solution these bands shift towards 3500 and 3390 cm$^{-1}$ respectively. On deuteration both bands disappear and four bands are observed in the 2650–2450 cm$^{-1}$ region corresponding to mono- and di-deuterated species. As remarked by Jensen and Nielsen, the bands at 1617 and 1598 cm$^{-1}$ are sensitive to deuteration which is implicative of a contribution of the δ(N—H) mode to both bands.

The infrared spectrum of **2** in KBr shows a band at 3340 cm$^{-1}$ which is commensurate with the presence of secondary NH group ruling out a Schiff base structure for this compound. In some solid samples another band or shoulder at 3305 cm$^{-1}$ appeared in the spectrum indicating differences in the surroundings of both N—H groups in the crystal. Characteristic bands of the 8-quinolyl group appear at 1592, 1579, 1508, 1477, 1429, 1377, 1337, 1098, 820, and 795 cm$^{-1}$. The bands due to the

Can. J. Chem. Downloaded from www.nrcresearchpress.com by 210.87.254.105 on 09/06/12
For personal use only.

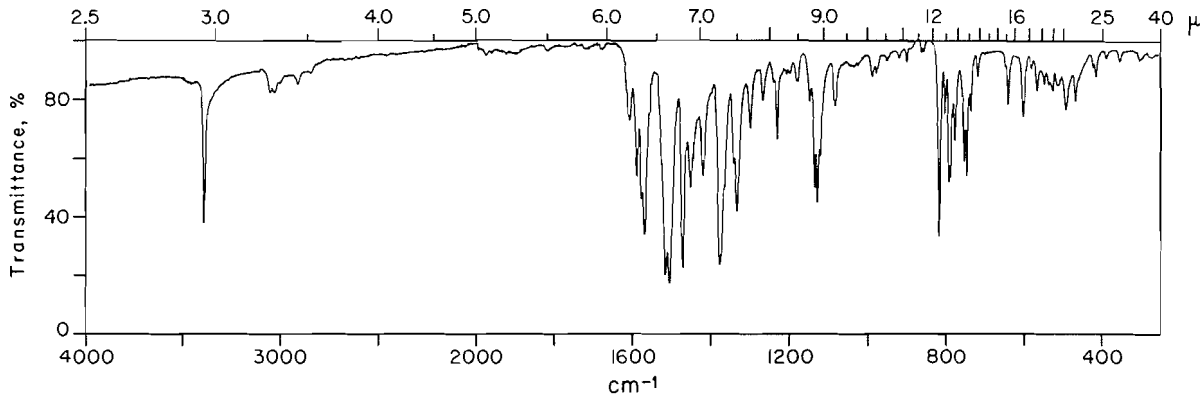


FIG. 3. Infrared spectrum of **4** in the solid state (KBr).

TABLE 1. Infrared frequencies ($cm^{-1}$) of compounds **1–4** in the NH stretching region

| | Infrared frequency[c] | | | | | | | |
|---|---|---|---|---|---|---|---|---|
| | **1** | | **2** | | **3** | | **4** | |
| Medium | Free | Bonded | Free | Bonded | Free | Bonded | Free | Bonded |
| KBr | 3450s | 3350s | | 3340m<br>3305w | | 3405m<br>3370m | | 3395s |
| $CDCl_3$[a] | 3495w | 3465sh<br>3390w | 3495vw | 3465sh<br>3355w | 3495w | 3465sh<br>3390m | 3495vw | 3465sh<br>3395m |
| $CCl_4$[b] | | | 3500vw | 3345w | 3495vw | 3390w | 3498vw | 3390w |

[a] 0.05 *M*.
[b] < 0.01 *M*.
[c] Abbreviations: s, strong; m, medium; w, weak; sh, shoulder; v, very.

di-2-pyridyl group are obscured in the spectrum probably due to overlapping by the predominant quinoline bands. The band at 1616 $cm^{-1}$ of 8-aminoquinoline (partly $\delta NH_2$) is shifted towards 1611 $cm^{-1}$ and its intensity decreases. This new band is not sensitive to deuteration. The spectra in $CCl_4$ and $CDCl_3$ showed only minor changes. The ν(N—H) band appears nearly at the same frequency in KBr as it does in solution (Table 1) and is consistent with the chelate structure. However, a new band at 3500 $cm^{-1}$ indicates the coexistence of free NH groups and a shoulder at 3385 $cm^{-1}$ can be attributed to the existence of other chelated species. All these bands disappear on deuteration, confirming the presence of N—H character.

In the case of **3** several crystalline forms were obtained giving slightly different spectra. Changes were observed in the N—H stretching region which revealed different types of hydrogen bonding. The spectrum given in Fig. 2 shows two ν(N—H) bands at 3405 and 3370 $cm^{-1}$, suggesting that one NH group is single bonded whilst the other takes part in a bifurcated hydrogen bond. In this spectrum the quinoline characteristic bands are observed at 1592, 1579, 1569, 1502, 1470, 1420, 1375, 1337, 1104, 816, 787, and 743 $cm^{-1}$. In very dilute $CCl_4$ solutions two bands at 3495 and 3390 $cm^{-1}$ are observed and support the existence of free NH groups as in compound **2**. The $CDCl_3$ solution spectra are similar and also reveal the presence of chelated species. In both solvents results are best interpretated if only single bonded NH groups exist.

Contrary to the case of compound **3**, only a crystalline form was obtained for **4**. Its KBr-spectrum (Fig. 3) shows a sharp ν(N—H) band at 3395 $cm^{-1}$ and bands due to the quinoline rings at 1591, 1580, 1571, 1517, 1508, 1473, 1423, 1380, 1337, 1131, 820, 797, 791, 758, and 750 $cm^{-1}$. Results in $CCl_4$ and $CDCl_3$ are comparable to those obtained for **3** and are interpreted in the same way.

*Nuclear magnetic resonance spectra*

The most significant features of the $^1H$ nmr spectra of **2–4** are listed in Table 2.

The spectrum of **3** shows a triplet at δ6.30 which converts into a singlet on deuteration. This signal is assigned to the methine proton coupled to the

Can. J. Chem. Downloaded from www.nrcresearchpress.com by 210.87.254.105 on 09/06/12
For personal use only.

Can. J. Chem. Downloaded from www.nrcresearchpress.com by 210.87.254.105 on 09/06/12
For personal use only.

TABLE 2. $^1$H nmr chemical shifts and multiplicities[a,b] for **2**–**4**

| Compound | $C_\alpha$—H | N—H | Me |
|---|---|---|---|
| **2** | | 9.90s | |
| | | 9.92[c] | |
| **3** | 6.25t,$^3J \sim 5$ | [d] | |
| **4** | 6.24t,$^3J$ 6 | [d] | 2.6s |
| | 6.52t,[c3] $J$ 7 | [d] | 2.5s |

[a]Spectra recorded at 90 MHz in $CDCl_3$ with internal TMS unless otherwise stated.
[b]Abbreviations: s, singlet; t, triplet.
[c]In DMSO-$d_6$.
[d]Not identified. See text.

amine protons. The existence of this coupling suggests that the amine hydrogens are bonded. Moreover, the triplet shape indicates that the amine signal appears at lower field than the signal of the methine proton and therefore must be overlapped by the heterocyclic proton signals. The data for compound **4** are similar to those found for **3** (see Table 2).

In the case of compound **2**, the signal at δ9.90 which disappears on deuteration is attributed to the amine protons. The high δ-value of this signal is attributed to the strong chelated hydrogen bonds in this compound.

Finally, the proton noise-decoupled $^{13}$C nmr spectrum of **2** which shows a signal at δ73.95 corresponding to a tetrahedral carbon unequivocally proves the aminal structure for compound **2**.

*Mass spectra*

The mean features of the mass spectrum of **2** are: a very weak $M^+$ peak at *m/e* 454, an intense peak at *m/e* 144, and a weak peak at *m/e* 310 which are originated from $M^+$ through a C—N cleavage with a simultaneous hydrogen rearrangement. The loss of a pyridinium radical ion (*m/e* 78) from the ion *m/e* 310 explains the base peak at *m/e* 232. Moreover, a metastable peak at *m/e* 173.3 confirms the transition 310→232. This fragmentation is in agreement with literature data (10). The peak at *m/e* 144 is attributed to an aminoquinolinium radical ion which originates the peaks at *m/e* 117, 116, 90, 89, 63, and 39 in accordance with the literature (11). The above data suggest the fragmentation pattern depicted by Scheme 1.

The mass spectra of compounds **3** and **4** presented similar features to those of compound **2**. In addition, an intense peak at *m/e* 129 and less abundant peaks at *m/e* 102, 76, 75, 51, and 50 were also observed. The ion of *m/e* 129 is due to quinolinium ion-radical $C_9H_7N^+$ which is originated from the molecular ion and/or from the amine ion through a cleavage with hydrogen rearrangement (see Scheme 1). Furthermore, in the mass spectra of **3** and **4** weak peaks at *m/e* 249 and 263 were respectively observed and are attributed to $(M - C_9H_6N)$.

Summarizing, the obtained results show that from the reaction of 8-aminoquinoline with pyridine-2-carboxaldehyde, 6-methyl-pyridine-2-carboxaldehyde, and di-2-pyridyl ketone aminals are obtained. The stability of these aminals is due to the occurrence of intramolecular hydrogen bonding which is also present even in polar solvents as was deduced from spectroscopic data. In this context it may be noted that when l-naphtylamine reacts with benzaldehyde the Schiff base is formed very easily (8).

The mechanism proposed for the formation of

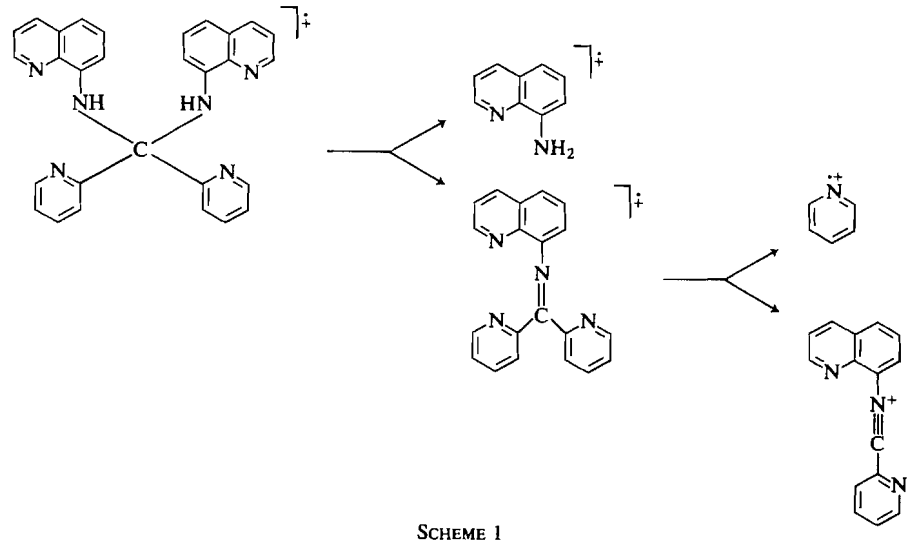

SCHEME 1

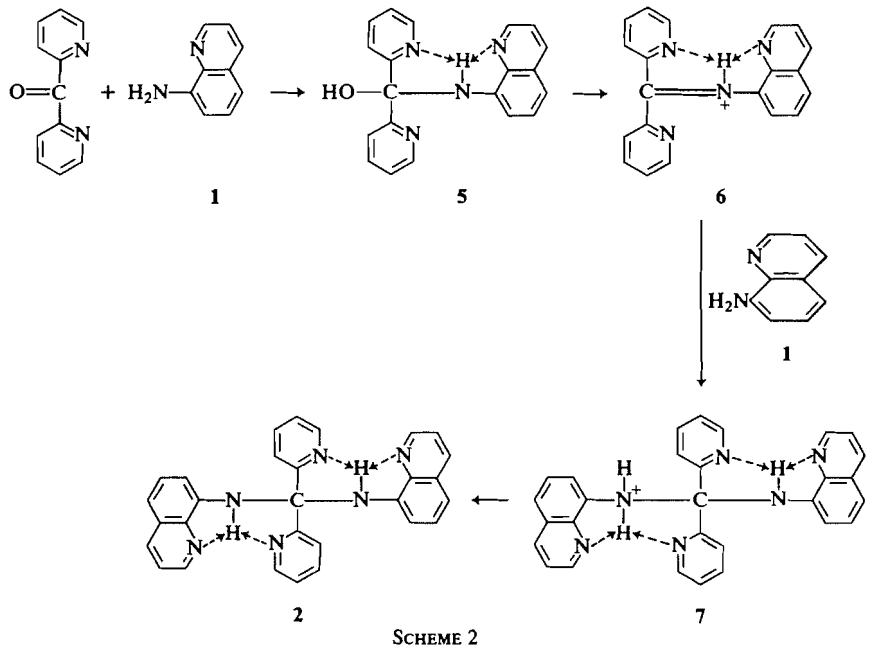

SCHEME 2

the aminals studied is given in Scheme 2 for compound **2**. The immonium cation **6** is stabilized by intramolecular hydrogen bonding; thus the nucleophilic addition of a second molecule of 8-aminoquinoline to **6** leads to **7** and finally to the aminal **2** by the loss of a proton.

The aminals **2–4** are good analytical reagents for transition metals, specially Fe(II), originating stable chelates (8). They can also be applied for the indirect determination of voluminous anions such as perchlorate, iodide, and others which form ionic pairs with the chelates allowing the extraction of these chelates.

Throughout the present work the complexes of the reagents with Fe(II), Ni(II), Co(II), and Cu(I) in the form of perchlorates or iodides have been isolated. The study of the relation between spectroscopic properties and structures of these complexes will be the subject of a future paper.

**Acknowledgements**

The authors thank Miss D. Casado for performing $^1$H nmr spectra and Dr. W. Ammann of Varian AG, Switzerland for the $^{13}$C nmr spectrum of a sample.

1. A. KIRPAL and E. REITER. Chem. Ber. **60**, 664 (1927).
2. R. TIOLLAIS, G. BOUGET, and H. BOUGET. C.R. Acad. Sci. **254**, 2957 (1962).
3. J. W. SUGGS. J. Am. Chem. Soc. **101**,489 (1979).
4. S. V. KESSAR. Private communication.
5. F. P. DWYER, N. S. GILL, E. C. GYARFAS, and F. LIONS. J. Am. Chem. Soc. **75**, 3834 (1953).
6. F. LIONS and K. V. MARTIN. J. Am. Chem. Soc. **79**, 2733 (1957).
7. H. A. GOODWIN and F. LIONS. J. Am. Chem. Soc. **81**, 6415 (1959).
8. R. ESCOBAR, J. M. CANO-PAVON, J. BELLANATO, E. GALVEZ, and F. PINO. Talanta. **29**, 135 (1982).
9. K. A. JENSEN and P. H. NIELSEN. Acta Chem. Scand. **18**, 1 (1964).
10. H. BUDZIKIEWIC, C. DJERASSI, and D. H. WILLIAMS. Mass spectrometry of organic compounds. Holden Day, San Francisco. 1967. pp. 393–394.
11. Eight peak index of mass spectra. 2nd ed. 1974. Mass Spectrometry Data Centre AWRE.

Can. J. Chem. Downloaded from www.nrcresearchpress.com by 210.87.254.105 on 09/06/12
For personal use only.

# Kinetics of solvolysis in water of four secondary alkyl nitrates

ROSS ELMORE ROBERTSON, KALVELIL MATTHEW KOSHY, ADRIANNE ANNESSA, AND JAN N. ONG
*Department of Chemistry, University of Calgary, Calgary, Alta., Canada T2N 1N4*
JOHN MARSHALL WILLIAM SCOTT
*Department of Chemistry, Memorial University, St. John's, Nfld., Canada A1C 5S7*
AND
MICHAEL JESSE BLANDAMER
*Department of Chemistry, The University, Leicester, England*

Received November 24, 1981

ROSS ELMORE ROBERTSON, KALVELIL MATTHEW KOSHY, ADRIANNE ANNESSA, JAN N. ONG, JOHN MARSHALL WILLIAM SCOTT, and MICHAEL JESSE BLANDAMER. Can. J. Chem. **60**, 1780 (1982).

Kinetic data are reported for the solvolysis in water of propane-2-nitrate, butane-2-nitrate, cyclopentyl nitrate, and cyclohexyl nitrate. In each case, the dependence of rate constant on temperature is analysed in terms of two mechanisms for the solvolytic reaction. First it is assumed that the rate constant describes a single step reaction, the analysis leading to estimates of the heat capacity of activation $\Delta C_p^{\neq}$. Three different analytical methods are discussed in this regard. Second it is assumed that the rate constant describes a two stage mechanism, the first stage being reversible. In this case the explanation of the $\Delta C_p^{\neq}$ term calculated according to the first mechanism is quite different. We comment on the alternative explanations of trends in activation parameters.

ROSS ELMORE ROBERTSON, KALVELIL MATTHEW KOSHY, ADRIANNE ANNESSA, JAN N. ONG, JOHN MARSHALL WILLIAM SCOTT et MICHAEL JESSE BLANDAMER. Can. J. Chem. **60**, 1780 (1982).

On rapporte des données cinétiques pour la solvolyse des nitrates de propyle-2, de butyle-2, de cyclopentyle et de cyclohexyle dans l'eau. Dans chaque cas, on analyse l'effet de la température sur la constante de vitesse en fonction de deux mécanismes pouvant régir la réaction de solvolyse. On admet premièrement que la constante de vitesse décrit une réaction en une seule étape, l'analyse conduisant à une évaluation de la capacité calorifique d'activation, $\Delta C_p^{\neq}$. De ce point de vue, on discute trois méthodes analytiques différentes. Deuxièmement, on admet que la constante de vitesse décrit un mécanisme en deux étapes, la première étant réversible. Dans ce cas, l'explication du terme $\Delta C_p^{\neq}$ calculé selon le premier mécanisme est tout à fait différente. Nous commentons d'autres explications relatives aux tendances des paramètres d'activation.

[Traduit par le journal]

Can. J. Chem. Downloaded from www.nrcresearchpress.com by 210.87.254.42 on 09/06/12
For personal use only.

An extensive body of information describes the kinetics of solvolysis of simple organic esters in water (1). For the most part, the dependence of rate constant, $k$, on temperature has been analysed using the Valentiner equation (2, 3) thereby leading to estimates of the thermodynamic activation parameters including the enthalpy of activation $\Delta H^{\neq}$ and the heat capacity of activation $\Delta C_p^{\neq}$. The latter quantity attracted considerable interest because, it was argued (1), a major contribution to the sign and magnitude of $\Delta C_p^{\neq}$ stems from reorganisation of solvent around the substrate on activation. However, certain features (4), previously unrecognised (1), of the Valentiner equation (2) prompted a reconsideration (5) of the methods of analysing the dependence of rate constant on temperature. We draw attention to these and other features of the Valentiner equation in this paper. A consequence of this reconsideration has been an investigation of other methods of data analysis with reference to the kinetics of solvolysis in water (5–7) and in mixed solvents (8) and to kinetic solvent isotope effects (9). For the most part this exercise has involved reexamining previously published data (1). In this communication, we report kinetic data for the solvolysis of four secondary nitrates in water. Originally, the experimental investigation was prompted by the need for a comparison between the activation parameters for these nitrates and those reported (10) for 2-adamantyl nitrate. However, as indicated above, the developments on the analytical side have overtaken events.

## Results

The rate constants were determined by the conductance method (1). First order rate constants at several temperatures are summarized in Tables 1–4. We report the averaged rate constants at each temperature but in the analysis we used the individual rate constants obtained from 3 or more determinations at each temperature.

### *Analysis*

In common with almost all solvolytic reactions of simple organic esters in water (1), plots of ln $k$ against $T^{-1}$ for the data given in Tables 1–4 are nonlinear. This observation can be accounted for in one of two ways; (A) the mechanism of reaction is a simple single-stage process but $\Delta C_p^{\neq}$ is nonzero (1), or (B) the mechanism of reaction is complex but

0008-4042/82/131780-06$01.00/0
©1982 National Research Council of Canada/Conseil national de recherches du Canada

Can. J. Chem. Downloaded from www.nrcresearchpress.com by 210.87.254.42 on 09/06/12
For personal use only.

TABLE 1. Kinetic data for solvolysis of propane-2-nitrate in water

| $T$ (K) | $10^5 k$ ($s^{-1}$) |
|---|---|
| 339.654 | 2.013 |
| 343.503 | 3.250 |
| 347.315 | 5.135 |
| 349.981 | 7.109 |
| 353.326 | 10.35 |
| 355.483 | 13.15 |
| 359.206 | 20.07 |
| 362.383 | 28.42 |
| 365.584 | 39.84 |
| 369.065 | 57.36 |

TABLE 2. Kinetic data for solvolysis of butane-2-nitrate

| $T$ (K) | $10^5 k$ ($s^{-1}$) |
|---|---|
| 334.543 | 2.700 |
| 336.811 | 3.590 |
| 342.770 | 7.570 |
| 344.274 | 9.020 |
| 345.562 | 10.63 |
| 348.837 | 15.65 |
| 351.254 | 20.64 |
| 354.371 | 29.55 |
| 357.360 | 41.14 |
| 359.866 | 54.15 |
| 363.583 | 80.55 |

TABLE 3. Kinetic data for the solvolysis in water of cyclopentyl nitrate

| $T$ (K) | $10^5 k$ ($s^{-1}$) |
|---|---|
| 322.832 | 2.098 |
| 327.809 | 4.034 |
| 331.021 | 6.185 |
| 334.323 | 9.370 |
| 338.546 | 15.84 |
| 342.463 | 25.24 |
| 346.308 | 39.41 |
| 349.835 | 58.71 |
| 352.791 | 81.28 |

TABLE 4. Kinetic data for solvolysis in water of cyclohexyl nitrate

| $T$ (K) | $10^5 k$ ($s^{-1}$) |
|---|---|
| 327.404 | 0.7694 |
| 337.844 | 3.278 |
| 343.284 | 6.648 |
| 346.405 | 9.887 |
| 348.845 | 13.41 |
| 351.083 | 17.54 |
| 352.514 | 20.86 |
| 355.503 | 29.70 |
| 356.707 | 34.13 |

the individual enthalpies of activation are independent of temperature (6, 7).

The mathematical analysis has been carried out using (*i*) computer programs (FORTRAN and GLIM (11) routines) for the CDC Cyber 73 at the University of Leicester and (*ii*) computer programs for a Hewlett–Packard 9825A desk-top computer.

A. *Single stage mechanism*

The underlying assumption is that the rate constant $k$ describes a single stage process;

[1] $\mathrm{R{-}NO_3} \xrightarrow{k}$ products

With this starting hypothesis, several methods can be used to fit the dependence of $k$ on $T$. We consider here three approaches to the evaluation of the activation parameters.

In the Valentiner equation (2), the dependence of $\ln k$ on $T$ is expressed as shown in eq. [2].

[2] $\ln k = a_1 + (a_2/T) + a_3 \ln T$

The outcome of the analysis for the four nitrates is summarized in Table 5. An estimate of the goodness of fit is provided by the quantity $\Omega$ defined by eq. [3] where $f$ is the number of degrees of freedom.

[3] $\Omega^2 = (\ln k(\mathrm{obs}) - \ln k(\mathrm{calc}))^2/f$

TABLE 5. Analysis of kinetic data using Valentiner equation

| Nitrate | $\hat{a}_1$ | $-10\hat{a}_2$ | $-\hat{a}_3$ | $10^3\,\Omega$ | $\Delta H^{\ddagger}$ at $T$ (K) (kJ $mol^{-1}$) | $\Delta H^{\ddagger}$ (298.15) (kJ $mol^{-1}$) | $\Delta Cp^{\ddagger}$ (J $mol^{-1}$ $K^{-1}$) |
|---|---|---|---|---|---|---|---|
| Propane-2- | 123.3 (20.4) | 1.902 (0.105) | 13.41 (2.97) | 4.688 | 115.8 353.326 (0.01) | 122.41 | −119.8 (24.7) |
| Butane-2- | 212.0 (25.9) | 1.877 (0.132) | 12.41 (3.78) | 4.202 | 115.51 ($1 \times 10^{-3}$) | 121.40 (1.60) | −107.9 (31.5) |
| Cyclopentyl | 175.5 (27.5) | 2.100 (0.136) | 20.98 (4.03) | 3.75 | 112.732 (0.02) | 120.11 (1.32) | −174.4 (33.5) |
| Cyclohexyl | 205.2 (13.2) | 2.365 (0.067) | 24.99 (1.9) | 3.97 | 122.454 (0.02) | 159.01 (2.97) | −207.8 (16.0) |

Can. J. Chem. Downloaded from www.nrcresearchpress.com by 210.87.254.42 on 09/06/12
For personal use only.

TABLE 6. Analysis using polynomial equation

| Nitrate | θ (K) | $-a_1$ | $a_2$ | $-10^3 a_3$ | $10^3\Omega$ | $\Delta H^{\ddagger}$ (θ) (kJ mol$^{-1}$) | $-\Delta Cp^{\ddagger}$ (θ) (J mol$^{-1}$ K$^{-1}$) | $(d\Delta Cp^{\ddagger}(\theta)/dT)$ (J mol$^{-1}$ K$^{-1}$) | $-10^2(d^2\Delta Cp^{\ddagger}/dT^2)$ (J mol$^{-1}$ K$^{-3}$) |
|---|---|---|---|---|---|---|---|---|---|
| Propane-2- | 355.483 | 8.9293 (0.0013) | 0.11293 (0.00011) | 0.37505 (0.012) | 4.851 | 115.69 (0.12) | 128.8 (26.4) | −6.99 (0.28) | 3.74 (0.01) |
| Butane-2- | 348.837 | 8.7665 (0.0014) | 0.11725 (0.00013) | 0.3917 (0.014) | 3.890 | 115.73 (0.13) | 120.8 (30.0) | −7.14 (0.34) | 3.908 (0.014) |
| Cyclopentyl | 338.54 | 8.7535 (0.0019) | 0.121503 (0.00013) | 0.455 (0.015) | 3.827 | 112.96 (0.13) | 191.5 (22) | −8.225 (0.36) | 4.50 (0.01) |
| Cyclohexyl | 343.284 | 9.6167 (0.0011) | 0.12820 (0.00008) | 0.42832 (0.0084) | 4.0712 | 125.60 (0.08) | 223.4 (16.9) | −8.902 (0.19) | 4.82 (0.01) |

In all four cases $\Delta C_p^{\ddagger}$ is negative. A common feature of the data for 17 alkyl nitrates is shown in Fig. 1 which shows plots of $a_2$ against $a_3$ and $a_1$ against $a_3$. We have commented elsewhere (4) on this phenomenon and examined the statistical significance underlying the linear dependences (12).

We have applied the polynomial suggested by Eyring and co-workers (13) to the analysis of kinetic data (7), eq. [4]:

$$[4] \quad \ln k = \sum_{i=1}^{i=m} a_i (T - \theta)^{i-1}$$

For the systems described here it was only significant to include all terms up to $m = 5$. The derived parameters are summarized in Table 6, together with the corresponding standard errors and estimates of $\Delta H^{\ddagger}(\theta)$, $\Delta C_p^{\ddagger}(\theta)$, $d\Delta C_p^{\ddagger}/dT$, and $d^2\Delta C_p^{\ddagger}/dT^2$.

The Clarke–Glew equation (14) uses a reference temperature but is based on a Taylor expansion of the enthalpy term about this reference temperature;

$$[5] \quad \ln\left(\frac{k}{T}\right) = \ln(k(\theta)/\theta) + \frac{\Delta H^{\ddagger}(\theta)}{R}\left[\frac{1}{\theta} - \frac{1}{T}\right] + \frac{\Delta C_p^{\ddagger}(\theta)}{R}\left[\frac{\theta}{T} - 1 + \ln\left(\frac{T}{\theta}\right)\right] + \frac{d\Delta C_p^{\ddagger}(\theta)/dT}{R} \times \left[\frac{T}{\theta} - \frac{\theta}{T} - 2\ln\left(\frac{T}{\theta}\right)\right]$$

The outcome of the analysis is summarized in Table 7.

B. *Two stage mechanism*

The assumption is that the mechanism of solvolysis follows the scheme (15) shown in eq. [6].

$$[6] \quad RX \underset{k_2}{\overset{k_1}{\rightleftharpoons}} (int) \xrightarrow{k_2} products$$

The measured first order rate constant $k$ is related to $k_1$ and $\alpha$ ($= k_2/k_3$) where $k = k_1/(1 + \alpha)$. The simplification introduced here is that $\ln k_1$ and $\ln \alpha$ are linear functions of $T^{-1}$. Hence

$$[7] \quad \ln k = (g_1/T) + g_2 - \ln[1 + \exp(g_3/T + g_4)]$$

The temperature at which $\alpha = 1$ is given by $-g_3/g_4$.

We have discussed elsewhere (12) the technique of fitting the data to eq. [7] using the Wentworth method (16). The results are summarized in Table 8. For each set of kinetic data there are two sets of solutions (17). Included in Table 8 are the calculated activation parameters, $\Delta H_1^{\ddagger}$ and $\Delta\Delta H^{\ddagger}$ ($= \Delta H_3^{\ddagger} - \Delta H_2^{\ddagger}$).

TABLE 7. Clarke–Glew equation

| Nitrate | θ | $10^3\ \Omega^*$ | $\Delta H^{\neq}$ (θ) (kJ mol$^{-1}$) | $-\Delta Cp^{\neq}$ (θ) (J mol$^{-1}$ K$^{-1}$) |
|---|---|---|---|---|
| Propane-2- | 355.483 | 4.6883 | 118.481 | 111.5 |
| | | | (0.015) | (24.7) |
| Butane-2- | 348.837 | 4.20 | 118.452 | 107.9 |
| | | | (0.014) | (31.5) |
| Cyclopentyl | 338.54 | 4.33 | 115.56 | 174.4 |
| | | | (0.014) | (33.5) |
| Cyclohexyl | 343.284 | 3.97 | 125.341 | 207.8 |
| | | | (0.008) | (16.0) |

*Based on ln $k$.

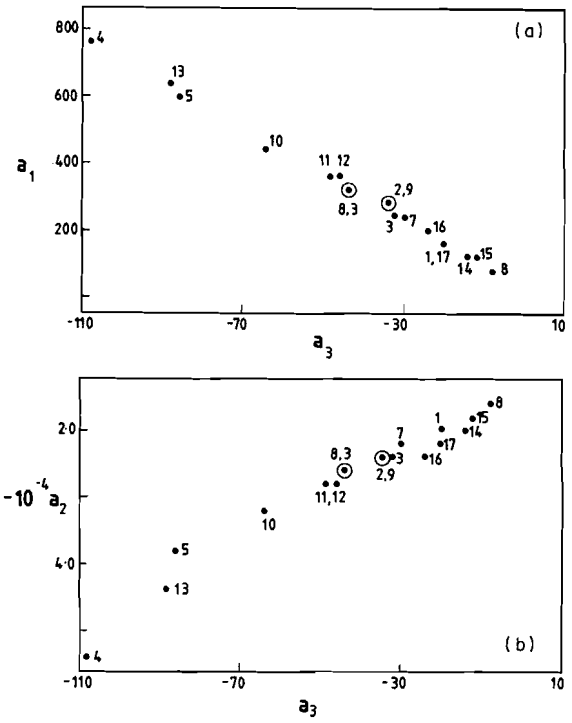


FIG. 1. Parameters obtained using the Valentiner equation; (a) dependence of $a_1$ on $a_3$, and (b) dependence of $a_2$ on $a_3$; the substrates are 1. Methyl nitrate (21); 2. allyl nitrate;[1] 3. benzyl nitrate ($D_2O$);[2] 4. 1-adamantyl nitrate (10); 5. 2-adamantyl nitrate (10); 6. *p*-trifluoromethylbenzyl nitrate (22); 7. *p*-nitrobenzyl nitrate (22); 8. *p*-methylbenzyl nitrate (22); 9. *p*-chlorobenzyl nitrate (22); 10. 2,6-dimethylbenzyl nitrate (23); 11. *m*-methylbenzyl nitrate (23); 12. *o*-methylbenzyl nitrate (23); 13. *m*-trifluoromethylbenzyl nitrate (22); 14. propane-2-nitrate; 15. butane-2-nitrate; 16. cyclohexyl nitrate; 17. cyclopentyl nitrate.

## Discussion

Details of the analysis in terms of the Valentiner equation are presented for comparison with the results obtained for other substrates (1). Our reservations over this approach stem from the plots shown in Fig. 1. We attribute these patterns to the fact that both $T^{-1}$ and ln $T$ are close to linear functions of $T$ (11). For this reason the Clarke–Glew equation has merit in that the equation contains different functions of $T$, ln $T$, and θ. Both sets of derived parameters (Tables 7 and 8) are in reasonable agreement. The value for $\Delta C_p^{\neq}$ (θ) provides an important clue here in that the estimates and their standard errors overlap for each substrate. However, the polynomial equation leads to estimates of $\Delta C_p^{\neq}$ (θ), together with the corresponding first and second temperature derivatives. Indeed, in all four systems, the analysis suggests that $\Delta C_p^{\neq}$ decreases with increase in temperature.

Granted that method A is a satisfactory explanation of the kinetic data, it is noteworthy that the calculated heat capacities of activation are significantly smaller than those previously reported for systems where the solvolysis involves a unimolecular process with extensive charge development in the transition state (10). The activation parameters are consistent with direct solvent participation in the activation process. In one extreme the data, here and in ref. 10, can be understood in terms of relatively little charge separation in the substrate but considerable nucleophilic involvement by solvent. At the same time it is possible that, in contrast to halides, there are special steric and related factors involved with the solvation of the leaving group in the case of alkyl nitrates. Hence it is possible to evolve numerous schemes such that the calculated activation parameters are composite quantities. Here is the link with mechanism B which breaks down the solvolytic reaction into component parts. Analysis in these terms raises new problems as indicated in Table 8. Thus for each nitrate there are two almost statistically equivalent solutions. For butane-2-nitrate and cyclopentyl nitrate results, solution (b) offers an intuitively reasonable set of parameters where the ratio

[1]R. E. Robertson and E. C. F. Ko. Unpublished data.
[2]K. M. Koshy and R. E. Robertson. Unpublished data.

Can. J. Chem. Downloaded from www.nrcresearchpress.com by 210.87.254.42 on 09/06/12
For personal use only.

Can. J. Chem. Downloaded from www.nrcresearchpress.com by 210.87.254.42 on 09/06/12
For personal use only.

TABLE 8. Analysis based on step-wise mechanism

| Nitrate | | $10^{-4}\,g_1$ | $g_2$ | $10^{-4}\,g_3$ | $g_4$ | $10^3\,\Omega\,(\ln k)$ | $10^7\,\Omega\,(k)$ | $T\,(\alpha = 1)$ (K) | $\Delta H_1^{\neq}$ (kJ mol$^{-1}$) | $\Delta\Delta H^{\neq}$ (kJ mol$^{-1}$) |
|---|---|---|---|---|---|---|---|---|---|---|
| Propane-2- | (a)* | −2.652 | 70.54 | −1.240 | 39.72 | 4.6835 | 6.613 | 312 | 218.04 | 103.0 |
| | (b) | −1.143 | 30.82 | 1.240 | −39.72 | 4.6844 | 6.591 | 312 | 114.99 | −103.0 |
| Butane-2- | (a) | 0.3293 | −12.73 | 1.765 | −45.13 | 3.952 | 5.025 | 391 | −29.85 | −146.8 |
| | (b)* | −1.436 | 32.41 | −1.765 | 45.13 | 3.952 | 5.025 | 391 | 116.92 | 146.8 |
| Cyclopentyl | (a) | −0.4905 | 9.285 | 0.9302 | −23.95 | 4.170 | 5.129 | 388 | 38.30 | −77.3 |
| | (b)* | −1.4207 | 33.239 | −0.9302 | 23.95 | 4.170 | 5.084 | 388 | 115.64 | 77.3 |
| Cyclohexyl | (a)* | −1.6547 | 39.136 | −0.3486 | 9.845 | 4.035 | 4.704 | 354 | 135.10 | 29.0 |
| | (b) | −1.3064 | 29.300 | 0.3486 | −9.845 | 4.036 | 4.710 | 354 | 106.14 | −29.0 |

*Favoured solution, see text.

$\alpha$ is $< 1.0$ over the experimental range of temperatures. More importantly, $\Delta\Delta H^{\neq}$ is positive and because we anticipate no marked difference between the four substrates, we favour solution (a) for propane-2-nitrate and solution (a) for cyclohexyl nitrate. However, for this latter system the two solutions are not wildly different because the temperature $T(\alpha = 1)$ falls within the experimental range. Indeed this system, cyclohexyl nitrate provides an important clue to a major problem in this work.

According to Model A, the heat capacity of activation is a true heat capacity term. Because the partial molar heat capacities of apolar solutes in water are positive, it is not altogether surprising that $\Delta C_p^{\neq}$ is negative. According to Model B, the $\Delta C_p^{\neq}$ term is an apparent quantity and no allowance is made for a contribution arising from the changes in real heat capacity of the substrate. Clearly this approximation is too sweeping and some compromise is sought. A line of argument would proceed as follows. Where the calculated $|\Delta C_p^{\neq}|$ quantity is large, a major part of that calculated heat capacity of activation stems from kinetic complexity. We anticipate that in these circumstances, the temperature T ($\alpha = 1$) is close to or within the experimental range (of cyclohexyl nitrate). Where the calculated $|\Delta C_p^{\neq}|$ is small (cf. propane-2-nitrate), the mechanism of solvolysis is controlled by one step. Moreover, $T$ ($\alpha = 1$) where calculated according to method B lies some way removed from the experimental range. This compromise view has much to commend it.

## Experimental

The alkylnitrates were prepared using methods based on published procedures (18–20) combined with nmr measurements as a confirmation of purity.

*Products*

In each study a separate experiment with the nitrate in water in the ratio 1:4–1:6 was sealed in a glass ampoule and reacted in a constant temperature bath in the experimental range for about 10 half-lives. The product was extracted with ether and identified by vpc on a FFAP column. In each case the only significant product was the corresponding alcohol. In the case of cyclohexyl nitrate, traces of cyclohexene in the original sample also appeared in the product.

## Acknowledgement

We thank the Royal Society for a travel award to MJB.

1. R. E. ROBERTSON. Prog. Phys. Org. Chem. **4**, 213 (1967).
2. S. VALENTINER. Z. Physik. Chem. **42**, 853 (1907).
3. D. H. EVERETT and W. F. K. WYNNE-JONES. Trans. Faraday Soc. **35**, 1380 (1932).

4. M. J. BLANDAMER, R. E. ROBERTSON, and J. M. W. SCOTT. Can. J. Chem. **58**, 772 (1980).
5. M. J. BLANDAMER, R. E. ROBERTSON, J. M. W. SCOTT, and A. VRIELINK. J. Am. Chem. Soc. **102**, 2585 (1980).
6. M. J. BLANDAMER, R. E. ROBERTSON, P. D. GOLDING, J. M. MACNEIL, and J. M. W. SCOTT. J. Am. Chem. Soc. **103**, 2415 (1981).
7. M. J. BLANDAMER, J. BURGESS, P. P. DUCE, J. M. W. SCOTT, and R. E. ROBERTSON. J. Chem. Soc. Perkin Trans. II, 1157 (1981).
8. M. J. BLANDAMER, J. BURGESS, P. P. DUCE, J. M. W. SCOTT, and R. E. ROBERTSON. J. Chem. Soc. Faraday Trans. I, **77**, 1999 (1981).
9. M. J. BLANDAMER, J. BURGESS, D. P. CLARE, P. P. DUCE, R. P. GRAY, R. E. ROBERTSON, and J. W. M. SCOTT. J. Chem. Soc. Faraday Trans. I. In press.
10. K. M. KOSHY, R. K. MOHANTY, and R. E. ROBERTSON. Can. J. Chem. **55**, 1314 (1977).
11. Royal Statistical Society, London. 1977.
12. M. J. BLANDAMER, J. BURGESS, R. E. ROBERTSON, and J. M. W. SCOTT. Chem. Rev. In press.
13. J. C. MAGEE, T. RI, and H. EYRING. J. Chem. Phys. **9**, 419 (1941).
14. E. C. W. CLARKE and D. N. GLEW. Trans. Faraday Soc. **62**, 539 (1966).
15. J. ALBERY and B. H. ROBINSON. Trans. Faraday Soc. **65**, 980 (1969).
16. J. E. WENTWORTH. J. Chem. Educ. **42**, 96 (1965).
17. N. W. ALCOCK, D. J. BENTON, and P. MOORE. Trans. Faraday Soc. **66**, 2210 (1970).
18. J. W. BAKER and D. M. EASTY. J. Chem. Soc. 1193 (1952).
19. A. F. FERRIS, K. W. MCLEAN, I. G. MARKS, and W. D. EMMONS. J. Am. Chem. Soc. **75**, 4078 (1973).
20. J. W. BAKER and T. G. HEGGS. J. Chem. Soc. 616 (1955).
21. J. A. LLEWELLYN, R. E. ROBERTSON, and J. W. M. SCOTT. Can. J. Chem. **38**, 222 (1960).
22. K. M. KOSHY and R. E. ROBERTSON. Can. J. Chem. **52**, 2485 (1974).
23. K. M. KOSHY, R. E. ROBERTSON, G. S. DYSON, and S. SINGH. Can. J. Chem. **54**, 3614 (1976).

Can. J. Chem. Downloaded from www.nrcresearchpress.com by 210.87.254.42 on 09/06/12
For personal use only.

# The entropy of formation of the mercury/methanol interface

Z. BORKOWSKA

*Institute of Physical Chemistry, Polish Academy of Sciences, Kasprzaka 44, 01-224 Warsaw, Poland*

AND

W. R. FAWCETT

*Guelph-Waterloo Centre for Graduate Work in Chemistry (Guelph Campus), Department of Chemistry, University of Guelph, Guelph, Ont., Canada N1G 2W1*

Received September 18, 1981

Z. BORKOWSKA and W. R. FAWCETT. Can. J. Chem. **60**, 1787 (1982).

The entropy of formation of the mercury/methanol interface has been calculated from double layer capacity and interfacial tension measurements. In contrast to results for aqueous and propylene carbonate solutions, the plot of entropy against electrode charge density passes through a minimum at negative charge densities and a maximum at positive charge densities in the same regions where a minimum and maximum are found on the capacity curve. The excess surface entropy of methanol is negative for all charge densities, indicating that the solvent is more structured at the mercury surface than in the bulk. The results have been discussed in terms of the three state model in which the charge dependence of the entropy is attributed to reorientation of solvent dipoles at the interface.

Z. BORKOWSKA et W. R. FAWCETT. Can. J. Chem. **60**, 1787 (1982).

On a calculé l'entropie de formation de l'interface mercure–méthanol à partir de mesures de la capacité de la couche double et de la tension interfaciale. Contrairement aux résultats obtenus pour des solutions aqueuses et dans le carbonate de propylène, la courbe d'entropie en fonction de la densité de charge passe par un minimum pour des densités de charge négative et par un maximum pour des densités de charge positive dans la région où l'on trouve un minimum et un maximum pour la courbe de capacité. L'excès d'entropie de surface du méthanol est négatif pour toutes les densités de charge indiquant ainsi que le solvant est plus structuré à la surface du mercure que dans l'ensemble de la solution. On discute des résultats en fonction d'une modèle à trois états dans lequel on attribue l'effet de la charge sur l'entropie à une réorientation des dipoles du solvant à l'interface.

[Traduit par le journal]

## Introduction

In a previous paper (1), the dielectric properties of the Hg/methanol (MeOH) interface in the presence of KF, $NaClO_4$, and $LiBF_4$ were discussed. Ionic specific adsorption could not be detected at charge densities in the range $-0.11 \leq \sigma \leq 0.04$ C m$^{-2}$ but the interfacial capacity was a function of the counter ion nature at higher charge densities. The main shape of the capacity curve, that is, the appearance of a maximum at positive charge densities and minimum at negative charge densities, was the same for all investigated solutions. Moreover, the coordinates of the minimum were independent of counter ion nature. These results suggested that, at least in the limited range of charge densities around the minimum ($\sigma = -0.05$ C m$^{-2}$), the dielectric properties of the Hg/solution interface are determined by the solvent.

The inner layer capacity curves for the electrolytes studied at various temperatures in methanol (1) and the temperature dependence of the surface potential (2) have been satisfactorily described by a three state model for unassociated solvents (3), although it is well known that methanol is to some extent hydrogen-bonded in the bulk (4).

In this paper, an attempt is made to answer the question of the extent of MeOH association in the surface layer as compared with the bulk solution and to test in more detail the applicability of the three state model. In this regard the entropy of formation of the Hg/MeOH interface has been evaluated on the basis of the measured temperature dependence of the surface tension at the point of zero charge (pzc), and the previously published temperature dependence of the inner layer capacity (1) and the surface potential (2) for a 0.1 *M* $NaClO_4$ solution in MeOH. The results have been compared with the entropy of formation of the free surface calculated from data in the literature (4) and with that calculated according to the three state model.

The Gibbs surface excess entropy and the entropy of formation have been reported for the mercury/aqueous solution interface (5–8). The only other data available for a mercury/nonaqueous interface are those for the mercury/propylene carbonate (PC) interface in the presence of $KPF_6$ (9).

## Experimental

MeOH and $NaClO_4$ were purified as described previously (1). Solutions were prepared in a dry box and transferred to the cell under an argon atmosphere. The water content in 0.1 *M* $NaClO_4$

0008-4042/82/141787-06$01.00/0

©1982 National Research Council of Canada/Conseil national de recherches du Canada

Can. J. Chem. Downloaded from www.nrcresearchpress.com by 210.87.254.105 on 09/06/12
For personal use only.

Can. J. Chem. Downloaded from www.nrcresearchpress.com by 210.87.254.105 on 09/06/12
For personal use only.

solutions in MeOH was about 0.02% as determined by Karl Fischer titration. The solutions were deaerated with argon which had been presaturated with the vapour of the solution under study.

Surface tension was measured in 0.1 *M* $NaClO_4$ solutions in the temperature range −5 to 50°C using the maximum bubble pressure method (10). The cell and the mercury column were kept at the same temperature by pumping ethylene glycol from a thermostated bath through external jackets. The temperature was measured directly in the cell, the difference between the solution and the top of the mercury column being less than 0.5°C. The electrometer was calibrated by measurements in an aqueous solution of 0.05 *M* $Na_2SO_4$ assuming $\gamma = 426.2 \pm 0.2$ mN $m^{-1}$ at 25°C for the interfacial tension at the pzc (11). The performance of the capillary in the investigated solution was checked by comparing the results with literature data for 0.1 *M* $NaClO_4$ in MeOH at 25°C ($\gamma = 392.7 \pm 0.2$ mN $m^{-1}$) (12). The check was repeated after each measurement at a temperature different than 25°C. The temperature dependence of the surface tension at the electrocapillary maximum was calculated taking into account the change in the density of mercury (13). The electrocapillary measurements were carried out with the position of the interface being kept constant in the capillary and with constant solution volume. The electrode potential was measured with respect to a saturated KCl calomel electrode in MeOH (1).

## Data analysis and results

The entropy of formation of the interface, $\Delta S^{m-s}$, was calculated following the method of Harrison *et al.* (7) on the basis of the system

[1] Hg/$NaClO_4$ in MeOH/Na(Hg)

The appropriate isobaric electrocapillary equation is

$$[2] \quad -d\gamma = \Gamma_s dT + \Gamma_- d\mu_{salt} + \sigma d\varepsilon_+$$

or

$$[3] \quad -d\xi_+ = \Gamma_s dT + \Gamma_- d\mu_{salt} - \varepsilon_+ d\sigma$$

where $\xi_+ = \gamma + \sigma\varepsilon_+$ and $\varepsilon_+ = E_+ - \mu_{Na(Hg)}/F$. $\Gamma_s$ is the surface excess of entropy, $\Gamma_-$, that of the anions and $E_+$, the potential of the Hg electrode measured against the Na amalgam reference electrode. It follows that

$$[4] \quad \Gamma_s = -\left(\frac{\partial\gamma}{\partial T}\right)_{E_+,\mu_{salt}} = -\left(\frac{\partial\xi_+}{\partial T}\right)_{\sigma,\mu_{salt}}$$

The entropy of formation of the interface may be calculated by comparing the entropy of the components in the surface phase $\alpha$ with the values they would have if they were in the bulk of their respective phases, $\beta$, metal and solution. Accordingly,

$$[5] \quad \Delta S^{m-s} = \sum_i m_i^{\alpha}\tilde{s}_i^{\alpha} - \sum_i m_i^{\alpha}\tilde{s}_i^{\beta}$$

where $m_i^{\alpha}$ is the concentration of component $i$ in the surface phase, $\tilde{s}_i^{\alpha}$, its molar entropy in the surface phase, and $\tilde{s}_i^{\beta}$, its value in the bulk phase.

On the other hand, the surface excess of entropy is given by (14)

$$[6] \quad \Gamma_s = \sum_i m_i^{\alpha}\tilde{s}_i^{\alpha} - m_{Hg}^{\alpha}\tilde{s}_{Hg}^{\beta} - m_{MeOH}^{\alpha}(\tilde{s}_{MeOH}^{\beta} + \tilde{s}_{salt}^{\beta} m_{salt}^{\beta}/m_{MeOH}^{\beta})$$

Keeping in mind the definition of the relative ionic surface excess $\Gamma_{\pm}$, namely,

$$[7] \quad \Gamma_{\pm} = m_{\pm}^{\alpha} - m_{MeOH}^{\alpha} m_{\pm}^{\beta}/m_{MeOH}^{\beta}$$

it is easily shown that

$$[8] \quad \Delta S^{m-s} = \Gamma_s - \Gamma_+\tilde{s}_+^{\beta} - \Gamma_-\tilde{s}_-^{\beta} = \Gamma_s - \Gamma_-\tilde{s}_{salt}^{\beta} + \sigma\tilde{s}_+^{\beta}/F$$

Since $d\mu_{salt} = -\tilde{s}_{salt}^{\beta} dT$ at constant electrolyte concentration, on combining eqs. [3] and [8], one obtains

$$[9] \quad -d\xi_+ = (\Delta S^{m-s} - \sigma\tilde{s}_+^{\beta}/F)dT - (E_+ - \mu_{Na(Hg)}/F)d\sigma$$

By cross-differentiation

$$[10] \quad \left(\frac{\partial\Delta S^{m-s}}{\partial\sigma}\right)_{m,P,T} = -\left(\frac{\partial E_+}{\partial T}\right)_{m,P,\sigma} + \frac{\tilde{s}_+^{\beta} - \tilde{s}_{Na(Hg)}}{F}$$

The potential drop across the Hg/solution interface is given by (2)

$$[11] \quad \Delta\phi^{m-s} = E_+ + (\mu_+ - \mu_{Na(hg)})/F$$

Differentiating this expression with respect to temperature, one finds the simple relationship

$$[12] \quad \left(\frac{\partial\Delta S^{m-s}}{\partial\sigma}\right)_{m,P,T} = -\left(\frac{\partial\Delta\phi^{m-s}}{\partial T}\right)_{m,P,\sigma}$$

$\Delta\phi^{m-s}$ is simply related to the differential capacity of the interface which may be measured experimentally:

$$[13] \quad \Delta\phi^{m-s} = \int_0^{\sigma}(1/C)d\sigma$$

where $C$ is the differential capacity. The temperature derivative of $\Delta\phi^{m-s}$ is given by

$$[14] \quad \left(\frac{\partial\Delta\phi^{m-s}}{\partial T}\right)_{m,P,\sigma} = \left(\frac{\partial\Delta\phi_0{}^{m-s}}{\partial T}\right)_{m,P} + \int_0^{\sigma}\left(\frac{\partial(1/C)}{\partial T}\right)_{m,P,\sigma} d\sigma$$

where $\Delta\phi_0{}^{m-s}$ is the potential drop at the pzc. It is convenient to consider separately the contributions to these quantities from the inner and diffuse

Can. J. Chem. Downloaded from www.nrcresearchpress.com by 210.87.254.105 on 09/06/12
For personal use only.

TABLE 1. Interfacial tension and entropy of formation of the mercury/methanol interface at the point of zero charge in the temperature range −5 to 40°C

| Temperature (°C) | Interfacial tension* $\gamma_0$ (mN m$^{-1}$) | Entropy of formation $\Delta S_0^{m-s} \times 10^5$ (J m$^{-2}$ K$^{-1}$) | Potential of zero charge† (V) | |
|---|---|---|---|---|
| | | | (*a*)‡ | (*b*)§ |
| −5 | 394.2 | 3.4 | −0.320$_5$ | 1.7234( 6°C) |
| 10 | 393.6 | 4.8 | −0.325 | 1.7169(15°C) |
| 25 | 392.7 | 6.6 | −0.330 | 1.7069 |
| 40 | 391.5 | 8.2 | −0.335 | 1.7024(35°C) |

*Precision = ±0.1 mN m$^{-1}$.
†Precision = ±0.5 mV; $E$(sce in MeOH) − $E$(sce in $H_2O$) = 0.0152 V at 25°C, the liquid junction being made in 0.1 $M$ $NaClO_4$ in MeOH.
‡Against sce in methanol.
§Against Na(Hg) with $X_{Na}$ = 0.0077 and [$NaClO_4$] = 0.049 $M$ (2).

parts of the double layer, for example,

$$[15]\quad \left(\frac{\partial \Delta\phi^{m-s}}{\partial T}\right)_{m,P,\sigma} = \left(\frac{\partial \Delta\phi^{m-d}}{\partial T}\right)_{m,P,\sigma} + \left(\frac{\partial \Delta\phi^{d-s}}{\partial T}\right)_{m,P,\sigma}$$

where $m - d$ designates the inner layer and $d - s$ the diffuse layer. The entropy of formation of the inner layer is then

$$[16]\quad \Delta S^{m-d} = \Delta S_0^{m-d} - \int_0^{\sigma}\left(\frac{\partial \Delta\phi^{m-d}}{\partial T}\right)_{m,P,\sigma} d\sigma$$
$$= \Delta S_0^{m-d} - \int_0^{\sigma}\left(\frac{\partial \Delta\phi_0^{m-d}}{\partial T}\right)_{m,P,\sigma} d\sigma - \int_0^{\sigma}\int_0^{\sigma}\left(\frac{\partial (1/C_i)}{\partial T}\right)_{m,P,\sigma} (d\sigma)^2$$

where $\Delta S_0^{m-d}$ is the entropy of formation of the inner layer at the pzc and $C_i$, the capacity of the inner layer. A similar equation can be written for the entropy of formation of the diffuse layer, $\Delta S^{d-s}$. The separation of the experimental capacity into inner layer and diffuse layer contributions is based on Gouy–Chapman theory with the assumption that ionic specific adsorption is absent.

Values of the temperature coefficient of the inner layer capacity for the Hg/MeOH interface as a function of electrode charge density were reported earlier (1). The coefficient $\partial(1/C_i)/\partial T$ was found to have a minimum value at $\sigma = -0.05$ C m$^{-2}$, coincident with the minimum on the capacity against charge density curve. The corresponding values of the coefficient $\partial \Delta S^{m-d}/\partial\sigma$ calculated on the basis of eqs. [12]–[14], and using the previously determined values of $\partial(1/C_i)/\partial T$ (1) and the temperature coefficient of the surface potential, $\partial \Delta\phi_0^{m-s}/\partial T$ (2) are shown in Fig. 1. As expected, this coefficient has a maximum at the charge density where $\partial(1/C_i)/\partial T$ is zero (−0.019 C m$^{-2}$).

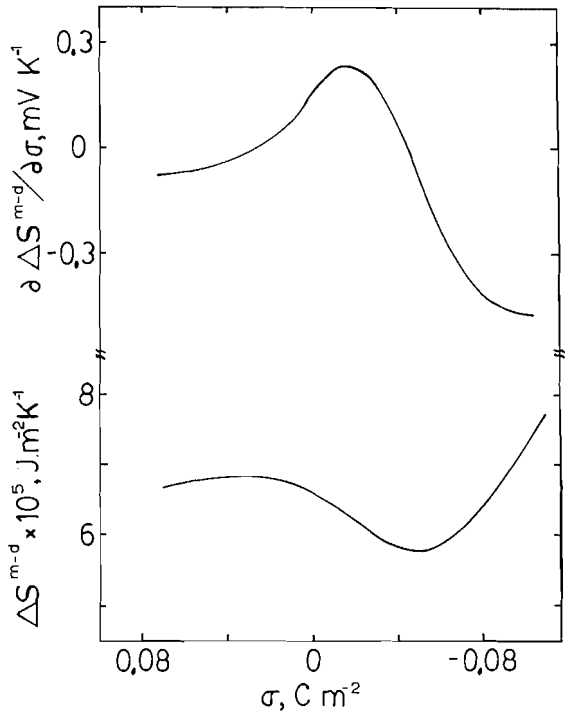


FIG. 1. Thermodynamic properties of the mercury/methanol interface as a function of electrode charge density σ with 0.1 $M$ $NaClO_4$ as electrolyte: (*a*) the coefficient $\partial \Delta S^{m-d}/\partial\sigma$ where $\partial \Delta S^{m-d}/\partial\sigma = -\partial \Delta\phi^{m-d}/\partial T$ and the superscript $(m-d)$ refers to the inner layer; and (*b*) the entropy of formation of the inner layer, $\Delta S^{m-d}$.

The data obtained for the interfacial tension in the temperature range −5 to 40°C and calculated values of $\Delta S^{m-s}$ at the pzc are recorded in Table 1. In the absence of specific adsorption, $\Gamma_+$ and $\Gamma_-$ are zero at the pzc and the temperature derivative of the surface tension gives directly the entropy of formation of the interface, $\Delta S^{m-s}$. Furthermore, since the entropy of formation of the diffuse layer is zero at the pzc, $\Delta S^{m-s}$ is identical with $\Delta S^{m-d}$, the entropy of formation of the inner layer. It was

Can. J. Chem. Downloaded from www.nrcresearchpress.com by 210.87.254.105 on 09/06/12
For personal use only.

noted that $\Delta S^{m-s}$ is a function of temperature. On the basis of eq. [16], the entropy of formation of the inner layer was calculated as a function of electrode charge density. The results presented in Fig. 1 show that there is a minimum in $\Delta S^{m-d}$ at $-0.05\,C\,m^{-2}$, the same charge density as the minimum on the inner layer capacity curve and the curve of $\partial(1/C_i)/\partial T$ against $\sigma$. A shallow maximum is also found at $\sigma = 0.028\,C\,m^{-2}$. The extrema on the entropy curve appear at charge densities where $\partial \Delta S^{m-d}/\partial\sigma$ is zero as one would expect (15).

The present results can be compared with those obtained earlier for the mercury/aqueous (5–8) and mercury/PC solution interfaces (9). In both cases, $\Delta S^{m-d}$ passes through a maximum at negative charge densities. It is interesting to note that MeOH is the only known solvent for which the temperature dependence of surface potential is negative (2) and also for which the predominant extremum on the curve of $\partial(1/C_i)/\partial T$ against $\sigma$ is a minimum (16).

Finally, one would expect $\Delta S^{m-d}$ to depend on the nature of the counter ion at charge densities outside of the range $-0.03 \leq \sigma \leq 0.03\,C\,m^{-2}$, that is, in the region where the diffuse layer contribution is negligible. However, it seems unlikely that the main features of the entropy curve would change. Therefore, the results presented here are considered to be typical for the Hg/MeOH interface.

## Discussion

According to the present data, the most ordered structure of the Hg/MeOH interface occurs at a negative charge density ($\sigma = -0.05\,C\,m^{-2}$) where a minimum is observed on the capacity curve. Maximum disorder exists at a positive charge density ($\sigma = 0.028\,C\,m^{-2}$). The position of the entropy minimum follows the predictions of the three state model according to which $\partial \Delta\phi^{m-d}/\partial T$ is zero at the extrema on the capacity curve. The entropy maximum occurs at a less positive charge density than the capacity maximum observed in the $NaClO_4$ system at $\sigma = 0.05\,C\,m^{-2}$. The difference could be due to weak specific adsorption of the perchlorate anion and suggests that the capacity hump is due partly to solvent reorientation and partly to ionic adsorption. However, the capacity minimum is due entirely to the orientation of solvent dipoles.

According to the three state model (1, 3), the solvent dipoles in a monolayer at the interface can take up three orientations, namely, with the positive end of the dipole towards the metal ("up"), the negative end towards the metal ("down"), and the dipole vector parallel to the electrode ("parallel"); the fractions in each of these orientations are $f_1$ ("up"), $f_2$("down"), and $f_3$ ("parallel"). The average orientation of dipoles surrounding a given dipole and the field due to the charge on the metal, $E$, define the reaction field $X$. Thus, the fraction of solvent molecules in a given orientation is determined by the local field $\mathscr{E} = E + X$ and a non-electrostatic residual energy $U_{ri}$ accounting for chemical interactions between the dipole in a given orientation and the metal. From the equations defining $f_1, f_2$, and $f_3$ given previously (1, 3), one may derive a set of simultaneous equations for calculating the temperature coefficients $\partial f_i/\partial T$ at constant field $E$:

$$[17]\quad \frac{\partial f_1}{\partial T} + \frac{\partial f_2}{\partial T} + \frac{\partial f_3}{\partial T} = 0$$

$$[18]\quad \frac{kT}{f_1}\left(\frac{\partial f_1}{\partial T}\right) - \frac{kT}{f_2}\left(\frac{\partial f_2}{\partial T}\right) = -k\ln\left(\frac{f_1}{f_2}\right) - 2p\frac{\partial X}{\partial T}$$

and

$$[19]\quad \frac{kT}{f_1}\left(\frac{\partial f_1}{\partial T}\right) - \frac{kT}{f_3}\left(\frac{\partial f_3}{\partial T}\right) = -k\ln\left(\frac{f_1}{f_3}\right) - p\frac{\partial X}{\partial T}$$

The temperature coefficient of the reaction field is given by

$$[20]\quad \frac{\partial X}{\partial T} = \frac{c_e}{Ad^3}\left[p\left(\frac{\partial f_1}{\partial T} - \frac{\partial f_2}{\partial T}\right)\right]$$

where $p$ is the magnitude of the dipole moment, $c_e$ the effective coordination number, $d$ the molecular diameter of the solvent molecule represented as a sphere, $\alpha$ its polarizability, and $A = 1 + c_e\alpha/d^3$. According to this model the free energy of the monolayer is given by (3)

$$[21]\quad F_i = \frac{N_T d^3 A \mathscr{E}^2}{2c_e} - \frac{N_T d^3 E^2}{2c_e} + \sum_i N_T f_i U_{ri} + \sum_i kTN_T f_i \ln f_i$$

where $N_T = 2/(\sqrt{3}d^2)$ is the number of solvent dipoles in hexagonal close packing per unit area. The expression for the entropy is then

$$[22]\quad S_i = \frac{-N_T d^3 A \mathscr{E}}{c_e}\frac{\partial X}{\partial T} - \sum_i N_T\left(\frac{\partial f_i}{\partial T}\right)U_{ri} - \sum_i kN_T f_i \ln f_i - \sum_i kTN_T\left(\frac{\partial f_i}{\partial T}\right)\ln f_i - \sum_i kTN_T\left(\frac{\partial f_i}{\partial T}\right)$$

Can. J. Chem. Downloaded from www.nrcresearchpress.com by 210.87.254.105 on 09/06/12
For personal use only.

and that for the temperature coefficient of the potential drop across the monolayer,

$$[23]\quad \frac{\partial \Delta\phi}{\partial T} = \frac{4\pi N_T d^3}{c_e}\left(\frac{\partial X}{\partial T}\right)$$

where $\partial\Delta\phi/\partial T = -\partial S_i/\partial\sigma$.

Curves of $S_i$ and $\partial S_i/\partial\sigma$ against electrode charge density were calculated on the basis of parameters found previously to describe representative capacity curves (1).[1] The molecular diameter was set equal to 0.335 nm and the effective coordination number $c_e$ to 13.95. The dipole moment ($5.54 \times 10^{-30}$ C m) and polarizability ($3.26 \times 10^{-3}$ nm$^3$) were taken from the literature. The results of these calculations are illustrated in Fig. 2. Comparison of the experimental data (Fig. 1) and theoretical curves (Fig. 2) reveals that the theory gives a reasonable qualitative description of the temperature coefficients concerned. However, just as was found with $\partial(1/C_i)/dT$ (1), the magnitude of the calculated values of $\partial S_i/\partial T$ is greater than that obtained experimentally. It is also apparent that the theory is only capable of predicting curves which are symmetrical with respect to the principal extremum on the capacity curve. The nonsymmetrical nature of the experimental curves is attributed to effects due to the specific counter ions which are not considered in either the three state model of the inner layer or the Gouy–Chapman model of the diffuse layer.

The contribution of the solvent to the entropy of formation of the electrode/solution interface was calculated on the basis of two assumptions (7–9): (*1*) the entropy of formation of an isolated Hg surface is not affected by being brought into contact with the solution and is not altered by the electrical field across the interface; on the basis of the temperature coefficient of the surface tension of the Hg/air interface, $m^{\alpha}_{Hg}(\tilde{s}^{\alpha}_{Hg} - \tilde{s}^{\beta}_{Hg})$ is equal to $2.1 \times 10^{-4}$ J m$^{-2}$ K$^{-1}$ (9); (*2*) the charge dependence of $\Delta S^{m-d}$ is due chiefly to reorientation of the solvent dipoles; the change in the surface concentration of MeOH is assumed to be quite small. On the basis of eq. [5], one may define the surface excess entropy of MeOH as follows:

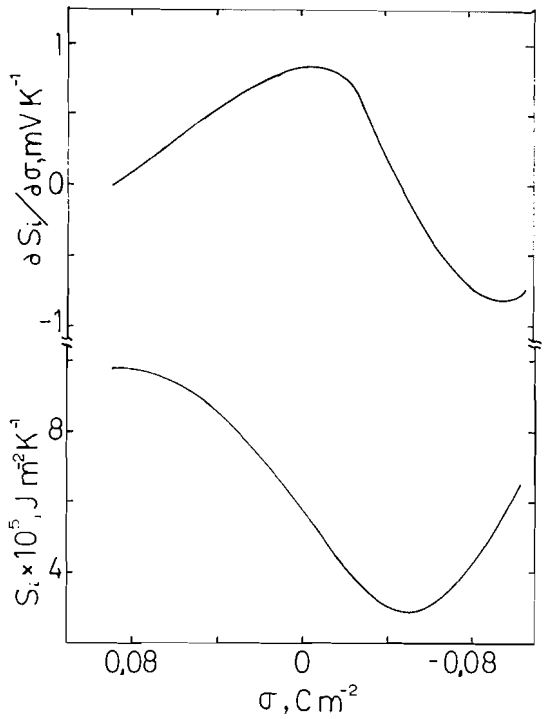


FIG. 2. Thermodynamic properties of the inner layer according to the three state model: (*a*) the coefficient $\partial S_i/\partial\sigma = -\partial\Delta\phi/\partial T$ where $S_i$ is the entropy of the dipole monolayer and $\Delta\phi$, the potential drop across it, and (*b*) $S_i$ as functions of electrode charge density $\sigma$. The parameters assumed are $d = 0.335$ nm, $c_e = 13.95$, $p = 1.66$ D, $\alpha = 3.26 \times 10^{-3}$ nm$^3$, $U_{r1} - U_{r3} = 18.05$ kJ mol$^{-1}$ and $U_{r2} - U_{r3} = 0.97$ kJ mol$^{-1}$. $U_{r1}$, $U_{r2}$, and $U_{r3}$ correspond to the residual energies for dipoles in the "up", "down", and "parallel" orientations, respectively. See the text for definition of the remaining symbols.

$$[24]\quad \Delta S^{m-d}_{MeOH} = m^{\alpha}_{MeOH}(\tilde{s}^{\alpha}_{MeOH} - \tilde{s}^{\beta}_{MeOH}) = \Delta S^{m-d} - m^{\alpha}_{Hg}(\tilde{s}^{\alpha}_{Hg} - \tilde{s}^{\beta}_{Hg})$$

According to the present results, $\Delta S^{m-d}_{MeOH}$ is equal to $-14.4 \times 10^{-5}$ J m$^{-2}$ K$^{-1}$ at the pzc and, to $-15.4 \times 10^{-5}$ J m$^{-2}$ K$^{-1}$ at the minimum on the entropy curve. These values cannot be compared directly with the results from the three state model which assumes that the solvent monolayer is in vacuum with the exception that the imaging roles of the contiguous metal and solution phases are considered (3). However, the difference in the values of $S_i$ between the pzc and minimum on the entropy curve is $3 \times 10^{-5}$ J m$^{-2}$ K$^{-1}$, a result which compares favorably with experiment.

Assuming the surface monolayer of solvent consists of a hexagonally closepacked layer of spheres of diameter equal to 0.335 nm (1), the surface concentration is $1.7 \times 10^{-5}$ mol m$^{-2}$. Accordingly, the molar surface excess entropy of MeOH, $\tilde{s}^{\alpha}_{MeOH} - \tilde{s}^{\beta}_{MeOH}$ at the pzc is $-8.5$ J mol$^{-1}$ K$^{-1}$. The negative result suggests that MeOH is more structured at the

[1]It should be noted that plots of $S_i$, $\partial\Delta\phi/\partial T$, and $\partial(1/C_i)/\partial T$ against $\sigma$ were presented earlier (1). These quantities were calculated by estimating the free energy, $\Delta\phi$ and $1/C_i$, respectively at three different temperatures. The temperature coefficient was estimated by assuming the latter quantities are linear functions of temperature, the temperature coefficient being calculated by linear regression. This procedure for obtaining the temperature coefficients is clearly not as precise as that based on the analytical expressions used here. It should also be noted that the quantity plotted in Fig. 7 of ref. 1 is $-S_i$ not $S_i$ as stated in the figure legend.

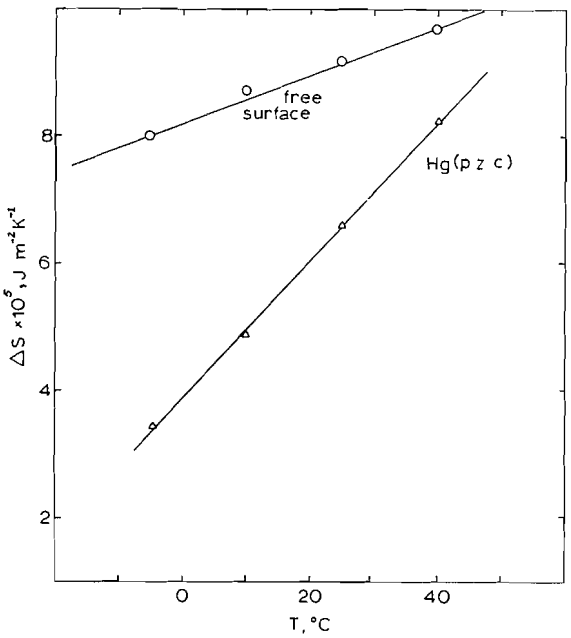


FIG. 3. Entropies of formation of the free methanol surface and of the uncharged mercury/methanol interface (0.1 *M* $NaClO_4$ in methanol) as a function of temperature.

electrode surface than in the bulk. The corresponding results for aqueous systems is $\tilde{s}^{\alpha}_{H_2O} - \tilde{s}^{\beta}_{H_2O} = -6.3\,J\,K^{-1}\,mol^{-1}$.

One possible explanation of the charge dependence of $\Delta S^{m-d}_{MeOH}$ is that the surface concentration of MeOH is also changing. On the basis of the observed change in $\Delta S^{m-d}_{MeOH}$ in the region $-0.05 \leq \sigma \leq -0.085\,C\,m^{-2}$, the change in solvent concentration in the monolayer should be $\sim 7 \times 10^{-7}$ mol $m^{-2}$. Although change in solvent concentration may affect $\Delta S^{m-d}_{MeOH}$ in some ranges of the polarizability of the electrode (17), it does not seem probable that it could account for all the features of the entropy against charge density curve.

On the basis of the above analysis, it is concluded that the charge dependence of the surface entropy is due to reorientation of MeOH molecules. According to the three state model, most solvent molecules are in the "parallel" orientation at the pzc, with a small excess of negatively oriented dipoles over positively oriented ones. The minimum on the entropy curve at $-0.05\,C\,m^{-2}$ corresponds to maximum coverage by the "parallel" species. As the charge is changed in either direction from this value, the entropy increases, the stability of the "parallel" species decreases and that of the "up" or "down" species increases. At the charge density where the probability of the "up" or "down" orientation is equal to that of the "parallel" one, maxima are observed on the entropy curve. The entropy decreases at the extremes of polarization due to the tendency for the dipoles in the surface monolayer to orient totally in either the "up" or "down" direction.

Finally, it is interesting to compare the entropy of formation of the uncharged Hg/MeOH interface, $\Delta S^{m-d}_0$ with the entropy of formation of the free methanol surface $\Delta S_0$. These data are presented in Fig. 3, the results for the free surface having been presented in the literature earlier (18). The entropy values obtained are remarkably similar in spite of the fact that $\Delta S^{m-d}_0$ includes a contribution from the entropy of formation of the mercury surface. A similar observation was made for aqueous solutions (8). If the entropy of formation of the mercury surface is independent of the nature of the solvent, then the entropies of surface formation for both MeOH and water are negative at all charge densities at the Hg/solution interface and positive at the free surface. This implies that both solvents are more structured at the mercury interface.

**Acknowledgement**

The financial support of the Natural Sciences and Engineering Research Council of Canada is gratefully acknowledged.

1. Z. BORKOWSKA, W. R. FAWCETT. Can. J. Chem. **59**, 710 (1981).
2. Z. BORKOWSKA, W. R. FAWCETT, and S. ANANTAWAN. J. Phys. Chem. **84**, 2769 (1980).
3. W. R. FAWCETT. J. Phys. Chem. **82**, 1385 (1978).
4. E. J. KING. *In* Physical chemistry of organic solvent systems. *Edited by* A. K. Covington and T. Dickinson. Plenum Press, New York. 1973. Chapt. 3.
5. G. J. HILLS and R. PAYNE. Trans. Faraday Soc. **61**, 326 (1965).
6. J. HILLS and S. HSIEH. Chem. Ing. Tech. **44**, 216 (1972).
7. J. A. HARRISON, J. E. B. RANDLES, and D. J. SCHIFFRIN. J. Electroanal. Chem. **48**, 359 (1973).
8. H. C. NGUYEN, C. V. D'ALKAINE, A. JENARD, and H. D. HURWITZ. J. Electroanal. Chem. **51**, 377 (1974).
9. H. C. NGUYEN, A. JENARD, and H. D. HURWITZ. J. Electroanal. Chem. **103**, 399 (1979).
10. D. J. SCHIFFRIN. J. Electroanal. Chem. **23**, 168 (1969).
11. E. M. DUYVIS and C. A. SMOLDERS. Rec. Trav. Chim. **80**, 636 (1963).
12. J. TARASZEWSKA. J. Electroanal. Chem. **49**, 443 (1974).
13. CRC Handbook of Chemistry and Physics, 57th edition, CRC Press Inc., 1976–1977.
14. R. PARSONS. Can. J. Chem. **37**, 308 (1959).
15. G. HILLS and F. SILVA. Can. J. Chem. **59**, 1835 (1981).
16. Z. BORKOWSKA and W. R. FAWCETT. Elektrokhimia, **16**, 1692 (1980).
17. A. BEWICK and J. ROBINSON. J. Electroanal. Chem. **71**, 131 (1976).
18. B. YA TEITELBAUM, T. A. GORTALOVA, and E. E. SIDOROVA. Zhur. Fiz. Khim. **25**, 911 (1951).

Can. J. Chem. Downloaded from www.nrcresearchpress.com by 210.87.254.105 on 09/06/12
For personal use only.

# Asymmetric homogeneous hydrogenation of olefins catalyzed by alkylphosphine complexes of rhodium(I)

WILLIAM R. CULLEN AND J. DEREK WOOLLINS

*Chemistry Department, University of British Columbia, Vancouver, B.C., Canada V6T 1Y6*

Received December 9, 1981

WILLIAM R. CULLEN and J. DEREK WOOLLINS. Can. J. Chem. **60**, 1793 (1982).

The cationic rhodium(I) complexes of the optically active ferrocenes, $C_5H_5FeC_5H_3[CH(CH_3)N(CH_3)_2][ER_2]$-1,2, catalyze the asymmetric hydrogenation of acetamidoacrylic acid derivatives, itaconic acid and styrene, when $ER_2$ is $P(C_6H_5)_2$ or $P(C(CH_3)_3)_2$. The configuration of the product is reversed on substituting $C_6H_5$ for $C(CH_3)_3$ groups. The catalyst with the *tert*-butyl groups can afford higher optical yields and is faster overall. The rhodium(I) complexes of the arsenic derivatives $ER_2 = As(C_6H_5)_2$ or $As(CH_3)_2$ do not catalyze the hydrogenation reactions. The nmr spectrum of the arsenic complex ($ER_2 = As(C_6H_5)_2$) is temperature dependent which seems to be due to a process involving the making and breaking of the Rh—N bond. The unsuccessful use of the MEM group (β-methoxyethoxymethyl) to protect an alcohol function α to a ferrocene ring is described. The hydrogenation results are discussed in the light of models which are currently used to predict the results of rhodium(I) catalyzed reactions but which are inapplicable to this work.

WILLIAM R. CULLEN et J. DEREK WOOLLINS. Can. J. Chem. **60**, 1793 (1982).

Les complexes cationiques du rhodium(I) avec des ferrocènes optiquement actifs du type $C_5H_5FeC_5H_3[CH(CH_3)N(CH_3)_2][ER_2]$-1,2, catalysent l'hydrogénation asymétrique des dérivés de l'acide acétamidoacrylique, de l'acide itaconique et du styrène lorsque le groupe $ER_2 = P(C_6H_5)_2$ ou $P(C(CH_3)_3)_2$. On observe une inversion de la configuration du produit lorsqu'on remplace le groupe $C(CH_3)_3$ par le groupe $C_6H_5$. Le catalyseur portant un groupe *tert*-butyle conduit à des rendements optiques plus élevés et agit d'une façon plus rapide. Les complexes du rhodium(I) des dérivés de l'arsenic $ER_2 = As(C_6H_5)_2$ ou $As(CH_3)_2$ ne catalysent pas les réactions d'hydrogénation. Le spectre de rmn du complexe de l'arsenic ($ER_2 = As(C_6H_5)_2$) dépend de la température et ceci semble être dû à un processus impliquant la formation et la rupture d'une liaison Rh—N. On décrit un essai qui n'a pas porté fruit d'utiliser le groupe MEM (β-méthoxyéthoxyméthyle) pour protéger la fonction alcool en α du cycle du ferrocène. On discute des résultats de l'hydrogénation en se basant sur les modèles couramment utilisés pour prédire les résultats de la catalyse par le rhodium(I) mais qui ne peuvent pas s'appliquer à ce travail.

[Traduit par le journal]

## Introduction

The spectacular success in achieving nearly 100% enantiomeric excess in the homogeneous hydrogenation of α-acetamidoacrylic acids, using cationic rhodium(I) complexes of chelating ligands as catalysts, eq. [1], has generated considerable interest (1–15). One mechanism of the reaction, based on studies of the commonly used substrates and catalysts, appears to be as depicted in eqs. [2]–[5] (3). However, as discussed below, this need not apply to all systems.

The source of the stereospecificity in these reactions is of particular importance. On the basis of the crystal structures of several catalyst precursors, all of which have ditertiary phosphines as ligands, Knowles and co-workers (6, 7) have suggested that the absolute configuration of the amino acid product can be predicted in terms of a model which requires the square planar intermediate **1** to have the structure shown in **4**. Here the COOH group (R′ = H) is located above the *face* of a phenyl group on the ligand.[1]

[1] 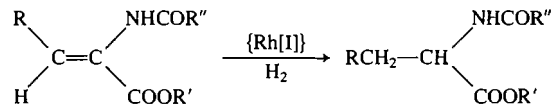

[2] $[Rh(L\text{-}L')(solvent)_2]^+ + substrate \leftrightarrows [Rh(L\text{-}L')substrate]^+$ **1** + 2 solvent

[3] $[Rh(L\text{-}L')(substrate)]^+ + H_2 \rightarrow [Rh(H)_2(L\text{-}L')(substrate)]^+$ **2**

[4] $[Rh(H)_2(L\text{-}L')(substrate)]^+ \rightarrow (Rh(H)(L\text{-}L')(Hsubstrate)]^+$ **3**

[5] $Rh(H)(L\text{-}L')(Hsubstrate) \rightarrow [Rh(L\text{-}L')(solvent)_2]^+ + (H)_2substrate$

Halpern and co-workers (3, 4) have recently determined the structure of two square planar intermediates **4** (L-L′ = $Ph_2P(CH_2)_2PPh_2$, $Ph_2P\overset{*}{C}HMeCH_2PPh_2$, R′ = Me, R = Ph). The olefin is bound as indicated but in both solids the COOR group lies over an *edge* of a phenyl ring. This, in the case of the optically active complex, hydrogenation would give the amino acid product of opposite configuration to that actually observed. These and other results led to the suggestion that the discrimination arises because of differences in the rates of reaction of the diasterotopic complexes **1** (or **4**) (eq.

[1]The four aromatic groups bound to phosphorus on the ditertiary phosphine, (L-L′), in **1** (or **4**) are "seen" by the incoming substrate as an alternating set of edge-on or face-on rings.

0008-4042/82/141793-07$01.00/0

©1982 National Research Council of Canada/Conseil national de recherches du Canada

TABLE 1. Analytical data for new ligands and complexes[a]

| | Complex | Found (%) | | | Calcd. (%) | | |
|---|---|---|---|---|---|---|---|
| | | C | H | N | C | H | N |
| 7 | $C_5H_5FeC_5H_3[CH(CH_3)N(CH_3)_2][As(C_6H_5)_2]$-1,2 | 64.37 | 5.93 | 2.86 | 64.43 | 5.82 | 2.89 |
| 8 | $C_5H_5FeC_5H_3[CH(CH_3)N(CH_3)_2][As(CH_3)_2]$-1,2 | 52.47 | 6.73 | 3.95 | 53.21 | 6.70 | 3.88 |
| 9 | $C_5H_5FeC_5H_3[CH(CH_3)N(CH_3)_2][P(C(CH_3)_3)_2]$-1,2 | 65.64 | 8.85 | 3.41 | 65.84 | 8.97 | 3.49 |
| 10 | $C_5H_5FeC_5H_3[CH(CH_3)OCOCH_3][P(C_6H_5)_2]$-1,2 | 68.27 | 5.67 | — | 68.44 | 5.52 | — |
| 11 | $C_5H_5FeC_5H_3[CH(CH_3)OH][P(C_6H_5)_2]$-1,2 | 69.62 | 5.90 | — | 69.58 | 5.60 | — |
| 12 | $C_5H_5FeC_5H_4CH(CH_3)OCH_2OC_2H_4OCH_3$ | 60.29 | 6.96 | — | 60.34 | 6.97 | — |
| 13 | $\{C_7H_8RhC_5H_5FeC_5H_3[CH(CH_3)N(CH_3)_2][As(C_6H_5)_2]$-1,2$\}ClO_4$[b] | 50.32 | 4.93 | 1.78 | 50.83 | 4.65 | 1.79 |
| 14 | $\{C_7H_8RhC_5H_5FeC_5H_3[(CH(CH_3)N(CH_3)_2][As(CH_3)_2]$-1,2$\}ClO_4$[c] | 37.34 | 5.21 | 2.00 | 37.92 | 4.70 | 1.92 |
| 15 | $[C_7H_8RhC_5H_5FeC_5H_3[CH(CH_3)N(CH_3)_2][P(C(CH_3)_3)_2]$-1,2$\}ClO_4$ | 50.08 | 6.82 | 2.00 | 50.06 | 6.37 | 2.01 |

[a]All derivatives are orange-red oils except for **7**, **13–15** which are orange-red solids.
[b]Cl Found: 4.90; calcd.: 4.55.
[c]$CH_2Cl_2$ solvate.

[3]). It should be noted that these rate differences could arise because of steric effects in the 6-coordinate *cis* hydride intermediate (13). In this connection Knowles *et al.* (7) have implied that the rate of subsequent reactions of **1** is a function of the flexibility of the ligand.

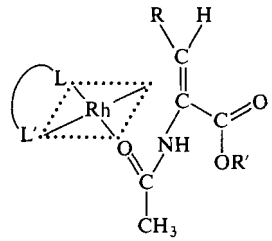


**4**

This paper describes some further studies with complexes of some ferrocenylphosphines **6–9**. The results indicate that some of the currently accepted models are not applicable to these systems. In particular, unexpectedly high optical yields are achieved using complexes of the bulky phosphine **9**.

## Experimental

Air sensitive reagents and products were manipulated in a nitrogen or argon atmosphere. Optical rotations were monitored on a Perkin Elmer 141 polarimeter. A cell length of 10 cm was used and the light source was the sodium D line (589 nm). *N,N*-dimethyl-α-ferrocenylethylamine **5** was prepared and resolved using (*R*)-(+)-tartaric acid as previously described (16). Microanalyses were done by Mr. Peter Borda, Chemistry Department, University of British Columbia. Data are given in Table 1.

*Preparation of the Group V derivatives* ***7–9***

The procedure for the preparation of **7–9** from **5** is essentially the same as that described for the preparation of **6** (13) (eq. [6]).

The resolved amine (or the racemic mixture) (0.01 mol) was placed in a Schlenck tube together with 15 mL of dry diethyl ether. The solution was treated with *n*-butyllithium (0.01 mol) and stirred for 1.5 h. The reaction is exothermic. The appropriate halide $XER_2$ ($ClAs(C_6H_2)_2$, $IAs(CH_3)_2$, $ClP(C(CH_3)_3)_2$) (0.01 mol) was added slowly and the solution stirred a further 3 h. An aqueous slurry of sodium bicarbonate (5 g in 10 mL) was added and the mixture was stirred for a further 1 h before it was filtered. The precipitate was washed with ether and the filtrate and washings were washed with water (2 × 30 mL). The organic layer, dried over $K_2CO_3$, was evaporated to leave an oily residue which was purified by recrystallization from absolute ethanol (**7**, 56% yield) or chromatography on an alumina column. Both **8** (40% yield) and **9** (40% yield) were eluted with 40:60 petroleum ether/diethyl ether; the first band was the desired product.

*Preparation of the rhodium(I) perchlorate complexes (**13–15**)*

The perchlorate salts of the ligands **7–9** were prepared essentially using the procedure of Schrock and Osborn (17) as described by Cullen *et al.* (13). Recrystallization required very little solvent. Thus at the ~1 m*M* scale the first formed cationic perchlorate salt was dissolved in ~1.5 mL of dichloromethane and treated with 5 mL of ethanol and 0.1 mL of diethyl ether to give crystals.

*Preparation of the acetate, **10***

The amine, **5**, (0.0125 mol) was sealed in a Carius tube with acetic anhydride (0.025 mol). The tube was heated to 100°C for 12 h. The reaction mixture was treated with $K_2CO_3$ (15 g in 50 mL of water) and extracted with diethyl ether. The ether extract was washed with dilute HCl (5%), $K_2CO_3$ (5%), and water, and dried over $K_2CO_3$. Evaporation of the solvent gave a 93% yield of **10**.

*Preparation of the alcohol, **11***

The acetate **10** in diethyl ether was treated with a slight excess of butyllithium and the mixture was stirred for 1 h. Water was added and the ether layer separated, washed with water, and dried over $K_2CO_3$. Removal of the solvent gave a 100% yield of **11**. The product can be recrystallized from heptane.

*Preparation of the MEM derivative of ferrocenylethanol, **12***

Ferrocenylethanol (11.7 g, 0.05 mol) was dissolved in dry dichloromethane (50 mL). To this solution was added diisopropylethylamine (9.7 g, 0.075 mol) and MEM chloride (9.35 g, 0.075 mol) was slowly added to the cooled stirred mixture (0°C). The temperature was slowly raised to 20°C (4 h). The resulting reaction mixture was washed with 5% HCl (2 × 50 mL), water (50 mL), and dried over $K_2CO_3$. Removal of solvent gave a brown liquid, **12**, in 88% yield. The liquid decomposed on distillation.

*Hydrogenation reactions*

A standard gas uptake apparatus was used for all hydrogenation reactions (13). The appropriate conditions are given in Table 3.

TABLE 2. The $^1H$ nmr spectra of new compounds[a]

| Compound | $CH(CH_3)(J(H,CH_3))$ | $N(CH_3)_2$ | $C_5H_5$ | Other |
|---|---|---|---|---|
| **7** | 1.21 (7) | 1.78 | 3.97 | — |
| **8** | 1.28 (6) | 2.11 | 4.10 | 1.22 (s), 1.03 (s), $(As(CH_3)_2)$ |
| **9** | [b] | 2.14 | 4.14 | 1.45(d), 0.88(d), $J(P,H) = 11$, $(P(C(CH_3)_3)_2)$ |
| **10** | 1.60 (6) | — | 4.03 | 1.15 $(C(O(CH_3)$ |
| **11** | 1.20 (7) | — | 4.24 | 1.10(d) (C—OH), 5.6 (qd)(C—H) |
| **12** | 1.56 (6.5) | — | 4.12 | 4.12(s)$(OCH_3)$, 4.78(2)(—O—$CH_2$—O—), 3.6(m)(—O—$CH_2CH_2$—$OCH_3$), 3.4(m)(—O—$CH_2CH_2$—$OCH_3$) |
| **13** | 1.74 (6) | 2.78 | 3.65 | See Fig. 1 |

[a] Principal features only at ambient temperature. Chemical shifts are given in ppm downfield from TMS. Coupling constants are in Hz.
[b] Under $C(CH_3)_3$ signals.

## Results and discussion

The lithiation of optically pure **5** is almost stereospecific (18), which allows the preparation of disubstituted derivatives **6–9** in reasonable yield. The products have the (*R,S*)-configurations as shown in eq. [6]. The (*S*)-isomer of **5** affords (*S,R*)-products. The phosphine **6** has been described previously (13, 15, 19) but the other derivatives **7–9** are new. The analytical results, Table 1, and the nmr spectra, Table 2, confirm their formulation. In particular, all show the singlet at about 4 ppm characteristic of an unsubstituted $C_5H_5$ ring. The most interesting feature of these spectra is the appearance of two signals for the alkyl groups in the $—P(C(CH_3)_3)_2$ and $—As(CH_3)_2$ derivatives. This could be due to inter- or intramolecular complex formation with the amine acting as a donor, however, since the $—N(CH_3)_2$ signal is a singlet this explanation seems unlikely. Probably the doubling arises because the groups are diastereotopic. The spectrum of the corresponding $—P(CH_3)_2$ derivative is reported to show inequivalent methyl groups (doublets at 1.08 and 1.31 ppm) (19).

[6]

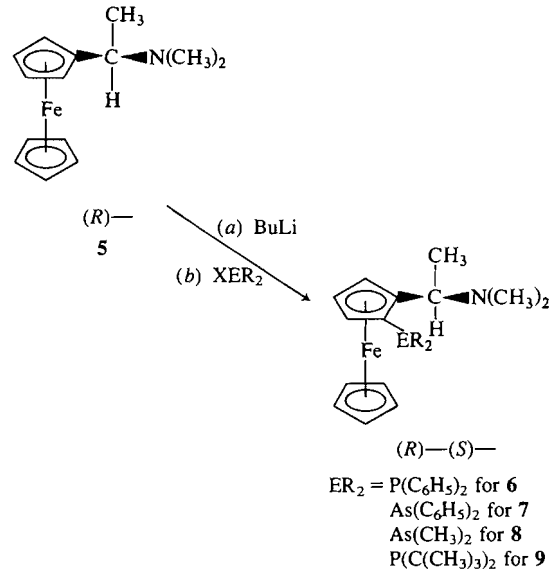


$ER_2$ = $P(C_6H_5)_2$ for **6**
$As(C_6H_5)_2$ for **7**
$As(CH_3)_2$ for **8**
$P(C(CH_3)_3)_2$ for **9**

The action of acetic anhydride in the amine **6** affords the acetate **10**. This compound has been prepared by others, also in high yield, using essentially the same conditions (19) and the spectroscopic data are in good agreement. The acetate **10** is readily converted to the alcohol **11** by reaction with butyllithium, a procedure which has been used to prepare this and related derivatives (19). The nmr spectrum of **11** is different from that previously described. The OH absorption is actually a doublet due to coupling with the C—H proton which itself is shifted downfield to 5.6 ppm and, because of the approximate equality of the couplings $J(CH_3,H)$ and $J(HO,H)$, it is seen as a sextet (a quartet of doublets).

In order to extend the chemistry of the phosphine **11** it was desirable to be able to protect the alcohol function. The β-methoxyethoxymethyl (MEM) group described by Corey *et al.* (20) seemed to offer many advantages, so preliminary experiments were carried out on α-ferrocenylethanol.

The MEM derivative, **12**, is formed easily from MEM chloride and the alcohol in the presence of diisopropylethylamine as described in the literature (20) (other suggested procedures involving, for example, butyl lithium are less desirable).

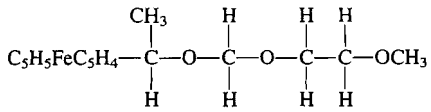


**12**

A number of unsuccessful experiments were attempted to establish if the MEM group would direct lithiation in ferrocene derivatives. Typically when **12** is treated with 1 equivalent of TMEDA and 1 equivalent of butyllithium a dark solution is obtained. Nuclear magnetic resonance investigation of the product following hydrolysis of this solution with $D_2O$ shows no lithiation reaction

takes place. Seemingly the MEM derivative complexes with the butyllithium. If excess butyllithium is used (three equivalents), cleavage occurs and an 80% yield of $C_5H_5FeC_5H_4C(CH_3)HOD$ can be isolated following treatment of the reaction mixture with $D_2O$.

Thus it seems that the MEM group is not as useful in ferrocene chemistry as could be hoped and no attempts were made to investigate the MEM derivative of **11**.

*Cationic rhodium(I) complexes*

The phosphines and arsines **6–9** all form derivatives $[(L\text{-}L')RhNBD]^+CO_4^-$ (L-L′ = bidentate ligand, and NBD=norbornadiene). The analytical results in Table 1 confirm the formulation of the new derivatives of **7–9**, however, the nmr spectra of the complexes are not straightforward. Some spectra of the perchlorate derivative of the arsine **7** are shown in Fig. 1. At ambient temperature, the phenyl region of the spectrum is more spread out than usual indicating that the two rings are in different environments and are, perhaps, held in a fixed orientation relative to each other. This difference in orientation is obvious in the crystal structure of the similar cation obtained from the $—P(C_6H_5)_2$ analogue **6** (13). The spectrum (Fig. 1) also shows a broad signal for the $N(CH_3)_2$ group which collapses and becomes the expected two singlets on cooling. The separation between the two signals is 72 Hz at −30°C. At this temperature the specturm is very similar to that of the analogous complex of **6** measured at ambient temperature.

It is difficult to account for this temperature effect by any simple exchange process such as conformational averaging because the methyl groups will always be inequivalent if the ring structure is preserved. The steps which seem to be necessary are as follows. (*i*) The Rh—N bond breaks. (*ii*) Rotation about the $C—N(CH_3)_2$ bond and inversion at nitrogen occurs. (*iii*) The Rh—N bond reforms.

A number of investigators have been attracted to work with ligands containing both hard and soft donor atoms in the hope that their metal complexes might show bond lability. This result could be the first clear demonstration of this expectation.

Work is now in progress to establish the validity of these proposals and hopefully the results will also enable an interpretation of the nmr spectra of complexes **15** and **16** which show similar features.

*Hydrogenation studies*

The results of a number of catalyzed hydrogenation reactions are given in Table 3.

The two phosphine derivatives **6** and **9** form rhodium complexes which are catalyst precursors but the arsine analogues **7** and **8** do not. Furthermore, the arsines **7** and **8** do not give catalytically active solutions when mixed with $[Rh(1,5\text{-}COD)Cl]_2$ (COD = cyclooctadiene).

The failure of the arsines to afford catalytic systems is yet a further example of the unpredictability of experiments of this type and no good rationalization is available. Thus, in related work, the rhodium(I) complexes (produced *in situ*) of the

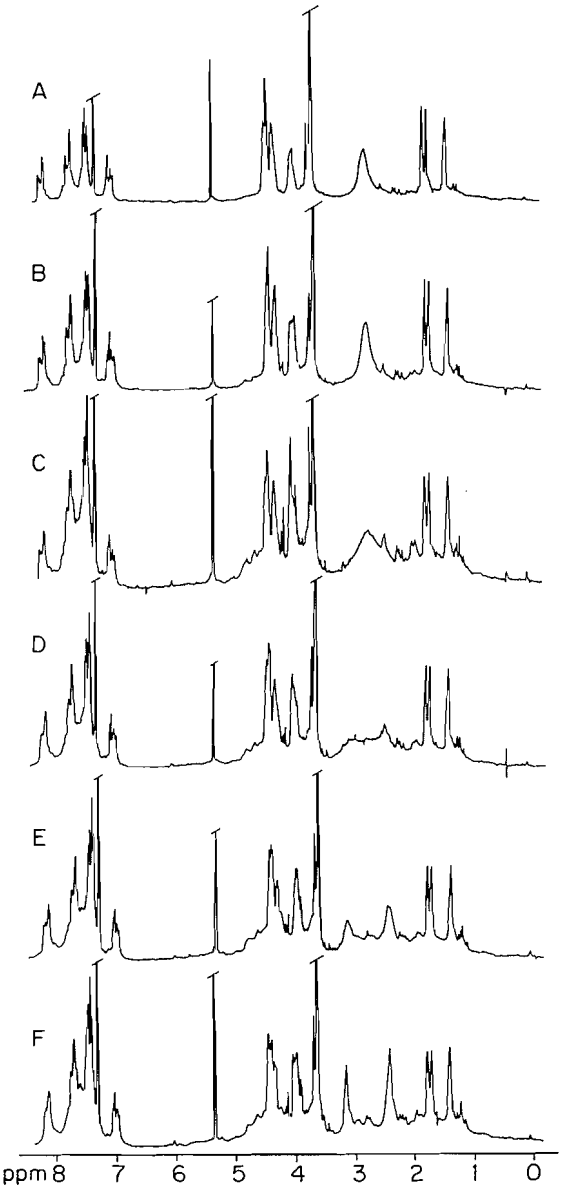


FIG. 1. The $^1H$ nmr spectrum of the arsine complex **13** (100 MHz). A, at ambient temperature; B, 10°C; C, 0°C; D, −10°C; E, −20°C; F, −30°C.

TABLE 3. Homogeneous hydrogenation of some olefins catalyzed by $[Rh(L\text{-}L')(NBD)]^+ ClO_4^-$[a]

| L-L′ of the catalyst precursor | Substrate | Time (h) | Optical yield (%) | Configuration |
|---|---|---|---|---|
| **9** | Acetamidocinnamic acid | 16 | 84 | *S* |
| | Acetamidoacrylic acid | 12 | 24 | *S* |
| | Itaconic acid | 16 | 43 | *R* |
| | Styrene | 6 | — | — |
| **6** | Acetamidocinnamic acid | 24 | 76 | *R* |
| | Acetamidoacrylic acid | 18 | 49 | *R* |
| | Itaconic acid[b] | 72 | 33 | *S* |
| | Styrene | 12 | — | — |

[a] Reactions were carried out at 1 atm $H_2$ and 30°C. The concentration of the catalyst was $5 \times 10^{-4}$ *M* and the substrate $5 \times 10^{-2}$ *M*. Optical yields are based on the rotation of the isolated products. All reductions were quantitative (by nmr or gas chromatography) except [b] which was only 21% completed after 72 h.

arsenic analogue of DIOP (**16**, $ER_2 = As(C_6H_5)_2$) catalyze reductions such as shown in eq. [1]. The rates are slower than with phosphine based catalysts (21, 22) and the optical yields are low. The products also have the opposite configuration. The same *in situ* catalyst can also be used for the reduction of ketones via hydrosilylation. The yields, chemical and optical, are similar to those obtained from DIOP based catalysts but this time no reversal of product configuration is found.

In the case of the unsymmetrical ligands **17** ($ER_2 = P(C_6H_5)_2$ or $As(C_6H_5)_2$, $R' = CH_3$), *in situ* rhodium(I) catalysts prepared from the phosphine give high chemical and optical yields for the hydrosilylation of ketones, with the optical yields being higher than those obtained from DIOP (**16**) based catalysts in some cases. However, even though the arsine **17** ($ER_2 = As(C_6H_5)_2$, $R' = CH_3$) affords an *in situ* catalyst for the hydrosilylation reaction the optical yields are very low or zero in spite of very similar chemical yields.[2]

The catalyst precursor based on **6** has a known crystal structure and, using this as model, it is apparent that in an intermediate like **1** the two, and only two, phenyl rings would have an edge-on face-on arrangement with respect to the bound substrate (13). The face-on ring is adjacent to the cyclopentadiene rings and from models its motion appears to be restricted.

As mentioned in the Introduction, Knowles and co-workers (6, 7) have pointed out that the absolute configuration of the products from reactions of this type can be predicted by requiring the intermediate **1** to have a structure with the COOR group lying above the face of an aromatic ring attached to phosphorus. If this model is applied to the present results (L-L′ = **6**) then the opposite configuration to that actually obtained is predicted.

[2] N. C. Payne and D. W. Stephan. Personal communication.

It is worth noting that using ligands like **6** with P and N donor atoms the Knowles requirement would ensure that the olefin C=C bond would have to be *trans* to the nitrogen in **4** ($L' = N(CH_3)_3$). This apparently is a favourable situation for binding since the crystal structure of (P-N)Ir(CO)Cl, when P-N is the closely related ligand *o*-diphenylphosphino-*N*,*N*-dimethylaniline, (**17**, $ER_2 = P(C_6H_5)_2$, $R' = H$) shows that the CO group is *trans* to N and that the Ir—(CO) and Ir—P bonds are unusually short and presumably strong (23).

A further striking feature of these new results (Table 3) is that changing the $-P(C_6H_5)_2$ group to $-P(C(CH_3)_3)_2$ results in an effective hydrogenation catalyst which gives products of the opposite absolute configuration. Furthermore, the reactions go to completion in a shorter time and, in one case, a higher optical yield is obtained. Clearly, aromatic rings on the ligand donor atom are not needed to achieve good optical yields and fast rates can be obtained in spite of the bulk of the *tert*-butyl groups. (The noteworthy reversal of product configuration should be considered with the same effect caused by changing the $ER_2$ group in **16** from $P(C_6H_5)_2$ to $P(C_6H_4OCH_3\text{-}o)_2$ (24).)

There are only a few reports of asymmetric catalysis by metal complexes of aliphatic phosphines. Thus, Kumada and co-workers (25) showed that a closely related ferrocene derivative to **6–9** in which the $ER_2$ group is $P(CH_3)_2$ can be used to prepare an *in situ* rhodium(I) catalyst for the hydrosilylation of ketones. The optical yields are moderate (~50%). This same reaction and reactions such as [1] are reported (26) to be catalyzed by rhodium(I) complexes of ditertiary phosphines related to DIOP (**16**, $ER_2 = P(alkyl)_2$). It should also be mentioned that alkyl sulfoxides with the DIOP skeleton (**16**, $ER_2 = S(O)CH_3$) form ruthenium complexes which catalyze hydrogenations like [1]. However, the optical yields are low (27).

The hydrogenations reported by Otsuka (26) appear to proceed via a hydride intermediate $[(L\text{-}L)Rh(H)_2\ (solvent)_x]^+$ rather than the simple solvate **1** described in eq. [2]. Brown *et al.* (28) also described cationic rhodium hydrides which have phosphines such as $(C_6H_5)_2P(CH_2)_5P(C_6H_5)_2$ as ligands. Thus it is certainly possible that the pathway of some of the reactions described in Table 3 also involves the formation of a stable hydride. This will be checked by kinetic and spectroscopic measurements.

When itaconic acid is the substrate (Table 3) the hydrogen uptake is slower than observed for the other substrates. The optical yields are in the same range reported for similar catalyzed hydrogenations. It seems that the hydrogen bonding in the acid needs to be disrupted in some way before high optical yields are achieved (29).

Kumada and co-workers have found that rhodium(I) complexes of the amine and alcohol **18** (R =

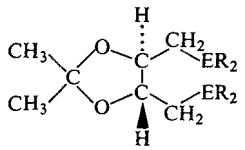

**16**

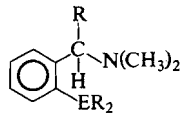

**17**

DIOP $ER_2 = P(C_6H_5)_2$

OH or $N(CH_3)_2$) are excellent hydrogenation catalysts (15, 19, 30, 31). In view of the result that the closely related **6** gives complexes which are as effective, it was of interest to establish if the same would hold for the alcohol **11**. The results of a number of experiments can be summarized as follows. For olefin reductions (eq. [1]) reaction is slow and optical yields are low. Thus acetamidocinnamic acid is 25% reduced after 3 days at 30°C (1 atm $H_2$). The optical yield is 17%. Ketones are not reduced under the same conditions.

These results could well be due to lack of chelate formation by **11**. Both P and N are bound in complexes of **6** (13) and both P atoms are bound in complexes of **18** ($R' = N(CH_3)_2$).[3]

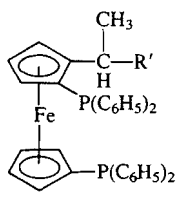

**18**

[3]W. R. Cullen and T.-J. Kim. Unpublished results.


## Acknowledgments

We thank Johnson Matthey Chemical Limited for the loan of rhodium, Drs. B. R. James and M. D. Fryzuk for discussion, Drs. D. W. Stephan and N. C. Payne for sending results prior to publication, and the Natural Sciences and Engineering Research Council of Canada for financial support.



1. B. R. James. Adv. Organomet. Chem. **17**, 319 (1970), and references therein.
2. H. B. Kagan. Ann. N.Y. Acad. Sci. **333**, 1 (1980).
3. A. S. C. Chan, J. J. Pluth, and J. Halpern. J. Am. Chem. Soc. **102**, 5952 (1980).
4. A. S. C. Chan, J. J. Pluth, and J. Halpern. Inorg. Chim. Acta, **37**, L477 (1979).
5. J. M. Brown and P. A. Chaloner. J. Chem. Soc. Chem. Commun. **344** (1980).
6. K. E. Koenig, M. J. Sabacky, G. L. Bachman, W. C. Christopfel, H. D. Barnstorff, R. B. Friedman, W. S. Knowles, R. B. Stults, B. D. Vineyard, and D. J. Weinkauff. Ann. N.Y. Acad. Sci. **333**, 16 (1980).
7. W. S. Knowles, B. D. Vineyard, M. J. Sabacky, and B. R. Stults. *In* Fundamental research in homogeneous catalysis. Vol. 3. *Edited by* M. Tsutsui. Plenum Press, New York. 1979. p. 537.
8. D. A. Slack, I. Greveling, and M. C. Baird. *In* Fundamental research in homogeneous catalysis. Vol. 3. *Edited by* M. Tsutsui. Plenum Press, New York. 1979. p. 983.
9. R. G. Ball and N. C. Payne. Inorg. Chem. **16**, 1187 (1977).
10. M. D. Fryzuk and B. Bosnich. J. Am. Chem. Soc. **100**, 5491 (1978).
11. I. Ojima, T. Kogure, and N. Yoda. Chem. Lett. 495 (1979).
12. J. M. Brown and P. A. Chaloner. J. Am. Chem. Soc. **102**, 3040 (1981).
13. W. R. Cullen, F. W. B. Einstein, C-H. Huang, A. C. Willis, and E-S Yeh. J. Am. Chem. Soc. **102**, 988 (1980).
14. K. Yamamoto, J. Wakatsuki, and R. Sugimoto. J. Chem. Soc. Jpn. **53**, 1132 (1980).
15. T. Hayashi, T. Mise, S. Mitachi, K. Yamamoto, and M. Kumada. Tetrahedron Lett. 1133 (1976).
16. S. W. Gokel and I. K. Ugi. J. Chem. Educ. **49**, 249 (1972).
17. R. R. Schrock and J. A. Osborn. J. Am. Chem. Soc. **98**, 2143 (1976).
18. L. F. Battelle, R. Bau, G. W. Gokel, R. T. Oyakawa, and I. K. Ugi. J. Am. Chem. Soc. **95**, 482 (1973).
19. T. Hayashi, T. Mise, M. Fukushima, M. Kogatani, N. Nagashima, Y. Hamada, A. Matsumoto, S. Kawakami, M. Konishi, K. Yamamoto, and M. Kumada. Bull Chem. Soc. Jpn. **53**, 1138 (1980).
20. E. J. Corey, J-L. Gras, and P. Ulrich. Tetrahedron Lett. 809 (1976).
21. A. D. Calhoun, W. J. Kobos, T. A. Nile, and C. A. Smith. J. Organometal. Chem. **170**, 175 (1979).
22. B. A. Murrer, J. M. Brown, P. A. Chaloner, P. N. Nicholson, and D. Parker. Synthesis, 350 (1979).
23. D. M. Roundhill, R. A. Bechtold, and S. G. N. Roundhill. Inorg. Chem. **19**, 284 (1980).
24. J. M. Brown and B. A. Murrer. Tetrahedron Lett. 581 (1980).
25. T. Hayashi, K. Yamamoto, and M. Kumada. Tetrahedron Lett. 4405 (1974).

26. S. OTSUKA. International Conference on the Chemistry of the Platinum Group Metals. Bristol, England. July, 1981. Abstract C1.
27. B. R. JAMES and R. S. MCMILLAN. Can. J. Chem. **55**, 3927 (1977).
28. J. M. BROWN, P. A. CHALONER, A. G. KENT, B. A. MURRER, P. N. NICHOLSON, D. PARKER and P. J. SIDEBOTTOM. J. Organometal. Chem. **216**, 263 (1981).
29. W. C. CHRISTOPHEL and B. C. VINEYARD. J. Am. Chem. Soc. **101**, 4406 (1979).
30. T. HAYASHI, T. MISE, and M. KUMADA. Tetrahedron Lett. 4351 (1976).
31. T. HAYASHI, A. KATSUMURA, M. KONISHI, and M. KUMADA. Tetrahedron Lett. 425 (1979).

# The mass spectra of pyrimidines: 2(1H)-pyrimidinone and some N(1)-substituted derivatives

EVA M. KAZDAN, ROBIN T. B. RYE,[1] AND OSWALD S. TEE

*Department of Chemistry, Concordia University, 1455 de Maisonneuve Blvd., W., Montreal, P.Q., Canada H3G 1M8*

Received December 16, 1981

EVA M. KAZDAN, ROBIN T. B. RYE, and OSWALD S. TEE. Can. J. Chem. **60**, 1800 (1982).

The EI induced fragmentation of 2-pyrimidinone (**1**) and several N(1)-substituted derivatives has been studied. Principal fragmentation pathways have been identified using $^2H$ labelling, metastable defocussing, and exact mass measurements.

The fragmentation of **1** parallels that of cytosine. The hydrogen atom at C(4), and not the tautomeric hydrogen, is involved in the formation of the prominent $[M - H]^+$ peak in the spectrum of **1**; subsequent fragmentations of the $[M - H]^+$ moiety contribute significantly to the spectrum.

Side chain eliminations predominate in the mass spectra of the N(1)-substituted derivatives, but peaks characteristic of the pyrimidinone nucleus are observable in every case. Alternative structures for the $[M - H]^+$ entity formed by $H^\cdot$ loss from the substituent are proposed for the *N*-phenyl and *N*-benzyl compounds.

EVA M. KAZDAN, ROBIN T. B. RYE et OSWALD S. TEE. Can. J. Chem. **60**, 1800 (1982).

On a étudié la fragmentation IE de la pyrimidinone-2 (**1**) et de plusieurs dérivés substitués sur le N(1). On a identifié le mécanisme principal de fragmentation en faisant appel au marquage au $^2H$, à l'étude des ions métastables et à des mesures de masses exactes.

La fragmentation du composé **1** ressemble à celle de la cytosine. C'est l'atome d'hydrogène sur le carbone en position 4 et non l'hydrogène tautomère qui est impliqué dans la formation du pic intense $[M - H]^+$ du spectre de ce composé **1**; des fragmentations ultérieures de l'unité $[M - H]^+$ apportent une contribution appréciable au spectre.

Des éliminations dans la chaîne latérale prédominent dans le spectre de masse des dérivés substitués sur le N(1) mais on observe dans chaque cas les pics caractéristiques du noyau pyrimidinone. Dans le cas des composés *N*-phényle et *N*-benzyle, on propose une autre structure pour l'unité $[M - H]^+$ qui se forme par élimination d'un $H^\cdot$ du substituant.

[Traduit par le journal]

## Introduction

Interest in the mass spectrometry of pyrimidines and related compounds has focussed primarily on the naturally occurring nucleosides and nucleotides. Mass spectra of nucleosides containing the pyrimidine moiety were first reported by Biemann and McClosky (1); the utility of mass spectrometry as a probe of nucleoside structure has since been firmly established. The electron impact induced fragmentation of the biologically imortant pyrimidines uracil, thymine, and cytosine has been well documented (2).

Derivatives of 2-pyrimidinone (**1**), while not naturally occurring, are receiving increased attention because of their wide-ranging biological activity. Oyen (3) and Holy and co-workers (4) showed that 1-(β-D-ribofuranosyl)-2-pyrimidinone is an efficient inhibitor of DNA synthesis in *E. coli*, and the latter group subsequently studied a number of other synthetic nucleosides derived from **1** (5). McCormack *et al.* (6) have recently reported that 2-pyrimidinone riboside and related compounds are inhibitors of the enzyme cytidine deaminase, and 5-halo derivatives of **1** are reported (7) to have potential value as metaphase inhibitors. Aspects of the chemistry of **1** in aqueous solution have been studied in our laboratory (8). Our ongoing interest in pyrimidinones and pyrimidine nucleosides has prompted us to examine the mass spectra of **1** and a number of N-substituted derivatives; the compounds studied are listed in Table 1.

## Experimental

*Synthesis*[2]

The majority of the compounds employed in this study were synthesized by literature procedures (9), with appropriate variations to make the N(1)-substituted compounds bearing deuterium in the substituent. Synthesis of 5-deuterio-2-pyrimidinones is possible by direct exchange in deuterated aqueous acid at elevated temperatures (10), but this route is time consuming and sometimes suffers from poor yields due to product decomposition. Furthermore, such a procedure would not be applicable to the synthesis of the 5-deuterio-2-thio analogues, compounds in which we are also interested. To avoid these problems we developed the modified cyclization route shown in Scheme 1. In this the unlabelled *bis*-acetal (1,1,3,3-tetramethoxypropane) is hydrolysed in *deuterated* aqueous acid so that the resulting malondialdehyde undergoes facile exchange of the methylene hydrogens. After 5 minutes, to allow for completion of these two processes, the appropriate urea (or thiourea) is added and condensation is achieved in the normal way. This procedure gives, after work-up, the desired labelled pyrimidinone (or pyrimidinthione) in acceptable yields (40–50%). We note that a similar approach has been used by Beak and Bonham (11) to prepare deuterium labelled 4-pyridones.

[1]Author to whom correspondence may be addressed.

[2]Full details of all synthetic procedures can be found in refs. 20 and 21.

0008-4042/82/141800-06$01.00/0

©1982 National Research Council of Canada/Conseil national de recherches du Canada

Can. J. Chem. Downloaded from www.nrcresearchpress.com by 210.87.254.40 on 09/06/12
For personal use only.

Can. J. Chem. Downloaded from www.nrcresearchpress.com by 210.87.254.40 on 09/06/12
For personal use only.

TABLE 1. Compounds studied

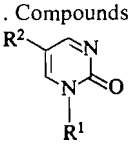

| Compound | $R^1$ | $R^2$ | Compound | $R^1$ ($R^2$ = H) |
|---|---|---|---|---|
| **1** | H | H | **9** | $CH(CH_3)_2$ |
| **2** | D | H | **10** | $CD(CH_3)_2$ |
| **3** | H | D | **11** | $CH(CD_3)_2$ |
| **4** | $CH_3$ | H | **12** | Phenyl |
| **5** | $CD_3$ | H | **13** | Phenyl-2,4,6-$d_3$ |
| **6** | $CH_3$ | D | **14** | Benzyl |
| **7** | $C_2H_5$ | H | **15** | Benzyl-α,α-$d_2$ |
| **8** | $C_2D_5$ | H | | |

*Spectra*

The mass spectra were taken on a Hitachi–Perkin–Elmer RMU-7 instrument using 70 V ionizing electrons and the lowest practicable source temperature. First field free region metastables were observed by the accelerating voltage scan method, using an instrument modification described by McGillivray and co-workers (12). Exact mass measurements at high resolution were made on a Kratos-AEI MS-902S instrument.

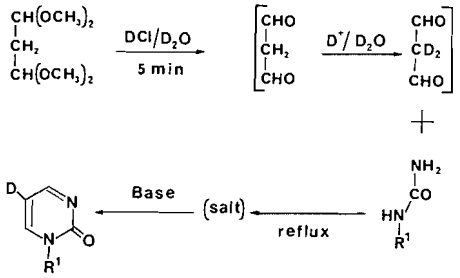


SCHEME 1. Synthetic route to 5-deuterio-2-pyrimidinones.

## Results and discussion

The 70 eV mass spectra of the compounds studied are reported in Table 2. Fragmentation pathways leading to the principal daughter ions have been deduced from exact mass measurements and from observed first field free region (FFFR) metastable decompositions.

(a) *2(1H)-Pyrimidinone* (**1**)

The partial mass spectrum of **1** has been reported by Undheim and co-workers (13) in connection with vapour phase tautomer analysis. In aqueous or ethanolic solution, **1** exists predominantly in the keto form **1***a*, whereas at equilibrium in the gas phase the enol form, **1***b*, is favoured by a factor of at least 10:1 (14). On the basis of ionization energy measurements it was concluded that **1***b* is the predominant tautomer even under the nonequilibrium conditions prevailing in the ion source. Since **1***a* is present to a significant extent in the solid state

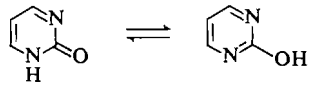

**1***a* **1***b*

(15), it has been suggested that the enol form evaporates preferentially in the inlet system of the mass spectrometer. Little information as to the tautomeric form of **1** could be obtained from the electron impact induced fragmentation pattern.

An intense molecular ion peak is characteristic of all the compounds studied, and in the mass spectrum of **1** it gives the base peak at *m/z* 96. Other major peaks of interest are found at *m/z* 95, 69–67, and 51–53. Loss of a hydrogen atom from the molecular ion to give the peak at *m/z* 95 can be rationalized in terms of either tautomer. If the enol form **1***b* is indeed predominant, it would be anticipated that loss of deuterium from **2** would be minimal and that loss of H• would be comparable to that observed from **1**. The spectrum of **2** is consistent with this view, but a comparison of the two spectra indicates that a quantitative measurement of the [H• loss]/[D• loss] ratio for **2** is not possible because of significant back exchange in the inlet system and ion source and an isotope effect of unknown magnitude. Calculations based on the relative intensity ratio for $[M^{+\bullet}]/[M - H]^+$ in the spectrum of **1** do show, however, that the relative intensity of the *m/z* 95 peak in the spectrum of **2** is entirely consistent with the presence of unlabelled and/or back exchanged material and the noninvolvement of the tautomeric hydrogen. On this basis we propose that the tautomeric hydrogen is not lost in the fragmentation leading to the [M − H] ion and infer that the enolic form of the molecular ion is involved. The absence of significant D• loss from **3** confirms C(4) and/or C(6) as the principal site(s) of H• loss from **1**, **2**, and **3**. Metastable peaks for these H•(D•) losses were not observed.

The peaks at *m/z* 69, 68, and 67 in the spectrum of **1** shift to *m/z* 70, 69, and 68, respectively, in **2** and **3**, confirming that the tautomeric hydrogen and the hydrogen at C(5) are retained in these fragment ions. Exact mass measurements show that the peak at *m/z* 69 in the spectrum of **1** is due solely to $[C_3H_3NO]^{+\bullet}$ (found: 69.0212, calcd.: 69.0215), corresponding to loss of HCN from the molecular ion. By analogy with the fragmentation of 2-pyridone (16, 17) and cytosine (2), the intense peak at *m/z* 68 was assumed to arise by loss of CO from $M^{+\bullet}$; high resolution measurements confirmed this assignment. Maquestiau *et al.* (17) have shown that CO loss from the molecular ion of 2-pyridone is from

Can. J. Chem. Downloaded from www.nrcresearchpress.com by 210.87.254.40 on 09/06/12
For personal use only.

TABLE 2. Major fragment ions in the mass spectra of compounds **1–15**

| Compound | *m/z* (relative intensity, %) |
|---|---|
| **1** | 96($M^{+\cdot}$, 100), 95(32), 69(27), 68(93), 67(18), 54(5), 53(24), 52(43), 51(21) |
| **2** | 97($M^{+\cdot}$, 99), 96(76), 95(12), 70(25), 69(100), 68(79), 67(14), 54(12), 53(38), 52(56), 51(39) |
| **3** | 97($M^{+\cdot}$, 100), 96(46), 95(8), 70(24), 69(94), 68(37), 54(10), 53(28), 52(19), 51(21) |
| **4** | 110($M^{+\cdot}$, 100), 109(79.3), 82(59), 81(28), 69(7), 68(16), 67(6), 55(19), 54(23), 52(17), 42(64) |
| **5** | 113($M^{+\cdot}$, 100), 112(87), 111(3), 85(71), 84(21), 82(45), 69(13), 45(78) |
| **6** | 111($M^{+\cdot}$, 100), 110(85), 109(12), 83(67), 82(45), 81(9), 69(18), 42(74) |
| **7** | 124($M^{+\cdot}$, 100), 123(12), 109(55), 97(11), 96(60), 95(43), 82(48), 81(37), 80(11), 69(24), 68(75), 67(12), 56(27), 54(41), 52(27), 42(27) |
| **8** | 129($M^{+\cdot}$, 100), 128(8), 127(4), 111(80), 101(4), 97(60), 96(47), 87(8), 84(40), 83(53), 69(87), 68(13), 56(23), 55(22), 52(22), 40(47) |
| **9** | 138($M^{+\cdot}$, 93), 137(9), 123(41), 97(100), 96(25), 96(25), 95(28), 82(13), 80(9), 68(44), 54(15), 43(38) |
| **10** | 139($M^{+\cdot}$, 56), 138(9), 124(40), 98(35), 97(100), 96(41), 95(22), 83(20), 81(26), 69(19), 68(73), 44(93), 42(89) |
| **11** | 144($M^{+\cdot}$, 100), 143(6), 142(6), 126(64), 99(84), 98(56), 97(30), 96(21), 82(24), 80(11), 69(34), 49(39), 45(39) |
| **12** | 172($M^{+\cdot}$, 100), 171(42), 144(32), 143(7), 130(6), 117(13), 104(13), 90(4), 78(8), 77(83), 51(38) |
| **13** | 175($M^{+\cdot}$, 100), 174(59), 173(20), 147(32), 146(14), 133(5), 120(10), 119(6), 107(8), 106(5), 80(48), 79(19), 53(15), 52(14) |
| **14** | 186($M^{+\cdot}$, 100), 185(19), 157(14), 144(13), 130(7), 92(10), 91(88), 81(16), 80(10), 77(4), 65(17) |
| **15** | 188($M^{+\cdot}$, 48), 187(11), 186(11), 94(14), 93(100), 92(8), 91(22), 83(13), 82(10), 81(13), 80(63), 77(4), 68(9), 67(10), 66(25), 65(25) |

the enolic tautomer, with a prior rate determining migration of the hydroxylic hydrogen to C(3). Because of molecular symmetry the equivalent process in **1** is indistinguishable from keto–enol tautomerism. A second route to *m/z* 68 in the spectrum of **1** involves loss of HCN from the $[M - H]^+$ ion; the analogous process is observed for cytosine but not for 2-pyridine.

The relative intensities of the $[C_3H_4N_2]^{+\cdot}$ and $[C_3H_2NO]^+$ peaks are in a ratio of 6:1, and the appropriate metastable peak was observed in each case. The peak at *m/z* 67 was also shown to be doublet under high resolution. Loss of H$^\cdot$ from $[M - CO]^{+\cdot}$ to give $[C_3H_3N_2]^+$ (found: 67.0298, calcd.: 67.0296) generates the major component of the peak; the fragmentation path leading to the minor component, $[C_3HNO]^\cdot$ (found: 62.0057, calcd.: 67.0058), has not been identified. The peaks at *m/z* 54–52 can be rationalized in terms of the retro-Diels–Alder mechanism proposed for cytosine, i.e. loss of NCO from $M^{+\cdot}$ (*m/z* 54), loss of HNCO from $M^{+\cdot}$ (*m/z* 53), and elimination of HNCO from $[M - H]^+$ (*m/z* 52). After correction for back exchange the spectrum of **2** gives very similar relative abundances for these peaks, indicating that N(1) is lost along with the tautomeric hydrogen in the elimination of HNCO. An alternative to the retro-Diels–Alder mechanism, involving ring opening prior to loss of HCO or HNCO, cannot be ruled out; the spectrum of **3** shows that the deuterium at C(5) is involved to some extent in these fragmentations, although we are unable to formulate an adequate mechanism at the present time. Owing to limitations in the range over which it was possible to scan the accelerating voltage, the fragmentations leading to the *m/z* 54–52 peaks are not confirmed by observed FFFR metastable peaks.

The principal fragmentation pathways for **1** are summarized in Scheme 2.

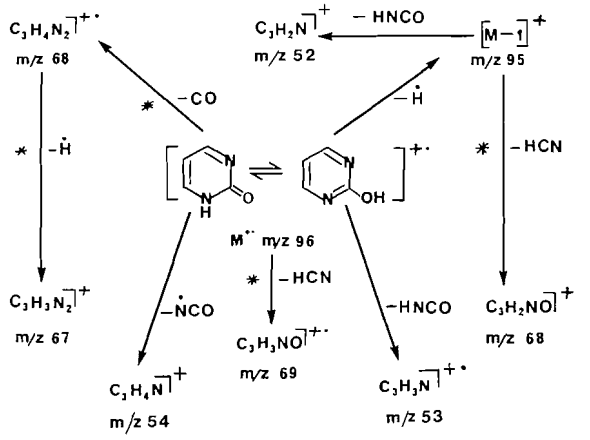


SCHEME 2. Principal fragmentation pathways for the molecular ion of **1**.

(b) N-*R*$^1$-*2-Pyrimidinones*

In common with the fragmentation of **1**, **4** ($R^1 = CH_3$) has the molecular ion as the base peak in the spectrum and an intense $[M - H]^+$ peak. The spectrum of **5** ($R^1 = CD_3$) indicates that there is

Can. J. Chem. Downloaded from www.nrcresearchpress.com by 210.87.254.40 on 09/06/12
For personal use only.

only minor involvement of the methyl group hydrogens in formation of the $[M - H]^+$ ion, with the relative intensities of $[M - H]^+$ and $[M - D]^+$ being in the ratio of approximately 30:1. The spectrum of the 5-$d_1$ analogue, **6**, indicates that some loss of the hydrogen at C(5) does occur. Loss of CO from $M^{+\cdot}$ and loss of HCN from $[M - H]^+$ give rise to the peak at *m/z* 82, parallelling the formation of *m/z* 68 from **1**. The peak at *m/z* 68 in the spectrum of **4** results from the loss of NCO from $M^{+\cdot}$; the analogous processes in **5** and **6** give peaks at *m/z* 71 and *m/z* 69, respectively. Observation of the appropriate metastable peak confirms that, at least in part, the abundant peak at *m/z* 42 in the spectrum of **4** arises by loss of 26 daltons, possibly as $C_2H_2$, from $[M - NCO]^+$. In the spectrum of **5** the corresponding fragmentation generates *m/z* 45, confirming the absence of significant mixing of ring and methyl hydrogens, whereas for **6** the analogous fragment ion occurs at *m/z* 42, corresponding to loss of $C_2HD$ from $[M - NCO]^+$. Plausible ion structures consistent with these results are given in Scheme 3.

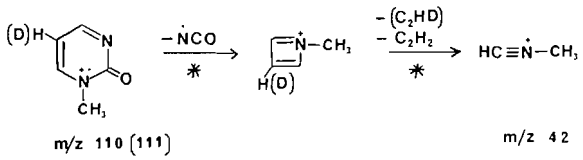


SCHEME 3. Origin and plausible structure of *m/z* 42 in the spectrum of **4**.

Fragmentations involving the *N*-alkyl substituent dominate the spectra of **7** ($R^1 = C_2H_5$) and **9** ($R^1 = CH(CH_3)_2$). Loss of ethylene from **7** via a McLafferty rearrangement is the main route to the intense *m/z* 96 peak, with loss of CO from $M^{+\cdot}$ making now only a minor (<10%) contribution. The $[M - C_2H_4]^{+\cdot}$ daughter ion, assumed to have the 2-pyrimidinone structure, fragments by loss of CO and H$^\cdot$ to generate the peaks at *m/z* 68 and *m/z* 95, respectively. Facile loss of $CH_3^\cdot$ from $M^{+\cdot}$ is followed by fragmentation of the *m/z* 109 ion to give peaks at *m/z* 81 (—CO) and *m/z* 82 (—HCN). Loss of H$^\cdot$ from the molecular ion is a relatively minor process but, in contrast with the fragmentation of **4**, there is significant involvement of the *N*-alkyl hydrogens; for **8** ($R^1 = C_2D_5$) the relative intensity ratio for $[M - H]^+/[M - D]^+$ is 2:1. The fragment ion resulting from loss of a ring hydrogen subsequently eliminates ethylene, but fragmentation of the ion formed by loss of H$^\cdot$ from the *N*-ethyl group has not been confirmed (Scheme 4).

The fragmentation of **9** parallels that of **7** but with the base peak at *m/z* 97 generated by a double

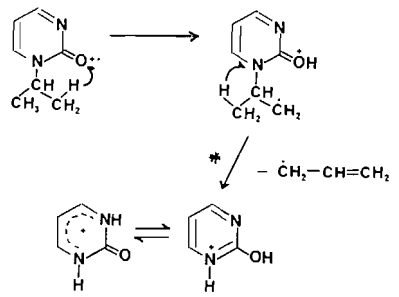


SCHEME 4. Principal fragmentation pathways for the molecular ion of **7**.

rearrangement and elimination of $C_3H_5$ from the molecular ion (Scheme 5). Consistent with this mechanism, the peak shifts to *m/z* 99 for **11** ($R^1 = CH(CD_3)_2$), but is unchanged in the spectrum of **10** ($R^1 = CD(CH_3)_2$). Loss of $C_3H_6$ from **9** via the McLafferty rearrangement and loss of $CH_3^\cdot$ from **9** give rise to peaks at *m/z* 68 and *m/z* 123, respectively; subsequent decomposition of these fragment ions parallels the corresponding processes observed for **7**. The $[M - H]^+$ peak is of minor intensity, and arises by loss of both ring and alkyl group hydrogen atoms as was the case for **7**. The spectra of **10** and **11** confirm that only methyl hydrogens are lost from the alkyl substituent, with a relative intensity ratio for $[M - H]^+/[M - D]^+$ of 1:1 in the spectrum of **11**.

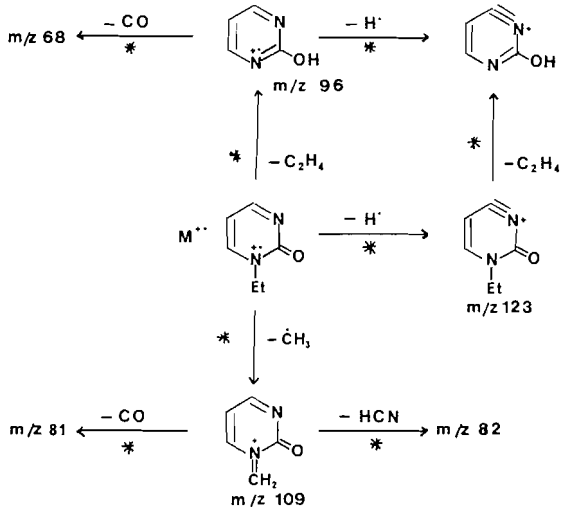


SCHEME 5. Origin of base peak in the spectrum of **9**.

The mass spectra of **12** ($R^1$ = phenyl) and **14** ($R^1$ = benzyl) are characterized by base peak molecular ions and intense peaks at *m/z* 77 and *m/z* 91, respectively, the latter peaks corresponding to N—C bond cleavage with the formation of the stable 2-oxypyrimidine radical and the appropriate

Can. J. Chem. Downloaded from www.nrcresearchpress.com by 210.87.254.40 on 09/06/12
For personal use only.

aryl cation. Other major peaks in the spectrum of **12** originate by cleavage of the substituent-bearing pyrimidine ring, with loss of CO from $M^{+\cdot}$ and HCN loss from $[M - H]^+$ generating the doublet at *m/z* 144; subsequent elimination of a 27 dalton fragment presumably involves HCN loss from the $[M - CO]^{+\cdot}$ moiety to give *m/z* 117. The trend towards decreasing H· loss from the molecular ion with increasing size of the N-substituent is markedly reversed in **12**, with a relative intensity of 41.7% for $[M - H]^+$. Interpretation of the spectrum of **13** ($R^1$ = 2,4,6-$d_3$-phenyl) is complicated by incomplete labelling (ca. 70% $d_3$) but the relative abundances of the FFFR metastable peaks for H· and D· loss indicate that involvement of phenyl ring hydrogens is of minor importance (see below). Some departure from the usual pattern is seen in the spectrum of **14**, with CO and HCNCO being lost from $[M - H]^+$ and elimination of NCO from the molecular ion. Formation of $[M - H]^+$ involves the benzylic hydrogens as well as those on the phenyl and pyrimidine rings, with the relative abundance ratio for $[M - H]^+/[M - D]^+$ being 1:1 for the α,α-$d_2$-benzyl pyrimidinone, **15**.

Intense FFFR metastable peaks are observed for H· loss from **12** and **13**. Since hydrogen atom elimination from C(4) of the pyrimidine ring is, typically, a fast simple cleavage process for which a metastable peak is not observed, we associate the observed metastable decompositions with a slow rearrangement process involving either the phenyl ring hydrogens or the C(6) hydrogen in the heterocycle. By analogy with 1-phenyl pyridone (16), loss of H· from the *ortho* position of the phenyl ring combined with new bond formation to the carbonyl oxygen would generate a $[M - H]^+$ ion with the stable oxazolium structure **16**. Aryl-oxygen bond formation in odd-electron ions with H· elimination has been postulated in the fragmentation of β-diketones and α,β-unsaturated esters and acids (18), and an analogous process has been proposed in the mass spectra of pyridinium oxides (19). However, the absence of metastable peaks of significant intensity for D· loss from **13** leads us to suggest that formation of **16** is, at best, a minor process in the fragmentation of **12** in the metastable time frame. An alternative structure, **17**, can be formulated in terms of an *ortho*-hydrogen transfer to oxygen followed by H· loss and new bond formation at C(6) of the pyrimidine ring. It is of interest to note that a very intense metastable peak is observed for D· loss from the molecular ion of 1-(2,4,6-$d_3$-phenyl)-pyrimidinthione (20).

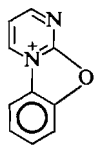

**16**

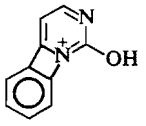

**17**

In the absence of further labelling studies, interpretation of H· loss from **14** ($R^1$ = benzyl) is speculative. Although the conventional spectrum of **15** indicated that the benzylic hydrogens are involved in formation of $[M - H]^+$, the corresponding metastable peaks were not observed. Thus the FFFR metastable peaks for H· loss observed for **14** and **15** can be associated with H· loss from the phenyl ring; by analogy with the phenyl derivative, structures corresponding to new bond formation to oxygen or to C(6), **18** and **19**, respectively, are plausible. Given the importance of $[M - H]^+$ ion fragmentations in the mass spectra of the 2-pyrimidinones, the characterization of the structure of these ions would be of considerable interest.

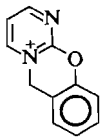

**18**

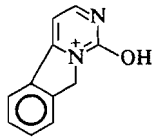

**19**

**Acknowledgements**

We thank the Natural Sciences and Engineering Research Council of Canada for operating grants and Dr. J. Krause for high resolution measurements. We thank Prof. J. L. Holmes for making the mass spectrometry facilities of the University of Ottawa available to us.

1. K. Biemann and J. A. McCloskey. J. Am. Chem. Soc. **84**, 2005 (1962).
2. J. M. Rice, G. O. Dudek, and M. Barber. J. Am. Chem. Soc. **87**, 4569 (1965).
3. T. B. Oyen. Biochim. Biophys. Acta, **186**, 237 (1969).
4. I. Votruba, A. Holy, and H. Pischel. Collect. Czech. Chem. Commun. **17**, 237 (1969).
5. D. Cech, H. Beerbaum, and A. Holy. Collect. Czech. Chem. Commun. **42**, 2694 (1977), and references cited therein.
6. J. J. McCormack, V. E. Marquez, P. S. Liu, D. T. Vistica, and J. S. Driscoll. Biochem. Pharmacol. **29**, 830 (1980).
7. M. Gacek, K. Undheim, R. Oftebro, and S. G. Laland. FEBS Lett. **98**, 355 (1979).
8. O. S. Tee and M. Paventi. J. Org. Chem. **45**, 2072 (1980), and references cited therein.
9. (*a*) R. R. Hunt, J. F. W. McOmie, and E. R. Sayer. J. Chem. Soc. 525 (1959); (*b*) J. J. Fox and D. Van Praag. J. Am. Chem. Soc. **82**, 486 (1960); (*c*) D. J. Brown and R. V. Foster. J. Chem. Soc. 4911 (1965); (*d*) G. C. Hopkins, J.

P. JONAK, H. TIECKELMANN, and H. J. MINNEMEYER. J. Org. Chem. **31**, 3969 (1966); (*e*) D. J. BROWN and T. C. LEE. Aust. J. Chem. **21**, 243 (1968).
10. A. R. KATRITZKY, M. KINGSLAND, and O. S. TEE. J. Chem. Soc. B, 1484 (1968).
11. P. BEAK and J. BONHAM. J. Am. Chem. Soc. **87**, 3365 (1965).
12. T. K. DAVIES, D. L. MCGILLIVRAY, and T. W. WILEY. Int. J. Mass Spectrom. Ion Phys. **15**, 350 (1974).
13. M. GACEK, O. THORSTAD, L. ONGSTAD, and K. UNDHEIM. Chem. Scripta, **13**, 99 (1978).
14. P. BEAK, F. S. FRY, J. LEE, and F. STEELE. J. Am. Chem. Soc. **98**, 171 (1976).
15. A. R. KATRITZKY and J. M. LAGOWSKI. Adv. Heterocycl. Chem. **1**, 339 (1963).
16. R. LAWRENCE and E. S. WAIGHT. J. Chem. Soc. B, 3 (1968).
17. A. MAQUESTIAU, Y. VAN HAVERBEKE, C. DE MEYER, A. R. KATRITZKY, M. J. COOK, and A. D. PAGE. Can. J. Chem. **53**, 490 (1975).
18. R. G. COOKS. Org. Mass Spectrom. **2**, 481 (1969).
19. K. UNDHEIM and G. HVISTENDHAL. Org. Mass Spectrom. **5**, 325 (1971).
20. E. M. KAZDAN. Ph.D. Thesis, Concordia University, Montreal (1980).
21. E. M. KAZDAN. M.Sc. Thesis, Concordia University, Montreal (1976).

Can. J. Chem. Downloaded from www.nrcresearchpress.com by 210.87.254.40 on 09/06/12
For personal use only.

# Formation of unusual side-products from succinimidyl esters of fatty acids during the acylation of amino acids[1]

ALENKA PAQUET AND MICHEL BERGERON

*Food Research Institute, Canada Department of Agriculture, Ottawa, Ont., Canada K1A 0C6*

Received December 7, 1981

ALENKA PAQUET and MICHEL BERGERON. Can. J. Chem. **60**, 1806 (1982).

A new side-product, succinohydroxamic decanoic anhydride, was isolated from the reaction mixture during the acylation of lysine by succinimidyl decanoate in the presence of aqueous sodium hydroxide. Lauric and palmitic acid derivatives were also obtained. It is shown that these compounds can be used for acylation of amino acids. The hydroxamic acid derivatives were also detected when the acylations by succinimidyl esters of fatty acids were carried out under anhydrous conditions. Preparation of *N*-lauroyl-L-tyrosine methyl ester from tyrosine methyl ester and succinimidyl laurate is also described.

ALENKA PAQUET et MICHEL BERGERON. Can. J. Chem. **60**, 1806 (1982).

On a isolé un nouveau produit secondaire, l'anhydride succino-hydroxamique décanoique, du mélange réactionnel obtenu lors de l'acylation de la lysine par le décanoate de succinimidyle en présence d'hydroxyde de sodium aqueux. On a également obtenu des dérivés des acides laurique et palmitique. On montre que l'on peut utiliser ces composés pour acyler des acides aminés. On a également décelé des dérivés de l'acide hydroxamique lorsqu'on réalise les acylations des acides gras par les esters succinimidyles en milieu anhydre. On décrit également la préparation de l'ester méthylique de la *N*-lauroyl-L tyrosine à partir du tyrosinate de méthyle et du laurate de succinimidyle.

[Traduit par le journal]

There have been several reports in the literature on formation of various side-products arising during the peptide synthesis where the activation of the carboxyl group is promoted by *N*-hydroxysuccinimide. Thus, the presence of succinimidoxycarbonyl-β-alanine-*N*-hydroxysuccinimide ester arising from *N*-hydroxysuccinimide in the presence of dicyclohexylcarbodiimide was observed in some dicyclohexylcarbodiimide/*N*-hydroxysuccinimide mediated couplings (1, 2). Another type of side-product is *O*,*N*-diacylhydroxylamine derivative formed from Boc-proline-*N*-hydroxysuccinimide ester and proline during the coupling of these two amino acids under anhydrous conditions (3).

This paper deals with the side-products arising from succinimidyl esters of fatty acids during the acylation of lysine in the presence of aqueous sodium hydroxide. In the previous communication (4) we have shown that good yields (72–84%) of $N^6$-substituted lysine derivatives can be obtained by acylation of lysine by succinimidyl esters of fatty acids in water – organic solvent in the presence of triethylamine. The use of aqueous sodium hydroxide as an alternative possibility was described for the work with decanoic acid ester. In such a procedure a large excess of reagent had to be used but the yield was lower (69%). Here we show that the presence of aqueous sodium hydroxide gives rise to mixed succinohydroxamic anhydrides from succinimidyl esters of fatty acids.

The hydrolysis of cyclic *N*-hydroxyimides in the form of their salts to hydroxamic acids has been reported in the literature (5). To our knowledge, this type of hydrolysis has not yet been observed with O-acylated *N*-hydroxyimides. It would be expected that the ester group would undergo saponification under such conditions faster than hydrolysis of the cyclic imide structure. The long chain of fatty acid hinders the ester group and gives rise to a hydroxamic acid derivative instead. In the previously reported syntheses, where excess of triethylamine was used (4), hydroxamic acid derivatives were also formed in all cases. They were separated from the products by extraction with organic solvent and characterized by infrared spectroscopy. Their isolation in pure form could not be achieved. We suggest that precautions should be taken in peptide synthesis when the excess of base is used during work with succinimidyl esters.

Thus, when lysine was acylated by succinimidyl decanoate in 2 *N* sodium hydroxide in dioxane (4), the by-product was isolated in 30% yield by extracting the crude $N^6$-decanoyl-L-lysine with ethanol. It was crystallized from chloroform–ether and identified as *O*-succinohydroxamic decanoic anhydride (**1**) on the basis of its elemental analysis, infrared and nmr spectra. By treating succinimidyl decanoate with 2 *N* sodium hydroxide in dioxane in the absence of lysine, 56% of the identical com-

[1]Contribution No. 484 from the Food Research Institute, Agriculture Canada, Ottawa, Ont., Canada.

0008-4042/82/141806-03$01.00/0

©1982 National Research Council of Canada/Conseil national de recherches du Canada

Can. J. Chem. Downloaded from www.nrcresearchpress.com by 210.87.254.5 on 09/06/12
For personal use only.

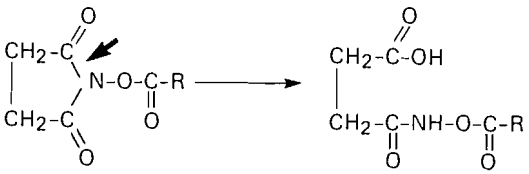

**1** R = $C_9H_{19}$
**2** R = $C_{11}H_{23}$
**3** R = $C_{15}H_{31}$

pound was obtained, besides decanoic acid, which was easily separated by extraction with chloroform–hexane. This serves as a further proof that the amino acid was not implicated in the formation of this compound.

When lysine was acylated by an excess of succinimidyl palmitate, succinohydroxamic palmitic anhydride (**3**) was isolated in 60% yield, besides the desired $N^6$-palmitoyl-L-lysine (57%). An identical hydroxamic acid derivative was obtained in 40% yield from succinimidyl palmitate in the absence of lysine. An additional amount of triethylamine was added to the reaction mixture during the work with this reagent. The same conditions served for the conversion of succinimidyl laurate into succinohydroxamic lauric anhydride (**2**) (absence of substrate).

Because hydroxamic acid derivatives have been known as acylating agents useful in peptide synthesis (6–8), it was of interest to explore the possibility of using these side-products for acylation of amino acids. Succinohydroxamic lauric anhydride and β-alanine in water–acetone mixture in the presence of three equivalents of triethylamine gave 76% of *N*-lauroyl-β-alanine. When 1 equivalent of triethylamine or sodium bicarbonate was used, the reaction was slow and impractical. No product was obtained when the acylation was carried out in the presence of 2 *N* sodium hydroxide. This fact explains the reason why these side-products accumulate in the reaction mixture during the acylation of lysine and do not react further with the substrate to give the desired product.

In selective acylations by succinimidyl esters of fatty acids carried out under the anhydrous conditions, namely acylation of the amino group in tyrosine methyl ester in chloroform–triethylamine mixture, only small amounts of hydroxamic acid derivatives could be detected (infrared spectra showed 1800 $cm^{-1}$, indicating the *O*-acylhydroxylamine bond) even in experiments where excess of reagent was used. The isolation of the side-products in the pure state from these reactions could not be achieved. However, we report in this paper the isolation and structure determination of the main product of the reaction, *N*-lauroyl-L-tyrosine methyl ester, as this structure was unexpected in the light of the results published by other authors. Recently Girin and Shvachkin reported the synthesis of *O*-(Boc-glycyl)-L-tyrosine ethyl ester from L-tyrosine ethyl ester and Boc-glycine-*p*-nitrophenyl ester in chloroform in the presence of an excess of triethylamine (9–11). Upon treating L-tyrosine methyl ester with succinimidyl laurate under such conditions we have obtained *N*-lauroyl-L-tyrosine methyl ester, identified on the basis of its elemental analysis, ir and nmr spectra, and its identity with the compound obtained from the reaction between tyrosine methyl ester and succinimidyl laurate in the absence of base. Its hydrolysis furnished *N*-lauroyltyrosine in 89% yield.

## Experimental

Melting points were taken by the capillary method. The nmr spectra were recorded on a Varian T-60 spectrometer. The ir spectra were recorded on a Beckman IR-20 instrument.

Succinimidyl esters of fatty acids were prepared as described previously (4). Amino acids were purchased from Sigma Chemical Company (Saint Louis, Missouri, U.S.A.).

*Succinohydroxamic decanoic anhydride (1)*

A. *From the acylation of lysine by succinimidyl decanoate*

To a stirred solution of L-lysine hydrochloride (456 mg, 2.5 mmol) in 2 *N* sodium hydroxide (7 mL) was added succinimidyl decanoate (2.01 g, 7.5 mmol) in dioxane (10 mL). A further amount of 2 *N* sodium hydroxide was added to keep the pH at 11–11.5. After 0.5 hour the mixture was acidified with concentrated hydrochloric acid to pH 3 and evaporated to a smaller volume. Then pH was brought up to 6 and the mixture was chilled; the precipitated $N^6$-substituted lysine derivative was filtered off and washed with water, chloroform–ether (to remove decanoic acid), and with ethanol. The ethanolic extract was evaporated to dryness and the residue crystallized from chloroform–ether to give 735 mg (25%, related to starting succinimidyl ester) of the title compound, mp 153–155°C; ir (Nujol): 1680, 1710–1720, 1795 $cm^{-1}$; nmr (DMSO) δ: 0.96 (m, 3H, $CH_3$-decanoic acid), 1.26 (s, 14H, $CH_2$-decanoic acid), 2.53 (m, 6H, $CH_2$-succinic acid, α-$CH_2$-decanoic acid). *Anal.* calcd. for $C_{14}H_{25}NO_5$: C 58.51, H 8.77, N 4.87; found: C 59.32, H 8.49, N 4.80.

B. *From succinimidyl decanoate and aqueous sodium hydroxide*

A solution of succinimidyl decanoate (808 mg, 3 mmol) in 2 *N* sodium hydroxide (3 mL) and dioxane (2 mL) was stirred for 2 hours. The mixture was chilled and acidified to pH 4 and concentrated to a small volume. The solid was separated by filtration, washed with ice-cold water, chloroform–ether mixture (1:4), and recrystallized from chloroform–ether to give 483 mg (56%) of the title compound, mp 155°C. The ir spectrum of this compound was identical with the product obtained from the acylation of lysine.

Can. J. Chem. Downloaded from www.nrcresearchpress.com by 210.87.254.5 on 09/06/12
For personal use only.

*Succinohydroxamic palmitic anhydride (3)*

This compound was obtained from succinimidyl palmitate using procedures A and B described for the preparation of the decanoyl derivative in 60 and 40% yields respectively, mp 153–155°C; ir (Nujol): 1680, 1715–1720, 1795–1800 $cm^{-1}$; nmr (DMSO) δ: 0.95 (m, 3H, $CH_3$-palmitic acid), 1.26 (s, 26H, $CH_2$-palmitic acid), 2.50 (m, 6H, $2CH_2$-succinic and α-$CH_2$-palmitic acid). *Anal.* calcd. for $C_{20}H_{37}NO_5$: C 64.65, H 10.03, N 3.76; found: C 64.75, H 10.00, N 3.83.

*Succinohydroxamic lauric anhydride (2)*

This compound was prepared from succinimidyl laurate in 1 mmol scale as described for decanoic derivative (procedure B) to give 162 mg (54%) of the product, mp 152–155°C; ir: 1680, 1710, and 1790 $cm^{-1}$. *Anal.* calcd. for $C_{16}H_{29}NO_5$: C 60.93, H 9.27, N 4.44; found: C 60.92, H 9.03, N 4.76.

N-*lauroyl-β-alanine*

To a stirred solution of β-alanine (89 mg, 1 mmol) and triethylamine (0.42 mL, 3 mmol) in acetone (1 mL) and water (1 mL) was added 315 mg (1 mmol) succinohydroxamic lauric anhydride. The mixture was stirred overnight, water was added, and concentrated hydrochloric acid to pH 2. The mixture was chilled, the solid separated, washed with water, and recrystallized from ethanol yielding 329 mg (76%) of the title compound. The ir spectrum in Nujol was identical with the spectrum of an authentic sample (1530–1550, 1660–1680 (amide), 1715 (carboxyl)).

N-*lauroyl-L-tyrosine methyl ester in an excess of base*

A solution of 195 mg (1 mmol) of L-tyrosine methyl ester, 297 mg (1 mmol) of succinimidyl laurate, and 1.4 mL (10 mmol) of triethylamine in chloroform (3 mL) was stirred at room temperature overnight (the analysis did not show any laurate present). The mixture was evaporated *in vacuo* till dryness, dissolved in chloroform (5 mL), and washed with 5% hydrochloric acid (2 times, 2 mL), water, and dried over sodium sulfate. The solvent was removed *in vacuo* and the residue was recrystallized from methanol–water and then from chloroform–ether mixture giving 304 mg (80%) of the title compound, mp 82–83°C; $[\alpha]_D^{25}$ +34.5° (*c* 1.0, ethyl acetate); ir ($CHCl_3$): 1510, 1665, 1740 $cm^{-1}$; nmr ($CHCl_3$) δ: 1.3 (s, 18H), 2.23 (m, 2H), 3.06 (m, 2H), 3.73 (s, 3H), 4.9 (m, 1H), 6.16 (broad s, 1H), 6.9 (m, 4H). *Anal.* calcd. for $C_{22}H_{35}NO_4$: C 69.99, H 9.34, N 3.70; found: C 69.91, H 9.11, N 3.47.

N-*lauroyl-L-tyrosine methyl ester in absence of base*

88% of the product was obtained from this reaction which was carried out as described for the acylation in an excess of base, with the exception that no triethylamine was added and the reaction time was extended to 3 days; mp 83°C; $[\alpha]_D^{25}$ +34.4° (*c* 1.16, ethyl acetate). Infrared and nmr spectra were identical with the product obtained in an excess of base.

N-*lauroyltyrosine*

To a solution of 19.8 mg of *N*-lauroyl-L-tyrosine methyl ester (obtained in the presence of an excess of triethylamine) in methanol (0.2 mL) was added 3% aqueous solution of sodium hydroxide (0.2 mL). The mixture was kept overnight at 0°C, diluted with water, and acidified with concentrated hydrochloric acid to pH 2 and kept at 0°C for two hours. The crystalline solid was collected by filtration, washed with water, and dried, giving 16.8 mg (88%) of the title compound, mp 134–135°C (Koffler block); ir: 1715 (carboxyl), 1660, and 1530 $cm^{-1}$ (amide). *Anal.* calcd. for $C_{21}H_{33}NO_4$: C 69.39, H 9.15; found: C 69.37, H 9.22.

## Acknowledgement

The authors thank Mr. G. Morris (Analytical Services, C.B.R.I., Agriculture Canada) for carrying out the microanalyses.

1. H. Gross and L. Bilk. Tetrahedron, **24**, 6935 (1968).
2. F. Weygand, W. Steglich, and N. Chytil. Z. Naturforsch. Teil B, **23**, 1391 (1968).
3. T. Šavrda. J. Org. Chem. **42**, 3199 (1977).
4. A. Paquet. Can. J. Biochem. **58**, 573 (1980).
5. L. Bauer and O. Exner. Angew. Chem. Int. Ed. Engl. **13**, 376 (1974).
6. S. M. Beaumont, B. O. Handford, J. H. Jones, and G. T. Young. Chem. Commun. 53 (1965).
7. T. R. Govindachari, S. Rajappa, A. S. Akerkar, and V. S. Iyer. Tetrahedron, **23**, 4811 (1967).
8. H. Jeschkeit. Z. Chem. **9**, 266 (1969).
9. S. K. Girin and Yu. P. Shvachkin. Zh. Obshch. Khim. **47**, 1182 (1977).
10. S. K. Girin and Yu. P. Shvachkin. Zh. Obshch. Khim. **47**, 2139 (1977).
11. S. K. Girin and Yu. P. Shvachkin. Zh. Obshch. Khim. **48**, 902 (1978).

Can. J. Chem. Downloaded from www.nrcresearchpress.com by 210.87.254.5 on 09/06/12
For personal use only.

# Effect of alkylation of ammonia on the optical band shape of solvated electrons[1]

FANG-YUAN JOU AND GORDON R. FREEMAN
*Department of Chemistry, University of Alberta, Edmonton, Alta., Canada T6G 2G2*

Received November 24, 1981

FANG-YUAN JOU and GORDON R. FREEMAN. Can. J. Chem. **60**, 1809 (1982).

At 200 K the width at half height, $W_{1/2}$, of the $e^-_{solv}$ optical absorption band in *n*-propyl amine is 2.1-fold greater than that in ammonia. Three quarters of the broadening occurs on the high energy side of the band. The energy $E_r$ at half height on the low energy side of the band is nearly the same in the amine as in ammonia, while $E_b$, the energy at half height on the high energy side, is 42% greater in the amine. The temperature coefficient $dE_{Amax}/dT$ is 1.8-fold greater in the amine than in ammonia. The larger width is consistent with there being a less uniform distribution of localization sites in the system, and the larger temperature coefficient implies that the sites are more easily disturbed by thermal agitation. A quantum statistical mechanical model, such as the one begun by Simons, is needed to extend the theoretical treatment of $e^-_{solv}$ spectra. The correlation between optical absorption energies of $e^-_{solv}$ and the structure of the solvent, as partially reflected in the Kirkwood correlation factor, is re-emphasized.

FANG-YUAN JOU et GORDON R. FREEMAN. Can. J. Chem. **60**, 1809 (1982).

A 200 K, la largeur à la mi-hauter, $W_{1/2}$, de la bande d'absorption optique de l'$e^-_{solv}$ dans la *n*-propyl amine est 2,1 fois plus grande que dans l'ammoniac. Les trois quarts de l'élargissement se produisent du côté de haute énergie de la bande. L'énergie $E_r$ à mi-hauteur du côté de faible énergie de la bande est presque la même dans l'amine et dans l'ammoniac, tandis que $E_b$, l'énergie à mi-hauteur du côté de haute énergie, est 42% plus élevée dans l'amine. Le coefficient de température $dE_{Amax}/dT$ est 1,8 fois plus élevé dans l'amine que dans l'ammoniac. La plus grande largeur est en accord avec le fait que la distribution des sites de localisation est moins uniforme dans le système; le coefficient de température plus élevé implique que les sites sont plus facilement perturbés par l'agitation thermique. Un modèle de mécanique statistique quantique tel que celui commencé par Simons est nécessaire pour développer l'étude théorique des spectres de $e^-_{solv}$. On a de nouveau mis l'accent sur la corrélation entre les énergies d'absorption optique de $e^-_{solv}$ et la structure du co-solvant, telle que reflétée partiellement dans le facteur de corrélation de Kirkwood.

[Traduit par le journal]

## Introduction

The optical absorption spectrum of solvated electrons in a primary alcohol (1–5) is about twice as wide as, and more asymmetric than, that in water (3–7). At a given temperature and pressure the hydroxy group determines the approximate energy of the absorption maximum $E_{Amax}$, while the alkyl group increases the band width. The shift of the band with temperature is also larger in alcohols than in water (7).

The situation is similar for electrons in ammonia (8–12) and primary amines (13–15), the optical bands being broader in the amines. The absorption energies are 2–3 times lower in the nitrogen compounds than in their oxygen analogs. The lower absorption energies are attributed to shallower potential wells, which are rationalized in terms of the lower polarity and less orderly structure of the former liquids (16). The degree of structure in the liquids is reflected in the Kirkwood molecular correlation factor $g_K$ (17), which can be calculated from physical properties of the liquid (18–21). The values of $g_K$ at 298 K are 2.7–3.3 in water and methyl to *n*-propyl alcohol, while they are 1.3–1.6 in ammonia and methyl to *n*-propyl amine (Table 1).

Oster and Kirkwood suggested that as a basis for classification of liquids according to their thermodynamic behavior, the correlation parameter $g_K$ is more significant than the molecular dipole moment (17). The value of $g_K$ reflects the degree of orderliness or intermolecular structure in the liquid. The correlation of $E_{Amax}$ with $g_K$, and the lack of correlation with dielectric constant $\varepsilon_s$ or dipole moment $\mu$ (Table 1), indicate that the details of liquid structure have a dominating influence on the energy levels of solvated electrons as well. In the estimation of $g_K$ values the spacial and optical anisotropies of the molecules were neglected. Refinements would be difficult to make and may not be worthwhile for our purposes. The present stage of development is sufficient to indicate that calculations of solvated electron spectra require a quantum statistical mechanical model that includes the liquid structure. An excellent beginning has been made (22, 23). Fluctuations in solvent properties were introduced in an early stage of the model, rather than being added on at the end of the calculation in the usual manner. However, multibody interactions were still handled as sums of pair interactions, and it was not possible to include the orientational disorder and the optical and electrical anisotropies of the molecules in a real calculation. Much work remains to be done to overcome these

[1]Assisted financially by the Natural Sciences and Engineering Research Council of Canada.

0008-4042/82/141809-06$01.00/0
©1982 National Research Council of Canada/Conseil national de recherches du Canada

Can. J. Chem. Downloaded from www.nrcresearchpress.com by 210.87.254.105 on 09/06/12
For personal use only.

TABLE 1. Solvent properties and electron excitation energies[a]

| Solvent | $n_D$[b] | $d$ (g/cm$^3$)[c] | $\mu_g$ (D)[d] | $\mu_l$ (D)[e] | $\varepsilon_s$[f] | $g_K$[g] | $E_{Amax}$ (eV)[h] | $W_{1/2}/E_{Amax}$[h] |
|---|---|---|---|---|---|---|---|---|
| $H_2O$ | 1.333 | 0.995 | 1.85 | 2.32 | 79 | 2.7 | 1.73[6,7] | 0.49 |
| $CH_3OH$ | 1.327 | 0.790 | 1.70 | 2.14 | 33.4 | 2.9 | 1.96[i] | 0.71 |
| $C_2H_5OH$ | 1.360 | 0.780 | 1.69 | 2.16 | 24.5 | 3.0 | 1.81[i] | 0.86 |
| $n$-$C_3H_7OH$ | 1.384 | 0.801 | 1.68 | 2.15 | 20.1 | 3.3 | 1.94[i] | 0.84 |
| $NH_3$ | 1.330 | 0.61 | 1.47 | 1.81 | 17.3 | 1.3 | 0.68[9] | 0.6[k] (0.46[l]) |
| $CH_3NH_2$ | 1.353 | 0.660 | 1.31 | 1.61 | 9.4 | 1.5 | 0.65[14] | 0.9[k] (0.61[l]) |
| $C_2H_5NH_2$ | 1.366 | 0.682 | 1.22 | 1.48 | 6.5 | 1.6 | 0.64[14] | 1.0[k] (0.66[l]) |
| $n$-$C_3H_7NH_2$ | 1.387 | 0.715 | 1.17 | 1.42 | 5.3 | 1.6 | 0.65[j] | 1.2[k] (0.85[l]) |

[a]296 ± 2 K, liquid under its vapor pressure.
[b]Refractive index for sodium D light, ref. 18.
[c]Reference 19.
[d]Electric dipole moment, gas phase, ref. 20.
[e]Electric dipole moment, liquid phase, calculated from the Onsager sphere formula, ref. 17.
[f]Static dielectric constant, ref. 21.
[g]Kirkwood molecular correlation factor, calculated as described in ref. 17.
[h]Energy at optical absorption maximum and band width at half height; superscript numbers are references.
[i]References 5 and 39.
[j]Present work.
[k]Extrapolated to 296 K.
[l]Experimental value at 200 K, because $W_{1/2}$ has not been measured at 296 K.

serious shortcomings, but the Simons approach (22), or something similar, seems to be the most promising for the next several years.

Calculations based upon the continuum, semicontinuum, and *ab initio* models of the past will yield little more information than they already have. Continuum models ignore the dominating short range interactions and the solvent structure. Semicontinuum models ignore the solvent structure and the extremely important structural connection between the first solvation layer and the rest of the solvent. The *ab initio* approach is the most basic, but current quantum mechanical methods are inadequate for the resolution of solvated electron structures. The optical and transport properties of solvated electrons would follow readily from the solution of the structure problem. The *ab initio* method cannot succeed with solvated electrons until it has been successful in describing the structures of the pure solvents.

To prepare for the arrival of a practical qsm model we are trying to obtain as complete as possible an empirical description of the behavior of electrons in liquids. The description includes both optical and transport properties. Reported below are details of the band shape and temperature dependence of the optical spectrum of electrons in *n*-propyl amine.

The temperature coefficients of $E_{Amax}$ in water (7) and ammonia (9, 12) are the same, −2.4 meV/K, and smaller than those in alcohols (2, 24) and amines (14). The reason for picking *n*-propyl to be the amine to be examined in more detail was through analogy with the alcohols. In *n*-alcohols the band width at half height, $W_{1/2}$, increases with alkyl length until *n*-propyl (5); longer alkyl groups do not increase $W_{1/2}$. Propyl amine may therefore provide an optimum band shape for contrast with that in ammonia.

## Experimental

The 2 MeV electron source and the optical system were described elsewhere (4, 25). The sizes of the radiation pulses used were 1 μs ($2 \times 10^{17}$ eV/g) for spectrum measurement, and 0.1 μs ($2 \times 10^{16}$ eV/g) for yield determination. The dosimeter was triple distilled water (distilled successively from acidic dichromate, basic permanganate, and no reagent, each time refluxing through a 50 cm column packed with glass beads) at 295 K, using $G\varepsilon_{715} = 50{,}000$ $e^-_s$/100 eV $M$ cm at 715 nm (26). A 15 mm Spectrosil cell was used at wavelengths $280 < \lambda < 1050$ nm, and a 3 mm Vitreosil cell at $800 < \lambda < 2200$ nm. The band pass of the monochromator in the present work was slightly larger than that for ammonia, and corresponded to an energy uncertainty of 10 meV throughout the band.

One half liter of *n*-propyl amine (Eastman) and 0.5 g of lithium aluminum hydride were refluxed under ultra high purity nitrogen (Linde) for 2 h. The middle 0.3 L was collected in a flask connected to a vacuum rack. When preparing a sample for irradiation, about 30 mL was vacuum distilled into a reservoir containing a mirror of triple distilled potassium, cooled by liquid nitrogen. The amine was melted and stirred for an hour at room temperature. The solubility of potassium in *n*-propyl amine is much less than in ammonia, but the solution was sky blue. The liquid was then distilled into a degassing trap cooled by liquid nitrogen, while pumping. When enough sample was collected, the reservoir was closed and pumping continued on the trap until pressure reached 0.3 mPa. The sample was then vacuum distilled into a cell reservoir.

## Results

The optical absorption spectra of electrons solvated in *n*-propyl amine at 190–295 K are shown in Fig. 1. The uncertainty in the reported temperatures is ±0.4 K. The variation of optical absorbance at the same wavelength per unit dose for consecutive pulses was <2%; the first and last points in a run were taken at the same wavelength and the variation in absorbance per unit dose was < 4%, after making a first order correction for the

Can. J. Chem. Downloaded from www.nrcresearchpress.com by 210.87.254.105 on 09/06/12
For personal use only.

TABLE 2. Optical spectrum parameters of solvated electrons in *n*-propyl amine[a]

| $T$ (K) | $E_{Amax}$ (eV) | $E_b$ (eV) | $E_r$ (eV) | $W_{1/2}$ (eV) | $\frac{W_{1/2}}{E_{Amax}}$ | $W_b$ (eV) | $W_r$ (eV) | $W_b/W_r$ | $I^b$ | $10^{-3}G\epsilon_{max}{}^c$ ($e^-_s$/100 eV $M$ cm) |
|---|---|---|---|---|---|---|---|---|---|---|
| 190 | 1.06 | 1.64 | 0.78 | 0.86 | 0.81 | 0.58 | 0.28 | 2.1 | 1.44 | 42.0 (9.8) |
| 200 | 1.03 | 1.62 | 0.75 | 0.87 | 0.85 | 0.59 | 0.28 | 2.1 | 1.45 | 41.8 (9.6) |
| 225 | 0.91 | 1.48 | 0.64 | 0.84 | 0.92 | 0.57 | 0.27 | 2.1 | 1.47 | 31.4 (9.4) |
| 265 | 0.76 | 1.29 | | | | 0.53 | | | | 15.2 (9.7) |
| 295 | 0.65 | 1.16 | | | | 0.51 | | | | 11.2 (9.5) |

[a]Uncertainty in $E$'s $\approx$ 0.01 eV.
[b]See text.
[c]At the end of 100 ns pulse. Free ion values in brackets, 9.6 $\pm$ 0.1 independent of temperature.

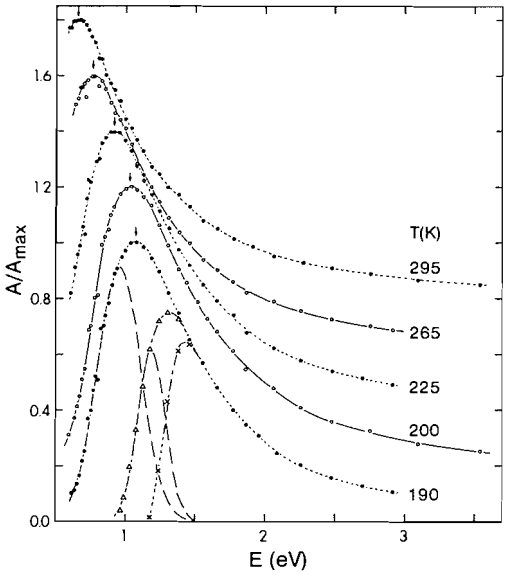


FIG. 1. Optical absorption spectra of solvated electrons in *n*-propyl amine at different temperatures. The points are experimental. The lines are empirical, except for 190 K (see text. $\Delta$, remainder after subtracting first Gaussian; $\times$, remainder after second Gaussian removed.). The arrows mark $E_{Amax}$. Successive spectra are displaced vertically by 0.2 units for clarity.

decay during the 1.0 μs pulse. The correction was only approximate, because at $T < 265$ K the geminate reaction was not complete at 1 μs and the total reaction was not first order.

At $\lambda < 650$ nm the first half life was longer than that at $\lambda > 650$, and it increases with decreasing wavelength. The longer lived species were presumably free radicals. A simple correction (25) was made to extract the absorbance due to solvated electrons.

The absorption band does not have a combined Gaussian–Lorenzian shape. The band can be well resolved into two Gaussians and a continuum remainder (5). For example, at 190 K one obtains $A_1 = 0.913$, $E_1 = 0.955$ eV, $g_1 = 0.185$ eV, and $A_2 = 0.612$, $E_2 = 1.19$ eV, $g_2 = 0.118$ eV (Fig. 1). However, the small temperature range does not warrant further analysis, because reliable temperature coefficients of these resolved parameters could not be obtained. The spectrum parameters listed in Table 2 were determined empirically. In a graph of $A/A_{max}$ against λ a smooth line was drawn through (near) the experimental points. At $A/A_{max} = 0.9$, 0.8, 0.7, and so on, the center point between the two sides of the band was marked. These points were then joined by a straight line, which was extrapolated to the band maximum to determine $\lambda_{Amax}$ and hence $E_{Amax}$. An example is shown in Fig. 2. This method was not applicable at 265 and 295 K, so $E_{Amax}$ was picked visually from the graphs for these temperatures.

The energies at half height on the red ($E_r$) and blue ($E_b$) sides of the band were used to calculate

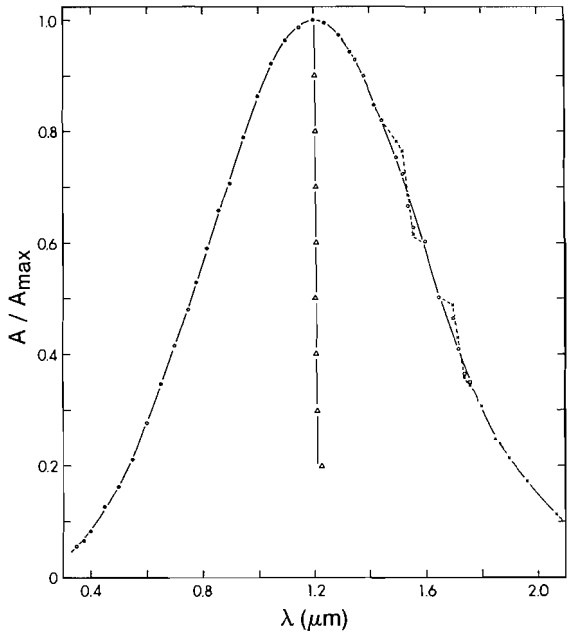


FIG. 2. Empirical location of $\lambda_{Amax}$ by extrapolation of middle points $\Delta$. Temperature = 200 K. Abnormal points near 1.45–1.60 μm and 1.65–1.77 μm were caused by increasing the optical slit width when light was absorbed by N—H and C—H stretching overtones, respectively, of the solvent. Band pass: ○, ≤ 26 nm; ×, 46 nm.

Can. J. Chem. Downloaded from www.nrcresearchpress.com by 210.87.254.105 on 09/06/12
For personal use only.

Can. J. Chem. Downloaded from www.nrcresearchpress.com by 210.87.254.105 on 09/06/12
For personal use only.

$W_{1/2} = E_b - E_r$, $W_r = E_{Amax} - E_r$, and $W_b = E_b - E_{Amax}$ (Table 2).

The zig–zags shown by dashed lines around 1.52 and 1.72 μm in Fig. 2 are artifacts caused by changing the optical slit width to compensate for absorption by solvent. The overtone of the N—H stretching band occurs at ~1.47–1.56 μm and that of the C—H stretching band is at 1.69–1.75 μm (27). When a measurement is made at wavelengths that are on a steep slope of a solvent absorption band, the transmitted light is not uniform across the monochromator band pass, but is distorted towards the less absorbed wavelengths. The effect is larger when the band pass is wider. The zig–zags occur on the long wavelength side of the $e^-_{solv}$ band in Fig. 2. The crest of each of these zig–zags corresponds to a measurement taken on the short wavelength slope of a solvent band, and the trough corresponds to a measurement on the long wavelength slope of a solvent band. Zig–zags were observed at the same wavelengths at all temperatures in the present work. They had also been observed but not mentioned in earlier studies with ammonia (12) and ethers (25), due to absorption by N—H and C—H stretching overtones, respectively.

The temperature effect on the spectrum parameters is shown in Fig. 3. All the characteristic energies, with the possible exception of $W_r$, decrease with increasing temperature.

The shift with temperature of the band at a given value of $A/A_{max}$ is approximately constant at −4.2 meV/K on the low energy side of $A_{max}$ (Fig. 4). The coefficient is somewhat more negative, −4.6 meV/K, on the high energy side at $A/A_{max} = 0.5$. The shift appears to be smaller in the high energy tail (Fig. 4), although the experimental uncertainty is greater at $A/A_{max} \leq 0.1$.

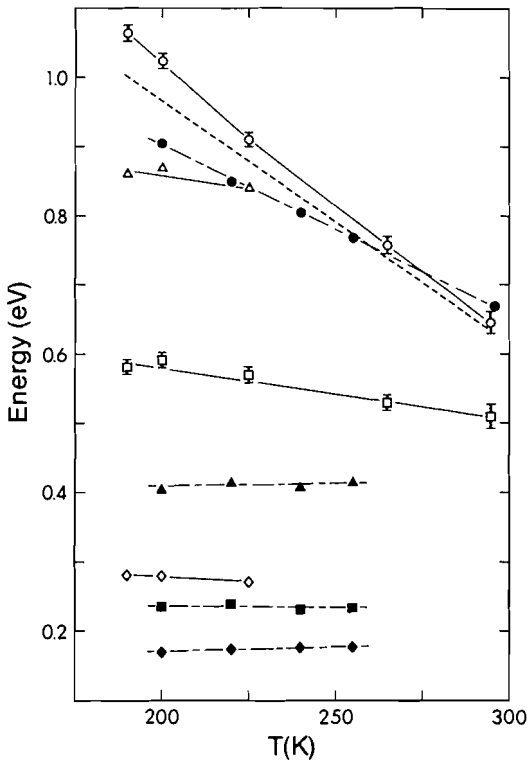


FIG. 3. Temperature dependence of spectrum parameters. Open symbols, $n$-$C_3H_7NH_2$, present work. Closed symbols, $NH_3$, refs. 10 and 12. Circles, $E_{Amax}$; triangles, $W_{1/2}$; squares, $W_b$; diamonds, $W_r$. ---, $E_{Amax}$ in methyl and ethyl amines, ref. 14.

## Discussion

*Comparison of band parameters*

Alkylation of ammonia has the same general effect upon the solvated electron optical spectrum as does alkylation of water, namely, to broaden the band (see ratio $W_{1/2}/E_{Amax}$ in Table 1) and increase the temperature dependence. The spectrum parameters in $n$-propyl amine and $n$-propyl alcohol are compared with those in ammonia and water in Table 3.

At 200 K, on going from ammonia to $n$-propyl amine $W_{1/2}$ broadens 2.1-fold and $dE_{Amax}/dT$ increases 1.8-fold. The broadening occurs mainly (3/4) on the high energy side of the band; the energy $E_r$ half way up the low energy side of the band is nearly the same in the two liquids, while $E_b$ is 42% greater in the amine than in ammonia (Table 3).

By comparison, at 298 K, on going from water to $n$-propyl alcohol $W_{1/2}$ broadens 1.9-fold and $dE_{Amax}/dT$ increases 1.4-fold. Three quarters of the broadening occurs on the high energy side of the band; the value of $E_r$ is nearly unshifted, while $E_b$ increases by 35% (Table 3).

The values of the above ratios are somewhat temperature dependent (Table 3). There is no single temperature at which the values of all the parameters are available for all four systems, so we picked temperatures that would give similar values of $T/T_c$ for each liquid while having the same temperature for the two liquids in a pair. The critical temperatures $T_c$ are 497 K for the amine, 406 K for ammonia, 537 K for the alcohol, and 647 K for water. The ratios $T/T_c$ are in the vicinity of 0.5 (Table 3). The reason for not picking a fixed $T/T_c$, say 0.50, for all liquids is that $T$ itself is important in determining the spectral parameter values, and $T_c$ of water is greatly different (1.6-fold) from that of ammonia.

The spectral parameter ratio that is most different for the two pairs of systems is $G_{fi}\varepsilon_{max}$ (Table 3). The value 0.28 for alcohol/water is due mainly to the higher dielectric constant of water (Table 1) and

Can. J. Chem. Downloaded from www.nrcresearchpress.com by 210.87.254.105 on 09/06/12
For personal use only.

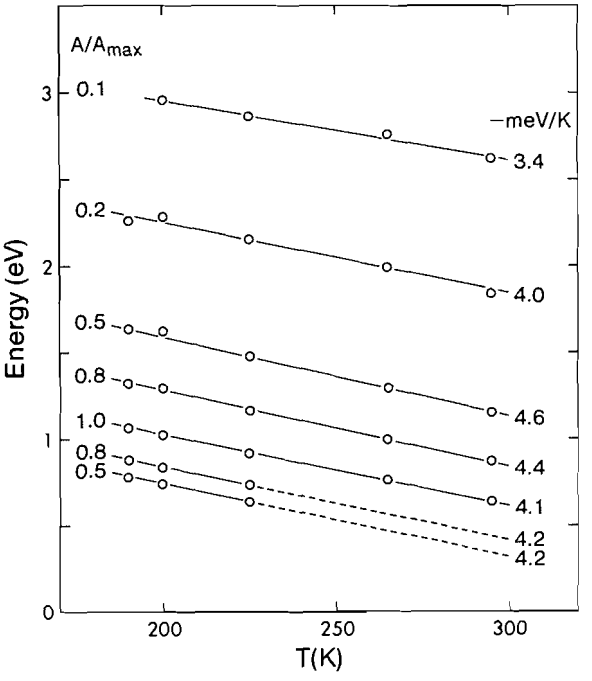


FIG. 4. Temperature dependence of the transition energy at various $A/A_{max}$.

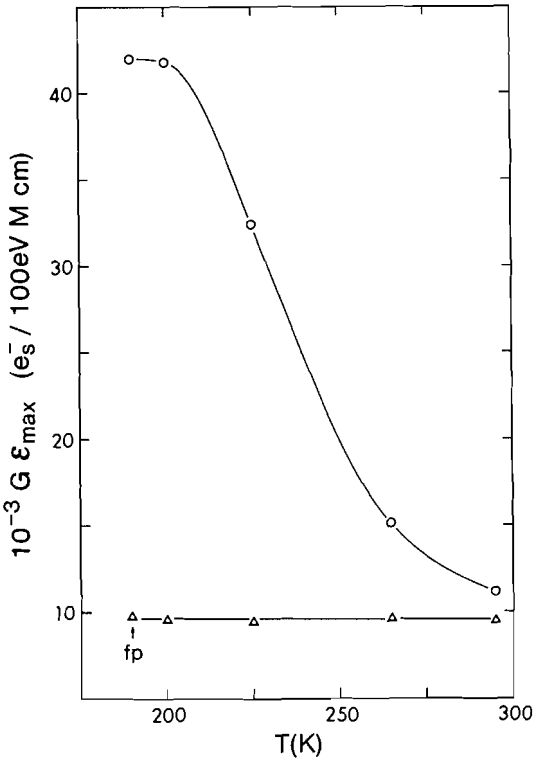


FIG. 5. Temperature dependence of $G\varepsilon_{max}$ for solvated electrons in *n*-propyl amine at the end of a 100 ns pulse (○), and for the free ions (△). Freezing point = 190 K.

TABLE 3. Comparison of effects on $e^-_{solv}$ spectra of propylating $NH_3$ and $H_2O$

| Ratio | *n*-$PrNH_2$[a] / $NH_3$[b] | | *n*-PrOH[c] / $H_2O$[c] | |
|---|---|---|---|---|
| $E_{Amax}$ | 1.03/0.90 | *= 1.14 (1.08)*[d] | 1.93/1.72 | *= 1.12* |
| $E_b$ | 1.62/1.14 | *= 1.42 (1.38)*[d] | 2.99/2.21 | *= 1.35* |
| $E_r$ | 0.75/0.73 | *= 1.02 (0.96)*[d] | 1.37/1.36 | *= 1.01* |
| $W_{1/2}$ | 0.87/0.41 | *= 2.12 (2.05)*[d] | 1.62/0.85 | *= 1.91* |
| $W_b$ | 0.59/0.24 | *= 2.46 (2.40)*[d] | 1.06/0.49 | *= 2.16* |
| $W_r$ | 0.28/0.17 | *= 1.6 (1.6)*[d] | 0.56/0.36 | *= 1.6* |
| $W_b/W_r$ | 2.1/1.4 | *= 1.5 (1.5)*[d] | 1.9/1.4 | *= 1.4* |
| $G_{fi}\varepsilon_{max}$[e] | 10k/167k | *= 0.06 (0.06)*[d] | 14k/50k | *= 0.28* |
| $-dE_{Amax}/dT$ | 4.3m/2.4m | *= 1.8 (1.8)*[d] | 3.3m[f]/2.4m | *= 1.4* |
| $T/T_c$ | 0.40/0.49(0.45/0.55)[d] | | 0.56/0.46 | |

[a] 200 K, present work.
[b] 200 K, ref. 12.
[c] 298 K, ref. 5.
[d] Ratio at 225 K.
[e] $G_{fi}$ = free ion yield, $\varepsilon_{max}$ = maximum molar absorptivity.
[f] Reference 40.

its effect on $G_{fi}$ (28). The value 0.06 for amine/ammonia is due mainly to the low encounter efficiency of the $e^-_{solv} + NH^+_{4,solv}$ reaction in ammonia and the consequent high free ion yield in that liquid (11).

The values of $G_{fi}\varepsilon_{max}$ are independent of temperature in *n*-propyl amine (Fig. 5), ammonia (12), water (7), and alcohols (29, 30). However, the spur reactions are greatly slowed at low temperatures, so the total observed yield at the end of a 100 ns pulse increases at low temperatures. The behavior in *n*-propyl amine (Fig. 5) is similar to that recorded earlier for alcohols (29, 30) and ethers (25).

*Asymmetry of the band*

The asymmetry factor $W_b/W_r$ for an F center is $1.2 \pm 0.1$ (31, 32). The factor is larger for solvated electrons, being 1.35 for electrons in water (7) and ammonia (12), 1.6 in tetrahydrofuran (5), and 1.8–2.4 in a variety of alcohols and diols (5) and propyl amine (Table 2). The greater asymmetry is consistent with the suggestion that both bound–bound and bound–continuum transitions make significant contributions to the optical band of solvated electrons. The large increase in asymmetry factor on going from water or ammonia to an alcohol or amine (Table 3) might indicate an extra bound–bound transition for electrons in the latter liquids. Photoconductivity measurements on trapped electrons in glassy MTHF (33), alcohol/water (34), and amines (35) also indicate that both bound–bound and bound–continuum transitions occur in these systems. Moment analysis of the spectra in water, ammonia, and MTHF (36) substantiates a substantial contribution from bound–continuum transitions.

*Oscillator strength*

The oscillator strength $f$ was estimated from eq. [1].

[1] $f = 3.5 \times 10^{-5}\ \varepsilon_{max} W_{1/2} I$

where

$$I = (1/W_{1/2}) \int_0^\infty (\varepsilon_E/\varepsilon_{max}) dE$$

The value of the integral was measured from the spectra shown in Fig. 1, and is ~1.45 (Table 2). Values of $I = 1.3$–$1.5$ have also been found in ammonia (12), water (7), and many alcohols (5).

Taking a typical value of $f = 0.7$ (5) one obtains $\varepsilon_{max} \approx \sim 1.7 \times 10^3$ m²/mol ($1.7 \times 10^4 M^{-1}$ cm$^{-1}$). The earlier reported value of $4.5 \times 10^3$ m²/mol in *n*-propyl amine at 293 K (15) is too high because it would give $f = 2.0$.

*Band shape stability*

The temperature coefficient $(\partial E/\partial T)_{A/A_{max}}$ for solvated electrons in *n*-propyl amine increases gently from the low energy side up to $E_b$, then decreases (Fig. 4). This shows a slight band shape instability. Using Golden and Tuttle's method (37, 38), the band at 190 K was chosen as a reference and that at another temperature was shifted to it by adding a fixed amount of energy which resulted in a minimum deviation between the reference and the shifted band. The root-mean-square (rms) deviation for the shifted bands was 0.04 eV/100 K. Similar values had been obtained for water, methanol, tetrahydrofuran, methyl amine, and ammonia (37, 38). This method of band analysis seems to be less sensitive than one which treats the high and low energy sides separately.


1. M. C. Sauer, Jr., S. Arai, and L. M. Dorfman. J. Chem. Phys. **42**, 708 (1965).
2. K. N. Jha, G. L. Bolton, and G. R. Freeman. J. Phys. Chem. **76**, 3876 (1972).
3. L. M. Dorfman, F.-Y. Jou, and R. Wageman. Ber. Bunsen.-Gesell. Phys. Chem. **75**, 68 (1971).
4. F.-Y. Jou and G. R. Freeman. J. Phys. Chem. **81**, 909 (1977).
5. F.-Y. Jou and G. R. Freeman. Can. J. Chem. **57**, 591 (1979).
6. B. D. Michael, E. J. Hart, and K. H. Schmidt. J. Phys. Chem. **75**, 2798 (1971).
7. F.-Y. Jou and G. R. Freeman. J. Phys. Chem. **83**, 2383 (1979).
8. I. Hurley, S. Golden, and T. R. Tuttle, Jr. Metal–ammonia solutions. Butterworths, London. 1970. p. 503.
9. G. Rubinstein, T. R. Tuttle, Jr., and S. Golden. J. Phys. Chem. 77, 2872 (1973).
10. Farhataziz and L. M. Perkey. J. Phys. Chem. **79**, 1651 (1975).
11. J. Belloni, F. Billiau, and E. Sait. Nouv. J. Chim. **3**, 157 (1979).
12. F.-Y. Jou and G. R. Freeman. J. Phys. Chem. **85**, 629 (1981).
13. J. F. Gavlas, F.-Y. Jou, and L. M. Dorfman. J. Phys. Chem. **78**, 2631 (1974).
14. W. A. Seddon, J. W. Fletcher, and F. C. Sopchyshyn. Can. J. Chem. **56**, 839 (1978).
15. J. A. Delaire and J. R. Bazouin. Can. J. Chem. **57**, 2013 (1979).
16. G. R. Freeman. J. Phys. Chem. 77, 7 (1973).
17. G. Oster and J. G. Kirkwood. J. Chem. Phys. **11**, 175 (1943).
18. R. W. Weast (*Editor*). Handbook of chemistry and physics. 50th edn., Chemical Rubber Co., Cleveland, OH. 1970.
19. R. W. Gallant. Physical properties of hydrocarbons. Vols. 1 and 2. Gulf Publishing Co., Houston, TX. 1968.
20. R. D. Nelson, Jr., D. R. Lide, Jr., and A. A. Maryott. Selected values of electric dipole moment for molecules in the gas phase. NSRDS-NBS 10, US Govt. Printing Office, Washington, DC. 1967.
21. A. A. Maryott and E. R. Smith. Table of dielectric constants of pure liquids. NBS Circular 514, US Govt. Printing Office, Washington, DC. 1951.
22. (*a*) J. McHale and J. Simons. J. Chem. Phys. **67**, 389 (1977); (*b*) A. Banerjee and J. Simons. J. Chem. Phys. **68**, 415 (1978).
23. (*a*) K. Funabashi, I. Carmichael, and W. H. Hamill. J. Chem. Phys. **69**, 2652 (1978); (*b*) N. R. Kestner, J. Logan, and J. Jortner. J. Phys. Chem. **78**, 2148 (1974).
24. S. Arai and M. C. Sauer, Jr. J. Chem. Phys. **44**, 2297 (1966).
25. F.-Y. Jou and G. R. Freeman. Can. J. Chem. **54**, 3693 (1976).
26. E. J. Hart and M. Anbar. The hydrated electron. Wiley-Interscience. 1970. p. 40.
27. K. Nakanishi and P. H. Solomon. Infrared absorption spectroscopy. 2nd ed. Holden-Day, Inc., San Francisco. 1977.
28. G. R. Freeman and J. M. Fayadh. J. Chem. Phys. **43**, 86 (1965).
29. J. H. Baxendale and P. Wardman. Chem. Commun. 429 (1971).
30. R. S. Dixon and V. J. Lopata. J. Chem. Phys. **62**, 4573 (1975).
31. J. D. Konitzen and J. J. Markham. J. Chem. Phys. **32**, 843 (1960).
32. W. Belhardt and H. Kühnert. Phys. Status. Solidi, **14**, 157 (1966).
33. T. Huang, I. Eisele, D. P. Lin, and L. Kevan. J. Chem. Phys. **56**, 4702 (1972).
34. S. A. Rice and L. Kevan. J. Phys. Chem. **80**, 847 (1977).
35. N. Kato, K. Akiyama, and K. Fueki. J. Phys. Chem. **85**, 3087 (1981).
36. I. Carmichael. Chem. Phys. Lett. **56**, 339 (1978).
37. T. R. Tuttle, Jr. and S. Golden. J. Chem. Soc. Faraday Trans. II, **77**, 873 (1981); **77**, 889 (1981).
38. S. Golden and T. R. Tuttle, Jr. J. Chem. Soc. Faraday Trans. II, **75**, 474 (1979).
39. A.-D. Leu, K. N. Jha, and G. R. Freeman. To be published.
40. A.-D. Leu and G. R. Freeman. To be published.


Can. J. Chem. Downloaded from www.nrcresearchpress.com by 210.87.254.105 on 09/06/12
For personal use only.

# Spectroscopic and chemical reactivity manifestations of strong hydrogen bonding: HCNH proton–proton coupling and alkylation reactions of amines[1]

JAMES H. CLARK AND JAMES D. PILE
*Department of Chemistry, University of York, York, England Y01 5DD*
AND
JACK M. MILLER,[2] SERGIO PAONE, AND SHWE Y. TAN
*Department of Chemistry, Brock University, St. Catharines, Ont., Canada L2S 3A1*
Received October 9, 1981

JAMES H. CLARK, JAMES D. PILE, JACK M. MILLER, SERGIO PAONE, and SHWE Y. TAN. Can. J. Chem. **60**, 1815 (1982).

Two useful but quite different manifestations of strong hydrogen bonding in systems containing NH groups are reported and discussed. The $pK_a$ limit for observation of proton–proton HNCH spin–spin coupling in *N*-methylanilines is shown to be related to the strength of added H-bond electron donors so that $Ph_3PO$, $Ph_3AsO$, and $F^-$ in particular are useful reagents for resolving this type of coupling. The mechanism of hydrogen exchange between anilines and water and the role of the added electron donors are discussed. Strong H-bonding between anilines or benzylamines and $F^-$ causes pronounced changes in the chemical reactivity of the amine. Results of experiments on the alkylation of these amines using potassium and tetra-*n*-butylammonium fluorides demonstrate the synthetic utility of this effect.

JAMES H. CLARK, JAMES D. PILE, JACK M. MILLER, SERGIO PAONE et SHWE Y. TAN. Can. J. Chem. **60**, 1815 (1982).

On rapporte, tout en les discutant, deux manifestations utiles mais très différentes de fortes liaisons hydrogènes dans des systèmes contenant des groupes NH. On montre que la limite du $pK_a$ pour observer le couplage spin proton–proton du HNCH dans les *N*-méthylaniline est reliée à la force des liaisons hydrogènes des électrodonneurs ajoutés de sorte que $Ph_3PO$, $Ph_3AsO$ et $F^-$ en particulier sont des réactifs utiles pour résoudre ce type de couplage. On discute du mécanisme de l'échange d'hydrogène entre les anilines et l'eau et du rôle des électrodonneurs ajoutés. De fortes liaisons hydrogènes entre les anilines ou les benzylamines et $F^-$ provoquent des changements importants de la réactivité chimique de l'amine. Les résultats des expériences sur l'alkylation de ces amines utilisant les fluorures de potassium et de tétra-*n*-butylammonium démontrent l'utilité de cet effet en synthèse.
[Traduit par le journal]

## Introduction

The concept of strong or very strong hydrogen bonding is not a new one, but it is only in the last few years that enough evidence has been accumulated to support its classification as a type of bonding quite distinct from normal or weak hydrogen bonding (1, 2). The identification of strong H-bonds in a large number of systems has enabled investigators to associate a number of interesting properties with this type of bonding. Ionic fluorides for example, are capable of forming strong H-bonds to a variety of H-bond electron acceptors and are known for their base-like reaction properties, but it is only through complementary spectroscopic and chemical reactivity studies that these properties are beginning to be linked (3, 4).

We report here what we believe to be two interesting and potentially useful examples of strong H-bonding in systems containing amines: changes in the exchange rate of the NH hydrogen in *N*-methylanilines facilitating the observation of proton–proton HNCH spin–spin coupling, and enhanced reactivities of some anilines and benzylamines.

[1] For preliminary communication, see ref. 19.
[2] Author to whom communications may be addressed.

## Experimental

The $^1H$ nmr spectra were recorded on a JEOL MH-100 (100 MHz), Bruker WP-60 (60 MHz), or Varian A60 (60 MHz) spectrometer. The $^1H$ nmr spectra of products from the alkylation reactions were recorded in $CDCl_3$ solution, while those of the solutions used to study proton–proton coupling were recorded in various solvents (see text). Reported coupling constants were recorded on at least two of the spectrometers. The $^{19}F$ nmr spectra were recorded on the Bruker spectrometer at 56.4 MHz. Mass spectra were determined with an AEI MS-30 double beam mass spectrometer interfaced via a Bieman separator to a 3% SE30 Chrom W (80–200 mesh) column in a Pye 104 gas chromatograph. Infrared spectra were recorded on Perkin Elmer 237B and 735 spectrophotometers.

Triphenylarsine oxide was prepared by treatment of an acetone solution of the parent arsine with aqueous permanganate. A solution of tetra-*n*-butylammonium fluoride (TBAF) was prepared by neutralization of 20% tetra-*n*-butylammonium hydroxide with hydrofluoride acid. The resulting solution was concentrated before use. Potassium fluoride was dried at 100°C under reduced pressure for several hours prior to use. All solvents were commercial grade dried over 5 Å molecular sieves before use. Other reagents were commercial grade samples used without further purification except as detailed below.

For the study of nmr coupling in the *N*-methylanilines, it was usually sufficient to dry the metal fluoride as described above, and to use fresh samples of 18-crown-6, analytical grade solvent, and the amine. Generally, however, and specifically for studies of the tolerance of the KF (18-crown-6) – *N*-methylaniline system to water content, we used 18-crown-6 that had been dried by the following method. The crown and freshly distilled nitromethane were mixed in equimolar proportions. The result-

0008-4042/82/141815-06$01.00/0
©1982 National Research Council of Canada/Conseil national de recherches du Canada

Can. J. Chem. Downloaded from www.nrcresearchpress.com by 210.87.254.6 on 09/06/12
For personal use only.

Can. J. Chem. Downloaded from www.nrcresearchpress.com by 210.87.254.6 on 09/06/12
For personal use only.

ing mixture was cooled to ca. −20°C and then evaporated on a rotary evaporator until all of the nitromethane had escaped. This process was repeated, and the final white solid pumped under high vacuum overnight. All subsequent manipulations were then carried out in a glove box operating under a dry nitrogen atmosphere.

*Reactions*

All reactions were carried out in ordinary glassware using efficient stirring techniques. All products are known compounds and gave satisfactory elemental analyses and $^1$H nmr, ir, and mass spectra consistent with their structure and, where reported data are available, consistent with those reported in the literature. Details of a representative reaction are given below.

*Preparation of* N-n-*butylaniline using KF–DMF*

1-Chlorobutane (0.01 mol) was added to a stirred mixture of KF (0.02 mol) and aniline (0.01 mol) in DMF (10 g) and the resulting mixture was stirred at 120°C for 12 h, after which time $^1$H nmr analysis showed no starting material remaining. Extraction of the cooled mixture with diethyl ether, aqueous washing (to remove the DMF), drying ($MgSO_4$), and evaporation under reduced pressure gave a brown viscous product. The product was purified by reduced pressure distillation giving *N-n*-butylaniline (0.0055 mol, 55%) bp 75–78°C/1 Torr (lit. (20) bp 118–120°C/20 Torr); $^1$H nmr δ: 7.3–6.5 (5H, m, ring CH), 3.45 (1H, s, N—H), 3.15 (2H, tr, $CH_2N$), 1.7–1.2 (4H, m, $(CH_2)_2$), 0.8 (3H, tr, $CH_3$) ppm; ms *m/e*: 149 ($M^+$). *Anal.* calcd. for $C_{10}H_{15}N$: C 80.54, H 10.07, N 9.40; found: C 79.78, H 10.03, N 10.00.

The above reaction may also be accomplished in a similar reaction time and with a slightly higher yield of product in the absence of DMF and using an excess of the aniline to make the mixture workable. Replacing KF by TBAF (the aqueous solution of which should be concentrated by evaporation at reduced pressure in the presence of the amine before use) produces similar results although reactions may now be accomplished at lower temperatures (> 80°C).

## Results and discussion

### *Proton–proton H—N—C—H spin–spin coupling in* N-*methylanilines*

The NH hydrogens of many secondary amines are labile on the nmr time scale, so that under normal conditions, proton–proton H—N—C—H spin–spin coupling will not be observed for such compounds. This problem is not limited to the nmr of secondary amines; alcohols, amides, and other compounds containing a fairly acidic hydrogen may not show short range coupling to that hydrogen (5).

In the case of *N*-methylanilines, a correlation between the lack of or presence of HNCH coupling, and the $pK_a$ of that amine has been established (6). Under normal conditions, coupling is observed only for those amines with $pK_a < 3.5$. Attempts to overcome the problems of fast hydrogen exchange in amines have been numerous (6–12) but have usually met with limited success. The most successful techniques that have been developed rely on the total removal of water from the amine–solvent systems (11, 12), although these methods inevitably demand very careful and often tedious experimentation and severe and highly reactive desiccants such as NaK alloy (11) or dimethylzinc (12). Of more interest here is the observation of Rae that use of pyridine as the nmr solvent allows the $pK_a$ limit to be extended by about 1 unit (6). This observation has been explained in terms of the ability of pyridine to effectively scavenge protons, but this does not seem to us to be the whole story as very weak bases such as DMSO have been used to extend the limit for observation of HNCH coupling in similar systems (13).

On the basis of the evidence available, the most probable mechanism for proton exchange in these systems would involve initial H-bonding of water to the amine NH nitrogen (eq. [1]). If this mecha-

[1] 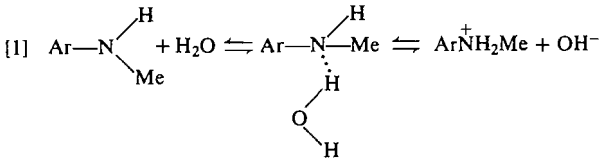

nism is correct, then it would seem that the best approach to solving the problem of fast exchange would be to attempt to control the H-bonding in the systems rather than introduce proton scavengers or powerful chemical desiccants. With this consideration in mind, we have studied the effects of a range of compounds of different H-bond electron donor abilities on the $^1$H nmr of solutions containing representative *N*-methylanilines. The amines we selected cover a $pK_a$ range up to 5.36 and the two higher $pK_a$ amines at least would normally require rigorous drying precautions for HNCH coupling to be observed at ambient temperatures. The results of our experiments are summarized in Table 1.

The results reported here reveal a definite correlation between the presence or absence of HNCH coupling and known H-bond electron donor abilities (1, 3, 14, 15) but not with aqueous basicities. Solutions containing the three powerful H-bond electron donors, $F^-$, $Ph_3PO$, and $Ph_3AsO$ show well-defined coupling for at least one of the amines. The medium strength donors DMSO, pyridine, and DMF do not produce defined coupling in any of the amines under the conditions used, but do reveal a broadening of the N—$CH_3$ proton resonance for the lowest $pK_a$ amine (*N*-methyl-*o*-toluidine). It has been reported that coupling in *N*-methyl-*o*-toluidine can be observed in pure pyridine (6) but we have generally used an electron donor to amine mole ratio of 2:1. Chloroform, a very weak donor, is totally ineffective. All $J_{HNCH}$ values observed here are consistent with those reported in the literature (12).

TABLE 1. H—N—C—H proton–proton coupling constants and chemical shifts for H-bond electron donor *N*-methylaniline systems[a]

| Electron donor | Aniline[b] | Solvent[c] | Temperature (K) | $J_{HNCH}$ (Hz) | $\delta(CH_3)$ (ppm) | $\Delta\delta(CH_2)$[d] (ppm) |
|---|---|---|---|---|---|---|
| KF(18-crown-6) | NMA | BB | 298 | 5.2 | 2.17 | 0.24 |
| | | | 323 | 5.2 | 2.22 | 0.21 |
| | | | 333 | 5.2 | 2.26 | 0.21 |
| | | | 343 | (br)[e] | 2.27 | 0.20 |
| RbF(18-crown-6) | NMA | BB | 298 | 5.2 | 2.19 | 0.26 |
| | | | 323 | 5.2 | 2.23 | 0.17 |
| | | | 333 | 5.2 | 2.24 | 0.11 |
| | | | 343 | 5.2 | 2.26 | 0.15 |
| | | | 353 | (br)[e] | 2.29 | 0.12 |
| CsF(18-crown-6) | NMA | BB | 298 | 5.2 | 2.20 | 0.18 |
| | | | 323 | 5.2 | 2.24 | 0.15 |
| | | | 333 | 5.2 | 2.26 | 0.20 |
| | | | 343 | 5.2 | 2.28 | 0.16 |
| | | | 353 | 5.2 | 2.31 | 0.18 |
| | | | 363 | (br)[e] | 2.35 | 0.15 |
| KF(18-crown-6) | NMA | B | 298 | 5.2 | 2.46 | −0.17 |
| RbF(18-crown-6) | NMA | B | 298 | 5.2 | 2.47 | −0.20 |
| CsF(18-crown-6) | NMA | B | 298 | 5.2 | 2.47 | −0.15 |
| KF(18-crown-6) | NMA | CB | 298 | 5.2 | 2.46 | 0.40 |
| RbF(18-crown-6) | NMA | CB | 298 | 5.2 | 2.50 | 0.26 |
| CsF(18-crown-6) | NMA | CB | 298 | 5.2 | 2.50 | 0.24 |
| KF(18-crown-6) | NMOT | BB | 298 | 5.1 | 2.21 | 0.21 |
| RbF(18-crown-6) | NMOT | BB | 298 | 5.1 | 2.30 | 0.27 |
| CsF(18-crown-6) | NMOT | BB | 298 | 5.2 | 2.30 | 0.23 |
| KF(18-crown-6) | NMPT | BB | 298 | 5.2 | 2.20 | 0.27 |
| RbF(18-crown-6) | NMPT | BB | 298 | 5.2 | 2.19 | 0.28 |
| CsF(18-crown-6) | NMPT | BB | 298 | 5.1 | 2.21 | 0.43 |
| KF(18-crown-6) | NMPT | $CCl_4$ | 298 | 5.2 | 2.78 | 0.63 |
| KF(18-crown-6) | NMPT | $CH_3CN$ | 298 | 5.2 | 2.55 | −0.44 |
| KF(18-crown-6) | NMPT | NB | 298 | 5.2 | 2.56 | 0.81 |
| KF(18-crown-6) | NMPT | $CH_3OH$ | 298 | — | 2.18 | ? |
| KF(18-crown-6) | NMA | $CH_3OH$ | 298 | — | 2.15 | ? |
| KF(18-crown-6) | NMOT | $CH_3OH$ | 298 | — | 2.17 | ? |
| $Ph_3PO$ | NMOT | B | 298 | 5.2 | 2.54 | — |
| $Ph_3PO$ | NMA | B | 298 | 5.2 | 2.40 | — |
| $Ph_3PO$ | NMPT | B | 298 | (br)[e] | 2.55 | — |
| $Ph_3AsO$ | NMOT | B | 298 | 5.1 | 2.56 | — |
| $Ph_3AsO$ | NMA | B | 298 | (br)[e] | 2.52 | — |
| $Ph_3AsO$ | NMPT | B | 298 | — | 2.53 | — |
| DMSO | NMOT | B | 298 | (br)[e] | 2.53 | — |
| DMSO | NMA | B | 298 | — | 2.41 | — |
| DMSO | NMPT | B | 298 | — | 2.56 | — |
| Pyridine | NMOT | B | 298 | (br)[e,f] | 2.38 | — |
| Pyridine | NMA | B | 298 | — | 2.35 | — |
| Pyridine | NMPT | B | 298 | — | 2.40 | — |
| DMF | NMOT | B | 298 | (br)[e] | 2.48 | — |
| DMF | NMA | B | 298 | — | 2.35 | — |
| DMF | NMPT | B | 298 | — | 2.48 | — |
| $CHCl_3$ | NMOT | $CHCl_3$ | 298 | — | 2.75 | — |
| $CHCl_3$ | NMA | $CHCl_3$ | 298 | — | 2.66 | — |
| $CHCl_3$ | NMPT | $CHCl_3$ | 298 | — | 2.70 | — |
| KOAc(18-crown-6) | NMOT | $CCl_4$ | 298 | (br)[e] | 2.60 | 0.70 |
| KCl(18-crown-6) | NMOT | $CCl_4$ | 298 | — | 2.56 | 0.70 |
| KI(18-crown-6) | NMOT | $CCl_4$ | 298 | — | 2.60 | 0.70 |

[a] A mole ratio of 2 electron donor: 1 aniline was used, unless stated otherwise. Aniline concentrations are ca. 0.1 molar.
[b] NMOT = *N*-methyl-*O*-toluidine ($pK_a$ 4.62); NMA = *N*-methylaniline ($pK_a$ = 4.85); NMPT = *N*-methyl-*p*-toluidine ($pK_a$ = 5.36).
[c] B = benzene, BB = bromobenzene, CB = chlorobenzene, NB = nitrobenzene.
[d] $\Delta\delta(CH_2) = \Delta\delta(CH_2$ of crown ether complex) − $\delta(CH_2$ of free crown); an accuracy of no better than ±0.1 ppm can be assumed for these values (see text).
[e] Broad unresolved peak.
[f] Coupling is observed in pure pyridine (ref. 6).

Can. J. Chem. Downloaded from www.nrcresearchpress.com by 210.87.254.6 on 09/06/12
For personal use only.

Can. J. Chem. Downloaded from www.nrcresearchpress.com by 210.87.254.6 on 09/06/12
For personal use only.

Solutions containing fluoride ions are particularly effective at revealing HNCH coupling in all three amines checked here. In all cases, coupling was very well-defined. No change was observed on replacing KF by RbF or CsF, but coupling was not observed when potassium acetate, KCl, or KI were used. These observations clearly point to the importance of the fluoride anion and are consistent with the concept of strong hydrogen bonding playing the major role in these systems. Changing the bulk solvent from benzene to bromobenzene, chlorobenzene, acetonitrile, or carbon tetrachloride also has no effect on the coupling. However, a single N—$CH_3$ proton resonance is observed in methanol suggesting that the fluoride anion is effectively masked by $CH_3OH\cdots F^-$ H-bonding in this solvent.

Normally, we did not take any special precautions before running the nmr's of the solutions (see Experimental) so as to determine the potential of the method as a routine analytical technique; but we did carry out a series of relative concentration and water tolerance studies using predried KF, 18-crown-6, benzene, and *N*-methylaniline. These studies showed that HNCH coupling is still clearly seen at amine to fluoride mole ratios of greater than 50 to 1, and water to fluoride mole ratios of about 10 to 1. These results strongly suggest that the function of the fluoride anion is to scavenge the water molecules rather than in some way block the amine NH sites. This is not unreasonable since OH groups are normally better H-bond electron acceptor sites than NH groups, and it is not immediately obvious how H-bonding to the NH hydrogen would inhibit hydrogen exchange with water molecules. It is not reasonable to suggest that fluoride, $Ph_3PO$, and $Ph_3AsO$ are acting as conventional desiccants and we believe that our observations confirm our suggested mechanism and, in particular, show that our H-bonding approach to the solution of the problem of observing coupling in rapidly exchanging systems of this type is a viable one. Our method would seem to compare very favourably in terms of ease, convenience, and efficiency with those methods employing rigorous drying techniques and highly reactive drying agents.

Results of raising the temperature in representative fluoride solutions are given in Table 1. Dried reagent systems withstand appreciable increases in temperature before the N—$CH_3$ proton doublet collapses. The coalescence temperatures for *N*-methylaniline systems are sensitive to fluoride concentration and to the identity of the cation so that $T_{coal}(CsF) > T_{coal}(RbF) > T_{coal}(KF)$.

It is not advisable to place too much emphasis on the absolute values for the N—$CH_3$ proton chemical shifts reported, as these values are rather sensitive to factors such as amine concentration and water content. But it is apparent that the maximum chemical shifts are observed in the very weakly associating solvents $CCl_4$ and $CHCl_3$, while the minimum values are observed in methanol and the aromatic solvents. Presumably, the high field chemical shift values observed in aromatic media are derived from an intermolecular interaction between the methyl group and the aromatic group of the solvent (12), while in methanol the effect is caused by actual molecular association.

The final column in Table 1 gives positions of the single resonances observed in almost all solutions containing salt – crown ether combinations (which we assume to be due to salt – crown ether complexes) relative to the position of uncomplexed crown. All of these solutions were made up with a large excess of crown (16) and relative intensities of the complex and free crown resonances suggest 1:1 or 2:1 crown/salt complexes. Too much emphasis should not be placed on the actual values quoted here for reasons similar to those given above, but it is interesting to note their solvent dependence and in particular the observation that in acetonitrile or benzene the complex resonances consistently occur upfield of that of the free crown, whereas in all other solvents the opposite effect is observed. This is obviously a subject of interest but a more detailed investigation is beyond the scope of this work and will be reported in a subsequent article.

The diffuse nature of the NH resonances of amine solutions which showed N—CH proton doublets made conventional decoupling experiments difficult and did not provide us with consistent results. We therefore decided to look at the $^{19}F$ nmr spectra of the fluoride-containing solutions in an attempt to rule out the possibility of coupling to the fluorine and to hopefully provide more information on these systems in general. In all of the solutions we investigated, $^{19}F$ nmr revealed an extremely broad resonance ($\omega_{1/2}$ = ca. 4 kHz) which was insensitive to the presence or absence of the amine and disappeared only on removal of the crown ether. A sample of KF (18-crown-6) in water showed a sharp signal characteristic of aqueous fluoride superimposed on the broad signal. The broad signal was centred at ca. 30 ppm downfield from $C_6F_6$, that is in the strong H-bonding to fluoride region of the spectrum, although it is extremely doubtful that such a wide band may be attributed to a simple H-bonding interaction. No

TABLE 2. Hydrogen bond assisted *N*-alkylation of anilines and benzylamines

| Amine | Alkylating agent | Solvent | Fluoride | Temperature (°C) | Time (h) | Alkylated product yield (%)[a] | Benzyl fluoride yield (%)[a] |
|---|---|---|---|---|---|---|---|
| $PhNH_2$ | $CH_3(CH_2)_3Cl$ | $PhNH_2$ | KF | 120 | 12 | 69 | — |
| $PhNH_2$ | $CH_3(CH_2)_3Cl$ | DMF | KF | 120 | 12 | 55 | — |
| $PhNH_2$ | $CH_3(CH_2)_3Cl$ | $PhNH_2$ | TBAF | 80 | 12 | 70 | — |
| $PhNH_2$ | $CH_3(CH_2)_3Cl$ | DMF | TBAF | 80 | 12 | 64 | — |
| $PhNH_2$ | $Cl(CH_2)_4Cl$ | $PhNH_2$ | KF | 120 | 12 | 88[b] | — |
| $PhNH_2$ | $Cl(CH_2)_4Cl$ | $PhNH_2$ | TBAF | 80 | 18 | 79[b] | — |
| $PhCH_2NHCH_3$ | $CH_3(CH_2)_3Br$ | $PhCH_2NHCH_3$ | KF | 120 | 12 | 92 | — |
| $PhCH_2NHCH_3$ | $CH_3(CH_2)_3Br$ | DMF | KF | 120 | 12 | 46 | — |
| $PhCH_2NHCH_3$ | $CH_3(CH_2)_3Br$ | $PhCH_2NHCH_3$ | TBAF | 80 | 18 | 74 | — |
| $PhCH_2NHCH_3$ | $CH_3(CH_2)_3Br$ | DMF | TBAF | 80 | 18 | 33 | — |
| $PhCH_2NHCH_3$ | $PhCH_2Br$ | $PhCH_2NHCH_3$ | KF | 120 | 28 | 87 | 10 |
| $PhCH_2NHCH_3$ | $PhCH_2Br$ | DMF | KF | 120 | 28 | 47 | 32 |
| $PhCH_2NHCH_3$ | $PhCH_2Br$ | $PhCH_2NHCH_3$ | TBAF | 80 | 28 | 67 | 21 |
| $PhCH_2NHCH_3$ | $PhCH_2Br$ | DMF | TBAF | 80 | 28 | 41 | 33 |
| $PhCH_2NHCH_3$ | $PhCH_2Cl$ | DMF | KF | 120 | 28 | 45 | 35 |
| $PhCH_2NHCH_3$ | $PhCH_2Cl$ | DMF | TBAF | 80 | 28 | 47 | 39 |

[a]Isolated yields.

[b]Product = PhN

effect was observed on applying proton decoupling power. We are carrying out further investigations on this phenomenon.

*Hydrogen bond assisted alkylations*

In the last section, we reported one spectroscopic manifestation of strong H-bonding in amine systems. On introducing powerful H-bond electron donors into solutions containing amines and water, the donor apparently preferentially H-bonded to water molecules although it seems certain that any excess donor molecules would H-bond to amine molecules. Here we turn our attention to possible chemical reactivity manifestations of strong H-bonding in amine systems. By using an excess of the electron donor (ionic fluorides have been chosen to exaggerate the effect), the effect of strong H-bonding to the amine should be readily observable.

There are relatively few examples in the literature of chemical reactivity manifestations of H-bonding at NH sites, although the biochemical as well as chemical importance of such reactions is clear. Since we reported our preliminary results on KF-promoted amine alkylations (3), related work elsewhere has confirmed the promise of the method (17). We here report a more comprehensive set of results for the reactions of anilines and benzylamines with alkylating agents in the presence of KF and, for comparison purposes, we have carried out the same reactions in the presence of TBAF which has become one of the more popular alternatives to its potassium counterpart (Table 2) (4).

The *N*-alkylation of the amino function to give a secondary or tertiary amine is an important, but often problematic, reaction. Conventional methods of *N*-alkylation require rather drastic conditions using powerful bases such as sodium hydride or potassium *tert*-butoxide, and are apt to produce complex mixtures containing unalkylated, partially alkylated, and quaternary products, as well as the required product. Our results would seem to confirm that ionic fluorides are a practicable alternative to conventional reagents for this type of reaction. It is also clear that the strong H-bond between the amine NH and the fluoride anion, established by us in our earlier article (3), provides a significant localization of charge at the NH nitrogen resulting in a synthetically useful increase in the amine nucleophilicity.

It should be noted from the results in the table that the use of DMF rather than an excess of the amine as the reaction solvent generally results in a smaller isolated yield. This is probably due to increased difficulties in separation and isolation of the pure products rather than any significant reduction in reactivity. The use of DMF as solvent does offer the advantages of easier working of the reaction systems, and allows for use of solid or highly viscous reagents.

Replacing KF by TBAF provided a homogeneous reaction system, but did not usually result in higher product yields although the temperature necessary for reaction was appreciably lower than before. As with all fluoride ion promoted reactions (4), the systems were found to be very sensitive to the amount of water present. This is likely to have a

Can. J. Chem. Downloaded from www.nrcresearchpress.com by 210.87.254.6 on 09/06/12
For personal use only.

much greater effect with those systems containing the extremely hygroscopic TBAF than with those using KF, which can be effectively dried before use and manipulated relatively easily. We did attempt to reduce the water present in the TBAF systems by coevaporation of the reactant amine with the aqueous TBAF (4) but it seems certain that our TBAF reaction systems contained significantly more water than those employing KF.

Reactions involving benzyl halides as the alkylating agents were the only reactions that we studied which produced significant quantities of side-products. Benzyl fluoride was isolated and identified in all such reactions (see Table 2). The competition between highly electrophilic carbons and H-bond electron acceptor sites for the fluoride anion is often a problem in fluoride-promoted reactions. Indeed recognition of this competition in attempted fluorination reactions led to the upsurge in interest in H-bond assisted reactions (4). While we were not able to overcome this problem, we did observe that the amount of fluorination that occurred could be kept to a minimum by using excess amine rather than DMF as solvent and by using KF rather than TBAF.

Tetraalkylammonium fluorides have been shown to be capable of promoting many reactions more efficiently than their alkali metal counterparts (4) but it does seem that, where fairly high reaction temperatures are required, the advantages of the former are less obvious. We believe that for *N*-alkylations, the advantages of using TBAF do not outweigh such disadvantages as higher cost, greater hygroscopicity, and increased yields of fluorine-containing side-products. We prefer the use of KF and suggest that useful improvements in reaction efficiency would be gained by achieving a better understanding of the importance of the physical characteristics of KF, as has been suggested by the recent work of Ishikawa, Ando and co-workers (18).

**Acknowledgements**

We thank the Natural Sciences and Engineering Research Council of Canada for financial support (to J.M.M.) and NATO for a collaborative research grant (to J.H.C. and J.M.M.).

1. J. EMSLEY. Chem. Soc. Rev. 91 (1980).
2. J. EMSLEY. Rev. Inorg. Chem. **3**, 105 (1981).
3. J. H. CLARK and J. M. MILLER. J. Am. Chem. Soc. **99**, 498 (1977).
4. J. H. CLARK. Chem. Rev. **80**, 429 (1980).
5. J. A. POPLE, W. G. SCHNEIDER, and H. J. BERNSTEIN. High-resolution nuclear magnetic resonance. McGraw-Hill, New York, NY. 1959.
6. J. D. RAE. Aust. J. Chem. **19**, 409 (1966).
7. L. PAOLILLO and E. D. BECKER. J. Magn. Reson. **3**, 200 (1970).
8. L. K. PETERSON and G. L. WILSON. Can. J. Chem. **49**, 3171 (1971).
9. B. BICHLMEIR and R. WEST. J. Organometal. Chem. **32**, 35 (1971).
10. J. D. RAE. Aust. J. Chem. **19**, 1983 (1966).
11. K. L. HENOLD. Chem. Commun. 1340 (1970).
12. K. P. SHRESTHA and K. L. HENOLD. J. Am. Chem. Soc. **95**, 6699 (1973).
13. P. LANCELIN, J. CHAMPY, and G. ALBERT. Method. Phys. Anal. **7**, 170 (1971).
14. R. W. TAFT, L. J. GURKA, L. JORIS, P. v. R. SCHLEYER, and J. W. RAKSHYS. J. Am. Chem. Soc. **91**, 4801 (1969).
15. M. D. JOESTEN and L. J. SCHAAD. Hydrogen bonding. Dekker, New York. 1974.
16. C. L. LIOTTA and H. P. HARRIS. J. Am. Chem. Soc. **96**, 2250 (1974).
17. T. ANDO and J. YAMAWAKI. Chem. Lett. 45 (1979); H. R. HANNA and J. M. MILLER. Can. J. Chem. **57**, 1011 (1979); K. K. OGILVIE, S. L. BEAUCAGE, M. F. GILLEN, D. W. ENTWHISTLE, and M. QUILLIAM. Nucleic Acids Res. **6**, 1695 (1979).
18. J. YAMAWAKI, T. ANDO, and T. HANAFUSA. Chem. Lett. 1143 (1981); N. ISHIKAWA, T. KITAZUME, and M. NAKOBAYASHI. Chem. Lett. 1089 (1980); T. KITAZUNE and N. ISHIKAWA. Chem. Lett. 1327 (1980); N. ISHIKAWA, T. KITAZUME, T. YAMAZAKI, Y. MOCHIDA, and T. TATSUNO. Chem. Lett. 761 (1980).
19. J. H. CLARK and J. M. MILLER. J. Chem. Soc. Chem. Commun. 63 (1982).
20. R. C. WEAST (*Editor*). Handbook of Chemistry and Physics. 52nd ed. Chemical Rubber Co., Cleveland. 1971.

Can. J. Chem. Downloaded from www.nrcresearchpress.com by 210.87.254.6 on 09/06/12
For personal use only.

# Some reactions of 3-cyano(diethylaminocarbonyl, methoxycarbonyl) pyridines with organolithium reagents. Synthesis of stabilized 1,2-, 1,4-, and 1,6-dihydropyridines

M. GAMAL EL DIN[1] AND EDWARD E. KNAUS[2]

*Faculty of Pharmacy and Pharmaceutical Sciences, University of Alberta, Edmonton, Alta., Canada T6G 2N8*

AND

CHOO-SENG GIAM

*Department of Chemistry, Texas A & M University, College Station, TX 77843, U.S.A.*

Received December 2, 1981

M. GAMAL EL DIN, EDWARD E. KNAUS, and CHOO-SENG GIAM. Can. J. Chem. **60**, 1821 (1982).

The reaction of 3-cyano **5***a*, 3-diethylaminocarbonyl **5***b*, and 3-methoxycarbonylpyridine **5***c* with alkyllithiums **6** has been investigated as a method of preparing stable dihydropyridines. Reaction of **5***a* with **6** affords a mixture of 1,2- and 1,6-dihydropyridines **10** and **11**, whereas reaction of **5***b* and **5***c* with **6** yields a mixture of 1,4- and 1,6-dihydropyridines **11** and **12**. The cyano and diethylaminocarbonyl substituents of **5***a* and **5***b* are relatively resistant toward attack by the alkyllithium whereas reaction of the methoxycarbonyl substituent of **5***c* is competitive with addition to the ring. The stabilities of the dihydropyridines prepared are described.

M. GAMAL EL DIN, EDWARD E. KNAUS et CHOO-SENG GIAM. Can. J. Chem. **60**, 1821 (1982).

On a examiné la possibilité d'utiliser la réaction des cyano-3 (**5***a*), diéthylaminocarbonyl-3 (**5***b*) et méthoxycarbonyl-3 pyridine (**5***e*) avec les alkyllithiums (**6**) pour préparer des dihydropyridines stables. La réaction du composé **5***a* avec le composé **6** conduit à un mélange de dihydro-1,2 et de dihydro-1,6 pyridines (**10** et **11**) tandis que les composés **5***b* et **5***c* dans les mêmes conditions fournissent un mélange des dihydro-1,4 et dihydro-1,6 pyridines (**11** et **12**). Les subsituants cyano et diéthylaminocarbonyle des composés **5***a* et **5***b* ne sont pas attaqués par l'alkyllithium tandis que le substituant méthoxycarbonyle réagit de façon compétitive avec l'addition sur le cycle. On décrit la stabilité des dihydropyridines ainsi préparées.

[Traduit par le journal]

Organolithium reagents add readily to the 2-position of pyridine to afford isolable *N*-lithio-2-alkyl(aryl)-1,2-dihydropyridines **1** (1). Reaction of **1** with acyl(aroyl) chlorides or esters gives predominately the *N*-substituted product **2** along with a low yield of **3** (2), whereas reaction with alkyl

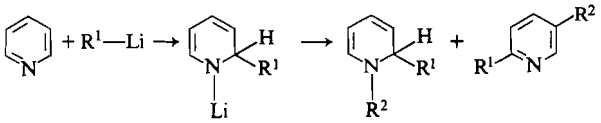

**1** **2** **3**

$R^1$ = *n*-Bu, *t*-Bu, Ph

halides yields only the β-substituted pyridines **3** (3). The 1,2-dihydropyridines **2** ($R^2$ = H), obtained by treatment of **1** with water (4), are very susceptible to oxidation, are thermally unstable, and undergo rapid conversion with acid catalysis to 1,2,3,6-tetrahydro-2,3[1]-dipyridyls **4** (4).

It is well documented that electron-attracting substituents capable of resonance interaction such as COOH, COMe, $CO_2Me$, $CONH_2$, $NO_2$, and CN in the C-3 and C-5 positions stabilize dihydropyridines by extending the conjugation (5). The reactions of 3,5-dicyano(dimethoxycarbonyl)pyridine with methyl(ethyl)lithium or methyl magnesium bromide yield a mixture of 1,2- and 1,4-dihydropyridines as well as products resulting from reaction of the nucleophilic reagent with the cyano or methoxycarbonyl substituent(s). Sodium borohydride reduction of these dinitriles (diesters) also affords 1,2- and 1,4-dihydropyridines even in protic solvents (5). On the other hand, sodium borohydride reduction of 3-cyanopyridine in aprotic solvents yields 3-cyano-1,4-dihydropyridine and 3-cyano-1,4,5,6-tetrahydropyridine in protic solvents (6). The regioselective nucleophilic addition of organolithium compounds to 3-(4,4-dimethyloxazolin-2-yl)pyridine was recently shown to yield stable crystalline 1,4-dihydropyridines in excellent yield (7). It is therefore of interest to develop preparatively useful procedures for the synthesis of 1,2-, 1,4-, and/or 1,6-dihydropyridines stabilized by a single electron-attracting substituent. These dihydropyridines could be used directly as the *N*-lithio-1,2-(1,4-, 1,6-)dihydropyridines to prepare stable *N*-substituted 1,2-(1,4-, 1,6-)dihydropyridines required in other studies or hydrolyzed with

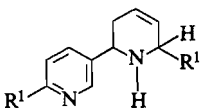

**4**

[1]Study Leave Fellow, Ain Shams University, Cairo, Egypt.
[2]Author to whom inquiries should be addressed.

0008-4042/82/141821-07$01.00/0

©1982 National Research Council of Canada/Conseil national de recherches du Canada

Can. J. Chem. Downloaded from www.nrcresearchpress.com by 210.87.254.6 on 09/06/12
For personal use only.

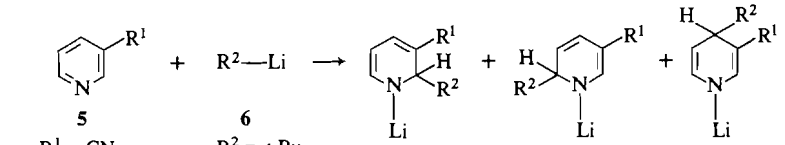

**5**

*a* $R^1 = CN$
*b* $R^1 = CONEt_2$
*c* $R^1 = CO_2Me$

**6**

*a* $R^2 = t\text{-Bu}$
*b* $R^2 = n\text{-Bu}$

**7** **8** **9**

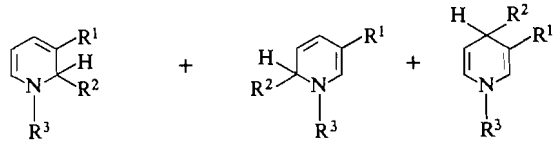

**10** **11** **12**

*a* $R^1 = CN, R^2 = t\text{-Bu}, R^3 = H$
*b* $R^1 = CN, R^2 = n\text{-Bu}, R^3 = H$
*c* $R^1 = CN, R^2 = t\text{-Bu}, R^3 = CO_2Me$
*d* $R^1 = CN, R^2 = n\text{-Bu}, R^3 = CO_2Me$
*e* $R^1 = CONEt_2, R^2 = t\text{-Bu}, R^3 = H$
*f* $R^1 = CONEt_2, R^2 = t\text{-Bu}, R^3 = CO_2Me$
*g* $R^1 = CONEt_2, R^2 = t\text{-Bu}, R^3 = Me$
*h* $R^1 = CO_2Me, R^2 = t\text{-Bu}, R^3 = H$
*i* $R^1 = CO\text{—}t\text{-Bu}, R^2 = t\text{-Bu}, R^3 = H$
*j* $R^1 = CO_2Me, R^2 = n\text{-Bu}, R^3 = H$
*k* $R^1 = CO_2Me, R^2 = n\text{-Bu}, R^3 = CO_2Me$
*l* $R^1 = CO\text{—}n\text{-Bu}, R^2 = n\text{-Bu}, R^3 = CO_2Me$

**13** **14**

*a* $R^1 = CN, R^2 = n\text{-Bu}$
*b* $R^1 = CONEt_2, R^2 = t\text{-Bu}$
*c* $R^1 = CO\text{—}t\text{-Bu}, R^2 = t\text{-Bu}$
*d* $R^1 = CO_2Me, R^2 = t\text{-Bu}$
*e* $R^1 = CO_2Me, R^2 = n\text{-Bu}$

*a* $R^1 = CO\text{—Bu-}n$
*b* $R^1 = CO\text{—Bu-}t$
*c* $R^1 = C(OH)\text{—}(n\text{-Bu})_2$

water to provide stable *N*-unsubstituted 1,2-(1,4-, 1,6-)dihydropyridines. The reaction of 3-cyano, 3-diethylaminocarbonyl, and 3-methoxycarbonylpyridines with alkyl lithiums now provides a useful reaction for the preparation of stabilized dihydropyridines.

Addition of 3-cyanopyridine (**5***a*) to an ethereal solution of *tert*-butyllithium (**6***a*) at −65°C results in the precipitation of a yellow solid, which is likely a mixture of **7** and **8**, since hydrolysis with water afforded a mixture which was separated by preparative hplc to give 1,2-dihydropyridine **10***a* (32.3%) and 1,6-dihydropyridine **11***a* (55.8%). No product **12***a* resulting from attack at the C-4 position was obtained. A similar reaction which involved addition of *n*-butyllithium (**6***b*) to **5***a* gave **10***b* (18.7%), **11***b* (51.4%), and 2-*n*-butyl-5-cyanopyridine **13***a* (6.9%). The aromatic product **13***a* arises from **11***b* during the hplc separation since it was not detected by $^1H$ nmr in the reaction product. A $^1H$ nmr study showed that a solution of **11***b* in $CDCl_3$ at 25°C oxidized slowly to **13***a* on standing with a **11***b*/**13***a* ratio of 15:100, 45:100, 55:100, and 77:100 after 2, 12, 18, and 25 days respectively. No product resulting from self condensation of **11***b* was observed.

The reaction of **7** and **8** with other electrophilic reagents was also investigated. Reaction of **7** and **8** ($R^1 = CN, R^2 = t\text{-Bu}$) with methyl chloroformate at −65°C gave a mixture of **10***c* and **11***c* (81.6%) in a ratio of 2:5 as determined from integration of the H-4 hydrogens at 7.24 and 6.58 δ for the respective compounds. A similar reaction of **7** and **8** ($R^1 = CN$, $R^2 = n\text{-Bu}$) afforded **10***d* (18.7%), **11***d* (48.1%), and **14***a* (14.1%) arising from reaction of *n*-butyl lithium with the 3-cyano substituent. The difficulty in separating **10***c* and **11***c* could be avoided by separating **10***a* and **11***a* by preparative hplc and regenerating the individual *N*-lithio derivatives prior to treatment with methylchloroformate.

The reaction of 3-diethylaminocarbonylpyridine **5***b* with *tert*-butyllithium was also studied with the

Can. J. Chem. Downloaded from www.nrcresearchpress.com by 210.87.254.6 on 09/06/12
For personal use only.

TABLE 1. Reactions of 3-substituted pyridines **5** with alkyllithiums **6** and electrophiles

| 3-Substituted pyridine **5** $R^1$ | Alkyllithium **6** $R^2$ | Electrophile $R^3$ | Yield (%) | | | | |
|---|---|---|---|---|---|---|---|
| | | | **10** | **11** | **12** | **13** | **14** |
| CN | *t*-Bu | H | 32.3 | 55.8 | | | |
| CN | *n*-Bu | H | 18.7 | 51.4 | | 6.9 (**13***a*)[a] | |
| CN | *t*-Bu | $CO_2Me$ | 23.3[b] | 58.3[b] | | | |
| CN | *n*-Bu | $CO_2Me$ | 18.7 | 48.1 | | | 14.1 (**14***a*) |
| $CONEt_2$[c] | *t*-Bu | H | | 11.5 | 14.1 | 27.0 (**13***b*)[d] | |
| $CONEt_2$ | *t*-Bu | $CO_2Me$ | | 26.3 | 39.8 | | |
| $CONEt_2$ | *t*-Bu | Me | | 44.5 | 39.5 | | |
| $CO_2Me$ | *t*-Bu | H | | 27.0 | 29.3 (**12***i*) | 13.4 (**14***c*) | 2.5 (**14***b*) |
| $CO_2Me$ | *n*-Bu | H | | 10.6 | 2.3 | 2.2 (**13***e*) | 11 (**14***a*) |
| | | | | | | | 35.5 (**14***c*) |
| $CO_2Me$ | *n*-Bu | $CO_2Me$ | | 16.9 | 3.2 (**12***l*) | | 18.2 (**14***c*) |

[a]Arises from the aromatization of **11***b* during preparative hplc.
[b]The percentage of **10***c* and **11***c* in the mixture was calculated from the integrals for the H-4 hydrogens at 7.24 and 6.58 δ for the respective compounds.
[c]Arises from dealkylative oxidation of **12***e* during preparative hplc (44.15% recovery).
[d]Arises from the oxidation of **11***e* during preparative hplc.

view of determining the influence of the 3-substituent upon the position of attack by the organolithium reagent and the stabilizing effect it imparts to the dihydropyridines produced. Reaction of *tert*-butyllithium with **5***b* followed by treatment with water afforded 1,6-dihydropyridine **11***e* (11.5%), 1,4-dihydropyridine **12***e* (14.1%), 3-diethylaminocarbonyl-6-*tert*-butylpyridine **13***b* (27%), and 3-diethylaminocarbonylpyridine **5***b* (44.15%). The $^1H$ nmr spectrum of the initial reaction mixture did not display aromatic pyridyl resonances and **5***b* could not be detected by tlc. Dihydropyridines usually undergo aromatization via a dehydrogenation reaction rather than loss of a substituent. However, dealkylative oxidation is particularly favoured when the substituent eliminated is capable of forming a stable carbonium ion and is assisted by relief of steric strain (8). For example, thermal or chemical oxidation of 3-(4, 4-dimethyloxazolin-2-yl)-4-*tert*-butyl-1,4-dihydropyridine was often accompanied by loss of the *tert*-butyl substituent (7). It is therefore expected that 3-dimethylaminocarbonylpyridine **5***b* arises due to dealkylative oxidation of **12***e* during preparative hplc, whereas **13***b* arises due to dehydrogenation of **11***e*. On the other hand, treatment of the *N*-lithio-1,2 and 1,6-dihydropyridyl intermediates **8** and **9** ($R^1 = CONEt_2$, $R^2 = t$-Bu) with methyl chloroformate gave only **11***f* (26.3%) and **12***f* (39.8%), whereas treatment with methyl iodide yielded **11***g* (44.5%) and **12***g* (39.5%). No product resulting from dealkylative oxidation was detected in these two latter reactions.

The reactions of 3-methoxycarbonylpyridine **5***c* with alkyllithiums **6***a* and **6***b* were more complex since products resulting from reaction with the methoxycarbonyl substituent were also produced. Thus reaction of *tert*-butyllithium with **5***c* and then treatment with water gave **11***h* (27%), **12***i* (29.3%), **13***c* (13.43%), **14***b* (2.5%), and a trace of **13***d*. It is not known whether **14***b* arises from reaction of *tert*-butyllithium with the methoxycarbonyl group of **5***c* and/or dealkylative oxidation of **12***i*. *n*-Butyllithium also reacted extensively with the methoxycarbonyl substituent of **5***c* to afford **11***j* (10.6%), **12***j* (2.3%), **13***e* (2.2%), **14***a* (11%), and **14***c* (35.5%) which arises from further reaction of **14***a* with *n*-butyllithium. A similar reaction of **5***c* with *n*-butyllithium and then with methyl chloroformate gave **11***k* (16.9%), **12***l* (3.2%), **14***c* (18.2%), and methyl nicotinate (33% recovery).

The 3-substituent of **5** influences the position of attack by alkyllithium reagents since 3-cyanopyridine undergoes attack at the C-2 and C-6 positions whereas 3-diethylaminocarbonylpyridine and 3-methoxycarbonylpyridine undergo addition to the C-4 and C-6 positions. The 3-cyano and 3-diethylaminocarbonyl substituents of **5** are quite stable toward alkyllithiums **6**, whereas a 3-methoxycarbonyl substituent competes readily with addition to the ring system. It is possible that reaction with the methoxycarbonyl substituent of **5***c* could be prevented by replacing the methyl by a bulky group such as *tert*-butyl, since it has been reported that Grignard reagents do not react with the carbonyl group of 3-mesityl(duryl)carbonylpyridine (9, 10).

The 3-cyano group appears to have a greater stabilizing effect than a 3-methoxycarbonyl or 3-diethylaminocarbonyl substituent for 1,6-dihydropyridines since 3-cyano-6-*tert*-butyl-1,6-dihydropyridine **11***a* was more stable toward oxygen and heat than the 3-methoxycarbonyl and 3-diethylaminocarbonyl analogs **11***h* and **11***e*. 3-Cyano-6-*tert*-butyl-1,6-dihydropyridine **11***a* was more stable than 3-cyano-6-*n*-butyl-1,6-dihydropyridine

Can. J. Chem. Downloaded from www.nrcresearchpress.com by 210.87.254.6 on 09/06/12
For personal use only.

**11***b*. On the other hand, 4-*n*-butyl-1,4-dihydropyridines appear to be more stable than the corresponding 4-*tert*-butyl-1,4-dihydropyridine analogs since the latter undergo dealkylative oxidation quite readily. The *N*-methoxycarbonyl and *N*-methyl 1,2-, 1,4-, and 1,6-dihydropyridines are more stable than the corresponding *N*-unsubstituted analogs.

## Experimental

Melting points were determined with a Büchi capillary apparatus and are uncorrected. Nuclear magnetic resonance spectra were determined for solutions in deuterochloroform with TMS as internal standard with a Varian EM-360A or Bruker WH-200 spectrometer. Infrared spectra (sodium chloride films unless otherwise noted) were taken on a Unicam SP-1000 or Perkin–Elmer-267 spectrometer. Preparative high pressure liquid chromatography was performed using a Water's Prep LC/System 500A using Prep Pak-500 silica cartridges. Mass spectra were measured with an AEI-MS-50 mass spectrometer and these exact mass measurements are used in lieu of elemental analysis. All of the products described gave rise to a single spot on tlc using a solvent system of low, medium, and high polarity. No residue remained after combustion of the products.

*2-*tert*-Butyl-3-cyano-1,2-dihydropyridine (**10**a) and 3-cyano-6-*tert*-butyl-1,6-dihydropyridine (**11**a)*

A solution of 3-cyanopyridine (1.04 g, 10 mmol) in 20 mL dry ether was added dropwise during 30 min to a solution of *tert*-butyllithium (0.768 g, 12 mmol) in 8 mL hexane under a nitrogen atmosphere, at −65°C with stirring. The resulting solution, in which a pale yellow precipitate forms, was allowed to stir for 30 min at −65°C prior to warming slowly to 25°C. Water (20 mL) was added and stirring was continued for 15 min. Extraction with ether (4 × 50 mL), drying ($Na_2SO_4$), and removal of the solvent *in vacuo* gave a pale yellow oil which was separated by preparative hplc using petroleum ether (bp 30–60°C) – ether (7:3 v/v) at a flow rate of 250 mL/min. Removal of the solvent from the peak having a retention time of 4.6–7.2 min gave **10***a* as a pale yellow oil (0.523 g, 32.3%); ir: 3380 (m, NH) and 2210 (s, C≡N) $cm^{-1}$; $^1H$ nmr δ: 0.96 (s, 9H, —C—$Me_3$), 3.92 (d, $J_{NH,2}$ = 4.8 Hz, 1H, H-2), 4.75 (br s, 1H, NH, exchanges with deuterium oxide), 4.75 (d, $J_{4,5}$ = 7.2 Hz of d, $J_{5,6}$ = 7.2 Hz of d, $J_{5,NH}$ = 1.8 Hz, 1H, H-5), 6.62 (d, $J_{5,6}$ = 7.2 Hz of d, $J_{NH,6}$ = 7.2 Hz of d, $J_{4,6}$ = 1.2 Hz, 1H, H-6), 6.84 (d, $J_{4,5}$ = 7.2 Hz of d, $J_{4,6}$ = 1.2 Hz, 1H, H-4). *Exact Mass* calcd. for $C_{10}H_{14}N_2$: 162.1155; found (high resolution ms): 162.1149. Collection of the peak with retention time of 12.4–16.4 min and removal of the solvent *in vacuo* gave **11***a* (0.91 g, 55.8%) as a pale yellow oil; ir: 3370 (m, NH) and 2205 (s, C≡N) $cm^{-1}$; $^1H$ nmr δ: 0.9 (s, 9H, C—$Me_3$), 3.95 (d, $J_{5,6}$ = 4.5 Hz of d, $J_{NH,6}$ = 2 Hz, 1H, H-6), 5.1 (d, $J_{4,5}$ = 9.75 Hz of d, $J_{5,6}$ = 4.5 Hz of d, $J_{NH,5}$ = 1.5 Hz, 1H, H-5), 5.8 (br s, 1H, NH, exchanges with deuterium oxide), 5.95 (d, $J_{4,5}$ = 9.75 Hz, 1H, H-4), 7.05 (d, $J_{NH,2}$ = 7 Hz, 1H, H-2, collapses to a singlet after exchange with deuterium oxide). *Exact Mass* calcd. for $C_{10}H_{14}N_2$: 162.1155; found (high resolution ms): 162.1156.

*2-n-Butyl-3-cyano-1,2-dihydropyridine (**10**b), 3-cyano-6-n-butyl-1,6-dihydropyridine (**11**b), and 2-n-butyl-5-cyanopyridine (**13**a)*

A solution of *n*-butyllithium (1.28 g, 20 mmol) in 9.2 mL hexane was added dropwise to a solution of 3-cyanopyridine (2.08 g, 20 mmol) in 75 mL dry tetrahydrofuran, under a nitrogen atmosphere, at −65°C with stirring. The resulting solution, in which a pale yellow precipitate forms, was allowed to stir for 1 h at −65°C prior to warming slowly to 25°C. Water (25 mL) was added. Extraction with ether (4 × 50 mL), drying ($Na_2SO_4$), and removal of the solvent *in vacuo* at 30–35°C afforded a pale yellow oil which was separated by preparative hplc using petroleum ether (bp 30–60°C) – ethyl acetate (9:1 v/v) at a flow rate of 250 mL/min. The eluant was collected in 100 mL fractions which were analyzed using $^1H$ nmr. Removal of the solvent from the 1200–1700 mL fractions gave **10***b* as a yellow oil (0.60 g, 18.7%); ir: 3360 (m, NH) and 2242 (s, C≡N) $cm^{-1}$; $^1H$ nmr δ: 0.95 (t, $J$ = 7 Hz, 3H, $CH_2CH_3$), 1.1–1.9 (m, 6H, $CH_2CH_2CH_2CH_3$), 4.2 (m, 1H, H-2), 4.8 (d, $J_{4,5}$ = 7 Hz of d, $J_{5,6}$ = 6 Hz of d, $J_{NH,5}$ = 1.5 Hz, 1H, H-5), 5.1 (br s, 1H, NH, exchanges with deuterium oxide), 6.4–6.85 (m, 2H, H-4, H-6). *Exact Mass* calcd. for $C_{10}H_{14}N_2$: 162.1155; found (high resolution ms): 162.1152. Collection of the 2000–3500 mL eluant gave a mixture of **11***b* as a yellow oil (1.566 g, 48.6%); ir: 3345 (s, NH) and 2210 (s, C≡N) $cm^{-1}$; $^1H$ nmr δ: 1.0 (t, $J$ = 7 Hz, 3H, $CH_2CH_3$), 1.15–1.9 (m, 6H, $CH_2CH_2CH_2CH_3$), 4.25 (m, 1H, H-6), 5.03 (d, $J_{4,5}$ = 9.75 Hz of d, $J_{5,6}$ = 4 Hz of d, $J_{5,NH}$ = 1.5 Hz, 1H, H-5), 5.55 (br s, 1H, NH, exchanges with deuterium oxide), 5.85 (d, $J_{4,5}$ = 9.75 Hz, 1H, H-4), 6.96 (d, $J_{2,NH}$ = 6.5 Hz, 1H, H-2, collapses to a singlet after addition of deuterium oxide). *Exact Mass* calcd. for $C_{10}H_{14}N_2$: 162.1155; found (high resolution ms): 162.1155; and **13***a* as a yellow oil (0.111 g, 3.45%); ir: 2240 (s, C≡N) $cm^{-1}$; $^1H$ nmr δ: 1.0 (t, $J$ = 7 Hz, 3H, $CH_2CH_3$), 1.15–2.1 (m, 4H, $CH_2CH_2CH_2CH_3$), 3.0 (t, $J$ = 7 Hz, $CH_2CH_2CH_2CH_3$), 7.38 (d, $J_{4,5}$ = 8 Hz, 1H, H-5), 8.0 (d, $J_{4,5}$ = 8 Hz of d, $J_{4,6}$ = 2 Hz, 1H, H-4), 8.9 (d, $J_{4,6}$ = 2Hz, 1H, H-6). *Exact Mass* calcd. for $C_{10}H_{12}N_2$: 160.0999; found (high resolution ms): 160.0998. The ratio of **11***b* and **13***a* was calculated from the integrals of the respective H-2 absorptions. Removal of the solvent from the 3600–3900 mL fractions also afforded a mixture of **11***b* (0.088 g, 2.8%) and **13***a* (0.111 g, 3.47%).

*1-Methoxycarbonyl-2-*tert*-butyl-3-cyano-1,2-dihydropyridine (**10**c) and 1-methoxycarbonyl-3-cyano-6-*tert*-butyl-1,6-dihydropyridine (**11**c)*

A solution of 3-cyanopyridine (1.04 g, 10 mmol) in 20 mL dry ether was added dropwise during 15 min to a solution of *tert*-butyllithium (0.768 g, 12 mmol) in 8 mL hexane, under a nitrogen atmosphere, at −65°C with stirring. The resulting solution, in which a pale yellow precipitate forms, was stirred for 30 min at −65°C after which methyl chloroformate (1.034 g, 11 mmol) was added. After an additional 30 min at −65°C, the reaction mixture was allowed to return to 25°C prior to addition of 20 mL water. Extraction with ether (4 × 50 mL), drying ($Na_2SO_4$), and removal of the solvent *in vacuo* gave a pale yellow oil (2.2 g). An aliquot of this product (0.512 g) was purified on ten 8 in. × 8 in. silica gel G plates, 1.0 mm in thickness, using petroleum ether – ether (5:5 v/v) as development solvent. Extraction of the band having $R_f$ 0.7 using warm absolute ethanol gave a mixture of **10***c* and **11***c* (1.79 g, 81.6%) in a ratio of 2:5 as determined by integration of the H-4 hydrogens at 7.24 and 6.58 δ for the respective compounds; ir: 2235 (s, C≡N), 1750 (s, CO), and 1730 (s, CO) $cm^{-1}$. The $^1H$ nmr spectrum of **10***c* showed the following absorptions, δ: 0.88 (s, 9H, C—$Me_3$), 3.9 (s, 3H, OMe), 4.84 (s, 1H, H-2), 5.6 (m, 1H, H-5), 6.92 (d, $J_{5,6}$ = 6 Hz, 1H, H-6), 7.24 (d, $J_{4,5}$ = 9.75 Hz, 1H, H-4), while **11***c* exhibited δ: 0.88 (s, 9H, C—$Me_3$), 3.9 (s, 3H, OMe), 4.74 (d, $J_{5,6}$ = 5.5 Hz, 1H, H-6), 5.6 (m, 1H, H-5), 6.15 (d, $J_{4,5}$ = 9.5 Hz, 1H, H-4), 7.68 (s, 1H, H-2). *Exact Mass* calcd. for $C_{12}H_{16}N_2O_2$: 220.1209; found (high resolution ms): 220.1207. Repeated attempts to separate **10***c* and **11***c* by hplc and glc were unsuccessful.

*1-Methoxycarbonyl-2-n-butyl-3-cyano-1,2-dihydropyridine (**10**d), 1-methoxycarbonyl-3-cyano-6-n-butyl-1,6-dihydropyridine (**11**d), and 3-pentanoylpyridine (**14**a)*

A solution of *n*-butyllithium (0.672 g, 10.5 mmol) in 4.3 mL

Can. J. Chem. Downloaded from www.nrcresearchpress.com by 210.87.254.6 on 09/06/12
For personal use only.

Can. J. Chem. Downloaded from www.nrcresearchpress.com by 210.87.254.6 on 09/06/12
For personal use only.

hexane was added dropwise to a solution of 3-cyanopyridine (1.04 g, 10 mmol) in 60 mL dry tetrahydrofuran, under an atmosphere of nitrogen, at −65°C with stirring. The mixture was allowed to stir for 30 min after which methyl chloroformate (0.87 g, 9.3 mmol) was added. The reaction was allowed to proceed for 30 min at −65°C with stirring prior to warming to 25°C. Water (20 mL) was added. Extraction with ether (4 × 50 mL), drying ($Na_2SO_4$), and removal of the solvent *in vacuo* gave a yellow oil which was purified by preparative hplc using hexane – ethyl acetate (9:1 v/v) at a flow rate of 250 mL/min. Removal of the solvent from the eluant having a retention time of 8.6–14 min gave a mixture of **10***d* and **11***d* as a pale yellow oil (1.47 g, 67.1%) in a ratio of 1:2.6 as determined by integration of the H-4 hydrogens at 7.08 and 5.96 δ for the respective compounds. Preparative glc of this hplc purified fraction, using a 6 ft × 1/4 in. column packed with 5% OV-101 on Chrom W (80–100 mesh) with a helium flow rate of 60 mL/min and a column temperature of 180°C, afforded a mixture of **10***d* and **11***d* in a ratio of 2:1 with a retention time of 9 min; ir: 2218 (s, C≡N) and 1735 (s, CO) $cm^{-1}$. The $^1H$ nmr spectrum of this mixture displayed the following absorptions for **10***d*: δ: 0.9 (t, $J$ = 7 Hz, 3H, $CH_2CH_2CH_2CH_3$), 1.2–1.8 (m, 6H, $CH_2CH_2CH_2CH_3$), 3.88 (s, 3H, OMe), 5.02 (m, 1H, H-2), 5.42 (m, 1H, H-5), 6.72 (d, $J_{5,6}$ = 6 Hz, 1H, H-6), 7.1 (d, $J_{4,5}$ = 9.75 Hz, 1H, H-4). *Exact Mass* calcd. for $C_{12}H_{16}N_2O_2$: 220.1210; found (high resolution ms): 220.1209. Collection of the peak with a retention time of 16 min gave a pure sample of **11***d*; ir: 2230 (s, C≡N) and 1745 (s, CO) $cm^{-1}$. $^1H$ nmr δ: 0.9 (t, $J$ = 7 Hz, 3H, $CH_2CH_2CH_2CH_3$), 1.2–1.8 (m, 6H, $CH_2CH_2CH_2$-$CH_3$), 3.88 (s, 3H, OMe), 4.84 (m, 1H, H-6), 5.66 (d, $J_{4,5}$ = 9.75 Hz of d, $J_{5,6}$ = 6 Hz, 1H, H-5), 5.96 (d, $J_{4,5}$ = 9.75 Hz, 1H, H-4), 7.52 (s, 1H, H-2). *Exact Mass* calcd. for $C_{12}H_{16}N_2O_2$: 220.1210; found (high resolution ms): 220.1211.

Removal of the solvent from the preparative hplc fraction having a retention time of 20.8–27.6 min gave a semi-solid product which was purified further using six 8 in. × 8 in. silica gel G plates, 1.0 mm in thickness, using chloroform – ethyl acetate (1:1 v/v) as development solvent. Extraction of the band having $R_f$ 0.4 using warm absolute ethanol afforded **14***a* (0.23 g, 14.1%); ir: 1690 (CO) $cm^{-1}$; $^1H$ nmr δ: 0.95 (t, $J$ = 7 Hz, 3H, $CH_2CH_2CH_2CH_3$), 1.1–2.1 (m, 4H, $CH_2CH_2CH_2CH_3$), 3.0 (t, $J$ = 7 Hz, CO—$CH_2$), 7.42 (d, $J_{4,5}$ = 8 Hz of d, $J_{5,6}$ = 5 Hz, 1H, H-5), 8.25 (d, $J_{4,5}$ = 8 Hz of d, $J_{2,4}$ = 2 Hz of d, $J_{4,6}$ = 2 Hz, 1H, H-4), 8.8 (d, $J_{5,6}$ = 5 Hz of d, $J_{4,6}$ = 2 Hz, 1H, H-6), 9.2 (d, $J_{2,4}$ = 2 Hz, 1H, H-2). *Exact Mass* calcd. for $C_{10}H_{13}NO$: 163.0995; found (high resolution ms): 163.0993.

*3-Diethylaminocarbonyl-6-*tert*-butyl-1,6-dihydropyridine (**11**e), 3-diethylaminocarbonyl-4-*tert*-butyl-1,4-dihydropyridine (**12**e), 3-diethylaminocarbonyl-6-*tert*-butylpyridine (**13**b), and 3-diethylaminocarbonylpyridine (**5**b)*

A solution of 3-diethylaminocarbonylpyridine (2.55 g, 15 mmol) in 60 mL dry tetrahydrofuran was added dropwise during 30 min to a solution of *tert*-butyllithium (0.43 g, 18 mmol) in 12 mL hexane, under a nitrogen atmosphere, at −65°C with stirring. The reaction mixture was stirred at −65°C for a further 30 min before warming to room temperature. Water (30 mL) was added. Extraction with ether (4 × 50 mL), drying ($Na_2SO_4$), and removal of the solvent *in vacuo* gave 3.40 g of a yellow viscous oil. The $^1H$ nmr spectrum of this oil did not exhibit any aromatic pyridine absorptions. Trituration of the above product with 3 mL ether resulted in the precipitation of **12***e* as a white solid (0.15 g, 4.24%); mp 111°C; ir (KBr): 1672 (s, $CONEt_2$) and 3290 (s, NH) $cm^{-1}$; $^1H$ nmr δ: 0.75 (s, 9H, *t*-Bu), 1.15 (t, $J$ = 7 Hz, 6H, $CH_2CH_3$), 3.1–3.9 (m, 5H, $CH_2CH_3$, H-4), 4.64 (d, $J_{5,6}$ = 8 Hz of d, $J_{4,5}$ = 6 Hz of d, $J_{5,NH}$ = 2 Hz, 1H, H-5), 5.86 (broad s, 1H, NH, exchanges with deuterium oxide), 6.16 (d, $J_{5,6}$ = 8 Hz of d, $J_{NH,6}$ = 4.5 Hz, 1H, H-6), 6.48 (d, $J_{NH,2}$ = 5.5 Hz, 1H, H-2, collapses to a singlet after deuterium oxide exchange). *Exact Mass* calcd. for $C_{14}H_{24}N_2O$: 236.1892; found (high resolution ms): 236.1888. The remainder of the product was separated by preparative hplc using petroleum ether (bp 30–60°C) – ethyl acetate (8.5:1.5 v/v) at a flow rate of 250 mL/min. One hundred mL fractions were collected. Fractions 7–17 contained **13***b* (0.153 g, 4.32%) which arises from aromatization of **11***e* on the column; ir: 1640 (s, $CONEt_2$) $cm^{-1}$; $^1H$ nmr δ: 1.22 (t, $J$ = 7 Hz, 6H, $CH_2CH_3$), 1.38 (s, 9H, *t*-Bu), 3.48 (m, 4H, $CH_2CH_3$), 7.42 (d, $J_{4,5}$ = 8 Hz, 1H, H-5), 7.7 (d, $J_{4,5}$ = 8 Hz of d, $J_{2,4}$ = 2.5 Hz, 1H, H-4), 8.66 (d, $J_{2,4}$ = 2.5 Hz, 1H, H-2). *Exact Mass* calcd. for $C_{14}H_{22}N_2O$: 234.1728; found (high resolution ms): 234.1726. Removal of the solvent from fractions 18–26 gave a mixture of **12***e* (0.349 g, 9.86%) and **5***b* (0.931 g, 34.9%) as determined by integration of H-5 for **12***e* at 4.64 δ and H-2 and H-6 for **5***b* at 8.56 δ. The $^1H$ nmr spectrum of this mixture was identical to an authentic mixture of the two pure products. Fractions 27–30 contained **5***b* (0.247 g, 9.25%), identical (ir, $^1H$ nmr) with an authentic sample. Removal of the solvent from fractions 31–46 gave additional **13***b* (0.197 g, 5.62%), whereas fractions 47–57 were composed of a mixture of **13***b* (0.305 g, 8.67%) and **11***e* (0.407 g, 11.5%) as shown by $^1H$ nmr integration of H-2 for **13***b* at 8.66 δ and of H-4 for **11***e* at 6.13 δ. The 1,6-dihydropyridine **11***e* exhibited the following spectral data; ir: 3350 (m, NH) $cm^{-1}$; $^1H$ nmr δ: 0.88 (s, 9H, *t*-Bu), 1.12 (t, $J$ = 7, 6H, $CH_2CH_3$), 3.1–3.62 (m, 4H, $CH_2CH_3$), 3.82 (d, $J_{5,6}$ = 4.5 Hz of d, $J_{NH,6}$ = 2 Hz, 1H, H-6), 4.93 (d, $J_{4,5}$ = 9.5 Hz of d, $J_{5,6}$ = 4.5 Hz of d, $J_{NH,5}$ = 1.5 Hz, 1H, H-5), 5.42 (broad s, 1H, NH, exchanges with deuterium oxide), 6.13 (d, $J_{4,5}$ = 9.5 Hz, 1H, H-4), 7.06 (d, $J_{2,NH}$ = 6 Hz, 1H, H-2, collapses to a singlet after exchange with deuterium oxide). Removal of the solvent from fractions 58–68 gave additional **13***b* (0.304 g, 8.64%).

*1-Methoxycarbonyl-3-diethylaminocarbonyl-6-*tert*-butyl-1,6-dihydropyridine (**11**f) and 1-methoxycarbonyl-3-diethylaminocarbonyl-4-*tert*-butyl-1,4-dihydropyridine (**12**f)*

A solution of 3-diethylaminocarbonylpyridine (2.55 g, 15 mmol) in 60 mL dry tetrahydrofuran was added dropwise during 30 min to a solution of *tert*-butyllithium (0.43 g, 18 mmol) in 12 mL hexane, under a nitrogen atmosphere, at −65°C with stirring. Stirring was continued at −65°C for 30 min after which methyl chloroformate (1.41 g, 15 mmol) was added. The reaction mixture was allowed to return to 25°C, after stirring at −65°C for 30 min, and 30 mL water was added. Extraction with ether (4 × 50 mL), drying ($Na_2SO_4$), and removal of the solvent *in vacuo* gave an oil (3.52 g) which was subjected to preparative hplc using petroleum ether (bp 30–60°C) – chloroform (7:3 v/v) with a flow rate of 250 mL/min. One hundred mL fractions were collected. Removal of the solvent from fraction 27 gave a mixture of two dihydropyridines **11***f* and **12***f* (3.105 g). An aliquot (0.528 g) of this mixture was separated by preparative tlc on eight 8 in. × 8 in. plates, 1.0 mm in thickness, using petroleum ether – ethyl acetate (7:3 v/v) as development solvent. Extraction of the band having $R_f$ 0.6 gave **12***f* (0.298 g, 39.8%) as a yellow oil; ir: 1730 (s, $CO_2Me$) $cm^{-1}$; $^1H$ nmr δ: 0.88 (s, 9H, *t*-Bu), 1.25 (t, $J$ = 7 Hz, 6H, $CH_2CH_3$), 3.24–3.83 (m, 5H, $CH_2CH_3$, H-4), 5.18 (d, $J_{5,6}$ = 8 Hz of d, $J_{4,5}$ = 5 Hz, 1H, H-5), 6.95 (d, $J_{4,5}$ = 8 Hz, 1H, H-4), 7.22 (s, 1H, H-2). *Exact Mass* calcd. for $C_{16}H_{26}N_2O_3$: 294.1928; found (high resolution ms): 294.1921. Extraction of the band having $R_f$ 0.4 afforded **11***f* (0.1982 g, 26.3%) as an oil; ir: 1730 (s, $CO_2Me$) $cm^{-1}$; $^1H$ nmr δ: 0.9 (s, 9H, *t*-Bu), 1.15 (t, $J$ = 7 Hz, 6H, $CH_2CH_3$), 3.42 (q, $J$ = 7 Hz, 4H, $CH_2CH_3$), 6.7 (d, $J_{5,6}$ = 5.5 Hz, 1H, H-6), 5.64 (d, $J_{4,5}$ = 9.75 Hz of d, $J_{5,6}$ = 5.5 Hz, 1H, H-5), 6.26 (d, $J_{4,5}$ = 9.75 Hz, 1H, H-4), 7.22 (s, 1H, H-2). *Exact Mass* calcd. for $C_{16}H_{26}N_2O_3$: 294.1928; found (high resolution ms): 294.1921.

*1-Methyl-3-diethylaminocarbonyl-6-*tert*-butyl-1,6-dihydropyridine (**11**g) and 1-methyl-3-diethylaminocarbonyl-4-*tert*-butyl-1,4-dihydropyridine (**12**g)*

A solution of 3-diethylaminocarbonylpyridine (2.55 g, 15

Can. J. Chem. Downloaded from www.nrcresearchpress.com by 210.87.254.6 on 09/06/12
For personal use only.

mmol) in 60 mL dry tetrahydrofuran was added dropwise during 30 min to a solution of *tert*-butyllithium (0.43 g, 18 mmol) in 12 mL hexane, under a nitrogen atmosphere, at −65°C with stirring. Stirring was continued at −65°C for 30 min after which methyl iodide (2.13 g, 15 mmol) was added. The reaction mixture was allowed to return to 25°C, after stirring at −65°C for 30 min, and then 30 mL water was added. Extraction with ether (4 × 50 mL), drying ($Na_2SO_4$), and removal of the solvent *in vacuo* gave 3.375 g of a yellow oil. An aliquot of this product (0.721 g) was purified by preparative tlc using ten 8 in. × 8 in. silica gel G plates, 1.0 mm in thickness, using petroleum ether (bp 30–60°C) – ethyl acetate (2:7 v/v) as development solvent. Extraction of the band having $R_f$ 0.7 using warm absolute ethanol gave **12***g* (0.316 g, 39.5%) as a yellow oil; ir: 1680 (s, $CONEt_2$) $cm^{-1}$; $^1H$ nmr δ: 0.78 (s, 9H, *t*-Bu), 1.18 (t, $J$ = 7 Hz, 6H, $CH_2CH_3$), 2.96 (s, 3H, N—Me), 3.1–3.9 (m, 5H, $CH_2CH_3$, H-4), 4.62 (d, $J_{5,6}$ = 8 Hz of d, $J_{4,5}$ = 5.5 Hz, 1H, H-5), 5.96 (d, $J_{5,6}$ = 8 Hz of d, $J_{4,6}$ = 1.5 Hz, 1H, H-6), 6.35 (d, $J_{2,4}$ = 1.5 Hz, 1H, H-2). *Exact Mass* calcd. for $C_{15}H_{26}N_2O$: 250.2043; found (high resolution ms): 250.2042. Extraction of the band having $R_f$ 0.5 yielded **11***g* (0.356 g, 44.5%) as a yellow oil; ir: 1650 (s, $CONEt_2$) $cm^{-1}$; $^1H$ nmr δ: 0.90 (s, 9H, *t*-Bu), 1.18 (t, $J$ = 7 Hz, 6H, $CH_2CH_3$), 3.12 (s, 3H, N—Me), 3.44 (q, $J$ = 7 Hz, 4H, $CH_2CH_3$), 3.70 (d, $J_{5,6}$ = 5.5 Hz of d, $J_{4,6}$ = 1.5 Hz, 1H, H-6), 4.94 (d, $J_{4,5}$ = 9.75 Hz of d, $J_{5,6}$ = 5.5 Hz, 1H, H-5), 6.33 (d, $J_{4,5}$ = 9.75 Hz of d, $J_{4,6}$ = 1.5 Hz, 1H, H-4), 7.02 (s, 1H, H-2). *Exact Mass* calcd. for $C_{15}H_{26}N_2O$: 250.2043; found (high resolution ms): 250.2031.

*3-Methoxycarbonyl-6-*tert*-butyl-1,6-dihydropyridine (**11**h), 3-*tert*-butylcarbonyl-4-*tert*-butyl-1,4-dihydropyridine (**12**i), 3-*tert*-butylcarbonyl-6-*tert*-butylpyridine (**13**c), 3-methoxycarbonyl-6-*tert*-butylpyridine (**13**d), and 3-*tert*-butylcarbonylpyridine (**14**b)*

A solution of 3-methoxycarbonylpyridine (2.74 g, 20 mmol) in 60 mL dry tetrahydrofuran was added dropwise during 30 min to a solution of *tert*-butyllithium (1.536 g, 24 mmol) in 16 mL hexane, under an atmosphere of nitrogen, at −65°C with stirring. The resulting solution was allowed to stir for 30 min at −65°C prior to warming slowly to 25°C. Water (30 mL) was added. Extraction with ether (4 × 50 mL), drying ($Na_2SO_4$), and removal of the solvent *in vacuo* gave a pale yellow oil which was separated by preparative hplc using methylene chloride – ethyl acetate (30:1 v/v) at a flow rate of 250 mL/min. One hundred mL fractions were collected. Fractions 4–7 contained **12***i* (1.3 g, 29.3%) which contained a trace of **14***b* arising from aromatization of **12***i*; ir: 3320 (m, NH) and 1665 (s, CO) $cm^{-1}$; $^1H$ nmr δ: 0.72 (s, 9H, $C_4$—*t*-Bu), 1.36 (s, 9H, CO—*t*-Bu), 3.5 (d, $J_{4,5}$ = 6 Hz, 1H, H-4), 4.9 (d, $J_{5,6}$ = 8 Hz of d, $J_{4,5}$ = 6 Hz of d, $J_{NH,5}$ = 2 Hz, 1H, H-5), 6.25 (d, $J_{5,6}$ = 8 Hz of d, $J_{NH,6}$ = 4.5 Hz, 1H, H-6), 6.8 (broad s, 1H, NH, exchanges with deuterium oxide), 7.5 (d, $J_{NH,2}$ = 5.5 Hz, 1H, H-2, collapses to a singlet after deuterium oxide exchange). The mass spectrum did not exhibit a molecular ion for $C_{14}H_{23}NO$ at *m/e* 221 but it did show a $M-2$ peak due to facile loss of $H_2$ and a $M-C_4H_9$ peak due to loss of a *tert*-butyl ion. *Exact Mass* calcd. for $C_{14}H_{21}NO$: 219.1602; found (high resolution ms): 219.1586. *Exact Mass* calcd. for $C_{10}H_{13}NO$: 164.1076; found (high resolution ms): 164.1075. The CI ms showed a $M+1$ ion at *m/e* 222 for the parent compound. Removal of the solvent from fraction 8 gave **14***b* (0.081 g, 2.5%); ir: 1690 (s, CO) $cm^{-1}$; $^1H$ nmr δ: 1.3 (s, 9H, *t*-Bu), 7.35 (d, $J_{4,5}$ = 8 Hz of d, $J_{5,6}$ = 6 Hz, 1H, H-5), 8.02 (d, $J_{4,5}$ = 8 Hz of d, $J_{4,6}$ = 2 Hz of d, $J_{2,4}$ = 2 Hz, 1H, H-4), 8.72 (d, $J_{5,6}$ = 6 Hz of d, $J_{4,6}$ = 2 Hz, 1H, H-6), 9.0 (d, $J_{2,4}$ = 2 Hz, 1H, H-2). *Exact Mass* calcd. for $C_{10}H_{13}NO$: 163.0993; found (high resolution ms): 163.0988. Fractions 12–24 were composed primarily of **11***h* along with a trace of **13***d* which arises from aromatization of **11***h* (1.05 g, 27.0%). The 1,6-dihydropyridine **11***h* exhibited ir: 3340 (m, NH) and 1735 (s, $CO_2$) $cm^{-1}$; $^1H$ nmr δ: 0.88 (s, 9H, *t*-Bu), 3.65 (s, 3H, OMe), 3.8 (m, 1H, H-6), 5.05 (d, $J_{4,5}$ = 9.75 Hz of d, $J_{5,6}$ = 4 Hz of d, $J_{NH,5}$ = 2 Hz, 1H, H-5), 5.35 (br s, 1H, NH, exchanges with deuterium oxide), 6.48 (d, $J_{4,5}$ = 9.75 Hz of d, $J_{2,4}$ = 2 Hz, 1H, H-4), 7.5 (d, $J_{NH,2}$ = 6 Hz of d, $J_{2,4}$ = 2 Hz, 1H, H-2, collapses to a d, $J_{2,4}$ = 2 Hz after exchange with deuterium oxide). The mass spectrum did not show a $M^+$ at *m/e* 195 for $C_{11}H_{17}NO_2$ but it did exhibit a $M-2$ peak due to the facile loss of $H_2$. *Exact Mass* calcd. for $C_{11}H_{15}NO_2$: 193.1099; found (high resolution ms): 193.1096. Compond **13***d* showed: $^1H$ nmr δ: 1.36 (s, 9H, *t*-Bu), 3.95 (s, 3H, OMe), 7.46 (d, $J_{4,5}$ = 8 Hz, 1H, H-5), 8.26 (d, $J_{4,5}$ = 8 Hz of d, $J_{2,4}$ = 2 Hz, 1H, H-4), 9.2 (d, $J_{2,4}$ = 2 Hz, 1H, H-2). *Exact Mass* calcd. for $C_{11}H_{15}NO_2$: 193.1099; found (high resolution ms): 193.1096. Fractions 24–30 contained **13***c* (0.588 g, 13.43%); ir: 1690 (s, CO) $cm^{-1}$; $^1H$ nmr δ: 1.36 (s, 18H, *t*-Bu), 7.42 (d, $J_{4,5}$ = 8 Hz, 1H, H-5), 8.08 (d, $J_{4,5}$ = 8.5 Hz of d, $J_{2,4}$ = 2 Hz, 1H, H-4), 9.08 (d, $J_{2,4}$ = 2 Hz, 1H, H-2). *Exact Mass* calcd. for $C_{14}H_{21}NO$: 219.1622; found (high resolution ms): 219.1621.

*3-Methoxycarbonyl-6-*n*-butyl-1,6-dihydropyridine (**11**j), 3-methoxycarbonyl-4-*n*-butyl-1,4-dihydropyridine (**12**j), 3-methoxycarbonyl-6-*n*-butylpyridine (**13**e), 3-pentanoylpyridine (**14**a), and 3-[1-(1-hydroxy-1-*n*-butyl pentyl)]pyridine (**14**c)*

A solution of *n*-butyllithium (1.34 g, 20.1 mmol) in 8.6 mL hexane was added dropwise to a solution of methyl nicotinate (2.74 g, 20 mmol) in 60 mL dry tetrahydrofuran, under an atmosphere of nitrogen, at −65°C with stirring. The reaction was allowed to proceed for 60 min at −65°C prior to warming to 25°C. Water (30 mL) was added. Extraction with ether (4 × 50 mL), drying ($Na_2SO_4$), and removal of the solvent *in vacuo* gave an oil which was separated by preparative hplc using ether–chloroform (1:1 v/v) at a flow rate of 250 mL/min. One hundred mL fractions were collected. Removal of the solvent from the 700–775 mL fraction gave a mixture of **12***j* (0.09 g, 2.3%) and **13***e* (0.03 g, 0.8%) in a ratio of 3:1 as determined by integration of H-6 of **12***j* and H-2 of **13***e* at 6.1 and 9.18 δ respectively. The 1,4-dihydropyridine **12***j*; exhibited the following spectra; ir: 3350 (m, NH) and 1732 (s, $CO_2$) $cm^{-1}$; $^1H$ nmr δ: 0.7–1.9 (m, 9H, *n*-Bu), 3.55 (m, 1H, H-4), 3.72 (s, 3H, OMe), 4.9 (d, $J_{5,6}$ = 8 Hz of d, $J_{4,5}$ = 5 Hz of d, $J_{NH,5}$ = 2 Hz, 1H, H-5), 6.1 (d, $J_{5,6}$ = 8 Hz of d, $J_{NH,6}$ = 4.5 Hz, 1H, H-6), 7.35 (br s, 1H, NH, exchanges with deuterium oxide), 7.35 (d, $J_{NH,2}$ = 5.5 Hz, 1H, H-2, collapses to a singlet after exchange with deuterium oxide). The mass spectrum did not exhibit a molecular ion for $C_{11}H_{17}NO_2$ at *m/e* 195; it did show a $M-2$ peak due to the facile loss of $H_2$. *Exact Mass* calcd. for $C_{11}H_{15}NO_2$: 193.1100; found (high resolution ms): 193.1098. Collection of the 800–1100 mL fractions gave **11***j* (0.41 g, 10.6%); ir: 3350 (m, NH) and 1732 (s, $CO_2Me$) $cm^{-1}$; $^1H$ nmr δ: 0.88 (t, $J$ = 7 Hz, 3H, —$CH_2CH_2CH_2CH_3$), 1.1–1.8 (m, 6H, $CH_2CH_2CH_2CH_3$), 3.7 (s, 3H, OMe), 4.25 (m, 1H, H-6), 5.0 (d, $J_{4,5}$ = 9.75 Hz of d, $J_{5,6}$ = 4 Hz of d, $J_{NH,5}$ = 2 Hz, 1H, H-5), 6.0 (br s, 1H, NH, exchanges with deuterium oxide), 6.35 (d, $J_{4,5}$ = 9.75 Hz of d, $J_{2,4}$ = 2 Hz, 1H, H-4), 7.42 (d, $J_{NH,2}$ = 6 Hz, 1H, H-2, collapses to a singlet after exchange with deuterium oxide). *Exact Mass* calcd. for $C_{11}H_{17}NO_2$: 195.1258; found (high resolution ms): 195.1256; and **13***e* (0.057 g, 1.4%), which likely arises during hplc chromatography; ir: 1735 ($CO_2Me$) $cm^{-1}$; $^1H$ nmr δ: 0.75–1.9 (m, 7H, $CH_2CH_2CH_2CH_3$), 2.9 (t, $J$ = 7 Hz, $CH_2CH_2CH_2CH_3$), 3.95 (s, 3H, OMe), 7.3 (d, $J_{4,5}$ = 8 Hz, 1H, H-5), 8.25 (d, $J_{4,5}$ = 8 Hz of d, $J_{2,4}$ = 2 Hz, 1H, H-4), 9.15 (d, $J_{2,4}$ = 2 Hz, 1H, H-2). *Exact Mass* calcd. for $C_{11}H_{15}NO_2$: 193.1102; found (high resolution ms): 193.1100. The yields of **11***j* and **13***e* were calculated from the integrals for the respective H-4 and H-2 protons at 6.35 and 9.15 δ. A pure sample of **13***e* was obtained by tlc separation of the above mixture. Collection of the 1200–1400 mL fraction gave **14***a* (0.36 g, 11%) which exhibited a $^1H$ nmr spectra identical to that previously described. Removal of the solvent from the

1500–2000 mL fraction gave **14***c* (1.57 g, 35.5%) as a pale yellow oil; ir: 3250 (br m, OH) $cm^{-1}$; $^1H$ nmr δ: 0.6–2.1 (m, 18H, *n*-Bu), 4.05 (br s, 1H, OH, exchanges with deuterium oxide), 7.28 (d, $J_{4,5}$ = 8 Hz of d, $J_{5,6}$ = 5 Hz, 1H, H-5), 7.86 (d, $J_{4,5}$ = 8 Hz of d, $J_{4,6}$ = 2 Hz of d, $J_{2,4}$ = 2 Hz, 1H, H-4), 8.46 (d, $J_{5,6}$ = 5 Hz, 1H, H-6), 8.7 (d, $J_{2,4}$ = 2 Hz, 1H, H-2). *Anal.* calcd. for $C_{14}H_{23}NO$·picrate: C 53.28, H 5.82, N 12.44; found: C 53.36, H 5.84, N 12.43.

*1,3-Dimethoxycarbonyl-6-*n*-butyl-1,6-dihydropyridine (**11**k), 1-methoxycarbonyl-3-pentanoyl-4-*n*-butyl-1,4-dihydropyridine (**12**l), and 3-[1-(1-hydroxy-1-*n*-butylpentyl)]pyridine (14*c*)*

A solution of *n*-butyllithium (1.28 g, 20 mmol) in 9.2 mL hexane was added dropwise to a solution of methyl nicotinate (2.74 g, 20 mmol) in 60 mL dry tetrahydrofuran, under an atmosphere of nitrogen, at −65°C with stirring. The reaction was allowed to proceed at −65°C for 30 min after which methylchloroformate (1.27 g, 20 mmol) was added dropwise. The mixture was stirred at −65°C for a further 30 min prior to warming to 25°C. Water (30 mL) was added and the reaction mixture was extracted with ether (4 × 50 mL), the extract dried ($Na_2SO_4$), and the solvent removed *in vacuo* to give an oil which was separated by preparative hplc using methylene chloride – chloroform (4:1 v/v) at a flow rate of 250 mL/min. Collection of the 900–1000 mL fraction afforded **12***l* (0.067 g, 1.2%) as a pale yellow oil; ir: 1735 (s, $CO_2$), 1680 (s, C=O), and 1620 (s, C=C) $cm^{-1}$; $^1H$ nmr δ: 0.7–2.0 (m, 16H, $C_4$-Bu, $COCH_2CH_2CH_2CH_3$), 2.68 (t, $J$ = 7 Hz, 2H, $COCH_2CH_2CH_2CH_3$), 3.48 (m, 1H, H-4), 3.92 (s, 3H, OMe), 5.2 (d, $J_{5,6}$ = 8 Hz of d, $J_{4,5}$ = 5 Hz, 1H, H-5), 6.85 (d, $J_{5,6}$ = 8 Hz, 1H, H-6), 7.95 (s, 1H, H-2). *Exact Mass* calcd. for $C_{16}H_{25}NO_3$: 279.1823; found (high resolution ms): 279.1817. The 1000–1100 mL fraction contained a mixture of **12***l* (0.11 g, 2.0%) and **11***k* (0.068 g, 1.34%). Removal of the solvent from the 1200–1600 mL fraction gave **11***k* as a viscous oil (0.767 g, 15.6%); ir: 1712 and 1734 (CO) $cm^{-1}$; $^1H$ nmr δ: 0.65–1.7 (m, 9H, Bu), 3.78 (s, 3H, OMe), 3.86 (s, 3H, OMe), 4.8 (m, 1H, H-6), 5.6 (d, $J_{4,5}$ = 9.75 Hz of d, $J_{5,6}$ = 5.5 Hz, 1H, H-5), 6.4 (d, $J_{4,5}$ = 9.75 Hz, 1H, H-4), 7.9 (s, 1H, H-2); *Exact Mass* calcd. for $C_{13}H_{19}NO_4$: 253.1314; found (high resolution ms): 253.1306. Elution with 1000 mL ethyl acetate gave a viscous oil which was purified using 1.0 mm silica gel G with chloroform–methanol (19:1 v/v) as development solvent. Extraction of the band having $R_f$ 0.4 using warm absolute ethanol gave **14***c* (0.84 g, 18.2%) identical ($^1H$ nmr) with the sample described previously. Extraction of the band having $R_f$ 0.7 afforded methyl nicotinate (0.90 g) identical ($^1H$ nmr) with an authentic sample.

## Acknowledgements

We are grateful to the Natural Sciences and Engineering Research Council of Canada (Grant A0531) for financial support of this work and to the Department of Chemistry, University of Alberta for providing some 200 MHz $^1H$ nmr spectra.

1. C. S. GIAM and J. L. STOUT. Chem. Commun. 142 (1969).
2. C. S. GIAM, E. E. KNAUS, and F. M. PASUTTO. J. Org. Chem. **39**, 3565 (1974).
3. C. S. GIAM and J. L. STOUT. Chem. Commun. 478 (1970).
4. T. A. ONDRUS, E. E. KNAUS, and C. S. GIAM. Can. J. Chem. **57**, 2342 (1979).
5. U. EISNER and J. KUTHAN. Chem. Rev. **72**, 1 (1972).
6. S. YAMADA, M. KURAMOTO, and Y. KIKUGAWA. Tetrahedron Lett. 3101 (1969).
7. A. E. HAUCK and C. S. GIAM. J. Chem. Soc. Perkin Trans. I, 2070 (1980).
8. B. LOEV and K. M. SNADER. J. Org. Chem. **30**, 1914 (1965).
9. R. C. FUSON and J. J. MILLER. J. Am. Chem. Soc. **79**, 3477 (1957).
10. R. E. LYLE and D. A. NELSON. J. Org. Chem. **28**, 169 (1963).

Can. J. Chem. Downloaded from www.nrcresearchpress.com by 210.87.254.6 on 09/06/12
For personal use only.

# Solute–solvent interactions in the association of hexacyanoferrate(III) with group II A cations. A calorimetric study

ROBERTO ARUGA

*Institute of Analytical Chemistry, University of Turin, via Giuria 5, 10125 Turin, Italy*

Received October 6, 1981

ROBERTO ARUGA. Can. J. Chem. **60**, 1828 (1982).

Enthalpy of association of hexacyanoferrate(III) ion with Mg(II), Ca(II), Sr(II), and Ba(II) cations has been determined by direct calorimetry. Using the equilibrium constants, Gibbs function and entropy were also obtained. Measurements were carried out in aqueous medium at 25°C and ionic strength $I = 0.1$ mol $L^{-1}$. Examination of the thermodynamic quantities obtained and calculation of the distance of closest approach between cation and anion show the presence of different desolvation processes for the metals studied. More particularly, solvent-separated ion pairs in the case of magnesium and contact pairs in the case of barium seem to be present. The presence of desolvation processes is uncertain for calcium and strontium. The $\Delta H^0$ and $\Delta S^0$ values show also an important influence from solvent-destructuring processes on ion pair formation.

ROBERTO ARUGA. Can. J. Chem. **60**, 1828 (1982).

On a déterminé, par calorimétrie directe, l'enthalpie d'association de l'ion hexacyanoferrate(III) avec les cations Mg(II), Ca(II), Sr(II) et Ba(II). On a également obtenu la fonction de Gibbs et l'entropie au moyen de la constante d'équilibre. On a effectué les mesures en milieu aqueux à 25°C et à une force ionique de $I = 0{,}1$ mol. $L^{-1}$. L'étude des quantités thermodynamiques obtenues et le calcul de la distance d'approche la plus faible entre le cation et l'anion révèle la présence d'un processus différent de désolvatation pour les métaux étudiés. Plus particulièrement, les paires d'ions séparés par le solvant dans le cas du magnésium et les paires de contact dans le cas du baryum semblent être présents. La présence du processus de dé solvatation est incertaine dans le cas du calcium et du strontium. Les valeurs de $\Delta H^0$ et de $\Delta S^0$ montrent également une influence marquée des processus de déstructuration par le solvant lors de la formation d'une paire d'ions.

[Traduit par le journal]

## Introduction

Desolvation processes of cation in complex formation and the factors which determine different orders of stability constants (1) are among the main points of interest in the study of associations of alkaline-earth metals with anions in aqueous solution.

More particularly, the problem of desolvation appears not sufficiently explained in the case of associations of these metals with hexacyanoferrate(II) and (III) anions. Jackman and Lister (2), by considering the thermodynamics of association, came to the conclusion that in the case of magnesium–hexacyanoferrate(II) pairs, the cation and anion are separated by solvent molecules, while for barium contact pairs are formed. On the contrary, in a previous paper (3), for associations of the same type, it was concluded that all pairs formed (those of barium included) are of outer-sphere type.[1] Other papers on the subject (4–6) do not seem to clarify this point.

By taking into account that enthalpy and entropy data are unavailable for the whole series from magnesium to barium with hexacyanoferrate(III) (7), it was thought interesting, in the present work, to determine these quantities by calorimetry, and to complete previous thermodynamic results for hexacyanoferrate(II) (2).

The data obtained refer to ionic strength $I = 0.1$ mol $L^{-1}$ and 25°C.

## Experimental

### *Reagents*

Mg(II), Ca(II), Sr(II), and Ba(II) nitrates were used (C. Erba RPE). The metal concentration was determined by complexometric titration with EDTA (0.1 *M* solution, C. Erba RPE). The ligand was used in the form of potassium salt (Fluka puriss. and C. Erba RPE ≥ 99%) without further purification. Its purity was checked iodometrically by Mohr's method (8). Hexacyanoferrate(III) solutions were prepared before each measurement and sheltered from light. Under these conditions they could be kept for some days without showing any evidence of decomposition. The background electrolyte was lithium nitrate for the measurement of the heat of dilution (C. Erba RPE).

### *Equipment*

Calorimetric measurements were performed at 25.00°C by an LKB 8700-2 Precision Calorimetry System and an LKB 8726-1 100 mL titration vessel, provided with a standard resistor (50 Ω) and a thermistor (2000 Ω). The accuracy of the instrument was checked by measuring the molar enthalpy of the reaction between tris(hydroxymethyl)methylamine and HCl in aqueous solution. The temperature of the titrant was kept at the temperature of the calorimeter by immersing (at least 12 h before the measure) the teflon reservoir of the titrant in the same thermostatic bath containing the calorimetric cell. The calorimeter was also equipped with a Radiometer ABU 12b autoburet for the titrant addition. The calorimetric experiments were

[1]The expression outer- or inner-sphere refers to the metal ion. With regard to the present anion all pairs, of course, are of outer-sphere type.

0008-4042/82/141828-04$01.00/0

©1982 National Research Council of Canada/Conseil national de recherches du Canada

Can. J. Chem. Downloaded from www.nrcresearchpress.com by 210.87.254.40 on 09/06/12
For personal use only.

TABLE 1. Experimental data for the mixing of metal nitrate and potassium hexacyanoferrate(III) aqueous solutions at 25°C*

| Metal | $C(MA^-) \times 10^3$ (mol $L^{-1}$) | $C(A^{3-}) \times 10^3$ (mol $L^{-1}$) | $C(KA^{2-}) \times 10^4$ (mol $L^{-1}$)† | $Q_{diss}$ (cal) | $-Q_c$ (cal) | $-Q_{cc}$ (cal) |
|---|---|---|---|---|---|---|
| Mg | 3.32 | 4.27 | 7.23 | 0.021 | 0.218 | 0.239 |
| | | | | | 0.213 | 0.234 |
| | | | | | 0.253 | 0.274 |
| | | | | | 0.180 | 0.201 |
| Ca | 3.51 | 4.10 | 6.95 | 0.022 | 0.195 | 0.217 |
| | | | | | 0.148 | 0.170 |
| | | | | | 0.158 | 0.180 |
| | | | | | 0.183 | 0.205 |
| Sr | 3.64 | 3.99 | 6.78 | 0.023 | 0.070 | 0.093 |
| | | | | | 0.068 | 0.091 |
| | | | | | 0.063 | 0.086 |
| | | | | | 0.060 | 0.083 |
| Ba | 3.75 | 3.89 | 6.62 | 0.023 | 0.127 | 0.150 |
| | | | | | 0.111 | 0.134 |
| | | | | | 0.124 | 0.147 |
| | | | | | 0.118 | 0.141 |

*Initial concentration of metal in the cell: 0.033 mol $L^{-1}$; concentration of hexacyanoferrate(III) in the titrant solution: 0.300 mol $L^{-1}$.
†Concentration of $KA^{2-}$ after the corresponding dilution experiment: $1.18 \times 10^{-3}$ mol $L^{-1}$.

performed in a room with temperature kept constant within ±0.3°C.

*Procedure*

For each metal–ligand system a set of measurements was carried out. Each measurement was performed by adding 2.507 ± 0.002 mL of potassium hexacyanoferrate(III) solution to 88.00 mL of metal nitrate solution contained in the calorimetric cell, and by measuring the corresponding heat (for the metal and ligand concentrations, see Table 1). The pH of all solutions had been previously brought to 6.0 ± 0.3. Under these conditions the following results were obtained: (*a*) the absence of hydrolysis processes of the metals; (*b*) no interaction of hexacyanoferrate(III) with proton (ferricyanic acid is completely dissociated above pH 1 (9)); (*c*) a negligible heat of neutralization between $H^+$ and $OH^-$; (*d*) an ionic strength constant at 0.1 mol $L^{-1}$ (the ionic strength variation during the addition of titrant was calculated, and was found to be lower than 0.02 mol $L^{-1}$); (*e*) the absence of triple ions of the type $M_2A^+$ ($A^{3-}$ = hexacyanoferrate(III) anion). Even with a strong excess of metal (up to 1.5 mol $L^{-1}$), the absence of these triple ions was previously demonstrated (6). Therefore, considering the weaker associating properties of $K^+$ ion with hexacyanoferrate(III) (10), species of the type KMA were also thought to be absent. For the $KA^{2-}$ pairs shown to be present, see below (Treatment of the experimental data).

The heat of dilution was measured by adding the same amount of titrant solution to 88.00 mL of lithium nitrate about 0.1 mol $L^{-1}$, at pH = 6. This salt was already used as background electrolyte in the study of associations of hexacyanoferrate(III) with several cations up to $I$ = 3 mol $L^{-1}$ (11). Tetraalkylammonium nitrate was not used, as it seems to associate more strongly with hexacyanoferrate(III) than alkaline metals (12).

*Treatment of the experimental data*

Hexacyanoferrate(III) associates to a certain extent with $K^+$. By knowing the concentration of $KA^{2-}$ after dilution and reaction (see Table 1), the heat of dissociation of these pairs was calculated, and found not negligible. So the experimental heats were corrected for both dilution and dissociation of the ligand. In these calculations the following values were used for the association between $K^+$ and $[Fe(CN)_6]^{3-}$: log $K$ = 0.85 at 25°C and $I$ = 0.1 mol $L^{-1}$ (10); $\Delta H^0$ = 0.5 kcal $mol^{-1}$. The latter value was obtained calorimetrically by Eaton *et al.* (13). Table 1 collects, as an example, the following experimental data for some measurements: concentration of species in the cell after the titrant addition ($C(MA^-)$, $C(KA^{2-})$, $C(A^{3-})$); dissociation heat of $KA^{2-}$ ($Q_{diss}$); heat corrected for dilution ($Q_c$), and for dilution and dissociation ($Q_{cc}$).

The molar enthalpies of association were obtained from the experimental heats ($Q_{cc}$) and from the concentration of the species $MA^-$, calculated using the stability constants in literature (4). These constants were obtained by conductance measurements at 25°C and $I$ = 0 mol $L^{-1}$. They were corrected to $I$ = 0.1 mol $L^{-1}$ by Davies' equation:

$$-\log f = Az^2[\sqrt{I}/(1+\sqrt{I}) - 0.2I]$$

where $A$ for water at 25°C is equal to 0.509. The $\Delta H^0$ values were calculated by the numerical method reported previously (14). The entropy variation was obtained from: $\Delta G^0 = \Delta H^0 - T\Delta S^0$.

## Results and discussion

The thermodynamics of complex formation of the present metals with hexacyanoferrate(III) and other quantities relating to the products of association are listed in Table 2.

Very few enthalpy and entropy data are available for the present associations. The following $\Delta H^0$ and $\Delta S^0$ were previously found for magnesium: −3.4 kcal $mol^{-1}$ and −16 cal $K^{-1}$ $mol^{-1}$; for barium: −3.7 and −15, respectively (5, 7). They refer to $T$ = 25°C and $I$ = 3 mol $L^{-1}$. The high ionic strength used in that work probably has a strong influence on the results, and may justify their large disagree-

Can. J. Chem. Downloaded from www.nrcresearchpress.com by 210.87.254.40 on 09/06/12
For personal use only.

TABLE 2. Thermodynamic quantities for the reaction: $M^{2+} + A^{3-} \rightarrow MA^-$ ($A^{3-}$ = hexacyanoferrate(III) ion) in aqueous solution at 25°C and $I$ = 0.1 mol $L^{-1}$*

| $M^{2+}$ | log $K$ | $-\Delta G^0$ (kcal $mol^{-1}$)† | $\Delta H^0$ (kcal $mol^{-1}$) | $\Delta S^0$ (cal $K^{-1}$ $mol^{-1}$) | $a$ (Å) | $a-(r_1+r_2)$ (Å) | $\bar{S}^0$ ($MA^-$, aq) (cal $K^{-1}$ $mol^{-1}$) | $n_M\bar{S}(H_2O)$ (cal $K^{-1}$ $mol^{-1}$) | $n_M$ |
|---|---|---|---|---|---|---|---|---|---|
| $Mg^{2+}$ | 1.44±0.01‡ | 1.96±0.01 | 0.79±0.10 | 9.2±0.4 | 7.1 | 2.0 | 51.8 | 0 | 0 |
| $Ca^{2+}$ | 1.48±0.01 | 2.02±0.01 | 0.60±0.10 | 8.8±0.2 | 6.8 | 1.3 | 71.6 | 20.4 | 1.2 |
| $Sr^{2+}$ | 1.50±0.01 | 2.04±0.01 | 0.27±0.02 | 7.8±0.1 | 6.6 | 1.0 | 74.6 | 23.9 | 1.4 |
| $Ba^{2+}$ | 1.53±0.01 | 2.09±0.01 | 0.42±0.02 | 8.4±0.1 | 6.4 | 0.6 | 84.9 | 34.5 | 2.1 |

*The $\bar{S}^0$($MA^-$, aq) values refer to $I$ = 0 mol $L^{-1}$.
†The results are expressed in terms of the thermochemical calorie, equal to 4.1840 J.
‡The uncertainty in each case is given as the estimated standard deviation.

ment (even in the sign) with the present ones. For calcium with hexacyanoferrate(III), Hanania and Israelian (15) obtained, by direct calorimetry, $\Delta H^0$ = 1.6 ± 0.2 kcal $mol^{-1}$ and $\Delta S^0$ = 17 ± 1 cal $K^{-1}$ $mol^{-1}$ at 25°C and $I$ = 0.07 mol $L^{-1}$. The agreement of these results with the present ones is only partial, since rather different values of log $K$ were used to calculate $\Delta H^0$ and $\Delta S^0$ in ref. 15 and in the present work.

Examination of the data in Table 2 shows that the stability of the species $M[Fe(CN)_6]^-$ is determined by the entropy factor, while enthalpy opposes association. This fact generally indicates the presence of electrostatic rather than covalent bonds. Furthermore, it indicates the prevalence of bond-breaking rather than bond-forming processes. In other words, solvent-destructuring external processes should prevail in the formation of these pairs. For both $\Delta H^0$ and $\Delta S^0$ the same sequence is followed: Mg > Ca > Sr < Ba. The same was previously observed in hexacyanoferrate(II) (2). Although it is difficult to draw certain conclusions from these data, the unexpectedly high values for barium could be due to desolvation processes of the cation (2).

For a more detailed investigation of desolvation processes of cations, the equations previously reported by Davies (16) may be useful. They allow one to correlate the association constant, $K$, with the distance of closest approach, $a$, of two ions in ion pair:

$$[1] \quad K = \frac{4\pi N}{1000}\left(\frac{|z_1z_2|e^2}{\varepsilon kT}\right)^3 Q(b)$$

$$[2] \quad Q(b) = \int_2^b x^{-4}\exp x \, dx$$

where: $x = |z_1z_2|e^2/(r\varepsilon kT)$, $b = |z_1z_2|e^2/(a\varepsilon kT)$, $N$ represents Avogadro's number, $z_1$ and $z_2$ the charge of cation and anion, $e$ the charge of electron, $k$ Boltzmann's constant, $r$ the distance between two ions in ion pair, $T$ the absolute temperature. By using the values of the thermodynamic constants of ref. 4 ($K$ = 613, 680, 709, 758 for Mg, Ca, Sr, and Ba respectively), and taking as reference $T$ = 298 K, the values of $a$ in Table 2 were obtained. The quantities $a - (r_1 + r_2)$ were determined by considering the crystal radii of cations, $r_1$, given by Pauling, and the value of 4.5 Å reported in literature (17) for the radius of hexacyanoferrate(III) ($r_2$). Then by taking into account ($a$), the water molecule has a tetrahedral structure with a center–vertex distance of about 1 Å (the O—H internuclear distance is 0.97 Å (18)); ($b$) Powell and Latimer (19) considered a thickness of 2 Å for the first hydration sphere of cations, the values of $a - (r_1 + r_2)$ in Table 2 are in accord with the presence of one water molecule between magnesium and hexacyanoferrate(III) in the corresponding pair, while they seem to indicate the presence of inner-sphere pairs for barium. The results for calcium and strontium appear more uncertain. Similar conclusions were drawn previously for the corresponding associations of hexacyanoferrate(II) (2).

Tanaka *et al.* (3), by considering the association constants of Mg, Ca, and Ba with hexacyanoferrate(III), and the corresponding interionic distances, suggested the presence of solvent separated pairs for all the metals studied. It must be noted, however, that instead of the radius of hexacyanoferrate(III), these authors considered the simple sum of Fe—C and C—N interatomic distances. In this manner, the contribution of the radius of the nitrogen atom of —C≡N group (about 1.5 Å (17)) was not taken into account.

The $\Delta S^0$ data in Table 2 provide another way of verifying these conclusions. More precisely, in order to calculate the water molecules displaced from a cation, the following empirical equation of Cobble may be used (20):

$$[3] \quad \bar{S}^0 = 49 - 99z[f/(r_1 + r_2)] + n\bar{S}(H_2O)$$

where $\bar{S}^0$ is the standard partial molal entropy of complex species; in the present case: $\bar{S}^0(MA^-, aq) = \Delta S_0{}^0 + \bar{S}^0(M^{2+}, aq) + \bar{S}^0(A^{3-}, aq)$; $z$ is the anion charge; $n$ is the number of water molecules re-

Can. J. Chem. Downloaded from www.nrcresearchpress.com by 210.87.254.40 on 09/06/12
For personal use only.

Can. J. Chem. Downloaded from www.nrcresearchpress.com by 210.87.254.40 on 09/06/12
For personal use only.

moved from the cationic sphere in complex formation; $\bar{S}(H_2O)$ is the partial molal entropy of water; $f$ is a structural constant; and $r_1$ and $r_2$ are the crystal radii of cation and anion. The expression $f/(r_1 + r_2)$ may be substituted by $1/r_{12}$, where $r_{12}$ is the actual interatomic crystal distance between cation and anion. The values of $\Delta S_0^0$ (the entropy variation referred to $I = 0$ mol $L^{-1}$) were obtained[2] from $\Delta S^0$ in Table 2. The results were as follows: 18.8, 18.4, 17.3, 18.0 cal $K^{-1}$ $mol^{-1}$ for Mg, Ca, Sr, and Ba, respectively. For $\overline{S^0}(M^{2+}, aq)$ the literature data were considered (21), while for $\overline{S^0}(A^{3-}, aq)$, from the absolute quantity previously reported (22), the value of 64.6 cal $K^{-1}$ $mol^{-1}$ was obtained. The resulting $\overline{S^0}(MA^-, aq)$ values are listed in Table 2. For the actual interatomic crystal distance ($r_{12}$) the $a$ values in Table 2 may be used.[3] Two observations must be made about the use of eq. [3]. (*a*) The $\overline{S^0}$ or $n$ values calculated by this equation are not always in agreement with the experimental results (20). (*b*) An uncertainty range exists for the calculated values of $\Delta S_0^0$. In order to eliminate the above causes of error, it seems more reasonable to calculate $n$ for the different metals by taking as reference a reaction of the same type, for which $n$ is known. Taking into account the results of the initial part in the discussion, we may assume that in the case of magnesium: $n_{Mg} = 0$, and write eq. [3] as follows:

$$[4] \quad (n_M - n_{Mg})\bar{S}(H_2O) = \overline{S^0}(MA^-, aq) - \overline{S^0}(MgA^-, aq) + 99z(1/a_{MA^-} - 1/a_{MgA^-})$$

Remembering that $\bar{S}(H_2O)$ is equal to 16.7 cal $K^{-1}$ $mol^{-1}$ (23), the values of $n_M\bar{S}(H_2O)$ and $n_M$ of Table 2 are obtained by eq. [4]. In accordance with the preceding conclusions, these values seem to suggest a contact-pair formation for barium, with the displacement of two water molecules. Desolvation processes could also take place for calcium and strontium, even though in a more limited form than for barium.

[2] $\Delta S_0^0$ was calculated by means of the equation:

$$\Delta S_0^0 = \Delta S^0 + R[T\Sigma\nu_i\partial(\ln\gamma_i)/\partial T - \Sigma\nu_i \ln\gamma_i]$$

reported by Austin, Matheson, and Parton (ref. 20, p. 370). For the values used in these calculations see also ref. 24.

[3] The present demonstration can be considered independent of the preceding one, even if the values of $a$ obtained by [1] and [2] are used. In fact, different values of $r_{12}$ ($r_{12} = a$, or $r_{12} = r_1 + r_2$) were found to have no substantial influence on the final conclusions.


1. R. Aruga. Inorg. Chem. **19**, 2895 (1980).
2. F. A. Jackman and M. W. Lister. J. Solution Chem. **4**, 1023 (1975).
3. N. Tanaka, Y. Kobayashi, and M. Kamada. Bull. Chem. Soc. Jpn. **39**, 2187 (1966).
4. C. W. Gibby and C. B. Monk. Trans. Faraday Soc. **48**, 632 (1952).
5. V. E. Mironov and Yu. I. Rutkovskii. Russ. J. Inorg. Chem. (English Transl.) **11**, 958 (1966).
6. A. N. Lazarev, Yu. A. Makashev, V. E. Mironov, and B. I. Lobov. Zh. Fiz. Khim. **49**, 2258 (1975).
7. J. J. Christensen, D. J. Eatough, and R. M. Izatt. Handbook of metal ligand heats. Marcel Dekker, New York. 1975. p. 175.
8. F. P. Treadwell. Chim. Anal. Vol. II. Analisi quantitativa. Francesco Vallardi, Milano. 1966. p. 585.
9. J. Jordan and G. T. Ewing. Inorg. Chem. **1**, 587 (1962).
10. R. W. Chlebek and M. W. Lister. Can. J. Chem. **44**, 437 (1966).
11. L. G. Sillén and A. E. Martell. Stability constants. Special Publication No 25. The Chemical Society, London. 1971. p. 50.
12. M. K. Basu and M. N. Das. Inorg. Chem. **9**, 2781 (1970).
13. W. A. Eaton, P. George, and G. I. H. Hanania. J. Phys. Chem. **71**, 2016 (1967).
14. L. G. Sillén. Acta Chem. Scand. **16**, 159 (1962).
15. G. I. H. Hanania and S. A. Israelian. J. Solution Chem. **3**, 57 (1974).
16. C. W. Davies. Ion association. Butterworths, London. 1962. p. 164.
17. R. A. Marcus. J. Chem. Phys. **26**, 867 (1957).
18. G. H. Nancollas. Interactions in electrolyte solutions. Elsevier, Amsterdam. 1966. p. 2.
19. R. E. Powell and W. M. Latimer. J. Chem. Phys. **19**, 1139 (1951).
20. J. M. Austin, R. A. Matheson, and H. N. Parton. The structure of electrolytic solutions (*Edited by* W. J. Hamer). Wiley, New York. 1959. p. 375.
21. W. M. Latimer, K. S. Pitzer, and W. V. Smith. J. Am. Chem. Soc. **60**, 1830 (1938).
22. H. E. Barner and R. V. Scheuerman. Handbook of thermochemical data for compounds and aqueous species. John Wiley, New York. 1978. p. 46.
23. D. D. Wagman, W. H. Evans, V. B. Parker, I. Halow, S. M. Bailey, and R. H. Schumm. National Bureau of Standards Technical Note 270-3. U.S. Government Printing Office, Washington, D.C. 1968.
24. H. S. Harned and B. B. Owen. The physical chemistry of electrolytic solutions. Reinhold, New York. 1950, pp. 116, 118.

# Thermochemistry of conjugation of simple cyclopropane derivatives

RICHARD FUCHS, JOHN H. HALLMAN, AND MICHAEL O. PERLMAN
*Department of Chemistry, University of Houston, Houston, TX 77004, U.S.A.*

Received January 6, 1982

RICHARD FUCHS, JOHN H. HALLMAN, and MICHAEL O. PERLMAN. Can. J. Chem. **60**, 1832 (1982).

Heats of vaporization of cyclopropyl cyanide and cyclopropylbenzene have been measured by vaporization calorimetry, and combined with liquid state heats of formation to give gaseous state heats of formation. When these compounds, cyclopropane, 1,1-dimethylcyclopropane, and cyclopropylamine are involved in (hypothetical) isodesmic reactions with ethane to give the isopropyl derivative and propane, the enthalpies of reaction are $-116.0 \pm 1.3$ kJ mol$^{-1}$, except for cyclopropylbenzene ($-103.7$ kJ mol$^{-1}$). The latter is less exothermic, in part, because of slight steric destabilization of the product, isopropylbenzene, but mainly due to 8 kJ mol$^{-1}$ stabilization of cyclopropylbenzene, which is the only of these cyclopropyl derivatives showing appreciable thermochemical stabilization.

RICHARD FUCHS, JOHN H. HALLMAN et MICHAEL O. PERLMAN. Can. J. Chem. **60**, 1832 (1982).

Faisant appel à la calorimétrie de vaporisation, on a mesuré les chaleurs de vaporisation du cyanure de cyclopropyle et du cyclopropylbenzène et on les a combinées aux chaleurs de formation à l'état liquide pour obtenir les chaleurs de formation à l'état gazeux. Quand ces composés: le cyclopropane, le diméthyl-1,1 cyclopropane et la cyclopropylamine sont impliqués dans des réactions isodesmiques (hypothétiques) avec l'éthane pour conduire au dérivé isopropylique et au propane, les enthalpies de réaction sont de $-116{,}0 \pm 0{,}3$ kJ mol$^{-1}$, sauf pour le cyclopropylbenzène ($-103{,}7$ kJ mol$^{-1}$). Ce dernier est moins exothermique, en partie à cause de la légère déstabilisation stérique du produit, l'isopropylbenzène, mais principalement à cause de la stabilisation de 8 kJ mol$^{-1}$ cyclopropylbenzène, qui est le seul de ces dérivés cyclopropyles à montrer une stabilisation thermochimique appréciable.
[Traduit par le journal]

Can. J. Chem. Downloaded from www.nrcresearchpress.com by 210.87.254.40 on 09/06/12
For personal use only.

There is a growing feeling among theorists that molecular parameters can be more accurately calculated than measured. The results of a calculation may indeed be closer to the "truth" than the corresponding experimental measurement, but the significance of the calculation may be limited by our inability to establish error limits accurately by experiment. It is therefore of the utmost importance that the best possible experimental measurements be performed. The alternative is devolution of chemistry from an experimentally verifiable science to the status of a religion, based on articles of nondemonstrable faith.

When a group, X, is substituted into a molecule, Y—H, we may consider the interactions between Y and X in the resulting molecule, Y—X, which lead to alteration in spectra, bond lengths, etc. But the most significant question is whether special interactions between X and Y lead to a *thermochemically demonstrable decrease in the energy of Y—X* relative to reasonable models.

For many years data have been presented suggestive of "double bond character" of the cyclopropane ring (1), but evidence for significant conjugation is strongest for cationic reaction intermediates (2) and excited states, rather than for the ground states of neutral cyclopropane derivatives. We have recently completed a decade of substantial theoretical interest in conjugative interactions of the cyclopropane ring. Variation in ring bond lengths with the nature of the attached group have been examined (3–8), and often indicate substantial substituent-ring conjugation (3–7). Hoffmann (9) attributed the stabilization of norcaradienes by cyano and phenyl substituents (relative to the isomeric cycloheptatrienes) to π-type cyclopropane-substituent conjugation. *Ab initio* calculations by Hehre (10) predicted a 13.4–14.6 kJ mol$^{-1}$ stabilization of vinylcyclopropane. Dill, Greenberg, and Liebman (11) recently made extensive calculations on small ring and bicyclic systems with a variety of substituents. They predict the following stabilizations of cyclopropane by substituents: $CH_3$, 10.0 kJ mol$^{-1}$; CN, 24.3 kJ mol$^{-1}$; and $NH_2$, 12.1 kJ mol$^{-1}$; but note that STO-3G calculations appear to overestimate stabilizations. It has been suggested (11) that stabilization or destabilization results not only from the ring-substituent bond character, but also from an increase or decrease in ring strain. It is the sum of these factors which is calculated, and is experimentally measurable.

What of the experimental thermochemical data previously available? We note several problems. (*a*) The data are few. (*b*) Some "experimental" values of gaseous state heats of formation ($\Delta H_f^0$(g)) are based on estimated heats of vaporization (11) (methylcyclopropane). (*c*) Some $\Delta H_g^0$(g) values are based on defective values of $\Delta H_v^0$ (12) (cyclopropyl cyanide).

It is the objective of the present study to provide $\Delta H_f^0$(g) data of sufficient accuracy that a critical assessment of cyclopropane-substituent thermo-

0008-4042/82/141832-04$01.00/0
©1982 National Research Council of Canada/Conseil national de recherches du Canada

Can. J. Chem. Downloaded from www.nrcresearchpress.com by 210.87.254.40 on 09/06/12
For personal use only.

chemical stabilization can be made. We will examine the results by two methods. The first involves the (hypothetical) isodesmic reaction (13), or group separation method, as recently modified (11, 14):

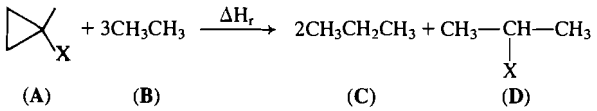


(A) (B) (C) (D)

where $\Delta H_r = 2\Delta H_f^0(g)$ (C) + $\Delta H_f^0(g)$ (D) − $\Delta H_f^0(g)$ (A) − $3\Delta H_f^0(g)$ (B). The reaction is exothermic due to the ring strain in (A), and $-\Delta H_r$ is the strain energy. $\Delta H_r$ will be the same where X = H and all other nonconjugating substituents, but $\Delta H_r$ will be less exothermic when a stabilizing interaction of X and the ring occurs, or more exothermic if (A) is destabilized.

The second method we term the metathetical relationship. Here substituents are exchanged by conjugating and equivalent, but nonconjugating systems:

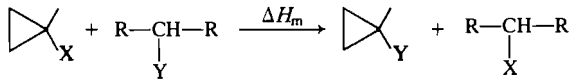


conjugated nonconjugated nonconjugated nonconjugated
(A) (B) (C) (D)

(B) can be the 2-propyl, cyclopentyl, or cyclohexyl derivative, with Y = H or other nonconjugating substituent, and $\Delta H_m = \Delta H_f^0(g)$ (C) + $\Delta H_f^0(g)$ (D) − $\Delta H_f^0(g)$ (A) − $\Delta H_f^0(g)$ (B). The reaction is thermoneutral if (A) is unstabilized, endothermic if (A) is stabilized, and exothermic if (A) is destabilized.

## Experimental

The technique and apparatus for measurement of calorimetric heats of vaporization (15) have been considerably changed in the present study, but the results with test substances are in excellent agreement with our earlier work, and with the best literature values (16). The vaporization calorimeter is again a coiled tube embedded in a copper disc heat sink fitted with a thermistor and heater, and enclosed in a vacuum jacketed solution calorimeter. The coiled tube is 0.476 cm (3/16 in.) od nickel tubing rather than copper, and the inlet and outlet stopcocks are Hamilton valves made of Teflon and Kel-F. Nitrogen flow is established by a low range digital mass flow controller (0–10 cc/min, Porter Instrument Co.). Vacuum below 1.3 kPa (10 Torr) is furnished by a vacuum pump, and by an aspirator with a drying column at higher pressures. Well dried 100 μL samples are introduced volumetrically (microliter syringe, constant stroke adapter), and the mass of separate samples is determined with a semimicro balance, using air buoyancy corrections. A major change from our earlier procedure (15) is introduction of the sample into the (25.00°C) calorimeter at a temperature at which no net heating or cooling effect occurs in the absence of vaporization. Surprisingly, these conditions are met with the sample and syringe jacket at 22.00 ± 0.01°C, and the 30 cm Teflon needle (air) temperature at 23.00 ± 0.05°C. We presume that the delivered sample is warmed by frictional heating and by handling of the needle. The previously used heat capacity correction for the sample is, therefore, no longer required. The validity of this procedure is verified not only by the excellent agreement of measured $\Delta H_v^0$ values of test substances with literature values, but also by the observation that nonvolatile samples (hexadecane introduced under conditions suitable for the evaporation of hexane) produce random temperature changes no greater than $1–2 \times 10^{-4}$ K. We have also observed that the overall cycle of closing the exit stopcock to the vacuum system, refilling the calorimeter with dried nitrogen or air to atmospheric pressure, opening the entrance stopcock to the atmosphere for 30 s (the time required for sample introduction) and reestablishment of the original nitrogen flow and vacuum produces negligible change ($< 1 \times 10^{-4}$ K) in the calorimeter temperature.

Sample evaporation occurs over a 14–20 min period, and the cooling effect is periodically compensated by short (8 or 10 s) heating periods (total 75–175 s), such that temperature excursions of 0.06–0.08 K occur symmetrically about the equilibrium temperature of the calorimeter. When no further evaporation cooling occurs, the block is brought to the original temperature ($\pm 1 \times 10^{-4}$ K). The calorimeter temperature is monitored for an additional 4 min to establish that the final and initial equilibrium temperatures are identical. The temperature measurement system consists of a thermistor (2000 Ω) imbedded in the copper heat sink, as the unknown resistance of a Wheatstone bridge, the output of which is displayed on a digital multimeter (Keithley 177, 19.999 mV full scale). The multimeter analog output is plotted on a potentiometer recorder. The heating system consists of a Type RN55C metal film resistor (822.8 Ω), a timed constant current source (17) with an output of 19.85 mA, and monitored by a digital milliammeter, and an adjustable interval timer based on the 555 integrated circuit. Operation of the vaporization calorimeter was verified by measurements of compounds with well established values of $\Delta H_v^0$ (16, 18): pentane, 26.61 ± 0.09 kJ mol$^{-1}$ (reported, 26.74 ± 0.21); hexane, 31.54 ± 0.18 (31.55 ± 0.04); octane, 41.44 ± 0.07 (41.51 ± 0.04); butanenitrile, 39.22 ± 0.11 (39.29 ± 0.08); butyl acetate, 43.66 ± 0.09 (43.60 ± 0.21); and isopropylbenzene, 45.12 ± 0.02 (45.15 ± 0.04).

Cyclopropyl cyanide (Fluka) and cyclopropylbenzene (Aldrich) were fractionally distilled. Purity was established by gas chromatography (99.90% and 99.70%, respectively), using a Shimadzu Mini 2 gc with a glass lined system, a 30 m × 0.25 mm id SE-30 silica capillary column, and a Hewlett-Packard 3390A integrator.

## Results and discussion

### *Heats of vaporization and gaseous heats of formation*

The standard heat of vaporization at 25°C of cyclopropyl cyanide (the mean of six determinations) is 41.94 ± 0.11 kJ mol$^{-1}$. A previously reported value based on vapor pressure measurements (12) is 39.8 ± 0.4 kJ mol$^{-1}$. However, a number of $\Delta H_v^0$ values published in this article appear to be considerably too low (by 12 kJ mol$^{-1}$ for ethyl benzoate, 8.3 kJ mol$^{-1}$ for cyclohexyl cyanide, etc.).

We are unaware of any previous $\Delta H_v^0$ measurements on cyclopropylbenzene. The mean of our

Can. J. Chem. Downloaded from www.nrcresearchpress.com by 210.87.254.40 on 09/06/12
For personal use only.

four determinations is 50.22 ± 0.10 kJ mol$^{-1}$ where the indicated uncertainty is twice the standard deviation.

Based on the liquid state heats of formation (16) of cyclopropyl cyanide (140.8 ± 0.7 kJ mol$^{-1}$), and of cyclopropylbenzene (100.5 ± 1.0 kJ mol$^{-1}$) one may derive gaseous state heats of formation of 182.7 ± 0.7 kJ mol$^{-1}$ and 150.7 ± 1.0 kJ mol$^{-1}$, respectively, where $\Delta H_f^0(g) = \Delta H_f^0(l) + \Delta H_v^0$. Other values of $\Delta H_f^0(g)$ below are taken from the Pedley–Rylance Tables (16).

*Enthalpies of isodesmic reactions*

The following are isodesmic reactions of cyclopropane and the four simply substituted cyclopropane derivatives for which *experimental* values of $\Delta H_f^0(g)$ are now known. The values are in kJ mol$^{-1}$.

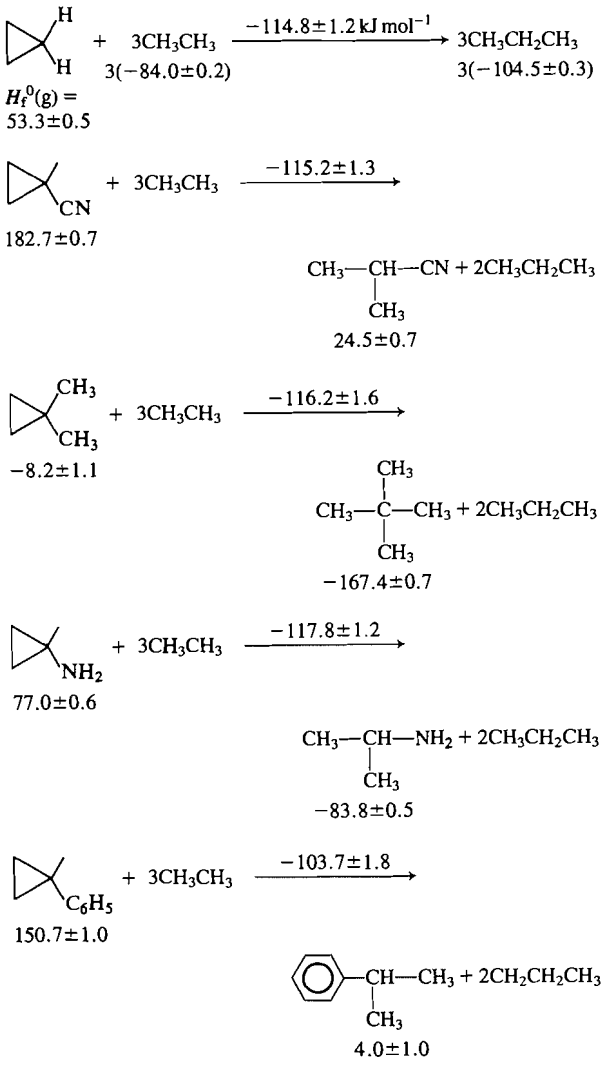


The mean of the first four heats of reaction is −116.0 ± 1.3 kJ mol$^{-1}$ (−27.7 ± 0.4 kcal/mol). Only the reaction of cyclopropylamine differs from the mean value by more than the experimental uncertainty; the difference is only 0.6 kJ mol$^{-1}$ (0.1 kcal/mol) larger than the uncertainty, and is of doubtful significance. By contrast, the reaction of cyclopropylbenzene is 12.3 kJ mol$^{-1}$ less exothermic than the mean of the other four reactions. Of this, 4.4 kJ mol$^{-1}$ results from steric strain in the product isopropylbenzene (the isodesmic reaction of isopropylbenzene with ethane to give isobutane and neopentane is more exothermic by this amount than the corresponding reactions of benzene, toluene, and ethylbenzene). The remaining 7.9 kJ mol$^{-1}$ results from conjugative stabilization in cyclopropylbenzene.

*Enthalpies of metathetical reactions*

An alternative but related method of detecting thermochemically significant interactions involves metathetical reactions. Exchange of substituents between two nonconjugated systems should be thermally neutral ($\Delta H = 0$), but destruction of a conjugated molecule leads to an endothermic reaction.

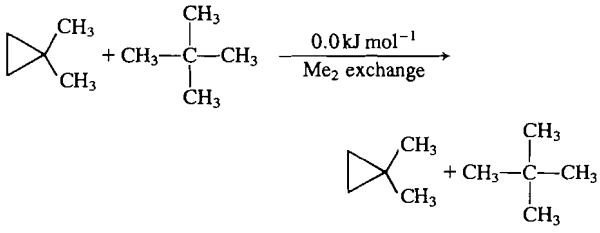


The other four cyclopropane derivatives can be similarly involved in metathetical reactions: cyclopropyl cyanide (CN, H exchanged for $Me_2$), $\Delta H$ = 1.0 ± 1.6; cyclopropane, 1.4 ± 1.4; cyclopropylamine, −1.6 ± 1.5; and cyclopropylbenzene, 12.5 ± 1.9 kJ mol$^{-1}$. The first four reactions have enthalpies which, essentially within the uncertainty limits, are zero. This again demonstrates that no stabilizing interactions occur in cyclopropyl cyanide, 1,1-dimethylcyclopropane, and cyclopropylamine, which are not also present in (unconjugated) cyclopropane. Similar conclusions would be drawn if cyclopropane substituents were exchanged with cyclopentane. Data for cyclopentane derivatives are less available and have larger uncertainties than the data for propane derivatives used above. The enthalpy of reaction of cyclopropylbenzene (12.5 kJ mol$^{-1}$) is in excellent agreement with the results of the isodesmic reaction, and indicates 8.1 kJ mol$^{-1}$ stabilization of cyclopropylbenzene.

Can. J. Chem. Downloaded from www.nrcresearchpress.com by 210.87.254.40 on 09/06/12
For personal use only.

## Conclusions

Studies of cyclopropane derivatives (3–7, 9–11) experimentally and by calculations have generally indicated appreciable ring-substituent interactions, and substantial stabilization has been predicted for many of the substituted compounds relative to unsubstituted cyclopropane. An exception is 1,1-dibromo-*trans*-2,3-diphenylcyclopropane (8), where the phenyl–cyclopropane interaction is apparently not strong enough to require a conjugating conformation in the crystal structure. However, *trans*-2-(*p*-nitrophenyl)cyclopropyl methyl ketone (19), the only unhindered cyclopropylbenzene derivative of known crystal structure, has the rings very close to the bisected (conjugated) conformation.

Many of the conclusions of previous studies regarding the stabilization of cyclopropane derivatives cannot be confirmed by the present experimental thermochemical measurements. Perhaps compounds such as cyclopropyl cyanide have a substituent-ring stabilizing $\pi$ interaction of 5–10 kJ $mol^{-1}$, together with destabilization of other orbitals and increased ring strain amounting to 4–9 kJ $mol^{-1}$. If this were the case, the very small net stabilization might not be observed thermochemically. We feel it is presently unwise to use calculations, structural data, and other nonthermochemical information to draw quantitative thermochemical conclusions about small effects.

## Acknowledgements

Acknowledgement is made to the donors of The Petroleum Research Fund, administered by the American Chemical Society, for partial support of this research, and to The Robert A. Welch Foundation (Grant E-136) for additional support.

1. M. CHARTON. *In* Chemistry of alkenes. *Edited by* J. Zabicky. Wiley Interscience, New York, NY. 1970.
2. D. G. GARRATT, A. MODRO, K. OYAMA, G. H. SCHMID, T. T. TIDWELL, and K. YATES. J. Am. Chem. Soc. **96**, 5295 (1974).
3. S. W. STALEY, A. E. HOWARD, M. D. HARMONY, S. N. MATHUR, M. KATTIJA-ARI, J.-I. CHOE, and G. LIND. J. Am. Chem. Soc. **102**, 3639 (1980).
4. R. PEARSON, A. CHOPLIN, and V. W. LAURIE. J. Chem. Phys. **62**, 4859 (1975).
5. A. SKANCKE and J. E. BOGGS. J. Mol. Struct. **51**, 267 (1979).
6. C. A. DEAKYNE, L. C. ALLEN, and V. W. LAURIE. J. Am. Chem. Soc. **99**, 1343 (1977).
7. S. DURMAZ and H. KOLLMAR. J. Am. Chem. Soc. **102**, 6942 (1980).
8. M. E. JASON and J. A. IBERS. J. Am. Chem. Soc. **99**, 6012 (1977).
9. R. HOFFMANN. Tetrahedron Lett. 2907 (1970).
10. W. J. HEHRE. J. Am. Chem. Soc. **94**, 6592 (1972).
11. J. D. DILL, A. GREENBERG, and J. F. LIEBMAN. J. Am. Chem. Soc. **101**, 6814 (1979).
12. H. K. HALL, JR. and J. H. BALDT. J. Am. Chem. Soc. **93**, 140 (1971).
13. W. J. HEHRE, R. DITCHFIELD, L. RADOM, and J. A. POPLE. J. Am. Chem. Soc. **92**, 4796 (1970).
14. P. GEORGE, M. TRACHTMAN, C. W. BOCK, and A. M. BRETT. Tetrahedron, **32**, 317 (1976).
15. R. FUCHS and L. A. PEACOCK. Can. J. Chem. **58**, 2796 (1980).
16. J. B. PEDLEY and J. RYLANCE. Sussex-N.P.L. computer analysed thermochemical data: organic and organometallic compounds. University of Sussex, Brighton, England. 1977.
17. R. FUCHS. J. Chem. Educ. **58**, 594 (1981).
18. J. D. COX and G. PILCHER. Thermochemistry of organic and organometallic compounds. Academic Press, New York, NY. 1970.
19. J. BORDNER, L. A. JONES, and R. L. JOHNSON. Cryst. Struct. Commun. **1**, 389 (1972).

# Polymer supported enantioselective reactions. II. α-Methylation of cyclohexanone[1]

COLIN R. MCARTHUR,[2] PAUL M. WORSTER, JI-LONG JIANG, AND CLIFFORD C. LEZNOFF[2]

*Department of Chemistry, York University, Toronto, Ont., Canada M3J 1P3*

Received January 4, 1982

COLIN R. MCARTHUR, PAUL M. WORSTER, JI-LONG JIANG, and CLIFFORD C. LEZNOFF. Can. J. Chem. **60**, 1836 (1982).

Insoluble cross-linked copolymers of styrene and 1% divinylbenzene with covalently bonded (*S*)-2-aminoalkoxy groups were used in the enantioselective α-methylation of cyclohexanone through the corresponding imines. Enantiomeric excesses of 94% of (*S*)-2-methylcyclohexanone were observed on methylation at 20°C. An analogous optically active 2-aminoalkyl benzyl ether, under otherwise identical conditions, resulted in a lower enantiomeric excess (49%) with selectivity approaching that of the polymer only at −78°C.

COLIN R. MCARTHUR, PAUL M. WORSTER, JI-LONG JIANG et CLIFFORD C. LEZNOFF. Can. J. Chem. **60**, 1836 (1982).

On a utilisé des copolymères de styrène et divinylbenzène réticulés à 1% et portant des groupes (*S*)-amino-2 alkoxy liés par des liaisons covalentes lors pour l'α méthylation énantiosélective de la cyclohexanone par l'intermédiaire des imines correspondantes. On a observé un excès énantiomérique de 94% de (*S*)-méthyl-2 cyclohexanone lors de la méthylation à 20°C. Un éther amino-2 alkyl benzylique analogue optiquement actif conduit dans des conditions identiques, à un excès énantiomérique de seulement 49%, la sélectivité ne se rapproche de celle du polymère qu'à −78°C.

[Traduit par le journal]

## Introduction

A number of advantages over the use of the solution phase have been identified in the use of solid, insoluble polymers as media for certain operations in synthesis. Considerable documentation exists on the usefulness of the property of insolubility of such media for facilitating separations and allowing for automated processes. In addition, other properties of these systems such as the decreased interaction between reactant moieties, a phenomenon which simulates high dilution, have been recognized (for reviews see ref. 1).

Speculation that a decrease in translational and conformational mobilities of moieties covalently bonded to cross-linked polymers, relative to their solution analogues, might enhance stereoselectivities of certain types of reactions led us to investigate the applicability of this type of medium to asymmetric syntheses (2). The situation might bear some general resemblance to that at the reactive sites of some enzymes. In the only research of which we are aware, prior to our work, into an example of an asymmetric synthesis on a polymer support, it was suggested that enhancement of the enantioselectivity observed relative to an analogous reaction in solution may result from conformational rigidity in the cross-linked polymer (3).

Enantioselectivities in solution may be considerably influenced by temperature (4). In particular, in the α-methylation of the metaloenamine formed by reaction of isopropylmagnesium bromide with the imine derived from cyclohexanone and (*R*)-1-butoxy-2-aminobutane, the enantiomeric excess of (*R*)-2-methylcyclohexanone formed after hydrolysis was 81% at −78°C, but only 20% at 65°C (5). In similar examples of the enantioselective alkylation of cyclohexanone imines, alkylation conditions routinely include temperatures of −98 and −78°C (6). Additional examples have been cited (7).

It seemed conceivable that the use of polymeric media might allow highly enantioselective reactions to occur at ambient temperatures, perhaps with concomitant increases in reaction rates relative to those observed in solution at low temperatures. Further, the separation of the optically active product after cleavage from the asymmetric induction sites on the polymer would be accomplished completely and easily by a simple filtration. At the same time, the insoluble polymer would be easily recovered and would be expected to be reusable.

In a preliminary article (2), we reported the use of a Merrifield polymer (**1**) bonded through ether linkages to (*S*)-2-amino-1-propyl groups. Condensation with cyclohexanone to give the corresponding polymer-bound ketimine followed by metalation, alkylation, and hydrolysis afforded optically active 2-alkylcyclohexanones in high enantiomeric excesses as well as high chemical yields and purities. In this paper we present the details of these and related studies on the enantioselective α-methylation of cyclohexanone using polymer-bound chiral amines.

[1]Presented in part at the 62nd Canadian Chemical Conference, Vancouver, June, 1979, and in part at the 64th Canadian Chemical Conference, Halifax, June, 1981.

[2]Authors to whom correspondence may be addressed.

0008-4042/82/141836-06$01.00/0

©1982 National Research Council of Canada/Conseil national de recherches du Canada

Can. J. Chem. Downloaded from www.nrcresearchpress.com by 210.87.254.40 on 09/06/12
For personal use only.

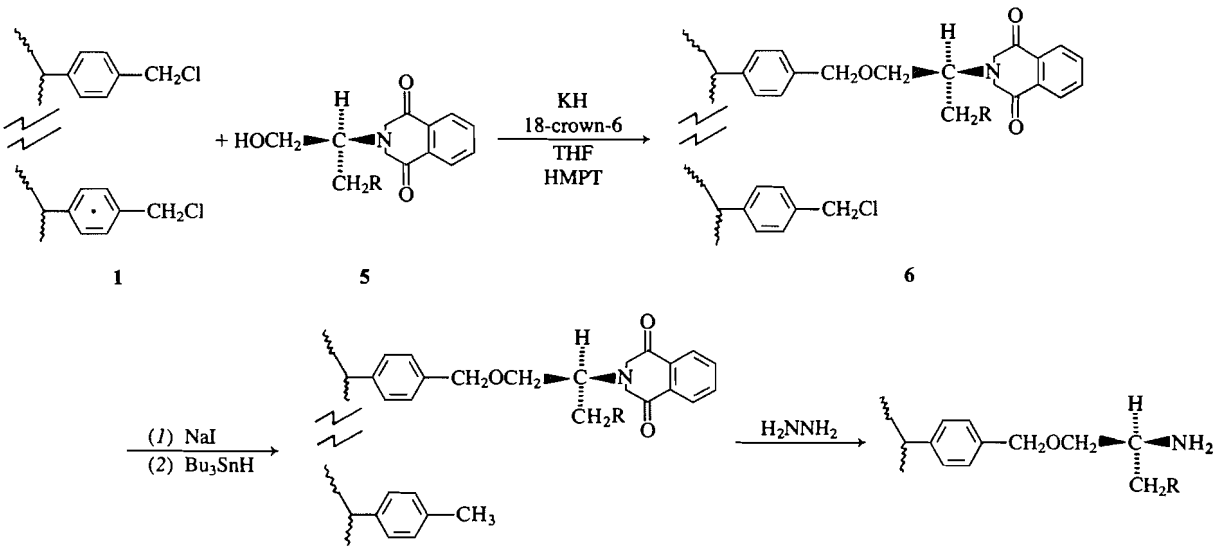


1 5 6 7 8

*a* R = H; *b* R = $CH_3$; *c* R = $\phi$

SCHEME 1

## Results and discussion

*Bonding* (S)-*2-aminoalkoxy groups to polystyrene*

(*S*)-2-Aminopropanol (**2**), (*S*)-2-aminobutanol (**3**), and (*S*)-2-amino-3-phenylpropanol (**4**) were converted, to prevent *N*-substitution by the polymer, to their corresponding *N*-phthaloyl derivatives (**5***a*, **5***b*, and **5***c* respectively) by reaction with *N*-(ethoxycarbonyl)phthalimide (8). The corresponding potassium alkoxides reacted with **1** to give the corresponding (*S*)-2-phthalimidoalkoxymethylated chloromethylated polystyrenes (**6***a*, **6***b*, and **6***c* respectively) as outlined in Scheme 1. The loadings of unreacted chloromethyl groups in **6** were determined quantitatively by reaction with pyridine, followed by analysis of the solution phase for chloride (9). These chloromethyl groups would be expected to become involved in subsequent steps in the reaction sequence to cause decreases in enantioselectivities. Such expectations were borne out experimentally as will be described.

Accordingly, the chloromethyl groups of **6** were converted to unreactive methyl groups by treatment with sodium iodide and then with tributyltin hydride. The resulting polymers (**7**) upon hydrazinolysis afforded polystyrene derivatives functionalized only with (*S*)-2-aminoalkoxy groups (**8**).

*Enantioselective methylation of cyclohexanone using polymers 8*

Condensation of polymers **8** with cyclohexanone gave the corresponding ketimines (**9**) (Scheme 2). The loadings of the ketimine functions on the polymers were in the range of 0.5 to 0.6 mmol/g as determined by hydrolysis to regenerate cyclohexanone and quantitative analysis of the solution phase by gas chromatography.[3]

Methylation of polymers **9** by reaction of the corresponding lithioenamines with iodomethane afforded the corresponding 2-(2-methylcyclohexyl-

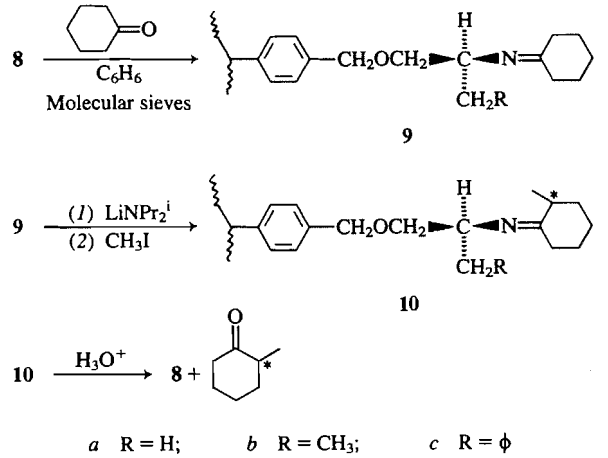


*a* R = H; *b* R = $CH_3$; *c* R = $\phi$

SCHEME 2

[3]Commercially available Merrifield polymer, used in numerous other reported syntheses, affords loadings in this range. Such loadings would be expected to minimize the potential complication of site to site interactions in interpreting results, a factor which we wished to avoid at this stage of our studies.

Can. J. Chem. Downloaded from www.nrcresearchpress.com by 210.87.254.40 on 09/06/12
For personal use only.

Can. J. Chem. Downloaded from www.nrcresearchpress.com by 210.87.254.40 on 09/06/12
For personal use only.

TABLE 1. Enantioselective α-methylations of polymeric imines, **9**, of cyclohexanone at 20°C

| Polymer | Loading of imine (mmol/g) | Yield of 2-methylcyclohexanones (%) | Enantiomeric excess* of (*S*)-2-methylcyclohexanone (%) |
|---|---|---|---|
| **9***a* | 0.57 | 32.5 | 92 |
| **9***b* | 0.56 | 86 | 94 |
| **9***c* | 0.54 | 87 | 94 |

*Based on optical rotation of pure (*R*)-2-methylcyclohexanone at −16.4°C (5).

TABLE 2. Comparison of **6***c* and **7***c* in subsequent enantioselectivities

| Parameter | Starting polymer **6***c* | Starting polymer **7***c* |
|---|---|---|
| $ClCH_2$ loading (mmol/g) | 0.4 | 0 |
| Imine loading (mmol/g) | 0.84 | 0.54 |
| Yield of 2-methylcyclohexanones (%) | 46 | 87 |
| Enantiomeric excess of (*S*)-2-methylcyclohexanone (%) | 32 | 94 |

idene)aminoalkoxymethylated polymers (**10**) which, on hydrolysis released (*R*)- and (*S*)-2-methylcyclohexanone to the solution phase. The predominant product under all of the variations in conditions studied (temperature, and the structure of R) was (*S*)-2-methylcyclohexanone[4] in enantiomeric excesses of >90%.

Results of methylation at ambient temperature (20°C) are shown in Table 1. In the methylation of **9***a* and subsequent hydrolysis, the chemical yield was much lower than was the case with **9***b* and **9***c* although, in all three systems, enantioselectivities appear in the same range (>90%).

The polymeric derivative **6***c* with chloro groups remaining after reaction of **1** with **5***c* was treated in the same sequence as that described above for polymers **7**. The 2-methylcyclohexanones were produced with the (*S*)-enantiomer in only 32% enantiomeric excess. The results are tabulated in Table 2. It would appear that the chloromethyl groups in **6***c* reacted in the hydrazinolysis step, and that the resulting hydrazyl groups formed polymer-bound cyclohexanone hydrazone functions which could methylate only non-enantioselectively.

*Comparison of polymer-bound systems with analogous systems in solution*

For quantitative comparison of asymmetric induction in the polymeric systems with analogous systems in solution, (*S*)-2-aminopropyl benzyl ether (**11***a*) and (*S*)-2-amino-3-phenylpropyl benzyl ether (**11***c*) were prepared. Conversion to the corresponding cyclohexanone imines (**12**) and then to their 2-methyl derivatives (**13**), followed by hydrolysis, afforded product mixtures from which the 2-methylcyclohexanones could be separated (Scheme 3). The separation, of course, was not as conveniently affected as was the case using the polymeric system.

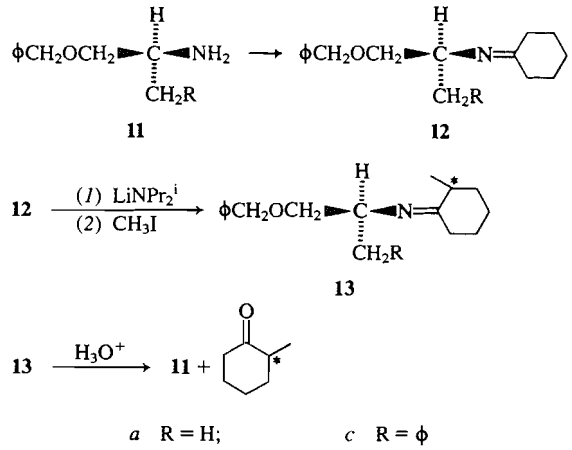


SCHEME 3

Much lower enantioselectivities (~50%) were observed from the methylations at 20°C using the systems in solution (Scheme 3) than were observed (>90%) using the analogous polymeric systems (Scheme 2). As might be expected, the enantioselectivities in solution increased as the temperature of the methylation reaction was decreased. Thus, for example, the enantiomeric excess of (*S*)-2-methylcyclohexanone from methylation of **11***c* in solution at −78°C was 85% compared with 49% at 20°C. In the polymeric systems, the enantioselectivities appeared to increase slightly (being of course already ~94% at ambient temperature) as the temperature was decreased. The chemical yields in solution at the temperatures required for enantioselectivities that approach those obtained using the polymer are much lower (compare 58%

[4]In all experiments, the identity of the 2-methylcyclohexanone produced was confirmed by comparison with an authentic sample through the use of ir, nmr, and vpc mass spectroscopy. The absence of polymethylated derivatives such as 2,6-dimethyl- and 2,2,6-trimethylcyclohexanone was confirmed by comparison of the vpc using authentic samples.

Can. J. Chem. Downloaded from www.nrcresearchpress.com by 210.87.254.40 on 09/06/12
For personal use only.

TABLE 3. Comparison of polymeric with solution systems

| Temperature (°C) | System | Yield of 2-methylcyclohexanones (%) | Enantiomeric excess of (*S*)-2-methylcyclohexanone (%) |
|---|---|---|---|
| 20 | Polymeric **9***c* | 87 | 94 |
| | Solution **11***c* | 62 | 49 |
| 0 | Polymeric **9***a* | 50 | 94 |
| | Polymeric **9***c* | 97 | 96 |
| −78 | Polymeric **9***c* | 72 | 98 |
| | Solution **11***c* | 58 | 85 |
| | Solution **11***a* | 43 | 71 |

TABLE 4. Enantioselectivities and yields from recycled polymer, **8***c*, compared with original **8***c*

| Recycle (No.) | Imine loading of **9***c* (mmol/g) | Yield (%) | Enantioselectivity (%) |
|---|---|---|---|
| 0 | 0.54 | 87 | 94 |
| 1 | 0.53 | 80 | 96 |

from **11***c* at −78°C with 87% from **9***c* at 20°C). The results are summarized in Table 3.

*Recycling the regenerated polymer* **8**c

The facile separation of the polymer used for the optical induction reaction is an obvious technical advantage over the homogeneous system in solution. The polymer may also be recycled. Preliminary experiments using recycled **8***c* indicated no decrease in the enantioselectivity of the methylation reaction (Table 4). There may be some decrease in chemical yield (87% to 80%) although this variation may be within experimental error. Additional experiments are required to examine more thoroughly this practical aspect of the use of polymeric systems in asymmetric syntheses.

## Conclusions

High enantioselectivities have been observed in the α-methylation, at 20°C, of cyclohexanone imines formed from cross-linked polystyrene functionalized with optically active 2-aminoalkoxy groups. Advantages over analogous systems in solution include facility in handling, separating, and recycling regenerated polymer, as well as higher enantioselectivities.

## Experimental

Optical rotations were determined using a Carl Zeiss polarimeter, no. 372140. All other instrumentation and general procedures are the same as described previously in a publication from these laboratories (10).

(S)-*2-Phthalimido-1-propanol (*5a)

A solution of (*S*)-2-amino-1-propanol (**2**) (4.625 g, 62.5 mmol) in tetrahydrofuran (10 mL) was added to a stirred slurry of *N*-(ethoxycarbonyl)phthalimide (**8**) (13.94 g, 62.74 mmol) in tetrahydrofuran (50 mL) at 0°C (ice–water bath). After 5 min, the bath was removed and the mixture stirred overnight at ambient temperature. After removal of the solvent under reduced pressure (boiling water bath), distillation (bulb-to-bulb, 0.1 Torr) gave ethyl carbamate (3.98 g, 71% yield). The residue was crystallized from a solution of toluene (25 mL) and hexane (10 mL) to give **5***a* (10.46 g, 74% yield); mp, 79–81°C; nmr, δ: 7.80 (d, 4H arom.), 4.30–4.66 (m, 1H), 3.80–4.10 (m, 2H), 3.10 (m, OH), and 1.40 (d, 2H) ppm. *Anal.* calcd. for $C_{11}H_{11}NO_3$: C 64.38, H 5.37, N 6.82; found: C 64.22, H 5.48, N 6.89.

(S)-*2-Phthalimido-1-butanol (*5b)

In a manner similar to that described above for **5***a*, (*S*)-2-amino-1-butanol (**3**) was converted to **5***b* (74% yield); oil; nmr, δ: 7.80 (d, 4H), 4.0–4.33 (m, 3H), 3.10 (m, OH), 1.70–2.10 (m, 2H), and 1.00 (t, 3H) ppm. *Anal.* calcd. for $C_{12}H_{13}NO_3$: C 65.75, H 5.94, N 6.39; found: C 65.69, H 6.31, N 6.43.

(S)-*2-Phthalimido-3-phenyl-1-propanol (*5c)

In a manner similar to that described for **5***a*, (*S*)-2-amino-3-phenyl-1-propanol (**4**) was converted to **5***c* (82% yield); mp 105–106°C; nmr, δ: 7.80 (d, 4H), 7.33 (s, 5H), 4.50–4.90 (m, 1H), 4.0–4.33 (m, 2H), 3.30 (d, 2H), and 2.90 (m, OH) ppm. *Anal.* calcd. for $C_{17}H_{15}NO_3$: C 72.59, H 5.34, N 4.98; found: C 72.64, H 5.57, N 4.94.

(S)-*2-Phthalimido-1-propoxymethylated chloromethylated polystyrene (*6a)

To a slurry of 1.006 g (25.02 mmol) of potassium hydride (washed with hexane) and tetrahydrofuran (100 mL) was added, with stirring, a solution of (*S*)-2-phlthalimido-1-propanol (**5***a*) (3.746 g, 18.27 mmol), dibenzo-18-crown-6 (200 mg, 0.56 mmol), and hexamethylphosphoric triamide (10 mL). After 1 h at ambient temperature, a slurry of chloromethylated polystyrene (**1**) (22.92 g, 23.30 mequiv. Cl) in tetrahydrofuran (50 mL) was added. The reaction mixture was stirred and heated under reflux for 48 h. The polymer was separated by filtration and washed successively with solutions of tetrahydrofuran and ethanol (1:1), tetrahydrofuran and methanol (1:1), and then with ether. The polymer was dried to constant weight under reduced pressure to give **6***a* (22.393 g); ir, ν(C=O): 1710 $cm^{-1}$; Cl(9), 0.5 mequiv./g.

(S)-*2-Phthalimido-1-butoxymethylated chloromethylated polystyrene (*6b)

In a manner similar to that described for **6***a*, chloromethylated polystyrene, using (*S*)-2-phthalimido-1-butanol (**5***b*), was converted to **6***b*; ir, ν(C=O): 1710 $cm^{-1}$; Cl(9), 0.45 mequiv./g.

(S)-*2-Phthalimido-3-phenylpropoxymethylated chloromethylated polystyrene (*6c)

In a manner similar to that described for **6***a*, chloromethylated polystyrene, using (*S*)-2-phthalimido-3-phenyl-1-propanol (**5***c*), was converted to **6***c*; ir, ν(C=O): 1710 $cm^{-1}$; Cl(9), 0.4 mequiv./g.

Can. J. Chem. Downloaded from www.nrcresearchpress.com by 210.87.254.40 on 09/06/12
For personal use only.

(S)-*2-Phthalimido-1-propoxymethylated methylated polystyrene (7*a)

To a solution of sodium iodide (13.182 g, 87.88 mmol) in acetone (150 mL) was added **6***a* prepared as described above (21.093 g, 10.55 mequiv. Cl). The mixture was stirred under reflux for 48 h and then allowed to cool to ambient temperature. The polymer was separated by filtration and washed successively with acetone, tetrahydrofuran, ethanol, methanol, aqueous methanol, methanol, and finally ether and then dried under reduced pressure to constant weight to give a polymer (22.018 g). To a stirred slurry of this polymer in tetrahydrofuran (150 mL) was added tributyltin hydride (6 mL, 22.74 mmol). The reaction mixture was heated under reflux for 48 h. The polymer was then removed by filtration and washed successively with the solvents described above and dried to constant weight to give **7***a* (21.903 g); ir, ν(C=O): 1710 $cm^{-1}$; Cl(9) not detected.

(S)-*2-Phthalimido-1-butoxymethylated methylated polystrene (7*b) *and (S)-2-phthalimido-3-phenyl-1-propoxymethylated methylated polystyrene (7*c)

Procedures similar to that described above for **7***a* were used to prepare **7***b* and **7***c* from **6***b* and **6***c*, respectively.

(S)-*2-Amino-1-propoxymethylated polystyrene (8*a), (S)-*2-amino-1-butoxymethylated polystyrene (8*b), *and* (S)-*2-amino-3-phenylpropoxymethylated polystyrene (8*c)

To a slurry of either polymer **7***a*, **7***b*, or **7***c* prepared as described above (ca. 20 g) in a solution of tetrahydrofuran (100 mL) and ethanol (100 mL) was added, with stirring, aqueous 95% hydrazine (10 mL). The reaction mixture was stirred for 16 h at ambient temperature. The insoluble polymer was then removed by filtration and washed successively with tetrahydrofuran, acetone, ethanol, methanol, aqueous methanol, and then ether to give, after drying under reduced pressure to constant weight (ca. 20 g), polymers **8***a*, **8***b*, or **8***c* respectively. Each exhibited an ir spectrum with absorptions at 3300 $cm^{-1}$ assignable to amino groups.

(S)-*2-Cyclohexylideneamino-2-propoxymethylated polystyrene (9a)*

A slurry of **8***a* prepared as described above (20 g, 10 mequiv. $NH_2$) in a solution of cyclohexanone (8.64 g, 88 mmol) in benzene (200 mL) was heated under reflux in a Soxhlet extractor in which the thimble contained 3 Å molecular sieves. The polymer was removed by filtration and washed successively with tetrahydrofuran, methanol, and then ether to give, after drying under reduced pressure to constant weight (20 g), **9***a*.

(S)-*2-Cyclohexylideneamino-1-butoxymethylated polystyrene (9*b) *and* (S)-*2-cyclohexylideneamino-3-phenyl-1-propoxymethylated polystyrene (9*c)

In a similar manner to that described above for the preparation of **9***a*, the polymers **8***b* and **8***c* were converted respectively to **9***b* and **9***c*.

*Determination of loadings of* **9**a, **9**b, *and* **9**c

A slurry of polymer **9***a* (2.983 g) in a buffer solution (14 mL) prepared from acetic acid (25 mL), sodium acetate (10.8 g), and water (25 mL), and methylene chloride (15 mL) was stirred at ambient temperature for 0.5 h. The methylene chloride layer was washed with water, then saturated sodium bicarbonate solution, and dried over magnesium sulfate. Removal of methylene chloride by distillation afforded a liquid residue (0.1667 g); gc, one sharp peak (tr, 2.5) assignable to cyclohexanone (>99% purity), and representing 0.57 mmol per g of **9***a*.

By the same method, cyclohexanone was obtained from polymers **9***b*, and **9***c* in amounts representing loadings of 0.56 mmol and 0.54 mmol/g of **9***b* and **9***c* respectively.

*2-(2-Methylcyclohexylideneamino)-1-propoxymethylated polystyrene (10a), 2-(2-methylcyclohexylideneamino)-1-butoxymethylated polystyrene (10*b), *and 2-(2-methylcyclohexylideneamino)-3-phenyl-1-propoxymethylated polystyrene (10*c)

To a stirred slurry of either **9***a*, **9***b*, or **9***c* (ca. 10 g, ca. 5.4 mequiv.) in tetrahydrofuran was added, *at 0°C* (ice–water bath), with stirring, diisopropylamine (2.0 mL, 14 mmol) followed by a solution of butyllithium (1.55 *M* in hexane, 10 mL, 15.5 mmol). The reaction mixture was stirred at either ambient temperature (*20°C*) or *0°C* (ice bath) for 20 h, or at *−78°C* (Dry-Ice bath) for 40 h. Then, iodomethane (2.0 mL, 40 mmol) was added, dropwise, and the reaction mixture stirred for 8 h while the same temperature was maintained. The polymer was removed by filtration and washed successively with tetrahydrofuran, methanol, and finally ether, and then dried under reduced pressure to constant weight (ca. 10 g) to give **10***a*, **10***b*, or **10***c* respectively.

*Formation of* (R)- *and* (S)-*2-methylcyclohexanone with regeneration of polymers 8*a, *8*b, *and 8*c

A slurry of polymer **10***a* prepared *at 20°C* as described above (5.231 g 2.98 mequiv.) in a buffer solution (15 mL) prepared from acetic acid (25 mL), sodium acetate (10.8 g), and water (25 mL), and methylene chloride (15 mL) was stirred at ambient temperature for 0.5 h. The methylene chloride layer was separated and washed successively with water (15 mL), saturated sodium bicarbonate solution (15 mL), 5% aqueous sodium chloride solution, and dried over magnesium sulfate. Removal of methylene chloride by distillation afforded a liquid residue (109 mg); gc, one sharp peak (>99%) assignable to (*R*)- and (*S*)-2-methylcyclohexanone (33% yield); polarimetric analysis $[\alpha]_D$ 15.2° (*c* 0.694, MeOH) (lit. (5) $[\alpha]_D$ 16.4°), 92% enantiomeric excess of (*S*)-2-methylcyclohexanone.

In a similar manner, polymer **10***a* prepared *at 0°C* as described above gave (*R*)- and (*S*)-2-methylcyclohexanone in 50% yield and 94% enantiomeric excess of the (*S*)-enantiomer.

In a similar manner, the polymer **10***b* prepared *at 20°C* as described above gave a liquid product; gc, one sharp peak (tr, 2.9) assignable to (*R*)- and (*S*)-2-methylcyclohexanones (86% yield calculated from the loading of **9***b*); polarimetric analysis, $[\alpha]_D$ 15.33° (lit. (5) $[\alpha]_D$ 16.4°), 93.5% enantiomeric excess of (*S*)-2-methylcyclohexanone.

Similarly, polymer **10***c* prepared *at 20°C* as described above gave essentially pure (*R*)- and (*S*)-2-methylcyclohexanone (87% yield calculated from loading of **9***c*); polarimetric analysis, $[\alpha]_D$ 15.40°, 93.8% enantiomeric excess of (*S*)-2-methylcyclohexanone.

In a similar manner, polymer **10***c* prepared *at 0°C* and −78°C as described above gave essentially pure (*R*)- and (*S*)-2-methylcyclohexanone in 97% and 72% yields respectively, and in 96 and 98% enantiomeric excesses of (*S*)-2-methylcyclohexanone respectively.

(S)-*2-Phthalimidopropyl benzyl ether*

To a slurry of potassium hydride (1.72 g, 43 mmol, washed with hexane) in tetrahydrofuran (100 mL) containing dibenzo-18-crown-6 (200 mg, 0.56 mmol) was added (*S*)-2-phthalimido-1-propanol (**5***a*) prepared as described above (8.27 g, 40.33 mmol). The reaction mixture was stirred at ambient temperature for 1 h and then cooled to, and maintained at, 0°C (ice–water bath) while benzyl bromide (10.07 g, 58.9 mmol) was added. After 0.5 h, the reaction mixture was allowed to warm to ambient temperature and stirred for 48 h. After addition of methanol (10 mL), the reaction mixture was concentrated under reduced pressure. To the residue was added ether (100 mL) and water (100 mL). The ether layer was washed with water, dried over magnesium sulfate, filtered, and concentrated. The residue was fractionated by column chromatography (Kieselgel 60,

Can. J. Chem. Downloaded from www.nrcresearchpress.com by 210.87.254.40 on 09/06/12
For personal use only.

Korngrösse 0.040–0.063 mm, 230–400 mesh ASTM). An eluent of 3% methanol in ether–hexane (1:1) gave, after evaporation of solvent, crystalline **11***a*, (6.71 g, 56.4% yield), mp 39–41°C; $[\alpha]_D$ +44.6° (*c* 1.0, MeOH); nmr, δ: 7.70 (d, 4H), 7.30 (s, 5H), 4.65–5.05 (m, 1H), 4.55 (s, 2H), 3.50–4.20 (m, 2H), and 1.40 (d, 3H) ppm. *Anal.* calcd. for $C_{18}H_{17}NO_3$: C 73.22, H 5.76, N 4.74; found: C 73.30, H 5.82, N 4.51.

(S)-*2-Phthalimido-3-phenylpropyl benzyl ether*

In a similar manner, *N*-2-phthaloyl-3-phenylpropanol was converted to **11***c*, 33% yield; mp 62–64°C; $[\alpha]_D$ −78.1° (*c* 0.267, MeOH); nmr, δ: 7.70 (d, 4H), 7.30 (d, 10H), 4.66–5.05 (m, 1H), 4.55 (s, 2H), 3.45–4.30 (m, 2H), and 3.20–3.35 (m, 2H) ppm. *Anal.* calcd. for $C_{24}H_{21}NO_3$: C 77.63, H 5.66, N 3.77; found: C 77.63, H 6.18, N 3.46.

(S)-*2-Aminopropyl benzyl ether (11*a)

A solution of (*S*)-2-phthalimidopropyl benzyl ether prepared as described above (2.155 g, 7.30 mmol) in ethanol (15 mL) was added to an excess of 95% aqueous hydrazine solution (1.5 g). The mixture was stirred at 30°C for 2 h and then treated with an excess of dilute hydrochloric acid. The insoluble phthalhydrazide was removed by filtration. The fitrate was concentrated, cooled, and filtered to remove additional phthalhydrazide. The filtrate was treated with dilute potassium hydroxide solution (to pH 14) and the mixture extracted with ether. The ether extract was dried over magnesium sulfate and concentrated. The residue was distilled (bulb-to-bulb, 0.5 Torr, 85–90°C) to give **11***a* (1.110 g, 92.3% yield); oil; $[\alpha]_D$ +16.35° (*c* 0.847, MeOH); nmr, δ: 7.50 (s, 5H), 4.65 (s, 2H); 4.50–4.90 (m, 1H), 3.10–3.45 (m, 2H), 2.10 (m, $NH_2$), 1.15 (d, 3H) ppm. Formation of the hydrochloride of **11***a* by reaction of a solution of **11***a* in ether with dry hydrogen chloride gave an analytical sample. *Anal.* calcd. for $C_{10}H_{16}ClNO$: C 59.6, H 7.94, N 6.94; found: C 60.06, H 8.16, N 6.84.

(S)-*2-Amino-3-phenylpropyl benzyl ether (11*c)

In a manner similar to that described above for **11***a*, (*S*)-2-phthalimido-3-phenylpropyl benzyl ether was converted to **11***c* (96.4% yield); oil; $[\alpha]_D$ + 5.59° (*c* 0.626, MeOH); nmr, δ: 7.30 (d, 10H), 4.55 (s, 2H), 3.00–3.55 (m, 3H), 2.55–2.80 (m, 2H), and 1.60 (m, $NH_2$) ppm. *Anal.* of the hydrochloride, calcd. for $C_{16}H_{20}ClNO$: C 69.18, H 7.21, N 5.04; found: C 69.11, H 7.36, N 4.93.

(S)-*2-Cyclohexylideneaminopropyl benzyl ether (12*a)

A solution of **11***a* (1.044 g, 6.33 mmol), and cyclohexanone (806.8 mg, 8.23 mmol) in benzene (100 mL) was heated under reflux for 8 h using a Dean–Stark trap for collection of water. Benzene was removed under reduced pressure and the residue distilled (bulb-to-bulb, 0.5 Torr, 165–170°C) to give crude **12***a* (1.488 g, 95% yield) which was redistilled to give a clear viscous oil; $[\alpha]_D$ +7.29° (*c* 1.007, MeOH); nmr, δ: 7.50 (s, 5H aromatic), 4.55 (s, 2H), 3.00–3.80 (m, 3H), 1.65–2.25 (m, 10H), and 1.20 (d, 3H) ppm.

(S)-*2-Cyclohexylideneamino-3-phenylpropyl benzyl ether (12*c)

In a manner similar to that described for **12***a*, **11***c* was converted to **12***c* (91% yield; bulb-to-bulb, 0.5 Torr, 190–195°C); $[\alpha]_D$ −15.9° (*c* 0.464, MeOH); nmr, δ: 7.20–7.50 (m, 10H aromatic), 4.55 (s, 2H), 3.80–4.20 (m, 1H), 3.30–3.60 (m, 2H), 2.65–3.00 (m, 2H), and 1.40–2.30 (m, 10H) ppm.

(R)- *and* (S)-*2-Methylcyclohexanones from 12*a *at −78°C*

To a solution of diisopropylamine (0.8 mL, 5.71 mmol) in tetrahydrofuran (15 mL) was added, with stirring at 0°C, a solution of butyllithium in hexane (1.6 *M*, 3.60 mL, 5.76 mmol). After 15 min, the reaction mixture was cooled to −30°C (Dry-Ice in acetone bath) and **12***a* (1.225 g, 5.0 mmol) was added. After 1.5 h, the solution was cooled to −78°C and a solution of iodomethane (0.4 mL, 6.42 mmol) in tetrahydrofuran (5 mL) was added dropwise over 0.5 h. The reaction mixture was stirred at −78°C for 2 h, and then poured into a saturated solution of sodium chloride (50 mL) and extracted with ether. The extract was washed with aqueous sodium chloride solution, dried over magnesium sulfate, and concentrated.

A solution of the residue in pentane (25 mL) was shaken for 0.5 h with a solution of sodium acetate (1.65 g) and acetic acid (3.75 mL) in water (17.5 mL). The aqueous layer was separated and washed with pentane. The combined pentane solutions were washed successively with hydrochloric acid (1 *N*), water, 5% aqueous sodium bicarbonate solution, water, and aqueous sodium chloride solution. Concentration of the pentane solution and distillation of the residue (bulb-to-bulb) gave a liquid product (241 mg); gc, one sharp peak assignable to (*R*)- and (*S*)-2-methylcyclohexanones (43% yield); polarimetric analysis, $[\alpha]_D$ 11.70° (*c* 0.573, MeOH) indicating an enantiomeric excess of (*S*)-2-methylcyclohexanone of 71.3%.

(R)- *and* (S)-*2-Methylcyclohexanones from 12*c *at −78°C*

In a manner similar to that described above for **12***a*, **12***c* produced (*R*)- and (*S*)-2-methylcyclohexanone in 58% yield and 85.3% enantiomeric excess of (*S*)-2-methylcyclohexanone.

(R)- *and* (S)-*2-Methylcyclohexanones from 12*c *at 20°C*

In a manner similar to that described above for **12***c* *at* −78°C, **12***c* was treated with lithium diisopropylamide at 20°C and iodomethane at 20°C to give 2-methylcyclohexanones in 62% yield, and 49% enantiomeric excess of (*S*)-2-methylcyclohexanone.

## Acknowledgements

We thank the Natural Sciences and Engineering Research Council of Canada and the Faculty of Science, York University, for financial support of this research.

1. (*a*) J. M. J. FRÉCHET. Tetrahedron, **37**, 663 (1981); (*b*) C. C. LEZNOFF. Acc. Chem. Res. **11**, 327 (1978); (*c*) N. K. MATHUR, C. K. NARANG, and R. E. WILLIAMS. Polymers as aids in organic chemistry. Academic Press, New York. 1980.
2. P. M. WORSTER, C. R. MCARTHUR, and C. C. LEZNOFF. Angew. Chem. Int. Ed. Engl. **18**, 221 (1979).
3. (*a*) M. KAWANA and S. EMOTO. Tetrahedron Lett. 4855 (1972); (*b*) M. KAWANA and S. EMOTO. Bull. Chem. Soc. Jpn. **47**, 160 (1974).
4. (*a*) J. D. MORRISON and H. S. MOSHER. Asymmetric organic reactions. American Chemical Society, Washington, D.C. 1976; (*b*) Y. IZUMI and A. TAI. Stereodifferentiating reactions. Academic Press, New York. 1977. Chapt. 8.
5. J. K. WHITESELL and M. A. WHITESELL. J. Org. Chem. **42**, 377 (1977).
6. A. I. MEYERS, D. R. WILLIAMS, and M. DRUELINGER. J. Am. Chem. Soc. **98**, 3032 (1976).
7. D. VALENTINE, JR. and J. W. SCOTT. Synthesis, 329 (1978).
8. P. M. WORSTER, C. C. LEZNOFF, and C. R. MCARTHUR. J. Org. Chem. **45**, 174 (1980).
9. J. H. STEWART and J. D. YOUNG [*Editors*). Solid phase Peptide syntheses. W. H. Freeman Co., San Francisco. CA. 1969 p. 55.
10. V. YEDIDIA and C. C. LEZNOFF. Can. J. Chem. **58**, 1144 (1980).

# The chemistry of thujone. V.[1] Thujone as a chiral synthon for the preparation of sesquiterpenes. Synthesis of (+)-carissone

JAMES P. KUTNEY AND ASHOK K. SINGH

*Department of Chemistry, University of British Columbia, 2036 Main Mall, University Campus, Vancouver, B.C., Canada V6T 1Y6*

Received February 2, 1982

JAMES P. KUTNEY and ASHOK K. SINGH. Can. J. Chem. **60**, 1842 (1982).

An efficient synthesis of (+)-carissone (**4**) from (+)-β-cyperone (**2**) is described. The latter sesquiterpene is readily available from thujone (**1**), via a previously described synthesis.

JAMES P. KUTNEY et ASHOK K. SINGH. Can. J. Chem. **60**, 1842 (1982).

On décrit une synthèse éfficace de la (+)-carissone (**4**) à partir de la (+)-β-cyperone. Ce dernier sesquiterpène est obtenu convenablement de la thujone (**1**) par une méthode de synthèse décrit antérieurement.

[Traduit par le journal]

Previous research in these laboratories has shown the uses of thujone (**1**)[2] in the preparation of acyclic insect juvenile hormone analogues(1,2), bicyclic natural products (e.g. (+)-β-cyperone **2**) (3), and of several pyrethroid analogues (4). In the synthesis of **2**, we have shown that thujone is an extremely efficient chiral synthon for the preparation of optically active sesquiterpenes possessing the eudesmane carbon skeleton (**3**) and (+)-β-cyperone with an optical purity of >98.8% was obtained. Here we wish to report the results of further chemical investigations to elaborate the isopropyl side chain in the basic skeleton. Of particular interest was the development of synthetic routes to eudesmane intermediates with hyroxyl groups at C7 and C11 (see **3**) and olefinic linkages at the C7—C11 or C11—C12 positions. Such studies have led to an effective synthesis of the bicyclic sesquiterpene (+)-carissone (**4**) from (+)-β-cyperone (**2**).

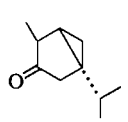

**1**

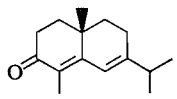

**2**

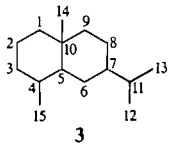

**3**

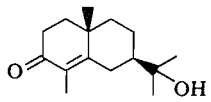

**4**

Treatment of **2** with *N*-bromosuccinimide in a tetrahydrofuran (THF)–water (1:1) mixture resulted in the formation of bromohydrin **5** in 76% yield. The ratio of THF to water was found to have an effect on the product composition. If a THF–water ratio of 7:3 was used, in addition to **5**, a dibromo product **6** was also obtained.

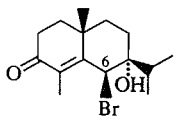

**5**

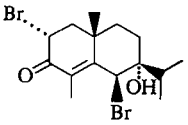

**6**

The stereochemistry of the bromohydrin was assigned on the basis of spectral data and consideration of the established mechanism of bromohydrin formation with $NBS/H_2O$ (5). In the $^1$Hmr spectrum of **5** the C6 proton which resonated at δ 4.87 appeared clearly as a doublet with a coupling constant of 2 Hz. This is consistent with a 1,3 di-equatorial coupling between the C6α-proton and the C8α-(equatorial) proton (6). Thus the *trans* configuration of the bromohydrin **5** is as depicted.

Attempts to introduce the C7—C11 double bond by conversion of the C7-hydroxyl group to the mesylate led to the exclusive formation of the epoxide **7**. Indeed the bromohydrin is quite labile under basic conditions and is readily converted to **7**. Reaction of **5** with thionyl chloride also failed to give the desired exocyclic double bond with (+)-β-cyperone being the final isolated product.

Debromination of **5** with triphenyl *or* tri-*n*-butyl tin hydride was ineffective for selective removal of the 6β-bromo group.

Treatment of **5** with "super hydride" resulted in

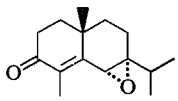

**7**

[1]For part IV, see ref. 4.

[2]Thujone is the major component (ca. 80%) of the steam distillate from the slash (waste) of Western red cedar.

0008-4042/82/141842-05$01.00/0

©1982 National Research Council of Canada/Conseil national de recherches du Canada

Can. J. Chem. Downloaded from www.nrcresearchpress.com by 210.87.254.42 on 09/06/12
For personal use only.

Can. J. Chem. Downloaded from www.nrcresearchpress.com by 210.87.254.42 on 09/06/12
For personal use only.

the initial conversion of the bromohydrin function to an epoxide with concomitant reduction of the C3-ketone to give **8**. Further reduction of the epoxide **8** by "super hydride" afforded the diol **9** while oxidation of **8** with $CrO_3$–pyridine complex provided an epoxyenone identical to **7** as obtained above. Oxidation of **9** under similar conditions gave the keto alcohol **10**. This compound was found to be very acid sensitive and hence attempts to dehydrate the tertiary hydroxyl group (or its derivatives) in a regiospecific manner, so as to furnish the exocyclic double bond, could not be realized.

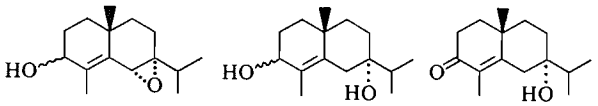

**8** **9** **10**

Reaction of **10** with thionyl chloride or methanesulfonyl chloride resulted only in the formation of (+)-β-cyperone (**2**). Further attempts to functionalize the isopropyl side chain employing intermediate **10** were abandoned when a convenient procedure to the trienone **11** directly from the bromohydrin **5** was discovered (Scheme 1).

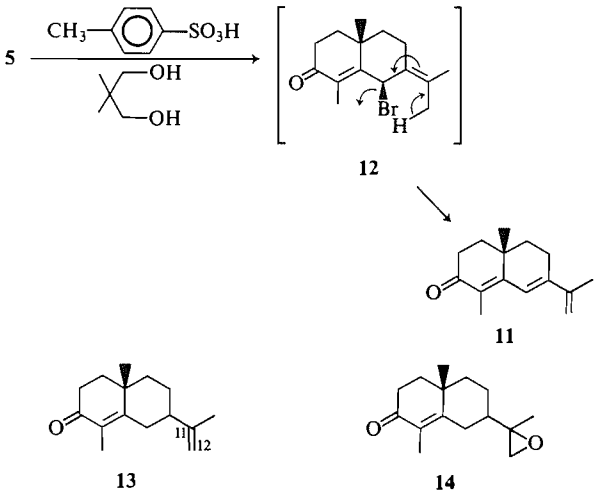

SCHEME 1

Treatment of **5** with a mixture of *p*-toluenesulfonic acid and 2,2-dimethyl-1,3-propanediol in anhydrous benzene at 75°C for 10 min afforded a high yield of **11**. Presumably the reaction proceeded by an initial dehydration to **12** which then underwent a facile dehydrobromination to form the trienone **11**. The fully conjugated trienone system was evident from the uv absorption chromophore with $\lambda_{max}$ at 320 nm and from ir spectrum with $\nu_{max}$ at 1636 and 1584 $cm^{-1}$. The $^1$Hmr spectrum is also in full agreement with the structure assigned (δ 1.88, C4 vinyl methyl; 2.02, C11 vinyl methyl; 6.60, C6H; 5.31, 5.15, C12(methylene)).

In their synthesis of (+)-carissone (**4**) from (+)-α-cyperone (**13**) Pinder and Williams (7) selectively converted the C11—C12 double bond into an epoxide **14** by means of perbenzoic acid.

Our attempts to carry out specific epoxidation of the same side chain double bond employing compound **11** were unsuccessful. However, this double bond can be selectively oxidized by osmium tetroxide or alkaline potassium permanganate to give a diastereomeric mixture of diols **15** (Scheme 2). Considerable efforts were expended in attempting to separate this mixture by various chromatographic methods. For example, preparative layer chromatography involving numerous (thirteen) developing solvents did afford several milligrams of the pure isomers but this separation was accompanied by large losses of materials and was therefore abandoned. The subsequent steps of the sequence (**15** ↠ **19**) were therefore performed on a mixture since **16**, **18**, and **19** were similarly difficult to separate and the eventual objective, the synthesis of **4**, was not restricted by this situation.

Hydrogenation of **15** with palladium on charcoal as catalyst under basic conditions afforded the partially reduced product **16** as the major component. The β-configuration of the side chain, as shown, became evident in subsequent studies when (+)-carissone (**4**) was obtained.

A minor product, the fully reduced intermediate **17**, was also isolated from the hydrogenation mixture. The characterization data for this compound, which is of no further use in the present synthetic work, are given in the Experimental section.

As expected, tosylation of the dihydroxy ketone **16** with tosyl chloride afforded only the monotosylate **18**. Lithium aluminium hydride reduction of the primary tosylate was accompanied by reduction of the C3 carbonyl function to give the diol **19**.

Finally oxidation (chromium trioxide, pyridine) converted **19** to a single product possessing all the physical properties of (+)-carissone (**4**) (see Experimental).

The above described route represents the most efficient synthesis of this natural product and represents an overall yield of **4** of 17% from β-cyperone (**2**).

Other syntheses of **4** (7–9) generally involve less readily available starting materials and proceed in lower yields.

Can. J. Chem. Downloaded from www.nrcresearchpress.com by 210.87.254.42 on 09/06/12
For personal use only.

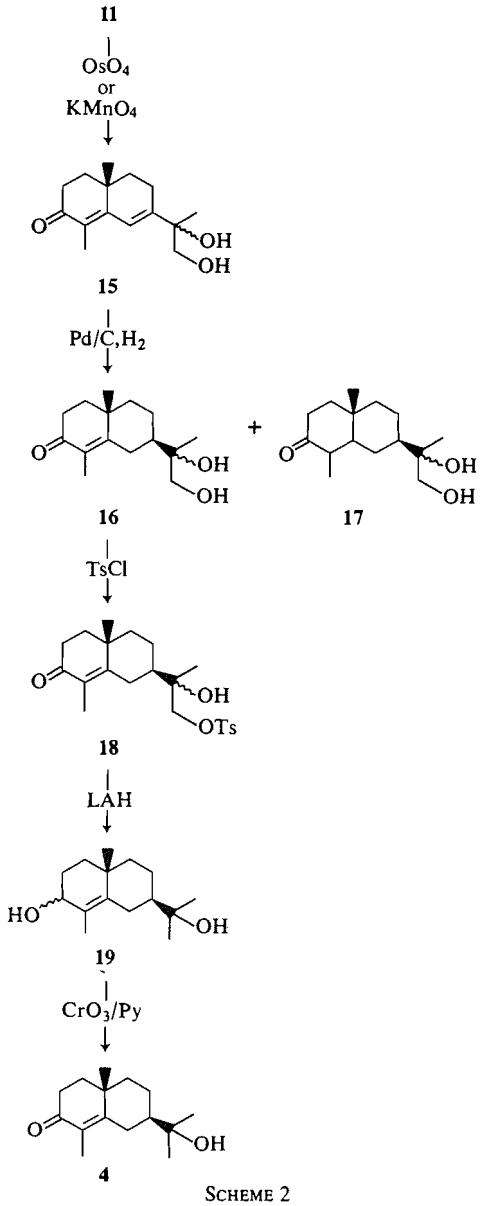


SCHEME 2

## Experimental

Ultraviolet spectra were recorded on a Cary 15 spectrophotometer using methanol as solvent. Infrared spectra were recorded on a Perkin–Elmer 710 spectrophtometer using chloroform as solvent. The $^1$Hmr spectra were recorded on either a Varian XL-100 or Nicolet Oxford H-270 or a 400 MHz instrument. Chemical shifts are reported as ppm from TMS, used as internal standard. Low resolution mass spectra were recorded on either an Atlas CH-4B or an AEI MS-902 spectrometer. High resolution mass measurements were made on an AEI MS-50 spectrometer. Optical rotations were recorded on a Perkin–Elmer 141 polarimeter. Rotations were obtained using a cell with a path length of 10 cm. Microanalyses were carried out by Mr. P. Borda, Microanalytical Laboratory, University of British Columbia. Column chromatography utilized Merck silica gel 60 (70–230 mesh). Preparative and thin layer chromatography utilized Merck silica gel $GF_{254}$. Petroleum ether refers to the fraction with boiling range 30–60°C.

*Bromohydrin* **5**

To a solution of **2** (500 mg) in THF and water (50 mL, 1:1 v/v) was added NBS (2 g) at room temperature and the mixture stirred for 22 h. The reaction mixture was diluted with water (50 mL), extracted with ether (2 × 100 mL), and the organic layer washed with water (3 × 50 mL), dried ($MgSO_4$), and concentrated. Crystallization of the residue from ether–petroleum ether gave colourless crystals **5** (550 mg, 76%); mp 114–115°C; $[\alpha]_D$ −118.5° (*c* 0.615, $CHCl_3$); ir $\nu_{max}$: 3486, 1666 cm$^{-1}$; uv $\lambda_{max}$: 249 (ε 12 372) nm; $^1$Hmr δ: 0.97 (3H, d, *J* = 7 Hz), 1.02 (3H, d, *J* = 7 Hz), 1.53 (3H, s), 1.59 (1H, s, $D_2O$ exchangeable), 1.72 (1H, ddd, *J* = 12, 5, 2 Hz), 1.81 (1H, ddd, *J* = 12, 5, 2 Hz), 1.87 (3H, s), 1.92 (1H, dt, *J* = 14, 4 Hz), 2.05 (1H, dt, *J* = 16, 4 Hz), 2.27 (1H, septet, *J* = 7 Hz), 2.49 (1H, ddd, *J* = 14, 6, 2 Hz), 2.66 (1H, ddd, *J* = 16, 14, 2 Hz), 4.87 (1H, d, *J* = 2 Hz); ms *m/e*: 316 ($M^+$), 314 ($M^+$), 298, 296, 273, 271, 234. High resolution molecular weight determination, calcd. for $C_{15}H_{23}O_2Br^{79}$: 314.0881; found: 314.0893; calcd. for $C_{15}H_{23}O_2Br^{81}$: 316.0861; found: 316.0866. *Anal.* calcd. for $C_{15}H_{23}O_2Br$: C 57.14, H 7.30, Br 25.39; found: C 56.94, H 7.41, Br 25.17.

A mixture of **2** and NBS stirred in THF and $H_2O$ (7:3 v/v) under the above condition gave **5** and **6** in the ratio 1:1 which were separated by silica gel column chromatography. The compound **6** was obtained as colourless crystals; mp 142–143°C; $[\alpha]_D$ −12.99° (*c* 0.231, $CHCl_3$); ir $\nu_{max}$: 3525, 1676 cm$^{-1}$; uv $\lambda_{max}$: 260 (ε 11 471) nm; $^1$Hmr δ: 0.97 (3H, d, *J* = 7 Hz), 1.02 (3H, d, *J* = 7 Hz), 1.60 (3H, s), 1.94 (3H, s), 4.81 (1H, d, *J* = 2 Hz), 5.00 (1H, dd, *J* = 12, 8 Hz); ms *m/e*: 396 ($M^+$), 392 ($M^+$), 315, 313. High resolution molecular weight determination, calcd. for $C_{15}H_{22}O_2Br_2^{79}$: 391.9986; found 391.9999; calcd. for $C_{15}H_{22}O_2Br_2^{81}$: 395.9946; found: 395.9940. *Anal.* calcd. for $C_{15}H_{22}O_2Br_2$: C 45.68, H 5.58, Br 40.60; found: C 45.49, H 5.42, Br 40.46.

*Epoxyenone* **7**

The bromohydrin **5** (50 mg) was dissolved in previously cooled pyridine (3 mL) to which methane sulfonyl chloride (0.02 mL) was added and stirred at 0°C for 3 h. It was poured into crushed ice, taken up in ether, and the organic layer washed successively with 10% HCl, 10% $NaHCO_3$ solution, and finally with water and dried ($MgSO_4$). After the removal of the solvent, the solid epoxyenone **7** (35 mg, 94%) was crystallized from petroleum ether as colourless crystals; mp 84–85°C; $[\alpha]_D$ +262.27° (*c* 0.6619, $CHCl_3$); ir $\nu_{max}$: 1666 cm$^{-1}$; uv $\lambda_{max}$: 249 (ε 14 549) nm; $^1$Hmr δ: 1.05 (3H, d, *J* = 7 Hz), 1.07 (3H, s), 1.08 (3H, d, *J* = 7 Hz), 1.28 (1H, ddd, *J* = 13.5, 5, 2 Hz), 1.46 (1H, dt, *J* = 13.5, 6 Hz), 1.6–1.72 (2H, m), 1.80 (1H, dt, *J* = 13.5, 5 Hz), 1.86–2.02 (5H, m, including 1.93 (3H, s)), 2.46 (1H, ddd, *J* = 17, 5, 2 Hz), 2.63 (1H, ddd, *J* = 17, 14.5, 5 Hz), 3.30 (1H, s); ms *m/e*: 234 ($M^+$), 219, 206, 136. High resolution molecular weight determination, calcd. for $C_{15}H_{22}O_2$: 234.1620; found: 234.1619. *Anal.* calcd. for $C_{15}H_{22}O_2$: C 76.92, H 9.40; found: C 77.09, H 9.43.

*Hydroxyenone* ***10***

To a reaction flask equipped with reflux condenser, magnetic stir bar, and rubber septum, was introduced super hydride ($LiEt_3BH$) (9.5 mL, 1 *M* in THF) by syringe under nitrogen. Bromohydrin **5** (448 mg) in THF (3 mL) was added in one portion by syringe. The resulting reaction mixture was stirred at ambient temperature for 24 h. The reaction mixture was diluted with ice water, extracted with ether, and dried ($MgSO_4$). Evaporation of solvent gave a solid which was chromatographed on silica gel (10 g). Elution with ether–petroleum ether (1:1 v/v) gave the hydroxyepoxide **8** (32 mg, 10%) as a viscous

Can. J. Chem. Downloaded from www.nrcresearchpress.com by 210.87.254.42 on 09/06/12
For personal use only.

oil; $[\alpha]_D$ +75.35 (*c* 0.215, $CHCl_3$); ir $\nu_{max}$: 3462 $cm^{-1}$; $^1$Hmr δ: 0.97 (3H, s), 1.03 (3H, d, *J* = 7 Hz), 1.05 (3H, d, *J* = 7 Hz), 1.08–1.85 (9H, m, including 1.80 (1H, s, $D_2O$ exchangeable)), 1.91 (3H, s), 2.06 (1H, m), 3.34 (1H, s), 4.13 (1H, dd, *J* = 10, 6 Hz); ms *m/e*: 236 ($M^+$), 218, 203, 193. High resolution molecular weight determination, calcd. for $C_{15}H_{24}O_2$: 236.1776; found: 236.1761. *Anal.* calcd. for $C_{15}H_{24}O_2$: C 76.27, H 10.17; found: C 76.34, H 10.28. Further elution with the same solvent furnished dihydroxy **9** (232 mg, 69%) as a colourless solid; mp 106–108°C; $[\alpha]_D$ −17.28° (*c* 0.162, $CHCl_3$); ir $\nu_{max}$: 3460 $cm^{-1}$; $^1$Hmr δ: 0.99 (6H, d, *J* = 7 Hz), 1.08 (3H, s), 1.30–1.73 (10H, m, including 1.54 (2H, s, $D_2O$ exchangeable)), 1.78 (3H, s), 1.94 (1H, m), 2.09 (1H, d, *J* = 14 Hz), 2.46 (1H, dd, *J* = 14, 3 Hz), 4.13 (1H, t, *J* = 8 Hz); ms *m/e*: 238 ($M^+$), 220, 205, 195, 167. High resolution molecular weight determination, calcd. for $C_{15}H_{26}O_2$: 238.1933; found: 238.1939. *Anal.* calcd. for $C_{15}H_{26}O_2$: C 75.63, H 10.92; found: C 75.42, H 10.86.

To the chromium–pyridine complex from chromium trioxide (310 mg) and pyridine (3 mL) was added a solution of dihydroxy **9** (153 mg) in pyridine (5 mL). The mixture was stirred at room temperature for 20 min and then diluted with cold water and extracted with benzene–ether (100 mL, 1:1 v/v), dried ($MgSO_4$), and evaporated to give a solid. Recrystallization from ether afforded hydroxyenone **10** (30 mg, 86%) as a colourless solid; mp 147–148°C; $[\alpha]_D$ +102.18° (*c* 0.321, $CHCl_3$); ir $\nu_{max}$: 3450, 1656, 1616 $cm^{-1}$; uv $\lambda_{max}$: 252 (ε 15 385) nm; $^1$Hmr δ: 0.98 (6H, d, *J* = 6.7 Hz), 1.20 (3H, s), 1.45–1.95 (11H, m, including 1.63 (1H, s, $D_2O$ exchangeable) and 1.80 (3H, s)), 2.20 (1H, d, *J* = 14 Hz), 2.36–2.60 (2H, m), 2.70 (1H, dd, *J* = 14, 2.7 Hz); ms *m/e*:236 ($M^+$), 218, 193, 138. High resolution molecular weight determination, calcd. for $C_{15}H_{24}O_2$: 236.1776; found: 236.1763. *Anal.* calcd. for $C_{15}H_{24}O_2$: C 76.27, H 10.16; found: C 76.15, H 10.26.

The compound **8** on $CrO_3$–pyridine oxidation afforded epoxyenone **7**, the same as described earlier.

*Trienone 11*

A mixture of bromohydrin **5** (1.5 g), 2,2-dimethyl-1,3-propanediol (7 g), and *p*-toluenesulfonic acid (20 mg) in dry benzene (60 mL) was heated at 74–79°C under argon for 10 min. It was then cooled, diluted with water (50 mL), and extracted with ether (3 × 50 mL). The combined extract was washed with water (2 × 50 mL), dried ($MgSO_4$), and concentrated *in vacuo*. Crude material was chromatographed on silica gel (100 g) eluted with 5% ether in petroleum ether to furnish a yellow oil (0.729 g, 71%) which solidified on standing; mp 35–36°C; $[\alpha]_D$ +622.74° (*c* 0.63975, $CHCl_3$); ir $\nu_{max}$: 1636, 1584 cm$^1$; uv $\lambda_{max}$: 320 (ε 33 469) nm; $^1$Hmr δ: 1.11 (3H, s), 1.48–1.88 (7H, m, including 1.88 (3H, s)), 2.02 (3H, s), 2.41–2.53 (3H, m), 2.67 (1H, ddd, *J* = 18, 14, 6 Hz), 5.15 (1H, s), 5.31 (1H, s), 6.60 (1H, s); ms *m/e*: 216 ($M^+$), 201, 188, 173. High resolution molecular weight, calcd. for $C_{15}H_{20}O$: 216.1514; found: 216.1517. *Anal.* calcd. for $C_{15}H_{20}O$: C 83.33, H 9.26; found: C 83.05, H 9.42.

*Hydroxydienone 15*

The trienone **11** (50 mg) in dioxane (3 mL) was treated with osmium tetroxide (64 mg) in dioxane (2 mL). The mixture was stirred for 18 h at ambient temperature under an atmosphere of nitrogen. The solution was saturated with $H_2S$, then filtered. After removal of the solvent it yielded solid which was recrystallized with ether–petroleum ether to afford a mixture of diols **15** (38 mg, 66%); mp 92–94°C. The diols were separated by preparative tlc plate developed several times in the same solvent, ether–petroleum ether–methanol (70:28:2). The less polar isomer gave: mp 114–115°C; $[\alpha]_D$ +392.48° (*c* 0.0665, $CHCl_3$); ir $\nu_{max}$: 3450, 1644, 1615 $cm^{-1}$; uv $\lambda_{max}$: 297 (ε 25 595) nm; $^1$Hmr δ: 1.10 (3H, s), 1.36 (3H, s), 1.51–1.81 (4H, m), 1.86 (3H, s), 2.18–2.76 (6H, m), 3.54 (1H, d, *J* = 10 Hz), 3.76 (1H, d, *J* = 10 Hz), 6.76 (1H, d, *J* = 2 Hz); ms *m/e*: 250 ($M^+$), 232, 219. High resolution molecular weight determination, calcd. for $C_{15}H_{22}O_3$: 250.1569; found: 250.1567. *Anal.* calcd. for $C_{15}H_{22}O_3$: C 72.00, H 8.80; found: C 71.86, H 8.96. The more polar isomer gave: mp 99–100°C; $[\alpha]_D$ +233.88° (*c* 0.0885, $CHCl_3$); ir $\nu_{max}$: 3450, 1645, 1616 $cm^{-1}$; uv $\lambda_{max}$: 297 (ε 25 000) nm; $^1$Hmr δ: 1.10 (3H, s), 1.36 (3H, s), 1.51–1.81 (4H, m), 1.86 (3H, s), 2.10–2.75 (6H, m), 3.57 (1H, d, *J* = 12 Hz), 3.75 (1H, d, *J* = 12 Hz), 6.74 (1H, d, *J* = 2 Hz); ms *m/e*: 250 ($M^+$), 232, 219. High resolution molecular weight determination, calcd. for $C_{15}H_{22}O_3$: 250.1569; found: 250.1569. *Anal.* calcd. for $C_{15}H_{22}O_3$: C 72.00, H 8.80; found: C 71.84, H 8.92.

A mixture of trienone **11** (28 mg), sodium hydroxide (20 mg), and potassium permanganate (55 mg) in aqueous *tert*-butanol (6 mL, 1:1 v/v) was stirred at 0°C for 1.5 h. Solid sodiumbisulfite was added until the solution became clear. This was concentrated and extracted with methylene chloride, washed with water, dried ($MgSO_4$), and evaporated to give **15** (16 mg, 50%), identical with that obtained above.

*Diols 16 and 17*

A solution of diols **15** (117 mg) and potassium hydroxide (18 mg) in ethanol (20 mL) containing 10% palladium/charcoal (32 mg) was stirred under an atmosphere of hydrogen at ambient temperature for 30 min. The solution was filtered and then evaporated. The residue was acidified with 10% HCl and extracted with ether (2 × 50 mL). The combined extract was washed with water, brine, and dried ($MgSO_4$), and concentrated to leave 118 mg of colourless oil. Preparative scale tlc gave pure diols **16** (85 mg, 72%) and **17** (28 mg, 24%) as viscous oils. The physical properties of **16** are as follows: $[\alpha]_D$ +147.92° (*c* 0.528, $CHCl_3$); ir $\nu_{max}$: 3464, 1652, 1617 $cm^{-1}$; uv $\lambda_{max}$: 249 (ε 14 560) nm; $^1$Hmr δ: 1.19, 1.21 (3H, s, two sets), 1.22 (3H, s), 1.40–1.77 (6H, m), 1.78, 1.80 (3H, s, two sets), 1.87–2.02 (3H, m, including 1.97 (2H, s, $D_2O$ exchangeable)), 2.41 (1H, dt, *J* = 16, 4 Hz), 2.53 (1H, ddd, *J* = 16, 14, 7 Hz), 2.76, 2.94 (1H, dt, *J* = 16, 4 Hz, two sets), 3.46–3.54 (2H, m), 3.66, 3.67 (1H, d, *J* = 11 Hz, two sets); ms *m/e*: 234 ($M^+-H_2O$), 221, 219, 203, 177. High resolution molecular weight determination, calcd. for $C_{15}H_{24}O_3-H_2O$ ($M^+-H_2O$): 234.1619; found 234.1618. *Anal.* calcd. for $C_{15}H_{24}O_3$: C 71.43, H 9.52; found: C 71.14, H 9.54. And for **17**, $[\alpha]_D$ −3.22° (*c* 0.4955, $CHCl_3$); ir $\nu_{max}$: 3450, 1706 $cm^{-1}$; uv $\lambda_{max}$: 284 (ε 60.27) nm; $^1$Hmr δ: 0.99, 1.02 (3H, d, *J* = 7 Hz, two sets), 1.08 (3H, s), 1.14, 1.16 (3H, s, two sets), 1.22–1.77 (10H, m), 1.85 (1H, ddd, *J* = 15, 5, 3 Hz), 1.96 (1H, b, $D_2O$, exchangeable), 2.22 (1H, m), 2.35 (1H, ddd, *J* = 15, 5, 3 Hz), 2.53 (1H, dt, *J* = 20, 6 Hz), 3.45, 3.46 (1H, d, *J* = 11 Hz, two sets); 3.60, 3.61 (1H, d, *J* = 11 Hz, two sets); ms *m/e*: 254 ($M^+$), 236, 223. High resolution molecular weight determination, calcd. for $C_{15}H_{26}O_3$: 254.1882; found: 254.1875. *Anal.* calcd. for $C_{15}H_{26}O_3$: C 70.87, H 10.24; found: C 71.06, H 10.19.

*Tosylates 18*

The diols **16** (85 mg) were dissolved in pyridine (5 mL) to which was added *p*-toluene sulfonyl chloride (192 mg) and the mixture stirred for 16 h. The solution was poured into ice water, extracted with ether, washed with water, dried ($MgSO_4$), evaporated to leave tosylates **18** (117 mg, 86%), mp 90–92°C; $[\alpha]_D$ +84.23° (*c* 0.6945, $CHCl_3$); ir $\nu_{max}$: 1656, 1616, 1380, 1190 $cm^{-1}$; uv $\lambda_{max}$: 227 (ε 17 585), 249 (15 678) nm; $^1$Hmr δ: 1.17, 1.20 (3H, s, two sets), 1.18 (3H, s), 1.35–1.70 (8H, m, including 1.67 (1H, s, $D_2O$ exchangeable)), 1.72, 1.75 (3H, s, two sets), 1.86, 1.94 (1H, d, *J* = 16 Hz, two sets), 2.39 (1H, dt, *J* = 16, 4 Hz), 2.47–2.56 (4H, m, including 2.47 (3H, s)), 2.68, 2.85 (1H, dt, *J* = 16, 4 Hz, two sets), 3.92, 3.93 (1H, d, *J* = 10 Hz, two sets), 4.00, 4.03 (1H, d, *J* = 10 Hz, two sets), 7.36 (2H, d, *J* = 8 Hz), 7.80 (2H, d, *J* = 8 Hz); ms *m/e*: 406 ($M^+$), 388, 234, 216, 190. High resolution molecular weight determination, calcd. for

$C_{22}H_{30}O_5S$: 406.1814; found: 406.1794. *Anal.* calcd. for $C_{22}H_{30}O_5S$: C 65.02, H 7.39; found: C 65.04, H 7.43.

*Diols* ***19***

A solution of tosylates **18** (58 mg) in anhydrous ether (25 mL) was added to LAH (100 mg) and the mixture refluxed for 4 h. It was cooled, poured onto ice, extracted with ether, and dried ($MgSO_4$). Removal of ether yielded crystalline diols **19** (30 mg, 88%); mp 31–33°C; $[\alpha]_D$ +50.51° (*c* 0.291, $CHCl_3$); ir $\nu_{max}$: 3442 $cm^{-1}$; $^1$Hmr δ: 1.19 (3H, s), 1.22 (6H, s), 1.25–1.70 (11H, m), 1.74 (3H, s), 1.92 (1H, m), 2.61 (1H, dt, $J$ = 14, 4 Hz), 4.04 (1H, t, $J$ = 6 Hz); ms *m/e*: 238 ($M^+$), 220, 205. High resolution molecular weight determination, calcd. for $C_{15}H_{26}O_2$: 238.1933; found: 238.1943. *Anal.* calcd. for $C_{15}H_{26}O_2$: C 75.63, H 10.92; found: C 75.61, H 10.89.

*(+)-Carissone* ***4***

Oxidation of diols **19** (30 mg) in pyridine (1 mL) with $CrO_3$ (70 mg) in pyridine (0.8 mL) gave **4** (26 mg, 86%); mp 78–79°C (lit. 7,10) mp 78–79°C); $[\alpha]_D$ +136.6° (*c* 0.1625, $CHCl_3$) (lit. (10) +136.6° ±2° (in chloroform); ir $\nu_{max}$: 3472, 1556, 1615 $cm^{-1}$; uv $\lambda_{max}$: 249 (ε 15652) nm; $^1$Hmr δ: 1.21 (3H, s), 1.25 (3H, s), 1.26 (3H, s), 1.36–1.60 (6H, m, including 1.56 (1H, s, $D_2O$ exchangeable)), 1.79 (3H, s), 1.67–1.77 (2H, m), 1.91 (1H, t, $J$ = 14 Hz), 2.40 (1H, dt, $J$ = 15, 3 Hz), 2.52 (1H, ddd, $J$ = 18, 12, 6 Hz), 2.87 (1H, dt, $J$ = 15, 3 Hz); ms *m/e*: 236 ($M^+$), 218, 203. High resolution molecular weight determination, calcd. for $C_{15}H_{24}O_2$: 236.1776; found: 236.1762. *Anal.* calcd. for $C_{15}H_{24}O_2$ C 76.27, H 10.16; found: C 76.38, H 10.22.

## Acknowledgements

Financial aid from the Science Council of British Columbia is gratefully acknowledged. The authors would also like to thank MacMillan Bloedel Limited and Mr. Alan Moss and Associates for generous samples of cedar leaf oil. We are grateful to Dr. Lewis S. L. Choi for helpful discussions and assistance.

1. J. P. KUTNEY, J. BALSEVICH, R. CARRUTHERS, A. MARKUS, M. J. MCGRATH, R. N. YOUNG, and B. R. WORTH. Bioorg. Chem. **7**, 289 (1979).
2. J. P. KUTNEY, M. J. MCGRATH, R. N. YOUNG, and B. R. WORTH. Can. J. Chem. **57**, 3145 (1979).
3. J. P. KUTNEY, J. BALSEVICH, and P. GRICE. Can. J. Chem. **58**, 2641 (1980).
4. J. P. KUTNEY, M. K. CHOUDHURY, J. M. DECESARE, H. JACOBS, A. K. SINGH, and B. R. WORTH. Can. J. Chem. **59**, 3162 (1981).
5. D. R. DALTON, V. P. DUTTA, and D. C. JONES. J. Am. Chem. Soc. **90**, 5498 (1968).
6. L. M. JACKMAN AND S. STERNHELL. Applications of nuclear magnetic resonance spectroscopy in organic chemistry. 2nd ed. Pergamon Press, Oxford, England. 1969. p. 334.
7. A. R. PINDER AND R. A. WILLIAMS. J. Chem. Soc. 2773 (1963).
8. S. M. MUKHERJI, S. SINGH, and O. P. VIG. Sci. Cult. Calcutta, **25**, 533 (1960).
9. V. M. SATHE AND A. S. RAO. Indian J. Chem. **9**, 95, (1971).
10. K. VON MOHR, O. SCHINDLER, and T. REICHSTEIN. Helv. Chim. Acta, **37**, 462 (1954).

Can. J. Chem. Downloaded from www.nrcresearchpress.com by 210.87.254.42 on 09/06/12
For personal use only.

# Synthesis and characterization of some oxidized derivatives of citronellal ethylene acetal

WESLEY G. TAYLOR

*Agriculture Canada Research Station, Lethbridge, Alta., Canada T1J 4B1*

Received October 26, 1981

WESLEY G. TAYLOR. Can. J. Chem. **60**, 1847 (1982).

Three pairs of geometrical isomers corresponding to allylic monooxidation products of the trisubstituted olefin, citronellal ethylene acetal (**3**), were synthesized. These compounds were the *E* and *Z* isomers of 7-(1,3-dioxolan-2-yl)-2,6-dimethyl-2-hepten-1-ol, -1-al, and -1-oic acid (methyl ester), precursors for identifying the biodegradation products from citronellal and some of its derivatives. The *E* aldehyde (**4**) was obtained from **3** by the Sharpless procedure with catalytic quantities of selenium dioxide. The *E* ester (**5**) and *E* alcohol (**6**) were prepared in high isomeric purity (97–99%) from **4** with activated manganese dioxide and sodium borohydride, respectively. Selective ozonolysis of the isobutenyl group in **3** gave 5-(1,3-dioxolan-2-yl)-4-methyl-1-pentanal (**7**). Under the conditions used, ozone did not react with the ethylene acetal group. Acetal aldehyde (**7**) was stereoselectively converted to the *Z* alcohol (**8**) by a Wittig reaction. Manganese dioxide oxidation of **8** (98–99% *Z* isomer) to the *Z* aldehyde (**9**) and of **9** to the *Z* ester (**10**) was accompanied by partial *Z* to *E* isomerization. The distribution of *E* and *Z* isomers in crude reaction mixtures was determined by gas chromatography with a glass capillary column or by proton magnetic resonance spectroscopy.

---

WESLEY G. TAYLOR. Can. J. Chem. **60**, 1847 (1982).

On a synthétisé trois paires d'isomères géométriques qui proviennent de la mono-oxydation allylique de l'oléfine trisubstitué, l'acétal éthylènique du citronellal (**3**). Ces composés sont les isomères *E* et *Z* du (dioxolanne-1,3 yl-2)-7 diméthyl-2,6 heptène-2 ol-1, de l'aldéhyde (al-1) et de l'acide (oique-1 sous forme d'ester méthylique) correspondants qui sont les précurseurs dans l'identification des produits de biodégradation du citronellal et de quelques-uns de ses dérivés. On a obtenu l'aldéhyde *E* (**4**) à partir du composé (**3**) en faisant appel au procédé de Sharpless avec des quantités catalytiques de bioxyde de sélénium. On a préparé l'ester *E*-(**5**) et l'alcool *E*-(**6**) avec une grande pureté isomérique (97–99%) en soumettant respectivement le composé **4** à une oxydation par le bioxyde manganèse activé et à une réduction au borohydrure de sodium. L'ozonolyse sélective du groupe isobuténylé du composé **3** donne le (dioxolanne-1,3 yl-2)-5 méthyl-4 pentanal-1 (**7**). Dans les conditions utilisées, l'ozone ne réagit pas avec l'acétal éthylènique. On a transformé d'une façon stéréosélective l'acétal-aldéhyde **7** en alcool *Z* (**8**) par une réaction de Wittig. L'oxydation du composé **8** (isomère *Z* à 98–99%) en aldéhyde *Z* (**9**) et du composé **9** en l'ester *Z* (**10**) par le bioxyde de manganèse s'accompagne d'une isomèrisation partielle de *Z* en *E*. On a déterminé la distribution des isomères *E* et *Z* des mélanges réactionnels bruts par chromatographie en phase vapeur avec un colonne capillaire en verre ou par la spectroscopie de rmn du proton.

[Traduit par le journal]

Several investigators have demonstrated that xenobiotics with the isobutenyl group are capable of undergoing metabolic oxidation in mammals according to eq. [1] (1–5). To explore such meta-

[1] $(CH_3)_2C{=}CHR \longrightarrow HOCH_2(CH_3)C{=}CHR + HC(=O)(CH_3)C{=}CHR + HOC(=O)(CH_3)C{=}CHR$

bolic transformations, authentic reference samples of the *E* (*trans*) and *Z* (*cis*) alcohols, aldehydes, and acids are required. In principle, these isomeric products are accessible from the substrate. Thus, it is known that *E* trisubstituted olefinic alcohols or aldehydes can usually be obtained by use of selenium dioxide chemistry (6–8) and that the cyanohydrins of conjugated *E* aldehydes have been converted to methyl esters of *E* trisubstituted olefinic acids with activated manganese dioxide in methanol (9). *Z* Trisubstituted alcohols of this particular type have been accessible with a special type of Wittig reaction (8), as demonstrated initially by Corey *et al.* (10, 11) and by Schlosser *et al.* (12–14). A new synthesis of *Z* trisubstituted olefinic alcohols by the Wittig reaction has also been reported (15).

The problem of obtaining reference oxidation products arose during investigations (unpublished) on the elucidation of metabolic pathways for citronellal (**1**) and stereoisomeric mixtures of its *N*-acetyloxazolidine derivative (**2**), two insect repellents with the isobutenyl group (16). However, it was evident that neither of these unsaturated monoterpenoids would withstand the reaction conditions necessary for stereoselective synthesis of both series of isomers, so a potentially versatile intermediate to **1** and **2** was selected instead. This paper describes the chemistry that has been explored during the synthesis of *E* and *Z* alcohols, aldehydes, and acids (as methyl esters) of citronellal ethylene acetal (**3**). It is planned to use these derivatives of **3** for identifying the biodegradation products from metabolic experiments with **1** and **2**.

## Results and discussion

### trans-*Oxidized derivatives of* 3

Clark *et al.* (17) had already prepared **4** by the regioselective oxidation of **3** with selenium dioxide in ethanol. In this work, a new procedure from Sharpless and co-workers (7, 18) was used in which **3** was oxidized in methylene chloride solution with

0008-4042/82/141847-06$01.00/0

©1982 National Research Council of Canada/Conseil national de recherches du Canada

Can. J. Chem. Downloaded from www.nrcresearchpress.com by 178.218.224.3 on 09/06/12
For personal use only.

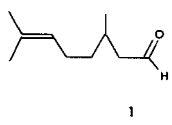

1

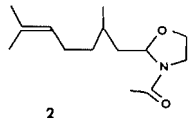

2

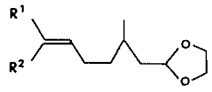

3 $R^1 = R^2 = CH_3$
4 $R^1 = CHO, R^2 = CH_3$
5 $R^1 = CO_2CH_3, R^2 = CH_3$
6 $R^1 = CH_2OH, R^2 = CH_3$

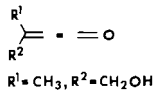

7
8 $R^1 = CH_3, R^2 = CH_2OH$
9 $R^1 = CH_3, R^2 = CHO$
10 $R^1 = CH_3, R^2 = CO_2CH_3$

a mixture of selenium dioxide and *tert*-butylhydroperoxide. The main product was **4**, as determined by spectral analysis of a sample from column chromatography. The *E* stereochemistry for **4** was indicated from the nmr spectrum because a signal for the unsaturated aldehyde proton was seen at 9.4 ppm. A signal for the aldehyde proton of the *Z* isomer would appear downfield near 10 ppm if it was present in detectable amounts (6, 19). The nmr analysis of the crude reaction product mixture gave no evidence for the presence of the *Z* aldehyde, so it was concluded that this reaction had proceeded with high (> 95%) stereoselectivity.

By employing a method from Crombie *et al.* (20) for converting related *E* trisubstituted olefinic aldehydes to *E* methyl esters, **4** gave the desired *E* acetal ester (**5**). The structure of **5** was confirmed by elemental and spectral analysis on a purified sample. Analysis of crude samples by glass capillary gas chromatography (capillary gc) showed **5** as a major component. A minor component, comprising 1–2% of the mixture, was also seen with a shorter retention time. It was apparent that the oxidation of **4** proceeded with little, if any, *E* to *Z* isomerization. In fact, only one olefinic proton was seen in the nmr spectrum of **5** and it resonated at the expected position (6.8 ppm) for an *E* trisubstituted olefinic ester of this type (6).

Alcohol (6) had previously been prepared by the incomplete oxidation of **3** with selenium dioxide in ethanol and pyridine (21). In the present investigation, **6** was obtained by reduction of **4** with sodium borohydride. The product from this reaction showed a major component and a minor component with a peak area ratio of 97:3 by capillary gc. Under conditions for electron impact mass spectrometry (ei-ms) combined with capillary gc, these two components gave nearly identical mass spectra, thus indicating that the *Z* isomer of **6** was probably present. Both components gave small $M - 1$ ions, which are characteristic ions in related ethylene acetals (22), and the base peak at *m/z* 73 was seen for the oxonium ($C_3H_5O_2$) ion (23). The latter ion was the base peak in the ei-ms of all of the compounds examined.

Confirmatory evidence for the presence of the *Z* isomer of **6** in samples from the reduction of **4** with sodium borohydride came from the independent synthesis of this isomer (discussed later). Additional evidence was also obtained by reducing the methyl ester function in **5** with lithium borohydride. The same isomeric alcohols, in approximately the same ratio (98:2), were found by capillary gc. This experiment also confirmed that **5** was formed from **3** with approximately 98% stereoselectivity.

Quasimolecular ions usually dominated the chemical ionization mass spectra (ci-ms) of these compounds and aided in confirming their structures. In the case of **3**, the loss of 60 amu from both the quasimolecular ion ($(M + 1) - 60$) and from the $M - 1$ ion ($(M - 1) - 60$) accounted for the major fragmentation pathways. With **4** and **6**, $(M - 1) - 60$ was more favorable. The most intense ion in **6** corresponded to $(M + 1) - 18$, a process observed in the ci-ms of saturated alcohols (24). Other prominent ions in **6** occurred at *m/z* 137 and *m/z* 135, which can be rationalized by $(M + 1) - 18 - 60$ and $(M - 1) - 18 - 60$ pathways. The most prominent fragment ion in **5** was seen at *m/z* 211, corresponding to $(M + 1) - CH_3OH$ (25).

*Ozonolysis of 3*

Synthetic approaches to the *Z* isomers of **4**, **5**, and **6** required that the olefinic bond in **3** first be cleaved and the product acetal aldehyde (**7**) subjected to a Wittig reaction. By employing a modification of the Wittig reaction for *Z* selectivity, where electrophilic substitution of intermediate β-oxido ylides with formaldehyde gave *Z* trisubstituted allylic alcohols directly (10–14), **7** should give the *Z* acetal alcohol (**8**).

A potential problem arose during the attempted synthesis of **7** by the ozonolysis of **3** (eq. [2]). This

[2] 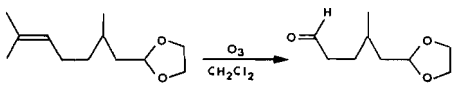

3 7

was because a number of acetals, including ethylene acetals, were known to react with ozone in ethyl acetate solution to give β-hydroxy esters (26–29). However, treatment of **3** with ozone at −78°C in methylene chloride solution gave one main product as detected by capillary gc. The nmr spectrum clearly indicated the formation of **7** since

Can. J. Chem. Downloaded from www.nrcresearchpress.com by 178.218.224.3 on 09/06/12
For personal use only.

Can. J. Chem. Downloaded from www.nrcresearchpress.com by 178.218.224.3 on 09/06/12
For personal use only.

an aldehyde signal (at 9.8 ppm), an acetal signal (at 4.9 ppm), and a four proton multiplet (at 3.6–4.1 ppm) for the methylene groups of the 1,3-dioxolane ring were present. The crude ozonolysis product was also examined by capillary gc in combination with ei-ms and ci-ms. By selected ion monitoring techniques, no evidence for the presence of β-hydroxy esters of **3** or **7** was obtained. The main component gave a weak molecular ion for **7** under ei conditions and the base peak (at *m/z* 73) suggested that the 1,3-dioxolane ring was present. Under ci-ms conditions, the most prominent ion of the main component occurred at *m/z* 173, which represented the quasimolecular ion for **7**. Ions were also seen at *m/z* 155 [(*M* + 1) − 18] and *m/z* 111 [(*M* − 1) − 60].

The crude material from ozonolysis experiments was purified by chromatography with silica gel and **7** was isolated in reasonable yields (40–80%). The use of high pressure liquid chromatography for purification of **7** was preferred. It was also important to stop the reaction as soon as **3** had disappeared and to use dimethylsulfide (30) as a reducing agent. The structure of **7** was confirmed by the synthesis of this aldehyde by reaction of **3** with osmium tetroxide and sodium periodate (Experimental section).

cis-*Oxidized derivatives of* **3**

The preparation of *Z* alcohol (**8**), and the subsequent conversion of **8** with manganese dioxide to *Z* aldehyde (**9**) and, via the cyanohydrin of **9**, to *Z* ester (**10**) depended on the functionalization of **7** with the hydroxyisopropenyl group. Since *Z* trisubstituted olefinic alcohols have been obtained from ketal aldehydes in this laboratory by a Wittig reaction (8), it was anticipated that acetal aldehyde (**7**) would behave analogously. In fact, the Wittig reaction on **7**, performed by adding **7** to a cold solution of ethylidenetriphenylphosphorane in THF, followed by the addition of *n*-butyllithium, formaldehyde, and water gave the desired **8**, in yields ranging from 0–50%. In comparison to dry paraformaldehyde or *s*-trioxane, gaseous formaldehyde, generated according to the procedure of Benkeser *et al.* (31), gave the best yield of **8**. The identity of **8** was confirmed from elemental analysis and from spectral comparisons to samples of the *E* alcohol (**6**). Noteworthy differences in nmr chemical shift values were apparent for the methyl, methylene, and vinyl protons of the isobutenyl group (Experimental section) and were in agreement with published values on isomers related to **6** and **8** (6, 8, 11). Capillary gc on samples of **8** showed that **6** was also present but only to the extent of 1–2%. Possible reasons for the remarkable stereoselectivity in this type of Wittig reaction have already been discussed (32).

For the preparation of **9**, pure samples of **8** were oxidized with activated manganese dioxide in hexane (9). Despite the high *Z* isomer content of **8** (98–99%), the nmr spectrum showed that the product was a mixture of isomeric aldehydes consisting predominantly of **9**. Thus, a main signal for the aldehyde proton in **9** resonated at 10.1 ppm and a minor signal was seen at 9.4 ppm which had the same chemical shift as the aldehyde proton for the *E* isomer (**4**). This *Z* to *E* isomerization, estimated at 25–30% in an experiment with a large excess of manganese dioxide, was reduced to 5–10% by the gradual addition of a minimum quantity of the reagent. Attempts to further suppress this isomerization were unsuccessful (Experimental section).

The **9** isolated from these experiments was an unstable compound and freshly isolated samples were used without purification for the synthesis of **10**. Cyanohydrin formation, followed by oxidation with manganese dioxide in methanol (as described for **5**), gave a mixture of **5** and **10**. This was confirmed by mass spectrometry. Capillary gc showed that there was from 15% to 32% of **5** in all samples of **10**. This amount was discernible in the nmr spectrum, particularly by comparison of chemical shifts for the vinylic proton. In **10**, this signal occurred at 5.9 ppm whereas the same signal for **5** was seen at 6.8 ppm.

The mass spectra of the isomeric pairs of esters and alcohols were very similar, especially under ei-ms conditions. A noteworthy difference in the ci-ms of **6** and **8** was apparent in the intensities of ions at *m/z* 153 [(*M* − 1) − 60] and *m/z* 197 [(*M* + 1) − 18]. Comparisons between the isomeric aldehydes were impractical because **9** was not amenable to capillary gc analyses.

The methodology described here illustrates a possible solution to the problem of obtaining authentic samples of the metabolites formed by eq. [1].

## Experimental

Proton nuclear magnetic resonance (nmr) spectra were obtained on a Varian EM-360 A spectrometer using tetramethylsilane as the internal standard. Infrared spectra were taken as liquid films on a Perkin–Elmer Model 137 Infracord spectrophotometer. For capillary gc, a Hewlett–Packard 5838A instrument equipped with a model 18835B capillary inlet system was used. The glass column (22 m × 0.31 mm id) was wall coated with Carbowax 20M-terephthalic acid according to the method of Grob and Grob (33). Helium at a velocity of 30 cm/s served as the carrier gas and nitrogen at a flow rate of 30 mL/min was used as a make-up gas for the flame ionization detector. Samples were

Can. J. Chem. Downloaded from www.nrcresearchpress.com by 178.218.224.3 on 09/06/12
For personal use only.

injected by the split technique. The injector and detector temperatures were 225°C and 250°C, respectively. For mass spectrometry, a Hewlett–Packard 5985B gc–ms computer system was used with a glass capillary column (55 m × 0.31 mm id) coated with Carbowax 20M-terephthalic acid. Electron-impact mass spectra were recorded at 70 eV whereas positive chemical ionization mass spectra were recorded using isobutane as the reagent gas at a source pressure of 0.5 Torr. High pressure liquid chromatography was performed with a Waters Prep LC/System 500 A instrument equipped with a Prep PAK Silica cartridge (Waters Associates, Inc.). Mallinckrodt cc-7 silica gel was used for column chromatography. Elemental analyses were obtained from Dr. C. Daessle, Montreal, Quebec. Melting points and boiling points are uncorrected.

Citronellal (Eastman P312), *tert*-butylhydroperoxide (Aldrich 18,471-3), selenium dioxide (K and K, 17660), activated manganese dioxide (K and K, 28107), and ethyl triphenylphosphonium bromide (Aldrich E5, 060-4) were used as received. *n*-Butyllithium (Aldrich 18,617-1) was standardized by titration (34) before use. Tetrahydrofuran (THF) was distilled from lithium aluminum hydride and then redistilled immediately before use from sodium and benzophenone. Evaporations were performed with a Büchi rotary evaporator at water aspirator vacuum and a bath temperature of 25–35°C.

*2-(2,6-Dimethyl-5-heptenyl)-1,3-dioxolane (3)*

This acetal was prepared from **1** (77 g, 0.5 mol), ethylene glycol (44.5 g, 0.72 mol), *p*-toluenesulfonic acid (0.1 g), and benzene as described in the literature (17). A center portion of the distillate gave **3** (57 g, 57.5% yield) as a colorless oil. Capillary gc (temperature programmed from 100°C to 130°C at 3°C/min) showed 78% of **3** with a retention time of 9.9 min. Pure samples of **3** were obtained in 48–52% overall yield by preparative hplc with 2% ethyl acetate in methylene chloride: bp 76–78°C (0.3 Torr) (lit (17) bp 125–130°C (18 Torr)); nmr ($CDCl_3$) δ: 5.17 (m, C=C*H*), 4.90 (t, $J$ = 4 Hz, acetal *H*), 4.10–3.53 (m, $OCH_2CH_2O$), 2.43–1.13 (m, 13 *H*), 0.96 (d, $J$ = 5 Hz, $CHCH_3$); ei-ms *m/z* (% relative abundance): 198 ($M^+$, 4), 197 (2), 121 (61), 113 (78), 73 (100); ci-ms: 199 ($MH^+$, 45), 197 (4), 139 (100), 137 (54).

*5-(1,3-Dioxolan-2-yl)-4-methyl-1-pentanal (7)*

Using an ozone-generating apparatus previously described in detail (8), **3** (14 g, 70 mmol) in methylene chloride solution (Caledon glass distilled, 300 mL) at −78°C was allowed to react with ozone until the starting material had just been consumed (gc evidence). With dual ozonizers and an oxygen flow rate of 12 L/h, the time of reaction was 7 h (± 30 min). The cold mixture was swept with nitrogen for 30 min and dimethylsulfide (10 mL) was added. The mixture was gradually allowed to approach room temperature with continuous stirring during 16–18 h. A crude oil (~ 18 g) was obtained by removing the volatiles on a rotary evaporator. Capillary gc (as described for **3**) showed a major component (> 70% of the mixture) with a retention time of 15.8 min. Samples of **7** (80–90% purity) were isolated in 40–60% yields by column chromatography with silicAR cc-7 and eluting with hexane–ether mixtures. Alternatively, **7** (75–95% purity) was obtained in 50–80% yields by preparative hplc using a solvent system of 4% ethyl acetate in methylene chloride: bp 72–76°C (0.3 Torr); ir: 1725 $cm^{-1}$ (C=O); nmr ($CDCl_3$) δ: 9.78 (m, aldehyde *H*), 4.90 (t, $J$ = 4 Hz, acetal *H*), 4.10–3.60 (m, $OCH_2CH_2O$), 2.70–2.10 (m, 2*H*), 2.06–1.20 (m, 5*H*), 0.98 (d, $J$ = 5.5 Hz, $CHCH_3$); ei-ms *m/z* (% relative abundance): 172 ($M^+$, 0.2), 171 (2), 73 (100); ci-ms: 173 ($MH^+$, 100), 171 (5), 155 (48), 111 (13), 93 (19). During ci-ms analyses, ions at *m/z* 215 and 189 were monitored but these ions, which correspond to quasi-molecular ions for β-hydroxy esters of **3** and **7**, were absent.

Aldehyde **7** (a colorless liquid) gave a crystalline, deep red 2,4-dinitrophenylhydrazone derivative, which was recrystallized from THF–water: mp 214–218°C. *Anal.* calcd. for $C_{15}H_{20}N_4O_6$: C 51.13, H 5.72, N 15.90; found: C 51.41, H 5.49, N 15.74.

Alternatively, **7** was prepared by stirring a mixture of **3** (9.915 g, 50 mmol), osmium tetroxide (0.051 g dissolved in ether, 0.2 mmol), dioxane, and water for 30 min at room temperature. Sodium periodate (20 g, 94 mmol) was added during 1 h and the mixture was heated at 50°C for 24 h (35). The mixture was filtered and the white precipitate was washed with ether. The aqueous layer was extracted with ether and the combined organic extracts were washed with 5% aqueous sodium carbonate and with water. The organic extract was dried ($Na_2SO_4$) and concentrated on a rotary evaporator to give 7.38 g of a crude product. Column chromatography with silicAR cc-7 and hexane–ether mixtures gave 1.9 g (22% yield) of **7** which had a purity of 70% by gc.

(E)*(4) and* (Z)*(9) isomers of 7-(1,3-dioxolan-2-yl)-2,6-dimethyl-2-hepten-1-al*

*By oxidation of 3 with selenium dioxide*

Following the literature method (7), **3** (11.9 g, 60 mmol) was allowed to react with a mixture of selenium dioxide (3.32 g, 30 mmol), *tert*-butylhydroperoxide (15.4 mL of a 70% aqueous solution, 120 mmol), and methylene chloride (60 mL) for 60 h. The reaction mixture was worked up as described (18) to give 8.78 g of a faint yellow oil. Capillary gc (160–180°C at 2°C/min) showed a major component (~ 60%) with a retention time of 10.75 min. A pure sample of **4** (2.3 g, 18% yield) was obtained by column chromatography with silicAR cc-7 and eluting with hexane–ether mixtures: ir: 1670 $cm^{-1}$ (C=O); nmr ($CDCl_3$) δ: 9.40 (s, aldehyde *H*), 6.48 (ragged t, $J$ = 7 Hz, C=C*H*), 4.88 (t, $J$ = 4 Hz, acetal *H*), 4.07–3.63 (m, $OCH_2CH_2O$), 2.63–2.10 (m, 2*H*), 1.93–1.20 (m, 8*H*), 0.98 (d, $J$ = 5.5 Hz, $CHCH_3$); ei-ms *m/z* (% relative abundance): 212 ($M^+$, O), 211 (1), 73 (100); ci-ms: 213 ($MH^+$, 100), 195 (3), 151 (35).

*By oxidation of 8 with activated manganese dioxide*

A mixture of **8** (2.143 g, 10 mmol), manganese dioxide (8.69 g, 100 mmol, added in portions during five days), and hexane (250 mL) was stirred at 20°C for 6 days and then filtered. A yellow oil (1.94 g) was obtained by removal of the solvent on a rotary evaporator. Capillary gc with Carbowax 20M-TPA and with SP 2300 (20 m × 0.29 mm id) showed a complex mixture of products, including a small peak with the same retention time as **4**. The mixture showed **9** and **4** by nmr ($CDCl_3$): δ: 10.15 (s, ~ 0.9 *H*, aldehyde *H* for *Z* isomer), 9.40 (s, ~ 0.1 *H*, aldehyde *H* for *E* isomer). This experiment was repeated at 0°C, by adding a total of 200 mmol of manganese dioxide in portions during two days to a suspension of **8** (4.2 g, 20 mmol) in hexane (400 mL). The product (3.30 g) contained **9** and **4** in an approximate ratio of 90:10 (nmr evidence). The same isomeric ratio was found on repeating this experiment with the Attenburrow grade of manganese dioxide (12.5-fold mole excess added during 2 days), which was prepared here by the literature method (36). When manganese dioxide (20-fold mole excess) was added in one portion to a mixture of **8** at 0°C, the reaction was completed in 4 h and the ratio of **9**/**4** was 70:30 (nmr evidence). Storage of neat samples resulted in a gradual decomposition of **9** to unidentified products. The aldehyde nmr signal for **9** had completely disappeared after storage of samples at 0°C for six months.

(E)*(5) and* (Z)*(10) isomers of the methyl ester of 7-(1,3-dioxolan-2-yl)-2,6-dimethyl-2-hepten-1-oic acid*

*By manganese dioxide oxidation of the cyanohydrin of 4*

A solution of **4** (2.16 g, 10.2 mmol) in methanol (150 mL) was stirred with sodium cyanide (2.5 g, 51 mmol) and glacial acetic acid (1.0 mL) for 1 h. Activated manganese dioxide (17.73 g, 204

Can. J. Chem. Downloaded from www.nrcresearchpress.com by 178.218.224.3 on 09/06/12
For personal use only.

mmol) was then added and the mixture was stirred at room temperature for 90 h. The mixture was filtered, the filtrate evaporated on a rotary evaporator, and the residue dissolved in chloroform. Washing with water and evaporating the dried ($MgSO_4$) organic phase gave 2.06 g (83% yield) of a yellow oil. The residue gave a main peak (98%) at 13.37 min and a minor peak (2%) at 10.05 min when analyzed by capillary gc (as described for **4**). The sample was purified by column chromatography (silicAR cc-7) with hexane–ether mixtures to give **5** as a colorless oil: bp 80–85°C (0.05 Torr); ir: 1720 $cm^{-1}$ (C=O); nmr ($CDCl_3$) δ: 6.77 (ragged t, $J$ = 7 Hz, C=C*H*), 4.92 (t, $J$ = 4 Hz, acetal *H*), 4.10–3.80 (m, $OCH_2CH_2O$), 3.75 (s, $OCH_3$), 2.47–2.00 (m, 2*H*), 1.93–1.13 (m, 8*H*), 0.99 (d, $J$ = 5.5 Hz, $CHCH_3$); ei-ms *m/z* (% relative abundance): 242 ($M^+$, O), 241 (1), 73 (100); ci-ms: 243 ($MH^+$, 100), 211 (25), 183 (4), 181 (7). *Anal.* calcd. for $C_{13}H_{22}O_4$: C 64.43, H 9.15; found: C 64.67, H 9.43.

*By manganese dioxide oxidation of the cyanohydrin of* **9**

A crude sample of **9** (1.9 g, ~ 9 mmol) in methanol (150 mL) was allowed to react with sodium cyanide (2.45 g, 50 mmol) and glacial acetic acid (1.0 mL), then with activated manganese dioxide (17.39 g, 200 mmol) for 160 h at 20°C as described for the preparation of **5**. A yellow oil (2.05 g, 90% yield) was isolated. Capillary gc (as described for **4**) showed **10** at 10.05 min and **5** at 13.37 min in a ratio of 82:18. Column chromatography (silicAR cc-7) with hexane–ether mixtures gave predominantly **10** as a colorless oil: bp 96–100°C (0.05 Torr); ir: 1720 $cm^{-1}$ (C=O); nmr ($CDCl_3$) δ: 5.93 (ragged t, $J$ = 7 Hz, C=C*H*), 4.93 (t, $J$ = 4 Hz, acetal *H*), 4.10–3.80 (m, $OCH_2CH_2O$), 3.76 (s, $OCH_3$), 2.73–2.10 (m, 2*H*), 2.00–1.00 (m, 8*H*), 0.98 (d, $J$ = 5.5 Hz, $CHCH_3$); ei-ms *m/z* (% relative abundance): 242 ($M^+$, 0.1), 241 (1), 73 (100); ci-ms: 243 ($MH^+$, 100), 211 (44), 183 (5), 181 (16). *Anal.* calcd. for $C_{13}H_{22}O_4$: C 64.43, H 9.15; found: C 64.17, H 9.16.

In three additional experiments on this oxidation (as described), crude samples of **10** contained from 15–25% of the *E* isomer (**5**) (capillary gc and nmr evidence). The ratio of **10/5** was 68:32 in another experiment with manganese dioxide prepared by the method of Attenburrow *et al.* (36).

(E)*(6) and* (Z)*(8) isomers of 7-(1,3-dioxolan-2-yl)-2,6-dimethyl-2-hepten-1-ol*

*By reduction of* **4** *with sodium borohydride*

A crude sample of **4** (1.83 g, 8.6 mmol) in 95% ethanol (30 mL) at 6°C was treated dropwise with a solution of sodium borohydride (1.085 g, 29.0 mmol) in 95% ethanol (30 mL; pH adjusted to 8 with NaOH) during 45 min. The mixture was stirred at room temperature for 18 h. Acetone (15 mL) was added and the solvents were evaporated on a rotary evaporator. The residue was dissolved in saturated brine and extracted with ether. The ether extract was dried ($MgSO_4$) and evaporated. There was obtained 1.636 g (88.6%) of **6** which eluted at 18.02 min under conditions of capillary gc analysis (as described for **4**). An analytically pure sample, as a colorless oil, was obtained by column chromatography (silicAR cc-7), eluting with hexane–ether mixtures: bp 82–84°C (0.1 Torr); ir: 3490 $cm^{-1}$ (OH); nmr ($CDCl_3$) δ: 5.40 (ragged t, $J$ = 7 Hz, C=C*H*), 4.90 (t, $J$ = 4 Hz, acetal *H*), 4.10–3.63 (m, $OCH_2CH_2O$ and $CH_2OH$), 1.93 (broad s, $CH_2OH$, exchanged with $D_2O$), 1.67 (s, $C=CCH_3$), 2.30–1.10 (m, 7*H*), 0.95 (d, $J$ = 5.5 Hz, $CHCH_3$); ei-ms *m/z* (% relative abundance): 214 ($M^+$, O), 213 (0.5), 113 (59), 73 (100); ci-ms: 215 ($MH^+$, 13), 213 (11), 197 (100), 155 (5), 153 (93), 137 (25), 135 (62). *Anal.* calcd. for $C_{12}H_{22}O_3$: C 67.25, H 10.35; found: C 67.34, H 10.46.

*By reduction of* **5** *with lithium borohydride*

To a mechanically stirred suspension of lithium borohydride (0.022 g, 1.0 mmol) in THF (5 mL) was added dropwise a solution of **5** (0.1 g, 0.41 mmol) in THF (3 mL). The mixture was stirred under an argon atmosphere for 16 h at 20°C, then heated under reflux for 21 h. Water was added and the pH was adjusted to 1 with 0.1 *N* hydrochloric acid. The product was isolated by extraction with ethyl acetate. The organic extracts were washed with water and saturated brine, then dried ($MgSO_4$) and concentrated on a rotary evaporator. The colorless oil (51 mg) when subjected to capillary gc (as described for **4**) and gc–ms showed the *E* alcohol (**6**, ~ 56% of the mixture) and the *Z* alcohol (**8**, ~ 1%). A component at 14.13 min (~ 27%) was identified by capillary gc–ms as the saturated alcohol, 7-(1,3-dioxolan-2-yl)-2,6-dimethyl-1-heptanol: ei-ms *m/z* (% relative abundance): 216 ($M^+$, O), 215 (1), 73 (100); ci-ms: 217 ($MH^+$, 100), 215 (5), 199 (8), 155 (44), 137 (11).

*By reaction of* **7** *in the Wittig reaction*

The preparation of ethylidenetriphenylphosphorane from ethyltriphenylphosphonium bromide (19.45 g, 52.4 mmol) and *n*-butyllithium (52.4 mmol) in THF (125 mL) was performed at 0°C as previously described (8). Aldehyde **7** (9.0 g from hplc, 52.4 mmol) was added by syringe at −78°C and, after 20 min of mechanical stirring, another 52.4 mmol of *n*-butyllithium was added. After 45 min, the Dry Ice bath was replaced by crushed ice. When the temperature was −5°C, formaldehyde gas (~ 3 g, freshly generated from 11.1 g of dried paraformaldehyde (31)) was delivered above the reaction mixture during 10 min. The color changed from deep red to creamy white during the delivery of formaldehyde. After stirring at 20°C for 12 h, the product was isolated as described (8). Distillation of the crude product *in vacuo* gave a volatile fraction (1.5 g, bp 57–98°C at 0.1 Torr) and another fraction (bp 98–120°C at 0.1 Torr) which was identified as **8** (4.86 g, 43.4%). Capillary gc (as described for **4**) on the first fraction showed several components. Two major components were seen with retention times of 2.8 and 2.9 min. These were tentatively identified by capillary gc–ms as 3-methyl-6-octen-1-al ethylene acetal (a 1:1 mixture of *E* and *Z* isomers); ei-ms *m/z* (% relative abundance); 184 ($M^+$, O), 183 (1), 73 (100) for both isomers; ci-ms showed prominent ions at 185, 125, and 123. Capillary gc on the second fraction from distillation showed a main peak (75–85% of the mixture) with a retention time of 15.85 min. This fraction was purified by column chromatography (silicAR cc-7) with hexane–ether mixtures, followed by redistillation. A pure sample of **8** was obtained as a colorless oil: bp 107°C (0.1 Torr); ir: 3490 $cm^{-1}$ (OH); nmr ($CDCl_3$) δ: 5.26 (ragged t, $J$ = 7 Hz, C=C*H*), 4.90 (t, $J$ = 4 Hz, acetal *H*), 4.11–3.63 (m, $OCH_2CH_2O$ and $CH_2OH$), 2.05 (broad s, $CH_2OH$, exchanged with $D_2O$), 1.80 (s, $C=CH_3$), 2.33–1.13 (m, 7*H*), 0.95 (d, $J$ = 5.5 Hz, $CHCH_3$), ei-ms *m/z* (% relative abundance): 214 ($M^+$ O), 213 (0.5), 113 (60), 73 (100); ci-ms: 215 ($MH^+$, 16), 213 (5), 197 (50), 153 (100), 137 (17), 135 (35). *Anal.* calcd. for $C_{12}H_{22}O_3$: C 67.25, H 10.35; found: C 67.05, H 10.60.

This reaction was repeated as described except gaseous formaldehyde (generated by heating paraformaldehyde in a vessel connected to the reaction flask by means of glass tubing) was used. Delivery of formaldehyde above the surface of the reaction, which was at −15°C, ultimately gave **8** in 43% yield. Delivery of formaldehyde below the surface of the reaction (at −78°C) resulted in the formation of a thick solid from which **8** was isolated in 25% yield. Addition of paraformaldehyde directly to the reaction mixture (at 0°C, −5°C, or −78°C) gave **8** in yields ranging from 11–29%. None of the desired **8** was isolated when excess *s*-trioxane (added at −5°C) was used as the source of formaldehyde. Volatile side products accounted for the majority of material in these experiments.

## Acknowledgements

I thank Mr. Art Hewitt for technical assistance and Mr. Jim Elder for recording the mass spectra.

1. K. A. PITTMAN, D. ROSI, R. CHERNIAK, A. J. MEROLA, and W. D. CONWAY. Biochem. Pharmacol. **18**, 1673 (1969).
2. K. A. PITTMAN. Biochem. Pharmacol. **19**, 1833 (1970).
3. K. UEDA, L. C. GAUGHAN, and J. E. CASIDA. Pestic. Biochem. Physiol. **5**, 280 (1975).
4. J. MIYAMOTO. Environ. Health Perspect. **14**, 15 (1976).
5. J. CHAMBERS. Residue Rev. **73**, 101 (1980).
6. U. T. BHALERAO and H. RAPOPORT. J. Am. Chem. Soc. **93**, 4835 (1971).
7. M. A. UMBREIT and K. B. SHARPLESS. J. Am. Chem. Soc. **99**, 5526 (1977).
8. W. G. TAYLOR. J. Org. Chem. **44**, 1020 (1979).
9. E. J. COREY, N. W. GILMAN, and B. E. GANEM. J. Am. Chem. Soc. **90**, 5616 (1968).
10. E. J. COREY, J. I. SHULMAN, and H. YAMAMOTO. Tetrahedron Lett. 447 (1970).
11. E. J. COREY and H. YAMAMOTO. J. Am. Chem. Soc. **92**, 226 (1970).
12. M. SCHLOSSER, F. K. CHRISTMANN, A. PISKALA, and D. COFFINET. Synthesis, 29 (1971).
13. M. SCHLOSSER and D. COFFINET. Synthesis, 380 (1971).
14. M. SCHLOSSER and D. COFFINET. Synthesis, 575 (1972).
15. C. SREEKUMAR, K. P. DARST, and W. C. STILL. J. Org. Chem. **45**, 4260 (1980).
16. W. G. TAYLOR. J. Agric. Food Chem. **30**, 409 (1982).
17. K. J. CLARK, G. I. FRAY, R. H. JAEGER, and R. ROBINSON. Tetrahedron, **6**, 217 (1959).
18. B. CHABAUD and K. B. SHARPLESS. J. Org. Chem. **44**, 4202 (1979).
19. K. C. CHAN, R. A. JEWELL, W. H. NUTTING, and H. RAPOPORT. J. Org. Chem. **33**, 3382 (1968).
20. L. CROMBIE, C. F. DOHERTY, and G. PATTENDEN. J. Chem. Soc. Sect. C, 1076 (1970).
21. F. CAMPS, J. COLL, and A. PARENTE. Synthesis, 215 (1978).
22. R. A. FRIEDEL and A. G. SHARKEY. Anal. Chem. **28**, 940 (1956).
23. H. BUDZIKIEWICZ, C. DJERASSI, and D. H. WILLIAMS. *In* Mass spectrometry of organic compounds. Holden-Day, Inc., San Francisco, CA. 1967. p. 263.
24. F. H. FIELD. J. Am. Chem. Soc. **92**, 2672 (1970).
25. A. G. HARRISON and H. ICHIKAWA. Org. Mass Spectrom. **15**, 244 (1980).
26. P. DESLONGCHAMPS and C. MOREAU. Can. J. Chem. **49**, 2465 (1971).
27. P. DESLONGCHAMPS, P. ATLANI, D. FREHEL, A. MALAVAL, and C. MOREAU. Can. J. Chem. **52**, 3651 (1974).
28. R. J. TAILLEFER, S. E. THOMAS, Y. NADEAU, S. FLISZAR, and H. HENRY. Can. J. Chem. **58**, 1138 (1980).
29. W. J. BAUMANN and T. H. MADSON. J. Lipid Res. **15**, 528 (1974).
30. R. M. COATES, D. A. LEY, and P. L. CAVENDER. J. Org. Chem. **43**, 4915 (1978).
31. R. A. BENKESER, W. DETALVO, and D. DARLING. J. Org. Chem. **44**, 225 (1979).
32. E. J. COREY, P. ULRICH, and A. VENKATESWARLU. Tetrahedron Lett. 3231 (1977).
33. K. GROB and G. GROB. J. Chromatogr. **125**, 471 (1976).
34. S. C. WATSON and J. F. EASTHAM. J. Organomet. Chem. **9**, 165 (1967).
35. I. NAKATSUKA, F. SHONO, and A. YOSHITAKE. J. Labelled Compd. Radiopharm. **13**, 561 (1977).
36. J. ATTENBURROW, A. F. B. CAMERON, J. H. CHAPMAN, R. M. EVANS, B. A. HEMS, A. B. A. JANSEN, and T. WALKER. J. Chem. Soc. 1094 (1952).

Can. J. Chem. Downloaded from www.nrcresearchpress.com by 178.218.224.3 on 09/06/12
For personal use only.

# Specific heats of polymer powders by differential scanning calorimetry

EVA I. VARGHA-BUTLER AND A. WILHELM NEUMANN
*Department of Mechanical Engineering, University of Toronto, 5 King's College Road, Toronto, Ont., Canada M5S 1A4*
AND
HASSAN A. HAMZA
*Western Research Laboratory, Department of Energy, Mines and Resources, CANMET, Edmonton, Alta., Canada T6G 2C2*
Received November 12, 1981

EVA I. VARGHA-BUTLER, A. WILHELM NEUMANN, and HASSAN A. HAMZA. Can. J. Chem. **60**, 1853 (1982).

The specific heats of five polymers were determined by differential scanning calorimetry (DSC) in the temperature range of 300 to 360 K. The measurements were performed with polymers in the form of films, powders, and granules to clarify whether or not DSC specific heat values are dependent on the diminution of the sample. It was found that the specific heats for the bulk and powdered form of the polymer samples are indistinguishable within the error limits, justifying the determination of specific heats of powders by means of DSC.

EVA I. VARGHA-BUTLER, A. WILHELM NEUMANN et HASSAN A. HAMZA. Can. J. Chem. **60**, 1853 (1982).

On a déterminé les chaleurs spécifiques de cinq polymères par calorimétrie à balayage différentiel (CBD) dans l'intervalle de température allant de 300 à 360 K. On effectué les mesures sur des polymères sous forme de film, de poudre ou de granules pour vérifier si les valeurs de chaleur spécifique déterminées par CBD dépendent de la diminution de l'échantillon. On a trouvé que les chaleurs spécifiques des échantillons sous forme encombrée et sous forme de poudre ne se distinguent pas à l'intérieur des limites d'erreurs, justifiant ainsi la détermination des chaleurs spécifiques des poudres par la CBD.

[Traduit par le journal]

## Introduction

Our studies of the specific heat of polymers were motivated by work on the wettability of coal and of other solid particles by means of a freezing front technique (1–3). Specific heat data are a prerequisite for the quantitative determination of contact angles on solid particles using the above technique. As such data were not available for coal in powdered form, it was decided to generate them by differential scanning calorimetry (DSC) (4). Since data for comparison were not available, it was also decided to measure the specific heats of several polymeric materials. The main concern in this connection is the question whether or not differential scanning calorimetry can be used to measure the specific heat of powders. The literature is not explicit on this point. Barrall and Johnson (5) state that "for very precise work, it is desirable to form the sample in the same shape as the sapphire standard". From this statement, as well as the rest of their review article, it seems that the possibility of studying the specific heat of a powder by DSC was not even considered as a possibility. These doubts are reinforced by McNaughton and Mortimer (6) in their discussion of the theory of DSC. They divide the total thermal resistance $R$ into two additive parts, $R_0$ and $R_s$, where $R_0$ represents the thermal resistance between pan and holder and $R_s$ between pan and sample. They base their further arguments on the assumption that for a close contact between sample and pan, $R_s$ will be very small compared to $R_0$. This assumption might well be incorrect in the case of powders where each particle in the bottom layer will normally be in contact with the pan only at a few points. In view of the fact that "the method is a dynamic method" (5), it thus is not *a priori* clear that DSC may be used to determine the specific heat independent of the degree of diminution of the sample. Therefore measurements were performed with several polymers in the form of films, powders, and granules. The results appear to be of sufficient interest to be reported here.

## Experimental

*Materials*

The specific heats of the following polymer samples were determined: (*1*) Poly(propylene), PP, powder (Polysciences Inc.). (*2*) Poly(styrene), PS, in both powder and film forms with a molecular weight of 20 400 and PS powder with a molecular weight of 200 000; $M_w/M_n$ less than 1.06 (Pressure Chemical Co., Pittsburgh, Mellon Institute, special PS standard). (*3*) Poly(hexamethylene adipamide), Nylon 66, PA 66, powder and film (Polysciences Inc.). (*4*) Poly(tetrafluoroethylene), Teflon, PTFE, granules and powder (Polysciences Inc.). (*5*) Tetrafluoroethylene–hexafluoropropylene copolymer, FEP, film (Commercial Plastics, Toronto).

The polymer films were prepared from the polymer powder either by heat pressing or by means of solvent casting (7). PTFE and FEP films were prepared by heat pressing, while the films of PP, PS, and PA were prepared by solvent casting.

*Method*

The specific heat measurements were performed in the temperature range from 300 to 360 K using a Perkin-Elmer Model DSC-2 calorimeter. The heating and cooling rate was

0008-4042/82/141853-04$01.00/0
©1982 National Research Council of Canada/Conseil national de recherches du Canada

Can. J. Chem. Downloaded from www.nrcresearchpress.com by 210.87.254.5 on 09/06/12
For personal use only.

Can. J. Chem. Downloaded from www.nrcresearchpress.com by 210.87.254.5 on 09/06/12
For personal use only.

TABLE 1. Temperature dependence of specific heats of polymers

| Temperature (K) | Specific heat $C_p$ (kJ/kg K) | | | | | | | | | | |
|---|---|---|---|---|---|---|---|---|---|---|---|
| | PS | | | | PA 66 | | PTFE | | | | FEP |
| | PP Powder | MW 20 400 Powder | MW 20 400 Film | MW 200 000 Powder | Powder | Film | Powder | Granules | Film |
| 300 | 1.680±0.089 | 1.188±0.077 | 1.193±0.092 | 1.185±0.010 | 1.574±0.079 | 1.591±0.047 | 1.098±0.286 | 1.074±0.042 | 1.022±0.055 |
| 310 | 1.782±0.152 | 1.232±0.050 | 1.239±0.062 | 1.275±0.067 | 1.711±0.169 | 1.722±0.070 | 1.155±0.102 | 1.146±0.105 | 1.046±0.097 |
| 320 | 1.843±0.139 | 1.285±0.104 | 1.271±0.057 | 1.399±0.022 | 1.824±0.166 | 1.830±0.065 | 1.176±0.216 | 1.190±0.015 | 1.065±0.094 |
| 330 | 1.978±0.152 | 1.327±0.109 | 1.300±0.119 | 1.445±0.084 | 1.993±0.147 | 1.939±0.109 | 1.239±0.146 | 1.256±0.010 | 1.093±0.062 |
| 340 | 2.051±0.099 | 1.412±0.089 | 1.401±0.060 | 1.564±0.005 | 2.021±0.037 | 1.991±0.109 | 1.355±0.089 | 1.359±0.037 | 1.104±0.084 |
| 350 | 2.120±0.142 | 1.481±0.047 | 1.447±0.070 | 1.660±0.037 | 2.054±0.030 | 2.052±0.147 | 1.349±0.164 | 1.358±0.027 | 1.128±0.025 |
| 360 | 2.159±0.147 | 1.515±0.032 | 1.518±0.142 | 1.698±0.057 | 2.145±0.052 | 2.098±0.117 | 1.362±0.226 | 1.372±0.032 | 1.147±0.022 |

selected as 10 K/min, the chart range as 5 mV, the range control as 5 mcal/s, and the chart speed as 20 mm/min. These settings were chosen on the recommendation of Perkin-Elmer for $C_p$ measurements. Lower rates give poor sensitivity, higher rates provide greater sensitivity but poorer temperature accuracy. Nitrogen gas of 99.99% minimum purity was used for purging the sample holders. A detailed discussion of the DSC-2 and the specific heat measurements are given in refs. 8–10.

An 8.21 mg synthetic sapphire ($\alpha$-$Al_2O_3$) standard was used for calibration; the specific heat values of sapphire were obtained from the work of Ginnings and Furukawa (11). The difference in the weights ($\Delta W$) of the aluminum sample–pans (in which the samples were encapsulated and weighed) were taken into account. The $\Delta W$ value defines an additional ordinate displacement ($\Delta D$ in mm) which has to be added to the displacement ($D$ in mm) caused by the material in the lighter pan. The $\Delta W$ values vary from 0.01 to 2.00 mg which, if not corrected, could cause errors in $C_p$ values up to 25%.

The specific heat of the polymer samples, $C_p$(sample), can be calculated after the calibration with the sapphire disc (ratio method (10)) using the formula

$$[1] \quad C_p(\text{sample}) = \frac{W(\text{sapphire})}{W(\text{sample})} \times \frac{D(\text{sample})}{D(\text{sapphire})} \times C_p(\text{sapphire})$$

where $C_p$(sapphire) is the specific heat of the sapphire standard in cal/g K, $W$(sapphire) and $W$(sample) are the weights of the standard and of the sample, respectively, in mg, $D$(sapphire) and $D$(sample) are the corrected ordinate displacements of the sapphire and that of the sample in mm. Finally, the specific heats were expressed in kJ/kg K.

The specific heat data presented here are the arithmetic mean values of at least three measurements. The standard deviation and the population mean were calculated from the sample mean assuming a $t$ distribution. The errors given in Tables 1–3 are 95% confidence limits.

The samples were reweighed after the experiments but no significant (less than 0.1 mg) change in weight was observed.

## Results and discussion

In Figs. 1 and 2 the specific heats of the various polymer samples are plotted as a function of temperature. For all of the polymers the specific heat increases linearly with temperature over the whole range investigated as expected for materials not undergoing conformational changes. However, Nylon 66 (PA 66) has a glass transition (12) around 323 K. Conceivably the slight deviation of our points at 330 K may be due to this conformational change, but this is of no concern for our present purposes.

As the plots in Figs. 1 and 2 are not adequate for recovering actual data, the results are summarized in Table 1, together with information on the accuracy.

A comparison of our results with literature data is shown in Tables 2 and 3. The data of the present work are given as the arithmetic mean of the specific heats obtained for the bulk and powdered forms of polymers. The $C_p$ values from the literature were selected for well defined systems only.

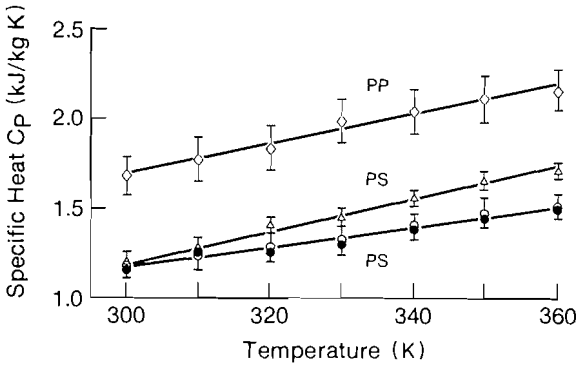


FIG. 1. Temperature dependence of specific heats of polypropylene and polystyrene: ◇ PP powder, ○ PS powder, MW 20 400, ● PS film, MW 20 400, △ PS powder, MW 200 000.

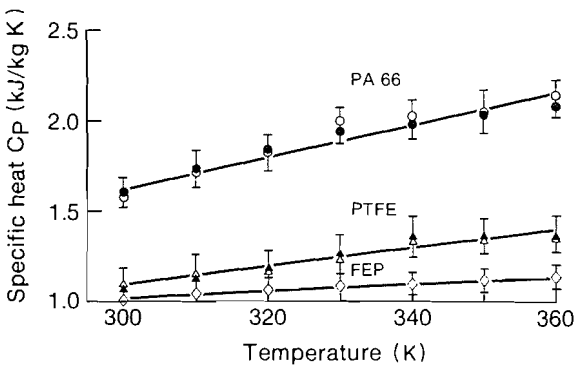


FIG. 2. Temperature dependence of specific heat of PA 66, PTFE, and FEP: ○ PA 66 powder, ● PA 66 film, △ PTFE powder, ▲ PTFE granules, ◇ FEP film.

In general, the agreement is satisfactory considering that the polymers used for the various specific heat measurements had different molecular weight, crystallinity, or pretreatment (annealing, molding, etc.). The specific heat of nylon 66 was found to be higher than that of the data given by Wilhoit and Dole (14), but their experimental results also showed some irregularity between 315 and 536 K. In Table 3, the temperature dependence of the specific heat of an atactic poly(propylene) and the average value of several sets of measurements averaged by Wunderlich (17) are compared with

TABLE 2. Comparison of the specific heats of polymers with literature data

| | Specific heat $C_p$ (kJ/kg K) | | |
|---|---|---|---|
| Sample | Literature data | References | Present work |
| Teflon | 0.960 at 298 K | 13 | 1.086±0.164 at 300 K |
| PTFE | 0.961 at 300 K | 12 | |
| | 0.996–1.021 at 310 K | 15 | 1.150±0.103 at 310 K |
| Poly(styrene) | 1.220 at 298 K | 13 | 1.191±0.084 at 300 K |
| PS | 1.194–1.220 at 298 K | 12 | |
| | 1.256 at 323 K | 12 | 1.278±0.080 at 320 K |
| Poly(propylene) | 1.630–1.760 at 298 K | 13 | 1.680±0.089 at 300 K |
| PP | 1.789–1.926 at 298 K | 12 | |
| Nylon 66 | 1.470 at 298 K | 13 | 1.583±0.063 at 300 K |
| PA 66 | 1.419 at 298 K | 12 | |
| | 1.536 at 310 K | 14 | 1.716±0.119 at 310 K |
| | 1.918 at 353 K | 14 | 2.053±0.088 at 350 K |

TABLE 3. Comparison of the specific heats of polymers with literature data at various temperatures

| | Specific heat $C_p$ (kJ/kg K) | | | | | | |
|---|---|---|---|---|---|---|---|
| | PP | | | PS | | | |
| Temperature (K) | Atactic (16) | Average value (17) | Present work | Atactic (18) | Atactic (19) | Average value (17) | Present work MW: 20 400 |
| 300 | 2.381 | 1.696 | 1.680±0.089 | 1.232 | 1.233 | 1.222 | 1.191±0.084 |
| 310 | 2.414 | — | 1.782±0.152 | 1.276 | 1.291 | — | 1.235±0.056 |
| 320 | 2.528 | — | 1.843±0.139 | 1.321 | 1.321 | 1.305 | 1.278±0.080 |
| 330 | 2.595 | — | 1.978±0.152 | 1.365 | — | — | 1.313±0.114 |
| 340 | 2.660 | — | 2.051±0.099 | 1.410 | 1.415 | 1.401 | 1.405±0.070 |
| 350 | 2.725 | 2.139 | 2.120±0.142 | 1.456 | 1.463 | — | 1.464±0.058 |
| 360 | — | — | 2.159±0.147 | — | — | — | 1.516±0.087 |

Can. J. Chem. Downloaded from www.nrcresearchpress.com by 210.87.254.5 on 09/06/12
For personal use only.

our results. The data of the present work agree with the average $C_p$ given for poly(propylene) (17); however, both are lower than the specific heat of the atactic poly(propylene) measured by Wilkinson and Dole (16). The specific heats of poly(styrene) agree with both the average data given for PS (17) and with the results from measurements of Chang *et al.* (18) and Karasz *et al.* (19). These authors used a commercial preparation and an N.B.S. standard sample of atactic poly(styrene) of a rather broad molecular weight distribution, respectively; the specific heat was determined by means of adiabatic calorimetry.

## Conclusions

From these measurements no differences were found between the results obtained for powdered and bulk polymers. On the other hand, relatively small differences in chemical structure (PTFE vs. FEP) as well as differences in molecular weight (PS powders with an MW of 20 400 vs. 200 000) show considerable differences in the specific heat.

The results found here agree well with literature values or at least fall within the spread typically found by different investigators, using different samples. This finding reinforces our main point, i.e. that DSC is an appropriate technique for determining the temperature dependence of polymer powders, and by implication, of powdered materials in general.

## Acknowledgement

This work was supported by Energy, Mines and Resources, CANMET, Canada, through contract No. 20SU-23440-0-9021.

1. E. I. VARGHA-BUTLER, M. R. SOULARD, H. A. HAMZA, and A. W. NEUMANN. CIM Bulletin, **74**, 54 (1981).
2. S. N. OMENYI and A. W. NEUMANN. J. Appl. Phys. **47**, 3956 (1976).
3. S. N. OMENYI, R. P. SMITH, and A. W. NEUMANN. J. Colloid Interface Sci. **75**, 117 (1980).
4. E. I. VARGHA-BUTLER, M. R. SOULARD, H. A. HAMZA, and A. W. NEUMANN. In press.
5. E. M. BARRALL and J. F. JOHNSON. Thermal characterization techniques. *In* Techniques and methods of polymer evaluation. Vol. 2. *Edited by* P. E. Slade and L. T. Jenkins. Marcel Dekker, New York. 1970. p. 18.
6. J. L. MCNAUGHTON and C. T. MORTIMER. Differential scanning calorimetry. Perkin-Elmer Co., pp. 1–16. *Reprinted from* "IRS", Physical Chemistry Series 2, Vol. 10. 1975. Butterworths, London.
7. S. N. OMENYI. Ph.D. Thesis, University of Toronto. 1978.
8. M. J. O'NEILL. Anal. Chem. **36**, 1238 (1964).
9. E. S. WATSON, M. J. O'NEILL, J. JUSTIN, and N. BRENNER. Anal. Chem. **36**, 1233 (1964).
10. M. J. O'NEILL. Anal. Chem. **38**, 1331 (1966).
11. D. C. GINNINGS and G. T. FURUKAWA. J. Am. Chem. Soc. **75**, 522 (1953).
12. J. BRANDRUP and E. H. IMMERGUT. Polymer handbook. 2nd ed. Wiley, New York. 1975.
13. D. V. VAN KREVELEN. Properties of polymers. Elsevier, Amsterdam. 1976. p. 84.
14. R. C. WILHOIT and M. DOLE. J. Phys. Chem. **57**, 14 (1953).
15. G. T. FURUKAWA, R. E. MCCOSKEY, and G. J. KING. J. Res. Natl. Bur. Stand. **49**, 273 (1952).
16. R. W. WILKINSON and M. DOLE. J. Polymer Sci. **58**, 1089 (1962).
17. B. WUNDERLICH. Adv. Polymer Sci. **7**, 151 (1970).
18. S. S. CHANG and A. B. BESTUL. J. Polymer Sci. Part A2, **6**, 849 (1968).
19. F. E. KARASZ, H. E. BAIR, and J. M. O'REILLY. J. Phys. Chem. **69**, 2657 (1965).

Can. J. Chem. Downloaded from www.nrcresearchpress.com by 210.87.254.5 on 09/06/12
For personal use only.

# Structure–sweetness relationships for fructose analogs. Part I. Synthesis and evaluation of sweetness of 5-deoxy-D-*threo*-hexulose

OLIVIER R. MARTIN, SIRKKA-LIISA KORPPI-TOMMOLA, AND WALTER A. SZAREK

*Carbohydrate Research Institute and Department of Chemistry, Queen's University, Kingston, Ont., Canada K7L 3N6*

Received December 28, 1981

OLIVIER R. MARTIN, SIRKKA-LIISA KORPPI-TOMMOLA, and WALTER A. SZAREK. Can. J. Chem. **60**, 1857 (1982).

5-Deoxy-D-*threo*-hexulose ("5-deoxyfructose", "5-deoxysorbose") has been prepared in six steps from D-fructose. The reaction of 2,3-*O*-isopropylidene-β-D-fructopyranose with sulfuryl chloride afforded exclusively 5-chloro-5-deoxy-2,3-*O*-isopropylidene-α-L-sorbopyranose in the key step. "5-Deoxyfructose" exists only in the $^2C_5$(D) pyranoid form in solution, and was found to be much sweeter than L-sorbose and nearly as sweet as D-fructose. Comments on this unexpected sweetness result are given.

OLIVIER R. MARTIN, SIRKKA-LIISA KORPPI-TOMMOLA et WALTER A. SZAREK. Can. J. Chem. **60**, 1857 (1982).

Le désoxy-5-D-*thréo*-hexulose ("désoxy-5-fructose", "désoxy-5-sorbose") a été préparé en six étapes à partir du D-fructose. La chloration de l'*O*-isopropylidène-2,3-β-D-fructopyrannose par le chlorure de sulfuryle conduit exclusivement au chloro-5-désoxy-5-*O*-isopropylidène-2,3-α-L-sorbopyrannose et constitue l'étape clé de la synthèse. Le "désoxy-5-fructose" adopte uniquement la forme pyrannique $^2C_5$(D) en solution, et se révéla beaucoup plus doux que le L-sorbose et presque aussi doux que le D-fructose. Le résultat inattendu des tests de douceur est commenté.

## Introduction

D-Fructose, the well-known fruit sugar, is the sweetest of the naturally occurring sugars;[1] however, the structural features responsible for its high sweetness have not yet been established with accuracy. Since the sweetness diminishes with the appearance of the furanose forms during mutarotation, the taste of D-fructose is thought to arise only from the β-D-fructopyranose form (1), the common form in the solid state. According to Shallenberger's theory of sweet taste based on intermolecular hydrogen bonding with the taste receptor of the tongue (2), the anomeric 2-OH and the $CH_2OH$ groups should correspond, respectively, to the H-donor, AH, and the H-acceptor, B, of the principal saporous unit of D-fructose (I); the stereochemical requirements between the AH and B groups are secured by the Lemieux effect (3). Since the physico-chemical interaction leading to sweet taste seems to need a lipophilic function (4), a third, hydrophobic component (γ) has been added to the AH,B system to form a tripartite site (see I).

Studies on modified forms by Birch and coworkers (5) seem to confirm Shallenberger's intuitive proposal for the sweetness of D-fructose; thus, "2-deoxyfructose" (II, 2,6-anhydro-D-mannitol) and β-D-arabinose (III) are indeed less sweet than D-fructose. However, L-sorbose, which adopts almost exclusively the α-L-pyranose form (IV) in solution (6), is far less sweet than D-fructose, although both of the ketoses are simply epimeric at C-5.

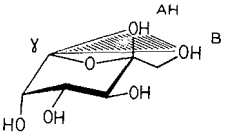


I

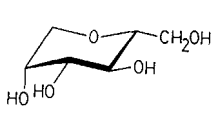


II

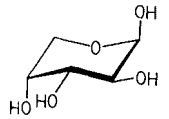


III

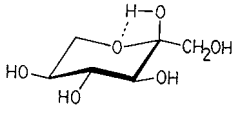


IV

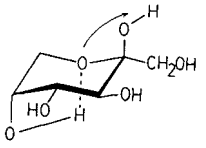


V

According to Birch (5), hydrogen bonding between HO-5 and the ring oxygen atom of β-D-fructopyranose (V) would release the anomeric hydroxyl group to participate in the AH,B system, whereas the HO-2 group of the C-5 epimer (IV) would be inhibited by an intramolecular H-bond. Further investigation proved to be necessary to explain this sweetness difference and to obtain more information about the origin of the high sweet taste of D-fructose.

Suppression of the 5-hydroxyl group of these ketoses would constitute a very interesting modification to examine the role played by this function. The corresponding 5-deoxyketose (5-

[1]Sweetness comparisons are normally made on a weight basis.

0008-4042/82/141857-06$01.00/0

©1982 National Research Council of Canada/Conseil national de recherches du Canada

Can. J. Chem. Downloaded from www.nrcresearchpress.com by 210.87.254.6 on 09/06/12
For personal use only.

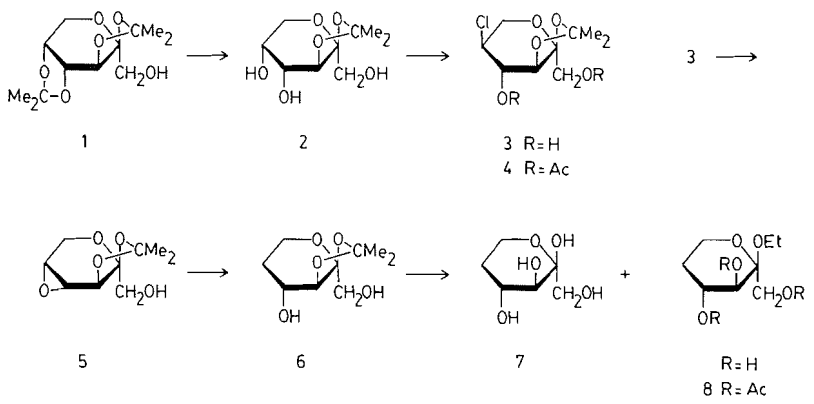

SCHEME 1

deoxy-D-*threo*-hexulose) was obtained 35 years ago as a by-product in the large scale biochemical oxidation of sorbitol to L-sorbose (7). Our synthesis involves six steps starting from D-fructose. The reaction of 2,3-*O*-isopropylidene-β-D-fructopyranose with sulfuryl chloride was anticipated (8) to give mainly the 5-chloro-5-deoxy derivative and constitutes the key step of the synthetic scheme.

## Results and discussion

In contrast to the facile selective hydrolysis of 1,2:4,5-di-*O*-isopropylidene-β-D-fructopyranose (9), partial hydrolysis of the 2,3:4,5-isomer **1** is known (10) to give a poor yield of 2,3-*O*-isopropylidene-β-D-fructopyranose (**2**), the desired starting material (Scheme 1). Treatment of **1** with a strongly acidic ion-exchange resin in 95% ethanol gave, after interruption of the reaction at the optimal time (tlc), **2** (11%), **1** (61%), and D-fructose. An overall yield of 27% of **2** could be obtained by repetition of the hydrolysis on the recovered **1** (four runs).

The reaction of **2** with sulfuryl chloride at low temperature afforded a two-component mixture ($R_f$ 0.67 and 0.76, solvent *B*). Displacement of the chlorosulfonyloxy group at C-5 by chloride ion is slow and the complete transformation of 2,3-*O*-isopropylidene-β-D-fructopyranose 1,4,5-tri(chlorosulfate) (A, $R_f$ 0.67) (Scheme 2) into 5-chloro-5-deoxy-2,3-*O*-isopropylidene-α-L-sorbopyranose 1,4-di(chlorosulfate) (B, $R_f$ 0.76) was achieved after 3 days at room temperature. Dechlorosulfation of B with methanolic sodium hydrogen carbonate gave **3** in 70% yield whereas dechlorosulfation after only 2 hours at 20°C afforded mainly the cyclic sulfate **9** (58%) and some chlorodeoxy derivative **3** (9%) (Scheme 2). The regiospecificity of the reaction arises from the fact that nucleophilic attack by chloride ion at C-4 of A would be highly unfavorable because of dipolar repulsion and steric interaction with the vicinal, axial OR substituent at C-3 of A (8), which adopts mainly (see below) the $^5C_2$(D) conformation.

Alkaline treatment of **3** gave readily 4,5-anhydro-2,3-*O*-isopropylidene-β-D-fructopyranose (**5**) which was specifically reduced at the less hindered site by lithium aluminum hydride to give the 2,3-acetonated form of "5-deoxyfructose" (**6**) in 94% yield. Deacetalation of **6** with $H^+$-resin in

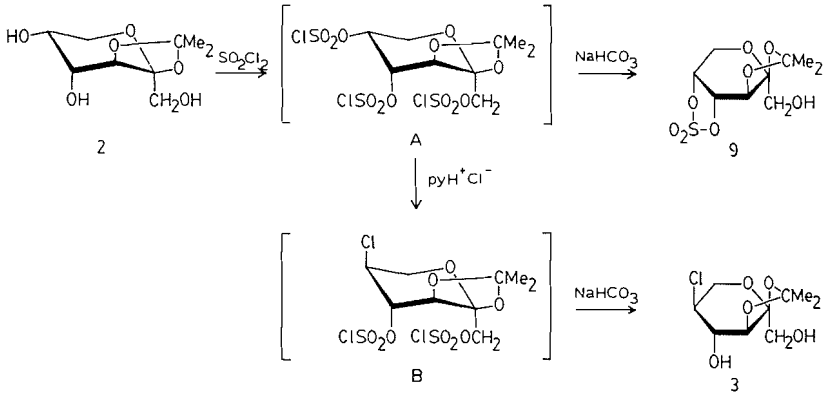

SCHEME 2

Can. J. Chem. Downloaded from www.nrcresearchpress.com by 210.87.254.6 on 09/06/12
For personal use only.

TABLE 1. Vicinal coupling constants for **4–9** (Hz)[a]

| Compound | $J_{3,4}$ | $J_{4,5A}$ | $J_{4,5B}$ | $J_{5A,6A}$ | $J_{5A,6B}$ | $J_{5B,6A}$ | $J_{5B,6B}$ |
|---|---|---|---|---|---|---|---|
| **4** | 2.9 | ? | — | ? | ? | — | — |
| **5** | 0.9 | 4.1 | — | 1.1 | <0.5 | — | — |
| **6** | 2.7 | 2.6 | 5.6 | 5.6 | 5.6 | 5.6 | 7.2 |
| **7** | 9.5 | 11.4 | 5.1 | 5.2 | 12.8 | 1.5 | 2.2 |
| **8** | 10 | 10 | 5 | 8 | 11 | ~2 | ~2 |
| **9** | 2.4 | 7.8 | — | 0.9 | 1.7 | — | — |

[a]A,B assignments made on basis of chemical shifts ($\delta_A < \delta_B$); for **6** and **7**: H-5A = H-$5_{axial}$, H-5B = H-$5_{equatorial}$; H-6A = H-$6_{equatorial}$, H-6B = H-$6_{axial}$.

aqueous ethanol gave "5-deoxyfructose" (**7**) in 78% yield together with some ethyl glycoside of **7** (6%) which was characterized as its acetylated derivative **8**.

Owing to the lack of a 5-OH group, **7** cannot exist in a furanose form and its constitutional equilibrium is much simpler than in the case of D-fructose. As in the case of L-sorbose, **7** does not show any mutarotation and was found on the basis of its nmr parameters to adopt exclusively the $^2C_5$(D) β-D-pyranoid form (*7a*) in solution. If the ethyl glycoside **8** has the same conformation, then the 2,3-*O*-acetonated precursors exhibit completely different types of conformations, as shown by the vicinal *J* values (see Table 1). Thus, the small $J_{3,4}$ coupling constants observed for the chlorodeoxy derivative **4** and the protected "5-deoxyfructose" indicate that these compounds adopt the unusual $^5C_2$ conformation (see *3a* and *6a*); however, according to the other coupling-constant values, the true conformation probably deviates from the ideal chair to a flattened chair, as in the case of 2,3-*O*-isopropylidene-β-D-fructopyranose (11).

Interestingly, the Lambert *R*-value (12), which accounts for the chair distortion of (hetero)cyclohexanes, can be calculated for the ethylene fragments of **6** and **7**. As expected, **7** exhibits an *R*-value (1.93) close to that of the *R*-parameter of an undistorted chair (2.16), whereas the *R*-value for **6** (1.14) is an indication of a considerable flattening of the pyranoid ring.

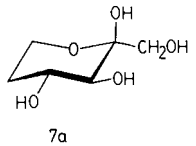

7a

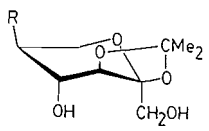

3a R = Cl
6a R = H

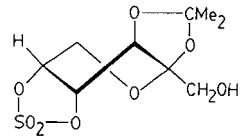

9a

The presence of the epoxide ring in **5** changes dramatically the conformation of the sugar ring which adopts an $^0H_2$- or $^2H_0$-type conformation (13). Furthermore, the cyclic sulfate **9** appears to exist in the same non-chair conformation as do 2,3:4,5-di-*O*-isopropylidene-β-D-fructopyranose (11) and di-*O*-isopropylidene-D-arabinose or di-*O*-isopropylidene-D-galactose derivatives (14), namely close to the $^6S_4$ skew conformation (see *9a*).

*Sweetness of "5-deoxyfructose"*

The sweetness of a 3% solution of **7** has been evaluated by four trained panelists and compared in several sessions to the tastes of 3% solutions of D-fructose and L-sorbose, and of water. All of the individual results showed clearly that "5-deoxyfructose" (**7**) is *much sweeter than* L-*sorbose and nearly as sweet as* D-*fructose*. In fact, the sweetness of D-fructose and of its 5-deoxy analog are very difficult to differentiate as two panelists found the latter sweeter than the common ketose. However, owing to the presence of other, non-sweet forms in D-fructose solutions, β-D-fructopyranose can still be considered as being slightly sweeter than the corresponding 5-deoxy-ketopyranose.

According to the existing theory (5), 5-deoxyfructose was expected to exhibit a sweetness close to that of L-sorbose. Our results show now that the axial, 5-hydroxyl group is not an indispensable component of the saporous unit of D-fructose and that the proposed mechanism of a "proton-releasing" effect on the HO-2 group by a competitive hydrogen bonding of HO-5 with the ring oxygen is not tenable. The large difference in

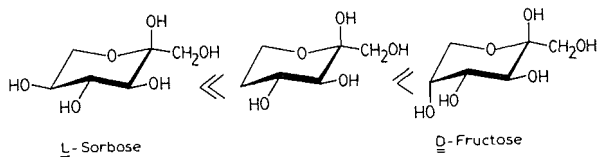

L-Sorbose D-Fructose

Can. J. Chem. Downloaded from www.nrcresearchpress.com by 210.87.254.6 on 09/06/12
For personal use only.

Can. J. Chem. Downloaded from www.nrcresearchpress.com by 210.87.254.6 on 09/06/12
For personal use only.

sweetness between the two ketoses epimeric at C-5 cannot arise only from a different degree of hydrogen bonding between HO-2 and the ring oxygen. It now appears that the equatorial 5-OH group exerts some detrimental influence on the saporous unit, possibly of a steric nature, which could preclude a correct alignment of the sugar on the taste receptor.

Further work is currently in progress to prepare new model compounds to gain more information about the intriguing problem of the sweetness of D-fructose.

## Experimental

Melting points were determined on a Fisher–Johns apparatus and are uncorrected. Optical rotations were measured with a Perkin–Elmer model 141 automatic polarimeter at 23 ± 3°C. Infrared spectra were recorded with a Perkin–Elmer 598 spectrophotometer. The $^1$Hmr spectra were recorded with a Bruker HX-60 (60 MHz) or a Bruker CXP-200 (200 MHz) spectrometer in chloroform-*d* with tetramethylsilane (TMS) as the internal standard, unless otherwise stated. The $^{13}$Cmr spectrum was obtained at 15.09 MHz on a Bruker HX-60 spectrometer equipped with an FT60M Fourier transform accessory; chemical shifts are given in parts per million downfield from TMS. Some of the coupling constants are given in Table 1. Thin-layer chromatography (tlc) was performed using silica gel G as the adsorbent in the following solvent systems (v/v): (*A*) ethyl acetate; (*B*) toluene – ethyl acetate, 2:1; (*C*) toluene – ethyl acetate, 1:1; (*D*) ethyl acetate – toluene, 3:1; (*E*) ethyl acetate – methanol–water, 7:1:0.2. The developed plates were dried and compounds located by spraying with 10% aqueous sulfuric acid containing 1% cerium sulfate and 1.5% molybdic acid, and heating at 150°C. Column chromatography was performed on silica gel 60 (70–230 mesh, Merck). The term "petroleum ether" refers to the fraction of bp 30–60°C.

*2,3;4,5-Di-*O*-isopropylidene-β-*D*-fructopyranose (1)*

This compound was prepared from D-fructose (72 g, 0.4 mol) by the method of Brady (15). The crude product (91.2 g, 87.7%) was recrystallized from ether–pentane to afford white needles (57 g, 55%), mp 97°C (lit. (15) mp 97°C), $[\alpha]_D^{23}$ −24.2° (*c* 0.6, $CHCl_3$) (lit. (15) $[\alpha]_D^{25}$ −24.7° (*c* 1.1, $CHCl_3$)). The $^1$Hmr spectrum is in agreement with the published spectrum (11).

*2,3-*O*-Isopropylidene-β-*D*-fructopyranose (2)*

This compound was prepared by a modification of the procedure of Wolfrom *et al.* (10). Compound **1** (45 g, 0.17 mol) was treated with Dowex 50W-X8 ($H^+$) resin (20 g) in 95% ethanol (160 mL) at room temperature. Thin-layer chromatographic analysis (solvent *A*) showed a slow formation of **2** ($R_f$ 0.40) together with D-fructose ($R_f$ 0, main product); after ~6 days the proportion of **2** was the greater. The resin was removed by filtration and the solvent evaporated. The residue was taken up in water and the resulting mixture extracted with methylene chloride (2 × 70 mL, 1 × 50 mL); the combined extracts were washed with water (3 × 25 mL), dried ($MgSO_4$), and concentrated to afford pure **1** (27.6 g, 61%).

The combined aqueous phases were concentrated to a yellowish syrup, which was chromatographed on a silica gel column using solvent *A* as eluent to give pure **2** as a syrup (4.1 g, 11%). The hydrolysis was repeated on the recovered **1** to yield finally 10.2 g (27%) of **2** from 45 g of **1** in four runs. The separation of **2** from D-fructose could also be achieved by continuous extraction of the aqueous solution with chloroform for three days, drying the organic phase ($MgSO_4$), evaporating the solvent, and treating the crude **2** with Darco, activated decolorizing charcoal in water. Compound **2** exhibited $[\alpha]_D^{23}$ +13.0° (*c* 1.5, water) (lit. (10) $[\alpha]_D$ +17.5° (*c* 2.3, water) after purification through the crystalline triacetate). The $^1$Hmr spectrum of 1,4,5-tri-*O*-acetyl-2,3-*O*-isopropylidene β-D-fructopyranose, prepared according to the procedure of Wolfrom *et al.* (10), was in agreement with the published spectrum (11).

*5-Chloro-5-deoxy-2,3-*O*-isopropylidene-α-L-sorbopyranose (3)*

This compound was prepared by a modification of the general procedure (16) for reactions with sulfuryl chloride. A solution of **2** (5.3 g, 24.1 mmol) in dry chloroform (100 mL) and pyridine (11.7 mL, 145 mmol, 2 equiv/OH) was cooled at −78°C (Dry Ice – acetone). Sulfuryl chloride (9.75 mL, 120.5 mmol) was added dropwise (1 h) to the viscous reaction mixture with vigorous stirring. The mixture was stirred at ~ −65°C for a further 5 h, then allowed to warm slowly to room temperature; stirring was continued at 20°C for 72 h after which time tlc revealed that all of the 2,3-*O*-isopropylidene-β-D-fructopyranose 1,4,5-tri(chlorosulfate) ($R_f$ 0.67, solvent *B*) had been converted into 5-chloro-5-deoxy-2,3-*O*-isopropylidene-α-L-sorbopyranose 1,4-di(chlorosulfate) ($R_f$ 0.76). The reaction mixture was poured into ice–water (150 mL) and the chloroform layer separated. The aqueous phase was extracted with chloroform (3 × 50 mL); the combined organic phases were washed with saturated aqueous sodium hydrogen carbonate (50 mL), then with water (50 mL), dried ($MgSO_4$), and concentrated. The residue was treated with sodium hydrogen carbonate (13 g) in methanol (150 mL) for 12 h at room temperature to achieve dechlorosulfation. The mixture was filtered and the filtrate was evaporated; the residue was dissolved in chloroform (100 mL) and water (10 mL). The aqueous layer was extracted with chloroform (3 × 10 mL) and the combined organic phases were dried ($MgSO_4$) and concentrated. The crude product was combined before purification with the product obtained from the same reaction using 2.1 g (9.6 mmol) of **2**; column chromatography (solvent *C*) afforded 38 mg (< 1%) of the cyclic sulfate derivative **9** and 5.59 g (69.7%) of **3** which was recrystallized from chloroform–ether – petroleum ether to give white crystals, mp 88–90°C; $R_f$ 0.14 (solvent *B*); $[\alpha]_D^{23}$ +24.0° (*c* 0.8, $CHCl_3$); $\nu_{max}$ (KBr): 3360, 3480 (OH) and 1373, 1384 $cm^{-1}$ ($CMe_2$); $^1$Hmr δ: 1.40 and 1.64 (2s, 2 × 3H, $CMe_2$), 3.34 (t, 1H, $J_{1A,OH}$ = 6.5 Hz, $J_{1B,OH}$ = 5.7 Hz, exchanged in $D_2O$, HO-1), 3.61 (dd, d after $D_2O$ exchange, 1H, $J_{1A,1B}$ = 11.5 Hz, H-1A), 3.85 (dd, d after $D_2O$ exchange, 1H, H-1B), 3.92–4.16 (m, 3H, H-6A, H-6B, H-3 or H-5), 4.24–4.37 (m, 3H, 2H after $D_2O$ exchange, H-4, HO-4, H-5 or H-3). *Anal.* calcd. for $C_9H_{15}ClO_5$: C 45.35, H 6.33, Cl 14.85; found: C 45.35, H 6.42, Cl 14.42.

*1,4-Di-*O*-acetyl-5-chloro-5-deoxy-2,3-*O*-isopropylidene-α-L-sorbopyranose (4)*

Acetylation of **3** (200 mg, 0.84 mmol) by the standard procedure afforded 250 mg (92%) of homogeneous **4** which was recrystallized from ether – petroleum ether, mp 47–49°C, $R_f$ 0.58 (solvent *B*), $[\alpha]_D^{23}$ +27.5° (*c* 1.16, $CHCl_3$); $\nu_{max}$ (KBr): 1745 (C=O), 1382 and 1390 $cm^{-1}$ ($CMe_2$); $^1$Hmr δ: 1.43 and 1.67 (2s, 2 × 3H, $CMe_2$), 2.15 and 2.16 (2s, 2 × 3H, 2 OAc), 3.98–4.10 (m, 3H, H-5, H-6's), 4.17 (d, 1H, $J_{3,4}$ = 2.9 Hz, H-3), 4.21 (d, 1H, $J_{1A,1B}$ = 12.2 Hz, H-1A), 4.32 (d, 1H, H-1B), 5.48 (narrow m, 1H, H-4). *Anal.* calcd. for $C_{13}H_{19}ClO_7$: C 48.38, H 5.93, Cl 10.99; found: C 48.54, H 6.14, Cl 11.09.

*2,3-*O*-Isopropylidene-β-*D*-fructopyranose 4,5-cyclic sulfate (9)*

A solution of compound **2** (2.0 g, 9.1 mmol) in chloroform

Can. J. Chem. Downloaded from www.nrcresearchpress.com by 210.87.254.6 on 09/06/12
For personal use only.

(60 mL) containing pyridine (4.4 mL, 55 mmol) was treated with sulfuryl chloride (3.7 mL, 45.6 mmol) at low temperature as described for the preparation of **3**, and the reaction was stopped after having been stirred for 2 h at room temperature. The reaction mixture was treated with sodium hydrogen carbonate in methanol for 70 h and processed; column chromatography afforded 1.5 g (58%) of syrupy **9** and 0.19 g (9%) of **3**. Compound **9** crystallized from ether – petroleum ether, mp 82.5–84°C, $R_f$ 0.46 (solvent *B*), $[\alpha]_D^{23}$ −23.8° (*c* 2.1, $CHCl_3$); $\nu_{max}$ (KBr): 3370 (OH), 1400 and 1205 $cm^{-1}$ ($SO_2$); $^1$Hmr δ: 1.46 and 1.60 (2s, 2 × 3H, $CMe_2$), 2.16 (t, 1H, $J_{1,OH}$ = 7 Hz, exchanged in $D_2O$, HO-1), 3.77 (d, s after $D_2O$ exchange, 2H, H-1's), 4.05 (dd, 1H, $J_{5,6A}$ = 0.9 Hz, $J_{6A,6B}$ = 14.7 Hz, H-6A), 4.15 (dd, 1H, $J_{5,6B}$ = 1.7 Hz, H-6B), 4.58 (d, 1H, $J_{3,4}$ = 2.4 Hz, H-3), 5.04 (ddd, 1H, $J_{4,5}$ = 7.8 Hz, H-5), 5.33 (dd, 1H, H-4). *Anal.* calcd. for $C_9H_{14}SO_8$: C 38.29. H 5.00; found: C 38.04, H 5.07.

*4,5-Anhydro-2,3-*O*-isopropylidene-*β*-*D*-fructopyranose (5)*

Compound **3** (4.95 g, 20.7 mmol) was treated with potassium hydroxide (1.4 g, 25 mmol) in ethanol (120 mL) at room temperature for 6 h. The mixture was neutralized with 1 *N* hydrochloric acid and concentrated. The residue was dissolved in methylene chloride (100 mL) and water (10 mL) the separated aqueous layer washed with methylene chloride (3 × 5 mL) and the combined organic phases dried over magnesium sulfate. Concentration of the solution afforded 4.1 g (98%) of crystalline **5**. An analytical sample was obtained from ether – petroleum ether, mp 114–116.5°C, $R_f$ 0.12 (solvent *B*); $[\alpha]_D^{23}$ −11.1° (*c* 0.8, $CHCl_3$); $\nu_{max}$ (KBr): 3460 (OH), 1377 and 1387 $cm^{-1}$ ($CMe_2$); $^1$Hmr δ: 1.45 and 1.55 (2s, 2 × 3H, $CMe_2$), 2.37 (broad s, 1H, exchanged in $D_2O$, HO-1), 3.28 (broad d, 1H, $J_{4,5}$ = 4.1 Hz, $J_{5,6A}$ = 1.1 Hz, $J_{5,6B}$ < 0.5 Hz, H-5), 3.39 (dd, 1H, $J_{3,4}$ = 0.9 Hz, H-4), 3.50 (broad dd, d after $D_2O$ exchange, 1H, $J_{1A,1B}$ = 11.7 Hz, $J_{1A,OH}$ ~ 7 Hz, H-1A), 3.64 (d, 1H, H-1B), 4.10 (d, 1H, H-6A), 4.21 (d, 1H, H-6B), 4.41 (s, 1H, H-3). *Anal.* calcd. for $C_9H_{14}O_5$: C 53.46, H 6.98: found: C 53.77, H 7.15.

*5-Deoxy-2,3-*O*-isopropylidene-*β*-*D*-threo-hexulopyranose (6)*

A solution of **5** (4.0 g, 19.8 mmol) in dry tetrahydrofuran (40 mL) was added, dropwise over a period of 45 min, under nitrogen to a suspension of lithium aluminum hydride (2.3 g, 61 mmol) in tetrahydrofuran (80 mL) at room temperature. Stirring was continued for 3.5 h at 20°C and 2 h at reflux temperature. Ice-water (20 mL) was then added carefully; the mixture was filtered, the filtrate neutralized with 0.5 *N* hydrochloric acid and concentrated. The residue was dissolved in chloroform (50 mL) and water (5 mL), the separated aqueous layer concentrated, and the crystalline residue triturated with chloroform (5 mL) and then with acetone (5 mL). The combined organic phases were dried ($MgSO_4$) and concentrated to afford 3.8 g (94%) of homogeneous (tlc) **6**. Pure **6** (3.1 g, 77%) was obtained by crystallization from chloroform–ether – petroleum ether followed by column chromatography (solvent *D*) and crystallization as before; mp 95–97°C, $R_f$ 0.22 (solvent *D*), $[\alpha]_D^{23}$ +28.6° (*c* 1.0, $CHCl_3$); $\nu_{max}$ (KBr): 3410 (OH), 1375 and 1384 $cm^{-1}$ ($CMe_2$); $^1$Hmr δ: 1.40 and 1.58 (2s, 2 × 3H, $CMe_2$), 1.72 (tdd, 1H, $J_{4,5A}$ = 2.6 Hz, $J_{5A,5B}$ = 14.3 Hz, $J_{5A,6A}$ = 5.6 Hz, $J_{5A,6B}$ = 5.6 Hz, H-5A), 2.12 (tdd, 1H, $J_{4,5B}$ = 5.6 Hz, $J_{5B,6A}$ = 5.6 Hz, $J_{5B,6B}$ = 7.2 Hz, H-5B), 3.47 (dd, 1H, $J_{1A,OH}$ = 5.0 Hz, $J_{1B,OH}$ = 7.5 Hz, exchanged in $D_2O$, HO-1), 3.67 (dd, d after $D_2O$ exchange, 1H, $J_{1A,1B}$ = 11.5 Hz, H-1A), 3.77 (d, 1H, $J_{4,OH}$ = 6.0 Hz, exchanged in $D_2O$, HO-4), 3.87 (obscured td, 1H, $J_{6A,6B}$ = 11.9 Hz, H-6A), 3.88 (dd, d after $D_2O$ exchange, 1H, H-1B), 3.97 (ddd, 1H, H-6B), 4.12 (d, 1H, $J_{3,4}$ = 2.7 Hz, H-3), 4.30 (tt, td after $D_2O$ exchange, 1H, H-4). *Anal.* calcd. for $C_9H_{16}O_5$: C 52.93, H 7.90; found: C 52.88, H 8.10.

*5-Deoxy-β-D-threo-hexulopyranose (7) ("5-deoxy-D-fructose" or "5-deoxy-L-sorbose")*

Compound **6** (2.7 g, 13.2 mmol) was treated with Dowex 50W-X8 ($H^+$) resin (75 g) in an ethanol (200 mL) – water (50 mL) mixture at room temperature for 7 days. The resin was removed by filtration and the filtrate concentrated. Resolution of the reaction mixture by column chromatography (solvent *E*) afforded 140 mg (5%) of **6**, 150 mg (6%) of the ethyl glycoside of **7** ($R_f$ 0.42), 200 mg of a mixture of the latter and **7**, and 1.69 g (78%) of homogeneous (tlc) **7**, which was recrystallized from methanol – acetate; mp 117.5–118.5°C, (lit. (7) mp 110°C); $R_f$ 0.23 (solvent *E*), $[\alpha]_D^{23}$ −65.8° (*c* 1.1, $H_2O$) (lit. (7) $[\alpha]_D$ −67.0° (*c* 1.0, $H_2O$)); $\nu_{max}$ (KBr): 3350 (very broad, OH), 1050, 1095, and 1150 $cm^{-1}$; $^1$Hmr ($CD_3OD$; a = axial,, e = equatorial) δ: 1.62 (tdd, 1H, $J_{5a,5e}$ = 12.8 Hz, $J_{5a,6a}$ = 12.8 Hz, $J_{4,5a}$ = 11.4 Hz, $J_{5a,6e}$ = 5.2 Hz, H-5a), 1.89 (dddd, 1H, $J_{4,5e}$ = 5.1 Hz, $J_{5e,6a}$ = 2.2 Hz, $J_{5e,6e}$ = 1.5 Hz, H-5e), 3.39 (d, 1H, $J_{3,4}$ = 9.5 Hz, H-3), 3.45 (d, 1H, $J_{1A,1B}$ = 11.1 Hz, H-1A), 3.63 (ddd, 1H, $J_{6a,6e}$ = 11.5 Hz, H-6e), 3.66 (d, 1H, H-1B), 3.87 (ddd, 1H, H-4), 3.95 (ddd, 1H, H-6a); ($D_2O$) δ: 1.71 (~qd, 1H, $J_{5a,5e}$ = 12 Hz, $J_{5a,6a}$ = 12 Hz, $J_{4,5a}$ = 12 Hz, $J_{5a,6e}$ = 5.5 Hz, H-5a), 2.05 (dm, 1H, $J_{4,5e}$ = 5 Hz, $J_{5e,6a}$ = 2 Hz, $J_{5e,6e}$ = 2 Hz, H-5e), 3.51 (d, 1H, $J_{3,4}$ = 9.5 Hz, H-3), 3.54 (d, 1H, $J_{1A,1B}$ = 11.7 Hz, H-1A), 3.79 (d, 1H, H-1B), 3.72–4.05 (m, 3H, H-4, H-6a, H-6e); $^{13}$Cmr ($D_2O$) δ: 33.9 (C-5), 59.8 (C-6), 64.8 (C-1), 69.4, 73.3 (C-3, C-4), 99.3 (C-2). *Anal.* calcd. for $C_6H_{12}O_5$: C 43.90, H 7.37; found: C 43.50, H 7.00.

*Ethyl 1,3,4-tri-*O*-acetyl-5-deoxy-*β*-*D*-threo-hexulopyranoside (8)*

The syrupy ethyl glycoside of **7** (150 mg) obtained as described above was acetylated by the standard procedure to afford 220 mg (89%) of **8**. An analytical sample of syrupy **8** was obtained by column chromatography (hexane – ethyl acetate, 2:1 (v/v)), $R_f$ 0.43 (solvent *B*); $[\alpha]_D^{23}$ −75.6° (*c* 1.11, $CHCl_3$); $\nu_{max}$ (film): 1750 $cm^{-1}$ (C=O); $^1$Hmr ($CD_3OD$; a = axial, e = equatorial) δ: 1.26 (t, 3H, $OCH_2CH_3$), 1.84 (m, 1H, $J_{4,5a}$ = 10 Hz, $J_{5a,5e}$ = 13 Hz, $J_{5a,6e}$ ~ 8 Hz, $J_{5a,6a}$ ~ 11 Hz, H-5a), 2.03, 2.09, and 2.12 (3s, 3 × 3H, 3 OAc), 2.18 (m, 1H, $J_{4,5e}$ = 5 Hz, $J_{5e,6a}$ ~ 2 Hz, $J_{5e,6e}$ ~ 2 Hz, H-5e), 3.51 (qd, 1H, $J_{H_A,CH_3}$ = 6.8 Hz, $J_{H_A,H_B}$ = 9.2 Hz, $OCH_AH_BCH_3$), 3.67 (qd, 1H, $J_{H_B,CH_3}$ = 7.2 Hz, $OCH_AH_BCH_3$), 3.8 (m, 2H, H-6a, H-6e), 4.04 (d, 1H, $J$ = 11.7 Hz, H-1A), 4.29 (d, 1H, H-1B), 5.19 (d, 1H, $J_{3,4}$ = 10 Hz, H-3), 5.28 (td, 1H, H-4). *Anal.* calcd. for $C_{14}H_{22}O_8$: C 52.83, H 6.97; found: C 52.78; H 7.35.

## Acknowledgements

The authors are grateful to the Natural Sciences and Engineering Research Council of Canada for its support of this work in the form of a grant (to W.A.S.), to the Fonds National Suisse de la Recherche Scientifique for its award of a fellowship (to O.R.M.), and to Queen's University for financial assistance (to S.-L. K.-T.).

1. R. S. Shallenberger. Pure Appl. Chem. **50**, 1409 (1978); Zuckerindustrie, **104**, 121 (1979).
2. R. S. Shallenberger. J. Food Sci. **28**, 584 (1963); New Sci. **407**, 569 (1964); R. S. Shallenberger and T. E. Acree. Nature, **216**, 480 (1967); J. Agric. Food Chem. **17**, 701 (1969).
3. R. U. Lemieux and J. T. Brewer. ACS Adv. Chem. Series, **117**, 121 (1973).
4. L. B. Kier. J. Pharm. Sci. **61**, 1394 (1972).
5. M. G. Lindley and G. G. Birch. J. Sci. Food Agr. **26**,

117 (1975); G. G. BIRCH. CRC Critical Rev. Food Sci. Nutr. **8**, 54 (1976).
6. S. J. ANGYAL and G. S. BETHELL. Aust. J. Chem. **29**, 1249 (1976).
7. P. P. REGNA. J. Am. Chem. Soc. **69**, 246 (1947).
8. W. A. SZAREK. Adv. Carbohydr. Chem. Biochem. **28**, 225 (1973).
9. J. C. IRVINE and C. S. GARRETT. J. Chem. Soc. **97**, 1277 (1910).
10. M. L. WOLFROM, W. L. SHILLING, and W. W. BINKLEY. J. Am. Chem. Soc. **72**, 4544 (1950).
11. T. MAEDA, K. TORI, S. SATOH, and K. TOKUYAMA. Bull. Soc. Chim. Jpn. **42**, 2635 (1969).
12. J. B. LAMBERT. Acc. Chem. Res. **4**, 87 (1971).
13. J. G. BUCHANAN, R. FLETCHER, K. PARRY, and W. A. THOMAS. J. Chem. Soc. B, 377 (1969).
14. C. CONE and L. HOUGH. Carbohydr. Res. **1**, 1 (1965).
15. R. F. BRADY, JR. Carbohydr. Res. **15**, 35 (1970).
16. H. J. JENNINGS and J. K. N. JONES. Can. J. Chem. **40**, 1408 (1962).

Can. J. Chem. Downloaded from www.nrcresearchpress.com by 210.87.254.6 on 09/06/12
For personal use only.

# The biosynthesis of *myo*-inositol and its isomers[1,2]

OTTO HOFFMANN-OSTENHOF[3] AND F. PITTNER

*Institut für Allgemeine Biochemie der Universität Wien and Ludwig-Boltzmann-Forschungsstelle für Biochemie, Vienna, Austria*

Received January 8, 1982

OTTO HOFFMANN-OSTENHOF and F. PITTNER. Can. J. Chem. **60**, 1863 (1982).

The present state of our knowledge about the biosynthetic processes leading to the inositols is reviewed. On the basis of experimental data obtained in the laboratory of the authors and by other groups working on the problem, a new mechanism of action for the mammalian *myo*-inositol-1-phosphate synthase is suggested. The central position of *myo*-inositol in the synthesis of the other inositols is described.

OTTO HOFFMANN-OSTENHOF et F. PITTNER. Can. J. Chem. **60**, 1863 (1982).

On passe en revue l'état actuel de nos connaissances sur les processus biosynthétiques conduisant aux inositols. En se basant sur des données expérimentales obtenues dans le laboratoire des auteurs et par d'autres groupes de chercheurs, on suggère un nouveau mécanisme d'action de la synthase du *myo*-inositol-phosphate-1 des mammifères. On décrit la position centrale du *myo*-inositol dans la synthèse des autres inositols.

[Traduit par le journal]

## Introduction

*myo*-Inositol is a natural compound with several important biological functions. It was first isolated by Scherer, a student of Wöhler, as a sugar-like compound from meat juice in 1850 (1). More than 30 years later Maquenne (2) found the compound to be a cyclohexanehexol. Its configuration was finally established almost simultaneously by Dangschat and Fischer (3) and by Posternak (4) in 1942.

Maquenne (2), as early as 1900, suggested that *myo*-inositol was the product of an intramolecular head-to-tail C—C cyclization of a hexose molecule, but more than half a century passed until this hypothesis could be confirmed. Fischer (5), realizing the analogy of four asymmetric centres in D-glucose and *myo*-inositol, considered D-glucose to be the most probable candidate for such a cyclization reaction and also supported his view by model experiments. However, the final establishment of this pathway was achieved much later with the use of radioactively labelled precursor substrates.

Employing selectively $^{14}$C-labelled D-glucose and a method of partial biological degradation of the product, Loewus and Kelly (6) showed it most probable that indeed a condensation between the carbon atoms 1 and 6 of D-glucose is the pathway to *myo*-inositol. Their conclusion was based on the assumption that *myo*-inositol incorporated into pectin producing plants yields D-galacturonyl residues via D-glucuronate without any fragmentation of the carbon chain during this transformation. A completely chemical degradation pathway for *myo*-inositol obtained from selectively labelled D-glucose in living organisms was developed in our laboratory (7); this method permitted the localization of radioactivity in all the carbon atoms of the molecule. The results also supported the correctness of the mechanisms suggested by Maquenne and Fischer.

Almost simultaneously with the establishment of the precursor function of D-glucose in the biosynthesis of *myo*-inositol, the first reports on cell-free homogenates capable of transforming D-glucose to *myo*-inositol appeared (8, 9). It soon was found that the overall reaction involves at least three stages (Scheme 1). Initially D-glucose is converted to D-glucose 6-phosphate by the well-known hexokinase. D-Glucose 6-phosphate is then transformed to 1 L-*myo*-inositol 1-phosphate which is finally dephosphorylated to *myo*-inositol by a rather specific phosphatase. It is probable that similar enzyme systems exist in all eucaryotes. On the other hand, this is not always the case in procaryotes since e.g. *E. coli* is not capable of producing or utilizing *myo*-inositol (10). On the other hand, *Streptomyces griseus*, which uses *myo*-inositol as a precursor of the antibiotic streptomycin, does synthesize it by an apparently analogous enzyme system (11).

## *myo*-Inositol-1-phosphate synthase, the key enzyme of inositol biosynthesis

Of the three steps concerned in the transforma-

[1] Presented at the 28th Congress of the International Union of Pure and Applied Chemistry, Vancouver, British Columbia, Canada, August 1981.

[2] Dedicated to Academician A. E. Braunstein on the occasion of his 80th birthday.

[3] Author to whom all correspondence should be addressed.

0008-4042/82/141863-09$01.00/0

©1982 National Research Council of Canada/Conseil national de recherches du Canada

Can. J. Chem. Downloaded from www.nrcresearchpress.com by 210.87.254.5 on 09/06/12
For personal use only.

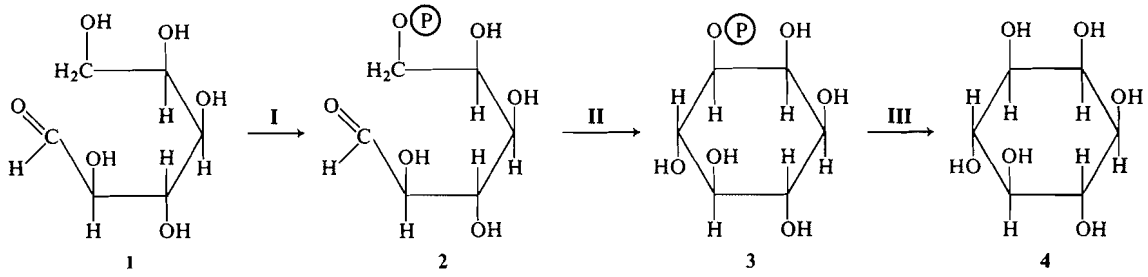

SCHEME 1. The pathway from D-glucose to *myo*-inositol. Enzyme I is hexokinase, enzyme II is *myo*-inositol-1-phosphate synthase, and enzyme III is a phosphatase.

tion of D-glucose to *myo*-inositol, the second one involving the cyclization of D-glucose 6-phosphate (**2**) to 1 L-*myo*-inositol 1-phosphate (**3**), attracted considerable interest among enzymologists. It was soon found that one enzyme only is responsible for this key reaction in *myo*-inositol synthesis, although apparently several intermediate steps are involved. The enzyme, originally called cyclase or cycloaldolase, now has the name *myo*-inositol-1-phosphate synthase (EC 5.5.1.4). The reaction is rather unusual, although it shows a certain analogy to the transformation of 3-deoxy-D-*arabino*-heptulosonate 7-phosphate (**5**) to 3-dehydroxyquinate (**6**), a reaction catalyzed by dehydroquinate synthase (EC 4.6.1.3). This enzyme requires $NAD^+$ for its action and plays a role in the biosynthesis of aromatic compounds (12). However, dehydroquinate synthase eliminates the phosphate moiety concomitantly with cyclization, whereas with *myo*-inositol-1-phosphate synthase the phosphate group is preserved in the product (Scheme 2).

*myo*-Inositol-1-phosphate synthase has been isolated from various animals, higher plants, yeasts, and some procaryotes. The enzyme proteins from these different sources vary considerably in their chemical and physical properties, such as metal content, molecular mass, and specific acitivity. They all, however, either contain more or less strongly bound $NAD^+$ or at least require this coenzyme for their action. Generally it seems to be established that the enzyme preparations from all sources catalyze a sequence of at least three reactions (Scheme 3). (1) The oxidation with $NAD^+$, as hydrogen acceptor, of the 5-hydroxyl group of D-glucose 6-phosphate to form L-*xylo*-hexosulose 1-phosphate, which remains bound to the enzyme. (2) This compound then undergoes an intramolecular aldol condensation to the cyclic product 2 L-2-phospho-2,4,6/3,5-pentahydroxycyclohexanone, which also remains bound to the enzyme. Concomitantly with the cyclization, one hydrogen atom, originally bound to the 6-position of the substrate, is set free as a proton. (3) Eventually, the last mentioned product is reduced to 1 L-*myo*-inositol 1-phosphate with the previously formed NADH acting as hydrogen donor.

There is good reason to assume that either the substrate itself or its oxidation product must exist in the open chain form to make the cyclization reaction possible. It is known that the spontaneous anomerization of α-glucose 6-phosphate within the physiological pH range is more than two orders of magnitude faster than that of α-glucose (13). It is debatable whether this anomerization that necessarily proceeds via the open chain form is sufficiently rapid in order not to be the limiting factor of the *myo*-inositol-1-phosphate synthase reaction, or whether we have to postulate an additional anomerizing activity for the enzyme.

Originally two possible mechanisms for the cyclization reactions catalyzed by *myo*-inositol-1-phosphate synthase were proposed, namely an aldol condensation corresponding to the reaction

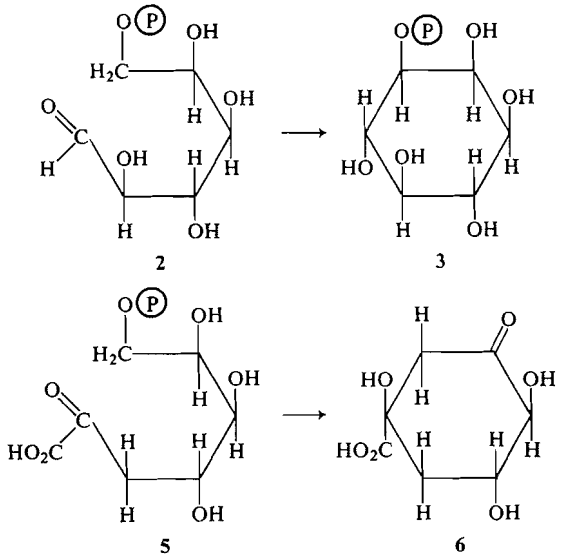

SCHEME 2. *myo*-Inositol-1-phosphate synthase and dehydroquinate synthase.

Can. J. Chem. Downloaded from www.nrcresearchpress.com by 210.87.254.5 on 09/06/12
For personal use only.

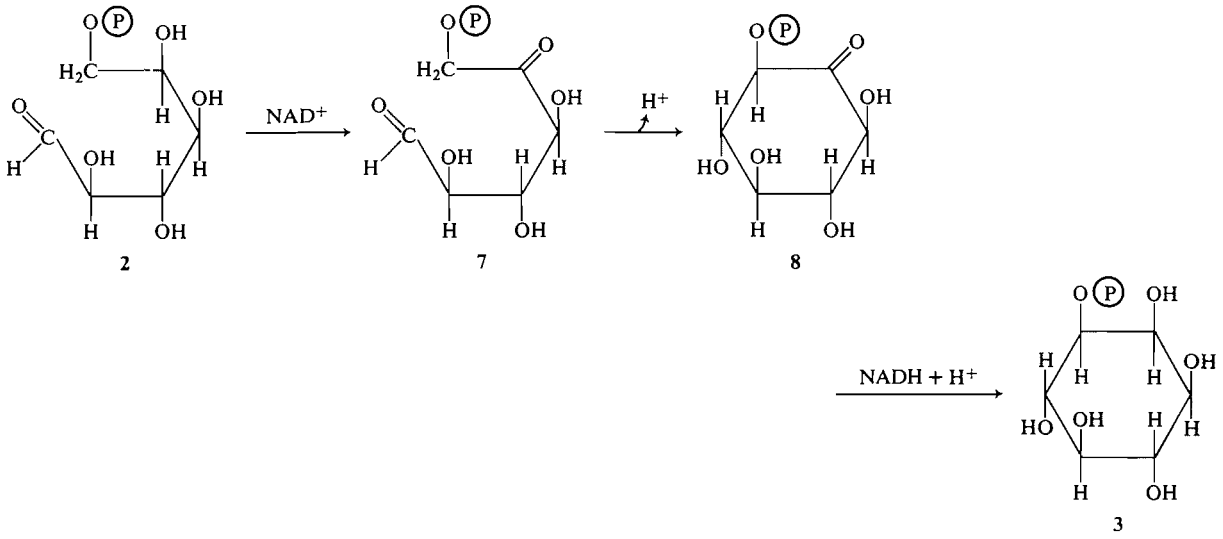


SCHEME 3. The general mechanism of action of *myo*-inositol-1-phosphate synthase; the intermediary compounds are bound to the enzyme.

scheme given in Scheme 3, and an acyloin condensation, where the carbon atom 6 of the substrate would be primarily hydroxylated by $NAD^+$ (14). However, especially through the work of Barnett and Corina (15), it seems to be established that it is indeed the aldol condensation mechanism that is responsible for the cyclization reaction. Although the two postulated intermediates have never been obtained in free form from the reaction mixture, there is ample evidence for their function as intermediates (16, 17).

The action of *myo*-inositol-1-phosphate synthase also poses some stereochemical problems. Quite recently it could be shown that, in contrast to an earlier report (18), it is the pro-*R* atom of C-6 of D-glucose 6-phosphate that is set free during the cyclization reaction (19). Another very recent paper (20) shows that in the first step of the reaction sequence the hydrogen from the 5-position of the substrate is transferred to $NAD^+$ to become the pro-*S* hydrogen at position 4 of the nicotinamide moiety of the reduced coenzyme. This pro-*S* hydrogen of NADH is also transferred to the keto group of 2 L-2-phospho-2,4,6/3,5-pentahydroxycyclohexanone in the third step of the sequence.

Whereas many enzymes of this specificity from plants or microorganisms are inhibited by EDTA and seem to contain bivalent ions or at least require them for their action, the animal enzymes so far investigated are metal-free and cannot be inhibited by EDTA. There is here a certain similarity to the situation encountered in the group of aldolases, where we can distinguish two types, namely the aldolases class I and the aldolases class II. The aldolases class I do not contain any bivalent metal ion and are characterized by the intermediate formation of a Schiff's base between the ε-amino group of a lysyl residue of the enzyme and a carbonyl group of the substrate. Aldolases class II require metal ions for their action. There is a marked similarity of the reactions catalyzed by *myo*-inositol-1-phosphate synthase to those by the aldolases.

In earlier papers by Naccarato *et al.* (21) and from our laboratory (22), experiments were reported that seemed to indicate that the *myo*-inositol-1-phosphate synthase from the rat (mammae, testes) is a Schiff's base forming enzyme. The main arguments for such a mechanism were that typical inhibitors of Schiff's base formation like pyridoxal phosphate or trinitrobenzenesulphonate acted as competitive inhibitors of the enzyme, furthermore $NaBH_4$ when added to the reaction mixture also had an inhibiting action. When radioactive substrate was used, reduction of the reaction mixture with $NaBH_4$ resulted in incorporation of radioactivity from the substrate into the enzyme protein; an analogous result was also obtained with cold substrate and tritiated $NaBH_4$. The affinity-labelled protein thus obtained was degraded by proteolytic enzymes and the resulting mixture was analyzed by paper chromatography. One single radioactive spot was found and the product was isolated.

According to the general reaction mechanism described above, this product can have two structures (Scheme 4). Two carbonyl groups can react with the ε-amino group of a lysyl residue, namely

Can. J. Chem. Downloaded from www.nrcresearchpress.com by 210.87.254.5 on 09/06/12
For personal use only.

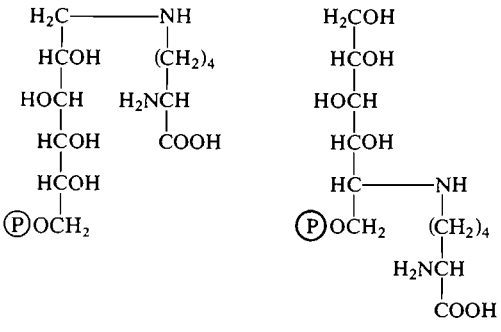

9 10

SCHEME 4

SCHEME 4. The two alternative possibilities for the structure of the reduced Schiff base between lysine and D-glucose 6-phosphate isolated after enzymic hydrolysis of the enzyme protein obtained from the incubation mixture treated with $NaBH_4$.

(a) the aldehyde group of the open chain of the substrate or of the first intermediate, L-*xylo*-hexosulose 1-phosphate, leading to product **9**, and (b) the oxo group on C-5 in this intermediate, which derives from the C-5 hydroxyl of the substrate by the dehydrogenation with $NAD^+$ as hydrogen acceptor. In this case **10** is produced.

For reasons of analogy to fructose-bisphosphate aldolase (EC 4.1.2.13), class I (Schiff's base forming), we originally considered mechanism (b) more probable, but in order to clarify this question, the product described above was analyzed for its structure by mass spectroscopy and by nmr. By comparison with a synthetically obtained sample it could be established that the compound is $N^{\varepsilon}$-1-D-glucityl-L-lysin, i.e. the product **10**, which means that mechanism (a) is operating (23). Thus, we have here no parallel to the aldolases class I.

Considering the bond formed between the lysyl residue of the enzyme and the substrate, we made some further interesting observations (23). Firstly the enzyme does not form the bond if $NAD^+$ is removed from the enzyme with the help of Norite; when $NAD^+$ is then added back, the ability of binding the substrate and with it the full activity of the enzyme is regained. From this result it can be concluded that in the absence of $NAD^+$ the enzyme shows very little affinity to the substrate; this may be due to a reversible change of conformation of the enzyme protein caused by the removal of $NAD^+$. Another set of experiments dealt with the incorporation of radioactivity into the enzyme from tritiated $NaBH_4$ when reduction of the reaction mixture took place at pH 6.0, the optimal conditions for the reduction of an —N=C— bond, and afterwards at pH 8.0, a condition favouring the reduction of a carbonyl bond. After isolation of the enzyme protein and preparation of the mentioned lysyl derivative from an aliquot reduced at pH 6.0 only and a second aliquot reduced at both pH 6.0 and 8.0, it was shown that the product from the second aliquot contained about twice as much activity as the product from pH 6.0 reduction. However, when the latter product was oxidatively degraded by means of periodate, about half of its activity was lost. This means that the activity lost was located in that part of the molecule which is split off by periodate oxidation, in our opinion most probably in the C-5 position of the substrate, which carries a keto group after the first oxidoreduction step of the reaction sequence.

It is not easy to explain these results. Firstly, it seems that the binding takes place before the first oxidoreduction step of the reaction sequence. Secondly, the binding may have the effect of fixing the enzyme to the substrate in such an orientation that the dehydrogenation step with $NAD^+$ as acceptor is made possible. A third possibility involves the mechanism of ring closure, as will be described further below.

Until quite recently, we thought that, in spite of some differences, the analogy with aldolases, class I, would hold at least as far as the nature of the bond between the enzyme protein and the substrate is concerned, namely that it should be a Schiff's base. Inhibition by typical inhibitors of Schiff's base formation, inhibition of the reaction by addition of $NaBH_4$ to the reaction mixture, the isolation of a reduction product that apparently derived from the reduction of Schiff's base, were all strong arguments for the involvement of this type of bond. However, it was Sherman and his group (24) who claimed that a Schiff's base could not participate in the reaction sequence. When the reaction takes place in a medium enriched with $H_2{}^{18}O$, an increased incorporation of $^{18}O$ into the product must be expected, because if a Schiff's base bond is intermediarily formed, a hydrolysis of this bond has to take place in order to make the ring closure possible, and this hydrolysis would cause an increased uptake of the isotope. Since Sherman *et al.* could not find such an effect, they suggest that an acid–base catalysis without any Schiff's base intermediate is operating.

Quite recently, Floss and co-workers (19) proposed some new ideas concerning the mechanism of our enzyme, partly based on their elucidation of the stereochemistry of the hydrogen removal from C-6 of the substrate during the reaction sequence. They suggest that a single base group of the enzyme acts alternately in the base form, abstracting the proton from C-6, and in the conjugate acid form,

Can. J. Chem. Downloaded from www.nrcresearchpress.com by 210.87.254.5 on 09/06/12
For personal use only.

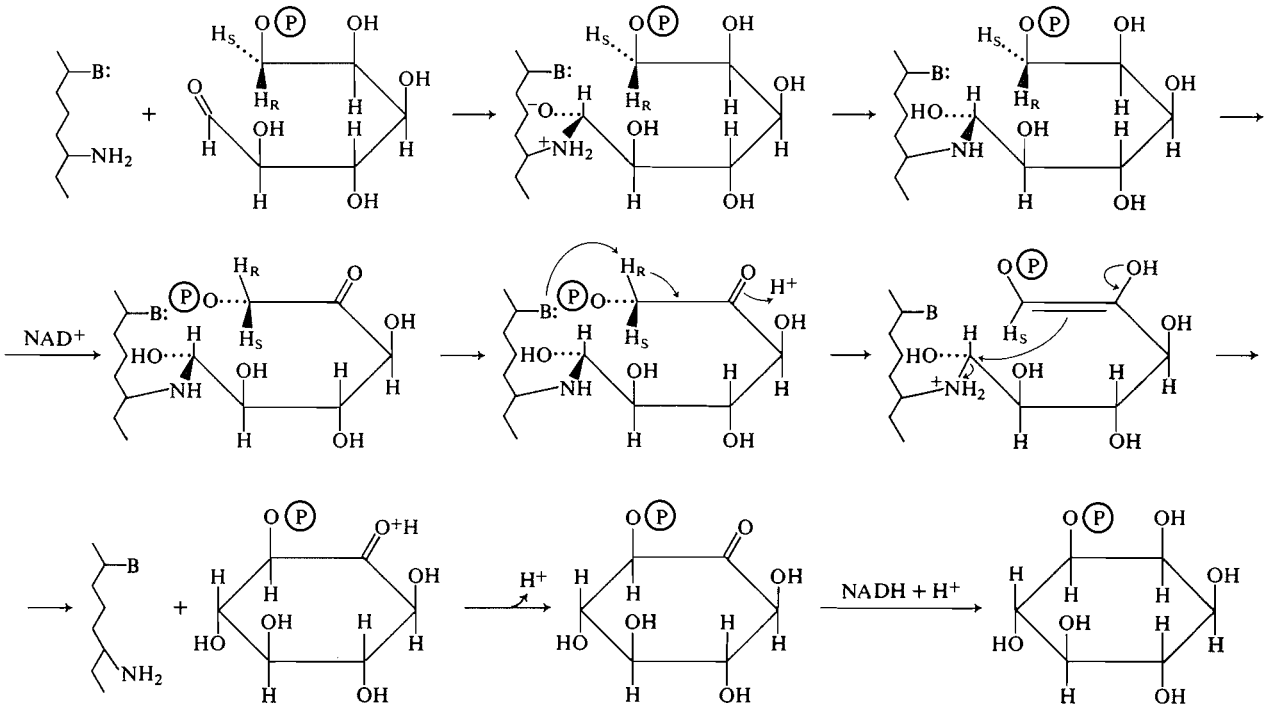

SCHEME 5. Suggested reaction scheme for *myo*-inositol-1-phosphate synthase from rat testes.

protonating the oxygen at C-1. This proposal is supported by the fact that the nucleophilic attack at C-1 occurs on the *Re* face of the carbonyl group, as evidenced by the configuration of the product.

In this context the same authors speculate that the base group may be the same lysine amino group that appears in the lysyl derivative isolated in our laboratory, and that the formation of a Schiff's base at C-1 may be a side reaction rather than an essential part of the reaction mechanism. Due to mutarotation such a side reaction would not bring about a measurable incorporation of $^{18}O$ from $H_2{}^{18}O$ into the product.

There is no doubt that the mechanism of Floss and co-workers represents a useful working hypothesis for the complex mechanisms of the reaction sequence of our enzyme. However, as enzymologists, we have considerable reservations concerning the existence of side reactions in enzyme-catalyzed processes; furthermore, some of our results are not easily brought to agree with the suggestions of the named authors.

We have now worked out a new mechanism that somewhat differs from that suggested by Floss and his group, but which seems to be in agreement with the data reported by them as well as with those of Sherman *et al.* (24).

As mentioned before, the data obtained by mass spectrometry by Sherman make a Schiff's base mechanism rather improbable, but on the other hand our reduction experiments and also the action of so-called Schiff's base inhibitors strongly support the idea that a binding between the ε-amino group of a lysyl residue of the enzyme with the aldehyde group of the substrate takes place. Such binding does not necessarily involve a Schiff's base. Another possibility is the formation of a carbinolamine, which on reduction would give the same products as a Schiff's base. Formation of a carbinolamine ought also to be inhibited by compounds inhibiting Schiff's base formation.

Some details of the proposed mechanism are represented in Scheme 5.

As shown there, a carbinolamine is formed as the aldehyde group of D-glucose 6-phosphate combines with the ε-amino group of a lysyl residue of the enzyme and a proton is transferred from N to O. The hydroxyl group at C-5 of the sugar is then oxidized by a $NAD^+$-mediated step to a keto group and a concomitant shift in the position of the substituents on C-6 takes place.

This is followed by a protonation of the keto oxygen and by an attack of a basic group of the enzyme to remove the pro-*R* hydrogen from C-6. This hydrogen is relatively acidic, as it is in an α-position to the carbonyl group. Due to steric

Can. J. Chem. Downloaded from www.nrcresearchpress.com by 210.87.254.5 on 09/06/12
For personal use only.

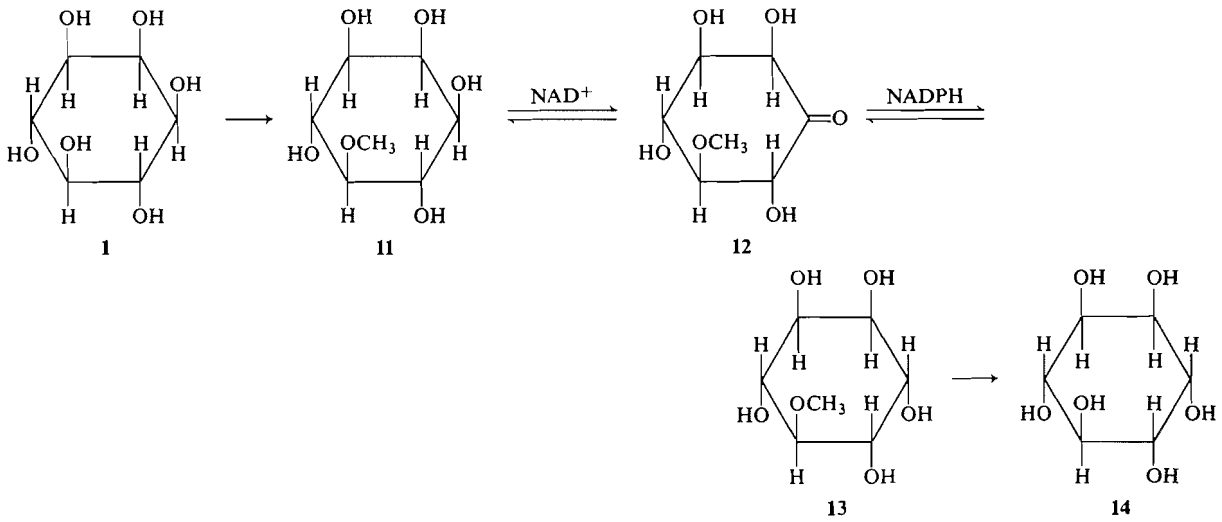


SCHEME 6. The pathway from *myo*-inositol to D-pinitol and D-*chiro*-inositol.

hindrance, the pro-*S* hydrogen could not react so easily. Following enol bond formation between C-5 and C-6, ring closure takes place as the resulting enol bond attacks C-1. As a consequence of this, the ammonium group of the enzyme is substituted by the carbanion, i.e. the electron pair of the enol bond, and consequently no hydrolysis is involved in the removal of the enzyme from the reactant.

The keto group in the product of the ring closure is finally reduced with NADH as hydrogen donor.

It has to be admitted that it will be difficult to find experimental ways to distinguish between the reaction mechanism suggested by Floss and co-workers and the one just reported. In any case, it must be stated here that the mechanism of action of the animal enzyme does not correspond to that of the aldolases, class I (cf. also Sherman *et al.* (25)).

The mechanism suggested here for the action of *myo*-inositol-1-phosphate synthase was elaborated for the mammalian enzyme only; it is probably not applicable to enzymes of the same specificity from higher plants, fungi, algae, or procaryotes. As mentioned before, some of these enzymes are metalloenzymes, which can be inhibited by EDTA. However, in a recent report (26) it is stated that the enzyme of pollen of *Lilium longiflorum* and possibly also that of *Neurospora crassa* are not metalloenzymes, although the latter enzyme is inhibited by EDTA. Anyhow, we have to agree with these authors (26) that, in the case of *myo*-inositol-1-phosphate synthase, a classification into two classes, analogous to that used for the aldolases, is not possible.

In our laboratory, three metalloenzymes with synthase activity, namely those from *Lemna gibba* (27), *Candida utilis* (unpublished), and *Streptomyces griseus* (11), have been studied. They all are strongly inhibited by EDTA and can be reactivated by either $Mn^{++}$ or $Mg^{++}$. It is to be noted that these metal-requiring *myo*-inositol-1-phosphate synthases exhibit a much stronger specific activity than the animal enzymes of the same specificity. Thus the enzyme from *Lemna gibba* is about 500 times more active than the enzyme from rat testes (27). This is the more surprising as usually plant enzymes are considerably less active than those from animal sources.

Investigations on the function of the metal in these enzymes have so far not led to a plausible picture of the reaction mechanism.

**Biosynthesis of the inositols other than *myo*-inositol**

Six of the nine inositol isomers occur in nature either as such or in the form of their methyl ethers. Most of them are found in higher plants. It was speculated that mechanisms similar to that of *myo*-inositol biosynthesis are responsible for their formation, in which case monosaccharides other than D-glucose would have to act as precursors for each of these inositols. For example, an intramolecular head-to-tail condensation of D-galactose would yield D-*chiro*-inositol (**14**).

It was soon found that such biosynthetic mechanisms for the inositols other than *myo*-inositol do not exist. With one minor exception, which may be without any biological significance, it could be established that all these compounds derive from *myo*-inositol via epimerization reactions. The one exception is also closely related to *myo*-inositol biosynthesis. It has been shown that *myo*-inositol-

Can. J. Chem. Downloaded from www.nrcresearchpress.com by 210.87.254.5 on 09/06/12
For personal use only.

Can. J. Chem. Downloaded from www.nrcresearchpress.com by 210.87.254.5 on 09/06/12
For personal use only.

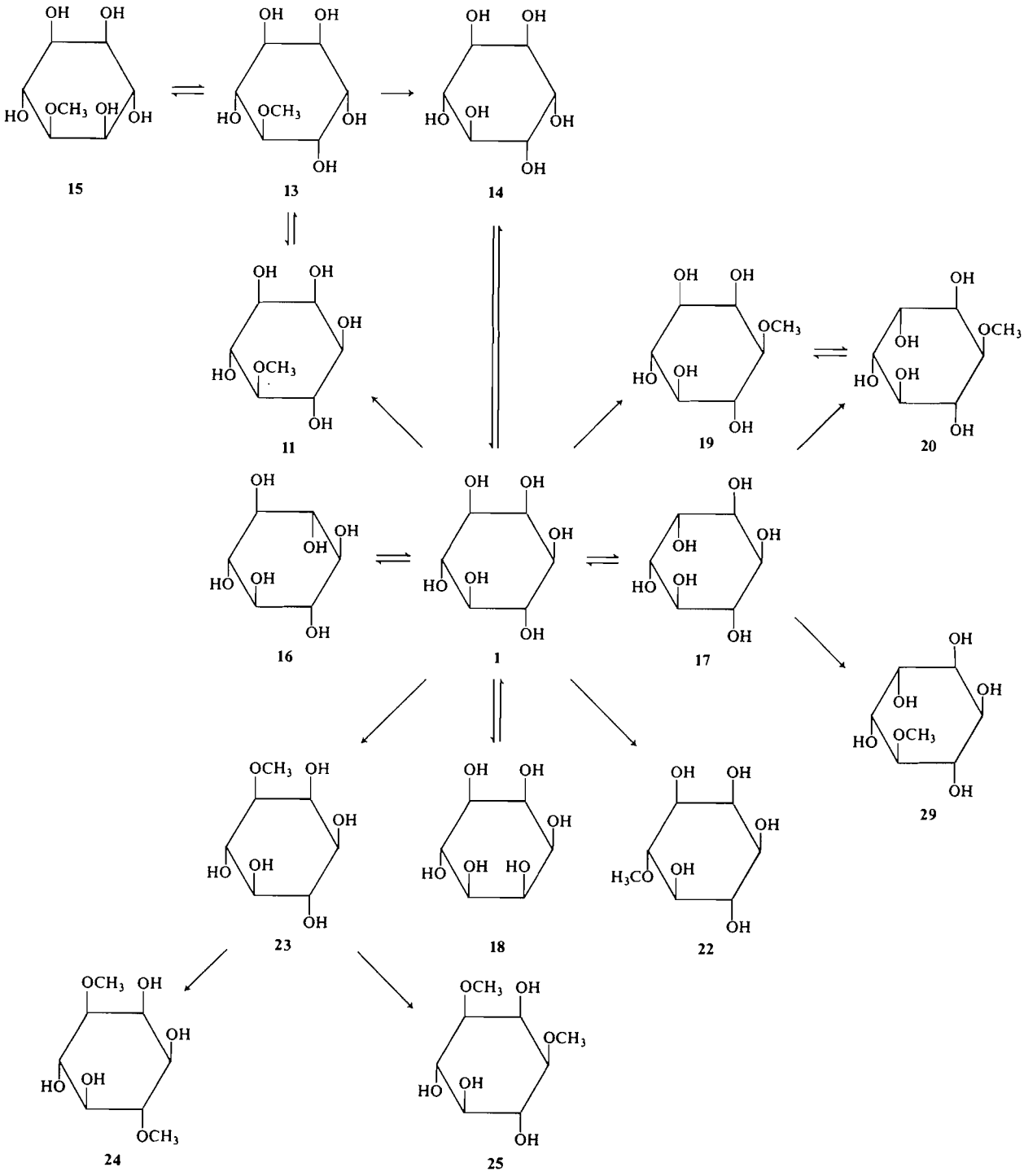


SCHEME 7. The central position of *myo*-inositol in the biosynthesis of its isomers and of the methyl ethers of the inositol series. **1**: *myo*-inositol, **11**: sequoyitol, **13**: D-pinitol, **14**: D-*chiro*-inositol, **15**: D-1-*O*-methyl-*muco*-inositol, **16**: *scyllo*-inositol, **17**: L-*chiro*-inositol, **18**: *neo*-inositol, **19**: L-bornesitol, **20**: L-quebrachitol, **21**: L-pinitol, **22**: ononitol, **23**: D-bornesitol, **24**: dambonitol, **25**: liriodenditol.

Can. J. Chem. Downloaded from www.nrcresearchpress.com by 210.87.254.5 on 09/06/12
For personal use only.

1-phosphate synthase acts on D-mannose 6-phosphate to yield *neo*-inositol 1-phosphate (**18**). This reaction, however, is several orders of magnitude slower than the reaction with D-glucose 6-phosphate (28). On the other hand, *neo*-inositol can also be the product of an enzymic epimerization of *myo*-inositol (29).

In some cases such epimerizations of *myo*-inositol do not take place directly but require a previous methylation of the substrate. Thus in many higher plants, e.g. the *Trifolium* species, D-*chiro*-inositol (**14**) is found in relatively small quantities. The plant also contains *myo*-inositol, sequoyitol (*myo*-inositol 5-methylether, **11**), and, in large quantities, D-pinitol (D-*chiro*-inositol 5-methylether, **13**). It could be shown that the reaction sequence leading to D-*chiro*-inositol (Scheme 6) starts with a methylation of *myo*-inositol to form sequoyitol, which in turn is epimerized to D-pinitol. Eventually, a small amount of D-pinitol is demethylated to D-*chiro*-inositol which, at least in higher plants, cannot be formed from *myo*-inositol by direct epimerization (30). Algae, however, can epimerize *myo*-inositol to D-*chiro*-inositol without intermediary formation of methyl ethers (31). The enzymes catalyzing the epimerization reaction in *Trifolium incarnatum* have been isolated and characterized (32); they are an NAD-specific sequoyitol dehydrogenase (EC 1.1.1.143) and an NADP-specific D-pinitol dehydrogenase (EC 1.1.1.142). The first enzyme oxidizes the equatorial hydroxyl group on C-3 of sequoyitol to a keto group, which then is reduced by the second enzyme to an axial hydroxyl group. It is interesting to note that these two enzymes show a different stereospecificity toward the nicotinamide part of their respective coenzymes.

Many epimerization reactions of this kind, acting on methylated and on nonmethylated inositols, are known, but not all of them have been thoroughly investigated with regard to their mechanism of action. It seems that two coenzymes are not always involved; animal systems of such epimerizations have been reported to act with $NAD^+$ or $NADP^+$ only (29, 33, 34).

Scheme 7 illustrates the central position of *myo*-inositol in the synthesis of the other inositols as well as the inositol methyl ethers, the formation of which is frequently required for the epimerization reaction to take place. The reactions shown in the scheme occur in different organisms, mostly in higher plants. Horizontal or perpendicular arrows represent epimerizations, whereas oblique arrows indicate methylations with *S*-adenosyl-L-methionine as methyl donor (cf. e.g. ref. 35). Thus whereas biogenetically all inositols seem to be closely interrelated, it should be noted that naturally occurring cyclitols, which do not belong to the inositol series, such as cyclohexanepentols (e.g. quercitol and viburnitol), the cyclohexenetetrols (conduritol, leucanthemitol), and the *C*-methylinositols (mytilitol, laminitol), are in general not synthesized via *myo*-inositol. The biosynthesis of these cyclitols seems to follow several independent pathways, some of them known to start also from monosaccharides (cf. ref. 36).

**Acknowledgements**

The authors are very grateful to Dr. I. D. Spenser (McMaster University, Hamilton) for the critical discussion of the results reported here and of the mechanism of action of the animal *myo*-inositol-1-phosphate synthase suggested. The experimental work of the authors reported here has been generously supported by the "Fonds zur Förderung der wissenschaftlichen Forschung in Österreich" (projects 2639, 3389, and 4067).

1. J. Scherer. Ann. Chem. **73**, 322 (1850).
2. L. Maquenne. Les sucres et principaux dérivés. Gauthier-Villars, Paris. 1900.
3. G. Dangschat and H. O. L. Fischer. Naturwissenschaften, **30**, 146 (1942).
4. T. Posternak. Helv. Chim. Acta, **25**, 746 (1942).
5. H. O. L. Fischer. Harvey Lectures, **40**, 156 (1944–1945).
6. F. A. Loewus and S. Kelly. Biochem. Biophys. Res. Commun. **7**, 204 (1962).
7. H. Kindl and O. Hoffmann-Ostenhof. Biochem. Z. **339**, 374 (1964).
8. I. W. Chen and R. Charalampous. J. Biol. Chem. **239**, 1905 (1964); **240**, 3507 (1965).
9. F. Eisenberg, Jr., A. H. Bolden, and F. A. Loewus. Biochem. Biophys. Res. Commun. **14**, 419 (1964).
10. V. Weisshäupl, O. Scheiner, P. Dworsky, and O. Hoffmann-Ostenhof. Z. Allgem. Mikrobiol. **16**, 81 (1976).
11. F. Pittner, I. I. Tovarova, E. Ya. Kornitskaya, A. S. Khokhlov, and O. Hoffmann-Ostenhof. Mol. Cell. Biochem. **25**, 43 (1979).
12. P. R. Srinivasan, J. Rothschild, and D. B. Sprinson. J. Biol. Chem. **238**, 3176 (1963).
13. M. Salas, E. Viñuela, and A. Sols. J. Biol. Chem. **240**, 561 (1965).
14. F. Eisenberg, Jr. J. Biol. Chem. **242**, 1375 (1967).
15. J. E. G. Barnett and D. L. Corina. Biochem. J. **108**, 125 (1968).
16. J. E. G. Barnett, A. Rasheed, and D. L. Corina. Biochem. J. **131**, 21 (1973).
17. C. H.-J. Chen and F. Eisenberg, Jr. J. Biol. Chem. **250**, 2963 (1975).
18. S. M. Buyn, R. Jenness, W. P. Ridley, and S. Kirkwood. Biochem. Biophys. Res. Commun. **54**, 961 (1973).
19. M. W. Loewus, F. A. Loewus, G. U. Brillinger, H. Otsuka, and H. G. Floss. J. Biol. Chem. **255**, 11710 (1980).
20. S. M. Buyn and R. Jenness. Biochemistry, **20**, 5174 (1981).

21. W. F. NACCARATO, R. E. RAY, and W. W. WELLS. Arch. Biochem. Biophys. **164**, 194 (1974).
22. F. PITTNER and O. HOFFMANN-OSTENHOF. Hoppe-Seylers Z. Physiol. Chem. **357**, 1667 (1976).
23. F. PITTNER and O. HOFFMANN-OSTENHOF. Hoppe-Seylers Z. Physiol. Chem. **359**, 1395 (1978).
24. W. R. SHERMAN, A. RASHEED, L. A. MAUCK, and J. WIECKO. J. Biol. Chem. **252**, 5672 (1977).
25. W. R. SHERMAN, P. P. HIPPS, L. A. MAUCK, and A. RASHEED. *In* Cyclitols and phosphoinositides. *Edited by* W. W. Wells and F. Eisenberg, Jr. Academic Press, New York. 1978. p. 279.
26. W. R. SHERMAN, M. W. LOEWUS, M. Z. PIÑA, and Y.-H. H. WONG. Biochim. Biophys. Acta, **660**, 299 (1981).
27. E. O. OGUNYEMI, F. PITTNER, and O. HOFFMANN-OSTENHOF. Hoppe-Seylers Z. Physiol. Chem. **252**, 613 (1978).
28. W. R. SHERMAN, M. A. STEWART, and K. D. GUNNELL. Biochemistry, **10**, 3491 (1971).
29. P. P. HIPPS, W. H. HOLLAND, and W. R. SHERMAN. Biochem. Biophys. Res. Commun. **77**, 340 (1977).
30. R. SCHOLDA, G. BILEK, and O. HOFFMANN-OSTENHOF. Monatsh. Chem. **95**, 611 (1964).
31. G. WÖBER, H. RUIS, and O. HOFFMANN-OSTENHOF. Monatsh. Chem. **102**, 459 (1971).
32. H. RUIS and O. HOFFMANN-OSTENHOF. Eur. J. Biochem. **7**, 442 (1969).
33. P. P. HIPPS, R. K. SEHGAL, W. H. HOLLAND, and W. R. SHERMAN. Biochemistry, **12**, 4705 (1973).
34. P. P. HIPPS, M. R. EVELAND, M. H. LAIRD, and W. R. SHERMAN. Biochem. Biophys. Res. Commun. **68**, 1133 (1976).
35. F. KOLLER and O. HOFFMANN-OSTENHOF. Hoppe-Seylers Z. Physiol. Chem. **357**, 1465 (1976).
36. W. WOLOSZCZUK and O. HOFFMANN-OSTENHOF. Hoppe-Seylers Z. Physiol. Chem. **355**, 633 (1974).

Can. J. Chem. Downloaded from www.nrcresearchpress.com by 210.87.254.5 on 09/06/12
For personal use only.

# Apparent molal heat capacities and volumes of aqueous hydrogen sulfide and sodium hydrogen sulfide near 25°C: the temperature dependence of $H_2S$ ionization

JOSÉ A. BARBERO[1]

*Department Quimica de Reactores, Comision Nacional de Energia Atomica, Avda del Libertador 8250, 1429 Buenos Aires, Argentina*

KEITH G. MCCURDY[1]

*Department of Chemistry, University of Lethbridge, Lethbridge, Alta., Canada T1K 3M4*

AND

PETER R. TREMAINE

*Oil Sands Research Department, Alberta Research Council, 11315-87 Avenue, Edmonton, Alta., Canada T6G 2C2*

Received December 23, 1981

JOSÉ A. BARBERO, KEITH G. MCCURDY, and PETER R. TREMAINE. Can. J. Chem. **60**, 1872 (1982).

A flow microcalorimeter and vibrating tube densimeter were used to obtain apparent molal heat capacities and volumes of aqueous NaHS and $Na_2S$ from 0.1 to 1.0 mol $kg^{-1}$ and of aqueous $H_2S$ from 0.03 to 0.08 mol $kg^{-1}$ at 10, 25, and 40°C. Standard state heat capacities and volumes for $H_2S$ and $HS^-$ were obtained by extrapolation to infinite dilution. Combining these results with 25°C enthalpy data yields an expression for the temperature dependence of the equilibrium constant for $H_2S$ neutralization at pressures near those of steam saturation, $H_2S + OH^- = HS^- + H_2O$, $\log K_1^b = 19.84 + 930.8/T - 2.800 \ln T$, with an estimated uncertainty of ±0.47 at 300°C. The heat capacity data for bulk aqueous $Na_2S$ suggest that the relative concentration of $S^{2-}$ at these molalities is small.

JOSÉ A. BARBERO, KEITH G. MCCURDY et PETER R. TREMAINE. Can. J. Chem. **60**, 1872 (1982).

On a utilisé un microcalorimètre à écoulement et un densimètre à tube vibrant pour obtenir les capacités calorifiques et les volumes molales apparents du NaHS et du $Na_2S$ aqueux à des concentrations allant de 0,1 à 1,0 mol $kg^{-1}$ et du $H_2S$ aqueux à des concentrations de 0,03 à 0.08 mol $kg^{-1}$ à −10, 25 et 40°C. On a obtenu les capacités calorifiques et les volumes de l'état standard du $H_2S$ et du $HS^-$ en extrapolant à dilution infinie. La combinaison de ces résultats avec les données d'enthalpie à 25°C donne une expression pour l'effet de la température sur la constante d'équilibre de la neutralisation du $H_2S$ à des pressions voisines de celles de la vapeur saturée, $H_2S + OH^- = HS^- + H_2O$, $\log K_1^b = 19{,}84 + 930{,}8/T^- 2{,}800 \ln T$ avec une incertitude évaluée à ±0.47 à 300°C. Les données de capacité calorifique pour la masse aqueuse de $Na_2S$ suggèrent que la concentration relative de $S^{2-}$ est petite à ces molalités.

[Traduit par le journal]

## Introduction

Accurate values for the temperature dependence of the first ionization constant of aqueous $H_2S$, $K_1$, are required to model steam-based methods for the in-situ extraction of bitumen and heavy oil, mass transport in Girdler-Sulfide heavy water plants, and hydrometallurgical procedures for treating sulfide ores. Low temperature measurements have been made by many workers using a variety of techniques (1) and the values for $K_1$ near 25°C are well established. Experiments above 100°C are difficult, largely because aqueous sulfide poisons the platinum electrodes commonly used to determine ionization constants in high temperature water. Ellis and co-workers (2) obtained data for $K_1$, up to 276°C using a spectrophotometric method, but noted that the results might be in error since their technique did not permit *in situ* pH measurements. Values to 150°C, reported by Tsonopoulos *et al.* (3), were also obtained by a spectrophotometric method and deviate from Ellis' results above 75°C. No other values for $K_1$ above 100°C have been reported.

The enthalpy of the ionization reaction at 25°C is known (4, 5) and has been used in the van't Hoff equation to extrapolate $K_1$ to high temperatures (1). The standard volume and heat capacity of ionization are required in such an extrapolation to account for the effects of pressure and, more important, changes in the enthalpy of reaction with temperature, respectively. As yet, no accurate values for these properties have been reported. We have now measured apparent molal heat capacities and volumes for aqueous NaHS and $H_2S$ at temperatures of 10°C, 25°C, and 40°C. The results yield both infinite dilution and excess partial molal heat capacities and volumes for these important species which can then be combined with existing low temperature enthalpy data to extrapolate $K_1$ to

[1]Visiting scientist at the Oil Sands Research Department, Alberta Research Council, 1981–1982.

0008-4042/82/141872-09$01.00/0

©1982 National Research Council of Canada/Conseil national de recherches du Canada

Can. J. Chem. Downloaded from www.nrcresearchpress.com by 210.87.254.6 on 09/06/12
For personal use only.

Can. J. Chem. Downloaded from www.nrcresearchpress.com by 210.87.254.6 on 09/06/12
For personal use only.

elevated pressures and temperatures. The results from such an extrapolation are also presented here, along with a detailed evaluation of uncertainties.

The many attempts to measure the equilibrium constant and other thermodynamic properties of the second ionization step have produced ambiguous results (1), possibly because of oxidation products or other impurities (6). Heat capacity measurements on $Na_2S$ solutions are included in our study and the experimental difficulties discussed.

## Experimental

The heat capacity and density of each solution were measured relative to water using a commerical Picker flow microcalorimeter and vibrating tube densimeter, both of which have been described previously (7, 8). Density determinations were made at the mean temperature of the calorimetric measurements. Kell's values (9) for the specific heat capacity and density of pure water were used in the calculation:

$$C_{p1}{}^0/\text{J g}^{-1}\text{ K}^{-1} = 4.1919,\ 4.1793,\text{ and } 4.1783,$$

$$d_1{}^0/\text{g cm}^{-3} = 0.999700,\ 0.997045,\text{ and } 0.992215$$

at 10°C, 25°C, and 40°C, respectively. The procedure of Desnoyers *et al.* (10) was used to correct for a small systematic difference in NaCl heat capacities obtained from our calorimeter and the values in ref. 10. Following this method, the average apparent molal heat capacity from calorimeter cells 1 and 2, $C_{p\phi}$, was multiplied by the mean heat leak correction factor $f = 1.009 \pm 0.003$, which we obtained from the calibration.

Water for these experiments was singly distilled, passed through a Milli-Q reagent grade mixed bed ion exchange and activated carbon system, then vigorously purged with He gas immediately before use. The conductivity of the final product was less than 1 $\mu$S cm$^{-1}$. Orion 0.1000 *M* $Pb(ClO_4)_2$ solutions, standardized by the manufacturer against standards traceable to NBS, were used for the sulfide determinations. Fisher "Full Range" glass electrodes standardized with commercial pH 7 and pH 10 buffers were used to measure pH.

Commercial purity $H_2S$ (Fisher) was bubbled through a saturated $Ba(OH)_2$ solution in a sealed glass system, which had been thoroughly purged with helium, then on into a sealed flask containing water or a 1 *m* NaOH solution to prepare stock solutions of $H_2S$ and NaHS, respectively. In the latter case, a sealed pH electrode allowed us to stop the gas flow when the pH fell to a value between 10 and 8, indicating that the composition was stoichiometric to within 0.01% in molality. Solutions of NaHS were also prepared from well defined crystals, synthesized in ethanol by reacting $H_2S$ with sodium ethoxide using the method of Stephens and Cobble (11). The crystals were then washed thoroughly in diethyl ether under a nitrogen atmosphere and stored in a vacuum desiccator (0.01 Pa). Well-formed crystals of analytical reagent grade $Na_2S$ (Mallinckrodt) were recrystallized twice from filtered hot aqueous solutions immediately before use. To minimize oxidation, the solutions were prepared by quickly removing large well-formed crystals from the recrystallization flask, washing in deoxygenated water, then dissolving them in a second flask of water, all in a nitrogen glove bag. The final clear colourless solutions had a pH of about 13.5 and the approximate concentration of $Na_2S$ in each was easily obtained by measuring the density. The NaHS solutions, which are less alkaline and hence less susceptible to oxidation, were prepared by weight using a $N_2$ glove bag for all transfers. During the calorimetric runs, the solutions of NaHS and $Na_2S$ were contained in closed 50 mL polythene bottles, which had been filled under nitrogen, and were siphoned into the calorimeter or densimeter via a short length of 0.8 mm i.d. Teflon tubing which passed through a small hole in the bottle cap. Immediately after each set of measurements, aliquots from each bottle were quickly pipetted into a flask containing the sulfide antioxidant buffer SAOB II (12) so that the sulfide concentration could be determined by titration with standardized $Pb(ClO_4)_2$ solution using an Orion model 94-16 sulfide ion electrode to detect the end point.

The $H_2S$ solutions, prepared by bubbling in a closed system at 1 atm, were handled and standardized in the same way except that the solutions were contained in closed Pyrex flasks to avoid $H_2S$ evaporation. Both the $H_2S$ solutions and the water reference solution were connected to the same cylinder of ultra high purity nitrogen so that manipulating a three-way stopcock allowed either to be pressurized. A second three-way stopcock allowed the $H_2S$ solution or the water to be forced into the calorimeter or densimeter by the overpressure of nitrogen. A needle valve downstream of the instruments controlled the flow rate. Before and after each run, the solutions were standardized by diverting the tubing so that the solution flowed directly under the surface of a weighed aliquot of SAOB II. The amount of solution which passed into the SAOB II was measured by noting the weight gain and the amount of sulfide determined by titration, as above.

Several preparations of the $H_2S$, NaHS, and $Na_2S$ solutions were made by each of the methods described above, to ensure that small changes in technique did not affect the heat capacity and density values.

## Results: Apparent molal heat capacities and volumes

Apparent molal heat capacities, $C_{p\phi}$, and volumes, $V_\phi$, are defined by the expression

$$[1] \qquad Y_\phi = (Y - n_1 Y_1{}^0)/n_2$$

where $Y$ is the extensive property of the aqueous solution, $n_1$ and $n_2$ are the number of moles of water and solute respectively (if $n_1 = 55.509$, $n_2 =$ molality, $m$), and $Y_1{}^0$ is the property of 1 mol of pure solvent.

Following Roux *et al.* (13), we used the least-squares method to fit expressions of the form

$$[2] \qquad Y_\phi = Y_\phi{}^\infty + A_Y(d_1{}^0 m)^{1/2} + B_Y m$$

to our $C_{p\phi}$ and $V_\phi$ data for aqueous NaHS. Here, $Y_\phi{}^\infty$ is the value of $Y_\phi$ at infinite dilution, $A_Y(d_1{}^0)^{1/2}$ is the Debye–Hückel limiting slope at the temperature in question on the molality scale and $B_Y$ is an adjustable parameter. We note that no significant concentrations of either $H_2S$ or $S^{2-}$ exist (1) in the pH range of 8 to 11, which was observed for all our NaHS solutions. The experimental data at 25°C from aqueous NaHS prepared both from synthesized crystals and by bubbling $H_2S$ through NaOH are plotted in Figs. 1 and 2. At 25°C, the results from solutions made using the synthesized NaHS

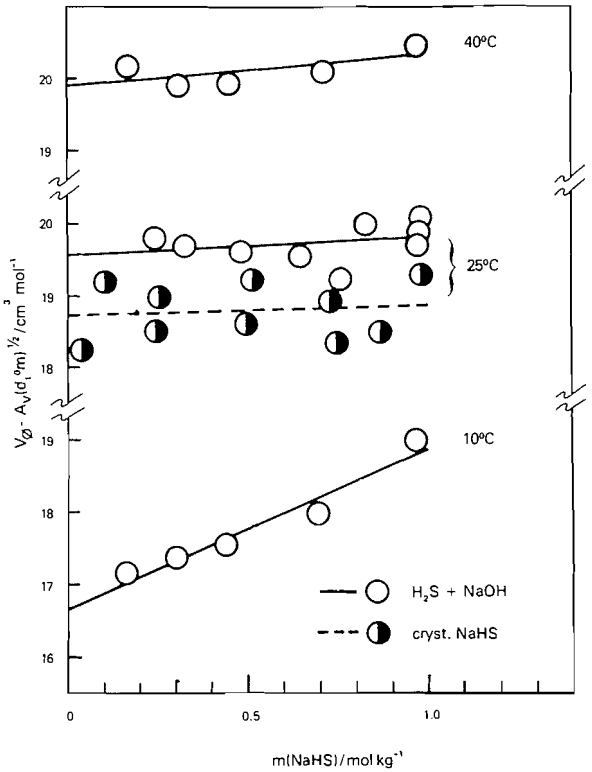


FIG. 1. Apparent molal volumes of aqueous NaHS from two preparation routes after subtracting the Debye–Hückel limiting slope. The lines are least squares fits.

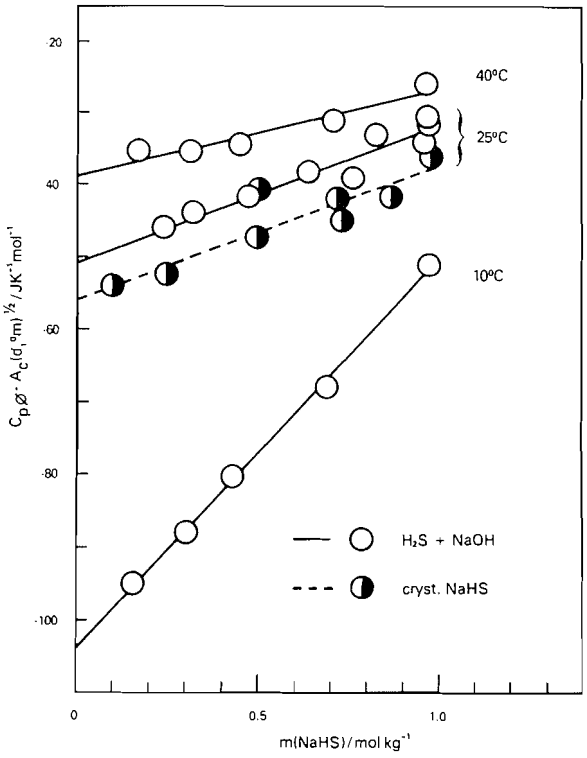


FIG. 2. Apparent molal heat capacities of aqueous NaHS from two preparation routes after subtracting the Debye–Hückel limiting slope. The lines are least squares fits.

crystals were more negative than those prepared from $H_2S$ and aqueous NaOH, by about 5 J $K^{-1}$ $mol^{-1}$ in $C_{p\phi}$ and smaller by about 1 $cm^3$ $mol^{-1}$ in $V_\phi$. Synthesized crystals which had been stored under a pumping vacuum for several days and washed commercial crystals produced solutions which yielded even more negative values. Thus, while the very similar values which were obtained from the two preparation routes confirm that no major impurities are present, we believe that the solutions prepared by bubbling $H_2S$ through aqueous NaOH yield superior results. The crystalline NaHS is probably slightly contaminated with sulfate or thiosulfate, which are known to have very negative aqueous heat capacities and volumes (14) or possibly by polysulfides.

Values of $C_{p\phi}^\infty$, $B_C$, $V_\phi^\infty$, and $B_V$ from NaHS solutions prepared from aqueous NaOH are listed in Table 1, along with the Debye–Hückel terms from Perron *et al.* (15), which were used in the fit.[2] Allred and Woolley's values for NaOH (16) are included for use in the ionization constant calculations presented below, as are Kell's data for water (9). The $V_\phi^\infty$ and $B_V$ values for NaHS are very similar to those for NaCl reported by Allred and Woolley, as might be expected since $Cl^-$ and $HS^-$ are isoelectronic ions. The $C_{p\phi}^\infty$ results are more positive than those for NaCl (16) by 24, 33, and 26 J $K^{-1}$ $mol^{-1}$ at 10, 25, and 40°C respectively. The substantial increase in $B_C$ with decreasing temperature is much like that reported for NaCl and NaOH (16).

The apparent molal properties of $H_2S$, also listed in Table 1, were obtained at the very low molalities, 0.03 to 0.08 mol $kg^{-1}$, which can be achieved by small overpressures of the gas. Solute–solute interactions are negligible at these concentrations, where $H_2S$ is known to obey Henry's law (17). Our measured values were therefore assumed to be equal to those at infinite dilution, $C_{p\phi}^\infty$ and $V_\phi^\infty$. Median values are reported in the table, along with the standard deviations of the median. Data obtained at 25°C were significantly more precise than those at 10°C and 40°C, because of temperature control problems and the nucleation of $H_2S$ bubbles in the instruments, respectively. The large

[2]Complete set of experimental data is available, at a nominal charge, from the Depository of Unpublished Data, CISTI, National Research Council of Canada, Ottawa, Ont., Canada K1A 0S2.

Can. J. Chem. Downloaded from www.nrcresearchpress.com by 210.87.254.6 on 09/06/12
For personal use only.

TABLE 1. Standard state heat capacities, volumes, and ionic strength parameters*

| Solute | $C_{p\phi}^{\infty}$ (J K$^{-1}$ mol$^{-1}$) | $B_C$ (J K$^{-1}$ mol$^{-2}$ kg) | $V_{\phi}^{\infty}$ (cm$^3$ mol$^{-1}$) | $B_V$ (cm$^3$ mol$^{-2}$ kg) | Molality range | $N$* |
|---|---|---|---|---|---|---|
| | | | $T$ = 10°C | | | |
| $H_2S$ | 187.4±10.3 | 0 | 34.04±2.33 | 0 | 0.034–0.073 | 3 |
| NaHS | −104.5±0.9 | 54.3±1.5 | 16.66±0.19 | 2.19±0.32 | 0.16 –0.97 | 5 |
| NaOH† | −167.4±0.8 | 82.4±4.1 | −7.54±0.03 | 2.24±0.16 | | |
| $H_2O$‡ | 75.517 | 0 | 18.020 | | | |
| | | | $T$ = 25°C | | | |
| $H_2S$ | 178.5±1.9 | 0 | 34.92±0.11 | 0 | 0.048–0.082 | 4 |
| NaHS | −50.9±0.7 | 19.0±0.8 | 19.54±0.3 | 0.26±0.33 | 0.24 –0.98 | 9 |
| NaOH† | −100.5±0.5 | 41.2±2.2 | −5.37±0.02 | 1.35±0.11 | | |
| $H_2O$‡ | 75.290 | 0 | 18.068 | 0 | | |
| | | | $T$ = 40°C | | | |
| $H_2S$ | 167.1±3.6 | 0 | 35.60±0.13 | 0 | 0.055–0.078 | 4 |
| NaHS | −38.9±1.2 | 12.07±2.0 | 19.89±0.17 | 0.47±0.29 | 0.17 –0.97 | 5 |
| NaOH† | −67.3±0.7 | 15.7 ±3.3 | −4.30±0.03 | 0.79±0.13 | | |
| $H_2O$‡ | 75.272 | | 18.156 | | | |

*$C_p^0 = C_{p\phi}^{\infty}$, $V^0 = V_{\phi}^{\infty}$ in eq. [2]. Debye–Hückel limiting slopes are $A_C(d_1^0)^{1/2}$ = 24.299, 28.945, and 33.805 J kg$^{1/2}$ K$^{-1}$ mol$^{-3/2}$ and $A_V(d_1^0)^{1/2}$ = 1.612, 1.865, and 2.131 cm$^3$ kg$^{1/2}$ mol$^{-3/2}$ at 10°C, 25°C, and 40°C, respectively (15). Error limits are the standard deviations of the median for $H_2S$ and of the coefficients for NaHS. $N$ is the number of experimental data points.
†From Allred and Woolley (16).
‡From Kell (9).

positive values of $C_{p\phi}$ are typical of neutral solutes in water.

Experimental values for the apparent molal properties of bulk aqueous $Na_2S$ are listed in Table 2. A functional representation, such as eq. [2], cannot be fitted easily to the data because both $HS^-$ and $S^{2-}$ may be present and their relative concentration is very uncertain (1). Since alkaline sulfide solutions are very easily contaminated (6), we tested two aliquots of solution for impurities by acidifying them to pH 9 with aqueous HCl to form mixed solutions (≈ 0.5 $m$ in both $Na_2S$ and HCl), then measuring the heat capacity of each. At this pH, hydrolysis of $S^{2-}$ to $HS^-$ is complete (1) so that the solutions contained only aqueous NaHS and NaCl. By analogy with Young's rule for enthalpies (18), $C_{p\phi}$ for this mixture can be calculated from the values for the pure components using the expression

$$[3]\quad C_{p\phi}(\text{NaHS} + \text{NaCl}) = \frac{1}{m(\text{NaCl}) + m(\text{NaHS})} \times [m(\text{NaHS})C_{p\phi}(\text{NaHS}) + m(\text{NaCl})\,C_{p\phi}(\text{NaCl})]$$

Here, each $C_{p\phi}$ is calculated from eq. [1] using $n_2 = n(\text{NaHS}) + n(\text{NaCl})$ and $\Delta C_{p\phi}$ of mixing at constant ionic strength is assumed to be zero. Our experimental values were more negative than those calculated using data from Table 1 and ref. 16 in eq. [3], by 11 and 21 J K$^{-1}$ mol$^{-1}$. As a result, the apparent molal heat capacities in Table 2 have been adjusted by 16 J K$^{-1}$ mol, on the assumption that the discrepancy was caused by impurities, present in concentrations proportional to the original $Na_2S$ molality. The uncertainty in this correction is estimated to be ±12 J K$^{-1}$ mol$^{-1}$. Bubbling air through the $Na_2S$ solutions for an hour did not affect the heat capacities so the effect was apparently not due to air oxidation.

TABLE 2. Experimental apparent molal properties for bulk aqueous $Na_2S$ at 25°C

| $m(Na_2S)$ | $C_{p\phi}$/J K$^{-1}$ mol$^{-1}$ | $V_{\phi}$/cm$^3$ mol$^{-1}$ |
|---|---|---|
| 0.157 | −183 | −5.1 |
| 0.222 | −165 | −3.7 |
| 0.280 | −151 | −2.9 |
| 0.305 | −152 | −3.2 |
| 0.372 | −140 | −3.1 |
| 0.439 | −138 | −4.6 |
| 0.799 | − 76 | −0.3 |
| 1.172 | − 40 | 0.5 |

## Discussion

*$H_2S$ vaporization below 50°C*

By definition, $C_{p\phi}^{\infty}$ is equal to $C_p^0$, the heat capacity of a solute in its hypothetical one molal standard state. McBride and Gordon (19) have calculated detailed ideal gas thermodynamic functions for $H_2S$, which are now accepted by several critical tabulations (20–24). Combining their results for $C_p^0(H_2S,g)$ with our $C_{p\phi}^{\infty}(H_2S)$ data yields the values for the heat capacity of vaporization, $\Delta C_{pR}^0$(vap), which are tabulated in Table 3. Values for $\Delta C_{pR}^0$(vap) can also be obtained by twice differentiating very accurate vapour pressure data with respect to temperature. Clark and Glew (17) have summarized the many

Can. J. Chem. Downloaded from www.nrcresearchpress.com by 210.87.254.6 on 09/06/12
For personal use only.

TABLE 3. The heat capacity change of vaporization for $H_2S(aq) = H_2S(g)$

| | | $\Delta C_{pR}^0$/J K$^{-1}$ mol$^{-1}$ | |
|---|---|---|---|
| $t$/°C | $C_p^0$(gas)* | This work | Clark and Glew |
| 10 | 34.07 | −153.3±10.3 | −154.2±5.0 |
| 25 | 34.24 | −144.3±1.9 | −146.2±1.4 |
| 40 | 34.40 | −132.7±3.6 | −138.2±5.0 |

*From McBride and Gordon (19).

$H_2S$ pressure measurements in the literature. Heat capacity data from their own very precise measurements are also tabulated in Table 3. The values from the calorimetric and vapour pressure measurements differ by no more than 5 J K$^{-1}$ mol$^{-1}$, well within the combined experimental uncertainty.

*$H_2S$ ionization versus temperature*

The thermodynamic expressions describing the temperature and pressure dependence of acid base ionization have been reviewed by Hepler and Hopkins (25). The key relationships are:

$$[4a] \quad (\partial \ln K/\partial T)_p = \Delta H_R^0/RT^2$$

$$[4b] \quad (\partial \Delta H_R^0/\partial T)_p = \Delta C_{pR}^0$$

$$[4c] \quad (\partial \ln K/\partial P)_T = -\Delta V_R^0/RT$$

where $T$ is the absolute temperature. Because $\Delta C_{pR}^0$ is related to the *second* derivative of $\ln K$ with respect to temperature and because compressibility effects are generally small, even a poor estimate of the temperature dependence of $\Delta C_{pR}^0$ and $\Delta V_R^0$ can yield quite accurate values of $K$ to rather high temperatures along the steam saturation curve of water providing that $\ln K$ and $\Delta H_R^0$ are known accurately at 25°C.

Rao and Hepler (1), and most other compilers (21–23) accept the value $\log K_1 = -6.99 \pm 0.10$ at 25°C for the acid dissociation reaction,

$$[5] \quad H_2S(aq) = H^+ + HS^-$$

This is slightly more positive than recent measurements by Tsonopoulos *et al.* (3) and by Ellis' group (2) but their values lie within the error limits, as do most of the many other measurements (1). Combining $\log K_1$ with $\log K_w$ (26) yields the value $\log K_1^b = 7.01 \pm 0.10$ for the neutralization reaction

$$[6] \quad H_2S + OH^- = H_2O + HS^-$$

Kury, Zielen, and Latimer (4) measured the value $\Delta H_R^0 = -33.7 \pm 0.3$ kJ mol$^{-1}$ for reaction [6] at 25°C by titration of $H_2S$ with a large excess of NaOH. Their result is based on Konopik and Leberl's value (27) for the second acid dissociation constant of $H_2S$, $\log K_2 = -12.7$. Recalculating their results in the region of the first end-point using Ellis and Giggenbach's much more negative value, $\log K_2 = -17$ (2), only slightly changes the result, $\Delta H_R^0 = -33.8$ kJ mol$^{-1}$. Using the same method, Zeumer and Roth obtained $\Delta H_R^0 = -34.2 \pm 0.2$ kJ mol$^{-1}$ at 20°C. The $\Delta C_{pR}^0$ values presented below can be used to correct this to 25°C with the result $\Delta H_R^0 = -33.9 \pm 0.2$ kJ mol$^{-1}$. We choose the median, $-33.8 \pm 0.3$ kJ mol$^{-1}$, as being consistent with both sets of results. We note that similar enthalpy of neutralization experiments with LiOH (28) yield a slightly more positive result, possibly because of the difficulty in purifying LiOH. Values of $\Delta C_{pR}^0$ and $\Delta V_R^0$ and their excess property terms can be calculated directly from the data in Table 1 since, by definition, $Y^0 = Y_\phi^\infty$. These are tabulated in Table 4, along with the other thermodynamic constants for $H_2S$ neutralization presented above.

Heat capacities and volumes of simple electrolytes are known (29–31) to increase with temperature to a maximum near 100°C, then to decrease as the temperature is raised further. Above 200°C, this decrease becomes dramatic, largely because of changes in the electrostatic properties of water along the steam saturation line (32, 33). The simple electrostatic effects tend to cancel when reactions are written symmetrically, so that the charge on each reactant species is equal to that on one of the product species, as in reaction [6]. Hence, for symmetric, or "isocoulombic" (31), reactions, $\Delta C_{pR}^0$ and $\Delta V_R^0$ might be expected to pass through only a shallow maximum or minimum depending on the relative magnitude of the electrostatic effect for each ion. This behavior has been observed for several systems (29, 31), and is well illustrated by the very accurate data recently reported for the neutralization of phosphoric acid and carbonic acid (34) at elevated temperatures. Below 250°C, values for $\Delta C_{pR}^0(T)$ for both systems vary by less than 50 J K$^{-1}$ mol$^{-1}$ from $\Delta C_{pR}^0$(25°C). Since the low temperature heat capacities in Table 4 decrease with temperature, $\Delta C_{pR}^0$ for reaction [6] probably passes through a minimum, shown schematically by curve $A$ in Fig. 3.

For the reasons outlined above, we believe the most appropriate extrapolation procedure for symmetric reactions is to assume that $\Delta C_{pR}^0$ and $\Delta V_R^0$ do not change substantially from their values at 25°C (curve $B$ in Fig. 3), and to assign error limits based on plausible estimates of the maximum and minimum values for $d\Delta C_{pR}^0/dT$ and $d\Delta V_R^0/dT$ which might be expected, averaged over the whole temperature range.

Can. J. Chem. Downloaded from www.nrcresearchpress.com by 210.87.254.6 on 09/06/12
For personal use only.

TABLE 4. Thermodynamic constants for $H_2S$ neutralization: $H_2S + OH^- = HS^- + H_2O$

| Parameter | Value | | |
|---|---|---|---|
| | 10°C | 25°C | 40°C |
| $\log K_1{}^b$ | — | 7.01±0.10* | — |
| $\Delta H_R{}^0$/J mol$^{-1}$ | — | −33800±300† | — |
| $\Delta C_{pR}{}^0$/J K$^{-1}$ mol$^{-1}$ | −49.0±12.0 | −53.6±3.1 | −63.4±5.5 |
| $\Delta V_R{}^0$/cm$^3$ mol$^{-1}$ | 8.18±2.6 | 8.06±0.4 | 6.75±0.3 |
| $\Delta B_C$/J K$^{-1}$ mol$^{-2}$ kg | −28.1±5.6 | −22.2±3.0 | −3.6±5.3 |
| $\Delta B_V$/cm$^3$ mol$^{-2}$ kg | −0.05±0.5 | −1.09±0.4 | −0.32±0.4 |

*Reference 1.
†Recalculated data from refs. 4 and 5.

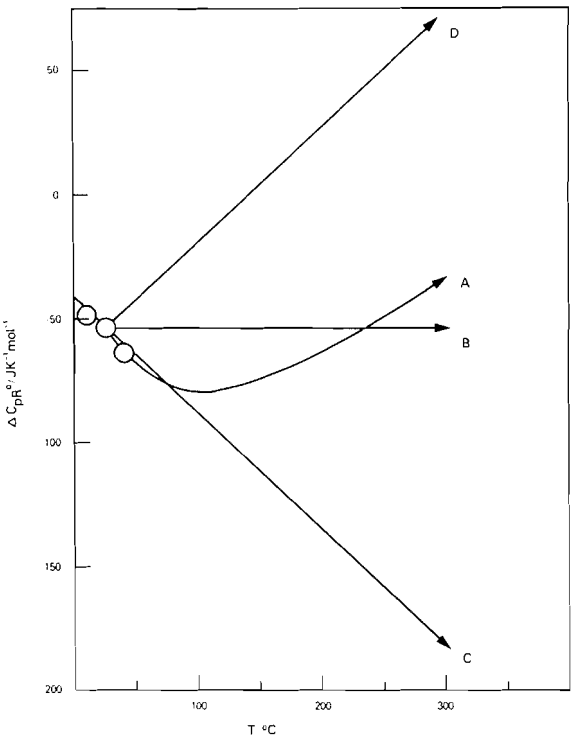


FIG. 3. A schematic drawing of the temperature dependence of $\Delta C_{pR}{}^0$ for reaction [6]: *A* is a plausible locus showing a shallow minimum; *B* is the locus if $\Delta C_{pR}{}^0$ is assumed constant; *C* and *D* are the values used to calculate the error limits in Table 5. Experimental data are shown.

Integrating eqs. [4*a*] and [4*b*] at constant pressure yields the result

$$[7]\quad \ln K_1{}^b(T) \approx \ln K_1{}^b(25°C) - [\Delta H_R{}^0(25°C)/R - 298.15\Delta C_{pR}{}^0(25°C)/R]\left[\frac{1}{T} - \frac{1}{298.15}\right] + \Delta C_{pR}{}^0(25°C)/R]\ln(T/298.15)$$

if $\Delta C_{pR}{}^0$ is temperature independent. Substituting the thermodynamic constants from Table 4 reduces this to the following equation,

$$[8]\quad \log K_1{}^b(T) = 19.840 + 930.8/T - 2.800\ln T$$

which was used to calculate the equilibrium constants tabulated in Table 5. The rather conservative error limits include the uncertainties in $\ln K_1{}^b$(25°C) and $\Delta H_R{}^0$(25°C), and also our estimate of the systematic error due to the unknown variation in $\Delta C_{pR}{}^0$ with temperature. This systematic error was calculated using a more general form of eq. [7] (35) in which $\Delta C_{pR}{}^0(T)$ varies with temperature, and by assuming that the value, $d\Delta C_{pR}{}^0/dT = 0.46$ J K$^{-2}$ mol$^{-1}$, observed between 10°C and 40°C, is the maximum positive or negative deviation from $\Delta C_{pR}{}^0$(25°C) which might be expected over the entire temperature range of 0 to 300°C (curves *C* and *D* in Fig. 3). Even if $\Delta V_R{}^0$ differs from the 25°C value by as much as ±50 cm$^3$ mol$^{-1}$, the effect of the vapour pressure of water (36) on $\log K_1{}^b$ is less than 0.05 at 300°C and so is negligible by comparison with the uncertainty in the extrapolation.

Results for the acid dissociation constant, $K_1$, were calculated from $K_1{}^b$ using Olofsson and Hepler's values for the dissociation constant of water (26). These are included in Table 5 and are also plotted in Fig. 4 for comparison with the

TABLE 5. Equilibrium constants for $H_2S$ neutralization and dissociation from eq. [8]

| *t*/°C | $\log K_1{}^b$ | $\log K_W$* | $\log K_1$ |
|---|---|---|---|
| 0 | 7.54±0.10 | −14.948 | −7.41±0.10 |
| 25 | 7.01±0.10 | −13.999 | −6.99±0.10 |
| 50 | 6.54±0.10 | −13.276 | −6.74±0.10 |
| 75 | 6.13±0.11 | −12.711 | −6.58±0.11 |
| 100 | 5.75±0.12 | −12.266 | −6.52±0.12 |
| 125 | 5.42±0.14 | −11.916 | −6.50±0.14 |
| 150 | 5.11±0.16 | −11.644 | −6.53±0.16 |
| 175 | 4.82±0.20 | −11.441 | −6.62±0.20 |
| 200 | 4.56±0.24 | −11.302 | −6.74±0.24 |
| 225 | 4.32±0.29 | −11.222 | −6.90±0.29 |
| 250 | 4.09±0.33 | −11.196 | −7.11±0.33 |
| 275 | 3.88±0.40 | −11.224 | −7.34±0.40 |
| 300 | 3.68±0.47 | −11.301 | −7.62±0.47 |

*From Olofsson and Hepler (26).

Can. J. Chem. Downloaded from www.nrcresearchpress.com by 210.87.254.6 on 09/06/12
For personal use only.

Can. J. Chem. Downloaded from www.nrcresearchpress.com by 210.87.254.6 on 09/06/12
For personal use only.

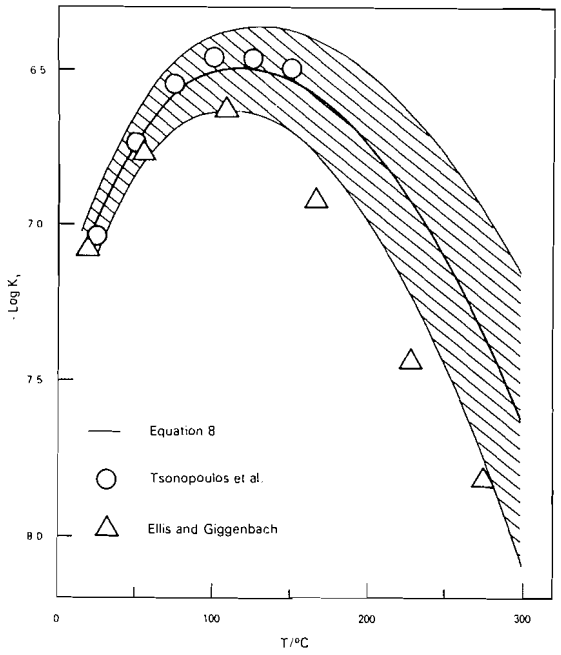


FIG. 4. The temperature dependence of the first ionization constant of $H_2S$, $H_2S \rightleftharpoons HS^- + H^+$. The shaded area represents the combined uncertainty from Table 5.

experimental data from refs. 2 and 3. Both sets of experimental values of $K_1$ (2, 3) may contain systematic errors, since neither apparatus provided a mechanism for measuring the equilibrium pH. Our results for log $K_1$ below 150°C deviate from those of Tsonopoulos *et al.* by no more than 0.05 at any temperature and therefore do not support the more negative values reported by Ellis and Giggenbach (2). Consequently, at higher temperatures, the extrapolated data in Table 5 are quite possibly more accurate than the direct measurements described in ref. 2.

The limiting law Debye–Hückel terms for $OH^-$ and $HS^-$ cancel out in reaction [6] so that $K_1{}^b$ can be expected to be independent of ionic strength up to about $0.1\,m$. The small but finite values for $\Delta B_C$ in Table 4 suggest that variations may occur at higher ionic strengths, at least at low temperatures. No excess free energies or enthalpies data for reaction [6] have been reported but when these become available, the $\Delta B_C$ and $\Delta B_V$ data can be used to extrapolate ionic strength effects to elevated temperatures and pressures (37). Variations in the acid dissociation constant, $K_1$, can readily be calculated from $K_1{}^b$ and values for the ionic strength dependence of $K_W$, which are well established over a wide range of temperatures and molalities (26, 38).

*$HS^-$ ionization*

Values ranging from log $K_2 = -12.5$ to $-17$ have been reported for the equilibrium constant of the second ionization reaction of $H_2S$ (1)

[9] $HS^- = H^+ + S^{2-}$

If little or no $S^{2-}$ is present and mixing effects are small (18), the apparent molal properties of $Na_2S$ are simply the sum of the values for NaHS and NaOH at ionic strength $I \approx 2\,m$ minus the value for the mole of water lost by the hydrolysis of $S^{2-}$, so that

[10] $$Y_\phi(Na_2S, m) = Y_\phi(NaOH, 2\,m) + Y_\phi(NaHS, 2\,m) - Y^0\,(H_2O)$$

The $C_{p\phi}(Na_2S)$ results from Table 2 are plotted in Fig. 5 along with the curve calculated by inserting the data from Table 1 into eq. [10]. The calculated and experimental results agree within the combined error limits below $0.5\,m$ (ionic strength $1.0\,m$), the highest ionic strength at which the NaHS and NaOH data were measured, and therefore provide no indication that the relative concentration of $S^{2-}$ is significant at these molalities. The

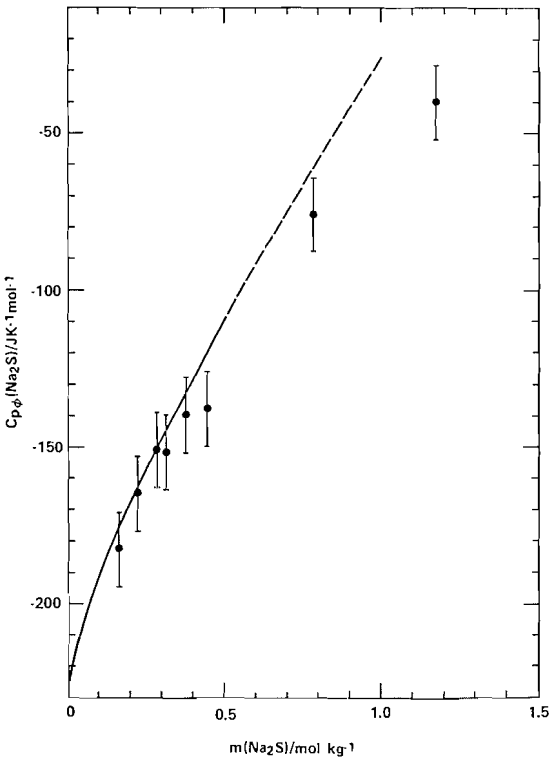


FIG. 5. Apparent molal heat capacities of bulk aqueous $Na_2S$. The solid curve corresponds to a solution containing only $Na^+$, $HS^-$, and $OH^-$ using data in Table 1.

Can. J. Chem. Downloaded from www.nrcresearchpress.com by 210.87.254.6 on 09/06/12
For personal use only.

extrapolation of eq. [10] to above 1.0 $m$ $Na_2S$ deviates significantly from the one experimental value, suggesting that some further ionization of $HS^-$ may have occurred above about 0.7 $m$. These observations are consistent with recent work (2, 3, 6, 11) which found log $K_2$ to be more negative than −13.5.

## Conclusions

The apparent molal volume and heat capacity results reported here yield standard state values for $HS^-$ and $H_2S$ and permit the extrapolation of low temperature equilibrium constants, as presented above. Equally important, the $H_2S$ heat capacities and high temperature values of $K_1$ calculated from $C_{p\phi}{}^0(H_2S)$ and $C_p{}^0(HS^-)$ provide a sensitive test of the results reported by Clark and Glew (17) and Tsonopoulos *et al.* (3), respectively. The agreement between data obtained using such very different techniques increases confidence in the accuracy of all these results and also of the other constants (3, 4, 19) used in the calculations, so that self-consistent thermodynamic functions for hydrogen sulfide and the hydrogen sulfide ion can easily be calculated (see Appendix). Finally, the $Na_2S$ heat capacities reinforce other evidence that, despite much uncertainty in its stability constant, the sulfide ion, $S^{2-}$, is at most a minor species in solutions less alkaline than pOH ≈ 0.5.

## Acknowledgements

We wish to express our appreciation to Drs. L. G. Hepler, J. Gulens, and D. W. Shoesmith for many helpful comments and suggestions, and to Dr. D. Smith-Magowan, Mr. M.-A. Simard, and Mr. L. Holloway for their assistance in setting up and calibrating the calorimeter. We are particularly grateful to Dr. Hepler and the University of Lethbridge for their long-term loan of the calorimetry system and to the Comisión Nacional de Energía Atómica of Argentina for awarding a CNEA Fellowship to A. Barbero. Funds for the project were provided jointly by the Alberta Research Council and the Alberta Oil Sands Technology and Research Authority.

1. S. Rao and L. G. Hepler. Hydrometallurgy, **2**, 293 (1976).
2. A. J. Ellis and W. Giggenbach. Geochim. Cosmochim. Acta, **35**, 247 (1971); A. J. Ellis and N. B. Milestone. Geochim. Cosmochim. Acta, **31**, 615 (1967).
3. C. Tsonopoulos, D. M. Coulson, and L. B. Inman. J. Chem. Eng. Data, **21**, 190 (1976).
4. J. W. Kury, A. J. Zielen, and W. M. Latimer. J. Electrochem. Soc. **100**, 468 (1953).
5. H. Zeumer and W. A. Roth. Z. Elektrochem. **40**, 777 (1934).
6. W. Giggenbach. Inorg. Chem. **10**, 1333 (1971).
7. P. Picker, P. A. Leduc, P. R. Philip, and J. E. Desnoyers. J. Chem. Thermodyn. **3**, 631 (1971).
8. P. Picker, E. Tremblay, and C. Jolicoeur. J. Solution Chem. **3**, 377 (1974).
9. G. S. Kell. *In* Water — a comprehensive treatise. Vol. 1. *Edited by* F. Franks. Plenum Press, New York. 1972.
10. J. E. Desnoyers, C. de Visser, G. Perron, and P. Picker. J. Solution Chem. **5**, 605 (1976).
11. H. P. Stevens and J. W. Cobble. Inorg. Chem. **10**, 619 (1971).
12. Orion Research Inc. Instruction manual — sulfide ion electrode Model 94-16.
13. A. Roux, G. M. Musbally, G. Perron, J. E. Desnoyers, P. P. Singh, E. M. Woolley, and L. G. Hepler. Can. J. Chem. **56**, 24 (1978).
14. I. V. Olofsson, J. J. Spitzer, and L. G. Hepler. Can. J. Chem. **56**, 1871 (1978).
15. G. Perron, N. Desrosiers, and J. E. Desnoyers. Can. J. Chem. **54**, 2163 (1976).
16. G. C. Allred and E. M. Woolley. J. Chem. Thermodyn. **13**, 147 (1981).
17. E. C. W. Clark and D. N. Glew. Can. J. Chem. **49**, 691 (1971).
18. T. F. Young and M. B. Smith. J. Phys. Chem. **58**, 716 (1954).
19. B. J. McBride and S. Gordon. J. Chem. Phys. **35**, 2198 (1961).
20. M. Sadiq and W. L. Lindsay. Selection of standard free energies of formation for use in soil chemistry. Colorado State University Tech. Bull. 134. 1979.
21. D. D. Wagman, W. H. Evans, V. B. Parker, I. Halow, S. M. Bailey, and R. H. Schumm. Selected values of chemical thermodynamic properties. U.S. National Bur. Stand. Tech. Note 270-3. 1968.
22. G. B. Naumov, B. N. Ryzhenko, and I. L. Khodakovsky. Handbook of thermodynamic data. Atomizdat, Moscow, 1971; English translation by G. J. Soleimani, U.S. Nat. Tech. Inform. Service PB-226 772. 1974.
23. R. A. Robie and D. R. Waldbaum. Thermodynamic properties of minerals and related substances at 298.15 K and one atmosphere pressure and at higher temperatures. U.S. Geol. Survey Bull. 1259. 1968.
24. H. C. Helgeson, J. M. Delany, H. W. Nesbitt, and D. K. Bird. Am. J. Sci. **278A**, 1 (1978).
25. L. G. Hepler and H. P. Hopkins. Rev. Inorg. Chem. **1**, 303 (1979).
26. G. Olofsson and L. G. Hepler. J. Solution Chem. **4**, 127 (1975).
27. N. Konopik and O. Leberl. Monatsh. Chem. **80**, 781 (1949).
28. R. Juza and W. Uphoff. Anorg. Allgem. Chem. **287**, 113 (1956).
29. R. C. Murray and J. W. Cobble. Proc. 41st International Water Conf. Eng. Soc. Western Penn., Pittsburgh, PA. 1980. pp. 295–310.
30. R. H. Wood and D. Smith-Magowan. *In* Thermodynamics of aqueous systems with industrial applications. *Edited by* S. A. Newman. A.G.S. Symposium Ser. **133** (Am. Chem. Soc., Washington D.C., 1980); D. Smith-Magowan. Ph.D. Thesis. University of Delaware. 1979.
31. W. T. Lindsay, Jr. Proc. 41st International Water Conf. Eng. Soc. Western Penn., Pittsburgh, PA. 1980. pp. 284–294.
32. J. W. Cobble and R. C. Murray. J. Chem. Soc. Faraday. Discuss. **64**, 144 (1978).

33. R. H. WOOD, J. R. QUINT, and J.-P. E. GROLIER. J. Phys. Chem. **85**, 3944 (1981).
34. (*a*) R. E. MESMER and C. F. BAES, JR. J. Solution Chem. **3**, 307 (1974); (*b*) C. S. PATTERSON, G. H. SLOCUM, R. H. BUSEY, and R. E. MESMER. Private communication.
35. H. C. HELGESON, J. M. DELANY, H. W. NESBITT, and D. K. BIRD. Am. J. Sci. **278**A, 1 (1978); I. M. KLOTZ. Chemical thermodynamics. Benjamin, New York. 1964. pp. 156–159.
36. H. C. HELGESON and D. H. KIRKHAM. Am. J. Sci. **274**, 1089 (1974).
37. J. L. FORTIER and J. E. DESNOYERS. J. Solution Chem. **5**, 297 (1976).
38. F. H. SWEETON, R. E. MESMER, and C. F. BAES, JR. J. Solution Chem. **3**, 191 (1974).
39. A. F. KAPUSTINSKII and R. T. KANAKOVSKII. Z. Fiz. Khim. **32**, 2810 (1958).

## Appendix

Table 6 is a tabulation of thermodynamic constants for $H_2S(g)$, $H_2S(aq)$, and $HS^-(aq)$ at 25°C based on the work presented above and consistent literature data. The values for $\Delta H_f^0$ (39), $S^0$ (19), and $C_p^0$ (19) for $H_2S(g)$ are identical to those in recent compilations (20–24) and lead to the value for $\Delta G_f^0(H_2S,g)$. Combining these with Clark and Glews' vapour pressure measurements (17) yields the values for $H_2S(aq)$, except for $V^0$ and $C_p^0$ which are from this work. Standard ionic heat capacities and volumes ($C_p^0(H^+) = 0$, $V^0(H^+) = 0$) were calculated for $HS^-$ using Allred and Woolley's data (16) and our results. Combining the data for $H_2S(aq)$ with log $K_1$[b] (7) and $\Delta H_R^0$ for reaction [6] (3, 4) yields $\Delta G_f^0(HS^-)$, $\Delta H_f^0(HS^-)$ and, hence, $S^0(HS^-)$. As in refs. 19–22, the standard state gas reference pressure is 101.325 kPa.

TABLE 6. Thermodynamic constants for hydrogen sulfide and the hydrogen sulfide ion at 25°C

| Parameter | Value | | |
|---|---|---|---|
| | $H_2S(g)$ | $H_2S(aq)$ | $HS^-(aq)$* |
| $\Delta G_f^0$/kJ mol$^{-1}$ | −33.56±0.4 | −27.92±0.4 | 11.98±0.5 |
| $\Delta H_f^0$/kJ mol$^{-1}$ | −20.63±0.4 | −38.11±0.4 | −16.10±0.5 |
| $S^0$/J K$^{-1}$ mol$^{-1}$ | 205.7±0.1 | 128.2±0.2 | 68.2±0.2 |
| $V^0$/cm$^3$ mol$^{-1}$ | — | 34.92±0.11 | 20.8±0.3* |
| $C_p^0$/J K$^{-1}$ mol$^{-1}$ | 34.24±0.02 | 178.5±1.9 | −92±1* |

*Based on $V^0(Na^+) = -1.26$ cm$^3$ mol$^{-1}$ and $C_p^0(Na^+) = 41$ J K$^{-1}$ mol$^{-1}$ (16) and a standard state pressure of 101.325 kPa for gases.

Can. J. Chem. Downloaded from www.nrcresearchpress.com by 210.87.254.6 on 09/06/12
For personal use only.

# Single crystal Raman spectra of an organic semiconductor: KTCNQ

ANDRÉ D. BANDRAUK AND K. D. TRUONG

*Groupe de Recherche sur les Semiconducteurs et Diélectriques, Département de chimie, Faculté des Sciences, Université de Sherbrooke, Sherbrooke (Qué.), Canada J1K 2R1*

AND

S. JANDL

*Groupe de Recherche sur les Semiconducteurs et Diélectriques, Département de physique, Faculté des Sciences, Université de Sherbrooke, Sherbrooke (Qué.), Canada J1K 2R1*

Received September 10, 1981

ANDRÉ D. BANDRAUK, K. D. TRUONG, and S. JANDL. Can. J. Chem. **60**, 1881 (1982).

Raman spectra are reported for single crystals of the organic salt KTCNQ (potassium tetracyanoquinodimethane) and its deuterated analogue. Intensities of intramolecular and intermolecular (phonons) vibrations exhibit strong variations at the phase transition temperature associated with a dimer–monomer transition. A simple model is presented to interpret and correlate these results with previously observed ir intensity anomalies in this and other organic semiconductors.

ANDRÉ D. BANDRAUK, K. D. TRUONG et S. JANDL. Can. J. Chem. **60**, 1881 (1982).

On rapporte les spectres Raman d'un monocristal du sel organique KTCNQ (tétracyanoquinodiméthane potassium) et de son analogue deutéré. Les intensités des vibrations intra et intermoléculaires (phonons) montrent de fortes variations à la température de transition de phase, associé à une transition dimère–monomère. On présente un modèle simple pour interpréter et faire correspondre ces résultats aux anomalies d'intensités observées en ir dans ce semi-conducteur organique ainsi que dans d'autres.

[Traduit par le journal]

## 1. Introduction

The charge transfer complexes of TCNQ (tetracyanoquinodimethane), besides providing us with new semiconducting materials, are important since their detailed study enables us to formulate general principles to correlate the high conductivity of such systems with their structural parameters (1–2). Torrance has recently pointed out the strong relationship that exists between various degrees of ionic bonding and conductivity (1). Thus, ionic complexes with complete charge transfer as in KTCNQ ($\rho = 1$) (3), and neutral covalent complexes ($\rho = 0$) such as perylene TCNQ (4–5) are highly insulating, whereas mixed valence complexes ($\rho < 1$, partial charge transfer) such as TTF—TCNQ are excellent conductors (6). The metallic nature of the highly conducting complexes is easily associated to their extreme optical anisotropy as a strong absorption band polarized parallel to the conduction axis, the molecular stacking axis, always appears in these systems. TTF—TCNQ, with the highest conductivity, has a very low electronic absorption band at $\sim 3000\ cm^{-1}$, which is displaced to $\sim 8000\ cm^{-1}$ in the less conductive salt such as RbTCNQ and others (1, 7). These bands are usually attributed to electron transfer between neighboring TCNQ anions along the stacking axis, i.e., perpendicular to the molecular axis, which therefore explains their polarization.

In single particle interpretations of the unusually high or low anisotropic conductivity of these systems, different scattering and interaction mechanisms have been proposed: electron–electron (8), electron–phonon (6, 9), electron–vibration (10, 11), and electron–libration (12, 13). In particular, the electron–vibration coupling effects show up dramatically at phase transitions, which are usually accompanied by large resistivity and magnetic susceptibility changes. These changes in physical properties are parallelled by *anomalous temperature* dependent absorptions in the *infrared region*. This anomalous infrared (ir) activity has been extensively studied by Pecile and co-workers in chloranil (14), TCNQ (15), and TTF salts (16, 17). A similar phenomenon has been recently observed in metal–dithiolene complexes (18) and in polyacetylene polymers (19). These infrared frequencies are usually attributed to symmetric $a_g$ molecular vibrations which become infrared active via a vibronic mechanism induced by the electron charge transfer (20, 21). These observations are consistent with a dimerization of the anionic columns with decreasing temperature (11). Furthermore, these $a_g$ infrared active modes shift to lower frequencies in the low temperature semiconducting or insulating phases when compared to the corresponding Raman frequencies which are unaffected by this mechanism. Such a behaviour has been predicted by Rice (10, 11, 22) with a theory based on a linear electron molecular vibration (emv) coupling mechanism in the dimer. Infrared studies have therefore been instrumental in identifying the

0008-4042/82/141881-10$01.00/0

©1982 National Research Council of Canada/Conseil national de recherches du Canada

Can. J. Chem. Downloaded from www.nrcresearchpress.com by 210.87.254.6 on 09/06/12
For personal use only.

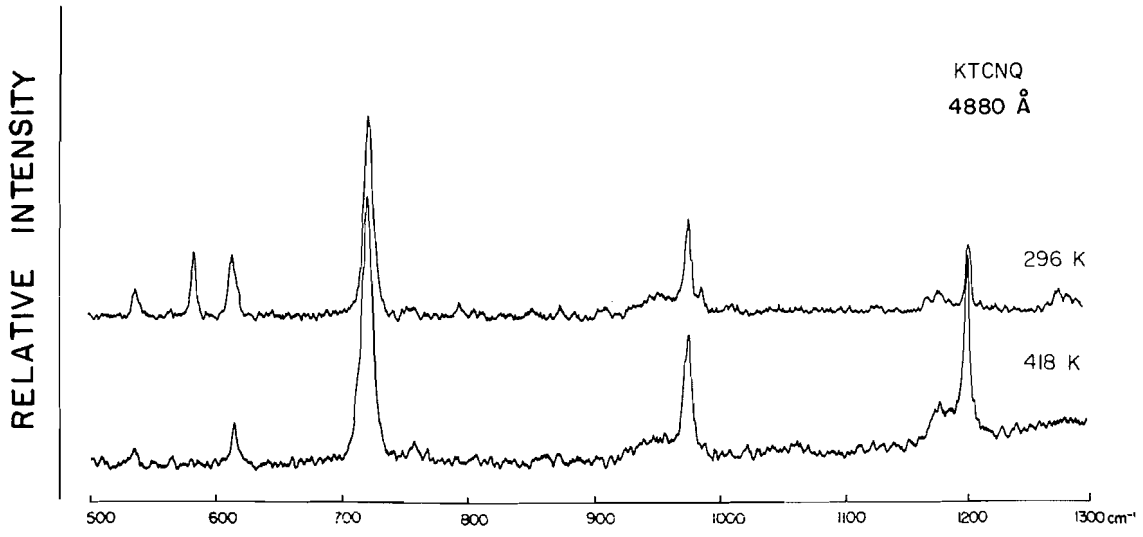


FIG. 1. Raman spectra of KTCNQ single crystal: intramolecular modes.

intramolecular modes which are coupled to the conduction electrons. Recently some attempt has been made to identify by ir spectroscopy the external modes which are activated by conduction electrons in the conductor TTF—TCNQ (23).

Since no previous Raman work exists on single crystals of TCNQ salts, we have undertaken a detailed study of the temperature dependence of the Raman spectra of intramolecular and intermolecular vibrations of single crystals of KTCNQ (24). This work is therefore motivated by the ir intensity anomalies observed in organic conducting and semiconducting salts by Pecile and others, as mentioned above (the ir measurements are usually done in KBr or mulls, and not on single crystals). We have found that such intensity anomalies indeed appear also in the Raman spectra and we propose a single dimer model to interpret these results in terms of the dimerization phase transition thought to occur in KTCNQ at 396 K (25, 26).

## 2. Experimental

The preparation of the crystals, the laser apparatus and spectrometer have been described in our previous Raman studies of this system at 25°C (27). The data in the present work were obtained from free standing single needles (in vacuum) of typical dimension 1 mm × 15 mm with the crystal axis (stacking axis) along the needle axis (26). Excitation of the Raman spectra was obtained with an argon-ion laser with typical power levels below 15 mW. Such low powers were necessary as crystals were found to rapidly deteriorate above this power level. Low frequencies were verified in the anti-Stokes region to confirm the assignments and eliminate errors due to plasma lines. All spectra were recorded, at 90° scattering geometry, on a strip recorder and simultaneously stored in a multichannel analyser. Normal speed of scanning was 1 $cm^{-1}$/min with 30S/channel being used particularly for low frequency modes and for comparison of line intensities. Slit width was maintained at 2 $cm^{-1}$ for simultaneous optimum power and resolution conditions.

## 3. Spectral results and assignments

Previous Raman work on KTCNQ and other alkali salts was done in KBr pellets (27, 28) and in solution (29, 30), to examine the resonance enhancement expected when one enters into an electronic absorption band (30, 31). In this work, we present results obtained on single crystals of KTCNQ and its deuterated analogue $KTCNQ_{d4}$. Partial Raman data were also obtained for the ammonium salt ($NH_4TCNQ$), the results being less complete for the latter due to its instability to laser irradiation (24).

### *(a) High frequency modes*

In Figs. 1 and 2 we present the Raman-active vibrations in the frequency range of 300 to 1300 $cm^{-1}$ for KTCNQ and $KTCNQ_{d4}$, taken at a laser wavelength of 488 nm, which gives intense lines for most modes (24). These spectra are reported at two temperatures, i.e., room temperature and one temperature above $T_c$, the phase transition temperature at 396 K as determined by X-ray diffraction (26). Clearly evident in these figures is the strong temperature dependence of the intensities of the lines at 585(568), 725, and 1204(875) $cm^{-1}$ for the $TCNQ^-$ ion (deuterated lines in parentheses). A more detailed study of the temperature dependence of the intensities of the close doublet at 585(568) and 618(612) $cm^{-1}$ is illustrated in Figs. 3 and 4. For both compounds, deuterated and undeuterated, the lower frequency component disappears progressively as the phase transition temperature is ap-

Can. J. Chem. Downloaded from www.nrcresearchpress.com by 210.87.254.6 on 09/06/12
For personal use only.

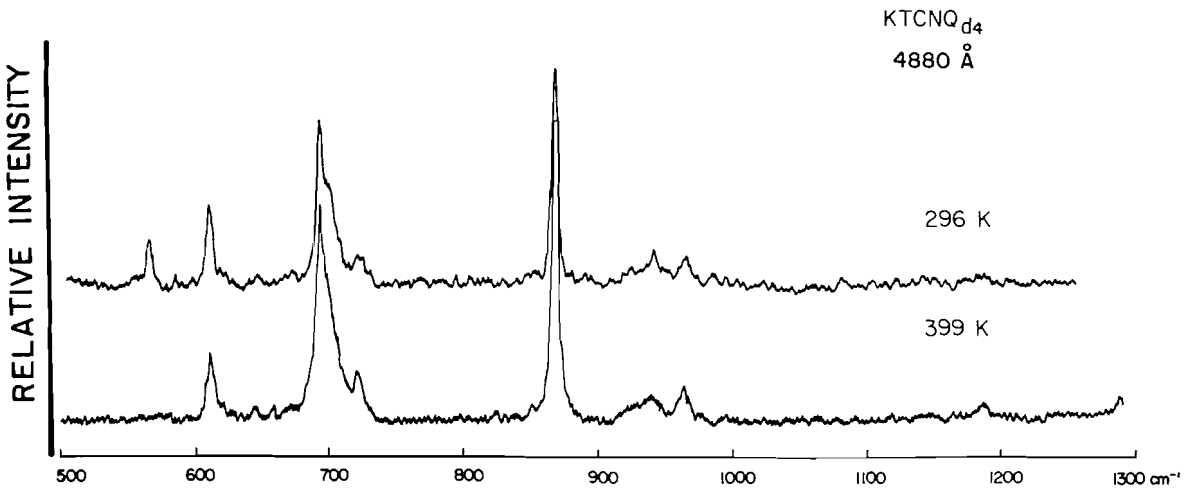


FIG. 2. Raman spectra of deuterated KTCNQ single crystal: intramolecular modes.

proached. In Figs. 5 and 6, for comparison, we illustrate the temperature-dependent intensities of the 725 and 1204(875) $cm^{-1}$ modes. The 699 $cm^{-1}$ line of $TCNQ_{d4}^-$ (Fig. 2), the equivalent of the undeuterated 725 $cm^{-1}$ line in $TCNQ^-$ (Fig. 1), also shows some intensity variation, but due to the presence of a sideband no quantitative measurements were possible. Of note is that the 585(568) $cm^{-1}$ mode vanishes at $T_c$ whereas the 725 and 1204(875) $cm^{-1}$ modes peak in intensity at $T_c$; the 618(612) $cm^{-1}$ vibration is relatively insensitive to the phase change. (The same results were found by exciting at different laser wavelengths (24).) This behaviour is related to the symmetries of these vibrations, as will be shown in detail in the next section. Thus, following Bozio *et al.*'s assignments (32), the 585(568) $cm^{-1}$ mode is an *out-of-plane* $\nu_{29}(b_{2g})$ mode whereas all the other modes are $a_g$, i.e., the strongest Raman-active modes.

*(b) Low frequency modes*

Low frequency modes, usually lattice modes such as translations and librations, are sensitive to changes in crystal structure and hence are a useful probe for phase transitions. With this view in mind, Raman spectra were taken in the region below 300 $cm^{-1}$ for single crystals with the incident light polarized perpendicular or parallel to the needle axis, *a*, which from X-ray work is known to be the stacking axis of the $TCNQ^-$ molecular planes (26). Thus in Figs. 7 and 8, with the incident light polarized perpendicular to the needle axis (i.e., in the plane of the TCNQ's) we observe the same low frequency mode distribution in $TCNQ^-$ and $TCNQ_{d4}^-$, the only noticeable isotope shift occurring for the 98(91) $cm^{-1}$ line which consequently is attributed as the in-plane $\nu_{49}(b_{3g})$ vibration following the normal mode analysis of Girlando and Pecile (33).

More detailed information is presented in Figs. 9 to 11 for the polarization dependence of the scattering of the low frequency modes. Thus Fig. 9 shows an exceptional resolution of the *bc–bc* scattering, i.e., in the plane of the TCNQ anions. In the high temperature phase, where from Konno's X-ray work (26), all TCNQ's are equivalent, only three main peaks remain in Fig. 9, at 98, 168, and 232 $cm^{-1}$. The 98 $cm^{-1}$ line is, as mentioned above, the in-plane $\nu_{49}(b_{3g})$ mode; the line at 168 $cm^{-1}$ is attributed to the out-of-plane $\nu_{17}(b_{1g})$ mode and the weak 300 $cm^{-1}$ line is assigned to $\nu_{31}(b_{2g})$, in agreement with the normal coordinate analysis of Girlando and Pecile (33). Recent high resolution infrared vibrational crystal spectra of TTF—TCNQ show the appearance of 95 and 165 $cm^{-1}$ modes only *below* the metal–semiconductor phase transition at 60 K for this compound (23). These have been assigned to $TCNQ^-$ Raman modes vibronically activated by the conduction electrons. Our results confirm these modes as being indeed $b_g$ modes. The vibration at 232 $cm^{-1}$ observed many times in $TCNQ^-$ powder salts can be now attributed as an $a_g$ out-of-plane mode (Fig. 11). Its temperature-dependent intensity suggests it is a fundamental strongly coupled to phonons (possibly a symmetric ring bending vibration).

Since no previous measurements of low frequency single crystal Raman modes of TCNQ salts exist, we therefore report in Table 1 these modes as observed by us in the dimerized low temperature phases for the two potassium salts as well as, for comparison, modes of $NH_4TCNQ$ which has a

Can. J. Chem. Downloaded from www.nrcresearchpress.com by 210.87.254.6 on 09/06/12
For personal use only.

Can. J. Chem. Downloaded from www.nrcresearchpress.com by 210.87.254.6 on 09/06/12
For personal use only.

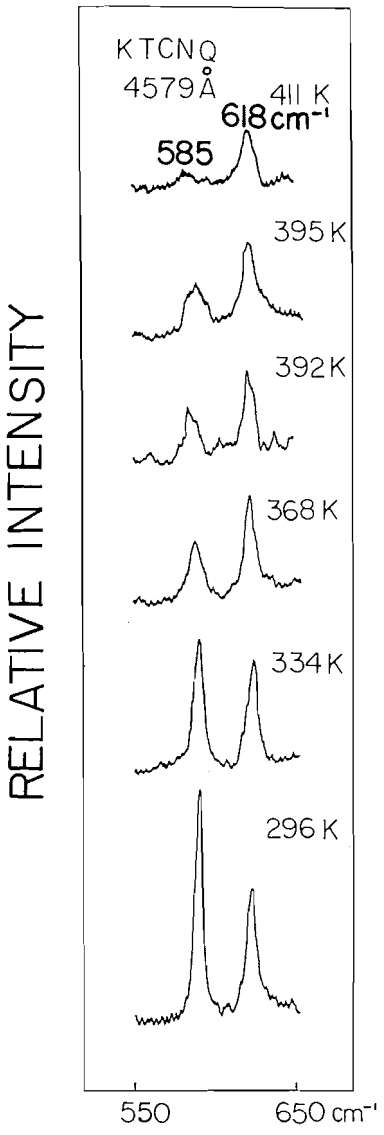


FIG. 3. Temperature dependent intensity of the out-of-plane $\nu_{29}(b_{2g})$ mode at 585 $cm^{-1}$ (618 $cm^{-1}$, $a_g$).

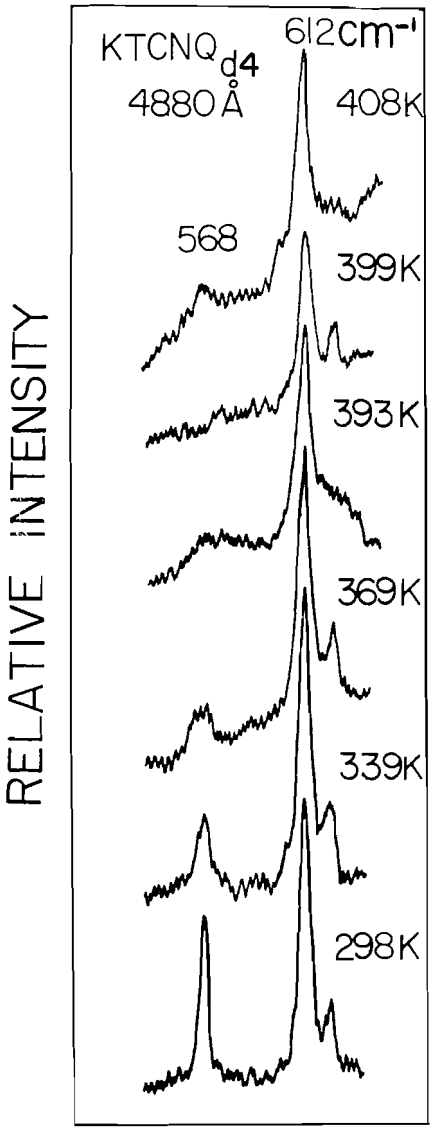


FIG. 4. Temperature dependent intensity of the deuterated out-of-plane $\nu_{29}(b_{2g})$ mode at 568 $cm^{-1}$ (612 $cm^{-1}$, $a_g$).

phase transition at 300 K (16, 25). For the latter salt, high temperature spectra were unobtainable due to crystal deterioration at laser powers even as low as 5 mW. One observes in Table 1 generally good correlation for the frequencies of the three different salts, even though the crystal structure of $NH_4$-TCNQ (orthorhombic) is slightly different from the potassium salt (monoclinic). This correlation permits us tentatively to conclude that vibrations of $K^+$ are absent in view of the disparity in mass of the two cations. In any case, as a result of the low temperature crystal structure of KTCNQ (space group $P2_1/n$, $Z = 8$ (26)), $K^+$ has approximate $C_i$ site symmetry as compared to $C_s$ for the dimerized $TCNQ^-$ ions; the $K^+$ translational modes therefore should be very weak.

In the high temperature phase (space group $P2_1/c$, $Z = 2$ (26)), all site symmetries now are $C_i$, so that in addition to the $C_{2h}$ crystal symmetry, one should observe above $T_c$ only librations of $a_g$ and $b_g$ symmetry for the $TCNQ^-$ anions. In the dimerized low temperature phase, translations of these anions ($C_s$ site) may now be Raman active. In Figs. 10 and 11 we notice from the polarization measurements

Can. J. Chem. Downloaded from www.nrcresearchpress.com by 210.87.254.6 on 09/06/12
For personal use only.

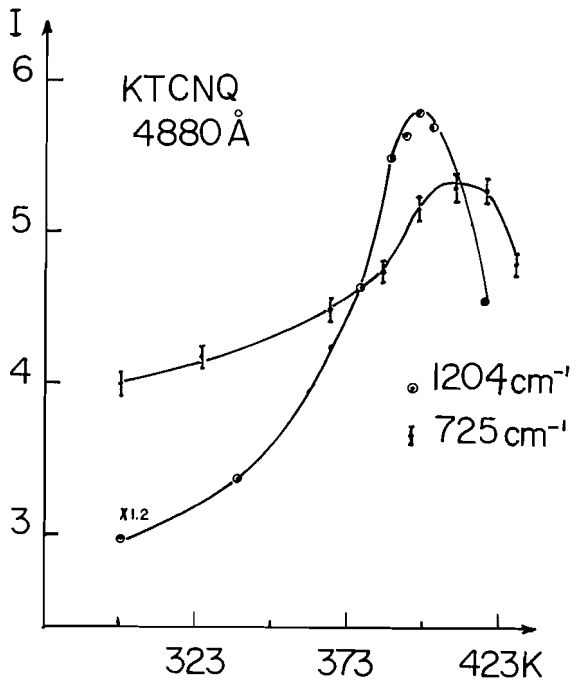


FIG. 5. Temperature dependent intensities of $a_g$ modes in KTCNQ single crystal (arbitrary scale).

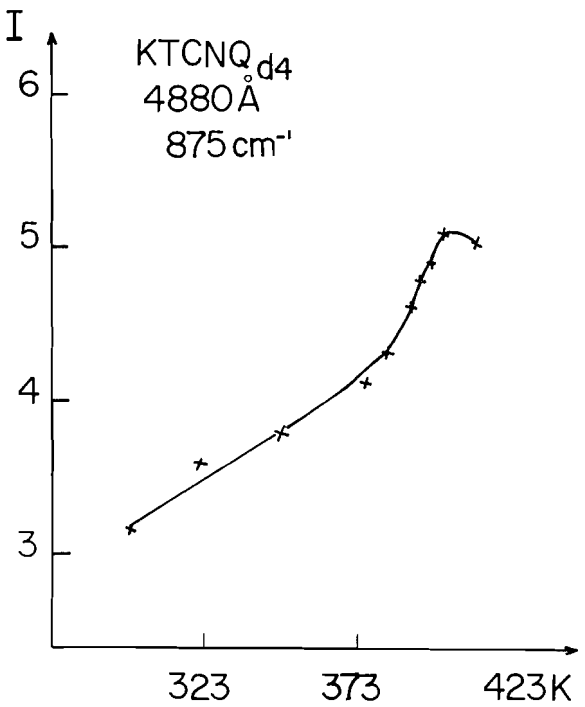


FIG. 6. Temperature dependent intensity of $a_g$ mode in deuterated KTCNQ single crystal (arbitrary scale).

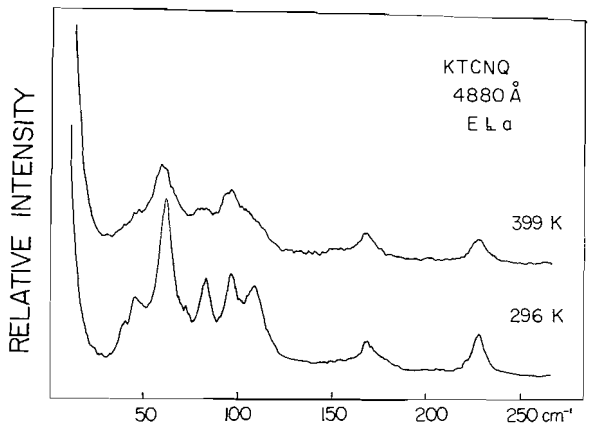


FIG. 7. Low frequency modes excited perpendicular to the stacking axis (in-plane scattering).

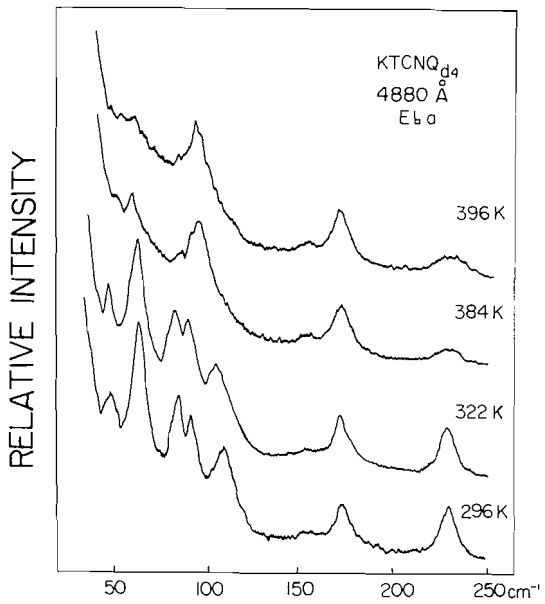


FIG. 8. Same as Fig. 7 for deuterated compound.

three broad bands in the low regions 45–50 $cm^{-1}$, 64–80 $cm^{-1}$, and the higher region 100–110 $cm^{-1}$. Since the moments of inertia of the TCNQ's are respectively 0.8 ($I_x$), 2.6 ($I_y$), 3.3 ($I_z$) $\times$ $10^{-37}$ g $cm^2$ where $x$ and $y$ are the long and short molecular axis, and $z$ is perpendicular to the molecular plane (9° off the stacking axis (26)), we readily obtain for the ratios of the reciprocals of the square roots of these moments — 2.1:1.2:1. The frequencies of librations should roughly follow (for equal force constants) this ratio so that we can expect three groups of frequencies as observed in Figs. 10 and 11. These three groups of frequencies broaden very

Can. J. Chem. Downloaded from www.nrcresearchpress.com by 210.87.254.6 on 09/06/12
For personal use only.

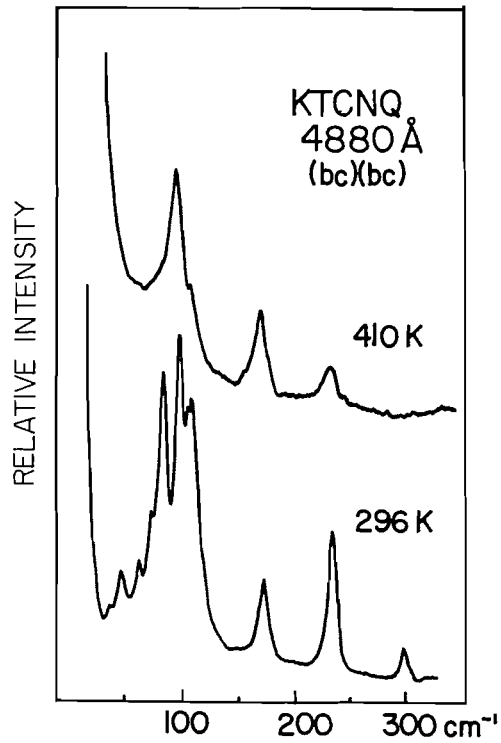


FIG. 9. Raman spectra of in-plane low frequency modes ($a_g + b_g$).

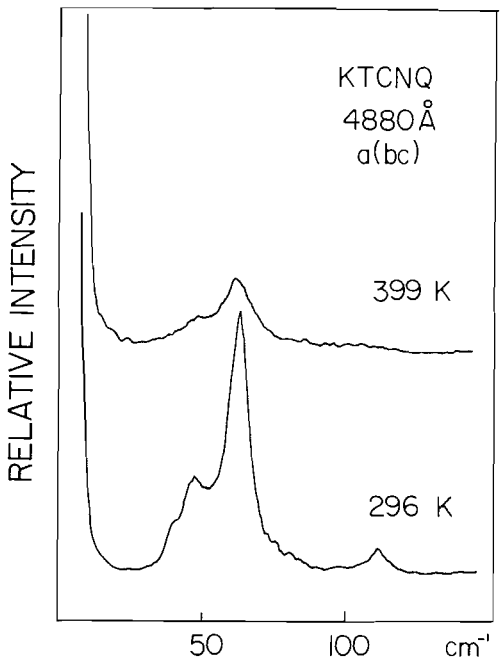


FIG. 10. Raman spectra of low frequency modes of $b_g$ symmetry.

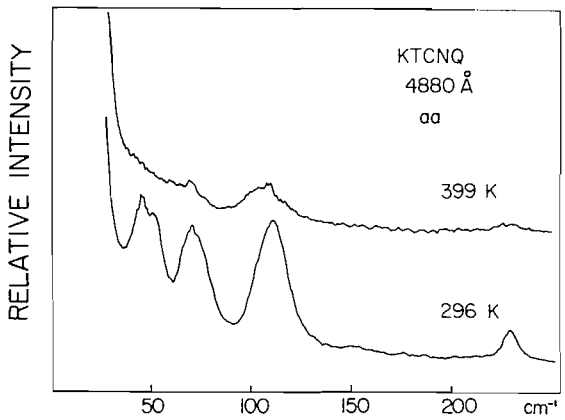


FIG. 11. Raman spectra of low frequency modes of $a_g$ symmetry.

rapidly as one approaches the transition temperature but are still identifiable. We therefore attribute these frequencies to the librations of the individual $TCNQ^-$ anions. In particular, the libration at 110 $cm^{-1}$ is strongly temperature dependent, appearing at 125 $cm^{-1}$ at low temperatures in all salts (Table 1), and seemingly converging to 100 $cm^{-1}$ at high temperatures as clearly seen in Fig. 8. Since it is polarized along the stack axis, Fig. 11, it is therefore easily influenced by the progressive elongation along that axis known to occur as the temperature increases (26).

## 4. Discussion

### *A. Theory*

The generally assumed simple model to explain spectral changes for the TCNQ salts consists of a dimerized unit which because of electron transfer parallel to the stacking axis activates $a_g$ modes in the infrared (11, 14). In order to apply this model to the discussion of our Raman spectra, we will rely on the theory developed by one of us for multiphoton vibrational processes in molecules (31).

Thus, for the dimer one can form linear combinations of molecular vibrations into symmetric, $Q_g$, and antisymmetric, $Q_u$, pairs, with respect to the inversion center of the dimer, i.e.,

$$[1] \quad Q_{g,u} = \frac{1}{\sqrt{2}} [Q_1 \pm Q_2]$$

where the +(−) sign is associated to the g(u) mode, and $Q_1$ and $Q_2$ are vibrations of the same symmetry on molecules 1 and 2. The total electronic Hamiltonian $H$ will be a function of $Q_g$, $Q_u$, and $d$, the distance between the monomer units. The dimer electronic molecular orbitals will also separate into

TABLE 1. Assignment of observed low frequency modes of $TCNQ^-$

| KTCNQ | | $KTCNQ_{d4}$ | $NH_4TCNQ$ | | |
|---|---|---|---|---|---|
| 37 K | 296 K | 296 K | 18 K | 77 K | Assignments |
| 45 | 42, 46 | 48 | 47 | 45 | $a_g,b_g$ |
| 52 | 52 | 56 | 53 | 55 | $a_g,b_g$ |
| 65 | 64 | 63 | 67 | | $b_g$ |
| 71 | 70 | | 72 | 70 | $a_g$ |
| 80 | | | | | |
| 88 | 85 | 84 | 87 | | $b_g$ |
| 105 | 98 | 91 | 90 | 90 | $b_g$ |
| 110 | | | 107 | | |
| 115 | 106 | | 114 | | |
| 124 | 110 | 108 | 125 | 114 | $a_g,b_g$ |
| 174 | 168 | 168 | 164 | 164 | $b_g$ |
| 232 | 232 | 232 | 232 | 230 | $a_g$ |

symmetric, $\psi_g$, and antisymmetric, $\psi_u$, combinations of the monomer orbitals $\psi_1$ and $\psi_2$, i.e.,

$$[2] \quad \psi_{g,u}(Q_g,Q_u,d) = \frac{1}{\sqrt{2}}[\psi_1(Q_1) \pm \psi_2(Q_2)]$$

Vibrations induce changes in the orbitals via the *Herzberg–Teller* effect, which for our two-state model is given exactly by (31)

$$[3] \quad \frac{\partial\psi_u}{\partial Q} = \frac{\langle g|\partial H/\partial Q|u\rangle}{E_u - E_g}$$

where $E$ is the dimer orbital energy. Thus for the antisymmetric mode $Q_u$, the electronic matrix element $\langle g|\partial H/\partial Q_u|u\rangle$ between the dimer orbitals $\psi_g$ and $\psi_u$ is, from eqs. [1] to [3], given by

$$[4] \quad \langle g|\partial H/\partial Q_u|u\rangle = \frac{1}{2\sqrt{2}}[\langle\psi_1|\partial H/\partial Q_1|\psi_1\rangle + \langle\psi_2|\partial H/\partial Q_2|\psi_2\rangle]$$

where we have used the relation $\partial H/\partial Q_u = +\partial H/\partial Q_1 - \partial H/\partial Q_2$ and cross terms have cancelled. By the Hellmann–Feynman theorem (31, 34), the energy derivative is the average force, i.e.,

$$[5] \quad \partial\varepsilon/\partial Q = \langle\psi|\partial H/\partial Q|\psi\rangle$$

so that eq. [4] becomes

$$[6] \quad \langle g|\partial H/\partial Q_u|u\rangle = \frac{1}{\sqrt{2}}(\partial\varepsilon/\partial Q)$$

where $\varepsilon$ is the *energy* of the *monomer* orbitals $\psi_1(Q_1)$ or $\psi_2(Q_2)$ and $Q$ is now $Q_1$ or $Q_2$ and must be of $a_g$ symmetry.

The infrared absorption amplitude can now be calculated by assuming an electronic virtual absorption into the state $|u\rangle$ from the ground state $|g\rangle$, followed by emission of a vibration (phonon) through the term $\partial\psi_u/\partial Q_u$, which corresponds to either nondiagonal electron–phonon coupling (35), or variation of the electronic transition moment (31). Thus,

$$[7] \quad T(\text{ir}) = \frac{\langle g|\boldsymbol{\mu}\cdot\boldsymbol{e}|u\rangle\langle u|\partial H/\partial Q_u|g\rangle}{(E_g + \hbar\omega - E_u)(E_u - E_g)}$$

where $\hbar\omega$ is the energy of the absorbed photon of polarization $\boldsymbol{e}$ and $\boldsymbol{\mu}$ is the electronic dipole operator (31). In view of relation [6], we now have the ir absorption intensity proportional to the square of the transition amplitude

$$[8] \quad T(\text{ir}) = \frac{1}{\sqrt{2}}\frac{\langle g|\boldsymbol{\mu}\cdot\boldsymbol{e}|u\rangle}{(E_g+\hbar\omega-E_u)(E_u-E_g)}\left(\frac{\partial\varepsilon}{\partial Q}\right)$$

To calculate the corresponding Raman intensities (31), we calculate the amplitude for absorption (emission), of a photon of energy $\hbar\omega_1$ ($\omega_2$) and polarization $e_1$ ($e_2$) with emission of vibrations, i.e., keeping account of symmetries we get,

$$[9] \quad T(\text{R}) = \frac{\langle g|\boldsymbol{\mu}\cdot\boldsymbol{e}_1|u\rangle\langle u|\partial H/\partial Q_g|u\rangle\langle u|\boldsymbol{\mu}\cdot\boldsymbol{e}_2|g\rangle}{(E_g+\hbar\omega_1 - E_u)(E_g+\hbar\omega_2 - E_u)}$$

By similar arguments which gave eq. [6] we can also show that

$$[10] \quad \langle u|\partial H/\partial Q_g|u\rangle \simeq \frac{1}{\sqrt{2}}(\partial\varepsilon/\partial Q)$$

Equations [8] and [9] illustrate that upon dimerization, both the ir and the Raman spectra are governed by a *common antisymmetric* dimer electronic state (orbital $\psi_u$). Since the absorption must be polarized along the stacking axis because of the inversion symmetry of the orbitals $\psi_g$ and $\psi_u$, we see that the monomer $Q(a_g)$ modes appear both in the ir and Raman by electronic excitations *perpendicular* to the monomer axis. This follows since $\partial\varepsilon/\partial Q$ is

Can. J. Chem. Downloaded from www.nrcresearchpress.com by 210.87.254.6 on 09/06/12
For personal use only.

Can. J. Chem. Downloaded from www.nrcresearchpress.com by 210.87.254.6 on 09/06/12
For personal use only.

nonvanishing only for symmetric modes, eq. [5], as it is a measure of the force on the nuclei giving rise to a displacement of their equilibria and therefore, to Franck–Condon excitation (31). Therefore this explains the appearance of the $a_g$ modes as seen by Pecile *et al.* (14–17). We note, however, that the ir and Raman bands can be made more intense by entering into near-resonance with the state $|u\rangle$, which corresponds to the electronic absorptions seen between 3000–8000 $cm^{-1}$ from TTF—TCNQ to KTCNQ (3). This therefore indicates the importance of infrared lasers to probe these states. In that case one would see, both by ir and Raman spectroscopy, the *same* $a_g$ modes.

*B. Correlation of intramolecular vibrations*

With the above theoretical model, we can now correlate our Raman results with the infrared studies of Pecile *et al.* of simple TCNQ salts. (We reiterate that our Raman spectra are for single crystals as opposed to the ir spectra.) In particular, these authors have found that the intensity of the 725 $cm^{-1}$ mode diminishes abruptly around $T_c$ (15) and have interpreted this effect as due to the dimer–monomer phase transition inferred from X-ray diffraction (25, 26). In the case of our Raman results, we first point out that the temperature dependence of the electronic absorption spectra may be ruled out as a mechanism for intensity variations, since the absorption has been observed to decrease with increasing temperature in KTCNQ (36) contrary to what we observe in the Raman intensities. These, we reiterate, peak at $T_c$ for the $a_g$ modes at 725 and 1204 $cm^{-1}$, Fig. 5, whereas the $b_{2g}$ mode at 585 $cm^{-1}$ disappears at the transition temperature, Figs. 3 and 4.

Previous resonance Raman experiments in KBr and solution (28, 29) show that the 725 $cm^{-1}$ mode is insensitive to the absorption to the localised electronic charge transfer band at 645 nm but responds rather to the higher energy band at 400 nm. The 1204 $cm^{-1}$ vibration is known to be enhanced when excited in the red so that contrary to the 725 $cm^{-1}$ vibration, it is coupled to the low wavelength absorption bands of $TCNQ^-$. *Ab initio* calculations (37) indicate that the 400 nm absorption corresponds to transfer out of the last occupied molecular orbital $b_{2g}$ to a highly delocalized $a_u$ orbital, whereas the 645 nm absorption increases the occupation of the $b_{2g}$ orbital by transferring electrons out of the C—H region from a $b_{1u}$ orbital. The large contribution of the C—H bond to the 1204 $cm^{-1}$ mode (shifted to 875 $cm^{-1}$ by deuteration) helps explain the strong coupling of this vibration to the $b_{2g}$ electron observed in conductivity measurements (22). Rice *et al.* have deduced from these measurements that the electron–vibration coupling is larger for the 1204 $cm^{-1}$ than the 725 $cm^{-1}$ vibration in KTCNQ. Our Raman studies, Fig. 5, correlate well with the conductivity experiments. We observe the 1204 $cm^{-1}$ vibration is much more sensitive to the phase transition than the 725 $cm^{-1}$ mode. In addition, the intensities of both vibrations peak at the phase transition temperature $T_c$, thus indicating a change in the nature of the excited electronic states and consequently a decrease in the electron–vibration interactions above $T_c$. We can explain this as due to the uniform spacing of the TCNQ's above $T_c$ which favors electron delocalization along the chain. This delocalization, by reducing the electron densities of the molecules, reduces the force $\partial H/\partial Q$, eq. [5], which is responsible for bond elongations and Franck–Condon excitations (31). We can conclude that as one approaches $T_c$ from below, electrons are returning to the molecular planes from the dimer overlap region, increasing $\partial\varepsilon/\partial Q$ and consequently the intensity. Above $T_c$, delocalization reduces these couplings and therefore the intensities. This interpretation does not take into account the variation of the energy $E_u$, of the dimer orbital $\psi_u$, on the dimer spacing $d$, eq. [3]. This presumably is negligible, since we did not observe translational modes in the low frequency region.

Contrary to the in-plane $a_g$ modes, the *out-of-plane* $\nu_{29}(b_{2g})$ mode at 585 $cm^{-1}$ disappears at and beyond $T_c$.[1] This mode has not been considered in previous ir (14–17) and conductivity measurements (22). The Raman intensity variations of this mode as a function of temperature, Figs. 1–4, clearly reflect the physical change along the stacking axis of the crystal. Since this mode contains a strong C—H component (568 $cm^{-1}$ in $TCNQ_{d4}$) and it is an out-of-plane bending mode, it must probe the overlap region between the TCNQ's. Furthermore, molecular orbital calculations (37) indicate an increase in electron distribution in the C—H region of $TCNQ^-$ as compared to $TCNQ^0$. We can therefore understand the sensitivity of this predominant out-of-plane C—H vibration to the phase transition. Thus, the return to a more symmetric electronic environment in approaching $T_c$ will decrease the force $\partial H/\partial Q_{b_{2g}}$ to zero at $T_c$, with the same effect on the intensity of that mode. We conclude therefore that these Raman spectroscopic results on single crystals confirm the model of a dimer–monomer phase transition proposed from

[1]It is not present in solution (24), thus confirming its presence only upon association (dimerization).

Can. J. Chem. Downloaded from www.nrcresearchpress.com by 210.87.254.6 on 09/06/12
For personal use only.

other physical measurements, and that at least one out-of-plane bending mode is strongly coupled to the conduction electrons. This has not been considered before.

*C. Temperature dependence of low frequency modes*

Temperature effects are much more pronounced for the modes below 100 $cm^{-1}$, a region normally attributed to the phonon region (translations + librations). Thus above $T_c$ (396 K), the modes at 64, 70, 85, 98, and 110 $cm^{-1}$ still remain in evidence although much broadened (Figs. 5–11). Measurements were done for the intensity of three lines 64, 85, and 98 $cm^{-1}$ as a function of temperature, since only for these, meaningful measurements were still feasible, i.e., they were still identifiable (Figs. 7, 10, 11). The results are illustrated in Fig. 12, where the 64 $cm^{-1}$ line, assigned as a libration, the 98 $cm^{-1}$ line (intramolecular $\nu_{49}(b_{3g})$), and the 85 $cm^{-1}$ (unassigned) decrease rapidly in intensity as one approaches $T_c$, the phase transition temperature. The similarity in temperature behaviour suggests the 85 $cm^{-1}$ line is probably a libration and that the 98 $cm^{-1}$ line must be strongly mixed with librations, a suggestion also made for TTF—TCNQ (23). (We have scaled down the 64 $cm^{-1}$ intensity by a half for convenience.) The temperature behaviour of these lines correlates rather well with the temperature dependence of the deviation from uniform spacing of the TCNQ's along their stacked column as determined from X-ray and magnetic susceptibility temperature data (26). Morawitz and Gutfreund *et al.* have indicated that librations (i.e., rotational displacements) should couple effectively to the electronic band motion in metal–insulator transitions which are a result of dimerization (12, 13). The strong temperature dependence observed in Figs. 10 to 12 is seen to be a reflection of this mechanism. The large linewidths, unfortunately, exclude any quantitative measurements, so that for these low frequency modes, a direct correlation of intensities and linewidths with electron–vibration couplings was not possible as for the intramolecular modes discussed previously.

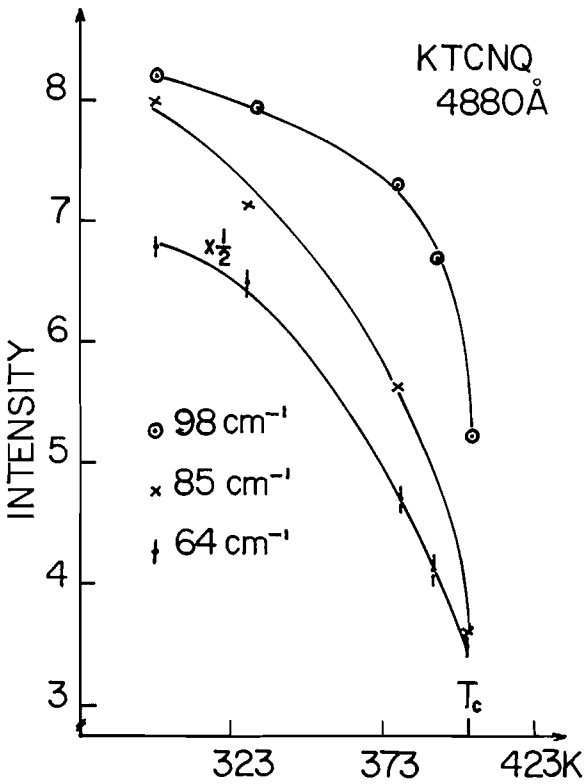


FIG. 12. Temperature dependent intensities of low frequency modes (arbitrary scale).

## Conclusion

The present work was motivated by the need to complement the important findings of Pecile *et al.* (14–17) on the infrared activation of the symmetric modes of TCNQ and TTF salts. We have found that the intensities of our Raman spectra correlate rather well with the dimerization phase transitions proposed for these salts (25, 26). Thus, we have found out-of-plane intramolecular modes which vanish at the phase transitions and sharp variations exist in the intensities of the in-plane symmetric modes at the transition temperature. We suggest that librations are important in describing the physical properties of these systems, a suggestion which has been made more than once (12, 13). We base our conclusions on the temperature effects observed in both the phonon and intramolecular regime of the spectrum. A simple theory, previous section, indicates that infrared lasers would be very useful in establishing the dominant electron–vibration (phonon) interactions. Since most of these organic salts have low electronic absorption bands (3000 ~ 8000 $cm^{-1}$ (6)), vibronic effects will be enhanced by near resonant optical excitations of these bands. The true nature of these electronic states is at the present not well known. Suffice it to mention that similar low energy charge transfer states are thought to be important in biological molecules (38), and organic radicals (39), so that similar electron–vibration effects should be anticipated in these systems.

## Acknowledgement

We thank both NSERC and DRB for supporting this research via instrument and operating grants.

1. J. B. TORRANCE. Acc. Chem. Res. **12**, 79 (1979); Ann. Acad. Sci. N.Y. **313**, 210 (1978).
2. W. E. HATFIELD. Molecular metals. Plenum Press, New York. 1979.
3. I. SHIROTANI, A. ONODERA, and N. SAKAI. Bull. Chem. Soc. Jpn. **48**, 167 (1975).
4. K. D. TRUONG and A. D. BANDRAUK. Chem. Phys. Lett. **44**, 232 (1976).
5. A. D. BANDRAUK, K. D. TRUONG, H. J. BERNSTEIN, and V. SALARES. J. Raman Spectrom. **8**, 5 (1979).
6. A. A. BRIGHT, A. F. GARITO, and A. J. HEEGER. Phys. Rev. B**10**, 1328 (1974).
7. J. TANAKA *et al*. Bull. Chem. Soc. Jpn. **49**, 2358 (1976).
8. S. KHANNA, A. A. BRIGHT, A. F. GARITO, and A. J. HEEGER. Phys. Rev. B**10**, 2139 (1974).
9. D. B. TANNER, C. J. JACOBSEN, A. F. GARITO, and A. J. HEEGER. Phys. Rev. B**13**, 3381 (1976).
10. M. J. RICE. Phys. Rev. Lett. **37**, 36 (1976).
11. M. J. RICE, V. M. YARTSEV, and C. J. JACOBSEN. Phys. Rev. B**21**, 3437 (1980).
12. H. MORAWITZ. Phys. Rev. Lett. **34**, 1096 (1975).
13. H. GUTFREUND, C. HARTZSTEIN, and M. WEGER. Solid State Commun. **36**, 647 (1980).
14. R. BOZIO, A. GIRLANDO, and C. PECILE. Chem. Phys. **21**, 257 (1977).
15. R. BOZIO and C. PECILE. J. Chem. Phys. **67**, 3864 (1977).
16. R. BOZIO, I. ZANON, A. GIRLANDO, and C. PECILE. J. Chem. Phys. **71**, 2282 (1979).
17. R. BOZIO and C. PECILE. J. Phys. C**13**, 6205 (1980).
18. L. C. ISETT, D. M. ROSSO, and G. L. BOTTGER. Phys. Rev. B**22**, 4739 (1980).
19. J. F. RABOLT, T. C. CLARK, and G. B. STREET. J. Chem. Phys. **71**, 4614 (1979).
20. H. B. FRIEDRICH and W. B. PERSON. J. Chem. Phys. **44**, 2161 (1966).
21. J. J. HINKEL and P. J. DEVLIN. J. Chem. Phys. **58**, 4750 (1973).
22. M. J. RICE, N. O. LIPARI, and S. STRASSLER. Phys. Rev. Lett. **39**, 1359 (1977).
23. F. E. BATES, J. E. ELDRIDGE, and M. R. BRYCE. Can. J. Phys. **59**, 339 (1981).
24. K. D. TRUONG. Ph.D. thesis. Faculty of Sciences, University of Sherbrooke. 1982.
25. J. G. VEGTER and J. KOMMANDEUR. Mol. Cryst. Liq. Cryst. **30**, 11 (1975).
26. M. KONNO, T. ISHII, and Y. SAITO. Acta Crystallogr. B**33**, 763 (1974).
27. K. D. TRUONG and C. CARLONE. Phys. Rev. B**20**, 2238 (1979).
28. C. K. CHI and E. R. NIXON. Spectrochim. Acta, **31**A, 1739 (1975).
29. W. T. WOZNIAK, G. DEPASQUALI, and M. V. KLEIN. Chem. Phys. Lett. **40**, 93 (1976).
30. D. L. JEANMAIRE and R. P. VAN DUYNE. J. Am. Chem. Soc. **98**, 4034 (1976).
31. A. D. BANDRAUK. Mol. Phys. **28**, 1259 (1974).
32. R. BOZIO, I. ZANON, A. GIRLANDO, and C. PECILE. Faraday Trans. II, **74**, 235 (1977).
33. A. GIRLANDO and C. PECILE. Spectrochim. Acta, **29**A, 1859 (1973).
34. A. C. HURLEY. Molecular orbitals in chemistry. *Edited by* P. O. Löwdin and B. Pullman. Academic Press, New York. 1964.
35. A. S. DAVYDOV. Theory of molecular excitons. Plenum Press, New York. 1971.
36. C. CARLONE, R. LAIDIG, E. KISELA, and N. K. HOTA. Solid State Commun. **37**, 253 (1981).
37. H. JOHANSEN. Int. J. Quant. Chem. **9**, 459 (1975).
38. M. REDI and J. J. HOPFIELD. J. Chem. Phys. **72**, 6651 (1980).
39. L. SALEM and C. ROWLAND. Angew. Chem. **11**, 92 (1972).


Can. J. Chem. Downloaded from www.nrcresearchpress.com by 210.87.254.6 on 09/06/12
For personal use only.

# Solid state decomposition studies on fluoroperoxo species of transition metals. Part XI. Kinetics of isothermal and photochemical decomposition of $K_2TaO_2F_5.H_2O$

GOPAL V. JERE,[1] LATHA SURENDRA, SURENDER M. KAUSHIK, AND MAHINDER K. GUPTA

*Department of Chemistry, Indian Institute of Technology Delhi, Hauz Khas, New Delhi 110 016, India*

Received September 24, 1981

GOPAL V. JERE, LATHA SURENDRA, SURENDER M. KAUSHIK, and MAHINDER K. GUPTA. Can. J. Chem. **60**, 1891 (1982).

The kinetics of the solid state isothermal and photochemical decompositions of $K_2TaO_2F_5.H_2O$ have been studied by measuring the pressure of oxygen evolved in a constant volume apparatus. Isothermal decomposition of the sample was carried out in the temperature range 528 to 553 K. The reaction is predominantly deceleratory. The initial stage of the decomposition can be described by the unimolecular decay law whereas the later stage obeys the contracting volume equation. The activation energy values of the two processes are 120 and 90 kJ $mol^{-1}$, respectively. The photolysis of the compound at different intensities yields a pressure–time curve which can be described by the rate equation $p = kt^{1/2}$. The rate of photolysis was found to be linearly dependent on intensity, indicating a monoexcitation process for peroxide decomposition.

GOPAL V. JERE, LATHA SURENDRA, SURENDER M. KAUSHIK et MAHINDER K. GUPTA. Can. J. Chem. **60**, 1891 (1982).

On a étudié la cinétique des décompositions photochimiques et isothermes du $K_2TaO_2F_5.H_2O$ à l'état solide en mesurant la pression d'oxygène dégagé dans un appareil à volume constant. On a réalisé la décomposition isotherme d'un échantillon dans un intervalle de température allant de 528 à 533 K. La réaction diminue de vitesse de façon prédominante. On peut décrire l'étape initiale de la décomposition selon la loi de désintégration unimoléculaire; la dernière étape obéit à l'équation de contraction de volume. Les valeurs des énergies d'activation des deux modes de réaction sont respectivement de 120 kJ $mol^{-1}$ et de 90 kJ $mol^{-1}$. La photolyse du composé à des intensités différentes conduit à une courbe de la pression en fonction du temps que l'on peut décrire par l'équation de vitesse $p = kt^{1/2}$. On a trouvé que la vitesse de photolyse dépend linéairement de l'intensité indiquant un processus de mono-excitation pour la décomposition du peroxyde.

[Traduit par le journal]

## Introduction

Peroxo compounds of transition metals have a wide range of utility because of their ability to release oxygen in active form either chemically, on heating, or on irradiation. These serve as reagents for the oxidation of various substrates (1, 2), epoxidation of olefins (1–5), and also serve as synthetic oxygen carriers in biological systems (6). However, due to the lack of solid state kinetic investigations on these compounds, as yet, no well-founded mechanism is established for the evolution of oxygen on decomposition. A kinetic study is a first important step in this direction. These factors prompted the authors to carry out the solid state thermal and photochemical decomposition of transition metal peroxo compounds on an elemental basis (7–12) to determine the generalities, trends, or differences in the mode of decomposition by changing the cation, anion, or the nature of peroxide linkages etc. This paper is a part of this series and reports the isothermal and photochemical decomposition of $K_2TaO_2F_5.H_2O$.

## Experimental

The title compound, potassium pentafluoroperoxotantalate(V) monohydrate, $K_2TaO_2F_5.H_2O$ (13), was prepared by heating 1 g of tantalum pentoxide in 25 mL of 40% hydrogen fluoride for a period of 10–12 h over a waterbath in a covered polythene beaker. To the clear solution, 20 mL of 30% hydrogen peroxide was added; the resulting solution was cooled. This was followed by the addition of potassium hydroxide solution in the stoichiometric amount. The compound was crystallized by adding alcohol to the above solution and was filtered, washed with alcohol and ether, and dried over phosphorus pentoxide. The dried solid was analysed for active oxygen, fluoride, and potassium contents. The analytical values are $O_A((1/2)O_2^{2-})$, 4.0%; F, 25.6%; K, 21.7%. The loss in weight in TGA run was 8% which is attributable to peroxy oxygen and water. Infrared and laser Raman spectra (530.9 nm laser irradiation) were recorded ($\nu_{O-O}$, at 875 $cm^{-1}$ (s)). The unground sample was used for decomposition studies.

The constant volume equipment and experimental procedures for thermal and photochemical decomposition remained the same as reported earlier (7–12). The kinetics were studied by measuring the pressure of oxygen evolved on decomposition; 4–5 mg (weighed on a Mettler H-54 balance) of compound was heated in a furnace electronically maintained at the desired temperature. Photolysis of the sample was carried out with a high pressure mercury arc lamp emitting principal lines at 365.5, 313.0, 265.3, and 253.7 nm along with a strong background of radiation in the near uv and visible region. Actinometry of the lamp was carried out with potassium trisoxalatoferrate(III) trihydrate and different intensities were obtained by changing the distance between the lamp and the sample. A liquid air trap was used in the system to condense the volatile vapour and water, if produced, during the decomposition reaction.

## Results

### *(a) Thermal decomposition*

Isothermal decomposition of the compound $K_2TaO_2F_5.H_2O$ was carried out in the temperature range of 528 K to 553 K. The values of fractional

0008-4042/82/141891-05$01.00/0

©1982 National Research Council of Canada/Conseil national de recherches du Canada

Can. J. Chem. Downloaded from www.nrcresearchpress.com by 210.87.254.5 on 09/06/12
For personal use only.

Can. J. Chem. Downloaded from www.nrcresearchpress.com by 210.87.254.5 on 09/06/12
For personal use only.

decomposition, $\alpha$, ranged from 0.45 to 0.60. The $\alpha$–time plots are presented in Fig. 1. This shows that the decomposition reaction is predominantly deceleratory. The initial stage of the reaction can be described by the unimolecular decay law, $-\log(1-\alpha) = k_1 t$, at all temperatures (Fig. 2). The activation energy, deduced from an Arrhenius plot (Fig. 3), is 120 kJ mol$^{-1}$. The subsequent decomposition at various temperatures obeys the contracting sphere equation, $1-(1-\alpha)^{1/3} = k_2 t$ (Fig. 4). The activation energy of this process is 90 kJ mol$^{-1}$ (Fig. 5).

*(b) Photochemical decomposition*

Photochemical decomposition studies, wherever feasible, are often complementary to thermal decomposition studies in understanding the mechanism of decomposition reactions. The diffuse reflectance spectrum of $K_2TaO_2F_5.H_2O$ shows a broad absorption band in the range 230–350 nm, similar to other fluoroperoxo species reported by us earlier (8, 10). It undergoes appreciable photochemical decomposition and is amenable for the study of photolysis kinetics. Unlike the thermal decomposition, water is not evolved during photolysis.

The pressure–time curves for the photodecomposition at different intensities and constant temperature (25°C) are parabolic in nature (Fig. 6) and $p$–$t$ data can be fitted to the equation, $p = kt^{1/2}$ (Fig. 7). To determine the effect of intensity on photodecomposition, the rate of photolysis $k$ was plotted against intensity, $I$ (Fig. 8). It was observed that temperature does not have a significant effect on

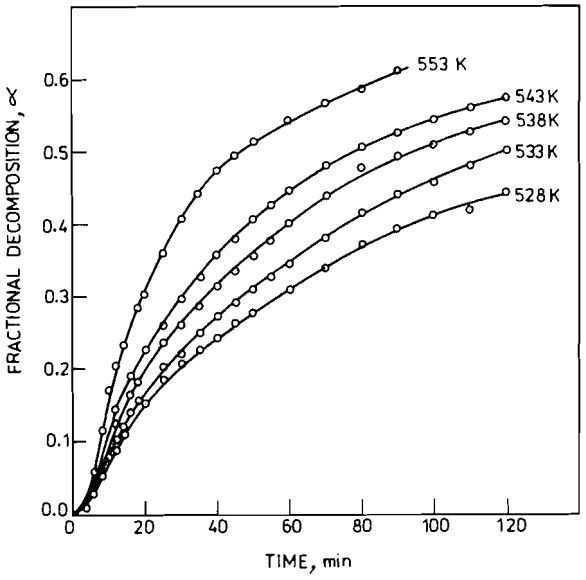


FIG. 1. Thermal decomposition curves for $K_2TaO_2F_5.H_2O$.

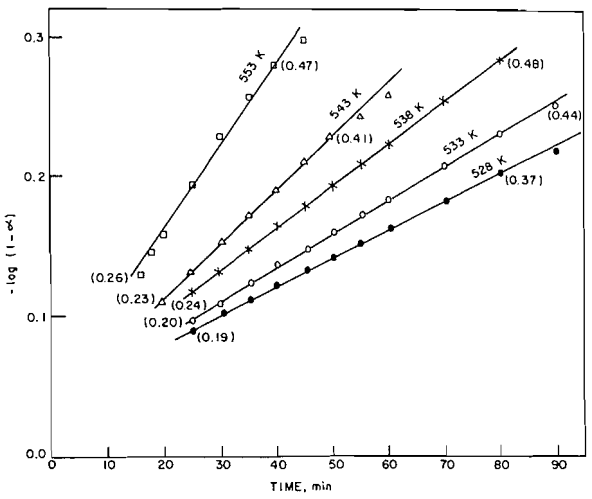


FIG. 2. Plot of the unimolecular decay law, $-\log(1-\alpha)$ vs. time for $K_2TaO_2F_5.H_2O$. The values of $\alpha$ in parentheses give the range over which this law is applicable.

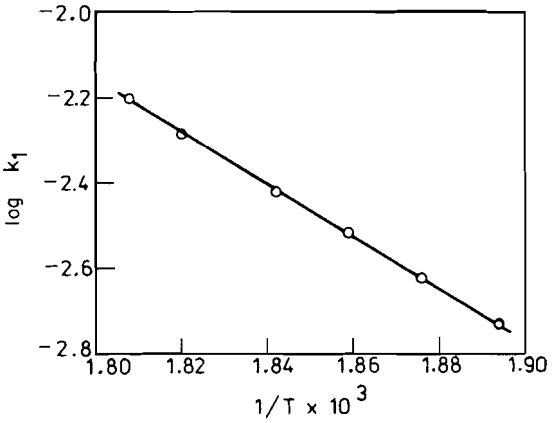


FIG. 3. Arrhenius plot of the unimolecular decay law rate constants, $\log k_1$ vs. $1/T \times 10^3$.

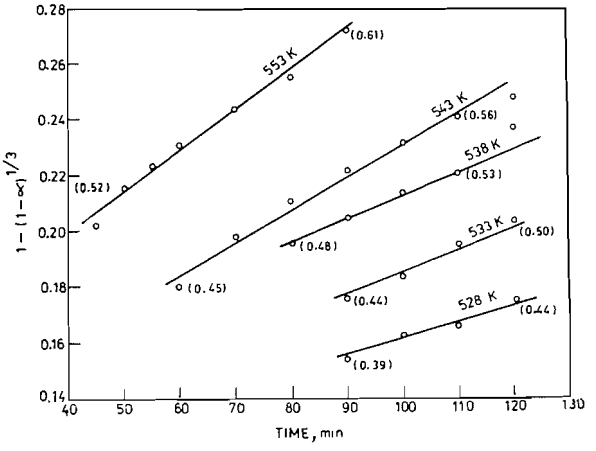


FIG. 4. Plot of contracting sphere equation, $1-(1-\alpha)^{1/3}$ vs. time for $K_2TaO_2F_5.H_2O$. The values of $\alpha$ in parentheses give the range over which this law is applicable.

Can. J. Chem. Downloaded from www.nrcresearchpress.com by 210.87.254.5 on 09/06/12
For personal use only.

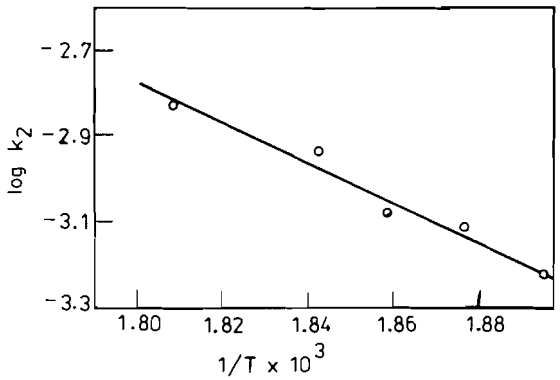


FIG. 5. Arrhenius plot of the contracting sphere rate constants $\log k_2$ vs. $1/T \times 10^3$.

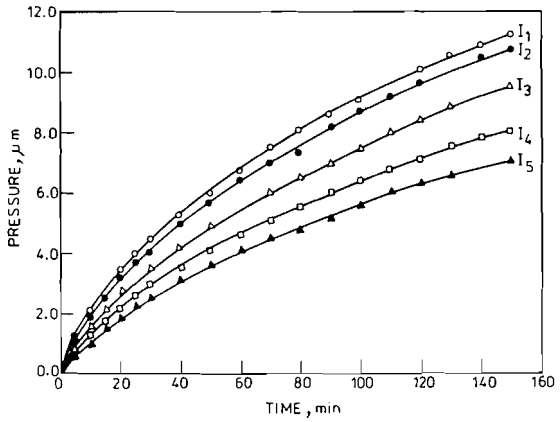


FIG. 6. Pressure–time plots for the photodecomposition of $K_2TaO_2F_5.H_2O$ at different intensities $I_1 = 19.09 \times 10^{15}$, $I_2 = 17.23 \times 10^{15}$, $I_3 = 15.63 \times 10^{15}$, $I_4 = 14.24 \times 10^{15}$, and $I_5 = 11.96 \times 10^{15}$ quanta/s cm$^2$ at constant temperature (25°C).

the photodecomposition of the solid and no dark reaction was detected.

## Discussion

The solid, potassium pentafluoroperoxotantalate(V) monohydrate, $K_2TaO_2F_5.H_2O$, is a typical coordination compound. In the anion, $[TaO_2F_5]^{2-}$, tantalum is surrounded by a pentagonal bipyramidal arrangement of ligands, the peroxo group and three fluorine atoms forming the equatorial plane and the two remaining fluorine atoms at the apices (14). The peroxo group is bidentate chelating in nature, forming a strained triangularly linked configuration

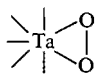


Water is lattice held.

The thermal decomposition of the solid is represented as below:

$$K_2TaO_2F_5.H_2O\ (s) \rightarrow K_2TaOF_5\ (s) + \tfrac{1}{2}O_2\ (g) + H_2O\ (g)$$

Potassium pentafluoroperoxotantalate(V) monohydrate — Potassium oxopentafluorotantalate(V) — Condensed in a cold trap

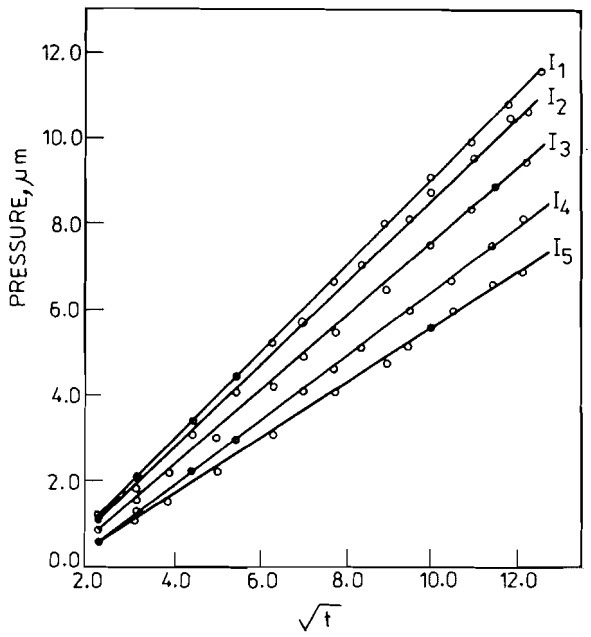


FIG. 7. Plots of $p$ vs. $t^{1/2}$ for $K_2TaO_2F_5.H_2O$ at different intensities $I_1 = 19.09 \times 10^{15}$, $I_2 = 17.23 \times 10^{15}$, $I_3 = 15.63 \times 10^{15}$, $I_4 = 14.24 \times 10^{15}$, and $I_5 = 11.96 \times 10^{15}$ quanta/s cm$^2$ at constant temperature (25°C).

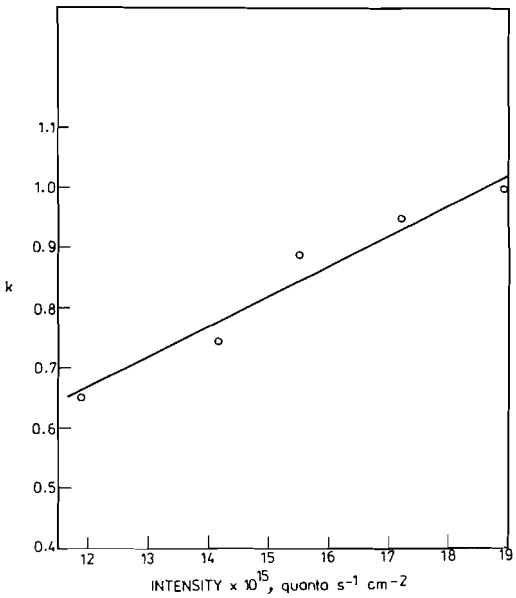


FIG. 8. The dependence of rate constant, $k$, on intensity for $K_2TaO_2F_5.H_2O$.

Can. J. Chem. Downloaded from www.nrcresearchpress.com by 210.87.254.5 on 09/06/12
For personal use only.

The weight loss calculated on the above basis agrees well with TGA data. Further, it is also seen that most of the lattice water is lost prior to peroxide decomposition. The reaction is irreversible and peroxide decomposition is exothermic. No melting of the solid is observed. It is also interesting to note that tantalum fluorine bonds are very stable and the only moiety undergoing decomposition in the anion, $[TaO_2F_5]^{2-}$, i.e. inside the coordination sphere, is the triangularly linked bidentate peroxo group.

Brown, Dollimore, and Galwey observe that, as with ionic solids, the reactivity and kinetic behaviour of coordination compounds can successfully be dealt with by invoking the rate equations and other ideas developed in dealing with model systems of simple inorganic ionic solids (15). Hence, the unimolecular decay law and contracting sphere equation have been used to describe the isothermal decomposition of the compound. The deceleratory nature of the reaction and kinetic obedience to a unimolecular decay law indicate instantaneous nucleation or facile nucleation followed by rapid surface growth of the product. As stated earlier the only moieties undergoing thermal decomposition in the title solid are the lattice water and peroxy oxygen from the coordination sphere. Hence the important factors leading to the instantaneous nucleation are probably the dehydration step, which occurs prior to the onset of peroxide decomposition and the inherent defects in this compound. Also, the decomposition reaction itself may initiate or generate large defects in the solid leading to instantaneous nucleation.

The later stage obeys the contracting volume equation (Fig. 4). This implies that the surface is completely transformed into the product and the interface progresses towards the centre of the crystal. The reaction is deceleratory since the interface progressively decreases.

The activation energies computed from the Arrhenius plots, 120 and 90 kJ $mol^{-1}$, are in agreement with the general finding that the $E_a$ value for the processes occurring on the surface of a crystal is higher than that of the reaction occurring at the interface (16).

The deceleratory nature of the photodecomposition can be explained in terms of "special sites" which assist photolysis and are present in the solid. These "special sites" are slowly consumed during photolysis leading to the decline of the rate of decomposition. This view point has been discussed by several workers (16–18). The rate equation, $p = kt^{1/2}$, describes a parabolic relationship between the pressure of oxygen evolved from peroxide decomposition and the duration of irradiation. Similar equations have been used in the photolysis of inorganic systems by Prout and Lownds (19), Morantz *et al.* (20), Yoganarasimhan and Sood (21), and Jere and Kaushik (10). It is seen from Fig. 8 that the photodecomposition is linearly dependent upon light intensity in the range studied, which shows that the peroxide photolysis probably involves a monoexcitation process (8, 10). However, a larger range of variation is desirable, if linear dependance of the rate on light intensity is to be demonstrated unequivocally. The absence of a dark rate indicates that entities induced by photolysis are either relatively stable or decay extremely rapidly resulting in a thermally stable product.

It is reasonable to assume that in the case of the title solid and other related fluoroperoxo species, the mechanism of the thermal and photochemical reactions appear the same except for the method of excitation. Probably the metal–peroxide ring system and peroxide–peroxide interaction at special sites play important roles in the evolution of oxygen in the decomposition of these solids. This has already been reported (8, 10) and can be visualized as below:

$$O_2^{2-} \xrightarrow{\text{Thermal or } h\nu} O_2^{2-*}$$

$$O_2^{2-} + O_2^{2-*} \rightarrow O_2 + 2O^{2-}$$

In coordination compounds the complexity of the ligands present in the anion increases the number of types of bond redistribution processes which are possible within and between the coordination spheres. This situation puts a severe restriction on kinetic studies of coordination compounds. The situation, however, is much more simple in the case of fluoroperoxo species of transition elements, like the title solid, wherein the only moiety undergoing either thermal or photochemical decomposition inside the coordination sphere of the anion $[TaO_2F_5]^{2-}$ is the peroxo group. The authors feel that these solids may serve as near ideal systems for examining the solid state reactivity and kinetic behaviour of coordination compounds. They also provide an easy route for the synthesis of oxofluorometallates (22) which are finding interesting applications as solid state materials (23).

**Acknowledgements**

The authors thank Dr. W. P. Griffith and his technicians for recording the laser Raman spectra. The authors (L.S., S.M.K., and M.K.G.) are grateful to CSIR and UGC for research fellowships.

1. H. MIMOUN, I. SEREE DE ROCH, and L. SAJUS. Bull. Soc. Chim. Fr. 1481 (1969).
2. H. MIMOUN, I. SEREE DE ROCH, and L. SAJUS. Tetrahedron, **26**, 37 (1970).
3. H. B. KAGAN, H. MIMOUN, C. MARK, and V. SCHURIG. Angew. Chem. **91**, 511 (1979).
4. H. B. KAGAN, H. MIMOUN, C. MARK, and V. SCHURIG. Angew. Chem., Int. Ed. Engl. **18**, 485 (1979).
5. W. WINTER, C. MARK, and V. SCHURIG. Inorg. Chem. **19**, 2045 (1980).
6. R. D. JONES, D. A. SUMMERVILLE, and F. BASOLO. Chem. Rev. **79**, 139 (1979).
7. G. V. JERE and S. M. KAUSHIK. J. Therm. Anal. **18**, 277 (1980).
8. G. V. JERE and S. M. KAUSHIK. J. Solid State Chem. **33**, 145 (1980).
9. G. V. JERE and S. M. KAUSHIK. Thermochim. Acta, **36**, 307 (1980).
10. G. V. JERE and S. M. KAUSHIK. J. Photochem. **16**, 1 (1981).
11. G. V. JERE, L. SURENDRA, S. M. KAUSHIK, and M. K. GUPTA. Thermochim. Acta, **42**, 115 (1980).
12. G. V. JERE, L. SURENDRA, S. M. KAUSHIK, and M. K. GUPTA. Thermochim. Acta, **43**, 379 (1981).
13. J. C. BAILAR, H. J. EMELEUS, SIR RONALD NYLHOLM, and A. F. TROTMAN-DICKENSON (*Editors*). Comprehensive inorganic chemistry. Vol. 3. Pergamon Press. 1973.
14. Z. RUŽIC-TOROŠ, B. KOJIC-PRODIC, and M. SLJUKIC. Acta Crystallogr. B**32**, 1096 (1976).
15. W. E. BROWN, D. DOLLIMORE, and A. K. GALWEY. Comprehensive chemical kinetics. Vol. 22. Reactions in solid state. *Edited by* C. H. Bamford and C. F. H. Tipper. Elsevier Scientific Publishing Company, Amsterdam. 1980. p. 231.
16. W. E. GARNER. Chemistry of the solid state. *Edited by* W. E. Garner. Butterworths, London. 1955. p. 57.
17. D. A. YOUNG. Prog. Solid State Chem. **5**, 427 (1971).
18. P. W. LEVY and P. J. HERLEY. 6th Int. Symp. on the Reactivity of Solids, Schenectady, New York. 1968. Wiley, New York. 1969. p. 75.
19. E. G. PROUT and C. M. LOWNDS. Inorg. Nucl. Chem. Lett. **9**, 377 (1973).
20. D. J. MORANTZ, R. A. M. SCOTT, and J. J. SHORTLAND. J. Phys. Chem. Solids, **33**, 1235 (1972).
21. S. R. YOGANARASIMHAN and R. K. SOOD. J. Solid State Chem. **10**, 323 (1974).
22. G. V. JERE, M. T. SANTHAMMA, S. M. KAUSHIK, L. SURENDRA, and M. K. GUPTA. Mat. Res. Bull. To be published.
23. B. KHAZAI, K. DWIGHT, E. KOSTINER, and A. WOLD. Inorg. Chem. **19**, 1670 (1980).

Can. J. Chem. Downloaded from www.nrcresearchpress.com by 210.87.254.5 on 09/06/12
For personal use only.

# Scaled particle theory of gas solubility — inclusion of the temperature dependent hard sphere term

BRUCE A. COSGROVE[1] AND JOHN WALKLEY[2]

*Department of Chemistry, Simon Fraser University, Burnaby, B.C., Canada V5A 1S6*

Received October 6, 1981

BRUCE A. COSGROVE and JOHN WALKLEY. Can. J. Chem. **60**, 1896 (1982).

The limiting behaviour of the scaled particle theory (spt) of gas solubility has been examined for the inert gases in a range of solvents. The hard sphere limit is shown to exhibit thermodynamic self-consistency only with the inclusion of an effective hard sphere diameter temperature dependence whereas the original spt (exclusion of a temperature dependence) fails to extrapolate to the correct hard sphere limit. Furthermore, inclusion of the temperature dependence yields correct thermodynamic properties for gases of small atomic diameter (and well depth potential) as would be expected from a hard sphere based theory.

BRUCE A. COSGROVE et JOHN WALKLEY. Can. J. Chem. **60**, 1896 (1982).

On a étudié le comportement limitant de la théorie de la particule graduée relative à la solubilité des gaz pour les gaz inertes dans divers solvants. On montre que la limite de sphère dure possède des propriétés thermodynamiques qui sont en accord entre elles uniquement lorsqu'on inclut l'effet de la température sur le diamètre effectif de la sphère dure, alors que la théorie originale (excluant l'effet de la température) ne peut être extrapolée vers la bonne limite de la sphère dure. De plus, l'introduction de l'effet de la température donne les bonnes propriétés thermodynamiques des gaz de faible diamètre atomique (et le potentiel de puit) tel qu'attendu à partir d'une théorie fondée sur la sphère dure.

[Traduit par le journal]

## Introduction

Recent work on the development of a theory of gas solubility based upon a hard sphere perturbation approach (1, 2) suggests that it is useful to take a further look at approaches based upon the use of scaled particle theory (spt) (3, 4). Like the perturbation approach, the leading terms (coming from spt) are rigorous for systems of hard spheres (5). With the future development of the perturbation approach, which will necessarily involve approximations for the application to systems even as complex as argon in benzene or water solvent, a comparison of the two theories should be mutually beneficial.

The scaled particle theory of gas solubility (6–8) has been used extensively over the past two decades and has been shown to give excellent agreement with experiment (9). The most surprising aspect of the theory is that it appears to predict the thermodynamic properties (Henry's law coefficient $K_H$, enthalpies of solution $\Delta H_S$, entropies of solution $\Delta S$) of gases dissolved in water as successfully as it does for less complex organic solvents. Despite some criticisms of the early theory (10–13), the formulation as put forward by Pierotti is still used. Basic to the theory is the use of terms derived by Reiss *et al.* (3, 4) for the calculation of the reversible work of making a cavity in a hard sphere solvent. The prescription used for the gas dissolution process is a very simple one. The gas solute is discharged to a hard sphere. As a hard sphere it makes a cavity in the real (undischarged) solvent. Finally, the solute is recharged and allowed to interact with the solvent molecules. This simple prescription has two important features. First is the recognition that when the (discharged) hard sphere solute makes a cavity in the real solvent the solute molecule interacts only with the effective hard sphere diameter of the solvent molecules. The second is that the retention of the solvent as an undischarged system has the not-negligible advantage of allowing the use of experimental solvent properties; for instance, the coefficient of thermal expansion, in the evaluation of the thermodynamic solubility terms.

In this paper we examine the criticism that the Pierotti theory neglects the temperature dependence of the "effective hard sphere diameter" of the solvent molecules (10, 12). Such a dependence is now well recognized and we shall show that without its inclusion the theory fails to extrapolate to the expected hard sphere limit.

## Theory

The spt of gas solubility is so well known and has been "rederived" so many times that we consider it necessary to quote only the required equations. We shall retain the notation as used by Pierotti (6) for all thermodynamic terms, using subscript 1 for solvent and subscript 2 for solute. For this theory the Henry's law coefficient for the dissolved gas

[1]Present address: Moli Energy Ltd., 4010 Myrtle Street, Burnaby, B.C., Canada.

[2]To whom all correspondence should be addressed.

0008-4042/82/141896-05$01.00/0

©1982 National Research Council of Canada/Conseil national de recherches du Canada

Can. J. Chem. Downloaded from www.nrcresearchpress.com by 210.87.254.105 on 09/06/12
For personal use only.

Can. J. Chem. Downloaded from www.nrcresearchpress.com by 210.87.254.105 on 09/06/12
For personal use only.

may be written:

[1] $$\ln K_H = \bar{G}_i/RT + \bar{G}_c/RT + \ln (RT/V_1)$$

where $\bar{G}_c$ is the reversible work required to make a cavity in a hard sphere solvent sufficient to accommodate a hard sphere solute molecule, and $\bar{G}_i$ is the free energy associated with the recharging step in the prescribed dissolution process. The assumption is made that this term is equivalent to the enthalpy of recharging, thus neglecting any entropy contribution from this step. Since the pressure of the system remains 1 atm (solvent is *not* discharged to an equivalent hard sphere system), the enthalpy of recharging $\bar{H}_i$ may be equated to the energy of interaction $\bar{E}_i$. This latter term may be written in terms of an appropriate potential of interaction and the radial distribution function of the solvent (a van der Waal's approximation is usually made (14)).

The enthalpy of solution may be written:

[2] $$\Delta H_S = \left(\frac{\partial \ln K_H}{\partial(1/RT)}\right)_P = \bar{H}_i + \bar{H}_c - RT + \alpha_p RT^2$$

(where $\alpha_p$ is the thermal expansion coefficient of the real solvent) and the entropy of solution, since $\bar{G}_i \equiv \bar{H}_i$, becomes

[3] $$T\Delta S = \bar{H}_c - RT + \alpha_p RT^2 - \bar{G}_c - RT \ln (RT/V_1)$$

In this paper we are interested primarily in those thermodynamic terms associated with the dissolution of a hard sphere solute into the real solvent. A hard sphere solute is one having a zero value for its molecular polarizability ($\alpha$) so for the dissolution of such a solute all terms arising from the recharging process must become zero. Thus, we may write:

[4] $$\lim_{\alpha \to 0} \ln K_H = \ln K_H{}^0 = \bar{G}_c/RT + \ln (RT/V_1)$$

[5] $$\lim_{\alpha \to 0} \Delta H_S = \Delta H_S{}^0 = \bar{H}_c - RT + \alpha_p RT^2$$

and, hence,

[6] $$\lim_{\alpha \to 0} T\Delta S^0 = \Delta H_S{}^0 - RT \ln k_H{}^0$$

Since spt gives us an expression for $\bar{G}_c$, we are concerned with the formulation of $\bar{H}_c$ from $\bar{G}_c$. That is, in obtaining the derivative

[7] $$\bar{H}_c = -RT^2[\partial(\bar{G}_c/RT)/\partial T]_p$$

where (3),

[8] $$\bar{G}_c/RT = A^2\{\tfrac{9}{2}[y/(1-y)]^2 + 3y/(1-Y)\} + 3yA/(1-y) - \ln(1-y) + n\pi Pa_2{}^3/6RT$$

If we recognise the effective hard sphere diameters ($a_i$) to be temperature dependent and define $l_i = 1/a_i(da_i/dT)_p$, then, since $y = \pi a_1{}^3 N/6V_1$,

[9] $$\bar{H}_c = yRT^2(\alpha_p - 3l_1)(1-y)^{-3}\{3(1+2y)A^2 + 3(1-y)A + (1-y)^2\} - N\pi Pa_2{}^3(3Tl_2 - 1)/6$$

We note that $A = a_2/a_1$ and, thus, $(\partial A/\partial T)_p$ is of negligible magnitude. For any real solvent the last term in eq. [9] is small and will henceforth be ignored. It is seen that eq. [9] differs from the expression for $\bar{H}_c$ given by Pierotti by the inclusion of the $3l_1$ term.

## Discussion

Pierotti (15) recognized that for the inert gas atoms a plot of the effective hard sphere diameter (that value of the inter-atomic separation at which the interaction potential is zero) against the atomic polarizability of the gas gave a smooth curve. The extrapolation of this curve to zero polarizability thus gives the hard sphere diameter ($a_2{}^0$) of a hard sphere (inert gas) atom ($a_2{}^0 = 2.55$ Å). If a similar plot is constructed for $\ln k_H$ (for the inert gases in a given solvent), then the extrapolation of this curve to zero polarizability will give the $\ln k_H{}^0$ value for the hard sphere solute in that solvent. It is easily seen from eqs. [4] and [8] that knowing $\ln k_H{}^0$ and $a_2{}^0$ allows $a_1$ to be determined.

Wilhelm later extended this technique and by examining $\ln k_H$ data over a range of temperatures, and hence obtaining $\ln k_H{}^0$ values at different temperatures, was able to show that the $a_1$ values so obtained did exhibit a sensible temperature dependence (16, 17). This approach to determining an $l_1$ value relies heavily upon the availability of accurate $k_H$ values over a wide temperature range. It is obvious, however, that if we obtain $\Delta H_S{}^0$ values from the extrapolation of a $\Delta H_S$ vs. atomic polarizability plot, then from eqs. [5] and [9] we may determine $l_1$ directly.

In Table 1 we present the extrapolated $\Delta H^0$ values (for the inert gases dissolved in a range of solvents). We compare these $\Delta H_S{}^0$ values to those calculated from eq. [5] when the Pierotti assumption of no hard sphere temperature dependence ($l_1 = 0$) is made (in eq. [9]). The agreement between these two sets of values is seen to be very poor, and certainly outside the $\pm 100$ cal mol$^{-1}$ error possible in the extrapolated $\Delta H_S{}^0$ values. A comparison is also made between the $l_1$ values calculated from these extrapolated $\Delta H_S{}^0$ values and those deter-

Can. J. Chem. Downloaded from www.nrcresearchpress.com by 210.87.254.105 on 09/06/12
For personal use only.

TABLE 1. Temperature dependence of the solvent effective hard sphere diameter

| Solvent | $\Delta H^0$ (extrap) (cal mol$^{-1}$) | $\Delta H^0$ (calcd, $l_1 = 0$) (cal mol$^{-1}$) | $10^3 l_1$, (K$^{-1}$) (eq. [5]) | $10^3 l_1$, (K$^{-1}$) Wilhelm[a] |
|---|---|---|---|---|
| Benzene | 2750 | 1929 | −0.15 | −0.16 |
| Water | 275 | −90 | −0.08 | −0.08 |
| $c$-$C_6H_{12}$ | 2550 | 1807 | −0.14 | −0.13 |
| $n$-$C_6H_{14}$ | 2250 | 1446 | −0.19 | −0.13 |

[a]Reference 16.

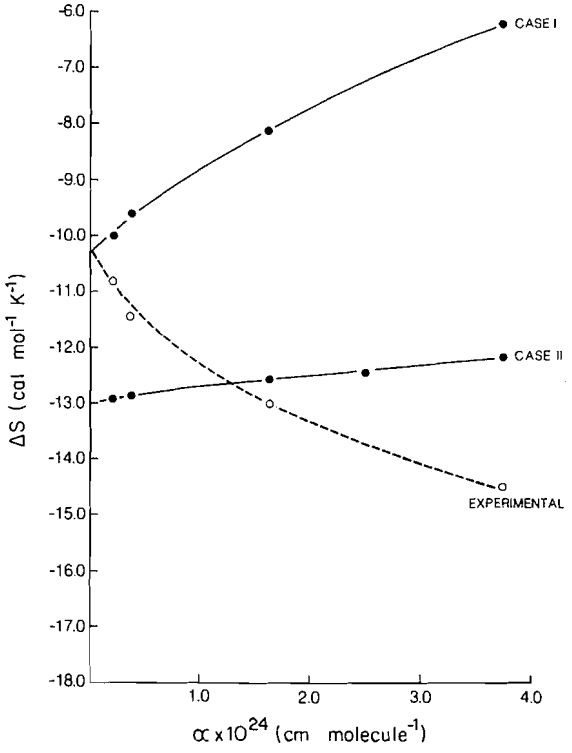


FIG. 1. Entropy of solution $\Delta S$ of inert gases in $C_6H_6$ vs. inert gases polarizability: case I, spt with $l_1 = -0.15 \times 10^{-3}$ K$^{-1}$; case II, original spt with $l_1 = 0$.

mined from the ln $K_H^0$ values (16). Here, the agreement is seen to be excellent.

It is of interest to examine the hard sphere limit of the entropy of solution term, eq. [6], since with the assumption that $\bar{G}_i \equiv \bar{H}_i \equiv \bar{E}_i$ the theoretical expression for $\Delta S$ (eq. [3]) itself contains no "interaction" term. In Fig. 1 we plot the entropy of solution as a function of the polarizability of the inert gas solutes in benzene. Only that theoretical curve calculated with the enthalpy term including the appropriate $l_1$ value agrees with the hard sphere extrapolation value of the experimental data. Using the Pierotti assumption, that $l_1 = 0$, the entropy plot again fails to give the correct limiting case value and though this data appears to give better agreement with experiment this is obviously the dominance of the $RT \ln (RT/V_1)$ term in the entropy expression ($\approx 12$ cal K$^{-1}$ mol$^{-1}$).

Ben-Naim and Friedman (10) suggested that a hard sphere temperature dependence should have been incorporated into the Pierotti theory. Pierotti examined the experimental gas solubility data then available and was unable to find any variation of $a_1$ with temperature for either water or benzene solvent (15). Wilhelm (16), using later data, showed a strong temperature dependence to exist. The fact that this term is not included in the Pierotti formulation for the enthalpy term seems to be based on the argument that although the solvent $a_1$ value is obtained from the ln $k_H^0$ and $a_2^0$ values at a given temperature the enthalpy term is that for the process of making a cavity in a system of hard spheres of *defined hard sphere radius* (at that temperature). That is to say $\Delta H$ is calculated using a different $a_1$ value at each temperature but not, however, incorporating an implicit temperature dependence for $a_1$ in the formulation of eq. [9]. Since the theory should work equally well for the dissolution of totally hard sphere solutes (i.e., of zero molecular polarizability) we can examine eqs. [1] and [2] for thermodynamic self-consistency for the dissolution of such a hypothetical solute molecule (i.e., for that case where $\bar{H}_i = \bar{G}_i = 0$). We chose hard sphere molecules of diameters corresponding to the $a_2$ values of the inert gases. We examine the enthalpy of solution term at 298 K calculated according to eq. [2] and an enthalpy calculated numerically from ln $k_H$ values (eq. [1]) at two temperatures spanning (±5 K) the 298 K value. Computer calculations show ln $k_H$ (298 K) to be the arithmetic mean of ln $k_H$ (293 K) and ln $k_H$ (303 K). We will define

$$[10] \quad \Delta H_S (\ln k_H) = -RT^2 \times \left( \frac{\ln k_H (303) - \ln k_H (293)}{10} \right)$$

and $\Delta H_S^p$(calcd) as that value calculated at 298 K using the Pierotti assumption that $l_1 = 0$ and $\Delta H_S^l$(calcd) as that value calculated using the "correct" $l_1$ value for that particular solvent. In Table 2 we present these enthalpy values for a

Can. J. Chem. Downloaded from www.nrcresearchpress.com by 210.87.254.105 on 09/06/12
For personal use only.

TABLE 2. Enthalpies of solution (cal $mol^{-1}$) inert gas type hard sphere solutes ($\bar{H}_1 = \bar{G}_1 = 0$)

| System | $\Delta H_S^p$ | $\Delta H_S$ (ln $k_H$) | $\Delta H_S^l$ (calcd) |
|---|---|---|---|
| $He/H_2O$ | −86.08 | $3.43\times10^2$ | $3.44\times10^2$ |
| $Ne/H_2O$ | −42.35 | $4.27\times10^2$ | $4.28\times10^2$ |
| $Kr/H_2O$ | $2.33\times10^2$ | $9.59\times10^2$ | $9.61\times10^2$ |
| $Xe/H_2O$ | $4.14\times10^2$ | $13.07\times10^2$ | $13.11\times10^2$ |
| $He/C_6H_6$ | $2.04\times10^3$ | $2.84\times10^3$ | $2.91\times10^3$ |
| $Ne/C_6H_6$ | $2.25\times10^3$ | $3.12\times10^3$ | $3.21\times10^3$ |
| $Kr/C_6H_6$ | $3.59\times10^3$ | $4.91\times10^3$ | $5.03\times10^3$ |
| $Xe/C_6H_6$ | $4.46\times10^3$ | $6.07\times10^3$ | $6.22\times10^3$ |
| $Ar/H_2O$ | $1.60\times10^2$ | $8.18\times10^2$ | $8.20\times10^2$ |
| $Ar/C_6H_6$ | $3.24\times10^3$ | $4.44\times10^3$ | $4.55\times10^3$ |
| $Ar/C_7H_{16}$ | $2.60\times10^3$ | $3.52\times10^3$ | $3.53\times10^3$ |
| $Ar/CCl_4$ | $2.83\times10^3$ | $3.89\times10^3$ | $3.93\times10^3$ |

range of hypothetical rare gas hard sphere solutes in water, in benzene and for hard sphere argon in a range of other solvents (18). It is seen that the necessary self-consistency is found only between the $\Delta H_S$ (ln $k_H$) and the $\Delta H_S^l$(calcd) values.

The interaction term in eqs. [1] and [2], representing the recharging step in the dissolution process, is necessarily approximate. It would not be expected that this term should represent the structural characteristics of the solvent surrounding the solute molecule as might terms beyond the hard sphere basis term of a perturbation approach. This term does, however, add a useful empirical element to the theory. In Figs. 2 and 3 we examine the predictive success of the theory in a plot of the difference term ($\Delta H_S$(calcd) − $\Delta H_S$(expt)) for the

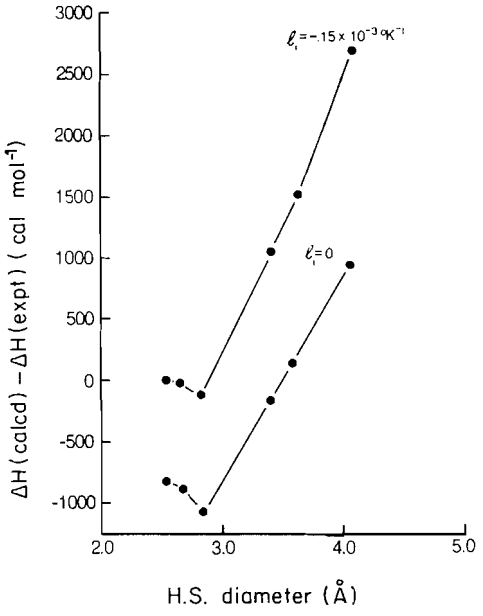


FIG. 2. $\Delta H_S$(calcd) − $\Delta H_S$(expt) for the inert gases in $C_6H_6$ vs. inert gases hard sphere diameters.

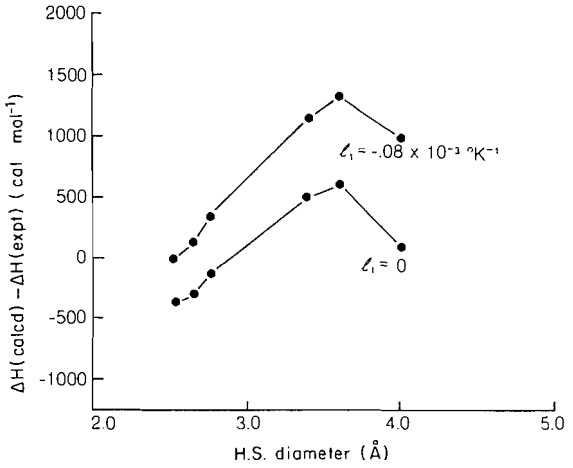


FIG. 3. $\Delta H_S$(calcd) − $\Delta H_S$(expt) for the inert gases in $H_2O$ vs. inert gases hard sphere diameters.

rare gases in benzene and water solvent, respectively. The pattern exhibited by those calculations made with the inclusion of the $l_1$ term again emphasises the correct limiting behaviour (as the molecular polarizability approaches zero) of this version of the theory, whereas calculations made with the assumption that $l_1 = 0$ appear only to give good agreement "around argon and krypton". To emphasise this we present in Table 3 ln $k_H$ and $\Delta H_S$ data for helium and neon in a range of solvents and it is seen that only those values calculated with the inclusion of the $l_1$ term give acceptable agreement with experiment.

We can summarise by noting that the original theory (with $l_1 = 0$) fails to give the expected hard sphere enthalpy value, fails to give thermodynamic self-consistency for the temperature variation of ln $k_H$ (for hard sphere solutes), and agrees with experiment only for gases of size and interaction well depth similar to argon and krypton. This is observed for all solvents (18). With the inclusion of the $l_1$ term the theory is observed to give excellent agreement with the hard sphere limiting enthalpy value, exhibits the correct thermodynamic self-

TABLE 3. Henry's law constants and enthalpies of solution

| System | ln $k_H$(expt) | ln $k_H$ (calcd) | $\Delta H_S^p$ (calcd) | $\Delta H_S$ (expt) | $\Delta H_S^l$ (calcd) |
|---|---|---|---|---|---|
| $He/H_2O$ | 11.82 | 11.64 | −486 | −182 | −56 |
| $Ne/H_2O$ | 11.72 | 11.10 | −1026 | −896 | −554 |
| $He/C_6H_6$ | 9.47 | 9.08 | 1521 | 2396 | 2400 |
| $Ne/C_6H_6$ | 9.09 | 8.05 | 931 | 1984 | 1889 |
| $He/c\text{-}C_6H_{12}$ | 9.01 | 8.69 | 1391 | 2421 | 2186 |
| $Ne/c\text{-}C_6H_{12}$ | 8.63 | 7.65 | 791 | 1461 | 1655 |
| $He/n\text{-}C_6H_{14}$ | 8.25 | 7.94 | 1084 | 1920 | 1913 |
| $Ne/n\text{-}C_6H_{14}$ | 7.90 | 7.04 | 563 | 1348 | 1461 |

TABLE 4. Values of parameters used in calculations

| | $\varepsilon/k$ (K) | $\sigma \times 10^8$ (cm) | Solvent dipole moment (D) | Solute polarizability $\alpha \times 10^{24}$ ($cm^3$/molecule) | $\beta_T \times 10^4$ $(atm)^{-1}$ | $\alpha_p \times 10^3$ $(K)^{-1}$ | Density ($g/cm^3$) at 298 K |
|---|---|---|---|---|---|---|---|
| He | 6.03[a] | 2.63[a] | — | 0.204[b] | — | — | — |
| Ne | 34.9[a] | 2.78[a] | — | 0.393[b] | — | — | — |
| Ar | 122[a] | 3.40[a] | — | 1.63[b] | — | — | — |
| Kr | 171[a] | 3.60[a] | — | 2.46[b] | — | — | — |
| Xe | 221[a] | 4.06[a] | — | 4.00[b] | — | — | — |
| $H_2O$ | 79.3[b] | 2.76[d] | 1.84[b] | — | 0.4583[e] | 0.257[e] | 0.9970[e] |
| $C_6H_6$ | 531[d] | 5.26[c] | 0 | — | 0.9808[e] | 1.235[f] | 0.8738[g] |
| $c$-$C_6H_{12}$ | 589[d] | 5.65[c] | 0 | — | 1.125[e] | 1.21[f] | 0.7738[g] |
| $CCl_4$ | 536[d] | 5.37[a] | 0 | — | 1.081[f] | 1.231[f] | 1.5842[f] |
| $n$-$C_6H_{14}$ | 517[d] | 5.92[b] | 0 | — | 1.627[e] | 1.30[f] | 0.6550[g] |

[a]Reference 6.
[b]Reference 8.
[c]Reference 20.
[d]Reference 18.
[e]Reference 21.
[f]Reference 22.
[g]Reference 23.

consistency, and gives agreement with the experimental data for gases of small interaction well depth. Thus, this latter version of the theory behaves in a manner expected of a theory based upon terms which are exact for hard sphere systems.

In Table 4 we give the values of the various physical parameters used in the above calculations. For experimental data values see refs. 9, 19.


1. S. GOLDMAN. J. Phys. Chem. **81**, 1428 (1977).
2. L. R. PRATT and D. CHANDLER. J. Chem. Phys. **67**, 3683 (1977).
3. H. REISS, H. L. FRISCH, and J. L. LEBOWITZ. J. Chem. Phys. **31**, 369 (1959).
4. H. REISS, H. L. FRISCH, E. HELFAND, and J. L. LEBOWITZ. J. Chem. Phys. **32**, 119 (1960).
5. N. M. DESROSIERS and J-P. MOREL. Can. J. Chem. **59**, 1 (1981).
6. R. A. PIEROTTI. J. Chem. Phys. **67**, 1840 (1963).
7. R. A. PIEROTTI. J. Chem. Phys. **69**, 281 (1965).
8. R. A. PIEROTTI. Chem. Rev. **76**, 717 (1976).
9. E. WILHELM, R. BATTINO, and R. J. WILCOCK. Chem. Rev. **77**, 219 (1977).
10. A. BEN-NAIM and H. L. FRIEDMAN. J. Phys. Chem. **71**, 448 (1967).
11. F. H. STILLINGER. J. Solution Chem. **2**, 141 (1973).
12. W.-Y. WEN and J. A. MUCCITELLI. J. Solution Chem. **8**, 225 (1979).
13. L. WOODCOCK. J. Chem. Soc. Faraday Trans. 2, **72**, 731 (1976).
14. N. S. SNIDER and T. M. HERRINGTON. J. Chem. Phys. **47**, 2248 (1967).
15. R. A. PIEROTTI. J. Phys. Chem. **71**, 2366 (1967).
16. E. WILHELM. J. Chem. Phys. **58**, 3558 (1973).
17. E. WILHELM. J. Chem. Phys. **60**, 3896 (1974).
18. B. A. COSGROVE. M.Sc. Thesis, Simon Fraser University. 1980.
19. B. COSGROVE and J. WALKLEY. J. Chromatogr. **216**, 161 (1981).
20. E. WILHELM and R. BATTINO. J. Chem. Phys. **58**, 3561 (1973).
21. M. DIAZ PENA, G. TARDAJOS, C. MENDUINA, and R. L. ARENOSA. J. Chem. Thermodyn. **11**, 67 (1979).
22. J. S. ROWLINSON. Liquids and liquid mixtures. Butterworths Scientific Press, London. 1959.
23. J. TIMMERMANS. J. physico-chemical constants of pure organic compounds. Vol. I. Elsevier Press, New York. 1965.


Can. J. Chem. Downloaded from www.nrcresearchpress.com by 210.87.254.105 on 09/06/12
For personal use only.

# Syntheses of N-substituted 3,3,4-triphenyl-4-benzoylazetidin-2-ones and 3′,3′-diphenyl spiro(acenaphthen-1-one-2,4′-azetidin-2′-ones); novel examples exhibiting a high reactivity of imino group in ketoimines

S. B. SINGH AND K. N. MEHROTRA

*Department of Chemistry, Banaras Hindu University, Varanasi-221005, India*

Received August 31, 1981[1]

S. B. SINGH and K. N. MEHROTRA. Can. J. Chem. **60**, 1901 (1982).

The reaction of 2-diazo-1,2-diphenylethanone (**1**) with 2-imino-1,2-diphenylethanones **2***a–e* gave new N-substituted 3,3,4-triphenyl-4-benzoylazetidin-2-ones **3***a–e*, together with 1,1′,2,2′-tetraphenyl-2,2′-azinodiethanone (**4**). Similar reaction of **1** with 2-iminoacenaphthenones **6***a*, *b* yielded N-substituted 3′,3′-diphenyl spiro(acenaphthen-1-one-2,4′-azetidin-2′-ones) **7***a*, *b* and ketazine **4**. Lithium aluminium hydride reduction of azetidinones **3***a*, *b* gave **4**-α-hydroxybenzylazetidin-2-ones **5***a*, *b*. The spiro azetidinones **7***a*, *b* on reduction with sodium borohydride yielded spiro(1-hydroxyacenaphthene-2,4′-azetidin-2-ones) **8***a*, *b*. The azetidinones **3***a–e* and **7***a*, *b* were found to be unaffected by either acid or base hydrolysis. The marked selective reactivity of the imino group as compared to the carbonyl group towards diphenylketene has been observed in the present studies. The comparative reactivity of carbonyl groups present in azetidinones **3***a*, *b* and **7***a*, *b* has been presented.

S. B. SINGH et K. N. MEHROTRA. Can. J. Chem. **60**, 1901 (1982).

La diazo-2 diphényl-1,2 éthanone (**1**) réagit avec les imino-2 diphényl-1,2 éthanones (**2***a–e*) en donnant les nouvelles triphényl-3,3,4 benzoyl-4 azétidinones-2 (**3***a–e*) substituées sur l'azote ainsi que la tétraphényl-1,1′,2,2′ azino-2,2 diéthanone (**4**). D'une manière analogue, le composé **1** réagit avec les imino-2 acénaphténones (**6***a*,*b*) en donnant les diphényl-3′,3′ spiro(acénaphténones-1 azétidine-2,4′ ones-2′) (**7***a*,*b*) substituées sur l'azote ainsi que la cétazine (**4**). La réduction des azétidinones (**3***a*,*b*) par $LiAlH_4$ conduit aux α-hydroxy benzyl-4 azétidinones-2 (**5***a*,*b*). La réduction des spiro(azétidinones) (**7***a*,*b*) par le borohydrure de sodium conduit aux spiro(hydroxy-1 acénaphthène-azétidine-2,4′ ones-2′) (**8***a*,*b*). On a trouvé que les azétidinones (**3***a–e* et **7***a*,*b*) ne s'hydrolysent pas en milieu acide ou en milieu basique. Dans cette étude, on a observé une réactivité sélective marquée du groupe imino, par comparaison au groupe carbonyle, envers le diphénylcétène. On présente une comparaison de la réactivité des groupes carbonyles présents dans les azétidinones **3***a*,*b* et **7***a*,*b*.

[Traduit par le journal]

The cycloaddition of diphenylketene with imines (1), diimines (2), azines (3), conjugated imines (4), and 1,3-diazabutadienes (5) is known to form β-lactams. Addition of dimethylketene to 2-*p*-tolyl-imino-1,2-diphenylethanone, having a ketoimine group, has been observed to give 4,4-dimethyl-1,5-diphenyl-2-*p*-tolyl-6-oxa-2-azabicyclo[3.1.0]-hexan-3-one (6). A few spiro(2-azetidinones) have been obtained from the reaction of isocyanates with olefins (7) or allenes (8), carbodiimides with 4,4-dicarboxy-2-azetidinones (9), and acid chlorides with anils (10). We now report the cycloaddition of diphenylketene, generated *in situ* by thermal decomposition of 2-diazo-1,2-diphenylethanone (**1**), with 2-imino-1,2-diphenylethanones **2***a–e* and 2-imino-acenaphthenones **6***a*, *b* leading to new azetidinones **3***a–e* and spiro azetidinones **7***a*, *b* in fair yields. This study has also revealed the marked selective reactivity of the imino group as compared to the carbonyl group in ketoimines **2***a–e* and **6***a*, *b* towards diphenylketene. The carbonyl group in the azetidinone ring in the products **3***a–e* and **7***a*, *b* is found to be unaffected either by hydrolysis or treatment with lithium aluminium hydride and sodium borohydride. The carbonyl group, not present in the azetidinone ring of the products **3***a*, *b*, is found to be less reactive than the corresponding carbonyl group in spiro azetidinones **7***a*, *b* as the former is reduced by lithium aluminium hydride while the latter is reduced even by sodium borohydride. Moreover, azetidinones **3***a–e* and **7***a*, *b* obtained in the present work could be used as precursors and their synthetic utility could be tapped as the carbonyl group left unattacked by diphenylketene could be developed to other desired functionalities.

## Results and discussion

The product mixture obtained by the reaction of 2-diazo-1,2-diphenylethanone (**1**) with 2-isopropyl-imino-1,2-diphenylethanone (**2***a*) was separated by fractional crystallization from *n*-hexane – ethanol (1:1) mixture and ethanol; it consisted of 1,1′,2,2′-tetraphenyl-2,2′-azinodiethanone (**4**, 4%) and 1-isopropyl-3,3,4-triphenyl-4-benzoyl-2-azetidinone (**3***a*, 44%). The structural assignment of **3***a* was made on the basis of analytical and spectral data given in Tables 1 and 2. The ir spectrum of **3***a* shows strong bands at 1740 (C=O, azetidinone) (11) and 1680 (C=O, benzoyl) $cm^{-1}$. The nmr

[1]Revision received February 15, 1982.

0008-4042/82/141901-06$01.00/0

©1982 National Research Council of Canada/Conseil national de recherches du Canada

Can. J. Chem. Downloaded from www.nrcresearchpress.com by 210.87.254.42 on 09/06/12
For personal use only.

TABLE 1. Conversion of ketoimines **2***a*–*e* to azetidinones **3***a*–*e*

| | | Product **3***a*–*e* | | | | | | | | |
|---|---|---|---|---|---|---|---|---|---|---|
| | | | | | Elemental Analysis (%) | | | | | |
| | | | | | Found | | | Calculated | | |
| Ketoimines | R | Yield (%) | Melting point (°C) | Molecular formula | C | H | N | C | H | N |
| **2***a* | $CH(CH_3)_2$ | 52 | 186–187 | $C_{31}H_{27}NO_2$ | 83.18 | 6.45 | 2.96 | 83.59 | 6.06 | 3.14 |
| **2***b* | $CH(C_6H_4—p\text{-}CH_3)CH_3$ | 31 | 155–156 | $C_{37}H_{31}NO_2$ | 84.72 | 6.20 | 3.22 | 85.22 | 5.96 | 2.68 |
| **2***c* | $CH(Ph)CH_3$ | 44 | 176–177 | $C_{36}H_{29}NO_2$ | 85.31 | 5.31 | 3.01 | 85.20 | 5.72 | 2.76 |
| **2***d* | $CH(Ph)_2$ | 11 | 198–199 | $C_{41}H_{31}NO_2$ | 86.90 | 5.47 | 2.77 | 86.46 | 5.45 | 2.46 |
| **2***e* | Ph | 47 | 177–178 | $C_{34}H_{25}NO_2$ | 84.96 | 5.40 | 2.97 | 85.18 | 5.22 | 2.92 |

spectrum of **3***a* displays the aromatic protons as multiplets at δ 7.33 (15H) and 6.97 (5H), the methine proton as a septet at δ 3.48 ($J$ = 7 Hz) and the methyl protons as a pair of doublets (11) at δ 1.70 and 1.23 (6H, $J$ = 7 Hz). The mass spectrum shows the molecular ion peak at $m/e$ 445. The authentic sample of **4** was prepared according to the reported method (12) for comparison (ir, nmr, and also mmp).

Similar treatment of ketoimines **2***b*–*e* with **1** gave azetidinones **3***b*–*e* (11–45%), identified on the basis of their analytical and spectral (uv, ir, and nmr) data (Tables 1 and 2), and ketazine **4** (5–10%).

The reduction of **3***a* with lithium aluminium hydride in dry ether gave 1-isopropyl-3,3,4-triphenyl-4-(α-hydroxybenzyl)-azetidin-2-one (**5***a*, 86%), characterized on the basis of analytical and spectral data. Its ir spectrum exhibits a medium intensity band at 3440 $cm^{-1}$, characteristic of the O—H group, and a strong band at 1735 $cm^{-1}$, characteristic of C=O (azetidinone) (11). The nmr spectrum displays the aromatic protons as multiplets at δ 7.93 (2H), 7.53 (4H), and 7.05 (14H), the benzylic proton as a doublet (collapses to a singlet on deuteration) at δ 4.89 ($J$ = 4 Hz), the methine proton as a septet at δ 2.69 ($J$ = 7 Hz), the hydroxy proton as a broad singlet at δ 2.00 (exchangeable on deuteration), and the methyl protons as a pair of

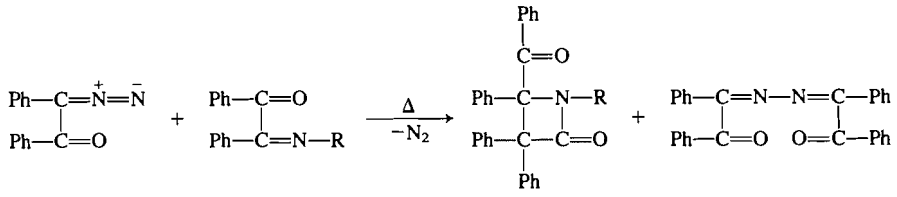

**1** **2***a*–*e* **3***a*–*e* **4**

*a* R = $CH(CH_3)_2$
*b* R = $CH(Ar)CH_3$; Ar = $C_6H_4—p\text{-}CH_3$
*c* R = $CH(Ph)CH_3$
*d* R = $CHPh_2$
*e* R = Ph

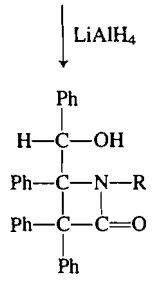

**5***a*,*b*

*a* R = $CH(CH_3)_2$
*b* R = $CH(Ar)CH_3$, Ar = $C_6H_4—p\text{-}CH_3$

SCHEME 1

Can. J. Chem. Downloaded from www.nrcresearchpress.com by 210.87.254.42 on 09/06/12
For personal use only.

Can. J. Chem. Downloaded from www.nrcresearchpress.com by 210.87.254.42 on 09/06/12
For personal use only.

doublets (11) at δ 1.54 and 1.20 (6H, $J$ = 7 Hz). When the product **3***b* was treated with LAH in a similar way, the reduced product **5***b* was obtained. The formation of products **3***a–e*, **4**, and **5***a*, *b* is shown in Scheme 1.

2-Imino-acenaphthenones **6***a*, *b* were prepared by the condensation of appropriate amines with acenaphthenequinone in dry toluene; ir (Nujol): 1730 (C=O, quinone) (13) and 1650 (C=N) $cm^{-1}$; uv (ethanol): 228, 305, 365, and 440 nm. The nmr spectra are in agreement with the proposed structures.[2]

The reaction between **1** and 2-phenylimino-acenaphthenone (**6***a*) gave ketazine **4** and 1′,3′,3′-triphenyl spiro(acenaphthen-1-one-2,4′-azetidin-2′-one) (**7***a*). The product **7***a* shows absorption maxima at 250, 318, and 345 nm in the uv spectrum. The ir spectrum exhibits strong bands at 1750 and 1730 $cm^{-1}$, characteristic of a spiro azetidinone (10) and a quinone (13), respectively. The sodium borohydride reduction of **7***a* afforded 1′,3′,3′-triphenyl spiro(1-hydroxyacenaphthene-2,4′-azetidin-2′-one)(**8***a*); ir (neat): 3580 (O—H), 1750 (C=O, spiro azetidinone) $cm^{-1}$ and absence of a band at 1730 $cm^{-1}$, characteristic of a quinone (13), revealing that the reduction of the carbonyl group at the 1-position of **7***a* has occurred. Similar treatment of **1** and **6***b* gave spiro azetidinone **7***b*, which on reduction with sodium borohydride gave **8***b* and ketazine **4**. The products **7***a*, *b* have been characterized by analytical and spectral (uv, ir, and nmr) data given in Tables 3 and 4. The formation of products **7***a*, *b* and **8***a*, *b* is depicted in Scheme 2.

The azetidinones **3***a–e* and spiro azetidinones **7***a*, *b* were found to be resistant to ordinary alkaline or acid hydrolysis supporting the above assigned structures. The bicyclic product, obtained earlier (6) by reaction of dimethylketene and 2-*p*-tolyl imino-1,2-diphenylethanone, undergoes hydrolysis quite readily (6).

Thermal decomposition of 2-diazo-1,2-diphenylethanone (**1**) may lead to benzoylphenylcarbene which may combine with **1** to form ketazine **4**. Benzoylphenylcarbene has been known to undergo Wolff rearrangement to give rise to diphenylketene (14) which may interact either with the C=N bond (15) or with the C=O (16) of ketoimines **2** and **6** leading to either azetidinones or β-lactones. The β-lactones, on decarboxylation, would have readily given rise to the corresponding olefins (16). The formation of azetidinones and not β-lactones has been supported on the basis of the analytical,

TABLE 2. Spectral data of azetidinones **3***a–e*

| Azetidinones | R | Ultraviolet $\lambda_{max}$ (EtOH) (nm) | Infrared (Nujol) ($cm^{-1}$) ν (C=O) azetidinone | Infrared (Nujol) ($cm^{-1}$) ν (C=O) benzoyl | Nuclear magnetic resonance ($CDCl_3$) δ (ppm) Aromatics | Nuclear magnetic resonance ($CDCl_3$) δ (ppm) Others |
|---|---|---|---|---|---|---|
| **3***a* | $CH(CH_3)_2$ | 230 | 1740 | 1680 | 7.33 (15H), 6.97 (5H) | 3.48 (sept, 1H, methine, isopropyl $J$ = 7 Hz), 1.70 and 1.23 (a pair of doublets, 6H, $CH_3$ isopropyl, $J$ = 7 Hz) |
| **3***b* | $CH(C_6H_4$—*p*-$CH_3)CH_3$ | 255 | 1740 | 1680 | 7.63 (4H), 7.28 (8H), 6.92 (12H) | 4.44 (q, 1H, methine, α-tolylethyl, $J$ = 7 Hz), 2.25 (s, 3H, $CH_3$, *p*-tolyl), 2.17 (d, 3H, $CH_3$, α-tolylethyl, $J$ = 7 Hz) |
| **3***c* | $CH(Ph)CH_3$ | 230 | 1745 | 1680 | 7.42 (20H), 6.79 (5H) | 4.17 (q, 1H, methine, α-phenylethyl, $J$ = 7 Hz), 1.61 (d, 3H, $CH_3$, α-phenylethyl, $J$ = 7 Hz) |
| **3***d* | $CH(Ph)_2$ | 255 | 1740 | 1680 | 7.42 (30H) | 5.53 (s, 1H, methine, benzhydryl) |
| **3***e* | Ph | 250 | 1750 | 1670 | 7.36 (H) | |

[2]Microanalyses for C, H, N are satisfactory, maximum error for C, ± 0.40; H, ± 0.20, N, ± 0.24.

Can. J. Chem. Downloaded from www.nrcresearchpress.com by 210.87.254.42 on 09/06/12
For personal use only.

TABLE 3. Conversion of ketoimines **6***a*, *b* to spiro azetidinones **7***a*, *b*

| | | Product **7***a*, *b* | | | | | | | | |
|---|---|---|---|---|---|---|---|---|---|---|
| | | | | | Elemental Analysis (%) | | | | | |
| | | | | | Found | | | Calculated | | |
| Ketoimines | R | Yield (%) | Melting point (°C) | Molecular formula | C | H | N | C | H | N |
| **6***a* | Ph | 76 | 235–236 | $C_{32}H_{21}NO_2$ | 85.41 | 4.88 | 3.18 | 85.14 | 4.66 | 3.10 |
| **6***b* | $C_6H_4$—*p*-$CH_3$ | 72 | 175–176 | $C_{33}H_{23}NO_2$ | 84.97 | 4.80 | 3.01 | 85.16 | 4.95 | 3.01 |

TABLE 4. Spectral data of spiro azetidinones **7***a*, *b*

| | | | Infrared (Nujol) ($cm^{-1}$) | | |
|---|---|---|---|---|---|
| Spiro azetidinones | R | Ultraviolet $\lambda_{max}$ (EtOH) (nm) | ν (C=O) (azetidinone) | ν (C=O) (quinone) | Nuclear magnetic resonance ($CDCl_3$) δ (ppm) |
| **7***a* | Ph | 250, 318, 345 | 1750 | 1730 | 8.17 (m, 4H, arom.), 7.25 (m, 16H, arom.), 6.67 (d, 1H, arom., *J* = 7 Hz) |
| **7***b* | $C_6H_4$—*p*-$CH_3$ | 255, 318, 345 | 1750 | 1730 | 7.98 (m, 4H, arom.), 7.28 (m, 11H, arom.), 6.85 (m, 3H, arom.), 6.59 (m, 2H, arom.), and 2.13 (s, 3H, $CH_3$) |

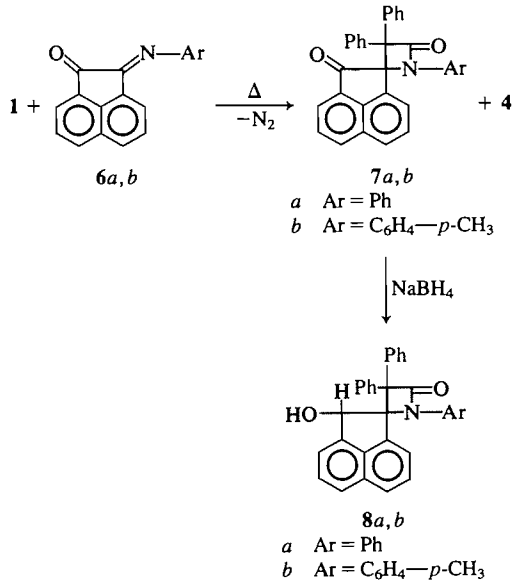


SCHEME 2

spectral, and chemical behaviour of the products. This reaction shows the high reactivity of the C=N in comparison with the C=O group towards diphenylketene. Since azetidinones **3***a*–*e* show their inertness towards sodium borohydride while the spiro azetidinones **7***a*, *b* undergo reduction with sodium borohydride, the carbonyl group present in the benzoyl moiety of azetidinones **3***a*–*e* is less reactive than the quinone carbonyl group of spiro azetidinones **7***a*, *b*. The azetidinone ring in **3***a*–*e* and **7***a*, *b* is unaffected on reduction ($NaBH_4$ or $LiAlH_4$) and thus appears to be quite stable. The formation of azetidinones takes place through the collapse of a possible zwitterionic intermediate (Scheme 3). A similar intermediate has been proposed in the reaction of diphenylketene and benzylideneaniline giving *N*-phenylimidate (15).

## Experimental

Melting points were determined on a Büchi apparatus (capillary method) and have been uncorrected. Ultraviolet spectra were obtained in 95% ethanol on a Cary-14 spectrophotometer. Infrared spectra were recorded in Nujol mull on a Perkin–Elmer 720 spectrophotometer. Proton nuclear magnetic resonance data were obtained on a Varian A-60D spectrometer in $CCl_4$ or $CDCl_3$ using TMS as internal standard.

*Materials*

Benzil, lithium aluminium hydride, and sodium borohydride were obtained from EGA chemicals, West Germany and 2-diazo-1,2-diphenylethanone (17), α-phenylethylamine (18), α-*p*-tolylethylamine (18), benzhydrylamine (19), and acenaphthenequinone (20) were prepared according to the reported methods.

*General procedure for preparation of ketoimines* **2**a–e *and* **6**a, b

The ketoimines **2***a*–*d* were prepared by dissolving a mixture containing 10 mmol of benzil and 10 mmol of corresponding freshly distilled amine in 30–40 mL of absolute ethanol at room temperature and keeping it for a week. The ketoimines **6***a*, *b* were obtained by refluxing a solution of 10 mmol of acenaphthenequinone and 10 mmol of corresponding amine in 60–80 mL of dry toluene for 2 h using a Dean–Stark separator to remove the water formed. The ketoimine **2***e* was obtained by heating a mixture of equimolecular amounts of benzil and aniline at 150°C for 2 h. The solvent in all cases was removed on a rotary evaporator and residual matter was triturated with ethanol. The

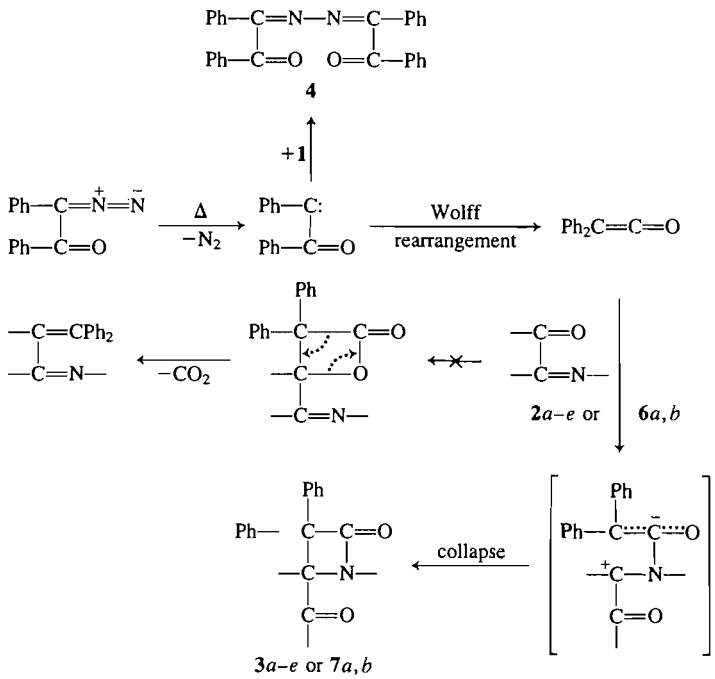


SCHEME 3

solid obtained was crystallized from ethanol to afford the product.

*General procedure for preparation of azetidinones* 3a–e *and spiro azetidinones* 7a, b

A mixture containing 10 mmol of 2-diazo-1,2-diphenylethanone (1) and 10 mmol of ketoimines 2*a–e* or 6*a*, *b* in 80 mL of dry benzene (thiophene free) was heated to reflux for 8 h under a nitrogen atmosphere. The reaction mixture was kept overnight at room temperature. The solvent was evaporated on a rotary evaporator and the residual matter was triturated with ethanol. The solid obtained was crystallized from ethanol to afford the products. The analytical and spectral data of the products 3*a–e* and 7*a*, *b* have been given in Tables 1–4. Evaporation of solvent from the mother liquor and crystallization from a *n*-hexane – ethanol (1:1) mixture gave a yellow crystalline solid identified as 1,1',2,2'-tetraphenyl-2,2'-azinodiethanone (4) on the basis of comparison (undepressed mixture melting point and identical ir spectrum) with an authentic sample prepared according to the reported method (12).

*Attempted hydrolysis of azetidinones* 3a–e *and spiro azetidinones* 7a, b

A mixture containing 0.02 g of 3*a*, 15 mL of 85% ethanol, and 1 mL of concentrated hydrochloric acid was heated to reflux for 30 h. After the usual work-up, 0.18 g (90%) of starting material was recovered. Similar treatment of 3*b–e* with concentrated HCl and 3*a–e* and 7*a*, *b* with either 40% aqueous alkali (potassium hydroxide or sodium hydroxide) or saturated ethanolic potassium hydroxide solution resulted in the recovery of starting material almost quantitatively.

*Preparation of 1-isopropyl-4-(α-hydroxybenzyl)-3,3,4-triphenyl-2-azetidinone (*5a)

To a suspension of 0.10 g of lithium aluminium hydride in 10 mL of dry ether was added slowly a solution of 0.23 g of 3*a* in 20 mL of dry ether. The reaction mixture was stirred for 3 h and kept overnight at room temperature. After the usual work-up, an oily material was obtained which on crystallization from ethanol gave 0.20 g (89%) of 5*a*; mp 177–178°C; ir (Nujol): 3440 (O—H) and 1735 (C=O, azetidinone) $cm^{-1}$; $uv_{max}$ (ethanol): 255 nm; nmr ($CCl_4$) δ: 7.93 (m, 2H, arom.), 7.53 (m, 4H, arom.), 7.05 (m, 14H, arom.), 4.89 (d, 1H, benzylic, $J$ = 4 Hz, collapses to a singlet on deuteration), 2.69 (septet, 1H, isopropyl, $J$ = 7 Hz), 2.00 (b, 1H, OH, $D_2O$ exchangeable), 1.54 and 1.20 (a pair of doublets, 6H, isopropyl, $J$ = 7 Hz). *Anal.* calcd. for $C_{31}H_{29}NO_2$: C 83.22, H 6.49, N 3.13; found: C 83.40, H 6.55, N 3.25.

*Preparation of 1-(α-p-tolylethyl)-3,3,4-triphenyl-4-(α-hydroxybenzyl)-azetidin-2-one (*5b)

Treatment of 0.26 g of 3*b* and 0.10 g of lithium aluminium hydride in a similar manner as described above gave 0.22 g (85%) of 5*b*, mp 75–76°C; ir (Nujol): 3400 (O—H) and 1730 (C=O, azetidinone) $cm^{-1}$; $uv_{max}$ (ethanol): 258 nm; nmr ($CDCl_3$) δ: 8.12 (m, 2H, arom.), 7.23 (m, 22H, arom.), 5.03 (s, 1H, benzylic), 3.33 (q, 1H, methine, $J$ = 7 Hz), 2.33 (s, 3H, $CH_3$—*p*-$C_6H_4$—), 2.33 (s, 1H, OH, $D_2O$ exchangeable), and 1.72 (d, 3H, methyl, $J$ = 7 Hz). *Anal.* calcd. for $C_{37}H_{33}NO_2$: C 84.89, H 6.31, N 2.67; found: C 84.65, H 6.21, N 2.71.

*Preparation of 1',3',3'-triphenyl spiro(1-hydroxyacenaphthene-2,4'-azetidin-2'-one) (*8a)

To a solution of 0.20 g of 7*a* in 20 mL of absolute ethanol (acetaldehyde free), 0.10 g of sodium borohydride was added. The reaction mixture was stirred for 30 min and kept overnight. After the usual work-up, 0.18 g (90%) of a white oily product 8*a* (which could not be further purified) was obtained; ir (neat): 3580 (O—H) and 1750 (C=O, azetidinone) $cm^{-1}$; the ir spectrum does not show a band at 1730 $cm^{-1}$, characteristic of quinone (13).

*Preparation of 1'-(*p*-tolyl)-3',3'-diphenyl spiro(1-hydroxyacenaphthene-2,4'-azetidin-2'-one) (*8b)

Treatment of 0.20 g of 7*b* with 0.10 g of sodium borohydride in a similar manner as described above gave 0.18 g (90%) of a white oily product 8*b* (which could not be further purified); ir (neat):

Can. J. Chem. Downloaded from www.nrcresearchpress.com by 210.87.254.42 on 09/06/12
For personal use only.

3520 (O—H) and 1750 (C=O, azetidinone) $cm^{-1}$. The ir spectrum does not show a band at 1730 $cm^{-1}$, characteristic of a quinone (13).


## Acknowledgements

We thank Professor B. M. Shukla for providing facilities and the Council of Scientific and Industrial Research, New Delhi, India for grant of a fellowship to S.B.S.



1. A. K. MUKERJEE and R. C. SRIVASTAVA. Synthesis, 327 (1973), and references cited therein.
2. M. SAKAMOTO and Y. TOMIMATSU. Yakugaku Zasshi, **90**, 1386 (1970); Chem. Abstr. **74**, 53357f (1971).
3. S. SATSUMABAYASHI, S. MOTOKI, and H. NAKANO. J. Org. Chem. **41**, 156 (1976).
4. F. DURAN and L. GHOSEZ. Tetrahedron Lett. 245 (1970).
5. I. MATSUDA, S. YAMAMOTO, and Y. ISHII. J. Chem. Soc. Perkin Trans. I, 1528 (1976).
6. R. D. BURPITT, K. C. BRANNOCK, R. G. NATIONS, and J. C. MARTIN. J. Org. Chem. **36**, 2222 (1971).
7. R. GRAF. Justus Leibigs Ann. Chem. **661**, 111 (1963).
8. E. J. MORICONI and J. F. KELLEY. J. Am. Chem. Soc. **88**, 3657 (1966).
9. A. K. BOSE, G. GARRATT, and J. J. PELOSI. J. Org. Chem. **28**, 730 (1963).
10. M. S. MANHAS, J. S. CHIB, Y. H. CHIANG, and A. K. BOSE. Tetrahedron, **25**, 4421 (1969).
11. K. N. MEHROTRA and S. B. SINGH. Bull. Chem. Soc. Jpn. **54**, 1838 (1981); Indian J. Chem. **19***B*, 702 (1980).
12. T. CURTIUS and R. KASTNER. J. Prakt. Chem. **83**, 215 (1911); Chem. Abstr. **5**, 2649 (1911).
13. O. TSUGE, T. SHINKAI, and M. KOGA. J. Org. Chem. **36**, 745 (1971).
14. V. FRANZEN. Justus Liebigs Ann. Chem. **614**, 31 (1958).
15. H. B. KAGAN and J. L. LUCHE. Tetrahedron Lett. 3093 (1968).
16. L. L. MULLER and J. HAMER. 1,2-Cycloaddition reactions. Interscience, New York. 1967. pp. 139–165.
17. C. D. NENITZESCU and E. SOLOMONICA. Org. Synth. Coll. Vol. II, 496 (1950).
18. A. W. INGERSOLL. Org. Synth. Coll. Vol. II, 503 (1950).
19. A. MICHAELIES. Chem. Ber. **26**, 2169 (1893).
20. C. F. H. ALLEN and J. A. VAN ALLAN. Org. Synth. Coll. Vol. III, 1 (1950).


Can. J. Chem. Downloaded from www.nrcresearchpress.com by 210.87.254.42 on 09/06/12
For personal use only.

## ADDITIONS AND CORRECTIONS/AJOUTS ET CORRECTIONS

Vol. 59, 1981

**John T. Edward.** Conformational effects on the enthalpy of formation of straight and branched-chain alkanes.

Page 3192. Professor P. v. R. Schleyer has brought to my attention that the essential arguments of the paper are to be found in the paper by P. v. R. Schleyer, J. E. Williams, and K. R. Blanchard, "The evaluation of the strain in hydrocarbons. The strain in adamantane and its origin" (J. Am. Chem. Soc. **92**, 2377 (1970)). The group increments for "skew-free conformations" calculated by Schleyer *et al.*, in kcal/mol, are as follows (corresponding values of Edward follow in parentheses): $CH_3$, −10.05 (−10.06); $CH_2$, −5.13 (−5.13); CH, −2.16 (−2.14); C, −0.30 (−0.11). I regret overlooking Professor Schleyer's paper.

**J. M. Stadlbauer, B. W. Ng, D. C. Walker, Y. C. Jean, and Y. Ito.** Muonium addition to vinyl monomers.

Page 3261. (*i*) The value of $k_H$ in Table 2 should be $4 \times 10^9$ not $4 \times 10^{10} M^{-1}$ $s^{-1}$; and (*ii*) $a_\mu$ should have been used for the hyperfine coupling constant on line 13 of p. 3263, rather than $A_\mu$ which is the muon asymmetry in eq. [1].

# Hydrogen bonding of O—H and C—H hydrogen donors to $Cl^-$. Results from mass spectrometric measurements of the ion–molecule equilibria $RH + Cl^- = RHCl^-$

M. A. FRENCH, S. IKUTA,[1] AND P. KEBARLE

*Department of Chemistry, University of Alberta, Edmonton, Alta., Canada T6G 2G2*

Received November 20, 1981

M. A. FRENCH, S. IKUTA, and P. KEBARLE. Can. J. Chem. **60**, 1907 (1982).

Equilibrium constants $K_1$ for reaction [1] $RH + Cl^- = RHCl^-$ in the gas phase were measured with a high pressure mass spectrometer under chemical ionization conditions. Data for some 40 compounds RH are presented. It is found that the binding free energies ($-\Delta G_1^0 = RT \ln K_1$) for RH = oxygen acids increase with the gas phase acidity of RH. The strongest bonds are formed with strong acids like $HCO_2H$, $CH_3CO_2H$, and phenol. Water and alkyl alcohols give much weaker interactions. A simple relationship between gas phase acidity and binding free energy does not occur for RH = carbon acids. Carbon acids like cyclopentadiene, whose high gas phase acidity is largely due to charge delocalization by conjugation in the completed anion, do not give $Cl^-$ adducts with stability commensurate with the acidity. A relationship between gas phase acidity and binding energy is found for carbon acids with carbonyl groups and for the substituted toluenes. Molecular orbital calculations with the STO-3G basis set provide insights to the bonding occurring in $RHCl^-$. For all cases investigated, hydrogen bonding to $Cl^-$ provides the most stable structure. Generally the hydrogen bond occurs through the hydrogen which has the highest net positive charge. The hydrogen bond strength is found approximately proportional to this positive charge. Another proportionality is found between the charge transferred from $Cl^-$ to RH, on formation of $RHCl^-$, and the strength of the hydrogen bond.

M. A. FRENCH, S. IKUTA et P. KEBARLE. Can. J. Chem. **60**, 1907 (1982).

On a mesuré la constante d'équilibre $K_1$ de la réaction [1] $RH + Cl^- = RHCl^-$ en phase gazeuse à l'aide d'un spectromètre de masse à haute pression et à ionisation chimique. On présente les données relatives à 40 composés du type RH. On a trouvé que les énergies libres de liaison, ($-\Delta G_1^0 = RT \ln K_1$), dans les cas où RH = acides oxygénés, augmentent avec l'acidité de la phase gazeuse de RH. Les liaisons hydrogènes les plus fortes s'établissent avec les acides forts, tels le $HCO_2H$, le $CH_3CO_2H$ et le phénol. L'eau et les alcools alkylés donnent lieu à des interactions beaucoup plus faibles. On n'obtient pas de relation simple entre l'acidité de la phase gazeuse et l'énergie libre de liaison dans les cas où RH = acides carbonés. Les acides carbonés du type cyclopentadiène, dont la forte acidité en phase gazeuse est due à une grande délocalisation de la charge par conjugaison de l'anion complété, ne donnent pas d'adduits avec $Cl^-$ qui auraient une stabilité proportionnelle à l'acidité. On a trouvé une relation entre l'acidité de la phase gazeuse et l'énergie de liaison dans le cas des acides carbonés ayant des groupes carbonylés et dans le cas des toluènes substitués. Les calculs d'orbitales moléculaires avec l'ensemble de base STO-3G fournissent des informations sur la liaison qui s'établit dans $RHCl^-$. Dans tous les cas étudiés, la liaison hydrogène avec $Cl^-$ conduit à la structure la plus stable. En général, la liaison hydrogène s'établit par l'intermédiaire de l'hydrogène qui a la plus forte charge positive totale. On a trouvé que la force de la liaison hydrogène est presque proportionnelle à sa charge positive. On a trouvé une autre proportionnalité entre la charge transferrée du $Cl^-$ au RH lors de la formation de $RHCl^-$ et la force de la liaison hydrogène.

[Traduit par le journal]

## Introduction

The association of molecules with negative ions is of interest in several disciplines. Strongly held adducts involving negative ions and acids like $HNO_2$, $HNO_3$, HCl, and HBr occur in the earth's atmosphere (1). The adducts of various molecular species of $Cl^-$ can be used for analytical purposes in negative ion chemical ionization mass spectrometry (2). Hydrogen bonded complexes between neutral hydrogen donors and negative ions have been observed and studied in aprotic solvents (3, 4). In a more general sense, information on the bonding of various neutral compounds to negative ions like $Cl^-$, etc. belongs to the large area of hydrogen bonding, since the interactions turn out to be predominantly hydrogen bonding ones. Improved understanding of the nature of bonding is of significance also to ion solvation and ion stabilization in different environments. For example, complexing positive ions with suitably designed compounds like crown ethers or cryptates (5) facilitates their passage into hydrophobic media, biological membranes, or liquid membranes in ion selective electrodes (6). Less developed is the design and synthesis of similar compounds which are to complex selectively with negative ions.

The present work provides information on the binding free energies of some 38 compounds with $Cl^-$. The information is obtained from the measurement of the ion–molecule equilibria [1] with a pulsed electron beam high pressure mass spectrometer. Measurement of the equilibrium con-

[1]Permanent address: Department of Chemistry, Tokyo Metropolitan University, Fukasawa, Setagaya-ku, Tokyo 158, Japan.

0008-4042/82/151907-12$01.00/0

©1982 National Research Council of Canada/Conseil national de recherches du Canada

Can. J. Chem. Downloaded from www.nrcresearchpress.com by 210.87.254.40 on 09/06/12
For personal use only.

Can. J. Chem. Downloaded from www.nrcresearchpress.com by 210.87.254.40 on 09/06/12
For personal use only.

stants $K_1$ at a given constant temperature $T$ leads to the free energy change $\Delta G_1^0 = -RT \ln K_1$. Measurement of the temperature dependence of $K_1$ leads also, via van't Hoff plots, to $\Delta H_1^0$ and $\Delta S_1^0$.

[1] $Cl^- + RH = RHCl^-$

[2] $R_0^- + RH = R_0H + R^-$

Several determinations of equilibria [1] have been published in previous reports from this laboratory. Measurements involving RH (HCOOH, $CH_3COOH$, $C_6H_5OH$, $HCCl_3$, $(CH_3)_3COH$, $CH_3OH$, $H_2O$) showed (7, 8) that the strong hydrogen bond $Cl^-\cdot\cdot HR$ (i.e. the chloride affinity of HR) increases approximately linearly with increase of the phase acidity of HR. A good linear relation is obtained for the case where the acids are more closely related, i.e. substituted phenols (9).

The early (1, 2) comparisons of chloride affinity and gas phase acidity were made on the basis of very incomplete and somewhat questionable data for the gas phase acidities of the RH compounds involved. Fortunately, since then, abundant data on gas phase acidities have become available from measurements in this (10) and other laboratories (11) of proton transfer equilibria [2] which provide accurate relative gas phase acidities. In the present work comparisons between the chloride affinities and gas phase acidities of the oxyacids are based on these newer and more accurate acidity data. The gas phase acidities of many nitrogen and carbon acids were part of the recent acidity determinations (10, 11). While only a few determinations of the chloride affinities of nitrogen acids have been made, it is to be expected that the relationships observed for oxygen acids will approximately hold also for nitrogen acids. The case of the carbon acids is quite different. Taking the term carbon acids in the broadest sense, carbon acids involve C—H hydrogens of all possible bonding environments, i.e. aromatic C—H hydrogens, allylic hydrogens, etc. Evidently, for some of the compounds involved, bonding to $Cl^-$ may not be occurring via a hydrogen bond, but by an electrostatic interaction with a whole group of atoms or by an interaction with a particular carbon atom, i.e. by the formation of a $\sigma$ complex. Even when the most stable adduct is hydrogen bonded, the parameters determining the strength of the bond are not so easily deduced. It is likely that a simple relationship with the gas phase acidity cannot be expected. For example, cyclopentadiene is a rather strong gas phase acid, its gas phase acidity is comparable to that of $p$-$NH_2$,phenol (10), yet this compound cannot be expected to have a high chloride affinity. The high acidity of the cyclopentadiene is largely due to the charge delocalization in the anion $C_5H_5^-$ in which the charge is evenly distributed on all five CH groups. Evidently, a compound whose gas phase acidity is achieved largely through delocalization of an electron pair from a former C—H bond cannot compete in hydrogen bonding with a compound whose acidity is largely due to a charge separation induced by an electronegative atom like oxygen.

In order to explore the chloride affinities of carbon acids, a number of determinations of equilibria [1] with RH = carbon acids were made in the present work. The measurements provide very useful thermochemical data, but of course no direct structural information. Considerable help in the bonding analysis can be obtained from molecular orbital calculations (STO-3G) of the energies of possible structures of the complexes $RHCl^-$.

## Experimental

The measurements of the equilibrium constants $K_1$ were made with a pulsed electron beam high ion source pressure mass spectrometer. The apparatus was the same as that used in earlier work on $Cl^-$ and phenols (9). It differed from that used in the earliest work (7) where pulsing of the electron beam was not employed. In the earliest work (7) neat gas RH was used in the ion source at pressures of 0.6 to 2 Torr. The use of the neat gas, in some cases, may lead to incorrect measurements due to unimolecular or collision-induced decomposition of the ion–molecule adduct in the mass analysis system (12). Therefore the present measurements were executed with methane as major gas. Generally, the methane contained 0.1 to 5% RH. The total ion source pressure was in the range 1–4 Torr.

The measurements with formic acid and phenol made in the earlier work (7) were repeated. The equilibrium constants for phenol at different temperatures as a function of phenol partial pressure are shown in Fig. 1. The equilibrium constants observed are seen to be quite independent of the phenol partial pressure. The phenol pressure is varied by a factor of 4. At low temperatures, where $K_1$ is large, low phenol partial pressures are used in order not to let the ion ratio $RHCl^-/Cl^-$ become much larger than unity.

van't Hoff plots for three determinations (HCOOH, PhOH, acetone) are shown in Fig. 2. The agreement with the earlier results for HCOOH is fairly good. The data points for the two determinations are very close; however, a deviation of the older data points (7) (see Fig. 2) at high temperature (low $K_1$) leads to a larger slope, i.e. a larger $-\Delta H_1$, for the earlier work. The present data, obtained with improved experimental conditions and extending over a wider temperature range, are believed to be the more reliable set. A considerably larger deviation between present and earlier data is observed for phenol (see Fig. 2). This disagreement must be due to some specific problem connected with the use of neat phenol in the earlier work. The very high molecular weight of phenol and its strong adsorption on metal surfaces may have led to an unusually high residual gas pressure in the acceleration and mass analysis system. Recent work (12, 13) has shown that under such conditions significant collision-induced decomposition (or $RHCl^-$ in the present case) can reduce the observed ion ratio $RHCl^-/Cl^-$. A recent redetermination[2] of the equilibrium $Cl^- + H_2O = Cl^-H_2O$, with methane as major gas, led to results in agreement with the earlier work (8*b*) which was undertaken with neat water. This observa-

[2]T. F. Magnera and P. Kebarle. Kinetics of the hydration of the $Cl^-$ ion. To be published.

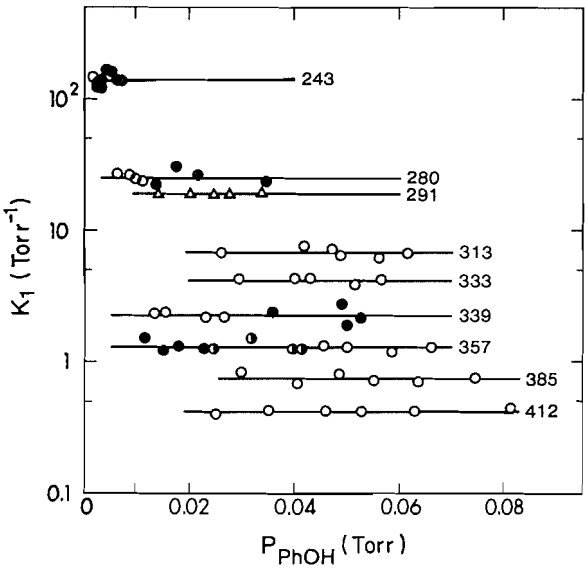


FIG. 1. Measured equilibrium constants for reaction: $Cl^-$ + PhOH = $PhOHCl^-$ at different constant temperatures given in degrees C. Equilibrium constant is found independent of phenol pressure. Experiments performed in the presence of a third gas methane at 1 to 5 Torr pressure. Different symbols for same temperature correspond to different ratios of phenol to methane.

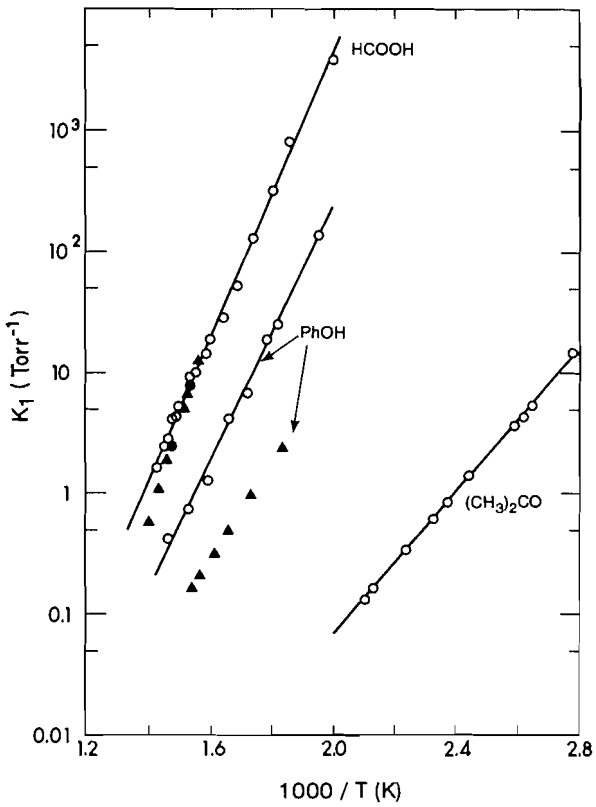


FIG. 2. van't Hoff plots for equilibria: RH + $Cl^-$ = $RHCl^-$. ○, present results with $CH_4$ as major gas. ▲, Yamdagni and Kebarle (7) with use of neat RH. ●, present results with neat formic acid.

tion also suggests that phenol represented a special problem in the earlier measurements. As will be shown in the next section, the present result for phenol is in better accord with theoretical predictions.

In order to cover a large number of compounds RH, determinations of the equilibrium constant $K_1$ were made only at one temperature. These data, shown in Figs. 3 and 4, will be discussed in the next section.

## Calculations

The $\Delta E$(STO-3G) data used in this work were obtained by calculating the total energies of the reactants in reaction [1] and obtaining $\Delta E$ from : $E(RHCl^-) - E(Cl^-) - E(RH)$. The STO-3G calculations of the total energies $E$ were performed with the Gaussian 70 and Hondo 5 programmes based on Pople's (14) STO-3G minimal basis set. The geometries used were standard geometries from Pople and Gordon (14) except: methanol, Harmony *et al.* (15*a*); acetone, J. E. Bel Bene (15*b*); pyrrole, Clementi *et al.* (16*a*); formic acid, Clementi *et al.* (16*b*). In the structures $RHCl^-$ shown in Fig. 6, only a few of the bond distances were optimized. These are shown in Table 3. In general, first the $Cl^-$ distance to the rigid R—H was optimized. Then for a fixed $Cl^-$ distance the O—H distance or C—H distance for oxygen or carbon acids was optimized.

## Results and discussion

*General description of results*

The present results consist of determinations of the equilibrium constants $K_1$ for the reaction [1], $Cl^- + RH = RHCl^-$. The experimental data are summarized in Figs. 2, 3, and 4. Shown in Fig. 2 are the few cases (formic acid, phenol, acetone) for which the temperature dependence of the equilibrium constants was measured. The resulting van't Hoff plots permit the determination of $\Delta H_1^0$ and $\Delta S_1^0$. In order to cover a large number of compounds, the remaining equilibrium constant determinations were made at a single temperature. Figure 3 summarizes the determinations at room temperature. This group consists of 18 compounds and covers equilibrium constants from $K_1 \approx 0.5$ to $K_1 = 1000$ (Torr$^{-1}$). Equilibrium constants much larger than 1000 are difficult to determine with the present apparatus. Therefore several equilibria of interest, involving more strongly bonding compounds, were measured at a temperature of 148°C. These are shown in Fig. 4.

Tables 1 and 2 summarize the available data. Table 1 contains the compounds for which van't Hoff plots are available. Present and previous determinations involving $Cl^-$ (7–9, 17) are included. Table 2 gives the free energy change $\Delta G_1^0 = -RT \ln K_1$ at 300 K of all the compounds for which

Can. J. Chem. Downloaded from www.nrcresearchpress.com by 210.87.254.40 on 09/06/12
For personal use only.

Can. J. Chem. Downloaded from www.nrcresearchpress.com by 210.87.254.40 on 09/06/12
For personal use only.

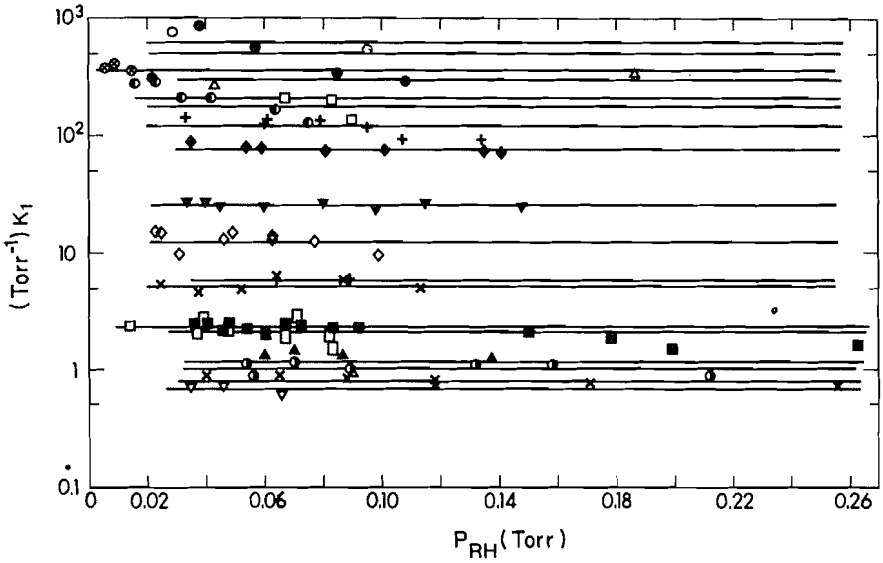


FIG. 3. Measured equilibrium constants for reaction [1]: $Cl^-$ + RH = $Cl^-$· RH at 26°C where RH is ○, acetone; ●, *m*-difluorobenzene; ⊗, *p*-nitrotoluene; △, diphenylmethane; ◐, iodobenzene; □, nitrobenzene; +, bromobenzene; ◆, chlorobenzene; ▼, fluorobenzene; ◇, cumene; +, *n*-propylbenzene; +, ethylbenzene; ⊡, mesitylene; [], *m*-xylene; ▲, toluene; ◑, *p*-xylene; ×, benzene; ▽, 1,4-pentadiene.

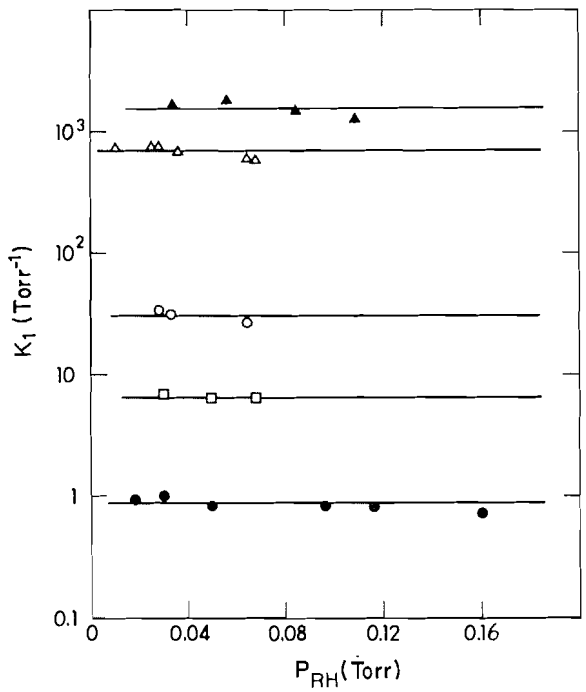


FIG. 4. Measured equilibrium constants for reaction [1]: RH + $Cl^-$ = $RHCl^-$ at 148°C, where RH is: pyrrole ▲; acetylacetone △; phenylacetone ○; acetopheonone □; and acetone ●.

determinations are available from the present and previous work. For the compounds shown in Fig. 4, determinations of the equilibrium constant $K_1$ are available only at 148°C. In order to obtain the free energy change $\Delta G_1^0$, at room temperature, one requires the entropy change $\Delta S_1^0$. We made a rough estimate of $\Delta S_1^0$ on the basis of the results in Table 1. These indicate that $-\Delta S_1^0$ decreases approximately with decreasing $-\Delta H_1^0$. The compounds in Fig. 1 include acetone, whose $\Delta S_1^0 = -19.6$ cal $K^{-1}$ was measured. The compounds in Fig. 4, which include acetone, fall in a not too broad bond strength range. Therefore a constant value of $\Delta S_1^0 = -20$ cal $K^{-1}$ was assumed for all of them. The $\Delta G_1^0$ data in Table 2 for these compounds are obviously only estimates.

*Hydrogen bonding of $Cl^-$ to oxygen acids*

As was mentioned in the introduction, earlier work (6–9, 17) showed that the hydrogen bond strength RH··$Cl^-$ increases as the gas phase acidity of RH increases. Most of the compounds involved in that relationship were oxygen acids.

The correlation was suggested before accurate and plentiful data for gas phase acidities were available. Fortunately, the present data can be examined with the help of recent comprehensive determinations of gas phase acidities (10, 11). The hydrogen bonds to $Cl^-$ ($-\Delta G_1^0$) of oxygen acids are shown in Fig. 5 plotted versus the corresponding gas phase acidities. The data fit quite well into a smooth curve which shows that the hydrogen bond free energies decrease with decrease of acidity of RH. It is interesting to note that the (negative) slope decreases gradually, i.e. the changes of hydrogen bonding with acidity are largest for the strongest

Can. J. Chem. Downloaded from www.nrcresearchpress.com by 210.87.254.40 on 09/06/12
For personal use only.

TABLE 1.[a] Thermodynamic data

| RH | $-\Delta G^0_1(300,g)$ | $-\Delta H^0_1(g)$ | $-\Delta S^0_{1(g)}$ | Reference[b] | $-\Delta H_{1(sl)}$[c] | $-\Delta H_{sl}(RH)$[d] | $\Delta H_4$[e] |
|---|---|---|---|---|---|---|---|
| HCOOH | 20.1 | 27.4 | 24.5 | — | 4.0 | 11 | 12.4 |
| Phenol | 19.2 | 26.0 | 25.0 | — | 3.7 | 14.6 | 7.7 |
| HCl | 16.7 | 23.7 | 23.5 | 8 | 8.1 | 5.8 | 9.8 |
| $CH_3OH$ | 9.8 | 14.2 | 14.8 | 8 | 3.2 | 7.5 | 3.5 |
| $CH_3CN$ | 9.2 | 13.4 | 14.3 | 8 | — | — | — |
| HOH | 8.2 | 13.1 | 16.5 | 8 | 2.6 | 8.9 | 1.6 |
| Acetone | 7.9 | 13.7 | 19.6 | — | — | — | — |

[a] Data relate to reaction [1]: RH + $Cl^-$ = $RHCl^-$. The abbreviation g stands for reaction in the gas phase, sl for reaction in solution. $\Delta G^0$ and $\Delta H^0$ are given in kcal $mol^{-1}$, $\Delta S$ in cal $K^{-1}$, standard state 1 atm. The errors are estimated at ± 2 kcal/mol for $\Delta H^0_{(g)}$ and $\Delta G^0_{(g)}$ and ± 5 cal $K^{-1}$ for $\Delta S^0_{(g)}$.
[b] Literature reference for gas phase reaction [1]; where no reference is given, determination was made in present work.
[c] $\Delta H_{1(sl)}$ for sulfolane from Benoit and co-workers (4).
[d] $\Delta H_{sl}(RH)$ corresponds to enthalpy change for reaction $HR_{(g)} \rightarrow HR_{(sl)}$ where solvent is sulfolane. Data from Benoit and co-workers (4).
[e] $\Delta H_{sl}(Cl^-HR) - \Delta H_{sl}(Cl^-) = \Delta H_4$ is obtained from cycle [2] and eq. [4]. $\Delta H_{sl}(Cl^-HR)$ corresponds to enthalpy change for reaction $ClHR^-_{(g)} \rightarrow ClHR^-_{(sl)}$ where solvent is sulfolane. $\Delta H_{sl}(Cl^-)$ for same process but involving $Cl^-$.

TABLE 2. Binding free energies $\Delta G^0_1$ of $Cl^-$ to compounds RH

| RH | $-\Delta G^0_1(300)$[a] | $\Delta H_D$[b] | RH | $-\Delta G^0_1(300)$[a] | $\Delta H_D$[b] |
|---|---|---|---|---|---|
| *p*-CN,phenol | 26.0[c] | 332.1[j] | *p*-$NO_2$,toluene | 7.5[d] | |
| *p*-Cl,phenol | 20.8[c] | 343.2[j] | Diphenylmethane | 7.4[d] | 364.5[k] |
| $HCO_2H$ | 20.1[d] | 345.2[j] | Anisole | 7.3[d] | |
| *p*-F,phenol | 19.3[c] | 347.2[j] | I-benzene | 7.2[d] | |
| $CH_3CO_2H$ | ~17.3[c] | 348.5[j] | $NO_2$-benzene | 7.1[d] | |
| Phenol | 17.2[c] | 349.8[j] | Br-benzene | 6.8[d] | |
| HCl | 16.7[f] | 333.6[j] | Cl-benzene | 6.5[d] | |
| *p*-Me,phenol | 16.6[c] | 351.1[j] | F-benzene | 5.9[d] | |
| Pyrrole | ~14.0[g] | 359.2[j] | *i*-Pr-benzene | 5.5[d] | 377.5[k] |
| $(CH_3CO)_2CH_2$ | ~13.4[g] | 343.7[j] | *n*-Pr-benzene | 5.0[d] | |
| *t*BuOH | 11.1[e] | 374[k] | Et-benzene | 5.0[d] | 378.3[k] |
| $PhCH_2COCH_3$ | ~10.7[g] | 351.8[j] | Mesitylene | 4.5[d] | |
| $CHCl_3$ | ~10.3[h] | | *m*-Xylene | 4.4[d] | |
| MeOH | 9.8 | 380[k] | Triphenylmethane | 4.1[d] | |
| MeCOPh | ~9.5[g] | 363[j] | Toluene | 4.0[d] | 379[k] |
| MeCN | 8.4[h] | 373.5[j] | *p*-Xylene | 3.9[d] | 380.5[k] |
| HOH | 8.2[i] | 390.8[k] | Benzene | 3.8[d] | |
| $Me_2CO$ | 7.9[d] | 370[j] | 1,4-Pentadiene | 3.7[d] | |
| *m*-diF,benzene | 7.7[d] | | Cyclopentadiene | <2.5[d] | 356[j] |

[a] Free energy change at 300 K for gas phase reaction $Cl^-$ + RH = $RHCl^-$ in kcal/mol, standard state 1 atm.
[b] Deprotonation enthalpy corresponding to gas phase reaction RH = $R^-$ + $H^+$. $\Delta H_D$ decreases with increase of gas phase acidity.
[c] From ref. 9 and phenol determination present work.
[d] Present work.
[e] Present work and ref.7.
[f] Reference 17.
[g] Present work, estimate of $\Delta G^0(300)$ from single determination at 421 K (see Fig. 4).
[h] References 7 and 8.
[i] Reference 8 and footnote 2.
[j] Reference 10.
[k] Reference 11.

acids for which, one could assume, the largest degree of proton transfer to $Cl^-$ occurs. This behavior is closely analogous to that observed in an earlier series (18) where the acids were oxonium and ammonium ions ($H_3O^+$, $EtOH_2^+$, $MeCO_2H_2^+$, $NH_4^+$, pyrridine $H^+$, etc.) and the proton acceptor was $H_2O$. In that case also, the slope was largest for the strongest acids ($H_3O^+$, $EtOH_2^+$) and decreased as the acids became weaker (pyridinium ions).

When the compounds were closely related, as is the case for the substituted pyridinium ions, the relationship between hydrogen bond energy (to $H_2O$) and acidity of the hydrogen donor was close to linear (18). It was also found that the hydrogen bond energies were proportional to the net positive charge on the acidic hydrogen of the pyridinium ions. The net positive charge was obtained from Mulliken electron population analysis with STO-3G basis sets by Reynolds *et al.* (19). These authors had shown that the acidity of the pyridinium ions is linearly related to the net atomic charge in the acidic hydrogen. Thus the relationship between hydrogen bond and net atomic charge could have been anticipated, once it was shown that the hydrogen bond energy increases with acidity.

It is interesting to note that the situation is exactly analogous for substituted phenols and $Cl^-$.

Can. J. Chem. Downloaded from www.nrcresearchpress.com by 210.87.254.40 on 09/06/12
For personal use only.

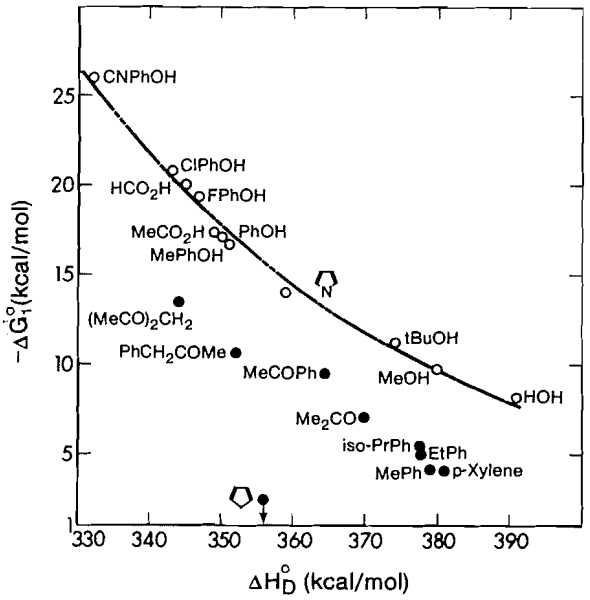


FIG. 5. Plot $\Delta G_1^0$ for gas phase reaction ($RH + Cl^- = RHCl^-$) versus gas phase acidity of RH. ○ RH are oxygen acids (and pyrrole); ● RH are carbon acids. The gas phase acidity is expressed as $\Delta H_D^0$, the deprotonation energy corresponding to enthalpy change for reaction $RH = R^- + H^+$. The gas phase acidity increases as $\Delta H_D^0$ decreases. The RH—$Cl^-$ binding free energies ($-\Delta G_1^0$) of the oxygen acids fit on a common curve. The binding energy increases as the acidity of RH increases. The carbon acids (except cyclopentadiene) also seem to fit on a common curve. Data in Fig. 5 are also given in Table 2.

There is a close to linear relationship between the hydrogen bond in $RHCl^-$ and the acidity of the phenols (see Fig. 5 and Fig. 3, ref. 9). The acidities and net atomic charges on the acidic hydrogen of substituted phenols have been calculated by Hehre *et al.* (20). These data, when plotted, demonstrate that a good linear dependence exists between the calculated acidity of the phenols and the net atomic charge on the acidic hydrogen. There is quite good agreement between the STO-3G calculated (20) and the experimental (21, 22) acidities of the substituted phenols. Since there is a near linear relationship between acidity and hydrogen bonding with $Cl^-$, it follows that the hydrogen bond energy in the phenol $Cl^-$ adducts is linearly related to the net atomic positive charge on the acidic hydrogen of the phenols.

*Hydrogen bonding of $Cl^-$ to carbon acids*

The bonding free energies $-\Delta G_1^0$ for $Cl^-$ association to carbon acids RH are shown in Fig. 5. None of these compounds falls on the correlation curve of the oxygen acids. All carbon acids have bonding free energies which are considerably lower than those for oxygen acids of the same gas phase acidity. The lowest chloride affinity is observed for cyclopentadiene (Fig. 3). The gas phase acidity for this compound is close to that of phenol and thus rather high. As already mentioned in the Introduction, the reason for the complete lack of correlation between acidity and chloride affinity in cyclopentadiene is easy to understand. The high acidity of cyclopentadiene is mostly due to the large stabilization by charge delocalization in the fully developed anion, in which each CH group carries one fifth of the negative charge. This stabilization is not available in the cyclo-$C_5H_6Cl^-$ adduct.

The remaining carbon acids (Fig. 5) seem to fall on a common curve which indicates a correlation between gas phase acidity and chloride affinity. For example, the chloride affinity order of the alkyl substituted toluenes: *p*-xylene, toluene, ethylbenzene, isopropylbenzene follows exactly the order of the gas phase acidities. For some of the toluenes, whose chloride affinities were measured in the present work, gas phase acidities are not available. However the acidity order can be inferred. For the series:

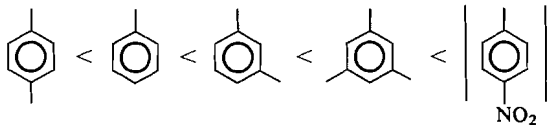


data from Table 2 show that the chloride affinities increase in the given orer. The gas phase acidities probably change also in the same order. The acidity order *para*-xylyl < toluene is experimentally observed. Methyl substitution on the aromatic ring, in *para* and *meta* position of phenols, leads to a decrease of acidity; however, the decrease is lower for the *meta* substituent (4, 12). This difference is expected because the π-like electron donation, from *para* methyl in the anion, brings destabilizing negative charge closer to the oxi group than is the case for the *meta* substituent. In the methyl substituted toluenes, *meta* substitution might in fact be slightly acidifying, since the favorable increase of the polarizability may be the overriding effect. This would lead to an acidity order which is the same as that shown above for the chloride affinities. The higher acidity for *p*-nitrotoluene is of course also expected.

The correlation of the chloride affinity with the gas phase acidity for the substituted toluenes and the carbonyl carbon acids (see Fig. 5) suggests that the chloride adducts of these compounds involve hydrogen bonding of the chloride to the most acidic hydrogen, i.e. the hydrogen that would be involved in the acid dissociation. In the next section, STO-

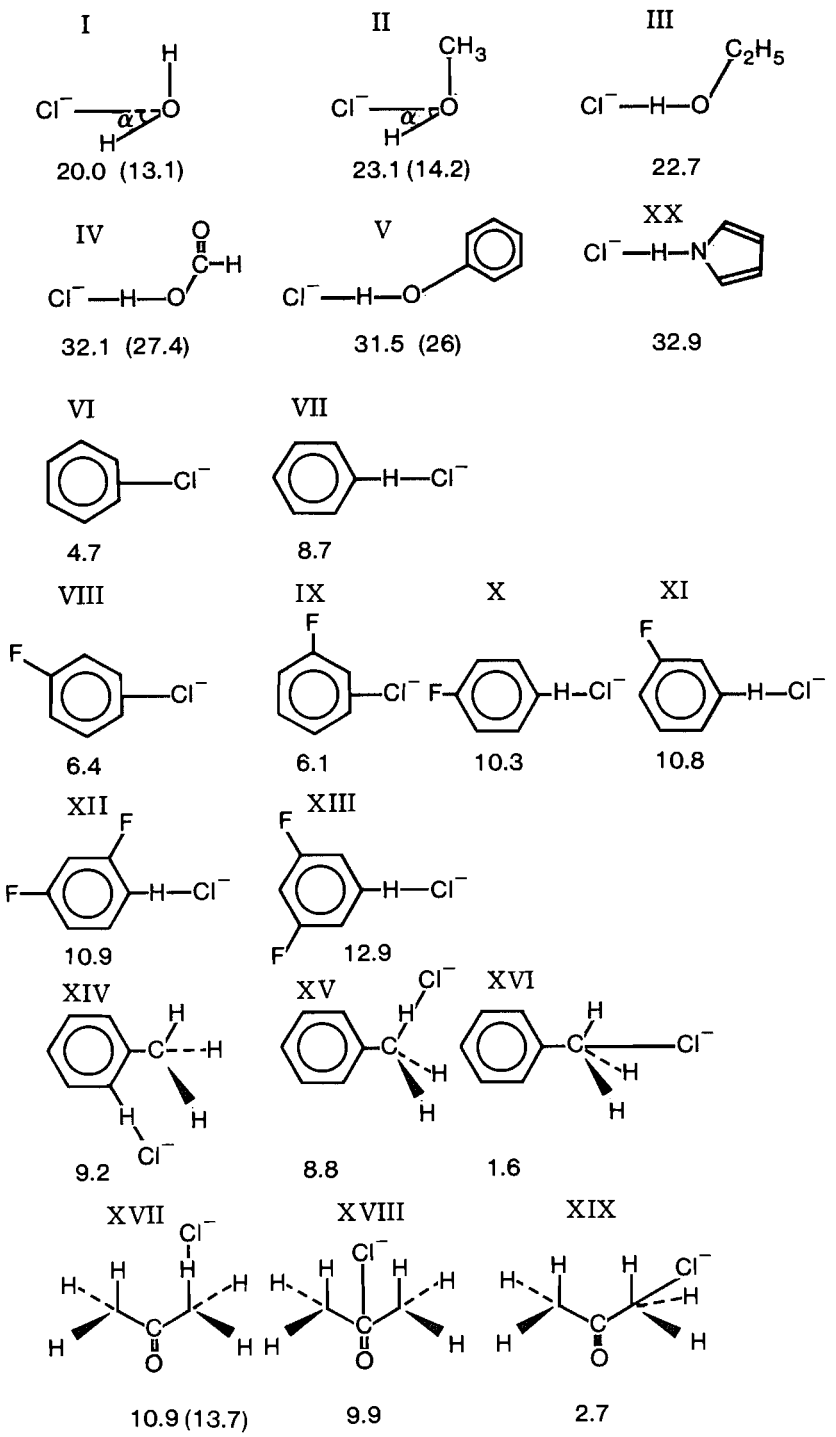


FIG. 6. Results from STO-3G calculations. The $-\Delta E$(STO-3G) calculated for the reaction [1]: RH + $Cl^-$ = $RHCl^-$ is given under the specific structure of $RHCl^-$. Whenever available, the $\Delta H_1^0$ measured experimentally are also given, these values are shown in brackets. Both results are in kcal/mol. In all structures shown, $Cl^-$ and the major bond frame of RH are in the same plane. For example, in the substituted benzenes $Cl^-$ and the benzene ring are in the same plane; in acetone, the $Cl^-$ is in the plane of the C—CO—C bonds. Other details of the calculations are given in Table 3.

Can. J. Chem. Downloaded from www.nrcresearchpress.com by 210.87.254.40 on 09/06/12
For personal use only.

Can. J. Chem. Downloaded from www.nrcresearchpress.com by 210.87.254.40 on 09/06/12
For personal use only.

TABLE 3. Results from STO-3G calculations for strucutres $RHCl^-$

| $(RHCl^-)^a$ | | R(O—Cl)[b] | R(O—H)[b] | α | $q(Cl^-)$[c] |
|---|---|---|---|---|---|
| $Cl^-HOH$ | I | 2.934 | 1.005 | 6.2° | −0.901 |
| $Cl^-HOCH_3$ | II | 2.887 | 1.015 | 3.3° | −0.880 |
| $Cl^-HOC_2H_5$ | III | 2.889 | 1.016 | 2.4° | −0.879 |
| $Cl^-HOC_6H_5$ | V | 2.830 | 1.030 | (0) | −0.835 |
| $Cl^-HOCOH$ | IV | 2.795 | 1.030 | (0) | −0.823 |
| | | R($Cl^-$..C) | R(C—H) | | |
| $Cl^-H—C_6H_5$ | VII | 3.203 | (1.084) | | −0.940 |
| $Cl^-H—C_6H_4F$ | XI | 3.186 | (1.084) | | −0.939 |
| $Cl^-H—C_6H_3F_2$ | XIII | 3.146 | (1.084) | | −0.930 |
| $Cl^-CH_3HH_5$ | XIV | 3.227 | 1.113 | | −0.936 |
| | XV | 3.26 | (1.113) | | −0.944 |
| $Cl^-CH_3COCH_3$ | XVII | 3.275 | (1.086) | | −0.952 |
| | XVIII | 3.67 | — | | −0.939 |
| | XIX | 3.54 | — | | −0.999 |

[a] Roman numerals correspond to structures shown in Fig. 6.
[b] Distance in Angstrom, distances shown without brackets were optimized, those with brackets were not optimized. For further details see section on calculations.
[c] Net atomic charge on Cl in $RHCl^-$. Charge on separated $Cl^-$ is −1.0.

3G calculations are used to explore further the nature of the bonding that occurs in the adducts $RHCl^-$.

*Comparison of chloride affinities with results from STO-3G calculations*

The results of the STO-3G calculations are summarized in Fig. 6 and Table 3. Some details concerning the calculations are given in the section Calculations.

The first five structures in Fig. 6 deal with the bonding of $Cl^-$ to the oxygen acids (HOH, $HOCH_3$, $HOC_2H_5$, HOPh, and HOCOH). Given in the figure are the STO-3G calculated binding energies and the experimentally determined $\Delta H$ values. Comparison between these two sets of results shows that the $-\Delta E$(STO-3G) are considerably larger than the experimental $-\Delta H$ values. The difference is most pronounced for the weak acids, HOH and $HOCH_3$. The calculated $\Delta E$ are closer to the experimental $\Delta H$ for the strong acids, phenol and formic acid.

It is well known that the basis set of STO-3G is too small and does not provide reliable stabilization energies even in the absence of electron correlation. Much closer agreement with the experimental result for $Cl^-HOH$, $\Delta H_1 = -13.1$ kcal/mol, has been obtained by Clementi and co-workers (23) who, using a large basis set, complete geometry optimization, correlation binding, and zero point difference correction, calculated $\Delta H_1 = -11.4$ kcal/mol. Kollman and Kunz (24), using the 431-G basis set, have obtained $\Delta E_1 = -19.9$ kcal/mol for the same comound, a value not significantly better than the $\Delta E_1 = -20$ kcal/mol obtained in the present work with the smaller STO-3G basis set. While the STO-3G basis set does not provide reliable absolute binding energies, the relative ordering of the binding energies is generally reliable. For example, the right order is predicted for the series HOH, $CH_3OH$, PhOH, and $HCO_2H$ (see Fig. 6). However, when the differences are very small, the predicted order cannot be trusted. Thus the slightly weaker binding predicted for ethanol relative to methanol is probably wrong, since a slightly stronger bonding for ethanol can be expected on the basis of the higher gas phase acidity of ethanol. The STO-3G energies for the isodesmic reactions are found to be fairly close to the observed enthalpy changes. Three examples are given below, where the energy changes quoted are in kcal/mol. It is probably safe to assume that STO-3G also gives approximately the correct chloride affinity ordering the approximate chloride affinity differences for the other structures given in Fig. 6.

| Reaction | $\Delta E$(STO-3G) | $\Delta H^0$ | $\Delta G^0(300)$ |
|---|---|---|---|
| $Cl^-HOH + CH_3OH = Cl^-CH_3OH + HOH$ | −3 | −1.1 | −1.6 |
| $Cl^-CH_3OH + HCO_2H = Cl^-HCO_2H + CH_3OH$ | −9 | −13.2 | −10.3 |
| $Cl^-PhOH + HCO_2H = Cl^-HCO_2H + PhOH$ | −0.6 | −1.4 | −2.9 |

The results for structures VI and VII show that stronger bonding with benzene is obtained in the hydrogen bonding position VII. The experimental $\Delta G^0_1$, for benzene is −3.8 kcal/mol (Table 2). Assuming the $\Delta S^0_1$ is in the neighbourhood of $-15$ cal $K^{-1}$ $mol^{-1}$ one obtains, from $\Delta G = \Delta H -$

Can. J. Chem. Downloaded from www.nrcresearchpress.com by 210.87.254.40 on 09/06/12
For personal use only.

$T\Delta S$, an estimate of $\Delta H_1^0 \approx -8$ kcal/mol. This value is close to the STO-3G result of 8.7 kcal mol$^{-1}$

Recently, we studied the equilibria of the potassium ion $K^+$ with benzene (25). The result given below shows that the bonding to potassium is much stronger than than to $Cl^-$. Calculations indicated that the most stable $K^+(C_6H_6)$ complex has an axial structure in which the $K^+$ lies on the symmetry axis of the benzene molecule. Benzene has a quadrupole moment of negative sign which is located on the symmetry axis in the centre of the molecule. The positive ion, when in the axial position, maximizes the attraction with the quadrupole and also achieves a substantial energy lowering due to the polarizability of the $\pi$ electron rings. For $Cl^-$, the axial position leads to a repulsive interaction with the quadrupole moment, and bonding that is considerably weaker than that calculated for structure VI.

$$K^+ + C_6H_6 = K^+(C_6H_6) \qquad -\Delta H^0 \approx 18 \text{ kcal mol}^{-1}$$

Structures VIII–XIII (Fig. 6) illustrate the bonding of fluorobenzenes to $Cl^{-1}$. The hydrogen atom *meta* to the fluorine substituent has the largest net atomic positive charge (based on Mullikan population analysis, STO-3G basis set). The strongest hydrogen bond with $Cl^-$ is obtained with that hydrogen. The stronger hydrogen bonding in the *meta* rather than *para* position to the fluorine substituent must be due to $\pi$ donation from the fluorine. While $\sigma$ withdrawal from the fluorine strengthens the hydrogen bond to $Cl^-$, $\pi$ donation weakens it. The effect of $\pi$ donation is smallest for the *meta* position. Increased fluorine substitution in the *meta* position in the series benzene, fluorobenzene, and 1,3-difluorobenzene can be expected to lead to increases of the chloride affinities. This in fact is observed experimentally (Table 2) and is also predicted by the calculations. The composite Fig. 7 shows that there is a linear relationship between the calculated and measured chloride binding energies and between the binding energies and the net atomic charge on the most positive hydrogen.

The chloride affinities of monosubstituted halobenzenes (see Table 2) increase in the order F, Cl, Br, I. The same order was found for the gas phase acidities of halosubstituted acetic acids (26). To explain the acidities of the acetic acids, the increased polarizability in the order F → I was invoked (26). In the present situation also, the increased polarizability should be the major effect, decreased $\pi$ donation in the F → I order may be another contributing factor.

The first report of hydrogen bonding involving an aromatic C—H as hydrogen donor was made by

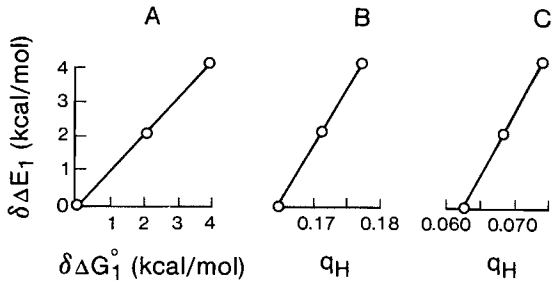


FIG. 7. Results for benzene, fluorobenzene, and difluorobenzene. Figure A shows STO-3G calculated ($\delta\Delta E_1$) versus measured ($\delta\Delta G_1^0$) energy of reaction: $FC_6H_5Cl^- + C_6H_6 = FC_6H_5 + C_6H_6{\cdot}Cl^-$. Figure B gives $\delta\Delta E$ versus net atomic positive charge on interacting hydrogen in complex $RHCl^-$. Figure C shows the same but for net positive charge on RH before formation of complex $RHCl^-$.

Allerhand and Schleyer (27). It was based on observation of an infrared association band for 1,3,5-trichlorobenzene and pyridine in carbon tetrachloride solvent. A hydrogen bonded complex with 1,3-dichlorobenzene was not observed under the same conditions (27). Unfortunately we did not make measurements with 1,3,5-trifluorobenzene or 1,3,5-trichlorobenzene. However, from the trends observed for the halobenzenes that were measured and calculated above, one may conclude that the chloride affinities of 1,3,5-trifluoro- and 1,3,5-trichlorobenzene should be higher than those for the 1,3 disubstituted compounds. Therefore our results are in line with the findings of Allerhand and Schleyer. The fact that they did not observe the more weakly bonded dichloro complex must be attributed to solvent effects. More recently Benoit and co-workers (4) reported that they did not observe a complex between 1,3,5-trichlorobenzene and $Cl^-$ in sulfolane solvent. Again this is obviously a solvent effect, the polar and abundant solvent displacing completely the trichlorobenzene from the $Cl^-$ complex.

Structures XIV, XV, and XVI provide an insight into the bonding of $Cl^-$ to toluene and by inference also for the substituted toluenes. In the lowest energy structure XIV, $Cl^-$ hydrogen bonds to one of the aromatic hydrogens. However, the structure XV, in which $Cl^-$ hydrogen bonds to one of the benzyl hydrogens, is less stable by only 0.4 kcal/mol. This suggests that, for the substituted toluenes with higher acidity than toluene, attachment of the $Cl^-$ will occur to the most acidic hydrogen, i.e. to a benzylic hydrogen. To this extent, one can say that the present STO-3G calculations are supportive of the findings based on the experimental chloride affinities, where the correlation of the affinities with the gas phase acidities of the toluene was

Can. J. Chem. Downloaded from www.nrcresearchpress.com by 210.87.254.40 on 09/06/12
For personal use only.

taken to imply that hydrogen bonding to the benzylic hydrogen occurs.

The results for structures XVII–XIX, dealing with $Cl^-$ and acetone, throw some light on the bonding of $Cl^-$ to carbon acids with carbonyl groups. The most stable structure is XVII where the $Cl^-$ is hydrogen bonded to one of the acidic hydrogens of the methyl group. The bond in XVIII, where $Cl^-$ is in line with the CO dipole is predicted to be of comparable but somewhat weaker strength. The correlation with the gas phase acidity observed for the carbonyl carbon acids in Fig. 5, i.e. progressively higher chloride affinities in the series $Me_2CO$, MeCOPh. $PhCH_2COMe$ and $(MeCO)_2CH_2$, taken together with the STO-3G prediction that the hydrogen bonded structure XVII is the most stable chloride, leads one to expect that, for the stronger acids also, the $Cl^-$ hydrogen bonds to the most acidic hydrogen. For example for $(CH_3CO)_2CH_2$ the $Cl^-$ attachment should be to one of the methylene hydrogens.

Acetone is another solvent molecule for which the bonding to the negative ion ($Cl^-$) $-\Delta H$ = 13.7 kcal $mol^{-1}$, is considerably weaker than that to the positive ion ($K^+$) of similar radius. Measurements from this laboratory (25) give a $-\Delta H$ = 24.4 kcal $mol^{-1}$ for the potassium ion. The reason for this difference is easily understood. The bonding is largely of an electrostatic nature. Most of the permanent dipole is in the CO bond. The positive ion can approach the CO dipole closely. On the other hand, the negative ion is kept from close approach by the presence of the methyl groups.

A comparison between the calculated $\Delta E_1$ (STO-3G) for the most stable structures and the measured $\Delta G^\circ_1$ is shown in Fig. 8. One may expect that the $\Delta S^\circ_1$ differences for the different RH are not very large. In such a case an approximately linear relationship between $\Delta E_1$ and $\Delta G^\circ_1$ should be observed. Such a relationship is indicated in Fig. 8, however, the data are quite scattered. This is probably due to the considerable difference in the nature of the compounds RH included in the figure.

In the preceding discussion it was noted that for related compounds there is a near linear relationship between the net atomic charge of the hydrogen in the RH and the hydrogen bond in the complex $RHCl^-$. This relationship is further explored in the data shown in Fig. 9, which contains the results for the substituted benzenes, the hydroxylic compounds, HOH, MeOH, EtOH, and phenol, and formic acid. It can be seen that the relationship does not hold up as well when strongly differing groups of compounds are included. Still, an approximate proportionality is observed, which suggests that the net atomic charges in the hydrogens of RH are a rough guide to the strength of the hydrogen bond with the negative ion. A much better relationship is observed when the hydrogen

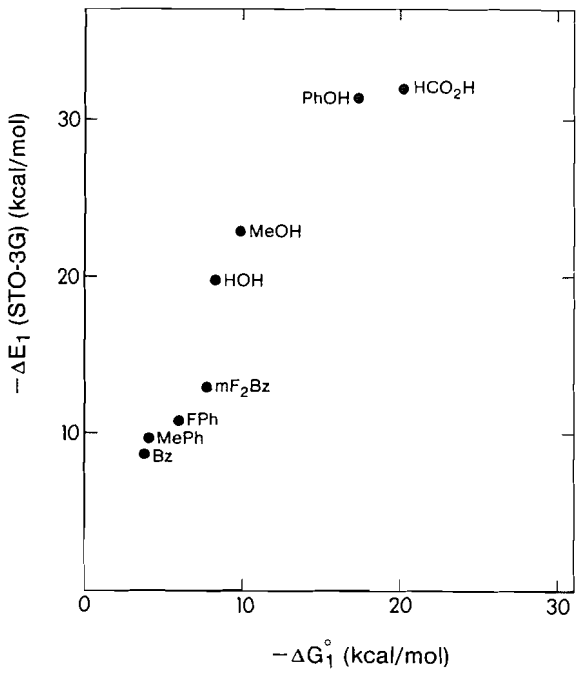


FIG. 8. Plot of calculated $\Delta E$(STO-3G) for reaction [1] (RH + $Cl^-$ = $RHCl^-$) versus measured $\Delta G^\circ_1$ for same reaction. $\Delta G^\circ_1$ values from Table 2.

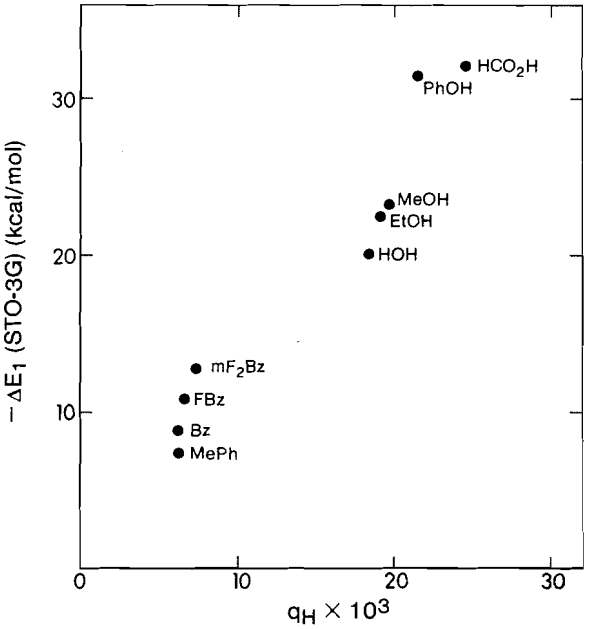


FIG. 9. Plot of $\Delta E$(STO-3G) for reaction [1] versus net positive charge on acidic hydrogen of RH before the reaction.

Can. J. Chem. Downloaded from www.nrcresearchpress.com by 210.87.254.40 on 09/06/12
For personal use only.

bond energies are plotted versus the charge on the chlorine in the complex $RHCl^-$. This is shown in Fig. 10. Since the charge in the separated $Cl^-$ is $-1$, the figure shows that the strength of the hydrogen bond in $RHCl^-$ increases in proportion with the negative charge transferred from $Cl^-$ to the molecule RH, on formation of the complex $RHCl^-$.

Benoit and co-workers (4) have determined the enthalpy change $\Delta H_{1(sl)}$ for reaction [1] occurring in sulfolane solution. These results are given in Table 1. Comparing the $\Delta H_1$ for gas phase and solution, we notice that the exothermicity is much attenuated in solution. The attenuation factor is not constant but is in the range 7 for the stronger acids $HCO_2H$ and phenol and 5 for the weaker HOH and $CH_3OH$. Benoit (4) has also determined the enthalpy of solvation of RH from gas phase to sulfolane (see Table 1) so that the cycle [2] can be set up, which leads to eqs. [3] and [4]. Equation [4] is of

[2]
$$\begin{array}{ccc} RH_{(g)} + Cl^-_{(g)} & \xrightarrow{\Delta H_{1(g)}} & RHCl^-_{(g)} \\ \uparrow\ -\Delta H_{sl}(RH) & & \downarrow\ \Delta H_{sl}(RHCl^-) \\ \uparrow\ -\Delta H_{sl}(Cl^-) & & \downarrow \\ RH_{(sl)} + Cl^-_{(sl)} & \xrightarrow{\Delta H_{1(sl)}} & RHCl^-_{(sl)} \end{array}$$

[3] $$\Delta H_{1(sl)} = -\Delta H_{sl}(RH) - \Delta H_{sl}(Cl^-) + \Delta H_{1(g)} + \Delta H_{sl}(RHCl^-)$$

[4] $$\Delta H_4 = \Delta H_{sl}(RHCl^-) - \Delta H_{sl}(Cl^-) = \Delta H_{1(sl)} - \Delta H_{1(g)} + \Delta H_{sl}(RH)$$

interest since it provides $\Delta H_4$, the solvation energy difference between the complex $RHCl^-$ and $Cl^-$. These results are given in Table 1. $\Delta H_4$ is always positive, as is to be expected. One might have also expected that $\Delta H_4$ will increase with the size of the RH molecule, i.e. $\Delta H_4$ should be larger for phenol than for formic acid. However this trend is not observed, $\Delta H_4$ (phenol) = 7.7 kcal/mol while $\Delta H_4(HCO_2H)$ = 12.4 kcal/mol. The clear trend observed is that $\Delta H_4$ increases with the acidity of RH. On reflection, the reason for this trend becomes clear. The solvation of $RHCl^-$ will decrease with the radius of RH only if substantial negative charge is delocalized onto RH. This delocalization depends on the extent of proton transfer from RH to $Cl^-$, i.e. on the acidity of RH. An even more direct measure is the STO-3G calculated charge transfer from $Cl^-$ to RH. Figures 5 and 9 demonstrate the proportionality between the charge transfer from $Cl^-$, the chloride affinity of RH, and the acidity of RH. Evidently, $\Delta H_4$ will depend on the extent of charge transfer from $Cl^-$ to RH, the sites on RH to which the charge is transferred, i.e. extent of delocalization within RH and the size of RH. The operation of some of these combined effects should be reflected in the available $\Delta H_4$.

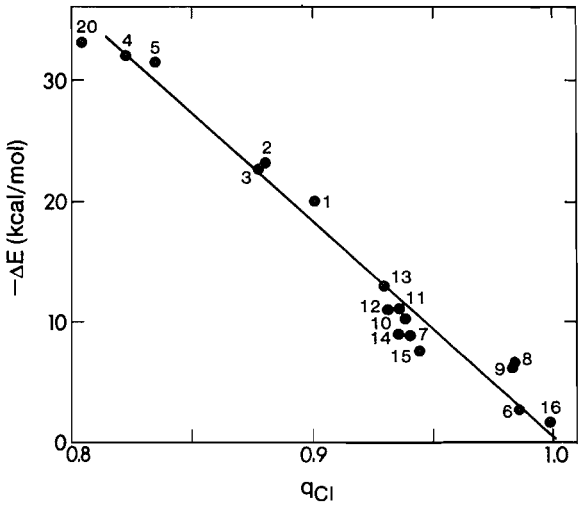


FIG. 10. Plot of $\Delta E$(STO-3G) from reaction [1] versus net negative charge on $Cl^-$ in $RHCl^-$. Numbers on data points correspond to structures (in roman numerals) in Fig. 7. Plot shows good correlation between the bonding in the complex $RHCl^-$ and the charge transferred from $Cl^-$ to RH on formation of the complex $RHCl^-$.

Unfortunately, these are very few and not of high accuracy. One case fits the expected trend. The extent of charge transfer in $ClHCl^-$ should be by far the largest, i.e. 0.5 electrons, since the two Cl atoms become equivalent, (for the other $\delta q Cl^-$, see Table 3). The observed $\Delta H_4$ for HCl is large but not by far the largest. This must be due to the small size of HCl, i.e. even though the charge transfer is large, the overall size of the ion $ClHCl^-$ is small, and this reduces the adverse effect on the solvation energy of the ion.

The attenuation of the observed hydrogen bonding in solution relative to the gas phase is closely analogous to the attenuation of substituent effects on acidity or basicity in the gas phase and solution. For example, a substituent which increases the gas phase acidity of benzoic acid delocalizes the charge in the benzoate anion and reduces the solvation energy of the substituted anion. This leads to an attenuation of the substituent effect in solution (21). In the hydrogen bonding complexes the role of the substituent is played by HR. An HR that forms a strong hydrogen bond, i.e. stabilizes $Cl^-$ strongly, decreases the solvation energy of $RHCl^-$ strongly and this leads to an attenuation of the hydrogen bonding in solution.

The gas phase hydrogen bonding energies could be useful in the design of multiligand complexing agents, i.e. crypts (5) for negative ions. Data from solutions often do not express the true available complexing power of a complexing group in a crypt. For example, the enthalpy changes $\Delta H_{1(l)}$ for

$CH_3OH$ and $CH_3CO_2H$ in sulfolane are equal, $\Delta H_{1(l)} = -3.2$ kcal/mol (4). Yet it is clear from the gas phase data that a carboxylic acid or a phenolic hydroxide group is vastly superior to the OH group from an aliphatic alcohol. Since the radius of the crypt as a whole is dictated largely by other considerations, it is clear that a great advantage in complexing is to be gained by selecting the most acidic hydroxide groups as ligands on the inside of the crypt.

The data in Table 2 give the order of stabilities of $RHCl^-$ gas phase complexes. Thus they have direct application to negative ion chemical ionization mass spectrometry of $Cl^-$ adducts (2). It is clear that adducts of a wide variety of compounds can be formed and that considerable selectivity can be obtained if the ion source temperature is varied from room temperature to 300°C. At room temperature, or below, adducts with all compounds in Table 2 will be formed. At the highest temperatures only adducts with the strongest acids will be observable.


1. J. L. PUCKETT and W. C. LINEBERGER. Phys. Rev. A, **1**, 1635 (1970); F. C. FEHSENFELD, C. J. HOWARD, and A. L. SCHMELLEKPF. J. Chem. Phys. **63**, 2835 (1975); J. A. DAVIDSON, F. C. FEHSENFELD, and C. J. HOWARD. Int. J. Chem. Kinet. **9**, 17 (1977).
2. H. P. TANNENBAUM, J. D. ROBERTS and R. C. DOHERTY. Anal. Chem. **47**, 49 (1975).
3. J. E. GORDON. J. Org. Chem. **26**, 738 (1961); I. M. KOLTHOFF and M. K. CHANTOONI, JR. J. Am. Chem. Soc. **91**, 4621 (1969).
4. S. Y. LAM, C. LOUIS, and R. L. BENOIT. J. Am. Chem. Soc. **98**, 1156 (1976).
5. J. M. LEHN. Pure Appl. Chem. **50**, 871 (1978).
6. R. A. DURST (*Editor*) Ion selective electrodes. NBS Special Publications 341. U. S. Government Printing Office, Washington, D. C. 1969.
7. R. YAMDAGNI and P. KEBARLE. J. Am. Chem. Soc. **93**, 7139 (1971).
8. (*a*) R. YAMDAGNI, J. D. PAYZANT, and P. KEBARLE. Can. J. Chem. **51**, 2507 (1973); (*b*) M. ARSHADI, R. YAMDAGNI, and P. KEBARLE. J. Phys. Chem. **74**, 1475 (1970); (*c*) P. Kebarle. Annu. Rev. Phys. Chem. **28**, 445 (1977).
9. M. A. FRENCH, J. CUMMING, and P. KEBARLE. J. Am. Chem. Soc. **99**, 6999 (1977).
10. J. B. CUMMING and P. KEBARLE. Can. J. Chem. **56**, 1 (1978).
11. J. E. BARTMESS, J. A. SCOTT, and R. T. MCIVER, JR. J. Am. Chem. Soc. **101**, 6045 (1979).
12. J. SUNNER and P. KEBARLE. J. Phys. Chem. **85**, 327 (1981).
13. Y. K. LAU, S. IKUTA, and P. KEBARLE. J. Am. Chem. Soc. **104**, 1062 (1982).
14. W. J. HEHRE, R. F. STEWART, and J. A. POPLE. J. Chem. Phys. **51**, 2657 (1969); J. A. POPLE and M. GORDON. J. Am. Chem. Soc. **89**, 4293 (1967); Gaussian 70: W. J. Hehre, W. A. Lathan, R. Ditchfield, M. D. Newton, and J. A. Pople. QCPE, **11**, 236 (1973); Hondo 5: M. King, M. Dupuis, and J. Rys. Nat. Resour. Comput. Chem. Software Cat. Vol. 1. Prog. No. QH02, Hondo 5 (1980).
15. (*a*) M. D. HARMONY, V. W. LAURIE, R. L. KUCZKOWSKI, R. H. SCHWEDEMAN, D. A. RAMSAY, F. J. LORAS, M. J. LAFFERTY, and A. G. MAKI. J. Phys. Chem. Ref. Data, **8**, 619 (1979); (*b*) J. E. DELBENE, F. T. MARCHESE, G. T. WORTH, and M. E. CONRAD. Theoret. Chim. Acta, **36**, 195 (1975).
16. (*a*) E. CLEMENTI, H. CLEMENTI, and D. R. DAVIS. J. Chem. Phys. **46**, 4725 (1967); (*b*) E. CLEMENTI, J. MEHL, and W. VON NIESSEN. J. Chem. Phys. **59**, 508 (1971).
17. R. YAMDAGNI and P. KEBARLE. Can. J. Chem. **52**, 2449 (1974).
18. W. R. DAVIDSON, J. SUNNER, and P. KEBARLE. J. Am. Chem. Soc. **101**, 1675 (1979).
19. W. F. REYNOLDS, P. G. MEZEY, W. J. HEHRE, R. D. TOPSOM, and R. H. TAFT. J. Am. Chem. Soc. **99**, 5821 (1977).
20. W. J. HEHRE, M. TAAGEPERA, R. W. TAFT, and R. D. TOPSOM. J. Am. Chem. Soc. **103**, 1344 (1981).
21. T. B. MCMAHON and P. KEBARLE. J. Am. Chem. Soc. **99**, 2222 (1977).
22. M. FUJIO, R. T. MCIVER, and R. W. TAFT. J. Am. Chem. Soc. **103**, 4017 (1981)
23. H. KISTENMACHER, H. POPKIE, and E. CLEMENTI. J. Chem. Phys. **59**, 5842 (1973).
24. P. KOLLMAN and I. KUNTZ. J. Am. Chem. Soc. **98**, 6820 (1976).
25. J. SUNNER, K. NISHIZAWA, and P. KEBARLE. J. Phys. Chem. **85**, 1814 (1981).
26. K. HIRAOKA, R. YAMDAGNI, and P. KEBARLE. J. Am. Chem. Soc. **95**, 6833 (1973).
27. A. ALLERHAND and P. V R. SCHLEYER. J. Am. Chem. Soc. **85**, 1715 (1963).


Can. J. Chem. Downloaded from www.nrcresearchpress.com by 210.87.254.40 on 09/06/12
For personal use only.

# Peroxide oxidation of $\Delta^4$-3-ketosteroids

HERBERT L. HOLLAND,[1] ELLY RIEMLAND, AND ULRICH DAUM
*Department of Chemistry, Brock University, St. Catharines, Ont., Canada L2S 3A1*

Received December 15, 1981

HERBERT L. HOLLAND, ELLY RIEMLAND, and ULRICH DAUM. Can. J. Chem. **60**, 1919 (1982).

Treatment of $\Delta^4$-3-ketosteroids with *tert*-butyl hydroperoxide in the presence of lithium hydroxide leads to the formation of the corresponding 4β,5β epoxides stereospecifically and in good yield. The stereospecificity of this reaction is explicable in terms of the accepted mechanism for the hydrogen peroxide epoxidation of $\Delta^4$-3-ketosteroids.

The use of aqueous sodium peroxide as oxidant leads to the production of the corresponding $\Delta^4$-3,6-diones. A mechanism for this reaction is proposed in which the key step is autoxidation of the corresponding deconjugated $\Delta^5$-3-ketone, produced from the starting material *in situ* by the action of the reagents. Lithium peroxide does not oxidize androst-4-ene-3,17-dione at C-6, but produces the 4,5 epoxides in low yield together with an *A*-nor-3,5-secoacid.

HERBERT L. HOLLAND, ELLY RIEMLAND et ULRICH DAUM. Can. J. Chem. **60**, 1919 (1982).

Les $\Delta^4$ céto-3 stéroïdes réagissent avec l'hydroperoxyde de *tert*-butyle en présence d'hydroxyde de lithium en donnant stéréospécifiquement les époxydes 4β,5β correspondants avec un bon rendement. On peut expliquer la stéréospécifité de cette réaction en fonction du mécanisme accepté pour l'époxydation des $\Delta^4$ céto-3 stéroïdes par le peroxyde d'hydrogène.

L'utilisation du peroxyde de sodium en solution aqueuse comme oxydant conduit à la formation des $\Delta^4$ diones-3,6 correspondantes. On propose, pour cette réaction, un mécanisme dans lequel l'étape fondamentale est l'auto-oxydation de la $\Delta^5$-cétone-3 déconjuguée correspondante, obtenue *in situ* à partir du produit de départ sous l'action des réactifs. Le peroxyde de lithium n'oxyde pas l'androstène-4 dione-3,17 en position C-6, mais il conduit à l'époxyde-4,5 avec un faible rendement en même temps qu'à un acide *A*-norseco-3,5.

[Traduit par le journal]

The epoxidation of α,β unsaturated ketones by basic hydrogen peroxide is a reaction which is tolerably well understood. Its mechanistic (1, 2) and stereoelectronic (3) requirements have been formulated, and, in the case of $\Delta^4$-3-ketosteroids (**1**) the details of the reaction leading to both β (**2**) and α (**3**) substituted products have been discussed (4–6). The predominance of the β isomer in the latter case is consistent within the known preference for attack from the β face at C-5 (*4b*) and intermediates for the formation of α and β products as shown in Fig. 1, in which formation of the α epoxide involves unfavourable 1,3 diaxial interactions between the hydroperoxide at C-5 and hydrogens at C-7 and C-9 (*4a*). The influence of long range electrostatic effects caused by a variation in substitution at C-17 on the α/β ratio obtained from reactions of $\Delta^4$-3-ketosteroids with hydrogen peroxide in the presence of sodium hydroxide has been examined by Henbest and Jackson (5, 6).

*tert*-Butyl hydroperoxide is known to epoxidize certain α,β unsaturated ketones in the presence of base (7, 8), but under the conditions employed (Triton B in benzene), was not reactive towards $\Delta^4$-3-ketosteroids (7). In the present study, we have obtained good yields of only β epoxide (**2**) from treatment of $\Delta^4$-3-ketosteroids (**1**) with *tert*-butyl hydroperoxide and lithium hydroxide in ethanol solution. These experiments are summarized in Table 1. Control experiments (Table 1) indicate that the substitution of lithium hydroxide for sodium hydroxide when using hydrogen peroxide as oxidizing agent has little effect on the ratio of α/β

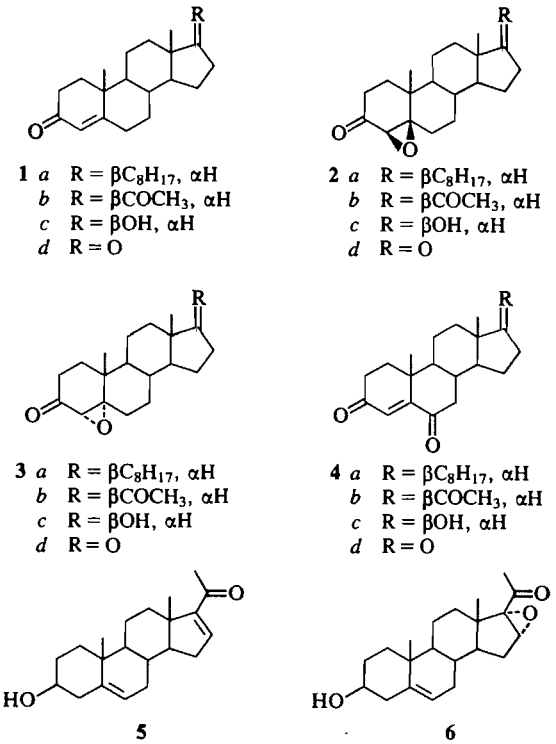


[1]Author to whom correspondence may be addressed.

0008-4042/82/151919-05$01.00/0

©1982 National Research Council of Canada/Conseil national de recherches du Canada

Can. J. Chem. Downloaded from www.nrcresearchpress.com by 210.87.254.5 on 09/06/12
For personal use only.

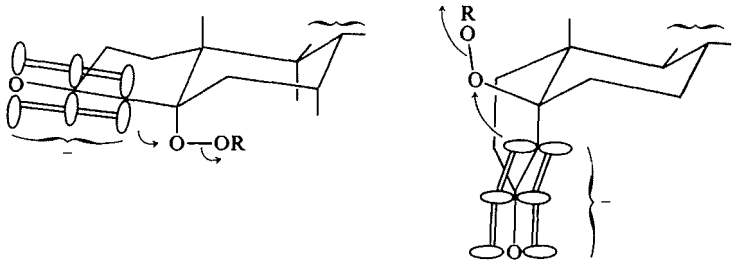


R = H, hydrogen peroxide oxidation
R = $C(CH_3)_3$, *tert*-butyl hydroperoxide oxidation

FIG. 1. The formation of α and β epoxides from $\Delta^4$-3-ketosteroids.

epoxides produced. The production of only the β epoxides (**2**) by *tert*-butyl hydroperoxide is entirely consistent with the accepted mechanism of hydrogen peroxide oxidation (1–6) shown in Fig. 1; for R = $C(CH_3)_3$, the 1,3 diaxial interactions leading to α epoxide are highly unfavourable.

We have also examined the reactions of lithium and sodium peroxides with α,β unsaturated ketosteroids. These are also summarized in the table. The use of aqueous sodium peroxide gave rise to products different from those obtained by treatment with sodium hydroxide/hydrogen peroxide mixtures. In only one case (**5** → **6**) was the expected product obtained (in low yield); the $\Delta^4$-3-ketosteroids **1** gave good yields of the corresponding $\Delta^4$-3,6-diones (**4**) as the sole isolable product. Variation of time and amount of reactants produced no evidence for the formation of any other product in significant amount. Lower yields were obtained with the $\Delta^5$-3-ketosteroid (**12**) and isophorone (**16***a*), whereas the simpler analogue 3-methylcyclohex-2-enone (**14**) gave only a trace of the corresponding oxidation product **15**.

The aqueous decomposition of commercial sodium peroxide, yielding oxygen and sodium hydroxide (9) appears to be a key feature in this reaction. The oxidation of **1***d* to **4***d* proceeded in good yield under a nitrogen atmosphere, but did not

TABLE 1. Products of peroxide oxidations

| Starting material | Oxidant | Base | Products | Isolated yield (%) | α:β ratio |
|---|---|---|---|---|---|
| **1***a* | $H_2O_2$ | NaOH | **2***a*,**3***a* | 55 | 1:5 |
| **1***a* | $H_2O_2$ | NaOH | **2***a*,**3***a* | — | β only (5, 6) |
| **1***a* | $H_2O_2$ | LiOH | **2***a*,**3***a* | 72 | 1:6 |
| **1***a* | *t*-Bu.OOH | LiOH | **2***a* | 76 | β only |
| **1***a* | $Na_2O_2$ | — | **4***a* | 56 | — |
| **1***b* | $H_2O_2$ | NaOH | **2***b*,**3***b* | 80 | 1:2.5 |
| **1***b* | $H_2O_2$ | NaOH | **2***b*,**3***b* | — | 1:3 (5, 6) |
| **1***b* | $H_2O_2$ | LiOH | **2***b*,**3***b* | 95 | 1:3 |
| **1***b* | *t*-Bu.OOH | LiOH | **2***b* | 80 | β only |
| **1***b* | $Na_2O_2$ | — | **4***b* | 63 | — |
| **1***c* | $H_2O_2$ | NaOH | **2***c*,**3***c* | — | 1:2.3 (5, 6) |
| **1***c* | *t*-Bu.OOH | LiOH | **2***c* | 73 | β only |
| **1***c* | $Na_2O_2$ | — | **4***c* | 43 | — |
| **1***d* | $H_2O_2$ | NaOH | **2***d*,**3***d* | 70 | 1:3 |
| **1***d* | *t*-Bu.OOH | LiOH | **2***d* | 78 | β only |
| **1***d* | $Na_2O_2$ | — | **4***d* | 55 | — |
| **1***d* | $Li_2O_2$ | — | **2***d*,**3***d* | 23 | 1:1 |
| | | | **18***a* | 33 | — |
| **2***b*,**3***b* | $Na_2O_2$ | — | Unidentified | — | — |
| **5** | *t*-Bu.OOH | LiOH | **6** | 95 | — |
| **5** | $Na_2O_2$ | — | **6** | 40 | — |
| **5** | $H_2O_2$ | NaOH | **6** | 90–95 (27) | 40:1 (28) |
| **2***b*,**7–11,17** | $Na_2O_2$ | — | No reaction | — | — |
| **2***b*,**8,11** | $Li_2O_2$ | — | No reaction | — | — |
| **12** | $Na_2O_2$ | — | **1***a* | Trace | — |
| | | | **4***a* | 20 | — |
| **14** | $Na_2O_2$ | — | **15** | Trace | — |
| **16***a* | $Na_2O_2$ | — | **16***a* | 5 | — |

Can. J. Chem. Downloaded from www.nrcresearchpress.com by 210.87.254.5 on 09/06/12
For personal use only.

Can. J. Chem. Downloaded from www.nrcresearchpress.com by 210.87.254.5 on 09/06/12
For personal use only.

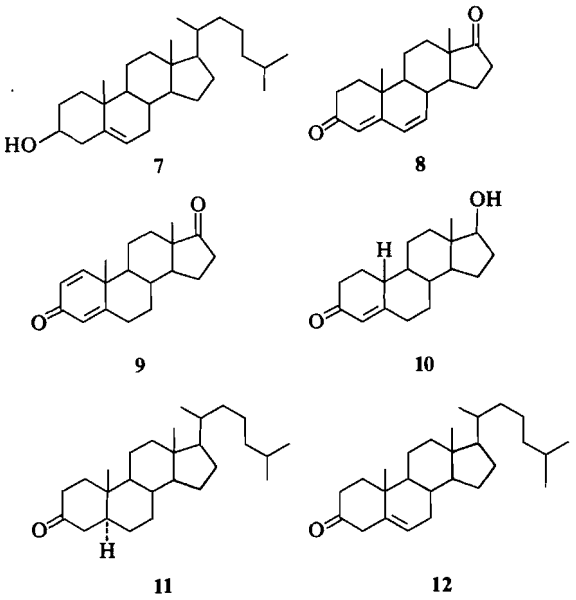


7 8 9 10 11 12

proceed appreciably under anhydrous conditions. The observed conversion of **12** into **4***a*, the known formation of the hydroperoxides **13** from **12** under autoxidative conditions (10, 11), and the established production of **4***a* from **13** under basic conditions (11) suggest the route for the conversion of **1** to **4** presented in Fig 2.

The simple base catalysed autoxidation of conjugated ketones **1** is known to proceed in poor yield, and give the 4-ol-$\Delta^{4,6}$-diene-3-ketones as the major product. However, the conditions reported herein differ appreciably from those described in the literature (12, 13). It has been proposed that the rapid autoxidation of **12** involves the formation of an enolate ion pair rather than the free enolate (11), and a similar mechanism may be operative in the present case (Fig. 2). If this is so, the structure of this intermediate presumably resembles **12** rather than **1**, for the following reasons. Firstly, the related ketosteroid **9**, inert to sodium peroxide oxidation, is only deconjugated under vigorous enolizing conditions (14), and the deconjugated compounds corresponding to **8** and **10** do not autoxidize rapidly at room temperature[2] under conditions where the autoxidation of **12** is fast. (11, 15, 16). The base catalyzed autoxidation of saturated 3-ketosteroids (e.g. **11**) requires 18–50 hours at room temperature before appreciable conversions are achieved (17). The low yields obtained from **14** and **16***a* are attributed to a low rate of autoxidation under basic conditions (18, 19).

The production of epoxide **6** (in low yield) from **5** by sodium peroxide suggested the possibility that the conversion of **1** to **4** may proceed via the 4,5 epoxide (**2** or **3**). However, treatment of **2***b* or **3***b* with aqueous sodium peroxide led only to a complex mixture of material more polar than starting material, of which **4***b* was not a component.

The possibility that singlet oxygen may be released in the decompositions of hydrogen peroxide (20) and potassium superoxide (21) led us to consider that this species may be involved in the oxidation of **12** to **13**. However, several factors militate against this: reaction of **12** with singlet oxygen gives, in addition to **4***a*, products derived from cholest-6-ene-3-one-5α-hydroperoxide (10), which were not produced in the present case; there is no precedent for the generation of singlet oxygen from sodium peroxide (22); and treatment of the singlet oxygen specific reagents cholesterol (**7**) (23) and 1,3-diphenylisobenzofuran (**17**) (24) with aqueous sodium peroxide did not result in the formation of oxidized products.

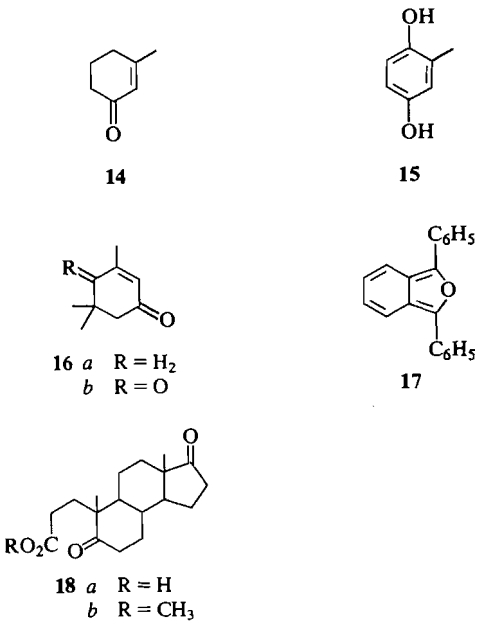


**14** **15**

**16** *a* R = $H_2$
*b* R = O

**17**

**18** *a* R = H
*b* R = $CH_3$

Treatment of lithium peroxide with water does not result in appreciable production of oxygen (9), and the $\Delta^4$-3,6-dione was not obtained on treatment of **1***d* with these reagents. Instead, the epoxides **2***d* and **3***d* were obtained, together with the *A*-nor-3,5-seco acid **18***a*, a classical oxidative degradation product of $\Delta^4$-3-ketones (25). The latter functionality has also been obtained by treatment of a 5β-3-ketone with potassium superoxide (26). The acid **18***a* may be produced via a mechanism similar to that proposed (26), but the details of its production have not been examined in the present study.

[2]H. L. Holland, G. J. Taylor, E. M. Thomas, and E. Riemland. Unpublished data.

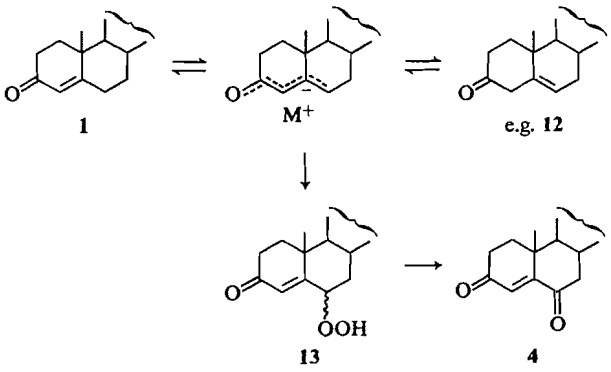


FIG. 2. Proposed routes for the conversions of $\Delta^4$- and $\Delta^5$-3-keto-steroids to $\Delta^4$-3,6-diketosteroids by sodium peroxide.

## Experimental

*Apparatus, materials, and methods*

Melting points were determined on a Kofler heating stage and are uncorrected. Infrared spectra were recorded with a Perkin–Elmer 237B spectrometer. Proton nmr spectra were obtained with a Varian A-60 or Bruker WP-60 at 60 MHz and $^{13}C$ nmr spectra with a Bruker WP-60 at 15.18 MHz, using $CDCl_3$ as solvent and TMS as internal standard. Mass spectra were obtained with an AEI MS30 spectrometer. Column chromatography was performed on silica gel (60–200 mesh) using a benzene/ether gradient as eluting solvent, and thin layer chromatography on Merck silica gel 60 F-254 (0.25 mm).

*Oxidations with hydrogen peroxide*

These were carried out by the literature procedure (6). The residue was examined by $^1H$ nmr to determine the ratio of α/β epoxides, using the C-4 hydrogen signal intensity (α 3.03; β 2.96 ppm) for a quantitative estimate, and then subjected to column chromatography. The isolated steroids so produced were identified by mp and spectral comparisons with literature values. Hitherto unreported spectral data and literature references are presented below.

*Oxidations with* tert-*butyl hydroperoxide*

*tert*-Butyl hydroperoxide (5 mL, 90%) was added dropwise over 15 min to a stirred solution of steroid (1 g) in ethanol (35 mL, 95%), and lithium hydroxide (4 mL, 4 *N*). The resulting solution was allowed to stand at room temperature for 48 h, and then worked up as described above.

*Oxidations with sodium peroxide*

Water (10 mL) was added dropwise over a 2 h period to a stirred mixture of starting material (1 g) and sodium peroxide (4 g) in ethanol (50 mL). The mixture was then acidified (dilute HCl) and extracted with chloroform. The extract was washed and evaporated. The product was isolated by chromatography and characterized by mp and spectral comparison with literature values. Hitherto unreported spectral data and literature references are presented below. Compounds **2***b*, **7**–**11**, and **17** were not affected by the treatment described above; starting material was recovered unchanged in these cases. The epoxide **2***b* was converted into a complex mixture of polar products of which **4***b* was not a component (tlc).

*Oxidations with lithium peroxide*

Treatment of **1***d* with lithium peroxide by the procedure described above for sodium peroxide, and workup as indicated, followed by chromatography, gave the epoxides **2***d* and **3***d* (1:1, total 23%) and a 33% yield of a compound identified as A-nor-3,5-seco-5,17-diketo-androstan-3-oic acid (**18***a*), mp 106–109°C (lit. (29) mp 108–110°C); ir $\nu_{max}$: 1705, 1730, 2500–3500 $cm^{-1}$; $^1H$ nmr included signals at δ 0.92 (3H, s, C-18H), 1.15 (3H, s, C-19H), 6.5–7.3 (br s, 1H, exchanges $D_2O$, –COOH); $^{13}C$ nmr, δ: 13.7 (C-18), 20.3 (C-19 or C-11), 20.7 (C-11 or C-19), 21.8 (C-15), 29.2 (C-1 or C-7), 29.9 (C-7 or C-1), 31.0 (C-12), 34.4 (C-8), 35.7 (C-16), 37.7 (C-2), 47.6 (C-10 and C-13 or C-6), 48.0 (C-10 and C-13 or C-6), 50.5 (C-9 or C-14), 50.7 (C-14 or C-9), 178.9 (C-3), 214.1 (C-5), and 220.1 (C-17) ppm; ms *m/z* (%): 306 (2), 288 (22), 273 (8), 260 (13), 234 (68), 219 (29) relative to *m/z* 55 (100); methyl ester (**18***b*) *m/z* (%): 320 (3), 305 (12), 302 (9), 289 (10), 273 (15), 261 (14), 247 (10), 234 (100). Compounds **2***b*, **8**, and **11** gave no detectable products (tlc) when treated by the above procedure.

*Physical and spectral data*

Only hitherto unreported data are listed. Other data obtained correspond to those given in the references listed.

*(4β,5)-Epoxy-5β-cholestan-3-one* (**2***a*) (30–32)

$^{13}C$ nmr, δ: 12.0 (C-18), 18.6 (C-21), 19.0 (C-19), 21.5 (C-11), 22.6 (C-26), 22.8 (C-27), 23.9 (C-23), 24.2 (C-15), 26.2 (C-7), 28.1 (C-16 and C-25), 29.9 (C-6), 30.5 (C-1), 32.6 (C-2), 35.1 (C-8), 35.8 (C-20), 36.2 (C-22), 37.2 (C-10), 39.6 (C-12 and C-24), 42.7 (C-13), 46.5 (C-9), 55.9 (C-14), 56.2 (C-17), 62.7 (C-4), 70.4 (C-5), and 206.9 (C-3) ppm.

*(4β,5)-Epoxy-5β-pregnan-3,20-dione* (**2***b*) (6)

$^{13}C$ nmr, δ: 13.3 (C-18), 18.9 (C-19), 21.5 (C-11), 22.8 (C-16), 24.4 (C-15), 26.2 (C-7), 29.8 (C-6), 30.3 (C-1), 31.4 (C-21), 32.6 (C-2), 35.1 (C-8), 37.2 (C-10), 38.5 (C-12), 44.1 (C-13), 46.4 (C-9), 56.0 (C-14), 62.7 (C-4), 63.5 (C-17), 70.2 (C-5), 206.6 (C-3), and 209.1 (C-20) ppm.

*(4β,5)-Epoxy-5β-androstan-17β-ol-3-one* (**2***c*) (6)

*(4β,5)-Epoxy-5β-androstan-3,17-dione* (**2***d*) (6)

*(4α,5)-Epoxy-5α-cholestan-3-one* (**3***a*) (30, 31, 33, 34)

*(4α,5)-Epoxy-5α-pregnan-3,20-dione* (**3***b*) (6)

*(4α,5)-Epoxy-5α-androstan-17β-ol-3-one* (**3***c*) (6)

*(4α,5)-Epoxy-5α-androstan-3,17-dione* (**3***d*) (6)

*Cholest-4-ene-3,6-dione* (**4***a*) (23, 35)

$^1H$ nmr included signals at δ 0.75 (3H, s, C-18H), 0.82 and 0.92 (9H, C-21, -26, -27 H's), 1.18 (3H, s, C-19H), and 6.20 (1H, s, C-4H) ppm.

*Pregn-4-ene-3,6,20-trione* (**4***b*) (35, 36)

$^1H$ nmr included signals at δ 0.70 (3H, s, C-18H), 1.18 (3H, s, C-19H), 2.06 (3H, s, C-21H), and 6.22 (1H, s, C-4H) ppm.

*Androst-4-ene-3,6-dione-17β-ol* (**4***c*) (35, 36)

$^1H$ nmr included signals at δ 0.81 (3H, s, C-18H), 1.18 (3H, s, C-19H), 3.5–3.8 (1H, m, C-17αH), and 6.20 (1H, s, C-4H) ppm.

*Androst-4-ene-3,6,17-trione* (**4***d*) (35–37)

$^1H$ nmr included signals at δ 0.92 (3H, s, C-18H), 1.19 (3H, s, C-19H), and 6.21 (1H, s, C-4H) ppm.

*(16α,17)-Epoxypregn-5-ene-3β-ol-20-one* (**6**) (27)

$^1H$ nmr included signals at δ 1.05 (6H, br s, C-18 and -19 H's), 2.05 (3H, s, C-21H), 3.25–3.7 (1H, m, C-3H), 3.73 (1H, s, C-16H), 5.37 (1H, m, C-6H) ppm.

*2,6,6,-Trimethylcyclohex-2-ene-1,4-dione* (**16***b*) (18, 38).

## Acknowledgements

We are grateful for financial support received from the Natural Sciences and Engineering Research Council of Canada, and to Mr. T. Jones for assistance in obtaining spectra.

1. C. A. BUNTON and G. J. MINKOFF. J. Chem. Soc. 665 (1949).
2. H. O. HOUSE and R. S. RO. J. Am. Chem. Soc. **80**, 2428 (1958).

Can. J. Chem. Downloaded from www.nrcresearchpress.com by 210.87.254.5 on 09/06/12
For personal use only.

3. J. KATSUHARA. Bull. Chem. Soc. Jpn. **42**, 2391 (1969).
4. D. N. KIRK and M. P. HARTSHORN. Steroid reaction mechanisms. Elsevier, Amsterdam. 1968. (*a*) p. 201; (*b*) p. 195.
5. H. B. HENBEST. Proc. Chem. Soc. 159 (1963).
6. H. B. HENBEST and W. R. JACKSON. J. Chem. Soc. C, 2459 (1967).
7. N. C. YANG and R. A. FINNEGAN. J. Am. Chem. Soc. **80**, 5845 (1958).
8. G. B. PAYNE. J. Org. Chem. **25**, 275 (1960).
9. S. H. COHEN and J. L. MARGRAVE. Anal. Chem. **29**, 1462 (1957).
10. A. NICKON and W. L. MENDELSON. J. Org. Chem. **30**, 2087 (1965).
11. P. B. D. DE LA MARE and R. D. WILSON. J. Chem. Soc. Perkin Trans. II, 157 (1977).
12. B. CAMERINO, B. PATELLI, and R. SCIAKY. Gazz. Chim. Ital. **92**, 676 (1962).
13. B. CAMERINO, B. PATELLI, and R. SCIAKY. Gazz. Chim. Ital. **92**, 693 (1962).
14. E. L. SHAPIRO, T. LEGATT, L. WEBER, E. P. OLIVETO, M. TANABE, and D. F. CROWE. Steroids, **3**, 183 (1964).
15. H. L. HOLLAND and P. R. P DIAKOW. Can. J. Chem. **57**, 436 (1979).
16. P. H. YU and L. TAN. J. Steroid Biochem. **8**, 825 (1977).
17. B. CAMERINO, B. PATELLI, and R. SCIAKY. Tetrahedron Lett. 554 (1961).
18. N. S. ZARGHAMI and D. E. HEINZ. Phytochemistry, **10**, 2755 (1971).
19. K. G. LEWIS and G. J. WILLIAMS. Tetrahedron Lett. 4573, (1965).
20. L. L. SMITH, M. J. KULIG, D. MILLER, and G. A. S. ANSARI. J. Am. Chem. Soc. **100**, 6206 (1978).
21. J. M. AUBRY, J. RIGAUDY, C. FERRADINI, and J. PUCHEAULT. J. Am. Chem. Soc. **103**, 4965 (1981).
22. H. H. WASSERMAN and R. W. MURRAY (*Editors*). Singlet oxygen. Academic Press, New York, NY. 1979.
23. M. J. KULIG and L. L. SMITH. J. Org. Chem. **38**, 3639 (1973).
24. N. I. KRINSKY. *In* Singlet oxygen. *Edited by* H. H. Wasserman and R. W. Murray. Academic Press, New York. 1979. p. 600.
25. A. WINDAUS. Chem. Ber. **39**, 2008 (1906).
26. E. ALVAREZ, C. BETANCOR, R. FRIERE, A. MARTIN, and E. SUAREZ. Tetrahedron Lett. 4335 (1981).
27. P. L. JULIAN, E. W. MEYER, W. J. KARPEL, and I. R. WALLER. J. Am. Chem. Soc. **72**, 5145 (1950).
28. B. LÖKEN, S. KAUFMANN, K. ROSENKRANZ, and F. SONDHEIMER. J. Am. Chem. Soc. **78**, 1738 (1956).
29. B. E. EDWARDS and P. N. RAO. J. Org. Chem. **31**, 324 (1966).
30. PL. A. PLATTNER, H. HENSER, and A. B. KULKARNI. Helv. Chim. Acta, **31**, 1822 (1948).
31. D. J. COLLINS, J. J. HOBBS, and S. STERNHALL. Tetrahedron Lett. 623 (1963).
32. J.-C. JACQUESY, R. JACQUESY, J. LEVISALLES, J.-P. PETE, and H. RUDLER. Bull. Soc. Chim. Fr. 2224 (1964).
33. D. COLLINS. J. Chem. Soc. 3919 (1959).
34. W. REUSCH and R. LEMAHIEU. J. Am. Chem. Soc. **85**, 1669 (1963).
35. C. DJERASSI, J. KARLINER, and R. T. ALPIN. Steroids, **6**, 1 (1965).
36. F. SONDHEIMER and G. ROSENKRANZ. U.S. Patent No. 2,786,855 (26 Mar. 1957). Chem. Abstr. **51**, 13947g (1957).
37. H. L. HOLLAND and E. M. THOMAS. Can. J. Chem. **57**, 3069 (1979).
38. J. N. MARX and F. SONDHEIMER. Tetrahedron Suppl. 8, part 1,1 (1966).

Can. J. Chem. Downloaded from www.nrcresearchpress.com by 210.87.254.5 on 09/06/12
For personal use only.

# The rotational angle dependence of $^5J_m{}^{H,SH}$ in benzenethiol

TED SCHAEFER, TIMOTHY A. WILDMAN, AND RUDY SEBASTIAN
*Department of Chemistry, University of Manitoba, Winnipeg, Man., Canada R3T 2N2*

Received February 11, 1982

TED SCHAEFER, TIMOTHY A. WILDMAN, and RUDY SEBASTIAN. Can. J. Chem. **60**, 1924 (1982).

It is suggested that the five-bond spin–spin coupling constant between the sulfhydryl proton and the ring proton in the *meta* position is given by $^5J = {}^5J^{\pi}_{90}\langle\sin^2\theta\rangle + {}^5J^{\sigma}_{180}\langle\sin^2(\theta/2)\rangle$. Here θ is the angle by which the S—H bond twists out of the benzene plane and angular brackets indicate expectation or average values, determined by the twofold barrier to internal rotation about the C—S bond. $^5J^{\pi}_{90}$ is the π electron contribution and has a maximum at θ = 90° and $^5J^{\sigma}_{180}$ is the σ electron contribution with a maximum at θ = 180° (zig-zag orientation). For eight *para* substituted derivatives of benzenethiol, the $^5J$ numbers can be reproduced by this equation, which also agrees with the observed couplings in 2-hydroxybenzenethiol. In this compound θ lies near 90°. It appears that this approach will allow an extension of the *J* method to the evaluation of two-term potential functions in, for example, *ortho* substituted benzene derivatives.

TED SCHAEFER, TIMOTHY A. WILDMAN et RUDY SEBASTIAN. Can. J. Chem. **60**, 1924 (1982).

On suggère que la constante de couplage spin–spin à travers cinq liaisons entre le proton du groupe sulfhydryle et le proton du cycle en position *méta* est donnée par la relation $^5J = {}^5J^{\pi}_{90}\langle\sin^2\theta\rangle + {}^5J^{\sigma}_{180}\langle\sin^2(\theta/2)\rangle$. Dans l'équation, θ est l'angle de torsion de la liaison S—H par rapport au plan du benzène et les parenthèse angulaires indiquent les valeurs prévues ou les valeurs moyennes déterminées par la barrière binaire à la rotation interne autour de la liaison C—S. $^5J^{\pi}_{90}$ est la contribution des électrons π et est maximum à θ = 90° et $^5J^{\sigma}_{180}$ est la contribution des électrons σ avec un maximum à θ = 180° (orientation en zig zag). Pour 8 dérivés du benzènethiol substitués en position *para*, on peut reproduire les valeurs de $^5J$ par cette équation qui est également en accord avec les couplages observés pour l'hydroxy-2 benzènethiol. Dans ce composé, θ se situe près de 90°. Il semble que cette approche permettra une extension de la méthode *J* à l'évaluation des fonctions de potentiel à deux termes dans, par exemple, des dérivés du benzène substitués en *ortho*.

[Traduit par le journal]

## Introduction

The *J* method (1) for the determination of small twofold internal rotational barriers in benzene derivatives depends on the $\sin^2\theta$ dependence of the spin–spin coupling over six bonds between *alpha* and *para* nuclei. When these nuclei are protons, one may write

$$[1] \quad {}^6J_p{}^{H,H} = {}^6J_{90}\langle\sin^2\theta\rangle$$

where $^6J_{90}$ is the value of $^6J_p$ when the bond of the sidechain lies in a plane perpendicular to the benzene plane. In particular, for benzenethiol, **1** (X

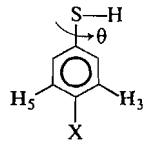


**1**

= H), a $^6J_{90}$ of −0.97 Hz and an observed $^6J_p{}^{H,H}$ of − 0.33 Hz (2) yields an expectation value for $\sin^2\theta$ of 0.345 and, via a hindered rotor model, a $V_2$ of 3.4 kJ/mol (3), in good agreement with microwave and far infrared results (4). In fact, the latter can be taken as a calibration of $^6J_{90}$.

Further, it has been shown (3) for *para* substituted derivatives of benzenethiol that $^4J_o{}^{H,H}$ can be used in an equation similar to [1] in order to derive $V_2$ numbers and that a value for $^4J_{90}{}^{H,H}$ of −1.10 Hz yields sensible barriers. In fact, this approach predicts that in *para* amino and *para* methoxybenzenethiols the perpendicular conformation (θ = 90°) becomes the stable form, allowing a rationalization of the contrasting conformation of 4-dimethylaminophenyl sulfide and 4-nitrophenyl sulfide observed in their crystals.

A present limitation of the *J* method is its restriction to twofold barriers, simply because there is only one observable, $^6J_p{}^{H,H}$. Therefore an *ortho* substituted benzenethiol cannot, in general, have the internal rotational potential of its S—H group characterized by $^6J_p$ alone. The internal potential must have at least two terms, $V_1$ and $V_2$ (5). In order to derive $V_1$ and $V_2$, an additional coupling parameter *and* its θ dependence are required.

$^5J_m{}^{H,H}$ may well be such a parameter. If its θ dependence were known, then $^5J$ should be relatable to $V_1$ and probably to $V_2$. It is known that $^5J_m{}^{XH,H_5}$ (θ = 0°) is essentially zero for a variety of X (C=O, O, $CR_2$, etc.) and that $^5J^{XH,H_3}$ (θ = 180°) is large (6). This knowledge has been used extensively in the deduction of conformational preferences for OH, CHO, $CHR_2$, and other sidechain moieties (7–10). However, if the internal barrier to rotation about the C($sp^2$)—X bond is comparable to $kT$ in magnitude (considerable out-of-plane mo-

0008-4042/82/151924-04$01.00/0
©1982 National Research Council of Canada/Conseil national de recherches du Canada

Can. J. Chem. Downloaded from www.nrcresearchpress.com by 210.87.254.40 on 09/06/12
For personal use only.

Can. J. Chem. Downloaded from www.nrcresearchpress.com by 210.87.254.40 on 09/06/12
For personal use only.

tion), then in principle the complete θ dependence of $^5J$ is required for a reliable conformational analysis. That is, just as in [1] the expectation value of $\sin^2\theta$ determines $^6J$ via $V_2$, so in the desired equation for $^5J$ the average value of the θ dependence of $^5J$ will determine the observed coupling. In other words, if the planar forms are not preferred by an energy large compared to $kT$, then $^5J^{XH,H_3}$ "borrows" some of $^5J^{XH,H_5}$ and vice versa, leading to an unknown error in conformational deductions.[1]

An indication of the θ dependence of $^5J_m$ comes from INDO MO FPT computations on toluene (14). The computed $^5J_m{}^{H,CH}$ can be written as a sum of two components: a π electron contribution varying as $\sin^2\theta$ (just as for $^6J^{H,CH}$) and a σ electron contribution varying as $\sin^2(\theta/2)$. Unpublished calculations for other sidechains in this laboratory, including the S—H groups, imply a similar θ dependence. Separation of the two components is facilitated by a substituent-induced change in one component only.

In *para* derivatives of benzenethiol the substituent perturbs $V_2$ and $\langle\sin^2\theta\rangle$ and therefore the π component of $^5J$ (3). It follows that $^5J$ in these compounds may allow a test of an assumed θ dependence and, by implication, suggest an eventual extension of $^5J$ to the derivation of two-term potential functions for asymmetrical benzene derivatives.

## Experimental

Most of the $^1$H nmr spectra of the compounds under discussion below have been analyzed previously (15). The spectrum of 4-*tert*-butylbenzenethiol could not be analyzed; the chemical shift dispersion was too small in any of the solvents utilized. However, the $^1$H nmr spectrum of 4-chlorobenzenethiol (Aldrich) in $C_6D_6$ solution, but not in $CCl_4$, displayed an analyzable pattern. A 3.0 mol% solution was degassed by a number of freeze–pump–thaw cycles. Its $^1$H nmr spectrum was recorded on an HA100 spectrometer. The calibration and analysis procedure followed that recently described in great detail (16). Figure 1 displays the observed and calculated spectrum of the sulfhydryl proton. Table 1 presents the spectral parameters.

## Discussion

### 1. *The θ dependence of* $^5J^{H,SH}$

The assumption, indicated theoretically and in agreement with observation at θ = 0° and 180°, is that $^5J_m{}^{H,SH}$ follows eq. [2].

$$[2]\quad {}^5J_m{}^{H,SH} = {}^5J^{\pi}_{90}\langle\sin^2\theta\rangle + {}^5J^{\sigma}_{180}\langle\sin^2(\theta/2)\rangle$$

In [2], $^5J^{\pi}_{90}$ is the π electron contribution to $^5J$ when the S—H bond lies in a plane perpendicular to that of the benzene ring, $^5J^{\sigma}_{180}$ is the maximum σ electron contribution to $^5J$ (zig-zag conformation, $^5J \equiv {}^5J^{SH,H_5}$ in the *planar* form **1**). Angular brackets indicate expectation or average values of the θ functions.

Now, $\langle\sin^2\theta\rangle$ is known from previous work (3) and $\langle\sin^2(\theta/2)\rangle$ is 0.5, independent of $V_2$ in these symmetrical compounds (see Appendix). Accordingly, a plot of $^5J_m{}^{H,SH}$ versus $\langle\sin^2\theta\rangle$ should yield a straight line, whose slope is $^5J^{\pi}_{90}$ and whose intercept is $^5J^{\sigma}_{180}/2$. In Table 2 the relevant data for a series of 4-X-benzenethiols are presented. These data give eq. [3]

$$[3]\quad {}^5J_m{}^{H,SH} = 0.196\langle\sin^2\theta\rangle + 0.360\,(0.5)\text{ Hz}$$

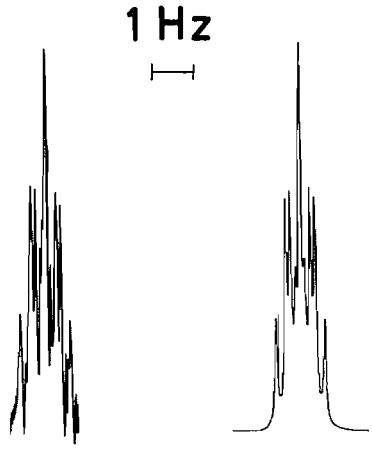


FIG. 1. The observed and calculated sulfhydryl proton $^1$H nmr spectrum at 100 MHz and 305 K for a 3 mol% solution of 4-chlorobenzenethiol in benzene-$d_6$ solution. The linewidth at half height in the calculated spectrum is 0.07 Hz (lorentzian), suggesting a similar linewidth for the observed spectrum.

TABLE 1. The $^1$H nmr spectral parameters for 4-chlorobenzenethiol as a 3.0 mol% solution in benzene-$d_6$ at 305 K

| Parameter | Value | Parameter | Value |
|---|---|---|---|
| $\nu_{SH}$ | 287.325(2)[a,b] | $^4J_o{}^{H,SH}$ | −0.370(3) |
| $\nu_2$ | 663.679(2) | $^5J_o{}^{H,SH}$ | 0.264(3) |
| $\nu_3$ | 681.917(2) | Transitions | 64[c] |
| $^3J_{23}$ | 8.358(4) | Assigned | 50 |
| $^4J_{26}$ | 2.433(4) | Peaks | 38 |
| $^4J_{35}$ | 2.430(4) | rms deviation | 0.008 Hz |
| $^5J_{36}$ | 0.406(3) | Largest deviation | 0.019 Hz |

[a] In Hz at 100.001$_2$ MHz to low field of internal tetramethylsilane.
[b] Numbers in parentheses are the standard deviations in the last significant figure.
[c] Those with a relative intensity greater than 0.05.

[1] The treatment of conformational preferences in terms of an equilibrium between or among rigid conformations has a long history because of its easy application. It has been emphasized recently (11–13) that such an approach, e.g. in the analysis of vicinal coupling constants by the Karplus curve or of temperature dependent band intensities, can lead to substantial errors in the derived equilibria.

TABLE 2. Relevant spin–spin coupling constants and internal barrier data for some *para* substituted benzenethiols[a]

| 4-X | $^4J_o^{H,SH}$ (Hz) | $^5J_m^{H,SH}$ | $\langle\sin^2\theta\rangle$ | $V_2$ (kJ) | $^5J_m^{H,SH}$ |
|---|---|---|---|---|---|
| $NO_2$ | −0.203 | 0.203 | 0.185 | 9.0±0.8 | 0.216[c] |
| Br | −0.333 | 0.231 | 0.303 | 4.8 | 0.240 |
| Cl | −0.370 | 0.264 | 0.335 | 3.7±0.4 | 0.246 |
| H | −0.380 | 0.250 | 0.345 | 3.4 | 0.248 |
| $CH_3$ | −0.439 | 0.271 | 0.399 | 2.2 | 0.258 |
| F | −0.531 | 0.270 | 0.483 | 0.4 | 0.275 |
| $OCH_3$ | −0.649 | 0.298 | 0.590 | −1.9[b] | 0.296 |
| $NH_2$ | −0.697 | 0.294 | 0.634 | −2.9±0.4 | 0.304 |

[a] For 5 mol% solutions in $CCl_4$ at 305 K, except for $NO_2$ (2 mol% in $CDCl_3$) and Cl (3 mol% in $C_6D_6$).
[b] A negative $V_2$ means that the perpendicular conformation is more stable than the planar form.
[c] These are calculated from eq. [3] of the text.

with a correlation coefficient of 0.935, significant at least at the 99% confidence level (17).[2] The standard deviations of the $^5J$ values in the spectral analysis were all considerably smaller than 0.01 Hz, so that at the 95% confidence limit an accuracy of about 0.01 Hz is probably a reasonable estimate (16). Such an error represents 10% of the variation in $^5J$ in Table 2. A $^5J^{\pi}_{90}$ of +0.195 Hz represents about 20% of the magnitude of $-^6J^{\pi}_{90}$ in benzenethiol, understandable in that, to zero order, the mobile bond order vanishes between *meta* carbons in benzene, while in a valence bond formulation the spin correlation function for atoms belonging to different classes is negative (18). In toluene it is estimated that $^5J^{\pi}_{90}$ amounts to about 30% of $-^6J^{\pi}_{90}$ (19, 20).

A test of [3] is available in 2-hydroxybenzenethiol (21), known to exist in a conformation in which stereospecific hydrogen bonding to a lone-pair on sulfur causes the S—H bond to lie in a plane *roughly* perpendicular to the benzene plane ($\theta \simeq 90°$). Therefore $\langle\sin^2\theta\rangle \simeq 1.0$ and $\langle\sin^2(\theta/2)\rangle \simeq 0.5$. Consequently $^5J_m^{H,SH} \simeq 0.195 + 0.180 = 0.376$ Hz from [3]. The observed values are 0.360 and 0.393 Hz, or a mean of 0.376 Hz. In this compound the perturbing hydroxy group lies roughly perpendicular to the C—S—H plane and intuition suggests that intrinsic substituent perturbations at the *ortho* position may not be negligible for other compounds.

In Fig. 2 the θ dependence of $^5J_m^{H,SH}$ in benzenethiol is plotted according to values deduced from eq. [3]. For comparison, the adjusted INDO MO FPT values of $^5J_m^{H,CH_3}$ for toluene (14) are shown. The INDO values of $^5J_m^{H,CH_3}$ are overestimates. To reach agreement with the experimental value of 0.36 Hz, i.e., when $\langle\sin^2\theta\rangle = \langle\sin^2(\theta/2)\rangle = 0.5$, the plotted numbers for $^5J_m^{H,CH_3}$ must be multiplied by 0.78.

[2] Omission of the data for X = Cl changes the slope and intercept by ca. 0.01 Hz and gives $r = 0.965$.

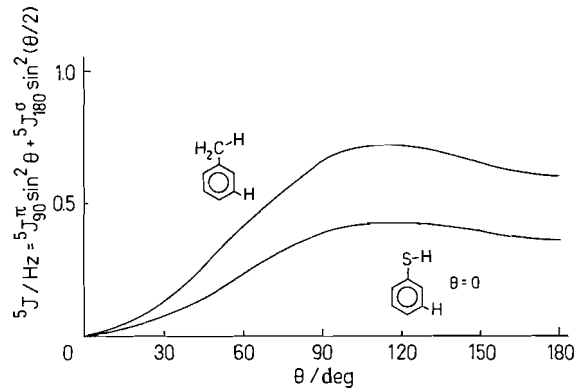


FIG. 2. A plot of $^5J_m^{H,SH}$ in benzenethiol and of $^5J_m^{H,CH_3}$ in toluene as a function of the conformational angle θ. The plot for $^5J_m^{H,SH}$ is inferred from the experimental numbers summarized in eq. [3] of the text. That for $^5J_m^{H,CH_3}$ comes from the MO calculations in ref. 14. The points for $^5J_m^{H,CH_3}$ must be reduced by a factor of 0.78 if the experimental value is to be reproduced.

2. *The internal barrier in 4-chlorobenzenethiol*

Following the procedure in ref. 3, a $V_2$ of 3.7 ± 0.4 kJ/mol is derived, compared to 3.4 ± 0.3 kJ/mol for benzenethiol. A recent dielectric relaxation study at 4 K or 77 K in paraffin solution gave the barrier in 4-chlorobenzenethiol as 0.4 kJ/mol lower than in benzenethiol (22). The dielectric data agreed with the *J* method for the 4-methyl but not for the 4-bromo derivative. Part of these disagreements may arise from solvent effects. According to coupling data for 4-aminobenzenethiol (15) $V_2$ varies by perhaps as much as 0.4 kJ/mol in going from $CCl_4$ to $C_6D_6$ or $CDCl_3$ as solvents.

**Acknowledgements**

We are grateful to the Natural Sciences and Engineering Research Council of Canada for financial assistance.

1. W. J. E. PARR and T. SCHAEFER. Acc. Chem. Res. **13**, 400 (1980).
2. W. J. E. PARR and T. SCHAEFER. J. Magn. Reson. **25**, 171 (1977).
3. T. SCHAEFER and T. A. WILDMAN. Chem. Phys. Lett. **80**, 280 (1981).
4. N. W. LARSEN and F. M. NICOLAISEN. J. Mol. Struct. **29**, 29 (1974).
5. G. L. CARLSON and W. G. FATELEY. J. Phys. Chem. **77**, 1157 (1973).
6. J. KOWALEWSKI. Prog. Nucl. Magn. Reson. Spectrosc. **11**, 1 (1978). See Section 8.5.
7. T. SCHAEFER, B. M. ADDISON, R. SEBASTIAN, and T. A. WILDMAN. Can. J. Chem. **59**, 1656 (1981), and references therein.
8. T. SCHAEFER, S. R. SALMAN, and T. A. WILDMAN. Can. J. Chem. **58**, 2364 (1980), and references therein.
9. M. BARFIELD and B. CHAKRABARTI. Chem. Rev. **69**, 757 (1969).
10. S. STERNHELL. Rev. Pure Appl. Chem. **14**, 15 (1964).
11. T. A. WILDMAN. Chem. Phys. Lett. **75**, 383 (1980); **80**, 210 (1981).

Can. J. Chem. Downloaded from www.nrcresearchpress.com by 210.87.254.40 on 09/06/12
For personal use only.

12. V. M. S. GIL and A. J. C. VARANDAS. J. Magn. Reson. **43**, 28 (1981).
13. E. HONEGGER and E. HEILBRONNER. Chem. Phys. Lett. **81**, 615 (1981).
14. R. WASYLISHEN and T. SCHAEFER. Can. J. Chem. **50**, 1852 (1972).
15. T. SCHAEFER and W. J. E. PARR. Can. J. Chem. **55**, 552 (1977).
16. T. SCHAEFER and R. SEBASTIAN. J. Magn. Reson. **41**, 395 (1980).
17. R. A. FISHER and F. YATES. Statistical tables for biological, agriculture, and medical research. 3rd ed. Hafner Publishing Co., New York. 1948. p. 46.
18. H. M. MCCONNELL. J. Chem. Phys. **30**, 126 (1959).
19. C. J. MACDONALD and W. F. REYNOLDS. Can. J. Chem. **48**, 1002 (1970).
20. J. B. ROWBOTHAM and T. SCHAEFER. Can. J. Chem. **52**, 489 (1974).
21. T. SCHAEFER, T. A. WILDMAN, and S. R. SALMAN. J. Am. Chem. Soc. **102**, 107 (1980).
22. J. LE G. GILCHRIST. Chem. Phys. **61**, 443 (1981).

## Appendix

The classical expectation value of $\sin^2(\theta/2)$ for a twofold barrier is given by:

$$\langle \sin^2(\theta/2)\rangle = \int_0^{\pi} \sin^2(\theta/2)\exp(-\beta V_2 \sin^2\theta)d\theta \times 1\Big/\int_0^{\pi}\exp(-\beta V_2\sin^2\theta)d\theta = I_1/I_2$$

where $\beta = 1/kT$. Let $a = \beta V_2/4$, $z = \exp(i\theta/2)$. Then

$$I_1 = -\exp(-2a)/8i \oint_{|z|=1} dz(z - 2/z + 1/z^3) \times (1 + az^4 + a^2z^8/2! + \ldots) \times (1 + a/z^4 + a^2/2!z^8 + \ldots)$$

Use of the residue theorem and the realization that only the term $-2/z$ of the first factor in the integral will contribute yields

$$I_1 = (-\exp(-2a)/8i)(2\pi i)(-2) \times (1 + a^2 + a^4/(2!)^2 + a^6/(3!)^2 + \ldots) = (\pi/2)\exp(-2a)\sum_{n=0}^{\infty}(a^n/n!)^2$$

Similarly,

$$I_2 = \pi\exp(-2a)\sum_{n=0}^{\infty}(a^n/n!)^2$$

The sums are absolutely convergent. Finally, $\langle \sin^2(\theta/2)\rangle = I_1/I_2 = 1/2$. This result is intuitively correct, of course. Suppose, for example, that $V_2 = \infty$. Then the two values of $\theta$ are 0 and $\pi$. If $V_2 = 0$, then the average value of $\theta$ is $\pi/2$.

Can. J. Chem. Downloaded from www.nrcresearchpress.com by 210.87.254.40 on 09/06/12
For personal use only.

# Kinetics and mechanism of the oxidation of 1-propane thiol by 2,6-dichlorophenolindophenol in acidic medium

M. KASHYAP, K. K. MISHRA,[1] AND N. K. PANDEY

*Department of Postgraduate Studies and Research in Chemistry, University of Jabalpur, Jabalpur 482001, (M.P.) India*

Received June 22, 1981[2]

M. KASHYAP, K. K. MISHRA, and N. K. PANDEY. Can. J. Chem. **60**, 1928 (1982).

The kinetics of oxidation of 1-propanethiol by 2,6-dichlorophenolindophenol have been studied in acetone–water medium and in the presence of phosphate buffer. The principal reactants interact in a molar ratio of 2:1 forming disulphide and dihydroindophenol. The reaction follows second order kinetics in indophenol while the order is unity in thiol. The rate increases linearly on increasing $[H^+]$. The rate of oxidation increases on increasing the ionic strength as well as the dielectric constant of the reaction system. The addition of reaction products has no effect on the rate. Activation parameters have been evaluated and a suitable mechanism consistent with kinetic data is suggested.

M. KASHYAP, K. K. MISHRA et N. K. PANDEY. Can. J. Chem. **60**, 1928 (1982).

On a étudié les cinétiques de l'oxydation du propanethiol-1 par le dichloro-2,6 phénolindophénol dans un milieu acétone–eau et en présence d'un tampon au phosphate. Les réactifs principaux dans un rapport molaire de 2:1 conduisent au disulfure et au dihydroindophénol. La réaction suit une cinétique d'ordre deux par rapport à l'indophénol et une cinétique d'ordre un par rapport au thiol. La vitesse augmente linéairement lorsqu'on augmente la concentration en ions $[H^+]$. La vitesse d'oxydation augmente avec la force ionique aussi bien qu'avec la constante diélectrique du système. L'addition des produits de réaction n'a aucun effet sur la vitesse. On a évalué les paramètres d'activation et on suggère un mécanisme convenable qui est en accord avec les données cinétiques.

[Traduit par le journal]

## Introduction

2,6-Dichlorophenolindophenol (2,6-dichloro *N*-(*p*-hydroxyphenyl) *p*-benzoquinone imine), a well known titrant for vitamin C in biochemical studies, has been used in a host of reactions of pharmaceutical and analytical importance (1, 2). Its reaction with thiols was first reported by Basford and Huennekens (3) and later by Hadler *et al.* (4). These investigations were exploited in biochemical researches to determine the membrane SH group (5). The importance of this reaction attracted our attention and, perhaps for the first time, mechanistic studies on such reactions were undertaken in this laboratory (6–15). In this paper, we now report the results obtained for the oxidation of 1-propanethiol by 2,6-dichlorophenolindophenol in acetone–water medium and in the presence of phosphate buffer.

## Experimental

The solution of 2,6-dichlorophenolindophenol (referred to later as indophenol, In) was prepared by dissolving an exactly weighed quantity of a BDH grade sample in double distilled water. The strength of the solution was checked by titrating it against ascorbic acid (16). The solution was stored in a cool, dark place since both light and temperature affect its stability (17). The solution of 1-propanethiol (symbolized later as 1-PT) was prepared by diluting the sample (obtained from Fluka A.G., Chemische Fabrick, Buchs S.G. Switzerland) in E. Merck's G.R. grade acetone. The thiol solution was standardized by employing a back iodimetric titration procedure (18). Freshly prepared thiol solutions were employed for each run to avoid the possibility of oxidation in air. As a precautionary measure, however, stock solutions were always kept under a nitrogen atmosphere. The corresponding disulphide was prepared by oxidizing thiol with iodine (19), while dihydroindophenol (leucodye) was prepared by passing pure $SO_2$ gas into the known solution of indophenol (6). The pH of the reaction system was maintained by adding phosphate buffer. The kinetics were studied in 50% (v/v) acetone–water medium because at this composition the runs give reproducible results. Other ingredients used in these investigations were either of BDH, AnalaR, or E. Merck's G.R. grade. Double distilled water was used throughout.

*Kinetic measurements*

The progress of the reaction was followed colorimetrically using a Klett–Summerson photoelectric colorimeter fitted with light filter No. 59 (spectral range 565–630 nm) because indophenol shows maximum absorbance at 610 nm ($\varepsilon_{max} = 8 \times 10^3\ cm^2\ mol^{-1}$) while the reaction products, viz. leucodye and the corresponding disulphide, absorb strongly at 282 (4) and 222 nm respectively. The products were characterized by recording the absorption spectra of the reaction mixture (marked with an asterisk in Table 1) after completion of the reaction. All the spectra were recorded by a Pye Unicam SP 8-100 spectrophotometer. The reaction flask made of Corning glass was coated with Black Japan from outside to minimize the photochemical effect. The flasks containing reaction mixture and indophenol were thermostated for a sufficiently long time (variation ± 0.1°C). The runs were made under a nitrogen atmosphere.

## Results and discussion

The stoichiometry of the reaction was determined by computing the residual concentration of

[1]Author to whom correspondence may be addressed.

[2]Revision received September 29, 1981.

0008-4042/82/151928-05$01.00/0

©1982 National Research Council of Canada/Conseil national de recherches du Canada

Can. J. Chem. Downloaded from www.nrcresearchpress.com by 210.87.254.5 on 09/06/12
For personal use only.

TABLE 1. Rate constants at different [RSH] and [In] values[a]

| | (A) | | (B) | |
|---|---|---|---|---|
| [1-PT] × $10^4$ $M$ | $k_2$, L $mol^{-1}$ $s^{-1}$ | $\frac{k_2}{[1\text{-PT}]} \times 10^{-4}$ | [In] × $10^5$ $M$ | $k_2$, L $mol^{-1}$ $s^{-1}$ |
| *4.50 | 20.71 | 4.60 | 4.50 | 20.71 |
| 5.50 | 24.34 | 4.42 | 4.00 | 20.20 |
| 7.50 | 34.06 | 4.54 | 3.50 | 21.90 |
| 9.50 | 42.55 | 4.48 | 3.00 | 22.51 |
| 11.50 | 52.86 | 4.59 | 2.50 | 22.40 |
| 13.50 | 62.99 | 4.66 | 2.00 | 22.93 |
| 16.50 | 80.78 | 4.89 | — | — |

[a]Acetone 50% (v/v); pH 6.8; ionic strength 0.132 $M$; temp. 30°C.
(A) $4.50 \times 10^{-5}$ $M$ Indophenol; (B) $4.50 \times 10^{-4}$ $M$ 1-PT.

indophenol in the reaction mixtures containing a known excess of oxidant (ca. $4.5 \times 10^{-5}$ $M$) over thiol. In the spectrophotometric method (20) the absorption spectra of the reaction mixture was recorded after completion of the reaction. Both the methods gave a stoichiometry of 2:1. Thus,

$$2RSH + In \rightarrow RSSR + H_2In$$

Here In and $H_2In$ denote indophenol and leucodye, respectively.

The quantitative formation of disulphide and the leucodye ($\varepsilon_{max} = 8.52 \times 10^4$ and 13 760 $cm^2$ $mol^{-1}$, respectively) was confirmed by using the relation $A = \varepsilon Cl$. The reaction follows second order kinetics in indophenol (Fig. 1). The order in indophenol was determined by Ostwald's isolation and van't Hoff's differential methods (21). Table 1 gives the values of the second order rate constant obtained at different [RSH].

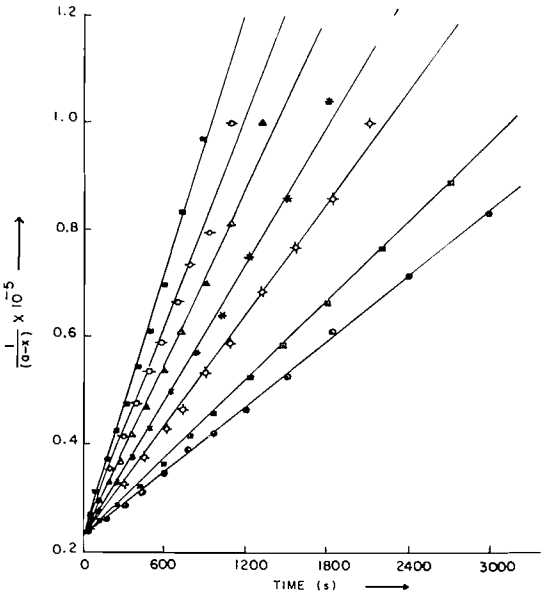


FIG. 1. [1-PT] ⊙ = $4.5 \times 10^{-4}$ $M$; ⊡ = $5.5 \times 10^{-4}$ $M$; ⊹ = $7.5 \times 10^{-4}$ $M$; ∗ = $9.5 \times 10^{-4}$ $M$; △ = $11.5 \times 10^{-4}$ $M$; ○ = $13.5 \times 10^{-4}$ $M$; ■ = $16.5 \times 10^{-4}$ $M$; [In] = $4.5 \times 10^{-5}$ $M$; acetone = 50% (v/v); pH = 6.8; I = 0.132 $M$; temp. = 30°C.

It is apparent from Table 1 that the reaction follows a first order kinetics in the substrate because the relation $k_2$/[RSH] gives nearly constant values. This was further confirmed by the initial rate measurement method. The rate of oxidation of 1-PT is not influenced by variation in [In] (Table 1).

The pH of the system was varied by adding different amounts of potassium dihydrogen phosphate and disodium hydrogen phosphate to the reaction mixtures. It may, however, be added that these variations could be done in a limited range only because, below pH 5.7 (equal to $pK_a$), the blue variety of indophenol changes into the red variety (22). The latter shows $\lambda_{max}$ at 514 nm ($\varepsilon_{max}$ = 6475 $cm^2$ $mol^{-1}$), which shows that there is a substantial change in the chromophoric character of the indophenol molecule with decrease in pH. Moreover, at lower pH (< 5.0), a substantial fading of indophenol is noticed during the course of the reaction and thus kinetic pursuit in this region was not possible. The rate increases on decreasing the pH of the system. The plots of log $k_2$ against log [$H^+$] give a straight line with a slope of unity (Fig. 2).

The ionic strength of the system was maintained constant (ca. 0.15 $M$) by adding the requisite amount of sodium perchlorate in these variations. The rate increases with increasing ionic strength (Table 2). Here only uni-univalent electrolytes could be added because higher valent cations are precipitated in the phosphate buffer as well as in 50% (v/v) acetone–water medium. These studies indicate that the rate-determining step involves the participation of similarly charged species (23).

In order to study the effect of dielectric constant,

Can. J. Chem. Downloaded from www.nrcresearchpress.com by 210.87.254.5 on 09/06/12
For personal use only.

Can. J. Chem. Downloaded from www.nrcresearchpress.com by 210.87.254.5 on 09/06/12
For personal use only.

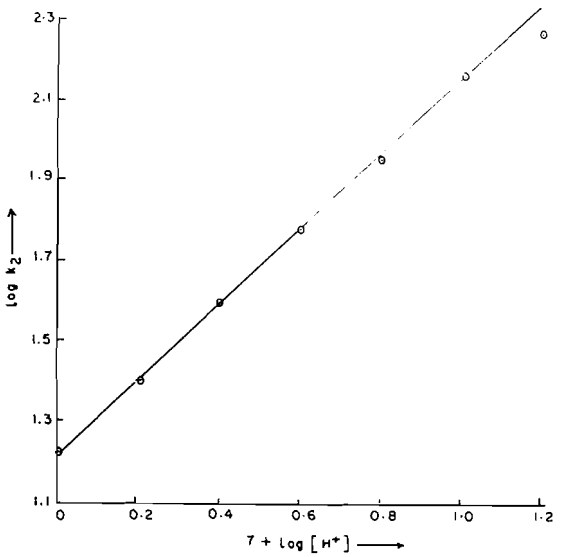


FIG. 2. [1-PT] = $4.5 \times 10^{-4}$ *M*; [In] = $4.5 \times 10^{-6}$ *M*; acetone = 50% (v/v); I = 0.15 *M*; temp. = 30°C.

the composition of the medium was changed by adding varying amounts of acetone. The latter could not be varied above 50% (v/v), because the phosphates are precipitated beyond this level. Table 3 gives a consolidated account of the rate constants obtained at different compositions of acetone along with the values of dielectric constant. The *D* values given here were obtained from the calibration plot using the value given by Kolthoff and co-workers (24).

The rate of oxidation was unaffected on addition of the reaction products, viz. dihydroindophenol and 1,1′-dipropyldisulphide (the disulphide), in the reaction system. The concentration, in both cases, was varied from $2.0 \times 10^{-5}$ *M* to $10.0 \times 10^{-5}$ *M*. This concludes that the end products are not involved in mass law terms. The activation parameters were determined by making the runs at different temperatures keeping other variables unchanged. The plots were drawn between log $k_2$ against $1/T$ and the slopes were measured. The heat of activation was calculated employing the

TABLE 2. Rate constants at different ionic strengths[a]

| Ionic strength (*M*) | $k_2$, L mol$^{-1}$ s$^{-1}$ | | | |
|---|---|---|---|---|
| | KCl | NaCl | $KNO_3$ | $NaNO_3$ |
| 0.15 | 26.04 | 27.85 | 26.73 | 28.86 |
| 0.20 | 36.51 | 40.72 | 37.53 | 43.40 |
| 0.25 | 40.50 | 54.47 | 48.48 | 59.73 |
| 0.30 | 54.27 | 72.14 | 60.78 | 74.71 |
| 0.35 | 63.11 | 91.72 | 71.38 | 96.44 |

[a]$4.50 \times 10^{-5}$ *M* Indophenol; $4.50 \times 10^{-4}$ *M* 1-PT; acetone 50% (v/v); pH 6.8; temp. 30°C.

TABLE 3. Rate constants at different dielectric constants[a]

| Acetone (% v/v) | *D* | $k_2$, L mol$^{-1}$ s$^{-1}$ |
|---|---|---|
| 50 | 49.50 | 20.71 |
| 45 | 52.50 | 31.92 |
| 40 | 56.00 | 47.79 |
| 35 | 59.00 | 65.71 |
| 30 | 62.00 | 84.78 |
| 25 | 65.00 | 130.87 |

[a]$4.50 \times 10^{-5}$ *M* Indophenol; $4.50 \times 10^{-4}$ *M* 1-PT; pH 6.8; ionic strength 0.132 *M*; temp. 30°C.

relation

$$\Delta H^* = -2.303 \times R \times \text{slope}$$

The entropy of activation was calculated from Eyring's equation

$$k_s = \frac{kT}{h} \cdot \exp(-\Delta H^*/RT) \cdot \exp(\Delta S^*/R)$$

(The notations have their usual meaning and $kT/h$ was assumed to be $10^{13}$ s$^{-1}$.) The free energy of activation was determined using the thermodynamic relation

$$\Delta F^* = \Delta H^* - T\Delta S^*$$

The second order rate constants obtained at different temperatures, along with the activation parameters, are given in Table 4.

*Mechanism*

As described previously, the reactions were investigated in acidic medium and thus the indophenol molecule (the sodium salt) may be presumed to be protonated, probably at nitrogen. The actual site of attack is, however, largely obscured owing to a complex geometry of the molecule.

[1] 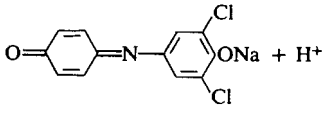


(I, In)

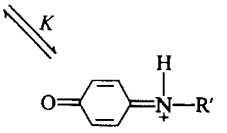


(II, $HIn^+$)

The protonated form of indophenol may combine with another indophenol molecule as shown in the proposed mechanism.

[2] $HIn^+ + In \underset{k_{-1}}{\overset{k_1}{\rightleftharpoons}} D$

[3] $D + RSH \xrightarrow{k_2} C^* + H^+$

Can. J. Chem. Downloaded from www.nrcresearchpress.com by 210.87.254.5 on 09/06/12
For personal use only.

TABLE 4. Rate constants at different temperatures and activation parameters of the reaction of 1-PT with indophenol[a]

| Temperature (K) | $k_2$, L mol$^{-1}$ s$^{-1}$ | $\Delta H^*$ kcal mol$^{-1}$ | $\Delta S^*$ e.u. | $\Delta F^*$ kcal mol$^{-1}$ |
|---|---|---|---|---|
| 293 | 19.26 | | | |
| 298 | 19.95 | 1.50 | −48.46 | 15.95 |
| 303 | 20.71 | ±0.4 | ± 1.0 | |
| 308 | 21.75 | | | |
| 313 | 22.48 | | | |
| 318 | 23.02 | | | |

[a] $4.50 \times 10^{-5}$ *M* Indophenol; $4.50 \times 10^{-4}$ *M* 1-PT; acetone 50% (v/v); pH 6.8; ionic strength 0.132 *M*.

Species D given in step [2] represents the indophenol dimer, while C* symbolizes the reactive intermediates (9, 10, 15). These intermediates may include free radicals such as RSIn· (25) and HIn· (26) which may combine with thiol molecules in a series of fast steps as given below:

[4] $$D + RSH \xrightarrow{k_2} RSIn^{\cdot} + HIn^{\cdot} + H^+$$

[5] $$RSIn^{\cdot} + RSH \xrightarrow{fast} RSSR + HIn^{\cdot}$$

[6] $$HIn^{\cdot} + RSH \xrightarrow{fast} H_2In + RS^{\cdot}$$

[7] $$2RS^{\cdot} \xrightarrow{fast} RSSR$$

Incidentally, the association of dye molecules in the presence of various electrolytes and in non-aqueous media has been widely reported in the literature (27). The participation of free radicals in the present case was qualitatively confirmed by the method of Kolthoff and Meehan (28).

The rate of reaction for the above scheme would be given by

[8] $$-d[In]/dt = k_1[HIn^+][In] - k_{-1}[D]$$

On applying steady state treatment for D

[9] $$[D] = \frac{k_1[HIn^+][In]}{k_{-1} + k_2[RSH]}$$

On substituting the value of [D] and $[HIn^+] = K[In][H^+]$, the rate of reaction would be given by the expression

[10] $$-\frac{d[In]}{dt} = \frac{k_1 k_2 K[In]^2[RSH][H^+]}{k_{-1} + k_2[RSH]}$$

If $k_{-1} \gg k_2[RSH]$;

[11] $$-\frac{d[In]}{dt} = \frac{k_1 k_2 K[In]^2[RSH][H^+]}{k_{-1}}$$

Equation [11] explains the second order kinetics in indophenol and first order with respect to thiol. Again, the proposed mechanism successfully explains the direct proportionality of the rate with $[H^+]$.

From eq. [11]

[12] $$k_{obs} = \frac{k_1 k_2 K[RSH][H^+]}{k_{-1}}$$

or

[13] $$\frac{1}{k_{obs}} = \frac{k_{-1}}{k_1 k_2 K[RSH][H^+]}$$

Thus, a plot of $1/k_{obs}$ against 1/[RSH] should give a straight line passing through the origin in conformity with eq. [13], which has actually been observed (Fig. 3). These plots were further exploited to calculate the pseudo-second order rate con-

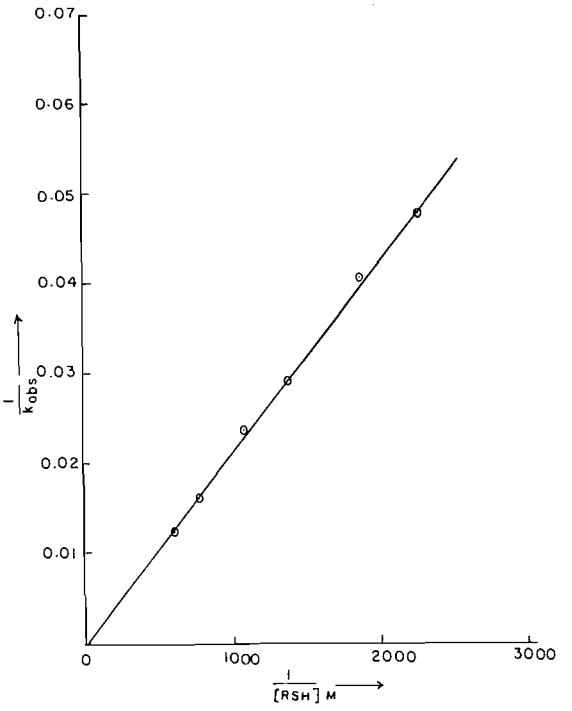


FIG. 3. $[In] = 4.5 \times 10^{-5}$ *M*; acetone = 50% (v/v); I = 0.132 *M*; temp. = 30°C.

TABLE 5. Calculated second order rate constants for the oxidation of 1-PT

| $[1\text{-PT}] \times 10^4$ *M* | Pseudo-second order rate constant ($k_{obs}$) |
|---|---|
| 4.50 | 20.93 |
| 5.50 | 25.58 |
| 7.50 | 34.88 |
| 9.50 | 44.18 |
| 11.50 | 53.48 |
| 13.50 | 62.79 |
| 16.50 | 76.74 |

stant ($k_{obs}$). From eq. [13]:

$$[14] \quad \text{slope} = \frac{k_{-1}}{k_1 k_2 K[H^+]}$$

Thus,

$$[15] \quad k_{obs} = 1/\text{slope} \times [RSH]$$

The values of the pseudo-second order rate constant calculated from eq. [15] are given in Table 5 (the slope from Fig. 3 is equal to $2.15 \times 10^{-5}$).

These values agree fairly well (except the last value) with those recorded in Table 1 for the corresponding concentrations of thiol and lend credence to the mechanistic approach to be advanced presently.

**Acknowledgements**

One of us (N.K.P.) is grateful to the University Grants Commission, New Delhi for the award of a Junior Research Fellowship.

1. L. GAMOLY and L. BRUNELOT. Chim. Anal. Paris, **45**, 641 (1963).
2. R. A. PATRICK, T. J. CARDWELL, and G. SVEHLA. Anal. Chem. Acta, (*a*) **88**, 155 (1977); (*b*) **88**, 163 (1977).
3. R. E. BASFORD and F. M. HUENNEKENS. J. Am. Chem. Soc. **77**, 3873 (1955).
4. I. M. HADLER, M. E. J. ERWIN, and H. A. LARDY. J. Am. Chem. Soc. **85**, 458 (1963).
5. P. C. JOCELYN. Biochemistry of the SH group. Academic Press, New York. 1972. p. 105.
6. B. P. SINHA and K. K. MISHRA. Indian J. Chem. **15A**, 1079 (1977).
7. K. K. MISHRA and B. P. SINHA. Proceedings of the symposium on chemical reactions in nonaqueous media and molten salts. Atomic Energy Commission, Government of India Osmania University, Hyderabad. March, 1978. p. 248.
8. P. H. GHATE, K. K. MISHRA, and B. P. SINHA. Indian J. Chem. **17A**, 375 (1979).
9. A. K. SHRIVASTAVA, K. K. MISHRA, and B. P. SINHA. Indian J. Chem. **17B**, 48 (1979).
10. K. K. MISHRA, A. K. SHRIVASTAVA, and B. P. SINHA. J. Phosphorus Sulfur, **10**, 99 (1981).
11. M. RASTOGI, K. K. MISHRA, and B. P. SINHA. Indian J. Chem. **20B**, 726 (1981).
12. M. SHRIVASTAVA, K. K. MISHRA, and B. P. SINHA. Int. J. Chem. Kinet. (1982). In press.
13. N. K. PANDEY, K. K. MISHRA, and B. P. SINHA. Indian J. Chem. (1982). In press.
14. N. K. PANDEY and K. K. MISHRA. Indian J. Chem. (1982). In press.
15. N. K. PANDEY, K. K. MISHRA, and M. KASHYAP. J. Phosphorus Sulfur, **12**, 179 (1982).
16. J. TILLMAN, P. HIRSCH, and E. REINSHAGEN. Z. Untersuch. Lebensmitt, **56**, 272 (1928).
17. W. LOJANDER. Chem. Abstr. **35**, 5055 (1941).
18. A. I. VOGEL. Quantitative inorganic analysis. Longmans Green & Co., Ltd., New York. 1962. p. 355.
19. I. M. KOLTHOFF, A. ANASTASI, and B. H. TAN. J. Am. Chem. Soc. **80**, 3235 (1958).
20. R. K. CHOHAN, B. P. SINHA, and R. C. KAPOOR. J. Phys. Chem. **76**, 3641 (1972).
21. K. J. LAIDLER. Chemical kinetics. Tata McGraw-Hill Publishing Company Ltd., New Delhi. 1978. pp. 15, 17.
22. W. M. CLARK. Topics in physical chemistry. The Williams and Wilkins Company, Baltimore. 1925. p. 467.
23. S. GLASSTONE, K. J. LAIDLER, and H. EYRING. The theory of rate processes. McGraw-Hill, Kogakusha International, Tokyo. 1941. p. 442.
24. E. J. MEEHAN, I. M. KOLTHOFF, and H. KAKIUCHI. J. Phys. Chem. **66**, 1238 (1962).
25. S. W. BENSON. The foundations of chemical kinetics. McGraw-Hill, New York. 1960. p. 611.
26. S. J. LEACH, J. H. BAXENDALE, and M. G. EVANS. Aust. J. Chem. **6**, 409 (1953).
27. A. K. GHOSH. Indian J. Chem. **12**, 313 (1974).
28. I. M. KOLTHOFF and E. J. MEEHAN. J. Polymer Sci. **11**, 71 (1953).

Can. J. Chem. Downloaded from www.nrcresearchpress.com by 210.87.254.5 on 09/06/12
For personal use only.

# Méthylhalogénocyclopropanation des éthoxy-alcènes diversement alkylés. Identification stéréochimique des adduits et étude de la stéréosélectivité

ROGER BARLET ET RAYMOND LE GOALLER

*Laboratoire d'Études Dynamiques et Structurales de la Sélectivité, Université Scientifique et Médicale de Grenoble, B.P. 53 X, 38041 Grenoble Cedex, France*

ET

CLAUDE GEY

*Centre d'Études et de Recherches sur les Macromolécules Végétales, B.P. 53 X, 38041 Grenoble Cedex, France*

Reçu le 3 septembre 1981

ROGER BARLET, RAYMOND LE GOALLER et CLAUDE GEY. Can. J. Chem. **60**, 1933 (1982).

Les éthoxy-alcènes s'avèrent d'excellents accepteurs de carbènes dans la réaction de *méthylmonohalogénocyclopropanation* au moyen du dichloro-1,1 éthane et du méthyllithium exempt d'ion iodure. A côté des adduits chlorés, on obtient une forte proportion d'adduits bromés grâce à un échange d'halogène au niveau du complexe carbène–sel intermédiaire. La stéréochimie des adduits est déterminée par rmn $^1H$ et $^{13}C$. La *syn*-stéréosélectivité de la réaction est discutée en termes électroniques et stériques.

ROGER BARLET, RAYMOND LE GOALLER, and CLAUDE GEY. Can. J. Chem. **60**, 1933 (1982).

Ethoxy-alkenes act as excellent carbene acceptors in the *methylmonohalogenocyclopropanation* reaction mediated by 1,1-dichloroethane and iodide-ion free methyl iodide. As well as chlorinated adducts, a large proportion of brominated products are obtained by means of halogen exchange at the carbene complex – salt intermediate stage. Adduct stereochemistry is determined by $^1H$ and $^{13}C$ nmr spectroscopy. The *syn*-stereoselectivity of the reaction is discussed in electronic and steric terms.

[Journal translation]

## Introduction

Nous avons récemment rendu compte de la formation, avec de hauts rendements et une nette stéréosélectivité, des éthoxy-1 halogéno-2 cyclopropanes (1). Cette réaction d'*halogénocyclopropanation* des éthoxy-alcènes s'inscrivait dans le cadre général de l'étude, menée par l'un d'entre nous, de la cycloaddition carbénique sur les oléfines désactivées par un groupement électroattracteur (2–4).

Nous présentons ici les résultats, dans la même perspective, de la *méthylhalogénocyclopropanation* des mêmes éthoxy-alcènes faiblement nucléophiles.

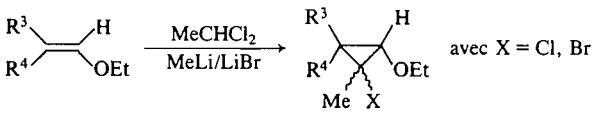


La détermination de la configuration *cis* ou *trans* des adduits,[1] rendue ici délicate en rmn par l'absence de couplages caractéristiques $^3J_{H-H}$ et l'absence d'effet nOe significatif, a cependant été obtenue de façon incontestable par la convergence de méthodes spectrographiques (rmn $^1H$, $^{13}C$) et chimiques (facilité d'ouverture disrotatoire). Une telle identification stéréochimique est également justifiée par la mise en évidence des effets d'anisotropie des méthyles, des éthoxy et des halogènes dans de telles structures. Elle permet en outre de mener une étude comparée de la stéréosélectivité de la méthylhalogénocyclopropanation présentée ici et de l'halogénocyclopropanation précédemment décrite.

Notons que nos résultats complètent ceux obtenus, à peu près simultanément, par Conia et coll. concernant l'addition du chlorométhyl carbène sur les siloxyalcènes et appliqués à la formation de systèmes cétoniques α-éthyléniques méthylés en α (5) et éventuellement inclus dans des produits naturels (6).

## Résultats expérimentaux

La réaction de cyclopropanation est obtenue avec un haut rendement (80 à 85%) pour les quatre éthers, d'énols **5–8** ci-dessous.[2] On observe la formation préférentielle des adduits chlorés et méthylés en position 2, de configuration *cis* et *trans*, accompagnés minoritairement des adduits bromés correspondants (Tableau 1).

[1]Comme dans le travail antérieur rendant compte des résultats d'halogénocyclopropanation des mêmes substrats (1), les termes *syn* et *anti* (ou *cis* et *trans*) précisent la position relative du groupement éthoxy et de l'halogène.

[2]Les substrats **5–8** sont identiques aux substrats **1–4** présentés dans notre travail antérieur (1). La numérotation différente est destinée à permettre la distinction des adduits **5***t*, **5***c*, etc ... résultant de la méthylhalogénocyclopropanation par rapport aux adduits homologues **1***t*, **1***c*, etc ... résultant de l'halogénocyclopropanation.

0008-4042/82/151933-09$01.00/0

©1982 National Research Council of Canada/Conseil national de recherches du Canada

Can. J. Chem. Downloaded from www.nrcresearchpress.com by 210.87.254.6 on 09/06/12
For personal use only.

TABLEAU 1. Méthylhalogénocyclopropanation des ethers α-éthyléniques au moyen de $CH_3CHCl_2$ et MeLi/LiBr (température ordinaire)

| Substrats[a] | % Adduits chlorés[b] | % Adduits bromés[b] | Répartition adduits chlorés: No ident. *trans* (*anti*) % | Répartition adduits chlorés: No ident. *cis* (*syn*) % | Répartition adduits bromés: No ident. *trans* (*anti*) % | Répartition adduits bromés: No ident. *cis* (*syn*) % |
|---|---|---|---|---|---|---|
| 5 | 60 (77) | 40 (23) | **5***t* *43* | **5***c* *57* | **5′***t* *49* | **5′***c* *51* |
| 6  | 73 (85) | 27 (15) | **6***t* *34* | **6***c* *66* | **6′***t* *5* | **6′***c* *95* |
| 7 | 75 (89) | 25 (11) | **7***t* *65* | **7***c* *35* | **7′***t* *43* | **7′***c* *57* |
| 8  | 64 (90) | 36 (10) | **8***t* *56* | **8***c* *44* | **8′***t* *48* | **8′***c* *52* |

[a]Les substrats **5**, **6**, **7**, **8** sont les mêmes que les substrats **1**, **2**, **3**, **4** mentionnés dans notre travail précédent (1) mais les adduits correspondants **5***t*, **5***c*, etc ... diffèrent des adduits **1***t*, **1***c*, etc ... par le méthyle géminé avec l'halogène.
[b]Les % indiqués entre parenthèses sont ceux des réactions de cycloaddition menés à −15°C. L'abaissement de température pratiquement sans effet sur la répartition des isomères *syn* et *anti* limite la formation des isomères bromés.

Par rapport à la réaction d'halogénocyclopropanation (1) conduisant aux adduits non méthylés en position 2 ($Me^2$ remplacé par H), nous avons observé un léger affaiblissement du rendement réactionnel, une moins bonne reproductibilité probablement due à une plus grande fragilité des adduits cyclopropaniques, la formation de sous-produits légers non identifiés et une augmentation sensible de la proportion d'adduits bromés.

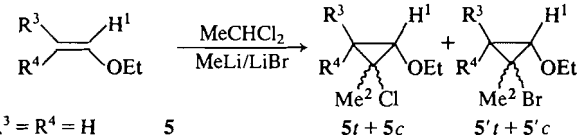


| | | | |
|---|---|---|---|
| $R^3 = R^4 = H$ | **5** | **5***t* + **5***c* | **5′***t* + **5′***c* |
| $R^3 = H$, $R^4 = Me$ | **6** | **6***t* + **6***c* | **6′***t* + **6′***c* |
| $R^3 = Me$, $R^4 = H$ | **7** | **7***t* + **7***c* | **7′***t* + **7′***c* |
| $R^3 = R^4 = Me$ | **8** | **8***t* + **8***c* | **8′***t* + **8′***c* |

L'addition de méthyllithium associé à un équivalent de bromure de lithium (lithien préparé par action de MeBr sur Li) et exempt d'ions iodures, est menée à faible reflux d'éther sur le mélange: accepteur de carbénoïde – générateur de carbénoïde. La formation des adduits bromés, produits primaires de réaction,[3] s'interprète comme dans la référence 1 par échange chlore–brome au niveau du complexe carbène–sel. Cet échange est bloqué à −80°C et seuls sont alors formés les adduits chlorés. L'existence de ce complexe carbène–sel expliquerait que seule soit mise en jeu la réactivité électrophile de tels carbènes sur la double liaison de cétones éthyléniques (7) alors que les carbénoïdes correspondants, stables à basse température (8), sont connus pour leur facile addition nucléophile sur les esters (9) et les composés carbonyls (10).

L'addition de $Bu_4N^+Br^-$, légèrement soluble, n'augmente pas la quantité de produits bromés ce qui indique, là encore, que la vitesse de formation des adduits est supérieure à celle de l'incorporation des bromures extérieurs au carbène–sel.

### Identification stéréochimique des adduits

Nous ne disposons pas, pour ces composés, de critères directs permettant de déterminer en rmn $^1H$ la stéréochimie *cis* ou *trans* des adduits: en effet, la position relative de $H^1$ et $Me^2$ ne donne pas lieu à un couplage $^4J$ spécifique de chacun des stéréoisomères puisque, même à 250 MHz, nous n'avons pas observé de couplage $^4J_{H^1H^2}$.

Nous nous sommes initialement tournés vers le "nuclear Overhauser effect", à priori la méthode de choix pour une telle détermination. En fait l'examen du signal de $H^1$, suffisamment distinct de tous les autres, avant et après irradiation de $Me^2$,

[3]Nous avons vérifié que la formation de composés bromés n'est pas due à une réaction de substitution nucléophile des adduits chlorés par les ions bromures présents dans le milieu. En effet, les adduits chlorés remis dans ces conditions de la réaction, mais en l'absence d'éthoxy-alcène accepteur, ne conduisent pas aux analogues bromés.

Can. J. Chem. Downloaded from www.nrcresearchpress.com by 210.87.254.6 on 09/06/12
For personal use only.

TABLEAU 2. Résonance magnétique nucléaire des adduits[a]

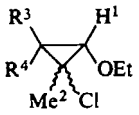


| | $\delta_{H^1}$ | $\delta_{Me^2}$ | $\delta_{R^3}$ | $\delta_{R^4}$ | $\delta_{OCH_2—CH_3}$ | $J_{H^1R^3}$ | $J_{H^1R^4}$ | $J_{R^3R^4}$ | $J_{R^3Me^2}$ | $J_{R^4Me^2}$ |
|---|---|---|---|---|---|---|---|---|---|---|
| **5***t* $R^3 = R^4 = H$ | 3,37 | 1,63 | 1,10 | 0,76 | 3,56 | 7,75 | 4,35 | 7,25 | 0,5[b] | 0[c] |
| **5***c* | 2,88 | 1,49 | 0,86 | 0,98 | 3,55<br>3,61 | 7,5 | 4,35 | 7,5 | 0 | 0,5[b] |
| **6***t* $R^3 = H, R^4 = Me$ | 3,34 | 1,49 | 1,10 | 1,08 | 3,58 | 7,6 | 0 | 6,5 | 0,5[b] | — |
| **6***c* | 2,81 | 1,50 | 0,83 | 1,10 | 3,52<br>3,60 | 7,5 | 0 | 6,5 | 0 | — |
| **7***t* $R^3 = Me, R^4 = H$ | 2,92 | 1,62 | 1,17 | 0,83 | 3,53 | 0 | 4 | 6,25 | — | 0 |
| **7***c* | 2,52 | 1,48 | 1,06 | 1,23 | 3,53<br>3,60 | 0 | 4 | 6 | — | 0,5[b] |
| **8***t* $R^3 = R^4 = Me$ | 2,93 | 1,52 | 1,22 | 1,04 | 3,52 | 0 | 0 | — | — | — |
| **8***c* | 2,54 | 1,54 | 1,07 | 1,15 | 3,52 | 0 | 0 | — | — | — |

[a]$\nu$ = 60 MHz, $CCl_4$, $\delta$ $10^6$, $J$(Hz).
[b]La mise en évidence de ces couplages $^4J$ a été obtenue à 250 MHz.
[c]Toutes les valeurs nulles figurant dans ce tableau signifient que ces $^4J$ n'ont jamais été observés même à 250 MHz.

ne permet pas de conclure. En effet les mesures multiples faites au spectrographe à onde continue Cameca 250 MHz ou Varian HA 100 donnent des évolutions du signal de $H^1$ quelque peu surprenantes: (a) l'effet nOe est négligeable sur le couple **8***c*/**8***t* dans tous les cas; (b) l'effet est minime sur les couples **5***t*/**5***c* (de 2 à 5% d'exaltation pour **5***t*, de 1 à 6% de diminution pour **5***c*) et **8***t*/**8***c* (de 1 à 4% d'exaltation pour **8***t*, de 1 à 6% de diminution pour **8***c*); (c) l'effet est relativement important dans le cas du couple **7***t*/**7***c*. De façon inattendue l'exaltation se manifeste aussi bien pour **7***t* (10% au minimum) que pour **7***c* (de l'ordre de 5%).

Dans tous les cas, l'effet nOe lorsqu'il se manifeste est faible mais va à l'encontre des hypothèses d'attributions faites par analogie avec les adduits non méthylés (1). Ce résultat nous a contraints par un travail spécifique sur cette série, à accumuler les observations expérimentales propres à étayer la détermination de ces structures.

L'identification stéréochimique des adduits a finalement pris appui sur un certain nombre de critères spectrographiques en rmn $^1H$: effets LIS, analyse des effets de blindage des alkyles et des halogènes; et en rmn $^{13}C$: examen du couplage $^{13}C—H$ entre le carbone de $Me^2$ et le proton $H^1$. Ces critères spectrographiques se sont révélés être convergents avec le critère chimique d'ouverture disrotatoire plus rapide des composés *trans* (11). En outre, nous avons pu ajouter à ces critères de configuration d'autres éléments de preuve cohérents dans toute la série et cohérents avec la série non méthylée ($H^2$ à la place de $Me^2$) (1).

1. *Effet LIS*

L'étude de l'effet LIS menée à partir du chélate de l'Europium $Eu(dpm)_3$ a eu un double objet: (*i*) *l'attribution directe des déplacements chimiques* $\delta R^3$ *et* $\delta R^4$ dans les adduits dérivés de **5** ($R^3 = R^4 =$ H) et de **8** ($R^3 = R^4$ Me), structures dans lesquelles, des deux substituants géminés identiques, le plus déplacé par le chélate est celui qui est en position *cis* par rapport à l'éthoxy complexant. L'ensemble de ces attributions est cohérent avec les attributions de déplacements chimiques des mêmes substituants $R^3$ et $R^4$ dans les adduits dérivés de **6** et de **7** (Tableau 2). (*ii*) *L'attribution des configurations par étude comparée de l'effet LIS sur ces couples* **5**t–**5**c *et* **8**t–**8**c. Dans ce dernier cas, on observe que $Me^4$ est nettement plus déplacé que $Me^2$ et $Me^3$ pour l'un des stéréoisomères. On en conclut alors que $Me^4$ se trouve du côté du OEt tandis que $Me^2$ et $Me^3$ sont du côté opposé. Cet isomère est donc **8***c* (Fig. 1). Dans l'autre isomère **8***t* $Me^2$ et $Me^4$, déplacés de façon voisine et trois à quatre fois plus que $Me^3$, sont donc l'un et l'autre du côté du OEt.

Pour le couple **5***t*–**5***c*, les rapports des pentes $a$ des droites $\Delta\delta = a(C_{Eu}/C_0)$ ($C_0$ concentration en adduit, $C_{Eu}$ concentration en chélate), permettent d'attribuer de façon nette les configurations (Tableau 3). Les rapports $a\,Me^2/a\,H^3$, $a\,Me^2/a\,H^4$, $a\,Me^2/a\,H^1$, $a\,Me^2/a\,OCH_2$ sont toujours supérieurs dans

Can. J. Chem. Downloaded from www.nrcresearchpress.com by 210.87.254.6 on 09/06/12
For personal use only.

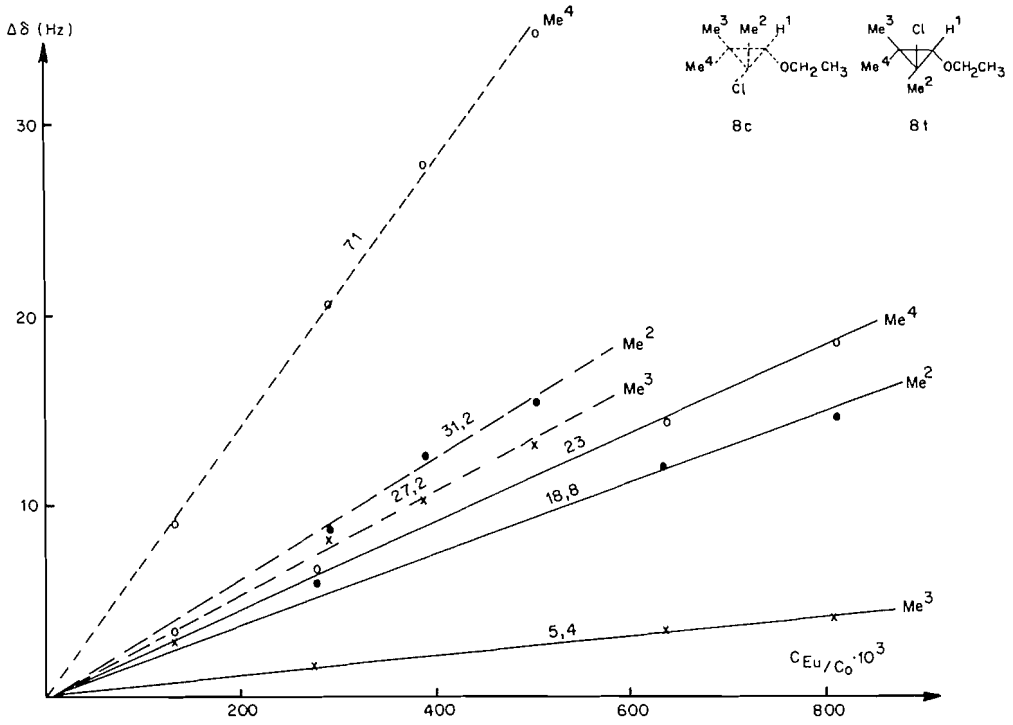


FIG. 1. Valeurs de Δδ et *a* pour les adduits **8***t* et **8***c*.

le cas ou $Me^2$ est plus proche du complexant, c'est-à-dire pour le stéréoisomère **5***t* où ces rapports sont respectivement de 1,14; 0,56; 0,38; 0,45 à opposer à 0,68; 0,31; 0,27 et 0,31 pour l'isomère **5***c*.

Ces attributions de configuration permettent de préciser, sans ambiguïté, les déplacements chimiques de $H^1$ pour chacun des stéréoisomères et par conséquent de prévoir les configurations des adduits dérivés de **6** et **7** (Tableau 2). Comme pour les adduits issus de **5** et **8**, il est en effet cohérent de penser que $\delta H^1$ est sensiblement plus élevé dans le cas du stéréoisomère *trans* (Δδ de l'ordre de 0,5 ppm) que dans celui du *cis*.

2. *Effets de blindage des méthyles et de déblindage des halogènes sur les protons cyclopropaniques*

L'étude des déplacements chimiques des protons $H^1$ (sur le carbone porteur de l'oxygène) et $H^2$ (sur le carbone porteur de l'halogène) dans les adduits de monohalogénation (1) montre que le groupe méthyle exerce sur $H^1$ un effet de blindage de 0,35 à 0,37 ppm pour les composés de la série *t* et 0,20 à 0,33 ppm pour ceux de la série *c*. Cet effet est encore plus grand pour $H^2$: 0,43 à 0,46 ppm pour les composés *t*, 0,35 à 0,36 ppm pour les adduits *c*. Ces valeurs moyennes recoupent sur un nombre de cas plus important celles obtenues antérieurement par Closs et coll. (12).

Ces observations transférées aux produits de méthyl monohalogénation étudiés ici confirment les attributions de configuration obtenues par effet LIS. Le tableau 2 met en évidence *les effets de déblindage attendus de* $Me^3$ *sur le proton* $H^1$ (0,45 ppm entre **5***t* et **7***t*, 0,36 entre **5***c* et **7***c*, 0,41 entre **6***t* et **8***t*, 0,27 entre **6***c* et **8***c*).

De plus, la comparaison des adduits *cis* et *trans*, de même structure alkylée, montre que $\delta H^1$ augmente de 0,39 à 0,53 ppm lorsqu'on passe du stéréoisomère *trans* au *cis* (0,49 de **5***t* à **5***c*, 0,53 de **6***t* à **6***c*, 0,40 de **7***t* à **7***c*, 0,39 de **8***t* à **8***c*). Ce Δδ est la somme en valeur absolue des effets de blindage de $Me^2$ et de déblindage de Cl, ce dernier chiffré comme dans les adduits non méthylés (1) à 0,1 ppm. *L'effet de blindage de* $Me^2$ *sur* $H^1$ *ressort donc dans la fourchette 0,29–0,43 ppm valeur tout-à-fait comparable à l'effet de* $Me^3$ *sur* $H^1$.

La cohérence de ces effets de blindage des méthyles dans l'ensemble des adduits, méthylés ou non, constitue un nouvel argument pour notre attribution de configuration. Une attribution inversée pour les adduits **5***t*–**5***c* .... **8***t*–**8***c* conduirait à des effets très atténués ou même des effets de déblindage des méthyles en opposition aux résul-

Can. J. Chem. Downloaded from www.nrcresearchpress.com by 210.87.254.6 on 09/06/12
For personal use only.

TABLEAU 3. Valeurs (en Hz) des deplacements (Δδ) induits par Eu (dpm)$_3$ et pente $a$ en Hz des droites $\Delta\delta = a(C_{Eu}/C_0)$

| | | $H^1$ | | $OC\underline{H}_2—CH_3$ | | $OCH_2—C\underline{H}_3$ | | $Me^2$ | | $H^3$ ou $Me^3$ | | $H^4$ ou $Me^4$ | |
|---|---|---|---|---|---|---|---|---|---|---|---|---|---|
| Adduits | $(C_{Eu}/C_0) \times 10^3$ | Δδ | $a$ | Δδ | $a$ | Δδ | $a$ | Δδ | $a$ | Δδ | $a$ | Δδ | $a$ |
| | 57 | 47,5 | | 37,5 | | 18,5 | | 16,2 | | 18 | | 35 | |
| **5***t* | 164 | 141 | 775 | 122 | 660 | 60 | 325 | 53,5 | 297 | 48 | 270 | 92 | 530 |
| | 232 | 170 | | 146 | | 74 | | 67 | | 59 | | 111,5 | |
| | 45 | 27 | | 22 | | 12 | | 6 | | 10 | | 21 | |
| **5***c* | 67 | 41 | 570 | 33 | 500 | 17 | 250 | 10,5 | 155 | 15 | 225 | 31 | 490 |
| | 103 | 64 | | 53 | | 27 | | 17 | | 23 | | 52 | |
| | 163 | 98 | | 82 | | 42 | | 26 | | 36 | | 79 | |
| | 278 | 10,2 | | 10,2 | | 4,2 | | 6 | | 1,8 | | 6,6 | |
| **8***t* | 636 | 21,6 | 29 | 20,4 | 32,8 | 7,8 | 12,8 | 12 | 18,8 | 3,6 | 5,4 | 14,4 | 23 |
| | 810 | 24,6 | | 24 | | 9 | | 14,4 | | 4,2 | | 18,6 | |
| | 132 | 12,6 | | 8,2 | | 4,5 | | 3,4 | | 3 | | 9 | |
| | 291 | 28 | | 19,8 | | 13,6 | | 8,8 | | 8,2 | | 20,6 | |
| **8***c* | 388 | 39,4 | 118 | 26 | 66 | 18,8 | 46,5 | 12,4 | 31,2 | 10,2 | 27,2 | 27,8 | 71 |
| | 502 | 50 | | 31,6 | | 23,6 | | 15,6 | | 13 | | 34,8 | |

tats précédemment observés dans notre série non méthylée (1) ou dans la littérature.

3. *Couplage $^{13}C—H$ entre $Me^2$ et $H^1$*

Il est admis que la valeur du couplage $^3J_{^{13}C—H}$ varie à peu près comme le couplage $^3J_{H—H}$ (13). Il a été montré récemment que dans une série de composés du type oxiranes, thiiranes, sulfones et cyclopropanes, le couplage du carbone substituant le $C^2$ du cycle et du proton porté par le carbone l'était toujours plus grand dans le cas d'une relation *cis* de ce carbone et ce proton que dans le cas d'une relation *trans*. La généralité d'une telle observation a d'ailleurs permis aux auteurs de faire de cette observation comparée de tels $^3J_{^{13}C—H}$ un critère d'attribution de configuration (14).

L'étude des spectres rmn $^{13}C$ des composés **8***t* et **8***c*, permet effectivement de distinguer un couplage $Me^2—H^1$ de 3,7 Hz pour **8***c* et de moins de 1,5 Hz pour **8***t*. Cette détermination comparée des couplages $^3J_{Me^2—H^1}$ constitue un élément de preuve supplémentaire pour notre attribution.

4. *Autres éléments de détermination des configurations*

Indépendamment des critères précédents de détermination des configurations, nous avons pu mettre en évidence d'autres caractères distinctifs entre les isomères *cis* et *trans*, parallèles à ceux que nous avions observés pour les adduits de monohalogénocyclopropanation.

(*i*) Les protons méthyléniques du groupe éthoxy présentent, ici encore, une légère inéquivalence, de l'ordre de 4 Hz, pour les isomères *cis* avec apparition d'un doublet de quadruplets. L'isomère *trans* ne présente, par contre, aucun dédoublement de son quadruplet. Nous interprétons, à nouveau, cette équivalence comme un effet de champ de l'halogène sur les deux hydrogènes voisins $OC\underline{H}_2—CH_3$. La généralisation de cette observation peut constituer un nouveau critère d'attribution de configuration pour les éthoxy-1 halogène-2 cyclopropanes, quel que soit, par ailleurs, leur degré d'alkylation.

(*ii*) Les temps de rétention en chromatographie en phase vapeur sont toujours supérieurs pour les isomères *cis* quelle que soit la nature de la colonne.

(*iii*) Les isomères *trans*, chauffés à reflux de toluène, disparaissent beaucoup plus rapidement que les isomères *cis* sauf dans le cas des adduits **7***t* et **7***c* où les vitesses d'ouverture sont voisines aussi bien dans $CCl_4$ que dans le toluène. Cette aptitude supérieure des isomères *trans* à l'ouverture disrotatoire, avec formation d'éthoxydiènes, est conforme aux règles de l'ouverture thermique de Woodward–Hoffman en série cyclopropanique (11).

(*iv*) Il faut noter un fait expérimental supplémentaire qui, sans être à priori un critère stéréochimique absolu, permet de fait une différenciation entre les isomères de la série *c* et ceux de la série *t*: la réalisation de spectres rmn H à 250 MHz nous a permis de mettre en évidence un léger mais net couplage $^4J$ entre $Me^2$ et $H^3$ ou $H^4$ selon la stéréochimie. Ce couplage à longue distance de 0,5 Hz (cf. Tableau 2) n'apparaît que lorsque le méthyle et l'hydrogène sont en position *trans*. On observe ainsi de tels couplages $^4J_{Me^2—H^3}$ dans les composés **5***t* et **6***t* et $^4J_{Me^2—H^4}$ dans les composés **5***c* et **7***c*. Par contre, à la limite de résolution de l'appareil à 250 MHz, on n'observe pas de coupla-

Can. J. Chem. Downloaded from www.nrcresearchpress.com by 210.87.254.6 on 09/06/12
For personal use only.

Can. J. Chem. Downloaded from www.nrcresearchpress.com by 210.87.254.6 on 09/06/12
For personal use only.

TABLEAU 4. Comparaison de la stéréosélection dans les reactions d'halogénocyclopropanation et de méthylhalogénocyclopropanation des ethers α-éthyléniques

| Substrats | Adduits | Halogenocyclopropanation | | Méthylhalogenocyclopropanation | |
|---|---|---|---|---|---|
| | | % Adduits chlorés | % Adduits bromés | % Adduits chlorés | % Adduits bromés |
| | *t* + *c* | 76 | 24 | 60 | 40 |
| | *t* | 33 | 28 | 43 | 49 |
| **1** ou **5** | *c* | 66 | 72 | 57 | 51 |
| | *t* + *c* | 77 | 23 | 73 | 27 |
| | *t* | 20 | 5 | 34 | 5 |
| **2** ou **6** | *c* | 80 | 95 | 66 | 95 |
| | *t* + *c* | 84 | 16 | 75 | 25 |
| | *t* | 47 | 45 | 65 | 43 |
| **3** ou **7** | *c* | 53 | 55 | 35 | 57 |
| | *t* + *c* | 93 | 7 | 64 | 36 |
| | *t* | 42 | 8 | 56 | 48 |
| **4** ou **8** | *c* | 58 | 92 | 44 | 52 |

ges analogues $^4J_{H^1—Me^3}$ ou $^4J_{H^1—Me^2}$. Dans ce dernier cas la raison en est sans doute que la présence d'atomes électronégatifs, géminés à la fois avec $H^1$ et $Me^2$, entraîne un abaissement, et en fait ici une disparition, du $^4J$ correspondant de la même façon que nous avions observé un abaissement des couplages $^3J_{H^1—H^2}$ dans les adduits de monohalogénocyclopropanation.

En conclusion, si les résultats obtenus par nOe nous ont fait douter du parallélisme entre la série méthylée et la série non méthylée, toutes les autres observations montrent au contraire une grande cohérence entre les deux. Dans le cas présent, l'effet nOe ne constitue pas un critère de distinction stéréochimique clair. Deux explications peuvent être retenues à ce sujet: d'une part la fréquence de découpleur, calée sur la résonance du $Me^2$, crée une fréquence harmonique très proche de la fréquence de résonance de $H^1$, d'autre part, le quadrupôle du chlore accélère la relaxation et rend l'effet nOe inobservable ou même quelques fois inversé (15). L'effet est dans cette série assez faible mais la tendance à l'inversion est nette.

## Discussion

*Effet* syn-*directeur des groupes méthylés. Absence d'effet stéréodirecteur sensible du groupe éthoxy*

En extension à l'utilisation de $CH_2Cl_2$ comme générateur de carbénoïde, l'*utilisation du générateur méthylé* $MeCHCl_2$, en présence de MeLi/LiBr et dans des conditions expérimentales proches de la température ordinaire, *autorise sur les éthoxyalcènes une réaction de méthylhalogénocyclopropanation facile à mettre en oeuvre et à haut rendement*.

Ce générateur de carbénoïde conduira à un intermédiaire très réactif, à mi-chemin entre le carbène libre singulet à carbone central $sp_2$ et le vrai carbénoïde tétraédrique à carbone central $sp_3$. Cet intermédiaire s'avère apte à ponter des structures désactivées par des groupements inductifs attracteurs comme le groupement éthoxy. L'interprétation de cette anomalie (l'assistance de l'agent de pontage par l'oxygène du substrat accepteur) déjà mise en avant antérieurement (1), nous paraît garder toute sa validité ici. La distance lithium–oxygène est d'ailleurs, dans le cas des éthers d'énols, particulièrement faible par rapport à d'autres substrats tels que cétones ou dioxolannes α-éthyléniques (4) puisque l'oxygène est alors directement lié au système éthylénique. Le pouvoir désactivant de l'éthoxy vis-à-vis d'un réactif électrophile pourrait ainsi être compensé par cette assistance.

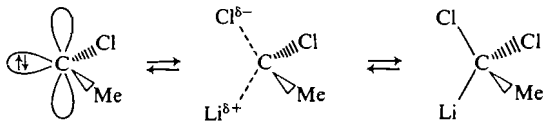


Carbène singulet électrophile — Complexe carbène–sel intermédiaire — Carbénoïde nucléophile

Une telle mise en oeuvre d'un carbène–sel de type carbénoïde est justifiée par la méthode de génération carbénique et l'observation de l'échange chlore–brome. Cela nous paraît exclure toute possibilité de formation primaire d'un ylure (où le carbène libre se serait associé au doublet de

Can. J. Chem. Downloaded from www.nrcresearchpress.com by 210.87.254.6 on 09/06/12
For personal use only.

l'oxygène) telle qu'elle a pu être invoquée ou discutée par Vogel et coll. (16) ou Moss (17).

Par rapport à la monohalogénocyclopropanation des mêmes substrats par $CH_2Cl_2$/MeLi, on observe ici le *maintien d'un net effet* syn-*directeur des méthyles de l'accepteur* et une *atténuation sensible de l'effet* syn-*directeur de l'éthoxy* (Tableau 4).

La cycloaddition sur **5** et **8**, permet d'isoler l'effet de l'éthoxy puisque **5** ne présente pas de méthyles et que **8** voit l'action des deux méthyles, de part et d'autre de la double liaison, se neutraliser. La présence d'une légère prépondérance de **5***c* avec renversement en faveur de **8***t* et la quasi disparition de cette prédominance au niveau des isomères bromés montrent que l'*effet de l'éthoxy est sensiblement nul*.

Par contre, l'obtention à partir de **6** et **7** d'environ 2/3 d'isomères **6***c* et **7***t*, stéréoisomères dans lesquels le méthyle est *cis* de l'halogène, montre *la persistance d'un net effet* syn-*directeur d'alkyle*. Par rapport aux adduits d'halogénocyclopropanation, nous observons une diminution globale de la stéréosélection lorsque le méthyle et l'éthoxy sont du même côté (**2***t*/**2***c* = 20:80, **6***t*/**6***c* = 34:66) et une augmentation lorsqu'ils sont de part et d'autre (**3***t*/**3***c* = 47:53, **7***t*/**7***c* = 65:35). Cette évolution est cohérente avec une forte atténuation de l'effet stéréodirecteur de l'éthoxy et un maintien de l'effet de l'alkyle.

Notons que la répartition des isomères bromés **6**′*t*/**6**′*c* et surtout **7**′*t*/**7**′*c* ne paraît pas compatible avec l'explication précédente. Nous pensons que ceci est dû à la forte sensibilité thermique de **6**′*t* et surtout **7**′*t*, qui entraine ainsi un abaissement de la proportion des isomères *trans* déterminée par chromatographie en phase vapeur.

Dans tous les cas la méthylhalogénocyclopropanation conduit à une plus grande quantité de stéréoisomère *trans* et une plus faible quantité d'isomère *cis* que l'halogénocyclopropanation. Ce fait montre que la distribution des isomères ne dépend pas prioritairement de l'interaction stérique attractive Me ... Me dans l'état de transition, tel que le décrivent Hofmann *et al.* (18). Si tel était le cas, le *trans* éthoxy propène devrait donner un accroissement de la quantité de l'isomère *cis*, au détriment du *trans*. Cette interaction secondaire joue donc un rôle mineur par rapport à l'interaction électronique alkyle–halogène habituellement invoquée dans ce type de réaction: *dans l'état de transition la position* cis *de l'halogène sera favorisée par interaction électrostatique entre l'halogène négatif et les alkyles légèrement positifs* lors du transfert d'électrons de la double liaison vers le

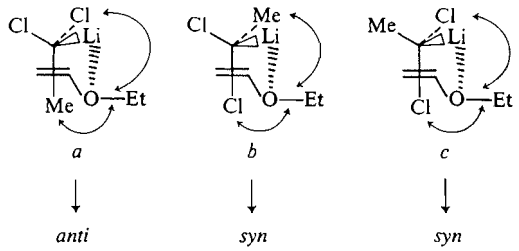


carbénoïde (19). A condition que l'effet stérique demeure, comme ici, modeste on obtiendra ainsi, de façon majoritaire, les adduits les plus encombrés.

L'interprétation de la disparition de l'effet *syn*-directeur de l'éthoxy est plus délicate. En conservant le même formalisme que pour les réactions de monohalogénocyclopropanation, les trois états de transition, *a*, *b* et *c* doivent conduire à un rapport *a*/*b* + *c* voisin de 1 et non plus inférieur à 1.

Ce résultat peut s'interpréter si l'on met en jeu, à nouveau, une forte intéraction Li ... O avec torsion dans l'état de transition et net rapprochement du lithium et de l'éthoxy et si l'on considère que Me est stériquement plus encombrant que Cl. Le remplacement de H par Me, sans effet au niveau de *c*, entrainera alors une déstabilisation de *b* (par augmentation de l'intéraction Me *anti* – OEt) supérieure à celle de *a* (intéraction Me *syn* – OEt supérieure à intéraction H *syn* – OEt mais minimisée par l'éloignement imposé par le rapprochement Li ... O).

Par rapport à la monohalogénocyclopropanation, à côté de la modification des éffets *syn*-directeurs, on peut noter une sensible augmentation de la proportion des adduits bromés (voir Tableau 4). Nous proposons l'explication suivante: la vitesse d'incorporation de l'ion bromure au complexe carbène–sel reste du même ordre tandis que les durées de vie de ce complexe sont accrues par l'effet donneur du méthyle. Cet accroissement laisse au brome un temps accru pour se substituer au chlore.

## Conclusion

Ce travail nous a permis d'obtenir des halogéno-2 méthyl-2 éthoxy-1 cyclopropanes, diversement alkylés en 3, par action du générateur de carbénoïde $MeCHCl_2$/MeLi/LiBr sur les éthoxy-alcènes correspondants. La réaction fournit, à côté des composés chlorés attendus, des analogues bromés d'accès réputé difficile (20).

La stéréochimie des adduits a été déterminée, en l'absence de critères absolus, à la fois par voie chimique et par convergence de divers arguments

Can. J. Chem. Downloaded from www.nrcresearchpress.com by 210.87.254.6 on 09/06/12
For personal use only.

spectrographiques: effet LIS, effet d'anisotropie des alkyles et des halogènes, couplages à longue distance en rmn $^1H$, couplage $^{13}C$—H en rmn $^{13}C$.

Par rapport à l'halogénocyclopropanation antérieurement rapportée (1), la méthylhalogénocyclopropanation des mêmes éthoxy-alcènes s'opère avec maintien d'un net effet *syn*-directeur des méthyles et disparition quasi-totale de l'effet *syn*-directeur de l'éthoxy. Cette différence est interprétée sur la base d'une grande sensibilité stérique de l'état de transition.

## Partie expérimentale

Les spectres de rmn $^1H$ ont été enregistrés dans $CCl_4$ sur appareils fonctionnant, dans la grande généralité des cas, à 60 MHz (Hitachi–Perkin–Elmer R 24) mais également à 100 voire 250 MHz (Varian HA 100, Caméca 250). L'étude de l'effet nOe a été menée à 100 HA 100, et 250 MHz (Caméca). Les spectres de rmn $^{13}C$ ont été enregistrés dans $CDCl_3$ sur un spectromètre à impulsion Brücker WP100 travaillant à 25,182 MHz. Les spectres infrarouge ont été réalisés sur Perkin–Elmer 397.

La cpv analytique a été effectuée sur Aérograph 600 D à ionisation de flamme, le plus souvent avec des colonnes Ucon Oil. La cpv préparative a été effectuée sur Autroprep A 700 et A 705 avec des colonnes Ucon Oil ou SE 30 de 90 cm à 2 m (1/8 po ou 3/8 po).

Les analyses élémentaires ont été réalisées par le Service Central de Microanalyses du C.N.R.S., Echangeur de Solaize, B.P. 22, 69390 Vernaison, France.

*Mode opératoire général*

La préparation du méthyllithium associé au bromure de lithium[4] de même que la mise en oeuvre de la réaction elle-même de *méthylhalogénocyclopropanation* sont entièrement conformes au mode opératoire décrit antérieurement (1) à ceci près que $MeCHCl_2$ remplace ici $CH_2Cl_2$ comme générateur de carbénoïde.

Les substrats soumis à la cycloaddition carbénique sont soit commerciaux (cas de **5**≡**1** et du mélange **6** + **7**≡**2** + **3**, produits Fluka) soit préparé, dans le cas de **8**≡**4** selon la méthode de Claisen (21). Le mélange **6**/**7** (environ 70:30) est séparé en cpv sur SE 30 20 pieds chargée à 30% ($t°$ de colonne = 40°C). Le mélange **6** + **7** soumis directement à la cycloaddition carbénique permet de mettre en évidence que le produit *cis* **6** réagit plus facilement que le produit *trans* **7** puisqu'au rapport de substrats **6**/**7** ≃ 2,5 correspond un rapport d'adduits ≃ 4,5.

*Caractérisation et identification des adduits*

*Caractérisation*

Les adduits de méthylhalogénocyclopropanation sont dans l'ensemble des composés plus fragiles que les adduits homologues non méthylés décrits dans notre travail antérieur (1). Tous ces composés sont des composés nouveaux. Les composés *trans*, aussi bien bromés que chlorés (sauf **5***t*), se décomposent plus ou moins rapidement même en solution (sensibilité plus grande à l'ouverture disrotatoire que les composés *cis*). Les composés *cis* sont relativement stables dans le cas des composés chlorés (sauf **7***c*). Par contre, seul parmi les composés *cis* bromés, **7**′*c* est séparable en chromatographie sans décomposition.

Par conséquent les composés fragiles ne donnent pas d'analyses élémentaires satisfaisantes et reproductibles car la libération d'halogène altère les compositions centésimales même si les spectres rmn restent pratiquement inchangés. Les seules analyses acceptables que nous avons pu obtenir (Cl ± 0,3%, Br ± 0,5%), à condition qu'elles soient faites rapidement après les séparations chromatographiques, sont les suivantes:

| Composé | | Analyse % |
|---|---|---|
| **5***t* | calculée pour $C_6H_{11}OCl$ | C% 53,55; H% 8,18; O% 11,90; Cl% 26,37 |
| | trouvée | C% 53,38; H% 8,25; O% 11,88; Cl% 26,29 |
| **5***c* | calculée pour $C_6H_{11}OCl$ | C% 53,55; H% 8,18; O% 11,90; Cl% 26,37 |
| | trouvée | C% 53,37; H% 8,26; O% 11,94; Cl% 26,24 |
| **6***c* | calculée pour $C_7H_{13}OCl$ | C% 56,58; H% 8,75; O% 10,78; Cl% 23,88 |
| | trouvée | C% 56,33; H% 8,83; O% 10,91; Cl% 23,62 |
| **7**′*c* | calculée pour $C_7H_{13}OBr$ | C% 43,54; H% 6,74; O% 8,29; Br% 41,42 |
| | trouvée | C% 43,37; H% 6,89; O% 8,37; Br% 41,07 |
| **8***c* | calculée pour $C_8H_{15}OCl$ | C% 59,09; H% 9,23; O% 9,85; Cl% 21,82 |
| | trouvée | C% 58,91; H% 9,34; O% 9,98; Cl% 21,56 |

Cependant, même pour les composés fragiles, l'ensemble des données spectrographiques ne laisse aucun doute sur la nature cyclopropanique de ces composés (valeurs des δ en rmn, présence de $\nu_{C-H}$ entre 3025 et 3040 $cm^{-1}$ en ir) et sur leur structure (Tableau 2 et Fig. 1 en rmn relatifs aux adduits chlorés). Les adduits bromés présentent des spectres très proches de ceux des adduits chlorés: les couplages restent inchangés, les déplacements chimiques voisins. Les seules modifications sensibles affectent $\delta H^1$ et $\delta Me^2$. Ainsi par rapport aux homologues chlorés $\delta H^1$ est abaissé de 0,1 à 0,2 ppm pour les bromés *cis* (2,75; 2,31; 2,67; 2,44 respectivement pour **5**′*c*, **6**′*c*, **7**′*c*, **8**′*c*) et de moins de 0,1 ppm pour les bromés *trans* (3,45; 2.98; 3,35; 2,99 respectivement pour **5**′*t*, **6**′*t*, **7**′*t*, **8**′*t*) tandis que $\delta Me^2$ est exalté dans tous les cas de plus de 0,1 ppm (1,74; 1,61; 1,70; 1,61; 1,55; 1,64; 1,63; 1,73 respectivement pour **5**′*t*, **5**′*c*, **6**′*t*, **6**′*c*, **7**′*t*, **7**′*c*, **8**′*t*, **8**′*c*).

*Séparation et détermination des pourcentages*

Les divers produits n'ont pas été séparés par distillation mais par cpv vu les faibles quantités sur lesquelles nous avons opéré (de 0,01 à 0,05 mole de substrat) et la complexité des mélanges obtenus. Les stéréoisomères *trans* sont moins retenus en cpv que les stéréoisomères *cis* aussi bien dans le cas des adduits bromés que des adduits chlorés et quelle que soit la colonne utilisée. Les adduits chlorés *cis* et *trans* sortent habituellement tous les deux avant les adduits bromés correspondants. La seule exception est constituée par les composés **8***t* et **8**′*t* qui sortent sous forme d'un pic unique sur Ucon Oil 30% LB 550 X de 200 cm tandis que, sur Ucon Polar 50 HB 2000 à 20% de 120 cm **8**′*t* est à nouveau bien distingué en 3è position. Sur ces deux colonnes **8**′*c* est totalement décomposé. Le composé **6***t* complètement décomposé sur SE 30 n'est pas affecté sur Ucon Oil tandis que **6***c* est séparé sans décomposition sur SE 30 de même que **7**′*c*.

La détermination des pourcentages d'adduits par cpv analytique n'est pleinement valable que si les températures de colonne sont suffisamment modérées pour empêcher toute décomposition liée à la fragilité de ces composés. La température de colonne pour de telles déterminations n'a jamais été supérieure à 60°C tandis que celle de l'injecteur était de l'ordre de 150°C. Il apparaît clairement qu'une température d'injecteur de 185°C suffit à modifier sensiblement les pourcentages.

[4]Les meilleurs résultats et la diminution des produits légers sont là encore obtenus avec un méthyllithium suffisamment concentré (solution dans l'éther de 0,7 à 1,0 *M*).

*Effet LIS*

L'effet LIS a été étudié sur les couples **5***t*/**5***c* et **8***t*/**8***c*. Le chélate Eu(dpm)$_3$ est additionné peu à peu sur le substrat dont la concentration est déterminée une fois pour toutes au départ. On mesure les déplacements chimiques induits $\Delta\delta$ et on représente les courbes $\Delta\delta = a(C_{Eu}/C_0)$ (Fig. 1) où $C_{Eu}$ et $C_0$ sont les concentrations en chélate et en substrat. Les valeurs de $\Delta\delta$ sont données dans le tableau 4.

*Spectres rmn $^{13}C$ de* **8***t et* **8***c*

Les spectres ont été enregistrés sur un spectromètre à impulsion Brücker WP 100. Les expériences ont été conduites en utilisant une fenêtre spectrale de 4500 Hz avec un temps d'acquisition de 0,9 s pour 8K points mémoire, une largeur d'impulsion de 5 μs (angle de 45°) avec un découplage par bruit de 3 W (mode BB, atténuateur 0,6 dB sur l'échelle 20 W). Les expériences de découplage sélectif ont été réalisées dans les mêmes conditions excepté le découpleur (mode CW, atténuation 20 dB sur l'échelle 20 W) à la fréquence exacte définie sur le spectre proton obtenu grâce à la bobine d'irradiation de la sonde $^{13}C$ (100, 132 MHz) avec taille mémoire de 8K, fenêtre spectrale de 1000 Hz, temps d'acquisition de 4,1 s, largeur d'impulsion de 2 μs). La détermination des constantes de couplage $^3J_{^{13}C-H}$ a été obtenue grâce à des expériences de "gated decoupling". Les conditions expérimentales restent identiques sauf pour le découpleur pulsé, en mode BB, pour lequel on a introduit un délai de 3 s. Les concentrations des solutions étudiées étaient les suivantes: **8***t* = 0,192 mol/l, **8***c* = 0,320 mol/l.

L'étude des spectres $^1H$ montre que $H^1$ et $Me^2$ sont bien isolés dans les deux composés. Les spectres rmn $^{13}C$ réalisés en découplage des protons par bruits montrent deux signaux très faibles correspondant aux carbones quaternaires $C^2$ et $C^3$. Les carbones porteurs de l'oxygène $C^1$ et $OCH_2$ apparaissent nettement plus déblindés, le méthyle de $OCH_2CH_3$ à champ le plus fort. Le découplage sélectif de $H^1$ permet de confirmer l'attribution du $C^1$ tandis que celui du $Me^2$ permet celle du $C^2$. Les carbones de $Me^3$ et $Me^4$ n'ont pas été attribués avec certitude mais il apparaît que le plus déblindé des deux est également le plus couplé. Les expériences de "gated decoupling" permettent ensuite d'analyser le signal du carbone du $Me^2$ et par conséquent d'observer les couplages $^3J_{^{13}C-H}$ entre $Me^2$ et $H^1$.

Résultats: δ de **8***t* (en ppm/TMS): $C^1$ (69,83), $C^2$ (49,97), $C^3$ (25,90), $Me^2$ (18,08), $Me^3$ et/ou $Me^4$ (23,08) et/ou (15,023), $OC\underline{H}_2$ (66,51), $OCH_2—C\underline{H}_3$ (14,63); $^3J_{^{13}C-H}$ ($Me^2—H^1$) ≤ 1.5 Hz. δ de **8***c*: $C^1$ (67,43), $C^2$ (50,35), $C^3$ (24,90), $Me^2$ (23,47), $Me^3$ et/ou $Me^4$ (21,07) et/ou (16,95), $OC\underline{H}_2$ (66,48), $OCH_2—C\underline{H}_3$ (14,98); $^3J_{^{13}C-H}$ ($Me^2—H^1$) = 3.7 Hz.


1. R. Barlet, R. Le Goaller et C. Gey. Can. J. Chem. **59**, 621 (1981).
2. R. Barlet. C.R. Acad. Sci. Ser. C, **278**, 621 (1974).
3. R. Barlet. Bull. Soc. Chim. Fr. 2767 (1975).
4. R. Barlet et M. Vincens. Tetrahedron, **33**, 1291 (1977).
5. L. Blanco, P. Amice et J. M. Conia. Synthesis, 289 (1981); 291 (1981).
6. L. Blanco, N. Slougui, G. Rousseau et J. M. Conia. Tetrahedron Lett. 645 (1981).
7. R. Barlet. Tetrahedron Lett. 4171 (1976).
8. J. Villieras, P. Pierrot et J. F. Normant. Bull. Soc. Chim. Fr. 765 (1977).
9. J. Villieras et M. Rambaud. C.R. Acad. Sci. Ser. C, **291**, 105 (1980).
10. J. Villieras et M. Rambaud. C.R. Acad. Sci. Ser. C, **290**, 295 (1980).
11. W. E. Parham, F. M. Parham, J. F. Dooley et M. K. Meilahn. J. Org. Chem. **33**, 3651 (1968).
12. G. L. Closs et J. J. Coyle. J. Am. Chem. Soc. **87**, 4270 (1965); D. T. Longone et A. H. Miller. Chem. Commun. 447 (1967).
13. J. B. Stothers. $^{13}C$ nmr spectroscopy organic chemistry. Vol. 24. Academic Press, New York, London. 1972. p. 350.
14. C. A. Kingsbury, D. L. Durham et R. Hutton. J. Org. Chem. **43**, 4696 (1978).
15. J. H. Noggle et R. E. Schirmer. The nuclear Overhauser effect. Academic Press, New York. 1971. pp. 24 et 58.
16. W. Grimme, J. Reisdorff, W. Jünemann et E. Vogel. J. Am. Chem. Soc. **92**, 6335 (1970).
17. R. A. Moss. J. Am. Chem. Soc. **94**, 6004 (1972).
18. R. Hoffmann, C. C. Levin et R. A. Moss. J. Am. Chem. Soc. **95**, 629 (1973).
19. (*a*) G. L. Closs et R. A. Moss. J. Am. Chem. Soc. **86**, 4042 (1964); (*b*) G. L. Closs et J. J. Coyle. J. Org. Chem. **31**, 2759 (1966).
20. (*a*) R. A. Moss. J. Org. Chem. **30**, 3261 (1965); (*b*) B. Martel et J. M. Hiriart. Synthesis, 201 (1972); (*c*) S. Miyano, Y. Matsumoto et H. Hashimoto. Chem. Commun. 364 (1975).
21. L. M. Claisen. Chem. Ber. **40**, 3903 (1970).


Can. J. Chem. Downloaded from www.nrcresearchpress.com by 210.87.254.6 on 09/06/12
For personal use only.

# Substituent effects in arosemibullvalene photochemistry: the methylcyclopropane rearrangement of 1,8-dimethylbenzosemibullvalene

CHRISTOPHER OWEN BENDER, DONALD LAVERNE BENGTSON, DOUGLAS DOLMAN, CAROLYN ELAINE L. HERLE, AND SEAMUS FRANCIS O'SHEA

*Department of Chemistry, University of Lethbridge, Lethbridge, Alta., Canada T1K 3M4*

Received January 11, 1982

CHRISTOPHER OWEN BENDER, DONALD LAVERNE BENGTSON, DOUGLAS DOLMAN, CAROLYN ELAINE L. HERLE, and SEAMUS FRANCIS O'SHEA. Can. J. Chem. **60**, 1942 (1982).

1,6- and 1,8-Dimethylbenzotricyclo[3.3.0.0$^{2,8}$]octa-3,6-diene (**16** and **14**) are the major semibullvalene products formed from acetophenone sensitized irradiations of the barrelenes 2,6- and 2,3-dimethyl-1,4-dihydro-1,4-ethenonaphthalene (**37** and **22**), respectively ($\Phi_{37\rightarrow16} = 0.65$; $\Phi_{22\rightarrow14} = 0.57$). The direct ($\Phi_{14} = 0.017$) or chlorobenzene sensitized ($\Phi_{14} = 0.12$) irradiation of **14** yields 2,3-benzo-5-methyl-6-methylenebicyclo[3.3.0]octa-2,7-diene (**17**), a transformation typical of methylcyclopropanes. Gas phase thermolysis (420°C/6 Torr) of **14** gives 6,7-dimethylbenzocyclooctatetraene (**15**). The direct irradiation ($\Phi_{39} = 0.003$) or the gas phase thermolysis (395°C/6 Torr) of **16** gives 6,9-dimethylbenzocyclooctatetraene (**39**). The rearrangement **14** → **17** is in accord with predictions based upon CNDO-CI calculations of changes in atom–atom interaction energies on excitation to the $S_1$ or $T_1$ excited states of **14**.

CHRISTOPHER OWEN BENDER, DONALD LAVERNE BENGTSON, DOUGLAS DOLMAN, CAROLYN ELAINE L. HERLE et SEAMUS FRANCIS O'SHEA. Can. J. Chem. **60**, 1942 (1982).

Diméthyl-1,6 et -1,8 benzotricyclo[3.3.0.0$^{2,8}$]octa-3,6-diène (**16** et **14**) sont les semibullvalènes principaux qui proviennent des irradiations sensibilisées par l'acétophénone des barrelènes dimethyl-2,6 et -2,3 dihydro-1,4 éthèno-1,4 naphtalène (**37** and **22**), respectivement ($\Phi_{37\rightarrow16} = 0.65$; $\Phi_{22\rightarrow14} = 0.57$). La photolyse directe ($\Phi_{17} = 0.017$) ou sensibilisée par le chlorobenzène ($\Phi_{17} = 0.12$) du **14** conduit au benzo-2,3 méthyl-5 méthylène-6 bicyclo[3.3.0]octa-2,7-diène (**17**), une transformation caractèristique des méthylcyclopropanes. La thermolyse en phase gazeuse (420°C/6 Torr) du **14** conduit au diméthyl-6,7 benzocyclooctatetraène (**15**). L'irradiation directe ($\Phi_{39} = 0.003$) ou la thermolyse en phase gazeuse du **16** (395°C/6 Torr) conduit au diméthyl-6,9 benzocyclooctatetraène (**39**). Le réarrangement **14** → **17** est en accord avec les prédictions qui proviennent de calculs des changements d'énergies d'interactions atome–atome de l'état excité singulet ou triplet de **14**.

## Introduction

Photoisomerizations of arosemibullvalenes (aro-SB's) have not been widely reported. Some rearrange efficiently to give cyclooctatetraene (COT) product (e.g. **1** → **2**, $\Phi = 0.4$ (1), **3** → **5**, $\Phi = 0.1$ (2); Scheme 1) while others show remarkable photostability (e.g. **7**, **8** (3), and **9** (4)), a property of current interest in connection with model organic photoisomer light energy storage devices (4).

In a previous paper we noted that the benzo-SB system was capable of undergoing an additional rearrangement, of the vinylcyclopropane type, to give isomeric SB, namely **10** → **12** (5), and more recently a further example has been found with the related derivative **11** (→ **13**).[1]

Since the photo-vinylcyclopropane rearrangement has thus far been observed only with benzo-SB's containing electron-withdrawing substituents at both C1 and C8, information on the effect of electron-donors at those positions was desired. Herein we report on the photochemistry of 3,4-benzo-1,8-dimethyltricyclo[3.3.0.0$^{2,8}$]octa-3,6-diene (**14**, i.e., 1,8-dimethylbenzo-SB). The selection of methyl as the donor group is additionally intriguing since it presents the opportunity for

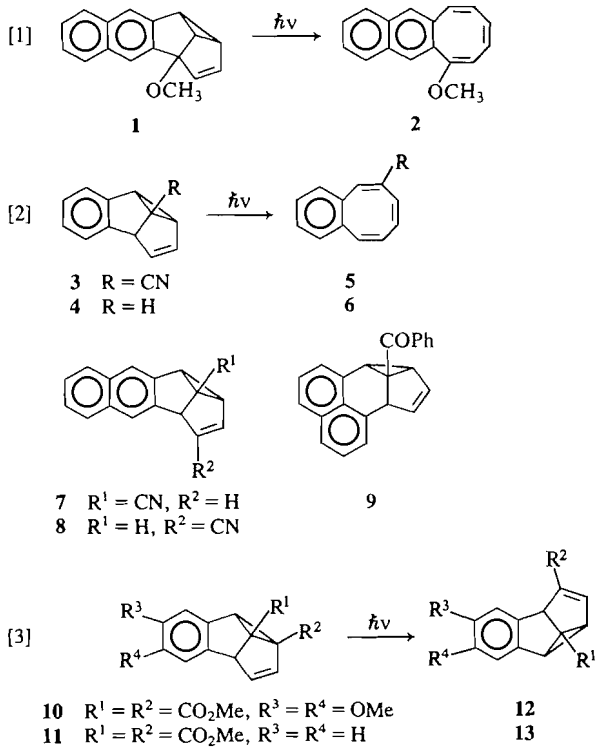


SCHEME 1

[1]C. O. Bender and D. Dolman, unpublished results.

0008-4042/82/151942-11$01.00/0

©1982 National Research Council of Canada/Conseil national de recherches du Canada

Can. J. Chem. Downloaded from www.nrcresearchpress.com by 210.87.254.5 on 09/06/12
For personal use only.

Can. J. Chem. Downloaded from www.nrcresearchpress.com by 210.87.254.5 on 09/06/12
For personal use only.

competition between three literature precedented photoisomerizations, each of which would lead to a different product. Transformation to COT **15** and/or SB **16** might be anticipated by analogy with the two known types of conversion discussed above (eqs. [2] and [3]; Scheme 1), and the third possibility is a methylcyclopropane 1,4-hydrogen migration to give conjugated diene **17** (Scheme 2). Although this latter type of isomerization has not been reported in an SB there are numerous examples of its occurrence in alkylphenylcyclopropanes (6), and of particular relevance are compounds **18** and **19** (7, 8) which are structurally similar to **14**.

## Results

Compound **14** was obtained as the major product from the acetophenone sensitized photolysis of 2,3-dimethylbenzobarrelene (**22**), the latter being the major of the two possible barrelene products from benzyne addition to *o*-xylene (Scheme 3). The structures assigned to the benzo-SB's **14** and **24** follow from analytical data and comparison of $^1$Hmr spectra with parent benzo-SB (**4**) (9) (see Table 1).

On direct and on chlorobenzene sensitized irradiations, **14** gave, at low conversions, the methylcyclopropane 1,4-hydrogen migrated product **17** as the only detectable product. Glass capillary gas chromatography (GC-2) analyses during the progress of photolyses indicated that possible photoproducts **15** and **16** were absent; **15** and **16** were independently prepared (*vide infra*) and used for GC-2 comparison.

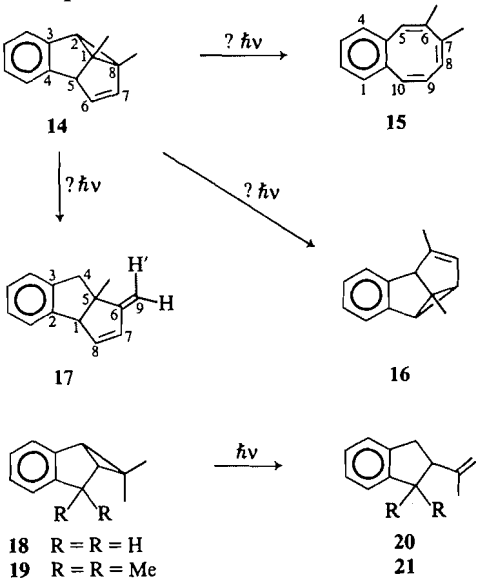


SCHEME 2

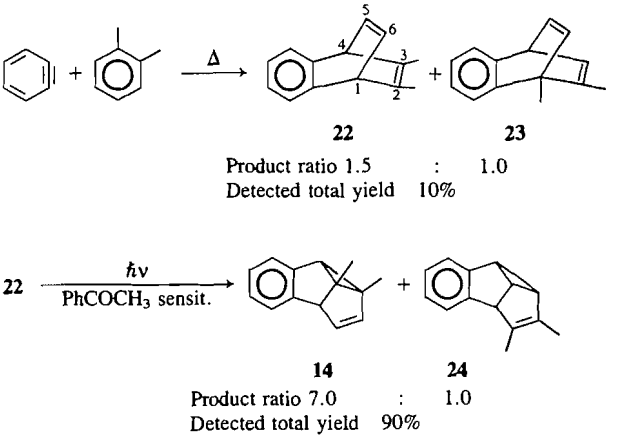


SCHEME 3

Attempts at sensitization with acetone led to the slow disappearance of **14** to give nonisomeric material. Both benzo-SB (**4**) (9) and 1-cyanobenzo-SB (**3**) (2) have been noted to behave similarly on attempted sensitization with acetone.

The structure of **17** was deduced from spectral data and from hydrogenation results. Mass spectral analysis indicated that the colourless oil **17** was isomeric with starting material **14**. The ir spectrum contains a moderately strong band at 1635 cm$^{-1}$ (cf. 1630 cm$^{-1}$ for the *exo*-conjugated model compound **25** (10)) and at 880 cm$^{-1}$, the latter band being characteristic for a 1,1-disubstituted vinyl. The uv spectrum shows strong absorption at $\lambda_{max}$ 237 nm (ε 11 700) which is attributed to the conjugated diene moiety (note $\lambda_{max}$ 234 nm (ε 17 900) for **25** (11)); this band is absent in uv spectra of the reduced compounds **29** and **30** (*vide infra*). The 400 MHz $^1$Hmr spectrum of **17** contains signals due to a methyl (s, δ1.39), two benzylic protons (AB q, δ3.13 and 3.01, $J_{AB}$ = 16.5 Hz), an allylic-benzylic proton (br s, δ3.98), and four olefinic protons centered at δ4.87, 4.97, 6.14, and 6.19. These olefinic chemical shift values compare well with those at lower resolution reported for the olefinic protons in **25** (11), i.e. δ4.79 (m, 2H) and δ6.12 (m, 2H). The $^1$Hmr data also provide additional support for the presence of a conjugated *s-trans* diene in **17**. Thus the large 1.4 Hz coupling between H-8 and H-9′ over a five bond conjugated zigzag pathway is close to the reported 1.3 Hz value between the corresponding protons in *s-trans*-butadiene (12).

It is to be noted that structures such as **26–28**, which are *a priori* alternatives for methylcyclopropane 1,4-hydrogen migration products from **14**, are not well accommodated by the uv and $^1$Hmr information. For example, **26** and **27** should show a

Can. J. Chem. Downloaded from www.nrcresearchpress.com by 210.87.254.5 on 09/06/12
For personal use only.

TABLE 1. The $^1$Hmr data of benzo-SB's

| Assignment | Description and signal position, $\delta$[a] | | | |
|---|---|---|---|---|
| | **4**[b] | **14**[c] | **24**[d] | **16**[e] |
| Aromatics | 6.80–7.33<br>m | 6.78–7.22<br>m | 6.97–7.36<br>m | 6.70–7.30<br>m |
| H-1 | 3.14<br>q, $J_{1,5} = J_{1,8} = J_{1,2} = 6.5$ | — | 3.18<br>q, $J_{1,5} = J_{1,2} = J_{1,8} = 6.5$ | — |
| H-2 | 2.96<br>t, $J_{1,2} = J_{2,8} = 6.0$ | 2.38<br>s | 2.82<br>t, $J_{1,2} = J_{2,8} = 6.5$ | 2.65<br>d, $J_{2,8} = 6.5$ |
| H-5 | 3.81<br>q, $J_{5,6} = 2.0, J_{1,5} = 6.0$ | 3.51<br>d, $J_{5,6} = 2.5$ | 3.54<br>d, $J_{1,5} = 6.5$ | 3.20<br>s |
| H-6 | 5.47<br>q, $J_{6,7} = 5.0, J_{5,6} = 2.0$ | 5.36<br>q, $J_{6,7} = 5.0, J_{5,6} = 2.5$ | — | — |
| H-7 | 5.08<br>q, $J_{6,7} = 5.0, J_{7,8} = 2.0$ | 4.92<br>d, $J_{6,7} = 5.0$ | — | 4.61–4.81<br>m |
| H-8 | 2.60<br>dxt, $J_{7,8} = 2.0, J_{1,8} = J_{2,8} = 6.5$ | — | 2.39<br>t, $J_{1,8} = J_{2,8} = 6.5$ | 2.28<br>q, $J_{2,8} = 6.5, J_{7,8} = 2.0$ |
| Methyls | — | 1.26 and 1.45<br>s s | 1.56<br>s | 1.35 and 1.65<br>s broad s<br>(C6—Me) |

[a]Run in $CCl_4$ with TMS as internal standard; coupling constants are given in Hz.
[b]Reference 9.
[c]Irradiation of H-6 collapsed H-5 and H-7 to singlets.
[d]Irradiation of H-1 collapsed H-5 to an s, and H-2 and H-8 to d's, $J_{2,8} = 6.5$. Irradiation of H-8 collapsed H-1 to a t, $J_{1,2} = J_{1,5} = 6.5$, and H-2 to a d, $J_{1,2} = 6.5$.
[e]Irradiation of H-7 collapsed H-8 to a d, $J_{2,8} = 6.5$, and changed the C6-methyl to a sharp s. Irradiation of the C6-methyl collapsed H-7 to a d, $J_{7,8} = 2.0$.

methyl doublet in the $^1$Hmr spectrum; **27** and **28** contain nonconjugated dienes.

**25** **26**

**27** **28**

Further evidence for structure **17** was obtained from its catalytic hydrogenation at room temperature and pressure. The stereoisomers *syn*- and *anti*-2,3-benzo-5,6-dimethylbicyclo[3.3.0]oct-2-ene (**29** and **30**), containing four more hydrogens than **17**, were the only detectable products (Scheme 4). They were readily separated via preparative gc and were shown to be identical with two of the four components isolated from the atmospheric hydrogenation of **14**. In an additional experiment the alkene double bond in **14** was first reduced with diimide and the resulting product **32** was then catalytically hydrogenated. This procedure was employed in order to preclude the possibility that **14** undergoes rearrangement on the catalytic surface prior to reduction. Either reduction methodology, however, led to the same major components, but product ratios were modified somewhat. For the purposes of comparison it is noted that Zimmerman *et al.* (9) obtained the indane **33** as the major reduction product of benzo-SB (**4**), together with two unidentified components.

The uv spectrum of **33** ($\lambda_{max}$ 273 nm ($\varepsilon$ 925), 266 (857), and 260sh (699)) is similar to those of both **29** ($\lambda_{max}$ 273 nm ($\varepsilon$ 1900), 267 (1500), 265sh (1100), and 261 (870)) and **30** ($\lambda_{max}$ 273 nm ($\varepsilon$1720), 267 (1360), 265sh (1050), and 261 (810)). The 400 MHz $^1$Hmr spectra of **29** and **30** closely resemble each other. For the minor product (**29**) the aliphatic ring protons occur as eight separate one proton resonances, although H-7 (? H-7′) is partially obscured by the C-5 methyl singlet peak. The benzylic methylene protons, H-4 and H-4′, occur as an AB quartet ($J_{AB}$ = 16.5 Hz), while the C-6 methyl is a doublet ($J$ = 7 Hz). Spin decoupling of the C-6 methyl readily enabled identification of H-6 which was then shown to be further coupled only to H-7 and H-7′ ($J$ = 6 and 11 Hz). H-1 occurs as a quartet and it too is coupled to only two protons (H-8 and H-8′, $J$ = 10.5 and 2.3 Hz). Further double irradiations revealed that H-7, -7′, -8, and -8′ are all intercoupled. Thus strong evidence is afford for the presence of isolated partial structure **34** in compound **29**.

Interpretation of the 400 MHz $^1$Hmr spectrum of the major reduction product **30** was made in

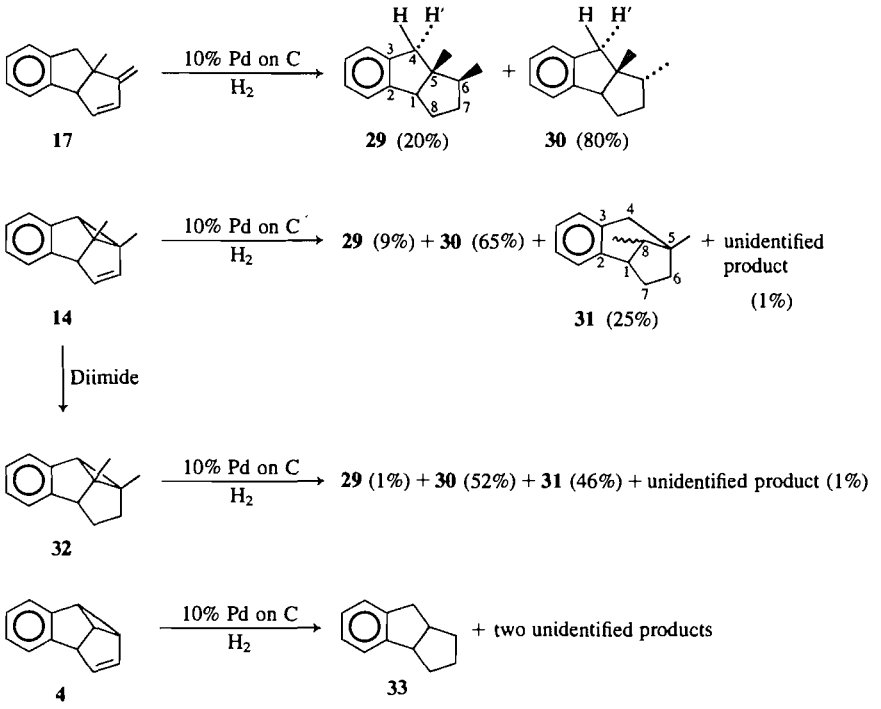


SCHEME 4

essentially the same manner as that used in the case of **29** (see Experimental), except that difficulties due to overlap of the H-7 and H-8′ signals in $CDCl_3$ solvent and of the H-6 and the H-8′ signals in $C_6D_6$ solvent did not permit definitive demonstration of coupling between H-7 and H-8′. Otherwise the double irradiation experiments are consistent with the presence of isolated partial structure **34** in **30**.

The major product **30** from the reduction of **17** is tentatively assigned the *anti* configuration of the

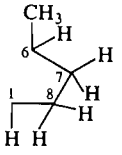

**34**

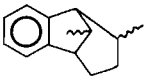

**35**

C-5 and C-6 methyls, and the minor product **29** the *syn* configuration, on the basis of the greater downfield shift of the H-4′ signal, due to *Van der Waals* deshielding by the C-6 methyl in the $^1$Hmr spectrum of **30** relative to that of H-4′ in **29**; the distance of closest approach of the C-6 methyl hydrogens to H-4′ is 0.9 Å in **30**, and 3.6 Å in **29** (Drieding Models).

The second major product from the reductions of SB **14** appears to be 2,3-benzo-5,8-dimethylbicyclo[3.2.1]oct-2-ene (**31**), arising from cleavage of the cyclopropyl C1—C2 bond. It cannot be **35**, which might result from C1—C8 cleavage, since the $^1$Hmr spectrum contains a methyl singlet and a methyl doublet.

In order to rule out the possible involvement of COT **15** and SB **16** (Scheme 2) in the direct and sensitized irradiations of **14**, their preparation and irradiation was undertaken.

*Preparation and photolyses of COT 15*

COT **15** was conveniently prepared in ca. 80% yield via flash gas phase thermolysis of **14** (ca. 420°C, nitrogen carrier gas at 6 Torr); minor (< 20%) amounts of cyclobutene **36** were also obtained, depending upon the precise conditions (Scheme 5). Note that Paquette *et al.* (13) have investigated the benzo-COT/benzobicyclo[4.2.0]-octatriene thermal interconvertibility and additionally have reported an alternative preparation of COT **15**. However, **15** was not obtained pure by their route (14).

The structure of COT **15** was assigned from $^1$Hmr data. Besides resonances for two methyls, the $^1$Hmr spectrum showed absorptions only in the aromatic-olefinic region; H-5 occurs as a broad singlet, being allylically coupled to the C-6 methyl, and strong coupling is found between H-8, -9, and -10. H-8 is additionally complexed due to allylic coupling to the C-7 methyl.

Both the direct and chlorobenzene sensitized photolysis of **15** gave cyclobutene **36** as the

Can. J. Chem. Downloaded from www.nrcresearchpress.com by 210.87.254.5 on 09/06/12
For personal use only.

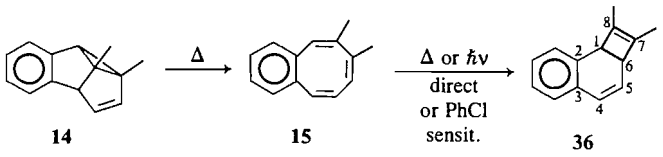


SCHEME 5

unique isomeric photoproduct at low conversions (Scheme 5).

*Preparation and photolyses of SB 16*

The preparation of **16** followed essentially the same procedure used above to obtain SB **14**, *o*-xylene being replaced by *m*-xylene in the benzyne addition stage (Scheme 6). The $^1$Hmr (Table 1) and analytical data are in full accord with structure **16**. The direct irradiation of **16** gave a single isomeric photoproduct, whose structure is assigned as **39** (see Experimental). Compound **39** was also obtained from the flash gas phase thermolysis of **16**.

The results of chlorobenzene sensitized photolysis of **16** are quite different to those obtained upon direct irradiation. No COT **39** was detected, but a single and presently unidentified photoproduct appeared as a shoulder on the GC-2 peak of starting material **16**. On the preparative scale, the photoproduct was not separable from **16**. However, the 400 MHz $^1$Hmr spectrum of the photolysate revealed no **17** to be present, nor any other $C_{14}H_{14}$ isomer (except **16**) identified in this study.

*Singlet and triplet energies of 14 and quantum yields*

Since neither fluorescence (room temperature, cyclohexane) nor phosphorescence (77 K, ethanol–ether 4:1 glass) were detected for **14**, $E_{S_1}$ and $E_{T_1}$ could not be obtained by emission techniques. However, inspection of the uv spectrum of **14** indicates that $94 \leq E_{S_1} \leq 101$ kcal/mol, the onset of absorption being ca. 305 nm and $\lambda_{max}$ for the lowest energy peak 283 nm.

For $E_{T_1}$, an "effective" triplet energy at room temperature of $78 \leq E_{T_1} \leq 82$ kcal/mol is suggested by triplet sensitization experiments; the conversion of **14** to **17** can be sensitized efficiently ($\Phi$ = 0.12) by chlorobenzene ($E_{T_1}$ = 82 kcal/mol), but not by acetone ($E_{T_1}$ = 78 kcal/mol) nor by acetophenone ($E_{T_1}$ = 74 kcal/mol). Interestingly, theoretical calculations (CNDO/2-CI, *vide infra*) for the lowest excited states of **14** give the relative energy ratio 1.000 ($S_1$) : 0.840 ($T_1$), and if the uv data range of $94 \leq E_{S_1} \leq 101$ kcal/mol is used as the scaling factor, then one obtains $79 \leq E_{T_1} \leq 85$ kcal/mol, i.e., the triplet energy of **14** is predicted to be above that of acetone.

Quantum yields for all transformations observed in this study were determined on an optical bench arranged for beam splitting into ferrioxalate actinometer (15). The $\Phi$'s for substrate disappearance and for product appearance are given in Table 2. Oxygen at $[O_2] \simeq 10^{-2}$ *M* was found to quench the rearrangement of **14** to **17** at room temperature by ca. 5 ± 3%, whereas 2,5-dimethyl-2,4-hexadiene at concentrations up to $0.5 \times 10^{-2}$ *M* showed no measurable quenching.

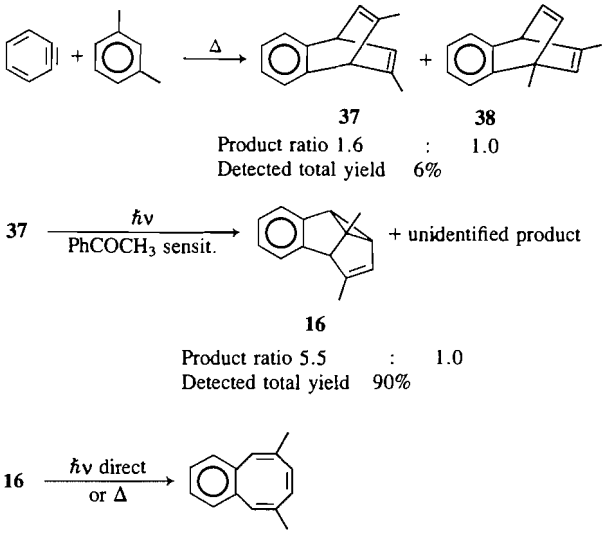


SCHEME 6

## Discussion

The observation that neither COT **15** nor SB **16** nor any of their respective photoproducts was detected in the direct and chlorobenzene sensitized irradiations of **14** rules out significant participation of the known benzo-SB photoisomerizations described by eqs. [2] and [3] (Scheme 1). Photochemically then, **14** behaves as a typical methylphenylcyclopropane.

The excited state of **14** yielding **17** upon irradiation in neat chlorobenzene[2] ($E_{T_1}$ = 82 kcal/mol) is assumed to be the triplet (probably $T_1$) since the photoisomer is formed seven times more efficiently than when generated from direct irradiation in

[2]The use of chlorobenzene as a high energy sensitizer–solvent has been discussed by Zimmerman and Samuelson (16).

Can. J. Chem. Downloaded from www.nrcresearchpress.com by 210.87.254.5 on 09/06/12
For personal use only.

TABLE 2. Quantum yield data[a]

| Compound | Light wavelength (nm) | Sensitizer | Quantum yields: Φ(Substrate disappearance) | Quantum yields: Φ(Product appearance) |
|---|---|---|---|---|
| **22** | 313 | PhCOMe | 0.62 | 0.57(**14**) and 0.08(**24**) |
| **37** | 313 | PhCOMe | 0.75 | 0.65(**16**) and 0.12[b] (unidentified) |
| **14** | 275 | None | 0.024 | 0.017(**17**) |
| **14** | 275 | PhCl(neat) | 0.20 | 0.12(**17**) |
| **16** | 275 | None | 0.007 | 0.003(**39**) |
| **16** | 275 | PhCl(neat) | 0.117 | 0.025[b] (unidentified) |
| **15** | 275 | None | 0.089 | 0.055(**36**) |
| **15** | 275 | PhCl(neat) | 0.166 | 0.047(**36**) |

[a]Ferrioxalate actinometry; cyclohexane solvent. Φ's given are extrapolated to zero conversion; product analyses by GC-2 (internal hydrocarbon standard) at several conversions of ≤ 8%. Experimental error for Φ(disappearance) is ± 10%, and for Φ(product appearance) is ± 5%. For sensitized runs, sensitizers absorb > 95% of the incident light.
[b]Quantum yield calculated on the assumption that unidentified product is isomeric with starting material.

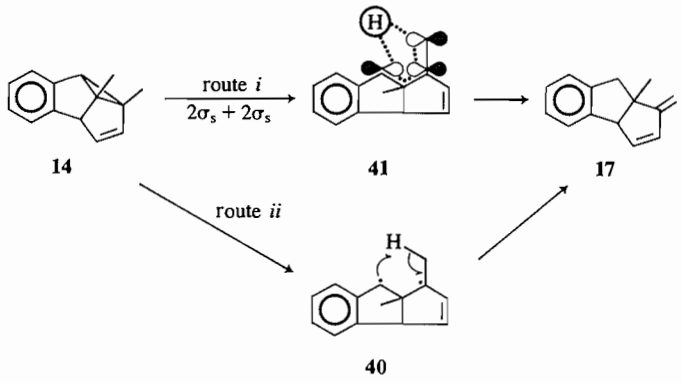


SCHEME 7

cyclohexane. If the quantum yield of intersystem crossing for chlorobenzene is taken to be 0.3 (17),[3] then the formation of **17** from $T_1$ of **14** appears to be a highly efficient process, i.e., $\Phi\, T_1\,(\mathbf{14}) \rightarrow \mathbf{17} = 0.4$.

In direct irradiations of **14**, the nature of the excited state species leading to **17** is not certain. Oxygen at $[O_2] \simeq 10^{-2}\,M$ showed only slight (≤5%) quenching of the reaction, suggesting a singlet excited state process. However, a short-lived $T_1$ state of lifetime ≃10 ns (at room temperature, with an assumed $k_q = 10^9\,M^{-1}\,s^{-1}$) cannot be ruled out.

With respect to mechanistic considerations, the formation of **17** from **14** can be accounted for in terms of a photo-allowed, concerted process involving a 4-electron (Möbius) cyclic array with zero nontrivial sign inversions (19), i.e., a $2\sigma_s + 2\sigma_s$ process (20), as shown in Scheme 7 (route *i*), or a two-step process beginning with homolysis of the C2—C8 bond of the cyclopropane ring, giving the benzylic and tertiary-allylic diradical intermediate (**40**), followed by intramolecular hydrogen atom transfer from the C-8 methyl to C-2 (route *ii*, Scheme 7). Note that mechanisms involving initial cleavage of the cyclopropane C1—C8 or C1—C2 bonds do not readily lead to the observed product **17**. Interestingly, CNDO/2-CI calculations of changes in atom–atom interaction energies for the lowest singlet and triplet excited states of **14** concur with the nonconcerted mechanistic analysis depicted by route *ii* (Scheme 7), i.e., the calculations indicate that the cyclopropane bond most weakened relative to the ground state is that between C2 and C8 (cf. cases 1, 3, and 5, Table 3; see Experimental for calculation details).

[3]Note that Bunce *et al.* (18) have recently obtained the value of $\Phi_{ISC} = 0.64$ for chlorobenzene, so that $\Phi T_1\,(\mathbf{14}) \rightarrow \mathbf{17}$ may be as low as 0.2.

## Experimental

The $^1$Hmr spectra were recorded on Bruker 200 or 400 MHz instruments or on a Varian (EM-360) 60 MHz instrument, with TMS as internal standard. The chemical shifts are in δ units and the coupling constants ($J$) in Hz. The abbreviations s, d, t, q, and m refer to singlet, doublet, triplet, quartet, and multiplet, respectively. The ir spectra were recorded on a Perkin–Elmer 337 spectrometer and are given in $cm^{-1}$. The uv spectra (run in cyclohexane solvent) were measured on a Cary 15 spectrometer; maxima are given in nm, with $\varepsilon_{max}$ values in parentheses; sh

Can. J. Chem. Downloaded from www.nrcresearchpress.com by 210.87.254.5 on 09/06/12
For personal use only.

Can. J. Chem. Downloaded from www.nrcresearchpress.com by 210.87.254.5 on 09/06/12
For personal use only.

TABLE 3. Changes[a,b] in atom–atom interaction energies (eV), between bound atoms, resulting from electronic excitation to the lowest singlet ($S_1$) and triplet ($T_1$) states of SB **14**

| Case | Atom–atom | $S_1$ | $T_1$ |
|---|---|---|---|
| 1 | 1–2 | 0.42 | −0.45 |
| 2 | 1–5 | 0.65 | 0.52 |
| 3 | 1–8 | 0.78 | 1.15 |
| 4 | 2–3 | −0.86 | 0.65 |
| 5 | 2–8 | 1.25 | 1.35 |
| 6 | 3–4 | 1.45 | 0.07 |
| 7 | 4–5 | 0.15 | 1.26 |
| 8 | 5–6 | −0.52 | −1.77 |
| 9 | 6–7 | 3.61 | 10.50 |
| 10 | 7–8 | −1.35 | −2.28 |

[a]Calculated by the CNDO/2-CI method using the theoretical parametization (21). Negative values are interpreted as "forces" tending to bring atoms together, while positive values cause the atoms to move further apart. Calculations on the full molecule **14** were performed; only values for the semibullvalene portion are given here. The underlined values are the most repulsive interactions (bond weakening) between the cyclopropane ring carbons.

[b]Relative theoretical energy ratios of the lower excited states of **14** are: $1.000(S_1):0.840(T_1):1.049(S_2):0.891(T_2)$.

= shoulder. Mass spectra were recorded on an MS 9 (A.E.I.) instrument at 70 eV. All melting points are uncorrected. Elemental analyses were performed by Galbraith Labs. Inc., Knoxville, TN. Fluorescence and phosphorescence studies were carried out on an Aminco–Bowman spectrometer. GC-2 analyses were made on a Varian 3700 instrument (FID) coupled to a Varian CDS 111 computing integrator, and fitted with an OV-101 glass capillary column, 50 m, with helium as carrier gas. Preparative gc separations were carried out on a Varian 2700 instrument (FID) on either a 20 ft × 0.375 in. 20% Carbowax 20M on 45–60 mesh Chromosorb W column or on a 20 ft × 0.375 in. 7.5% OV-101 on 45–60 mesh Chromosorb G column. Column chromatography was performed with Silicar CC-7 (100–200 mesh; Mallinckrodt), Silica Gel 60 (230–400 mesh; Merck), or Silica Gel H (100–200 mesh; Grace). Cyclohexane for photolyses was prepared by scrubbing with 10% of its volume of 30% fuming sulfuric acid, followed by washing with 10% aqueous sodium hydroxide, drying ($MgSO_4$), and finally distilling from calcium hydride. Chlorobenzene and acetophenone sensitizers and 2,5-dimethyl-2,4-hexadiene quencher were distilled prior to use.

*1,2- and 2,3-Dimethyl-1,4-dihydro-1,4-ethenonaphthalene (**23** and **22**)*

A 6 mL portion of isoamyl nitrite was added to a stirred, ice-cooled mixture of 3.5 g (25.5 mmol) of anthranilic acid and a catalytic quantity (70 mg) of trifluoroacetic acid in 35 mL of THF. The stirred mixture was allowed to warm to room temperature during 2 h. The resulting diazonium carboxylate salt was filtered under vacuum through a cotton plug fitted into a polypropylene funnel, washed with THF until the washings were colourless, and then with 1,2-dichloroethane (3 × 10 mL). The salt (WARNING! the dry solid is explosive), slurried in *o*-xylene (30 mL), was transferred to a 1 L round bottom flask and was diluted with 500 mL of *o*-xylene. The mixture was stirred at 50°C overnight under a dry nitrogen atmosphere, and then concentrated. The residue was dissolved in acetone (50 mL) and diluted with cyclohexane (500 mL). The resulting mixture was filtered, and the filtrate was concentrated. The residue was dissolved in benzene (20 mL) and column chromatographed on Silica Gel H (70 × 2 cm); elution was with 2.5% ether–cyclohexane. The first yellow band eluted was concentrated to give an oil which was analysed by GC-2; the ratio of the first and second major peaks eluted was 1.5 (**22**) : 1.0 (**23**), and corresponded to a total barrelene content of 449 mg (10%), as determined by calibration against standardized tridecane. Preparative gc (OV-101, 180°C) separation of the oil afforded 145.0 mg of **22**, mp 63–65°C and 70.3 mg of **23**, mp 36–38°C, after recrystallization of each from ethanol.

The spectral data for **22** were: ir (melt): 745 *o*-substituted benzenoid; uv: 247 sh (850), 257 (760), 264 (950), 271 (1 350), and 278 (1 470); $^1$Hmr (60 MHz, $CCl_4$): 6.58–7.08 (m, 6H, aromatic and vinyl), 4.24–4.48 (sym. m, 2H, H-1 and H-4), and 1.74 (s, 6H, methyls); spin decoupling experiments: irradiation of H-1(4) modified the 6.58–7.08 m, implanted in which was an s at 6.68 (H-5 and H-6); irradiation at 6.68 collapsed the H-1(4) m to an s. Mass spectrum showed molecular ion at *m/e* 182.1096 (92%); $C_{14}H_{14}$ requires 182.1096. *Anal.* calcd. for $C_{14}H_{14}$: C 92.26, H 7.74; found: C 92.43, H 7.78.

For **23**: ir (melt): 745 *o*-substituted benzenoid, 820 trisubstituted alkene; uv: 233 sh (1 070), 255 sh (630), 263 (660), 270 (890), and 277 (940); $^1$Hmr (400 MHz, $CDCl_3$): 7.14–7.19 (m, 2H, aromatics), 6.93–6.96 (m, 2H, aromatics), 6.93 (t, 1H, H-5, $J_{5,4}$ = 6.0, $J_{5,6}$ = 6.5), 6.50 (d × d, 1H, H-6, $J_{6,5}$ = 6.5, $J_{6,4}$ = 1.5), 6.48 (m, 1H, H-3), 4.74 (d × t, 1H, H-4, $J_{4,5} = J_{4,3}$ = 6.0, $J_{4,6}$ = 1.5), 1.94 (s, 3H, C1-methyl), and 1.83 (d, 3H, C2-methyl, $J_{3,Me}$ = 1.5); spin decoupling experiments: irradiation of the C2-methyl collapsed H-3 to a d ($J_{3,4}$ = 6.0); irradiation of H-4 collapsed H-3 to a broad s, and H-5 and H-6 to d's ($J_{5,6}$ = 6.5). Mass spectrum showed molecular ion at *m/e* 182.1096 (84%). *Anal.* found: C 92.25, H 7.83.

*1,3- and 2,6-Dimethyl-1,4-dihydro-1,4-ethenonaphthalene (**38** and **37**)*

Barrelenes **37** and **38** were prepared according to the procedure described above for the preparation of **22** and **23**, except that *o*-xylene was replaced by *m*-xylene. The crude mixture of barrelenes obtained from column chromatography was analysed by GC-2 which revealed the barrelenes to be eluted in the order and ratio of 1.6 (**37**) : 1.0 (**38**). Calibration via addition of standardized tridecane indicated 280 mg (6%) total barrelene production from 3.50 g of anthranilic acid. The barrelenes were difficult to separate from each other. On the preparative gc (OV-101, 180°C) the barrelene peaks coalesced, giving a broad envelope; the barrelenes were collected as one fraction (an oil, 244 mg). The oil was placed in a Craig tube (no solvent) and kept at −12°C for 7 days after which time 47.0 mg of **37**, mp 58–60°C (twice recrystallized from ethanol), were obtained upon centrifuging. The residual oil was resubmitted to preparative gc (Carbowax, 190°C) and **38** was obtained in small quantity from the tail of the barrelene envelope; short-path distillation (60°C/0.1 Torr) gave a colourless oil (GC-2 purity > 97%).

The spectral data of **37** were: ir (melt): 755 *o*-substituted benzenoid, 815 trisubstituted alkene; uv: 236 (1 190), 256 (740), 264 (810), 271 (1 130), and 278 (1 270); $^1$Hmr (60 MHz, $CCl_4$): 6.60–7.10 (m, 4H, aromatics), 6.10–6.35 (m, 2H, H-3 and H-5), 4.47 (t, 1H, H-4, $J_{3,4} = J_{5,4}$ = 5.5), 4.00–4.13 (m, 1H, H-1), and 1.87 (d, 6H, methyls, $J_{3(5),Me}$ = 1.5); spin decoupling experiment: irradiation of H-3(5) collapsed H-1, H-4 and the methyl signals to singlets. *Anal.* found: C 92.02, H 7.88.

For **38**: ir (film): 740 *o*-substituted benzenoid, 835 trisubstituted alkene; uv: 235 sh (1 120), 255 sh (660), 263 (690), 270 (920), and 277.5 (968); $^1$Hmr (400 MHz, $CDCl_3$): 7.14–7.18 (m, 2H, aromatics), 6.86–6.98 and 6.92 (m and t, 3H, remaining aromatics and H-5, $J_{5,4} = J_{5,6}$ = 6.5), 6.53 (d × d, 1H, H-6, $J_{6,4}$ = 1.5, $J_{6,5}$ = 6.5), 6.00–6.04 (m, 1H, H-2, $J_{2,4}$ = 2.0, $J_{2,C3\text{-}Me}$ = 1.7), 4.48–4.52 (m, 1H, H-4, $J_{4,5}$ = 6.5, $J_{4,2}$ = 2.0, $J_{4,6}$ = 1.5), 1.96 (s, 3H, C1-methyl), and 1.91 (d, 3H, C3-methyl, $J_{Me,2}$ = 1.7);

Can. J. Chem. Downloaded from www.nrcresearchpress.com by 210.87.254.5 on 09/06/12
For personal use only.

spin decoupling experiments: irradiation of H-2 collapsed the C3-methyl to an s and H-4 to a d × d ($J_{4,5}$ = 6.5, $J_{4,6}$ = 1.5); irradiation of H-4 collapsed both H-5 and H-6 to d's ($J_{5,6}$ = 6.5); irradiation of H-6 collapsed H-5 to a d ($J_{4,5}$ = 6.5) and H-4 to a d × d ($J_{4,5}$ = 6.5, $J_{2,4}$ = 2.0); irradiation of the C3-methyl collapsed H-2 to a d ($J_{2,4}$ = 2.0). *Anal.* found: C 92.39, H 7.67.

*Preparative photolysis apparatus*

*Apparatus I*

The apparatus consisted of a 450 W Hanovia medium pressure mercury arc surrounded by a water-cooled quartz immersion well. For direct and chlorobenzene sensitized irradiations the light was filtered through a Corex sleeve. For acetophenone sensitized irradiations a Pyrex sleeve was used. Sample solutions were deoxygenated by flushing with argon, before and during irradiations.

*Apparatus II*

On an optical bench arrangement, the arc from an Osram HBO 100W/2 lamp, located at the focus of an elliptical reflector contained in a water-cooled ALH-215 Arc Lamp Housing (P.R.A.), was focussed (image size ≃ 2 mm) onto the inlet slit of a high radiance monochromator (A 200, P.R.A.). The monochromator exit light was passed directly into a cylindrical quartz cell containing the sample solution. Prior to irradiations, the solutions were deoxygenated by flushing with argon. A positive pressure of argon was maintained over the stirred solutions throughout the course of the irradiations.

*Sensitized photolysis of barrelene* ***22***

A stirred solution of 397.7 mg (2.19 mmol) of **22** and 2.0 g of acetophenone in 250 mL of cyclohexane was irradiated for 30 min in apparatus I. The photolysate was concentrated and the residue chromatographed on Silicar (50 × 2.5 cm) with cyclohexane solvent. The first band contained 356.2 mg (90%) of a mixture of 1,8- and 6,7-dimethylbenzotricyclo[3.3.0.$0^{2,8}$]octa-3,6-diene (**14** and **24**) in the ratio of 7.0 : 1.0, respectively (GC-2 analysis). The SB's were separated by preparative gc (OV-101, 180°C), **14** being eluted before **24**. Compound **14** (219.3 mg) was obtained as a colourless oil after short-path distillation at 55°C/0.1 Torr (GC-2 purity > 98%); uv:269 sh (900), 275 (1060), and 282.5 (890); $^1$Hmr, see Table 1. Mass spectrum showed molecular ion at *m/e* = 182.1095 (24%). *Anal.* found: C 92.12, H 7.88.

Compound **24** (20.6 mg) was also obtained as a colourless oil after short-path distillation at 60°C/0.1 Torr (GC-2 purity > 98%); uv:266 sh (1160), 273 (1070), and 282 (860); $^1$Hmr, see Table 1. Mass spectrum showed molecular ion at *m/e* = 182.1093 (95%).

*Direct irradiation of SB* ***14***

A stirred solution of 121.2 mg (0.67 mmol) of **14** in 250 mL of cyclohexane was irradiated in apparatus I for 30 min. The photolysate was concentrated and the residue chromatographed on Silicar (100 × 2 cm) with cyclohexane solvent. The first 200 mL of eluent was discarded, and thereafter 5 mL fractions were collected: fractions 10–20 contained 26.5 mg (22%) of an oily mixture of 2,3-benzo-5-methyl-6-methylenebicyclo[3.3.0]-octa-2,7-diene (**17**) and **14**, in the ratio of 11 : 1, respectively (GC-2 analysis); fractions 21–53 contained 76.7 mg (63%) of a mixture of **14** and **17** in the ratio of 8 : 1, respectively. The contents of fractions 10–20 were separated by preparative gc (OV-101, 180°C) and short-path distilled at 60°C/0.1 Torr to give 15.2 mg of **17** as a colourless oil (GC-2 purity > 98%), **17** being eluted after **14**.

For **17**: ir (film): 1635 conj. C=C, and 880 C=$CH_2$; uv: 237 (11200), 265 sh (1200), 267 (1440), and 273 (1600); $^1$Hmr (400 MHz, $CDCl_3$): 7.14–7.25 (m, 4H, aromatics), 6.17–6.21 (m, 1H, H-8), 6.12–6.15 (broad d × d, 1H, H-7, $J_{7,1}$ = 1.8, $J_{7,8}$ = 5.5), 4.97 (broad s, 1H, H-9), 4.87 (broad s, 1H, H-9'), 3.98 (broad s, 1H, H-1), 3.13 (d, 1H, H-4, $J_{4,4'}$ = 16.5), 3.01 (d, 1H, H-4', $J_{4',4}$ = 16.5), and 1.39 (s, 3H, methyl); spin decoupling experiments: irradiation of H-1 modified H-8 (d of m, $J_{7,8}$ = 5.5), H-7 (broad d, $J_{7,8}$ = 5.5), H-9, and H-9'; irradiation of H-9 modified H-8 (d × q, $J_{7,8}$ = 5.5, $J_{1,8}$ = 2.7, and $J_{8,9'}$ = 1.4), H-7 (d × q, $J_{7,8}$ = 5.5, $J_{1,7}$ = 1.8, $J_{7,9'}$ = 0.7), H-9' and H-1; irradiation of H-9' modified H-8 (d × q, $J_{1,8}$ = 2.7, $J_{7,8}$ = 5.5, $J_{8,9}$ ≃ 0.5), H-7 (d × d, $J_{1,7}$ = 1.8, $J_{7,8}$ = 5.5, $J_{7,9}$ < 0.5), H-9 and H-1. Mass spectrum showed molecular ion at *m/e* = 182.1093 (95%). *Anal.* found: C 92.41, H 7.79.

*Sensitized irradiation of SB* ***14***

A stirred solution of 134.3 mg (0.74 mmol) of **14** in 250 mL of chlorobenzene was irradiated in apparatus I for 10 min. The photolysate was concentrated and the residue chromatographed on Silica Gel 60 (90 × 2 cm) with cyclohexane; the first 700 mL of eluent was discarded and thereafter 10 mL fractions were collected. Fractions 11–18 contained 9.7 mg (7%; GC-2 purity 98%) of colourless oil identical (GC-2, nmr, ir) to **17**; fractions 19–35 contained 104.8 mg (78%) of recovered **14** (GC-2 purity 97%).

*Catalytic reduction of SB* ***14***

A stirred mixture of 57.6 mg (0.32 mmol) of **14** and 28.4 mg of 10% Pd on C in 6 mL of methanol was hydrogenated at room temperature and pressure during 24 h. The catalyst was removed (centrifuge) and the resulting solution concentrated to give 56.9 mg of oil, gc (Carbowax, 160°C) analysis of which showed four peaks, eluted in the order: unidentified product (1%), **29** (9%), **30** (65%), and **31** (25%). The three major components of the oil were separated by preparative gc (Carbowax) giving 2.2 mg (4%) of **29**, 16.9 mg (29%) of **30**, and 7.7 mg (13%) of **31**, each being a colourless oil of GC-2 purity > 98%.

For **29**: uv: 212 (9250), 217 (8050), 247 sh (275), 254 sh (465), 261 (870), 265 sh (1100), 267 (1500), and 273 (1900); $^1$Hmr (400 MHz, $CDCl_3$): 7.07–7.18 (m, 4H, aromatics), 3.14 (q, 1H, H-1, *J* = 10.5 and 2.3), 2.98 (d, 1H, H-4, $J_{4,4'}$ = 16.5), 2.38 (d, 1H, H-4', $J_{4',4}$ = 16.5), 1.95–2.05 (m, 1H, H-8), 1.70–1.78 (m, 1H, H-6), 1.62–1.70 (m, 1H, H-7), 1.54–1.60 (m, 1H, H-8'), 1.14–1.26 and 1.17 (m and s, 4H, H-7' and C5-methyl), and 0.99 (d, 1H, C6-methyl, $J_{Me,6}$ = 7.0); spin decoupling experiments: irradiation of H-1 modified H-8 and H-8'; irradiation of H-4 collapsed H-4' to an s; irradiation of H-8 collapsed H-1 to a broad s and modified H-8', H-7, and H-7'; irradiation of H-6 collapsed the C6-methyl to an s and modified H-7 and H-7'; irradiation of H-7 modified H-6, -7', -8, and -8'; irradiation of H-8' collapsed H-1 to a d (*J* = 10.5), and modified H-7, -7', and -8; irradiation of H-7' modified H-6, -7, -8, and -8'; irradiation of C6-methyl collapsed H-6 to a q (*J* = 6 and 11). Mass spectrum showed molecular ion at *m/e* = 186.1412 (100%), $C_{14}H_{18}$ requires 186.1409.

For **30**: uv: 212 (8750), 216 (7550), 248 sh (220), 254 sh (440), 261 (810), 265 sh (1050), 267 (1360), and 273 (1720); $^1$Hmr (400 MHz, $CDCl_3$): 7.09–7.18 (m, 4H, aromatics), 3.21 (q, 1H, H-1, *J* = 10.0 and 4.0), 2.85 (d, 1H, H-4, $J_{4,4'}$ = 16.5), 2.73 (d, 1H, H-4', $J_{4',4}$ = 16.5), 2.21–2.31 (m, 1H, H-8), 1.70–1.79 (m, 1H, H-7), 1.60–1.70 (m, 2H, H-8' and H-8), 1.41–1.50 (m, 1H, H-7'), 1.07 (s, 3H, C5-methyl), and 0.95 (d, 3H, C6-methyl, $J_{Me,6}$ = 7.0); spin decoupling experiments: irradiation of H-1 modified H-8 and the overlapping H-6 and H-8' m's; irradiation of H-8 collapsed H-1 to a broad s, and modified H-7, H-7', and the overlapping H-6 and H-8' m's; irradiation of H-7' modified H-7, H-8, and the overlapping H-6 and H-8' m's; irradiation of the C6-methyl modified the overlapping H-6 and H-8' m's; $^1$Hmr (400 MHz, $C_6D_6$): 7.04–7.18 (m, 4H, aromatics), 3.07 (q, 1H, H-1, *J* = 10.0 and 3.5), 2.72 (d, 1H, H-4, $J_{4,4'}$ = 16.5), 2.57

Can. J. Chem. Downloaded from www.nrcresearchpress.com by 210.87.254.5 on 09/06/12
For personal use only.

(d, 1H, H-4', $J_{4',4}$ = 16.5), 2.07–2.16 (m, 1H, H-8), 1.56–1.66 (m, 2H, H-7 and H-8'), 1.47–1.56 (m, 1H, H-6), 1.27–1.37 (m, 1H, H-7'), 0.90 (s, 3H, C5-methyl), and 0.82 (d, 3H, C6-methyl, $J_{Me,6}$ = 7.0); spin decoupling experiments: irradiation of H-1 modified H-8 and the overlapping H-7 and H-8' m's; irradiation of H-8 collapsed H-1 to a broad s, and modified the overlapping H-7 and H-8' m's and H-7'; irradiation of H-7' modified H-6, H-8, and the overlapping H-7 and H-8' m's; irradiation of the C6-methyl collapsed H-6 to a q ($J$ = 11.0 and 6.0). Mass spectrum showed molecular ion at $m/e$ = 186.1410 (100%). *Anal.* calcd. for $C_{14}H_{18}$: C 90.26, H 9.74; found: C 90.08, H 9.93.

For **31**: uv: 213 (8700), 216 sh (7800), 249 sh (150), 254 sh (270), 259 (470), 262 (470), 266 (730), and 273 (900); $^1$Hmr (400 MHz, $CDCl_3$): 6.94–7.10 (m, 4H, aromatics), 2.90 (d, 1H, H-4, $J_{4,4'}$ = 16.5), 2.72 (d, 1H, H-1, $J_{1,7}$ = 6.5), 2.67 (d, 1H, H-4', $J_{4',4}$ = 16.5), 2.12–2.22 (m, 1H, H-7), 1.86 (q, 1H, H-8, $J_{8,Me}$ = 7.0), 1.52–1.68 (m, 3H, H-6, H-6' and H-7'), 1.12 (s, 3H, C5-methyl), and 0.98 (d, 3H, C8-methyl, $J_{Me,8}$ = 7.0); spin decoupling experiments: irradiation of the C8-methyl collapsed H-8 to an s; irradiation of H-7 collapsed H-1 to an s and modified the overlapping H-6, H-6', and H-7' m's; irradiation of H-4 collapsed H-4' to an s. Mass spectrum showed molecular ion at $m/e$ = 186.1407 (100%).

*Catalytic reduction of diene* ***17***

A stirred mixture of 13.0 mg (0.07 mmol) of **17** and 11.7 mg of 10% Pd on C in 5 mL of methanol was hydrogenated at room temperature and pressure during 4 h. The catalyst was removed (centrifuge) and the resulting solution concentrated to give 12.3 mg of an oil, gc (Carbowax, 160°C) analysis of which showed two peaks of relative area 1 (**29**) : 4 (**30**). Preparative gc separation gave 1.6 mg (12%) of colourless oil identical (gc, $^1$Hmr, ir) to **29**, and 6.2 mg (47%) of colourless oil identical (gc, $^1$Hmr, ir) to **30**.

*Diimide reduction of SB* ***14***

To a stirred mixture of 97.6 mg (0.54 mmol) of **14** and 1.0 g (5.16 mmol) of potassium azodicarboxylate in 20 mL of methanol at −30°C, 2 mL of acetic acid was added in one portion. The reaction mixture was allowed to warm to room temperature during 1.25 h after which time the solution was added to 200 mL of cyclohexane and was washed with 5% aqueous sodium hydroxide (200 mL) followed by water (2 × 200 mL). The cyclohexane solution was dried ($MgSO_4$), concentrated, and the residue column chromatographed on Silicar (35 × 2 cm) with cyclohexane solvent. The contents of the first band were short-path distilled (80°C/0.1 Torr) to give 72.4 mg (73%) of 3,4-benzo-1,8-dimethyltricyclo[3.3.0.$0^{2,8}$]oct-3-ene (**32**) as a colourless oil (GC-2 purity > 97%); uv: 229 (4350), 261 sh (470), 268 sh (790), 273 (1070), and 281.5 (1100); $^1$Hmr (400 MHz, $CDCl_3$): 6.95–7.18 (m, 4H, aromatics), 3.28 (broad d, 1H, H-5, $J_{5,6}$ = 5.5), 2.10–2.19 (m, 1H, H-6), 1.86 (s, 1H, H-2), 1.57 (d × q, 1H, H-6', $J_{6',5}$ = 1.5, $J_{6',6}$ = 12.0, $J_{6',7}$ = 8.5, $J_{6',7'} \simeq 0$), 1.37–1.50 and 1.39 (m and s, 5H, H-7, H-7', and methyl), and 1.24 (s, 3H, methyl); spin decoupling experiments: irradiation of H-5 collapsed H-6 to six lines (1;1;2;2;1;1; $J$ = 12.0, $J$ = 11.0, $J$ = 9.0) and H-6' to a q ($J$ = 12 and 8.5); irradiation of H-6 collapsed H-5 to a d ($J_{5,6'}$ = 1.5) and modified the overlapping H-7 and H-7' m's, and H-6' (incomplete decoupling). Mass spectrum showed molecular ion at $m/e$ = 184.1248 (26%), $C_{14}H_{16}$ requires 184.1253. *Anal.* calcd. for $C_{14}H_{16}$: C 91.25, H 8.75; found: C 91.49, H 8.51.

*Catalytic reduction of* ***32***

A stirred mixture of 47.3 mg (0.26 mmol) of **32** and 28.8 mg of 10% Pd on C in 8 mL of methanol was hydrogenated at room temperature and pressure during 24 h. The catalyst was removed (centrifuge) and the solution concentrated to give 42.3 mg of an oil, gc (Carbowax, 160°C) analysis of which showed the same four peaks as in the case of the catalytic reduction of **14**, the relative areas being 1 (unknown) : 1 (**29**) : 52 (**30**) : 46 (**31**). Preparative gc separation of the two major components followed by short-path distillation gave 15.7 mg (33%) of an oil identical (gc, $^1$Hmr, ir) to **30**, and 10.2 mg (22%) of an oil identical (gc, $^1$Hmr, ir) to **31**.

*Gas phase thermolysis of* ***14***

Over a 1 h period 94.4 mg (0.52 mmol) of **14** was sublimed into a Pyrex tube (30 × 2 cm) packed with glass beads (0.5 cm diameter) maintained at 420°C. The pressure in the system was kept at 6 Torr by the passage of nitrogen. The thermolysis product was collected in a cooled U-trap (Dry Ice – acetone) to give 92.6 mg of an oil, GC-2 analysis of which showed three major peaks, eluted in the order and ratio of 1 (**14**) : 8 (**15**) : 2 (**36**). The oil was chromatographed on Silica Gel 60 (90 × 2 cm) with cyclohexane solvent. The first 300 mL of eluent was discarded, and thereafter 10 mL fractions were collected: fractions 3–8 gave 12.4 mg (13%) of 2,3-benzo-7,8-dimethylbicyclo[4.2.0]-octa-2,4,7-triene (**36**) as a colourless oil after short-path distillation at 55°C/0.1 Torr (GC-2 purity 100%); uv: 273 (5650), 283 (5200), 290 sh (3250), 295 sh (2400), and 303 (1400); $^1$Hmr (400 MHz, $CDCl_3$): 6.95–7.13 (m, 4H, aromatics), 6.22 (d, 1H, H-4, $J_{4,5}$ = 10), 5.94 (q, 1H, H-5, $J_{5,4}$ = 10, $J_{5,6}$ = 4.5), 3.76 (broad s, 1H, H-1, $J_{1,6}$ = 4.5, $J_{1,C8\text{-}Me} \simeq$ 1.0), 3.43 (broad s, 1H, H-6, $J_{6,5}$ = $J_{6,1}$ = 4.5, $J_{6,C7\text{-}Me} \simeq$ 1.0), 1.65 (broad s, 3H, C8-methyl), and 1.55 (broad s, 3H, C7-methyl); spin decoupling experiments: irradiation of H-5 collapsed H-4 to an s; irradiation of H-1 modified both methyls; irradiation of H-6 collapsed H-5 to a d ($J_{4,5}$ = 10) and both methyl signals were modified; irradiation of the C8-methyl collapsed H-1 to a d ($J_{1,6}$ = 4.5) and modified the C7-methyl; irradiation of the C7-methyl collapsed H-6 to a t ($J_{1,6}$ = $J_{5,6}$ = 4.5) and modified the C8-methyl. Mass spectrum showed molecular ion at $m/e$ = 182.1093 (100%); fragmentation peak at 128 (76%) corresponding to the loss of dimethylacetylene from molecular ion.

Fractions 10–19 gave, after short-path distillation (55°C/0.1 Torr), 56.2 mg (60%) of 6,7-dimethylbenzocyclooctatetraene (**15**) as a colourless oil (GC-2 purity 98%); uv: 228 (19000), 268 sh (1550), and 280 sh (1350); $^1$Hmr (200 MHz, $CDCl_3$): 6.95–7.22 (m, 4H, aromatics), 6.52 (broad d, 1H, H-10, $J_{10,9}$ = 11.5, $J_{10,8}$ = 0.6), 6.28 (broad q, 1H, H-5, $J_{5,C6\text{-}Me}$ = 1.5), 6.03 (d × m, 1H, H-9, $J_{9,10}$ = 11.5, $J_{9,8}$ = 3.6, $J_{9,C7\text{-}Me}$ = 1.5), 5.53–5.59 (m, 1H, H-8, $J_{8,9}$ = 3.6, $J_{8,C7\text{-}Me}$ = 1.5, $J_{8,10}$ = 0.6), 1.94 (d, 3H, C6-methyl, $J_{C6\text{-}Me,5}$ = 1.5), and 1.78 (t, 3H, C7-methyl, $J_{C7\text{-}Me,8}$ = $J_{C7\text{-}Me,9}$ = 1.5); spin decoupling experiments: irradiation of H-9 collapsed H-10 to a broad s, the C7-methyl to a d ($J_{8,C7\text{-}Me}$ = 1.5), and modified H-8; irradiation of H-10 collapsed H-9 to a single m and modified H-8; irradiation of H-5 collapsed the C6-methyl to an s; irradiation of H-8 collapsed the C7-methyl to a d ($J_{9,C7\text{-}Me}$ = 1.5) and modified H-10 to a sharp d ($J_{9,10}$ = 11.5) and H-9 to a d × q ($J_{9,10}$ = 11.5, $J_{9,C7\text{-}Me}$ = 1.5); irradiation of the C6-methyl collapsed H-5 to an s; irradiation of the C7-methyl collapsed both H-9 to a d × d ($J_{9,10}$ = 11.5, $J_{8,9}$ = 3.6) and H-8 to a d × d ($J_{8,9}$ = 3.6, $J_{8,10}$ = 0.6). Mass spectrum showed molecular ion at $m/e$ = 182.1093 (98%).

*Direct irradiation of COT* ***15***

A stirred solution of 72.3 mg (0.40 mmol) of **15** in 250 mL of cyclohexane was irradiated in apparatus I for 12 min. The photolysate which contained two components in the ratio of 1 (**36**) : 8.5 (**15**) (GC-2 analysis) was concentrated *in vacuo* and the residue chromatographed on Silica Gel 60 (90 × 2 cm) with cyclohexane solvent. The first band off the column gave, after short-path distillation (55°C/0.1 Torr), 4.7 mg (6.5%) of an oil, identical to **36**. The second band gave 57.2 mg (79%) of recovered **15**.

Can. J. Chem. Downloaded from www.nrcresearchpress.com by 210.87.254.5 on 09/06/12
For personal use only.

*Sensitized irradiation of COT 15*

Because of extensive direct light absorption by **15** at wavelengths greater than 300 nm when neat chlorobenzene was used as sensitizer, the monochromator preparative apparatus II was used.

A solution of 47.1 mg (0.26 mmol) of **15** in 15 mL of chlorobenzene was photolysed for a total of 48 h with the monochromator settings of $\lambda$ = 275 nm, input slit = 2.5 mm, and bandwidth = 10 nm. The photolysate was concentrated and the residue was worked up as in the case of the direct irradiation of COT **15** to give 3.1 mg (7%) of an oil identical to **36** and 30.9 mg (66%) of recovered **15**.

*Sensitized photolysis of barrelene 37*

A stirred solution of 137.0 mg (0.75 mmol) of **37** and 2.5 g of acetophenone in 250 mL of cyclohexane was irradiated in apparatus I for 30 min. The photolysate was concentrated and the residue chromatographed on Silicar (50 × 2.5 cm) with cyclohexane. The first band contained 123.4 mg (90%) of an oily mixture of 1,6-dimethylbenzotricyclo[3.3.0.$0^{2,8}$]octa-3,6-diene (**16**) and an unidentified compound in the ratio of 5.5 : 1.0, respectively (GC-2 analysis). The first major band eluted from preparative gc (OV-101, 170°C) of the oil gave, after short-path distillation at 60°C/0.1 Torr, 82.7 mg of **16** as a colourless oil (GC-2 purity > 98%); ir (film): 815 trisubstituted alkene; uv: 268 sh (910), 274.5 (1 030), and 282 (860); $^1$Hmr, see Table 1. Mass spectrum showed molecular ion at $m/e$ = 182.1098 (77%).

*Gas phase thermolsis of 16*

Over a 1.5 h period, 85.0 mg (0.47 mmol) of **16** was thermolysed at 395°C and at 6 Torr of nitrogen in the apparatus described above for the gas phase thermolysis of **14**. An oil (82.3 mg) was obtained, GC-2 analysis of which showed two major components, eluted in the order and ratio of 1.5 (**16**) : 1.0 (**39**). The oil was separated by preparative gc (OV-101, 180°C) to give 32.9 mg (39%) of recovered **16**, and, after short-path distillation at 70°C/0.1 Torr, 19.6 mg (23%) of 6,9-dimethylbenzocyclooctatetraene (**39**) of GC-2 purity 100%; uv: 234.5 (19 000), 273 sh (1 300), and 283 sh (1 000); $^1$Hmr (60 MHz, $CCl_4$): 6.62–7.12 (m, 4H, aromatics), 6.21 (broad s, 2H, H-5(10)), 5.62 (s, 2H, H-7(8)), and 1.82 (d, 6H, methyls, $J_{5(10),Me}$ = 1.5); spin decoupling experiments: irradiation of the methyl doublet modified H-5(10) to a sharp s. Mass spectrum showed molecular ion at $m/e$ = 182.1094 (93%).

*Direct irradiation of SB 16*

A stirred solution of 78.3 mg (0.43 mmol) of **16** in 250 mL of cyclohexane was irradiated in apparatus I for 1.5 h. The photolysate, which contained two components in the ratio of 1 (**39**) : 6 (**16**) (GC-2 analysis) was concentrated *in vacuo*, passed down a short column of Silicar with cyclohexane solvent to remove polymeric material, and then separated by preparative gc (OV-101, 180°C). The first component gave 29.7 mg (38%) of recovered **16**, while the second gave 3.9 mg (5%) of an oil identical to **39**.

*Sensitized irradiation of SB 16*

A solution of 61.3 mg (0.34 mmol) of **16** in 15 mL of chlorobenzene was photolysed for a total of 72 h in apparatus II, with monochromator settings of $\lambda$ = 275 nm, input slit = 2.5 mm, and bandwidth = 10 nm. The progress of photolysis was followed by GC-2 analysis which revealed the buildup of a product eluting from the column as an after shoulder on the starting material (**16**) peak. The photolysis was stopped when the ratio of **16** to unknown product was 5 : 1. The photolysate was then concentrated *in vacuo* and the residue chromatographed on Silicar (75 × 1.5 cm) with cyclohexane solvent; no separation of the unknown photoproduct from **16** was apparent from GC-2 analysis of eluent fractions. Those fractions containing **16** and the unknown were combined and short-path distilled (65°C/0.1 Torr) to give 24 mg of colourless oil. The $^1$Hmr (400 MHz) spectrum of the oil contained no peaks characteristic of **17**. Preparative gc on Carbowax or on OV-101 columns provided no separation of the oil into its components.

*Quantum yield determinations*

Quantum yields were performed on an optical bench using the light source and monochromator system described for the preparative photolysis apparatus II. Attached to the exit slit of the monochromator was a black aluminum housing within which a portion of the radiation was reflected by a thin quartz beam splitter onto a 4 mL cylindrical quartz cell containing ferrioxalate actinometer (15), while the main radiation beam entered a 4 mL cylindrical cell containing the sample solution. Beam splitter ratios at 275 nm and at 313 nm were determined by placing actinometer solutions in both cells. Sample solutions at concentrations of ca. $2 \times 10^{-3} M$ were deoxygenated prior to irradiation by flushing with argon. A positive pressure of argon was maintained over the stirred solutions throughout the course of the irradiations. For further experimental details see Table 2.

*Quenching experiments*

Sample solutions of $5 \times 10^{-3} M$ **14** in cyclohexane in the presence of 0 to $0.5 \times 10^{-2} M$ 2,5-dimethyl-2,4-hexadiene (with argon flushing of solutions) or oxygen at ca. $10^{-2} M$ concentration were irradiated in a turntable reactor with Corex-filtered light provided by a 450 W Hanovia medium pressure mercury arc. The product formation (**17**) was determined by GC-2 analysis with *n*-pentadecane as internal standard. Quenching was discernible only in the case when oxygen was the quencher, to the extent of ca. 5 ± 3%.

*Calculations*

Although the calculations were performed as previously described (2, 23), two points require comment. Attempts to optimize the geometry of SB **14** led to unsatisfactory results, because the bridgehead angle, C4—C5—C6, closed to unreasonably small values. This is due to a well-known deficiency in the CNDO (and INDO) method, and results from the use of a single coulomb integral to represent the interaction between electrons on different atoms; by making the interaction between electrons in *p* orbitals the same as the interactions between electrons in *s* orbitals, the balance between $\sigma$ and $\pi$ type interactions is lost. In the present case the interaction between the unsaturated centres at C4 and C6 is overstabilized, causing the angle to be reduced at the bridgehead. To overcome this problem, the C4—C5—C6 angle was fixed at 101.3°, the value determined by X-ray techniques for 1-cyanosemibullvalene (22), and the remainder of the structure optimized. The other aspect requiring discussion is the conformation of the methyl groups in **14**. Because of their positions on the cyclopropyl ring, there is some possibility that they might influence the position at which the ring opens. However, a series of calculations for varying conformations shows clearly that the methyl groups influence neither the pattern of changes in the atom–atom energies nor the excitation energies. The data in Table 3 refer to a near optimum conformation of the methyl groups.

## Acknowledgements

The authors thank the Spectroscopic Services Laboratory of the University of Alberta for the 200 and 400 MHz $^1$Hmr and mass spectra, and the University of Lethbridge Computing Centre for the use of the DEC-20 system computer. Financial

support from the Natural Sciences and Engineering Research Council of Canada and The University of Lethbridge Research Committee is gratefully acknowledged.

1. C. O. BENDER, J. L. M. ELDER, A. J. HERBST, and L. E. MILLER. Can. J. Chem. **50**, 395 (1972).
2. C. O. BENDER, D. W. BROOKS, W. CHENG, D. DOLMAN, S. F. O'SHEA and S. S. SHUGARMAN. Can. J. Chem. **56**, 3027 (1978).
3. C. O. BENDER and H. D. BURGESS. Can. J. Chem. **51**, 3486 (1973).
4. M. DEMUTH, W. AMREIN, C. O. BENDER, S. E. BRASLAVSKY, U. BURGER, M. V. GEORGE, D. LEMMER, and K. SCHAFFNER. Tetrahedron, **37**, 3245 (1981).
5. C. O. BENDER and J. WILSON. Helv. Chim. Acta, **59**, 1469 (1976).
6. S. S. HIXSON. In Organic photochemistry. Vol. 4. *Edited by* A. Padwa. Marcel Dekker, Inc., New York and Basel. 1979. pp. 191–260.
7. J. MEINWALD and D. A. SEELEY. Tetrahedron Lett. 3739 (1970); 3743 (1970).
8. L. ULRICH, H.-J. HANSEN, and H. SCHMID. Helv. Chim. Acta, **53**, 1323 (1970).
9. H. E. ZIMMERMAN, R. S. GIVENS, and R. M. PAGNI. J. Am. Chem. Soc. **90**, 6096 (1968).
10. I. N. NAZAROV and N. V. KUZNETSOV. J. Gen. Chem. (U.S.S.R.), 754 (1959).
11. T. C. SHIELDS, W. E. BILLUPS, and A. R. LEPLEY. J. Am. Chem. Soc. **90**, 4749 (1968).
12. J. B. LAMBERT, H. R. SHURVELL, L. VERBIT, R. G. COOKS, and G. H. STOUT. Organic structural analysis. MacMillan Publishing Co., Inc., New York. 1976. pp. 74–75.
13. L. A. PAQUETTE, M. OKU, W. E. HEYD, and R. H. MEISINGER. J. Am. Chem. Soc. **96**, 5815 (1974).
14. L. A. PAQUETTE, J. M. PHOTIS, and R. P. MITCHELI. J. Am. Chem. Soc. **99**, 7899 (1977).
15. W. D. BOWMAN and J. N. DEMAS. J. Phys. Chem. **80**, 2434 (1976).
16. H. E. ZIMMERMAN and G. E. SAMUELSON. J. Am. Chem. Soc. **91**, 5307 (1969).
17. M.-A. FOX, W. C. NICOLS, JR., and D. M. LEMAL. J. Am. Chem. Soc. **95**, 8164 (1973).
18. N. J. BUNCE, J. P. BERGSMA, M. D. BERGSMA, W. DE GRAAF, Y. KUMAR, and L. RAVANAL. J. Org. Chem. **45**, 3708 (1980).
19. H. E. ZIMMERMAN. J. Am. Chem. Soc. **88**, 1565 (1966); **88**, 1566 (1966); Acc. Chem. Res. **4**, 272 (1972).
20. R. B. WOODWARD and R. HOFFMANN. The conservation of orbital symmetry. Verlag Chemie, Weinheim and Academic Press, New York. 1970.
21. J. DEL BENE and H. H. JAFFÉ. J. Chem. Phys. **48**, 1807 (1968); **48**, 4050 (1968); **49**, 1221 (1968); **50**, 1126 (1969).
22. L. A. PAQUETTE, W. E. VOLZ, M. A. BENO, and G. G. CHRISTOPH. J. Am. Chem. Soc. **97**, 2562 (1975).
23. C. O. BENDER and S. F. O'SHEA. Can. J. Chem. **57**, 2804 (1979).

Can. J. Chem. Downloaded from www.nrcresearchpress.com by 210.87.254.5 on 09/06/12
For personal use only.

# Enthalpies of interaction of polar and nonpolar molecules with aromatic solvents

RICHARD FUCHS, L. ALAN PEACOCK, AND W. KIRK STEPHENSON
*Department of Chemistry, University of Houston, Houston, TX 77004, U.S.A.*

Received February 9, 1982

RICHARD FUCHS, L. ALAN PEACOCK, and W. KIRK STEPHENSON. Can. J. Chem. **60**, 1953 (1982).

Enthalpies of solution of representative ketones, phenols, alcohols, and ethers have been determined in α,α,α-trifluorotoluene, benzene, toluene, and mesitylene, and combined with heats of vaporization to give enthalpies of transfer from vapor to the aromatic solvents [$\Delta H(v \rightarrow S)$]. Comparison of these values with $\Delta H(v \rightarrow S)$ of nonpolar model compounds provides an estimate of the special interactions (dipole – induced dipole or charge transfer, and hydrogen bonding) of the polar solutes with each aromatic solvent. Unless the model compound is perfectly matched, an alternative procedure, the pure base method, is superior for evaluating hydrogen bonding.

The special interactions of ketones and ethers with aromatic solvents increase with decreasing π electron density of the solvent. By contrast, *m*-cresol shows the strongest special interaction with the most electron-rich solvent (mesitylene > toluene > benzene > trifluorotoluene). These results demonstrate that —OH and —OR groups undergo quite different interactions, and that a distinctive interaction occurs between the hydroxyl group and the aromatic ring.

Calorimetric heats of vaporization have been measured for the solutes *n*-butyl ether (10.68 ± 0.02 kcal/mol), 2,2,4,4-tetramethylpentane (9.20 ± 0.03), *n*-pentane (6.36 ± 0.02), 1-butanol (12.46 ± 0.00), and 2-methyl-2-butanol (11.94 ± 0.02).

RICHARD FUCHS, L. ALAN PEACOCK et W. KIRK STEPHENSON. Can. J. Chem. **60**, 1953 (1982).

On a déterminé les enthalpies de solutions de cétones, de phénols, d'alcools et d'éthers représentatifs dans le α,α,α-trifluorotoluène, le benzène, le toluène et le mésytilène et on les a combinées aux chaleurs de vaporisation pour obtenir les enthalpies de transfert de la phase vapeur aux solvants aromatiques [$\Delta H(v \rightarrow S)$]. La comparaison de ces valeurs avec le $\Delta H(v \rightarrow S)$ de composés modèles non polaires fournit une évaluation des interactions spéciales (dipôle-dipôle induit ou transfert de charge, et liaison hydrogène) des solutés polaires avec chaque solvant aromatique. A moins que le composé modèle corresponde parfaitement, une méthode alternative, la méthode de base pure, est de loin la meilleure pour évaluer la liaison hydrogène. Les interactions spéciales des cétones et des éthers avec les solvants aromatiques augmentent lorsque diminue la densité des électrons π du solvant. Au contraire, le *m*-crésol montre les interactions spéciales les plus fortes avec les solvants les plus riches en électrons (mésitylène > toluène > benzène > trifluorotoluène). Ces résultats démontrent que les groupes OH et OR subissent des interactions très différentes et qu'une interaction distincte se produit entre le groupe hydroxyle et le cycle aromatique.

On a mesuré par calorimétrie les chaleurs de vaporisation des solutés: éther *n*-butylique (10,68 ± 0,02 kcal/mol), tétraméthyl-2,2,4,4 pentane (9,20 ± 0,03), *n*-pentane (6,36 ± 0,02), butanol-1 (12,46 ± 0,00) et méthyl-2 butanol-2 (11,94 ± 0,02).

[Traduit par le journal]

Hydrogen bonding of phenols to aromatic hydrocarbons is a phenomenon which has been examined by infrared spectroscopy and by the calorimetric pure base method (1). Calorimetric measurements of these weak interactions at *high dilution* in an inert solvent are essentially useless because the H-bond donor and acceptor are incompletely complexed, but this is not a problem in the pure base method (1, 2). Ordinarily, hydrogen bonding occurs to a nonbonding (n) electron pair of an electronegative element, but with benzene the π electron system is involved (3). Electron-releasing substituents should increase the ring π electron density, and make the substituted benzene a stronger H-bond acceptor. Conversely, electron attracting substituents should decrease the strength of H-bond formation, provided that the substituent itself lacks n electrons which are strongly H-bond accepting.

In studies by the pure base method, Arnett *et al.* (1) found the enthalpy of H-bond formation ($\Delta H_f$) of phenol and *p*-fluorophenol with aromatic hydrocarbons becomes more exothermic (favorable) in the order benzene < toluene < mesitylene. Here $\Delta H_f$ represents the interactions of phenol with the aromatic base, less the interactions of the non-hydrogen-bonding model compound, anisole, with the same base. It appeared possible to us that the trend in $\Delta H_f$ might reflect increasing steric hindrance to the approach of the model compound, rather than a true trend in H-bond acceptor strength. Furthermore, there is almost no variation of $\Delta H_f$ for 1-butanol (vs. 1-chlorobutane) with the same aromatic solvents, and this also seemed worthy of additional investigation.

We have chosen to examine the bases benzene, toluene, mesitylene, and α,α,α-trifluorotoluene (benzotrifluoride). The latter is nearly ideal for several reasons. (*a*) The $CF_3$ group is substantially electron attracting, but is not appreciably basic nor H-bond accepting. (*b*) Although benzotrifluoride has a dipole moment of about 2.6 D (4), there is little evidence from the boiling point (102°C), heat of vaporization (8.98 kcal/mol (5)) (1 kcal = 4.184 kJ), or cohesive energy density (68.3 cal/cm$^3$) that ap-

0008-4042/82/151953-06$01.00/0
©1982 National Research Council of Canada/Conseil national de recherches du Canada

Can. J. Chem. Downloaded from www.nrcresearchpress.com by 210.87.254.105 on 09/06/12
For personal use only.

Can. J. Chem. Downloaded from www.nrcresearchpress.com by 210.87.254.105 on 09/06/12
For personal use only.

preciable dipole–dipole association occurs in the liquid. (The corresponding values for toluene are 110.6°C, 9.08 kcal/mol, and 79.9 cal/cm$^3$.) (*c*) The $CF_3$ group is larger than methyl, but the benzotrifluoride ring is more electron-deficient than that of benzene. This will permit us to distinguish between steric and electronic effects on H-bonding.

The interactions of ketones with cyclohexane, benzene, methanol, and *N*,*N*-dimethylformamide have previously been examined calorimetrically (6), and the acetone–benzene system has been studied by nmr (7). The interactions of polar ketones and ethers with the essentially nonpolar aromatic solvents may be charge-transfer complexation or dipole – induced dipole forces.

Our previous approach has been somewhat different from the pure base method. We have calculated enthalpies of transfer from vapor to solvent for each solute:

$$[1] \quad \Delta H(v \rightarrow S) = \Delta H_s - \Delta H_v$$

where $\Delta H_s$ is the enthalpy of solution of a dilute ($10^{-3}$–$10^{-2}$ *M*) liquid sample in the solvent at 25°C, and $\Delta H_v$ is the solute heat of vaporization at 25°C. The assumption is made that the more exothermic value of $\Delta H(v \rightarrow S)$ for a hydrogen bond donor, relative to the value for a comparably polar nondonor model compound, can be attributed entirely to the enthalpy of hydrogen bond formation. Similarly, the enthalpy of polar interaction ($\Delta H_p$) of a polar solute incapable of H-bond donation (ketones, ethers) is taken as the difference in $\Delta H(v \rightarrow S)$ vs. that of a nonpolar model compound (hydrocarbon) ($\Delta\Delta H(v \rightarrow S)$ method).

In the pure base method (1) hydrogen bonding enthalpy is evaluated in a basic solvent with reference to a nonpolar solvent incapable of H-bonding ($CCl_4$):

$$[2] \quad \Delta H_f = (\Delta H_s^A - \Delta H_s^M)_B - (\Delta H_s^A - \Delta H_s^M)_{ref}$$

where A is the H-bond donating solute, M is the model compound, B is a basic (H-bond acceptor) solvent, and ref is the reference solvent. Using eq. [1] the above equation can be equated to:

$$[3] \quad \Delta H_f = (\Delta H^A(v \rightarrow B) - \Delta H^M(v \rightarrow B)) - (\Delta H^A(v \rightarrow ref) - \Delta H^M(v \rightarrow ref))$$

The two methods of evaluating $\Delta H_f$ will be equivalent *only* when $\Delta H^A(v \rightarrow ref) - \Delta H^M(v \rightarrow ref) = 0$. We will compare results by the two methods, and attempt to evaluate the characteristics of appropriate model compounds.

The required values of $\Delta H_v$ for calculation of $\Delta H(v \rightarrow S)$ are available (5, 8), except for di-*n*-butyl ether. This was measured using a recently developed vaporization calorimetry technique (9). Values for 2,2,4,4-tetramethylpentane, *n*-pentane, 1-butanol, and 2-methyl-2-butanol (for which only an estimate was available) were redetermined.

## Experimental

Solutes and solvents were commercial samples in excess of 99% purity, and dried over 4A molecular sieve. Heat of vaporization samples were di-*n*-butyl ether (99.85%), 2,2,4,4-tetramethylpentane (99.98%), *n*-pentane (99.9%), 1-butanol (99.92%), and 2-methyl-2-butanol (99.75%). Purities were established by gas chromatography using a Shimadzu Mini 2 gc with a glass lined system, a 30 m × 0.25 mm id SE-30 silica capillary column, and a Hewlett-Packard 3390A integrator.

The calorimetric procedure and apparatus have previously been described (10). The calorimeters were immersed in water baths at 25.0°C, with regulation to ±0.002°C. Liquid samples were introduced into the calorimeters from 10-, 20-, or 50-μL syringes with immersed tips. Heats of solution were corrected (0.01–0.03 kcal/mol less endothermic) to allow for the heat capacity of the sample which was introduced at 21–23°C. The uncertainties in $\Delta H_s$ (twice the standard deviation of three or more determinations) are 0.04–0.25 kcal/mol.

Heats of vaporization were determined by evaporating 100 μL samples into a slow stream of nitrogen (0.2–2.0 mL/min) under partial vacuum in a vacuum jacketed calorimeter at 25°C (9). The samples were injected under conditions producing no temperature change ($< 2 \times 10^{-4}$ K) in the absence of evaporation; no sample heat capacity corrections are therefore required. The evaporative cooling was compensated by an electrical heater powered by a timed constant current source (11). Determinations were made on 4–6 samples. The uncertainties listed in Table 1 are twice the standard deviations.

## Results and discussion

Enthalpies of solution of the polar and nonpolar solutes in α,α,α-trifluorotoluene, benzene, toluene, and mesitylene (in kcal/mol) are listed in Table 1, together with the molar volume and enthalpy of vaporization of each. In Table 2 the derived values of $\Delta H(v \rightarrow S)$ are presented, and enthalpies of hydrogen bond formation or other polar interactions are evaluated. The compound used as the non-hydrogen-bonding or nonplar model is identified by number. Table 3 lists polar interactions calculated by the pure base method. Values in Tables 2 and 3 based on two heats of solution and two heats of vaporization, or on four heats of solution, have estimated uncertainties of 0.1–0.3 kcal/mol.

The enthalpies of hydrogen bond formation of *m*-cresol with benzene, toluene, and mesitylene are quite similar to the values of Arnett *et al.* for phenol and *p*-fluorophenol (1), whether the cresol values are calculated from $\Delta H(v \rightarrow S)$ of cresol vs. anisole or by the pure base method. The difference calculated by the two methods (0.11 kcal/mol), is equal to the difference in $\Delta H(v \rightarrow CCl_4)$ between cresol and anisole. Arnett found $\Delta H_f = -1.18$ kcal/mol for the phenol–benzene system, using anisole as a model, by the pure base method.

Can. J. Chem. Downloaded from www.nrcresearchpress.com by 210.87.254.105 on 09/06/12
For personal use only.

TABLE 1. Heats of solution in aromatic solvents (kcal/mol)

| | Solute[a] | $\Delta H_v$[b] | MV, mL[c] | $\Delta H_s$ ($C_6H_5CF_3$) | $\Delta H_s$ ($C_6H_6$) | $\Delta H_s$ (toluene) | $\Delta H_s$ (mesit) | $\Delta H_s$ ($CCl_4$) |
|---|---|---|---|---|---|---|---|---|
| 1 | 1-Butanol | 12.46±0.00[d] | 91.5 | 4.32 | 4.05[e] | 4.05[e] | 3.88[e] | 4.60 |
| 2 | 1-Pentanol | 13.61±0.04 | 108.2 | 4.32 | 4.22 | 4.01 | 3.89 | 4.70 |
| 3 | 1-Octanol | 16.96±0.10 | 157.5 | 4.50 | 4.35 | 4.02 | 3.64 | 4.76 |
| 4 | 2-Me-2-butanol | 11.94±0.02 | 109.4 | 3.86 | 3.97 | 3.88 | 3.57 | 4.61 |
| 5 | *m*-Cresol | 14.75±0.25 | 104.6 | 3.54 | 2.58 | 2.50 | 2.29 | 4.08 |
| 6 | Phenol | 16.41±0.12 | 89.0 | — | 4.72[f] | 4.51[f] | 4.62[f] | 6.27[f] |
| 7 | Acetone | 7.48±0.02 | 73.5 | −0.05 | 0.29 | 0.32 | 0.70 | 0.74 |
| 8 | 2-Heptanone | 11.34±0.07 | 140.8 | −0.34 | 0.24 | −0.10 | 0.00 | 0.25 |
| 9 | 4-Heptanone | 11.10±0.09 | 139.7 | −0.23 | 0.16 | −0.09 | −0.11 | 0.25 |
| 10 | 2,2,4,4-$Me_4$-3-pentanone | 10.84±0.02 | 172.6 | −0.30 | 0.56 | 0.21 | 0.19 | 0.12 |
| 11 | Cyclohexanone | 10.77±0.05 | 103.6 | −0.40 | −0.26 | −0.16 | 0.19 | −0.06 |
| 12 | Pyridine | 9.61±0.01 | 80.6 | 0.26 | 0.01 | 0.18 | 0.73 | 0.31 |
| 13 | Aniline | 13.33±0.01 | 91.2 | 1.97 | 1.25 | 1.39 | 1.89 | 2.08 |
| 14 | Nitrobenzene | 13.15±0.05 | 102.3 | 0.36 | 0.56 | 0.36 | 0.39 | 1.27 |
| 15 | Et—O—Et | 6.49±0.06 | 103.8 | −0.29 | 0.20 | −0.10 | 0.09 | −0.42 |
| 16 | *n*-Bu—O—Me | 7.77±0.02 | 118.4 | −0.16 | 0.27 | −0.01 | 0.04 | −0.36 |
| 17 | *n*-Bu—O—*n*-Bu | 10.68±0.02[d] | 164.6 | 0.15 | 0.60 | 0.11 | 0.02 | −0.21 |
| 18 | *tert*-Bu—O—Me | 7.27±0.02 | 119.0 | 0.34 | 0.62 | 0.63 | 0.70 | 0.38 |
| 19 | Anisole | 11.19±0.05 | 108.6 | 0.24 | 0.05[g] | 0.08[g] | 0.38[g] | 0.41 |
| 20 | Benzene | 8.09±0.01 | 88.9 | 0.25 | 0.00 | 0.04 | 0.62 | 0.14 |
| 21 | Toluene | 9.08±0.01 | 106.3 | 0.05 | 0.12 | 0.00 | 0.13 | −0.03 |
| 22 | Mesitylene | 11.35±0.01 | 138.9 | 0.03 | 0.62 | 0.17 | 0.00 | — |
| 23 | Benzotrifluoride | 8.98±0.03 | 122.9 | 0.00 | 0.56 | 0.08 | 0.00 | — |
| 24 | Propane | — | 85.5[h] | 0.53[h] | 0.83[h] | 0.34[h] | 0.27[h] | 0.17[h] |
| 25 | Butane | — | 100.4 | 0.62[h] | 0.95[h] | 0.43[h] | 0.28[h] | 0.26[h] |
| 26 | Pentane | 6.36±0.02[d] | 115.2 | 0.71[h] | 1.07 | 0.52[h] | 0.29[h] | 0.35 |
| 27 | Hexane | 7.54±0.01 | 130.5 | 0.80 | 1.17 | 0.61 | 0.30 | 0.44 |
| 28 | Heptane | 8.74±0.01 | 146.5 | 0.91 | 1.33 | 0.69 | 0.30 | 0.51 |
| 29 | Octane | 9.92±0.01 | 162.6 | 1.01 | 1.44 | 0.78 | 0.30 | 0.57[h] |
| 30 | Nonane | 11.10±0.01 | 178.7 | 1.11 | 1.62 | 0.87 | — | 0.63 |
| 31 | Decane | 12.28±0.01 | 194.9 | — | 1.80 | 0.96 | 0.34 | 0.72 |
| 32 | Dodecane | 14.65±0.06 | 227.5 | — | 2.15 | — | 0.38 | 0.87 |
| 33 | Hexadecane | 19.45±0.08 | 292.9 | 2.01 | 2.70 | 1.48 | 0.52 | 1.12 |
| 34 | 2-Methylbutane | 6.03±0.05 | 116.4 | 0.72 | 1.13 | 0.67 | 0.33 | 0.31 |
| 35 | 2,2-$Me_2$butane | 6.62±0.01 | 132.9 | 0.79 | 1.15 | 0.74 | 0.41 | 0.43 |
| 36 | 2,2,4,4-$Me_4$pentane | 9.20±0.03[d] | 178.3 | 0.94 | 1.46 | 0.89 | 0.38 | 0.56 |
| 37 | Cyclohexane | 7.90±0.01 | 108.1 | 0.97 | 0.87 | 0.60 | 0.47 | 0.21 |
| 38 | 1-Hexene | 7.34±0.05 | 125.0 | 0.49 | 0.76 | 0.26 | 0.10 | 0.15 |
| 39 | 1-Octene | 9.70±0.05 | 157.0 | 0.65 | 0.97 | 0.39 | 0.10 | 0.24 |

[a] Me is methyl, Bu is butyl.
[b] Heat of vaporization and uncertainty, kcal/mol, from ref. 5 unless otherwise indicated, at 25°C.
[c] Molar volume.
[d] This study, see Experimental section.
[e] Reference 1 values are 3.93, 3.56, and 3.62 kcal/mol, respectively, in benzene, toluene, and mesitylene.
[f] Values from ref. 1.
[g] Reference 1 values are 0.00, −0.06, and 0.12 kcal/mol, respectively, in benzene, toluene, and mesitylene.
[h] Estimated by extrapolation.

The acetone–benzene interaction of 4.0 kcal/mol (Table 2) or 3.1 kcal/mol (Table 3) are both within the uncertainty limits of a value (3.6 ± 0.7 kcal/mol) determined from the temperature dependence of the association constant measured by nmr (7).

The $\Delta H(v \rightarrow S)$ method requires the availability or measurement of appropriate heats of vaporization or sublimation, which for highly associated high boiling substances such as phenols, may not be of high accuracy. The pure base method requires a nonpolar reference solvent in which the polar solutes are unassociated. Carbon tetrachloride serves well as the reference solvent for phenols (1), but $\Delta H_f$ for *m*-cresol in benzene (−1.1 kcal/mol) is appreciably affected if the reference solvent is heptane (−1.3 kcal/mol) or cyclohexane (−1.8 kcal/mol). ($\Delta H_s$ of *m*-cresol and anisole are 5.21 and 1.34 kcal/mol in heptane, and 6.02 and 1.72 kcal/mol in cyclohexane.) On the other hand, if one examines the ketone–benzene system for polar interactions ($\Delta H_p$), there is *no* reference solvent available totally devoid of polar interactions with the ketone dipole. Based on Spencer's estimates (2) of dipole – induced dipole interaction with the methylene group, one calculates an interaction of acetone ($\mu$ = 2.86 D) with cyclohexane at an assumed distance of 4 Å to be 0.7 kcal/mol. This could account for much of the difference in $\Delta H_p$ calculated for the

TABLE 2. Enthalpies of transfer from vapor to aromatic solvents (kcal/mol)

| | Solute | Model compound | $-\Delta H(v\rightarrow S)$, $-\Delta\Delta H(v\rightarrow S)^a$ | | | | | | | |
|---|---|---|---|---|---|---|---|---|---|---|
| | | | $C_6H_5CF_3$ | | Benzene | | Toluene | | Mesitylene | |
| 1 | 1-Butanol | **15** | 8.1[b] | 1.4[c] | 8.4[b] | 2.1[c] | 8.4[b] | 1.8[c] | 8.6[b] | 2.2[c] |
| | | **25** | | 3.6 | | 4.2 | | 3.7 | | 3.7 |
| 2 | 1-Pentanol | **16** | 9.3 | 1.4 | 9.4 | 1.9 | 9.6 | 1.8 | 9.7 | 2.0 |
| | | **26** | | 3.6 | | 4.1 | | 3.8 | | 3.7 |
| 3 | 1-Octanol | **17** | 12.5 | 1.9 | 12.6 | 2.5 | 12.9 | 2.4 | 13.3 | 2.7 |
| | | **29** | | 3.6 | | 4.1 | | 3.8 | | 3.7 |
| 4 | 2-Me-2-butanol | **18** | 8.1 | 1.2 | 8.0 | 1.3 | 8.1 | 1.4 | 8.4 | 1.8 |
| | | **34** | | 2.8 | | 3.1 | | 2.7 | | 2.7 |
| 5 | *m*-Cresol | **19** | 11.2 | 0.3 | 12.2 | 1.0 | 12.3 | 1.1 | 12.5 | 1.7 |
| | | **21** | | 2.2 | | 3.2 | | 3.2 | | 3.5 |
| 6 | Phenol | **19** | — | — | 11.7[d] | 0.6[e] | 11.9[d] | 0.8[e] | 11.8[d] | 1.0[e] |
| 7 | Acetone | **24** | 7.5 | 4.0 | 7.2 | 4.0 | 7.2 | 3.5 | 6.8 | 3.1 |
| 8 | 2-Heptanone | **28** | 11.7 | 3.9 | 11.1 | 3.7 | 11.4 | 3.4 | 11.3 | 2.9 |
| 9 | 4-Heptanone | **28** | 11.3 | 3.5 | 10.9 | 3.5 | 11.2 | 3.1 | 11.2 | 2.8 |
| 10 | 2,2,4,4-$Me_4$-3-pentanone | **36** | 11.1 | 2.9 | 10.3 | 2.5 | 10.6 | 2.3 | 10.7 | 1.8 |
| 11 | Cyclohexanone | **37** | 11.2 | 4.2 | 11.0 | 4.0 | 10.9 | 3.6 | 10.6 | 3.2 |
| 12 | Pyridine | **20** | 9.4 | 1.5 | 9.6 | 1.5 | 9.4 | 1.4 | 8.9 | 1.4 |
| 13 | Aniline | **20** | 11.4 | 3.5 | 12.1 | 4.0 | 11.9 | 3.9 | 11.4 | 4.0 |
| 14 | Nitrobenzene | **21** | 12.8 | 3.8 | 12.6 | 3.6 | 12.8 | 3.7 | 12.8 | 3.8 |
| 15 | Et—O—Et | **25** | 6.8 | 2.2 | 6.3 | 2.0 | 6.6 | 1.9 | 6.4 | 1.5 |
| 16 | *n*-Bu—O—Me | **26** | 7.9 | 2.3 | 7.5 | 2.2 | 7.8 | 2.0 | 7.7 | 1.7 |
| 17 | *n*-Bu—O—*n*-Bu | **29** | 10.5 | 1.6 | 10.1 | 1.6 | 10.6 | 1.4 | 10.7 | 1.0 |
| 18 | *tert*-Bu—O—Me | **34** | 6.9 | 1.6 | 6.7 | 1.8 | 6.6 | 1.3 | 6.6 | 0.9 |
| 19 | Anisole | **21** | 11.0 | 1.9 | 11.1 | 2.2 | 11.1 | 2.0 | 10.8 | 1.9 |
| 20 | Benzene | | 7.8 | | 8.1 | | 8.1 | | 7.5 | |
| 21 | Toluene | | 9.0 | | 9.0 | | 9.1 | | 9.0 | |
| 22 | Mesitylene | | 11.3 | | 10.7 | | 11.2 | | 11.4 | |
| 23 | Benzotrifluoride | | 9.0 | | 8.4 | | 8.9 | | 9.0 | |
| 24 | Propane | | 3.5[f] | | 3.2[f] | | 3.6[f] | | 3.7[f] | |
| 25 | Butane | | 4.6[f] | | 4.3[f] | | 4.7[f] | | 4.9[f] | |
| 26 | Pentane | | 5.7[f] | | 5.3 | | 5.8[f] | | 6.1[f] | |
| 27 | Hexane | | 6.7 | | 6.4 | | 6.9 | | 7.2 | |
| 28 | Heptane | | 7.8 | | 7.4 | | 8.1 | | 8.4 | |
| 29 | Octane | | 8.9 | | 8.5 | | 9.1 | | 9.6 | |
| 30 | Nonane | | 10.0 | | 9.5 | | 10.2 | | 10.8[f] | |
| 31 | Decane | | — | | 10.5 | | 11.3 | | 11.9 | |
| 32 | Dodecane | | — | | 12.5 | | — | | 14.3 | |
| 33 | Hexadecane | | 17.4 | | 16.8 | | 18.0 | | 18.9 | |
| 34 | 2-Methylbutane | | 5.3 | | 4.9 | | 5.4 | | 5.7 | |
| 35 | 2,2-$Me_2$butane | **27** | 5.8 | 0.91[g] | 5.5 | 0.90[g] | 5.9 | 1.05[g] | 6.2 | 1.03[g] |
| 36 | 2,2,4,4-$Me_4$pentane | **30** | 8.3 | 0.86[g] | 7.7 | 0.87[g] | 8.3 | 0.96[g] | 8.8 | 0.98[g] |
| 37 | Cyclohexane | | 6.9 | | 7.0 | | 7.3 | | 7.4 | |
| 38 | 1-Hexene | **27** | 6.9 | 0.1 | 6.6 | 0.2 | 7.1 | 0.2 | 7.2 | 0.0 |
| 39 | 1-Octene | **29** | 9.1 | 0.1 | 8.7 | 0.3 | 9.3 | 0.2 | 9.6 | 0.0 |

[a] $\Delta H(v\rightarrow S)$ of solute vs. indicated model compound.
[b] $\Delta H(v\rightarrow S)$.
[c] $\Delta\Delta H(v\rightarrow S)$.
[d] Calculated from $\Delta H_s$ from ref. 1.
[e] H-bonding vs. anisole.
[f] Estimated by extrapolation of alkane series.
[g] Loss in $\Delta H(v\rightarrow S)$ vs. *n*-isomer per quaternary carbon atom.

acetone–benzene interaction by the pure base method vs. the $\Delta H(v \rightarrow S)$ method, but for ethers, where the calculated differences are as large, the dipole – induced dipole interactions with cyclohexane are only 0.1–0.2 kcal/mol. One evaluates a quantity by the pure base method for non-hydrogen-bonding polar solutes, which is not the *total* polar interaction, but the *difference* in the polar interactions with the "basic" and reference solvents. This problem is avoided in the $\Delta\Delta H(v \rightarrow S)$ method, but the ambiguity here is whether $\Delta H(v \rightarrow S)^P - \Delta H(v \rightarrow S)^M$ results entirely from polar interactions of the polar solute, or whether substances P and M differ in other respects.

The choice of a model compound is a critical part of the $\Delta\Delta H(v \rightarrow S)$ procedure. An ideal model would probably have the same molar volume and dipole moment as the H-bond donor. We note from

Can. J. Chem. Downloaded from www.nrcresearchpress.com by 210.87.254.105 on 09/06/12
For personal use only.

TABLE 3. Enthalpies of hydrogen bond formation or polar interactions by the pure base method

| Solute | Model compound[a] | Type[b] | $-\Delta H_f$ or $-\Delta H_p$[c] $C_6H_5CF_3$ | Benzene | Toluene | Mesitylene | $\Delta H_f - \Delta\Delta H(v \rightarrow S)$[d] |
|---|---|---|---|---|---|---|---|
| 1-Butanol | **15** | H | 0.4 | 1.2 | 0.9 | 1.2 | 1.0 |
| 1-Pentanol | **16** | H | 0.6 | 1.1 | 1.0 | 1.2 | 0.8 |
| 1-Octanol | **17** | H | 0.6 | 1.2 | 1.1 | 1.4 | 1.3 |
| 2-Me-2-butanol | **18** | H | 0.7 | 0.9 | 1.0 | 1.4 | 0.4 |
| *m*-Cresol | **19** | H | 0.4 | 1.1 | 1.3 | 1.8 | −0.1 |
| Phenol | **19** | H | — | 1.2[e] | 1.3[e] | 1.6[e] | −0.6 |
| Acetone | **24** | P | 3.1 | 3.1[f] | 2.6 | 2.1 | 0.9 |
| 2-Heptanone | **28** | P | 2.9 | 2.7 | 2.4 | 1.9 | 1.0 |
| 4-Heptanone | **28** | P | 2.8 | 2.8 | 2.4 | 2.0 | 0.7 |
| 2,2,4,4-$Me_4$-3-pentanone | **36** | P | 2.2 | 1.8 | 1.6 | 1.1 | 0.7 |
| Cyclohexanone | **37** | P | 3.1 | 2.9 | 2.5 | 2.1 | 1.1 |
| Et—O—Et | **25** | P | 1.7 | 1.4 | 1.3 | 1.0 | 0.6 |
| *n*-Bu—O—Me | **26** | P | 1.3 | 1.2 | 1.0 | 0.7 | 1.0 |
| *n*-Bu—O—*n*-Bu | **29** | P | 1.6 | 1.6 | 1.4 | 1.0 | 0.8 |
| *tert*-Bu—O—Me | **34** | P | 1.7 | 1.9 | 1.4 | 1.0 | −0.1 |
| Anisole | **21** | P | 0.8 | 1.0 | 0.9 | 0.7 | 1.2 |

[a] See Table 2.
[b] H-bonding or (other) polar interactions.
[c] Enthalpy of H-bonding or of other polar interactions, kcal/mol.
[d] Difference between pure base method results and results of Table 2.
[e] Reference 1.
[f] A value of 3.6 ± 0.7 kcal/mol was reported in ref. 7.

Tables 2 and 3 the similarity of $\Delta H_f$ from the $\Delta\Delta H(v \rightarrow S)$ and pure base methods for the cresol vs. anisole comparison (MV 104.6 vs. 108.6 mL; dipole moments (4) 1.5 vs. 1.3 D). In the Arnett comparison of phenol (MV 89.0 mL) vs. anisole (1) $\Delta H_f$ differs by 0.6 kcal/mol by the two methods, resulting from the difference in $\Delta H(v \rightarrow CCl_4)$ of phenol (−10.14 kcal/mol) and anisole (−10.78 kcal/mol). If calculations (2) correspond at least roughly with reality, then the solvent cavity formation term in $CCl_4$ is 1.3 kcal/mol per $CH_2$, and the dispersion interactions are −2.1 kcal/mol per $CH_2$. A methylene group typically contributes 16.1 mL to the molar volume. Relative to anisole, phenol "saves" (19.6/16.1) × 1.3 = 1.6 kcal/mol in cavity formation energy, but loses the dispersion interactions of one methylene group, for an overall loss of 0.5 kcal/mol. The agreement with the experimental may be better than can be counted on, but this suggests the importance of the molar volume match.

We note that 1-butanol (MV 91.5 mL, μ = 1.8 D, $\Delta H(v \rightarrow CCl_4)$ = −7.90 kcal/mol) is better served by 1-chlorobutane as a model (1) (104.5 mL, 2.0 D, −7.93 kcal/mol) than by ethyl ether (103.8 mL, 1.3 D, −6.91 kcal/mol). Both models have larger molar volumes than 1-butanol, but this endothermic cavity contribution may be compensated in 1-chlorobutane by the larger dipole moment and polarizability, resulting in exothermic contributions from increased dipole – induced dipole and dispersion interactions. The ketones (Table 2) are appreciably smaller in molar volume than the hydrocarbon models, while the ethers are slightly larger.

While the factors which determine model compound suitability may be identified, we do not feel that perfect predictions can be made at this time. For this reason hydrogen bond formation enthalpies may be better determined by the pure base method. Estimates of other polar interaction enthalpies by the $\Delta\Delta H(v \rightarrow S)$ procedure should be regarded as only rough approximations.

Regardless of the method of estimation, certain trends in $\Delta H_f$ and $\Delta H_p$ as a function of solvent are evident from Tables 2 and 3. The enthalpy of hydrogen bond formation of *m*-cresol with aromatic solvents becomes more exothermic in the order benzotrifluoride < benzene < toluene < mesitylene, the order of increasing π electron density. Alcohols, by the pure base method are surprisingly comparable in $\Delta H_f$ with cresol. Our values in benzene, toluene, and mesitylene are all more exothermic than those previously reported (1) for 1-butanol. This may reflect our use of the isomeric ethers, rather than the chloroalkane, as model. It is somewhat disappointing to find that the results of the pure base method are so dependent on the choice of models. The general trend in alcohol $\Delta H_f$ with solvent variation resembles that of cresol, except for the unexpectedly strong interaction with benzene.

With both ketones and ethers the trend shows strongest interactions with benzotrifluoride and weakest with mesitylene. Since benzotrifluoride is

Can. J. Chem. Downloaded from www.nrcresearchpress.com by 210.87.254.105 on 09/06/12
For personal use only.

more hindered, less polarizable, and of lower electron density than toluene, the observed order probably results predominantly from charge transfer, rather than from steric factors or simple dipole – induced dipole interactions. The ketones in all cases interact more strongly than the ethers.

$\Delta\Delta H(v \rightarrow S)$ for 1-butanol, 1-pentanol, and 1-octanol vs. alkane models give crude estimates of the total $\Delta H_f + \Delta H_p$. In a given aromatic solvent these values are much more uniform than $\Delta H_f$ (or even $\Delta H_f$ derived from the pure base method). This suggests that ethyl ether, *n*-butyl methyl ether, and butyl ether are not equally well matched to the respective alcohols.

Aniline shows a trend in interaction enthalpies with aromatic solvents similar to the alcohols, suggesting that the principal interaction is hydrogen bond donation. Pyridine and nitrobenzene show almost no variation or trends.

The methylene increment in $\Delta H(v \rightarrow S)$ for alkane solutes in benzotrifluoride, benzene, toluene, and mesitylene are $-1.07$, $-1.04$, $-1.10$, and $-1.17$ kcal/mol, respectively. The latter is the largest we have observed except for *n*-heptane ($-1.18$ kcal/mol).

**Acknowledgement**

This study was supported by the Robert A. Welch Foundation (Grant E-136).

1. E. M. Arnett, L. Joris, E. Mitchell, T. S. S. R. Murty, T. M. Gorrie, and P. V. R. Schleyer. J. Am. Chem. Soc. **92**, 2365 (1970).
2. J. N. Spencer, J. E. Gleim, C. H. Blevins, R. C. Garrett, and F. J. Mayer. J. Phys. Chem. **83**, 1249 (1979).
3. W. G. Read, E. J. Campbell, G. Henderson, and W. H. Flygare. J. Am. Chem. Soc. **103**, 7670 (1981).
4. A. L. McClellan. Tables of experimental dipole moments. W. H. Freeman, San Francisco. 1963.
5. J. B. Pedley and J. Rylance. Sussex-N.P.L. computer analysed thermochemical data: organic and organometallic compounds. University of Sussex, Brighton. 1977.
6. P. P. S. Saluja, L. A. Peacock, and R. Fuchs. J. Am. Chem. Soc. **101**, 1958 (1979).
7. S.-M. Park and W. C. Herndon. Tetrahedron, **34**, 3201 (1978).
8. R. Fuchs and L. A. Peacock. Can. J. Chem. **57**, 2302 (1979).
9. R. Fuchs and L. A. Peacock. Can. J. Chem. **58**, 2796 (1980).
10. R. Fuchs and P. P. S. Saluja. Can. J. Chem. **54**, 3857 (1976).
11. R. Fuchs. J. Chem. Educ. **58**, 594 (1981).

Can. J. Chem. Downloaded from www.nrcresearchpress.com by 210.87.254.105 on 09/06/12
For personal use only.

# Competitive inclusion of chloro-substituted acetic acids into β-cyclodextrin monitored by rotational correlation frequencies of 4-hydroxy-2,2,6,6-tetramethylpiperidinyl-1-oxy radical

YOSHIAKI MOTOZATO, TSUKASA NISHIHARA, CHUICHI HIRAYAMA, AND YOSHIAKI FURUYA

*Department of Synthetic Chemistry, Faculty of Engineering, Kumamoto University, Kumamoto, Japan 860*

AND

YOSHIO KOSUGI

*Department of Synthetic Chemistry, Faculty of Engineering, Nagoya University, Nagoya, Japan 464*

Received October 9, 1981

YOSHIAKI MOTOZATO, TSUKASA NISHIHARA, CHUICHI HIRAYAMA, YOSHIAKI FURUYA, and YOSHIO KOSUGI. Can. J. Chem. **60**, 1959 (1982).

Competitive inclusion in β-cyclodextrin between 4-hydroxy-2,2,6,6-tetramethylpiperidinyl-1-oxy and chloro-substituted acetic acids has been monitored by esr spectroscopy. The temperature dependence of the rotational correlation frequencies calculated by Kivelson's equation, using esr spectra of the radical, suggests that a structural change of β-cyclodextrin occurs at about 30°C and that trichloroacetic acid is included extensively at 20–35°C, but significant inclusion of acetic acid is not observed. The degree of competitive inclusion is in the order of trichloro, dichloro, and monochloroacetic acids over the range of 20–80°C. Carbon-13 nmr studies also prove the inclusion of trichloroacetic acid showing an inclusion shift of the trichloromethyl carbon by 1.4 ppm.

YOSHIAKI MOTOZATO, TSUKASA NISHIHARA, CHUICHI HIRAYAMA, YOSHIAKI FURUYA et YOSHIO KOSUGI. Can. J. Chem. **60**, 1959 (1982).

Utilisant la spectroscopie de rpe, on a enregistré l'introduction compétitive de la β-cyclodextrine entre l'hydroxy-4 tétra méthyl-2,2,6,6 pipérideryloxy-1 et des acides acétiques chlorés. L'influence de la température sur les fréquences de corrélation vibrationnelle, calculées à l'aide des équations de Kivelson, suggère qu'un changement de structure de la β-cyclodextrine se produit à environ 30°C et que l'acide trichloroacétique est inclus de façon extensive à 20–35°C; on n'observe toutefois pas d'inclusion importante d'acide acétique. Le degré d'inclusion compétitive est dans l'ordre des acides trichloro, dichloro et monochloro acétiques dans l'intervalle de 20–80°C. Les études en rmn du $^{13}C$ prouvent également qu'il se produit une inclusion de l'acide trichloroacétique qui provoque un déplacement, dû à l'inclusion, du carbone portant le groupe trichlorométhyle de 1,4 ppm.

[Traduit par le journal]

Cycloheptaamylose or β-cyclodextrin (β-CD) has been used in various ways such as to accelerate or retard organic reactions or as simple models of enzymatic reactions. A number of physical methods to investigate the inclusion behavior have been proposed as β-CD has been applied to numerous reactions related to hydrolysis and decarboxylation. Electron spin resonance (esr) spectroscopy is one of those methods, but examples are few (1–4). Kaiser and co-workers (1–3) used nitroxyl radicals as spin-labels on acyl compounds and exemplified, using esr spectrometry, the deacylation reaction assisted by β-CD.

The mechanism of base catalyzed decarboxylation of trichloroacetic acid in the presence of β-CD has been discussed on the basis of kinetic data in our previous report (5). In the present studies, as a new method without labelling, competitive inclusion of a nitroxyl radical and chloro-substituted acetic acids into β-CD was examined, and rotational correlation frequencies of the spin probe were monitored by means of esr. In this way the high propensity for inclusion of trichloroacetic acid could be demonstrated.

## Results and discussion

Electron spin resonance spectra of an aqueous solution of 4-hydroxy-2,2,6,6-tetramethyl piperidinyl-1-oxy, **1**, consisted of triplet peaks whose hyperfine splitting constant ($a^N$) was 17 G (Fig. 1*a*).

Upon addition of a molar equivalent of β-CD to the solution, the triplet signal of intensity ratio 1:1:1 lost symmetry with a marked broadening (with decrease of the ratio of peak height to width) of the highest field peak ($m = -1$) (see Fig. 1*b*). Such a line broadening is ascribed to slow rotation in β-CD cavity or slow exchange in the equilibrium given by reaction [1].

[1] $\quad \mathbf{1} + \beta\text{-CD} \rightleftarrows [\mathbf{1}\cdots\ \beta\text{-CD}]_{complex}$

As a result of either or both factors, the observed rotational correlation time of the spin is prolonged. Slow rotation is illustrated using the present spin, **1**, by increasing solvent viscosities (6). When di-*tert*-butyl nitroxide is used as a spin in β-CD, free spin and complexed spin give independent peaks (7). Among three typical approximations to calculate rotational correlation time ($\tau_c$), Kivelson's equation (eq. [2]) (8) was employed for the

0008-4042/82/151959-03$01.00/0

©1982 National Research Council of Canada/Conseil national de recherches du Canada

Can. J. Chem. Downloaded from www.nrcresearchpress.com by 210.87.254.105 on 09/06/12
For personal use only.

Can. J. Chem. Downloaded from www.nrcresearchpress.com by 210.87.254.105 on 09/06/12
For personal use only.

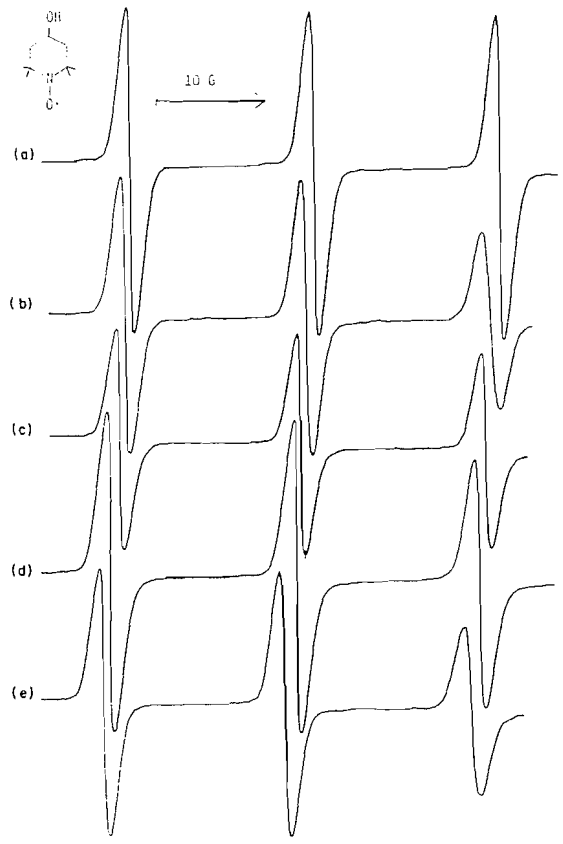


FIG. 1. Electron spin resonance spectra of nitroxy radical **1** in aqueous solutions. (*a*) **1** $3 \times 10^{-4}$ mol/L at 30°C, (*b*) **1** with β-CD at 30°C, (*c*) **1** with β-CD at 80°C, (*d*) **1**, β-CD, and TCAA at 30°C, (*e*) **1**, β-CD, and acetic acid (AA) at 30°C.

nitrogen triplets,

$$[2] \quad \tau_c = \{(h_0/h_{+1})^{1/2} + (h_0/h_{-1})^{1/2} - 2\}(4\pi\sqrt{3}/b^2)W_0$$

where $h$ and $W$ are peak height and peak width, subscripts $+1$, 0, and $-1$ correspond to magnetic spin quantum number $m = +1$, 0, and $-1$, respectively, and the term $(4\pi\sqrt{3}/b^2)$ equals $5.96626 \times 10^{-10}$.

Spectra of the triplet were examined at various temperatures in the presence or absence of β-CD. The line broadening decreased with increase of temperature (e.g. Fig. 1*c*) and a slight inflexion at about 30°C was observed in the temperature dependence of the log $(1/\tau_c)$ when **1** was complexed with β-CD (Fig. 2*b*).

The inflexion is suggestive of a structural change in the β-CD cavity at this temperature. Over the range of lower temperatures (20–35°C) it is known that water molecules of large enthalpy are retained in the cavity (9). At this stage, the hydrophobic radical, **1**, would tend to be more out of the cavity.

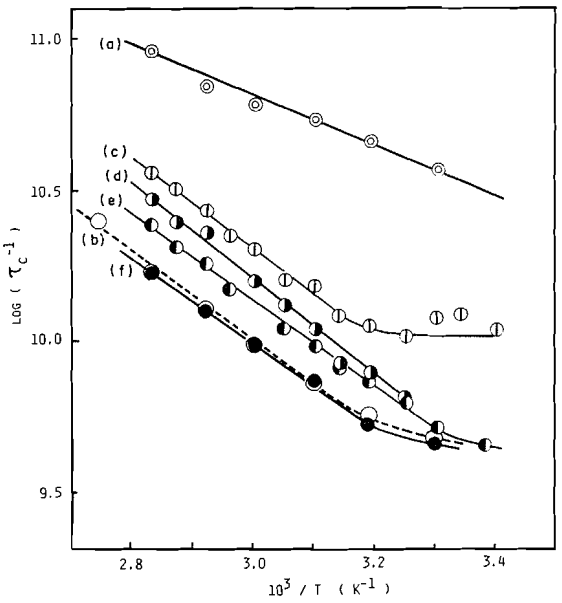


FIG. 2. Relationship between rotational correlation frequency ($\tau_c$) of nitroxy radical **1** and temperature ($T$). (*a*) **1** only, (*b*) **1** and β-CD, (*c*) **1**, β-CD, and TCAA, (*d*) **1**, β-CD, and DCAA, (*e*) **1**, β-CD, and MCAA, (*f*) **1**, β-CD, and AA.

In fact at the lower temperatures, the correlation line of log $(1/\tau_c)$ vs. $1/T$ of **1** with β-CD was almost parallel with that of **1** without β-CD (Fig. 2*a*). The increment of the slope, relative to that at higher temperature, is assigned to the energy of complex formation, calculated to be 2.7 kcal/mol.

The tendency was more evident when hydrophilic trichloroacetic acid (TCAA) was added (Fig. 2*c*). Competitive inclusion between **1** and TCAA according to reactions [1] and [3], respectively, is apparent.

$$[3] \quad \text{TCAA} + \beta\text{-CD} \rightleftarrows [\text{TCAA} \cdots \beta\text{-CD}]_{\text{complex}}$$

The relationship of Fig. 2*a* at six different temperatures did not change with addition of TCAA in the absence of β-CD. The spectrum of **1** (Fig. 1*d*) approached that of free **1** (Fig. 1*a*) and the inclusion of TCAA was much favored at the lower temperatures.

By increasing the amount of TCAA up to 10 times more than **1**, a similar correlation line with scattered points of maximum ±0.1 unit to that of **1** without β-CD was obtained. The scatter of log $(1/\tau_c)$ values from the line was probably caused by either too high concentrations ($3 \times 10^{-3}$ mol/L) of the solution or by partial hydrolysis of β-CD, which might have occurred in the strong acidic medium.

By contrast, acetic acid (AA) instead of TCAA did not alter significantly the correlation line of Fig. 2*b*. Although the spectrum (Fig. 1*e*) is like that of **1**

Can. J. Chem. Downloaded from www.nrcresearchpress.com by 210.87.254.105 on 09/06/12
For personal use only.

with β-CD only, the effect of α-CD on the $pK_a$ value of AA reported by Connors and Lipari (10) using a titration method suggests a slight inclusion is still taking place. Monochloroacetic acid (MCAA) (Fig. 2*e*) or dichloroacetic acid (DCAA) (Fig. 2*d*) decreased the correlation frequencies of **1**, not as much as TCAA, but more than AA did. Therefore the order of feasibility of inclusion is TCAA > DCAA > MCAA > AA. The order can be understood in terms of the order of van der Waals interactions and/or London dispersion forces between acetic acids and β-CD. In no cases at any temperatures investigated were interactions recognized without β-CD and the relationship of log $(1/\tau_c)$ vs. $1/T$ in the presence of acetic acids, but not β-CD, was the same as that of Fig. 2*a*.

Carbon-13 nmr spectra of TCAA in a mixed solvent of $H_2O$ and dimethyl sulfoxide-$d_6$ (DMSO-$d_6$) in the ratio of 1 to 1 showed at ambient temperature (27°C) two peaks at 164.4 and 94.0 ppm of carboxyl carbon ($\delta_{CO}$) and trichloromethyl carbon ($\delta_{CCl_3}$), respectively. Upon addition of β-CD in 1 to 1 ratio, $\delta_{CCl_3}$ moved to 95.4 ppm, while $\delta_{CO}$ remained at 164.4 ppm. The chemical shift change caused by β-CD was examined in cases of DCAA, MCAA, and AA in the same manner as was done for TCAA. No substantial shift changes were observed in all cases under the condition studied.

Thus the results of the nmr method also support the conclusion that the complex formation of TCAA with β-CD is the most favorable among chloro-substituted acetic acids. The inclusion shift of 1.4 ppm for the trichloromethyl carbon suggests that the trichloromethyl group is in or near the hydrophobic cavity of β-CD. The inclusion shift became smaller by 20% when α-CD, of smaller size cavity, was employed. The result is comparable with the fact that rate constants of the decarboxylation reaction (11) decrease, probably because of less stable complex formation with α-CD than β-CD.

## Experimental

All chemicals were of guaranteed grade and were used as purchased. Electron spin resonance sample solutions were made up with 3 mL of **1** ($3 \times 10^{-4}$ mol/L aqueous solution), acetic acids, and 100 mg of β-CD. A capillary tube of 1 mm inner diameter was filled with the sample solution and fixed in an esr sample tube of 3 mm inner diameter.

Electron spin resonance spectra were recorded on a JES-FAEX (JEOL) equipped with a JES-VT-3A2 for variable temperatures. Carbon-13 nmr spectra were taken on a Varian XL-100 spectrometer. Pulse conditions have been described elsewhere (12). Sample concentrations were $3 \times 10^{-4}$ mol/L in a solvent mixture of $H_2O$ and DMSO-$d_6$ in the ratio of 1 to 1 which increased solubilities and stabilized the magnetic field at the same time.

1. R. M. Paton and E. T. Kaiser. J. Am. Chem. Soc. **92**, 4723 (1970).
2. K. Flohr, R. M. Paton, and E. T. Kaiser. J. Chem. Soc. Chem. Commun. 1621 (1971).
3. K. Flohr, R. M. Paton, and E. T. Kaiser. J. Am. Chem. Soc. **97**, 1209 (1975).
4. N. M. Atherton and S. J. Strach. J. Magn. Reson. **17**, 134 (1975).
5. Y. Motozato, Y. Furuya, T. Matsumoto, and T. Nishihara. Bull. Chem. Soc. Jpn. **53**, 2578 (1980).
6. J. Hsia and L. Piette. Arch. Biochim. Biophys. **129**, 296 (1969).
7. N. M. Atherton and S. J. Strach. J. Chem. Soc. Faraday Trans. I, **71**, 357 (1975).
8. D. Kivelson. J. Chem. Phys. **25**, 709 (1956).
9. R. L. VanEtten, J. F. Sebastian, G. A. Clowes, and M. L. Bender. J. Am. Chem. Soc. **89**, 3243 (1967).
10. K. A. Connors and J. M. Lipari. J. Pharm. Sci. **65**, 379 (1976).
11. F. Cramer and W. Kampe. J. Am. Chem. Soc. **87**, 1115 (1965).
12. Y. Kosugi and T. Takeuchi. J. Magn. Reson. **32**, 83 (1978).

# Analyse conformationnelle d'acyl-5 dioxannes-1,3. Étude en rmn du proton de dioxannes-1,3 substitués en position 5 par un groupement acyle aliphatique ou aromatique

ALAIN DENIS, MICHEL DELMAS, ANTOINE GASET ET JEAN-PIERRE GORRICHON[1]

*Laboratoire du Chimie Organique et d'Agrochimie, École Nationale Supérieure de Chimie (INPT), 118, route de Narbonne, 31077 Toulouse Cedex, France*

Reçu le 1 mars 1982

ALAIN DENIS, MICHEL DELMAS, ANTOINE GASET et JEAN-PIERRE GORRICHON. Can. J. Chem. **60**, 1962 (1982).

L'étude en rmn du proton (basse température, sels de lanthanide) permet d'établir la conformation privilégiée des dioxannes-1,3 substitués en position 5 par un groupement acyle. Dans les acyl-5 alkyl-5 dioxannes-1,3 le groupe acyle est préférentiellement axial tandis que pour l'acétyl-5 dioxanne-1,3 ce substituant est équatorial. Un groupement acyle aromatique adopte préférentiellement la position équatoriale.

ALAIN DENIS, MICHEL DELMAS, ANTOINE GASET, and JEAN-PIERRE GORRICHON. Can. J. Chem. **60**, 1962 (1982).

This $^1$H nmr study (temperature-dependent nmr, lanthanide shift reagent) establishes the preferred conformations of 1,3-dioxans substituted at the five position by an acyl group. For 5-acyl-5-alkyl-1,3-dioxans, this group is preferentially axial whereas in 5-acetyl-1,3-dioxans this substituent is equatorial. An aromatic acyl group is preferentially equatorial.

## Introduction

Les composés cycliques à six chainons ont fait l'objet de travaux d'analyse conformationnelle importants et variés et, notamment, en rmn du proton (1 à 8). Néanmoins, les acyl-5 dioxannes-1,3, dont nous avons par ailleurs rapporté les méthodes de synthèse (9, 10), n'ont fait l'objet d'aucune étude structurale approfondie. Ces composés, du fait de la présence d'un groupement carbonyle en α du cycle dioxannique, sont des intermédiaires de synthèse pour des dérivés dont l'activité biologique dépend de la structure (11). On conçoit, donc, l'intérêt d'une analyse conformationnelle permettant de préciser l'orientation axiale ou équatoriale du groupement acyle sur de telles molécules.

## Résultats et discussion

Les valeurs de déplacements chimiques et des constantes de couplage des protons figurant dans les tableaux 1 et 2 sont en accord avec la structure dioxannique par comparaison avec les valeurs relevées dans la littérature (1 à 8).

Les valeurs des constantes de couplage ne permettent pas de déterminer l'orientation axiale ou équatoriale du substituant acyle. En effet, dans le composé **3***a*, par exemple, on relève des constantes de 7,8 et 4,1 Hz respectivement pour $^3J_{4a\text{-}5}$ et $^3J_{4e\text{-}5}$. Or, les valeurs généralement admises pour ce type de composés, en conformation chaise bloquée, sont de 10–12 Hz ($^3J_{4a-5a}$), 4–6 Hz ($^3J_{4e-5a}$), 4 Hz ($^3J_{4a-5e}$) et 1–2, 5 Hz ($^3J_{4e-5e}$) (2). Il semble donc logique de considérer qu'à température ambiante tous ces composés existent sous la forme d'un équilibre conformationnel entre les deux conformères représentés dans la figure 1.

Afin de mettre en évidence cet équilibre conformationnel, nous avons réalisé une étude à basse température de quelques uns de ces dioxannes. Nous avons appliqué la méthode décrite par Anteunis et coll. (6, 12).

### 1. *Étude en rmn à basse température de l'acétyl-5 méthyl-5 dioxanne-1,3, 3b*

L'allure générale des spectres de rmn correspondant à un abaissement de la température confirme l'existence d'un équilibre conformationnel et à −90°C, les spectres de deux conformères se différencient nettement.

Les valeurs des déplacements chimiques des protons du composé **3***b* à température ambiante et celles des deux formes à −90°C sont rassemblées dans le tableau 3.

Il a été démontré (13, 14) que, pour des dioxannes-1,3 disubstitués en position 5 ou l'un de ces substituants est un méthyle, ce groupement lorsqu'il est équatorial résonne à champ plus fort

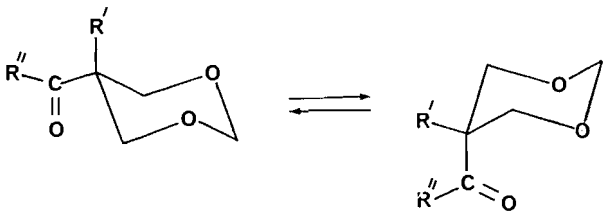

FIG. 1. Représentation des deux conformères des acyl-5 dioxannes-1,3 aliphatiques (R″ aliphatique, R′ aliphatique ou aromatique).

[1]Auteur auquel doit être adressée toute correspondance.

0008-4042/82/151962-07$01.00/0

©1982 National Research Council of Canada/Conseil national de recherches du Canada

Can. J. Chem. Downloaded from www.nrcresearchpress.com by 210.87.254.105 on 09/06/12
For personal use only.

TABLEAU 1. Déplacements chimiques des protons (en ppm/TMS) et constantes de couplage (en Hz) pour les dioxannes-1,3 **3***a*–**3***i* (60 MHz; $CDCl_3$)

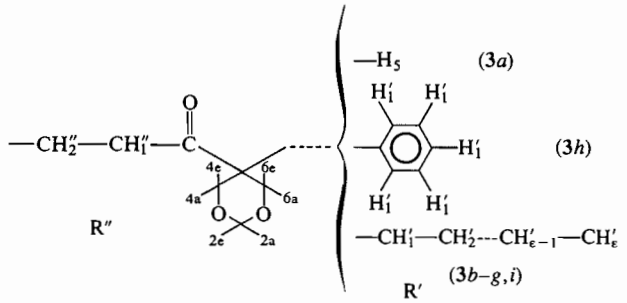


| | | | Cycle dioxannique | | | | | | | | | R'' | | | R' | | | |
|---|---|---|---|---|---|---|---|---|---|---|---|---|---|---|---|---|---|---|
| Produit | R'' | R' | $\delta_{2e}$ | $\delta_{2a}$ | $\delta_{4,6e}$ | $\delta_{4,6a}$ | $\delta_5$ | $^2J_{2e-2a}$ | $^2J_{\substack{4e-4a\\6e-6a}}$ | $\delta H''_1$ | $\delta H''_2$ | $^3J_{H''_1-H''_2}$ | $\delta H'_1$ | $\delta H'_\varepsilon$ | $\delta H'_{2-(\varepsilon-1)}$[a] | $^3J_{H_{\varepsilon-1}-H_\varepsilon}$ |
| **3***a*[d] | $CH_3$ | H | 4,88 | 4,67 | 4,15 | 3,94 | 2,83 | −6,2 | −11,8 | 2,19 | — | — | — | — | — | — |
| **3***b* | $CH_3$ | $CH_3$ | 4,90 | 4,71 | 4,31 | 3,56 | — | −6,2 | −12,0 | 2,26 | — | — | 0,96 | — | — | — |
| **3***c* | $CH_3$ | $C_2H_5$ | 4,89 | 4,70 | 4,33 | 3,59 | — | −6,2 | −12,0 | 2,25 | — | — | 1,53 | 0,76 | — | 7,5 |
| **3***d* | $CH_3$ | $i$-$C_3H_7$ | 4,95 | 4,63 | 4,53 | 3,63 | — | −6,2 | −12,0 | 2,33 | — | — | 1,77 | 0,90 | — | 7,0 |
| **3***e* | $CH_3$ | $n$-$C_4H_9$ | 4,90 | 4,68 | 4,35 | 3,58 | — | −6,2 | −12,0 | 2,25 | — | — | [b] | 0,87 | 1,21 | 4,8 |
| **3***f* | $CH_3$ | $n$-$C_7H_{15}$ | 4,88 | 4,68 | 4,35 | 3,58 | — | −6,2 | −12,0 | 2,23 | — | — | [b] | 0,88 | 1,25 | 4,5 |
| **3***g* | $CH_3$ | $n$-$C_9H_{19}$ | 4,90 | 4,68 | 4,35 | 3,58 | — | −6,2 | −12,0 | 2,24 | — | — | [b] | 0,87 | 1,45 | 4,5 |
| **3***h* | $CH_3$ | $C_6H_5$ | 5,00 | 4,73 | 4,84 | 3,96 | — | −6,2 | −12,0 | 2,12 | — | — | 7,33[c] | — | — | — |
| **3***i* | $C_2H_5$ | $CH_3$ | 4,91 | 4,70 | 4,37 | 3,53 | — | −6,2 | −12,0 | 2,65 | 1,05 | 7,3 | 0,97 | — | — | — |

[a] Massif élargi.
[b] Situé sous le massif $H'_2$-(ε-1).
[c] Singulet.
[d] $J_{4a-5} = 7,8$ Hz; $J_{4e-5} = 4,1$ Hz.

que son homologue axial. On peut déjà en conclure que le conformère majoritaire comporte un groupement méthyle équatorial.

Nous avons confirmé ce résultat en utilisant l'étude en rmn de l'acétyl-5 diméthyl-2,5 dioxanne-1,3 réalisée par Crabb et Newton (15).

En tenant compte de l'effet du méthyle en position 2 équatoriale (7) il est possible de se ramener aux valeurs des déplacements chimiques de l'acétyl-5 méthyl-5 dioxanne-1,3, c'est à dire aux deux formes du composé **3***b*. (cf. Tableau 4).

On note une bonne concordance pour les groupements méthyle et acétyle qui nous permet d'attribuer leur position équatoriale ou axiale sans ambiguité. Les écarts enregistrés pour les déplacements chimiques des protons du cycle dioxannique ne sont pas en désaccord avec cette attribution, car l'ordre de ces derniers est conservé et les différences observées sont probablement dues à un effet de solvant ($CCl_4$ à $CS_2$).

*La conformation privilégiée (A) du composé* **3**b *est donc celle qui comporte le groupement acétyle en position axiale et le groupement méthyle en position équatoriale.*

Un autre argument en faveur de cette attribution est apporté par une étude en rmn en double irradiation à 250 MHz. Il a été montré que pour des dioxannes-1,3 comportant un méthyle en position 5 axiale, il existe un couplage à longue distance entre ce méthyle et les protons en 4a ou 6a allant de 0,8 à 3,2 Hz (15 à 18). Or, même à 250 MHz, à température ambiante dans $CDCl_3$, nous n'observons pas de couplage entre le groupement méthyle et les protons. De plus, sur le spectre à −90°C enregistré à 100 MHz, on note pour la forme minoritaire (B) un couplage de l'order de 0,6 Hz sur le groupement méthyle et un élargissement des raies du massif des protons 4a et 6a. Le groupement méthyle de cette forme est donc bien en position axiale.

Signalons enfin, que le résultat ainsi obtenu apparait contradictoire avec celui rapporté par Anteunis et coll. (19). Ces auteurs indiquent l'existence d'un équilibre conformationnel mais précisent que les deux conformères ont des spectres identiques à −90°C dans $CS_2$. En fait, cette interprétation est certainement liée à un phénomène de cristallisation que nous avons observé. En dessous de la température de coalescence, la cristallisation du conformère B minoritaire est plus rapide que celle du conformère A et de ce fait, il disparait de la

Can. J. Chem. Downloaded from www.nrcresearchpress.com by 210.87.254.105 on 09/06/12
For personal use only.

Can. J. Chem. Downloaded from www.nrcresearchpress.com by 210.87.254.105 on 09/06/12
For personal use only.

TABLEAU 2. Déplacements chimiques (en ppm/TMS) et constantes de couplage (en Hz) pour les dioxannes-1,3 **3***j*-**3***v* (60 MHz; $CDCl_3$)

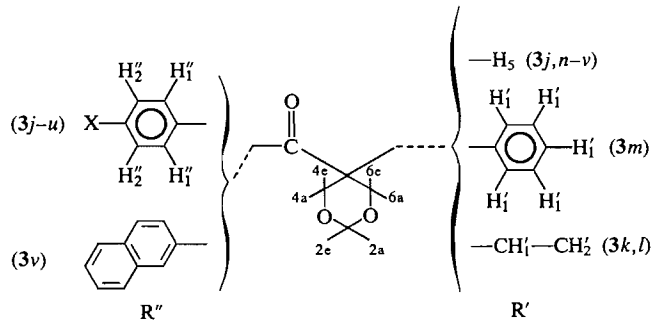


| | | | Cycle dioxannique | | | | | | R'' | | | | R' | |
|---|---|---|---|---|---|---|---|---|---|---|---|---|---|---|
| Produit | R'' | R' | $\delta_{2e}$ | $\delta_{2a}$ | $\delta_{4,6e}$[c] | $\delta_{4,6a}$[c] | $^2J_{2e-2a}$ | $^2J_{4e-4a}^{c}$ $_{6e-6a}$ | $\delta H''_1$ | $\delta H''_2$ | $\delta X$ | $^3J_{H''_1-H''_2}$ | $\delta H'_1/\delta H_5$[c] | $\delta H'_2$ |
| **3***j* | $C_6H_5$ | H | 5,06 | 4,67 | (4,25) | (3,94) | −6,2 | (−9,7) | 7,98 | 7,58 | | | (4,01) | — |
| **3***k* | $C_6H_5$ | $CH_3$ | 4,88 | 4,82 | 4,43 | 3,72 | −6,2 | −11,7 | 7,76 | 7,46 | | | 1,30 | — |
| **3***l*[a] | $C_6H_5$ | $C_2H_5$ | 4,84 | 4,77 | 4,37 | 3,77 | −6,2 | −12,0 | 7,70 | 7,45 | | | 1,83 | 0,84 |
| **3***m* | $C_6H_5$ | $C_6H_5$ | 4,99 | 4,81 | 4,72 | 4,22 | −6,2 | −12,0 | | 7,42** | | — | 7,42** | |
| **3***n*[b] | 4-F-$C_6H_4$ | H | 5,04 | 4,67 | (4,28) | (3,95) | −6,2 | (−9,7) | 7,98 | 7,14 | — | 8,7 | (3,99) | — |
| **3***o* | 4-Cl-$C_6H_4$ | H | 5,03 | 4,67 | (4,29) | (3,95) | −6,2 | (−9,7) | 7,83 | 7,39 | — | 8,5 | (4,03) | — |
| **3***p* | 4-CN-$C_6H_4$ | H | 5,08 | 4,73 | | | −6,2 | | 8,08 | 7,82 | — | 8,4 | | — |
| **3***q* | 4-$NO_2$-$C_6H_4$ | H | 5,05 | 4,73 | | | −6,4 | | 8,11 | 8,36 | — | 8,5 | | — |
| **3***r* | 4-$CH_3$-$C_6H_4$ | H | 5,02 | 4,63 | | | −6,0 | | 7,82 | 7,23 | 2,39 | 8,3 | | — |
| **3***s* | 4-$C_6H_5$-$C_6H_4$ | H | 5,07 | 4,68 | | | −6,2 | | 7,99 | 7,72 à 7,32*** | | 8,6 | | — |
| **3***t* | 4-$CH_3$-O-$C_6H_4$ | H | 5,09 | 4,71 | | | −6,4 | | 7,98 | 6,99 | 3,90 | 9,2 | | — |
| **3***u* | 4-$C_6H_5$-O-$C_6H_4$ | H | 5,04 | 4,65 | | | −6,2 | | 7,92 | 7,54 à 6,90*** | | 8,4 | | — |
| **3***v* | 2-$C_{10}H_7$ | H | 5,12 | 4,72 | | | −6,2 | | | 8,51 à 7,43*** | | — | | — |

[a] $^3J_{H'_1-H'_2} = 7,5$ Hz.
[b] $^4J_{H''_2-F} = 5,5$ Hz; $^5J_{H''_2-F} = 8,4$ Hz.
[c] Les valeurs entre parenthèses ont été obtenues par simulation à 250 MHz (voir texte).
** Singulet élargi.
*** Multiplet

TABLEAU 3. Effet de l'abaissement de la température sur les déplacements chimiques des protons du composé **3***b*.

| | Conformère[a] | | |
|---|---|---|---|
| Paramètre | A + B[c] | A | B |
| Température (°C) | +33 | −90 | −90 |
| $\delta_{2e}$ | 4,71 | 4,79 | — |
| $\delta_{2a}$ | 4,56 | 4,43 | — |
| $\delta_{4,6e}$ | 4,08 | 4,28 | 3,70 |
| $\delta_{4,6a}$ | 3,38 | 3,24 | 3,52 |
| $\delta_{CH_3-C(=O)}$ | 2,12 | 2,20 | 1,98 |
| $\delta_{CH_3}$ | 0,89 | 0,75 | 1,34 |
| Pourcentage des deux formes A/B[b] | 74/26 | 89 | 11 |

[a] Spectre enregistré à 100 MHz dans $CS_2$.
[b] Les pourcentages des deux formes sont calculés à partir des courbes $\Delta\nu$, $\Delta I$, $\Delta\Pi = f(T)$ et $\delta CH_3— = f(T)$ (6, 12). Ils sont en bon accord avec le calcul obtenu par intégration des signaux méthyle et acétyle enregistrés à −90°C.
[c] Les notations A et B *correspondent respectivement aux conformères majoritaire et minoritaire. L'attribution des ces deux formes pour chacun des composés étudiés sera précisée au cours de la discussion.*

phase liquide ne permettant pas l'enregistrement de son spectre dans un laps de temps relativement court à −90°C.

2. *Étude en rmn à basse température des composés* **3**a, **3**e, **3**i

Les données spectrales de ces composés, obtenues de manière identique à celle du produit **3***b*, sont regroupées dans le tableau 5.

En ce qui concerne les composés **3***e* et **3***i*, la comparaison des valeurs obtenues avec celle du tableau 3 montre que leur conformation privilégiée A est également celle pour laquelle le groupement acyle est en position axiale et le groupement alkyle en position équatoriale. D'autre part, d'après les pourcentages obtenus pour ces composés à température ambiante et à −90°C, l'allongement de la chaine alkyle (**3***e*) ne semble pas influencer l'équilibre conformationnel, alors que l'allongement de la chaine du groupement acyle (**3***i*) semble favoriser la conformation A déjà privilégiée.

Dans le cas du composé **3***a*, en se référant aux

TABLEAU 4. Comparaison des valeurs observées et calculées des déplacements chimiques des deux conformères A et B de l'acétyl-5 méthyl-5 dioxanne-1,3 **3***b*

| Conformère | | | Déplacement chimique $\delta_{2e}$ | $\delta_{2a}$ | $\delta_{4,6e}$ | $\delta_{4,6a}$ | $\delta_{CH_3-C(=O)-}$ | $\delta_{CH_3}$ |
|---|---|---|---|---|---|---|---|---|
| $CH_3-C(=O)-$ | ax. | Calculé[a] | — | 4,53 | 4,35 | 3,35 | 2,25 | 0,76 |
| $CH_3-$ | éq. | Observé (A) | 4,79 | 4,43 | 4,28 | 3,24 | 2,20 | 0,75 |
| $CH_3-C(=O)-$ | éq. | Calculé[a] | — | 4,42 | 3,75 | 3,69 | 1,98 | 1,37 |
| $CH_3-$ | ax. | Observé (B) | — | — | 3,70 | 3,52 | 1,98 | 1,34 |

[a] Ces valeurs sont calculées à partir des déplacements chimiques des protons des acétyl-5 diméthyl-2,5 dioxannes-1,3 (15) en soustrayant l'effet du méthyle équatorial en position 2 (7).

TABLEAU 5. Effet de l'abaissement de la température sur les déplacements chimiques des protons des dioxannes du type:

**3***a* $\begin{cases} R'' = CH_3 \\ R' = H \end{cases}$ **3***e* $\begin{cases} R'' = CH_3 \\ R' = n\text{-}C_4H_9 \end{cases}$ **3***i* $\begin{cases} R'' = C_2H_5 \\ R' = CH_3 \end{cases}$

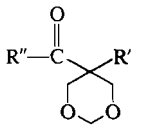

| Produit | Solvant[d] | Conformère[a] | $T$(°C) | $\delta_{2e}$ | $\delta_{2a}$ | $\delta_{4,6e}$ | $\delta_{4,6a}$ | $\delta_5$ | $\delta R''$ | $\delta R'$ | Pourcentage[b] des deux formes A/B |
|---|---|---|---|---|---|---|---|---|---|---|---|
| **3***a* | Acétone-$d_6$ | A + B | +33 | 4,84 | 4,61 | 4,14 | 3,87 | 2,83 | 2,18 | — | 68/32 |
| | | A | −90 | 5,01 | 4,54 | 4,30 | 3,63 | 3,21 | 2,18 | — | 75 |
| | | B | −90 | 4,92 | 4,69 | 4,56 | 3,89 | — | 2,35 | — | 25 |
| **3***e* | $CS_2$ | A + B | +33 | 4,71 | 4,55 | 4,11 | 3,44 | — | 2,10 | [c] | 73/17 |
| | | A | −90 | 4,77 | 4,43 | 4,33 | 3,26 | — | 2,18 | [c] | 88 |
| | | B | −90 | 4,74 | 4,24 | 3,82 | 3,42 | — | 1,90 | [c] | 12 |
| **3***i* | Acétone-$d_6$ | A + B | +33 | 4,80 | 4,68 | 4,31 | 3,54 | — | 2,67<br>0,97 | 0,93 | 80/20 |
| | | A | −90 | 4,97 | 4,63 | 4,53 | 3,50 | — | 2,82<br>0,93 | 0,80 | 92 |
| | | B | −90 | — | — | 3,95 | 3,80 | — | 2,57<br>0,92 | 1,41 | 8 |

[a] Spectre enregistré à 100 MHz.
[b] Même remarque que dans le tableau 2 sauf pour 3*a* dont les pourcentages à température ambiante ont été calculés à partir de ΔI, ΔII, Δν pour les protons 2e–2a et 4,6e–4,6a.
[c] Massif élargi.
[d] Les solvants ont été choisis en fonction de la solubilité des produits et de la résolution du spectre de rmn à basse température.

composés précédents, il semblerait d'après les valeurs des déplacements chimiques du groupement méthyle de l'acétyle dans les deux conformations A et B que celle qui est privilégiée soit celle ou *ce groupement est en position équatoriale*. Cette hypothèse est encore confirmée par les valeurs des constantes de couplage relevées pour les deux conformères:

$$A \begin{cases} {}^3J_{4a-5} = 11\,Hz \\ {}^3J_{4e-5} = 4\,Hz \end{cases}$$ en accord avec $H_5$ axial

$$B \begin{cases} {}^3J_{4a-5} = 3{,}8\,Hz \\ {}^3J_{4e-5} = 1\,Hz \end{cases}$$ en accord avec $H_5$ équatorial

De même, l'enregistrement du spectre du com-

Can. J. Chem. Downloaded from www.nrcresearchpress.com by 210.87.254.105 on 09/06/12
For personal use only.

TABLEAU 6. Déplacement chimique des carbones (en ppm/TMS) des dioxannes-1,3 **3***a*–**3***i*

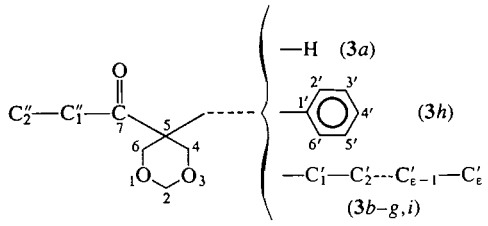


| Produit | R'' | R' | Cycle dioxannique δC2 | δC4,6 | δC5 | δC7 | C=O δC''1 | R'' δC''2 | δC'1 | R' δC'2 | δC'3 | δC'4 | δC'5 | δC'6 | δC'7 | δC'8 | δC'9 |
|---|---|---|---|---|---|---|---|---|---|---|---|---|---|---|---|---|---|
| **3***a* | $CH_3$ | H | 93,9 | 67,3 | 48,3 | 206,7 | 28,9 | — | — | — | — | — | — | — | — | — | — |
| **3***b* | $CH_3$ | $CH_3$ | 93,9 | 72,9 | 47,4 | 209,9 | 26,1 | — | 17,5 | — | — | — | — | — | — | — | — |
| **3***c* | $CH_3$ | $C_2H_5$ | 94,2 | 72,0 | 51,1 | 209,7 | 27,0 | — | 25,2 | 7,8 | — | — | — | — | — | — | — |
| **3***d* | $CH_3$ | *i*-$C_3H_7$ | 94,0 | 71,4 | 53,2 | 209,8 | 28,8 | — | 30,9 | 17,4 | — | — | — | — | — | — | — |
| **3***e* | $CH_3$ | *n*-$C_4H_9$ | 94,1 | 72,2 | 50,9 | 209,9 | 27,0 | — | 23,2 | 32,1 | 25,5 | 13,7 | — | — | — | — | — |
| **3***f* | $CH_3$ | *n*-$C_7H_{15}$ | 94,2 | 72,3 | 51,0 | 209,9 | 27,0 | — | 23,4 | 30,1 | 32,5 | 28,9 | 31,8 | 22,6 | 14,0 | — | — |
| **3***g* | $CH_3$ | *n*-$C_9H_{19}$ | 94,2 | 72,3 | 51,0 | 209,8 | 27,0 | — | 23,4 | 29,5 | 32,5 | 29,3 | 30,1 | 29,3 | 31,9 | 22,7 | 14,1 |
| **3***h* | $CH_3$ | $C_6H_5$ | 94,0 | 71,7 | 54,6 | 206,2 | 26,0 | — | 136,1 | 126,0 | 129,2 | 128,1 | 129,2 | 126,0 | — | — | — |
| **3***i* | $C_2H_5$ | $CH_3$ | 94,0 | 73,1 | 47,3 | 212,3 | 31,3 | 7,5 | 17,9 | — | — | — | — | — | — | — | — |

posé **3***a*, en présence de sel lanthanide dans le chloroforme, confirme que le conformère majoritaire a le groupement acétyle en position équatoriale. En utilisant le sel d'europium $Eu(fod)_3$ en quantités croissantes, les déplacements chimiques des divers protons varient linéairement pour un rapport ρ entre la concentration de ce sel et celle du composé **3***a* allant jusqu'à 0,45. Par ailleurs, on observe que les constantes de couplage vicinales $^3J_{4a-5}$ et $^3J_{4e-5}$ diminuent lorsque ρ augmente ce ceci d'une façon plus marquée quand ce rapport est supérieur à 0,45.

$$\rho = 0 \begin{cases} J_{4a-5} = 7{,}8\ \text{Hz} \\ J_{4e-5} = 4{,}1\ \text{Hz} \end{cases} \qquad \rho = 0{,}6 \begin{cases} {}^3J_{4a-5} = 6{,}4\ \text{Hz} \\ {}^3J_{4e-5} = 3{,}5\ \text{Hz} \end{cases}$$

La variation de ces constantes de couplage en fonction de la quantité de sel traduit une évolution de l'équilibre entre les deux conformations (20, 21). Cette évolution se fait dans le sens de la formation du complexe le plus stable, c'est-à-dire, dans ce cas, vers le complexe où le groupement acétyle du composé dioxannique est en position axiale. Ceci permettant ainsi (Fig. 2) une complexation tridentate, en général plus stable.

Ceci confirme que le conformère ayant les constantes de couplage vicinales les plus faibles est celui où le groupement acétyle est en position axiale, c'est-à-dire la forme **3***a* A.

3. *Étude des composés* **3**j *à* **3**v

Mis à part, les cas où R' est différent de H (**3***k–m*, Tableau 2) les spectres obtenus sont difficilement

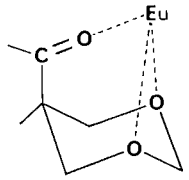


FIG. 2. Complexation tridentate de l'acétyl-5 dioxanne-1,3.

interprétables en ce qui concerne les protons 5, 4e, 4a, 6e, 6a car ils résonnent sous forme d'un massif complexe en raison de l'effet déblindant du groupe acyle aromatique sur le proton 5. Contrairement aux cas des dioxannes comportant un groupement acyle aliphatique, une étude à basse température ne nous a pas permis de déterminer la conformation privilégiée de ces dérivés. Leur température de coalescence, de l'ordre de −90°C, ne nous permet pas d'obtenir un spectre interprétable, compte tenu des limites de l'appareil utilisé (−100°C). Toutefois, en dessous de la température de coalescence (−95°C), nous n'observons pas l'apparition d'un deuxième conformère, ce qui semble indiquer que l'un des conformères est majoritaire à un pourcentage supérieur ou égal à 90%.

*Simulation des spectres (250 MHz) et utilisation d'un sel d'europium ($Eu(fod)_3$)*

En utilisant ces deux techniques, nous avons pu déterminer les déplacements chimiques (cf. Tableau 2) et les constantes de couplage pour les protons des dioxannes **3***j*, **3***n* et **3***o*. Le fait que les constantes $^3J_{4a-5}$ et $^3J_{4e-5}$ aient, pour ces trois composés, des valeurs de 8,8 et 3,6 Hz respec-

Can. J. Chem. Downloaded from www.nrcresearchpress.com by 210.87.254.105 on 09/06/12
For personal use only.

Can. J. Chem. Downloaded from www.nrcresearchpress.com by 210.87.254.105 on 09/06/12
For personal use only.



TABLEAU 7. Déplacement chimiques des carbones (en ppm/IMS) des dioxannes-1,3 **3***j*–**3***v* ($CDCl_3$: 15,08 MHz)

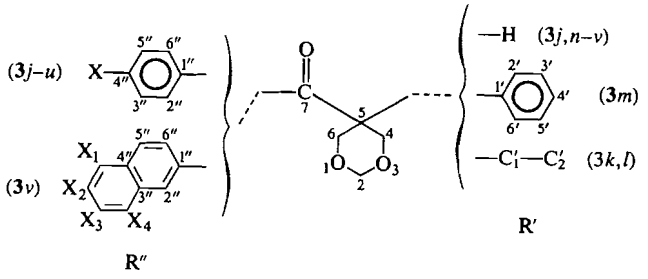


| Produit | R″ | R′ | Cycle dioxannique $\delta C_2$ | $\delta C_{4,6}$ | $\delta C_5$ | C=O $\delta C_7$ | R″ $\delta C''_1$ | $\delta C''_{2,6}$ | $\delta C''_{3,5}$ | $\delta C''_4$ | R′ $\delta C'_1$ | $\delta C'_2$ | $\delta C'_3$ | $\delta C'_4$ | X $\delta CX_1$ | $\delta CX_2$ | $\delta CX_3$ | $\delta CX_4$ |
|---|---|---|---|---|---|---|---|---|---|---|---|---|---|---|---|---|---|---|
| **3***j* | $C_6H_5$ | H | 94,0 | 68,6 | 43,8 | 198,1 | 135,9 | 129,0 | 128,3 | 133,7 | — | — | — | — | — | — | — | — |
| **3***k* | $C_6H_5$ | $CH_3$ | 94,0 | 73,4 | 47,6 | 205,3 | 138,1 | 127,5 | 128,4 | 131,4 | 18,9 | — | — | — | — | — | — | — |
| **3***l* | $C_6H_5$ | $C_2H_5$ | 94,0 | 71,9 | 51,5 | 204,7 | 138,7 | 127,2 | 128,4 | 131,3 | 25,2 | 8,1 | — | — | — | — | — | — |
| **3***m* | $C_6H_5$ | $C_6H_5$ | 94,0 | 72,8 | 53,8 | 200,6 | 137,4 | 128,7 | 128,3 | 131,9 | 136,8 | 126,5 | 129,4 | 127,5 | — | — | — | — |
| **3***n*[a] | 4-F-$C_6H_4$ | H | 94,0 | 68,6 | 43,8 | 196,5 | 132,3$_5$ | 131,0$_5$ | 116,1$_5$ | 166,1 | — | — | — | — | — | — | — | — |
| **3***o* | 4-Cl-$C_6H_4$ | H | 94,0 | 68,5 | 43,9 | 196,9 | 134,2 | 129,3 | 129,8 | 140,3 | — | — | — | — | — | — | — | — |
| **3***p* | 4-CN-$C_6H_4$ | H | 93,9 | 68,0 | 44,0 | 197,2 | 138,6 | 128,7 | 132,9 | 116,9 | — | — | — | — | 117,8 | — | — | — |
| **3***q* | 4-$NO_2$-$C_6H_4$ | H | 94,0 | 68,0 | 44,3 | 197,0 | 140,1 | 129,3 | 124,2 | 150,7 | — | — | — | — | — | — | — | — |
| **3***r* | 4-$CH_3$-$C_6H_4$ | H | 93,9 | 68,7 | 43,7 | 197,6 | 133,4 | 128,5 | 129,6 | 144,6 | — | — | — | — | 21,6 | — | — | — |
| **3***s* | 4-$C_6H_5$-$C_6H_4$ | H | 93,9 | 68,4 | 43,7 | 197,5 | 134,4 | 128,9 | 127,2 | 146,1 | — | — | — | — | 139,4 | 127,2 | 128,9 | 128,4 |
| **3***t* | 4-$CH_3$-O-$C_6H_4$ | H | 93,9 | 68,7 | 43,5 | 196,5 | 128,9 | 130,7 | 114,2 | 164,1 | — | — | — | — | 55,5 | — | — | — |
| **3***u* | 4-$C_6H_5$-O-$C_6H_4$ | H | 93,7 | 68,4 | 43,4 | 196,2 | 132,0 | 130,5 | 117,2 | 162,4 | — | — | — | — | 155,2 | 120,1 | 130,1 | 124,8 |
| **3***v* | 2-$C_{10}H_7$ | H | 93,9 | 68,6 | 43,8 | 197,8 | 132,9 | 2″ 128,8<br>6″ 126,9 | 3″ 132,5<br>5″ 128,8 | 135,7 | — | — | — | — | 130,1 | 123,6 | 127,7 | 129,6 |

[a] $^4J_{C''_1-F} = 2{,}7$ Hz; $^3J_{C''_2-F} = 9{,}9$ Hz; $^2J_{C''_3-F} = 21{,}7$ Hz; $^1J_{C''_4-F} = 255{,}9$ Hz.

tivement, permet de conclure que le groupement acyle aromatique est vraisemblablement en position équatoriale.

## Conclusion

D'après les résultats obtenus au cours de ce travail, nous pouvons conclure que pour un groupement acyle aliphatique (*i*) la conformation privilégiée des acyl-5 alkyl-5 dioxanne-1,3 a le groupement acyle en position axiale, et (*ii*) la conformation privilégiée de l'acétyl-5 dioxanne-1,3 a ce même groupement en position équatoriale.

Il est raisonnable de penser que cette inversion de conformation constatée pour l'acétyl-5 dioxanne-1,3 est liée au fait que, vu la faible polarité du carbonyle, la stabilisation de l'hétérocycle apportée par les interactions électroniques des trois oxygènes, lorsque ce groupement est en position axiale, n'est pas suffisante en l'absence d'un deuxième substituant en position 5 sur le cycle.

Pour un groupement acyle aromatique, la conformation ou ce groupement est équatorial est très fortement privilégiée. Par ailleurs, l'analyse cristallographique de quelques uns de ces composés (22) a montré, sans ambiguité, qu'à l'état solide, le groupement aroyle est équatorial.

## Partie expérimentale

Les spectres de rmn du proton ont été enregistrés sur un appareil Varian T60 travaillant à 60 MHz pour des solutions environ *M*/20 dans le chloroforme deutérié (sauf indication contraire) avec le TMS comme référence interne.

Les études particulières ont été effectuées dans les conditions suivantes.

*Les spectres de rmn à basse température*

Les spectres ont été enregistrés sur un appareil Varian HA100 travaillant à 100 MHz. Les solvants (sulfure de carbone ou acétone deutérié) ont été choisis en fonction de la solubilité respective à basse température des composés étudiés.

*Les spectres de rmn à 250 MHz*

Les spectres ont été obtenus sur un appareil Cameca 250 travaillant à 250 MHz pour des solutions *M*/40 dans le chloroforme deutérié.

*Les spectres de rmn en présence d'Eu (fod)*$_3$

Les spectres ont été enregistrés sur un appareil Bruker WH90 travaillant à 90 MHz en transformé de Fourier pour des solutions dans le chloroforme deutérié.

*Les spectres de rmn du carbone-treize*

Les spectres ont été enregistrés sur un appareil Bruker WP60 travaillant à 15,08 MHz pour des solutions environ *M* dans le chloroforme deutérié avec le TMS comme référence interne.

Les déplacements chimiques ainsi déterminés sont rassemblés dans les tableaux 6 et 7 ci-dessous.


1. E. L. Eliel, N. L. Allinger, S. J. Angyal et G. A. Morrison. Conformational analysis. Wiley Interscience, New York. 1965. p. 249.
2. E. L. Eliel. Bull. Soc. Chim. Fr. 517 (1970).
3. E. L. Eliel. Angew. Chim. Int. Ed. Engl. **11**, 739 (1972), et références citées.
4. K. Pihlaja. Acta Chim. Scand. **21**, 2430 (1967).
5. H. Friebolin, H. G. Schmid, S. Kabuss et W. Faisst. Org. Magn. Reson. **1**, 67 (1969).
6. M. J. O. Anteunis. Conformational analysis. Academic Press, New York. 1971. p. 31, et références citées.
7. P. Maroni, L. Cazaux, J. P. Gorrichon, P. Tisnes et J. G. Wolf. Org. Magn. Reson. **5**, 517 (1973); **5**, 523 (1973).
8. L. Cazaux, J. P. Gorrichon et P. Maroni. Can. J. Chem. **56**, 2998 (1978); **56**, 3006 (1978); **56**, 3016 (1978).
9. J. P. Gorrichon, A. Gaset et M. Delmas. Synthesis, 219 (1979).
10. M. Delmas, A. Denis, J. P. Gorrichon et A. Gaset. Synth. Commun. **10**, 517 (1980).
11. R. N. Booher, S. E. Smits, W. W. Turner et A. Pohland. J. Med. Chim. **20**, 885 (1977).
12. J. Gelan et M. J. O. Anteunis. Bull. Soc. Chim. Belg. **78**, 599 (1969).
13. E. L. Eliel et R. M. Enanoza. J. Am. Chem. Soc. **94**, 8072 (1972).
14. H. G. Schmid, H. Friebolin, S. Kabuss et R. Mecke. Spectrochim. Acta, **22**, 623 (1966).
15. T. A. Crabb et R. F. Newton. Tetrahedron, **26**, 693 (1968).
16. E. Coene et M. J. O. Anteunis. Bull. Soc. Chim. Belg. **79**, 25 (1970).
17. M. J. O. Anteunis, W. Vandenbroucke et N. Schamp. Bull. Soc. Chim. Belg. **76**, 552 (1967).
18. J. E. Anderson. J. Chem. Soc. B, 712 (1967).
19. E. Coene et M. J. O. Anteunis. Tetrahedron Lett. 595 (1970).
20. W. G. Bentrude, H. W. Tan et K. C. Yee. J. Am. Chem. Soc. **94**, 3264 (1972).
21. K. C. Yee et W. G. Bentrude. Tetrahedron Lett. 2775 (1971).
22. M. Delmas, J. P. Gorrichon, A. Gaset, R. Roques, J. P. deClerq et G. Germain. Acta Crystallogr. Sect. B, **37**, 621 (1980).


Can. J. Chem. Downloaded from www.nrcresearchpress.com by 210.87.254.105 on 09/06/12
For personal use only.

# Gas-phase infrared laser spectroscopy of bound hydrogen-bonded systems

FA-MEI WANG, KHALID IQBAL, HANS-GEORG KRAFT, MARK LUCKSTEAD, WILLIAM C. EUE, AND JOHN W. BEVAN

*Chemistry Department, Texas A&M University, College Station, TX 77843, U.S.A.*

Received February 1, 1982

FA-MEI WANG, KHALID IQBAL, HANS-GEORG KRAFT, MARK LUCKSTEAD, WILLIAM C. EUE, and JOHN W. BEVAN. Can. J. Chem. **60**, 1969 (1982).

Application of tunable infrared lasers to the spectroscopic investigation of equilibrium, gaseous hydrogen-bonded systems is demonstrated. Broadband spectra of the $n\nu_6 + \nu_1 - n\nu_6$ vibrations in HCN---HF and $CH_3CN$---HF have been recorded with a computer-controlled multimode color center laser using both conventional absorption and infrared-acoustic detection methods.

FA-MEI WANG, KHALID IQBAL, HANS-GEORG KRAFT, MARK LUCKSTEAD, WILLIAM C. EUE et JOHN W. BEVAN. Can. J. Chem. **60**, 1969 (1982).

On démontre l'application des lasers à infrarouge réglables à l'étude spectroscopique de l'équilibre des systèmes gazeux ayant des liaisons hydrogènes. On a enregistré les larges bandes des spectres des vibration $n\nu_6 + \nu_1 - n\nu_6$ des systèmes HCN---HF et $CH_3CN$---HF à l'aide d'un laser multimode à centre coloré contrôlé par ordinateur et utilisant comme méthodes de détection tant l'absorption conventionnelle que l'acoustique infrarouge.

[Traduit par le journal]

## Introduction

Infrared spectroscopy has long been recognized as a physico-chemical technique capable of providing fundamental information concerning the nature of bound chemically important hydrogen-bonded systems (1, 2). The majority of these studies have been conducted in the condensed phase where these weakly bound species are sensitive to environmental perturbations which have limited the extent of information which can be determined from this data. Spectroscopic investigations of gaseous equilibrium mixtures (3–5), molecular beam (6), or supersonic jet (7) hydrogen-bonded species offer the opportunity of studying these species in an isolated situation. Infrared spectroscopic studies have been limited to investigations involving classical instrumentation on gas-phase mixtures. However, sensitive high resolution spectroscopic techniques are necessary to resolve the fine structure of vibrational bands associated with these hydrogen-bonded species.

The recent availability of tunable infrared lasers provides the opportunity to observe Doppler-limited and sub-Doppler spectra for such systems. The latter being fundamental to a detailed analysis of the nature of proton dynamics in hydrogen-bonded systems. Broadband laser spectra of these vibrations are an important preliminary to such high resolution Doppler-limited or sub-Doppler analysis and subsequent investigation of proton dynamics in these systems.

## Experimental

Spectra were obtained using a Burleigh Instruments FCL-20 color center laser operating multimode pumped by a Spectra Physics 171-01 Krypton ion laser (Fig. 1). The KCl:Li color center laser crystal used in this research has a maximum output power of 70 mW per watt at 2.69 μm when pumped single line with the 6471 Å output of the pump laser. The multimode infrared laser output has a linewidth of approximately 0.2 $cm^{-1}$ and is tunable from 3448 to 4167 $cm^{-1}$.

The optical cavity of a color center laser is an astigmatically compensated folded mirror system. The end and folding mirrors are enclosed in an evacuated crystal chamber and the output coupler, a precision diffraction grating, served also as a tuning element. The linewidth of the color center laser is homogeneously broadened at liquid nitrogen temperature, oscillation consisting of a fundamental and one or more spatial hole burning modes with a frequency separation of 6.0 GHz

$$\Delta\nu_M = \frac{nc}{4z} \text{ where } n = 1,3,5,\cdots$$

and $z$ is the separation between the crystal and the closest cavity end mirror and $c$ the speed of light.

A North-American Philips K82430 Stepper Motor was connected to the grating drive of the color center laser to scan it. A Micromation Z-64 microcomputer was chosen to control the laser system. An interface board was designed using 4N33 optical isolators to prevent voltage spikes from entering the computer and an SAA-1027 driver for bi-directional control.

The photovoltaic detector in conventional absorption studies utilized an Infrared Industries 2304 PbS detector and LM004 precision operational amplifiers. The infrared-acoustic detector employed was a small-volume non-resonant detector utilizing a BT-1834 Knowles miniature microphone (8). The microphone was carefully prepared to be resistant to the highly corrosive hydrogen-fluoride gas. Output signals of these detectors were applied to a PARC HR-8 lock-in amplifier. The outputs produced from the latter were either applied directly to the recorder or collected by the computer, processed, and then presented.

The hydrogen fluoride was obtained from Matheson and used with purification while spectrograde $CH_3CN$ was used following drying and distillation over calcium hydride. HCN was prepared under vacuum from the action of 50% $H_2SO_4$:$H_2O$ mixtures on KCN. It was collected and dried over $P_2O_5$ following trap-to-trap distillation to remove $CO_2$.

Vacuum lines, cells, and valves were constructed of stainless steel or Teflon with Viton "O" rings to prevent corrosive action

0008-4042/82/151969-03$01.00/0

©1982 National Research Council of Canada/Conseil national de recherches du Canada

Can. J. Chem. Downloaded from www.nrcresearchpress.com by 210.87.254.6 on 09/06/12
For personal use only.

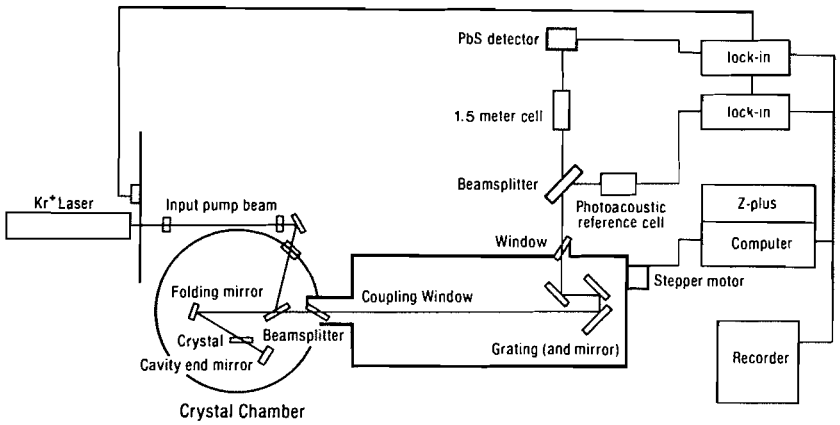


FIG. 1. Experimental arrangement for recording broadband gas-phase hydrogen-bonded spectra.

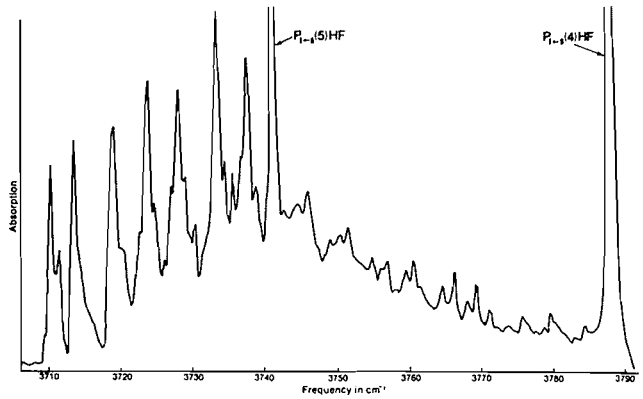


FIG. 2. Broadband laser absorption spectrum of the $n\nu_6 + \nu_1 - n\nu_6$ vibrational band in HCN---HF. $n = 7$ is overlapped by $P_{1\leftarrow 0}(5)$ transition of free HF.

by HF. Conventional absorption studies were carried out with a 1.5 m cell with $CaF_2$ windows.

## Results and discussion

A tunable-laser conventional absorption scan from 3700 to 3800 $cm^{-1}$ is shown in Fig. 2 for an equilibrium gaseous mixture of HCN (50 Torr) and HF (50 Torr) at 300 K. The frequencies of the major features have been measured previously and interpreted as P bandheads associated with the $n\nu_6 + \nu_1 - n\nu_6$ vibration of the HCN---HF hydrogen-bonded complex (5). A better resolved spectrum of the first seven members of this series is shown in Fig. 3. The frequencies of the most prominent of these features at peak maximum have been measured and included in Table 1 with an estimated absolute accuracy of 0.05 $cm^{-1}$. Certain P bandheads are sufficiently resolved from each other to permit rotational–vibrational parameters to be fitted to their experimentally observed spectral profiles. Lorentzian intensity-profiles chosen to represent individual unresolved rotational–vibrational transitions are integrated in these model calculations and molecular parameters varied to simulate the data. Neglecting centrifugal distortion and utilizing (9):

$$\nu = \nu_0 + (B_1 + B_0)m + (B_1 - B_0)m^2 \quad (2)$$

with $B_0 = 0.1197\ cm^{-1}$ (determined from microwave spectroscopy (10)); $B_1$ can be estimated as $0.1219 \pm 0.0003\ cm^{-1}$ for the first P bandhead within the limits of this approximation. The fit also permits a corrected $\nu_0$ frequency to be evaluated as $3714.2 \pm 0.5\ cm^{-1}$ at the band origin.

Other resolved features are apparent (Table 1, Column 2) in the spectrum and are under current investigation.

The infrared-acoustic spectrum (11) of an equilibrium gas mixture of $CH_3CN$ and HF (10 Torr of each, $T = 300$ K) is shown in Fig. 4. The P bandheads are numbered for the first eight members although an extensive number of additional members can be discerned (Table 1). Substructure is also evident in this spectrum for the initial members of the series. The effective interaction pathlength used to record this spectrum is less than 1 cm, indicating that infrared-acoustic laser spec-

Can. J. Chem. Downloaded from www.nrcresearchpress.com by 210.87.254.6 on 09/06/12
For personal use only.

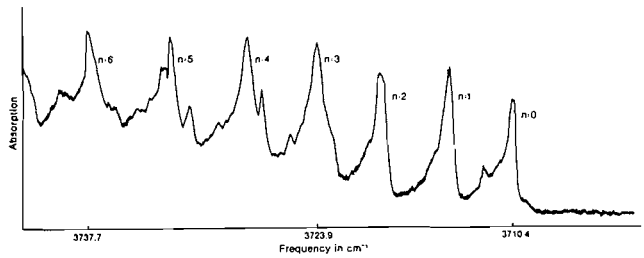


FIG. 3. P-bandheads associated with first seven members of the $n\nu_6 + \nu_1 - n\nu_6$ vibrational band in HCN---HF.

TABLE 1. Frequencies* of $n\nu_6 + \nu_1 - n\nu_6$ bandheads in HCN---HF and $CH_3CN$---HF

| | HCN—HF | | $CH_3CN$—HF |
|---|---|---|---|
| $n$ | Primary series | Subseries | Primary series |
| 0 | 3710.4 | 3711.8 | 3673.5 |
| 1 | 3714.6 | | 3676.1 |
| 2 | 3719.2 | | 3678.5 |
| 3 | 3723.9 | 3724.8 | 3681.4 |
| 4 | 3728.2 | 3729.1 | 3683.7 |
| | | 3730.8 | |
| 5 | 3733.5 | 3734.6 | 3687.2 |
| 6 | 3737.7 | 3739.1 | 3689.6 |
| 7 | — | — | 3692.0 |
| 8 | 3746.2 | 3744.6 | |
| 9 | 3751.8 | 3749.3 | |
| | | 3750.4 | |
| 10 | 3757.3 | 3755.2 | |
| | | 3756.4 | |
| 11 | 3760.7 | 3759.9 | |
| 12 | 3766.6 | 3764.8 | |

*Frequencies are in wavenumber ($cm^{-1}$). The accuracy is $\pm 0.5 cm^{-1}$.

troscopy has considerable potential in the investigation of gas-phase hydrogen-bonded species.

## Conclusion

The $n\nu_6 + \nu_1 - n\nu_6$ bandheads in the hydrogen-bonded complexes HCN---HF and $CH_3CN$---HF have been recorded using conventional absorption and infrared-acoustic spectroscopy with a tunable infrared laser respectively. In both cases there is significant improvement in resolution in these pressure-broadened spectra relative to those recorded previously using classical spectroscopic techniques. The reported results form an important preliminary to spectroscopic investigations at much higher resolution using the laser system. Introduction of an intracavity etalon into the color center laser enables its output linewidth to be reduced to $\leq 7$ MHz, permitting application of Doppler-limited and sub-Doppler techniques. Such experiments are in progress.

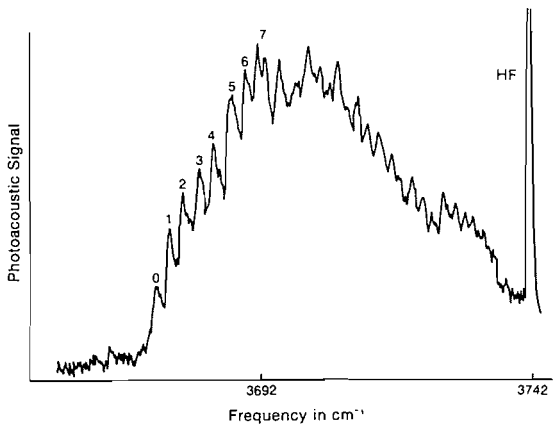


FIG. 4. Broadband infrared-acoustic spectrum of $n\nu_6 + \nu_1 - n\nu_6$ vibrational band of $CH_3CN$---HF.

## Acknowledgements

We would like to express our appreciation to the National Science Foundation (CHE 79-23237), The Robert A. Welch Foundation (Grant A747), and The Research Corporation for supporting this research. M. Eliades is also thanked for technical assistance.

1. D. HADZI and H. W. THOMPSON (*Editors*). Hydrogen bonding. Proceedings of the First International Conference on Hydrogen Bonding, Ljubljana. Pergamon Press, New York. 1957.
2. P. SCHUSTER, G. ZUNDAL, and C. SANDORFY (*Editors*). The hydrogen bond. North Holland, New York. 1976.
3. J. E. BERTIE and D. J. MILLEN. J. Chem. Soc. 497 (1965); 514 (1965).
4. R. K. THOMAS and SIR H. THOMPSON. Proc. R. Soc. London, **316**A, 303 (1970).
5. R. K. THOMAS. Proc. R. Soc. London, **325**A, 133 (1971).
6. T. E. GOUGH, R. E. MILLER, and G. SCOLES. Appl. Phys. Lett. **30**, 338 (1977).
7. D. N. TRAVIS, J. C. MCGURK, D. MCKEOWN, and D. G. DENNING. Chem. Phys. Lett. **45**, 287 (1977).
8. H. G. KRAFT and J. W. BEVAN. Infrared Phys. To be published.
9. G. M. HERZBERG. Infrared and Raman spectra. Van Nostrand. 1945.
10. A. C. LEGON, D. J. MILLEN, and S. C. ROGERS. Proc. R. Soc. A**370**, 213 (1980).
11. Y. H. PAO. Optoacoustic spectroscopy and detection. Academic Press, New York. 1977.

Can. J. Chem. Downloaded from www.nrcresearchpress.com by 210.87.254.6 on 09/06/12
For personal use only.

# Infrared spectra of the ammonium ion in crystals. Part XII. Low-temperature transitions in ammonium dichromate, $(NH_4)_2Cr_2O_7$[1,2]

GÁBOR KERESZTURY[3] AND OSVALD KNOP

*Department of Chemistry, Dalhousie University, Halifax, N.S., Canada B3H 4J3*

AND

MICHAEL FALK

*Atlantic Research Laboratory, National Research Council of Canada, Halifax, N.S., Canada B3H 3Z1*

Received December 11, 1981

GÁBOR KERESZTURY, OSVALD KNOP, and MICHAEL FALK. Can. J. Chem. **60**, 1972 (1982).

Examination of the infrared spectra of the probe ions $NH_3D^+$ and $NHD_3^+$ in ammonium dichromate confirms the existence of the lowest ($T_{tr} \sim 125$ K) of the three transitions that are known, from nonspectroscopic evidence, to occur in this crystal below room temperature. Below $T_{tr}$ the ammonium ions are of two types, in an abundance ratio of 1:1 and both of symmetry $C_1$. Above $T_{tr}$ the probe ion spectra are difficult to interpret in detail. The strength of the hydrogen-bonding interactions covers a wide range, as indicated by the difference between the highest and the lowest values of the isotopically isolated ND stretching frequencies at 10 K, 2392 and 2234 $cm^{-1}$.

GÁBOR KERESZTURY, OSVALD KNOP et MICHAEL FALK. Can. J. Chem. **60**, 1972 (1982).

L'examen des spectres infrarouges des ions $NH_3D^+$ et $NHD_3^+$, étudiés dans le dichromate d'ammonium, confirme l'existence de la plus basse ($T_{tr} \approx 125$ K) des trois transitions qui, d'après des preuves non spectroscopiques, se produisent dans ce cristal à basse température. En dessous de $T_{tr}$, les ions ammonium sont de deux types, avec un rapport d'abondance de 1:1 et les deux ont une symétrie $C_1$. En dessus de $T_{tr}$, il est difficile d'interpréter en détail les spectres de l'ion étudié. La force des interactions des liaisons hydrogènes s'étend sur un large domaine, telle que l'indique la différence entre les plus grandes et les plus faibles valeurs des fréquences de vibration ND isolé d'une façon isotopique à 10 K, 2392 et 2234 $cm^{-1}$.

[Traduit par le journal]

At room temperature the $(NH_4)_2Cr_2O_7$ crystal ($C2/c$, $Z = 4$) contains a single type of ammonium ion, at sites of symmetry $C_1$ (2, 3). The positions of the H atoms have not been determined, but the ammonium ion must be regarded as hydrogen-bonded: each N atom is surrounded irregularly by eight oxygens at distances ranging from ca. 2.83 to ca. 3.17 Å, all of them different, and there is another oxygen at ca. 3.50 Å. On cooling, three transitions have been detected (4) by DTA, calorimetry, and dilatometry, at 268(3), 155(5), and 128(5) K. The total volume of a $(NH_4)_2Cr_2O_7$ crystal varied smoothly on passage through the three transition temperatures, but at 128 K there was an anisotropic discontinuity in the individual dimensions of the crystal; the energy changes associated with the transitions were judged to be small, and the transitions at 155 and 268 K were described as second-degree.

The transition at 268 K appears to correspond to a change of slope in the spin–lattice relaxation time vs. temperature plot for the dichromate (5). Evidence from ir (6–8) and $^2H$ nmr (9) spectra in support of the existence of low-temperature transitions in $(NH_4)_2Cr_2O_7$ and $(ND_4)_2Cr_2O_7$ has also been presented, but no information on the symmetry of any of the low-temperature phases. In the following we report on such observations and conclusions as are obtainable from the temperature variation of the ir spectra of the $NH_3D^+$ and $NHD_3^+$ probe ions in $(NH_4)_2Cr_2O_7$ and $(ND_4)_2Cr_2O_7$, respectively, between 10 and 293 K.

*Spectrum of $NH_3D^+$ in $(NH_4)_2Cr_2O_7$*

For a single type of ammonium ion of symmetry $C_1$ the ir spectrum of the $NH_3D^+$ probe ion, if fully resolved, should contain four $\nu_1(NH_3D^+)$ absorptions in the ND stretching region and eight $\nu_{4bc}(NH_3D^+)$ absorptions in the ND bending region (cf. refs. 10–12), and this would be the situation if the room-temperature crystal structure of the dichromate remained unchanged on cooling. However, at 10 K the ND stretching region of $(NH_4)_2Cr_2O_7$ (4% D) was found to consist of eight clearly resolved $\nu_1$ component bands (Fig. 1), indicative of *two* types of ammonium ion of symmetry $C_1$ in a 1:1 abundance ratio. The octet persisted up to 80 K, at which temperature it began to broaden and collapse to a quartet. This collapse was complete at 120(15) K (Fig. 2*A*), coincident with the transition at 128(5) K detected by calorimetry (4).

[1] For Part XI, see ref. 1.

[2] NRCC No. 20231.

[3] Permanent address: Central Research Institute for Chemistry, Hungarian Academy of Sciences, Pusztaszeri út 59-67, Budapest, H-1025, Hungary.

0008-4042/82/151972-06$01.00/0

©1982 National Research Council of Canada/Conseil national de recherches du Canada

Can. J. Chem. Downloaded from www.nrcresearchpress.com by 210.87.254.6 on 09/06/12
For personal use only.

Can. J. Chem. Downloaded from www.nrcresearchpress.com by 210.87.254.6 on 09/06/12
For personal use only.

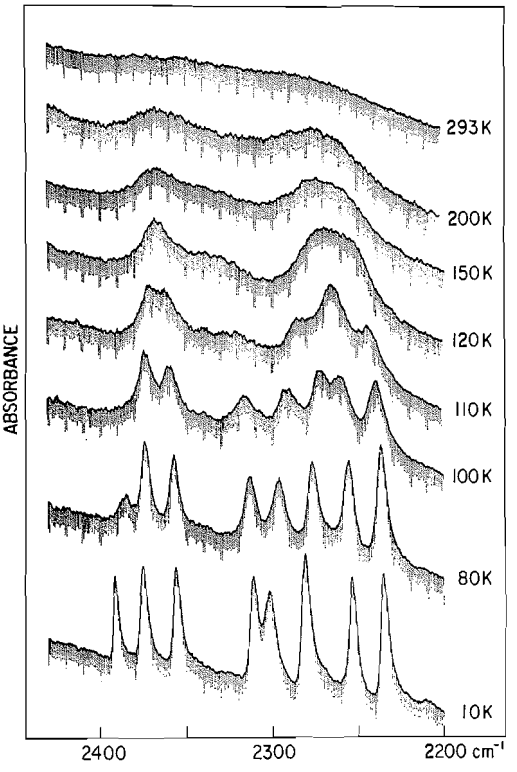


FIG. 1. Spectra of $(NH_4)_2Cr_2O_7$ (4% D) in the region of the ND stretching fundamental $\nu_1(NH_3D^+)$ of the $NH_3D^+$ probe ion at different temperatures.

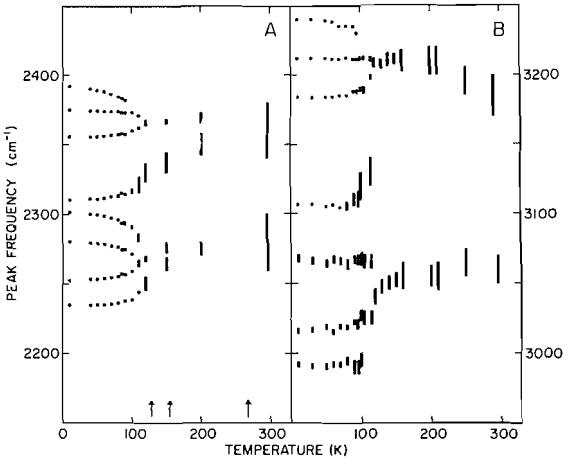


FIG. 2. Temperature variation of peak frequencies of (*A*) the ND stretching fundamental (from Fig. 1) and (*B*) the NH stretching fundamental (from Fig. 5). The arrows correspond to the calorimetrically etc. detected transitions in $(NH_4)_2Cr_2O_7$ (4).

The four bands remained resolved up to 150 K, but on further heating they gradually merged until only two very broad bands were observed at room temperature. The spectra above 120 K were consistent with the expectation from the room-temperature crystal structure; the large halfwidths and the increasingly poor quality of the spectra precluded any conclusions regarding the transitions at 155 and 168 K.

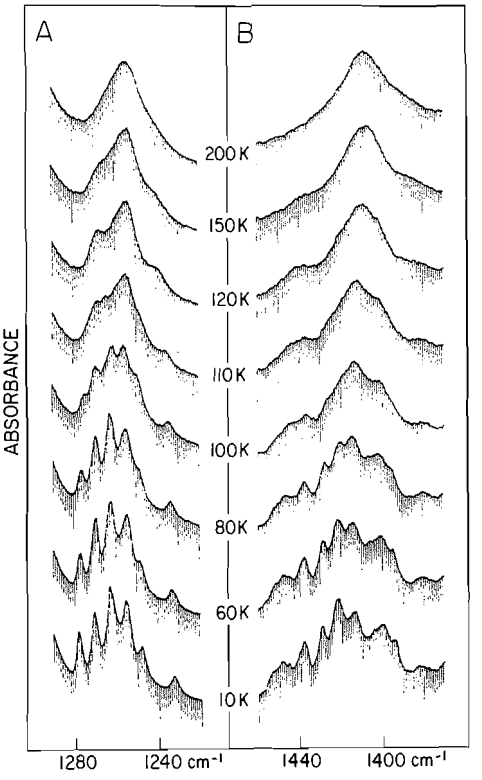


FIG. 3. Spectra in the region of (*A*) the ND bending fundamental $\nu_{4bc}(NH_3D^+)$ of $NH_3D^+$ in $(NH_4)_2Cr_2O_7$ (4% D) and (*B*) the NH bending fundamental $\nu_2(NHD_3^+)$ of $NHD_3^+$ in $(NH_4)_2Cr_2O_7$ (95% D).

The $\nu_{4bc}(NH_3D^+)$ absorption in the ND deformation region (Fig. 3*A*) consisted of six resolved components up to 100 K; these broadened with increasing temperature until only one broad band remained above about 200 K. The resolution of this composite absorption was inadequate for a specific conclusion but not incompatible with the better resolved $\nu_1$ absorption from which one would expect 16 $\nu_{4bc}$ components at low temperatures and 8 $\nu_{4bc}$ components at the higher temperatures. As shown in the plot of the resolved frequencies vs. temperature (Fig. 4), the six-band system collapsed at first, fairly sharply, to a triplet at 120(10) K and then, more gradually, to a singlet at 175(25) K. These spectral changes appear to correspond to the transitions at 128 and 155 K. No conclusion can be made regarding the transition at 268 K.

Can. J. Chem. Downloaded from www.nrcresearchpress.com by 210.87.254.6 on 09/06/12
For personal use only.

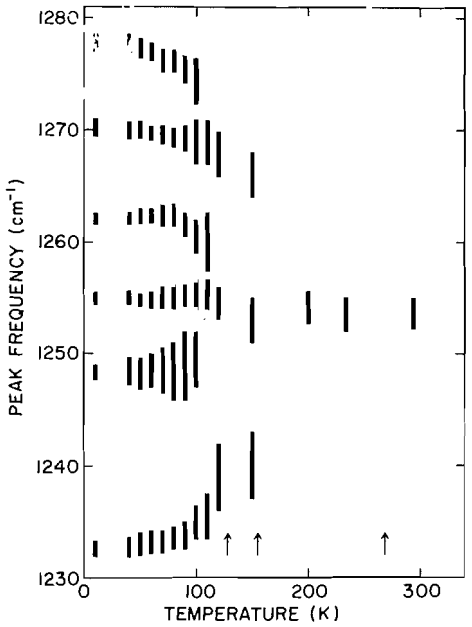


FIG. 4. Temperature variation of the peak frequencies of the ND bending fundamental $\nu_{4bc}(NH_3D^+)$ (from Fig. 3*A*).

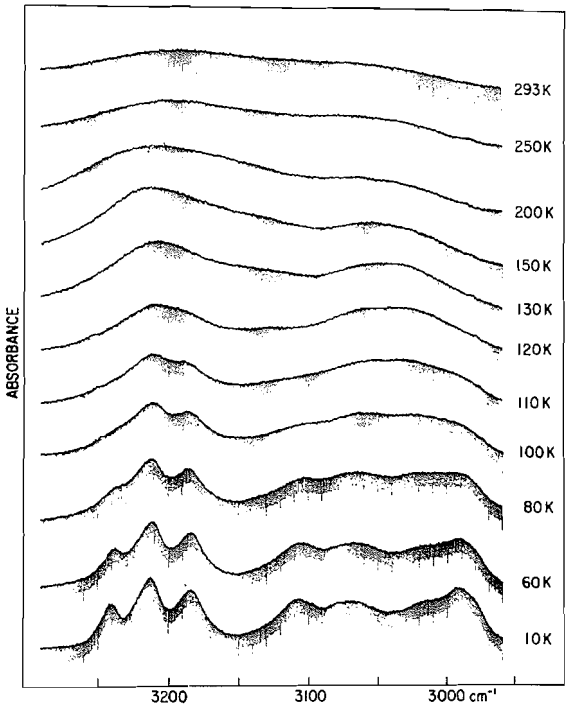


FIG. 5. Spectra in the region of the NH stretching fundamental $\nu_1(NHD_3^+)$ of the $NHD_3^+$ probe ion in $(NH_4)_2Cr_2O_7$ (95% D).

*Spectrum of $NHD_3^+$ in $(ND_4)_2Cr_2O_7$*

The spectra of the $NHD_3^+$ probe ion in $(ND_4)_2Cr_2O_7$ in the NH stretching and deformation regions corresponded closely to the ND stretching and deformation bands of $NH_3D^+$ in $(NH_4)_2Cr_2O_7$. In the NH stretching region at 10 K the $\nu_1(NHD_3^+)$ multiplet consisted of seven resolved peaks (Fig. 5) which clearly correspond to the $\nu_1(NH_3D^+)$ components in $(NH_4)_2Cr_2O_7$ (Table 1). The plot of the $\nu_1(NHD_3^+)$ component frequencies vs. temperature (Fig. 2*B*) parallels the corresponding $\nu_1(NH_3D^+)$ vs. *T* plot of Fig. 2*A*. The collapse of the low-temperature multiplet, which occurred at about 125 K, indicates that the temperature of the lowest transition in the undeuterated and the deuterated dichromate cannot differ by any substantial amount.

The counterpart, in the NH bending region, of $\nu_{4bc}(NH_3D^+)$ is $\nu_2(NHD_3^+)$ (cf. ref. 13). At 10 K at least 12 partially resolved components were discernible in the $\nu_2(NHD_3^+)$ absorption of $(NH_4)_2Cr_2O_7$ (95% D) (Fig. 3*B*). These broadened and collapsed with increasing temperature to a single broad band at room temperature. The collapse occurred in the same temperature region, 130(10) K, as the collapse of the low-temperature $\nu_1(NHD_3^+)$ multiplet.

*Comparison of the NH and ND features*

The NH/ND frequency ratio for the $\nu_1(NH_3D^+)$ and $\nu_1(NHD_3^+)$ absorptions decreased significantly and regularly with frequency (Table 1). This decrease is attributed to the gradually increasing anharmonicity of the NH stretching frequency with the increasing strength of the hydrogen bonding. A similar behaviour has been found for the OH/OD vibrational frequencies of HDO in a number of crystals (14) and solvents (M. Falk, unpublished results).

TABLE 1. Frequencies ($cm^{-1}$) of the $NH_3D^+$ and $NHD_3^+$ probe ions in $(NH_4)_2Cr_2O_7$ and $(ND_4)_2Cr_2O_7$, respectively, at 10 K

| $\nu_1(NH_3D^+)$ | $\nu_1(NHD_3^+)$ | Ratio |
|---|---|---|
| 2391.7(2) | 3240.8(5) | 1.3550(3) |
| 2374.5(2) | 3212.8(5) | 1.3530(3) |
| 2355.5(3) | 3184.5(12) | 1.3519(7) |
| 2310.3(3)<br>2301.2(3) | 3106.0(15) | 1.3471(8) |
| 2280.3(3) | 3067.0(30) | 1.3450(15) |
| 2252.4(3) | 3015.0(50) | 1.3386(22) |
| 2234.2(3) | 2991.0(20) | 1.3387(11) |

The NH stretching bands had much larger halfwidths than the corresponding ND stretching bands, 16 $cm^{-1}$ for the narrowest $\nu_1(NHD_3^+)$ component at 10 K compared with 3 $cm^{-1}$ for the narrowest $\nu_1(NH_3D^+)$ component at the same temperature. We are currently investigating to what

Can. J. Chem. Downloaded from www.nrcresearchpress.com by 210.87.254.6 on 09/06/12
For personal use only.

extent this difference is due to an intrinsically larger bandwidth of the NH absorptions (over and above that arising from the difference in the relative frequency scale for NH and ND) and hope to discuss our findings elsewhere.

*Temperature dependence of $\nu_4(NH_4^+)$ and $\nu_4(ND_4^+)$*

Although our concern was with the probe ion spectra, we used the opportunity to record the spectra of $(NH_4)_2Cr_2O_7$ in the region of $\nu_4(NH_4^+)$ and those of $(ND_4)_2Cr_2O_7$ in the region of $\nu_4(ND_4^+)$ (Fig. 6), i.e. the absorptions described in refs. 6–8. The $\nu_4(ND_4^+)$ spectra were found to resemble closely those of Fig. 1 of ref. 7 and Fig. 9 of ref. 8, allowing for an improved instrumental resolution. At 10 K five well-resolved peaks and a shoulder[4] were present, their frequencies agreeing within 0.5 $cm^{-1}$ with the frequencies at 17 K reported in Table 3 of ref. 8. The $\nu_4(NH_4^+)$ spectra, however, differed from those reported in refs. 6 and 8. Unlike the latter, they were very similar to the $\nu_4(ND_4^+)$ spectra. At 10 to 70 K, six resolved peaks and two shoulders are seen in our spectra (Fig. 6*A*), in contrast to Fig. 7 of ref. 8, which shows two peaks and some poorly resolved shoulders at 17 K and a different intensity distribution across the composite band. The origin of these differences is not likely to be in the lower instrumental resolution. A possible explanation of this discrepancy might be sought in an incomplete transformation on cooling of the higher phase (i.e. residual supercooling of the 128 K transition) in the sample studied in refs. 6 and 8.

Temperature increase produced broadening and collapse of both the $\nu_4(NH_4^+)$ and $\nu_4(ND_4^+)$ multiplets until at room temperature only one broad absorption was observed. The spectral changes occurred most rapidly around 130 K (Fig. 7), and there was no substantial difference between $(NH_4)_2Cr_2O_7$ and $(ND_4)_2Cr_2O_7$. The gradual changes observed in our $\nu_4(ND_4^+)$ spectra between 50 and 100 K do not support the existence of a transition around 80 K in $(ND_4)_2Cr_2O_7$, tentatively proposed in refs. 7 and 8.

*Thermal collapse of isotopically isolated NH and ND absorptions*

The gradual broadening and eventual collapse of multiplets with increasing temperature were seen particularly clearly in the case of the NH and ND stretching absorptions (Fig. 2). Examples of this

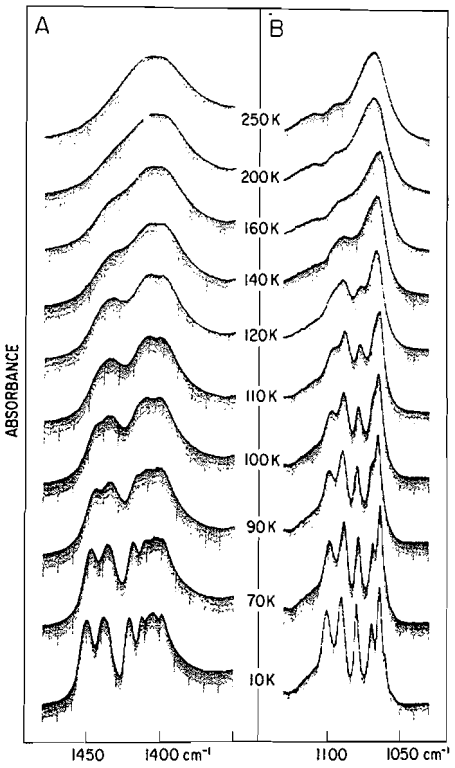


FIG. 6. Spectra in the region of (*A*) the $\nu_4(NH_4^+)$ fundamental of $NH_4^+$ in $(NH_4)_2Cr_2O_7$ (0% D) and (*B*) the $\nu_4(ND_4^+)$ fundamental of $ND_4^+$ in $(NH_4)_2Cr_2O_7$ (95% D). The small bands near 1095 and 1110 $cm^{-1}$ visible at the higher temperatures are probably due to $NHD_3^+$.

behaviour have been reported previously (for $\nu_1(NH_3D^+)$ in $NH_4SnF_3$ and $NH_4CuSO_3$, ref. 15), and several more instances have been noted since (1, 12, 16), including a particularly striking one in the ND stretching region of the spectrum of $NH_4ClO_4$ (results to be published).

It has been suggested (15) that the most important mechanism of such gradual collapse of NH and ND stretching multiplets involves the rapidly increasing thermal amplitude of certain low-frequency motions (mainly librations) of the ammonium ion. This mechanism is characteristic of potential energy functions with very flat, possibly multiple minima; it was invoked earlier (17, 18) to account for a similar thermal collapse of multiplets observed in the spectra of HDO in crystalline hydrates. A quantitative treatment of the phenomenon has recently been proposed by Corn and Strauss (ref. 19 and personal communication).

*Strength of hydrogen bonding*

The frequencies of the $\nu_1(NH_3D^+)$ components at 10 K (Table 1) span a range of 2234–2392 $cm^{-1}$, i.e. almost as wide as the ranges observed in

[4]This shoulder (at 1060 $cm^{-1}$) is not included in Fig. 7, as its frequency cannot be determined with any certainty even at 50 K.

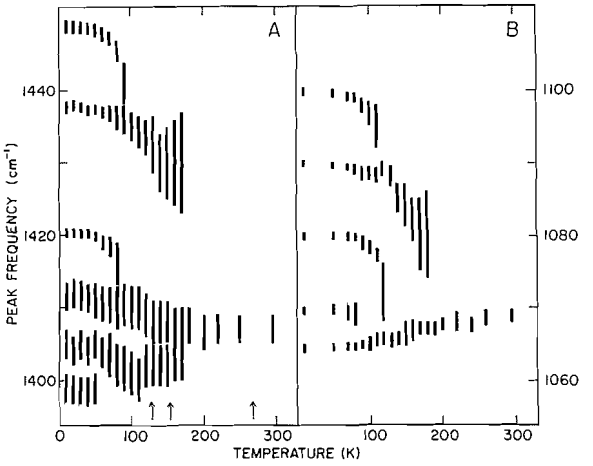


FIG. 7. Temperature variation of the frequencies from Fig. 6.

$NH_4CuSO_3$ (15), $NH_4SnF_3$ (15), and $(NH_4)_2SO_4$ (G. Keresztury, O. Knop, and M. Falk, to be published), which are the widest (~2230 – ~2430 $cm^{-1}$) noted for an ammonium salt to date. This frequency spread indicates a considerable difference in the strength of the individual N—H···O bonds in the lowest-temperature form of the dichromate. The statement (20) that the hydrogen bonding in ammonium dichromate is weak is thus inaccurate, for while the frequency of the highest $\nu_1(NH_3D^+)$ component corresponds clearly to a very weak hydrogen bond, the frequency of the lowest $\nu_1(NH_3D^+)$ component approaches that observed for this fundamental in the strongly hydrogen-bonded $NH_4F$, ~2181 $cm^{-1}$ at 10 K (11). Judging by the clearly discernible anomalous temperature dependence of the frequencies of the 2392, 2374, 2301, and 2280 $cm^{-1}$ absorptions the corresponding hydrogen bonds must be strongly bent and to more than one oxygen acceptor each (cf. ref. 16). This is not surprising if one considers the room-temperature crystal structure; the environments of the ammonium ions in the lowest phase are not likely to be less complicated.

Although the diffuseness of the $\nu_1$ spectra above 130 K makes a precise statement difficult, the evolution of the $\nu_1$ component frequencies with temperature (Fig. 2) does appear to support a general improvement of the hydrogen bonding on cooling through the lowest $T_{tr}$, with some bonds being weakened but others appreciably strengthened. The $\nu_1$ frequency vs. $T$ plots are also suggestive of a specific hydrogen-bonding scheme: at room temperature two of the N—H bonds of the ammonium ion engage in a weaker and the other two in a stronger hydrogen bonding. On cooling through the lowest transition temperature the single set of ammonium ions splits into two nonequivalent sets, but in both sets an ion again contains a pair of weakly and a pair of more strongly engaged N—H bonds.

It is not clear how such a hydrogen-bonding scheme can be reconciled with a mechanism of reorientation of the ammonium ion between 130 K and room temperature that operates with an activation energy of only 4.5 kJ/mol (ref. 5; cf. also refs. 20–22), i.e. about one-third that in simple cubic $NH_4I$, and in particular with the reorientation taking place about "random" axes, as proposed in ref. 20.

## Conclusions

Infrared spectra of the $NH_3D^+$ and $NHD_3^+$ probe ions recorded between 10 and 293 K confirm the existence, in $(NH_4)_2Cr_2O_7$, of a transition the temperature of which had been previously (4) determined as 128(5) K by nonspectroscopic methods. The corresponding transition in $(ND_4)_2Cr_2O_7$ occurs at a similar temperature. The number of components of the $\nu_1(NH_3D^+)$ and $\nu_1(NHD_3^+)$ absorptions between 10 K and this transition temperature indicates the existence of two nonequivalent sets of ammonium ions of $C_1$ symmetry in the low-temperature phase, in a 1:1 abundance ratio. The temperature coefficients of the $\nu_1$ component frequencies suggest that some of the N—H···O bonds are strongly bent and to more than one oxygen acceptor each. The strength of the hydrogen bonding has a wide range.

Above 130 K the well-defined absorptions in the probe-ion spectra of the low-temperature phase merge and the spectra become diffuse. The spectral features persisting above 130 K are compatible with a single set of ammonium ions of $C_1$ symmetry, as required by the room-temperature crystal structure, but they do not permit conclusions as to the nature of the other two transitions detected by nonspectroscopic methods, at 155(5) and 268(3) K.

## Experimental

Reagent-grade $(NH_4)_2Cr_2O_7$ was deuterated by recrystallization from solutions in $H_2O$–$D_2O$ mixtures of the appropriate composition. Nujol or fluorocarbon mulls were sandwiched between $CaF_2$, AgCl, or Irtran-2 windows. The ir spectra were recorded with a Perkin-Elmer model 180 spectrophotometer fitted with a closed-cycle He refrigerator (Displex model 202, Air Products and Chemicals Co.).

The error bars in Figs. 2, 4, and 7 correspond to standard errors calculated from several duplicate sets of spectra in some cases and estimated from the noise level and peak sharpness in others.

## Acknowledgment

This investigation was supported by a research grant from the Natural Sciences and Engineering Research Council of Canada to one of the authors (O.K.).

Can. J. Chem. Downloaded from www.nrcresearchpress.com by 210.87.254.6 on 09/06/12
For personal use only.

1. O. KNOP, I. A. OXTON, W. J. WESTERHAUS, and M. FALK. J. Chem. Soc. Faraday 2, **77**, 811 (1981).
2. A. BYSTRÖM and K. A. WILHELMI. Acta Chem. Scand. **5**, 1003 (1951).
3. G. A. P. DALGAARD, A. C. HAZELL, and R. GRØNBÆK HAZELL. Acta Chem. Scand. **28**, 541 (1974).
4. J. JAFFRAY. C.R. **241**, 1114 (1955).
5. F. KÖKSAL and S. BAHÇELİ. J. Chem. Soc. Faraday 2, **74**, 1844 (1978).
6. C. J. H. SCHUTTE and A. M. HEYNS. Chem. Phys. Lett. **1**, 487 (1968).
7. C. J. H. SCHUTTE and A. M. HEYNS. Chem. Phys. Lett. **1**, 515 (1968).
8. C. J. H. SCHUTTE and A. M. HEYNS. J. Mol. Struct. **5**, 37 (1970).
9. S. D. DAMLE, L. C. GUPTA, and R. VIJAYARAGHAVAN. Chem. Phys. Lett. **37**, 614 (1976).
10. I. A. OXTON, O. KNOP, and M. FALK. J. Phys. Chem. **80**, 1212 (1976).
11. O. KNOP, I. A. OXTON, and M. FALK. Can. J. Chem. **57**, 404 (1979); **57**, 2003 (1979).
12. O. KNOP, I. A. OXTON, W. J. WESTERHAUS, and M. FALK. J. Chem. Soc. Faraday 2, **77**, 309 (1981).
13. I. A. OXTON, O. KNOP, and M. FALK. Can. J. Chem. **53**, 2675 (1975).
14. B. BERGLUND, J. LINDGREN, and J. TEGENFELD. J. Mol. Struct. **43**, 169 (1978).
15. O. KNOP, W. J. WESTERHAUS, and M. FALK. Can. J. Chem. **58**, 270 (1980).
16. O. KNOP, W. J. WESTERHAUS, and M. FALK. Can. J. Chem. **58**, 867 (1980).
17. G. BRINK and M. FALK. Can. J. Chem. **48**, 2096 (1970).
18. G. BRINK and M. FALK. Can. J. Chem. **49**, 347 (1971).
19. R. M. CORN and H. L. STRAUSS. J. Chem. Phys. In press.
20. R. E. RICHARDS and T. SCHAEFER. Trans. Faraday Soc. **57**, 210 (1961).
21. J. J. RUSH, T. I. TAYLOR, and W. W. HAVENS, JR. J. Chem. Phys. **37**, 234 (1962).
22. P. S. LEUNG, J. J. RUSH, and T. I. TAYLOR. J. Chem. Phys. **57**, 175 (1972).

Can. J. Chem. Downloaded from www.nrcresearchpress.com by 210.87.254.6 on 09/06/12
For personal use only.

# The least-squares intersection of a family of lines and its application to phase equilibria

JOHN W. LORIMER

*Department of Chemistry, University of Western Ontario, London, Ont., Canada N6A 5B7*

Received January 19, 1982

JOHN W. LORIMER. Can. J. Chem. **60**, 1978 (1982).

A generalized least-squares method is described for finding the point of intersection of a family of straight lines, each of which is defined by two experimental points. It is shown that the method of the least-squares triangle (Can. J. Chem. **59**, 3076 (1981)) is a good first approximation to the general method. An example demonstrates the method of iteration of both parameters and observations for a problem involving evaluation of solid phase compositions from solubility measurements.

JOHN W. LORIMER. Can. J. Chem. **60**, 1978 (1982).

On décrit une méthode des moindres carrés généralisés qui permet de calculer les coordonnées d'intersection d'une famille de lignes droites, dont chacune est définie par deux points expérimentaux. On démontre que la méthode des triangles moindres carrés (Can. J. Chem. **59**, 3076 (1981)) est une assez bonne approximation initiale de la méthode générale. Un exemple numérique démontre la méthode d'itération à la fois des observations et des paramètres dans un calcul pour évaluer les compositions de phases solides à partir de données de solubilité.

Can. J. Chem. Downloaded from www.nrcresearchpress.com by 210.87.254.40 on 09/06/12
For personal use only.

## Introduction

In a previous paper (1) (referred to hereafter as **I**), a least-squares method was developed for finding the coordinates of the common point of intersection of a family of straight lines, each member of which is defined by two points only. An example is provided by tie-lines which pass through experimental solubility and wet residue composition points in a multicomponent system. The method fixed the point of intersection by minimizing the sum of squares of the areas of all triangles formed by the point of intersection and pairs of solubility and wet residue points. In this paper, another method (referred to briefly in **I**) is investigated. It is based on standard non-linear least-squares procedures (2, 3) that are used widely in surveying and photogrammetry, but do not appear to be well known in other fields. Although the basic equations seem at first glance to differ from those for the least-squares triangle, it will be shown that the least-squares triangle, as described in **I**, is a first (and reasonably good) approximation to the more general method. For simplicity, only lines in two-dimensional space will be considered. Generalization to multi-dimensional space is straightforward, but as pointed out in **I**, is usually not necessary for practical calculations involving solubility equilibria.

## Theory

### *(a) The generalized least-squares equations*

The equation of the straight line through the points $x_{k1}'$, $x_{k2}'$ (representing the solubility), $x_{k1}''$, $x_{k2}''$ (representing the wet residue or initial composition), and $x_1$, $x_2$ is

$$[1]\quad f_k = (x_{k2}' - x_{k2}'')(x_{k1}' - x_1) - (x_{k1}' - x_{k1}'')(x_{k2}' - x_2) = 0 \qquad k = 1, \ldots, p$$

If $x_1, x_2$ are the coordinates of the common point of intersection of $p$ such lines, then there are $p - 2$ degrees of freedom. In practice, each point has an associated error, so that eq. [1] is written as

$$[2]\quad f_k = (x_{k2}'^{0} + \delta x_{k2}' - x_{k2}''^{0} - \delta x_{k2}'')(x_{k1}'^{0} + \delta x_{k1}' - x_1^{0} - \delta x_1) - (x_{k1}'^{0} + \delta x_{k1}' - x_{k1}''^{0} - \delta x_{k1}'')(x_{k2}'^{0} + \delta x_{k2}' - x_2^{0} - \delta x_2) = 0 \qquad k = 1, \ldots, p$$

where the superscript zero signifies an approximate value. To the first order in small quantities, this equation can be written as

$$[3]\quad f_k^{0} + \mathbf{E}_k \delta \mathbf{l}_k + \mathbf{G}_k \delta = 0 \qquad k = 1, \ldots, p$$

where the matrices (with their orders) are

$$[4]\quad \mathbf{E}_k = [x_2^{0} - x_{k2}''^{0}\; x_{k1}''^{0} - x_1^{0}\; x_{k2}'^{0} - x_2^{0}\; x_1^{0} - x_{k1}'^{0}] \qquad (1 \times 4)$$

$$[5]\quad \delta \mathbf{l}_k = [\delta x_{k1}'\quad \delta x_{k2}'\quad \delta x_{k1}''\quad \delta x_{k2}'']^{t} \qquad (4 \times 1)$$

$$[6]\quad \mathbf{G}_k = [x_{k2}''^{0} - x_{k2}'^{0}\quad x_{k1}'^{0} - x_{k1}''^{0}] \qquad (1 \times 2)$$

$$[7]\quad \delta = [\delta x_1\quad \delta x_2]^{t} \qquad (2 \times 1)$$

In these equations, superscript t indicates the transpose. The equations can also be obtained by the more general method (2, 3) of expanding $f_k$ in a Taylor series about $f_k^{0}$ and computing the derivatives. Matrix $\mathbf{E}_k$ is the Jacobian matrix of $f_k$ with respect to $\mathbf{l}_k$. If $\hat{\mathbf{l}}_k$, $\mathbf{l}_k$ are the matrices of least-square estimates of the observations and the observations

0008-4042/82/151978-04$01.00/0

©1982 National Research Council of Canada/Conseil national de recherches du Canada

Can. J. Chem. Downloaded from www.nrcresearchpress.com by 210.87.254.40 on 09/06/12
For personal use only.

themselves, their difference defines the deviation matrix $\mathbf{v}_k$. Similarly, the difference between $\hat{\mathbf{l}}_k$ and $\mathbf{l}_k{}^o$ defines matrix $\delta\mathbf{l}_k$. Thus,

[8] $\hat{\mathbf{l}}_k = \mathbf{l}_k + \mathbf{v}_k = \mathbf{l}_k{}^o + \delta\mathbf{l}_k$

and eq. [3] can be rewritten in terms of $\mathbf{v}_k$ as

[9] $\mathbf{E}_k\mathbf{v}_k + \mathbf{G}_k\delta = -f_k{}^o - \mathbf{E}_k(\mathbf{l}_k - \mathbf{l}_k{}^o) \equiv F_k{}^o$

For all $p$ equations of this type,

[10] $$\begin{bmatrix} \mathbf{E}_1 & \mathbf{0} & \cdots & \mathbf{0} \\ \mathbf{0} & \mathbf{E}_2 & \cdots & \mathbf{0} \\ \vdots & \vdots & & \vdots \\ \mathbf{0} & \mathbf{0} & \cdots & \mathbf{E}_p \end{bmatrix} \begin{bmatrix} \mathbf{v}_1 \\ \mathbf{v}_2 \\ \vdots \\ \mathbf{v}_p \end{bmatrix} + \begin{bmatrix} \mathbf{G}_1 \\ \mathbf{G}_2 \\ \vdots \\ \mathbf{G}_p \end{bmatrix} \delta = \begin{bmatrix} F_1{}^o \\ F_2{}^o \\ \vdots \\ F_p{}^o \end{bmatrix}$$

or

[11] $$\underset{p\times 4p}{\mathbf{E}} \quad \underset{4p\times 1}{\mathbf{v}} + \underset{p\times 2}{\mathbf{G}} \quad \underset{2\times 1}{\delta} = \underset{p\times 1}{\mathbf{F}^o}$$

To obtain least-squares estimates of the correction matrices $\mathbf{v}$ and $\delta$, the function

[12] $\phi = \mathbf{v}^t\mathbf{W}\mathbf{v} - 2\mathbf{k}^t(\mathbf{E}\mathbf{v} + \mathbf{G}\delta - \mathbf{F}^o)$

is minimized with respect to $\mathbf{v}$ and $\delta$. In eq. [12], $\mathbf{W}$ is the $4p \times 4p$ weight matrix of the observations $\mathbf{l}$, and $\mathbf{k}$ is a $p \times 1$ matrix of Lagrange multipliers, so that $\phi$ is the weighted sum of squares of deviations modified by the constraints given by eq. [11]. Equation [12] is now in standard form, and the minimization results are as deduced in ref. 3:

[13] $\delta = \mathbf{N}^{-1}\mathbf{T}$ $(2 \times 1)$

where

[14] $\mathbf{N} = \mathbf{G}^t(\mathbf{E}\mathbf{W}^{-1}\mathbf{E}^t)^{-1}\mathbf{G}$ $(2 \times 2)$

[15] $\mathbf{T} = \mathbf{G}^t(\mathbf{E}\mathbf{W}^{-1}\mathbf{E}^t)^{-1}\mathbf{F}^o$ $(2 \times 1)$

The deviation matrix is

[16] $\mathbf{v} = \mathbf{W}^{-1}\mathbf{E}^t(\mathbf{E}\mathbf{W}^{-1}\mathbf{E}^t)^{-1}(\mathbf{F}^o - \mathbf{G}\delta)$

and an unbiased estimate of the variance is

[17] $\hat{\sigma}^2 = \mathbf{v}^t\mathbf{W}\mathbf{v}/(p - 2)$
$= \{\mathbf{F}^{ot}(\mathbf{E}\mathbf{W}^{-1}\mathbf{E}^t)^{-1}\mathbf{F}^o - \delta^t\mathbf{T}\}/(p - 2)$

The estimated covariance matrix is the same for the corrections $\delta$ and the parameters $\mathbf{x}$:

[18] $\hat{\mathbf{M}}_\delta = \hat{\mathbf{M}}_x = \hat{\sigma}^2\mathbf{N}^{-1}$

The covariance matrix of the functions $\mathbf{F}^o$ follows from the facts that (as noted above) $\mathbf{E}$ is the Jacobian matrix $\partial\mathbf{F}^o/\partial\mathbf{l}$ and that the covariance matrix of the l-values is $\langle\mathbf{v}\mathbf{v}^t\rangle = \sigma^2\mathbf{W}^{-1}$, where $\sigma^2$ is the variance of an observation of unit weight and $\mathbf{W}_F$ is the weight matrix of $\mathbf{F}^o$:

[19] $\mathbf{M}_{F^o} = \langle\mathbf{F}^o\mathbf{F}^{ot}\rangle = \sigma^2\mathbf{E}\mathbf{W}^{-1}\mathbf{E}^t = \sigma^2\mathbf{W}_F{}^{-1}$

This matrix will be diagonal with $p$ scalar elements $\sigma^2(\mathbf{E}\mathbf{W}^{-1}\mathbf{E}^t)_k$ if $\mathbf{W}$ is diagonal (i.e., the observations are uncorrelated) (3). Matrixes $\mathbf{N}$ and $\mathbf{T}$ can be shown easily to be the sums

[20] $\mathbf{N} = \sum_{k=1}^{p} \{\mathbf{G}^t(\mathbf{E}\mathbf{W}^{-1}\mathbf{E}^t)^{-1}\mathbf{G}\}_k$

[21] $\mathbf{T} = \sum_{k=1}^{p} \{\mathbf{G}^t(\mathbf{E}\mathbf{W}^{-1}\mathbf{E}^t)^{-1}\mathbf{F}^o\}_k$

*(b) Practical equations for computations*

Although the above equations can be used as given, it is more useful to calculate the various matrices explicitly. Equation [4] gives

[22] $(\mathbf{W}_F{}^{-1})_k \equiv (\mathbf{E}\mathbf{W}^{-1}\mathbf{E}^t)_k = (x_2{}^o - x_{k2}{}''{}^o)^2 W_{x_{k1}'}{}^{-1} + (x_1{}^o - x_{k1}{}''{}^o)^2 W_{x_{k2}'}{}^{-1} + (x_2{}^o - x_{k2}{}'{}^o)^2 W_{x_{k1}''}{}^{-1} + (x_1{}^o - x_{k1}{}'{}^o)^2 W_{x_{k2}''}{}^{-1}$

while matrices $\mathbf{N}$ and $\mathbf{T}$ are found to be identical to matrices $\mathbf{B}$ and $\mathbf{C} - \mathbf{B}\mathbf{x}^o$, respectively, as defined in eqs. [12] and [14] of **I**, provided that $\sigma_{Ak}{}^2$ in **I** is interpreted as $\sigma^2(\mathbf{W}_F{}^{-1})_k$ in eq. [22] (see below for justification), the matrix $\mathbf{l}$ is taken as the matrix $\mathbf{l}^o$, and $y_{ki} = x_{ki}{}'{}^o - x_{ki}{}''{}^o$. Thus, eq. [13] gives

[23] $\delta = \mathbf{B}^{-1}\mathbf{C} - \mathbf{x}^o$

so that the matrix product $\mathbf{B}^{-1}\mathbf{C}$ gives a direct least-squares estimate of the parameters $\mathbf{x}$, just as in **I**.

In most problems in phase equilibria, $\mathbf{W}^{-1} = \mathbf{I}$ is a reasonable assumption. As a first approximation, it is assumed that $\mathbf{l} = \mathbf{l}^o$ (i.e., $\mathbf{v} = \Delta\mathbf{l}$), $(\mathbf{W}_F{}^{-1})_k = 1$. Next, $\mathbf{x}^o = \mathbf{B}^{-1}\mathbf{C}$ is calculated, this value is used in eq. [22] to compute the weights, and a further iteration gives the corrections $\delta$ and $\mathbf{v}$. Updated approximations

[24] $\mathbf{x}^o = \mathbf{x}^o + \delta$, $\hat{\mathbf{l}} = \mathbf{l} + \mathbf{v}$

are then found, and the equations are iterated until convergence is reached. Note that the corrections $\delta$

Can. J. Chem. Downloaded from www.nrcresearchpress.com by 210.87.254.40 on 09/06/12
For personal use only.

are applied to the previous values of $\mathbf{x}^o$, but that the corrections $\mathbf{v}$ are applied to the initial values $\mathbf{l}$. For problems in phase equilibria, a satisfactory criterion of convergence is $\delta_{max} < \varepsilon$, where $\varepsilon$ is the maximum incremental correction to any parameter; a reasonable value is often 0.005 mass%. The computation is completed by finding the final values of $\hat{\sigma}^2$ and $\hat{\mathbf{M}}_x$, noting that the second term in eq. [17] should be negligible compared to the first when convergence is reached.

In **I**, the effect of the distance between the points $\mathbf{x}_k'$ and $\mathbf{x}_k''$ was investigated by taking

$$[25] \quad \mathbf{y}_k = \mathbf{x}_k' - \mathbf{x}_k'' = L(\mathbf{x}_k' - \mathbf{x}) + \delta\mathbf{y}_k$$

where $L$ is the distance between these points divided by the distance between points $\mathbf{x}_k'$ and $\mathbf{x}$, and $\delta\mathbf{y}_k$ is a random error. If $\delta\mathbf{y}_k \ll L(\mathbf{x}_k' - \mathbf{x})$, substitution of eq. [25] into eq. [22] shows that (for $\mathbf{W} = \mathbf{I}$) the weights $(\mathbf{W}_F^{-1})_k$ each contain the factor $L^2 - 2L + 2$. Matrices $\mathbf{N}$ and $\mathbf{T}$ each contain the factor $L^2/(L^2 - 2L + 2)$, so that $\delta$ is independent of $L$, $\hat{\sigma}^2$ (eq. [17]) is independent of $L$, but $\hat{\mathbf{M}}_x$ (eq. [18]) varies as $1 - 2/L + 2/L^2$. This latter variation is roughly the same as $1/L^2$, so that the standard deviations of the parameters are roughly inversely proportional to $L$, just as in **I**.

*(c) Relation to the least-squares triangle*

Equation [11] can be written as

$$[26] \quad \mathbf{Ev} = \mathbf{F}$$

where

$$[27] \quad \mathbf{F} = \mathbf{F}^o - \mathbf{G}\delta$$

is the matrix with elements

$$[28] \quad F_k = -\mathbf{E}_k(\mathbf{l}_k - \mathbf{l}_k^o) - y_{k2}^o(x_{k1}'^o - x_1) + y_{k1}^o(x_{k2}'^o - x_2)$$

Using the fact that $\mathbf{M}_{F^o}$ is diagonal, it is found from eqs. [16] and [27] that

$$[29] \quad \mathbf{v}^t\mathbf{W}\mathbf{v} = \sigma^2\mathbf{F}^t\mathbf{M}_F^{-1}\mathbf{F} = \mathbf{F}^t\mathbf{W}_F\mathbf{F}$$

where, from eq. [26],

$$[30] \quad \mathbf{M}_F \simeq \sigma^2\mathbf{E}\mathbf{W}^{-1}\mathbf{E}^t = \mathbf{M}_{F^o}$$

is the variance matrix for $\mathbf{F}$. Equations [29] and [30] complete the demonstration that minimizing the weighted sum of squares of the deviations $\mathbf{v}$ is equivalent to minimizing the weighted sum of squares of the functions $\mathbf{F}$. Furthermore, if $\mathbf{l}_k = \mathbf{l}_k^o$, the functions $\mathbf{F}_k$ are each equal to twice the area of the triangle formed by points $\mathbf{x}_k'$, $\mathbf{x}_k''$, and $\mathbf{x}$, so that eq. [29] is also four times the weighted sum of squares of these areas. In **I**, it should be noted that the variance matrix of area $\alpha$ (or $\pm\mathbf{F}/2$ in the present notation) was given as $\langle\alpha\alpha^t\rangle$, while the correct value is eq. [30], which can also be calculated directly as

$$[31] \quad \mathbf{M}_F = \sigma^2\mathbf{J}_l\mathbf{W}^{-1}\mathbf{J}_l^t \simeq \sigma^2\mathbf{E}\mathbf{W}^{-1}\mathbf{E}^t$$

where $\mathbf{J}_l$ is the Jacobian matrix with elements $\partial\alpha/\partial\mathbf{l}$.

When $\mathbf{l}$ and $\mathbf{l}^o$ are not equal, the function $\mathbf{F}^t\mathbf{W}_F\mathbf{F}$ in eq. [29] has to be minimized with respect to both $\mathbf{x}$ and $\mathbf{v}$, subject to the constraint of eq. [26]. This procedure is relatively complicated, because matrices $\mathbf{F}$ and $\mathbf{E}$ are both functions of $\mathbf{x}$. Therefore, the practical theory for iterations on both parameters and observations is that based on eq. [12]. If iterations on the parameters only are to be carried out, eq. [26] is no longer a constraint, and the minimization problem is that solved in **I**, using the weights of eq. [31]. The generalized least-squares procedure gives identical results in this case.

## A numerical example

In **I**, selected solubility and wet residue data (4) were used to illustrate use of the least-squares triangle. These same data can be used to illustrate calculations with iterations on: (*a*) the parameters only; (*b*) both parameters and observations. The procedures are those described in section (*b*) of the Theory, and the results are given in Table 1, where the original data and the first approximation to the parameters are exactly as in **I**. When iterations are performed on the parameters only, convergence is obtained after two iterations to $1 \times 10^{-4}$ mass% for the coordinates $\mathbf{x}$ and for their estimated standard deviations. In this case, the final values of $\mathbf{x}$ do not differ significantly from the initial values. Identical results are obtained using the least-squares triangle with weights given by eq. [22] or [31]. When iterations are performed on both parameters and observations, three iterations are sufficient to obtain convergence to $1 \times 10^{-4}$ mass% for $\mathbf{x}$. The largest corrections to the observations are for the wet residue data points, all of which lie close to the point of intersection. Again, the values of $\mathbf{x}$ do not differ significantly from the values found by the least-squares with $\mathbf{W}_F = \mathbf{I}$, and this is likely to be the case in most problems in phase equilibria. In general, iterations on both parameters and observations should be carried out, because the equations for $\mathbf{F}^o$ are non-linear in the observations $\mathbf{l}$. The least-squares triangle method provides a convenient starting point for these iterations.

TABLE 1. Generalized least-squares analysis of solubility data*

| | Composition of saturated solutions, mass% | | Composition of wet residues, mass% | | Point of intersection, mass% | |
|---|---|---|---|---|---|---|
| | $Cs_2SO_4$ | $MgSO_4$ | $Cs_2SO_4$ | $MgSO_4$ | $Cs_2SO_4$ | $MgSO_4$ |
| (*a*) Original data (4) | 60.02 | 6.831 | 62.28 | 18.65 | 63.1631 | 20.8170 |
| (1st approx. to *x*) | 53.02 | 10.37 | 62.49 | 19.30 | (0.5302) | (0.2530) |
| | 41.35 | 17.02 | 61.18 | 20.57 | | |
| | 36.43 | 19.16 | 59.68 | 20.64 | | |
| (*b*) Iteration on parameters only | | | | | | |
| 1st iteration | | | | | 63.1028 | 20.6993 |
| | | | | | (0.5339) | (0.3911) |
| 2nd iteration | | | | | 63.1014 | 20.6971 |
| | | | | | (0.5337) | (0.3930) |
| (*c*) Iteration on parameters | 59.9641 | 6.84375 | 62.6440 | 18.5676 | 63.1365 | 20.7232 |
| and observations | 53.0577 | 10.3338 | 62.1117 | 19.6664 | (0.5313) | (0.3971) |
| 3rd iteration | 41.3475 | 17.0351 | 61.2092 | 20.3966 | | |
| | 36.4291 | 19.1750 | 59.6867 | 20.5228 | | |

[a]Solid phase: $Cs_2SO_4 \cdot MgSO_4 \cdot nH_2O$; see ref. 1. Quantities in parentheses are estimated standard deviations.

## Acknowledgement

This research was supported in part by a grant from the Natural Sciences and Engineering Research Council of Canada.

1. J. W. LORIMER. Can. J. Chem. **59**, 3076 (1981).
2. A. BJERHAMMER. Theory of errors and generalized matrix inverses. Elsevier Scientific Publishing Co., Amsterdam, London, New York. 1973. Chapt. 11, sect. 11.6, 11.7.
3. E. M. MIKHAIL and F. ACKERMANN. Observations and least squares. IEP: New York. 1976. Chapt. 6; sect. 6.1, 6.2; Chapt. 11, sect. 11.1.
4. V. G. SHEVCHUK, D. A. STOROZHENKO, and N. M. LAZORENKO. Zh. Neorg. Khim. **24**, 3140 (1979); Russ. J. Inorg. Chem. (Engl. Transl.) **24**, 1747 (1979).

Can. J. Chem. Downloaded from www.nrcresearchpress.com by 210.87.254.40 on 09/06/12
For personal use only.

# Stereochemistry of the conventional and modified Bucherer–Bergs reactions of 2-substituted cyclohexanones

GUERINO SACRIPANTE AND JOHN T. EDWARD

*Department of Chemistry, McGill University, 801 Sherbrooke St. West, Montreal, P.Q., Canada H3A 2K6*

Received January 18, 1982

GUERINO SACRIPANTE and JOHN T. EDWARD. Can. J. Chem. **60**, 1982 (1982).

The configurations of the spiro-hydantoins produced from 2-methyl- and 2-phenylcyclohexanone, 2,6-dimethylcyclohexanone, and *dl*-menthone by either the conventional Bucherer–Bergs (B.–B.) reaction, or a variant employing COS or $CS_2$ in place of $CO_2$, have been established by $^{13}C$ nmr. In all cases the conventional B.–B. reaction gave the hydantoin having the 4′-carbonyl group equatorial, and the COS or $CS_2$ variant, the mono- or dithiohydantoin having the 4′-thiocarbonyl group, axial.

GUERINO SACRIPANTE et JOHN T. EDWARD. Can. J. Chem. **60**, 1982 (1982).

Faisant appel à la rmn du $^{13}C$, on a établi les configurations des spiro-hydantoines provenant soit de la réaction conventionnelle de Bucherer–Bergs (B.–B.) des méthyl-2, phényl-2 et diméthyl-2,6 cyclohexanones avec la *dl*-menthone, soit en utilisant une variante de cette réaction faisant intervenir le COS ou le $CS_2$ au lieu du $CO_2$. Dans tous les cas, la réaction conventionnelle de B.–B. conduit à l'hydantoine ayant le groupe carbonyle-4′ en position équatoriale, tandis que l'utilisation du COS ou du $CS_2$ conduit au mono ou au dithiohydantoine ayant le groupe thiocarbonyle-4′ en position axiale.

[Traduit par le journal]

Munday (1) obtained two isomeric amino-acids from 2-methylcyclohexanone (**3**; R = Me): the first, to which he assigned the structure **1** (R = Me), by hydrolysis of the aminonitrile **2** (R = Me) given by the Strecker reaction; the second, to which he assigned the structure **8** (R = Me), by hydrolysis of the hydantoin **4** (R = Me) given by the Bucherer–Bergs reaction (Scheme 1).

Munday's configurational assignments in these and other cases were based on the resistance of the nitrile groups to hydrolysis (indicating axial configurations as in **2** (R = Me)); infrared spectra; and dissociation constants. However, the evidence could not be considered unequivocal, and indeed Cremlyn and Chisholm (2) argued for a reversal of Munday's assignments on the basis of the effect of changing solvent on the two dissociation constants of the various isomeric amino-acids. However, Edward and Jitsrangsri (3), using $^{13}C$ nmr, showed that Munday's assignments of structures for the isomeric amino-acids obtained from 4-*tert*-butylcyclohexanone were correct. Furthermore, they showed that the results in this and other cases in which configurational assignments were based on unequivocal evidence (X-ray crystallography (4, 5), chemical transformations (6)) all accorded with the assignments to be expected from a detailed consideration of steric effects on either a thermodynamically-determined product (the Strecker product) or a kinetically-determined product (the Bucherer–Bergs product). These considerations showed that the amino-acid derived by the Strecker route (e.g. **1**) should have its carboxyl group in the axial orientation, and that the amino-acid derived by the conventional Bucherer–Bergs route (e.g. **8**) should have this group in the equatorial orientation (the EJ rule). Mechanistic considerations also explained why two modifications of the Bucherer–Bergs reaction introduced by Carrington (one using carbon disulfide in place of carbon dioxide, and affording 2,4-dithiohydantoins (7); a second using carbonyl sulphide and affording 4-thiohydantoins (8)) gave products (β-series (9)) having the "Strecker" rather than the conventional Bucherer–Bergs (α-series (9)) configurations.

In view of the success of the EJ rule, it was curious to find that it ran counter to the configurational assignments of Ansell *et al.* (10) for the amino-acids obtained by the Strecker and Bucherer–Bergs routes from 2-phenylcyclohexanone (**3**; R = Ph). These assignments were based on variations in the chemical shift of the benzylic proton nmr band when the amino-acids were converted to *O*-methyl or *N*-acetyl derivatives. Previously Ansell *et al.* had shown that the shifts of the benzylic proton of 2-phenylcyclohexane carboxylic acids when they underwent *O*-methylation, and of 2-phenylcyclohexylamines when they underwent *N*-acetylation, depended on whether the compounds were *cis* or *trans*, and hence proceeded to use the shifts to determine configurations of the amino-acids **1** and **8** (R = Ph).

Because of this apparent failure of the EJ rule, we have investigated by $^{13}C$ nmr the configurations of the α- and β-products obtained from

0008-4042/82/151982-06$01.00/0

©1982 National Research Council of Canada/Conseil national de recherches du Canada

Can. J. Chem. Downloaded from www.nrcresearchpress.com by 210.87.254.42 on 09/06/12
For personal use only.

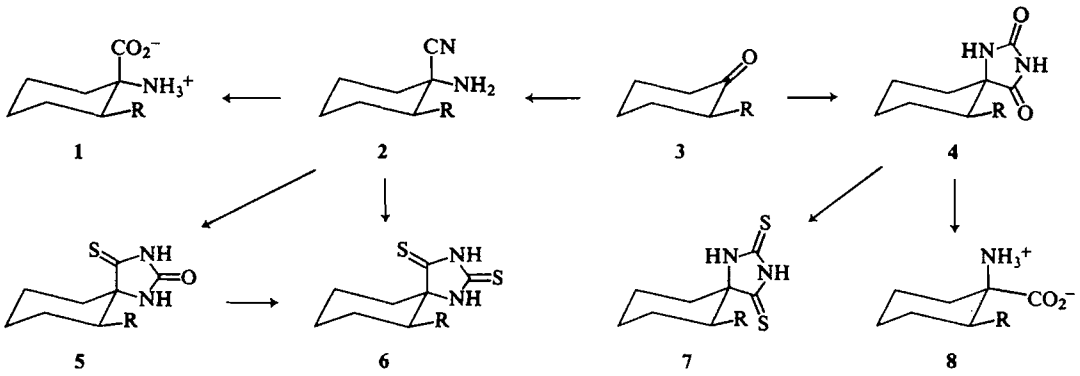

SCHEME I

2-methylcyclohexanone, 2-phenylcyclohexanone, 2,6-dimethylcyclohexanone, and 2-isopropyl-5-methylcyclohexanone (*dl*-menthone) by using either the conventional Bucherer–Bergs reaction (α-series) or its modification employing carbonyl sulfide or carbon disulfide (β-series).

## Experimental

All melting points are in degrees Celsius and are not corrected. The $^{13}C$ nmr spectra were determined on a Varian XL-200 spectrometer. Infrared spectra were measured on a Perkin–Elmer 297 spectrophotometer, and ultraviolet spectra on a Unicam SP800 spectrophotometer. Analyses were by G. Sinclair at Guelph Chemical Laboratories.

*1-Amino-2-phenylcyclohexanenitrile (2; R = Ph)*

A solution of 2-phenylcyclohexanone (5.2 g), ammonion chloride (1.6 g), sodium cyanide (1.5 g), ethanol (28 mL), and water (12 mL) was heated for 9 h at 45–50°C in a pressure bottle. The crude product was removed by filtration and recrystallized from methanol: pale yellow-orange crystals (3.0 g, 47%), mp 110°C; ir (Nujol): 3480, 3415 (NH), 2180 (C≡N) $cm^{-1}$. *Anal.* calcd. for $C_{13}H_{16}N_2$: C 77.96, H 8.03; found; C 78.01, H 8.13.

*2-Phenylcyclohexane-1-spiro-5'-hydantoin (α isomer; 4; R = Ph)*

A solution of 2-phenylcyclohexanone (8.3 g), sodium cyanide (4.6 g), ammonium carbonate (17.0 g), ethanol (37 mL), and water (37 mL) was stirred in a pressure bottle for 6 h at 50–55°C, acidified, and left overnight. The crude product was removed by filtration, washed with water, and crystallized from methanol to yield several crops: 1.65 g, mp 246°C; 1.2 g, mp 240–242°C; and 2.85 g (total yield 49%). Recrystallization from methanol raised the mp of all crops to 246°C; ir (Nujol): 3430, 3280 (NH), 1720 (C=O) $cm^{-1}$. *Anal.* calcd. for $C_{14}H_{16}N_2O_2$: C 68.83, H 6.60; found: C 68.50, H 6.87.

*2-Phenylcyclohexane-1-spiro-5'-(2',4'-dithiohydantoin) (α isomer; 7; R = Ph)*

2-Phenylcyclohexane-1-spiro-5'-hydantoin (α isomer) (1.0 g), phosphorous pentasulfide (1.0 g), and tetralin (20.0 mL) were stirred under reflux for 4 h at 210°C. The hot solution was decanted from some tar and cooled. The solid product was removed by filtration, washed with cold benzene, and found from its uv spectrum (11) to be a mixture of its monothio and dithio derivatives (approx. 80% and 20% respectively). The crude mixture (0.7 g) was therefore allowed to react with *p*-methoxyphenylthionophosphine (12) (1.0 g) in tetralin (20 mL) under reflux for 2 h. The hot solution was decanted from some tar and cooled down, and the product was removed by filtration, washed with cold benzene, and recrystallized from methanol: colorless crystals (0.5 g, 44%), mp 270°C; ir (Nujol): 3240 (NH), 1565, 1545 (thioamide) $cm^{-1}$. *Anal.* calcd. for $C_{14}H_{16}N_2S_2$: C 60.86, H 5.84; found: C 60.66, H 5.89.

*2-Phenylcyclohexane-1-spiro-5'-(4'thiohydantoin) (β isomer; 5; R = Ph)*

A solution of 2-phenylcyclohexanone (2.9 g), sodium cyanide (0.95 g), ammonia (6.3 mL), ethanol (17.3 mL), and water (1.5 mL) was stirred in a three-necked flask immersed in an icebath. Carbon oxysulfide was bubbled into the solution until 3.2 g had been absorbed. The solution was then transferred into a pressure bottle and heated to 50–55°C for 4.4 h. The mixture was cooled, and the crude product was removed by filtration and recrystallized from methanol: 2.5 g, mp 260–265°C, and a second crop, 0.5 g, mp 260–262°C (total yield 69%); ir (Nujol): 3400, 3220 (N—H), 1730 (C=O). *Anal.* calcd. for $C_{14}H_{16}N_2OS$: C 64.60; H 6.20; found: C 64.40, H 6.30.

*2-Phenylcyclohexane-1-spiro-5'-(2',4'-dithiohydantoin) (β isomer; 6; R = Ph)*

(a) *Carbon disulfide modification of the Bucherer–Bergs hydantoin synthesis*

A solution of 2-phenylcyclohexanone (5.2 g), sodium cyanide (1.5 g), ammonion chloride (1.6 g), carbon disulfide (3.0 g), ethanol (28 mL), and water (12 mL) was stirred in a pressure bottle at 50°C for 24 h. The solution was acidified, and the crude product removed by filtration and crystallized from methanol: yellow crystals (0.1 g), mp 242°C; ir (Nujol): 3160 (NH), 1570, 1540 (thioamide) $cm^{-1}$. *Anal.* calcd. for $C_{14}H_{16}N_2S_2$: C 60.86, H 5.84; found: C 60.52, H 5.95.

(b) *Replacement of oxygen in 2-phenylcyclohexane-1-spiro-5'-(4'-thiohydantoin) (β isomer) by sulfur*

2-Phenylcyclohexane-1-spiro-5'-(4'-thiohydantoin) (1.0 g), and phosphorus pentasulfide (1.0 g) in tetralin (20 mL) were heated under reflux for 5 h. The hot solution was decanted from some tar, cooled, and the yellow solid removed by filtration and washed with cold benzene. Crystallization from methanol gave yellow crystals, yield 0.8 g (85%), mp 242°C; identical (mp, uv spectrum) with the compound above.

*2,6-Dimethylcyclohexane-1-spiro-5'-hydantoin (α isomer; 9; X = Y = O)*

A solution of 2,6-dimethylcyclohexanone (4.0 g), potassium cyanide (2.3 g), and ammonium carbonate (15.0 g) in ethanol

Can. J. Chem. Downloaded from www.nrcresearchpress.com by 210.87.254.42 on 09/06/12
For personal use only.

Can. J. Chem. Downloaded from www.nrcresearchpress.com by 210.87.254.42 on 09/06/12
For personal use only.

(50 mL) and water (40 mL) was heated in a pressure bottle at 50–60°C for 24 h. The mixture was worked up in the usual way, and the hydantoin crystallized from ethanol as colourless needles (3.2 g, 51%), mp 254°C; ir (KBr): 3170, 3100 (NH) 1760, 1710 (C=O) $cm^{-1}$. *Anal.* calcd. for $C_{10}H_{16}N_2O_2$: C 61.20, H 8.22; found: C 61.10, H 8.64.

*2,6-Dimethylcyclohexane-1-spiro-5'-(2',4'-dithiohydantoin) (α isomer; **9**; X = Y = S)*

2,6-Dimethylcyclohexane-1-spiro-5-hydantoin (α isomer) (1.0 g) was heated with phosphorus pentasulfide (1.0 g) in boiling tetralin (20 mL) for 7 h, and the reaction mixture then worked up as usual to give, after crystallization from methanol, yellow crystals (0.5 g, 43%), mp 274°C; ir (KBr): 3240, 3100 (NH), 1525 (thioamide) $cm^{-1}$. *Anal.* calcd. for $C_{10}H_{16}N_2S_2$: C 52.60, H 7.06; found: C 52.84, H 7.40.

*2,6-Dimethylcyclohexane-1-spiro-5'-(4'-thiohydantoin) (β isomer; **10**; X = O, Y = S)*

A solution of 2,6-dimethylcyclohexanone (6.0 mL), potassium cyanide (2.3 g), and concentrated ammonium hydroxide (15.6 mL) in ethanol (50 mL)–water (4 mL) was cooled in an ice-bath. Carbonyl sulfide was passed into the solution until 8.0 g had been absorbed. The solution was transferred to a pressure bottle and heated to 45°C with stirring for 4.2 h. The product, obtained after the usual work-up, was crystallized from methanol and obtained as yellow crystals (2.0 g, 20%), mp 159°C; ir (KBr): 3220, 3130 (N—H), 1735 (C=O) $cm^{-1}$. *Anal.* calcd. for $C_{10}H_{16}N_2OS$: C 56.57, H 7.80, N 13.20; found: C 56.42, H 7.80, N 13.47.

*2,6-Dimethylcyclohexane-1-spiro-5'-(2',4'-dithiohydantoin) (β isomer; **10**; X = Y = S)*

2,6-Dimethylcyclohexane-1-spiro-5'-(4'-thiohydantoin) (β isomer) (1.0 g) was heated with phosphorus pentasulfide (1.0 g) in tetralin (20 mL) to 180–200°C for 7 h, and then worked up as usual. The product crystallization from ethanol as pale yellow crystals (0.5 g, 46%), mp 234–236°C; ir (KBr): 3130 (NH), 1550, 1520 (thioamide) $cm^{-1}$; *Anal.* calcd. for $C_{10}H_{16}N_2S_2$: C 52.60, H 7.10; found: C 52.64, H 7.40.

dl-*Menthane-1-spiro-5'-hydantoin (α isomer; **11**; X = Y = O)*

A solution of *dl*-menthone (5.0 g), potassium cyanide (2.3 g), and ammonium carbonate (15.0 g) in ethanol (50 mL)–water (50 mL) was heated in a pressure bottle to 50–60°C for 9 h. The reaction mixture was worked up in the usual way, and the product crystallized from ethanol: colourless crystals (3.9 g, 54%), mp 233°C; ir (KBr): 3280, 3170 (NH), 1720 (C=O) $cm^{-1}$. *Anal.* calcd. for $C_{12}H_{20}N_2O_2$: C 64.25, H 8.99; found: C 64.00, H 9.20.

dl-*Menthane-1-spiro-5'-(2',4'-dithiohydantoin) (α isomer; **11**; X = Y = S)*

*dl*-Menthane-1-spiro-5'-hydantoin (α isomer) (1.0 g) was heated with phosphorus pentasulfide (1.0 g) in boiling tetralin (40 mL) for 5 h. The product, after the usual work-up, was crystallized from ethanol: pale yellow crystals (0.5 g, 33%), mp 261°C; ir (KBr): 3120 (NH), 1525 (thioamide) $cm^{-1}$. *Anal.* calcd. for $C_{12}H_{20}N_2S_2$: C 56.18, H 7.80; found: 56.10, H 8.14.

dl-*Menthane-1-spiro-5'-(4'-thiohydantoin) (β isomer; **12**; X = O, Y = S)*

A solution of *dl*-menthone (7.1 g), potassium cyanide (2.3 g), and concentrated ammonium hydroxide (15.6 mL) in ethanol (43 mL)–water (3 mL) was cooled in an ice-bath. Carbon oxysulfide was passed into the solution until 8.0 g had been absorbed. The solution was transferred to a pressure bottle, and heated to 50–60°C with stirring for 4.2 h. The product, after the usual work-up, was crystallized from methanol: yellow crystals (7.4 g, 70%), mp 203°C, ir (Nujol): 3240 (NH). *Anal.* calcd. for $C_{12}H_{20}N_2OS \cdot 0.5H_2O$: C 57.78, H 8.48, N 11.27; found: C 58.07, H 7.97, N 11.00.

dl-*Menthane-1-spiro-5'-(2',4'dithiohydantoin) (β isomer; **12**; X = Y = S)*

*dl*-Menthane-1-spiro-5'-(4'-thiohydantoin) (β isomer) (1.0 g) was heated with phosphorus pentasulfide (1.0 g) in boiling tetralin (30 mL) for 5 h. The product crystallized from ethanol in yellow crystals (1.0 g, 94%), mp 150°C[1]; ir (KBr): 3130 (NH), 1550 (thioamide) $cm^{-1}$. *Anal.* calcd. for $C_{12}H_{20}N_2S_2$: C 56.23, H 7.87, N 10.93; found: C 56.32, H 7.70, N 10.91.

## Results and discussion

### *Preparation of 2,4-dithiohydantoins of the α and β series*

Ansell *et al.* (10), in studying the stereochemistry of the Strecker and Bucherer–Bergs reactions of 2-phenylcyclohexanone (**3**, R = Ph), converted the reaction products to the epimeric amino-acids **1** and **8** (R = Ph). We found the amino-nitrile **2** (R = Ph) unusually resistant to acid hydrolysis, perhaps because of the presence of the large phenyl group *gauche* to the axial nitrile, and so for convenience chose as our "Strecker" product the 2,4-dithiohydantoin **6** (R = Ph), produced by the modified reaction using $CS_2$. This reaction went in very poor yield (another indication of hindrance), and the dithiohydantoin **6** (R = Ph) was more readily available by preparing first the monothiohydantoin **5** (R = Ph) by the COS modification of the Bucherer–Bergs reaction (8) (a reaction known to go well with hindered ketones such as adamantanone (13)), followed by sulfuration of the monothiohydantoin to the dithiohydantoin by phosphorus pentasulfide (14). The corresponding 2,4-dithiohydantoin **7** (R = Ph) of the α-series was prepared by sulfuration of the normal Bucherer–Bergs product **4** (R = Ph). This reaction also proved difficult, sulfuration by phosphorus pentasulfide being incomplete after six hours. Sulfuration was accordingly completed by using the more reactive *p*-methoxyphenylthionophosphine (12).

The configurations of the products from 2-phenylcyclohexanone shown in Scheme 1, and assumed in the account above, are those predicted by the EJ rule, and up to this point are only tentative. The same is true for the configurations of the epimeric 2,4-dithiohydantoins **6** and **7** (R = Me) obtained from 2-methylcyclohexanone (**3**; R = Me); the preparation of these products has already been described in the literature (9).

Similar routes were used to prepare the epimeric

[1]Carrington (7) reported obtaining this compound, mp 209°C, in 5% yield by the $CS_2$-modification of the Bucherer–Bergs reaction, but his product had a poor analysis and may have been impure. The purity of our own product follows from its $^{13}C$ nmr spectrum (see below).

TABLE 1. $^{13}C$ chemical shifts (ppm, downfield from TMS) of carbon atoms of epimeric hydantoins and 2,4-dithiohydantoins in DMSO-$d_6$

| Compound | Isomer | Structure | Cyclohexane ring carbons C-1 | C-2 | C-3 | C-4 | C-5 | C-6 | Other carbons $CH_3$ | C-2′ | C-4′ | Σ[a] |
|---|---|---|---|---|---|---|---|---|---|---|---|---|
| 2-Methylcyclohexane-1-spiro-5′-hydantoin | α[b] | **4**, R = Me | 65.7 | 35.5 | 29.2[c] | 20.4 | 24.5[c] | 31.1 | 14.9[d] | 157.0 | 178.1 | 556.4 |
| | β[b] | **5**, R = Me (O in place of S) | 63.8 | 35.5 | 28.9[c] | 20.8 | 24.2[c] | 31.3 | 14.7[d] | 156.4 | 177.0 | 552.6 |
| 2-Methylcyclohexane-1-spiro-5′-(2′,4′-dithiohydantoin) | α[b] | 7, R = Me | 80.5 | 36.4 | 29.0[c] | 20.3 | 24.3[c] | 31.2 | 14.7[d] | 180.6 | 211.1 | 628.1 |
| | β[b] | **6**, R = Me | 77.4 | 33.6 | 28.8[c] | 19.2 | 24.8[c] | 29.6 | 14.4[d] | 179.2 | 208.9 | 615.9 |
| 2,6-Dimethylcyclohexane-1-spiro-5′-(2′,4′-dithiohydantoin) | α | **9**, X = Y = S | 84.3 | 41.1 | 28.9 | 24.7 | 28.9 | 41.1 | 14.9[d,e] | 181.4 | 210.7 | 670.9 |
| | β | **10**, X = Y = S | 81.7 | —[f] | 26.9 | 24.5 | 26.0 | —[f] | 13.8[d,e] | 179.9 | 206.7 | — |
| 2-Phenylcyclohexane-1-spiro-5′-(2′,4′-dithiohydantoin) | α[g] | 7, R = Ph | 80.4 | 50.7 | 27.6[c] | 20.0 | 25.0[c] | 35.0 | — | 180.2 | 209.3 | 628.2 |
| | β[h] | **6**, R = Ph | 77.3 | 49.6 | 24.8 | 18.7 | 24.8 | 35.7 | — | 178.6 | 208.0 | 617.5 |
| *dl*-Menthane-1-spiro-5′-(2′,4′-dithiohydantoin) | α[i] | **11**, X = Y = S | 81.6 | 49.7 | 33.9 | 20.4 | 27.3 | 47.4 | 17.2[k] | 180.0 | 211.2 | 668.7 |
| | β[j] | **12**, X = Y = S | 77.9 | 50.3 | 34.0 | 19.6 | 25.9 | 45.1 | 18.1[k] | 179.0 | 209.7 | 659.6 |

[a] Summation of chemical shifts shown in the table, but omitting values in footnotes.
[b] Prepared following ref. 9.
[c] Present evidence compatible with an interchange of the two values.
[d] Substituent on C-2.
[e] Value also for methyl group at C-6.
[f] These bands hidden by solvent peak.
[g] Peaks due to phenyl: C-1, 138.9; C-2 and C-6, 127.6; C-3 and C-5, 128.6; C-4, 127.5.
[h] Peaks due to phenyl: C-1, 138.7; C-2 and C-6, 127.3; C-3 and C-5, 128.5; C-4, 127.0.
[i] Peaks due to isopropyl: CH, 26.7; $CH_3$, 23.5; $CH_3$, 21.7
[j] Peaks due to isopropyl: CH, 24.8; $CH_3$, 23.7; $CH_3$, 21.7
[k] Substituent on C-5.

2,4-dithiohydantoins **9** and **10** (X = Y = S) from 2,6-dimethylcyclohexanone and **11** and **12** (X = Y = S) (only one enantiomer shown in each case) from *dl*-menthone. The preparation of the latter compounds encountered no difficulty, the steric hindrance of the isopropyl group (conformational free energy difference of 2.1 kcal mol$^{-1}$ (15) for equatorial–axial change) evidently being much less than that of the phenyl group (conformational free energy difference 2.87 ± 0.09 kcal mol$^{-1}$ (16)).

### $^{13}C$ *nuclear magnetic resonance of* α *and* β *isomers*

Carbon-13 nmr spectroscopy has proved a powerful tool for revealing the presence of minor isomeric impurities in supposedly pure compounds (5). In the present instance it shows that compounds of Table 1 are free from any appreciable quantity of isomeric impurity, which would be revealed by additional peaks in the spectra. It had been considered possible that the reaction products **9–12** might be contaminated by small quantities of epimers having an axial methyl group, because of epimerization of the starting ketones under the alkaline reaction conditions, but such compounds, if formed, were evidently removed by the isolation and purification procedures followed.

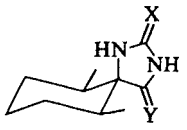


**9**

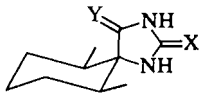


**10**

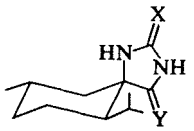


**11**

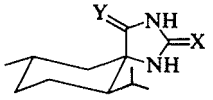


**12**

The nmr peaks of the carbon atoms of the various epimeric hydantoins and 2,4-dithiohydantoins are shown in Table 1. As before (3) the peaks at lowest field can be assigned to C-4′ carbon atoms, and at next lowest field to C-2′ carbons. Peaks at higher field due to cyclohexyl, methyl, phenyl, and isopropyl carbons can be assigned on the basis of splitting patterns in the coupled spectra, although not always unambiguously.

As before (3, 5) the strongest evidence for a particular configuration came from the half-widths of the coupled C-4′ peaks. When C-4′ is axial, as in **6**, **10**, and **12**, it will be coupled with *anti* hydrogen atoms at C-2 and C-6 of the cyclohexane ring, and the vicinal coupling constants, $^3J_{(^{13}C-^1H)}$, should be large. When C-4′ is equatorial, as in the epimers **7**, **9**, and **11**, it will be coupled with *gauche* hydrogens

Can. J. Chem. Downloaded from www.nrcresearchpress.com by 210.87.254.42 on 09/06/12
For personal use only.

TABLE 2. Ultraviolet absorption bands of mono- and dithiohydantoins in ethanol

| | | Band I | | Band II | | Band IV | |
|---|---|---|---|---|---|---|---|
| Compound | Series | $\lambda_{max}$(nm) | $\varepsilon_{max}$ | $\lambda_{max}$(nm) | $\varepsilon_{max}$ | $\lambda_{max}$(nm) | $\varepsilon_{max}$ |
| **5**, R = Me | β | 389 | 18 | 282 | 12 600 | 233 | 6 150 |
| **6**, R = Me | β | 407 | 39 | 301 | 23 300 | 225 | 6 240 |
| **7**, R = Me | α | 386 | 47 | 300 | 25 400 | 226 | 6 280 |
| **6**, R = Ph | β | 406 | 45 | 304 | 56 200 | 226 | 27 400 |
| **7**, R = Ph | α | 387 | 50 | 302 | 85 300 | 228 | 28 000 |
| **9**, X = Y = S | α | 390 | 45 | 300 | 24 500 | 226 | 7 240 |
| **10**, X = Y = S | β | 410 | 43 | 302 | 26 300 | 226 | 7 140 |
| **11**, X = Y = S | α | 388 | 37 | 300 | 19 500 | 225 | 6 020 |
| **12**, X = Y = S | β | 411 | 44 | 304 | 26 000 | 226 | 8 010 |

at C-2 and C-6, and the vicinal coupling constants should be small. Because of the complexity of the coupled C-4′ peaks, the width at half-height, $W_{1/2}$, was used as an indication of $^3J_{(^{13}C-^1H)}$. The half-widths (in Hz) for the various compounds were as follows:

| β-Series | $W_{1/2}$ | α-Series | $W_{1/2}$ |
|---|---|---|---|
| **6**, R = Me | 20.0 | **7**, R = Me | 10.0 |
| **6**, R = Ph | 26.0 | **7**, R = Ph | 13.5 |
| **10**, X = Y = S | 28.0 | **9**, X = Y = S | 13.6 |
| **12**, X = Y = S | 21.0 | **11**, X = Y = S | 11.3 |

In all cases, the half-widths of the coupled C-4′ peaks of the β epimers were about twice as great as the half-widths for the α epimers. This shows that the β compounds have C-4′ predominantly in the axial position, and the α compounds C-4′ predominantly in the equatorial position, and justifies the various structural assignments in Table 1, and the tentative assignments in Scheme 1. These are all in conformity with the EJ rule.

Further support for these configurational assignments comes from the fact, evident in Table 1, that for **4/5** (O in place of S), **6/7** (R = Me and Ph), and **11/12** the summed values Σ of the $^{13}C$ chemical shifts of the β compounds are smaller than the summed values of the shifts of the α compounds (i.e. the average chemical shift of a β compound is at higher field than the average shift of its corresponding α epimer). That indicates the β compounds to be more strained than the α compounds (17), which is expected from the assignments above. In the β compounds a bulky oxygen or sulfur atom attached to C′-4′ is pushing inward towards the axial hydrogen atoms of the cyclohexane ring, while in the α compounds a smaller hydrogen atom attached to N′-1′ is pushing inwards.

*Ultraviolet absorption spectra of α and β isomers*

The ultraviolet absorption characteristics in ethanol solution of the mono- and dithiohydantoins prepared in this investigation are given in Table 2, the absorption bands being classified according to Janssen's scheme (18). The results for the most part are unexceptional, although the high intensities of Band II and Band IV for **6** and **7** (R = Ph) are noteworthy in indicating the effect of proximate phenyl on what are probably $\pi \rightarrow \pi^*$ transitions (18). However, for our present purposes we need consider only Band I at longest wavelength, which is due to the $n \rightarrow \pi^*$ transition of the 4-thiocarbonyl group. In any epimeric pair the band of the β compound was at longer wavelength (see Table 2), which supports the configurational assignments given above (see ref. 3 for detailed argument).

## Conclusion

We are compelled by the nmr and uv evidence marshalled above to conclude that the stereochemistry of the products obtained from 2-substituted cyclohexanones by the conventional Bucherer–Bergs reaction, on the one hand, and by the Strecker or modified Bucherer–Bergs reactions, on the other hand, are in conformity with the EJ rule. It might seem reassuring to find that Nature is not capricious, and that 2-substituted cyclohexanones behave like other ketones. But the change in the chemical shift of the benzylic proton of the amino-acids **1** and **8** (R = Ph) on formation of *N*-acetyl or *O*-methyl derivatives (10) *is* decidedly capricious and misleading, if the changes in the chemical shifts of this proton in the monofunctional cyclohexylamines and cyclohexane carboxylic acids on formation of the same derivatives are considered normal. The same remarks apply to the very reasonable generalizations of Cremlyn and Chisholm, which were based on the effect of changing solvent composition on the dissociation constants of cyclohexylamines and cyclohexane carboxylic acids of known configuration, and which fail for geminal amino carboxylic acids (19). Evidently the

Can. J. Chem. Downloaded from www.nrcresearchpress.com by 210.87.254.42 on 09/06/12
For personal use only.

proximity of amino and carboxylic groups causes simple additive schemes to break down.

**Acknowledgements**

We are most grateful to Dr. Francoise Sauriol for the $^{13}C$ nmr spectra, to Dr. F. L. Chubb and Dr. S. C. Wong for much help and advice, and to the Natural Sciences and Engineering Research Council of Canada for financial support.

1. L. MUNDAY. J. Chem. Soc. 4372 (1961).
2. R. J. W. CREMLYN and M. CHISHOLM. J. Chem. Soc. 2269 (1967).
3. J. T. EDWARD and C. JITSRANGSRI. Can. J. Chem. **53**, 3339 (1975).
4. H. S. TAGER and H. N. CHRISTENSEN. J. Am. Chem. Soc. **94**, 968 (1972).
5. G. G. TRIGO, C. AVENDAÑO, E. SANTOS, J. T. EDWARD, and S. C. WONG. Can. J. Chem. **57**, 1456 (1979).
6. Y. MAKI and T. MASUGI. Chem. Pharm. Bull. (Tokyo) **21**, 685 (1973).
7. H. C. CARRINGTON. J. Chem. Soc. 681 (1947).
8. H. C. CARRINGTON, C. H. VASEY, and W. S. WARING. J. Chem. Soc. 396 (1959).
9. H. C. BRIMELOW, H. C. CARRINGTON, C. H. VASEY, and W. S. WARING. J. Chem. Soc. 2789 (1962).
10. J. ANSELL, P. MORGAN, and H. C. PRICE. Tetrahedron Lett. 4615 (1978).
11. J. T. EDWARD and J. K. LIU. Can. J. Chem. **47**, 1117 (1969).
12. S. SCHEIBE, B. S. PEDERSEN, and S. O. LAWESSON. Bull. Soc. Chim. Belg. **87**, 229 (1978).
13. F. L. CHUBB, J. T. EDWARD, and S. C. WONG. J. Org. Chem. **45**, 2315 (1980).
14. H. C. CARRINGTON and W. S. WARING. J. Chem. Soc. 354 (1950).
15. E. L. ELIEL, N. L. ALLINGER, S. J. ANGYAL, and G. A. MORRISON. Conformational analysis. Interscience, New York. 1965. p. 44.
16. E. L. ELIEL and M. MANOHARAN. J. Org. Chem. **46**, 1959 (1981).
17. A. S. PERLIN and H. J. KOCH. Can. J. Chem. **48**, 2639 (1970).
18. M. J. JANSSEN. Recl. Trav. Chim. Pays-Bas, **79**, 454 (1960); **79**, 464 (1960); **79**, 1066 (1960).
19. J. T. EDWARD, P. G. FARRELL, J. KIRCHNEROVA, J.-C. HALLÉ, and R. SCHAAL. Can. J. Chem. **54**, 1899 (1976).

Can. J. Chem. Downloaded from www.nrcresearchpress.com by 210.87.254.42 on 09/06/12
For personal use only.

# Ambident nucleophiles. II. Nitrogen-bonded and carbon-bonded σ-complex formation in the reaction of pyrrolide anions with 1,3,5-trinitrobenzene[1,2]

J. C. HALLE, M. J. POUET, AND M. P. SIMONNIN

*Laboratoires de Physicochimie des solutions et de Spectrographie, E.N.S.C.P., 11 rue Pierre et Marie Curie, 75231 Paris Cédex 05, France*

AND

F. DEBLEDS AND F. TERRIER[3]

*Laboratoire de Chimie Organique Physique, Faculté des Sciences de Rouen, 76130 Mont Saint Aignan, France*

Received February 3, 1982

Can. J. Chem. Downloaded from www.nrcresearchpress.com by 210.87.254.5 on 09/06/12
For personal use only.

J. C. HALLE, M. J. POUET, M. P. SIMONNIN, F. DEBLEDS, and F. TERRIER. Can. J. Chem. **60**, 1988 (1982).

Reaction of 1,3,5-trinitrobenzene (TNB) with pyrrole, 2,5-dimethyl pyrrole, and 2,4-dimethyl-3-ethyl pyrrole in the presence of a strong base ($CH_3O^-$) yields nitrogen- and/or carbon-bonded 1:1 σ-complexes in dimethylsulphoxide (DMSO). Depending on the stoichiometry of the reagents, 1:2 and 2:1 pyrrole–TNB diadducts are also formed. Identification of all complexes was effected by nmr. The reactive species are shown to be the pyrrolide ions and the results emphasize the ambident character of these anions towards an aromatic electrophile. Some of the complexes have been isolated as crystalline potassium salts when experiments are performed in acetonitrile. Among the isolable complexes, the *kinetically but not thermodynamically favored* nitrogen adduct of pyrrole (**5***a*) is remarkably unreactive. The second-order rate constant $k^{H^+}$ for is $H^+$-catalyzed decomposition in aqueous solution is only 1 L mol$^{-1}$ s$^{-1}$ ($t$ = 25°C).

J. C. HALLE, M. J. POUET, M. P. SIMONNIN, F. DEBLEDS et F. TERRIER. Can. J. Chem. **60**, 1988 (1982).

Dans le diméthylsulfoxyde (DMSO) et en présence d'une base forte ($CH_3O^-$), le trinitro-1,3,5-benzène (TNB) réagit avec le pyrrole, le diméthyl-2,5 pyrrole et le diméthyl-2,4 éthyl-3 pyrrole pour donner des complexes-σ azotés et/ou carbonés 1:1. En fonction de la stoechiométrie des réactifs, des diadduits pyrrole–TNB 1:2 et 2:1 sont également formés. L'identification des complexes a été faite par rmn. Les résultats montrent que les espèces réactives sont les ions pyrrolate et mettent en évidence le caractère ambident de ces anions vis-à-vis d'un électrophile aromatique. Quelques complexes ont pu être isolés à l'état solide sous forme de sels de potassium. Parmi ces complexes, et bien qu'il se forme seulement sous contrôle cinétique, l'adduit azoté **5***a* du pyrrole présente une "stabilité" remarquable. La constante $k^{H^+}$ relative à sa dissociation catalysée par les ions $H^+$ est seulement de 1 L mol$^{-1}$ s$^{-1}$ en solution aqueuse ($t$ = 25°C).

## Introduction

Much interest has been devoted to the reactions of aliphatic, alicyclic, and aromatic amines with electron-deficient aromatics like 1,3,5-trinitrobenzene (TNB) to give the nitrogen bonded σ-complexes of general structure **1** (2–7). Equation [1] describes the interaction which proceeds through the initial formation of the zwitterionic complexes **1**, $H^+$. In contrast, but in accord with their much lower basicity, heteroaromatic amines like pyrrole derivatives are not known to react with TNB. In this regard, one can wonder that the reactivity of the corresponding anions, e.g. pyrrolide anions, towards electron-deficient aromatics has received no attention so far. In fact, the behaviour of such anions is of interest for two reasons: (*1*) they are known to react as ambident nucleophiles with most common electrophiles (acyl and alkyl halides), yielding usually N-1 and/or C-2 or C-3 substituted products (8–10); (*2*) they can offer the possibility of forming nitrogen-bonded σ-adducts of type **1** by another route than that depicted in eq. [1], i.e. by direct attack of the anion on the aromatic. We report our observation that N-bonded adducts, C-bonded adducts, and various 1:2 and 2:1 diadducts form in the reactions of TNB with different pyrrolide anions. The results, which are very dependent on the substituents bonded to the pyrrole ring, emphasize the ambident character of pyrrolide anions.

## Results

While no reaction occurs in adding pyrrole (**2***a*), 2,5-dimethyl pyrrole (**2***b*), or 2,4-dimethyl-3-ethyl pyrrole (**2***c*, kryptopyrrole) to a DMSO or acetonitrile solution of TNB, strong colors typical of σ-complexes develop immediately in the presence of methoxide ion. Similar adducts form when the amines are added to a DMSO solution of the TNB–methoxide complex **4**. As will be discussed below, the reactive species are the pyrrolide ions **3***a*, **3***b*, and **3***c*. The structures of the various adducts have been determined by $^1$H nmr.

[1]Part I is ref. 1.

[2]Presented in part at the Fifth IUPAC Conference on Physical Organic Chemistry, Santa Cruz, California, August, 1980.

[3]Author to whom correspondence may be addressed.

0008-4042/82/151988-08$01.00/0

©1982 National Research Council of Canada/Conseil national de recherches du Canada

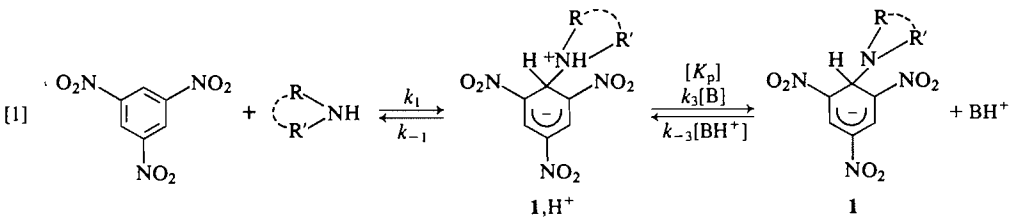


*Pyrrole 2a*

Addition of an equimolar mixture of pyrrole and methoxide ion (1 equiv.) in DMSO to a DMSO solution of TNB (1 equiv.) results in the formation

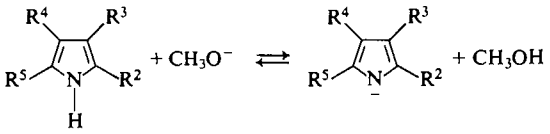


**2a** $R^2 = R^3 = R^4 = R^5 = H$ **3a**
**2b** $R^2 = R^5 = Me$; $R^3 = R^4 = H$ **3b**
**2c** $R^2 = R^4 = Me$; $R^3 = Et$; $R^5 = H$ **3c**

of the N-adduct **5a**. The symmetrical structure of the pyrrole moiety was confirmed by the presence of an AA'BB' system in the $^1H$ nmr spectrum of **5a** which also shows the $AX_2$ system ($\delta H_{1'} = 6.89$; $\delta H_{3',5'} = 8.51$; $^4J = 0.8$) characteristic of the cyclohexadienylide ring (Table 1). The chemical shifts of the $H_{1'}$ and $H_{3',5'}$ protons are consistent with those previously reported for other N-bonded complexes (1). No NH signal is observed. Further confirmation of the structure of **5a** comes from its $^{13}C$ nmr spectrum which consists of six signals, only two of them belonging to fully substituted carbons ($C_{4'}$ and $C_{2',6'}$): $\delta C_{1'} = 52.5$ (d); $\delta C_{2',6'} = 131.6$ (s); $\delta C_{3',5'} = 125.8$ (d); $\delta C_{4'} = 120.6$ (s); $\delta C_{2,5} = 120.2$ (d); $\delta C_{3,4} = 107.6$ (d).

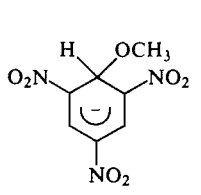

**4**

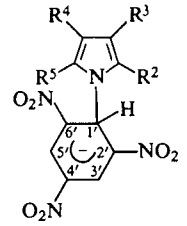

**5a**: $R^2 = R^3 = R^4 = R^5 = H$
**5b**: $R^2 = R^5 = Me$; $R^3 = R^4 = H$
**5c**: $R^2 = R^4 = Me$; $R^3 = Et$; $R^5 = H$

Compound **5a** is very stable and was isolated as a crystalline potassium salt by carrying out similar experiments in acetonitrile and evaporating the solvent (see experimental section). Dissolution of this salt in DMSO-$d_6$ gives a spectrum similar to that observed from the *in situ* generation of **5a** (Fig. 1).

Despite the high stability of **5a**, a slow evolution of the spectra occurs over an extended period of time, i.e. several months. One thus observes the progressive disappearance of the signals of **5a** and the concomitant appearance of pyrrole, the C-2 adduct **6**, the C-2, C-5 1:2 diadduct **7**, and a small amount of the C-2, C-4 1:2 diadduct **8**. Figure 2 shows the spectrum obtained after seven months when the N-adduct **5a** is no longer observed.

The structure of the C-2 adduct **6** has been established from the following observations: (*1*) the presence of a low-field NH signal ($\delta = 10.51$); (*2*) an

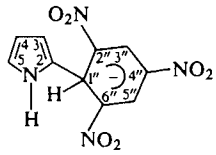

**6**

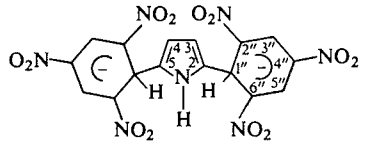

**7**

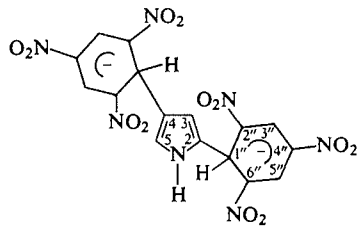

**8**

$AX_2$ system ($\delta H_{1''} = 5.73$, $\delta H_{3'',5''} = 8.31$); (*3*) three pyrrolic protons forming an AMX system. In agreement with the lower electronegativity of a carbon atom relative to a nitrogen atom, the chemical shifts of the cyclohexadienylic $H_{1''}$ and $H_{3'',5''}$ protons are at higher field than those of the analogous $H_{1'}$ and $H_{3',5'}$ protons of the N-adduct **5a**. They are also consistent with those previously reported for other TNB C-bonded complexes (1, 4). Double resonance experiments indicate that the three protons of the AMX system are coupled with the amino proton. The various coupling constants of the pyrrolic protons are of the same order of magnitude as those observed for pyrrole itself, allowing an unambiguous assignment of these protons (11, 12) (Table 1).

The nmr spectrum of the symmetrical C-2, C-5

Can. J. Chem. Downloaded from www.nrcresearchpress.com by 210.87.254.5 on 09/06/12
For personal use only.

Can. J. Chem. Downloaded from www.nrcresearchpress.com by 210.87.254.5 on 09/06/12
For personal use only.

TABLE 1. Nuclear magnetic resonance parameters of pyrrole and its TNB-adducts in DMSO-$d_6$[a]

| Compounds | $\delta NH_1$ | $\delta H_2$ | $\delta H_3$ | $\delta H_4$ | $\delta H_5$ | $\delta H_{1'}$ | $\delta H_{3'/5'}$ | $^4J_{1'\text{-}3'/5'}$ | $\delta H_{1''}$ | $\delta H_{3''/5''}$ | $^4J_{1''\text{-}3''/5''}$ | $\delta H_A$ | $\delta H_X$ | $J$ |
|---|---|---|---|---|---|---|---|---|---|---|---|---|---|---|
| **2***a* | 10.8 | 6.75 | 6.06 | 6.06 | 6.75 | | | | | | | | | |
| **5***a* | | 6.59 | 5.89 | 5.89 | 6.59 | 6.89 | 8.51 | 0.8 | | | | | | |
| **6** | 10.51 | | 5.67 | 5.84 | 6.51 | | | | 5.73 | 8.31 | 0.5 | | | $J_{3,4} = 3.3$ $J_{3,5} = 1.6$ $J_{4,5} = 2.7$ $J_{1,5} = 2.6$ |
| **7** | 9.72 | | 5.44 | 5.44 | | | | | 5.69 | 8.29 | 0.5 | | | $J_{1\text{-}3/4} = 2.6$ |
| **8** | 10.20 | | 5.52 | | 6.18 | | | | (2) 5.65<br>(4) 5.53 | (2) 8.27<br>(4) 8.23 | (2) 0.6<br>(4) 0.6 | | | $J_{3,5} = 1.6$ |
| **9** | | 6.43 | 5.65 | 5.65 | 6.43 | | | | | | | 8.85 | 6.88 | $^4J_{AX} \simeq 0.2_7$ |

[a]Chemical shifts in ppm relative to TMS as internal standard, $J$ in Hertz.

diadduct **7** exhibits a single cyclohexadienylic $AX_2$ system at δ 8.29 and 5.69, a broad NH signal at δ 9.72, and a high-field doublet at δ 5.44 which coalesces to a *singlet* when irradiating the NH signal. Integration shows that these two latter resonances are in a 1:2 ratio. The chemical shift of the two equivalent protons indicates that they are located in the positions β to the nitrogen. The symmetrical structure of **7** is further supported by the absence of a vicinal coupling constant.

The minor product is the dissymmetrical C-2, C-4 diadduct **8** since its spectrum shows two $AX_2$ cyclohexadienylic systems very close to those observed for **6** and **7** and that the NH proton (δ = 10.20) is coupled with two pyrrolic protons ($\delta H_3$ = 5.52; $\delta H_5$ = 6.18). The large chemical shift difference between these two latter protons confirms that they are located in the positions β and α to the nitrogen atom, respectively.

Another type of diadduct, i.e. **9**, may be obtained in using a 2:1 stoichiometry of the reagents (2 equiv. of pyrrole and $CH_3O^-$ ion, 1 equiv. TNB) or adding a second equivalent of the basic mixture to a solution of the N-adduct **5***a*. In agreement with the structure **9**, the $^1H$ nmr spectrum shows four different resonances in a 1:2:4:4 ratio when going from low to high-field. That both pyrrole moieties in **9** are bonded by their nitrogen atom is evidenced by the presence of a single AA'BB' system. Whether **9** has a *cis* or *trans* configuration (13–15) cannot be deduced from nmr data recorded between 22 and 37°C. The $^4J_{AX}$ coupling constant in **9** is unresolved and has been determined, using Sardella's method, by double resonance experiments (16).

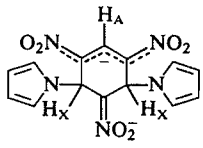


**9**

*2,5-Dimethyl pyrrole (***2**b**) and 2,4-dimethyl-3-ethyl pyrrole (***2**c**)*

Addition of an equimolar mixture of methoxide ion and **2***b* or **2***c* (1 equiv.) to a DMSO solution of TNB (1 equiv.) results in the initial formation of the oxygen adduct **4** which is subsequently converted into a C-adduct. Various attempts to detect the N-bonded complexes **5***b* and **5***c*, even as transient species, have failed. The results in Tables 2 and 3 are consistent with the formation of the C-3 and C-5 complexes **10** and **12** respectively.[4] The nmr spec-

[4]For simplicity, the numbering of the pyrrolic ring of **12** is the same as that of its parent, **2***c*.

Can. J. Chem. Downloaded from www.nrcresearchpress.com by 210.87.254.5 on 09/06/12
For personal use only.

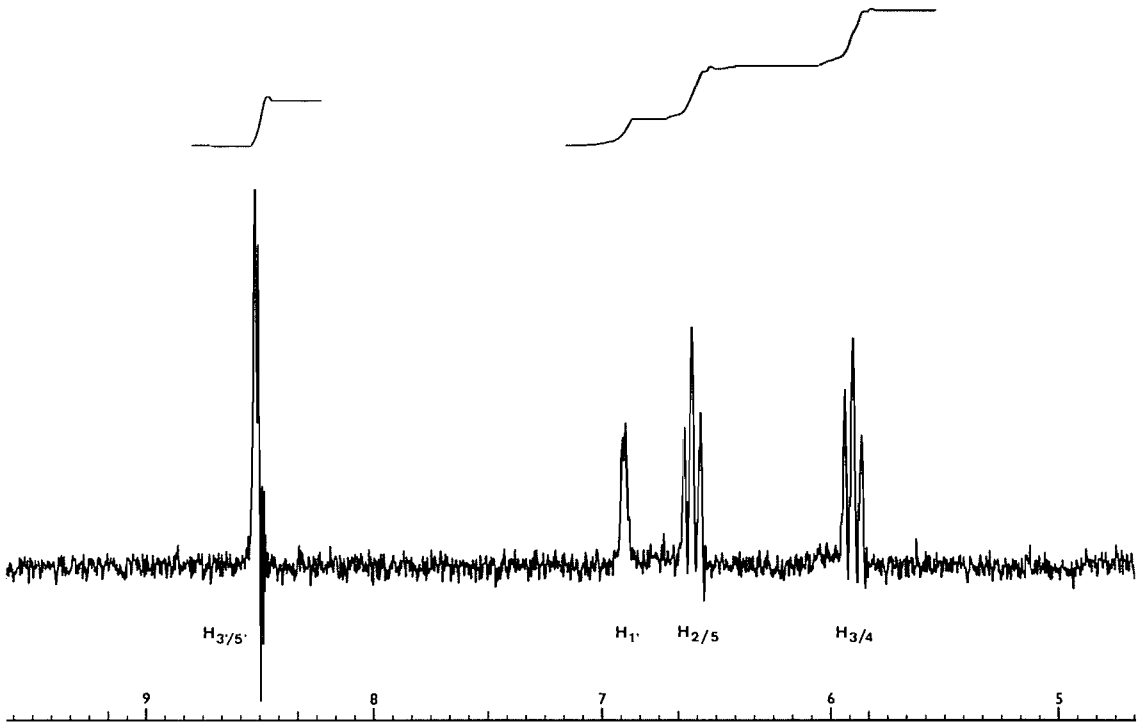


FIG. 1. The $^1H$ nmr spectrum of the potassium salt of the N-adduct **5***a* of pyrrole in DMSO-$d_6$.

trum of **10** shows in particular that the resonance of the 2-methyl group is a singlet while that of the 5-methyl group is a doublet, due to the allylic coupling constant $^4J_{H_4Me_5}$. In the case of **12**, both 2- and 4-methyl groups give a singlet, thus confirming the absence of the H-5 proton.

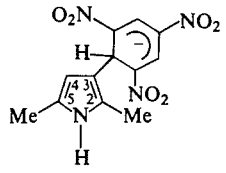

**10**

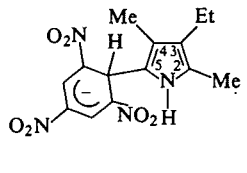

**12**

The use of a 2:1 2,5-dimethyl pyrrole (or kryptopyrrole)/$CH_3O^-$–TNB stoichiometry leads to the formation of the C-bonded diadduct **11** (or **13**). Both nmr spectra exhibit a low-field $AX_2$ system. In addition, the spectrum of **11** shows the presence of one pyrrolic β proton ($\delta H_4$ = 5.21) and two different methyl groups, the most shielded being coupled with $H_4$. On the other hand, and in agreement with a tetrasubstituted pyrrole ring, the spectrum of **13** exhibits no $H_\alpha$ resonance but shows two singlets corresponding to the 2- and 4-methyl groups and the multiplets expected for the ethyl group.

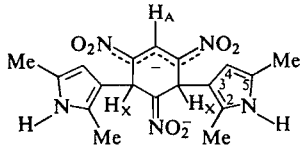

**11**

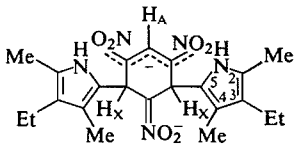

**13**

## Discussion

*Mechanism of complex formation*

It is well-known that addition of primary and secondary aliphatic and alicyclic amines to TNB and related derivatives in DMSO and acetonitrile obeys eq. [1], the overall interaction requiring two equivalents of amine (B = RR'NH) to form the anionic σ-complex **1** (5, 7, 17–21). Equation [1] also holds for less basic aromatic amines like aniline (7, 22, 23). However, the formation of the anilide zwitterion is thermodynamically so unfavorable that, despite a large $K_p$ value for its deprotonation by aniline, no reaction occurs in only the presence of aniline itself. In this case, addition of a stronger base like $MeO^-$ or diazabicyclo[2,2,2]octane (DABCO) is necessary for the reaction to proceed. The effect of this stronger base is to increase the equilibrium constant $K_p$ for deprotonation of **1**, $H^+$ to the extent that the overall interaction becomes feasible (7, 22, 23).

Can. J. Chem. Downloaded from www.nrcresearchpress.com by 210.87.254.5 on 09/06/12
For personal use only.

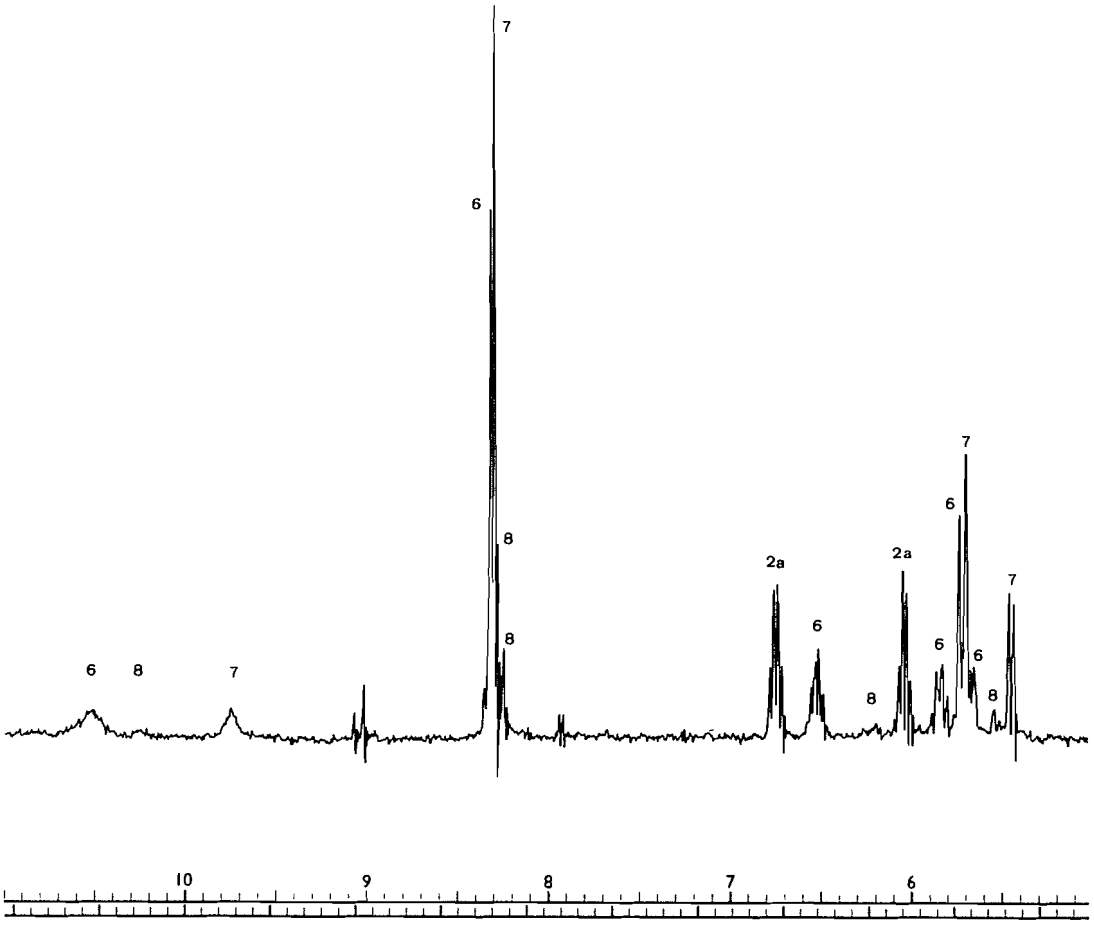


FIG. 2. The $^1$H nmr spectrum of the C-adduct **6** and the C-diadducts **7** and **8** of pyrrole in DMSO-$d_6$. Resonances are identified by structure numbers.

TABLE 2. Nuclear magnetic resonance parameters of 2,5-dimethyl pyrrole and its TNB-adducts in DMSO-$d_6$[a]

| Compounds | $\delta NH_1$ | $\delta Me(2)$ | $\delta Me(5)$ | $\delta H_3$ | $\delta H_4$ | $\delta H_{1''}$ | $\delta H_{3''/5''}$ | $^4J_{1''\text{-}3''/5''}$ | $\delta H_A$ | $\delta H_X$ | $J$ |
|---|---|---|---|---|---|---|---|---|---|---|---|
| **2***b* | 10.10 | 2.12 | 2.12 | 5.54 | 5.54 | | | | | | $^4J_{1-3/4} = 2.5$ |
| **10** | 9.72 | 2.18 | 2.00 | | 5.34 | 5.45 | 8.27 | 0.5 | | | $^4J_{4-Me(5)} = 0.8$ |
| **11** | | 2.16 | 1.99 | | 5.21 | | | | 8.41 | 5.01 | $^4J_{4-Me(5)} = 0.8$ |

[a]Chemical shifts in ppm relative to TMS as internal standard, $J$ in Hertz.

TABLE 3. Nuclear magnetic resonance parameters of 2,4-dimethyl-3-ethyl pyrrole and its TNB-adducts in DMSO-$d_6$[a]

| Compounds | $\delta NH_1$ | $\delta Me(2)$ | $\delta Me(4)$ | $\delta_{CH_2(Et(3))}$ | $\delta_{CH_3(Et(3))}$ | $\delta H_5$ | $\delta H_{1''}$ | $\delta H_{3''/5''}$ | $^4J_{1''\text{-}3''/5''}$ | $\delta H_A$ | $\delta H_X$ | $J$ |
|---|---|---|---|---|---|---|---|---|---|---|---|---|
| **2***c* | 9.77 | 2.07 | 1.92 | 2.30 | 0.99 | 6.25 | | | | | | $^4J_{5-Me(4)} = 1$ |
| **12** | 9.63 | 1.98 | 1.83 | 2.18 | 0.94 | | 5.64 | 8.28 | $0.3_2$ | | | |
| **13** | | 1.86 | 1.81 | 2.19 | 0.93 | | | | | 8.70 | 5.72 | $^4J_{AX} \simeq 0.1_2$ |

[a]Chemical shifts in ppm relative to TMS as internal standard, $J$ in Hertz.

In the case of pyrrole derivatives, the basicity of the nitrogen atom is very low because the lone pair is part of the aromatic sextet: a $pK_a^{H_2O}$ of $\sim -10$ has been estimated for unsubstituted pyrrole (24). Consequently, protonation and other electrophilic reactions occur preferentially at the α carbon atoms (pyrrole: $pK_a^{H_2O}$ ($C_\alpha$) = −3.8) or, if these positions are blocked, at the β carbon atoms (10, 25). In such conditions, direct nucleophilic attack of neutral pyrroles on TNB to give a zwitterion of

Can. J. Chem. Downloaded from www.nrcresearchpress.com by 210.87.254.5 on 09/06/12
For personal use only.

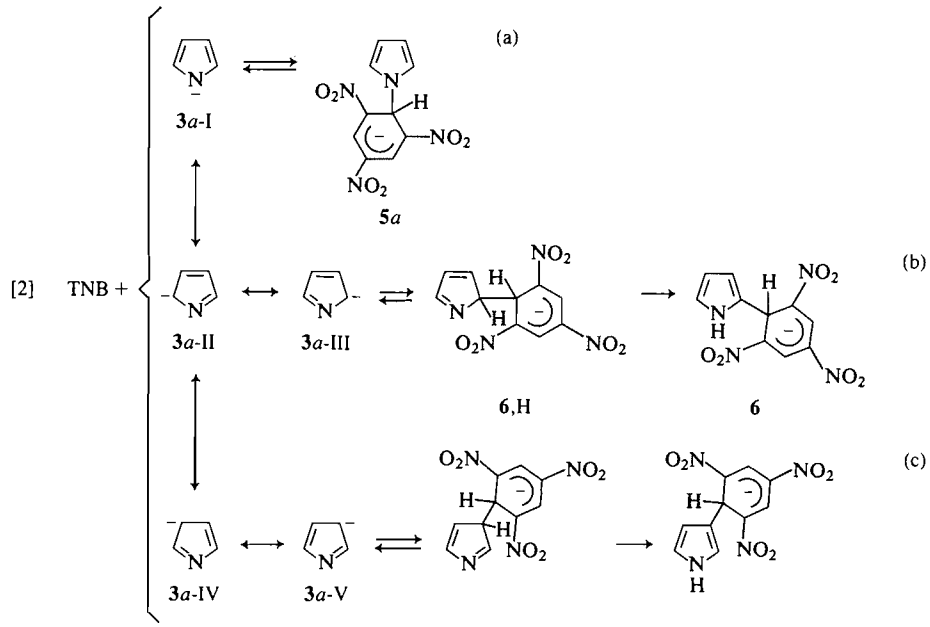


the **1**, $H^+$ type is totally unrealistic. In contrast, substitution on nitrogen is known to normally occur in basic media via the anions **3** and is often followed by isomerization to a C-substituted product, due to the contribution of the mesomeric forms **3***a*-I ·· **3***a*-V (see eq. [2]) (8–10). In accord with these results, there is no doubt that the formation of the N-bonded complex **5***a* reflects the attack of the highly nucleophilic pyrrolide ions, as shown in path (a) of eq. [2]. Support for this mechanism is provided by potentiometric hydrogen electrode measurements which show that ionization of unsubstituted pyrrole occurs to a notable extent in basic MeOH–DMSO and $H_2O$–DMSO mixtures with more than 95% DMSO by volume.[5] With time, and in agreement with a greater contribution of the resonance form **3***a*-II/III over **3***a*-IV/V, **5***a* is converted into the thermodynamically more stable C-2 complex **6**, according to paths (a) and (b) of eq. [2].

Due to the presence of electron-donating alkyl groups, 2,5-dimethyl and 2,4-dimethyl-3-ethyl pyrroles are much less acidic than pyrrole itself (10, 25). Potentiometric hydrogen electrode measurements show that they don't ionize to a great extent in our mixtures, preventing reliable $pK_a$ determinations. In this case, the equilibrium concentrations of the pyrrolide ions **3***b* and **3***c* are small and the methoxy complex **4** is first generated as a result of the highly favorable kinetic and thermodynamic factors associated with the formation of **4** from TNB and $CH_3O^-$ (7, 27). Then, the C-complexes **10** and **12** are formed from **4** according to eq. [3] (shown for 2,5-dimethyl pyrrole). The N-adducts **5***b* and **5***c*, which one would expect to form under kinetic control relative to **10** and **12**, cannot be detected.

The formation of the 1:2 diadducts **7** and **8** may be explained by the fact that the C-2 complex **6** behaves as a 2-substituted pyrrole and should ionize to some extent to give the corresponding pyrrolide ion **14**. In principle, such an anion may

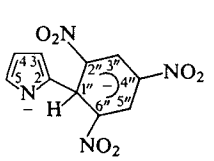

**14**

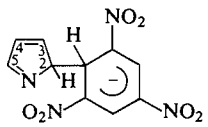

**12**,H

react with TNB at N-1, C-3, or C-4 and C-5. As for alkyl pyrroles **2***b* and **2***c*, attack at N-1 is not favored so that only the C,C-diadducts **7** and **8** are observed. The largely favored formation of **7** over **8** again reflects the preferential occurrence of electrophilic attack at the α-position in pyrroles (8–10).

It should be noted that the formation of the various C-adducts (**6**, **10**, and **12**) must be preceded by that of the corresponding C—H pyrrolenine adducts such as **6**, *H* (see eq. [2]), **10**, *H* (see eq. [3]), and **12**, *H*. A similar remark holds for diadducts **7** and **8**. That pyrrolenine adducts are not observed suggests they are not stable and rearrange very fast to **6**, **10**, and **12** or **7** and **8**. Indeed this behaviour is similar to that encountered in the

[5]For example, the $pK_a$ for formation of pyrrolide ion **3***a* is 21.9 in 5% $H_2O$ – 95% DMSO (J. C. Halle, unpublished results) while a 0.01 *M* tetramethylammonion hydroxide solution in this mixture has a pH of 22 (26).

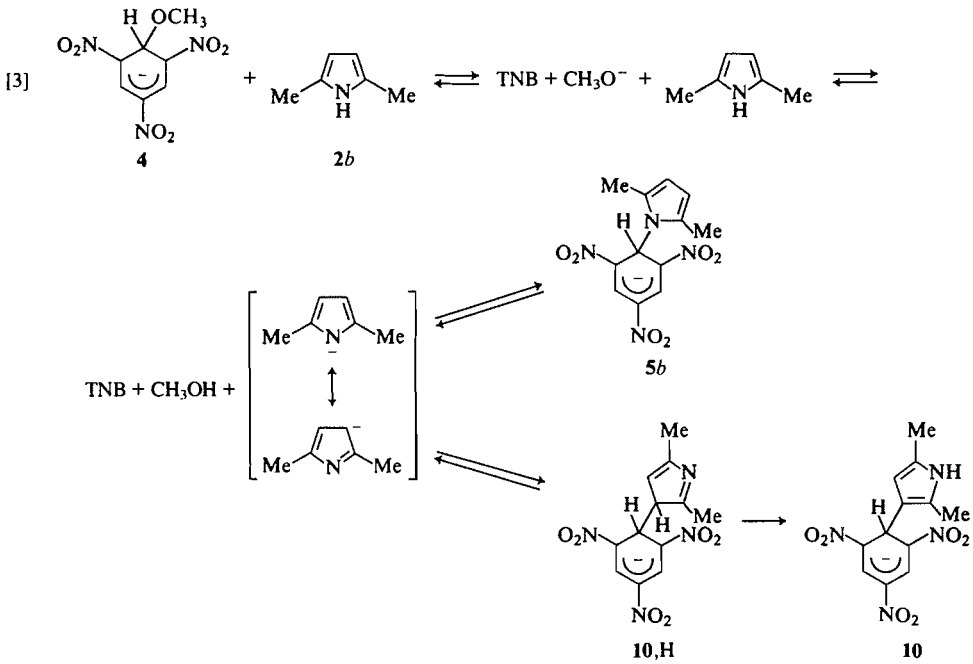


reactions of TNB with indoles to give the C-3 complexes **15** (1).

Although it is not a thermodynamically stable product, the N-adduct **5***a* may be isolated as a crystalline potassium salt. This is because its decomposition is remarkably slow. Thus, no appreciable dissociation of **5***a* into TNB and pyrrole occurs at pH 7 in aqueous solution. However, in dilute hydrochloric acid solutions, the decomposition occurs at measurable rates. The $H^+$-catalyzed second-order rate constant $k^{H^+}$ associated with eq. [4] is equal to $1\,L\,mol^{-1}\,s^{-1}$ ($t$ = 25°C, $I$ = 0.2 *M* KCl). It is one of the slowest rates ever measured for such a process (7). For comparison, the C-adducts **10** and **12** decompose faster: $k^{H^+}$ is equal to 3.09 and $70\,L\,mol^{-1}\,s^{-1}$ for **10** and **12**,

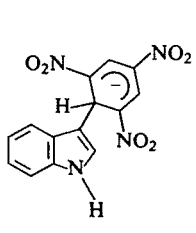
15

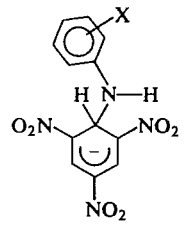
16

respectively. However, such $k^{H^+}$ values are in the range of those typically measured for very stable carbon-bonded complexes (7, 28). The exact mechanism of these $H^+$-catalyzed decompositions is currently under investigation.

[4] **5***a* + $H^+$ $\xrightarrow{k^{H^+}}$ TNB + pyrrole

*Nuclear magnetic resonance chemical shifts*

Tables 1, 2, and 3 show that all the protons of the pyrrole moieties move upfield on going from pyrroles **2***a*, *b*, *c* to the monoadducts **5***a*, **6**, **10**, and **12**. These protons undergo an additional high-field shift when substituting an α or β position by a second cyclohexadienyl ring to form the diadducts **7** and **8**. Thus, the NH and H-3 protons in pyrrole and its various adducts have chemical shifts decreasing in the order **2***a* > **5***a* (H-3) > **6** > **8** > **7**. An explanation of this phenomenon on only the basis of anisotropy effects due to either the cyclohexadienyl ring or the nitro groups is not satisfactory since similar upfield shifts are observed for the α and β protons in **5***a*. Also, such behaviour is apparently not consistent with the fact that the trinitrocyclohexadienyl moiety is known to be electron-withdrawing relative to a proton (29–33). It has thus been observed that all the protons of the aniline moiety in the various anilide complexes **16** resonate at lower field than their analogs in the parent anilines (30). In this instance, the electron-demanding cyclohexadienyl ring reduces the electron-releasing capability of the nitrogen in **16** as compared with that in the anilines. Another evidence of the electron-withdrawing effect of the cyclohexadienyl ring is that the zwitterions **1**, $H^+$ are, regardless of the amine, 100 to 400 times more acidic than the parent $RR'NH_2^+$ alkyl or aryl ammonium ions (31–33). In the pyrrole derivatives, the nitrogen lone pair is part of an aromatic sextet, so that the observed upfield shifts suggest that the

Can. J. Chem. Downloaded from www.nrcresearchpress.com by 210.87.254.5 on 09/06/12
For personal use only.

cyclohexadienyl moiety diminishes the electron density of the pyrrolic ring, thereby decreasing the ring current. It should be noted that the only case where a downfield shift is observed is the 2-Me group in the C-complex **10**. This is probably because this group is spatially located close to the cyclohexadienyl ring and suggests that the preferred conformation of **10** is different from that of **12**.

## Experimental

*Nuclear magnetic resonance experiments*

The $^1$H nmr spectra were recorded at 60 (Varian A-60; $T$ = +37°C) and 100 MHz (Varian XL-100; $T$ = +31°C) using TMS as an internal standard. The $^{13}$C spectra were collected at 25.17 MHz, using the Fourier transform technique (Varian XL-100) and the solvent $^2$H signal (DMSO-$d_6$) for internal field-frequency lock.

*Isolable complexes*

Potassium salts of **5***a*, **10**, and **12** were prepared by the addition of an equimolar mixture of pyrrole (**2***a*, **2***b*, or **2***c*) and potassium methoxide ion in 1 mL acetonitrile to an acetonitrile solution of TNB (100 mg in 1 mL). The reaction mixtures turned immediately dark red or purple and were allowed to stand at room temperature for one hour (**5***a*) or two days (**10** and **12**). Then some anhydrous ether $Et_2O$ was added to the solutions. The crystals which formed were filtered, ground to a fine powder, washed with copious amounts of ether, and dried *in vacuo* to eliminate any associated solvent. The three complexes decompose from 180 to 200°C. The $^1$H nmr spectra of the salts in DMSO-$d_6$ are similar to those observed in the *in situ* generation of **5***a*, **10**, and **12**.

*Rate measurements*

The kinetics of the decomposition of the complexes **5***a*, **10**, and **12** was followed spectrophotometrically at 480 nm on a Beckman Acta 3 spectrophotometer, the cell compartment of which was thermostated to 25 ± 0.5°C. All kinetic runs were carried out under pseudo first-order conditions with an acid (HCl) or buffer ($HCOO^-$/HCOOH, $CH_3COO^-$/$CH_3COOH$) concentration in large excess over the complex concentration ($2 \times 10^{-5}$ *M*). The reported rate constants represent average values obtained from two or three independent determinations.


1. J. C. Halle, F. Terrier, M. J. Pouet, and M. P. Simonnin. J. Chem. Res. (S), 360 (1980).
2. R. Foster and C. A. Fyfe. Rev. Pure Appl. Chem. **16**, 1 (1966).
3. E. Buncel, A. R. Norris, and K. E. Russell. Q. Rev. Chem. Soc. **22**, 123 (1968).
4. M. J. Strauss. Chem. Rev. **70**, 667 (1970).
5. C. F. Bernasconi. Acc. Chem. Res. **11**, 147 (1978).
6. S. Sekiguchi. Yuki Gosei Kagaku Kyokai Shi **36**, 633 (1978).
7. F. Terrier. Chem. Rev. In press.
8. P. A. Cantor and C. A. van der Werf. J. Am. Chem. Soc. **80**, 970 (1958).
9. C. F. Hobbs, C. K. McMillin, E. P. Papadopoulos, and C. A. van der Werf. J. Am. Chem. Soc. **84**, 43 (1962).
10. A. H. Jackson. *In* Comprehensive organic chemistry. Vol. 4. *Edited by* D. Barton, W. D. Ollis, and P. G. Sammes. Pergamon Press, Oxford. 1979. p. 275.
11. R. J. Abraham and H. J. Bernstein. Can. J. Chem. **37**, 1056 (1969); **39**, 905 (1961).
12. G. F. Katekar and A. G. Moritz. Aust. J. Chem. **22**, 1199 (1969).
13. C. F. Bernasconi and R. G. Bergstrom. J. Am. Chem. Soc. **95**, 3603 (1973).
14. M. J. Strauss and S. P. B. Taylor. J. Am. Chem. Soc. **95**, 3813 (1973).
15. M. R. Crampton and M. J. Willison. J. Chem. Soc. Perkin Trans. II, 160 (1976).
16. D. J. Sardella. J. Magn. Reson. **10**, 188 (1973).
17. J. A. Orvik and J. F. Bunnett. J. Am. Chem. Soc. **92**, 2417 (1970).
18. C. F. Bernasconi. Chimia (Aarau), **34**, 1 (1980).
19. M. R. Crampton and B. Gibson. J. Chem. Soc. Perkin Trans. II, 533 (1981).
20. T. O. Bamkole, J. Hirst, and J. Onyido. J. Chem. Soc. Perkin Trans. II, 1201 (1981).
21. S. Sekiguchi and J. F. Bunnett. J. Am. Chem. Soc. **103**, 4871 (1981).
22. E. Buncel, J. G. K. Webb, and J. F. Wiltshire. J. Am. Chem. Soc. **99**, 4429 (1977).
23. E. Buncel and W. Eggimann. J. Am. Chem. Soc. **99**, 5958 (1977).
24. H. J. Chen, L. E. Hakka, R. L. Hinman, A. J. Kresge, and E. B. Whipple. J. Am. Chem. Soc. **93**, 5102 (1971).
25. Y. Chiang and E. B. Whipple. J. Am. Chem. Soc. **85**, 2763 (1963).
26. H. Achassi Sorkhabi, J. C. Halle, and F. Terrier. (*a*) J. Chem. Res. (S), 108 (1978); (M), 1371 (1978); (*b*) J. Chem. Res. (S), 196 (1978); (M), 2345 (1978).
27. M. R. Crampton. J. Chem. Soc. (B), 1208 (1968).
28. R. A. Renfrow, M. J. Strauss, and F. Terrier. J. Org. Chem. **45**, 471 (1980).
29. M. R. Crampton. J. Chem. Soc. (B), 2112 (1971).
30. E. Buncel and J. G. K. Webb. Can. J. Chem. **52**, 630 (1974).
31. C. F. Bernasconi and C. L. Gehriger. J. Am. Chem. Soc. **96**, 1092 (1974).
32. C. F. Bernasconi, C. L. Gehriger, and R. H. de Rossi. J. Am. Chem. Soc. **98**, 8451 (1976).
33. C. F. Bernasconi, M. C. Muller, and P. Schmid. J. Org. Chem. **44**, 3189 (1979).


Can. J. Chem. Downloaded from www.nrcresearchpress.com by 210.87.254.5 on 09/06/12
For personal use only.

# Xanthocyclines: 5-oxaanthracyclines (7,8,9,10-tetrahydrobenzo[*b*]xanthen-12-one)

JAMES L. CHARLTON, VILAYAT A. SAYEED, AND GERALD N. LYPKA
*Department of Chemistry, University of Manitoba, Winnipeg, Man., Canada R3T 2N2*

Received February 2, 1982

JAMES L. CHARLTON, VILAYAT A. SAYEED, and GERALD N. LYPKA. Can. J. Chem. **60**, 1996 (1982).

The anthracycline antibiotics daunorubicin and adriamycin are potent antitumor agents. It has recently been suggested that 5-oxaanthracycline analogs of these compounds might show reduced cardiotoxicity, a property that limits the clinical use of the anthracyclines. In this paper we describe the condensation–cyclization reactions of 2-methylchromone-3-carboxylate with cyclohexanones, a reaction that leads ultimately to the xanthocycline skeleton.

JAMES L. CHARLTON, VILAYAT A. SAYEED et GERALD N. LYPKA. Can. J. Chem. **60**, 1996 (1982).

Les antibiotiques du type anthracycline tels la daunorubicine et l'andriamicyne sont des agents puissants contre les tumeurs. On a suggéré récemment que les oxa-5 anthracycline analogues de ces composés, peut exhiber une cardiotoxicité réduite; cette propriété limite l'utilisation clinique des anthracyclines. Dans cette publication, nous décrivons les réactions de condensation–cyclisation du méthyl-2 chromone carboxylate-3 avec les cyclohexanones qui conduisent éventuellement au squelette de la xanthocycline.
[Traduit par le journal]

## Introduction

The anthracycline antibiotics daunorubicin, **1**, and adriamycin, **2**, have been the subject of extensive synthetic effort due to their use in the treatment of several human cancers (ref. 1, and for reviews of synthetic methods, see ref. 2). Unfortunately, these drugs also exhibit a cardiotoxicity which limits their clinical use (3). Although some analogs show a reduced cardiotoxicity (4), the search continues for drugs with a higher therapeutic index. It has been suggested that the cardiotoxicity of the anthracycline antibiotics may be related to the electron transport properties of the quinone function within these molecules (5). This in turn led to the suggestion by Wong *et al.* that modification of the C ring might reduce the cardiotoxicity (6).

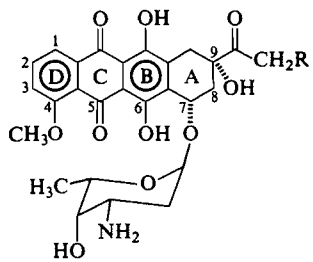

**1** R = H
**2** R = OH

Wong suggested replacing the 5-carbonyl group with an oxygen in order to alter the reduction potential of the C ring. He referred to the 5-oxa-adriamycin analog **3** as xanthoadriamycin (6). We propose the more general name xanthocycline for this class of compounds, that is, compounds having the 7,8,9,10-tetrahydrobenzo[*b*]xanthen-12-one skeleton.

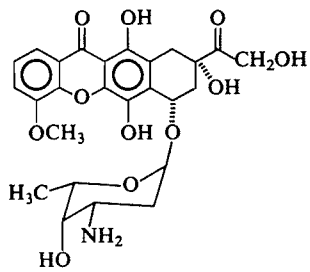

**3**

Xanthones, and especially hydroxyxanthones, have long been known to produce pharmacological and biological effects (7), although few examples of compounds having the general tetracyclic carbon skeleton of compound **3** are known. The one exception is bikaverin **4**, which has been the subject of three independent synthetic studies (8).

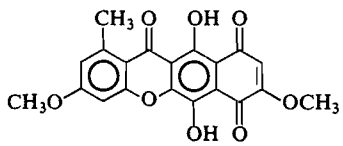

**4**

Although bikaverin is reported to show only antiprotozoal activity, we were intrigued to find that other derivatives of 1-hydroxyxanthone were active against Sarcoma 180 tumor cells (9). This further encouraged us to seek a synthetic route to the xanthocyclines, since they contain both the 1-hydroxyxanthone functionality and the major structural features of the anthracycline antibiotics.

In this paper we report the synthesis of the tetracyclic compound **5**

0008-4042/82/151996-06$01.00/0
©1982 National Research Council of Canada/Conseil national de recherches du Canada

Can. J. Chem. Downloaded from www.nrcresearchpress.com by 210.87.254.6 on 09/06/12
For personal use only.

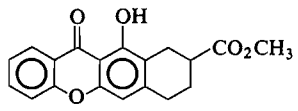

5

beginning from methyl 2-methylchromone-3-carboxylate **6**.

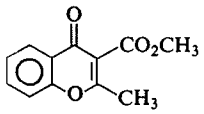

6

## Results and discussion

Several methods for the synthesis of xanthones have been described in the literature (7, 8). Most of these involve condensation between two aromatic precursors as illustrated in the example below (10). The latest two papers on the synthesis of bikaverin incorporate similar aromatic condensation methods involving two steps, a photo-Fries followed by cyclization (8*a*, *b*). Although these routes are

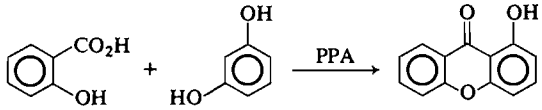

convenient for simple derivatives of xanthones, the possible lack of specificity in coupling, and the difficulty in obtaining the proper aromatic precursors makes this approach less attractive as a general method. The method used by Barton *et al.* in the first successful synthesis of bikaverin (8*c*) requires the A ring to be aromatic and is not suitable for the tetrahydrosubstitution pattern of **5**.

As an alternate to the existing methods for tetracyclic xanthone synthesis, we have attempted to condense 2-methylchromone-3-carboxylic acid derivatives with cyclohexanones in order to form the B ring of the tetracyclic compound from the preformed DC and A ring precursors.

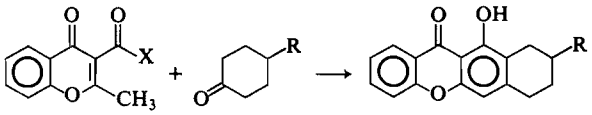

Ethyl 2-methylchromone-3-carboxylate was prepared by the condensation of salicyloyl chloride and the enamine of ethyl acetoacetate (11). Hydrolysis (11) and reesterification with methanol gave the methyl ester **6**. An alternate high yield synthesis of the chromone esters from *o*-fluorobenzoyl chloride has also been recently reported (12).

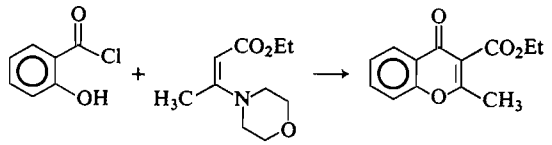

We anticipated that the condensation of the chromone acid chloride **7** with the enamine of cyclohexanone **8** would yield the acylated cyclohexanone which could be easily cyclized to the tetracyclic skeleton **9**. The acid chloride **7** was therefore reacted with cyclohexanone morpholine enamine in methylene chloride using triethylamine as an acid scavenger at several different temperatures. Despite considerable effort the major prod-

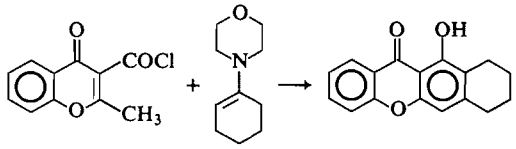

7 8 9 3%

ucts were always the chromone acid and/or its morpholine amide. Under optimum conditions a 3% yield of tetracyclic compound **9** was obtained from chromatography of the reaction mixture on silica gel. Whereas aromatic acid chlorides normally acylate enamines readily at carbon, it appears that the chromone acid chloride reacts primarily at the nitrogen center.

Since it appeared difficult to form a bond to the acyl group of the chromone acid, we investigated the possibility of condensation at the 2-methyl group of the chromone. The anion at this center should be stabilized by delocalization of the charge onto the two carbonyls and a reactivity similar to that of the malonate anion might be expected.

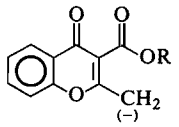

Several attempts to condense the chromone methyl ester **5** with cyclohexanone under conditions suitable for malonic ester condensations (Knoevenagel conditions) led to no appreciable reaction. The use of potassium *tert*-butoxide in *tert*-butyl alcohol/dimethoxyethane, did, however, lead to the spirolactone **10** in high yield as illustrated below.

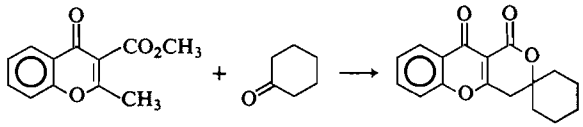

6 10 ~90%

Can. J. Chem. Downloaded from www.nrcresearchpress.com by 210.87.254.6 on 09/06/12
For personal use only.

Can. J. Chem. Downloaded from www.nrcresearchpress.com by 210.87.254.6 on 09/06/12
For personal use only.

The use of the stronger base apparently allowed the intermediate oxy anion to be trapped intramolecularly. The reaction time had to be kept very short as the product was not stable to the reaction conditions.

The spirolactone had a very low mobility on thin layer chromatography (tlc) and we suspected that, in polar media, it existed in equilibrium with the acid form **11**. Indeed, treating the lactone with diazomethane in diethyl ether led to the cyclohexylidene ester **12**.

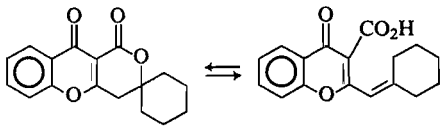

**10** **11**

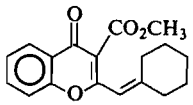

**12**

This same alkene ester could be obtained from treatment of the lactone with methyl iodide and potassium carbonate in acetone. Rather surprisingly though, treatment of the lactone with dry HCl in methanol appeared to give the unconjugated ester **13**. Apparently the double bond is thermodynamically more stable in the unconjugated position. Although the unconjugated ester **13** was not characterized fully, it could also be prepared by treating the ester **12** with *p*-toluenesulfonic acid in benzene, substantiating the structural assignment. The isomerization of the conjugated ester **12** to the unconjugated ester **13** under acidic conditions led to the proposal that the tetracyclic skeleton might be obtained by intramolecular acylation of the double bond. Treatment of the ester **12** with polyphosphoric acid converted it to the tetracyclic compound **9**. In view of this success, the spirolactone itself was treated with various acid catalysts to convert it directly to the tetracyclic xanthone. It was found that both phosphorus pentoxide and trifluoromethane sulfonic acid could convert the lactone directly to the xanthone **9** in approximately 40% yield. The latter reagent is preferred, as the phosphorus pentoxide complexes the product strongly and work-up must include extensive hydrolysis in aqueous acid.

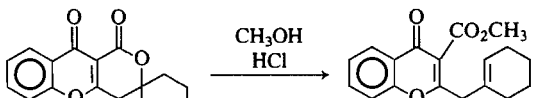

**10** **13**

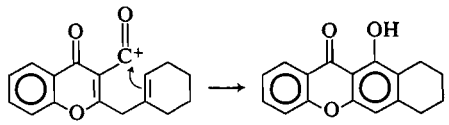

**9**

Since we were interested in the preparation of xanthocyclines with substituents in the A ring, we attempted to modify the cyclohexano ring in **9**. NBS bromination of **9** led primarily to substitution *para* to the hydroxyl and NBS bromination of the *O*-methyl ether of **9** gave a mixture of products with apparent aromatization of the cyclohexano ring.

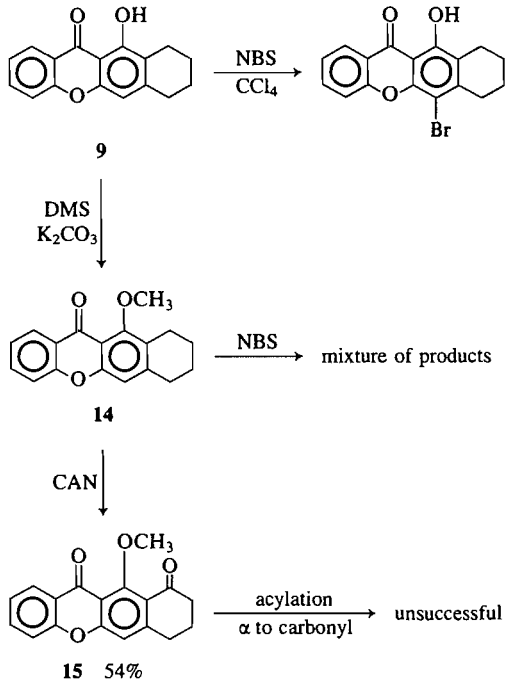

**9** **14** **15** 54%

Treatment of the ether **14** with ceric ammonium nitrate (CAN) led to the methoxy ketone **15** in 54% yield. The structure **15** was assigned on the basis of our expectation that position 10 will be activated towards oxidation by the methoxyl group and the ring oxygen, whereas position 7 would be deactivated by the xanthone carbonyl. The spectral and analytical data alone were not sufficient to distinguish **15** from the isomeric ketone **16**.

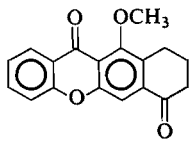

**16**

Can. J. Chem. Downloaded from www.nrcresearchpress.com by 210.87.254.6 on 09/06/12
For personal use only.

Unfortunately, we were unable to find conditions which would allow the introduction of an acetyl group α to the carbonyl in compound **15** and this approach to further substitution in the cyclohexano ring was abandoned.

An alternate method of introducing substituents into the cyclohexano ring of **9** begins with the substituent in place, prior to the condensation with the chromone ester **6**. We therefore attempted the condensation of methyl 4-oxocyclohexane carboxylate **17** with the chromone ester **6**. The cyclohexanone was prepared from methyl *p*-hydroxybenzoate (13).

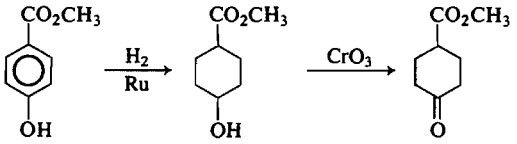


**17**

The synthesis of the final product **5** was analogous to the procedure already described for **9** except that the final step could not be catalysed by trifluoromethane sulfonic acid. Phosphorus pentoxide was successful, and gave the carbomethoxyxanthocycline **5** in 25% yield. Compound **5** was difficult to purify by recrystallization although the mass spectrum and nuclear magnetic resonance spectrum were consistent with the proposed structure. Conversion to the methyl ether **19** and recrystallization to a constant melting point gave a material which gave a satisfactory elemental analysis and the expected spectra for the ether.

The condensation–cyclization reactions of 2-methylchromone-3-carboxylic acid esters with cyclohexanones provide a convenient two step synthesis to the tetracyclic xanthones. The further elaboration of these precursors to daunorubicin analogs will be the object of future work.

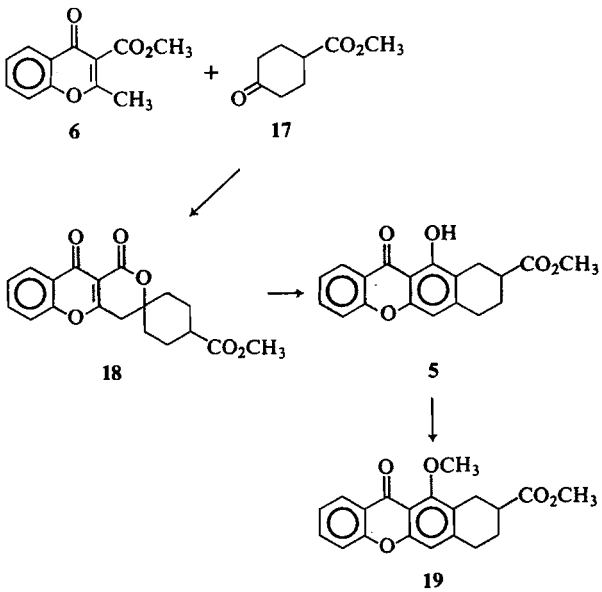


## Experimental

Melting points were determined on a Kofler hot stage and are uncorrected. Infrared spectra were obtained with a Beckman IR-10 instrument and nuclear magnetic resonance spectra were recorded on a Varian EM-360 or a Bruker WH90-DS instrument. Chemical shifts are reported in ppm downfield from tetramethylsilane. Mass spectra were recorded on a Finnigan 1015 mass spectrometer. Silica gel column chromatography was carried out on Merck silica gel 60 (230–400 mesh).

*2-Methyl-4-oxo-4H-1-benzopyran-3-carboxylic acid (2-methylchromone-3-carboxylic acid)*

The chromone was synthesized from salicyloyl chloride and the morpholine enamine of ethyl acetoacetate according to the published procedure (11).

*2-Methylchromone-3-carboxylic acid chloride, 7*

The acid chloride was prepared by refluxing the acid (16.0 g) in an excess of thionyl chloride (400 mL) and chlorform (200 mL) for 15 h, followed by evaporation to dryness to leave yellow-brown crystalline material which was used without further purification; nmr ($CDCl_3$) δ: 2.56 (s, 3H), 7.53 (m, 3H), 8.18 (d, 1H); ms *m/e*: 222/224, 187.

*Methyl 2-methylchromone-3-carboxylate, 6*

The acid (33.1 g) was stirred at room temperature overnight in an excess of 3% HCl in methanol (prepared from 10 mL of acetyl chloride and 200 mL of anhydrous methanol). The solvent was removed *in vacuo*, the residue dissolved in chloroform, washed with dilute aqueous bicarbonate, dried ($MgSO_4$), and evaporated *in vacuo* to leave the crystalline ester (31.4 g); nmr ($CDCl_3$) δ: 2.50 (s, 3H), 3.92 (s, 3H), 7.42 (m, 3H), 8.08 (d, 1H).

*Spirolactone, 10*

To a solution of methyl 2-methylchromone-3-carboxylate **6** (0.887 g, 0.004 mol) and cyclohexanone (1.995 g, 0.020 mol) in dimethoxyethane (5 mL) was added a solution of potassium *tert*-butoxide in *tert*-butyl alcohol (35 g of 0.11 *M*). The solution was stirred for one minute at room temperature, poured into 300 mL of 2 *N* HCl, and extracted into chlorform. The extracts were dried ($MgSO_4$) and evaporated *in vacuo* to yield an orange solid (1.187 g). Nuclear magnetic resonance of the crude material indicated that it was greater than 90% lactone. Recrystallization from acetone gave white crystals, mp 164–166.5°C (dec.); ir ($CHCl_3$): 1740, 1655 $cm^{-1}$; nmr ($CDCl_3$) δ: 1.1–2.2 (m, 10H), 3.08 (s, 2H), 7.25–7.85 (m, 3H), 8.10–8.45 (m, 1H); ms *m/e* (relative intensity): 284(20), 261(28), 228(57), 213(23), 200(48), 186(100). *Anal.* calcd. for $C_{17}H_{16}O_4$: C 71.81, H 5.67; found: C 72.14, H 5.89.

*Cyclohexylidenechromone ester, 12*

*Method A*

To a solution of the lactone **10** (0.348 g, 0.0012 mol) in methanol (10 mL) was added an excess of diazomethane in ether (50 mL). The reaction mixture was stirred for 48 h, washed with dilute HCl, dried ($MgSO_4$), and evaporated to give a yellow oil (0.425 g). Chromatography on silica gel (eluent, benzene–ether, 60:40) gave pale yellow crystals (0.190 g, 52%). Recrystallization from isopropanol gave white crystals, mp 154.5–156.5°C; ir ($CHCl_3$): 1640, 1735 $cm^{-1}$; nmr ($CDCl_3$) δ: 1.45–1.95 (m, 6H), 2.1–2.55 (m, 2H), 2.55–2.9 (m, 2H), 3.93 (s, 3H), 6.13 (s, 1H),

Can. J. Chem. Downloaded from www.nrcresearchpress.com by 210.87.254.6 on 09/06/12
For personal use only.

7.2–7.22 (m, 3H), 8.1–8.32 (q, 1H); ms *m/e* (relative intensity): 298(45), 266(71), 255(45), 251(49), 238(57), 225(67), 121(100). *Anal.* calcd. for $C_{18}H_{18}O_4$: C 72.47, H 6.08; found: C 72.28, H 6.22.

*Method B*

A mixture of the lactone **10** (0.124 g), anhydrous potassium carbonate (0.1 g), and methyl iodide (0.226 g) in acetone (10 mL) was stirred at room temperature for 72 h. The reaction mixture was poured into dilute HCl, extracted with chloroform, and the extracts dried ($MgSO_4$) and evaporated *in vacuo* to yield yellow crystals of the ester.

*11-Hydroxy-7,8,9,10-tetrahydrobenzo*[b]*xanthene-12-one, **9***

*Method A*

A solution of the chromone acid chloride 7 (1.52 g, 0.007 mol) in chloroform (20 mL) was slowly added to a stirred, cooled (0°C) solution of 1-morpholinocyclohex-1-ene (5.85 g, 0.035 mol) in chloroform (30 mL). The mixture was refluxed 45 h, cooled, washed with 1 *N* HCl, dried ($MgSO_4$), and evaporated *in vacuo* to leave an oil. Chromatography on silica gel (eluent, benzene/ether, 95:5) gave an early crystalline fraction (45 mg) (for properties see below).

*Method B*

To a solution of the spirolactone **10** in toluene (1.48 g in 100 mL) was added $P_2O_5$ (20 g) and the mixture refluxed, with stirring, for three hours. The toluene was decanted off and a slurry of 2 *N* HCl in crushed ice added to the residue. The toluene was returned to the flask and the mixture heated to distill off the toluene. Extraction of the remaining aqueous solution with chloroform, drying ($MgSO_4$), evaporation, and chromatography on silica gel (eluent, benzene) gave yellow crystals (0.533 g, 38%). Recrystallization from ethanol gave yellow crystals (for properties see below).

*Method C*

The spirolactone **10** (80 mg) was heated in trifluoromethanesulfonic acid (4 mL) in an oil bath at 100–110°C for 42 h. After cooling, addition of water (40 mL), and extraction with chloroform, the extracts were dried and evaporated to give a crystalline residue. Chromatography as above gave pale yellow crystals (32 mg, 43%), mp (ethanol) 199.5–201.5°C; ir ($CHCl_3$): 1616, 1652 $cm^{-1}$; nmr ($CDCl_3$) δ: 1.55–2.04 (m, 4H), 2.50–3.00 (m, 4H), 6.65 (s, 1H), 7.15–7.90 (m, 3H), 8.12–8.35 (q, 1H), 12.63 (s, 1H); ms *m/e* (relative intensity): 266 (100), 265 (38), 251 (55), 238 (37). *Anal.* calcd. for $C_{17}H_{14}O_3$: C 76.67, H 5.30; found: C 76.73, H 5.45.

*11-Methoxy-7,8,9,10-tetrahydrobenzo*[b]*xanthene-12-one, **14***

A mixture of the hydroxycyclohexanoxanthone **9** (0.335 g, 0.00125 mol), anhydrous potassium carbonate (0.35 g), dimethyl sulfate (3 mL), and acetone (20 mL) was refluxed for 18 h. Filtration and evaporation *in vacuo* yielded the methoxyanthone, mp (isopropyl alcohol) 148–149°C; ir ($CHCl_3$): 1625, 1663 $cm^{-1}$; nmr ($CDCl_3$) δ: 1.65–1.95 (m, 4H), 2.65–3.0 (m, 4H), 3.93 (s, 3H), 6.95 (s, 1H), 7.05–8.0 (m, 3H), 8.15–8.40 (m, 1H); ms *m/e* (relative intensity): 294 (100), 276 (57), 265 (71), 236 (71), 139 (90). *Anal.* calcd. for $C_{18}H_{16}O_3$: C 77.12, H 5.75; found: C 76.88, H 5.75.

*11-Methoxy-7,8,9,10-tetrahydrobenzo*[b]*xanthene-10,12-dione, **15***

The methoxyketoxanthocycline **15** was prepared using a modification of the procedure of Trahanovsky and Young (14).

Six equivalents (4.76 g) of ceric ammonium nitrate were added to the methoxyxanthone **14** (0.405 g, 0.0015 mol) dissolved in a mixture of acetic acid, water, and ether (1:1:1, 100 mL). The mixture was heated on a steam bath until it turned a pale yellow (5–10 min) and then poured into water. The product was extracted into chloroform, dried ($MgSO_4$), and the solvent removed *in vacuo* to yield a yellow oil (0.438 g). Chromatography on silica gel (eluent, benzene/ether, 50:50) gave 0.240 g of product which crystallized from isopropyl alcohol in pale yellow needles, mp 186.5–188°C; ir ($CHCl_3$): 1605, 1672, 1698 $cm^{-1}$; nmr ($CDCl_3$) δ: 1.9–2.4 (m, 2H), 2.5–3.2 (m, 4H), 4.07 (s, 3H), 7.05 (s, 1H), 7.18–7.88 (m, 3H), 8.15–8.37 (m, 1H); ms *m/e* (relative intensity): 294(100), 276(97), 265(72), 236(87). *Anal.* calcd. for $C_{18}H_{14}O_4$: C 73.46, H 4.79; found: C 73.52, H 4.98.

*Methyl 4-oxocyclohexane carboxylate, **17***

The procedure of Finnegan and Bachman (13) was used. Methyl *p*-hydroxybenzoate (20 g) and 5% rhodium on alumina (400 mg) were mixed in 95% ethanol (150 mL) and hydrogenated at 45 psi for 96 h. Work-up gave the saturated alcohol in quantitative yield. The alcohol (36 g) was oxidized in ether (200 mL) with aqueous chromic acid (20 g $CrO_3$ in 200 mL of 25% $H_2SO_4$, v/v) at 10°C (cooling), adding the chromic acid over 40 min, followed by stirring at room temperature (4 h). Work-up yielded the ketone **17** (16.5 g, 46%); ir ($CHCl_3$): 1683, 1730 $cm^{-1}$; nmr ($CDCl_3$) δ: 2.0–3.0 (m, 9H), 3.72 (s, 3H); ms *m/e* (relative intensity): 156(22), 128(17), 125(21), 100(100).

*Carbomethoxy spirolactone, **18***

To a solution of methyl 2-methylchromone-3-carboxylate (1.09 g, 0.005 mol) and methyl 4-oxocyclohexane carboxylate (3.44 g, 0.02 mol) in dimethoxyethane (7 mL), was added 0.1 *M* potassium *tert*-butoxide in *tert*-butyl alcohol (55 g). The mixture was stirred one minute at room temperature, poured into 2 *N* HCl (300 mL), and extracted into chloroform. The extracts were dried ($MgSO_4$) and evaporated at high vacuum to remove the excess cyclohexanone ester. The residue was crystallized from $CCl_4$/isopropyl alcohol/hexane to yield brown crystals (0.81 g, 47%). Recrystallization from isopropyl alcohol gave white crystals, mp 153.5–154.5°C; ir ($CHCl_3$) 1662, 1742 $cm^{-1}$; nmr ($CDCl_3$) δ: 1.82–2.42 (m, 8H), 3.01 (s, 2H), 3.69 (s, 3H), 7.33–7.82 (m, 3H), 8.25–8.36 (m, 1H); ms *m/e* (relative intensity): 342(15), 311(7), 265(32), 241(100), 186(62). *Anal.* calcd. for $C_{19}H_{18}O_6$: C 66.66, H 5.30; found: C 66.44, H 5.57.

*9-Carbomethoxy-11-hydroxy-7,8,9,10-tetrahydrobenzo*[b]*xanthene-12-one, **5***

$P_2O_5$ (10 g) was added to a solution of the carbomethoxy lactone **18** (1.17 g, 0.0034 mol) in toluene (100 mL) and the mixture heated, with stirring, in an 130°C oil bath for two hours. The toluene was decanted from the residue, a slurry of 2 *N* HCl in crushed ice added (200 mL), and the toluene returned to the flask and heated until the toluene had distilled off. The aqueous solution was extracted with chloroform, the extracts washed with dilute bicarbonate, dried ($MgSO_4$), and evaporated *in vacuo* to yield 0.565 g. Chromatography on silica gel (eluent, benzene/ether, 60:40) gave 0.277 g of yellow crystals (25%). Recrystallization from ethanol was accomplished with difficulty, mp 160–164°C; ir ($CHCl_3$): 1618, 1650, 1735 $cm^{-1}$; nmr ($CDCl_3$) δ: 2.67–3.29 (m, 7H), 3.75 (s, 3H), 6.69 (s, 1H), 7.33–7.87 (m, 3H), 8.21–8.34 (m, 1H), 12.97 (s, 1H); ms *m/e* (relative intensity): 324(55), 265(100), 249(14), 238(24).

*9-Carbomethoxy-11-methoxy-7,8,9,10-tetrahydrobenzo*[b]*xanthene-12-one, **19***

The carbomethoxy hydroxyxanthocycline **19** (100 mg, $3.09 \times 10^{-4}$ mol), methyl iodide (2 mL), potassium carbonate (400 mg), and dry acetone (25 mL) were refluxed together for 36 h. After cooling and filtering the acetone was evaporated *in vacuo*. The residue was dissolved in chloroform, washed with 1 *N* HCl, dried ($MgSO_4$), and evaporated to give 90 mg (86%) yellow crystals. Recrystallization from 2-propanol cyclohexane gave mp 155–157°C; ir ($CHCl_3$): 1670, 1740 $cm^{-1}$; nmr ($CDCl_3$) δ:

3.10–1.50 (m, 7H), 3.77 (s, H), 3.96 (s, 3H), 7.05 (s, 1H), 7.14–8.00 (m, 3H), 8.15–8.53 (d, 1H); ms *m/e* (relative intensity): 388(88), 323(100), 309(70), 279(82). *Anal.* calcd. for $C_{20}H_{18}O_5$: C 71.01, H 5.32; found: C 70.84, H 5.64.


1. J. R. BROWN. Prog. Med. Chem. **15**, 126 (1978); A. C. SARTORELLI (*Editor*). Cancer chemotherapy. Am. Chem. Soc. Symposium Series No. 30, Am. Chem. Soc., Washington, DC. 1976.
2. T. R. KELLY. Annu. Rep. Med. Chem. **14**, 288 (1979); T. R. KELLY, J. VAYA, and L. ANANTHASUBRAMANIAN. J. Am. Chem. Soc. **102**, 5983 (1980), and references cited.
3. R. T. CHEWBOWSKI. West. J. Med. **131**, 364 (1979), and references cited.
4. G. L. TONG, H. Y. WU, T. H. SMITH, and D. W. HENRY. J. Med. Chem. **22**, 918 (1979).
5. J. GOODMAN and P. HOCHSTEIN. Biochem. Biophys. Res. Commun. **77**, 797 (1977); I. B. AFANAS'EV, N. I. POLOZOVA, and G. I. SAMOKHVALOV. Bioorg. Chem. **9**, 434 (1980).
6. C. M. WONG, W. HAQUE, H. Y. LAM, and K. MARAT. Presented at the Chemical Institute of Canada conference in Ottawa, Canada, June 1980.
7. M. AFZAL and J. M. AL-HASSAN. Heterocycles, **14**, 1173 (1980).
8. (*a*) J. R. LEWIS and J. G. PAUL. J. Chem. Soc. Perkin. Trans. I, 770 (1981); (*b*) T. KATO, N. KATAGIRI, J. NAKANO, and H. KAWAMURA. J. Chem. Soc. Chem. Commun. 645 (1977); (*c*) D. H. R. BARTON, L. COTTIER, K. FREUND, F. LUINI, P. D. MAGNUS, and I. SALAZAR. J. Chem. Soc. Perkin Trans. I, 499 (1976).
9. R. A. FINNEGAN, K. E. MERKEL, and J. K. PATEL. J. Pharm. Sci. **62**, 483 (1973).
10. B. M. DESAI, P. R. DESAI, and R. D. DESAI. J. Indian Chem. Soc. **37**, 53 (1960).
11. J. L. CHARLTON, G. LYPKA, and V. SAYEED. J. Heterocycl. Chem. **17**, 593 (1980).
12. G. M. COPPOLA and R. W. DODSWORTH. Synthesis, 523 (1981).
13. R. A. FINNEGAN and P. L. BACHMAN. J. Org. Chem. **30**, 4145 (1965).
14. W. S. TRAHANOVSKY and L. B. YOUNG. J. Org. Chem. **31**, 2033 (1966).


Can. J. Chem. Downloaded from www.nrcresearchpress.com by 210.87.254.6 on 09/06/12
For personal use only.

# The reaction of heptachlor on alumina impregnated with sulfuric acid in the presence of various aromatic compounds[1]

FOR ERRATA SEE
V.60 #2419.82 ...P.3084

JOHN W. APSIMON[2]
*Department of Chemistry, Carleton University, Ottawa, Ont., Canada K1S 5B6*

ALFRED S. CHAU,[2] ROBIN SAMPSON, AND HUNG TZE
*Water Quality Board, Canada Centre for Inland Waters, Environment Canada, Burlington, Ont., Canada L7R 4A6*

AND

ALAIN FRUCHIER
*Centre de Chimie Organique, Université des Sciences et Techniques de Languedoc, 34060 Montpellier, France*

Received January 14, 1982

JOHN W. APSIMON, ALFRED S. CHAU, ROBIN SAMPSON, HUNG TZE, and ALAIN FRUCHIER. Can. J. Chem. **60**, 2002 (1982).

Solid phase-matrix catalysed ($H_2SO_4$ on alumina) substitution of heptachlor (**1**) by a variety of aromatic species has been studied and the structures of the compound obtained using benzene, toluene, phenol, *o*-dichlorobenzene, and nitrobenzene have been determined by extensive use of 250 MHz proton nmr spectroscopy and mass spectrometry.

Preliminary comments are made concerning the variety of orientation modes noted.

JOHN W. APSIMON, ALFRED S. CHAU, ROBIN SAMPSON, HUNG TZE et ALAIN FRUCHIER. Can. J. Chem. **60**, 2002 (1982).

On a étudié la substitution, catalysée par une matrice en phase solide ($H_2SO_4$ sur alumine), de l'heptachlore (**1**) par une série de produits aromatiques et on a déterminé les structures des composés obtenus, par réaction avec le benzène, le toluène, le phénol, l'*o*-dichlorobenzène et le nitrobenzène, en faisant appel à la spectroscopie de rmn du proton à 250 MHz et à la spectrométrie de masse.

On fait des commentaires préliminaires au sujet de la diversité des modes d'orientation observés.

[Traduit par le journal]

We have recently reported in preliminary form (1) the formation of 1-aryl-chlordene **2** by the reaction of heptachlor **1** with aromatic species on an alumina/sulfuric acid solid matrix. In this article we present our evidence for the structures of compounds arising from the above reaction of heptachlor in the presence of benzene, toluene, phenol, *ortho*-dichlorobenzene, and nitrobenzene as being **2**, **3**, **4**, **5**, and **6** respectively.

The impetus for this work arises from one of the procedures reported for the confirmation of heptachlor identity in trace amounts using the technique of solid matrix derivatization (2) and the need to isolate the derivatives formed as analytical standards together with the search for more sensitive analytical methods.

All of the products obtained have been examined thoroughly using spectral methods, in particular by the use of proton and carbon-13 nuclear magnetic resonance (nmr). Tables 1 and 2 present the data obtained and analysed with attribution of signals to particular nuclei and include data for chlordene **7** and heptachlor **1** for comparison purposes. Table 3 presents substituent effects on the $^{13}C$ chemical shifts of the compounds studied.

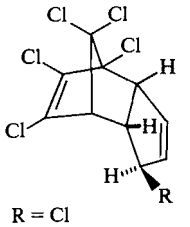

**1** R = Cl
**2** R = ϕ
**3** R = *p*-tolyl
**4** R = *o*-hydroxyphenyl
**5** R = 2′,3′-dichlorophenyl
**6** R = —O-3-*exo*-chlordene
**7** R = H

The nmr spectra and the mass spectra of all compounds studied indicate that no skeletal rearrangements have occurred during the solid matrix reaction but rather that allylic substitution has taken place. Thus all of the mass spectra in this series show, as the base peak, a fragment resulting from the reverse Diels–Alder process as shown

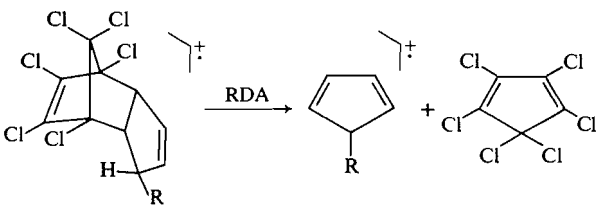


[1]Part XII in the CCIW series, Confirmation of Pesticide Residue Identities. For Part XI see ref. 1.

[2]Author to whom inquiries may be addressed.

0008-4042/82/152002-05$01.00/0

©1982 National Research Council of Canada/Conseil national de recherches du Canada

Can. J. Chem. Downloaded from www.nrcresearchpress.com by 210.87.254.5 on 09/06/12
For personal use only.

Can. J. Chem. Downloaded from www.nrcresearchpress.com by 210.87.254.5 on 09/06/12
For personal use only.

TABLE 1. Proton chemical shifts (ppm from internal TMS) and coupling constants (Hz) for compounds **1–7** in $CDCl_3$ solutions at 250 MHz

| | Compound | | | | | | |
|---|---|---|---|---|---|---|---|
| Parameter | **7**[b] | **1** | **2** | **3**[c] | **4**[c] | **5**[d] | **6** |
| $\delta_4$ | 5.838 | 5.958 | 5.923 | 5.892 | 5.882 | 5.901 | 5.962 |
| $\delta_5$ | 5.638 | 5.919 | 5.879 | 5.848 | 5.846 | 5.757 | 5.942 |
| $\delta_6$ | 3.865 | 4.080 | 3.992 | 3.976 | 4.056 | 4.058 | 3.998 |
| $\delta_2$ | 3.464 | 3.650 | 3.283 | 3.252 | 3.344 | 3.277 | 3.188 |
| $\delta_3$ | 2.363 | 4.826 | 3.876 | 3.854 | 4.148 | 4.504 | 4.564 |
| $J_{4,5}$ | 5.8 | 5.6 | 5.7 | 5.7 | 5.7 | 5.5 | 5.7 |
| $J_{4,6}$ | −2.1 | −2.0 | −1.9 | −1.9 | −1.9 | −2.1 | −1.5 |
| $J_{4,2}$ | 0.0 | 0.0 | 0.0 | 0.0 | 0.0 | 0.0 | 0.0 |
| $J_{4,3}$ | 2.1 | 2.1 | 2.3 | 2.3 | 2.3 | 2.2 | 2.1 |
| $J_{5,6}$ | 2.2 | 2.0 | 2.0 | 2.0 | 2.0 | 2.0 | 1.9 |
| $J_{5,2}$ | 0.0 | 0.0 | 0.0 | 0.0 | 0.0 | 0.0 | 0.0 |
| $J_{5,3}$[a] | −2.4 | −1.3 | −2.2 | −2.2 | −2.2 | −2.1 | −2.0 |
| $J_{6,2}$ | 8.2 | 7.5 | 8.0 | 8.0 | 8.0 | 7.9 | 7.3 |
| $J_{6,3}$ | 3.1 | 2.8 | 3.1 | 3.1 | 3.1 | 3.3 | 2.8 |
| $J_{2,3}$ | 3.5 | 2.1 | 3.2 | 3.2 | 3.2 | 3.3 | 1.6 |

[a]These signs have not been determined. Nevertheless they have been introduced in the calculations as allylic couplings are normally negative.
[b]$\delta_{3exo} = 2.507$ ppm, $J_{4,3exo} = 2.1$ Hz, $J_{5,3exo} = -2.2$ Hz, $J_{6,3exo} = 2.1$ Hz, $J_{2,3exo} = 9.9$ Hz, $J_{3endo,3exo} = 18.4$ Hz.
[c]$\delta_{3'} = 6.794$ ppm, $\delta_{4'} = 7.145$ ppm, $\delta_{5'} = 6.904$ ppm, $\nu_{6'} = 6.988$ ppm, $J_{3'4'} = 8.0$ Hz, $J_{3'5'} = 1.0$ Hz, $J_{3'6'} = 0.0$, $J_{4'5'} = 7.5$ Hz, $J_{4'6'} = 1.5$ Hz, $J_{5'6'} = 7.6$ Hz.
[d]$\nu_{4'} = 7.369$ ppm, $\nu_{5'} = 7.144$ ppm, $\delta_{6'} = 6.926$ ppm, $J_{4'5'} = 7.7$ Hz, $J_{4'6'} = 1.9$ Hz, $J_{5'6'} = 7.7$ Hz.
[e]$\delta_{2'} = \delta_{6'} = 7.04$ ppm, $\delta_{3'} = \delta_{5'} = 7.14$ ppm; this AA'BB' system has not been analysed because insufficient small transitions are observable, $5_{Me} = 2.334$ ppm.

TABLE 2. Carbon-13 chemical shifts (ppm from internal TMS) measured in $CDCl_3$ solutions for the compounds studied

| | Compound | | | | | | |
|---|---|---|---|---|---|---|---|
| Carbon | **1** | **2** | **3** | **4** | **5** | **6** | **7** |
| 1[a] | 80.3 | 81.5 | 81.5 | 81.7 | 81.3 | 80.0 | 81.9 |
| 2 | 60.5 | 58.7 | 58.9 | 58.1 | 58.9 | 58.2 | 49.3 |
| 3 | 60.1 | 50.9 | 50.5 | 45.4 | 48.5 | 81.2 | 32.4 |
| 4 | 137.7 | 138.8 | 139.1 | 139.2 | 138.9 | 136.3 | 136.1 |
| 5 | 131.1 | 127.6 | 127.4 | 127.7 | 128.2 | 132.2 | 126.4 |
| 6 | 60.8[c] | 61.2 | 61.2 | 61.7 | 61.8 | 60.6 | 61.2 |
| 7 | 82.1 | 82.2 | 82.3 | 82.4 | 82.2 | 81.7 | 82.5 |
| 8[b] | 132.3 | 131.9 | 131.8 | 132.1 | 132.1 | 131.6 | 132.0 |
| 9[b] | 128.9 | 129.2 | 129.2 | 129.2 | 129.8 | 128.8 | 129.3 |
| 10 | 103.7 | 103.4 | 103.5 | 103.8 | 103.7 | 103.9 | 103.8 |
| 1′ | — | 143.2 | 140.3 | 129.6 | 142.9 | — | — |
| 2′ | — | 127.2 | 127.1 | 153.2 | 132.0 | — | — |
| 3′ | — | 128.8 | 129.5 | 116.5 | 134.1 | — | — |
| 4′ | — | 127.1 | 136.7 | 136.7 | 129.5 | — | — |
| 5′ | — | 128.8 | 129.5 | 121.5 | 127.7 | — | — |
| 6′ | — | 127.2 | 127.1 | 128.6 | 127.3 | — | — |
| $CH_3$ | — | — | 21.0 | — | — | — | — |

[a], [b], [c]Assignments can be reversed.

below. A rapid detection of the carbon skeleton present is therefore available.

Two structural questions have to be answered for the isolated compounds: (a) the site and stereochemistry of substitution on the chlordane nucleus, and (b) the substitution site on the aromatic moiety, if this is not phenyl.

The first point is readily answered in part by the mass spectral information described above (i.e. at C-3 or C-5, both sites are identical after allylic substitution occurs) and the stereochemical fate of substitution is evident from the nmr studies where $J_{2,3}$ indicates that no change in geometry at C-3[3] takes place. Thus substitution occurs in all cases with retention of configuration at C-3, not a surprising observation when the geometry of heptachlor and access to any derived allylic carbonium ions at C-10 is considered.[4]

The site of substitution on the benzene ring in compounds **2–5** was solved by an analysis of the 250 MHz $^1H$ nmr spectra of these compounds using LAOCN 3 (3) and summarized in Table 1 in footnotes *b–e*. These assignments are unequivocal and

[3]The numbering system for the chlordene skeleton that we use here is based on the *endo*-tricyclo[5,2,1,$0^{2,6}$]deca-4,8-diene skeleton **i** following the IUPAC nomenclature system.

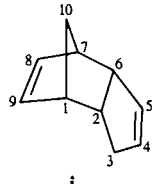


**i**

Thus, heptachlor is named as 1-*exo*-3,7,8,9,10,10-heptachloro-*endo*-tricyclo[5,2,1,$0^{2,6}$]deca-4,8-diene.

[4]Of course $S_N2'$ reactions with retention of configuration are also possible.

Can. J. Chem. Downloaded from www.nrcresearchpress.com by 210.87.254.5 on 09/06/12
For personal use only.



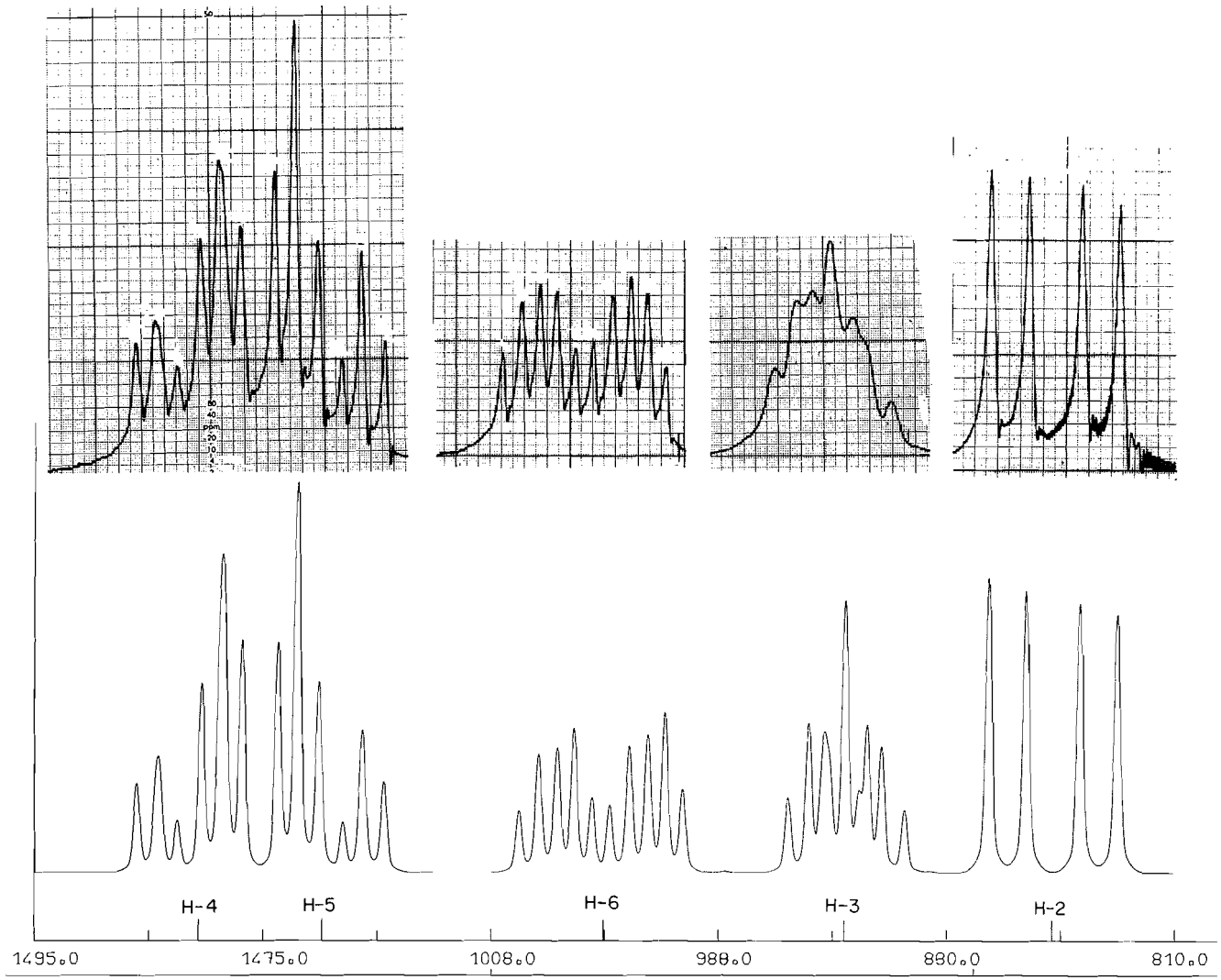


FIG. 1. Comparison of the 250 MHz experimental proton nmr spectrum of 3-*exo*-γ-phenylchlordene (**2**) (phenyl signals excluded) compared to the simulated spectrum (lower trace).

Can. J. Chem. Downloaded from www.nrcresearchpress.com by 210.87.254.5 on 09/06/12
For personal use only.

TABLE 3. Influence of the substituent R on the carbon-13 chemical shifts of the chlordene skeleton

| | Compound | | | | | |
|---|---|---|---|---|---|---|
| Carbon | 1 | 2 | 3 | 4 | 5 | 6 |
| 1[a] | −1.6 | −0.4 | −0.4 | −0.2 | −0.6 | −1.9 |
| 2 | 11.2 | 9.4 | 9.6 | 8.8 | 9.6 | 8.9 |
| 3 | 27.7 | 18.5 | 18.1 | 13.0 | 16.1 | 48.8 |
| 4 | 1.6 | 2.7 | 3.0 | 3.1 | 2.8 | 0.2 |
| 5 | 4.7 | 1.2 | 1.0 | 1.3 | 1.8 | 5.8 |
| 6 | −0.4 | 0.0 | 0.0 | 0.5 | 0.6 | −0.6 |
| 7[a] | −0.4 | −0.3 | −0.2 | −0.1 | −0.3 | −0.8 |
| 8[b] | 0.3 | −0.1 | −0.2 | 0.1 | 0.1 | −0.4 |
| 9[b] | 0.6 | −0.1 | −0.1 | −0.1 | 0.5 | −0.5 |
| 10 | −0.2 | −0.4 | −0.3 | 0.0 | −0.1 | 0.1 |

[a,b] Assignments can be reversed.

lead to the derivation of the structures depicted herein.

The power of this method is exemplified by Fig. 1 where portions of the experimental and calculated spectra for 1-*exo*-phenylchlordene (**2**) are compared. In the experimental spectrum the signal for H-5 centred at 3.926 ppm is broadened compared to the simulated spectrum because of small long-range benzylic couplings that we did not include in the simulation but are present as indicated by double irradiation.

Compound **6**, prepared by the use of nitrobenzene in this reaction, does not fall into the category of substituted chlordenes. Inspection of its nmr spectra indicates no aromatic substitution has occurred, rather only chlordene type protons (see Table 1) and carbon atoms (see Table 2) appear to be present. For some time this compound presented a problem, until we were able to obtain a satisfactory mass spectrum under conditions of low electron impact energy, showing a molecular ion at 686 together with chlorine isotope peaks, indicating a molecular formula of $C_{20}H_{10}OCl_{12}$. In addition, a major fragment of *m/e* 335 corresponding to $C_{10}H_5Cl_6^+$ was observed. The mass spectral and nmr data are best reconciled by dimeric structure **6**; in particular, the C-3—O—C′-3 moiety accounts for the chemical shift of 81.2 ppm for the two C-3 positions in this compound, a substituent shift of 48.8 ppm. At this stage we have not pursued the mode of formation of this material.

The formation of compounds **2–5** appears to be a Friedel–Crafts type process with the alumina supported acid acting as a catalyst (4), the precedent for this process appearing once in the patent literature (5) using the standard Friedel–Crafts conditions. In our hands this latter process proved less convenient for the preparation of substituted chlordenes, from the point of view of yield, product homogeneity, and isolation, although it must be stressed that we have only pursued a limited number of examples.[5]

There remain some intriguing questions to be answered concerning the mode of formation of compounds **3**, **4**, and **5**. Thus formation of **3** results from exclusive *para* attack of toluene, whereas **4** arises from exclusive *ortho* attack of phenol.[6] If a steric argument is involved it is difficult to reconcile formation of **4**. It therefore appears reasonable to us to suggest that **3** arises via a normal electrophilic substitution of toluene in the *para*-position, the bulk of the chlordene allylic cationic species precluding *ortho* attack, whereas **4** arises via prior O-alkylation to **8** followed by a rapid thermal

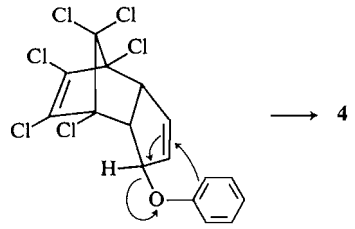


**8**

oxy-Cope rearrangement to **4** as shown. This possibility is being presently explored using *ortho*-substituted phenols.

The formation of **5** is a direct alkylation, *ortho* to one of the chlorine atoms of *o*-dichlorobenzene. Here the previously used steric argument for the formation of **3** falls down.

Our continuing work includes an investigation of the questions raised by the formation of the above compounds and attempts to include, in the aromatic substituents, groups that are photochemically active that could lead to ready degradation of the chlordene skeleton. The agricultural implications of such a course are tantalizing.

## Experimental

Proton nmr spectra were determined in the C.W. mode at 250 MHz on a Camera spectrometer at la Faculté de Pharmacie, Marseille, and analysed with the help of the LAOCN 3 program (3) or with a Varian XL-100 spectrometer at C.C.I.W. Carbon-13 spectra were determined in the FT mode on JEOL PS-100-FT and Bruker WP-80-DS spectrometers working at 25.03 and 20.11 MHz respectively in the Laboratoire de Mesures Physiques at U.S.T.L. The nmr data for the compounds described are presented in Tables 1 and 2. The ir spectra were recorded on a Unicon SP 110 spectrophotometer. Mass spectra were obtained

[5]Benzene, toluene, and phenol have been reacted with heptachlor under the usual Friedel–Crafts conditions ($AlCl_3$) yielding **2**, **3**, and **4** in low yield (< 20%) in each case.

[6]We have been unable to detect minor amounts of materials resulting from alternate modes of attack.

on a JEOL JMS-D100 at U.S.T.L. or at C.C.I.W. The chlorine isotope patterns confirm the molecular formula for all fragments. Mass spectral molecular weights are calculated using the $^{35}Cl$ isotope.

Heptachlor was kindly provided by the Velsicol Chemical Corporation. Microanalyses were carried out by the Guelph Chemical Laboratories.

*Alumina/sulfuric acid matrix*

Precooled concentrated sulfuric acid (10 mL) and alumina (50 g) (Woelm neutral grade 1) were mixed rapidly in a mortar and pestle at 0°C in a dry nitrogen atmosphere. The mixture was then transferred to a tightly capped bottle and stored in a desiccator until used.

exo-*3-Phenylchlordene (2)*

Pure heptachlor (2 g) in benzene (200 mL) was shaken with alumina/sulfuric acid solid matrix (50 g) (2) to ensure uniform mixing. Enough benzene was removed under vacuum on a rotary evaporator to ensure that the alumina remained moist. The mixture was heated under reflux on a steam bath overnight when, after cooling to room temperature, the moist mass was extracted with warm acetone (3 × 80 mL). The combined acetone extracts were evaporated to dryness and the solid residue was recrystallized from hexane/benzene (5:1) to yield colorless prisms (1.9 g), mp 76–77°C (lit. (5) mp 77–78°C); ir ($CHCl_3$): 3080, 2020 (C—H), 1610 (Cl—C=C—Cl), 1495, and 1415 ($C_6H_5$) $cm^{-1}$. Mass spectra: $M^+$ 412 (5%) ($C_{16}H_{10}Cl_6$), 270 (10%) ($M - C_5Cl_6$, retro Diels–Alder), 142 (100%) ($C_{11}H_{10}$ retro Diels–Alder). *Anal.* calcd. for $C_{16}H_{10}Cl_6$: C 46.60, H 2.43, Cl 50.97; found: C 46.79, H 2.1, Cl 50.5.

*3-Aryl-chlordenes*

The above procedure was followed using, in separate experiments, toluene (200 mL), *o*-dichlorbenzene (200 mL), nitrobenzene (200 mL), or phenol (4 g) dissolved in isooctane/ether (8:2) (300 mL).

The following materials were obtained. (1) 3-(*p*-Tolyl)-chlordene (**3**), 70% yield, mp 127–128°C; ir (KBr): 1610 (Cl—C=C—Cl), 1512 (aromatic) $cm^{-1}$. Mass spectra: $M^+$ 426 (3%) ($C_{17}H_{12}Cl_6$); *m/e* 156 (100%) ($M - C_5Cl_6$, retro Diels–Alder). *Anal.* calcd. for $C_{17}H_{12}C_6$: C 47.89, H 2.81, Cl 49.30; found: C 47.65, H 2.62, Cl 48.88. (2) 3-(*o*-Hydroxyphenyl)-chlordene (**4**), 50% yield, mp 105°C; ir (KBr): 3300 (O—H), 1605 (Cl—C=C—Cl), 1500 (aromatic) $cm^{-1}$. Mass spectra: $M^+$ 428 (4%) ($C_{16}H_{10}Cl_6O$); *m/e* 158 (100%) ($M - C_5Cl_6$, retro Diels–Alder). *Anal.* calcd. for $C_{16}H_{10}Cl_6O$: C 44.85, H 2.33, Cl 49.07; found: C 44.73, H 2.08, Cl 48.76. (3) 3-(2′,3′-Dichlorophenyl)-chlordene (**5**), 25% yield, mp 153°C; ir (KBr): 1600 (Cl—C=C—Cl) $cm^{-1}$. Mass spectra: $M^+$ 480 (2%) ($C_{16}H_8Cl_8$); *m/e* 210 (100%) ($M - C_5Cl_6$, retro Diels–Alder). *Anal.* calcd. for $C_{16}H_8Cl_8$: C 40.00; H 1.66, Cl 58.33; found: C 39.82, H 1.30, Cl 57.97. (4) Dichlordene ether **6**, 8% yield, mp 258°C; ir (KBr): 1605 (Cl—C=C—Cl) $cm^{-1}$. Mass spectrum: $M^+$ 686 (5%) ($C_{20}H_{10}OCl_{12}$), 335 (100%) ($C_{10}H_5Cl_6$), 65 (95%) ($C_{10}H_5Cl_6$-$C_5Cl_6$, reverse Diels–Alder). *Anal.* calcd. for $C_{20}H_{10}Cl_{12}O$: C 34.98, H 1.46, Cl 61.22; found: C 34.62, H 1.13, Cl 61.54.

## Acknowledgements

We thank the National Research Council of Canada and Le Centre National de la Recherche Scientifique de France for support of this work under the auspices of a joint research program (J.W.A., A.F.). We thank the Velsicol Corporation for a generous gift of pure heptachlor. One of us (J.W.A.) acknowledges the continued generous support of the Natural Sciences and Engineering Research Council of Canada in the form of a Grant-in-Aid of Research.

1. J. W. ApSimon, A. S. Y. Chau, and A. Fruchier. Synth. Commun. **12**, 249 (1982).
2. A. S. Y. Chau and K. Terry. J. Am. Assoc. Anal. Chem. **57**, 394 (1974); A. S. Y. Chau. J. Am. Assoc. Anal. Chem. **55**, 1232 (1972).
3. A. A. Bothner By and S. M. Castellano. *In* Computer progress for chemistry. *Edited by* De Los F. De Tar. W. A. Benjamin Inc., New York. 1968. p. 10.
4. A. McKillop and D. W. Young. Synthesis, 481 (1979).
5. A. Goldman. U.S. Patent No. 2,709,180 (1955).

Can. J. Chem. Downloaded from www.nrcresearchpress.com by 210.87.254.5 on 09/06/12
For personal use only.

# Enzymes in organic synthesis. 26.[1] Synthesis of enantiomerically pure grandisol from an enzyme-generated chiral synthon

J. Bryan Jones, Mark A. W. Finch, and Ignac J. Jakovac

*Department of Chemistry, University of Toronto, Toronto, Ont., Canada M5S 1A1*

Received February 16, 1982

J. Bryan Jones, Mark A. W. Finch, and Ignac J. Jakovac. Can. J. Chem. **60**, 2007 (1982).

The synthesis of enantiomerically pure (+)-grandisol has been achieved from an enzymically generated chiral synthon. The synthesis is an efficient one, the yield of optically pure material being 12% up to the penultimate step and 3% overall.

J. Bryan Jones, Mark A. W. Finch et Ignac J. Jakovac. Can. J. Chem. **60**, 2007 (1982).

On a réalisé la synthèse du (+)-grandisol énatiomèrement pur à partir d'un synthon chiral produit enzymatiquement. C'est une synthèse efficace dont le rendement en produit optiquement pur est de 12% jusqu'à l'avant dernière étape et de 3% pour l'ensemble.

[Traduit par le journal]

Can. J. Chem. Downloaded from www.nrcresearchpress.com by 210.87.254.40 on 09/06/12
For personal use only.

Grandisol (**1**), the major component of the four synergistic compounds of the male boll weevil sex pheromone (**2**), has attracted considerable attention and several successful syntheses have been reported (3). Of these, two have led to optically active grandisol (4) but neither approach afforded enantiomerically pure material. The elegant synthesis of Hobbs and Magnus (*4a*) was limited in this regard by the 90% ee of the (−)-β-pinene starting material available at that time, while a difficult resolution step in the route followed by Mori (*4b*) restricted the optical purity of his product to 80%.

The ready availability of the cyclobutyl lactone **3** of 100% purity, obtained via horse liver alcohol dehydrogenase-catalyzed oxidation of the *meso*-diol **2** (*5a*), prompted us to convert it into natural (+)-(1*R*,2*S*)-grandisol (**1**) in order to provide a further demonstration of the asymmetric synthetic value of enzymically produced chiral synthons (*5b*). As the paper shows, the use of lactone **3** as starting material enables grandisol to be prepared enantiomerically pure for the first time.

The route followed is summarized in Scheme 1. The initial target was the δ-lactone **10**, which in its racemic form had previously been converted to (±)-grandisol by Gueldner and co-workers (6). The lactone ring of the starting material **3** was opened with potassium hydroxide, and the resulting potassium carboxylate solution was acidified carefully to pH 3 at 0°C in order to prevent reformation of the lactone. The hydroxyacid obtained was immediately esterified with diazomethane and then treated with *tert*-butyldimethyl silyl chloride to give the protected ester **4** in 83% yield. No epimerization at the ring junction of **3** occurred during the

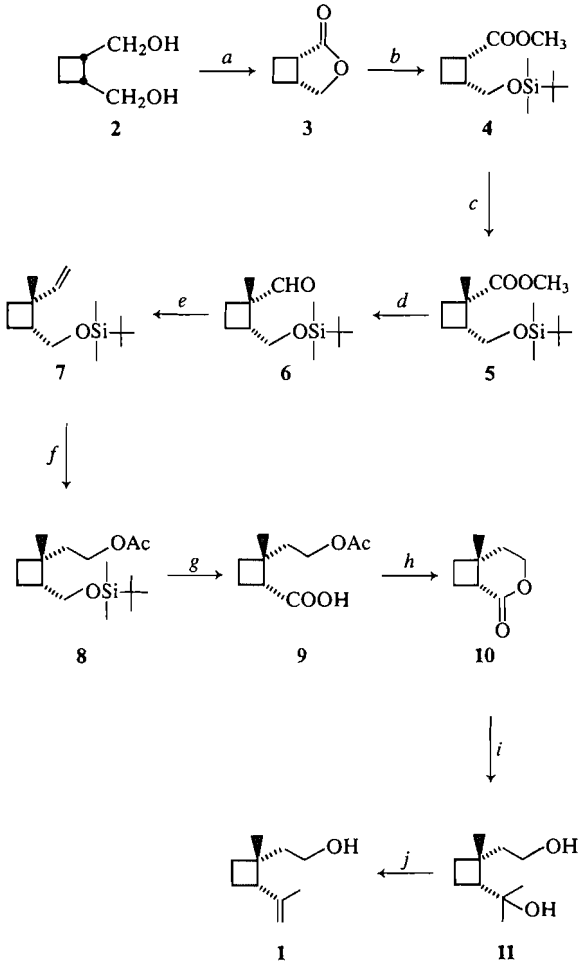


Scheme 1. Reagents: (*a*) horse liver alcohol dehydrogenase; (*b*) 1, KOH; 2, $CH_2N_2$; 3, *t*-Bu(Me)$_2$SiCl; (*c*) 1, LDA; 2, MeI; (*d*) 1, Dibal; 2, Collins; (*e*) $Ph_3P{=}CH_2$; (*f*) 1, $B_2H_6/H_2O_2$; 2, $Ac_2O$; (*g*) 1, HF; 2, Jones; (*h*) 5% $H_2SO_4$; (*i*) MeLi; (*j*) 1, $Ac_2O$; 2, $LiAlH_4$.

[1]For Part 25, see ref. 1.

0008-4042/82/152007-05$01.00/0

©1982 National Research Council of Canada/Conseil national de recherches du Canada

Can. J. Chem. Downloaded from www.nrcresearchpress.com by 210.87.254.40 on 09/06/12
For personal use only.

base-mediated lactone opening step.[2] This was established by glc analysis. Introduction of the angular methyl group into **4** was readily accomplished by treatment with lithium diisopropylamide followed by methyl iodide (7). The methylated ester **5** was isolated in 89% yield. The methylation reaction was stereospecific. No trace of the (1*R*, 2*R*)-diastereomer of **5** could be detected spectroscopically or by glc or tlc analysis. The controlled insertion of the methyl group to give **5** possessing only the desired 1*S*-chirality is attributed to the steric effect of the large *tert*-butyldimethylsilyloxy group in the region of the 2*R*-centre of **4** that precludes approach of methyl iodide to the hindered (*Re*,*Si*)-face of the intermediate enolate.[3]

Conversion of the ester **5** to the aldehyde **6** was achieved in 68% yield and the subsequent Wittig reaction proceeded smoothly to give the alkene **7** in 63% yield. Hydroboration of **7** gave the expected alcohol, which was converted directly to its acetate **8** (60% yield).

The silyl protecting group of **8** was removed with hydrofluoric acid and the exposed alcohol function oxidized with Jones reagent. The carboxyl acetate **9** so obtained (83% yield) was then hydrolyzed in dilute sulfuric acid to give an excellent (90%) yield of the δ-lactone **10**.

Having achieved the preparation of our initial target **10**, known (6) to be transformable into grandisol, we examined the possibility of converting the intermediate **9** into the pheromone more directly via Wittig reaction (9) of the methyl ester **13**. Esterification of **9** with diazomethane yielded **13** quantitatively. Unfortunately, however, all attempts to convert the carbomethoxy group to the desired isopropylidene function using a salt-free (to avoid epimerization) methylene triphenylphosphorane (10) were not fruitful. Accordingly, attention was refocussed on the Scheme 1 route.

Lactone **10** was converted into the diol **11** in 87% yield using the procedure of Gueldner *et al.* (6). The spectral characteristics of the diol were identical with those of the racemic material prepared previously (6). In fact, the intermediacy of this compound in the penultimate stage of the synthesis had a significant influence on our formulation of the Scheme 1 approach, since it was known that the diol functionalities of **11** would permit its enantiomeric purity to be readily determined (11). The $^1$H nmr examination of the diastereotopic methyl groups of **11** in the presence of Eu(tfc)$_3$ showed the diol to be optically pure. The racemic sample of **11** required for the reference spectra was obtained by treatment of (±)-**13** with methyl lithium.

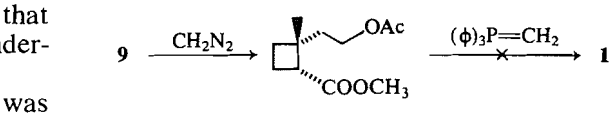


**13**

In the final step, dehydration of **11** was accomplished with acetic anhydride followed by lithium aluminum hydride reduction of the resulting acetate. The product consisted of a 2:1 mixture of grandisol and its isopropylidene isomer **14**. After purification by preparative glc, (+)-(1*R*,2*S*)-grandisol (**1**) was obtained in 25% yield. Its spectral properties were identical with those reported by Gueldner *et al.* (6) and those of its *p*-nitrobenzoate with those recorded by Hobbs and Magnus (4*a*). No enantiomeric contamination could be detected from $^1$H nmr examination of its MTPA ester (12) in the presence of Eu(fod)$_3$.

The preparation of optically pure grandisol was achieved in 3.1% overall yield from the enzymically generated starting lactone **3**. This compares very favourably with the 3.5% overall yield of Magnus and Hobbs' (4*a*) route. In fact, the overall yield of the Scheme 1 route could undoubtedly be markedly improved by optimization of the conditions in the final step, since the cumulative yield up to the penultimate intermediate **11** is a remarkably high 12.3%. Furthermore, the synthetic approach is a versatile one in that its modification to provide the other enantiomer of grandisol can be readily envisaged. All that is required is the conversion of the starting lactone (1*S*,5*R*)-**3** to its enantiomer (1*R*, 5*S*)-**3** by straightforward chemical transposition of the CO and $CH_2$ functionalities of the lactone ring.

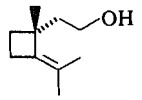


**14**

## Experimental

All compounds were purified at least until pure by glc. The glc analyses were performed on a Varian 2700 instrument using 5% Carbowax or QF-1 on Chromosorb GHP columns. Preparative

[2]In order to effect such epimerization, lactone **2** requires heating with sodium hydroxide in a sealed stainless-steel tube for several days (5*a*).

[3]In an initial approach to grandisol, direct alkylation of **3** to the methylated lactone **12** by the LDA–MeI method was explored. However, all attempts to effect the desired methylation were unsuccessful, presumably as a result of the reluctance of such cyclobutyl systems to form the carbanion intermediate required (8). Lactone **12** can be obtained by treatment of **5** with hydrochloric acid.

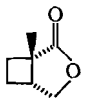

**12**

Can. J. Chem. Downloaded from www.nrcresearchpress.com by 210.87.254.40 on 09/06/12
For personal use only.

glc separations were effected on a Varian 920 chromatograph with a 5% Carbowax on Chromosorb GHP column. The ir spectra were determined on liquid films with a Unicam SP 1025 spectrometer. The $^1$H nmr spectra were measured on chloroform solutions (TMS internal standard) on a Varian T 60 machine and enantiomeric purity determinations were made with a Bruker WP 80 instrument. Optical rotations were obtained with a Perkin–Elmer 141 polarimeter. Low resolution and high resolution mass spectra were determined on Dupont 21-490 and AEI MS-30 spectrometers respectively.

*(−)-(1*S,2R)-cis-2-tert-*Butyldimethylsilyloxymethyl-1-carboxymethylcyclobutane (4)*

(+)-(1*S*,5*R*)-3-Oxabicyclo[3.2.0]heptan-2-one (**3**, 5.0 g, 44.6 mmol, $[\alpha]_D^{25}$ +118.7° (*c* 10, $CHCl_3$), 100% ee, obtained by horse liver alcohol dehydrogenase-catalyzed oxidation (5*a*) of *cis*-1,2-bis(hydroxymethyl)cyclobutane (**2**)) in methanol (20 mL) was added to KOH (4.5 g, 0.8 mol) in methanol (50 mL). The mixture was refluxed for 1 h, then cooled (20°C) and the methanol removed by rotoevaporation. The resulting white solid was dissolved in ethyl acetate (30 mL) and the cooled (0°C) solution acidified to pH 3 with 2 *N* hydrochloric acid. The aqueous layer was separated and extracted with ethyl acetate (3 × 25 mL). Ethereal diazomethane was then added to the combined ethyl acetate solutions until a yellow color just persisted. The reaction solution was then dried ($K_2CO_3$) and evaporated to yield an orange oil (5 g). This was immediately dissolved in dry dimethylformamide (20 mL) and imidazole (7.5 g, 0.11 mol) and *tert*-butyldimethylsilyl chloride (8.0 g, 53 mmol) added. The mixture was stirred for 12 h at 20°C and then diluted with water (50 mL) and extracted with hexane (2 × 50 mL). The hexane solution was washed with water (50 mL), dried ($MgSO_4$), and evaporated. The crude product obtained was Kugelrohr-distilled to give (−)-(1*S*,2*R*)-*cis-tert*-butyldimethylsilyloxymethyl-1-carboxymethylcyclobutane (**4**) as a colorless oil (10.0 g), bp 70°C (0.7 Torr); $[\alpha]_D^{25}$ −10.7° (*c* 1, $CHCl_3$); ir: 1740 cm$^{-1}$; $^1$H nmr δ: 0.10 (6H, s), 0.93 (9H, s), 1.6–3.3 (6H, m), 3.63 (3H, s), and 3.75 (2H, d, *J* = 5 Hz) ppm; high resolution mass spectrum,[4] *Exact Mass* calcd. for $C_{12}H_{23}O_3Si$ ($M^+ - CH_3$): 243.1416; found: 243.1428; *Exact Mass* calcd. for $C_9H_{17}O_3Si$ ($M^+ - C(CH_3)_3$): 201.0947; found: 201.0970.

*(−)-(1*S,2R)-2-tert-*Butyldimethylsilyloxymethyl-1-carboxymethyl-1-methylcyclobutane (5)*

*n*-Butyllithium (3.3 g, 52 mmol, 1.5 *M* solution in hexane) was added slowly under $N_2$ with stirring to diisopropylamine (6 g, 60 mmol) in dry tetrahydrofuran (50 mL) at −78°C. After stirring the mixture for a further 30 min at −78°C, (−)-(1*S*,2*R*)-*cis*-2-*tert*-butyldimethylsilyloxymethyl-1-carboxymethylcyclobutane (**4**, 10.0 g, 39 mmol) in dry tetrahydrofuran (20 mL) was added and the mixture stirred for 15 min. Methyl iodide (9.4 g, 67 mmol) was added and stirring at −78°C continued for 2 h more. The reaction was then quenched with water (50 mL) and the mixture warmed to 20°C. The aqueous solution was extracted with ether (3 × 50 mL) and the ether solution washed with 2 *N* hydrochloric acid (100 mL), then with 10% aqueous sodium thiosulphate, followed by water (100 mL). The dried ($MgSO_4$) ether layer was rotoevaporated and the residue Kugelrohr-distilled to give (−)-(1*S*,2*R*)-2-*tert*-butyldimethylsilyloxymethyl-1-carboxymethyl-1-methylcyclobutane (**5**) as a colorless oil (9.3 g), bp 80°C (0.6 Torr); $[\alpha]_D^{25}$ −40.4° (*c* 1, $CHCl_3$); ir: 1740 cm$^{-1}$; $^1$H nmr δ: 0.05 (6H, s), 0.95 (9H, s), 1.22 (3H, s), 1.6–2.8 (5H, m), and 3.60–3.70 (3H, s, and 2H, d, *J* = 5 Hz) ppm; high resolution mass spectrum,[4] *Exact Mass* calcd. for $C_{13}H_{25}O_3Si$ ($M^+ - CH_3$): 257.1573; found: 257.1570; *Exact Mass* calcd. for $C_{10}H_{19}O_3Si$ ($M^+ - C(CH_3)_3$): 215.1103; found: 215.1099.

*(−)-(1*S,2R)-2-tert-*Butyldimethylsilyloxymethyl-1-formyl-1-methylcyclobutane (6)*

Diisobutylaluminum hydride (8.6 g, 60.6 mmol, 20% solution in hexane) was added at −78°C under $N_2$ to the above ester **5** (5.5 g, 20.2 mmol) in dry hexane (100 mL). The reaction mixture was stirred for 2 h at −78°C, then quenched with water (50 mL) and warmed to 20°C. The solution was acidified with 2 *N* hydrochloric acid and then extracted with ether (3 × 75 mL). The ether extract was washed with water (100 mL), dried ($MgSO_4$), and evaporated to give (1*S*,2*R*)-2-*tert*-butyldimethylsilyloxymethyl-1-hydroxymethyl-1-methylcyclobutane (5 g, 20 mmol), ir: 3450 cm$^{-1}$; $^1$H nmr δ: 0.05 (6H, s), 0.95 (9H, s), 1.22 (3H, s), 1.3–2.4 (5H, m), and 3.0–3.8 (5H, m) ppm. This material in dry $CH_2Cl_2$ (50 mL) was oxidized at 20°C for 30 min with a solution of chromium trioxide (12.4 g, 124 mmol) and pyridine (9.5 g, 124 mmol) in dry $CH_2Cl_2$ (200 mL). The solvent was then evaporated and the residual black tar dissolved in ether, filtered through Celite, and washed with 2 *N* hydrochloric acid (100 mL), then with water (100 mL) and dried ($MgSO_4$). Evaporation of the solvent yielded, after Kugelrohr distillation, (−)-(1*S*,2*R*)-2-*tert*-butyldimethylsilyloxymethyl-1-formyl-1-methylcyclobutane (**6**) as a colorless oil (3.3 g), bp 70°C (0.5 Torr); $[\alpha]_D^{25}$ −38.0° (*c* 0.6, $CHCl_3$); ir: 2720 and 1720 cm$^{-1}$; $^1$H nmr δ: 0.07 (6H, s), 0.97 (9H, s), 1.38 (3H, s), 1.4–2.7 (5H, m), 3.66 (2H, d, *J* = 5 Hz), and 9.82 (1H, s) ppm; high resolution mass spectrum,[4] *Exact Mass* calcd. for $C_8H_{15}O_2Si$ ($M^+ - CH_3 - C(CH_3)_3$): 171.0841; found: 171.0842.

*(−)-(1*R,2R-2-tert-*Butyldimethylsilyloxymethyl-1-methyl-1-vinylcyclobutane (7)*

The aldehyde (**6**, 3.0 g, 12.5 mmol) in dry tetrahydrofuran (30 mL) was added at −78°C under $N_2$ to the methylene Wittig reagent obtained from methyltriphenylphosphonium bromide (8.9 g, 25 mmol) and *n*-butyllithium (1.44 g, 22.5 mmol, 1.5 *M* solution in hexane) in dry tetrahydrofuran (50 mL). After stirring for 2 h at −78°C, the reaction was quenched with water (100 mL) and extracted with ether (3 × 50 mL). The combined ether extracts were washed with water (50 mL), dried ($MgSO_4$), and evaporated. The residue was distilled to give (−)-(1*R*,2*R*)-2-*tert*-butyldimethylsilyloxymethyl-1-methyl-1-vinylcyclobutane (**7**) as a colorless oil (1.9 g), bp 105°C (25 Torr); $[\alpha]_D^{25}$ −23.6° (*c* 1.2, $CHCl_3$); ir: 3070 and 1640 cm$^{-1}$; $^1$H nmr δ: 0.05 (6H, s), 0.95 (9H, s), 1.26 (3H, s), 1.4–2.5 (5H, m), 3.45–3.75 (2H, m), and 4.7–6.3 (1H, m) ppm; high resolution mass spectrum,[4] *Exact Mass* calcd. for $C_{10}H_{19}OSi$ ($M^+ - C(CH_3)_3$): 183.1205; found: 183.1202.

*(+)-(1*R,2R)-1-(2′-Acetoxyethyl)-2-tert-*butyldimethylsilyloxymethyl-1-methylcyclobutane (8)*

Diborane (7.8 mmol, 7.8 mL of 1 *M* solution in tetrahydrofuran) was added at 0°C with stirring under $N_2$ to the above vinylcyclobutane 7 (2.8 g, 11.7 mmol) in dry tetrahydrofuran (60 mL). The mixture was then allowed to warm to 20°C and stirred for 1 h. Water (5 mL) was added and the mixture cooled to 0°C. 15% Aqueous NaOH (3.5 mL) and 30% hydrogen peroxide (3.0 mL) were added and the mixture warmed to 55°C for 1 h. The mixture was saturated with NaCl at 20°C and extracted with ether (3 × 50 mL). The ether solution was washed with water (50 mL), dried ($MgSO_4$), and evaporated to yield (1*R*,2*R*)-*tert*-butyldimethylsilyloxymethyl-1-(2′-hydroxyethyl)-1-methylcyclobutane (2.5 g), ir: 3350 cm$^{-1}$; $^1$H nmr δ: 0.05 (6H, s), 0.95 (9H, s), 1.20 (3H, s), 1.3–2.4 (7H, m), and 3.5–3.8 (4H, two t, *J* = 7 Hz) ppm. This alcohol was dissolved in dry pyridine (20 mL) and excess acetic anhydride (5 mL) added at 0°C. After keeping

[4]The molecular ions of the silyl derivatives **4–8** were unstable and the fragmentation patterns observed were those of ions resulting from loss of methyl or *tert*-butyl groups. Combustion analyses were not performed for these intermediates since the subsequent compounds, and grandisol itself, had been fully characterized previously.

Can. J. Chem. Downloaded from www.nrcresearchpress.com by 210.87.254.40 on 09/06/12
For personal use only.

for 12 h at 20°C, the mixture was diluted with water (25 mL) and extracted with ether (2 × 50 mL). The ether solution was washed with 2 *N* hydrochloric acid (50 mL), then with water (50 mL) and dried ($MgSO_4$). Evaporation gave (+)-(1*R*,2*R*)-1-(2′-acetoxyethyl)-2-*tert*-butyldimethylsilyloxymethyl-1-methylcyclohexane (**8**) which was Kugelrohr-distilled to give a colorless oil (2.1 g), bp 80°C (0.2 Torr); $[\alpha]_D^{25}$ +10.2° (*c* 0.32, $CHCl_3$); ir: 1740 $cm^{-1}$; $^1H$ nmr δ: 0.05 (6H, s), 0.95 (9H, s), 1.10 (3H, s), 1.5–2.2 (7H, m), 2.08 (3H, s), 3.54–3.75 (2H, m), and 4.12 (2H, t, *J* = 7 Hz) ppm; high resolution mass spectrum,[4] *Exact Mass* calcd. for $C_{12}H_{23}O_3Si$ ($M^+ - C(CH_3)_3$): 243.1417; found: 243.1418.

*(−)-(1*R*,2*R*)-6-Methyl-3-oxabicyclo[4.2.0]octan-2-one (**10**)*

10% Hydrofluoric acid (20 mL, prepared by dissolving 40% aqueous hydrofluoric acid in acetonitrile) was added to the above silyl acetate **8** (0.9 g, 3 mmol) and the solution stirred for 1 h at 20°C. Water (20 mL) was then added and the mixture extracted with chloroform (3 × 50 mL). The chloroform solution was washed with water (50 mL), dried ($MgSO_4$), and evaporated to give (1*R*,2*R*)-1-(2′-acetoxyethyl)-2-hydroxymethyl-1-methylcyclobutane (0.6 g), ir: 3400 and 1740 $cm^{-1}$; $^1H$ nmr δ: 1.98 (3H, s), 1.4–2.3 (7H, m), 2.05 (3H, s), 3.2–3.75 (3H, m including O*H*), and 4.15 (2H, t, *J* = 6 Hz) ppm. This material was dissolved in acetone (30 mL) and Jones reagent (13) (5 mL) added. The mixture was stirred for 1 h at 20°C and water (30 mL) then added. The mixture was extracted with ether (3 × 50 mL), and the ether solution then extracted with saturated aqueous sodium bicarbonate (2 × 50 mL). The bicarbonate solution was acidified with 6 *N* hydrochloric acid and then extracted with ether (3 × 50 mL). The combined ethereal layers were washed with water (50 mL), dried ($MgSO_4$), and evaporated to yield (−)-(1*R*,2*R*)-2-(2′-acetoxyethyl)-1-carboxy-2-methylcyclobutane (**9**) as a colorless oil (0.5 g), $[\alpha]_D^{25}$ −2.5° (*c* 0.4, $CHCl_3$); ir: 3750–3100, 1740, and 1715 $cm^{-1}$; $^1H$ nmr δ: 1.27 (3H, s), 1.6–2.2 (6H, m), 2.05 (3H, s), 2.65–3.1 (1H, m), 4.10 (2H, t, *J* = 6 Hz), and 10.9 (1H, s) ppm.

The acid **9** (0.6 g, 3 mmol) was dissolved directly in 5% aqueous sulfuric acid (20 mL) and the solution refluxed for 1 h and then cooled to 20°C, diluted with water (20 mL), and extracted with ethyl acetate (3 × 50 mL). The ethyl acetate solution was washed with water (50 mL), dried ($MgSO_4$), and evaporated to give an oil which was chromatographed on silica gel (ethyl acetate/hexane (20:1) elution) to give (−)-(1*R*,2*R*)-6-methyl-3-oxabicyclo[4.2.0]octan-2-one (**10**) (6*a*) as a colorless oil (0.38 g), $[\alpha]_D^{25}$ −43.1° (*c* 0.4, $CHCl_3$); ir: 1730 $cm^{-1}$; $^1H$ nmr δ: 1.27 (3H, s), 1.6–3.05 (7H, m), and 4.1–4.6 (2H, m) ppm; high resolution mass spectrum, *Exact Mass* calcd. for $C_8H_{12}O_2$ ($M^+$): 140.0837; found: 140.0842.

*(+)-(1*R*,2*R*)-1-(2′-Hydroxyethyl)-2-(1′-hydroxy-1′-methylethyl)-1-methylcyclobutane (**11**)*

The lactone **10** (0.35 g, 2.5 mmol) in dry ether (10 mL) was added with stirring to methyl lithium (0.25 g, 11 mmol) in dry ether (20 mL) at 0°C. The mixture was stirred at 0°C for 2 h and saturated aqueous ammonium chloride (20 mL) then added. The mixture was extracted with chloroform (3 × 30 mL) and the organic solution dried ($MgSO_4$) and evaporated. The crude diol product was purified by thick layer chromatography on silica gel (chloroform development) to give (+)-(1*R*,2*R*)-1-(2′-hydroxyethyl)-2-(1′-hydroxy-1′-methylethyl)-1-methylcyclobutane (**11**, 0.4 g), mp (after recrystallization from cyclohexane) 87°C (lit. (6*b*) (±) mp 87–87.5°C); $[\alpha]_D^{25}$ +17.3° (*c* 0.3, $CHCl_3$); ir: 3300 (broad) $cm^{-1}$; $^1H$ nmr δ: 1.06 (3H, s), 1.12 (3H, s), 1.20 (3H, s), 1.4–2.2 (9H, m), and 3.68 (2H, t, *J* = 7 Hz) ppm.

The 100 ± 3% ee of the diol **11** was established by its $^1H$ nmr examination in $CCl_4$ in the presence of 0.3 equiv. $Eu(tfc)_3$ shift reagent (11). No splitting of the diastereotopic methyl groups of the 2-(1′-hydroxy-1′-methylethyl) side chain was observed, while under the same conditions the corresponding signals in the spectrum of the (±)-diol were clearly separated into doublets (ΔΔδ 0.14 ppm).

*(+)-(1*R*,2*S*)-1-(2′-Hydroxyethyl)-1-methyl-2-isopropenylcyclobutane (**1**, grandisol)*

The diol **11** (0.4 g, 2.3 mmol) was treated with acetic anhydride (3 mL), and the acetate so obtained reduced with lithium aluminum hydride (1.5 g, 39 mmol) as described by Gueldner *et al.* (6*a*). The mixture of grandisol and its isopropylidene isomer isolated was separated by preparative glc to give (+)-(1*R*,2*S*)-1-(2′-hydroxyethyl)-1-methyl-1-isopropenylcyclobutane (**1**, 85 mg), $[\alpha]_D^{25}$ +14.8° (*c* 1, *n*-hexane) (lit. (4*a*) $[\alpha]_D^{21.5}$ +15.9° (*c* 1, *n*-hexane, highly purified +18.4°; lit. (4*b*) $[\alpha]_D^{20}$ +19.6° (*c* 0.23, *n*-hexane)); ir: 3320, 3060, 1650, 1450, 1375, 1260, 1050, 1000, and 885 $cm^{-1}$; $^1H$ nmr ($CCl_4$) δ: 1.18 (3H, s), 1.66 (3H, s), 1.3–2.3 (4H, m), 2.40 (1H, s, OH), 2.52 (1H, t, *J* = 8 Hz), 3.53 (1H, t, *J* = 7.5 Hz), 4.60 (1H, s), and 4.78 (1H, s) ppm. The spectra matched those of grandisol provided by Drs. R. C. Gueldner (6) and P. D. Magnus (4*a*). The *p*-nitrobenzoate (4*a*) had mp 64–65°C; ir: 1725, 1605, 1535, 1350, 1272, 1117, 1100, 1070, 837, 785, and 718 $cm^{-1}$; $^1H$ nmr ($CCl_4$) δ: 1.26 (3H, s), 1.4–2.8 (7H, m), 4.36 (2H, t, *J* = 7.5 Hz), 4.66 (1H, s), 4.82 (1H, s), and 8.18 (4H, s) ppm, also identical with an authentic spectrum provided by Dr. P. D. Magnus (4*a*).

Both (±)- and (+)-(1*R*,2*S*)-**1** were reacted with (+)-(2*R*)-α-methoxy-α-trifluoromethylphenylacetyl chloride and the MeO-groups of the MTPA-esters subjected to 100 MHz $^1H$ nmr examination in the presence of up to 2 equiv. of $Eu(fod)_3$ (12). No enantiomeric contamination could be detected in the MTPA-ester from (+)-**1**. (For the MTPA ester of (±)-**1**, ΔΔδ for the MeO-doublet was 0.05 ppm with 2 equiv. of shift reagent.)

## Acknowledgements

We thank the National Sciences and Engineering Research Council of Canada for generous financial support. We are also grateful to Drs. R. C. Gueldner and P. D. Magnus for their invaluable assistance in providing comparison spectra of (±)-grandisol, and of the natural enantiomer and its *p*-nitrobenzoate.

1. J. A. Haslegrave and J. B. Jones. J. Am. Chem. Soc. In press.
2. J. H. Tumlinson, D. D. Hardee, R. C. Gueldner, A. C. Thompson, P. A. Hedin, and J. P. Minyard. Science, **166**, 1010 (1969).
3. (*a*) J. A. Katzenellenbogen. Science, **194**, 139 (1976); (*b*) F. Wenkert, D. A. Berges, and N. F. Golob. J. Am. Chem. Soc. **100**, 1263 (1978); (*c*) R. D. Clark. Synth. Commun. **9**, 325 (1979); (*d*) H. Kosugi, S. Sekiguchi, R. Sekita, and H. Uda. Bull. Soc. Chem. Jpn. **49**, 520 (1976); (*e*) G. Rosini, A. Salomoni, and F. Squarcia. Synthesis, **12**, 942 (1979).
4. (*a*) P. D. Hobbs and P. D. Magnus. J. Am. Chem. Soc. **98**, 4594 (1976); (*b*) K. Mori. Tetrahedron, **34**, 915 (1978).
5. (*a*) I. J. Jakovac, G. Ng, K. P. Lok, and J. B. Jones. Chem. Commun. 515 (1980); I. J. Jakovac, H. B. Goodbrand, K. P. Lok, and J. B. Jones. J. Am. Chem. Soc. In press; (*b*) J. B. Jones. *In* Enzymic and nonenzymic catalysis. *Edited by* P. Dunnill, A. Wiseman, and N. Blakeborough. Ellis Horwood/J. Wiley, Chichester/New York. 1980. pp. 54–83.
6. (*a*) R. C. Gueldner, A. C. Thompson, and P. A. Hedin. J. Org. Chem. **37**, 1854 (1972); (*b*) J. H. Tumlinson, R. C.

GUELDNER, D. D. HARDEE, A. C. THOMPSON, P. A. HEDIN, and J. P. MINYARD. J. Org. Chem. **36**, 2616 (1971).
7. J. L. HERRMANN and R. H. SCHLESSINGER. Chem. Commun. 711 (1973).
8. P. E. EATON, G. D. ANDREWS, E-P. KREBS, and A. KUNAI. J. Org. Chem. **44**, 2824 (1979).
9. A. P. VIGTTEWAAL, F. L. JONKERS, and A. VANDERGEN. J. Org. Chem. **44**, 3157 (1979).
10. H. SCHMIDBAUR, H. STÜHLER, and W. VORNBERGER. Chem. Ber. **105**, 1084 (1972).
11. I. J. JAKOVAC and J. B. JONES. J. Org. Chem. **44**, 2165, (1979).
12. J. A. DALE, D. L. DULL, and H. S. MOSHER. J. Org. Chem. **34**, 2543 (1969).
13. K. BOURDEN, I. M. HEILBRON, E. R. H. JONES, and B. C. L. WEEDON. J. Chem. Soc. 39 (1946).

Can. J. Chem. Downloaded from www.nrcresearchpress.com by 210.87.254.40 on 09/06/12
For personal use only.

# Temperature profiles for reactions with self-heating

AVYGDOR MOISE AND HUW O. PRITCHARD
*Centre for Research in Experimental Space Science, York University, Downsview, Ont., Canada M3J 1P3*

Received August 14, 1981

AVYGDOR MOISE and HUW O. PRITCHARD. Can. J. Chem. **60**, 2012 (1982).

It is shown that the steady temperature distribution for an exothermic reaction taking place in a sphere can be approximated by a simple function for values of the dimensionless heat production rate $\delta \leq 2$. Further, for $2 < \delta \leq 3$, a simple iterative correction to this function yields temperature profiles, $\theta$, which are nowhere in error by more than 1%, the error increasing to 5% at $\delta = 3.3$.

AVYGDOR MOISE et HUW O. PRITCHARD. Can. J. Chem. **60**, 2012 (1982).

On montre que la distribution de température stationnaire pour une réaction exothermique se produisant dans une sphère, peut-être évaluée à l'aide d'une fonction simple pour des valeurs de vitesse de production de chaleur qui sont sans dimensions de $\delta \leq 2$. De plus, pour $2 < \delta \leq 3$, une correction itérative simple de cette fonction fournit les profils de température, $\theta$, avec une erreur maximale de 1%; l'erreur augmente à 5% pour $\delta = 3{,}3$.

[Traduit par le journal]

## Introduction

A long-established method for estimating the steady-state temperature rise at the centre of a sphere for an exothermic reaction is an interpolation based upon the tables of Chandrasekhar and Wares (1), as suggested by Chambre (2); however, this method is cumbersome when it is required to calculate the temperature rise for points other than at the centre of the sphere. In this paper we establish a very simple function which gives accurate estimates for the complete temperature profile at low values of the temperature rise, and which can easily be corrected with a hand-held programmable calculator for temperature profiles right up to the critical one.

In an Appendix, we describe briefly an alternative power-series expansion solution to this problem, since it illuminates the nature of the mathematical difficulty in defining the critical point, a matter which is discussed elsewhere in some detail (3).

The Frank-Kamenetskii heat equation for an exothermic reaction taking place in a sphere may be written as (4–6)

$$[1] \quad \frac{\partial^2\theta}{\partial x^2} + \frac{2}{x}\frac{\partial\theta}{\partial x} = -\delta\, e^{\theta}$$

where $\theta$ (the dimensionless temperature excess) and $\delta$ (the dimensionless heat production rate) have their usual definitions (4–6), and $x$ is the (dimensionless) distance from the centre of the vessel, i.e. $0 \leq x \leq 1$. A solution for $\theta$ will have the properties that $\partial\theta/\partial x|_{x=0} = 0$ and $\theta|_{x=1} = 0$.

Let $\psi = x\theta$, whence it follows that $x^{-1}\partial^2\psi/\partial x^2$ is equal to the left-hand side of [1]; consequently

$$[2] \quad \frac{\partial^2\psi}{\partial x^2} = -\delta x \exp(\psi/x)$$

Expanding the exponential, and retaining only the first term in $x$, we find that

$$\frac{\partial^2\psi}{\partial x^2} \approx \frac{\partial^2\psi^0}{\partial x^2} = -\delta(x + \psi^0)$$

This equation, together with the appropriate boundary conditions $\psi^0|_{x=0} = \psi^0|_{x=1} = 0$, has the solution

$$[3] \quad \psi^0 = \frac{\sin(x\sqrt{\delta})}{\sin\sqrt{\delta}} - x$$

which is, therefore, an approximate solution to the original Frank-Kamenetskii heat equation.

We now write

$$[4] \quad \psi = \psi^0 + \sum_{n=1}^{\infty} b_n \sin.(n\pi x)$$

where $b_n \equiv b_n(\delta)$ is a function of the parameter $\delta$. Substitution of [4] into [2] leads, after some manipulation, to

$$[5] \quad \sum_{n=1}^{\infty} b_n[(n\pi)^2 - \delta]\sin(n\pi x) = \delta x[e^{\theta} - 1 - \theta]$$

Differentiating [5] with respect to $x$ gives

$$[6] \quad \sum_{n=1}^{\infty} b_n[(n\pi)^2 - \delta]n\pi\cos(n\pi x) = \delta[e^{\theta} - 1 - \theta] + \delta x[e^{\theta} - 1]\frac{\partial\theta}{\partial x}$$

and from [4] we get

$$[7] \quad \theta = \frac{1}{x}\left[\frac{\sin(x\sqrt{\delta})}{\sin\sqrt{\delta}} - x + \sum_{n=1}^{\infty} b_n \sin(n\pi x)\right]$$

0008-4042/82/152012-05$01.00/0
©1982 National Research Council of Canada/Conseil national de recherches du Canada

Can. J. Chem. Downloaded from www.nrcresearchpress.com by 210.87.254.42 on 09/06/12
For personal use only.

Can. J. Chem. Downloaded from www.nrcresearchpress.com by 210.87.254.42 on 09/06/12
For personal use only.

$$[8]\quad \frac{\partial\theta}{\partial x}=\frac{1}{x}\left[\frac{\sqrt{\delta}\cos(x\sqrt{\delta})}{\sin\sqrt{\delta}}-1-\theta+\sum_{n=1}^{\infty}b_n n\pi\cos(n\pi x)\right]$$

Equations [5]–[8] hold for all $x$, so for convenience we choose to examine the solution $\theta_{1/2}$ at $x = 1/2$, whence $n\pi x$ becomes $n\pi/2$; replacing $n$ by $2n + 1$ in [5] and by $2n$ in [6], they may now be rewritten, respectively, as

$$[9]\quad \sum_{n=1}^{\infty}b_{2n+1}(-1)^n\{[(2n+1)\pi]^2-\delta\}=\frac{\delta}{2}[e^{\theta_{1/2}}-1-\theta_{1/2}]$$

$$[10]\quad \sum_{n=1}^{\infty}b_{2n}(-1)^n(2n\pi)[(2n\pi)^2-\delta]=\delta\left[(e^{\theta_{1/2}}-1)\left(1+\frac{1}{2}\left.\frac{\partial\theta}{\partial x}\right|_{x=1/2}\right)-\theta_{1/2}\right]$$

$$[11]\quad \theta_{1/2}=2\left[\frac{\sin((1/2)\sqrt{\delta})}{\sin\sqrt{\delta}}-\frac{1}{2}+\sum_{n=0}^{\infty}b_{2n+1}(-1)^n\right]$$

$$[12]\quad \left.\frac{\partial\theta}{\partial x}\right|_{x=1/2}=2\left[\frac{\sqrt{\delta}\cos((1/2)\sqrt{\delta})}{\sin\sqrt{\delta}}-1-\theta_{1/2}+\sum_{n=1}^{\infty}b_{2n}(2n\pi)(-1)^n\right]$$

These equations are all exact.

## An approximate solution

Comparison with the exact numerical solution shows that equation [3] *alone* gives a good approximation for the temperature excess $\theta = \psi/x$ provided that $\delta \leq 2$; this is shown in the first five columns of Table 1, and arises because the $b_n$ of eq. [4] are small for all $n$ in this range. We set ourselves the target of trying to find a simple formula for $\theta$ which would be accurate to within 5% right up to the critical point; we felt that this was realistic in view of our experience in a slightly different case, where it was possible to find a subcritical profile to within this accuracy simply by scaling the critical temperature profile by an appropriate factor (7).

We show in the Appendix that the $b_n$ of eq. [4] form a decreasing series, and we assume for the present purposes that we can truncate the series at two terms, whence

$$[13]\quad \psi\approx\psi^0+\sum_{n=1}^{2}b_n\sin(n\pi x)$$

$$\text{i.e.}\quad \psi=\theta x\approx\frac{\sin(x\sqrt{\delta})}{\sin\sqrt{\delta}}-x+b_1\sin\pi x+b_2\sin 2\pi x$$

With this truncation, we have four eqs. [9]–[12] with four unknowns and can solve them without resorting to any integration: the solution is

$$[14]\quad b_1=\frac{\delta}{2(\pi^2-\delta)}(e^{\theta_{1/2}}-1-\theta_{1/2})+O(b_3)=\tfrac{1}{2}(\theta_{1/2}+1)-\frac{\sin((1/2)\sqrt{\delta})}{\sin\sqrt{\delta}}+O(b_3)$$

$$[15]\quad b_2=\frac{\beta\left[(e^{\theta_{1/2}}-1)\left(\frac{\sqrt{\delta}\cos((1/2)\sqrt{\delta})}{\sin\sqrt{\delta}}-\theta_{1/2}\right)-\theta_{1/2}\right]}{1+2\pi\beta(e^{\theta_{1/2}}-1)}+O(b_4)$$

where

$$\beta=\delta/[2\pi(\delta-4\pi^2)]$$

Equations [11]–[15] now constitute a complete solution: substitution of [14] into [11] gives an implicit equation in $\theta_{1/2}$ which can be solved easily by iteration. Once $\theta_{1/2}$ is known, the complete solution is available in this approximation for the given value of $\delta$.

## Properties of the approximate solution

We begin by comparing the formal behaviour of the present solution with the known properties of other solutions. Most illuminating from the point of view of illustrating the general difficulty in solving eq. [1] is a plot of $\partial\theta/\partial x|_{x=1}$ as a function of $\delta$. For the polynomial expansion method described in the Appendix, Fig. 1 shows this behaviour for expansion lengths of 10, 14, 16, and 20: clearly this plot would become a step function at $\partial\theta/\partial x|_{x=1} = -2$ and $\delta = \delta_c$ if a sufficient expansion length could be

TABLE 1. Comparison of exact and approximate solutions of eq. [1] for various values of $\delta$[a]

| $\delta$ | $\psi_0^0/x$ eq. [3] | $\theta_0$* | $\psi_0/x$ eq. [13] | $\theta_0$ | $b_1$* | $b_1$ | $b_2$* | $b_2$ | $b_3$ |
|---|---|---|---|---|---|---|---|---|---|
| 0.5 | $0.088_4$ | $0.088_7$ | $0.088_7$ | $0.088_7$ | $5.95 \times 10^{-5}$ | $5.67 \times 10^{-5}$ | $1.71 \times 10^{-6}$ | $2.22 \times 10^{-6}$ | $-3.5 \times 10^{-7}$ |
| 1.0 | 0.188 | 0.190 | 0.190 | 0.190 | $5.85 \times 10^{-4}$ | $5.57 \times 10^{-4}$ | $1.82 \times 10^{-5}$ | $2.28 \times 10^{-5}$ | $-3.3 \times 10^{-6}$ |
| 1.5 | 0.302 | 0.310 | 0.310 | 0.310 | $2.50 \times 10^{-3}$ | $2.38 \times 10^{-3}$ | $8.49 \times 10^{-5}$ | $1.03 \times 10^{-4}$ | $-1.3 \times 10^{-5}$ |
| 2.0 | 0.432 | 0.458 | 0.457 | 0.457 | $7.79 \times 10^{-3}$ | $7.43 \times 10^{-3}$ | $2.93 \times 10^{-4}$ | $3.41 \times 10^{-4}$ | $-3.6 \times 10^{-5}$ |
| 2.5 | 0.581 | 0.655 | 0.652 | 0.651 | $2.15 \times 10^{-2}$ | $2.05 \times 10^{-2}$ | $9.14 \times 10^{-4}$ | $1.02 \times 10^{-3}$ | $-8.4 \times 10^{-5}$ |
| 3.0 | 0.755 | 0.967 | 0.960 | 0.958 | $6.12 \times 10^{-2}$ | $5.85 \times 10^{-2}$ | $3.13 \times 10^{-3}$ | $3.33 \times 10^{-3}$ | $-1.6 \times 10^{-4}$ |
| 3.3 | 0.873 | 1.409 | 1.417 | 1.417 | $1.51 \times 10^{-1}$ | $1.52 \times 10^{-1}$ | $9.86 \times 10^{-3}$ | $1.06 \times 10^{-2}$ | $-3.8 \times 10^{-5}$ |
| 3.322 | 0.882 | 1.496 | 1.603 | 1.606 | $1.72 \times 10^{-1}$ | $1.99 \times 10^{-1}$ | $1.18 \times 10^{-2}$ | $1.52 \times 10^{-2}$ | $+2.2 \times 10^{-4}$ |

[a]In column 3, $\theta_0$* is the iterated solution found by using eqs. [11]–[15]; $\theta_0$ is the exact numerical solution found by the method described in ref. 7. The $b_n$ are the exact values of the expansion coefficients found from eq. [16] and the $b_n$* are the approximate values found by iteration, eqs. [14] and [15].

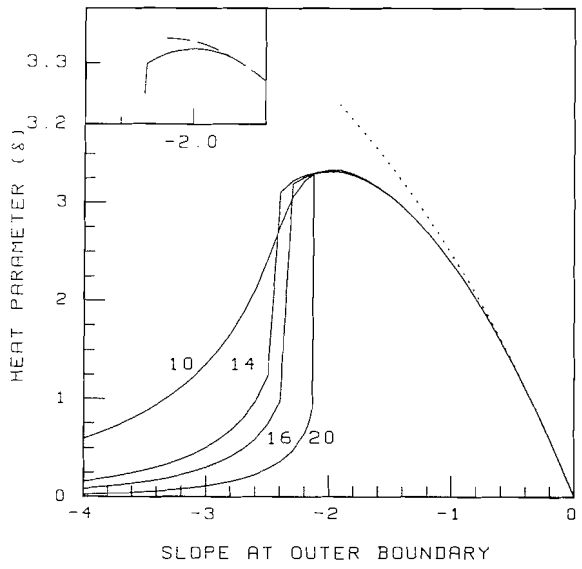


FIG. 1. Plots of $\partial\theta/\partial y|_{y=0}$ vs. $\delta$ for polynomial expansion lengths of $n$ = 10, 14, 16, and 20 for an exothermic reaction taking place in a sphere. Dotted line is eq. [3]. Dashed line (in inset) compares to present approximate solution (eq. [13]) with the 20-term polynomial expansion (eq. [A4]).

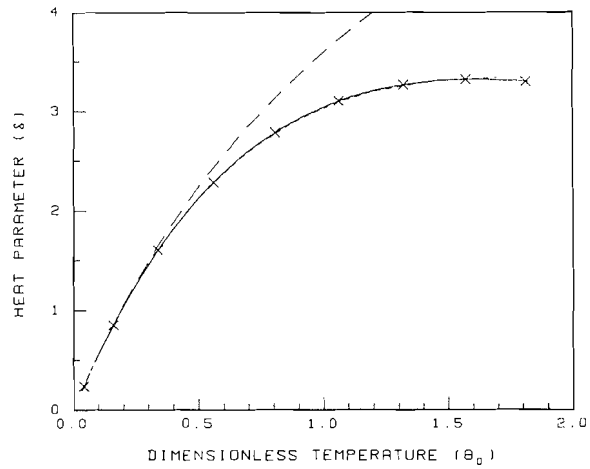


FIG. 2. Plots of $\theta_0$ vs. $\delta$ for the 20-term polynomial expansion and for the present approximate solution: solid line from equation [A4], dashed line from eq. [3], dotted line from eq. [13]; crosses are points from the tabulation of Chandrasekhar and Wares (1).

used. Since a common approach to the determination of $\delta_c$ is to find the maximum of such a curve (3, 4), the observed variability of $\delta_c$ around 3.32 in various solutions is not surprising.

The results of our approximate iterative method are also shown as the dashed line in Fig. 1; the agreement is very close up until about $\delta = 3.2$, and no solutions could be found beyond critical values of $\delta_c^* = 3.341$, $\partial\theta_c^*/\partial x|_{x=1} = -2.074$ (where the asterisk is used to denote the approximate solution by the present method). These approximate critical values may be accounted for easily by making an alternative plot, that of $\delta$ against $\theta_0$; this is shown in Fig. 2. By putting $\partial\delta/\partial\theta_{1/2} = 0$, we obtain for the critical condition $\delta_c^* = \pi^2/e^{\theta_{1/2,c}}$; substitution of this back into [11] leads to the critical solution $\theta_{1/2,c}^* = 1.08325$, from which then follow $\delta_c^* = 3.340_8$, $\theta_{0,c}^* = 1.697$, and $\partial\theta_c^*/\partial x|_{x=1} = -2.074$. Considering the simplicity of eq. [13], these are excellent approximations to the true critical parameters.

Figure 2 makes a comparison of the various methods showing the extent of the agreement between them. The solid line is derived from the 20-term polynomial expansion described in the Appendix; it is extended beyond the critical value of $\theta_0$ for the purposes of evaluating the stationary point in the curve, although there is no physical meaning to this solution beyond $\theta_{0,c}$. Our numerical solution (7) is indistinguishable from the solid line up as far as the critical point. The crosses denote a selection of points (approximately every fifth point) calculated from the tables of Chandrasekhar and Wares (1); our numerical solution (7) confirms the numerical values given in these tables to nine

Can. J. Chem. Downloaded from www.nrcresearchpress.com by 210.87.254.42 on 09/06/12
For personal use only.

Can. J. Chem. Downloaded from www.nrcresearchpress.com by 210.87.254.42 on 09/06/12
For personal use only.

decimal places up as far as the critical point. The dashed line is the simple function $\psi^0/x$, eq. [3], and the dotted line is the iterated function $\psi/x$, eq. [13].

In conclusion, we give in Table 1 a selection of values of $b_1$* and $b_2$* obtained by this method, and the true values of $b_1$ and $b_2$ (also $b_3$) obtained from the 20-term polynomial solution by evaluating the integral

$$[16] \quad b_n = 2\int_0^1 (\psi - \psi^0)\sin(n\pi x)\,dx$$

Notice the magnitude of $b_3$ is always significantly smaller than that of $b_1$ or $b_2$, justifying our original assumption, and in fact it passes through zero near $\delta = 3.3$; $b_4$ onwards become progressively smaller (see Table 2(*b*) in the Appendix for more details), and generally alternate in sign. Moreover, it is only at the critical point itself that we fail to achieve a calculation of $\theta_0$* within 1% of the correct value, $\theta_0$.

We present this method of calculating approximate temperature profiles for an exothermic reaction taking place in a sphere as an alternative to the method of Chambre, via the tables of Chandrasekhar and Wares (1, 2). Our formula is much simpler for low values of $\delta$; on the other hand, the older method is somewhat easier to use for larger values of $\delta$ if the central temperature *only* is required, but when the complete profile is needed, the present method is much quicker, although not quite as accurate. In the unlikely event that more accurate profiles are required near the critical point, we may use our earlier observation (7) that temperature profiles can be scaled by the ratio of $\theta_{0,\text{exact}}/\theta_{0,\text{approx}}$ with considerable confidence; alternatively, the poor performance of $\theta$* at values of $\delta > 3.3$ can be improved empirically by multiplying the right-hand side of [11] by an arbitrary correction factor of 1.0043, which improves $\theta_{0,c}$* to 1.596 without destroying the agreement at lower values of $\delta$.

**Acknowledgement**

We are grateful to Raj Vatsya for many helpful comments.

1. S. Chandrasekhar and G. W. Wares. Astrophys. J. **109**, 551 (1949).
2. P. L. Chambre. J. Chem. Phys. **20**, 1795 (1952).
3. S. R. Vatsya. J. Math. Phys. **22**, 2977 (1981).
4. D. A. Frank-Kamenetskii. Diffusion and heat exchange in chemical kinetics. Princeton University Press. 1955.
5. B. J. Tyler and T. A. B. Wesley. Eleventh Symposium (International) on Combustion. The Combustion Institute, 1967. p. 1115.
6. T. Boddington and P. Gray. Proc. R. Soc. London, A**320**, 71 (1970).
7. A. Moise and H. O. Pritchard. Can. J. Chem. **60**, 165 (1982).
8. P. Gray and M. E. Sherrington. Specialist Periodical Reports. Kinetics and Energy Transfer, **2**, 331 (1977).

## Appendix

We present here an outline of a general power series solution to eq. [1], which was used in generating Fig. 1. The function $\theta(x)$ is almost linear in the region near $x = 1$; consequently, we express $\theta(x)$ as a Taylor expansion about the point $x = 1$, viz.

$$[A1] \quad \theta(x) = \sum_{n=0}^{\infty} a_n (x-1)^n$$

Let $y = x - 1$ so that the limits $x = 0$, 1 become $y = -1$, 0, whence

$$[A2] \quad a_n = \frac{1}{n!}\frac{\partial^n\theta}{\partial x^n}\bigg|_{x=1} = \frac{1}{n!}\frac{\partial^n y}{\partial y^n}\bigg|_{y=0}$$

and

$$\theta(y) = \sum_{n=0}^{\infty}\frac{1}{n!}\frac{\partial^n\theta}{\partial y^n}\bigg|_{y=0} y^n$$

$$\frac{\partial\theta}{\partial y} = \sum_{n=1}^{\infty}\frac{1}{(n-1)!}\frac{\partial^n\theta}{\partial y^n}\bigg|_{y=0} y^{n-1}$$

The boundary conditions are $\theta_{y=0} = 0$ and $\partial\theta/\partial y|_{y=-1} = 0$ giving

$$[A3] \quad 0 = \sum_{n=1}^{\infty} n a_n (-1)^{n-1} = \sum_{n=1}^{\infty}\frac{1}{(n-1)!}\frac{\partial^n\theta}{\partial y^n}\bigg|_{y=0}(-1)^{n-1}$$

with $a_0 = 0$ and $a_1 = \partial\theta/\partial y|_{y=0}$. We may now construct a recursive relation for the expansion coefficients in terms of the $a_1$, viz.

$$[A4] \quad \theta(y) = \sum_{n=1}^{\infty} a_n y^n = \sum_{n=1}^{\infty} f_n(\delta, a_1) y^n$$

The first few members of this series are

$$f_1(\delta, a_1) = \partial\theta/\partial y|_{y=0} = a_1$$

$$f_2(\delta, a_1) = \frac{1}{2!}\partial^2\theta/\partial y^2|_{y=0} = -\frac{1}{2!}(2a_1 + \delta)$$

$$f_3(\delta, a_1) = \frac{1}{3!}\partial^3\theta/\partial y^3|_{y=0} = \frac{1}{3!}[6a_1 + (2 - a_1)\delta] \text{ etc.}$$

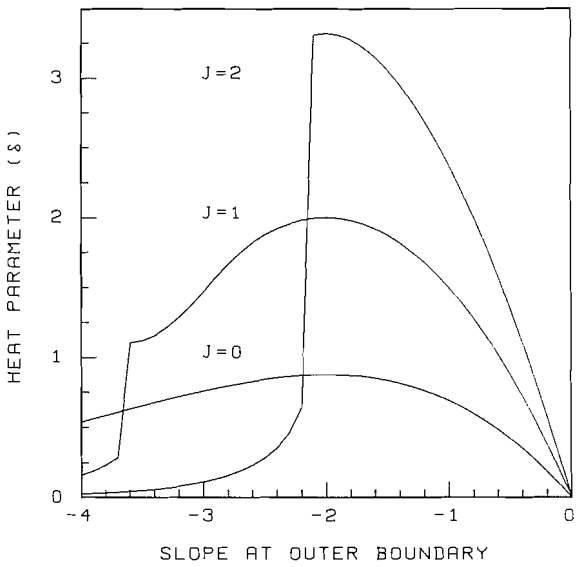


FIG. 3. Plots of $\partial\theta/\partial y|_{y=0} = a_1$ vs. $\delta$ for the 20-term expansion (eq. [A4]) for the sphere ($j = 2$), the infinite cylinder ($j = 1$), and the infinite slab ($j = 0$) (see ref. 6 for the definition of $j$).

This method was used to generate plots of $a_1 = \partial\theta/\partial y|_{y=0}$ vs. $\delta$ and of $\theta_0$ vs. $\delta$ as shown in Figs. 1 and 2, for expansion lengths up to $n = 20$. For $n = 20$, the maximum in the curve of $a_1$ vs. $\delta$ occurred at $a_1 = -2.000 \pm 0.001$ and $\delta_c = 3.322640$ for the case of a sphere, with a corresponding value of $\theta_{0,c} = 1.60569_5$. For the infinite cyclinder and for the infinite slab respectively, our $\theta_{0,c}$ values for a 20-term expansion are 1.38630 and 1.1868, in good agreement with the accepted ones (6, 8); notice that the degree of convergence of this method is poorest for the slab and best for the sphere, as evidenced by the behaviour of these plots, shown in Fig. 3.

In Table 2*a*, we list the first 20 values of $f_n(\delta, a_1)$ required for the expansion [A4] at $\delta = \delta_c = 3.322640$ and $a_1 = -2$ exactly (2); it is a very slowly converging series. This is in contrast with the

TABLE 2[a]

(*a*) Coefficients $f_n(\delta, a_1)$ in the Taylor expansion [A4] for the critical temperature profile in a sphere

| Coefficient | Value | Coefficient | Value |
|---|---|---|---|
| $f_1$ | $-2$ | $f_{11}$ | $-9.412533 \times 10^{-3}$ |
| $f_2$ | $3.386800 \times 10^{-1}$ | $f_{12}$ | $-4.387559 \times 10^{-3}$ |
| $f_3$ | $2.150933 \times 10^{-1}$ | $f_{13}$ | $9.811017 \times 10^{-3}$ |
| $f_4$ | $-3.088693 \times 10^{-1}$ | $f_{14}$ | $-8.819543 \times 10^{-3}$ |
| $f_5$ | $2.186463 \times 10^{-1}$ | $f_{15}$ | $4.871653 \times 10^{-3}$ |
| $f_6$ | $-9.313060 \times 10^{-2}$ | $f_{16}$ | $-9.033602 \times 10^{-4}$ |
| $f_7$ | $6.664293 \times 10^{-4}$ | $f_{17}$ | $-1.529783 \times 10^{-3}$ |
| $f_8$ | $4.204102 \times 10^{-2}$ | $f_{18}$ | $2.191259 \times 10^{-3}$ |
| $f_9$ | $-4.557776 \times 10^{-2}$ | $f_{19}$ | $-1.637864 \times 10^{-3}$ |
| $f_{10}$ | $2.918359 \times 10^{-2}$ | $f_{20}$ | $6.401175 \times 10^{-4}$ |

(*b*) Coefficients $b_n$ in the Fourier expansion [4] for the same temperature profile

| Coefficient | Value | Coefficient | Value |
|---|---|---|---|
| $b_1$ | $1.933 \times 10^{-1}$ | $b_6$ | $6.097 \times 10^{-6}$ |
| $b_2$ | $1.510 \times 10^{-2}$ | $b_7$ | $-8.808 \times 10^{-6}$ |
| $b_3$ | $1.938 \times 10^{-4}$ | $b_8$ | $4.801 \times 10^{-7}$ |
| $b_4$ | $1.103 \times 10^{-4}$ | $b_9$ | $-3.014 \times 10^{-6}$ |
| $b_5$ | $-3.560 \times 10^{-5}$ | $b_{10}$ | $-1.155 \times 10^{-7}$ |

[a]The critical parameters for these functions are $\delta_c = 3.322640$; $\partial\theta/\partial x|_{x=1} = \partial\theta/\partial y|_{y=0} = -2$; $\theta_{0,c} = 1.60569_5$.

Fourier series expansion [4]: Table 2*b* gives the first 10 $b_n$ coefficients, calculated by [16] from the critical profile described in Table 2*a*. In fact, if the last 8 coefficients $b_3 - b_{10}$ are ignored altogether, it makes very little difference, changing the calculated value of $\theta_{0,c}$ from 1.6058 to 1.6033, whereas the correct value is 1.6057.

Finally, we note that our Taylor expansion method also works for the case we have already treated numerically (7), that of variable thermal conductivity; however, we have insufficient computer storage space in which to calculate the required analytic forms for the derivatives beyond the 10th, and at this point, the expansion [A4] is only converged to about $\pm 10\%$.

Can. J. Chem. Downloaded from www.nrcresearchpress.com by 210.87.254.42 on 09/06/12
For personal use only.

# Synthesis, structure, and properties of poly-bis(μ-diethylphosphinato)copper(II)

KATHERINE W. OLIVER, STEVEN J. RETTIG, ROBERT C. THOMPSON, AND JAMES TROTTER
*Department of Chemistry, University of British Columbia, 2036 Main Mall, Vancouver, B.C., Canada V6T 1Y6*
Received November 25, 1981

KATHERINE W. OLIVER, STEVEN J. RETTIG, ROBERT C. THOMPSON, and JAMES TROTTER. Can. J. Chem. **60**, 2017 (1982).

The preparation, magnetic properties, electronic and infrared spectra, and molecular structure of poly-bis(μ-diethylphosphinato)copper(II) are described. Crystals of poly-bis(μ-diethylphosphinato)copper(II) are triclinic, $a = 7.700(1)$, $b = 9.807(1)$, $c = 10.101(1)$ Å, $\alpha = 90.48(1)$, $\beta = 104.77(1)$, $\gamma = 112.21(1)°$, $Z = 2$, space group $P\bar{1}$. The structure was solved by direct methods and was refined by full-matrix least-squares procedures to $R = 0.025$ and $R_w = 0.032$ for 3491 reflections with $I \geq 3\sigma(I)$. The polymeric structure consists of Cu atoms with flattened tetrahedral coordination geometry linked by double phosphinate bridges. Mean bond lengths (corrected for libration) are: Cu—O, 1.924(3), P—O, 1.526(4), and P—C, 1.807(4) Å. Assignment of the electronic spectrum using a crystal field model gives $Dq = 1665$ cm$^{-1}$ and $Cp = 1800$ cm$^{-1}$. Magnetic susceptibility studies give no evidence for magnetic concentration over the temperature range 80 to 300 K.

KATHERINE W. OLIVER, STEVEN J. RETTIG, ROBERT C. THOMPSON et JAMES TROTTER. Can. J. Chem. **60**, 2017 (1982).

On décrit la préparation les propriétés magnétiques, les spectres électronique et infrarouge et la structure moléculaire de poly-bis (μ-diéthyle phosphinato) cuivre (II). Les cristaux sont tricliniques $a = 7.700(1)$, $b = 9.807(1)$, $c = 10.101(1)$ Å, $\alpha = 90.48(1)$, $\beta = 104.77(1)$, $\gamma = 112.21(1)°$, $Z = 2$, groupe d'espace $P\bar{1}$. La structure a été résolve à l'aide des méthodes directes et affinée par la méthode des moindres carrés (matrices entières) jusqu'à des valeurs de $R = 0.0025$ et $R_w = 0.032$ pour 3491 réflexions avec $I \geq 3\sigma(I)$. La structure polymérique consiste en atomes de cuivre avec une géométrie de coordination tétraédrique aphatie et liés de ponts phosphinates doubles. Des longueurs moyennes de liaison (corrigées pour la libration) sont: Cu—O, 1.924(3), P—O, 1.526(4), et P—C, 1.807(4) Å. On a analysé le spectre électronique en faisant appel à un modèle de champs de cristal et on a obtenu $Dq = 1665$ cm$^{-1}$ et $Cp = 1800$ cm$^{-1}$. Des études de la susceptibilité magnétique ne donnant aucune indication d'une concentration magnétique dans l'intervale de température de 80 à 300 K.

[Traduit par le journal]

## Introduction

Because of their potential industrial use, metal phosphinates have attracted attention over the last few years (1). Although these materials are generally thought to be highly polymeric, with metal atoms joined by O—P—O bridges, the structures of relatively few have been established with certainty by X-ray diffraction methods (2–5). We report here the synthesis and crystal structure determination of poly-bis(μ-diethylphosphinato)copper(II). The vibrational and electronic spectra have been recorded and assigned and magnetic susceptibilities have been measured over the temperature range 80 to 300 K. The magnetic properties of this material are of particular interest because of the possibility of the propagation of magnetic exchange via the bridging phosphinate groups (5–7).

## Experimental

*Synthesis*

Poly-bis(μ-diethylphosphinato)copper(II), $Cu[(C_2H_5)_2PO_2]_2$, was prepared by a route which involved the synthesis of silver(I) diethylphosphinate followed by the reaction of the silver salt with copper(II) chloride in aqueous solution. The silver salt was prepared by Kosolapoff's procedure (8) with the minor change of using reagent grade acetone rather than aqueous ethanol in the final precipitation. An aqueous solution of copper(II) chloride dihydrate (27 mmol) was added to an excess of silver(I) diethylphosphinate (71 mmol) dissolved in water. Silver(I) chloride was removed by filtration, then dilute aqueous HCl was added until no further precipitation of AgCl occurred. The solution was filtered then evaporated under vacuum to yield a gummy solid consisting of the product contaminated with diethylphosphinic acid (an oil at room temperature). This material was washed with acetone. Most of the copper salt remained on the filter while some dissolved in the acetone together with the diethylphosphinic acid. Slow evaporation in air of the acetone washings yielded a deep blue oil in which blue crystals developed over about a week. The crystals used in the X-ray study were separated from the bulk of the oil and residual oil on the crystals was removed by washing with cold acetone. The crude product which remained after washing with acetone was dissolved in methanol; this solution was filtered and then evaporated to dryness. The resulting light blue powder (40% yield) was the desired poly-bis(μ-diethylphosphinato)copper(II) (melting point, 227–228.5°C). *Anal.* calcd. for $CuC_8H_{20}P_2O_4$: Cu 20.78, C 31.43, H 6.59; found: Cu 20.92, C 31.19, H 6.16. Carbon and hydrogen were determined by P. Borda of the Department of Chemistry, The University of British Columbia. Copper was determined by EDTA titration.

*Solubility*

Qualitative solubility tests showed the compound to be quite soluble (in excess of 0.1 g in 100 mL) in water, methanol, chloroform, and carbon tetrachloride; and only slightly soluble in ethanol, acetone, and benzene.

0008-4042/82/152017-06$01.00/0
©1982 National Research Council of Canada/Conseil national de recherches du Canada

Can. J. Chem. Downloaded from www.nrcresearchpress.com by 210.87.254.42 on 09/06/12
For personal use only.

Can. J. Chem. Downloaded from www.nrcresearchpress.com by 210.87.254.42 on 09/06/12
For personal use only.

*Infrared spectrum*

Data for the range 1400 to 300 $cm^{-1}$: 1279 sh, 1270 m br, 1245 w br, 1237 sh, 1188 m, 1110 vs, 1049 vs, 997 w sh, 976 w sh, 780 s, 771 s, 757 sh, 728 m, 655 vw, 673 vw, 508 m sh, 487 m, 422 m, 375 w, 335 m (w = weak, m = medium, s = strong, v = very, br = broad, sh = shoulder). Infrared spectra were obtained on Nujol mulls as described previously (9).

*Electronic spectrum*

The electronic spectrum of a Nujol mull obtained using a Cary 14 spectrophotometer (range 3800 to 30000 $cm^{-1}$) showed a broad band centered at 12000 $cm^{-1}$ with a broad shoulder at 14300 $cm^{-1}$.

*Magnetic susceptibilities*

These were obtained using equipment described previously (9). The magnetic susceptibility was corrected for the diamagnetism of all atoms ($155 \times 10^{-6}$ $cm^3$ $mol^{-1}$). A total of twenty measurements made over the temperature range 80 to 300 K gave magnetic moments which were independent of temperature, lying within the narrow range of 1.89 to 1.91 BM.

*X-ray crystallographic analysis of poly-bis(μ-diethylphosphinato)copper(II)*

A crystal ca. $0.12 \times 0.30 \times 0.40$ mm in size was mounted in a general orientation. Unit-cell parameters were refined by least-squares on $2\sin\theta/\lambda$ values for 25 reflections measured on a diffractometer with Mo Kα Radiation ($\lambda = 0.71073$ Å). Crystal data at 22°C are:

$C_8H_{20}CuO_4P_2$ fw = 305.74

Triclinic, $a = 7.700(1)$, $b = 9.807(1)$, $c = 10.101(1)$ Å, $\alpha = 90.48(1)$, $\beta = 104.77(1)$, $\gamma = 112.21(1)°$, $V = 678.2(2)$ Å$^3$, $Z = 2$, $\rho_c = 1.497$ g $cm^{-3}$, $F(000) = 316$, $\mu$(Mo Kα) = 18.4 $cm^{-1}$. Absent reflections: none, space group $P\bar{1}$ ($C_i^1$, No. 2, reduced cell) from structure analysis.

Intensities were measured with graphite-monochromatized Mo Kα Radiation on an Enraf-Nonius CAD4-F diffractometer. An ω–2θ scan at 1.12–10.06° $min^{-1}$ over a range of $(0.72 + 0.35\tan\theta)$ degrees in ω (extended by 25% on both sides for background measurement) was employed. Data were measured to $2\theta = 65°$. The intensities of 3 check reflections, measured every 3600 s throughout the data collection, decreased uniformly by 5% during the data collection. An isotropic decay correction was applied. After data reduction, an absorption correction was applied using the Gaussian integration method (10, 11). Transmission factors ranged from 0.598 to 0.811 for 188 sampling points. Of the 4891 independent reflections measured, 3491 (71.4%) had intensities greater than $3\sigma(I)$ above background where $\sigma^2(I) = S + 2B + (0.025(S-B))^2$ with $S$ = scan count and $B$ = background count.

The centrosymmetric space group $P\bar{1}$ was indicated by the $E$-statistics. The structure was solved by direct methods, the coordinates of the Cu, P, and O atoms being determined from an $E$-map and those of the carbon atoms from a subsequent difference map. After full-matrix least-squares refinement of the non-hydrogen atoms with anisotropic thermal parameters to $R = 0.037$, a difference map revealed the positions of all 20 hydrogen atoms which were refined with isotropic thermal parameters in subsequent least-squares cycles. The scattering factors of ref. 12 were used for non-hydrogen atoms and those of ref. 13 for hydrogen atoms. Anomalous scattering factors from ref. 14 were used for the Cu and P atoms. The weighting scheme, $w = 1/\sigma^2(F)$ where $\sigma^2(F)$ is derived from the previously defined $\sigma^2(I)$ gave uniform average values of $w(|F_o|-|F_c|)^2$ over ranges of $|F_o|$ and was employed in the final stages of refinement. Convergence was reached at $R = 0.025$ and $R_w = 0.032$ for 3491 reflections with $I \geq 3\sigma(I)$. For all 4891 reflections $R = 0.048$ and $R_w = 0.033$. The function minimized was $\Sigma w(|F_o|-|F_c|)^2$, $R = \Sigma||F_o|-|F_c||/\Sigma|F_o|$ and $R_w = (\Sigma w(|F_o|-|F_c|)^2/\Sigma w|F_o|^2)^{1/2}$.

TABLE 1. Final positional (fractional: C × $10^4$, Cu, P, and O × $10^5$, H × $10^3$) and isotropic thermal parameters ($U \times 10^3$ Å$^2$) with estimated standard deviations in parentheses

| Atom | $x$ | $y$ | $z$ | $U_{eq}/U_{iso}$* |
|---|---|---|---|---|
| Cu | 23567( 2) | 25977( 2) | 51902( 2) | 29 |
| P(1) | 14361( 5) | −1713( 4) | 68056( 4) | 30 |
| P(2) | 35286( 5) | 49660( 4) | 31273( 4) | 29 |
| O(1) | 28359(17) | 12912(12) | 65019(12) | 40 |
| O(2) | 3632(15) | −13622(11) | 55821(11) | 33 |
| O(3) | 25850(18) | 34068(12) | 34918(11) | 40 |
| O(4) | 57350(16) | 56604(11) | 36271(12) | 36 |
| C(1) | −301( 3) | 153( 2) | 7521( 2) | 43 |
| C(2) | 2890( 3) | −844( 2) | 8108( 2) | 46 |
| C(3) | 2543( 3) | 6152( 2) | 3738( 2) | 48 |
| C(4) | 2810( 3) | 4792( 2) | 1270( 2) | 44 |
| C(5) | 573( 5) | 1378( 3) | 8724( 3) | 64 |
| C(6) | 4424( 5) | −1147( 4) | 7657( 4) | 77 |
| C(7) | 325( 4) | 5573( 5) | 3280( 4) | 80 |
| C(8) | 3480( 5) | 6247( 3) | 654( 2) | 69 |
| H(1a) | −134( 3) | 45( 2) | 671( 2) | 57( 6) |
| H(1b) | −109( 4) | −79( 3) | 781( 3) | 79( 9) |
| H(2a) | 350( 4) | −24( 3) | 885( 3) | 65( 7) |
| H(2b) | 190( 4) | −177( 3) | 842( 3) | 76( 8) |
| H(3a) | 288( 4) | 613( 3) | 453( 3) | 59( 7) |
| H(3b) | 299( 4) | 706( 3) | 338( 3) | 62( 7) |
| H(4a) | 317( 4) | 410( 3) | 102( 3) | 69( 8) |
| H(4b) | 159( 4) | 444( 3) | 97( 3) | 59( 7) |
| H(5a) | 135( 5) | 125( 4) | 941( 4) | 92(11) |
| H(5b) | 144( 3) | 231( 2) | 836( 2) | 54( 6) |
| H(5c) | −54( 6) | 154( 4) | 874( 4) | 127(14) |
| H(6a) | 503( 5) | −144( 3) | 837( 3) | 78( 9) |
| H(6b) | 391( 5) | −182( 4) | 664( 4) | 106(12) |
| H(6c) | 515( 5) | −18( 4) | 720( 3) | 90(10) |
| H(7a) | −30( 5) | 609( 4) | 368( 3) | 86( 9) |
| H(7b) | −5( 9) | 580( 6) | 199( 6) | 217(23) |
| H(7c) | −32( 5) | 474( 3) | 348( 3) | 91(11) |
| H(8a) | 470( 4) | 681( 3) | 100( 3) | 76( 9) |
| H(8b) | 331( 4) | 599( 3) | −16( 3) | 77( 9) |
| H(8c) | 290( 6) | 692( 5) | 81( 4) | 131(17) |

*$U_{eq}$ = (1/3) trace ($U_{diag}$).

On the final cycle of refinement the mean and maximum parameter shifts corresponded to 0.16 and 0.98σ respectively. The mean error in an observation of unit weight was 1.985. A final difference map showed no unusual features. The final positional and thermal parameters appear in Tables 1 and 2[1] respectively. Measured and calculated structure factors have been placed in the Depository of Unpublished Data.[1]

The ellipsoids of thermal motion for the non-hydrogen atoms are shown in Fig. 1. The thermal motion has been analysed in terms of the rigid-body modes of translation, libration, and screw motion (15). The rms standard error in the temperature factors $\sigma U_{ij}$ (derived from the least-squares analysis) is 0.0009 Å$^2$. Analysis of all unique atoms of the asymmetric unit indicated significant independent motion of the two bridging phosphinate groups which were then analysed separately (rms $\Delta U_{ij}$ = 0.0006, 0.0007, 0.0016, and 0.0023 Å$^2$ for first five-atom and then seven-atom rigid-groups containing P(1) and P(2) respectively). Since derived parameters were very similar for the five- and seven-atom groups, corrections were based on the better-

[1]The structure factor table, Table 2 (anisotropic thermal parameters) and other material mentioned in the text are available, at a nominal charge, from the Depository of Unpublished Data, CISTI, National Research Council of Canada, Ottawa, Ont., Canada K1A 0S2.

Can. J. Chem. Downloaded from www.nrcresearchpress.com by 210.87.254.42 on 09/06/12
For personal use only.

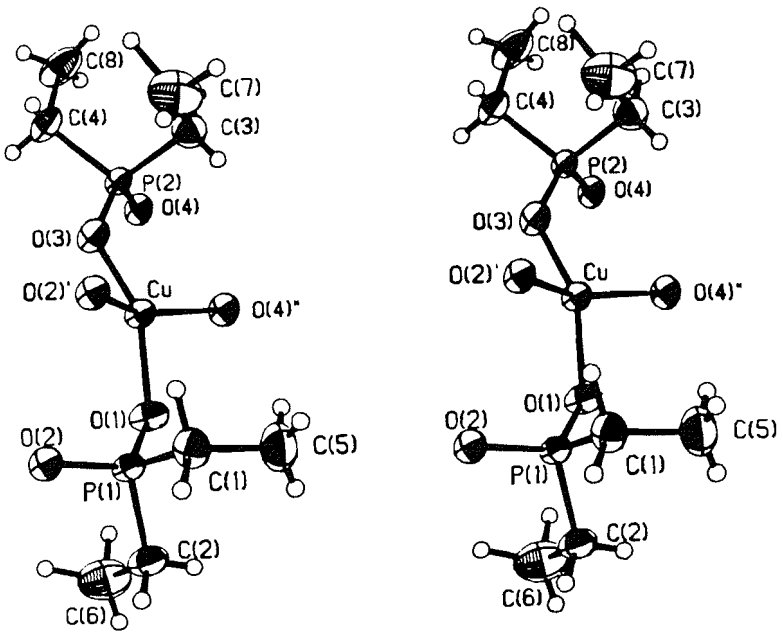


FIG. 1. Stereoview of $Cu[(C_2H_5)_2PO_2]_2$ showing atom numbering scheme and the coordination about Cu. Primed and double primed atoms are related to those in Table 1 by inversion through centres of symmetry at 0,0,1/2 and 1/2,1/2,1/2 respectively.

TABLE 3. Bond lengths (Å) with estimated standard deviations in parentheses*

| | Length | | | Length | |
|---|---|---|---|---|---|
| Bond | Uncorr. | Corr. | Bond | Uncorr. | Corr. |
| Cu —O(1) | 1.9158(11) | 1.922 | P(2)—O(3) | 1.5191(10) | 1.528 |
| Cu —O(3) | 1.9171(11) | 1.923 | P(2)—O(4) | 1.5125(11) | 1.521 |
| Cu —O(2)′ | 1.9224(10) | 1.928 | P(2)—C(3) | 1.790(2) | 1.801 |
| Cu —O(4)″ | 1.9177(10) | 1.924 | P(2)—C(4) | 1.802(2) | 1.812 |
| P(1)—O(1) | 1.5233(10) | 1.531 | C(1)—C(5) | 1.524(3) | 1.529 |
| P(1)—O(2) | 1.5164(11) | 1.524 | C(2)—C(6) | 1.492(4) | 1.499 |
| P(1)—C(1) | 1.795(2) | 1.804 | C(3)—C(7) | 1.521(3) | 1.527 |
| P(1)—C(2) | 1.800(2) | 1.809 | C(4)—C(8) | 1.521(3) | 1.527 |

*Atoms denoted by prime and double prime are related to those in Table 1 by the centres of symmetry at 0,0,1/2 and 1/2,1/2,1/2 respectively.

fitting five-atom groups. The appropriate bond distances have been corrected for libration (15, 16), using shape parameters $q^2$ of 0.08 for all atoms involved. Corrected bond lengths appear in Table 3 along with the uncorrected values; corrected bond angles do not differ by more than 1σ from the uncorrected values given in Table 4. Intra-annular torsion angles defining the conformations of the eight-membered rings are listed in Table 5. Distances and angles involving hydrogen atoms and a complete list of torsion angles (Tables 6–8) are included as supplementary material.[1]

## Results and discussion

### *The crystal structure of $Cu[(C_2H_5)_2PO_2]_2$*

The crystal structure of $Cu[(C_2H_5)_2PO_2]_2$ consists of well-separated infinite chains of centrosymmetric spiro-fused eight-membered rings extending along the crystallographic [110] direction (see Fig. 2). Each of the eight-membered rings consists of two copper atoms bridged by two phosphinate groups. The two crystallographically independent rings have qualitatively similar conformations which are best described as distorted chairs (torsion angles are given in Table 5). The structure is very similar to that of $Cu[(n\text{-}C_4H_9)_2PO_2]_2$ (5) and analogous to that of $Pb[(C_6H_5)_2PO_2]_2$ (4) which also contains double phosphinate bridges. The other metal phosphinate structures (2, 3) contain tetrahedrally coordinated metal atoms linked alternately by single and triple phosphinate bridges.

The Cu atoms have the same $D_{2d}$ flattened tetrahedral coordination geometry observed pre-

Can. J. Chem. Downloaded from www.nrcresearchpress.com by 210.87.254.42 on 09/06/12
For personal use only.

TABLE 4. Bond angles (deg) with estimated standard deviations in parentheses

| Bonds | Angle (deg) | Bonds | Angle (deg) |
|---|---|---|---|
| O(1)—Cu —O(3) | 149.85(6) | O(3)—P(2)—C(3) | 110.00(9) |
| O(1)—Cu —O(2)′ | 94.88(5) | O(3)—P(2)—C(4) | 105.11(7) |
| O(1)—Cu —O(4)″ | 93.20(5) | O(4)—P(2)—C(3) | 109.76(8) |
| O(3)—Cu —O(2)′ | 92.74(5) | O(4)—P(2)—C(4) | 108.30(8) |
| O(3)—Cu —O(4)″ | 96.00(5) | C(3)—P(2)—C(4) | 108.03(10) |
| O(2) —Cu—O(4)″ | 147.24(6) | Cu —O(1)—P(1) | 130.08(7) |
| O(1)—P(1)—O(2) | 114.99(6) | P(1)—O(2)—Cu′ | 132.30(7) |
| O(1)—P(1)—C(1) | 109.72(8) | Cu —O(3)—P(2) | 133.70(7) |
| O(1)—P(1)—C(2) | 106.37(8) | P(2)—O(4)—Cu″ | 135.45(8) |
| O(2)—P(1)—C(1) | 109.51(7) | P(1)—C(1)—C(5) | 115.3(2) |
| O(2)—P(1)—C(2) | 108.26(8) | P(1)—C(2)—C(6) | 113.6(2) |
| C(1)—P(1)—C(2) | 107.69(10) | P(2)—C(3)—C(7) | 114.4(2) |
| O(3)—P(2)—O(4) | 115.31(7) | P(2)—C(4)—C(8) | 114.84(15) |

viously for $Cu[(n\text{-}C_4H_9)_2PO_2]_2$ (5). The mean[2] libration-corrected Cu—O, P—O, and P—C distances of 1.924(3), 1.526(4), and 1.807(4) Å as well as bond angles at Cu, P, and O atoms (Table 4) are in excellent agreement with corresponding values found for $Cu[(n\text{-}C_4H_9)_2PO_2]_2$ (5). The Cu···Cu separation of 4.9555(8) Å is slightly longer than the value of 4.938(2) Å in the *n*-butyl analog (5).

*Infrared spectrum*

A detailed assignment of all bands was not attempted; however, by comparison of the observed spectrum with published data for tetra(ethyl)diphosphine disulfide (17) and related phosphinate derivatives (18, 19) it was possible to assign the principal modes associated with the $C_2PO_2$ part of the compound. Two very strong bands at 1110 and 1049 $cm^{-1}$ may be readily assigned as the antisymmetric and symmetric $PO_2$ stretching frequencies (18, 19). A medium intensity absorption at 728 $cm^{-1}$ is assigned to the symmetric $PC_2$ stretching mode with a shoulder at 757 $cm^{-1}$ assigned to the corresponding antisymmetric stretch. For comparison, these vibrations occur at 700 and 738 $cm^{-1}$ in the spectrum of $(CH_3)_2PO_2Na$ (18). Bands at 472 and 440 $cm^{-1}$ in the infrared spectrum of $(CH_3)_2PO_2Na$ were suggested by Nyquist to result from fundamental modes associated with angle bending of both the $PC_2$ and $PO_2$ groups (18). The medium intensity bands observed at 487 and 422 $cm^{-1}$ in the spectrum of $Cu[(C_2H_5)_2PO_2]_2$ are tentatively assigned to these vibrations. The remaining bands in the spectrum, with the possible exception of the absorption at 335 $cm^{-1}$, doubtless arise primarily from internal vibrations of the $C_2H_5$ moieties. The medium intensity band at 335 $cm^{-1}$ may arise from Cu—O stretching. For comparison, bands at 336 $cm^{-1}$ in anhydrous copper(II) nitrate and 345 $cm^{-1}$ in anhydrous copper(II) sulfate have been previously assigned to ν(Cu—O) (20, 21).

It is interesting to note that although the crystal structure of the title compound shows the presence of two structurally distinct phosphinate groups, the difference is not sufficient to result in band duplication or splitting in the infrared spectrum. This clearly illustrates the limitations of infrared spectroscopy as a tool for detailed structure assessment. In spite of such limitations, attempts have been made, for example, to correlate features such as the separation between $\nu_{as}(PO_2)$ and $\nu_{sym}(PO_2)$ with the nature of the bridging groups in phosphinate polymers (22, 23). This may be a useful criterion since we note that the separation of 61 $cm^{-1}$ observed here is of a magnitude expected for symmetrical phosphinate bridging, a result consistent with the X-ray study.

*Electronic spectrum*

To assign this spectrum we considered the crystal field model as described by Gerloch and Slade (24). The copper in the title compound is in a

TABLE 5. Intra-annular torsion angles (deg) standard deviations in parentheses*

| Atoms | Value (deg) |
|---|---|
| O(1)—Cu —O(2)′—P(1)′ | −93.26(9) |
| O(2)′—Cu —O(1)—P(1) | −2.39(12) |
| O(2)—P(1)—O(1)—Cu | 57.64(13) |
| O(1)—P(1)—O(2)—Cu′ | −129.07(9) |
| O(3)—Cu —O(4)″—P(2)″ | −79.73(11) |
| O(4)″—Cu —O(3)—P(2) | −13.30(13) |
| O(4)—P(2)—O(3)—Cu | 67.94(14) |
| O(3)—P(2)—O(4)—Cu″ | −120.60(10) |

*Symmetry related torsion angles have the opposite sign.

[2]Here and elsewhere in this report mean values refer to weighted means with rms deviations from the mean in parentheses.

Can. J. Chem. Downloaded from www.nrcresearchpress.com by 210.87.254.42 on 09/06/12
For personal use only.

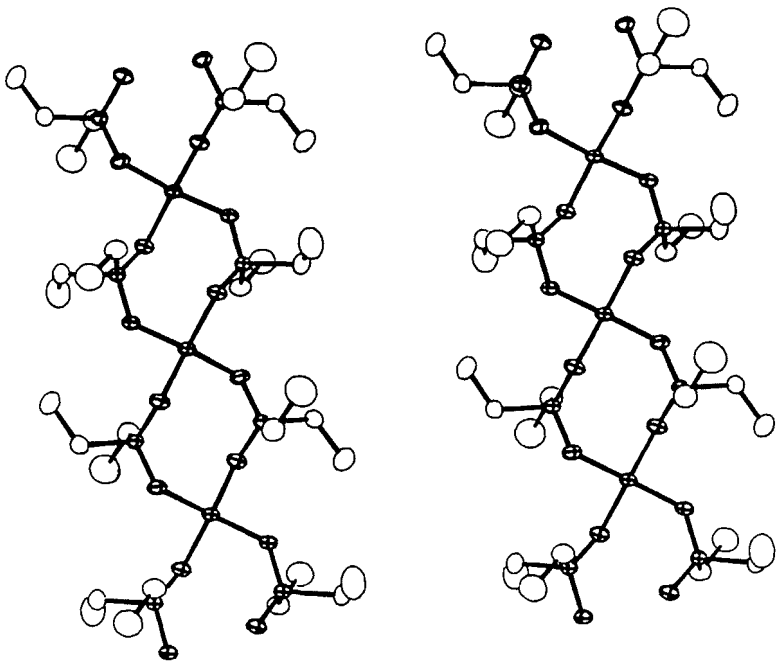

FIG. 2. Stereoview of the structure of poly-bis(μ-diethylphosphinato)copper(II).

compressed tetrahedral environment of four oxygens (approximate $D_{2d}$ symmetry) with the two larger angles 149.85 and 147.24°. The ground electronic state in such a case is $^2B_2$ with $^2E$, $^2B_1$, and $^2A_1$ excited states. Point charge crystal field calculations give the energies of these levels in terms of two crystal field parameters, *Dq* and *Cp* (the fourth-and second-order radial parameters respectively), and a distortion parameter, α (half of the largest O—Cu—O bond angle) (24).

Setting α at 74.3° (as obtained from the structure data) we were able to obtain two fits to the observed spectral data. Setting the crystal field parameters *Dq* and *Cp* at 700 and 3800 $cm^{-1}$ respectively gives $^2B_2 \rightarrow {}^2B_1, \rightarrow {}^2E, \rightarrow {}^2A_1$ transition energies of 6000, 12400, and 14400 $cm^{-1}$. Since the $^2B_2 \rightarrow {}^2B_1$ transition is formally symmetry forbidden, this might account for the fact that we observe no band at 6000 $cm^{-1}$. A major difficulty with this assignment is, however, that the value of *Dq* is unreasonably small (note the definition of *Dq* which is given in ref. 24; these *Dq* values should be regarded as $(9/4)\Delta_{tet}$), smaller even than the *Dq* value for $CuCl_4^{2-}$ (24). *Dq* values for oxygen bonding ligands are usually significantly greater than those for $Cl^-$ (25).

The second and more favored fit involves setting *Dq* and *Cp* at 1665 and 1800 $cm^{-1}$ respectively. This gives $^2B_2 \rightarrow {}^2A_1, \rightarrow {}^2E$, and $\rightarrow {}^2B_1$ transition energies of 11600, 12500, and 14300 $cm^{-1}$. The observed band at 12000 $cm^{-1}$, according to this fit, is reasonably assigned to the unresolved $^2B_2 \rightarrow {}^2A_1, {}^2E$ transition with the shoulder observed at 14300 $cm^{-1}$ assigned to the $^2B_2 \rightarrow {}^2B_1$ transition. The value of *Dq* obtained from this fit is quite reasonable, being of the order of 30–40% greater than the *Dq* for $CuCl_4^{2-}$ (24). For comparison we note that the ligand field "*f*-value" for water is 25% greater than the value for $Cl^-$ (25). To our knowledge this is the first estimate of crystal field *Dq* and *Cp* parameters in phosphinate compounds.

*Magnetic susceptibilities*

We were interested in examining the bulk magnetic properties of $Cu[(C_2H_5)_2PO_2]_2$ because of the possibility of magnetic concentration resulting from exchange interactions propagated by the bridging phosphinate groups. Antiferromagnetic exchange of this type has been observed in some chromium phosphinates (6, 7) and in a related phosphate-bridged copper(II) dimer (26). One interesting feature of this earlier work discussed by Lambert *et al.* (26) is that, although the (approximately) tetrahedral geometries of the bridging groups lead to a hybridization at the central atom that could result in a net ferromagnetic exchange, the observed exchange is, in fact, antiferromagnetic.

Our measurements on poly-bis(μ-diethylphosphinato)copper(II) give no evidence for mag-

netic exchange over the temperature range 80 to 300 K. The temperature independent moment of $1.90 \pm 0.01$ BM is comparable to the temperature independent value of 1.97 BM calculated from the Curie constant reported for the di-*n*-butylphosphinato derivative over the same temperature range (5). The magnetic moment is also similar to that observed for the structurally related $Ca[Cu(CH_3CO_2)_4]\cdot 6H_2O$, although in the latter case the moment varies slightly from 1.93 BM at room temperature to 1.88 BM at 80 K (27). If there is magnetic exchange in the copper(II) phosphinate compounds under discussion here, magnetic susceptibility evidence for it will have to come from measurements at lower temperatures.

## Acknowledgments

We thank the Natural Sciences and Engineering Research Council of Canada and the Xerox Corporation of Canada for financial support and the University of British Columbia Computing Centre for assistance. K.W.O. also thanks the UBC Graduate Scholarship Committee and NSERC for scholarship awards.

1. B. P. Block. Inorg. Macromol. Rev. **1**, 115 (1970).
2. F. Giordano, L. Randaccio, and A. Ripamonti. J. Chem. Soc. Chem. Commun. 19 (1967).
3. F. Giordano, L. Randaccio, and A. Ripamonti. Acta Crystallogr. Sect. B, **25**, 1057 (1969).
4. P. Colamarino, P. L. Orioli, W. D. Benzinger, and H. D. Gillman. Inorg. Chem. **15**, 800 (1976).
5. R. Cini, P. Colamarino, P. L. Orioli, L. S. Smith, P. R. Newman, H. D. Gillman, and P. Nannelli. Inorg. Chem. **16**, 3223 (1977).
6. J. C. Scott, A. F. Garito, A. J. Heeger, P. Nannelli, and H. D. Gillman. Phys. Rev. Sect. B, **12**, 356 (1975).
7. T. S. Wei, J. C. Scott, A. F. Garito, A. J. Heeger, H. D. Gillman, and P. Nannelli. Phys. Rev. Sect. B, **12**, 5297 (1975).
8. G. M. Kosolapoff and R. M. Watson. J. Am. Chem. Soc. **73**, 5466 (1951).
9. R. M. Morrison and R. C. Thompson. Can. J. Chem. **56**, 985 (1978).
10. P. Coppens, L. Leiserowitz, and D. Rabinovich. Acta Crystallogr. **18**, 1035 (1965).
11. W. R. Busing and H. A. Levy. Acta Crystallogr. **22**, 457 (1967).
12. D. T. Cromer and J. B. Mann. Acta Crystallogr. Sect. A, **24**, 321 (1968).
13. R. F. Stewart, E. R. Davidson, and W. T. Simpson. J. Chem. Phys. **42**, 3175 (1965).
14. D. T. Cromer and D. Liberman. J. Chem. Phys. **53**, 1891 (1970).
15. V. Schomaker and K. N. Trueblood. Acta Crystallogr. Sect. B, **24**, 63 (1968).
16. D. W. J. Cruickshank. Acta Crystallogr. **9**, 747 (1956); **9**, 754 (1956); **14**, 896 (1961).
17. A. H. Cowley and W. D. White. Spectrochim. Acta, **22**, 1431 (1966).
18. R. A. Nyquist. J. Mol. Struct. **2**, 111 (1968).
19. E. A. Robinson. Can. J. Chem. **41**, 173 (1963).
20. J. R. Ferraro and A. Walker. J. Chem. Phys. **42**, 1273 (1965).
21. J. R. Ferraro and A. Walker. J. Chem. Phys. **42**, 1278 (1965).
22. H. D. Gillman. Inorg. Chem. **13**, 1921 (1974).
23. H. D. Gillman and J. L. Eichelberger. Inorg. Chem. **15**, 840 (1976).
24. M. Gerloch and R. C. Slade. Ligand-field parameters. The University Press, Cambridge. 1973.
25. B. N. Figgis. Introduction to ligand fields. Interscience, London. 1966.
26. S. L. Lambert, T. R. Felthouse, and D. N. Hendrickson. Inorg. Chim. Acta, **29**, L223 (1978).
27. M. Gerloch. J. Chem. Soc. Sect. A, 2023 (1968).

Can. J. Chem. Downloaded from www.nrcresearchpress.com by 210.87.254.42 on 09/06/12
For personal use only.

# A kinetic study of the interaction of hydrous aluminum oxide colloids with a well-characterized soil fulvic acid[1]

MARK K. S. MAK AND COOPER H. LANGFORD[2]

*Departments of Chemistry, Concordia University, 1455 de Maisonneuve Blvd., West, Montreal, P.Q., Canada H3G 1M8 and Carleton University, Ottawa, Ont., Canada K1S 5B6*

Received January 11, 1982

MARK K. S. MAK and COOPER H. LANGFORD. Can. J. Chem. **60**, 2023 (1982).

Models of the species arising from the interaction of hydrous aluminum oxide colloids with humic substances have been prepared by neutralizing Al(III) stock solutions in the presence of a well-characterized fulvic acid and aging for 24 h. These samples have been examined kinetically using the fluorimetric Al(III) reagent calcein blue. The rates of formation of Al(III) calcein blue complexes allows recognition of five kinetically distinguishable components in the mixtures. Some are similar in lability to simple organic chelates of Al(III). Others are much less labile. Evidence for non-labile colloidal "ternary" complexes of Al(III) ion species complexed to fulvic acid, and bound to hydrous aluminum oxide colloid is presented. The polydisperse mixture character of fulvic acid is seen in patterns of complex lability much as it is seen in patterns of complex stability.

MARK K. S. MAK et COOPER H. LANGFORD. Can. J. Chem. **60**, 2023 (1982).

On a préparé des modèles de l'espèce provenant de l'interaction de colloides d'oxyde d'aluminium hydraté avec des substances humiques en neutralisant des solutions de réserve de Al(III) en présence de l'acide fulvique bien caractérisé et vielli pendant 24 h. On a examiné cinétiquement ces échantillons en utilisant le réactif fluorimétrique de Al(III), le bleu de calcéine. Les vitesses de formation des complexes du bleu de calcéine de Al(III) permettent de reconnaître les cinq composantes du mélange que l'on peut distinguer cinétiquement. Certains de ces composants sont semblables, du point de vue labilité, aux chélates organiques du Al(III). D'autres sont beaucoup moins labiles. On présente la preuve de l'existence des complexes colloidaux "ternaires" de Al(III) non labiles complexés avec l'acide pulvique et liés à des colloides d'oxyde d'aluminium hyraté. On se rend compte du caractère polydipersif du mélange d'acide fulvique dans les processus de labilité des complexes beaucoup plus que dans les processus de stabilité des complexes.

[Traduite par le journal]

## Introduction

The hydrolytic precipitation of Al(III) is unquestionably influenced by the organic acids present in the soil solution and other natural waters (1). This may be important to phenomenon as diverse as aluminum toxicity in plants and fish kills in lakes undergoing acidification. Central among the relevant organic acids are the "soluble" natural soil organic acid mixtures called fulvic acids. (These are the humic substances not precipitated by neutralization of the NaOH extract from a soil.) An especially well-characterized fulvic acid sample is the one obtained by Schnitzer and colleagues at Agriculture Canada (2) from a poorly drained $B_h$ horizon Podsol near Charlottetown, P.E.I., Canada. This sample has been studied extensively and a variety of reports comment on its functional group content, molecular weight, degradation products, and titration functions. (Note especially that we speak of titration functions since the mixture is *not* correctly described by discrete equilibrium constants (3).) The properties are summarized in refs. 2 and 3. The purpose of the present paper is to explore interactions of this fulvic acid with hydrous aluminum oxide colloids. The point of view is kinetic.

Hydrolytic precipitation of Al(III) is a complex subject even without attention to organic ligands (4). Laboratory studies designed to inform studies of natural systems must be carried out at sufficiently *low* total Al(III) concentrations. Turbidity curves reported by Matijevic *et al.* (5, 6) show that a maximum occurs at $10^{-5}$ *M* Al(III). At low Al(III) concentrations, the sol stability was attributed to adsorption of polyhydroxo cations of Al(III). At higher concentration, anion adsorption is taken to stabilize the colloid. This determines a central aspect of our experimental approach. We use a fluorescent reagent, calcein blue, to determine aluminum accurately at concentrations below $10^{-6}$ *M*. We shall see that our studies reflect phenomena related to the turbidity maxima reported by Matijevic *et al.*

The kinetic method of analysis employed has been used successfully to study distinguishable components of colloidal mixtures of Fe(III) hydrous oxides and the corresponding fulvic acid – iron colloids (7, 8). The technique involves the addition of an excess concentration of the metal detection reagent and sufficient buffer to impose

[1]We thank the Natural Sciences and Engineering Research Council of Canada for support.

[2]To whom correspondence should be addressed at Concordia University.

0008-4042/82/152023-06$01.00/0

©1982 National Research Council of Canada/Conseil national de recherches du Canada

Can. J. Chem. Downloaded from www.nrcresearchpress.com by 210.87.254.40 on 09/06/12
For personal use only.

Can. J. Chem. Downloaded from www.nrcresearchpress.com by 210.87.254.40 on 09/06/12
For personal use only.

pseudo first order kinetics and to follow the *first order* grow-in of the detection complex, in this case the Al – calcein blue. The number of distinguishable components in the kinetics provides a means of identifying a distinguishable set of components of the colloids. It must be emphasized, however, that the kinetic components are not necessarily (at all!) structurally homogeneous chemical species.

The kinetic data are treated by the expression

$$[1] \quad P = A_0 [1 - \exp(-k_A t)] + B_0 [1 - \exp(-k_B t)] + \ldots + X$$

where $P$ is the product parameter (fluorescence intensity in this case), $A_0$, $B_0$ ... are appropriately scaled (to the same dimension) measures of the initial concentrations of the kinetically distinguishable components of the analytic mixture. The parameters $k_A$, $k_B$ ... are the pseudo first order rate constants. The term $X$ is a time-independent term including blank and any fast reacting components. A standard library nonlinear regression package based on the Marquardt algorithm is used (9, 10). However, we do exploit one unconventional technique. A limit on simple application of nonlinear regression is that one needs to know how many components it is reasonable to try to resolve from the data and one needs physically reasonable *initial* values of total concentrations and rate constants to put into the iterative process. One could assume a *continuum* of rate constants for the mixture called fulvic acid and examine the form of the distribution. Instead, we look for a *minimum* number of parameters needed to *accurately* fit the data. We recognize that the resulting parameters will most probably be averages over parts of the distribution. We have used Guggenheim plots (which should be linear for a single component) to identify the minimum number of resolvable components (the number of linearizable segments in the plots) and to supply initial approximations of parameters for the nonlinear regression. This approach has been evaluated elsewhere in a kinetic study of the complexation of Al(III) by citrate (11, 12).

## Experimental

*Materials*

Stock solutions of Al(III) in 0.1 *M* $HClO_4$ were prepared from $AlCl_3 \cdot 6H_2O$ (B.D.H. Reagent grade) twice recrystallized. The formula of the precipitate was verified gravimetrically by precipitation of Al(III) with 8-hydroxyquinoline. Solutions at various Al(III) concentrations were obtained by diluting a 0.2 *M* stock with $HClO_4$. Calcein blue was obtained from G.F. Smith Chemical Company and used as received. Fulvic acid was a gift of Dr. D.S. Gamble, Agriculture Canada, Ottawa (2). It is metal-free so that Al is the only metal in these experiments. The sample is assumed here to have a molecular weight of (wt. avg.) ~900 (2, 3). This value is subject to significant error and it should be noted that for many purposes it may be wise to convert results to a mg FA per mL basis in preference to molar. Molar units are used here because they allow clearer discussion of some chemically interesting matters. Sodium hydrogen carbonate was obtained from Nichols Chemical company and reagent grade sodium acetate from Fisher Scientific. Water was redistilled in an all glass apparatus from alkaline $KMnO_4$.

*Sample preparations*

Stock solutions of aluminum fulvates were initially prepared at pH = 3.00 from Al(III) stocks and *fresh* fulvic acid solutions. The Al/fulvate ratio and Al concentration ($2 \times 10^{-6} - 2 \times 10^{-5}$) were adjusted at this pH. Then solutions were slowly neutralized with $NaHCO_3$. The pH change was monitored with an Orion Research (701A) digital four place pH meter. After titration, the samples were adjusted to volume with small additions and allowed to "equilibrate" for 24 h. The final pH of the solutions after equilibration was rechecked and found to be within less than ±0.15 pH units of the initial (and nominal) levels.

*Kinetic analysis*

The fluorescence reagent, calcein blue, solution was prepared at pH = 5.00 in a 0.2 *M* acetic acid – sodium acetate buffer. Calcein blue was always chosen to be in excess over Al(III) by a factor of $10^2$. Since equal volumes of this solution and the equilibrated Al(III) sample were mixed, the ionic strength and pH are *determined* during the kinetic run by the components of this reagent. The conditions render component steps pseudo first order.

Kinetic runs were carried out manually on a Perkin-Elmer Model 204S spectrofluorimeter equipped with a strip chart recorder. Samples were contained in 1.00 cm square cross section cuvettes. Excitation was at 377 nm and emission from the Al–CB complex was monitored at 450 nm. Theoretical infinity time values were obtained by reacting Al(III) solutions prepared at pH = 3.00 with calcein blue. This is because recoveries of Al(III) were frequently below 100% and appropriate experimental infinities were not available — some Al(III) reacts extremely slowly if at all! A kinetic experiment was initiated by mixing the Al(III) sample from a syringe into the thermostatted (19.5°C) spectrofluorimeter cell containing an equal volume of reagent solution. Reactions were initially followed for periods up to 2 weeks. However, it was found that no significant changes could be analyzed beyond 24 h. (Perhaps some reaction is occurring on a longer time scale but the instability of the instrument does not permit acquisition of meaningful data. In any event, reaction in the period between 24 h and 2 weeks is not large.) Consequently, all reactions were followed for 24 h.

*Data treatment*

Records from the chart recorder were manually digitized and entered as a data file in the Carleton University computer system. First the data were analyzed and plotted according to the Guggenheim method (11, 12) (where no experimental infinity is required and each well-resolved component may be recognized by a linear segment in a plot). Figures 1 and 2 illustrate the results of this step for a first case where at least two kinetically distinguishable components are clearly recognizable and a second case where only one component is evident.

From slopes and intercepts of the Guggenheim plots preliminary estimates of the rate constants and initial concentrations of the kinetically distinguishable components were obtained. These values were used as *initial* estimates for the nonlinear regression library program which obtained best fit of the data to the model expressed by eq. [1] using the Marquardt algorithm (11, 12). No more than two components were considered

TABLE 1. Summary of kinetically distinguishable components

| Sample | $[Al]_{total}$ $\times 10^6$ $M$ | $[FA]_{total}$ $\times 10^5$ $M$ | pH of mixture | $[CB]_{total}$ $\times 10^4$ $M$ | $k_{(Al)}$ $M^{-1}$ $s^{-1}$ | $k_{(Al—FA(I))}$ $\times 10^2$ $s^{-1}$ (obs) | $k_{(Al—FA(II))}$ $\times 10^3$ $s^{-1}$ (obs) | $k_{(Al—FA(III))}$ $\times 10^4$ $s^{-1}$ (obs) | Equilibrium (24 h) recovery % | Total kinetic recovery % |
|---|---|---|---|---|---|---|---|---|---|---|
| a | 20.0 | Zero | 5.0 | 20.0 | $2.81 \times 10^2$ | — | — | — | 86.28 | 78.51 |
| b | 20.0 | 2.0 | 5.0 | 20.0 | — | 2.71 | 3.36 | — | 65.22 | 61.44 |
| c | 20.0 | 5.0 | 5.0 | 20.0 | — | 2.62 | 3.30 | — | 33.33 | 35.13 |
| d | 20.0 | 2.0 | 6.0 | 20.0 | — | 2.35 | 1.98 | — | 56.52 | 48.02 |
| e | 20.0 | 5.0 | 6.0 | 20.0 | — | 2.64 | 3.54 | — | 33.33 | 31.31 |
| f | 2.00 | Zero | 5.0 | 2.00 | $6.24 \times 10$ | — | — | — | 51.11 | 40.96 |
| g | 2.00 | 0.10 | 6.0 | 2.00 | — | 2.34 | 3.57 | — | 17.41 | 15.91 |
| h | 2.00 | 0.20 | 6.0 | 2.00 | — | 1.85 | 1.92 | — | 40.00 | 26.16 |
| i | 2.00 | 0.50 | 6.0 | 2.00 | — | 1.66 | 1.76 | — | 51.85 | 39.39 |
| j | 2.00 | 2.0 | 6.0 | 2.00 | — | 1.35 | 1.53 | — | 75.93 | 56.95 |
| k | 2.00 | 5.0 | 6.0 | 2.00 | — | — | — | 5.51 | 37.06 | 35.07 |
| l | 2.00 | 5.0 | 5.0 | 2.00 | — | — | — | 7.77 | 38.46 | 42.04 |
| m | 2.00 | 0.20 | 8.0 | 2.00 | — | 16.6 | 30.9 | — | 35.09 | 31.69 |
| n | 2.00 | 2.0 | 8.0 | 2.00 | — | — | — | 18.7 | 29.83 | 20.29 |

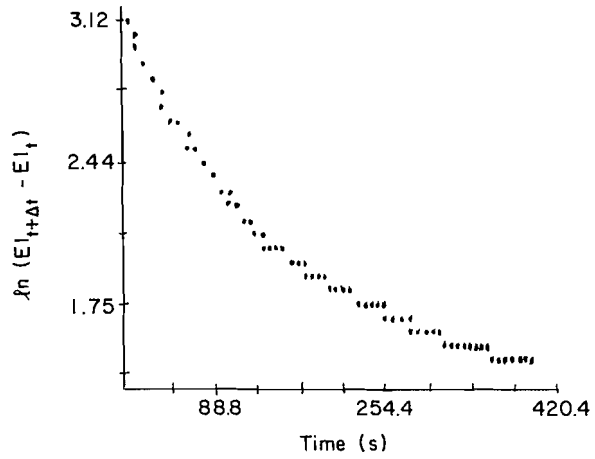


FIG. 1. Guggenheim plot of a typical 2-component system in an aluminum/fulvic acid mixture. System under observation is: $\{2 \times 10^{-5}$ $M$ $[Al^{3+}]/2 \times 10^{-5}$ $M$ [FA]$\}$ mixture at pH = 6.0 + $2 \times 10^{-3}$ $M$ [CB]; in 0.1 $M$ acetate buffer at pH = 5.0. EI designates emission intensity.

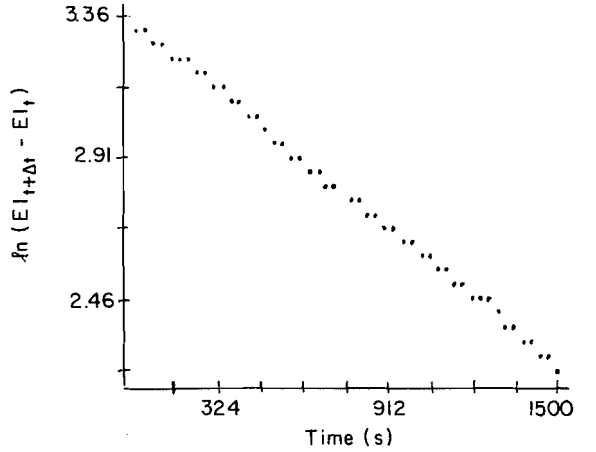


FIG. 2. Guggenheim plot of a typical 1-component system in an aluminum/fulvic acid mixture. System under observation is: $\{2 \times 10^{-6}$ $M$ $[Al^{3+}]/5 \times 10^{-5}$ $M$ [FA]$\}$ mixture at pH = 5.0 + $2 \times 10^{-4}$ $M$ [CB]; in 0.1 $M$ acetate buffer at pH = 5.0. EI designates emission intensity.

because the data for cases like those shown in Fig. 1 were fit within experimental error by two components. The addition of more would not be subject to objective test. Nevertheless, since FA is a mixture, the parameters are probably averages over a relatively narrow segment of the distribution.

## Results

All values reported in the results section are averages of at least five runs. Standard deviation on rate constants is less than 10%. The sums of component concentrations are reproducible to less than 5% of the total. A grand summary of kinetically distinguishable components characterized by their rate constants is shown in Table 1. No single run had more than two objectively demonstrable components but "kinetic" aluminum recovery was generally less than "equilibrium" recovery. That is, the sum of parameters $A_0$ and $B_0$ extracted from the good nonlinear regression fits of data to eq. [1] using components recognizable from Guggenheim plots did not account for all of the Al(III) found from the emission after 24 h. It seems quite plausible and almost necessary to postulate an additional slowly reacting component which is not represented by rate constants in Table 1. This was confirmed by examination of fluorescence after 2 h to that after 24 h. Note that the half-times associated with recognizable components vary from about 5 s to a little over 20 min. The slowest of these is "complete" in less than 2.5 h. The postulated relatively small additional slower component need not react too slowly.

On the basis of three distinguishable relatively

Can. J. Chem. Downloaded from www.nrcresearchpress.com by 210.87.254.40 on 09/06/12
For personal use only.

TABLE 2. Distribution of Al(III)

| Sample | Equilibrium | | Kinetic | | |
|---|---|---|---|---|---|
| | Unrecoverable nonlabile Al—FA(A) % | Recoverable kinetically very slow Al—FA(B) % | Recoverable Al—FA(I) % | Recoverable Al—FA(II) % | Recoverable Al—FA(III) % |
| b | 34.78 | 3.780 | 29.50 | 31.94 | |
| c | 66.67 | (−1.800) | 14.46 | 20.67 | |
| d | 43.48 | 8.500 | 18.21 | 29.81 | |
| e | 66.67 | 2.020 | 12.70 | 18.61 | |
| g | 82.59 | 1.500 | 10.67 | 5.240 | |
| h | 60.00 | 13.84 | 12.51 | 13.65 | |
| i | 48.15 | 12.46 | 16.80 | 22.59 | |
| j | 24.07 | 18.98 | 16.10 | 40.85 | |
| k | 62.94 | 1.990 | — | — | 35.07 |
| l | 61.54 | (−3.580) | — | — | 42.04 |
| m | 64.91 | 3.400 | 11.79 | 19.90 | |
| n | 70.17 | 9.540 | — | — | 20.29 |

labile forms of Al(III) fulvates plus a slow but reactive component and with the addition of an entirely unreactive and unrecoverable fraction of Al(III), we can summarize Al(III) distribution in five classes. Parameters for these classes, it should be emphasized, are probably averages. The shares to each of the five classes are summarized in Table 2. The coding of samples in Table 2 follows Table 1. The patterns indicated by Tables 1 and 2 are very complex. The individual entries in Table 2 corresponding to fractions smaller than 20% also must be recognized as being associated with quite large uncertainties. It is worth remarking the non-recoverable fractions are large in all cases. These fractions could not be rendered accessible to the calcein blue reagent by boiling with added $HClO_4$. Precipitated hydrous oxides of aluminum are very difficult to redissolve.

## Discussion

We can begin by commenting on samples (a) and (f) of Table 1. These samples, our controls, contained *only* Al(III) and no fulvic acid at pH = 5.00. The second order rate constants obtained are to be compared to values of $2.5 \times 10^2 M^{-1}\ s^{-1}$ reported for unhydrolyzed (pH = 3) Al(III) samples mixed with the present reagent (11, 12). That these values are significantly smaller for the lower Al(III) concentration here suggests that this sample is more extensively hydrolyzed. Such a result, though a bit surprising, is in agreement with the equilibrium recoveries where more Al(III) has disappeared into non-reactive hydrous oxide precipitate at the lower concentration. It is also in agreement with the turbidity maximum result of Matijevic *et al.* It may be appropriate to cautiously suggest an implication. Perhaps labile Al(III) in these studies has some relation to biochemically available metal. If so, availability will be a complex, non-monotonic, function of concentration and pH.

Turning to the aluminum fulvates, two initial comments are important. First, the range studied spans 0.9–45 mg/L, a range appropriate to modeling DOC of natural fresh waters. Second, a $6.67 \times 10^{-6} M$ fulvic acid solution has, according to Gamble and Schnitzer (2), about $2 \times 10^{-5}$ equiv. /L of phenol carboxylate sites and at least $3.3 \times 10^{-5}$ equiv./L of total bidentate chelating sites providing a 1:1 binding capacity for at least $2 \times 10^{-5} M$ Al(III). All experiments use excess fulvic acid as is appropriate to a majority of waters.

Turning next to rate constants associated with objectively distinguishable fractions of the FA mixture, one sees two well-defined sets in the pH range 5–6. These are designated Al—FA(I) with an average $k$ of $2.2 \pm 0.5 \times 10^{-2}\ s^{-1}$ and Al—FA(II) with an average $k$ of $2.6 \pm 0.9 \times 10^{-3}\ s^{-1}$. These values are probably representative of the distribution of components of the fulvic acid mixture which behave most nearly like simple complexes of Al(III). (It is important to remember here that the thrust of a number of recent studies has been to underline the mixture character of fulvic acid and to demonstrate that its complexing behaviour cannot be modeled by a single small molecule ligand (3, 13).)

Given the functional groups identified on fulvic acid samples (2), chelating sites analogous to salicylate (phenol carboxylate) and phthalate (aromatic dicarboxylate) are very probably present in the fulvic acid sample. Secco and Venturini (14) have reported a dissociation rate constant of $7.9 \times$

Can. J. Chem. Downloaded from www.nrcresearchpress.com by 210.87.254.40 on 09/06/12
For personal use only.

Can. J. Chem. Downloaded from www.nrcresearchpress.com by 210.87.254.40 on 09/06/12
For personal use only.

$10^{-3}$ $s^{-1}$ for aluminum salicylate at 25°C (higher than our $T = 19.5$°C). This value is actually similar to that we determined for dissociation of aluminum citrate, namely $4.8 \times 10^{-3}$ $s^{-1}$ (11, 12). It is reasonable to associate Al—FA(II) with reasonably strong simple chelating sites such as salicylate or carbohydrate-derived types in the fulvic acid mixture. Dissociation of the chelate is rate determining as was the case in the aluminum citrate study.

The phthalate-like sites on fulvic acid might be expected to be more labile. If formation rate constants for Al(III) complexes are similar for salicylate, oxalate, and phthalate, as is common for the largely dissociative substitution mechanism, the order of stability constants (15) suggests that dissociation rates would decrease in the order phthalates > oxalates > salicylates. However, we cannot overlook the probability that an increase of a factor of 10 in rate constant to about $2.2 \times 10^{-2}$ $s^{-1}$ merely reflects similar chelating groups to those of Al—FA(II) but with neighboring electron-withdrawing groups. Nevertheless, it may be useful to think of Al—FA(I) sites as analogous to simple phthalate chelates of aluminum.

It might be noted here that a comparison with an ion of similar lability to Al(III), namely $Fe(OH_2)_6^{3+}$, and the same fulvic acid in acid media where only one single kinetic component was observed supports the above ideas. The acid dissociation rate constant of Fe(III)—FA was found to be $7 \times 10^{-3}$ $s^{-1}$ at 25°C (16). This is intermediate between the two Al(III) values.

The above analysis is not contradicted by the observation of less labile Al(III) in the cases (k and l) where the FA/Al(III) ratio is largest. The binding constants of metals to fulvic acid mixtures decrease with increasing coverage of sites by the metal (3, 13). At low coverage some especially strong binding sites are resolved. We assign the quantities labelled Al—FA(III) to these sites. The distribution of labilities of sites is similar to that described recently for copper fulvates by Shuman (17). Shuman's work reveals copper fulvates of very widely varying lability. If the slow reacting component which is not represented by rate constants in Table 1 but is represented by the difference between "kinetic" and "equilibrium" (24 hr) recovery in Table 2 is considered, the distribution of labilities of aluminum fulvate sites probably covers as many orders of magnitude as copper fulvate sites.

The complicated pattern of distribution of amounts of material associated with the various lability categories as summarized in Table 2 must now be considered. In most cases, a substantial fraction of the total Al(III) is not recoverable. This is true in the absence of fulvic acid and is attributed to precipitation of hydrous aluminum oxides. Samples a and f already show that the quantity of non-labile Al(III) is a complex function of concentration and pH. This can be understood only in conjunction with the results on a turbidity maximum at Al(III) = $1 \times 10^{-5}$ $M$ already discussed (5, 6).

The presence of fulvic acid introduces additional complexity. Recently, in the context of a study of adsorption on alumina, Bourg (18) has obtained unequivocal evidence for ternary surfaces complexes involving: (*i*) groups from the alumina surface, (*ii*) humic substances, and (*iii*) metal ions from the solution. In the present case, Al(III) can play both the first and third role with the fulvic acid in the second. Such ternary complexes are most probably responsible for the elaborate pattern of variation in the distribution of Al(III) between kinetically recoverable and non-recoverable form found in Table 2. Compare the pairs b, c; d, e; j, k; and even m, n in Table 2. In each of these cases, we see an increase of fulvic acid leading to an increase of unrecoverable Al(III). The simplest explanation is ternary complexes with the hydrous oxide although formation of complexes at the least labile sites may also be significant.

## Conclusions

The distribution of labilities found for aluminum fulvates is qualitatively similar to that found with copper fulvates, and less spectacularly, for iron fulvates. They reinforce the mixture model of fulvic acid and emphasize the variety of sites involved in metal binding. If, as has long been suspected, labilities have a determining influence on bioavailability of Al(III), the complexities hydrous oxide precipitation presents to interpretation are not reduced but instead increased by complexation in binary and ternary forms involving humic organic matter.

1. K. F. Ng Kee Kwong and P. M. Huang. Soil Sci. **128**, 337 (1979).
2. D. S. Gamble and M. Schnitzer. *In* Trace organic and metal organic interactions in natural waters. *Edited by* P. Singer. Ann Arbor Science, Ann Arbor, MI. 1974, Chapt. 9.
3. C. H. Langford, D. S. Gamble, A. W. Underdown, and S. Lee. Terrestrial and aquatic humic substances. *Edited by* E. Gjessing and R. F. Christman. Ann Arbor Science, Ann Arbor, MI. 1982. In press.
4. C. F. Baes, Jr. and R. C. Mesmer. The hydrolysis of cations. John Wiley and Sons, New York. 1976. Chapt. 6.
5. E. Matijevic, K. G. Mathai, R. H. O. Hewill, and M. Kerker. J. Phys. Chem. **65**, 826 (1961).
6. E. Matijevic, E. F. Jananer, and M. Kerker. J. Colloid Sci. **19**, 333 (1964).

7. C. H. LANGFORD, G. W. QUANCE, R. KAY, and T. R. KHAN. Anal. Lett. **10**, 1249 (1977).
8. C. H. LANGFORD, S. M. WONG, and A. W. UNDERDOWN. Can. J. Chem. **59**, 181 (1981).
9. D. W. MARQUARDT. Chem. Eng. Prog. **55**, 66 (1959).
10. A guide to the program "NONLINEAR". Carleton University Computing Services, Careleton University, Ottawa. 1976.
11. M. K. S. MAK. Ph.D. Thesis, Carleton University, Ottawa, Ont. 1980.
12. M. K. S. MAK and C. H. LANGFORD. To be published.
13. R. A. SAAR and J. H. WEBER. Can. J. Chem. **57**, 1263 (1979).
14. F. SECCO and M. VENTURINI. Inorg. Chem. **14**, 1978 (1975).
15. L. G. SILLEIN and A. E. MARTELL. Stability constants of metal–ion complexes. The Chemical Society Special Publication #17, The Chemical Society, London. 1964.
16. C. H. LANGFORD and T. R. KHAN. Can. J. Chem. **53**, 2979 (1975).
17. M. S. SHUMAN. *In* Terrestrial and aquatic humic substances. *Edited by* E. Gjessing and R. F. Christman. Ann Arbor Science, Ann Arbor, MI. 1982. In press.
18. A. BOURG. Proc. International Conf. Heavy Metals in the Environment, Amsterdam. 1981.

Can. J. Chem. Downloaded from www.nrcresearchpress.com by 210.87.254.40 on 09/06/12
For personal use only.

# Metal carbonyl complexes of some aromatic *ortho* bis(methylthio)ethers

MICHAEL E. PEACH[1] AND CHRISTIAN BURSCHKA

*Institut für Anorganische Chemie der Universität Würzburg, Am Hubland, 8700 Würzburg, West Germany*

Received January 7, 1982

MICHAEL E. PEACH and CHRISTIAN BURSCHKA. Can. J. Chem. **60**, 2029 (1982).

Various complexes of the type $M(CO)_4L$ and $[M(CO)_4]_2L$, M = Cr, Mo, W, have been prepared and characterized. A series of aromatic *ortho* bis(methylthio)ethers were used as the ligand L. The crystal structures of the free ligand $C_6(SCH_3)_6$ and of the complex $Cr(CO)_4C_6(SCH_3)_6$ are reported.

MICHAEL E. PEACH et CHRISTIAN BURSCHKA. Can. J. Chem. **60**, 2029 (1982).

On a préparé divers complexes du type $M(CO)_4L$ et $[M(CO)_4]_2L$, où M = Cr, Mo, W, et on les a identifiés. On a utilisé une série d'*ortho* bis (méthylthio) éthers aromatiques comme ligand L. On rapporte la structure cristalline du ligand libre $C_6(SCH_3)_6$ et celle du complexe $Cr(CO)_4C_6(SCH_3)_6$.

[Traduit par le journal]

Can. J. Chem. Downloaded from www.nrcresearchpress.com by 210.87.254.105 on 09/06/12
For personal use only.

The ligating properties of several chelating sulfur ligands, particularly with various metal carbonyls and the platinum group metals, are the subject of continuing study (1–13). It has been shown that aromatic *ortho* bisthioethers form complexes with a number of metal ions (1). All of the complexes with simple metal ions were polymeric and could not be purified by recrystallization.

Various chromium, molybdenum, and tungsten carbonyl complexes can be formed by potentially chelating sulfur ligands. The aliphatic bisthioethers, $RS(CH_2)_xSR(L)$, give the complexes $M(CO)_5L$, $[M(CO)_5]_2L$, and $M(CO)_4L$ (2–6). However, the latter complex, $M(CO)_4L$, is only obtained when $x = 2$, and the complex contains a five-membered ring. Similar complexes have been prepared with some *ortho* bisthioethers (L1, L3, L9, L10) (1, 7, 8) and tetrakis(alkylthio)ethenes (9). The tetrakis(alkylthio)ethenes could form two five-membered chelate rings in complexes such as $[M(CO)_4]_2L$, although these were not reported (9). The crystal structure of $W(CO)_4L$, L = *o*-$(MeS)_2C_6H_4$, has been noted (7).

Molybdenum and tungsten hexacarbonyls react with the macrocyclic ligand 2,6,15,19-tetrathia-[7.7]paracyclophane (TTPH) to form the complexes $TTPH[M(CO)_4]_2.2C_6H_6$ (M = Mo, W) and $TTPH[W(CO)_5]_2$ (10). The former two involve the coordination of the $M(CO)_4$ unit to two sulfur atoms and the formation of a six-membered ring, basically $M(CO)_4RS(CH_2)_3SR'$. However, with chromium hexacarbonyl several products are formed, the main one being the $\pi$ complex ($\eta^6$TTPH) chromium tricarbonyl (11). Other products characterized include elimination of the 1,3-propanedithia unit, and coordination of $Cr(CO)_4$ or $Cr(CO)_5$ units to sulfur atoms.

A further series of potential sulfur containing ligands of formula $C_6(SMe)_xH_{6-x}$ has been prepared (14). This paper is an extension of previous studies of the ligand properties of aromatic *ortho* bis(methylthio)ethers (1), with particular reference to the chromium, molybdenum, and tungsten carbonyl complexes. The ligands studied (L1, L2, L3, L4, L5, L6, L7, and L8) are shown below.

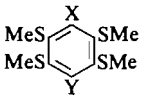

L1, X = Y = SMe
L2, X = SMe, Y = H
L3, X = Y = F
L4, X = Y = Cl
L5, X = Y = H

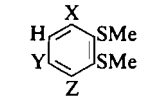

L6, X = Z = SMe, Y = H
L7, X = Y = SMe, Z = H
L8, Y = Z = H, Y = SMe
L9, X = Z = F, Y = SMe
L10, X = Z = F, Y = H

Various carbonyl complexes can be postulated, depending on the specific ligand. All the ligands should form the simple complexes $M(CO)_4L$ (1),

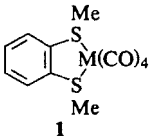

1

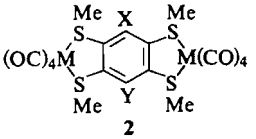

2

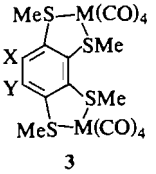

3

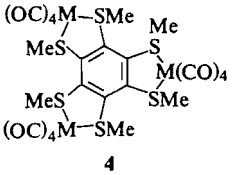

4

whereas the ligands L1, L2, L3, L4, L5, and L6 have two potentially chelating functions and the

[1]On leave from Acadia University, Wolfville, N.S., Canada B0P 1X0 and to whom correspondence should be addressed at Acadia University.

0008-4042/82/152029-09$01.00/0

©1982 National Research Council of Canada/Conseil national de recherches du Canada

TABLE 1. Products and analyses

| Product | Color | Decomp. temp. (°C) | Method | Ratio M:L | Solvent† | Time | Yield‡ (%) | Found (%) C | Found (%) H | Calcd. (%) C | Calcd. (%) H |
|---|---|---|---|---|---|---|---|---|---|---|---|
| $Cr(CO)_4L$ | Yellow | 113 | A | 2:1 | tol | 20d | 32 | 37.2 | 3.37 | 37.1 | 3.50 |
| $Mo(CO)_4L$ | Green–yellow | 95 | A | 1:1 | tol | 16h | 77 | 34.6 | 3.06 | 34.2 | 3.22 |
| | | | | 2:1 | hex | 2d | 56 | | | | |
| $W(CO)_4L1$ | Lemon | 110–111* | B | 1.2:1 | THF | 12m | 4 | 30.2 | 3.00 | 29.5 | 2.79 |
| | | | C | 1.2:1 | THF | 1.5h | 25 | | | | |
| | | | C | 1:1 | $CH_2Cl_2$ | 5h | 11 | | | | |
| $[Cr(CO)_4]_2L1$ | Orange | 170 | D | 2:1 | EtOH,P | 18h | 62 | 33.6 | 2.92 | 35.2 | 2.64 |
| $[Mo(CO)_4]_2L1$ | Yellow | 155 | A | 2:1 | tol | 2d | 80 | 31.0 | 2.83 | 31.2 | 2.35 |
| $[W(CO)_4]_2L1$ | Yellow–brown | 130 | C | 3:1 | THF | 2h | 9 | 26.3 | 2.11 | 25.4 | 1.92 |
| $Cr(CO)_4L2$ | Yellow | 135 | A | 1:1 | tol | 6d | 33 | 38.0 | 3.56 | 38.1 | 3.41 |
| | | | B | 2:1 | THF | 45m | 54 | | | | |
| | | | D | 2:1 | EtOH,P | 21h | 83 | | | | |
| $Mo(CO)_4L2$ | Green–yellow | 125 | A | 2:1 | hex,P | 2d | 31 | 34.8 | 2.79 | 34.9 | 3.12 |
| | | | A | 2:1 | tol,P | 1d | 23 | | | | |
| $W(CO)_4L2$ | Yellow–brown | 130 | C | 1:1 | THF | 1h | 24 | 29.4 | 3.46 | 29.8 | 2.67 |
| $Mo(CO)_4L3$ | Light brown | 66–68* | A | 1:1 | tol | 1d | 70 | 33.4 | 2.41 | 33.1 | 2.39 |
| $[Cr(CO)_4]_2L3$ | Orange | 115 | D | 2:1 | EtOH | 2d | 25 | 34.4 | 2.17 | 34.5 | 1.93 |
| $[Mo(CO)_4]_2L3$ | Yellow–brown | 120 | A | 4:1 | $CH_2Cl_2$ | 10d | 77 | 30.1 | 1.94 | 30.3 | 1.69 |
| $Cr(CO)_4L4$ | Yellow | 135 | A | 1:1 | tol | 5d | 50 | 33.5 | 3.40 | 33.9 | 2.44 |
| $Cr(CO)_4L5$ | Yellow | 145 | A | 2:1 | tol | 5d | 38 | 39.7 | 3.47 | 39.4 | 3.31 |
| | | | D | 2:1 | EtOH,P | 22h | 84 | | | | |
| $Mo(CO)_4L5$ | Pale green | 70 | A | 1:1 | tol,P | 2d | 43 | 35.4 | 2.94 | 35.7 | 3.00 |
| $W(CO)_4L5$ | Lemon | 135 | C | 1:1 | THF | 1h | 10 | 30.4 | 3.19 | 30.1 | 2.53 |
| $Cr(CO)_4L6$ | Yellow | 130 | A | 1:1 | tol | 4d | 23 | 39.6 | 3.38 | 39.4 | 3.31 |
| | | | D | 2:1 | EtOH,P | 1d | 30 | | | | |
| $Mo(CO)_4L6$ | Yellow–brown | 125 | A | 1:1 | tol | 5h | 53 | 35.3 | 3.19 | 35.7 | 3.00 |
| $W(CO)_4L6$ | Lemon | 130 | C | 1.2:1 | THF | 2h | 37 | 30.3 | 2.80 | 30.1 | 2.53 |
| $Cr(CO)_4L7$ | Orange | 122–124* | A | 1:1 | tol | 2d | 43 | 39.5 | 3.30 | 39.4 | 3.31 |
| $Mo(CO)_4L7$ | Brown–yellow | 128 | A | 1:1 | tol | 20h | 75 | 36.6 | 3.15 | 35.7 | 3.00 |
| $W(CO)_4L7$ | Yellow | 120 | C | 1.2:1 | THF | 2h | 49 | 30.7 | 2.61 | 30.1 | 2.53 |
| $Cr(CO)_4L8$ | Orange–yellow | 75–77* | A | 1:1 | tol | 5d | 55 | 41.0 | 3.30 | 41.0 | 3.18 |

*Melting point.
†tol = toluene, hex = *n*-hexane, P = precipitate formed.
‡Based on amount of ligand taken.

complexes $[M(CO)_4]_2L$, structure **2** or **3**, can be postulated. Similarly, it might be possible to prepare the complexes $[M(CO)_4]_3L$ (**4**) from L1.

The complexes $M(CO)_4L$ were readily prepared. Several attempts, mostly unsuccessful, were made to prepare the complexes $[M(CO)_4]_2L$ using an excess of the carbonyl reactant. Although analogous complexes with one polyfunctional sulfur ligand bonded to two metals are not known, some similar complexes with two metals and two ligands have been prepared, such as $Rh_2Cl_2(\mu\text{-CO})(PhSCH_2SPh)_2$ (13) and the group V ligand complexes, $(OC)_4M(EMe_2{-}{-}EMe_2)_2M(CO)_4$, M = Cr, W, Mo; E = P, As, with six-membered rings (15).

The complexes were obtained from *cis* metal tetracarbonyls, $M(CO)_4X_2$, specifically norbornadiene chromium and molybdenum tetracarbonyls and bis(acetonitrile)tungsten tetracarbonyl and the desired ligand in hexane, toluene, or THF solution (tungsten complexes). Some complexes were also prepared by irradiation of chromium hexacarbonyl to form $Cr(CO)_5$.THF, which then reacted with the ligand or from $Et_4N[Cr(CO)_5Cl]$ in ethanol. The yields were very low when tungsten hexacarbonyl was irradiated. The tungsten complexes could not be prepared from *cis*-bis(piperidine)molybdenum tetracarbonyl (16) as the free piperidine generated in the reaction reacted with the sulfur-containing ligand, presumably nucleophilically displacing a methylthio group.

The complexes isolated were mainly of the type $M(CO)_4L$, see Table 1, and did not usually depend on the reactant stoichiometry. Although the chromium complex $Cr(CO)_4L$ was readily prepared the complex $[Cr(CO)_4]_2L$ was not obtained from an excess of $C_7H_8Cr(CO)_4$ or $Cr(CO)_5$THF with L. The complexes $[Cr(CO)_4]_2L$ (L = L1, L3) were precipitated from ethanol solutions of $Et_4N[Cr(CO)_5Cl]$ and L, in stoichiometry 2:1; under the same conditions with L2, L5, and L6 the complex $Cr(CO)_4L$ precipitated. Even with reactant stoichiometry 3:1 $W(CO)_4(MeCN)_2$:L in THF solution

Can. J. Chem. Downloaded from www.nrcresearchpress.com by 210.87.254.105 on 09/06/12
For personal use only.

Can. J. Chem. Downloaded from www.nrcresearchpress.com by 210.87.254.105 on 09/06/12
For personal use only.

it was generally only possible to isolate or detect in solution the complexes $[W(CO)_4L]$. However, depending on the stoichiometry, the complexes $W(CO)_4C_6(SMe)_6$ and $[W(CO)_4]_2C_6(SMe)_6$ could be prepared. The reactions of $C_7H_8Mo(CO)_4$ with the various ligands were usually studied in toluene solution where precipitation of $Mo(CO)_4L$ sometimes occurred. The reactions with molar ratios $C_7H_8Mo(CO)_4$:L, 2:1, were studied in either toluene or methylene chloride, depending on the solubility of $Mo(CO)_4L$. The nmr spectra of the initial products indicated that although small amounts of $[Mo(CO)_4]_2L$ may have been formed in several reactions, it was only possible to isolate this product when L = L1 or L3. The molybdenum complexes were often formed with incorporation of some solvent in the crystal lattice. This was detected in the nmr spectra and thermal analysis showed a loss of weight (less than 5%) accompanied by an endothermic change before decomposition. Incorporation of solvent benzene in some molybdenum complexes $Mo(CO)_4L$ with sulfur-containing ligands has been noted previously (10).

The formation of the complexes $Cr(CO)_4L$ clearly depends on the bulk of the methyl group. When $p$-$F_2C_6(SBu^t)_4$ was used as a potential ligand no reaction occurred in four days at 45°C with $C_7H_8Cr(CO)_4$, although $C_7H_8Cr(CO)_4$ reacted within 2 days with other ligands containing the methyl group at 45°C. It can be inferred that the large tertiary butyl group blocks the coordination of the metal to the sulfur.

The number of *ortho* methylthio groups in a ligand also determines the ease of the reaction. In a reaction of 1 mmol of $C_7H_8Cr(CO)_4$ with 1 mmol of each of L1 and L5 in toluene at 45°C, the $C_7H_8Cr(CO)_4$ had all reacted within one day. The nmr spectrum of the product, after removal of the solvent, showed that approximately 75% of L1 had formed the complex $Cr(CO)_4L1$. The ligand L1 with six possible *ortho* bis(methylthio) sites for coordination clearly forms the complex $Cr(CO)_4L$ more readily than L5 which has only two *ortho* bis(methylthio) sites.

The structures of the products in solution were determined from their infrared and nmr (H-1) spectra. The spectroscopic data cannot, however, distinguish between the simple monomeric complex, $M(CO)_4L$, and a dimer, such as **5**. However, as the solutions used in the preparations were relatively concentrated ($0.05\,M \sim 0.02\,M$), the possibility of the formation of **5** can be excluded. The crystal structure of $Cr(CO)_4L1$ shows that it is monomeric in the solid state.

The carbonyl vibrations, tabulated in Table 2,

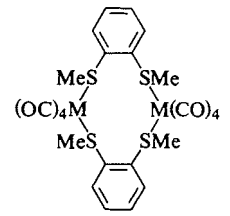


**5**

are all consistent with the established values for *cis*-tetracarbonyl complexes, *cis*-$M(CO)_4X_2$ (1, 9). The proton nmr spectra were normally recorded in benzene or methylene chloride solutions (see Table 2). The complexes decomposed readily in solvents such as deuterochloroform in which they are readily soluble. The structure **1** is clearly indicated for the complexes $M(CO)_4L1$ as three distinct methyl groups are observed in the proton nmr spectra with intensity ratio 1:1:1. Similarly, with the ligands L3, L4, L5, L7, and L8 where only one isomeric product is possible, the structure **1** is clearly indicated by the nmr spectra. The possibility of a $\pi$ complex, as occurs in bis(methylthio-$\eta$-benzene) chromium (18) and the $\eta^6$ arene compound $Cr(CO)_3C_6H_5$—$SC_6H_5$ (19) can be excluded.

Comparison of the nmr spectra of the complexes and the free ligand in $CH_2Cl_2$ or $CDCl_3$ solution shows that the protons of the methyl group bonded to the ligand sulfur in the complexes $M(CO)_4L$ are deshielded by approximately 0.30 ppm (Cr), 0.38 ppm (Mo), and 0.57 ppm (W) and that there is somewhat greater deshielding in the complexes $[M(CO)_4]_2L$. Similar deshielding has been observed in the complexes $M(CO)_5SRR^1$ (M = Cr, Mo, W), with the magnitude of the deshielding Cr < Mo < W (19, 20). The chemical shifts of the other methyl protons are relatively unchanged in comparison with the free ligand. This deshielding effect is not as clearly observed in benzene solution, with respect to the free ligand, but the magnitude of the deshielding is still Cr < Mo < W.

With the ligands L2 and L6, two isomeric products $M(CO)_4L$ can be postulated, **6** and **7**.

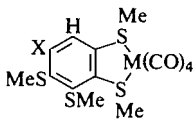


**6**

L2, X = SMe
L6, X = H

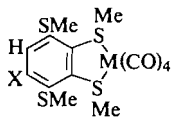


**7**

The nmr spectra of both the $M(CO)_4L$ (L = L2, L6) complexes indicate that only one isomeric product is formed. The structure **7** is clearly shown in the spectrum of the L6 complexes as only two methyl proton signals are observed. Similarly, it can be postulated from the observed spectrum of L2 and

TABLE 2. CO absorptions and summary of nmr data

| Compound | CO absorptions ($cm^{-1}$)* | H nmr chemical shifts (ppm) and intensity ratios† |
|---|---|---|
| L1 | | 2.49s |
| $Cr(CO)_4L1$ | 2014s, 1912sh, 1902vs, 1881s | 2.76s, 2.54s, 2.52s(1:1:1) |
| $Mo(CO)_4L1$ | 2021s, 1915sh, 1910vs, 1886s | 2.83s, 2.53s, 2.51s(1:1:1) |
| $W(CO)_4L1$ | 2018s, 1905sh, 1901vs, 1882($C_6H_6$) | 2.99s, 2.55s, 2.54s(1:1:1) |
| $[Cr(CO)_4]_2L1$ | 2015s, 1915sh, 1908vs, 1878($CH_2Cl_2$) | 2.90s, 2.65s(2:1) |
| $[Mo(CO)_4]_2L1$ | 2024s, 1923vs, 1920s, 1881s($CH_2Cl_2$) | 2.92s, 2.61s(2:1) |
| $[W(CO)_4]_2L1$ | 2016s, 1912sh, 1905vs, 1883s(THF) | 3.16s, 2.65s(2:1) |
| L2 | | 2.49s, 2.45s, 2.37s, 6.41s(3:6:6:1) |
| $Cr(CO)_4L2$ | 2015s, 1915sh, 1902vs, 1880s | 2.79s, 2.64s, 2.57s, 2.49s, 2.40s, 6.90s(3:3:3:3:3:1) |
| $Mo(CO)_4L2$ | 2022s, 1914sh, 1911vs, 1884s | 2.85s, 2.74s, 2.57s, 2.48s, 2.40s, 6.91s(3:3:3:3:3:1) |
| $W(CO)_4L2$ | 2018s, 1910sh, 1901vs, 1877s($C_6H_6$) | 3.01s, 2.90s, 2.55s, 2.46s, 2.37s, 6.84s(3:3:3:3:3:1) |
| L3 | | 2.45T($J$(H—F) 1.0Hz)‡ |
| $Cr(CO)_4L3$ | 2020s, 1925s, 1910s, 1890s(ref. 1) | 2.77s, 2.59T($J$(H—F)0.55Hz) (ref. 1) (1:1) |
| $Mo(CO)_4L3$ | 2028s, 1920sh, 1916vs, 1891s | 2.81s, 2.55T($J$(H—F)1.1Hz) (1:1)‡ |
| $W(CO)_4L3$ | 2018s, 1925m, 1907m, 1901m(ref. 1) | 2.98s, 2.54T($J$(H—F)1.3Hz) (ref. 1) (1:1) |
| $[Cr(CO)_4]_2L3$ | 2022s, 1922sh, 1918vs, 1886s($CH_2Cl_2$) | 2.81s |
| $[Mo(CO)_4]_2L3$ | 2026s, 1926vs, 1920sh, 1887s($CH_2Cl_2$) | 2.87s |
| L4 | | 2.47s |
| $Cr(CO)_4L4$ | 2018s, 1920sh, 1902vs, 1888s | 2.74s, 2.50s(1:1) |
| L5 | | 2.46s, 7.05s(6:1) |
| $Cr(CO)_4L5$ | 2016s, 1915sh, 1903vs, 1879s | 2.72s, 2.54s, 7.42s(3:3:1) |
| $Mo(CO)_4L5$ | 2024s, 1916sh, 1913vs, 1884s | 2.77s, 2.51s, 7.42s(3:3:1) |
| $W(CO)_4L5$ | 2018s, 1903sh, 1899vs, 1876s(THF) | 2.94s, 2.52s, 7.45s(3:3:1) |
| L6 | | 2.39s, 7.05s(6:1) |
| $Cr(CO)_4L6$ | 2012s, 1913sh, 1904vs, 1880s | 2.71s, 2.55s, 7.25s(3:3:1) |
| $Mo(CO)_4L6$ | 2022s, 1915sh, 1911vs, 1883s | 2.75s, 2.51s, 7.23s(3:3:1) |
| $W(CO)_4L6$ | 2017s, 1908sh, 1901vs, 1879s($C_6H_6$) | 2.95s, 2.54s, 7.27s(3:3:1) |
| L7 | | 2.47s, 2.39s, 2.24s, 6.67s(3:6:3:2) |
| $Cr(CO)_4L7$ | 2017s, 1907sh, 1904vs, 1879s | 2.72s, 2.60s, 2.25s, 7.25d, 6.95d(3:3:6:1:1)§ |
| $Mo(CO)_4L7$ | 2024s, 1920sh, 1910vs, 1883s | 2.83s, 2.70s, 2.55s, 7.26d, 6.94d(3:3:6:1:1)§ |
| $W(CO)_4L7$ | 2019s, 1908sh, 1901vs, 1874s | 2.97s, 2.86s, 2.54s, 7.28d, 6.96d(3:3:6:1:1)§ |
| L8 | | 2.44s, 2.42s, 2.39s, 7.06m(1:1:1:1) |
| $Cr(CO)_4L8$ | 2016s, 1920sh, 1902vs, 1888s | 2.72s, 2.67s, 2.50s, 7.50m(1:1:1:1) |

*Measured in toluene solution.
†Measured in $CH_2Cl_2$ solution.
‡F-19 L3, 101.4s ($CFCl_3/CCl_4$ ref. 17); $Mo(CO)_4L3$, 99.84s($CFCl_3/CDCl_3$).
§$M(CO)_4L7$, $J$(H—H) (Hz): M = Cr, 2.0; M = Mo, 1.8; M = W, 1.7.

the magnitude of the deshielding found in the other complexes that the probable structure of the $M(CO)_4L2$ complexes is also **7**, rather than **6**.

In the free ligand L3, the methyl protons are coupled to the fluorine, and appear as a triplet (17). This can be attributed to steric through space coupling, with free rotation about both the aromatic carbon–sulfur and the methyl carbon–sulfur bonds. In the complexes there is increasing rigidity of the aromatic carbon–sulfur bond, so that no coupling to fluorine is observed in $[M(CO)_4]_2L3$. However, in the complexes $M(CO)_4L3$, two distinct methyl groups are observed. The methyl group bonded to the coordinated sulfur is a singlet, whereas the methyl group bonded to non-coordinated sulfur still appears as a triplet.

While the structures of the complexes $[M(CO)_4]_2L3$ must be unambiguously assigned as **2**, it is not clear from the nmr spectra whether the complexes $[M(CO)_4]_2L1$ have structure **2** or **3**. Two distinct methyl groups are observed in the proton nmr spectrum, with intensity ratio 2:1.

Similarly, any complexes of the type $[M(CO)_4]_2L$ could have structure **2**, when L = L2, L5, and structure **3**, when L = L2 or L6. There was no indication of any complexes $[M(CO)_4]_2L$ being formed with L2, L5, or L6. If the complexes were formed with L6, some rearrangement must have occurred in the solution as the complexes $M(CO)_4L6$ all have structure **7**. The different abilities of the somewhat analogous ligands L3 and L5 to form the $[M(CO)_4]_2L$ complexes may be due to the differences in size of hydrogen and fluorine.

The crystal structures of the free ligand $C_6(SCH_3)_6$, L1, and the chromium complex $Cr(CO)_4L1$ have been examined and compared.

Can. J. Chem. Downloaded from www.nrcresearchpress.com by 210.87.254.105 on 09/06/12
For personal use only.

Can. J. Chem. Downloaded from www.nrcresearchpress.com by 210.87.254.105 on 09/06/12
For personal use only.

They are shown in Figs. 1, 2, and 3 and some bond lengths and angles are tabulated in Tables 3 and 4.

In the crystal all $C_6(SCH_3)_6$ molecules are found to have a crystallographic centre of symmetry in their middle. The $C_6S_6$ fragment is only roughly planar. With the carbon atoms deviating from a best plane through the origin by ±0.03 Å (signs alternating) the benzene ring is slightly puckered. Deviations of the sulfur atoms from this plane are considerably higher (S1: 0.22 Å, S2: 0.25 Å; S3: 0.24 Å), probably caused by short non-bonding S...S-contacts (Table 3).

While the low temperature nmr spectrum of $C_6(SCH_3)_6$ (−75°C in $CS_2$) indicates that all the methyl groups are equivalent, in the solid state three adjacent methyl groups are situated above the plane, the other three below. The aromatic C—S bond length and S—$CH_3$ bond lengths are as expected, but the aromatic C—S bond length, average 1.78 Å, is approximately 0.05 Å lower than the anticipated sum of the covalent radii (21); however, values of 1.74 and 1.76 Å are reported in di-*p*-toly sulfide (22).

The structure of $Cr(CO)_4C_6(SCH_3)_6$ does not show fundamental changes within the ligand. Still some changes in the SCCS torsion angles can be observed, possibly due to complexation, though it cannot be excluded that intermolecular packing gives rise to similar effects. Bonding to the chromium atom apparently reduces the angle S1C1C2S2 from the range of 11.7°–13.6° in the free ligand to 5.4° in the complex, thus enabling the chelate ring to be more planar. Contrary to that, the carbon–sulfur bonds to S4 and S5 opposite the bonded part of the ligand enclose a torsion angle of 19.8° which is unusual for adjacent $sp^2$-centres normally being coplanar. As for the aromatic carbon-bridging sulfur bond lengths, however, there is virtually no change from those observed in the free ligand.

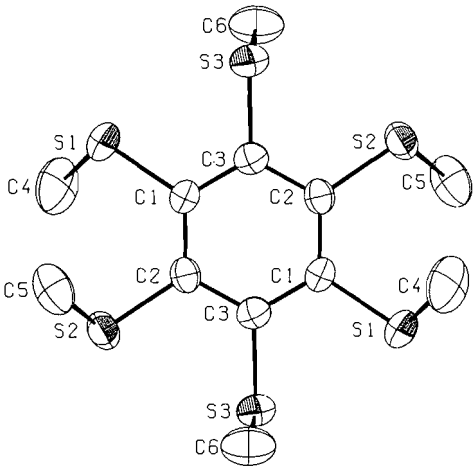


FIG. 1. ORTEP-plot (50% probability) of the molecule $C_6(SCH_3)_6$ direction of view perpendicular to the $C_6$-plane.

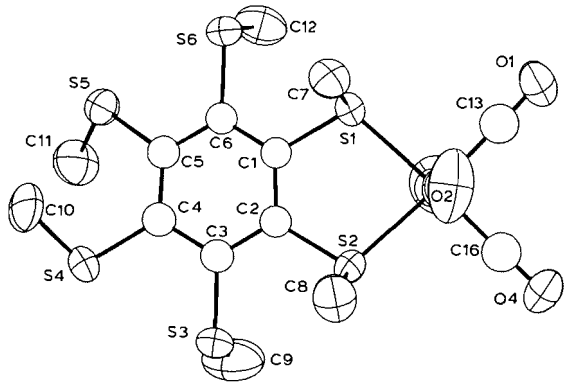


FIG. 2. ORTEP-plot (50% probability) of the complex $Cr(CO)_4L1$ showing the atomic numbering scheme. Direction of view perpendicular to the plane CrS1S2 (C14 and C15 axial: C14 above, C14 and O3 below the projection plane).

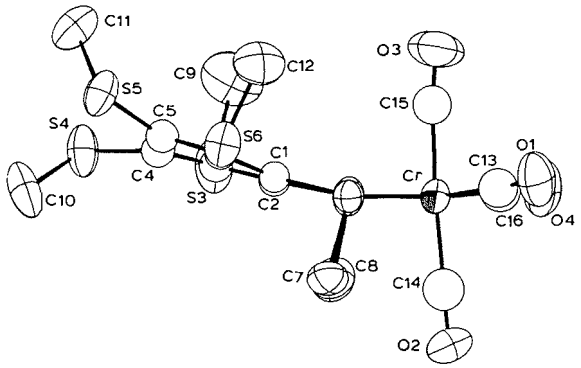


FIG. 3. ORTEP-plot (50% probability) of the complex $Cr(CO)_4L1$ direction of view from atom S1 to atom S2.

In the crystal three of the methyl groups bonded to non-coordinated sulfur are on one side of the ligand plane and only one on the other. This may be due to packing as the room temperature nmr spectrum ($CH_2Cl_2$) shows that there are three distinct methyl groups of equal intensity. On cooling the peaks broaden somewhat and below −25°C the peaks due to the methyl attached to non-coordinated sulfur coalesce and a single broad peak is observed.

The methyl groups bonded to the coordinated sulfur are on the same side of the ligand plane. This was also observed in $W(CO)_4L$ where L = *o*-$(MeS)_2C_6H_4$ (7) and in the complex $Cr(CO)_4L$, where L is tetrakis(methylthio)ethene (9). However, in the complexes $Cr(CO)_4L$ where L is $RS(CH_2)_nSR$ ($n = 2, 3$) and the bridging $(CH_2)_n$ unit is saturated the groups R are *anti* (5, 6).

Can. J. Chem. Downloaded from www.nrcresearchpress.com by 210.87.254.105 on 09/06/12
For personal use only.

TABLE 3. Some bond lengths and angles in $C_6(SMe)_6$

| Bond | Length (Å) | Bond | Angle (deg) |
|---|---|---|---|
| S1—C1 | 1.778(2) | C1—S1—C4 | 103.8(2) |
| S1—C4 | 1.805(4) | C2—S2—C5 | 102.4(1) |
| S2—C2 | 1.778(2) | C3—S3—C6 | 101.8(1) |
| S2—C5 | 1.795(3) | C1—C2—S2 | 123.5(2) |
| S3—C3 | 1.779(2) | C3—C2—S2 | 117.2(2) |
| S3—C6 | 1.794(4) | C2—C1—S1 | 124.3(2) |
| C1—C2 | 1.402(3) | C3—C1—S1 | 116.4(2) |
| C1—C3 | 1.403(3) | C1—C3—S3 | 119.4(2) |
| C2—C3 | 1.405(3) | C2—C3—S3 | 119.7(2) |

| Non-bonding S...S-contacts | Distance | Atoms | Dihedral angle (deg) |
|---|---|---|---|
| S1...S3 | 3.083(1) | S1C1C2S2 | 13.2 |
| S2...S3 | 3.119(1) | S2C2C3S3 | 13.4 |
| S1...S2 | 3.401(1) | S3C3C1S1 | 12.3 |

As there is an angle of 13.3° between the plane S1CrS2 and a best plane S1C1C2S2 the chelate ring is envelope shaped. Although it would be tempting to attribute this angle to the space requirements of the methyl groups at C7 and C8, this is apparently not justified, since the chelate ring in $Cr(CO)_4L$, L = bis(*t*-butylthio)ethene, with far more bulky groups in the same positions is reported to be planar.[2] The structure with L = tetrakis(methylthio)ethene (9), however, exhibits an angle of 7.03° between corresponding planes in the ring.

The coordination around chromium in the present structure is octahedral with relatively little distortion. The S—Cr—S angle of 84.5° is in good agreement with that reported in $Cr(CO)_4L$, when L = tetrakis(methylthio)ethene (83.8°) (9) or L = 3,6-dithiaoctane (85.1°) (5).

Influence of the substituents at the sulfur atom on the environment of the metal may be detected from the S—Cr—C angles, which are greater when C = C14 and smaller when C = C15 (see Table 3). A corresponding observation has been made in similar compounds (9).[2] The carbonyl group closest to sulfur is bent to an angle O3—C15—Cr of 173.3(6)° and thus distorted most from 180° with respect to the other three. It was suggested that repulsion from lone pairs of the sulfur atom might be responsible for such a distortion (5). The angle C14—Cr—C15 (176.6°) is significantly larger than that in some other $Cr(CO)_4L$ complexes, when L = bis(*t*-butylthio)ethane (169.8°) (6), L = 3,6-dithiaoctane (174.7°) (5), or L = bis(*t*-butylthio)ethene (173.5°).[2]

Much discussion has been presented about Cr—S and Cr—C(O) distances in similar compounds. Values found in the present structure fit quite well with those already reported. A shortening of the average Cr—S bond (2.39 Å) (2.38 Å when L = tetrakis(methylthio)ethene, 2.42 Å when L = 2,6-dithiaoctane, and 2.44 Å when L = 2,2,7,7-tetramethyl-3,6-dithiaoctane) compared to the sum of the assumed covalent radii (1.48 Å for $Cr^0$ (23) and 1.04 Å for sulfur (21)) has been attributed to multiple bonding between Cr and S (5, 9). Differences in the bond lengths Cr—C(O) of carbonyl groups mutually *trans* and those *trans* to sulfur have been taken as an indicator for the lack of π-interaction in the Cr—S bond compared to the Cr—C(O) bond (5). Similar differences are observed in the present complex, Cr—C(O) mutually *trans* being slightly longer (1.878 Å ave) than Cr—C(O) *trans* to sulfur (1.842 Å ave). Corresponding, though less significant, variations of the C—O bond lengths are found as expected.

[2]G. M. Reisner, I. Bernal, and G. R. Dobson. To be published.

TABLE 4. Some bond lengths and angles in $Cr(CO)_4$-$C_6(SCH_3)_6$

| Bond | Length (Å) | q Bonds | Angle (deg) |
|---|---|---|---|
| C1—S1 | 1.794(5) | C6—C1—S1 | 119.1(4) |
| C2—S2 | 1.788(5) | C2—C1—S1 | 119.5(4) |
| S1—C7 | 1.826(6) | C1—C2—S2 | 120.8(4) |
| S2—C8 | 1.827(7) | C3—C2—S2 | 119.7(4) |
| S1—Cr | 2.368(2) | C1—S1—Cr | 106.7(2) |
| S2—Cr | 2.388(2) | C2—S2—Cr | 106.2(2) |
| Cr—C13 | 1.834(6) | S1—Cr—S2 | 84.55(6) |
| Cr—C14 | 1.893(7) | C1—S1—C7 | 99.9(3) |
| Cr—C15 | 1.863(6) | C2—S2—C8 | 101.7(3) |
| Cr—C16 | 1.849(7) | C14—Cr—S1 | 93.6(2) |
| C1—C2 | 1.396(7) | C14—Cr—S2 | 94.1(2) |
| C1—C6 | 1.384(7) | C14—Cr—C13 | 91.6(3) |
| C2—C3 | 1.404(6) | C14—Cr—C16 | 89.6(3) |
| C3—C4 | 1.416(8) | C15—Cr—S1 | 88.6(2) |
| C4—C5 | 1.403(8) | C15—Cr—S2 | 88.6(2) |
| C5—C6 | 1.409(6) | C15—Cr—C13 | 85.8(3) |
| C3—S3 | 1.771(6) | C15—Cr—C16 | 88.2(3) |
| C4—S4 | 1.770(6) | C14—Cr—C15 | 176.6(3) |
| C5—S5 | 1.765(5) | C13—Cr—C16 | 90.3(3) |
| C6—S6 | 1.775(5) | O1—C13—Cr | 176.3(6) |
| S3—C9 | 1.832(9) | O2—C14—Cr | 178.8(7) |
| S4—C10 | 1.825(8) | O3—C15—Cr | 173.3(6) |
| S5—C11 | 1.817(8) | O4—C16—Cr | 177.5(6) |
| S6—C12 | 1.801(7) | | |
| C13—O1 | 1.151(7) | | |
| C14—O2 | 1.140(10) | | |
| C15—O3 | 1.134(9) | | |
| C16—O4 | 1.163(9) | | |

| Non-bonding atoms | Distance (Å) | Atoms | Dihedral angle (deg) |
|---|---|---|---|
| S1...S2 | 3.199(2) | S1C1C2S2 | −5.4 |
| S2...S3 | 3.203(3) | S2C2C3S3 | +2.4 |
| S3...S4 | 3.103(3) | S3C3C4S4 | +13.8 |
| S4...S5 | 3.419(3) | S4C4C5S5 | −19.8 |
| S5...S6 | 3.089(3) | S5C5C6S6 | +10.3 |
| S6...S1 | 3.170(2) | S6C6C1S1 | +1.5 |

Can. J. Chem. Downloaded from www.nrcresearchpress.com by 210.87.254.105 on 09/06/12
For personal use only.

TABLE 5. Some data of the crystals, the data set, and the refinement

| Parameter | Value* $C_6(SCH_3)_6$ | Value* $(CO)_4Cr \cdot C_6(SCH_3)_6$ |
|---|---|---|
| Crystal dimensions (mm) | 0.3 × 0.2 × 0.15 | Sphere with $r = 0.17$ |
| Space group, molecules/unit cell | $P2_1/n, Z = 2$ | $P2_1/n, Z = 4$ |
| $a$ (Å) | 9.513(1) | 10.542(1) |
| $b$ (Å) | 6.218(1) | 10.764(1) |
| $c$ (Å) | 14.404(1) | 20.526(1) |
| $\beta$ (deg) | 106.95(1) | 101.58(1) |
| $V$ (Å$^3$) | 815.0 | 2281.8 |
| $\rho_{exp}$ (Mg m$^{-3}$) | 1.40 | 1.49 |
| $\rho_{calcd}$ (Mg m$^{-3}$) | 1.45 | 1.51 |
| 2$\theta$ range | 5°–46° | 5°–43° |
| Number of reflections | | |
| Symmetrically independent | 1119 | 2447 |
| Observed | 1027 | 2260 |
| Number of variables refined | 109 | 194 |
| $R_1$ (obs. refl. only) | 0.028 | 0.048 |
| (incl. unobs. refl.) | 0.031 | 0.050 |
| $R_2$ (obs. refl. only) | 0.035 | 0.068 |

*Data collection: Syntex $P2_1$-Diffractometer, Mo $K_\alpha$-radiation, graphite monochromator, $\lambda = 0.71069$ Å, $\omega$-scan, $\Delta\omega = 0.8°$, $T$ = ca. 298 K.

## Experimental

All reactions are studied in dry solvents, under $N_2$. The ligands were prepared by literature methods (14, 24). The carbonyl complexes were available commercially or were prepared by slightly modified known procedures, $C_7H_8M(CO)_4$ (M = Cr, Mo), $Et_4N[Cr(CO)_5Cl]$ from $Et_4NCl$ and $Cr(CO)_6$, and $(MeCN)_2W(CO)_4$ from MeCN and $W(CO)_6$.[3]

Infrared spectra were recorded in solution on a Perkin Elmer Infrared Spectrophotometer Model 283 and nmr spectra were recorded on a Varian T-60 (H-1) or XL-90 (F-19). Thermal analyses were studied on a DuPont Thermal Analyser 990.

Details of the reaction conditions, yields, analyses of products, and ir and nmr spectra are shown in Tables 1 and 2, respectively. Microanalyses were performed either by the Mikroanalytical Laboratory, University of Würzburg, or Mikroanalytisches Laboratorium Beller, Göttingen, W. Germany.

*Structure investigation by X-ray methods*

The crystals examined were grown from methanol (L1) and toluene/hexane (1:2 volume ratio) $(Cr(CO)_4L1)$, respectively. Some of the crystal data are given in Table 5. The lattice constants and estimated standard deviations are derived from least-squares calculations based on 19 (20) centered reflections in a 2$\theta$ range of 23°–28° (23°–26°) in the case of the free ligand L1 (the complex $Cr(CO)_4L1$). Systematic extinction was observed for reflections $h0l$ with $h + l = 2n + 1$ and $0k0$ with $k = 2n + 1$ leading to the space group $P2_1/n$ (non standard setting of $P2_1/c$, No. 19 of the International Tables) with the equivalent positions $x, y, z; -x, -y, -z; x + 1/2, 1/2 - y, z + 1/2; 1/2 - x, y + 1/2, 1/2 - z$. X-ray intensity data were measured on a Syntex P $2_1$-diffractometer. They were corrected for Lorentz and polarisation factors but not for absorption. The structure L1 was solved by direct methods (program MULTAN (25)). After refining positional parameters and anisotropic temperature factors[4] for the non-hydrogen atoms by full-matrix least-squares the following $R$-values were obtained: $R_1 = 0.047$, $R_2 = 0.074$ (observed reflections only). The quantity minimized was $\Sigma(|F_{obs}| - |F_{calc}|)^2 \cdot W$ with $W = 1/\sigma^2$ and $\sigma$ derived from counting statistics. Those reflections with $I/\sigma(I) < 3.0$ were classified as unobserved and not included in the refinement.

At this stage all of the 9 hydrogen atoms could be localized among the 12 highest peaks of a difference electron density map at reasonable positions. Including these in the structure factor calculations yielded $R_1 = 0.038$. Further refinement, with hydrogens kept tied to a common isotropic temperature factor, converged at $R_1 = 0.028$ and $R_2 = 0.035$. Positional parameters are listed in Table 6.

During the last cycle change/esd was less than 0.1 for all parameters.

Concerning the complex $(CO)_4CrL1$ the position of the Cr

TABLE 6. Positional parameters for the crystal structure of the free ligand L1 $C_6(SCH_3)_6$*

| Atom | $x$ | $y$ | $z$ |
|---|---|---|---|
| S1 | −0.20869(8) | 0.35051(13) | 0.12475(5) |
| S2 | 0.14793(7) | 0.19090(11) | 0.17760(4) |
| S3 | 0.34537(6) | 0.44239(10) | 0.07583(4) |
| C1 | −0.0884(2) | 0.4202(3) | 0.0554(2) |
| C2 | 0.0621(2) | 0.3730(3) | 0.0828(2) |
| C3 | 0.1508(2) | 0.4643(4) | 0.0305(2) |
| C4 | −0.1073(5) | 0.4247(7) | 0.2471(2) |
| C5 | 0.0315(4) | −0.0415(5) | 0.1477(2) |
| C6 | 0.3794(4) | 0.1984(6) | 0.0195(3) |
| H41 | −0.186(4) | 0.433( 6) | 0.277(3) |
| H42 | −0.060(4) | 0.310( 6) | 0.277(2) |
| H43 | −0.066(4) | 0.562( 7) | 0.247(3) |
| H51 | 0.098(4) | −0.156( 6) | 0.188(2) |
| H52 | −0.021(4) | −0.063( 5) | 0.077(3) |
| H53 | −0.051(4) | −0.016( 7) | 0.162(3) |
| H61 | 0.336(4) | 0.208( 6) | −0.049(2) |
| H62 | 0.490(4) | 0.177( 6) | 0.037(2) |
| H63 | 0.336(4) | 0.079( 5) | 0.048(3) |

*Estimated standard deviations are given in parentheses and correspond to the least significant digits.

[3] W-D. Schenk. Private communication.

[4] Tables of the observed and calculated structure amplitudes and temperature factors are available, at a nominal charge, from the Depository of Unpublished Data, CISTI, National Research Council of Canada, Ottawa, Ont., Canada K1A 0S2.

Can. J. Chem. Downloaded from www.nrcresearchpress.com by 210.87.254.105 on 09/06/12
For personal use only.

atom in the unit cell could be found from a Patterson synthesis. Successive structure factor, Fourier and difference Fourier calculations revealed the positions of the lighter atoms except hydrogen. All atoms except C1, ..., C6 and C13, ..., C16 were made anisotropic. Positional parameters as resulting from full-matrix least-squares refinement are given in Table 7. The maximum change/esd during the last cycle was 0.01 and there were no values above 0.5 e/Å$^3$ in the final difference electron density map. *R*-values are given in Table 5.

All calculations were carried out by means of the XTL-programme (26) package on a NOVA 1200 minicomputer with structure factors for uncharged atoms as given in ref. 27. Effects of anomalous dispersion were not taken into account.

*Methods*

*Reactions with $C_7H_8M(CO)_4$, M = Cr, Mo (Method A)*

Equimolecular amounts (1 mmol) of $C_7H_8M(CO)_4$ and ligand were dissolved in ~20 mL toluene and heated to approximately 45°C. The reaction was monitored by observing changes in the ir spectrum in the 2100–1750 cm$^{-1}$ region. When the reaction was approximately 90% complete, any precipitate was filtered off, and further product precipitated by addition of an equal volume of hexane. The products were recrystallized from toluene/hexane.

The nmr spectra and thermal analysis of the Mo products, $Mo(CO)_4L$, showed that they contained some solvent which was lost before the product decomposed. The excess solvent was removed by carefully heating in vacuum.

Reactions with stoichiometry 2:1 $C_7H_8Mo(CO)_4$:L were studied in either toluene at 45°C, or methylene chloride (~35°C) when precipitation had occurred in toluene. The reaction was monitored by ir or nmr spectra. In the reactions with L2, L5, and L6 in $CH_2Cl_2$, the infrared spectrum showed that approximately 50% of the $C_7H_8Mo(CO)_4$ had reacted within 20 h, and that any subsequent reaction was very slow, probably a decomposition generating increasing amounts of $Mo(CO)_6$. After 4 or 5 days, the nmr spectrum showed that the main product formed was $Mo(CO)_4L$ and only traces of possible $[Mo(CO)_4]_2L$ could be detected.

TABLE 7. Positional parameters (× 10$^4$, for Cr × 10$^5$) for non-hydrogen atoms in the crystal structure of the complex $Cr(CO)_4L1$ with esd's in parentheses

| Atom | *x* | *y* | *z* |
|---|---|---|---|
| Cr | 25965(9) | 22032(8) | 718(4) |
| S1 | 4233(1) | 3179(1) | −385(1) |
| S2 | 2116(1) | 1121(1) | −964(1) |
| S3 | 2376(2) | −365(2) | −2283(1) |
| S4 | 4493(2) | 389(2) | −3062(1) |
| S5 | 7212(1) | 1671(2) | −2110(1) |
| S6 | 6773(2) | 3416(1) | −981(1) |
| C1 | 4382(5) | 2304(4) | −1110(2) |
| C2 | 3420(5) | 1450(4) | −1376(2) |
| C3 | 3536(5) | 773(5) | −1946(2) |
| C4 | 4599(5) | 1008(5) | −2254(3) |
| C5 | 5657(5) | 1697(5) | −1914(2) |
| C6 | 5505(5) | 2407(4) | −1358(2) |
| C7 | 3744(6) | 4681(5) | −768(3) |
| C8 | 745(6) | 1826(8) | −1529(3) |
| C9 | 3129(10) | −1751(7) | −1852(5) |
| C10 | 5145(8) | 1633(8) | −3502(3) |
| C11 | 7468(7) | 45(7) | −2284(4) |
| C12 | 7635(7) | 2418(7) | −337(3) |
| C13 | 3152(6) | 2960(6) | 879(3) |
| C14 | 1373(7) | 3478(7) | −210(3) |
| C15 | 3776(6) | 954(6) | 399(3) |
| C16 | 1362(7) | 1335(6) | 412(3) |
| O1 | 3547(5) | 3382(4) | 1395(2) |
| O2 | 651(6) | 4261(6) | −373(3) |
| O3 | 4493(6) | 239(5) | 658(3) |
| O4 | 614(5) | 794(5) | 649(2) |

*Reactions with $M(CO)_6$, M = Cr, W (Method B)*

The experimental details have been described previously (1).

*Reactions with $W(CO)_4(MeCN)_2$ (Method C)*

A solution of approximately 1.7 mmol $W(CO)_4(MeCN)_2$ in 20 mL THF was filtered into a solution of the ligand (1.0 mmol) in 10 mL THF. The infrared spectrum showed that the reaction was complete at room temperature within less than 2 h, i.e. specifically the band at 1853 cm$^{-1}$ attributed to $W(CO)_4(MeCN)_2$ (28) had disappeared. Any $W(CO)_5MeCN$ did not react, as no change was observed in the band at 1840 cm$^{-1}$ (28). The solvent was removed and the product extracted with 20 ~ 30 mL toluene. The product was precipitated on addition of an equal volume of hexane. It was recrystallized from a mixture of hexane and toluene.

In the reactions with approximately 3 mmol $W(CO)_4(MeCN)_2$ and 1 mmol ligand, the residue after the toluene extraction to remove $W(CO)_4L$ was further extracted with $CH_2Cl_2$. The product $[W(CO)_4]_2L$ was precipitated on slow addition of toluene. In reactions with L3 and L5, $W(CO)_4L$ was the only complex detected in the nmr spectra of the products.

*Reactions with $Et_4N[Cr(CO)_5Cl]$ (Method D)*

Approximately 1 mmol of $Et_4N[Cr(CO)_5Cl]$ was added to a solution of 0.5 mmol of ligand in 60 mL EtOH at room temperature. The solution was stirred. If precipitation had not occurred within 1 day, approximately 5 mL of $H_2O$ was added. The volume of the solution was reduced until a precipitate had formed. The precipitate was extracted with toluene to remove $Cr(CO)_4L$ and the residue with $CH_2Cl_2$. The product $[Cr(CO)_4]_2L$ reprecipitated on addition of toluene.

## Acknowledgements

One of the authors (M. E. P.) wishes to thank Prof. Dr. Max Schmidt for the hospitality in Würzburg and the Alexander von Humboldt Stiftung (Bonn) for a fellowship while on leave from Acadia University. Dr. W-D. Schenk is thanked for many helpful discussions.

1. W. J. FRAZEE and M. E. PEACH. Phosphorus Sulfur, **6**, 407 (1978).
2. J. A. CONNOR and G. A. HUDSON. J. Chem. Soc. Dalton Trans. 1025 (1975).
3. E. W. AINSCOUGH, E. J. BIRCH, and A. M. BRODIE. Inorg. Chim. Acta, **20**, 187 (1976).
4. G. R. DOBSON. Inorg. Chem. **8**, 80 (1969).
5. E. N. BAKER and N. G. LARSEN. J. Chem. Soc. Dalton Trans. 1769 (1976).
6. G. M. REISNER, I. BERNAL, and G. R. DOBSON. Inorg. Chim. Acta, **50**, 227 (1981).
7. R. ROS, M. VIDALI, and R. GRAZIANI. Gazz. Chem. Ital. **100**, 407 (1970).
8. E. W. AINSCOUGH, A. M. BRODIE, N. G. LARSEN, and R. G. MATTHEWS. Inorg. Chim. Acta, **49**, 159 (1981).
9. M. F. LAPPERT, D. B. SHAW, and G. M. MCLAUGHLIN. J. Chem. Soc. Dalton Trans. 427 (1979).
10. B. K. BALBACH, A. R. KORAY, A. OKUR, P. WUELKNITZ, and M. L. ZIEGLER. J. Organomet. Chem. **212**, 77 (1981).

11. A. R. KORAY and M. L. ZIEGLER. J. Organomet. Chem. **202**, 13 (1980).
12. D. SEVIČ and H. MEIDER. J. Inorg. Nucl. Chem. **43**, 153 (1981).
13. A. R. SANGER, C. G. LOBE, and J. E. WEINER-FEDORAK. Inorg. Chim. Acta, **53**, L123 (1981).
14. M. E. PEACH and E. S. RAYNER. J. Fluorine Chem. **13**, 447 (1979).
15. A. TRENKLE and H. VAHRENKAMP. Chem. Ber. **114**, 1343 (1981).
16. D. J. DARENSBOURG and R. L. KUMP. Inorg. Chem. **17**, 2680 (1978).
17. M. E. PEACH and A. M. SMITH. J. Fluorine Chem. **4**, 341 (1974).
18. H. BURDORF and C. EISCHENBROICH. Z. Naturforsch. **36**b, 94 (1981).
19. M. HERBERHOLD and G. SUSS. J. Chem. Res.(S), 246 (1977).
20. H. G. RAUBENHEIMER, J. C. A. BOYENS, and S. LOTZ. J. Organomet. Chem. **112**, 145 (1976).
21. L. PAULING. Nature of the chemical bond. 3rd ed. Cornell University Press, Ithaca, New York. 1960. p. 225.
22. W. R. BLACKMORE and S. C. ABRAHAMS. Acta Crystallogr. **8**, 329 (1955).
23. F. A. COTTON and D. C. RICHARDSON. Inorg. Chem. **5**, 1851 (1966).
24. K. R. LANGILLE and M. E. PEACH. J. Fluorine Chem. **1**, 407 (1971/2).
25. G. GERMAIN, P. MAIN, and M. M. WOOLFSON. Acta Crystallogr. **27**A, 368 (1971).
26. Syntex-XTL-Systems (1976), Syntex Analytical Instruments, Cupertino, CA.
27. D. T. CROMER and J. T. WABER. International tables for X-ray crystallography. Vol. IV. Kynoch Press, Birmingham. 1974. pp. 99–101.
28. G. R. DOBSON, M. F. AMIR EL SAYER, I. W. STOLZ, and R. K. SHELINE. Inorg. Chem. **1**, 526 (1962).

Can. J. Chem. Downloaded from www.nrcresearchpress.com by 210.87.254.105 on 09/06/12
For personal use only.

# Discreteness-of-charge effects in electrode kinetics. I. The electroreduction of tetrathionate anion in the presence of specifically adsorbed iodide anions

W. Ronald Fawcett and Kveta Markušová[1]

*Guelph-Waterloo Centre for Graduate Work in Chemistry (Guelph Campus), Department of Chemistry, University of Guelph, Guelph, Ont., Canada N1G 2W1*

Received September 28, 1981

W. Ronald Fawcett and Kveta Markušová. Can. J. Chem. **60**, 2038 (1982).

The kinetics of electroreduction of tetrathionate anion have been studied at a Hg electrode in aqueous solutions of NaI + NaF and KI + KF with an ionic strength of 0.25 *M*. The rate of reaction was observed to decrease as the iodide ion concentration was increased, and when the cation was changed from $K^+$ to $Na^+$ at constant electrode potential. Analysis of the double layer effects on the basis of the Frumkin model results in an overestimation of the repulsive effect of the adsorbed iodide anions. This result is interpreted on the basis of the discreteness-of-charge effect and the possible non-coincidence of the reaction plane and outer Helmholtz plane.

W. Ronald Fawcett et Kveta Markušová. Can. J. Chem. **60**, 2038 (1982).

On a étudié la cinétique de l'électroréduction de l'anion tétrathionate au niveau d'une électrode au Hg dans des solutions aqueuses de NaI + NaF et de KI + KF avec une force ionique de 0,25 *M*. On a observé que la vitesse de réduction décroît lorsqu'on augmente la concentration en ion iodure et lorsqu'on passe du cation $K^+$ au cation $Na^+$ à potentiel d'électrode constant. L'analyse des effets de la couche double en fonction du modèle de Frumkin conduit à une surévaluation très marquée de l'effet répulsif des anions iodures absorbés. On interprète ce résultat en fonction du caractère discret de l'effet de charge et de la non-coincidence possible du plan de la réaction et du plan extérieur de Helmholtz.

[Traduit par le journal]

## Introduction

Discreteness-of-charge effects in electrode kinetics have been discussed in detail in recent literature (1–14). One essential feature of the theory for these effects is that the rate of a simple redox process at an inert electrode is changed less than one would predict on the basis of the classical Frumkin theory of double layer effects (15, 24) in the presence of specifically adsorbed non-reacting ions. For example, the rate of electroreduction of an anion such as tetrathionate at a mercury electrode is slower in the presence of specifically adsorbed iodide anions than in their absence (16, 17), but the extent of deceleration is less than that estimated on the basis of the corresponding shift in the potential drop across the diffuse layer in the negative direction.

The electroreduction of tetrathionate was first studied by Žežula (18–20) who showed that a minimum occurs on the current–potential curve at potentials negative of the point of zero charge (pzc) similar to that found in the electroreduction of other anions (21). The presence of a large double layer effect over a wide potential range for this system makes it a good candidate for more detailed examination. Foresti and Guidelli (16) studied the effects of adsorbed ions on the electroreduction of tetrathionate; however, these experiments were not carried out at constant ionic strength so that detailed interpretation of the results on the basis of the theory of discreteness-of-charge effects is not possible (14). Žežula *et al.* (17) reported similar data at constant ionic strength; their analysis could not be completed because of the lack of double layer data at all the ionic strengths considered. Double layer data for the adsorption of iodide ion at an ionic strength of 0.25 *M* have been obtained for the NaI + NaF and KI + KF systems (22). These electrolytes are particularly convenient for investigating the above phenomena in that the double layer effect is reasonably large at this ionic strength, and the effects of the cations $Na^+$ and $K^+$ can be compared. The results of these experiments are reported in the present paper.

## Experimental

The kinetic data were obtained by dc polarography with a dropping mercury electrode as the working electrode. The counter electrode was a Pt cylinder of large area, and the reference electrode, a saturated calomel electrode. The current–voltage curves were recorded with a PAR model 174A polarographic analyzer. The drop time of the mercury electrode was controlled at 2 s and the mercury flow rate was 0.39 mg $s^{-1}$. The temperature of the cell was maintained at 25°C via an external jacket through which water at controlled temperature was pumped. The fluoride and iodide salts were purified as described previously (22). Reagent grade potassium tetrathionate (K and K Laboratories) was recrystallized twice from triply distilled water before use.

The rate constant was calculated from the ratio of the

[1]On leave from Šafárik University, Košice, Czechoslovakia.

0008-4042/82/152038-08$01.00/0

©1982 National Research Council of Canada/Conseil national de recherches du Canada

Can. J. Chem. Downloaded from www.nrcresearchpress.com by 210.87.254.42 on 09/06/12
For personal use only.

Can. J. Chem. Downloaded from www.nrcresearchpress.com by 210.87.254.42 on 09/06/12
For personal use only.

observed current to its diffusion limited value according to the theory of Koutecký for an irreversible electrode process with inclusion of the correction of electrode sphericity (23).

## Results

Kinetic data were obtained in twenty different electrolyte solutions of composition $xM$ NaI + $(0.25 - x)M$ NaF or $xM$ KI + $(0.25 - x)M$ KF where $x = 0, 0.0063, 0.01, 0.016, 0.025, 0.04, 0.063, 0.1, 0.16$, and $0.25\,M$. Representative data for the $Na^+$ and $K^+$ systems at potentials negative of the pzc in the pure fluoride electrolyte are shown in Figs. 1 and 2, respectively. As one would expect, the rate constant decreases at constant potential with increase in bulk iodide concentration, that is, with increase in the extent that iodide is adsorbed on the electrode. As the electrode potential is made more negative, the surface excess of iodide decreases and the rate constants in a given system become independent of bulk solution composition. In any system of given bulk iodide and fluoride concentration, the rate constant in the potassium system is higher than that in the sodium system. The latter result agrees with similar observations with a variety of anionic reactants at negatively charged electrodes (21).

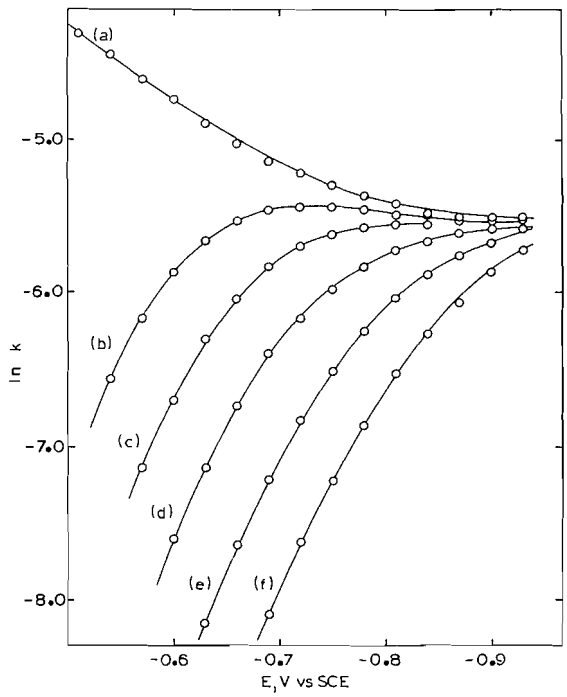


FIG. 1. Logarithm of the rate constant for electroreduction of tetrathionate anion ($S_4O_6^{2-} + 2e \rightarrow 2S_2O_3^{2-}$) at Hg against electrode potential with respect to a saturated calomel electrode. The electrolyte solution contained $x$ mol dm$^{-3}$ KI + $(0.25 - x)$ mol dm$^{-3}$ KF with the following values of $x$: (*a*) 0, (*b*) 0.0063, (*c*) 0.016, (*d*) 0.04, (*e*) 0.10, and (*f*) 0.25 mol dm$^{-3}$.

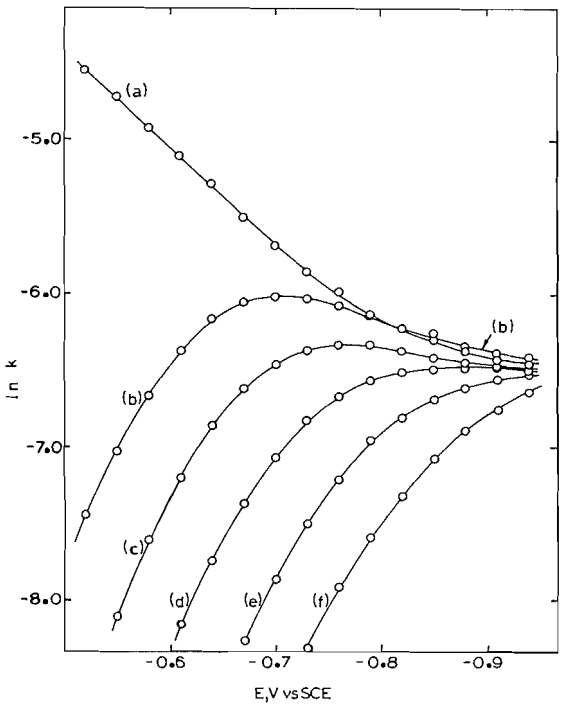


FIG. 2. Kinetic data for the electroreduction of tetrathionate anion as in Fig. 1 except that the electrolyte solution contained $x$ mol dm$^{-3}$ NaI + $(0.25 - x)$ mol dm$^{-3}$ NaF with the following values of $x$: (*a*) 0, (*b*) 0.0063, (*c*) 0.016, (*d*) 0.04, (*e*) 0.10, and (*f*) 0.25 mol dm$^{-3}$.

According to Frumkin's theory for double layer effects in electrode kinetics (15), the reaction site in the double layer is the outer Helmholtz plane (oHp), the potential at the reaction site being the average potential on that plane, $\phi^d$. The kinetic parameters are obtained from corrected Tafel plots (cTp) (24) on the basis of the relationship

$$[1] \quad \ln k + zf\phi^d = \ln k_0 - \alpha_a f(\phi^m - \phi^d)$$

where $k$ is the rate constant for reduction, $z$, the charge on the reacting species, $\phi^m$, the electrode potential on the rational scale, $k_0$, the value of the rate constant at a potential where both $\phi^m$ and $\phi^d$ are zero, $\alpha_a$, the apparent transfer coefficient, and $f = F/RT$. The oHp potential is calculated from Gouy–Chapman theory according to the equation

$$[2] \quad \phi^d = \frac{2}{f}\sinh^{-1}\left(\frac{\sigma_m + \sigma_a}{2A}\right)$$

where $\sigma_m$ is the charge density on the electrode and $\sigma_a$, that due to adsorbed ions, in the present case, iodide anions. The constant $A$ is equal to $(2RT\varepsilon\varepsilon_0 c_s)^{1/2}$ where $\varepsilon$ is the dielectric constant of the solvent, $\varepsilon_0$, the permittivity of free space, and $c_s$, the concentration of electrolyte (ionic strength

Can. J. Chem. Downloaded from www.nrcresearchpress.com by 210.87.254.42 on 09/06/12
For personal use only.

in the case of 1–1 electrolytes). On the basis of eq. [1], $y = \ln k + zf\phi^d$ should be independent of solution composition provided that $\phi^m - \phi^d$ is held constant.

The kinetic results obtained here were corrected for the double layer effect on the basis of the data for the adsorption of iodide obtained earlier (22). Values of $y$ were estimated as a function of electrode potential and solution composition. These data are plotted in Fig. 3 for the system with $K^+$ as a function of $\sigma_a$ for constant $\phi^m - \phi^d$. It is readily apparent that $y$ does depend on solution composition, its value increasing with $\sigma_a$ for low adsorbed charge densities and then decreasing. Similar results were obtained with $Na^+$ as the cation. It should be noted that the corresponding change in $\ln k$ at constant $\phi^m - \phi^d$ is of the same order of magnitude. For instance, at $\phi^m - \phi^d = 0.25$ V for the $K^+$ system, $\ln k$ decreases by 1.5 units when the iodide concentration is changed from 0 to 0.25 $M$; at the same time, $y = \ln k + zf\phi^d$ increases by 0.9 units. Thus, correction of the double layer effect on the basis of the Frumkin model results in an overestimation of the electrostatic effect of the adsorbed anions by approximately 50% of the observed decrease in the logarithm of the rate constant.

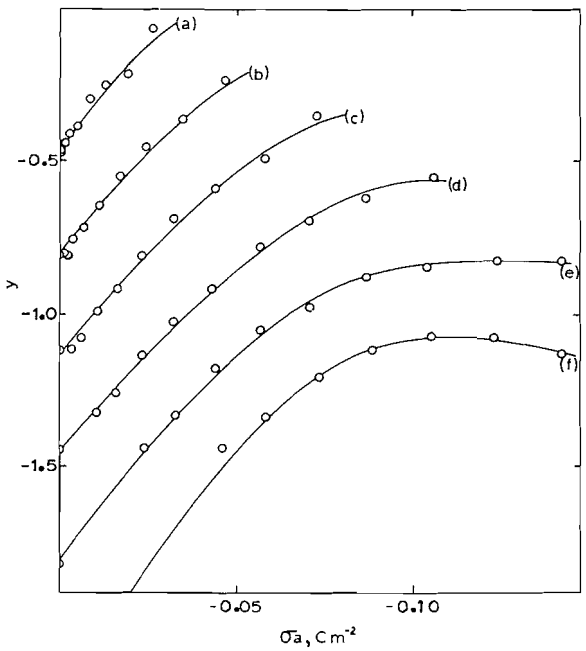


FIG. 3. Corrected logarithm of the rate constant for electroreduction of tetrathionate anion, $y = \ln k - 2f\phi^d$ against adsorbed charge density due to $I^-$ anions, $\sigma_a$ in an electrolyte solution containing KI + KF (ionic strength = 0.25 mol dm$^{-3}$) for constant potential drop across the inner layer, $\phi^m - \phi^d$. The values of $\phi^m - \phi^d$ for each of the curves are (*a*) −0.40, (*b*) −0.35, (*c*) −0.30, (*d*) −0.25, (*e*) −0.20, and (*f*) −0.15 V.

The double layer effect observed in the presence of strongly adsorbed ions is rather complex because of the fact that the reactant has both cations and anions in its immediate environment. In the present case, a negatively charged anion is reduced at a negatively charged electrode in an atmosphere composed predominantly of cations at the oHp with anions on the inner Helmholtz plane (iHp). It follows that one expects some interaction between the reacting species and its atmosphere in the diffuse layer (4, 5, 14, 15, 21). According to the theory of discreteness-of-charge effects (14), the change in the corrected logarithm of the rate constant, $y$ with respect to its value in the absence of adsorbed anions at constant $\phi^m - \phi^d$ is given by

$$[3] \quad y - y_0 = \frac{(\alpha - z)f(1-\lambda)(1-g)\sigma_a}{K_2} + \frac{(a_{\neq}\sigma_d)_0}{RT} - \frac{a_{\neq}\sigma_d}{RT} + p_{\neq}\ln(1 - \sigma_a/\sigma_{am})$$

The parameter $\lambda$ is equal to $K_i/K_{rd}$ where $K_i$ is the integral capacity of the inner layer and $K_{rd}$, that of the region between the reaction plane and the oHp, the reaction site being assumed to be located within the inner layer. $g$ is a dimensionless factor related to the degree that repulsive interactions between adsorbed anions are screened; it is given by (25)

$$[4] \quad g = \frac{C_d + K_2}{C_d + K_i}$$

where $C_d$ is the differential capacity of the diffuse layer and $K_2$, the integral capacity of the region between the iHp and the oHp. $\sigma_d$ is the charge density of cations in the diffuse layer whose distance from the reactant is such that attractive interaction is possible and $a_{\neq}$, the interaction parameter in the activated state (14). $\sigma_d$ and $a_{\neq}$ both vary with electrode potential, $\sigma_d$ being strongly dependent on the value of $\phi^d$. $\sigma_{am}$ is the maximum possible coverage by adsorbed iodide ions and $p_{\neq}$, the number of solvent molecules displaced by the reactant at the surface in the transition state. Since there is no evidence for surface coverage being significant in the analysis of data for iodide adsorption (22, 26, 27), the last term in eq. [3] may be disregarded, especially considering the extent of iodide adsorption under the present experimental conditions. It should also be noted that $\alpha$ is the true transfer coefficient which is obtained after correction for double layer effects, not the apparent value. This follows from the fact

Can. J. Chem. Downloaded from www.nrcresearchpress.com by 210.87.254.42 on 09/06/12
For personal use only.

that eq. [3] is based on the assumption that the reaction plane is not necessarily coincident with the oHp and that the local potential rather than the average value on the reaction plane is considered (14).

On the basis of the above discussion, the expression for $y - y_0$ becomes

$$[5] \quad y - y_0 = \frac{(\alpha - z)f(1-\lambda)(1-g)\sigma_a}{K_2} + \frac{(a_{\mp}\sigma_d)_0}{RT} - \frac{a_{\mp}\sigma_d}{RT}$$

Since $z$ is negative, the first term increases with increase in $|\sigma_a|$ provided that $g$ is less than unity. This term accounts for the fact that the repulsive effect of the adsorbed anions is overestimated on the basis of the average potential on the reaction plane. The interaction term $(a_{\mp}\sigma_d)_0 - (a_{\mp}\sigma_d)$ also depends on $\sigma_a$ as a result of the corresponding change in inner layer properties. According to Grahame's model of the inner layer (26), one may write that

$$[6] \quad \phi^m - \phi^d = \frac{\sigma_m}{K_i} + \frac{\sigma_a}{K_2}$$

Thus, as the amount of adsorbed iodide increases at constant $\phi^m - \phi^d$, $\sigma_m$ becomes more positive. At the same time, $K_i$ and $K_2$ increase so that ion–ion interactions become less strong because of the increase in average dielectric constant between interacting species (4). Since the anionic reactant is stabilized by the cationic atmosphere at the electrode, $a_{\mp}$ is negative; it depends in a complex way on the local dielectric properties at the reaction site and imaging conditions in the electrode and diffuse layer (4). On the other hand, $\sigma_d$ increases with increase in $|\sigma_a|$ due to the concomitant change in $\sigma_a + \sigma_m$, and thus, $\phi^d$ in the negative direction. However, if the concentration of cations in the vicinity of a reacting anion is sufficiently high, further increase in $\sigma_d$ is not expected to result in reaction acceleration in the case that there is a fixed number of cations associated with one anion (4). On the basis of the experimental results (Fig. 3), it is apparent that $(a_{\mp}\sigma_d)_0 - (a_{\mp}\sigma_d)$ decreases with increase in $|\sigma_a|$ indicating that attractive ion–ion interactions are becoming less important at high adsorbed charge densities.

The two influences on $y - y_0$ may be separated if the variation in this function at constant potential drop across the diffuse layer, $\phi^d$, is considered; under these circumstances, one expects $a_{\mp}\sigma_d$ to be approximately constant since the ionic atmosphere in the diffuse layer is not changing. Plots of $\Delta = (y - y_0)_{\phi^m - \phi^d}$ against $\sigma_a$ at constant $\sigma_a + \sigma_d$ (constant $\phi^d$) are shown in Figs. 4 and 5 for the $Na^+$ and $K^+$ systems, respectively. From these results, it is apparent that $\Delta$ is approximately a linear function of $\sigma_a$ at constant $\phi^d$. The slopes of the plots which are equal to $(\alpha - z)f(1-\lambda)(1-g)/K_2$ decrease with increase in $|\sigma_m + \sigma_a|$, and also, with change in the nature of the counter ion from $K^+$ to $Na^+$. Values of $(\alpha - z)(1-\lambda)(1-g)/K_2$ vary from $9.6 \times 10^{-4}$ to $2.5 \times 10^{-3}$ cm$^2$ $\mu$F$^{-1}$ for variation in $\sigma_m + \sigma_a$ from $-11.5$ to $-9.0$ $\mu$C cm$^{-2}$ in the $Na^+$ system; the corresponding data for the $K^+$ system vary from $2.6 \times 10^{-3}$ to $3.8 \times 10^{-3}$ cm$^2$ $\mu$F$^{-1}$. The larger values of this parameter in the $K^+$ system reflect chiefly a lower value of $\lambda$. This trend has been interpreted as being the result of differences in the distance of closest approach to the electrode of the reacting system, and the predominant non-reacting counter ion, the more weakly solvated $K^+$ ion approaching more closely than the $Na^+$ ion (28). Similar results have been observed previously in the case of electroreduction of other anions (29, 30), neutral molecules (28), and cations (31).

The slopes of the plots in Figs. 4 and 5 may be interpreted further on the basis of the adsorption isotherm for the iodide anions. Neglecting the coverage term, the adsorption isotherm may be written

$$[7] \quad \ln(|\sigma_a|) = \Phi + \ln c_a + f(\phi^a + \zeta_d{}^a)$$

where $\Phi$ is the isotherm constant, $c_a$, the concen-

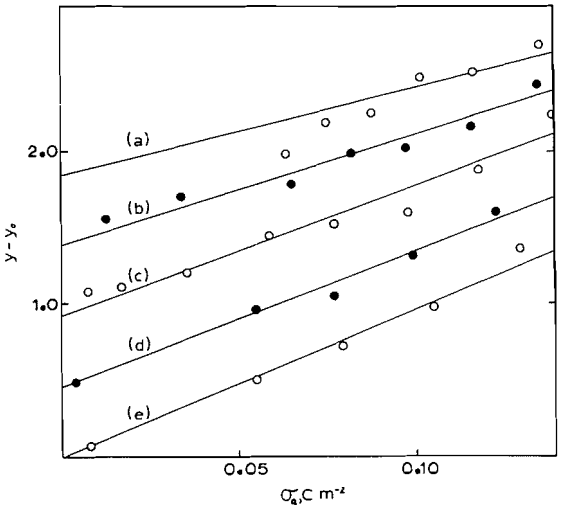


FIG. 4. Corrected logarithm of the rate constant for electroreduction of tetrathionate anion in a solution of NaI + NaF with respect to that in pure NaF at constant $\phi^m - \phi^d$, $y - y_0$ plotted against the adsorbed charge density due to $I^-$ anion, $\sigma_a$ for constant charge density in the diffuse layer, $-(\sigma_m + \sigma_a)$. The values of $\sigma_m + \sigma_a$ are (*a*) $-0.11$, (*b*) $-0.105$, (*c*) $-0.10$, (*d*) $-0.095$, and (*e*) $-0.09$ C m$^{-2}$. The ordinate scale is correct for curve (e); for the others it has been shifted up by (*a*) 2.0, (*b*) 1.5, (*c*) 1.0, and (*d*) 0.5 units.

Can. J. Chem. Downloaded from www.nrcresearchpress.com by 210.87.254.42 on 09/06/12
For personal use only.

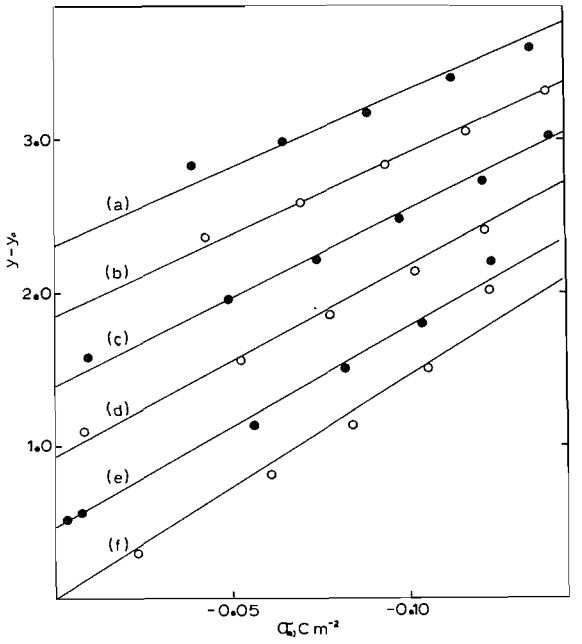


FIG. 5. Kinetic data for the electroreduction of tetrathionate anion as in Fig. 4 except that the electrolyte solution contained KI + KF. The values of $\sigma_m + \sigma_a$ are (*a*) −0.115, (*b*) −0.11, (*c*) −0.105, (*d*) −0.10, (*e*) −0.095, and (*f*) −0.09 C m$^{-2}$. The ordinate scale is correct for curve (f); for the others it has been shifted up by (*a*) 2.5, (*b*) 2.0, (*c*) 1.5, (*d*) 1.0, and (*e*) 0.5 units.

tration of adsorbing anions in the bulk, $\phi^a$, the average potential on the adsorption pt plane, and $\zeta_d{}^a$, the exclusion disc potential on the same plane (25). The average potential $\phi^a$ is given by

$$[8] \quad \phi^a = \phi^d + \frac{\sigma_m + \sigma_a}{K_2}$$

It is easily shown (14) that it can also be expressed as follows

$$[9] \quad \phi^a = \phi^d + \lambda'(\phi^m - \phi^d) + \frac{(1-\lambda')\sigma_a}{K_2}$$

where $\lambda' = K_i/K_2$. The exclusion disc potential is given by (25)

$$[10] \quad \zeta_d{}^a = \frac{-K_i g \sigma_a}{K_1 K_2} = \frac{(1-\lambda')g\sigma_a}{K_2}$$

where $K_1$ is the integral capacity of the region between the electrode surface and the adsorption plane. Combining eqs. [7], [9], and [10] one may write

$$[11] \quad \ln(|\sigma_a|/c_a) - f\phi^d = \Phi + f\lambda'(\phi^m - \phi^d) + \frac{f(1-\lambda')(1-g)\sigma_a}{K_2}$$

The parameters $\lambda'$, $g$, and $K_2$ all vary with electrode charge density (22, 25). However, an approximate value of the parameter $(1-\lambda')(1-g)/K_2$ can be obtained from plots of the function $\ln(|\sigma_a|/c_a) - f\phi^d$ against $\sigma_a$ at constant $\phi^m - \phi^d$.

Plots of data obtained earlier for the $K^+$ system (22) according to eq. [11] are shown in Fig. 6. The average slopes of the plots were determined by least squares and yielded values of $(1-\lambda')(1-g)/K_2$ varying from $6.7 \times 10^{-4}$ cm$^2$ μF$^{-1}$ at $\phi^m - \phi^d = -0.3$ V to $2.2 \times 10^{-3}$ cm$^2$ μF$^{-1}$ at $\phi^m - \phi^d = -0.1$ V. Assuming $\alpha - z$ is equal to 2.5, the corresponding values of $(\alpha - z)(1-\lambda')(1-g)/K_2$ are in the range $1.7 \times 10^{-3}$ to $5.5 \times 10^{-3}$ cm$^2$ μF$^{-1}$. These results are comparable to the values of $(\alpha - z)(1-\lambda')(1-g)/K_2$ obtained from the kinetic data. Thus we conclude that the discreteness-of-charge effect observed in the kinetic data is of the same order of magnitude as that observed for the equilibrium adsorption of the iodide ions. It also follows that the reaction site is in the inner layer but it is not possible to make any estimate of where it is with respect to the iHp on the basis of the present results.

The above analysis ignores the possible change in $(a_{\mp}\sigma_d)_0$ associated with change in Δ at constant $\sigma_m + \sigma_a$. On the basis of eq. [6], and recognizing that $1/K_i = 1/K_1 + 1/K_2$, one may write

$$[12] \quad \phi^m - \phi^d = \frac{\sigma_m + \sigma_a}{K_i} - \frac{\sigma_a}{K_1}$$

Thus, at constant $\sigma_m + \sigma_a$, as $\sigma_a$ increases in the negative direction, $\phi^m - \phi^d$ becomes more positive. The extent that $a_{\mp}\sigma_d$ changes with $\phi^m - \phi^d$ in the absence of specific adsorption is unknown; however, considering the fact that the corrected Tafel plots of kinetic data for tetrathionate anion reduction in NaF and KF media are linear, any change in $(a_{\mp}\sigma_d)_0$ is a linear function of $\phi^m - \phi^d$. The extent that this effect changes the present analysis is probably small but impossible to assess on the basis of the data obtained.

## Discussion

It is interesting to compare the double layer effects obtained in the present study with those reported earlier (16, 17, 19, 20, 33). Foresti and Guidelli analyzed data obtained in NaF and KF using the graphical procedure devised by Gierst (34). They concluded that the charge on the reacting species is −1.5. The apparent transfer coefficients were 0.07 and 0.17 in the presence of NaF and KF, respectively. Fedorovich *et al.* (33) studied the kinetics of electroreduction of $S_4O_6{}^{2-}$ at Bi, Sn, Pb, and Cd electrodes in aqueous solutions of

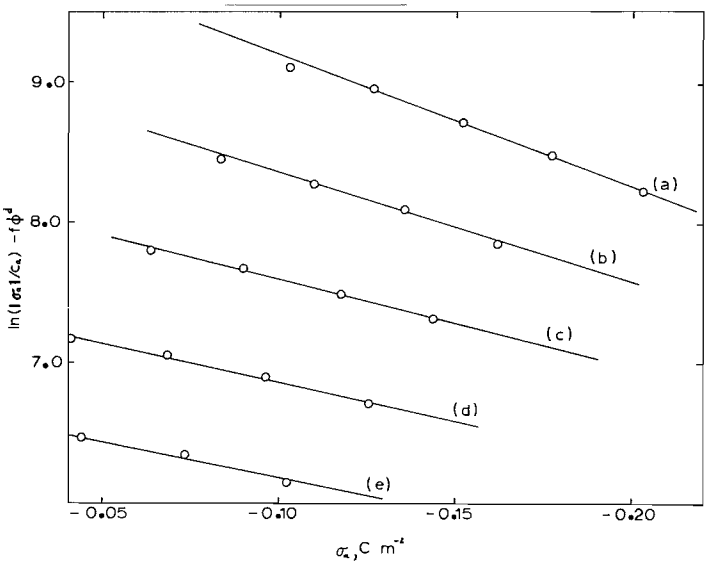


FIG. 6. Isotherms for the adsorption of $I^-$ anion at Hg from solutions of $x$ mol dm$^{-3}$ KI + (0.25 − $x$) mol dm$^{-3}$ KF plotted as ln $(|\sigma_a|/c_a) - f\phi^d$ against $\sigma_a$ at constant $\phi^m - \phi^d$. The values of $\phi^m - \phi^d$ are (*a*) −0.10, (*b*) −0.15, (*c*) −0.20, (*d*) −0.25, and (*e*) −0.30 V.

NaF. On the basis of an analysis of the dependence of ln $k$ on base electrolyte concentration, they determined the charge on the reacting species to be −1.9; furthermore, the apparent transfer coefficient, $\alpha_a$ was independent of the nature of the electrode and equal to 0.24. The great discrepancy between these results can be understood by examining corrected Tafel plots (cTp) in non-adsorbing electrolytes over a wide potential range. These plots for the present data obtained in 0.25 *M* NaF and KF and assuming $z = -2$ are shown in Fig. 7. At negative potentials the slopes of the cTp are linear in the region $-0.1 \geq \phi^m - \phi^d \geq -0.6$ V and yield values of $\alpha_a$ equal to 0.13 and 0.18 for the NaF and KF systems, respectively. However, at more positive potentials, the corrected logarithm of the rate constant is independent of the nature of the base electrolyte cation and the slope of the cTp increases, becoming approximately constant at the most positive values of $\phi^m - \phi^d$. The kinetic parameters at potentials positive of the pzc are probably influenced by specific adsorption of the reactant (35). If a graphical procedure is used to determine $z$ and $\alpha_a$ and data obtained near the pzc are involved, then some error in the analysis will result from the potential dependence of $\alpha_a$ in this potential region. For this reason, the values of $\alpha_a$ reported by Foresti and Guidelli are somewhat low. On the other hand, it is difficult to understand why the value of $\alpha_a$ reported by Fedorovich *et al.* (33) at other polarizable electrodes is so much higher than that reported here at Hg.

According to the analysis of double layer effects

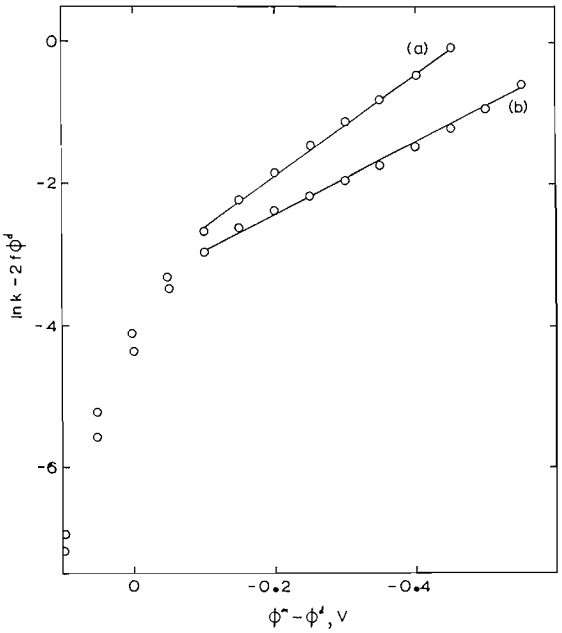


FIG. 7. Corrected Tafel plots of kinetic data for the electroreduction of tetrathionate anion in (*a*) 0.25 mol dm$^{-3}$ KF and (*b*) 0.25 mol dm$^{-3}$ NaF.

given earlier (14), the apparent transfer coefficient for a process involving the reduction of an anion at a negatively charged electrode in the absence of ionic specific adsorption may be written

$$[13] \quad \alpha_a = \alpha + \lambda(z - \alpha) + \frac{\partial(a_{\neq}\sigma_d)}{F\partial(\phi^d - \phi^m)}$$

Can. J. Chem. Downloaded from www.nrcresearchpress.com by 210.87.254.42 on 09/06/12
For personal use only.

Can. J. Chem. Downloaded from www.nrcresearchpress.com by 210.87.254.42 on 09/06/12
For personal use only.

On the basis of previous discussion (29), the parameter $\lambda$ is expected to depend on the solvated size of the counter ion at the electrode, being greater for $Na^+$ than for $K^+$. Since $z - \alpha$ is negative, $\alpha_a$ is less than $\alpha$ by an amount which depends on the counter ion nature. However, $a_{\pm}\sigma_d$ is also negative and may decrease with increase in $|\phi^m - \phi^d|$. Thus, the term $\partial(a_{\pm}\sigma_d)/\partial(\phi^d - \phi^m)$ may also result in a decrease in $\alpha_a$ with respect to $\alpha$; in addition, if $K^+$ interacts more strongly with the reactant than $Na^+$, the effect may be dependent on the nature of the counter ion. The change in the nature of the counter ion from cation to anion and on the onset of specific adsorption of $S_4O_6^{2-}$ results in potential dependence of $\alpha_a$ in the vicinity of the pzc.

The analysis of the effects of specifically adsorbed anions on the electrode kinetics used by Foresti and Guidelli (16) is somewhat different than that presented here. For the present system, $\ln k$ is given by (14)

$$[14] \quad \ln k = \ln(\gamma_A^s k_c) + \frac{(\alpha - z)f(1-\lambda)(1-g)\sigma_a}{K_2} - a_{\pm}\sigma_d/RT - zf\phi^d - \alpha' f(\phi^m - \phi^d)$$

where $k_c$ is the potential independent part of the rate constant, $\gamma_A^s$, the activity coefficient of the reactant in the bulk of the solution, and $\alpha' = \alpha - \lambda(\alpha - z)$. Foresti and Guidelli (16) defined the logarithm of the rate constant corrected for all explicit effects due to the potential drop across the diffuse layer, $\phi^d$, as follows:

$$[15] \quad y' = \ln k + (z - \alpha')f\phi^d = \ln(\gamma_A^s k_c) + \frac{(\alpha - z)f(1-\lambda)(1-g)\sigma_a}{K_2} - a_{\pm}\sigma_d/RT - \alpha' f\phi^m$$

Considering the fact that $\alpha_a$ and, thus, $\alpha'$ are rather low for the present system, the difference between $y'$ and $y$, the corrected value of the logarithm of the rate constant discussed above, is not expected to be great. However, these authors observed that $y'$ decreased at constant $\phi^m$ with increase in $|\sigma_a|$ in the range $-3 \geq \sigma_a \geq -12\ \mu C\ cm^{-2}$. This observation is very different from that reported here, namely, that $y$ increases at constant $\phi^m - \phi^d$ and then decreases with increase in $|\sigma_a|$. The difference can be attributed to the fact that the data of Foresti and Guidelli (16) were obtained in solutions of varying ionic strength. Under these circumstances, one expects to find a concomitant change in the extent of interaction of the reactant with cations in its environment, that is, in the term $a_{\pm}\sigma_d$. As the ionic strength increases, $|\sigma_a|$ increases and $|\phi^d|$ decreases; at the same time, there is a decrease in $\sigma_d$ (14). Thus, the difference between the present results and those obtained at varying ionic strength (16) is attributed to the fact that the latter data were obtained under conditions in which ion–ion interactions vary greatly with adsorbed charge density, $\sigma_a$.

An analysis of the effect of adsorbed $I^-$ anions on the kinetics of electroreduction of $S_4O_6^{2-}$ was carried out by Žežula *et al.* (17) in solutions of constant ionic strength containing NaI and NaF. In this case, the analysis involved plotting $y' - y_0'$ against $\sigma_a$ where $y_0'$ is the value of $y'$ in a solution of pure NaF (eq. [15]). For values of $\sigma_a$ up to $-6\ \mu C\ cm^{-2}$, the slopes of these plots were negative, indicating a net increase in $y'$ with increase in $|\sigma_a|$.[2] The values of the slope, which is approximately equal to $(\alpha - z)f(1-\lambda)(1-g)/K_2$ if one ignores the contribution of the term in $a_{\pm}\sigma_d$, vary between $-0.33$ and $-0.21\ cm^2\ \mu C^{-1}$ for ionic strengths in the range 0.05 to 0.50 *M*. Considering the fact that their analysis differs from that given above, the agreement with the present data is satisfactory.

In conclusion, the present results show clearly that discreteness-of-charge effects must be considered in analyzing the effects of specifically adsorbed ions on electron transfer reactions. Assessment of these effects should be based on data obtained at constant ionic strength; otherwise it becomes exceedingly difficult to separate the various contributions, specifically, the exclusion disc effect and the effects of attractive ion–ion interactions. Finally, it should be recognized that the above analysis is based on the Gouy–Chapman theory of the diffuse layer. On the basis of recent theoretical work (32), it is clear that $|\phi^d|$ is overestimated by the Gouy–Chapman model but to an extent of less than 10% for the range of charge densities and ionic strength involved here. This model is used in the analysis of both the equilibrium adsorption data and the kinetic data. Thus, the error introduced in these analyses is not estimated to be large so that the magnitude of the discreteness-of-charge effect is not expected to change significantly if an improved model of the diffuse layer were used.

**Acknowledgement**

The financial assistance of the Natural Sciences and Engineering Research Council is gratefully acknowledged.

1. W. R. Fawcett and S. Levine. J. Electroanal. Chem. **43**, 175 (1973).

[2]In the paper of Žežula *et al.* (17), there is a contradiction with respect to sign between the data presented in Table 1 and Fig. 2. We have assumed that the sign given in Table 1 is correct.

2. R. GUIDELLI. J. Electroanal. Chem. **53**, 205 (1974).
3. W. R. FAWCETT. J. Chem. Phys. **61**, 3842 (1974).
4. W. R. FAWCETT and S. LEVINE. J. Electroanal. Chem. **65**, 505 (1975).
5. R. GUIDELLI. J. Electroanal. Chem. **74**, 347 (1976).
6. V. S. KRYLOV, W. R. FAWCETT, and V. A. KIR'YANOV. Elektrokhimiya, **12**, 424 (1976).
7. V. S. KRYLOV, W. R. FAWCETT, and V. A. KIR'YANOV. Elektrokhimiya, **12**, 543 (1976).
8. R. R. DOGONADZE and A. M. KUZNETSOV. Kinetics and catalysis, Itogi Nauki i Tekhniki. Vol. 5. Moscow. 1978.
9. M. A. VOROTYNTSEV. Electrochemistry, Itogi Nauki i Tekhniki. Vol. 14. Moscow. 1979. Chapt. 2.
10. V. S. KRYLOV, V. A. KIR'YANOV, and I. F. FISHTIK. Elektrokhimiya, **16**, 340 (1980).
11. I. F. FISHTIK and V. S. KRYLOV. Elektrokhimiya, **16**, 636 (1980).
12. I. F. FISHTIK and V. S. KRYLOV. Elektrokhimiya, **16**, 641 (1980).
    Nauka. Moscow. 1979. Chapt. 9.
13. V. S. KRYLOV, V. A. KIR'YANOV, and I. F. FISHTIK. J. Electroanal. Chem. **109**, 115 (1980).
14. W. R. FAWCETT. Can. J. Chem. **59**, 1844 (1981).
15. A. N. FRUMKIN. Potentials of zero charge, Izdatelstvo Nauka, Moscow. 1979. Chapt. 9.
16. M. L. FORESTI and R. GUIDELLI. J. Electroanal. Chem. **53**, 219 (1974).
17. I. ŽEŽULA, V. RYCHNAVSKÁ, and E. ALEXYOVÁ. J. Electroanal. Chem. **86**, 433 (1978).
18. I. ŽEŽULA. Chem. listy. **47**, 485 (1953); **47**, 492 (1953).
19. I. ŽEŽULA. Coll. Czech. Chem. Commun. **33**, 18 (1968).
20. I. ŽEŽULA. Coll. Czech. Chem. Commun. **33**, 2327 (1968).
21. A. N. FRUMKIN and N. NIKOLAEVA-FEDOROVICH. *In* Progress in polarography. Vol. 1. *Edited by* P. Zuman and I. M. Kolthoff. Wiley-Interscience, New York. 1962. p. 223.
22. W. R. FAWCETT and T. A. MCCARRICK. J. Electrochem. Soc. **123**, 1325 (1976).
23. J. KOUTECKÝ and J. ČIŽEK. Coll. Czech. Chem. Commun. **21**, 836 (1956).
24. P. DELAHAY. Double layer and electrode kinetics. Wiley-Interscience, New York. 1965. Chapt. 9.
25. S. LEVINE. J. Colloid Interfac. Sci. **37**, 619 (1971).
26. D. C. GRAHAME. J. Am. Chem. Soc. **80**, 4201 (1958).
27. E. DUTKIEWICZ and R. PARSONS. J. Electroanal. Chem. **11**, 100 (1966).
28. A. BARANSKI and W. R. FAWCETT. J. Electroanal. Chem. **100**, 185 (1979).
29. W. R. FAWCETT. J. Electroanal. Chem. **22**, 19 (1969).
30. W. R. FAWCETT and Y. C. KUO LEE. Can. J. Chem. **49**, 2657 (1971).
31. A. S. BARANSKI and W. R. FAWCETT. J. Chem. Soc. Faraday Trans. I, **76**, 1962 (1980).
32. D. HENDERSON and L. BLUM. Can. J. Chem. **59**, 1906 (1981).
33. N. V. FEDOROVICH, A. N. FRUMKIN, and KH. E. KEYS. Coll. Czech. Chem. Commun. **36**, 722 (1971).
34. L. GIERST. *In* Trans. Symp. on Electrode Processes. *Edited by* E. Yeager. Philadelphia, 1959; Wiley, New York. 1961. p. 109.
35. T. OHSAKA and R. DE LEVIE. J. Electroanal. Chem. **99**, 255 (1979).

Can. J. Chem. Downloaded from www.nrcresearchpress.com by 210.87.254.42 on 09/06/12
For personal use only.

Can. J. Chem. Downloaded from www.nrcresearchpress.com by 210.87.254.105 on 09/06/12
For personal use only.

COMMUNICATION

# The structure of demethoxyrapamycin

JOHN A. FINDLAY, JIA-SEN LIU, AND D. JEAN BURNELL

*Department of Chemistry, University of New Brunswick, Bag Service #45222, Fredericton, N.B., Canada E3B 6E2*

AND

THOMAS T. NAKASHIMA

*Department of Chemistry, University of Alberta, Edmonton, Alta., Canada T6G 2G2*

Received April 6, 1982

JOHN A. FINDLAY, JIA-SEN LIU, D. JEAN BURNELL, and THOMAS T. NAKASHIMA. Can. J. Chem. **60**, 2046 (1982).

The structure **2**, 29-demethoxyrapamycin, is proposed for a new antibiotic from *Streptomyces hygroscopicus* and has been deduced by comparison of high field $^1H$ and $^{13}C$ nmr spectra, ir, uv, and mass spectra, and ORD/CD curves with those of the known antifungal antibiotic rapamycin **1**.

JOHN A. FINDLAY, JIA-SEN LIU, D. JEAN BURNELL et THOMAS T. NAKASHIMA. Can. J. Chem. **60**, 2046 (1982).

On propose la structure **2**, déméthoxy-29 rapamycine, pour le nouvel antibiotique obtenu à partir du *Streptomyces hygroscopicus*. On a déduit cette structure en comparant les spectres de rmn à haut champ du $^1H$ et du $^{13}C$, les spectres ir, uv, les spectres de masse et les courbes de ORD/DC du produit à ceux de l'antibiotique antifongique connu: la rapamycine **1**.

We reported (1, 2) recently on the structure, absolute configuration, chemistry, and high field nmr spectroscopy of the macrolide antifungal antibiotic rapamycin **1**, $C_{51}H_{79}NO_{13}$, isolated from cultures of *Streptomyces hygroscopicus*. In this paper we propose structure **2**, 29-demethoxyrapamycin, for a new crystalline (mp 107–108°C) antibiotic isolated (3) from the same source.

The uv spectrum ($CH_3OH$) of the latter ($\lambda_{max}$: 288, 276, 266; $E^{1\%}_{1cm}$: 423, 549, 421) is virtually identical with that of the triene rapamycin while the ir ($CHCl_3$) showing 3500 (OH), 1730, 1712 (ester, ketones), and 1640 (broad, amide/triene) $cm^{-1}$ is very similar to that of **1** (4). Elemental analysis, while not definitive, is reasonably consistent with $C_{50}H_{77}NO_{12}$ (calcd.: C 67.95, H 8.72, N 1.58, O 21.74; found: C 67.86, H 8.94, N 1.68, O 21.52). Attempts to obtain supportive mass spectral data for the molecular formula of demethoxyrapamycin have met with limited success. High resolution EI spectra of **1** and **2** are similar in that neither shows a molecular ion but both feature the base peak *m/e* 175.112 ($C_{12}H_{15}O$) and a prominent higher mass ion at *m/e* 304.2035 (28, $C_{19}H_{28}O_3$), both ions originating from the fragmentation and aromatization of a moiety derived by cleavage of the C20—C21 and C28—C29 bonds of rapamycin as proposed (2) by us earlier. The highest ion observed in the EI spectrum of rapamycin **1** at *m/e* 541.3051 (7.4, $C_{31}H_{43}NO_7$) corresponds to the larger fragment ($C_{20,19,\ldots} \rightarrow C_{29}$ incl.) derived by the same two bond cleavages accompanied by the net loss of 4H. The EI spectrum of demethoxyrapamycin **2** shows a highest and isolated ion at *m/e* 511.2944 (1.8, $C_{30}H_{41}NO_6$), readily explained via cleavages at the same C20—C21 and C28—C29 bonds and clearly supporting the contention that rapamycin and demethoxyrapamycin have the

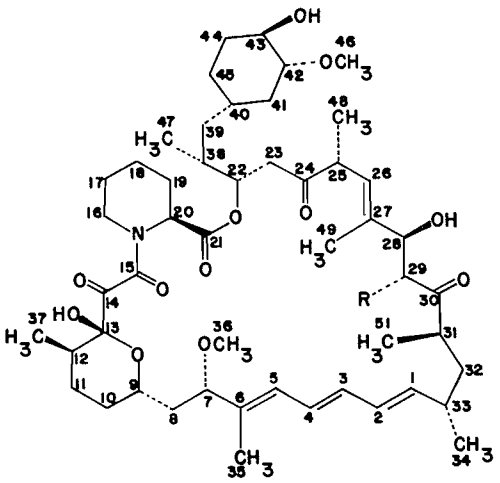

**1** R = $^{50}CH_3O$

**2** R = H

0008-4042/82/152046-02$01.00/0

©1982 National Research Council of Canada/Conseil national de recherches du Canada

TABLE 1. ORD/CD data

| Compound | ORD maxima ($CH_3OH$) | CD maxima ($CH_3OH$) |
|---|---|---|
| **1** | $[\theta]_{315} = -90\,000$<br>$[\theta]_{260} = +77\,000$ | $[\theta]_{296} = -143\,000$<br>$[\theta]_{215} = +90\,000$ ($c = 0.0005$) |
| **2** | $[\theta]_{305} = -80\,000$<br>$[\theta]_{260} = +34\,000$ | $[\theta]_{290} = -112\,000$<br>$[\theta]_{210} = +87\,000$ ($c = 0.00043$) |

identical structural features at all sites except C29 and that they differ in elemental composition by the increment of $CH_2O$.

Corroborative evidence for the elemental composition of rapamycin **1** is available from its CI ($NH_3$) spectrum which displays an ion at *m/e* 931 ($913 + \overset{+}{N}H_4$). The comparable spectrum of demethoxyrapamycin shows its highest mass ion cluster around *m/e* 901 ($883 + \overset{+}{N}H_4$); however, this peak is less intense than the accompanying *m/e* 900 and 902 ions in some scans.

The FD mass spectrum of demethoxyrapamycin shows an ion at *m/e* 883 (69, $C_{50}H_{77}NO_{12}$) but this is complicated by the appearance of a base peak *m/e* 888 as well as an ion at *m/e* 1234 (62.5). In several FD scans rapamycin displays the correct molecular ion *m/e* 913 (100) while in others it shows *m/e* 913 (75) and 882 (100), the latter corresponding to $M^+ - OCH_3$.

The 100.6 MHz $^{13}C$ nmr spectrum ($C_6D_6$) of the new metabolite **2** contains fifty signals all of which have their counterparts in the $^{13}C$ nmr of rapamycin (2). The notable differences are the absence of a signal corresponding to the rapamycin C50 methoxyl and the chemical shift of the signal corresponding to C29, which in the new compound is found at higher field (δ 47.49) than in rapamycin (δ 84.87). These differences are in complete agreement with formulation **2**.

The 400 MHz $^1H$ nmr spectra ($CDCl_3$) of **2** and **1** (2) are remarkably similar except for the absence in the former of a signal corresponding to H-50 and the concomitant presence of signals for two H-29 protons, δ 2.64 ppm ($J_{28,29A} = 9.2$ Hz, $J_{29A,20B} = 17.4$ Hz) and 2.52 ppm ($J_{28,29B} = 2.8$, $J_{29A,29B} = 17.4$ Hz), whose assignments were confirmed by $^1H$–$^1H$ decoupling experiments.

The ORD and CD curves of **1** and **2** (Table 1) are not superimposable but very similar, consistent with the proposal that these molecules, originating from the same organism, are most probably configurationally identical at all common chiral centres but differ in some conformational aspects.

As in the case of rapamycin **1**, the $^{13}C$ and $^1H$ nmr spectra of **2** are complicated by the presence in solution of a minor (~ 20%) isomer component. Additional experiments are in progress to determine the nature of this isomerism and to complete the analysis of nmr spectral data.

We thus conclude that the new metabolite is 29-demethoxyrapamycin, **2**, that it exists in two isomeric forms in solution, and that the absolute configuration is as portrayed in **2** by analogy with rapamycin.

**Acknowledgements**

The authors are grateful to Ayerst Laboratories, Montreal, for providing material (AY-24,668), some spectral data (ir, uv), and financial assistance. The cooperation of Gordon Wood, University of Windsor, in obtaining FD mass spectra and Alan Hogg, Spectral Services Laboratory, Department of Chemistry, University of Alberta, in furnishing CI and EI spectra is much appreciated. The ORD/CD curves were obtained from the Spectral Services Laboratory, University of Alberta. This work was supported, in part, by a grant from the Natural Sciences and Engineering Research Council of Canada.

1. D. C. NEIL SWINDELLS, PETER S. WHITE, and JOHN A. FINDLAY. Can. J. Chem. **56**, 2491 (1978).
2. JOHN A. FINDLAY and LAJOS RADICS. Can. J. Chem. **58**, 579 (1980); JOHN A. FINDLAY and LAJOS RADICS. Can. J. Chem. **59**, 49 (1981).
3. CLAUDE VEZINA, ALICIA KUDELSKI, and S. N. SEGHAL. J. Antibiot. **XXVIII**, 721 (1975).
4. S. N. SEGHAL, H. BAKER, and C. VEZINA. J. Antibiot. **XXVIII**, 727 (1975).

Can. J. Chem. Downloaded from www.nrcresearchpress.com by 210.87.254.105 on 09/06/12
For personal use only.

# Dipole moments and conformation energies for substituted ethanes

VICTOR M. S. GIL
*Department of Chemistry, University of Aveiro, 3800 Aveiro, Portugal*
AND
ANTÓNIO J. C. VARANDAS
*Department of Chemistry, University of Coimbra, 3000 Coimbra, Portugal*

Received September 25, 1981[1]

VICTOR M. S. GIL and ANTÓNIO J. C. VARANDAS. Can. J. Chem. **60**, 2049 (1982).

By using simple model potential energy functions for internal rotation of ethane derivatives ($CH_2X$–$CH_2X$ and $CHX_2$–$CHX_2$), a comparison was made between the continuum and the rotational isomeric state models for obtaining conformation information (especially energy differences for the staggered conformers) from electric dipole moments. It is found that the results obtained by the two procedures may be appreciably different, depending on the features of the conformational energy function and on the temperature considered.

VICTOR M. S. GIL et ANTÓNIO J. C. VARANDAS. Can. J. Chem. **60**, 2049 (1982).

Faisant appel à un modèle simple de fonctions d'énergie potentielle pour la rotation interne des dérivés de l'éthane ($CH_2X$–$CH_2X$ et $CHX_2$–$CHX_2$), on a établi une comparaison entre le modèle continium et le modèle d'état de l'isomère de rotation pour obtenir des informations sur les conformations (spécialement les différences d'énergie entre les conformères décalés) à partir des moments dipolaires électriques. On a trouvé que les résultats obtenus par les deux méthodes peuvent différer de façon appréciable en fonction des caractéristiques de la fonction d'énergie conformationnelle et de la température considérée.

[Traduit par le journal]

## Introduction

The use of electric dipole moments to obtain conformational information on molecules possessing rapid internal rotation, especially substituted ethanes, is well known (1, 2). The most widely used method assumes, namely, that (a) bond and group dipole moments (or atomic charges) are invariant to internal rotation, and (b) the mean-square dipole moment $\overline{\mu^2}$, which is an average for all possible

$$[1] \quad \overline{\mu^2} = \int_0^{2\pi} \mu^2(\theta) \exp[-E(\theta)/RT]d\theta \Big/ \int_0^{2\pi} \exp[-E(\theta)/RT]d\theta$$

conformations of rotation angle $\theta$ (in a classical view of an internally rotating molecule, $E(\theta)$ being the corresponding potential energy function) can be treated as a weighted (populations $p_i$) average of the discrete $\mu_i^2$ values which correspond to the three most stable conformers (the so-called rotational isomeric state approximation):

$$[2] \quad \overline{\mu^2} = \sum_{i=1,2,3} \mu_i^2 p_i$$

In a theoretical work essentially aiming at determining the main features of the conformational energy functions for chloroethanes, Mark and Sutton (3) have found that (for those chloroethanes where dipole moments are a function of the rotation angle, and for temperatures ranging from 298 K to 400 K) assumption (b) is a valid one as far as the calculated root-mean-square dipole moment $(\overline{\mu^2})^{1/2}$ is concerned, providing the discrete rotational isomeric states are taken at the actual minima in the conformation potential energy function, instead of the classical staggered conformers corresponding to $\theta = 60°$, 180°, and 300°, as in ethane. A different result was later found by Vaughan (4) using a slightly different potential function. He also discussed the limits on the application of the rotational isomeric state method to the study of dynamic properties.

In order to establish how the agreement between the continuum and the rotational isomeric state models depends on the features of the conformation energy function and to investigate the validity of this approximation as far as calculated $\Delta E$ values for the most stable conformers are concerned, we have initiated a series of simple calculations using model potential energy functions of increasing complexity. We have previously found that, when vicinal H—H nuclear spin coupling constants are used as the conformational dependent property, the continuum and the discrete approaches (ignoring entropy differences) give significantly different results, the differences being temperature dependent (5). Assumption (a), which is also questionable, is not, however, dealt with in the present study.

[1]Revision received March 18, 1982.

0008-4042/82/162049-08$01.00/0
©1982 National Research Council of Canada/Conseil national de recherches du Canada

Can. J. Chem. Downloaded from www.nrcresearchpress.com by 210.87.254.6 on 09/06/12
For personal use only.

Can. J. Chem. Downloaded from www.nrcresearchpress.com by 210.87.254.6 on 09/06/12
For personal use only.

We start by considering the most symmetrical systems $CH_2X$–$CH_2X$ and $CHX_2$–$CHX_2$ where only two different conformational energy minima occur; we further consider the dipole moment vector to be given as a sum of two local dipoles of equal magnitude $\mu_0$. Accordingly, for the staggered conformations of $CH_2X$–$CH_2X$

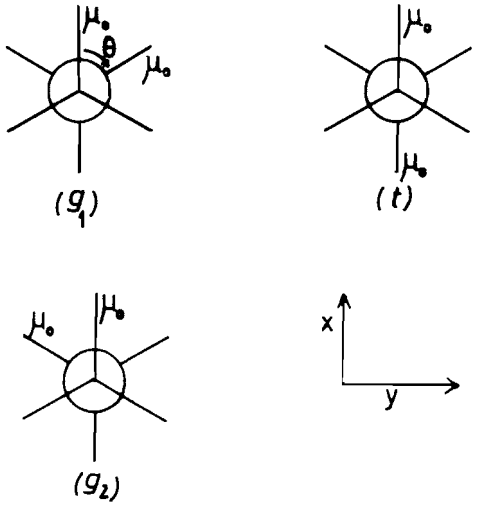


(and similarly for the $CHX_2$–$CHX_2$ system) we have

[3] $\Delta E = E_g - E_t$

the dependence of $\mu^2$ on $\theta$ being given by

[4] $\mu^2 = \mu_x^2 + \mu_y^2 = m_0^2 (1 + \cos\theta)^2 + m_0^2 \times \sin^2\theta = 2m_0^2 (1 + \cos\theta)$

where $m_0$ is the magnitude of the projected local dipoles on the plane perpendicular to the CC bond ($z$ axis). We will, in particular, compare the "true" $\Delta E$ values obtained directly from the minima of the potential energy curves with the corresponding apparent $\Delta E'$ values which are obtained using the discrete average approach, ignoring entropy differences. We will also compare $\overline{\mu^2}$ and $\overline{\mu'^2}$ values obtained by the continuum and the discrete procedures.

The simplest type of energy functions we have used are given by curves *a* and *b* in Fig. 1, that is, we assume that all eclipsed conformations have the same energy (a condition that is relaxed later, curve *c*) and that the conformational energy minima correspond exactly to $\theta = 60$, 180, and 300°. The form of the $E(\theta)$ function in the interval 0–120° has been taken as $E(60°) \times (1\text{-}\cos 3\theta)/2$ and similarly for the intervals 120–240° and 240–360°; this is the

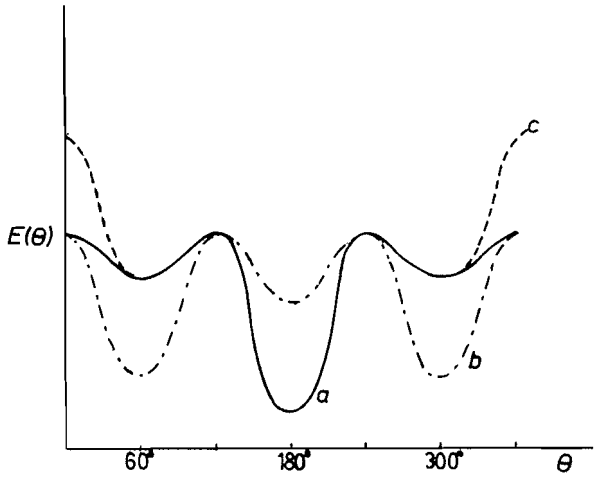


FIG. 1. Types of potential energy functions used.

form of the leading term in the potential energy function for ethane (6).

In a second set of calculations we have taken curves of type *c* in Fig. 1. This is derived from *a* by increasing the energy of the *cis* conformation (the case, for instance, of 1,2-dichloroethane (3)) and keeping the same type of function in the intervals 0–60° and 300–360°. For simplicity the minima have been supposed to occur at the same $\theta$ values. We note that the estimated deviation in such minima is only of the order of 10° in 1,2-dichloroethane where the energy of the *cis* conformation is well above that for the other eclipsed conformations (3).

Using [4] and [1], we simulate "observed" $\overline{\mu^2}$ values (by direct numerical integration of [1]) for various well depths and temperatures. These values are then used to calculate the effective populations, $t$, $g_1 = g_2$, of the three rotational isomers, by applying [2]:

[5] $\overline{\mu^2} \equiv 2m_0^2 \quad \overline{(1 + \cos\theta)} = \mu_t^2 . t + 2\mu_{g_1}^2 . g_1 = 2\mu_{g_1}^2 . g_1 = 6m_0^2 g_1$

(where $\mu_t^2 = 0$ and $\mu_{g_1}^2 = 3m_0^2$ for $\theta = 60°$) in conjunction with the relationship

[6] $t + 2g_1 = 1$

The calculated $\Delta E'$ value is

[7] $\Delta E' = E'_{g_1} - E'_t = RT \ln t/g_1$

which is to be compared with the original $\Delta E$ value.

We also compare the "observed" $\overline{\mu^2}$ values with the corresponding $\overline{\mu'^2}$ quantities which would be obtained if only the staggered conformations, with

Can. J. Chem. Downloaded from www.nrcresearchpress.com by 210.87.254.6 on 09/06/12
For personal use only.

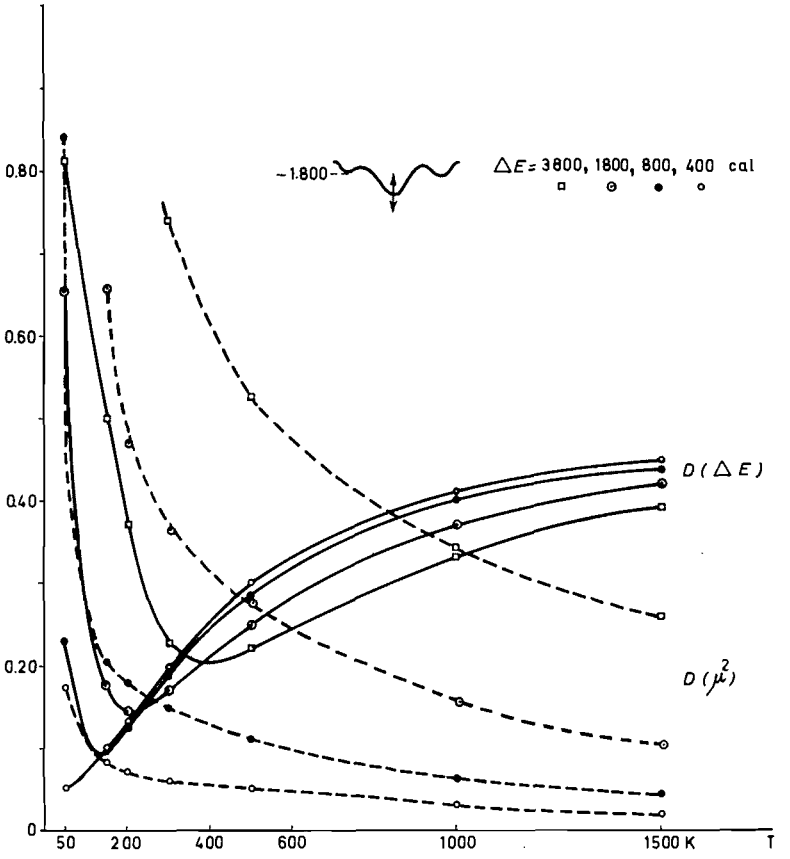


FIG. 2. The deviations $D(\Delta E)$ and $D(\mu^2)$ as a function of $T$ and $\Delta E$, for various $E(\theta)$ functions of type (a) differing in $E_t$ from each other.

energies given by the potential energy functions used, were populated (populations $t'$, $g_1' = g_2'$). The general scheme is illustrated below.

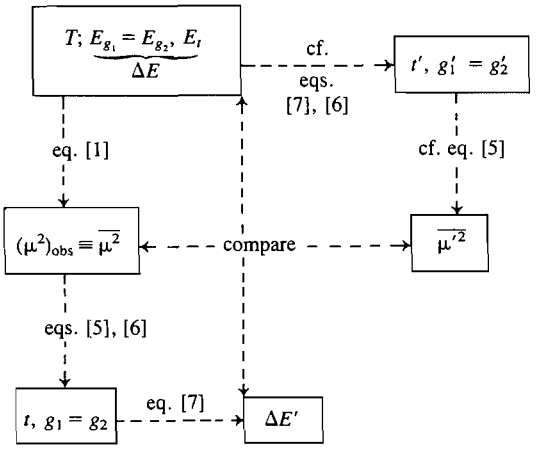


The differences between $\Delta E$ and $\Delta E'$ and between $\overline{\mu^2}$ and $\overline{\mu'^2}$ stem, in a related manner, from the difference between populations $t$ and $t'$ (or $g$ and $g'$).

## Results and discussion

### (a) *Simple* E(θ) *functions*

Figures 2 and 3 show the deviations $D(\Delta E) = (\Delta E - \Delta E')/\Delta E$ and $D(\mu^2) = |\overline{\mu^2} - \overline{\mu'^2}|/\overline{\mu^2}$ as a function of $T$, obtained with energy functions of type (a) (see Fig. 1) and keeping $E(60°) = E(300°)$ constant while varying $E(180°)$, or vice versa. The corresponding $D(\Delta E)$ and $D(\mu^2)$ curves for functions of type (b) are shown in Figs. 4 and 5.

Whereas these figures essentially show the effect of $\Delta E$ on $D(\Delta E)$ and $D(\mu^2)$ as a function of $T$, Fig. 6 illustrates the effect of the depth of the potential wells, while keeping $\Delta E$ the same. We note that the addition of a constant to $E(\theta)$ does not lead to any changes, as can be directly seen from eq. [1]. Multiplication of a given $E(\theta)$ by a constant $\lambda$, thus changing simultaneously $\Delta E$ and the depth of the energy wells, leads to $D(\Delta E)$ and $D(\mu^2)$ curves that

Can. J. Chem. Downloaded from www.nrcresearchpress.com by 210.87.254.6 on 09/06/12
For personal use only.

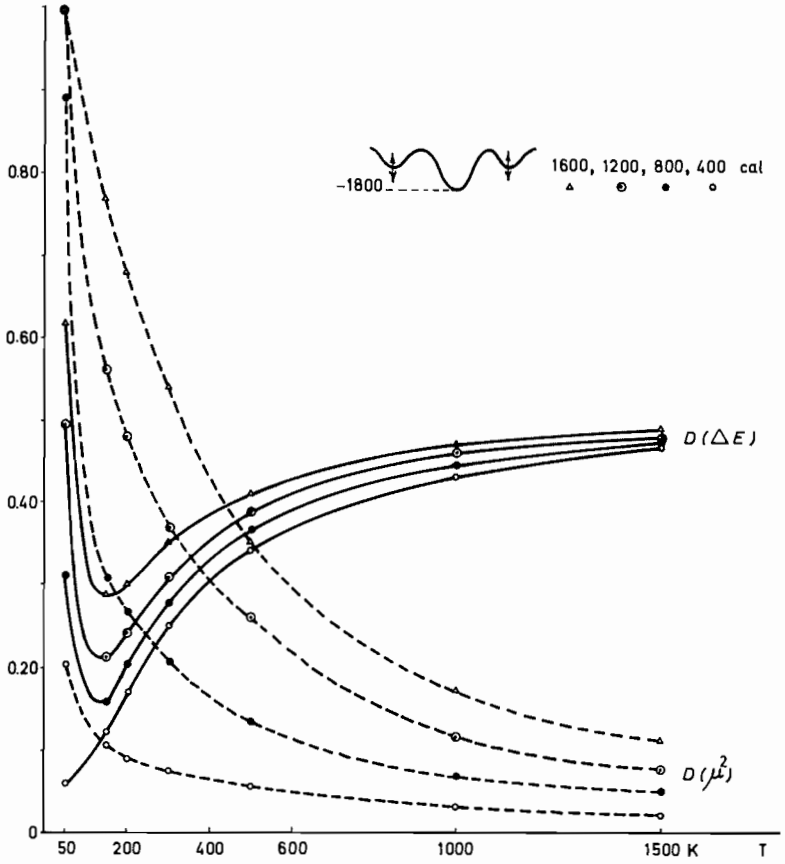


FIG. 3. The deviations $D(\Delta E)$ and $D(\mu^2)$ as a function of $T$ and $\Delta E$, for various $E(\theta)$ functions of type (a) differing in $E_g$ from each other.

can be easily related to the original curves using eq. [1] (5):

[8] $D(\Delta E)\ [E(\theta), T] = D(\Delta E)\ [\lambda E(\theta), \lambda T]$

[9] $D(\mu^2)\ [E(\theta), T] = D(\mu^2)\ [\lambda E(\theta), \lambda T]$

The crossing observed in the $D(\Delta E)$ curves of Figs. 2 and 5 but not in Figs. 3 and 4 can be rationalized as was done in ref. 5. As a matter of fact, the $D(\Delta E)$ curves now obtained are very similar to those constructed on the basis of H—H nuclear spin coupling constants $J$ (5).

As in the work with $J_{HH}$ (5), $|\Delta E'|$ is always smaller than $|\Delta E|$ for a given temperature. The same explanation can be given. Going from a continuum procedure to the rotational isomeric state approximation corresponds to a "transfer" of part of the population from the intermediate conformations into the three minimal energy rotamers; as a result, a bigger increase in the effective population is produced in the case of the upper minima ($g_1$ and $g_2$ for curves $a$) which then appear to be stabilized with respect to the lower minima ($g_1 > g_1'$, $t < t'$ for energy functions $a$). In parallel with these results, one finds $\overline{\mu'^2} < \overline{\mu^2}$ for situations of type $a$ (Figs. 2, 3) and the opposite for curves of type $b$ (Figs. 4, 5).

The discriminating effect of such a "transfer" of population is, of course, expected to decrease as the potential wells become deeper or the $|\Delta E|$ value becomes smaller. This is observed for the $D(\Delta E)$ values in Figs. 3 and 4, and for lower temperatures in the cases of Figs. 2 and 5. It is noted that, in the latter, a decrease of $|\Delta E|$ is accompanied by a raising of the lower minima (um), giving rise to two opposite effects whose relative importance depends on the temperature.

Now, $D(\Delta E)$ and $D(\mu^2)$ can be written as follows:

[10] $D(\Delta E) = 1 - (\ln t/g_1)/(\ln t'/g_1')$

[11] $D(\mu^2) = 1 - g_1'/g_1$

For energy functions of type $a$ (Figs. 2 and 3) the following rationalization of the shapes of $D(\Delta E)$ and $D(\mu^2)$ as a function of $T$ can be offered. When $T \to \infty$, $t$, $g_1$, $t'$, and $g_1'$ all tend to a common value:

Can. J. Chem. Downloaded from www.nrcresearchpress.com by 210.87.254.6 on 09/06/12
For personal use only.

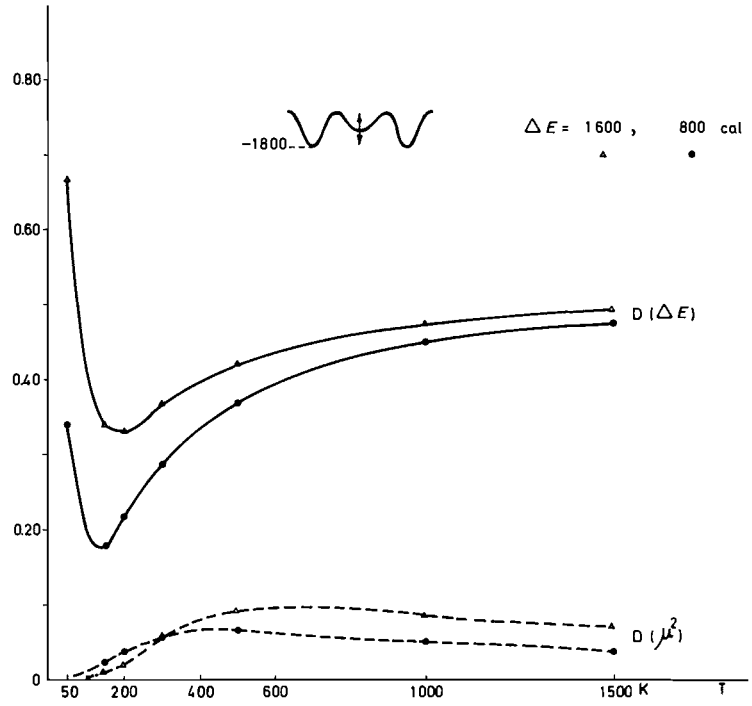


FIG. 4. The deviations $D(\Delta E)$ and $D(\mu^2)$ as a function of $T$ and $\Delta E$, for various $E(\theta)$ functions of type (b) differing in $E_t$ from each other.

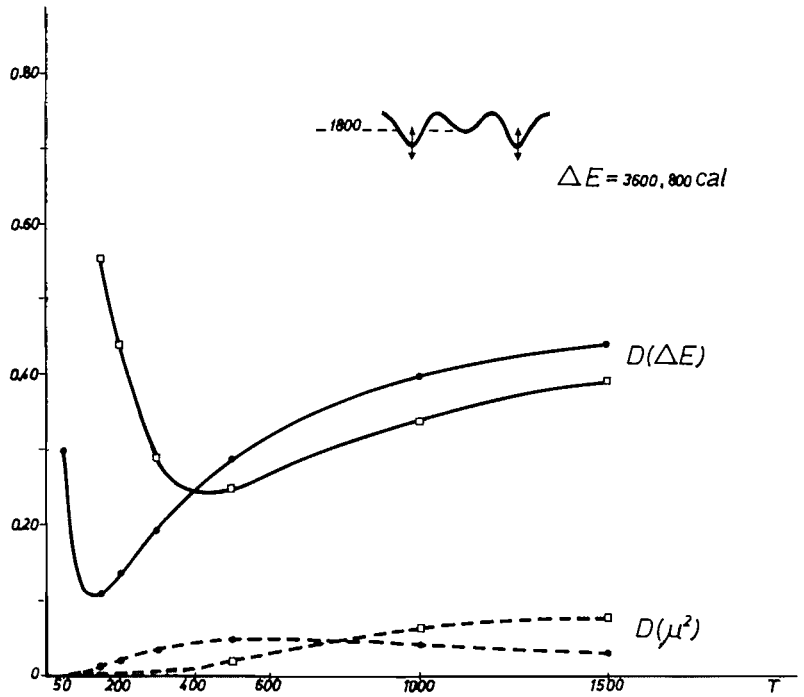


FIG. 5. The deviations $D(\Delta E)$ and $D(\mu^2)$ as a function of $T$ and $\Delta E$, for various $E(\theta)$ functions of type (b) differing in $E_a$ from each other.

Can. J. Chem. Downloaded from www.nrcresearchpress.com by 210.87.254.6 on 09/06/12
For personal use only.

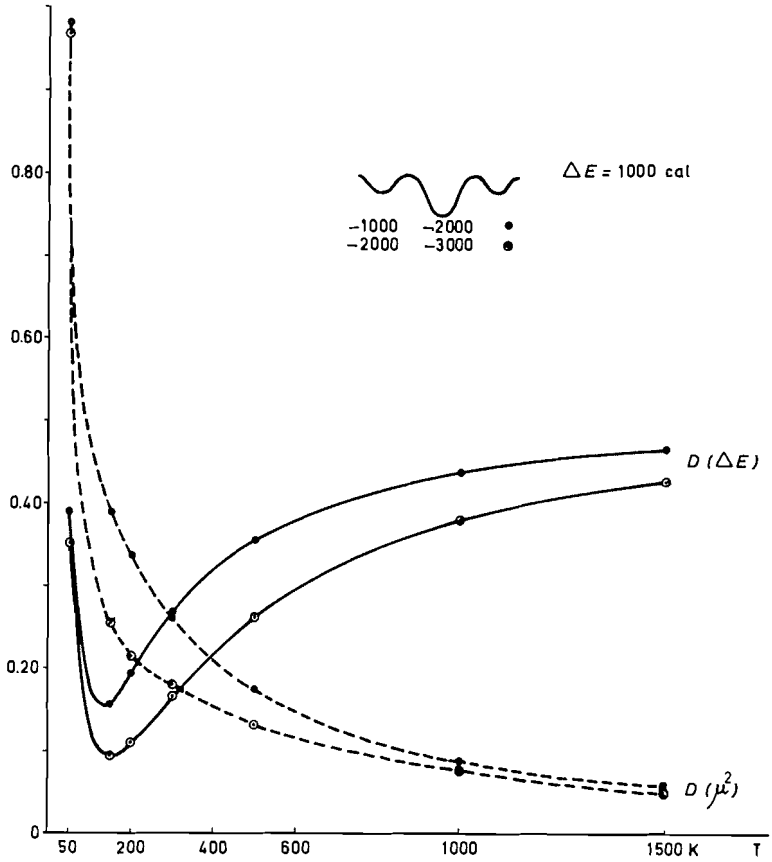


FIG. 6. The effect on $D(\Delta E)$ and $D(\mu^2)$ of the depth of the potential wells (energy functions of type (a)).

1/3; as a result, $D(\Delta E)$ goes to a constant and $D(\mu^2)$ goes to zero. When $T \rightarrow 0$, only the *trans* conformation becomes populated, that is $g_1$ and $g_1'$ go to zero; since $g_1' < g_1$ ($t' > t$), $D(\Delta E)$ and $D(\mu^2)$ both go to 1. For curves of type *b*, a similar reasoning applies; now, when $T \rightarrow 0$, $g_1', g_1 \rightarrow 1$ and $D(\mu^2) \rightarrow 0$ (Figs. 4 and 5).

At this stage we can already conclude that the $\Delta E'$ values calculated from observed dipole moments, using the rotational isomeric state approximation, may be affected by appreciable (temperature-dependent) errors. The same is true of the averaged dipole moments calculated from local dipoles (or atomic charges) and $\Delta E$ values, especially in the cases when the *trans* conformation is more stable than the *gauche* ones; it should be noted, however, that the discrepancy is not as dramatic as Figs. 2 and 3 might suggest, because when the large percentual errors occur the dipole moments are small.

(b) *More realistic* E(θ) *functions*

The conclusion above regarding the deviations of calculated dipole moments is at variance with the calculations of Mark and Sutton (3), namely for 1,2-dichloroethane. Taking a given $E(\theta)$ function, the values they have obtained for the dipole moment are practically the same when using the continuum model and the rotational isomeric state model for $T = 298$ K; the same can be said of the temperature coefficients of the dipole moment in the vicinity of 298 K.

An important difference with respect to the calculations we have done above is that the $E(\theta)$ function they have used is of type *c* in Fig. 1, and not of type *a*. We anticipate that the decrease of population for the *cis* conformation (and for those of $300° < \theta < 60°$) has the effect of reducing the apparent stabilization of the *gauche* conformations with respect to *trans*, on going from a continuum procedure to a discrete one. That is, $\Delta E'$ will become closer to $\Delta E$ and so will the calculated dipole moments, up to the point $\Delta E = \Delta E'$ and $\overline{\mu^2} = \overline{\mu'^2}$. Continuing to increase the energy of the *cis* conformation, the *trans* conformation will become stabilized, $\Delta E' > \Delta E$ and $\overline{\mu^2} < \overline{\mu'^2}$.

These conclusions are corroborated by the calculations using *c* energy functions of variable $E(0°)$

Can. J. Chem. Downloaded from www.nrcresearchpress.com by 210.87.254.6 on 09/06/12
For personal use only.

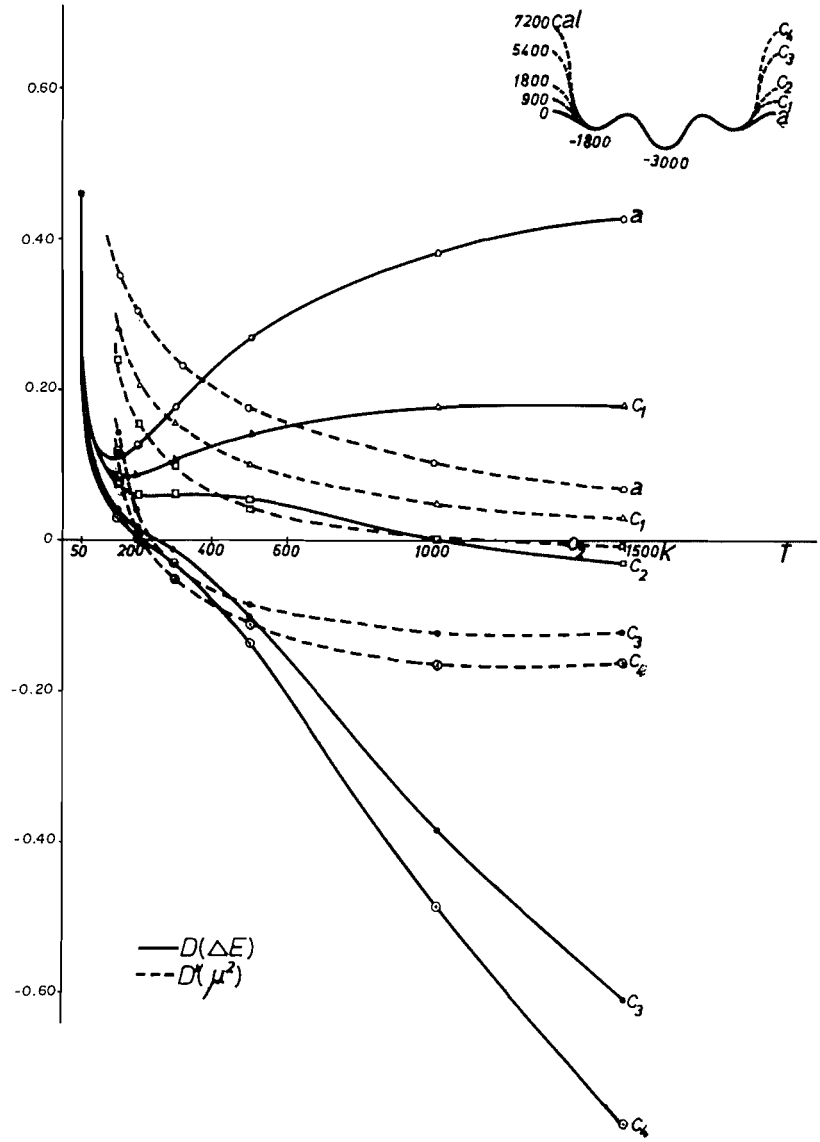


FIG. 7. The effect on $D(\Delta E)$ and $D'(\mu^2)$ of increasing the energy of conformation *cis* with respect to an energy function of type (a). $D'(\mu^2)$ is defined as $(\mu^2 - \overline{\mu'^2})/\mu^2$.

values, as shown in Fig. 7. The $E(\theta)$ function $c_4$ is close to that calculated by Mark and Sutton (3) for 1,2-dichloroethane; in this case, in fact, the deviations $D(\Delta E)$ and $D'(\mu^2)$ for $T = 298$ K are very small ($D'(\mu^2)$ is defined as $(\mu^2 - \mu'^2)/\mu^2$). Further insight is obtained by comparing the ratio of populations $t'/g'$ and $\mu'^2$ for 298 K, for example, calculated from a $\Delta E$ value of 1200 cal,

[12] $\Delta E = 1200 = RT \ln t'/g'$

[13] $t'/g' = 7.59$

[14] $\overline{\mu'^2} = 0.625\, m_0^2$

with the ratios of the total populations (at 298 K) corresponding to the intervals 120°–240° and 0–120°, respectively $t^*$ and $g^*$, for the various $E(\theta)$ functions of Fig. 7:

$$t^*(a)/g^*(a) = 5.58$$
$$t^*(c_1)/g^*(c_1) = 6.26$$
$$t^*(c_2)/g^*(c_2) = 6.71$$
$$t^*(c_3)/g^*(c_3) = 7.67$$
$$t^*(c_4)/g^*(c_4) = 7.95$$

The corresponding $\Delta E^*$ and $\overline{\mu^{*2}}$ values obtained using the discrete average approach are as follows (the $\Delta E'$ and $\mu^2$ values are given in brackets):

| | | | |
|---|---|---|---|
| $\Delta E^*(a)$ = 1018 cal | (989) | $\overline{\mu^{*2}}(a)$ = 0.792 $m_0^2$ | (0.821) |
| $\Delta E^*(c_1)$ = 1086 | (1074) | $\overline{\mu^{*2}}(c_1)$ = 0.726 | (0.737) |
| $\Delta E^*(c_2)$ = 1127 | (1126) | $\overline{\mu^{*2}}(c_2)$ = 0.689 | (0.690) |
| $\Delta E^*(c_3)$ = 1206 | (1220) | $\overline{\mu^{*2}}(c_3)$ = 0.620 | (0.609) |
| $\Delta E^*(c_4)$ = 1228 | (1245) | $\overline{\mu^{*2}}(c_4)$ = 0.603 | (0.584) |

## Conclusion

We can thus conclude that, apart from other sources of error, the use of the rotational isomeric state approximation in conformational studies of internally rotating molecules, based on molecular dipole moments, may lead to appreciable errors, especially as far as the computation of $\Delta E$ values is concerned, depending on the features of the conformational energy function and on the temperature considered. Those cases referred to in the literature (3), where the continuum and the discrete average methods lead to very similar results, are accidental.

After this work was completed, Honegger and Heilbronner (7) published a similar criticism of the rotational isomeric state model when used in conjunction with photoelectron spectral bands.

Further work is in progress regarding other molecular systems. In addition, a general study of the rotational isomeric state method is being carried out, aiming at the identification of the main sources of error affecting enthalpy and entropy values according to the θ-variation of the conformation-dependent property, the form of the potential function, and the temperature.

## Acknowledgements

This work is also a contribution of the Centro de Investigação Química (INIC) at the University of Coimbra. The principal results were presented at the 4th Meeting of the Portuguese Chemical Society, Lisbon, April, 1981. The authors thank Professor John N. Murrell for helpful discussions.

1. S. MIZUSHIMA. The structure of molecules and internal rotation. Academic Press, New York. 1954, and references therein.
2. W. J. ORVILLE-THOMAS (*Editor*). Internal rotation in molecules. Wiley, London. 1974, and references therein.
3. J. E. MARK and C. SUTTON. J. Am. Chem. Soc. **94**, 1083 (1972).
4. W. E. VAUGHAN. Adv. Mol. Relaxation Processes, **13**, 171 (1978).
5. V. M. S. GIL and A. J. C. VARANDAS. J. Magn. Reson. **43**, 28 (1981).
6. E. B. WILSON. Chem. Soc. Rev. **1**, 293 (1972), and references therein.
7. E. HONEGGER and E. HEILBRONNER. Chem. Phys. Lett. **81**, 615 (1981).

Can. J. Chem. Downloaded from www.nrcresearchpress.com by 210.87.254.6 on 09/06/12
For personal use only.

# Preparation, properties, and X-ray crystal structure of a 1:1 complex of tetrathiafulvalene and *p*-dinitrobenzene

MARTIN R. BRYCE, ANTHONY S. SECCO, JAMES TROTTER,[1] AND LARRY WEILER[1]

*Department of Chemistry, University of British Columbia, Vancouver, B.C., Canada V6T 1Y6*

Received February 22, 1982

MARTIN R. BRYCE, ANTHONY S. SECCO, JAMES TROTTER, and LARRY WEILER. Can. J. Chem. **60**, 2057 (1982).

A crystalline complex of tetrathiafulvalene and *p*-dinitrobenzene has been prepared and characterised by esr and ir spectroscopy, bulk magnetic susceptibility, dc conductivity, and an X-ray diffraction analysis. It is a neutral 1:1 complex which is an insulator at room temperature, $\sigma_{RT} = 2.5 \times 10^{-7}$ ohm$^{-1}$ cm$^{-1}$. The complex crystallizes in the triclinic system, space group $P\bar{1}$ with cell constants $a = 6.915(1)$, $b = 7.615(1)$, $c = 8.149(1)$ Å, $\alpha = 79.39(1)$, $\beta = 69.55(1)$, $\gamma = 70.81(1)°$, $Z = 1$. Data were collected on an Enraf-Nonius CAD-4 diffractometer. The structure was solved by direct methods and refined to an *R*-value of 0.028 for 1222 observed reflections. The structure consists of molecules stacked in an alternating donor–acceptor fashion along the *c*-axis. Mixed sheets parallel to $(01\bar{2})$ are comprised of tetrathiafulvalene and *p*-dinitrobenzene molecules arranged end-on in the [021] direction.

MARTIN R. BRYCE, ANTHONY S. SECCO, JAMES TROTTER et LARRY WEILER. Can. J. Chem. **60**, 2057 (1982).

On a préparé un complexe cristallin du tétrathiafulvalène et du *p*-dinitrobenzène et on l'a caractérisé par la rpe, la spectroscopie ir, la susceptibilité magnétique de groupe, la conductivité cd, et par l'analyse de diffraction de rayons X. C'est un complexe neutre 1:1 qui est un isolant à la température ambiante, $\sigma_{RT} = 2{,}5 \times 10^{-7}$ ohm$^{-1}$ cm$^{-1}$. Le complexe cristallise dans le système triclinique et appartient au groupe d'espace $P\bar{1}$ avec $a = 6{,}915(1)$, $b = 7{,}615(1)$, $c = 8{,}149(1)$ Å, $\alpha = 79{,}39(1)$, $\beta = 69{,}55(1)$, $\gamma = 70{,}81(1)°$, $Z = 1$. On a recueilli les données à l'aide d'un diffractomètre Enraf-Nonuis CAD-4. On a résolu la structure par des méthodes directes et on l'a affiné jusqu'à une valeur de *R* de 0,028 pour 1222 réflexions observées. La structure comporte alternativement des molécules de donneur et de receveur qui sont entassées suivant l'axe *c*. Les couches mixtes paralèlles à $(01\bar{2})$ comprennent des molécules de tétrathiafulvalène et de *p*-dinitrobenzène arrangées en positions tête-queue dans la direction [021].

[Traduit par le journal]

Since the discovery of metallic conductivity in the complex of tetrathiafulvalene (**1**) and tetracyanoquinodimethane (**2**) (TTF–TCNQ), great interest has been focussed on the synthesis and properties of related organic charge transfer complexes (1). Many new donors have been prepared; the majority are sulphur and selenium heterocycles, and their complexes with TCNQ have certainly contributed to our understanding of this field (2). Recently, certain salts of tetramethyltetraselenofulvalene (**3**) have exhibited superconductivity at low temperature (3).

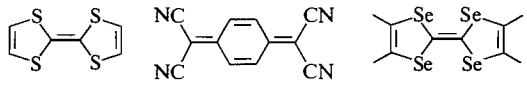

**1** **2** **3**

It is noticeable that there has been considerably less work reported on new electron acceptors. Substitution on the basic TCNQ skeleton has been shown generally to lower the conductivity of charge-transfer complexes formed (4). An alternative approach has been to vary the TCNQ skeleton by extending the conjugated $\pi$ system while retaining the high degree of symmetry and the dicyanomethylene groups of the TCNQ. Accordingly, the acceptors TNAP (**4**) (5), TCNDQ (**5**) (6), and the pyrene analogues **6** (6*c*, 7) and **7** (8) have been synthesized and their charge-transfer complexes studied, but none has room temperature conductivity substantially above that of TTF–TNCQ.

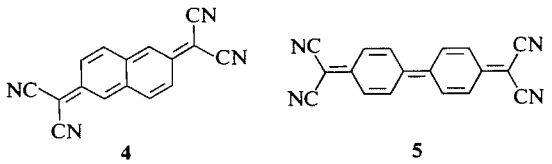

**4** **5**

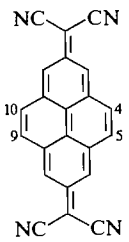

**6**

**7** 4,5,9,10-tetrahydro

It has become apparent that the range of electron acceptors should be extended and Torrance *et al.* have recently reported that the tetrahalo-*p*-benzoquinones form both metallic and semi-conducting complexes with TTF and its derivatives (9). These complexes were the first, that do not contain TCNQ or a TCNQ-like molecule, to display the

[1]Authors to whom correspondence may be addressed.

0008-4042/82/162057-05$01.00/0

©1982 National Research Council of Canada/Conseil national de recherches du Canada

Can. J. Chem. Downloaded from www.nrcresearchpress.com by 210.87.254.105 on 09/06/12
For personal use only.

Can. J. Chem. Downloaded from www.nrcresearchpress.com by 210.87.254.105 on 09/06/12
For personal use only.

two essential prerequisites for high conductivity; namely, segregated stacks of donors and acceptors, and incomplete charge transfer. They also exhibit several striking new phenomena that have increased our knowledge of intermolecular interactions in the solid state (*9b*).

We now report the preparation, properties, and an X-ray diffraction analysis of a complex of TTF with the electron acceptor *p*-dinitrobenzene (DNB). DNB was chosen as an acceptor because it resembles TCNQ in two important ways. Both molecules are of similar size; it is possible that the failure of some of the larger acceptors to form complexes with TTF may be due to their incompatible molecular dimensions. DNB has the same high symmetry as TCNQ ($D_{2h}$); the key role of the symmetry of the TCNQ radical anion in dictating stacking arrangements in TTF–TCNQ has been shown (10). Electron spin resonance studies of the radical anions of aromatic compounds show that the electronegativity of the nitro group is similar to that of the dicyanomethylene group (11). Thus the two acceptors, TCNQ and DNB, should have similar spin and charge distributions in their radical ions.

A 1:1 complex was obtained quantitatively by evaporation of a toluene solution of TTF and DNB. All the data obtained suggest that TTF–DNB is a neutral, insulating complex. The solid state esr signal has a *g*-value at 2.0018 consistent with a free electron of a π-radical, but the signal is very weak. The esr signal was about 7 G wide and no proton hyperfine splitting could be detected in this signal. The ir spectrum of TTF–DNB consists of sharp peaks typical of insulating complexes; organic metals are characterised by very broad bands in the infrared region (12). The magnetic susceptibility of the complex between 78 and 295 K is constant, again suggesting a diamagnetic complex with no unpaired electrons. The single crystal conductivity is that of an insulator, $\sigma = 2.5 \times 10^{-7}$ ohm$^{-1}$ cm$^{-1}$ at 300 K.

The crystal structure of TTF–DNB consists of stacks along the *c*-axis of alternating TTF and DNB molecules (Fig. 1). It is further characterised by mixed sheets of TTF and DNB molecules which are parallel to $(01\bar{2})$. Peculiar to this structure is the end-on packing arrangement (... TTF ... DNB ... TTF ...) in the [021] direction within the sheets. The intrastack interplanar spacing between TTF and DNB averages 3.64 Å, where the averaging is between the plane of the benzene ring and the two (S(1), C(2), C(3), S(2)) planes in the "chair-like" TTF molecule (*vide infra*); furthermore, the planes of the DNB ring and S(1), C(2), C(3), S(2) moieties are not parallel but subtend angles of 2.6(2)°. Generally, the above structural features are common in donor–acceptor charge-transfer complexes, although the interplanar spacing of 3.64 Å is larger than in even the weak CT-complexes TTF–X, where X is chloranil, fluoranil (13), or bromanil (14).

In view of the apparent lack of charge-transfer properties in the present structure, it is interesting to compare the overlap of TTF and DNB within the stacks. Figure 2 shows the projection of the TTF molecule onto the plane of the DNB ring. All intermolecular contacts are at least the sum of the van der Waals radii for any two atoms, indicating a minimum energy crystal packing. The angle between the long molecular axes of TTF and DNB is 126°. This is in contrast to the suggestion, based on crystal packing arguments in TTF–bromanil and TTF–chloranil by Mayerle, Torrance, and Crowley (13), that in donor–acceptor complexes, if both donor and acceptor molecules have a long molecular axis, they tend to line up. In light of the present study of the TTF–DNB complex, where crystal packing forces appear to be the controlling factor affecting the relative orientations of molecules, the above suggestion by Mayerle *et al.* should perhaps stress an increased role of orbital overlap in determining relative molecular orientations in D–A complexes.

Both the interplanar separation and relative molecular orientation in the present complex seem to prohibit any experimentally observable charge transfer interactions (i.e. conductivity and spectroscopic measurements). However, it is interesting to note the differences between the internal angles (122.5° at C(5) and averaging 118.8° at C(4) and C(6)) in the DNB ring in TTF–DNB (Fig. 3) and the corresponding angles (123.4° and 118.3°) in the neutral *p*-DNB structure (15). The fact that these angles are slightly closer to 120° in the current structure implies an increased electron density in the benzene ring relative to neutral *p*-DNB. The short C—N bond of 1.467(2) Å in the present complex compared to 1.478(2) Å in neutral *p*-DNB is consistent with this implication. Increased electron density in the DNB ring is not explicable on the basis of the electron-withdrawing $NO_2$ substituents and therefore, some interaction between DNB and TTF is inferred. However, the extent of this interaction must be small when considering the other physical properties of the complex.

The C—C bond lengths in the present DNB molecule are not significantly different from those in the neutral *p*-DNB structure. The geometry of the $NO_2$ group is essentially the same in both compounds. Noteworthy is the slightly skewed

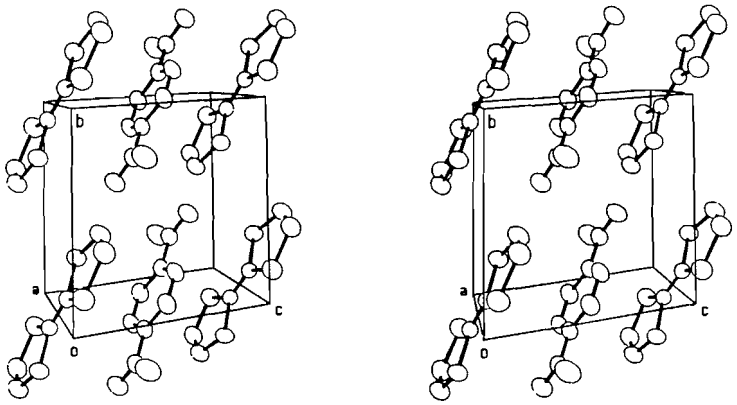


FIG. 1. Stereoview approximately down *a* of the unit cell contents.

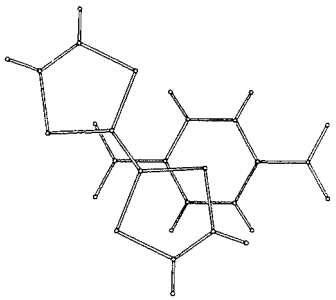

FIG. 2. Projection of the TTF molecule onto the plane of the DNB ring.

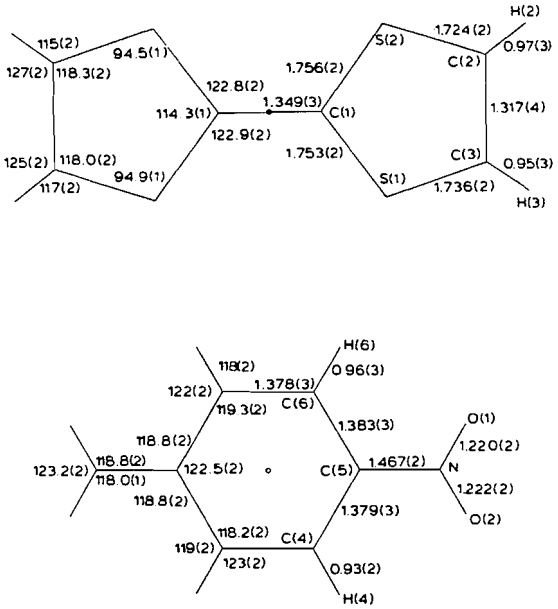


FIG. 3. Bond lengths (Å) and angles (deg) in TTF (top) and *p*-DNB (bottom).

orientation of the $NO_2$ plane with respect to the benzene ring plane; the two planes are twisted about the C—N bond by 1.1° (Table 1), considerably less than the 10° twist in neutral *p*-DNB.

The TTF molecule can be described by three planes (Table 1) forming a "chair-like" structure. In liquid crystals TTF was also found to adopt a non-planar conformation (16). Bond lengths and angles compare favorably with neutral TTF (17) and are generally not significantly different from those in TTF–chloranil and TTF–bromanil (13).

## Experimental

Infrared spectra were run on a Perkin-Elmer model 710 spectrometer; solid spectra were run as KBr discs. Electron spin resonance spectra were obtained on a Varian E-3 spectrometer operating at 9.1 GHz. Bulk magnetic susceptibility data were obtained using a Gouy magnetic balance (18).

Tetrathiafulvalene was purified by gradient sublimation. *p*-Dinitrobenzene was recrystallized from ethanol. Toluene was freshly distilled from sodium under nitrogen.

*TTF–DNB complex*

A solution of TTF (204 mg, 1.0 mmol) in 5 mL of hot toluene was added to a solution of DNB (168 mg, 1.0 mmol) in 5 mL of hot toluene. The resulting dark solution was allowed to cool to room temperature and evaporated to dryness under a stream of nitrogen to give 372 mg (100%) of the complex as long black needles, mp 134°C. *Anal.* calcd. for $C_{12}H_8N_2O_4S_4$: C 38.70, H 2.15, N 7.53; found: C 38.89, H 2.15, N 7.62. Ir (KBr) $\nu_{max}$: 1529, 1324, 1260, 1129, 1050, 1001, 836, 795, 782, 720, 658 $cm^{-1}$; esr (powder) very weak singlet, $g = 2.0018$ (7 G wide).

A crystal with well-defined faces along the *c*-axis and measuring 0.22 × 0.07 × 0.42 $mm^3$ was employed in the crystallographic study. Preliminary Weissenberg and precession photographs indicated a triclinic structure. The crystal data (at 22°C) are:

$C_6H_4S_4.C_6H_4N_2O_4$ fw = 372.5

Triclinic, $a = 6.915(1)$, $b = 7.615(1)$, $c = 8.149(1)$ Å, $\alpha = 79.39(1)$, $\beta = 69.55(1)$, $\gamma = 70.81(1)°$, $V = 378.5(2)$ $Å^3$, $Z = 1$, $\rho_c = 1.634$ g $cm^{-3}$, $\mu(MoK_\alpha; \lambda = 0.71073$ Å) = 5.75 $cm^{-1}$, space group $P\bar{1}$ from structure analysis.

Intensities were measured on an Enraf-Nonius CAD-4 dif-

Can. J. Chem. Downloaded from www.nrcresearchpress.com by 210.87.254.105 on 09/06/12
For personal use only.

Can. J. Chem. Downloaded from www.nrcresearchpress.com by 210.87.254.105 on 09/06/12
For personal use only.

TABLE 1

(*a*) Least-squares planes by Hamilton's method*

(*x*, *y*, and *z* are fractional coordinates referred to the unit cell)

Plane *1* defined by atoms S(1), C(2), C(3), and S(2)
Equation: $-0.5498x + 2.7683y - 6.8871z + 0.2302 = 0$
Distances from the plane (Å): S(1), 0.0000; C(2), −0.0007; C(3), 0.0006; S(2), 0.0000

Plane *2* defined by atoms S(1), C(1), and S(2)
Equation: $0.4801x - 2.5908y + 6.9751z - 0.2485 = 0$

Plane *3* defined by atoms N, O(1), O(2), and C(5)
Equation: $-0.4632x + 2.9958y - 6.7448z + 3.6166 = 0$
Distances from the plane (Å): N, 0.0003; O(1), −0.0002; O(2), −0.0001; C(5), −0.0001

Plane *4* defined by C(4), C(5), and C(6)
Equation: $-0.5473x + 3.0622y - 6.7125z + 3.6354 = 0$

*Reference 21.

(*b*) Dihedral angles between planes

| Planes | Angle (deg) |
|---|---|
| *1,2* | 178.2(2) |
| *1,3* | 1.8(2) |
| *1,4* | 2.6(2) |
| *2,3* | 176.5(2) |
| *2,4* | 175.8(2) |
| *3,4* | 1.1(2) |

TABLE 2. Final positional (fractional × $10^5$, H × $10^3$) and isotropic thermal parameters ($U$ × $10^3$ Å$^2$) with estimated standard deviations in parentheses

| Atom | *x* | *y* | *z* | $*U_{eq}/U_{iso}$ |
|---|---|---|---|---|
| S(1) | 15021( 8) | 12607( 7) | 7211( 8) | 54 |
| S(2) | 49943( 8) | 25209( 7) | 9488( 7) | 49 |
| O(1) | 77946(24) | 26346(24) | 59971(24) | 67 |
| O(2) | 44230(24) | 41012(20) | 68800(20) | 57 |
| N | 59136(25) | 27938(22) | 61962(21) | 45 |
| C(1) | 42723(27) | 7812(23) | 3523(23) | 38 |
| C(2) | 23874(40) | 39205(30) | 17205(30) | 60 |
| C(3) | 8249(38) | 33616(31) | 16186(30) | 61 |
| C(4) | 71207(29) | −1106(28) | 47684(26) | 45 |
| C(5) | 54338(26) | 13377(24) | 55831(22) | 38 |
| C(6) | 33076(28) | 14828(28) | 58227(25) | 44 |
| H(2) | 219( 4) | 507( 4) | 219( 3) | 78( 8) |
| H(3) | −67( 5) | 400( 4) | 199( 3) | 78( 8) |
| H(4) | 855( 4) | −18( 3) | 458( 3) | 65( 7) |
| H(6) | 220( 4) | 254( 3) | 637( 3) | 66( 7) |

*$U_{eq}$ is one third the trace of the diagonalized anisotropic temperature factor matrix.

fractometer in the θ range 1.0–27.0° with an ω–2θ scan and graphite monochromatized $MoK_\alpha$ radiation; scan speeds ranged from 1.01 and 10.06 deg min$^{-1}$. The ω scan angle, (1.00 + 0.35 tan θ)°, was extended 25% on both sides for background measurement. A variable horizontal aperture (2.00 + 0.50 tan θ) mm was employed and the vertical aperture remained constant at 4 mm. Crystal orientation and intensity controls were monitored periodically throughout data collection.

Data processing included the application of Lorentz and polarization corrections in the usual manner. An additional correction was made to account for the slight variation (±3%) in the intensities over the duration of data collection. Of the 1640 accessible data, 1222 (74.5%) had $I \geq 3\sigma(I)$, where $\sigma^2(I) = S + 2B + (0.04(S - B))^2$, $S$ = scan count and $B$ = time-averaged background.

On the basis of the *E*-statistics, the centrosymmetric space group $P\bar{1}$ was chosen and later confirmed to be correct by the subsequent structure refinement. MULTAN (19) yielded the positions of all non-hydrogens in the asymmetric unit which consisted of half a TTF molecule and half a DNB molecule. Following several cycles of full-matrix least-squares refinement, a difference-Fourier synthesis provided the hydrogen positions. The remainder of the refinement included 11 non-hydrogen atoms with anisotropic thermal parameters and 4 hydrogen atoms with isotropic temperature factors yielding a total of 116 variables. Anomalous scattering factors, from ref. 20*a*, were used for S atoms; all other scattering factors were taken from ref. 20*b*. On the final cycle of refinement the mean and maximum parameter shifts were 0.017 and 0.141 σ, respectively; the standard error in an observation of unit weight was 1.207. *R*-values, defined as $R = \Sigma||F_o| - k|F_c||/\Sigma|F_o|$ and $R_w = [\Sigma w(|F_o| - k|F_c|)^2/\Sigma w|F_o|^2]^{1/2}$, were 0.028 and 0.037, respectively, for the 1222 observed data with $I > 3\sigma(I)$ employed in the refinement, whereas for the complete data set $R = 0.047$ and $R_w = 0.037$. The quantity $\Sigma w(|F_o| - k|F_c|)^2$ was minimized in the refinement where $w = 1/\sigma^2(F_o)$, $\sigma^2(F_o)$ being derived from the previously defined $\sigma^2(I)$. The suitability of the chosen weights was confirmed by a weighting analysis program. A difference-map, calculated after convergence, showed random fluctuations in electron density up to 0.25 e/Å$^3$. Final atomic positional parameters and temperature factors are presented in Table 2.[2]

## Acknowledgements

We are grateful to the Natural Sciences and

[2]Tables of observed and calculated structure factor amplitudes, anisotropic thermal parameters for non-H atoms, and torsion angles are available, at a nominal charge, from the Depository of Unpublished Data, CISTI, National Research Council of Canada, Ottawa, Ont., Canada K1A 0S2.

Engineering Research Council of Canada for financial support, to the University of British Columbia Computing Centre for assistance, to R. C. Thompson for assistance with the susceptibility measurement, to J. F. Carolan for the conductivity measurement, and to J. B. Torrance for several discussions and reprints.

1. Organic conductors and semiconductors. *Edited by* L. Pal, G. Gruner, A. Janossy, and J. Solyon. Springer-Verlag, Berlin. 1977; The physics and chemistry of low dimensional solids. *Edited by* L. Alcacer and D. Reidel. Dordrecht, Holland. 1980.
2. P. SHU, L. CHIANG, T. EMGE, D. HOLT, T. KISTENMACHER, M. LU, J. STOKES, T. POEHLER, A. BLOCK, and D. COWAN. J. Chem. Soc. Chem. Commun. 920 (1981); F. WUDL and D. NALEWAJCK. J. Chem. Soc. Chem. Commun. 866 (1980); L. Y. CHIANG, T. O. POEHLER, A. N. BLOCK, and D. O. COWAN. J. Chem. Soc. Chem. Commun. 866 (1980); F. WUDL, R. C. HADDON, E. T. ZELLERS, and F. B. BRAMWELL. J. Org. Chem. **44**, 2491 (1979).
3. D. JEROME, A. MAZAND, M. RIMBAULT, and K. BECHGAARD. J. Phys. (Paris) Lett. **41**, L-95 (1980); N. THORUP, G. RINDORF, H. SOLING, and K. BECHGAARD. Acta Crystallogr. B**37**, 1236 (1981).
4. R. C. WHELAND and J. L. GILLSON. J. Am. Chem. Soc. **98**, 3916 (1976); R. C. WHELAND. J. Am. Chem. Soc. **98**, 3926 (1976).
5. P. A. BERGLER, D. J. DAHM, G. R. JOHNSON, M. G. MILES, and J. D. WILSON. Phys. Rev. B, **12**, 4085 (1975).
6. (*a*) W. R. HERTLER. U.S. Patent 3,153,658 (1967); (*b*) A. W. ADDISON, N. S. DALAH, Y. HOYANO, S. HUIZINGA, and L. WEILER. Can. J. Chem. **55**, 4191 (1977); (*c*) E. AHARON-SHALOM, J. Y. BECKER, and I. AGRANAT. Nouv. J. Chem. **3**, 643 (1979).
7. M. MAXFIELD, D. O. COWAN, A. N. BLOCK, and T. O. POEHLER. Nouv. J. Chem. **3**, 647 (1979).
8. M. MAXFIELD, S. M. WILLI, D. O. COWAN, A. N. BLOCK, and T. O. POEHLER. J. Chem. Soc. Chem. Commun. 947 (1980).
9. (*a*) J. B. TORRANCE, J. J. MAYERLE, V. Y. LEE, and K. BECHGAARD. J. Am. Chem. Soc. **101**, 4747 (1979); (*b*) J. B. TORRANCE, J. E. VAZQUEZ, J. J. MAYERLE, and V. Y. LEE. Phys. Rev. Lett. **46**, 253 (1981).
10. A. J. BERLINSKY, J. F. CAROLAN, and L. WEILER. Solid State Commun. **19**, 1165 (1976); J. P. LOWE. J. Am. Chem. Soc. **102**, 1262 (1980).
11. P. H. RIEGER and G. K. FRAENKEL. J. Chem. Phys. **39**, 609 (1963); P. H. RIEGER and G. K. FRAENKEL. J. Chem. Phys. **37**, 2759 (1962); D. A. LOWITZ. J. Chem. Phys. **46**, 4698 (1967).
12. J. B. TORRANCE. Acc. Chem. Res. **12**, 79 (1979) and references therein.
13. J. J. MAYERLE, J. B. TORRANCE, and J. I. CROWLEY. Acta Crystallogr. B**35**, 2988 (1979).
14. J. J. MAYERLE and J. B. TORRANCE. Acta Crystallogr. B**37**, 2030 (1981).
15. F. DI RIENZO, A. DOMENICANO, and L. RIVA DI SANSEVERINO. Acta Crystallogr. B**36**, 586 (1980).
16. T. C. WONG, E. E. BURNELL, and L. WEILER. Chem. Phys. Lett. **50**, 243 (1977).
17. W. F. COOPER, N. C. KENNY, J. W. EDMONDS, A. NAGEL, F. WUDL, and P. COPPENS. Cryst. Struct. Comm. **3**, 23 (1974).
18. J. M. PAYLOR and R. C. THOMPSON. Can. J. Chem. **49**, 511 (1971).
19. P. MAIN, S. E. HULL, L. LESSINGER, G. GERMAIN, J. P. DECLERQ, and M. M. WOOLFSON. MULTAN 78–a system of computer programs for the automatic solution of crystal structures from X-ray diffraction data. Universities of York, England and Louvain, Belgium.
20. J. A. IBERS and W. C. HAMILTON (*Editors*). International Tables for X-ray Crystallography. Vol. IV. Kynoch Press, Birmingham, 1974. (*a*) pp. 148–151; (*b*) pp. 71–98.
21. W. C. HAMILTON. Acta Crystallogr. **14**, 185 (1968).

Can. J. Chem. Downloaded from www.nrcresearchpress.com by 210.87.254.105 on 09/06/12
For personal use only.

# On the synthesis of cryptosporiopsin: stereochemistry of early intermediates

GEORGE M. STRUNZ

*Canadian Forestry Service, P.O. Box 4000, Fredericton, N.B., Canada E3B 5P7*

AND

PETER S. WHITE

*Department of Chemistry, University of New Brunswick, Fredericton, N.B., Canada E3B 6E2*

Received March 15, 1982

GEORGE M. STRUNZ and PETER S. WHITE. Can. J. Chem. **60**, 2062 (1982).

The relative configurations of two intermediates in the synthetic route to cryptosporiopsin are clarified through the structure of 3,5-dichloro-1,4-dihydroxy-2-methylcyclopent-2-ene-1-carboxylic acid methyl ester, which was determined by single crystal X-ray techniques. The crystal was monoclinic, space group $P2_1/c$, $a = 7.352(1)$, $b = 8.868(3)$, $c = 16.300(7)$ Å; $\beta = 96.49(2)°$. The structure was solved by direct methods and refined to a final $R$ of 0.057.

GEORGE M. STRUNZ et PETER S. WHITE. Can. J. Chem. **60**, 2062 (1982).

Les configurations rélatives de deux intermédiaires dans la synthèse de cryptosporiopsin sont clarifiées par la structure de l'ester méthylique de l'acide dichloro-3,5 dihydroxy-1,4 méthylcyclopent-2 ene-2 carboxylique-1, qu'on a déterminé par diffraction de rayons-X sur un monocristal. Le cristal était monoclinique et appartenait au groupe d'espace $P2_1/c$, $a = 7.352(1)$, $b = 8.868(3)$, $c = 16.300(7)$ Å; $\beta = 96.49(2)°$. On a résolu la structure au moyen de méthodes directes, et on l'a affinée jusqu'à $R = 0.057$.

The reaction of phenol or 2,4,6-trichlorophenol with alkaline hypochlorite gives rise to a complex mixture of products, from which 3,5,5-trichloro-1,4-dihydroxycyclopent-2-ene-1-carboxylic acid, **1** (R = H), may be isolated in yields up to 50 or 60% (1–3). This compound and the homologue **1** (R = *n*-propyl) derived from 3-*n*-propylphenol have provided useful synthetic entries to some natural products (3, 4), including the fungal metabolite cryptosporiopsin **2** (5).

In the course of the latter synthesis, **1** (R = *n*-propyl) was reduced with sodium amalgam (1–3) to the dichloro product **3** (R = *n*-propyl) (5). The newly introduced hydrogen at C-5 was considered to be *cis* with respect to the hydrogen at C-4 on the basis, *inter alia*, of the magnitude of the coupling between them ($J = 6.5$ Hz) (2, 3, 5). Assuming then the *trans* relationship of the hydroxyl groups of **1** (R = H) tentatively favored by earlier authors (3), it seemed likely that the C-1 hydroxyl group and the C-5 hydrogen of **3** (R = *n*-propyl) were *cis*. The stage thus appeared to be set stereochemically for completion of the synthesis of (±) cryptosporiopsin, and this was duly accomplished (5).

Subsequently, X-ray studies by Rickards and co-workers (6) on the lactone **4**, obtained in low yield from 2,4,6-trichlorophenol or from **1** (R = H) by reaction with alkaline hypochlorite, established that the stereochemistry of **1** (R = H) is as depicted in **5** (R = H), i.e., with *cis* rather than *trans* hydroxyl groups.

The present study was undertaken in order to clarify the stereochemical ramifications bearing on the successful synthesis of cryptosporiopsin.

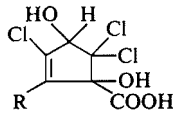


**1**

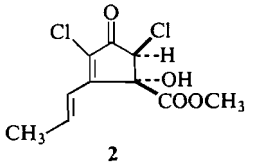


**2**

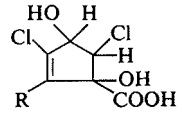


**3**

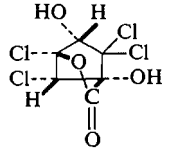


**4**

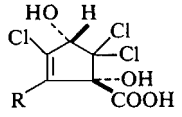


**5**

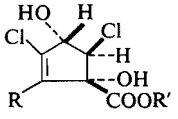


**6**

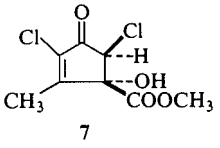


**7**

If sodium amalgam reduction of a precursor **5** (R = *n*-propyl), with *cis* hydroxyl groups, indeed introduces a hydrogen at C-5 *cis* to the C-4 hydrogen, then the (desired) *cis* configuration of C-1 hydroxyl and C-5 hydrogen observed in later intermediates in the synthesis must result from epimerization at C-5 after oxidation of the C-4 hydroxyl group. (The possibility of epimerization of a C-5 epimer of cryptosporiopsin was demon-

0008-4042/82/162062-03$01.00/0

©1982 National Research Council of Canada/Conseil national de recherches du Canada

Can. J. Chem. Downloaded from www.nrcresearchpress.com by 210.87.254.5 on 09/06/12
For personal use only.

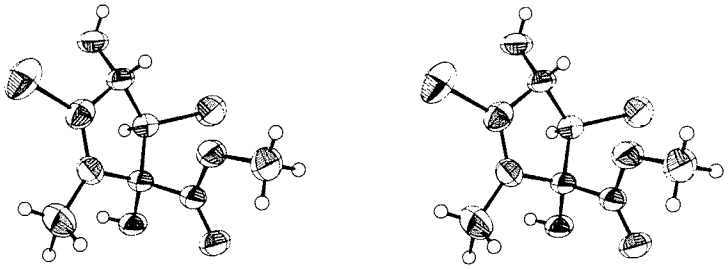

FIG. 1. Ortep (12) stereoplot of **6**, thermal ellipsoids are drawn at 50% probability.

TABLE 1. Fractional atomic coordinates (esd's) for non-hydrogen atoms

| Atom | *X* | *Y* | *Z* |
|---|---|---|---|
| Cl(1) | 0.64758(10) | 0.15429(8) | 0.05417(5) |
| Cl(2) | 0.37230(9) | 0.44836(11) | −0.22859(4) |
| C(1) | 0.49689(29) | 0.24434(23) | −0.01667(15) |
| C(2) | 0.56386(26) | 0.31204(26) | −0.09200(13) |
| C(3) | 0.40101(25) | 0.41219(23) | −0.12108(13) |
| C(4) | 0.23291(24) | 0.34513(22) | −0.08625(12) |
| C(5) | 0.32013(28) | 0.26048(22) | −0.01132(13) |
| O(6) | 0.72193(18) | 0.40112(20) | −0.07395(12) |
| O(7) | 0.10791(18) | 0.45631(17) | −0.06820(10) |
| C(8) | 0.12320(25) | 0.23535(23) | −0.14387(12) |
| O(9) | −0.03931(21) | 0.23794(18) | −0.15875(12) |
| O(10) | 0.23018(20) | 0.13434(19) | −0.17326(10) |
| C(11) | 0.14070(37) | 0.02498(32) | −0.22987(19) |
| C(12) | 0.20693(41) | 0.20434(35) | 0.05279(16) |

TABLE 2. Bond lengths (esd's)

| Bond | Length (Å) |
|---|---|
| Cl(1)—C(1) | 1.706(2) |
| Cl(2)—C(3) | 1.770(2) |
| C(1)—C(2) | 1.499(3) |
| C(1)—C(5) | 1.320(3) |
| C(2)—C(3) | 1.523(3) |
| C(2)—O(6) | 1.409(2) |
| C(3)—C(4) | 1.537(3) |
| C(4)—C(5) | 1.513(3) |
| C(4)—O(7) | 1.402(2) |
| C(4)—C(8) | 1.520(3) |
| C(5)—C(12) | 1.493(3) |
| C(8)—O(9) | 1.192(2) |
| C(8)—O(10) | 1.318(2) |
| O(10)—C(11) | 1.445(3) |

TABLE 3. Bond angles (esd's)

| Bond | Angle (°) |
|---|---|
| Cl(1)—C(1)—C(2) | 119.6(2) |
| Cl(1)—C(1)—C(5) | 125.1(2) |
| C(2)—C(1)—C(5) | 115.3(2) |
| C(1)—C(2)—C(3) | 99.7(2) |
| C(1)—C(2)—O(6) | 113.2(2) |
| C(3)—C(2)—O(6) | 109.8(2) |
| Cl(2)—C(3)—C(2) | 114.5(2) |
| Cl(2)—C(3)—C(4) | 115.2(2) |
| C(2)—C(3)—C(4) | 107.2(2) |
| C(3)—C(4)—C(5) | 101.8(2) |
| C(3)—C(4)—O(7) | 112.3(2) |
| C(3)—C(4)—C(8) | 114.4(2) |
| C(5)—C(4)—O(7) | 114.1(2) |
| C(5)—C(4)—C(8) | 109.1(2) |
| O(7)—C(4)—C(8) | 105.4(2) |
| C(1)—C(5)—C(4) | 109.3(2) |
| C(1)—C(5)—C(12) | 129.9(2) |
| C(4)—C(5)—C(12) | 120.8(2) |
| C(4)—C(8)—O(9) | 124.3(2) |
| C(4)—C(8)—O(10) | 111.3(2) |
| O(9)—C(8)—O(10) | 124.4(2) |
| C(8)—O(10)—C(11) | 116.2(2) |

strated during other studies after completion of the synthetic work (7).)

Alternatively, the correct stereochemistry would be established at C-1 and C-5 if sodium amalgam reduction of **5** (R = *n*-propyl) yielded **6** (R = *n*-propyl, R′ = H), with C-4 and C-5 hydrogens *trans*.

To distinguish between these possibilities, an X-ray crystal structure analysis of 3,5-dichloro-1,4-dihydroxy-2-methylcyclopent-2-ene-1-carboxylic acid methyl ester[1] was undertaken. This compound, derived from *m*-cresol via the corresponding "Hantzsch acid", has been converted to the cryptosporiopsin analogue **7** in model studies (8).

The structure established by X-ray analysis, **6** (R, R′ = $CH_3$) (*vide infra*), confirms that the 2-alkyl Hantzsch acid **5** (R = $CH_3$) possesses the same relative configuration at C-1 and C-4 as its 2-desalkyl analogue (6), and indicates that the hydrogen introduced at C-5 in the sodium amalgam product is *trans* with respect to the C-4 hydrogen, contrary to the earlier assignment based on interpretation of nmr data (*vide supra*).

Accordingly, by analogy, early intermediates in the cryptosporiopsin synthetic route (5) possess

[1]Selected for study because it afforded crystals suitable for X-ray analysis more readily than its 2-*n*-propyl homologue, the actual synthetic intermediate.

Can. J. Chem. Downloaded from www.nrcresearchpress.com by 210.87.254.5 on 09/06/12
For personal use only.

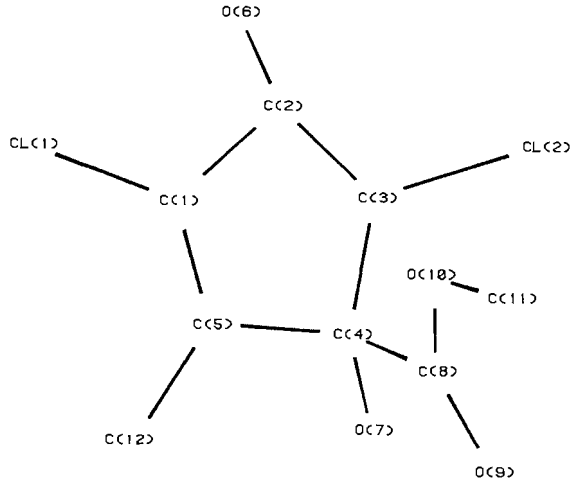


FIG. 2. Labelling scheme for **6** used in the X-ray investigation.

the relative stereochemistry depicted as **5** (R = *n*-propyl) and **6** (R = *n*-propyl, R′ = H or $CH_3$).

A stereo view of **6** (R, R′ = $CH_3$) is presented in Fig. 1. Tables 2 and 3 give the relevant bond lengths and angles and Fig. 2 shows the labelling scheme used in the X-ray determination.

### X-ray structure determination

A preliminary photographic investigation of a suitable crystal showed it to be monoclinic, space group $P2_1/c$. The crystal was mounted onto a Picker FACS-I diffractometer and graphite monochromated Mo $K_\alpha$ radiation was used. After preliminary alignment the cell parameters and an orientation matrix were determined from a least squares fit to the centered coordinates of 12 Friedel pairs of reflections in the range $35° < 2\theta < 50°$. Intensity data were collected, using an $\omega - 2\theta$ scan with a scan rate of 2 deg ($2\theta$) $min^{-1}$, for $2\theta \leq 50°$. The background intensity was estimated by standing counts of 1/10 of the scantime at each end of the scan; if the reflection was considered significant ($I > 2\sigma(I)$) an analysis of the scan profile was performed in order to provide a better estimate of the background. The relevant crystallographic data are:

$C_8H_{10}O_4Cl_2$ fw = 241.07

Monoclinic, space group $P2_1/c$, $a = 7.352(1)$, $b = 8.868(3)$, $c = 16.300(7)$ Å, $\beta = 96.49(2)°$, $V = 1056$ Å$^3$, $Z = 4$, $D_{calc} = 1.52$ Mg m$^{-3}$, crystal size = 0.30 × 0.35 × 0.12 mm, $\mu = 0.60$ mm$^{-1}$.

Two independent sets of data were collected and averaged, the agreement between sets ($\Sigma|\Delta I|\Sigma|I|$) was 0.026. This resulted in 1866 unique reflections of which 1706 were considered observed ($I \geq 3\sigma(I)$) and included in the subsequent refinement.

The structure was solved by multiple solution direct methods using a version of the program MULTAN (9) modified for use on the PDP 8/A computer. The resulting *E*-map revealed the positions of all non-hydrogen atoms. The structure was refined by least squares methods minimizing the function $\Sigma\omega(|F_o| - |F_c|)^2$. The weighting scheme was of the form $\omega = 1/(\sigma^2(F) + pF^2)$ where $\sigma(F)$ was derived from counter statistics and a value of $p = 0.005$ was determined from the statistics of the standard reflections. Scattering factors were taken from the International Tables for Crystallography (10) and were corrected for anomalous dispersion. After the initial cycles of refinement the hydrogen positions were located from a difference synthesis. In the final refinement non-hydrogen atoms were refined with anisotropic thermal parameters and the hydrogens were varied with isotropic thermal parameters. The final agreement indices were $R = 0.057$, $R_w = 0.117$ (0.060 and 0.125 respectively for the complete data set). The final coordinates for the non-hydrogen atoms are given in Table 1.[2] The computer programs used were those of Larson and Gabe for the PDP 8/A computer (11).

1. A. HANTZSCH. Chem. Ber. **20**, 2780 (1887); **22**, 1238 (1889).
2. C. J. MOYE and S. STERNHELL. Tetrahedron Lett. 2411 (1964); Aust. J. Chem. **19**, 2107 (1966).
3. A. W. BURGSTAHLER, T. B. LEWIS, and M. O. ABDEL-RAHMAN. J. Org. Chem. **31**, 3516 (1966).
4. M. GILL and R. W. RICKARDS. J. Chem. Soc. Chem. Commun. 121 (1979).
5. G. M. STRUNZ and A. S. COURT. Experientia, **26**, 714 (1970); **26**, 1054 (1970); J. Am. Chem. Soc. **95**, 3000 (1973).
6. R. M. CHRISTIE, R. W. RICKARDS, K. J. SCHMALZL, and D. TAYLOR. Aust. J. Chem. **30**, 2195 (1977).
7. G. M. STRUNZ, P. I. KAZINOTI, and M. A. STILLWELL. Can. J. Chem. **52**, 3623 (1974).
8. G. M. STRUNZ, A. S. COURT, and J. KOMLOSSY. Tetrahedron Lett. 3613 (1969).
9. G. GERMAIN, P. MAIN, and M. M. WOOLFSON. Acta Crystallogr. Sect. A, **27**, 368 (1971).
10. International Tables for X-ray Crystallography. Vol. IV. Kynoch Press, Birmingham. 1974.
11. A. C. LARSON and E. J. GABE. Minimum computer system for complete crystal structure determination. *In* Computing in crystallography. *Edited by* H. Schenk, R. Olthof-Hazekamp, H. van Koningsveld, and G. C. Bass. Delft University Press, The Netherlands. 1978. pp. 81–89.
12. C. K. JOHNSON. ORTEP. Report ORNL-3794 Oak Ridge National Laboratory, Tennessee. 1965.

[2]Tables of hydrogen atom coordinates and isotropic thermal parameters, anisotropic thermal parameters, and observed and calculated structure factors are available, at nominal charge, from the Depository of Unpublished Data, CISTI, National Research Council of Canada, Ottawa, Ont., Canada K1A 0S2.

Can. J. Chem. Downloaded from www.nrcresearchpress.com by 210.87.254.5 on 09/06/12
For personal use only.

# The molecular structure of 1-(2′-triphenylphosphonio-3′,3′,4′,4′-tetrafluorocyclobutenyl)(3,3-difluorocyclobutene-2,4-dionate)·chloroform solvate

F. W. B. EINSTEIN AND T. JONES

*Department of Chemistry, Simon Fraser University, Burnaby, B. C., Canada V5A 1S6*

Received January 26, 1982

F. W. B. EINSTEIN and T. JONES. Can. J. Chem. **60**, 2065 (1982).

The title compound, $C_{26}F_{15}O_2F_6P(0.5CHCl_3)$ (**A**), crystallizes as pale yellow crystals in the monoclinic system $C2/c$ with $a$ = 29.624(6), $b$ = 10.224(3), $c$ = 18.576(4) Å; $\beta$ = 116.26(2)°, $Z$ = 8. On the basis of 1652 observed reflections ($I \geq 2.3\sigma(I)$) in the range 3° ≤ 2θ ≤ 42° the structure was solved and refined by least-squares methods to $R$ = 0.042 and shown to be a zwitterion consisting of a phosphonium cation and a delocalised anion. The bond parameters of the cation are normal; P—C distances range from 1.773(5)–1.786(5) Å and C—P—C angles range from 106.4(2)–111.7(2)°. Within the delocalised anionic fragment of the molecule C—C distances range from 1.388(7)–1.440(8) Å and C—O distances are 1.216(7) and 1.208(7) Å.

F. W. B. EINSTEIN et T. JONES. Can. J. Chem. **60**, 2065 (1982).

Les cristaux du composé (**A**) mentionné dans le titre, $C_{26}F_{15}O_2F_6P(0,5CHCl_3)$ sont monocliniques de couleur jaune pâle et appartiennenet au groupe d'espace $C2/c$ avec $a$ = 29,624(6), $b$ = 10,224(3), $c$ = 18,576(4) Å; $\beta$ = 116,26(2)°, $Z$ = 8. A partir de 1652 réflexions observées ($I \geq 2{,}3\sigma(I)$) dans l'intervalle 3° ≤ 2θ ≤ 42°, on a résolu la structure par la méthode des moindres carrés et on l'a ajusté jusqu'à une valeur de $R$ = 0,042. Cette structure indique qu'il s'agit d'un Zwitterion constitué d'un cation phosphonium et d'un anion délocalisé. Les paramètres de liaison du cation sont normaux; les distances P—C se situent entre 1,773(5) et 1,786(5) Å et les angles C—P—C varient de 106,4(2) à 111,7(2)°. A l'intérieur de plus fragment anionique délocalisé de la molécule, les distances C—C se situent entre 1,388(7) et 1,440(8) Å et les distances C—O sont 1,216(7) et 1,208(7) Å.

[Traduit par le journal]

## Introduction

The title compound, formulated as $C_{26}F_{15}O_2F_6P(0.5CHCl_3)$, was believed to exist as one of two possible structures; either (*a*), as a cyclic structure (**i**) involving a five-coordinate phosphorus atom, an oxygen atom, and four carbon atoms in a novel, potentially aromatic, heterocyclic ring system or (*b*), as a zwitterion (**ii**), containing a phosphonium cation and an oxyanion, derived from one of the carbonyl groups attached to ring 2 of the fluorocarbon ligand.

To determine which of these two structures does, in fact, prevail, full crystallographic analysis was carried out.

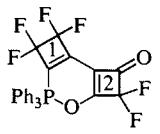


i

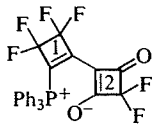


ii

## Experimental

Crystal data:

$C_{26}F_{15}O_2F_6P(0.5CHCl_3)$ fw = 564.06

Monoclinic, $a$ = 29.624(6), $b$ = 10.224(3), $c$ = 18.576(4) Å, $\beta$ = 116.26(2)°, $V$ = 5045.57 Å$^3$, $\rho_c$ = 1.485 Mg/m$^3$, $Z$ = 8, $\mu$ = 33.1 mm$^{-1}$, $\lambda(MoK_{\alpha_1})$ = 0.70926 Å. $F(000)$ = 2279.8.

Bright yellow crystals (10) of **A** were crystallized from $CHCl_3$. A single crystal suitable for data collection (0.45 × 0.25 × 0.28 mm) was mounted in a Lindemann glass tube. Precession and Weissenberg methods were used to determine approximate cell dimensions and the space group as being $Cc$ or $C2/c$ (subsequent structure solution showed $C2/c$ to be the correct space group). Accurate cell dimensions were determined by least-squares refinement of 16 accurately centred reflections (2θ = 16–23°, $\lambda(Mo\text{-}K_\alpha)$ = 0.71069 Å). Data were collected at 298 K, using a Picker FACS-I automatic four-circle diffractometer with a graphite monochromator and a scintillation counter with pulse height discrimination. Symmetrical θ–2θ scans (2° in 2θ min$^{-1}$) were taken for (1.6 + tanθ)°, whilst stationary-crystal, stationary-counter background counts were taken for 10% of the scan time at each scan limit. The background-corrected intensity and associated error of each reflection was determined by the peak profile method of Gabe and Grant (1). Intensity measurement of two standards every 70 reflections showed no evidence of crystal deterioration during data collection. Intensities (3.0–42.0° in 2θ) were measured for 2720 independent reflections, of which 1652 were classed observed ($I \geq 2.3\sigma(I)$).

The structure was solved using MULTAN. The tangent refinement solution with best agreement factors was used to phase an $E$-map which revealed most of the atoms, remaining atoms being located in subsequent difference-Fourier syntheses. After location of what were thought to be all the atoms of the unit cell, the preceding difference map revealed a chloroform molecule of crystallization which lay across the two-fold axis along $b$ alternately in one of the two symmetry-related orientations. This arrangement results in a 50% occupancy for the molecule. A mass spectrum later confirmed the presence of chloroform in the crystals.

The final difference map was very clean apart from the solvent region, where a number of residual peaks and troughs appeared (approximately five times the error associated with the map). In order to account for these peaks, our simple model of alternate two-fold related chloroform molecules was substituted by other more complex models. Despite considerable effort, no chemically reasonable alternative was found. The model which gave best agreement was achieved by allowing the three chlorines

0008-4042/82/162065-04$01.00/0

©1982 National Research Council of Canada/Conseil national de recherches du Canada

Can. J. Chem. Downloaded from www.nrcresearchpress.com by 210.87.254.105 on 09/06/12
For personal use only.

Can. J. Chem. Downloaded from www.nrcresearchpress.com by 210.87.254.105 on 09/06/12
For personal use only.

and one carbon to refine anisotropically. It is clear that this description is not totally satisfactory. Phenyl hydrogen atoms were included as fixed contributions in their calculated positions and given isotropic temperature factors related to the carbon atoms to which they are attached. Gausse-Seidel block-diagonal least-squares refinement (3) of all non-hydrogen atoms with anisotropic temperature factors gave final agreement values of $R = 0.042$ and $R_w = 0.039$.

Lorentz and polarisation corrections have been applied, but no absorption correction has been made ($\mu = 33.1\ mm^{-1}$). Unit weights were used. The agreement factors quoted are of the form: $R = \Sigma\ ||F_o| - |F_c||/\Sigma|F_o|$ and $R_w = (\Sigma w(|F_o| - |F_c|)^2/\Sigma w|F_o|^2)^{1/2}$. Scattering factors were taken from International tables for X-ray crystallography (2). The computer programs used were those belonging to "The NRC pdp-8e crystal structure system" (3).

Final positional and thermal parameters are listed in Table 1. Anisotropic thermal parameters and structure factor listings have been deposited.[1]

## Discussion

The true structure of **A** was found to be a modification of **ii**; viz., a zwitterion, in which the cationic species is a phosphonium ion, and the negative counter ion is delocalised over both carbonyl oxygen atoms, and a portion of the fluorocarbon ligand (**iii**).

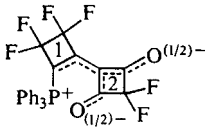


**iii**

The molecular structure of **A** is shown in Fig. 1, whilst the bond parameters are given in Table 2. The P—C distances, which range from 1.773(5)–1.786(5) Å, and C—P—C angles, which range from 106.4(2)–111.7(2)°, are very similar to the values found in other phosphonium ions; e.g., triphenylmethylphosphonium bis((3)-1,2-dicarbollyl)cuprate(III) (4) (P—C = 1.79(2)–1.80(2) and C—P—C angles = 105–112°). The geometries of the phenyl rings also appear to be normal. The bond distances within the cyclobutanone ring in the present compound are compared with those of the analogous rings found in perfluoro-1,2-3,4-5,6-triethanobenzene (**B**) (5) and perfluorotetracyclooctatetraene (**C**) (6) (Table 3). It can be seen that C(19)—C(22) in ring 1 is not a formal double bond, suggesting that it is part of a delocalised system as is the case in **B**, as opposed to the cyclobutene type system found in **C**. Consideration of the bond distances in the fragment

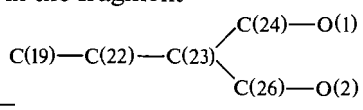


suggests that it is partially if not completely delocalised. The C—C distances in the fragment range from 1.388(7)–1.440(8) Å and are intermediate between the double (1.342(2) Å) and single (1.508(1) Å) bonds formed between $sp^2$ hybridized carbon atoms in this type of compound (7); the C—O distances[2] of 1.216(7) and 1.208(7) Å, which within error are equivalent to one another, are intermediate between the value of 1.259(7) Å found by the crystallographic study of the completely delocalised squarate ion in $K_2[C_4O_4]\cdot H_2O$ (8) and the value of 1.204(6) Å determined by a microwave study of cyclobutanone (9).

The angles within the fragment P(1)—

TABLE 1. Final positional parameters and isotropic equivalents for **A** (coordinates are multiplied by $10^5$ for P; by $10^4$ for all other atoms)

| Atom | $x$ | $y$ | $z$ | $B_{eq}$[a] |
|---|---|---|---|---|
| P | 37107(5) | 4616(13) | 4660(8) | 7.11(6) |
| F(1) | 3713(2) | 2112(4) | 2117(2) | 16.3(3) |
| F(2) | 2944(1) | 1931(3) | 1216(2) | 17.6(3) |
| F(3) | 3714(2) | 4617(3) | 1678(2) | 16.8(3) |
| F(4) | 2958(1) | 4405(3) | 748(2) | 16.9(3) |
| F(5) | 4332(2) | 5720(4) | −685(3) | 25.9(4) |
| F(6) | 3570(2) | 5512(4) | −1563(3) | 22.0(4) |
| O(1) | 4013(2) | 2740(4) | −854(2) | 13.2(3) |
| O(2) | 3633(2) | 6404(4) | 124(3) | 26.3(6) |
| C(1) | 4366(2) | 289(5) | 760(3) | 7.2(3) |
| C(2) | 4687(2) | 1355(5) | 961(3) | 9.1(3) |
| C(3) | 5187(2) | 1200(6) | 1157(4) | 11.2(4) |
| C(4) | 5375(2) | −36(7) | 1144(4) | 12.0(4) |
| C(5) | 5065(2) | −1100(6) | 948(4) | 10.9(3) |
| C(6) | 4565(2) | −954(5) | 761(3) | 9.0(3) |
| C(7) | 3518(2) | −689(5) | 995(3) | 7.2(3) |
| C(8) | 3852(2) | −1146(5) | 1750(3) | 9.3(3) |
| C(9) | 3690(2) | −2009(6) | 2156(3) | 11.3(4) |
| C(10) | 3193(2) | −2407(6) | 1818(3) | 12.6(4) |
| C(11) | 2858(2) | −1946(6) | 1085(3) | 11.2(3) |
| C(12) | 3017(2) | −1094(5) | 665(3) | 9.5(3) |
| C(13) | 3348(2) | 220(5) | −588(3) | 7.1(3) |
| C(14) | 3421(2) | −908(5) | −941(3) | 9.2(3) |
| C(15) | 3146(2) | −1116(6) | −1744(3) | 10.3(3) |
| C(16) | 2800(2) | −225(6) | −2216(3) | 10.5(4) |
| C(17) | 2722(2) | 881(6) | −1879(3) | 11.0(4) |
| C(18) | 2996(2) | 1116(5) | −1070(3) | 9.3(3) |
| C(19) | 3582(2) | 2033(5) | 735(3) | 8.0(3) |
| C(20) | 3399(2) | 2382(5) | 1341(3) | 10.0(3) |
| C(21) | 3408(2) | 3829(5) | 1093(3) | 10.4(3) |
| C(22) | 3602(2) | 3322(5) | 516(3) | 8.1(3) |
| C(23) | 3725(2) | 4029(5) | −21(3) | 10.2(3) |
| C(24) | 3901(2) | 3718(5) | −597(3) | 9.9(3) |
| C(25) | 3898(3) | 5171(6) | −803(4) | 14.9(4) |
| C(26) | 3716(3) | 5418(6) | −155(4) | 15.3(4) |
| C(SOL) | 4788(6) | 5399(13) | 2254(18) | 27.0(28) |
| Cl(1) | 5026(3) | 5224(5) | 1489(3) | 28.1(6) |
| Cl(2) | 4913(6) | 6604(5) | 2221(5) | 31.1(10) |
| Cl(3) | 5117(4) | 3904(5) | 2334(5) | 25.6(7) |

[a] $B_{eq} = 8\pi^2(U_{11}^2 + U_{22}^2 + U_{33}^2)^{1/2}$.

[1] Complete set of data may be obtained, at a nominal charge, from the Depository of Unpublished Data, CISTI, the National Research Council of Canada, Ottawa, Ont., Canada K1A 0S2.

[2] The C—O distances quoted here have not been corrected for thermal motion and are possibly slightly larger than reported.

Can. J. Chem. Downloaded from www.nrcresearchpress.com by 210.87.254.105 on 09/06/12
For personal use only.

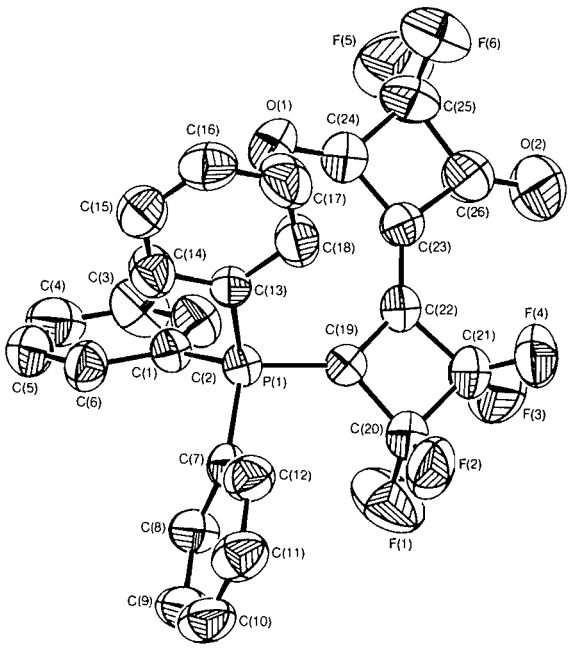


FIG. 1. Molecular structure and labelling scheme for **A** (ORTEP diagram; 50% probability contours for all atoms).

TABLE 2.
(*a*) Interatomic distances for **A**[a]

| Bonds | Distance (Å) | Bonds | Distance (Å) |
|---|---|---|---|
| P(1)—C(1) | 1.779(5) | C(19)—C(20) | 1.494(7) |
| P(1)—C(7) | 1.781(5) | C(20)—C(21) | 1.553(8) |
| P(1)—C(13) | 1.786(5) | C(21)—C(22) | 1.513(7) |
| P(1)—C(19) | 1.773(5) | C(22)—C(19) | 1.388(7) |
| | | C(22)—C(23) | 1.405(7) |
| C(1)—C(2) | 1.385(7) | C(23)—C(24) | 1.418(7) |
| C(2)—C(3) | 1.368(8) | C(24)—C(25) | 1.533(8) |
| C(3)—C(4) | 1.386(9) | C(25)—C(26) | 1.541(9) |
| C(4)—C(5) | 1.365(9) | C(26)—C(23) | 1.440(8) |
| C(5)—C(6) | 1.372(7) | | |
| C(6)—C(1) | 1.401(7) | C(20)—F(1) | 1.355(6) |
| | | C(20)—F(2) | 1.343(7) |
| C(7)—C(8) | 1.391(7) | C(21)—F(3) | 1.335(6) |
| C(8)—C(9) | 1.377(7) | C(21)—F(4) | 1.335(6) |
| C(9)—C(10) | 1.383(9) | C(25)—F(5) | 1.329(8) |
| C(10)—C(11) | 1.366(9) | C(25)—F(6) | 1.357(8) |
| C(11)—C(12) | 1.383(7) | C(24)—O(1) | 1.216(7) |
| C(12)—C(7) | 1.393(7) | C(26)—O(2) | 1.208(7) |
| C(13)—C(14) | 1.389(7) | C(SOL)—Cl(1) | 1.86(3) |
| C(14)—C(15) | 1.363(7) | C(SOL)—Cl(2) | 1.58(2) |
| C(15)—C(16) | 1.362(8) | C(SOL)—Cl(3) | 1.78(2) |
| C(16)—C(17) | 1.360(9) | | |
| C(17)—C(18) | 1.377(8) | | |
| C(18)—C(13) | 1.379(7) | | |

[a] Analysis of the internal consistency of the phenyl rings in **A** suggests that the errors determined from least-squares are underestimated by a factor as large as 0.5.

(*b*) Interatomic angles for **A**

| Bonds | Angle (deg) | Bonds | Angle (deg) |
|---|---|---|---|
| C(1)—P(1)—C(7) | 109.8(2) | P(1)—C(1)—C(2) | 122.0(4) |
| C(1)—P(1)—C(13) | 111.7(2) | P(1)—C(1)—C(6) | 119.5(4) |
| C(1)—P(1)—C(19) | 110.2(2) | C(1)—C(2)—C(3) | 120.9(5) |
| C(7)—P(1)—C(13) | 109.2(2) | C(2)—C(3)—C(4) | 119.9(5) |
| C(7)—P(1)—C(19) | 106.4(2) | C(3)—C(4)—C(5) | 120.2(5) |
| C(13)—P(1)—C(19) | 109.5(2) | C(4)—C(5)—C(6) | 120.3(5) |
| | | C(5)—C(6)—C(1) | 120.4(5) |
| P(1)—C(7)—C(8) | 121.3(4) | C(6)—C(1)—C(2) | 118.4(5) |
| P(1)—C(7)—C(12) | 119.5(4) | | |
| C(7)—C(8)—C(9) | 120.2(5) | C(22)—C(23)—C(24) | 135.9(5) |
| C(8)—C(9)—C(10) | 119.9(5) | C(22)—C(23)—C(26) | 129.8(5) |
| C(9)—C(10)—C(11) | 120.6(5) | C(23)—C(24)—C(25) | 90.4(4) |
| C(10)—C(11)—C(12) | 120.0(5) | C(24)—C(25)—C(26) | 86.0(4) |
| C(11)—C(12)—C(7) | 120.1(5) | C(25)—C(26)—C(23) | 89.3(4) |
| C(12)—C(7)—C(8) | 119.1(5) | C(26)—C(23)—C(24) | 94.3(4) |
| | | C(23)—C(24)—O(1) | 137.5(5) |
| P(1)—C(13)—C(14) | 119.2(4) | C(25)—C(24)—O(1) | 132.1(5) |
| P(1)—C(13)—C(18) | 122.3(4) | C(23)—C(26)—O(2) | 137.8(6) |
| C(13)—C(14)—C(15) | 120.3(5) | C(25)—C(26)—O(2) | 132.9(6) |
| C(14)—C(15)—C(16) | 121.0(5) | C(24)—C(25)—F(5) | 118.0(6) |
| C(15)—C(16)—C(17) | 119.5(5) | C(24)—C(25)—F(6) | 115.6(6) |
| C(16)—C(17)—C(18) | 120.7(5) | C(26)—C(25)—F(5) | 116.7(6) |
| C(17)—C(18)—C(13) | 120.2(5) | C(26)—C(25)—F(6) | 115.7(6) |
| C(18)—C(13)—C(14) | 118.4(5) | F(5)—C(25)—F(6) | 104.9(5) |
| P(1)—C(19)—C(20) | 128.6(4) | C(21)—C(20)—F(2) | 115.1(4) |
| P(1)—C(19)—C(22) | 137.4(4) | F(1)—C(20)—F(2) | 106.1(4) |
| C(19)—C(20)—C(21) | 86.8(4) | C(19)—C(22)—C(23) | 139.0(5) |
| C(20)—C(21)—C(22) | 86.9(4) | C(21)—C(22)—C(23) | 128.7(5) |
| C(21)—C(22)—C(19) | 92.3(4) | C(20)—C(21)—F(3) | 115.4(5) |
| C(22)—C(19)—C(20) | 94.0(4) | C(20)—C(21)—F(4) | 114.6(5) |
| C(19)—C(20)—F(1) | 116.5(4) | C(22)—C(21)—F(3) | 116.8(5) |
| C(19)—C(20)—F(2) | 115.1(4) | C(22)—C(21)—F(4) | 115.0(5) |
| C(21)—C(20)—F(1) | 114.6(5) | F(3)—C(21)—F(4) | 107.4(4) |

C(19)—C(22)—C(23)—C(24)—O(1) which range from 135.9(5)–137.4(4)° reflect the angular distortion caused by the adjacent four-membered rings and are similar to the equivalent angles observed in the cyclooctenyl ring in **C** (6).

The C—F distances in both fluorocarbon rings 1 and 2 (1.329(8)–1.355(6) Å) are similar to those found in other fluorocarbon systems; e.g., 1.33(1)–1.36(1) in **C** (6) and 1.336(2) in perfluorocyclobutene (7).

The six-membered rings and the four-membered rings in this compound are all planar as one might expect. The largest deviation of any atom out of its least-squares plane is 0.008(6) Å (information concerning least-squares planes has been deposited). The two four-membered rings are virtually coplanar (interplanar angle = 0.8°) which is consistent with a delocalised system. There is no significant solvent/zwitterion interaction, the shortest distance between the two species is 2.98 Å for C(SOL)—F(3).

TABLE 3. Comparison of the bond distances of some perfluorocyclobutenyl rings

| Bond | Distance | | |
|---|---|---|---|
| | Ring 1[a] | *B* | *C* |
| C(19)—C(22) | 1.388(7) | 1.383(9) | 1.342(2) |
| C(19)—C(20) | 1.494(7) | 1.502(9) | 1.508(1) |
| C(22)—C(21) | 1.513(7) | 1.500(10) | 1.508(1) |
| C(20)—C(21) | 1.553(8) | 1.594(9) | 1.595 |
| *ave.* C—F | 1.342(9) | 1.335(5) | 1.336(2) |

[a]Present compound; the numbering scheme used here is different from that used in the original publications of **B** and C.

## Acknowledgements

We would like to thank Drs. W. Cullen and R. Soulen for their gift of crystals and for the suggestion of the problem. Also, we thank the Natural Sciences and Engineering Research Council of Canada for financial assistance.

1. D. F. GRANT and E. J. GABE. J. Appl. Crystallogr. **11**, 114 (1977).
2. International tables for X-ray crystallography. Vol. IV, Birmingham, Kynoch Press. 1974.
3. E. J. GABE, A. C. LARSON, F. L. LEE, and Y. WANG. The NRC pdp-8e crystal structure system. Chemistry Division, NRC, Canada. 1980.
4. R. M. WING. J. Am. Chem. Soc. **90**, 4828 (1968).
5. R. E. COBBLEDICK and F. W. B. EINSTEIN. Acta Crystallogr. B**32**, 1908 (1976).
6. F. W. B. EINSTEIN, A. C. WILLIS, W. R. CULLEN, and R. L. SOULEN. J. Chem. Soc. Chem. Commun. 526 (1981).
7. C. H. CHANG, R. F. PORTER, and S. N. BAUER. J. Mol. Struct. **7**, 89 (1971).
8. W. M. MACINTYRE and M. S. WEKEMA. J. Chem. Phys. **40**, 3563 (1964).
9. A. F. PERDEMAN, J. P. C. HOLST, L. HORNER, and H. WINKLER. Tetrahedron Lett. 811 (1965).
10. W. R. CULLEN and R. L. SOULEN. Private communication.

Can. J. Chem. Downloaded from www.nrcresearchpress.com by 210.87.254.105 on 09/06/12
For personal use only.

# A rapid semiquantitative approach to the calculation of net group charge (q)

WARREN KENNETH JARDINE, RICHARD FRANCIS LANGLER,[1] AND JOHN ATLEE MACGREGOR

*Department of Chemistry, Mount Allison University, Sackville, N.B., Canada E0A 3C0*

Received January 20, 1982

WARREN KENNETH JARDINE, RICHARD FRANCIS LANGLER, and JOHN ATLEE MACGREGOR. Can. J. Chem. **60**, 2069 (1982).

Huheey's approach to the calculation of partial charges on groups is extended and some group electronegativity parameters modified. The modified form of Huheey's method is shown to provide rapid access to net group charges (population numbers) in cations, radicals, anions, and sulfur trigonal bipyramids. Results obtained by substituent electronegativity calculations are shown to be comparable to those obtained by *ab initio* calculations.

WARREN KENNETH JARDINE, RICHARD FRANCIS LANGLER et JOHN ATLEE MACGREGOR. Can. J. Chem. **60**, 2069 (1982).

On a élargi l'approche de Huheey relative au calcul des charges partielles des groupes et on a modifié quelques paramètres d'électronégativité de groupe. On montre que la forme modifiée de la méthode de Huheey permet d'accéder rapidement aux charges globales des groupes (indice de population) des cations, des radicaux, des anions et des bipyramides trigonales du soufre. On montre que dans le cas des calculs d'électronégativité du substituant, les résultats obtenus sont comparables à ceux obtenus par les calculs *ab initio*.

[Traduit par le journal]

## Introduction

Organic chemists commonly utilize information about partial charges in a given species to speculate on the course of a particular ionic reaction. Such information may be obtained, these days, from molecular orbital calculations which can be both expensive and time consuming. Traditionally, qualitative analyses have employed valence bond theory (1, 2).

We wish to propose an extended form of Huheey's method for calculating partial charges by way of substituent electronegativities (3, 4) to the problem of obtaining rapid, inexpensive, and semiquantitative net group charge information about ions, radicals, and ground state molecules. Such calculations may be supplemented by traditional resonance analyses or a variant which has been discussed in detail elsewhere (5, 6).

## Atomic electronegativity parameters

According to Huheey (3, 4), the Mulliken electronegativity[2] of an atom can be defined as shown in eq. [2]:

$$[2] \quad X_M = a + b\delta$$

where $a$ corresponds (approximately) to the old invariant Pauling electronegativity in Mulliken units, $b$ is the charge coefficient and $\delta$ is the partial charge on the atom. Huheey (3) has reported $a$ and $b$ values for some 19 elements. By plotting Huheey's $a$ values against % orbital $p$ character, it has been possible to obtain some useful $a$ values which have not been previously reported. A similar procedure affords the corresponding $b$ values. These new $a$ and $b$ values are presented as entries 1–6 in Table 1.

## Group electronegativity parameters

In 1945, Sanderson (7) proposed that the electronegativity of two atoms is equalized upon covalent bond formation. Sanderson's assumption, in conjunction with eq. [2], permits one to formulate simultaneous eqs. [3] and [4] for the hypothetical covalent molecule AB.

$$[3] \quad \delta_A + \delta_B = \text{total charge on AB}$$

$$[4] \quad a_A + b_A\delta_A = a_B + b_B\delta_B$$

Provided the $a$ and $b$ values are known for the atoms A and B, the partial charges ($\delta_A$,$\delta_B$) are

TABLE 1. Atomic electronegativity parameters

| | Element | Hybridization | $a$ | $b$ |
|---|---|---|---|---|
| 1. | C | $sp^{2.5}$ | 8.38 | 13.47 |
| 2. | N | $sp$ | 13.94 | 15.91 |
| 3. | N | $sp^2$ | 13.46 | 15.58 |
| 4. | N | $sp^{2.5}$ | 12.50 | 15.18 |
| 5. | O | $sp^2$ | 15.65 | 18.94 |
| 6. | O | $sp^{2.5}$ | 15.45 | 18.61 |
| 7. | S | *$sp^2$ } $sp^3d$ | −1.01 | 10.73 |
| | | $pd$ } $sp^3d$ | −16.93 | 10.73 |
| 8. | S | Average $sp^3d$ | −20.665 | 10.73 |

*These parameters cannot be used for a sulfur atom which is simply $sp^2$ hybridized.

[1]Author to whom correspondence should be directed at: Department of Chemistry and Chemical Engineering, Florida Institute of Technology, 150 West University Boulevard, Melbourne, FL 32901, U.S.A.

[2]The relationship between the Mulliken and Pauling scales is:

$$[1] \quad X_P = 0.336(X_M - 0.615) \text{ (ref. 3)}$$

0008-4042/82/162069-06$01.00/0

©1982 National Research Council of Canada/Conseil national de recherches du Canada

Can. J. Chem. Downloaded from www.nrcresearchpress.com by 210.87.254.42 on 09/06/12
For personal use only.

Can. J. Chem. Downloaded from www.nrcresearchpress.com by 210.87.254.42 on 09/06/12
For personal use only.

readily found. AB constitutes a new group which may be combined with another atom Q. The $a$ and $b$ values for AB are obtained as follows:

$$[5] \quad a_{AB} = \frac{a_A b_B + a_B b_A}{b_A + b_B}$$

$$[6] \quad b_{AB} = \frac{b_A \cdot b_B}{b_A + b_B}$$

Huheey (3, 4) has tabulated electronegativity parameters for 196 groups. Both SH and $PH_2$ have incorrect $a$ values in Huheey's table (3) and are corrected in Table 2. Two commonly occurring groups require modified electronegativity parameters.

Since carbene is a neutral species ($\delta_{CH_2} = 0$), its Mulliken electronegativity is 7.43 (cf. Table 2 and eq. [2]). However, the Mulliken electronegativity of the methyl cation is 10.80 (cf. Table 2 and eq. [2]). These numbers do not appear to be self consistent for species which are isoelectronic. While Huheey's $a$ value for $CH_2$ is quite satisfactory for the calculation of electronegativity parameters for a host of substituted methyl groups, it is much too small for carbene itself.

The importance of the $CH_2$ group arises from a consideration of the hypothetical reaction between carbene and an anion to give a carbanion. When the resultant carbanionic centre bears an inductive stabilizer, the very low partial charge on $CH_2$ (obtained with Huheey's $a$ value) implicates virtually complete loss of σ bonding to the substituent. Thus the resistance of carbon to the loss of an octet (in inductively stabilized carbanions) provides a second route to the conclusion that the $a$ value for carbene is too small.

Reformulating eq. [2], the electronegativity of carbene can be expressed as shown in eq. [7].

$$[7] \quad X_M{}^{CH_2} = (a_{CH_2} + n b_{CH_2}) + b_{CH_2}\delta_{CH_2}$$

A comparison of calculated partial charges on $CH_2$ in a variety of inductively stabilized carbanions and ylides with results obtained from *ab initio* calculations (presented later), indicate that the value of $n$ should be 0.64. The resultant $a$ and $b$ values are shown in Table 2 for $\cdot\ddot{C}H_2^-$. *These parameters only apply to carbanions and ylides where conventional resonance interactions involving* p *orbitals are not possible*. The application of eq. [7] to alkyl substituted carbanions $CH_3\ddot{C}H^-$—, $CH_3CH_2\text{-}\ddot{C}H^-$—, etc. (with $n = 0.64$) will permit the calculation of partial charges in more complex carbanionic species which lack π bonding interactions.

TABLE 2. Group electronegativity parameters

| Group | Element/Hybridization | $a$ | $b$ |
|---|---|---|---|
| SH | S/unhybridized | 7.29 | 5.62 |
| $PH_2$ | P/unhybridized | 6.72 | 3.80 |
| $CH_2$ | C/$sp^3$ | 7.43 | 4.32 |
| $\underline{C}H_3$ | C/$sp^2$ | 7.55 | 3.25 |
| $\cdot\ddot{C}H_2$* | C/$sp^3$ | 10.19 | 4.32 |
| Ph | — | 7.81 | 26.67 |

*These parameters should only be used for carbanions and ylides in which the atom attached to $\cdot\ddot{C}H_2$ does not have a $p$ orbital available for a conventional resonance interaction.

The second group for which the parameters need modification is the phenyl group. The parameters Huheey has reported (4) for the phenyl group can be obtained by iterative use of eqs. [5] and [6]. No consideration was given to the special nature of aromatic groups in general or the phenyl group in particular. As we have pointed out previously (5), the phenyl group is particularly resistant to resonance interactions which necessarily disrupt the aromatic sextet. Not surprisingly, calculated partial charges on phenyl for such neutral aromatics as toluene and phenol, using Huheey's parameters, are approximately an order of magnitude larger than those obtained with *ab initio* calculations by Hehre *et al.* (8). The general formula for partial charge on phenyl in the generalized molecule PhZ is:

$$[8] \quad \delta_{Ph} = \frac{a_Z - a_{Ph}}{b_{Ph} + b_Z}$$

It is clear from inspection of eq. [8] that phenyl will only acquire small partial charges if $b_{Ph}$ is relatively large. By setting up simultaneous linear equations for toluene and phenol (*vide* eq. [4]), using Huheey's parameters for methyl and hydroxyl and the partial charges obtained by Hehre *et al.* (8), one can obtain the phenyl parameters shown in Table 2. These parameters represent a small decrease for $a_{Ph}$ and a very large increase for $b_{Ph}$.

## Results and discussion

This approach requires the calculation of partial charges using Huheey's method which affords net group charges due to *both* inductive and resonance effects and may be supplemented by the elaboration of a set of resonance contributors which permits an assessment of resonance effects. Since isomeric groups will have the same electronegativity parameters regardless of the arrangement of the atoms within them, *it is prudent to simplify the species as much as possible before carrying out partial charge calculations*.

### (i) *Carbocations*

The simplest carbocation is the methyl cation. A

Can. J. Chem. Downloaded from www.nrcresearchpress.com by 210.87.254.42 on 09/06/12
For personal use only.

TABLE 3. Partial charges in the methyl cation

| Method | $\delta_C$* | $\delta_H$ | Reference |
|---|---|---|---|
| This paper | +0.148 | +0.283 | — |
| *ab initio* | +0.000 | +0.340 | 9 |
| INDO | +0.523 | +0.159 | 10 |

*Carbon-$sp^2$ hybridized.

TABLE 4. Partial charges in CXY-Z]$^+$

| Method | X* | Y* | Z* | $\delta_{CXY}$ | $\delta_Z$ | Reference |
|---|---|---|---|---|---|---|
| This paper | H | H | $CH_3$ | +0.383 | +0.616 | — |
| This paper | H | H | $NH_2$ | +0.628 | +0.371 | — |
| *ab initio* | H | H | $NH_2$ | +0.614 | +0.368 | 11 |
| This paper | H | H | OH | +0.874 | +0.125 | — |
| *ab initio* | H | H | OH | +0.734 | +0.226 | 11 |
| *ab initio* | H | H | OH | +0.970 | +0.030 | 9, 12 |
| This paper | H | H | F | +1.005 | −0.005 | — |
| INDO | H | H | F | +0.941 | +0.059 | 10 |
| *ab initio* | H | H | F | +0.912 | +0.098 | 11 |
| *ab initio* (STO-3G) | H | H | F | +1.090 | −0.090 | 12 |
| *ab initio* (4-31G) | H | H | F | +1.200 | −0.200 | 12 |
| This paper | H | H | $SiH_3$ | +0.333 | +0.666 | — |
| *ab initio* | H | H | $SiH_3$ | +0.433 | +0.567 | 11 |
| This paper | H | H | $PH_2$ | +0.347 | +0.652 | — |
| This paper | H | H | SH | +0.523 | +0.476 | — |
| *ab initio* (STO-3G) | H | H | SH | +0.340 | +0.660 | 12 |
| *ab initio* (4-31G) | H | H | SH | +0.320 | +0.680 | 9 |
| This paper | H | H | Cl | +0.829 | +0.170 | — |
| *ab initio* (STO-3G) | H | H | Cl | +0.720 | +0.280 | 12 |
| *ab initio* (4-31G) | H | H | Cl | +0.620 | +0.380 | 12 |
| This paper | H | F | F | +0.921 | +0.078 | — |
| INDO | H | F | F | +1.004 | −0.004 | 10 |
| This paper | F | F | F | +0.823 | +0.176 | — |
| INDO | F | F | F | +1.028 | −0.028 | 10 |
| This paper | H | H | $C_2H$ | +0.685 | +0.314 | — |
| INDO | H | H | $C_2H$ | +0.577 | +0.423 | 13 |

*Heteroatoms hybridized: N-$sp^{2.5}$; O-$sp^{2.5}$; F-unhybridized; Si-$sp^3$; P-unhybridized; S-unhybridized; Cl-unhybridized.

comparison of the present approach with *ab initio* and INDO results is presented in Table 3. These results appear to indicate what we find in practice, namely, that results obtained by this method match *ab initio* results better than they match semi-empirical results.

Table 4 presents results for calculations on a variety of carbocations obtained by Huheey's method, INDO calculations, and *ab initio* calculations. Provided that one can select the hybridizations appropriate to the atoms in a given structure,

TABLE 5. Partial charges in radicals $\dot{Y}—\ddot{X}]^n$

| Y* | X* | $n$ | $\delta_Y$ | $\delta_X$ |
|---|---|---|---|---|
| $CH_2$ | $CH_3$ | 0 | −0.042 | +0.042 |
| $CH_2$ | $NH_2$ | 0 | +0.120 | −0.120 |
| $CH_2$ | OH | 0 | +0.239 | −0.239 |
| $CH_2$ | F | 0 | +0.206 | −0.206 |
| $CH_2$ | $SiH_3$ | 0 | −0.065 | +0.065 |
| $CH_2$ | $PH_2$ | 0 | −0.117 | +0.117 |
| $CH_2$ | SH | 0 | −0.039 | +0.039 |
| $CH_2$ | Cl | 0 | +0.107 | −0.107 |
| $CH_2$ | O | −1 | −0.466 | −0.533 |
| $NH_2$ | OH | +1 | +0.775 | +0.224 |
| HS | OH | +1 | +0.820 | +0.179 |

*Calculations with present method utilized atoms hybridized as follows: C-$sp^{2.5}$; N-$sp^{2.5}$; O-$sp^{2.5}$; F-unhybridized; Si-$sp^3$; P-unhybridized; S-unhybridized; Cl-unhybridized.

TABLE 6. Partial charges in $CH_2$=Z systems

| Method | Z* | $\delta_{CH_2}$ | $\delta_Z$ | Reference |
|---|---|---|---|---|
| This paper | NH | +0.203 | −0.203 | — |
| This paper | O | +0.341 | −0.341 | — |
| *ab initio* | O | +0.490 | −0.490 | 9 |
| MNDO | O | +0.290 | −0.290 | † |
| This paper | S | −0.020 | +0.020 | — |
| *ab initio* | S | −0.080 | +0.080 | 9 |
| MNDO | S | +0.150 | −0.150 | † |
| This paper | PH | −0.117 | +0.117 | — |

*Heteroatoms hybridized: N-$sp^2$; O-$sp^2$; S-unhybridized; P-unhybridized.
†Personal communication from Professor J. Ginsburg.

unusual geometries present no special problems for this approach to partial group charges. This point is illustrated by the results for protonated ethylene[3] **1** and the ethyl cation (first entry in Table 4).

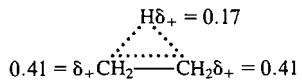


**1**

(ii) *Radicals*

In general, radicals present no special problems for Huheey's method. A representative selection of partial charges on groups in simple radicals with and without direct heteroatom substitution is presented in Table 5.

(iii) *Neutral molecules*

Amongst the simple molecules of general interest are those molecules containing a simple carbonyl group or an heteroatomic analogue. Table 6 presents results of Huheey's approach along with those obtained by modern computational methods.

As we have suggested earlier in this paper, the

[3]Carbon hybridization for this case is $sp^2$.

Can. J. Chem. Downloaded from www.nrcresearchpress.com by 210.87.254.42 on 09/06/12
For personal use only.

TABLE 7. Partial charges for Ph—Z

| Method | Z* | $\delta_{Ph}$ | $\delta_Z$ | Reference |
|---|---|---|---|---|
| This paper | $CH_3$ | −0.014 | +0.014 | — |
| *ab initio* | $CH_3$ | −0.015 | +0.015 | 8 |
| This paper | $C_2H_3$ | −0.004 | +0.004 | — |
| *ab initio* | $C_2H_3$ | −0.009 | +0.009 | 8 |
| This paper | $NH_2$ | +0.030 | −0.030 | — |
| *ab initio* | $NH_2$ | +0.060 | −0.060 | 8 |
| This paper | OH | +0.080 | −0.080 | — |
| *ab initio* | OH | +0.080 | −0.080 | 8 |
| *ab initio* | OH | +0.080 | −0.080 | 12 |
| This paper | F | +0.099 | −0.099 | — |
| *ab initio* | F | +0.135 | −0.135 | 8 |
| This paper | SH | −0.015 | +0.015 | — |
| *ab initio* | SH | −0.110 | +0.110 | 12 |
| This paper | $PH_2$ | −0.035 | +0.035 | — |

*Heteroatom hybridization: N-$sp^{2.5}$; O-$sp^{2.5}$; F-unhybridized; P-unhybridized.

TABLE 8. Partial charges in $CH_2$=CH—Z

| Method | Z* | $\delta_{C_2H_3}$ | $\delta_Z$ | Reference |
|---|---|---|---|---|
| This paper | OH | +0.269 | −0.269 | — |
| *ab initio* (STO-3G) | OH | +0.080 | −0.080 | 12 |
| *ab initio* (4-31G) | OH | +0.330 | −0.330 | 12 |
| This paper | SH | −0.060 | +0.060 | — |
| *ab initio* (STO-3G) | SH | −0.120 | +0.120 | 12 |
| *ab initio* (4-31G) | SH | −0.170 | +0.170 | 12 |

*Heteroatom hybridization: O-$sp^{2.5}$; S-unhybridized.

phenyl ring is somewhat unusual in that its aromaticity precludes substantial interactions with substituents, despite the ease with which one can draw conventional resonance contributors. Application of our revised parameters for the phenyl group (see Table 2) affords the results for monosubstituted benzenes shown in Table 7.

Calculations on a pair of vinyl substituted heteroatomics are presented in Table 8.

(iv) *Carbanions and ylides*

Since resonance stabilized carbanions may have relatively low partial charge on carbon without the implication of loss of σ bonding, such systems can be treated routinely using the *a* and *b* values given for $CH_2$ in Table 2, as shown in Table 9.

Inductively stabilized carbanions and ylides are readily treated using the *a* and *b* values given in Table 2 for $\cdot\ddot{C}H_2^-$. No attempt[4] has been made to resolve $d_\pi$–$p_\pi$ back-bonding and inductive transfer of electrons in anions or ylides stabilized by third row heteroatoms (Si, S, P, and Cl). Results obtained from the present approach are presented, along with those from *ab initio* calculations, in Table 10.

TABLE 9. Partial charges in $\overline{C}H_2$—C(=O)—R

| R | $\delta_{CH_2}$* | $\delta_{COR}$ |
|---|---|---|
| H | −0.272 | −0.727 |
| $CH_3$ | −0.187 | −0.812 |
| $C_2H_5$ | −0.146 | −0.853 |
| $C_3H_7$ | −0.122 | −0.877 |

*$CH_2$ carbon hybridized $sp^{2.5}$.

(v) *Beyond tetrahedra*

As Huheey (3) has pointed out, isomeric groups have the same electronegativity parameters, provided all of the corresponding atoms are hybridized the same way in all isomers. For species containing only second row elements, one can often circumvent the ensuing difficulties. For example, a series

TABLE 10. Partial charges in $\overline{C}H_2$—Z

| Method | Z* | $\delta_{CH_2}$ | $\delta_Z$ | Reference |
|---|---|---|---|---|
| This paper | H | −0.920 | −0.080 | — |
| *ab initio* | H | −1.156 | +0.078 | 14 |
| This paper | $C_2H_5$ | −0.752 | −0.248 | — |
| *ab initio* | $C_2H_5$ | −0.719 | −0.281 | 15 |
| This paper | $NH_2$ | −0.713 | −0.286 | — |
| This paper | OH | −0.631 | −0.369 | — |
| *ab initio* | OH | −0.666 | −0.334 | 15 |
| This paper | $OCH_3$ | −0.615 | −0.385 | — |
| *ab initio* | $OCH_3$ | −0.639 | −0.361 | 15 |
| This paper | F | −0.709 | −0.291 | — |
| *ab initio* | F | −0.571 | −0.429 | 14 |
| This paper | $SiH_3$ | −0.814 | −0.186 | — |
| This paper | $PH_2$ | −0.895 | −0.105 | — |
| This paper | SH | −0.835 | −0.165 | — |
| This paper | $SCH_3$ | −0.700 | −0.300 | — |
| *ab initio* | $SCH_3$ | −0.724 | −0.276 | 15 |
| This paper | Cl | −0.775 | −0.225 | — |
| This paper | $^+NH_3$ | −0.278 | +0.278 | — |
| *ab initio* | $^+NH_3$ | −0.315 | +0.315 | 17 |
| This paper | $H_2O^+$ | −0.122 | +0.122 | — |
| *ab initio* | $H_2O^+$ | −0.175 | +0.175 | 17 |
| This paper | $^+PH_3$ | −0.446 | +0.446 | — |
| *ab initio* | $^+PH_3$ | −0.526 | +0.526 | 17 |
| This paper | $^+SH_2$ | −0.356 | +0.356 | — |
| *ab initio* | $^+SH_2$ | −0.448 | +0.448 | 17 |

*Hybridization: N-$sp^3$; O-$sp^3$; F-unhybridized; Si-$sp^3$; P-unhybridized; S-unhybridized; Cl-unhybridized.

[4]Lehn and Wipff (15) have found that sulfur does not stabilize an adjacent carbanionic site by $d_\pi$–$p_\pi$ back bonding.

TABLE 11. Partial charges in: 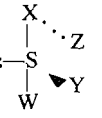

| W | X | Y | Z | $\delta_s$ | $\delta_w$ | $\delta_x$ | $\delta_y$ | $\delta_z$ |
|---|---|---|---|---|---|---|---|---|
| F | F | F | F | +2.18 | −0.75 | −0.75 | −0.34 | −0.34 |
| Cl | Cl | Cl | Cl | +2.21 | −0.79 | −0.79 | −0.31 | −0.31 |
| $OCH_3$ | $OCH_3$ | $OCH_3$ | $OCH_3$ | +2.59 | −0.94 | −0.94 | −0.35 | −0.35 |
| Cl | $OCH_3$ | $CH_3$ | $CH_3$ | +2.51 | −0.47 | −1.49 | −0.27 | −0.27 |
| Cl | $OCH_3$ | Cl | $CH_3$ | +3.04 | −0.50 | −1.95 | −0.19 | −0.39 |
| Cl | Cl | $OCH_3$ | $CH_3$ | +2.12 | −0.50 | −0.50 | −0.73 | −0.39 |
| F | F | $CH_3$ | $CH_3$ | +1.94 | −0.57 | −0.57 | −0.39 | −0.39 |
| Cl | Cl | $CH_3$ | $CH_3$ | +2.13 | −0.58 | −0.58 | −0.48 | −0.48 |
| $OCH_3$ | $OCH_3$ | $CH_3$ | $CH_3$ | +2.85 | −1.23 | −1.23 | −0.19 | −0.19 |
| $NH_2$ | $NH_2$ | $CH_3$ | $CH_3$ | +2.48 | −0.94 | −0.94 | −0.29 | −0.29 |
| $CF_3$ | $CF_3$ | $CH_3$ | $CH_3$ | +3.19 | −1.48 | −1.48 | −0.11 | −0.11 |

containing 1-chloropropyl, 2-chloropropyl, and 3-chloropropyl groups can be examined in an approximate way by utilizing a chloromethyl, a 2-chloroethyl, and a 3-chloropropyl group.

However, third row elements can form species which involve more complex geometries such as rectangular pyramidal and trigonal bipyramidal. Huheey (3) has not provided parameters for atoms which are $sp^3d$ hybridized. Recent semi-empirical calculations[5] (18) provided net charge data for fluorine and sulfur in $SF_4$. By resolving $SF_4$ into two hypothetical components, $SF_2$ ($pd$ hybridized) and $SF_2$ ($sp^2$ hybridized), and reversing the usual substituent electronegativity calculations using the partial charges given elsewhere (18), one can obtain the sulfur parameters listed in Table 1. The problem with using these parameters for sulfur trigonal bipyramids is that they preclude interactions between the apical and equatorial substituents. By reversing the usual substituent electronegativity calculations, utilizing the average net charge on fluorine in $SF_4$ (18), one can obtain electronegativity parameters for sulfur which represent five identical $sp^3d$ orbitals (see Table 1). Utilizing these parameters will permit the calculation of net charge on a substituent which represents the average of what it would bear in an equatorial position and what it would bear in an apical position.

One can now utilize the $pd$ and $sp^2$ parameters given in Table 1 to obtain the following expression for the partial charges of apical and equatorial groups in $SX_4$.

$$[9] \quad \frac{\delta_x^{equ.}}{\delta_x^{ap}} = \frac{-1.01 - a_x}{-16.93 - a_x}$$

[5]Semi-empirical calculations furnish quite different partial charges than do *ab initio* calculations (*vide* Table 6).

Assuming that the ratio of partial charges a given group will bear in an equatorial position to that which it will bear in an apical position is roughly constant from sulfur trigonal bipyramid to sulfur trigonal bipyramid, one can utilize the ratio in eq. [9] to modify the average partial charge $\bar{\delta}_x$ obtained by employing the sulfur $sp^3d$ parameters. The complete expressions for partial charge on X in any SWXYZ (sulfur-$sp^3d$) are given below:

$$[10] \quad \delta_x^{equ.} = \bar{\delta}_x \left[\frac{1.01 + a_x}{8.97 + a_x}\right]$$

$$[11] \quad \delta_x^{ap} = \bar{\delta}_x \left[\frac{16.93 + a_x}{8.97 + a_x}\right]$$

Thus it is now possible to calculate partial charges on substituents in sulfur trigonal bipyramids, which permit interactions between the substituents as well as allowing for the impact consequent upon equatorial or apical disposition.

Table 11 depicts the results of calculations carried out on a variety of sulfur trigonal bipyramids. While these results should be in reasonable agreement with those obtained by the methods used in ref. 18, other methods may give quite different results. For instance Cowley *et al.* (18) obtain a partial charge of +2.18 on the sulfur atom in $SF_4$, while Jolly *et al.* (19) obtain +0.79. Although the sulfur parameters in Table 1 can be modified to yield greater or smaller charges on the substituents, the trends tabulated (Table 11) are a function of the parameters of the substituents and will not be altered significantly by modifying the sulfur parameters.

## Conclusions

The application of Huheey's approach to the

Can. J. Chem. Downloaded from www.nrcresearchpress.com by 210.87.254.42 on 09/06/12
For personal use only.

calculation of partial charges using variable electronegativities for atoms and groups has been shown to afford reasonable semiquantitative net group charges. It has also been shown that Huheey's method can be extended to treat more complex geometries such as the trigonal bipyramid.

**Acknowledgements**

The authors are indebted to Dean P. Bogaard and Mount Allison University for generous financial support. We thank Dr. J. Ginsburg for stimulating discussions about the calculation of partial charges in trigonal bipyramids and C. M. Milley for some technical assistance.

1. K. HIGASI, H. BABA, and A. REMBAUM. Quantum organic chemistry. Wiley, New York, NY. 1965.
2. L. PAULING. The nature of the chemical bond. 3rd ed. Cornell University Press, Ithaca, NY. 1960.
3. J. E. HUHEEY. J. Phys. Chem. **69**, 3284 (1965).
4. J. E. HUHEEY. J. Phys. Chem. **70**, 2086 (1966).
5. R. F. LANGLER, J. E. TRENHOLM, and J. S. WASSON. Can. J. Chem. **58**, 780 (1980), and references therein.
6. W. JENSEN. Can. J. Chem. **59**, 807 (1981).
7. R. T. SANDERSON. J. Chem. Educ. **31**, 2 (1945).
8. W. J. HEHRE, L. RADOM, and J. A. POPLE. J. Am. Chem. Soc. **94**, 1496 (1972).
9. F. BERNARDI, I. G. CSIZMADIA, H. B. SCHLEGEL, and S. WOLFE. Can. J. Chem. **53**, 1144 (1975).
10. L. D. KISPERT, C. U. PITTMAN, JR., D. L. ALLISON, T. B. PATTERSON, JR., C. W. GILBERT, JR., C. F. HAINES, and J. PRATHER. J. Am. Chem. Soc. **94**, 5979 (1972).
11. Y. APELOIG, P. v. R. SCHLEYER, and J. A. POPLE. J. Am. Chem. Soc. **99**, 1291 (1977).
12. F. BERNARDI, A. MANGINI, N. E. EPIOTIS, J. R. LARSON, and S. SHAIK. J. Am. Chem. Soc. **99**, 7465 (1977).
13. C. U. PITTMAN, JR., G. WILEMON, J. E. FOJTASEK, and L. D. KISPERT. J. Phys. Chem. **79**, 2443 (1975).
14. J. BURDON, D. W. DAVIES, and G. DEL CONDE. J. Chem. Soc. Perkin Trans II, 1205 (1979).
15. J. M. LEHN and G. WIPFF. J. Am. Chem. Soc. **98**, 7498 (1976).
16. F. BERNARDI, I. G. CSIZMADIA, A. MANGINI, H. B. SCHLEGEL, M. Y. WHANGBO, and S. WOLFE. J. Am. Chem. Soc. **97**, 2209 (1975).
17. G. BERNARDI, H. B. SCHLEGEL, M. Y. WHANGBO, and S. WOLFE. J. Am. Chem. Soc. **99**, 5633 (1977).
18. A. H. COWLEY, M. LATTMAN, and M. L. WALKER. J. Am. Chem. Soc. **101**, 4074 (1979).
19. W. L. JOLLY, M. S. LAZARUS, and O. GLEMSER. Z. Anorg. Allg. Chem. **406**, 209 (1974).

Can. J. Chem. Downloaded from www.nrcresearchpress.com by 210.87.254.42 on 09/06/12
For personal use only.

# The preparation of thiolato bridged platinum dimers; the crystal and molecular structure of *cis*-μμ′-bis(phenylmethanethiolato)bis(phenylmethanethiolatomethyldiphenylphosphineplatinum(II)), *cis*-[$(PMePh_2)Pt(SCH_2Ph)(\mu\text{-}SCH_2Ph)]_2$

PETER H. BIRD[1] AND UPALI SIRIWARDANE
*Department of Chemistry, Concordia University, Montreal, P.Q., Canada*
AND
RABIN D. LAI AND ALAN SHAVER[2]
*Department of Chemistry, McGill University, 801 Sherbrooke St. W., Montreal, P.Q., Canada H3A 2K6*

Received September 24, 1981

PETER H. BIRD, UPALI SIRIWARDANE, RABIN D. LAI, and ALAN SHAVER. Can. J. Chem. **60**, 2075 (1982).

Fusion *in vacuo* of complexes of the type $P_2Pt(SR)_2$ is a facile route to dimers of the type $[PPt(SR)(\mu\text{-}SR)]_2$; thus, the compounds *cis*-$P_2Pt(SR)_2$, where P = $PPh_3$, $PMePh_2$, R = $CH_2Ph$ and *trans*-$P_2Pt(SR)_2$, where P = $PPh_3$, $PMePh_2$, $PMe_2Ph$, R = 4-$C_6H_4CH_3$ gave the appropriate dimers **1–5**. A three-dimensional X-ray structure analysis of the complex $[(PMePh_2)Pt(SCH_2Ph)(\mu\text{-}SCH_2Ph)]_2$, **2**, has shown that it has *cis* geometry with the benzyl groups of the bridging thiolato ligands oriented *anti* with respect to each other. The dihedral angle between the two square planes is 138.8°. Crystals of **2** are triclinic, space group $P\bar{1}$, with two molecules in a cell of dimensions $a$ = 10.856(3) Å, $b$ = 19.935(5) Å, $c$ = 12.202(4) Å, $\alpha$ = 82.52(2)°, $\beta$ = 105.18(2)°, and $\gamma$ = 92.35(2)°. Full-matrix least-squares refinement converged at $R$ = 0.052.

PETER H. BIRD, UPALI SIRIWARDANE, RABIN D. LAI et ALAN SHAVER. Can. J. Chem. **60**, 2075 (1982).

La fusion sous vide des complexes du type $P_2Pt(SR_2)$ conduit facilement aux dimères du type $[PPt(SR)(\mu\text{-}SR)]_2$; ainsi les composés $P_2Pt(SR)_2$-*cis* où P = $PPh_3$, $PMePh_2$, R = $CH_2Ph$ et $P_2Pt(SR)_2$-*trans*, où P = $PPh_3$, $PMePh_2$, R = $C_6H_4CH_3$-4 donnent les dimères appropriés **1–5**. Une analyse de structure en trois dimensions aux rayons X du complexe $[(PMePh_2)Pt(SCH_2Ph)(\mu\text{-}SCH_2Ph)]_2$, **2**, a montré que ce composé a une géométrie *cis*, avec les groupes benzyles des ligands thiolato du pont orientés en *anti* l'un par rapport à l'autre. L'angle dièdre entre les deux plans carrés est de 138,8°. Les cristaux sont tricliniques, groupe d'espace $P\bar{1}$ avec deux molécules par maille et les dimensions de la maille seul: $a$ = 10,856(3) Å, $b$ = 19,935(5) Å, $c$ = 12,202(4) Å, $\alpha$ = 82,52(2)°, $\beta$ = 105,18(2)° et $\gamma$ = 92,35(2)°. On a affiné la structure par la méthode des moindres carrés (matrice complète) jusqu'à une valeur de $R$ de 0,052.

[Traduit par le journal]

## Introduction

Recently we reported the effect of oxygen on the reaction of the dichlorides $P_2PtCl_2$ with thiols in the presence of triethylamine, where P is a phosphine ligand (1). The *cis* isomers of the dithiolato complexes $P_2Pt(SR)_2$ are isolated cleanly and in high yield if oxygen is absent and when R is an alkyl group. However, the presence of oxygen leads to a mixture of products which often included the *trans* isomer plus dimers of the type $[PPt(SR)(\mu\text{-}SR)]_2$ in addition to the *cis* isomer. When R is an aryl group the *trans* isomer is isolated regardless of the presence or absence of oxygen. While studying the stability of the new *cis* complexes the effect of heating them came to our attention. During melting point determinations crystals or clear liquids (phosphines) condensed in the top of the capillary tube. Scaled up to preparative amounts, the fusion *in vacuo* of both *cis* and *trans* monomers is a facile route to a series of the dimers $[PPt(SR)(\mu\text{-}SR)]_2$, some of which were also observed in the solution decomposition of the monomers.

Dimeric platinum complexes with bridging thiolato ligands have been known for many years (2). Previously reported routes to these complexes involve multi-step procedures (3). The fusion method represents a significant simplification in obtaining these dimers. These complexes may occur as *cis* and *trans* isomers or even as the asymmetrical isomer $P_2Pt(\mu\text{-}SR)_2Pt(SR)_2$. It was

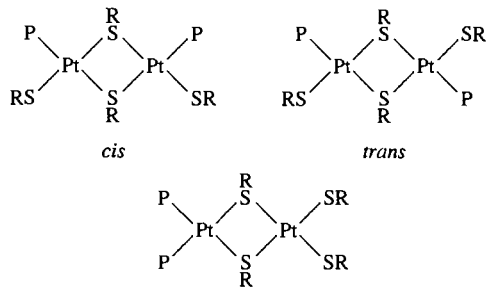


not possible from routine spectroscopic characterization to determine which geometry was obtained. An X-ray structural determination found the *cis*

[1]Author to whom correspondence concerning the X-ray structural determination should be sent.

[2]Author to whom correspondence concerning the preparations should be sent.

0008-4042/82/162075-07$01.00/0
©1982 National Research Council of Canada/Conseil national de recherches du Canada

Can. J. Chem. Downloaded from www.nrcresearchpress.com by 210.87.254.40 on 09/06/12
For personal use only.

geometry for the complex $[(PMePh_2)Pt(SCH_2Ph)(\mu\text{-}SCH_2Ph)]_2$. Our earlier $^{31}P$ nmr study of the *cis* and *trans* monomers (1) indicated that the nmr *trans*-influences (4) of the phosphine and thiolato ligands were similar. Therefore, it was of interest to compare the structural *trans*-influences of these ligands.

## Experimental

The fusion reactions were performed *in vacuo* ($\leq 10^{-1}$ Torr) and subsequent isolation and characterization was conducted in air. All solvents were of spectrograde quality. Melting points were determined in air on a Thomas-Hoover Uni-melt apparatus and are uncorrected. Proton nmr spectra were obtained on a Varian T-60 spectrometer, using $CDCl_3$ (Merck, Sharpe and Dohme of Montreal) as solvent and TMS as internal standard. Phosphorus nmr spectra were recorded by Mrs. Elva Heyge of McGill University using a Bruker WH-90 instrument operating in the pulsed Fourier Transform mode. The $^{31}P$ chemical shifts of the samples in $CDCl_3$ solution are reported in ppm downfield (positive) from 85% $H_3PO_4$ as external standard, using $D_2O$ as the lock signal. Elemental analyses were performed by Midwest Microlab Ltd., Indianapolis, IN. The midrange infrared spectra (Perkin Elmer 297) of the dimers were almost superimposable on those of the corresponding monomers (1) and were uninformative. The monomers were prepared by reported methods (1, 5).

*A.* *μμ′-Bis(phenylmethanethiolato)bis(phenylmethanethiolatotriphenylphosphineplatinum(II)), [(PPh$_3$)Pt(SCH$_2$Ph)(μ-SCH$_2$Ph)]$_2$*, **1**

The monomor *cis*-$(PPh_3)_2Pt(SCH_2Ph)_2$ (0.24 g, 0.25 mmol) was placed in a 50 mL flask connected to a trap-to-trap vacuum distillation apparatus. The flask was heated to 200°C with a wax bath and the yellow crystals melted (~150°C), effervesced briefly, and resolidified. The upper regions of the apparatus were warmed by pouring the hot wax over it by means of a small pipette or were warmed with a hot-air gun. The phosphine was distilled into the liquid nitrogen cooled collecting flask. The complex was kept at 200°C for 15 min, cooled to room temperature, and extracted in $CH_2Cl_2$. The solution was filtered and evaporated to dryness and the residue recrystallized from $Ch_2Cl_2$/ether to give yellow crystals (0.12 g, 69%).

In a similar experiment, *trans*-$(PPh_3)_2Pt(SCH_2Ph)_2$ (0.48 g, 0.50 mmol) was heated to 230°C *in vacuo*. Recrystallization of the residue from $CH_2Cl_2$/ether gave yellow crystals (0.25 g, 86%).

This dimer was also obtained from the decomposition of the monomer *cis*-$(PPh_3)_2Pt(SCH_2Ph)_2$ in toluene. This complex was formed *in situ* by treating the dichloride *cis*-$(PPh_3)_2PtCl_2$ (6) (3.0 g, 3.8 mmol), suspended in 200 mL toluene, with phenylmethanethiol (0.9 mL, 7.7 mmol) and triethylamine (3 mL, 21.6 mmol) in 100 mL $CH_2Cl_2$ added dropwise. The mixture was stirred at room temperature in air for 22 h and the solvents evaporated on a rotary evaporator. The residue was dissolved in $CH_2Cl_2$ and the solution was washed with 4 × 100 mL portions of distilled water and dried over $MgSO_4$. Recrystallization from hot $CH_2Cl_2$/ether gave yellow crystals of the *trans*-monomer. The mother liquors were evaporated to dryness, the residue boiled in hexane for 1 h and filtered. The insoluble yellow powder was recrystallized as above to give yellow crystals (0.73 g, 33%) of the dimer.

*B.* cis-*μμ′-Bis(phenylmethanethiolato)bis(phenylmethanethiolatomethyldiphenylphosphineplatinum(II))*, cis-*[(PMePh$_2$)Pt(SCH$_2$Ph)(μ-SCH$_2$Ph)]$_2$*, **2**

The complex *cis*-$(PMePh_2)_2Pt(SCH_2Ph)_2$ (0.82 g, 0.97 mmol) was placed in a vacuum microdistillation apparatus and heated for 0.5 h at 210°C with a wax bath as in A. After cooling, the light orange glassy solid was recrystallized from $CH_2Cl_2$/ hexane to give yellow crystals (0.43 g, 70%).

*C.* *μμ′-Bis(4-methylphenylthiolato)bis(4-methylphenylthiolatotriphenylphosphineplatinum(II)), [(PPh$_3$)Pt(4-SC$_6$H$_4$Me)(μ-4-SC$_6$H$_4$Me)]$_2$*, **3**

The monomer *trans*-$(PPh_3)_2Pt(4\text{-}SC_6H_4Me)_2$ (0.81 g, 0.84 mmol) was heated *in vacuo* as in A at 255°C for 0.5 h. After cooling, the clear red glassy residue was extracted with 150 mL of hot $CH_2Cl_2$ and filtered. The filtrate was reduced in volume and excess hexane was added. The resulting yellow powder was filtered, washed with hexane, and pumped on (0.27 g). The product was contaminated by the monomer. Chromatography on alumina failed to separate the two.

*D.* *μμ′-Bis(4)methylphenylthiolato)bis(4-methylphenylthiolatomethyldiphenylphosphineplatinum(II)), [(PMePh$_2$)Pt(4-SC$_6$H$_4$Me)(μ-4-SC$_6$H$_4$Me)]$_2$*, **4**

As in B, *trans*-$(PMePh_2)_2Pt(4\text{-}SC_6H_4Me)_2$ (0.40 g, 0.48 mmol) was heated to 235°C for 5 min. The cooled orange solid was dissolved in toluene and chromatographed on activated alumina. The column was eluted with toluene first, followed by $CH_2Cl_2$ after removal of the first band (*trans*-monomer). The second yellow band was collected, evaporated to dryness, and recrystallized from $CH_2Cl_2$/hexane (0.076 g, 25%).

*E.* *μμ′-Bis(4)methylphenylthiolato)bis(4)methylphenylthiolatodimethylphenylphosphineplatinum(II)), [(PMe$_2$Ph)Pt(4-SC$_6$H$_4$Me)(μ-4-SC$_6$H$_4$Me)]$_2$*, **5**

Again, as in B, *trans*-$(PMe_2Ph)_2Pt(4\text{-}SC_6H_4Me)_2$ (0.51 g, 0.71 mmol) was heated at 250°C for 10 min. The cooled orange glass which contains both the monomer and the dimer in equal proportions was extracted with 10 mL of toluene and filtered. The yellow filtrate was evapoarted to dryness and the residue recrystallized from $Ch_2Cl_2$/ether to give the dimer (0.23 g, 57%).

*X-ray structure determination*

*Crystal data*

$C_{54}H_{54}P_2Pt_2S_4$ fw = 1283.67

Triclinic, $a$ = 10.856(3), $b$ = 19.935(5), $c$ = 12.202(4) Å, $\alpha$ = 82.52(2), $\beta$ = 105.18(2), $\gamma$ = 92.35(2)°, $V$ = 2526.8, $Z$ = 2, $\rho_0$ = 1.69(3), $\rho_c$ = 1.687 g/cm$^3$ (Mo K$\alpha$ $\lambda$ = 0.71069 Å, 20°C, $\mu$ = 60.79 cm$^{-1}$).

The crystal used in the structure determination was grown from methylene chloride. It was approximately a parallelepiped with dimensions 0.30 × 0.25 × 0.20 mm. Preliminary Weissenberg and precession photographs led to the assignment of space groups $P1$ (No. 1) or $P\bar{1}$ (No. 2). The latter choice yielded a successful structure solution. Accurate cell dimensions were obtained by least-squares refinements from the setting angles of 12 reflections on a fully automated Picker FACS-1 diffractometer. Each reflection was centred at both positive and negative 2θ values, and the 2θ, $w$, $\chi$, and $\phi$ values were appropriately averaged before the least-square calculation.

Intensity measurements were made using the θ–2θ scan method. The scanning speed was 2° per min with a scan length of (2.5 + 0.692 tan θ)°. Backgrounds were measured for 20 s on either side of the peak. A hemisphere of data defined by $3.5° < 2\theta < 40°$ and $\pm h$, $\pm k$, $+l$ was collected yielding 6078 intensities. Every 50 cycles, 3 standard reflections were remeasured to check instrumental and crystal stability. These varied randomly by less than 4%.

*Data collection*

Data reduction using locally written programs computed the net intensity $I$ and its estimated standard deviation $\sigma(I)$ as:

Can. J. Chem. Downloaded from www.nrcresearchpress.com by 210.87.254.40 on 09/06/12
For personal use only.

Can. J. Chem. Downloaded from www.nrcresearchpress.com by 210.87.254.40 on 09/06/12
For personal use only.

$$I = [N - B \cdot t_s/t_b]$$
$$\sigma(I) = [N + B(t_s/t_b)^2 + (0.02N)^2]^{1/2}$$

where $N$ is the total count accumulated during the scan time $t_s$ and $B$ is the total background count accumulated in time $t_b$.

The reflections having $I > 3\sigma(I)$ (4444 intensities) were considered "observed": the remainder were discarded. The observed data were corrected for Lorentz and polarization effects:

$$(Lp)^{-1} = \sin 2\theta_s(\cos^2 2\theta_n + 1)/(\cos^2 2\theta_m + \cos^2 2\theta_s)$$

where $2\theta_m$ and $2\theta_s$ are the diffraction angles at the graphite monochromator and sample crystal respectively. An absorption correction was applied using the program GNABS by Burnham (7) (transmission factors ranged between 0.30 and 0.55).

*Structure determination*

A three-dimensional Patterson synthesis yielded the positions of the two platinum atoms. The remaining non-hydrogen atoms were found from successive structure factor calculations and Fourier synthesis (FORDAP by A. Zalkin). Structure factor and least-squares calculations were performed using NUCLS in its rigid body version by J. A. Ibers. The scattering factors were taken from the compilation of Cromer and Waber (8). Full-matrix least-squares refinement of the fractional atomic coordinates, anisotropic thermal parameters for the Pt, S, and P atoms and isotropic thermal parameters for the remaining non-hydrogen atoms with the eight phenyl rings refined as rigid groups (C—C = 1.39 Å), resulted in convergence after 7 cycles with $R = 0.052$ and $R_w = 0.066$ ($R = \Sigma(||F_o| - |F_c||)/\Sigma|F_o|$; $R_w = [\Sigma w(|F_o| - |F_c|)^2/\Sigma w|F_o|^2]^{1/2}$, where $w = [\sigma(F_o)]^{-2}$ and $\sigma(F_o) = \sigma(I)/2Lp F_o$). A final difference Fourier showed no significant residual electron density.

The final atomic parameters are listed in the Table 1.[3]

## Results

Fusion *in vacuo* of complexes of the type $P_2Pt(SR)_2$, where P is a phosphine, is a facile route to dimers of the type $[PPt(SR)(\mu\text{-}SR)]_2$. Thus the compounds *cis*-$P_2Pt(SR)_2$, where P = $PPh_3$, $PMePh_2$, R = $CH_2Ph$, and *trans*-$P_2Pt(SR)_2$ where P = $PPh_3$, $PMePh_2$, $PMe_2Ph$, R = 4-$C_6H_4Me$ gave the appropriate dimers **1–5**. Repeated attempts to dimerize the complex *cis*-$(PMe_2Ph)_2Pt(SCH_2Ph)_2$ (containing about 15% of the *trans* isomer) led to decomposition while fusion of *trans*-$(PMe_2Ph)_2Pt(4\text{-}SC_6H_4Me)_2$ gave its dimer. The *trans*-monomers are very stable to decomposition in solution; *trans*-$(PMePh_2)_2Pt(4\text{-}SC_6H_4Me)_2$ was refluxed in decahydronaphthalene for 15 h without any appreciable dimerization or degradation. On the other hand, the *cis*-monomers dimerize slowly in solution in air (1). Since $[(PMe_2Ph)Pt(SCH_2Ph)(\mu\text{-}SCH_2Ph)]_2$ was not obtained by fusion, the appropriate *cis*-monomer was refluxed in decalin. However, extensive decomposition resulted and the dimer was not isolated. Thus, the combination of the $PMe_2Ph$ and $PhCH_2S^-$ ligands appears to be unsuitable for some

[3]Tables of observed and calculated structure amplitudes and of temperature factors are available, at a nominal charge, from the Depository of Unpublished Data, CISTI, National Research Council of Canada, Ottawa, Ont., Canada K1A 0S2.

TABLE 1. Final positional parameters for *cis*-$[(PMePh_2)Pt(SCH_2Pt)(\mu\text{-}SCH_2Ph)]_2$[a]

| Atom | x/a | y/b | z/c |
|---|---|---|---|
| Pt1 | 1203.7(6) | 2209.6(3) | 3886.4(5) |
| Pt2 | −374.3(6) | 2676.5(3) | 1160.1(5) |
| S1 | 775(5) | 2288(2) | 5649(4) |
| P1 | 2386(4) | 1270(2) | 4532(4) |
| SB1 | −83(4) | 3152(2) | 2906(3) |
| SB2 | 1651(4) | 2273(2) | 2116(3) |
| S2 | −2459(4) | 3031(2) | 360(4) |
| P2 | −558(4) | 2206(2) | −449(4) |
| CB1 | −1562(16) | 3065(8) | 3357(14) |
| CB2 | 2743(15) | 3015(8) | 2234(14) |
| CS1 | 1511(18) | 3135(9) | 5973(16) |
| CP1 | 2987(15) | 1051(8) | 6093(15) |
| CS2 | −2352(18) | 3961(10) | 262(16) |
| CP2 | −611(15) | 2849(9) | −1729(14) |
| C11 | 2908(9) | 3167(6) | 5972(10) |
| C12 | 3810(13) | 2823(6) | 6875(9) |
| C13 | 5098(11) | 2872(7) | 6896(10) |
| C14 | 5483(9) | 3264(7) | 6014(13) |
| C15 | 4581(13) | 3608(6) | 5111(10) |
| C16 | 3294(11) | 3559(6) | 5090(9) |
| C21 | 1490(11) | 525(5) | 4028(10) |
| C22 | 1919(9) | −124(6) | 4494(9) |
| C23 | 1236(12) | −683(4) | 4077(11) |
| C24 | 124(12) | −593(5) | 3194(11) |
| C25 | −305(9) | 56(6) | 2729(9) |
| C26 | 378(11) | 615(5) | 3146(10) |
| C31 | 3808(9) | 1297(5) | 4001(9) |
| C32 | 4745(12) | 1753(5) | 4463(9) |
| C33 | 5868(10) | 1823(6) | 4112(11) |
| C34 | 6055(9) | 1437(7) | 3299(11) |
| C35 | 5118(12) | 982(6) | 2836(9) |
| C36 | 3995(10) | 0912(5) | 3188(9) |
| C41 | 3066(11) | 3248(6) | 1143(8) |
| C42 | 3886(11) | 2863(5) | 777(10) |
| C43 | 4240(10) | 3087(6) | −225(10) |
| C44 | 3775(12) | 3697(6) | −862(8) |
| C45 | 2955(12) | 4082(5) | −496(10) |
| C46 | 2600(10) | 3858(6) | 506(10) |
| C51 | 728(8) | 1629(4) | −407(9) |
| C52 | 1714(10) | 1821(4) | −918(9) |
| C53 | 2686(9) | 1370(6) | −836(9) |
| C54 | 2674(9) | 726(5) | −243(10) |
| C55 | 1688(10) | 533(4) | 269(9) |
| C56 | 716(8) | 985(5) | 187(9) |
| C61 | −1972(8) | 1664(5) | 9170(9) |
| C62 | −2680(10) | 1473(5) | 9961(7) |
| C63 | −3764(10) | 1070(5) | 9671(9) |
| C64 | −4140(9) | 858(5) | 8590(10) |
| C65 | −3433(11) | 1048(6) | 7799(7) |
| C66 | −2348(10) | 1451(5) | 8089(8) |
| C71 | −2035(14) | 4278(6) | −796(10) |
| C72 | −765(12) | 4419(7) | −780(11) |
| C73 | −449(11) | 4708(8) | −1771(15) |
| C74 | −1403(17) | 4857(7) | −2779(11) |
| C75 | −2673(14) | 4716(7) | −2795(10) |
| C76 | −2989(10) | 4426(7) | −1803(13) |
| C81 | −2207(10) | 3740(4) | 3305(10) |
| C82 | −1610(8) | 4241(6) | 3957(9) |
| C83 | −2260(12) | 4831(5) | 3938(10) |
| C84 | −3507(11) | 4920(4) | 3267(11) |
| C85 | −4104(8) | 4419(6) | 2615(10) |
| C86 | −3454(11) | 3829(5) | 2633(9) |

[a]The estimated standard deviations given in parentheses are right justified to the least significant digit of the preceding numbers, which have been multiplied by $10^4$.

Can. J. Chem. Downloaded from www.nrcresearchpress.com by 210.87.254.40 on 09/06/12
For personal use only.

TABLE 2. Analytical and physical data

| Compound | Melting point (°C) | % Carbon | | % Hydrogen | | % Sulfur | |
|---|---|---|---|---|---|---|---|
| | | Calcd. | Found | Calcd. | Found | Calcd. | Found |
| $[(PPh_3)Pt(SCH_2Ph)(\mu\text{-}SCH_2Ph)]_2$, **1** from *cis* monomer | 205–7 | 54.6 | 54.9 | 4.13 | 4.40 | 9.10 | 8.77 |
| **1** + $0.5CH_2Cl_2$, from *trans* monomer | 172–4 | 53.4 | 53.7 | 4.07 | 3.99 | 8.84 | 8.15 |
| *cis*-$[(PMePh_2)Pt(SCH_2Ph)(\mu\text{-}SCH_2Ph)]_2$ | 169–70 | 50.5 | 50.2 | 4.21 | 4.35 | 9.98 | 10.1 |
| $[(PPh_3)Pt(4\text{-}SC_6H_4Me)(\mu\text{-}4\text{-}SC_6H_4Me)]_2\cdot CH_2Cl_2$ | >250 | 52.3 | 52.3 | 4.02 | 4.01 | 8.58 | 8.74 |
| $[(PMePh_2)Pt(4\text{-}SC_6H_4Me)(\mu\text{-}4\text{-}SC_6H_4Me)]_2$ | 126–8 | 50.5 | 49.9 | 4.21 | 4.37 | 9.98 | 10.2 |
| $[(PMe_2Ph)Pt(4\text{-}SC_6H_4Me)(\mu\text{-}4\text{-}SC_6H_4Me)]_2$ | 168–70 | 45.6 | 45.4 | 4.32 | 4.56 | 11.1 | 11.2 |

TABLE 3. $^1H$ and $^{31}P$ nmr data for tetrathiolato platinum dimers[a]

| Compound | P—$CH_3$[b] | | | S—R[b] | | P[c] | |
|---|---|---|---|---|---|---|---|
| | τ | $J$(Pt—H) | $J$(P—H) | τ | $J$(Pt—H) | α | $^1J$(Pt—P) |
| $[(PPh_3)Pt(SCH_2Ph)(\mu\text{-}SCH_2Ph)]_2$ | | | | 4.79(tt)[d,e] | 36 | −18.6(t) | 3611 |
| | | | | 6.73(t) | 37 | | |
| | | | | 6.81(t) | 33 | | |
| *cis*-$[(PMePh_2)Pt(SCH_2Ph)(\mu\text{-}SCH_2Ph)]_2$ | 8.31(td) | 36 | 11 | 4.71(tt)[d,e] | 34 | − 3.5(t) | 3543 |
| | | | | 6.55(t) | 48 | | |
| | | | | 6.77(t) | 34 | | |
| $[(PPh_3)Pt(4\text{-}SC_6H_4Me)(\mu\text{-}4\text{-}SC_6H_4Me)]_2$ | | | | 7.8 (s)[f] | | [g] | |
| $[(PMePh_2)Pt(4\text{-}SC_6H_4Me)(\mu\text{-}4\text{-}SC_6H_4Me)]_2$ | 8.27(td) | 36 | 11 | 7.8 (s)[f] | | − 2.1(t) | 3423 |
| $[(PMe_2Ph)Pt(4\text{-}SC_6H_4Me)(\mu\text{-}4\text{-}SC_6H_4Me)]_2$ | 8.54(td) | 36 | 11 | 7.8 (s)[f] | | 12.1(t) | 3354 |

[a] In $CDCl_3$ solvent, all $J$ values in Hz, s = singlet, d = doublet, t = triplet, tt = triplet of triplets.
[b] Phenyl resonances in the range 2–3 τ, R = $CH_2Ph$ or 4-$C_6H_4CH_3$ where appropriate.
[c] All $^{31}P$ chemical shifts in ppm upfield (negative) from 85% $H_3PO_4$.
[d] The relative ratio of the three signals is 1:2:1.
[e] The separation of the lines of the small apparent triplet is 5 Hz.
[f] Broad singlet centered at ~7.9–7.85 τ.
[g] Too insoluble to be detected.

reason with respect to the preparation of the dimer by this method. The *trans*-monomers were also much more resistant to dimerization via fusion than the *cis*-monomers. The dimer was always contaminated by starting *trans*-monomer which made isolation of the former difficult and reduced yields. Prolonging the fusion time or elevating the temperature reduced overall yields. The greater stability of the *trans*-monomer compared to the *cis* during fusion is consistent with the relative stability of the two complexes in solution. The dimers also undergo facile cleavage by phosphines to give the monomers. Thus, nmr tube scale reactions of $[(PMe_2Ph)Pt(4\text{-}SC_6H_4Me)(\mu\text{-}4\text{-}SC_6H_4Me)]_2$ and $[(PMePh_2)Pt(SCH_2Ph)(\mu\text{-}SCH_2Ph)]_2$ with the appropriate phosphine in $CDCl_3$ gave the *trans*- and *cis*-monomers, respectively, identified by their nmr spectra.

The five dimers produced by fusion of the monomeric complexes were obtained as stable yellow–orange materials. Their melting ponts and analytical data are given in Table 2. The solubility of the complexes varied: the benzylthiolato dimers are quite soluble in $CH_2Cl_2$ while $[(PPh_3)Pt(4\text{-}SC_6H_4Me)_2]_2$ is not. The $^1H$ and $^{31}P$ nmr data for the dimers are given in Table 3. The $J$(P—H) coupling patterns for the appropriate monomers permitted the assignment of their geometry with respect to being *cis* or *trans*. However, the phosphine ligands in the dimers are well removed from each other and virtual coupling (9) is not observed. The peaks due to the methyl groups of the 4-methylphenylthiolato ligands were simple singlets and were not helpful for assigning the structures of the dimers containing this ligand. The peaks for the methylene protons in the dimers containing the phenylmethane thiolato ligand should in principle be indicative of the geometry of the complex. In the *cis* geometry there are three different environments for these methylene protons in the ratio 1:1:2, while the in *trans* there are two different types in the ratio 1:1. Three signals in the proper ratio were observed for the methylene protons of both complexes consistent with *cis* geometry. The resonance with double the intensity of the other two is assigned to the terminal thiolato ligands. It is interesting to note the large difference in the chemical shifts of the methylene protons of the two bridging ligands (2 ppm) and that while the high field signal is a slightly broadened singlet with satellites due to $^{195}$platinum coupling, the low field signal is an apparent triplet with a spacing of 5 Hz

Can. J. Chem. Downloaded from www.nrcresearchpress.com by 210.87.254.40 on 09/06/12
For personal use only.

accompanied by platinum satellites. This triplet of triplets thus observed occurs at much lower field than has been previously observed for the methylene protons of terminal phenylmethane thiolato ligands in the monomeric complexes (1). Irradiation of the triplet in the spectrum of the $PMePh_2$ complex did not decouple any other peaks; however, a slight sharpening of some of the peaks in the phenyl region was observed. Irradiation of these did not decouple the triplet. The value of the coupling (5 Hz) is close to that observed for the monomer *cis*-$(PMePh)_2Pt(SCH_2Ph)_2$ (6 Hz) (1) whereas no coupling could be detected for the latter's *trans* isomer. Thus, it seems reasonable to assign the low field triplet to the bridging thiolato ligand *trans* to the two phosphine ligands. The peaks are broad and difficult to detect at room temperature. The spectrum of the complex containing the $PMePh_2$ ligand undergoes a series of very complicated changes when the sample is cooled wherein the signals due to the phosphine methyl groups, the methylene protons and even some of the phenyl rings are involved. Explanations of the origins of: (*1*) the low field shift of one of the methylene groups and (*2*) the temperature dependence of the spectrum of the $PMePh_2$ derivative are not readily apparent and may require more intensive study.

Such explanations are likely to be related to the possibility of geometrical isomerism in addition to the *cis–trans* type already mentioned. The bridging sulfur atoms are tetrahedral and can generate *syn* and *anti* type geometries depending on the relative arrangement of the organic groups. Since the dimers are bent along the axis joining the bridging sulfur atoms this generates *syn–exo* and *syn–endo*

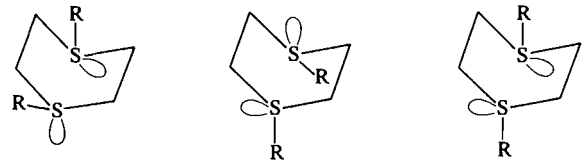


isomers. Such isomers have been observed for other dimers and their interconversion via inversion at sulfur has been studied (2*a*). It seems possible that at least some of the properties of the nmr spectra of the dimers reported here are due to the interconversion of these types of conformers in solution (10).

There is only one type of environment for the two phosphine ligands in either the *cis*- or *trans*-isomer. The $^{31}P$ nmr spectra reflect this with the chemical shifts and $J$(Pt—P) values being similar for all the complexes and not helpful in the structural assignments. This is consistent with the observation (1) that the $^{31}P$ nmr spectra of the monomers were not very sensitive to the geometry of those complexes either. The spectra of the dimers show additional long range P—P and Pt—P coupling which are being examined (11) to determine if these would be useful structural probes of this type of molecule.

Earlier studies concluded that alkylthiolato bridged dimers have *cis*-geometry while arylthiolato bridged dimers were *trans* (3, 12). X-Ray data has tended to confirm this with the complexes $[(P(C_3H_7)_3)PtCl(\mu\text{-}SC_2H_5)]_2$ (13) and $[(PPh_3)Pd(SC_6F_5)(\mu\text{-}SC_6F_5)]_2$ (14) having *cis* and *trans* geometries, respectively. The crystal and molecular structure of $[(PMePH_2)Pt(SCH_2PH)(\mu\text{-}SCH_2PH)]_2$ has been determined and shows that this alkylthiolato bridged platinum dimer also has the *cis* geometry in agreement with the assignment based on its nmr spectrum.

The molecular configuration and numbering scheme for **2** is shown in Fig. 1. The principal molecular distances and angles are listed in Table 4. A packing diagram of the triclinic unit cell containing two molecules of **2** is shown in Fig. 2. The complex is dimeric with two square planar platinum units joined by two mercaptide bridges, as expected (Fig. 3). The dihedral angle between the two square planes is 138.8°. This compares to a value of 130° for the same angle in the similar complex *cis*-$[(PPr_3)PtCl(\mu\text{-}SEt)]_2$ (13). The angles Pl—Pt1—SB2, S1—Pt1—SB1, P2—Pt2—SB2, and S2—Pt2—SB2 are 91°, 94°, 92°, and 96°,

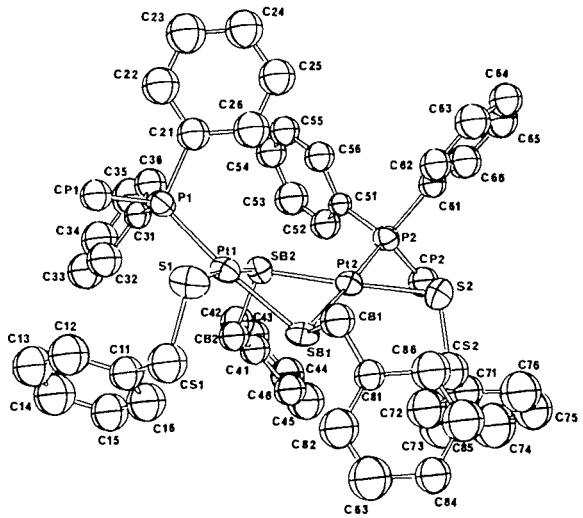


FIG. 1. The molecular configuration and the numbering scheme for **2**.

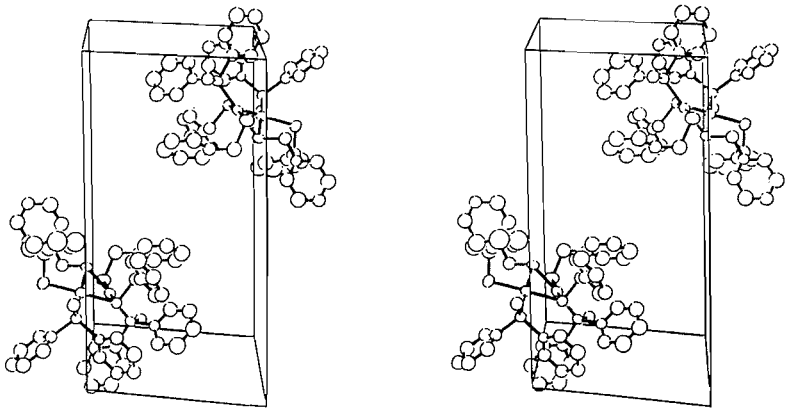

FIG. 2. An illustration of the unit cell packing diagram containing two molecules of **2** as viewed down the *b* axis.

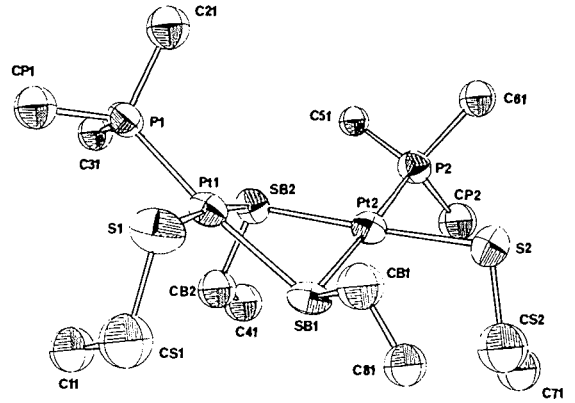


FIG. 3. The configuration of **2** excluding phenyl rings for clarity.

respectively. The adoption of the *anti*-configuration for the benzyl groups of the bridging thiolato ligands with the one *trans* to the two phosphines in the *endo* position (Fig. 3) tends to minimize crowding. The angles at the bridging sulfur atoms Pt1—SB1—Pt2 and Pt1—SB2—Pt2 are 89° and 92°, respectively; expanded slightly from the values of 85° and 89° for the same angles in $[(PPr_3)PtCl(\mu\text{-}SEt)]_2$ (13).

The platinum-to-bridging-sulfur distances *trans* to the terminal thiolato ligands (Pt1—SB2, 2.322(4) Å and Pt2—SB2, 2.323(4) Å) are shorter than those *trans* to the phosphine ligands (Pt1—SB1, 2.380(4) Å and Pt2—SB1, 2.380(4) Å). This would tend to indicate that the structural *trans*-influence of the terminal $PhCH_2S^-$ ligand was less than that of $PMePh_2$ as has been noted (4). This, however, is not reflected in the relative nmr *trans*-influences of the two ligands which have been shown to be very similar (1).

TABLE 4. Principal bond lengths (Å) and angles (deg) for **2**

| Bond | Length | Bond | Length | Bond | Length |
|---|---|---|---|---|---|
| Pt1—P1 | 2.250(4) | P1—CP1 | 1.84(2) | SB1—CB1 | 1.82(2) |
| Pt2—P2 | 2.245(4) | P2—CP2 | 1.88(2) | SB2—CB2 | 1.85(2) |
| Pt1—S1 | 2.342(5) | P1—C21 | 1.82(1) | CB1—C81 | 1.53(2) |
| Pt2—S2 | 2.317(5) | P1—C31 | 1.82(1) | CB2—C41 | 1.48(2) |
| | | P2—C51 | 1.83(1) | CS1—C11 | 1.52(2) |
| Pt1—SB1 | 2.380(4) | P2—C61 | 1.83(1) | CS2—C71 | 1.48(2) |
| Pt2—SB1 | 2.380(4) | | | | |
| Pt1—SB2 | 2.322(4) | S1—CS1 | 1.88(2) | | |
| Pt2—SB2 | 2.322(4) | S2—CS2 | 1.84(2) | | |

| Bonds | Angle | Bonds | Angle |
|---|---|---|---|
| Pt1—SB1—Pt2 | 89.3(1) | Pt1—SB1—CB1 | 106.5(6) |
| Pt1—SB2—Pt2 | 92.2(1) | Pt2—SB1—CB1 | 109.9(5) |
| | | Pt1—SB2—CB2 | 98.7(5) |
| P1—Pt1—SB2 | 91.3(2) | Pt2—SB2—CB2 | 106.9(5) |
| P2—Pt2—SB2 | 97.0(1) | | |
| P1—Pt1—SB1 | 170.8(2) | SB1—CB1—C81 | 113(1) |
| P2—Pt—SB1 | 177.3(2) | SB2—CB2—C41 | 111.8(1) |
| S1—Pt1—SB1 | 94.5(2) | Pt1—P1—CP1 | 117.9(5) |
| S2—Pt2—SB1 | 96.5(2) | Pt1—P1—C21 | 110.8(4) |
| S1—Pt1—SB2 | 173.1(2) | Pt1—P1—C31 | 112.2(4) |
| S2—Pt2—SB2 | 174.4(2) | Pt2—P2—CP2 | 112.8(5) |
| | | Pt2—P2—C51 | 115.2(4) |
| P1—Pt1—S1 | 94.1(2) | Pt2—P2—C61 | 114.1(4) |
| P2—Pt2—S2 | 86.2(2) | | |
| SB1—Pt1—SB2 | 80.4(1) | S1—CS1—C11 | 111(1) |
| SB1—Pt2—SB2 | 80.2(1) | S2—CS2—C71 | 113(1) |

## Discussion

The bridging abilities of thiolato ligands are well known. Early reports of monomeric thiolato platinum complexes (2) are now thought to describe thiolato bridged dimers or polymers (15). Analytical methods for determining the concentration of platinum in aqueous solution (16) very likely pro-

Can. J. Chem. Downloaded from www.nrcresearchpress.com by 210.87.254.40 on 09/06/12
For personal use only.

Can. J. Chem. Downloaded from www.nrcresearchpress.com by 210.87.254.40 on 09/06/12
For personal use only.

duced $RS^-$ bridged polymers. Relatively recently Chatt and co-workers carried out extensive studies on the preparation of such complexes (3, 12, 17). Their preparations involved the step-wise replacement of terminal and bridging chloride ligands (3). The method has remained popular (11, 15, 17, 18), although sulfide (19) or hydride bridges (20) have also been displaced. A conceptually simpler route to preparing thiolato bridged dimers is the condensation of monomeric thiolato complexes. Examples include the monomers $(Me_2S)_2WCl_3(SEt)$, $[(MeC_5H_4)Mn(SEt)(CO)_2]^-$, $CpFe(SR)(CO)_2$, *trans*-$(PPh_3)_2Pd(SC_6F_5)_2$, and *cis*-$(PPh_3)_2Pt(SCF_3)Cl$ which dimerized to $[(Me_2S)WCl_2(\mu\text{-}SEt)]_2$ (21), $[(MeC_5H_4)Mn(CO)_2]_2(\mu\text{-}SEt)^-$ (22), $[CpFe(\mu\text{-}SR)(CO)]_2$ (23), *trans*-$[(PPh_3)Pd(SC_6F_5)(\mu\text{-}SC_6F_5)]_2$ (14), and $[(PPh_3)_2Pt(\mu\text{-}SCF_3)]_2^{2+}$ (18*d*), respectively. Eighteen-electron complexes such as $CpFe(SR)(CO)_2$ probably dimerize via a dissociative pathway. More relevant to our work is the dimerization of *trans*-$(PPh_3)_2Pd(SC_6F_5)_2$ by warming in ethanol (24). It is reasonable to assume that this reaction and the fusions reported here proceed via an associative pathway (25). Such a route might involve bridged five-coordinate complexes such as are observed for dithiolene dimers (26); however, the details of the mechanism require further study.

## Acknowledgements

This research was supported by grants from the Natural Sciences and Engineering Research Council of Canada and the Quebec Department of Education. We thank the Imperial Oil Co. of Canada for the award of a research grant to A. S. Predoctoral fellowships awarded to R.D.L. by McGill University are gratefully acknowledged. We thank Mrs. Elva Heyge of McGill University for the $^{31}P$ nmr spectra. The authors acknowledge Dr. Gordon Hamer of Xerox Canada for very helpful discussions concerning the nmr spectra of the dimers and for performing the preliminary variable temperature nmr experiments.

1. R. D. Lai and A. Shaver. Inorg. Chem. **20**, 477 (1981).
2. (*a*) P. Klason. Chem. Ber. **28**, 1493 (1895); (*b*) P. C. Ray. J. Chem. Soc. **133** (1923).
3. J. Chatt and F. A. Hart. J. Chem. Soc. (*a*) 2363 (1953); (*b*) 2807 (1960).
4. T. G. Appleton, H. C. Clark, and L. E. Manzer. Coord. Chem. Rev. **10**, 335 (1973).
5. D. M. Roundhill. Inorg. Chem. **19**, 557 (1980).
6. (*a*) K. A. Jensen. Z. Anorg. Allg. Chem. **229**, 237 (1936); (*b*) L. Malatesta and C. Cariello. J. Chem. Soc. 2323 (1958); (*c*) R. Ugo, F. Cariati, and G. LaMonica. Inorg. Synth. **11**, 105 (1968).
7. C. W. Burnam. Am. Mineral. **51**, 159 (1966).
8. D. T. Cromer and J. T. Waber. Acta Crystallogr. **18**, 104 (1965).
9. J. M. Jenkins and B. L. Shaw. (*a*) J. Chem. Soc. A, 770 (1966); (*b*) Proc. Chem. Soc. 279 (1963).
10. M. P. Brown, R. J. Puddephatt, and C. E. E. Upton. J. Chem. Soc. Dalton, 2490 (1976).
11. G. Hamer and A. Shaver. To be published.
12. H. Chatt and J. M. Davidson. J. Chem. Soc. 2433 (1964).
13. M. C. Hall, J. A. J. Jarvis, B. T. Kilbourn, and P. G. Owston. J. Chem. Soc. Dalton, 1544 (1972).
14. R. H. Fenn and G. R. Segrott. (*a*) J. Chem. Soc. A, 3197 (1970); (*b*) J. Chem. Soc. Dalton, 330 (1972).
15. P. L. Goggin, R. J. Goodfellow, and F. J. S. Reed. J. Chem. Soc. A, 2031 (1971).
16. (*a*) J. E. Currah, W. A. E. McBryde, A. J. Cruikshank, and F. E. Beamish. Indust. Eng. Chem. **18**, 120 (1946); (*b*) P. Champ, P. Fauconnier, and C. Duval. Anal. Chim. Acta, **10**, 443 (1954).
17. H. Chatt, L. M. Vallarino, and L. M. Venanzi. J. Chem. Soc. 2496 (1957).
18. (*a*) R. B. King and A. Efraty. Inorg. Chem. **10**, 1376 (1971); (*b*) C. Eaborn, K. J. Odell, and A. Pidcock. J. Organomet. Chem. **170**, 105 (1979); (*c*) J. Chatt, D. M. P. Mingos. J. Chem. Soc. A, 1770 (1969); (*d*) K. R. Dixon, K. C. Moss, and M. A. R. Smith. J. Chem. Soc. Dalton, 971 (1974).
19. J. Chatt and D. M. Mingos. J. Chem. Soc. A, 1243 (1970).
20. (*a*) M. P. Brown, J. R. Fisher, R. J. Puddephatt, and K. R. Seddon. Inorg. Chem. **18**, 2808 (1979); (*b*) M. P. Brown, J. R. Fisher, L. Manojlovic-Muir, K. W. Muir, R. J. Puddephatt, M. A. Thomson, and K. R. Seddon. J. Chem. Soc. Chem. Commun. 931 (1979).
21. P. M. Boorman and V. D. Patel. Inorg. Chim. Acta, **44**, L85 (1980).
22. J. C. T. R. Burckett-St. Laurent, M. R. Caira, R. B. English, R. J. Haines, and L. R. Nassimbeni. J. Chem. Soc. Dalton, 1077 (1977).
23. M. Ahmad, R. Bruce, and G. R. Knox. J. Organomet. Chem. **6**, 1 (1966).
24. W. Beck, K. H. Stetter, S. Tadros, and K. E. Schwarzhans. Chem. Ber. **100**, 3944 (1967).
25. F. Basolo and R. G. Pearson. Mechanisms of inorganic reactions. 2nd ed. J. Wiley and Sons, New York. 1968. Chapt. 5.
26. A. Herrmann and R. M. Wing. Inorg. Chem. **11**, 1415 (1972).

# Fast, mild, and convenient procedures for iodination and bromination of carbohydrates: reactions of organoboranes with iodine monochloride, sodium iodide, bromine, and bromine chloride

LAURANCE D. HALL AND JEAN-RICHARD NEESER

*Chemistry Department, University of British Columbia, Vancouver, B.C., Canada V6T 1Y6*

Received February 2, 1982

LAURANCE D. HALL and JEAN-RICHARD NEESER. Can. J. Chem. **60**, 2082 (1982).

5,6-Dideoxy-1,2-*O*-isopropylidene-3-*O*-methanesulfonyl-α-D-*xylo*-hexofuranosene-5 (**1**), reacts with $BH_3$–THF to form the tris(glycosyl)borane (**2**) and with dicyclohexylborane to form the dicyclohexylglycosylborane (**3**). The iodination and bromination of **2** and **3** has been investigated using a variety of electrophiles. Iodination of either **2** or **3** with NaI–Chloramine-T/NaOAc is complete within one minute with high percentage uptake of iodine (70–90%) and recovery of the iodinated sugar (**4**). Bromination of **2** in 15 minutes with NaBr–Chloramine-T permits a high percentage uptake of bromine (75%), and bromination of **3** in 15 minutes with $Br_2$/NaOAc gives the brominated sugar (**5**) with a reasonably good yield (60%) with respect to the starting material (**1**).

LAURANCE D. HALL et JEAN-RICHARD NEESER. Can. J. Chem. **60**, 2082 (1982).

Le didéoxy-5,6 *O*-isopropylidène-1,2 *O*-méthanesulfonyl-3 α-D-*xylo*-hexofurannosène-5 (**1**) réagit avec le complexe $BH_3$ –THF pour donner accès au tris(glycosyl)borane (**2**), tandis que face au dicyclohexylborane, il conduit au dicyclohexylglycosylborane (**3**). L'iodation et la bromation des composés **2** et **3** ont été étudiées en utilisant divers agents électrophiles. En présence de NaI–Chloramine-T/NaOAc, l'iodation des composés **2** ou **3** est complète au bout d'une minute, le fort pourcentage d'incorporation d'iode (70–90%) conduisant sucre iodé (**4**). La bromation du composé **2** par NaBr–Chloramine-T requiert 15 minutes et donne lieu à un fort pourcentage d'incorporation de brome par le sucre (75%); la bromation du composé **3** par $Br_2$/NaOAc s'effectue en 15 minutes et permet d'obtenir le sucre bromé (**5**) avec un rendement acceptable (60%) par rapport au produit de départ (**1**).

## Introduction

In recent years, a very wide variety of radiohalogen-containing radiopharmaceuticals have been developed (1) for use in diagnostic nuclear medicine and positron emission tomography (PET). Much interest has been aroused in the search for rapid methods of halogenation, compatible with the use of very short half-life radiohalogens. Very recently a new, mild, and rapid method for fluorination of aromatic compounds by treatment of aryl-tin derivatives with $^{18}F$-$F_2$ (2) was developed and similar reactions of other aryl-metal derivatives have been evaluated. Continuing in this general field, we have now adapted new, fast, and mild methods for the iodination and bromination of carbon–boron bonds to the area of carbohydrate chemistry. Recently, Kabalka and co-workers have developed two methods for the iodination (3, 4) and two for the bromination (5) of organoboranes, which work under conditions so mild that they are compatible with a wide range of functional groups.

Kabalka and co-workers have observed that when trialkylboranes, derived from the hydroboration of terminal alkenes, are activated in an electron-rich organoborane–acetate complex, two of the three groups on boron react instantaneously when treated with iodine monochloride (3), or with iodide ion in the presence of an oxidizing agent such as Chloramine-T (4). This latter reaction permits the selective cleavage of a primary alkylboron bond when mixed organoboranes, prepared with dicyclohexylborane, react with iodonium ion (4). Without activation of the trialkylborane, one of the three primary alkyl groups on boron reacts instantaneously when treated with bromine in the presence of water, or with bromine chloride prepared *in situ* (5). This latter reaction permits the preferential cleavage (70%) of a primary alkyl–boron bond, when dicyclohexylborane is used as the hydroborating agent (5). All these reactions are postulated to proceed in an ionic fashion, via an $S_E2$ mechanism.

Prior to this study, organoborane technology had been successfully used in carbohydrate chemistry in hydroboration–oxidation sequences (6). The success generally observed in these applications of organoborane technology in carbohydrate chemistry, and the recent interest in research for very fast methods for the synthesis of halogenosugar derivatives, has prompted us to adapt the new "Kabalka" procedures to an unsaturated carbohydrate model, namely 5,6-dideoxy-1,2-*O*-isopropylidene-3-*O*-methanesulfonyl-α-D-*xylo*-hexosene-5 (7) (**1**).

## Results and discussion

The triglycosylborane (**2**), obtained by reaction

0008-4042/82/162082-05$01.00/0

©1982 National Research Council of Canada/Conseil national de recherches du Canada

Can. J. Chem. Downloaded from www.nrcresearchpress.com by 210.87.254.6 on 09/06/12
For personal use only.

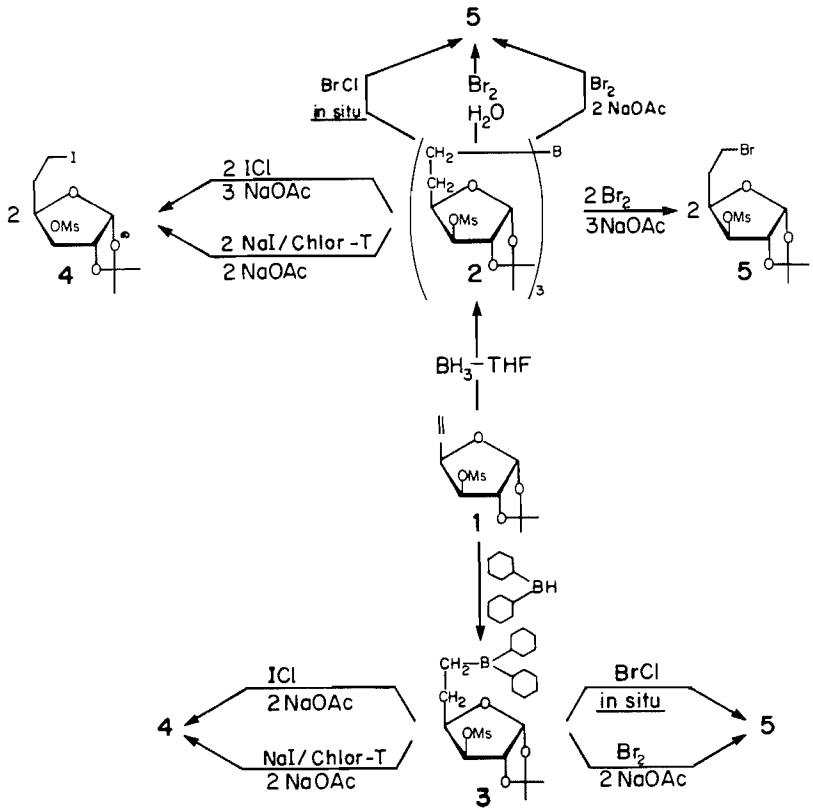


SCHEME 1

of the starting unsaturated carbohydrate (**1**) with $BH_3$–THF, readily reacts in the presence of sodium acetate with two equivalents of ICl, or with two equivalents of sodium iodide and Chloramine-T; under these conditions 74 and 72%, respectively, of the added iodine is consumed. It seems reasonable to speculate that the first carbohydrate moiety attached on the boron atom reacts quantitatively, whereas the reaction of the second group is incomplete. It was possible to confirm this hypothesis by using dicyclohexylborane as the hydroborating agent. It was found that the dicyclohexylglycosylborane (**3**) reacts quantitatively with one equivalent either of the iodide/Chloramine-T reagent or the ICl reagent, the carbohydrate-containing primary alkyl group being selectively iodinated within one minute by the former reagent to produce the iodo derivative (**4**) in excellent yield (ca. 90%). The results for the iodination reactions are summarized in Table 1.

The triglycosylborane (**2**) reacts readily with one equivalent of BrCl prepared *in situ* from bromide/Chloramine-T, and permits the isolation of the bromo derivative (**5**), in 75% yield with respect to the bromide reagent. However, the fact that, in this reaction, only one of the three carbohydrate groups attached to the boron atom is able to react reduces the yield with respect to the unsaturated starting carbohydrate to 25%. Unfortunately the above reaction conditions appear not to discriminate efficiently between bromination of a glycosyl–boron bond and that of a cyclohexyl–boron bond. Thus it was found that the organoboron derivative (**3**) reacted with one equivalent of BrCl *in situ* to give only 36% of the bromo-sugar (**5**) (mixed with an unidentified carbohydrate-containing by-product) and an equivalent yield of bromocyclohexane. Under the same reaction conditions, Kabalka *et al.* (5) report that tricyclohexylborane utilized 67% of the added halogen.

With one equivalent of $Br_2$ in aqueous medium, **2** is converted to **5**, utilizing less than half of the bromine in the reaction. In addition, an unresolved mixture of by-products was isolated by lcc (liquid column chromatography); these contain no carbohydrate and probably come from the tetrahydrofuran present in the reaction medium. Consequently, it seems necessary to activate the

Can. J. Chem. Downloaded from www.nrcresearchpress.com by 210.87.254.6 on 09/06/12
For personal use only.

TABLE 1. Halogenations of organoboranes derived from **1**

| Substrate | Product | Hydroborating agent | Halogenating agent/ Equiv. of organoborane intermediate | Halogenation time (min) | % Isolated yield[a] |
|---|---|---|---|---|---|
| | 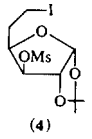 (4) | $BH_3$: THF | 2 ICl/3NaOAc | 45 | 74 (49) |
| | | 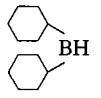 | 1 ICl/2NaOAc | 45 | 88 (88) |
| 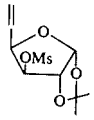 (1) | | $BH_3$: THF | 2 NaI/2Chlor-T/2NaOAc | 1 | 72 (48) |
| | | 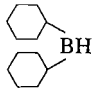 | 1 NaI/2Chlor-T/2NaOAc | 1 | 91 (91) |
| | 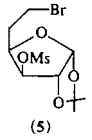 (5) | $BH_3$: THF | 1 BrCl *in situ* | 15 | 75 (25) |
| | | | 1 BrCl *in situ* | 15 | 36 (36)[b] |
| | | $BH_3$: THF | 1 $Br_2/H_2O$ | 30 | 48 (16) |
| | | $BH_3$: THF | 1 $Br_2$/2NaOAc | 15 | 93 (31) |
| | | $BH_3$: THF | 2 $Br_2$/3NaOAc | 15 | 62 (41) |
| | | | 1 $Br_2$/2NaOAc | 15 | 60 (60) |

[a]Isolated yields based on the halogenating agent. The numbers in parentheses refer to isolated yields based on starting unsaturated carbohydrate (**1**).
[b]The product (**5**) isolated from this procedure is mixed with an unidentified carbohydrate-containing by-product.

organoboron intermediate (**2**) to obtain a specific reaction with molecular bromine. By analogy with our iodination experiments, **2** was activated with methanolic sodium acetate, and under these conditions one equivalent of $Br_2$ reacts quantitatively with one sugar moiety to give **5**. However, we observe that under the same conditions, two equivalents of $Br_2$ are utilized with a 62% yield of **5**, showing that this reaction permits fast cleavage of two of the three primary alkyl groups attached to the boron atom, but with an incomplete migration of the second group in this case. Fortunately, when treated with one equivalent of $Br_2$, the activated dicyclohexylglycosylborane (**3**) utilizes 60% of the halogen for bromination of the glycosyl group. Thus this latter procedure is more selective for the preferential cleavage of the primary alkyl carbohydrate-containing group than is the BrCl *in situ*. Our results are summarized in Table 1.

In principle, three different products could arise from the hydroboration of **1**: the two, C-5 epimeric 5-bora-5,6-dideoxy-1,2-*O*-isopropylidene-3-*O*-methanesulfonyl-α-D-glucofuranose and β-L-iodofuranose, and the 6-bora-5,6-dideoxy-1,2-*O*-isopropylidene-3-*O*-methanesulfonyl-α-D-*xylo*-hexose (**2** or **3**). The latter is the expected product arising from the normal, anti-Markovnikov hydroboration. Although the fact that only the 6-iodo and 6-bromo derivatives were obtained from the halogenation reactions provides supportive evidence for C-6 boronation, this is not conclusive since it is known that these halogenation methods *preferentially* cleave primary alkyl groups; thus, if small amounts of 5-bora derivatives had been produced by the hydroboration reactions, these products might not be halogenated. The structures of **4** and **5** were unambiguously assigned on the basis of their nmr spectra.

## Conclusion

By the standards of conventional organic syntheses the reactions described here are reasonably efficient, but probably not sufficiently so to warrant their selection in preference to other methods for introducing halogen at a primary centre. However, their merit is somewhat more obvious in the context of the constraints of radiolabelling chemistry, where yields are based on the uptake of halogen rather than consumption of the organic substrate, and where time limitations

Can. J. Chem. Downloaded from www.nrcresearchpress.com by 210.87.254.6 on 09/06/12
For personal use only.

Can. J. Chem. Downloaded from www.nrcresearchpress.com by 210.87.254.6 on 09/06/12
For personal use only.

require that the halogenation reaction plus work-up be completed within the equivalent of 2–3 half-lives; this latter limit requires that the halogen be used in essentially the same atomic form in which it is generated in the cyclotron.

Given such constraints and considering the known ease of generating $^{120}$I-iodide, the synthesis of **4** from **1** via dicyclohexylboronation and NaI–Chloramine-T/NaOAc, with essentially quantitative uptake of iodine and quantitative yield of **4**, is very encouraging; that the reaction is completed within 1 minute which amounts to ca. 1% of one radioactive half-life for $^{120}$I (81 min) is exemplary. The synthesis of the bromo-derivative (**5**) is somewhat less satisfactory, but the yields based on the bromine uptake (75%) in the $BH_3$–THF/NaBr–Chloramine-T procedure is again encouraging ($^{75}$Br-bromide being easily generated), as is the time of the reaction, 15 min, 15% of one half life for $^{75}$Br (97 min).

## Experimental

The nmr spectra were run at 270 MHz using a home-built, pulse Fourier transform nmr spectrometer. All chemical shifts are reported in parts per million downfield from $Me_4Si$. The mass spectra were recorded at low resolution, on a Varian MAT Atlas CH4-B mass spectrometer. The specific optical rotation $[\alpha]_D$ values were obtained with a Perkin–Elmer 241 MC polarimeter.

*5,6-Dideoxy-1,2-*O*-isopropylidene-3-*O*-methanesulfonyl-α-*D*-xylo-hexosene-5* (**1**) was prepared according to a published procedure (7), modified as follows: 1,2-*O*-isopropylidene-3,5,6-tri-*O*-methanesulfonyl-α-D-glucose (10 g) and NaI (26 g) were dissolved in 500 mL of 2-butanone and heated under reflux (3.5 h). After work-up using the published procedure (7), the crude product was crystallized from methanol to yield pure **1** (5.35 g, 92%).

*Hydroborations*

Commercially available (Alfa) $BH_3$–THF (1 *M* solution) was used. Reagent Grade THF was deoxygenated according to a published procedure (8*a*) and kept under $N_2$ in a bottle stoppered with a septum. Syringes were purged before each use with $N_2$, according to a published technique (8*b*).

*$BH_3$–THF procedure (synthesis of 1 mmol of 2)*

Compound **1** (792 mg, 3 mmol) was introduced under a blanket of $N_2$ in a round-bottomed flask equipped with magnetic stirrer and septum inlet, which had been flushed hot with $N_2$. THF (1.5 mL) was added via a syringe, the resultant solution cooled to 0°C and $BH_3$–THF (1.05 mL of a 1 *M* solution) added via a syringe. The mixture was stirred for 1.5 h at 25°C.

*Dicyclohexylborane procedure (synthesis of 2 mmol of 3)*

A suspension of dicyclohexylborane in THF at 0°C (4.2 mL of 0.5 *M*) was prepared according to the published procedure (8*c*). During the same time period a solution of **1** (528 mg, 2 mmol) in THF (1 mL) was prepared as above. This solution was added via a syringe to the dicyclohexylborane suspension at 0°C and the mixture was stirred at 25°C for 2 h.

*Iodinations:*

*Iodinations of two groups on boron from 1 mmol of 2 {or one group on boron from 2 mmol of 3}*

The published procedures of Kabalka and Gooch (3, 4) were followed. After quenching, the mixtures were poured into water (20 mL) and extracted with 4 × 10 mL of ether. The combined ether extracts were dried ($MgSO_4$) and ether was removed under reduced pressure. Column chromatography on silica with ether/hexane (2:1) as eluant yielded 580 mg (74%) {or 690 mg (88%)} of pure **4** from the *iodine monochloride procedure*, and 565 mg (72%) {or 715 mg (91%)} of pure **4** from the *iodide/Chloramine-T procedure*.

*Brominations:*

*Brominations of 1 group on boron from 1 mmol of 2 {or 2 mmol of 3}*

The published procedures of Kabalka *et al.* (5) were followed. After reacting, the mixtures were extracted with 15 mL of ether; the ether solutions were washed with two 7.5 mL portions of water, dried over $MgSO_4$, and concentrated. Column chromatography on silica with ether/hexane (2:1) as eluant yielded 260 mg (75%) of pure **5** {or 250 mg (36%) of **5** mixed with an unidentified carbohydrate-containing by-product} from the *BrCl* in situ *procedure*, and 165 mg (48%) of pure **5** from the *molecular bromine/water procedure*.

*Molecular bromine/methanolic sodium acetate procedure*

Methanol (1 mL {or 2 mL}), followed by 2 mL {or 4 mL} of 1 *M* methanolic sodium acetate were added to the organoborane solution in THF. The mixture was cooled to 0°C and shielded from light. Bromine (1 mmol {or 2 mmol}) was added and the mixture stirred 15 min at 0°C; 2 mL of saturated $K_2CO_3$ solution were added and the mixture poured into 15 mL of water. The mixture was extracted with 4 × 10 mL of ether, the combined ether layers were washed with 2 × 7.5 mL of water and 2 × 7.5 mL of saturated NaCl solution, and dried over anhydrous $MgSO_4$. The product was isolated as described before and 320 mg {or 415 mg} of pure **5** was obtained. The yield was 93% {or 60%}.

*Bromination of two groups on boron from 1 mmol of 2*

*Molecular bromine/methanolic sodium acetate procedure*

Three milliliters of 1 *M* methanolic sodium acetate were added to the organoborane solution in THF. The mixture was treated as described previously using 2 mmol of bromine. This method permitted isolation of 430 mg (62%) of pure **5**.

*Characterization of 4 and 5*

*5,6-Dideoxy-6-iodo-1,2-*O*-isopropylidene-3-*O*-methanesulfonyl-α-*D*-xylo-hexose* (**4**) was recrystallized from methanol; mp 70–71°C; $[\alpha]_D^{22}$ +4.06° (*c* 1, $CHCl_3$); $^1$H nmr δ ($CDCl_3$): 1.33 and 1.54 (2s, 2 × 3H, $CMe_2$), 2.12 and 2.22 (2m, 2 × 1H, $H_A$- and $H_B$-C5), 3.08 (s, 3H, $SO_2Me$), 3.30 (m, 2H, H-C6), 4.43 (ddd, 1H, H-C4, $J_{4,5}$ = 8.1 and 4.0 Hz, $J_{4,3}$ = 3 Hz), 4.77 (d, 1H, H-C2, $J_{2,1}$ = 3.8 Hz), 4.98 (d, 1H, H-C3), 5.92 (d, 1H, H-C1); *m/e*: 377(25) ($M^+$ − Me), 239(33), 83(16), 79(18), 59(46), 57(16), 55(20), 43(100), 41(26), 32(23), 28(97). *Anal.* calcd. for $C_{10}H_{17}IO_6S$: C 30.62, H 4.37, I 32.36; found: C 30.51, H 4.35, I 32.30.

*6-Bromo-5,6-dideoxy-1,2-*O*-isopropylidene-3-*O*-methanesulfonyl-α-*D*-xylo-hexose* (**5**) was recrystallized from methanol; mp 74–75°C; $[\alpha]_D^{22}$ +6.50° (*c* 1, $CHCl_3$); $^1$H nmr, δ ($CDCl_3$): 1.34 and 1.54 (2s, 2 × 3H, $CMe_2$), 2.14 and 2.29 (2m, 2 × 1H, $H_A$- and $H_B$- C5), 3.11 (s, 3H, $SO_2Me$), 3.54 (m, 2H, H-C6), 4.52 (ddd, 1H, H-C4, $J_{4,5}$ = 8.2 Hz and 3.8 Hz, $J_{4,3}$ = 2.9 Hz), 4.78 (d, 1H, H-C2, $J_{2,1}$ = 3.8 Hz), 4.99 (d, 1H, H-C3), 5.94 (d, 1H, H-C1); *m/e*: 331–329 (18-18) ($M^+$ − Me), 193–191 (23-23), 79(17), 59(53), 55(14), 43(100), 41(22), 28(20). *Anal.* calcd. for $C_{10}H_{17}BrO_6S$: C 34.79, H 4.96, Br 23.15; found: C 34.95, H 5.02, Br 22.95.

**Acknowledgements**

This work was supported by a grant from the Fonds National Suisse de la Recherche Scientifique (to J.R.N.) and by operating funds from the Natural Sciences and Engineering Research Council of Canada (A 1905 to L.D.H.). It is a pleasure to thank Dr. M. J. Adam for helpful discussions and Dr. S. Sukumar for recording the nmr spectra.

1. (*a*) J. K. MAZAITIS, R. E. GIBSON, T. KOMAI, W. C. ECKELMAN, B. FRANCIS, and R. C. REBA. J. Nucl. Med. **21**, 142 (1980); (*b*) G. SCHROBILGEN, G. FIRNAU, R. CHIRAKAL, and E. S. GARNET. J. Chem. Soc. Chem. Commun. 198 (1981); (*c*) G. W. KABALKA, E. E. GOOCH, and K. A. R. SASTRY. J. Nucl. Med. **22**, 908 (1981); (*d*) G. W. KABALKA and E. E. GOOCH. J. Labelled Compd. Radiopharm. **18**, 117 (1981); (*e*) G. W. KABALKA, E. E. GOOCH, and C. A. OTTO. J. Radioanalyt. Chem. **65**, 115 (1981); (*f*) W. KORYTNYK and S. VALENTEKOVIC-HORVAT. Tetrahedron Lett. 1493 (1980); (*g*) J. S. FOWLER, R. R. MACGREGOR, A. P. WOLF, A. A. FARRELL, K. I. KARLSTROM, and T. J. RUTH. J. Nucl. Med. **22**, 376 (1981); (*h*) J. R. BARRIO, N. S. MACDONALD, G. D. ROBINSON, JR., A. NAJAFI, J. S. COOK and D. E. KUHL. J. Nucl. Med. **22**, 372 (1981).
2. M. J. ADAM, B. D. PATE, J. R. THOMAS, J. M. BERRY, and L. D. HALL. J. Chem. Soc. Chem. Commun. 733 (1981).
3. G. W. KABALKA and E. E. GOOCH. J. Org. Chem. **45**, 3578 (1980).
4. G. W. KABALKA and E. E. GOOCH. J. Org. Chem. **46**, 2582 (1981).
5. G. W. KABALKA, K. A. R. SASTRY, H. C. HSU, and M. D. HYLARIDES. J. Org. Chem. **46**, 3113 (1981).
6. (*a*) M. L. WOLFROM, K. MATSUDA, F. KOMITSKY, JR., and T. E. WITHELEY. J. Org. Chem. **28**, 3551 (1963); (*b*) F. E. ZIEGLER and P. J. GILLIGAN. Tetrahedron Lett. 3371 (1979); (*c*) K. C. NICOLAOU, M. R. PAVIA, and S. P. SEITZ. Tetrahedron Lett. 2327 (1979); (*d*) H. REDLICH and H. G. NEUMANN. Chem. Ber. **114**, 2029 (1981); (*e*) H. PAULSEN and H. BEHRE. Carbohydr. Res. **2**, 80 (1966); (*f*) C. L. STEVENS and D. CHITHARANJAN. J. Org. Chem. **40**, 2474 (1975); (*g*) W. MEYER ZU RECKENDORF and H. HEHENBERGER. Chem. Ber. **113**, 3089 (1980); (*h*) J. LEHMANN. Carbohydr. Res. **2**, 1 (1966); (*i*) A. ROSENTHAL and M. SPRINZL. Can. J. Chem. **47**, 4477 (1969); (*j*) A. ROSENTHAL and M. SPRINZL. Carbohydr. Res. **16**, 337 (1971); (*k*) J. H. JORDAAN and S. SMEDLEY. Carbohydr. Res. **18**, 303 (1971); (*l*) T. SUAMI and S. OGAWA. Japan Kokai 7863353 (1978); Chem. Abstr. **89**, 197888n (1978); (*m*) D. HORTON, A. LIAV, and S. E. WALKER. Carbohydr. Res. **28**, 201 (1973).
7. J. K. N. JONES and J. L. THOMPSON. Can. J. Chem. **35**, 955 (1957).
8. H. C. BROWN. Organic syntheses via boranes. Wiley, New York. 1975. (*a*) pp. 251–254; (*b*) p. 206; (*c*) p. 29, note 2.

Can. J. Chem. Downloaded from www.nrcresearchpress.com by 210.87.254.6 on 09/06/12
For personal use only.

# Préparation stéréosélective de méthyle cétones α-bromées: stéréochimie de l'addition d'anions en α d'un groupe sulfone sur des cyclohexanones monocycliques et stéroïdiques

JEAN-PIERRE BÉGUÉ,[1] DANIÈLE BONNET-DELPON, MICHELINE CHARPENTIER-MORIZE ET JEAN SANSOULET

*GR 12, Centre National de la Recherche Scientifique, 2–8, rue Henri Dunant, B.P. 28, 94320 Thiais, France*

Reçu le 16 décembre 1981

JEAN-PIERRE BÉGUÉ, DANIÈLE BONNET-DELPON, MICHELINE CHARPENTIER-MORIZE et JEAN SANSOULET. Can. J. Chem. **60**, 2087 (1982).

La méthode décrite par Durst et coll. pour la préparation de méthyle cétones α-bromées ou d'aldéhydes α-bromés a été appliquée en série cyclohexane, notamment en série stéroïde à l'obtention de composés *gem*-bromocarbonylés. Le bilan stéréochimique du processus réactionnel a été précisé: dans tous les cas étudiés, le composé carbonylé à brome équatorial se forme très sélectivement. Toutefois, en série monocyclique, cette méthode se trouve limitée par l'existence d'une réaction compétitive d'élimination.

JEAN-PIERRE BÉGUÉ, DANIÈLE BONNET-DELPON, MICHELINE CHARPENTIER-MORIZE, and JEAN SANSOULET. Can. J. Chem. **60**, 2087 (1982).

This work describes stereochemical results obtained for the preparation of α-bromomethyl ketones or α-bromoaldehydes starting from monocyclic and steroid cyclohexanones, using the Durst method. In all the cases studied here, the bromine is introduced selectively in the equatorial position. However, for monocyclic compounds, the yields of α-bromocarbonyl compounds are limited by the competitive formation of α-ethylenic carbonyl compounds.

Lors d'études de déshalogénations de composés carbonylés α-bromés effectuées dans notre laboratoire (2), la préparation de méthyle cétones α-bromées a souvent été source de difficultés. Parmi les méthodes susceptibles d'être utilisées (notamment refs. 3 et 4), celle récemment publiée par Durst *et al.* (1) a attiré notre attention par sa facilité de mise en œuvre.

La méthode décrite par Durst *et al.* (1) consiste à additionner, dans les conditions de transfert de phase liquide–liquide, les chlorosulfones **1** sur des cétones ou des aldéhydes: la cyclisation *in situ* de l'anion intermédiairement formé **2** mène à l'époxysulfone **3**. Celle-ci isolée, puis traitée par $MgBr_2$ conduit aux méthyle cétones α-bromées (R = $CH_3$) ou aux aldéhydes α-bromés (R = H).

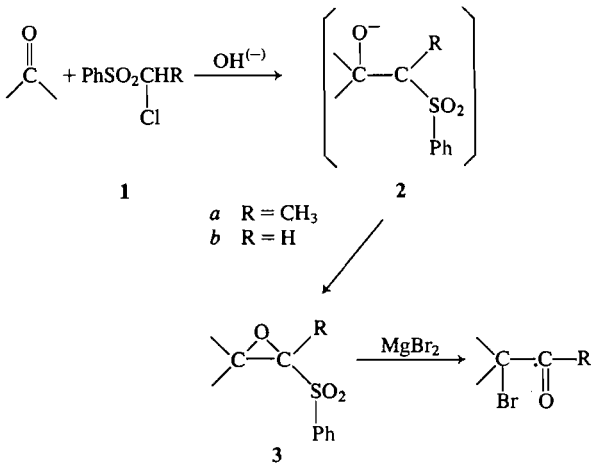


**1** **2**

*a* R = $CH_3$
*b* R = H

**3**

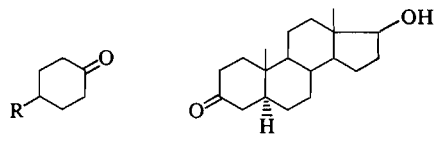

**4** R = H
**5** R = $CH_3$
**6** R = *t*Bu



**7** (Androstanolone-5α)

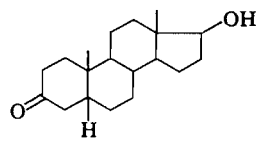

**8** (Androstanolone-5β)

Toutefois, les modèles étudiés par Durst *et al.* n'avaient pas permis de préciser le bilan stéréochimique de la réaction.

## Résultats

Le présent travail décrit l'addition de l'α-chloroéthylsulfone **1***a* sur les cétones **4**, **5**, **6**, **7** et **8** (Tableau 1) et celle de l'α-chlorométhylsulfone **1***b* sur les cétones **4** et **6** (Tableau 2).

A priori toutes ces cétones (sauf **4**) peuvent conduire à un mélange de cétones bromées stéréoisomères (Tableaux 1 et 2).

Dans le cas des expériences **b**, **c** et **d**, effectuées

[1] Auteur à qui toute correspondance doit être envoyée.

0008-4042/82/162087-06$01.00/0
©1982 National Research Council of Canada/Conseil national de recherches du Canada

Can. J. Chem. Downloaded from www.nrcresearchpress.com by 210.87.254.6 on 09/06/12
For personal use only.

Can. J. Chem. Downloaded from www.nrcresearchpress.com by 210.87.254.6 on 09/06/12
For personal use only.

TABLEAU 1. Préparation de méthyle cétones α-bromées (Addition de **1***a*)

| Cétones | N° expérience | Cétones α-bromées (Rendement)[a] | | Stéréosélectivité[b] | Cétones α-éthylénique (Rendement)[a] |
|---|---|---|---|---|---|
| **4** | **a** | 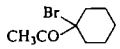 | (≥90%) | — | 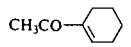 (~10%) |
| **5** | **b** | 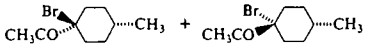 **12** + **13** | (38%) | **12/13** = 85:15 | 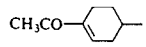 (61%) |
| **6** | **c** | 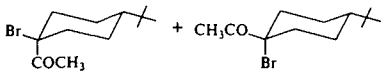 **14** + **15** | (39%) | **14/15** = 90:10 | 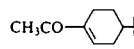 (42%) |
| **7** | **d** | 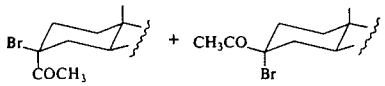 **16** + **17** | (38%) | **16/17** = 99:1 | 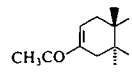 **18** (8%) |
| **8** | **e** | 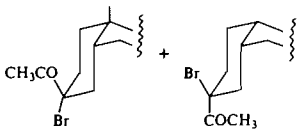 **19** + **20** | (51%) | **19/20** = 96:4 | 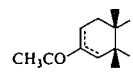 **21** (6%) |

[a]Les rendements en produits isolés sont calculés par rapport aux cétones de départ et sont la moyenne de plusieurs expériences.
[b]Les pourcentages relatifs des stéréoisomères sont la moyenne de plusieurs expériences et varient d'environ ±5%.

TABLEAU 2. Préparation d'aldéhydes α-bromées (Addition de **1***b*)

| Cétones | N° expérience | Aldéhyde α-bromée (Rendement)[a] | | Stéréosélectivité[b] | Aldéhyde α-éthylénique (Rendement)[a] |
|---|---|---|---|---|---|
| **4** | **f** | 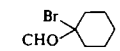 **23** | (23%) | — | 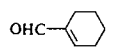 **24** (28%) |
| **6** | **g** | 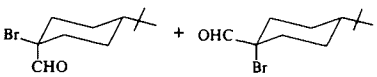 **25** + **26** | (28%) | **25/26** = 70:30 | 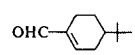 **27** (41%) |

[a]Les rendements en produits isolés sont calculés par rapport aux cétones de départ et sont la moyenne de plusieurs expériences.
[b]Le pourcentage relatif des stéréoisomères est la moyenne de plusieurs expériences et varie d'environ ±5%.

respectivement à partir des cétones **5**, **6** et **7**, l'examen des spectres rmn $^{13}C$ des époxysulfones **3** (produits bruts de réaction), montre que dans les trois cas, un stéréoisomère est très majoritaire (≥90%). Sur la base de cette seule donnée, il n'a toutefois pas été possible de déterminer la configuration de cet isomère majoritaire. Par contre, l'attribution de configuration des cétones bromées a pu être faite par corrélation des spectres de rmn $^{13}C$ et par voie chimique[2] (voir partie expérimentale). L'isomère à brome équatorial est toujours obtenu très majoritairement. (Le pourcentage relatif des stéréoisomères correspond soit à une analyse par cpg (expériences **b**, **c** et **g**), soit aux proportions de produits isolés (expériences **d** et **e**).)

Dans toutes les expériences, à côté des cétones ou aldéhydes α-bromés se forment les composés α-éthyléniques correspondants. La proportion de ces derniers varie de 6% (expérience **e**) à 52% (expérience **b**).

Nous avons repris les conditions décrites par Durst (1) uniquement dans le cas de l'époxysulfone dérivée de la cyclohexanone (3 h, −30°C) pour le traitement par $MgBr_2$ de l'époxysulfone dérivant de la méthyl-4 cyclohexanone. Dans ces conditions, cette époxysulfone est récupérée inchangée; lorsqu'on remonte la température (−15°C) on

[2]Dans le cas des expériences **c** et **g** la configuration des composés bromés était déjà connue (5). Par ailleurs, au laboratoire, il a été montré, à partir d'une importante série de composés cyclohexaniques *gem*-bromocarbonylés que le carbone porteur du brome axial résonne à champ plus faible que celui porteur du brome équatorial, la différence étant toujours de l'ordre de 5 ppm (14).

Can. J. Chem. Downloaded from www.nrcresearchpress.com by 210.87.254.6 on 09/06/12
For personal use only.

observe la formation d'éthylénique et de cétones bromées. Pour avoir une réaction complète dans un temps assez bref, nous avons effectué la réaction à 0°C.

Evidemment, pour voir si la température avait un effet sur la compétition entre la formation de cétone bromée et l'élimination, nous avons répété l'expérience décrite par Durst avec la cyclohexanone mais en effectuant la réaction à 0°C (c'est l'expérience qui est décrite en partie expérimentale). Nous avons obtenu le même rendement (90%) que Durst *et al.* en acétyl bromocyclohexane.[3]

À notre sens, la compétition entre la réaction d'élimination et la formation de cétones bromées est liée essentiellement à la structure de l'époxysulfone et non pas à un effet de température.

## Discussion

L'obtention stéréosélective de cétones (ou aldéhydes) α-bromés et la formation compétitive dans cette réaction de cétones (ou aldéhydes) α-éthyléniques sont les deux faits marquants rapportés dans ce travail. Ils sont la conséquence et de la stéréosélectivité de formation des époxysulfones **3** et du mécanisme d'ouverture de ces dernières sous l'action de $MgBr_2$.

(a) *Stéréosélectivité de formation des époxysulfones 3*

Les époxysulfones **3** se forment par cyclisation *in situ* des anions **2** résultant eux-mêmes de l'addition sur les cyclohexanones du carbanion correspondant à la sulfone **1**. Dans les conditions de transfert de phase utilisées, cette addition est vraisemblablement irréversible.[4] La configuration des époxysulfones **3** serait donc déterminée par le sens de l'attaque du carbanion $Ph—SO_2—C^-(Cl)R$ sur les cyclohexanones (face α ou face β).[5]

Dans le cas des cétones **5** et **6**, il a été montré (7) que les carbanions $ClC^-(CH_3)COR$ et $ClC^-(CH_3)CN$ attaquent très préférentiellement le carbonyle par la face β. Dans le cas de la cétone **7**, les carbanions $C^-(Cl_2)—CO_2$ isoprop. (8)[6] et

$(CH_3)_2—S—CH_2^-$ (9) attaquent exclusivement la face β. Il est donc raisonnable d'admettre que le carbanion $Ph—SO_2—C^-(Cl)R$ de structure et de taille assez voisines attaque les trois cétones **5**, **6** et **7** par la même face β et conduise aux époxysulfones **9** et **10** de configuration α (Schéma 1).

En ce qui concerne la cétone **8**, il n'existe dans la littérature que peu de données concernant la stéréochimie de l'attaque nucléophile du carbonyle en 3 d'un stéroïde en série A/B *cis* 5β. Toutefois, en comparant les résultats obtenus lors de la réduction par les hydrures et lors de l'addition de réactifs de Grignard (10), il semble raisonnable de conclure que, plus le réactif est volumineux, plus l'attaque α est favorisée. Selon cette séquence le carbanion $Ph—SO_2—C^-(Cl)CH_3$ devrait attaquer **8** par la face α et conduire à l'époxysulfone **11** de configuration β.

(b) *Ouverture des époxysulfones 3 sous l'action de $MgBr_2$*

Le mécanisme d'ouverture d'un époxyde sous l'action d'un acide de Lewis est généralement considéré comme un mécanisme limite: dans l'intermédiaire (ou dans l'état de transition) le carbone de la liaison C—O qui se rompt, possède un caractère carbocationique plus ou moins prononcé. Toutefois les réactions de substitution observées s'effectuent très sélectivement avec inversion (11). Selon ce mécanisme, l'attaque par $Br^-$ des époxysulfones **9**, **10** et **11** a donc lieu avec inversion de configuration et conduit aux cétones α-bromées comportant un brome équatorial (Schéma 1).

En ce qui concerne la formation parallèle des composés α-éthyléniques, il est intéressant de rapporter des observations antérieures rapportées par Durst *et al.* (1) puis par Taber et Gunn (12). Ces auteurs ont constaté que les époxysulfones **3** sous l'action de $BF_3$ dans l'éther, conduisent exclusivement aux composés carbonylés α-éthyléniques correspondants. L'observation de la même réaction, lorsque $MgBr_2$ est utilisé à la place de $BF_3$ n'est donc pas surprenante. Toutefois, la proportion substitution–élimination en fonction de la structure des époxysulfones **3** est, avec les données dont nous disposons, difficilement interprétable. Cependant à notre sens, il est bien clair que les deux époxysulfones isomères ont un com-

[3] En fait, dans leur texte, Durst *et al.* (1) ne précisent pas s'il y a ou non élimination compétitive à −30°C. En effet la nature des 10% manquant au bilan de la réaction n'est pas précisée. Nous avons montré que dans notre cas, il s'agit de 10% d'acétylcyclohexène.

[4] Seyden et coll. (6, 7*b*) ont montré sur un exemple analogue que, dans ces conditions réactionnelles, la cyclisation en époxyde de l'oxyanion intermédiaire est beaucoup plus rapide que sa transformation en produits de départ.

[5] Pour faciliter la discussion, nous avons étendu à la série cyclohexane monocyclique, la nomenclature α et β utilisée en série stéroïde (voir Schéma 1).

[6] L'attribution de l'halohydrine (2) doit être inversée (B. Castro, communication personnelle à J. Seyden; voir réf. 7*b*).

Can. J. Chem. Downloaded from www.nrcresearchpress.com by 210.87.254.6 on 09/06/12
For personal use only.

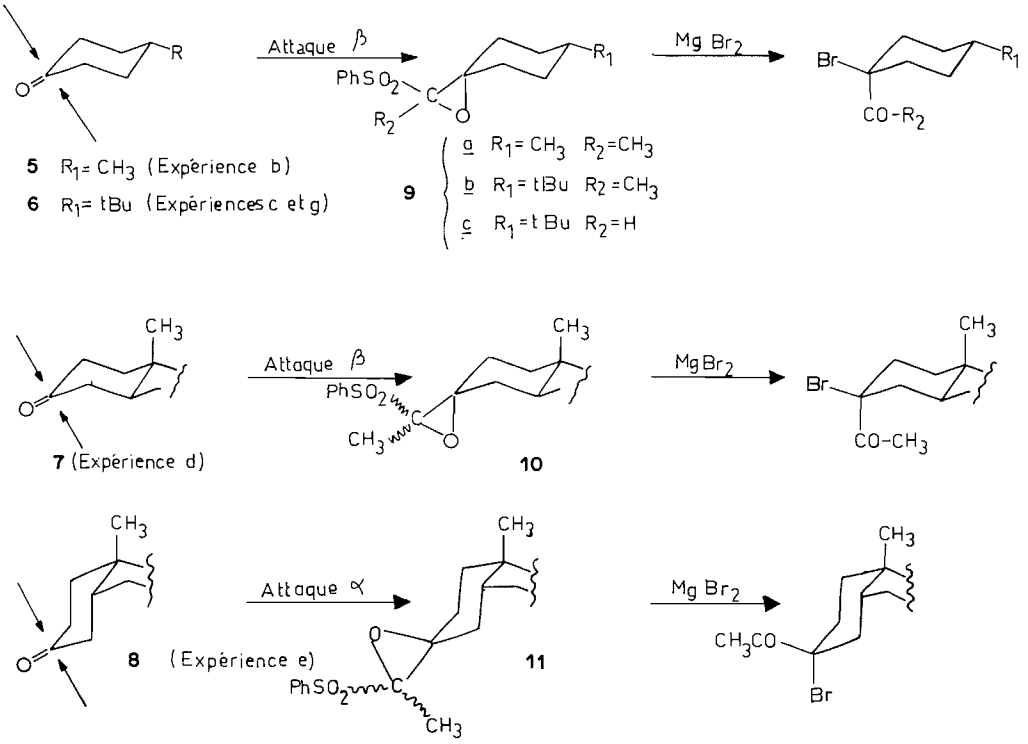


SCHÉMA 1

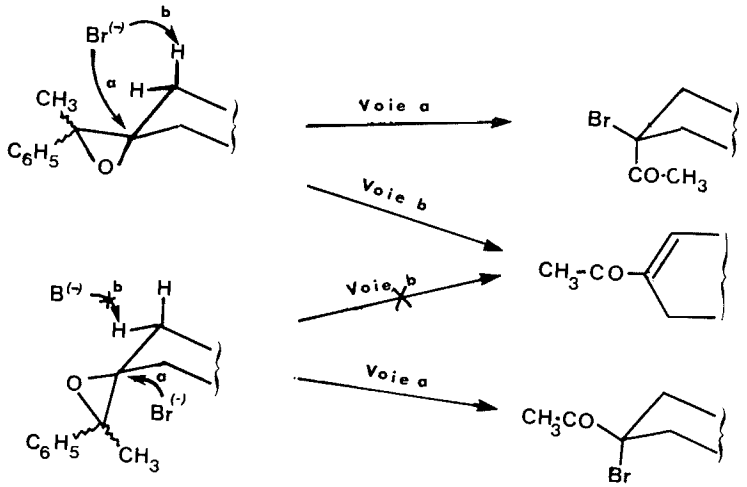


SCHÉMA 2

portement différent vis à vis de la réaction d'élimination (les deux cétones bromées sont stables dans les conditions de la réaction). L'époxysulfone majoritaire (provenant de l'attaque équatoriale) possède un hydrogène axial *trans* antipériplanaire à la liaison C—O, elle est donc susceptible de conduire à la cétone éthylénique (et à la cétone bromée à brome équatorial). Par contre, l'autre époxysulfone minoritaire (provenant de l'attaque axiale) doit conduire uniquement à la cétone bromée à brome axial.

Ceci est bien en accord avec le fait que le rapport entre les deux époxysulfones (> 90:10 dans le cas de **5** ou **6**) soit plus grand que celui entre les deux cétones bromées correspondantes (~ 85:15).

Cela veut donc dire que le degré de stéréosélectivité au niveau de la stéréochimie de l'attaque de la cétone par l'anion de la sulfone est supérieur ou

égal à la valeur des rapports des deux cétones bromées.

Le contraste frappant entre la série cyclohexane monocyclique et la série stéroïde ne conduisant, elle, qu'à une très faible proportion de composés éthyléniques, a récemment été confirmé par d'autres auteurs (13).

## Conclusion

Ce travail montre que la méthode de préparation de méthyle cétones α-bromées par ouverture d'époxysulfones sous l'action de $MgBr_2$ peut constituer pour ces composés une voie d'accès privilégiée et fortement stéréosélective, notamment en série stéroïde où la réaction secondaire d'élimination est très minoritaire.

## Partie expérimentale

*Commentaires généraux*

Les analyses par cpg ont été effectuées sur un appareil Girdel "75 FS" (colonne 1,60 m, Chromosorb 5% SE 30).

Les spectres rmn $^1H$ ont été enregistrés sur un spectromètre Varian T-60 ou A-60 D; les déplacements chimiques sont exprimés en ppm avec comme référence interne le TMS.

Les spectres rmn $^{13}C$ ont été enregistrés à 20 MHz sur un spectromètre Varian CFT-20, avec une largeur spectrale de 5000 Hz.

Les spectres ir (solvant $CCl_4$) ont été enregistrés sur un appareil Perkin–Elmer 157. Les pouvoirs rotatoires ont été mesurés avec un polarimètre Perkin–Elmer 141.

*Modes opératoires généraux*

1. *Époxysulfones*

Une quantité (0,024 mol) d'α-cholorophénylsulfone **1** (1) et 0,029 mol de cyclohexanone sont maintenues pendant 20 h sous agitation à température ambiante en présence de 20 mL de soude à 50% et 200 mg de sulfate acide de tetrabutylammonium. Après dilution dans l'eau, le mélange réactionnel est extrait avec $CH_2Cl_2$. La solution organique est lavée à l'eau, séchée sur $Na_2SO_4$, filtrée sur Florisil et évaporée sous pression réduite.

2. *Ouverture des époxysulfones par $MgBr_2$*

On prépare une solution de $MgBr_2$ et faisant réagir 5,50 g (0,23 mol) de Mg sur 37,6 g (0,2 mol) de dibromoéthane en solution dans 80 mL d'éther anhydre. On ajoute à cette solution refroidie à 0°C, 0,024 mol d'époxysulfone en solution dans 30 mL d'éther anhydre. Après 1 h sous agitation, la solution est hydrolysée ($H_2O$ + glace) puis décantée, séchée et évaporée.

*Description des expériences*

*Expérience **a***

L'expérience décrite par Durst *et al.* (1) a été répétée: il a été montré que le complément à 100% de cette réaction est la cyclohexényl-1 méthyle cétone (comparaison avec un échantillon authentique).

*Expérience **b***

*Époxysulfone* **9**a: 3,3 g (0,029 mol) de méthyl-4 cyclohexanone et 5 g (0,024 mol) de **1***a* conduisent à 6,5 g d'époxysulfone brute (85%); rmn $^1H$ ($CCl_4$) δ ppm: 1,0 (s, 3H, $CH_3$), 1,33 (m, 3H, $CH_3$), 7,6 (m, 3H) et 7,93 (m, 2H) ($C_6H_5$); rmn $^{13}C$, isomère très majoritaire, δ ppm: 15,3 (q, $CH_3$), 21,7 (q, $CH_3$-4), 69,9 (s, C-1), 79,4 (C—$SO_2$); isomère très minoritaire, δ ppm: 74,1 (s, C-1).

*Cétones bromées **12** et **13***: 6,5 g de **5***b* conduisent après traitement habituel et chromatographie sur une colonne de Florisil (pentane) à 1,74 g (38%) de **12** + **13** (**12/13** = 85:15, analyse cpg) et à 1,8 g (61%) de méthyl-4 cyclohexényl-1 méthyle cétone identifiée par rapport à un échantillon authentique. Composé **12**: ir ($CCl_4$): ν C=O: 1695 $cm^{-1}$; rmn $^1H$ ($CCl_4$) δ ppm: 0,88 (d, 3H, $CH_3$), 2,39 (s, 3H, $COCH_3$); rmn $^{13}C$ ($CDCl_3$) δ ppm: 206,4 (C=O), 68,5 (s, C-1), 37,4 (t, C-2), 33,4 (t, C-3), 30,8 (d, C-4), 23,9 ($COCH_3$), 21,3 (q, $CH_3$-4); *m/e*: 219 ($M^+$); sm (ion. chim., $C_4H_{10}$) *m/e*: 219 et 221 $(MH)^+$, 139 $(M - Br)^+$. Composé **13**: rmn $^1H$ ($CCl_4$) δ ppm: 1,0 (d, 3H, $CH_3$), 2,42 (s, 3H, $COCH_3$); rmn $^{13}C$ ($CDCl_3$) δ ppm: 72,5 (s, C-1), 35,5 (t, C-2), 31,5 (t, C-3), 30,5 (d, C-4), 24,4 ($COCH_3$), 21,9 (q, $CH_3$-4), C=O non visible; sm (ion. chim., $C_4H_{10}$) *m/e*: 219 et 221 $(MH)^+$, 139 $(M-Br)^+$.

*Expérience **c***

*Époxysulfone* **9**b: 3,6 g (0,023 mol) de 4-*t*Bu-cyclohexanone et 4 g (0,019 mol) de **1***a* conduisent à 4,6 g d'époxysulfone cristallisée (77%); rmn $^1H$ ($CCl_4$) δ ppm: 0,9 (s, 9H, *t*Bu), 1,43 (s, 3H, $CH_3$), 7,7 et 8,06 (m, 5H, $C_6H_5$); rmn $^{13}C$ ($CDCl_3$) δ ppm: 15,3 (q, $CH_3$), 25,1 (q, *t*Bu), 31,7 (d, C-2), 32,4 (s, $C(CH_3)_3$), 47,0 (d, C-4), 70,1 (s, C-1), 79,5 (*C*—$SO_2Ph$). Dans les eaux mères on isole un isomère minoritaire; rmn $^{13}C$: 15,3 (q, $CH_3$), 25,2 (t, C-3), 27,6 (q, *t*Bu), 30,9 (t, C-2), 32,4 (s, *C*—$CH_3)_3$), 46,7 (d, C-4), 72,0 (s, C-1), 79,4 (*C*—$SO_2$).

*Cétones bromées **14** et **15***: 4 g d'époxysulfone **9***b* brute, sous l'action de $MgBr_2$ conduisent après chromatographie sur Florisil (pentane) à 1,3 g (39%) de **4** + **15** (**14/15** = 90:10, analyse cpg) et à 0,99 g (42%) de 4*t*Bu-cyclohexenyl méthyle cétone. Les produits ont été identifiés par rapport à des échantillons authentiques (5, 14).

*Expérience **d***

*Époxysulfone **10***

Préparée à partir de 8,7 g d'androstan-5α-ol-17β-one-3 et de 6,2 g de **1***a*. Après traitement habituel, la solution finale $CH_2Cl_2$) est concentrée jusqu'à un volume d'environ 50 mL.

*Cétones bromées **16**, **17** et cétone α-éthylénique **18***

La solution précédente est ajoutée dans les conditions habituelles à $MgBr_2$. Après traitement, le produit est filtré sur Florisil (hexane–ether 80:20), concentré puis acétylé par 100 mL de pyridine et 20 mL d'anhydride acétique pendant 20 h. La mélange réactionnel est versé dans l'eau, le précipité est essoré et sèché. Le produit est chromatographié sur Florisil (hexane–$Et_2O$ 90:10); 5 g de **16** sont isolés (38%); on élue ensuite 0,9 g (8%) d'acétate de Δ-2 acétyl-3 androsténol-17β **18** (la cétone bromée **17**, très minoritaire, a pu être mise en évidence à l'état de traces). Composé **16**: pf = 171–172,5°C (EtOH); $R_f$ = 0,72 ($Et_2O$–hexane 40:60); $[\alpha]_{540}^{19}$ +24,8° ($CH_2Cl_2$); ir ($CCl_4$) ν(C=O): 1705 et 1730 $cm^{-1}$; rmn $^1H$ ($CDCl_3$) δ ppm: 0,73 (s, 3H, ME-18), 0,86 (s, 3H, Me-19), 1,99 (s, 3H, $OCOCH_3$), 2,35 (s, 3H, $COCH_3$), 4,53 (t, 1H, H-17); $^{13}C$ ($CDCl_3$) δ ppm: 67,9 (s, C-3), 170,9 ($OCOCH_3$), 201,6 ($COCH_3$). Composé **17**: $R_f$ = 0,56 ($Et_2O$–hexane 40:60); rmn $^{13}C$ ($CDCl_3$) δ ppm: 73,3 (s, C-3), 203,2 ($COCH_3$). Composé **18**: pf: 138–145°C (ether de pétrole); $R_f$ = 0,50 ($Et_2O$–hexane 40:60); $[\alpha]_{546}^{21}$ +3,86° ($CH_2Cl_2$); ir ν(C=O): 1735 et 1670 $cm^{-1}$; ν(C=C): 1640 $cm^{-1}$; rmn $^1H$ ($CDCl_3$) δ ppm: 0,70 (s, 3H, Me-18), 0,78 (s, 3H, Me-19), 2,02 (s, 3H, $OCOCH_3$), 2,26 (s, 3H, $COCH_3$), 4,57 (t, 1H, H-17), 6,8 (m, 1H, H-2); rmn $^{13}C$ ($CDCl_3$) δ ppm: 82,7 (d, C-17), 139,5 (d, C-2), 138,7 (d, C-3), 170,9 ($OCOCH_3$), 199,0 (*C*O—$CH_3$). *Anal.* calc. pour $C_{23}H_{35}O_3Br$: C 62,80, H 7,96, Br 18,18; trouvé: C 63,02, H 8,27, Br 52,52.

*Expérience **e***

*Époxysulfone **11***

Préparée à partir de 10 g d'acétate d'androstan-5β-ol-17β-one-3 et de 6,2 g de **1***a*. Comme dans l'expérience précédente **d**, l'époxysulfone n'a pas été isolée.

Can. J. Chem. Downloaded from www.nrcresearchpress.com by 210.87.254.6 on 09/06/12
For personal use only.

Can. J. Chem. Downloaded from www.nrcresearchpress.com by 210.87.254.6 on 09/06/12
For personal use only.

*Cétones bromées* ***19*** *et* ***20*** *et cétones éthyléniques* ***21***

Comme dans l'expérience **d**, le produit brut est acétylé puis chromatographié sur gel de silice (hexane–ether 93:7). On isole 6,45 g (49%) de **19**, 0,26 g (2%) de **20** et 0,6 g (6%) d'un mélange des acétates de Δ-2 et Δ-3 acétyl-3 androstanol-17 **21**. Composé **19**: pf = 110–111°C puis 123–125°C (pentane); $R_f$ = 0,61 ($Et_2O$–hexane 25:75); $[\alpha]_{546}^{20}$ 50,4° ($CH_2Cl_2$); ir ($CCl_4$) ν (C=O): 1705 et 1730 $cm^{-1}$; rmn $^1H$ ($CDCl_3$) δ ppm: 0,77 (s, 3H, Me-18), 0,87 (s, 3H, Me-19), 2,04 (s, 3H, $OCOCH_3$), 2,38 (s, 3H, $CO—CH_3$), 4,61 (t, 1H, H-17); rmn $^{13}C$ ($CDCl_3$) δ ppm: 69,0 (s, C-3), 82,6 (d, C-17), 170,0 ($OCOCH_3$), 204,0 ($COCH_3$). *Anal.* calc. pour $C_{23}H_{35}O_3Br$: C 62,80, H 7,96, Br 18,18; trouvé: C 62,31, H 8,14, Br 18,08. Composé **20**: pf = 149–151,5°C (EtOH); $R_f$ = 0,42 ($Et_2O$–hexane 25:75); $[\alpha]_{546}^{23}$ 2,4° ($CH_2Cl_2$); ir ($CCl_4$) ν(C=O): 1705 et 1730 $cm^{-1}$; rmn $^1H$ ($CDCl_3$) δ ppm: 0,77 (s, 3H, Me-18), 1,05 (s, 3H, Me-19), 2,04 (s, 3H, $OCOCH_3$), 2,43 (s, 3H, $CO—CH_3$); rmn $^{13}C$ ($CDCl_3$) δ ppm: 12,6 (q, Me-18), 74,8 (s, C-3), 170,7 ($OCO—CH_3$), 202,7 ($COCH_3$). Composé **21**: $R_f$ = 0,42 ($Et_2O$–hexane 25:75); ir ($CCl_4$): ν(C=O): 1735 et 1667 $cm^{-1}$; ν(C=C): 1645 et 1640 $cm^{-1}$; rmn $^1H$ ($CDCl_3$) δ ppm: 0,78 (s, 3H, Me-18), 1,03 (s, 3H, Me-19), 2,02 (s, 3H, $OCOCH_3$), 2,28 (s, 3H, $COCH_3$), 4,54 (t, 1H, H-17), 6,58 (m, $\Delta\nu_{1/2}$ = 5 Hz, $HC$=C), 6,75 (m, $\Delta\nu_{1/2}$ = 11 Hz, $HC$=C); rmn $^{13}C$ ($CDCl_3$) δ ppm: 82,8 (d, C-17), 138,8 (d) et 139,8 (d) (C-2 et C-4), 145,9 (d, C-3), 171,1 ($O=COCH_3$), 199,2 ($COCH_3$).

*Expérience f*

*Époxysulfone* ***22***: 1,96 g (0,02 mol) de cyclohexanone et 4 g (0,02 mol) de **1***b* conduisent à 4,25 g (84%) de **22**, pf = 56–57°C (hexane – 10% éther); rmn $^1H$ ($CCl_4$) δ ppm: 3,63 (s, 1H, $CH—O$), 7,73 (m, 3H, $C_6H_5$), 8,03 (m, 2H, $C_6H_5$).

*Aldéhyde bromé* ***23***: 4 g d'époxysulfone **22** sous l'action de $MgBr_2$ conduisent après chromatographie sur Florisil (pentane) à 0,95 g (27%) de **23** et à 0,65 g (33%) de cyclohexényl 1-carboxaldéhyde **24** (1). Composé **23**: rmn $^1H$ ($CCl_4$) δ ppm: 9,36 (s, 1H, *CHO*). *Composé* **24**: rmn $^1H$ ($CCl_4$) δ ppm: 6,80 (m, 1H, $CH$—C), 9,43 (S, 1H, *CH*O).

*Expérience g*

*Époxysulfone* ***9***c: 3,7 g (0,052 mol) de *t*Bu-4 cyclohexanone et 10 g (0,052 mol) de **1***b* conduisent à 13 g (84%) d'époxysulfone ***9c***; pf = 56–57°C (hexane – 10% éther); rmn $^1H$ ($CCl_4$) δ ppm: 3,63 (s, 1H, $CH$—O), 7,73 (m, 3H, $C_6H_5$), 8,03 (m, 2H, $C_6H_5$).

*Aldéhydes bromés* ***25*** *et* ***26***: 3,3 g (0,01 mol) d'époxysulfone ***9c*** "brute", sous l'action de $MgBr_2$ conduisent après chromatographie sur Florisil (pentane) à 0,75 g (28%) de **25** + **26** (**25**/**26** = 70:30, analyse cpg) et à 0,74 g (41%) d'aldéhyde éthylénique **27**. Les produits ont été identifiés par rapport à des échantillons authentiques (5).

1. T. Durst, K. C. Tin, F. de Reinach-Hirtzbach, J. M. Decesare et M. D. Ryan. Can. J. Chem. **57**, 258 (1979).
2. J. P. Bégué et M. Charpentier-Morize. Acc. Chem. Res. **13**, 207 (1980).
3. G. Stork, W. S. Worrall et J. J. Pappas. J. Am. Chem. Soc. **82**, 4315 (1960).
4. M. Gaudry et A. Marquet. Tetrahedron, **26**, 5611 (1970).
5. M. Bettahar et M. Charpentier-Morize. Tetrahedron, **30**, 1373 (1974).
6. E. d'Incan et J. Seyden-Penne. C. R., Acad. Sci. Paris, Ser. C, **281**, 1031 (1975).
7. (*a*) Y. Maroni-Barnaud, M. C. Roux-Schmitt et J. Seyden-Penne. Tetrahedron Lett. 3129 (1974); (*b*) N. Idriss, M. Perry, Y. Maroni-Barnaud, M. C. Roux-Schmitt et J. Seyden-Penne. J. Chem. Res. (S), 128 (1978), et références citées.
8. B. Castro et J. Amos. Bull. Soc. Chim. Fr. 2559 (1974).
9. C. E. Cook, R. C. Corley et M. E. Wall. J. Org. Chem. **33**, 6789 (1968).
10. J. Fried et J. A. Edwards (*Editeurs*). Organic reactions in steroid chemistry. van Nostrand-Reinhold Company. (1972). Vol. I. pp. 75–81; Vol. II. p. 58.
11. D. N. Kirk. Chem. Ind. 109 (1973).
12. D. F. Taber et B. P. Gunn. J. Org. Chem. **44**, 450 (1979).
13. W. Gschwendtner, V. Hoppen et H. J. Schneider. J. Chem. Research (S), 96 (1981).
14. J. P. Bégué et D. Bonnet-Delpon. Org. Magn. Reson. **18**, 190 (1982).

# Synthèse de pyranno[*f* et *g*]indoles

PHIEO TA KIM ET ROGER GUILARD

*Laboratoire de Synthèse et d'Electrosynthèse organométallique associé au C.N.R.S., Faculté des Sciences "Gabriel", 21100 Dijon, France*

ET

PATRICE RENAUT

*Centre de Recherche des Laboratoires Fournier, 42, rue de Longvic, 21300 Chenôve, France*

Reçu le 2 février 1982

PHIEO TA KIM, ROGER GUILARD et PATRICE RENAUT. Can. J. Chem. **60**, 2093 (1982).

La réaction de l'azidoacétate d'éthyle avec les formyl-6 chromannes, suivie par la cyclisation des azides obtenus conduit aux tetrahydro-1,7,8,9 pyranno[2,3-*g*]indoles et tetrahydro-2,3,4,8 pyranno[3,2-*f*]indoles. Quelques aspects de la réactivité chimique de ces nouveaux systèmes tricycliques sont décrits. Les structures de tous les composés synthétisés sont établies sur la base des données de rmn protonique.

PHIEO TA KIM, ROGER GUILARD, and PATRICE RENAUT. Can. J. Chem. **60**, 2093 (1982).

Reaction of ethyl azidoacetate with 6-formylchromans, followed by cyclisation of the azides obtained, leads to 1,7,8,9-tetrahydropyrano[2,3-*g*]indoles and 2,3,4,8-tetrahydropyrano[3,2-*f*]indoles. Some aspects of the chemical reactivity of these new tricyclic systems are described. The structures of all products synthesized are established on the basis of $^1$H nmr data.

## Introduction

Les systèmes pyrannoindoliques ont été relativement peu étudiés et si un certain nombre de pyranno[*e*]indoles ont été décrits (1–4) depuis environ une décennie, ce n'est que très récemment que les pyranno[*b*]indoles ont été synthétisés (5, 6). Les méthodes préconisées pour l'accès aux pyranno[*e*] et [*b*] indoles ne pouvaient être utilisées pour la synthèse des pyranno[*f*] et [*g*] indoles que nous désirions préparer, ces produits pouvant servir de synthons pour l'obtention de composés à intérêt pharmacologique.[1]

Nous avons pensé que la réaction de Hemetsberger, utilisée avec succès pour la synthèse de nouveaux dérivés indoliques (7), pouvait au départ de formyl chromannes conduire à des pyrannoindoles. Nous nous sommes exclusivement intéressés aux produits porteurs d'un groupe aldéhyde en position 6:

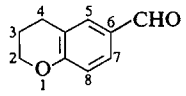


Ces composés étaient *a priori* susceptibles de donner naissance soit à des pyranno[*f*]indoles soit à des pyranno[*g*]indoles.

Nous examinerons tout d'abord les modalités mises en œuvre pour l'accès aux pyrannoindoles recherchés et nous indiquerons ensuite quelques aspects de la réactivité chimique des produits obtenus.

[1]Les dérivés décrits dans ce mémoire font l'objet du brevet français no 80-14246 déposé en juin 1980.

## Synthèses

La série de transformations réalisée au départ des formyl-6 chromannes peut être ainsi schématisée (voir Schéma 1).

La condensation de l'azidoacétate d'éthyle sur les aldéhydes **1** s'effectue de façon classique en présence de méthanolate de sodium; le rendement de la réaction est de l'ordre de 50% et les azides obtenus se cyclisent partiellement au cours de la purification. La cyclisation est totale lorsqu'on traite à ébullition une solution xylénique (ou trichlorobenzénique) d'azide; cette réaction conduit toujours aux pyranno[*g*]indoles substitués **3**, cependant lors de la cyclisation de **2***b* ($R^1$ = Cl) on observe également la formation conjointe du pyranno[*f*]indole **4***b* ($R^1$ = Cl). L'hydrolyse des esters **3** et **4***b* donne naissance (rendement de 90%) aux acides correspondants **5** et **6***b* ($R^1$ = Cl). Leur décarboxylation effectuée selon des conditions classiques (chromite de cuivre activé au baryum comme catalyseur et quinoléine comme solvant) conduit aux pyrannoindoles **7** ou **8** avec des rendements de l'ordre de 60 à 80%. Toutefois au cours du traitement de l'acide **5***a* ($R^1$ = H) apparaît, conjointement au pyranno[*g*]indole attendu **7***a*, le pyranno[*f*]indole **8***a*. Les pourcentages respectifs en produits **7***a* et **8***a* sont de 90 et 10%. Toujours dans le cas où $R^1$ = H, les diverses méthodes d'analyse (rmn, ir ...) utilisées ne nous ont pas permis de mettre en évidence la formation d'un ester correspondant à un arrangement pyranno[*f*]indolique. L'apparition du dérivé **8***a* doit donc résulter soit d'une ouverture du cycle pyrrolique,

0008-4042/82/162093-06$01.00/0
©1982 National Research Council of Canada/Conseil national de recherches du Canada

Can. J. Chem. Downloaded from www.nrcresearchpress.com by 210.87.254.5 on 09/06/12
For personal use only.

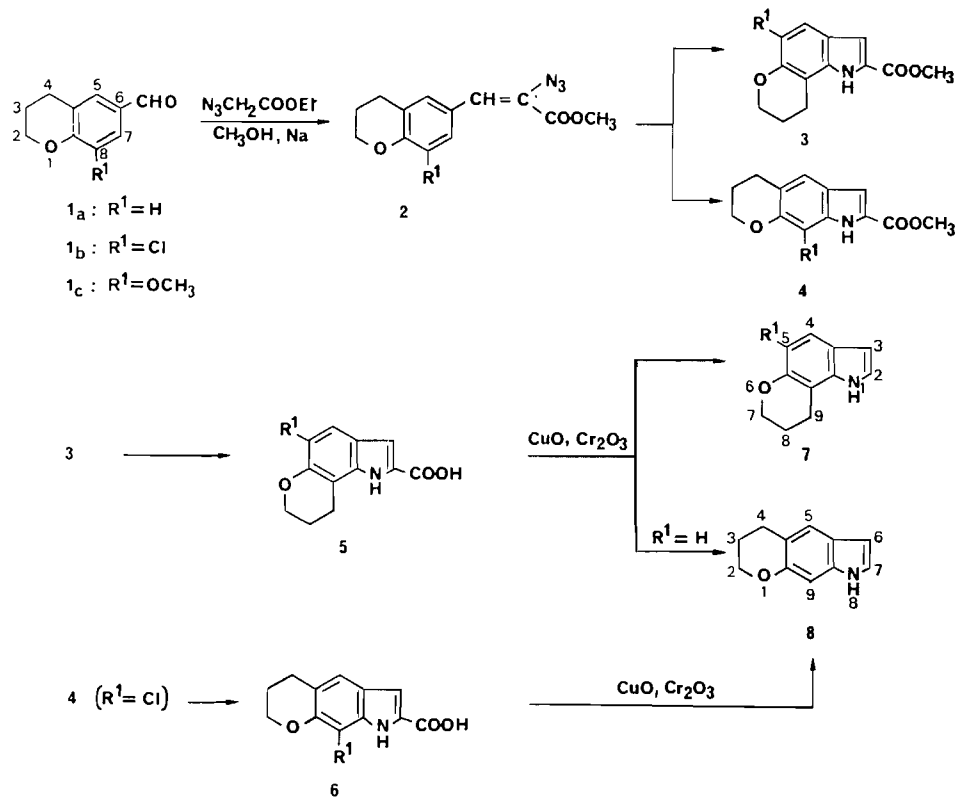

SCHÉMA 1

qui n'a jamais été observée lors des réactions de décarboxylation, soit plus vraisemblablement d'un réarrangement du cycle pyrannique.

*Quelques aspects de la réactivité des hydropyranno[f ou g]indoles obtenus*

Les tétrahydropyranno[3,2-*f* ou 2,3-*g*]indoles éventuellement substitués en 9 ou 5, **7** et **8** ont été traités selon Vilsmeier; quel que soit le substrat pyrannoindolique de départ, un seul dérivé formylé est obtenu (dérivé **9** pour la série *g* et **10** pour la série *f*) avec un rendement de l'ordre de 40% et le groupe formyle se fixe sur le sommet β pyrrolique.

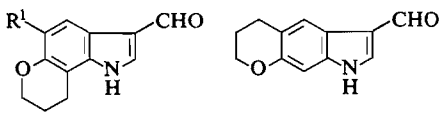

**9** $R^1 = H, Cl, OCH_3$ **10***a*

L'action du chlorure d'oxalyle sur **7***a* suivie de celle de la diméthylamine conduit au dérivé **11***a* avec un rendement global de 70%. La réaction de Mannich appliquée au même produit **7***a* permet d'obtenir **11***b* (rendement de 58%). Dans les deux cas l'on observe la substitution de l'hydrogène en β de l'atome d'azote.

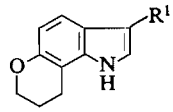

**11***a*: $R^1 = COCON(CH_3)_2$
**11***b*: $R^1 = CH_2N(CH_3)_2$

## Établissement des structures

La structure de chacun des produits obtenus a pu être établie par analyse des spectres de rmn protonique. Les caractéristiques relevées pour les produits [*g*] et [*f*] ont été regroupées respectivement sur les tableaux 1 et 2.

Avant d'aborder l'analyse des spectres obtenus, rappelons les valeurs moyennes des glissements des protons pyranniques des chromannes situés en position α, β et γ de l'atome d'oxygène (8, 9): $\delta(CH_2)_\alpha \simeq 4{,}3$ ppm; $\delta(CH_2)_\beta \simeq 2{,}0$ ppm et $\delta(CH_2)_\gamma \simeq 2{,}8$ ppm. Les protons méthyléniques en α et γ de l'atome d'oxygène apparaissent sous la forme d'un triplet, ceux du méthylène en β sous celle d'un multiplet. Par ailleurs, les protons du noyau benzé-

Can. J. Chem. Downloaded from www.nrcresearchpress.com by 210.87.254.5 on 09/06/12
For personal use only.

Can. J. Chem. Downloaded from www.nrcresearchpress.com by 210.87.254.5 on 09/06/12
For personal use only.



TABLEAU 1. Caractéristiques rmn de tétrahydro-1,7,8,9 pyranno[2,3-*g*]indoles

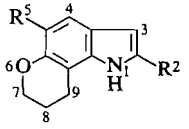

| | | | Déplacement chimique des protons (ppm) | | | | | | | | |
|---|---|---|---|---|---|---|---|---|---|---|---|
| Composés | $R^2$ | $R^5$ | H1 | $R^2$ | H3 | H4 | $R^5$ | $(CH_2)_7$ | $(CH_2)_8$ | $(CH_2)_9$ | Constante de couplage (Hz) |
| **3***a* | $COOCH_3$ | H | 8,64 (m) | 3,92 (s) | 7,14 (d) | 7,38 (m) | 6,70 (d) | 4,23 (m) | 2,16 (m) | 2,84 (m) | 2,20($J_{13}$) 0,73($J_{14}$) 8,61($J_{45}$) 0,73($J_{49}$) |
| **3***b* | $COOCH_3$ | Cl | 8,71 (m) | 3,92 (s) | 7,08 (d) | 7,52 (m) | | 4,35 (m) | 2,17 (m) | 2,88 (m) | 2,20($J_{13}$) 0,73($J_{14}$) 0,73($J_{49}$) |
| **3***c* | $COOCH_3$ | $OCH_3$ | 8,64 (m) | 3,92 (s) | 7,11 (d) | 6,91 (m) | 3,90 (d) | 4,34 (m) | 2,14 (m) | 2,86 (m) | 2,20($J_{13}$) 0,73($J_{14}$) 0,73($J_{49}$) |
| **5***a* | COOH | H | 8,63 (m) | | 7,31 (d) | 7,42 (m) | 6,72 (d) | 4,26 (m) | 2,14 (m) | 2,86 (m) | 2,20($J_{13}$) 0,73($J_{14}$) 8,79($J_{45}$) 0,73($J_{49}$) |
| **5***b* | COOH | Cl | 11,55 (m) | 12,66 (m) | 7,01 (d) | 7,53 (s) | | 4,24 (m) | 2,00 (m) | 2,94 (m) | 2,01($J_{13}$) |
| **5***c* | COOH | $OCH_3$ | 11,26 (m) | 12,51 (m) | 6,96 (d) | 6,90 (s) | 3,72 (s) | 4,14 (m) | 2,01 (m) | 2,87 (m) | 2,01($J_{13}$) |
| **7***a* | H | H | 7,88 (m) | 7,06 (2d) | 6,46 (2d) | 7,35 (m) | 6,67 (d) | 4,21 (m) | 2,11 (m) | 2,82 (m) | 2,01($J_{13}$) 2,38($J_{12}$) 3,30($J_{23}$) 0,73($J_{14}$) 8,61($J_{45}$) 0,73($J_{49}$) |
| **7***b* | H | Cl | 10,98 (m) | 7,21 (2d) | 6,30 (2d) | 7,38 (m) | | 4,21 (m) | 2,01 (m) | 2,87 (m) | 1,83($J_{13}$) 2,38($J_{12}$) 3,11($J_{23}$) 0,73($J_{14}$) 0,73($J_{49}$) |
| **7***c* | H | $OCH_3$ | 7,84 (m) | 7,06 (2d) | 6,44 (2d) | 6,95 (m) | 3,90 (d) | 4,31 (m) | 2,12 (m) | 2,85 (m) | 2,08($J_{13}$) 2,44($J_{12}$) 3,17($J_{23}$) 0,73($J_{14}$) 0,24($J_{45}$) 0,73($J_{49}$) |

TABLEAU 2. Caractéristiques rmn de tétrahydro-2,3,4,8 pyranno[3,2-*f*]indoles

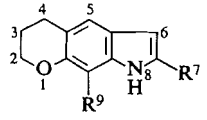

| | | | Déplacement chimique des protons | | | | | | | | |
|---|---|---|---|---|---|---|---|---|---|---|---|
| Composés | $R^7$ | $R^9$ | H5 | H6 | $R^7$ | H8 | $R^9$ | $(CH_2)_2$ | $(CH_2)_3$ | $(CH_2)_4$ | Constantes de couplage (Hz) |
| **8***a* | H | H | 7,25 (m) | 6,37 (3d) | 7,03 (2d) | 7,85 (m) | 6,79 (2d) | 4,19 (m) | 2,02 (m) | 2,93 (m) | 3,11($J_{67}$) 0,92($J_{69}$) 0,55($J_{59}$) |
| **4***b** | $COOCH_3$ | Cl | 7,24 (m) | 7,10 (d) | 3,92 (s) | 8,81 (m) | | 4,34 (m) | 2,14 (m) | 2,94 (m) | 2,30($J_{68}$) – ($J_{58}$) |
| **6***b* | COOH | Cl | 7,30 (s) | 7,06 (d) | 11,35 (m) | | | 4,26 (m) | 1,94 (m) | 2,89 (m) | 3,11($J_{78}$) 2,30($J_{68}$) 3,11($J_{67}$) |
| **8***b** | H | Cl | 7,19 (d) | 6,43 (2d) | 7,11 (2d) | 8,11 (m) | | 4,32 (m) | 2,05 (m) | 2,94 (m) | 3,10($J_{67}$) |

*Spectres relevés dans le $CDCl_3$.

Can. J. Chem. Downloaded from www.nrcresearchpress.com by 210.87.254.5 on 09/06/12
For personal use only.

nique ne se différencient pas, tant pour les valeurs de leur déplacement chimique que pour celles de leurs constantes de couplage, de celles observées normalement en série benzénique; cependant on peut noter que de façon générale le proton H8 proche de l'atome d'oxygène est plus blindé que le proton H7.

L'interprétation des données de rmn des pyrannoindoles obtenus découle d'un examen comparatif des spectres des dérivés [*f*] et [*g*] et les pyrannoindoles non substitués **7***a* et **8***a* présentent des spectres caractéristiques de ces deux séries. Pour les deux composés étudiés les protons pyranniques apparaissent aux valeurs attendues soit $\delta(CH_2)_\alpha \simeq 4{,}2$, $\delta(CH_2)_\beta \simeq 2{,}0$ et $\delta(CH_2)_\gamma \simeq 2{,}8$ ppm. De plus et à moyenne résolution les signaux des protons méthyléniques en position α et γ par rapport à l'atome d'oxygène donnent bien un triplet, ceux de $(CH_2)_\beta$ un multiplet. En fait, à plus haute résolution on note, logiquement, que par suite de l'inéquivalence des protons des groupes méthyléniques chaque signal présente la morphologie d'un multiplet. Les protons α et β pyrroliques sont couplés entre eux, la constante de couplage observée correspond à celle signalée en série indolique ($J_{\alpha\beta} \simeq 3{,}2$ Hz) (*7d*, *7e*) et couplés avec l'hydrogène iminique avec des constantes de couplage de l'ordre de 2 Hz.

Les protons benzéniques des deux isomères se manifestent respectivement vers 7,3 et 6,7 ppm et quel que soit le composé envisagé, les protons benzéniques sont couplés entre eux: pour **7***a*, la constante de couplage est 8,6 Hz, c'est-à-dire celle d'un couplage "*ortho*", le produit est donc de type [*g*]; pour **8***a* la constante vaut 0,9 Hz soit celle de protons en "*para*" et le composé **8***a* est [*f*].

Les spectres obtenus au départ de l'un ou l'autre de ces pyrranoindoles présentent les caractéristiques indiquées précédemment, la position en 3 du substituant découlant du fait que le signal du proton pyrrolique restant est celui d'un proton α ($7{,}4 < \delta < 7{,}9$ ppm).

En ce qui concerne les pyrannoindoles obtenus au départ des formyl-6 chromannes substitués, le cycle benzénique ne porte plus qu'un atome d'hydrogène. La position du signal relatif à ce proton implique que l'hydrogène est en 5 pour un composé [*f*] et en 4 pour un produit [*g*]. Pour des composés [*g*] ne différant que par l'absence du proton 5 les déplacements chimiques observés pour H4 sont conformes à l'effet inductif de chacun des substituants et ne s'interprétent raisonnablement que si l'atome de chlore et le groupe méthoxy sont voisins du proton considéré. Cette déduction est confirmée par l'existence, pour les produits méthoxylés ($R^1 = OCH_3$), d'un faible couplage entre proton benzénique et protons méthyliques ($J \simeq 0{,}24$ Hz). En effet, ce couplage ($^5J$ classique ou interaction dans l'espace) apparaît sur les spectres des produits méthoxylés (**3***c*, **5***c*, **7***c*) et il ne peut logiquement se manifester que si l'atome d'hydrogène et le groupe méthoxy sont relativement proches, ce qui n'est réalisé que dans un arrangement [*g*].

La morphologie des spectres des composés **4***b*, **6***b* et **8***b* se rapproche de celle du composé [*f*] que nous avons analysé.

## Partie expérimentale

Les analyses élémentaires ont été effectuées par le Laboratoire Central de Microanalyse du C.N.R.S. Les spectres rmn ont été relevés sur un appareil JEOL FX 100 en utilisant le TMS comme référence interne et, sauf indication contraire, le DMSO-$d_6$ comme solvant. Le couplage des protons avec l'hydrogène iminique a été supprimé par ajout d'eau lourde. Les points de fusion ont été pris sur banc Kofler.

Certains produits de départ ont été préparés par les méthodes citées en référence: bromo-6 dihydro-3,4 2*H*-benzopyranne-1, (10), $Eb_{16}$ 141°C; cyano-6 dihydro-3,4 2*H*-benzopyranne-1, (11); formyl-6 dihydro-3,4 2*H*-benzopyranne-1, **1***a*, (réf. 12, et selon la méthode décrite dans réf. 13), $Eb_{20}$ 160–163°C; bromo-6 chloro-8 dihydro-2,3 4*H*-benzopyranne-1 one-4 (14), pf 109°C; bromo-6 méthoxy-8 dihydro-2,3 4*H*-benzopyranne-1 one-4 (14), pf 137°C.

*Bromo-6 chloro-8 dihydro-3,4 2*H*-benzopyranne-1*

À l'amalgame de zinc (préparé à partir de 1280 g (19,7 at. g.) de zinc, 128 g (0,54 mol) de chlorure mercureux, 64 cm³ d'acide chlorhydrique concentré et 1900 cm³ d'eau) on ajoute dans l'ordre 1000 cm³ d'eau, 1500 cm³ d'acide chlorhydrique concentré, 3500 cm³ de toluène et 640 g (2,45 mol) de bromo-6 chloro-8 chromannone-4. Le mélange est porté à reflux durant 1 h et après refroidissement et décantation il est extrait à l'éther et lavé à l'eau jusqu'à neutralité. On isole ainsi 305 g (50%) de bromo chloro chromanne, $Eb_{0,01}$ 128°C. *Anal.* calc. pour $C_9H_8OBrCl$: C 43,68, H 3,23, Br 32,29; trouvé: C 43,51, H 3,20, Br 31,98.

*Bromo-6 méthoxy-8 dihydro-3,4 2*H*-benzopyranne-1*

Selon le mode de préparation décrit pour le dérivé précédent, au départ de l'amalgame de zinc préparé à partir de 915 g (14 at. g.) de zinc, 91 g (0,38 mol) de chlorure mercureux dans 46 cm³ d'acide chlorhydrique concentré et 1350 cm³ d'eau, après ajout de 700 cm³ d'eau, 1100 cm³ d'acide chlorhydrique concentré, 2500 cm³ de toluène et 450 g (1,8 mol) de bromo méthoxy chromannone, on obtient 200 g (47%) de bromo méthoxy chromanne, pf 67°C. *Anal.* calc. pour $C_{10}H_{11}O_2Br$: C 49,42, H 4,52, O 13,16, Br 32,88; trouvé: C 49,41, H 4,42, O 13,96, Br 31,68.

*Chloro-8 dihydro-3,4 2*H*-benzopyranne-1 carbaldéhyde-6 **1**b*

À 72 g (0,29 mol) de bromo-6 chloro-8 chromanne dissous dans 250 cm³ d'éther anhydre sont ajoutés lentement et sous agitation à 0,29 mol de *n*-butyllithium dans 320 cm³ d'éther anhydre. La température est maintenue à −70°C durant 6 h puis on additionne goutte à goutte 31 g (0,38 mol) de *N*,*N*-diméthylformamide dissous dans 150 cm³ d'éther anhydre. Le mélange réactionnel est encore maintenu sous agitation à la même température durant 12 h puis, après retour à la température ambiante, il est versé sur de l'eau glacée. Après acidification avec l'acide chlorhydrique 5 *N*, extraction à l'éther et évapora-

Can. J. Chem. Downloaded from www.nrcresearchpress.com by 210.87.254.5 on 09/06/12
For personal use only.

tion, on isole 54 g (95%) de **1***b*, pf 51°C. *Anal.* calc. pour $C_{10}H_9O_2Cl$: C 61,11, H 4,57, O 16,27, Cl 18,03; trouvé: C 61,20, H 4,60, O 16,37, Cl 17,99.

*Méthoxy-8 dihydro-3,4 2*H*-benzopyranne-1 carbaldéhyde-6* **1***c*

On procède selon la méthode décrite précédemment mais en maintenant la température à −50°C. Au départ de 186 g (0,77 mol) de bromo-6 méthoxy-8 chromanne dans 500 cm³ d'éther anhydre et de 0,77 mol de *n*-butyllithium dans 650 cm³ d'éther anhydre on isole après ajout de 78 g (1,1 mol) de *N*,*N*-diméthylformamide dans 200 cm³ d'éther anhydre et recristallisation dans l'éther isopropylique, 75 g (51%) de composé **1***c*, pf 81°C. *Anal.* calc. pour $C_{11}H_{12}O_3$: C 68,77, H 6,24, O 24,97; trouvé: C 69,00, H 6,37, O 25,15.

*Synthèses*

*Tétrahydro-1,7,8,9 pyranno[2,3-g]indolecarboxylate-2 de méthyle* **3**a

À une solution méthanolique de méthylate de sodium (1,4 g de Na (0,06 at. g.) dans 30 cm³ de méthanol absolu), on ajoute, à 0°C, 4,5 g (0,028 mol) de formyl-6 chromanne **1***a*, dissous dans 10 cm³ de méthanol absolu. On verse alors, goutte à goutte, à 0°C et sous agitation 7,2 g (0,056 mol) d'azidoacétate d'éthyle dans 10 cm³ de méthanol absolu. Après avoir maintenu la température durant 6 h à 0°C on verse le mélange réactionnel sur l'eau glacée et retient par filtration l'azide **2***a*. À 30 cm³ de xylène porté à ébullition, on ajoute sous agitation l'azide dissous dans 150 cm³ de xylène. L'addition terminée, agitation et reflux sont maintenus durant 5 h. Après élimination du xylène, le résidu solide obtenu est recristallisé dans un mélange éther isopropylique – benzène et on obtient 2,7 g (42%) du pyrannoindole **3***a*, pf 163°C. *Anal.* calc. pour $C_{13}H_{13}O_3N$: C 67,55, H 5,62, O 20,75, N 6,05; trouvé: C 67,60, H 5,74, O 20,75, N 6,05.

*Chloro-5 tétrahydro-1,7,8,9 pyranno[2,3-g]indolecarboxylate-2 de méthyle* **3**b *et chloro-9 tétrahydro,2,3,4,8 pyranno [3,2-f]indolecarboxylate-7 de méthyle* **4**b

Selon la méthode décrite pour l'obtention du composé précédent et au départ de 16 g (0,69 at. g.) de Na dissous dans 600 cm³ de méthanol absolu, 59 g (0,3 mol) du chloroformyl chromanne **1***b* dans 250 cm³ de méthanol absolu et 77 g (0,6 mol) d'azidoacétate d'éthyle dans 100 cm³ de méthanol absolu, on isole 44 g d'azide **2***b*. Une fraction du composé précédent (5 g (0,017 mol)) est dissoute dans 100 cm³ de trichloro-1,2,4 benzène et ajouté à 150 cm³ de trichloro-1,2,4 benzène portés à 110°C. Le mélange est agité et maintenu à 110°C durant 20 min. Après élimination du solvant, on ajoute quelques cm³ d'éthanol et un solide jaune apparaît (2,28 g). Les eaux mères sont évaporées et le résidu chromatographié sur acide silicique (éluant: toluène – acétate d'éthyle 4:1). Or, après recristallisation dans l'alcool éthylique, on isole 2,27 g d'ester méthylique **3***b*, fraction identique au solide jaune précédent (55,5% globalement), pf 238°C et 0,99 g (22%) d'ester méthylique **4***b*, pf 130°C. *Anal.* calc. pour $C_{13}H_{12}O_3NCl$: C 58,79, O 18,06, N 5,27, Cl 13,34; trouvé pour **3***b*: C 58,73, O 18,35, N 5,39, Cl 13,46; trouvé pour **4***b*: C 59,39, N 5,28, Cl 13,42.

*Méthoxy-5 tétrahydro-1,7,8,9 pyranno[2,3-g]indolecarboxylate-2 de méthyle* **3**c

Selon le mode de préparation décrit pour **3***a* et à partir de 19 g (0,8 at. g.) de Na dissous dans 1250 cm³ de méthanol absolu, 73 g (0,38 mol) de méthoxy formyl chromanne **1***c* dans 50 cm³ de méthanol et 98 g (0,76 mol) d'azidoacétate d'éthyle dans 100 cm³ de méthanol, on isole l'azide **2***c*. Après cyclisation de l'azide dans le xylène, on obtient 38 g (38%) d'ester **3***c*, pf 231°C. *Anal.* calc. pour $C_{14}H_{15}O_4N$: C 64,39, H 5,74, O 24,49, N 5,36; trouvé: C 64,35, H 5,85, O 24,27, N 5,17.

*Acide tétrahydro-1,7,8,9 pyranno[2,3-g]indolecarboxylique-2* **5**a

On porte à reflux durant 3 h 30 une solution de 17 g (0,074 mol) d'ester **3***a* et 8,3 g (0,15 mol) de KOH dans 300 cm³ d'eau. Après retour à la température ambiante, acidification à 0°C par l'acide chlorhydrique 5 *N*, le précipité obtenu est filtré, lavé à l'eau jusqu'à neutralité et recristallisé dans un mélange éthanol–eau. On isole 13,2 g (83%) d'acide **5***a*, pf 228°C. *Anal.* calc. pour $C_{12}H_{11}O_3N$: C 66,38, H 5,06, O 22,09, N 6,44; trouvé: C 66,50, H 5,20, O 22,12, N 6,43.

*Acide chloro-5 tétrahydro-1,7,8,9 pyranno[2,3-g]indolecarboxylique-2* **5**b

On procède selon la méthode précédente; au départ de 22,6 g (0,085 mol) d'ester **3***b*, 14 g (0,26 mol) de potasse dans 300 cm³ d'eau, on obtient 20 g (93%) d'acide **5***b*, pf 308°C. *Anal.* calc. pour $C_{12}H_{10}O_3NCl$: C 57,29, H 3,97, O 19,07, N 5,56, Cl 14,09; trouvé: C 57,11, H 4,07, O 19,20, N 5,67, Cl 13,71.

*Acide chloro-9 tétrahydro-2,3,4,8 pyranno[3,2-f]indolecarboxylique-7* **6**b

Selon la même méthode et à partir de 5 g (0,019 mol) d'ester **4***b* dans 15 cm³ de méthanol et 3,2 g (0,055 mol) de soude dans 30 cm³ d'eau, on obtient 4,52 g (95%) d'acide **6***b*, pf (déc.) 270°C.

*Acide méthoxy-5 tétrahydro-1,7,8,9 pyranno[2,3-g]indolecarboxylique-2* **5**c

Selon la même méthode et à partir de 10 g (0,038 mol) d'ester **3***c* dans 150 cm³ de méthanol et 6,4 g (0,11 mol) de potasse dans 15 cm³ d'eau portés à ébullition durant 1 h 30, on isole 9,3 g (98%) d'acide **5***c*, pf 268°C. *Anal.* calc. pour $C_{13}H_{13}O_4N$: C 63,18, H 5,26, O 25,88, N 5,66; trouvé: C 63,12, H 5,33, O 26,00, N 5,82.

*Tétrahydro-1,7,8,9 pyranno[2,3-g]indole* **7**a *et tétrahydro-2,3,4,8 pyranno[3,2-f]indole* **8**a

On chauffe à 190–195°C durant 7 h 30 120 cm³ de quinoléine distillée, 5 g (0,023 mol) d'acide **5***a* et 0,08 g de chromite de cuivre. Après retour à la température ambiante, on retient le catalyseur par filtration, étend par le chloroforme et élimine la quinoléine par lavage à l'acide chlorohydrique 5 *N*. La phase chloroformique est ensuite lavée à l'eau jusqu'à neutralité, évaporée et le résidu obtenu est chromatographié sur acide silicique (éluant: chloroforme–hexane 2:1). On isole après évaporation des fractions d'élution convenables et recristallisation dans l'éther isopropylique 3,3 g (83%) du pyranno[*g*]indole **7***a*, pf 115°C et 0,3 g (7%) du pyranno[*f*]indole isomère **8***a*, pf 97°C. *Anal.* calc. pour $C_{11}H_{11}ON$: C 76,32, H 6,35, O 9,23, N 8,08; trouvé pour **7***a*: C 76,87, H 6,54, O 9,36, N 8,00; trouvé pour **8***a*: C 75,67, H 6,51, O 9,16, N 8,03.

*Chloro-5 tétrahydro-1,7,8,9 pyranno[2,3-g]indole* **7**b

Selon la même méthode et au départ de 9 g (0,036 mol) d'acide **5***b*, 0,18 g de chromite de cuivre dans 240 cm³ de quinoléine, après chromatographie sur acide silicique (éluant: chloroforme) et recristallisation dans un mélange éther isopropylique – hexane, on isole 5,5 g (74%) du pyranno[2,3-*g*]indole **7***b*, pf 108°C. *Anal.* calc. pour $C_{11}H_{10}ONCl$: C 63,65, H 4,81, O 7,70, N 6,74, Cl 17,08; trouvé: C 63,82, H 4,93, O 7,98, N 6.80, Cl 17,18.

*Chloro-9 tétrahydro-2,3,4,8 pyranno[3,2-f]indole* **8**b

Selon la même méthode et au départ de 1,2 g (0,0048 mol) d'acide **6***b*, 0,18 g de chromite de cuivre dans 6 cm³ de quinoléine, après chromatographie sur acide silicique (éluant: hexane–acétone 7:4) et recristallisation dans l'alcool éthylique, on isole 0,45 g (45%) du pyranno[3,2-*f*]indole **8***b*, pf 117°C. *Anal.* calc. pour $C_{11}H_{10}ONCl$: C 63,65, H 4,81, N 6,74; trouvé: C 63,74, H 4,83, N 6,73.

Can. J. Chem. Downloaded from www.nrcresearchpress.com by 210.87.254.5 on 09/06/12
For personal use only.

*Méthoxy-5 tétrahydro-1,7,8,9 pyranno[2,3-g]indole* **7**c

De même, mais avec une durée de décarboxylation réduite (4 h), à partir de 12 g (0,049 mol) d'acide **5***c*, 0,24 g de chromite de cuivre et 240 cm³ de quinoléine, après chromatographie sur acide silicique (éluant: chloroforme) et recristallisation dans le benzène, on isole 6 g (60%) du produit **7***c*, pf 138°C. *Anal.* calc. pour $C_{12}H_{13}O_2N$: C 70,96, H 6,40, O 15,74, N 6,89; trouvé: C 71,03, H 6,42, O 15,89, N 6,79.

*Tétrahydro-1,7,8,9 pyranno[2,3-g]indolecarbaldéhyde-3* **9**a

À 0,3 g (0,002 mol) d'oxytrichlorure de phosphore dans 0,12 g (0,0016 mol) de *N,N*-diméthylformamide, on verse à 5°C 10 cm³ de dichloro-1,2 éthane puis 0,27 g (0,0015 mol) du pyranno[*g*]indole **7***a* dissous dans 10 cm³ de dichloro-1,2 éthane. Le mélange est maintenu à 5°C durant 2 h 30 puis porté à reflux pendant 30 min. Après refroidissement on ajoute 1,2 g (0,009 mol) d'acétate de sodium trihydraté dissous dans 10 cm³ d'eau et on porte à ébullition 15 min. Après retour à la température ambiante, neutralisation, lavage à l'eau, on obtient, après recristallisation dans l'éthanol, 0,2 g (64%) de l'aldéhyde **9***a*, pf 232°C; rmn (DMSO-$d_6$, $D_2O$) δ: 8,50 (m, $J_{12}$ = 2,93 et $J_{14}$ = 0,73, H1), 7,72 (d, $J_{12}$ = 2,93 Hz, H2), 9,99 (s, $H_a$), 7,88 (m, $J_{14}$ = 0,73, $J_{45}$ = 8,61 et $J_{49}$ = 0,73 Hz, H4), 6,83 (d, $J_{45}$ = 8,61 Hz, H5), 4,23 (m, $(CH_2)_7$), 2,13 (m, $(CH_2)_8$), 2,87 (m, $(CH_2)_9$). *Anal.* calc. pour $C_{12}H_{11}O_2N$: C 71,66, H 5,46, O 15,90, N 6,96; trouvé: C 71,55, H 5,41, O 15,87, N 7,01.

*Tétrahydro-2,3,4,8 pyranno[3,2-f]indolecarbaldéhyde-6* **10**a

En mettant en œuvre les modalités opératoires précédentes, à partir de 0,2 g (0,0013 mol) d'oxytrichlorure de phosphore, 0,09 g (0,0012 mol) de *N,N*-diméthylformamide, 0,2 g (0,0011 mol) de l'isomère [*f*] **8***a* et 1 g (0,007 mol) d'acétate de sodium trihydraté, on isole, après recristallisation dans le benzène, 0,075 g (31%) de l'aldéhyde **10***a*, pf 195°C; rmn (DMSO-$d_6$, $D_2O$) δ: 8,77 (m, $J_{12}$ = 3,11 et $J_{14}$ = 0,73, H1) 7,70 (d, $J_{12}$ = 3,11 Hz, H2), 9,94 (s, $H_a$), 7,96 (m, $J_{14}$ = 0,73 et $J_{49}$ = 0,92 Hz, H4), 6,82 (2d, $J_{49}$ = 0,92 Hz, H9), 2,96 (m, $(CH_2)_5$), 2,03 (m, $(CH_2)_6$), 4,21 (m, $(CH_2)_7$). *Anal.* calc. pour $C_{12}H_{11}O_2N$: C 71,66, H 5,46, O 15,90, N 6,96; trouvé: C 71,85, H 5,53, O 15,94, N 7,03.

*Chloro-5 tétrahydro-1,7,8,9 pyranno[2,3-g]indole-carbaldéhyde-3* **9**b

À partir de 0,3 g (0,002 mol) d'oxytrichlorure de phosphore, 0,12 g (0,0016 mol) de *N,N*-diméthylformamide dans 10 cm³ de dichloro-1,2 éthane et 0,3 g (0,00145 mol) de pyranno[*g*]indole chloré **7***b*, on obtient après chromatographie sur acide silicique (éluant: chloroforme–acétone 3:1) et recristallisation dans un mélange benzène–hexane 0,1 g (29%) de l'aldéhyde **9***b*, pf 214°C; rmn (DMSO-$d_6$, $D_2O$) δ: 7,73 (d, $J_{23}$ = 2,93 Hz, H2), 9,98 (s, $H_a$), 8,16 (m, H4), 4,36 (m, $(CH_2)_7$), 2,18 (m, $(CH_2)_8$), 2,98 (m, $(CH_2)_9$). *Anal.* calc. pour $C_{12}H_{10}O_2NCl$: C 61,18, H 4,24, N 5,94, Cl 15,04; trouvé: C 59,81, H 4,34, N 5,91, Cl 14,68.

*Méthoxy-5 tétrahydro-1,7,8,9 pyranno[2,3-g]indole-carbaldéhyde-3* **9**c

On opère de même au départ de 0,3 g (0,00147 mol) de pyranno[*g*]indole méthoxylé **7***c*, on isole après chromatographie sur acide silicique (éluant: chloroforme–acétone 3:1) et recristallisation dans le benzène 0,11 g (31%) de l'aldéhyde **9***c*, pf 107°C; rmn (DMSO-$d_6$, $D_2O$) δ: 8,91 (m, $J_{12}$ = 3,22 et $J_{14}$ = 0,73 Hz, H1), 7,69 (d, $J_{12}$ = 3,22 Hz, H2), 9,96 (s, $H_a$), 7,62 (m, $J_{14}$ = 0,73 et $J_{4\text{-}OCH_3}$ = 0,29 Hz, H4), 3,94 (d, $J_{4\text{-}OCH_3}$ = 0,29 Hz, $OCH_3$), 4,32 (m, $(CH_2)_7$), 2,14 (m, $(CH_2)_8$), 2,88 (m, $(CH_2)_9$). *Anal.* calc. pour $C_{13}H_{13}O_3N$: C 67,55, H 5,62, O 20,75, N 6,05; trouvé: C 67,08, H 5,57, O 20,84, N 6,00.

*Tétrahydro-1,7,8,9 pyranno[2,3-g]indolyl-3* N,N-*diméthylglyoxamide* **11**a

À 1 g (0,0057 mol) de pyranno[*g*]indole **7***a* dans 25 cm³ d'éther anhydre, on verse, sous courant d'azote et à 0°C, une solution de 1 cm³ de chlorure d'oxalyle dans 5 cm³ d'éther anhydre. On maintient 30 min à 0°C puis porte 15 min à reflux; après refroidissement à 0°C on ajoute rapidement une solution de diméthylamine jusqu'à ce que le milieu réactionnel soit basique. On abandonne 12 h à température ambiante, filtre le précipité apparu et le recristallise dans le méthanol. On isole 1,1 g (70 %) du dérivé oxamoylé **11***a*, pf 290°C; rmn (DMSO-$d_6$, $D_2O$) δ: 11,91 (m, H1), 7,91 (s, H2), 2,88 et 2,98 (s, $N(CH_3)_2$), 7,78 (d, $J_{45}$ = 8,61 Hz, H4), 6,69 (d, $J_{45}$ = 8,61 Hz, H5), 4,15 (m, $(CH_2)_7$), 2,00 (m, $(CH_2)_8$), 2,92 (m, $CH_2)_9$). *Anal.* calc. pour $C_{15}H_{16}O_3N_2$: C 66,20, H 5,87, N 10,28; trouvé: C 65,33, H 6,06, N 10,06.

*Tétrahydro-1,7,8,9 pyranno[2,3-g]indolyl-3* N,N-*diméthylamine* **11**b

On porte à ébullition durant 3 jours un mélange de 0,46 g (0,0057 mol) de formaldéhyde à 37%, 0,65 g (0,0057 mol) de diméthylamine à 40% et 1 g (0,0057 mol) de pyrannoindole **7***a* dans 30 cm³ de méthanol. Après évaporation du solvant, dissolution du produit huileux obtenu dans l'acétate d'éthyle, on traite par l'acide chlorhydrique 5 *N*, lave au chloroforme et rend la phase aqueuse alcaline par ajout de soude à 20%. On extrait alors par l'éther et isole 0,77 g (58%) d'une huile **11***b*; rmn (DMSO-$d_6$, $D_2O$) δ: 11,21 (m, H1), 7,38 (d, $J_{23}$ = 2,38 Hz, H2), 2,71 (s, $N(CH_3)_2$), 4,36 (s, $CH_2N$), 7,43 (d, $J_{45}$ = 8,61 Hz, H4), 6,58 (d, $J_{45}$ = 8,61 Hz, H5), 4,12 (m, $(CH_2)_7$), 2,46 (m, $(CH_2)_8$), 2,82 (m, $(CH_2)_9$). On ajoute 0,8 g (0,0034 mol) d'acide picrique dissous dans 15 cm³ d'éthanol à température ambiante, agite durant 12 h le mélange réactionnel, filtre le précipité formé, le lave à l'éthanol et obtient ainsi 1,4 g (93%) de picrate, pf 160°C. *Anal.* calc. pour $C_{20}H_{21}O_8N_5$: C 52,31, H 4,57, O 27,86, N 15,24; trouvé: C 52,33, H 4,53, O 27,99, N 15,28.

1. F. Troxler. Helv. Chim. Acta, **51**, 1214 (1968).
2. H. Meyer. Acta Chem. Scand. Ser. B, **29**, 133 (1975).
3. M. A. Khan et M. L. de B. Morley. J. Heterocycl. Chem. **16**, 997 (1979).
4. L. Mosti, P. Schenone et Cr. Menozzi. J. Heterocycl. Chem. **16**, 913 (1979)
5. T. Hino, H. Miura, R. Murata et M. Nakagawa. Chem. Pharm. Bull. **26**, 1978 (1978).
6. L. Capuana, T. Tammer et R. Zander. Chem. Ber. **109**, 3497 (1976).
7. (*a*) H. Hemetsberger, D. Knittel et H. Weidmann. Monatsh. Chem. **100**, 1599 (1969); (*b*) H. Hemetsberger, D. Knittel et H. Weidmann. Monatsh. Chem. **101**, 161 (1970); (*c*) H. Hemetsberger et D. Knittel. Monatsh. Chem. **103**, 194 (1972); (*d*) P. Ta Kim, R. Guilard, P. Dodey et R. Sornay. J. Heterocycl. Chem. **18**, 1365 (1981); (*e*) P. Ta Kim, R. Guilard, S. Samreth et R. Sornay. J. Heterocycl. Chem. **18**, 1373 (1981).
8. T. J. Batterham. NMR spectra of simple heterocycles. Wiley Interscience, New York. 1976. (*a*) p. 394; (*b*) p. 385.
9. G. Brancaccio, G. Lettieri et R. Viterbo. J. Heterocycl. Chem. **5**, 745 (1968).
10. P. Maitte. Ann. Chim. **9**, 431 (1954).
11. G. Chatelus. Ann. Chim. **4**, 505 (1949).
12. J. N. Chatterjea. J. Indian Chem. Soc. **36**, 76 (1959).
13. A. Hofmann et F. Troxler. Brevet d'Invention Sandoz S.A., PV no 969 464 no 1394371 (2/04/1964, application suisse: 4/04/1963).
14. P. Ta Kim, P. Cocolios et R. Guilard. Can. J. Chem. **60**, 2099 (1982).

# Synthèse d'oxopyranno[*g*]indoles

PHIEO TA KIM, PANAYOTIS COCOLIOS ET ROGER GUILARD

*Laboratoire de Synthèse et d'Electrosynthèse organométallique associé au C.N.R.S., Faculté des Sciences "Gabriel", 21100 Dijon, France*

Reçu le 2 février 1982

PHIEO TA KIM, PANAYOTIS COCOLIOS et ROGER GUILARD. Can. J. Chem. **60**, 2099 (1982).

La réaction de l'azidoacétate d'éthyle avec les formyl-6 chromannones, suivie par la cyclisaton des azides obtenus conduit aux dihydro-7,8 pyranno[2,3-*g*] 1*H*-indolone-9. Un aspect de la réactivité de ces nouveaux systèmes tricycliques est décrit. La structure des composés isolés au cours des diverses synthèses réalisées est précisée par spectroscopie rmn protonique.

PHIEO TA KIM, PANAYOTIS COCOLIOS, and ROGER GUILARD. Can. J. Chem. **60**, 2099 (1982).

Reaction of ethyl azidoacetate with 6-formyl-4 chromanones, followed by cyclization of the azides obtained leads to 7,8-dihydropyrano[2,3-*g*]indol-9 (1*H*)-one. One aspect of the chemical reactivity of these new tricyclic systems is described. The structure of the compounds isolated from various syntheses is established by proton nmr data.

Si les pyranno[*f* et *g*]indoles (1) apparaissaient aptes à conduire à des composés susceptibles de présenter une activité pharmacologique intéressante, il en était de même des oxopyranno[*f* ou *g*]indoles et nous avons cherché à synthétiser ces composés au départ des chromannones-6 via la réaction de Hemetsberger. La plupart des synthons nécessaires à la réalisation de ce travail étaient inconnus, notre premier objectif a été de les préparer.

## Synthèses

Nous décrivons ici la préparation des synthons indispensables à notre étude; le Schéma 1 ci-dessous rend compte du mode de synthèse utilisé pour accéder aux formyl-6 chromannones. La bromation des phénols orthosubstitués **1** conduit exclusivement aux dérivés trisubstitués **2**; ces composés soumis à l'action de la β-propiolactone en milieu alcalin permettent d'accéder aux acides **3**. La cyclisation de ces acides en chromannones est totale lorsqu'on traite à ébullition la solution benzénique des acides **3** en présence du mélange $P_2O_5$–$H_3PO_4$. Le groupe carbonyle des chromannones **4** est alors bloqué à l'etat de dioxolanne, l'action ultérieure du *n*-butyllithium suivie de celle du diméthylformamide conduit aux aldéhydes dioxolannes **6**. La fonction carbonyle de ces derniers composés est libérée par traitement acide et l'on isole les chromannones formylées en 6, **7**, le rendement de chacune des transformations étant compris entre 80 et 90%.

En présence de méthanol, l'azidoacétate d'éthyle ne se condense pas sur les aldéhydes **7**, il se forme les hémiacétals **8**. Aussi, avons-nous mis en oeuvre les aldéhydes dioxolanes **6**, les trans-

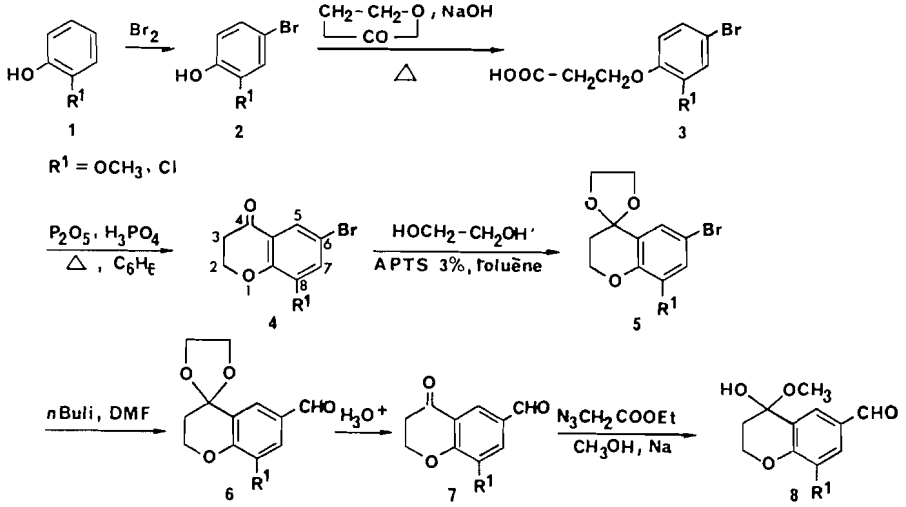


SCHÉMA 1

0008-4042/82/162099-05$01.00/0

©1982 National Research Council of Canada/Conseil national de recherches du Canada

Can. J. Chem. Downloaded from www.nrcresearchpress.com by 210.87.254.40 on 09/06/12
For personal use only.

formations alors effectuées pouvant être ainsi traduites:

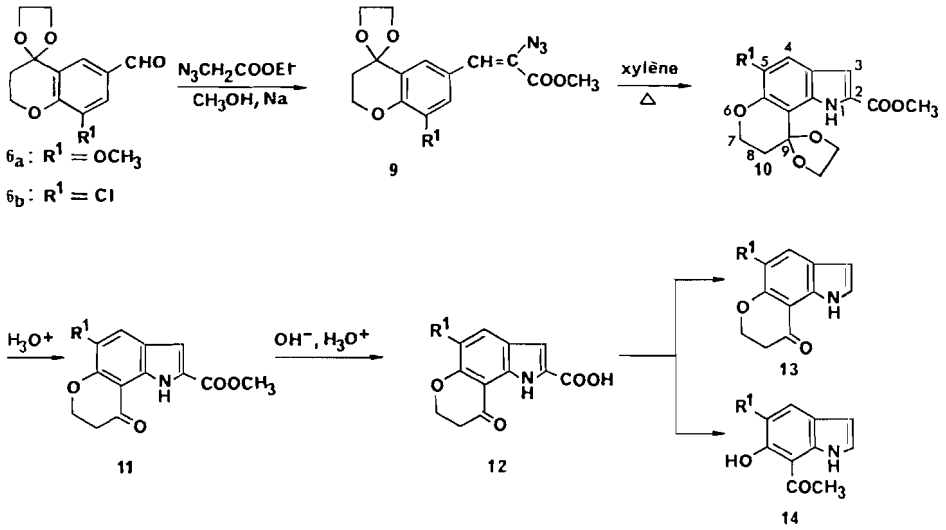

SCHÉMA 2

Les composés **6** se condensent aisément sur l'azidoacétate d'éthyle et les azides obtenus **9** se cyclisent totalement en les composés **10**. Après avoir libéré la fonction carbonyle, l'hydrolyse des esters **11** conduit avec un rendement voisin de 90% aux acides **12**. Lorsque le cycle benzénique porte un groupe méthoxy, la décarboxylation de l'acide **12***a* s'effectue dans de bonnes conditions (60%) et donne naissance à l'oxopyrannoindole attendu **13***a*, mais il se forme également le dérivé indolique trisubstitué en 5, 6, 7, **14***a*; les proportions relatives des produits **13***a* et **14***a* sont respectivement de 92 et 8%. Si le substituant en 5 est un atome de chlore, apparaît exclusivement l'indole trisubstitué **14***b*. Par élévation de température le cycle pyrannique des acides **12** a donc tendance à s'ouvrir et ce résultat est à rapprocher de celui observé lors de l'hydrolyse alcaline des chromones (2) selon:

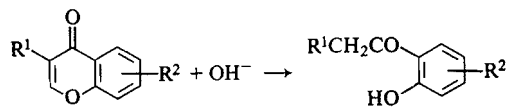

La mise en évidence de la formation d'une cétone benzénique orthohydroxylée après hydrolyse est d'ailleurs considérée comme un test de caractérisation des chromones.

Nous avons examiné un des aspects de la réactivité chimique des oxopyranno[*g*]indoles. Traité selon Vilsmeier, le méthoxy-5 dihydro-7,8 pyranno[2,3-*g*] 1*H*-indolone-9 **13***a* conduit à l'aldéhyde **15***a* selon:

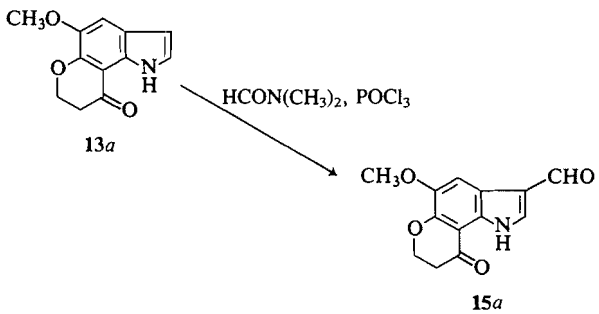

Le groupe formyle se fixe exclusivement sur le sommet β pyrrolique et, comme dans le cas des trihydropyrannoindoles (1), la réactivité du squelette indolique ne semble pratiquement pas affectée par la présence du cycle hydropyrannique orthocondensé au cycle benzénique.

### Établissement des structures

La structure des divers produits préparés a été établie sur la base des données de l'analyse élémentaire et des résultats de rmn protonique. L'ensemble des caractéristiques de rmn observées est regroupé sur le Tableau 1.

Les spectres de rmn des oxopyrannoindoles ont été interprétés sur la base des données de rmn de la chromannone-4 et de ses dérivés de substitution (3–6). Les protons méthyléniques en 2 résonnent vers 4,5 ppm et ceux en 3 vers 2,8 ppm (solvant $CDCl_3$) et l'ensemble donne un système $A_2X_2$. Les signaux des protons benzéniques s'observent à 8,0 ppm pour $H_5$, à 7,6 ppm pour $H_6$ et vers 7,2 pour $H_7$ et $H_8$, le déblindage de $H_5$ étant raisonnablement

Can. J. Chem. Downloaded from www.nrcresearchpress.com by 210.87.254.40 on 09/06/12
For personal use only.

Can. J. Chem. Downloaded from www.nrcresearchpress.com by 210.87.254.40 on 09/06/12
For personal use only.



TABLEAU 1. Caractéristiques rmn des dihydro-7,8 pyranno[2,3-*g*]-1*H*-indolones-9

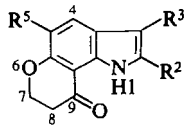


| Composés | $R^2$ | $R^3$ | $R^5$ | Déplacement chimique des protons (ppm)* H1 | $R^2$ | $R^3$ | H4 | $R^5$ | $(CH_2)_7$ | $(CH_2)_8$ | Constantes de couplage (Hz) | |
|---|---|---|---|---|---|---|---|---|---|---|---|---|
| **11***a* | $COOCH_3$ | H | $OCH_3$ | 10,38 (m) | 3,93 (s) | 7,12 (d) | 7,32 (m) | 3,94 (d) | 4,73 (m) | 2,90 (m) | 2,49($J_{13}$)<br>0,29($J_{45}$) | 0,73($J_{14}$) |
| **11***b* | $COOCH_3$ | H | Cl | 10,46 (m) | 3,94 (s) | 7,12 (d) | 7,89 (d) | | 4,74 (m) | 2,92 (m) | 2,34($J_{13}$) | 0,73($J_{14}$) |
| **12***a*† | COOH | H | $OCH_3$ | 10,24 (m) | | 7,08 (d) | 7,53 (s) | 3,83 (s) | 4,66 (m) | 2,88 (m) | 2,38($J_{13}$) | |
| **12***b*† | COOH | H | Cl | 10,96 (m) | | 7,11 (d) | 8,05 (s) | | 3,88 (m) | 3,33 (m) | 2,19($J_{13}$) | |
| **13***a* | H | H | $OCH_3$ | 9,91 (m) | 7,18 (2d) | 6,45 (2d) | 7,38 (m) | 3,94 (d) | 4,69 (m) | 2,88 (m) | 2,34($J_{12}$)<br>0,73($J_{14}$)<br>0,29($J_{45}$) | 2,20($J_{13}$)<br>3,22($J_{23}$) |
| **15***a* | H | CHO | $OCH_3$ | 10,44 (m) | 7,78 (d) | 10,01 (d) | 8,03 (m) | 4,00 (d) | 4,72 (m) | 2,91 (m) | 2,93($J_{12}$)<br>0,29($J_{34}$) | 0,73($J_{14}$)<br>0,29($J_{45}$) |

*s, singulet; d, doublet; m, multiplet.
†Spectres relevés en utilisant le DMSO-$d_6$ comme solvant.

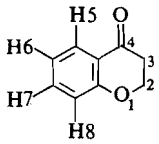


attribuable à l'effet électroaccepteur du carbonyle en *péri*. Les protons pyranniques des produits que nous avons préparés présentent bien ces caractéristiques (voir Tableau 1) et les protons pyrroliques sont couplés entre eux ($J_{23} \simeq 3{,}22$ Hz) et avec $H_1$ ($J_{12} \simeq 2{,}3$ et $J_{13} \simeq 2{,}1$ Hz).

## Partie expérimentale

Les analyses élémentaires ont été effectuées par le Laboratoire Central de Microanalyse du C.N.R.S. Les spectres rmn ont été relevés sur un appareil JEOL FX 100 en utilisant le TMS comme référence interne et, sauf indication contraire, le $CDCl_3$ comme solvant. Le couplage des protons pyrroliques avec l'hydrogène iminique a été supprimé par ajout d'eau lourde. Les points de fusion ont été pris sur banc Kofler.

*Matières premières*

Les produits de départ ont été préparés par les méthodes citées en référence: bromo-4 méthoxy-2 phénol **2***a* (7, 8), $Eb_{16}$ 133°C, pf 36–37°C; bromo-4 chloro-2 phénol **2***b* (8), pf 48–49°C.

*Préparation des synthons*

*Acide (bromo-4 méthoxy-2 phénoxy-1)-3 propionique* **3**a

On porte à ébullition un mélange de 203 g (1 mol) de bromo-4 méthoxy-2 phénol **2***a* et 40 g (1 mol) de soude dans 400 cm³ d'eau. Après 15 min d'ébullition on ajoute lentement 72 g (1 mol) de β-propiolactone et maintient l'ébullition durant 50 min. Après refroidissement on acidifie le mélange réactionnel par 100 cm³ d'acide chlorhydrique concentré, extrait le produit à l'éther et lave la phase organique jusqu'à neutralité. On isole, après évaporation du solvant 216 g (79%) de l'acide **3***a*, pf 98°C. *Anal.* calc. pour $C_{10}H_{11}O_4Br$: C 43,67, H 4,00, O 23,26; trouvé: C 43,54, H 3,94, O 22,67.

*Acide (bromo-4 chloro-2 phénoxy-1)-3 propionique* **3**b

Selon la même méthode 311 g (1,5 mol) de bromo-4 chloro-2 phénol **2***b* et 60 g (1,5 mol) de soude dans 600 cm³ d'eau permettent d'obtenir 126 g (30%) de l'acide **3***b*, pf 125°C. *Anal.* calc. pour $C_9H_8O_3BrCl$: C 38,68, H 2,86, O 17,16; trouvé: C 38,72, H 2,83, O 17,25.

*Bromo-6 méthoxy-8 dihydro-2,3 4H-benzopyranne-1 one-4* **4**a

On ajoute, à 0°C, 34 g (0,35 mol) d'acide phosphorique dans un mélange contenant 475 cm³ de benzène anhydre et 56 g (0,4 mol) d'anhydride phosphorique. Après avoir porté 4 h à ébullition on additionne, lentement, 83 g (0,3 mol) d'acide **3***a*. Le mélange est maintenu à ébullition durant 12 h puis, après refroidissement, versé sur l'eau glacée, traité par l'acide chlorhydrique 5 *N* et extrait à l'éther. Après traitement habituel et recristallisation du solide obtenu dans l'éthanol, on isole 67 g (86%) de la chromannone **4***a*, pf 137°C. *Anal.* calc. pour $C_{10}H_9O_3Br$: C 46,73, H 3,50, O 18,66, Br 31,09; trouvé: C 46,74, H 3,53, O 18,76, Br 31,30.

*Bromo-6 chloro-8 dihydro-2,3 4H-benzopyranne-1 one-4* **4**b

On porte durant 2 h à 70–80°C, un mélange de 279 g (1 mol) de l'acide **3***b* et 127 g (1,3 mol) d'acide sulfurique concentré. Le mélange réactionnel est ensuite versé sur l'eau glacée, extrait à l'éther, lavé avec une solution diluée d'ammoniaque puis à l'eau. On obtient finalement 183 g (70%) de chromannone-4 **4***b*, pf 109°C. *Anal.* calc. pour $C_9H_6O_2BrCl$: C 41,34, H 2,29, O 12,23; trouvé: C 41,32, H 2,41, O 12,14.

*Dioxolanne de la bromo-6 méthoxy-8 dihydro-2,3 4H-benzopyranne-1 one-4* **5**a

Un mélange de 10 g (0,039 mol) de chromannone-4 **4***a*, 24 g (0,39 mol) d'éthylène glycol et 0,3 g (0,0017 mol) d'acide paratoluènesulfonique dans 200 cm³ de toluène anhydre est porté à ébullition durant 7 h dans un appareil Dean et Stark. Le mélange réactionnel est ensuite versé sur l'eau glacée, extrait à l'éther et le solide obtenu est recristallisé dans un mélange alcool éthylique–éther. On obtient 9,6 g (82%) du dioxolanne **5***a*, pf 104°C. *Anal.* calc. pour $C_{12}H_{13}O_4Br$: C 47,88, H 4,31, O 21,25, Br 26,54; trouvé: C 47,87, H 4,53, O 21,39, Br 26,44.

*Dioxolanne de la bromo-6 chloro-8 dihydro-2,3 4H-benzopyranne-1 one-4* **5**b

De même 30 g (0,11 mol) de chromannone-4 **4***b*, 71 g (1,1 mol) d'éthylène glycol et 0,2 g (0,0011 mol) d'acide paratoluènesulfonique dans 200 cm³ de toluène conduisent après recristallisation dans un mélange benzène–éther isopropylique à 34 g (97%) du dioxolanne **5***b*, pf 94°C. *Anal.* calc. pour $C_{11}H_{10}O_3BrCl$: C 43,25, H 3,27, O 15,75; trouvé: C 43,20, H 3,21, O 15,60.

*Dioxolanno-4 méthoxy-8 dihydro-2,3 4H-benzopyranne-1 carbaldéhyde-6* **6**a[1]

À 177 g (0,59 mol) de dioxolanne **5***a* (177 g, 0,59 mol) dissous dans 500 cm³ d'éther anhydre est ajouté lentement à −70°C 0,59 mol de *n*-butyllithium dans 570 cm³ d'éther anhydre. Après addition, on maintient le milieu durant 6 h à −70°C et ajoute goutte à goutte 56 g (0,77 mol) de *N,N*-diméthylformamide dissous dans 300 cm³ d'éther anhydre. Le mélange réactionnel est maintenu durant 12 h à −70°C puis après retour à la température ambiante versé sur l'eau glacée. Après extraction au chloroforme, recristallisation du solide obtenu dans l'éthanol, on isole 133 g (90%) de l'aldéhyde dioxolanne **6***a*, pf 167°C.

*Chloro-8 dioxolanno-4 dihydro-2,3 4H-benzopyranne-1 carbaldéhyde-6* **6**b[1]

En opérant de même à partir de 45 g (0,15 mol) du dioxolanne **5***b*, on obtient après recristallisation dans le benzène 31 g (84%) de l'aldéhyde dioxolanne **6***b*, pf 133°C.

*Méthoxy-8 oxo-4 dihydro-2,3 4H-benzopyranne-1 carbaldéhyde-6* **7**a

À 34 g (0,14 mol) du dioxolanne **6***a* dans 700 cm³ d'alcool éthylique on ajoute, lentement et à température ambiante, 90 cm³ d'acide chlorhydrique concentré. Le mélange est maintenu sous agitation durant 1 h, puis versé sur l'eau glacée et extrait à l'éther. Après recristallisation du solide obtenu dans l'alcool éthylique on obtient 26 g (91%) de l'aldéhyde méthoxylé **7***a*, pf 139°C. *Anal.* calc. pour $C_{11}H_{10}O_4$: C 64,10, H 4,85, O 31,03; trouvé: C 64,48, H 4,91, O 30,06.

*Hémiacétal du méthoxy-8 oxo-4 dihydro-2,3 4H-benzopyranne-1 carbaldéhyde-6* **8**a

À une solution méthanolique de méthylate de sodium (3 g de Na (0,13 at. g.) dans 200 cm³ de méthanol absolu), on ajoute, à 0°C, 8,7 g (0,042 mol) de l'aldehyde **7***a* puis, goutte à goutte, 16 g (0,12 mol) d'azidoacétate d'éthyle dans 30 cm³ de méthanol absolu. Le mélange réactionnel est maintenu durant 6 h à 0°C puis versé sur l'eau froide et acidifié par l'acide chlorhydrique 5 *N*. Après extraction par le chloroforme, chromatographie sur colonne d'acide silicique (éluant: chloroforme) et recristallisation dans un mélange benzène–hexane, on obtient 4,8 g (41%) d'hémiacétal **8***a*, pf 110°C. *Anal.* calc. pour $C_{12}H_{14}O_5$: C 60,53, H 5,88, O 33,58; trouvé: C 60,47, H 6,13, O 33,37.

[1]Les dérivés **6***a* et **6***b* ont pu être isolés à l'état de pureté analytique (points de fusion, rmn ...); cependant par suite de leur instabilité due à l'hydrolyse de la fonction dioxolanne, les résultats des analyses élémentaires ne sont pas corrects.

Can. J. Chem. Downloaded from www.nrcresearchpress.com by 210.87.254.40 on 09/06/12
For personal use only.

Can. J. Chem. Downloaded from www.nrcresearchpress.com by 210.87.254.40 on 09/06/12
For personal use only.

*Méthoxy-5 oxo-9 dihydro-7,8 pyranno[2,3-g]indolecarboxylate-2 de méthyle* ***11****a*

À 0,7 g (0,03 at. g.) de Na dans 30 cm³ de méthanol absolu on ajoute 3 g (0,012 mol) d'aldéhyde dioxolanne **6***a* et 3,7 g (0,029 mol) d'azidoacétate d'éthyle dans 10 cm³ de méthanol absolu. On maintient 7 jours à 0°C et extrait à l'éther. L'azide obtenu **9***a* est ensuite dissous dans 70 cm³ de xylène portés à ébullition durant 3 h et le produit cyclisé ainsi obtenu **10***a* est traité après dissolution dans 50 cm³ d'éthanol par 5 cm³ d'acide chlorhydrique concentré. On abandonne durant 18 h et isole après recristallisation dans le benzène 0,52 g (16%) de l'ester **11***a*, pf 188°C. *Anal.* calc. pour $C_{14}H_{13}O_5N$: C 61,12, H 4,72, O 29,06, N 5,08; trouvé: C 60,87, H 4,63, O 29,29, N 5,10.

*Chloro-5 oxo-9 dihydro-7,8 pyranno[2,3-g]indolecarboxylate-2 de méthyle* ***11****b*

À partir de 26 g de l'aldéhyde dioxolanne **6***b* et selon le protocole expérimental décrit pour la préparation du produit précédent, on obtient après cyclisation de l'azide **9***b* (temps de reflux 8 h) et hydrolyse du dioxolanne ester **10***b* 15 g (54%) de l'ester **11***b*, pf 194°C (recristallisation dans le benzène). *Anal.* calc. pour $C_{13}H_{10}O_4NCl$: C 55,85, H 3,57, O 22,88, N 5,00, Cl 12,68; trouvé: C 55,92, H 3,76, O 22,86, N 5,04, Cl 12,84.

*Acide méthoxy-5 oxo-9 dihydro-7,8 pyranno[2,3-g]indolecarboxylique-2* ***12****a*

En utilisant une méthode de saponification classique à partir de 34 g (0,12 mol) d'ester **11***a* et 14 g (0,25 mol) de potasse dans 700 cm³ d'eau, on isole 30 g (93%) d'acide **12***a*, pf 312°C. *Anal.* calc. pour $C_{13}H_{11}O_5N$: C 59,80, H 4,21, O 30,62, N 5,36; trouvé: C 58,93, H 4,29, O 30,87, N 5,31.

*Acide chloro-5 oxo-9 dihydro-7,8 pyranno[2,3-g]indolecarboxylique-2* ***12****b*

De même 26 g (0,093 mol) d'ester **11***b* permettent l'obtention de 27 g (90%) d'acide **12***b*, pf 227–230°C. *Anal.* calc. pour $C_{12}H_8O_4NCl$: C 54,27, H 3,01, O 24,08, N 5,27; trouvé: C 54,24, H 3,67, O 24,75, N 4,95.

*Méthoxy-5 dihydro-7,8 pyranno[2,3-g] 1H-indolone-9* ***13****a et acétyl-7 hydroxy-6 méthoxy-5 indole* ***14****a*

À partir de 31 g (0,12 mol) d'acide **12***a* et 0,77 g de chromite de cuivre dans 500 cm³ de quinoléine, on isole après 13 h de réaction, chromatographie sur acide silicique (éluant: chloroforme) et recristallisation dans le benzène, 14 g (54%) de pyrannoindole **13***a*, pf 123°C. *Anal.* calc. pour $C_{12}H_{11}O_3N$: C 66,38, H 5,06, O 22,09, N 6,44; trouvé: C 66,39, H 5,08, O 22,27, N 6,32.

On obtient conjointement, après recristallisation dans un mélange benzène–hexane, 1,1 g (4,3%) de dérivé indolique **14***a*, pf 130°C; rmn (DMSO-$d_6$, $D_2O$) δ: 10,02 (m, $J_{12}$ = 2,38, $J_{13}$ = 2,19 et $J_{15}$ = 0,73 Hz, H1), 7,11 (2d, $J_{12}$ = 2,38 et $J_{23}$ = 3,22 Hz, H2), 6,33 (2d, $J_{23}$ = 3,22 et $J_{13}$ = 2,19 Hz, H3), 7,40 (d, $J_{15}$ = 0,73 Hz, H5), 10,88 (m, OH), 3,84 (s, $OCH_3$), 2,69 (s, $COCH_3$). *Anal.* calc. pour $C_{11}H_{11}O_3N$: C 64,41, H 5,36, O 23,39, N 6,82; trouvé: C 64,45, H 5,42, O 23,50, N 6,73.

*Acétyl-7 chloro-5 hydroxy-6 indole* ***14****b*

La décarboxylation de 2,7 g (0,01 mol) de l'acide **12***b* conduit, après chromatographie sur acide silicique (éluant: hexane–chloroforme 1:2) puis recristallisation dans un mélange benzène–hexane–éther isopropylique à 0,11 g (5%) du dérivé indolique **14***b*, pf 150°C; rmn (DMSO-$d_6$, $D_2O$) δ: 11,04 (m, $J_{12}$ = 2,38, $J_{13}$ = 2,19 et $J_{15}$ = 0,73 Hz, H1), 7,26 (2d, $J_{12}$ = 2,38 et $J_{23}$ = 3,22 Hz, H2), 6,45 (2d, $J_{13}$ = 2,19 et $J_{23}$ = 3,22 Hz, H3), 7,92 (d, $J_{15}$ = 0,73 Hz, H5), 11,86 (m, OH), 2,78 (s, $COCH_3$). *Anal.* calc. pour $C_{10}H_8O_2NCl$: C 57,31, H 3,81, O 15,26, N 6,68, Cl 16,91; trouvé: C 57,71, H 4,16, O 15,16, N 6,68, Cl 16,91.

*Méthoxy-5 oxo-9 dihydro-7,8 pyranno[2,3-g]indolecarbaldèhyde-3* ***15****a*

Selon les modalités opératoires de la réaction de Vilsmeier et au départ de 0,4 g (0,0018 mol) du produit **13***a* on obtient, après chromatographie sur acide silicique (éluant chloroforme–acétone 3:1) puis recristallisation dans un mélange éthanol–benzène–hexane 0,19 g (42%) d'aldéhyde **15***a*, pf 236°C. *Anal.* calc. pour $C_{13}H_{11}O_4N$: C 63,70, H 4,48, O 26,09, N 5,71; trouvé: C 63,42, H 4,61, O 25,81, N 5,70.

## Remerciements

L'un d'entre nous, Phieo Ta Kim, remercie les laboratoires Fournier, 42, rue de Longvic, 21300 Chenôve, France, pour leur soutien financier.

1. P. Ta Kim, R. Guilard et P. Renaut. Can. J. Chem. **60**, 2093 (1982).
2. W. Baker. J. Chem. Soc. **127**, 2349 (1925).
3. T. J. Batterham. NMR spectra of simple heterocycles. Wiley Interscience. New York. 1976. p. 385.
4. A. R. Katritzky et B. Ternai. J. Heterocycl. Chem. **5**, 745 (1968).
5. G. Grandolini, A. Ricci, N. P. Buuhoï et F. Perin. J. Heterocycl. Chem. **5**, 133 (1968).
6. G. P. Ellis. Chromanes, chromanones and chromones. John Wiley and Sons, New York. 1977. p. 215.
7. R. H. Rosenwald. J. Am. Chem. Soc. **74**, 4602 (1952).
8. L. C. Raiford et G. R. Miller. J. Am. Chem. Soc. **55**, 2125 (1933).

# Apparent octanol/water partition coefficients of pentachlorophenol as a function of pH

KLAUS L. E. KAISER AND ILZE VALDMANIS

*Environmental Contaminants Division, National Water Research Institute, Burlington, Ont., Canada L7R 4A6*

Received October 6, 1981

KLAUS L. E. KAISER and ILZE VALDMANIS. Can. J. Chem. **60**, 2104 (1982).

The apparent 1-octanol/water partition coefficient (log $P_{App}$) of pentachlorophenol (PCP) varies in non-linear function with pH of the aqueous solution. In the range of pH 1.2 to 13.5 extreme values of log $P_{App}$ 4.84 at pH 1.2 and log $P_{App}$ 1.3 at pH 10.5 were observed. In the alkaline regime, log $P_{App}$ increases strongly with the ionic strength. The ion-corrected partition coefficient of PCP was found to be log $P$ 5.05 in good agreement with literature values.

KLAUS L. E. KAISER et ILZE VALDMANIS. Can. J. Chem. **60**, 2104 (1982).

Le coefficient de partage apparent entre octanol-1/eau, log $P_{app}$, du pentachlorophénol (PCP) varie d'une façon non-linéaire avec le pH de la solution aqueuse. Dans l'intervalle de pH de 1,2 à 13,5, les valeurs extrêmes sont log $P_{app}$ = 4,84 à un pH de 1,2 et de log $P_{app}$ = 1,3 à un pH de 10,5. En régime alcalin, le log $P_{app}$ augmente fortement avec la force ionique. Pour le PCP, on a trouvé que le coefficient de partage corrigé pour les ions est le log $P$ 5,05 qui est en bon accord avec les valeurs publiées dans le littérature.

[Traduit par le journal]

Can. J. Chem. Downloaded from www.nrcresearchpress.com by 210.87.254.6 on 09/06/12
For personal use only.

Partition coefficients (log $P$) of organic solutes in the 1-octanol/water system are very useful physicochemical parameters for the correlation and prediction of the solutes' biological activities (1). The fungicidal properties of pentachlorophenol (PCP) and its resistance to degradation make it an important wood preservative (2). Consequently, it is frequently found to be present in industrial waste water effluents and has been observed as contaminant of water, sediment, and biota of many lakes and rivers (2, 3).

The rates of biological magnification of contaminants correlate with their effective partition coefficients (4). For ionizing compounds, such as PCP, the effective or apparent partition coefficient (log $P_{App}$)[1] is pH dependent. Therefore, it is of interest to determine log $P_{App}$ for the wide range of pH as found in the waste effluents and receiving waters. This paper reports on such measurements for PCP in 1-octanol/water over a range of pH 1.2 to 13.5.

## Experimental

*Materials*

Pentachlorophenol (Aldrich, Gold Label, lot #081587 KC) was twice recrystallized from ethanol/water. 1-Octanol (MCB, Reagent Grade) was fractionated over a 0.6 m glass column; the distillate of bp 194 to 195°C was collected and found free of impurities by gas chromatography – flame ionization detector. Double distilled water was passed through a mixed bed of Amberlite XAD-4 and XAD-8 resins to remove trace organic impurities. Purity was checked by extraction with hexane and gas chromatography on a 3% Dexsil-300 column at 175°C with an electron capture detector. Other solvents were of pesticide grade, acetic anhydride (ANALAR, double distilled), sulfuric acid (ARISTAR).

*Standards and procedure*

Octanol-saturated water and water-saturated octanol were prepared by stirring mixtures of 200 mL octanol with 10 mL water and of 200 mL water with 2 mL octanol, respectively, for 1 h at high speed, centrifugating each mixture for 1.5 h at 2300 rpm and removing the excess octanol, respectively water, with a Pasteur pipette.

A 250 mL stock solution of pentachlorophenol (PCP) in water-saturated octanol was prepared with a PCP concentration of 1.0 mg/mL. This stock solution was diluted with water-saturated 1-octanol to give stock solutions of 0.100 mg/mL PCP (*A*) and 0.010 mg/mL PCP (*B*) in octanol. As standards for the recovery tests, 10 mL volumes of 20.0 mg/mL PCP (*C*) and 0.2 mg/mL PCP (*D*) were also prepared.

The pH of 2 L of octanol-saturated water was determined with a pH meter and adjusted to the desired value with $H_2SO_4$ or NaOH solution. To each four of eight 200 mL aliquots in 250 mL centrifuge flasks, 2.0 mL stock solution *A*, or 10.0 mL stock solution *B* were added. The flasks were covered with acetone-washed aluminum foil, stirred at high speed for 1 h, centrifugated at 2300 rpm for 1.5 h, and allowed to stand for 12 h. After removal of octanol layers with glass pipettes, the aqueous phases were transferred to 250 mL Erlenmeyer flasks and approximately 1.0 g solid NaOH added to each. After dissolution, 1.5 mL acetic anhydride and 5.0 mL toluene were added to each. The flasks were covered with aluminum foil, sealed with screw top caps, stirred gently for 1 h, then at high speed for 0.2 h. The toluene layers were separated with glass pipettes and analyzed directly.

*Analysis*

The toluene phases were analyzed for PCP-acetate by gas chromatography of 1.0 μL volumes, in some cases after dilution with toluene, using a Tracor Microtek 220 with a 1.8 m × 3.1 mm (i.d.) glass column packed with 3% Dexsil-300 on Gas Chrom O and $^{63}Ni$ electron capture detector. The operating conditions were: carrier gas, prepurified $N_2$ at 66 mL/min flow; detector purge gas, 5% $CH_4$ in Ar at 10 mL/min flow; temperatures: injector, 240°C; column, 175°C isothermal; detector, 295°C. The

[1]Normally, the partition coefficients (log $P$), also for ionizing compounds are determined for the non-ionized solute species only. The apparent partition coefficients (log $P_{App}$), as reported here, represent the distribution of the sums of both ionized and non-ionized solute molecules between the two phases of the test system.

0008-4042/82/162104-03$01.00/0

©1982 National Research Council of Canada/Conseil national de recherches du Canada

Can. J. Chem. Downloaded from www.nrcresearchpress.com by 210.87.254.6 on 09/06/12
For personal use only.

chromatograms were recorded with both a Hewlett-Packard strip chart recorder and a Spectra-Physics SP-4000 data system.

In separate tests, the recovery of PCP as PCP-acetate was determined for several PCP concentrations in the aqueous phase. The recovery was found to be 35.5% with a standard deviation of 1.9%. All test data were corrected for this recovery rate and the concentrations of PCP in the octanol phases were determined by difference. As the determination of $P_{App}$ at each pH value, each octanol/water ratio, and each PCP concentration was made in duplicate, the mean of those data pairs were calculated for each test condition. The means and standard deviations reported in Table 1 are those of the four duplicate means at each pH level. The mean of the relative standard deviations of all 136 tests was found to be 10.7%.

## Results and discussion

The apparent octanol/water partition coefficients of PCP were determined at 16 selected pH values between pH 1.2 and 13.5. At each pH value, the four concentrations of 0.02, 0.1, 0.2, and 1.0 mg PCP per test system of 200 mL water and 2 or 10 mL octanol were tested in duplicate. In general, the duplicate measurements were within 5% of each other. Over the entire pH range, the apparent partition coefficient varies by more than three orders of magnitude between log $P_{App}$ 4.84 and 1.30. The means of the duplicate determinations for each pH value and test system are given in Table 1. Except possibly in the range of pH 1.2 to 4.7, no significant differences are found between the test systems with the lower (*A*, *B*) and those with the higher (*C*, *D*) PCP concentrations. This indicates

TABLE 1. Apparent octanol/water partition coefficient (log $P_{App}$) of pentachlorophenol as function of pH, PCP, and octanol concentrations

| | Test system[a] | | | | | |
|---|---|---|---|---|---|---|
| pH | *A* | *B* | *C* | *D* | Mean | s.d. |
| 1.2 | 4.74 | 4.81 | 4.83 | 4.99 | 4.84 | 0.11 |
| 2.4 | 4.68 | 4.64 | 4.77 | 4.79 | 4.72 | 0.07 |
| 3.4 | 4.56 | 4.52 | 4.76 | 4.64 | 4.62 | 0.11 |
| 4.7 | 4.51 | 4.26 | 4.90 | 4.62 | 4.57 | 0.27 |
| 5.9 | 3.82 | 3.68 | 3.68 | 3.78 | 3.72 | 0.07 |
| 6.5 | 3.55 | 3.38 | 3.57 | 3.74 | 3.56 | 0.15 |
| 7.2 | 3.34 | 3.36 | 3.23 | 3.36 | 3.32 | 0.06 |
| 7.8 | 3.27 | 3.11 | 3.17 | 3.23 | 3.20 | 0.07 |
| 8.4 | 3.03 | 3.11 | 3.04 | 3.23 | 3.10 | 0.09 |
| 8.9 | 2.74 | 2.81 | 2.71 | 2.74 | 2.75 | 0.04 |
| 9.3 | 1.66 | 1.19 | 1.58 | 1.37 | 1.45 | 0.21 |
| 9.8 | 1.34 | 1.07 | 1.70 | 1.33 | 1.36 | 0.26 |
| 10.5 | 1.43 | 1.31 | 1.40 | 1.07 | 1.30 | 0.16 |
| 10.5[b] | 2.57 | 2.48 | 2.36 | 2.25 | 2.42 | 0.14 |
| 11.5 | 1.38 | 1.02 | 1.57 | 1.21 | 1.30 | 0.24 |
| 12.5 | 1.74 | 1.64 | 1.71 | 1.57 | 1.67 | 0.08 |
| 13.5 | 3.88 | 3.64 | 4.00 | 3.91 | 3.86 | 0.15 |

[a]Composition of the test systems in mg PCP, mL octanol ($H_2O$ presaturated), mL $H_2O$ (*n*-octanol presaturated): *A*, 0.02, 2, 200; *B*, 0.1, 10, 200; *C*, 0.2, 2, 200; *D*, 1.0, 10, 200.
[b]Determination at elevated ionic strength of $\mu = 1.0$.

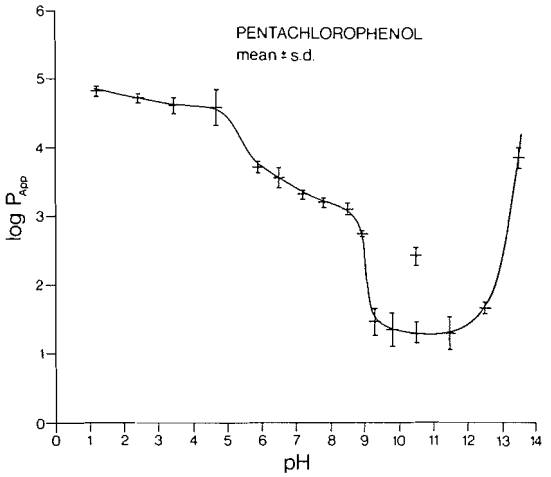


FIG. 1. Apparent octanol/water partition coefficient of pentachlorophenol vs. pH of the aqueous phase. Means and standard deviations of eight determinations in four test systems at each pH value given. The single, high value at pH 10.5 observed at high ionic strength ($\mu = 1.0$).

the absence of any appreciable association of the solute molecules in the organic phase as generally known to occur at higher concentrations. Therefore, the results for the four test systems were combined to the means ± s.d. at each of the pH values and are also given in Table 1.

As is to be expected, the apparent partition coefficient of PCP varies strongly with the pH of its aqueous solution. Figure 1 shows the means and standard deviations of log *P* vs. pH, using the data of Table 1. In the range of pH 1 to 5, the apparent partition coefficient declines slightly from log $P_{App}$ 4.84 to ≈4.5. At increasing values above pH 5, the apparent partition coefficient of PCP is declining more steeply, presumably this is caused by the ionization of this weak acid ($pK_a$ 4.8). At pH ≈9, another strong decrease of log $P_{App}$ is found for a relatively small increase in the pH. The cause of this drop, approximately 1.5 log *P* units, is not clear at this time. According to the general relation between ionization, $pK_a$ and pH (5), at pH 9, PCP is ionized in excess of 99.99% compared with 99.94% of pH 8. This minor change in ionization cannot account for the observed change in log $P_{App}$. Hypotheses which may explain the phenomenon include a change in the specific PCP–octanol solvation complex (6) or the formation of PCP–sodium complexes. The apparent partition coefficient of PCP reaches a minimum of log $P_{App}$ ≈ 1.3 at approximately pH 10.5. Further increase of pH results in a steeply increasing coefficient. At the highest pH investigated, pH 13.5, the partition

coefficient rose to log $P_{App}$ 3.9. This strong rise appears to result from the increase in ionic strength of the aqueous solution with pH. This interpretation is supported by a separate determination of the partition coefficient at pH 10.5 at the higher ionic strength of $\mu$ 1.0 which results in log $P_{App} \approx 2.4$ compared to log $P_{App}$ 1.3 at $\mu \approx 0.01$.

In literature, several values are reported for the ion-corrected partition coefficient of PCP. Values for the 1-octanol/water system are log $P$ 5.01 and log $P$ 5.12 (1), log $P$ 5.86 (7), and log $P$ 3.81 (4). We observed the highest log $P_{App}$ values in the range of pH 3.4 to 1.2. In this pH range, results of the test system $D$ (Table 1) are likely to be more accurate than those of $A$ to $C$ due to the analytical constraints as the PCP concentration in the aqueous phase approached $10^{-10}$ $M$ (0.2 $\mu$g $L^{-1}$). As it has been suggested to measure log $P$ at least 4 pH units away from the p$K$ values (1), it may be reasonable to calculate the partition coefficient for the non-ionized PCP for pH 0.8 from the data for the test system $D$ at the three lowest pH values measured (Table 1). This extrapolation results in log $P$ 5.05 which appears in good agreement with the data presently considered to be most reliable (1).

Our results demonstrate the strong dependence of the apparent partition coefficient of PCP on the pH and, in basic medium, on the ionic strength. As pH and ionic strengths of effluents containing PCP as well as those of the receiving waters vary widely, the environmental effects and pathways of ionizing compounds such as PCP may vary accordingly. In particular, it would appear that the bioconcentration factors, which generally correlate well with the partition coefficients (4, 8), could vary between different aquatic systems by several orders of magnitude. Specifically, the observed variation of log $P_{App}$ of PCP will affect fugacity calculations (9) and may also explain the disagreement between the experimental bioconcentration factor and that calculated from the partition coefficient of the un-ionized PCP moiety (8, 10).

1. C. HANSCH and A. J. LEO. Substituent constants for correlation analysis in chemistry and biology. John Wiley and Sons, New York, 1979 and references therein.
2. P. A. JONES. Chlorophenols and their impurities in the Canadian Environment. Environment Canada, Economic and Technical Review Report EPS 3-EC-81-2. 1981.
3. D. KONASEWICH, W. TRAVERSY, and H. ZAR. Great Lakes Water Quality. Status Report on organic and heavy metal contaminants in the Lakes Erie, Michigan, Huron and Superior basins to the Implementation Committee of the Great Lakes Water Quality Board. International Joint Commission. Windsor (1978).
4. P.-Y LU and R. L. METCALFE. Environ. Health Persp. **10**, 269 (1975).
5. R. F. REKKER. The hydrophobic fragmental constant. Elsevier Scientific Publ. Co., Amsterdam. 1977.
6. Y. I. KORENMAN. Russ. J. Phys. Chem. **46**, 42 (1972).
7. L. S. YAGUZHINSKII, E. G. SMIRNOVA, L. RATNIKOVA, G. M. KOLESOVA, and I. P. KRASINSKAYA. J. Bioenerg. **5**, 163 (1973).
8. D. MACKAY. Environ. Sci. Technol. **16**, 274 (1982).
9. D. MACKAY and S. PATERSON. Environ. Sci Technol. **15**, 1006 (1981).
10. G. D. VEITH, D. L. DEFOE, and B. V. BERGSTEDT. J. Fish. Res. Board Can. **36**, 1040 (1979).

Can. J. Chem. Downloaded from www.nrcresearchpress.com by 210.87.254.6 on 09/06/12
For personal use only.

# Fragmentations des cétones aliphatiques métastables. II.[1] Compétition entre éliminations de radicaux hydrocarbonés et d'alcanes.

GUY BOUCHOUX ET YANNIK HOPPILLIARD

*Laboratoire de Synthèse Organique, École Polytechnique, 91128, Palaiseau Cedex, France.*

Reçu le 18 décembre 1981

GUY BOUCHOUX et YANNIK HOPPILLIARD. Can. J. Chem. **60**, 2107 (1982).

Les fragmentations des ions moléculaires métastables de six cétones aliphatiques sont étudiées. Les ions $[M - R^{\bullet}]$ et [M–RH] ($R^{\bullet}$ étant une chaîne latérale à la fonction carbonyle) sont formés par des mécanismes pour lesquels l'énergie d'activation de la réaction retour ($\Delta H_R^0$) est nulle. Seuls les ions moléculaires de la méthyléthylcétone et de la méthylisopropylcétone n'évoluent pas conformément aux prédictions thermodynamiques: les ions fragments détectés $[M–CH_3^{\bullet}]$ ne correspondent pas à l'état final le plus stable. Ce résultat est expliqué ici en terme de durée de vie de l'ion moléculaire.

GUY BOUCHOUX and YANNIK HOPPILLIARD. Can. J. Chem. **60**, 2107 (1982).

The fragmentation of the metastable molecular ions of six aliphatic ketones is studied. The ion fragment abundances $[M - R^{\bullet}]$ and [M–RH] ($R^{\bullet}$ being a lateral radical) can be predicted from the thermochemical stability of the corresponding final states. Exceptions to this behavior are found for metastable molecular ions of methylethylketone and methylisopropylketone where it is demonstrated that the lifetime of these ions is too short to permit significant decompositions via the low energy channel after $10^{-5}$ s.

Can. J. Chem. Downloaded from www.nrcresearchpress.com by 210.87.254.6 on 09/06/12
For personal use only.

Les fragmentations des cétones aliphatiques métastables peuvent conduire aussi bien à des ions à nombre pair d'électrons $[M - R^{\bullet}]$ qu'aux ions radicaux $[M - C_nH_{2n}]^{\bullet+}$ et $[M - C_nH_{2n+2}]^{\bullet+}$. Le radical hydrocarboné $R^{\bullet}$ éliminé n'est pas nécessairement une des chaînes adjacentes à la fonction carbonyle. Ainsi la pentanone-2 (1), l'hexanone-2 (2, 3) et les méthyl cétones isomères (3) éliminent un radical méthyle dont l'origine n'est pas exclusivement la position 1.

Les ions $[M - C_nH_{2n}]^{\bullet+}$ sont généralement issus d'un réarrangement de McLafferty, tandis que l'alcane éliminé pour conduire à l'ion $[M - C_nH_{2n+2}]^{\bullet+}$ contient une des chaînes latérales complétée par un atome d'hydrogène.

Les résultats présentés ici concernent six cétones (**1–6**, schéma 1) qui possèdent la particularité d'être inaptes à engendrer des ions $[M - C_nH_{2n}]^{\bullet+}$.

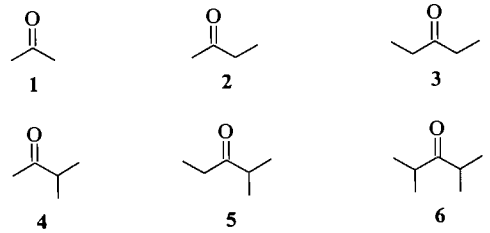


SCHÉMA 1

En effet, seules les réactions d'élimination des chaînes latérales sont observées sur les spectres des ions **1–6** métastables (Tableau 1). Elles se produisent, soit par simple rupture d'une liaison carbone–carbone ($M^{\bullet+} \rightarrow [M - R^{\bullet}]^+$), soit simultanément au transfert d'un atome d'hydrogène ($M^{\bullet+} \rightarrow [M - RH]^{\bullet+}$); cette dernière réaction étant généralement plus facile que l'élimination du radical R correspondant.

Les caractéristiques énergétiques de ces deux réactions compétitives sont présentées dans les deux premiers paragraphes de cette étude. Il est ainsi établi que les ions **1–6** métastables produisent les fragments possédant la meilleure stabilité thermodynamique. Deux ions moléculaires (**2** et **4**) semblent néanmoins faire exception à cette règle, l'examen de leur situation sera complété par une étude particulière.

## *I. Fragmentation $M^{\bullet+} \rightarrow [M - R^{\bullet}]^+$*

De nombreux résultats expérimentaux (4–6) démontrent que l'état de transition de la fragmentation $M^{\bullet+} \rightarrow [M - R^{\bullet}]^+$ possède une enthalpie de formation voisine de celle de l'état final $[M - R]^+ + R^{\bullet}$. Ces résultats sont en faveur d'une élimination du radical $R^{\bullet}$ des cétones ionisées **1–4** par simple rupture d'une liaison carbone–carbone.

Le premier type d'argument est apporté par la valeur de l'énergie cinétique $T$ de séparation des fragments. Pour l'acétone **1** la distribution expérimentale de $T$ est reproduite par un calcul statistique dans lequel il est implicitement admis que le $\Delta H_f^0$ de l'état de transition est égal à celui de l'état final $[CH_3CO]^+ + CH_3^{\bullet}$ (4, 5).

La valeur de $T$ n'a donc pour origine que l'excès d'énergie vibrationnelle de l'ion métastable, au-dessus de l'état de transition. La largeur à

[1] Première partie (I), référence 1.

0008-4042/82/162107-06$01.00/0

©1982 National Research Council of Canada/Conseil national de recherches du Canada

Can. J. Chem. Downloaded from www.nrcresearchpress.com by 210.87.254.6 on 09/06/12
For personal use only.

TABLEAU 1. Spectres de masse des ions $[R^1COR^2]^{\bullet+}$ métastables[a], intensités de pics (%) et énergie cinétique $T_{0,5}$[b] (meV)

| Composé | $R^1$ | $R^2$ | $[M-R^1]^+$ | $T$ | $[M-R^1H]^{\bullet+}$ | $T$ | $[M-R^2]^+$ | $T$ | $[M-R^2H]$ | $T$ |
|---|---|---|---|---|---|---|---|---|---|---|
| **1** | $CH_3$ | $CH_3$ | < 10 | | 100 | 3 | | | | |
| **2** | $CH_3$ | $C_2H_5$ | 100 | 13[d] | < 1 | | 70 | 32[d] | — | — |
| **3** | $C_2H_5$ | $C_2H_5$ | < 9 | 29[e] | 100 | 14 | | | | |
| **4**[c] | $CH_3$ | i-$C_3H_7$ | 100 | 23 | < 2 | | < 1 | | — | — |
| **5** | $C_2H_5$ | i-$C_3H_7$ | — | | 100 | 15 | — | | 15 | 9 |
| **6** | i-$C_3H_7$ | i-$C_3H_7$ | — | | 100 | 12 | | | | |

[a] Technique MIKE, spectrométrie VG.ZAB.2F.
[b] L'erreur relative sur les valeurs de $T_{0,5}$ est de l'ordre de 5%.
[c] Un ion $m/z$ 58 est également détecté (≈ 20%), son origine est attribuée à une fragmentation de McLafferty après isomérisation de **4** en pentanone-2 (réf. 1). Notons que le réarrangement de la chaîne isopropyle en *n*-propyle ne peut pas être suspecté pour **5** et **6** puisqu'aucune élimination de 28 unités de masse n'est observée à partir de ces cétones.
[d] Référence 7.
[e] Référence 8.

mihauteur $T_{0,5}$ de la fonction de distribution de $T$, est une valeur de comparaison commode. Dans le cas de l'acétone $T_{0,5} \leq 15$ meV (5), des valeurs de $T_{0,5}$ similaires sont associées aux éliminations des radicaux $CH_3$, $C_2H_5$ et même $iC_3H_7$ des cétones **2**, **3** et **4** (Tableau 1).

Le second élément en faveur de la formation directe des ions acylium $[RCO]^+$ est leur grande stabilité. Les valeurs expérimentales des $\Delta H_f^0$ montrent que les ions $[CH_3CO]^+$ et $[C_2H_5CO]^+$ sont plus stables que leurs isomères (9, 10), leur apparition est donc privilégiée. En ce qui concerne les ions $[C_4H_7O]^+$, le $\Delta H_f^0$(exp) de $[(CH_3)_2CHCO]^+$ (556 kJ mol$^{-1}$) est peu éloigné de celui de $[CH_2CHC(OH)CH_3]^+$ (569 kJ mol$^{-1}$, réf. 11).

L'élimination d'un $CH_3^{\bullet}$ à partir du groupement isopropyle de l'ion **4** est exclue, un calcul MINDO/3 situe l'ion$[CH_3CHCOCH_3]^+$ 201 kJ mol$^{-1}$ au-dessus de l'ion $[(CH_3)_2CHCO]^+$.

Le troisième apport expérimentale est la détermination des énergies d'apparition des ions $[RCO]^+$. La récente investigation de Maccol (6) démontre clairement que les méthylcétones ionisées, de faible énergie interne, produisent directement les ions acylium.

Notons enfin la caractérisation de la structure $[CH_3CO]^+$ par son spectre de décomposition induite par collision (12). Il est ainsi démontré que l'ion fragment $C_2H_3O$ est le même qu'il soit issu de **1** ou de **2**.

Cet ensemble de résultats démontre donc que les cétones **1**–**4** conduisent par un mécanisme simple à l'état final $[M-R^{\bullet}]^+ + R^{\bullet}$.

Aucune élimination de radical n'est observée sur le spectre des composés **5** et **6**. La fragmentation correspondante est éclipsée par la réaction $M^{\bullet+} \rightarrow [M-RH]^{\bullet+}$.

*II. Fragmentation* $M^{\bullet+} \rightarrow [M-RH]^{\bullet+}$

La substitution isotopique des hydrogènes occupant les positions α (schéma 2) met en

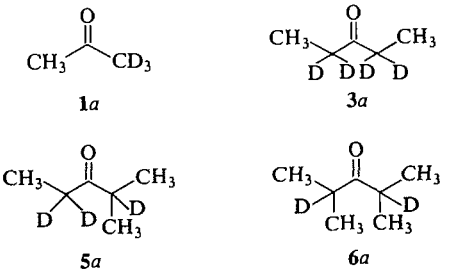


SCHÉMA 2

évidence la grande spécificité de cette réaction ainsi que l'absence à peu près complète d'échanges d'hydrogène avant la fragmentation. Lifshitz et Tzidony (6) observant des éliminations de $CH_3$, $CH_3D$, $CD_3$ et $CD_3H$ à partir de **1***a* dans les proportions 16:1, 1:5:77. Un effet isotopique notable est donc associé à l'élimination de méthane mais aussi à celle du radical méthyle. Une étude de Cooks *et al.* (13) mentionne que **3***a* élimine $CD_3CH_3$ avec une spécificité de l'ordre de 95%. Enfin le Tableau 2 rassemble les résultats obtenus ici pour les composés **5***a* et **6***a*. Il s'avère là encore que seuls les hydrogènes des positions α sont impliqués dans le mécanisme de fragmentation, les échanges d'hydrogène entre les positions α et β sont inférieurs à 1% dans le cas de **5** et à 6% pour **6**.

TABLEAU 2. Spectres de masse des cétones deutériées **5***a* et **6***a* métastables[a]

| Composé | $m/z$ | Intensité (%) |
|---|---|---|
| **5***a* | 72 | 3 |
| $CH_3CD_2COCD(CH_3)_2$ | 71 | 1 |
| $m/z$ 103 | 70 | 20 |
| | 59 | 1 |
| | 58 | 1 |
| | 57 | 100 |
| **6***a* | 72 | 2 |
| $(CH_3)_2CDCOCD(CH_3)_2$ | 71 | 6 |
| $m/z$ 116 | 70 | 100 |

[a] Technique MIKE (VG.ZAB.2F).

Can. J. Chem. Downloaded from www.nrcresearchpress.com by 210.87.254.6 on 09/06/12
For personal use only.

La spécificité de cette réaction suggère un mécanisme concerté dont une représentation est donnée sur le schéma 3:

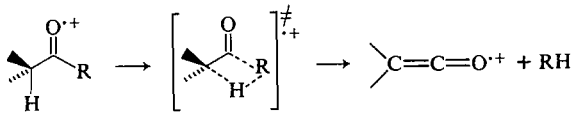

SCHÉMA 3

L'évolution vers un état final constitué d'un céténe ionisé et d'un alcane est également la plus favorable au sens thermodynamique. Les enthalpies standards de formation de quelques ions $[C_nH_{2n-2}O]^{\bullet+}$ sont présentées sur le Tableau 3. Les valeurs de $\Delta H_f^0$ expérimentales résultent pour la plupart de l'addition: $\Delta H_f^0$ $(C_nH_{2n-2}O^{\bullet+})$ = $\Delta H_f^0$ $(C_nH_{2n-2}O)$ + $I$ $(C_nH_{2n-2}O)$. Seule l'énergie d'ionisation est d'origine expérimentale (spectroscopie de photoélectrons), l'enthalpie standard de formation des molécules a été estimée (Tableau 3) par la méthode des incréments de Benson (17); il en résulte nécessairement une incertitude de plusieurs kJ mol$^{-1}$. La comparaison avec des valeurs de $\Delta H_f^0$ calculées par une toute autre méthode (MNDO) permet de contrôler la validité de ces estimations. Les valeurs obtenues par la méthode MNDO (19) ont été calculées après optimisation complète de la géométrie des ions.

Les résultats des calculs sont en bon accord avec l'expérience dans une marge d'erreur inférieure à 20 kJ mol$^{-1}$. La méthode permet donc, en cas de nécessité, de combler certaines lacunes expérimentales. L'ensemble des résultats prouve sans ambiguïté que les ions de formule brute $[C_nH_{2n-2}O]^{\bullet+}$ les plus stables sont des cétènes ionisés. Cette stabilisation représente un gain de plus de 100 kJ mol$^{-1}$ par rapport aux structures de type $[RC{\equiv}COH]^{\bullet+}$. L'acroléine et ses homologues supérieurs sont encore plus défavorisés.

TABLEAU 3. Enthalpies standards de formation (kJ mol$^{-1}$) des ions $[C_nH_{2n-2}O]^{\bullet+}$

| $n$ | Structure | MNDO | Valeurs expérimentales | |
|---|---|---|---|---|
| 2 | $CH_2{=}C{=}O$ | 827 | 879[a] | |
| | H—C≡C—OH | 977 | — | |
| 3 | $CH_3$—CH=C=O | 763 | — | 770[c,e] |
| | $CH_3$—C≡C—OH | 885 | — | |
| | $CH_2$=CH—CHO | 900 | 900[b] | |
| 4 | $(CH_3)_2C{=}C{=}O$ | 713 | — | 686[d,e] |
| | $CH_3$—CH—C—C—OH | 859 | — | |
| | $CH_2$=CH—CO—$CH_3$ | 868 | 816[b] | |
| | $CH_3$—CH=CH—CHO | 833 | 833[b] | |
| | $CH_2{=}C(CH_3)$—CHO | 846 | 849[b] | |

[a] Valeur calculée à partir de $\Delta H_f^0$ $[CH_2CO]$ = −48 kJ mol$^{-1}$ (14) et de l'énergie d'ionisation du cétène 9,607 eV (15).
[b] Référence 16.
[c] $\Delta H_f^0$neutre = $\Delta H_f^0$ $[CH_2CO]$ + [Cd − (H) (C) − Cd − $(H)_2$] + [C − $(H)_3$ (C)] = −48 + 10 − 42 = −80 kJ mol$^{-1}$ (14 et 17).
[d] $\Delta H_f^0$neutre = −48 + 17 − 42 − 42 = −115 kJ mol$^{-1}$ (14 et 17).
[e] Référence 18.

La présence ou l'absence d'un $\Delta H_R^0$ pour la fragmentation $M^{\bullet+} \rightarrow [M-RH]^{\bullet+}$ peuvent être démontrées. En effet, la thermochimie comparée des deux éliminations concurrentes de R$^{\bullet}$ et de RH permet d'évaluer les chances d'existence d'un $\Delta H_R^0$ pour la seconde réaction.

La Figure 1 résume l'ensemble des données thermodynamiques concernant ces deux fragmentations. Les valeurs des $\Delta H_f^0$ nécessaires à cette discussion sont rassemblées dans les Tableaux 3 et 4.

On constate par exemple (Fig. 1) que l'acétone élimine $CH_3^{\bullet}$ et $CH_4$, cette dernière réaction étant dix fois plus aisée (Tableau 1). Le pic métastable le plus intense correspondant à la réaction de plus faible énergie critique, l'état de transition conduisant à $[C_2H_2O]^{\bullet+}$ + $CH_4$ possède nécessairement une enthalpie inférieure à celle de $[CH_3CO]^+$ + $CH_3$. En conséquence le $\Delta H_R^0$ associé à l'élimination de méthane s'il existe, est inférieur à 17 kJ mol$^{-1}$. Un raisonnement analogue s'applique aux réactions compétitives: **3** → $[C_3H_4O]^{\bullet+}$ et $C_2H_6$ et **3** → $[C_3H_5O]^+$ + $C_2H_5$. La valeur limite du $\Delta H_R^0$ éventuel correspondant à l'élimination d'éthane est, ici encore, très faible ($\Delta H_R^0 \leq 20$ kJ mol$^{-1}$).

Si les énergies critiques des deux réactions en compétition sont très différentes, un seul type d'ion fragment est détecté. C'est ainsi que, pour les cétones **5** et **6**, les éliminations des radicaux $C_2H_5^{\bullet}$ et i-$C_3H_7^{\bullet}$ ne sont pas observées. La compétition favorise nettement la formation des méthylcétènes:

$$\mathbf{5} \rightarrow [CH_3CHCO]^{\bullet+} + C_3H_8$$
$$\mathbf{5} \rightarrow [(CH_3)_2CCO]^{\bullet+} + C_2H_6$$
$$\mathbf{6} \rightarrow [(CH_3)_2CCO]^{\bullet+} + C_3H_8$$

les $\Delta H_R^0$ étant respectivement inférieurs à 0, 9 et 6 kcal mol$^{-1}$. De la même manière la perte de $C_2H_6$ à partir de **2** et celle de $C_3H_8$ à partir de **3** ne sont pas observées, les états finals sont en effet trop énergétiques.

Il ressort clairement de ces comparaisons que l'élimination d'alcane se déroule sans $\Delta H_R^0$ appréciable. Un argument complémentaire vient étayer cette conclusion: les valeurs de $T_{0,5}$ associées à la formation des ions $[M-RH]^{\bullet+}$ sont

Can. J. Chem. Downloaded from www.nrcresearchpress.com by 210.87.254.6 on 09/06/12
For personal use only.





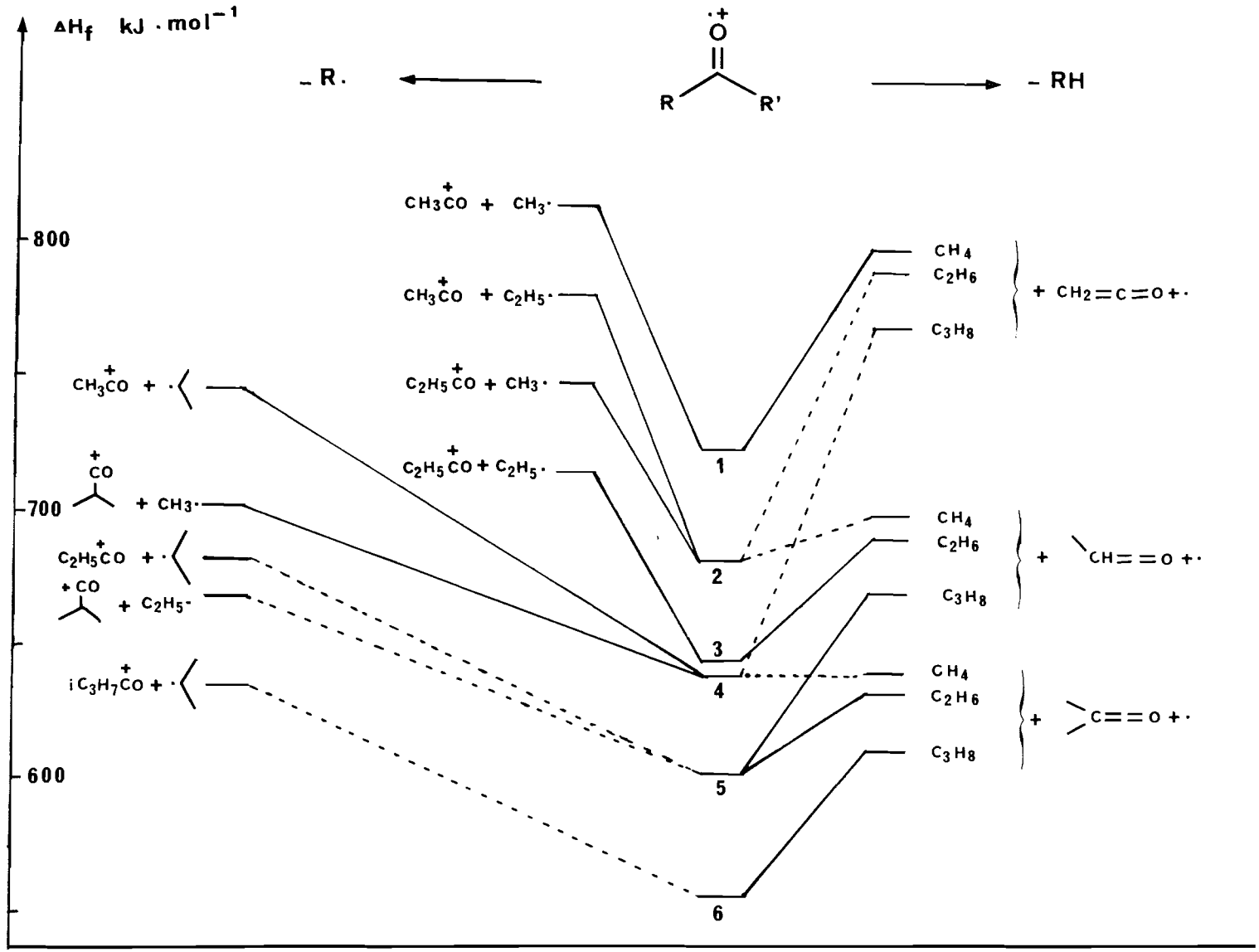


FIG. 1. Diagramme d'énergie associé aux éliminations de R et RH à partir des cétones ionisées métastables. Les états finals correspondant à un pic observé sont connectés à l'ion moléculaire par un trait plein, les lignes pointillées sont associées aux filiations non observées.

TABLEAU 4. Enthalpies standards de formation ($kJ\,mol^{-1}$) utilisées lors de l'établissement de la Figure 1[a]

| $R^1$ | $R^2$ | $\Delta H_f^0(R^1COR^2)^{\bullet+}$ | $\Delta H_f^0(R^1CO)^+$ | $\Delta H_f^0(R^{1\bullet})$ | $\Delta H_f^0(R^1H)$ |
|---|---|---|---|---|---|
| $CH_3$ | $CH_3$ | 720 | 669 | 142 | −75 |
| $CH_3$ | $C_2H_5$ | 678 | — | — | — |
| $C_2H_5$ | $C_2H_5$ | 640 | 602 | 109 | −84 |
| $CH_3$ | i-$C_3H_7$ | 636 | — | — | — |
| $C_2H_5$ | i-$C_3H_7$ | 598 | — | — | — |
| i-$C_3H_7$ | i-$C_3H_7$ | 552 | 556 | 75 | −105 |

[a]Référence 12.

très faibles, de l'ordre d'une dizaine de meV. Ce chiffre est cohérent avec une absence de $\Delta H_R^0$.

L'état de transition de l'élimination de RH est peu éloigné de l'état final, en énergie et par conséquent en structure (20). Cette similitude structurale revient à considérer l'état de transition comme étant une association ion– molécule ([cétène]$^{\bullet+}$–alcane). A cet égard, il convient de noter le rôle important tenu par l'hydrogène transféré dans le complexe intermédiaire. Un fort effet isotopique est observé pour **1** → $[CH_2CO]^{\bullet+}$ + $CH_4$ par Lifshitz et Tzidony (5), une constatation semblable peut être mentionnée ici pour **5**. La comparaison entre **5** et ***5a*** (Tableaux 1 et 2) montre que le rapport $[M-C_2H_6]^{\bullet+}/[M-C_3H_8]$ est égal à 6,7 tandis que $[M-C_2H_3D_3]^{\bullet+}/[M-C_3H_6C_2]^{\bullet+}$ n'atteint plus que 0,2.

En conclusion de cette première partie les deux réactions étudiées $[M]^{\bullet+} \rightarrow [M-R^{\bullet}]^+ + R^{\bullet}$ et $[M]^{\bullet+} \rightarrow [M-RH]^{\bullet+} + RH$ obéissant strictement aux critères de stabilité thermodynamique. Dans les deux cas, aucune énergie d'activation apprèciable ne semble associée aux réactions de recombinaison des fragments.

Deux fragmentations semblent échapper à ces critères: l'élimination de méthane à partir de la méthyléthylcétone et de la méthylisopropylcétone.

*Durée de vie maximum des ions moléculaires*

Bien que les deux réactions:

$$\mathbf{2} \rightarrow [CH_3CHCO]^{\bullet+} + CH_4$$

et

$$\mathbf{4} \rightarrow [(CH_3)_2CCO]^{\bullet+} + CH_4$$

n'aient besoin que d'une très faible énergie d'activation (respectivement 0 et 4 kcal $mol^{-1}$) les pics correspondants au méthylcétène ($C_3H_4O^{\bullet+}$) et au diméthylcétène ($C_4H_6O^{\bullet+}$) n'apparaissent pas. Si la fragmentation est extrêmement rapide, elle devient indétectable à partir d'ions ayant quitté la chambre d'ionisation depuis plusieurs μs.

La durée de vie τ d'une entité se décomposant de façon unimoléculaire avec une constante de vitesse $k$ est donnée simplement par $\tau = 1/k$. La durée de vie maximum d'un ion moléculaire sera donc:

$$\tau_{max} = 1/k(E_0)$$

Si l'énergie d'activation $E_0$ est très basse, $\tau_{max}$ peut devenir inférieur à $10^{-6}$ s. Les évaluations de $\tau_{max}$ portées sur le Tableau 5 montrent que pour un ensemble de 24 oscillateurs (comme l'acétone **1**), $E_0$ doit atteindre environ 1 eV pour que la fragmentation de l'ion métastable soit détectée. Par contre, dans le cas de 42 oscillateurs (**3** et **4**) la valeur de $E_0$ limite est abaissée à 0,6 eV environ. Les deux éliminations de $CH_4$ à partir de **2** et **4** possèdent des valeurs de $\tau_{max}$ nettement inférieures à $10^{-6}$ s. Ce phénomène est donc vraisemblablement responsable du comportement "anormal" des ions **2** et **4**.

Il faut ajouter que le peuplement initial des niveaux d'énergie de l'ion moléculaire proches de l'état fondamental est généralement pauvre. Dans l'hypothèse d'une très faible énergie d'activation, un très petit nombre d'ions fragments est formé au seuil thermodynamique.

TABLEAU 5. Durée de vie maximum $\tau_{max}$ (s) d'ions comportant $s$ oscillateurs[a]

| | $E_0$ (eV) | | |
|---|---|---|---|
| $s$ | 0,2 | 0,5 | 1,0 |
| 24[b] | $3,6\times10^{-11}$ | $8,5\times10^{-9}$ | $4,1\times10^{-6}$ |
| 42[b] | $2,2\times10^{-10}$ | $3,2\times10^{-7}$ | $1,6\times10^{-3}$ |

[a]$\tau_{max}$ est calculé à l'aide de l'approximation proposée par Whitten et Rabinovitch (21) pour un ensemble de $s$ oscillateurs, soit:

$$\tau_{max} = \frac{h(E_0 + a\,E_z)^{s-1}}{(s-1)!\,\frac{s}{\pi}\,h\nu_1}$$

[b]Les fréquences utilisées sont réparties en six groupes de $n$ valeurs: $n\times3000\,cm^{-1}$; $n\times1500\,cm^{-1}$; $n\times1100\,cm^{-1}$; $n\times900\,cm^{-1}$; $n\times600\,cm^{-1}$ et $n\times300\,cm^{-1}$. ($n = 4$ pour $s = 24$ et $n = 7$ pour $s = 42$.)

## Conclusion

Les décompositions des cétones ionisées étudiées obéissent à des critères thermodynamiques. Deux sortes de réaction ont été étudiées, l'élimination de radicaux et l'élimination d'alcanes.

Can. J. Chem. Downloaded from www.nrcresearchpress.com by 210.87.254.6 on 09/06/12
For personal use only.

Dans les deux cas, l'énergie de l'état de transition est quasiment égale à l'énergie de l'état final. Les fragmentations qui apparaissent sont celles qui conduisent aux états finals les plus stables.

Il existe deux situations où la fragmentation de plus basse énergie critique n'est pas observée après un laps de temps de plusieurs μs.

Dans le premier cas, présenté ici, les ions précurseurs sélectionnés après plusieurs μs ne sont plus susceptibles de se decomposer par la voie de plus basse énergie. Seule la fragmentation de haut facteur de fréquence sera observée.

Le second exemple correspond à une isomérisation préalable conduisant à un ion précurseur riche en énergie. Si la réaction de plus basse énergie d'activation possède également le plus bas facteur de fréquence, la compétition la défavorise à haute énergie. Ainsi la fragmentation **1** → $[CH_2CO]^{\cdot+}$ + $CH_4$ n'est pas observée si **1** provient de la réaction d'isomérisation de l'énol $[CH_2{=}C(OH)CH_3]^{\cdot+}$ (6).

## Partie expérimentale

La méthyl-2 trideutéro-2,4,4 pentanone **5***a* et la diméthyl-2,4 bideutéro-2,4 pentanone **6***a* ont été préparées à partir des cétones non marquées correspondantes par échange dans $D_2O$ en présence de $K_2CO_3$ (10%). Après 3 heures de chauffage à reflux, les produits organiques sont isolés par décantation. Le composé **5** conduit ainsi à 67% de composé trideutérié, 24% de deutérié, 5% de monodeutérié et 4% de produit non marqué tandis que les pourcentages de 28, 27 et 45 sont obtenus respectivement pour les molécules **6** di, mono et non deutériées.

Les spectres MIKE ont été enregistrés sur le spectromètre VG-ZAB 2F de l'École Polytechnique de Palaiseau. Les conditions d'utilisation de la source à impact électronique sont: courant d'émission = 100 μA, tension d'accélération des électrons = 70 eV, température = 200°c.

Les valeurs des énergies cinétiques $T_{0,5}$ sont calculées à partir des largeurs de pics mesurées à mi-hauteur, la résolution en énergie est de l'ordre de 1500.

Les intensités portées dans les Tableaux 1 et 2 sont déterminées à partir des hauteurs des pics des spectres de masse.


1. J. J. Zwinselman, N. M. M. Nibbering, N. E. Middlemiss, J. H. Vajda et A. G. Harrison. Int. J. Mass Spectrom. Ion Phys. **38**, 163 (1981).
2. G. Bouchoux et Y. Hoppilliard. Int. J. Mass Spectrom. Ion Phys. Sous presse.
3. A. Maquestiau, P. Meyrant et R. Flammang. 2ème Congrès de Spectrométrie de Masse Fondamentale et Appliquée, Toulouse, 23–25 Septembre 1981.
4. D. M. Mintz et T. Baer. Int. J. Mass Spectrom. Ion Phys. **25**, 39 (1977).
5. C. Lifshitz et E. Tzidony. Int. J. Mass Spectrom. Ion Phys. **39**, 181 (1981).
6. A. Maccoll. Org. Mass Spectrom. **16**, 297 (1981).
7. D. J. McAdoo, C. E. Hudson et D. N. Witiak. Org. Mass Spectrom. **14**, 350 (1979).
8. D. J. McAdoo, W. Farr et C. E. Hudson. J. Am. Chem. Soc. **102**, 5165 (1980).
9. Y. Hoppilliard, G. Bouchoux et P. Jaudon. Nouv. J. Chim. **6**, 43 (1982).
10. D. R. Yarkony et H. F. Schaefer III. J. Chem. Phys. **63**, 4317 (1975).
11. J. H. Vajda et A. G. Harrison. Int. J. Mass Spectrom. Ion Phys. **30**, 293 (1979).
12. J. K. Terlouw, W. Heerma et J. L. Holmes. Org. Mass Spectrom. **16**, 306 (1981).
13. R. G. Cooks, A. N. H. Yeo et D. H. Williams. Org. Mass Spectrom. **2**, 985 (1969).
14. M. Pedley et P. Rylance. Computer analysed thermochemical data for organic and organometallic compounds. University of Sussex Press. 1977.
15. H. M. Rosenstock, K. Draxl, B. W. Steiner et J. T. Herron. J. Phys. Chem. Ref. Data, **6**, Suppl. 1 (1977).
16. P. Masclet et G. Mouvier. J. Electron Spectrosc. Relat. Phenom. **14**, 77 (1978).
17. S. W. Benson. Thermochemical kinetics. J. Wiley & Sons, New York. 1968.
18. H. Bock, T. Hirabayashi et S. Mohmano. Chem. Ber. **114**, 2595 (1981).
19. M. J. S. Dewar et W. Thiel. J. Am. Chem. Soc. **99**, 4899 (1977).
20. J. S. Hammond. J. Am. Chem. Soc. **77**, 334 (1955).
21. G. Z. Whitten et B. S. Rabinovitch. J. Chem. Phys. **38**, 2466 (1963).


Can. J. Chem. Downloaded from www.nrcresearchpress.com by 210.87.254.6 on 09/06/12
For personal use only.

# Mercury-199 nuclear magnetic resonance relaxation in some mercury(II) compounds

RODERICK E. WASYLISHEN[1]

*Department of Chemistry, University of Winnipeg, Winnipeg, Man., Canada R3B 2E9*

ROBERT E. LENKINSKI

*Department of Chemistry, University of Guelph, Guelph, Ont., Canada N1G 2W1*

AND

CHARLES RODGER

*Bruker Spectrospin, Mississauga, Ont., Canada L5L 1J9*

Received March 12, 1982

RODERICK E. WASYLISHEN, ROBERT E. LENKINSKI, and CHARLES RODGER. Can. J. Chem. **60**, 2113 (1982).

Mercury-199 spin-lattice relaxation times are reported for several mercury(II) compounds at 5.875 and 9.40 T. From the field dependence of $T_1$ in $Hg(CN)_2$, $Hg(CH_3)_2$, and $Hg(C_6H_5)_2$, $^{199}Hg$ chemical shielding anisotropies of 3800, 5820, and 5800 ppm are calculated. The errors in these of estimates of $\Delta\sigma$ are at least 10%. Some implications of the large $\Delta\sigma(^{199}Hg)$ values in high field nmr studies are discussed.

RODERICK E. WASYLISHEN, ROBERT E. LENKINSKI et CHARLES RODGER. Can. J. Chem. **60**, 2113 (1982).

On rapporte les temps de relaxation spin-réseau du mercure-199 dans plusieurs composés du mercure(II) à 5,875 et 9,40 T. A partir de l'influence du champ sur $T_1$ dans les composés $Hg(CN)_2$, $Hg(CH_3)_2$ et $Hg(C_6H_5)_2$, on a calculé les anisotropies de blindage chimique du $^{199}Hg$ qui sont respectivement de 3800, 5820 et 5800 ppm. Les erreurs dans ces évaluations sont au moins de 10%. On discute des quelques implications des grandes valeurs $\Delta\sigma(^{199}Hg)$ dans les études de rmn à haut champ.

[Traduit par le journal]

## Introduction

While investigating the high field ($B_0$ = 9.40 T) $^{13}C$ nmr spectra of several organomercury(II) compounds, we observed $^{199}Hg$ satellites due to $^{199}Hg$—$^{13}C$ scalar coupling which were significantly broader than the central uncoupled $^{13}C$ resonance. Of the naturally occurring mercury isotopes, only $^{199}Hg$ (natural abundance 16.84%) has a spin $I$ = 1/2. Although $^{201}Hg$ has $I$ = 3/2, its large quadrupole moment generally leads to extremely efficient quadrupole relaxation for this nucleus, resulting in "self-decoupling" from any spin 1/2 nucleus such as $^{13}C$. In this paper we show that chemical shielding anisotropy relaxation is very efficient for $^{199}Hg$ at applied fields of 9.40 T and that this mechanism can lead to significant $^{199}Hg$ line broadening, thus broadening $^{199}Hg$ satellites in spectra of spin 1/2 nuclei which are scalar coupled to $^{199}Hg$. Values of the $^{199}Hg$ chemical shielding anisotropy, CSA, are estimated from $^{199}Hg$ $T_1$ values measured at applied fields of 5.875 T and 9.40 T and the implications of these values are discussed.

Previously, $^{199}Hg$ $T_1$ values have been reported for neat dimethylmercury (1, 2), divinylmercury (1), and $HgCl_2$ (1.4 $M$ in ethanol) (3). These measurements were carried out in electromagnets where $B_0 \leq 2.35$ T. Both spin rotation and CSA relaxation mechanisms were found to contribute to $^{199}Hg$ relaxation in dimethylmercury (1, 2) and divinylmercury (1) at these applied fields. The mechanism for $^{199}Hg$ relaxation in $HgCl_2$ was not investigated. While this study was being completed, Gillies *et al.* (4) reported the results of a $^{199}Hg$ $T_1$ study on diphenylmercury. At $B_0$ = 7.05 T the $^{199}Hg$ $T_1$ is completely dominated by CSA relaxation. The CSA mechanism is also extremely efficient for several other heavy metal nuclides (5), including $^{195}Pt$ (6), $^{205}Tl$ (7), and $^{207}Pb$ (8).

## Theory

The rate of spin-lattice relaxation observed for a particular spin 1/2 nucleus can generally be expressed as a sum of rates (eq. [1]) due to four distinct mechanisms: dipole–dipole, $T_1(DD)^{-1}$; spin rotation, $T_1(SR)^{-1}$; chemical shielding anisotropy, $T_1(CSA)^{-1}$; and scalar coupling, $T_1(SC)^{-1}$ (9). Of the mechanisms in eq. [1], only the CSA

$$[1]\quad \frac{1}{T_1}(\text{obs.}) = \frac{1}{T_1}(\text{DD}) + \frac{1}{T_1}(\text{SR}) + \frac{1}{T_1}(\text{CSA}) + \frac{1}{T_1}(\text{SC})$$

mechanism becomes more efficient with increasing applied magnetic field, $B_0$. This mechanism is

[1]Author to whom all correspondence should be addressed. Address as of August 1, 1982: Department of Chemistry, Dalhousie University, Halifax, Nova Scotia, Canada B3H 4J3.

0008-4042/82/162113-05$01.00/0

©1982 National Research Council of Canada/Conseil national de recherches du Canada

Can. J. Chem. Downloaded from www.nrcresearchpress.com by 210.87.254.40 on 09/06/12
For personal use only.

Can. J. Chem. Downloaded from www.nrcresearchpress.com by 210.87.254.40 on 09/06/12
For personal use only.

expected to be most important for isotopes which have a large chemical shift range and for nuclei in an environment with less than tetrahedral symmetry. For a nucleus with axial symmetry, the efficiency of the CSA mechanism depends on the square of the applied magnetic field, $B_0$, as shown in eq. [2]:

$$[2a]\quad \frac{1}{T_1}(\mathrm{CSA}) = \frac{1}{15}(\gamma_I B_0)^2(\Delta\sigma)^2\left(\frac{2\tau_2}{1+\omega_I^2\tau_2^2}\right)$$

$$[2b]\quad \frac{1}{T_2}(\mathrm{CSA}) = \frac{1}{90}(\gamma_I B_0)^2(\Delta\sigma)^2 \times \left(\frac{6\tau_2}{1+\omega_I^2\tau_2^2} + 8\tau_2\right)$$

where $\gamma_I$ is the gyromagnetic ratio, $\omega_I = \gamma_I B_0$, $\tau_2$ is the rotational correlation time, $\Delta\sigma$ is the shielding anisotropy, $\sigma_{||} - \sigma_\perp$, $\sigma_{||}$ is the component of the shielding tensor parallel to the symmetry axis, and $\sigma_\perp$ is the component perpendicular to the symmetry axis (10, 11). For linear mercury(II) compounds $\Delta\sigma$ varies between 3500–8000 ppm (see Results and discussion, which follows). For $\Delta\sigma$ = 6000 ppm in eqs. [2*a*] and [2*b*], Fig. 1 shows the dependence of $\log_{10} T_1$(CSA) and $\log_{10} T_2$(CSA) on the rotational correlation time ($\log_{10}\tau_2$) with $\nu_I$ = 71.67 MHz ($B_0$ = 9.40 T) and $\nu_I$ = 44.80 MHz ($B_0$ = 5.875 T). Under conditions of extreme narrowing, $\omega_I^2\tau_2^2 \ll 1$, $T_1/T_2$ = 7/6 at constant $B_0$ and $T_1(B_0 = 5.875\ \mathrm{T})/T_1(B_0 = 9.40\ \mathrm{T})$ = 2.56 (10, 11). At $B_0$ = 9.40 T, the $T_1$ is a minimum, 0.93 ms, for $\tau_2 = 2.2 \times 10^{-9}$ s. Also at the $T_1$ minimum, $T_2$ = 0.55 ms; hence the line-width at half height, $\nu_{1/2} \geq [\pi T_2(\mathrm{CSA})]^{-1}$ = 580 Hz. Figure 2 shows the dependence of $\log_{10} T_1$(CSA) and $\log_{10} T_2$(CSA) on $\log_{10}\tau_2$ for $\Delta\sigma$ = 5000 ppm and 7000 ppm assuming $B_0$ = 9.40 T. For any value of $\tau_2$, relaxation of a nucleus with $\Delta\sigma$ = 7000 ppm is almost twice as effective as it is for one where $\Delta\sigma$ = 5000 ppm.

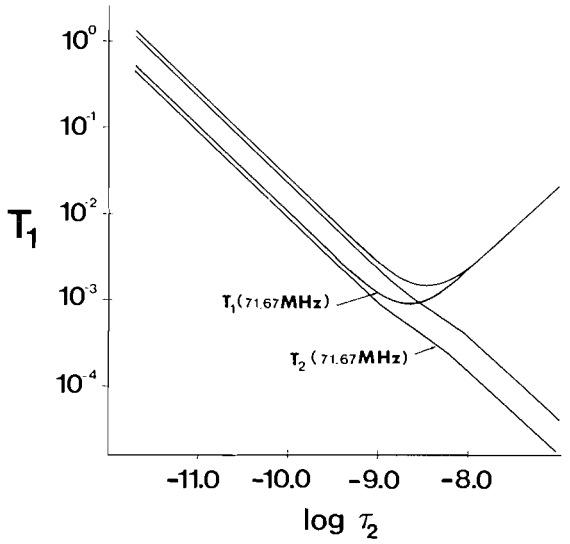


FIG. 1. Plot of $\log_{10} T_1$(CSA) and $\log_{10} T_2$(CSA) vs. $\log_{10}\tau_2$ for $\Delta\sigma$ = 6000 ppm at $\nu_I$ = 71.67 MHz and 44.80 MHz.

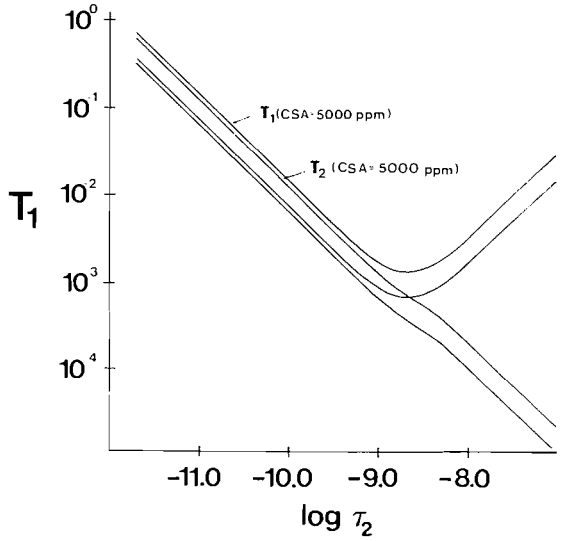


FIG. 2. Plot of $\log_{10} T_1$(CSA) and $\log_{10} T_2$(CSA) vs. $\log_{10}\tau_2$ for $\Delta\sigma$ = 5000 ppm and 7000 ppm. $\nu_I$ = 71.67 MHz.

## Experimental

All mercury compounds were commercially available from Aldrich and Alfa. Mercury cyanide was recrystallized from methanol and dried under vacuum. All other compounds were used as received. Deuterated solvents were obtained from Merck, Sharp and Dohme (Canada). All solutions with the exception of $HgCl_2$, $HgCl_4^{2-}$, and $Hg(CN)_4^{2-}$ were degassed by the freeze–pump–thaw technique. A 0.5 *M* aqueous solution of $HgCl_4^{2-}$ was prepared by mixing equal volumes of 1 *M* $HgCl_2$ and 4 *M* LiCl (12). Similarly a 0.5 *M* $Hg(CN)_4^{2-}$ (aqueous) solution was prepared from equal volumes of 1 *M* $Hg(CN)_2$ and 2.3 *M* KCN (13).

Mercury-199 nmr spectra were recorded at 9.40 T (71.67 MHz) and at 5.875 T (44.80 MHz) on Bruker WH-400 and WM-250 spectrometers respectively. Nitrogen-14 and carbon-13 nmr spectra were obtained at 28.9 MHz and 100.6 MHz respectively (9.40 T). All spin-lattice relaxation times were measured using the inversion–recovery technique (10) and calculated using a 3-parameter fitting procedure (14). All measurements were carried out at 297 ± 2 K.

## Results and discussion

### (a) $^{199}Hg$ Spin-lattice relaxation; $\Delta\sigma(^{199}Hg)$

Measured relaxation times are given in Table 1. The errors in all $T_1$ values are estimated to be less than 15% unless otherwise indicated. For the $^{199}$Hg spin-lattice relaxation times, the ratio $T_1(B_0 = 5.875\ \mathrm{T})/T_1(B_0 = 9.40\ \mathrm{T})$ is given in Table 2.

Can. J. Chem. Downloaded from www.nrcresearchpress.com by 210.87.254.40 on 09/06/12
For personal use only.

TABLE 1. Nuclear magnetic resonance relaxation data for some mercury(II) compounds

| Compound | $B_0$ (T) | $T_1$ ($^{199}$Hg) (s) | $T_1$ (other) (s) |
|---|---|---|---|
| $Hg(CN)_2$ saturated solution in methanol-$d_4$ | 9.40<br>5.875 | 0.0627<br>0.184 | $^{14}$N $1.06 \times 10^{-4}$ [a] |
| $K_2Hg(CN)_4$ 0.5 *M* in $H_2O$ | 9.40<br>5.875 | ≥6.5<br>6.97±0.42 | — |
| $Hg(CH_3)_2$ neat | 9.40<br>5.875<br>1.41 | 0.148<br>0.308<br>1.176[b] | |
| $Hg(C_6H_5)_2$ saturated solution in $CDCl_3$ | 9.40<br>5.875 | 0.0356<br>0.0866 | C2 3.57<br>C3 3.68<br>C4 1.43 |
| $Hg(CH_2C_6H_5)_2$ saturated solution in $CDCl_3$ | 9.40<br>5.875 | 0.0267<br>0.0737 | |
| $HgCl_2$ in EtOH | 9.40<br>5.875<br>2.114 | 0.113<br>0.281<br>1.4[c] | — |
| $HgCl_4^{2-}$ in $D_2O$ | 5.875 | 6.50±0.50 | |

[a] Measured from the $^{14}$N line-width assuming $T_2^* = T_1$, estimated error of 15%.
[b] Reference 2.
[c] Measured for a 1.4 *M* solution in EtOH (ref. 3).

(i) *Hg(CN)*$_2$

For a spin 1/2 nucleus, the $^{199}$Hg $T_1$'s measured for $Hg(CN)_2$ are exceedingly short. The $T_1$'s are field dependent; at applied fields of 9.40 T, spin-lattice relaxation is more efficient than relaxation at 5.875 T by a factor of 2.9 ± 0.4. This strong dependence on the applied field indicates that the chemical shielding anisotropy mechanism completely dominates. If relaxation mechanisms other than CSA make significant contributions to the observed $T_1$'s, then the ratio of the $T_1$'s at 5.875 and 9.40 T would be less than 2.56; and in the limit where CSA relaxation is unimportant the ratio is 1.0. With the exception of scalar coupling of the second kind (10, 11), all other spin-lattice relaxation mechanisms are field independent under conditions of extreme narrowing. Substitution into standard expressions (10, 11) indicates that the scalar coupling mechanism is unimportant because $T_1$ increases with increasing $B_0$ if this mechanism dominates.

The effective rotational correlation time, $\tau_2$, for mercury(II) cyanide can be estimated from the $^{14}$N line-width at half height, $\nu_{1/2} = 3.0 \pm 0.5$ kHz. Assuming $T_1^{-1} = (T_2^*)^{-1} = \pi\nu_{1/2}$ and that nuclear quadrupolar relaxation is the major relaxation mechanism operative (10, 11),

$$[3] \quad \frac{1}{T_1} = \frac{3}{2}\pi^2\left(\frac{e^2qQ}{h}\right)^2\tau_2$$

TABLE 2. Ratio of observed $^{199}$Hg spin-lattice relaxation times at $B_0$ = 5.875 and 9.40 T

| Compound | $\frac{T_1(5.875\text{ T})}{T_1(9.40\text{ T})}$ |
|---|---|
| $Hg(CN)_2$ | 2.9±0.3 |
| $K_2Hg(CN)_4$ | 1.1±0.1 |
| $Hg(CH_3)_2$ | 2.1±0.2 |
| $Hg(C_6H_5)_2$ | 2.4±0.2 |
| $Hg(CH_2C_6H_5)_2$ | 2.8±0.3 |
| $HgCl_2$ | 2.5±0.2 |

where $(e^2qQ/h) = 3.9513$ MHz (15) is the $^{14}$N nuclear quadrupole coupling constant. Substitution into eq. [3] leads to a value of 40.8 ps for $\tau_2$. Using this value of $\tau_2$ in eq. [2] and the $^{199}$Hg $T_1$ measured at 9.40 T, we calculated $\Delta\sigma = 3800$ ppm. The value of $\Delta\sigma$ obtained by the procedure outlined here may be dependent on the solvent. The mercury atom of $Hg(CN)_2$ is known to interact strongly with nitrogen containing ligands such as ammonia (16) and pyridine (17). Strong mercury–solvent interactions are expected to decrease $\Delta\sigma$ relative to the value one would measure for an isolated molecule in the gas phase.

(ii) *Hg(CN)*$_4^{2-}$

At $B_0 = 9.40$ T, $^{199}$Hg spin-lattice relaxation is less efficient in $Hg(CN)_4^{2-}$ than it is in $Hg(CN)_2$ by a factor of at least 100. The tetracyanomercury(II) ion is known to be tetrahedral (18); thus the chemical shielding anisotropy, $\Delta\sigma$, is expected to be approximately zero. This is supported by the observation that the $^{199}$Hg $T_1$ is independent of $B_0$. Spin-rotation and/or intermolecular dipole–dipole relaxation with protons or unpaired electrons (e.g. dissolved $O_2$ or paramagnetic transition metal impurities) are the most likely relaxation mechanisms for $^{199}$Hg in $Hg(CN)_4^{2-}$.

(iii) *Hg(CH*$_3$*)*$_2$

Nuclear magnetic resonance relaxation in dimethylmercury has been studied in detail by Lassigne and Wells (2) and by Sens *et al.* (1). Over the temperature range studied by Lassigne and Wells (2), 234 to 333 K, the $^{199}$Hg $T_1$'s at 1.41 T decreased with increasing temperature ($E_a = -1.1 \pm 0.2$ kcal/mol), indicating that the spin-rotation mechanism is the most important relaxation mechanism at this applied field. Assuming that the CSA mechanism makes a small contribution to the $^{199}$Hg $T_1$ at 297 K and $B_0 = 1.41$ T, one can calculate lower limits for $T_1(\text{CSA})^{-1}$ at 5.875 and 9.40 T using eq. [4]

$$[4] \quad \frac{1}{T_1}(\text{CSA}) \geq \frac{1}{T_1}(\text{obs.}) - \frac{1}{T_1}(1.41\text{ T})$$

Can. J. Chem. Downloaded from www.nrcresearchpress.com by 210.87.254.40 on 09/06/12
For personal use only.

For $B_0$ values of 5.875 and 9.40 T, $T_1(\text{CSA}) \leq 0.417$ and 0.169 s respectively. On the basis of $^1H$ and $^2H$ $T_1$'s, Lassigne and Wells (2) estimate $\tau_2 = 6.7$ ps at 300 K. Substitution of the above values of $T_1(\text{CSA})$ and $\tau_2$ into eq. [2] leads to $\Delta\sigma$ values of 5720 ppm and 5820 ppm. Assuming CSA is the only mechanism at 9.40 T leads to a value of 6100 ppm for $\Delta\sigma$. These values for $\Delta\sigma$ are significantly lower than those of 7475 ± 80 ppm (19) and 7325 ± 55 ppm (20) obtained from liquid crystal data. The main source of error in our calculated value of $\Delta\sigma$ probably results from inaccuracy in $\tau_2$ (2). $\tau_2$ must be less than 4.7 ps in order for the $T_1$ data to be compatible with the liquid crystal data (19, 20).

(iv) *$Hg(C_6H_5)_2$*

The field dependent $^{199}Hg$ $T_1$ data (Table 2) indicate that the chemical shielding anisotropy mechanism must completely dominate at $B_0$ = 9.40 T. The appropriate correlation time for $^{199}Hg$ spin-lattice relaxation in diphenylmercury can be obtained from the $^{13}C$ $T_1$ of the carbon *para* (C4) to mercury (21). This carbon is relaxed entirely by the dipole–dipole mechanism with directly attached protons. Assuming $r_{CH}$ = 108 pm, substitution into eq. [5] yields $\tau_2$ (C2) = 30.8 ps.

$$[5]\quad \frac{1}{T_1} = \frac{\gamma_C^2 \gamma_H^2 \hbar^2}{r_{CH}^6}\ \tau_2$$

Use of this correlation time and $T_1(^{199}Hg) = 0.0356$ s at 9.40 T in eq. [2] gives $\Delta\sigma$ 5800 ± 600 ppm, in fair agreement with the value 6800 ± 680 ppm reported by Gillies *et al.* (4).

Using the rotational diffusion model of Woessner and Snowden (21*a*) and the carbon-13 relaxation data in Table 1, we calculated $D_{\|}/D_{\perp} = 6.8$, where $D_{\|}$ and $D_{\perp}$ are the rotational diffusion constants parallel and perpendicular to the major symmetry axis which passes through the Hg, directly bonded carbons (C1), and the carbon atoms *para* (C4) to the Hg.

(v) *$Hg(CH_2C_6H_5)_2$*

The $^{199}Hg$ $T_1$ data for dibenzylmercury indicate that the CSA mechanism completely dominates at high field. In this case, the absence of axial symmetry precludes calculation of $\Delta\sigma$ using eq. [2].

(vi) *$HgCl_2$ and $HgCl_4^{2-}$*

The decrease in $T_1(^{199}Hg)$ with increasing $B_0$ observed for the linear dichloride indicates that the CSA mechanism completely dominates at high field. We were unable to observe the $^{35}Cl$ or $^{37}Cl$ resonance of $HgCl_2$; thus an estimate of $\tau_2$ and $\Delta\sigma$ is not possible at this time. The relatively long $T_1$ value for the tetrahedral $HgCl_4^{2-}$ ion indicates that the CSA mechanism is not efficient in this species.

(b) *Implications of efficient $^{199}Hg$ CSA relaxation*

There are two main implications of the extremely efficient CSA $^{199}Hg$ relaxation observed for two-coordinate Hg(II) compounds at 9.40 T. Firstly, if mercury is essentially two-coordinate in a macromolecule (for example, see refs. 22–26) which has a rotational correlation time greater than $10^{-9}$ s, it may be difficult to observe the $^{199}Hg$ resonance because of its large line-width ($\nu_{1/2}$ = 335 Hz for $\Delta\sigma$ = 6000 ppm). Secondly, the scalar coupled $^{199}Hg$ satellites (doublet) generally observed in the nmr spectrum of a slowly relaxing nucleus, X, will be significantly broadened. The minimum line-width of the satellites will be $1/\pi T_2(^{199}Hg)$ (27). Figure 3 shows the $^{13}C$ nmr spectrum of $Hg(CN)_2$ at 9.40 T. Whereas the central resonance has a line-width of 15 ± 4 Hz, the satellites are characterized by $^1J(^{199}Hg, ^{13}C)$ = 3158 ± 15 Hz and line-widths of 55 ± 15 Hz. The contributions of CSA relaxation to the $^{199}Hg$ and hence $^{13}C$ line-widths of the compounds studied here are given in Table 3. The large $^{13}C$ line-width of the $^{199}Hg$ satellites in $Hg(CN)_2$ arises at least in part from both CSA relaxation and scalar relaxation of the second kind ($^{199}Hg$—$^{14}N$ scalar coupling). From eq. [2] it is

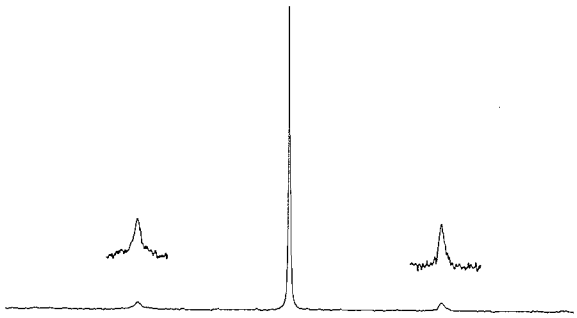

FIG. 3. Carbon-13 nmr spectrum of $Hg(CN)_2$ at $B_0$ = 9.40 T.

TABLE 3. Contribution of CSA relaxation to $^{199}Hg$ line-widths at half-height ($\nu_{1/2}$) at $B_0$ = 9.40 and 5.875 T[a]

| Compound | $B_0$ (T) | $\nu_{1/2}$ (Hz) |
|---|---|---|
| $Hg(CN)_2$ | 9.40 | 5.9 |
| | 5.875 | 2.0 |
| $Hg(CH_3)_2$ | 9.40 | 2.5 |
| | 5.875 | 1.2 |
| $Hg(C_6H_5)_2$ | 9.40 | 10.4 |
| | 5.875 | 4.3 |
| $Hg(CH_2C_6H_5)_2$ | 9.40 | 13.9 |
| | 5.875 | 5.0 |
| $HgCl_2$ | 9.40 | 3.3 |
| | 5.875 | 1.3 |

[a]Minimum $^{199}Hg$ nmr line-widths. Calculated assuming extreme narrowing and CSA relaxation, $T_2 = 6/7\,T_1$.

apparent that for molecules with rotational correlation times greater than $5 \times 10^{-9}$s, the $^{199}$Hg will be essentially "self-decoupled" from nucleus X at applied fields of 9.40 T.


## Acknowledgements

The nmr spectra recorded at 9.40 T were obtained at the Southwestern Ontario NMR Center funded by a Major Installation Grant from the Natural Sciences and Engineering Research Council of Canada. We wish to thank Werner Danchura for his assistance in preparing Figs. 1 and 2. R.E.W. and R.E.L. wish to thank N.S.E.R.C. for financial support in the form of operating grants.



1. M. A. Sens, N. K. Wilson, P. D. Ellis, and J. D. Odom. J. Magn. Reson. **19**, 323 (1975).
2. C. R. Lassigne and E. J. Wells. Can. J. Chem. **55**, 1303 (1977).
3. G. E. Maciel and M. Borzo. J. Magn. Reson. **10**, 388 (1973).
4. D. C. Gillies, L. P. Blaauw, G. R. Hays, R. Huis, and A. D. H. Clague. J. Magn. Reson. **42**, 420 (1981).
5. R. E. Wasylishen, C. Rodger, and R. E. Lenkinski. Relaxation in multinuclear systems. Presented at the 28th Canadian Spectroscopy Symposium, Ottawa, Canada, September 28–30, 1981.
6. J.-Y. Lallemand, J. Soulié, and J.-C. Chottard. J. Chem. Soc. Chem. Commun. 436 (1980).
7. F. Brady, R. W. Matthews, M. J. Forster, and D. G. Gillies. Inorg. Nucl. Chem. Lett. **17**, 155 (1981).
8. G. R. Hays, D. G. Gillies, L. P. Blaauw, and A. D. H. Clague. J. Magn. Reson. **45**, 102 (1981).
9. H. W. Spiess. *In* NMR – basic principles and progress. Vol. 15. *Edited by* P. Diehl, E. Fluck, and R. Kosfeld. Springer Verlag, New York. 1978. p. 104.
10. T. C. Farrar and E. D. Becker. Pulse and Fourier transform nmr. Academic Press, New York. 1971.
11. A. Abragam. The principles of nuclear magnetism. Oxford Press, Clarendon. 1961.
12. P. D. Godfrey, M. L. Heffernan, and D. F. Kerr. Aust. J. Chem. **17**, 701 (1964).
13. (*a*) F. Wagenknecht and R. Juza. *In* Handbook of preparative inorganic chemistry. Vol. II. 2nd ed. *Edited by* G. Brauer. Academic Press, New York. 1965; (*b*) K. G. Ashurst, N. P. Finkelstein, and L. A. Goold. J. Chem. Soc. A, 1899 (1971).
14. M. Sass and D. Ziessow. J. Magn. Reson. **25**, 263 (1977).
15. R. Ikeda, D. Nakamura, and M. Kubo. J. Phys. Chem. **72**, 2982 (1968).
16. D. J. Gardiner, A. H. Haji, and B. P. Stranghan. J. Mol. Struct. **49**, 301 (1978).
17. I. S. Ahuja and A. Garg. J. Inorg. Nucl. Chem. **34**, 2681 (1972).
18. (*a*) R. G. Dickinson. J. Am. Chem. Soc. **44**, 774 (1922); (*b*) A. G. Sharpe. The chemistry of cyano complexes of the transition metals. Academic Press, New York. 1976.
19. J. D. Kennedy and W. McFarlane. J. Chem. Soc. Faraday Trans. **2**, 72 (1976); **2**, 1653 (1976).
20. J. Jokisaari and P. Diehl. Org. Magn. Reson. **13**, 359 (1980).
21. (*a*) D. E. Woessner and B. S. Snowden. Adv. Mol. Relaxation Processes, **3**, 181 (1972); (*b*) G. C. Levy, J. D. Cargioli, and F. A. L. Anet. J. Am. Chem. Soc. **95**, 1527 (1973).
22. S. Mansy and R. S. Tobias. Biochemistry, **14**, 2952 (1975).
23. N. J. Taylor and A. J. Carty. J. Am. Chem. Soc. **99**, 6143 (1977).
24. C. A. Evans, D. L. Rabenstein, G. Geier, and I. W. Erni. J. Am. Chem. Soc. **99**, 8106 (1977).
25. N. W. Alcock, P. A. Lampe, and P. Moore. J. Chem. Soc., Dalton Trans. 1471 (1980).
26. R. D. Bach, S. J. Rajan, N. B. Vardhan, T. J. Lang, and N. G. Albrecht. J. Am. Chem. Soc. **103**, 7727 (1981).
27. J. W. Emsley, J. Feeney, and L. H. Sutcliffe. High resolution nuclear magnetic resonance spectroscopy. Vol. 1. Section 9.1.3. Pergamon Press, New York. 1965.


Can. J. Chem. Downloaded from www.nrcresearchpress.com by 210.87.254.40 on 09/06/12
For personal use only.

# Formation of acid–water hydrogen bonds with large proton polarizability and molecular processes with dissociation of acids in the p$K_a$ range 0–4

MARTIN LEUCHS AND GEORG ZUNDEL

*Physikalisch-Chemisches Institut der Universität München, Theresienstr. 41, D-8000 München 2, West Germany*

Received September 25, 1981

MARTIN LEUCHS and GEORG ZUNDEL. Can. J. Chem. **60**, 2118 (1982).

Aqueous solutions of fourteen acids in the p$K_a$ region 0–4 were studied by ir spectroscopy as a function of concentration. All data are summarized in a table. The degree of dissociation was determined from bands of the anions. The removal of the protons from the anions decreases in the following series of the acids $CF_3COOH$, $H_2CrO_4$, $(HIO_3)$, $CF_2HCOOH$, $HPO(OH)_2$, $HSO_4^-$, $(HSeO_4^-)$, $H_2POOH$, $PO(OH)_3$, $AsO(OH)_3$ (Table 1, columns 3 and 4). Continua indicate the formation of hydrogen bonds with large proton polarizabilities. In the case of $H_3PO_3$, $H_3PO_4$, and $H_3AsO_4$, the acid–acid hydrogen bonds are still polarizable although they have relatively asymmetrical proton potentials. The acid–water hydrogen bonds (**I**) $AH\cdots OH_2 \rightleftharpoons A^-\cdots H^+OH_2$ (**II**) may show considerable proton polarizability, as indicated by strong continuous absorptions. The proton potential, and thus the proton polarizability of the acid–water hydrogen bonds, are discussed taking into consideration the intensity and the wave number range of the continuum (column 7), as well as the line width of the vibration with δ OH character (column 9). With increasing asymmetry of the hydrogen bonds, the continuum changes to the bands observed with asymmetrical hydrogen bonds. The sequence of acids in the series arranged according to the degree of dissociation is not the same as the sequence according to the intensity of the continuum and proton polarizability. This is explained by the fact that the proton polarizability is mainly determined by the shape of the proton potential, whereas the dissociation equilibrium is also influenced by entropy effects associated with hydrate structure formation.

It is shown that the following molecular processes are of significance for the dissociation of the acids: the formation of acid–water hydrogen bonds with proton polarizability, whereby the weight of the polar proton-limiting structure $A^-\cdots H^+OH_2$ increases with increasing addition of water molecules. Besides the shape of the proton potential, the entropy effects mentioned influence the degree of dissociation, too. Finally, the positive charge transfers from the acid–water into water–water hydrogen bonds, i.e., $H_5O_2^+$ is formed.

---

MARTIN LEUCHS et GEORG ZUNDEL. Can. J. Chem. **60**, 2118 (1982).

Utilisant la spectroscopie ir, on a étudié, en fonction de la concentration, solutions aqueuses de quatorze acides dans le domaine de p$K_a$ allant de 0 à 4. On résume toutes les données dans un tableau. On a déterminé le degré de dissociation à partir des bandes des anions. L'élimination des protons des anions diminue dans la série suivante d'acides: $CF_3COOH$, $H_2CrO_4$, $(HIO_3)$, $CF_2HCOOH$, $HPO(OH)_2$, $HSO_4^-$, $(HSeO_4^-)$, $H_2POOH$, $PO(OH)_3$, $ASO(OH)_3$ (col. 3 et 4 du tableau). Les continua indiquent la formation de liaisons hydrogènes avec de grandes polarisabilités protonique. Dans les cas des acides suivants: $H_3PO_3$, $H_3PO_4$ et $H_3AsO_4$, les liaisons hydrogènes acide–acide sont encore polarisables bien qu'elles aient des potentiels de proton relativement asymétriques. Les liaisons hydrogènes acide–eau (**I**) $AH\cdots OH_2 \rightleftharpoons A^-\cdots H^+OH_2$ (**II**) peuvent montrer une polarisabilité considérable protonique comme l'indiquent les fortes absorptions continues. On discute du potentiel du proton et, par conséquent, de la polarisabilité du proton des liaisons hydrogènes acide–eau, en considérant l'intensité et l'intervalle du nombre d'onde du continuum (col. 7), ainsi que la largeur des bandes de vibration ayant un caractère de δ OH (col. 9). En augmentant l'asymétrie des liaisons hydrogènes, le continuum change pour donner les bandes observées avec les liaisons hydrogènes asymétriques. L'ordre des acides, établi suivant le degré de dissociation, n'est pas le même que celui établi selon l'intensité du continuum et selon la polarisabilité protonique. On explique ceci par le fait que la polarisabilité protonique est principalement déterminée par la forme du potentiel protonique alors que l'équilibre de dissociation est de plus influencé par les effets d'entropie associés à la formation d'une structure d'hydratée.

On montre que les processus moléculaires suivants sont significatifs pour la dissociation des acides: la formation des liaisons hydrogènes acide–eau avec polarisabilité protonique, alors que le poids de la structure limite du proton polaire $A^-\cdots H^+OH_2$ augmente avec l'addition de molécules d'eau. En plus de la forme du potentiel du proton, les effets d'entropie mentionnés influencent également le degré de dissociation. Finalement charge positive des liaisons hydrogène acide–eau transfert en liaisons hydrogènes eau–eau c'est-à-dire $H_5O_2^+$.

[Traduit par le journal]

## I. Introduction

In the case of aqueous solutions of acids with p$K_a < 1$, acid–water hydrogen bonds of the type

$$\underset{\textbf{(I)}}{AH\cdots OH_2} \rightleftharpoons \underset{\textbf{(II)}}{A^-\cdots H^+OH_2}$$

with large proton polarizabilities are observed if these acids can be studied at very high concentrations. The large proton polarizability of these hydrogen bonds is indicated by strong ir continua. In these hydrogen bonds, double minimum proton potentials are present, whereby with the very strong acids the deeper well occurs preferentially at the water molecule (proton-limiting structure **II** has larger weight), and with the less strong acids it occurs preferentially at the anion (proton-limiting structure **I** has larger weight). With increasing $n$ (number of water molecules per acid molecule), i.e., increasing amount of water in the solutions, the weight of proton-limiting structure **II** increases, and more and more protons transfer into the water–water hydrogen bonds, i.e., $H_5O_2^+$ is

0008-4042/82/162118-14$01.00/0

©1982 National Research Council of Canada/Conseil national de recherches du Canada

Can. J. Chem. Downloaded from www.nrcresearchpress.com by 210.87.254.6 on 09/06/12
For personal use only.

Can. J. Chem. Downloaded from www.nrcresearchpress.com by 210.87.254.6 on 09/06/12
For personal use only.

formed. The hydrogen bond in this grouping also shows large proton polarizability and causes strong continuous absorption. All these results were obtained from the ir data (for details see ref. 1). The proton polarizability of hydrogen bonds, interactions of these bonds with their environment, and the occurrence of ir continua are discussed in detail in refs. 1–10.

One should expect that with aqueous solutions of acids with $pK_a > 0$, such acid–water hydrogen bonds with large proton polarizabilities should also be found at higher dilution. In the study presented here, ir spectra of aqueous solutions of fourteen acids (Table 1) with $pK_a$ in the region 0–4 are studied and discussed with regard to the degree of asymmetry of the acid–acid and acid–water hydrogen bonds.

## II. Materials and methods

The acids were purchased from Merck in Darmstadt, Germany, Riedl-de-Haen in Seelze, Germany, and Fluka in Buchs, Switzerland. The purity was analytical grade except difluoroacetic acid, iodoacetic acid, and monochloroacetic acid which were for synthesis.

The solutions were studied in a cell with Si windows. Because of the high reflectivity of these windows, considerable interferences would superimpose the spectra when the windows were parallel. Therefore, a wedge-shaped layer with a mean thickness of 9.5 μm was used. This layer is obtained by milling a wedge-shaped groove into one of the windows. With this equipment the reproducibility of the layer is better than 0.2 μm.

This mean layer thickness was calibrated from benzene bands at 1950 and 1815 $cm^{-1}$. However, in the case of a wedge-shaped layer, Lambert–Beer's law is no longer valid. The necessary calibration curve was obtained from the spectra of solutions of cyclohexane in $CCl_4$.

The spectra were taken with a spectrophotometer model 325, Bodenseewerk Perkin-Elmer, Überlingen (slit program 6.5, time response 2, gain 2.5).

The absorbance of the continuum was evaluated at 1900 $cm^{-1}$. It is referred to the same absorbance at 4500 $cm^{-1}$. The quantitative determination of the absorbance of the continuum is described in ref. 11.

The degrees of dissociation were obtained from the characteristic bands of the non-dissociated acids. The intensity of these bands in the spectrum of the water-free acids yields the molar absorbance of these bands. With this molar absorbance, the concentration of the non-dissociated acid molecules in each solution could be determined, and thus the degree of dissociation.

## III. Results and discussion

Figure 1 shows selected spectra. The data are summarized in Table 1. For $H_3PO_2$, $H_3PO_3$, $H_3PO_4$, and $H_3AsO_4$ these data are taken from detailed discussions in ref. 11,[1] and for $CF_3COOH$, $CF_2HCOOH$, and HCOOH from detailed discussions in ref. 13. The acids not studied in detail up to now will be discussed in section III.2.

### *III.1 Fundamentals of discussion*

Information is obtained from the following spectral features:

(*1*) The degree of dissociation can be determined, as in ref. 1 and in many other ir and Raman studies performed by various authors (12–27), from the bands of the acid molecules (Table 1, col. 3). The molarities and $n$ values ($n$ = number of water per acid molecule) at which, with increasing dilution, anion bands begin to appear, i.e. proton-limiting structure **II** becomes noticeable (Table 1, col. 4), in weakly dissociating acids will be discussed.

The presence of acid bands (Table 1, col. 5) indicates that a still non-dissociated species is present, it is also present in dilute solutions.

(*2*) The continua indicate the presence of hydrogen bonds with large proton polarizability, i.e., hydrogen bonds with double minimum proton potential wells. (*a*) If continua are observed, even at $n = 0$, or do not decrease if $n$ becomes $< 1$, then the acid–acid hydrogen bonds are also polarizable (Table 1, col. 6). (*b*) If the intensity of the continuum is zero in the pure acid, and increases on dilution from $n = 0$ to $n = 1$, or if the continuum is observed in the pure acid, and remains with addition of the first water molecules per acid molecule, then the continuum indicates the formation of acid–water hydrogen bonds with large proton polarizability. (*c*) If the intensity of the continuum continues to increase with increasing $n$ for $n > 1$, it indicates that either the degree of asymmetry of the proton potential of the acid–water hydrogen bonds decreases or that positive charge has already transferred into water–water hydrogen bonds, i.e., $H_5O_2^+$ groupings are formed. (*d*) From theoretical calculations, as well as from experimental results, it is known that with increasing degree of asymmetry of the proton potentials in the hydrogen bonds, the continua change as follows: With increasing degree of asymmetry the intensity of the continua should decrease, and they should decrease more strongly at smaller wave numbers (see, for instance, Fig. 6 in ref. 28), i.e., the continua should recede from smaller wave numbers (see Table 1, col. 7). The continuum is still observed in the region of larger wave numbers, however, when the residence time of the protons at one side of the hydrogen bonds is much greater than at the other one, as has been shown theoretically (29, 30) as well as experimentally (25*a*, 26). From theory it is

[1]Some of the data given in ref. 12 are improved due to more exact measurements.

TABLE 1. Data of aqueous

| | Column 1, acid | Column 2, spectra see figure | Column 3, degree of dissociation determined from band at $cm^{-1}$ | | Column 4, bands of dissociated species begin to appear | | | Column 5, band of non-dissociated species | | Column 6, continuum has noticeable intensity for $n < 1$ |
|---|---|---|---|---|---|---|---|---|---|---|
| | | | | | $M$ | $n$ | Fig. | | | |
| **7** | $CF_3COOH$ | 1*a* | $\nu_s CO_2^-$ | 1440 | 7.4 | 3.6 | 2*a* | νC=O | 1770 | No |
| **8** | $H_2CrO_4$ | 1*b* | $\nu_s CrO_3^-$ | 880 | 6.5 | 5.5 | 2*b* | | 900 | Are not soluble at very high concentrations |
| **9** | $HIO_3$ | 1*c* | See text | | | | — | | | |
| **10** | $NaHSO_4$ | 1*d* | $\nu_{as} SO_4^{2-}$ | 1100 | 5.7 | 8.4 | 2*c* | $\nu_{as} SO_3$ | 1200 | |
| **11** | $NaHSeO_4$ | 1*e* | See text | | | | | $\nu_{as}$ $SeO_3$ | 920 | |
| **12** | $H_3PO_2$ | — | $\nu_s PO_2$ | 1040 | 4.1 | 11.0 | — | νP—OH | 975 | Yes |
| **13** | $H_3PO_3$ | — | $\nu_s PO_2$ | 1065 | 5.0 | 8.3 | — | | | Yes |
| **14** | $H_3PO_4$ | 1*f* | $\nu_s PO_2$ | 1065 | 2.5 | 19.4 | — | νP=O | 1170 | Yes |
| **15** | $CF_2HCOOH$ | 1*i* | $CF_2HCOO^-$ | 1320 | 6.0 | 5.8 | — | νC=O | 1752 | No |
| | | | with the following acids no bands of dissociated species are found even in relatively dilute solutions: | | | | | | | |
| **16** | $H_3AsO_4$ | 1*g* | | | 0.8 | 57 | | νAs=O | 925 | Yes |
| **17** | $OSe(OH)_2$ | 1*h* | | | 1.0 | 55 | | νSe=O | 890 | — |
| **18** | $CClH_2COOH$ | — | | | 0.95 | 55 | | νC=O | 1730 | — |
| **19** | $ClH_2COOH$ | 1*j* | | | 1.7 | 28 | | νC=O | 1705 | — |
| **20** | $HCOOH$ | — | | | 1.2 | 44 | | νC=O | 1720 | — |

*Band pair caused by νC—O and δ OH (see ref. 27).

known that with increasing degree of asymmetry of the double minimum proton potential, the residence time in the higher well decreases much more strongly than the fluctuation frequency of the protons. Even when the residence time of the proton in the higher well is very short, the polarizability is smaller but still appreciable. This theoretical result was confirmed experimentally with carboxylic acid – *N* base (25*a*) and with phenol–amine (26) systems. It was shown that even when the proton is largely located at one side of the hydrogen bond the absorbance of the continuum in the region of higher wave numbers is weaker, but a less intense continuum can still be observed.

Furthermore, in the region 3000–1500 $cm^{-1}$, band-like structures of the continua are sometimes observed (Table 1, col. 8). These band-like structures become more pronounced with increasing degree of asymmetry of the proton potentials, and the continua finally vanish, and the spectral features change to the bands observed with asymmetrical hydrogen bonds in this region. In considering such band-like structures of continua, one has to take into account that they occur not only with increasing degree of asymmetry of the proton potentials, but also with increasing length of the polarizable hydrogen bonds (25*a*). It was shown theoretically that long hydrogen bonds with large proton polarizabilities show a broad band-like structure in the region 2500–2000 $cm^{-1}$ (see Fig. 5 in ref. 8).

Hadži and co-workers (31, 32) explained band splitting in this region (A, B, C bands) on the basis of Fermi resonance of the fundamental transition of the hydrogen bonds with the overtones of the bending vibrations. With long $N^+H\cdots N \rightleftharpoons N\cdots H^+N$ bonds, band splitting and band-like structures of the continua were explained by various authors (28, 32–35) as being caused by Fermi resonance of the fundamental transitions of the hydrogen bonds with combinational vibrations. Finally, Wolff and co-workers (36, 37) explained the fine structure of bands observed with carboxylic acids on the same basis. Thus, splitting of the band-like structures of the continua and splitting of bands, given in Table 1, col. 8, must be explained by such resonance effects.

(*3*) If bands of vibrations with δ OH character caused by the acid–water hydrogen bonds are observed in the spectra (Table 1, col. 9), one can conclude that the residence time of the proton at the anion is long enough for these vibrations to occur, whereby the half width gives additional information.

Can. J. Chem. Downloaded from www.nrcresearchpress.com by 210.87.254.6 on 09/06/12
For personal use only.

solutions of acids with $pK_a > 0$

| | Column 7, continuum extends toward smaller wave numbers | Column 8, maxima of band-like structures of the continuum and bands in the region 3000–1500 $cm^{-1}$ | | | Column 9, δ OH in acid–water H-bonds | $pK_a$ | Reference |
|---|---|---|---|---|---|---|---|
| **7** | Yes | Band with structure in the region 2800–2500 | | 1980 | 1450* br<br>1332* br | 0.22 | 49 |
| **8** | Yes | | | | 1170 extremely broad | 0.74 | 43 |
| **9** | Yes | 2800–2700 | 2300 | | 1200 extremely broad | 0.77 | 43 |
| **10** | Yes | 2900–2800 | 2450 | | Very broad shoulder in the region 1400–1380, the rest masked | 1.9 | 43 |
| **11** | Yes | 2700 | 2350 | | 1270 vbr | 1.9 | 43 |
| **12** | Yes | 2750 | Masked | 1700 | Masked | 1.1 | 48 |
| **13** | Yes | 2800 | 2350 | 1700 | Masked | 1.8 | 48 |
| **14** | Weak | 2900 | 2350 | 1700 | Masked | 2.1 | 48 |
| **15** | If at all, extremely weak | Band with structure in the region 2800–2450 | | 1950 | 1458* less broad than with 1262* $CF_3COOH$ | 1.3 | 49 |
| **16** | No | 2850 pronounced | 2350 | 1700 vbr | 1235 vbr | 2.3 | 48 |
| **17** | No | 2900 very pronounced | 2420 | | 1225 br | 2.5 | 43 |
| **18** | No | Band with structure in the region 2900–2400 | | 1950 | | 2.85 | 48 |
| **19** | No | | | 2100 | | 3.16 | 48 |
| **20** | No | | | 2050 | | 3.75 | 48 |

(*4*) Finally, in more dilute solutions, the hydrogen bond with large proton polarizability in $H_5O_2^+$ groupings may also contribute to the continuum.

From the plots in Fig. 3*a*, *b*, and *d*, it can be decided whether, in addition to these hydrogen bonds, acid–water hydrogen bonds with large proton polarizability are still present, and whether they are also present in the more dilute solutions. As discussed in detail in ref. 27, p. 10, this can be concluded from these figures as follows: the dashed lines shown in Fig. 3 give the absorbance of the continuum which would be expected if all protons removed from the anions were present in $H_5O_2^+$ groupings. The observed intensities of the continuum (solid lines) are, however, greater, thus an additional type of hydrogen bond with large proton polarizability must contribute to the continuum.

(*5*) Finally, the following viewpoint must be mentioned: the proton polarizability is determined by the proton potential, i.e., the potential energy dependent on the proton position. The $AH\cdots OH_2 \rightleftharpoons A^-\cdots H^+OH_2$ equilibrium is, however, determined by free energy and hence also influenced by the entropy term of the Gibbs–Helmholtz equation. It is known from other systems (38–41) that entropy effects are highly significant with proton transfer equilibria in solutions. This viewpoint must be taken into account when considering the molecular processes involving dissociation, as described in sections III.6 and III.7.

### *III.2 Discussion of various acids*

#### *$H_2CrO_4$ (spectra Fig. 1b)*

In the spectrum of the 10.3 *M* solution ($n = 2.6$), only bands of non-dissociated acid molecules are observed. With increasing dilution, beginning with the 6.5 *M* solution, the presence of $HOCrO_3^-$ anions is indicated by $\nu_s CrO_3^-$ at 880 $cm^{-1}$ (42) (see spectrum of the $KHCrO_4$ solution). Hence, the degree of dissociation (first step) can be determined from the absorbance of this band (the band of $\nu_{as} CrO_3^-$ at 950 $cm^{-1}$ cannot be used since it overlaps with a band of the non-dissociated molecules). The degree of dissociation (first step) is plotted in Fig. 2*b* as a function of the molarity, *M*, and of *n*. Also in the spectrum of the most dilute solution (1.0 *M*) studied, no bands of $CrO_4^-$ are observed.

Figures 1*b* and 3*b* show that a continuum arises with increasing molarity of the acid. It is most intense in the saturated solution ($M = 10.3$, $n = 2.6$, at 293 K). This continuum cannot be caused by $H_5O_2^+$ groupings, since under these conditions no dissociated species is present (see also Fig. 2*b*).

Can. J. Chem. Downloaded from www.nrcresearchpress.com by 210.87.254.6 on 09/06/12
For personal use only.

Can. J. Chem. Downloaded from www.nrcresearchpress.com by 210.87.254.6 on 09/06/12
For personal use only.

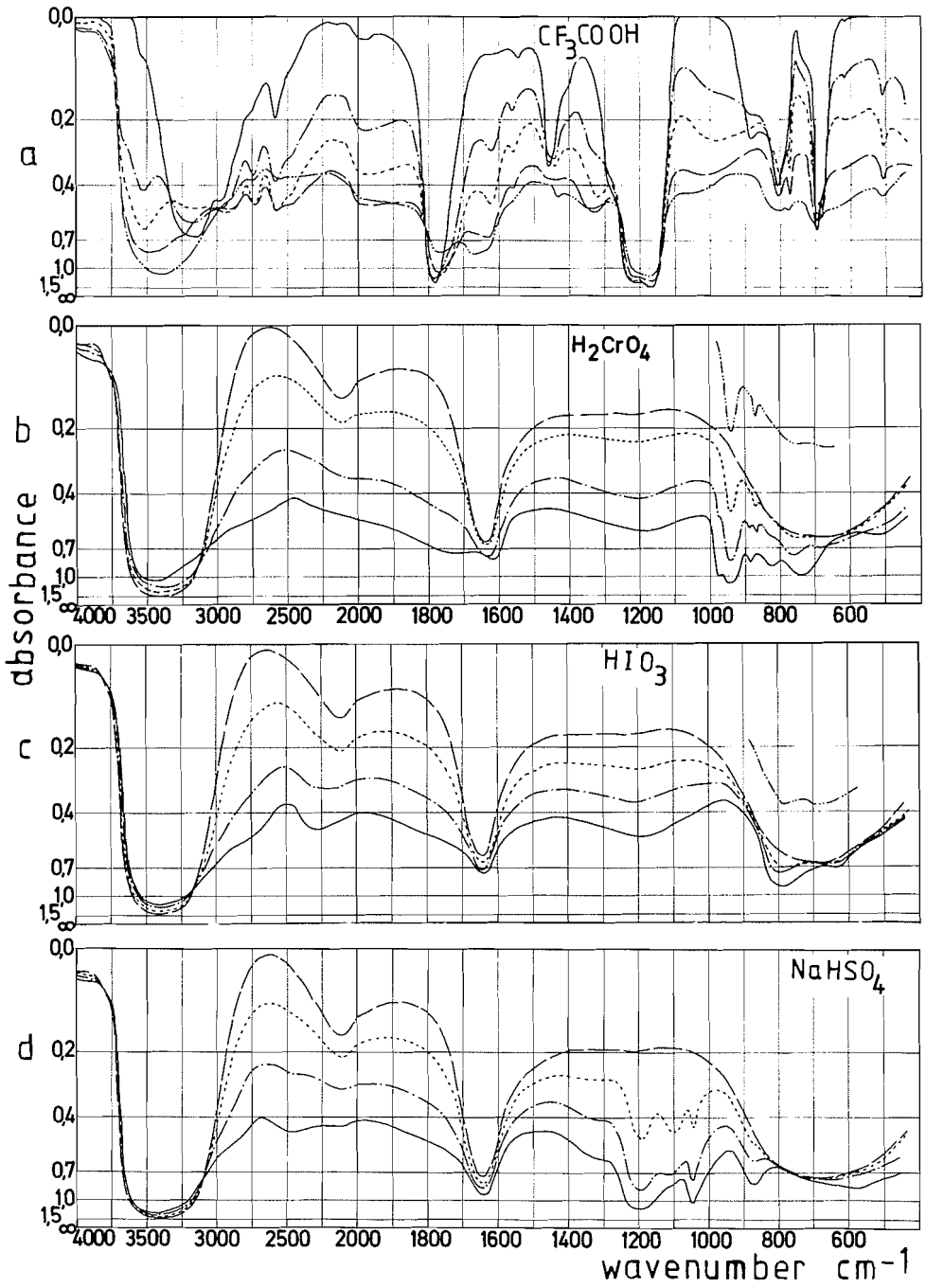


FIG. 1. (*a*) $CF_3COOH$: — 13.0 *M* (*n* = 0.0); ····· 12.1 *M* (*n* = 0.42); --- 11.2 *M* (*n* = 0.88); – – – 9.3 *M* (*n* = 2.0); ····· 6.3 *M* (*n* = 5.1). (*b*) $H_2CrO_4$: — 10.3 *M* (*n* = 2.6); ····· 2.9 *M* (*n* = 16.5); --- 1.0 *M* (*n* = 53); – – – $H_2O$; ····· $KHCrO_4$ solution. (*c*) $HIO_3$: — 8.1 *M* (*n* = 4.8) ····· 4.6 *M* (*n* = 10.2); --- 1.1 *M* (*n* = 49); – – – $H_2O$; ····· $NaIO_3$ solution. (*d*) $NaHSO_4$: — 5.7 *M* (*n* = 8.4); ····· 2.8 *M* (*n* = 17); --- 0.9 *M* (*n* = 57); – – – $H_2O$.

Thus, the continuum must be caused by an acid–water hydrogen bond, and it indicates that these bonds

$$\underset{\textbf{(I)}}{CrOH\cdots OH_2} \rightleftharpoons \underset{\textbf{(II)}}{CrO^-\cdots H^+OH_2}$$

show large proton polarizability. At *n* = 2.6, almost all protons are present at the anions (Fig. 2*b*). Thus, the weight of proton-limiting structure **I** is much larger than that of proton-limiting structure **II**, and hence the deeper well of the double mini-

Can. J. Chem. Downloaded from www.nrcresearchpress.com by 210.87.254.6 on 09/06/12
For personal use only.

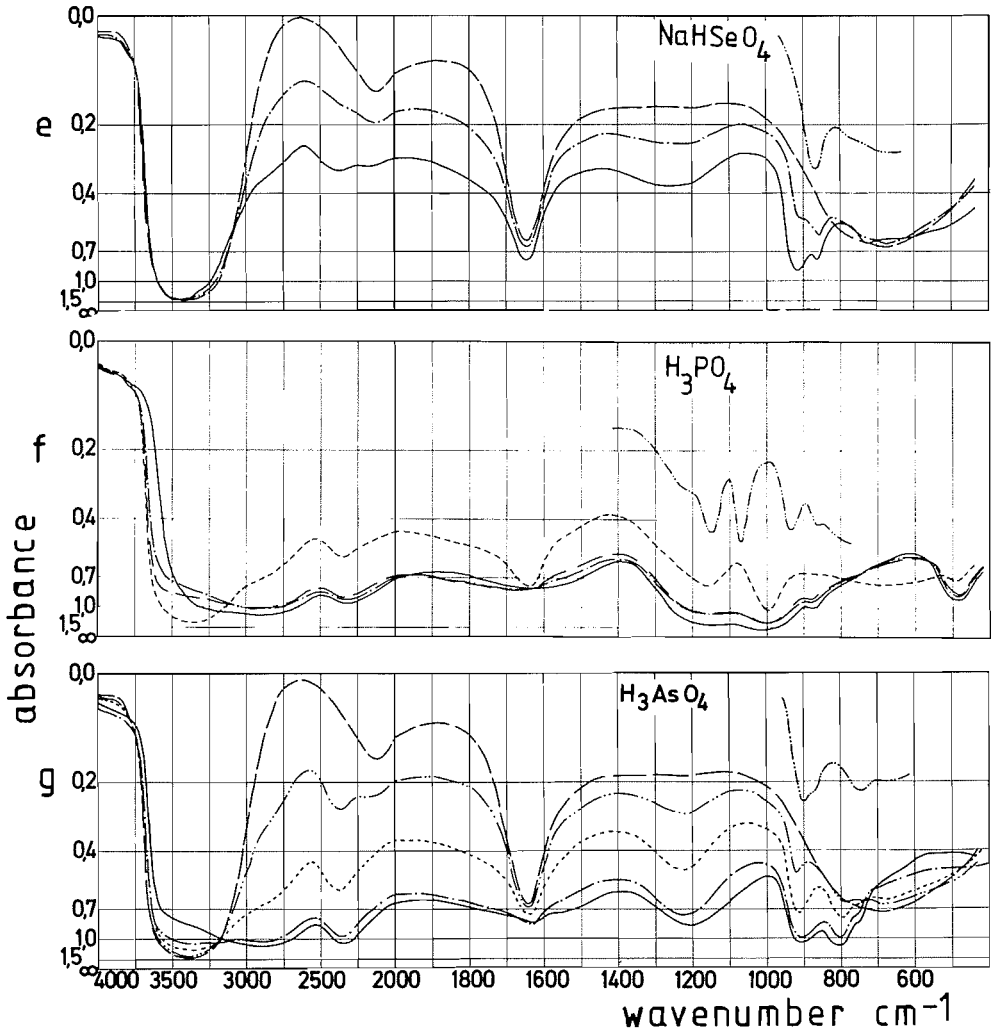


FIG. 1. (*Continued*). (*e*) $NaHSeO_4$: — 5.0 *M* (*n* = 8.5); ····· 1.6 *M* (*n* = 33.8); – – – $H_2O$; ·–·–·–· $Na_2SeO_4$ solution. (*f*) $H_3PO_4$: — 18.6 *M* (*n* = 0.1); ·–·–· 14.7 *M* (*n* = 1.0); – – – 12.2 *M* (*n* = 1.8); — 4.5 *M* (*n* = 9.6); ·–·–·–· $NaH_2PO_4$ solution. (*g*) $H_3AsO_4$: — 14.8 *M* (*n* = 0.49); – – – 10.8 *M* (*n* = 1.9); — 7.5 *M* (*n* = 9.5); ····· 1.4 *M* (*n* = 35.6); – – – $H_2O$; ·–·–·–· $NaH_2AsO_4$ solution.

mum proton potential is preferentially present at the anion. Figure 1*b* shows that the continuum also extends towards smaller wave numbers, indicating that these acid–water hydrogen bonds are still considerably polarizable. The residence time of the protons at the anions is sufficiently long that the δ OH vibration is found with maximum at 1170 $cm^{-1}$, whereby the broadening of this band, however, is extremely strong (Fig. 1*b*).

With increasing dilution, more and more protons are removed from the anions (Fig. 2*b*). The weight of proton-limiting structure **II** increases, and excess protons transfer into the network of hydrogen-bonded water molecules, i.e., $H_5O_2^+$ is formed. The comparison (solid and dashed lines in Fig. 3*b*) of the observed continuum with the continuum which one would expect, if all protons were removed from the anions, and present in $H_5O_2^+$, shows that even in solutions with molarities < 1, protons are still present in polarizable acid–water hydrogen bonds, contributing to the continuum.

*$HIO_3$ (spectra Fig. 1c)*

Two intense bands caused by $IO_2OH$ are observed in the spectrum of concentrated solutions, one at 800 $cm^{-1}$ and one at 650 $cm^{-1}$. $IO_3^-$ is indicated by a band at 790 $cm^{-1}$, as shown by the spectrum of the salt solution. The degree of dissociation, however, cannot be determined from these bands, since the bands of the non-dissociated and dissociated species overlap too strongly.

The spectra in Fig. 1*c* and Fig. 3*c* show that with

Can. J. Chem. Downloaded from www.nrcresearchpress.com by 210.87.254.6 on 09/06/12
For personal use only.

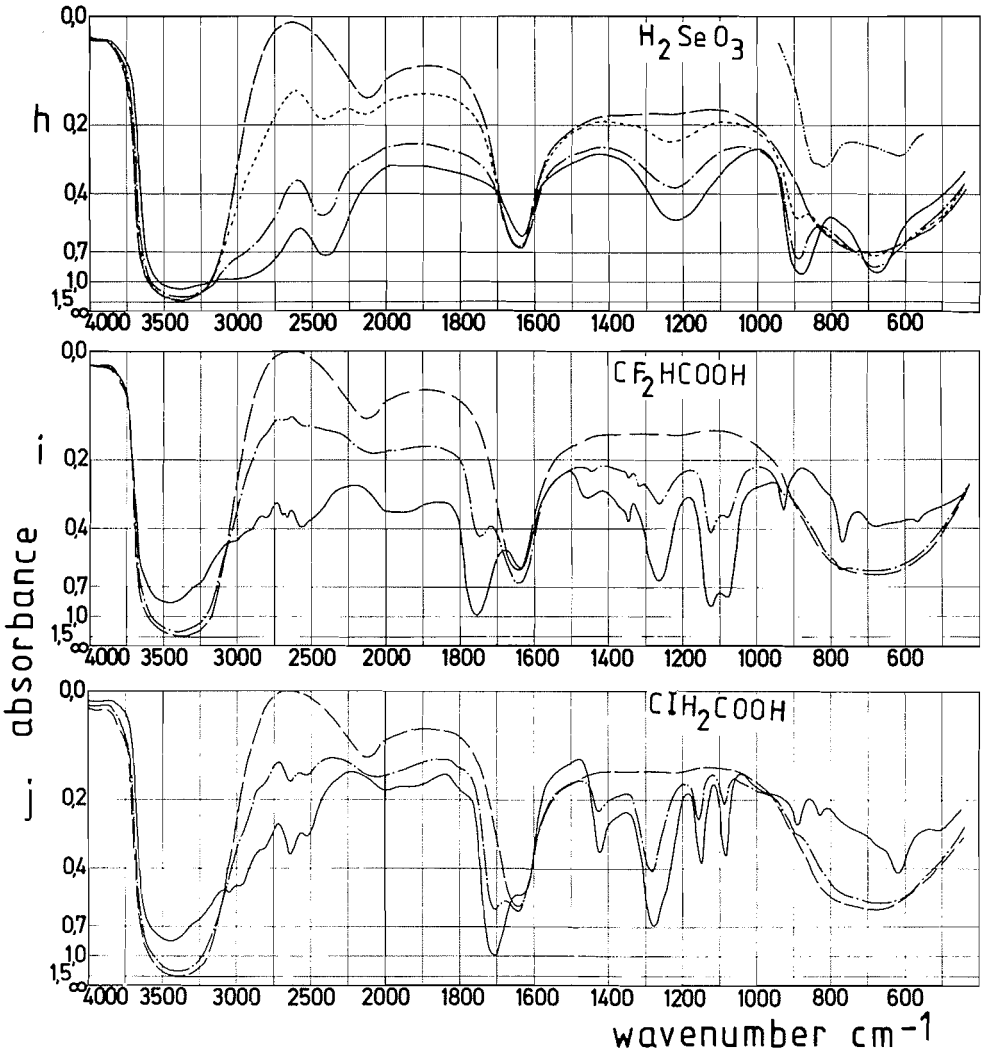


FIG. 1. (*Concluded*). (*h*) $H_2SeO_3$: — 12.3 *M* (*n* = 2.1); ····· 5.6 *M* (*n* = 7.6); --- 1.8 *M* (*n* = 29.2); – – – $H_2O$; ····· $NaHSeO_3$ solution. (*i*) $CF_2HCOOH$: — 9.3 *M* (*n* = 2.6); ····· 2.4 *M* (*n* = 19); – – – $H_2O$. (*j*) $ClH_2COOH$: — 7.9 *M* (*n* = 2.8); ····· 2.8 *M* (*n* = 1.3); – – – $H_2O$.

increasing molarity, a continuum arises which also extends toward the smaller wave numbers. The criteria considered above show that the proton potential in the acid–water hydrogen bonds is similar to that with chromic acid. The $pK_a$ value of $HIO_3$ is 0.77 (43), and hence it is also similar to the $pK_a$ value of the first dissociation step of $H_2CrO_4$, 0.74 (43). Thus, the continuum observed with iodic acid is also mainly caused by acid–water hydrogen bonds with large proton polarizabilities.

*$NaHSO_4$ (spectra Fig. 1*d)

Three bands of the non-dissociated $HOSO_3^-$ molecules are observed, the degenerated $\nu_{as}SO_3$ vibration at 1200 $cm^{-1}$, $\nu_sSO_3$ at 1050 $cm^{-1}$, and νS—O at 990 $cm^{-1}$. With increasing dilution, the band of the triply degenerated antisymmetrical stretching vibration of the $SO_4^{2-}$ anions (42) at 1100 $cm^{-1}$ arises. This band was separated by a computer program. From the absorbance of this band, the degree of dissociation is determined and plotted in Fig. 2*c* as a function of molarity and of *n*. These data do not agree with the Raman data from refs. 21 or 44, however the results in refs. 21 and 44 are also not in agreement with each other.

Figures 1*d* and 3*d* (solid line) show that a continuum arises with increasing molarity of the acid. For comparison, in Fig. 3*d* (dashed line) the absorbance of the continuum is plotted which would be observed if all protons removed from the anions were present in $H_5O_2^+$ groupings. Comparison of the solid and dashed curves in Fig. 3*d*

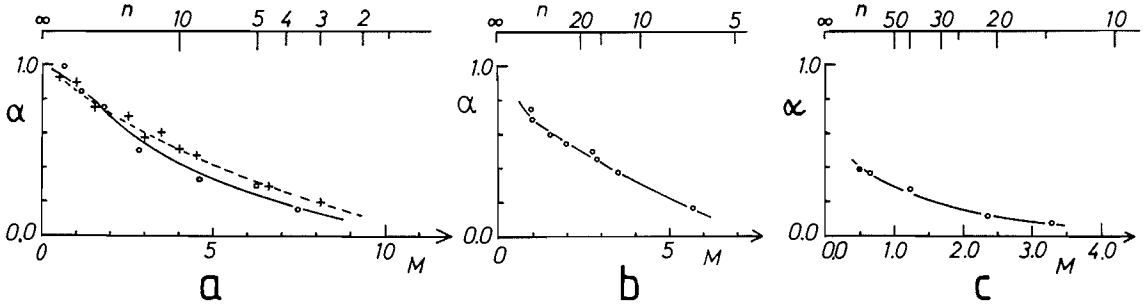


FIG. 2. Degree of dissociation, determined from the ir spectra: (*a*) $CF_3COOH$ (+ values from ref. 20); (*b*) $H_2CrO_4$; (*c*) $NaHSO_4$.

demonstrates that the continuum is not preferentially caused by $H_5O_2^+$ groupings, but by another type of hydrogen bond with large proton polarizability. The only type of hydrogen bond which would be sufficiently symmetrical are acid–water hydrogen bonds.

$$\underset{\text{(I)}}{O_3SO^-H\cdots OH_2} \rightleftharpoons \underset{\text{(II)}}{O_3SO^{2-}\cdots H^+OH_2}$$

Thus, these hydrogen bonds show large proton polarizabilities.

With increasing dilution, more and more protons are removed from the anions (Fig. 2*c*). Thus, the weight of proton-limiting structure **II** increases, and excess protons transfer into the network of hydrogen-bonded water molecules, i.e., $H_5O_2^+$ is formed. But also in solutions less concentrated than 0.5 *M*, acid–water hydrogen bonds with large proton polarizabilities are still present. This is demonstrated by the results presented in Fig. 2*c* and Fig. 3*d*.

*$NaHSeO_4$ (spectra Fig. 1e)*

Three bands of the non-dissociated $HOSeO_3^-$ molecules are observed in the spectra, the degenerated $\nu_{as}SeO_3$ vibration at 920 $cm^{-1}$, $\nu_sSeO_3$ at 865 $cm^{-1}$, and νSe—O at 730 $cm^{-1}$. The triply degenerated antisymmetric stretching vibration of the $SeO_4^{2-}$ anions occurs at 870 $cm^{-1}$ (45), as shown by the spectrum of the salt solution. With decreasing concentration, the intensity of the band at 920 $cm^{-1}$ decreases much faster than that of the band at 865 $cm^{-1}$. The larger intensity at 865 $cm^{-1}$ is caused by $\nu_{as}SeO_4^-$, arising at this position with increasing dilution, indicating dissociation. A quantitative evaluation is not possible, due to the strong overlapping of these bands. The proton acceptor strength of the $SeO_4^-$ ions, however, should be greater than that of the $SO_4^-$ ions (45). Hence, the degree of dissociation of $HOSeO_3^-$ should be a little less than that of $HOSO_3^-$.

Figures 1*e* and 3*e* show that with increasing molarity of this acid, a continuum arises which is only a little weaker than that observed with hydrogen sulfate solutions (cf. Figs. 3*d* and *e*). Paetzold (45) has shown that the affinity of $SeO_4^{2-}$ ions for protons is greater than that of $SO_4^{2-}$ ions. Thus the weight of proton-limiting structure **I** of the acid–water hydrogen bonds is a little greater and, therefore, the well of the double minimum in the average a little deeper at the anion, than with $HSO_4^-$. This larger degree of asymmetry explains the smaller intensity of the continuum. Nevertheless, the continuum also extends toward smaller wave numbers (Fig. 1*e*). The very broad band, with maximum at about 1270 $cm^{-1}$, superimposed on the continuum, is the OH bending vibration in the acid–water groupings. The appearance of this band demonstrates that the residence time of the proton at the anion is sufficiently long for the occurrence of this OH bending vibration.

*$H_2SeO_3$ (spectra Fig. 1h)*

Simon and Paetzold (46) demonstrated that this acid is present in the form $O{=}Se(OH)_2$. At 890 $cm^{-1}$, νSe=O is found, and at 680 $cm^{-1}$ the stretching vibration of the $Se(OH)_2$ groups is observed (46). No bands of dissociated groupings can be found even in the spectrum of the 1 *M* ($n = 55$) solution. This is shown by comparison with the spectrum of the aqueous $NaHSeO_3$ solution.

The intensity of the continuum is much weaker than with arsenic acid (cf. Fig. 1 *h* and *g*). It no longer extends toward smaller wave numbers. Very pronounced bands, however, with maxima at about 2900 $cm^{-1}$ and 2420 $cm^{-1}$, caused by the OH stretching vibration and the overtone of the OH bending vibration of the acid–water hydrogen bonds are observed. The latter is intensified by Fermi resonance with the stretching vibration (31, 32). The bending vibration itself is observed as a broad intense band with maximum at 1225 $cm^{-1}$. With increasing dilution, no bands of $HSeO_3^-$ are found. All these observations together demonstrate that the degree of asymmetry of the acid–water hydrogen bonds is already so large that the continuum has vanished to a large degree, and only

Can. J. Chem. Downloaded from www.nrcresearchpress.com by 210.87.254.6 on 09/06/12
For personal use only.

Can. J. Chem. Downloaded from www.nrcresearchpress.com by 210.87.254.6 on 09/06/12
For personal use only.

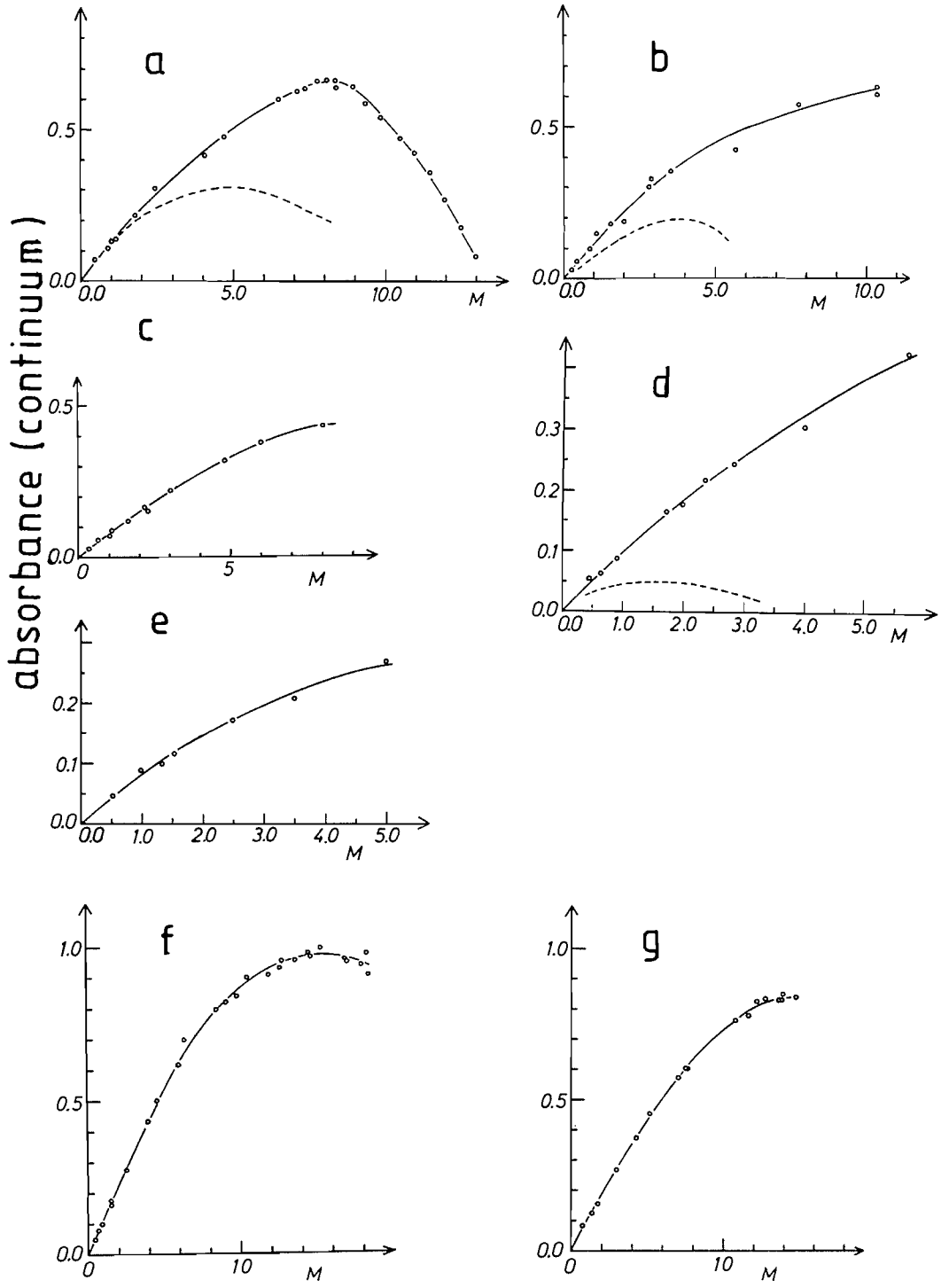


FIG. 3. Continuous absorption at 1900 $cm^{-1}$ as function of molarity $M$: (*a*) $CF_3COOH$; (*b*) $H_2CrO_4$; (*c*) $HIO_3$; (*d*) $NaHSO_4$; (*e*) $NaHSeO_4$; (*f*) $H_3PO_4$; (*g*) $H_3AsO_4$.

Can. J. Chem. Downloaded from www.nrcresearchpress.com by 210.87.254.6 on 09/06/12
For personal use only.

the usual bands observed with asymmetrical hydrogen bonds are found. Thus, the polarizability of the acid–water bonds with selenous acid is very weak.

*$CClH_2COOH$, $ClH_2COOH$ (spectra Fig. 1j), $CHOOH$ (Fig. 1e and f in ref. 13)*

Even in 0.95 *M* solution of $CClH_2COOH$, and in 1.7 *M* aqueous solutions of $ClH_2COOH$, no shoulders of bands of dissociated molecules can be observed, as shown by comparison with the spectra of the sodium salt solutions (with $ClH_2COO^-$, $\nu_{as}CO_2^-$ at 1595 $cm^{-1}$ and $\nu_sCO_2^-$ at 1370 $cm^{-1}$).

With these acids, various bands are observed in the region 3200–1750 $cm^{-1}$ which raise the background slightly. These bands are caused by the OH stretching vibration of the acid–water hydrogen bonds and by overtones and combinational vibrations which are intensified by Fermi resonance with the OH stretching vibration, as discussed by Wolff and co-workers (36, 37). No rise of background is observed below 1600 $cm^{-1}$. Also in the diluted solution, no bands of dissociated acid molecules are observed. Thus, the proton potentials in the acid–water hydrogen bonds with these carboxylic acids are single minima with the well at the anions. These hydrogen bonds are asymmetrical and show no anomalous proton polarizabilities due to proton motion.

*III.3 Degree of dissociation*

In the case of acids **7–15**, bands of the dissociated species (Table 1, col. 3) appear with increasing dilution (Table 1, col. 4). This demonstrates that the proton-limiting structure **II** of the acid–water hydrogen bonds (see section III.5)

$$\underset{\textbf{(I)}}{AH\cdots OH_2} \rightleftharpoons \underset{\textbf{(II)}}{A^-\cdots H^+OH_2}$$

acquire noticeable weight. Thus, addition of water molecules, i.e., a more polar environment, increases the weight of the polar proton-limiting structure $A^-\cdots H^+OH$. This result is in very good agreement with the findings obtained from other systems (25, 26, 50–52).

The spectroscopically-observed removal of the protons from the anions decreases in the following series of acids (Table 1, col. 4): $CF_3COOH$ **7**, $H_2CrO_4$ **8**, ($HIO_3$ **9**), $CF_2HCOOH$ **15**, $HPO(OH)_2$ **12**, $HSO_4^-$ **10**, ($HSeO_4^-$ **11**), $H_2POOH$ **13**, $PO(OH)_3$ **14**, $AsO(OH)_3$ **16**. With $AsO(OH)_3$, no bands of the dissociated species are observed, even in the 0.8 *M* ($n = 57$) solution.

With these spectroscopically-determined degrees of dissociation, one must always keep in mind that the acid molecules observed as dissociated are not only those from which the protons have been removed from the anions and are present in $H_5O_2^+$ groupings, but also those with which the proton is present in the proton-limiting structure **II** in the acid–water hydrogen bonds.

*III.4 Polarizable acid–acid hydrogen bonds*

In the case of strong acids, such as $HClO_4$ (1, 27) or $HNO_3$ (1, 47), no continua are observed with the pure acids. In contrast to this finding, $H_3PO_2$, $H_3PO_3$, $H_3PO_4$, and $H_3AsO_4$ show intense continuous absorption, even for $n < 1$, and if they could be studied pure, also in the pure liquid acid (see Fig. 1*f* and figures in ref. 12). This result demonstrates that with these acids, the acid–acid hydrogen bonds

$$\underset{\textbf{(I)}}{POH\cdots OP} \rightleftharpoons \underset{\textbf{(II)}}{PO^-\cdots H^+OP}$$

$$\underset{\textbf{(I)}}{AsOH\cdots OAs} \rightleftharpoons \underset{\textbf{(II)}}{AsO^-\cdots H^+OAs}$$

show still noticeable proton polarizabilities. No bands of anionic groupings, i.e. bands caused by proton-limiting structure **II**, can be observed in the spectra (cf., for instance, in Fig. 1*f* the spectrum drawn with solid line with the spectrum of the sodium salt solution ·····). Thus, the weight of proton-limiting structure **II** is very small, and the double minimum proton potential present in these hydrogen bonds largely asymmetrical, with the deeper well preferentially at the anion. As already mentioned in section III.1, when the proton is largely located at one side of the hydrogen bond its proton polarizability is much weaker and the continuum is less intense, but it can still be observed in the region of larger wave numbers. Thus, as already discussed in detail in ref. 12, the proton polarizabilities of these acid–acid hydrogen bonds are much smaller than those of structurally symmetrical hydrogen bonds with a double minimum, but still much larger than the proton polarizabilities of asymmetrical hydrogen bonds with single minimum.

Some acids in this $pK_a$ region, as, for instance, $CF_3COOH$ and $CF_2HCOOH$, which can also be studied pure, show no continuum when no water molecules are present. This fact is understandable, since these acids form dimers via two hydrogen bonds. With these dimers, a symmetrical total proton potential is present when both protons transfer simultaneously in the hydrogen bonds. The barrier for such a cooperative proton transfer is, however, high, since both protons repel each other. Furthermore, with the transfer of both protons, no considerable change of the dipole

Can. J. Chem. Downloaded from www.nrcresearchpress.com by 210.87.254.6 on 09/06/12
For personal use only.

moments occurs. Therefore, no continua are observed.

The question arises then, why, in this $pK_a$ region, do the hydrogen bonds between the acid molecules become so symmetrical that they show noticeable proton polarizability? The degree of asymmetry of the acid–acid bonds should decrease, if the proton is less easily removed from the anions, and if the hydrogen bond acceptor strength of the acceptor sites at the acid molecules increases. Hence, with increasing $pK_a$ of the acids, a $pK_a$ region should occur in which the degree of asymmetry of the acid–acid hydrogen bonds is low. The prevailing results show that this is the case with the above-mentioned acids in the $pK_a$ region 1–2.5.

*III.5 Acid–water hydrogen bonds with large proton polarizability*

With $CF_3COOH$ **7**, $H_2CrO_4$ **8**, $HIO_3$ **9**, $NaHSO_4$ **10**, and $NaHSeO_4$ **11**, intense continua are observed even in the concentrated solutions in which, as shown by the results presented in Fig. 3*a*, *b*, and *d*, the concentration of $H_5O_2^+$ can be neglected. Thus, these continua are caused by acid–water hydrogen bonds, and indicate that these hydrogen bonds are of the type

$$\underset{\textbf{(I)}}{AH\cdots OH_2} \rightleftharpoons \underset{\textbf{(II)}}{A^-\cdots H^+OH_2}$$

and show large proton polarizabilities. At high concentrations, no bands of the dissociated species are found (Fig. 1*a*–*e*, data given in Table 1, col. 3 and col. 4). Thus, the weights of proton-limiting structure **II** are still very low. The result that the continua also extend toward smaller wave numbers (Table 1, col. 7), however, indicates that these acid–water hydrogen bonds still show considerable proton polarizability. Thus, a relatively asymmetrical double minimum proton potential, with the deeper well preferentially at the anion, is present in these acid–water hydrogen bonds. The band with δ OH bending character of the OH groups in these hydrogen bonds is found in the region 1350–1150 $cm^{-1}$, indicating that the residence time of the protons at the anions is long enough for this vibration to occur (Table 1, col. 9). With the exception of $CF_3COOH$, however, this band is extremely or at least very strongly broadened, indicating that the residence time of the protons at the anions is comparable to that necessary for the occurrence of this vibration.

It is known from studies of acids with $pK_a < 0$ (1) that increasing weight of the polar proton-limiting structure in the acid–water hydrogen bonds favors the transfer of the positive charge into water–water hydrogen bonds, i.e., the $H_5O_2^+$ formation. Therefore, in more dilute solutions of stronger acids of the above series, for instance, $CF_3COOH$, $H_2CrO_4$, and $NaHSO_4$, the hydrogen bond in the $H_5O_2^+$ groupings with large proton polarizability contribute to the continuous absorption. The question arises, whether, even in the most dilute solutions of these acids, acid–water hydrogen bonds are still present. Comparison of the solid with the dashed curve in Fig. 3*a*, *b*, and *d* shows (see section III.1, point 4) that with these acids, even in relatively dilute solutions, acid–water hydrogen bonds with large proton polarizability occur. This result is confirmed by the observation that even in relatively dilute solutions of these acids, bands of nondissociated acid molecules are still found (see Table 1, col. 5).

The series of acids, $H_3PO_4$ **14**, $H_3AsO_4$ **16**, $OSe(OH)_2$ **17**, $ClH_2COOH$ **18**, $ClH_2COOH$ **19**, CHOOH **20** (Fig. 1*f*–*h* and *j* and Table 1, col. 8), shows that with increasing degree of asymmetry of the acid–water hydrogen bonds, the continuum vanishes and the usual bands of strong hydrogen bonds occur in the region 3000–1600 $cm^{-1}$. With $H_3PO_4$, a relatively intense continuum is still observed in the region 3000–1500 $cm^{-1}$, showing a band-like structure with maxima at 2900 $cm^{-1}$, 2350 $cm^{-1}$ and 1700 $cm^{-1}$. With $H_3AsO_4$, the intensity of the continuum in this region is already weaker, but the bands with maxima at 2850 $cm^{-1}$ and 2350 $cm^{-1}$ are much more pronounced, and the continuum is no longer observed below 1600 $cm^{-1}$. With $OSe(OH)_2$, the intensity of the continuum vanishes almost completely, also in the region above 1600 $cm^{-1}$, and two pronounced bands are observed with maxima at 2900 $cm^{-1}$ and 2420 $cm^{-1}$, whereby the band at the higher wave number is the stretching vibration of the OH groups in the acid–water hydrogen bonds, and the band at lower one, the overtone of the OH bending vibration, which is intensified by Fermi resonance with the former vibration (32). Thus, in the series of acids, **14**, **16** to **20**, the double minimum proton potential in the acid–water hydrogen bonds changes to an asymmetrical single minimum with the well at the anion.

In summary we can state: with increasing asymmetry of the double minimum proton potential in the acid–water hydrogen bonds, as expected (see section III.1, point 2), the absorbance of the continuum per acid–water hydrogen bond decreases, vanishing first at smaller wave numbers.

The sequence of the acids in the series arranged according to the degree of dissociation discussed in sec III.3 is not the same as the sequence of the acids arranged according to the intensity of the continuum which they cause. The most striking

example is $CF_2HCOOH$. The polar proton-limiting structure $O^-\cdots H^+OH_2$ begins to be observed when only $n = 5.8$ water molecules per acid molecule are present, whereas almost no continuum is observed with this acid at smaller wave numbers (cf. the spectra in Fig. 1*i* with the spectra in Fig. 1*b–f*). This different behavior regarding degree of dissociation and continuum will be explained in the next section.

*III.6 Polarizable acid–water hydrogen bonds as a function of $pK_a$ and intensity of the continua*

In Fig. 4, the absorbance of the continuum at 1900 $cm^{-1}$ is plotted as a function of the $pK_a$ of the respective acids. For comparison, results with acids having $pK_a < 0$, taken from ref. 1, are also given in this figure.

As previously discussed in ref. 1, the absorbance of the continuum with the 1 *M* solutions is the same with all acids having $pK_a < 0$, since it is always the same hydrogen bond, the easily polarizable hydrogen bond in $H_5O_2^+$ groupings, which causes the continuum. With the acids having $pK_a > 0$, the absorbance of the continuum decreases with increasing $pK_a$. This decrease of the continuum has two causes: (*1*) With increasing $pK_a$, fewer protons transfer in the network of hydrogen bonds formed between water molecules, i.e., the concentration of the hydrogen bond with large proton polarizability in $H_5O_2^+$ groupings decreases. (*2*) The degree of asymmetry of the proton potentials in the acid–water hydrogen bonds increases, and hence the proton polarizability of these bonds and thus the intensity of the continuous absorbance caused by these hydrogen bonds decreases.

Figure 4 shows that two different types of acids with regard to the absorbance of the continuum as a function of $pK_a$ are observed. The absorbance of the continuum decreases at lower $pK_a$ values with the following acids (type **I**): $CF_3COOH$ **7**, $IO_2OH$ **9**, $H_2POOH$ **12**, $CF_2HCOOH$ **15**, $CClH_2COOH$ **18**, $ClH_2COOH$ **19**, $HCOOH$ **20**. In contrast to this result, it decreases at higher $pK_a$ values with the following acids (type **II**): $CrO_2(OH)_2$ **8**, $(SO_3OH)^-$ **10**, $(SeO_3OH)^-$ **11**, $HPO(OH)_2$ **13**, $PO(OH)_3$ **14**, $AsO(OH)_3$ **16**, $SeO(OH)_2$ **17**. The first type of acid has only one OH group, and these acids are not charged when non-dissociated. The second type of acid has either more than one OH group as hydrogen bond donor (**8**, **13**, **14**, **16**, **17**), or the acid is charged, i.e. the acid has strong hydrogen bond acceptor groupings (**10**, **11**). These different properties of the two types of acids may explain their different behavior.

As already mentioned in sec. III.1 point 5, the

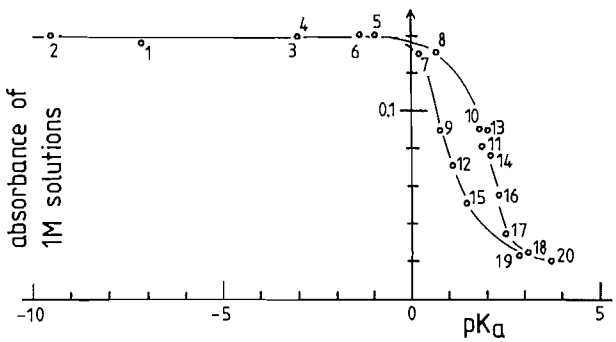


FIG. 4. Absorbance of the continuum of 1 *M* solutions at 1900 $cm^{-1}$ as a function of $pK_a$: **1** $HClO_4$; **2** HI; **3** $H_2SO_4$; **4** $H_2SeO_4$; **5** HCl; **6**, $HNO_3$; **7** $CF_3COOH$; **8** $H_2CrO_4$; **9** $HIO_3$; **10** $HSO_4^-$; **11** $HSeO_4^-$; **12** $H_2POOH$; **13** $HPO(OH)_2$; **14** $PO(OH)_3$; **15** $CF_2HCOOH$; **16** $AsO(OH)_3$; **17** $SeO(OH)_2$; **18** $CClH_2COOH$; **19** $ClH_2COOH$; **20** $HCOOH$.

proton potential is mainly determined by enthalpy effects, whereas the dissociation equilibrium is also determined by entropy effects. These are highly significant with proton transfer processes (38–41). Thus, the $AH\cdots OH_2 \rightleftharpoons A^-\cdots HOH_2$ equilibrium is also significantly determined by entropy effects caused by interaction effects of these hydrogen bonds with their environments. With regard to the fact that the continuum and the position of the $AH\cdots OH_2 \rightleftharpoons A^-\cdots H^+OH_2$ equilibria are determined by two different thermodynamic quantities, it is not surprising that, with systems showing the same intensity of the continuum (determined by the proton potential), another position of the dissociation equilibrium (determined by the free energy) is observed. Furthermore, it is not surprising that types with similar interaction properties show a similar relation between intensity of the continuum and of the position of the equilibrium

$$AH\cdots OH_2 \rightleftharpoons A^-\cdots H^+OH_2$$

*III.7 Molecular processes on dissociation of acids*

The following molecular processes are decisive on the dissociation of an acid (16):

(*a*) The formation of acid–water hydrogen bonds

$$AH\cdots OH_2 \rightleftharpoons A^-\cdots H^+OH_2$$

with large proton polarizability. The position of this equilibrium is determined by the hydrogen bond donor strength of the acid and by the hydrogen bond acceptor strength of the lone pairs at the water molecules as well as by the polarity of the environment, i.e., on the polarity of non-dissociated acid molecules and anions as well as on the presence of water molecules.

(*b*) With the addition of more than one water molecule per acid molecule, this equilibrium is

Can. J. Chem. Downloaded from www.nrcresearchpress.com by 210.87.254.6 on 09/06/12
For personal use only.

shifted to the right hand side, since polar environments favor the polar proton-limiting structure. The reason for this is that an additional negative enthalpy contribution occurs, caused by the stronger dipole–dipole interaction of structure **II** with the more polar environment, i.e., the interaction of the dipole of the $A^-\cdots H^+OH_2$ structure with the reaction field induced by this dipole in its environment.

(*c*) Entropy effects associated with the hydrate structure formation, however, shift this proton transfer equilibrium in the opposite direction, i.e., to the left hand side.

(*d*) Increasing weight of structure **II** favors the transfer of the positive charge from the acid–water into water–water hydrogen bonds, i.e., the $H_5O_2^+$ formation.

(*e*) If the free energy of solvation of the separated species $A^-$ and $H^+OH_2$ due to non-dissociated acid molecules is high enough, then the $A^-\cdots H^+OH_2$ groupings may dissociate, even in very concentrated solutions, before the processes *b*–*d* occur. Of course, also in this case, with the addition of more water molecules, $H_5O_2^+$, and more-extended hydrogen-bonded networks around this structure, are formed.

Thus, for the acids discussed in this paper, the formation of acid–water hydrogen bonds with large proton polarizability, and the interaction of these hydrogen bonds with their environments are highly important for the molecular processes on dissociation with these acids.


## Acknowledgements

We thank Professor G. S. Denisov, Dr. V. M. Schreiber, and Dr. N. S. Golubev of the University of Leningrad for very valuable discussion regarding proton transfer and entropy effects. Furthermore, our thanks are due to the Deutsche Forschungsgemeinschaft and the Fonds der Deutschen Chemischen Industrie for providing facilities for this work.



1. M. Leuchs and G. Zundel. Can. J. Chem. **58**, 311 (1980).
2. E. G. Weidemann and G. Zundel. Z. Naturforschg. **25**a, 627 (1970).
3. G. Zundel. Allgem. Prakt. Chem. Wien, **21**, 329 (1970).
4. R. Janoschek, E. G. Weidemann, H. Pfeiffer, and G. Zundel. J. Am. Chem. Soc. **94**, 2387 (1972).
5. G. Zundel. *In* The hydrogen bond — recent developments in theory and experiments. Vol. II. *Edited by* P. Schuster, G. Zundel, and C. Sandorfy. North Holland Publ. Co., Amsterdam. 1976.
6. R. Janoschek, E. G. Weidemann, and G. Zundel. J. Chem. Soc. Faraday Trans. II, **69**, 505 (1973).
7. R. Janoschek, A. Hayd, E. G. Weidemann, M. Leuchs, and G. Zundel. J. Chem. Soc. Faraday Trans. II, **74**, 1238 (1978).
8. A. Hayd, E. G. Weidemann, and G. Zundel. J. Chem. Phys. **70**, 86 (1979).
9. H. Pfeiffer, G. Zundel, and E. G. Weidemann. J. Phys. Chem. **83**, 2544 (1979).
10. (*a*) N. B. Librovich, V. P. Sakun, and N. D. Sokolov. Chem. Phys. **39**, 351 (1979); (*b*) G. Zundel and E. G. Weidemann. Chem. Phys. **44**, 427 (1979).
11. D. Schiöberg and G. Zundel. Can. J. Chem. **54**, 2193 (1976).
12. M. Leuchs and G. Zundel. Can. J. Chem. **57**, 487 (1979).
13. M. Leuchs and G. Zundel. J. Chem. Soc. Faraday Trans. II, **76**, 14 (1980).
14. T. F. Young, L. F. Meranville, and H. M. Smith. *In* The structure of electrolytic solutions. *Edited by* W. Hamer, Wiley, New York. 1959.
15. W. R. Busing and D. F. Hornig. J. Phys. Chem. **65**, 284 (1961).
16. T. F. Young and G. E. Walrafen. Trans. Faraday Soc. **57**, 34 (1961).
17. G. E. Walrafen. J. Chem. Phys. **39**, 1479 (1963).
18. J. H. R. Clarke and C. A. Woodward. Trans. Faraday Soc. **62**, 2226 (1966); **62**, 3022 (1966).
19. K. Stoperka. Z. Anorg. Allg. Chem. **344**, 263 (1966).
20. A. K. Covington, J. G. Freeman, and Th. Liley. J. Phys. Chem. **74**, 3773 (1970).
21. H. Chen and D. E. Irish. J. Phys. Chem. **75**, 2672 (1971).
22. G. Zundel. Hydration and intermolecular interaction. Academic Press, New York. 1969. p. 116 ff; Mir Moscov 1972.
23. V. D. Maiorov and N. B. Librovich. Russ. J. Phys. Chem. **47**, 1295 (1973).
24. V. D. Maiorov and N. B. Librovich. Russ. J. Phys. Chem. **49**, 1661 (1975).
25. R. Lindemann and G. Zundel. (*a*) J. Chem. Soc. Faraday Trans. II, **73**, 788 (1977); (*b*) Biopolymers, **16**, 1407 (1977); (*c*) Biopolymers, **17**, 1285 (1978).
26. A. Nagyrevi and G. Zundel. J. Phys. Chem. **82**, 687 (1978).
27. M. Leuchs and G. Zundel. J. Chem. Soc. Faraday Trans. II, **74**, 2256 (1978).
28. B. Brzezinski and G. Zundel. J. Chem. Soc. Faraday Trans. II, **72**, 2127 (1976).
29. E. G. Weidemann and G. Zundel. Z. Naturforschg. **28**a, 236 (1973).
30. E. G. Weidemann. *In* The hydrogen bond — recent developments in theory and experiments. Vol. I. *Edited by* P. Schuster, G. Zundel, and C. Sandorfy. North Holland Publ. Co., Amsterdam. 1976. pp. 245 ff.
31. D. Hadži. Pure Appl. Chem. **11**, 435 (1965).
32. D. Hadži and N. Kobilarov. J. Chem. Soc. A, 439 (1966).
33. D. H. Bonsor, B. Borah, R. L. Dean, and J. L. Wood. Can. J. Chem. **54**, 2458 (1976).
34. B. Borah and J. L. Wood. Can. J. Chem. **54**, 2470 (1976).
35. E. Grech, Z. Malarski, and L. Sobczyk. Polish J. Chem. **52**, 131 (1978).
36. H. Wolff, H. Müller, and E. Wolff. J. Chem. Phys. **64**, 2192 (1976).
37. H. Wolff, H. Müller, and E. Wolff. J. Chem. Phys. **65**, 3394 (1976).
38. H. Baba, A. Matsuyama, and H. Kokubun. Spectrochim. Acta, **25**A, 1709 (1969).
39. G. S. Denisov and V. M. Schreiber. News of the University of Leningrad, **4**, 61 (1976).
40. N. S. Golubev, N. A. Sofarov, and A. S. Tanasiitschuk. Kinet. Katal. **14**, 302 (1978).
41. A. I. Kulbida and V. M. Schreiber. Dokl. Akad. Nauk, **250**, 889 (1980).


Can. J. Chem. Downloaded from www.nrcresearchpress.com by 210.87.254.6 on 09/06/12
For personal use only.

42. H. SIEBERT. Anwendungen der Schwingungsspektroskopie in der anorganischen Chemie. Springer, Berlin. 1966.
43. R. C. WEAST (*Editor*). Handbook of chemistry and physics. 49 ed., The Chemical Rubber Co., Cleveland, OH. 1968.
44. D. J. TURNER. International Symposium on The Structure of Water and Aqueous Solutions, Marburg, 1973.
45. R. PAETZOLD and H. AMOULONG. Z. Anorg. Allg. Chem. **317**, 288 (1962).
46. A. SIMON and R. PAETZOLD. Z. Anorg. Allgem. Chem. **301**, 246 (1959).
47. M. LEUCHS and G. ZUNDEL. J. Phys. Chem. **82**, 1632 (1978).
48. A. ALBERT and E. P. SERJEANT. Ionization constants of acids and bases. Wiley Publ. Co., New York. 1962.
49. J. J. CHRISTENSEN, L. D. HANSEN, and R. M. IZATT (*Editors*). Handbook of proton ionization heats. Wiley Publ. Co., New York. 1976.
50. J. JADŻYN and J. MAŁECKI. Acta Phys. Polon. A**41**, 599 (1972).
51. L. SOBCZYK. *In* The hydrogen bond — recent developments in theory and experiments. Vol. III. *Edited by* P. Schuster, G. Zundel, and C. Sandorfy. North Holland Publ. Co., Amsterdam. 1976.
52. V. M. SCHREIBER. A. KOLL, and L. SOBCZYK. Bull. Akad. Polon. Sci. Ser. Sci. Chim. **26**, 651 (1978).

Can. J. Chem. Downloaded from www.nrcresearchpress.com by 210.87.254.6 on 09/06/12
For personal use only.

# Thermochemical study of adducts of methylurea with zinc, cadmium, and mercury halides

CLAUDIO AIROLDI,[1] AÉCIO P. CHAGAS, AND FRANCISCO P. ASSUNÇÃO[2]

*Instituto de Química, Universidade Estadual de Campinas, Caixa Postal 6154–13.100–Campinas, São Paulo, Brasil*

Received January 14, 1982

CLAUDIO AIROLDI, AÉCIO P. CHAGAS, and FRANCISCO P. ASSUNÇÃO. Can. J. Chem. **60**, 2132 (1982).

The adducts $Zn(mu)_2X_2$ (X = Cl, Br), $M(mu)X_2$ (M = Cd, Hg and X = Cl, Br) have been characterized. The CO and NH stretching frequencies indicate that methylurea (mu) is bound to metals through oxygen. Enthalpies of dissolution of the adducts in ethanol or methanol have been measured calorimetrically. Combination with the enthalpies of solution of metal halides and ligand in the same solvents at 298.15 K yielded the standard enthalpy ($\Delta H_R^\ominus$/kJ mol$^{-1}$) for the reaction: $MX_2(s) + n\,mu(s) \rightarrow M(mu)_nX_2$ (s): $Zn(mu)_2Cl_2$, (−36.27±0.51); $Zn(mu)_2Br_2$, (−37.52±0.97); $Cd(mu)Cl_2$, (−22.78±0.26); $Cd(mu)Br_2$, (−9.58±0.26); $Hg(mu)Cl_2$, (−13.91±0.41); and $Hg(mu)Br_2$, (−13.29±0.48). The standard enthalpies of formation of the adducts in the same sequence as above, $\Delta H_f^\ominus$ (s, 298.15 K): −1024, −938, −701, −612, −524, and −470 kJ mol$^{-1}$, were determined from these values, the standard enthalpy of the ligand (−285±15 kJ mol$^{-1}$) being obtained via combustion calorimetry, and literature values of the standard enthalpies of metal halides being used. With the determination of the standard enthalpy of sublimation of the ligand (78.2 kJ mol$^{-1}$) it was possible to determine the standard enthalpies of the reactions $MX_2(g) + n\,mu(g) \rightarrow M(mu)X_2$ (s) and $M(mu)_nX_2$ (s) → $MX_2$ (s) + $n$mu(g). The enthalpies of metal–oxygen bonds were also estimated.

CLAUDIO AIROLDI, AÉCIO P. CHAGAS et FRANCISCO P. ASSUNÇÃO. Can. J. Chem. **60**, 2132 (1982).

On a caractérisé les adduits $Zn(mu)_2X_2$ (X = Cl, Br), $M(mu)X_2$ (M = Cd, Hg et X = Cl, Br). Les fréquences de vibration du CO et du NH indiquent que la méthylurée (mu) est liée au métal par l'intermédiaire de l'oxygène. On a mesuré par calorimétrie les enthalpies de dissolution des adduits dans l'éthanol ou le méthanol. La combinaison avec des enthalpies de solution des halogénures métalliques et du ligand dans les mêmes solvants à 298,15 K donne l'enthalpie standard ($\Delta H_R^\ominus$/kJ mol$^{-1}$) de la réaction: $MX_2(s) + n\,mu(s) \rightarrow M(mu)_nX_2$ (s): $Zn(mu)_2Cl_2$, (−36,27±0,51); $Zn(mu)_2Br_2$, (−37,52±0,97); $Cd(mu)Cl_2$, (−22,78±0,26); $Cd(mu)Br_2$, (−9,58±0,26); $Hg(mu)Cl_2$, (−13,91±0,41) et $Hg(mu)Br_2$, (−13,29±0,48). En se basant sur ces valeurs, sur l'enthalpie standard du ligand (−285±15 kJ) obtenue par calorimétrie de combustion et sur des valeurs d'enthalpie standard des halogénures métalliques tirées de la littérature, on a déterminé l'enthalpie de formation des adduits $\Delta H_F^\ominus$ (s, 298,15 K) dans la même ordre que ci-dessus: −1024, −938, −701, −612, −524 et −470 kJ mol$^{-1}$. La détermination de l'enthalpie standard de sublimation du ligand (78,2 kJ mol$^{-1}$) rend possible la détermination des enthalpies standards des réactions: $MX_2(g) + n\,mu(g) \rightarrow M(mu)X_2$ (s) et $M(mu)_nX_2$ (s) → $MX_2$ (s) + $n$mu(g). On a également évalué les enthalpies des liaisons métal–oxygène.

[Traduit par le journal]

## Introduction

Our interest in the thermochemistry of adducts of halides of the zinc family with urea derivatives as ligand is now focused on methylurea (mu). The determinations of crystallographic parameters for $Cd(mu)_nX_2$ (X = Cl, Br, I and $n$ = 1, 2) and $Zn(mu)_6Br_2$ were the pioneer studies involving methylurea as a ligand (1, 2). Moreover, a complete X-ray diffraction pattern for $Cd(mu)Cl_2$ illustrates an interesting structure (3) where the metal is octahedrally coordinated, with the participation of methylurea as a monodentate ligand. This polymer structure shows one site of coordination occupied by oxygen of the ligand carbonyl with the other positions being occupied by chloride bridges.

The coordination characteristic of methylurea is expected to be the same as that of *N*,*N*′-dimethylurea (dmu) where both molecules resemble the urea molecule (4, 5) in structure. From infrared studies methylurea has a nearly planar configuration of the N—C(O)—N moiety with the C—N bonds possessing appreciable double bond character and a tendency to form hydrogen bonds (4). It can act as a ligand utilizing either nitrogen or oxygen as the donor atom.

From the results on thermal decomposition of $CdLCl_2$ (L = urea, methylurea, and *N*,*N*′-dimethylurea) adducts by thermogravimetric analysis in air and vacuum, the following order of stability was established: urea > methylurea > *N*,*N*′-dimethylurea (6). This sequence clearly indicates an influence of ligand substituents on stability. This is the only thermochemical datum dealing with the methylurea ligand.

In our study, the $Zn(mu)_2X_2$ (X = Cl, Br) and $M(mu)X_2$ (M = Cd, Hg and X = Cl, Br) adducts were synthesized and characterized, with special concern being devoted to obtaining thermochemical data of these adducts and ligand. Nevertheless, bearing in mind the systematic behavior observed for the urea derivatives, a comparison of the present results will be made with tetramethylurea

[1]To whom all correspondence should be addressed.

[2]Permanent address: Departamento de Química, Universidade Federal do Pará, 66.000–Belém, Pará, Brasil.

0008-4042/82/162132-05$01.00/0

©1982 National Research Council of Canada/Conseil national de recherches du Canada

Can. J. Chem. Downloaded from www.nrcresearchpress.com by 210.87.254.40 on 09/06/12
For personal use only.

Can. J. Chem. Downloaded from www.nrcresearchpress.com by 210.87.254.40 on 09/06/12
For personal use only.

(7) and *N*,*N'*-dimethylurea (8), mainly in relation to the thermochemical data.

Broadly speaking, in any kind of systematic study, attention is always pointed toward well- or badly-behaved systems and correlations are used to illustrate the adjustment of the experimental data. To exemplify our very well-behaved systems, considering the enthalpies of combustion of urea (9), methylurea, *N*,*N'*-dimethylurea (dmu) (8), trimethylurea (10), and tetramethylurea (tmu) (11), a correlation $\Delta U_C^{\ominus}$(ureas)/kJ mol$^{-1}$ = $-49.14\,M + 2305.15$ is observed with less than 1% of error, $M$ being the molar mass of the urea and its derivatives. Moreover, the basicity order, tmu > dmu > mu, could be established from our experimental results. These results indicate that the sequence of basicity follows the inductive effect of the methyl groups, in agreement with the successive replacement of the hydrogen on the nitrogen of urea. Other thermochemical results involving mu and adducts will be reported here.

## Experimental

*Materials*

Only reagent grade materials were used throughout. Methylurea (Aldrich) was recrystallized twice in anhydrous ethanol at −5°C (12). After crystallization the amide was filtered in a dry nitrogen atmosphere, washed with a cold ethanol–ether (1:5) mixture, and dried *in vacuo* for 6 h. Nitromethane, acetone, and ethanol for conductance measurements as well as methanol and ethanol for calorimetric measurements were rigorously dried. Anhydrous chlorides and bromides of zinc and cadmium were prepared as before (7). The commercial mercury chloride (E. Merck) and bromide (Baker) were dried *in vacuo* for 3 h before use.

*Preparation of $Zn(mu)_2Cl_2$*

7.2 mmol of $ZnCl_2$ were dissolved in 10 mL of acetone. This was poured into a solution of 14.2 mmol of methylurea dissolved in 5 mL of acetone. This mixture was stirred at room temperature and a viscous product resulted after evaporation of the solvent *in vacuo*. The prolonged vacuum for 6 h produced crystals which were washed with a cold mixture of ethanol–ether (1:5) and dried *in vacuo* for 6 h.

*Preparation of $Zn(mu)_2Br_2$*

A solid mixture of 8.9 mmol of $ZnBr_2$ and 17.8 mmol of ligand was ground in a mortar with 0.3 mL of ethanol. The resulting paste was dissolved in ethylacetate and after evaporation of this solvent, the adduct crystallized, and was dried *in vacuo*.

*Preparations of $M(mu)X_2$ (M = Cd, Hg and X = Cl, Br)*

A solution of methylurea in 15 mL of ethanol was added dropwise to a solution of $MX_2$ dissolved in 50 mL of ethanol in a stoichiometric ratio 4:1. After evaporation of half of the solvent, the adduct started to settle, and was then filtered, washed, and dried as before.

*Analysis*

Weighed samples of the product were analysed for halide, metal, and nitrogen. The metals were spectrophotometrically titrated by EDTA. Halides were determined by potentiometric titration. Nitrogen was determined by the micro-Kjeldahl method (8).

*Calorimetry*

A LKB 8700 precision calorimetric system was used for all measurements of the enthalpies of the process of dissolution at (298.15±0.02) K, and operation and calibration have been described previously (7, 8). The measurements were carried out using 90 mL of solvent and the ampoules varied from 6 to 65 mg. Each enthalpy value was obtained from at least five independent runs.

The enthalpy of combustion of methylurea was determined from a conventional static bomb – calorimeter system (Veb Apparatenbau Babelsberg of the type Berthelot-Thomsen), for which the calibration and procedure have been described previously (13). The sample of ligand was ignited in an oxygen atmosphere of ~3 MPa in a calorimetric bomb of 250 mL internal capacity containing 1 mL of distilled water. The energy equivalent of the calorimeter, $E = -(10\,211 \pm 12)$ J K$^{-1}$, was determined from the combustion of benzoic acid on $\Delta U = -(26\,435.1 \pm 2.9)$ J g$^{-1}$. The auxiliary data used are $\Delta H_f^{\ominus}(HNO_3,l) = 59.7$; $\Delta H_f^{\ominus}(H_2O,l) = -(285.83 \pm 0.04)$; and $\Delta H_f^{\ominus}(CO_2,g) = -(393.51 \pm 0.31)$ kJ mol$^{-1}$ (14, 15).

The enthalpy of fusion, heat capacity of solid and liquid forms of methylurea were determined in a Perkin-Elmer DSC-2 differential scanning calorimeter. For the first determination seven measurements were made and the range of masses varied between 1 to 4 mg. The heat capacities of solid and liquid were determined from three and four runs, respectively, and in this case the masses varied in the 9–15 mg range. The calibration constant of the instrument, $k = 0.0394$ cm$^{-1}$ s$^{-1}$, was obtained from seven measurements of the fusion of indium (16, 17).

*Other measurements*

Melting point, infrared, conductance, mass spectra, and thermogravimetry of the ligand and adducts were performed as before (7, 8).

## Results

The new compounds are listed in Table 1, together with analytical data, melting point, and conductivities. The melting points are not reproducible due to decomposition of the adducts during the heating. The $Cd(mu)X_2$ (X = Cl, Br) adducts did not show a liquid phase when heated up to 210°C. However, the thermograms demonstrate the loss of ligand below this temperature, which characterizes a real interval of decomposition. The $Cd(mu)X_2$ (X = Cl, Br) adducts presented a low solubility in nitromethane and acetone; for this reason their conductance values were obtained in ethanol. In comparing adducts of the same stoichiometry, the conductance data in nitromethane revealed a higher conductance of the chloride adducts, which is opposite to that found in acetone.

In observing the thermograms of the zinc and cadmium adducts, two distinct steps can be seen. First of all, the adducts lose the ligands followed by the sublimation of the halides, leaving no residue, except in the case of the zinc chloride adduct which leaves an unidentified 10% of residue. Similar

TABLE 1. Elemental analysis, conductance in nitromethane and acetone, and melting point of the adducts

| Adduct | Analysis (%)[a] M | X | N | Conductance Nitromethane (c/mmol) | Nitromethane ($\Lambda/\Omega^{-1}\,cm^2\,mol^{-1}$) | Acetone (c/mmol) | Acetone ($\Lambda/\Omega^{-1}\,cm^2\,mol^{-1}$) | Melting point (K) |
|---|---|---|---|---|---|---|---|---|
| $Zn(mu)_2Cl_2$ | 22.88(22.98) | 24.75(24.93) | 20.42(19.69) | 0.90 | 7.97 | 1.04 | 1.30 | 322–325 |
| $Zn(mu)_2Br_2$ | 17.62(17.50) | 42.73(42.80) | 15.21(15.00) | 0.98 | 3.98 | 0.99 | 2.21 | 325–328 |
| $Cd(mu)Cl_2$ | 43.49(43.67) | 27.10(27.54) | 11.20(10.89) | 1.03 | 4.45[b] | — | — | >483 |
| $Cd(mu)Br_2$ | 32.34(32.46) | 46.18(46.15) | 8.15 (8.09) | 1.20 | 2.58[b] | — | — | >483 |
| $Hg(mu)Cl_2$ | 57.84(58.04) | 19.64(19.71) | 8.63 (8.11) | 1.00 | 5.73 | 1.00 | 0.75 | 403–406 |
| $Hg(mu)Br_2$ | 45.91(46.16) | 36.53(36.78) | 6.66 (6.44) | 1.00 | 2.76 | 1.00 | 1.01 | 421–423 |

[a]Calculated values are given in parentheses.
[b]Conductance in ethanol.

thermograms are displayed for the adducts of mercury, in which the total mass loss is observed in only one step. All thermograms showed a loss of mass very well correlated with the stoichiometry of the adducts.

The mass spectrum of the ligand (18) showed the peak of the parent ion at $m/e$ 74 and the fragments: 58 $CH_3NHCO$ and 44 $HN(CH_3)_2$. These same peaks appeared in the spectra of the zinc and cadmium adducts, while in the mercury adducts the peaks of the mercury halides and metal were also observed.

The standard enthalpy of the reaction in the condensed phase, $MX_2(s) + n\,mu(s) = M(mu)_n X_2(s)$; $\Delta H_R^\ominus$, was obtained in ethanol or methanol. $\Delta H_R^\ominus$ values are derived from the individual enthalpies of solution of reactions 1, 2, and 3 of Table 2.

The standard enthalpy of formation of the adducts ($\Delta H_f^\ominus$) can be determined from the enthalpy of formation of metal halides (19), the enthalpy of formation of the ligand, and the enthalpy of the reaction in condensed phase, $\Delta H_R^\ominus$. The enthalpy of formation of mu was obtained by six measurements of the enthalpy of combustion: $C_2H_6N_2O(s) + 3O_2(g) = 2CO_2(g) + 3H_2O(l) + N_2(g)$; $\Delta H_c^\ominus = -(1358.3\pm7.6)$ kJ mol$^{-1}$ which gave the standard enthalpy of formation $\Delta H_f^\ominus(mu,s) = -(286\pm15)$ kJ mol$^{-1}$. In all those determinations the error quoted is twice the standard deviation of the mean and included all the uncertainty of the auxiliary data used.

A sharp peak at 373 K which corresponds to fusion and yields the value $\Delta H_{fus}^\ominus = (14.9\pm0.2)$ kJ mol$^{-1}$ was observed from the dsc thermograms of methylurea. The heat capacities of the solid and liquid forms of the ligand were also obtained and gave 0.093 and 0.184 kJ mol$^{-1}$ K$^{-1}$, respectively. Attempts were made to measure the enthalpy of vaporization ($\Delta H_v^\ominus$) of the ligand, but it decomposes at its temperature of normal ebulition. Thus, $\Delta H_v^\ominus$ was calculated by means of Riedel–Plack–Miller equations (20) and the obtained value was 58.8 kJ mol$^{-1}$. The heat capacity in the gas phase of mu was estimated by the method of generalized vibrational assignment (21) by means of the expression:

$$Cp(g) = -10 \times 10^{-3} + 2.96 \times 10^{-4}T - 11.9 \times 10^{-8}T^2$$

Now the standard enthalpy of sublimation of the ligand can be obtained from

$$\Delta H_{sub}^\ominus(298\ K) = \int_{298}^{373} Cp(s)dT + \Delta H_{fus}^\ominus(373\ K) + \int_{373}^{453} Cp(l)dT + \Delta H_{vap}^\ominus(453\ K) - \int_{298}^{453} Cp(g)dT$$

giving the value, $\Delta H_{sub}^\ominus = 78.2$ kJ mol$^{-1}$.

TABLE 2. Standard enthalpy of dissolution necessary to calculate the standard enthalpy of reaction in condensed phase, $\Delta H_R^\ominus = \Delta H_1^\ominus + \Delta H_2^\ominus - \Delta H_3^\ominus$

| Reaction[a] | $\Delta H^\ominus$/kJ mol$^{-1}$ |
|---|---|
| (1) $ZnCl_2(s) + EtOH = ZnCl_2(EtOH)$ | −43.33±0.77 |
| (2) $ZnCl_2(EtOH) + 2mu(s) = Zn(mu)_2Cl_2(EtOH)$ | 31.98±0.28 |
| (3) $Zn(mu)_2Cl_2(s) + EtOH = Zn(mu)_2Cl_2(EtOH)$ | 24.92±0.33 |
| (1) $ZnBr_2(s) + MeOH = ZnBr_2(MeOH)$ | −56.98±0.93 |
| (2) $ZnBr_2(MeOH) + 2mu(s) = Zn(mu)_2Br_2(MeOH)$ | 28.85±0.23 |
| (3) $Zn(mu)_2Br_2(s) + MeOH = Zn(mu)_2Br_2(MeOH)$ | 9.39±0.16 |
| (1) $CdCl_2(s) + EtOH = CdCl_2(EtOH)$ | −11.96±0.16 |
| (2) $CdCl_2(EtOH) + mu(s) = Cd(mu)Cl_2(EtOH)$ | 12.38±0.15 |
| (3) $Cd(mu)Cl_2(s) + EtOH = Cd(mu)Cl_2(EtOH)$ | 23.20±0.15 |
| (1) $CdBr_2(s) + EtOH = CdBr_2(EtOH)$ | −6.13±0.12 |
| (2) $CdBr_2(EtOH) + mu(s) = Cd(mu)Br_2(EtOH)$ | 15.52±0.12 |
| (3) $Cd(mu)Br_2(s) + EtOH = Cd(mu)Br_2(EtOH)$ | 18.97±0.20 |
| (1) $HgCl_2(s) + MeOH = HgCl_2(MeOH)$ | −1.60±0.01 |
| (2) $HgCl_2(MeOH) + mu(s) = Hg(mu)Cl_2(MeOH)$ | 15.10±0.11 |
| (3) $Hg(mu)Cl_2(s) + MeOH = Hg(mu)Cl_2(MeOH)$ | 27.41±0.40 |
| (1) $HgBr_2(s) + EtOH = HgBr_2(EtOH)$ | 3.14±0.03 |
| (2) $HgBr_2(EtOH) + mu(s) = HgBr_2(EtOH)$ | 14.73±0.08 |
| (3) $Hg(mu)Br_2(s) + EtOH = Hg(mu)Br_2(EtOH)$ | 31.16±0.48 |

[a]MeOH = methanol, EtOH = ethanol.

Can. J. Chem. Downloaded from www.nrcresearchpress.com by 210.87.254.40 on 09/06/12
For personal use only.

TABLE 3. Summary of thermochemical (kJ mol$^{-1}$) and infrared (cm$^{-1}$) data for methylurea and adducts

| Compound | $\Delta H_R^\ominus$ | $\Delta H_f^\ominus$ | $\Delta H_D^\ominus$ | $\Delta H_M^\ominus$ | $\Delta H_{M-O}^\ominus$ | $\nu_{CO}$ | $\nu_{CN}$ | $\nu_{NH}$ |
|---|---|---|---|---|---|---|---|---|
| mu | | −286±15 | | | | 1650 | 1570 | 3420,3325,3200,3110 |
| $Zn(mu)_2Cl_2$ | −36.27±0.51 | −1024 | 192.7 | −341.7 | 132 | 1635 | 1600 | 3440,3400,3340 |
| $Zn(mu)_2Br_2$ | −37.52±0.97 | − 938 | 194.0 | −325.0 | 123 | 1620 | 1598 | 3450,3400,3350 |
| $Cd(mu)Cl_2$ | −22.78±0.26 | − 701 | 101.0 | −182.2 | 204 | 1632 | 1605 | 3475,3420,3370 |
| $Cd(mu)Br_2$ | − 9.58±0.26 | − 612 | 87.8 | −239.3 | 161 | 1630 | 1605 | 3475,3420,3365 |
| $Hg(mu)Cl_2$ | −13.91±0.41 | − 524 | 92.1 | −175.0 | 97 | 1620 | — | 3440,3338,3305 |
| $Hg(mu)Br_2$ | −13.29±0.48 | − 470 | 91.5 | −175.6 | 97 | 1620 | — | 3458,3338 |

From thermodynamic cycles, the standard enthalpies of reactions $M(mu)_nX_2(s) = MX_2(s) + n\,mu(g)$; $\Delta H_D^\ominus$ and $MX_2(g) + n\,mu(g) = M(mu)_nX_2(s)$; $\Delta H_M^\ominus$ could also be calculated and these values are summarized in Table 3. In this table only the infrared bands which indicate the coordination of the ligand to the metal, i.e., the CO and NH stretching vibrations, are listed.

## Discussion

The infrared spectrum of methylurea (4) exhibits a large splitting of the NH stretching frequency due to the presence of hydrogen bonding, whose presence is also revealed in the adducts, but at higher frequencies, see Table 3. The very strong bands at 1650 and 1570 cm$^{-1}$ in the free ligand are assigned to CO stretching frequency and CN stretching vibration or amide II, respectively. After coordination both bands remain with their same intensities; however, their frequencies shift in opposite directions (22). The decrease of νCO and the increase of νCN and νNH frequencies are evidence that the carbonyl group of the ligand is coordinated to the metal. It is worthwhile to mention that the CO out-of-plane deformation, which appeared at 655 cm$^{-1}$ in the free ligand, did not change its position in the adducts.

The molar conductivities of the new adducts are typical for non-electrolytes. The conductance for a 1:1 electrolyte type in nitromethane, acetone, and ethanol should be in the intervals 75–95, 100–140, and 35–45 Ohm$^{-1}$ cm$^2$ mol$^{-1}$, respectively (23). The low values listed in Table 1 suggest that the halides are coordinated to the metal and their conductivities are probably due to a small degree of solvolysis of the adduct in this solvent (24).

The heats of formation of the adducts in the condensed phase ($\Delta H_R^\ominus$) have been used to compare the acidity of metals and the basicity of ligands for adducts of the same structure (13, 25). In our results it is difficult to establish an order of acidity for all elements of the family because of the variation of the stoichiometry of the adducts. Nevertheless, the acidity order, $CdCl_2 > HgCl_2$, is observed, but the inverse order appeared with the bromides (Table 3), assuming that these adducts have the same crystal structures. The apparent anomaly observed for Cd and Hg can be explained through the effects of lattice energy. This fact is demonstrated by the enthalpy of dissolution of the adduct of mercury (31.16±0.48) which is somewhat higher than that of the cadmium adduct (18.97±0.20), see Table 2.

In connection with other urea derivatives it is worthwhile to consider the $\Delta H_R^\ominus$ values for adducts of tetramethylurea (7), dimethylurea (8), and methylurea. For example, $ZnL_2Br_2$ showed $\Delta H_R^\ominus$/kJ mol$^{-1}$: −88.68±1.32; −55.87±0.97, and −37.52±0.97, for L = tmu, dmu, and mu, respectively. These results enable us to establish the basicity order, tmu > dmu > mu. This sequence reflects that the donor ability of the ligand is associated with the electronic density of the oxygen, which is derived from the inductive effect of the methyl groups linked to the nitrogen atoms. Bearing in mind that these ligands involve a gradual decrease in $\Delta H_R^\ominus$ from tmu to mu, the great difference between tmu and dmu (compare 33 kJ mol$^{-1}$ from tmu to dmu and 18 kJ mol$^{-1}$ dmu to mu) can be attributed to the absence of trimethylurea results.

The adduct lattice enthalpy ($\Delta H_M^\ominus$) and $\Delta H_D^\ominus$, which is the enthalpy of the inverse of the decomposition reaction (Table 3), decrease from zinc to mercury. Both thermochemical parameters have been used to compare and systematize adducts which do not sublime without decomposition (7, 8, 26, 27). The enthalpy of formation of the adducts also presents the same trend in variation.

Under the conditions of the physical measurements such as melting point, thermogravimetry, and mass spectrometry one knows that the adducts decompose during the heating and the enthalpy of sublimation of the adduct is not accessible experimentally (26). In this case, the enthalpy of metal–ligand bond can be estimated (7, 8, 26). For that evaluation the enthalpy of reaction in the gas phase: $MX_2(g) + n\,mu(g) = M(mu)_nX_2(g)$; $\Delta H_g^\ominus$, was considered and this enthalpy was calculated by means of an appropriate thermochemical cycle. In

Can. J. Chem. Downloaded from www.nrcresearchpress.com by 210.87.254.40 on 09/06/12
For personal use only.

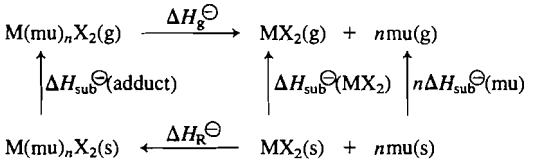


such a way, it was assumed that the enthalpy of 1 mol of ligand is equal to the enthalpy of sublimation of the adduct (26). It is clearly known from infrared spectra that the metal is bound to oxygen, so $\Delta H_g^\ominus/n = \Delta H_{(M-O)}^\ominus$ and its value is higher for monoadducts, as was observed previously. For adducts of the same stoichiometry, $\Delta H_{(M-O)}^\ominus$ presents high values for Cd. The small $\Delta H_{(M-O)}^\ominus$ value for mercury should reflect its different bonding characteristics in relation to the other elements within the family, also it does not correlate with the shift in frequency of CO stretching frequency upon coordination. Of course, it must be remembered that this vibration is probably subject to extensive coupling. Of further interest, the large shift of νCO is observed with adducts of mercury, which have small $\Delta H_{(M-O)}^\ominus$.

**Acknowledgement**

The authors express their gratitude to FINEP for financial support and CNPq for the award of a fellowship (to F.P.A.).

1. M. Nardelli and L. Coghi. Ric. Sci. **28**, 379 (1958).
2. M. Nardelli and L. Coghi. Ric. Sci. **29**, 134 (1959).
3. M. Nardelli, L. Coghi, and G. Azzoni. Gaz. Chim. Ital. **88**, 235 (1958).
4. C. N. R. Rao, G. C. Chaturvedi, and R. K. Gosavi. J. Mol. Spectrosc. **28**, 526 (1968).
5. Y. Saito, K. Machida, and T. Uno. Spectrochim. Acta, **31A**, 1237 (1975).
6. R. A. Bailey and W. J. Tangredi. J. Inorg. Nucl. Chem. **38**, 2221 (1976).
7. C. Airoldi, A. P. Chagas, and F. P. Assunção. J. Chem. Soc. Dalton Trans. 1823 (1980).
8. F. P. Assunção, A. P. Chagas, and C. Airoldi. J. Chim. Phys. In press.
9. J. D. Cox and G. Pilcher. Thermochemistry of organic and organometallic compounds. Academic Press, London. 1970.
10. P. Tavernier and M. Samouroux. Mem. Poudres, **38**, 65 (1956), Chem. Abstr. **51**, 14403h (1957).
11. A. Luttringhaus and H. W. Dirksen. Angew. Chem. Internat. Ed. **3**, 260 (1964).
12. T. A. Zordan, D. G. Hurkot, M. Peterson, and L. G. Hepler. Thermochim. Acta, **5**, 21 (1972).
13. A. S. Gonçalves, A. P. Chagas, and C. Airoldi. J. Chem. Soc. Dalton Trans. 159 (1979).
14. M. Colomina, P. Jimenez, M. V. Roux, and C. Turrion. J. Chem. Thermodyn. **10**, 661 (1978).
15. Codata, J. Chem. Thermodyn. **4**, 331 (1971).
16. M. J. O'Neill. Anal. Chem. **38**, 1331 (1966).
17. W. W. Wendlandt. Thermal methods of analysis. John Wiley and Sons, New York. 1974.
18. M. A. Baldwin, A. M. Kirkien-Konasiewicz, A. G. London, A. Maccol, and D. Smith. J. Chem. Soc. B, 34 (1968).
19. D. D. Wagman, W. H. Evans, V. B. Parker, I. Halow, S. W. Baley, and R. H. Schumm. Selected values of chemical thermodynamic properties. Tech. Note 270-3 and 270-4. Natl. Bur. Stand. Washington DC. 1968.
20. R. C. Reid and T. K. Sherwood. The properties of gases and liquids. 2nd. ed. McGraw-Hill, New York. 1968.
21. G. J. Janz. Thermodynamic properties of organic compounds. Revised ed. Academic Press, New York. 1968.
22. J. Maslowska and K. Cedzynska. J. Mol. Struct. **19**, 521 (1973).
23. W. J. Geary. Coord. Chem. Rev. 7, 81 (1971).
24. G. Marcotrigiano, G. Peyronel, and R. Battistuzzi. J. Inorg. Nucl. Chem. **37**, 1675 (1975).
25. J. W. Wilson and I. J. Worral. J. Inorg. Nucl. Chem. **31**, 1357 (1969).
26. R. A. Jorge, C. Airoldi, and A. P. Chagas. J. Chem. Soc. Dalton Trans. 1102 (1978).
27. J. Barnes and C. S. Ducan. J. Chem. Soc. Dalton Trans. 1732 (1972).

Can. J. Chem. Downloaded from www.nrcresearchpress.com by 210.87.254.40 on 09/06/12
For personal use only.

# A low-temperature structural phase transition in aqueous dimyristoyl phosphatidylcholine bilayers observed by Raman scattering[1]

PATRICK T. T. WONG AND HENRY H. MANTSCH

*Division of Chemistry, National Research Council of Canada, Ottawa, Ont., Canada K1A 0R6*

Received April 15, 1982

PATRICK T. T. WONG and HENRY H. MANTSCH. Can. J. Chem. **60**, 2137 (1982).

A new structural phase change at −60°C and atmospheric pressure was observed in the gel phase of aqueous DMPC dispersions. This gel–gel phase transition exhibits first-order characteristics and is equivalent to the phase transition observed at 2.6 kbar and 30°C. The decrease in temperature has analogous effects on the ordering of the acyl chains in DMPC as has the increase in pressure. The rigid interchain reorientational fluctuations in the gel phase are gradually damped with decreasing temperature and below −60°C the interchain orientation becomes highly ordered.

PATRICK T. T. WONG et HENRY H. MANTSCH. Can. J. Chem. **60**, 2137 (1982).

On a observé un nouveau changement structural de phase à 60°C et à la pression atmosphérique dans la phase gel des dispersions aqueuses du CDMP. Cette transition de phase gel–gel a des caractéristiques d'ordre un et équivaut à la transition de phase observée à 2,6 kbar et à 30°C. La diminution de température a des effets analogues sur l'agencement des chaînes acyles du CDMP lorsque la pression augmente. Les fluctuations dans la réorientation entre chaînes rigides de la phase gel sont amorties graduellement lorsque la température diminue; et en-dessous de −60°C, l'orientation entre les interchaines devient fortement ordonnée.

[Traduit par le journal]

## Introduction

Temperature-induced phase transitions in dimyristoyl phosphatidylcholine (DMPC) – water dispersions have been extensively studied (1–5). Two first-order phase transitions have been found at 24°C and 14°C and are generally referred to as the main transition and the pretransition, respectively. In a recent study (6) we have shown that the temperature of the main transition ($T_m$) and that of the pretransition ($T_p$) can be raised to 30°C by increasing the hydrostatic pressure to 0.15 and 1 kbar, respectively. In addition, a third first-order gel–gel phase transition was found at 2.6 kbar and 30°C. According to the thermodynamic Clausius–Clapeyron relationship, one may predict that this latter gel–gel phase transition should also occur at low temperature and atmospheric pressure. Yellin and Levin (7) have studied the temperature dependence of the Raman spectrum of DMPC–water dispersions from temperatures slightly below that of the pretransition to about −180°C. No cooperative phase transition was found in this temperature region; however, an inflection point at −40°C in the plot of the peak height ratio between the antisymmetric and the symmetric $CH_2$ stretching bands was observed in their study and was attributed to the onset of the *gauche–trans* isomerization in the acyl chains.

In the present work we have performed a detailed study of the temperature dependence of the frequencies and widths of various Raman bands of DMPC–water dispersions in the gel phase with the hope to detect a phase transition at low-temperature and atmospheric pressure, which would correspond to that observed at high pressure (6). We were aided considerably by instrumental and computational improvements with our Raman system, which enabled us to detect discontinuities in frequency of less than 1 $cm^{-1}$ (6).

## Experimental

DMPC–water dispersions containing 33.5 wt% water was prepared as previously described (6). The DMPC sample was placed in a quartz capillary which was mounted in a low-temperature system cooled by boiling liquid nitrogen. A chromel–alumel thermocouple was taped on the capillary tube as close as possible to the laser beam transit. Temperature control was maintained within ±1°C.

The Raman spectra were excited by using the 5145 nm argon line with a power of 200 mW at the sample from a CRL model 12 argon ion laser. The temperature increase due to the local heating by the 200 mW laser beam was estimated to be 2°C (6). The Raman spectra with a resolution of 2 $cm^{-1}$ were recorded with a Spex Model 14018 double monochromator having 1800 lines/mm holographic gratings and a cooled RCA C31034 photomultiplier. The data acquisition system and the data treatment have been described previously (6).

## Results

Raman spectra of DMPC–water dispersions in the gel phase were measured in the C—H stretching (2770–3100 $cm^{-1}$), the $CH_2$ bending (1350–1520 $cm^{-1}$), the $CH_2$ twisting (1270–1350 $cm^{-1}$), and the C—C skeletal stretching (960–1270 $cm^{-1}$) regions, at various temperatures between 9 and −120°C. Representative spectra are shown in Fig. 1.

[1]NRCC No. 20060.

0008-4042/82/162137-04$01.00/0

©1982 National Research Council of Canada/Conseil national de recherches du Canada

Can. J. Chem. Downloaded from www.nrcresearchpress.com by 210.87.254.105 on 09/06/12
For personal use only.

Can. J. Chem. Downloaded from www.nrcresearchpress.com by 210.87.254.105 on 09/06/12
For personal use only.

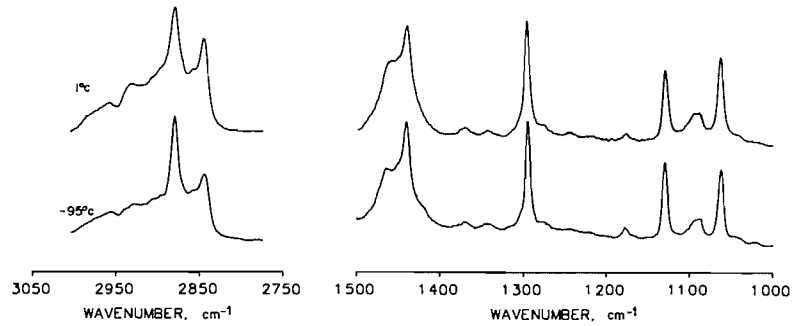


FIG. 1. Representative Raman spectra above (1°C) and below (−95°C) the GII to GIII phase transition.

The temperature dependencies of the frequencies and band-widths of these Raman bands are shown in Fig. 2. Discontinuities near −60°C are observed in the temperature–frequency plots for all these modes. The widths of most of the Raman bands decrease considerably with decreasing temperature between 9 and −60°C. Below −60°C the band-widths are constant or decrease only slightly with decreasing temperature. An exception is the symmetric $CH_2$ stretching vibration, the width of which increases with decreasing temperature, reaches a maximum at −60°C, and decreases thereafter.

The ratio of peak heights between the antisymmetric and the symmetric $CH_2$ stretching bands, H2885/H2845, is plotted against temperature in Fig. 3. This ratio first increases with decreasing temperature but becomes almost constant below −60°C.

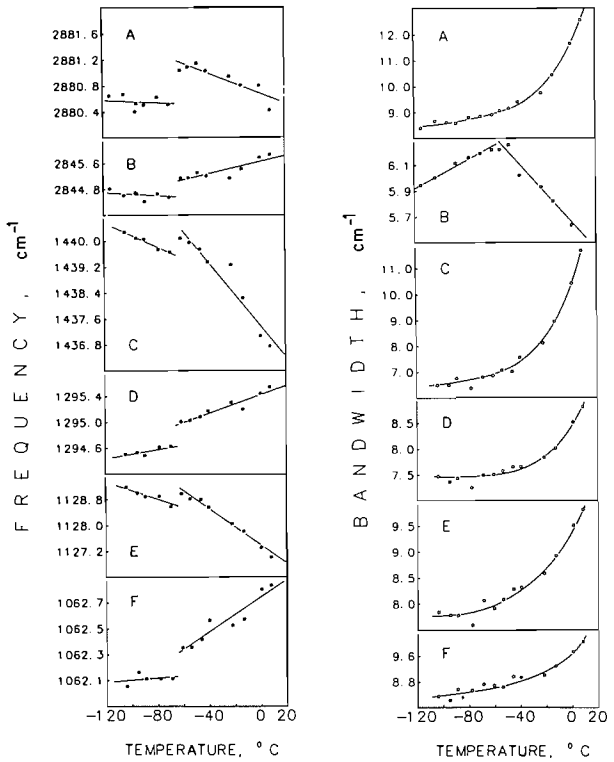


FIG. 2. Frequencies (closed symbols) and band-widths (open symbols) of selected Raman bands of DMPC as a function of temperature. *A*: antisymmetric $CH_2$ stretch; *B*: symmetric $CH_2$ stretch; *C*: $CH_2$ bend; *D*: $CH_2$ twist; *E*: asymmetric C—C stretch; *F*: symmetric C—C stretch. Band-widths were measured at different peak-heights: *A* (0.75), *B* (0.9), *C* (0.8), and *D*, *E*, *F* (0.5).

## Discussion

The changes near −60°C in the temperature dependencies of the band-frequencies, band-widths, and the peak height ratio, H2880/H2845, shown in Figs. 2 and 3 clearly indicate that a structural phase transition takes place at this temperature. The Raman spectra at temperatures between 9 and −60°C are similar to those observed at pressures between 1 and 2.6 kbar (6); the spectra in the C—H stretching region resemble those observed in *n*-alkanes with hexagonal interchain packing (8). Below −60°C, the Raman spectra are similar to those observed at pressures above 2.6 kbar and the spectra in the C—H stretching region resemble those of *n*-alkanes with orthorhombic or monoclinic interchain packing (8). Furthermore,

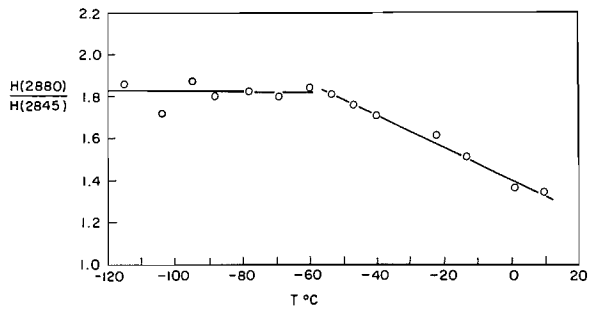


FIG. 3. Temperature dependence of the peak height ratio H2880/H2845.

Can. J. Chem. Downloaded from www.nrcresearchpress.com by 210.87.254.105 on 09/06/12
For personal use only.

the correlation field component of the $CH_2$ bending mode near 1410 $cm^{-1}$, which is a characteristic band for *n*-alkanes and polyethylene with the orthorhombic subcell structure, appears in the spectra immediately below −60°C. As the spectral features observed at temperatures below and above −60°C are similar to those observed at pressures above and below 2.6 kbar, respectively, the gel phases above and below −60°C can be identified with the gel phases below and above 2.6 kbar, designated in ref. 6 as GII and GIII phases, respectively. Thus, the phase transition at −60°C can be associated with a structural change from the GII gel phase at temperatures above −60°C to the GIII gel phase at temperatures below −60°C. From X-ray studies the GII phase has been correlated with distorted hexagonal (9) or quasi-orthorhombic (10) chain packing. However, diffraction studies of the GIII phase are required to determine the exact nature of the structural change at this phase transition. Although the phase behaviour of DMPC–water has not been explored at temperatures below −10°C, the changes observed at −60°C could possibly be correlated with a transition between the two lamellar gel phases $L_{\beta'}$ and L (9).

The change in band-width observed in the depolarized and weakly polarized bands when the temperature was decreased from 9 to −60°C is comparable with that observed at constant temperature when the pressure was increased from 1 to 2.6 kbar. For instance, the half-width of the 1295 $cm^{-1}$ band decreases in the GII phase from 8.8 $cm^{-1}$ at 9°C to 7.5 $cm^{-1}$ at −60°C while it decreases from 8.5 $cm^{-1}$ at ~ 1 kbar to 7.4 $cm^{-1}$ at ~ 2.6 kbar (6). This decrease in band-width is largely due to the damping of the large angle reorientational fluctuation about the long axis of the acyl chains. At temperatures near $T_p$ (9, 11) or at pressures near 1 kbar (6) there are rapid reorientational fluctuations about the long axis of the acyl chains. It is well documented (12, 13) that the narrowing of the depolarized and weakly polarized Raman bands mainly arises from the decrease in the rate of such reorientational fluctuations. Below −60°C the widths of the depolarized and weakly polarized bands are much less sensitive to temperature, a situation similar to that observed in the high pressure GIII phase (6), indicating that the acyl chains are highly orientationally ordered in this phase. On the other hand, the width of the highly polarized 2845 $cm^{-1}$ band (symmetric $CH_2$ stretch), which is not affected by the reorientational fluctuation but is strongly affected by intermolecular interactions and vibrational relaxation (14–16), increases in the GII phase with decreasing temperature (Fig. 2*B*). The same effect was observed when the pressure was increased throughout the GII phase (6). However, below −60°C the width of this polarized band decreases slightly with decreasing temperature. This indicates that in the GIII phase the contribution of the intramolecular anharmonicity, which would narrow the width of this polarized band (16) as the temperature decreases, dominates that of the interchain interaction.

Isotopic dilution studies at constant temperature (8, 17, 18) have shown that the peak height ratio H2880/H2845 represents a measure of the magnitude of interchain interactions. We found earlier (6) that at constant temperature the H2880/H2845 ratio, and thus the interchain interaction, increased in the GII phase with increasing pressure due to the pressure damping of the reorientational fluctuation. In the present study we found that at constant pressure the H2880/H2845 ratio increases linearly with decreasing temperature in the GII phase. The total change observed in this ratio in the temperature range of the GII phase is comparable with that observed in the pressure range of the GII phase (6). We therefore conclude that the increase in the H2880/H2845 ratio observed in the present work is largely due to the increased interchain interaction rather than the decrease in the number of the *gauche* conformers in the acyl chains (7). The increase in interchain interaction with decreasing temperature is undoubtedly the result of the damping of the reorientational fluctuation as demonstrated by the temperature dependence of the widths of the depolarized and weakly polarized Raman bands. The increase in interchain coupling with decreasing temperature is also evident from the increase in the width of the highly polarized 2845 $cm^{-1}$ Raman band with decreasing temperature. In the GIII phase the H2880/H2845 ratio is almost independent of temperature, which implies that due to the highly ordered structure of the acyl chains in this phase, the interchain coupling does not increase by further lowering the temperature. Thus, the changes observed in DMPC–water dispersions at −60°C have all the characteristics of the GII to GIII phase transition previously found to occur at 2.6 kbar and 30°C.

**Acknowledgement**

We wish to thank Dr. D. G. Cameron for helpful discussions.

1. M. J. JANIAK, D. M. SMALL, and G. G. SHIPLEY. Biochemistry, **15**, 4575 (1976).
2. N. YELLIN and I. W. LEVIN. Biochemistry, **16**, 642 (1977).
3. J. F. NAGLE and D. A. WILKINSON. Biophys. J. **23**, 159 (1978).

4. R. M. EPAND and R. F. EPAND. Chem. Phys. Lipids, **27**, 139 (1980).
5. S. C. CHEN and J. M. STURTEVANT. Biochemistry, **20**, 713 (1981).
6. P. T. T. WONG, W. F. MURPHY, and H. H. MANTSCH. J. Chem. Phys. **76**, 5230 (1982).
7. N. YELLIN and I. W. LEVIN. Biochim. Biophys. Acta, **489**, 177 (1977).
8. R. G. SNYDER, S. L. HSU, and S. KRIMM. Spectrochim. Acta, **34A**, 395 (1978).
9. M. J. JANIAK, D. M. SMALL, and G. G. SHIPLEY. J. Biol. Chem. **254**, 6068 (1979).
10. M. RUOCCO and G. G. SHIPLEY. Biochim. Biophys. Acta, **684**, 59 (1982).
11. A. TARDIEU, V. LUZZATI, and F. C. REMAN. J. Mol. Biol. **75**, 711 (1973).
12. A. V. RAKOV. Opt. Spectrosc. **7**, 128 (1959).
13. F. J. BARTOLI and T. A. LITOVITZ. J. Chem. Phys. **56**, 404 (1972).
14. M. KOBAYASHI and H. TODOKORO. J. Chem. Phys. **73**, 3635 (1980).
15. D. F. HORNIG. J. Chem. Phys. **16**, 1063 (1948).
16. R. J. ABBOTT and D. W. OXTOBY. J. Chem. Phys. **70**, 4703 (1979).
17. B. P. GABER and W. L. PETICOLAS. Biochim. Biophys. Acta, **465**, 260 (1977).
18. R. MENDELSOHN and C. C. KOCH. Biochim. Biophys. Acta, **598**, 260 (1980).

Can. J. Chem. Downloaded from www.nrcresearchpress.com by 210.87.254.105 on 09/06/12
For personal use only.

# Heat capacities and volumes of dissociation of phosphoric acid (1st, 2nd, and 3rd), bicarbonate ion, and bisulfate ion in aqueous solution

JOHN W. LARSON,[1] KEVIN G. ZEEB, AND LOREN G. HEPLER

*Department of Chemistry and Oil Sands Research Laboratory, University of Lethbridge, Lethbridge, Alta., Canada T1K 3M4*

Received January 18, 1982

JOHN W. LARSON, KEVIN G. ZEEB, and LOREN G. HEPLER. Can. J. Chem. **60**, 2141 (1982).

Measurements at 25°C with a flow calorimeter and a flow densimeter have led to heat capacities and densities of aqueous solutions of $H_3PO_4$, $NaH_2PO_4$, $Na_2HPO_4$, $Na_3PO_4$, $NaHCO_3$, $Na_2CO_3$, $H_2SO_4$, and various buffer solutions. Results are presented in terms of apparent molar heat capacities ($\phi_C$) and apparent molar volumes ($\phi_V$). Analysis of the experimental $\phi_V$ values to obtain the desired standard state $\phi_V^0$ values for single electrolytes requires that allowance be made for hydrolysis and dissociation reactions of certain solutes, along with extrapolation to zero concentration. Analysis of $\phi_C$ values requires similar considerations of hydrolysis and dissociation reactions, allowance for enthalpy and equilibrium changes ("relaxation") during calorimetric measurements, and extrapolation to zero concentration. Procedures for these calculations are presented. The $\phi_C^0$ and $\phi_V^0$ values that result from all of these measurements and calculations are used to obtain $\Delta C_p^0$ and $\Delta V^0$ values for acid dissociation reactions, which are then related to effects of temperature and pressure on other thermodynamic properties.

JOHN W. LARSON, KEVIN G. ZEEB et LOREN G. HEPLER. Can. J. Chem. **60**, 2141 (1982).

Des mesures à 25°C, à l'aide d'un calorimètre à écoulement et d'un densimètre à écoulement, ont conduit aux capacités calorifiques et aux densités des solutions aqueuses de $H_3PO_4$, $NaH_2PO_4$, $Na_2HPO_4$, $Na_3PO_4$, $NaHCO_3$, $H_2SO_4$ et de plusieurs solutions tampons. On présente les résultats en termes de capacités calorifiques molaires apparentes, ($\phi_C$), et de volumes molaires apparents, ($\phi_V$). Lorsqu'on effectue une analyse des valeurs expérimentales de $\phi_V$, en vue d'obtenir les valeurs $\phi_V^0$ de l'état standard d'électrolytes spécifiques, on doit tenir compte des réactions d'hydrolyse et de dissociation de certains solutés en plus de faire une extrapolation à dilution infinie. Pour faire une analyse des valeurs $\phi_C$, on doit aussi prendre en considération les réactions d'hydrolyse et de dissociation, on doit tenir compte des variations d'enthalpie et d'équilibre ("relaxation") pendant les mesures calorimétriques et faire une extrapolation à concentration zéro. On présente les marches à suivre pour ces calculs. On a utilisé les valeurs de $\phi_C^0$ et de $\phi_V^0$ qui résultent de toutes ces mesures et de tous ces calculs, pour obtenir les valeurs de $\Delta C_p^0$ et de $\Delta V^0$ pour les réactions de dissociation des acides que l'on peut alors relier aux effets de température et de pression sur d'autres propriétés thermodynamiques.

[Traduit par le journal]

## Introduction

The thermodynamic properties of the aqueous acids listed in the title are important in such fields as boiler water chemistry, interaction of aqueous solutions with minerals, biochemistry, marine science, and analytical chemistry. The research to be described in this paper was undertaken to provide information about changes in heat capacity ($\Delta C_p^0$) and volume ($\Delta V^0$) accompanying dissociation of these acids and then to use these values in calculations of the thermodynamics of dissociation over ranges of temperature and pressure. Obtaining the desired standard state changes in volume from measured densities of solutions requires appropriate extrapolations to zero concentration and also "corrections" for such chemical reactions as hydrolysis and dissociation, for which we have developed convenient methods. Evaluation of standard state changes in heat capacities involves similar "corrections" and extrapolations and also requires that allowance be made for "relaxation" effects that are associated with the changes in equilibrium states that occur with changing temperature during the course of calorimetric measurements of heat capacities.

## Experimental

Our heat capacity measurements have been made with a Picker flow calorimeter of the type previously described (1). A *small* systematic error in measurements with this calorimeter has been detected and corrected on the basis of measurements (2–4) on NaCl (aq) solutions. Densities of solutions were measured with a flow densimeter (5). Results of all of these measurements refer to (25.0 ± 0.1)°C.

BDH AnalaR grade $Na_2CO_3$ was dried at 270°C. BDH reagent grade $NaH_2PO_4$ and $Na_3PO_4$ were recrystallized from water–ethanol and dried at 150°C. Fisher certified $Na_2HPO_4 \cdot 7H_2O$ and Baker reagent grade $NaHCO_3$ were used as received. The $Na_2HPO_4 \cdot 7H_2O$ was analyzed for water by heating to constant weight at 150°C.

All compounds mentioned above were titrated with standardized HCl or NaOH and found to contain no appreciable acid–base impurities and had overall purities of not less than 99.7%.

Stock solutions of sulfuric acid and phosphoric acid were prepared from ACS reagent grade concentrated acids and distilled water, and were then analyzed by titration with standardized NaOH solutions.

Buffer solutions of $NaHCO_3/Na_2CO_3$ and $NaH_2PO_4/Na_2H$-

[1]Visiting scientist from Department of Chemistry, Marshall University, Huntington, W. VA. 25701, U.S.A.

0008-4042/82/162141-10$01.00/0

©1982 National Research Council of Canada/Conseil national de recherches du Canada

Can. J. Chem. Downloaded from www.nrcresearchpress.com by 210.87.254.40 on 09/06/12
For personal use only.

Can. J. Chem. Downloaded from www.nrcresearchpress.com by 210.87.254.40 on 09/06/12
For personal use only.

TABLE 1. Apparent molar heat capacities and volumes of aqueous $NaH_2PO_4/Na_2HPO_4$ buffers at 25.0°C

| $m$ | $\phi_C$ | $\phi_V$ | $m$ | $\phi_C$ | $\phi_V$ |
|---|---|---|---|---|---|
| mol kg$^{-1}$ | J K$^{-1}$ mol$^{-1}$ | cm$^3$ mol$^{-1}$ | mol kg$^{-1}$ | J K$^{-1}$ mol$^{-1}$ | cm$^3$ mol$^{-1}$ |
| | $F_2 = 0.900$ | | | $F_2 = 0.500$ | |
| 0.0440 | 2.2 | 27.95 | 0.0501 | −61.2 | 17.73 |
| 0.0820 | 5.0 | 28.28 | 0.0719 | −53.1 | 17.80 |
| 0.1235 | 11.7 | 28.78 | 0.1004 | −43.9 | 18.68 |
| 0.1558 | 12.7 | 28.50 | 0.1177 | −37.9 | 18.85 |
| 0.2206 | 20.4 | 28.76 | 0.1565 | −30.2 | 19.58 |
| 0.2394 | 26.7 | 29.63 | 0.2028 | −19.9 | 20.00 |
| 0.3185 | 30.9 | 29.35 | 0.2460 | −12.1 | 20.40 |
| 0.3951 | 41.6 | 30.48 | 0.2792 | 2.5 | 20.78 |
| 0.4823 | 45.1 | 30.10 | 0.3500 | 6.8 | 21.42 |
| 0.6921 | 60.9 | 30.99 | 0.4189 | 15.9 | 22.01 |
| 0.8286 | 73.2 | 32.34 | 0.4931 | 26.9 | 22.58 |
| | $F_2 = 0.100$ | | | | |
| 0.0366 | −116.1 | 7.27 | | | |
| 0.0538 | −112.2 | 7.63 | | | |
| 0.0641 | −106.5 | 7.96 | | | |
| 0.1025 | −93.1 | 8.74 | | | |
| 0.1030 | −91.3 | 8.86 | | | |
| 0.1450 | −76.6 | 9.63 | | | |
| 0.1681 | −69.8 | 9.78 | | | |
| 0.2035 | −58.0 | 10.52 | | | |
| 0.2410 | −49.2 | 10.81 | | | |
| 0.2870 | −35.9 | 11.63 | | | |
| 0.3504 | −21.7 | 12.17 | | | |

$PO_4$ were prepared from known masses of the solids and distilled water. These buffer solutions were made with mole ratios equal to 9/1, 1/1, and 1/9. Solutions of $Na_3PO_4$ were prepared from known masses of solid and distilled water. Further solutions were prepared by quantitative dilutions of several of these solutions.

## Experimental results and analyses of data

Results of measurements with the Picker flow calorimeter are heat capacities per unit volume of solution. Combination of these heat capacities with the densities that we have also measured leads to heat capacities per unit mass of solution. Further combination of these latter heat capacities with the already known (6) heat capacity of water (4.1793 J K$^{-1}$ g$^{-1}$) leads to apparent molar heat capacities. Similarly, densities of solutions in combination with the already known density of water (0.997044 g cm$^{-3}$) lead to apparent molar volumes. These apparent molar properties are defined according to

$$[1] \quad \phi_Y = Y(\text{sol'n}) - n_1 Y_1^0 / \sum_{i>1} n_i$$

in which $Y$ is the extensive property (heat capacity or volume) of a specified quantity of solution, $n_1$ is the number of moles of water in the specified quantity of solution, $Y_1^0$ is the molar property of pure water, and $n_i$ for $i > 1$ represents the numbers of moles of solutes. Results of our measurements of heat capacities and densities, expressed in terms of apparent molar heat capacities and volumes, are listed in Tables 1, 2, and 3. Treatment of these experimental results is described in the following paragraphs.

Our principal interest in this investigation has been to obtain the $\phi_C^0$ and $\phi_V^0$ values for zero concentration that are identical to the corresponding partial molar quantities that then lead to $\Delta C_p^0$ and $\Delta V^0$ values for various dissociation reactions. Analysis of our apparent molar volumes for this purpose requires that appropriate allowance be made for hydrolysis and dissociation reactions of certain solutes along with extrapolation to zero concentration. Analysis of our apparent molar heat capacities requires similar considerations of hydrolysis and dissociation reactions, allowance for enthalpy and equilibrium changes during calorimetric measurements, along with extrapolations to zero concentration. Because of their relative simplicity, we consider volumes first.

Apparent molar volumes of reasonably dilute solutions of electrolytes are accurately represented by equations of the form

$$[2] \quad \phi_V = \phi_V^0 + A_V (d_1^0)^{1/2} (\omega)^{3/2} (m)^{1/2} + B_V \omega m$$

in which $A_V$ and $\omega$ come from the Debye–Hückel theory and $B_V$ is an adjustable parameter for each solute. We have used

$$A_V (d_1^0)^{1/2} = 1.865 \text{ cm}^3 \text{ mol}^{-3/2} \text{ kg}^{1/2}$$

Can. J. Chem. Downloaded from www.nrcresearchpress.com by 210.87.254.40 on 09/06/12
For personal use only.

TABLE 2. Apparent molar heat capacities and volumes of aqueous $NaHCO_3/Na_2CO_3$ buffers at 25.0°C

| $m$ | $\phi_C(\phi_C^{sp})$ | $\phi_V$ | $m$ | $\phi_C(\phi_C^{sp})$ | $\phi_V$ |
|---|---|---|---|---|---|
| mol kg$^{-1}$ | J K$^{-1}$ mol$^{-1}$ | cm$^3$ mol$^{-1}$ | mol kg$^{-1}$ | J K$^{-1}$ mol$^{-1}$ | cm$^3$ mol$^{-1}$ |
| | $F_2 = 0.900$ | | | $F_2 = 0.500$ | |
| 0.0660 | −25.2(−25.7) | 20.85 | 0.0568 | −82.7(−87.7) | 10.30 |
| 0.0788 | −15.9(−16.9) | 21.60 | 0.0844 | −82.2(−85.3) | 9.95 |
| 0.1418 | −12.3(−12.5) | 21.44 | 0.1021 | −74.8(−77.3) | 10.39 |
| 0.1621 | −7.3(−7.5) | 21.93 | 0.1518 | −68.5(−70.1) | 10.72 |
| 0.2435 | −2.4(−2.5) | 21.96 | 0.1847 | −61.2(−62.5) | 11.14 |
| 0.2837 | 3.6(3.5) | 22.50 | 0.2376 | −57.1(−58.1) | 11.39 |
| 0.3887 | 9.7(9.6) | 22.53 | 0.2903 | −45.5(−46.3) | 11.95 |
| 0.4556 | 15.7(15.6) | 22.86 | 0.3172 | −43.2(−44.0) | 12.04 |
| 0.5127 | 17.7(17.7) | 22.96 | 0.3872 | −31.9(−32.5) | 12.56 |
| 0.6023 | 25.5(25.5) | 23.37 | 0.4265 | −27.5(−28.0) | 12.69 |
| 0.7080 | 32.6(32.6) | 23.54 | 0.5227 | −16.5(−17.0) | 13.31 |
| 0.8369 | 39.2(39.2) | 24.03 | | | |
| | $F_2 = 0.100$ | | | | |
| 0.0326 | −121.0(171.1) | −2.60 | | | |
| 0.0584 | −127.5(−158.1) | −1.44 | | | |
| 0.0815 | −123.1(−145.6) | −1.01 | | | |
| 0.0958 | −123.6(−142.8) | −0.60 | | | |
| 0.1293 | −116.6(−131.1) | −0.19 | | | |
| 0.1526 | −115.9(−128.2) | 0.24 | | | |
| 0.2063 | −101.9(−111.1) | 0.79 | | | |
| 0.2150 | −99.5(−108.4) | 1.06 | | | |
| 0.2904 | −83.2(−90.0) | 1.79 | | | |
| 0.3048 | −81.7(−88.2) | 2.02 | | | |
| 0.4148 | −60.6(−65.7) | 2.96 | | | |

TABLE 3. Apparent molar heat capacities and volumes of aqueous acids and salts at 25.0°C

| $m$ | $\phi_C(\phi_C^{sp})$ | $\phi_V$ | $m$ | $\phi_C(\phi_C^{sp})$ | $\phi_V$ |
|---|---|---|---|---|---|
| mol kg$^{-1}$ | J K$^{-1}$ mol$^{-1}$ | cm$^3$mol$^{-1}$ | mol kg$^{-1}$ | J K$^{-1}$ mol$^{-1}$ | cm$^3$ mol$^{-1}$ |
| | $H_3PO_4$ | | | $Na_3PO_4$ | |
| 0.1055 | 70.4(61.4) | 43.78 | 0.0203 | −3.3(−341.7) | −18.19 |
| 0.3206 | 80.1(74.2) | 45.32 | 0.0405 | −39.4(−301.8) | −17.22 |
| 0.5450 | 84.5(79.8) | 45.89 | 0.0617 | −56.6(−270.8) | −16.29 |
| 0.7782 | 89.3(85.3) | 46.18 | 0.0825 | −65.1(−249.5) | −15.42 |
| 1.0214 | 90.0(86.4) | 46.39 | 0.1028 | −70.4(−235.1) | −14.68 |
| 1.2763 | 93.8(90.6) | 46.50 | 0.1295 | −70.3(−217.2) | −13.88 |
| | | | 0.1746 | −66.7(−195.2) | −12.84 |
| | $H_2SO_4$ | | | $Na_3PO_4$ in 0.020 $m$ NaOH | |
| 0.0520 | 47.6(−53.5) | 29.73 | | | |
| 0.1521 | 51.9(−14.9) | 32.81 | 0.0150 | 35.5(−315.5) | −16.73 |
| 0.1973 | 55.3(−3.2) | 33.15 | 0.0234 | −7.4(−309.0) | −18.27 |
| 0.2432 | 52.9(0.4) | 33.97 | 0.0499 | −42.0(−260.9) | −15.96 |
| 0.2960 | 55.5(9.7) | 33.93 | 0.0766 | −55.3(−234.3) | −14.82 |
| 0.3538 | 53.0(12.6) | 34.50 | 0.1035 | −61.7(−217.3) | −13.90 |
| 0.3990 | 56.0(19.1) | 34.39 | 0.1310 | −60.5(−200.8) | −13.03 |
| 0.4568 | 55.5(22.3) | 34.92 | 0.1671 | −56.6(−183.9) | −12.02 |
| 0.5628 | 56.3(28.9) | 35.21 | | | |

from Millero (7) and the "valence factor" $\omega$ as commonly defined (8) is

$$[3] \quad \omega = I/m = (0.5\,\Sigma\nu_i z_i^2 m_i)/m$$

in which $I$ is the molal ionic strength, $m_i$ is the molality of a particular solute, and $m$ is the total molality. For non-electrolytes and undissociated weak electrolytes such as $H_3PO_4$(aq) we have [2′] instead of [2]:

$$[2'] \quad \phi_V = \phi_V^0 + B_V m$$

Many of our measurements have been made on

Can. J. Chem. Downloaded from www.nrcresearchpress.com by 210.87.254.40 on 09/06/12
For personal use only.

buffer solutions that are described as containing component solutes in ratios equal to 9/1, 1/1, and 1/9. We now define solute mole fractions $F_2$ and $F_3$ according to

[4] $$F_2 = n_2/(n_2 + n_3)$$

and

[5] $$F_3 = n_3/(n_2 + n_3)$$

in which subscript 2 refers to a 1:1 electrolyte and subscript 3 refers to a 2:1 electrolyte. For $F_2$ values of 0.9, 0.5, and 0.1 we have ω values equal to 1.2, 2.0, and 2.8, respectively. As shown in Tables 1 and 2, we have made measurements on solutions having three different $F_2$ values at several different total molalities.

For our $NaH_2PO_4/Na_2HPO_4$ and $NaHCO_3/Na_2CO_3$ buffer solutions we find that hydrolysis and dissociation corrections are negligible. We have therefore obtained values of $\phi_V^0$ and $B_V$ by least-squares fitting of $\phi_V - A_V(d_1^0)^{1/2}(\omega)^{3/2}(m)^{1/2}$ against $\omega m$, as suggested by eq. [2], with results that are given in Table 4. Further linear least-squares fits of $\phi_V^0$ values for buffers against corresponding $F_2$ values lead to $\phi_{V,2}^0$ and $\phi_{V,3}^0$ values for single electrolyte components of the buffers, as reported in Table 5. Using

$$\phi_V^0(Na^+) = -1.2\,cm^3\,mol^{-1}$$

from Millero (7), based on the useful convention that

$$\phi_V^0(H^+) \equiv 0$$

we then obtain the conventional ionic volumes for $H_2PO_4^-(aq)$, $HPO_4^{2-}(aq)$, $HCO_3^-(aq)$, and $CO_3^{2-}(aq)$ that are listed in Table 6.

For solutions of phosphoric acid we need consider only the first dissociation as in

[6] $$H_3PO_4(aq) = H^+(aq) + H_2PO_4^-(aq)$$

for which we have the equilibrium constant $K_6$ from a recent review (9). We calculate the fraction dissociated (α) from $K_6$ and the Davies equation for activity coefficients (γ):

[7] $$\log \gamma = (-Az^2I^{1/2})/(1 + I^{1/2}) + 0.1z^2I$$

The apparent molar volumes of solutions of phosphoric acid are expressed as

[8] $$\phi_V = (1-\alpha)\phi_V(H_3PO_4) + \alpha\phi_V(H^+ + H_2PO_4^-)$$

Substitution of the appropriate version of eq. [2] and [2′] in [8] leads us to obtain the desired apparent molar volume of undissociated phosphoric acid, $\phi_V^0(H_3PO_4)$, by extrapolating

$$\frac{\phi_V - \alpha\phi_V^0(H^+ + H_2PO_4^-) - (\alpha)^{3/2}A_V(d_1^0)^{1/2}(m)^{1/2}}{(1-\alpha)}$$

to zero concentration. Our value for $\phi_V^0(H_3PO_4)$ is listed in Table 6.

The hydrolysis of solutions of sodium phosphate is represented by

[9] $$PO_4^{3-}(aq) + H_2O(liq) = HPO_4^{2-}(aq) + OH^-(aq)$$

We have calculated α (fraction hydrolyzed) values from the equilibrium constant (9) and activity coefficients (10). The apparent molar volumes of solutions of sodium phosphate are then expressed as

[10] $$\phi_V = (1-\alpha)\phi_V(3Na^+ + PO_4^{3-}) + \alpha\phi_V(2Na^+ + HPO_4^{2-}) + \alpha\phi_V(Na^+ + OH^-) - \alpha V^0(H_2O)$$

Substitution of appropriate versions of eq. [2] in [10] and rearrangement of the resulting complicated expression has led us to extrapolate

$$[\phi_V - \alpha\phi_V^0(2Na^+ + HPO_4^{2-}) - \alpha\phi_V^0(Na^+ + OH^-) + \alpha V^0(H_2O) - (6-2\alpha)A_V(d_1^0)^{1/2}(I)^{1/2}]/(1-\alpha)$$

to zero ionic strength to obtain the desired $\phi_V^0(3Na^+ + PO_4^{3-})$ that is listed in Table 5 and thence the conventional $\phi_V^0(PO_4^{3-})$ that is listed in Table 6.

TABLE 4. Parameters for eqs. [2] and [16] for aqueous $NaH_2PO_4/Na_2HPO_4$ and $NaHCO_3/Na_2CO_3$ buffers at 25.0°C

| | $\phi_C^0$ | $B_C$ | $\phi_V^0$ | $B_V$ |
|---|---|---|---|---|
| $F_2$ | $J\,K^{-1}\,mol^{-1}$ | $J\,K^{-1}\,mol^{-2}\,kg$ | $cm^3\,mol^{-1}$ | $cm^3\,mol^{-2}\,kg$ |
| | | $NaH_2PO_4/Na_2HPO_4$ | | |
| 0.900 | −8.9 | 48.0 | 27.3 | 2.5 |
| 0.500 | −80.0 | 51.5 | 16.6 | 2.5 |
| 0.100 | −150.3 | 49.5 | 5.5 | 1.7 |
| | | $NaHCO_3/Na_2CO_3$ | | |
| 0.900 | −32.7 | 39.1 | 20.5 | 1.2 |
| 0.500 | −112.1 | 35.9 | 8.4 | 1.1 |
| 0.100 | −195.8 | 38.7 | −3.8 | 1.2 |

TABLE 5. Standard state heat capacities and volumes of aqueous solutes at 25.0°C

| Solute | $\phi_C^0$ $J\,K^{-1}\,mol^{-1}$ | $\phi_V^0$ $cm^3\,mol^{-1}$ |
|---|---|---|
| $H_3PO_4$(aq, undiss.) | 94.5 | 48.1 |
| $NaH_2PO_4$(aq) | 8.6 | 30.1 |
| $Na_2HPO_4$(aq) | −168.1 | 2.8 |
| $Na_3PO_4$(aq) | −367 | −22.4 |
| $NaHCO_3$(aq) | −11.6 | 23.6 |
| $Na_2CO_3$(aq) | −215.5 | −6.8 |
| $H^+(aq) + HSO_4^-(aq)$ | 21.7 | 35.2 |

Can. J. Chem. Downloaded from www.nrcresearchpress.com by 210.87.254.40 on 09/06/12
For personal use only.

TABLE 6. Standard state heat capacities and volumes for aqueous species at 25.0°C, based on $\phi_V^0(H^+) \equiv 0$ for ions

| Species | $\phi_C^0$ / J K$^{-1}$ mol$^{-1}$ | $\phi_V^0$ / cm$^3$ mol$^{-1}$ |
|---|---|---|
| $H_3PO_4$(aq) | 94 | 48.1 |
| $H_2PO_4^-$(aq) | −34 | 31.3 |
| $HPO_4^{2-}$(aq) | −254 | 5.2 |
| $PO_4^{3-}$(aq) | −496 | −18.8 |
| $HCO_3^-$(aq) | −55 | 24.8 |
| $CO_3^{2-}$(aq) | −302 | −4.4 |
| $HSO_4^-$(aq) | 22 | 35.2 |
| $SO_4^{2-}$(aq) | −278[a] | 14.0[b] |

[a] From ref. 19.
[b] From ref. 7.

Sulfuric acid in our solutions is completely dissociated into $H^+$(aq) and $HSO_4^-$(aq) and some of the bisulfate ions are further dissociated as in

[11] $HSO_4^-(aq) = H^+(aq) + SO_4^{2-}(aq)$

We have calculated α (fraction of $HSO_4^-$ dissociated) values from the equilibrium constant (9) and the Davies equation (10). The apparent molar volumes of sulfuric acid solutions are expressed as

[12] $\phi_V = (1 - \alpha)\phi_V(H^+ + HSO_4^-) + \alpha\phi_V(2H^+ + SO_4^{2-})$

Substitution of the appropriate forms of eq. [2] in [12] and rearrangement lead us to obtain $\phi_V^0(H^+ + HSO_4^-)$ by extrapolation of

$$\phi_V - \alpha\phi_V^0(2H^+ + SO_4^{2-}) - (1 + 2\alpha)A_V(d_1^0)^{1/2}I^{1/2}/(1 - \alpha)$$

to zero ionic strength to obtain the $\phi_V^0(H^+ + HSO_4^-)$ that is listed in Table 5. The conventional $\phi_V^0(HSO_4^-)$ is listed in Table 6.

Analysis of experimental apparent molar heat capacities for reactive systems to obtain the desired $\phi_C^0$ values of specified solute species requires that we allow for the temperature dependent state of equilibrium and related thermal effects. These "relaxation" effects have been considered previously for other systems by Woolley and Hepler (11) and by Jolicoeur, Lemelin, and Lapalme (12). As these earlier investigations have shown, experimental apparent molar heat capacities ($\phi_C$) can be regarded as a sum of two kinds of contributions. One contribution is from the solute species present in the solution of interest and is designated $\phi_C^{sp}$; it is this contribution that we will relate to the desired standard state heat capacities of various solute species. The other contribution to the total experimental apparent molar heat capacity is from the thermal effects associated with changes in chemical equilibrium ("relaxation") and is designated $\phi_C^{rel}$. We therefore have

[13] $\phi_C = \phi_C^{sp} + \phi_C^{rel}$

The contribution of "relaxation" to the apparent molar heat capacity is given (11, 12) by

[14] $\phi_C^{rel} = \Delta H(d\alpha/dT)$

Thus the desired contributions due to the aqueous solute species can be obtained as

[15] $\phi_C^{sp} = \phi_C - \Delta H(d\alpha/dT)$

Procedures for calculating $(d\alpha/dT)$ from equilibrium constants, enthalpies, and activity coefficients for systems of various charge types follow those previously described (11, 12) and recently extended (13). The required equilibrium constants and enthalpies have been taken from a recent review (9).

The "relaxation" effects on heat capacities of the $NaH_2PO_4/Na_2HPO_4$ buffer systems are very small compared with the experimental uncertainties. We have therefore taken $\phi_C = \phi_C^{sp}$ for these solutions and used the $\phi_C$ values in Table 1 for our subsequent calculations for this system. For all other systems we have calculated $\phi_C^{sp}$ values by way of experimental $\phi_C$ values and eq. [15], which has involved calculation of $\Delta H(d\alpha/dT)$ as described in detail elsewhere (11–13), with results presented in parentheses in Tables 2 and 3.

The next step has been to analyse the $\phi_C^{sp}$ values in Tables 2 and 3 and the $\phi_C$ ($= \phi_C^{sp}$) values in Table 1 on the basis of the equation

[16] $\phi_C^{sp} = \phi_C^0 + A_C(d_1^0)^{1/2}(\omega)^{3/2}(m)^{1/2} + B_C\omega m$

in which $A_C$ is derived from the Debye–Hückel theory and $B_C$ is an adjustable parameter. We have used

$$A_C(d_1^0)^{1/2} = 28.95\,\text{J K}^{-1}\,\text{mol}^{-3/2}\,\text{kg}^{1/2}$$

from Desnoyers (14, 15). In this connection we note that there is recent evidence (16, 17) for a slightly larger value of $A_C(d_1^0)^{1/2}$, but the difference is not enough to be significant for our present purposes.

We have used our $\phi_C^{sp}$ results with eq. [16] in carrying out calculations and extrapolations to zero concentration in ways that are equivalent to those already described in detail for our $\phi_V$ values. The resulting $\phi_C^0$ values are listed in Tables 4 and 5. These $\phi_C^0$ values have been combined with the conventional $\phi_C^0(H^+) \equiv 0$ and $\phi_C^0(Na^+) = 43\,\text{J K}^{-1}\,\text{mol}^{-1}$ and $\phi_C^0(SO_4^{2-}) = -278\,\text{J K}^{-1}\,\text{mol}^{-1}$ from earlier work (18, 19) to obtain the conventional $\phi_C^0$ values listed in Table 6.

Can. J. Chem. Downloaded from www.nrcresearchpress.com by 210.87.254.40 on 09/06/12
For personal use only.

TABLE 7. Standard state changes in heat capacity and volume for acid dissociation reactions at 25.0°C, from $\phi_C^0$ and $\phi_V^0$ values in Table 6

| Reaction | $\Delta C_p^0$ / J K$^{-1}$ mol$^{-1}$ | $\Delta V^0$ / cm$^3$ mol$^{-1}$ |
|---|---|---|
| $H_3PO_4 = H^+ + H_2PO_4^-$ | −128 | −16.8 |
| $H_2PO_4^- = H^+ + HPO_4^{2-}$ | −220 | −26.1 |
| $HPO_4^{2-} = H^+ + PO_4^{3-}$ | −242 | −24.0 |
| $HCO_3^- = H^+ + CO_3^{2-}$ | −247 | −29.2 |
| $HSO_4^- = H^+ + SO_4^{2-}$ | −300 | −21.2 |

We have used the conventional standard state heat capacities and volumes listed in Table 6 for calculation of $\Delta C_p^0$ and $\Delta V^0$ for the acid dissociation reactions listed in Table 7. It should be emphasized that the arbitrariness in setting $\phi_Y^0(H^+) \equiv 0$ to obtain the conventional values in Table 6 cancels out of the calculations leading to Table 7 so that the reported $\Delta C_p^0$ and $\Delta V^0$ values are independent of the conventional values chosen for $\phi_Y^0(H^+)$.

We estimate that uncertainties in most of our $\phi_V^0$ and $\phi_C^0$ values are about $\pm 0.6$ cm$^3$ mol$^{-1}$ and about $\pm 4$ J K$^{-1}$ mol$^{-1}$, respectively; exceptions are $Na_3PO_4$(aq), $PO_4^{3-}$(aq), and $HSO_4^-$(aq) for which uncertainties are larger than for the other solutes. Our further estimates for uncertainties in $\phi_V^0$ are about $\pm 3$ cm$^3$ mol$^{-1}$ for $Na_3PO_4$(aq) and $PO_4^{3-}$(aq) and about $\pm 0.8$ cm$^3$ mol$^{-1}$ for $HSO_4^-$(aq). We also estimate that uncertainties in $\phi_C^0$ are about $\pm 20$ J K$^{-1}$ mol$^{-1}$ for $Na_3PO_4$(aq) and $PO_4^{3-}$(aq) and about $\pm 8$ J K$^{-1}$ mol$^{-1}$ for $HSO_4^-$(aq). As shown in the next section, results of several earlier investigations provide evidence that most of our $\phi_V^0$ values (Tables 5 and 6) and related $\Delta V^0$ values (Table 7) are reliable to within the estimated uncertainties; the only exceptions are $Na_3PO_4$(aq) and $PO_4^{3-}$(aq) and the related $\Delta V^0$ for dissociation of $HPO_4^{2-}$(aq), for which the true uncertainties may be larger than our estimates above. Uncertainties in most earlier $\Delta C_p^0$ values are so large that they provide little evidence for or against our $\Delta C_p^0$ values and our estimates of their uncertainties.

## Comparisons of results

There have been many investigations of partial molar volumes and also dissociation constants at various pressures that have yielded volumes to be compared with our values in Tables 6 and 7. Nearly all such results obtained before 1973 have been cited and summarized in Hamann's excellent review (20). Now we also have some useful results from more recent investigations.

Hamann (20) has listed $\Delta V^0 = -16.6$ and $-16.2$ cm$^3$ mol$^{-1}$ for the first dissociation of phosphoric acid. More recently, Lo Surdo, Bernstrom, Jonsson, and Millero (21) have reported $\Delta V^0 = -16.26$ cm$^3$ mol$^{-1}$ for this dissociation. All of these results are in good agreement with our $\Delta V^0 = -16.8$ cm$^3$ mol$^{-1}$.

Hamann (20) has listed $\Delta V^0 = -24.0$ and $-24.1$ cm$^3$ mol$^{-1}$ for the second dissociation of phosphoric acid, for which Lo Surdo *et al.* (21) have recently reported $\Delta V^0 = -25.85$ cm$^3$ mol$^{-1}$. Our $\Delta V^0 = -26.1$ cm$^3$ mol$^{-1}$ for this dissociation provides support for the value from Lo Surdo *et al.* (21) in preference to the earlier values.

Lo Surdo *et al.* (21) have also reported $\Delta V^0 = -35.96$ cm$^3$ mol$^{-1}$ for the third dissociation of phosphoric acid, for which we found $\Delta V^0 = -24.0$ cm$^3$ mol$^{-1}$. There is no obvious explanation for the difference in these values.

We also note that the $\phi_V^0$ values reported by Lo Surdo *et al.* (21) for $H_3PO_4$(aq), $NaH_2PO_4$(aq), and $Na_2HPO_4$(aq) are all in good agreement with our corresponding values in Table 5. On the other hand, their $\phi_V^0$ for $Na_3PO_4$(aq) is in poor agreement with our value.

Previous reviews by Millero (7) and by Hamann (20) have led to a choice of $\Delta V^0 = -27.7$ cm$^3$ mol$^{-1}$ for dissociation of $HCO_3^-$(aq). The more recently reported partial molar volumes of Perron, Desnoyers, and Millero (8) lead to $\Delta V^0 = -28.4$ cm$^3$ mol$^{-1}$. As shown in Table 7, our measurements lead to $\Delta V^0 = -29.2$ cm$^3$ mol$^{-1}$ for this dissociation. We suggest that both of the latter two values are more accurate than the first value quoted above.

Both Millero (7) and Hamann (20) chose $\Delta V^0 = -21.7$ cm$^3$ mol$^{-1}$ for dissociation of $HSO_4^-$(aq). More recent volumetric measurements by Rohwer, Brink, and Cruywagen (22) lead to $\Delta V^0 = -20.0 \pm 1.0$ cm$^3$ mol$^{-1}$. These earlier values are in good agreement with our $\Delta V^0 = -21.2$ cm$^3$ mol$^{-1}$ for this dissociation.

We now turn to some comparisons of our heat capacities with earlier results.

Bates (23) has evaluated the first dissociation constant of $H_3PO_4$(aq) at 5° intervals from 0 to 60°C. An equation of type $\log K = f(T)$ has been fitted to the results; two differentiations with respect to $T$ have led to a reported $\Delta C_p^0 = -154 \pm 5$ J K$^{-1}$ mol$^{-1}$ at 25°C. More recently, Mesmer and Baes (24) have investigated the first dissociation of $H_3PO_4$(aq) at 25° intervals from 0 to 300°C. Their results have led to $\Delta C_p^0 = 34 \pm 29$ J K$^{-1}$ mol$^{-1}$ for the neutralization reaction

[17] $H_3PO_4(aq) + OH^-(aq) = H_2PO_4^-(aq) + H_2O(liq)$

Can. J. Chem. Downloaded from www.nrcresearchpress.com by 210.87.254.40 on 09/06/12
For personal use only.

Combination of this result with $\Delta C_p^0 = -215\,J\,K^{-1}\,mol^{-1}$ for dissociation of water from a recent review (9) leads to $\Delta C_p^0 = -186 \pm 30\,J\,K^{-1}\,mol^{-1}$ for the first dissociation of $H_3PO_4(aq)$. Because of the well-known magnification of uncertainties and errors associated with double differentiation and also because of the difficulties in evaluating accurately the relatively small $pK$ of $H_3PO_4(aq)$ as reviewed recently by Pitzer and Silvester (25), we believe that our $\Delta C_p^0 = -128\,J\,K^{-1}\,mol^{-1}$ is the best available for the first dissociation of $H_3PO_4(aq)$.

For the second dissociation of phosphoric acid we have four separate values of $\Delta C_p^0$ to compare with our value. Bates and Acree (26) have determined this dissociation constant at 5° intervals from 0 to 60°C; two differentiations of the derived $\log K = f(T)$ have led to $\Delta C_p^0 = -226\,J\,K^{-1}\,mol^{-1}$. Bates and Acree (26) also calculated $\Delta C_p^0 = -189\,J\,K^{-1}\,mol^{-1}$ from the earlier dissociation constants of Nims (27), determined over the temperature range 20 to 50°C. Grzybowski (28) has determined dissociation constants at 5°C intervals from 5 to 50°C and has similarly calculated $\Delta C_p^0 = -200 \pm 9.5\,J\,K^{-1}\,mol^{-1}$ for the second dissociation. Finally, Mesmer and Baes (23) have determined equilibrium constants for

[18] $H_2PO_4^-(aq) + OH^-(aq) = HPO_4^{2-}(aq) + H_2O(liq)$

at 25° intervals from 0 to 300°C and have calculated $\Delta C_p^0 = 32 \pm 25\,J\,K^{-1}\,mol^{-1}$ for this neutralization reaction. Combination of this result with $\Delta C_p^0$ for dissociation of water (9) leads to $\Delta C_p^0 = -183 \pm 26\,J\,K^{-1}\,mol^{-1}$ for the second dissociation of phosphoric acid. We suggest that our $\Delta C_p^0 = -220\,J\,K^{-1}\,mol^{-1}$ is the best available value. Although we are generally skeptical of $\Delta C_p^0$ values based on double differentiation of $\log K = f(T)$, we note that the equilibrium constants of Bates and Acree (26) and Grzybowski (28) appear to have been determined with considerable skill and accuracy; it is therefore gratifying to note that their (26, 28) $\Delta C_p^0$ values are in good agreement with our value.

We do not know of any earlier results that permit calculation of the heat capacity change for the third dissociation of phosphoric acid to compare with our $\Delta C_p^0 = -242\,J\,K^{-1}\,mol^{-1}$.

For the dissociation of $HCO_3^-(aq)$ we have several $\Delta C_p^0$ values to compare with our value. Harned and Scholes (29) have determined the equilibrium constant at 5° intervals from 0 to 50°C and by double differentiation of the resulting equation of type $\log K = f(T)$ have obtained $\Delta C_p^0 = -276\,J\,K^{-1}\,mol^{-1}$. Nakayama (30) has treated the experimental results of Harned and Scholes (29) slightly differently to obtain $\Delta C_p^0 = -282\,J\,K^{-1}\,mol^{-1}$ for this dissociation. More recently, Plummer and Busenberg (31) have analyzed equilibrium data over a wider range of temperature; double differentiation of their $\log K = f(T)$ now leads us to $\Delta C_p^0 = -291\,J\,K^{-1}\,mol^{-1}$ at 298.15 K. Plummer (31) has also found that different selection and treatment of the equilibrium constants leads to less negative $\Delta C_p^0$ values. Perron, Desnoyers, and Millero (8) have measured heat capacities of aqueous solutions of $NaHCO_3$ and $Na_2CO_3$. We have used their *reported* $\phi_C^0$ values in calculating $\Delta C_p^0 = -214\,J\,K^{-1}\,mol^{-1}$ for the dissociation of $HCO_3^-(aq)$. We know, however, that their *reported* $\phi_C^0$ values for these salts and this calculated $\Delta C_p^0$ value are incorrect because of neglect of the chemical relaxation effect (11–13), which had not yet been recognized (11) at the time Perron, Desnoyers, and Millero (8) wrote their paper. We have therefore made use of eqs. [13]–[15] with their experimental results to obtain a corrected $\Delta C_p^0 = -249\,J\,K^{-1}\,mol^{-1}$ for the dissociation of $HCO_3^-(aq)$. We also note that Peiper and Pitzer (32) have independently and by a slightly different procedure (also using slightly different auxiliary data) made "relaxation corrections" to the results of Perron, Desnoyers, and Millero (8) to obtain $\Delta C_p^0 = -260\,J\,K^{-1}\,mol^{-1}$ for the dissociation of $HCO_3^-(aq)$. These "corrected" $\Delta C_p^0$ values from the measurements of Perron, Desnoyers, and Millero (8) are in good agreement with our $\Delta C_p^0 = -247\,J\,K^{-1}\,mol^{-1}$ for this dissociation.

For dissociation of $HSO_4^-(aq)$ we have several values for $\Delta C_p^0$ as follows. Lietzke, Stoughton, and Young (33) have determined equilibrium constants at temperatures from 25 to 225°C and have obtained an equation of type $\ln K = f(T)$ from which we now calculate $\Delta C_p^0 = -209\,J\,K^{-1}\,mol^{-1}$ for the dissociation of $HSO_4^-(aq)$ at 298.15 K. Marshall and Jones (34) have determined equilibrium constants from 25 to 350°C and have calculated $\Delta C_p^0 = -238\,J\,K^{-1}\,mol^{-1}$. Young, Singleterry, and Klotz (35) have reported results of their determinations of equilibrium constants at 10° intervals from 5 to 55°C and have calculated two values for the heat capacity change associated with dissociation of $HSO_4^-(aq)$: $\Delta C_p^0 = -192$ and $-238\,J\,K^{-1}\,mol^{-1}$. Readnour and Cobble (36) have measured enthalpies of solution of $Na_2SO_4(c)$ in water and in dilute hydrochloric acid at several temperatures and have calculated $\Delta C_p^0 = -356\,J\,K^{-1}\,mol^{-1}$ for dissociation of $HSO_4^-(aq)$ at 25°C. More recently, Criss (37) has used the experimental results of Readnour and Cobble (36) in some improved calculations and has

TABLE 8. Selected standard state thermodynamic properties for acid dissociation reactions in aqueous solution at 298.15 K and 1 atm

| Reaction | $K^a$ | $\Delta H^0$ / J mol$^{-1}$ | $\Delta S^0$ / J K$^{-1}$ mol$^{-1}$ | $\Delta C_p{}^0$ / J K$^{-1}$ mol$^{-1}$ | $\Delta V^0$ / cm$^3$ mol$^{-1}$ |
|---|---|---|---|---|---|
| $H_3PO_4 = H^+ + H_2PO_4^-$ | $7.13 \times 10^{-3}$ | $-7.74 \times 10^3$ | $-67.06$ | $-128$ | $-16.3$ |
| $H_2PO_4^- = H^+ + HPO_4^{2-}$ | $6.31 \times 10^{-8}$ | $3.60 \times 10^3$ | $-126.82$ | $-220$ | $-25.9$ |
| $HPO_4^{2-} = H^+ + PO_4^{3-}$ | $4.22 \times 10^{-13}$ | $17.2 \times 10^3$ | $-179.2$ | $-242$ | |
| $HCO_3^- = H^+ + CO_3^{2-}$ | $4.69 \times 10^{-11}$ | $14.70 \times 10^3$ | $-148.45$ | $-250$ | $-28.7$ |
| $HSO_4^- = H^+ + SO_4^{2-}$ | $1.05 \times 10^{-2}$ | $-22.6 \times 10^3$ | $-113.7$ | $-300$ | $-21.0$ |

[a] All $K$ values here are based on compositions of solutions expressed in terms of molalities (mol kg$^{-1}$) of solutes and the hypothetical one molal standard state so that activity coefficients approach unity as $m$ approaches zero.

obtained $\Delta C_p{}^0 = -280$ J K$^{-1}$ mol$^{-1}$ for dissociation of $HSO_4^-$(aq) at 25°C. We believe that our $\Delta C_p{}^0 = -300$ J K$^{-1}$ mol$^{-1}$, supported by the value from Criss (37), is the best value available for the dissociation of $HSO_4^-$(aq) at 25°C.

## Thermodynamic calculations

A principal purpose of this research has been to obtain $\Delta V^0$ and especially $\Delta C_p{}^0$ values for acid dissociation reactions with a view toward using these values in calculating the dependences of other thermodynamic properties on pressure and temperature. For these calculations we want the "best" available values for the equilibrium constant $K$, $\Delta H^0$, $\Delta S^0$, $\Delta C_p{}^0$, and $\Delta V^0$ for dissociation reactions at 298.15 K and 1 atm. Our selected values for these quantities are given in Table 8; sources of these values are as follows.

Equilibrium constants for the first and second dissociations of phosphoric acid have already been cited (23–28). For the third dissociation we select the $K$ value from Quist and Vanderzee (38). Enthalpies for these dissociations have been selected from values calculated with $d \ln K/dT = \Delta H^0/RT^2$ (23, 24, 26–28) and from results of calorimetric measurements (39–43). The selected $\Delta C_p{}^0$ values are all based on our calorimetric results as reported in this paper. Selected $\Delta V^0$ values are based on our results and on other values already cited (20, 21).

We take the equilibrium constant at 298.15 K for dissociation of $HCO_3^-$(aq) from Harned and Scholes (29) and the enthalpy of dissociation from Berg and Vanderzee (44). Our selected $\Delta C_p{}^0$ is based on the present calorimetric results and the "corrected" results from Perron, Desnoyers, and Millero (8). The selected $\Delta V^0$ is a weighted average of the values cited earlier in this paper.

For the dissociation of $HSO_4^-$(aq) we have equilibrium constants from investigations already cited (33–35) and many others, especially including Covington, Dobson, and Srinivasan (45) and Pitzer, Roy, and Silvester (46). We select the $K_{298.15}$ value in Table 8 from this last investigation (46). Pitzer, Roy, and Silvester (46) have also calculated a $\Delta H_{298.15}{}^0$ value for dissociation of $HSO_4^-$(aq), which we have considered along with values derived from investigations already cited (33–35) and from several calorimetric investigations (47). Our selected value is given in Table 8. We have also selected $\Delta C_p{}^0$ from our results, in good agreement with the recalculated $\Delta C_p{}^0$ from Criss, Readnour, and Cobble (36, 37). The selected $\Delta V^0$ is based on our results and those cited earlier (7, 20, 22).

A first approximation to the effect of temperature on thermodynamic properties associated with chemical reactions is to take $\Delta C_p{}^0 = 0$. In this approximation both $\Delta H^0$ and $\Delta S^0$ are independent of temperature and the effect of temperature on the equilibrium constant is expressed as follows:

$$[19] \quad \ln K_T = -(\Delta H^0/RT) + (\Delta S^0/R)$$

$$[20] \quad \ln K_T = \ln K_{298.15} + (\Delta H^0/298.15RT)(T - 298.15)$$

$$[21] \quad \ln K_T = (298.15/T) \ln K_{298.15} + (\Delta S^0/RT)(T - 298.15)$$

The $\Delta C_p{}^0$ values in Table 8 show that $\Delta C_p{}^0 = 0$ is a poor approximation for the reactions of interest in this paper; hence eqs. [19]–[21] can be regarded as useful only when $T$ is very close to 298.15 K. We therefore go on to the next approximation, a non-zero $\Delta C_p{}^0$ that is considered to be independent of temperature.

Integration of $(d\Delta H^0/dT) = \Delta C_p{}^0$ with $\Delta C_p{}^0$ taken to be independent of temperature leads to

$$[22] \quad \Delta H_T{}^0 = \Delta H_{298.15}{}^0 + \Delta C_p{}^0(T - 298.15)$$

and similar integration of $(d\Delta S^0/dT) = \Delta C_p{}^0/T$ leads to

$$[23] \quad \Delta S_T{}^0 = \Delta S_{298.15}{}^0 + \Delta C_p{}^0 \ln(T/298.15)$$

Combinations of eqs. [22] and [23] with

$$\Delta G_T{}^0 = \Delta H_T{}^0 - T\Delta S_T{}^0 = -RT \ln K_T$$

Can. J. Chem. Downloaded from www.nrcresearchpress.com by 210.87.254.40 on 09/06/12
For personal use only.

Can. J. Chem. Downloaded from www.nrcresearchpress.com by 210.87.254.40 on 09/06/12
For personal use only.

or integration of

$$d\ln K/dT = \Delta H^0/RT^2$$

with [22] leads to the following:

[24] $$\ln K_T = \ln K_{298.15} + (\Delta H_{298.15}{}^0/298.15RT) \times (T - 298.15) - (\Delta C_p{}^0/RT)(T - 298.15) + (\Delta C_p{}^0/R)\ln(T/298.15)$$

[25] $$\ln K_T = (298.15/T)\ln K_{298.15} + (\Delta S_{298.15}{}^0/RT) \times (T - 298.15) - (\Delta C_p{}^0/RT)(T - 298.15) + \Delta C_p{}^0/R)\ln(T/298.15)$$

[26] $$\ln K_T = -(\Delta H_{298.15}{}^0/RT) + (\Delta S_{298.15}{}^0/R) - (\Delta C_p{}^0/RT)(T - 298.15) + (\Delta C_p{}^0/R)\ln(T/298.15)$$

Calculations with eqs. [24]–[26] and comparisons with experimental $K$ values for several reactions show (48) that these equations yield very accurate $K$ values over the temperature range 0-100°C (273–373 K) and yield moderately accurate $K$ values at temperatures to 200°C (473 K) or even higher.

According to eqs. [19]–[21], $\ln K$ should be a linear function of $1/T$, with no minimum or maximum. It is, however, known that $\ln K$ is *not* generally a linear function of $1/T$ and that $\ln K$ versus $1/T$ or $T$ often passes through a minimum or maximum. Equations [24]–[26] are substantial improvements over eqs. [19]–[21] in that the equations containing $\Delta C_p{}^0$ allow for non-linearity of plots of $\ln K$ versus $1/T$ and also permit a minimum or maximum. Consideration of

$$d\ln K/dT = \Delta H^0/RT^2$$

shows that $\ln K$ will go through a minimum or maximum at the temperature where $\Delta H^0 = 0$. We therefore set $\Delta H_T{}^0 = 0$ in eq. [22] and solve to obtain

[27] $$T_m = 298.15 - (\Delta H_{298.15}{}^0/\Delta C_p{}^0)$$

in which we have used $T_m$ to represent the temperature corresponding to a minimum or maximum in $\ln K$ (or $K$). No minima nor maxima have been observed for $\ln K$ values for dissociation of $H_3PO_4$(aq) and $HSO_4^-$(aq), in accord with the $T_m < 273$ K values that we calculate using $\Delta H_{298.15}{}^0$ and $\Delta C_p{}^0$ values from Table 8. For dissociation of $H_2PO_4^-$(aq) and $HCO_3^-$(aq) we calculate $T_m$ = 314 K and 357 K, respectively. Both these values are in satisfactory accord with experimental results (24, 26–28, 31). For dissociation of $HPO_4^-$(aq) we calculate $T_m$ = 369 K, but have no high temperature experimental results to compare with this value.

Effects of pressure on enthalpies and entropies of reaction can be calculated with

[28] $$(d\Delta H^0/dP)_T = \Delta V_T{}^0 - T(d\Delta V^0/dT)_P$$

and

[29] $$(d\Delta S^0/dP)_T = -(d\Delta V^0/dT)_P$$

Of more immediate use to us in relation to the data that we have available ($\Delta V^0$, but not usually $d\Delta V^0/dT$) is

[30] $$(d\ln K/dP)_T = -\Delta V^0/RT$$

Integration of eq. [30] taking $\Delta V^0$ to be independent of pressure leads to

[31] $$\ln K_P = \ln K_1 - (\Delta V^0/RT)(P - 1)$$

in which $K_1$ represents the equilibrium constant at 1 atm and $P$ is the pressure of interest expressed in atm. Use of $K$ and $\Delta V^0$ values from Table 8 in eq. [31] leads to calculated $K_P$ values that are in good agreement with experimental results (20) over moderate ranges of pressure. Better accuracy over wide ranges of pressure can be obtained by considering $\Delta V^0$ to be dependent on pressure (non-zero partial molar compressibility changes) as summarized elsewhere (7, 20, 21).

## Acknowledgments

We are grateful to the Alberta Oil Sands Technology and Research Authority and the Natural Sciences and Engineering Research Council of Canada for support of this research. We also thank Dr. Gregory Allred for his helpful advice. Finally, we thank Dr. K. S. Pitzer and Dr. L. N. Plummer for sending us manuscript copies of their papers (31, 32) and Dr. C. M. Criss for sending us the results of his recent calculations.

1. P. Picker, P.-A. Leduc, P. R. Philip, and J. E. Desnoyers. J. Chem. Thermodyn. **3**, 631 (1971).
2. G. Perron, N. Desrosiers, and J. E. Desnoyers. Can. J. Chem. **54**, 2163 (1976).
3. J. E. Desnoyers, C. de Visser, G. Perron, and P. Picker. J. Solution Chem. **5**, 605 (1976).
4. I. V. Olofsson. J. Chem. Thermodyn. **11**, 1005 (1979).
5. P. Picker, E. Tremblay, and C. Jolicoeur. J. Solution Chem. **3**, 377 (1974).
6. D. D. Wagman, W. H. Evans, V. B. Parker, I. Halow, S. M. Bailey, and R. H. Schumm. NBS Technical Note 270–3, U. S. Gov't. Printing Office, Washington, DC (1968).
7. F. J. Millero. *In* Water and aqueous solutions: structure, thermodynamics, and transport processes. *Edited by* R. A. Horne. Wiley-Interscience, New York. 1972. Chapt. 13.
8. G. Perron, J. E. Desnoyers, and F. J. Millero. Can. J. Chem. **53**, 1134 (1975).
9. L. G. Hepler and H. P. Hopkins, Jr. Rev. Inorg. Chem. **1**, 303 (1979).

10. R. A. ROBINSON and R. H. STOKES. Electrolyte solutions. 2nd ed. revised. Butterworths, London. 1965.
11. E. M. WOOLLEY and L. G. HEPLER. Can. J. Chem. **55**, 158 (1977).
12. C. JOLICOEUR, L. L. LEMELIN, and R. LAPALME. J. Phys. Chem. **83**, 2806 (1979).
13. J. W. LARSON and L. G. HEPLER. To be published.
14. P. R. PHILIP and J. E. DESNOYERS. J. Solution Chem. **1**, 353 (1972).
15. P.-A. LEDUC, J.-L. FORTIER, and J. E. DESNOYERS. J. Phys. Chem. **78**, 1217 (1974).
16. D. J. BRADLEY and K. S. PITZER. J. Phys. Chem. **83**, 1599 (1979).
17. J. J. SPITZER, I. V. OLOFSSON, P. P. SINGH, and L. G. HEPLER. Can. J. Chem. **57**, 2798 (1979).
18. A. ROUX, G. M. MUSBALLY, G. PERRON, J. E. DESNOYERS, P. P. SINGH, E. M. WOOLLEY, and L. G. HEPLER. Can. J. Chem. **56**, 24 (1978).
19. I. V. OLOFSSON, J. J. SPITZER, and L. G. HEPLER. Can. J. Chem. **56**, 1871 (1978).
20. S. D. HAMANN. *In* Modern aspects of electrochemistry. No. 9. *Edited by* B. E. Conway and J. O'M. Bockris. Plenum Press, New York. 1974. Chapt. 2.
21. A. LO SURDO, K. BERNSTROM, C.-A. JONSSON, and F. J. MILLERO. J. Phys. Chem. **83**, 1255 (1979).
22. E. F. C. H. ROHWER, J. A. BRINK, and J. J. CRUYWAGEN. J. South African Chem. Inst. **28**, 1 (1975).
23. R. G. BATES. J. Res. Natl. Bur. Stds. **47**, 127 (1951).
24. R. E. MESMER and C. F. BAES, JR. J. Solution Chem. **3**, 307 (1974).
25. K. S. PITZER and L. F. SILVESTER. J. Solution Chem. **5**, 269 (1976).
26. R. G. BATES and S. F. ACREE. J. Res. Natl. Bur. Stds. **30**, 129 (1943).
27. L. F. NIMS. J. Am. Chem. Soc. **55**, 1946 (1933).
28. A. K. GRZYBOWSKI. J. Phys. Chem. **62**, 555 (1958).
29. H. S. HARNED and S. R. SCHOLES, JR. J. Am. Chem. Soc. **63**, 1706 (1941).
30. F. S. NAKAYAMA. J. Inorg. Nucl. Chem. **33**, 1287 (1971).
31. L. N. PLUMMER and E. BUSENBERG. To be published.
32. J. C. PEIPER and K. S. PITZER. To be published.
33. M. H. LIETZKE, R. W. STOUGHTON, and T. F. YOUNG. J. Phys. Chem. **65**, 2247 (1961).
34. W. L. MARSHALL and E. V. JONES. J. Phys. Chem. **70**, 4028 (1966).
35. T. F. YOUNG, C. R. SINGLETERRY, and I. M. KLOTZ. J. Phys. Chem. **82**, 671 (1978).
36. J. M. READNOUR and J. W. COBBLE. Inorg. Chem. **8**, 2174 (1969).
37. C. M. CRISS. Personal communication.
38. C. E. VANDERZEE and A. S. QUIST. J. Phys. Chem. **65**, 118 (1961).
39. K. S. PITZER. J. Am. Chem. Soc. **59**, 2365 (1937).
40. F. J. MILLERO, W. C. DUER, E. SHEPARD, and P. V. CHETIRKIN. J. Solution Chem. **7**, 877 (1978).
41. J. J. CHRISTENSEN and R. M. IZATT. J. Phys. Chem. **66**, 1030 (1962).
42. R. R. IRANI and T. A. TAULLI. J. Inorg. Nucl. Chem. **28**, 1011 (1966).
43. J. J. CHRISTENSEN, R. M. IZATT, L. D. HANSEN, and J. A. PARTRIDGE. J. Phys. Chem. **70**, 2003 (1966).
44. R. L. BERG and C. E. VANDERZEE. J. Chem. Thermodyn. **10**, 1049 (1978).
45. A. K. COVINGTON, J. V. DOBSON, and K. V. SRINIVASAN. J. Chem. Soc. Faraday Trans. I, **69**, 94 (1973).
46. K. S. PITZER, R. N. ROY, and L. F. SILVESTER. J. Am. Chem. Soc. **99**, 4930 (1977).
47. J. J. CHRISTENSEN, L. D. HANSEN, and R. M. IZATT. Handbook of proton ionization heats and related thermodynamic quantities. Wiley-Interscience, New York. 1976.
48. L. G. HEPLER and P. R. TREMAINE. To be published.

Can. J. Chem. Downloaded from www.nrcresearchpress.com by 210.87.254.40 on 09/06/12
For personal use only.

# Les équations cinétiques pour les systèmes réactifs. Initiation photochimique et thermique. Les coefficients de vitesse

JUAN VEGUILLAS, MIGUEL ANGEL DIAZ ARMENTIA ET ANGEL MARIA GUTIERREZ TERRON

*Departamento de Química-Física, Facultad de Ciencias, Universidad del Pais Vasco, Apdo. 644 Bilbao, Espagne*

Reçue le 10 avril 1981[1]

JUAN VEGUILLAS, MIGUEL ANGEL DIAZ ARMENTIA et ANGEL MARIA GUTIERREZ TERRON. Can. J. Chem. **60**, 2151 (1982).

Dans une publication antérieure, on a mis au point une méthode permettant d'obtenir des équations cinétiques pour un système en réaction. Dans la présente publication, on applique cette méthode au système $Br_2 + H_2 \rightleftharpoons 2HBr$ pour lequel l'initiation est une photodissociation. On a trouvé l'Hamiltonien du réactif par l'intermédiaire d'une transformation généralisée de Tani. On a utilisé l'équation cinétique généralisée. On a développé le superopérateur de collision "en cluster" à l'aide du développement du superopérateur résolvant en faisant l'hypothèse que les collisions sont instantanées. On a obtenu les équations généralisées de Boltzman. À l'aide des équations cinétiques, nous avons obtenu l'équation maîtresse et, grâce à elle, on a identifié les coefficients de vitesse. [Traduit par le journal]

JUAN VEGUILLAS, MIGUEL ANGEL DIAZ ARMENTIA, and ANGEL MARIA GUTIERREZ TERRON. Can. J. Chem. **60**, 2151 (1982).

In a previous publication a method was developed for obtaining kinetic equations for a reacting system. In this publication that method is applied to a system $Br_2 + H_2 \rightleftharpoons 2\,HBr$ whose initiation is a photodissociation. The reactive Hamiltonian has been found through Tani's generalized transformation. The generalized kinetic equation has been used. The cluster expansion of the collision superoperator has been obtained from the cluster expansion of the resolvent superoperator, by assuming that collisions are instantaneous. The generalized Boltzmann equations have been obtained. From the kinetic equations we have found the master equations and from them the rate coefficients have been identified.

## I. Introduction

L'un des principaux questions que l'on pose par rapport aux systèmes chimiques réactifs consiste à exprimer les coefficients de vitesse des différentes réactions en fonction des propriétés microscopiques des particules.

Pour les réactions chimiques à l'initiation thermique des gaz dilués, on a déjà résolu cette question (1–4). Pourtant, l'étude des réactions à l'initiation non thermique est encore sans réponse, bien que l'on a proposé des équations cinétiques à l'initiation photochimique (5, 6).

Dans cet article, on obtient les équations cinétiques, valables pour des systèmes homogènes, qui rapportent l'évolution statistique des particules d'un système réactif constitué par les atomes Br et H, les molécules $Br_2$, $H_2$ et BrH, et le champ électromagnétique. Les interactions réactives que l'on prend en considération sont:

[1.1] $Br_2 + \hbar\nu \xrightarrow{k_{i1}} Br + Br$

[1.2] $Br_2 + Br_2 \xrightarrow{k_{i2}} Br + Br + Br_2$

[1.3] $Br + H_2 \xrightarrow{k_1} HBr + H$

[1.4] $H + Br_2 \xrightarrow{k_2} HBr + Br$

[1.5] $HBr + H \xrightarrow{k_{-1}} Br + H_2$

[1.6] $Br + HBr \xrightarrow{k_{-2}} H + Br_2$

[1.7] $Br + Br \xrightarrow{k_{t1}} Br_2 + \hbar\nu$

[1.8] $Br + Br + Br_2 \xrightarrow{k_{t2}} Br_2 + Br_2$

qui composent le schéma cinétique d'une réaction en chaîne. Dans ce mécanisme, on tient compte de deux façons d'initiation, c'est-à-dire, l'ouverture de la molécule de $Br_2$ est realisée à l'aide du rayonnement d'un champ électromagnétique convenable ou d'une forme thermique. De la même façon, la rupture a

[1]Revision reçue le 15 mars 1982.

0008-4042/82/162151-08$01.00/0

©1982 National Research Council of Canada/Conseil national de recherches du Canada

Can. J. Chem. Downloaded from www.nrcresearchpress.com by 210.87.254.6 on 09/06/12
For personal use only.

aussi ces deux possibilités. L'ouverture et la rupture thermique sont réalisées en présence d'une troisième particule qui peut être une molécule de $Br_2$ comme dans le présent schéma cinétique.

Le but final de cet étude est exprimer les coefficients de vitesse, rattachés aux differéntes interactions élémentaires prises en considération dans le schéma cinétique, en fonction des propriétés microscopiques (3).

L'article a été organisé de la forme suivante.

Dans la section II, on commence avec un Hamiltonien, dans la quantification secondaire, exprimé en fonction des constituants élémentaires (noyaux de H, noyaux de Br, électrons et photons). Les forces d'interactions entre les noyaux de H, noyaux de Br et électrons sont de Coulomb. A l'aide de la transformation généralisée de Tani (7–10), on obtient un Hamiltonien où les termes rattachés aux atomes, molécules, interactions non réactives et réactives apparaissent explicitement. Les termes d'interaction sont considerés sous deux formes: les interactions entre atomes ou/et molécules qui seront appelées interactions matière–matière et les interactions entre atomes ou molécules et le champ électromagnétique qui seront appelées interactions lumière–matière.

Dans la Section III, on commence avec l'équation cinétique sous la forme proposée par le Groupe de Bruxelles (11, 12). La superopérateur de collision du système est dévéloppé en "cluster" à l'aide du dévéloppement en "cluster" du superopérateur résolvante (13, 14) où l'on suppose la statistique de Boltzmann pour les atomes et les molécules. Ce dévéloppement en "cluster" du superopérateur résolvante nous permet de faire une séparation du superopérateur de collision de telle sorte qu'il apparaît le superopérateur de transition rattaché aux collisions matière–matière celui-ci satisfaisant à l'équation de Lippmann–Schwinger du "scattering" formel, et un superopérateur de collision rattaché aux collisions lumière–matière à l'approximation du faible couplage.

En définant les matrices densité réduite, on obtient les équations cinétiques reliées à l'évolution statistique des particules du système. Ensuite, on exprime les superopérateurs de transition en fonction des matrices de transition au cas des interactions matière–matière (3, 4, 15, 16) et le superopérateur de collision lumière–matière à l'approximation du faible couplage en fonction de la matrice du Hamiltonien de l'interaction lumière–matière.

Dans la section IV, on obtient les équations "master" en appliquant la trace convenable aux équations cinétiques. De cette façon, on identifie les coefficients de vitesse.

La section V est consacrée aux discussions.

## II. Hamiltonien réactif

Le système considéré est constitué par les atomes H, Br, les molécules $Br_2$, $H_2$, HBr et le champ électromagnétique.

Pour commencer l'étude de ce système, on va faire usage d'un représentation où seulement les noyaux de brome ($Z$), les noyaux d'hydrogène ($Y$), les électrons ($X$) et les photons apparaissent.

Telles variables ont vraiment la forme suivante $Z \equiv (R_z, \sigma_z)$, $Y \equiv (R_y, \sigma_y)$ et $X \equiv (r, \sigma_x)$ où $R_z$, $R_y$ et $r$ sont les rayons vecteurs et $\sigma_z$, $\sigma_y$, $\sigma_x$ sont les variables de "spin".

Dans cette représentation, le Hamiltonien dans la quantification secondaire est:

$$[2.1] \quad H = T_z + T_y + T_x + V_{zy} + V_{zx} + V_{yx} + V_{zz} + V_{yy} + V_{xx} + H_1 + H_{l-m}$$

où $T$ est l'opérateur énergie cinétique, $V$ est l'opérateur énergie potentielle d'interaction qui a une nature coulombienne, $H_1$ est le Hamiltonien de la lumière non perturbé et $H_{1-m}$ est le Hamiltonien relié à l'interaction entre la lumière et les constituants élémentaires.

Dans cette représentation, les propriétés des atomes et molécules n'apparaissent pas explicitement et elles doivent être inclues dans les conditions de contour des vecteurs état.

Pourtant, on peut trouver une transformation unitaire $\mathbf{U}$ (7–10) telle que $\mathbf{U}^{-1}\mathbf{H}\,\mathbf{U}$, qui a d'abord la même information que $\mathbf{U}$, contienne les variables dynamiques atomiques et moléculaires.

Le résultat d'appliquer la transformation unitaire généralisée de Tani est un Hamiltonien transformé que l'on approxime de telle sorte qu'il doit contenir les termes réactifs proposés au schéma cinétique. De cette façon, on écrit:

Can. J. Chem. Downloaded from www.nrcresearchpress.com by 210.87.254.6 on 09/06/12
For personal use only.

$$[2.2]\quad \mathbf{U}^{-1}\mathbf{H}\mathbf{U} = H_{H} + H_{Br} + H_{H_2} + H_{Br_2} + H_{I} + H_{H_2-H_2} + H_{Br_2-Br_2} + H_{HBr-HBr} + H_{H-H} + H_{Br-Br} + H_{H-Br} + H_{H-H_2} + H_{H-Br_2} + H_{H-HBr} + H_{Br-H_2} + H_{Br-Br_2} + H_{Br-HBr} + H_{H_2-Br_2} + H_{H_2-HBr} + H_{Br_2-Br_2} + H(HBr + H \leftarrow H_2 + Br) + H(H_2 + Br \leftarrow HBr + H) + H(HBr + Br \leftarrow Br_2 + H) + H(Br_2 + H \leftarrow HBr + Br) + V(Br + Br \leftarrow Br_2 + \hbar\nu) + V(Br_2 + \hbar\nu \leftarrow Br + Br) + H(Br + Br + Br \leftarrow Br_2 + Br_2) + H(Br_2 + Br_2 \leftarrow Br + Br + Br)$$

où, par exemple:

$$[2.3]\quad H_{Br} = \sum_i E_{Br_i} a^+_{Br_i} a_{Br_i}$$

$$H_I = \sum_i \bar{h}\omega_i b^+_i b_i$$

$$H_{H-Br} = \sum_{iklm} \langle br_i h_k | V | h_l br_m \rangle a^+_{Br_i} a^+_{H_k} a_{H_l} a_{Br_m}$$

$$H(HBr + H \leftarrow H_2 + Br) = \sum_{iklm} \langle hbr_i h_k | V | h_{2_l} br_m \rangle a^+_{HBr_i} a^+_{H_k} a_{H_{2_l}} a_{Br_m}$$

$$V(Br + Br \leftarrow Br_2 + \hbar\nu) = \frac{1}{2} \sum_{ijkl} V_{ikjl} a^+_{Br_i} a^+_{Br_i} b_j a_{Br_{2_l}}$$

$$H(Br + Br + Br_2 \leftarrow Br_2 + Br_2) = \frac{1}{4} \sum_{iklmn} \langle br_i br_k br_{2_l} | V | br_{2_m} br_{2_n} \rangle a^+_{Br_i} a^+_{Br_k} a^+_{Br_{2_l}} a_{Br_{2_m}} a_{Br_{2_n}}$$

où par exemple $a^+_{Br_i}$, $a_{Br_i}$, $b^+_j$ et $b_j$ sont les opérateurs idéals de création de annihilation du brome et des photons respectivement. L'indice $i$ représente l'état quantique et l'indice $j$ représente le vecteur d'onde et la polarisation simultanément.

Ces opérateurs satisfont aux conditions de commutation de Bose. Il faut remarquer que les éléments matriciels de la première et la troisième relation de [2.3] sont coulombiens et que $V_{ikjl}$ est l'élément matriciel rattaché à l'interaction réactive entre la molécule de $Br_2$ et la lumière. Les expressions de ces éléments matriciels ont été déjà calculés (17, 18).

## III. Équations cinétiques

L'équation cinétique proposée par le Groupe de Bruxelles est:

$$[3.1]\quad i\partial_t P\rho(t) = \Omega\Psi(+i0)P\rho(t)$$

où $P$ est le superopérateur projettant les éléments diagonaux, $\Psi(+i0)$ est le limite lorsque $z \rightarrow +i0$ du superopérateur de collision irréductible $\Psi(z)$ dont l'expression formelle est:

$$[3.2]\quad \Psi(z) = PLQ \frac{1}{z - QLQ} QLP$$

où $L$ est le superopérateur de Liouville et $Q = I - P$.

Le superopérateur $\Omega$ prend en considération la durée finite des collisions et il peut être exprimé sous la forme:

$$[3.3]\quad \Omega = 1 + \Psi'(+i0) + \ldots$$

Les collisions peuvent être considerées instantanées au limite du faible couplage pour l'interaction lumière–matière (19) et puis pour les systèmes dilués les collisions matière–matière peuvent aussi être considerées instantanées (11).

Si l'on considère les conditions ci-dessous on peut écrire $\Omega = 1$ et l'équation [3.1] devient:

$$[3.4]\quad i\partial_t P\rho(t) = \Psi(+i0)P\rho(t)$$

Can. J. Chem. Downloaded from www.nrcresearchpress.com by 210.87.254.6 on 09/06/12
For personal use only.

Can. J. Chem. Downloaded from www.nrcresearchpress.com by 210.87.254.6 on 09/06/12
For personal use only.

Pour les systèmes homogènes, on peut écrire les suivantes relations:

[3.5] $L_0P = 0 \quad PL'P = 0$

où $L_0$ et $L'$ sont les parties non perturbée et perturbée de superopérateur de Liouville $L$, respectivement.

On peut trouver une rélation très simple, pour les systèmes dilués et homogènes, entre le superopérateur de collision, $\Psi(z)$, et le superopérateur de transition, $W(z)$, rattaché aux collisions matière–matière celui-ci satisfaisant à l'équation de Lippman–Schwinger:

[3.6] $W(z) = L' + L'R(z)L'$

où $R(z)$ est le superopérateur résolvante dont l'expression formelle est:

[3.7] $R(z) = 1/(z - L)$

Cette rélation est:

[3.8] $PW(z)P = \Psi(z)$

On a pris en considération les rélations [3.5] valables pour les systèmes homogènes.

Ensuite, on fait le dévéloppement du superopérateur de collision (13, 14), $\Psi(z)$, en négligeant tous les termes réactifs non inclus dans le schéma cinétique.

Le vecteur état dans la quantification secondaire est:

[3.9] $|h_1..h_{N_H}br_1..br_{N_{Br}}h_{2_1}..h_{2_{N_{H_2}}}..br_{2_1}..hbr_1..hbr_{N_{HBr}}n_{f_1}..n_{f_m})$

où l'on a supposé la statistique de Boltzmann pour les atomes et molécules ce qui veut dire que les nombres de remplissage peuvent prendre deux valeurs, $n_i = 0,1$. Les symboles de $N_H, N_{Br}, N_{H_2}, N_{Br_2}, N_{HBr}$ représentent le nombre d'atomes de H, atomes de Br, molécules de $H_2$, $Br_2$ et HBr. Le nombre de photons est $\Sigma_m n_{f_m}$.

Le vecteur état [3.9] peut être exprimée d'une forme symbolique:

[3.10] $|h, br, h_2, br_2, hbr, n_f)$

Le superopérateur résolvante peut être développé en "cluster".

$$
\begin{aligned}
[3.11]\quad (h,br,h_2,br_2,hbr,n_f;h,br,h_2,br_2,hbr,n_f|R(z)|h',br',h_2',br_2',hbr',n_f';h',br',h_2',br_2',hbr',n_f') \\
= (h,br,h_2,br_2hbr,n_f;h,br,h_2,br_2hbr,n_f|R_0(z)|h',br',h_2',br_2',hbr',n_f';h',br',h_2',br_2',hbr',n_f') \\
+ (h,br,h_2,br_2,hbr;h,br,h_2,br_2,hbr|R_0(z)WR_0(z)|h',br',h_2',br_2',hbr;h',br',h_2',br_2',hbr') \\
+ \sum_{i<j;k,l} (br_ibr_j;br_ibr_j|R_0(z)\Psi^{(2)}_{l-m}(z)R_0(z)|f_k'br_{2_l}';f_k'br_{2_l})\delta \\
+ \sum_{i,j;k<l} (f_ibr_{2_j};f_ibr_{2_j}|R_0(z)\Psi^{(2)}_{l-m}(z)R_0(z)|br_k'br_l';br_k'br_l')\delta
\end{aligned}
$$

où $W$ est le superopérateur de transition pour les collisions matière–matière, $\Psi^{(2)}_{l-m}(z)$ est le superopérateur de collision pour l'interaction lumière–matière à l'approximation du faible couplage, et $\delta$ est la delta de Kronecker pour les états qui n'apparaissent pas dans les vecteurs ci-dessus.

L'expression formelle de $\Psi^{(2)}_{l-m}(z)$ est:

[3.12] $$\Psi^{(2)}_{l-m}(z) = PL'Q \frac{1}{z - L_0} QL'P$$

où $L'$ est le superopérateur de Liouville pour l'interaction réactive entre la lumière et la molécule de $Br_2$.

Ensuite, on exprime les éléments diagonaux du superopérateur résolvante en fonction du superopérateur irréductible de collision.

[3.13] $$PR(z)P = \frac{1}{z - \Psi(z)} P$$

On peut exprimer l'équation [3.13] à l'aide d'une série formelle de $1/z$:

[3.14] $$PR(z)P = \sum_{n=0}^{\infty} \frac{1}{z^{n+1}} |\Psi(z)|^n$$

Pour les collisions instantanées (11), il est suffisant d'écrire seulement les deux premiers termes de [3.14]:

[3.15] $$PR(z)P = \frac{1}{z} + \frac{1}{z} \Psi(z) \frac{1}{z}$$

Le dévéloppement global du superopérateur de collision est obtenu en prenant en considération les rélations [3.11] et [3.15], et en tenant compte du dévéloppement en "cluster" du superopérateur de transition pour les collisions matière–matière.

Un terme de ce dévéloppement du superopérateur de collision rattaché aux collisions matière–matière a la forme:

[3.16] $$\sum_{i,j} (br_i hbr_j; br_i hbr_j | W | h_i' br_j'; h_i' br_j') \delta$$

et l'un autre rattaché aux collisions lumière–matière a la forme:

[3.17] $$\sum_{i<j;kl} (br_i br_j; br_i br_j | \Psi^{(2)}_{l-m} | f_k' br_{2_l}'; f_k' br_{2_l}') \delta$$

Dans ce dévéloppement, il faut introduire le terme:

[3.18] $$\sum_{i<j;k} (br_i br_j br_{2_k}; br_i br_j br_{2_k} | W' | br_i' br_j' br_{2_k}'; br_i' br_j' br_{2_k}') \delta$$

rattaché à une collision non réactive de trois particules afin d'obtenir le terme de perte dans l'équation cinétique qui se rapporte à l'interaction réactive de trois particules pour en donner deux, en étant $W'$ la partie connectée du superopérateur de transition des collisions de trois particules, qui peut être exprimée sous la forme:

[3.19] $$W_{ijk}' = W_{ijk} - W_{ij} - W_{ik} - W_{jk}$$

Les autres termes non réactives considerées dans le dévéloppement en "cluster" appartiennent à l'approximation binaire puisque seulement les collisions binaires ont importance à cause des conditions diluées du système.

La matrice densité est normalisée de la forme suivante:

[3.20] $$\mathrm{Tr}\, \rho^{(N)} = N_{\mathrm{H}}! N_{\mathrm{Br}}! N_{\mathrm{H_2}}! N_{\mathrm{Br_2}}! N_{\mathrm{HBr}}! N_{\mathrm{F}}!$$

on définit les matrices densité réduite:

[3.21] $$\rho_\alpha^{(n)} = \left\{ (N_\alpha - n)! \prod_{\beta \neq \alpha; a} N_\beta! N_a! \right\}^{-1} \mathrm{Tr}'_{1..n\varepsilon\alpha} \rho^{(N)}$$

[3.22] $$\rho_a^{(2n)} = \left\{ (N_a - n)! \prod_{\alpha; b \neq a} N_\alpha! N_a! \right\}^{-1} \mathrm{Tr}'_{1..2n\varepsilon a} \rho^{(N)}$$

[3.23] $$\rho_{\alpha a}^{(2n+m)} = \left\{ (N_\alpha - m)!(N_a - n)! \prod_{\substack{\beta \neq \alpha \\ b \neq a}} N_\beta! N_b! \right\}^{-1} \mathrm{Tr}'_{\substack{1..m\varepsilon\alpha \\ m+1..2n\varepsilon a}} \rho^{(N)}$$

où "$\alpha$" représente les atomes H, Br et les photons, et "$a$" représente les molécules $H_2$, $Br_2$ et HBr. La trace Tr′ est appliquée sur toutes les particules sauf celles qui sont indiquées par les indices.

Les superopérateurs de transition peuvent être reliés avec les matrices de transition à l'aide des suivantes rélations (3, 4, 15, 16).

[3.24] $$(a_i b_j; a_i b_j | W | a_i' b_j'; a_i' b_j') = 2\pi i \delta(E_{a_i} + E_{b_j} - E_{a_{i'}} - E_{b_{j'}}) |\langle a_i b_j | T | a_i' b_j' \rangle|^2$$

$$(a\alpha; a\alpha | W | b\beta; b\beta) = 2\pi i \delta(E_a + E_\alpha - E_b - E_\beta) |\langle a\alpha | T | b\beta \rangle|^2$$

où $T$ est l'opérateur de transition.

Can. J. Chem. Downloaded from www.nrcresearchpress.com by 210.87.254.6 on 09/06/12
For personal use only.

Can. J. Chem. Downloaded from www.nrcresearchpress.com by 210.87.254.6 on 09/06/12
For personal use only.

Par rapport à l'interaction de la lumière avec les particules composées, le formalisme de la matrice de transition $T$ ne peut pas être appliqué (21), et c'est pourquoi la méthode à employer n'est pas le même. Pour le superopérateur de collision lumière–matière, à l'approximation du faible couplage, on a:

$$[3.25]\quad (br_i br_j; br_i br_j|\Psi^{(2)}_{l-m}|f_i' br_{2_j}; f_i' br_{2_j}) = 2\pi i\delta(E_{br_i} + E_{br_j} - \bar{h}\omega_{f_i'} - E_{br_{2_j}'})|\langle br_i br_j|V|f_i' br_{2_j}'\rangle|^2$$

En tenant compte des considérations ci-dessus, on peut écrire les équations cinétiques de chacun des composants du système. On écrit seulement l'équation cinétique de l'atome de brome, puisque cette équation nous rapporte tous les coefficients de vitesse des processus élémentaires considerés dans le schéma cinétique.

$$\begin{aligned}[3.26]\quad i\partial_t(br_i|\rho^{(1)}_{Br}|br_i) = &\sum_{br_i' br_{j'}} \sum_{br_j} 2\pi i\delta(E_{br_i} + E_{br_j} - E_{br_{i'}} - E_{br_{j'}})|\langle br_i br_j|T|br_i' br_j'\rangle|^2 \\
&\{(br_i'|\rho^{(1)}_{Br}|br_i')(br_j'|\rho^{(1)}_{Br}|br_j') - (br_i|\rho^{(1)}_{Br}|br_i)(br_j|\rho^{(1)}_{Br}|br_j)\} \\
&+ \sum_{br_i' h_{j'}} \sum_{h_j} 2\pi i\delta(E_{Br_i} + E_{h_j} - E_{Br_{i'}} - E_{h_{j'}})|\langle br_i h_j|T|br_i h_j\rangle|^2 \\
&\times \{(br_i'|\rho^{(1)}_{Br}|br_i')(h_j'|\rho^{(1)}_{H}|h_j') - (br_i|\rho^{(1)}_{Br}|br_i)(h_j|\rho^{(1)}_{H}|h_j)\} \\
&+ \sum_{br_i' h_{2'}} \sum_{h_2} 2\pi i\delta(E_{br_i} + E_{h_{2_j}} - E_{br_{i'}} - E_{h_{2_j}'})|\langle br_i h_{2_j}|T|br_i' h_{2_j}'\rangle|^2 \\
&\times \{(br_i'|\rho^{(1)}_{Br}|br_i')(h_{2_j}'|\rho^{(2)}_{H_2}|h_{2_j}') - (br_i|\rho^{(1)}_{Br}|br_i)(h_{2_j}|\rho^{(2)}_{H_2}|h_{2_j})\} \\
&+ \sum_{br_i' br_{2_{j'}}} \sum_{br_{2_j}} 2\pi i\delta(E_{br_i} + E_{br_{2_j}} - E_{br_{i'}} - E_{br_{2_{j'}}})|\langle br_i br_{2_j}|T|br_i' br_{2_j}'\rangle|^2 \\
&\times \{(br_i'|\rho^{(1)}_{Br}|br_i')(br_{2_j}'|\rho^{(2)}_{Br_2}|br_{2_j}') - (br_i|\rho^{(1)}_{Br}|br_i)(br_{2_j}'|\rho^{(2)}_{Br_2}|br_{2_j}')\} \\
&+ \sum_{br_i' hbr_{j'}} \sum_{hbr_j} 2\pi i\delta(E_{br_i} + E_{hbr_j} - E_{br'} - E_{hbr_{j'}})|\langle br_i hbr_j|T|br_i' hbr_j'\rangle|^2 \\
&\times \{(br_i'|\rho^{(1)}_{Br}|br_i')(hbr_j'|\rho^{(2)}_{HBr}|hbr_j') - (br_i|\rho^{(2)}_{Br}|br_i)(hbr_j|\rho^{(2)}_{HBr}|hbr_j)\} \\
&+ \sum_{hbr_i' h_{j'}} \sum_{h_{2_j}} 2\pi i\delta(E_{br_i} + E_{h_{2_j}} - E_{hbr_{i'}} - E_{h_{j'}})|\langle br_i h_{2_j}|T|hbr_i' h_{j'}\rangle|^2 \\
&\times \{(hbr_i'|\rho^{(2)}_{HBr}|hbr_i')(h_j'|\rho^{(1)}_{H}|h_j') - (br_i|\rho^{(1)}_{Br}|br_i)(h_{2_j}|\rho^{(2)}_{H_2}|h_{2_j})\} \\
&+ \sum_{h_i' br_{2_{j'}}} \sum_{hbr_j} 2\pi i\delta(E_{br_i} + E_{hbr_j} - E_{h_{i'}} - E_{br_{2_{j'}}})|\langle br_i hbr_j|T|h_i' br_{2_j}'\rangle|^2 \\
&\times \{(h_i'|\rho^{(1)}_{H}|h_i')(br_{2_j}'|\rho^{(2)}_{Br_2}|br_{2_j}') - (br_i|\rho^{(1)}_{Br}|br_i)(hbr_j|\rho^{(2)}_{HBr}|hbr_j)\} \\
&+ \sum_{f_i' br_{2_{j'}}} \sum_{br_j} 2\pi i\delta(E_{br_i} + E_{br_j} - \hbar\omega_{f_i'} - E_{br_{2_{j'}}})|\langle br_i br_j|V|f_i' br_{2_{j'}}\rangle|^2 \\
&\times \{(f_i'|\rho^{(1)}_{F}|f_i')(br_{2_j}'|\rho^{(2)}_{Br_2}|br_{2_j}') - (br_i|\rho^{(1)}_{Br}|br_i)(br_j|\rho^{(1)}_{Br}|br_j)\} \\
&+ \sum_{br_{2_i}' br_{2_{j'}}} \sum_{br_j br_{2_k}} 2\pi i\delta(E_{br_i} + E_{br_j} + E_{br_{2_k}} - E_{br_{2_{i'}}} - E_{br_{2_{j'}}})|\langle br_i br_j br_{2_k}|T|br_{2_{i'}} br_{2_{j'}}\rangle|^2 \\
&\qquad \times \{(br_{2_i}'|\rho^{(2)}_{Br_2}|br_{2_i}')(br_{2_j}'|\rho^{(2)}_{Br_2}|br_{2_j}') - (br_i|\rho^{(1)}_{Br}|br_i)(br_j|\rho^{(1)}_{Br}|br_j)(br_{2_k}|\rho^{(3)}_{Br_2}|br_{2_k})\}\end{aligned}$$

En obtenant l'équation [3.26], on a fait usage de l'expression [3.8], et de la suivante rélation (22)

$$[3.27]\quad \sum_{n_1', n_2'} (n_1 n_2..; n_1 n_2..|\Psi(+10)|n_1' n_2'..; n_1' n_2'..) = 0$$

et on a utilisé l'approximation du chaos moléculaire.

## IV. Équation master. Coefficients de vitesse

L'équation "master" est obtenue en appliquant la trace sur l'expression [3.26], sur les états $br_i$ de l'atome de Br.

A l'aide des définitions des matrices densité réduite, la trace de telles matrices devient le nombre du particules:

[4.1] $\mathrm{Tr}\,\rho_{\mathrm{Br}}^{(1)} = N_{\mathrm{Br}}$

En tenant compte de la réversibilité microscopique, les termes non réactifs deviennent nuls lorsqu'on applique les traces; on a, par exemple:

$$[4.2]\quad \sum_{br_i'br_j'}\sum_{br_ibr_j} 2\pi i\delta(E_{br_i}+E_{br_j}-E_{br_i'}-E_{br_j'})|\langle br_ibr_j|T|br_i'br_j'\rangle|^2 \times\{(br_i'|\rho_{\mathrm{Br}}^{(1)}|br_i')(br_j'|\rho_{\mathrm{Br}}^{(1)}|br_j')-(br_i|\rho_{\mathrm{Br}}^{(1)}|br_i)(br_j|\rho_{\mathrm{Br}}^{(1)}|br_j)\}=0$$

L'équation "master" est:

$$[4.3]\quad \partial_t N_{\mathrm{Br}} = k_{i,1}(h\omega,\mathrm{Br}_2;\mathrm{Br},\mathrm{Br})N_{\mathrm{Br}_2} - k_{t,1}(\mathrm{Br},\mathrm{Br};\mathrm{Br}_2,h\omega)|N_{\mathrm{Br}}|^2 + k_{i,2}(\mathrm{Br}_2,\mathrm{Br}_2;\mathrm{Br},\mathrm{Br},\mathrm{Br})|N_{\mathrm{Br}_2}|^2 - k_{t,2}(\mathrm{Br},\mathrm{Br},\mathrm{Br}_2;\mathrm{Br}_2,\mathrm{Br}_2)N_{\mathrm{Br}_2}|N_{\mathrm{Br}}|^2 + k_1(\mathrm{HBr},\mathrm{H};\mathrm{Br},\mathrm{H}_2)N_{\mathrm{HBr}}N_{\mathrm{H}} - k_{-1}(\mathrm{Br},\mathrm{H}_2;\mathrm{HBr},\mathrm{H}) \times N_{\mathrm{Br}}N_{\mathrm{H}_2} + k_2(\mathrm{H},\mathrm{Br}_2;\mathrm{HBr},\mathrm{Br})N_{\mathrm{H}}N_{\mathrm{Br}_2} - k_{-2}(\mathrm{HBr},\mathrm{Br};\mathrm{H},\mathrm{Br}_2)N_{\mathrm{HBr}}N_{\mathrm{Br}}$$

A l'intérieur des parenthèses des coefficients de vitesse on montre le réaction qui a lieu, en apparaissant d'abord les réactifs et après les produits.

En vertu de l'équation [4.3], on obtient pour les coefficients de vitesse les suivantes expressions:

$$[4.4]\quad k_{i,1}(\hbar\nu,\mathrm{Br}_2;\mathrm{Br},\mathrm{Br}) = \sum_{f_i'br_{2_j}'}\sum_{br_ibr_j} 2\pi\delta(E_{br_i}+E_{br_j}-h\omega_{f_i'}-E_{br_{2_j}'})|\langle br_ibr_j|V|f_i'br_{2_j}'\rangle|^2 \times (f_i'|\rho_{\mathrm{F}}^{(1)}|f_i')(br_{2_j}'|\rho_{\mathrm{Br}_2}^{(2)}|br_j')|N_{\mathrm{Br}_2}|^{-1}$$

$$[4.5]\quad k_1(\mathrm{Br},\mathrm{H}_2;\mathrm{HBr},\mathrm{H}) = \sum_{hbr_i'h_j'}\sum_{br_ih_{2_j}} 2\pi\delta(E_{br_i}+E_{h_{2_j}}-E_{h_j'}-E_{hbr_i'})|\langle br_ih_{2_j}|T|hbr_i'h_j'\rangle|^2 \times (br_i|\rho_{\mathrm{Br}}^{(1)}|br_i)(h_{2_j}|\rho_{\mathrm{H}_2}^{(2)}|h_{2_j})|N_{\mathrm{Br}}|^{-1}|N_{\mathrm{H}_2}|^{-1}$$

$$[4.6]\quad k_{t,2}(\mathrm{Br},\mathrm{Br},\mathrm{Br}_2;\mathrm{Br}_2,\mathrm{Br}_2) = \sum_{br_{2_i}'br_{2_j}'}\sum_{br_ibr_jbr_{2_k}} 2\pi\delta(E_{br_i}+E_{br_j}+E_{br_{2_k}}-E_{br_{2_i}'}-E_{br_{2_j}'}) \times|\langle br_ibr_jbr_{2_k}|T|br_{2_i}'br_{2_j}'\rangle|^2(br_i|\rho_{\mathrm{Br}}^{(1)}|br_i)(br_j|\rho_{\mathrm{Br}}^{(1)}|br_j)(br_{2_k}|\rho_{\mathrm{Br}_2}^{(2)}|br_{2_k})|N_{\mathrm{Br}}|^{-2}|N_{\mathrm{Br}_2}|^{-1}$$

Pour les autres coefficients que l'on obtient, les expressions sont pareilles.

## V. Discussion

Dans cet article, on obtient les équations cinétiques d'un système gazeux homogène dilué réactif, qui interactionne avec un champ électromagnétique.

Les différents processus réactifs, considérés dans cet étude, sont exposés dans le schéma cinétique, où on fait inclusion de deux formes d'initiation et de rupture; de cette façon, l'ouverture de la molécule de $Br_2$ a deux possibilités: l'initiation photochimique et l'initiation thermique.

Par analogie, la rupture a aussi deux possibilités. On peut penser que, dans les conditions du milieu ambiant et en présence de lumière convenable, l'initiation sera préférablement photochimique et la rupture sera thermique.

Le Hamiltonien réactif permet d'obtenir, explicitement, tous les termes réactifs proposés dans le schéma cinétique, et on y inclut les interactions réactives de deux particules pour donner trois particules et de trois particules pour en donner deux.

Le dévéloppement du superopérateur de collision est realisé à l'aide d'un dévéloppement en "cluster" du superopérateur résolvante. C'est ici qu'il apparaît le superopérateur de collision rélié à l'interaction lumière–matière à l'approximation du faible couplage.

L'obtention d'une seule équation cinétique, rattachée à l'atome de brome, nous permet de trouver tous les coefficients de vitesse. Pourtant, la méthode employée permet d'obtenir, de la même façon, les équations cinétiques des autres composants du système.

Enfin, il faut remarquer que l'on a choisi la réaction de $Br_2$ avec $H_2$ dans cet étude, du fait qu'elle a la possibilité de trois formes d'initiation: l'initiation thermique, photochimique et hétérogène. Pourtant, la méthode employé n'est pas exclusive de ce système mais elle est complètement générale et elle nous permet d'écrire les équations cinétiques aux cas d'autres systèmes gazeux homogènes et dilués. De la même façon, on veut indiquer que des prochaines articles, se rapportant a l'initiation hétérogène, seront publiés.

Can. J. Chem. Downloaded from www.nrcresearchpress.com by 210.87.254.6 on 09/06/12
For personal use only.

1. B. C. EU. J. Chem. Phys. **63**, 303 (1975).
2. C. I. IVANOV. Physica A, **94**, 571 (1978).
3. J. VEGUILLAS et M. RIVAS. Envoyé au J. Chem. Phys.
4. J. LOWRY et R. F. SNIDER. J. Chem. Phys. **61**, 2320 (1974).
5. M. S. JHON et J. S. DAHLER. J. Chem. Phys. **69**, 819 (1978).
6. M. S. JHON et J. S. DAHLER. J. Chem. Phys. **70**, 5292 (1979).
7. M. D. GIRARDEAU. J. Math. Phys. **16**, 1901 (1975).
8. M. D. GIRARDEAU. J. Math. Phys. **19**, 2605 (1978).
9. M. D. GIRARDEAU. Physica A, **95**, 609 (1979).
10. M. D. GIRARDEAU et J. D. GILBERT. Physica A, **97**, 42 (1979).
11. I. PRIGOGINE. Non equilibrium statistical mechanics. Wiley, New York. 1962.
12. R. BALESCU. Equilibrium and non equilibrium statistical mechanics. Wiley, New York. 1975.
13. S. WEINBERG. Phys. Rev. B, **133**, 232 (1964).
14. B. C. EU. J. Chem. Phys. **55**, 4613 (1971).
15. B. C. EU. J. Chem. Phys. **63**, 298 (1975).
16. I. PRIGOGINE et F. MAYNE. Transport phenomena. *Edité par* G. Kirczenow et J. Marro. Springer-Verlag, New York. 1974.
17. M. A. DIAZ. Thèse de Licence, 1980. Université du Pays Basque, Espagne.
18. A. M. GUTIERREZ. Thèse de Licence, 1980. Université du Pays Basque, Espagne.
19. F. HENIN. Physica, **39**, 599 (1968).
20. F. MAYNE et I. PRIGOGINE. Physica, **63**, 1 (1973).
21. W. HEITLER. The quantum theory of radiation. Clarendon Press, Oxford. 1953.
22. R. ZWANZIG. Physica, **30**, 1109 (1964).

Can. J. Chem. Downloaded from www.nrcresearchpress.com by 210.87.254.6 on 09/06/12
For personal use only.

Can. J. Chem. Downloaded from www.nrcresearchpress.com by 210.87.254.105 on 09/06/12
For personal use only.



# Topochemical photodimerization of 7-acetoxycoumarin: the acetoxy group as a steering agent

N. RAMASUBBU, K. GNANAGURU, K. VENKATESAN, AND V. RAMAMURTHY[1]

*Department of Organic Chemistry, Indian Institute of Science, Bangalore 560012, India*

Received March 19, 1982

N. RAMASUBBU, K. GNANAGURU, K. VENKATESAN, and V. RAMAMURTHY. Can. J. Chem. **60**, 2159 (1982).

Among the various substituted coumarins investigated only 7-acetoxycoumarin is observed to photodimerize topochemically in the crystalline state and this observation may be of importance in the context of "crystal engineering".

N. RAMASUBBU, K. GNANAGURU, K. VENKATESAN et V. RAMAMURTHY. Can. J. Chem. **60**, 2159 (1982).

Des diverses coumarines substituées étudiées, seule l'acétoxy-7 coumarine se photodimérise topochimiquement à l'état cristallin; cette observation peut avoir de l'importance dans le contexte de "l'ingénierie des cristaux".

[Traduit par le journal]

The photochemical and photophysical processes of many organic compounds are a function of the environment in which they are present. In this connection, we have chosen to investigate the environmental perturbations on the photodimerization of coumarins and the results of our study in the crystalline state are presented here. Coumarins have been chosen for our investigation as their fascinating photochemical behaviour has been fairly well understood (1) and therefore the environmental influence, which is the subject of our concern, would more easily be understandable. The type of bimolecular photochemical process which has been investigated extensively in the solid state is $[\pi_{2s} + \pi_{2s}]$ cycloaddition (2). It has been established that the success of this process in the solid state requires a packing arrangement in which the reacting double bonds are parallel to one another with mean interplanar distances < ca. 4.1 Å. The utility of such photoreactions as a synthetic tool is limited by the difficulty of achieving the desired type of crystal structure in any given case, for the factors that control the crystal packing are not fully understood. However, attempts to design molecules wherein the potentially reactive chromophores are brought into favourable orientation have been reported. So far as dimerization of olefins is concerned, the utilization of dichlorophenyl substituents has been of great value (3). A similar strategy, involving the strong tendency for oxygen atoms of ester groups to pack over the centre of the benzene ring of a neighbouring molecule, has been utilized to "engineer" crystals (4). Scope undoubtedly exists for "engineering" many other crystals and the results presented below are important in this context.

Coumarin is known to be photostable in the solid state (5) although it readily dimerizes in solution (1).[2] Therefore, this appeared to be a good molecular framework to study the role of substituents in bringing about the preferred molecular packing for photodimerization. Of the several coumarins examined by us only a few underwent photodimerization in the solid state upon uv irradiation (450 W medium pressure mercury lamp) as illustrated in Table 1. X-ray crystallographic studies of the monomers of 7-methoxy, 8-methoxy, and 4-chlorocoumarins completed in our laboratory reveal that packing arrangements in these crystals do not allow favorable orientation of the potentially reactive double bonds for dimerization to occur. These appear to be defect-initiated dimerizations (6). In this communication, we present our results on the solid state photodimerization of 7-acetoxycoumarin which is interesting in the context of crystal engineering. The mechanism of dimerization and the nature of the dimer are yet to be characterized in the case of other coumarins listed in Table 1.

The dimer (mp 215–217°C) formed in quantitative yield upon irradiation of 7-acetoxycoumarin

[1]Author to whom correspondence may be addressed.

[2]Although coumarin is established to be photostable in the solid state, its unstable modification and its complex with mercuric chloride give *syn* head–head dimers in the solid state upon uv exposure.

0008-4042/82/162159-03$01.00/0

©1982 National Research Council of Canada/Conseil national de recherches du Canada

Can. J. Chem. Downloaded from www.nrcresearchpress.com by 210.87.254.105 on 09/06/12
For personal use only.

TABLE 1. Photoreactivity of coumarins in the solid state

| Sl. No. | Compound | Solvent of crystallization | Dimerization solid state (yield)[a] | Nature of the dimer |
|---|---|---|---|---|
| 1. | Coumarin | Ethanol | No | — |
| 2. | 4-Hydroxycoumarin | Water | No | — |
| 3. | 4-Methoxycoumarin | Benzene | No | — |
| 4. | 4-Acetoxycoumarin | Ethanol | No | — |
| 5. | 4-Chlorocoumarin | Ethanol | Yes (40%) | *syn* Head–tail<br>*anti* Head–tail |
| 6. | 7-Hydroxycoumarin | Ethanol | No | — |
| 7. | 7-Methoxycoumarin | Benzene | Yes (~90%) | *syn* Head–tail |
| 8. | 7-Acetoxycoumarin | Chloroform | Yes (~90%) | *syn* Head–head |
| 9. | 7-Chlorocoumarin | Ethanol | Yes | [b] |
| 10. | 7-Methylcoumarin | Ethanol–water | Yes | [b] |
| 11. | 6-Chlorocoumarin | Ethanol | Yes | [b] |
| 12. | 6-Methoxycoumarin | Water | Yes | [b] |
| 13. | 8-Methoxycoumarin | Benzene | Yes (~50%) | *anti* Head–tail |
| 14. | 4-Methyl-7-hydroxycoumarin | Ethanol | No | — |
| 15. | 4-Methyl-7-methoxycoumarin | Benzene | No | — |
| 16. | 4-Methyl-7-chlorocoumarin | Chloroform – carbon tetrachloride | Yes | [b] |
| 17. | 4-Methyl-7-acetoxycoumarin | Acetone | Yes | [b] |

[a]Irradiated using 450 W medium pressure mercury lamp; yields were measured by nmr integration.
[b]Nature of the dimer is yet to be characterized.

was shown to have the *syn* head–head configuration based on its spectral properties: ir (Nujol): 1750 $cm^{-1}$; $^1$Hmr (DMSO-$d_6$) δ: 2.21 (3H, s), 4.22 (2H, m, AA′BB′ pattern), 6.66 (1H, d, $J$ = 2 cps), 6.73 (1H, d × d, $J$ = 2 and 8.5 cps) and 6.92 (1H, d, $J$ = 8.5 cps); ms (CI, $NH_3$): 426 (M + $NH_4^+$). Comparison of the above nmr spectral data with those published for the *anti* head–head dimer of 7-acetoxycoumarin and the *syn* head–head dimers of polymethylene-dicarboxylic acid (7-coumarinyl) diesters (7) revealed that the above dimer is *syn* head–head.

In order to elucidate the nature of the intermolecular packing which leads to the formation of the observed dimer, a crystal structure analysis of 7-acetoxycoumarin was carried out.[3] The packing thus obtained is displayed in Fig. 1.

[3]7-Acetoxycoumarin crystallizes from chloroform solution in the space group $P2_1/c$ with $a$ = 3.833(2), $b$ = 22.665(4), $c$ = 10.975(3) Å, β = 96.27(2)°, and $Z$ = 4. A total of 1789 reflections were collected on an Enraf Nonius CAD-4 diffractometer (λ = 1.5418 Å, ω/2θ scan) out of which 1016 were unique and significant [$|F_o| > 3\sigma(|F_o|)$]. The direct methods programme package MULTAN-80 was used for the structure solution (9). Full matrix least-squares refinement of positional and anisotropic thermal parameters of non-hydrogen atoms (treating hydrogen atoms isotropically) led to an $R$ value of 0.056. The computer data on which this calculation is based are available, at a nominal charge, from the Depository of Unpublished Data, CISTI, National Research Council of Canada, Ottawa, Ont., Canada K1A 0S2.

The 7-acetoxycoumarin possesses so-called β-type packing which is characterized by the close packing of parallel and nearly planar reactive double bonds (8) with a separation distance of 3.833 Å along the $a$-axis. Thus the *syn* head–head dimer obtained is the direct consequence of this packing arrangement. It is noteworthy that coumarin which does not undergo dimerization in its stable modification (5) in the solid state undergoes a clean topochemical photoreaction when substituted by an acetoxy group. Thus it is evident that the acetyl group plays a strategic role in steering coumarin rings to pack themselves into a β stacked structure. Earlier, interaction involving overlap of an ester group of one molecule with a benzene ring of another had been utilized to steer diacrylic acids into structures suited for solid state polymerization (4). However, perusal of the figure reveals no such interaction in our case.

Photostability of some of the coumarins (Table 1) in the solid state is not due to any inherent electronic or steric properties of these molecules as they all dimerize readily in solution. It must be attributed to unfavourable packing of these molecules in the crystal lattices. The results of our study on 7-acetoxycoumarin reveal that electronic and steric aspects play, if any, only a minor role in the solid state reactions. It is significant that 7-acetoxycoumarin does not dimerize in solution (7), probably owing to the deactivation of the active

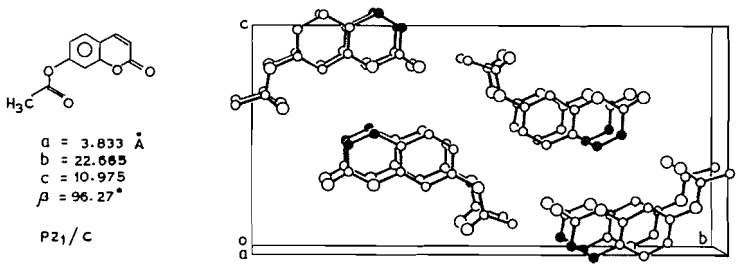


β-TYPE PACKING OF 7-ACETOXYCOUMARIN DOWN a AXIS

FIG. 1.

double bond by the electron withdrawing acetoxy group. Therefore, it appears that adoption of a crystal packing arrangement favourable for bimolecular reaction can overcome the disadvantageous inherent electronic factors. Attempts are underway to explore the generality of acetoxy group effects in "crystal engineering".

**Acknowledgements**

The University Grants Commission and Council of Scientific and Industrial Research, Government of India are thanked for financial assistance. We are grateful to Dr. S. Chandrasekaran for mass spectra.

1. H. MORRISON, H. CURTIS, and T. MCDOWELL. J. Am. Chem. Soc. **88**, 5415 (1966); R. HOFFMAN, P. WELLS, and H. MORRISON. J. Org. Chem. **36**, 102 (1971).
2. G. M. J. SCHMIDT *et al.* Solid state photochemistry. *Edited by* D. Ginsburg. Verlag Chemie. 1976; J. M. THOMAS, S. E. MORSI, and J. P. DESVERGNE. Adv. Phys. Org. Chem. **15**, 63 (1977).
3. G. M. J. SCHMIDT. Pure Appl. Chem. **27**, 647 (1971).
4. H. NAKANISHI, W. JONES, J. M. THOMAS, M. HASEGAWA, and W. L. REES. Proc. R. Soc. London Ser. A, **369**, 307 (1980).
5. J. BERGMAN, K. OSAKI, G. M. J. SCHMIDT, and F. I. SONNTAG. J. Chem. Soc. 2021 (1964).
6. N. RAMASUBBU, T. N. GURU ROW, K. VENKATESAN, V. RAMAMURTHY, and C. N. R. RAO. J. Chem. Soc. Chem. Commun. 178 (1982).
7. L. H. LEENDERS, E. SCHOUTEDEN, and F. C. DE SCHRYVER. J. Org. Chem. **33**, 957 (1973).
8. G. M. J. SCHMIDT. J. Chem. Soc. 2014 (1964).
9. P. MAIN, S. J. FISKE, S. E. HULL, L. LESSINGER, G. GERMAIN, J. P. DECLERCQ, and M. M. WOOLFSON. MULTAN-80. System of Computer Programmes, University of York, York, England. 1980.

Can. J. Chem. Downloaded from www.nrcresearchpress.com by 210.87.254.105 on 09/06/12
For personal use only.

# On cardioactive steroids. IX. The conversion of digitoxigenin to bufalin

THOMAS Y. R. TSAI AND KAREL WIESNER

*Natural Products Research Centre, University of New Brunswick, Bag Service #45222, Fredericton, N.B., Canada E3B 6E2*

Received May 20, 1982

THOMAS Y. R. TSAI and KAREL WIESNER. Can. J. Chem. **60**, 2161 (1982).

A conversion of digitoxigenin **I** to bufalin **7** via a novel furan-to-pyrone transformation is described. It is hoped that this process will be useful in a simple and efficient total synthesis of bufalin, as well as various other synthetic problems.

THOMAS Y. R. TSAI et KAREL WIESNER. Can. J. Chem. **60**, 2161 (1982).

On décrit une transformation de la digitoxigénine (**I**) en bufaline (**7**) par l'intermédiaire d'une nouvelle transformation du furanne en pyrone. On espère que ce procédé sera utile dans le cas d'une synthèse simple et efficace de la bufaline et également dans d'autres synthèses.

[Traduit par le journal]

A few years ago we reported a novel and very efficient methodology for the synthesis of cardenolides featuring furan-containing intermediates (1, 2). In order to use this methodology for the synthesis of bufadienolides, an equally efficient furan-to-pyrone transformation is required. We have worked out recently (using a model system) four different transformations of this type (3, 4). In the

0008-4042/82/162161-03$01.00/0
©1982 National Research Council of Canada/Conseil national de recherches du Canada

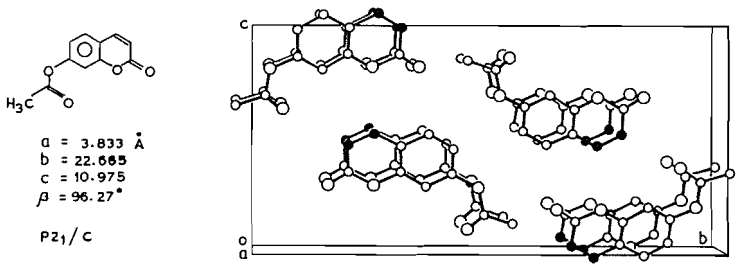


β-TYPE PACKING OF 7-ACETOXYCOUMARIN DOWN a AXIS

FIG. 1.

double bond by the electron withdrawing acetoxy group. Therefore, it appears that adoption of a crystal packing arrangement favourable for bimolecular reaction can overcome the disadvantageous inherent electronic factors. Attempts are underway to explore the generality of acetoxy group effects in "crystal engineering".

**Acknowledgements**

The University Grants Commission and Council of Scientific and Industrial Research, Government of India are thanked for financial assistance. We are grateful to Dr. S. Chandrasekaran for mass spectra.

1. H. MORRISON, H. CURTIS, and T. MCDOWELL. J. Am. Chem. Soc. **88**, 5415 (1966); R. HOFFMAN, P. WELLS, and H. MORRISON. J. Org. Chem. **36**, 102 (1971).
2. G. M. J. SCHMIDT *et al.* Solid state photochemistry. *Edited by* D. Ginsburg. Verlag Chemie. 1976; J. M. THOMAS, S. E. MORSI, and J. P. DESVERGNE. Adv. Phys. Org. Chem. **15**, 63 (1977).
3. G. M. J. SCHMIDT. Pure Appl. Chem. **27**, 647 (1971).
4. H. NAKANISHI, W. JONES, J. M. THOMAS, M. HASEGAWA, and W. L. REES. Proc. R. Soc. London Ser. A, **369**, 307 (1980).
5. J. BERGMAN, K. OSAKI, G. M. J. SCHMIDT, and F. I. SONNTAG. J. Chem. Soc. 2021 (1964).
6. N. RAMASUBBU, T. N. GURU ROW, K. VENKATESAN, V. RAMAMURTHY, and C. N. R. RAO. J. Chem. Soc. Chem. Commun. 178 (1982).
7. L. H. LEENDERS, E. SCHOUTEDEN, and F. C. DE SCHRYVER. J. Org. Chem. **33**, 957 (1973).
8. G. M. J. SCHMIDT. J. Chem. Soc. 2014 (1964).
9. P. MAIN, S. J. FISKE, S. E. HULL, L. LESSINGER, G. GERMAIN, J. P. DECLERCQ, and M. M. WOOLFSON. MULTAN-80. System of Computer Programmes, University of York, York, England. 1980.

Can. J. Chem. Downloaded from www.nrcresearchpress.com by 210.87.254.105 on 09/06/12
For personal use only.

# On cardioactive steroids. IX. The conversion of digitoxigenin to bufalin

THOMAS Y. R. TSAI AND KAREL WIESNER

*Natural Products Research Centre, University of New Brunswick, Bag Service #45222, Fredericton, N.B., Canada E3B 6E2*

Received May 20, 1982

THOMAS Y. R. TSAI and KAREL WIESNER. Can. J. Chem. **60**, 2161 (1982).

A conversion of digitoxigenin **I** to bufalin **7** via a novel furan-to-pyrone transformation is described. It is hoped that this process will be useful in a simple and efficient total synthesis of bufalin, as well as various other synthetic problems.

THOMAS Y. R. TSAI et KAREL WIESNER. Can. J. Chem. **60**, 2161 (1982).

On décrit une transformation de la digitoxigénine (**I**) en bufaline (**7**) par l'intermédiaire d'une nouvelle transformation du furanne en pyrone. On espère que ce procédé sera utile dans le cas d'une synthèse simple et efficace de la bufaline et également dans d'autres synthèses.

[Traduit par le journal]

A few years ago we reported a novel and very efficient methodology for the synthesis of cardenolides featuring furan-containing intermediates (1, 2). In order to use this methodology for the synthesis of bufadienolides, an equally efficient furan-to-pyrone transformation is required. We have worked out recently (using a model system) four different transformations of this type (3, 4). In the

0008-4042/82/162161-03$01.00/0
©1982 National Research Council of Canada/Conseil national de recherches du Canada

Can. J. Chem. Downloaded from www.nrcresearchpress.com by 210.87.254.105 on 09/06/12
For personal use only.

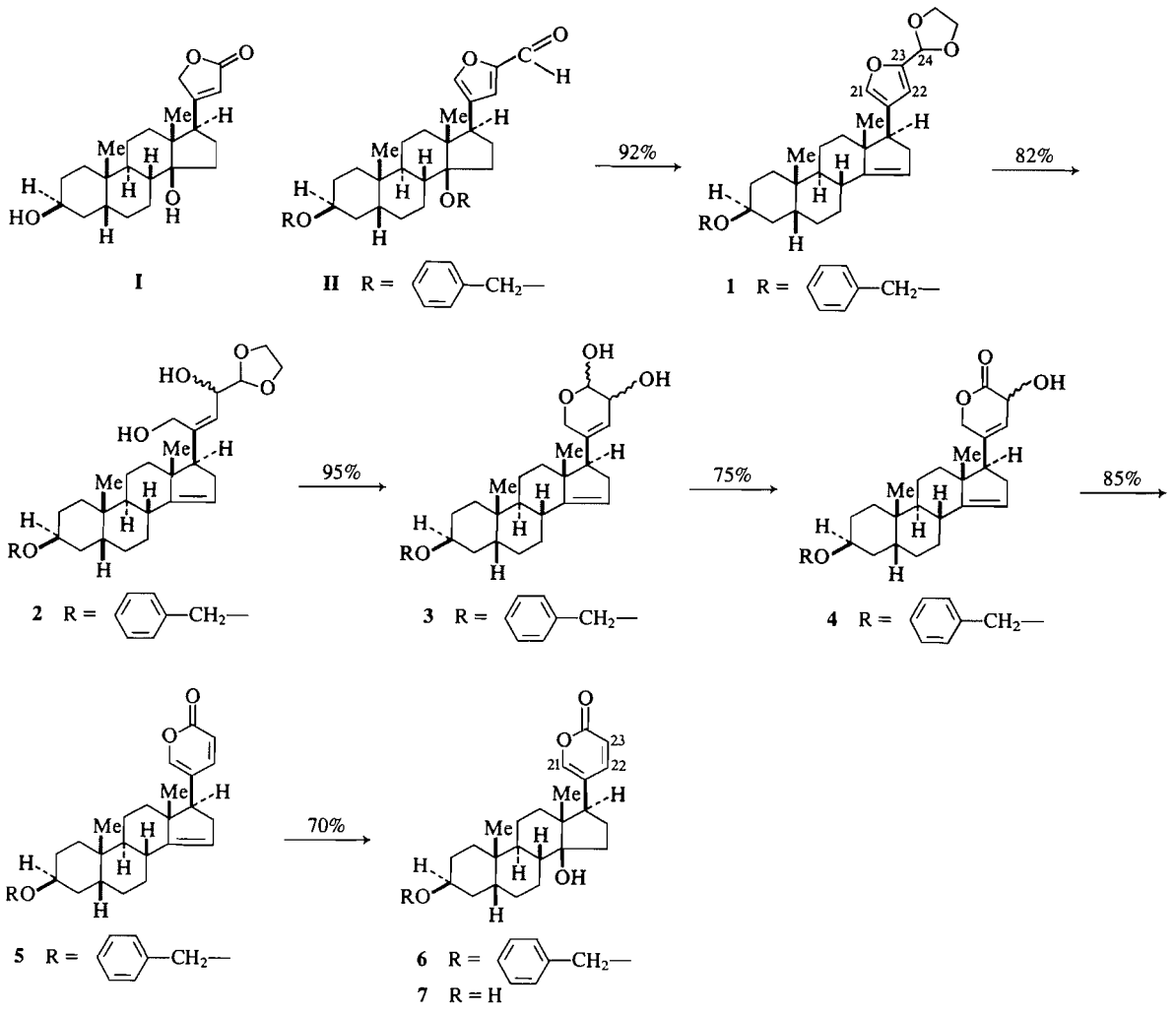


present Communication we wish to disclose a high yield preparation of bufalin from digitoxigenin using still another such transformation. The direct synthesis of bufalin from testosterone, which is in progress, will be the subject of a separate paper. A lengthy transformation of digitoxigenin to bufalin was reported some time ago by Pettit *et al.* (5).

The starting material was the dibenzyl aldehyde **II** easily prepared from digitoxigenin **I** (3). Acetalization by the standard method with benzene and *p*-toluenesulfonic acid yielded 92% of the oily Δ-14,15 acetal **1**;[1] $^1$H nmr ($CDCl_3$) δ: 7.18 (br s, 1H, C21-H), 6.33 (br s, 1H, C22-H), 5.83 (s, 1H, C24-H), 5.23 (m, 1H, C15-H), 3.88–4.20 (m, 4H, O—$CH_2$—$CH_2$—O).

[1]All compounds gave correct molecular ions in mass spectrometry and all spectral data consistent with the structures assigned to them. All crystalline compounds gave acceptable C/H analyses.

The acetal **1** was irradiated with a 100 W high pressure mercury lamp at −70°C in $CH_2Cl_2$ in the presence of mesotetraphenylporphine (6) (0.4%) while oxygen was bubbled through the solution. The resulting endoperoxide solution was treated with a large excess of dimethylsulfide and the solvent was evaporated to dryness. the residue was taken up in aqueous tetrahydrofuran (THF) and 2 *N* NaOH and reduced with an excess of $NaBH_4$. Purification by preparative thin layer chromatography (tlc) yielded 82% of the pure oily acetal **2**; $^1$H nmr ($CDCl_3$) δ: 5.52, 5.56 (2 sets, d, $J$ = 8 Hz, 1H, C22-H), 4.90 (d, $J$ = 4 Hz, 1H, C24-H), 4.12 (br s, 2H, C21-H), 3.93 (br s, 4H, —O—$CH_2$—$CH_2$—O—).

Compound **2** was heated under reflux for 5 h in a mixture of THF and 3 *N* HCl. The crude hemiacetal **3** was obtained in a yield of 95% and it was used without further purification. Compound **3**

Can. J. Chem. Downloaded from www.nrcresearchpress.com by 210.87.254.105 on 09/06/12
For personal use only.

was heated under reflux with silver carbonate on Celite in benzene for 30 min (7). Purification by preparative tlc yielded 75% of the hydroxy lactone **4** which crystallized from ether–hexane (mp 117–119°C); ir ($CHCl_3$) $\nu_{max}$: 3550 (OH), 1735 (C=O) $cm^{-1}$; $^1H$ nmr ($CDCl_3$) δ: 5.88 (m, 1H, C22-H), 4.60–4.87 (m, 3H, C21-H + C23-H).

The hydroxy lactone **4** was dissolved in $CH_2Cl_2$ and stirred on the ice-bath with mesyl chloride and triethylamine. The crude mesylate was isolated in the usual manner and it was heated under reflux with DBN in benzene. The α-pyrone **5** was isolated by preparative tlc and crystallization from ether–hexane in a yield of 85% (mp 115–116°C).

The introduction of the C14-β hydroxy group was performed as described previously (cf. ref. 1). The benzyl derivative **6** was isolated in a yield of 70% and recrystallized from ether–$CHCl_3$ (mp 198–200°C). Debenzylation with palladium hydroxide on carbon as described previously (ref. 8, see also ref. 3) finally yielded 70% of semi-synthetic bufalin **7**. It was recrystallized from $CHCl_3$–hexane and melted at 235–237°C; ir ($CHCl_3$) $\nu_{max}$: 3600, 3450 (OH), 1710, 1635 (pyrone) $cm^{-1}$; uv (EtOH) $\lambda_{max}$ nm (log ε): 298 (3.77); $^1H$ nmr ($CDCl_3$) δ: 7.83 (dd, $J$ = 10, 2 Hz, 1H, C22-H), 7.23 (d, $J$ = 2 Hz, 1H, C21-H), 6.25 (d, $J$ = 10 Hz, 1H, C23-H).

The semi-synthetic compound **7** was identical with natural bufalin by melting point, mixture melting point, uv, ir, $^1H$ nmr, and mass spectrometry and by tlc in several systems.

**Acknowledgements**

We wish to thank the Natural Sciences and Engineering Research Council of Canada, the Canadian Heart Foundation, and Advance Biofactures Corporation, New York, for the support of this work.

1. T. Y. R. Tsai, A. Minta, and K. Wiesner. Heterocycles, **12**, 1397 (1979).
2. R. Marini-Bettòlo, P. Flecker, T. Y. R. Tsai, and K. Wiesner. Can. J. Chem. **59**, 1403 (1981).
3. F. J. Jäggi, T. Y. R. Tsai, and K. Wiesner. Heterocycles, **19**, 647 (1982).
4. F. J. Jäggi, M. Tsubuki, T. Y. R. Tsai, and K. Wiesner. To be published.
5. G. P. Pettit, L. E. Houghton, J. C. Knight, and F. Bruschweiler. Chem. Commun. 93 (1970).
6. W. Adam and K. Takayama. J. Org. Chem. **44**, 1727 (1979).
7. H. J. J. Loozen, E. F. Godefroi, and J. S. M. Besters. J. Org. Chem. **40**, 892 (1975).
8. A. M. Felix, E. P. Heimer, T. J. Lambros, C. Tzougraki, and J. Meienhofer. J. Org. Chem. **43**, 4194 (1978).

# Thermochemical parameters for organic radicals and radical ions. Part 1. The estimation of the p$K_a$ of radical cations based on thermochemical calculations

A. MARTIN DE P. NICHOLAS AND DONALD R. ARNOLD[1]

*Department of Chemistry, Dalhousie University, Halifax, N.S., Canada B3H 4J3*

Received November 30, 1981

A. MARTIN DE P. NICHOLAS and DONALD R. ARNOLD. Can. J. Chem. **60**, 2165 (1982).

Three methods for estimating the p$K_a$ of a radical cation using thermochemical cycles are discussed. These methods enable the calculations of the p$K_a$ of radical cations which have not been determined experimentally. Radical cation acids are classified according to the nature of their respective conjugate bases. The application of these methods is illustrated for a σ-acid (the benzene radical cation) and π-acid (the toluene radical cation). The potential of these methods to estimate relative and absolute solvation energies is also discussed. The use of thermochemical cycles in estimating standard oxidation potentials of organic compounds is outlined.

Calculations show that the toluene radical cation is an extremely strong acid and the benzene radical cation a moderately strong acid in acetonitrile solution. Difficulties in directly determining the p$K_a$ value of aromatic hydrocarbon radical cations are also discussed.

A. MARTIN DE P. NICHOLAS et DONALD R. ARNOLD. Can. J. Chem. **60**, 2165 (1982).

On discute de trois méthodes d'évaluation du p$K_a$ d'un cation radicalaire en utilisant les cycles thermochimiques. Ces méthodes permettent de calculer le p$K_a$ des cations radicalaires que l'on ne peut pas déterminer expérimentalement. Les cations radicalaires acides sont classés selon la nature de leurs bases conjuguées respectives. On illustre l'application de ces méthodes dans le cas d'un acide σ (le cation radicalaire du benzène) et dans le cas d'un acide π (le cation radicalaire du toluène). On discute également du potentiel de ces méthodes en ce qui a trait à l'évaluation des énergies de solvatation relatives et absolues. On souligne l'utilisation des cycles thermochimiques dans l'évaluation des potentiels standard d'oxydation des composés organiques.

Les calculs indiquent que le cation radicalaire du toluène est un acide extrêmement fort et que le cation radicalaire du benzène est un acide moyennement fort en solution dans l'acétonitrile. On discute également des difficultés rencontrées lors de la détermination directe de la valeur du p$K_a$ des cations radicalaires des hydrocarbures aromatiques.

[Traduit par le journal]

## Introduction

A radical cation can be described as the species obtained upon removal of an electron from a neutral molecule (1, 2). These oxidations have been achieved by chemical oxidants (e.g., concentrated sulphuric acid (3), $SO_4^{-\cdot}$ (4), the metal ion oxidants (5), Mn(III) (5*a*), Co(III) (5*b*, *c*), Ce(IV) (5*d*, *e*), and Ag(II) (5*f*), and Lewis acids $AlCl_3$ and $SbCl_5$ (6)), physical methods (e.g., photoionization, pulse radiolysis, and electron impact) (7), anodic oxidation (2, 8), and photosensitization (electron transfer) (9).

The deprotonation of radical cations has been found to be an important reactive pathway, for example, in the oxidation of alkyl aromatics (5, 10, 11). The Co(III) ion catalysed oxidation of toluene (5*b*) is believed to involve the sequence shown in reactions [1] and [2].

$$[1] \quad C_6H_5CH_3 \xrightarrow{\text{Co(III)}} (C_6H_5CH_3)^{+\cdot} \xrightarrow{(a)} \text{Products}$$

$$[2] \quad (C_6H_5CH_3)^{+\cdot} \xrightarrow{\text{base}} C_6H_5CH_2^{\cdot} \xrightarrow{(b)} \text{Products}$$

One of the factors that determines the ratio of products obtained from paths (*a*) and (*b*) will obviously be the acidity of the radical cation of toluene. This makes the study of the acidities of these reactive radical ions in general, of interest, and it is surprising that so little is, in fact, known.

The p$K_a$ of neutral hydrocarbons has been expressed in terms of standard oxidation potentials and bond dissociation energies (12*a*, *b*). The p$K_a$ of a radical cation can be related to several important thermochemical parameters (13) via simple thermochemical cycles which will be discussed below. Conversely, such relationships make possible the estimation of a related thermochemical parameter if the p$K_a$ of the radical cation can be obtained by an independent method.

Differences in solvation energies of ions cause deviations in the linear correlation observed between gas phase ionization potential data and solution phase standard oxidation potentials (14, 15). The relationship between acidities of radical ions in the gas phase and in solution should make possible the estimation of the solvation energies of organic radical ions.

Various types of radical cations have been recognised and described in the literature (1*a*). For the purposes of this discussion of the acidity of radical cations it is convenient to subclassify these

[1]To whom all correspondence should be addressed.

0008-4042/82/172165-15$01.00/0

©1982 National Research Council of Canada/Conseil national de recherches du Canada

Can. J. Chem. Downloaded from www.nrcresearchpress.com by 210.87.254.42 on 09/06/12
For personal use only.

Can. J. Chem. Downloaded from www.nrcresearchpress.com by 210.87.254.42 on 09/06/12
For personal use only.

species according to the nature of their conjugate bases. Thus, the benzene radical cation can be considered a σ-acid since the deprotonation yields a phenyl σ-radical. The toluene radical cation yielding the benzyl radical would be a π-acid, whereas the radical cation of phenol would be classed as a hetero-π-acid, since the radical of the conjugate base (the phenoxyl radical) is delocalised. If the unpaired electron was localised on oxygen it would be a hetero-σ-acid. The aminylium radical cations of the type $RNH_2^{+\cdot}$ (R = alkyl) will thus be considered as hetero-σ-acids.

Recent studies (16) of the behaviour of the tertiary aminylium radicals, $R_3N^{+\cdot}$, seem to indicate that these species can undergo fast proton exchange with other protic species in solution as a result of the following resonance structures of their conjugate bases (reaction [3]).

[3] $$\rangle N^{+\cdot}-CH_2- \underset{H^+}{\overset{-H^+}{\rightleftharpoons}} \rangle \overset{+}{N}-\overset{-}{C}H- \leftrightarrow \rangle \dot{N}-\dot{C}H-$$
$$(a) \qquad (b)$$

These radical cations can be considered as *p*-acids, albeit profoundly stabilized by the nitrogen substituent which allows 3-electron bonding ((*a*) ↔ (*b*)).

So few studies of the $pK_a$ of radical cations have been reported that in the next few paragraphs we can provide a complete review of this area. In fact all of the radical cations whose $pK_a$'s have been determined are of the hetero-σ or π-acid type. The $pK_a$ of the radical cation of durohydroquinone was estimated to be −1 by Bridge, Land, and Porter (17*a*, *b*). They also estimated a $pK_a$ of −5 for the radical cation of 2,4,6-triphenylphenol (7*c*, 17*c*). The phenoxyl radicals were generated by flash photolysis, chemical oxidation, and photolysis of rigid solutions. The $pK_a$'s were estimated by observing the absorption spectrum of the phenoxyl radicals as a function of pH. Dixon and Murphy (13, 18) generated phenoxyl radicals in aqueous solution using cerium(IV) oxidation in a flow esr system, and, followed the equilibrium shown in reaction [4] as a function of $H_0$.

[4] $$ArO^{\cdot} \underset{-H^+}{\overset{H^+}{\rightleftharpoons}} (ArOH)^{+\cdot}$$

The $pK_a$'s of a number of phenol radical cations were determined in this manner ($pK_a(PhOH)^{+\cdot}$ = −2.0).

The acidities of a few hetero-σ-acids have been determined (19). For example, a study of the intermediates produced in the one-electron oxidation and reduction of hydroxylamines enabled the determination of the $pK_a$ of $NH_3^{+\cdot}$ (6.7 ± 0.2), $HONH_2^{+\cdot}$ (4.2 ± 0.1), and $CH_3ONH_2^{+\cdot}$ (2.9 ± 0.2) (19*a*). Pulse radiolysis was used to generate the radical cations and their conjugate bases. The $pK_a$ of the radical cations was determined by observing the pH dependence of the optical absorption spectra of the intermediates formed.

The determination of the $pK_a$ of radical cations of aromatic hydrocarbons in solution has not been reported. An equilibrium constant for the acid–base equilibrium of the radical cation of hexamethylbenzene (HMB) and its conjugate base, a benzylic radical, in the solvent system dichloromethane – trifluoroacetic acid was estimated from kinetic data obtained in an anodic oxidation of HMB (20) (see reaction [5]).

[5] $$ArCH_3^{+\cdot} + B \rightleftarrows ArCH_2^{\cdot} + BH^+$$

However, a $pK_a$ value for $(HMB)^{+\cdot}$ could not be obtained from the deduced $K_5$ value because the nature of the base (B) in reaction [5] was unknown. Further work by this group seems to indicate that the assumptions made are in error. Hence the equilibrium constant value they deduced is not reliable (21*a*, *b*). In a study by Sehested and Holcman, radical ions of polyalkylbenzenes were generated in solution by pulse radiolysis. They then attempted to correlate relative rates of deprotonation of the radical cations with the ionization potentials of the corresponding neutral compounds (10*d*, 22). These kinetic indications of acidity are informative with regard to the reactivity of radical cations; however, it is clearly desirable to know the thermodynamic acidities of these and other π- and σ-acids.

For the sake of completeness it should be mentioned that an electrochemical (potentiometric) determination of the $pK_a$ of radical cations is possible in principle (23). However, such a potentiometric determination requires that $RH^{+\cdot}/(R^{\cdot} + \frac{1}{2}H_2)$ be a reversible redox couple. In general, the high reactivity of these species precludes the establishment of an equilibrium. Refinements in current methods of studying equilibrium systems and/or new experimental techniques are needed to directly determine the $pK_a$ of aromatic hydrocarbon radical cations. With presently available methods and techniques even attaining measurable steady state concentrations of acid–base forms is not easy. Thus, we feel that an empirical approach to estimate the $pK_a$'s of radical cations is useful in that it enables the prediction of the fate of these radical ions in solution.

In the following section, three empirical methods to estimate the $pK_a$ of radical cations will be discussed. These methods have been applied to the radical cations of benzene and toluene.

Can. J. Chem. Downloaded from www.nrcresearchpress.com by 210.87.254.42 on 09/06/12
For personal use only.

## Results and discussion

*Method I (eq. [19]), based upon the standard oxidation potential of RH ($E^0_{RH}$) and the free energy of bond dissociation of RH ($\Delta G_{BDE}$)*

The p$K_a$ of the radical cation $RH^{+\bullet}$ in solution is related to the standard oxidation potential of RH ($E^0_{RH}$) and the free energy change associated with the homolytic cleavage of the R—H bond ($\Delta G_{BDE(RH)}$) in the gas phase. This relationship can be defined using the thermochemical cycle summarised in Fig. 1, which shows that the p$K_a$ of the radical cation is dependent upon the free energy change $\Delta G_6$ (eq. [6]) and is given by eq. [7].

[6] $RH^{+\bullet}_{sol} \rightarrow R^{\bullet}_{sol} + H^{+}_{sol}$

[7] $pK_a(RH^{+\bullet})_{sol} = \Delta G_6/2.303RT$

$G$, the Gibbs free energy, is a thermodynamic property:

[8] $\oint \Delta G = 0$

Application of eq. [8] to the thermochemical cycle in Fig. 1 gives eq. [9].

[9] $$\Delta G_6 = -\Delta G_{10} + \Delta G_{14} + \Delta G_{16} + \Delta G_{13} - \Delta G_{17} - \Delta G_{11} + \Delta G_{18}$$

The quantity, $\Delta G_{10} + \Delta G_{11}$, can be expressed in terms of the standard oxidation potential of RH referred to the standard hydrogen electrode (S.H.E.) (eq. [12]).

[10] $RH_{sol} \rightarrow RH^{+\bullet}_{sol} + e^-$

[11] $e^- + H^+_{aq} \rightarrow \frac{1}{2}H_{2(g)}$

[12] $\Delta G_{10} + \Delta G_{11} = FE^0_{RH(sol)}$

The free energies of solvation of gaseous neutral compounds and radicals are known to be small compared with the solvation energies of ions. It has also been shown that the difference in the free energy of solvation of a neutral compound RH and its corresponding radical, R$^\bullet$, is likely to be very small (24).[2] This energy difference has been neglected in previous studies (2*a*, *b*). Thus, by considering the following reactions ([13] and [14]) it is reasonable to assume that eq. [15] is valid.

[13] $R^{\bullet}_g \rightarrow R^{\bullet}_{sol}$

[14] $RH_{sol} \rightarrow RH_g$

[15] $$\Delta G_{13} + \Delta G_{14} = \Delta G_{solvation(R^\bullet)} - \Delta G_{solvation(RH)} \approx 0$$

$\Delta G_{16}$ is the standard free energy associated with the homolytic cleavage of the R—H bond in the gas phase ($\Delta G^0_{BDE(RH)}$), where the H atom removed is the acidic H of its radical cation. In reaction [16] all species are in their standard state of 1 atm pressure.

[16] $RH_g \rightarrow R^{\bullet}_g + H^{\bullet}_g$

The other free energy terms required to complete the cycle in Fig. 1 are given by reactions [17] and [18].

[17] $\frac{1}{2}H_{2(g)} \rightarrow H^{\bullet}_g$

[18] $H^+_{aq} \rightarrow H^+_{sol}$

$\Delta G_{17}$ is the standard free energy of formation of the hydrogen atom ($\Delta G^0_{f(H)g}$) using the convention that the standard free energy of formation of the gaseous hydrogen molecule is zero. $\Delta G_{18}$ is the standard free energy associated with the transfer of a proton from water to the solution of interest ($\Delta G^0_{tr(H^+)}$)$_{sol}$. Substitution of eqs. [7], [12], and [15] in eq. [9] and rearranging terms gives eq. [19].

[19] $$pK_{a(RH^{+\bullet})sol} = \frac{1}{2.303RT}(-FE^0_{RH} + \Delta G^0_{tr(H^+)sol} + \Delta G^0_{BDE(RH)g} - \Delta G^0_{f(H)g})$$

The standard free energy of formation of the hydrogen atom, $\Delta G^0_{f(H)g}$, can be calculated (25). The free energy of transfer of a proton from water to other solvents has been estimated (26). Thus if the standard oxidation potential ($E^0_{RH}$) and the free energy associated with the homolytic cleavage of the R—H bond ($\Delta G_{BDE(RH)}$) (27) are known, the p$K_a$ of the radical cation $RH^{+\bullet}$ can be estimated.

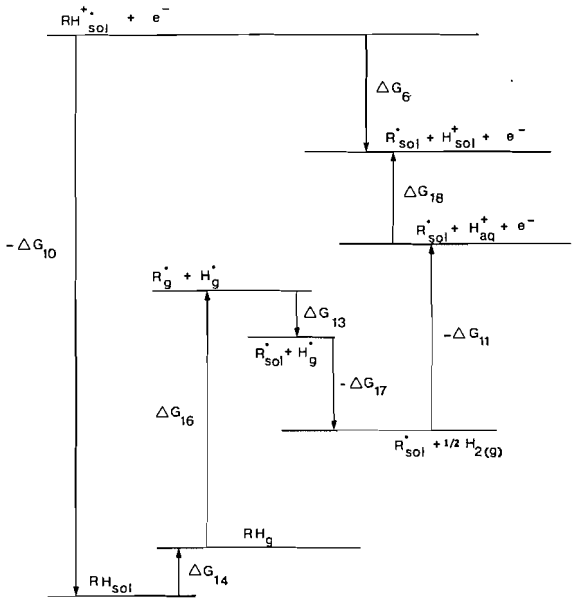


FIG. 1. The relationship between the p$K_a$ of a radical cation ($RH^{+\bullet}$), the standard oxidation potential ($E^0_{RH}$), and the standard free energy of bond dissociation ($\Delta G^0_{BDE(RH)}$).

[2]This approximation may not be valid for hetero acids of low molecular weight (e.g. $NH_3$ and $NH_2^\bullet$) and/or where strong hydrogen bonding is possible.

Can. J. Chem. Downloaded from www.nrcresearchpress.com by 210.87.254.42 on 09/06/12
For personal use only.

*Method II (eq. [27]), based upon the standard oxidation potential and free energy of bond dissociation of R—H ($\Delta G_{BDE(RH)}$) in comparison with the standard oxidation potential of $B^-$ and free energy of bond dissociation of the B—H bond ($\Delta G_{BDE(BH)}$)*

Protolytic or proton transfer reactions can be used to determine the $pK_a$ of an acid relative to a standard. Similarly the $pK_a$ of a radical cation can be obtained by considering the proton transfer reaction from radical cation to the conjugate base of an acid, BH, with a known $pK_a$ (eq. [20]).[3] It is useful to define this relationship:

[20] $RH^{+\cdot}_{sol} + B^-_{sol} \rightleftarrows R^{\cdot}_{sol} + BH_{sol}$

in terms of the thermochemical cycle summarised in Fig. 2 where $pK_{a(RH^{+\cdot})}$ is expressed by eq. [21]

[21] $$pK_{a(RH^{+\cdot})} = \frac{\Delta G_{20}}{2.303RT} + pK_{a(BH)}$$

$\Delta G_{20}$ is related to the standard oxidation potentials of RH and $B^-$ and the free energies associated with homolytic cleavage of the R—H and B—H bonds (eqs. [22]–[27]).

The oxidation of anion $B^-$ will result in the formation of $B^{\cdot}_{sol}$:

[22*a*] $B^-_{sol} - e^- \rightarrow B^{\cdot}_{sol}$

Combining eq. [22*a*] with the reduction of $H^+$ ions to hydrogen gas, eq. [11]:

[22*b*] $$\Delta G_{22a} + \Delta G_{11} = FE^0_{B^-/B^{\cdot}(sol)}$$

where $E^0_{B^-/B^{\cdot}(sol)}$ is the standard oxidation potential of the anion $B^-$. Combining eqs. [12] and [22*b*] we obtain an expression for the free energy associated with the indirect electron transfer from anion $B^-_{sol}$ to radical cation $RH^{+\cdot}_{sol}$ (eq. [23]).[4]

[23] $RH^{+\cdot}_{sol} + B^-_{sol} \rightarrow RH_{sol} + B^{\cdot}_{sol}$

$\Delta G_{23}$ can be given in terms of standard oxidation potentials of $B^-$ and RH as shown in eq. [24].

[24] $$\Delta G_{23} = \Delta G_{22a} - \Delta G_{10} = F[E^0_{B^-/B^{\cdot}(sol)} - E^0_{RH(sol)}]$$

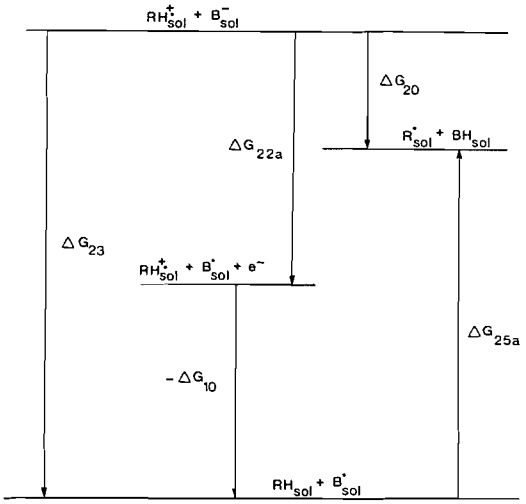


FIG. 2. The relationship between the $pK_a$ of a radical cation ($RH^{+\cdot}$), relative to a standard acid (BH), and the comparison of the standard oxidation potential ($E^0_{RH}$) and the standard free energy of bond dissociation ($\Delta G^0_{BDE(RH)}$) with the standard oxidation potential of $B^-$ ($E^0_{B^-}$) and the standard free energy of bond dissociation of the B—H bond ($\Delta G^0_{BDE(BH)}$).

If $\Delta G_{23}$ can be determined by independent measurements of $E^0_{B^-/B^{\cdot}(sol)}$ and $E^0_{RH(sol)}$, the only term required for obtaining $\Delta G_{20}$ is the free energy associated with the indirect hydrogen atom transfer between $RH_{sol}$ and $B^{\cdot}_{sol}$ to form $R^{\cdot}_{sol}$ (the conjugate base of the radical cation $RH^{+\cdot}$) and $BH_{sol}$ (reaction [25*a*]).

[25*a*] $RH_{sol} + B^{\cdot}_{sol} \rightarrow R^{\cdot}_{sol} + BH_{sol}$

$\Delta G_{25a}$ can be expressed in terms of the free energies associated with the homolytic cleavage of the R—H bond (reaction [25*b*]) and B—H bond (reaction [25*c*]), where the H atom removed is the acidic H of the radical cation $RH^{+\cdot}$

[25*b*] $RH_{sol} \rightarrow R^{\cdot}_{sol} + H^{\cdot}_{sol}$

[25*c*] $BH_{sol} \rightarrow B^{\cdot}_{sol} + H^{\cdot}_{sol}$

[25*d*] $$\Delta G_{25a} = \Delta G_{25b} - \Delta G_{25c} = \Delta G^0_{BDE(RH)sol} - \Delta G^0_{BDE(BH)sol}$$

As before, it is assumed that the difference in the free energy of solvation will be the same for the pairs RH/R$^{\cdot}$ and BH/B$^{\cdot}$ without the introduction of any serious error (eq. [25*e*]).

[25*e*] $$\Delta G^0_{solvation(RH)} - \Delta G^0_{solvation(R^{\cdot})} = \Delta G^0_{solvation(BH)} - \Delta G^0_{solvation(B^{\cdot})}$$

Substituting the equality expressed in eq. [25*e*] into eq. [25*d*] we get eq. [25*f*].

[25*f*] $$\Delta G_{25a} = \Delta G^0_{BDE(RH)g} - \Delta G^0_{BDE(BH)g}$$

[3]It is assumed that the only interaction between the radical cation and base is proton transfer. Thus effects of counter ions on the stability of ions in solution are ignored. It is also assumed that all ions are solvated but remain as discrete species in solution. The above assumptions are reasonable, as Method II is not based on results of a single experiment involving equilibrium [20] but on data related by a thermochemical cycle.

[4]$\Delta G_{23}$ is not the free energy associated with direct homogeneous electron transfer between $RH^{+\cdot}_{sol}$ and $B^-_{sol}$. Thus the free energy associated with bringing ions to encounter distance is not considered.

Can. J. Chem. Downloaded from www.nrcresearchpress.com by 210.87.254.42 on 09/06/12
For personal use only.

From Fig. 2 we see that

[26] $$\Delta G_{20} = \Delta G_{22a} - \Delta G_{10} + \Delta G_{25a} = F(E^0_{B^-/B^{\cdot}(sol)} - E^0_{RH}) + \Delta G^0_{BDE(RH)g} - \Delta G^0_{BDE(BH)g}$$

By substituting the result obtained in eq. [26] into eq. [21], eq. [27] which gives $pK_a(RH^{+\cdot})$ is obtained.

[27] $$pK_{a(RH^{+\cdot})sol} = \frac{F\delta E^0 + \delta\Delta G^0_{BDE}}{2.303RT} + pK_{a(BH)sol}$$

where

$$\delta E^0 = E^0_{B^-/B^{\cdot}(sol)} - E^0_{RH}$$

and

$$\delta\Delta G^0_{BDE} = \Delta G^0_{BDE(RH)g} - \Delta G^0_{BDE(BH)g}$$

If all the terms of the right hand side of eq. [27] can be estimated, $pK_{a(RH^{+\cdot})}$ can be obtained. However, if $pK_{a(BH)sol}$ is unknown, BH can be chosen as a standard and the acidity of a radical cation can be expressed relative to this standard.

An approximate $pK_a$ value can be obtained in the absence of $\Delta G$ data if $\Delta H$ data are available using eq. [29].[5]

Equation [27] allows derivation of two other useful relationships from Fig. 2.

*Case (i)*

If BH ≡ RH and the acidic hydrogen of RH and its radical cation $RH^{+\cdot}$ are the same, from eq. [25*f*]

[30] $$\delta\Delta G^0_{BDE} = \Delta G_{25a} = 0$$

eq. [30] is obtained. Substitution of eq. [30] into eq. [27] gives eq. [31]

[31*a*] $$pK_{a(RH^{+\cdot})sol} = \frac{F\delta' E^0}{2.303RT} + pK_{a(RH)sol}$$

or

[31*b*] $$\delta' pK_a = \frac{F\delta' E^0}{2.303RT}$$

where

$$\delta' pK_a = pK_{a(RH^{+\cdot})sol} - pK_{a(RH)sol}$$

and

$$\delta' E^0 = (E^0_{R^-/R^{\cdot}} - E^0_{RH})$$

*Case (ii)*

If BH ≡ $RH_2^+$, $B^-$ ≡ RH, and $B^{\cdot}$ ≡ $RH^{+\cdot}$ from eq. [24] we obtain eq. [32].

[32] $$\delta E^0 = E^0_{B^-/B^{\cdot}(sol)} - E^0_{RH} = 0$$

Substitution of eq. [32] in eq. [27] gives eq. [33],

[33*a*] $$pK_{a(RH^{+\cdot})sol} = \frac{\delta''\Delta G^0_{BDE}}{2.303RT} + pK_{a(RH_2^+)sol}$$

or

[33*b*] $$\delta'' pK_a = pK_{a(RH^{+\cdot})sol} - pK_{a(RH_2^+)sol} = \frac{\delta''\Delta G^0_{BDE}}{2.303RT}$$

where

$$\delta''\Delta G^0_{BDE} = \Delta G^0_{BDE(RH)g} - \Delta G^0_{BDE(RH_2^+)g}$$

The free energy of bond dissociation considered in $RH_2^+$ is associated with the bond that when cleaved gives the same radical cation $RH^{+\cdot}$ as obtained on oxidizing RH in solution.

From eq. [31] it is evident that a knowledge of the standard oxidation potentials of an organic compound RH and its anion $R^-$ along with the $pK_a$ of RH in the solvent of interest provides a direct estimate of the $pK_a$ of its radical cation $RH^{+\cdot}$. Similarly, eq. [33] shows that if the bond dissociation free energies of $RH_2^+$ and RH are known along with the $pK_a$ of $RH_2^+$, the $pK_a$ of $RH^{+\cdot}$ can be estimated.

*Method III (eq. [39]), based upon the gas phase acidity and free energies of solvation of the species involved in the acid–base equilibrium (i.e. $RH^{+\cdot}$, $R^{\cdot}$, and $H^+$)*

Solvation factors have a profound influence on the acid–base properties of any species in solution. Recently considerable effort has been applied to the determination of gas phase acidities of organic molecules (28), where intrinsic molecular properties free of solvation effects will be reflected. Determinations of gas phase acidities of radical cations are, however, of additional interest because they constitute further means of estimating $pK_a$'s in solution.

The $pK_a$ of a radical cation $RH^{+\cdot}$ in solution is related to its gas phase acidity and the free energy of solvation of the species $RH^{+\cdot}_g$, $R^{\cdot}_g$, and $H^+_g$. It is useful to define this relationship in terms of Figs. 3 and 4.

The gas phase acidity of a radical cation can be

---

[5]An approximate value of the $pK_a$ can be obtained if we assume [28].

[28] $$S^0_{RH(g)} - S^0_{R^{\cdot}(g)} \approx S^0_{BH(g)} - S^0_{B^{\cdot}(g)}$$

Substitution of [28] in [27] gives [29]

[29] $$pK_{a(RH^{+\cdot})sol} \approx \frac{F\delta E^0 + \delta\Delta H^0_{BDE}}{2.303RT} + pK_{a(BH)sol}$$

where $\delta\Delta H^0_{BDE} = \Delta H^0_{BDE(RH)} - \Delta H^0_{BDE(BH)}$.

Can. J. Chem. Downloaded from www.nrcresearchpress.com by 210.87.254.42 on 09/06/12
For personal use only.

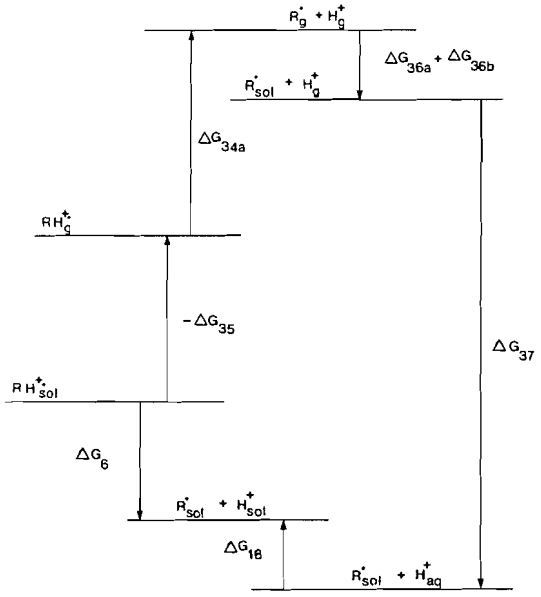


FIG. 3. The $pK_a$ of a radical cation ($RH^{+\cdot}$) in solution in relation to its gas phase acidity and the standard free energy of solvation of the species $RH^{+\cdot}_g$, $R^{\cdot}_g$, and $H^+_g$.

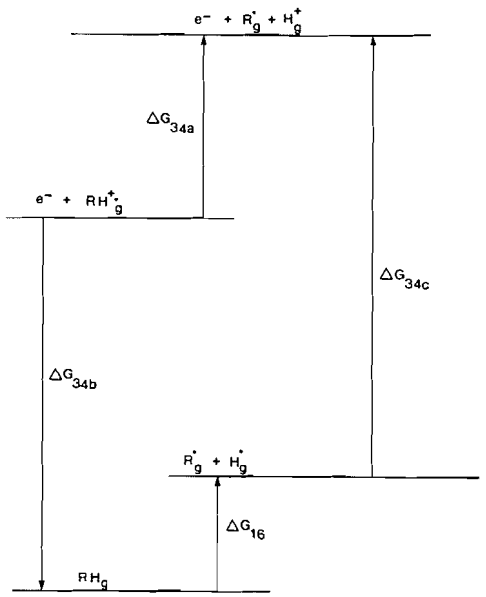


FIG. 4. The relationship between the $pK_a$ of a radical cation ($RH^{+\cdot}$) in the gas phase, the adiabatic ionization potential ($IP_{adiabatic(RH)}$), and the standard free energy of bond dissociation ($\Delta G^0_{BDE(RH)}$).

expressed in terms of the free energy change $\Delta G_{34a}$ for its deprotonation in the gas phase by eq. [34*a*]. This quantity, $\Delta G_{34a}$, can be calculated for many species

[34*a*] $RH^{+\cdot}_g \rightarrow R^{\cdot}_g + H^+_g$

using existing data from the relationship summarised in Fig. 4 and expressed by eqs. [34*a*] to [34*f*] and eq. [16].

[34*b*] $e^- + RH^{+\cdot}_g \rightarrow RH_g$

[16] $RH_g \rightarrow R^{\cdot}_g + H^{\cdot}_g$

[34*c*] $R^{\cdot}_g + H^{\cdot}_g \rightarrow R^{\cdot}_g + H^+_g + e^-$

[34*d*] $\Delta G_{34a} = \Delta G_{34b} + \Delta G_{16} + \Delta G_{34c}$

$\Delta G_{34b}$ is assumed to be equal to $\Delta H_{34b}$ because $\Delta S_{34b}$ has been shown to be negligible (29, 30).[6] $\Delta H_{34b}$ is given by eq. [34*e*].

[34*e*] $\Delta H_{34b} = -\text{IP(adiabatic)}_{RH} - \Delta\int C_p\,dT$

where IP(adiabatic), the adiabatic ionization potential, is the energy difference between the ground vibrational and rotational level of the lowest electronic state of the radical cation and the ground vibrational and rotational level of the lowest electronic state of the molecule. This is rigorously equal to the difference in the enthalpies of formation of $RH^{+\cdot}$ and RH at 0 K. For most aromatic compounds the heat capacities of the molecule and the corresponding radical cation are effectively the same, so that $\Delta\int C_p\,dT$ is negligible and $\Delta H_{34b} \approx -\text{IP(adiabatic)}_{RH}$ (30).

Assuming $\Delta S_{34b}$ and $\Delta\int C_p\,dT$ are both negligible we can write eq. [34*f*].

[34*f*] $\Delta G_{34b} \approx -\text{IP(adiabatic)}_{RH}$

$\Delta G_{16}$ can be calculated from the existing thermochemical data (27) (see Table 3). $\Delta G_{34c}$ is calculable because $\Delta H^0_{f(H^+)g}$, $\Delta H^0_{f(H)g}$, $S^0_{H^+(g)}$, and $S^0_{H\cdot(g)}$ are well known (25, 31); $\Delta G_{34a}$ can therefore be calculated using eq. [34*d*].

The solvation of the species in eq. [34*a*] can be expressed by the following reactions [35]–[37] and [18].

[35] $RH^{+\cdot}_g \rightarrow RH^{+\cdot}_{sol}$

[36*a*] $R^{\cdot}_g \rightarrow R^{\cdot}_{aq}$

[36*b*] $R^{\cdot}_{aq} \rightarrow R^{\cdot}_{sol}$

[37] $H^+_g \rightarrow H^+_{aq}$

[18] $H^+_{aq} \rightarrow H^+_{sol}$

From Fig. 3 we get eq. [38].

[38] $\Delta G_6 = -\Delta G_{35} + \Delta G_{34a} + \Delta G_{36a} + \Delta G_{37} + \Delta G_{36b} + \Delta G_{18}$

[6]The benzene radical cation undergoes a Jahn–Teller distortion and shows a difference in symmetry compared to benzene. Thus there will be a change in rotational entropy on forming the radical cation. However, this change has been neglected because it will introduce only a small error compared to the uncertainty in the estimated value of $pK_a$.

Can. J. Chem. Downloaded from www.nrcresearchpress.com by 210.87.254.42 on 09/06/12
For personal use only.

Substitution of the result of eq. [38] in eq. [7] gives eq. [39].

$$[39] \quad pK_{a(RH^{+\cdot})sol} = pK_{a(RH^{+\cdot})g} + \frac{\Sigma\Delta G^0_{solvation}}{2.303RT}$$

where

$$pK_{a(RH^{+\cdot})g} = \frac{\Delta G_{34a}}{2.303RT}$$

and

$$\Sigma\Delta G^0_{solvation} = \Delta G^0_{solvation(H^+)g} + \Delta G^0_{solvation(R\cdot)g} - \Delta G^0_{solvation(RH^{+\cdot})g}$$

Application of eq. [39] to estimate $pK_a$ is limited because the free energies of solvation of most organic radical cations have not been determined. However, the free energies of solvation of radical cations of a series of alternant aromatic hydrocarbons have been estimated (15*a*, *b*), permitting the estimation of $pK_a$ values for these radical ions (eq. [39]).

*In addition, since an experimental $pK_a$ value has been determined for the phenol radical cation it is possible to estimate acidities of radical cations relative to the phenol radical cation (eq. [41]).*

The acidity of the phenol radical cation has been determined in aqueous solution (13). A measure of the acidity of a radical cation relative to the phenol radical cation enables an estimate of its $pK_a$ to be made.

Using eq. [39] the $pK_a$ of the phenol radical cation in aqueous solution can be expressed by eq. [40].

$$[40] \quad pK_{a(C_6H_5OH)^{+\cdot}{}_{aq}} = pK_{a(C_6H_5OH)^{+\cdot}{}_g} + \Sigma\Delta G^0_{solvation(RH\equiv C_6H_5O-H)}$$

where

$$pK_{a(C_6H_5OH)^{+\cdot}{}_g} = \Delta G_{34a(RH^{+\cdot}\equiv(C_6H_5OH)^{+\cdot})}/2.303RT$$

and

$$\Sigma\Delta G^0_{solvation} = \Delta G^0_{solvation(H^+)} + \Delta G^0_{solvation(C_6H_5O\cdot)} - \Delta G^0_{solvation(C_6H_5OH)^{+\cdot}}$$

Subtraction of eq. [40] from eq. [39] gives, on rearrangement, eq. [41].

$$[41] \quad pK_{a(RH^{+\cdot})aq} = [pK_{a(RH^{+\cdot})g} - pK_{a(C_6H_5OH)^{+\cdot}{}_g}] + \frac{\delta\Delta G^0_{solvation}}{2.303RT} + pK_{a(C_6H_5OH)^{+\cdot}{}_{aq}}$$

It is convenient to summarise the relationship in eq. [41] in terms of Fig. 5 using the following reactions [42]–[44].

$$[42] \quad C_6H_5O^{\cdot}{}_g + RH^{+\cdot}{}_g \rightarrow (C_6H_5OH)^{+\cdot}{}_g + R^{\cdot}{}_g$$

$$[43a] \quad (C_6H_5OH)^{+\cdot}{}_g \rightarrow (C_6H_5OH)^{+\cdot}{}_{aq}$$

$$[43b] \quad C_6H_5O^{\cdot}{}_g \rightarrow C_6H_5O^{\cdot}{}_{aq}$$

$$[36a] \quad R^{\cdot}{}_g \rightarrow R^{\cdot}{}_{aq}$$

$$[43c] \quad RH^{+\cdot}{}_g \rightarrow RH^{+\cdot}{}_{aq}$$

$$[44] \quad C_6H_5O^{\cdot}{}_{aq} + RH^{+\cdot}{}_{aq} \rightarrow (C_6H_5OH)^{+\cdot}{}_{aq} + R^{\cdot}{}_{aq}$$

The difference in the acidities of the radical cations of phenol and RH in the gas phase can be expressed by eq. [45],

$$[45] \quad pK_{a(RH^{+\cdot})g} - pK_{a(C_6H_5OH)^{+\cdot}g} = \frac{\Delta G_{42}}{2.303RT}$$

and the other term of interest in eq. [41], $\delta\Delta G^0_{solvation}$, can be expressed by eq. [46].

$$[46] \quad \delta\Delta G^0_{solvation} = \Delta G_{43a} + \Delta G_{36a} - \Delta G_{43b} - \Delta G_{43c}$$

The free energy of solvation of neutral radicals is known to be small (24) and the approximation [47] may be made.

$$[47] \quad \Delta G_{43b} \approx \Delta G_{36a}$$

If RH is an aromatic hydrocarbon, its radical cation $RH^{+\cdot}$ will be less extensively hydrated in solution as compared to the phenol radical cation (14*b*). This can be expressed by the inequality [48].

$$[48] \quad (-\Delta G_{43a}) > (-\Delta G_{43c})$$

Substitution of eqs. [47] and [48] into eq. [41] gives the inequality [49]

$$[49] \quad pK_{a(RH^{+\cdot})aq} < (pK_{a(RH^{+\cdot})g} - pK_{a(C_6H_5OH)^{+\cdot}g} + pK_{a(C_6H_5OH)^{+\cdot}aq}$$

Thus, the inequality [49] can be used to estimate an upper value for the $pK_a$ of an aromatic hydrocarbon radical cation in aqueous solution. However, if the difference in solvation energies of the radical cations of phenol and the aromatic hydrocarbon can be estimated the $pK_a$ can be obtained using eq. [41].

### *An empirical approach to the estimation of standard oxidation potentials*

The estimation of the $pK_a$ of radical cations by methods I and II require standard oxidation potentials of RH. ($E_{1/2}$ values do not have the same thermodynamic significance.) In addition, method II requires the standard oxidation potential of the $B^-$ anion. We have also shown that a knowledge of the standard oxidation potential ($E^0$) of $R^-$ can give an independent route to the estimation of radical

Can. J. Chem. Downloaded from www.nrcresearchpress.com by 210.87.254.42 on 09/06/12
For personal use only.

cation acidities. Furthermore, standard redox potentials are of general interest as they have been used extensively in calculating other thermochemical parameters (32). The estimation of the $pK_a$ values of weakly acidic hydrocarbons (12*a*, *b*, 33*a*) and the solvation energies of aromatic hydrocarbon radical ions (15*b*) are recent examples. Other applications of redox potentials are determining the energetics and establishing the mechanism of electrode reactions (24*b*, 33*b*, *c*). Unfortunately, with the present methods and techniques $E^0$ values cannot be experimentally determined for most compounds.

The direct measurement of standard redox potentials using a conventional electroanalytical technique such as cyclic voltammetry will give accurate results only where both the substrate and intermediates formed at the electrode are relatively stable (34). Recent studies have shown that second harmonic AC voltammetry at high frequencies is capable of providing standard redox potentials even when very reactive intermediates are formed at the electrode (35). This method too has inherent limitations in its use, since theoretical calculations show that reversible potentials are measurable only as long as $k < 3\omega$, where $k$ is the first order or pseudo first order rate constant for the reaction of the intermediate and $\omega$ is the angular frequency of the applied AC signal (35*a*). Use of thermochemical cycles to estimate standard redox potentials constitutes a useful method of obtaining these thermodynamically significant parameters when they cannot be measured directly (24*b*, *c*). The basis for the use of redox potentials in thermochemical calculations is their direct relationship to equilibrium constants eq. [51]. The $E^0$ of the redox couple Ox/Red can be related to the free energy change (hence equilibrium constant) of reaction [50] by eq. [51].

[50] $\quad Ox + \frac{1}{2}H_{2(g)} \rightarrow Red + H^+_{aq}$

$$[51] \quad E^0_{Red/Ox} = \frac{-\Delta G_{50}}{F} = \frac{RT \ln K_{50}}{F}$$

In the section that follows two empirical methods to estimate the standard oxidation potential of organic compounds are discussed. This approach has been applied to benzene and toluene to compare the estimated values with the experimental values obtained recently (2*a*, *b*, 15*b*).

*Method A (eq. [67]), based upon the $pK_a$ of RH (or $RH_2^+$) and the free energy of dissociation of the R—H bond in RH, $\Delta G_{BDE(RH)}$ (or $RH_2^+$, $\Delta G_{BDE(RH_2^+)}$)*

The following thermochemical cycle summarised by eqs. [52]–[57] is similar to that used by Berdinikov and Bazhin (24*a*) to estimate the standard redox potentials of the inorganic radicals $^{\bullet}OH$, $HO_2^{\bullet}$, $O_2$, and $NO_3$, in an aqueous solution. It is extended here to be applicable in any solvent (reaction [56]).

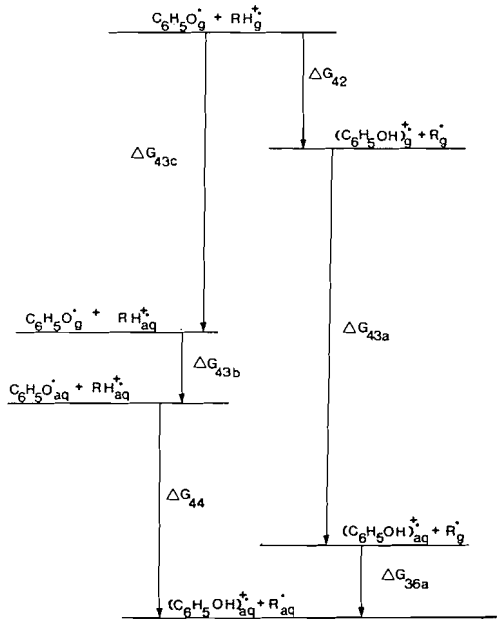


FIG. 5. The relationship between the $pK_a$ of a radical cation ($RH^{+\bullet}$) relative to the $pK_a$ of the phenol radical cation in the gas phase and in solution.

[52] $\quad R^{\bullet}_{sol} \rightarrow R^{\bullet}_g$

[53] $\quad \frac{1}{2}H_{2(g)} + R^{\bullet}_g \rightarrow RH_g$

[54] $\quad RH_g \rightarrow RH_{sol}$

[55] $\quad RH_{sol} \rightarrow R^-_{sol} + H^+_{sol}$

[56] $\quad H^+_{sol} \rightarrow H^+_{aq}$

[57] $\quad R^{\bullet}_{sol} + \frac{1}{2}H_{2(g)} \rightarrow R^-_{sol} + H^+_{aq}$

Application of the result expressed in eq. [51] to eq. [57] gives eq. [58].

$$[58] \quad E^0_{R^{\bullet}/R^-} = -\Delta G_{57}/F$$

where $\Delta G_{57}$ can be expressed by eq. [59].

$$[59] \quad \Delta G_{57} = \Delta G_{52} + \Delta G_{53} + \Delta G_{54} + \Delta G_{55} + \Delta G_{56}$$

Substitution of the value of $\Delta G_{57}$ in eq. [59] gives eq. [60].

$$[60] \quad E^0_{R^{\bullet}/R^-} = -(\Delta G_{52} + \Delta G_{53} + \Delta G_{54} + \Delta G_{55} + \Delta G_{56})/F$$

In the absence of accurate data for the solvation energies of organic radicals in solution, the assumption is made that for neutral species $R^{\bullet}$ and

Can. J. Chem. Downloaded from www.nrcresearchpress.com by 210.87.254.42 on 09/06/12
For personal use only.

RH, which are of similar size, the free energies of solvation are equal (24) as in eq. [61]. This approximation has been shown to be reasonable by comparing physical characteristics of the radicals (R) and corresponding molecules (RH) (2*a*, *b*, 24).

[61*a*] $\Delta G^0_{\text{solvation}(R^{\cdot}_g)} = \Delta G^0_{\text{solvation}(RH)g}$

or expressed as [61*b*]

[61*b*] $\Delta G_{52} + \Delta G_{54} = 0$

Values for $\Delta G_{53}$ and $\Delta G_{55}$ are available in the literature. However, $\Delta G_{55}$ values have been reported mostly in aqueous solution. $\Delta G_{56}$ values have been estimated for a few solvents (26); but if the $E^0$ value in aqueous solution is required $\Delta G_{56}$ will be zero. Substitution of eq. [61*b*] in eq. [60] gives eq. [62].

[62*a*] $E^0_{R^{\cdot}/R^-} = -(\Delta G_{53} + \Delta G_{55} + \Delta G_{56})/F$

and in aqueous solution

[62*b*] $E^0_{R^{\cdot}/R^-} = -(\Delta G_{53} + \Delta G_{55})/F$

From eq. [62] the standard oxidation potential of $R^-$ in solution is estimated.

To estimate the standard oxidation potential of RH, $RH^{+\cdot}$ and $RH_2^+$ are substituted for $R^{\cdot}$ and RH respectively in eqs. [52] to [57].[7] This gives eqs. [63*a*–*d*], [64] which are summarised in Fig. 6.

[63*a*] $RH^{+\cdot}_{sol} \rightarrow RH^{+\cdot}_g$

[63*b*] $\frac{1}{2}H_{2(g)} + RH^{+\cdot}_g \rightarrow RH_2^+{}_g$

[63*c*] $RH_2^+{}_g \rightarrow RH_2^+{}_{sol}$

[63*d*] $RH_2^+{}_{sol} \rightarrow RH_{sol} + H^+_{sol}$

[56] $H^+_{sol} \rightarrow H^+_{aq}$

[64] $RH^{+\cdot}_{sol} + \frac{1}{2}H_{2(g)} \rightarrow RH_{sol} + H^+_{aq}$

The standard redox potential $E^0$ for the redox couple $RH^{+\cdot}/RH$ is obtained by application of eq. [51] to eq. [64] and is expressed by eq. [65].

[65] $$E^0_{RH^{+\cdot}/RH} = -(\Delta G_{63a} + \Delta G_{63b} + \Delta G_{63c} + \Delta G_{63d} + \Delta G_{56})/F = -\Delta G_{64}/F$$

If we assume that the free energies of solvation for organic ions of equal charge and similar size are equal and express it by eq. [66], substitution of eq. [66] into eq. [65] gives eq. [67].

[66*a*] $\Delta G^0_{\text{solvation}(RH^{+\cdot})g} = \Delta G^0_{\text{solvation}(RH_2^+)g}$

or

[7]This method is applicable only if the protonation of RH in the gas phase and in solution yield the same $RH_2^+$ species.

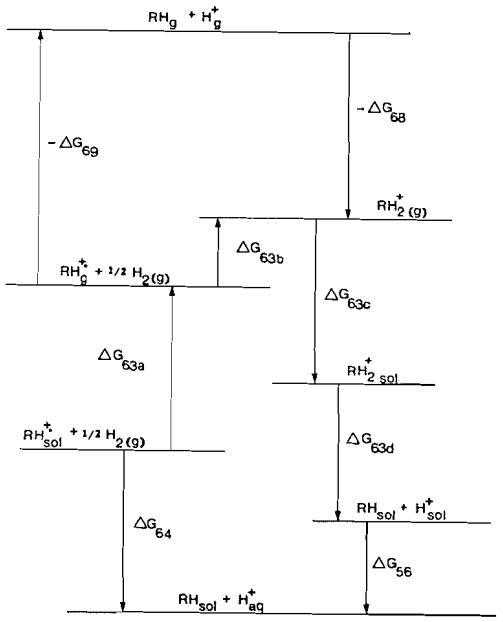


FIG. 6. The standard oxidation potential of RH ($E^0_{RH}$) in relation to the standard free energy of bond dissociation ($\Delta G^0_{BDE(RH_2^+)}$) and the $pK_a$ of its conjugate acid $RH_2^+$.

[66*b*] $\Delta G_{63a} + \Delta G_{63c} = 0$

[67] $$E^0_{RH^{+\cdot}/RH} = -(\Delta G_{63b} + \Delta G_{63d} + \Delta G_{56})/F = (\Delta G^0_{BDE(RH_2^+)g} - \Delta G^0_{f(H)g} - 2.303RTpK_{a(RH_2^+)sol} + \Delta G^0_{tr(H^+)sol})/F$$

Values for $\Delta G_{63b}$ are not available in the literature. But reasonable estimates can be made using the following reactions [68]–[70].

[68] $RH_2^+{}_{(g)} \rightarrow RH_g + H^+_g$

[69] $RH_g + H^+_g \rightarrow RH^{+\cdot}_g + \frac{1}{2}H_{2(g)}$

[70] $RH_2^+{}_{(g)} \rightarrow RH^{+\cdot}_g + \frac{1}{2}H_{2(g)}$

Thus, if the free energy values $\Delta G_{63d}$ and $\Delta G_{56}$ are available the standard oxidation potential of RH in solution can be estimated using eq. [67].

*Method B (eq. [77]), based on ionization potentials and free energies of solvation*

The free energies of solvation for a series of radical cations of alternant aromatic hydrocarbons (including benzene) have been estimated (15*b*). This makes possible the use of the thermochemical cycle summarised in Fig. 7 (eqs. [71]–[74], [54], [37]) to estimate redox potentials of alternant aromatic hydrocarbons.

[71] $RH^{+\cdot}_{sol} + \frac{1}{2}H_{2(g)} \rightarrow RH^{+\cdot}_g + \frac{1}{2}H_{2(g)}$

[72] $RH^{+\cdot}_g + \frac{1}{2}H_{2(g)} \rightarrow RH^{+\cdot}_g + H^{\cdot}_g$

Can. J. Chem. Downloaded from www.nrcresearchpress.com by 210.87.254.42 on 09/06/12
For personal use only.

[73] $RH^{+\cdot}{}_g + H^{\cdot}{}_g \rightarrow RH_g + H^+{}_g$

[54] $RH_g \rightarrow RH_{sol}$

[37] $H^+{}_g \rightarrow H^+{}_{aq}$

---

[74] $RH^{+\cdot}{}_{sol} + \frac{1}{2}H_{2(g)} \rightarrow RH_{sol} + H^+{}_{aq}$

and $E^0$ for the redox couple $RH^{+\cdot}/RH$ is given by eq. [75].

[75] $$E^0{}_{RH^{+\cdot}/RH} = \frac{-(\Delta G_{71} + \Delta G_{72} + \Delta G_{73} + \Delta G_{54} + \Delta G_{37})}{F} = \frac{-\Delta G_{74}}{F}$$

Thus, if the $\Delta G$ terms in eq. [75] are known the standard oxidation potential of an alternant aromatic hydrocarbon can be estimated.

The free energy change ($\Delta G_{72} + \Delta G_{73}$) can be expressed as:

$$\Delta G_{72} + \Delta G_{73} = \Delta G^0{}_{f(RH)g} + \Delta G^0{}_{f(H^+)g} - \Delta G^0{}_{f(RH^{+\cdot})g}$$

$\Delta G^0{}_{f(H^+)g}$ can be calculated (25, 31). In the absence of changes in entropy and heat capacity of RH on ionization eq. [76] can be assumed (29, 30).

[76] $$\Delta G^0{}_{f(RH^{+\cdot})g} - \Delta G^0{}_{f(RH)g} = IP(adiabatic)_{RH}$$

Substitution of eq. [76] in eq. [75] gives eq. [77].

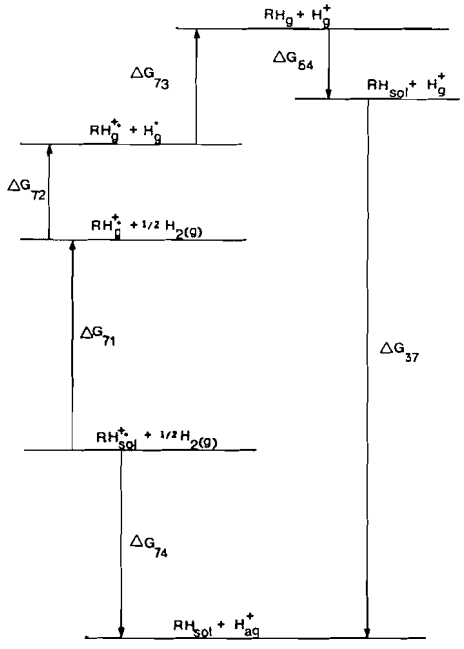


FIG. 7. The standard oxidation potential of RH ($E^0{}_{RH}$) in relation to its adiabatic ionization potential ($IP_{adiabatic(RH)}$) and the standard free energies of solvation of $RH^{+\cdot}{}_g$, $RH_g$, and $H^+{}_g$.

[77] $$E^0{}_{RH^{+\cdot}/RH} = IP(adiabatic)_{RH} + (\Delta G^0{}_{solvation(RH^{+\cdot})g} - \Delta G^0{}_{hydration(H^+)g} - \Delta G^0{}_{solvation(RH)g} - \Delta G^0{}_{f(H^+)g})/F$$

where $E^0$ and IP are expressed in eV.

It has been shown recently that $\Delta G^0{}_{solvation(RH^{+\cdot})g}$ is approximately constant over a series of alternant aromatic hydrocarbons (15*b*). Similarly if $\Delta G^0{}_{solvation(RH)g}$ is assumed to be constant, eq. [77] will simplify to eq. [78].

[78] $$E^0 = IP + \text{constant}$$

Equation [78] is applicable to a series of compounds where the free energies of solvation of the radical cations and the parent compounds are both constants.

## Applications and conclusions

We now apply methods I, II, and III to estimate the $pK_a$ of the radical cations of benzene and toluene. The results are tabulated in Table 1. Whenever possible, experimentally determined thermochemical quantities have been used.[8] In the

---

[8]The data required to estimate the $pK_a$ values are given in Tables 2 to 4. In addition, the following data at 300 K have been used. The stationary electron convention has been used in this work (31*a*).

$\Delta G^0{}_{f(H)g} = 203.2\ kJ\ mol^{-1}$ (25)

$\Delta G^0{}_{f(H_2)g} = 0$ (25)

$\Delta G^0{}_{tr(H^+)CH_3CN} = 46.0\ kJ\ mol^{-1}$ (26)

$\Delta G^0{}_{tr(Cl^-)CH_3CN} = 42.3\ kJ\ mol^{-1}$ (26)

$\Delta G^0{}_{tr(Br^-)CH_3CN} = 32\ kJ\ mol^{-1}$ (26)

$\Delta G^0{}_{hydration(H^+)g} = -1090 \pm 4\ kJ\ mol^{-1}$ (36)

$\Delta G^0{}_{solvation(C_6H_6)^{+\cdot}{}_g} = -186\ kJ\ mol^{-1}$ (15*b*)

$\Delta G^0{}_{solvation(C_6H_6)g} = \Delta G^0{}_{hydration(C_6H_6)g} + \Delta G^0{}_{tr(C_6H_6)CH_3CN} = 0.2\ kJ\ mol^{-1}$

$\Delta G^0{}_{hydration(benzene)}$ was calculated from ref. 24*b* and $\Delta G^0{}_{tr(benzene)}$ was calculated as suggested in ref. 37*a* using the Raoult's Law activity coefficients, $\gamma_x$: 2.7 (in MeCN (37*b*)) and $2.4 \times 10^3$ (in $H_2O$ (37*c*)). $\Delta G^0{}_{solvation}$ of the benzyl and phenyl radicals were assumed to be equal to that of benzene.

$pK_{a(HCl)}$ in $CH_3CN = 8.9$ (38)

$pK_{a(HBr)}$ in $CH_3CN = 5.5$ (38)

$pK_a$ of cyclohexadienyl cation (protonated benzene) in aqueous solution $= -23.0 \pm 1$ (39)

$pK_{a(C_6H_5OH)^{+\cdot}{}_{aq}} = -2.0$ (13)

$\Delta H^0{}_{f(H^+)g} - \Delta H^0{}_{f(H)g} = 1312\ kJ\ mol^{-1}$ (31*a*)

$\Delta G^0{}_{f(H^+)g} = 1517\ kJ\ mol^{-1}$ (31)

The free energy of bond dissociation of protonated benzene

TABLE 1. Estimates of the p$K_a$ of the radical cations of benzene and toluene at 300 K

| Parent compound | Method I (eq. [19]), solvent = MeCN | Method I (eq. [19]), solvent = $H_2O$ | Method II (eq. [27]), solvent = MeCN (BH = HCl) | Method II (eq. [27]), solvent = MeCN (BH = HBr) | Method II (eq. [27]), solvent = MeCN eq. [31] | Method II (eq. [27]), solvent = $H_2O$, eq. [33] | Method III (eq. [39]), solvent = MeCN | Method III (eq. [39]), solvent = $H_2O$, eq. [49] |
|---|---|---|---|---|---|---|---|---|
| Benzene | −3.8±2 | −3±4[a] | −2.7±3 | −1.9±3 | — | −3±4[b] | −2.3±2 | <2.0±3 |
| Toluene | −13 ±2 | — | −11 ±3 | −10 ±3 | >−16±?[c] | — | −10 ±2[d] | <−6.0±3 |

[a] Obtained using the $E^0$ estimated in this work and given in Table 2.
[b] Obtained using $\Delta G^0_{BDE(RH_2^+)}$ estimated in this work.
[c] $E^0$ for the benzyl anion from ref. 12*a* ($E^0 \simeq -1.6$ V vs. S.H.E.) is only an upper estimate as shown in ref. 43. The p$K_a$ of toluene was taken from ref. 12*a*. This p$K_a$ value is not reliable because it also depends on the $E^0$ values for the benzyl anion (12*a*) and was obtained using the assumption that the p$K_a$ of triphenylmethane is the same in both cyclohexylamine and acetonitrile.
[d] Estimated assuming the free energies of solvation of the radical cations of toluene and benzene are equal.

TABLE 2. Standard oxidation potentials in acetonitrile and aqueous solutions at 300 K

| Species | $E^0_{MeCN}$/(V) Literature | Reference | Estimated, this work | Method | $E^0_{aqueous}$/(V) Literature | Reference | Estimated, this work | Method |
|---|---|---|---|---|---|---|---|---|
| Benzene | 3.0 | [a] | 2.9 ±0.2 | [c] | — | — | 2.4±0.2 | [g] |
| Toluene | 2.6 | [b] | 2.5 ±0.2 | [d] | — | — | — | — |
| $Br^-$ | — | — | 1.7 ±0.1 | [e] | 2.0 ±0.1 | [f] | | |
| $Cl^-$ | — | — | 2.11±0.1 | [e] | 2.55±0.1 | [f] | | |

[a] References 2*a* and 15*b*.
[b] Reference 2*a* where $E^0$ was determined at −40°C. We have assumed that the temperature effect on the $E^0$ value is negligibly small.
[c] Estimated using method B.
[d] Estimated using method B and assuming the solvation energies of the radical cations of benzene and toluene are equal.
[e] Estimated using $E^0_{ac} = E^0_{aq} - (\Delta G^0_{tr(B^-)ac} - \Delta G^0_{tr(B\cdot)ac})/F$, where ac ≡ MeCN; $\Delta G^0_{tr(B\cdot)ac}$ was taken as zero (see ref. 2*a*, *b*) and $\Delta G^0_{tr(B^-)ac}$ was obtained from ref. 26.
[f] Reference 24*a*.
[g] Estimated using method A.

absence of oxidation potentials for benzene and toluene in aqueous solution, values estimated in this work were used in the calculation of the p$K_a$ of the radical cations.

From Table 1, we see that there is general agreement in the estimated p$K_a$ values by the three methods, within the limits of error.

These estimates indicate that the radical cations of benzene and toluene should deprotonate even in moderately acidic media if alternative pathways for decay do not exist.

Application of Methods I–III indicates that the radical cation of benzene is a strong acid in acetonitrile solution,[9] with p$K_a$ between −1 and −4. This is indeed a surprising result, for there are no known examples where unambiguous evidence for the deprotonation of the benzene radical cation in acidic media have been reported (41). The Co(III) oxidation of benzene in trifluoroacetic acid (TFA) is believed to occur via the radical cation. Proton incorporation was not observed during the Co(III) oxidation of perdeutero-benzene ($C_6D_6$) in TFA where the only trifluoroacetate ester formed was $C_6D_5O_2CCF_3$; conversely, $C_6H_6$ in TFA-$d_1$ produced only $C_6H_5O_2CCF_3$ (5*c*). Under these conditions, there was no evidence for an acid–base equilibrium between the benzene radical cation and the phenyl radical. Even evidence for the phenyl radical formed by deprotonation of the radical cation was absent. When stoichiometric amounts of the reagents were used biphenyl and other oxidative condensation products, which would result if phenyl radicals were formed, were not detected. However, the deprotonation of the benzene radical cation and subsequent biphenyl formation in acetonitrile solution has been

($\Delta G^0_{BDE(RH_2)^+}$) was estimated from free energies associated with eqs. [68], [69], and [70] where RH = benzene.

The free energy change for eq. [68] was obtained from $\Delta G^0_{300}$ for the proton transfer reaction $C_6H_{6(g)} + NH_4^+{}_{(g)} \rightarrow C_6H_7^+{}_{(g)} + NH_{3(g)}$ (40*a*) and $\Delta G^0_{300}$ for $NH_4^+{}_g \rightarrow NH_{3(g)} + H^+{}_g$. The free energy change for the latter reaction was obtained by adjusting the $\Delta G^0$ value in ref. 40*b* and using the $\Delta H^0$ value in ref. 40*c*.

$$C_6H_{6(g)} + NH_4^+{}_{(g)} \rightarrow C_6H_7^+{}_{(g)} + NH_{3(g)} \qquad \Delta G^0{}_{300} = 79.5\ \text{kJ mol}^{-1}$$

$$NH_4^+{}_{(g)} \rightarrow NH_{3(g)} + H^+{}_{(g)} \qquad \Delta G^0{}_{300} = 812 \pm 8\ \text{kJ mol}^{-1}$$

From the above equations

$$\Delta G^0_{BDE(C_6H_7^+)g} = 305 \pm 8\ \text{kJ mol}^{-1}$$

where $C_6H_7^+$ is the cyclohexadienyl cation.

[9] Whether acetonitrile would be appreciably protonated by the benzene radical cation cannot be predicted because the p$K_a$ of protonated acetonitrile in acetonitrile is not known.

Can. J. Chem. Downloaded from www.nrcresearchpress.com by 210.87.254.42 on 09/06/12
For personal use only.

Can. J. Chem. Downloaded from www.nrcresearchpress.com by 210.87.254.42 on 09/06/12
For personal use only.

TABLE 3. Gas phase bond dissociation data at 300 K

| Species | $\Delta H^0_{BDE}$/kJ mol$^{-1}$ | Ref. | $\Delta S^0_{BDE}$/J mol$^{-1}$ K$^{-1}$ | Ref. | $\Delta G^0_{BDE}$/kJ mol$^{-1}$ |
|---|---|---|---|---|---|
| Benzene | 464± 6 | [a] | 136±4 | [a] | 423±7 |
| Toluene | 368± 6 | [b,g] | 109±4 | [a] | 335±7 |
| HCl | 431.6 | [c] | 92.9 | [c] | 403.7 |
| HBr | 366.2 | [c] | 90.9 | [c] | 338.9 |
| Phenol | 362± 8 | [d] | 108±4 | [d] | 330±9 |
| $NH_3$ | 456± 4 | [a] | 117 | [a] | 421±4 |
| Aniline | 335±13 | [e] | 115±? | [f] | 301±? |

[a] Calculated from ref. 27.
[b] Reference 45.
[c] Calculated from ref. 25.
[d] Reference 46.
[e] Reference 47.
[f] Assuming $S^0_{(C_6H_5NH_2)g} = S^0_{(C_6H_5NH)g}$.
[g] Recent results (44) indicate that $\Delta H^0_{BDE} = 372$ kJ mol$^{-1}$. This will increase the p$K_a$ values for the toluene radical cation given in Table 1 by 0.7 p$K_a$ units.

TABLE 4. Estimated gas phase acidities of the radical cations of benzene, toluene, phenol, ammonia, and aniline at 300 K

| Species | IP(adiabatic)/eV[a] | $\Delta G_{34b}$/kJ mol$^{-1}$ [b] (eq. [34f]) | $\Delta G_{34a}$/kJ mol$^{-1}$ [c] | p$K_{a(RH^{+\cdot})g}$ [d] |
|---|---|---|---|---|
| Benzene | 9.247±0.002 | −892 | 845± 7 | 147±1 |
| Toluene | 8.82 ±0.01 | −851±1 | 798± 8 | 139±1 |
| Phenol | 8.50 ±0.01 | −820±1 | 824±10 | 143±2 |
| $NH_3$ | 10.16 ±0.02 | −980±2 | 755± 6 | 131±1 |
| Aniline | 7.70 ±0.02 | −743±2 | 872± ? | 152±? |

[a] Reference 31*a*.
[b] $\Delta G_{34b} \approx IP_{adiabatic}$ (see text).
[c] $\Delta G_{34a} = \Delta G_{34b} + \Delta G_{16} + \Delta G_{34c}$; $\Delta G_{16}$ values were taken from Table 3 and $\Delta G_{34c} = \Delta G^0_{f(H^+)g} - \Delta G^0_{f(H)g} = 1314$ kJ mol$^{-1}$ (see text).
[d] p$K_{a(RH^{+\cdot})g} = 0.174\Delta G_{34a}$ at 300 K where $\Delta G$ is in kJ mol$^{-1}$.

suggested (41*a*). Recent studies of the oxidation of benzene by $SO_4^{-\cdot}$ demonstrate the reactivity of the benzene radical cation in aqueous solution (41*d*). Product analysis shows the formation of phenol in greater yield than biphenyl. This indicates that the formation of the hydroxycyclohexadienyl radical is preferred to the formation of the phenyl radical. However, the formation of biphenyl does not prove that deprotonation of the radical cation has occurred; for example, it can arise from the attack of the benzene radical cation on benzene. In fact, such a reaction of benzene with its radical cation has been suggested to explain the increase in yield of biphenyl with an increasing initial benzene concentration (5*c*).

The apparent reluctance of the benzene radical cation to deprotonate may be due to competition from even more rapid reactions, reaction with nucleophile, for example. However, there may be an activation barrier in forming the σ-radical from a π-delocalised radical cation. Also, rapid deprotonation generally requires a pre-formed hydrogen bond.

The toluene radical cation is an extremely strong acid in acetonitrile solution with a p$K_a$ between −9 and −13. When we compare this value to the reported p$K_a$ value of toluene in acetonitrile (12*a*), *a difference of over 60 p$K_a$ units is indicated.* Although this may appear surprising at first, it can easily be understood in terms of eq. [31]. The standard oxidation potential of the benzyl anion is between −1.1 V and −1.6 V vs. S.H.E.; ($E_{1/2}$ = −1.1 V (12*b*) and $E^0 > -1.6$ (12*a*, *b*)); this difference of about 3.5 to 4 V in the standard oxidation potentials of toluene and the benzyl anion corresponds to a difference of 60–70 units in the acidities of toluene and its radical cation.

In the case of phenol the corresponding difference is only 12 p$K_a$ units since the difference between the standard oxidation potentials of phenol and the phenoxide anion will not be as great as it is for toluene. Phenol will be expected to have a considerably lower oxidation potential than toluene and the phenoxide anion should have a considerably higher oxidation potential than that of the benzyl anion.

From Methods I and II it is evident that the extremely low p$K_a$ value estimated for the toluene radical cation is the result of both the relatively low bond dissociation free energy of toluene and its high oxidation potential. A comparison of standard oxidation potentials shows that the toluene radical

Can. J. Chem. Downloaded from www.nrcresearchpress.com by 210.87.254.42 on 09/06/12
For personal use only.

cation is somewhat more stable than the benzene radical cation relative to their respective parent compounds. However, the conjugate base of the toluene radical cation, the benzyl radical, a $\pi$-radical, is resonance stabilized. This is shown by the large difference in the bond dissociation free energy of toluene and benzene ($\delta\Delta G_{BDE} \approx 88\,kJ\,mol^{-1}$). This difference far outweighs the lower oxidation potential of toluene as compared to that of benzene ($\delta E^0 \approx 40\,kJ\,mol^{-1}$).

In general, for compounds with very similar standard oxidation potentials a difference in their respective bond dissociation free energies of $\approx 10\,kJ\,mol^{-1}$ corresponds to a difference of $\approx 2\,pK_a$ units in the acidities of their respective radical cations. Conversely, for compounds with very similar bond dissociation free energies a difference in their respective standard oxidation potentials of $\approx 0.1$ V corresponds to a difference of $\approx 2\,pK_a$ units in the acidities of their radical cations.

The comparison between gas phase and solution phase acidities of radical cations provides a means of obtaining free energies of solvation of radical cations. We have shown how the gas phase acidity of a radical cation of an aromatic hydrocarbon, relative to that of the phenol radical cation, can give an upper estimate for its $pK_a$ in solution. The difference in the gas phase acidities of the radical cations of aniline and phenol ($\delta pK_a \approx 9$; see Table 4) is very similar to their difference in aqueous solution ($\delta pK_a \approx 9$; see refs. 7*c* and 13). This indicates that the solvation energies of the radical cations of phenol and aniline are very similar in aqueous solution.

A comparison of the difference in the $pK_a$'s of $NH_4^+$ and $NH_3^{+\cdot}$ in the gas phase ($\delta pK_a \approx 10$) with that in aqueous solution ($\delta pK_a \approx 2.5$; see ref. 19*e*) indicates a significant difference in solvation energies of these ions. Extensive studies of the solvation of aliphatic amines have shown that the extent of solvation decreases in the series $NH_4^+ > RNH_3^+ > R_1R_2NH_2^+ > R_1R_2R_3NH^+$ (40*b* and 42). Further work is required before the difference in the solvation energies of $NH_4^+$ and $NH_3^{+\cdot}$ is completely understood.

From eq. [19], it is possible to obtain the standard oxidation potentials of phenol ($E^0 \approx 1.4 \pm 0.1$), aniline ($E^0 \approx 0.6 \pm 0.2$), and $NH_3$ ($E^0 \approx 1.9$) in aqueous solution. However, the effects of hydrogen bonding in the solvation of phenol and aniline can introduce an error in the estimated $E^0$ values using eq. [19]; this error may be considerable for ammonia.

The present article is an attempt to illustrate the usefulness of thermochemical cycles to obtain thermodynamically significant parameters not directly determinable by experiment. Wherever possible, experimentally determined quantities have been used in the calculations. We note that there may be a greater uncertainty than has been reported in some of the thermochemical data used. Thus the derived results may have a larger uncertainty than is shown in Table 1. We hope the above applications will encourage more accurate determinations of some of these useful thermochemical parameters in future.

**Acknowledgements**

This work was supported by a grant from the Natural Sciences and Engineering Research Council of Canada. D.R.A. is grateful for a Fellowship from the Guggenheim Foundation and A.M.N. is grateful for the award of an Izaac Walton Killam Memorial scholarship.

1. (*a*) G. A. Russel and R. K. Norris. Organic reactive intermediates. *Edited by* S. P. McManus. Academic Press, New York. 1973. pp. 423–448; (*b*) A. J. Bard, A. Ledwith, and H. J. Shine. Adv. Phys. Org. Chem. **13**, 156 (1976); (*c*) H. J. Shine. Organic free radicals. *Edited by* W. A. Pryor. Am. Chem. Soc. Symposium Series. Vol. 69. 1978. pp. 359–375; (*d*) E. T. Kaiser and L. Kevan (*Editors*). Radical ions. Interscience, New York, NY. 1968; (*e*) J. K. Kochi. Free radicals Vol. 1. *Edited by* J. K. Kochi. Wiley, New York. 1973. Chapt. 11; (*f*) L. L. Miller. J. Chem. Educ. **48**, 168 (1971).
2. (*a*) L. Eberson and K. Nyberg. Acta Chem. Scand. B**32**, 235 (1978); (*b*) L. Eberson, L. Jonsson, and L-G. Wistrand. Acta Chem. Scand. B**32**, 520 (1978) and references therein; (*c*) A. Bewick, J. M. Mellor, and B. S. Pons. Electrochim. Acta, **25**, 931 (1980) and references therein.
3. (*a*) G. J. Hoijtink and W. P. Weijland. Rec. Trav. Chim. **76**, 836 (1957); (*b*) H. Kon and M. S. Blois. J. Chem. Phys. **28**, 743 (1958); (*c*) W. I. Aalbersberg, G. J. Hoijtink, E. L. Mackor, and W. P. Weijland. J. Chem. Soc. 3049 (1959); (*d*) S. I. Weissman, E. de Boer, and J. J. Conradi. J. Chem. Phys. **26**, 963 (1957); (*e*) A. Carrington, F. Dravnieks, and M. C. R. Symons. J. Chem. Soc. 947 (1959).
4. (*a*) A. Ledwith and P. J. Russell. J. Chem. Soc. Chem. Commun. 291 (1974); 959 (1974); (*b*) A. Ledwith and P. J. Russell. J. Chem. Soc. Perkin II, 582 (1974).
5. (*a*) P. J. Andrulis, Jr., M. J. S. Dewar, R. Dietz, and R. L. Hunt. J. Am. Chem. Soc. **88**, 5473 (1966); (*b*) E. I. Heiba, R. M. Dessau, and W. J. Koehl, Jr. J. Am. Chem. Soc. **91**, 6830 (1969); see, however, K. Sakata, Y. Kamiya, and N. Ohta. Can. J. Chem. **47**, 387 (1969); (*c*) J. K. Kochi, R. T. Tang, and T. J. Bernath. J. Am. Chem. Soc. **95**, 7114 (1973); (*d*) R. O. C. Norman, C. B. Thomas, and P. J. Ward. J. Chem. Soc. Perkin I, 2914 (1973); (*e*) H. P. Fritz and H. J. Kremer. Z. Naturforsch. **316**, 1565 (1976); (*f*) K. Nyberg and L-G. Wistrand. J. Org. Chem. **43**, 2613 (1978); (*g*) D. Benson. Mechanism of oxidation by metal ions. Elsevier, New York. 1976. p. 2; (*h*) J. S. Littler. Essays on free radical chemistry. Special publication No. 24. The Chemical Society London, 1970. Chapt. 15, pp. 383–408.

Can. J. Chem. Downloaded from www.nrcresearchpress.com by 210.87.254.42 on 09/06/12
For personal use only.


6. (*a*) I. C. LEWIS and L. S. SINGER. J. Chem. Phys. **43**, 2712 (1965) and references therein; (*b*) I. C. LEWIS and L. S. SINGER. J. Chem. Phys. **44**, 2082 (1966).
7. (*a*) G. N. LEWIS and D. LIPKIN. J. Am. Chem. Soc. **64**, 2801 (1942); (*b*) G. N. LEWIS and J. BIGELEISEN. J. Am. Chem. Soc. **65**, 2419 (1943); (*c*) E. J. LAND and G. PORTER. Trans. Faraday Soc. **59**, 2016, 2027 (1963); (*d*) H. D. BURROWS, D. GREATOREX, and T. J. KEMP. J. Phys. Chem. **76**, 20 (1972).
8. (*a*) S. D. ROSS, M. FINKELSTEIN, and E. J. RUDD. Anodic oxidation. Academic Press, New York. 1975; (*b*) N. L. WEINBERG. Technique of electroorganic synthesis. *Edited by* N. L. Weinberg. Wiley, New York. 1974. Part I. Chapt. 4; (*c*) L. EBERSON and K. NYBERG. Acc. Chem. Res. **6**, 106 (1973); (*d*) L. EBERSON and K. NYBERG. Adv. Phys. Org. Chem. **12**, 1 (1976); (*e*) L. EBERSON and K. NYBERG. Tetrahedron Report No. 21. Tetrahedron, **32**, 2185 (1976); (*f*) G. MANNING, V. D. PARKER, and R. N. ADAMS. J. Am. Chem. Soc. **91**, 4584 (1969); (*g*) K. NYBERG. Acta Chem. Scand. **25**, 2499 (1971); (*h*) U. SVANHOLM and V. D. PARKER. Tetrahedron Lett. 471 (1972); (*i*) A. BEWICK, G. J. EDWARDS, J. M. MELLOR, and S. PONS. J. Chem. Soc. Perkin II, 1952 (1977).
9. (*a*) A. WELLER. Nobel Symp. n5, Fast React. Primary Processes Chem. Kinet. 413 (1967); (*b*) D. REHM and A. WELLER. Israel J. Chem. **8**, 259 (1970).
10. (*a*) A. ONOPCHENKO, J. G. D. SCHULZ, and R. SEEKIRCHER. J. Org. Chem. **37**, 1414 (1972); (*b*) P. O'NEILL, S. STEENKEN, and D. SCHULTE-FROHLINDE. J. Phys. Chem. **79**, 2773 (1975); (*c*) M. K. EBERHARDT. J. Org. Chem. **42**, 832 (1977); (*d*) K. SEHESTED and J. HOLCMAN. J. Phys. Chem. **82**, 651 (1978); (*e*) P. J. WAGNER and A. E. PUCHALSKI. J. Am. Chem. Soc. **100**, 5948 (1978).
11. (*a*) J. M. MANCILLA, D. C. NONHEBEL, and I. SCULLION. J. Chem. Res. S, 100 (1980) and references therein; (*b*) E. BACIOCCHI, C. ROL, and L. MANDOLINI. J. Am. Chem. Soc. **102**, 7597 (1980) and references therein; (*c*) L. EBERSON and L-G. WISTRAND. Acta Chem. Scand. B**34**, 349 (1980); (*d*) C. GIORDANO, A. BELLI, A. CITTERIO, and F. MINISCI. Tetrahedron, **36**, 3559 (1980).
12. (*a*) R. BRESLOW and J. GRANT. J. Am. Chem. Soc. **99**, 7745 (1977); (*b*) B. JAUN, J. SCHWARZ, and R. BRESLOW. J. Am. Chem. Soc. **102**, 5741 (1980).
13. W. T. DIXON and D. MURPHY. J. Chem. Soc. Faraday II, **72**, 1221 (1976).
14. (*a*) E. S. PSYCH and N. C. YANG. J. Am. Chem. Soc. **85**, 2124 (1963); (*b*) L. L. MILLER, G. D. NORDBLOM, and E. A. MAYEDA. J. Org. Chem. **37**, 916 (1972).
15. (*a*) V. D. PARKER. J. Am. Chem. Soc. **96**, 5656 (1974); (*b*) V. D. PARKER. J. Am. Chem. Soc. **98**, 98 (1976); (*c*) B. CASE, N. S. HUSH, R. PARSONS, and M. E. PEOVER. J. Electroanal. Chem. **10**, 360 (1965).
16. G. P. GARDINI and J. BARGON. J. Chem. Soc. Chem. Commun. 757 (1980).
17. (*a*) N. K. BRIDGE and G. PORTER. Proc. R. Soc. A, **244**, 259 (1958); (*b*) E. J. LAND and G. PORTER. Proc. Chem. Soc. 84 (1960); (*c*) E. J. LAND, G. PORTER, and E. STRACHAN. Trans. Faraday Soc. **57**, 1885 (1961).
18. (*a*) W. T. DIXON and D. MURPHY. J. Chem. Soc. Faraday II, **74**, 432 (1978); (*b*) D. M. HOLTON and D. MURPHY. J. Chem. Soc. Faraday II, **75**, 1637 (1979).
19. (*a*) M. SIMIC and E. HAYON. J. Am. Chem. Soc. **93**, 5982 (1971); (*b*) R. W. FESSENDEN and P. NETA. J. Phys. Chem. **76**, 2857 (1972); (*c*) E. HAYON and M. SIMIC. Acc. Chem. Res. **7**, 114 (1974); (*d*) P. NETA. Adv. Phys. Org. Chem. **12**, 223 (1976); (*e*) Y. L. CHOW, W. C. DANEN, S. F. NELSON, and D. H. ROSENBLATT. Chem. Rev. **78**, 243 (1978).
20. J. BAREK, E. AHLBERG, and V. D. PARKER. Acta Chem. Scand. B**34**, 85 (1980).
21. (*a*) R. S. BAUMBERGER and V. D. PARKER. Acta Chem. Scand. B**34**, 537 (1980); (*b*) V. D. PARKER. Acta Chem. Scand. B**35**, 123 (1981).
22. (*a*) J. HOLCMAN and K. SEHESTED. Nukleonika, **24**, 887 (1979); (*b*) K. SEHESTED and J. HOLCMAN. Nukleonika, **24**, 941 (1979); (*c*) J. HOLCMAN. Risø-M-1947, Risø National Laboratory, DK-4000 Roskilde, Denmark. 1977; (*d*) J. HOLCMAN and K. SEHESTED. Nukleonika, **24**, 879 (1979).
23. (*a*) R. P. BELL. The proton in chemistry. 2nd ed. Cornell University Press, New York. 1973. Chapt. 3, p. 43; (*b*) E. WIBERG. Z. Phys. Chem. **171**A, 1 (1934); (*c*) A. ALBERT and E. P. SERJEANT. The determination of ionization constants. 2nd ed. Chapman and Hall, London. 1971. Chapt. 2, p. 9.
24. (*a*) V. M. BERDNIKOV and N. M. BAZHIN. Russ. J. Phys. Chem. **44**, 395 (1970); (*b*) L. EBERSON. Acta Chem. Scand. **18**, 2004 (1963); (*c*) W. H. WOODRUFF and D. W. MARGERUM. Inorg. Chem. **12**, 962 (1973).
25. CODATA Bulletin No. 28, ICSU CODATA, Paris 1978. J. Chem. Thermodynamics, **10**, 903 (1978).
26. B. G. COX, G. R. HEDWIG, A. J. PARKER, and D. W. WATTS. Aust. J. Chem. **27**, 477 (1974).
27. S. W. BENSON. Thermochemical kinetics. 2nd ed. Wiley Interscience, New York. 1976.
28. J. E. BARTMESS, J. A. SCOTT, and R. T. MCIVER, JR. J. Am. Chem. Soc. **101**, 6046 (1979); **101**, 6056 (1979) and references therein.
29. M. MEOT-NER and F. H. FIELD. Chem. Phys. Lett. **44**, 484 (1976).
30. S. G. LIAS and P. AUSLOOS. J. Am. Chem. Soc. **100**, 6027 (1978).
31. (*a*) H. M. ROSENSTOCK, K. DRAXL, B. W. STEINER, and J. T. HERRON. J. Phys. Chem. Ref. Data, Suppl. 1, **6** (1977); (*b*) D. R. STULL and H. PROPHET. JANAF thermochemical tables. 2nd ed. NSRDS-NBS 37, U.S. Government Printing Office, Washington D.C., 1971.
32. W. M. LATIMER. The oxidation states of the elements and their potentials in aqueous solution. Prentice-Hall, Inc., New York. 1952.
33. (*a*) R. BRESLOW and W. CHU. J. Am. Chem. Soc. **95**, 411 (1973); (*b*) S. BANK, C. L. EHRLICH and J. A. ZUBIETA. J. Org. Chem. **44**, 1454 (1979); (*c*) S. BANK, C. L. EHRLICH, M. MAZUR, and J. A. ZUBIETA. J. Org. Chem. **46**, 1243 (1981).
34. (*a*) D. H. EVANS. Acc. Chem. Res. **10**, 313 (1977); (*b*) O. HAMMERICH and V. D. PARKER. Electrochim. Acta, **18**, 537 (1973); (*c*) B. S. JENSEN and V. D. PARKER. J. Am. Chem. Soc. **97**, 5211 (1975); (*d*) R. J. KLINGLER and J. K. KOCHI. J. Phys. Chem. **85**, 1731 (1981); (*e*) K. J. VETTER. Electrochemical kinetics. Academic Press, New York. 1967. Chapt. 1; (*f*) V. D. PARKER. Pure Appl. Chem. **51**, 1021 (1979).
35. (*a*) T. G. MCCORD and D. E. SMITH. Anal. Chem. **41**, 1423 (1969); (*b*) A. M. BOND and D. E. SMITH. Anal. Chem. **46**, 1946 (1974); (*c*) E. AHLBERG, B. SVENSMARK, D. PARKER, and V. D. PARKER. Acta Chem. Scand. B**32**, 363 (1978); (*d*) E. AHLBERG and V. D. PARKER. Acta Chem. Scand. B**34**, 91 (1980).
36. (*a*) H. L. FRIEDMAN and V. C. KRISHNAN. Water: a comprehensive treatise. Vol. 3. *Edited by* F. F. Franks. Plenum Press, New York. NY. 1973. Chapt. 1; (*b*) J. E. B. RANDLES. Trans. Faraday Soc. **52**, 1573 (1956).
37. (*a*) M. H. ABRAHAM. Prog. Phys. Org. Chem. **11**, 1 (1974); [*b*) J-P. MONFORT, J. VIDAL, and H. RENON. J. Chim. Phys. **67**, 748 (1970); (*c*) M. H. ABRAHAM and G. F. JOHNSTON. J. Chem. Soc. (A), 1610 (1971).

38. J. F. COETZEE. Prog. Phys. Org. Chem. **4**, 45 (1967).
39. (*a*) A. J. KRESGE, H. J. CHEN, L. E. HAKKA, and J. E. KOUBA. J. Am. Chem. Soc. **93**, 6174 (1971); (*b*) O. A. REUTOV, I. P. BELETSKAYA, and K. P. BUTIN. "CH-Acids", Pergamon, London. 1978. Chapt. I.
40. (*a*) J. F. WOLF, R. H. STALEY, I. KOPPEL, M. TAAGEPERA, R. T. MCIVER, JR., J. L. BEAUCHAMP, and R. W. TAFT. J. Am. Chem. Soc. **99**, 5417 (1977); (*b*) D. H. AUE, H. M. WEBB, and M. T. BOWERS. J. Am. Chem. Soc. **98**, 318 (1976); (*c*) P. KEBARLE. Ann. Rev. Phys. Chem. **28**, 445 (1977).
41. (*a*) T. OSA, A. YILDIZ, and T. KUWANA. J. Am. Chem. Soc. **91**, 3994 (1969); (*b*) E. B. MANO and L. A. ALVES. J. Polym. Sci. Polym. Chem. Ed. A-1 **10**, 655 (1972); (*c*) L-S. WEN and P. KOVACIC. Tetrahedron, **34**, 2723 (1978); (*d*) M. K. EBERHARDT. J. Am. Chem. Soc. **103**, 3876 (1981).
42. (*a*) E. M. ARNETT. Proton-transfer reactions. *Edited by* E. Caldin and V. Gold. 1975. Chapt. 3, p. 79; (*b*) F. M. JONES, III, and E. M. ARNETT. Prog. Phys. Org. Chem. **11**, 263 (1974); (*c*) K. M. DYUMAEV and B. A. KOROLEV. Russ. Chem. Rev. **49**, 1021 (1980).
43. A. J. BARD and A. MERZ. J. Am. Chem. Soc. **101**, 2959 (1979).
44. W. TSANG. Shock tubes in chemical technology. *Edited by* A. Lipschitz. Marcel Dekker, New York. In press.
45. M. ROSSI and D. M. GOLDEN. J. Am. Chem. Soc. **101**, 1230 (1979).
46. A. J. COLUSSI, F. ZABEL, and S. W. BENSON. Int. J. Chem. Kinet. **9**, 161 (1977).
47. J. A. KERR. Chem. Rev. **66**, 465 (1966).

Can. J. Chem. Downloaded from www.nrcresearchpress.com by 210.87.254.42 on 09/06/12
For personal use only.

# Solution carbocation stabilities measured by internal competition for a hydride ion

NANCY E. OKAZAWA AND TED S. SORENSEN[1]

*Department of Chemistry, University of Calgary, Calgary, Alta., Canada T2N 1N4*

Received November 20, 1981

NANCY E. OKAZAWA and TED S. SORENSEN. Can. J. Chem. **60**, 2180 (1982).

Although many techniques are known which allow one to compare the stabilities of solution carbocations, that involving the intermolecular competition for a hydride ion is conceptually (but not experimentally) the simplest procedure. This paper describes a variant of this which is experimentally more reliable and which uses intramolecular equilibria where the two competing systems are held together by a $-(CH_2)_n-$ chain, e.g.

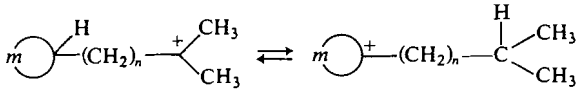

By systematically varying "$n$" in this example ($n$ = 0, 1, 2, or 3), it has been found that a methylene chain of two or more carbons is necessary in order to minimize steric interactions between the end "systems". It has also been found that all cycloalkyl rings studied (except cyclohexyl) stabilize a cation centre much better than an aliphatic equivalent, i.e. $-\overset{+}{C}(CH_3)_2$, in agreement with solvolysis rate studies. The same situation was found when comparing this aliphatic "system" against the 2-norbornyl cation (bicyclic) or against the tricyclic 2-adamantyl cation. In fact, in these cases the equilibria are too lop-sided to obtain numerical values for the equilibrium constants concerned. Finally, three carbocations were looked at where the 2-norbornyl cation structure was pitted against the structurally very related cyclopentyl, bicyclo[2.1.1]hexyl, and bicyclo[3.2.1]octyl cations. In all cases, the 2-norbornyl cation is the more stable. $^{13}C$ nmr spectroscopy was used as the analytical tool to measure (or attempt to measure) the equilibrium constants. Depending on the *rate* of the equilibration process, three different techniques are involved and the relative merits of these are discussed in the latter part of the paper.

NANCY E. OKAZAWA et TED S. SORENSEN. Can. J. Chem. **60**, 2180 (1982).

Parmi toutes les techniques connues qui permettent de comparer les stabilités des carbocations en solution, celle qui implique la compétition intramoléculaire de l'ion hydrure est conceptuellement (mais non expérimentalement) la plus simple. Ce travail décrit une variante de cette technique qui est plus fiable expérimentalement et qui utilise les équilibres intramoléculaires lorsque les deux systèmes en compétition sont maintenus ensembles par une chaîne de $-(CH_2)_n-$, comme dans

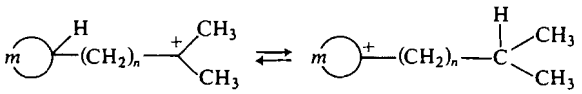

En faisant varier "$n$" d'une façon systématique dans cet exemple ($n$ = 0, 1, 2 ou 3) on a trouvé qu'une chaîne contenant au moins deux unités méthylènes est nécessaire afin de minimiser les interactions stériques entre les systèmes terminaux. On a également trouvé que tous les cycloalkyles étudiés (à l'exception du cyclohexyle) stabilisent mieux le centre cationique que les équivalents aliphatiques c'est-à-dire $-\overset{+}{C}(CH_3)_2$; ceci est en accord avec les études de vitesse de solvolyse. On a trouvé la même situation en comparant ce "système" aliphatique avec le cation norbornyle-2 (bicyclique) ou avec le cation tricyclique adamantyle-2. En fait, dans ces cas les équilibres sont trop dissymétriques pour obtenir les valeurs numériques des constantes d'équilibres concernées. Finalement, on a étudié trois carbocations où la structure du cation norbornyle-2 est opposée aux cations cyclopentyle, bicyclo[2.1.1]hexyle et bicyclo[3.2.1]octyle qui sont structurellement très reliés. Dans tous les cas, le cation norbornyle-2 est le plus stable. On a utilisé la spectroscopie de rmn du $^{13}C$ pour mesurer (ou pour essayer de mesurer) les constantes d'équilibre. Dépendant de la vitesse du processus d'équilibration, on utilise trois techniques différentes et on discute de leurs mérites relatifs dans la dernière partie de cette publication.

[Traduit par le journal]

## Introduction

The comparative base strengths of anions in general, and carbanions in particular, can be measured by setting up solution equilibria in which two anions compete for a proton, e.g.

$$[1]\quad R_1{-}H + R_2^- \underset{}{\overset{K}{\rightleftharpoons}} R_1^- + R_2H$$

This classic procedure (1) has an opposite charge analogy, in which solution cations formally compete for a hydride ion, e.g.

$$[2]\quad R_1{-}H + R_2^+ \overset{K}{\rightleftharpoons} R_1^+ + R_2H$$

[1]To whom all correspondence should be addressed.

0008-4042/82/172180-14$01.00/0

©1982 National Research Council of Canada/Conseil national de recherches du Canada

Can. J. Chem. Downloaded from www.nrcresearchpress.com by 210.87.254.105 on 09/06/12
For personal use only.

Can. J. Chem. Downloaded from www.nrcresearchpress.com by 210.87.254.105 on 09/06/12
For personal use only.

Where $R^+$ is a carbocation, one can in principle use this procedure to study the relative stabilities of carbocations. However, it should be noted that while the proton transfer process (reaction [1]) can be defined in terms of $pK_a$'s, this is not true of reaction [2]. Furthermore, much information relating to relative carbocation stabilities is available from a host of other techniques, such as solvolysis rate comparisons, calorimetry of ionization processes (2), mass spectrometry and ion cyclotron resonance (3) (reaction [2]-type *gas-phase* equilibria are now accurately known for a large number of systems), $pK_a$-type equilibria (4), kinetics of various acid-catalyzed reactions, ionization equilibria (5), etc. Nevertheless, reaction [2] solution equilibria, if the measurements could be made general for a wide variety of cation structures, would be unsurpassed as a "true" measure of solution cation stability since the hydrogen being competed for is the smallest transfer "group" possible, minimizing as much as one can steric contributions. This can be contrasted, for example, with the simplest traditional $pK_a$ equilibrium (reaction [3])

[3] $\text{>C=C<} + (H^+) \rightleftarrows \text{>C(H)—C}^+\text{<}$

Not only are these equilibria very hard to measure (6) (because of polymerization) but we believe that one must take account of more steric factors in this case.

Although many studies involving [2]-type reactions have appeared in the past, they have focussed primarily on kinetics (7) or synthetic applications, the numerical equilibrium constant being of secondary concern. However, Kramer and co-workers have reported some studies devoted entirely to measuring [2]-type equilibria (8).

A serious drawback to intermolecular equilibria involves experimental difficulties associated with an oxidation of the hydrocarbon component (9) of these equilibria by the excess strong acid solvent system used in generating the cation component, leading to "messy" nmr spectra. Furthermore, in choosing solvent systems where both cation and hydrocarbon are soluble, one is reduced to solvents such as dichloromethane, where extensive ion-pairing may result, coincidentally, also a problem with some carbanion equilibria. For example, in the study by Kramer *et al.* (8), the results quoted are markedly influenced by the choice of both the solvent and the Lewis acid.

Our approach to the above problems is to link the $R_1$ and $R_2$ fragments, modifying reaction [2] as follows:

[4] $R_1—H + R_2^+ \overset{K}{\rightleftharpoons} R_1^+ + R_2H$

Each species is now a cation so that solubility problems no longer exist and oxidation is certainly a less serious problem.

Other studies have in the past used the position of a suitable *intramolecularly-generated* carbocation equilibrium in order to probe various phenomena related to carbocation stabilities, e.g. the hyperconjugative order (10). However, the recent availability of routine $^{13}C$ nmr spectroscopy now makes it potentially possible to study a wider variety of such equilibria.

We were therefore interested in looking at intramolecular equilibria related to the above intermolecular processes and as a consequence of this in: (*a*) the design of suitable carbocation systems for such equilibrium measurements and (*b*) an examination of the relative practical merits of various $^{13}C$ nmr techniques needed to obtain the equilibrium constant numerical data.

The design of the desired organic systems can be schematically represented as follows:

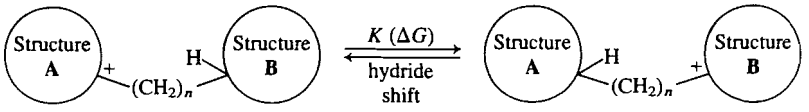


I II

The major uncertainty initially was in knowing how large to make "*n*" so that structures **A** and **B** would not directly interfere with each other, the aim being of course to mimic intermolecular equilibria as closely as possible. We therefore prepared a number of systems in which only "*n*" was allowed to vary.

A consequence of changing "*n*" is that the *rate* for the equilibration will also change (based on the known behavior of simple model systems) (11, 12).

Can. J. Chem. Downloaded from www.nrcresearchpress.com by 210.87.254.105 on 09/06/12
For personal use only.

Depending on how fast this equilibration rate is, there are three separate $^{13}C$ nmr techniques which could be used to measure the equilibrium constant $K$: (A) for very fast rates, only averaged nmr peaks will be observed and $K$ can be calculated if reasonable estimates can be made for the chemical shifts of the individual components. Also, these averaged peaks will be measureably temperature-dependent if $K$ is not too large or too small. (B) for intermediate exchange rates, an nmr line-broadening technique could be used, in particular the application of techniques designed to detect potentially very lop-sided equilibria (13), and (C) for moderately slow rates, one could expect to quantitatively detect peaks characteristic of both ions **I** and **II**.

In evaluating these three techniques, we will be concerned with two factors: (*a*) the potential ability of the technique to detect very large and very small $K$ values and (*b*) a confidence factor which ultimately comes into play when pushing these techniques to their practical limits.

## Results

All of the carbocations were prepared *in situ* from the corresponding alcohol using previously described techniques (14). The alcohols were prepared by standard Grignard or alkyl lithium reactions. Nuclear magnetic resonance procedures for determining $K$'s will be discussed later. Each specific cation is given an arabic number, but when we wish to discuss the series in a general way we use the Roman numerals **I** ⇄ **II**.

*Effect of varying "*n*" in* ***I*** ⇄ ***II***

A series of cations were prepared in which one end was simply

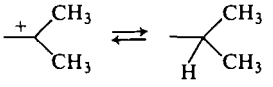

and this "structure" we equate as being equivalent to a normal acyclic tertiary carbocation, e.g. *t*-butyl. In this study, the other "structure" was a cycloalkyl group (ring size = 4–8) (monocyclic), or 2-norbornyl (bicyclic) or 2-adamantyl (tricyclic). For the purposes of investigating the effect of $n$, only the cyclohexyl system **1** ⇄ **2** (structures in Table 1) was suitable, all other systems involving at least some equilibria which were too lop-sided to quantitatively measure. The data are summarized in Table 1.

There is an increase in $K$ as $n$ is increased, but the change from $n = 2$ to $n = 3$ is minimal and we conclude that direct proximity effects between the two "structures" have become insignificant for $n = 2$ and 3.

*Effect of ring size*

A series of cations were prepared, where $n = 0$, 1, and 2 and the ring size $m + 1 = 5$, 7, and 8 (general structures **3** and **4**, see Table 2). The alcohols for the $m + 1 = 4$ series were also prepared but the corresponding cations could not be prepared, a ring expansion to a cyclopentyl or a cyclohexyl ring occurring too fast. The data are summarized in Table 2.

For the $n = 0$ series, equilibrium constants could be measured for $m + 1 = 5$ and 7, but not 8. However, for $n = 1$ or 2, only minimum estimates were obtained. This situation is not unexpected if one looks at the Table 1 data.

The 2-norbornyl comparisons (cations **5** and **6** in Table 3) were also made for the $n = 0$, 1, and 2 series and are summarized in Table 3. These equilibria are even more lop-sided than those in Table 2 and even the $n = 0$ equilibrium constant cannot be obtained.

Finally the tricyclic 2-adamantyl comparisons (cations **7** and **8** in Table 4) were made. In this case only the $n = 1$ equilibrium constant could be measured.

As it turns out, most of the presently chosen equilibria are too lop-sided to obtain numerical $K$ values, i.e. the combination of the $sp^2$ $C^+$ centre in the cyclic, bicyclic, or tricyclic ring and the CH $sp^3$ centre in

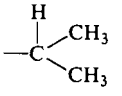

is much better than the alternative. In principle, it would probably be possible to devise a series of overlapping equilibria which would permit one to evaluate all of the $K$'s looked at here, but this would require more study. However, since the tertiary 2-norbornyl cation "structure" has been the subject of numerous studies, it seemed worthwhile to look at cation equilibria in which the 2-norbornyl cation was pitted against the structurally-related cyclopentyl cation, and also against related tertiary bicyclic frameworks, in the hope that this closer similarity of the two "structures" would yield measurable $K$'s. The comparisons are shown below with dark lines emphasizing the similarities in the two "structures". An $n = 2$ connection was used to minimize direct interactions.

For **9** ⇄ **10**, the equilibrium constant was 15 at −90°C, while for **11** ⇄ **12**, only ion **12** was observed at equilibrium, $K \geq 30$ at −90°C. Similarly, it can be

Can. J. Chem. Downloaded from www.nrcresearchpress.com by 210.87.254.105 on 09/06/12
For personal use only.

TABLE 1. Effect of varying "$n$" on the **1** ⇄ **2** equilibrium

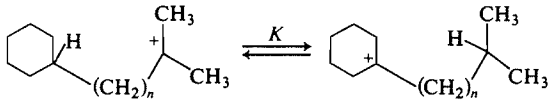

**1** **2**

| Ion | $n$ | $K$ | $-G$ (kcal) | Temperature (°C) | Nmr method used |
|---|---|---|---|---|---|
| **1***a*–**2***a* | 0 | 0.045 | −1.0 | −105 | A |
| **1***b*–**2***b* | 1 | 0.33 | −0.35 | −113 | C |
| **1***c*–**2***c* | 2 | 1 | 0.00 | −106 | C |
| **1***d*–**2***d* | 3 | 1.2 | 0.09 | −74 | A |

TABLE 2. Equilibrium constants (or minimum estimates) for the equilibria **3** ⇄ **4**, where $m + 1 = 5$, 7, and 8 and $n = 0$, 1, or 2

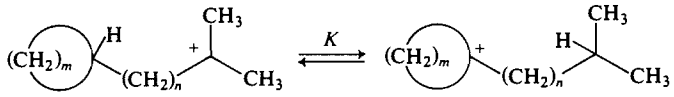

**3** **4**

| Ion | $m$ | $n$ | $K$ | $-\Delta G$ (kcal) | Temperature (°C) | Nmr method used |
|---|---|---|---|---|---|---|
| **3***a*–**4***a* | 4 | 0 | 25 | 1.1 | −105 | A |
| **3***b*–**4***b* | 4 | 1 | ≥1000 | ≥2.6 | −85 | B |
| **3***c*–**4***c* | 4 | 2 | ≥35 | ≥1.2 | −116 | C |
| **3***d*–**4***d* | 6 | 0 | 50–100 | 1.2–1.4 | −123 | A |
| **3***e*–**4***e* | 6 | 1 | ≥20 | ≥1.0 | −110.5 | C |
| **3***f*–**4***f* | 6 | 2 | ≥35 | ≥1.2 | −102 | C |
| **3***g*–**4***g* | 7 | 0 | ≥200 | ≥1.8 | −128 to −102 | A |
| **3***h*–**4***h* | 7 | 1 | ≥1000 | ≥2.6 | −81 | B ($K \geq 20$, method C) |
| **3***i*–**4***i* | 7 | 2 | ≥35 | ≥1.2 | −105 | C |

TABLE 3. Minimum equilibrium constant estimates for the equilibria **5** ⇄ **6**

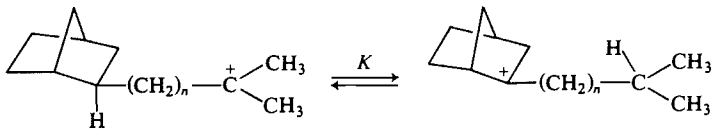

**5** **6**

| Ion | $n$ | $K$ | $-\Delta G$ (kcal) | Temperature (°C) | Nmr method used |
|---|---|---|---|---|---|
| **5***a*–**6***a* | 0 | ≥200 | ≥2.2 | −119 to −63 | A |
| **5***b*–**6***b* | 1 | ≥1000 | ≥2.6 | −118 to −61 | B |
| **5***c*–**6***c* | 2 | ≥50 | ≥1.8 | −117 to −40 | C |

deduced that the **13** ⇄ **14** equilibrium lies completely on the side of **14**, $K \geq 400$ at −90°C. This case is somewhat complicated by another equilibrium involving cation **15** and this is discussed later.

## Discussion

As with carbanion equilibria, the equilibrium constant for **I** ⇄ **II** is *not* necessarily a direct measure of the stability of the two cation "structures" in **I** and **II**. One must also consider the two $sp^3$ CH centres and their relative stabilities, although these will not normally be expected to be the dominant factors involved.

The situation in kinetic solvolysis work is also related, although this involves a variety of larger leaving groups and transition-state developed "cations". Nevertheless, the rather incomplete equilibrium constant data (or limits) for the cycloalkyl vs. acyclic carbocation "structures" is completely in accord with previous solvolysis rate comparisons. These are shown in Table 5.

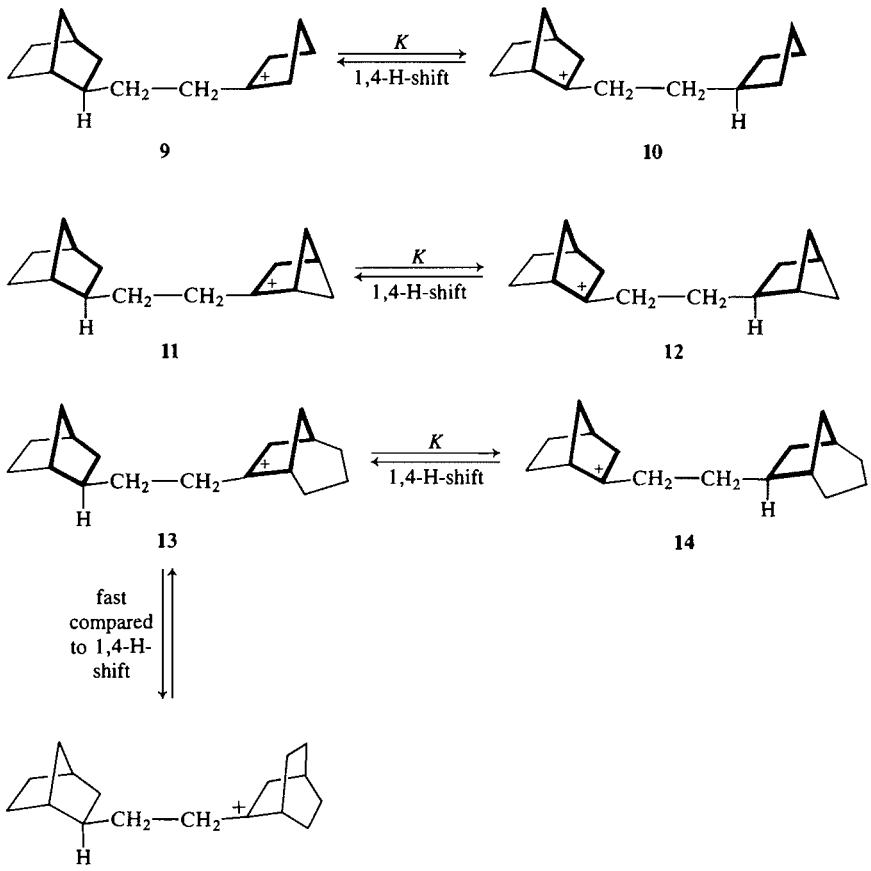


The equating of the *t*-Bu solvolysis data in Table 5 with our

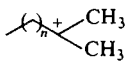

"structure" can be justified by noting the similarity of the solvolysis data for *t*-BuCl, 2-methyl-2-chlorobutane, and 2-methyl-2-chloropentane (less than a factor of two difference among these) (15).

The $K$ equilibrium constant data for $n = 2$ in Table 5 employs the nmr method C and, as will be discussed subsequently, this is not very sensitive. It is entirely possible, based on the more sensitive (nmr method B) $n = 1$ data, that these $K$ values are indeed much larger than the lower limits quoted in Table 5. It is entirely reasonable, of course, that the present $K$ equilibrium constant data would be larger than $k_{cyclic}/k_{t\text{-Bu}}$ because the temperature of the $K$ measurements is quite low (favoring larger $K$'s) and in addition, fully developed cations are involved. The "I-strain" concept (16) generally accounts for both the internal solvolysis comparisons and the equilibrium constant data; however, other factors like C—H hyperconjugation are probably involved as well.

The 2-norbornyl results in ions **5** ⇄ **6**, **9** ⇄ **10**, **11** ⇄ **12**, and **13** ⇄ **14** are also interesting in the context of comparisons to solvolysis data. Both *exo*- and *endo*-2-methyl-2-norbornyl esters or halides lead, of course, to the same carbocation intermediate. They typically differ greatly in solvolysis rate, however, and it is not immediately obvious which comparisons, if any, one should make. The data in Table 6 are illustrative.

The first column shows that tertiary cyclopentyl solvolysis rates typically fall between tertiary *exo*- and *endo*-2-norbornyl. Column two shows that the $k_{exo}/k_{endo}$ difference also applies to a chloride-leaving group and column three shows the solvolysis comparison of acyclic, monocyclic, and *exo*-bicyclic chlorides.

In view of the 1:355 solvolysis ratio, the complete dominance of ion **6** in the **5** ⇄ **6** equilibrium is to be expected. Ion **5**, although not present in detectable amounts, would be expected

Can. J. Chem. Downloaded from www.nrcresearchpress.com by 210.87.254.105 on 09/06/12
For personal use only.

TABLE 4. Equilibrium constants (or minimum estimates) for the equilibria **7** ⇄ **8**

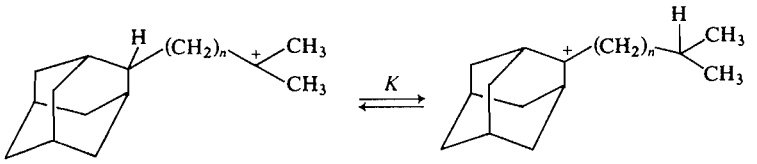

**7** **8**

| Ion | $n$ | $K$ | $-\Delta G$ (kcal) | Temperature (°C) | Nmr method used |
|---|---|---|---|---|---|
| **7a–8a** | 0 | ≥200 | ≥2.2 | −120 to −68 | A |
| **7b–8b** | 1 | 330 | 2.2 | −79 | B |
| **7c–8c** | 2 | ≥50 | ≥1.4 | −88 | C |

TABLE 5. Solvolysis data for 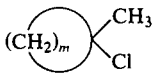 vs. $K$ data from this work

| Ring size ($m$ + 1) | $k$ (cyclic)[a] / $k$ (acyclic) (tBu) | $K$ ($n$ = 1 data) nmr method B | $K$ ($n$ = 2 data) nmr method C |
|---|---|---|---|
| 5 | 43.7 | ≥1000 | ≥35 |
| 6 | 0.35 | 0.33 | 1.0 |
| 7 | 38.0 | [b] | ≥35 |
| 8 | 100.0 | ≥1000 | ≥35 |

[a]Data from ref. 42.
[b]Ion too unstable to use method B.

TABLE 6. Solvolysis data for various tertiary 2-norbornyl compounds

| Compound | Relative $k$[a] | Compound | Relative $k$[b] | Compound | Relative $k$[c] |
|---|---|---|---|---|---|
| 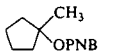 | 1 | 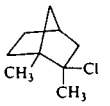 | 178 | *t*-BuCl | 1 |
| 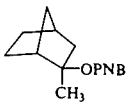 | 4.75 | 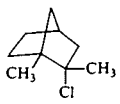 | 1 | 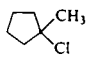 | 66 |
| 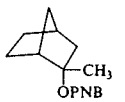 | 0.00536 | | | 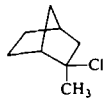 | 355 |

[a]In 80% acetone, data of ref. 43.
[b]In ethanol, data of ref. 18.
[c]In ethanol, data of ref. 44.

to have the *exo* stereochemistry on steric grounds and this can actually be verified for the **9** ⇄ **10** equilibrium.

The comparisons in **9** ⇄ **10**, **11** ⇄ **12**, and **13** ⇄ **14** are more relevant since one is comparing rather similar structures. The stability of **10** over **9** seems to clearly involve an "extra" stability associated with the tertiary 2-norbornyl cation. For example, having the $sp^3$ centre (as in **10**) should preferentially disfavor the simple cyclopentyl ring (more eclipsing interactions), but this is obviously more than made up for by some favorable effect, presumably associated with the 2-norbornyl cation "structure".

An even closer comparison comes from the rather exotic **11** ⇄ **12** equilibrium and this serves to

Can. J. Chem. Downloaded from www.nrcresearchpress.com by 210.87.254.105 on 09/06/12
For personal use only.

show that ring strain *per se* is not involved in stabilizing the 2-norbornyl cation, the 2-bicyclo-[2.1.1]hexyl "structure" being much more strained and also clearly disfavored as a cation site in the **11** ⇄ **12** comparison.

A three-carbon "backside" bridge is also much less favorable than the two-carbon one in 2-norbornyl, as shown by the **13** ⇄ **14** equilibrium. This equilibrium is somewhat more complicated than the others since we do not actually see cation **13**. Even carrying out the addition of the alcohol **16** to the acid solution at −120°C, the initially expected **13** has rearranged to **15** ($K \geq 20$). Model system experiments starting with alcohol **17** confirm this observation, i.e. ionization of **17** at −120°C gives "immediately" >90% of the known (14) 2-methylbicyclo[2.2.2]octyl cation **18**.

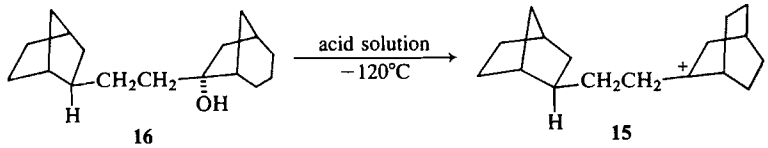


**16** **15**

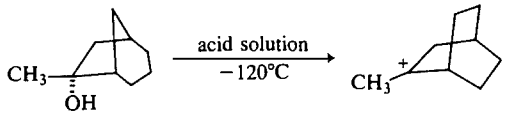


**17** **18**

At about −90 to −100°C, cation **15** rearranges to **14** (via **13** and a 1,4-H-shift) since a *neutral* bicyclo[3.2.1]octane skeleton is more stable than the [2.2.2] skeleton (17). The **15** ⇄ **14** equilibrium lies completely to the right ($K \geq 20$), but since one already knows that **13** is less stable than **15**, one has a combined result giving a minimum $K$ of 400 for the **13** ⇄ **14** equilibrium.

Overall, the $K$'s for the 2-norbornyl "structures" correlate much better with *exo*-leaving-group solvolyses, the implication being that these are "normal" and that factors *other* than the intrinsic cation stability are involved in the transition-state for *endo*-solvolyses. This has been a point of contention for a number of years and our results are consistent with the arguments of Brown (18). These "interpretation problems" also point out the advantages of using equilibria as a measure of cation stability.

The 2-adamantyl equilibria also correlate with solvolysis data, i.e. *t*-BuBr/2-methyl-2-adamantyl bromide rates are about 1:10 (19). These enhanced rates are usually attributed to the removal of 1,3-diaxial interactions in going to the $sp^2$ carbocation intermediate and are also found in dehydration studies (20). However, in the ion equilibria where the 2-position of adamantane is $sp^3$-hybridized, i.e. ion **7**, only one 1,3-diaxial interaction is important (hydrogen occupying the other position) and this is balanced in the $sp^2$-hybridized case, structure **8**, by eclipsing interactions of the 2-alkyl group with hydrogens on the 1- and 3-carbons of the adamantyl ring, as shown below:

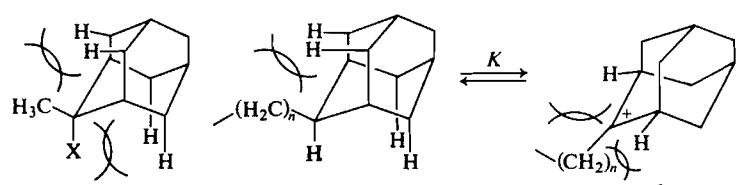


solvolysis starting material **7** **8**

However, interactions in **7** may be the dominant factor and it is significant in this regard that in the one case where a $K$ could be measured (Table 4, $n = 1$, the isobutyl group), molecular mechanics calculations (20) suggest the least steric gain in going from the $sp^3$-hybridized adamantane to the corresponding $sp^2$-hybridized cation. The calculated relief in the isopropyl case ($n = 0$) is

Can. J. Chem. Downloaded from www.nrcresearchpress.com by 210.87.254.105 on 09/06/12
For personal use only.

Can. J. Chem. Downloaded from www.nrcresearchpress.com by 210.87.254.105 on 09/06/12
For personal use only.

considerably larger and would account for the fact that $K$ is larger here than in the $n = 1$ case.

It is somewhat surprising that one sees no 1-adamantyl cations in the equilibria. Although a 1,2-hydride shift in **8** is probably proscribed (21), there is ample opportunity to form a 1-adamantyl cation by a 1,3-hydride shift from **7***a*, a 1,4-shift from **7***b*, or a 1,5-shift from **7***c*.

*Overall conclusions on the equilibrium results*

Solvolysis rate comparisons, when used to probe cation stabilities, are obviously capable of a much greater range than the equilibria looked at in this study. However, as previously noted, solvolysis data are more complex and, besides cation stability and steric effects associated with $sp^3 \rightarrow sp^2$ hybridization changes, are also concerned with internal return (ion-pairing), stereoelectronic participation, solvent effects, leaving group effects, etc., as witnessed by comparing *exo*- and *endo*-2-norbornyl solvolysis rates (which lead to the same cation). The equilibrium method described in this work is restricted at present to subtle comparisons such as cyclopentyl vs. 2-norbornyl in cations **9** $\rightleftarrows$ **10**. Eventually, of course, one could probably devise overlapping equilibria which would allow one to compare quantitatively all of the "systems" looked at in this study, as well as a host of others.

An even better approach is suggested by the elegant work of Arnett and co-workers (2), who have developed calorimetric techniques to measure cation stabilities, including methods for measuring the heat of isomerization of cations, e.g. 4-methyl-2-norbornyl → 2-methyl-2-norbornyl (22). The cations described in this work which are related by 1,4-H shifts rearrange slowly enough to be potential candidates for such calorimetry. Direct $K$ ($\Delta G$) measurements and $\Delta H_{\text{isom.}}$ measurements tend to be complementary techniques, since the latter are best applied where energy differences are relatively large, the former where they are small.

With regard to comparisons to gas-phase ion work, we do not feel that we have enough data yet to make very many meaningful comparisons, i.e. the effect of solvation on cation stabilities.

**Discussion of the nmr methods used to determine $K$**

As mentioned in the Introduction, three $^{13}C$ nmr methods were used in determining $K$ (methods A, B, and C).

*Method A*

For the 1,2-hydride shift equilibria ($n = 0$ case), the associated rate constant is very fast over the temperature range of our measurements. One sees only averaged spectra for ions **I** and **II**. In those cases where there is no temperature dependence of the chemical shift and where the spectrum "fits" a single isomer, we obviously cannot measure any $K$ value and only a lower limit has been estimated. It does not matter which alcohol one starts with to prepare the cation (both were used for **1***a* $\rightleftarrows$ **2***a* and for **3***a* $\rightleftarrows$ **4***a*) and one has to determine the presence of **I** or **II** from the detailed analysis of the actual $^{13}C$ shifts (easily done by looking at the methyl signals in ions **1–8**).

A detectable equilibrium for the $n = 0$ case is signalled by noting a temperature dependence for the "averaged" $C^+$—CH and CH—$C^+$ carbon peaks in **I–II**, the higher field combination moving downfield on increasing the temperature and the other moving upfield. Other peaks will possibly shift as well but to a much smaller extent. There are four unknowns here: (*1*) the chemical shift separation $\Delta_1$ for the $C^+$ carbon in **I** and the CH carbon in **II**; (*2*) $\Delta_2$ for the $C^+$ of **II** and the CH of **I**; (*3*) $\Delta H$ (assumed independent of temperature); and (*4*) $\Delta S$. Normally, one assumes that $\Delta_1 = \Delta_2 = \Delta$, and then adjusts $\Delta$ to give a good ln $K$ vs. $1/T$ van't Hoff plot, $K = \Delta - \delta/\Delta + \delta$, where $\delta$ = the observed separation of the $C^+$—CH and CH—$C^+$ peaks at a given temperature.

In the cyclohexyl vs. dimethyl case, ions **1***a* $\rightleftarrows$ **2***a*, there is no question but that an observable equilibrium exists. The data for these ions are shown in Table 7.

The best fit van't Hoff plot gives $K = 0.045$ at $-105°C$, $\Delta H = 1.2$ kcal/mol, and $\Delta = 254$ ppm (Fig. 1). Since the peaks being averaged in Table 7 are ca. 5700 Hz apart, the temperature dependence is large. For the remaining peaks in **1***a*–**2***a*, only small changes are observed (nevertheless providing enough information to assign **1***a* as the major species).

The data for the cyclopentyl vs. dimethyl case, ions **3***a* $\rightleftarrows$ **4***a*, are shown in Table 8. A van't Hoff plot gives $\Delta = 285$ ppm, $K = 25$ at $-105°C$, and $\Delta H = -1.9$ kcal/mol. One has uncertainties in $K$ because this number is very dependent on the $\Delta$ value used.

As expected, there are situations, for example **3***d* $\rightleftarrows$ **4***d*, where one sees even smaller changes and in the right directions. One knows that $K$ cannot be smaller than a certain value but one cannot be very certain that the actual value calculated is correct. In general, one should be able to detect $K$'s between 200 and 0.005 by this procedure but the confidence factor will be lower as one approaches these extremes.

Can. J. Chem. Downloaded from www.nrcresearchpress.com by 210.87.254.105 on 09/06/12
For personal use only.

TABLE 7. Chemical shift values for the averaged $C^+$—CH and CH—$C^+$ peaks in $1a \rightleftarrows 2a$[a]

| Temperature (°C) | $^{13}C$ shift (ppm) | | δ separation (ppm) |
|---|---|---|---|
| | $C^+$ (1*a*)—CH (2*a*) | $C^+$ (2*a*)—CH (1*a*) | |
| −133 | 320.9 | 77.3 | 243.6 |
| −126 | 319.5 | 78.2 | 241.3 |
| −116 | 317.7 | 80.0 | 237.7 |
| −105 | 314.9 | 82.8 | 232.1 |
| −96 | 313.3 | 84.7 | 228.6 |
| −84 | 310.2 | 87.5 | 222.7 |

[a]Saunders and Lloyd have also looked at this equilibrium and the one shown in Table 8; their results are similar to ours (ref. 45, ref. 46, footnote 31).

TABLE 8. Chemical shift values for the averaged $C^+$—CH and CH—$C^+$ peaks in $3a \rightleftarrows 4a$

| Temperature (°C) | $^{13}C$ shift (ppm) | | δ separation (ppm) |
|---|---|---|---|
| | $C^+$ (4*a*)—CH (3*a*) | $C^+$ (3*a*)—CH (4*a*) | |
| −128 | 336.2 | 60.5 | 275.7 |
| −116 | 333.1 | 63.5 | 269.6 |
| −105 | 329.1 | 66.8 | 262.3 |

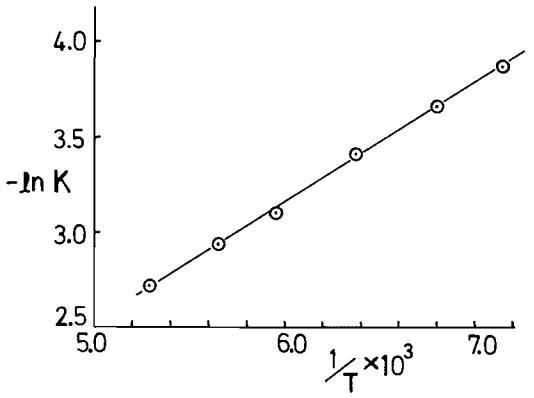


FIG. 1. Van't Hoff plot for the equilibrium 1*a*–2*a*, using the data in Table 7.

For the single $n = 3$ case studied, ions $1d \rightleftarrows 2d$, a 1,5-hydride shift is involved. Over a large temperature range from about −80 to −120°C, intermediate exchange kinetics made the averaged $C^+$—CH and CH—$C^+$ signals too broad to detect. Eventually, at about −70°C, they sharpen sufficiently to detect and using nmr method A, an equilibrium constant was calculated.

Standard deviation type errors for method A are very small.

*Method B*

Equilibrium in the $n = 1$ cases involves a 1,3-hydride shift. From previous work by Brouwer and Saunders (11, 12), it was expected that these shifts would be moderately fast on the nmr time scale (very fast on a conventional kinetic time scale). Consequently, either of the alcohols related, for example, to cations 1*b* and 2*b* can be used to prepare the equilibrium mixture. To determine the equilibrium constant, one could in principle use methods A, B, or C (see subsequent discussion). However, the temperature where averaged spectra would be obtained (method A) is too high for the survival of any of the cations studied in this work. Method C will apply at low temperatures under "frozen-out" exchange conditions. This procedure is the method of choice where both isomers can in fact be detected, but only in the cyclohexyl vs. dimethyl case (1*b*–2*b*) was this situation found. In all other cases, we have applied (or tried) method B.

Method B involves cases where one sees only one isomer at low temperatures (frozen-out conditions). As one warms the solution, one looks for line-broadening due to exchange with the "hidden" equilibrium partner. This method has been discussed in detail elsewhere (13). Cations **I** ⇄ **II** are particularly suitable for such a treatment if one focuses on the $C^+$ and CH carbons of the major isomer. The corresponding minor exchange partners (CH and $C^+$ respectively) are separated by about 6000 Hz in each case (there is very little uncertainty involved in estimating this separation using model systems). Since the potential line-broadening is a linear function of this separation, one should see *selective* broadening of these two peaks and much smaller changes, if any, in the others. In addition, these peaks should resharpen at still higher temperatures. This method is capable

Can. J. Chem. Downloaded from www.nrcresearchpress.com by 210.87.254.105 on 09/06/12
For personal use only.

of detecting much larger or smaller $K$'s than either A or C, and this is nicely shown in the 2-adamantyl vs. dimethyl case, ions **7***b* ⇄ **8***b*. In this system, the peaks for the $C^+$ and CH (in isobutyl) carbons each reach a maximum broadness, in excess of the natural line-width, of ca. 20 Hz at −79°C, corresponding to a $K$ of ca. 330. The rate constant for **8***b* → **7***b* is ca. 120 $s^{-1}$, $\Delta G^{\ddagger}$ = 9.3 kcal/mol at −79°C. No other peaks are significantly broadened and a subsequent resharpening of the $C^+$ and CH carbon peaks was also observed. Selected spectra are shown in Fig. 2.

This method is quite capable of detecting $K$'s between 1000 and 0.001 using a 22.63 MHz instrument (and even wider ranges with higher fields). In those cases where we still have detected no line-broadening, e.g. 2-norbornyl vs. dimethyl, **5***b* ⇄ **6***b*, one can place a lower limit on $K$ *providing one is willing to accept that we have passed through a temperature where the equilibrium rate would have maximized the line-broadening if it had been detectable*. In the two cases where detectable changes were observed, $\Delta G^{\ddagger}$ for the 1,3-hydride shift was 8.9 and 9.3 kcal/mol (cf. 8.5 for the 2,4-dimethylpentyl cation) (11). It therefore appears reasonable to expect a similar $\Delta G^{\ddagger}$ (and temperature of maximum broadness) for all of these ions, particularly since the 1,3-hydride shift is not constrained by unfavorable geometries.

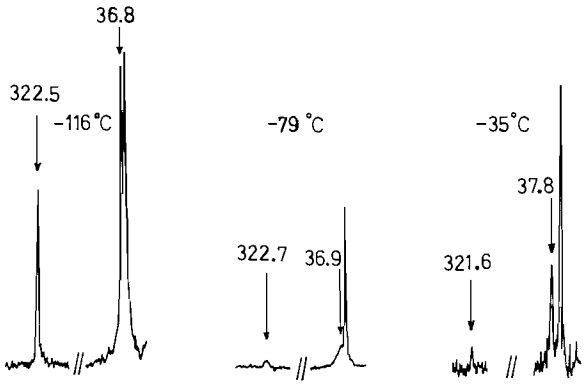


FIG. 2. Three (partial) $^{13}C$ nmr spectra of cation **8***b* taken at three temperatures (others are not shown). The spectrum at the left is the "frozen out" spectrum of **8***b* showing the $C^+$ and isobutyl CH peaks. The spectrum at −79°C (maximum broadness) shows the *specific* line-broadening caused by the dynamic exchange with cation **7***b* (which is "hidden" in the spectrum at −116°C because its concentration is very small). The peak to the right of the one at 36.9 ($C_6$) is included in the diagram to illustrate that the other peaks in **8***b* are *not* broadened. At −35°C, the peaks are "resharpened" and are from the averaged **7***b*–**8***b* situation. However, they have remained at almost the same chemical shift because of the very small concentration of **7***b* involved here.

In the case of the cycloheptyl vs. dimethyl cation, we were unable to reach −80°C (ring-contraction), so this can place a restriction on the use of method B.

Method B requires some faith that one understands the rearrangement under consideration since, as mentioned, one often does not directly "see" the minor equilibrium partner. However, the selectivity involved in the line-broadening would be very difficult to interpret in any alternative way and we believe that this method has a good confidence factor over the $K$ range that we quote. The error limits are probably within ±20% of the quoted $K$ values.

*Method C*

Equilibrium via a 1,4-hydride shift (either direct or a combination of 1,2-shifts) was already known from model systems to be a slow process on an nmr time scale (11). Therefore, this nmr method is simply involved in trying to "see" peaks from both isomers. Ultimately for large or small $K$'s the limitation is determined by signal/noise considerations. In order to verify that a 1,4-shift is reasonably fast on a conventional kinetic time scale, we prepared both alcohols related to cations **1***c* and **2***c* and to **3***c* and **4***c* and found the same $^{13}C$ nmr spectrum for the ions at −100°C, i.e. equilibration has occurred. The equilibration reaction was directly observed in the case of **9** ⇄ **10** and **11** ⇄ **12**, where the less stable cations **9** and **11** were first prepared at −120°C and the isomerization to **10** and **12**, respectively, could be followed at ca. −90 to −100°C. That **10** and **12** are the species formed is clear from a detailed analysis of the $^{13}C$ peak positions and comparisons to the $^{13}C$ shifts and reactivity of model systems, for example, the ring expansion of **11** was shown to be slow by preparing the 2-ethyl-2-bicyclo[2.1.1]hexyl cation **19** and noting that the quantitative expansion to the 2-methyl-2-norbornyl cation **20** occurred only at much higher temperatures than that involved in a 1,4-hydride shift.

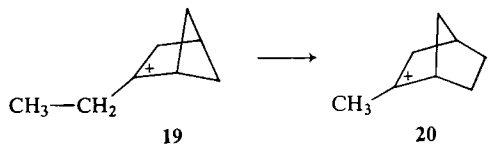


**19** **20**

In the case of cations **3***f*–**4***f*, **3***i*–**4***i*, **5***c*–**6***c*, and **7***c*–**8***c*, only one species was observed, but one can confidently presume equilibration conditions were present based on the near constancy of the 1,4-hydride shift rate in the four cases where this was checked.

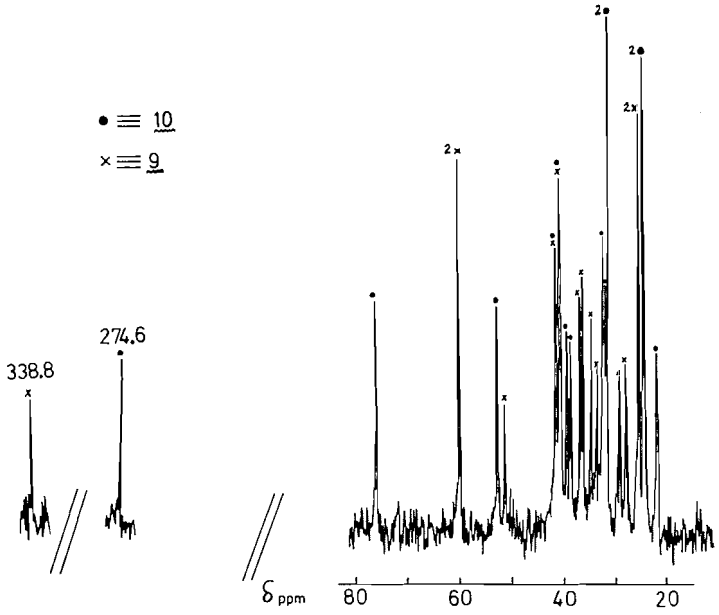


FIG. 3. Illustration of the "Method C" procedure for determining $K$ values. This spectrum (1000 scans at −90°C) was recorded at an intermediate point in the rearrangement of **9** to **10** to show the "fingerprinting" capabilities of the $^{13}C$ nmr spectra (only two lines are overlapped in the two ions). With longer times, the **9** ⇄ **10** equilibrium is reached.

The S/N limits for the *absence* of detectable amounts of the minor partners in the above cases employed a search for the characteristic methyl signals from

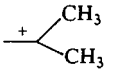

which occur (or would occur) at about 45 ppm, a region fairly free of other $^{13}C$ peaks. In most cases, spectra were obtained after about 4000 accumulations, which has sufficient S/N to place an upper limit of about 3% on the maximum possible minor isomer. Thus, this method is not as sensitive as A or B, depending of course on how many accumulations one is able or willing to obtain.

Where equilibrium constants can be measured, one has a high confidence rating. For example, in ions **9** and **10**, there are fourteen peaks possible for each ion and in mixtures, twenty-two of these are completely resolved, i.e. "fingerprinting" comparisons have numerous peaks to use. This is shown in Fig. 3. The error limits are probably within ±10% of the reported $K$ values.

*Carbocation structures*

All of the ions prepared in this work are new, but in all cases, the corresponding methyl-substituted species has been reported. In the ions prepared in this work, only in the case of cation **4***g* are any anomalies noted in the expected (based on the methyl-substituted species) $^{13}C$ peak positions and this case has been discussed elsewhere (23). The $^{13}C$ shifts which are relevant to determining $K$'s or for structure assignment are given in Table 9.

Like the methyl analog, the cyclohexyl cations show evidence of a chair – twist boat conformational equilibrium and the cyclooctyl cations show a conformational line-broadening for some of the $^{13}C$ peaks.

*Carbocation rearrangements*

All of the cations eventually irreversibly rearrange. In the monocyclic cations, ring expansions or contractions readily occur, leading to cyclohexyl cations. Thus, none of the cyclobutyl ions could even be prepared, the cyclopentyl cations ring expand at ca. −80°C, a rate rather similar to the simple 1-ethyl analog (24), the cycloheptyl cations readily contract at about −90°C to −100°C, again similar to the 1-methyl analog (24), and the cyclooctyl cations also ring contract. In most cases, the products of these reactions were the same 1-isoalkylcyclohexyl cations which had already been characterized.

The 2-norbornyl cations are stable to about −30°C and the initial ring-expanded product is likely a 2-bicyclo[2.2.2.]octyl cation system. The 2-adamantyl cations are also stable to about −30°C. In the one case where rearrangement peaks were recorded, peaks characteristic of 1-adamantyl

Can. J. Chem. Downloaded from www.nrcresearchpress.com by 210.87.254.105 on 09/06/12
For personal use only.

TABLE 9. Diagnostic $^{13}C$ chemical shifts in the carbocations which were used to identify or calculate equilibrium constants

| Cation | $^{13}C$ chemical shifts and assignments | $T$ (°C)[m] | Comments |
|---|---|---|---|
| **1***a*–**2***a* | See Table 7 | | |
| **1***b* | 331.3 ($C^+$), 46.1 ($CH_3$'s), 42.9 (CH) | −113 | *a* |
| **2***b* | 328.4 ($C^+$), 22.9 ($CH_3$'s), 31.4 (CH) | −113 | *a* |
| **1***c* | 332.9 ($C^+$), 38.2 (CH), 45.2 ($CH_3$'s) | −119 | *b* |
| **2***c* | 328.6 ($C^+$), 29.3 (CH), 22.2 ($CH_3$'s) | −119 | *b* |
| **1***d*–**2***d* | ~204 (broad), ~160 (broad), 32.0 ($CH_3$'s) | −74 | *c* |
| **3***a*–**4***a* | See Table 8 | | |
| **4***b* | 337.1 ($C^+$), 30.8 (CH), 22.5 ($CH_3$'s) | −112 | *d* |
| **4***c* | 338.1 ($C^+$), 28.2 (CH), 21.7 ($CH_3$'s) | −116 | |
| **3***d*–**4***d* | 331.1 ($C^+$—CH), 58.4 (CH—$C^+$), 21.7 ($CH_3$'s) | −123 | *e* |
| **4***e* | 327.3 ($C^+$), 32.0 (CH), 23.0 ($CH_3$'s) | −124 | *f* |
| **4***f* | 332.8 ($C^+$), 28.7 (CH), 21.9 ($CH_3$'s) | −117 | |
| **4***g* | 313.7 ($C^+$), 53.7 (CH), 25.3 ($CH_3$'s) | −93 | *g*, *h* |
| **4***h* | 333.5 ($C^+$), 23.1 ($CH_3$'s) | −89 | *h* |
| **4***i* | 331.8 ($C^+$), 30.6 (CH), 21.8 ($CH_3$'s) | −81 | *h* |
| **6***a* | 269.0 ($C^+$), 76.6 (C-1), 41.7 (CH of *i*Pr), 20.7 ($CH_3$'s) | −80 | *i* |
| **6***b* | 278.2 ($C^+$), 77.1 (C-1), 29.4 (CH of *i*Bu), 22.4, 22.6 ($CH_3$'s) | −95 | *i* |
| **6***c* | 275.0 ($C^+$), 76.4 (C-1), 28.4 (CH of *i*Pent), 21.9 ($CH_3$'s) | −87 | *i* |
| **8***a* | 319.2 ($C^+$), 54.3 (CH of *i*Pr), 19.0 ($CH_3$'s) | −109 | |
| **8***b* | 322.7 ($C^+$), 36.9 (CH of *i*Bu), 24.1 ($CH_3$'s) | −79 | *j* |
| **8***c* | 320.5 ($C^+$), 30.3 (CH of *i*Pent), 22.0 ($CH_3$'s) | −105 | |
| **9** | 338.8 ($C^+$), 60.9 and 26.4 (both 2C), α and β-C of C-5 ring | −80 | |
| **10** | 274.6 ($C^+$), 76.7 (C-1 of 2-norbornyl), 25.4 and 32.5 (both 2C), α and β-C of neutral C-5 ring | −80 | |
| **11** | 326.4 ($C^+$), 79.4 (C-1 of bicyclo[2.1.1.]hexyl) | −100 | *k* |
| **12** | 275.1 ($C^+$), 76.7 (C-1 of 2-norbornyl) | −90 | *k* |
| **14** | 276.6 ($C^+$), 76.4 (C-1 of 2-norbornyl), 20.1 (C-6 of a neutral bicyclo[3.2.1]octyl system) | −90 | *l* |
| **15** | 333.8 ($C^+$), 61.9 (C-1 of 2-bicyclo[2.2.2]octyl), 29.5 and 23.7 (both 2C), the C-6, C-7 and C-5, C-8, carbons of the 2-bicyclo[2.2.2] system | −108 | |
| **19** | 329.1 ($C^+$), 78.8 (C-1), 57.1 (C-5, C-6), 55.7 ($CH_2$ of Et), 48.3 (C-3), 36.2 (C-4), 9.1 ($CH_3$ of Et) | −90 | |

[a]Dynamic line-broadening occurs at higher temperatures due to the **1***b* ⇄ **2***b* rate process becoming fast on the nmr time-scale.
[b]At other temperatures one sees changes in the ratio of **1***c* and **2***c*.
[c]The methyl carbons move to lower field at lower temperatures, indicating that while enthalpy favors **1***d*, entropy favors **2***d*.
[d]The $C^+$ and CH peaks did not broaden up to −85°C.
[e]Total chemical shift vs. temperature changes were only about 2 ppm over a 25°C span.
[f]Rearranges before the temperature needed for the 1,3-H-shift to show dynamic nmr line-broadening.
[g]See ref. 23 for a full description of this system.
[h]A dynamic chair–twist boat ⇄ twist boat–chair conformational interchange broadens some of the peaks. See ref. 14 for an analysis of the 1-methyl analog.
[i]Line-broadening, due to the well-known (25) 6,2-H-WM-6,2-H rearrangement, begins to show up at the higher temperatures.
[j]See Fig. 2, showing the line-broadening due to the exchange with the "hidden" **7***b*.
[k]See Fig. 3, showing an intermediate spectrum in the rearrangement of **11** to **12**.
[l]The peak at δ 20.1 is not compatible with a bicyclo[2.2.2]octane ring (26).
[m]In all cases, the spectra were also run at a number of other temperatures.

cations were observed, although the rearrangement appears to be "deep-seated".

## Experimental

*General procedures*

Mass spectra were obtained on a Varian CH-5 mass spectrometer. $^1H$ nmr spectra of neutral precursors were obtained on a Varian HA-100, Varian A-60, or Hitachi Perkin-Elmer R24B spectrometer. $^{13}C$ nmr spectra were obtained using a Bruker WH-90 or Varian XL-200 spectrometer, in $CDCl_3$ unless otherwise stated. Boiling points and melting points are uncorrected.

*Preparation of alcohol precursors*

Alkyl lithium reagents were prepared by standard procedures. The appropriate ketone, dissolved in ether, was added dropwise under argon at 0°C and then the mixture was refluxed for several hours. After work-up, the alcohols were isolated by fractional distillation. Yields using isopropyl lithium were generally poor (enolization) but purity of product was the main concern. $^{13}C$ and/or $^1H$ nmr spectroscopy and mass spectrometry were used to characterize the liquid products and to check the alcohol purity.

*1-(1-Methylethyl)-1-cyclobutanol*, bp 51°C/12 mm, *m/e* = 114.

*1-(1-Methylethyl)-1-cyclopentanol*, bp 63–66°C/11 mm, lit. (27), 53°C/6 mm, $^{13}C$ nmr ($CFCl_3$): δ 84.9, 38.8, 37.8, 24.4, and 18.0.

*1-(1-Methylethyl)-1-cyclohexanol*, bp 70–77°C/11 mm, lit. (27), 77°C/13 mm, $^{13}C$ nmr ($CFCl_3$): δ 72.8, 38.3, 34.7, 26.5, 22.3, and 17.0.

*1-(1-Methylethyl)-1-cycloheptanol*, bp 42°C/0.09 mm, lit. (28), 96°C/12 mm, $^{13}C$ nmr ($CFCl_3$): δ 76.9, 39.7, 38.8, 30.2, 23.3, and 17.7.

*1-(1-Methylethyl)-1-cyclooctanol*, bp 133–135°C/26 mm, reported in patent literature (29), $^{13}C$ nmr ($CFCl_3$): δ 75.5, 36.2, 34.7, 28.5, 25.5, 22.5, and 17.0.

*2-(1-Methylethyl)-2-bicyclo[2.2.1]heptanol*, bp 85–89°C/13 mm, *m/e* = 154, reported with no details (30), $^{13}C$ nmr ($CFCl_3$): δ 81.3, 45.8, 44.9, 39.0, 38.0, 36.7, 28.6, 23.3, 17.7, and 16.3.

*2-(1-Methylethyl)-2-tricyclo[3.3.0.0$^{3,7}$]decanol*, mp 59°C, lit. (31), 72.8–73.8°C, $^{13}C$ nmr ($CFCl_3$): δ 75.4, 39.0, 35.2, 34.4, 33.8, 30.0, 27.8, and 15.5.

Isobutyl lithium reactions also gave generally poor yields

Can. J. Chem. Downloaded from www.nrcresearchpress.com by 210.87.254.105 on 09/06/12
For personal use only.

Can. J. Chem. Downloaded from www.nrcresearchpress.com by 210.87.254.105 on 09/06/12
For personal use only.

because of the facile reduction of ketones by this particular reagent.

*1-(2-Methylpropyl)-1-cyclobutanol*, bp 58°C/10 mm, *m/e* = 128.

*1-(2-Methylpropyl)-1-cyclopentanol*, bp 69–71°C/10 mm, lit. (32), 120°C/22 mm, $^{13}C$ nmr ($CFCl_3$): δ 82.6, 50.9, 40.8, 25.3, 24.8, and 23.9.

*1-(2-Methylpropyl)-1-cyclohexanol*, bp 80–83°C/10 mm, lit. (32), 95°C/15 mm, $^{13}C$ nmr ($CFCl_3$): δ 71.7, 52.3, 38.5, 26.3, 25.1, 23.8, and 22.6.

*1-(2-Methylpropyl)-1-cycloheptanol*, bp 98–102°C/10.5 mm, lit. (32), 120°C/16 mm.

*1-(2-Methylpropyl)-1-cyclooctanol*, bp 116–118°C/9 mm, *m/e* = 184.

*2-(2-Methylpropyl)-2-bicyclo[2.2.1]heptanol*, bp 91–93°C/10 mm, *m/e* = 168.

*2-(2-Methylpropyl)-2-tricyclo[3.3.0.0$^{3,7}$]decanol*, mp 51°C, lit. (33), 57°C.

Isopentyl alcohols were prepared using the Grignard reagent or where noted, the lithium reagent, and yields were good in most cases.

*1-(3-Methylbutyl)-1-cyclobutanol*, isolated on a small scale by molecular distillation, bath temperature 50–75°C at 10 mm, *m/e* = 142, $^{13}C$ nmr: δ 75.8, 37.5, 36.0, 32.5, 28.5, 22.7, and 12.3.

*1-(3-Methylbutyl)-1-cyclopentanol*, bp 88–89°C/11 mm, *m/e* = 156, $^{13}C$ nmr: δ 82.5, 39.7, 39.3, 33.8, 28.6, 23.9, and 22.7.

*1-(3-Methylbutyl)-1-cyclohexanol*, bp 60–62°C/0.025 mm, reported in patent literature (34), $^{13}C$ nmr: δ 71.4, 40.2, 37.5, 32.0, 28.6, 26.0, 22.7, and 22.4.

*1-(3-Methylbutyl)-1-cycloheptanol*, using Li reagent, bp 115–121°C/10 mm, reported in patent literature (29).

*1-(3-Methylbutyl)-1-cyclooctanol*, using Li reagent, bp 86–92°C/0.25 mm, *m/e* = 198.

*2-(3-Methylbutyl)-2-bicyclo[2.2.1]heptanol*, bp 58–60°C/0.05 mm, *m/e* = 182, $^{13}C$ nmr: δ 79.5, 46.8, 45.8, 40.2, 38.7, 37.2, 32.3, 28.6, 22.7, and 22.2.

*2-(3-Methylbutyl)-2-tricyclo[3.3.0.0$^{3,7}$]decanol*, using Li reagent, mp 65°C, *m/e* = 204 (M − 18).

Cation solutions **1***a*–**2***a*, **1***c*–**2***c*, **3***a*–**4***a*, and **3***c*–**4***c* were also prepared from the corresponding sidechain alcohols.

*2-Cyclohexyl-2-propanol*, bp 76–78°C/9 mm, lit. (27), 85°C/15 mm, $^{13}C$ nmr ($CFCl_3$): δ 72.5, 50.0, 28.1, 27.3, and 27.2.

*4-Cyclohexyl-2-methyl-2-butanol* was prepared from 3-cyclohexylpropanoic acid by reaction of the acid chloride with 2 mol of methyl lithium, bp 108–110°C/11 mm, lit. (35), 96–97°C/7 mm.

*2-Cyclopentyl-2-propanol*, bp 35–36°C/0.35 mm, lit. (27), 50°C/3 mm, $^{13}C$ nmr ($CFCl_3$): δ 71.9, 51.8, 28.4, 27.7, and 26.6.

*4-Cyclopentyl-2-methyl-2-butanol*, prepared like the cyclohexyl analog, bp 90–93°C/11 mm, *m/e* = 138 (M − 18).

Cation **1***d*–**2***d* solutions were prepared from *5-Cyclohexyl-2-methyl-2-pentanol*, bp 70–76°C/0.09 mm, $^{13}C$ nmr ($CFCl_3$): δ 70.5, 44.7, 38.5, 38.1, 33.9, 29.4, 27.0, 26.8, and 22.0. This alcohol was prepared from the known (36) 3-cyclohexyl-1-bromopropane and acetone via the lithium reagent of the former.

Cations **9** and **10** both originated from the alcohol related to **9**.

*1-[2-(*exo*-2-bicyclo[2.2.1]heptyl)ethyl]-1-cyclopentanol*, bp 125–130°C/0.5 mm, solidifying at 25°C. *Anal.* calcd. for $C_{14}H_{24}O$: C 80.7, H 11.6; found: C 80.9, H 12.0. This alcohol was prepared by adding cyclopentanone at 0°C to the Grignard reagent from 1-bromo-2-(*exo*-2-bicyclo[2.2.1]heptyl)ethane and was formed in near quantitative yield.

*1-Bromo-2-(*exo*-2-bicyclo[2.2.1]heptyl)ethane*, bp 45–46°C/0.6 mm, was prepared from the known (37) alcohol ($Br_2$, triphenylphosphine, in acetonitrile) (38). In our case, the alcohol was prepared by esterification and $LiAlH_4$ reduction of the commercially-available carboxylic acid. The bromide had $^{13}C$ nmr: δ 62.4 ($CH_2$—Br), 40.8 (CH), 40.0 ($CH_2$), 37.6 ($CH_2$), 36.5 (CH), 35.5 (CH), 32.0 ($CH_2$), 30.0 ($CH_2$), and 28.7 ($CH_2$).

*2-[2-(*exo*-2-Bicyclo[2.2.1]heptyl)ethyl]-2-bicyclo[2.1.1]hexanol* was prepared like the cyclopentyl analog and was used to prepare both cations **11** and **12**, bp 103–106°C/0.3 mm, solidifies to a slightly oily solid at 25°C. *Anal.* calcd. for $C_{15}H_{24}O$: C 81.8, H 11.0; found: C 82.0, H 11.6. The alcohol is expected to be a mixture of two diastereomers and the $^{13}C$ nmr spectrum indicates this. The 2-bicyclo[2.1.1]hexanone was prepared by the method of Bond (39).

*6-[2-(*exo*-2-Bicyclo[2.2.1]heptyl)ethyl]-6-bicyclo[3.2.1]octanol* was prepared like the cyclopentyl analog using 6-bicyclo-[3.2.1]octanone (40) as the ketone, bp 128–140°C/0.6 mm, solidifies at room temperature. *Anal.* calcd. for $C_{17}H_{28}O$: C 82.2, H 11.5; found: C 82.0, H 11.7. This alcohol is likewise a mixture of diastereomers, but is expected to have the *endo*-alcohol configuration at C-6 (40).

*Preparation of the cations*

All of the cations were prepared by adding the weighed alcohol (80–200 mg dissolved in 200–500 μL of $CFCl_3$) to 2 mL of a 1:4 mixture of Magic acid (1:1 $SbF_5$–$FSO_3H$) and $SO_2ClF$. The acid solution was cooled to ca. −130°C in a liquid $N_2$ slush bath prior to the alcohol addition. In all cases, except the cyclobutanols, carbocations were obtained with unrearranged alcohol carbon skeleton (although H-shifts often occurred). 1-(1-Methylethyl)-1-cyclobutanol gave the 1,2-dimethylcyclopentyl cation (41), 1-(2-methylpropyl)-1-cyclobutanol gave mainly the cations **3***a*–**4***a*, and 1-(3-methylbutyl)-1-cyclobutanol gave **1***a*–**2***a* cleanly.

*Nuclear magnetic resonance spectra of the cations*

All $^1H$ and $^{13}C$ nmr spectra were obtained on a Bruker WH-90 FT-NMR spectrometer and previously described procedures were used for temperature calibration, lock, etc. (14). $^1H$ nmr spectra were obtained in a few cases but are not very useful for determining *K* values and are not further reported. $^{13}C$ nmr spectra were obtained at approximately 10–15°C intervals and generally involved about 4000 accumulations. Complete $^{13}C$ assignments were made for each cation, except for **11**, **12**, **14**, and **15** which are very complex, from off-resonance spectra and comparisons to the known 1-methyl analogs. Table 9 records the peaks of importance to the actual or attempted *K* determinations. Complete $^{13}C$ nmr assignments are available on request or are in the thesis of N.E.O. Any special observations on the $^{13}C$ spectra, such as dynamic line-broadening, are given in Table 9. Nuclear magnetic resonance procedures used to determine the *K*'s have already been discussed.

## Acknowledgements

We thank Mr. A. Joffe and Dr. K. Ranganayakulu for their help. The Natural Sciences and Engineering Research Council of Canada is thanked for a Studentship award to N.E.O.

1. (*a*) J. B. Conant and G. W. Wheland. J. Am. Chem. Soc. **54**, 1212 (1932); (*b*) W. K. McEwan. J. Am. Chem. Soc. **58**, 1124 (1936).
2. E. M. Arnett and C. Petro. J. Am. Chem. Soc. **100**, 2563 (1978); **100**, 5402 (1978); **100**, 5408 (1978).
3. M. T. Bowers (*Editor*). Gas phase ion chemistry. Vol. II. Academic Press, New York. 1979.
4. E. M. Arnett. Prog. Phys. Org. Chem. **1**, 223 (1963).
5. N. N. Lichtin. *In* Carbonium ions. Vol. 1. *Edited by* G. A.

Olah and P. von R. Schleyer. Interscience Publishers, New York. 1968. Chapt. 4.
6. N. C. DENO. Prog. Phys. Org. Chem. **2**, 129 (1964).
7. N. C. DENO, G. SAINES, and M. SPANGLER. J. Am. Chem. Soc. **84**, 3295 (1962).
8. D. MIRDA, D. RAPP, and G. M. KRAMER. J. Org. Chem. **44**, 2619 (1979) and earlier papers.
9. G. A. OLAH and J. LUKAS. J. Am. Chem. Soc. **89**, 2227 (1967).
10. K. RANGANAYAKULU and T. S. SORENSEN. Can. J. Chem. **50**, 3534 (1972) and earlier papers.
11. M. SAUNDERS and J. S. STOFKO, JR. J. Am. Chem. Soc. **95**, 252 (1973).
12. D. M. BROUWER and J. A. VAN DOORN. Rec. Trav. Chim. Pays-Bas, **88**, 573 (1969).
13. (*a*) N. OKAZAWA and T. S. SORENSEN. Can. J. Chem. **56**, 2737 (1978); (*b*) F. A. L. ANET and V. J. BASUS. J. Mag. Reson. **32**, 339 (1978).
14. R. P. KIRCHEN and T. S. SORENSEN. J. Am. Chem. Soc. **100**, 1487 (1978).
15. H. C. BROWN and R. S. FLETCHER. J. Am. Chem. Soc. **71**, 1845 (1949).
16. H. C. BROWN, R. S. FLETCHER, and R. B. JOHANESEN. J. Am. Chem. Soc. **73**, 212 (1951).
17. P. V. R. SCHLEYER, K. R. BLANCHARD, and C. D. WOODY. J. Am. Chem. Soc. **85**, 1358 (1963).
18. H. C. BROWN, M. RAVINDRANATHAN, C. G. RAO, F. J. CHLOUPEK, and M-H REI. J. Org. Chem. **43**, 3667 (1978).
19. J. L. FRY, J. M. HARRIS, R. C. BINGHAM, and P. V. R. SCHLEYER. J. Am. Chem. Soc. **92**, 2540 (1970).
20. J. S. LOMAS, P. K. LUONG, and J. E. DUBOIS. J. Am. Chem. Soc. **99**, 5478 (1977).
21. P. VOGEL, M. SAUNDERS, W. THIELECKE, and P. V. R. SCHLEYER. Tetrahedron Lett. 1429 (1971).
22. E. M. ARNETT, N. PIENTA, and C. PETRO. J. Am. Chem. Soc. **102**, 398 (1980).
23. R. P. KIRCHEN, N. OKAZAWA, K. RANGANAYAKULU, A. RAUK, and T. S. SORENSEN. J. Am. Chem. Soc. **103**, 597 (1981).
24. R. P. KIRCHEN, T. S. SORENSEN, and K. WAGSTAFF. J. Am. Chem. Soc. **100**, 5134 (1978).
25. R. HASELTINE, E. HUANG, K. RANGANAYAKULU, T. S. SORENSEN, and N. WONG. Can. J. Chem. **53**, 1876 (1975).
26. J. B. STOTHERS, J. R. SWENSON, and C. T. TAN. Can. J. Chem. **53**, 581 (1975).
27. G. S. SKINNER and F. P. FLORENTINE, JR. J. Am. Chem. Soc. **76**, 3200 (1954).
28. R. BORSDORF and B. OLESCH. J. Prakt. Chem. **36**, 165 (1967).
29. Chem. Abstr. **83**, P136919*c* (1975).
30. W. C. AGOSTA and S. WOLFF. J. Org. Chem. **41**, 2605 (1976).
31. J. L. FRY, E. M. ENGLER, and P. V. R. SCHLEYER. **94**, 4628 (1972).
32. R. PALLAUD and J. PLEAU. C.R. Acad. Sci. Ser. C, **265**, 1479 (1967).
33. S. LANDA, J. VAIS, and J. BURKHARD. Collect. Czech. Chem. Commun. **32**, 570 (1967).
34. Chem. Abstr. **80**, P41042*k* (1974).
35. I. N. NAZAROV and T. D. NAGIBINA. Bull. Acad. Sci. URSS, 83 (1946).
36. J. M. PABIOT and R. PALLAUD. C. R. Acad. Sc., Ser C, **273**, 475 (1971).
37. E. L. ALLRED and T. J. MARICICH. Tetrahedron Lett. 949 (1963).
38. Organic Synthesis, Coll. Vol. V, p. 249.
39. F. T. BOND, H. L. JONES, and L. SCERBO. Org. Photochem. Synth. **1**, 33 (1971).
40. A. D. WOLF and D. G. FARNUM. J. Am. Chem. Soc. **96**, 5175 (1974).
41. H. HOGEVEEN and G. J. GAASBECK. Red. Trav. Shim. Pays-Bas, **88**, 1305 (1969).
42. H. C. BROWN and M. BARKOWSKI. J. Am. Chem. Soc. **74**, 1894 (1952).
43. H. C. BROWN and S. IKEGAMI. J. Am. Chem. Soc. **90**, 7124 (1968).
44. H. C. BROWN and F. J. CHLOUPEK. J. Am. Chem. Soc. **85**, 2322 (1963).
45. J. R. LLOYD. Diss. Abstr. Int. B, **40**, 1720 (1979).
46. B. B. SNIDER, D. J. RODINI, and J. VAN STRATEN. J. Am. Chem. Soc. **102**, 5872 (1980).

Can. J. Chem. Downloaded from www.nrcresearchpress.com by 210.87.254.105 on 09/06/12
For personal use only.

# Carbon-13/carbon-12 isotope effects on nitrogen-15 chemical shielding in some diamagnetic cyano complexes

RODERICK E. WASYLISHEN[1]

*Department of Chemistry, University of Winnipeg, Winnipeg, Man., Canada R3B 2E9*

Received February 22, 1982

RODERICK E. WASYLISHEN. Can. J. Chem. **60**, 2194 (1982).

Carbon-13/carbon-12 isotope-induced $^{15}N$ chemical shifts of 0.06 to 0.10 ppm have been observed for the cyanide ion and several transition metal cyanides. In each case, the $^{15}N$ resonance of the $^{13}C$ labelled isotopomers is to high field of that in the corresponding carbon-12 species. The sensitivity of the $^{15}N$ and $^{13}C$ shielding constants in the cyanide ion to small changes in the CN bond length are evaluated using the theoretical formulation of Jameson: $(\partial\sigma(^{15}N)/\partial r)_e = -872 \pm 160$ ppm/Å and $(\partial\sigma(^{13}C)/\partial r)_e = -473 \pm 90$ ppm/Å. Nitrogen-15 chemical shifts in the metal complexes exhibit basically the same behaviour as do the $^{13}C$ chemical shifts in these same complexes.

RODERICK E. WASYLISHEN. Can. J. Chem. **60**, 2194 (1982).

Dans les cas d'ions cyanures et de plusieurs cyanures de métaux de transition, on a observé des déplacements chimiques de 0,06 à 0,10 ppm pour des $N^{15}$ soumis à des inductions provoquées par des carbone-13/carbone 12. Dans chaque cas, la résonance du $^{15}N$ des composés marqués au $^{13}C$ se situe vers les champs forts par rapport à celle des substances correspondantes contenant du $^{12}C$. On a évalué la sensibilité des constantes de blindage du $^{15}N$ et du $^{13}C$ de l'ion cyanure vis à vis des petites variations dans la longueur de la liaison CN, en utilisant la formulation théorique de Jameson: $(\partial\sigma(^{15}N)/\partial r)_e = -872 \pm 160$ ppm/Å et $(\partial\sigma(^{13}C)/\partial r)_e = -473 \pm 90$ ppm/Å. Les déplacements chimiques du $^{15}N$ des complexes métalliques se comportent sensiblement de la même manière que les déplacements chimiques du $^{13}C$ dans ces mêmes complexes.

[Traduit par le journal]

## Introduction

With the availability of high resolution multinuclear nmr systems, particularly those equipped with superconducting magnets ($B_0$ = 5 to 12 T) there appears to be renewed interest in the effects of isotope substitution on chemical shielding constants (1). A part of this interest stems from the utility of isotope-induced shifts in studying reaction mechanisms, most notably $^{18}O$-induced shifts in $^{31}P$, $^{15}N$, and $^{13}C$ nmr (1*c*, 2–4).

Here we report $^{15}N$ chemical shifts and $^{13}C/^{12}C$ isotope effects on $^{15}N$ chemical shifts in the cyanide ion and several diamagnetic cyano complexes. Previously, $^{13}C/^{12}C$ isotope effects have been observed in $^{1}H$, $^{13}C$, $^{19}F$, $^{59}Co$, $^{113}Cd$, and $^{199}Hg$ nmr (5–10). Observed chemical shifts are generally to high field when $^{12}C$ is replaced by $^{13}C$; however, in dimethylcadmium and dimethylmercury downfield shifts are observed (9, 10). Also, several examples of downfield deuterium-induced $^{13}C$ chemical shifts, once considered rare, have recently been reported (11–13).

The magnitude of isotope effects is observed to depend on a number of factors including the chemical shift range of the nucleus under observation, the fractional change in mass upon isotopic substitution, and the remoteness of the nucleus under observation from the point of substitution (11, 14). These general empirical observations are reasonably well accounted for by an approximate theoretical model developed by Jameson (15). For a diatomic molecule, she has shown that the magnitude of the isotopic shift, $\Delta\sigma$, is determined entirely by anharmonic vibrational averaging.

$$[1]\quad \Delta\sigma = \langle\sigma^i\rangle^T - \langle\sigma\rangle^T \simeq -\frac{(\mu^i - \mu)}{2\mu} f_{anh}(T) \left(\frac{\partial\sigma}{\partial r}\right)_e$$

where

$$f_{anh}(T) = \frac{3h\ (1 + \alpha\omega/6B_e^2)}{16\pi^2 c r_e \mu\omega} \coth\left(\frac{hc\omega}{2kT}\right)$$

The $\mu$'s are the reduced masses of the two isotopomers, $B_e$ is the rotational constant, $\omega$ is the vibrational frequency, $\alpha$ is the rotational–vibrational interaction constant, $(\partial\sigma/\partial r)_e$ is a measure of the dependence of the shielding constant, $\sigma$, on internuclear distance in the neighbourhood of the equilibrium bond length, $r_e$, and the other symbols are standard. Observed $^{13}C/^{12}C$ and $^{15}N/^{14}N$ secondary isotope effects on $^{15}N$ and $^{13}C$ chemical shifts in the cyanide ion are discussed in terms of this theory.

## Experimental

Isotopically enriched $KC^{15}N$ (95% $^{15}N$) and $K^{13}C^{15}N$ (90% $^{13}C$ and 90% $^{15}N$) were obtained from Merck, Sharp, and Dohme and Prochem., respectively. Metal complexes, $M(CN)_4^{2-}$ (M =

[1]As of August 1, 1982: Department of Chemistry, Dalhousie University, Halifax, Nova Scotia, Canada B3H 4J3.

0008-4042/82/172194-04$01.00/0

©1982 National Research Council of Canada/Conseil national de recherches du Canada

Can. J. Chem. Downloaded from www.nrcresearchpress.com by 210.87.254.6 on 09/06/12
For personal use only.

Can. J. Chem. Downloaded from www.nrcresearchpress.com by 210.87.254.6 on 09/06/12
For personal use only.

TABLE 1. $^{15}N$ chemical shifts and $^{13}C/^{12}C$ isotope effects on $^{15}N$ chemical shifts in some diamagnetic cyano complexes

| Species | $\delta(^{15}N)$, ppm[a] | Isotope shift, ppm[b] | $^1J(^{15}N, ^{13}C)$, Hz[c] |
|---|---|---|---|
| $CN^-$ | 274.3 (0.0) | 0.075±0.005 | 6.1±0.1 |
| HCN | 252.4[d] (−21.9) | — | 18.5±0.1[e] |
| $Ni(CN)_4^{2-}$ | 290.2 (15.9) | 0.066±0.010 | 9.8±0.2 |
| $Pd(CN)_4^{2-}$ | 281.1 (6.8) | 0.101±0.025 | 8.3±1.0 |
| $Pt(CN)_4^{2-}$ | 270.8 (−3.5) | 0.077±0.010 | 11.4±0.2 |
| $Zn(CN)_4^{2-}$ | 274.4 (0.1) | 0.069±0.010 | 8.9±0.2 |
| $Cd(CN)_4^{2-}$ | 277.7 (3.4) | 0.081±0.020 | 7.4[5]±0.2 |
| $Hg(CN)_4^{2-}$ | 278.3 (4.0) | 0.067±0.010 | 7.2±0.2 |

[a]All chemical shifts were measured relative to external 0.4 *M* $KC^{15}N$ which is taken to be 106.1 ppm to high field of neat nitromethane (17) or 274.3 ppm to low field of liquid ammonia (18). Values in brackets are relative to $CN^-$, negative values are high field shifts.
[b]Here the isotope shift is defined as $\Delta\sigma = \sigma(^{15}N^{13}C) - \sigma(^{15}N^{12}C)$. Positive values indicate greater shielding in the heavier isotopomer.
[c]The sign of $^1J(^{15}N, ^{13}C)$ is probably negative in all these compounds (19).
[d]Reference 18.
[e]Reference 19.

Ni, Zn, Cd, and Hg) were prepared by treating 0.30 mmol of $M(CN)_2$ with stoichiometric amounts of $KC^{15}N$ (0.30 mmol) and $K^{13}C^{15}N$ (0.30 mmol) (16). $Pd(CN)_4^{2-}$ and $Pt(CN)_4^{2-}$ were prepared by dissolving 0.30 mmol $K_2MCl_4$ in 1.50 mL $D_2O$ and adding stoichiometric quantities of KCN (0.60 mmol), $KC^{15}N$ (0.30 mmol), and $K^{13}C^{15}N$ (0.30 mmol) (16). All $M(CN)_4^{2-}$ solutions were prepared in 1.50 mL $D_2O$, therefore the concentration of all complexes is 0.20 molal.

Nitrogen-15 nmr spectra were obtained at 40.55 MHz using a Bruker WH-400 spectrometer. Computer acquisition times of 8.192 s were used to collect all spectra. The probe temperature was 297 ± 2 K.

## Results and discussion

Nitrogen-15 chemical shifts and $^{13}C/^{12}C$ isotope-induced $^{15}N$ chemical shifts are given in Table 1. The $^{15}N$ nmr spectrum of 0.20 *m* $KC^{15}N$ and 0.20 *m* $K^{13}C^{15}N$ in $D_2O$ is shown in Fig. 1. The $^{15}N$ chemical shift of the $^{13}C^{15}N^-$ ion is approximately 3.04 Hz (0.075 ppm) upfield of that in $^{12}C^{15}N^-$. The low field line of the doublet in $^{13}C^{15}N^-$, for which $^1J(^{15}N, ^{13}C) = 6.08 \pm 0.10$ Hz, is coincident with the singlet observed for $^{12}C^{15}N^-$. The nitrogen-15 spectra of $Zn(CN)_4^{2-}$ and $Pt(CN)_4^{2-}$ are shown in Figs. 2 and 3. The $^{15}N$ nmr spectrum of $Pt(CN)_4^{2-}$ shows additional splittings due to scalar coupling with $^{195}Pt$ ($I = \frac{1}{2}$, natural abundance, 33.8%), giving $^2J(^{195}Pt, ^{15}N) = 61.2 \pm 0.2$ Hz. To our knowledge, this is the first reported $^2J(^{195}Pt, ^{15}N)$ value (20).

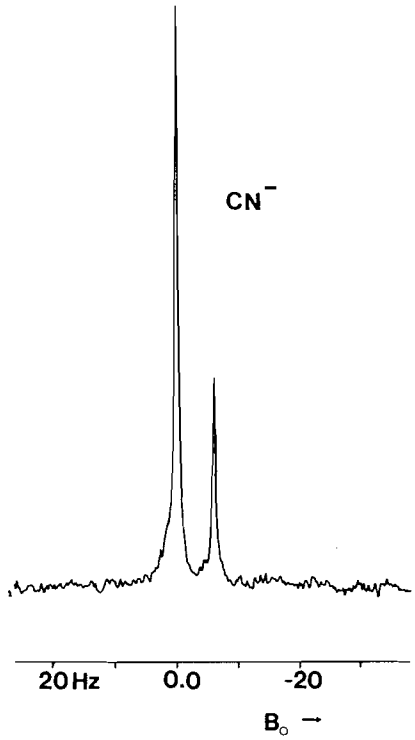


FIG. 1. Nitrogen-15 nmr spectrum of 0.20 *m* $KC^{15}N$ and 0.20 *m* $K^{13}C^{15}N$ in $D_2O$ at 40.55 MHz. All frequencies are relative to the chemical shift of $^{12}C^{15}N^-$.

### *(i) Isotope effects*

The $^{13}C/^{12}C$ isotope effects on $^{15}N$ chemical shifts in the cyanide ion and the complexes studied here range from 0.066 to 0.10 ppm. The magnitudes of the $^{13}C/^{12}C$ isotope effects are intermediate between those observed in $^{13}C$ nmr (0.01–0.03 ppm (6)) and $^{19}F$ nmr (0.067–0.192 ppm (7)). They are more than twice the $^{15}N/^{14}N$ isotope effect on $^{13}C$ chemical shifts (0.02–0.04 ppm) observed in these same complexes (21). $^2H/^1H$ isotope effects on nitrogen shielding in $^{15}NH_2D$ (0.68 ± 0.03 ppm relative to $NH_3$ (22)) are also large compared to the $^2H/^1H$ isotope-induced $^{13}C$ chemical shift in $^{13}CH_3D$ (0.187 ppm relative to $CH_4$ (23)). The greater sensitivity to isotopic substitution of $^{15}N$ compared with $^{13}C$ chemical shifts results mainly from the relative values of the last factor in eq. [1]. For example, in the isoelectronic molecules $N_2$ and

Can. J. Chem. Downloaded from www.nrcresearchpress.com by 210.87.254.6 on 09/06/12
For personal use only.

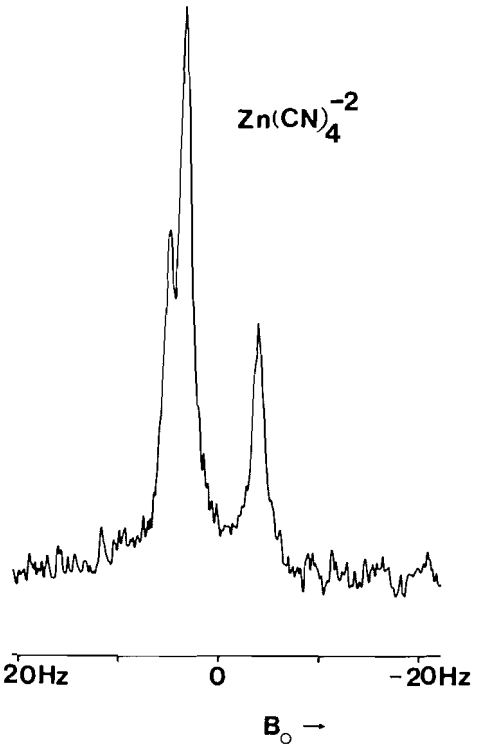


FIG. 2. Nitrogen-15 nmr spectrum of 0.20 *m* $K_2Zn(CN)_4$ in $D_2O$ at 40.55 MHz. The sample contains approximately equal concentrations of $^{15}N$ and $^{13}C^{15}N$ labelled cyanide. All frequencies are relative to the chemical shift of external 0.4 *m* $KC^{15}N$ (aq).

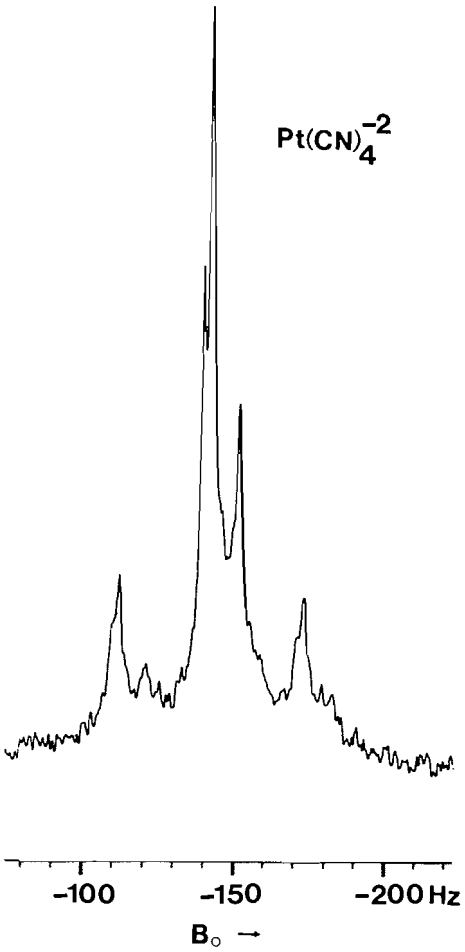


FIG. 3. Nitrogen-15 nmr spectrum of 0.20 *m* $K_2Pt(CN)_4$ in $D_2O$ at 40.55 MHz. The sample contains approximately equal concentrations of $^{15}N$ and $^{13}C^{15}N$ labelled cyanide. All frequencies are relative to the chemical shift of external 0.4 *m* $KC^{15}N$ (aq).

CO, $(\partial\sigma/\partial r)_e$ has been measured to be $-776 \pm 118$ ppm/Å($^{15}N$) and $-226 \pm 44$ ppm/Å($^{13}C$), respectively (24).

Since most of the variables in eq. [1] are available for the cyanide ion, we have calculated $(\partial\sigma(^{15}N)/\partial r)_e$ and $(\partial\sigma(^{13}C)/\partial r)_e$ from the $^{15}N$ (this work) and $^{13}C$ (ref. 21) isotope shifts in the cyanide ion. Taking values of $r_e$, $B_e$, $\omega_e$, and $\alpha_e$ for the cyanide ion from the *ab initio* CI calculations of Ha and Zumofen (25), $(\partial\sigma(^{15}N)/\partial r)_e = -872$ ppm/Å and $(\partial\sigma(^{13}C)/\partial r)_e = -473$ ppm/Å. The error in these derivatives is probably 20% or more.[2] The value of $(\partial\sigma(^{15}N)/\partial r)_e$ calculated here for the cyanide ion is within experimental error of the value recently measured in the isoelectronic molecule $N_2$ (24); however, the values of $(\partial\sigma(^{13}C)/\partial r)_e$ in the cyanide ion and CO differ by a factor of approximately 2. These calculations indicate that the isotope shifts in $CN^-$ (aq) result from mass-substitution effects on the anharmonic vibrational averages over the dependence of the chemical shifts on internuclear separation. The fact that the analogous isotope shifts for the $M(CN)_4^{-2}$ (aq) complexes are within experimental error of the $CN^-$ (aq) values implies that complexation of $CN^-$ does not significantly affect this configurational average.

Both positive and negative $^{15}N/^{14}N$ isotope-induced $^{15}N$ chemical shifts have been reported in $N_2O_3$ and $N_2O_3^{2-}$ respectively (27). These isotope shifts, $-0.24$ to 0.37 ppm, are much larger than those reported here. Also, the $^{18}O/^{16}O$ isotope-induced $^{15}N$ shift for the nitrate ion, 0.138 ppm/$^{18}O$ (3), is somewhat larger than those reported here. Unfortunately, the model of Jameson (1*a*, 15) is difficult to apply to these polyatomic species.

[2]Using spectroscopic data ($r_e$, $B_e$, $\omega_e$, and $\alpha_e$) for the cyanide radical (26) we obtain $(\partial\sigma(^{15}N)/\partial r)_e = -800$ ppm/Å and $(\partial\sigma(^{13}C)/\partial r)_e = -434$ ppm/Å.

*(ii) $^{15}N$ chemical shifts*

Nitrogen-14 chemical shifts for several diamagnetic complexes have been previously reported (27–29), however, very efficient $^{14}N$ quadrupole relaxation in these complexes leads to broad resonances precluding accurate nitrogen chemical shift data.

The cyano complexes studied here show substantial downfield $^{15}N$ chemical shifts relative to those measured in hydrogen cyanide and acetonitrile, $\delta(^{15}N)$ = 244 ppm and 264 ppm (18), respectively. In fact, $\delta(^{15}N)$ for all of the complexes in Table 1 is within 16 ppm of the value observed for the cyano ion in KCN (aq). The $^{13}C$ chemical shifts in the same complexes are all 15 to 42 ppm downfield relative to $\delta(^{13}C)$ in HCN and 13 to 40 ppm upfield of $\delta(^{13}C)$ in $CN^-$ (aqueous) (30, 31).

In the previous $^{13}C$ nmr studies it was noted that, in cyanide metal complexes with partly filled *nd* levels, there is an upfield $^{13}C$ shift as *n* increases, while for complexes in which the *d* shell is filled, small downfield shifts were observed (30, 31). This trend also holds for the $^{15}N$ shifts. On going from $Ni(CN)_4^{2-}$ to $Pd(CN)_4^{2-}$ to $Pt(CN)_4^{2-}$ (all square planar $nd^8$ complexes, $n$ = 3, 4, and 5 respectively) the $^{15}N$ chemical shifts are 290.2, 281.1, and 270.8 ppm. For the tetrahedral cyanides of the zinc family there are small downfield shifts as one proceeds down the group. The origin of these shifts is not clear at this time.

**Acknowledgements**

The nmr spectra reported here were obtained at the Southwestern Ontario NMR Center funded by a Major Installation Grant from the Natural Sciences and Engineering Research Council of Canada. I wish to thank Dr. Robert Lenkinski for making instrument time available for this study, Brian A. Pettitt for his encouragement and comments, and N.S.E.R.C. for financial support.

1. (*a*) C. J. JAMESON. Bull, Magn. Reson. **3**, 3 (1980); (*b*) C. J. JAMESON. Theoretical and physical aspects of nuclear shielding. *In* Specialist Periodical Reports – Nuclear Magnetic Resonance. Vol. 10. *Edited by* G. A. Webb. The Royal Society of Chemistry, London. 1981. p. 1, and earlier reports in this series; (*c*) G. E. HAWKES. Applications of nuclear shielding. *In* Specialist Periodical Reports – Nuclear Magnetic Resonance. Vol. 10. *Edited by* G. A. Webb. The Royal Society of Chemistry, London. 1981. p. 18.
2. (*a*) M. COHN and A. HU. J. Am. Chem. Soc. **102**, 913 (1980); (*b*) D. G. GORENSTEIN and R. ROWELL. J. Am. Chem. Soc. **102**, 6165 (1980); (*c*) M. COHN and B. D. NAGESWARA RAO. Bull. Magn. Reson. **1**, 38 (1979).
3. R. L. VAN ETTEN and J. M. RISLEY. J. Am. Chem. Soc. **103**, 5633 (1981).
4. (*a*) J. M. RISLEY and R. L. VAN ETTEN. J. Am. Chem. Soc. **101**, 252 (1979); (*b*) J. M. RISLEY and R. L. VAN ETTEN. J. Am. Chem. Soc. **102**, 6699 (1980), and references therein; (*c*) J. C. VEDERAS and T. T. NAKASHIMA. J. Chem. Soc. Chem. Commun. 183 (1980); (*d*) R. N. MOORE, J. DIAKUR, T. T. NAKASHIMA, S. L. MCLAREN, and J. C. VEDERAS. J. Chem. Soc. Chem. Commun. 501 (1981); (*e*) D. J. DARENBOURG and B. J. BALDWIN. J. Am. Chem. Soc. **101**, 6447 (1979).
5. E. A. V. EBSWORTH and J. J. TURNER. J. Chem. Soc. Faraday Trans. **60**, 256 (1964).
6. F. J. WEIGERT and J. D. ROBERTS. J. Am. Chem. Soc. **94**, 6021 (1972).
7. (*a*) N. MULLER and D. T. CARR. J. Phys. Chem. **67**, 112 (1963); (*b*) S. G. FRANKISS. J. Phys. Chem. **67**, 752 (1963).
8. (*a*) P. C. LAUTERBUR. J. Chem. Phys. **42**, 799 (1965); (*b*) A. LOEWENSTEIN and M. SHPORER. Mol. Phys. **9**, 293 (1965).
9. J. JOKISAARI, K. RAISANEN, L. LAJUNEN, A. PASSOJA, and P. PYYKKO. J. Magn. Reson. **31**, 121 (1978).
10. J. JOKISAARI and K. RAISANEN. Mol. Phys. **36**, 113 (1978).
11. R. AYDIN and H. GÜNTHER. J. Am. Chem. Soc. **103**, 1301 (1981), and references therein.
12. P. E. HANSEN and J. J. LED. Org. Magn. Reson. **15**, 288 (1981).
13. K. L. SERVIS and F.-F. SHUE. J. Am. Chem. Soc. **102**, 7233 (1980).
14. H. BATIZ-HERNANDEZ and R. A. BERNHEIM. Prog. Nucl. Magn. Reson. Spectrosc. **3**, 63 (1967).
15. C. J. JAMESON. J. Chem. Phys. **66**, 4983 (1977).
16. G. GRAUER (*Editor*). Handbook of preparative inorganic chemistry. Vol. II. 2nd ed. Academic Press, New York. 1965.
17. M. WITANOWSKI, L. STEFANIAK, S. SZYMAŃSKI, and H. JANUSZEWSKI. J. Magn. Reson. **28**, 217 (1977).
18. C. J. JAMESON, A. K. JAMESON, D. OPPUSUNGGU, S. WILLE, P. M. BURRELL, and J. MASON. J. Chem. Phys. **74**, 81 (1981).
19. K. J. FRIESEN and R. E. WASYLISHEN. J. Magn. Reson. **41**, 189 (1980); **48**, 152 (1982).
20. (*a*) G. J. MARTIN, M. L. MARTIN, and J.-P. GOUESNARD. $^{15}N$ NMR spectroscopy. Vol. 18. *Edited by* P. Diehl, E. Fluck, and R. Kosfeld. Springer Verlag, New York. 1981; (*b*) M. WITANOWSKI, L. STEFANIAK, and G. A. WEBB. Nitrogen NMR spectroscopy. Vol. 11B. *Edited by* G. A. Webb. Academic Press, New York. 1981.
21. R. E. WASYLISHEN, D. H. MULDREW, and K. J. FRIESEN. J. Magn. Reson. **41**, 341 (1980).
22. W. M. LITCHMAN, M. ALEI, and A. E. FLORIN. J. Chem. Phys. **50**, 1897 (1969).
23. M. ALEI and W. E. WAGEMAN. J. Chem. Phys. **68**, 783 (1978).
24. C. J. JAMESON, A. K. JAMESON, S. WILLE, and P. M. BURRELL. J. Chem. Phys. **74**, 853 (1981).
25. T.-K. HA and G. ZUMOFEN. Mol. Phys. **40**, 445 (1980).
26. G. HERZBERG. Molecular spectra and molecular structure – spectra of diatomic molecules. Vol. 1. Van Nostrand Reinhold Co., New York. 1950. p. 520.
27. D. HERBISON-EVANS and R. E. RICHARDS. Mol. Phys., **8**, 19 (1964).
28. M. SHPORER, G. RON, A. LOEWENSTEIN, and G. NAVON. Inorg. Chem. **4**, 358 (1965).
29. R. BRAMLEY, B. N. FIGGIS, and R. S. NYHOLM. J. Chem. Soc. A, 861 (1967).
30. M. HIROTA, Y. KOIKE, H. ISHIZUKA, A. YAMASAKI, and S. FUJIWARA. Chem. Lett. 853 (1973).
31. J. J. PESEK and W. R. MASON. Inorg. Chem. **18**, 924 (1979).

Can. J. Chem. Downloaded from www.nrcresearchpress.com by 210.87.254.6 on 09/06/12
For personal use only.

# Detection limitations of photomultiplier tubes in pulsed-laser emission spectroscopy: time-resolved fluorescence spectra of chlorophyll solutions[1]

A. DE WILTON, L. V. HALEY, AND J. A. KONINGSTEIN

*The Ottawa-Carleton Institute for Research and Graduate Studies in Chemistry, Carleton University, Department of Chemistry, Ottawa, Ont., Canada K1S 5B6*

Received January 12, 1982

A. DE WILTON, L. V. HALEY, and J. A. KONINGSTEIN. Can. J. Chem. **60**, 2198 (1982).

An experimental method is described for determination of the onset of saturation effects on the performance of photomultiplier tubes (PMTs) used in time-resolved pulsed-laser spectroscopy. Changes in the dark level response in time (on the 0–100 ns time scale) of the PMT were observed to indicate saturation of the tube. At low repetition rates conditions were found for which an RCA 8850 PMT and an RCA 7102 PMT can be used to obtain reliable fluorescence decays on the 0–100 ns time scale while operating at high anode currents, without modification of interdynode voltages.

Results for time-resolved fluorescence studies of Chl *a* in solution, in benzene and in pyridine, are discussed. The fluorescence decays at ~680 nm indicate that several Chl *a* species are present in each solution. In pyridine, the main fluorescence process at 677 nm, characterised by a lifetime of ~7 ns, is assigned as arising from ligated monomeric species of Chl *a*. A second longer-lived and weaker component ($\tau \simeq 75$ ns) is assigned to the ligated monomeric species of Chl *a'*. A third, and even weaker process characterised by a lifetime $\tau \simeq 145$ ns is also observed. The time-resolved fluorescence spectral band shape of this component has a unique narrow profile, and is assigned to a dimeric or more highly aggregated species of Chl *a*. The time-resolved measurements also indicate that another emission band occurs at 740 nm, and that this process has a lifetime 75 ns $< \tau <$ 145 ns.

A. DE WILTON, L. V. HALEY et J. A. KONINGSTEIN. Can. J. Chem. **60**, 2198 (1982).

On décrit une méthode expérimentale pour déterminer le début des effets de saturation sur la performance des tubes photomultiplicateurs (TPM) utilisés dans la spectroscopie laser à impulsion, à résolution en fonction du temps. On a observé des variations dans la réponse au niveau sombre dans le temps (dans l'échelle de temps allant de 0 à 100 ns) du TMP indiquant ainsi la saturation du tube. A de faibles vitesses de répétition, on a trouvé les conditions dans lesquelles on peut utiliser des tubes photomultiplicateurs RCA8850 et RCA7102 pour obtenir des valeurs sures pour la désintégration de la fluorescence à des échelles de temps allant de 0 à 100 ns lorsqu'on opère avec de forts courants anodiques sans modification des voltages interdynodes.

On discute des résultats obtenus lors d'études de fluorescence, résolue en fonction du temps, du composé Chl *a* en solution dans le benzène et dans la pyridine. Les désintégrations de la fluorescence à 680 nm indiquent que plusieurs espèces de Chl *a* sont présents dans chaque solution. Dans la pyridine, on attribue le mode principal de fluorescence à 677 nm, caractérisé par un temps de vie d'environ 7 ns, à des espèces monomères de Chl *a* reliées entre elles. On attribue une deuxième composante plus faible et d'une durée de vie plus longue ($\tau = 75$ ns) à des espèces monomères de Chl *a'* reliées entre elles. On a également observé un troisième processus qui est encore plus faible et qui est caractérisé par un temps de vie $\tau \simeq 145$ ns. La forme de la bande spectrale de fluorescence, résolue en fonction du temps, de ce composé a un profil étroit caractéristique et on l'attribue à une espèce dimère ou à une espèce plus fortement agrégée de Chl *a*. Les mesures, résolues en fonction du temps, indiquent également qu'une autre bande d'émission apparaît à 740 nm et que ce processus a une durée de vie de 75 ns $< \tau <$ 145 ns.

[Traduit par le journal]

## I. Introduction

The measurement and interpretation of fluorescence decay curves has been simplified by the introduction of pulsed lasers to induce the fluorescence processes. The emitted radiation, after passing through a monochromator, reaches a photomultiplier tube (PMT), and the signal generated by this "square-law" detector is processed by either a boxcar integrator or by a photon-counting system. The former has the advantage that the fluorescence decay can be studied on the 0–100 ns time scale, with a gate width of $\gtrsim$2 ns. On the other hand, while photon-counting systems are more easily adapted to multichannel analysis, with the advantage of improved S/N of the fluorescence decay curve obtained by increasing the sampling time per channel, the gate width is in general >20 ns.

Of relevance to both systems is the ability of the detector (PMT) to process intense light pulses of short duration. There are two important quantities to consider. The first is the time response of the PMT, and the second is the light level which should be chosen so that saturation of the PMT does not occur. In fact, saturation can result in a change of the response time in addition to non-linear response with regard to the signal generated by the radiation incident on the photocathode (1). These effects can lead to erroneous determination of lifetimes from fluorescence and phosphorescence data (2), particularly when a weak emission with a longer lifetime follows a shorter-lived and more intense emission process.

[1]Research supported by the Natural Sciences and Engineering Research Council of Canada.

0008-4042/82/172198-09$01.00/0

©1982 National Research Council of Canada/Conseil national de recherches du Canada

Can. J. Chem. Downloaded from www.nrcresearchpress.com by 210.87.254.6 on 09/06/12
For personal use only.

Can. J. Chem. Downloaded from www.nrcresearchpress.com by 210.87.254.6 on 09/06/12
For personal use only.

Gating the PMT high voltage supply can overcome this difficulty in certain cases (3, 4). For some PMT's the maximum average anode current can be increased by modification of the resistors of the dynode chain (5, 6). When employing a conventional dc PMT power supply with the detection system exposed to high intensity pulsed radiation, it is necessary to carry out a series of calibrations to detect the onset of saturation effects at higher light levels, before analysis of the decay of fluorescence (1).

Because our detection system utilizes a boxcar, we are interested in the ways in which saturation effects influence fluorescence decay curves on the 0–100 ns time scale. In this paper we describe a study of such effects for the fluorescence of Chlorophyll *a* (Chl *a*) in pyridine and benzene solutions, which is characterised by processes with lifetimes of $\gtrsim 10$ ns, induced by laser pulses having a FWHM of $\sim 4$ ns at a repetition rate of 25 Hz.

## II. Experimental

A detailed description of the experimental set up has been given in an earlier publication (7). Of relevance to the present work are the PAR boxcar integrator and the PMT which are the fundamental electronic components in the detection system. The PAR boxcar (main frame Model 162) is equipped with gated integrators (Model 165 and 164) which allow one to achieve 2 ns temporal resolution. In experiments for detection of fluorescence radiation in the red ($\sim 680$ nm) from Chl *a* in benzene and in pyridine, one of each of the following PMT's was used: RCA C31034A, RCA 7102, RCA 8850, and ITT FW130. In the case of weak signals a preamplifier was placed between the PMT and the input of the boxcar. This preamplifier consists of one or two cascading fast-pulsed amplifiers (Le Croy 101a) with gains of $\sim 10$ and $\sim 100$ respectively.

Fluorescence decay curves were recorded by setting the wavelength of the monochromator at the position of maximum intensity of a fluorescence band, and the aperture of the boxcar was scanned over the 0–100 ns scale. Since the boxcar does not integrate at the repetition rate (25 Hz) of the $N_2$-pumped tunable-dye laser, scans were recorded over a period of 15 min. In some cases 2 or 3 scans were averaged. The intensity data were corrected for a background level and the fluorescence decay time was obtained from a semi-log plot of intensity versus time. The background is due to noise from (*i*) the electronics of the boxcar (and preamplifier) and (*ii*) the PMT. In the following we shall refer to this background, when the PMT is not exposed to light, as the dark level.

In order to be able to use the 0–100 ns scale of the boxcar, care was taken to avoid the dead time of the instrument. This was achieved by delaying the PMT signal, so that the peak of the laser pulse appeared at $t \simeq 30$ ns on the 0–100 ns time scale of the boxcar. This time is defined as $t_0$.

The fluorescence in the red of chlorophyll *a* (Chl *a*) in solution was excited by pulsed radiation at 447 nm. Chl *a* was obtained from Sigma Chemical Co. and dried by codistillation with dried benzene. Benzene (Fisher ACS Reagent grade) and pyridine (BDH Aristar) were dried over neutral activated alumina (Woelm Activity 1). All solutions were deoxygenated and sample handling took place in a dry-nitrogen-purged glovebag. The water content of the Chl *a* solutions was estimated from a combination absorption band of $H_2O$ in the near infrared at $\sim 1940$ nm.

## III. Time-dependent photomultiplier response at the onset of saturation

Although the effects of saturation of PMT's due to strong light levels are well known in ordinary spectroscopy (1–3, 8, 9) (non-linear response), there is a lack of information on how saturation influences the time response of these light detectors. In order to study such saturation effects, a series of experiments were carried out as described below.

An uncooled RCA 7102 PMT (with S-1 response) was left for several days in the dark at 1500 V and its dark level in real time was recorded as shown in Fig. 1*C*. This figure shows a pattern of peaks and valleys in the dark level which occur at specific

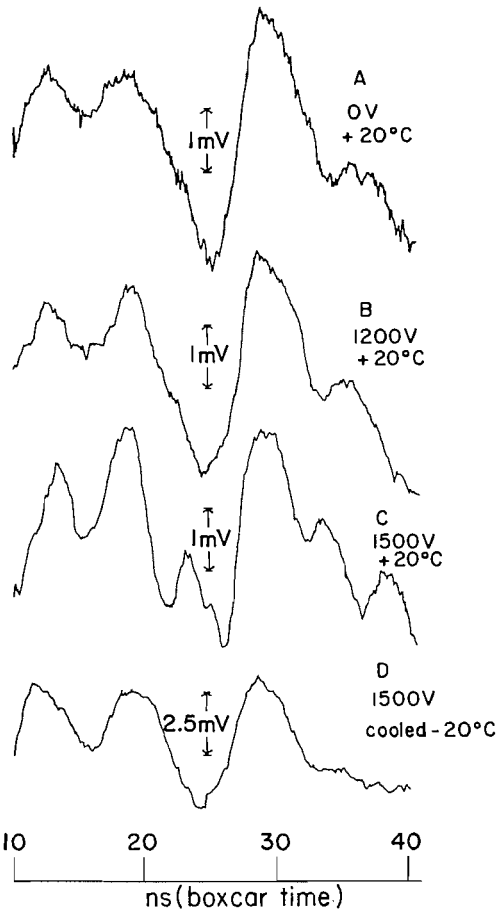


FIG. 1. Part of the dark level of a RCA 7102 PMT recorded on the 0–100 ns scale of the boxcar.

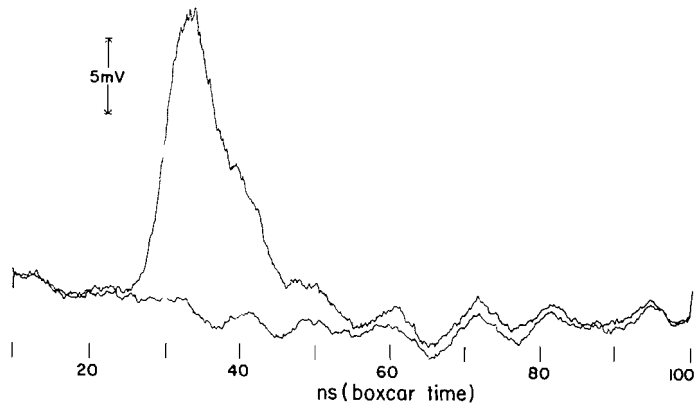


FIG. 2. Dark level and decay of fluorescence signal at 678 nm from $10^{-5}$ *M* Chl *a* in pyridine as recorded using RCA 7102 PMT.

points in time on the 0–100 ns scale of the boxcar. These peaks and valleys are characteristic for the system (PMT + boxcar) because they are reproducible. A change in the high voltage from 1500 V to 1200 V, and finally to 0 V does not result in drastic changes in the dark-level pattern, although one notes that there are more changes between the patterns of Fig. 1*B* and 1*C* than between Fig. 1*B* and 1*A*. The pattern of Fig. 1*D* is that of a cooled (−20°C) 7102 PMT, also at 1500 V. The peaks and valleys occur at approximately the same positions as those of Fig. 1*A*, 1*B*, and 1*C*. The contributions to the dark level from the PMT become clear if one compares Fig. 1*A* with 1*B*, 1*C*, and 1*D*, when one notices the absence in Fig. 1*D* of peaks at $t \approx 14$ ns, $t \approx 23$ ns, and $t \approx 34$ ns. We conclude that the latter are due to the PMT and the rest of the pattern is due to boxcar noise and/or rf pick up. The effect of the rf radiation was minimized by (*i*) shielding of the PMT and input and output joints of the PMT housing and (*ii*) by introducing a common ground for all components of the system. Although only a part of the dark level on the 0–100 ns scale is shown, similar patterns were recorded over the full range examined, from 0 to 1000 ns.

In the next series of experiments we exposed the cooled PMT (at 1500 V) to fluorescence of Chl *a* in pyridine at 678 nm at low light levels. Figure 2 shows traces of dark and signal levels and we find that the fluorescence decay is modulated with the same characteristic pattern as the dark level. Subtraction of the latter from the former results in the decay curve of Fig. 3. Also shown is the position and shape of the laser pulse in real time. This pulse has decayed to zero intensity at $t \approx 40$ ns. The fluorescence decay curve reveals short- and longer-lived fluorescence processes (Fig. 4). The short-lived process was found from Fig. 4 to be characterised by $\tau = 7 \pm 1$ ns, which is typical for Chl *a* in pyridine (10). Immediately after exposure of the PMT to the low-level light signal, the dark level was recorded and found to be identical to that before the tube was exposed to pulsed light. However, if exposed to light levels which were 100 times that of the run shown in Fig. 2, it was found that the modulations in the fluorescence decay curves no longer followed those present in the dark level *before* the PMT was exposed to the pulsed-fluorescence light at 678 nm (Fig. 5). A semilog plot of the fluorescence intensity versus time for the same Chl *a* solution now resulted in a non-linear plot. Such behaviour is to be expected if the PMT is saturated. On continued exposure of the PMT to high light levels, we found that the modulation of the fluorescence decay curves remained while that of the dark level diminished (see Fig. 6). The longer the tube was exposed to high light levels, the flatter the dark-level curve. Figure 6 shows that the oscillations in the signal intensity (versus time) bear no relation to the modulation in the dark level. The proper dark level recorded before the onset of saturation is shown in Fig. 2. It was found that the PMT required at least 24 h in the dark (cooled and at 500 V) to recover from saturation. The modulation in the dark level returned gradually, from the flat baseline (Fig. 6) to the pattern shown in Fig. 2. The recovery time was shorter if the PMT was not fully saturated, i.e., some modulation in the dark level was still visible. The above observations pertain to a RCA 7102 PMT, but we recorded similar behaviour for the following PMT's: RCA C31034A, RCA 8850, and ITT FW130.

The well-known red-sensitive C31034A PMT was found to saturate at lower light levels than the 7102 PMT. In order that the signal be displayed at the 100 mV scale, cascading amplifiers have to be

Can. J. Chem. Downloaded from www.nrcresearchpress.com by 210.87.254.6 on 09/06/12
For personal use only.

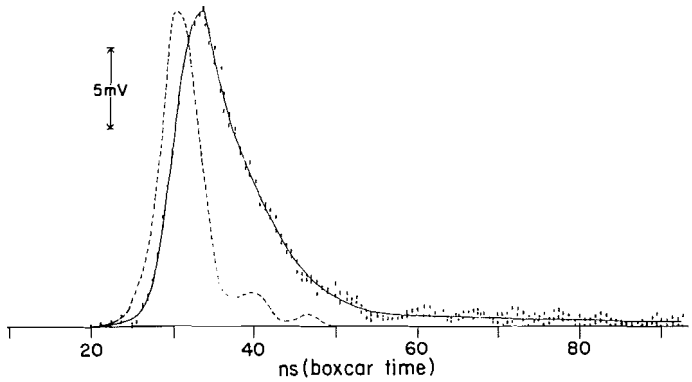


FIG. 3. Fluorescence decay (solid line) at 678 nm for $10^{-5}$ *M* Chl *a* in pyridine, corrected for the dark level (average of 2 runs, RCA 7102 PMT). Position and shape of the laser pulse (dashed line) in time as recorded by the boxcar, corrected for the dark level. The time at which the pulse reaches maximum intensity is defined as $t_0$.

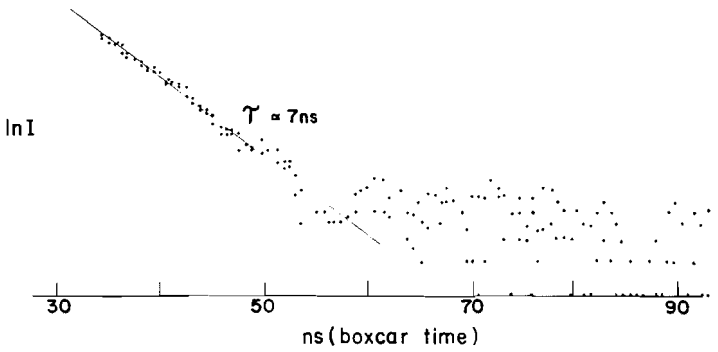


FIG. 4. Semilog plot of fluorescence intensity vs. time for the data shown in Fig. 3.

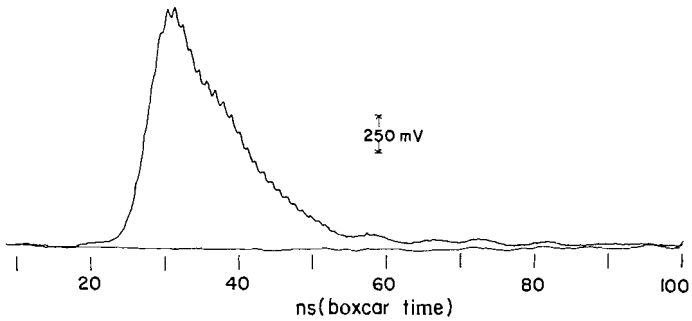


FIG. 5. Dark level and decay of the fluorescence signal at 678 nm for $10^{-5}$ *M* Chl *a* in pyridine recorded with saturated RCA 7102 PMT.

employed with the RCA C31034A, but they broaden the signal and introduce noise. We conclude that the RCA 7102 PMT is the better tube for pulsed-laser spectroscopy in the red spectral regions. This is because signals can be directly recorded on the 100 mV scale of the boxcar whilst its noise characteristics, as recorded with the boxcar (with a 2 ns gate), are in fact very small (see Fig. 1). The 7102 PMT does not require a preamplifier and consequently any broadening of the laser pulse, due to the detection system, is limited to that caused by the response time of the tube and the gate width of the boxcar.

The ITT FW130 should not be used in pulsed work, because its response time is too slow. If exposed to a laser pulse with a FWHM of 3.2 ns, we record an output signal which has a FWHM of 40 ns!

Can. J. Chem. Downloaded from www.nrcresearchpress.com by 210.87.254.6 on 09/06/12
For personal use only.

TABLE 1. Selected parameters of PMT's under pulsed and continuous illumination

| PMT | High voltage supply (V) | Anode pulse rise time (ns) | Anode pulse decay time (experimental) (ns) | Maximum average anode current (continuous illumination) (A) |
|---|---|---|---|---|
| RCA 7102[a] | 1500 | 2.4 | 2.5 | $10 \times 10^{-6}$ |
| RCA C31034A[b] | 2000 | 2.6 | 2.5 | $100 \times 10^{-9}$ |
| RCA 8850[c] | 2500 | 2.5 | 4.5 | $0.2 \times 10^{-3}$ |
| ITT FW130[d] | 1800 | 10 | ~25 | $0.3 \times 10^{-3}$ |

[a]RCA Technical Report 7102 S-65.
[b]RCA Data Sheet C31034A.
[c]RCA Electronic Components Data Sheet 8850.
[d]Electron Tube Division (ITT). Data sheet FW 130.

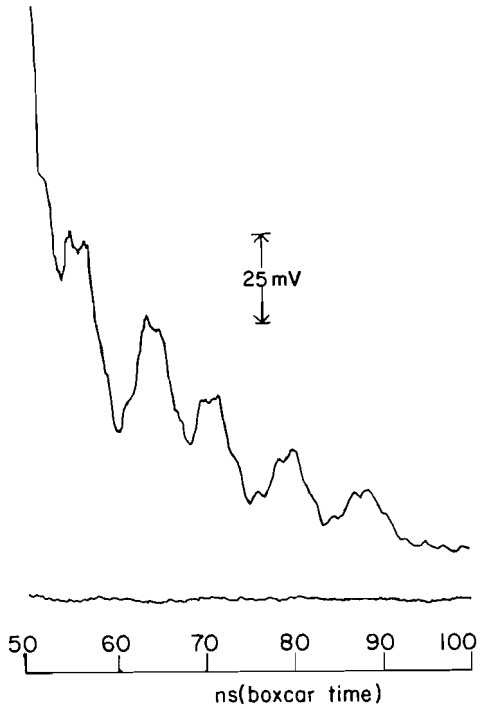


FIG. 6. Part of the dark level and signal level shown in Fig. 5, under higher gain.

The cathode sensitivity of the RCA 8850 PMT is better than that of the 7102 PMT in the blue spectral region. The former has a longer anode pulse decay time (~4 ns), but if it is operated at 2500 V, this PMT does not require a preamplifier to display the signals at the 100 mV scale of the integrator and was found to be very effective for investigation of fluorescence decay curves on the 0–100 ns scale, in the spectral region of 400–550 nm.

Some characteristic parameters of the PMT's used in these investigations are shown in Table 1. Of importance here is the maximum value of the average anode current which is generated by the incident photons. Keeping in mind that the input impedance of the boxcar (and preamplifiers) is 50 Ω, one calculates that for the 7102 PMT, under continuous radiation, the maximum input voltage into the amplifier should be 0.5 mV. In reality, we found that effective saturation in the pulsed mode, without preamplification of the signal, takes place on the 250 mV scale of the Model 165 integrator (PMT cooled and at 1500 V). Thus, it appears that this PMT behaves extremely well in the pulsed mode, without changing the resistors of the dynode chain. However, the laser operates at only 25 Hz. It may be that an increase in the repetition rate could cause saturation at lower input levels.

The low value for the maximum average anode current of 100 nA for the C31034A PMT is responsible for the fact that preamplifiers or an increase in high voltage are required to meet the input requirements of the boxcar. The RCA 8850 PMT would theoretically saturate if the input signal to the boxcar is 10 mV (continuous radiation). If cooled and operated at 2200 V, we find that pulsed signals can be processed safely at the 250 mV scale. This appears to be the same for the ITT FW130 PMT, but, as already indicated, this tube should not be used for time-resolved spectroscopic studies on the 0–100 ns time scale.

To conclude this section, we note that in pulsed spectroscopy with low repetition rates, certain PMT's commonly used in fluorescence and Raman spectroscopy seem to perform rather well in processing strong light signals without modification to their interdynode voltages. In addition, we emphasize the usefulness of recording the dark level in time both before and after running a fluorescence decay or time-resolved spectrum.

## IV. Decay of fluorescence and time-resolved emission spectrum of chlorophyll *a* in solution

Having found the experimental conditions for time-resolved studies with our pulsed-laser system, we discuss in this section some relevant experimental data for Chl *a* in solution and offer possible explanations in terms of simple models.

Can. J. Chem. Downloaded from www.nrcresearchpress.com by 210.87.254.6 on 09/06/12
For personal use only.

Can. J. Chem. Downloaded from www.nrcresearchpress.com by 210.87.254.6 on 09/06/12
For personal use only.

Due to the complexity of the chemical equilibria, particularly those involving water, the interpretation of time-resolved fluorescence spectra and fluorescence decay curves of Chl *a* in solution is not a straightforward matter.

*Chl* a *in pyridine solution*

In an earlier publication, we reported on the observation of fluorescence at 680 nm of Chl *a* in pyridine (11). The solutions used in the experiments were not free of water; in fact, the number of $H_2O$ molecules exceeded the number of chlorophyll molecules by more than two orders of magnitude. Because chlorophyll *a* in wet pyridine may form penta- and hexa-coordinated complexes with pyridine and water (12, 13), only a small amount (if any) of free monomer chlorophyll *a* molecules may be found in these solutions. Also of importance to this work is the knowledge that an equilibrium exists between Chl *a* and Chl *a'*. Chl *a'* is the C10 epimer of Chl *a*. This alteration results in a strain in the ring, thus the *a'* isomer is less stable and is the minority species in the equilibrium between Chl *a* – Chl *a'* in solution. In pyridine solutions a substantial amount (~20%) of Chl *a'* may be present (14). However, the ratio of concentrations of the penta- to the hexa-coordinated complexes for the two isomers does not necessarily have to be the same, because of steric effects.

We assume that due to the great abundance of pyridine, chlorophyll is present predominantly as the hexacoordinated species (12) Chl *a*.$pyr_2$, with only a small amount of Chl *a*.$pyr_1$ and that transitions from these species dominate the fluorescence spectrum, as discussed below. The ligand-free Chl *a* has both axial positions above and below the plane of the molecule unoccupied. Chl *a*.$pyr_1$ has one pyridine ligand which is bonded through the pyridine nitrogen atom. In Chl *a*.$pyr_2$, the remaining axial position is occupied, thus completing the maximum coordination of six for the central magnesium atom. The interpretation of the spectral information can furthermore be influenced by the presence of emission from chlorophyll dimers or aggregates. Such aggregates can be subdivided into those which do or do not contain $H_2O$ molecules. It is well known that the predicted fluorescence intensity from a theoretical symmetrical dimer is approximately identical to that of the monomer (16, 17, 21, 22), although dynamical processes in the real aggregates may quench this fluorescence.

Analysis of the fluorescence decay curve of a $10^{-5}$ *M* solution of Chl *a* in wet pyridine (~1200 ppm $H_2O$) resulted in the following observations. The main fluorescence at 677 nm is due to a process with a lifetime $\tau = 7 \pm 1$ ns which we assign to the combined fluorescence from the monomer species Chl *a*.$pyr_1$ and Chl *a*.$pyr_2$. We reported previously the presence of a fluorescence process characterised by $\tau = 45 \pm 5$ ns (Fig. 7 of ref. 11). A more careful analysis of the decay, taking into account the contribution to the intensity from a longer-lived species, yields a corrected value of $75 \pm 10$ ns. This is assigned to a combined fluorescence from Chl *a'*.$pyr_1$ and Chl *a'*.$pyr_2$ because (*i*) we anticipate a considerable amount of Chl *a'* to be present and (*ii*) this fluorescence, like that characterised by $\tau = 7 \pm 1$ ns, is observed even under very high intensity laser radiation where the dimeric species are expected to dissociate. Lastly, a process having $\tau = 145 \pm 10$ ns was observed, and this fluorescence was found to disappear if the sample was exposed to high light levels (11). Time-resolved spectra are depicted in Fig. 7. The gradual disappearance of fluorescence due to Chl *a*.$(pyr)_{1,2}$ and the appearance of that due to Chl *a'*.$(pyr)_{1,2}$ is observable if one compares the spectra which are recorded at $t = 3$ ns (the peak of the fluorescence signal) at $t \simeq 200$ ns and at $t \simeq 300$ ns, all times being measured from $t_0$, the peak of the laser excitation pulse. The existence of fluorescence from a process characterised by $\tau = 145 \pm 10$ ns becomes clear if one compares these spectra with those recorded at times $t = 325$ ns and $t = 360$ ns. Finally, the fluorescence spectrum observed at $t = 360$ ns is free from interference from the other spectra. We note that the band has a unique profile. Since this fluorescence can be made to disappear if too much laser radiation enters the solution, one may conclude that the chemical species from which the fluorescence originates is more easily destroyed than the monomeric species. We assign the long-lived fluorescence as originating from chemical species composed of two or more chlorophyll molecules. Such an assignment is supported by the line shape as recorded, because presently available theoretical information (17) predicts that the stronger the interaction between the component molecules of a dimer (or aggregate), the narrower the line width of the fluorescence band in comparison to that of the monomer.

Time-resolved spectra in the time range from 300–500 ns reveal that the intensity of the vibronic side band at 740 nm shows a peculiar behaviour in time when compared to the intensity in the wing of the main band at 665 nm. In this time region, contributions to the intensity from the processes characterised by lifetimes $\tau \simeq 7$ ns have vanishing

Can. J. Chem. Downloaded from www.nrcresearchpress.com by 210.87.254.6 on 09/06/12
For personal use only.

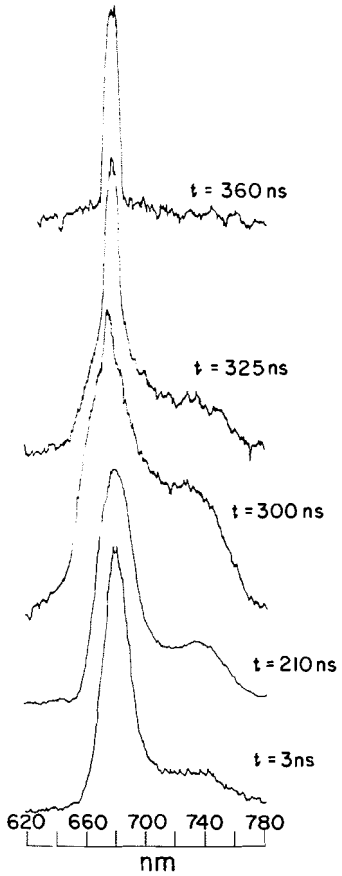


FIG. 7. Time-resolved fluorescence spectra of $10^{-5}$ *M* Chl *a* in wet pyridine. Relative intensities are not to scale, the spectrum recorded at $t = 360$ ns is ~100 times weaker than the spectrum recorded at $t = 3$ ns.

intensity, while the shape of the emission band having a lifetime $\tau \simeq 145$ ns is such that the intensities at 740 nm and at 665 nm are zero.

The fluorescence decay measurements indicate that at 665 nm, in the wing of the main band, the intensity is due to the two processes governed by lifetimes of $\tau \simeq 7$ ns and $\tau \simeq 75$ ns, also present in the intensity at the peak of the main band. The intensity at 740 nm is also related to those two processes, but in addition, examination of the time-resolved spectra shows that a third process, characterised by a lifetime 75 ns $< \tau <$ 145 ns, contributes to the intensity. This component was also found in solutions having a higher concentration of chlorophyll than the original solution, and apparently higher concentrations of the aggregates, because they did not appear to photodissociate at high laser powers. Although the presence of this fluorescence process is even more evident in the more concentrated solutions we failed to obtain a more accurate value for the lifetime. This is because there are three competing processes in the fluorescence decay. This component of the fluorescence at 740 nm is assigned to a dimer or higher aggregate for the following reasons. The species could not be destroyed by photodissociation in the more concentrated solution. Previous experiments on chlorophyll aggregates in solid solutions revealed the appearance of a red-shifted fluorescence band (15), and because this band was assigned to the aggregate, we believe that the same assignment belongs to the process at 740 nm characterised by a lifetime 75 ns $< \tau <$ 145 ns. Furthermore, the position of the two excited states of the aggregate and their lifetimes, as determined by the present study, are in agreement with the predictions made by Fong for an asymmetric dimer (16).

*Chl* a *in benzene solution*

We have also investigated the time-resolved fluorescence spectrum and fluorescence decay of chlorophyll *a* in benzene. The decay curve for the peak of the fluorescence at 14880 $cm^{-1}$ (672 nm) for a $10^{-5}$ *M* solution containing ~100 ppm $H_2O$ is shown in Fig. 8. Again, we found an indication of fluorescence processes which are characterised by short (6–8 ns) and longer (> 30 ns) lifetimes. Because of weak signals, it was not possible to probe the time-resolved spectrum at times greater than $t \simeq 100$ ns. In benzene solutions containing higher concentrations of water (~1200 ppm and ~2000 ppm $H_2O$), a red shift of 20 $cm^{-1}$ was observed in the peak of the fluorescence relative to that in the drier (100 ppm $H_2O$) solution (Fig. 9).

Time-resolved fluorescence spectra recorded for the benzene solution containing ~100 ppm $H_2O$ are displayed in Fig. 10. While the peak of the fluorescence at $t = 5$ ns (the time at which the maximum fluorescence intensity is observed) centres around 14880 ± 10 $cm^{-1}$, the position of the peaks in the fluorescence spectra at $t = 0$ ns and $-2$ ns is at 14860 ± 10 $cm^{-1}$. Time-resolved measurements on the wetter solution (~1200 ppm $H_2O$) yielded only one fluorescence band at 14860 ± 10 $cm^{-1}$, the position of which is equal to the position of the fluorescence at $t = 0$ ns for the drier solution.

It is well known that there exists a time delay between the time at which a laser pulse reaches its maximum intensity and the time at which the fluorescence intensity induced by the laser pulse has maximum intensity, which is related to such properties as the lifetime $\tau$ of the excited state from which the fluorescence transition originates and the

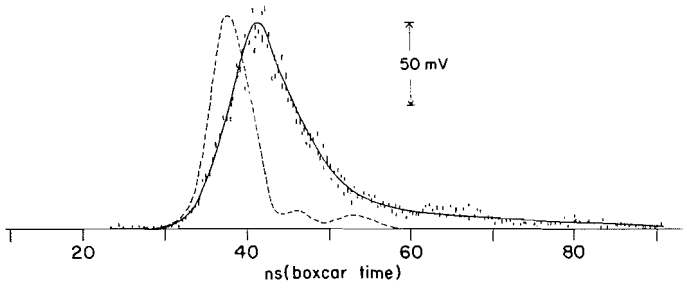


FIG. 8. Fluorescence decay (solid line) at 672 nm for $10^{-5}$ *M* Chl *a* in benzene (containing ~ 100 ppm $H_2O$) corrected for the dark level (with × 10 preamplification). Position and shape (dashed line) of the laser pulse in time as recorded with boxcar and × 10 preamplification (corrected for dark level).

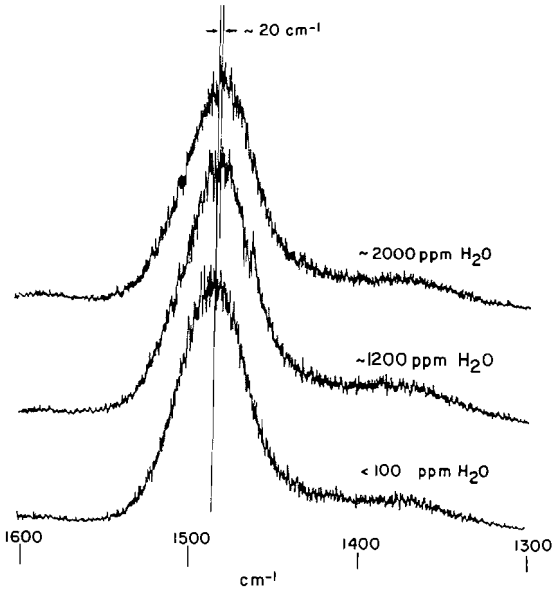


FIG. 9. Fluorescence spectra at 672 nm of $10^{-5}$ Chl *a* in benzene solutions containing different water concentrations, recorded at $t$ = 5 ns, the time at which maximum fluorescence intensity is observed. Wavenumber scale should be multiplied by a factor of 10.

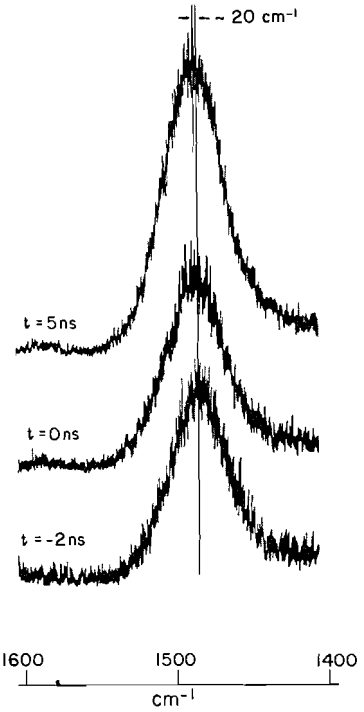


FIG. 10. Time-resolved fluorescence spectra of $10^{-5}$ *M* Chl *a* in benzene containing ~ 100 ppm $H_2O$. Wavenumber scale should be multiplied by a factor of 10.

cross section of the absorption transition from ground to excited state (18, 19). Thus, for equal absorption cross sections, one finds that the build up of fluorescence of a short-lived excited state occurs more rapidly than that of a longer-lived fluorescence process. We took advantage of this knowledge to explain the data displayed in Fig. 10. Apparently, they suggest that apart from a fluorescence transition which originates in an excited state having $\tau$ = 6–8 ns there also exists another excited state which must have a lifetime $\tau < 7 \pm 1$ ns. We conclude that this short-lived species ($\tau < 7$ ns), which is present in the drier solution, is the major component in the wetter solutions, because the position of the fluorescence transitions from these species are both at 14860 ± 10 $cm^{-1}$. It is known that dimers exist in solutions of Chl *a* in dry benzene. However, in our driest solution (100 ppm $H_2O$), the number of water molecules is two orders of magnitude larger than the number of Chl *a* molecules. Consequently, it is believed that the spectral features shown in Figs. 9 and 10 are due to hydrated monomeric species.

We complete this section with a remark on the overall fluorescence intensity of these solutions. The smaller the concentration of $H_2O$, the weaker this overall intensity. This observation suggests that for drier solutions even weaker fluorescence

Can. J. Chem. Downloaded from www.nrcresearchpress.com by 210.87.254.6 on 09/06/12
For personal use only.

signals can be expected (20). Because the concentration of dimers is higher in such solutions, it could well be that the fluorescence of dimers (which do *not* contain water) is weak indeed.

## V. Concluding remarks

In this work an experimental method is described which allows one to determine the onset of saturation effects on the performance of PMT's in time-resolved pulsed laser spectroscopy. At low repetition rates, conditions were found under which certain PMT's can be used to obtain reliable fluorescence decay measurements on the 0–100 ns time scale, without modification of the PMT for use in the pulsed mode.

From the fluorescence decays of Chl *a* in pyridine and in benzene solutions, and time-resolved spectroscopic measurements of this fluorescence, it is concluded that several chemical species are present. Long-lived fluorescence processes at 677 nm and 740 nm from these species in pyridine are assigned to chlorophyll dimers or higher aggregates. The position of one of the fluorescence bands of the aggregate is within experimental error equal to that of the monomeric species and the position of the other is red shifted by 1250 $cm^{-1}$. The intensities of the aggregate bands are approximately two orders of magnitude weaker than that of the monomeric species. It is reasonable to assume that only small amounts of dimers and higher aggregates are present in the $\sim 10^{-5}$ *M* solution of Chl *a* in pyridine. This would lead to the conclusion that the intrinsic fluorescence intensity of the aggregated and monomeric species are not all that different. Simple exciton theory predicts that for a symmetric dimeric chlorophyll species, one fluorescence transition should have non-vanishing intensity and the position of the transition could indeed be close to that of the ligated monomer (donor and acceptor) species (12). On the other hand, if the dimer is asymmetric we expect non-vanishing intensity for both components in the fluorescence spectrum. It appears that the time-resolved studies presented in this work contribute to the knowledge of chlorophyll dimers or higher aggregates in solution. It is equally clear that the present work indicates that any detailed understanding of the time-resolved fluorescence from chlorophyll in solution requires further studies.


1. D. H. Hartman. Rev. Sci. Instrum. **49**, 1130 (1978).
2. P. F. Jones and A. R. Calloway. Rev. Sci. Instrum. **44**, 1393 (1973).
3. G. G. Albach and J. Meyer. Rev. Sci. Instrum. **44**, 615 (1973).
4. T. Araki, T. Uchida, and S. Minami. Jpn. J. Appl. Phys. **15**, 2421 (1976).
5. J. M. Harris, F. E. Lytle, and T. C. McCain. Anal. Chem. **48**, 2095 (1976).
6. G. Beck. Rev. Sci. Instrum. **47**, 537 (1976).
7. D. Nicollin, P. Bertels, and J. A. Koningstein. Can. J. Chem. **58**, 1334 (1980).
8. J. P. Keene. Rev. Sci. Instrum. **34**, 1220 (1963).
9. A. Fenster, J. C. LeBlanc, W. B. Taylor, and H. E. Johns. Rev. Sci. Instrum. **44**, 689 (1973).
10. M. J. Yuen, L. L. Shipman, J. J. Katz, and J. C. Hindman. Photochem. Photobiol. **32**, 281 (1980).
11. M. Asano and J. A. Koningstein. Chem. Phys. **57**, 1 (1981).
12. L. L. Shipman, T. M. Cotton, J. R. Norris, and J. J. Katz. J. Am. Chem. Soc. **98**, 8222 (1976).
13. K. Ballschmiter and J. J. Katz. J. Am. Chem. Soc. **91**, 2661 (1969).
14. P. H. Hynninen, M. R. Wasielewski, and J. J. Katz. Acta Chim. Scand. **B33**, 637 (1979).
15. F. K. Fong and V. J. Koester. Biochim. Biophys. Acta, **423**, 52 (1976).
16. F. K. Fong. Appl. Phys. **6**, 151 (1975).
17. M. Kasha. Radiation Res. **20**, 55 (1963).
18. J. M. Friedman and R. M. Hochstrasser. Chem. Phys. **6**, 155 (1974).
19. J. O. Berg, C. A. Langhoff, and G. W. Robinson. Chem. Phys. Lett. **29**, 305 (1974).
20. R. Livingston, W. F. Watson, J. McArdle. J. Am. Chem. Soc. **71**, 1542 (1949).
21. L. L. Shipman, J. R. Norris, and J. J. Katz. J. Phys. Chem. **80**(8), 877 (1976).
22. K. F. Freed. J. Am. Chem. Soc. **102**(9), 3130 (1980).


Can. J. Chem. Downloaded from www.nrcresearchpress.com by 210.87.254.6 on 09/06/12
For personal use only.

# Time-resolved pulsed-laser Raman studies at the nanosecond level of an aqueous solution of $UO_2(NO_3)_2$[1]

M. ASANO AND J. A. KONINGSTEIN

*The Ottawa-Carleton Institute for Research and Graduate Studies in Chemistry, Carleton University, Ottawa, Ont., Canada K1S 5B6*

Received January 13, 1982

M. ASANO and J. A. KONINGSTEIN. Can. J. Chem. **60**, 2207 (1982).

The pulsed-laser Raman spectrum of aqueous solution of $UO_2(NO_3)_2 \cdot 6H_2O$ is reported. Raman shifts were observed which could be assigned to the $\nu_1$ mode of the $UO_2$ unit in species $(UO_2)_3(OH)_5^+$, $(UO_2)_2(OH)_2^{2+}$, and $UO_2^{2+}$. Vibrational ground and excited level transitions were induced, where part of the laser radiation at 22350 $cm^{-1}$ was used as an optical pump while the remaining part served as Raman probe. The lifetimes of the excited states were 7 μs and 1.5 μs for the trinuclear and dinuclear species, respectively. An analysis of the population characteristics of the ground and electronic excited states of the trinuclear species was performed and compared with the time evolution of the scattered light due to vibrational Raman processes in the ground and electronic excited states

M. ASANO et J. A. KONINGSTEIN. Can. J. Chem. **60**, 2207 (1982).

On rapporte le spectre Raman par laser à impulsion d'une solution aqueuse de $UO_2(NO_3)_2 \cdot 6H_2O$. On a observé des déplacements Raman qui peuvent être attribuées au mode $\nu_1$ de la portion $UO_2$ des espèces $(UO_2)_3(OH)_5^+$, $(UO_2)_2(OH)_2^{2+}$ et $UO_2^{2+}$. On a déduit les niveaux vibrationnels de transition de l'état fondamental et de l'état excité lorsqu'on utilise une partie de la radiation du laser à 22350 $cm^{-1}$ comme une pompe optique tandis que la partie restante sert de sonde Raman. Les temps de vie des états excités sont respectivement de 7 μs et de 1,5 μs pour les espèces trinucléaires et dinucléaires. On a réalisé une analyse des caractéristiques de la population des états électroniques fondamental et excité des espèces trinucléaires et on les a comparé au temps d'émission de la lumière diffuse due aux processus vibrationnels Raman dans les états électroniques fondamental et excité.

[Traduit par le journal]

## I. Introduction

With the availability of pulsed tunable lasers it has become possible to induce Raman transitions from excited states of ions in solids or molecules in solution. These excited states were prepared by absorption of laser radiation at specific wavelength and the light scattering spectra were induced by that part of the laser radiation which is not used in the optical pumping process. Experiments have also been carried out with two lasers and in that case the optical pump and Raman probe (*i*) can be delayed in time, and (*ii*) their wavelengths do not have to be the same.

In this paper emphasis is placed on part of the excited level vibrational Raman spectrum of the trinuclear species $(UO_2)_3(OH)_5^+$ in aqueous solution. Time-resolved measurements of the Raman intensities for this species — using one laser — were performed which are related to the time evolution of the ground and excited state populations, and the results were compared with theoretical calculations. The species mentioned above occurs in aqueous solutions of the uranyl salt $UO_2(NO_3)_2$ with a specific pH. In order to carry out the time-resolved measurements, light scattering spectra of the solutions having different pH values were investigated and Raman bands of the spectra were assigned. These assignments were based on the knowledge of the emission and absorption spectra, not only of the trinuclear species but also of the mononuclear $UO_2^{2+}$ and dinuclear $(UO_2)_2(OH)_2^{2+}$ species. The absorption and emission spectra are discussed in section III and the time-resolved aspects of the light scattering spectra in sections IV and V.

## II. Experimental methods

All solutions used in the present spectroscopic investigations were prepared from a reagent grade $UO_2(NO_3)_2.6H_2O$ (99.8% pure). In a 0.02 *M* solution of the salt, hydrolysis of the uranyl ion occurs and, by adjusting the pH, the species $UO_2^{2+}$, $(UO_2)_2(OH)_2^{2+}$, and $(UO_2)_3(OH)_5^+$ are formed in different concentrations (5, 6). Using values of equilibrium constants pertaining to the chemical equilibrium of some of these species their concentrations may be calculated (5) — see Table 1. The species $UO_2NO_3^+$ too can be present in these 0.02 *M* solutions, but its concentration is negligibly small (7, 8).

Absorption, fluorescence, and Raman spectra were obtained. A pulsed-Raman apparatus was used to record the emission spectra, which were induced by radiation of a $N_2$ laser-pumped tunable-dye laser (pulsed). The duration of the pulse was 3.2 ns (FWHM) with its peak power ~100 kW. The emitted light was dispersed by a Jobin Yvon monochromator and detected by a RCA 8850 photomultiplier. The signals generated by this PMT were fed into a PAR model 162 boxcar equipped with a model 165 gated integrator. The light scattering apparatus (9) allowed us to carry out lifetime measurements of weak fluorescence while time-resolved Raman and fluorescence spectra could be recorded by adjusting the 2 ns gate of the boxcar at different

[1]Research supported by the Natural Sciences and Engineering Research Council of Canada.

0008-4042/82/172207-09$01.00/0

©1982 National Research Council of Canada/Conseil national de recherches du Canada

Can. J. Chem. Downloaded from www.nrcresearchpress.com by 210.87.254.5 on 09/06/12
For personal use only.

TABLE 1. Hydrolysis products and their concentration at different pH values for a 0.020 *M* aqueous $UO_2(NO_3)_2$ solution

| pH | $UO_2^{2+}$ | $(UO_2)_2(OH)_2^{2+}$ | $(UO_2)_3(OH)_5^{+}$ |
|---|---|---|---|
| 0.9 | 0.020 (100) | 0 (0) | 0 (0) |
| 3.6 | $1.25 \times 10^{-2}$ (63) | $3.5 \times 10^{-3}$ (35) | $1.3 \times 10^{-4}$ (2) |
| 4.2 | $3.6 \times 10^{-3}$ (16) | $4.6 \times 10^{-3}$ (43) | $2.9 \times 10^{-3}$ (41) |
| 4.5 | $1.4 \times 10^{-3}$ (6) | $3.0 \times 10^{-3}$ (25) | $4.6 \times 10^{-3}$ (69) |

points in time. Except otherwise stated, the recorded Raman spectra were obtained with the gate fixed at a point in time at which the intensity of the laser pulse had reached a maximum value. Measurements were performed making sure that the PMT was operating in its linear regime and photochemical decomposition of the uranyl species was prevented by moving the 50 × 10 × 10 mm quartz cell — which contained the solutions — up and down with respect to the laser beam. The frequency of the lateral displacement was 1/5 Hz and solutions could be studied for 2 h before the effect of photodecomposition became noticeable.

The excitation spectra of the green phosphorescence of some solutions were recorded with a Perkin-Elmer Fluorescence Spectrophotometer 204-S and absorption spectra were recorded with a Carry model 14 spectrometer.

## III. Results

### *A. Absorption and emission spectra of uranyl nitrate solutions*

It shall be shown in section III*B* that the pulsed-laser Raman spectra of some of the solutions of the uranyl nitrate salt exhibit, besides Raman transitions of the electronic ground state, transitions between vibrational levels of an electronic excited state. In order to assign the spectra it is necessary to consider part of the electronic energy level diagrams of the $UO_2$ unit which is present in some of the species mentioned in section II (Table 1). Some information regarding the energy level diagram can be obtained if one considers the absorption and fluorescence spectra of the aqueous solutions with a pH = 0.9, 4.2, and 4.5. Spectra are shown in Figs. 1 and 2 and a short discussion is given below regarding some relevant features.

The absorption spectrum of the solution with pH = 0.9 is very similar to that of an aqueous solution of the uranyl perchlorate salt (10), which is known to contain a high concentration of the mononuclear uranyl ion $UO_2^{2+}$. The spectrum shown in Fig. 1 of the solution with pH = 0.9 is also assigned to spectroscopic transitions of the $UO_2^{2+}$ ion. An analysis of the vibronic progression present in the absorption and fluorescence spectrum reveals that the frequency of a vibrational mode of $UO_2^{2+}$ in an electronic excited state has a value of 720 $cm^{-1}$ while the frequency of this mode of the electronic ground state is 875 $cm^{-1}$. The mode is assigned to the symmetric stretching vibration ($\nu_1$) and the 0–0 transition between the electronic surfaces occurs at 20550 $cm^{-1}$. The electronic transition is between the $S_0$ ground state and the $T_0$ excited state and the latter is split into spin–orbit components for the $UO_2^{2+}$ ion in the solid state (11, 12).

The solutions with pH = 4.5 and 4.2 contain more than one species and, according to Table 1, the trinuclear species $(UO_2)_3(OH)_5^{+}$ has the highest concentration at pH 4.5. We note that the extinction coefficients of the absorption bands of this solution (Fig. 2) are stronger than those of the solution (pH = 0.9) which contains only the mononuclear species. The vibrational progression in the spectra of the pH = 4.5 solution is less distinct than that shown in Fig. 1 of $UO_2^{2+}$ and is even less distinct for the pH 4.2 solutions (absorption spectrum, not shown here). We assign features of absorption and fluorescence spectra of the pH = 4.5 solution to transitions between electronic states of the $UO_2$ unit present in the trinuclear species. The frequency $\nu_1^{T_0} = 710\ cm^{-1}$ for a mode in the excited state is obtained from the vibrational progression visible in the absorption spectrum and the frequency $\nu_1^{S_0} = 840\ cm^{-1}$ for this mode in the ground state is obtained from the emission spectrum. The mode is assigned to the symmetric stretching vibration of the $UO_2$ unit and the 0–0 transition between the electronic surface $S_0$ and $T_0$ is at 19600 $cm^{-1}$. The structure of this trinuclear species has been discussed in the literature (7, 8). Three $UO_2$ units and three hydroxy ions are arranged in a ring with the $UO_2$ bridged to two hydroxy ions and vice versa. The other two $OH^-$ ions are situated above and below this ring and they are bound to the three uranium atoms. From Table 2 one can see that small differences exist between the frequencies $\nu_1^{T_0}$ and $\nu_1^{S_0}$ for the $UO_2$ unit in the trinuclear species and those of the mononuclear $UO_2^{2+}$ ion. In addition it can be said that for both the mono- and trinuclear species Raman scattering of the $\nu_2$ or $\nu_3$ mode was not observed. As a result we assume that the $UO_2$ unit is also linear in the trinuclear species. The chemical bond between $OH^-$ and the $UO_2$ in the latter has a marked effect on the strength of the absorption bands as was mentioned above.

The energy level diagrams shown in Fig. 3 are for the trinuclear species and the assignment of the electronic states is based on that of the $UO_2^{2+}$ ion, although of course the energy and labelling of each state in terms of the $UO_2^{2+}$ molecular orbital diagram is not valid.

In previous publications from this laboratory we emphasised the importance of the measurement of the transmission value of a sample (at a given wavelength) as a function of the intensity of the laser beam in relation to carrying out excited level

Can. J. Chem. Downloaded from www.nrcresearchpress.com by 210.87.254.5 on 09/06/12
For personal use only.

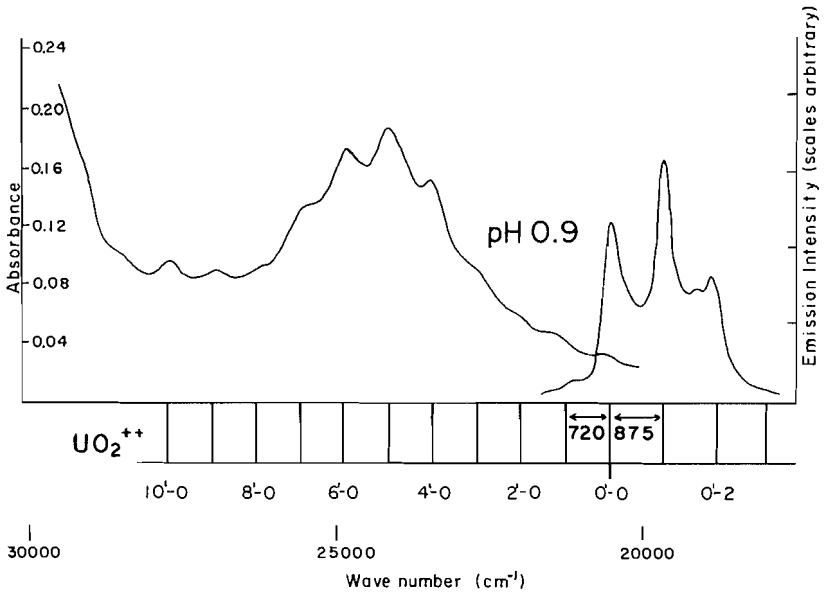


FIG. 1. The absorption (left) and pulsed laser induced emission spectrum (right) of a 0.02 $M$ aqueous solution of $UO_2(NO_3)_2$ at 300 K. The value of pH = 0.9 suggests that the species $UO_2^{2+}$ dominates over that of others containing the $UO_2$ unit — see also Table 1. Band spacings due to a vibrational mode in the $T_0$ excited state and those due to the mode in the $S_0$ ground state are indicated in the bottom part.

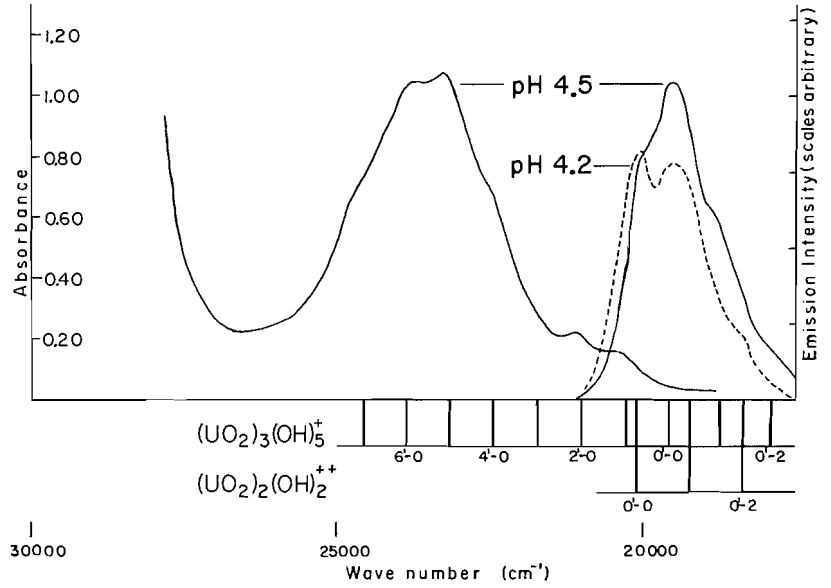


FIG. 2. The absorption (left) and pulsed laser induced emission spectra (right) of the pH = 4.5 (solid line) and pH = 4.2 (dashed line) aqueous solutions of $UO_2(NO_3)_2$. The assignment of the vibrational progressions due to a normal mode of the trinuclear $(UO_2)_3(OH)_5^+$ and dinuclear $(UO_2)_2(OH)_2^{2+}$ species is shown at the bottom.

Raman spectroscopy. Part of the photons of the laser beam are absorbed by the sample and causes the creation of population of an electronic excited state and part of the radiation not involved in optical pumping serves as a Raman probe. For low light levels one finds that excited states are not populated and the value of the transmission $T$ is due to the excited state ← ground state absorption at $\lambda_l$. Upon an increase of $I_l$ — which is achieved by focussing the laser beam in the solution — a situation could occur where the number of photons actually exceeds the number of molecules (in the

Can. J. Chem. Downloaded from www.nrcresearchpress.com by 210.87.254.5 on 09/06/12
For personal use only.

Can. J. Chem. Downloaded from www.nrcresearchpress.com by 210.87.254.5 on 09/06/12
For personal use only.

TABLE 2. A comparison of spectroscopic data of the mono-, di-, and trinuclear species

| Species | Band spacings* in emission spectroscopy | $\nu_1 S_0$ recorded* in Raman spectroscopy | Band spacings* in absorption spectroscopy | $\nu_1 T_0$ recorded* in Raman spectroscopy | 0–0′ transitions ($T_0$–$S_0$) ($cm^{-1}$) |
|---|---|---|---|---|---|
| $UO_2^{2+}$ | 875±10 | 873 | 720±15 | — | 20550 |
| $(UO_2)_2(OH)_2^{2+}$ | 860±20 | 856 | — | 716 | 20100 |
| $(UO_2)_3(OH)_5^{+}$ | 840±20 | 842 | 710±20 | 704 | 19600 |

*Values of the $\nu_1$ mode of the $UO_2$ unit in the ground ($S_0$) and electronic excited ($T_0$) state of each of the species (in $cm^{-1}$).

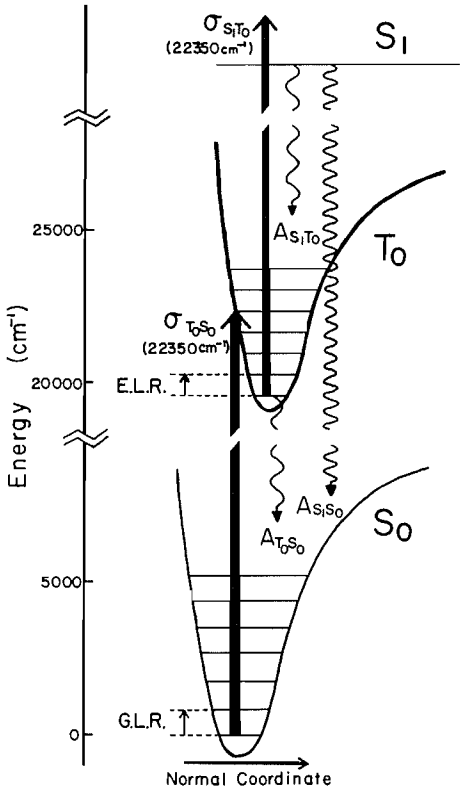


FIG. 3. Part of the energy level diagrams of the trinuclear species $(UO_2)_3(OH)_5^+$ appropriate to the present study. The excited level Raman (ELR) and ground level Raman (GLR) transitions are indicated, together with the energy of the optical pump and that of the Raman probe. The pump and probe induces several emission processes which are designated by their Einstein coefficients (for spontaneous emission).

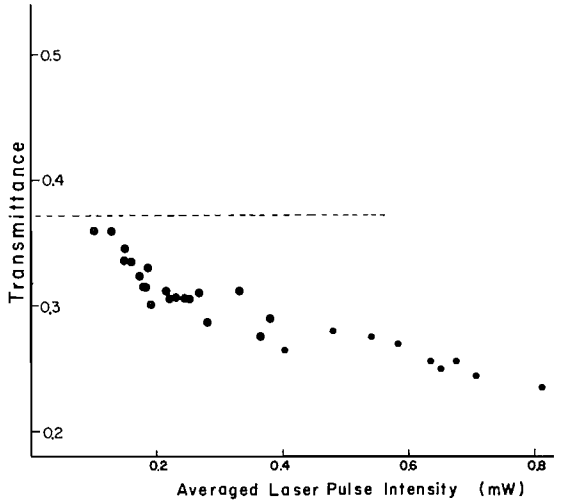


FIG. 4. Transmission studies at 22350 $cm^{-1}$ (see Fig. 3) of the 0.02 $M$ $UO_2(NO_3)_2$ aqueous solution with pH = 4.5. The dashed line represents the value of $T$ for low light levels (encountered in a normal absorption experiment) and is primarily due to $T_0 \leftarrow S_0$ transitions of the trinuclear species. Focusing of the laser beam causes population of $T_0$ and consecutive absorption of laser photon (with an energy of 22350 $cm^{-1}$) due to $S_1 \leftarrow T_0$ transitions reduces the value of $T$. The value of $T$ for high (pulsed) laser power levels does not reach a constant value. This suggests that — during the 3.2 ns duration of the laser pulse — effective saturation of $T_0$ does not occur. The average value of 0.8 mW corresponds to $0.72 \times 10^{14}$ photons per pulse.

irradiated area). Depending on the lifetime of the excited state, population of that state can take place. Consecutive absorption of other laser photons can now result in a change of the value of the transmissions. The results shown in Fig. 4 of the solution with a pH = 4.5 is a case in point. If laser radiation at $\lambda_l$ = 447 nm (22350 $cm^{-1}$) is allowed to enter the solution in the 1 cm long quartz cell, then this radiation is primarily absorbed by the $(UO_2)_3(OH)_5^+$ species. This energy reaches the $v' = 0$ level of the $T_0$ state via vibrational relaxation from $v' = 4$ (see Fig. 3). For unfocused radiation, saturation of this excited state does not take place and the transmission is independent of $I_l$. Focusing the laser beam leads to a different situation. Apparently the $v' = 0$ level of $T_0$ of a large number of the trinuclear species becomes populated and consecutive absorption of other photons with $\lambda_l$ = 447 nm takes place. The cross section $\sigma_{S_1T_0} > \sigma_{T_0S_0}$ and consequently the value of $T$ decreases upon an increase of $I_l$. Relevant to the transmission studies are the results of lifetime measurements of the green emission (induced by the laser radiation at 447 nm) of this solution — see Fig. 5. The upper trace of this figure shows the decay of the emission intensity in time if the sample is exposed to the non-focused laser beam. The lower trace was recorded for emission which emerged from the

Can. J. Chem. Downloaded from www.nrcresearchpress.com by 210.87.254.5 on 09/06/12
For personal use only.

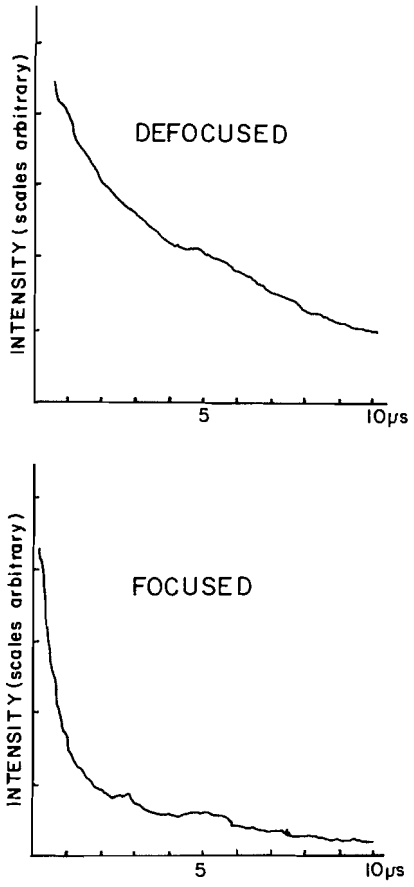


FIG. 5. Top: the decay of phosphorescence induced by a defocused laser beam at $\nu_l = 22350\,cm^{-1}$ propagating through the pH = 4.5 aqueous solution recorded with the 162 Model P.A.R. boxcar averager with 165 Model gated integrator. The curve is a single exponential decay characterised with a lifetime of 7 μs, which is thought to belong to the $T_0$ state of the trinuclear species $(UO_2)_3(OH)_5^+$. Bottom: decay curve for the emission recorded from the focused part of the laser beam in the solution. This curve shows double exponential decays characterised by lifetimes of 7 μs and 1.5 μs. Due to the population of $T_0$ of the trinuclear species a competition occurs between the processes $T_0 \rightarrow S_0$ and $S_1 \leftarrow T_0$. The competition is in favour of the latter, hence the reduction in the intensity of the former process. The emission characterised by a lifetime of 1.5 μs is assigned to the process $T_0 \rightarrow S_0$ of the dinuclear species $(UO_2)_2(OH)_2^{2+}$ which, according to Table 1, is present in the solution.

focused part of the laser beam at 447 nm, which induced the emission spectrum. Both traces reveal the presence of a short- ($\tau \sim 1.5\,\mu s$) and long-lived ($\tau \sim 7\,\mu s$) phosphorescence process although the intensity of the latter appears to be much weaker in the focused case. This reduction in intensity can be understood if one considers the results of the transmission experiments in conjunction with the energy level diagram of Fig. 3. The $T_0$ excited state of the trinuclear species becomes populated with $\lambda_l = 447$ nm (focused beam) for high laser intensity and a competition takes place between the spontaneous emission $T_0 \rightarrow S_0$ and the induced absorption process $S_1 \leftarrow T_0$ at $22350\,cm^{-1}$. This competition favours the $S_1 \leftarrow T_0$ process (stimulated emission $T_0 \rightarrow S_0$ cannot occur (13) because of the behaviour of $T$ at high laser intensity levels) and a decrease in the green phosphorescence intensity takes place, which can be observed with the unaided eye. The short-lived phosphorescence is not due to the trinuclear species and is assigned to the dinuclear species. The mononuclear species which is present in the solution with pH = 4.5 does not interfere with the interpretation of the transmission experiment. Measurements of $T$ versus $I_l$ of the pH = 0.9 solutions for focused and unfocused laser radiation at $\lambda_l = 447$ nm does *not* cause a change in $T$. The transmission measurement yields the following values of the cross section for the trinuclear species at 447 nm: $\sigma_{T_0S_0} = 4.4 \times 10^{-19}\,cm^2$ and $\sigma_{S_1T_0} = 1.5 \times 10^{-18}\,cm^2$ (see also section IV).

### *B, Pulsed-laser Raman spectra of uranyl nitrate solutions*

Parts of the pulsed-laser Raman spectrum of the 0.02 *M* $(UO_2)(NO_3)_2$ solution in water is shown in Fig. 6. The intensity level of the pulsed laser operating at 447.4 nm ($23350\,cm^{-1}$) was so chosen that population of an excited state could take place. The recording of good quality Raman spectra was difficult as a result of the generation of (*i*) green phosphorescence and (*ii*) the Rayleigh background. Spectral shifts were recorded in the region of $550\,cm^{-1} < \Delta\tilde{\nu} < 1100\,cm^{-1}$. The Raman shift of $\Delta\tilde{\nu} = 1046\,cm^{-1}$ is due to the $\nu_1$ mode of the $NO_3^-$ ion and the spectrum of the solution with pH = 0.9 (lower trace, Fig. 6) clearly shows Stokes scattering to the first vibrational level at $873\,cm^{-1}$ of the $\nu_1$ mode of the $UO_2^{2+}$ ion. The polarisation of the incident laser beam was such that polarised and depolarised lines could be recorded but neither scattering to the $\nu_2$ mode nor the $\nu_3$ mode was observed. Vibrational light scattering of the $\nu_1$ mode at $842\,cm^{-1}$ of the $UO_2$ unit of the trinuclear species dominates the spectrum of the solution with pH = 4.5 (upper trace, Fig. 6). This species is not present in the solution with pH = 3.6 (middle trace, Fig. 6), but other bands are observed with a shift of 856 and $871\,cm^{-1}$. This former band has vanishing intensity in the pH = 0.9 solution and is assigned to the shift of the $\nu_1$ mode of the $UO_2$ unit of $(UO_2)_2(OH)_2^{2+}$. Besides these shifts, one observes in the upper and middle spectra shifts at $\sim 704\,cm^{-1}$ and $716\,cm^{-1}$. The frequencies are close

Can. J. Chem. Downloaded from www.nrcresearchpress.com by 210.87.254.5 on 09/06/12
For personal use only.

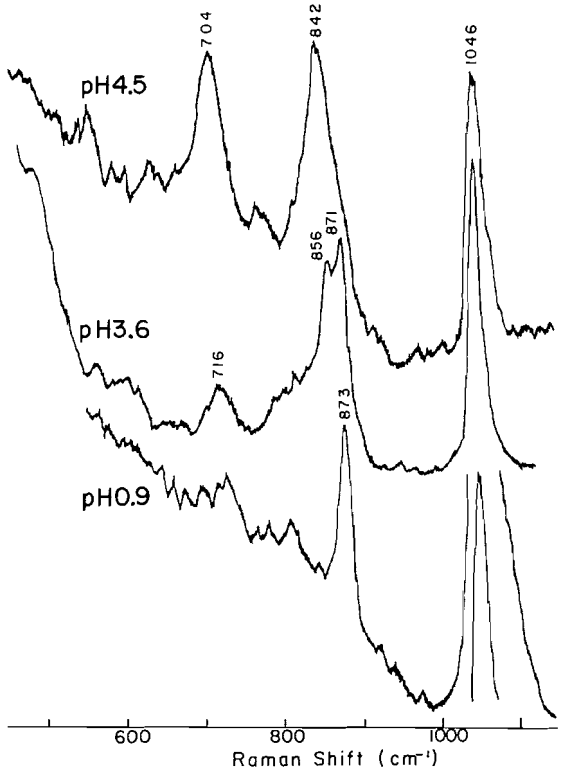


FIG. 6. Part of the pulsed-laser Raman spectra of the solutions with different pH of $UO_2(NO_3)_2$ induced by $\nu_l = 22350\,cm^{-1}$. The assignment of the spectra — see text and Table 2 — is: Lower trace: $\nu_1{}^{S_0} = 873\,cm^{-1}$ of $UO_2^{2+}$ and $\nu_1$ of $NO_3^-$ at $1046\,cm^{-1}$. Middle trace: $\nu_1{}^{S_0} = 871\,cm^{-1}$ of $UO_2^{2+}$ and $\nu_1{}^{S_0} = 856\,cm^{-1}$ of the $UO_2$ unit of $(UO_2)_2(OH)_2^{2+}$. The shift at $716\,cm^{-1}$ is assigned to vibrational scattering of $\nu_1{}^{T_0}$ in the $T_0$ excited state from the dinuclear species. Upper trace: $\nu_1{}^{S_0} = 842\,cm^{-1}$ and $\nu_1{}^{T_0} = 704\,cm^{-1}$ of $(UO_2)_3(OH)_5^+$.

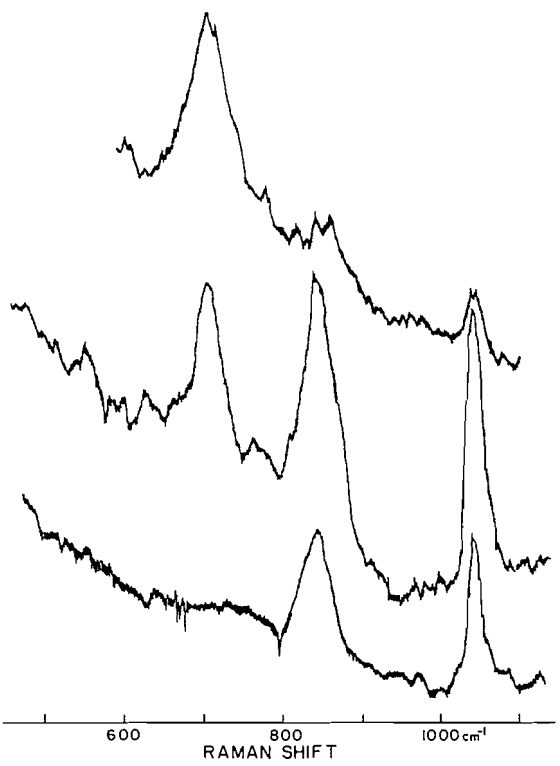


FIG. 7. Part of the Raman spectrum of the pH = 4.5 solution. Lower trace: recorded from the defocused part of the laser beam, hence indicating the ground state Raman scattering only. Middle trace: recorded from the defocused and focused parts of the path of the laser beam; ground and excited level Raman scattering from the trinuclear species are recorded. Upper trace: spatial filtering of the focused part of the laser beam, hence primarily the ELR spectrum.

to those found for the frequency $\nu_1{}^{T_0}$ of the symmetric stretching mode of the $UO_2$ unit in the tri- and dinuclear species (compare Table 1). The assignment of the Raman band to that of scattering of the $\nu_1{}^{T_0}$ mode becomes unambiguous if one considers the spectra shown in Fig. 7. These spectra are taken from the solution with pH = 4.5 under the following experimental conditions. The lower trace was recorded with the laser beam defocused and the middle trace with the beam focused (see also upper trace of Fig. 6). As explained in section III*A*, the green phosphorescence of this solution disappears in the small focused part of the path of laser beam. This part is 0.5 mm long and occurs before and behind the focal point of the $f = 30$ mm microscope objective lens. The focal point was adjusted to occur in the middle of the 10 mm long quartz cell. The density of electronically excited trinuclear species has reached maximum values in that short (0.5 mm) part of the path of the focused laser beam. The spectrum shown in the upper trace of Fig. 7 was recorded from scattered light which emerged from the 0.5 mm path only. The $S_0$ ground state spectrum has nearly completely vanished and scattering from the $\nu_1{}^{T_0}$ mode of the $UO_2$ unit of the trinuclear species in the $T_0$ electronic excited state only remains visible.

Returning to the middle trace of Fig. 6, we find that the solution with pH = 3.6, which revealed the presence of Raman scattering of the dinuclear species, exhibits a shift at $716\,cm^{-1}$ which was not observed in the spectrum obtained with the defocused beam. The value of $716\,cm^{-1}$ is higher than that observed for the $\nu_1$ mode in the $T_0$ excited state of the trinuclear species. It could well be that the Raman band at $716\,cm^{-1}$ (or part of it) is due to scattering from the $T_0$ electronic excited state of the dinuclear species. In that case we conclude from intensity comparisons that the concentration of these excited states is much smaller than those of the trinuclear species.

Can. J. Chem. Downloaded from www.nrcresearchpress.com by 210.87.254.5 on 09/06/12
For personal use only.

## IV. Time evolution of the Raman pulse due to scattering in ground and electronic excited state

In this section, a comparison is made of the intensity of the laser pulse at different points in time $I_l(t)$ and that of the pulse due to Raman scattered light at the same points in time. The scattering is induced by the laser pulse of the $\nu_1$ vibrational mode of the $UO_2$ unit of the trinuclear species in ground and electronic excited states. The temporal shape of the laser pulse recorded with the boxcar (gate width 2 ns) is shown in Fig. 8. The true shape of the laser pulse is different from the one recorded with the boxcar because both the response time of the PMT and the 2 ns gate affect the shape of the original pulses (14) (the true FWHM of 3.2 ns of the pulse is broadened to 5.6 ns). However, this difference does not affect the comparison of intensities of time-resolved spectra mentioned above because the instrumental time base for both laser and Raman pulse is identical.

The experimental data of interest here is the integrated area of the Raman band of the $\nu_1$ mode of the trinuclear species in the $S_0$ ground and $T_0$ electronic excited states, which are denoted here by respectively $\nu_1{}^{S_0}$ and $\nu_1{}^{T_0}$. The integrated intensities of Raman scattering to these modes measured at time $t$ are denoted by $I_{\nu_1}{}^{S_0}(t)$ and $I_{\nu_1}{}^{T_0}(t)$ and the following expressions apply:

[1] $$I_{\nu_1}{}^{S_0}(t) = n_{S_0}(t)\phi l Q_{\nu_1}{}^{S_0} I_l(t)$$

and

[2] $$I_{\nu_1}{}^{T_0}(t) = n_{T_0}(t)\phi l Q_{\nu_1}{}^{S_0} I_l(t)$$

where the Raman cross section

$$Q_{\nu_1}{}^{S_0} = \frac{2^7\pi^5}{3^2C^5}(\nu_l - \nu_1{}^{S_0})^4 |\alpha|^2$$

is independent of time in the non-resonance case (a corresponding expression can be written for $\nu_1{}^{T_0}$). Also $n_{S_0}(t)$ and $n_{T_0}(t)$ are the time-dependent concentrations of species in the states $S_0$ and $T_0$ respectively, $\phi$ is the cross sectional area of the focused laser beam, and $l$ is the length of the focused part of the laser beam (0.5 mm) as discussed in the previous section. The area $\phi$ is assumed to be constant over the $l$ = 0.5 mm distance and the number of scattering centers in the electronic ground and excited states are equal to $n_{S_0}(t)\phi l$ and $n_{T_0}(t)\phi l$. The time evolution of the intensity of the laser pulse is represented by $I_l(t)$. One obtains from eqs. [1] and [2] the expressions

[1a] $$n_{S_0}(t) \propto I_{\nu_1}{}^{S_0}(t)/I_l(t)$$

and

[2a] $$n_{T_0}(t) \propto I_{\nu_1}{}^{T_0}(t)/I_l(t)$$

Values of $n_{S_0}(t)$ and $n_{T_0}(t)$ — calculated from eqs. [1*a*] and [1*b*] — at specific points in time (in arbitrary units) are shown in Fig. 8.

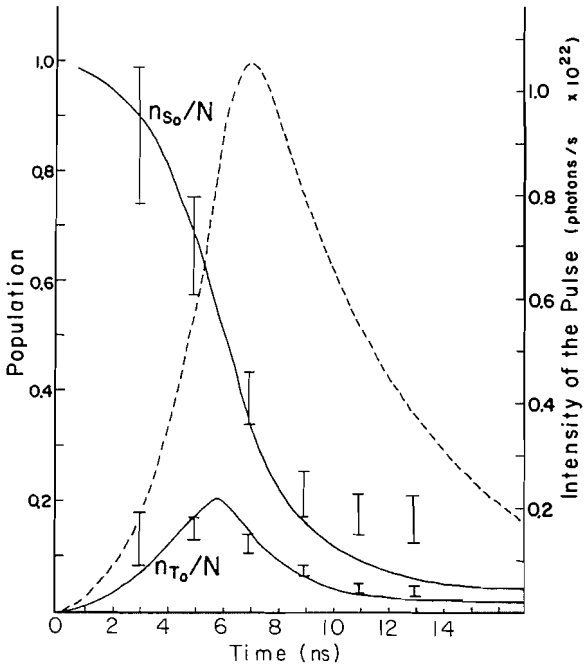


FIG. 8. The dashed curve represents the laser pulse as recorded with the boxcar. The vertical bars are data for $I_{\nu_1}{}^{S_0}/I_l$ (upper) and $I_{\nu_1}{}^{T_0}/I_l$ (lower) at different points in time. The solid lines are calculated for the depopulation of the ground state $S_0$ (upper) and the population of the excited state $T_0$ (lower) of the trinuclear species $(UO_2)_3(OH)_5{}^+$ during the time of the pulse.

The recorded spectra are resonance Raman spectra because the frequency of the exciting radiation is coincident with that of absorption transitions $T_0 \leftarrow S_0$ and $S_1 \leftarrow T_0$. In fact, the laser radiation with $\nu_l$ = 22350 $cm^{-1}$ is in resonance with the fourth vibrational level of $\nu_1{}^{T_0}$. Because we are dealing with a vibrational Raman effect in resonance one predicts that the rise and decay time of the Raman scattered light pulse could be very much different from that of the pulse in the non-resonance case (1–4). The ratios $I_{\nu_1}{}^{S_0}(t)/I_l(t)$ and $I_{\nu_1}{}^{T_0}(t)/I_l(t)$ would in that case not be proportional to the concentrations $n_{S_0}(t)$ and $n_{T_0}(t)$. Instead, these ratios would show a gradual increase upon an increase of $t$. The results shown in Fig. 8 are not in agreement with the above; rather it appears that the ratio $I_{\nu_1}{}^{S_0}(t)/I_l(t)$ decreases upon an increase of $t$. This behaviour is expected if we assume that the concentration of ground states $S_0$ decreases during optical pumping with $I_l(t)$. Consequently we assume that the resonance Raman effects are small

Can. J. Chem. Downloaded from www.nrcresearchpress.com by 210.87.254.5 on 09/06/12
For personal use only.

and that eq. [1*a*] is valid. The ratio $I_{\nu_1}^{T_0}(t)/I_l(t)$ as function of $t$ is different from $I_{\nu_1}^{S_0}/I_l(t)$. The intensity $I_{\nu_1}^{T_0}(t)$ can also be affected by resonance. But, because the lifetime $\tau_{S_1}$ of the state $S_1$ is thought to be shorter than $\tau_{T_0} = 7\,\mu s$ of $T_0$, we predict that the shape of the Raman scattered light pulse due to $\nu_1^{T_0}$ approaches that of $I_l(t)$. However, the maximum intensity of the scattered light should occur after a point in time at which the laser pulse has reached its maximum value. This again is not observed and we therefore assume that eq. [2*a*] is applicable.

In addition to the above, another complication could arise if we assume that the vibrational relaxation process between levels of the $T_0$ electronic surface is slow. This could result in a situation where the vibrational levels up to $v' = 4$ of $T_0$ are populated, which in turn means that the Boltzman statistics cannot be applied to calculate population numbers for these levels. It has previously been shown that a deviation from Boltzman statistics also can change the Raman scattered light pulse (15). This effect, however, can be neglected because it is known that the vibrational relaxations occur in the picosecond time scale (e.g., see refs. 16, 17, and 18). In order to populate the vibrational levels with such short lifetimes, a larger cross section than the value $\sigma_{T_0S_0} = 4.4 \times 10^{-19}\,cm^2$ is required (15).

As explained in section III*A*, light scattering spectra were recorded from the central part ($l$ = 0.5 mm) of the laser beam trace. The concentrations $n_{S_0}(x, t)$, $n_{T_0}(x, t)$, and $n_{S_1}(x, t)$ are taken to be independent of the coordinate $x$ of the travelling light wave, where $0 < x < 0.5$ mm, because the number of photons at the central focused part of the laser beam, $I_l^0(t)$, and the cross section of the beam there, are assumed to be constant. In that case, we can use a series of expressions which pertain to the calculation of the temporal behaviour of the population members of a three level system ($S_0$, $T_0$, and $T_1$ shown in Fig. 3).

Thus

$$[3]\quad \frac{dn_{S_0}(t)}{dt} = -\frac{1}{\phi}\sigma_{T_0S_0}n_{S_0}(t)I_l^0(t) + A_{T_0S_0}n_{T_0}(t) + A_{S_1S_0}n_{S_1}(t)$$

$$[4]\quad \frac{dn_{T_0}(t)}{dt} = \frac{1}{\phi}(\sigma_{T_0S_0}n_{S_0}(t) - \sigma_{S_1T_0}n_{T_0}(t))I_l^0(t) - A_{T_0S_0}n_{T_0}(t) + A_{S_1T_0}n_{S_1}(t)$$

$$[5]\quad \frac{dn_{S_1}(t)}{dt} = \frac{1}{\phi}\sigma_{S_1T_0}n_{T_0}(t)I_l^0(t) - (A_{S_1S_0} + A_{S_1T_0})n_{S_1}(t)$$

In these expressions $\sigma$ are absorption cross sections, the $A$ coefficients are those for spontaneous emission, and $\phi$ is the area of the laser beam in the focused part of the beam.

The lifetime of the state $T_0$ is 7 μs ($\tau_{T_0} = 1/A_{T_0S_0}$) which is much longer than the 3.2 ns duration of the laser pulse. Consequently the system does *not* achieve a steady state. In addition to the above we have

$$[6]\quad N = n_{S_0}(t) + n_{T_0}(t) + n_{S_1}(t)$$

Equations [3]–[5] can be simplified if the following is taken into account. Because $\tau_{T_0}$ is much longer than 3.2 ns (and thus $A_{T_0S_0}$ is very small), we neglect all terms which contain $A_{T_0S_0}$. Shown in Fig. 9 is the excitation spectrum for the green fluorescence ($T_0 \rightarrow S_0$) at 515 nm. From this spectrum, one concludes that pumping near 42000 $cm^{-1}$ does not result in energy transfer into $T_0$. This energy difference of 42000 $cm^{-1}$ is equal to that of the (pseudo) consecutive two photon absorption process (with pulsed laser radiation at 22350 $cm^{-1}$) via the channel $T_0(v = 5) \leftarrow S_0(v = 0)$ at 22350 $cm^{-1}$; $T_0(v = 5) \rightarrow T_0(v = 0)$ followed by $S_1 \leftarrow T_0(v = 0)$ also at 22350 $cm^{-1}$. Because energy transfer from $S_1 \rightarrow T_0$ does not take place, the coefficient $A_{S_1T_0}$ also can be dropped from eqs. [4] and [5]. Furthermore we assume that the lifetime of $S_1$ is also longer than 3.2 ns and after integration we get:

$$[7]\quad n_{S_0}(t) = N \exp\left\{-\frac{1}{\phi}\sigma_{T_0S_0}F(t)\right\}$$

$$[8]\quad n_{T_0}(t) = \frac{1}{\phi}\sigma_{T_0S_0}\exp\left\{-\frac{1}{\phi}\sigma_{S_1T_0}F(t)\right\}G(t)$$

where

$$F(t) = \int_0^t I_l^0(t')dt'$$

and

$$G(t) = \frac{1}{N}\int_0^t n_{S_0}(t')I_l^0(t')\exp\left\{\frac{1}{\phi}\sigma_{S_1T_0}F(t')\right\}dt'$$

The temporal aspects of $n_{S_0}(t)$ and $n_{T_0}(t)$ are calculated with these expressions. First, numerically integrated values of $F(t)$ at different $t$ were obtained and with the known value of $\sigma_{T_0S_0} = 4.4 \times 10^{-19}\,cm^2$, values of $n_{S_0}(t)/N$ as a function $\phi$ were calculated and compared with the experimental data of Fig. 8. Then, numerically integrated values of $G(t)$ were obtained from a best fit of $n_{S_0}(t)_N$ with experiment in combination with values of $\sigma_{S_1T_0}$. Finally, the best fit was made with the experimental values of $n_{T_0}(t)/N$ by varying the value of $\sigma_{S_1T_0}$. The

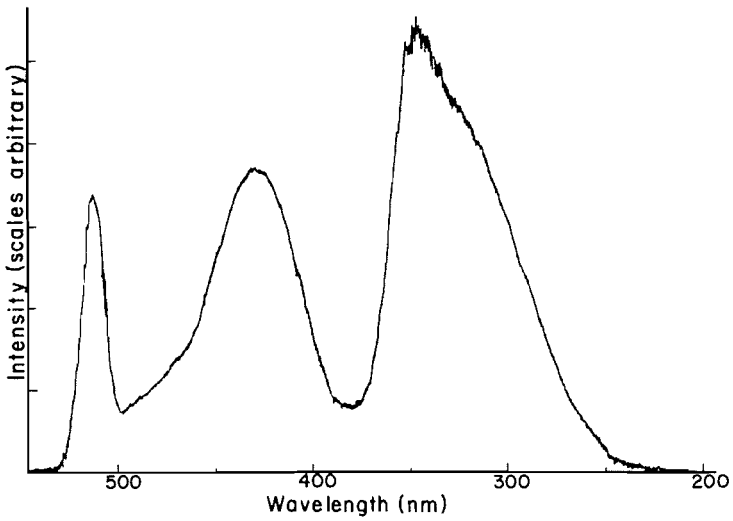


FIG. 9. Excitation spectrum of the phosphorescence of $(UO_2)_3(OH)_5^+$ detected at 515 nm.

best possible fit to the experimental data with $\phi = 8.5 \times 10^{-6}\,cm^2$ and $\sigma_{S_1T_0} = 1.5 \times 10^{-18}\,cm^2$ are shown as solid lines in Fig. 8. The differences between the calculated populations (solid lines) and experimental data are small. Finally using the intensity of the $\nu_1$ mode of $NO_3^-$ as an internal standard we obtain $Q_{\nu_1}{}^{T_0}/Q_{\nu_1}{}^{S_0} \approx 9$.

## V. Concluding remarks

In this paper, an example is given in which the radiation of a pulsed laser can be used to produce excited states of the $UO_2$ unit of the species $(UO_2)_3(OH)_5^+$ and $(UO_2)_2(OH)_2^{2+}$, while part of the radiation not used for optical pumping can serve as a Raman probe to induce light scattering transitions from 7 μs and 1.5 μs lived excited states of these species. By employing standard expressions for the temporal behaviour of population numbers of ground and excited states, an attempt was made to compute these numbers and to compare them with experimental data. Due to the fact that the lifetime of the excited states is longer than the duration of the laser pulse we employed expressions for a *non*-steady-state situation. The comparison is reasonable and can be used for other systems which permit the observation of their excited level Raman spectra.

## VI. Acknowledgement

The authors wish to thank Dr. L. V. Haley for discussions and technical assistance.

1. P. F. WILLIAMS, D. L. ROUSSEAU, and S. H. DIWORETSKY. Phys. Rev. Lett. **32**, 196 (1974).
2. J. M. FRIEDMAN and R. M. HOCHSTRASSER. Chem. Phys. **6**, 155 (1974).
3. D. L. ROUSSEAU and P. F. WILLIAMS. J. Chem. Phys. **64**, 3519 (1976).
4. J. O. BERG, C. A. LANGHOFF, and G. W. ROBINSON. Chem. Phys. Lett. **29**, 305 (1974).
5. C. F. BAES and R. E. MESMER. The hydrolysis of cations. Wiley, New York. 1976. pp. 177–182.
6. I. M. TOTH and G. M. BEGUN. J. Phys. Chem. **85**, 547 (1981).
7. M. H. BROOKER, C.-H. HUANG, and J. SYLWESTROWICZ. J. Inorg. Nucl. Chem. **42**, 1431 (1980).
8. M. D. MARCANTONATOS, M. DESCHAUX, and F. CELARDIN. Chem. Phys. Lett. **69**, 144 (1980).
9. D. NICOLLIN, P. BERTELS, and J. A. KONINGSTEIN. Can. J. Chem. **58**, 1334 (1980).
10. (*a*) J. T. BELL and R. E. BIGGERS. J. Mol. Spectrosc. **18**, 247 (1965); **22**, 262 (1967); **25**, 312 (1968); (*b*) S. P. MCGLYNN and J. K. SMITH. J. Mol. Spectrosc. **6**, 164 (1961).
11. J. B. NEWMAN. J. Chem. Phys. **47**, 85 (1967).
12. R. G. DENNING, T. R. SNELLGROVE, and D. R. WOODWARK. Mol. Phys. **32**, 419 (1976); **37**, 1109 (1979); R. G. DENNING, D. N. P. FOSTER, T. R. SNELLGROVE, and D. R. WOODWARK. Mol. Phys. **37**, 1089 (1979).
13. B. HALPERIN and J. A. KONINGSTEIN. Can. J. Chem. **59**, 2792 (1981).
14. A. E. MCKINNON, A. G. SZABO, and D. R. MILLER. J. Phys. Chem. **81**, 1564 (1977).
15. M. ASANO, J. A. KONINGSTEIN, and D. NICOLLIN. J. Chem. Phys. **73**, 688 (1980).
16. R. M. HOCHSTRASSER and J. E. WESSEL. Chem. Phys. **6**, 19 (1974).
17. B. I. GREENE, R. M. HOCHSTRASSER, and R. B. WEISMAN. J. Chem. Phys. **70**, 1247 (1979).
18. K. J. CHOI and M. R. TOPP. Chem. Phys. Lett. **69**, 441 (1980).

Can. J. Chem. Downloaded from www.nrcresearchpress.com by 210.87.254.5 on 09/06/12
For personal use only.

# Vibrations moléculaires du nitrate de di-μ-hydroxo-bis(diammine) platine (II)[1] $[(NH_3)_2Pt(OH)_2Pt(NH_3)_2]$ $(NO_3)_2$. Partie 1: étude spectroscopique Raman et infrarouge[2]

MICHEL MANFAIT[3] ET ALAIN J. P. ALIX

*Laboratoire de Recherches Optiques, Faculté des Sciences, B.P. 347, 51062 Reims-Cedex, France*

JACQUELINE DELAUNAY-ZECHES

*Laboratoire de Chimie Minérale, Faculté des Sciences, B.P. 347, 51062 Reims-Cedex, France*

ET

THÉOPHILE THEOPHANIDES[3]

*Laboratoire de Chimie de Coordination, Faculté des Arts et Sciences, Université de Montréal, C.P. 6210, Montréal (Qué.), Canada H3C 3V1*

Reçu le 19 octobre 1981

MICHEL MANFAIT, ALAIN J. P. ALIX, JACQUELINE DELAUNAY-ZECHES et THÉOPHILE THEOPHANIDES. Can. J. Chem. **60**, 2216 (1982).

Les spectres Raman laser des complexes dimères pontés du nitrate de di-μ-hydroxo-bis(diammine) platine(II): $[(NH_3)_2Pt(OH)_2Pt(NH_3)_2](NO_3)_2$ et des dérivés isotopiques (substitutions H/D, $^{16}O/^{18}O$) ont été obtenus à l'état solide dans le domaine 0–4000 $cm^{-1}$. Les spectres infrarouge de ces complexes ont été obtenus à l'état solide dans KBr (200–4000 $cm^{-1}$). Les attributions des différentes fréquences de vibration de l'ion nitrate, des ligands $NH_3$, des groupes hydroxo et du squelette carré plan sont discutées en détail pour le complexe et ses dérivés isotopiques.

MICHEL MANFAIT, ALAIN J. P. ALIX, JACQUELINE DELAUNAY-ZECHES, and THÉOPHILE THEOPHANIDES. Can. J. Chem. **60**, 2216 (1982).

The laser Raman spectra of the hydroxo-bridged platinum(II) complexes, di-μ-hydroxo-bis(diammine) platinum(II)-nitrate $[(NH_3)_2Pt(OH)_2Pt(NH_3)_2](NO_3)_2$, and isotopic derivatives involving the atoms H/D and $^{16}O/^{18}O$ are recorded in the solid state in the range 0–4000 $cm^{-1}$. The infrared spectra of the complexes are recorded in KBr pellets in the range 200–4000 $cm^{-1}$. Assignments of the different lines for the nitrate ion, the ammonia molecules, the hydroxo groups, and the square planar skeleton vibrations of the complex and its isotopic analogs are given.

## Introduction

Il est maintenant bien reconnu que le complexe de platine *cis*-dichlorodiammine platine(II) (*cis*-DDP, *cis*-platine) est un agent antitumoral très efficace contre plusieurs types de cancers (1). L'étude des réactions d'hydrolyse du *cis*-platine a conduit à la synthèse de nouveaux composés di- et tri-nucléaires hydroxo-pontés (2, 3).

Nous nous sommes intéressés en particulier au complexe dimère du nitrate de di-μ-hydroxo-bis-(diammine platine(II)) de formule $[(NH_3)_2Pt(II)-(OH)_2Pt(II)(NH_3)_2](NO_3)_2$ dont la structure a été résolue récemment par Faggiani *et al.* (2). Ces auteurs ont donné également une première attribution très incomplète des spectres de vibration du dimère, surtout en ce qui concerne les vibrations du squelette $[N_2PtO_2PtN_2]$.

Nous avons entrepris l'étude des vibrations moléculaires (4) du dimère et de ses dérivés isotopiques H/D, $^{16}O/^{18}O$ par spectroscopie Raman et infrarouge ainsi qu'une analyse en coordonnées normales complète du squelette (voir partie 2, réf. 5). Dans ce travail nous donnons les spectres Raman et infrarouge du complexe à l'état solide et de ses divers isotopes (D, $^{18}O$). Les attributions des différentes fréquences sont discutées en détail en termes de vibrations de l'anion (ion nitrate $NO_3^-$) et de vibrations du cation dinucléaire pour lequel une distinction adéquate est faite pour les parties ammines, hydroxydes et squelette. En particulier, nous avons attribué les modes de vibrations mettant en jeu les liaisons platine–oxygène (ν(Pt—O), δ(PtOPt)) dans le cycle biponté carré-plan $Pt_2O_2$ (voir Fig. 1).

Ces résultats, obtenus sur les attributions des vibrations impliquant les liaisons Pt—O, sont d'une grande importance quant à l'interprétation

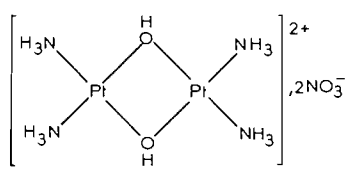


FIG. 1. Nitrate de di-μ-hydroxo-bis(diammine platine (II)).

[1]Suivant nouvelle nomenclature de UICPA: le nitrate de tétraammine-μ-dihydroxo-diplatine (2+).

[2]Présentée au 28ème Symposium Canadien de Spectroscopie, Ottawa, Canada, 28–30 septembre 1981.

[3]Auteur à qui toute correspondance doit être adressée.

0008-4042/82/172216-06$01.00/0

©1982 National Research Council of Canada/Conseil national de recherches du Canada

Can. J. Chem. Downloaded from www.nrcresearchpress.com by 210.87.254.5 on 09/06/12
For personal use only.

Can. J. Chem. Downloaded from www.nrcresearchpress.com by 210.87.254.5 on 09/06/12
For personal use only.

des mécanismes d'interactions des complexes du platine(II) avec les acides nucléiques intervenant dans les processus cancéreux: voir en particulier l'étude des drogues anticancéreuses, comme le *cis*-platine, en interaction avec l'ADN (6, 7).

## Matériels et méthodes

*Préparation des composés*

Le complexe dimère du nitrate de di-μ-hydroxo-bis(diammine platine(II)) est préparé à partir du *cis*-dichlorodiammine platine(II) (Johnson-Matthey Co.) suivant la méthode décrite par Faggiani *et al*. (2). Le complexe deutérié est obtenu par dissolution du dimère dans $D_2O$ (99.8% Merck) suivie d'une évaporation lente sous vide, dans le noir et à température ambiante. Cette procédure est répétée trois fois. Le complexe substitué $^{18}O$ a été préparé comme le deutérié à partir d'une évaporation sous vide d'une solution dans $H_2{}^{18}O$, à température ambiante. L'examen des différents spectres montre qu'il y a bien eu une substitution isotopique.

*Instrumentation*

Les spectres Raman du complexe et de ses dérivés isotopiques sous forme solide ont été obtenus sur un spectromètre triple monochromateur Coderg modèle T800 avec un laser à argon ionisé Coherent Radiation modèle 52B (488.0 nm, puissance 200 mW). La technique de la cellule tournante a été utilisée afin d'éviter une dégradation thermique des échantillons (caractère explosif de ces composés). Les spectres infrarouge des complexes dans le KBr ont été enregistrés sur un spectromètre Perkin Elmer 521 pour le domaine 200–4000 $cm^{-1}$. Les fréquences des raies sont mesurées avec une précision de ± 2 $cm^{-1}$. L'intensité des raies est mesurée par la hauteur de crête.

## Résultats et discussions

La structure cristalline a été déterminée par diffraction de rayons X par Faggiani *et al*. (2). Le dimère cristallise dans le groupe d'espace triclinic $P\bar{1}$ avec une molécule par maille ($Z = 1$). La symétrie moléculaire du cation $[(NH_3)_2Pt(OH)_2Pt(NH_3)_2]^{2+}$ se rapproche de la symétrie idéale $D_{2h}$ (protons omis). La symétrie de site est $C_i$. Il en résulte, quelque soit la symétrie considérée (molécule libre $D_{2h}$, molécule dans le cristal $C_i$), une non-coincidence des fréquences Raman et infrarouge.

Les spectres Raman à l'état solide des complexes, $[(NH_3)_2Pt(OH)_2Pt(NH_3)_2](NO_3)_2$, $[(NH_3)_2Pt(^{18}OH)_2Pt(NH_3)_2](NO_3)_2$ et $[(ND_3)_2Pt(OD)_2Pt(ND_3)_2](NO_3)_2$ sont représentés respectivement sur les Figs. 2a, 2b, 2c. Les spectres infrarouge de ces mêmes composés sont donnés dans les Figs. 3a, 3b, 3c. Les fréquences Raman et infrarouge des divers complexes sont reportées dans le Tableau 1.

Les différents critères d'attribution des fréquences ont été les suivants.

(*i*) Attribution des fréquences de l'ion nitrate $NO_3^-$; elles sont en général séparées des fréquences du complexe et ne varient pas par substitution isotopique (H/D, $^{16}O/^{18}O$).

(*ii*) Attribution des fréquences du ligand $NH_3$ (respectivement $ND_3$); cette attribution est assez classique (2, 8, 9) et ne pose pas de problème.

(*iii*) Attribution des fréquences du groupe hydroxo; les fréquences d'élongation ν(OH) et de balancement $\rho_w$(OH) ont été attribuées par comparaison avec des résultats équivalents obtenus pour des complexes binucléaires pontés du même type (10–13).

(*iv*) Attribution des fréquences du squelette du complexe; les vibrations normales du cation binucléaire sont considérées dans l'approximation du point (les groupes hydroxo et les ammines sont réduits respectivement aux points O′ ($m_{O'} = m_O + m_H$) et N′ ($m_{N'} = m_N + 3m_H$):

$$\Gamma(D_{2h}) = 4A_g(\mathrm{R}) + B_{1g}(\mathrm{R}) + B_{2g}(\mathrm{R}) + 3B_{3g}(\mathrm{R}) + A_u(—) + 3B_{1u}(\mathrm{ir}) + 3B_{2u}(\mathrm{ir}) + 2B_{3u}(\mathrm{ir})$$

(*v*) Attribution des fréquences des vibrations du couplage squelette–ligands $NH_3$; les couplages Pt—$NH_3$ (rocking) donnent lieu à des mouvements de fréquences bien séparées de celles du squelette et/ou des ligands libres (faibles couplages cinématiques et dynamiques justifiés par l'approximation du point).

*Ion nitrate $NO_3^-$*

Les quatre fréquences de vibration observées, reportées dans le Tableau 1, confirment une structure $D_{3h}$ pour l'ion $NO_3^-$ ($A_1' + A_2'' + 2E'$) (14) qui de ce fait n'apparaît pas être coordonné (la symétrie serait dans ce dernier cas soit $C_{2v}$ soit $C_s$ et on observerait une levée de dégénérescence).

*Ligands $NH_3/ND_3$*

L'attribution des modes de vibration des ligands $NH_3$ et $ND_3$ est directe (voir pour comparaison notre travail sur $[Pt(NH_3)_4]^{2+}$ (8, 9)). Les bandes dans le domaine 3107–3253 $cm^{-1}$ (Raman) et 3100–3245 $cm^{-1}$ (infrarouge) correspondent aux modes d'élongation symétriques et antisymétriques ($\nu_{as}(NH) > \nu_s(NH)$). Ces bandes se déplacent à 2275–2467 $cm^{-1}$ (Raman) et à 2380–2425 $cm^{-1}$ (infrarouge) pour le complexe deutérié. Ces fréquences semblent ne pas se modifier dans le cas du complexe $^{18}O$.

Les modes de déformation $\delta_s(NH_2)$ et $\delta_{as}(NH_2)$ sont observés respectivement dans les domaines 1318–1396 $cm^{-1}$ et 1573–1596 $cm^{-1}$ (Raman), 1312–1322 $cm^{-1}$ et 1551–1608 $cm^{-1}$ (infrarouge) pour $NH_3$. Les modes correspondants $\delta_s(ND_2)$ et $\delta_{as}(ND_2)$ sont déplacés à environ 1023 $cm^{-1}$ (raie masquée par la $\nu_s(NO) = 1046\ cm^{-1}$) et 1105–1168

Can. J. Chem. Downloaded from www.nrcresearchpress.com by 210.87.254.5 on 09/06/12
For personal use only.

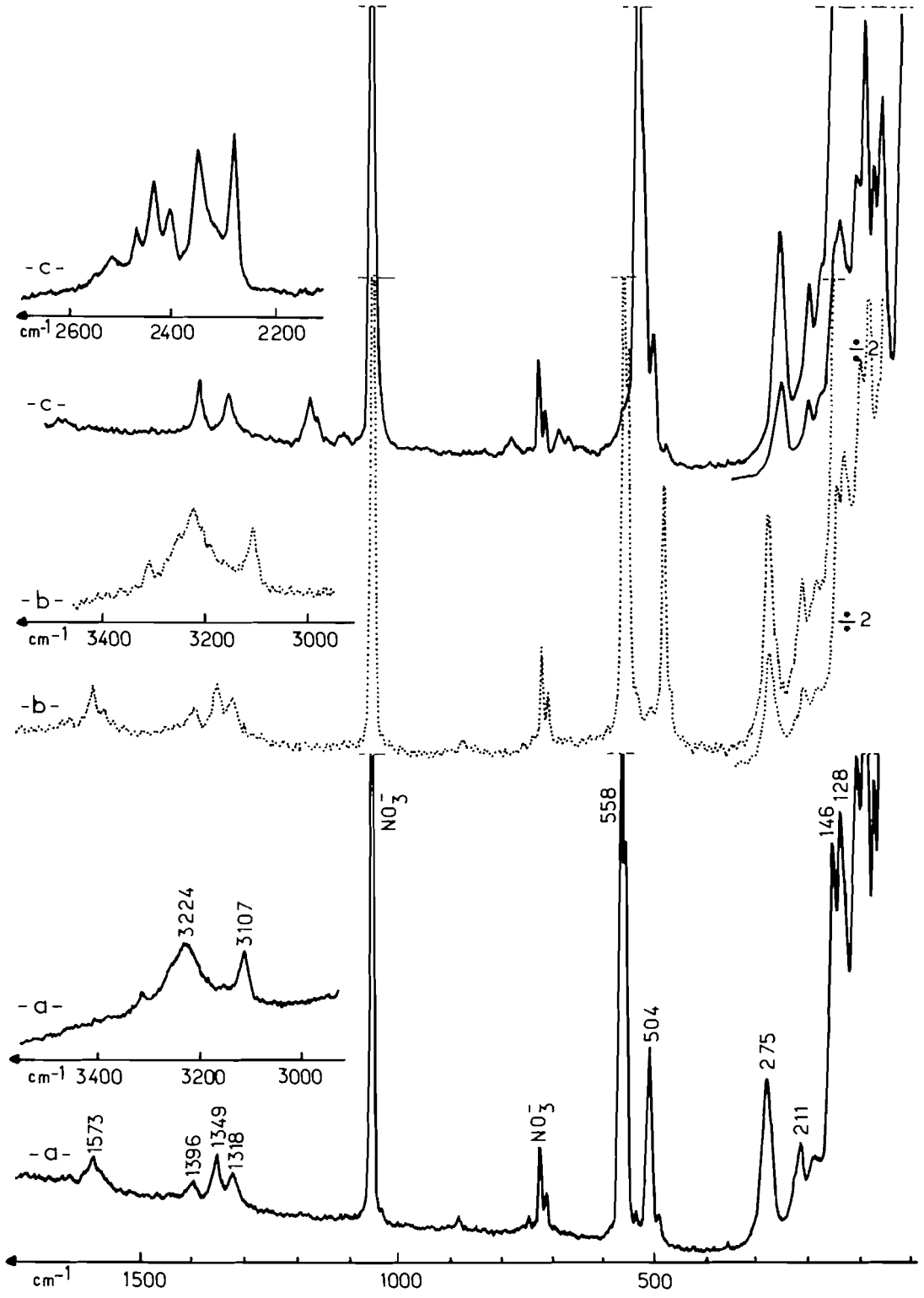


FIG. 2. Spectres Raman à l'état solide: (a) $[(NH_3)_2Pt(II)(OH)_2\ Pt(II)(NH_3)_2](NO_3)_2$, (b) $[(NH_3)_2Pt(II)(^{18}OH)_2Pt(II)(NH_3)_2](NO_3)_2$ et (c) $[(ND_3)_2Pt(II)(OD)_2Pt(II)(ND_3)_2](NO_3)_2$. Excitation laser 488.0 nm. Largeur des fentes 4 $cm^{-1}$.

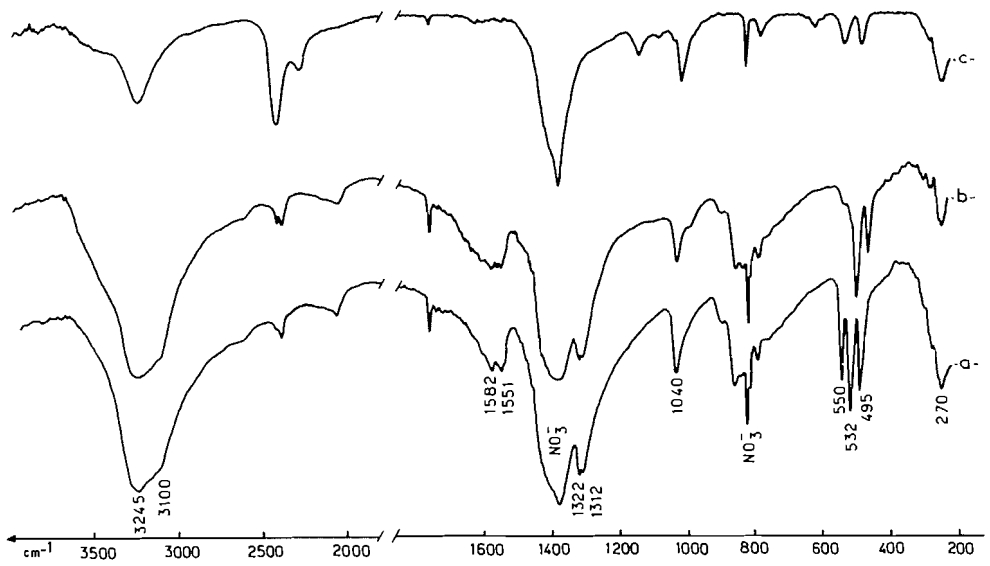


FIG. 3. Spectres infrarouge dans KBr: (a) $[(NH_3)_2Pt(II)(OH)_2Pt(II)(NH_3)_2](NO_3)_2$, (b) $[(NH_3)_2Pt(II)(^{18}OH)_2Pt(II)(NH_3)_2](NO_3)_2$ et (c) $[(ND_3)_2Pt(II)(OD)_2Pt(II)(ND_3)_2](NO_3)_2$.

$cm^{-1}$ (Raman), 1021–1041 $cm^{-1}$ et 1082–1165 $cm^{-1}$ (infrarouge). L'ensemble des déplacements isotopiques des fréquences satisfait au rapport $\nu(H)/\nu(D) = 1{,}3–1{,}4$.

*Groupes hydroxo OH/OD/$^{18}$OH*

Les modes d'élongation $\nu$(OH), $\nu$(OD) sont attribués aux raies 3310 $cm^{-1}$ (R), 3460 $cm^{-1}$ (ir) et 2515 $cm^{-1}$ (R), respectivement. Bien que l'ensemble des modes d'élongation $\nu$(NH) et $\nu$(OH) soient relativement superposés, il nous paraît malgré tout raisonnable de distinguer les différents domaines (c'est-à-dire, $\nu_s$(NH), $\nu_{as}$(NH) et $\nu$(OH)) comme présentés ci-dessus.

Le mode de vibration de déformation $\delta$(Pt—OH) est pointé à 1040 $cm^{-1}$ (ir) et se déplace à 780 $cm^{-1}$ dans le complexe deutérié; rapport $\nu(OH)/\nu(OD) = 1.33$. Ce mode est complètement masqué dans le spectre Raman du complexe par la bande très intense $\nu_1$(NO) = 1046 $cm^{-1}$ du nitrate, mais apparaît clairement à 773 $cm^{-1}$ dans le spectre Raman du deutérié.

*Squelette $[N_2PtO_2PtN_2]$ ($D_{2h}$)*

La localisation des raies correspondant aux mouvements des atomes d'azote dans le squelette (c'est-à-dire relativement aux atomes lourds de platine) est faite compte tenu de nos résultats antérieurs sur l'ion $[Pt(NH_3)_4]^{2+}$ (8, 9) et ceux sur le nitrate de *cis*-diaquo diammine platine(II) (15).

Les mouvements d'élongation des quatre liaisons PtN donnent lieu à quatre fréquences de vibration. Les modes symétriques sont pointés à 558 $cm^{-1}$ (Raman, très intense) et 550 $cm^{-1}$ (infrarouge) pour le complexe et se déplacent respectivement à 525 $cm^{-1}$ (R) et 532 $cm^{-1}$ (ir) pour le deutérié. Les modes antisymétriques sont vus à 552 $cm^{-1}$ (R, peu intense) et 532 $cm^{-1}$ (ir, forte) pour le complexe et à 515 $cm^{-1}$ (R) et 494 $cm^{-1}$ (ir) pour le deutérié. Ces déplacements isotopiques ($\Delta\nu$-(Pt—N)) de l'ordre de 30 $cm^{-1}$ sont assez caractéristiques de la substitution H/D dans les complexes platine–ammines (8). Il nous a été très difficile d'obtenir le spectre Raman du complexe en solution dans l'eau. Cependant, nous avons pu observer la raie $\nu_s$(PtN) de type $A_g$ à 550 $cm^{-1}$ (polarisée) et la raie $\nu_{as}$(PtN) de type $B_{3g}$ à 545 $cm^{-1}$ (dépolarisée).

Les mouvements de déformations angulaires planes des deux groupements $PtN_2$ donnent lieu à quatre fréquences de vibration. Les modes de déformation d'angle de type ciseau symétrique $\delta_s$-($PtN_2$) et antisymétrique $\delta_{as}$($PtN_2$) sont pointés à 275 $cm^{-1}$ (Raman, large et peu intense) et 270 $cm^{-1}$ (ir, moyenne); ils se déplacent à 248 $cm^{-1}$ (R et ir) par deutération. Le mode de déformation de type rotation plane $\rho_{r,s}$($PtN_2$) est attribué à la raie 211 $cm^{-1}$ (R) et à 193 $cm^{-1}$ (R) pour le complexe et son homologue deutérié. Le mode antisymétrique $\rho_{r,as}$-($PtN_2$) (actif en ir, $B_{2u}$) n'a pas été observé.

Le mode de déformation de type torsion angulaire (hors du plan) $\rho_{t,as}$($PtN_2$) est attribué à la raie 128 $cm^{-1}$ (R). Le mode $\rho_{t,s}$ ($PtN_2$) (ir, $A_u$) étant inactif, n'est pas observable. Le mode de déformation de type balancement (hors du plan) $\rho_{w,as}$($PtN_2$) est attribué à la raie 146 $cm^{-1}$ (R). Le mode $\rho_{w,s}$($PtN_2$) (ir, $B_{3u}$) n'est pas observé. Les précédentes attribu-

Can. J. Chem. Downloaded from www.nrcresearchpress.com by 210.87.254.5 on 09/06/12
For personal use only.

Can. J. Chem. Downloaded from www.nrcresearchpress.com by 210.87.254.5 on 09/06/12
For personal use only.

TABLEAU 1. Fréquences Raman et infrarouge du complexe $[(NH_3)_2Pt(OH)_2Pt(NH_3)_2](NO_3)_2$ et de ses dérivés isotopiques (H/D, $^{16}O/^{18}O$) sous forme solide[a]

| Dimère | | Dimère $^{18}O$ | | Dimère deutérié | | Attributions | |
|---|---|---|---|---|---|---|---|
| Raman | Infrared | Raman | Infrared | Raman | Infrared | Descriptions | $D_{2h}$[b] |
| 40 f | | 40 | | | | | |
| 50 TF | | 50 F | | 49 F | | Vibrations du réseau | |
| 56 f | | 55 f | | 54 ep | | | |
| 66 F | | 67 m | | 65 m | | | |
| 83 TF | | 85 TF | | 83 TF | | $\delta_s(Pt_2O_2)$ def. cycle | $A_g$ |
| 100 F | | 103 F | | 90 F | | | |
| 128 F | | 130 F | | 130 F | | $\rho_{\tau,as}(PtN_2)$ | $B_{1g}$ |
| 146 F | | 147 F | | 143 F | | $\rho_{w,as}(PtN_2)$ | $B_{2g}$ |
| | | | | 168 | | | |
| 181 | | | | | | | |
| 211 | | 210 | | 193 | | $\rho_{r,s}(PtN_2)$ | $B_{3g}$ |
| 222 ep | | | | | | | |
| | 270 m | | | | 248 m | $\delta_{as}(PtN_2)$ | $B_{1u}$ |
| 275 f,l | | 276 f,l | | 248 f,l | | $\delta_s(PtN_2)$ | $A_g$ |
| 353 | | | | | | | |
| | 410 | | 410 | | | | |
| 488 | | 468 | | 473 | | $\nu_{as}$(PtO) cycle | $B_{3g}$ |
| | 495 F | | 471 | | 482 m | $\nu$(PtO) cycle | $B_{1u}$, $B_{2u}$ |
| 504 f | | 481 f | | 495 | | $\nu_s$(PtO) resp. cycle | $A_g$ |
| | 532 F | | 505 F | | 494 ep | $\nu_{as}^{op}(PtN) + \nu(PtO)$ | $B_{2u}$ |
| 532 | | | 520 ep | | 520 ep | | |
| | 550 m | | 540 f | | 532 m | $\nu_s^{op}(PtN) + \nu(PtO)$ | $B_{1u}$ |
| 552 | | 552 | | 515 | | $\nu_{as}^{ip}(PtN)$ | $B_{3g}$ |
| 558 TF | | 559 TF | | 525 TF | | $\nu_s^{ip}(PtN)$ | $A_g$ |
| | | | | 533 ep | | | |
| 706 | | 706 | | 707 | | $\nu_4 NO_3^-$ | |
| 718 | 724 | 716 | 730 | 718 | | | |
| | 759 | | 762 | | | | |
| | 794 f | | 795 | | | | |
| | 819 F | | 820 F | | | $\nu_2 NO_3^-$ | |
| | 824 F | | 827 F | | 825 F | | |
| | 843 m | | 840 m | 660 | 600 m | | |
| 879 | 863 m | 871 | 864 m | 679 | 622 m | $\rho_r(NH_3)$ | |
| | 908 | | 904 | | 650 | | |
| | 1000 ep | | 1003 ep | | | | |
| | 1040 m | | 1038 m | 773 | 780 m | $\delta$(Pt-OH) | |
| 1046 TF | | 1046 TF | | 1046 TF | | $\nu_1 NO_3^-$ | |
| 1318 | 1312 F | 1319 | 1312 F | 1023 ep | 1021 F | | |
| 1349 | 1322 F | 1350 | 1325 F | | 1041 ep | $\delta_s(NH_2)$ | |
| 1396 | | 1396 | 1360 ep | | | | |
| | 1385 F | | 1384 TF | 1381 | 1386 TF | $\nu_3 NO_3^-$ | |
| | | | | 1105 | | | |
| 1573 | 1551 m | 1571 | 1552 m | 1152 | 1082 | | |
| 1596 | 1582 m | 1592 | 1584 m | 1168 | 1145 f | $\nu_{as}(NH_2)$ | |
| | 1608 f | | 1610 f | | 1165 ep | | |
| | | | | 1325 | | | |
| | | | | 2275 f | | | |
| 3107 | 3100 TF | 3108 | 3110 TF | 2310 f | | $\nu_s$(NH) | |
| | 3160 TF | | 3160 TF | 2344 f | 2380 F | | |
| | | | | 2372 | | | |
| | | 3186 ep | | 2400 | | | |
| 3224 | 3245 TF | 3226 f | 3342 TF | 2434 | 2425 TF | $\nu_{as}$(NH) | |
| 3253 ep | | 3254 ep | 3315 ep | 2467 | | | |
| 3310 | 3460 ep | 3311 | 3460 m,ep | 2515 | | $\nu$(OH) | |

[a]Abréviations: ep, épaulement; l, large; TF, très forte; F, forte; m, moyenne; f, faible; ip, en phase; op, en opposition de phase. Les raies non libellées ont une intensité très faible.
[b]Symétrie locale du squelette $[N_2PtO_2PtN_2]$.

Can. J. Chem. Downloaded from www.nrcresearchpress.com by 210.87.254.5 on 09/06/12
For personal use only.

tions proposées sont confirmées par l'analyse en coordonnées normales du squelette des complexes (voir partie 2 (5)).

L'attribution précise des différentes raies associées aux divers mouvements de vibration d'un cycle biponté est dans le cas présent assez complexe étant donné que les groupes hydroxo et les ligands $NH_3$ ont des masses similaires $m(OH) \simeq m(NH_3)$, que les liaisons PtN et PtO ont des longueurs pratiquement égales ($PtN = 2.03_0$ Å $\simeq PtN = 2.01_5$ Å (2)) et que les mouvements impliquant les liaisons platine–oxygène et platine–azote sont de même symétrie. Le problème a cependant été résolu sans trop de difficultés, en particulier par l'obtention des spectres Raman et infrarouge du complexe $^{18}O$.

En accord avec les analyses en coordonnées normales d'un cycle biponté quadriatomique plan (15, 16), les fréquences de vibration d'élongation sont exprimées en termes de fréquences symétriques et antisymétriques du pont simple. La fréquence de respiration du cycle $\nu_s(PtO)$ est observée à 504 $cm^{-1}$, 495 $cm^{-1}$ et 481 $cm^{-1}$ (Raman) pour les complexes H, D, $^{18}O$. Le mouvement de type antisymétrique $B_{3g}$ est attribué à la raie $\nu_{as}(PtO)$ pointée à 488 $cm^{-1}$, 473 $cm^{-1}$ et 468 $cm^{-1}$ (Raman, H, D, $^{18}O$). Pour l'infrarouge, la bande forte à 495 $cm^{-1}$ (482 $cm^{-1}$: D; 471 $cm^{-1}$: $^{18}O$) est attribuée à la fois à $\nu_s(PtO)$ et $\nu_{as}(PtO)$. Cette coïncidence des deux modes de vibration actifs en infrarouge, de symétrie $B_{1u}$, $B_{2u}$, est observée en particulier dans les cycles *carrés* plans (c'est-à-dire PtOPt = 90°) (voir l'analyse théorique dans les travaux de Baran (17)).

On constate (voir Tableau 1) que la substitution $^{18}O$ conduit à un déplacement des fréquences infrarouge $\nu_s(PtN)$ et $\nu_{as}(PtN)$ de l'ordre d'une dizaine de $cm^{-1}$ alors que les fréquences Raman associées aux $\nu(PtN)$ ne sont pas affectées. Cette anomalie trouve une explication dans le cadre de l'analyse en coordonnées normales (5) qui indique en fait, que les fréquences ir $\nu_s(PtO)$ et $\nu_s(PtN)$ d'une part et $\nu_{as}(PtO)$ et $\nu_{as}(PtN)$ d'autre part sont fortement couplées. Seul le mode $A_g$ de déformation angulaire du cycle $\delta_s(Pt_2O_2)$ est observé à 83 $cm^{-1}$ (R) dans le complexe. Cette fréquence ne bouge pas dans les complexes D ou $^{18}O$.

*Couplages squelette–ligands*

Les bandes des modes "rocking", $\rho_r(NH_3) = \rho_r(PtNH)$, sont vues à 879 $cm^{-1}$ (R), 843, 863, 908 $cm^{-1}$ (ir) pour le dimère et se déplacent à 660, 679 $cm^{-1}$ (R), 600, 622, 650 $cm^{-1}$ (ir) pour le deutérité. Il s'avère qu'il est quasiment impossible d'attribuer les modes de torsion de type $\tau(HNPtO)$ et $\tau(HNPtN')$ (ce dernier est observé aux environs de 200 $cm^{-1}$ dans les complexes carrés plans tétraammines (8)).

1. B. Rosenberg. Cancer Chemother. Rep. **59**, 589 (1975).
2. R. Faggiani, B. Lippert, C. J. L. Lock et B. Rosenberg. J. Am. Chem. Soc. **99**, 77 (1977).
3. R. Faggiani, B. Lippert, C. J. L. Lock et B. Rosenberg. Inorg. Chem. **16**, 1192 (1977).
4. A. J. P. Alix, M. Manfait, J. Delaunay-Zeches et T. Theophanides. 28ème Symposium Canadien de Spectroscopie, 28–30 Sept., Ottawa (1981).
5. A. J. P. Alix, M. Manfait, O. Krug et T. Theophanides. Can. J. Chem. **60**, 2222 (1982).
6. A. J. P. Alix, L. Bernard, M. Manfait, P. K. Ganguli et T. Theophanides. Inorg. Chim. Acta, **55**, 147 (1981).
7. T. Theophanides. Applied Spectrosc. **35**, 461 (1981).
8. M. Manfait, A. J. P. Alix, L. Bernard et T. Theophanides. J. Raman Spectrosc. **7**, 143 (1978).
9. A. J. P. Alix, M. Manfait, B. N. Cyvin, S. J. Cyvin, B. J. Van Der Veken et T. Theophanides. J. Chim. Phys. (France), **76**, 475 (1979).
10. J. R. Ferraro et W. R. Walker. Inorg. Chem. **4**, 1382 (1965).
11. J. R. Ferraro, R. Driver, W. R. Walker et W. Wozniak. Inorg. Chem. **6**, 1586 (1967).
12. P. A. Bulliner, V. A. Maroni et T. G. Spiro. Inorg. Chem. **8**, 1023 (1969).
13. P. A. Bulliner, V. A. Maroni et T. G. Spiro. Inorg. Chem. **9**, 1887 (1970).
14. K. Nakamoto. Infrared spectra of inorganic and coordination compounds. John Wiley & Sons, New York. 1963.
15. M. Manfait, A. J. P. Alix et T. Theophanides. En préparation.
16. R. M. Wing et K. P. Callahan. Inorg. Chem. **8**, 871 (1969).
17. V. Baran. J. Mol. Struct. **13**, 4 (1972); **13**, 11 (1972); **29**, 335 (1975).

# Vibrations moléculaires du nitrate de di-μ-hydroxo-bis(diammine) platine (II) $[(NH_3)_2Pt(OH)_2Pt(NH_3)_2](NO_3)_2$. Partie 2: analyse en coordonnées normales[1]

ALAIN J. P. ALIX,[2] MICHEL MANFAIT ET ODILE KRUG

*Laboratoire de Recherches Optiques, Faculté des Sciences, B.P. 347, 51062 Reims-Cedex, France*

ET

THÉOPHILE THEOPHANIDES[2]

*Laboratoire de Chimie de Coordination, Faculté des Arts et Sciences, Université de Montréal, C.P. 6210, Montréal (Qué.), Canada H3C 3V1*

Reçu le 10 mars 1982

ALAIN J. P. ALIX, MICHEL MANFAIT, ODILE KRUG et THÉOPHILE THEOPHANIDES. Can. J. Chem. **60**, 2222 (1982).

Une analyse complète en coordonnées normales a été conduite pour le squelette [$N_2'$ Pt $O_2'$ Pt $N_2'$] du nitrate de di-μ-hydroxo-bis(diammine) platine(II) dans le cadre de l'approximation du point et en assumant une configuration de symétrie $D_{2h}$.

La méthode de construction d'une base de 18 coordonnées de symétrie indépendantes repose sur la théorie des vibrations moléculaires dans le système de coordonnées rectilignes dépendantes. Un champ de forces général de valence est obtenu par raffinement et reproduit d'une façon satisfaisante les fréquences de la molécule mère et de son dérivé deutérié. Le calcul de toutes les distributions énergétiques permet la description des modes normaux et spécialement ceux impliqués dans les vibrations du cycle carré plan ($Pt_2O_2$) qui présentent des coulages importants.

Additionnellement, nous avons calculé indépendamment certains fragments du complexe dimère entier qui peuvent être ainsi comparés avec des molécules de même type.

ALAIN J. P. ALIX, MICHEL MANFAIT, ODILE KRUG, and THÉOPHILE THEOPHANIDES. Can. J. Chem. **60**, 2222 (1982).

A full normal coordinate analysis of the skeleton [$N_2'$ Pt $O_2'$ Pt $N_2'$] of the di-μ-hydroxo-bis(diammine) platinum(II) nitrate has been performed according to the Point Mass Model approximation and assuming a $D_{2h}$ molecular symmetry.

The method of construction of a set of 18 independent symmetry valence coordinates was based on the theory of molecular vibrations in dependent rectilinear coordinates. A refined general valence force field which reproduces satisfactorily the frequencies of the molecule and its deuterated analog has been obtained. Calculations of all distributions of vibrational energy allow us to describe all normal modes of vibration and especially the ones related to the square planar ring modes ($Pt_2O_2$) showing evidence of strong couplings.

In addition we have calculated independently some fragments of the whole dimeric complex, which may be used for comparison with related compounds.

## Introduction

Dans la première partie de ce travail (1), nous avons présenté en détail l'analyse par spectroscopie Raman et infrarouge du complexe dinucléaire ponté: nitrate de di-μ-hydroxo-bis(diammine platine(II)) de formule $[(NH_3)_2$ Pt $(OH)_2$ Pt $(NH_3)_2)]$ $(NO_3)_2$ et de certains de ses dérivés isotopiques (substitution H/D, $^{16}O/^{18}O$).

Dans le présent travail, nous reportons l'analyse complète en coordonnées normales du complexe dans l'approximation du point massique (PMM: "point mass model" (2, 3)); c'est-à-dire que les groupes ($NH_3$) et (OH) sont respectivement réduits aux points N′ et O′ de masse $m(N') = m(NH_3)$ et $m(O') = m(OH)$. Le calcul de l'édifice [$N_2'$ Pt $O_2'$ Pt $N_2'$], de symétrie $D_{2h}$, correspond alors au calcul du squelette du complexe considéré.

L'utilisation du formalisme de la théorie des vibrations moléculaires en coordonnées rectilignes dépendantes (pour détails voir réfs. 4–8), conduit à la définition d'une base de 18 coordonnées internes de valence et/ou de 18 coordonnées symétriques indépendantes n'impliquant pas les relations de redondances. Ce système se révèle ainsi particulièrement adéquat pour décrire les vibrations du complexe entier ou de ses divers fragments pris indépendemment tels que: pont simple Pt O Pt, double pontage $Pt_2O_2'$, monomère $O_2'$ Pt $N_2'$...

Un champ de forces général de valence est obtenu par raffinement et reproduit d'une façon exacte les fréquences observées pour le complexe (H) et assez satisfaisante pour le dérivé deutérié (D). Le calcul de l'ensemble des distributions d'énergie: potentielle (PED), cinétique (KED), totale (TED) et vibrationnelle (PKTED) donne la description des modes normaux de vibration et révèle les couplages (cinématiques et dynamiques) entre les mouvements du cycle carré plan ($Pt_2O_2'$) et des édifices terminaux ($PtN_2'$).

## Expérimentation

*Paramètres structuraux* (voir Fig. 1)

Les distances Pt—N = 2,01$_5$ Å et Pt—O = 2,03 Å sont issues des résultats de diffraction des rayons X de Faggiani *et al.* (9). Le cycle $Pt_2$ $O_2$ est supposé parfaitement plan et carré. Les

[1]Présentée au 28ème Symposium Canadien de Spectroscopie, Ottawa, Ontario, Canada, 28–30 septembre 1981.

[2]Auteur à qui toute correspondance doit être adressée.

0008-4042/82/172222-07$01.00/0

©1982 National Research Council of Canada/Conseil national de recherches du Canada

Can. J. Chem. Downloaded from www.nrcresearchpress.com by 210.87.254.42 on 09/06/12
For personal use only.

Can. J. Chem. Downloaded from www.nrcresearchpress.com by 210.87.254.42 on 09/06/12
For personal use only.

angles $\beta = \widehat{NPtN}$ sont fixés à la valeur 90° ce qui implique la définition des angles plats $\delta = \widehat{NPtO}$ (hors du plan).

L'analyse en coordonnées normales du complexe entier sera effectué dans le cadre de l'approximation du modèle des masses ponctuelles (PMM = "Point Mass Model" (2, 3)). Les groupes OH et $NH_3$ sont rassemblés aux points O′ et N′ de masses respectives $m(O') = m(O) + m(H)$ et $m(N') = m(N) + 3m(H)$.

On constate ainsi dans le cas du squelette non deutéré que, non seulement l'ensemble des distances relatives aux liaisons de pont (PtO) et terminales (PtN) sont sensiblement identiques, mais que les masses des atomes réduits sont presque égales ($m(O') \simeq m(N')$). Il est alors prévisible que les mouvements correspondants du cycle $Pt_2O_2'$ et des groupements terminaux $Pt\,N_2'$ seront d'énergie comparable et donc qu'il est à envisager d'importants couplages (au moins du type cinématique) entre les différents mouvements.

*Spectres Raman et infrarouge* (fréquences observées)

Les spectres Raman et infrarouge du complexe $[(NH_3)_2\,Pt(OH)_2\,Pt\,(NH_3)_2](NO_3)_2$ et de ses dérivés isotopiques (substitutions H/D, $^{16}O/^{18}O$) ont été décrits en détail dans la première partie de ce travail (1). L'attribution des fréquences observées a été faite dans réf. 1 conjointement au présent travail, c'est-à-dire que dans tous les cas possibles d'ambiguité (voir par exemple les raies Raman à 83 $cm^{-1}$ ($A_g$), 128 $cm^{-1}$ ($B_{1g}$), 146 $cm^{-1}$ ($B_{2g}$) et 211 $cm^{-1}$ ($B_{3g}$)), l'analyse en coordonnées normales a été conduite pour chaque cas de permutation des fréquences. Les valeurs excessives ou même aberrantes des constantes de force internes de valence obtenues pour l'un ou l'autre de ces calculs nous ont permis de rejeter les permutations correspondantes hormis l'attribution finale qui est reportée dans le Tableau 1.

## Coordonnées internes de valence

La figure 1 représente le squelette $[N_2'\,Pt\,O_2'\,Pt\,N_2']$ du complexe, ainsi que l'ensemble des coordonnées internes de valence qui permettent de décrire les différentes variations des liens et angles valenciels.

Le système complet de coordonnées internes $\mathbf{R}^c$ comprend ainsi 26 coordonnées internes soit 8 coordonnées surabondantes. Un système plus simple peut-être défini en ne prenant pas en compte les angles $\alpha_i$ et $\varepsilon_i$ et conduit au système tronqué $\mathbf{R}^t$ comprenant 22 coordonnées (dont 4 surabondantes). Ce système a l'avantage de ne pas faire intervenir directement les paramètres reliés aux coordonnées $\alpha_i$ et $\varepsilon_i$ tels que par exemple $f_\varepsilon = f(\widehat{Pt\,O'\,Pt}), f_\alpha = f(\widehat{O'PtO'})$... dont on trouve peu de données dans la littérature.

Le système de 18 coordonnées internes de valence indépendantes $\mathbf{R}^{ind}$ est obtenu en prenant des combinaisons symétriques $t$ et $\tau$ des coordonnées du système $\mathbf{R}^t$, soit $\mathbf{R}^{ind} = \{4r_i, 4R_i, 4\gamma_i, 4\delta_i, t, \tau\}$ ou: $t = 2^{-1/2}(\beta_1 + \beta_2)$ et $\tau = 2^{-1}(\tau_1 - \tau_2 + \tau_3 - \tau_4)$.

Les relations de redondances sont alors implicitement exprimées dans la relation:

$$[1] \quad \mathbf{R}^{ind} = \mathbf{T}\mathbf{R}^c$$

faisant intervenir le formalisme de la matrice $\mathbf{T}$ reliant les systèmes dépendant $\mathbf{R}^c$ et indépendant $\mathbf{R}^{ind}$ (pour détails et expressions analytiques de $\mathbf{T}$, voir réfs. 4–8).

TABLEAU 1. Fréquences du squelette $[N_2'\,Pt\,O_2'\,Pt\,N_2']$, distribuées suivant les espèces de $D_{2h}$ et utilisées pour le calcul des constantes de force

| Espèce | $k^a$ | $\nu_k{}^b$ | Description$^c$ |
|---|---|---|---|
| | 2 | 558 | $\nu_s^{ip}$(Pt—N) |
| $A_g$(R) | 1 | 504 | $\nu_s$(Pt—O) |
| | 3 | 275 | $\delta_s$(Pt $N_2$) |
| | 4 | 83 | $\delta_s$($Pt_2O_2$) |
| $B_{1g}$(R) | 5 | 128 | $\rho_{t,as}$(Pt $N_2$) |
| $B_{2g}$(R) | 6 | 146 | $\rho_{w,as}$(Pt $N_2$) |
| | 8 | 552 | $\nu_{as}^{ip}$(Pt N) |
| $B_{3g}$(R) | 7 | 488 | $\nu_{as}$(Pt O) |
| | 9 | 211 | $\rho_{r,as}$(Pt $N_2$) |
| $A_u$(—) | 10 | (108)$^d$ | $\rho_{t,s}$(Pt $N_2$) |
| | 12 | 550 | $\nu_s^{op}$(Pt N) |
| $B_{1u}$(ir) | 11 | 495 | $\nu_{as}$(Pt O) |
| | 13 | 270 | $\delta_{as}$(Pt $N_2$) |
| | 15 | 532 | $\nu_{as}^{op}$(Pt N) |
| $B_{2u}$(ir) | 14 | 495 | $\nu_s$(Pt O) |
| | 16 | (150)$^d$ | $\rho_r$(Pt $N_2$) |
| $B_{3u}$(ir) | 17 | (150)$^d$ | $\rho_{w,s}$(Pt $N_2$) |
| | 18 | (40)$^d$ | $\tau$($Pt_2$ $O_2$) |

$^a$Cette colonne donne la numérotation des fréquences en accord avec celle des coordonnées de symétrie (voir Tableau 2).
$^b$Fréquence observées en $cm^{-1}$ (R et ir solide).
$^c$Description préliminaire; ip en phase; op en opposition de phase (voir aussi Tableau 2).
$^d$Fréquences assumées, voir texte.

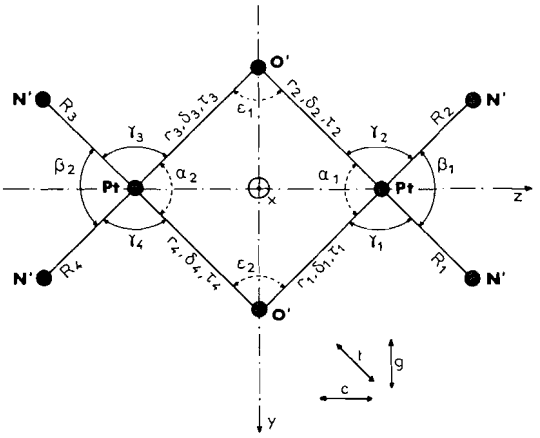


FIG. 1. Modèle moléculaire pour le squelette $[N_2'\,Pt\,O_2'\,Pt\,N_2']$ ($D_{2h}$). Coordonnées internes de valence ($i$ = 1–4; $j$ = 1–2): $t = 2^{-1/2}(\beta_1 + \beta_2)$, $\tau = 2^{-1}(\tau_1 - \tau_2 + \tau_3 - \tau_4)$; $\mathbf{R}^c = \{r_i, R_i, \alpha_j, \beta_i, \gamma_i, \delta_i, \varepsilon_j, \tau_i\}$; $\mathbf{R}^t = \{r_i, R_i, —, \beta_i, \gamma_i, \delta_i, —, \tau_i\}$; $\mathbf{R}^{ind} = \{r_i, R_i, —, t, \gamma_i, \delta_i, —, \tau\}$.

## Coordonnées de symétrie indépendantes

Le squelette du complexe est supposé parfaitement plan et de symétrie idéalisée $D_{2h}$. Il lui

TABLEAU 2. Coordonnées de symétrie du squelette $[N_2^t\ Pt\ O_2^t\ Pt\ N_2^t]$ $(D_{2h})$

| Espèce | $N_0{}^a$ | $N^b$ | $c$ | Combinaison$^d$ | Description$^e$ |
|---|---|---|---|---|---|
| $A_g$ | $S_1$ | $2^{-1}$ | | $r_1+r_2+r_3+r_4$ | $Pt_2O_2$: respiration du cycle |
| | $S_2$ | $2^{-1}$ | | $R_1+R_2+R_3+R_4$ | Pt $N_2$: élongation, symétrique |
| | $S_3$ | 1 | $R$ | $t$ | Pt $N_2$: ciseau, symétrique |
| | $S_4$ | $2^{-1}$ | $(Rr)^{1/2}$ | $\gamma_1+\gamma_2+\gamma_3+\gamma_4$ | $Pt_2O_2/PtN_2$: déformation, symétrique |
| $B_{1g}$ | $S_5$ | $2^{-1}$ | $(Rr)^{1/2}$ | $\delta_1-\delta_2-\delta_3-\delta_4$ | Pt $N_2$: torsion angulaire O.P. (g,as) |
| $B_{2g}$ | $S_6$ | $2^{-1}$ | $(Rr)^{1/2}$ | $\delta_1+\delta_2-\delta_3-\delta_4$ | Pt $N_2$: balancement O.P. (g,as) |
| $B_{3g}$ | $S_7$ | $2^{-1}$ | | $r_1-r_2+r_3-r_4$ | $Pt_2O_2$: élongation anti-symétrique en phase |
| | $S_8$ | $2^{-1}$ | | $R_1-R_2+R_3-R_4$ | Pt $N_2$: élongation anti-symétrique en phase |
| | $S_9$ | $2^{-1}$ | $(Rr)^{1/2}$ | $\gamma_1-\gamma_2+\gamma_3-\gamma_4$ | Pt $N_2$: rotation plane (g,s) |
| $A_u$ | $S_{10}$ | $2^{-1}$ | $(Rr)^{1/2}$ | $\delta_1-\delta_2+\delta_3-\delta_4$ | Pt $N_2$: torsion angulaire (u,s) |
| $B_{1u}$ | $S_{11}$ | $2^{-1}$ | | $r_1+r_2-r_3-r_4$ | $Pt_2O_2$: élongation (u,s) |
| | $S_{12}$ | $2^{-1}$ | | $R_1+R_2-R_3-R_4$ | Pt $N_2$: élongation (u,s) |
| | $S_{13}$ | $2^{-1}$ | $(Rr)^{1/2}$ | $\gamma_1+\gamma_2-\gamma_3-\gamma_4$ | $Pt_2O_2$: déformation du cycle |
| $B_{2u}$ | $S_{14}$ | $2^{-1}$ | | $r_1-r_2-r_3+r_4$ | $Pt_2O_2$: élongation anti-symétrique |
| | $S_{15}$ | $2^{-1}$ | | $R_1-R_2-R_3+R_4$ | Pt $N_2$: élongation anti-symétrique |
| | $S_{16}$ | $2^{-1}$ | $(Rr)^{1/2}$ | $\gamma_1-\gamma_2-\gamma_3+\gamma_4$ | Pt $N_2$: rotation plane (u,as) |
| $B_{3u}$ | $S_{17}$ | $2^{-1}$ | $(Rr)^{1/2}$ | $\delta_1+\delta_2+\delta_3+\delta_4$ | Pt $N_2$: balancement O.P. (u,s) |
| | $S_{18}$ | 1 | $r$ | $\tau$ | $Pt_2O_2$: torsion dy cycle |

[a] Coordonnées de symétrie indépendantes.
[b] Facteur de normalisation.
[c] Facteur d'échelle (coordonnées homogènes à des longueurs).
[d] Combinaison symétrique des coordonnées internes de valence indépendantes.
[e] Description du mouvement correspondant à la coordonnée de symétrie.
g: gerade, u: ungerade, s: symétrique/X,Y, as: anti-symétrique/X,Y; O.P. hors du plan.

correspond alors 18 fréquences fondamentales de représentation:

$$\Gamma = 4A_g(\mathrm{R}) + B_{1g}(\mathrm{R}) + B_{2g}(\mathrm{R}) + 3B_{3g}(\mathrm{R}) + A_u(—) + 3B_{1u}(\mathrm{ir}) + 3B_{2u}(\mathrm{ir}) + 2B_{3u}(\mathrm{ir})$$

On construit un système **S** de 18 coordonnées de symétrie indépendantes à partir du système $\mathbf{R}^{ind}$, par les méthodes classiques de théorie des groupes (10), soit:

[2] $\quad \mathbf{S} = \mathbf{U}\mathbf{R}^{ind}$

où, **U** est une matrice orthogonale. Le Tableau 2 donne les coordonnées de symétrie du squelette ainsi que la description des mouvements correspondants.

## Champ de forces général de valence

*Principes de la méthode*

La méthode standard des matrices **G** et **F** de Wilson *et al.* (10) et le formalisme de la matrice **T** (4–8) permet de définir un champ de forces général de valence symétrique sous la forme:

[3] $\quad \mathbf{F} = \mathbf{U}\mathbf{F}^{ind}\tilde{\mathbf{U}}$

où, $\mathbf{F}^{ind}$ représente la matrice des constantes de force internes de valence définit dans le système indépendant $\mathbf{R}^{ind}$. Les relations entre $\mathbf{R}^c$ et $\mathbf{R}^{ind}$ conduisent à l'expression:

[4] $\quad \mathbf{F}^{ind} = \tilde{\mathbf{T}}\mathbf{F}^c\mathbf{T}$

La matrice **F** est obtenue par raffinement, à partir d'une solution initiale $\mathbf{F}^{(0)}$ de l'équation séculaire

[5] $\quad |\mathbf{G}\mathbf{F}^{(0)} - \lambda\mathbf{E}| = 0$

où $\mathbf{F}^{(0)}$ est définie par le modèle cinématique de la méthode de couplage pas à pas (introduction linéaire des éléments extradiagonaux de **G**: pour détails voir la revue sur les méthodes d'approximations du champ de forces Alix *et al.* (11) et réfs. 12 et 13).

Les constantes de forces internes de valence $\mathbf{F}^{ind}$ sont alors calculées à partir de [3] sous la forme:

[6] $\quad \mathbf{F}^{ind} = \tilde{\mathbf{U}}\mathbf{F}\mathbf{U}$

La connaissance des paramètres du système complet $\mathbf{R}^c$ passe ainsi par la définition des compliances définies selon (4–8):

[7] $\quad \mathbf{n}^{ind} = [\mathbf{F}^{ind}]^{-1}$

[8] $\quad \mathbf{n}^c = \mathbf{T}\mathbf{n}^{ind}\tilde{\mathbf{T}}$

Ainsi que démontré par Alix (7, 8), seules les constantes de force $\mathbf{F}_{ij}{}^c$ associées aux coordonnées internes indépendantes sont déductibles directement des constantes correspondantes $\mathbf{F}_{ij}{}^{ind}$. Toutes les autres constantes $\mathbf{F}_{ij}{}^c$ associées à une ou deux coordonnées de redondances restent indéterminées (i.e., la matrice $\mathbf{F}^c$ reste indéterminable à

Can. J. Chem. Downloaded from www.nrcresearchpress.com by 210.87.254.42 on 09/06/12
For personal use only.

Can. J. Chem. Downloaded from www.nrcresearchpress.com by 210.87.254.42 on 09/06/12
For personal use only.

partir de $\mathbf{F}^{ind}$ car la relation [4] ne peut être inversée, **T** étant rectangulaire). Il en résulte que nous ne donnerons dans ce travail que les valeurs numériques des constantes de forces indépendantes $\mathbf{F}_{ij}^{ind}$.

*Détermination pratique des constantes de force*

La résolution de l'équation séculaire [5] nécessite au préalable la définition complète de la matrice Λ des valeurs $\lambda_k$ reliées aux fréquences observées par la relation:

$$[9] \quad \lambda_k = \frac{4\pi^2 \nu_k^2}{c^2 \mathcal{N}} = \left[\frac{\nu_k(\text{cm}^{-1})}{1303{,}16}\right]^2$$

Les fréquences non observées $\nu_{16}$, $\nu_{17}$ et $\nu_{18}$ (infrarouge) ont été fixées aux valeurs respectives 150, 150 et 40 $cm^{-1}$. Ce choix repose sur la comparaison des résultats obtenus pour des composés soit de même type, soit de même symétrie (14–19).

Les mouvements hors du plan Pt $N_2$ peuvent ainsi être classés de la façon suivante:

torsion angulaire: [100–130 $cm^{-1}$]; $\rho_{t,as} = 128\ cm^{-1}$(R)

balancement: [≃150 $cm^{-1}$]; $\rho_{\omega,as} = 146\ cm^{-1}$(R)

rotation plane: [150–200 $cm^{-1}$]; $\rho_{r,s} = 211\ cm^{-1}$(R)

La torsion du cycle $Pt_2O_2$ est assumée à 40 $cm^{-1}$.

La fréquence $\nu_{10}(A_u)$ étant inactive, a été calculée en imposant la condition $f_{\delta\delta}{}^t = 0$. Il en résulte que le mouvement hors du plan de torsion angulaire symétrique ($\rho_{t,s}$(Pt $N_2$)) a une fréquence calculée à 108 $cm^{-1}$.

Le champ de forces raffiné, symétrique de valence est reporté dans le Tableau 3. Le Tableau 4 présente les constantes de force internes de valence indépendantes ($F_{ij}^{ind}$) les plus significatives. Les constantes n'apparaissant pas dans le Tableau 4 peuvent être considérées comme nulles (i.e., $F_{rr}{}^t$, $F_{RR}{}^t$, $F_{RR}{}^c$, $F_{\beta R}$, $F_{\delta\delta}{}^g$, $F_{\delta\delta}{}^t$, $F_{\delta\tau}$, $F_{r\gamma}$, $F_{R\gamma}$ etc.).

Le Tableau 5 donne les fréquences calculées pour le complexe (H) et son dérivé deutérié (D). Le champ de forces raffiné reproduit ainsi d'une façon parfaite les fréquences de la molécule mère et d'une façon satisfaisante, celles de son isotopomère.

Le Tableau 6 présente les distributions d'énergie vibrationnelle en termes de contribution des diverses coordonnées de symétrie $S_i$ aux modes normaux de vibration $Q_k$ de fréquence $\nu_k$ (pour détails voir réfs. 20–24). Pour des raisons d'économie d'impression,[3] nous ne donnerons pas les

TABLEAU 3. Constantes de forces symétriques de valence[a] (champ de forces raffiné)

$$F(A_g) = \begin{vmatrix} 2{,}502_5 & & & \\ 0{,}048_2 & 2{,}799_3 & & \\ 0{,}098_6 & 0{,}015_2 & 0{,}406_2 & \\ 0{,}168_5 & 0{,}024_8 & 0{,}124_2 & 0{,}255_8 \end{vmatrix}$$

$$F(B_{1g}) = |0{,}0531|$$

$$F(B_{2g}) = |0{,}125_3|$$

$$F(B_{3g}) = \begin{vmatrix} 2{,}158_9 & & \\ -0{,}003_9 & 2{,}753_9 & \\ -0{,}064_1 & 0{,}017_5 & 0{,}280_0 \end{vmatrix}$$

$$F(A_u) = |(0{,}115_1)^b|$$

$$F(B_{1u}) = \begin{vmatrix} 2{,}346_7 & & \\ -0{,}018_2 & 2{,}670_3 & \\ -0{,}360_4 & -0{,}034_7 & 0{,}739_1 \end{vmatrix}$$

$$F(B_{2u}) = \begin{vmatrix} 2{,}339_5 & & \\ -0{,}032_5 & 2{,}506_6 & \\ 0{,}106_2 & 0{,}010_2 & 0{,}215_7 \end{vmatrix}$$

$$F(B_{3u}) = \begin{vmatrix} 0{,}063_3 & \\ 0{,}009_4 & 0{,}023_9 \end{vmatrix}$$

[a] Toutes les constantes $F_U$ sont exprimées en mdyn/Å.
[b] $f_{\delta\delta}{}^t = 0$ implique $F(A_u) = F(B_{1u}) + F(B_{2g}) - F_{11}(B_{3u})$.
[c] Les calculs ont été effectués avec 7 chiffres significatifs; seules les 4 premières décimales sont reportées dans le tableau.

TABLEAU 4. Constantes de force internes de valence indépendantes ($f_{ij}^{ind}$)

| Constantes[a] | Types[b] | Valeurs[c] |
|---|---|---|
| $f_r$ | $f$(Pt O) | $2{,}33_7$ |
| $f_{rr}^g$ | $f$(Pt O, Pt O') | $0{,}08_8$ |
| $f_{rr}^c$ | $f$(Pt O, Pt O) | $0{,}08_4$ |
| $f_R$ | $f$(Pt N) | $2{,}68_3$ |
| $f_{RR}^g$ | $f$(Pt N, Pt N') | $0{,}05_2$ |
| $f_\beta$ | $f$(Pt $N_2$) | $0{,}40_6$ |
| $f_{\beta r}$ | $f$(Pt $N_2$, Pt O) | $0{,}05_0$ |
| $f_{\beta\gamma}$ | $f$(Pt $N_2$, N Pt O) | $0{,}06_2$ |
| $f_\gamma$ | $f$(N Pt O) | $0{,}37_3$ |
| $f_{\gamma\gamma}^g$ | $f$(N Pt O, N'Pt O') | $0{,}12_5$ |
| $f_{\gamma\gamma}^t$ | $f$(N Pt O, N'Pt'O') | $-0{,}10_5$ |
| $f_{\gamma\gamma}^c$ | $f$(N Pt O, N'Pt'O) | $-0{,}13_7$ |
| $f_\delta$ | $f(\overline{\text{N Pt O}})$ | $0{,}08_9$ |
| $f_{\delta\delta}^c$ | $f(\overline{\text{N Pt O}}, \overline{\text{N'Pt'O}})$ | $-0{,}05_1$ |
| $f_\tau$ | $f$(Pt O Pt O') | $0{,}02_4$ |
| $f_{r\gamma}^g$ | $f$(Pt O, O'Pt N) | $-0{,}05_9$ |
| $f_{r\gamma}^t$ | $f$(Pt O, O'Pt'N') | $0{,}09_0$ |
| $f_{r\gamma}^c$ | $f$(Pt O, OPt'N') | $0{,}12_2$ |

[a] Les indices supérieurs c, g, t sont utilisés respectivement pour definir les intéractions *cis*, *gem* et *trans* (voir Fig. 1).
[b] Le symbole prime est utilisé pour distinguer deux atomes de même nature; ex. PtO,PtO' = $r_1, r_2$ et/ou $r_3, r_4$ etc.
[c] Valeurs en mdyn/Å; excepté pour $f_\tau$, les valeurs inférieures à |0,05| ne sont pas reportées.

[3] L'ensemble des calculs tels que matrices **G**, **F**, **L**, **Λ** et les distributions d'énergie DEP, DEC, DET sont à la disposition de tout lecteur qui en ferait la demande.

Can. J. Chem. Downloaded from www.nrcresearchpress.com by 210.87.254.42 on 09/06/12
For personal use only.

distributions d'énergie potentielle, cinétique et totale définies selon:

[10] DEP: $V_{ij}^{(k)} = F_{ij} L_{ik} L_{jk}/\lambda_k$ (PED)

[11] DEC: $T_{ij}^{(k)} = (\mathbf{G}^{-1})_{ij} L_{ik} L_{jk}$ (KED)

[12] DET: $E_{ij}^{(k)} = [V_{ij}^{(k)} + T_{ij}^{(k)}]/2$ (TED)

L'étude détaillée de ces diverses distributions indique que les couplages cinématiques sont très importants (DEC), et ceci essentiellement pour les vibrations associées aux mouvements du cycle carré plan: voir pour détails la correspondance entre les Tableaux 2 et 6.

On retiendra en particulier de la détermination du champ de forces général de valence raffiné pour la molécule et son dérivé deutérié, les valeurs suivantes des constantes de force internes de valence indépendantes (mdyn/Å):

$$F_r(\mathrm{PtO}) = 2{,}33_7 \qquad F_R(\mathrm{Pt\ N}) = 2{,}68_3 \qquad F_r/F_R = 0{,}87$$
$$F_\beta(\widehat{\mathrm{NPtN}}) = 0{,}40_7 \qquad F_\gamma(\widehat{\mathrm{NPtO}}) = 0{,}37_3 \qquad F_\delta(\widehat{\mathrm{NPtO}}) = 0{,}08_9$$

## Calculs additionnels

*Champ de forces des divers fragments du complexe*

Indépendamment de la détermination du champ de forces raffiné pour le complexe [$N_2'$ Pt $O_2'$ Pt $N_2'$], $\mathscr{D}_{2h}$, nous avons calculé les constantes de force associées aux divers fragments du complexe pour lesquels nous avons transféré ou attribué les fréquences de vibration en fonction de la nature et de la symétrie propre (locale) du fragment considéré (voir Tableau 7).

*(i) Pont [Pt O' Pt]:* $\mathscr{C}_{2v}(2a_1 + b_1)$

Le transfert des fréquences $\nu_1 = 504 = \nu_s(\mathrm{PtO})$; $\nu_4 = 83 = \nu_s(\mathrm{O'Pt_2})$ et $\nu_7 = 488\,\mathrm{cm^{-1}} = \nu_{as}(\mathrm{PtO})$, conduit à la valeur $f_r(\mathrm{PtO}) = 2{,}44\,\mathrm{mdyn/Å}$. Les autres constantes de force ont cependant des valeurs inacceptables (i.e., $f_{rr}^c, f_\varepsilon$).

*(ii) Double pont: [cycle $Pt_2O_2'$]:* $\mathscr{D}_{2h}(2a_g + b_{3g} + b_{1u} + b_{2u} + b_{3u})$

L'étude des cycles bipontés de type [$M_2L_2$] (M = métal, L = ligand) a fait l'objet de travaux théoriques précis, en particulier pour le cas du pontage par l'oxygène (25–28). Il a ainsi été mis en évidence par Baran (25, 26), une forte corrélation entre les valeurs des fréquences infrarouges d'élongations symétrique et anti-symétrique $\nu_s(\mathrm{MO})$, $\nu_{as}(\mathrm{MO})$ et celle de l'angle $\widehat{\mathrm{MOM}}$. Pour un cycle carré plan, $\widehat{\mathrm{MOM}} = 90°$, les fréquences tombent en parfaite coïncidence, ce qui est le cas effectivement observé pour le dimère ($\nu_s = \nu_{as} = 495\,\mathrm{cm^{-1}}$).

Les constantes de force significatives ont été

TABLEAU 5. Fréquences calculées pour le complexe et son dérivé deutérié (champ de forces raffiné)

| Espèces | Complexe (H) | | Complexe (D) | |
|---|---|---|---|---|
| | $\nu_k$(calculées) | $\nu_k$(obs.) | $\nu_k$(calculées) | $\nu_k$(obs.) |
| $A_g$(R) | 504 | 504 | 484 | 495 |
| | 558 | 558 | 525 | 525 |
| | 273 | 273 | 253 | 248 |
| | 83 | 83 | 82 | 83 |
| $B_{1g}$(R) | 128 | 128 | 120 | 130 |
| $B_{2g}$(R) | 146 | 146 | 140 | 143 |
| $B_{3g}$(R) | 488 | 488 | 471 | 473 |
| | 552 | 552 | 517 | 515 |
| | 211 | 211 | 200 | 193 |
| $A_u$(—) | 107,6 | — | 99 | — |
| $B_{1u}$(ir) | 495 | 495 | 473 | 482 |
| | 550 | 550 | 520 | 527 |
| | 270 | 270 | 251 | 248 |
| $B_{2u}$(ir) | 495 | 495 | 469 | 482 |
| | 532 | 532 | 507 | 494 |
| | 150 | — | 139 | — |
| $B_{3u}$(ir) | 150 | — | 145 | — |
| | 40 | — | 38 | — |

TABLEAU 6. Distributions d'énergie vibrationnelle[a] $(\mathrm{PKTED})_i^k = L_{ik}(\mathbf{L}^{-1})_{ki}$

| Fréquences calculées[b] | Distributions[c] |
|---|---|
| $\nu_1 = 504$ | 81% $S_1$ + 14% $S_2$ |
| $\nu_2 = 558$ | 86% $S_2$ + 14% $S_1$ |
| $\nu_3 = 273$ | 93% $S_3$ + 6% $S_4$ |
| $\nu_4 = 83$ | 92% $S_4$ + 6% $S_3$ |
| $\nu_5 = 126$ | 100% $S_5$ |
| $\nu_6 = 146$ | 100% $S_6$ |
| $\nu_7 = 488$ | 84% $S_7$ + 8% $S_8$ + 8% $S_9$ |
| $\nu_8 = 552$ | 92% $S_8$ + 8% $S_7$ |
| $\nu_9 = 211$ | 92% $S_9$ + 8% $S_7$ |
| $\nu_{10} = 108$ | 100% $S_{10}$ |
| $\nu_{11} = 495$ | 60% $S_{11}$ + 22% $S_{12}$ + 18% $S_{13}$ |
| $\nu_{12} = 550$ | 78% $S_{12}$ + 19% $S_{11}$ |
| $\nu_{13} = 270$ | 79% $S_{13}$ + 23% $S_{11}$ |
| $\nu_{14} = 495$ | 65% $S_{14}$ + 31% $S_{15}$ |
| $\nu_{15} = 532$ | 69% $S_{15}$ + 28% $S_{14}$ |
| $\nu_{16} = 150$ | 93% $S_{16}$ + 7% $S_{14}$ |
| $\nu_{17} = 150$ | 94% $S_{17}$ + 6% $S_{18}$ |
| $\nu_{18} = 40$ | 94% $S_{18}$ + 6% $S_{17}$ |

[a] $\mathrm{PKTED}_i^{(k)} = V_i^{(k)} = T_i^{(k)} = E_i^{(k)}$.
[b] Fréquences calculées en $\mathrm{cm^{-1}}$ (champ de forces raffiné).
[c] Seules les contributions supérieures à 5% sont reportées ici.

Can. J. Chem. Downloaded from www.nrcresearchpress.com by 210.87.254.42 on 09/06/12
For personal use only.

calculées aux valeurs suivantes: $F_r(\mathrm{PtO}) = 2{,}26$, $f_\tau(\mathrm{Pt_2\,O_2}) = 0{,}00_7$.

Les interactions de type $f_{rr}$ ont des valeurs négligeables, ce qui justifie la proximité des fréquences d'élongation du cycle $Pt_2O_2$ (c.-à-d., 504, 488 et 495 $cm^{-1}$).

*(iii) "Monomère" [$O_2'$ Pt $N_2'$]:* $\mathscr{C}_{2v}$ $(4a_1 + a_2 + b_1 + 3b_2)$

L'étude indépendante de la moitié de l'édifice global conduit à des résultats très intéressants dans la mesure ou les constantes de force obtenues ont des valeurs parfaitement acceptables et comparables avec celles du complexe entier (voir Tableau 4):

$F_r(\mathrm{PtO}) = 2{,}36_7$ $\quad F_R(\mathrm{PtN}) = 2{,}67_3$ $\quad F_r/F_R = 0{,}88_6$

$F_\beta(\mathrm{NPtN}) = 0{,}34_4$ $\quad f_\gamma(\mathrm{NPtO}) = 0{,}08_3$ $\quad f_\delta(\overline{\mathrm{NPtO}}) = 0{,}06_9$

$F^g_{RR}(\mathrm{PtN,PtN'}) = 0{,}13_0$ $\quad F^g_{rR} = 0{,}04_8$

On constate que le champ de forces symétrique de valence est sensiblement diagonal. Les seuls termes non diagonaux sont relatifs aux interactions $F_{12}(A_1)$ et $F_{12}(B_2)$.

*Champ de forces symétrique simplifié pour le complexe entier*

A partir des résultats préliminaires issus de l'étude des différents fragments, il a été recherché par raffinement la possibilité de déterminer un champ de forces de valence symétrique simplifié pour le squelette complet. Ce champ diagonal est défini par $F_{ij} = 0\ \forall_i, \forall_j$. Les calculs montrent qu'il n'est pas possible de reproduire correctement les fréquences des espèces $A_g$ et $B_{1u}$ sans introduire de constantes d'interaction ou sans obtenir de valeurs aberrantes pour les constantes de force principales.

Les valeurs $F_{ii}$ obtenues pour le champ de forces simplifié sont les suivantes: $A_g$: 1,90, 2,80, $0{,}22_5$, 0,45; $B_{3g}$: 2,00, 2,75, 0,30; $B_{1u}$: 1,60, 2,40, 1,00; $B_{2u}$: 2,07, 2,43, 0,25.

Les autres constantes correspondant aux espèces de dimension 1 ($B_{1g}$, $B_{2g}$, $A_u$) sont les mêmes que celles obtenues pour le champ de forces général de valence symétrique (voir Tableau 3).

On déduit du champ de forces symétrique de valence diagonal, les valeurs suivantes des constantes de force internes de valence:

$f_r(\mathrm{Pt\ O}) = 1{,}90$ $\quad f_R(\mathrm{PtN}) = 2{,}60$ $\quad F_r/F_R = 0{,}73$

$f_\beta(\mathrm{NPtN}) = 0{,}22_6$ $\quad f_\gamma(\mathrm{NPtO}) = 0{,}50$ $\quad f_\delta(\overline{\mathrm{NPtO}}) = 0{,}09$

## Discussion et conclusion

Dans ce travail nous avons pu déterminer un champ de forces général de valence raffiné pour un complexe du type [$Z_2$ X $Y_2$ X $Z_2$], de symétrie $D_{2h}$, présentant un cycle carré plan $X_2$ $Y_2$. Il existe assez peu d'exemples dans la littérature d'analyses en coordonnées normales complètes de complexes dinucléaires de même types ou de même symétries.

Nous tenons à souligner l'importance pratique de la méthode de travail proposée, c.-à-d., la détermination des constantes de forces dans un système de coordonnées indépendantes ($\mathbf{R}^{ind}$ et/ou **S**), n'impliquant pas les redondances d'une façon explicite. Les calculs des divers fragments du complexe sont parfaitement cohérents avec ceux du squelette complet, et peuvent ainsi servir de base à un raffinement d'un champ de forces général (surtout dans les cas où il existe peu de données dans la littérature, et où il s'avère difficile de transférer des valeurs de constantes de force; c'est le cas des composés comportant des liaisons platine–oxygène).

Les travaux d'Adams *et al.* (29, 30), sur les composés $[M_2X_6]^{2-}$, (M = Pt, Pd, Au, Al; X = Br, Cl, I), conduisent à la détermination de quelques constantes de force internes de valence (champ de forces symétrique diagonal), dont en particulier $f_r$ et $f_R$, satisfaisant le rapport $f_r/f_R$ = 75–100% (X = Cl → Br → I.).

Les résultats présentés dans ce travail sont cohérents avec ceux d'Adams *et al.* Les rapports $f_r/f_R = f(\mathrm{Pt—O})/f(\mathrm{Pt—N}) = f_r(\mathrm{cycle})/f_R(\mathrm{terminal})$ sont respectivement égaux à: 0,87: champ de forces général du squelette entier; 0,89: champ de forces général du "monomère"; et 0,73: champ de forces simplifié (diagonal) du squelette entier.

Les valeurs finales $f_r(\mathrm{Pt—O}) = 2{,}34$ et $f_R(\mathrm{Pt—N}) = 2{,}68$ mettent en évidence le caractère prononcé de la liaison platine–oxygène. Ce résultat fondamental tend à corroborer l'existence d'un méca-

TABLEAU 7. Correspondances entre les espèces des fréquences du complexe entier et de ses divers fragments

| Complexe entier | | | Fragments | | | | | |
|---|---|---|---|---|---|---|---|---|
| | | | [PtO'Pt] | | [$Pt_2O_2$] | | [$O_2'PtN_2'$] | |
| $\nu_k$ | $k$ | $\mathscr{D}_{2h}$ | $k$ | $C_{2v}$ | $k$ | $D_{2h}$ | $k$ | $C_{2v}$ |
| 504 | 1 | $A_g$ | 1 | $a_1$ | 1 | $a_g$ | 1 | $a_1$ |
| 558 | 2 | $A_g$ | | | | | 2 | $a_1$ |
| 273 | 3 | $A_g$ | | | | | 3 | $a_1$ |
| 83 | 4 | $A_g$ | 2 | $a_1$ | 2 | $a_g$ | 4 | $a_1$ |
| 128 | 5 | $B_{1g}$ | | | | | | |
| 146 | 6 | $B_{2g}$ | | | | | 6 | $b_1$ |
| 488 | 7 | $B_{3g}$ | 3 | $b_1$ | 3 | $b_{3g}$ | | |
| 552 | 8 | $B_{3g}$ | | | | | | |
| 211 | 9 | $B_{3g}$ | | | | | | |
| 108 | 10 | $A_u$ | | | | | 5 | $a_2$ |
| 495 | 11 | $B_{1u}$ | | | 4 | $b_{1u}$ | | |
| 550 | 12 | $B_{1u}$ | | | | | | |
| 270 | 13 | $B_{1u}$ | | | | | | |
| 495 | 14 | $B_{2u}$ | | | 5 | $b_{2u}$ | 7 | $b_2$ |
| 332 | 15 | $B_{2u}$ | | | | | 8 | $b_2$ |
| 150 | 16 | $B_{2u}$ | | | | | 9 | $b_2$ |
| 150 | 17 | $B_{3u}$ | | | | | | |
| 40 | 18 | $B_{3u}$ | | | 6 | $b_{3u}$ | | |

nisme d'interaction *cis*-platine-ADN impliquant des ponts platine–oxygène Pt—O6 (guanine) et/ou Pt—O (ribose phosphate) (voir nos travaux (31–33) sur les interactions complexes du platine(II) – acides nucléiques).

## Remerciements

A.J.P.A. tient à remercier le Département de Chimie de l'Université de Montréal pour toutes les facilités offertes.

1. M. MANFAIT, A. J. P. ALIX, J. DELAUNAY-ZECHES et T. THEOPHANIDES. Can. J. Chem. **60**, 0000 (1982).
2. T. SHIMANOUCHI. J. Chem. Phys. **17**, 245 (1949); J. Chem. Soc. Jpn. Pure Chem. Sect. **74**, 266 (1953); Pure Appl. Chem. **7**, 131 (1963).
3. T. SHIMANOUCHI et J. NAKAGAWA. Spectrochim. Acta, **18**, 89 (1962).
4. S. J. CYVIN. Molecular structures and vibrations. Elsevier, Amsterdam. 1972. Chapt. 6.
5. A. J. P. ALIX et O. KRUG. C. R. Acad. Sci. Ser. B, **288**, 347 (1979).
6. O. KRUG. Thèse doctorat 3° cycle, Reims, octobre 1980.
7. A. J. P. ALIX. 2[d] World/European Conference on Spectroscopy, Antwerpen, juin 1981.
8. A. J. P. ALIX. En préparation.
9. R. FAGGIANI, B. LIPPERT, C. J. L. LOCK et B. ROSENBERG. J. Am. Chem. Soc. **99**, 777 (1977).
10. E. B. WILSON, JR., J. C. DECIUS et P. C. CROSS. Molecular vibrations, McGraw-Hill, New York. 1955.
11. A. J. P. ALIX, H. H. EYSEL, B. JORDANOV, R. KEBABCIOGLU, N. MOHAN et A. MÜLLER. J. Mol. Struct. **27**, 1 (1975).
12. A. J. P. ALIX et L. BERNARD. J. Mol. Struct. **20**, 51 (1974); C.R. Acad. Sci. Ser. B, **276**, 933 (1973).
13. A. J. P. ALIX et B. J. VAN DER VEKEN. Bull. Soc. Chem. Belg. **84**, 111 (1975); J. Chem. Phys. **74**, 81 (1977).
14. M. MANFAIT, A. J. P. ALIX, L. BERNARD et T. THEOPHANIDES. J. Raman Spectrosc. **7**, 143 (1978).
15. A. J. P. ALIX, M. MANFAIT, B. N. CYVIN, S. J. CYVIN, B. J. VAN DER VEKEN et T. THEOPHANIDES. J. Chim. Phys. **76**, 475 (1979).
16. D. M. ADAMS, P. J. CHANDLER et R. G. CHURCHILL. J. Chem. Soc. A, 1272 (1967); D. M. ADAMS et R. G. CHURCHILL. J. Chem. Soc. A, 2141 (1968).
17. I. R. BEATIE, T. GILSON et G. A. OZIN. J. Chem. Soc. A, 813 (1968).
18. R. FORNERIS, J. HIRAISHI, F. A. MILLER et M. UEHARA. Spectrochim. Acta, Part A, **26**, 581 (1970).
19. J. R. FERRARO et W. R. WALKER. Inorg. Chem. **4**, 1382 (1965); J. R. FERRARO, R. DRIVER, W. R. WALKER et W. WOZNIAK. Inorg. Chem. **6**, 1586 (1967).
20. A. J. P. ALIX. Thèse doctorat ès Sciences Physiques, Reims, octobre 1973 (no A.O. CNRS 9063).
21. A. J. P. ALIX et L. BERNARD. C. R. Acad. Sci. Ser. B, **278**, 525 (1974); A. J. P. ALIX et A. MÜLLER. J. Mol. Struc. **24**, 229 (1975).
22. A. J. P. ALIX, D. E. FREEMAN et A. MÜLLER. Z. Naturforsch. Teil A, **29**, 1454 (1974).
23. A. J. P. ALIX et E. RYTTER. Z. Naturforsch. Teil A, **35**, 463 (1980); **35**, 1142 (1980).
24. A. J. P. ALIX. Spectrosc. Lett. **14**, 441 (1981).
25. V. BARAN. Inorg. Nucl. Chem. Lett. **6**, 375 (1970).
26. V. BARAN. J. Mol. Struct. **13**, 1 (1972); **13**, 11 (1972); **29**, 335 (1975).
27. J. S. ANDERSON et J. S. OGDEN. J. Chem. Phys. **51**, 4189 (1969).
28. J. S. OGDEN et M. J. RICKS. J. Chem. Phys. **52**, 352 (1970); **53**, 896 (1970).
29. D. M. ADAMS, P. J. CHANDLER et R. G. CHURCHILL. J. Chem. Soc. A, 1272 (1967).
30. D. M. ADAMS et R. G. CHURCHILL. J. Chem. Soc. A, 2141 (1968).
31. A. J. P. ALIX, L. BERNARD, M. MANFAIT, P. K. GANGULI et T. THEOPHANIDES. Inorg. Chim. Acta, **55**, 147 (1981).
32. T. THEOPHANIDES. Appl. Spectrosc. **35**, 461 (1981).
33. M. MANFAIT. Thèse de Doctorat ès Sciences, Reims, décembre 1981.

Can. J. Chem. Downloaded from www.nrcresearchpress.com by 210.87.254.42 on 09/06/12
For personal use only.

# Synthesis of metal-chelates of amino sugars: Schiff's base complexes[1]

MICHAEL J. ADAM[2] AND LAURANCE D. HALL

*Department of Chemistry, University of British Columbia, Vancouver, B.C., Canada V6T 1Y6*

Received February 25, 1982

MICHAEL J. ADAM and LAURANCE D. HALL. Can. J. Chem. **60**, 2229 (1982).

Metal-complexing, salicylaldimine ligands **4**, **7**, **8**, and **9** have been synthesized from 2-amino-2-deoxy-D-glucopyranose and some of its derivatives with salicylaldehyde and 3-formyl-2-hydroxybenzoic acid. Copper(II), zinc, and cobalt(II) complexes were formed from ligand **7**, whereas only copper(II) would complex with ligand **8**. The sugar ligand **4** forms a water-soluble complex with copper(II) and ligand **9** forms a binuclear copper(II) complex. These products have been studied by $^1$H nmr, visible absorption, and esr spectroscopy, mass spectrometry, and by their magnetic moment data.

MICHAEL J. ADAM et LAURANCE D. HALL. Can. J. Chem. **60**, 2229 (1982).

Utilisant l'amino-2 désoxy-2 D-glucopyrannose ainsi que quelques-uns de ses dérivés et la salicylaldéhyde ainsi que l'acide formyl-3 hydroxy-2 benzoïque, on a préparé les ligands du type salicylaldimine, **4**, **7**, **8** et **9**, qui sont des complexants métalliques. On a préparé les complexes de cuivre(II), de zinc et de cobalt(II) à partir du ligand **7**, tandis que seul le cuivre(II) peut être complexé par le ligand **8**. Le ligand **7** forme un complexe soluble dans l'eau avec le cuivre(II) et le ligand **9** forme un complexe binucléaire de cuivre(II). On a caractérisé ces produits par la rmn du $^1$H, par les spectres d'absorption dans le visible, par les spectres de rpe et de masse et par leurs données de moment magnétique.

[Traduit par le journal]

## Introduction

In spite of the fact that it has been known for about 100 years (2, 3) that sugars can form complexes with metals, the field of sugar–metal complexes is still largely unexplored. For example, although at least 70 crystalline complexes which contain a sugar and an inorganic salt have been reported (2) since 1973, these complexes are mainly restricted to group IA and IIA metals, and their structures are, for the most part, unknown. Literature on the complexation of sugars with transition metals and metals other than those in groups IA and IIA is in comparison much more recent (4) and less abundant.

The ability of sugars to sequester metals is of current interest for a wide variety of reasons, some of the more important of which include the possible development of novel classes of metal-based affinity chromatography materials (5), chiral homogeneous catalysts (6), metal-chelators for clinical use (7), and of models for biologically important chelates (8). Further interests include nuclear magnetic resonance studies of the interactions of many metals with sugars (9, 10). These and many other studies would be advanced by the development of general methods whereby metals can be readily attached to sugars.

Metal complexes of Schiff's bases have occupied a central role in the development of coordination chemistry (11) and, since 1840, a tremendous variety of stable chemical species have been synthesized containing either transition or nontransition metals. That amino sugars form Schiff's bases readily with salicylaldehyde and other aromatic aldehydes (12) has been known since 1922 (13) when Irvine and Earl first showed that sparingly water-soluble Schiff's bases of 2-amino-2-deoxy-D-glucopyranose (glucosamine) could be formed with salicylaldehyde. Prompted by this knowledge, we have explored the formation of metal complexes from such amino sugar – Schiff's base ligands. We start this by discussing the synthesis of Schiff's base ligands of salicylaldehyde and 3-formyl-2-hydroxybenzoic acid with both alkylamine and glucosamine derivatives, along with their metal complexes. Then visible absorption spectroscopy, esr and nmr spectroscopy, mass spectrometry, and magnetic moments are examined as tools for the structure determination of the compounds synthesized.

## Results and discussion

### *Synthesis*

#### *Schiff's base formation*

The Schiff's base ligands considered here are derived from 2-hydroxybenzaldehyde (salicylaldehyde) **1** and 3-formyl-2-hydroxybenzoic acid (3-aldehydro-salicylic acid) **2**. The reaction between 2-amino-2-deoxy-D-glucopyranose hydrochloride **3** and salicylaldehyde is very easily accomplished, using sodium bicarbonate in aqueous methanol, with the water-insoluble product **4** being obtained

[1]For a preliminary communication see ref. 1.

[2]Present Address: TRIUMF, University of British Columbia, Vancouver, B.C., Canada V6T 2A3.

0008-4042/82/172229-09$01.00/0

©1982 National Research Council of Canada/Conseil national de recherches du Canada

Can. J. Chem. Downloaded from www.nrcresearchpress.com by 210.87.254.5 on 09/06/12
For personal use only.

Can. J. Chem. Downloaded from www.nrcresearchpress.com by 210.87.254.5 on 09/06/12
For personal use only.

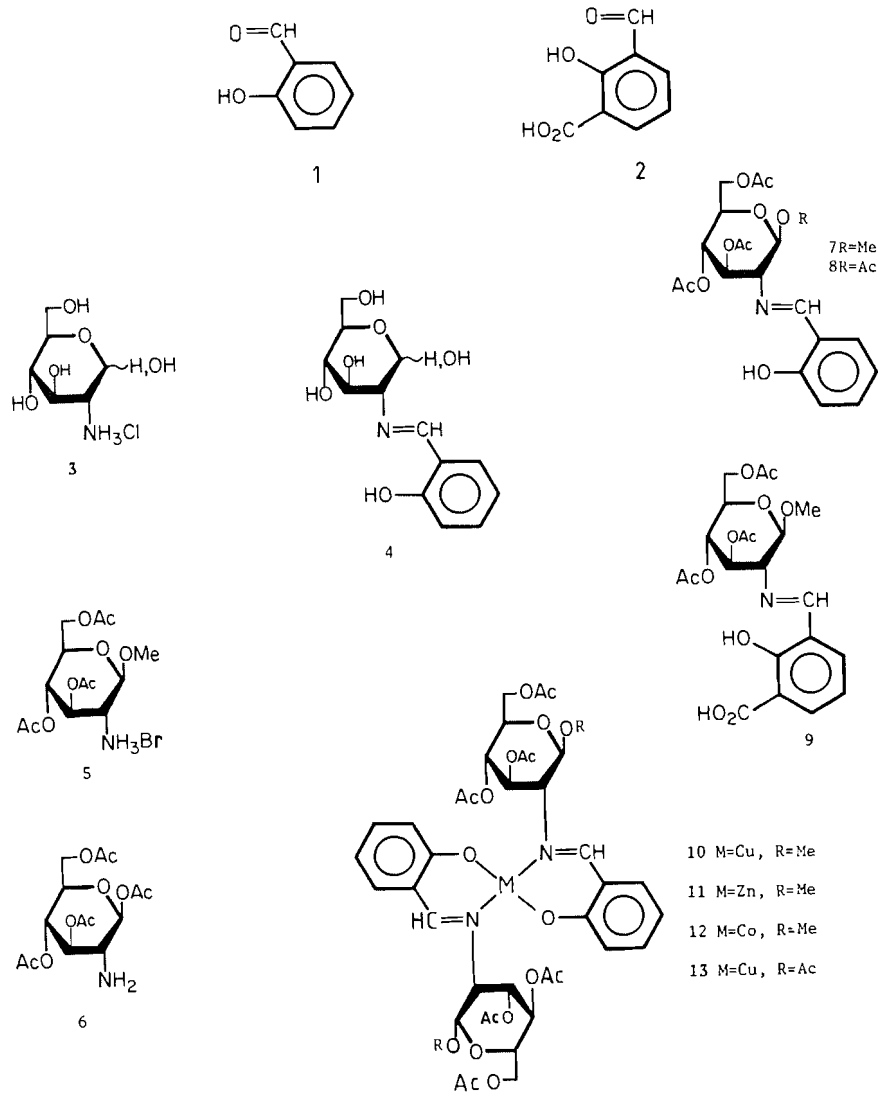


in a high yield (13). As well as the parent sugar, glucosamine derivatives such as methyl 3,4,6-tri-*O*-acetyl-2-amino-2-deoxy-β-D-glucopyranoside hydrobromide **5** (14) and 1,3,4,6-tetra-*O*-acetyl-2-amino-2-deoxy-β-D-glucopyranose **6** (15) also condense with salicylaldehyde to form the Schiff's bases **7** and **8** respectively.

Schiff's bases formed from 3-aldehydo-salicylic acid **2**, in comparison to the salicylaldehyde derivatives, previously have received very little attention and, to our knowledge, syntheses of such derivatives from amino sugars have not before been reported. The formation of the Schiff's base between the blocked glucosamine sugar **5** and this aldehyde readily afforded compound **9** in high yield.

The sugar – Schiff's base compounds **4**, **7**, **8**, and **9** are crystalline stable compounds (as are their alkyl counterparts) and are bright yellow in color. These compounds are, however, acid- and base-labile due to their azomethine linkage.[3]

*Schiff's base – metal complexes*

Salicylaldimine–metal complexes are generally readily prepared by reaction, in alcoholic solution, of the salicylaldimine with a metal ion (usually acetate salt) or by the condensation of an amine with the preformed salicylaldehyde–metal complex. The products usually precipitate and can be easily purified by recrystallization.

[3]Sugar Schiff's bases are, fortunately, stable to cold anhydrous acylating reagents. Thus, the amino sugar **6** was prepared by using *p*-methoxybenzaldehyde as an amino blocking group with subsequent acetylation and Schiff's base cleavage.

Can. J. Chem. Downloaded from www.nrcresearchpress.com by 210.87.254.5 on 09/06/12
For personal use only.

Although the latter synthetic method has been used by other workers more often than the former, it was found in this study that the first method was more suitable for the formation of sugar complexes. Thus, when a methanol solution of cupric acetate was added to a methanol solution of **7** at room temperature, the copper–sugar complex **10** precipitated immediately as a brown solid in 90% yield.[4]

The ir spectrum showed a shift in the —C=N— absorption to lower frequency compared with the parent ligand (**7**, 1630 $cm^{-1}$; **10**, 1590 $cm^{-1}$), indicating the coordination of the nitrogen atom to the copper ion.

Both zinc and cobaltous acetate also complexed with the ligand **7** in methanol to form the yellow and green bis-complexes, **11** and **12**, respectively; the yields for these complexes were, however, lower than that obtained for the copper analogue, being 41% and 51% respectively. Surprisingly, nickel(II) complexes could not be formed using any of the sugar ligands, even though most simple alkyl salicylaldimine ligands readily complex with nickel(II). When Ni(II) acetate was mixed with a methanol solution of the sugar ligand no colour change could be seen, and both starting materials were recovered upon volume reduction. If the sugar amine was condensed with the preformed salicylaldehyde–nickel complex, the sugar–salicylaldimine was isolated after work-up, indicating that condensation takes place, but that the metal dissociates from the ligand. This lack of complexation may be due to the combined effects of a normally lower stability constant for nickel–salicylaldimine complexes compared to the analogous copper(II) complexes, and the possibility that the sugar–salicylaldimines are poorer ligands. Although stability constants were not determined for these sugar complexes, some evidence of the suggestions that they are more labile than their alkyl counterparts is derived from the observation that the sugar complexes decomposed back to their parent ligands when run on silica gel thin-layer chromatography (tlc), whereas alkyl complexes such as Cu(cyclohexyl-sal)$_2$ are stable on silica gel. Furthermore, the zinc and cobalt complexes **11** and **12** decomposed when dissolved in hot methanol, and had to be recrystallized under cold conditions (see Experimental). Upon heating the green cobalt complex in methanol the solution turned orange, and after cooling and volume reduction the salicylaldehyde–cobalt complex was isolated, indicating that Schiff's base cleavage had occurred. In contrast, the copper complex **10** was stable to this treatment; thus, it seems that the zinc and cobalt complexes are more labile than the copper complex.

The sugar–salicylaldimine ligand **8** also forms a complex **13** with copper, subsequently proven to be Cu(SugII – sal)$_2$; this was obtained as shiny olive-green crystals in 90% yield when a hot, ethanolic solution of cupric acetate and ligand **8** were mixed and allowed to cool. This complex could be recrystallized from hot ethanol and decomposed only partially on silica gel tlc. However, attempted complexation of **8** with zinc and cobaltous acetate failed to yield any product.

One of the more interesting complexes prepared was the copper complex **15** of the free sugar–salicylaldimine ligand **4** which was highly water soluble. Although the structure **15** proposed for this complex was consistent with the evidence obtained from elemental analysis and mass spectrometry, the esr spectrum of this material indicates a mixture of compounds is present. This material also decomposed readily by Schiff's base cleavage and was, therefore, not successfully purified.

Complexes derived from 3-aldehydo-salicylic acid can be prepared by mixing the ligand and metal salt, usually the metal acetate, in an alcohol solution, and then filtering the precipitated product from the reaction mixture. For example, the reaction of the sugar ligand **9** and cupric acetate in ethanol resulted in a leaf-green product **16** in 80% yield. As will be discussed in more detail later, mass spectrometry and esr spectroscopy lead to the conclusion that this product has the binuclear copper structure as shown. The structure proposed previously by Poddar (16) for such complexes, where the nitrogen substituent R is nonbridging, is shown for **17**. We feel that this type of structure is highly unlikely in light of our own findings and also from simple model building (see below).

### *Proof of structure*

#### *Nuclear magnetic resonance spectroscopy*

In order for metal complexation to occur with the ligands **4**, **7**, **8**, and **9**, the hydroxyl function on the aromatic ring should be in close proximity with the nitrogen atom of the sugar group and probably strongly hydrogen bonded to it. Evidence for such hydrogen bonding comes from the characteristically low field shifts of the hydroxyl protons of **7**, **8**,

[4]For convenience the sugar unit shown in **10**, **11**, and **12** will be abbreviated as Sug I. In complexes incorporating the sugar units derived from compounds **6** and **3**, the sugar moiety will be abbreviated to Sug II and III respectively. Also, the metal complexes themselves will be abbreviated $M_x$(R-sal)$_y$ or $M_x$(R-salicylic)$_y$ where M is the metal, R is the amine group, $x$ or $y$ can be either one or two, sal = **1** and salicylic = **2**.

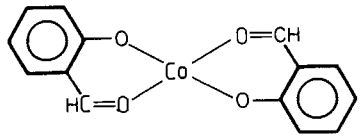

14

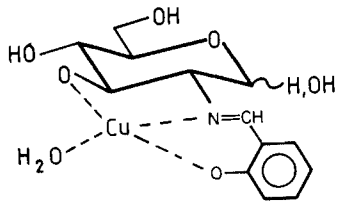

15

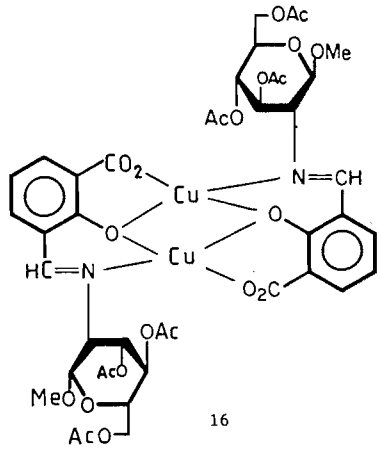

16

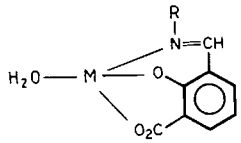

17

and **9**, (12.4 ppm, 12 ppm, and 14 ppm respectively).

Compound **9** has a very interesting proton nmr spectrum which provides additional evidence for the existence of a strong hydrogen bond in this molecule. The resonances of the imine-proton and H-2 are both broader than one would expect, and it can be shown by spin decoupling that this is a result of vicinal spin–spin coupling of these protons to the hydrogen-bonded hydroxyl protons; thus, irradiation of the hydroxyl resonance at 14 ppm results in sharpening of the imine and H-2 resonances. That these resonances show broadening rather than a clearly resolved coupling implies that the hydroxyl-proton is exchanging at an intermediate rate.

*Visible absorption studies*

Visible absorption spectroscopy was used to investigate the coordination geometry of the sugar–copper complexes Cu(SugI – sal)$_2$ **10**, and Cu(SugII – sal)$_2$ **13**, and the cobalt complex Co(SugI – sal)$_2$ **12**.

Although the visible absorption spectra of the Cu(R-sal)$_2$ complexes (where R = *n*-Bu, *i*-Pr, and *t*-Bu) have been reported elsewhere (17, 18), they have been remeasured here for comparison purposes, along with those of the sugar complexes, in order to obtain systematic information about their coordination geometry; all of the observed spectra are shown in Fig. 1.

The crystal structure of the complex Cu(R-sal)$_2$, where R = *n*-Bu, shows that this complex adopts a "normal" planar configuration (19). In contrast, complexes where R = *i*Pr and *t*-Bu are distorted toward tetrahedral configuration, and the inference is that this is due to the presence of bulky R groups because the *t*-Bu complex has more tetrahedral character than does the isopropyl complex.

When the *t*-Bu complex is dissolved, no structural change is observed (18), whereas when R = *i*-Pr or cyclohexyl, these complexes appear to exist in solution as an equilibrium mixture of square planar and pseudotetrahedral complexes as revealed by $^1$H nmr (20) and esr (17) studies.

All the visible spectra (*d–d* transitions) in Fig. 1 appear as shoulders on the long wavelength side of the intense bands in the near-ultraviolet, except for that of the Cu(*t*-Bu-sal)$_2$ derivative which appears as a broad peak. Although these spectra do not lend themselves to detailed discussion, one important observation concerning the three alkyl complexes, where R = *n*-Bu, *i*-Pr, and *t*-Bu, can be made; namely, the tendency for the intensities of the *d–d* spectra to increase and to shift to longer wavelengths, in the order *n*-Bu to *t*-Bu. This trend is consistent with a progressive distortion of the

Can. J. Chem. Downloaded from www.nrcresearchpress.com by 210.87.254.5 on 09/06/12
For personal use only.

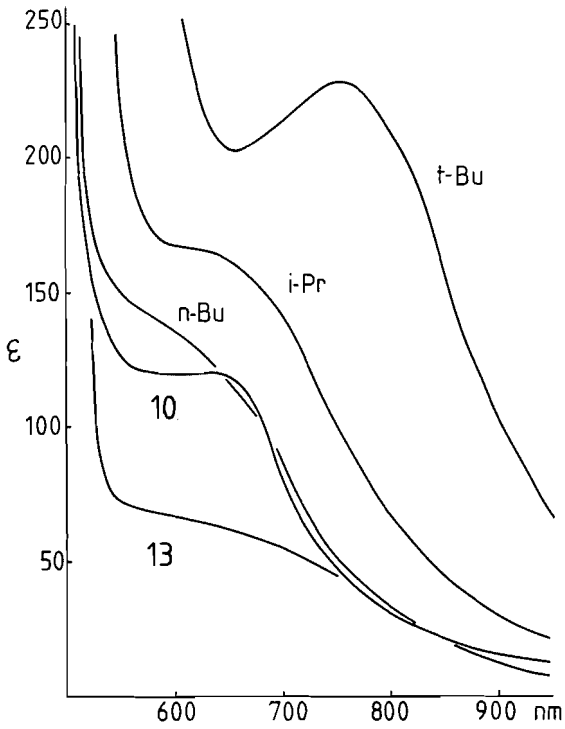


FIG. 1. Visible absorption spectra ($CHCl_3$), comparing the sugar–copper complexes **10** and **13** with the previously known analogous *N*-alkyl complexes where the nitrogen substituent is either *n*-butyl, *i*-propyl, or *tert*-butyl. As the alkyl group is changed from *n*-Bu to *t*-Bu (made more bulky) the intensity of the *d–d* spectra increases along with a shift to longer wavelength. The sugar complexes, however, do not fit into this sequence.

coordination geometry towards a tetrahedron (17, 18) with increase in the bulk of the R-group; the greater the tetrahedral distortion, the greater the spectral change.

That the spectra for the two sugar complexes **10** and **13** are not more similar to the spectrum of the *t*-Bu complex implies that the sugar substituents are effectively less bulky than the *t*-Bu group, possibly due to their lower effective symmetry. Of course, it may simply be that, due to the very different nature of sugar substituents, it is not possible to compare these complexes to those complexes in which R is an alkyl group.

The solid-mull visible spectrum of Cu(Sug I-sal)$_2$ **10** consists of three bands at 9500, 13500, and 20000 $cm^{-1}$ which is characteristic of a pseudotetrahedral Cu(R-sal)$_2$ complex (11, 17, 18). Therefore, the visible absorption spectra in the solid state and solution suggest that, when dissolved, this complex loses a significant amount of its tetrahedral character.

The visible spectrum of the cobalt–sugar complex Co(SugI-sal)$_2$ is straightforward and consists of three bands at 7300, 11250, and 17240 $cm^{-1}$. This suggests that it has the tetrahedral geometry expected for a cobalt(II)–salicylaldimine complex (18).

*Electron spin resonance spectroscopy*

All of the esr spectral parameters acquired in this work for the copper–sugar complexes and for the Cu(R-sal)$_2$ complexes where R = *n*-butyl, isopropyl, and *tert*-butyl are shown in Table 1. Here $g_0$ and $a_0$ are parameters from the room temperature solution spectrum and the $g_{||}$ and $A_{||}$ values are from the frozen 77 K solution or spin dilute powder spectrum. The room temperature solution spectra and the polycrystalline spectra for all of the complexes in Table 1 are shown in Figs. 2 and 3 respectively.

A classification of the Cu(R-sal)$_2$ complexes can be made on the basis of esr results in the same way as previously described for the visible absorption spectra (17). As the geometry becomes more tetrahedral in nature, the $A_{||}$ value becomes smaller, and at the same time $g_{||}$ and $g_0$ begin to increase while $a_0$ decreases, as does $A_{||}$. The Cu(R-sal)$_2$ complexes with R = *n*-butyl, isopropyl, and *tert*-butyl have esr parameters which clearly show the effect of tetrahedral distortion on these spectral parameters. As R changes from *n*-Bu to *t*-Bu, the *A* values decrease and the *g* values increase (Table 1 (c), (d), and (e)). The $g_{||}$ and $A_{||}$ parameters for the isopropyl complex are only approximate because this complex exists as a mixture of geometrical isomers in solution, which broadens the $g_{||}$ components, making them difficult to measure.

As was the case with the visible absorption data, it is not clear just where the sugar complexes Cu(Sug I-sal)$_2$ **10** and Cu(Sug II-sal)$_2$ **13** fall within the series of alkyl complexes. The *A* values suggest that the sugar complexes are square planar, but the *g* values put them about midway between the *n*-alkyl planar and *tert*-butyl pseudotetrahedral complexes.

When the copper complex **10** was cocrystallized in the Zn(sug I-sal)$_2$ matrix it was found to adopt the tetrahedral structure of the zinc complex. The characteristic tetrahedral $Cu^{2+}$ esr spectrum obtained (f) is quite different from that of the pure copper complex, which implies that the latter has little tetrahedral character.

Additional information concerning these complexes could be obtained from direct inspection of their esr spectra. The rate of tumbling of the complexes in solution (designated by the correlation time $\tau_c$) can affect the esr spectra dramatically,

Can. J. Chem. Downloaded from www.nrcresearchpress.com by 210.87.254.5 on 09/06/12
For personal use only.

Can. J. Chem. Downloaded from www.nrcresearchpress.com by 210.87.254.5 on 09/06/12
For personal use only.

TABLE 1. Electron spin resonance parameters for copper(II) complexes

| Complex | $g_0$ | $a_0 \times 10^{-4}$ cm$^{-1}$ | $g_{\|\|}$ | $A_{\|\|} \times 10^{-4}$ cm$^{-1}$ |
|---|---|---|---|---|
| (a) Cu(Sug I-sal)$_2$[a] | 2.129 | 64.6 | 2.246 | 167.8 |
| (b) Cu(Sug II-sal)$_2$[a] | 2.130 | 66.6 | 2.259 | 177.2 |
| (c) Cu(*n*-butyl-sal)$_2$[a] | 2.112 | 73.9 | 2.223 | 162.9 |
| (d) Cu(isopropyl-sal)$_2$[a] | 2.119 | 66.3 | ~2.23 | ~166 |
| (e) Cu(*t*-Bu-sal)$_2$[a] | ~2.14 | <50 | 2.271 | 135.7 |
| (f) Cu(Sug I-sal)$_2$[b] 0.5% in Zn(Sug I-sal)$_2$ | | | 2.258 | 129.7 |
| (g) Cu(Sug III-sal)[c] | 2.136 | ~65 | 2.263 | 176.4 |

[a]$CHCl_3$ solution.
[b]Powder.
[c]$H_2O$ solution.

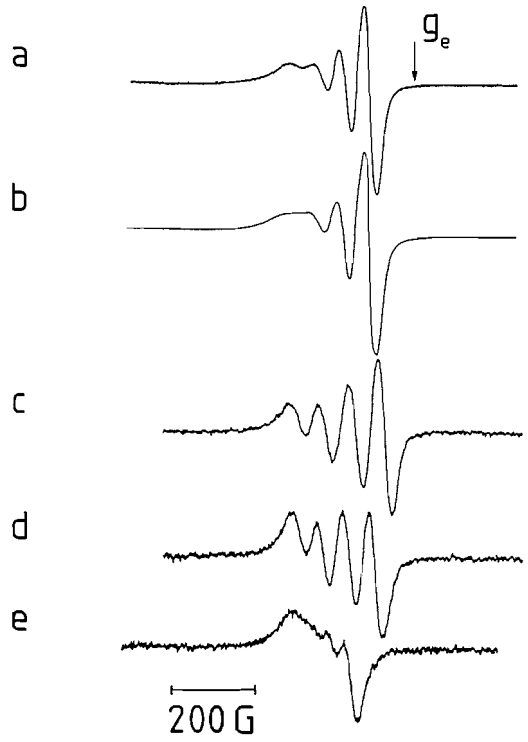


FIG. 2. Ambient temperature chloroform solution esr spectra of (a) compound **10**, (b) compound **13**, (c) the *n*-butyl complex, (d) the isopropyl complex, and (3) the *tert*-butyl complex at $< 10^{-4}$ *M*.

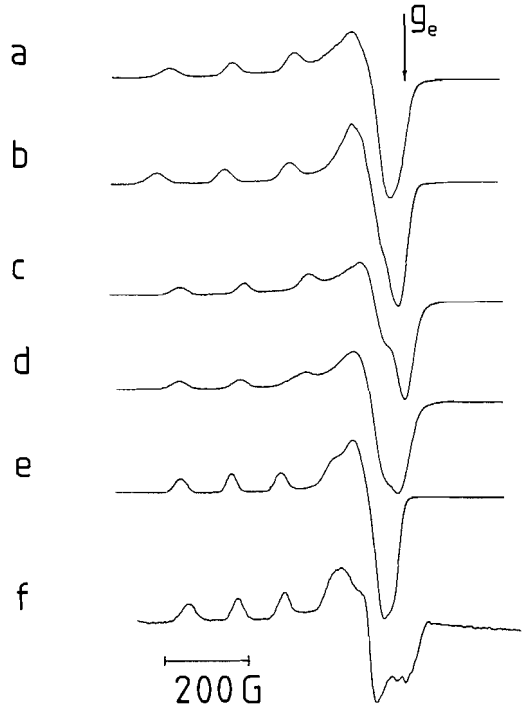


FIG. 3. 77 K liquid $N_2$ frozen solution esr spectra of (a) compound **10**, (b) compound **13**, (c) the *n*-butyl complex, (d) the isopropyl complex, (e) the *tert*-butyl complex, and in (f) the room temperature powder spectrum of 0.5% **10** doped in the zinc complex **11**.

as shown in Fig. 2 (a)–(d). As the molecule tumbles more and more slowly, the low field transitions (lines) broaden to a greater extent than do the high field lines; this is because incomplete averaging of the $g$ and $A$ anisotropies affects the low field lines before the high field line. This information can then be used to compare the effective "size" of copper complexes. From the spectra in Fig. 2, it is clear that the suger complexes are much "larger" than their alkyl counterparts. The esr spectrum of the *t*-Bu complex is very broad and poorly resolved due to its high tetrahedral character (21).

The polycrystalline spectra shown in Fig. 3 also contain additional information; insofar that they all have an axial type of line shape, this implies that in each case the copper centre possesses an axial, or near axial symmetry. Spectrum (d) of the isopropyl complex also reveals that a mixture of geometries is present for this molecule in solution. This deduction is based on the observation of the broad $g_{\|}$ components in this spectrum which have been previously attributed (17) to overlapping lines of a mixture of planar and pseudotetrahedral species. This has an important corollary in that it now seems

Can. J. Chem. Downloaded from www.nrcresearchpress.com by 210.87.254.5 on 09/06/12
For personal use only.

safe to assume from the spectra in Fig. 3 that the other sugar and alkyl complexes exist as a single structural species in solution. That the binuclear copper complex **16** did not give either a room temperature or a 77 K solution spectrum can be explained on the basis of exchange coupling between the two copper ions to product singlet ($S = 0$) and triplet ($S = 1$) electronic states. Since the singlet state is expected to have zero magnetic moment, only molecules in the triplet state can give rise to an esr signal. Therefore, if the triplet state is not populated, which is most likely the case here, no esr spectrum will be seen.

*Magnetic moments*

Often associated with red spectral shifts, as seen for the alkyl complexes of Cu(R-Sal)$_2$ with pseudotetrahedral structures, are large magnetic moments; a $\mu_{eff}$ value of $\geq$ 1.89 BM has been considered characteristic of nonplanar geometry (20). This does not, however, appear to be a reliable structural criterion; for example, recent measurements (20) of solid Cu(*i*-Pr-sal)$_2$ and Cu(*t*-Bu-sal)$_2$, which are known to be pseudotetrahedral, have yielded values of 1.84 and 1.83 BM respectively compared to 1.90–1.93 BM obtained earlier (20). The magnetic moments calculated from the esr and Faraday methods for the copper complexes shown previously are given in Table 2. Initially it was thought that the change in $\mu_{eff}$ for the solid complex Cu(Sug I-sal)$_2$ (1.91 BM) upon dissolution of the solid reflected a change in geometry. However, in light of the recent data (20) cited above for Cu(*i*-Pr-sal)$_2$ and Cu(*t*-Bu-sal)$_2$, it does not seem wise to be too dogmatic on this conclusion.

*Mass spectrometry*

Copper has two isotopes ($^{63}$Cu, 69.09% and $^{65}$Cu, 30.91%) which confer defined isotope patterns to the mass spectral fragmentation of copper-containing complexes and thereby make this a useful tool for structure determination. Using the relative ratios of 7:3 for the two copper isotopes, and taking into account the 1.08% isotope effect for each $^{13}$C of a molecule which has 42 carbon atoms, one can calculate the simulated spectrum shown below for the binuclear copper complex **16**.

TABLE 2. Magnetic moments of copper complexes

| Complex | $\mu_{eff}$ from esr (BM) | $\mu_{eff}$ Faraday (BM) |
|---|---|---|
| (a) Cu(Sug I-sal)$_2$ **10** | 1.84 | 1.91 |
| (b) Cu(Sug II-sal)$_2$ **13** | 1.84 | |
| (c) Cu(*n*-Bu-sal)$_2$ | 1.83 | |
| (d) Cu(*i*-Pr-sal)$_2$ | 1.84 | |
| (e) Cu(*t*-Bu-sal)$_2$ | 1.85 | |
| (f) Cu(Sug III-sal)$_2$ **15** | 1.85 | |

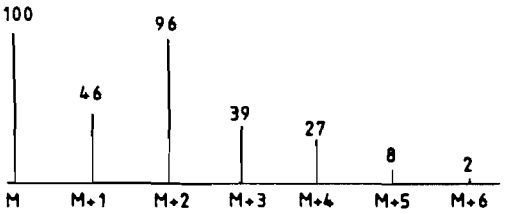


This simulation gives exactly the same molecular ion pattern as that obtained experimentally (see Experimental). This evidence, along with the parent mass of 1056 and the lack of an esr spectrum, provides good evidence for the assignment of a binuclear structure for the copper complex **16**. Obviously, such isotope patterns were also very useful for characterizing the mononuclear copper complexes.

Zinc has four isotopes in natural abundance ($^{64}$Zn, 48.89%, $^{66}$Zn, 27.81%; $^{67}$Zn, 4.11%; and $^{68}$Zn, 18.57%) which also confer well defined isotope patterns to the mass spectrum of zinc complexes. The zinc–sugar complex **11** did indeed reveal this well defined isotope pattern.

## Conclusions

It is obvious that this study has done no more than prove the existence of a new area of metal-chelation chemistry based on ligands derived from amino-containing monosaccharides. Given the ease with which the solubility of sugars can be manipulated, it should be relatively easy to tailor the physical properties of the resultant metal-chelates, and by choice of the appropriate amino-sugar it is also feasible to control their geometry. A recent extension of this work describes (22) the formation of metal complexes from amine-containing polysaccharides.

## Experimental

All solutions were concentrated using a Buchi rotary evaporator. All melting points were determined using a Thomas Hoover Unimelt instrument (Model 6404-K) and are corrected. All optical rotations were determined using a Perkin–Elmer Polarimeter (model 241-MC).

Thin-layer chromatography (tlc) was performed on silica gel plates (Baker-flex Silica gel 1B2-F) using 1:1 toluene – ethyl acetate.

Sources for the key chemicals used in the synthesis of compounds in this chapter are as follows: salicylaldehyde was obtained from Fisher and was vacuum distilled before use; salicylic acid (Malinckrodt); hexamethylenetetramine (Matheson, Coleman and Bell); cyclohexylamine, *tert*-butylamine, *n*-butylamine, and *i*-propylamine (Eastman); D-glucosamine hydrochloride (Sigma); benzyl chloroformate (Aldrich); anisaldehyde (Matheson, Coleman and Bell); cupric and cobaltous acetate (Fisher); zinc acetate (Matheson, Coleman and Bell); nickel acetate (Baker).

Electron spin resonance spectra were recorded at X-band using a Varian E-3 instrument in the derivative absorption mode. Spectrometer settings – modulation amplitude, filter time

Can. J. Chem. Downloaded from www.nrcresearchpress.com by 210.87.254.5 on 09/06/12
For personal use only.

constant, and scan rate – were chosen in each case to avoid distortion of the spectral lines, and power levels were nonsaturating. The ambient temperature was always 25°C ± 1, and the field was always increased from left to right.

The field was calibrated using a proton nmr magnetometer and the X-band microwave frequency was monitored on a Hewlett–Packard 5245-L electronic counter equipped with a 8–18 GHz frequency converter.

Spectra at 77 K were obtained using a Dewar-insert containing liquid nitrogen, at 0.16 mW microwave power, the lowest available. Oxygen was prevented from condensing in the sample tube by sealing the top with a rubber septum cap. All low temperature spectra were recorded in 3 mm id quartz tubes when nonpolar organic solvents were used, and in 1 mm id Pyrex tubes for aqueous solutions. At room temperature, both these types of tubes were used. The 3 mm id tube was preferred for use with the dilute chloroform solutions of the copper complexes since more sample could be placed in the esr cavity, thereby giving a better signal-to-noise ratio. Powder samples of metal complexes were run inside melting point capillary tubes placed inside a 3 mm id quartz tube.

Proton nmr spectra were measured at 270 MHz with a prototype of a home-built spectrometer based on a Bruker WP-60 console, a Nicolet 1180 computer (32K), a Nicolet 293A pulse controller unit, a Diablo Disk model 30, and an Oxford Instruments Superconducting solenoid. The concentration of most samples ranged from 0.01 to 0.10 *M*. All deuterated solvents were obtained from Merck Sharp and Dohme (Montreal, Canada) and tetramethylsilane was used as an internal standard.

Infrared spectra were run on a Perkin–Elmer 137 spectrometer. Samples were prepared as the Nujol mull and polystyrene film was used to calibrate the spectra.

All visible absorption spectra were run on a Cary 14 spectrometer and solutions were made in chloroform at approximately 0.01 *M* concentrations.

The solution magnetic moments were determined from the esr solution spectra and were calculated from $g_0$ by the relationship

$$\mu_{eff} = g_0 \sqrt{S(S+1)}$$

where $S$ is $\frac{1}{2}$ for copper(II). The single, solid magnetic moment determination was performed on a Faraday instrument by Professor R. C. Thompson of this department.

All microanalysis was performed by Mr. P. Borda, of this department. The mass spectra were obtained using an Atlas CH-4B mass spectrometer by Dr. G. Eigendorf.

The compound, 3-formyl-2-hydroxybenzoic acid **2**, was prepared by the method of Duff and Bills (23).

Methyl 3,4,6-tri-*O*-acetyl-2-amino-2-deoxy-β-D-glucopyranoside hydrobromide **5** was prepared by a combination of the methods by Chargraff and Bovarnick (24), Fodar and Otvos (25), and Irvine and Earl (13).

1,3,4,6-Tetra-*O*-acetyl-2-amino-2-deoxy-β-D-glucopyranose **6** was prepared by the method of Bergman and Zervas (15), using *p*-methoxybenzaldehyde to protect the amino function.

The sugar salicylaldimines **4**, **7**, and **8** were all prepared readily by the method of Irvine and Earl (14) by mixing vigorously the amino sugar and salicylaldehyde together in water, or in a methanol–water mixture, with one equivalent of sodium bicarbonate added in the preparation of compounds **4** and **7**.

The preparation of the salicylaldimine–metal complexes Cu(cyclohexyl-sal)$_2$, Cu(*n*-Bu-sal)$_2$, Cu(*t*-Bu-sal)$_2$, and Cu(*i*-Pr-sal)$_2$ was readily carried out by the original method of Schiff and repeated from a more recent reference by Holm and Swaminathan (26). Both copper(II) and nickel(II) complexes were prepared in ≥ 60% yield by heating under reflux an ethanolic solution of 0.1 mol of the appropriate nickel or copper salicylaldehyde complex together with a 10% mol excess of the amine. The products were obtained by cooling the reaction mixture and filtration of the precipitate.

*Preparation of methyl-3,4,6-tri-*O*-acetyl-2-deoxy-2-(3-carboxylsalicylaldimino)-β-D-glucopyranoside* **9**

To a solution of amino sugar **5** (0.51 g, 1.27 mmol) in methanol (4 mL) was added a solution of sodium bicarbonate (0.25 g, 3 mmol) in $H_2O$ (4 mL) and a solution of 3-formyl-2-hydroxybenzoic acid (0.22 g, 1.28 mmol) in methanol (4 mL). The mixture was stirred at room temperature for 1 h and then evaporated to dryness and a small amount of ethanol added. The resulting precipitate was filtered, washed with cold ethanol, and dried under vacuum to give the product in 70% yield. The compound was recrystallized from ethanol; mp 251–252°C, $[\alpha]_D^{22}$ +245.0° (*c* 2, $CHCl_3$). *Anal.* calcd. for $C_{21}H_{25}N_1O_{11}$: C 53.94, H 5.39, N 2.99; found: C 53.52, H 5.54, N 2.80.

*Preparation of Schiff's base metal complexes from ligands* **4**, **7**, **8**, *and* **9**

Ligand **4** was dissolved in methanol at room temperature and ligands **7**, **8**, and **9** were dissolved in hot ethanol. To these stirred mixtures was then added an alcoholic solution of the appropriate metal acetate (molar equivalents). The complex precipitated either immediately or upon cooling and was separated by filtration and purified as shown below.

*Bis-{N-(methyl-3,4,6-tri-*O*-acetyl-2-deoxy-β-D-glucopyranosyl-2-salicylaldimino)} Cu(II)* **10** was obtained in 90% yield and was analytically pure directly from the reaction mixture. Slow crystallization from an acetone solution yielded dark-brown cubic crystals, mp 250–251°C, $[\alpha]_D^{22}$ +777° (*c* 0.74, $CHCl_3$). *Anal.* calcd. for $C_{40}H_{49}CuN_2O_{18}$: C 52.91, H 5.29, N 3.08; found: C 53.08, H 5.21, N 3.02; ms (low resolution) calcd. for $C_{40}H_{48}CuN_2O_{18}$: 907 ($Cu^{63}$), 909 ($Cu^{65}$) amu (M:M+1:M+2:M+3; 100:40:50:20); found: 907 and 909 amu (M:M+1:M+2:M+3; 100:40:50:20).

*Bis-{N-(methyl-3,4,6-tri-*O*-acetyl-2-deoxy-β-D-glucopyranosyl-2-salicylaldimino)} Zn(II)* **11** was obtained in 41% yield from acetone–chloroform, mp 272–273°C, $[\alpha]_D^{22}$ +240.3° (*c* 0.77, $CHCl_3$). *Anal.* calcd. C for $_{40}H_{48}N_2O_{18}Zn$: C 52.80, H 5.28, N 3.08; found: C 53.00, H 5.40, N 3.07; ms (low resolution) calcd. for $C_{40}H_{48}N_2O_{18}Zn$: 908 ($Zn^{64}$), 910 ($Zn^{66}$), 911 ($Zn^{67}$), 912 ($Zn^{68}$) amu (M:M+1:M+2:M+3:M+4; 100:44:65:33:46); found: 908, 910, 911, 912 amu (M:M+1:M+2:M+3:M+4; 100:50:70:30:45).

*Bis-{N-(methyl-3,4,6-tri-*O*-acetyl-2-deoxy-β-D-glucopyranosyl-2-salicylaldimino)} Co(II)* **12** was obtained in 58% yield from chloroform, mp 260–261°C, $[\alpha]_D^{22}$ −25.6° (*c* 0.39, $CHCl_3$). *Anal.* calcd. for $C_{40}H_{48}CoN_2O_{18}$: C 53.18, H 5.31, N 3.10; found: C 53.06, H 5.39, N 3.20; ms (low resolution) calcd. for $C_{40}H_{48}CoN_2O_{18}$: 903 amu; found 903 amu.

*Bis-{N-(1,3,4,6-tetra-*O*-acetyl-2-deoxy-β-D-glucopyranose-2-salicylaldimino)} Cu(II)* **13** was obtained in 90% yield from ethanol, mp. 125–126°C, $[\alpha]_D^{22}$ +194° (C 0.5 $CHCl_3$). *Anal.* calcd. for $C_{42}H_{48}CuN_2O_{20}$: C 52.30, H 4.98, N 2.90; found: C 51.9, H 5.03, N 2.84; ms (low resolution) calcd. for $C_{42}H_{48}CuN_2O_{20}$: 963 ($Cu^{63}$), 965 ($Cu^{65}$) amu (M:M+1:M+2:M+3; 100:40:50:20); found: 963, 965 amu (M:M+1:M+2:M+3; 100:40:50:20).

*(N-2-amino-2-deoxy-α,β-D-glucopyranose-salicylaldimino)-Cu(II)* **14** was prepared in 65% yield, mp, 150°C (dec.), $[\alpha]_D^{22}$ +244.7° (*c* 0.76, $H_2O$). *Anal.* calcd. for $C_{13}H_{18}CuNO_7$: C 42.90, H 4.95, N 3.85; found: C 43.50, H 4.82, N 3.68; ms (low resolution) calcd. for $C_{13}H_{18}CuNO_7$: 363 ($Cu^{63}$), 365 ($Cu^{65}$) amu (M:M+2; 10:4); found: 363, 365, 420 amu.

*Bis-{N-(methyl-3,4,6-tri-O-acetyl-2-deoxy-2-[3-carboxyl-salicylaldimino])} $Cu_2$(II)* **16** was obtained in 80%

yield, mp > 270°C, $[\alpha]_D^{22}$ +100.0° (*c* 0.16, $CHCl_3$). *Anal.* calcd. for $C_{42}H_{46}Cu_2N_2O_{22}$: 1056 ($Cu^{63}$ $Cu^{63}$), 1058 ($Cu^{63}$ $Cu^{65}$), 1060 ($Cu^{65}$ $Cu^{65}$) amu (M:M+1:M+2:M+3:M+4:M+5:M+6; 100:46:96:39:27:8:2); found: 1056, 1058, 1060 amu (M:M+1:M+2:M+3:M+4:M+5:M+6; 100:50:95:40:30:10:2).

## Acknowledgements

It is a pleasure to thank the Natural Sciences and Engineering Research Council of Canada for their support of this work via operating grants to L.D.H. (A-1905) and a Postgraduate Scholarship to M.A. (1977–1979). The authors would also like to thank Drs. R. C. Thompson and R. Morrison of this department for many helpful discussions relating to coordination chemistry and to Dr. Jeremy K. M. Sanders, on sabbatical leave from Cambridge University, for his thoughts on several aspects of this work.

1. M. J. ADAM and L. D. HALL. J. Chem. Soc. Chem. Commun. 234 (1979); M. J. ADAM. Ph.D. Thesis. University of B.C., Vancouver. 1980.
2. J. A. RENDLEMAN, JR. Adv. Carbohydr. Chem. **21**, 209 (1966).
3. S. J. ANGYAL. Pure Appl. Chem. **35**, 131 (1973).
4. M. MIYAZAKI, S. NISHIMURA, A. YOSHIDA, and N. OKUBO. Chem. Pharm. Bull. **27**, 532 (1979); V. GIBB and L. D. HALL. Carbohydr. Res. **55**, 239 (1977); **63**, C1(1978); L. D. HALL, P. R. STEINER, and D. C. MILLER. Can. J. Chem. **57**, 38 (1979).
5. B. LONNERDAL, J. CARLSSON, and J. PORATH. FEBS Lett. **75**, 89 (1977); J. P. LEBRETON. FEBS Lett. **80**, 351 (1977).
6. W. R. CULLEN and Y. SUGI. Tetrahedron Lett. 1635 (1978).
7. W. F. ANDERSON and M. C. MILLER. (*Editors*). Proceedings of Symposium on Development of Iron Chelators for Clinical Use, U.S. Department of Health, Education, and Welfare. 1975.
8. YU, A. ZHDANOV *et al*. Carbohydr. Res. **38**, C1(1974).
9. S. HANNESSIAN and G. PATIL. Tetrahedron Lett. 1031 (1978); J. J. WRIGHT, A. COOPER, P. J. L. DANIELS, T. L. NAGABUSHAN, D. ROME, W. N. TURNER, and J. WEINSTEIN. J. Antibiot. **29**, 714 (1976).
10. I. ARMITAGE and L. D. HALL. Carbohydr. Res. **24**, 221 (1972); D. HORTON and J. D. WANDER. Carbohydr. Res. **39**, 141 (1975); L. D. HALL and C. M. PRESTON. Carbohydr. Res. **41**, 53 (1975); B. CASU, G. GATTI, N. CYR, and A. S. PERLIN. Carbohydr. Res. **41**, C6 (1975); S. J. ANGYAL. Carbohydr. Res. **26**, 271 (1973); R. F. BUTTERWORTH, A. G. PERNET, and S. HANNESSIAN. Can. J. Chem. **49**, 981 (1971); P. GIRARD, H. KOGAN, and S. DAVID. Bull. Soc. Chim. Fr. **12**, 4515 (1970).
11. R. H. HOLM, G. W. EVERETT, JR., and A. CHAKRAVORTY. Prog. Inorg. Chem. **7**, 83 (1966).
12. D. HORTON. The amino sugars. Vol. 1A. *Edited by* R. W. Jeanloz. Academic Press, New York. 1969. p. 70.
13. J. C. IRVINE and J. C. EARL. J. Chem. Soc. **121**, 2376 (1922).
14. J. C. IRVINE, D. MCNICOLL, and A. HYND. **99**, 250 (1911).
15. M. BERGMANN and L. ZERVAS. Chem. Ber. B, **64**, 975 (1931).
16. S. N. PODDAR. Z. Angorg Allg. Chem. **322**, 326 (1963).
17. H. YOKOI. Bull. Chem. Soc. Jpn. **47**, 3037 (1974).
18. T. P. CHEESMAN, D. HALL, and T. N. WATERS. J. Chem. Soc. A, 694 (1966).
19. D. HALL, R. H. SUMMER, and T. N. WATERS. J. Chem. Soc. A, 420 (1969).
20. R. H. HOLM and M. J. O'CONNOR. Prog. Inorg. Chem. **14**, 241 (1971).
21. H. P. FRITZ, B. M. GOLLA, H. J. KELLER, and K. E. SCHWARZHANS. Z. Naturforsch. Teil B, **21**, 725 (1966).
22. L. D. HALL and M. YALPANI. Carbohydr. Res. **83**, C5–C7 (1980).
23. J. C. DUFF and E. J. BILLS. J. Chem. Soc. 1987 (1932).
24. E. CHARGAFF and M. BOVARNICK. J. Biol. Chem. **118**, 421 (1937).
25. G. FODOR and L. OTVOS. Ann. Chem. **604**, 29 (1957).
26. R. H. HOLM and K. SWAMINATHAN. Inorg. Chem. **2**, 181 (1963).

Can. J. Chem. Downloaded from www.nrcresearchpress.com by 210.87.254.5 on 09/06/12
For personal use only.

# Synthèse de nucléosides pyrimidiques à partir de bromures de désoxy-4-pentopyranosyles non totalement protégés[1]

CHRISTIAN H. GAGNIEU, ANNIE V. GROUILLER ET HENRI PACHECO

*Service de Chimie Biologique, Bât. 406, INSA, 20 av. Albert Einstein, 69621 Villeurbanne, France*

Reçue le 11 décembre 1981

CHRISTIAN H. GAGNIEU, ANNIE V. GROUILLER et HENRI PACHECO. Can. J. Chem. **60**, 2238 (1982).

La synthèse des nucléosides **15–19** a été réalisée avec de très bons rendements selon la méthode de Hilbert–Johnson, par condensation de la diméthoxy-2,4-pyrimidine avec des bromo désoxy-4-pentopyranosides dont l'hydroxyle en C-3 est libre. La présence de ce groupement augmente la réactivité des bromures mais ne semble pas jouer de rôle important dans la stéréochimie de la réaction; celle-ci étant surtout influencée par l'encombrement stérique et la nature du substituant en C-2.

CHRISTIAN H. GAGNIEU, ANNIE V. GROUILLER, and HENRI PACHECO. Can. J. Chem. **60**, 2238 (1982).

The synthesis of nucleosides **15–19** has been completed in high yield following the method of Hilbert–Johnson, by condensation of 2,4-dimethoxypyrimidine with bromo-4-deoxypento pyranosides in which the C-3 hydroxyl group is free. The presence of this group augments the reactivity of the bromides but does not appear to play an important role in the stereochemistry of the reaction, which is above all influenced by steric factors and the nature of the C-2 substituent.

[Journal translation]

## Introduction

L'obtention de nucléosides pyrimidiques à structure désoxy-4-pentopyranosique, présentant un groupement hydroxyle libre en C-3′, constitue une étape importante dans le développement de nos travaux sur l'application de la réaction de Neber à la synthèse de nucléosides aminés en C-4′(1). En particulier, la préparation de nucléosides porteurs de groupements O-alkylés ou O-acylés, aromatiques et aliphatiques en C-2′, et d'un hydroxyle libre en C-3′ est nécessaire pour l'étude de l'influence des substituants de la partie osidique des nucléosides sur la stéréochimie de cette réaction. Lors des essais de synthèse des nucléosides O-acylés en C-2′ par les méthodes classiques de condensation de bases pyrimidiques avec des sucres totalement protégés (2), nous nous sommes heurtés à d'importants problèmes quant au choix des groupements protecteurs des pentopyranosides de départ. Ainsi, nous avons été amené à envisager la synthèse de ces nucléosides directement à partir de sucres possédant un hydroxyle non protégé en C-3. Ces synthèses ont été réalisées par la méthode de Hilbert–Johnson, dans laquelle des halogénoses sont condensés en l'absence de catalyseur avec des dialkoxy-2,4-pyrimidines (3).

Le type de synthèse que nous rapportons ici est un premier exemple de l'application de cette réaction à la préparation directe de nucléosides pyrimidiques non totalement protégés. Le présent article décrit la synthèse des méthylglycosides de départ hydroxylés en C-3, la préparation de leurs dérivés bromoglycosidiques et les résultats obtenus lors de la condensation de ces derniers avec la diméthoxy-2,4-pyrimidine.

## Résultats et discussion

*Synthèse des méthylglycosides*

Ces synthèses ont été réalisées à partir de deux composés connus: le désoxy-4-*O*-isopropylidène-1,2-β-DL-*thréo*-pentopyranose(4) et les méthyl *O*-benzyl-3-désoxy-4-α et β-DL-*thréo*-pentopyranosides (5).

L'acétylation et la benzoylation du désoxy-4-*O*-isopropylidène-1,2-β-DL-*thréo*-pentopyranose par les chlorures d'acétyle et de benzoyle dans la pyridine conduisent avec des rendements quasi quantitatifs aux acétyl et benzoyl-3-*O*-isopropylidène-1,2-désoxy-4-β-DL-*thréo*-pentopyranoses **1** et **2**. La méthanolyse du groupement isopropylidène du composé **2**, catalysée par de la résine Dowex 50H$^+$ en suspension dans du méthanol bouillant conduit très rapidement aux méthyl *O*-benzoyl-3-désoxy-4-α et β-DL-*thréo*-pentopyranosides **4** avec un rendement de 80%. Cette méthanolyse appliquée au composé **1** doit être réalisée à plus basse température (40°C) afin de minimiser la réaction de désacétylation qui se produit lorsque les conditions sont trop drastiques. Les méthyl *O*-acétyl-3-désoxy-4-α et β-DL-*thréo*-pentopyranosides (**3**) ont été obtenus avec un rendement de 65%. La benzylation en C-2 des composés **3** et **4** par le bromure de benzyle dans le *N*, *N* diméthylformamide en présence d'oxyde d'argent à été obtenue avec des rendements accep-

[1] Travail présenté en partie au 4th International Round Table Nucleoside, Nucleotide and their Biological Applications, 4–6 février 1981, Anvers, Belgique.

0008-4042/82/172238-08$01.00/0

©1982 National Research Council of Canada/Conseil national de recherches du Canada

Can. J. Chem. Downloaded from www.nrcresearchpress.com by 210.87.254.5 on 09/06/12
For personal use only.

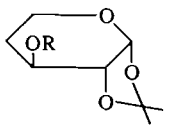

**1** R = Ac
**2** R = Bz

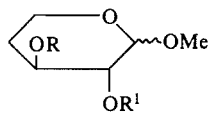

**3** α,β R = Ac, $R^1$ = H
**4** α,β R = Bz, $R^1$ = H
**5** α,β R = Ac, $R^1$ = Bn
**6** α,β R = Bz, $R^1$ = Bn
**7** α,β R = Ac, $R^1$ = Me
**8** α,β R = Bz, $R^1$ = Me
**9** α,β R = Bn, $R^1$ = Ac
**10** α,β R = Bn, $R^1$ = Bz

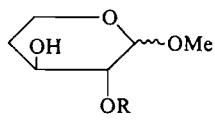

**11** α,β R = Ac
**12** α,β R = Bz
**13** α,β R = Bn
**14** α,β R = Me

tables (env. 70%) grâce à l'adjonction dans le milieu réactionnel de quantités catalytiques d'iodure de potassium. Les méthyl *O*-acétyl et *O*-benzoyl-3-*O*-benzyl-2-désoxy-4-α et β-DL-*thréo*-pentopyranosides **5** et **6** obtenus ont été désacylés par du méthylate de sodium en solution méthanolique pour donner les méthyl *O*-benzyl-2-désoxy-4-α et β-DL-*thréo*-pentopyranosides (**13**).

La méthylation en C-2 des composés **3** et **4** par l'iodure de méthyle dans le *N,N* diméthylformamide en présence d'oxyde d'argent conduit avec d'excellents rendements aux méthyl *O*-acétyl et *O*-benzoyl-3-*O*-méthyl-2-désoxy-4-α et β-DL-*thréo*-pentopyranosides **7** et **8** qui sont désacylés comme précédemment pour donner les méthyl *O*-méthyl-2-désoxy-4-α et β-DL-*thréo*-pentopyranosides (**14**).

L'acétylation et la benzoylation en C-2 du méthyl *O*-benzyl-3-désoxy-4-α et β-DL-*thréo*-pentopyranosides par la méthode précédemment décrite conduisent avec de très bons rendements aux méthyl *O*-acétyl et *O*-benzoyl-2-*O*-benzyl-3-désoxy-4-α et β-DL-*thréo*-pentopyranosides **9** et **10** qui sont soumis à une hydrogénolyse en présence de palladium sur charbon pour donner les méthyl *O*-acétyl et *O*-benzoyl-2-désoxy-4-α et β-DL-*thréo*-pentopyranosides **11** et **12**.

Tous les composés cités sont nouveaux; leurs structures ont été déterminées en rmn du proton (tableaux 1 et 2) et confirmées par micro-analyse.

*Synthèse des bromoglycosides*

Les bromoglycosides sont synthétisés de façon classique par action d'un excès d'acide bromhydrique gazeux anhydre sur les méthylglycosides **11–14** dissous dans du dichlorométhane fraîchement distillé sur hydrure de sodium. Dans les conditions optimales, la réaction est rapide et quantitative, mais les bromures qui ne sont stables qu'au sein de leur milieu de synthèse ne peuvent être facilement isolés. En effet, leur réactivité inhabituelle, dont la cause reste à déterminer, est à l'origine de la création d'un équilibre réactionnel dépendant de la concentration de la solution en acide bromhydrique (schéma 1). Ainsi, l'élimination de l'acide en excès, qu'il est nécessaire d'effectuer avant la condensation des bromures avec la diméthoxy-2,4-pyrimidine, conduit à une resynthèse partielle mais toujours importante des produits de départ. La grande réactivité des bromures est à mettre en relation avec la présence de

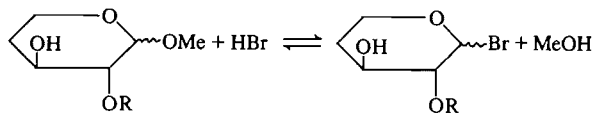

SCHÉMA 1

l'hydroxyle libre en C-3 puisque nous avons pu isoler des bromures relativement stables en présence de traces de méthanol à partir de méthylglycosides de la même série totalement protégés.

L'obtention de solutions neutres de bromoglycosides est conditionnée par l'élimination simultanée de l'acide bromhydrique en excès et du méthanol réactionnel. Cette élimination a été réalisée par dégazage partiel des solutions avec un courant d'azote anhydre suivi d'un traitement par du tamis moléculaire 10 Å en poudre. Ce composé, à l'égal des autres tamis moléculaires, piège très efficacement les acides minéraux (6) tel que l'acide bromhydrique mais il a également la propriété d'adsorber de petites molécules polaires telles que le méthanol.

Les solutions obtenues à l'issue de ces traitements sont utilisées directement comme milieu de synthèse des nucléosides.

*Synthèse des nucléosides*

Les solutions de bromoglycosides sont traitées par un excès de diméthoxy-2,4-pyrimidine et portées à reflux pendant 10 minutes. Après divers traitements du milieu réactionnel, les nucléosides sont obtenus purs avec de bons rendements (77 à

Can. J. Chem. Downloaded from www.nrcresearchpress.com by 210.87.254.5 on 09/06/12
For personal use only.

Can. J. Chem. Downloaded from www.nrcresearchpress.com by 210.87.254.5 on 09/06/12
For personal use only.





TABLEAU 1. $^1$H résonance magnétique nucléaire des glycosides **1–10**

| Composé | H-1[a] | H-2[b] | H-3[c] | H-4,4′[c] | H-5,5′[c] | $J_{1,2}$ | $J_{2,3}$ | $J_{3,4}$ et $J_{3,4'}$ | Autres protons |
|---|---|---|---|---|---|---|---|---|---|
| **1** | 5,25 | 3,70 | 5,22 | 2,25–1,50 | 3,85–3,75 | 3,6 | 3,6 | 3,6 et 3,9 | 2,10(s,3H,$COCH_3$), 1,37 et 1,57(2s,6H,$2CH_3$) |
| **2** | 5,37 | 4,03 | 5,53 | 2,23 et 1,83 | 3,90–3,65 | 3 | 3,3 | 4 | 8,00 et 7,50(2m,5H,$C_6H_5$), 1,37 et 1,57(2s,6H,$2CH_3$) |
| **3α** | 4,15 | 3,65–3,20 | 4,82 | 2,20–1,50 | 4,00 et 3,45 | 7,2 | 9 | 5,5 et 10,5 | 3,53(s,3H,$OCH_3$), 3,30(d,1H,OH), 2,10(s,3H,$COCH_3$) |
| **3β** | 4,66 | 3,71 | 5,00 | 2,10–1,70 | 3,90–3,65 | 3,6 | 10,5 | 5 et 10,5 | 3,45(s,3H,$OCH_3$), 2,50(d,1H,OH), 2,10(s,3H,$COCH_3$) |
| **4α** | 4,25 | 3,63 | 5,12 | 2,45–1,60 | 4,00 et 3,50 | 6,8 | 8,8 | 5,3 et 10,3 | 8,05 et 7,47(2m,5H,$C_6H_5$), 3,55(s,3H,$OCH_3$), 3,47 (d,1H,OH) |
| **4β** | 4,80 | 3,73 | 5,28 | 2,30–1,50 | 3,85–3,55 | 3,7 | 10,5 | 5,3 et 9,7 | 8,05 et 7,43(2m,5H,$C_6H_5$), 3,43(s,3H,$OCH_3$), 2,40 (s,1H,OH) |
| **5α** | 4,28 | 3,27 | 4,91 | 2,10–1,40 | 3,91 et 3,40 | 6,9 | 9 | 5 et 10,5 | 7,29(s,5H,$C_6H_5$-benzyl), 4,80 et 4,59(2d,2H,$CH_2$-benzyl) 3,53(s,3H,$OCH_3$), 2,00(s,3H,$COCH_3$) |
| **5β** | 4,66 | 3,46 | 5,20 | 2,15–1,40 | 3,70–3,30 | 3,3 | 10 | 4,5 et 10,5 | 7,30 et 4,63(2s,7H,benzyl), 3,36(s,3H,$OCH_3$), 2,97 (s,3H,$COCH_3$) |
| **6α** | 4,38 | 3,60–3,30 | 5,22 | 2,30–1,50 | 4,25–3,80 | 1,7 | 8,7 | | 8,00 et 7,47(2m,5H,benzoyl), 7,23 et 4,77(2s, 7H, benzyl), 3,57(s,3H,$OCH_3$) |
| **6β** | 4,77 | 3,63 | 5,47 | 2,25 et 1,75 | 3,90–3,30 | 3,5 | 9,7 | 5,3 et 10,5 | 8,00 et 7,47(2m,5H,benzoyl), 7,27 et 4,70(2s, 7H benzyl), 3,40(s,3H,$OCH_3$) |
| **7α** | 4,18 | 3,00 | 4,79 | 2,25–1,50 | 3,90 et 3,45 | 7,2 | 8,4 | 5,4 et 10,2 | 3,50(s,6H,$2OCH_3$), 2,07(s,3H,$COCH_3$) |
| **7β** | 4,79 | 3,25 | 5,08 | 2,00 et 1,65 | 4,00–3,25 | 3,6 | 9,3 | 5,4 et 10,8 | 3,48 et 3,43(2s,6H,$2OCH_3$), 2,04(s,3H,$COCH_3$) |
| **8α** | 4,32 | 3,20 | 5,12 | 2,30–1,50 | 4,00–3,35 | 6,3 | 8,2 | 5,4 et 9,7 | 8,07 et 7,50(2m,5H,benzoyl), 3,53(s,6H,$2OCH_3$) |
| **8β** | 4,90 | 4,00–3,30 | 5,37 | 2,30–1,50 | 4,00–3,30 | 3,3 | 9,7 | 5,5 et 10,7 | 8,07 et 7,47(2m,5H,benzoyl), 3,53 et 3,43(2s,6H, $2OCH_3$) |
| **9α** | 4,22 | 4,85 | 4,00–3,30 | 2,35–1,40 | 4,00–3,35 | 6,3 | 7,7 | | 7,28 et 4,56(2s,7H,benzyl), 3,43(s,3H,$OCH_3$), 2,05 (s,3H,$COCH_3$) |
| **9β**[d] | 4,97 | 5,02 | 4,00–3,30 | 1,80–1,30 | 4,00–3,30 | 3,3 | 10,3 | | 7,12 et 4,47(2s,7H,benzyl), 3,13(s,3H,$OCH_3$), 1,76 (s,3H,$OCH_3$) |
| **10α** | 4,36 | 5,13 | 3,66 | 2,20–1,50 | 4,00–3,30 | 6,3 | 7,5 | 5 et 8,7 | 8,00 et 7,43(2m,5H,benzoyl), 7,17 et 4,57(2s,7H, benzyl), 3,40(s,3H,$OCH_3$) |
| **10β** | 4,98 | 5,03 | 3,80–3,30 | 2,20–1,50 | 4,20–3,50 | 3,5 | 10,2 | | 8,00 et 7,43(2m,5H,benzoyl), 7,20 et 4,63(2s,7H, benzyl), 3,33(s,3H,$OCH_3$) |

[a] Doublet.
[b] Doublet de doublet.
[c] Multiplet.
[d] Solvant: $C_6H_5$, tous les autres spectres sont réalisés dans $CDCl_3$. Les déplacements chimiques sont exprimés en δ ppm par rapport à $Me_4Si$ et les constantes de couplage en Hz.

Can. J. Chem. Downloaded from www.nrcresearchpress.com by 210.87.254.5 on 09/06/12
For personal use only.

90%) par cristallisation ou chromatographie sur colonne de gel de silice (voir schéma 2).

Il est bien connu que le degré de stéréospécificité des réactions de glycosylation est dépendant pour une grande part de la nature du substituant en C-2 du sucre de départ. Ceci est vrai en particulier pour la réaction de Hilbert–Johnson avec laquelle les nucléosides sont très souvent obtenus sous forme de mélange anomérique (7). La réaction de glycosylation de sucres non protégés en C-3, telle que nous l'avons réalisée ne fait pas exception à ces règles générales.

Lors de la synthèse des nucléosides **17** et **18**, benzylés ou méthylés en C-2′, des mélanges d'anomères ont été obtenus avec prédominance nette des isomères *cis* 1′,2′, ce qui correspond dans notre série osidique à une configuration β majoritaire. Dans le cas des composés benzylés en C-2′, le rapport des anomères α et β est d'environ 1:5, alors que dans le cas des composés méthylés ce rapport est de 1:3. Cette différence de proportion, qui découle d'une augmentation de la quantité relative de l'isomère α dans le mélange des anomères du composé méthylé **18**, nous permet de dire que l'approche de la diméthoxy-2,4-pyrimidine au moment de la condensation avec les bromoglycosides n'est pas influencée par l'encombrement stérique de substituants en C-2 de ces derniers. En effet, si cet encombrement intervenait à ce niveau dans la stéréochimie de la réaction, il serait logique d'obtenir le résultat inverse, c'est-à-dire une proportion plus importante de l'isomère *trans* 1′,2′ pour les composés benzylés puisque le groupement benzyle a un volume moléculaire très supérieur au groupement méthyle. En revanche, cet encombrement stérique peut influer sur l'équilibre d'anomérisation des composés bromés de départ, car l'absence de substituants en C-4 et C-5 crée un déséquilibre stérique au niveau du site anomérique, variable suivant la taille du substituant en C-2 et de nature à renforcer l'effet stérique de ce dernier. De ce fait il est logique de penser que l'équilibre existant entre les paires d'ions **A** et **B**, (schéma 3) qui sont considérées comme des intermédiaires dans les réactions de glycosylation à partir d'halogénosucres (8), est déplacé préférentiellement dans le sens de la formation du composé **A** dont l'ion bromure est en relation *trans* avec le groupement en C-2. L'attaque nucléophile de type $S_N2$ des paires d'ion **A** et **B** par la base aboutit à la formation préférentielle de nucléosides *cis* 1′,2′.

La formation d'un ion carbonium à partir des bromures peut être également envisagée; mais les paramètres stériques que nous venons de citer

TABLEAU 2. $^1$H résonance magnétique nucléaire des glycosides hydroxylés en C-3 (**11–14**)

| Composé | H-1[a] | H-2[b] | H-3[c] | H-4,4′[c] | H-5,5′[c] | $J_{1,2}$ | $J_{2,3}$ | Autres protons |
|---|---|---|---|---|---|---|---|---|
| **11α** | 4,40 | 4,65 | 4,00–3,30 | 2,15–1,30 | 4,25–3,25 | 4,4 | 5,7 | 3,40(s,3H,$OCH_3$), 3,17(s,1H,OH), 2,10(s,3H,$COCH_3$) |
| **11β** | 4,89 | 4,63 | 4,08 | A[e] | 3,80–3,50 | 3,9 | 9,9 | 2,25–1,50(m,2H,$J_{3,4}$ = 5,8,$J_{3,4'}$ = 10,5, H-4,4′), 3,38(s,3H, $OCH_3$), 2,25(s,1H,OH), 2,10(s,3H,$COCH_3$) |
| **12α**[d] | 4,36 | 4,83 | 4,10–3,75 | 2,00–1,50 | A | 7 | 8,1 | 3,50(m,1H,$J_{5,5'}$ = −12,5,$J_{5',4'}$ = 11,$J_{5',4}$ = 3,3 H-5′), 4,10–3,75(m,1H,H-5), 7,95 et 7,43(2m,5H,benzoyl), 4,25(d,1H,OH), 3,35(s,3H,$OCH_3$) |
| **12β**[d] | 4,89 | 4,73 | 4,13 | 2,00–1,50 | 3,90–3,50 | 3,9 | 9,7 | 7,43 et 7,97(2m,5H,benzoyl), 4,30(d,1H,OH), 3,28(s,3H,$OCH_3$) |
| **13α** | 4,32 | 3,17 | 4,00–3,40 | 2,00–1,50 | 4,00–3,40 | 5,7 | 7,3 | 7,30(s,5H,$C_6H_5$-benzyl), 4,87 et 4,60 (2d,2H,$CH_2$-benzyl), 3,53(s,3H,$OCH_3$), 2,50(s,1H,OH) |
| **13β** | 4,63 | 3,30 | 4,20–3,50 | 2,00–1,50 | 4,00–3,50 | 3,3 | 8,5 | 7,33 et 4,63(2s,7H,benzyl), 3,35(s,3H,$OCH_3$), 2,70(s,1H,OH) |
| **14α** | 4,30 | 2,94 | 4,00–3,50 | 2,00–1,50 | 4,00–3,50 | 6 | 7,5 | 3,56 et 3,50(2s,6H,2$OCH_3$), 3,18(s,1H,OH) |
| **14β** | 4,91 | 3,10 | 4,25–3,50 | 2,00–1,50 | 4,25–3,50 | 3,6 | 9,6 | 3,54 et 3,45(2s,6H,2$OCH_3$), 2,87(s,1H,OH) |

[a]Doublet.
[b]Doublet de doublet.
[c]Multiplet.
[d]Solvant: $CD_3COCD_3$, tous les autres spectres sont réalisés dans $CDCl_3$.
[e]A: voir "autres protons." Les déplacements chimiques sont exprimés en δ ppm par rapport à $Me_4Si$ et les constantes de couplage en Hz.

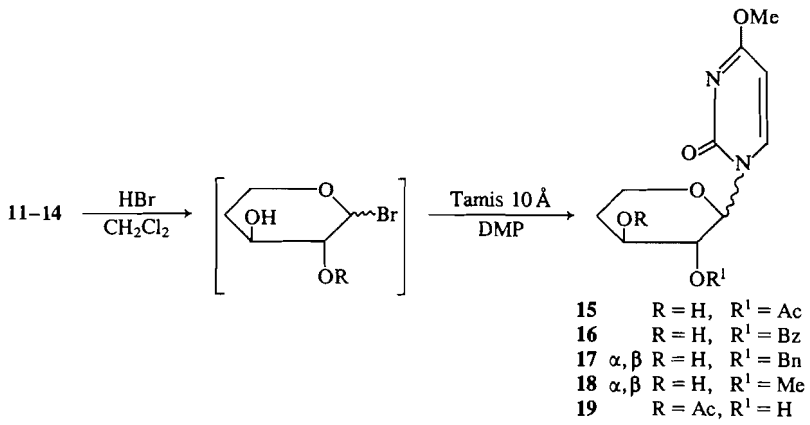


**15** R = H, $R^1$ = Ac
**16** R = H, $R^1$ = Bz
**17** α,β R = H, $R^1$ = Bn
**18** α,β R = H, $R^1$ = Me
**19** R = Ac, $R^1$ = H

SCHÉMA 2

orienteraient la réaction de condensation vers la formation de nucléosides *trans* 1′,2′. Enfin, il n'est pas exclu que l'hydroxyle libre en C-3 ait une influence sur la stéréochimie de la réaction. Des travaux de recherche sur l'existence et le cas échéant sur la nature de cette influence sont en cours.

Lors de la synthèse des nucléosides **15** et **16**, acétylés et benzoylés en C-2′, seuls les isomères *trans* 1′,2′ ont été obtenus, ce qui est en accord avec l'hypothèse d'une réaction assistée par le groupement acyle via un ion acyloxonium; celui-ci étant connu pour orienter la réaction de glycosylation vers la formation préférentielle et souvent exclusive de nucléosides *trans* (2).

Notons que dans la synthèse du nucléosides dérivant du méthylglycoside **11** acétylé en C-2, le composé majoritaire obtenu ne correspond pas à la structure **15** attendue, mais à la structure **19** dans laquelle le groupement acétyle est en C-3. Ce résultat ne peut être expliqué que par l'existence d'une transestérification intramoléculaire liée à la présence de l'hydroxyle libre en C-3 du sucre de départ et catalysée par les conditions acides de la réaction de bromuration. Ce type de transestérification acide-catalysée est très courant en chimie des sucres (9).

Les configurations anomériques de tous les nucléosides synthétisés ont été déterminées sans ambiguité en rmn du proton sur la base des valeurs des constantes de couplage $^3J_{1',2'}$ et des déplacements chimiques des protons anomériques (tableau 3).

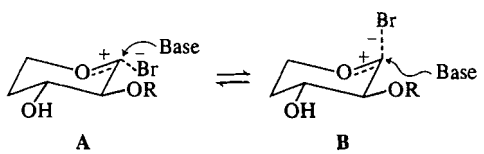


**A** **B**

SCHÉMA 3

## Partie expérimentale

*Méthodes générales*

Le déroulement des réactions a été suivi en ccm sur gel de silice (Kieselgel 60 $F_{254}$, Merck 5535) et la révélation des chromatogrammes a été réalisée par pulvérisation de réactif phosphomolybdique suivie d'un chauffage à 100°C. La purification des composés a été réalisée par chromatographie liquide sous basse pression avec des colonnes Lobar (Merck, Lichroprep Si60) ou sur gel de silice (Kieselgel 60 et 60 $F_{254}$, Merck 7734 et 10757). Les points de fusion, mesurés sur banc Kofler ne sont pas corrigés. Les indices de réfraction ont été mesurés sur un réfractomètre OPL et les spectres ir ont été enregistrés sur le spectrophotomètre Beckman Acculab-4. Les spectres de rmn ont été enregistrés à 80 et 60 MHz sur les spectromètres Brüker WP 80 et Perkin Elmer R 24 B. Les déplacements chimiques sont exprimés en ppm, le tétraméthylsilane étant pris comme référence zéro. Les microanalyses ont été effectuées par le service central de microanalyse du C.N.R.S., division de Lyon. Le dichlorométhane utilisé dans les réactions de bromuration a été distillé sur hydrure de sodium afin d'éliminer l'alcool éthylique utilisé commercialement comme stabilisant de ce solvant. L'acide bromhydrique gazeux a été séché par barbotage dans de l'acide orthophosphorique à 85% puis traité par de la tournure de cuivre afin de piéger d'éventuelles traces de brome. L'azote utilisé pour le dégazage des solutions de bromuration a été Séché sur acide sulfurique à 98% et le tamis moléculaire 10 Å (Merck 5703) a été réduit en poudre puis activé 3 h à 130°C. La diméthoxy-2,4-pyrimidine a été préparée par la méthode de Bhat et Munson (10) et distillée deux fois pour éliminer toute trace de méthanol.

*Méthode générale d'acylation*

A une solution du composé à acyler (10 mmol) dans un mélange de $CH_2Cl_2$ anhydre (20 mL) et de pyridine (5 mL), refroidie à −15°C, est ajouté goutte à goutte et sous forte agitation, du chlorure de benzoyle (25 mmol, 3,5 g, 2,9 mL) ou d'acétyle (25 mmol, 2 g, 1,8 mL) en solution dans $CH_2Cl_2$ (5 mL). Après addition complète, le vase à réaction est sorti du bain réfrigérant et la solution est ramenée progressivement à température ambiante (20°C) en 15 min. On rajoute alors de l'eau (20 mL) et on décante la phase organique. On extrait la phase aqueuse par 20 mL de $CH_2Cl_2$ et on lave les phases organiques réunies par une solution saturée de $NaHCO_3$. Après séchage sur $Na_2SO_4$, l'extrait organique est évaporé sous vide et le résidu huileux obtenu est coévaporé avec du toluène (2 × 30 mL) pour donner les dérivés acylés, soit sous forme d'huiles jaunâtres qui sont purifiées par chromatographie sur gel de silice, soit sous forme de pâtes semi-cristallines qui sont purifiées par recristallisation.

Can. J. Chem. Downloaded from www.nrcresearchpress.com by 210.87.254.5 on 09/06/12
For personal use only.

Can. J. Chem. Downloaded from www.nrcresearchpress.com by 210.87.254.5 on 09/06/12
For personal use only.

O-*acétyl-3-désoxy-4*-O-*isopropylidène*-1,2-β-DL-*thréo-pentopyranose (1)*

Synthèse à partir du désoxy-4-*O*-isopropylidène-1,2-β-DL-*thréo*-pentopyranose (**4**) (1,5 g, 8.7 mmol); *le composé* **1** est obtenu sous forme cristalline (1,740 g, 97%): pf 58–59°C; $R_f$ 0,65 (AcOEt–hexane, 1:1); $\nu_{max}$ (KBr): 2880 ($CH_3$), 1730 et 1240 (ester), 1370 et 1390 (isopropylidène) $cm^{-1}$. *Anal.* calc. pour $C_{10}H_{16}O_5$: C 55,56, H 7,41; trouvée: C 55,67, H 7,55.

*Méthyl* O-*acétyl-2*-O-*benzyl-3-désoxy-4*-α *et* β-DL-thréo-*pentopyranosides (9α et 9β)*

Synthèse à partir des méthyl *O*-benzyl-3-désoxy-4-α et β-DL-*thréo*-pentopyranosides (**5**) (2 g, 8,4 mmol). La chromatographie des extraits réactionnels dans le solvant AcOEt–hexane 2:1 permet d'isoler les isomères α et β de **9** (2,282 g, rendement global: 97%). *Le composé* **9α** est une huile: $R_f$ 0,41 (AcOEt–hexane, 2:1); $\nu_{max}$ (film): 3040, 3060, 740 et 700 (benzyle), 1735 et 1240 (ester) $cm^{-1}$. *Le composé* **9β** est cristallisé: pf 84–86°C; $R_f$ 0,46 (AcOEt–hexane, 2:1); $\nu_{max}$ (KBr): caractéristiques identiques à **9α**. *Anal.* calc. pour $C_{15}H_{20}O_5$ (**9α** + **9β**): C 64,29, H 7,14; trouvée: C 64,00, H 7,13.

O-*benzoyl-3-désoxy-4*-O-*isopropylidène-1,2*-β-DL-*thréo-pentopyranose (2)*

Synthèse à partir du désoxy-4-*O*-isopropylidène-1,2-β-DL-*thréo*-pentopyranose (**4**) (1,5 g, 8,7 mmol). L'extrait réactionnel cristallise spontanement; des recristallisations successives dans le solvant hexane–$CH_2Cl_2$ fournissent *le composé* **2** sous forme de plaquettes nacrées (1,65 g, 96%): pf 91–93°C; $R_f$ 0,53 (AcOEt–hexane, 1:3); $\nu_{max}$ (KBr): 3070, 3030, 1610 et 710 (phényle), 1730 et 1230 (ester), 1380 et 1370 (isopropylidène) $cm^{-1}$. *Anal.* calc. pour $C_{15}H_{18}O_5$: C 64,75, H 6,47; trouvée: C 64,48, H 6,35.

*Méthyl* O-*benzoyl-2*-O-*benzyl-3-désoxy*-4-α *et* β-DL-thréo-*pentopyranosides (10α et 10β)*

Synthèse à partir des méthyl *O*-benzyl-3-désoxy-4-α et β-DL-*thréo*-pentopyranosides (1,5 g, 6,3 mmol); l'huile obtenue après traitement du milieu réactionnel est purifiée par chromatographie sur gel de silice dans le solvant AcOEt–hexane 1:3 pour donner les composés **10α** et **10β** (2,07 g, 96%); *le composé* **10β** est recristallisé dans le mélange éther–pentane 1:5 pour donner des cristaux blancs: pf 65–70°C; $R_f$ 0,57 (AcOEt–hexane, 1:2); $\nu_{max}$ (KBr): 3060, 3020, 1600, 1580, 725 et 740 (phényles), 1720 et 1285 (ester) $cm^{-1}$. *L'isomère* **10α** est une huile: $R_f$ 0,47 (AcOEt–hexane, 1:2); $\nu_{max}$ (film): caractéristiques identiques à **10β**. *Anal.* calc. pour $C_{20}H_{22}O_5$ (**10α** + **10β**): C 70,18, H 6,43; trouvée: C 70,27, H 6,28.

*Méthanolyse des groupements isopropylidène*

Les composés **1** et **2** (10 mmol) sont dissous dans du méthanol (20 mL) contenant de la résine Dowex 50 $H^+$ (env. 1 g) fraîchement activée par HCl. Les suspensions obtenues sont chauffées à 40°C pour le composé **1** et à 65°C pour le composé **2** pendant 1 h et 0,5 h respectivement. Après filtration de la suspension et lavage de la résine par du méthanol à 40°C, le solvant est évaporé et les résidus huileux obtenus sont chromatographiés sur colonne de gel de silice.

*Méthyl* O-*acétyl-3-désoxy-4*-α *et* β-DL-thréo-*pentopyranosides (3α et 3β)*

Les isomères **3α** et **3β** sont obtenus dans le rapport 1:1; ils sont séparés par chromatographie dans le solvant AcOEt–hexane 1:1; rendement global 65%; *le composé* **3β** est isolé sous forme d'une huile qui cristallise très lentement dans le mélange éther–hexane 1:5: pf 49–50°C; $R_f$ 0,25 (AcOEt–hexane, 1:1); $\nu_{max}$ (KBr): 3280 (OH), 2860 (OMe), 1740 et 1240 (ester) $cm^{-1}$. *Le composé* **3α** est une huile: $R_f$ 0,18 (AcOEt–hexane, 1:1); $\nu_{max}$ (film): caractéristiques identiques à **3β**. *Anal.* calc. pour $C_8H_{14}O_5$ (**3α** + **3β**): C 50,53, H 7,37; trouvée: C 50,67, H 7,30.

TABLEAU 3. $^1H$ résonance magnétique nucléaire des nucléosides **15–19**

| Composé | H-1′[a] | H-2′[b] | H-3′[c] | H-4′,4″[c] | H-5′,5″[c] | $J_{1',2'}$ | $J_{2',3'}$ | Autres protons |
|---|---|---|---|---|---|---|---|---|
| **15** | 5,62 | 4,77 | 4,00–3,50 | 2,00–1,50 | 4,00–3,50 | 9 | 9 | 7,97 et 6,00(2d,2H,$J_{5,6}$ = 7,3, H-6,H-5), 5,33(d,1H,OH), 3,82(s,3H,$OCH_3$), 1,88(s,3H,$COCH_3$) |
| **16** | 5,80 | 5,05 | 4,25–3,75 | 2,10–1,75 | 4,25–3,75 | 9,3 | 9,3 | 8,07 et 6,00(2d,2H,$J_{5,6}$ = 7,5, H-6,H-5), 7,83 et 7,55 (2m,5H,$C_6H_5$), 5,50(d,1H,OH), 3,73(s,3H,$OCH_3$) |
| **17α** | 5,50 | 3,50 | 4,15–3,50 | 2,10–1,50 | 4,15–3,50 | 8,8 | | 7,83 et 5,93(2d,2H,$J_{5,6}$ = 7,3, H-6,H-5), 7,17(s,5H,$C_6H_5$-benzyl), 4,77 et 4,37(2d,2H,$CH_2$-benzyl), 3,73(s,3H,$OCH_3$) |
| **17β** | 5,83 | 3,42 | 4,10 | 2,00 et 1,45 | 3,87 et 3,77 | 1 | 1 | 7,74 et 5,90(2d,2H,$J_{5,6}$ = 7,5, H-6,H-5), 7,17(m,5H,$C_6H_5$-benzyl), 5,25(d,1H,OH), 4,47 et 4,25(2d,2H,$CH_2$-benzyl), 3,82(s,3H,$OCH_3$) |
| **18α** | 5,44 | 3,28 | 3,53 | 1,84 et 1,61 | 3,87 et 3,68 | 9 | 9,8 | 8,03 et 6,00(2d,2H,$J_{5,6}$ = 7,5, H-6,H-5), 5,23(d,1H,OH), 3,82(s,3H,$OCH_3$-base), 3,27(s,3H,$OCH_3$-sucre) |
| **18β** | 5,83 | 3,10 | 3,15 | 1,93 et 1,43 | 4,10–3,80 | 1 | 1 | 7,75 et 5,95(2d,2H,$J_{5,6}$ = 7,5, H-6,H-5), 5,25(d,1H,OH), 3,93(s,3H,$OCH_3$-base), 3,25(s,3H,$OCH_3$-sucre) |
| **19** | 5,46 | 4,00–3,58 | 4,83 | 2,10–1,60 | 4,00–3,58 | 9,5 | 9,5 | 7,96 et 5,96(2d,2H,$J_{5,6}$ = 7,6, H-6,H-5), 5,43(d,1H,OH), 3,81(s,3H,$OCH_3$), 2,02(s,3H,$COCH_3$) |

[a] Doublet.
[b] Doublet de doublet.
[c] Multiplet. Solvant: $Me_2SO$-$d_6$. Les déplacements chimiques sont exprimés en δ ppm par rapport à $Me_4Si$ et les constantes de couplage en Hz.

Can. J. Chem. Downloaded from www.nrcresearchpress.com by 210.87.254.5 on 09/06/12
For personal use only.

*Méthyl* O-*benzoyl-3-désoxy-4-α et* β-DL-thréo-*pentopyranosides (4α et 4β)*

Les isomères α et β sont obtenus dans le rapport 55:45, et sont séparés de la même manière que les composés **3**; rendement global 80%; *le composé* **4β** est cristallisé: pf 95–98°C; $R_f$ 0,42 (AcOEt–hexane, 1:1); $\nu_{max}$ (KBr): 3270 (OH), 3060, 3040, 1600, 1585 et 715 (phényle), 2870 (OMe), 1730 et 1285 (ester) $cm^{-1}$. *Le composé* **4α** est une huile: $R_f$ 0,36 (AcOEt–hexane, 1:1); $\nu_{max}$ (film): caractéristiques identiques à **4β**. *Anal.* calc. pour $C_{13}H_{16}O_5$ (**4α** + **4β**): C 61,90, H 6,35; trouvée: C 61,94, H 6,50.

*Méthylation*

Les composés à méthyler (10 mmol) sont dissous dans du DMF (25 mL) contenant de l'oxyde d'argent (20 mmol) et de l'iodure de méthyle (50 mmol, 7,1 g, 3,1 mL). La suspension obtenue est agitée pendant 18 h à température ambiante puis les sels sont filtrés et lavés à l'éther (3 × 25 mL). Le filtrat est alors additionné d'eau (30 mL) et la phase aqueuse est extraite à l'éther (3 × 25 mL). La solution éthérée est lavée à l'eau (25 mL), séchée sur $Na_2SO_4$ et évaporée sous pression réduite pour donner les composés méthylés sous forme d'une huile jaune.

*Méthyl* O-*acétyl-3-désoxy-4-*O-*méthyl-2-α et* β-DL-thréo-*pentopyranosides (7α et7β)*

Synthèse à partir des composés **3α** et **3β**; la purification des produits est réalisée par chromatographie liquide sous basse pression dans le solvant pentane–éther 1:5; rendement: 91%. *Le composé* **7β** cristallise dans le mélange éther–hexane 1:5: pf 32,5°C; $R_f$ 0,65 (pentane–éther, 1:5); $\nu_{max}$ (KBr): 2850 (OMe), 1740 et 1245 (ester) $cm^{-1}$. *Le composé* **7α** est un liquide incolore: $n_D^{20}$ 1,4455; $R_f$ 0,49 (pentane–éther, 1:5); $\nu_{max}$ (film): caractéristiques identiques à **7β**. *Anal.* calc. pour $C_9H_{16}O_5$ (**7α** + **7β**): C 51,94, H 7,84; trouvée: C 52,10, H 7,71.

*Méthyl* O-*benzoyl-3-désoxy-4-*O-*méthyl-2-α et* β-DL-thréo-*pentopyranosides (8α et 8β)*

Synthèse à partir de **4α** et **4β**; la purification des composés est réalisée par chromatographie sur colonne sèche de gel de silice dans le solvant pentane–éther 1:1; rendement: 89%. Les deux composés sont isolés sous forme d'huiles incolores. *Composé* **8α**: $R_f$ 0,48 (pentane–éther, 1:1); $\nu_{max}$ (film): 2850 (OMe), 1720 et 1270 (ester) $cm^{-1}$. *Composé* **8β**: $R_f$ 0,34 (pentane–éther, 1:1); $\nu_{max}$ (film): caractéristiques identiques à **8α**. *Anal.* calc. pour $C_{14}H_{18}O_5$ (**8α** + **8β**): C 63,16, H 6,77; trouvée: C 63,34, H 6,91.

*Benzylation*

Le composé à benzyler (10 mmol) est dissous dans du DMF anhydre (10 mL) et à la solution obtenue sont ajoutés successivement: du bromure de benzyle (25 mmol, 4,3 g, 3 mL) et de l'oxyde d'argent (14 mmol, 3,25 g). La suspension ainsi formée est agitée à température ambiante pendant 5 min puis de l'iodure de potassium (0,4 mmol, 70 mg) est ajouté. Le mélange est agité pendant 6 h puis dilué par AcOEt (40 mL). Le précipité qui se forme instantanément est filtré et rincé par AcOEt (20 mL); le filtrat est évaporé à 50°C sous pression réduite et le résidu huileux obtenu est purifié pour donner les composés benzylés attendus.

*Méthyl* O-*acétyl-3-*O-*benzyl-2-désoxy-4-α et* β-DL-thréo-*pentopyranosides (5α et 5β)*

Synthèse à partir de **3α** et **3β**; les produits sont purifiés par chromatographie sur colonne de gel de silice dans le solvant AcOEt–hexane 1:3; rendement: 72%. Les deux composés sont recristallisés dans le mélange éther–pentane 1:5. *Composé* **5α**: pf 84°C; $R_f$ 0,39 (AcOEt–hexane, 1:3); $\nu_{max}$ (KBr): 3030, 3015, 3000, 740 et 705 (benzyle), 1740 et 1250 (ester) $cm^{-1}$. *Composé* **5β**: pf 68–69°C; $R_f$ 0,31 (AcOEt–hexane, 1:3); $\nu_{max}$ (KBr): caractéristiques identiques à **5α**. *Anal.* calc. pour $C_{15}H_{20}O_5$ (**5α** + **5β**): C 64,29, H 7,14; trouvée: C 64,53, H 6,97.

*Méthyl* O-*benzoyl-3-*O-*benzyl-2-désoxy-4-α et* β-DL-thréo-*pentopyranosides (6α et 6β)*

Synthèse à partir de **4α** et **4β**; les produits sont purifiés par chromatographie sur colonne de gel de silice dans le solvant AcOEt–hexane, 1:3; rendement: 65–75%. *Le composé* **6α** qui est obtenu sous forme d'huile après chromatographie, peut être recristallisé dans le mélange éther–hexane 1:6: pf 67–69°C; $R_f$ 0,43 (AcOEt–hexane, 1:3); $\nu_{max}$ (KBr): 3060, 3030, 1600, 1580, 710 et 690 (phényle), 1720 et 1270 (ester) $cm^{-1}$. *Le composé* **6β** est une huile; $R_f$ 0,33 (AcOEt–hexane, 1:3); $\nu_{max}$ (KBr): caractéristiques identiques à **6α**. *Anal.* calc. pour $C_{20}H_{22}O_5$ (**6α** + **6β**): C 70,18, H 6,43; trouvée: C 70,29, H 6,57.

*Hydrogénolyse des groupements benzyles*

Tous les oses soumis à l'hydrogénolyse ont été purifiés de façon à éliminer toute trace de pyridine pouvant provenir des réactions d'acylation; ce composé ayant entraîné dans quelques cas un ralentissement ou un blocage de la réaction.

Une solution éthanolique dégazée (45 mL) de composés benzylés (10 mmol) contenant de l'acide acétique pur (8 mL) et du palladium à 10% sur charbon (300 mg) est mise en contact à température ambiante avec de l'hydrogène gazeux sous faible pression hydrostatique. La solution est agitée pendant 18 h, filtrée sur Célite, évaporée sous pression réduite à 50°C et coévaporée 3 fois avec du toluène pour éliminer l'acide acétique. Le liquide sirupeux obtenu est purifié pour donner les composés débenzylés attendus.

*Méthyl* O-*acétyl-2-désoxy-4-α et* β-DL-thréo-*pentopyranosides (11α et 11β)*

Synthèse à partir de **9α** et **9β**; les produits sont purifiés sur colonne de gel de silice dans le solvant AcOEt–hexane 1:1; rendement: 96%. Les composés **11α** et **11β** sont recristallisés, après chromatographie, dans l'éther éthylique à −20°C. *Composé* **11α**: pf 61–62°C; $R_f$ 0,22 (AcOEt–hexane, 1:1); $\nu_{max}$ (KBr): 3390 (OH), 2870 (OMe), 1750, 1715 et 1270 (ester) $cm^{-1}$. *Composé* **11β**: pf 69–70°C; $R_f$ 0,27 (AcOEt–hexane, 1:1); $\nu_{max}$ (KBr): 3420 (OH), 2850 (OMe), 1745 et 1260 (ester) $cm^{-1}$. *Anal.* calc. pour $C_8H_{14}O_5$ (**11α** + **11β**): C 50,53, H 7,37; trouvée: C 50,76, H 7,65.

*Méthyl* O-*benzoyl-2-désoxy-4-α et* β-DL-thréo-*pentopyranosides (12α et 11β)*

Synthèse à partir de **10α** et **10β**; les purifications sont effectuées sur colonne de gel de silice dans le solvant AcOEt–hexane 1:1; rendement: 93%. Les composés **12α** et **12β** sont recristallisés dans un mélange AcOEt–hexane. *Composé* **12α**: pf 77°C; $R_f$ 0,26 (AcOEt–hexane, 1:1); $\nu_{max}$ (KBr): 3500 et 3400 (OH), 1730 et 1710, 1285 et 1260 (ester); 1600, 1580, 715 et 690 (phényle) $cm^{-1}$. *Composé* **12β**: pf 85–87°C; $R_f$ 0,35 (AcOEt–hexane, 1:1); $\nu_{max}$ (KBr): 3440 (OH), 3110, 3070, 3040, 1600, 1580 et 725 (phényle), 1730 et 1270 (ester) $cm^{-1}$. *Anal.* calc. pour $C_{13}H_{16}O_5$ (**12α** + **12β**): C 61,90, H 6,35; trouvée: C 61,99, H 6,48.

*Méthanolyse des groupements acyles*

À une solution méthanolique (50 mL) des sucres acétylés ou benzoylés (10 mmol) est ajoutée une solution de MeONa obtenue par dissolution de sodium (5 mmol, 115 mg) dans du méthanol (5 mL). Le mélange obtenu est chauffé à reflux 0,5 h, neutralisé à température ambiante par de la résine Dowex 50 $H^+$ méthanolique et filtré. Le filtrat est évaporé à sec et le résidu pâteux obtenu est purifié par chromatographie sur colonne de gel de silice.

*Méthyl* O-*benzyl-2-désoxy-4-α et* β-DL-thréo-*pentopyranosides (13α et 13β)*

Synthèse à partir de **5α**, **5β** et **6α** et **6β**; les produits sont purifiés par chromatographie dans le solvant AcOEt–hexane 1:1; rendement moyen: 94%. Les composés **13α** et **13β** sont obtenus sous forme d'huiles incolores. *Composé* **13α**: $R_f$ 0,46

Can. J. Chem. Downloaded from www.nrcresearchpress.com by 210.87.254.5 on 09/06/12
For personal use only.

(AcOEt–hexane, 1:1); $\nu_{max}$ (film): 3470 (OH), 3100, 3070, 3040, 740 et 700 (benzyle), 2840 (OMe) $cm^{-1}$. *Composé* **13β**: $R_f$ 0,36 (AcOEt–hexane, 1:1); $\nu_{max}$ (film): caractéristiques identiques à **13α**. *Anal.* calc. pour $C_{13}H_{18}O_4$ (**13α** + **13β**): C 65,55, H 7,56; trouvée: C 65,50, H 7,82.

*Méthyl désoxy-4-*O*-méthyl-2-α et* β-DL-threo-*pentopyranosides (**14α** et **14β**)*

Synthèse à partir de **7α**, **7β** et **8α**, **8β**; les produits sont purifiés par chromatographie dans le solvant AcOEt pur; rendement moyen: 84%. Les composés **14α** et **14β** sont des liquides incolores. *Composé* **14α**: $n_D^{20}$ 1,4510; $R_f$ 0,40 (AcOEt); $\nu_{max}$ (film): 3470 (OH), 2840 (OMe) $cm^{-1}$. *Composé* **14β**: $n_D^{20}$ 1,4525; $R_f$ 0,32 (AcOEt); $\nu_{max}$ (film): caractéristiques identiques à **14α**. *Anal.* calc. pour $C_7H_{14}O_4$ (**14α** + **14β**): C 51,85, H 8,64; trouvée: C 51,59, H 8,76.

*Méthode générale de bromuration*

Dans les réactions de bromuration, l'acide bromhydrique a été utilisé sous forme de solution à demi saturation dans $CH_2Cl_2$ à 0°C (environ 500 mg/10 mL $CH_2Cl_2$). Cet acide est ajouté à une solution de méthylglycoside (10 mmol) dans $CH_2Cl_2$ (60 mL) à raison de 5 équivalents par équivalent de sucre. La solution obtenue est agités à 0°C jusqu'à disparition complète des produits de départ (10–15 min). Le vase à réaction est alors sorti du bain refrigérant et la solution est dégazée par un fort courant d'azote anhydre. Ce dégazage, suivi en ccm, est stoppé dès l'apparition des premiers indices de resynthèse des produits de départ (5–10 min.); on ajoute alors en une seule fois le tamis moléculaire 10 Å en poudre (10 g) et la suspension orange obtenue est agitée jusqu'à disparition totale des vapeurs d'HBr dans le vase à réaction (environ 2 min).

*Condensation des bromoglycosides avec la diméthoxy-2,4-pyrimidine*

À la solution neutre de bromoglycoside obtenue précédemment est ajoutée en une seule fois de la DMP (2 équivalents par équivalent de bromure) et le mélange obtenu est porté à reflux pendant 10 min. Le solvant est évaporé pour donner un résidu pâteux qui est trituré dans du méthanol chaud (50°C). La suspension obtenue est filtrée, le gâteau de filtration est rincé 2 fois par du méthanol chaud et le filtrat est évaporé à sec. L'huile résiduelle orange obtenue est diluée avec le mélange acétone–méthanol 10:1 (10 mL/g de résidu) et le précipité blanc cristallin d'uracyle qui se forme en faible quantité est filtré puis rincé par de l'acétone pure. Le filtrat est évaporé et le concentré réactionnel huileux obtenu est purifié pour donner les nucléosides attendus.

*(O-acétyl-2 et O-acétyl-3-désoxy-4-α-DL-threo-pentopyranosyl)-1-méthoxy-4-pyrimidinone-2 (**15** et **19**)*

Synthèse à partir de **11**; le concentré réactionnel est dilué par le mélange acétone–hexane 1,5:1 (5 mL/g de concentré); il se forme lentement à température ambiante un précipité blanc de composé **19** (51%). La solution de cristallisation est chromatographiée sur colonne de gel de silice dans le solvant acétone–hexane 1,5:1 pour donner le composé **15** (30%) et un peu de nucléoside **19** (6%); rendement global: 87%. Ces composés peuvent être recristallisés dans le mélange $CH_3OH$–éther 1:10. *Composé* **15**: pf 152–154°C; $R_f$ 0,25 (acétone–hexane, 1,5:1); $\nu_{max}$ (KBr): 3380 (OH), 2900 (OMe), 1740 et 1240 (ester), 1670, 1640, 1550 et 1485 (base) $cm^{-1}$. *Anal.* calc. pour $C_{12}H_{16}N_2O_6$: C 50,70, H 5,63, N 9,36; trouvée: C 50,92, H 5,79, N 9,27. *Composé* **19**: pf 203–204°C; $R_f$ 0,30 (acétone–hexane 1,5:1); $\nu_{max}$ (KBr): 3110 (OH), 2890 (OMe), 1740 et 1260 (ester), 1645, 1550 et 1480 (base) $cm^{-1}$. *Anal.* calc. pour $C_{12}H_{16}N_2O_6$: C 50,70, H 5,63, N 9,36; trouvée: C 50,61, H 5,72, N 9,73.

*(O-benzoyl-2-désoxy-4-α-DL-threo-pentopyranosyl)-1-méthoxy-4-pyrimidinone-2 (**16**)*

Synthèse à partir de **12**; le concentré réactionnel est dilué par de l'acétate d'éthyle pur (6 mL/g de concentré); et le précipité blanc de *composé* **16** qui se forme est filtré puis rincé par AcOEt pur; rendement: 80–85%: pf 195–197°C; $R_f$ 0,40 (AcOEt); $\nu_{max}$ (KBr): 3300 (OH), 1720 et 1260 (ester), 1650, 1635, 1540 et 1480 (base), 710 (phényle) $cm^{-1}$. *Anal.* calc. pour $C_{17}H_{18}N_2O_6$: C 58,96, H 5,20, N 8,09; trouvée: C 59,10, H 5,30, N 7,87.

*(O-benzyl-2-désoxy-4-α et* β-DL-threo-*pentopyranosyl)-1-méthoxy-4-pyrimidinone-2 (**17α** et **17β**)*

Synthèse à partir de **13**; le concentré réactionnel ne cristallise pas par adjonction de solvants, il est chromatographié sur gel de silice dans le solvant acétone–hexane 1,5:1 pour donner le composé **17β** pur (67%) et le composé **17α** (10%) contenant des traces du composé β. Ces nucléosides sont obtenus sous forme de laques qui cristallisent par trituration dans l'éther éthylique anhydre. *Composé* **17α**: pf 155–165°C; $R_f$ 0,23 (acétone–hexane, 1,5:1); $\nu_{max}$ (KBr): 3420 (OH), 2900 (OMe), 1660, 1635, 1550 et 1490 (base), 700 (phényle) $cm^{-1}$. *Anal.* calc. pour $C_{17}H_{20}N_2O_5$: C 61,45, H 6,02, N 8,43; trouvée: C 61,51, H 6,12, N 8,56. *Composé* **17β**: pf 137°C; $R_f$ 0,32 (acétone–hexane, 1,5:1); $\nu_{max}$ (KBr): 3370 (OH), 2890 (OMe), 1640, 1620, 1540 et 1470 (base), 700 (phényle) $cm^{-1}$. *Anal.* calc. pour $C_{17}H_{20}N_2O_5$: C 61,45, H 6,02, N 8,43; trouvée: C 61,25, H 6,05, N 8,38.

*(Désoxy-4-*O*-méthyl-2-α et* β-DL-threo-*pentopyranosyl)-1-méthoxy-4-pyrimidinone-2 (**18α** et **18β**)*

Synthèse à partir de **14**; le concentré réactionnel est chromatographié sur gel de silice dans le solvant acétone–hexane 5:1 pour donner les composés **18β** (55%) et **18α** (23%) sous forme de laques qui cristallisent dans l'éther éthylique; rendement global: 77%. *Composé* **18α**: pf 205–206°C; $R_f$ 0,45 (acétone–hexane, 5:1); $\nu_{max}$ (KBr): 3400 (OH), 2845 (OMe), 1680, 1620, 1540 et 1480 (base) $cm^{-1}$. *Anal.* calc. pour $C_{11}H_{16}N_2O_5$: C 51,56, H 6,25, N 10,94; trouvée: C 51,54, H 6,42, N 10,79. *Composé* **18β**: pf 178–179°C; $R_f$ 0,60 (acétone–hexane, 5:1); $\nu_{max}$ (KBr): 3470 (OH), 1665, 1630, 1540 et 1480 (base) $cm^{-1}$. *Anal.* calc. pour $C_{11}H_{16}N_2O_5$: C 51,56, H 6,25, N 10,94; trouvée: C 51,45, H 6,32, N 11,05.

## Remerciements

Nous tenons à remercier le C.N.R.S. (ERA 560) et l'I.N.S.E.R.M. (U 205) pour l'aide financière qu'ils nous ont apportée.

1. C. H. Gagnieu et A. V. Grouiller. Travail présenté en partie au Xth International Symposium on Carbohydrate Chemistry. 7–11 juillet 1980, Sydney, Australie.
2. K. A. Watanabe, D. H. Hollenberg et J. J. Fox. J. Carbohydr. Nucléosides-Nucléotides, **1**, 1 (1974).
3. G. E. Hilbert et T. B. Johnson. J. Am. Chem. Soc. **52**, 4489 (1930).
4. C. H. Gagnieu et A. V. Grouiller. Carbohydr. Res. **84**, 61 (1980).
5. D. Descours. Thèse de doctorat d'état, Institut National des Sciences appliquées de Lyon, France. 27 mars 1979.
6. L. M. Weinstock, S. Karady, F. E. Roberts, A. M. Hoinowski, G. S. Brenner, T. B. K. Lee, W. C. Lumma et M. Sletzinger. Tetrahedron Lett. 3979 (1975).
7. J. Pliml et M. Prystas. Adv. Heterocycl. Chem. **8**, 115 (1967).
8. S. Hanessian et A. G. Pernet. Can. J. Chem. **52**, 1266 (1974).
9. A. H. Haines. *Dans* Advances in carbohydrate chemistry and biochemistry, Vol. 33. *Edité par* R. S. Tipson et D. Horton. Academic Press, New York. 1976.
10. C. C. Bhat et H. R. Munson. *Dans* Synthetic procedures in nucleic acid chemistry. Vol. 1. *Edité par* W. W. Zorbach et R. S. Tipson. Interscience, New York. 1968.

# Isomeric and tautomeric $[C_4H_4O]^{+\cdot}$ ions; their thermochemistry and collisionally induced fragmentation characteristics

PETER C. BURGERS, JOHN L. HOLMES,[1] and F. P. LOSSING
*Department of Chemistry, University of Ottawa, Ottawa, Ont., Canada K1N 9B4*

AND

ALEXANDER A. MOMMERS, FRANK R. POVEL, and JOHAN K. TERLOUW
*Analytical Chemistry Laboratory, University of Utrecht, Croesestraat, 77A, Utrecht, 3522AD, The Netherlands*

Received February 25, 1982

PETER C. BURGERS, JOHN L. HOLMES, F. P. LOSSING, ALEXANDER A. MOMMERS, FRANK R. POVEL, and JOHAN K. TERLOUW. Can. J. Chem. **60**, 2246 (1982).

Ionic heats of formation and collisional activation (CA) mass spectra for fifteen isomeric or tautomeric $[C_4H_4O]^{+\cdot}$ ions are described. Twelve of these species can be characterised by means of their CA mass spectra alone. The relative thermodynamic stabilities of keto–enol tautomers and the ease of interconversion of some ions are discussed. It is emphasised that CA spectra *alone* (i.e. in the absence of other information, such as heat of formation, etc.) may not easily be correlated with the appropriate ion structures.

PETER C. BURGERS, JOHN L. HOLMES, F. P. LOSSING, ALEXANDER A. MOMMERS, FRANK R. POVEL et JOHAN K. TERLOUW. Can. J. Chem. **60**, 2246 (1982).

On a déterminé les chaleurs de formation ionique et les spectres de masse d'activation de collision (AC) de quinze ions isomères ou tautomères $[C_4H_4O]^+$. On peut caractériser douze de ces espèces en faisant appel uniquement à leur spectre de masse AC. On discute des stabilités thermodynamiques relatives des tautomères céto–énol et de la facilité d'interconversion de quelques ions. On souligne le fait que les spectres de AC seuls (i.e. en l'absence d'autres informations, tels la chaleur de formation, etc.) ne peuvent être facilement reliés aux structures appropriées de l'ion.

[Traduit par le journal]

## Introduction

Attempts to understand qualitatively the unimolecular decomposition of organic ions in the gas phase were, in the 1960's, concentrated upon identifying which atoms actively participated in the transition-state — by the classical method of isotopic labelling (1). Interpretation of results then leaned heavily upon analogies drawn from reactions of neutral organic compounds in solution or in the gas phase. The confirmation of proposed mechanisms in the majority of cases still awaits unequivocal methods for the identification of the reacting configurations (RC) of precursor ions (the structure which leads directly to the transition state (2)) and the structures of the product ions and neutral fragments.

In recent years considerable progress has been made towards this end and it is now often possible to obtain a detailed description of a reaction pathway provided that several complementary techniques are used. Such methods include (*i*) the accurate determination of appearance energies (AE) in order to evaluate the energy barrier for the fragmentation and thus to permit a choice between possible daughter ion structures; (*ii*) the study of metastable ion (MI) phenomena which arise from dissociations of ions of low internal energy (2) having lifetimes of the order of μs; (*iii*) collisional activation (CA) and collisional ionisation (charge stripping [CS]) mass spectra of mass-selected ions may be used to characterise product ion structures and also as a probe for the possible isomerisation of the precursor ion prior to fragmentation (3). Each of these methods, in contrast with observations derived from normal mass spectra, focuses attention on restricted ranges of ion internal energy and in *combination* provide a powerful (although still largely empirical) tool for the study of gas phase ion fragmentations.

In general, these advances in technique have established the existence of many isomeric (radical) cations as stable entities in the gas phase. Of these, relatively few have been observed in condensed phases as either neutral or charged species and so analogies cannot readily be drawn from solution chemistry for the behaviour of such ions.

Some years ago we employed these methods to investigate a longstanding problem in gas phase ion chemistry, namely, the identity of the $[C_4H_4O]^{+\cdot}$ daughter ion produced by loss of CO from ionised 2- and 4-pyrone and which generates the base peak in their normal mass spectra. It was shown (4),

[1]To whom all correspondence should be addressed.

0008-4042/82/172246-10$01.00/0
©1982 National Research Council of Canada/Conseil national de recherches du Canada

Can. J. Chem. Downloaded from www.nrcresearchpress.com by 210.87.254.105 on 09/06/12
For personal use only.

Can. J. Chem. Downloaded from www.nrcresearchpress.com by 210.87.254.105 on 09/06/12
For personal use only.

contrary to earlier conclusions, that the $[C_4H_4O]^{+\cdot}$ ions from both precursors mainly had the [furan]$^{+\cdot}$ structure and that some ionised vinyl ketene $[CH_2{=}CH{-}CH{=}C{=}O]^{+\cdot}$ was also generated. The properties of the only five readily accessible isomeric $[C_4H_4O]^{+\cdot}$ ions were studied in this early work. Other stable configurations undoubtedly exist and further investigation is warranted to provide the necessary reference ions whose MI and CA mass spectra would permit the ready identification of unknown $[C_4H_4O]^{+\cdot}$ product ions. Of particular interest are isomers containing a hydroxyl group. It has been shown that enol ions have lower $\Delta H_f$ values than their tautomers derived from ionised saturated (5) and unsaturated aldehydes and ketones (6). $[C_4H_4O]^{+\cdot}$ ions considered in the present work include some highly unsaturated keto–enol pairs and also an —OH substituted alkene–yne for which no keto counterpart exists. It should be noted that such species also provide information as to the stabilising effects of substituents in $\pi$-bonded systems and additional basic data for methods for the estimation of ionic heats of formation (7).

We here present evidence for the identification of fifteen isomeric (or tautomeric) $[C_4H_4O]^{+\cdot}$ radical cations.

## Results and discussion

The CA mass spectra and ionic heats of formation of the $[C_4H_4O]^{+\cdot}$ ions are shown in Table 1. The ions will be discussed by group, in the order of their presentation in Table 1, namely the ethers (furan and vinyloxy ethyne, $HC{\equiv}C{-}O{-}CH{=}CH_2$), the three ketenes (vinylketene, $CH_2{=}CH{-}CH{=}C{=}O$; dimethylene ketene

and buta-1,2-dienone, $CH_3{-}CH{=}C{=}C{=}O$), the hydroxy-containing species (1-hydroxybuta-1-en-3-yne, $HOCH{=}CH{-}C{\equiv}CH$; 2-hydroxybuta-1-en-3-yne, $CH_2{=}C(OH){-}C{\equiv}CH$; 4-hydroxybuta-1-en-3-yne, $CH_2{=}CH{-}C{\equiv}C(OH)$; and hydroxybutatriene, $CH_2{=}C{=}C{=}CHOH$), the aldehydes and ketones (buta-2,3-dien-al, $CH_2{=}C{=}CH{-}CHO$; 2-butynal, $CH_3{-}C{\equiv}C{-}CHO$; 3-cyclopropenecarbaldehyde,

methylethynyl ketone, $CH_3{-}CO{-}C{\equiv}CH$; methylcyclopropenone,

and 3-butynal).

The CA mass spectra are tabulated so as clearly to emphasise those peaks whose significant intensity differences permit the characterisation of ion structures. In a number of cases the CA mass spectra were only readily assigned to specific ion structures with the aid of ancillary observations. All structure assignments are given in the detailed discussions which follow.

*Ether ions*

The CA mass spectrum of furan agrees well with our previously reported (partial) CA mass spectrum (4); it is dominated by the peak at *m/z* 39 $[C_3H_3]^+$ (corresponding to CHO loss) and is readily distinguished from the other isomers by the *B* and *D* ion clusters (see Table 1). Vinyloxyethyne has the highest $\Delta H_f$ of any of the $[C_4H_4O]^+$ ions so far investigated, 251 kcal mol$^{-1}$ (IE = 9.40 eV, $\Delta H_f$ [$HC{\equiv}C{-}O{-}CH{=}CH_2$] = 34 kcal mol$^{-1}$ (8)). Its CA mass spectrum is highly characteristic, being dominated by the reactions

$$HC{\equiv}C{-}O{-}CH{=}CH_2^{+\cdot} \longrightarrow \underset{m/z\ 42}{CH_2C\overset{+\cdot}{O}} + C_2H_2$$

$$\longrightarrow \underset{m/z\ 27}{CH_2CH^+} + HC_2O^{\cdot}$$

showing that this molecular ion does not readily rearrange to any of its thermodynamically more stable structures prior to collision-induced fragmentation. Similarly furan, which must ring open before fragmenting, does not communicate with the linear ether.

*Ketene ions*

Thermal decomposition of the en–yne ether, $CH_2{=}CH{-}C{\equiv}C{-}O{-}CH_2CH_3$, was proposed in our earlier study (9) to produce vinylketene plus ethene. This has been confirmed by microwave and infrared spectroscopy (10, 11), which in addition showed that the *trans*-rotamer is generated. Ionised vinylketene remains the $[C_4H_4O]^{+\cdot}$ isomer of lowest $\Delta H_f$ (see Table 1). The CA mass spectrum agrees well with that previously reported (4, 9).

CA mass spectra identical with that of [vinylketene]$^{+\cdot}$ were obtained from the *m/z* 68 ions produced by the dissociative ionisation of 5,6-dihydro-2-pyrone



and 2-cyclohexen-1-one. Loss of $CH_2O$ and $C_2H_4$ respectively, via a $4\pi + 2\pi$ cycloreversion reaction, readily rationalises the production of [vinylketene]$^{+\cdot}$. The heats of formation of the $[C_4H_4O]^{+\cdot}$ daughter ions were found to be 200 $\pm$ 2 kcal mol$^{-1}$ (AE *m/z* 68 = 10.56 eV, $\Delta H_f$[lactone]

Can. J. Chem. Downloaded from www.nrcresearchpress.com by 210.87.254.105 on 09/06/12
For personal use only.

TABLE 1. Ionic heats of formation ($\Delta H_f$) and collisional

| $[Ion]^{+\cdot}$ | $\Delta H_f$ (kcal mol$^{-1}$) | 67 | 66 | 65 | $E$ | 54 | 53 | 52 | 51 | 50 | 49 | $D$ |
|---|---|---|---|---|---|---|---|---|---|---|---|---|
| Furan | 197 | 91 | 8 | 1 | 10 | 9 | 9 | 2 | 11 | 34 | 34 | 4 |
| HC≡C—O—CH=CH$_2$ | 251 | 87 | 11 | 2 | 2 | 5 | 76 | 4 | 2 | 7 | 5 | 2 |
| CH$_2$=CH—CH=C=O | 194 | 65 | 29 | 5 | 4 | 21 | 17 | 4 | 13 | 28 | 17 | 9 |
| ▷C=C=O | 198±2 | 69 | 26 | 5 | 3 | 31 | 27 | 5 | 10 | 17 | 10 | 14 |
| CH$_3$—CH=C=C=O | 202 | 87 | 12 | 1 | 11 | 1 | 44 | 8 | 10 | 21 | 15 | 8.5 |
| | 240 | 89 | 9 | 2 | 7 | 1 | 44 | 8 | 9 | 23 | 15 | 7 |
| CH$_3$—CO—C≡CH | 244 | 80 | 11 | 9 | 8 | — | 94 | 2 | 0.5 | 2 | 1 | 300 |
| HC≡C—C(OH)=CH$_2$ | 217 | 78 | 20 | 2 | 70 | 3 | 30 | 2 | 18 | 31 | 17 | 76 |
| H$_2$C=C=CH—CHO | 236 | 43 | 51 | 6 | 9 | 2 | 7 | 2 | 15 | 48 | 27 | 14 |
| CH$_3$—C≡C—CHO | 246 | 96 | 4 | — | 250 | 1 | 17 | 15 | 16 | 33 | 19 | 14 |
| HC≡C—CH$_2$CHO | 247 | See text | | | | | | | | | | |
| HC≡C—CH=CH(OH) | 222 | 38 | 56 | 7 | 12 | 3 | 6 | 1 | 14 | 50 | 27 | 19 |
| H$_2$C=C=C=CH(OH) | 222 | 53 | 43 | 4 | 58 | 3 | 6 | 2 | 21 | 47 | 21 | 38 |
| H$_2$C=CH—C≡C—OH | See text | 85 | 14 | 1 | 80 | 4 | 30 | 5 | 12 | 30 | 19 | 19 |
| ▷CHO | See text | 86 | 11 | 3 | 7 | 10 | 12 | 3 | 12 | 37 | 26 | 2 |

*The sum of the relative abundances of ions in each $m/z$ series (e.g. $m/z$ 54 → 49) have been normalized to 100 units. The relative abundances of each *group* of ions ($A$–$E$) have also been normalized, but relative to group $C$ = 100 units.

= −69 ± 2 kcal mol$^{-1}$,[2] $\Delta H_f$[CH$_2$O] = −25.9 kcal mol$^{-1}$ (12)) and 194 kcal mol$^{-1}$ (9), respectively.

In an earlier study (13), it was concluded that [vinylketene]$^{+\cdot}$ was the predominant $m/z$ 68 ion generated by the loss of H$_2$O from *cis* and *trans* crotonic acids and cyclopropanecarboxylic acid. However, the metastable peaks for these reactions were of composite shape and it was considered that the [C$_4$H$_4$O]$^{+\cdot}$ isomer ionised cyclobutenone might be cogenerated. Accordingly, the behaviour of 4-cyclopenten-1,3-dione was investigated, because the simple dissociative ionisation thereof might well be expected to generate [cyclobutenone]$^{+\cdot}$ ions, i.e.

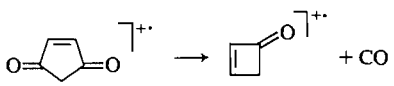

The $\Delta H_f$[C$_4$H$_4$O]$^{+\cdot}$ from this dione was found to be 224 kcal mol$^{-1}$ (AE $m/z$ 68 = 10.88 eV, $\Delta H_f$[4-cyclopenten-1,3-dione] = −53 kcal mol$^{-1}$ (8), $\Delta H_f$[CO] = −26.4 kcal mol$^{-1}$ (12)). This must represent an *upper limit* for the $\Delta H_f$ because the metastable peak for the above reaction was of dished shape. The approximate minimum kinetic energy release (calculated from the width of the metastable peak across its maxima (2)) $T_{min}$ = 0.19 eV. Our revised estimated value for $\Delta H_f$ [cyclobutenone]$^{+\cdot}$ = 223 ± 3 kcal mol$^{-1}$,[3] reinforced the suggestion that it may be generated from the dione as described above.

However, the CA mass spectrum of the $m/z$ 68 daughter ions was closely similar to that of [vinylketene]$^{+\cdot}$, as indeed were those of the [C$_4$H$_4$O]$^{+\cdot}$ daughter ions from the three isomeric acids referred to above. It is therefore concluded that *if* it is generated, [cyclobutenone]$^{+\cdot}$ has a CA mass spectrum essentially indistinguishable from that of its valence isomer [vinylketene]$^{+\cdot}$, i.e. although the cyclic ion could be generated at threshold, it readily ring-opens with little energy requirement.

The mass spectral properties of the unsaturated ether, CH$_2$=CH—C≡C—OCH$_2$CH$_3$, which readily yields vinylketene at ca. 150°C, were studied under conditions at which thermolysis was negligible. $m/z$ 68 is the base peak in the normal mass spectrum of the compound and there is an intense metastable peak for its generation from the molecular ion, $m/z$ 96. The CA mass spectrum of $m/z$ 68 ions generated in the first field-free region was clearly that of [vinylketene]$^{+\cdot}$ and this dissociative ionisation therefore must parallel the thermal decomposition. Surprisingly, however, the ion-source generated [C$_4$H$_4$O]$^{+\cdot}$ ions cannot have this structure alone, because their CA mass spec-

[2]By additivity (ref. 8) and assuming a ring-strain correction of +3±2 kcal mol$^{-1}$. The values of +26 and −34 kcal mol$^{-1}$ were assumed for C$_t$—(O) and O—(C$_t$)(C), respectively.

[3]Ionisation energy ≃ 9.3 eV (estimated), $\Delta H_f$[cyclobutenone] = +8 kcal mol$^{-1}$ by additivity (ref. 8) and assuming ring strain is the same as for cyclobutene and that CO—(C$_d$)(C) = −33 kcal mol$^{-1}$.

activation mass spectra for $[C_4H_4O]^{+\cdot}$ ions*

| 43 | 42 | 41 | 40 | 39 | 38 | 37 | C | 29 | 28 | 27 | 26 | 25 | 24 | B | 15 | 14 | 13 | 12 | A |
|---|---|---|---|---|---|---|---|---|---|---|---|---|---|---|---|---|---|---|---|
| — | 5 | 1 | 8 | 54 | 18 | 13 | 100 | 50 | 6 | 4 | 24 | 11 | 4 | 18 | — | 43 | 30 | 26 | 2 |
| — | 61 | 10 | 6 | 19 | 2 | 2 | 100 | 6 | 2 | 74 | 11 | 5 | 1 | 35 | 31 | 32 | 31 | 7 | 3 |
| — | 8 | 3 | 16 | 45 | 15 | 10 | 100 | 6 | 10 | 23 | 40 | 16 | 5 | 10 | 4 | 38 | 38 | 20 | 1 |
| — | — | — | 40 | 32 | 16 | 11 | 100 | 5 | 13 | 5 | 48 | 22 | 6 | 7.5 | 2 | 58 | 19 | 21 | 1 |
| — | 0.5 | 2 | 49 | 29 | 11 | 9 | 100 | 7 | 15 | 16 | 28 | 28 | 8 | 6.5 | 28 | 23 | 31 | 19 | 1 |
| — | 1 | 2 | 57 | 24 | 9 | 7 | 100 | 6 | 19 | 19 | 24 | 24 | 7 | 6 | 26 | 24 | 29 | 21 | 1 |
| 31 | 9 | 2 | 34 | 11 | 6 | 7 | 100 | 7 | 7 | 5 | 11 | 55 | 16 | 18 | 57 | 23 | 10 | 10 | 7 |
| 2 | 19 | 3 | 7 | 40 | 16 | 13 | 100 | 35 | 4 | 9 | 20 | 23 | 8 | 17 | 45 | 25 | 15 | 15 | 4 |
| — | 2 | 0.5 | 30 | 42 | 16 | 11 | 100 | 64 | 5 | 4 | 15 | 10 | 3 | 13 | 20 | 40 | 20 | 20 | 1 |
| — | — | — | 41 | 29 | 17 | 13 | 100 | 46 | 8 | 9 | 17 | 14 | 6 | 12 | 28 | 19 | 26 | 26 | 1 |
| — | 3 | 1 | 27 | 43 | 16 | 11 | 100 | 69 | 3 | 5 | 12 | 9 | 2 | 12 | 30 | 40 | 15 | 15 | 1 |
| — | 5 | 1 | 8 | 52 | 19 | 15 | 100 | 64 | 5 | 4 | 11 | 10 | 6 | 13 | — | 40 | 30 | 30 | 1 |
| — | 7 | 2 | 11 | 41 | 21 | 16 | 100 | 28 | 9 | 16 | 27 | 18 | 7 | 15 | — | 33 | 33 | 33 | 2 |
| — | 3 | 1 | 5 | 75 | 10 | 6 | 100 | 61 | 4 | 4 | 22 | 7 | 1 | 9 | — | 50 | 33 | 17 | 1 |

trum is wholly different from that of [vinylketene]$^{+\cdot}$. These observations are further discussed below under hydroxy-containing ions.

Dimethyleneketene can conveniently be generated via the dissociative ionisation of α-methylene-γ-butyrolactone. Loss of $CH_2O$ produces $[C_4H_4O]^{+\cdot}$ ions, base peak in the normal mass spectrum, and can reasonably be expected to produce the desired species:

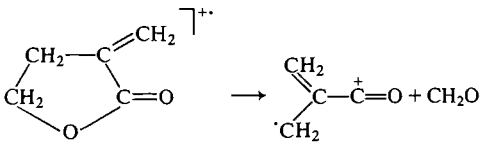


The AE $m/z$ 68 from this lactone, 10.44 ± 0.05 eV, leads to $\Delta H_f[C_4H_4O]^{+\cdot}$ = 198 ± 2 kcal mol$^{-1}$ ($\Delta H_f$[lactone] = −69 ± 2 kcal mol$^{-1}$ (8); $\Delta H_f$ [$CH_2O$] = −25.9 kcal mol$^{-1}$ (12)). This fragmentation is accompanied by an intense Gaussian-type metastable peak, with a kinetic energy release calculated from the width of the peak at half-height, $T_{0.5}$ = 0.006 eV, and thus there is no evidence to indicate that this reaction involves a significant reverse energy barrier. The CA mass spectrum was independent of electron energy and that derived from the ion source generated $[C_4H_4O]^{+\cdot}$ ions was the same as that for ions produced in the first field-free region, indicating that more than one structure is unlikely to be involved. It is concluded from the above evidence that these $[C_4H_4O]^{+\cdot}$ ions are *not* merely slightly energy-rich [vinylketene]$^{+\cdot}$, but represent a different structure, namely dimethyleneketene. The most pronounced differences from the CA mass spectrum of [vinylketene]$^{+\cdot}$ are: the absence of $m/z$ 42, $[CH_2{=}C{=}O]^{+\cdot}$, the much lower intensity of $m/z$ 27 $[C_2H_3]^+$, and the enhanced intensity of $m/z$ 40, $[C_3H_4]^{+\cdot}$. The latter process is that of lowest energy requirement ($\Delta H_f$(products) = $\Delta H_f(CH_2CCH_2)^{+\cdot}$ + $\Delta H_f$(CO) = 243 kcal mol$^{-1}$ (14)). In the normal mass spectrum this fragmentation generates an intense metastable peak and analysis (15) of the $[C_3H_4]^{+\cdot}$ daughter ions shows them to have, as expected, the [allene]$^{+\cdot}$ structure, i.e. [propyne]$^{+\cdot}$ is not produced at higher internal energies of the fragmenting ions. All of these differences are in keeping with the ion generated from this lactone having the *branched* ketene structure shown above, in contrast with the *linear* [vinylketene]$^{+\cdot}$.

The above results permit further analysis of observations of the elimination of $H_2O$ from ionised methacrylic acid (13) where it had been proposed that metastable molecular ions rearrange to [crotonic acid]$^{+\cdot}$ via a 1,2-methyl shift, yielding [vinylketene]$^{+\cdot}$ (and [cyclobutenone]$^{+\cdot}$) on loss of $H_2O$. The apparent $\Delta H_f$ of the $[C_4H_4O]^{+\cdot}$ daughter ion, 215 kcal mol$^{-1}$ (AE $m/z$ 68 = 10.64 eV; $\Delta H_f$ [$CH_2{=}C(CH_3)COOH$] = −88.2 kcal mol$^{-1}$ (8), $\Delta H_f[H_2O]$ = −57.8 kcal mol$^{-1}$ (14)), is a maximum value (the reaction has a reverse energy barrier (13)) and so in principle permits the cogeneration of

Can. J. Chem. Downloaded from www.nrcresearchpress.com by 210.87.254.105 on 09/06/12
For personal use only.

Can. J. Chem. Downloaded from www.nrcresearchpress.com by 210.87.254.105 on 09/06/12
For personal use only.

the *branched* ketene; e.g., via the reaction:

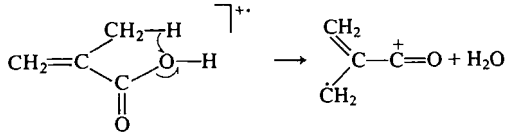

This proposal cannot be demonstrated by labelling experiments, but the CA mass spectrum of the *ion-source* generated $[C_4H_4O]^{+\cdot}$ ions from this reaction can most satisfactorily be reproduced from a 2:3 mixture of the CA mass spectra of [vinylketene]$^{+\cdot}$ and the branched ketene. $[C_4H_4O]^{+\cdot}$ ions of lower internal energy, derived from molecular ions fragmenting in the first field-free region, display CA mass spectra for which a respective 3:2 summation suffices, indicating a higher proportion of the thermodynamically more stable species.

*[Buta-1,2-dienone]*$^{+\cdot}$

Identification of this ion proved difficult because of the lack of precursor molecules which might predictably yield it upon dissociative ionisation. The neutral ketene has not been described, but its homologue, propadienone, $CH_2{=}C{=}C{=}O$, resulted from the gas phase pyrolysis of the mixed anhydride of acrylic and trifluoroacetic acids.[4] By analogy, the anhydride of crotonic and trifluoroacetic acid might be expected to yield the desired ketene. However, the IE of the $C_4H_4O$ species derived from the pyrolysis of $CH_3CH{=}CH{-}CO{-}O{-}COCF_3$ was only 8.07 eV, i.e. *lower* than the IE of vinylketene (8.31 eV (9)) and thus excluding *its* generation. Consequently this pyrolysis may well yield the expected product whose IE should be lower than that of vinylketene. So far, however, the characterisation of the ionised $C_4H_4O$ pyrolysis product by its CA mass spectrum could not be performed because of the lack of a pyrolytic inlet system for the instrument (ZAB-2F) with which CA mass spectra were measured. However, three precursor molecules were examined which have major *m/z* 68 $[C_4H_4O]^{+\cdot}$ ions in their mass spectra whose structure may indeed be that of ionised buta-1-2-dienone. Loss of $CH_2O$ from $[CH_2{=}C{=}CHCOOCH_3]^{+\cdot}$ and loss of $CO_2$ from itaconic and citraconic anhydrides produce $[C_4H_4O]^{+\cdot}$ ions with identical CA mass spectra (see Table 1) which we propose is that of $[CH_3CH{=}C{=}C{=}O]^{+\cdot}$. The assignment is based on the following arguments. Consider the two *direct* $CO_2$ eliminations from ionised itaconic anhydride.

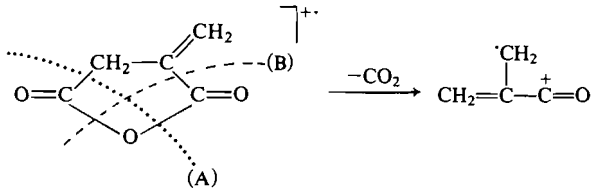

Only mode A leads *directly* to a stable product ion as shown above. However, this $[C_4H_4O]^{+\cdot}$ ion is *not* generated because its CA mass spectrum (and its charge-stripping [CS] mass spectrum, see below) is markedly different from that of the observed product ion. Note for example, the absence of *m/z* 54 (loss of $:CH_2$) and the relative prominence of *m/z* 53 (loss of $CH_3{\cdot}$). Mode B would yield, at least initially, a highly unstable linear ion and would not be expected to compete with mode A; it could also generate $[O{=}CH{-}CH{=}C{=}CH_2]^{+\cdot}$ but the observed CA mass spectrum rules this out. However, the following two simple *rearrangements* in ionised itaconic and citraconic anhydrides would yield product ions having $\Delta H_f$ lower than that of the branched ketene:

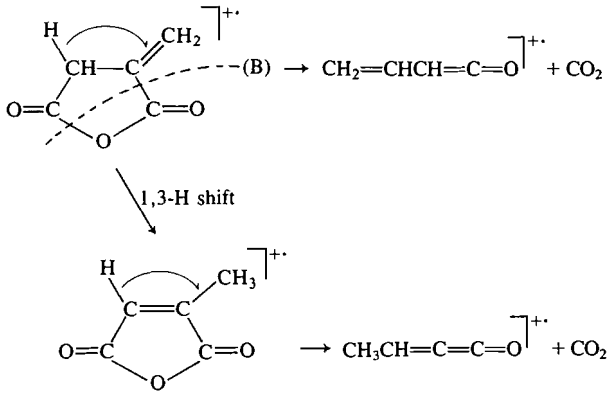

Route B, the formation of [vinylketene]$^{+\cdot}$, can be rejected (CA and CS mass spectra). The second reaction proceeds via ionised citraconic anhydride and thereby accounts for the observed daughter ions from the two anhydrides having the same characteristics; the 1,2-H shift shown in the second step leads to [buta-1,2-dienone]$^{+\cdot}$. Note that *without* rearrangement, loss of $CO_2$ from citraconic anhydride would generate [methylcyclopropenone]$^{+\cdot}$,

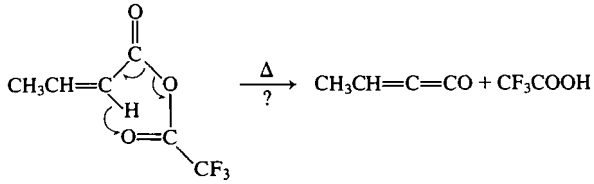

[4]This was obtained by measurement of the AE for the metastable peak *m/z* 112 → *m/z* 68 by a comparative method (34).

Can. J. Chem. Downloaded from www.nrcresearchpress.com by 210.87.254.105 on 09/06/12
For personal use only.

a reference ion whose CA mass spectrum is closely similar to that of the observed daughter ion. The latter, however, *cannot* have the cyclic structure because the $\Delta H_f[C_4H_4O]^{+\cdot}$ values derived from AE measurements (AE *m/z* 68 from citraconic anhydride = 10.68 eV. $\Delta H_f$(neutral) = −106.8 kcal mol$^{-1}$ (12), $\Delta H_f(CO_2)$ = −94.1 kcal mol$^{-1}$ (14). $T_{min}$ from metastable peak *m/z* 112 → *m/z* 68 = 0.3 eV, whence $\Delta H_f[C_4H_4O]^{+\cdot} \leq 226$ kcal mol$^{-1}$. AE *m/z* 68 from itaconic anhydride = 10.95 ± 0.15 eV,[3] $\Delta H_f$(neutral) = −104 kcal mol$^{-1}$ (8), $T_{min}$ = 0.36 eV, whence $\Delta H_f[C_4H_4O]^{+\cdot} \leq 234$ kcal mol$^{-1}$) are all significantly below that of ionised [methylcyclopropenone] ($\Delta H_f$ = 240 kcal mol$^{-1}$ (4)). This conclusion is reinforced by the observation that CS mass spectra of the $[C_4H_4O]^{+\cdot}$ ions generated from the ester and the anhydrides are dissimilar — see Table 2. It should be noted that CS mass spectra have successfully been used to differentiate between cyclic and acyclic isomers which are indistinguishable by means of their CA mass spectra (3, 16). That [methylcyclopropenone]$^{+\cdot}$ and the proposed product ion $[CH_3—CH=C=C=O]^{+\cdot}$ have some closely related characteristics is also exemplified by observations on their loss of CO, where the $[C_3H_4]^{+\cdot}$ product ions in both cases consist largely of [propyne]$^{+\cdot}$, rather than the more stable [allene]$^{+\cdot}$ ion. A recent CA study (15) showed how these isomeric $[C_3H_4]^{+\cdot}$ ions may be distinguished from both their CA and CS mass spectra; additional work by ourselves (17) leads us to conclude that the presence of a methyl group within an unsaturated $C_3$ system is a prerequisite for [propyne]$^{+\cdot}$ generation.

Another route to $[CH_3CH=C=C=O]^{+\cdot}$ involves the loss of $CH_2O$ from the ionised methyl ester of allene carboxylic acid (base peak in the normal mass spectrum), for which we propose the following mechanism:

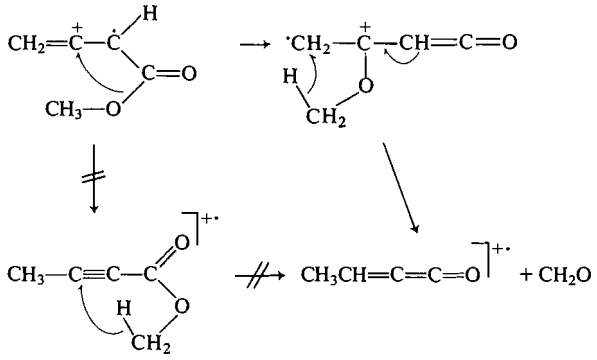

The 1,3-methoxy shift is analogous to the 1,3-hydroxy migration in $[CH_2=C=CHCH_2OH]^{+\cdot}$ (6) and yields [buta-1,2-dienone]$^{+\cdot}$ as shown above. The alternative route via an allene–yne rearrangement (see also below) cannot be involved, because directly ionised $CH_3C{\equiv}CCOOCH_3$ does not lose $CH_2O$. Note that a simple reaction mechanism yielding [vinylketene]$^{+\cdot}$ could be envisaged:

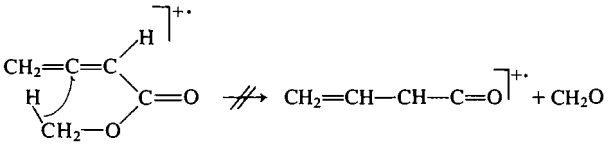

but is unable to compete with the methoxy shift.

The remaining ions will be grouped as keto–enol tautomeric pairs.

*Ionised methylethynylketone and its enol [HC≡C—C(OH)=CH$_2$]*

The $\Delta H_f$[ketone]$^{+\cdot}$ was obtained from its IE = 10.25 eV, $\Delta H_f[CH_3COC{\equiv}CH]$ = +7.4 kcal mol$^{-1}$,[5] leading to $\Delta H_f[CH_3COC{\equiv}CH]^{+\cdot}$ = 244 kcal mol$^{-1}$. The CA mass spectrum is dominated by ions resulting from simple bond cleavages, *m/z* 53 $[HC{\equiv}C—\overset{+}{C}O]$ and *m/z* 43 $[CH_3\overset{+}{C}O]$.[6]

For the enol, $\Delta H_f[HC{\equiv}C—C(OH)=CH_2]^{+\cdot}$ = 217 kcal mol$^{-1}$ was obtained from the AE *m/z* 68 from $HC{\equiv}C—COCH_2CH_2CH_3$, the method normally used to obtain $\Delta H_f$ values for enol ions (5) (AE *m/z* 68 = 10.08 eV, $\Delta H_f[HC{\equiv}CCOCH_2CH_2CH_3]$ = −2.6 kcal mol$^{-1}$,[4] $\Delta H_f[C_2H_4]$ = +12.4 kcal mol$^{-1}$ (12)). That there is little, if any, communication between the tautomeric ions follows from a comparison of the CA mass spectrum of the keto ion with that of the enol ion (Table 1). The latter was also generated via a 2π + 2π cycloreversion reaction from ionised 1-ethynyl cyclobutanol (loss $C_2H_4$) and similarly from 1-ethynylcyclopentanol (loss $C_3H_6$).

*Aldehyde ions and their enols*

Scheme 1 shows these ions and their proposed interrelationships. $\Delta H_f$ values and CA mass spectra are shown in Table 1. From their CA mass spectra it can be seen that allene aldehyde (**1**) does not communicate with its isomer (**2**); this is in keeping with the behaviour of the analogous allenic and acetylenic esters discussed above. The CA mass spectrum of (**2**) is dominated by H atom loss, a simple cleavage having an energy requirement

[5]Values for $C_t$—(CO), CO—($C_l$)(C), and CO—($C_l$)(H) of +25.6, −35, and −33 kcal mol$^{-1}$ were used in these $\Delta H_f$ estimations.

[6]AE *m/z* 53 = 11.14 eV, which with $\Delta H_f[CH_3^{\cdot}]$ = 34 kcal mol$^{-1}$ (14) leads to $\Delta H_f[C_3HO^+]$ = 230 kcal mol$^{-1}$.

TABLE 2. Charge stripping spectra of some $[C_4H_4O]^{+\cdot}$ ions

| m/z | $68^{2+}$ | $67^{2+}$ | $66^{2+}$ | $65^{2+}$ | $40^{2+}$ | $39^{2+}$ | $38^{2+}$ |
|---|---|---|---|---|---|---|---|
| | 100 | 23 | 32 | 3.5 | 5.5 | 2.5 | 8 |
| $[C_4H_4O]^{+\cdot}$[a] | 100 | 45 | 46 | 5 | 8 | 3 | 10 |

[a]Derived from loss of $CH_2O$ from $CH_2{=}C{=}CHCOOCH_3$ and from loss of $CO_2$ from ionised itaconic and citraconic anhydrides.

Can. J. Chem. Downloaded from www.nrcresearchpress.com by 210.87.254.105 on 09/06/12
For personal use only.

($\Delta H_f[CH_3C{\equiv}C{-}\overset{+}{C}{=}O] + \Delta H_f[H]^{\cdot} = 254$ kcal mol$^{-1}$)[7] similar to that for the rearrangement leading to $[CH_3{-}C{\equiv}CH]^{+\cdot} + CO$ ($\Delta H_f[C_3H_4]^{+\cdot} + \Delta H_f[CO] = 257$ kcal mol$^{-1}$ (14)). The latter daughter ion in the normal mass spectrum of **2** was shown to have the structure $[CH_3{-}C{\equiv}CH]^{+\cdot}$ from its CA and CS mass spectra (15) (see also above).

Allene aldehyde, **1**, shows little $H^{\cdot}$ loss in its CA mass spectrum, in which *m/z* 40 is the second most abundant ion. It is noteworthy that for **1**, *m/z* 40 in its normal mass spectrum has the $[allene]^{+\cdot}$ structure.

Aldehyde **3** could not be studied directly; all attempts at synthesis failed. However, several related compounds of general formula

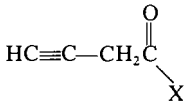

X = $CH_3$, $C_2H_5$, OH, and $OCH_3$, displayed mass spectral characteristics which indicated that a facile rearrangement to their allenic analogue preceded fragmentation; such behaviour has also been observed in the

$$HC{\equiv}C{-}CH_2{-}OCH_3^{+\cdot} \rightleftharpoons H_2C{=}C{=}CHOCH_3^{+\cdot}$$

system (18). The $\Delta H_f$ for ion **3** can be estimated by assuming that the IE will be typically aldehydic, similar to that of butanal = 9.85 eV (14), $\Delta H_f[HC{\equiv}CCH_2CHO] = 20.1$ kcal mol$^{-1}$ (8), whence $\Delta H_f[HC{\equiv}CCH_2CHO]^{+\cdot} \simeq 247$ kcal mol$^{-1}$. We propose that the CA mass spectrum of **3** will be closely similar to that of **1**.

The CA mass spectrum of the ionised cyclic aldehyde, **4**, is clearly very different from that of all other isomers and is characteristic of its structure (Table 1). Unfortunately a reliable value for its IE could not be measured; the compound polymerised very readily and it could only be introduced into a mass spectrometer in small quantities from dilute solution in $CH_2Cl_2$.

Two of the aldehydes, **3** and **1**, have enol tautomers, **5** and **6** respectively. The two ethyl ethers $HC{\equiv}C{-}CH{=}CH{-}O{-}CH_2CH_3$ and $CH_2{=}C{=}C{=}CH{-}OCH_2CH_3$ have intense *m/z* 68, $[C_4H_4O]^{+\cdot}$ peaks in their normal mass spectra. By analogy with the behaviour of $[CH_2{=}CH{-}O{-}CH_2CH_3]^{+\cdot}$, which generates $[CH_2{=}CHOH]^{+\cdot} + C_2H_4$ via a β-hydrogen shift, it may be argued that the above ethers will generate the desired enols upon loss of $C_2H_4$ by dissociative ionisation. $\Delta H_f[C_4H_4O]^{+\cdot}$ from $HC{\equiv}C{-}CH{=}CH{-}OCH_2CH_3 = 220$ kcal mol$^{-1}$ (from AE = 9.22 eV; $\Delta H_f[HC{\equiv}CCH{=}CH{-}OCH_2CH_3] = 20.1$ kcal mol$^{-1}$ (8), $\Delta H_f[C_2H_4] = 12.5$ kcal mol$^{-1}$ (14)). Note that the narrow metastable peak for this process is of simple Gaussian-type with $T_{0.5} = 0.024$ eV, indicating that the reverse reaction is unlikely to have any appreciable energy requirement and thus the derived $\Delta H_f$ will not be significantly greater than the thermochemical $\Delta H_f$. The CA mass spectra of this ion generated both metastably and in the ion source are the same and remarkably close to that of **1**; furthermore, the same composite metastable peaks, shown in Fig. 1, are observed for CO loss from **1** and the $[C_4H_4O]^{+\cdot}$ ions derived from $[HC{\equiv}C{-}CH{=}CH{-}OCH_2CH_3]$. We conclude that the latter $[C_4H_4O]^{+\cdot}$ ions have the enol-structure **5** and that **1** must be able rapidly to rearrange to **5** at or very close to the [allene–aldehyde] IE. This rearrangement could readily take place via a 1,5-H shift rather than via enolisation of **3**.

**6**, the enol of **1**, generated as described above, has $\Delta H_f = 222$ kcal mol$^{-1}$ (AE *m/z* 68 from $CH_2{=}C{=}C{=}CHOCH_2CH_3 = 8.74$ eV; $\Delta H_f$[neutral] = 33.4 kcal mol$^{-1}$ (8), $\Delta H_f[C_2H_4] = 12.4$ kcal mol$^{-1}$ (14)). The metastable peak for the fragmentation *m/z* 96 → *m/z* 68 was of simple Gaussian type, $T_{0.5} = 0.045$ eV, and so no significant correction for excess energy is likely to be necessary. Its CA mass spectrum is significantly different from those of **1** and **5**, as is the metastable peak shape for CO loss (see Fig. 1). We conclude therefore that this ion exists as a stable species in the gas phase. The molecule $HC{\equiv}C{-}CH(C_3H_7)CHO$ does not generate **5** by dissociative ionisation (loss of $C_3H_6$ via a McLafferty rearrangement) but produces a $[C_4H_4O]^{+\cdot}$ ion whose CA mass spectrum is identi-

[7]AE *m/z* 67 from $CH_3C{\equiv}CCOOCH_3 = 10.70$ eV; $\Delta H_f[CH_3C{\equiv}CCOOCH_3] = -43.3$ kcal mol$^{-1}$ (8[4]), $\Delta H_f[CH_3O] = 1.4$ kcal mol$^{-1}$, $\Delta H_f[H^{\cdot}] = 52.1$ kcal mol$^{-1}$ (14).

Can. J. Chem. Downloaded from www.nrcresearchpress.com by 210.87.254.105 on 09/06/12
For personal use only.

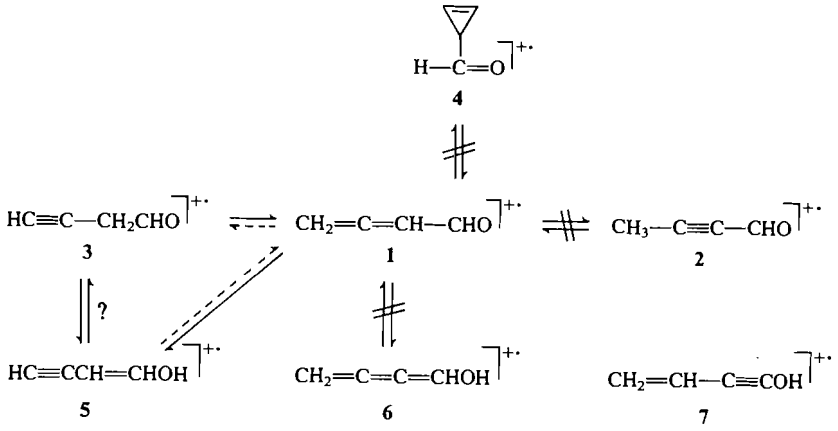


SCHEME 1

cal with that of **6**. It is concluded that the molecular ion undergoes an -yne to allene isomerisation before dissociation.

Generation of the last ion shown in Scheme 1, $[CH_2{=}CH{-}C{\equiv}C{-}OH]^{+\cdot}$, **7**, was achieved by the dissociative ionisation of $CH_2{=}CH{-}C{\equiv}C{-}OCH_2CH_3$, by analogy with the behaviour of the two ethers described above. Although the metastably fragmenting ions from this ether clearly produced ionised [vinylketene]$^{+\cdot}$ (as described above), the CA mass spectrum of the ion-source generated ions was completely different from all others shown in Table 1, and we propose that at the higher energies, the desired species is produced.

We have attempted in this study to develop criteria for the identification of fifteen isomeric $[C_4H_4O]^{+\cdot}$ ions, using many of the currently available techniques for investigating ion structures in the gas phase. Although the CA mass spectra shown in Table 1 may be readily explained in terms of the given ion structures, identification of the latter relied heavily on the establishing of ionic heats of formation to assist in their proper designation. The CA mass spectra *alone* would have been very difficult to interpret. Only two pairs of isomers showed closely similar CA mass spectra, namely, $[CH_3{-}CH{=}C{=}C{=}O]^{+\cdot}$ and [methylcyclopropenone]$^{+\cdot}$, $[H_2C{=}C{=}CH{-}CHO]^{+\cdot}$ and $[HC{\equiv}C{-}CH{=}CH(OH)]^{+\cdot}$. The similarity of the former pair may well result from there being only a small (or no) energy requirement for opening the strained cyclopropene ring; a concomitant H-shift would readily produce $[CH_3{-}CH{=}C{=}C{=}O]^{+\cdot}$, via an exothermic reaction. The second pair of isomers could be envisaged as interconverting via a single 1,5-H shift, the acetylenic enol being thermochemically the more stable species.

The differences in $\Delta H_f$ for the keto–enol pairs deserve comment. For example, $\Delta(\Delta H_f)$ for the ions $[HC{\equiv}C{-}CH_2CHO]^{+\cdot}$ and $[HC{\equiv}C{-}CH{=}$

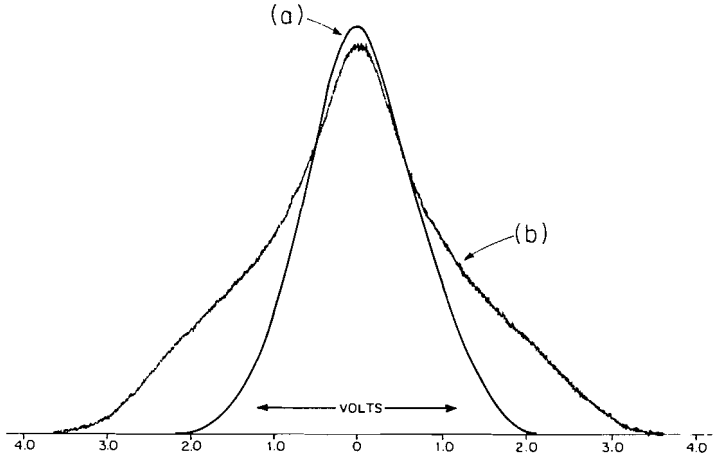


FIG. 1. Metastable peaks for loss of CO from (*a*) $[CH_2{=}C{=}C{=}CHOH]^{+\cdot}$ and (*b*) $[HC{\equiv}C{-}CH{=}CHOH]^{+\cdot}$ and/or $[CH_2{=}C{=}CHCHO]^{+\cdot}$.

Can. J. Chem. Downloaded from www.nrcresearchpress.com by 210.87.254.105 on 09/06/12
For personal use only.

$CHOH]^{+\cdot}$, 25 kcal mol$^{-1}$, is very similar to that for the analogous pair $[CH_2{=}CH{-}CH_2CHO]^{+\cdot}$ ($\Delta H_f$[ion]$^{+\cdot} \simeq 202$ kcal mol$^{-1}$ from IE $\sim$ 9.6 eV, $\Delta H_f$(neutral) = $-19.7$ kcal mol$^{-1}$, by additivity (8)) and $[CH_2{=}CH{-}CH{=}CHOH]^{+\cdot}$, $\Delta H_f$ = 176 kcal mol$^{-1}$ (6). For the ketone $[CH_3COC{\equiv}CH]^{+\cdot}$ and its enol a stabilisation of similar magnitude was observed. The relatively small stabilisation found between $[CH_2{=}C{=}CH{-}CHO]^{+\cdot}$ and $[CH_2{=}C{=}C{=}CHOH]^{+\cdot}$ is in keeping with the loss of conjugative stabilisation in going from the en–al to the cumulene–ol. This situation is analogous to that of ionised acrolein, $[CH_3{=}CHCHO]^{+\cdot}$, and its enol $[CH_2{=}C{=}CHOH]^{+\cdot}$; $\Delta H_f[CH_2{=}CHCHO]^{+\cdot}$ = 215 kcal mol$^{-1}$; from IE = 10.11 eV (19), $\Delta H_f[CH_2{=}CHCHO]$ = $-17.7$ kcal mol$^{-1}$ (8). For the enol $\Delta H_f[CH_2{=}C{=}CHOH] = 4 \pm 1$ kcal mol$^{-1}$ (by additivity (8)) and an IE of $9.1 \pm 0.1$ eV (assumed to be similar to that of vinyl alcohol, 9.1 eV (20)) whence $\Delta H_f[CH_2{=}C{=}CHOH]^{+\cdot} = 214 \pm 3$ kcal mol$^{-1}$. For this pair, the enol ion may have a higher $\Delta H_f$ than its keto tautomer, the first example of reversed thermodynamic stability between such ionised tautomers. The situation arises from the large difference between the $\Delta H_f$ values for the neutral compounds.

## Experimental

*Synthesis of compounds*

The purity and, where necessary, the structure of the compounds synthesized was checked by nmr spectroscopy.

*Vinyloxyethyne* ($CH_2{=}CHOC{\equiv}CH$) was prepared by the method of Brandsma and Arens (21).

*5,6-Dihydro-2-pyrone* ($\overline{CH_2{-}CH_2{-}CH{=}CH{-}COO}$) was prepared from 3-butenoic acid and paraformaldehyde as described in ref. 22.

*Trifluoroacetic*-trans-*crotonic anhydride* ($CF_3{-}COO{-}CO{-}CH{=}CH{-}CH_3$) was prepared from *trans*-crotonic acid chloride and the sodium salt of trifluoroacetic acid by the general procedure of ref. 23.

The *methylester of butadienecarboxylic acid* ($CH_2{=}C{=}CHCOOCH_3$) was synthesized from the acid and diazomethane (24). The acid was prepared from allene, *n*-butyllithium, and $CO_2$ (25).

*Methylcyclopropenone* ($\overline{CO{-}C(CH_3){=}CH}$) was synthesized by the method of Breslow and Altman (26).

*Hex-1-yn-3-one* ($CH_3CH_2CH_2COC{\equiv}CH$) was prepared by oxidation of hex-1-yn-3-ol (27).

*1-Ethynylcyclobutanol* ($\overline{CH_2{-}CO(C{\equiv}CH)CH_2{-}CH_2}$) was prepared by the reaction of ethynylmagnesium bromide with cyclobutanone (25).

*1-Ethynylcyclopentanol* ($\overline{CH_2{-}CO(C{\equiv}CH)CH_2CH_2CH_2}$) was synthesized similarly using cyclopentanone.

*1-Ethoxybut-1-en-3-yne* ($HC{\equiv}C{-}CH{=}CHOC_2H_5$) was prepared from 1,4-diethoxybut-2-yne with sodium amide in liquid ammonia (27).

*Buta-2,3-dienal* ($CH_2{=}C{=}CHCHO$) was prepared by adding 1-ethoxybut-1-en-3-yne to excess 2 *N* ortho-phosphoric acid at $-10$°C. The reaction is complete in about 5 min, after which the crude aldehyde (containing water, ethanol, and traces of starting material) was collected in a $CO_2$/acetone trap at reduced pressure (15 mm Hg). The purified aldehyde (repetitive trap-to-trap distillations) has physical properties identical with the sample prepared in ref. 28 by a more laborious procedure.

*1-Ethoxybut-3-en-1-yne* ($CH_2{=}CH{-}C{\equiv}C{-}O{-}C_2H_5$) was prepared by elimination of *p*-toluene sulfuric acid from 1-ethoxybut-1-yn-4-tosylate (25, 29).

*Cycloprop-3-ene carboxaldehyde* ($\overline{HC{=}CHCHCHO}$) was prepared by irridation of pyridazine-*N*-oxide (30). The sample was purified by gas chromatography using a 10% OV-17 column at room temperature.

*Ethoxybutatriene* ($CH_2{=}C{=}C{=}CHOC_2H_5$) was synthesized from 1,4-diethoxybut-2-yne and ethyllithium in ether followed by hydrolysis (25).

*(2-n-Propyl)-butadienal* ($CH_2{=}C{=}C(CHO)C_3H_7$) was obtained by treatment of dilithiated hex-1-yne (31) with dimethyl formamide at $-50$°C. After 30 min the reaction mixture was hydrolysed with 1 equiv. of 1 *N* HCl and extracted with ether. Evaporation of the solvent yielded the desired product b.p. 55°/10 mm in a 50% yield.

(2-*n*-Propyl)-but-3-yne-1-al ($HC{\equiv}C{-}CH(CHO)C_3H_7$) was obtained by the same reaction using excess of 2 *N* HCl.

The propargylic aldehyde easily isomerises into the allenic form (see above) with traces of base formed during hydrolysis. This isomerisation is prevented by slowly pouring the reaction mixture into vigorously stirred excess of acid. However, this procedure yields a large amount of polymer from which the desired aldehyde was isolated in low yield (10%).

All other compound were commercially available and checked by gcms and nmr analysis.

Ionisation and appearance energies were measured using energy selected electrons (32). Metastable peaks (33) and collisional activation mass spectra (18) were measured by conventional means.

CA spectra of metastably generated ions were obtained using a ZAB-2F mass spectrometer; metastable peaks arising from dissociations in the first field-free region were selected by their apparent mass and the transmitted species were then subjected to collisional excitation in the second field-free region.

## Acknowledgements

J. L. Holmes thanks the Natural Sciences and Engineering Research Council of Canada for financial support. J. K. Terlouw gratefully acknowledges the continuing support of the Netherlands Organisation for the advancement of pure research (Z.W.O.).

1. J. L. Holmes. *In* M.T.P. international review of science, physical chemistry series two. Vol. 5. Mass spectrometry. *Edited by* A. Maccoll. Butterworths, London. 1975. Chapt. 6.
2. J. L. Holmes and J. K. Terlouw. Org. Mass Spectrom. **15**, 383 (1980).
3. R. D. Bowen, M. P. Barbalas, F. P. Pagano, P. G. Todd, and F. W. McLafferty. Org. Mass Spectrom. **15**, 51 (1980); J. L. Holmes, J. K. Terlouw, P. C. Burgers, and R. T. B. Rye. Org. Mass Spectrom. **15**, 149 (1980).
4. J. L. Holmes and J. K. Terlouw. J. Am. Chem. Soc. **101**, 4973 (1979).
5. J. L. Holmes and F. P. Lossing. J. Am. Chem. Soc. **102**, 1591 (1980).
6. J. K. Terlouw, W. Heerma, J. L. Holmes, and P. C. Burgers. Org. Mass Spectrom. **15**, 582 (1980).
7. J. L. Holmes, M. Fingas, and F. P. Lossing. Can. J. Chem. **59**, 80 (1981).

8. S. W. BENSON, F. R. CRUICKSHANK, D. M. GOLDEN, G. R. HAUGEN, H. E. O'NEAL, A. S. RODGERS, R. SHAW, and R. WALSH. Chem. Rev. **69**, 279 (1969).
9. J. K. TERLOUW, P. C. BURGERS, and J. L. HOLMES. J. Am. Chem. Soc. **101**, 225 (1979).
10. R. D. BROWN, P. D. BODFREY, and M. WOODRUFF. Austral. J. Chem. **33**, 279 (1980).
11. E. BJARNOV. Z. Naturforsch. **34A**, 1269 (1979).
12. J. B. PEDLEY and J. RYLANCE. Computer analysed thermochemical data; organic and organometallic compounds. University of Sussex. 1977.
13. J. L. HOLMES, J. K. TERLOUW, P. C. VIJFHUIZEN, and C. A'CAMPO. Org. Mass Spectrom. **14**, 204 (1979).
14. H. M. ROSENSTOCK, K. DRAXL, B. W. STEINER, and J. T. HERRON. J. Phys. Chem. Ref. Data Suppl. **6**, 1 (1977).
15. W. WAGNER, K. LEVSEN, and C. LIFSHITZ. Org. Mass Spectrom. **15**, 271 (1980).
16. A. MAQUESTIAU, Y. V. VAN HAVERBEKE, R. FLAMMANG, C. DE MEYER, and A. MENU. Org. Mass Spectrom. **11**, 706 (1977).
17. J. K. TERLOUW and J. L. HOLMES. To be published.
18. J. K. TERLOUW, P. C. BURGERS, and H. HOMMES. Org. Mass Spectrom. **14**, 387 (1979).
19. P. MASCLET and G. MOUVIER. J. Electron Spectrosc. Rel. Phen. **14**, 77 (1978).
20. J. L. HOLMES and F. P. LOSSING. J. Am. Chem. Soc. **104**, 2648 (1982).
21. L. BRANDSMA and J. F. ARENS. Recl. Trav. Chim. Pays-Bas, **79**, 1307 (1960).
22. M. NAKAGUMA, M. TONOZUKA, M. OBI, M. KIUCHI, and T. HIRO. Synthesis, 510 (1974).
23. A. I. VOGEL. Textbook of practical organic chemistry. Longmans, Green and Co., New York. 1978.
24. L. CROMBIE, P. A. JENKINS, and D. MITCHARD. J. Chem. Soc. Perkin Trans. I, 1081 (1975).
25. L. BRANDSMA and H. D. VERKRUIJSSE. Synthesis of acetylenes, allenes and cumulenes: a laboratory manual. Elsevier Publishing Company, Amsterdam. 1981.
26. R. BRESLOW and L. J. ALDMAN. J. Am. Chem. Soc. **88**, 504 (1966).
27. L. BRANDSMA. Preparative acetylenic chemistry. Elsevier Publishing Company, Amsterdam. 1971.
28. C. AUGÉ, S. DAVID, and A. LUBINEAU. J. Chem. Soc. Chem. Commun. 568 (1980).
29. J. LINK, P. VERMEER, J. G. A. KOOIMAN, J. MEIJER, L. BRANDSMA, and J. F. ARENS. Recl. Trav. Chim. Pays-Bas, **93**, 92 (1974).
30. T. TSUCHIJA, H. ARAI, and H. IGETA. Tetrahedron, **29**, 2947 (1973).
31. H. HOMMES, H. D. VERKRUIJSSE, and L. BRANDSMA. Recl. Trav. Chim. Pays-Bas, **99**, 113 (1980).
32. K. MAEDA, G. P. SEMELUK, and F. P. LOSSING. Int. J. Mass Spectrom. Ion Phys. **1**, 395 (1968).
33. J. L. HOLMES and J. K. TERLOUW. Can. J. Chem. **53**, 2076 (1975).
34. J. L. HOLMES and P. C. BURGERS. Org. Mass. Spectrom. **17**, 123 (1982).

Can. J. Chem. Downloaded from www.nrcresearchpress.com by 210.87.254.105 on 09/06/12
For personal use only.

# $^{125}$Te Fourier transform nuclear magnetic resonance studies of tellurium compounds

RAJ K. CHADHA AND JACK M. MILLER[1]

*Chemistry Department, Brock University, St. Catharines, Ont., Canada L2S 3A1*

Received February 24, 1982

RAJ K. CHADHA and JACK M. MILLER. Can. J. Chem. **60**, 2256 (1982).

$^{125}$Te nmr spectra of a number of organotellurium compounds and inorganic tellurium salts are reported. The tellurium shielding has been found to be dependent upon the nature and number of electronegative substituents bonded to tellurium and where applicable, upon the *para* substituents on the phenyl ring. Possible reasons for the observed broad line widths are discussed.

RAJ K. CHADHA et JACK M. MILLER. Can. J. Chem. **60**, 2256 (1982).

On rapporte les spectres de RMN du $^{125}$Te de plusieurs composés organotelluriques et de plusieurs sels inorganiques du tellure. On a trouvé que le blindage du tellure dépend de la nature et du nombre de substituants électronégatifs liés au tellure et des substituants en position *para* du cycle phényle, quand le cas se présente. On discute des raisons éventuelles qui expliquent la largeur des lignes observées.

[Traduit par le journal]

Can. J. Chem. Downloaded from www.nrcresearchpress.com by 210.87.254.42 on 09/06/12
For personal use only.

## Introduction

Studies in the field of $^{77}$Se nmr of inorganic and organic selenium compounds are rapidly increasing (1–8). In contrast, $^{125}$Te nmr investigations have received little attention (9–14), though the nuclear properties of $^{125}$Te are more favourable for nmr studies than those of $^{77}$Se. For example, $^{125}$Te is approximately 4.5 times more sensitive than $^{77}$Se and spin–lattice relaxation times for the $^{125}$Te are 4 to 6 times shorter than those for the $^{77}$Se (15). $^{125}$Te nmr spectroscopy has recently been utilised to study the exchange reactions (16) and the characterisation of metal complexes (17) in solution. These studies demonstrate the usefulness of this technique for the understanding of grossly complex and relatively unknown solution nature of the tellurium compounds (13, 14, 18). Examination of literature shows that $^{125}$Te chemical shift values of only limited categories of organotellurium compounds with different environments of tellurium have been reported (14, 19, 20), and more results are required before there is a thorough understanding of the trends in the chemical shifts. We, therefore, present the $^{125}$Te chemical shift data of some unsymmetric diaryltellurium dichlorides, aryltellurium trihalides, and some ionic tellurium salts, the categories which have received relatively less attention.

## Results and discussion

$^{125}$Te chemical shifts, using neat $Me_2Te$ as an external reference, are recorded in Table 1. Data already available in the literature have established the chemical shift range to be ~5000 ppm (13, 14, 21). The compounds studied here cover a range of 1530 ppm. Inspection of Table 1 reveals that $^{125}$Te chemical shifts are sensitive to the oxidation state of tellurium, amount of the ionic character in the Te—X bond, and the *para* substituent present in the phenyl ring. Similar trends were shown by selenium compounds (6), though the tellurium shifts are much more sensitive to the nature of substituents than are the selenium shifts. This observation is similar to the one made earlier (20). It is suggested that for heavy atom nuclei including selenium, the paramagnetic contribution ($\sigma_p$) to the shielding is dominant. The expression used for the paramagnetic term also involves the mean inverse cubes of the valence *p*- and *d*-electron–nuclear distances. Since this distance increases on going from selenium to tellurium, it may account for larger chemical shift values for tellurium than for selenium, and consequently, the tellurium shifts appear to be more sensitive than the selenium shifts to the nature of the substituents. However, the chemical shift values change significantly with *para* substituents on the aromatic ring, separated from tellurium by five interatomic bonds and about 6.2 Å (22) in space. This suggests that neighbouring atom electronic effects contribute significantly to the paramagnetic shielding. The chemical shifts show slight dependence upon solvent and concentration. Therefore, the solute–solvent interaction also has a slight contribution to the $\sigma_p$. This is consistent with earlier observation (21).

The downfield shift of *p*-$BrC_6H_4(Ph)Te$ and highfield shift of *p*-$MeOC_6H_4(Ph)Te$ as compared to $Ph_2Te$ (19) suggest that the tellurium nucleus is strongly deshielded (or shielded) by electron-withdrawing (or releasing) substituents on the phenyl

[1]To whom all correspondence should be addressed.

0008-4042/82/172256-03$01.00/0

©1982 National Research Council of Canada/Conseil national de recherches du Canada

TABLE 1. $^{125}$Te nmr parameters for tellurium compounds

| Compound | Solvent | δ $^{125}$Te (ppm)[a] | | Δν (Hz)[b] | |
|---|---|---|---|---|---|
| | | 27°C | −80°C | 27°C | −80°C |
| **1**, $(p\text{-}BrC_6H_4)(Ph)Te$ | $CH_2Cl_2$ | 698.7 | | 38 | |
| **2**, $Ph_2Te$[c] | $CH_2Cl_2$ | 688.0 | | — | |
| **3**, $(p\text{-}MeOC_6H_4)(Ph)Te$ | $CH_2Cl_2$ | 668.0 | | 75 | |
| **4**, $(p\text{-}BrC_6H_4)(Ph)TeCl_2$ | $CH_2Cl_2$ | 1079.6 | | 47 | |
| **5**, $Ph_2TeCl_2$[c] | $CH_2Cl_2$ | 981.0 | | — | |
| **6**, $(p\text{-}MeOC_6H_4)(Ph)TeCl_2$ | $CH_2Cl_2$ | 1070.6 | | 80 | |
| **7**, $Ph(Et_2N)TeCl_2$ | $CH_2Cl_2$ | 1242.1 | | 70 | |
| **8**, $(p\text{-}MeOC_6H_4)(Et_2N)TeCl_2$ | $Ch_2Cl_2$ | 1249.6 | | 60 | |
| **9**, $(p\text{-}PhOC_6H_4)(Et_2N)TeCl_2$ | $CH_2Cl_2$ | 1219.0 | | 32 | |
| **10**, $PhTeCl_3$ | $CH_2Cl_2$:DMSO (1:1) | 1228.5 | 1235.2 | 80 | 30 |
| | DMSO | 1237.9 | | 35 | |
| **11**, $PhTeBr_3$ | $CH_2Cl_2$:DMSO (1:1) | 1192.9 | 1203.9 | 160 | 105 |
| **12**, $PhTeI_3$ | $CH_2Cl_2$:DMSO (2:1) | — | 1101.4 | — | 120 |
| **13**, $(p\text{-}MeOC_6H_4)TeCl_3$ | $CH_2Cl_2$:DMSO (1:1) | — | 1244.9, 1253.8 | — | 120, 80 |
| | DMSO | 1246.1 | | 375 | |
| **14**, $(p\text{-}MeOC_6H_4)TeBr_3$ | $CH_2Cl_2$:DMSO (2:1) | — | 1204.3 | — | 88 |
| **15**, $(p\text{-}MeOC_6H_4)TeI_3$ | $CH_2Cl_2$:DMSO (1:1) | — | 1078.2 | — | 550 |
| **16**, $(p\text{-}MeC_6H_4)TeCl_3$ | $CDCl_3$:DMSO (1:1) | 1233.8 | 1236.5 | 400 | 166 |
| **17**, $(p\text{-}PhOC_6H_4)TeCl_3$ | $CH_2Cl_2$:DMSO (1:1) | 1226.2 | 1229.6 | 200 | 78 |
| **18**, $(p\text{-}BrC_6H_4)TeCl_3$ | $CH_2Cl_2$:DMSO (1:1) | 1208.1 | 1218.4 | 80 | 90 |
| **19**, $(p\text{-}ClC_6H_4)TeCl_3$ | $CH_2Cl_2$:DMSO (1:1) | — | 1208.0 | — | 120 |
| **20**, $OC{-}Me_2TeI_2$ | DMSO | 675.0 | | 155 | |
| **21**, $Et_3Te^+Br^-$ | $CH_2Cl_2$ | 570.5 | | 115 | |
| **22**, $(Et_3Te)_2^+(TeCl_4Br_2)^{2-}$ | $CH_2Cl_2$:DMSO (1:2) | 598.4, 1365.4 | | 150, 11 | |
| **23**, $(Et_3Te)_2^+(TeBr_6)^{2-}$ | $CH_2Cl_2$:DMSO (1:2) | 603.5, 1347.7 | | 325, 95 | |
| **24**, $(Et_2NH_2)^+(PhTeCl_4)^-$ | $CH_2Cl_2$ | 1264.6 | | 47 | |
| **25**, $(Et_4N)^+(p\text{-}MeOC_6H_4TeBr_4)^-$ | $CH_2Cl_2$:DMSO (1:1) | 1206.2 | | 70 | |
| **26**, $(Et_4N)^+(PhTeBr_3Cl)^-$ | $CH_2Cl_2$:DMSO (1:1) | 1226.0 | | 90 | |
| **27**, $(Et_4N)^+(PhTeCl_3Br)^-$ | $CH_2Cl_2$:DMSO (1:2) | 1253.4 | | 50 | |
| **28**, $(Et_4N)_2^+(TeBr_4Cl_2)^{2-}$ | $CH_2Cl_2$:DMSO (1:2) | 1336.5 | | 70 | |
| **29**, $(Et_2NH_2)_2^+(TeCl_6)^{2-}$ | DMSO | 1531.7 | | 200 | |

[a]From neat $Me_2Te$.
[b]Line width.
[c]Taken from ref. 19.

ring. Similar observation was made in case of tellurol esters (23). No clear trend is observed in diaryltellurium dichlorides, or in diaryl ditellurides (21), while an opposite order is found in aryltellurium trichlorides. Figure 1 shows that there is an approximately linear relationship between $^{125}$Te chemical shifts of aryltellurium trichlorides and Swain and Lupton parameter, $\sigma_p^+$, of the *para* aromatic substituents (24) except for the *p*-phenoxy derivative for which resonance effect may be important. Downfield chemical shifts for electron-releasing substituents are observed. It is not clear why the two series should have completely opposite orders. Organotellurium trichlorides are known to be capable of forming stable solvates (25) in strongly donating solvents, such as $CH_3CN$ and DMSO, and subsequent change in solute–solvent interaction might have affected the observed difference. These compounds are not sufficiently soluble in other organic solvents. Therefore, nmr studies of unsolvated or weakly solvated species are not easily possible.

The line widths vary from 10 to several hundred Hz for the compounds studied here. Large line widths for organotellurium trihalides may be due to the association in solution (25). The spectra taken at −80°C in an attempt to observe separate signals from monomer and halogen-bridged dimer species resulted in, in many cases, the sharpening of the signals, but for only one compound, viz. $p\text{-}MeOC_6H_4TeCl_3$, could the splitting of the signal be observed. However, $^{125}$Te chemical shifts show a slight downfield shift (of the order of 0.05 ppm/°C) when measured at −80°C. The consistency with which reduced temperature gave narrower lines indicates that relaxation is predominantly by the spin-rotation mechanism, as was concluded by Granger and Chapelle (26). A slight component of the line broadening can also arise from the fluctuations of the temperature during long accumulation,

Can. J. Chem. Downloaded from www.nrcresearchpress.com by 210.87.254.42 on 09/06/12
For personal use only.

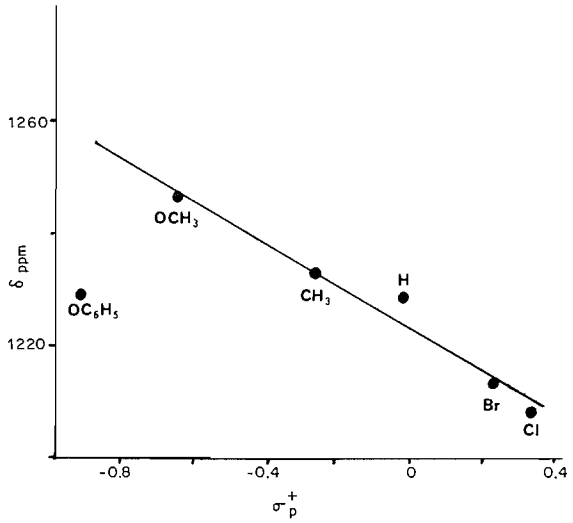


FIG. 1. Substituent effects on the $^{125}$Te chemical shifts of *para*-substituted aryltellurium trichlorides.

particularly when the superconducting magnets are used (21). A temperature variation of ±1°C, which is likely in our experimentation, can contribute line broadening of the order of 12 Hz.

The tellurium atom attached to the phenyl ring having a *para* substituent can be coupled only to *ortho* or remotely separated *meta* protons. However, fine structure due to three or four bond couplings could not be observed because $^3J_{Te-H}$ or $^4J_{Te-H}$ is expected to be smaller (~6 Hz) (21) than the observed line widths.

## Experimental

$^{125}$Te nmr spectra were recorded at 126.2413643 MHz on a Bruker WH-400 Fourier Transform Multinuclear Magnetic Resonance Spectrometer using 50 kHz sweep widths (6.1 Hz/pt), using 50° pulses and repetition rate of 2 s for 100 scans. Typically 100–300 scans were obtained. The shifts were determined with an accuracy of ±0.1 ppm. The samples were saturated solutions in $CH_2Cl_2$ or 1:1 mixture of $CH_2Cl_2$ and DMSO in 10 mm tubes. No deuterium lock was necessary since the lines were relatively broad and acquisition time short. In some cases 27° spectra were not observed because of fast exchange between monomers and dimers.

The compounds, **1**, **3**, **4** (27), **6–9** (28), **10–19** (29, 30), **20** (31), **21–29** (32, 33), were prepared by the methods described earlier.

## Acknowledgements

The authors thank the Natural Sciences and Engineering Research Council of Canada for support (J.M.M.) and the Southwestern Ontario NMR Centre for time on the Bruker WH-400.

1. W. MCFARLANE and R. J. WOOD. J. Chem. Soc. Dalton Trans. 1397 (1972).
2. L. CHRISTIAENS, J. L. PIETTE, L. LAITEM, M. BAIWIR, J. DENOEL, and G. LLABRÈS. Org. Magn. Reson. **8**, 354 (1976).
3. S. GRONOWITZ, A. KONAR, and A. B. HÖRNFELDT. Org. Magn. Reson. **9**, 213 (1977).
4. G. A. KALABIN, D. F. KUSHNAREV, V. M. BZESOVSKY, and G. A. TSCHMUTOVA. Org. Magn. Reson. **12**, 598 (1979).
5. M. A. LARDON. Organic selenium compounds: their chemistry and biology. *Edited by* D. L. Klayman and W. H. H. Günther. Wiley Interscience, New York. 1972. p. 933.
6. G. LLABRÈS, M. BAIWIR, J. L. PIETTE, and L. CHRISTIAENS. Org. Magn. Reson. **15**, 152 (1981).
7. W. H. PAN and J. P. FACKLER. J. Am. Chem. Soc. **100**, 5783 (1978).
8. E. R. CULLEN, F. S. GUZIEC, C. J. MURPHY, T. C. WONG, and K. K. ANDERSON. J. Am. Chem. Soc. **103**, 7055 (1981).
9. C. MCFARLANE and W. MCFARLANE. NMR and the periodic table. *Edited by* R. K. Harris and B. E. Mann. Academic Press, New York. 1978. Chapt. 12.
10. W. W. DU MONT and H. J. KROTH. Z. Naturforsch. **36**, 332 (1981).
11. T. DRAKENBERG, A. B. HÖRNFELDT, S. GRONOWITZ, J. M. TALBOT, and J. L. PIETTE. Chem. Scr. **13**, 152 (1979).
12. W. LOHNER and K. PRAEFCKE. J. Organomet. Chem. **208**, 39 (1981).
13. G. V. FAZAKERLEY and M. CELOTTI. J. Magn. Reson. **33**, 219 (1979).
14. N. ZUMBULYADIS and H. J. GYSLING. J. Organomet. Chem. **192**, 183 (1980).
15. D. B. DENNEY, D. Z. DENNEY, P. J. HAMMOND, and Y. F. HSU. J. Am. Chem. Soc. **103**, 2340 (1981).
16. P. GRANGER, S. CHAPELLE, and W. R. MCWHINNIE. J. Organomet. Chem. **220**, 149 (1981).
17. H. J. GYSLING, N. ZUBMULYADIS, and J. A. ROBERTSON. J. Organomet. Chem. **209**, C41 (1981).
18. N. S. DANCE, W. R. MCWHINNIE, and C. H. W. JONES. J. Organomet. Chem. **125**, 291 (1977).
19. W. MCFARLANE, F. J. BERRY, and B. C. SMITH. J. Organomet. Chem. **113**, 339 (1976).
20. H. C. E. MCFARLANE and W. MCFARLANE. J. Chem. Soc. Dalton Trans. 2416 (1973).
21. P. GRANGER. General aspects of the nmr of tellurium. Proceedings of the Third International Symposium on Organic Selenium and Tellurium Compounds. Metz, France. July 9–12, 1979. p. 305.
22. P. H. BIRD, V. KUMAR, and B. C. PANT. Inorg. Chem. **19**, 2487 (1980).
23. B. KOHNE, W. LOHNER, K. PRAEFCKE, H. J. JAKOBSEN, and B. VILLADSEN. J. Organomet. Chem. **166**, 373 (1979).
24. C. G. SWAIN and E. C. LUPTON. J. Am. Chem. Soc. **90**, 4328 (1968).
25. K. J. WYNNE and P. S. PEARSON. Inorg. Chem. **9**, 106 (1970).
26. P. GRANGER and S. CHAPELLE. J. Magn. Reson. **39**, 329 (1980).
27. R. K. CHADHA and J. M. MILLER. Can. J. Chem. **60**, 596 (1982).
28. J. M. MILLER and R. K. CHADHA. J. Organomet. Chem. **216**, 177 (1981).
29. J. BERGMAN. Tetrahedron, **28**, 3323 (1972).
30. R. C. PAUL, K. K. BHASIN, and R. K. CHADHA. J. Inorg. Nucl. Chem. **37**, 2337 (1975).
31. A. SCOTT. Proc. Chem. Soc. **20**, 156 (1904).
32. G. A. OZIN and A. VAN DER VOET. J. Mol. Struct. **13**, 435 (1972).
33. R. K. CHADHA and G. SINGH. Unpublished results.

Can. J. Chem. Downloaded from www.nrcresearchpress.com by 210.87.254.42 on 09/06/12
For personal use only.

# Membrane transport systems. III. A mechanistic study of cation–proton coupled countertransport[1]

THOMAS M. FYLES,[2] VIRGINIA A. MALIK-DIEMER, CYNTHIA A. MCGAVIN, AND DENNIS M. WHITFIELD

*Department of Chemistry, University of Victoria, P.O. Box 1700, Victoria, B.C., Canada V8W 2Y2*

Received March 8, 1982

THOMAS M. FYLES, VIRGINIA A. MALIK-DIEMER, CYNTHIA A. MCGAVIN, and DENNIS M. WHITFIELD. Can. J. Chem. **60**, 2259 (1982).

The rate of extraction and transport of potassium ions from a basic aqueous solution into a chloroform membrane containing a macrocyclic polyether (crown ether) – carboxylic acid has been investigated as a function of the following variables: stirring rate, potassium ion concentration, crown ether concentration, proton concentration, buffer concentration and composition, and crown ether-to-potassium ion ratio. Two rate regimes are found, a "zero order" regime where transport rate depends only on the carrier concentration and a "consecutive first order" regime where transport rate depends on the concentration of a crown ether – potassium complex. The kinetic data, together with partition coefficient and interfacial surface tension data, indicate that the rate determining steps in ion extraction occur at the interface. A mechanism involving rate limiting adsorption of carrier or desorption of complex, depending on the experimental conditions, is shown to be consistent with all available data.

THOMAS M. FYLES, VIRGINIA A. MALIK-DIEMER, CYNTHIA A. MCGAVIN et DENNIS M. WHITFIELD. Can. J. Chem. **60**, 2259 (1982).

On a étudié la vitesse de l'extraction et de la transport des ions de potassium d'une phase aqueuse basique à travers une membrane chloroformique, qui contient un macrocycle (ether-couronne) – acide carboxylique, en fonction des paramétres suivants: la vitesse d'agitation des phases, la concentration de potassium, la concentration de macrocycle, la concentration de proton, la concentration et la composition de tampon et le rapport des concentrations de potassium et macrocycle. Il y a deux régimes cinétiques; celui d'un "ordre zero" où la vitesse n'est en fonction que de la concentration de macrocycle et celui d'un "ordre premier consécutif" où la vitesse est en fonction de la concentration d'un complex du macrocycle et potassium. Ces faits, avec les coefficients de partage chloroforme–eau et la tension de la surface d'interface, indiquent l'interface comme site des étapes lentes. On propose une mécanisme où les étapes lentes sont, soit l'adsorption du macrocycle, soit la désorption du complex selon des conditions expérimentaux. Toutes les observations sont consistantes à une telle mécanisme.

Can. J. Chem. Downloaded from www.nrcresearchpress.com by 210.87.254.5 on 09/06/12
For personal use only.

We have recently described an artificial membrane transport system based upon derivatives of macrocyclic polyethers (crown ethers) which utilizes the coupled countertransport of cations and protons to "pump" alkali metal ions from dilute, basic solution, across a liquid membrane, to a more concentrated, acidic solution (1, 2). The system is presumed to function according to the schematic mechanism outlined in Fig. 1. Starting at the basic interface, proton–cation exchange occurs, the liposoluble complex diffuses to the acidic interface, and the reverse cation–proton exchange occurs to regenerate the carrier. The net result is the transport of a metal ion from the basic to the acidic side of the membrane coupled to the transport of a proton in the opposite direction. The system can act as a cation pump if the gradient in protons exceeds the gradient in the transported cation.

Our previous studies were concerned with the synthesis and characterization of the carriers and their alkali metal cation complexes (1) and with a general examination of the transport behaviour of

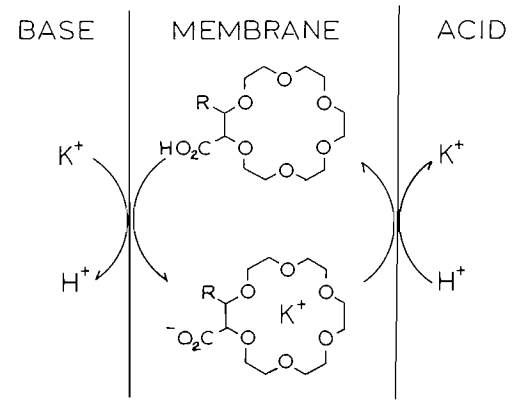


FIG. 1. A schematic mechanism for the carrier mediated countertransport of a metal ion and a proton.

the system (2). This report presents a kinetic examination of potassium ion transport by membrane systems incorporating one of the carriers previously described (**1**). Our goal was to develop a mechanism for ion extraction and transport by carriers of this type which would be useful in designing other carriers for cation–proton coupled countertransport membranes. It was assumed that the important step in the transport cycle is the

[1]Presented, in part, at the 29th congress of the I.U.P.A.C., Vancouver, B.C., August 1981.

[2]Author to whom correspondence may be addressed.

0008-4042/82/172259-09$01.00/0

©1982 National Research Council of Canada/Conseil national de recherches du Canada

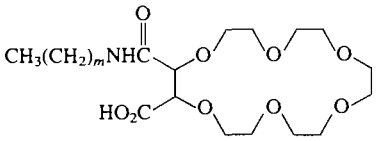

**1** $m = 13$
**2** $m = 3$
**3** $m = 7$

initial extraction of the ion from the aqueous phase; previously it was shown that extraction is typically, but not necessarily, rate limiting (2). The extraction kinetics of potassium picrate into 1,2-dichloroethane by dibenzo-18-crown-6 have been studied, and the process was shown to occur by an interfacial chemical reaction involving as intermediates the crown ether and its complex adsorbed to the interface (3). Although no other detailed studies have been reported for crown ether extractions nor for artificial membrane transport systems, it has been widely assumed that the key step in the extraction occurs at the interface with the carrier (extractant) in the organic phase and the ion in the aqueous phase (2, 4–6). A recent review concludes that interfacial chemical reactions are rate limiting for a wide variety of extractants and metal ions (7). We have therefore undertaken an examination of the kinetics of the ion extraction half of the transport cycle with a view to identifying the location and nature of the rate limiting step(s) in the process occurring within our transport system.

## Results and discussion

*Initial rate studies*

The transport of potassium by **1** exhibits two types of kinetic behaviour depending upon the initial ratio of carrier and metal ion (2). When the concentration of cation exceeds the concentration of carrier, the transport of metal ion is independent of the metal ion concentration ("zero order" regime). When the concentrations of cation and carrier are comparable, the kinetic behaviour can be described as a pair of consecutive first order reactions ("consecutive first order" regime).[3] At intermediate ratios, mixed order behaviour can be found. The rate of cation transport is not limited by diffusion (2) but is controlled by the rates of the extraction reactions (the "kinetic regime" of ref. 7). This conclusion was further tested by measuring the transport rate at various stirring rates for the three phases in the U-tube cell. Between 200 and 800 rpm, no variation in the observed rate could be detected provided the interface remained quiescent. At the standard rate of 400 rpm, the extraction is thus "kinetically controlled".[4]

The extraction may thus be regarded as a chemical reaction. In general, the rate of extraction as a function of observable concentrations is given by eq. [1].

$$[1] \quad \text{rate} = k[K^+(aq)]^p[HCr(org)]^c[H^+(aq)]^h$$

where $p$, $c$, and $h$ are the orders of the reaction for potassium, carrier, and protons respectively. In the zero order regime, $p = 0$ by definition and $h = 0$ from previously reported experiments (2); the value of $c$ was unknown (eq. [2]). In the consecutive first order regime, $p = 1$ by definition but the values of $c$ and $h$ were unknown (eq. [3]).

$$[2] \quad \text{rate} = k[HCr(org)]^c$$

$$[3] \quad \text{rate} = k[K^+(aq)][HCr(org)]^c[H^+(aq)]^h$$

The value of $c$ in eq. [2] was determined from a series of experiments in which the initial rates of reaction were determined as a function of the initial concentration of carrier. Taking the logarithms of both sides of [2] at $t = 0$ gives

$$[4] \quad \log(\text{rate}_0) = c \log([HCr(org)]_0) + \text{const}$$

where the subscript indicates initial values. This approach is feasible for the zeroth order regime as the system behaviour is relatively insensitive to the magnitude of the excess of potassium. Proton concentration was fixed by buffering. The cell thus consisted of: variable concentration of KCl (ten-fold excess over **1**); 0.125 *M* Tris,[5] 0.125 *M* Tris HCl[5] || variable concentration of **1** in $CHCl_3$ || variable concentration of KCl (ten-fold excess over **1**), 0.125 *M* $H_3PO_4$, 0.125 *M* $TEAH^+H_2PO_4^-$.[5] A graph of the initial transport rate data according to eq. [4] is given in Fig. 2 and shows a line of slope 1.02 ($r^2 = 0.995$) clearly indicating that, in the zero order regime, the transport of potassium is first order in carrier.

The situation for the consecutive first order regime is substantially more complex. Not only does the rate vary with carrier and proton concentrations, but the system collapses towards the zero

[3]Extraction of potassium from the basic phase is first order in potassium and is followed by a release step which is first order in "$[K^+(org)]$". Thus $[K^+(aq)] \xrightarrow{k_1} [KCr(org)] \xrightarrow{k_2} [K^+(aq)]$ describes the transport cycle.

[4]Two sets of experiments were performed; one was typical of the zeroth order regime ($[K^+]_0 = 5 \times 10^{-3}$ *M*, $[HCr]_0 = 5 \times 10^{-4}$), the other was typical of the consecutive first order regime ($[K^+]_0 = 1 \times 10^{-3}$ *M* = $[HCr]_0$). Both sets led to similar conclusions.

[5]Tris = tris(hydroxymethyl)amino methane, Tris HCl = hydrochloride salt of Tris, $TEAH^+ H_2PO_4^-$ = dihydrogenphosphate salt of triethanolammonium. pH of basic buffer = 8.25; pH of acidic buffer = 2.30.

Can. J. Chem. Downloaded from www.nrcresearchpress.com by 210.87.254.5 on 09/06/12
For personal use only.

Can. J. Chem. Downloaded from www.nrcresearchpress.com by 210.87.254.5 on 09/06/12
For personal use only.

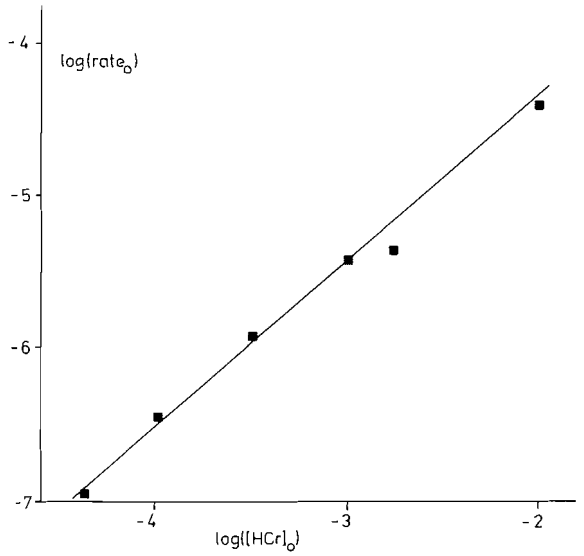


FIG. 2. A plot of log ($rate_0$) as a function of log ($[HCr]_0$) for the zero order transport of potassium by **1**. Log ($rate_0$) = −2.38 + 1.02 log ($[HCr]_0$); $r^2 = 0.995$. Units of rate are μmol $h^{-1}$, units of concentration are mol $L^{-1}$.

order regime if the potassium excess exceeds three-fold. The order in potassium is known by definition. Thus rearrangement of [3] and taking logarithms yields eq. [5].

$$[5] \quad \log\left(\frac{\text{rate}_0}{[K^+(aq)]_0}\right) = c \log([HCr(org)]_0) + h \log([H^+(aq)]_0) + \text{const}$$

The proton concentration may be imposed as constant by buffers, thus

$$[6] \quad \log\left(\frac{\text{rate}_0}{[K^+(aq)]_0}\right) = c \log([HCr(org)]_0) + \text{const}'$$

Furthermore, for a first order process, the initial rate is related to the first order rate constant for uptake of potassium ion ($k_1$obs) by definition [7] to give, on substitution, eq. [8].

$$[7] \quad \text{rate}_0 = k_1 \text{ obs } [K^+(aq)]_0$$

$$[8] \quad \log(k_1 \text{ obs}) = c \log([HCr(org)]_0) + \text{const}'$$

Equation [8] permits an evaluation of the order in carrier even though the concentration of potassium is allowed to vary. Experimentally, this permits the consecutive first order regime to be maintained by balancing the potassium and carrier concentrations. The cell thus consisted of: KCl, 0.125 *M* Tris, 0.125 *M* Tris HCl || variable concentration of **1** || KCl, 0.125 *M* $H_3PO_4$, 0.125 *M* $TEAH^+ H_2PO_4^-$ where $[K^+(aq)]_0 = [HCr(org)]_0$ or $[K^+(aq)]_0 = 1/3$

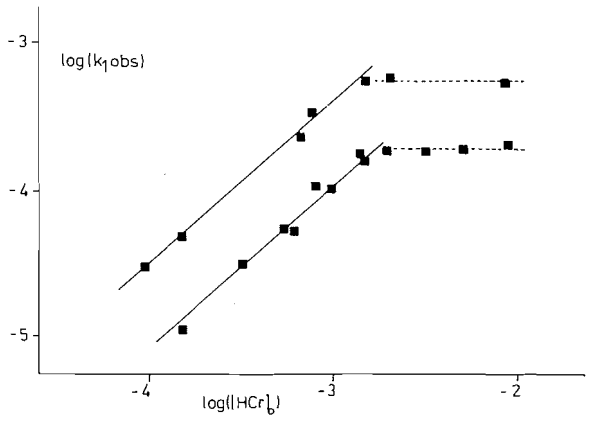


FIG. 3. A plot of log ($k_1$obs) as a function of log ($[HCr]_0$) for the consecutive first order transport of potassium by **1**. Upper curve: log ($k_1$obs) = −0.15 + 1.08 log ($[HCr]_0$); $r^2 = 0.995$; $3[K^+]_0 = [HCr]_0$. Lower curve: log ($k_1$obs) = −0.70 + 1.09 log $[HCr]_0$; $r^2 = 0.983$; $[K^+]_0 = ([HCr]_0)$. Units of $k_1$obs are $s^{-1}$, units of ($[HCr]_0$) are mol $L^{-1}$.

$[HCr(org)]_0$. A graph of the data according to eq. [8] is given as Fig. 3. The curves consist of two regions; the upper horizontal portions correspond to cells where potassium ion release on the acidic side of the membrane is rate limiting. The other portions have slopes of 1.08 ($r^2 = 0.995$) and 1.09 ($r^2 = 0.983$) indicating that uptake is first order in carrier. The separation between the curves corroborates this conclusion; a three-fold increase in the excess of carrier increases the observed rate constant by three-fold resulting in a log 3 separation of the curves at every point. This also indicates that potassium ion release is probably first order in carrier as well, since the log 3 separation continues between the upper portions of the curves.

By a similar analysis to that presented above, [5] may be rewritten as:

$$[9] \quad \log(k_1 \text{ obs}) = h \log([H^+(aq)]_0) + \text{const}'' = -h \log \text{pH}_0 + \text{const}''$$

if the initial carrier concentration is held constant. In principle the initial potassium ion concentration could vary, but this is not necessary as the consecutive first order regime is not as sensitive to pH as to changes in the carrier-to-potassium ion ratio. The cell consisted of: $1.5 \times 10^{-3}$ *M* KCl, Tris/Tris HCl buffers at various pH, Tris (total) = 0.25 *M* || $1.5 \times 10^{-3}$ *M* **1** in $CHCl_3$ || $1.5 \times 10^{-3}$ *M* KCl, 0.125 *M* $H_3PO_4$, 0.125 *M* $TEAH^+ H_2PO_4^-$. A graph of the transport data according to [9] is given as Fig. 4. At higher pH the cells had ion release as the rate determining step, hence were apparently zeroth order in pH. Below pH 8.2 the slope is 0.955 ($r^2 = 0.985$) indicating that in the consecutive first order

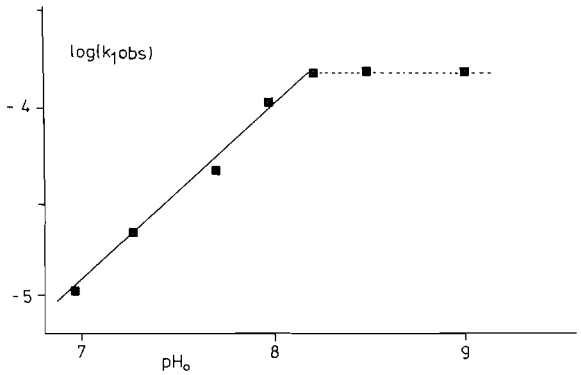


FIG. 4. A plot of log ($k_1$obs) as a function of $pH_0$ for the consecutive first order transport of potassium by **1**. Log ($k_1$obs) $= -11.64 + 0.995\ pH_0$; $r^2 = 0.985$.

regime, the uptake of potassium is inversely proportional to the proton concentration. Thus:

$$[10] \quad \text{rate} = k\,\frac{[K^+(aq)][HCr(org)]}{[H^+(aq)]}$$

for the consecutive first order regime. Equation [10] may be rearranged to an equivalent, but more revealing, form by consideration of two hypothetical partition equilibria, eqs. [11] and [12], which sum to the exchange equilibrium [13].

$$[11] \quad HCr(org) \rightleftharpoons Cr^-(org) + H^+(aq)$$

$$[12] \quad Cr^-(org) + K^+(aq) \rightleftharpoons KCr(org)$$

$$[13] \quad HCr(org) + K^+(aq) \rightleftharpoons KCr(org) + H^+(aq)$$

Equation [11] defines a type of acidity constant $K_a^*$ while [12] defines a type of complex formation constant $K_s^*$. The exchange equilibrium constant $K_e$ of [13] is thus given by [14].

$$[14] \quad K_e = K_a^* K_s^* = \frac{[H^+(aq)][KCr(org)]}{[K^+(aq)][HCr(org)]}$$

Rearrangement of [14] and substitution into [10] gives finally

$$[15] \quad \text{rate} = \frac{k[KCr(org)]}{K_a^* K_s^*} = k'[KCr(org)]$$

The result of this analysis is to demonstrate that in the consecutive first order regime, the rate of potassium ion uptake depends directly upon the concentration of the carrier–potassium complex. This is essentially the mechanism implied by Fig. 1. Additional checks were made of the effect of buffer type (phosphate, TEA, glycinate) and concentration (0.01 to 0.5 *M*) on observed transport rates in both kinetic regimes. There is no discernible effect of either of these variables.

*Partition equilibria and interfacial surface tension*

Several fundamental steps may be envisaged for the movement of an ion from water to within a complex in the organic phase and in principle any one could be rate limiting. However, complexation–decomplexation rates of crown ethers and other ionophores with alkali metal cations are known to be rapid in a variety of media (8–10), hence it is unlikely that the actual complexation step would be the slowest in this particular case. This is particularly true if the complexation occurs in a predominantly aqueous environment. Similarly, deprotonation of the ligand is unlikely to be rate limiting. More likely candidates for the rate limiting steps are reactions involving transfer across a phase boundary (partition) or adsorption–desorption reactions at an interface. Similar processes occur in extraction (7) and in phase transfer catalysis (11); in both cases the extractant remains within the organic phase and ion exchange reactions occur at the interface (12, 13).

Partition of the carrier between the two phases has been examined by two indirect methods. All partition equilibria strongly favour the carrier and its complexes in the organic phase, hence a direct determination of the partition coefficient **1** is analytically difficult. Direct determinations for a lower homolog of **1** (i.e. **2**) have been possible.

Consider the following equilibria:

$$[16] \quad HCr(aq) \rightleftharpoons HCr(org) \qquad P_{HCr} = \frac{[HCr(org)]}{[HCr(aq)]}$$

$$[17] \quad KCr(aq) \rightleftharpoons KCr(org) \qquad P_{KCr} = \frac{[KCr(org)]}{[KCr(aq)]}$$

$$[18] \quad HCr(aq) \rightleftharpoons Cr^-(aq) + H^+(aq)$$

$$[19] \quad K^+(aq) + Cr^-(aq) \rightleftharpoons KCr(aq)$$

Equations [16] and [17] define partition coefficients for HCr and KCr respectively, while [18] and [19] define the acidity and stability constants for complexation in the aqueous phase. For **2**, $pK_a = 3.60 \pm 0.2$ and $\log K_s(K^+) = 2.6 \pm 0.2$ in 0.1 *M* $(CH_3)_4NCl$ as determined from pH-metric titration using procedures previously described (1).

At a pH less than the $pK_a$, the carrier in the aqueous phase will be predominantly as the protonated form, and eq. [16] will describe the system to a first approximation. Solutions of **2** in chloroform were equilibrated with aqueous phosphoric acid and the equilibrium concentrations of HCr in both phases were determined by acid–base titration. In this manner $\log P_{HCr}$ was found to be $1.50 \pm 0.2$.

Can. J. Chem. Downloaded from www.nrcresearchpress.com by 210.87.254.5 on 09/06/12
For personal use only.

Can. J. Chem. Downloaded from www.nrcresearchpress.com by 210.87.254.5 on 09/06/12
For personal use only.

Manipulation of eqs. [16]–[19] (14) leads to an expression for the distribution of metal ions between two phases (eq. [20]).

$$[20] \quad \frac{[KCr(org)]}{[K^+(aq)]} \cong \frac{P_{KCr}K_sK_a}{P_{HCr}} \frac{[HCr(org)]}{[H^+(aq)]}$$

Values of $P_{HCr}$, $K_s$, and $K_a$ are given above, [HCr(org)] may be determined as described above by titration, $[H^+(aq)]$ may be calculated from the pH, and the metal ion distribution may be determined by atomic absorption analysis for potassium ion in the two phases, $P_{KCr}$ is the only unknown. Under conditions which closely resembled the initial conditions in a transport experiment, log $P_{KCr}$ was found to be $-0.7 \pm 0.3$.

The values of log $P_{HCr}$ and $P_{KCr}$ for **1** may be estimated by assuming a constant increment of log $P = +0.54$ per additional methylene group (15). Thus for **1** log $P_{HCr} = 6.9$ and log $P_{KCr} = 4.7$. One other value in this series has been directly determined; log $P_{HCr}$ for **3** was found to be $3.8 \pm 0.2$ (1). The calculated value for **3** is 3.66. The agreement is quite good although the extrapolation required for **1** may lead to greater errors (15).

Returning to the central question; is the carrier partitioned into the aqueous phase kinetically important under the transport conditions? The answer is likely not. At pH 8.25, $[K^+(aq)]_0 = 1.0 \times 10^{-3}\,M$ and $[HCr(org)]_0 = 1.0 \times 10^{-3}\,M$, the maximum concentration of KCr(aq) is calculated to be ca. $10^{-8}\,M$. In order to achieve μmol $h^{-1}$ transfer rates the partition equilibria would have to be established at rates of about $10^3\,h^{-1}$ (ca. $s^{-1}$). This is clearly not the case, as some distribution experiments required days to reach limiting values.

Further evidence ruling out kinetically important roles for HCr(aq) and KCr(aq) may be obtained from experiments conducted in H-tube cells (16). In the base of one arm was a solution of **1** in chloroform and in the other, chloroform with no carrier. Floating on these, and filling the cross of the H, was placed $1 \times 10^{-3}\,M$ KCl in pH 8.25 buffer. All compartments were stirred. The approach to equilibrium of the potassium in the aqueous phase was followed by analysis of aliquots for potassium. This process was complete within 8 h. However, even after 80 h, the two chloroform phases had not achieved equilibrium as determined by analysis of the two chloroform solutions by atomic absorption (for potassium) and acid–base titration (for carrier). By either criterion, virtually none of the carrier was transferred through the aqueous phase in this time. It follows that a partitioning of the carrier is insufficiently rapid to explain the transport rates.

Since the kinetically important carrier form is membrane bound, it is reasonable to suppose that the site of extraction is at the interface. Other extractants are known to be surfactants (7, 17) and the interfacial activity of simple crown ethers has been investigated (3, 18). The surfactant properties of **1**, under conditions similar to those encountered in the transport experiments, have been determined by measurement of the interfacial surface tension ($\gamma_i$) by the de Nöuy ring method (19). Due to the large amount of organic solute in the buffers, the value of $\gamma_i$ between pH 8.25 buffer and chloroform is low (5 dyne $cm^{-1}$). Quantitative data are thus rather imprecise but serve to give a qualitative insight into the behaviour of **1** at the interface. In the absence of potassium ions, the interfacial surface tension between pH 8.25 buffer and chloroform falls to less than 1 dyne $cm^{-1}$ at concentrations of **1** greater than $10^{-6}\,M$. The change in $\gamma_i$ occurs abruptly between $10^{-6}$ and $10^{-7}\,M$ in **1**. In the presence of $10^{-2}\,M$ KCl the abrupt decrease in $\gamma_i$ occurs at slightly higher concentrations of **1**, between $10^{-6}$ and $10^{-5}\,M$. At the concentrations used for transport the interface is likely to be completely saturated by the surfactant carrier, either as the anion $Cr^-$(i) or as the complex KCr(i).

The Gibbs equation [21] (19) relates the change in $\gamma_i$ with concentration to the surface excess of the surfactant (Γ).

$$[21] \quad \Gamma = -\frac{1}{RT}\left(\frac{d\gamma_i}{d \ln c}\right)$$

where Γ is the surface excess of the solute considered and $c$ is its concentration. The data are insufficiently reliable to give accurate values for the final term in [21]; they are, however, sufficient to provide an estimate of about $-5$ dyne $cm^{-1}$ per decade as a minimum value. The surface excess of **1** is calculated to be ca. $9 \times 10^{-11}$ mol $cm^{-2}$ by [21] which can be converted to a value of 185 $Å^2$/molecule as the area occupied at the interface. The area per molecule may be estimated from CPK models to be about 200 Å for an "edge-on" orientation and about 250 $Å^2$ for a "face-on" orientation. The interface probably consists of a fully condensed monolayer of carrier between the aqueous and chloroform phases, with the alkyl chains extending to the organic solvent.

If the carboxylate and the complex are both strongly adsorbed to the interface, the protonated carrier is much less strongly adsorbed. Interfacial

surface tension measurements for pH 2.3 buffer and chloroform reveal that $\gamma_i$ remains constant to carrier concentrations above $10^{-3}\,M$ and only reaches a limiting value at $5 \times 10^{-2}\,M$. Under the transport conditions the acidic interface is unlikely to be saturated with carrier. At the basic interface the situation is more complex. The carrier, HCr, will have little tendency to adsorb; once at the interface, deprotonation and complexation can occur and the tendency for *desorption* will be small. The basic interface remains saturated throughout, *but not with the species whose concentration is experimentally varied.*

*Extraction mechanism*

The extraction mechanism likely in the case of ion extraction and transport by **1** is similar to those observed with other amphiphilic extractants (7). It involves adsorption of the carrier to the interface, a series of exchange equilibria, and desorption of the adsorbed complex into the organic phase. The sequence of primary steps is given below.

[22] $\mathrm{HCr(org)} \underset{k_{-1}}{\overset{k_1}{\rightleftharpoons}} \mathrm{HCr(i)}$

[23] $\mathrm{HCr(i)} \overset{K_a'}{\rightleftharpoons} \mathrm{Cr^-(i)} + \mathrm{H^+(aq)}$

[24] $\mathrm{Cr^-(i)} + \mathrm{K^+(aq)} \overset{K_s'}{\rightleftharpoons} \mathrm{KCr(i)}$

[25] $\mathrm{KCr(i)} \underset{k_{-2}}{\overset{k_2}{\rightleftharpoons}} \mathrm{KCr(org)}$

In principle any of the steps could be rate limiting; as argued above, protonation and complexation are likely to be fast. Thus the interfacial "concentration" of the various carrier species are interrelated through the equilibrium constants $K_a'$ and $K_s'$; i.e.

$$[26] \quad [\mathrm{HCr(i)}] = \frac{[\mathrm{KCr(i)}][\mathrm{H^+(aq)}]}{K_a' K_s' [\mathrm{K^+(aq)}]}$$

Further, for an interfacial area of 1.54 $\mathrm{cm^2}$ and an area per molecule of ca. 200 Å, the various interfacial species can never exceed one part in $10^{11}$ of the total amount of carrier present in a typical experiment. Thus, the interfacial species may be treated as steady-state intermediates, which gives an expression for the "concentration" of KCr(i) in terms of bulk concentrations; i.e.

$$[27] \quad [\mathrm{KCr(i)}] = \frac{k_1[\mathrm{HCr(org)}] + k_{-2}[\mathrm{KCr(org)}]}{\dfrac{k_{-1}[\mathrm{H^+(aq)}]}{K_a' K_s' [\mathrm{K^+(aq)}]} + k_2}$$

The rate of disappearance of potassium from the aqueous phase must equal the rate of formation of the complex in the memebrane, hence

$$[28] \quad \frac{-\mathrm{d}[\mathrm{K^+(aq)}]}{\mathrm{d}t} = \frac{\mathrm{d}[\mathrm{KCr(org)}]}{\mathrm{d}t} = (k_1 k_2 K_a' K_s' [\mathrm{K^+(aq)}][\mathrm{HCr(org)}] - k_{-1} k_{-2} [\mathrm{H^+(aq)}][\mathrm{KCr(org)}])/(k_{-1}[\mathrm{H^+(aq)}] + k_2 K_s' K_a' [\mathrm{K^+(aq)}])$$

The concentration of the complex in the bulk organic phase is initially zero and, by mass balance calculation, rarely exceeds 15% of the total amount of carrier present under normal transport conditions (2). The proton concentration is also low; thus the second numerator term of [28] is likely to be negligible for most circumstances. Two limiting cases are thus possible; one in which $k_{-1}[\mathrm{H^+(aq)}]$ is large with respect to $k_2[\mathrm{K^+(aq)}]\ K_a'\ K_s'$, giving eq. [29], and the converse, which leads to eq. [30].

$$[29] \quad \frac{-\mathrm{d}[\mathrm{K^+(aq)}]}{\mathrm{d}t} \approx \frac{k_1 k_2 K_a' K_s' [\mathrm{K^+(aq)}][\mathrm{HCr(org)}]}{k_{-1}[\mathrm{H^+(aq)}]}$$

$$[30] \quad \frac{-\mathrm{d}[\mathrm{K^+(aq)}]}{\mathrm{d}t} \approx k_1[\mathrm{HCr(org)}]$$

The result of this analysis is to show the relationship of the experimentally observed rate constants to the individual steps in the extraction process. Equation [29] corresponds to the consecutive first order regime. A comparison of [29] and [10] shows that the observed first order rate constant, $k_1$obs, is equal to the constants in [29]; i.e., $k_1 k_2 K_a' K_s'/k_{-1}$. In this regime, complex desorption is rate limiting. The absorption–desorption of HCr appears as an equilibrium constant given by $k_1/k_{-1}$.

Equation [30] corresponds to the zero order regime and a comparison with eq. [3] shows that the observed zero order rate constant $k_0$obs is equal to $k_1$. In this regime it is the adsorption of HCr to the interface which is rate limiting. As outlined above, the interface is likely to be saturated with $\mathrm{Cr^-(i)}$ and KCr(i); the rate limiting step may thus be the penetration of the protonated carrier into the monolayer of adsorbed carrier complex at the interface.

Can. J. Chem. Downloaded from www.nrcresearchpress.com by 210.87.254.5 on 09/06/12
For personal use only.

Can. J. Chem. Downloaded from www.nrcresearchpress.com by 210.87.254.5 on 09/06/12
For personal use only.

*Comparison with other transport systems*

To what degree is the mechanism presented above applicable to the numerous other membrane transport systems, both artificial and natural, which are known? Many artificial membrane transport systems have been shown to be rate limited by diffusion of the carrier and its complexes within the membrane (4, 20). The rate determining steps applicable to the mechanism above are thus sufficiently rapid to be treated as equilibria in the kinetic analysis (20). Although there have been no detailed studies of these systems under "kinetic control" (7), the behaviour of a typical transport system in which potassium picrate is transported by dibenzo-18-crown-6 (21) may be inferred from the extraction data (3). In this case two separate rate behaviours were noted. In the concentration range of $10^{-3}$ to $10^{-2}$ *M* in dibenzo-18-crown-6, the extraction closely resembles the consecutive first order regime of **1**, i.e., extraction apparently depends on the formation of a carrier–potassium complex. To higher concentration the extraction becomes zero order in carrier while data at lower carrier concentrations are not presented. Neither of the mechanisms discussed by the authors of ref. 3 will fit with the data presented above for the carrier **1**. However, the data of ref. 3 are consistent with a mechanism similar to the one presented above in which desorption of an interfacial carrier complex is rate limiting. Further study will reveal if the proposed mechanism is generally applicable in other cases as well. It is potentially a candidate in any case where the surfactant properties of the carrier alter on complex formation (22) and where the complexation rates are likely to be fast.

Comparisons with naturally occurring transport systems are unlikely to reveal any mechanistic similarities. There are, nonetheless, considerable kinetic similarities. Transport data in naturally occurring transport systems are commonly analysed using the Michealis–Menton equation developed for use in enzyme kinetics (23). The basic equation has many forms; the one due to Eadie and Hofstee (24, 25) (eq. [31]) gives the most reliable estimates of the parameters $V_{max}$ and $K_m$ (26, 27).

$$[31] \quad \text{rate}_0 = V_{max} - \frac{K_m(\text{rate})_0}{[K^+(aq)]}$$

where $V_{max}$ is the maximal rate of transport for a given concentration of carrier and $K_m$ is an apparent dissociation constant for the carrier complex. Initial rate data were obtained for the cell: variable concentration of KCl, 0.125 *M* Tris, 0.125 *M* Tris HCl || $5.0 \times 10^{-4}$ *M* in $CHCl_3$ || variable concentration of KCl, 0.125 *M* $H_3PO_4$, 0.125 *M* $TEAH^+$ $H_2PO_4^-$. The data are plotted according to [31] (Fig. 5). The intercept gives a value of $V_{max}$ = 4.1 μmol $h^{-1}$ ($4.1 \times 10^{-4}$ *M* $h^{-1}$)[6] and the slope gives $K_m = 6.1 \times 10^{-4}$ mol $L^{-1}$. Although this value of $K_m$ would be typical for a wide range of natural transport systems for potassium (23), the value of $V_{max}$ is several orders of magnitude lower than those found for biological systems. This is doubtless due to the difference between a thin bilayer membrane and the large volumes of the U-tube.

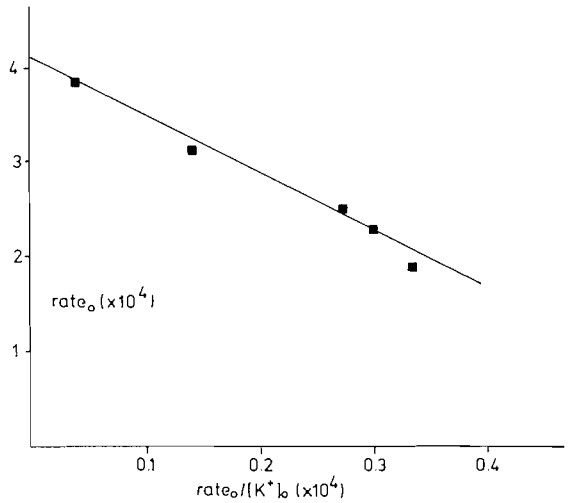


FIG. 5. A plot of initial transport rate of potassium as a function of $\text{rate}_0/[K^+]_0$ by $5 \times 10^{-4}$ *M* **1**. $\text{Rate}_0 = 4.10 \times 10^{-4} - 6.1 \times 10^{-4}$ ($\text{rate}_0/[K^+]_0$); $r^2 = 0.981$. Units of $\text{rate}_0$ are mol $L^{-1}$ $h^{-1}$, units of concentration are mol $L^{-1}$.

TABLE 1. Initial transport rates for the zero order transport of potassium by **1**[a]

| Entry | $[K^+(aq)]_0$[b] | $[HCr(org)]_0$[b] | Initial rate[c] |
|---|---|---|---|
| 1 | $1.0 \times 10^{-1}$ | $1.02 \times 10^{-2}$ | 41.2 |
| 2 | $3.0 \times 10^{-2}$ | $1.77 \times 10^{-3}$ | 4.22 |
| 3 | $1.0 \times 10^{-2}$ | $1.02 \times 10^{-3}$ | 3.91 |
| 4 | $5.0 \times 10^{-3}$ | $5.50 \times 10^{-4}$ | 1.34 |
| 5 | $3.0 \times 10^{-3}$ | $3.40 \times 10^{-4}$ | 1.24 |
| 6 | $1.0 \times 10^{-3}$ | $1.02 \times 10^{-4}$ | 0.332 |
| 7 | $5.0 \times 10^{-4}$ | $3.40 \times 10^{-5}$ | 0.114 |
| 8 | $5.0 \times 10^{-4}$ | $5.0 \times 10^{-4}$ | 1.91[d] |
| 9 | $7.5 \times 10^{-4}$ | $5.0 \times 10^{-4}$ | 2.25[d] |
| 10 | $1.0 \times 10^{-3}$ | $5.0 \times 10^{-4}$ | 2.54 |
| 11 | $2.25 \times 10^{-3}$ | $5.0 \times 10^{-4}$ | 3.12 |
| 12 | $1.0 \times 10^{-2}$ | $5.0 \times 10^{-4}$ | 3.89 |

[a]Basic buffer = 0.125 *M* Tris, 0.125 *M* Tris HCl, pH 8.25. Acidic buffer = 0.125 *M* $H_3PO_4$, 0.125 *M* $TEAH^+$ $H_2PO_4^-$, pH 2.30. Initial concentrations of potassium equal on both sides of the cell. Temperature = 25°C.[e]
[b]Units mol $L^{-1}$.
[c]Units μmol $h^{-1}$.
[d]Order mixed for the complete reaction, predominantly first order initially.
[e]Entries 1–6 appear in Fig. 1, entries 7–12 appear in Fig. 5.

[6]Note that the initial volume of 10 mL introduces a factor of 100 in the initial rate in terms of *concentration* compared to the initial rate in terms of *amount*.

Can. J. Chem. Downloaded from www.nrcresearchpress.com by 210.87.254.5 on 09/06/12
For personal use only.

As noted, $K_m$ is an apparent dissociation constant for the carrier complex. The apparent *association* constant, the reciprocal of $K_m$, has a value of log $(1/K_m) = 3.2$. This may be compared to the stability constants for complex formation in water (log $K_s = 2.6$) and in 90:10 methanol–water (log $K_s = 5.6$) (1). This serves to further corroborate the assertion that complexation occurs in a predominantly aqueous environment.

The values of $K_m$ and $V_{max}$ are of little fundamental importance as they depend on the concentration of the carrier. They do, however, provide a simple way to summarize the kinetic and thermodynamic behaviour of a carrier under a specified set of conditions. A more complete analysis would involve an evaluation of all the constants in eq. [28].

TABLE 2. First order rate constants for the transport of potassium by **1**[a]

| Entry | $[K^+]_0$[b] | $[HCr]_0$[b] | $k_1$[c] | $k_2$[c] |
|---|---|---|---|---|
| 1 | $1.50 \times 10^{-4}$ | $1.50 \times 10^{-4}$ | $1.16 \times 10^{-5}$ | — |
| 2 | $3.00 \times 10^{-4}$ | $3.00 \times 10^{-4}$ | $3.33 \times 10^{-5}$ | — |
| 3 | $5.00 \times 10^{-4}$ | $5.01 \times 10^{-4}$ | $5.47 \times 10^{-5}$ | $8.63 \times 10^{-5}$ |
| 4 | $6.00 \times 10^{-4}$ | $6.00 \times 10^{-4}$ | $5.50 \times 10^{-5}$ | $6.86 \times 10^{-5}$ |
| 5 | $7.50 \times 10^{-4}$ | $7.52 \times 10^{-4}$ | $1.15 \times 10^{-4}$ | $1.39 \times 10^{-4}$ |
| 6 | $1.00 \times 10^{-3}$ | $1.00 \times 10^{-3}$ | $1.00 \times 10^{-4}$ | $1.88 \times 10^{-4}$ |
| 7[d] | $1.00 \times 10^{-3}$ | $1.37 \times 10^{-3}$ | $1.27 \times 10^{-4}$ | $3.16 \times 10^{-4}$ |
| 8[e] | $1.00 \times 10^{-3}$ | $1.14 \times 10^{-3}$ | $1.22 \times 10^{-4}$ | $2.63 \times 10^{-4}$ |
| 9[f] | $1.00 \times 10^{-3}$ | $1.14 \times 10^{-3}$ | $1.36 \times 10^{-4}$ | $3.30 \times 10^{-4}$ |
| 10 | $1.50 \times 10^{-3}$ | $1.50 \times 10^{-3}$ | $1.43 \times 10^{-4}$ | $2.91 \times 10^{-4}$ |
| 11 | $1.00 \times 10^{-3}$ | $1.87 \times 10^{-3}$ | $1.89 \times 10^{-4}$ | $1.50 \times 10^{-4}$ |
| 12 | $4.00 \times 10^{-3}$ | $2.00 \times 10^{-3}$ | $1.75 \times 10^{-4}$ | — |
| 13 | $3.30 \times 10^{-3}$ | $3.26 \times 10^{-3}$ | $1.78 \times 10^{-4}$ | $1.33 \times 10^{-4}$ |
| 14 | $5.00 \times 10^{-3}$ | $5.01 \times 10^{-3}$ | $1.96 \times 10^{-4}$ | $2.45 \times 10^{-4}$ |
| 15 | $1.00 \times 10^{-2}$ | $1.00 \times 10^{-2}$ | $2.09 \times 10^{-4}$ | — |
| 16 | $5.00 \times 10^{-5}$ | $1.56 \times 10^{-4}$ | $4.75 \times 10^{-5}$ | — |
| 17 | $3.00 \times 10^{-5}$ | $9.33 \times 10^{-5}$ | $1.81 \times 10^{-5}$ | $2.60 \times 10^{-5}$ |
| 18 | $2.00 \times 10^{-4}$ | $6.56 \times 10^{-4}$ | $2.30 \times 10^{-4}$ | — |
| 19 | $2.50 \times 10^{-4}$ | $7.50 \times 10^{-4}$ | $3.25 \times 10^{-4}$ | — |
| 20 | $5.00 \times 10^{-4}$ | $1.50 \times 10^{-3}$ | $5.80 \times 10^{-4}$ | — |
| 21 | $2.50 \times 10^{-3}$ | $7.50 \times 10^{-3}$ | $5.35 \times 10^{-4}$ | $6.96 \times 10^{-5}$ |
| 22 | $5.00 \times 10^{-3}$ | $1.50 \times 10^{-2}$ | $6.16 \times 10^{-4}$ | $7.32 \times 10^{-5}$ |
| 23[g] | $1.50 \times 10^{-3}$ | $1.50 \times 10^{-3}$ | $1.70 \times 10^{-4}$ | — |
| 24[h] | $1.50 \times 10^{-3}$ | $1.50 \times 10^{-3}$ | $1.56 \times 10^{-4}$ | — |
| 25[i] | $1.50 \times 10^{-3}$ | $1.50 \times 10^{-3}$ | $1.15 \times 10^{-4}$ | — |
| 26[j] | $1.50 \times 10^{-3}$ | $1.50 \times 10^{-3}$ | $4.45 \times 10^{-5}$ | — |
| 27[k] | $1.50 \times 10^{-3}$ | $1.50 \times 10^{-3}$ | $2.13 \times 10^{-5}$ | — |
| 28[l] | $1.50 \times 10^{-3}$ | $1.50 \times 10^{-3}$ | $1.15 \times 10^{-5}$ | — |
| 29[m] | $1.00 \times 10^{-3}$ | $1.00 \times 10^{-3}$ | $4.56 \times 10^{-5}$ | $9.19 \times 10^{-5}$ |
| 30[n] | $1.00 \times 10^{-3}$ | $1.00 \times 10^{-3}$ | $5.33 \times 10^{-5}$ | $1.17 \times 10^{-4}$ |
| 31[o] | $1.00 \times 10^{-3}$ | $1.00 \times 10^{-3}$ | $4.62 \times 10^{-5}$ | $1.07 \times 10^{-4}$ |

[a] Basic buffer = 0.125 *M* Tris, 0.125 *M* Tris HCl, pH 8.25. Acidic buffer = 0.125 *M* $H_3PO_4$, 0.125 *M* $TEAH^+ H_2PO_4^-$, pH 2.30 (unless otherwise specified). Initial concentrations of potassium equal on both sides of the cell. Temperature = 25°C.[p]
[b] Units mol $L^{-1}$.
[c] Units $s^{-1}$.
[d] Basic pH = 8.60 (2).
[e] Basic pH = 8.60, acidic pH = 1.40 (2).
[f] Basic pH = 8.60, acidic pH = 3.30 (2).
[g] Basic pH = 9.02, Tris (total) = 0.25 *M*.
[h] Basic pH = 8.52, Tris (total) = 0.25 *M*.
[i] Basic pH = 8.02, Tris (total) = 0.25 *M*.
[j] Basic pH = 7.70, Tris (total) = 0.25 *M*.
[k] Basic pH = 7.25, Tris (total) = 0.25 *M*.
[l] Basic pH = 7.02, Tris (total) = 0.25 *M*.
[m] Basic pH = 8.01, Tris (total) = 0.01 *M*.
[n] Basic pH = 8.02, Tris (total) = 0.025 *M*.
[o] Basic pH = 7.96, Tris (total) = 0.10 *M*.
[p] Entries 1–6 and 10–15 appear as the lower line in Fig. 3, entries 16–21 appear as the upper line. Previous values (7–9) are included for comparison. Entry 22 lies on the upper line of Fig. 3 but outside the boundary of the graph. Entries 23–28 and entry 10 appear in Fig. 4. The negligible buffer effect is indicated by entries 29–31.

## Experimental

General methods for purification of carriers, kinetic analyses, and thermodynamic measurements were as previously described (1, 2). The reported kinetic data were usually determined in duplicate and in some cases triplicate. In addition, most experiments were conducted once in a preliminary fashion to determine optimal sampling times and analytical procedures; none of these experiments is included in the final values. Kinetic data are appended in Tables 1 and 2.

*Extraction equilibria*

An aqueous phase, 10 mL, with or without added potassium, and a chloroform solution of the carrier were stirred in a jacketed test tube at 25°C for a minimum of 48 h. The equilibrated phases were analysed for potassium ion content by atomic absorption and for carrier by acid–base titration. Aliquots of the aqueous phase were directly titrated with standard base. Endpoints were determined from the maxima in plots of the first derivative of the pH–volume curve. Separate endpoints for the carrier and $H_3PO_4$ were clearly identifiable. Aliquots of the organic phase were evaporated, taken up in 0.1 *M* KCl(aq), and titrated with standard base. Partition coefficients were calculated from this data as described in the text.

*Interfacial surface tension*

The aqueous phase (20 mL) and the chloroform solution of the carrier (20 mL) were allowed to stand at 20°C overnight before measurements were performed. The interfacial surface tension was measured using a Fisher Surface tensiometer. The scale was calibrated with standard weights and scale readings were corrected for buoyancy (28). Final values were the average of several measurements. Typical values were 0.125 *M* Tris, 0.125 *M* Tris HCl/chloroform: 5.0 ± 0.6 dyne $cm^{-1}$; 0.125 *M* Tris, 0.125 *M* Tris HCl/1 × $10^{-3}$ *M* **1** in chloroform: 0.9 ± 0.5 dyne $cm^{-1}$. Due to the low magnitude and large uncertainty the values obtained were of qualitative interest only.

## Acknowledgements

We thank V. A. Harris and M. E. Robinson for analytical assistance in the preliminary work and the Natural Sciences and Engineering Research Council of Canada and the University of Victoria for support of this project.

1. L. A. FREDERICK, T. M. FYLES, N. P. GURPRASAD, and D. M. WHITFIELD. Can. J. Chem. **59**, 1724 (1981).
2. T. M. FYLES, V. A. MALIK-DIEMER, and D. M. WHITFIELD. Can. J. Chem. **59**, 1734 (1981).
3. P. R. DANESI, R. CHIARIZIA, M. PIZZICHINI, and A. SALTELLI. J. Inorg. Nucl. Chem. **40**, 1119 (1978).
4. E. M. CHOY, D. F. EVANS, and E. L. CUSSLER. J. Am. Chem. Soc. **96**, 7085 (1974).
5. N. N. LI. J. Membrane Sci. **3**, 265 (1978).
6. R. W. BAKER, M. E. TUTTLE, D. J. KELLY, and H. K. LONSDALE. J. Membrane Sci. **2**, 213 (1977).
7. P. R. DANESI and R. CHIARIZIA. C. R. C. Crit. Rev. Anal. Chem. **10**, 1 (1980).

8. E. SHCHORI, J. JAGUR-GRODZINSKI, and M. SHPORER. J. Am. Chem. Soc. **95**, 3842 (1973).
9. H. HOLLAND, J. A. RINGSETH, and T. S. BRUN. J. Solution Chem. **8**, 779 (1979).
10. H. DIEBLER, M. EIGEN, G. ILGENFRITZ, G. MASS, and R. WINKLER. Pure Appl. Chem. **20**, 93 (1969).
11. E. V. DEHMLOW and S. S. DEHMLOW. Phase transfer catalysis. Verlag Chemie, Weinheim. 1980.
12. D. LANDINI, A. MAIA, and F. MONTANARI. J. Am. Chem. Soc. **100**, 2796 (1978).
13. P. E. STOTT, J. S. BRADSHAW, and W. W. PARISH. J. Am. Chem. Soc. **102**, 4810 (1980).
14. D. G. PETERS, J. M. HAYES, and G. H. HIEFTJE. Chemical separations and measurements. W. B. Saunders Co., Philadelphia. 1974. pp. 508–510.
15. C. HANSCH and A. LEO. Substituent constants for correlation analysis in chemistry and biology. J. Wiley & Sons, New York. 1979. pp. 18–25.
16. N. YAMAZAKI, S. NAKAHAMA, A. HIRAO, and S. NEGI. Tetrahedron Lett. 2429 (1978).
17. G. F. VANDEGRIFT and E. P. HORWITZ. J. Inorg. Nucl. Chem. **39**, 1425 (1977).
18. G. F. VANDEGRIFT and W. H. DELPHIN. J. Inorg. Nucl. Chem. **42**, 1359 (1980).
19. D. C. HILMENZ. Principles of colloid and surface science. Marcel Dekker, New York. 1977.
20. J. D. LAMB, J. J. CHRISTENSEN, J. L. OSCARSON, B. L. NIELSEN, B. W. ASAY, and R. M. IZATT. J. Am. Chem. Soc. **102**, 6820 (1980).
21. J. L. CHRISTENSEN, J. D. LAMB, S. R. IZATT, S. E. STARR, G. C. WEED, M. S. ASTIN, B. C. STITT, and R. M. IZATT. J. Am. Chem. Soc. **100**, 3219 (1978).
22. J. LEMOIGNE and J. SIMON. J. Phys. Chem. **84**, 170 (1980).
23. A. KOTYK and K. JANACEK. Cell membrane transport. Plenum Press, New York. 1975.
24. G. S. EADIE. J. Biol. Chem. **146**, 85 (1942).
25. B. H. J. HOFSTEE. Nature, **184**, 1296 (1959).
26. J. E. DOWD and D. S. RIGGS. J. Biol. Chem. **249**, 863 (1965).
27. G. L. ATKINS and I. A. NIMMO. Biochem. J. **149**, 775 (1975).
28. W. D. HARKINS and H. F. JORDAN. J. Am. Chem. Soc. **52**, 1751 (1930).

Can. J. Chem. Downloaded from www.nrcresearchpress.com by 210.87.254.5 on 09/06/12
For personal use only.

# The electrophilic addition of dimethylbromosulfonium bromide to conjugated enones: efficient synthesis of α-bromo enones

YUAN L. CHOW AND BERT H. BAKKER

*Department of Chemistry, Simon Fraser University, Burnaby, B.C., Canada V5A 1S6*

Received January 21, 1982

YUAN L. CHOW and BERT H. BAKKER. Can. J. Chem. **60**, 2268 (1982).

Dimethylbromosulfonium bromide reacted readily with many enones at 0°C or lower to precipitate α-bromo-β-sulfonium conjugated enones. These salts eliminate a proton and dimethylsulfide readily with aqueous potassium carbonate to give excellent yields of α-bromo conjugated enones cleanly. The mechanism of the addition was explained by the bromonium ion initiated 1,4-addition followed by tautomerization of enol hypobromites.

YUAN L. CHOW et BERT H. BAKKER. Can. J. Chem. **60**, 2268 (1982).

Le bromure de diméthylbromosulfonium réagit facilement avec plusieurs énones à 0°C ou à une température plus basse pour donner un précipité formé d'énones conjuguées α-bromo-β-sulfonium. Ces sels, en présence de carbonate de potassium en solution aqueuse, perdent facilement un proton et le diméthylsulfure en donnant des α-bromo énones conjuguées à l'état pur, avec un excellent rendement. On explique le mécanisme d'addition par l'ion bromonium qui initie une addition 1,4 suivie d'une tautomérisation des hypobromites d'énol.

[Traduit par le journal]

Can. J. Chem. Downloaded from www.nrcresearchpress.com by 210.87.254.5 on 09/06/12
For personal use only.

Dialkylbromosulfonium bromides are readily prepared from dialkylsulfides and bromine as relatively stable crystalline compounds (1–5) and their structures have been determined by X-ray analysis to have a S—Br bond (6). Dimethylbromosulfonium bromide is also formed from the interaction of dimethylsulfoxide with bromine or *N*-bromosuccinimide (7) in alcohols. This obviously involves an oxidation reaction by DMSO since it has been shown that HBr can catalyze the reduction of DMSO in the presence of $H_2O$ to give dimethylsulfide and bromine.

In recent years, much interest has been directed toward dialkylhalosulfonium halides, in particular $(CH_3)_2SBr^+Br^-$ because of its ready availability, as synthetic reagents for various transformations. Pummerer type rearrangement is probably the earliest known reaction in which α-halosulfides are the product (1). The reaction type involving nucleophilic substitution at the α-carbon has been reported (1, 7).

$$R-\overset{\overset{Br}{|}}{\underset{+}{S}}-CH_3 \quad X^- \rightarrow R-SBr + CH_3X$$

$$X = RO^-,\ OH^-,\ Br^-$$

However, nucleophilic attack at the cationic sulfur center is the more commonly observed reaction (3, 4, 8, 9). The reagent is also proposed as the donor of bromonium ion to electron-rich centers (5, 9). As shown by the reaction patterns, the reagents are versatile, but that also causes diversity of products. In some cases, control of the reaction conditions can promote a single reaction pathway enabling the reagents to be useful in synthetic chemistry.

$$Me_2\overset{+}{S}-Br + XH \rightarrow Me_2\overset{+}{S}-X + HBr$$

$$XH = R-OH\ (3);\ R_2NH\ (8),\ H_2C(CO_2R)_2\ (4),\ \text{epoxide}\ (9)$$

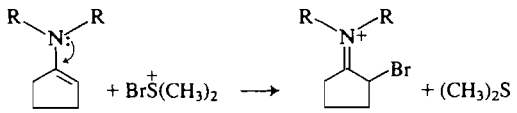


In pursuit of the application of dimethylbromosulfonium bromide in synthesis, we quite unexpectedly found that the reagent reacted efficiently and cleanly with certain α,β-unsaturated carbonyl compounds but not so efficiently with others. Our curiosity was further aroused by the fact that while the reagent was assumed to be an electrophile, it added efficiently to a so-called electron-poor conjugated double bond, in a manner very similar to electrophilic reactions. The addition reaction also led us to discover a simple way of preparing certain α-bromo-α,β-unsaturated carbonyl compounds in high yields and purity. This paper describes the chemistry pertaining to the synthetic processes and discusses the mechanism of the reactions.

## Results

While the yellow solid bromodimethylsulfonium bromide, $(CH_3)_2S \cdot Br_2$ (**1**), could be prepared by mixing dimethyl sulfide and bromine in an inert solvent, it was more convenient to make it in acetonitrile and react it with α,β-unsaturated

0008-4042/82/172268-06$01.00/0
©1982 National Research Council of Canada/Conseil national de recherches du Canada

Can. J. Chem. Downloaded from www.nrcresearchpress.com by 210.87.254.5 on 09/06/12
For personal use only.

carbonyl compounds (**2**) *in situ* at temperatures lower than zero degrees. The rate of the reaction varied under these conditions depending on the degree of steric crowding and could be visually monitored by the changing of the yellow precipitate to a colorless solid which was identified as an α-bromo-β-dimethylsulfonium carbonyl compound (**3**). The sulfonium adducts **3** were stable enough at room temperature to be isolated and characterized by spectroscopic methods but not sufficiently stable for recrystallization. In aqueous solution the sulfonium adducts **3** underwent decomposition giving α-bromo enones **4** as the sole or the major product. However, simple dissolution of sulfonium adducts **3** in aqueous sodium bicarbonate solution resulted in a base catalyzed elimination of the α-proton and dimethylsulfide to provide, after extraction, excellent yields of practically pure α-bromo enones **4**.

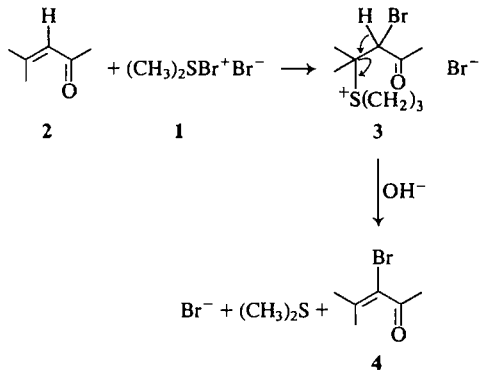


The overall reaction could be represented by the scheme shown above. The yields and spectroscopic parameters of the sulfonium adducts **3** and bromo enones **4** prepared by this process are summarized in Tables 1 and 2. Simplicity of operation, good yields of products, and the absence of by-products characterize this procedure as a superior method over the direct addition of bromine and base-catalyzed elimination to introduce the α-bromo group into certain α,β-unsaturated carbonyl compounds. The latter method (10–13) generally yields some by-products and requires distillation and recrystallization to obtain the reasonably pure products. In addition, several stereochemical features associated with the course and the products of the addition and elimination require some comments.

The reactions of $(CH_3)_2S \cdot Br_2$ with vinylmethyl ketone and acrolein were instantaneous even at −40°C, as judged by the disappearance of the yellow solid, whereas those with mesityl oxide and 2-cyclohexenenone were slow and only reasonably rapid in the vicinity of 0°C. The reaction with other enones 3-penten-2-one, crotonaldehyde, and 2-cyclopentenone was rapid at intermediate temperatures, e.g., at −10°C to ≈ −20°C. These observations clearly indicated the operation of steric crowding during the course of addition. The sulfonium adducts derived from acrolein and crotonaldehyde showed no (or superficial) carbonyl peaks but strong hydroxyl absorptions in the 3500 $cm^{-1}$ region and were consistent with the *gem*-diol structure shown in **6** and **8**. This conclusion was supported by the lack of aldehydic signals in the 9–10 ppm region of the nmr spectra. However, in both cases, the sulfonium group was eliminated easily in the presence of bicarbonate, presumably occurring from the minor component of the aldehydic form in equilibrium with the hydrated form in solution. In aqueous solution, most of the sulfonium adducts **3** eliminated the sulfonium group slowly over a period of several days, except for **11** which, under nmr measurement conditions, did so rapidly to give 2-bromo-2-cyclopentenone **18**. While **9** is stable in storage, the copious amounts of **9** formed during the addition slowly decomposed when stirred at room temperature, by elimination of the sulfonium group, to give **16**, indicating steric acceleration. This may account for a lower yield of **18** (30–40%) when reaction was run at room temperature for a longer period.

The rates of $(CH_3)_2S \cdot Br_2$ addition to conjugated enones were significantly slower in less polar solvents. For example, the addition to acrolein in methylene chloride did not take place unless warmed to room temperature and took ten hours for the yellow color to disappear. It gave poorer yields of adduct **6**. In carbon tetrachloride the reaction was too slow at room temperature to be practical. The same trend was noted in the addition to mesityl oxide. In these cases, trimethylsulfonium bromide ($(CH_3)_3S^+Br$, singlet at 2.90 ppm) was formed in significant amounts.

The addition of $(CH_3)_2S \cdot Br_2$ to some conjugated enones naturally led to the question of the stereochemistry of the resulting sulfonium adducts which were, in turn, related to the stereochemical course of the reaction. While the stereochemistry of sulfonium adduct **11** could not be determined due to its instability in solution, that of 2-bromo-3-sulfonium cyclohexanone **10** obviously had the *trans*-configuration (diequatorial) as shown by the nmr doublet at 4.38 ppm with $J = 10$ Hz. However, the presence of ≈5% of

TABLE 1. The addition of $(CH_3)_2SBr^+ \cdot Br^-$ to enones

| Olefins | Adducts[a] | % Yields Melting point (°C) | Infrared ($cm^{-1}$)[b] | Nuclear magnetic resonance (ppm)[c] |
|---|---|---|---|---|
| Vinylmethyl ketone | $CH_2$—$CHBrCOCH_3$ <br> $^+S(CH_3)_2$ <br> **5** | 84 <br> 103–106 (dec.) | 1720 | 5.24 (t, 1H, 6Hz), 4.02 (d, 2H, 6 Hz), 3.08 (s, 3H), 3.02 (s, 3H), 2.47 (s, 3H) |
| Acrolein | $CH_2$—$CHBrCHO$[d] <br> $^+S(CH_3)_2$ <br> **6** | 88 <br> 70–75 (dec.) | 3500 | 5.25 (d, 1H, 4 Hz), 4.45 (m, 1H), 3.96 (m, 2H), 3.06 (s, 3H), 3.02 (s, 3H) |
| 3-Penten-2-one | $CH_3CH$—$CHBrCOCH_3$[f] <br> $^+S(CH_3)_2$ <br> **7** | 92 <br> 58–61 (dec.) | 1735 | 5.34 (d, 1H, 4 Hz), 4.25 (dq, 1H, 6.5 and 4 Hz), 3.02 (s, 3H), 3.00 (s, 3H), 2.52 (s, 3H), 1.59 (d, 3H, 7 Hz) |
| Crotonaldehyde | $CH_3CH$—$CHBrCH(OH)_2$[e] <br> $^+S(CH_3)_2$ <br> **8** | 91 <br> 51–54 (dec.) | 3500 | 5.27 (d, 1H, 5 Hz), 4.45 (m, 1H), 4.15 (m, 1H), 3.00 (s, 6H), 1.65 (d, 3H, 6.5 Hz) |
| Mesityloxide | $(CH_3)_2C$—$CHBrCOCH_3$ <br> $^+S(CH_3)_2$ <br> **9** | 68 <br> 95–98 (dec.) | 1715 | 5.15 (s, 1H), 2.92 (s, 3H), 2.90 (s, 3H), 2.50 (s, 3H), 1.74 (s, 6H) |
| 2-Cyclohexenone | 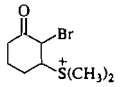 <br> **10** | 96 <br> 45–47 | 1730 | 4.38 (d, 1H, 10 Hz), 4.03 (m, 1H), 2.97 (s, 3H), 2.86 (s, 3H), 1.6–2.4 (m, 6H) |
| 2-Cyclopentenone | 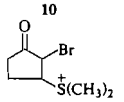 <br> **11** | 96 <br> 51–52 | 1755 | 3.32 (s), 3.11 (s)[g] |

[a] The adducts were isolated as sulfonium bromides and their ir and nmr spectra were given.
[b] The ir spectra were taken in Nujol or as KBr pellets.
[c] The nmr spectra were taken in $D_2O$ using DSS as an internal standard.
[d] In $CF_3CO_2H$, it showed signals at 9.38 (broad s, 1H), 5.19 (t, 1H, 5 Hz), 4.10 (d, 2H, 5 Hz), 3.25 (s, 3H), 3.18 (s, 3H).
[e] The spectrum also showed weak signals at 5.30 (d, $J = 5$ Hz), 2.92 (s), 1.65 (s) for the minor isomer. In $CF_3CO_2H$ it showed two sets of signals in a 1:1 ratio.
[f] On standing at the room temperature, there emerged another set of signals at 5.18 (d, 4 Hz), 4.10 (m), 3.02 (s), 2.88 (s), 2.52 (3), 1.64 (d, 7 Hz).
[g] On dissolution in $D_2O$, the compound eliminated $(CH_3)_2S$ spontaneously and showed weak signals of these two singlets corresponding to the dimethylsulfonium group.

another isomer was suggested by a small spike at 3.00 ppm (for a $CH_3S^+$-signal). Sulfonium adduct **8** showed a major and minor set of nmr signals in $D_2O$ corresponding to the *erythro* and *threo* diastereoisomers. In trifluoroacetic acid, however, the two sets of signals were in the ratio of nearly 1:1. While 3-penten-2-one contained *trans* and *cis* isomers in a 10:1 ratio as shown by the nmr spectra, its sulfonium adduct **7** showed only one set of $^1H$ nmr signals in $D_2O$. This solution developed another set of signals, reaching a 1:1 ratio in two weeks. In trifluoroacetic acid solution, the change was much faster, reaching the equilibrium in four days. Assuming that the two sets of signals were derived from *erythro* and *threo* diastereoisomers, we must conclude isomerization occurred in solution. *It was noteworthy that the isomerization of 7 in $D_2O$ solution was not accompanied by deuterium exchanges at the α- and β-position.*

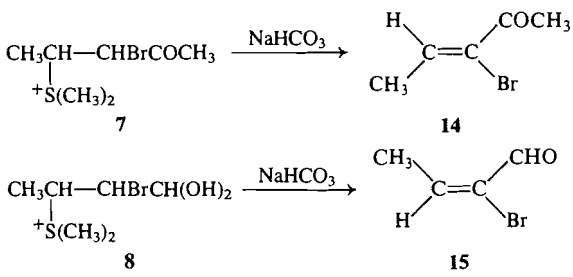


7 **14**

8 **15**

The base-promoted elimination of sulfonium adducts **7** and **8** also generates geometrical isomers of α-bromo enones **14** and **15**. The crude product obtained from base treatment of **8** showed a clear nmr spectrum in carbon tetrachloride for the single isomer **15**. The doublet at 2.14 ppm and the quartet at 7.18 ppm allowed us to assign the structure as shown. Another set of nmr signals developed gradually, reaching a 1:1 ratio after 3 days. This set

Can. J. Chem. Downloaded from www.nrcresearchpress.com by 210.87.254.5 on 09/06/12
For personal use only.

TABLE 2. Spectral data of α-bromo enones[a]

| Compounds | Yield (%) | Infrared ($cm^{-1}$) | $^1H$ nuclear magnetic resonance (ppm) | $^{13}C$ nuclear magnetic resonance (ppm) | Mass spectra (*m/e*, %) |
|---|---|---|---|---|---|
| $CH_2$=CBrCOCH$_3$ **12** | 85 | 1710<br>1614 | 6.80 (d, 1H, 2 Hz),<br>6.32 (d, 1H, 2 Hz),<br>2.44 (s, 3H) | 190.3 (s),<br>132.1 (s),<br>128.6 (t), 26.4 (q) | 150(100), 148(99),<br>135(25), 133(27),<br>107(50), 105(52),<br>43(74) |
| $CH_2$=CBrCHO **13** | 51[f] | 1716<br>1603<br>2760 | 9.22 (s, 1H), 6.83,<br>6.77 (ABq, 1.9 Hz) | 184.4 (d),<br>133.4 (s),<br>134.8 (t) | 136(92), 135(17),<br>134(100), 133(14),<br>108(21), 106(17),<br>107(23), 105(25),<br>54(14) |
| 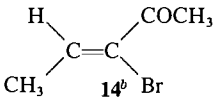 **14**[b] | 84 | 1700<br>1615 | 7.18 (q, 1H, 6.8<br>Hz), 2.39 (s, 3H),<br>1.99 (d, 3H, 6.8<br>Hz) | 190.0 (s),<br>129.1 (s),<br>139.2 (d),<br>27.0 (q), 18.5 (q) | 164(93), 162(100),<br>149(93), 147(89),<br>121(42), 119(40),<br>43(69), 39(41) |
| 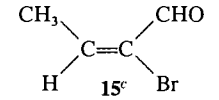 **15**[c] | 86 | 1720<br>1630<br>2730 | 9.17 (s, 1H), 7.18<br>(q, 1H, 6.8 Hz),<br>2.14 (d, 3H, 6.8<br>Hz) | 184.8 (d),<br>131.0 (s),<br>149.2 (d), 18.3 (q) | 150(100), 148(95),<br>149(22), 147(20),<br>121(16), 119(18),<br>69(33), 41(25),<br>39(45) |
| $(CH_3)_2$C=CBrCOCH$_3$ **16** | 94 | 1690 | 2.42 (s, 3H),<br>2.08 (s, 3H), 2.03<br>(s, 3H) | 194.4 (s),<br>118.7 (s),<br>144.7 (s), 30.1 (q),<br>27.6 (q), 23.5 (q) | 178(76), 176(73),<br>163(92), 161(100),<br>135(20), 133(22),<br>67(18), 53(46),<br>43(50) |
| **17**[d] | 92 | 1705<br>1605 | 7.26 (6, 1H, 4.5<br>Hz), 2.50 (m, 4H),<br>2.08 (m, 2H) | 188.6 (s),<br>125.1 (s),<br>149.4 (d),<br>38.7 (t), 28.8 (t),<br>23.9 (t) | 176(80), 174(80),<br>148(92), 146(100),<br>135(25), 133(28),<br>120(32), 118(36),<br>67(60), 55(26),<br>39(20) |
| **18**[e] | 93 | 1732<br>1597 | 7.27 (t, 1H, 3<br>Hz), 2.67 (m,<br>2H), 2.44(m,<br>2H) | 199.1 (s),<br>127.4 (s),<br>160.3 (d), 32.4 (t),<br>28.4 (t) | 162(100), 160(95),<br>134(38), 132(35),<br>81(23), 43(91) |

[a]The ir and nmr spectra were recorded in $CCl_4$ solution; for the latter TMS was used as an internal standard. The molecular ion peaks gave the correct molecular weight by high resolution mass spectrometry.
[b]In $CCl_4$ solution, the $^1H$ nmr spectrum exhibited weak signals (10%) for the minor component at 6.42 (q, 6.8 Hz), 2.60 (s), 2.00 (d, 6.8 Hz); no isomerization occurred under the conditions (10).
[c]In $CCl_4$ solution, the $^1H$ nmr spectrum showed signals for the minor component at 9.40 (s), 7.50 (q, 7 Hz), 2.01 (d, 7 Hz); the ratio of the corresponding signals reached 1:1 in 3 days.
[d]Melting point 68–69°C (lit. (11) mp 69–71°C).
[e]Melting point 34–35°C (lit. (12) mp 39–39.5°C).
[f]The low yield arose from volatility of **13** (13).

showed a singlet at 9.40 ppm, a quartet at 7.50, and a doublet at 2.01 ppm, and was assigned to the structure with alternative geometry isomeric to **15**. On the contrary, the elimination of the sulfonium group from **7** gave **14** as the major product, with about 10% of the alternative isomer as shown by gc–ms and $^1H$ nmr. The latter was more volatile and easily removed by evaporation. Compound **14** was stable in $CCl_4$ solution.

The reagent $(CH_3)_2S \cdot Br_2$ reacted with cinnamaldehyde slowly at 0°C (but not at −30°C) and with ethyl cinnamate only at room temperature to give dibromo adducts without a trace of the sulfonium adducts. The reagent failed to add to isophorone and maleic anhydride and reacted sluggishly with 4-cholesten-3-one. In the presence of ethyl acrylate, the reagent reacted very slowly at 0°C and gave a complex mixture.

## Discussion

The addition of $(CH_3)_2S \cdot Br_2$ to α,β-unsaturated carbonyl compounds is characterized by some unusual observations. Firstly, the addition occurs very rapidly even at −40°C in solid–solution mixture. Secondly, the rates of the addition are very sensitive to steric control, as seen by the failure to add to isophorone and 4-cholesten-3-one, and to electronic factors, as seen by the sluggish addition to conjugated esters. Thirdly, the reagent behaves as a bromine addition reagent with phenyl

Can. J. Chem. Downloaded from www.nrcresearchpress.com by 210.87.254.5 on 09/06/12
For personal use only.

Can. J. Chem. Downloaded from www.nrcresearchpress.com by 210.87.254.5 on 09/06/12
For personal use only.

conjugated α,β-unsaturated carbonyl compounds. Fourthly, the reagent completely fails to react with maleic anhydride which is brominated readily by $Br_2$ in carbon tetrachloride (14). Fifthly, the addition is dramatically retarded in less polar solvents such as methylene chloride. Finally, the addition is regiospecific, giving α-bromo-β-sulfonium carbonyl compounds, and stereoselective, giving predominantly one isomer where relevant. The evidence described above appears to indicate that the addition occurs by a mechanism of brominium ion initiated electrophilic addition to the conjugated double bond (15), or that of dimethylsulfide initiated nucleophilic attack at the β-carbon similar to the Michael type 1,4-addition. However, the attack of bromonium ion at the electron deficient olefinic bond of enones is not likely, nor is the manifested reactivity order in agreement with such an assumption. The latter idea suffers from the assumption that dimethylsulfide attacks at a disubstituted β-olefinic carbon in the mesityl oxide case; indeed, dimethylsulfide initiated addition is unknown as far as we are aware.

Alternatively, one may consider the sulfide cation radical (16) as the reactive species which initiates the addition by a chain process. Such a radical mechanism also suffers from inadequacy to explain dramatic solvent effects. Nor is it reasonable to use the sulfide cation radical to attack the β-carbon of a conjugated enone system. We have observed that the presence of air does not substantially alter the addition product pattern; this observation rules out the possibility of a radical mechanism.

The clue to the addition mechanism may rest on the reactivity order in which conjugated aldehydes react faster than conjugated ketones which, in turn, react faster than conjugated esters; that is, the more basic substrates react faster. It has been demonstrated that the addition of bromine to α,β-unsaturated ketones, aldehydes, and esters (and also other electron withdrawing groups) is catalyzed by acids involving the attack of the bromide (or an anionoid) at the β-carbon as the rate determining step (17). Reactivity is in the order of acrolein > crotonaldehyde >> cinnamaldehyde > ethyl cinnamate (18). We propose a similar mechanism as shown below to account for the addition. The reaction is initiated by the electrophilic attack of the brominium ion at the carbonyl oxygen to give the intermediate **19**. Such a mechanism can account for the observed regiospecificity and acceleration of the addition in polar solvent. In this mechanism the stereochemistry of the sulfonium adduct **3** is determined by tautomerization of the enol hypobromite **20** to **3** and may involve the attack of a bromide anion as a possible pathway. Therefore, irrespective of the *cis–trans* geometry of conjugated enones, the stereochemistry of the adducts **3** should be the same as determined by the tautomerization process as shown in the addition to 3-penten-2-one to give the single isomer **14**. It follows that the carbonyl group of conjugated esters is not as electron rich as that of conjugated enones to interact with $(CH)_2S—Br^+$ and therefore does not lead to a successful addition. Recently, the addition of bromine to conjugated enones has been reinvestigated in methylene chloride and from the reactivity pattern a similar mechanism has been proposed (19).

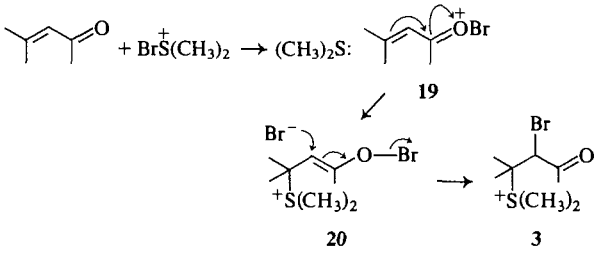


20 3

The observed isomerization of sulfonium adducts **7** and **8** from one diastereoisomer to the other in $D_2O$ solution must involve the breaking and reformation of a bond at a chiral center. That this bond is not a C—H bond at the α and β chiral carbon centers is demonstrated by the lack of deuterium exchange in $D_2O$. A mechanism involving unsymmetrically bridged bromonium ions **21** and **22** may account for the isomerization. The isomerization of **7** occurs much faster in trifluoroacetic acid and, indeed, **8** also isomerizes in this solvent.

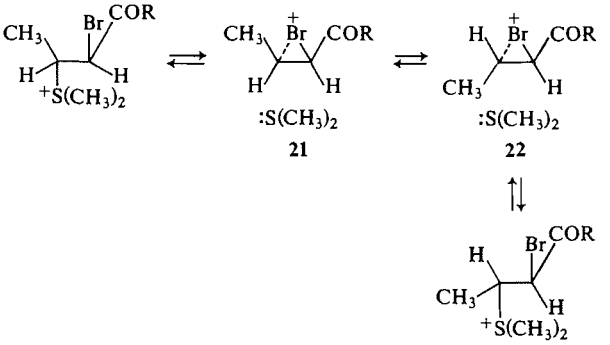


21 22

The base-promoted elimination of sulfonium adduct **3** is most likely to occur by an E1cb mechanism via the anion **23** and, thus, the stereochemistry of α-bromoenone **4** is determined by the stereoelectronic balance around the developing double bond. This mechanism can account for the elimination of diastereomeric

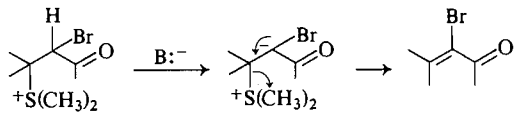


3 23 4

mixtures of **8** to give only one isomer **15** which rearranged slowly in carbon tetrachloride solution. In contrast, **14** is stable under similar conditions. Conjugated enones with the α-bromo group are versatile dienophiles in the Diels–Alder reaction, giving highly regiospecific adducts (20–24).

## Experimental

Melting points were uncorrected. Reported nmr spectra were recorded on a Varian EM-360 or a Varian XL-100 and ir spectra with a Perkin–Elmer 457 spectrophotometer. Mass spectra were obtained with a Hewlett–Packard 5985 spectrometer. Gas chromatography was performed on a Varian 1400 instrument equipped with a SE-30 capillary column (45 ft × 0.28 mm). Reagent grade solvents were redistilled, and other chemicals were C.P. grade materials as supplied from commercial sources.

*Preparation of dimethylbromosulfonium bromide*

To a solution of dimethylsulfide (10 mL, 130 mmol) in methylene chloride (100 mL) cooled to −40°C under nitrogen, a bromine (15.01 g, 94 mmol) solution in methylene chloride (30 mL) was added in 30 min. A yellow precipitate formed immediately. The mixture was stirred for 10–20 min and ether (100 mL) was added. The precipitate was filtered, and washed with ether and pentane to afford bromodimethylsulfonium bromide (19.0 g, 91%).

*Addition of dimethylbromosulfonium bromide to conjugated enones*

Generally, the salt was formed *in situ* for the addition reaction. To a solution of dimethyl sulfide (1 to 2 mol equivalent) in acetonitrile (50–100 mL), cooled under nitrogen, a solution of bromine (≈ 20–100 mmol) in carbon tetrachloride (5 mL) was added, dropwise, at −40°C. The yellow precipitate was stirred at this temperature for 5 min and an enone (≈ 1–1.5 equivalent) was injected. Unhindered enones, such as vinylmethyl ketone or acrolein, reacted immediately at this temperature to give a colorless precipitate. Hindered carbonyl compounds, such as mesityloxide and 2-cyclohexenone, reacted at 0°C in 10–20 min to afford a colorless precipitate. To the mixture, ether (100 mL) was added. The precipitate was filtered and washed with ether and pentane and dried. The solid was generally stored in a freezing compartment.

*Preparation of 2-bromo-α,β-unsaturated carbonyl compounds*

A sulfonium salt (5–20 mmol) obtained from the above preparation was dissolved in 5% sodium bicarbonate solution (50–100 mL). The mixture was warmed for 10–15 min at room temperature and was extracted with methylene chloride. The methylene chloride solution was washed with water, dried, and evaporated to give the α-bromo enone. The product was pure enough to obtain the spectra shown in Table 2, but could be recrystallized or distilled. All α-bromo enones showed very intense molecular ion peaks which showed correct molecular weight by high resolution mass spectrometry.

*Synthesis of α-bromoacrolein (an example)*

Dimethylsulfide (5 mL) in acetonitrile (100 mL) was cooled at −40°C under nitrogen. Bromine (6 g) in carbon tetrachloride (5 mL) was added at −40°C to give the yellow precipitate. To this mixture acrolein (3 mL) was injected at −40°C, at which the yellow precipitate was changed to a white precipitate immediately. Ether (100 mL) was added to the mixture. The precipitate was filtered, washed, and dried on filter paper to give a white solid (8.0 g), mp 70–75°C(dec.). The solid was dissolved in water (50 mL) containing sodium bicarbonate (4.0 g). After warming up to 35°C for 15 min, the mixture was extracted with methylene chloride. The methylene chloride solution was worked up as usual and distilled over a short Vigreux column. The residue was distilled under a water pump vacuum to afford colorless α-bromoacrolein (1.85 g, 48% based on bromine); 45°C/25 Torr.

## Acknowledgement

The authors are indebted to the Natural Sciences and Engineering Research Council of Canada for generous support of this project.

1. C. F. Boberg, C. Winter, and G. R. Schultz. Chem. Ber. **89**, 160 (1965).
2. H. Bohme and E. Ball. Z. Anorg. Allg. Chem. **290**, 17 (1957).
3. N. Furukawa, T. Inoue, T. Aida, and S. Oae. J. Chem. Soc. Chem. Commun. 212 (1973).
4. N. Furukawa, T. Inoue, T. Aida, T. Akasaka, and S. Oae. Phosphorus Sulphur, **4**, 15 (1978).
5. G. A. Olah, Y. D. Vankar, M. Arvanaghi, and G. K. Surya Prakash. Synthesis, 721 (1979).
6. G. Allegra, G. E. Wilson, Jr., E. Beneketti, C. Pedone, and R. Albert. J. Am. Chem. Soc. **92**, 4002 (1970).
7. R. Manavu. J. Org. Chem. **45**, 3361 (1980).
8. P. G. Gassman, T. J. van Bergen, and G. Gruetzmacher. J. Am. Chem. Soc. **95**, 6508 (1973).
9. G. A. Olah, Y. D. Vankar, and M. Arvanaghi. Tetrahedron Lett. 3653 (1979).
10. C. H. Nield. J. Am. Chem. Soc. **67**, 1145 (1945).
11. F. G. Bordwell and K. M. Wellman. J. Org. Chem. **28**, 2544 (1963).
12. G. L. Dunn, V. J. DiPasquo, and J. R. E. Hoover. J. Org. Chem. **33**, 1454 (1968).
13. R. H. Baker, S. W. Tinsley, D. Butler, and B. Rigel. J. Am. Chem. Soc. **72**, 393 (1950); V. Rosnati and A. Salimbeni. Gazz. Chim. Ital. **107**, 271 (1977).
14. R. P. Bell and M. Pring. J. Chem. Soc. B, 1119 (1966).
15. F. C. Fahey. Top. Stereochem. **3**, 237 (1968).
16. Y. L. Chow and K. Iwai. J. Chem. Soc. Perkin Trans. II, 931 (1980).
17. P. B. D. de la Mare and P. W. Robertson. J. Chem. Soc. 889 (1945); H. P. Rothbaum, I. Ting, and P. W. Robertson. J. Chem. Soc. 980 (1945).
18. P. B. D. de la Mare and R. Bolton. Electrophilic additions to unsaturated systems. Elsevier Publishing Co., Amsterdam. 1966. p. 22.
19. V. L. Heasley, D. F. Shellhamer, T. L. Carter, D. E. Gipe, R. R. Gipe, R. C. Green, J. Nordeen, T. D. Rampel, and D. W. Spaite. Tetrahedron Lett. 2467 (1981).
20. B. B. Snider. J. Org. Chem. **38**, 3961 (1973).
21. R. Lee and K. Undheim. J. Chem. Soc. Perkin Trans. I, 2049 (1973).
22. E. J. Corey and B. B. Snider. J. Am. Chem. Soc. **94**, 2549 (1972).
23. K. S. Ayyar, R. C. Cookson, and D. A. Kagi. J. Chem. Soc. Chem. Commun. 161 (1973).
24. A. Enger and J. P. Pete. Bull. Soc. Chim. Fr. 1681 (1975).

Can. J. Chem. Downloaded from www.nrcresearchpress.com by 210.87.254.5 on 09/06/12
For personal use only.

# Spin–spin coupling constants as indicators of the conformation of anthrone in solution

TED SCHAEFER, RUDY SEBASTIAN, TIMOTHY A. WILDMAN, AND HEATHER DETTMAN
*Department of Chemistry, University of Manitoba, Winnipeg, Man., Canada R3T 2N2*

Received March 17, 1982

TED SCHAEFER, RUDY SEBASTIAN, TIMOTHY A. WILDMAN, and HEATHER DETTMAN. Can. J. Chem. **60**, 2274 (1982).

The analyses of the $^1$H nmr spectra of fluorene, 2,7-dibromofluorene, and anthrone are reported. The benzylic couplings in these compounds are compared with those in indene and toluene. It is argued that the six-bond and five-bond couplings in anthrone are more compatible with a nonplanar than a planar central ring. The spectrum of the 2,7-dibromofluorene suggest that couplings between protons in different benzenoid rings are small, perhaps no larger than 0.05 Hz.

TED SCHAEFER, RUDY SEBASTIAN, TIMOTHY A. WILDMAN et HEATHER DETTMAN. Can. J. Chem. **60**, 2274 (1982).

On rapporte l'analyse des spectres de rmn du $^1$H du fluorène, du dibromo-2,7 fluorène et de l'anthrone. On a comparé les couplages benzyliques dans ces composés à ceux de l'indène et du toluène. On démontre que les couplages à travers six et cinq liaisons dans l'anthrone sont plus compatibles avec un cycle non plan qu'avec un cycle ayant un plan central. Le spectre du dibromo-2,7 fluorène suggère que les couplages entre protons de différents cycles benzénoides sont petits, peut-être pas plus grands que 0,05 Hz.

[Traduit par le journal]

## Introduction

The recent report of the complete analysis of the $^1$H nmr spectrum of indene, **1**, at 270 MHz (1) prompts an account of our analyses of the $^1$H nmr spectra of fluorene, **2**, and anthrone, **3**, (9,(10H)-anthracenone) at 100 MHz. Although the heavy atom skeletons of **1** and **2** are planar, and although **3**

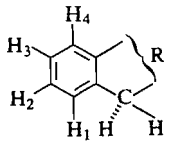


**1** R = HC = CH
**2** R = $C_6H_4$
**3** R = $C_6H_4C$ = O

has been judged as planar by X-ray diffraction (2, 3), and as planar or very nearly planar by Kerr effect studies (4), the long-range spin–spin couplings to the methylene protons reported here for anthrone are most easily interpreted in terms of an inverting boatlike structure for the central ring.

## Experimental

The $^1$H nmr spectrum of a degassed, 10 mol% solution of fluorene in $CS_2$ was calibrated on an HA 100 spectrometer at a probe temperature of 350 K. The calibration and subsequent, interpolated peak frequency, procedure followed that described in detail recently (5). The $^1$H nmr spectrum of a degassed, 3.9 mol% solution of anthrone in $CDCl_3$ was also calibrated in the frequency sweep mode, as was that of a 2.0 mol% solution of 2,7-dibromofluorene in $CS_2$. No nmr evidence was found for anthrol in the former solution.

## Results and discussion

### *Spectral analyses*

The benzenoid ring proton spectra for fluorene and anthrone were analyzed with the computer program LAME (6, 7) with the assumption of no cross-ring coupling. Previous analyses of fluorene, fluorenone, and 1-methylfluorene also made this assumption with success (8–12). For 2,7-dibromofluorene this assumption was unnecessary (LAME-8 analysis) yet no strong evidence for cross-ring couplings could be found,. i.e., between protons in different benzenoid rings.

Figure 1 displays the calculated and observed ring proton spectra for 2,7-dibromofluorene. The observed peaks are somewhat broader (0.15 Hz) than normal and this *may* arise from some cross-ring coupling. The calculated spectrum with no cross-ring coupling agrees well with the observed peaks. Presumably any coupling across the five-membered ring is not larger than ca. 0.05 Hz.

The spectral parameters are found in Table 1.

### *The proton coupling constants within the benzenoid rings*

These couplings for fluorene in Table 1 agree very closely with those in indene (1), the mean difference being $0.04_4$ Hz for six couplings. The corresponding parameters for anthrone are quite different from those in fluorene. Recent rough analyses (13) of the $^1$H nmr spectra of a series of anthracene derivatives suggested that $^3J_{12}$ is 7.99 ± 0.15 Hz for nonplanar and 8.67 ± 0.10 Hz for planar molecules. For anthrone, $^3J_{12}$ was given as 7.5 Hz although nothing was stated about its conformation. In Table 1, the value of $^3J_{12}$ is 7.79(1) Hz, the error being taken as twice the standard deviation.

The benzenoid ring proton couplings expected for a relatively unstrained anthrone molecule might be approximated by those in 2-methylacetophenone (14). Acetophenone is probably planar in

0008-4042/82/172274-04$01.00/0
©1982 National Research Council of Canada/Conseil national de recherches du Canada

Can. J. Chem. Downloaded from www.nrcresearchpress.com by 210.87.254.5 on 09/06/12
For personal use only.

Can. J. Chem. Downloaded from www.nrcresearchpress.com by 210.87.254.5 on 09/06/12
For personal use only.

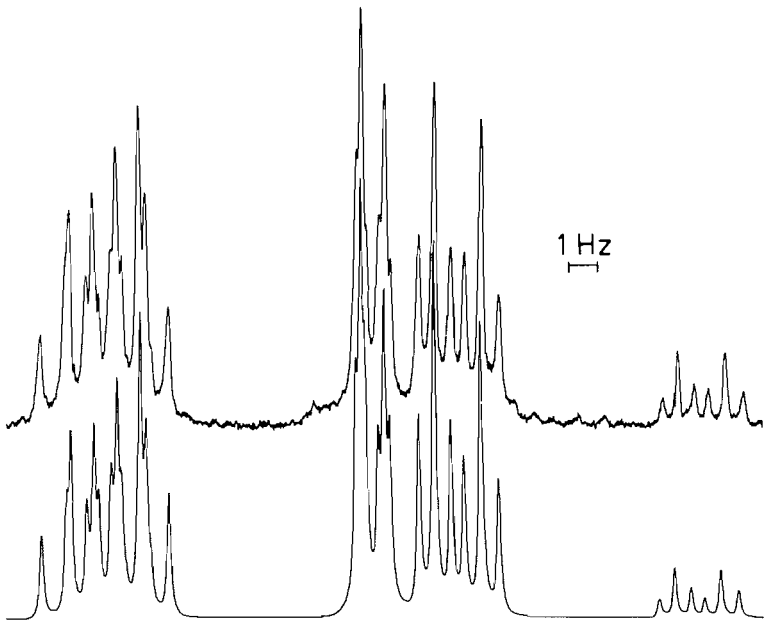


FIG. 1. The observed and calculated benzenoid ring proton spectra of a 2.0 mol% solution of 2,7-dibromofluorene in $CS_2$ at 100 MHz and 305 K. The linewidths at half height are 0.15 Hz, suggesting rather small, $\leq 0.05$ Hz, couplings between protons in different benzenoid rings.

TABLE 1. $^1$H nuclear magnetic resonance spectral parameters for fluorene, 2,7-dibromofluorene, and anthrone at 100 MHz and 305 K

| Parameter | Value | | | Parameter | Value | | |
|---|---|---|---|---|---|---|---|
| $\upsilon_1$ | 729.708(5)[a] | 751.132(3)[b] | 739.116(3)[c] | $^5J_{14}$ | 0.765(6)[a] | 0.538(6)[b] | 0.591(4)[c] |
| $\upsilon_2$ | 710.498(7)[d] | — | 752.692(4) | $^4J_o^{H,CH_2}$ | −0.994(6) | −0.983(5) | −0.927(4) |
| $\upsilon_3$ | 717.235(4) | 737.061(5) | 740.394(3) | $^5J_2^{H,CH_2}$ | 0.159(8) | — | 0.290(5) |
| $\upsilon_4$ | 758.885(4) | 744.395(5) | 831.965(2) | $^5J_4^{H,CH_2}$ | 0.389(6) | 0.371(6) | 0.397(3) |
| $\upsilon CH_2$ | 364.1 | $375.53_2$ | $425.5_8$ | $^6J_p^{H,CH_2}$ | −0.777(10) | −0.741(6) | −0.723(4) |
| $^3J_{12}$ | 7.497(8) | — | 7.790(4) | Peaks | 61 | 30 | 106 |
| $^3J_{23}$ | 7.394(8) | — | 7.269(4) | Transitions | 141 | 53 | 156 |
| $^3J_{34}$ | 7.621(8) | 8.123(5) | 7.947(4) | Assigned | 68 | 49 | 136 |
| $^4J_{13}$ | 1.082(10) | 1.811(6) | 1.235(3) | Rms deviation | 0.015 | 0.012 | 0.014 |
| $^4J_{24}$ | 1.179(9) | — | 1.465(4) | | | | |

[a]Fluorene as a 10 mol% solution in $CS_2$ and shifts in Hz at $100.001_2$ MHz to low field of internal TMS.
[b]A 2.0 mol% solution of 2,7-dibromofluorene in $CS_2$.
[c]Anthrone as a 3.9 mol% solution in $CDCl_3$.
[d]Numbers in parentheses are the standard deviations in the last one or two significant figures.

the ground state (15) but some degree of non-planarity of the heavy-atom skeleton is very likely induced by an *ortho* methyl substituent. The coupling constants (those for anthrone in parentheses) are 7.64(7.79), 7.39(7.27), 7.87(7.94), 1.30 (1.23), 1.44(1.46), and 0.47(0.59) Hz.

*Benzylic couplings*

In toluene the coupling over six bonds, $^6J_p^{H,CH_3}$, is represented by $-1.24 \sin^2\theta$, where $\theta$ is the angle by which the $\alpha$ C—H bond twists out of the benzene plane (16). This behaviour is reproduced almost exactly by INDO MO FPT calculations (17). In ref. 17 it is also implied that $^5J_m^{H,CH_3}$ consists of $\sigma$ and $\pi$ electron components and one may write

$$[1] \qquad {}^5J_m{}^{H,CH_3} = {}^5J^{\pi}{}_{90}\langle \sin^2\theta \rangle + {}^5J^{\sigma}{}_{180}\langle \sin^2(\theta/2) \rangle$$

Experimental data on toluene (18) and *m*-xylene (19,20) suggest $^5J^{\pi}{}_{90}$ as 0.38(4) Hz and $^5J^{\sigma}{}_{180}$ as 0.34(4) Hz. $^5J^{\pi}{}_{90}$ is the counterpart of $^6J^{\pi}{}_{90} = -1.24$ for the six-bond coupling, whereas $^5J^{\sigma}{}_{180}$ is the coupling for an all-*trans* arrangement of the five

Can. J. Chem. Downloaded from www.nrcresearchpress.com by 210.87.254.5 on 09/06/12
For personal use only.

bonds intervening between the *meta* ring proton and the α proton. In toluene both averages over θ in [1] are 0.5.

In indene and fluorene θ is fixed to within small vibrational motions. For fluorene, simple trigonometry and the heavy-atom structure (21) allow the statement that θ varies between 57.9° and 61.5° as the methylene HCH angle ranges between 103.5° and 111.5°. For present purposes, θ will be assigned a value of 60° in fluorene. The same number will be assumed for indene.

$^6J$ in indene is $-0.66_2$ Hz (1), implying $^6J_{90}$ as $-0.88_3$ Hz, whereas in fluorene $^6J$ is $-0.77_7$ Hz, suggesting $^6J_{90}$ as $-1.04$ Hz, $\sin^2\theta$ being 0.75. Both values of $^6J_{90}$ are substantially smaller in magnitude than in toluene. This we take as an indication of ring strain rather than of a reduction caused by the electronegativity of the additional carbon atom attached to the methylene group (there is good evidence (16) that $^6J_{90}$ should not be reduced in magnitude by more than about 0.03 Hz by the presence of a second carbon).

Turning to $^5J$, for fluorene one may write (Table 1)

$$[2] \quad {}^5J_m{}^{H_2,CH_2} = 0.159 = {}^5J^{\pi}{}_{90} \sin^2 60° + {}^5J^{\sigma}{}_{180} \sin^2(60°/2)$$

$$[3] \quad {}^5J_m{}^{H_4,CH_2} = 0.389 = {}^5J^{\pi}{}_{90} \sin^2 120° + {}^5J^{\sigma}{}_{180} \sin^2(120°/2)$$

with the result that $^5J^{\pi}{}_{90}$ is $0.05_9$ Hz and $^5J^{\sigma}{}_{180} = 0.46_0$ Hz. Apparently the π electron contribution to $^5J$ is much smaller than in toluene. Again, the analogous couplings in indene are < 0.05 Hz and 0.20 Hz (1). If the former coupling is zero, then $^5J^{\pi}{}_{90}$ necessarily vanishes and equations of the type [2] and [3] are incompatible. For compatibility, one has $^5J^{\pi}{}_{90} + {}^5J^{\sigma}{}_{180} = 0.27$ Hz and the minimum magnitude of $^5J^{\pi}{}_{90}$ must be $0.06_6$ Hz if it is to be positive. However, the two couplings are then calculated as $0.10_0$ and $0.20_4$ Hz. Now, INDO MO FPT calculations on indene (1) yield reasonable values for $^4J_o{}^{H,CH_2}$ and $^6J_p{}^{H,CH_2}$. Normally, such calculations overestimate the *magnitude* of $^5J_m{}^{H,CH_2}$. For indene, they yield the two couplings as 0.21 and 0.55 Hz. Then $^5J_{90}$ and $^5J_{180}$ follow as 0.05 and 0.68 Hz, again emphasizing the very small π electron contributions to $^5J$ in indene and fluorene in contrast to experimental and theoretical indications for toluene. Whether peculiar coupling paths or some other mechanism could account for these results is unknown. It may be noted that the ratios of $^4J_o/^6J_p$ for these π electron dominated couplings are 0.80 ± 0.02 for indene, fluorene, toluene, and anthrone.

For anthrone, $^6J_p{}^{H,CH_2}$ is $-0.72_3$ Hz. If the molecule is planar, then $^6J_{90}$ is $-0.96_4$ Hz, a value much smaller in magnitude than in toluene, $-1.2_4$ Hz, or even fluorene, $-1.0_4$ Hz. Such a situation seems rather unlikely. However, if anthrone exists in the boat form which inverts rapidly on the nmr time scale, as does 9,10-dihydroanthracene (22, 23), then the extreme boat conformation is one in which one C—H bond of the methylene group has θ as ca. 90° and the other C—H bond has θ as ca. 30°. Rapid inversion between the two equivalent boat forms yields $\langle \sin^2\theta \rangle$ as 0.5 ($\sin^2 90° + \sin^2 30°$) or 0.625. Then $^6J_{90}$ becomes $-0.723/0.625$ or $-1.1_6$ Hz, a value much more consistent with that expected for an α-alkyl toluene (16) and for a central six-membered ring in anthrone.

Equations of type [2] and [3] yield $^5J^{\pi}{}_{90}$ as $0.35_2$ Hz and $^5J^{\sigma}{}_{180}$ as $0.24_7$ Hz for an inverting boat structure of anthrone. These numbers predict $^5J^{H,CH_3}$ as 0.30 Hz in toluene, whereas the observed value is 0.36 ± 0.02 Hz. Of course, according to the arguments above, this observed value should be somewhat larger because of the larger π (and possibly σ) electron contribution in toluene.

Again, in ethylbenzene $^5J_m{}^{H,CH_2}$ is 0.28 Hz (24). $^6J_p{}^{H,CH_2}$ is (−)0.45 Hz, implying (16) $\langle \sin^2\theta \rangle$ as 0.45/1.22 or 0.369. The π contribution to $^5J$ is then 0.369 × 0.352 or 0.130 Hz. This molecule prefers a conformation in which the $CH_3$ group lies in a plane perpendicular to the benzene plane (25*a*). If this were a fixed conformation, $\sin^2(\theta/2)$ averaged over the two methylene protons would be $\{\sin^2(150°/2) + \sin^2(30°/2)\}/2$ or 0.500. Free rotation would also yield an average of 0.5. Approximately then, the σ contribution to $^5J_m$ is 0.5 × 0.247 or 0.123 Hz, yielding a total $^5J_m{}^{H,CH_2}$ of $0.25_3$ Hz, perhaps within or very near the combined experimental error of all the measurements.

By way of contrast, assumption of a planar anthrone molecule yields $^5J^{\pi}{}_{90}$ and $^5J^{\sigma}{}_{180}$ as $0.31_5$ and $0.21_4$ Hz, respectively, a $^5J_m{}^{H,CH_3}$ in toluene of 0.26 Hz, and a $^5J_m{}^{H,CH_2}$ of 0.22 Hz in ethylbenzene, rather far from the observed couplings.

Now, as emphasized by a referee, the preceding derivation of $^6J_{90}$ as $-1.1_6$ Hz in anthrone assumes rapid inversion between boat conformations and also that conformations lying on the inversion path have negligible populations. An alternative hypothesis assumes a planar conformation with large amplitude vibrations, of the sort implied by recent molecular mechanics calculations on 9,10-dihydroanthracene (25*b*). Were anthrone to behave similarly, the molecular mechanics results in Fig. 3 of ref. 25*b* imply that the proper average value of $\sin^2\theta$ is, approximately, $\int_{\pi/6}^{\pi/2} \sin^2\theta d\theta$ or 0.740. Then

Can. J. Chem. Downloaded from www.nrcresearchpress.com by 210.87.254.5 on 09/06/12
For personal use only.

$^6J_{90}$ is $-0.723/0.740$ or $0.97_7$ Hz. The arguments above would reject this hypothesis. Similar remarks apply to the somewhat steeper energy profiles calculated by molecular orbital methods (25*b*).

Our central assumption, that $^6J_{90}$ in anthrone is larger in magnitude than in fluorene and that, indeed, it is closer to the magnitudes in toluene and its α-substituted derivatives, therefore suggests a double minimum potential for the inversion of anthrone in solution. Furthermore, the assumption implies that the barrier to inversion be somewhat larger than $kT$ at ambient temperatures.

This rather bold suggestion may be wrong. Nevertheless, it may have sufficient merit to interest those spectroscopists specializing in the interpretation of relatively low frequency vibrational bands.

*The X-ray data*

The anthrone crystal, although structurally disordered, has been studied extensively by X-ray diffraction (2, 3). Apparently, the molecule is planar in the solid. A large out-of-plane libration of the oxygen atom occurs (3). A boatlike central ring exists in crystals of 10-bromoanthrone (26). In 9,10-dihydroanthracene, successive substitution at the 9,10 positions can induce increased flattening of the central ring (23, 27). Packing forces in the crystal could be sufficient to perturb derivatives of 1,4-dihydrobenzene from their equilibrium geometry (28). Whether such perturbations occur for anthrone is a point of interest.

## Conclusions

The benzylic couplings in anthrone are most naturally interpreted in terms of an inverting, nonplanar, central ring. Additional evidence might be provided by experiments on geminal proton–proton coupling constants of the kind performed by Fraser and co-workers (29) on related compounds. The benzylic couplings in 9,10-dihydroanthracenes and 1,4-dihydronaphthalenes are needed to provide a necessary complement to homoallylic couplings (23, 30, 31) as conformational markers. Their extraction requires a more powerful spectrometer than used in this study.

## Acknowledgments

We are grateful to the Natural Sciences and Engineering Research Council of Canada for financial assistance and also thank a referee for some cogent criticism.

1. H. Nies and D. Rewicki. J. Magn. Reson. **46**, 138 (1982).
2. S. N. Srivastava. Indian. J. Phys. **46**, 56 (1972).
3. H. D. Flack. Philos. Trans. R. Soc. London Ser. A, **266**, 561 (1970); 583 (1970).
4. M. J. Aroney, G. Cleaver, R. J. W. LeFèvre, and R. K. Pierens. J. Chem. Soc. London B, 82 (1971).
5. T. Schaefer and R. Sebastian. J. Magn. Reson. **41**, 395 (1980).
6. S. Castellano and A. A. Bothner-By. J. Chem. Phys. **41**, 3863 (1964).
7. C. W. Haigh. Ann. Rep. NMR Spectrosc. **4**, 311 (1971).
8. J. Douris and A. Mathieu. Bull. Soc. Chim. Fr. 3365 (1971).
9. D. W. Jones, R. S. Mathews, and K. D. Bartle. Spectrochim. Acta Part A, **28**, 2053 (1972).
10. J. A. G. Drake and D. W. Jones. Spectrochim. Acta Part A, **36**, 23 (1980).
11. J. B. Stothers, C. T. Tan, and N. K. Wilson. Org. Magn. Reson. **9**, 408 (1977).
12. J. A. G. Drake and D. W. Jones. Org. Magn. Reson. **14**, 272 (1980).
13. N. E. Sharpless, R. B. Bradley, and J. A. Ferretti. Org. Magn. Reson. **6**, 115 (1974).
14. W. B. Smith, D. L. Deavenport, and A. M. Ihrig. J. Am. Chem. Soc. **94**, 1959 (1972).
15. D. Mirarchi and G. L. D. Ritchie. Aust. J. Chem. **34**, 1443 (1981).
16. W. J. E. Parr and T. Schaefer. Acc. Chem. Res. **13**, 400 (1980).
17. R. Wasylishen and T. Schaefer. Can. J. Chem. **50**, 1852 (1972).
18. M. P. Williamson, R. Castellano, and S. M. Castellano. J. Chem. Phys. **49**, 2218 (1968).
19. C. J. Macdonald and W. F. Reynolds. Can. J. Chem. **48**, 1002 (1970).
20. J. B. Rowbotham and T. Schaefer. Can. J. Chem. **52**, 489 (1974).
21. D. M. Burns and J. Iball. Proc. R. Soc. London Ser. A, **227**, 200 (1955).
22. W. B. Smith and B. A. Shoulders. J. Phys. Chem. **69**, 2022 (1965).
23. P. W. Rabideau. Acc. Chem. Res. **11**, 141 (1978), and references therein.
24. W. E. Hull. To be published.
25(*a*). T. Schaefer, L. Kruczynski, and W. Niemczura. Chem. Phys. Lett. **38**, 498 (1976). (*b*) K. B. Lipkowitz, P. W. Rabideau, D. J. Raber, L. E. Hardee, P. v. R. Schleyer, A. J. Kos, and R. A. Kahn. J. Org. Chem. **47**, 1002 (1982).
26. R. Destro, T. B. D'Alfonso, and M. Simonetta. Acta Crystallogr. Part B, **29**, 2214 (1973).
27. D. K. Dalling, K. W. Zilm, D. M. Grant, W. A. Heeschen, W. J. Horton, and R. J. Pugmire. J. Am. Chem. Soc. **103**, 4817 (1981).
28. M. J. Bennett, J. T. Purdham, S. Takada, and S. Masamune. J. Am. Chem. Soc. **93**, 4063 (1971).
29. R. N. Renaud, J. W. Bovenkamp, R. R. Fraser, and R. Capoor. Can. J. Chem. **55**, 2642 (1977).
30. M. C. Grossel and M. J. Perkins. J. Chem. Soc. Perkin Trans. II, 1544 (1975).
31. A. K. Cheetham, M. C. Grossel, and D. James. J. Org. Chem. **47**, 566 (1982).

# Use of the absolute method in neutron activation analysis: application to National Bureau of Standards coal and spinach

J. ST-PIERRE AND L. ZIKOVSKY

*Nuclear Engineering Institute, École Polytechnique, P.O. Box 6079, Stn. A, Montreal, P.Q., Canada H3C 3A7*

Received November 10, 1981[1]

J. ST-PIERRE and L. ZIKOVSKY. Can. J. Chem. **60**, 2278 (1982).

Absolute neutron activation analysis, which consists of gamma-ray counting and direct calculation of weights from nuclear constants, was applied to two National Bureau of Standards materials: coal (SRM 1632a) and spinach (SRM 1570). Al, As, Br, Cl, Co, Cr, Cs, Eu, Fe, Ga, K, La, Mg, Na, Sb, Sc, Sr, Ti, V, W, and Zn were instrumentally determined in these samples with accuracy ranging from −18 to +21% among elements for which reference values were available.

J. ST-PIERRE et L. ZIKOVSKY. Can. J. Chem. **60**, 2278 (1982).

L'analyse par activation neutronique absolue qui consiste à calculer directement des masses à partir des constantes nucléaires et des données obtenues par spectrométrie gamma a été utilisée pour analyser deux étalons du National Bureau of Standards: charbon (SRM 1632a) et épinard (SRM 1570). Dans ces étalons, nous avons dosé 21 éléments (Al, As, Br, Cl, Co, Cr, Cs, Eu, Fe, Ga, K, La, Mg, Na, Sb, Sc, Sr, Ti, V, W et Zn) d'une façon non-destructive et avec une exactitude qui a variée de −18 à +21% pour les éléments pour lesquels les valeurs certifiées étaient connues.

## Introduction

In our laboratory, the semi-absolute method (1) is used to analyze a great variety of samples by neutron activation. One drawback of this technique is the necessity of measuring the activation constants (1) for each gamma-ray peak, detector, and counting position used. Our gamma-ray library contains 2000 peaks and we are using 4 different detectors with 3 or more counting positions. This means that there are 24 000 values to be determined – a life-long endeavour. In order to eliminate this tedious work we started 2 years ago to develop an "absolute" method. This technique consists of absolute gamma-ray measurement and direct calculation of weights or concentrations from nuclear constants. Such a technique had been used earlier (2, 3) but, judging from the number of researchers which were using this method, it did not enjoy wide acceptance by neutron activation analysts, we believe, mostly because of the limited accuracy of the nuclear data (cross sections, isotopic abundances, etc.) at that time. This method was given a new impetus with the introduction of the $k_0$ standardization method (4, 5). Presently, the nuclear constants are much more reliable, which should rekindle a new interest in this technique. In this paper, the demonstration of the capability of this rejuvenated standardization method is described.

## Theory

In the absolute method, the weight $W$ of the element of interest is calculated from the corresponding gamma peak area $A$ using eq. [1]:

$$[1] \quad W = \frac{MA\lambda}{NF\sigma IG\eta\,(1 - \exp(-\lambda t_i))\,(1 - \exp(-\lambda t_c))\exp(-\lambda t_d)}$$

where $M$ is the atomic weight of the element, $\lambda$ is the radioactive constant, $N$ is Avogadro's number, $F$ is the neutron flux, $\sigma$ is the reaction cross section, $I$ is the isotopic abundance of the target nuclide, $G$ is the abundance of the gamma-ray counted, $\eta$ is the absolute counting efficiency for a given gamma-ray energy, and $t_i$, $t_d$, $t_c$ are the irradiation, decay, and counting times. In this equation $M$, $\lambda$, $N$, $\sigma$, $I$, $G$ are nuclear constants and only the detector efficiency $\eta$ needs to be measured, for different energies and counting positions. About 20 experimental points are needed for each detector efficiency curve, which reduces the 24 000 measurements to 240. The advantage of such an approach is evident.

## Experimental

The efficiency curves were established by using a calibrated source of $^{60}$Co and sources with well known gamma-ray intensities, in our case $^{152}$Eu, $^{75}$Se, $^{182}$Ta, and $^{165}$Dy.

An example of two such efficiency curves is shown in Fig. 1.

For the next step, a computer program called ANAS (Absolute Neutron Activation with SLOWPOKE) was written.

[1]Revision received February 23, 1982.

0008-4042/82/172278-03$01.00/0

©1982 National Research Council of Canada/Conseil national de recherches du Canada

Can. J. Chem. Downloaded from www.nrcresearchpress.com by 210.87.254.6 on 09/06/12
For personal use only.

TABLE 1. Trace element concentrations in NBS coal (SRM 1632a) and spinach (SRM 1570) in ppm

| | Coal SRM 1632a | | | Spinach SRM 1570 | | |
|---|---|---|---|---|---|---|
| Element | This work | NBS value (10) | Reference 11 | This work | NBS value (12) | References 13, 14 |
| Al | 26 050±1930 | (30 700)* | — | 838±83 | 870±50 | — |
| As | 7.7±1.6 | 9.3±1 | 9 | — | 0.15±0.05 | — |
| Br | 40±3 | — | — | 44±3 | (54) | — |
| Cl | 616±44 | — | — | 6460±547 | — | — |
| Co | 7.4±0.2 | (6.8) | 6.8 | 7.8±1 | (1.5) | — |
| Cr | 41±22 | 34.4±1.5 | 26 | — | 4.5 | — |
| Cs | 2.4±0.2 | (2.4) | 2.5 | — | — | — |
| Eu | 0.47±0.1 | (0.54) | 0.5 | — | (0.02) | — |
| Fe | 11 600±2160 | 11 100±200 | 11 200 | — | 550±20 | 551 |
| Ga | 7.1±0.6 | (8.49) | — | 0.36±0.24 | — | — |
| K | 4 313±205 | — | — | 35 000±1 300 | 35 600±300 | — |
| La | 14±1 | — | 10.9 | — | (0.37) | — |
| Mg | 5 727±373 | — | — | 10 070±2 000 | — | — |
| Mn | 28±1 | 28±2 | — | 165±40 | 165±6 | 118, 156 |
| Na | 779±17 | — | — | 12 940±2 000 | — | — |
| Sb | 1.7±1.5 | (0.58) | 0.53 | — | — | (0.04) |
| Sc | 4.53±1.68 | (6.3) | 6.3 | 0.47±0.3 | — | — |
| Sr | 117±81 | — | — | — | 87±2 | — |
| Ti | 1 848±240 | (1750) | — | — | — | — |
| V | 46±5 | 44±3 | — | — | — | 1.2 |
| W | 0.9±0.7 | — | — | — | — | — |
| Zn | 29±6 | 28±2 | 30 | 41±22 | 50±2 | 47 |

*Non-certified value.

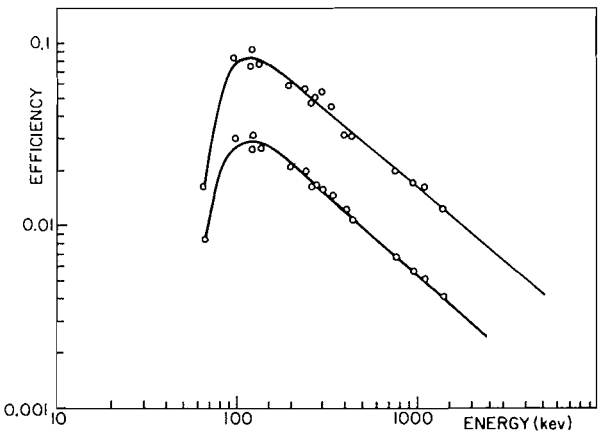


FIG. 1. Efficiency curves for the Ge(Li) detector at two sample–detector distances.

This program incorporates basic routines developed earlier (6) for the semi-absolute method but instead of activation constants it uses published nuclear data (7, 8) and the measured efficiency curves.

In order to assess the accuracy and precision of the absolute method, we applied this technique to two NBS standards: coal (SRM 1632a) and spinach (SRM 1570). Three aliquots of each of these standards were placed in 1 mL polyethylene vials and irradiated in the SLOWPOKE reactor for 30 s, 2 minutes, and 1 h with a neutron flux of $10^{11}$ or $10^{12}$ n/cm$^2$/s depending on the activity desired.

The decay times used vary from 20 s to 440 days and the irradiated capsules were counted for 30 to 30 000 s using a Ge(Li) detector with an active volume of 114 cm$^3$.

The counting positions were made reproducible by using plastic sample holders which keep the sample always at the same distance from the detector and on its axis.

## Results and discussion

Altogether 19 gamma-ray spectra were analyzed by the ANAS program and a large number of results were obtained. For some nuclides which emit gamma-rays of different energies, up to 16 values of the concentration were generated. These data were analyzed by another computer program which calculates an average and the standard deviation and where each value is weighted by the inverse of its statistical error.

Using these, it tries to identify subpopulations of results. If any can be found, it would indicate that at least some results are subject to a systematic error. The complete description of this program will be published later.

The final results are listed in Table 1; the values listed are the arithmetic means of the measured concentrations with the standard deviations of the measured values.

The results obtained agree reasonably well with the NBS certified values whenever these are available. A significant deviation from those values could be caused by a systematic error in the calibration curves and/or incorrect nuclear data. Since the differences are small, one can conclude

Can. J. Chem. Downloaded from www.nrcresearchpress.com by 210.87.254.6 on 09/06/12
For personal use only.

Can. J. Chem. Downloaded from www.nrcresearchpress.com by 210.87.254.6 on 09/06/12
For personal use only.

that these factors do not affect significantly the accuracy of the method for the samples studied and that the nuclear data used are of high quality.

The precision of the absolute method is somewhat lower than the precision obtained in the same conditions by the semi-absolute or relative methods. This is due mainly to the coincidence effects for certain gamma-rays. Some nuclides emit two gamma-rays in cascade. One such example is $^{56}$Mn with 1811 and 846 keV gamma-rays which can penetrate simultaneously into the detector and produce a sum pulse. Consequently, the concentration calculated from cascade gamma-rays will be lower than the real concentration because the counting efficiency is lower than the tabulated one. This effect diminishes with greater sample-to-detector distance but the sensitivity is also reduced, so it is better to apply corrections to the results. This problem was discussed by Crouthamel (9) and Girardi *et al.* (3).

On the other hand, when a peak with energy equal to the sum of the energies of cascade gamma-rays is used, the calculated concentration will be too high and hence corrections must also be applied.

Another fact that can affect the precision of the method is an error in the slope of the calibration curves. A small deviation in that slope can produce two different concentrations calculated from two peaks of the same radioisotope.

Matrix effects such as self-shielding and self-absorption can yield erroneous results and the method, as described, applies only to samples which are relatively transparent to neutrons and gamma-rays. We plan to take into account these two effects in a subsequent version of ANAS.

The method is valid for a standard sample volume of 1 mL and the sample shape which is determined by the inner dimensions of the irradiation vials. These have a diameter of 8 mm and height of 20 mm; for a different sample shape or volume counting geometry corrections would also be needed.

Despite these drawbacks, the absolute method can be a valuable tool in neutron activation analysis, particularly in conjunction with a very stable nuclear reactor such as SLOWPOKE. When this reactor is used, it is not necessary to measure the neutron flux for each irradiation, since it is very stable.

The irradiation positions in the reactor are very reproducible because of its design which is based on the pneumatic transport and gravity positioning of samples. This feature combined with negligible axial and small longitudinal variations of the neutron flux, makes SLOWPOKE a very suitable reactor for absolute neutron activation.

## Conclusion

The absolute method was used with accuracy ranging from −18 to +21% to determine nondestructively 22 elements in two NBS standards. This technique in conjunction with neutron activation constitutes a useful analytical tool by reducing considerably the number of tedious measurements which would be otherwise necessary. By better characterization of counting particularities of this method of standardization (gamma-ray coincidence), precision similar to that which is presently attainable with the semi-absolute or relative methods should be achievable. A very stable nuclear reactor such as SLOWPOKE is distinctly preferable for this technique.

1. C. Bergerioux, G. Kennedy, and L. Zikovsky. J. Radioanal. Chem. **50**, 229 (1979).
2. G. E. Boyd. Anal. Chem. **21**, 355 (1949).
3. F. Girardi, G. Guzzi, and J. Pauly. Anal. Chem. **36**, 1588 (1964).
4. A. Simonits, F. de Corte, and J. Hoste. J. Radioanal. Chem. **24**, 31 (1975).
5. L. Moens, F. de Corte, and J. Hoste. Anal. Chem. Acta, **88**, 319, (1977).
6. L. Zikovsky and J. St-Pierre. J. Radioanal. Chem. **54**, 391 (1979).
7. G. Erdtmann and W. Soyka. J. Radioanal. Chem. **26**, 375 (1975).
8. N. E. Holden and F. W. Walker. Chart of the nuclides. General Electric Co., San Jose, CA. 1977.
9. C. E. Crouthamel. Applied gamma-ray spectrometry. Pergamon Press. 1960. p. 94.
10. J. P. Cali. SRM 1632a – Trace elements in coal. Natl. Bur. Stand., Washington, DC. 1978.
11. K. N. Kostadinov and R. G. Djingova. Radiochem. Radional. Lett. **45**, 297 (1980).
12. J. P. Cali. SRM 1570 – Trace elements in spinach. Natl. Bur. Stand., Washington, DC. 1976.
13. M. Gallorini, M. di Casa, R. Stella, N. Genova, and E. Orvini. J. Radioanal. Chem. **32**, 17 (1976).
14. M. Hoenig, P. van Hoeweghen, and J. Liboton. Analysis, **7**, 104 (1979).

# The electronic structure of the tetrasulphur tetranitride dication, $S_4N_4^{2+}$: an *ab initio* molecular orbital study

MILAN TRSIC

*Instituto de Física e Química de São Carlos, Universidade de São Paulo, C.P. 369, 13560, São Carlos, S.P., Brazil*

AND

WILLIAM G. LAIDLAW AND RICHARD T. OAKLEY[1]

*Department of Chemistry, University of Calgary, Calgary, Alta, Canada T2N 1N4*

Received March 4, 1982

MILAN TRSIC, WILLIAM G. LAIDLAW, and RICHARD T. OAKLEY. Can. J. Chem. **60**, 2281 (1982).

*Ab initio* Hartree–Fock–Slater molecular orbital calculations on the planar tetrasulphur tetranitride dication $S_4N_4^{2+}$ reveal that it can be described as a fully delocalised 10 π-electron system. Overlap populations for the NS bonds suggest a bond order substantially stronger than in neutral $S_4N_4$. The strong uv/visible absorptions observed for $S_4N_4^{2+}$ at 346 and 262 nm are assigned to $n\pi_S \rightarrow \pi^*$ and $n\pi_N \rightarrow \pi^*$ excitations. The Hartree–Fock–Slater π-molecular orbital manifold is discussed in relation to simple HMO concepts.

MILAN TRSIC, WILLIAM G. LAIDLAW et RICHARD T. OAKLEY. Can. J. Chem. **60**, 2281 (1982).

Des calculs *ab initio* d'orbitales moléculaires de Hartree–Fock–Slater sur les dications planaires de tétraazoture de soufre, $S_4N_4^{2+}$, révèlent qu'on peut décrire ce cation comme étant un système pleinement délocalisé à 10 électrons π. Le recouvrement de populations des liaisons NS suggère un ordre de liaison substantiellement plus fort que dans le composé neutre $S_4N_4$. On attribue les fortes absorptions uv/visible observées pour le $S_4N_4^{2+}$ à 346 et 262 nm à des excitations $n\pi_S \rightarrow \pi^*$ et $n\pi_N \rightarrow \pi^*$. On discute des multiples d'orbitales moléculaires π de Hartree–Fock–Slater en relation avec des concepts simples de OMH.

[Traduit par le journal]

## Introduction

The unusual cage-like structure of tetrasulphur tetranitride **1** has long been of central interest in the study of binary SN species. A little over a decade ago Gleiter presented an intuitively appealing rationalization of its molecular structure by considering the π-system of an idealised planar $S_4N_4$ ring **2**

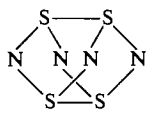

**1**

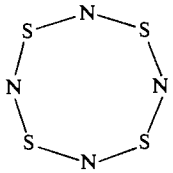

**2**

(1). In this view the 12 π-electron ground state of **2** would be orbitally degenerate and, as such, unstable with respect to Jahn–Teller distortion. Of the several possible symmetry changes that will break the orbital degeneracy of the ground state, the $D_{2d}$ conformation is the most attractive since, in the extended Hückel description, two antibonding π-MO's of **2** would be converted into cross-ring S—S σ-interactions. With the discovery of the planar $S_4N_4^{2+}$ dication in 1977 by Gillespie and co-workers (2), the structure/bonding relationships of Gleiter were strengthened. Implicit in his original analysis was the concept that a planar $S_4N_4^{2+}$ system, with 10 π-electrons, would be stable. In 1978, Michl recognized the spectroscopic consequences of such a π-electron distribution, and predicted the appearance of the MCD spectrum of $S_4N_4^{2+}$ (3). Very recently Sharma, Aubke, and Paddock have provided a specific and quantitative molecular orbital analysis of the $S_4N_4^{2+}$ species (4). Their extended Hückel and CNDO calculations yield orbital eigenvalues and Mulliken overlap populations which are crucial to the understanding of the system. Although these studies have enhanced our knowledge of the electronic make-up of $S_4N_4^{2+}$, it nevertheless has seemed appropriate to us to undertake an investigation of the species at the *ab initio* level. Our Hartree–Fock–Slater (HFS) calculations not only provide a confirmation, within the *ab initio* context, of many of the concepts developed by previous workers, but also allow the prediction of electronic excitation and total energies. In addition, a more detailed analysis of the charge density distribution and overlap populations permits a discussion of the HFS results in terms of elementary considerations of electronegativity and simple Hückel MO theory.

## Theoretical method

The Hartree–Fock–Slater method has been well documented in the literature, and efficient procedures for its implementation have been outlined and tested extensively by Baerends and co-

[1]To whom all correspondence should be addressed.

0008-4042/82/172281-05$01.00/0

©1982 National Research Council of Canada/Conseil national de recherches du Canada

Can. J. Chem. Downloaded from www.nrcresearchpress.com by 210.87.254.5 on 09/06/12
For personal use only.

Can. J. Chem. Downloaded from www.nrcresearchpress.com by 210.87.254.5 on 09/06/12
For personal use only.

TABLE 1. Eigenvalues and Mulliken population analysis of $S_4N_4^{2+}$

| Orbital | Eigenvalue (au) | Overlap and self-atom populations SN | $S_1S_3$ | $S_1S_5$ | N | S | Designation |
|---|---|---|---|---|---|---|---|
| $2a_{2u}$ | −0.4537 | −0.042 | 0.008 | 0.001 | 0.183 | 0.217 | π* |
| $2e_g$ (LUMO) | −0.5399 | −0.019 | −0.003 | −0.001 | 0.128 | 0.202 | π* |
| $2b_{1g}$ (HOMO) | −0.6612 | 0.010 | 0.000 | 0.000 | 0.214 | 0.014 | $n\sigma_N$ |
| $1b_{1u}$ | −0.6618 | 0.000 | −0.014 | 0.002 | 0.000 | 0.276 | $n\pi_S$ |
| $4e_u$ | −0.6627 | −0.027 | 0.005 | 0.000 | 0.209 | 0.138 | σ* |
| $1b_{2u}$ | −0.6992 | 0.013 | 0.001 | 0.000 | 0.196 | 0.010 | $n\pi_N$ |
| $2b_{2g}$ | −0.7001 | −0.007 | −0.006 | 0.003 | 0.034 | 0.252 | $n\sigma_S$ |
| $3a_{1g}$ | −0.7404 | −0.043 | 0.011 | 0.002 | 0.227 | 0.168 | σ* |
| $3e_u$ | −0.7859 | 0.005 | 0.001 | −0.001 | 0.072 | 0.161 | $n\sigma_S$ |
| $1e_g$ | −0.7880 | 0.017 | 0.001 | −0.001 | 0.094 | 0.088 | π |
| $1a_{2u}$ | −0.8300 | 0.019 | 0.003 | 0.000 | 0.083 | 0.079 | π |
| $2a_{1g}$ | −0.8430 | −0.003 | 0.001 | 0.000 | 0.062 | 0.183 | $n\sigma_S$ |
| $1a_{2g}$ | −0.9863 | 0.023 | −0.004 | 0.000 | 0.106 | 0.067 | σ |
| $2e_u$ | −1.0745 | 0.019 | −0.005 | 0.000 | 0.104 | 0.089 | σ |
| $1b_{2g}$ | −1.1923 | 0.022 | −0.008 | 0.001 | 0.040 | 0.134 | σ |
| $1b_{1g}$ | −1.2234 | 0.023 | 0.002 | 0.000 | 0.139 | 0.029 | σ |
| $1e_u$ | −1.3142 | 0.024 | 0.003 | 0.000 | 0.082 | 0.068 | σ |
| $1a_{1g}$ | −1.3580 | 0.023 | 0.002 | 0.000 | 0.080 | 0.062 | σ |
| | Ground state overlap and self-atom populations | | | | | | |
| π-Contribution | | 0.26 | −0.03 | 0.00 | 0.93 | 1.08 | |
| σ-Contribution | | 0.35 | 0.01 | 0.02 | 3.67 | 3.64 | |
| Total | | 0.61 | −0.02 | 0.02 | 4.60 | 4.72 | |
| | Ground state charges | | | | | | |
| π-Contribution | | | | | −0.19 | 0.69 | |
| σ-Contribution | | | | | 0.00 | 0.00 | |
| Total | | | | | −0.19 | 0.69 | |

workers (5). Our application of the method to a variety of $S_xN_y^{z\pm}$ cages (6), rings (7), and chains (8) has provided satisfactory results. The calculations reported here were carried out using a single determinant closed shell state function and the double ζ basis of Clementi and Roetti (9) augmented with a sulphur 3*d* orbital with exponent 1.68 (10). Throughout the SCF calculations the core electrons were kept "frozen" in the manner described by Baerends and co-workers (11). An idealized planar $D_{4h}$ geometry with $d$(S—N) = 1.545 Å, $\hat{S}$ = 120°, and $\hat{N}$ = 150° was assumed for $S_4N_4^{2+}$. These parameters represent an average of those observed in a variety of $S_4N_4^{2+}$ salts (2*b*).

## Results and discussion

*Orbital energy levels*

The HFS molecular orbital energies (eigenvalues), atomic charges, and Mulliken overlap populations calculated for $S_4N_4^{2+}$ are shown in Table 1. Figure 1 illustrates the upper energy levels of the valence shell of $S_4N_4^{2+}$ along with the corresponding levels for the neutral $S_4N_4$ molecule (6). Since the representations $a_{2u}$, $b_{1u}$, $b_{2u}$, and $e_g$ are antisymmetric with respect to the molecular plane, it is clear that the ground state of the $S_4N_4^{2+}$ dication is a 10 π-system in our *ab initio* calculations. The calculated atomic charges on sulphur (0.69) and nitrogen (−0.19) indicate that the positive charge resides primarily on sulphur, as expected on electronegativity grounds. However, an analysis of the σ- and π-electron distributions of $S_4N_4^{2+}$ shows that the transfer of electrons is entirely within the π-system; in the σ-system $\rho_S^\sigma = \rho_N^\sigma = 4.0$, while for the π-MO's $\rho_S^\pi = 1.31$ and $\rho_N^\pi = 1.21$.[2] Thus if one arbitrarily assumes that 0.5 electron is lost from each sulphur atom in the ionization process $S_4N_4 \rightarrow S_4N_4^{2+} + 2e$ (1, 2), then an additional transfer of ~0.2 π-electron occurs during the formation of the $S_4N_4^{2+}$ π-bonding network.

The total NS overlap population of 0.61 is significantly larger than in $S_4N_4$ (0.49) and illustrates the strengthening of the skeletal bonds caused by oxidation of the neutral molecule (cf. NS → $NS^+$ + e effects the removal of a π*-electron and increases the net NS bond order from 2.5 to 3 (12)). Analysis of the orbital overlap populations reveals a π-contribution of 0.26 (approximately ½ of a π-bond), which is clearly larger than in $S_3N_3^-$ (0.16). By contrast, the σ-contributions for both species (0.35 in $S_4N_4^{2+}$ vs. 0.36 in $S_3N_3^-$) are almost identical.

[2]The lack of polarity in the σ-framework imparts to it a pseudo $D_{8h}$ symmetry. Thus several energy levels (e.g., $1b_{1g}$ and $1b_{2g}$) are approximately degenerate.

Can. J. Chem. Downloaded from www.nrcresearchpress.com by 210.87.254.5 on 09/06/12
For personal use only.

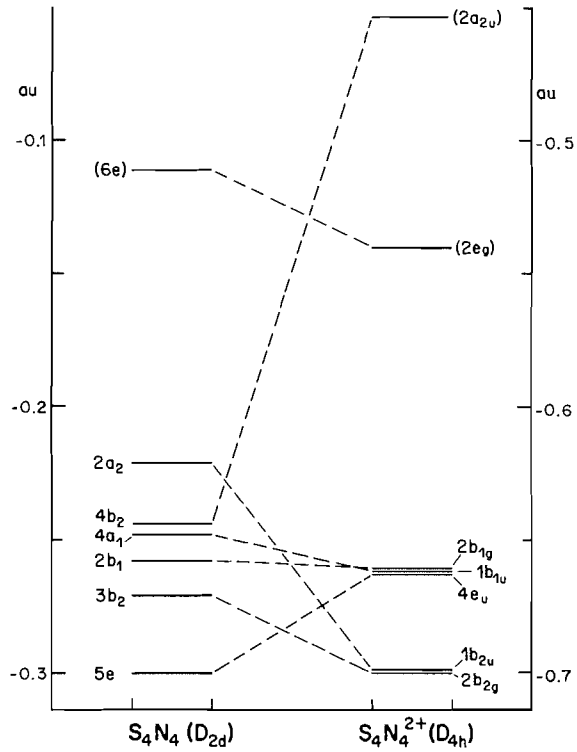


FIG. 1. Correlation diagram between the upper part of the energy level stack of $S_4N_4$ ($D_{2d}$) and planar $S_4N_4^{2+}$ ($D_{4h}$). Virtual orbitals are indicated by parentheses.

Thus the stronger bond in $S_4N_4^{2+}$ ($d$(S—N) = 1.53–1.57 Å) compared to $S_3N_3^-$ ($d$(S—N) = 1.58–1.62 Å) can be attributed to the strengthened π-network of the former, i.e. there are fewer occupied anti-bonding levels. Gillespie and co-workers (2*b*) have suggested the presence of a partial π-bond between nearest neighbour sulphurs, but little or no cross-ring interaction. However, our calculations indicate that there is essentially zero overlap between adjacent and remote pairs of sulphur atoms. Indeed, the highest occupied π-orbital $1b_{1u}$, which would presumably be a candidate for 1,3-SS-overlap in a valence bond approach, is strongly localised on sulphur, and the very weak overlap population that it has is anti-bonding in character.

Comparison of the HFS energy levels with the CNDO results of Paddock and co-workers reveals major similarities. In both cases there is a sulphur lone pair orbital $1b_{1u}$ at the Fermi surface (because of the choice of axes their subscripts 1 and 2 on the $b_u$ and $b_g$ representations are interchanged with ours), and at somewhat lower energy lies a nitrogen lone pair orbital $1b_{2u}$. The remaining occupied π-orbitals $1a_{2u}$ and $1e_g$ are well buried in the upper σ-levels and the two lowest unoccupied levels are the π-orbitals $2e_g$ and $2a_{2u}$. Perhaps the major distinction between the CNDO results and ours is the accumulation of several energy levels near the Fermi surface in the HFS case. This grouping of lone pair and antibonding orbitals at the top of the filled energy level stack seems typical of *ab initio* calculations on SN compounds.[3] This difference in the position of the σ-energy levels is reflected in a somewhat different characterization of the σ-orbitals themselves. We find a total of eight σ-bonding orbitals $1a_{1g}$, $1a_{2g}$, $1b_{1g}$, $1b_{2g}$, $1e_u$, and $2e_u$, with the eight remaining σ-orbitals divided between five lone pairs ($2a_{1g}$, $2b_{1g}$, $2b_{2g}$, and $3e_u$) and three anti-bonding orbitals ($3a_{1g}$ and $4e_u$). This description is reminiscent of Gillespie's characterization (2*b*) of the σ-system into eight bonding pairs and eight lone pairs (valence bond parlance does not recognize anti-bonding orbitals), but is in contrast to the CNDO picture of a dozen σ-bonding orbitals (4).

### Ab initio *vs. Hückel MO description*

Partitioning of the electrons of planar ring systems into σ- and π-networks, as we have done above, has a long history in carbocyclic systems, and retains its appeal in the present context. Indeed, the implications of simple Hückel molecular orbital (HMO) theory pervade much of the current understanding of the π-structure of cyclic SN systems. In any HMO treatment of the π-system of a cyclic molecule of general formula $(AB)_n$, the energy levels of the system are given by the roots of the secular determinant (14):

$$\begin{vmatrix} \alpha_A - E & 2\beta \cos l\pi/n \\ 2\beta \cos l\pi/n & \alpha_B - E \end{vmatrix} = 0$$

where $l = 0, \pm 1, \pm 2, \cdots \pm (n-1)/2$ ($n$ odd)

$l = 0, \pm 1, \pm 2, \cdots \pm n/2$ ($n$ even)

However, the form of the MO's will depend critically on the values of the Coulomb parameters $\alpha_A$ and $\alpha_B$, their relative magnitudes reflecting the electronegativity difference between the A and B sites. In sulphur–nitrogen rings, the choice of $\alpha_S$ and $\alpha_N$ is not obvious. Gleiter (1, 15) has proposed "a higher electronegativity of nitrogen compared to sulphur" (i.e. $\alpha_N < \alpha_S$) and refers to the atomic electronegativity scale of Pauling (16). By contrast, Gimarc and Trinajstić (17) have pointed out the potential applicability of the orbital electronegativities proposed by Streitweiser (18) (i.e. $\alpha_N > \alpha_S$). From our *ab initio* calculations (and from Paddock's CNDO work) it is apparent that the sulphur

[3]See, for example, our own results (6) and those of Palmer *et al.* (13) for $S_4N_4$.

Can. J. Chem. Downloaded from www.nrcresearchpress.com by 210.87.254.5 on 09/06/12
For personal use only.

lone pair π-orbital $1b_{1u}$ lies above the corresponding nitrogen-based orbital $1b_{2u}$. From this energy level ordering one would conclude that nitrogen is more electronegative than sulphur ($\alpha_N < \alpha_S$). However, upon examination of the HFS π-electron density distribution, one finds (as mentioned earlier) a greater π-charge on sulphur ($\rho_S^\pi = 1.31$) than on nitrogen ($\rho_N^\pi = 1.21$). At the HMO level such a result can only be reproduced by choosing Coulomb parameters such that $\alpha_S < \alpha_N$, i.e. a sulphur which is more electronegative than nitrogen.

It is therefore apparent that the π-MO's of $S_4N_4^{2+}$ respond to a potential field that cannot be modelled by a single Hückel parameterization. This is not really surprising insofar as the lower π-levels are well buried in the stack and consequently sense a potential more characteristic of the core. By contrast the higher lying and more diffuse frontier orbitals $1b_{2u}$ and $1b_{1u}$ and the virtual levels $2e_g$ and $2a_{2u}$ see a potential which is more characteristic of a complete nitrogen and sulphur valence shell, for which the atomic electronegativity scale (i.e. $\alpha_N < \alpha_S$) is more appropriate. Simple Hückel concepts must therefore be used with caution. However, bearing this caveat in mind, useful information can be obtained by a suitable choice of parameters. If properties such as π-charge densities are desired, the *ab initio* charge distribution is best described at the Hückel level by setting $\alpha_S < \alpha_N$. However, if information concerning the composition and ordering of the frontier orbitals is required, as would be the case in the study of pericyclic reactions, the ratio $\alpha_S > \alpha_N$ will provide more meaningful results.

*Ionization of $S_4N_4$*

Before leaving the discussion of the molecular orbitals of $S_4N_4^{2+}$ we should comment on the proposition (1, 4, 15) that ionization of $S_4N_4$ to $S_4N_4^{2+}$ involves the $2a_{2u}$ orbital. Certainly this orbital has SS-bonding character in $S_4N_4$; removal of electrons from it would weaken the cross-ring interaction and could lead to the formation of a planar $S_4N_4^{2+}$. This concept is consistent with Fig. 1, which shows that the $2a_{2u}$ orbital of $S_4N_4^{2+}$, to which the $4b_2$ orbital of $S_4N_4$ has evolved, is noticeably destabilized. However, such a description has certain shortcomings. For example, upon oxidation of $S_4N_4$ with chlorine to give $S_4N_4Cl_2$, **3**, one of the S—S bonds of $S_4N_4$ is retained (19). As we have already noted, $S_4N_4$ itself has several orbitals located very near the surface which could be involved in the attack of electrophiles (e.g. $Cl^+$), and the retention of the cage shape in $S_4N_4Cl_2$ implicates the use of orbitals other than the $4b_2$ in the formation of the S—Cl σ-bonds. The structures of the Lewis acid adducts of $S_4N_4$, e.g. $S_4N_4.L$ (**4**, $L = BF_3$ (20), $SbCl_5$ (21), $FeCl_3$ (22), $AsF_5$ (23), $SO_3$ (24)) also pose an interesting question. Adduct formation through nitrogen effects structural changes similar to those caused by ionization, i.e. both cross-ring S—S bonds are lost, but it is hard to conceive of the $4b_2$ orbital being significantly perturbed by the N → L interaction. Instead the nitrogen lone pairs $2b_1$ and $4e$ seem more likely candidates for adduct formation.

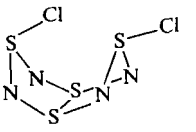


3

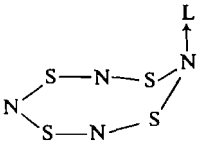


4

In order to understand better the thermodynamics of the structural change which occurs upon the ionization of $S_4N_4$, we have calculated the energy of the $S_4N_4^{2+}$ cage ($D_{2d}$) formed by removing the two electrons from one of the three uppermost orbitals of $S_4N_4$: $2a_2$, $4a_1$, and $4b_2$. Although we have had difficulty in obtaining a fully converged state in the case of an empty $4b_2$ orbital, the energy of all of these cage dications is over 100 kcal/mol above that of the planar form. This rather significant stabilization of the latter reflects the energetic importance of the well developed π-system found in it. The high π-bond energy achieved in the planar structure is more than sufficient to offset the loss of cross-ring SS-bonding (25).

*Electronic spectrum of $S_4N_4^{2+}$*

The uv/visible spectrum of $S_4N_4^{2+}$ contains two major peaks with $\lambda_{max}$ at 346 and 262 nm (4). There is also a small shoulder near 300 nm on the latter peak. In order to assign the electronic excitations responsible for these absorptions we have calculated the oscillator strengths[4] of all symmetry-allowed transitions which correspond to a $\lambda_{max} > 200$ nm. Of these the $1b_{1u}$ ($n\pi_S$) → $2e_g$ ($\pi^*$) and $1b_{2u}$ ($n\pi_N$) → $2e_g(\pi^*)$ are dominant (see Table 2). There is in addition another allowed transition $4e_u$ ($\sigma^*$) → $2e_g$ ($\pi^*$) which has an oscillator strength of about 1% of the two major absorptions. The calculated energies[5] for the two intense transitions are 334 nm ($1b_{1u}$ → $2e_g$) and

[4]The dipole length – dipole velocity formula was employed for the calculation of transition moments. See ref. 26.

[5]Excitation energies have been obtained by adding 0.4 eV to the corresponding one-electron energy differences; this correction reproduces well the total energy differences calculated by the more expensive, and exact, transition state method (27) we used in refs. 7, 8. Theoretical and numerical justification for this correction will be published elsewhere.

TABLE 2. Electronic spectrum of $S_4N_4^{2+}$

| Transition | Polarization | $\lambda_{max}$ (nm) Observed[a] | $\lambda_{max}$ (nm) Calculated | Calculated oscillator strength (au) |
|---|---|---|---|---|
| $1b_{1u} \rightarrow 2e_g$ | Molecular plane | 346 | 334 | $2 \times 10$ |
| $4e_u \rightarrow 2e_g$ | $C_4$ axis | 300 | 331 | $1 \times 10^{-1}$ |
| $1b_{2u} \rightarrow 2e_g$ | Molecular plane | 262 | 262 | $1 \times 10$ |

[a]From ref. 4.

262 nm ($1b_{2u} \rightarrow 2e_g$), both of which compare remarkably well with the observed $\lambda_{max}$ values. The weak transition $4e_u \rightarrow 2e_g$ has a calculated energy of 331 nm, and we presume that the weak absorption near 300 nm corresponds to this excitation.

The above assignments provide theoretical confirmation of Michl's prediction for the MCD spectrum of $S_4N_4^{2+}$ (3). Treating $S_4N_4^{2+}$ as an 8-atom 10 $\pi$-electron perimeter one would expect two $\pi \rightarrow \pi^*$ transitions to be symmetry-allowed. These are indeed the two excitations which, according to our calculations, dominate the electronic spectrum. Both transitions give rise to a degenerate excited state and, according to the perimeter model (3), should give rise to a pair of positive *A*-terms in the MCD spectrum.

## Summary

*Ab initio* Hartree–Fock–Slater molecular orbital calculations on the $S_4N_4^{2+}$ dication confirm the description of its electronic structure in terms of a fully delocalised 10 $\pi$-electron system. The preference for the planar form of $S_4N_4^{2+}$ over a cage structure can be rationalized in terms of the strong $\pi$-network of the former, which is more than sufficient to counterbalance the loss of cross-ring sulphur–sulphur bonding in the cage. The electronic spectrum of $S_4N_4^{2+}$ provides a classic example of an 8-atom 10 $\pi$-electron perimeter, the two intense uv/visible absorptions being assigned to $n\pi_S \rightarrow \pi^*$ and $n\pi_N \rightarrow \pi^*$ transitions.

## Acknowledgements

We thank the Natural Sciences and Engineering Research Council of Canada and FINEP of Brazil for financial support and for an NSERC University Research Fellowship (to R.T.O.). The use of a set of $X_\alpha$ programs provided by Dr. T. Ziegler is acknowledged, as are several stimulating conversations with Dr. T. Chivers.

1. R. GLEITER. J. Chem. Soc. **A**. 3174 (1970).
2. (*a*) R. J. GILLESPIE, D. R. SLIM, and J. D. TYRER. J. Chem. Soc. Chem. Commun. 253 (1977); (*b*) R. J. GILLESPIE, J. P. KENT, J. R. SAWYER, D. R. SLIM, and J. D. TYRER. Inorg. Chem. **20**, 3799 (1981).
3. J. MICHL. J. Am. Chem. Soc. **100**, 6801 (1978).
4. R. J. SHARMA, F. AUBKE, and N. L. PADDOCK. Can. J. Chem. **59**, 3157 (1981).
5. (*a*) E. J. BAERENDS and P. ROS. Intl. J. Quantum Chem. Symp. **12**, 169 (1978); (*b*) T. ZIEGLER and A. RAUK. Theoret. Chim. Acta, **46**, 1 (1977).
6. T. CHIVERS, L. FIELDING, W. G. LAIDLAW, and M. TRSIC. Inorg. Chem. **18**, 3379 (1979).
7. (*a*) J. BOJES, T. CHIVERS, W. G. LAIDLAW, and M. TRSIC. J. Am. Chem. Soc. **101**, 4517 (1979); (*b*) N. BURFORD, T. CHIVERS, A. W. CORDES, W. G. LAIDLAW, M. C. NOBLE, R. T. OAKLEY, and P. N. SWEPSTON. J. Am. Chem. Soc. **104**, 1282 (1982); T. CHIVERS, P. W. CODDING, W. G. LAIDLAW, S. W. LIBLONG, R. T. OAKLEY, and M. TRSIC. J. Am. Chem. Soc. To be published.
8. (*a*) T. CHIVERS, W. G. LAIDLAW, R. T. OAKLEY, and M. TRSIC. J. Am. Chem. Soc. **102**, 5773 (1980); (*b*) J. BOJES, T. CHIVERS, W. G. LAIDLAW, and M. TRSIC. Inorg. Chem. To be published.
9. E. CLEMENTI and C. ROETTI. At. Data Nucl. Data Tables, **14**, 177 (1974).
10. W. G. LAIDLAW and M. TRSIC. Chem. Phys. **36**, 323 (1979).
11. E. J. BAERENDS, D. E. ELLIS, and P. ROS. Chem. Phys. **2**, 41 (1973).
12. J. M. DYKE, A. MORRIS, and I. R. TRICKLE. J. Chem. Soc. Faraday Trans. II, 147 (1977).
13. R. H. FINDLAY, M. H. PALMER, A. J. DOWNS, R. G. EGDELL, and R. EVANS. Inorg. Chem. **19**, 1307 (1980).
14. (*a*) K. A. R. MITCHELL. Chem. Rev. **69**, 157 (1969); (*b*) D. P. CRAIG. J. Chem. Soc. 997 (1959); (*c*) D. P. CRAIG. *In* Theoretical organic chemistry. Kekulé Symposium. Butterworth and Co., Ltd. London. 1959. p. 20.
15. R. GLEITER. Ang. Chem. Int. Ed. Engl. **20**, 444 (1981).
16. L. PAULING. The nature of the chemical bond. Cornell University Press, Ithaca. 1960.
17. B. M. GIMARC and N. TRINAJSTIĆ. Pure Appl. Chem. **52**, 1443 (1980).
18. A. STREITWEISER. Molecular orbital theory for organic chemists. John Wiley, New York. 1961.
19. Z. ZAK. Acta Crystallogr. B**37**, 23 (1981).
20. M. G. B. DREW, D. H. TEMPLETON, and A. ZALKIN. Inorg. Chem. **6**, 1906 (1967).
21. D. NEUBAUER and J. WEISS. Z. Anorg. Allg. Chem. **303**, 28 (1960).
22. U. THEWALT. Z. Naturforsch. B**35**, 855 (1980).
23. R. J. GILLESPIE, J. P. KENT, and J. F. SAWYER. Acta Crystallogr. B**36**, 655 (1980).
24. A. GIEREN and B. DEDERER. Z. Anorg. Allg. Chem. **440**, 119 (1978).
25. N. BURFORD, T. CHIVERS, P. W. CODDING, and R. T. OAKLEY. Inorg. Chem. **21**, 982 (1982).
26. M. TRSIC, T. ZIEGLER, and W. G. LAIDLAW. Chem. Phys. **15**, 383 (1976).
27. T. ZIEGLER, A. RAUK, and E. J. BAERENDS. Theoret. Chim. Acta, **46**, 1 (1977).

Can. J. Chem. Downloaded from www.nrcresearchpress.com by 210.87.254.5 on 09/06/12
For personal use only.

# Diazonium salts in photochemistry. I. Quenching of triplet photosensitizers[1]

J. C. SCAIANO AND NGUYEN KIM-THUAN[2]

*Division of Chemistry, National Research Council of Canada, Ottawa, Ont., Canada K1A 0R6*

Received March 11, 1982

J. C. SCAIANO and NGUYEN KIM-THUAN. Can. J. Chem. **60**, 2286 (1982).

Aromatic diazonium tetrafluoroborates have been shown to be excellent triplet quenchers. Typical rate constants obtained using laser flash photolysis are in the $1-10 \times 10^9 M^{-1} s^{-1}$ range in acetonitrile at 300 K. With most sensitizers the interaction leads to the dediazoniation reaction, via either energy transfer or electron transfer mechanisms. In the case of anthracene, where the rate constant for benzenediazonium tetrafluoroborate is $(5.4 \pm 0.3) \times 10^9 M^{-1} s^{-1}$, the reaction involves the transfer of an electron, leading to the formation of anthracene radical-cation, which has been characterized by absorption spectroscopy. High energy sensitizers, such as benzophenone, are believed to lead to aryl cations and nitrogen; the process may involve some degree of charge transfer, since it is somewhat faster when electron donating substituents are present in the diazonium salt.

J. C. SCAIANO et NGUYEN KIM-THUAN. Can. J. Chem. **60**, 2286 (1982).

On montre que les tétrafluoroborates de diazonium aromatiques sont d'excellents pièges à triplet. Les constantes typiques de vitesse obtenues en utilisant la photolyse flash au laser sont de l'ordre de 1 à $10 \times 10^9 M^{-1} s^{-1}$ dans l'acétonitrile à 300 K. Avec la plupart des sensibilisateurs, l'interaction conduit à une réaction de perte d'une molécule d'azote par l'intermédiaire de mécanismes de transfert d'énergie ou de transfert d'électrons. Dans le cas de l'anthracène, où la constante de vitesse du tétrafluoroborate de benzènediazonium est de $(5{,}4 \pm 0{,}3) \times 10^9 M^{-1} s^{-1}$, la réaction implique le transfert d'un électron et conduit à la formation d'un cation radicalaire anthracène, que l'on a identifié par la spectroscopie d'absorption. On pense que les sensibilisateurs à haute énergie, tels la benzophénone, conduisent à des cations aryliques et à l'azote; la réaction peut impliquer un certain degré de transfert de charge puisqu'elle est en quelque sorte plus rapide quand des substituants électrodonneurs sont présents dans le sel de diazonium.

[Traduit par le journal]

## Introduction

The involvement of diazonium salts in photochemical reactions has been the subject of a number of studies (1–22); however, many fundamental aspects remain, at best, obscure. For example, we find that, while photosensitized processes have been examined in several systems (8, 10–12, 14, 17, 19, 21–23), only in the case of singlet pyrene have a few rate constants been determined (12).

We have recently started work on a project involving the study of the mechanism and kinetics of a wide range of photoreactions of diazonium salts. We find that the total lack of knowledge of quenching rates, particularly in the case of the triplet state, makes any serious analysis of reaction mechanisms virtually impossible. Most photosensitizers induce the loss of molecular nitrogen from the diazonium salt; however, several mechanisms can lead to this result. For instance, energy transfer can lead to an heterolytic mechanism involving the intermediacy of aryl cations. On the other hand, electron transfer can lead to homolytic pathways via diazenyl radicals which decompose to give phenyl radicals and nitrogen. The photoreduction of diazonium salts can take place via a direct electron transfer from the excited sensitizer in the primary photochemical step, or through the involvement of photogenerated radical intermediates. For example, with sensitizers such as benzophenone (21), it is necessary to establish whether the primary photoprocesses involve the solvent (in cases such as methanol) or a direct interaction of the triplet sensitizer with the diazonium salt.

This study was undertaken in order to examine the kinetics of the interaction of a variety of triplet sensitizers, covering a range of molecular structures and triplet energies, with a few diazonium tetrafluoroborates having representative ring substituents. Rate constants were measured using nanosecond laser flash photolysis techniques. In a few cases we have also been able to gather some information concerning the detailed nature of the interaction; while mechanistic aspects are still poorly understood, our experiments provide a glimpse at some of the details, and perhaps complications, that can be expected in these systems.

## Results

All the experiments reported herein have been carried out in deaerated solution, using the pulses from a nitrogen or, occasionally, an excimer laser for excitation. In each system a complete transient spectrum (usually 300 to 760 nm) was recorded in the absence of quencher, as well as in the presence

[1]NRCC No. 20255.
[2]NRCC Research Associate.

0008-4042/82/172286-06$01.00/0
©1982 National Research Council of Canada/Conseil national de recherches du Canada

of sufficient diazonium salt to make decay-via-quenching the predominant decay mode. Kinetic measurements were carried out by monitoring T–T absorptions at or near the corresponding maximum.

A few preliminary experiments with representative sensitizers showed that the tetrafluoroborate anion (sodium salt) is a very poor quencher by comparison with the diazonium salts (*vide infra*). For example, experiments with benzophenone and anthracene in acetonitrile–water at 300 K led to $k_q = (1.5 \pm 0.7) \pm 10^7$ and $< 3.6 \times 10^5 M^{-1} s^{-1}$, respectively. Thus, the rate constants discussed below cannot be attributed to quenching by free tetrafluoroborate anion, with the possible exception of benzil.

When attempting to carry out experiments on a variety of substituent and solvent effects, it is clear that all possible combinations cannot be examined, and little would be gained by trying to do so. Our systems were selected so that the quenching of all sensitizers used by the "parent" substrate, benzenediazonium tetrafluoroborate, was examined. The sensitizers used were mostly the same employed in other studies from this laboratory (24, 25); this should make the comparison of diazonium salts with other quenchers readily available. Substituent effects were examined mostly using benzophenone and anthracene as sensitizers. Acetonitrile was used as a "base" solvent, with a few experiments in other media. Experiments were carried out either using a flow system or static samples; the former are definitely more accurate, but they are also far more time consuming.

The measurement of the rate constant for benzophenone triplet quenching by benzenediazonium tetrafluoroborate in acetonitrile at 300 K is the only one described in detail here; the same approach was followed in all other systems. A $0.014 M$ solution of benzophenone in acetonitrile was examined in the laser photolysis system using the nitrogen laser; the choice of laser was based on the favorable ratio of extinction coefficients at 337.1 nm, which makes selective excitation of benzophenone possible. The transient spectrum (at 5 nm intervals) recorded immediately following the laser pulse was in full agreement with that reported for the benzophenone triplet (26) and which had already been recorded numerous times in our laboratory. When the full laser dose was used for excitation, the decay of the triplet, monitored at 525 nm, followed mixed first and second order kinetics, the latter reflecting triplet–triplet annihilation. Usage of suitable neutral density filters to attenuate the excitation laser dose led to predominant first order decay. The diazonium salts proved to be excellent quenchers, and in their presence the decay of the triplet followed clean pseudo-first order kinetics, with rate constant $k_{obs}$ given by:

[1] $$k_{obs} = \tau_0^{-1} + k_q[DS]$$

where $\tau_0$ is the triplet lifetime in the absence of quencher, $k_q$ is the rate constant for triplet quenching, and [DS] the concentration of diazonium salts. Figure 1 shows a plot according to eq. [1] and the insert a representative decay trace. As in most of the systems examined, the spectrum in the presence of diazonium salt, and after triplet decay was complete, was also recorded. A residual signal was detected at 375 nm. This signal is not due to benzophenone radical-cation and could be due to nitrylium ion (15), but it has not been characterized in detail yet. We note that in most cases these studies are limited to wavelengths at least 10 nm longer than that of the laser used for excitation, since most samples are not transparent at shorter wavelengths.

One exception to the problems mentioned above is the case of xanthone, which is strongly absorbing at 337 nm, but presents a window in the 300 nm region. For example, in the xanthone – *p*-methoxybenzenediazonium tetrafluoroborate system, it is possible to observe the bleaching of the quencher. Figure 2 illustrates this effect; the top part shows the decay of the triplet ketone, while the bottom part shows that the destruction of the diazonium salt is concurrent with the quenching process. At 300 nm the diazonium salt and triplet xanthone have significant absorption.

Another system where it is possible to monitor the bleaching of the diazonium salts is in the case of *p*-diethylaminobenzenediazonium tetrafluoroborate, where the absorption maximum is located at ~380 nm. Experiments with benzophenone showed, as in the case of xanthone described above, that bleaching of the quencher occurs concurrently with triplet decay.

Another type of transient phenomena that one can hope to detect in experiments of this type is the transfer of an electron from the sensitizer to the diazonium salt, i.e., reaction [5],

[2] $$S^* \xrightarrow{k_d} S$$

[3] $$S^* + DS \xrightarrow{k_3} S + DS$$

[4] $$S^* + DS \xrightarrow{k_4} S + Ar^+ + N_2$$

[5] $$S^* + DS \xrightarrow{k_5} S^{+\cdot} + Ar^\cdot + N_2$$

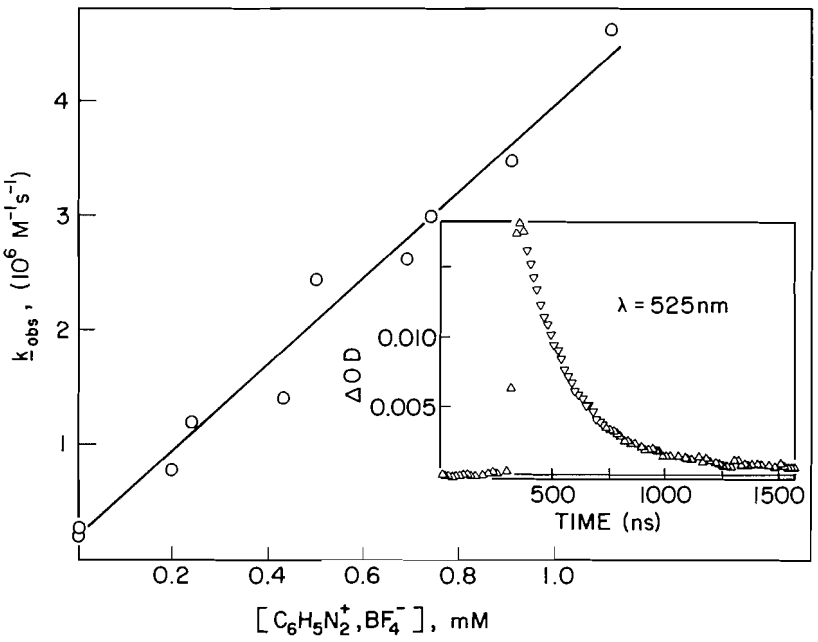


FIG. 1. Quenching of benzophenone triplets by benzenediazonium tetrafluoroborate in acetonitrile at 300 K, according to eq. [1]. *Insert*: Decay of benzophenone triplet monitored at 525 nm in the presence of 1.12 m*M* diazonium salt.

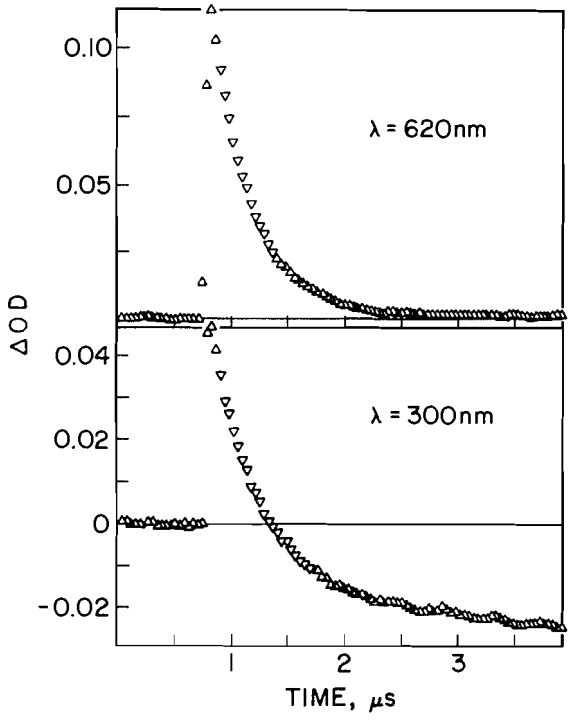


FIG. 2. Transient phenomena observed in the xanthone – *p*-methoxybenzenediazonium tetrafluoroborate (0.26 m*M*), monitored at two different wavelengths. *Top*: Decay of the triplet state. *Bottom*: Triplet decay with concurrent bleaching of the diazonium salt. The slow bleaching at the tail of this trace may be due to relatively minor free radical processes induced in this system.

where S* stands for triplet sensitizer, and reactions [3]–[5] have been written as a single step for simplicity. In fact, reactions [3] and [4] may involve an electronically excited diazonium salt, while reaction [5] probably involves a diazenyl radical (12, 27), which then loses molecular nitrogen. Further, the aryl cation produced in reaction [4] may not be initially in its ground state since, depending upon substitution, these may have singlet or triplet ground states (28, 29).

Occurrence of reaction [5] should lead to the formation of sensitizer-derived radical-cations. This has been observed in the case of anthracene, where the radical-cation shows a very characteristic absorption band at 720 nm (30). Figure 3 shows the transient spectra recorded before significant triplet decay and after the decay (predominantly via quenching) was complete. Time resolved studies showed that the formation of anthracene$^{+\cdot}$ occurred concurrently with triplet decay. From a knowledge of the extinction coefficients of the triplet state (31) and the radical-cation (30) it is possible to estimate the yield of the latter. From an estimated ratio of extinction coefficients of 4 or 5 (triplet-to-radical-cation, at the corresponding maxima (30, 31)), we estimate that the yields of electron transfer are close to quantitative in acetonitrile at 300 K, for benzene- and *p*-methoxybenzenediazonium tetrafluoroborates. It should be noted that estimates are not quantum yields, but rather, the fraction of quenching events that lead to

TABLE 1. Quenching of triplet sensitizers by diazonium tetrafluoroborates at 300 K

| Sensitizer ($E_T$)[a,b] | Diazonium salt[c] | Solvent | $\lambda_{ex}$, $\lambda_{mon}$, method[d] | $k_q$, $M^{-1}$ $s^{-1}$[e] |
|---|---|---|---|---|
| Benzophenone (69) | Benzene | Acetonitrile | 337, 525, flow | $(3.8\pm0.5)\times10^9$ |
| | Benzene | Acetone | 337, 525, flow | $(3.0\pm0.3)\times10^9$ |
| | *o*-Toluene | Acetonitrile | 337, 525, flow | $(1.6\pm0.4)\times10^9$ |
| | *p*-Methoxybenzene | Acetonitrile | 337, 525, flow | $(8.2\pm1.3)\times10^9$ |
| | *p*-Diethylaminobenzene | Acetonitrile | 308, 525, flow | $(7.6\pm2.7)\times10^9$ |
| | 1-Naphthalene | Acetonitrile | 308, 525, flow | $(8.4\pm1.0)\times10^9$ |
| Xanthone (74) | Benzene | Acetonitrile | 337, 620, flow | $(9.8\pm0.9)\times10^9$ |
| | Benzene | Water | 337, 620, static | $(2.8\pm0.8)\times10^9$ |
| | *p*-Methoxybenzene | Acetonitrile | 337, 620, flow | $(6.9\pm2.0)\times10^9$ |
| *p*-Methoxyacetophenone (72) | Benzene | Acetonitrile | 337, 375, static | $(1.3\pm0.4)\times10^{10}$ |
| | Benzene | Acetone | 337, 400, static | $(5.2\pm1.6)\times10^9$ |
| | *o*-Toluene | Acetonitrile | 337, 400, static | $(5.4\pm0.3)\times10^9$ |
| Anthracene (42) | Benzene | Acetonitrile | 337, 420, flow | $(5.4\pm0.3)\times10^9$ |
| | *p*-Methoxybenzene | Acetonitrile | 337, 420, flow | $(2.3\pm0.7)\times10^9$ |
| α,α,α-Trifluoroacetophenone (71)[f] | Benzene | Acetonitrile | 337, 370, static | $(6.7\pm0.5)\times10^9$ |
| Benzil (54) | Benzene | Acetonitrile | 337, 475, static | $\leq2\times10^6$ |
| Phenanthrene (62) | Benzene | Acetonitrile | 337, 483, static | $(3.3\pm0.4)\times10^9$ |
| Pyrene (48) | Benzene | Acetonitrile | 337, 410, static | $(6.1\pm0.8)\times10^8$ |

[a] Triplet energy in kcal $mol^{-1}$, rounded up to the closest unit.
[b] Reference 38.
[c] All tetrafluoroborates, e.g. in the first line: $C_6H_5N_2^+$, $BF_4^-$.
[d] Excitation and monitoring wavelengths in nanometers.
[e] Only random errors (95% confidence limits) are included.
[f] Reference 39.

complete electron transfer, i.e.,

$$[6]\quad \text{yield of radical-cation} = \frac{k_5}{k_3+k_4+k_5}$$

Other systems where the detection of $S^{+\cdot}$ could have been expected to be simple are the cases of phenanthrene and pyrene. For the former we could not detect any significant concentrations of radical-cation, suggesting that reaction [5] is unimportant.

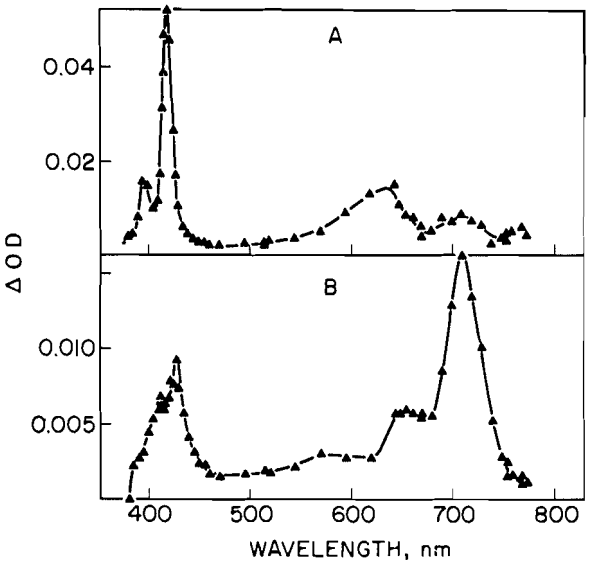


FIG. 3. Transient spectra recorded in the anthracene – *p*-methoxybenzenediazonium tetrafluoroborate (0.88 m*M*) in acetonitrile at 300 K. *Top*: Immediately after laser excitation. *Bottom*: 2.5 μs after excitation.

In the case of pyrene, the radical-cation can be detected, but the problem is complicated by the efficient biphotonic ionization of pyrene (32). This problem can be reduced by working at very low excitation doses, although this leads to a decrease in the signal-to-noise ratio. After a detailed study of the yields of radical cations as a function of laser dose, our conclusion is that $pyrene^{+\cdot}$ is formed rather inefficiently and that some of this radical-cation may in fact be the result of singlet quenching as suggested by Becker *et al.* (14), although overall ion formation is rather inefficient.

We have also carried out a detailed study of the uv–vis spectra of sensitizer – diazonium salt mixtures, since it has been reported that these systems can form electron donor–acceptor complexes (12). Typical equilibrium constants at 293 K in acetonitrile are somewhat below $1\,M^{-1}$ (e.g. for pyrene, anthracene, and phenanthrene). Our studies indicate no complex formation under the conditions of our experiments, typically involving both reagents in millimolar (and occasionally lower) concentrations.

## Discussion

The data in Table 1 clearly show that diazonium tetrafluoroborates are, in most cases, excellent triplet quenchers. Our studies using sodium tetrafluoroborate show that this property reflects the

behaviour of aryldiazonium cations, since the anion, $BF_4^-$, shows only very inefficient quenching. Our results also indicate a true intermolecular process, since complex formation has been shown to be unimportant in these systems.

The only example where the anion is likely to play a role is the case of benzil, where the quenching process is quite slow. The result is perhaps not surprising; benzil has a tendency to show very peculiar behaviour as a sensitizer (24), and it has been suggested that this may be the result of the dramatic structural differences between the ground and triplet states (24).

While one could be tempted to try to offer a comprehensive explanation for the triplet quenching mechanism, this seems rather difficult in view of the rather contradictory spectroscopic evidence on the triplet level of the diazonium compounds. For example, Zharkov and Kondratenko (33) have studied the absorption spectra of *para*-substituted benzenediazonium salts between 4.2 and 300 K; they claim that the long wave edge of the main absorption band is due to absorption to the lowest triplet level, which is a predissociative state. If this is correct, then one can expect the mechanism of triplet quenching to be similar to that proposed in the case of peroxides (24, 34), involving the transfer of energy to a dissociative state of the acceptor. The spectroscopic evidence does not seem consistent with the observation by Sukigara *et al.* (6) of well defined triplet phosphorescence in the case of the unsubstituted substrate, benzenediazonium tetrafluoroborate, with $\lambda_{max} = 412$ nm (77 K). Our own evidence indicates that if excited triplet diazonium salts are formed at all in solution at room temperature, their lifetimes must be extremely short, probably in the subnanosecond range, since the diazonium salt is bleached concurrently with triplet decay (see Fig. 2) and no new transients are observed following it. This is true of all systems examined, including 1-naphthalenediazonium tetrafluoroborate, where the presence of the naphthalene chromophore could be expected to lead to easily detectable triplets.

Our data suggest that electronic effects (see *para*-substituted substrates in Table 1) do not play a major role in determining the rate constants for triplet quenching, while steric effects (see *o*-toluene diazonium data in Table 1) could be of importance. Some small electronic effects are in fact observable; for example, in electron transfer processes, as is the case for anthracene triplet, the rate for benzenediazonium ion is ~2.3 faster than for the methoxy substituted derivative, while in the case of the electrophilic benzophenone triplet the situation is reversed. Solvent effects do not seem extensive; only water seems to reduce significantly the rate constants, at least in the case of xanthone. Futher studies in this area are certainly needed.

While it may be tempting to use free energy relationships to further interpret the data, these may be of very limited applicability in many of these systems. The majority of the rate constants measured are close to diffusion controlled, a fact that will tend to mask substituent effects. Further, some of the more informative substituents (such as nitro) can lead to enough absorption at the excitation wavelength (35) to make selective sensitizer excitation difficult, and ground state complex formation a definite possibility.

In the case of the sensitizers examined, we believe that the most common pathway is probably the fragmentation of the diazonium salt according to reaction [4], which occurs concurrently with the decay of the triplet sensitizer. Figure 2 illustrates this effect.

Full electron transfer from the sensitizer triplet seems to be a less common process, observed as an efficient reaction in the case of anthracene and to some degree in pyrene. It is possible that reaction [5] will be a favoured process for triplets with relatively low triplet energy and substantial electron donor ability. Naturally, anthracene is precisely a good representative of this group.

While electron transfer may not be a common pathway with high energy sensitizers, charge transfer may play a role in the transition state during the quenching process. As pointed out earlier, the reactivity changes observed in the case of benzophenone point in this direction; even the intermediacy of an exciplex is a definite possibility. Many sensitizers can form electron donor–acceptor complexes with the diazonium salts under favorable conditions (14), and this property is expected to be enhanced in the excited state.

Finally, as pointed out above, we have observed residual absorption signals in a number of systems after the quenching event and triplet decay are complete. Benzophenone and xanthone are two examples of this behaviour; these signals are likely to arise from reactions of aryl cations or of transients derived from them. The complete characterization of these species is beyond the scope of this report, but we hope to undertake the detailed study of some of these problems in the near future.

## Experimental

*Materials*

*p*-Diethylaminobenzenediazonium tetrafluoroborate was an Aldrich product, and was purified by recrystallization from acetonitrile by precipitation with ether. All other diazonium compounds were prepared from the corresponding amines by

standard procedures (36) and purified as indicated above. The solid samples were stored at −20°C, and freshly prepared solutions were used in the experiments.

*Spectra*

The uv–vis spectra of the samples were recorded in Varian 219 or Hewlett Packard 8450-A spectrometers.

*Laser flash photolysis*

The samples (under oxygen-free conditions) were excited with the pulses from a Molectron UV-24 nitrogen (337.1 nm, ~8 ns, up to 10 mJ) or a Lumonics TE-860-2 excimer (308 nm with Xe/HCl mixtures, ~4 ns, up to 80 mJ) laser. The samples were contained or flowed through Suprasil cells. In the case of the excimer laser the optical path was 7 mm and a flow system was essential because of its high power. In the case of the nitrogen laser the energy per pulse is considerably less and fresh static samples were, in some cases (see Table 1) regarded as acceptable; in these experiments the optical path was 3 mm. The signal from an RCA-4840 photomultiplier tube was terminated into 93 ohms. Each trace was initially stored in an R7912 Tektronix transient digitizer, and later transferred to a PDP 11/23 computer which controlled the experiment and provided suitable processing, storage, and hardcopy facilities. Further details have been given elsewhere (37).


1. W. Ando. *In* The chemistry of diazonium and diazo compounds. *Edited by* S. Patai. Wiley, New York. 1978. Chapt. 9.
2. W. E. Lee, J. G. Calvert, and E. W. Malmberg. J. Am. Chem. Soc. **83**, 1928 (1961).
3. J. G. Calvert and J. N. Pitts, Jr. Photochemistry. Wiley, New York. 1966. p. 471.
4. D. Schulte-Frohlinde and H. Blume. Z. Physik. Chem. (Frankfurt) **59**, 282 (1968).
5. E. S. Lewis, R. E. Holliday, and L. D. Hartung. J. Am. Chem. Soc. **91**, 430 (1969).
6. M. Sukigara, K. Honda, and S. Kikuchi. J. Photogr. Sci. **18**, 38 (1970).
7. R. C. Petterson, A. DiMaggio III, A. L. Herbert, T. J. Haley, J. P. Mykytka, and I. M. Sarkar. J. Org. Chem. **36**, 631 (1971).
8. T. Yamase, T. Ikawa, H. Kokado, and E. Inoue. Photogr. Sci. Eng. **17**, 268 (1973).
9. H. Boettcher, H. G. O. Becker, V. L. Inanov, and M. G. Kuzmin. Chimia, **27**, 437 (1973).
10. T. Yamase, T. Ikawa, H. Kokado, and E. Inoue. Photogr. Sci. Eng. **18**, 647 (1974).
11. E. Inoue, H. Kokado, T. Ikawa, T. Yamase, and Y. Inoue. Bull. Chem. Soc. Jpn. **47**, 3181 (1974).
12. H. G. O. Becker, G. Schukat, and M. G. Kuzmin. J. Prakt. Chem. **317**, 229 (1975).
13. A. Cox, T. J. Kemp, D. R. Payne, M. C. R. Symons, D. M. Allen, and P. P. de Moira. J. Chem. Soc. Chem. Commun. 693 (1976).
14. H. G. O. Becker, R. Ebisch, G. Israel, G. Kroha, O. Brede, and R. Mehnert. J. Prakt. Chem. **319**, 98 (1977).
15. N. V. Kupletskaya, T. N. Tikhonova, V. V. Shirkova, M. M. Oreshin, and L. A. Kazitsyna. Zh. Org. Khim. **13**, 229 (1976).
16. A. Cox, T. J. Kemp, D. R. Payne, and P. P. de Moira. J. Photogr. Sci. **25**, 208 (1977).
17. H. G. O. Becker, G. Hoffmann, and G. Israel. J. Prakt. Chem. **319**, 1021 (1977).
18. H. B. Ambroz and T. J. Kemp. J. Chem. Soc. Perkin Trans. II, 1420 (1979).
19. P. A. Kondratenko and I. P. Zharkov. Teor. Eksp. Khim. **15**, 723 (1979).
20. H. B. Ambroz and T. J. Kemp. Pol. J. Chem. **53**, 2093 (1979).
21. G. V. Fomin, P. I. Mordvintsev, R. A. Mkhitarov, and T. A. Gordina. Russ. J. Phys. Chem. **54**, 135 (1980); **54**, 137 (1980); **54**, 138 (1980).
22. J. Jirkorsky, A. Fojtik, and H. G. O. Becker. Collect. Czech. Chem. Commun. **46**, 1560 (1981).
23. G. Smets, A. Aerts, and J. Van Erum. Polym. J. **12**, 539 (1980).
24. J. C. Scaiano and G. G. Wubbels. J. Am. Chem. Soc. **103**, 640 (1981).
25. G. D. Mendenhall, L. C. Stewart, and J. C. Scaiano. J. Am. Chem. Soc. In press.
26. M. R. Topp. Chem. Phys. Lett. **32**, 144 (1975); T. S. Godfrey, J. W. Hilpern, and G. Porter. Chem. Phys. Lett. **1**, 490 (1967).
27. N. A. Porter, G. B. Dubay, and J. G. Green. J. Am. Chem. Soc. **100**, 920 (1978).
28. J. D. Dill, P. v. R. Schleyer, and J. A. Pople. J. Am. Chem. Soc. **99**, 1 (1977).
29. H. B. Ambroz and T. J. Kemp. Wiad. Chem. **34**, 773 (1980).
30. T. Shida and W. H. Hamill. J. Chem. Phys. **44**, 2375 (1966); W. Ij. Aalbersberg, G. J. Hoijtink, E. L. Mackor, and W. P. Weijland. J. Chem. Soc. 3055 (1959).
31. R. H. Compton, K. T. V. Grattan, and T. Morrow. J. Photochem. **14**, 61 (1980).
32. J. T. Richards, G. West, and J. K. Thomas. J. Phys. Chem. **74**, 4137 (1970).
33. I. P. Zharkov and P. A. Kondratenko. Opt. Spektrosk. **47**, 877 (1979); English version **47**, 484 (1979).
34. M. V. Encinas and E. A. Lissi. J. Photochem. In press.
35. E. S. Lewis and H. Suhr. J. Am. Chem. Soc. **80**, 1367 (1958).
36. A. Roe. *In* Organic reactions. Vol. V. *Edited by* R. Adams. Wiley, New York. 1949. Chapt. 4.
37. J. C. Scaiano. J. Am. Chem. Soc. **102**, 7747 (1980).
38. S. L. Murov. Handbook of photochemistry. Dekker, New York. 1973. Table 1-1.
39. P. J. Wagner and H. M. H. Lam. J. Am. Chem. Soc. **102**, 4167 (1980).

Can. J. Chem. Downloaded from www.nrcresearchpress.com by 210.87.254.105 on 09/06/12
For personal use only.

COMMUNICATION

# The total, stereocontrolled synthesis of a chemical precursor to (+)-thienamycin. A formal synthesis of the antibiotic[1]

STEPHEN HANESSIAN, DENIS DESILETS,[2] GEORGES RANCOURT,[3] AND REJEAN FORTIN

*Department of Chemistry, University of Montreal, Montreal, Qué., Canada H3C 3V1*

Received May 7, 1982

STEPHEN HANESSIAN, DENIS DESILETS, GEORGES RANCOURT, and REJEAN FORTIN. Can. J. Chem. **60**, 2292 (1982).

A total synthesis of a key lactone intermediate in the synthesis of (+)-thienamycin is described, based on a strategy that uses "chiral templates" derived from D-glucose.

STEPHEN HANESSIAN, DENIS DESILETS, GEORGES RANCOURT et REJEAN FORTIN. Can. J. Chem. **60**, 2292 (1982).

Il s'agit de la description d'une synthèse globale d'un intermédiaire lactone principal dans la synthèse du (+)-thiénamycine qui s'étaye sur une stratégie qui utilise des "matrices chirales" dérivées du D-glucose.

[Traduit par le journal]

Thienamycin (1) and related naturally occurring compounds are new-generation β-lactam antibiotics which are endowed with unique structures (2) and unusually potent antibacterial activity (3). Synthetic efforts in this area, mainly by the Merck group, have resulted in a number of elegant contributions culminating with the total synthesis of the racemic (4), as well as optically active (5) antibiotic. A number of other groups (6), including one at Merck (7), have reported on other approaches to the chiral backbone (in racemic form) of this intriguing structure.

We wish to report on the total synthesis of an optically active six-carbon segment encompassing the functionality and chirality represented by the upper half of the molecule. Our synthesis is based on the recognition of *hidden carbohydrate-type symmetry* in the target (8) as illustrated by the analysis in Scheme 1. Thus, successive bond disconnection at the double bond (C-2—C-3) and the β-lactam function (N-4—C-7) generates a six-carbon β-amino acid which can be related to a "chiral template" derived from a carbohydrate (8). Our synthesis starts with D-glucose and converges on a known lactone which has been previously used in the total synthesis of the racemic antibiotic (7). With the decoding of the hidden symmetry in the target, as depicted in Scheme 1, it is clear that the generation of a segment which encompasses all three asymmetric centers entails systematic modification of the original carbohydrate framework. Consideration of the chemistry involved presents a unique challenge in devising a regio- and stereospecific method for incorporating a carboxyl group or its equivalent at C-4 (carbohydrate numbering).

The starting material **1** for our synthesis already contains a 2-deoxy function (C-1 of the target) and can be prepared in large quantities via crystalline intermediates from D-glucose (9)[4] (Scheme 2). Deoxygenation at the terminal position as well as introduction of the potential amino group were effected via the bromo derivative **2**, $[\alpha]_D$ +140.2° (10), to give compound **3**, $[\alpha]_D$ +133°[5] in excellent overall yield. Thus, the desired deoxygenation pattern as well as the necessary functionality with the correct sense of chirality corresponding to C-5 and C-8 of the target were achieved by virtue of the highly predictive nature of the transformations. We were now faced with the deceptively simple task of introducing a carboxyl group or its equivalent at C-4 of "template" **3**. This proved to be a challenging goal, which we were able to achieve by considering ketenedithioacetals as carboxyl equivalents (12). Thus, oxidation (13) of **3** afforded the azidoketone derivative **4** which was treated with the anion from *O*,*O*-dimethyl formylphosphonate

[1]Portions of this work, including its conceptual design, were previously communicated, S. Hanessian and R. Fortin, Abstr. Papers Am. Chem. Soc. Meeting, 181 (1981), CARB, 27.

[2]NSERCC predoctoral fellow.

[3]Summer postdoctoral associate.

[4]New compounds had spectroscopic (¹H nmr 400 and 90 MHz) and mass spectral characteristics that were in accord with their structure. Crystalline samples gave correct microanalyses. Optical rotations were measured in chloroform unless otherwise stated.

[5]Reported for the L-series, $[\alpha]_D$ −131.8°, see ref. 11.

0008-4042/82/172292-03$01.00/0

©1982 National Research Council of Canada/Conseil national de recherches du Canada

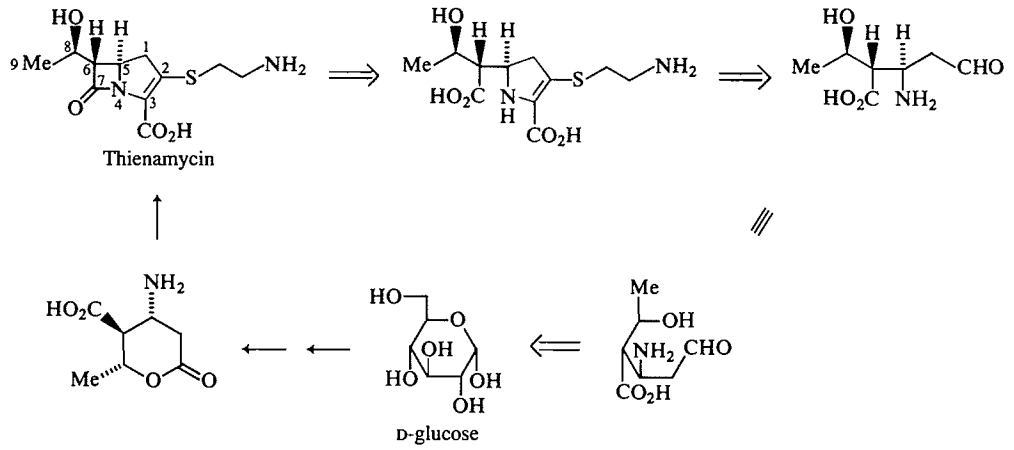


SCHEME 1

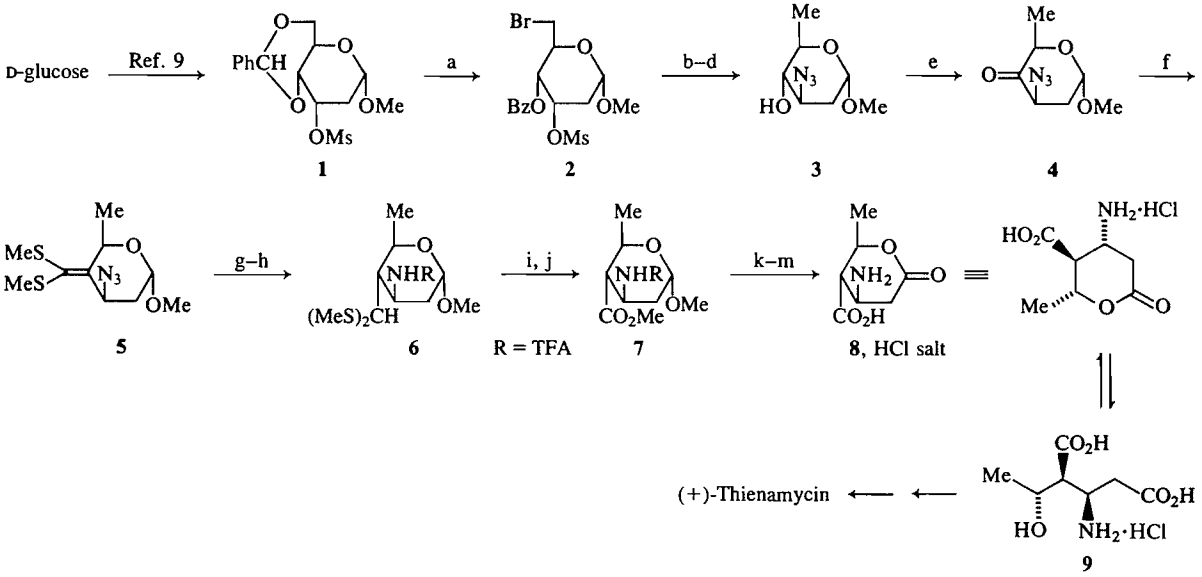


SCHEME 2. (a) NBS, $CCl_4$, $BaCO_3$, reflux, 95%; (b) Pd/C,$H_2$, EtOAc, 90%; (c) $n$-$Bu_4NN_3$, benzene, reflux, 85%; (d) NaOMe, MeOH, 93%; (e) pyridinium chlorochromate, $CH_2Cl_2$, 4 Å sieves, 95%; (f) $(MeO)_2POCH(SMe)_2$, BuLi, THF, −78°C → 25°C, 60%; (g) $LiAlH_4$, THF, 84%; (h) $(CF_3CO)_2O$, pyr., $CH_2Cl_2$, 87%; (i) $HgCl_2$, HgO, aqueous acetone, 76%; (j) $CrO_3$, acetone, $H_2SO_4$, 88%, then $CH_2N_2$, 90%; (k) 12 $N$ HCl, THF (2:5), 68%; (l) aqueous $Br_2$, MeCN, $CaCO_3$, 80%; (m) 12 $N$ HCl, reflux, then azeotropic evaporation from toluene at 50°C, 73%; evaporation at low temperature gave **9**.

$S$,$S$-dimethyl thioacetal (14) to give the ketenedithioacetal derivative **5** in a nonoptimized yield of 60%. With the incorporation of this useful functionality in regiospecific manner we were now ready to address the problem of selective functional group transformations and more importantly to achieve this with a high measure of stereocontrol. We reasoned that treatment of **5**, $[\alpha]_D$ +185.6°, with a reducing agent such as lithium aluminum hydride would reduce the ketenedithioacetal function[6] virtually stereospecifically from the β-side by virtue of prior coordination with the initially formed amine. Indeed, reduction of the azide function in **5** with lithium aluminum hydride followed by derivatization gave the $N$-trifluoroacetyl derivative **6**, $[\alpha]_D$ +120°, in good overall yield. With the regio- and stereochemical problems solved, there remained to change the oxidation

[6]For a related case, see ref. 15.

Can. J. Chem. Downloaded from www.nrcresearchpress.com by 210.87.254.105 on 09/06/12
For personal use only.

state of the dithioacetal derivative **6**. Routine manipulations led to the crystalline ester **7**, mp 174–175°C, $[\alpha]_D$ +112°, which was subjected to selective hydrolysis, oxidation, and deprotection to give the crystalline Melillo lactone **8**, mp 192–193°C (dec.) in optically active form.[7] Interestingly, in aqueous solution the lactone hydrochloride **8** was converted in major part to the open-chain acid form **9**, mp 136–138°C (from acetone), $[\alpha]_D$ +4.2° → +6.7°, 20 h ($H_2O$).[8]

As previously mentioned, the racemic form of lactone **8**, mp 184–186°C (dec.) and its open-chain monobenzyl ester were previously used in a total synthesis of (±)-thienamycin (7). The presently described synthesis should therefore provide access to the optically active thienamycin and constitutes a formal synthesis of the antibiotic.[9]

**Acknowledgements**

We thank the Natural Sciences and Engineering Council of Canada and le Ministère de l'éducation du Québec for financial support.

1. J. S. KAHAN, F. M. KAHAN, R. GOEGELMAN, S. A. CURRIE, M. JACKSON, E. O. STAPLEY, T. W. MILLER, A. K. MILLER, D. HENDLIN, S. MOCHALES, S. HERNANDEZ, H. B. WOODRUFF, and J. BIRNBAUM. J. Antibiot. **32**, 1 (1979).
2. G. ALBERS-SCHONBERG, B. H. ARISON, O. D. HENSENS, J. HIRSHFIELD, K. HOOGSTEEN, E. A. KACZKA, R. E. RHODES, J. S. KAHAN, F. M. KAHAN, R. W. RATCLIFFE, E. WALTON, L. J. RUSWINKLE, R. B. MORIN, and B. G. CHRISTENSEN. J. Am. Chem. Soc. **100**, 6491 (1978).
3. H. KROPP, J. S. KAHAN, F. M. KAHAN, J. SUNDELOF, G. DARLAND, and J. BIRNBAUM. 16th Intersci. Conf. Antimr. Agents and Chemother. Abstract 228, Chicago, IL. 1976.
4. S. M. SCHMITT, D. B. R. JOHNSTON, and B. G. CHRISTENSEN. J. Org. Chem. **45**, 1142 (1980).
5. T. N. SALZMANN, R. W. RATCLIFFE, B. G. CHRISTENSEN, and F. A. BOUFFARD. J. Am. Chem. Soc. **102**, 6161 (1980).
6. J. J. TUFARIELLO, G. E. LEE, P. A. SENARATINE, and M. AL-NURI. Tetrahedron Lett. 4359 (1979); T. KAMETANI, S.-P. HUANG, S. YOKOHAMA, Y. SUZUKI, and M. IHARA. J. Am. Chem. Soc. **107**, 2060 (1980); M. SHIOZAKI and T. HIRAOKA. Tetrahedron Lett. **21**, 4473 (1980); T. KAMETANI, S. P. HUANG, T. NAGAHARA, and M. IHARA. J. Chem. Soc. Perkin Trans. I, 2282 (1981); R. V. STEVENS and K. ALBIZATI. J. Chem. Soc. Chem. Commun. 104 (1982).
7. D. G. MELILLO, T. LIU, K. RYAN, M. SLETZINGER, and I. SHINKAI. Tetrahedron Lett. **22**, 913 (1981); D. G. MELLILO, I. SHINKAI, T. LIU, K. RYAN, and M. SLETZINGER. Tetrahedron Lett. **21**, 2783 (1980).
8. S. HANESSIAN. Acc. Chem. Res. **12**, 159 (1979).
9. J. KOVAR, V. DIENSTBIEROVA, and J. JARY. Collect. Czech. Chem. Commun. **32**, 2498 (1967).
10. S. HANESSIAN and N. R. PLESSAS. J. Org. Chem. **34**, 1045 (1969).
11. S. K. GUPTA. Carbohydr. Res. **37**, 381 (1974).
12. E. J. COREY and G. MÄRKL. Tetrahedron Lett. 3201 (1967); P. F. JONES and M. F. LAMPERT. J. Chem. Soc. Chem. Commun. 526 (1972).
13. J. HERSCOVICI and K. ANTONAKIS. J. Chem. Soc. Chem. Commun. 561 (1980).
14. M. MIKOLAJCZYK, D. GRZEJSZCZAK, and M. ZATORSKI. Tetrahedron Lett. 2731 (1976).
15. M. Y. H. WONG and G. R. GRAY. J. Am. Chem. Soc. **100**, 3548 (1978).
16. M. DURETTE. Carbohydrate Res. **100**, C27 (1982).

[7]The optical rotation measured in DMSO shows $[\alpha]_D$ +15.5° (unchanged after 1 h).

[8]The nmr analysis of the solution indicated the presence of **8** and **9** in a ratio of 1:6.

[9]After completion of this manuscript, a report appeared which described the synthesis of a D-glucose-derived "chiral template" (8) via **3**, and involving a double inversion at C-4, followed by displacement of a triflate ester with cyanide ion in modest yield, see ref. 16.

Can. J. Chem. Downloaded from www.nrcresearchpress.com by 210.87.254.105 on 09/06/12
For personal use only.

# Synthesis of 1,2-dihydro-3*H*-pyrrolo[1,2-*a*]pyrrole-1-carboxylic acids[1] and homologous pyridine and azepine analogues thereof[2]

HUMBERTO CARPIO, EDVIGE GALEAZZI, ROBERT GREENHOUSE, ANGEL GUZMÁN, ESPERANZA VELARDE, YULIA ANTONIO, FIDENCIO FRANCO, ALICIA LEON, VIRGINIA PÉREZ, RAQUEL SALAS, AND DAVID VALDÉS

*Syntex, S.A., División de Investigación, Apartado Postal 10-820, México 10, D.F.*

AND

JACK ACKRELL, DIANE CHO, PASQUALE GALLEGRA, OTTO HALPERN, RICHARD KOEHLER, MICHAEL L. MADDOX, JOSEPH M. MUCHOWSKI,[3] ANTHONY PRINCE, DEREK TEGG, T. CRAIG THURBER, ALBERT R. VAN HORN, AND DOUG WREN

*Syntex Research, Institute of Organic Chemistry, Palo Alto, CA 94304, U.S.A.*

Received December 31, 1981

HUMBERTO CARPIO, EDVIGE GALEAZZI, ROBERT GREENHOUSE, ANGEL GUZMÁN, ESPERANZA VELARDE, YULIA ANTONIO, FIDENCIO FRANCO, ALICIA LEON, VIRGINIA PÉREZ, RAQUEL SALAS, DAVID VALDÉS, JACK ACKRELL, DIANE CHO, PASQUALE GALLEGRA, OTTO HALPERN, RICHARD KOEHLER, MICHAEL L. MADDOX, JOSEPH M. MUCHOWSKI, ANTHONY PRINCE, DEREK TEGG, T. CRAIG THURBER, ALBERT R. VAN HORN, and DOUG WREN. Can. J. Chem. **60**, 2295 (1982).

Several syntheses of the previously unknown 1,2-dihydro-3*H*-pyrrolo[1,2-*a*]pyrrole-1-carboxylic acid and various 5- and 6-substituted derivatives thereof have been devised. Some of these processes have been extended to the heretofore unreported 5,6,7,8-tetrahydropyrrolo[1,2-*a*]pyridine-8-carboxylic acid and 5,6,7,8-tetrahydro-9*H*-pyrrolo[1,2-*a*]azepine-9-carboxylic acid derivatives.

Two new processes were developed for the conversion of pyrroles into the corresponding pyrrol-2-acetic acid esters. Both processes were based on the use of the readily available ethoxalylpyrrole derivatives as the starting material. One sequence involved saponification of the α-keto ester, followed by Wolff–Kishner reduction of the crude α-keto acid salt and subsequent esterification of the acetic acid derivative thus produced. The second synthesis commenced with reduction of the 2-ethoxalpyrrole with sodium borohydride to the α-hydroxy ester, which was further reduced to the acetic acid ester with an equimolar mixture of triphenylphosphine and triphenylphosphine diiodide.

HUMBERTO CARPIO, EDVIGE GALEAZZI, ROBERT GREENHOUSE, ANGEL GUZMÁN, ESPERANZA VELARDE, YULIA ANTONIO, FIDENCIO FRANCO, ALICIA LEON, VIRGINIA PÉREZ, RAQUEL SALAS, DAVID VALDÉS, JACK ACKRELL, DIANE CHO, PASQUALE GALLEGRA, OTTO HALPERN, RICHARD KOEHLER, MICHAEL L. MADDOX, JOSEPH M. MUCHOWSKI, ANTHONY PRINCE, DEREK TEGG, T. CRAIG THURBER, ALBERT R. VAN HORN et DOUG WREN. Can. J. Chem. **60**, 2295 (1982).

On a réalisé plusieurs synthèses de l'acide dihydro-1,2 3*H*-pyrrolo-[1,2-*a*] pyrrole carboxylique-1 inconnu jusqu'à présent et de plusieurs de ses dérivés substitués en position 6. On a étendu quelques-unes de ces synthèses aux dérivés de l'acide tétrahydro-5,6,7,8 pyrrolo[1,2-*a*] pyridine carboxylique-8 et de l'acide tétrahydro-5,6,7,8 9*H*-pyrrolo[1,2-*a*] azépine carboxylique-9 non rapportés antérieurerement.

On a mis au point deux nouveaux procédés pour transformer des pyrroles en esters d'acides pyrroleacétique-2 correspondants. Les deux méthodes s'appuient sur l'utilisation, comme produit de départ, des dérivés de l'éthoxalylpyrrole facilement disponible. Une méthode fait appel à la saponification de l'α-cétoester suivi d'une réduction de Wolff–Kishner du sel de l'α-cétoacide brut et d'une estérificatin du dérivé d'acide acétique. La deuxième synthèse débute par la réduction de l'éthoxalyl-2 pyrrole, par le borohydrure de sodium, en α-hydroxy ester que l'on réduit ensuite en ester d'acide acétique avec un mélange équimolaire de triphénylphosphine et d'iodure de triphénylphosphine.

[Traduit par le journal]

In connection with a program related to the development of certain nonsteroidal antiinflammatory agents (1), methods were required for the synthesis of bicyclic carboxylic acids of the structural types encompassed by formula **1** ($n$ = 2–4). No examples of these specific compounds, with or without substituents in the aromatic ring, have ever been reported in the literature.[4] This publication describes several ways in which the synthesis of such compounds can be achieved.

Central to the synthetic studies described herein was the observation that the iodoethyl pyrrole derivative **3**,[5] obtained in very low overall yield

[1]Alternative nomenclature: 1,2-dihydro-3*H*-pyrrolizine-1-carboxylic acids.

[2]Contribution No. 600 from the Syntex Institute of Organic Chemistry.

[3]Author to whom enquiries concerning this paper should be addressed.

[4]Certain aspects of the research described in this paper have appeared in the patents cited in ref. 1.

[5]The synthesis of this compound was effected by the copper catalysed reaction of the THP ether corresponding to **2***a* with ethyl diazoacetate, followed by hydrolysis of the protecting group, conversion of the alcohol into the methanesulfonate, and displacement with sodium iodide.

0008-4042/82/182295-18$01.00/0

©1982 National Research Council of Canada/Conseil national de recherches du Canada

Can. J. Chem. Downloaded from www.nrcresearchpress.com by 210.87.254.5 on 09/06/12
For personal use only.

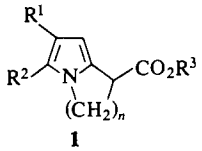

1

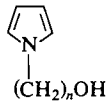

2*a* $n = 2$
2*b* $n = 3$
2*c* $n = 4$

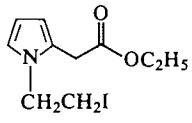

3

from 1-(2-hydroxyethyl)pyrrole **2***a*, readily underwent cyclization to the pyrrolopyrrole derivative **1** ($n = 1$; $R^1$, $R^2$ = H, $R^3$ = $C_2H_5$) on reaction with sodium hydride in dimethylformamide (DMF) solution. Therefore the strategy was to devise efficient preparative routes to compound **3** and derivatives and homologues thereof.

The first successful approach to the desired compounds was based on a Hantzsch pyrrole synthesis. When bromocetaldehyde was added to an acetonitrile solution of the enamine derived from dimethyl acetonedicarboxylate and ethanolamine, and the solution thus obtained was heated at reflux temperature, the crystalline 1-substituted pyrrole dicarboxylic acid ester **4***a* was formed in 38–43% yield. This compound was converted into the methanesulfonate **4***b* which, after nucleophilic displacement with sodium iodide in acetonitrile, gave the iodide **4***c* in 90% overall yield from the alcohol. As expected, cyclization of the iodide to the bicyclic diester **5***a* was effected rapidly, and in high yield, in the presence of sodium hydride in DMF solution. The removal of the unwanted carboxyl group from **5***a* was accomplished by a three-step sequence which took advantage of the differing steric environment of the two ester moieties. Saponification of **5***a* with excess potassium hydroxide gave the dicarboxylic acid **5***b* which was selectively esterified at the less hindered

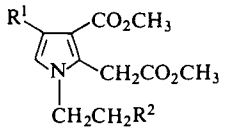

**4***a* $R^1$ = H, $R^2$ = OH
**4***b* $R^1$ = H, $R^2$ = $OSO_2CH_3$
**4***c* $R^1$ = H, $R^2$ = I
**4***d* $R^1$ = $CH_3$, $R^2$ = OH
**4***e* $R^1$ = $CH_3$, $R^2$ = $OSO_2CH_3$
**4***f* $R^1$ = $CH_3$, $R^2$ = I
**4***g* $R^1$ = $C_2H_5$, $R^2$ = OH
**4***h* $R^1$ = $C_2H_5$, $R^2$ = $OSO_2CH_3$
**4***i* $R^1$ = $C_2H_5$, $R^2$ = I
**4***j* $R^1$ = $CH_3O(CH_2)_2$, $R^2$ = OH
**4***k* $R^1$ = $CH_3O(CH_2)_2$, $R^2$ = $OSO_2CH_3$
**4***l* $R^1$ = $CH_3O(CH_2)_3$, $R^2$ = OH
**4***m* $R^1$ = $CH_3O(CH_2)_3$, $R^2$ = $OSO_2CH_3$

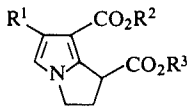

**5***a* $R^1$ = H, $R^2$, $R^3$ = $CH_3$
**5***b* $R^1$, $R^2$, $R^3$ = H
**5***c* $R^1$, $R^2$ = H, $R^3$ = $CH(CH_3)_2$
**5***d* $R^1$, $R^2$, $R^3$ = $CH_3$
**5***e* $R^1$ = $CH_3$, $R^2$, $R^3$ = H
**5***f* $R^1$ = $CH_3$, $R^2$ = H, $R^3$ = $CH(CH_3)_2$
**5***g* $R^1$ = $C_2H_5$, $R^2$, $R^3$ = $CH_3$
**5***h* $R^1$ = $C_2H_5$, $R^2$, $R^3$ = H
**5***i* $R^1$ = $C_2H_5$, $R^2$ = H, $R^3$ = $CH(CH_3)_2$
**5***j* $R^1$ = $CH_3O(CH_2)_2$, $R^2$, $R^3$ = $CH_3$
**5***k* $R^1$ = $CH_3O(CH_2)_2$, $R^2$, $R^3$ = H
**5***l* $R^1$ = $CH_3O(CH_2)_2$, $R^2$ = H, $R^3$ = $CH(CH_3)_2$
**5***m* $R^1$ = $CH_3O(CH_2)_3$, $R^2$, $R^3$ = $CH_3$
**5***n* $R^1$ = $CH_3O(CH_2)_3$, $R^2$, $R^3$ = H
**5***o* $R^1$ = $CH_3O(CH_2)_3$, $R^2$ = H, $R^3$ = $CH(CH_3)_2$

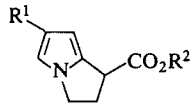

**6***a* $R^1$ = H, $R^2$ = $CH(CH_3)_2$
**6***b* $R^1$, $R^2$ = H
**6***c* $R^1$ = $CH_3$, $R^2$ = $CH(CH_3)_2$
**6***d* $R^1$ = $C_2H_5$, $R^2$ = $CH(CH_3)_2$
**6***e* $R^1$ = $CH_3O(CH_2)_2$, $R^2$ = $CH(CH_3)_2$
**6***f* $R^1$ = $CH_3O(CH_2)_2$, $R^2$ = H
**6***g* $R^1$ = $CH_3O(CH_2)_3$, $R^2$ = $CH(CH_3)_2$
**6***h* $R^1$ = H, $R^2$ = $CH_3$
**6***i* $R^1$, $R^2$ = $CH_3$
**6***j* $R^1$ = $CH_3OCH_2$, $R^2$ = $CH_3$
**6***k* $R^1$ = Cl, $R^2$ = $CH_3$
**6***l* $R^1$ = Br, $R^2$ = $CH_3$

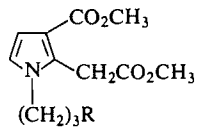

**7***a* R = OH
**7***b* R = $OSO_2CH_3$
**7***c* R = I

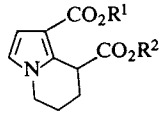

**8***a* $R^1$, $R^2$ = $CH_3$
**8***b* $R^1$, $R^2$ = H
**8***c* $R^1$ = H, $R^2$ = $CH(CH_3)_2$

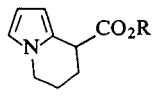

**9***a* R = $CH(CH_3)_2$
**9***b* R = H
**9***c* R = $CH_3$

Can. J. Chem. Downloaded from www.nrcresearchpress.com by 210.87.254.5 on 09/06/12
For personal use only.

Can. J. Chem. Downloaded from www.nrcresearchpress.com by 210.87.254.5 on 09/06/12
For personal use only.

carboxyl group with 2-propanol under Fischer conditions. Thermal decarboxylation of the mono carboxylic acid **5***c* took place in a manner typical of pyrrole-3-carboxylic acids (2) to give *i*-propyl 1,2-dihydro-3*H*-pyrrolo[1,2-*a*]pyrrole-1-carboxylate **6***a* in 55% yield from the diester **5***a*. Alkaline hydrolysis of the air-sensitive ester gave the corresponding carboxylic acid **6***b* which was characterized as the stable, crystalline dicyclohexylammonium salt.

When propanolamine was substituted for ethanolamine in the Hantzsch pyrrole synthesis, the 1-(3-hydroxypropyl) diester **7***a* was obtained in 43–58% yield. This compound was subjected to a sequence of reactions analogous to that described above to provide 5,6,7,8-tetrahydropyrrolo[1,2-*a*]-pyridine-8-carboxylic acid **9***b* (see Tables 1 and 2).

One of the significant aspects of the above reaction sequences was that when a bromomethyl ketone was used as the halocarbonyl component, then depending on the conditions utilized to effect the Hantzsch reaction, pyrroles substituted in the 4- or the 5-position could be prepared. For example, slow addition of bromoacetone (2 equiv.) to a mixture of aqueous ethanolamine (10 equiv.) and dimethyl acetonedicarboxylate (1 equiv.) gave the pyrrole diester **4***d*, bearing a methyl group at C-4, as the major product. This substance was converted into *i*-propyl 6-methyl-1,2-dihydro-3*H*-pyrrolo[1,2-*a*]pyrrole-1-carboxylate **6***c*. Similarly, commencing with 1-bromo-2-butanone, 1-bromo-4-methoxy-2-butanone, and 1-bromo-5-methoxy-2-pentanone, the 6-substituted bicyclic acid esters **6***d*, **6***e*, and **6***g*, respectively (see Tables 1 and 2), were synthesized. In contrast, when the Hantzsch pyrrole synthesis was effected under nonaqueous conditions with bromoacetone or phenacyl bromide as the halocarbonyl components, the 5-substituted pyrrole diesters **10***a* and **10***d* were obtained as the principal products. These compounds were converted into the corresponding 5-substituted pyrrolopyrrole carboxylic acid derivatives **12***a* and **12***c*, via the usual reaction sequence.

The formation of isomeric pyrroles from a single set of starting materials merely through a minor variation of the reaction conditions indubitably is a reflection of a mechanistic change in the Hantzsch reaction. While it is probable that the pyrroles **4***a*, **7***a*, **10***a*, and **10***d* result from carbon alkylation of the enamine **13** in the expected sense, the mechanism of formation of the abnormal Hantzsch products (i.e., with the substituent at C-4) is less apparent. In this connection, it has recently been shown (3) that the optimum conditions for the formation of the 4-methyl compound **14** involve the simultaneous addition of a 1.5:1 molar ratio of chloracetone and dimethyl acetonedicarboxylate to a considerable excess (≥3.5 equiv.) of aqueous methylamine in a two phase system. Although other explanations are possible, it may be that these conditions favor the generation of a low concentration of a reactive intermediate, such as methylaminoacetone, which might be efficiently trapped in the Knorr sense (see ref. 2, pp. 52–57) to yield the vinylogous urethane **15**. This intermediate would be especially prone to a base catalyzed internal aldolization to the alcohol **16**, followed by an equally facile base catalyzed elimination of water therefrom, to yield the observed product.

The distinguishing feature of a second synthetic route to 1,2-dihydro-3*H*-pyrrolo[1,2-*a*]pyrrole-1-carboxylic acid derivatives was the sequential attachment of two carbon units, suitable for closure

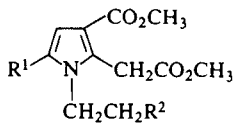

**10***a* $R^1 = CH_3$, $R^2 = OH$
**10***b* $R^1 = CH_3$, $R^2 = OSO_2CH_3$
**10***c* $R^1 = CH_3$, $R^2 = I$
**10***d* $R^1 = C_6H_5$, $R^2 = OH$
**10***e* $R^1 = C_6H_5$, $R^2 = OSO_2CH_3$
**10***f* $R^1 = C_6H_5$, $R^2 = I$

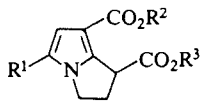

**11***a* $R^1, R^2, R^3 = CH_3$
**11***b* $R^1 = CH_3$, $R^2, R^3 = H$
**11***c* $R^1 = CH_3$, $R^2 = H$, $R^3 = CH(CH_3)_2$
**11***d* $R^1 = C_6H_5$, $R^2, R^3 = CH_3$
**11***e* $R^1 = C_6H_5$, $R^2, R^3 = H$
**11***f* $R^1 = C_6H_5$, $R^2 = H$, $R^3 = CH(CH_3)_2$

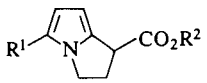

**12***a* $R^1 = CH_3$, $R^2 = CH(CH_3)_2$
**12***b* $R^1 = C_6H_5$, $R^2 = CH(CH_3)_2$
**12***c* $R^1 = C_6H_5$, $R^2 = H$

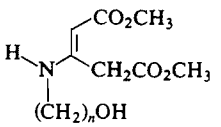

**13**

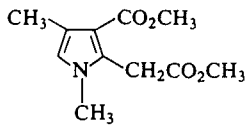

**14**

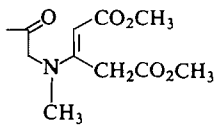

**15**

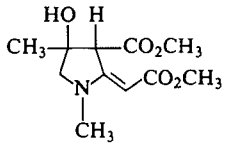

**16**

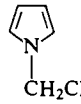

**17***a* R = OTHP
**17***b* R = $OCOCH_3$
**17***c* R = Cl

Can. J. Chem. Downloaded from www.nrcresearchpress.com by 210.87.254.5 on 09/06/12
For personal use only.



TABLE 1. Synthetic conditions, yields, and physical constants for 1-substituted pyrroles

| Compound No. | Reaction temp. °C | Reaction time, h | Yield (%) | Melting point (°C) boiling point °C/Torr | Cryst. solvent | Calcd. C | Calcd. H | Calcd. N | Found C | Found H | Found N |
|---|---|---|---|---|---|---|---|---|---|---|---|
| **4***a* | Reflux (MeCN) | 1 | 38–43 | 68–69 | Ether–hexane | 54.76 | 6.27 | 5.81 | 54.50 | 6.18 | 5.66 |
| **4***b* | −10 to −5 | 1 | 99 | 102–103 | EtOAc–hexane | 45.14 | 5.37 | 4.39 | 44.93 | 5.27 | 4.40 |
| **4***c* | Reflux (MeCN) | 1 | 90 | 137–138 | MeCN–water | 37.60 | 3.98 | 3.98 | 37.66 | 4.07 | 4.02 |
| **4***d* | −10 to rt | 1 | 35 | 78 | $CH_2Cl_2$–hexane | 56.45 | 6.71 | | 56.41 | 6.73 | |
| **4***e* | 0 to rt | 0.25 | 95 | 81 | MeOH | 46.83 | 5.74 | | 46.99 | 5.85 | |
| **4***f* | Reflux (MeCN) | 8 | 92 | 103 | Ether–hexane | 39.46 | 4.41 | | 39.57 | 4.44 | |
| **4***g* | −10 to rt | 1 | 78 | 64–65 | Ether–hexane–acetone | 57.98 | 7.11 | 5.20 | 58.08 | 7.35 | 5.11 |
| **4***h* | −10 to rt | 1 | 88 | 82–83 | Acetone–hexane | 48.40 | 6.09 | 4.03 | 48.49 | 6.02 | 4.02 |
| **4***i* | Reflux (MeCN) | 5 | 100 | 86 | Ether–hexane | 41.17 | 4.78 | | 41.05 | 4.79 | |
| **4***j* | 35 | 0.25 | 30 | 65–66 | $CH_2Cl_2$–ether–hexane | 56.18 | 7.07 | | 56.02 | 7.01 | |
| **4***k* | 0 to rt | 0.25 | 82 | 105–106 | $CH_2Cl_2$–hexane | 47.75 | 6.14 | | 47.56 | 5.97 | |
| **4***l* | rt | 0.25 | 27 | Oil | — | 57.49 | 7.40 | | 57.23 | 7.33 | |
| **4***m* | 0 | 0.5 | 88 | 74–75 | Acetone–hexane | 49.10 | 6.44 | | 48.94 | 6.43 | |
| **7***a* | rt | 16 | 43–58 | 52 | $CH_2Cl_2$–hexane | 56.46 | 6.71 | 5.48 | 56.52 | 6.70 | 5.39 |
| **7***b* | 0 | 0.25 | 66–69 | 53–54 | $CH_2Cl_2$–ether | 46.86 | 5.75 | 4.21 | 46.79 | 5.76 | 4.23 |
| **7***c* | Reflux (MeCN) | 25 | 60–73 | 64–65 | $CH_2Cl_2$–hexane | 39.48 | 4.42 | 3.80 | 39.68 | 4.46 | 3.79 |
| **10***a* | rt | 120 | 16 | Oil[a] | — | | | | | | |
| **10***b* | −10 to rt | 0.25 | 92 | 112 | $CHCl_3$–hexane | 46.83 | 5.74 | | 46.60 | 5.67 | |
| **10***c* | Reflux (MeCN) | 5 | 95 | 86 | Hexane | 39.46 | 4.41 | | 39.61 | 4.23 | |
| **10***d* | Reflux (MeCN) | 1.75 | 40[b] | 160–162[c] | $CH_2Cl_2$–MeOH[c] | 63.15 | 4.59 | 9.82 | 63.10 | 4.59 | 9.85 |
| **10***e* | −10 to 0 | 0.5 | 100 | 82–84 | Ether–hexane | 54.67 | 5.35 | 3.54 | 54.69 | 5.34 | 3.43 |
| **10***f* | Reflux (MeCN) | 8.5 | 100 | 102–103 | Acetone–hexane | 47.79 | 4.24 | 5.27 | 47.76 | 4.21 | 3.17 |
| **18***a* | −20 to 0 | 24 | 80–86 | Oil | — | 61.07 | 7.18 | 4.75 | 61.28 | 7.18 | 4.85 |
| **18***b* | −25 to rt | 18 | 71 | Oil | — | 56.96 | 5.98 | 5.54 | 56.84 | 5.80 | 5.46 |
| **18***c* | Reflux (MeOH–$H_2O$) | 1 | 93[d] | 170–172[e] | Ether–MeOH[e] | 65.90 | 8.85 | 7.69 | 66.13 | 8.58 | 7.68 |
| **18***d* | Reflux ($ClCH_2CH_2Cl$) | 0.25 | 68 | Oil | — | 55.56 | 5.38 | 4.99 | 55.14 | 5.40 | 4.70 |
| **18***e* | rt | 14 | 44 | 125–127 | Acetone | 51.23 | 4.30 | 6.64 | 51.41 | 4.44 | 6.31 |
| **18***f* | See experimental | — | —[f] | Oil | — | 56.61 | 6.45 | 4.72 | 56.42 | 6.53 | 4.55 |
| **18***g* | See experimental | — | 12–26 | 56–57 | Hexane | 55.16 | 6.82 | 5.36[g] | 54.81 | 6.57 | 5.36 |
| **18***h* | −20 to rt | 20 | 74 | 104–6/0.075 | — | 52.59 | 5.26 | 6.09[h] | 52.10 | 5.33 | 5.73 |
| **18***i* | See experimental | — | 51–52 | 28–29 | Ether | 52.69 | 5.90 | 5.12[i] | 52.90 | 5.90 | 4.92 |
| **18***j* | See experimental | — | 4–7 | 70–72 | Methanol | 50.89 | 5.43 | 5.40[j] | 50.88 | 5.31 | 5.33 |
| **18***k* | See experimental | — | 7–18 | 65–68 | Ether | 50.89 | 5.43 | 5.40[k] | 50.94 | 5.42 | 5.28 |
| **18***l* | See experimental | — | 50 | Oil | — | 48.12 | 4.92 | 4.92[l] | 47.84 | 4.85 | 4.86 |
| **18***m* | −70 to rt | 2 | 41 | Oil | — | 50.09 | 4.90[m] | | 50.12 | 4.92 | |
| **18***n* | −75 to rt | 2.5 | 56 | Oil | — | 43.38 | 4.24[n] | | 43.33 | 4.29 | |
| **19***a* | See experimental | — | 94[o] | 132–134[e] | $CH_2Cl_2$–ether[e] | 68.53 | 9.87 | 7.99 | 68.72 | 9.87 | 8.19 |
| **19***b* | See experimental | — | 49–66[p] | Oil | — | 59.07 | 7.16 | 7.65 | 59.38 | 7.23 | 7.44 |
| **19***c* | −5 | 1 | 93 | 51–53 | EtOAc–hexane | 45.97 | 5.79 | 5.36 | 46.03 | 5.86 | 5.48 |
| **19***d* | Reflux (MeCN) | 1 | 97 | Oil | — | 36.89 | 4.13 | 4.78[q] | 37.06 | 4.07 | 4.67 |
| **19***f* | See experimental | — | 60[r] | Oil[s] | — | | | | | | |
| **19***g* | −5 | 1 | 94 | 44–45 | Ether–hexane | 48.04 | 6.23 | 5.09 | 48.16 | 6.24 | 5.08 |
| **19***h* | Reflux (MeCN) | 2 | 97 | Oil | — | 39.12 | 4.60 | 4.56 | 39.42 | 4.70 | 4.39 |
| **19***j* | See experimental | — | 57–59[t] | 145–150[c] | $CH_2Cl_2$[c] | 59.99 | 5.03 | 11.66 | 59.83 | 5.13 | 11.74 |
| **19***k* | −10 | 0.5 | 88 | 43–44 | Ether | 47.25 | 6.28 | 4.59 | 47.00 | 5.96 | 4.65 |

Can. J. Chem. Downloaded from www.nrcresearchpress.com by 210.87.254.5 on 09/06/12
For personal use only.



TABLE 1 (*Concluded*)

| Compound No. | Reaction temp. °C | Reaction time, h | Yield (%) | Melting point (°C) boiling point °C/Torr | Cryst. solvent | Calcd. C | Calcd. H | Calcd. N | Found C | Found H | Found N |
|---|---|---|---|---|---|---|---|---|---|---|---|
| **19***l* | Reflux (benzene) | 2.5 | 83 | Oil | — | 52.65 | 5.89 | 5.11 | 52.57 | 5.90 | 5.09 |
| **19***m* | rt | 6 | 97 | Oil | — | 49.66 | 5.55 | 6.43 | 49.63 | 5.46 | 6.53 |
| **19***n* | 0 to rt | 1 | 100 | Oil | — | 40.60 | 4.77 | 4.73 | 40.75 | 4.74 | 4.65 |
| **19***o* | Reflux (MeCN) | 2 | 81 | Oil[u] | — | | | | | | |
| **19***p* | rt | 18 | 86 | Oil[v] | — | | | | | | |
| **19***q* | rt | 18 | 88 | Oil[w] | — | | | | | | |
| **19***r* | 0 to rt | 0.5 | 80 | Oil[x] | — | | | | | | |
| **20** | 65 | 40 | 12 | Oil | — | 60.81 | 6.38 | 5.91 | 60.67 | 6.41 | 5.99 |
| **21** | 0 | 0.5 | 56 | Oil | — | 56.38 | 7.10 | 6.58 | 56.11 | 7.30 | 6.30 |
| **22***a* | −70 to rt | 2 | 34 | Oil[y] | — | | | | | | |
| **22***b* | −75 | 2.5 | 20 | 79 | Hexane | 35.06 | 3.18[z] | | 35.15 | 3.15 | |
| **23***a* | −20 to −30 | 3 | 100 | 60–61[aa] | $CH_2Cl_2$–hexane | | | | | | |
| **23***b* | −40 | 1 | 67 | 59[bb] | Ether | | | | | | |
| **24***a* | See experimental | — | 63 | 95–100/0.2[cc] | — | | | | | | |
| **24***b* | See experimental | — | 62 | 129/0.15 | — | 65.89 | 9.95 | 15.37 | 65.78 | 10.10 | 15.09 |
| **24***c* | See experimental | — | 88 | Oil | — | 67.30 | 10.27 | 14.27 | 67.33 | 10.32 | 13.93 |
| **26***a* | See experimental | — | 72 | Oil | — | 63.98 | 6.71 | 18.66 | 63.91 | 6.76 | 18.91 |
| **26***b* | −8 to 0 | 1 | 100 | Oil[dd] | — | 47.35 | 5.30 | 12.27 | 47.78 | 5.32 | 12.20 |
| **26***c* | Reflux (MeCN) | 0.67 | 92 | Oil[ee] | — | | | | | | |
| **26***d* | See experimental | — | 74 | 146/0.15 | — | 65.82 | 7.37 | 17.06 | 65.70 | 7.57 | 16.81 |
| **26***e* | −8 to 0 | 1 | 76 | Oil | — | 49.57 | 5.82 | 11.56 | 49.46 | 5.81 | 11.60 |
| **26***f* | See experimental | — | 36[ff] | 125–126[c] | $CH_2Cl_2$–MeOH[c] | 64.30 | 4.91 | 16.23 | 63.98 | 4.91 | 16.46 |
| **26***g* | 0 | 1.25 | 87 | Oil | — | 51.49 | 6.29 | 10.93 | 51.69 | 6.37 | 10.74 |

[a] *m/e* 255.1111 (calcd. for $C_{12}H_{17}NO_5$: 255.1107).
[b] Yield of the alcohol, an oil.
[c] These data and the elemental analysis are for the 4-(4-nitrophenylazo)benzoate.
[d] Yield of unstable carboxylic acid, mp 85–90°C (ether – ethyl acetate).
[e] These data and the elemental analysis refer to the dicyclohexylammonium salt.
[f] Yield, 10–17% from **18***b*; 35–46% from **18***h*.
[g] Calcd. for $C_{12}H_{17}NO_5$: 0.33 $H_2O$.
[h] Calcd. for $C_{10}H_{12}ClNO_3$: Cl 15.43; found: Cl 15.27.
[i] Calcd. for $C_{12}H_{16}ClNO_4$: Cl 12.96; found: Cl 12.86.
[j] Calcd. for $C_{11}H_{14}ClNO_4$: Cl 13.66; found: Cl 13.42.
[k] Calcd. for $C_{11}H_{14}ClNO_4$: Cl 13.66; found: Cl 13.49.
[l] Calcd. for $C_{11}H_{13}Cl_2NO_3$: 0.5 $H_2O$.
[m] Calcd. for $C_{12}H_{14}ClNO_5$: Cl 12.32; found: Cl 12.35.
[n] Calcd. for $C_{12}H_{14}BrNO_5$: Br 24.06; found: Br 24.01.
[o] Yield of the carboxylic acid, an oil.
[p] Overall yield from **18***b* of ester obtained with methyl iodide on salt of **19***a*.
[q] Calcd. for $C_9H_{12}INO_2$: I 43.32; found: I 43.38.
[r] Yield from **18***d*.
[s] *m/e* 197.1053 (calcd. for $C_{10}H_{15}NO_3$: 197.1052).
[t] Overall yield of **19***j* from **18***g* (methyl iodide process).
[u] *m/e* 326.9528; 328.9495 (calcd. for $C_9H_{11}{}^{35}Cl\,INO_2$: 326.9523; $C_9H_{11}{}^{37}Cl\,INO_2$: 328.9494).
[v] *m/e* 317.0274; 319.0256 (calcd. for $C_{12}H_{16}{}^{79}Br\,NO_4$: 317.0263; $C_{12}H_{16}{}^{81}Br\,NO_4$: 319.0242).
[w] *m/e* 261.0002; 262.9990 (calcd. for $C_9H_{12}{}^{79}Br\,NO_3$: 261.0001; $C_9H_{12}{}^{81}Br\,NO_3$: 262.9980).
[x] *m/e* 338.9780; 340.9761 (calcd. for $C_{10}H_{14}{}^{79}BrNO_5S$: 338.9796; $C_{10}H_{14}{}^{81}BrNO_5S$: 340.9756).
[y] *m/e* 287.0574; 289.0540 (calcd. for $C_{12}H_{14}{}^{35}ClNO_5$: 287.0561; $C_{12}H_{14}{}^{37}ClNO_5$: 289.0531).
[z] Calcd. for $C_{12}H_{13}Br_2NO_5$: Br 38.88; found: Br 38.75.
[aa] *m/e* 289.0716; 291.0697 (calcd. for $C_{12}H_{16}{}^{35}ClNO_5$: 289.0717; $C_{12}H_{16}{}^{37}ClNO_5$: 291.0688).
[bb] *m/e* 333.0217; 335.0205 (calcd. for $C_{12}H_{16}{}^{79}Br\,NO_5$: 333.0212; $C_{12}H_{16}{}^{81}Br\,NO_5$: 335.0191).
[cc] *m/e* 168.1261 (calcd. for $C_9H_{16}N_2O$: 168.1263).
[dd] *m/e* 228.0573 (calcd. for $C_9H_{12}N_2O_3S$: 228.0569).
[ee] *m/e* 259.9813 (calcd. for $C_8H_9IN_2$: 259.9810).
[ff] Yield of nitrile, bp 196°C/0.15 Torr).

Can. J. Chem. Downloaded from www.nrcresearchpress.com by 210.87.254.5 on 09/06/12
For personal use only.





TABLE 2. Synthetic conditions, yields, and physical constants for the bicyclic pyrrole derivatives

| Compound No. | Reaction temp. °C | Reaction time, h | Yield (%) | Melting point (°C) boiling point °C/Torr | Cryst. solvent | Calcd. C | Calcd. H | Calcd. N | Found C | Found H | Found N |
|---|---|---|---|---|---|---|---|---|---|---|---|
| **5***a* | 0 to rt | 1 | 95 | 70–71 | EtOAc–hexane | 59.18 | 5.87 | 6.28 | 59.10 | 5.99 | 6.27 |
| **5***b* | Reflux (MeOH–$H_2O$) | 3 | 89 | 200 dec. | MeOH | 55.38 | 4.65 | 7.18 | 55.15 | 4.58 | 7.00 |
| **5***c* | 0 to 25 | 1.5 | 91 | 144–145 | EtOAc–hexane | 60.75 | 6.37 | 5.90 | 60.54 | 6.46 | 5.82 |
| **5***d* | 0 to rt | 3 | 77 | 71 | Ether–hexane | 60.74 | 6.37 | | 60.74 | 6.48 | |
| **5***e* | Reflux (MeOH–$H_2O$) | 8 | 76 | 200–230 dec. | MeOH | 57.40 | 5.30 | | 57.53 | 5.53 | |
| **5***f* | −10 to rt | 3 | 82 | 160 | Water–acetone | 62.13 | 6.82 | | 62.19 | 6.81 | |
| **5***g* | 0 to rt | 24 | 99 | 42–43 | Ether–hexane | 62.13 | 6.82 | | 62.20 | 6.63 | |
| **5***h* | Reflux (MeOH–$H_2O$) | 18 | 79 | 160–200 dec. | MeOH–ether | 59.18 | 5.87 | | 59.27 | 5.89 | |
| **5***j* | 0 | 1 | 76[a] | | | | | | | | |
| **5***k* | Reflux (EtOH–$H_2O$) | 48 | 89 | 180.5–181.5 | MeOH–acetone | 56.90 | 5.97 | | 56.88 | 5.96 | |
| **5***l* | rt | 24 | 90 | 124–125 | $CH_2Cl_2$–ether | 61.00 | 7.17 | | 60.83 | 7.12 | |
| **5***m* | 0 | 3 | 72 | Oil | — | 61.00 | 7.17 | | 60.97 | 7.02 | |
| **5***n* | Reflux (EtOH–$H_2O$) | 24 | 92 | 153–154 | Acetone–hexane | 58.42 | 6.41 | | 58.46 | 6.38 | |
| **5***o* | rt | 6 | 86 | 122 | EtOAc–hexane | 62.11 | 7.49 | | 62.14 | 7.42 | |
| **6***a* | 270 | 1 | 68 | Oil | — | 68.37 | 7.82 | 7.25 | 68.13 | 7.65 | 7.08 |
| **6***b* | Reflux (MeOH–$H_2O$) | 4 | 77 | 152–153[b] | EtOAc–hexane | 72.25 | 9.70 | 8.43 | 72.28 | 9.68 | 8.29 |
| **6***c* | 240 | 1 | 70 | Oil[c] | — | | | | | | |
| **6***d* | rt (see text) | 24.5 | 61 | Oil[d] | — | | | | | | |
| **6***e* | 165/40 Torr | — | 88 | Oil[e] | — | | | | | | |
| **6***f* | Reflux (MeOH–$H_2O$) | 24 | 80 | 132–133[b] | Benzene–hexane | 70.73 | 9.81 | | 70.91 | 9.73 | |
| **6***g* | 230/22 Torr | — | 90 | Oil[f] | — | | | | | | |
| **6***h* | 0 to rt | 0.75 | 63 | Oil | — | 65.44 | 6.73 | 8.48 | 65.35 | 6.70 | 8.42 |
| **6***i* | 0 | 1 | 49 | 35–36.5[g] | — | 67.03 | 7.31 | 7.82 | 67.14 | 7.26 | 7.82 |
| **6***j* | 0 | 1 | 43 | 55–56 | Ether | 63.21 | 7.23 | 6.70 | 63.19 | 7.31 | 6.87 |
| **6***k* | 0 to rt | 2 | 75 | Oil[h] | — | | | | | | |
| **6***l* | 0 | 3 | 49 | Oil[i] | — | | | | | | |
| **8***a* | 0 to rt | 1 | 67–86 | 107–108 | Benzene–hexane | 60.75 | 6.37 | 5.90 | 60.81 | 6.28 | 5.83 |
| **8***b* | Reflux (MeOH–$H_2O$) | 24 | 96 | 236–237 | MeOH | 57.41 | 5.30 | | 57.21 | 5.39 | |
| **8***c* | 0 to rt | 48 | 28–33 | 160 | Acetone–hexane | 62.14 | 6.82 | | 61.89 | 6.91 | |

Can. J. Chem. Downloaded from www.nrcresearchpress.com by 210.87.254.5 on 09/06/12
For personal use only.



TABLE 2 (*Concluded*)

| Compound No. | Reaction temp. °C | Reaction time, h | Yield (%) | Melting point (°C) boiling point °C/Torr | Cryst. solvent | Calcd. C | Calcd. H | Calcd. N | Found C | Found H | Found N |
|---|---|---|---|---|---|---|---|---|---|---|---|
| **9***a* | 230–245 | — | 60–75 | Oil[j] | — | | | | | | |
| **9***b* | Reflux (EtOH–$H_2O$) | 18 | 50 | 94–95 | Benzene | 65.43 | 6.71 | 8.48 | 65.42 | 6.52 | 8.59 |
| **9***c* | See text | — | 51 | Oil | — | 67.02 | 7.31 | 7.82 | 66.95 | 7.43 | 7.62 |
| **11***a* | 0 to rt | 5 | 64 | 105 | $CH_2Cl_2$–hexane | 60.74 | 6.37 | | 60.54 | 6.29 | |
| **11***b* | Reflux (MeOH–$H_2O$) | 30 | 93 | 213 | MeOH–$H_2O$ | 57.90 | 5.30 | | 57.31 | 5.18 | |
| **11***c* | −10 to rt | 2 | 75 | 160 | EtOAc–hexane | 62.13 | 6.82 | | 62.19 | 6.81 | |
| **11***d* | 0 | 0.5 | 93 | 98–100 | Acetone–hexane | 68.21 | 5.72 | 4.69 | 68.13 | 5.63 | 4.57 |
| **11***e* | Reflux (MeOH–$H_2O$) | 7 | 80 | 203–206 | EtOAc–ether | 66.41 | 4.82 | 5.16 | 66.36 | 4.91 | 4.94 |
| **11***f* | −10 to rt | 2 | 95 | 157–159 | Acetone–hexane | 68.99 | 6.11 | 4.46 | 68.80 | 5.96 | 4.34 |
| **12***a* | 250 | — | 50–60 | Oil[k] | — | | | | | | |
| **12***b* | 270 | 0.75 | 50 | 52–54 | MeOH | 75.80 | 7.11 | 5.19 | 76.00 | 7.18 | 5.22 |
| **12***c* | Reflux (MeOH–$H_2O$) | 1 | 56 | 162–163 | EtOAc–hexane | 73.99 | 5.76 | 6.16 | 74.15 | 5.62 | 6.32 |
| **27***a* | 15 to rt | 2 | 84 | 44–45 | EtOH | 72.70 | 6.10 | 21.20 | 72.72 | 6.25 | 21.17 |
| **27***b* | −5 to rt | 2 | 65 | 47–49 | Acetone–hexane | 73.94 | 6.89 | 19.17 | 73.67 | 6.92 | 19.30 |
| **27***c* | −5 to 15 | 1 | 69 | 70–72 | Acetone–hexane | 74.96 | 7.55 | 17.49 | 75.25 | 7.47 | 17.63 |
| **28***a* | 118 (see text) | 3 | 92 | 129–130 | Benzene | 67.02 | 7.31 | 7.81 | 67.30 | 7.53 | 7.86 |
| **28***b* | See text | — | 89 | 56–57 | Acetone–hexane | 68.36 | 7.82 | 7.24 | 68.16 | 7.83 | 7.17 |

[a] *m/e* 281.1263 (calcd. for $C_{14}H_{19}NO_5$: 281.1263).
[b] Analysis and physical constants for dicyclohexylammonium salt.
[c] *m/e* 207.1275 (calcd. for $C_{12}H_{17}NO_2$: 207.1259).
[d] *m/e* 221.1398 (calcd. for $C_{13}H_{19}NO_2$: 221.1416).
[e] *m/e* 251.1521 (calcd. for $C_{14}H_{21}NO_3$: 251.1521).
[f] *m/e* 265.1641 (calcd. for $C_{15}H_{23}O_3N$: 265.1678).
[g] Melting point of material which crystallized on standing.
[h] *m/e* 199.0404; 201.0378 (calcd. for $C_9H_{10}{}^{35}ClNO_2$: 199.0400; $C_9H_{10}{}^{37}ClNO_2$: 201.0371).
[i] *m/e* 242.9888; 244.9879 (calcd. for $C_9H_{10}{}^{79}BrNO_2$: 242.9895; $C_9H_{10}{}^{81}BrNO_2$: 244.9874).
[j] *m/e* 207.1258 (calcd. for $C_{12}H_{17}NO_2$: 207.1259).
[k] *m/e* 207.1251 (calcd. for $C_{12}H_{17}NO_2$: 207.1259).

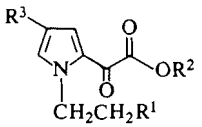

**18a** $R^1$ = OTHP, $R^2$ = $C_2H_5$, $R^3$ = H
**18b** $R^1$ = $OCOCH_3$, $R^2$ = $C_2H_5$, $R^3$ = H
**18c** $R^1$ = OH, $R^2$, $R^3$ = H
**18d** $R^1$ = $OCOCH_3$, $R^2$ = $CH_3$, $R^3$ = CHO
**18e** $R^1$ = OH, $R^2$ = H, $R^3$ = CHO
**18f** $R^1$ = $OCOCH_3$, $R^2$ = $C_2H_5$, $R^3$ = $CH_3OCH_2$
**18g** $R^1$ = OH, $R^2$ = $C_2H_5$, $R^3$ = $CH_3OCH_2$
**18h** $R^1$ = Cl, $R^2$ = $C_2H_5$, $R^3$ = H
**18i** $R^1$ = Cl, $R^2$ = $C_2H_5$, $R^3$ = $CH_3OCH_2$
**18j** $R^1$ = Cl, $R^2$ = $CH_3$, $R^3$ = $CH_3OCH_2$
**18k** $R^1$ = Cl, $R^2$ = $C_2H_5$, $R^3$ = $HOCH_2$
**18l** $R^1$ = Cl, $R^2$ = $C_2H_5$, $R^3$ = $ClCH_2$
**18m** $R^1$ = $OCOCH_3$, $R^2$ = $C_2H_5$, $R^3$ = Cl
**18n** $R^1$ = $OCOCH_3$, $R^2$ = $C_2H_5$, $R^3$ = Br

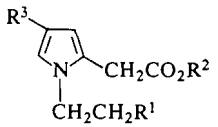

**19a** $R^1$ = OH, $R^2$, $R^3$ = H
**19b** $R^1$ = OH, $R^2$ = $CH_3$, $R^3$ = H
**19c** $R^1$ = $OSO_2CH_3$, $R^2$ = $CH_3$, $R^3$ = H
**19d** $R^1$ = I, $R^2$ = $CH_3$, $R^3$ = H
**19e** $R^1$ = OH, $R^2$ = H, $R^3$ = $CH_3$
**19f** $R^1$ = OH, $R^2$, $R^3$ = $CH_3$
**19g** $R^1$ = $OSO_2CH_3$, $R^2$, $R^3$ = $CH_3$
**19h** $R^1$ = I, $R^2$, $R^3$ = $CH_3$
**19i** $R^1$ = OH, $R^2$ = H, $R^3$ = $CH_3OCH_2$
**19j** $R^1$ = OH, $R^2$ = $CH_3$, $R^3$ = $CH_3OCH_2$
**19k** $R^1$ = $OSO_2CH_3$, $R^2$ = $CH_3$, $R^3$ = $CH_3OCH_2$
**19l** $R^1$ = $OCOCH_3$, $R^2$ = $C_2H_5$, $R^3$ = Cl
**19m** $R^1$ = OH, $R^2$ = $CH_3$, $R^3$ = Cl
**19n** $R^1$ = $OSO_2CH_3$, $R^2$ = $CH_3$, $R^3$ = Cl
**19o** $R^1$ = I, $R^2$ = $CH_3$, $R^3$ = Cl
**19p** $R^1$ = $OCOCH_3$, $R^2$ = $C_2H_5$, $R^3$ = Br
**19q** $R^1$ = OH, $R^2$ = $CH_3$, $R^3$ = Br
**19r** $R^1$ = $OSO_2CH_3$, $R^2$ = $CH_3$, $R^3$ = Br

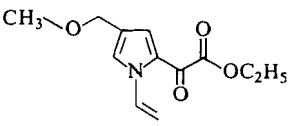

**20**

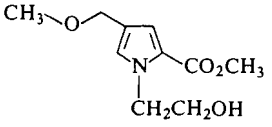

**21**

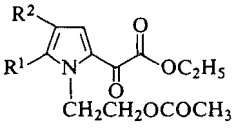

**22a** $R^1$ = Cl, $R^2$ = H
**22b** $R^1$, $R^2$ = Br

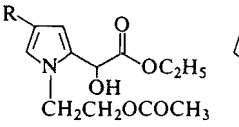

**23a** R = Cl
**23b** R = Br

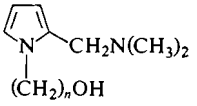

**24a** $n$ = 2
**24b** $n$ = 3
**24c** $n$ = 4

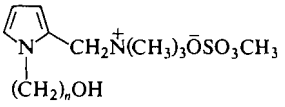

**25**

to a 5-membered ring, at positions -1 and -2 of pyrrole. For the parent system the process commenced with the preparation of the known (4) 1-(2-hydroxyethyl)pyrrole **2***a* from 2,5-dimethoxytetrahydrofuran and ethanolamine, a synthesis which was much more convenient, and better yielding, than that described by Blicke and Blake (4). The alcohol was converted into the tetrahydropyranyl ether **17***a* which, on acylation with ethoxalyl chloride in the presence of pyridine, gave the α-keto ester **18***a*. This compound could also be prepared, in good yield, by the sodium hydride mediated alkylation of 2-ethoxalyl pyrrole (5) with the tetrahydropyranyl ether of bromoethanol. In addition, acylation of 1-(2-acetoxyethyl)pyrrole **17***b* (4) with ethoxalyl chloride provided the acetate **18***b*, a particularly useful precursor of the required bicyclic systems. Saponification of either **18***a* or **18***b*, followed by careful acidification at 0°C, permitted the isolation of the unstable α-keto acid **18***c*. In general, however, the crude carboxylic acid salt was directly subjected to the Huang–Minlon modification of the Wolff–Kishner reduction. The pyrrole acetic acid derivative **19***a* thus produced was converted, without purification, into the corresponding methyl ester **19***b* with methyl iodide, in DMF containing potassium carbonate (50–70% overall yield from α-keto esters **18***a* or **18***b*), or with ethereal diazomethane (53% overall from **18***a*). The transformation of this substance into the bicyclic methyl ester **6***h* was then accomplished, in the usual manner, via the methanesulfonate **19***c* and the iodide **19***d*.

The versatility of the above process proved to be considerable since, by appropriate modification of the reaction sequence, it was also possible to prepare analogues of **6***h* incorporating a methyl, methoxymethyl, chloro, or a bromo group at C-6. For example, the carbon atom destined to be the 6-methyl group in **6***i* was introduced by a Vilsmeier–Haack reaction on the keto ester **18***b*. Saponification of the 4-formyl-α-keto ester **18***d* so produced gave the carboxylic acid **18***e* which was transformed, in one step, into the 4-methylpyrrole-2-acetic acid derivative **19***e* by the modified Wolff–Kishner reduction.

The introduction of the methoxymethyl group was first effected by the hydrogen chloride promoted reaction of dimethoxymethane with the ethoxalyl pyrrole **18***b*, and subsequent methanolysis of a presumed (see below) intermediate chloromethyl compound. This reaction gave varying amounts of the expected 4-methoxymethyl pyrrole **18***f* and the corresponding alcohol **18***g* in

Can. J. Chem. Downloaded from www.nrcresearchpress.com by 210.87.254.5 on 09/06/12
For personal use only.

Can. J. Chem. Downloaded from www.nrcresearchpress.com by 210.87.254.5 on 09/06/12
For personal use only.

combined yields of 30–36%. Because of the capricious nature of the above reaction, an alternative route to the desired compounds, based on the methoxymethylation of 1-(2-chloroethyl)-2-ethoxyalylpyrrole **18***h* (prepared by acylation of 1-(2-chloroethyl)pyrrole **17***c*), was devised. This reaction sequence gave the expected 4-methoxymethyl pyrrole derivative **18***i* as the major product, together with minor amounts of the methyl ester **18***j* and the 4-hydroxymethyl compound **18***k* (converted into **18***i* by acid catalyzed methanolysis). The process was shown to proceed via the intermediate 4-chloromethyl compound **18***l* by elimination of the methanolysis step. Nucleophilic displacement of chloride ion in **18***i* with excess sodium acetate, in the presence of sodium iodide, gave a mixture of the 1-acetoxyethyl and 1-hydroxyethyl pyrrole derivatives **18***f* and **18***g* in a combined overall yield of 35–47% from 1-(2-chloroethyl)-2-ethoxalylpyrrole **18***h*. A small amount of the *N*-vinyl compound **20** was also formed in this reaction. Careful saponification of either **18***f* or **18***g* with potassium hydroxide in ethylene glycol at −5°C, followed by sequential Wolff–Kishner reduction and esterification of the crude potassium salt of the acetic acid **19***i* with methyl iodide, gave the methyl ester **19***j* in 58% yield overall.[6]

The introduction of chlorine or bromine at the required position was accomplished by the low temperature halogenation of the oxalyl compound **18***b* with sulfuryl chloride or bromine. In each case, in addition to the desired 4-substituted pyrrole derivatives **18***m* and **18***n*, lesser amounts of the pyrroles **22***a* and **22***b*, substituted at C-5 or at C-5 and C-6, were also isolated. Because of the concern that the halo moiety in **18***m* and **18***n* would not survive the drastic conditions of the Wolff–Kishner reduction, an alternative means of converting these α-keto esters into the corresponding acetic acid derivatives was devised. Thus, reduction with sodium borohydride at low temperature gave the secondary alcohols **23***a* and **23***b*, which were then reacted with equimolar amounts of triphenylphosphine and triphenylphosphine diiodide in boiling benzene (6). Whereas this resulted in the clean conversion of the 4-chloro alcohol **23***a* into the acetic acid ethyl ester **19***l*, under the same conditions **23***b* suffered the loss of the nuclear bromine atom as well. This difficulty was obviated, however, when the reaction was conducted at room temperature.[7] Finally, the acetates **19***l* and **19***p* were subjected to 1,5-diazabicyclo[4.3.0]non-5-ene (DBN) catalyzed transesterification with methanol, which resulted in the formation of the *N*-hydroxyethyl methyl esters **19***m* and **19***q*.

The 4-substituted 1-(2-hydroxyethyl)pyrrole acetic acid esters **19***f*, **19***j*, **19***m*, and **19***q*, described above, were converted into the corresponding 6-substituted 1,2-dihydro-3*H*-pyrrolo[1,2-*a*]pyrrole-1-carboxylic acid derivatives **6***i* to **6***l*, in the usual manner, via the respective *N*-methanesulfonyloxyethyl or *N*-iodoethyl compounds.

A third and final approach to the desired bicyclic compounds was tactically identical to the second synthetic route, described above, except for the manner of the attachment of the two-carbon unit to C-2 of the pyrrole moiety. This operation was accomplished in a three-step sequence (7) which is exemplified below for the synthesis of the parent pyrrolopyrrole carboxylic acid derivative **6***h*. Thus, reaction of *N*-hydroxyethylpyrrole **2***a* with formaldehyde and dimethylamine hydrochloride gave the Mannich base **24***a* which was quaternized with dimethyl sulfate. The quaternary ammonium salt **25** ($n = 2$) was converted, without isolation, into the acetonitrile derivative **26***a* with hot aqueous sodium cyanide. The cyclization of this compound to **27***a* was then carried out in the usual

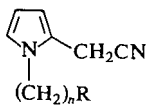


**26***a* $n = 2$, R = OH
**26***b* $n = 2$, R = $OSO_2CH_3$
**26***c* $n = 2$, R = I
**26***d* $n = 3$, R = OH
**26***e* $n = 3$, R = $OSO_2CH_3$
**26***f* $n = 4$, R = OH
**26***g* $n = 4$, R = $OSO_2CH_3$

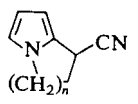


**27***a* $n = 1$
**27***b* $n = 2$
**27***c* $n = 3$

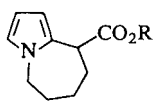


**28***a* R = H
**28***b* R = $CH_3$

manner via the methane sulfonate **26***b* and the iodide **26***c*. Alkaline hydrolysis of the nitrile **27***a*, followed by reaction of the crude salt with methyl iodide, provided the previously described methyl ester **6***h*. In a similar manner, but commencing with *N*-hydroxypropylpyrrole **2***b* and *N*-hydroxybutylpyrrole **2***c*, were prepared 5,6,7,8-tetrahydropyrrolo[1,2-*a*]pyrrole-8-carbonitrile **27***b*, 5,6,7,8-tetrahydro-9*H*-pyrrolo[1,2-*a*]azepine-9-carbonitrile **27***c*, and the corresponding acid methyl esters **9***c* and **28***b*.

[6]A small amount of the decarbonylation product **21** was also isolated. If the saponification of **18***f* was effected with aqueous methanolic potassium hydroxide at 0°C, it became the major product.

[7]This synthesis of pyrrole acetic acid derivatives, which doubtless proceeds via the α-iodo ester and the enol phosphonium salt (8) corresponding thereto, has a considerable degree of generality.[8]

[8]Y. Antonio and R. Greenhouse. Unpublished data.

TABLE 3. Nuclear magnetic resonance spectra of some bicyclic pyrrole derivatives[a]

| Compound | Chemical shifts (δ ppm)[b] | Coupling constants (Hz)[b] Aliphatic | | Aromatic | |
|---|---|---|---|---|---|
| 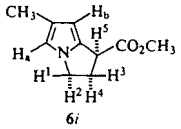 *6i* | 2.10 ($CH_3$) | $J_{1,2}$ | −10.07 | | |
| | 2.66 (H-4) | $J_{1,3}$ | 8.14 | | |
| | 2.80 (H-3) | $J_{1,4}$ | 6.10 | | |
| | 3.72 ($OCH_3$) | $J_{2,3}$ | 5.18 | | |
| | 3.88 (H-2) | $J_{2,4}$ | 8.43 | | |
| | 3.97 (H-5) | $J_{3,4}$ | −13.06 | | |
| | 4.05 (H-1) | $J_{3,5}$ | 5.00 | | |
| | 5.81 ($H_b$) | $J_{4,5}$ | 8.56 | | |
| | 6.40 ($H_a$) | $J_{5,b}$ | 0.83 | | |
| 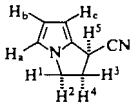 *27a* | 2.82 (H-3) | $J_{1,2}$ | −10.46 | $J_{a,b}$ | 2.65 |
| | 2.92 (H-4) | $J_{1,3}$ | 8.60 | $J_{a,c}$ | 1.11 |
| | 3.99 (H-2) | $J_{1,4}$ | 5.84 | $J_{b,c}$ | 3.55 |
| | 4.11 (H-5) | $J_{2,3}$ | 5.90 | | |
| | 4.13 (H-1) | $J_{2,4}$ | 7.84 | | |
| | 6.07 ($H_c$) | $J_{3,4}$ | −13.35 | | |
| | 6.25 ($H_b$) | $J_{3,5}$ | 5.50 | | |
| | 6.66 ($H_a$) | $J_{4,5}$ | 8.24 | | |
| | | $J_{5,c}$ | 1.00 | | |
| 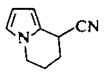 *27b* | 1.93–2.05 (m, 1H) | | | | |
| | 2.08–2.25 (m, 3H) | | | | |
| | 3.96 (m, 2H) | | | | |
| | 4.07 (m, 1H) | | | | |
| | 6.18 (m, 2H) | | | | |
| | 6.59 (m, 1H) | | | | |
| 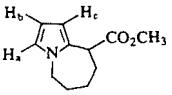 *28b* | 1.60–1.91 (m, 5H) | | | $J_{a,b}$ | 2.79 |
| | 2.10–2.24 (m, 1H) | | | $J_{a,c}$ | 1.91 |
| | 3.73 ($OCH_3$) | | | $J_{b,c}$ | 3.38 |
| | 3.88–4.08 (m, 3H) | | | $J_{9,c}$ | 0.44 |
| | 5.90 ($H_c$) | | | | |
| | 6.00 ($H_b$) | | | | |
| | 6.59 ($H_a$) | | | | |

[a]Measured on a Bruker WM300 spectrometer operating at 300.133 MHz (spectral width 3600 Hz; pulse width 4 μs; pulse interval 5.4 s; scans 4; line broadening function −0.1 Hz; data points 32 000).
[b]The chemical shifts and coupling constants of the aliphatic protons of *6i* and *27a* were simulated as indicated in the experimental section.

The compounds described in this manuscript were fully characterized by the usual spectroscopic techniques (see introduction to experimental section), which included nmr spectra. A selection of the latter are found in Table 4 or in the experimental part. A complete compilation of the spectra (Tables 5 and 6) can be obtained from the Depository of Unpublished Data.[9] The nmr spectra of the nitriles **27***a* and **27***b* and the methyl esters **6***i* and **28***b* were also measured at 300 MHz. The absorptions for the protons of the ester **6***i* and the nitrile **27***a* were sufficiently chemically shifted from one another to permit a complete analysis of the spectra (see Table 3). This was not true for compounds **27***b* and **28***b*, and little useful information could be derived from the aliphatic region of these spectra.

Molecular models predict that the ring system of the 1-substituted 1,2-dihydro-3*H*-pyrrolo[1,2-*a*]-pyrroles should be nearly planar. The vicinal coupling constants, listed in Table 3, at the least show the expected trend of $J_{cis} > J_{trans}$, which is consistent with this prediction. Nevertheless, the *cis* and *trans* coupling constants do not differ as much as might be anticipated for a planar 5-membered ring, a situation which has been observed and discussed in detail elsewhere (9).

Finally, it is of some interest that the proton α to the carbomethoxy or the cyano substituent in compounds **6***i*, **27***a*, and **28***b* is long range coupled (0.5–1 Hz) to the adjacent pyrrole proton, a phenomenon which has previously been reported for various substituted pyrroles (10).

## Experimental

The melting points were determined in a Mel-Temp melting point apparatus and are corrected. The infrared spectra were measured with a Perkin–Elmer Model 237 grating infrared

[9]These tables are available at a nominal charge from the Depository of Unpublished Data, CISTI, National Research Council of Canada, Ottawa, Ont., Canada K1A 0S2.

Can. J. Chem. Downloaded from www.nrcresearchpress.com by 210.87.254.5 on 09/06/12
For personal use only.

Can. J. Chem. Downloaded from www.nrcresearchpress.com by 210.87.254.5 on 09/06/12
For personal use only.

TABLE 4. Nuclear magnetic resonance spectra of some pyrrole derivatives[a]

| Compound | Chemical shifts δ (ppm) |
|---|---|
| **4***a* | 3.68 (s, 3H, $OCH_3$), 3.75 (s, 3H, $OCH_3$), 3.81–3.99 (m, 4H, $CH_2CH_2$), 4.11 (s, 2H, $CH_2CO$), 6.61 (q, 2H, $J_{AB}$ = 2.9 Hz, H-3,4) |
| **4***d* | 2.20 (s, 3H, $CH_3$), 3.62–3.97 (m, 4H, $CH_2CH_2$), 3.68 (s, 3H, $OCH_3$), 3.73 (s, 3H, $OCH_3$), 4.00 (s, 2H, $CH_2$), 6.35 (s, 1H, H-5) |
| **5***a* | 2.48–3.08 (m, 2H, $CH_2$), 3.71 (s, 3H, $OCH_3$), 3.74 (s, 3H, $OCH_3$), 3.93–4.31 (m, 3H, CH, $CH_2N$), 6.47 (m, 2H, H-5, 6) |
| **5***d* | 2.23 (s, 3H, $CH_3$), 2.42–3.07 (m, 2H, $CH_2$), 3.67 (s, 6H, 2 × $OCH_3$), 3.73–4.32 (m, 3H, CH, $CH_2N$), 6.27 (s, 1H, H-5) |
| **6***j* | 2.40–2.79 (m, 2H, $CH_2$), 3.25 (s, 3H, $CH_3OCH_2$), 3.63 (s, 3H, $OCH_3$), 3.75–4.05 (m, 3H, CH, $CH_2N$), 4.20 (s, 2H, $CH_3OCH_2$), 5.90 (s, 1H, H-7), 6.52 (s, 1H, H-5) |
| **6***k* | 2.37–2.75 (m, 2H, $CH_2$), 3.62 (s, 3H, $OCH_3$), 3.53–4.07 (m, 3H, CH, $CH_2N$), 5.85 (m, 1H, H-7), 6.45 (m, 1H, H-5) |
| **10***a* | 2.19 (s, 3H, 5-$CH_3$), 3.65 (s, 3H, $OCH_3$), 3.70 (s, 3H, $OCH_2$), 3.82 (m, 4H, $CH_2CH_2$), 4.03 (s, 2H, $CH_2$), 6.23 (m, 1H, H-4) |
| **11***a* | 2.13 (s, 3H, $CH_3$), 2.50–2.90 (m, 2H, $CH_2$), 3.63–4.22 (m, 3H, CH, $CH_2N$), 3.66 (s, 6H, 2 × $OCH_3$), 6.18 (s, 1H, H-6) |
| **18***i* | 1.40 (t, 3H, $J$ = 7.2 Hz, $CH_3$), 3.40 (s, 3H, $CH_3O$), 3.84 (t, 2H, $J$ = 5.7 Hz, $CH_2Cl$), 4.37 (s, 2H, $CH_3OCH_2$), 4.43 (q, 2H, $J$ = 7.2 Hz, $CH_2$), 4.63 (t, 2H, $J$ = 5.7 Hz, $CH_2N$), 7.16 (d, 1H, $J$ = 1.8 Hz, H-3 or H-5), 7.34 (d, 1H, $J$ = 1.3 Hz, H-5 or H-3) |
| **18***m* | 1.44 (t, 3H, $J$ = 7.2 Hz, $CH_3$), 2.07 (s, 3H, $CH_3CO_2$), 4.23–4.70 (m, 6H, 3 × $CH_2$), 7.00 (d, 3H, $J$ = 1.8 Hz, H-3 or H-5), 7.27 (d, 1H, $J$ = 1.8 Hz, H-5 or H-3) |
| **19***n* | 2.84 (s, 3H, $SO_2CH_3$), 3.60 (s, 2H, $CH_2CO$), 3.70 (s, 3H, $OCH_3$), 4.00–4.47 (m, 4H, $CH_2CH_2$), 5.98 (d, 1H, $J$ = 2.0 Hz, H-3), 6.64 (d, 1H, $J$ = 2.0 Hz, H-5) |

[a] Measured in deuteriochloroform. OH and NH groups were exchanged with deuterium oxide.

spectrophotometer. The ultraviolet spectra were recorded on a Perkin–Elmer Model 402 ultraviolet visible spectrometer. The $^1H$ nmr spectra were measured with a Varian T-60, a Varian HA-100, or a Bruker WM 300 nmr spectrometer and are expressed as parts per million (δ) from internal tetramethylsilane. The low resolution mass spectra were measured on Atlas CH-4, Varian-MAT CH-7, and AEI MS-9 spectrometers. The high resolution mass spectra were obtained with a Varian-MAT 311A mass spectrometer.

The 300 MHz nmr spectra of compounds **6***h* and **27***a* were simulated with an Aspect 2000 computer using the PANIC computer program (Bruker-Physik AG, Rheinstetten, Germany).

The term "dried" signifies dried over $Na_2SO_4$ throughout the experimental section.

*Synthesis of the 1-bromoalkan-2-ones*

(a) *1-Bromobutan-2-one*

This compound was prepared in the manner described by Catch *et al.* (11).

(b) *1-Bromo-4-methoxybutan-2-one*

A solution of the known (12) 3-methoxypropionyl chloride (1 mol) in dry $CH_2Cl_2$ (25 mL/g) was added to an ethereal solution of $CH_2N_2$ (2.5 mol, prepared from nitrosomethylurea) at −10°C. After 1 h at this temperature, the solvent was removed at 0°C by means of a stream of $N_2$. The crude diazoketone (ir ($CHCl_3$): 2120, 1636 $cm^{-1}$) was dissolved in $CH_2Cl_2$ (50 mL/g) and the solution was cooled to −70°C. A saturated solution of HBr gas in $CH_2Cl_2$ was then added dropwise, care being taken that excess HBr solution was not added. When the diazoketone had been consumed (tlc analysis), the temperature was lowered to −75°C and a stream of $N_2$ was passed through the solution until the solvent volume had been reduced to about one-third of the original. The remainder of the solvent was then removed *in vacuo* (≤25 mm) at room temperature. The residue was subjected to column chromatography on silica gel using EtOAc–hexane (5:95) as the eluting solvent. A lachrymatory, volatile oil (74% yield) remained; ir ($CHCl_3$): 1716 $cm^{-1}$; nmr ($CDCl_3$) δ: 2.87 (t, 2H, $J$ = 6.0 Hz), 3.33 (s, 3H), 3.67 (5, 2H, $J$ = 6.0 Hz), 3.94 (s, 2H). This compound was not characterized further.

(c) *1-Bromo-5-methoxy-2-pentanone*

To a solution of 4-methoxybutyric acid (ref. 13; 20.0 g, 169 mmol), in dry $CH_2Cl_2$ (50 mL), was added anhydrous DMF (0.5 mL) and $SOCl_2$ (21.4 g, 180 mmol). The solution was left at room temperature for 2 h and then the solvent was removed *in vacuo* (≤25°C). The residual oil was then added to excess ethereal $CH_2N_2$ at 0°C as described above. After the usual work-up the crude diazoketone was dissolved in ether and an ethereal solution of HBr gas was added thereto in the manner described above. When the diazoketone was no longer present the solvent was removed *in vacuo* (≤20°C) and the residue was subjected to column chromatography on silica gel (400 g) using $CH_2Cl_2$ (15:85) to elute the product. The eluate was evaporated at ≤20°C (≈20 Torr) to minimize loss of the volatile bromoketone (25.0 g, 76%); ir ($CHCl_3$): 1715 $cm^{-1}$; nmr ($CDCl_3$) δ: 1.88 (quin., 2H, $J$ = 6.8 Hz), 2.74 (t, 2H, $J$ = 6.0 Hz), 3.29 (s, 3H), 3.37 (t, 2H, $J$ = 6.0 Hz), 3.88 (s, 2H). This compound (light sensitive) was not characterized further.

*1-(2-Hydroxyethyl)pyrrole* **2**a

Ethanolamine (400 g, 6.55 mol) was added with efficient agitation to glacial HOAc (720 mL), cooled in an ice–salt mixture at a rate such that the temperature was maintained at 15–25°C. When the addition was completed, 2,5-dimethoxytetrahydrofuran (200 g, 1.51 mol) was added in one portion, the reaction vessel was removed from the cooling bath and set up for downward distillation. The reaction flask was placed in an oil bath and the temperature was raised to 110–120°C, at which point distillation of a liquid commenced. After ca. 1.5 h at this temperature about 250 mL of a distillate had been collected. The residual liquid in the reaction vessel was cooled to room temperature, it was diluted with $H_2O$ (1.2 L), and extracted with $CH_2Cl_2$. The extract was washed successively with saturated aqueous solutions of NaCl and $Na_2CO_3$, it was dried, and then the solvent was removed *in vacuo*. The residue, which consisted mainly of the desired alcohol **2***a* and a lesser amount of the corresponding acetate **17***b*, was dissolved in MeOH (250 mL), 20 wt.% NaOH (200 mL) was added, and the solution was left at room temperature for 1 h. The solution was poured into saturated aqueous NaCl solution (2.5 L), the product was extracted into $CH_2Cl_2$, and the extract was dried. The solvent was removed *in vacuo* leaving an oil (117 g, 70%) which was spectroscopically identical to a specimen which had been prepared by the method of Blicke and Blake (4); uv (MeOH): 223 nm (ε 3900); ir ($CHCl_3$): 3605, 3490 $cm^{-1}$; nmr ($CDCl_3$) δ: 2.23 (s, 1H, OH), 3.50–3.93 (m, 4H, $CH_2CH_2$), 6.04 (m, 2H, H-3,4), 6.55 (m, 2H, H-2,5).

Can. J. Chem. Downloaded from www.nrcresearchpress.com by 210.87.254.5 on 09/06/12
For personal use only.

*1-(3-Hydroxypropyl)pyrrole* 2b

This compound was prepared from 3-aminopropanol (300 g, 3.99 mol) and 2,5-dimethoxytetrahydrofuran (150 g, 1.14 mol), in HOAc solution (540 mL), in the manner described above for compound **2***a*. After alkaline hydrolysis of the crude product obtained from this condensation, the hydrolysate was subjected to column chromatography on Florisil. The product (79.6 g, 45.6%) was eluted from the column with hexane–$CH_2Cl_2$ (3:1, then 1:1) and was of sufficient purity for use in subsequent reactions. For analysis a small amount of the material was distilled *in vacuo*, bp 65–67°C/0.2 Torr; uv (MeOH): 223 nm (ε 4570); ir ($CHCl_3$): 3436 $cm^{-1}$; nmr ($CDCl_3$) δ: 2.00 (m, 2H, $CH_2$), 3.55 (m, 2H, $CH_2O$), 3.95 (m, 2H, $CH_2N$), 6.10 (m, 2H, H-3,4), 6.61 (m, 2H, H-2,5); *Anal.* calcd. for $C_7H_{11}NO$: C 67.17, H 8.86, N 11.15; found: C 67.04, H 8.93, N 11.12.

*1-(4-Hydroxybutyl)pyrrole* 2c

This alcohol was prepared from 4-aminobutanol (ref. 14; 76.8 g, 860 mmol) and 2,5-dimethoxytetrahydrofuran (38.4 g, 290 mmol), in glacial HOAc solution (150 mL), in the manner described above. The product was obtained in 61% yield after purification by distillation *in vacuo*, bp 69°C/0.075 Torr; uv (MeOH): 224 nm (ε 3800); ir ($CHCl_3$): 3597, 3460 $cm^{-1}$; nmr ($CDCl_3$) δ: 1.66 (m, 4H, $CH_2CH_2$), 3.56 (m, 2H, $CH_2O$), 3.86 (m, 2H, $CH_2N$), 6.10 (m, 2H, H-3,4), 6.60 (m, 2H, H-2,5); mass spectrum *m/e*: 139 ($M^+$); *Anal.* calcd. for $C_8H_{13}NO$: C 69.02, H 9.41, N 10.06; found: C 68.55, H 9.48, N 10.03.

This compound was further characterized by conversion into the 4-(4-nitrophenylazo) benzoate. To a stirred solution of the alcohol **2***c* (0.450 g, 3.2 mmol) in dry $C_6H_6$ (50 mL) containing pyridine (0.51 g, 6.4 mmol) was added 4-(4-nitrophenylazo) benzoyl chloride (ref. 15; 1.03 g, 3.5 mmol). After 40 min the mixture was evaporated to dryness *in vacuo* and the residue was passed through a column of neutral alumina (30 g, Fluka, Act. I) using $C_6H_6$ as the solvent. The product, after crystallization from $CH_2Cl_2$–MeOH, was obtained in 68% yield. A further crystallization from EtOAc gave the analytical specimen, mp 108–110°C; ir ($CHCl_3$): 1710, 1610, 1520, 1340 $cm^{-1}$; *Anal.* calcd. for $C_{21}H_{20}N_4$: C 64.27, H 5.14, N 14.28; found: C 63.97, H 5.15, N 14.24.

*1-(2-Tetrahydropyran-2-yloxyethyl)pyrrole* 17a

A solution of the alcohol **2***a* (3.0 g, 2.7 mmol) in anhydrous $CH_2Cl_2$ (50 mL), containing dihydropyran (6.8 g, 8.1 mmol), was cooled to −20°C and *p*-TsOH (0.073 g) was added. After 45 min at this temperature, pyridine (5 drops) was added, and then the mixture was partitioned between $H_2O$ and ether. The organic phase was washed with saturated NaCl solution, it was dried, and then the solvent was removed *in vacuo*. The residue was purified by column chromatography on Florisil (150 g) using hexane and hexane–ether (95:5) to elute the product (4.2 g, 81%) which had bp 87°C/2 Torr (slight dec.); uv (MeOH): 220 nm (ε 5130); nmr ($CDCl_3$) δ: 1.60 (m, 6H, $(CH_2)_3$ of THP), 3.25–4.12 (m, 6H, $NCH_2CH_2O$ and $OCH_2$ of THP), 4.43 (m, 1H, H-2 of THP), 6.03 (m, 2H, H-3,4), 6.60 (H-2,5); *Anal.* calcd. for $C_{11}H_{17}NO_2$: C 67.75, H 8.79, N 7.18; found: C 67.79, H 8.79, N 6.98.

*1-(2-Acetoxyethyl)pyrrole* 17b

A solution of the crude 1-(2-hydroxyethyl)pyrrole **2***a* (147 g; which contained some of the acetate **17***b*) in pyridine (415 mL), containing $Ac_2O$ (139 mL), was heated on a steam bath for 0.5 h. The solution was poured into $H_2O$ (1 L) and the product was extracted into EtOAC (3 × 1 L). The extract was washed successively with dilute HCl solution, brine, dilute $Na_2CO_3$ solution, and brine again. The extract was dried, the solvent was removed *in vacuo* and the residue was purified by column chromatography on Florisil using 1:1 hexane–$CH_2Cl_2$ as the developing solvent. The product (128 g) was identical to a sample prepared by the method of Blicke and Blake (4); uv (MeOH): 223 nm (ε 4170); ir ($CHCl_3$): 1741 $cm^{-1}$; nmr ($CDCl_3$) δ: 2.02 (s, 3H, $CH_3CO$), 3.92–4.37 (m, 4H, $CH_2CH_2$), 6.07 (m, 2H, H-3,4), 6.60 (m, 2H, H-2,5).

*1-(2-Chloroethyl)pyrrole* 17c

A mixture of 2,5-dimethoxytetrahydrofuran (150 g, 1.13 mol), 2-chloroethylamine hydrochloride (450 g, 3.88 mol), anhydrous NaOAc (450 g, 5.5 mol), and HOAc (560 mL) was heated with an oil bath, with mechanical stirring, in an apparatus set up for distillation. The oil bath was heated to 110°C, at which temperature distillation of a liquid took place. After 15 min at 110°C the mixture was cooled, poured into saturated salt solution, and the product was extracted into $CH_2Cl_2$. The extract was washed successively with saturated salt solution, saturated $Na_2CO_3$ solution, and saturated salt solution. The extract was dried, the solvent was removed *in vacuo*, and the residue was passed through a column of Florisil (800 g) using hexane as the solvent. The product (84 g, 57%) obtained in this way was sufficiently pure for synthetic purposes. For analysis, a small portion was distilled at 50°C/1.2 Torr; uv (MeOH): 219 nm (ε 4790); nmr ($CDCl_3$) δ: 3.66 (m, 2H, $CH_2Cl$), 4.06 (m, 2H, $CH_2N$), 6.10 (m, 2H, H-3,4), 6.63 (m, 2H, H-2,5); *Anal.* calcd. for $C_6H_8ClN$: C 55.60, H 6.22, Cl 27.36; found: C 55.44, H 6.23, Cl 27.11.

*Hantzsch pyrrole synthesis*

A. *Use of bromoacetaldehyde as α-halo carbonyl component. Synthesis of methyl 1-(2-hydroxyethyl)-3-methoxycarbonylpyrrol-2-acetate* 4a

A 250 mL 3-necked round bottomed flask containing a magnetic stirring bar and fitted with a $CaCl_2$-filled drying tube was connected directly (via one of the outer necks) by means of a receiver adapter and a 3 in. Liebig condensor to the acetal pyrolysis apparatus. This latter apparatus consisted of a 100 mL round bottomed flask topped with a 6 in. Vigreux column (bearing a thermometer) connected to the above-mentioned condensor.

The acetal pyrolysis flask was charged with oxalic acid dihydrate (15.6 g, 124 mmol) and bromoacetaldehyde diethyl acetal (11.82 g, 60 mmol). Ethanolamine (3.36 g, 55 mmol) was placed in the 3-necked flask, which was immersed in an ice bath. Dimethyl acetonedicarboxylate (8.7 g, 0.05 mol) was then added with stirring at 0–10°C. The enamine formed immediately. When the addition was completed, the cooling bath was removed and dry MeCN (100 mL) was added. The acetal pyrolysis part of the apparatus was now placed in an oil bath and the temperature thereof was raised to 150–160°C. The bromoacetaldehyde solution, which formed (bp 80–83°C/ca. 580 Torr pressure in Mexico City), distilled directly into the three-necked flask. When the temperature of the distillate had dropped below 80°C, the pyrolysis part of the apparatus was replaced by a reflux condensor fitted with a drying tube containing $CaCl_2$. The solution was heated at reflux temperature for 1 h. The solvent was removed *in vacuo*, MeOH (200 mL) and silica gel (20 g) were added to the residue, the MeOH was removed *in vacuo*, and the solid mixture was placed on top of a column of silica gel (200 g) packed in hexane. The column was eluted with hexane–EtOAc (4:1, 1 × 500 mL) and hexane–EtOAc (1:1, 9 × 500 mL). Fractions 2 and 3 contained dimethyl acetonedicarboxylate and nonpolar impurities, fractions 4–8 contained the crystalline pyrrole **4***a* (38–43%), which was recrystallized from ether–hexane. The physical constants for this compound are found in Tables 1 and 2.

The yield of the product was very dependent on the scale of

Can. J. Chem. Downloaded from www.nrcresearchpress.com by 210.87.254.5 on 09/06/12
For personal use only.

the reaction. Thus, doubling the scale gave the pyrrole in about half the yield stated above.

*Methyl 1-(3-hydroxypropyl)-3-methoxycarbonylpyrrol-2-acetate* **7**a

This compound was prepared in the same manner as described above for the synthesis of **4***a* except that 3-amino-1-propanol was used in place of ethanolamine and the condensation between the dimethyl acetonedicarboxylate – 3-amino-1-propanol adduct and bromoacetaldehyde was conducted at room temperature for 16 h. The crude product was purified by column chromatography on silica gel, the column being developed successively with hexane, hexane–ether (4:1), and hexane–ether (1:4). The product was eluted from the column with the last solvent system, and then crystallized from $CH_2Cl_2$–hexane. See Tables 1 and 2 for physical constants.

B. *Utilization of 1-bromoalkan-2-ones as the α-halo carbonyl component*

(a) *Aqueous conditions*

The experimental procedures for the synthesis of compounds **4***d* and **4***g* were identical, except that 60% aqueous HOAc was used as the reaction solvent for the preparation of **4***g*. Compounds **4***j* and **4***l* were obtained by processes which differed somewhat from that used for **4***d* and **4***g* (see below) but were identical to each other, except that hexane–EtOAc (1:1) was used as the eluting solvent in the column chromatographic purification of **4***l*.

*Methyl 1-(2-hydroxyethyl)-3-methoxycarbonyl-4-methylpyrrol-2-acetate* **4**d

Dimethyl acetonedicarboxylate (1.74 g, 10 mmol) was added in one portion to ethanolamine (6 mL, 100 mmol) and $H_2O$ (5 mL) and the mixture was rapidly cooled to −10°C at which point bromoacetone (1.67 mL, 0.02 mol) was added in a dropwise manner. The temperature was allowed to rise, but not above 45°C. When the addition was completed the deeply colored solution was stirred at room temperature for 1 h and then the reaction was quenched by pouring it onto a mixture of crushed ice and 25% HCl. The solution was saturated with NaCl and the product was extracted into EtOAc. The extract was washed to neutrality with $H_2O$, dried, and then the solvent was removed *in vacuo*. The residue was subjected to column chromatography on silica gel using hexane–EtOAc (7:3) as the eluting solvent. The solid product (0.89 g, 35%) was crystallized from $CH_2Cl_2$–hexane for analysis. See Tables 1 and 2.

*Methyl 1-(2-hydroxyethyl)-3-methoxycarbonyl-(2-methoxyethyl)pyrrol-2-acetate* **4**j

To a stirred solution of ethanolamine (10 equiv.) and $H_2O$ (0.33 g/g ethanolamine) was added a mixture of 1-bromo-4-methoxybutan-2-one (1 equiv.) and dimethyl acetonedicarboxylate (1 equiv.) in a dropwise manner. A vigorous reaction took place but the temperature was not permitted to exceed 35°C. Fifteen minutes after the addition was completed, the reaction was worked up in the usual way. The desired pyrrole was obtained from the product mixture by column chromatography on silica gel using ether–hexane (5:1) as the eluting solvent.

(b) *Nonaqueous conditions*

*Methyl 1-(2-hydroxyethyl)-3-methoxycarbonyl-5-methylpyrrol-2-acetate* **10**a

A mixture of dimethyl acetonedicarboxylate (1 equiv.) and ethanolamine (1 equiv.) was stirred at room temperature for 10 min and then bromoacetone (3 equiv.) was added. The mixture was left at room temperature for 5 days, after which time it was subjected to column chromatography on silica gel. The desired product was eluted as an oil with a 1:1 EtOAc–hexane mixture.

*Methyl 1-(2-hydroxyethyl)-3-methoxycarbonyl-5-phenylpyrrol-2-acetate* **10**d

Ethanolamine (1 equiv.) and phenacyl bromide (2 equiv.) were added in succession to dimethyl acetonedicarboxylate (2 equiv.) in MeCN (1 mL/mmol phenacyl bromide) and the solution was heated at reflux temperature for 1.75 h. The solvent was removed *in vacuo* and a 1:1 mixture of $H_2O$ and HCl was added to the residue. After the usual work-up, the crude product was subjected to column chromatography on silica gel and the desired pyrrole was eluted with 1:1 EtOAc–hexane.

*Synthesis of the methanesulfonates*

All of the methanesulfonates described in this paper were prepared by the general procedure outlined below.

To a stirred solution of the hydroxy compound (1 equiv.) in anhydrous $CH_2Cl_2$ (10–20 mL/g of the alcohol), cooled to 0°C or lower (see Table 1), and containing triethylamine (1 equiv.), was added $CH_3SO_2Cl$ (1 equiv.) at a rate such that the temperature was maintained at 0°C or below. When the addition was completed, the mixture was stirred for the time and at the temperature specified in Table 1. The solution was washed successively with $H_2O$ and saturated salt solution, dried, and evaporated *in vacuo*. The residue was then purified by crystallization from the appropriate solvent system, or by column chromatography on silica gel. For the 6-chloro and 6-bromo compounds **19***n* and **19***r*, respectively, the methanesulfonate was eluted with hexane–EtOAc (7:3). The cyano methanesulfonates **26***e* and **26***g* were removed from the column with 9:1 and 7:2 hexane–$CH_2Cl_2$ mixtures.

*Synthesis of the 4-(4-nitrophenylazo) benzoate esters*

The syntheses of the 4-(4-nitrophenylazo) benzoate esters of compounds **10***d*, **19***j*, and **26***f* were effected in exactly the same manner as described for 1-(4-hydroxybutyl)pyrrole **2***c*, except that compound **19***j* was purified by column chromatography on Act. II neutral alumina and the ester was eluted with $C_6H_6$–EtOAc (9:1).

*Synthesis of the 1-(ω-iodoalkyl)pyrroles*

A solution of the methanesulfonate (1 equiv.) in anhydrous MeCN (10–40 mL/g methanesulfonate) containing dry NaI (2.3 equiv. for compounds **7***b*, **26***b*, and **26***e*; 10 equiv. for **4***h*; all others, 5 equiv.) was heated at reflux temperature for the time specified in Table 1. The solvent was evaporated to dryness *in vacuo*, $H_2O$ was added to the residue, and the product was extracted into $CH_2Cl_2$. The extract was washed with $H_2O$, dried, and evaporated *in vacuo*. The residue in some cases was analytically pure, in others the crude product was purified by crystallization from the appropriate solvent system or by column chromatography on silica gel using hexane–EtOAc (3:2 for **7***c* and 95:5 for **19***o*).

*Acylation of 1-substituted pyrroles with ethoxalyl chloride*

The α-keto esters **18***a*, **18***b*, and **18***h* were synthesized in the manner described below.

A solution of pyridine (1.1 equiv.) in anhydrous $CH_2Cl_2$ (25 mL/g) was added to a stirred solution of ethoxalyl chloride (1 equiv.) in $CH_2Cl_2$ (15 mL/g) at a rate such that the temperature was maintained at −20 to −25°C. Immediately thereafter, a solution of the 1-substituted pyrrole (1 equiv.) in $CH_2Cl_2$ (15 mL/g) was added at the same temperature. The solution was then stirred for the time and at the temperature specified in Table 1, after which time it was washed successively with dilute HCl and saturated aqueous NaCl solution. The $CH_2Cl_2$ solution was dried and evaporated *in vacuo*. The residue was subjected to column chromatography on Florisil. For compounds **18***a* and **18***h* the column was eluted successively with hexane, and hexane–ether (95:5, then 90:10); for compound **18***b* the product was eluted with hexane–EtOAc mixtures (95:5, then 80:20).

Can. J. Chem. Downloaded from www.nrcresearchpress.com by 210.87.254.5 on 09/06/12
For personal use only.

*Synthesis of 1-(2-tetrahydropyran-2-yloxy)-2-ethoxalylpyrrole* ***18a*** *by alkylation of 2-ethoxalylpyrrole with the tetrahydropyranyl ether of bromoethanol (ref. 16)*

To a stirred suspension of NaH (prepared by washing 50% NaH in mineral oil (7.9 g, 165 mmol) with hexane) in dry DMF (150 mL), maintained in a $N_2$ atmosphere, was added 2-ethoxalylpyrrole (5) (25.0 g, 150 mmol) in portions. After 0.75 h, the tetrahydropyranyl ether of bromoethanol (46.7 g, 224 mmol) was added and the solution was left at room temperature for 16 h. The solution was diluted with $C_6H_6$ and the mixture was washed well, first with $H_2O$ and then with saturated aqueous NaCl solution. The organic phase was dried and evaporated *in vacuo*. The residue was chromatographed on silica gel (600 g) using EtOAc–hexane (9:1) to elute the product (36.0 g, 81%) which was identical to that obtained by the acylation of 1-(2-tetrahydropyran-2-yloxy)pyrrole with ethoxalyl chloride.

*1-(2-Hydroxyethyl)pyrrole-2-glyoxylic acid* ***18c***

A solution of the tetrahydropyranyloxy ether **18***a* (10.0 g, 33.8 mmol) in 65% HOAc (150 mL) was stirred at 55°C for 2 h. The solvent was evaporated *in vacuo* and the residue was subjected to column chromatography on silica gel (300 g). The free hydroxy compound (6.1 g, 85%), which was eluted with hexane–EtOAc (4:1), was obtained as an oil (uv (MeOH): 303 nm (ε 9120); ir ($CHCl_3$): 3615, 3420, 1737, 1643 $cm^{-1}$; mass spectrum *m/e*: 211 ($M^+$)). The hydroxy compound was not characterized further; instead, it was converted directly to the carboxylic acid **18***c* as follows. A mixture of the above ester (4.75 g, 22.5 mmol) and $K_2CO_3$ (6.54 g), in 80% MeOH (100 mL), was heated at reflux temperature for 1 h. The mixture was evaporated to dryness *in vacuo*; $H_2O$ (4 mL) was added to the residue; the solution which resulted was cooled to 0°C and made acidic with concentrated HCl. The product was extracted into EtOAc, the extract was washed with saturated NaCl solution and dried. The solvent was removed *in vacuo* leaving a solid (3.84 g, 93%), which was crystallized from ether–EtOAc to give the very unstable α-oxocarboxylic acid **18***c*, mp 85–90°C (dec.), which was best characterized as the stable dicyclohexylammonium salt. This salt was prepared by adding the carboxylic acid (0.590 g, 3.2 mmol) to a stirred 1:1 MeOH–ether (10 mL) solution of dicyclohexylamine (0.634 g, 3.5 mmol). After 0.5 h, ether (25 mL) was added and the precipitated salt, mp 170–172°C (0.935 g, 80%), was collected by filtration, washed with ether, and dried *in vacuo*. It was recrystallized from ether–MeOH for analysis.

*Ethyl 1-(2-acetoxyethyl)-4-formylpyrrole-2-glyoxalate* ***18d***

Phosphorus oxychloride (35.1 g, 229 mmol) was added to dry DMF (17.3 g, 237 mmol), with stirring and cooling, at a rate such that the internal temperature was maintained at 10–20°C. When the addition was completed, the solution was stirred at room temperature for 15 min, and then it was mixed with anhydrous 1,2-dichloroethane (50 mL) and the mixture was cooled in an ice bath. When the internal temperature had reached 5°C, a solution of 1-(2-acetoxyethyl)-2-ethoxalylpyrrole **18***b* (10.0 g, 39.5 mmol) in 1,2-dichloroethane (50 mL) was added over a 0.5 h period. The mixture was then stirred at reflux temperature for 8 h, cooled to room temperature, and a solution of NaOAc·3 $H_2O$ (161 g, 1.18 mol) in $H_2O$ (220 mL) was added cautiously. The mixture was heated at reflux temperature with stirring for 15 min and after cooling the organic phase was separated and the aqueous phase was extracted with ether (3 × 100 mL). The combined organic phases were washed with saturated $Na_2CO_3$ solution and then dried. The solvent was removed *in vacuo* and the residue was chromatographed on Florisil (300 g) using hexane–EtOAc (95:5 and 90:10) to elute the oily product (7.5 g, 68%).

*1-(2-Hydroxyethyl)-4-formylpyrrole-2-glyoxylic acid* ***18e***

This carboxylic acid was obtained by hydrolysis of the ester **18***d* in the same manner as described for the synthesis of **18***c*, except that the reaction was conducted at room temperature for 14 h. The crude product (44% yield) was crystallized from acetone for analysis.

*1-(2-Acetoxyethyl)-2-ethoxalyl-4-methoxymethylpyrrole* ***18f*** *and 1-(2-hydroxyethyl)-2-ethoxalyl-4-hydroxymethylpyrrole* ***18g*** *from* ***18b***

Concentrated HCl (1.5 mL) was cooled to 0–5°C and $Ac_2O$ (6 mL) was added, at a rate such that the temperature did not exceed 5°C, over a 1.5 h period. The mixture was stirred at room temperature for 16 h and then dimethoxymethane (3 mL) and a solution of 1-(2-acetoxyethyl)-2-ethoxalylpyrrole **18***b* (1.00 g) in anhydrous $C_6H_6$ (6 mL) were added and the solution was heated at 63°C for 1.5 h. The solution was cooled to room temperature, MeOH (10 mL) was added, and the solution was stirred at room temperature for 16 h. The solvent was evaporated *in vacuo* and a saturated solution of $Na_2CO_3$ was added to the residue. The mixture was extracted with EtOAc, the extract was washed well with $H_2O$ and dried over $MgSO_4$. The solvent was removed *in vacuo* and the residue was subjected to tlc on silica gel using hexane–EtOAc (65:35) as the developing solvent. The acetate **18***f* (0.115 g, 10%) was obtained as an oil, while the alcohol **18***g* (0.255 g, 26%) was isolated as a solid which was crystallized from hexane.

When this reaction was carried out on a 158 mmol scale, compounds **18***f* and **18***g* were isolated in 17% and 12% yields, respectively.

*1-(2-Chloroethyl)-2-ethoxalyl-4-methoxymethylpyrrole* ***18i***, *1-(2-chloroethyl)-2-methoxalyl-4-methoxymethylpyrrole* ***18j***, *and 1-(2-chloroethyl)-2-ethoxalyl-4-hydroxymethylpyrrole* ***18k***

The reaction of 1-(2-chloroethyl)-2-ethoxalyl pyrrole with dimethoxymethane was carried out in exactly the same manner as described above for the synthesis of **18***f* and **18***g*. The mixture was separated by tlc on silica gel using hexane–EtOAc (4:1) as the developing solvent.

*1-(2-Chloroethyl)-2-ethoxalyl-4-chloromethylpyrrole* ***18l***

To isolate the title compound, a reaction was carried out in the normal manner but the MeOH treatment was not carried out. Instead, the reaction mixture was poured into dilute $Na_2CO_3$ solution. The mixture was extracted into EtOAc, the extract was washed to neutrality with $H_2O$, dried over $MgSO_4$, and evaporated *in vacuo*. The crude product was then subjected to tlc on silica gel (hexane–EtOAc (4:1)), which gave the 4-chloromethyl compound **18***l* as well as a small amount (9%) of the 4-hydroxymethyl compound **18***k* which resulted from the hydrolysis of the chloro compound during the chromatographic process.

*Synthesis of 1-(2-chloroethyl)-2-ethoxalyl-4-methoxymethylpyrrole* ***18i*** *by acid catalyzed reaction of* ***18k*** *with methanol*

A solution of the hydroxymethyl compound **18***k* (0.150 g) in anhydrous MeOH (5 mL) containing *p*-TsOH·$H_2O$ (0.005 g) was heated at reflux temperature for 1.5 h. The MeOH was removed *in vacuo* and $H_2O$ (5 mL) was added to the residue. The product was extracted into ether, the extract was washed with $H_2O$, dried over $MgSO_4$, and evaporated *in vacuo*. The crude product was purified by tlc on silica gel (hexane–EtOAc (4:1)), followed by crystallization from ether to give the 4-methoxymethyl compound **18***i* (0.110 g, 70%) identical to the material obtained as described above.

Can. J. Chem. Downloaded from www.nrcresearchpress.com by 210.87.254.5 on 09/06/12
For personal use only.

*Acetolysis of 1-(2-chloroethyl)-2-ethoxalyl-4-methoxymethylpyrrole* ***18****i*

A mixture of the title compound **18***i* (40 g, 146 mmol), fused NaOAc (59.9 g, 730 mmol), and NaI (65.7 g, 438 mmol) in anhydrous DMF (500 mL) was heated at 65°C for 40 h. The reaction mixture was cooled to room temperature, poured into $H_2O$, and then extracted with $C_6H_6$. The extract was washed well with $H_2O$, dried over $MgSO_4$, and evaporated *in vacuo*. The residue (35 g) was subjected to column chromatography on silica gel (1.05 kg). Elution with hexane–EtOAc (85:15) gave, in succession, 1-vinyl-2-ethoxalyl-4-methoxymethylpyrrole **20** (4.3 g, 12%) as an oil, the 1-(2-acetoxyethyl) compound **18***f* (15.0 g, 35%), and the 1-(2-hydroxyethyl) compound **18***g* (7.0 g, 21%).

*1-(2-Acetoxyethyl)-2-ethoxalyl-4-chloropyrrole* ***18****m* *and 1-(2-acetoxyethyl)-2-ethoxalyl-5-chloropyrrole* ***22****a*

Recently distilled $SO_2Cl_2$ (13.7 mL, 170 mmol) was added at −70°C to a stirred solution of 1-(2-acetoxyethyl)-2-ethoxalylpyrrole **18***b* (40.5 g, 160 mmol) in anhydrous $CH_2Cl_2$ (900 mL). When the addition was completed, the solution was left to come to room temperature and after 2 h the solvent was removed *in vacuo*. The oily residue was taken up in $CH_2Cl_2$, the solution was washed to neutrality with $H_2O$ and dried. The solvent was evaporated *in vacuo* and the residual mixture (63 g) was separated by column chromatography on silica gel (800 g) using hexane–EtOAC (9:1) as the eluting solvent. In this way there was obtained the desired 4-chloro compound **18***m* (19.0 g, 41%) as an oil, the isomeric oily 5-chloro compound **22***a* (16.0 g, 34%), as well as some starting material (2.3 g).

*1-(2-Acetoxyethyl)-2-ethoxalyl-4-bromopyrrole* ***18****n* *and 1-(2-acetoxyethyl)-2-ethoxalyl-4,5-dibromopyrrole* ***22****b*

Bromine (3.0 mL, 58.3 mmol) was added in a dropwise manner to a stirred solution of 1-(2-acetoxyethyl)-2-ethoxalylpyrrole **18***b* (14.8 g, 58.3 mmol) in anhydrous $CH_2Cl_2$ (200 mL) at −75°C. After 2.5 h at this temperature, the temperature was left to reach ambient and the solvent was removed *in vacuo*. $CH_2Cl_2$ was added to the residue and the solution was washed successively with $H_2O$, 10% $NaHCO_3$ solution, and $H_2O$. The solution was dried, evaporated *in vacuo*, and the mixture (18.3 g) was separated by column chromatography on Florisil (1 kg) using hexane–EtOAc (9:1) as the eluting solvent. This gave the mono bromo compound **18***n* (10.9 g, 56%) as an oil, as well as lesser amounts of the crystalline dibrominated pyrrole **22***b* (4.8 g, 20%) and the starting material (2.1 g). These compounds were eluted from the column in the order **22***b*, **18**n, **18***b*. See Tables 1 and 2 for other data concerning the products.

*1-(2-Hydroxyethyl)pyrrol-2-acetic acid* ***19****a* *and methyl 1-(2-hydroxyethyl)pyrrol-2-acetate* ***19****b*

A solution of 85% KOH (85 g, 1.29 mol), in $H_2O$ (150 mL), was added with stirring to a cooled solution of the ester **18***b* (151 g, 0.597 mol), in MeOH (550 mL), at a rate such that the temperature did not exceed 15°C. The cooling bath was removed and after the mixture had reached ambient temperature it was stirred for a further 2 h. The solution was evaporated to dryness *in vacuo*, $C_6H_6$ was added to the residue, and the mixture was again evaporated *in vacuo*. This process was repeated 3–4 times to remove the $H_2O$. To the solid thus obtained was added diethylene glycol (500 mL) and 85% hydrazine hydrate (209 mL), and the mixture was heated in an oil bath at 100–110°C for 2 h in a nitrogen atmosphere. The solution was cooled to 40–50°C and solid 85% KOH (pellets, 225 g) was added carefully in small portions (vigorous foaming). The apparatus was set up for distillation and the mixture was slowly heated in an oil bath to 170–180°C. This temperature (internal temperature rose to 145°C) was maintained for 1 h 10 min, during which time a distillate (300 mL) was collected. The apparatus was then changed to allow boiling under reflux, at which temperature the reaction was maintained for 2 h. The mixture was cooled to room temperature, $H_2O$ (1.5 L) was added, and the solution was cooled to 0°C. Concentrated HCl (530 mL) was added in a dropwise manner at 0°C, which gave a solution with pH ca. 4. The product was extracted with EtOAc (3 × 2 L), the extract was washed with saturated salt solution, dried, and evaporated *in vacuo* to give the crude acetic acid **19***a* (105 g) as an oil.

A small portion of the crude carboxylic acid was converted into the crystalline dicyclohexylammonium salt, in ether, in the manner described for **18***c*. The crude salt was crystallized from $CH_2Cl_2$–ether (see Table 1).

To a solution of the above crude carboxylic acid in dry DMF (500 mL) was added $K_2CO_3$ (93.3 g) and MeI (180 g). The mixture was stirred at room temperature for 18 h, after which time it was poured into a large volume of saturated salt solution and ice. The product was extracted with $C_6H_6$ (3 × 2 L); the extract was washed with salt solution, dried, and evaporated *in vacuo*. The residue was purified by column chromatography on Florisil (1.2 kg). The product began to come off the column on elution with hexane–EtOAc (9:1) and was completely removed with a 3:2 mixture of these solvents. The ester was obtained as an oil (49–66% yield from **18***b*).

This ester could also be obtained by reaction of the crude carboxylic acid with excess ethereal $CH_2N_2$ (52–54% overall from **18***b*).

*1-(2-Hydroxyethyl)-4-methylpyrrol-2-acetic acid* ***19****e* *and methyl 1-(2-hydroxyethyl)-4-methylpyrrol-2-acetate* ***19****f*

The carboxylic acid **19***e* was prepared from the 4-formyl compound **18***d* in exactly the same manner as described above for the synthesis of **19***a*, except that ethylene glycol was used as the solvent for the Huang–Minlon version of the Wolff–Kishner reduction, and the ethylene glycol was removed *in vacuo*. The residual solid was dissolved in $H_2O$ and then worked up in the usual way to give the crude unstable carboxylic acid **19***e*, which was immediately converted into the methyl ester **19***f* with ethereal $CH_2N_2$.

Alternatively, it was not necessary to isolate the unstable acid **19***e*. Instead, after removal of the ethylene glycol *in vacuo*, the residual solid, containing the potassium salt of the carboxylic acid **19***e* (obtained from **18***d* (4.81 g)), was dissolved in DMSO (20 mL) and $H_2O$ (5 mL). MeI (31 mL) was added and, after 14 h at room temperature, water was added and the product was extracted with ether. The extract was washed with saturated salt solution, dried, and evaporated *in vacuo*. The product was purified by column chromatography on Florisil using hexane–EtOAc (95:5) to elute the desired ester **19***f*.

*Methyl 1-(2-hydroxyethyl)-4-methoxymethylpyrrol-2-acetate* ***19****j* *and methyl 1-(2-hydroxyethyl)-4-methoxymethylpyrrole-2-carboxylate* ***21***

A solution of 85% KOH (1.36 g, 20.7 mmol) in $H_2O$ (4 mL) was added to a stirred and cooled mixture of the α-keto ester **18***f* (3.00 g, 10.1 mmol) and ethylene glycol (120 mL, argon atmosphere) at a rate such that the reaction temperature did not exceed 0°C. The hydrolysis was complete in about ten minutes. At this stage, 85% hydrazine hydrate (1.7 mL) was added, the cooling bath was removed, and the mixture was heated at 100–110°C for 2.5 h. The solution was cooled to 40°C and 85% KOH (2.32 g) was added cautiously. The apparatus was set up for distillation, placed in an oil bath, and slowly heated to 170°C. During a 0.5 h period distillation occurred (90–120°C) and then vacuum was applied and ca. 10 mL of ethylene glycol was

Can. J. Chem. Downloaded from www.nrcresearchpress.com by 210.87.254.5 on 09/06/12
For personal use only.

removed. The apparatus was set up for heating under reflux and the solution was heated at 145°C for 3 h. At the end of this time the major portion of the ethylene glycol was removed *in vacuo*, the mixture was cooled to 0°C, DMSO (40 mL) and MeI (8 mL) were added, and the solution was stirred at room temperature for 6 h. The solution was poured into $H_2O$, extracted with an EtOAC–ether mixture (1:1), and the extract was washed with saturated NaCl solution and dried over $MgSO_4$. The solvent was removed *in vacuo* and the residue was separated by tlc on silica gel using hexane–EtOAc (3:2) as the developing solvent. There was thus obtained the pyrrole carboxylic acid derivative **21** (0.160 g, 7%) and the desired pyrrole acetic acid derivative **19***j* (1.30 g, 57%), both as oils. The latter compound was characterized as the crystalline 4-(4-nitro)phenylazobenzoate.

*Sodium borohydride reduction of ethyl 1-(2-acetoxyethyl)-4-chloropyrrole-2-glyoxalate* ***18***m

$NaBH_4$ (23.7 g, 624 mmol) was added to 8% aqueous MeOH (325 mL) with stirring at −30°C. When the vigorous reaction had subsided, a solution of the α-keto ester **18***m* (40.0 g, 139 mmol) in MeOH (400 mL) was added at a rate such that the reaction temperature did not exceed −20°C. When the addition was completed, the solution was stirred for 2 h at −30°C and then a solution of HOAc (21.5 mL) in $H_2O$ (320 mL) was added. After an additional 1 h at −30°C the precipitated solid was collected by filtration and dissolved in $CH_2Cl_2$. This solution was washed with saturated NaCl solution, dried, and evaporated *in vacuo*. The solid alcohol **23***a* (33.2 g, 83%; homogeneous by tlc), which was obtained, was of sufficient purity to be used directly in the next step.

*Sodium borohydride reduction of ethyl 1-(2-acetoxyethyl)-4-bromopyrrole-2-glyoxalate* ***18***n

$NaBH_4$ (3.07 g, 81.2 mmol) was added at −50°C to 2.5% aqueous methanol (103 mL) and after 5 min a solution of the 4-bromo compound **18***n* (8.90 g, 26.7 mmol) in MeOH (40 mL) was added, with stirring, at a rate such that the reaction temperature did not exceed −40°C. After 1 h at −40°C, 50% HOAc was added until the solution was weakly acidic. The MeOH was removed *in vacuo*, the residue was shaken with EtOAc, and the organic phase was washed with saturated NaCl solution. After drying, the solvent was removed *in vacuo* and the residue was crystallized at low temperature from ether to give the alcohol **23***b* (6.0 g, 67%). This solid is very unstable at room temperature and must be stored in an evacuated vessel at −10°C.

*Synthesis of the ethyl 1-(2-acetoxyethyl)-4-halopyrrol-2-acetates* ***19***l *and* ***19***p *by reduction of the α-hydroxy esters* ***23***a *and* ***23***b

Triphenylphosphine (2 equiv.) was added to a stirred solution of $I_2$ (1 equiv.) in anhydrous $C_6H_6$ (15–25 mL/g $I_2$) maintained in an inert atmosphere. After 5–10 min, the α-hydroxy ester (1 equiv.) was added all at once. The mixture was then heated at reflux temperature for 2.5 h (**23***a*) or stirred at room temperature for 18 h (**23***b*). The mixture was filtered, the filtrate was washed well with NaCl solution, dried, and evaporated *in vacuo*. The chloro compound **19***l* was purified by column chromatography on Florisil using hexane–EtOAc (9:1) as the eluting solvent. The oily ester **19***l* (83% yield) must be stored in the cold in the presence of a few drops of $Et_3N$.

The bromo compound **19***p* was purified by column chromatography on silica gel using hexane–EtOAc (1:1 and 4:1) as the eluting solvent system. An oil (86% yield) was obtained which was even less stable than the chloro compound. It was best used immediately in the next step but could be stored safely at Dry-Ice temperature in the presence of a few drops of $Et_3N$.

*Methyl 1-(2-hydroxyethyl)-4-halopyrrol-2-acetates* ***19***m *and* ***19***q

A solution of the acetoxyethylpyrrole in anhydrous MeOH (10–15 mL/g of pyrrole) containing 1,5-diazabicyclo[4.3.0]non-5-ene (1–2 drops/5 mmol substrate) was left at room temperature in an inert atmosphere for the specified time. The solvent was removed *in vacuo*; the residue was taken up in EtOAc; the solution was washed with saturated salt solution, dried, and evaporated *in vacuo*. The residual oil was unstable at room temperature but could be stored at low temperature in an inert atmosphere if a few drops of $Et_3N$ was added.

*1-(ω-Hydroxyalkyl)-2-dimethylaminomethylpyrroles* ***24***a–c

The 1-(ω-hydroxyalkyl)pyrrole (1 equiv.) was heated to 50°C in an oil bath and a solution of $Me_2NH{\cdot}HCl$ (1.2–1.35 equiv.) in 37% aqueous HCHO (7–10 g/100 mmol pyrrole), which was prewarmed to 45°C, was added with stirring at a rate such that the reaction temperature did not exceed 60°C (ca. 1 h). The reaction mixture was then allowed to reach room temperature and stirring was continued for a further 2 h. At the end of this period, 20% NaOH (15.5–19 mL/100 mmol pyrrole) and $H_2O$ (40–60 mL/100 mmol starting pyrrole) were added and the product was extracted into $CH_2Cl_2$. The extract was washed with saturated salt solution, then with $H_2O$, and finally it was dried. The solvent was removed *in vacuo* and the residue was purified by distillation (**24***a*), by column chromatography on silica gel (**24***c*, hexane–EtOAc (1:1)), or by column chromatography on silica gel ($CH_2Cl_2$–MeOH (95:5)) followed by distillation (**24***b*).

*1-(ω-Hydroxyalkyl)pyrrol-2-acetonitriles* ***26***a, ***26***d, *and* ***26***f

Dimethyl sulfate (1.03–1.18 equiv.) was added to a stirred and cooled (0°C) solution of the 1-hydroxyalkylated-2-dimethylaminomethylpyrrole (1 equiv.) in acetone (5 mL/g pyrrole), maintained in a nitrogen atmosphere, at a rate such that the reaction temperature did not exceed 4°C. When the addition was completed, the solution was stirred at room temperature for 1 h and then a solution of NaCN (2.0–2.4 equiv.) in $H_2O$ (2.2 mL/g NaCN) was added. The apparatus containing the reaction mixture was set up for distillation and the reaction mixture was heated on a steam bath. Distillation was continued until the temperature of the reaction mixture reached 90–95°C. At this point the solution was heated at reflux temperature for 0.5 h. The reaction mixture was cooled to room temperature, and after dilution with $H_2O$ it was extracted with $CH_2Cl_2$. The extract was washed with half-saturated NaCl solution and after drying it was evaporated *in vacuo*. The residue was subjected to column chromatography on silica gel using hexane–EtOAc (3:2 for **26***a*, 85:15 for **26***d*, and 4:1 for **26***f*) to elute the product. Compounds **26***d* and **26***f* were further purified by distillation.

*Cyclization of the 1-(ω-iodoalkyl or ω-methanesulfonyloxyethyl)pyrrole diesters* ***4***c, ***4***f, ***4***i, ***4***k, ***4***m, ***7***c, ***10***c, *and* ***10***f *to the bicyclic diesters* ***5***a, ***5***d, ***5***g, ***5***j, ***5***m, ***8***a, ***11***a, *and* ***11***d, *respectively*

NaH (50% in mineral oil, or 100%; 1–1.2 equiv.) was suspended in anhydrous DMF (100–300 mL/g of NaH) and the mixture was cooled with stirring (inert atmosphere) to 0°C. The iodide or the methanesulfonate (1 equiv.) was added neat, in small portions, or as a solution in dry DMF for compound **10***f* (10 mL/g iodide). A vigorous evolution of hydrogen, in some cases accompanied by considerable foaming, took place. The solution was then stirred at the temperature and for the time indicated in Table 2. The reaction mixture was poured into a large volume of $H_2O$ and the product was extracted into $C_6H_6$ or EtOAc (compounds **5***j*, **5***m*, and **11***d*). The extract was washed successively with $H_2O$ and saturated salt solution and then it was dried and evaporated *in vacuo*. The residue was purified by

Can. J. Chem. Downloaded from www.nrcresearchpress.com by 210.87.254.5 on 09/06/12
For personal use only.

crystallization (compounds **5***a* and **8***a*) or by column chromatography or tlc followed by crystallization. The following compounds were first purified by column chromatography on silica gel using the solvent systems indicated: **5***d*, **5***m*, **11***a* (hexane–EtOAc (7:3)); **5***j* (hexane–ether (4:1 to 1:4)). Compound **5***g* was purified by column chromatography on Florisil (hexane–EtOAc (9:1)) and the bicyclic diester **11***d* was obtained pure by tlc on silica gel using hexane–EtOAc (7:3) as the developing solvent.

The yields, physical constants, and spectroscopic properties of these compounds are given in Tables 2 and 5.

*Cyclization of the 1-(ω-iodoalkyl or ω-iodomethanesulfonyloxyalkyl)pyrrole acetic esters and acetonitriles* ***19***d, ***19***h, ***19***k, ***19***o, ***19***r, ***26***c, ***26***e, *and* ***26***g *to the bicyclic monoesters and bicyclic nitriles* ***6***h–l *and* ***27***a–c, *respectively*

A solution of the iodide or the methanesulfonate (1 equiv.) in dry DMF (1–10 mL/g substrate) was added with stirring at −5–15°C (inert atmosphere) to a suspension of NaH (1–1.2 equiv.) in dry DMF (20–120 mL/g of NaH). The reaction mixture was then stirred for the time and at the temperature shown in Table 2 and the reaction was worked up in the manner described above. $CH_2Cl_2$ was used as the extracting solvent for **27***a*, while $C_6H_6$ was utilized as the extractant for all of the other reaction products. Compounds **6***h*, **6***j*, and **6***l* were purified by tlc on silica gel using hexane–EtOAc (7:3 for **6***i* and **6***j*, 4:1 for **6***l*) as the developing solvent. Methyl 6-methyl-1,2-dihydro-3*H*-pyrrolo[1,2-*a*]pyrrole-1-carboxylate **6***i* was purified by column chromatography on Florisil using hexane–EtOAc (95:5) as the developing solvent. All of the other compounds were purified by column chromatography on silica gel using hexane–EtOAc to elute the desired material (9:1 for **6***k*, 10:1 for **27***a*, and 95:5 for **27***b*,*c*). Compounds **6***h*–*l* could be stored for extended periods at ≤ −20°C in the presence of a trace of $Et_3N$. The nitriles **27***a*–*c* were stable at ambient temperature.

*Saponification of the diesters* **5**a, **5**d, **5**g, **5**j, **5**m, **8**a, **11**a, *and* **11**d

A solution of the diester (1 mol) in MeOH or EtOH (10–50 mL/g of ester) containing $H_2O$ (5–20 mL/g of ester) and 85% KOH (3.8 mol) was heated at reflux temperature for the time stipulated in Table 2. The alcoholic solvent was removed *in vacuo* and the residual aqueous phase was extracted with ether. The basic aqueous layer was then cooled to 0°C and made acidic with 5 *N* HCl solution. If the dicarboxylic acid precipitated, it was collected by filtration, washed with $H_2O$, and dried *in vacuo*. If the dicarboxylic acid did not precipitate from solution, it was extracted with EtOAc. The extract was washed well with $H_2O$, dried, and evaporated *in vacuo*. The crystalline residue was recrystallized from a suitable solvent system for analysis (see Table 4).

*Synthesis of the monoisopropyl esters* **5**c, **5**f, **5**l, **5**o, **8**c, **11**c, *and* **11**f *by selective esterification of the corresponding dicarboxylic acids*

A solution or a suspension of the dicarboxylic acid in anhydrous *i*-PrOH (15–50 mL/g of diacid) was cooled to 0 to −10°C and HCl gas was bubbled through the *i*-PrOH until saturation was achieved. The solution was then left at ambient temperature for the time indicated in Table 2 and then the solvent was evaporated *in vacuo*. $C_6H_6$ was added to the residue and the mixture was evaporated to dryness *in vacuo* again. This process was repeated a total of three times and the solid residue was then crystallized from a suitable solvent.

Alternatively, after removal of the *i*-PrOH, the residue was dissolved in EtOAc, the resulting solution was washed well with $H_2O$, dried, and evaporated *in vacuo*. The residual solid was purified by crystallization.

Under the conditions described, the 6-ethyl substituted dicarboxylic acid **5***h* did not give the expected monoacidic ester **5***i*. Instead, *i*-propyl 6-ethyl-1,2-dihydro pyrrolo[1,2-*a*]pyrrole-1-carboxylate **6***d* was obtained directly, presumably as a result of the acid catalyzed decarboxylation of **5***i*.

*Decarboxylation of the dicarboxylic acid monoisopropyl esters* **5**c, **5**f, **5**l, **5**o, **8**c, **11**c, *and* **11**f

The carboxylic acid was heated, in an inert atmosphere, to a temperature (see Table 2) at which decarboxylation occurred at a rapid but controllable rate. In most cases the decarboxylation was effected in a distillation apparatus (in some cases, under a vacuum of 20–40 Torr) and the product distilled as it was formed. The purity of material obtained in this way was usually at least 95%. In some cases, it was more convenient to effect the decarboxylation without simultaneous distillation of the product. The product obtained in this way could then be purified by tlc on silica gel (e.g., **12***b*; hexane–ether (4:1)) or by column chromatography on silica gel (e.g., **6***a*; 200 mL fractions; elution with hexane (2 fractions), hexane–$C_6H_6$ (7:3, four fractions), hexane–$C_6H_6$ (1:1, eight fractions); product in fractions 7–14).

As mentioned above, the 6-ethyl substituted dicarboxylic acid monoisopropyl ester **5***i* was not observed, decarboxylation to **6***d* occurred during the acid catalyzed esterification. This compound was purified by tlc on silica gel using hexane–EtOAc (85:15) as the developing solvent.

All of these compounds were unstable to varying degrees in the presence of air and light. They could, however, be kept without decomposition for extended periods of time at low temperature (< −10°C) in the presence of a trace of $Et_3N$.

*1,2-Dihydro-3*H*-pyrrolo[1,2-*a*]pyrrole-1-carboxylic acid* **6**b *and 6-(2-methoxyethyl)-1,2-dihydro-3*H*-pyrrolo[1,2-*a*]pyrrole-1-carboxylic acid* **6**f

A solution of the *i*-propyl ester (1 equiv.) in MeOH (20 mL/g) and $H_2O$ (10 mL/g) containing 85% KOH (4 equiv.) was heated at reflux temperature for the time shown in Table 2. The MeOH was removed *in vacuo* and the aqueous alkaline residue was made acidic with 20% HCl. The product was extracted into EtOAc; the extract was washed with $H_2O$, dried, and evaporated *in vacuo*. The residual oil was dissolved in dry $C_6H_6$ and an equimolar amount of dicyclohexylamine was added. The solid which separated on standing was collected by filtration and crystallized from a suitable solvent system.

*5-Phenyl-1,2-dihydro-3*H*-pyrrolo[1,2-*a*]pyrrole-1-carboxylic acid* **12**c

A solution of the *i*-propyl ester **12***b* (0.60 g, 2.23 mmol) in MeOH (20 mL) and $H_2O$ (5 mL) containing $K_2CO_3$ (0.20 g, 1.45 mmol) was heated at reflux temperature in a nitrogen atmosphere for 1 h. After removal of the solvent *in vacuo*, $H_2O$ (20 mL) was added to the residue and the alkaline solution was extracted with ether. The aqueous phase was cooled to 0°C and made acidic with 4 *N* HCl. The product was extracted with saturated salt solution, dried, and evaporated *in vacuo*. Crystallization of the residue from EtOAc–hexane gave the pure carboxylic acid **12***c* (0.284 g, 56%), mp 162–163°C.

*Synthesis of methyl 1,2-dihydro-3*H*-pyrrolo[1,2-*a*]pyrrole-1-carboxylate* **6**h *and methyl 5,6,7,8-tetrahydropyrrolo[1,2-*a*]pyridine-8-carboxylate* **9**c *from nitriles* **27**a *and* **27**b, *respectively*

A solution of the nitrile (1 equiv.) in 95% EtOH (15–50 mL/g of nitrile) and $H_2O$ (1–2 mL/g of nitrile) containing 85% KOH (3–6 equiv.) was heated at reflux temperature for 3–9 hours. The

solvent was removed *in vacuo* and the residue was processed in a manner which depended on the substrate.

For the synthesis of **6***h* the above residue was dissolved in DMSO (5 mL/g of nitrile taken), the solution was cooled to 0°C, and MeI (4 mL/g of nitrile taken) was added. After stirring for 18.5 h at room temperature, the solution was poured into saturated NaCl solution and the product was extracted into $CH_2Cl_2$. The extract was washed with $H_2O$, dried, and evaporated *in vacuo*. The residual oil was subjected to column chromatography on Florisil using hexane–EtOAc (95:5) to elute the product (82%). The ester thus produced was identical to a sample prepared as described previously.

To prepare the methyl ester **9***c*, the residue described above, which in this case was mainly the crude, unstable carboxylic acid **9***b*, was diluted with $H_2O$ and the solution was made acidic with dilute HCl. The product was extracted with EtOAc, the extract was washed with $H_2O$, dried, and evaporated *in vacuo*. The residue was dissolved in $CH_2Cl_2$ and excess ethereal $CH_2N_2$ was added. The solvent was removed *in vacuo* and the residue was subjected to column chromatography as described above for **6***h*. The oily ester **9***c* (51%) was purified for analysis by tlc on silica gel using hexane–ether (1:1) as the developing solvent.

*5,6,7,8-Tetrahydro-9*H*-pyrrolo[1,2-*a*]azepine-9-carboxylic acid **28**a and methyl ester **28**b*

A solution of the nitrile **27***c* (1.00 g) in ethylene glycol (11 mL) and $H_2O$ (1.2 mL) containing 85% KOH (2.02 g) was heated in an oil bath at 118°C for 3 h. $H_2O$ was added, the solution was extracted with ether, and the aqueous phase was cooled to 5°C and made acidic with concentrated HCl. The product was extracted with EtOAc, the extract was washed with $H_2O$, dried, and evaporated *in vacuo*. The residue was recrystallized from EtOAc–ether to give the carboxylic acid **28***a* (1.03 g, 92%), mp 129–130°C.

The methyl ester was prepared by dissolving the carboxylic acid (2.9 g) in DMSO (25 mL) and $H_2O$ (5 mL), containing 85% KOH (1.11 g), and adding MeI (15 equiv.). After 18 h at room temperature, the reaction was worked up as described for **9***c* and the crude product was crystallized from $CH_2Cl_2$–hexane to give a solid (2.7 g, 89%), mp 56–57°C.


1. J. M. Muchowski and A. F. Kluge. U.S. Patents 4,087,539 (1978); 4,089,969 (1978); 4,097,579 (1978); 4,232,038 (1980).
2. R. A. Jones and G. P. Bean. The chemistry of pyrroles. Academic Press, London. 1977. pp. 329–335.
3. D. A. Robinson and J. C. Chen. Belgian Patent 879,538 (1980).
4. F. F. Blicke and E. S. Blake. J. Am. Chem. Soc. **53**, 1015 (1931).
5. D. Behr, S. Brandage, and B. Landstrom. Acta Chem. Scand. **27**, 2411 (1973).
6. F. Bohlmann, J. Staffoldt, and W. Skuballa. Chem. Ber. **109**, 1586 (1976).
7. K. E. Wiegand. U.S. Patent 3,882,146 (1975); Chem. Abstr. **83**, 79071u (1975).
8. I. J. Borowitz and L. I. Grossman. Tetrahedron Lett. 421 (1962).
9. R. A. Bothner-By. *In* Advances in magnetic resonance. Vol. 1. *Edited by* J. S. Waugh. Academic Press, New York. 1965. pp. 205, 239, 242; H. Booth. *In* Progress in nuclear magnetic resonance spectroscopy. Vol. 5. *Edited by* J. W. Emsley, J. Feeney, and L. H. Sutcliffe. Pergamon Press, New York. 1969. pp. 224–225.
10. J. W. Emsley, J. Feeney, and L. H. Sutcliffe. High resolution nuclear magnetic resonance spectroscopy. Vol. 2. Pergamon Press, New York. 1966. p. 788; H. J. Anderson and C. W. Huang. Can. J. Chem. **45**, 897 (1967).
11. J. R. Catch, D. F. Elliot, D. H. Hey, and E. R. H. Jones. J. Chem. Soc. 278 (1948).
12. L. W. Jones and D. H. Powers. J. Am. Chem. Soc. **46**, 2518 (1924).
13. M. H. Paloma and A. Kenetti. Chem. Ber. **64**, 800 (1931).
14. P. F. Alewood, M. Benn, and R. Reinfred. Can. J. Chem. **52**, 4083 (1974).
15. W. H. Nutting, R. A. Jewel, and H. Rapoport. J. Org. Chem. **35**, 505 (1970).
16. W. E. Parham and E. L. Anderson. J. Am. Chem. Soc. **70**, 4187 (1948).


Can. J. Chem. Downloaded from www.nrcresearchpress.com by 210.87.254.5 on 09/06/12
For personal use only.

# The synthesis, characterization, and thermal isomerization of some 1,1,2,2-tetraarylcyclopropanes

DONALD R. ARNOLD,[1] DANIAL D. M. WAYNER, AND MASATO YOSHIDA
*Department of Chemistry, Dalhousie University, Halifax, N.S., Canada B3H 4J3*

Received March 9, 1982

DONALD R. ARNOLD, DANIAL D. M. WAYNER, and MASATO YOSHIDA. Can. J. Chem. **60**, 2313 (1982).

The synthesis and spectral characterization of an extensive series of 1,1,2,2-tetraarylcyclopropanes are reported. The effects of substituents on the $^{13}$Cmr and $^{1}$Hmr chemical shifts are examined in detail. In a series of symmetrically substituted derivatives, the $^{13}$Cmr chemical shifts correlate with $\Sigma\sigma_R^0$. This correlation is only observed in cases where the $C_\alpha$—$C_\beta$ bond has no net polarity. Details of the thermal isomerization of those derivatives for which the possibility of *cis* and *trans* configurations exists are also reported. Trends in the Arrhenius parameters provide evidence for the biradical character of the transition state. Other data supporting the biradical character of the transition state are discussed.

DONALD R. ARNOLD, DANIAL D. M. WAYNER et MASATO YOSHIDA. Can. J. Chem. **60**, 2313 (1982).

On rapporte la synthèse et les caractéristiques spectrales d'une série importante de tétraaryl-1,1,2,2 cyclopropanes. On a examiné en détail l'effet des substituants sur les déplacements chimiques en rmn du $^{13}$C et du $^{1}$H. Dans les séries de dérivés substitués d'une façon symétrique, les déplacements chimiques du $^{13}$C correspondent à $\Sigma\sigma_R^0$. On observe cette corrélation uniquement dans les cas où la liaison C—$C_\beta$ n'a pas de polarité nette. On rapporte également les détails relatifs à l'isomérisation thermique de ces dérivés pour lesquels existe la possibilité de configuration *cis* et *trans*. La tendance des paramètres d'Arrhénius fournit la preuve du caractère biradicalaire de l'état de transition. On discute d'autres données qui appuient le caractère biradicalaire de l'état de transition.

[Traduit par le journal]

## Introduction

We have reported the characterization of the ground and excited state surfaces for twisting about the double bond in tetraphenylethylene, and the effect of substituents on these surfaces (1). The results provided additional evidence for the 1,2-biradical character of the transition state for the thermal *cis–trans* isomerization of symmetrically substituted alkenes (1*a*, *c*, *e*, *g*, *i*, *l*).

The enhanced rate and significantly lower (8 kJ mol$^{-1}$) activation barrier for the thermal isomerization of the unsymmetrically substituted derivative 1*l* was attributed to merostabilization (1*a*). Direct irradiation of 1*a*, *c*, and *g* brought about efficient *cis–trans* isomerization. The sum of the quantum yields for *cis* to *trans* plus *trans* to *cis*

| | X | Y |
|---|---|---|
| *a* | $CH_3$ | H |
| *c* | $OCH_3$ | H |
| *e* | $OCH_3$ | $OCH_3$ |
| *g* | CN | H |
| *i* | CN | CN |
| *l* | $OCH_3$ | CN |

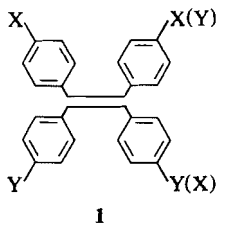


1

isomerization was essentially unity and the excited state ($S^1$) partitioned almost equally to the two isomers. In the case of 1*l*, however, the photostationary state significantly favoured the *trans* isomer and the efficiency of the *cis–trans* isomerization was greatly reduced. These differences were attributed to attractive dipolar forces between the methoxy and cyano substituted rings in the singlet excited state of this derivative (1*b*). The photosensitized (triplet–triplet energy transfer) isomerization of 1*a*, *c*, *g*, and *l* led to the same photostationary state, equal amounts of both isomers, for all four derivatives. However, the triplet energy of 1*l* was estimated to be about 8 kJ mol$^{-1}$ lower than the triplet energy of 1*a*, *c*, and *g*. This difference again was attributed to merostabilization (1*b*). The half-wave oxidation and reduction potentials of 1*a*, *c*, *e*, *g*, *i*, and *l* were found to correlate with the sum of the substituent parameters $\sigma^+$ and $\sigma^-$, respectively. These electrochemical data provided further information about the HOMO and LUMO of these alkenes, as well as further illustrating the effect of merostabilization on the stability of these radical-like (i.e. radical ion) species (1*a*).

This study has now been extended to the 1,1,2,2-tetraarylcyclopropane series. Our objective is to define the nature of the intermediates or transition states (the 1,3-biradicals and radical ions) that are involved in reactions of the 1,1,2,2-tetraarylcyclopropanes analogous to the previously studied tetraarylethylenes. Some of the

[1]Author to whom correspondence may be addressed.

0008-4042/82/182313-08$01.00/0
©1982 National Research Council of Canada/Conseil national de recherches du Canada

Can. J. Chem. Downloaded from www.nrcresearchpress.com by 210.87.254.105 on 09/06/12
For personal use only.

Can. J. Chem. Downloaded from www.nrcresearchpress.com by 210.87.254.105 on 09/06/12
For personal use only.

TABLE 1. Melting points of 1,1,2,2-tetraarylcyclopropanes (2)

| 2 | $X_1$ | $X_2$ | $Y_1$ | $Y_2$ | mp (°C) |
|---|---|---|---|---|---|
| *a* | H | H | H | H | 167.5–168(165–165.5)[a] |
| *b* | $OCH_3$ | H | H | H | 145 |
| *c cis* | $OCH_3$ | $OCH_3$ | H | H | 205–206 |
| *c trans* | $OCH_3$ | H | H | $OCH_3$ | 139–141 |
| *d* | $OCH_3$ | H | $OCH_3$ | H | 107–108 |
| *e* | $OCH_3$ | $OCH_3$ | $OCH_3$ | $OCH_3$ | 215.5–216 |
| *f* | CN | H | H | H | 175 |
| *g cis* | CN | CN | H | H | 201–202 |
| *g trans* | CN | H | H | CN | 106–109 |
| *h* | CN | H | CN | H | 217–218 |
| *i* | CN | CN | CN | CN | 233–234.5 |
| *j cis* | CN | $OCH_3$ | H | H | 158 |
| *j trans* | CN | H | H | $OCH_3$ | 134 |
| *k* | CN | H | $OCH_3$ | H | 191–192 |
| *l cis* | CN | CN | $OCH_3$ | $OCH_3$ | 157 |
| *l trans* | CN | $OCH_3$ | $OCH_3$ | CN | 95 |
| *m* | CN | $OCH_3$ | CN | $OCH_3$ | 203–204 |

[a]See reference 14.

preliminary results have been published (2). In this paper we report the details of the synthesis, separation, purification, and spectral characterization of an extensive series of substituted 1,1,2,2-tetraarylcyclopropanes **2***a–m* (Table 1). All of these cyclopropanes, with the exception of the unsubstituted tetraphenyl derivative, are new compounds. In addition, this paper includes the details of the results of a study of the *cis–trans* thermal isomerization of the derivatives **2***c*, *g*, *j*, and *l* which were summarized in the preliminary communication (2*a*).

## Results and discussion

The tetraarylcyclopropanes were synthesized from the corresponding diaryldiazomethanes (3) and the 1,1-diarylethylenes (4), eq. [1].

In some cases, two routes were possible and both were tried. A better yield was obtained when the diarylmethylene bore the electron-donating substituents and the diarylethylene was substituted with the electron-withdrawing groups. For example, the yield of **2***j* was increased from 20% to 70% when the reactant pair was 4-methoxyphenylphenyldiazomethane and 1-(4-cyanophenyl)-1-phenylethylene. This relative reactivity is as expected (5).

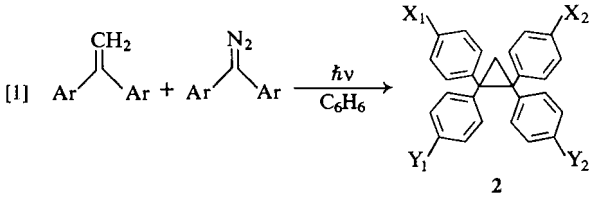


**2**

Whenever configurational isomers were possible (**2***c*, *g*, *j*, and *l*), both *cis* and *trans* were obtained as an approximately equimolar mixture. Purification and separation of the isomers was achieved by medium pressure column chromatography on silica gel and/or by recrystallization. The composition of the isomeric mixtures could be determined conveniently by high pressure liquid chromatography.

The gross structures of the compounds **2***b–m* were inferred from their $^{13}$Cmr, $^1$Hmr, ir, and uv spectra and elemental analyses (or exact mass determination). Establishing the configuration of the isomeric pairs was straightforward in the case of **2***c*, *g*, and *l*. The cyclopropyl hydrogens are identical in the *trans* isomer of these derivatives, while an AB pair of doublets for these nonequivalent protons indicates the *cis* configuration.

Distinguishing *cis* from *trans* (**2***j*) was not trivial. The cyclopropyl hydrogens are obviously not equivalent in either isomer and the expected multiplet was observed for both. It seemed likely that an analysis of the nmr spectra, both $^{13}$C and $^1$H (Table 2), of this extensive series of analogous compounds would reveal some correlation upon which an assignment could be made. Furthermore, the nmr spectra of these compounds are of interest (6, 7). However, no correlation useful for assigning configuration to the isomers of **2***j* was evident.

The initial distinction between the *cis* and *trans* isomers of **2***j* rested on their relative thermodynamic stability (ref. 2*a* and Table 3). We knew that the thermal equilibrium in the case of **2***l* favoured the *trans* isomer. Therefore, the *cis* configuration was assigned to the more stable isomer of **2***j*. It

Can. J. Chem. Downloaded from www.nrcresearchpress.com by 210.87.254.105 on 09/06/12
For personal use only.

seems likely that through-space donor–acceptor interactions (8) between the cyano and methoxy substituted phenyl rings will stabilize the *cis* configuration of **2***j*. The magnitude of the equilibrium constant for **2***j* was, however, so small that the assignment was considered tentative (2*a*).

Confirmation of the structural assignment was provided by a complete X-ray analysis[2] of a single crystal of the less stable isomer (mp 134°C) which was shown to have the *trans* configuration of **2***j*.

*Substituent effects on the* $^{13}$*Cmr chemical shift*

The effect of ring substituents on the $^{13}$Cmr chemical shift (C-SCS) of a carbon α or β to the phenyl ring has been studied previously (6). It has been suggested that, in general, the $C_\alpha$-SCS are influenced primarily by the substituent Pauling electronegativity, $X_p$ (9), and to a lesser extent by resonance, $\sigma_R^0$ (6*c*–*e*). The data were treated in terms of a two parameter correlation plotting the $C_\alpha$-SCS against the substituent electronegativity and $\sigma_R^0$. The absolute magnitudes of the contribution of electronegativity ($\rho_{X_p}$) and resonance ($\rho_R$) cannot be compared since the substituent parameters $X_p$ and $\sigma_R^0$ are based on completely different energy scales. We can, however, obtain information about the relative importance of the two by comparing the ratios of $\rho_{X_p}$ to $\rho_R$. The results of Inamoto and co-workers (6*c*–*e*) clearly show that the relative magnitude of $\rho_{X_p}$ is much larger when $C_\alpha$ is *sp* or $sp^2$ than when $C_\alpha$ is $sp^3$ hybridized. Although they found a reasonable correlation using the two parameter approach for the *para*-substituted toluenes (**3**) ($r = 0.907$), we find that an even better correlation is obtained (Table 4) when their $C_\alpha$-SCS are plotted against $\sigma_R^0$ alone. Similar correlations were also observed for the 2-arylpropanes (**4**) and the arylcyclopropanes (**5**). We conclude that substituent electronegativity has some contribution to the $C_\alpha$-SCS for *sp* or $sp^2$ hybridized $C_\alpha$ but has a negligible effect when $C_\alpha$ is $sp^3$ hybridized. The effect of substitution on the $C_\beta$-SCS, on the other hand, has been interpreted as being dependent on the π-character of the $C_\alpha$—$C_\beta$ bond (6*e*) and on the dihedral angle between the plane of the aromatic ring and the $C_\alpha$—$C_\beta$ bond (6*b*).

Examination of the effect of aryl substituents on the $^{13}$C-SCS in the tetraarylcyclopropane series (Table 2) reveals that a complex mechanism for transmission of the substituent effects exists. Several important features can be pointed out. When all the data are considered, it is not surprising that no correlation is observed with $\Sigma\sigma_R^0$ in a one parameter Hammett plot. A two parameter Hammett plot, accommodating the effects of the α- and β-aryl substituents, also gives a poor correlation ($r = 0.80$). One surprising feature is that the $^{13}$C-SCS for the *cis* and *trans* isomers **2***c*, *g*, *j*, and *l* are virtually identical (at least for the quaternary cyclopropyl ring carbons). This implies that the influence of preferred conformations of the aryl rings is not as important as we had anticipated. If the series is limited to the symmetrically substituted derivatives **2***a*, *c*, *e*, *g*, *i*, and *l*, a good correlation is observed ($r = 0.97$) for a one parameter Hammett plot (Fig. 1). The slope of the correlation line in this case would actually be a composite ρ-value (i.e. $\rho = \rho_\alpha + \rho_\beta$ of a two parameter Hammett plot). Since the magnitude of ρ

[2]T. S. Cameron, unpublished results.

TABLE 2. Nuclear magnetic resonance spectroscopic data for **2**[a]

| **2** | $\delta^{13}C(CAr_2)$ | $\delta^{13}C(CH_2)$ | $\delta^1H(CH_2)$ |
|---|---|---|---|
| *a* | 44.1 | 25.1 | 2.54 (s) |
| *b* | 44.8, 43.8 | 25.3 | 2.46, 2.50 (AB, $J = 0.1$ Hz) |
| *c cis* | 43.2 | 25.3 | 2.40, 2.46 (AB, $J = 5$ Hz) |
| *c trans* | 43.2 | 25.3 | 2.44 (s) |
| *d* | 43.8, 42.6 | 25.3 | 2.45 (s) |
| *e* | 42.6 | 25.7 | 2.34 (s) |
| *f* | 43.9, 43.3 | 25.2 | 2.56, 2.65 (AB, $J = 5$ Hz) |
| *g cis* | 44.5 | 25.2 | 2.57, 2.71 (AB, $J = 6$ Hz) |
| *g trans* | 44.5 | 25.6 | 2.64 (s) |
| *h* | 45.4, 43.4 | 25.3 | 2.64 (s) |
| *i* | 44.7 | 25.5 | 2.68 (s) |
| *j cis* | 44.2, 43.7 | 25.4 | 2.47, 2.57 (AB, $J = 6$ Hz) |
| *j trans* | 44.2, 43.7 | 25.4 | 2.53 (s)[b] |
| *k* | 44.9, 43.3 | 25.6 | 2.53 (s) |
| *l cis* | 43.9 | 25.6 | 2.43, 2.66 (AB, $J = 7$ Hz) |
| *l trans* | 43.9 | 26.1 | 2.58 (s) |
| *m* | 44.2, 43.5 | 25.7 | 2.53 (s) |

[a]Data are reported in ppm downfield from TMS in $CDCl_3$ solution. The error limits are estimated to be 0.1 ppm for the $^{13}$Cmr chemical shifts and 0.02 ppm for the $^1$Hmr chemical shifts.
[b]Appears as AB pair of doublets in benzene-$d_6$.

TABLE 3. Arrhenius activation energies ($E_a$)[a] and pre-exponential factors ($A$) for the thermal isomerization of **1** and **2** in benzene solution

| $K_e$ (*cis*/*trans*) | $E_a$ (kJ mol$^{-1}$)[b] | log $A$ (s$^{-1}$)[b] |
|---|---|---|
| (**2***c*) 0.992[c] | 127±5 | 13.1±0.6 |
| (**1***c*) 0.938[d] | 148±3 | 12.5±0.3 |
| (**2***g*) 0.602[c] | 127±3 | 13.4±0.4 |
| (**1***g*) 0.730[d] | 147±2 | 12.3±0.2 |
| (**2***j*) 1.105[c] | 127±4 | 13.3±0.5 |
| (**2***l*) 0.685[c] | 118±5 | 12.5±0.7 |
| (**1***l*) 0.610[d] | 138±5 | 11.8±0.5 |

[a]Obtained by linear least-squares analysis of the Arrhenius equation $(k_{t\to c} + k_{c\to t}) = A \exp(-E_a/RT)$. The quantity $(k_{t\to c} + k_{c\to t})$ is the sum of the rate constants for the forward and reverse reactions; therefore, the Arrhenius factors refer to the approach to equilibrium and not to individual processes.
[b]Error limits obtained from least-squares analysis.
[c]At 120°C.
[d]At approx. 205°C (see ref. 1*a*).

Can. J. Chem. Downloaded from www.nrcresearchpress.com by 210.87.254.105 on 09/06/12
For personal use only.

TABLE 4. Hammett $\rho_R$ values ($^{13}$C-SCS versus $\Sigma\sigma_R^0$)

| Compound | $\rho_R$ | $r^a$ |
|---|---|---|
| **2** | 1.95±0.18 | 0.98 |
| **3** | 1.96±0.20 | 0.97 |
| **4** | 1.78±0.21 | 0.97 |
| **5** | 2.00±0.27 | 0.96 |

[a]Correlation coefficient obtained from linear least-squares analysis.

is close to the ρ-value obtained for mono-arylcyclopropanes (Table 4), we are tempted to conclude that $\rho_\alpha$ is much greater than $\rho_\beta$. Although this may be the case, the evidence is not strong, since the absolute magnitude of $\rho_\alpha$ and $\rho_\beta$ is not known, only their sum is known; hence, the similarity may be fortuitous.

The $C_\alpha$—$C_\beta$ bond, in the symmetric derivatives, has no net polarity, thus the effect of a bond moment may account for the poor correlation obtained (10) when all of the derivatives are considered. The similarity in the trends observed for the tetraarylcyclopropane series and the toluene series indicates that the interaction of the cyclopropyl ring carbons with the aromatic ring is not fundamentally different than those interactions in the toluene series.

The $C_\beta(CH_2)$-SCS are much less sensitive to substitution (Table 2). Although the variation in chemical shift is only 1 ppm over the entire series, note that the $C_\beta(CH_2)$-SCS of the unsubstituted derivative **2***a* is at highest field, a result expected

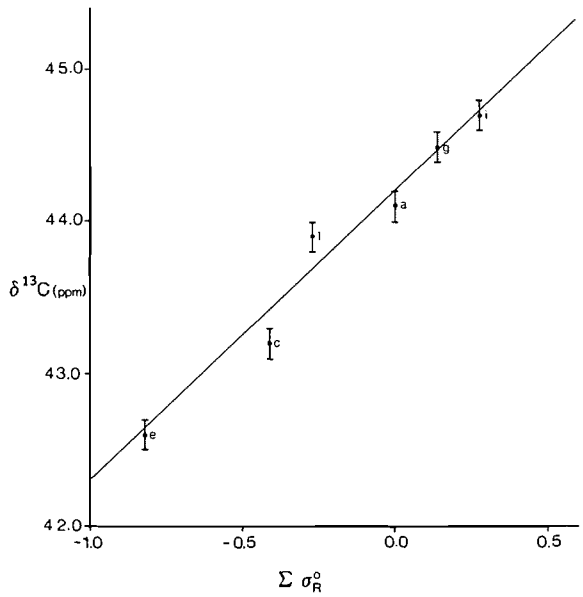


FIG. 1. Hammett plot of the $^{13}$C- CS of the symmetrical tetraarylcyclopropanes versus $\Sigma\sigma_R^0$.

considering the substituent electronegativity. This dependence is not observed for the less heavily arylated cyclopropane derivatives (**5**), or for the other phenylalkanes (**3**, **4**). The complex steric restrictions intrinsic to the tetraaryl series may be responsible for this anomalous behavior.

*Substituent effects on $^1$Hmr spectra*

The effect of the aryl substituents on the cyclopropyl ring proton chemical shifts has been studied previously (7) and our results are qualitatively similar. While correlation with substituent parameters is inadequate, the general trend observed is that the electron-donating substituents shield both methylene protons while the electron-withdrawing substituents deshield both. Table 2 shows the variation in chemical shift is only 0.3–0.4 ppm (~20 Hz) over the entire series. This effect is somewhat less than that reported for a series of *trans*-2-arylcyclopropanecarboxylic acids (7). This may be a result of different preferred conformations of the aryl ring with respect to the cyclopropane ring in the two series. The effect of the *para* substituents on the chemical shift of the cyclopropane methylene protons is additive. The *para*-methoxy substituent shifts the *cis*-methylene proton upfield by 0.07 ppm while the *trans*-methylene proton is shifted upfield by 0.04 ppm relative to the unsubstituted derivative (δ 2.54). In the case of the *para*-cyano substituent, the *cis*-methylene proton is shifted downfield by 0.1 ppm while the *trans*-methylene proton is shifted downfield by 0.02 ppm. The calculated values agree with the observed values to within 0.02 ppm (except **2***i* which appears 0.1 ppm upfield from the calculated value).

*Thermal isomerization*

The results for the thermal isomerization of **2***c*, *g*, *j*, and *l* have been summarized (ref. 2*a* and Table 3). The thermal *cis*–*trans* isomerization of **2** can be compared to the corresponding olefins (**1**), inasmuch as both involve the cleavage of a weak bond, a σ-bond for **2** and a π-bond for **1**. The trends in the activation energies as a function of substituent in **1** and **2** are remarkably similar. The lower activation barriers for **2** indicate a lower cyclopropane σ-bond strength compared to the olefin π-bond strength, about 20 kJ mol$^{-1}$ difference for these derivatives. Evidence for the biradical character of the transition state is obtained from an analysis of the substituent effects on the activation energy. If charge separation was involved at the transition state, the activation barrier of **2***j* would be expected to be lowered relative to the others. The lower barrier (9 kJ mol$^{-1}$) for **2***l* (and **1***l*) may be attributed to merostabiliza-

TABLE 5. The relationship between spin delocalization in the 1,3-biradical and the activation energy for thermal isomerization

| Compound | Hydrocarbon radical | $\rho_\alpha$[a] | $\Sigma\rho_\alpha$ | $E_a$ (kJ mol$^{-1}$) |
|---|---|---|---|---|
| Cyclopropane-1,2-$d_2$ (7) | $CH_3$· | 0.944 | 1.888 | 272.0[b] |
| 1-Phenylcyclopropane-2-*d* (5*d*) | $PhCH_2$· | 0.654 | 1.598 | 220.9[c] |
| | $CH_3$· | 0.944 | | |
| *trans*-1,2-Diphenylcyclopropane (6) | $PhCH_2$· | 0.654 | 1.308 | 145.6[d] |
| 2 | $Ph_2CH$· | 0.588 | 1.176 | 126.8[e] |

[a]Calculated from experimental hyperfine constants from "Landolf-Börnstein" (ref. 16); $a = Q\rho$ $Q = 25$G.
[b]See ref. 10.
[c]See ref. 17; estimated from the rate of isomerization at 309.5 K assuming a preexponential factor of $10^{14}$.
[d]See ref. 18.
[e]This work.

tion of the 1,3- (and 1,2-) biradical. The decrease in the preexponential factor (log *A*) in **2***l* is also consistent with the involvement of merostabilization. The merostabilized radical requires coplanarity of both rings and substituents; therefore, a decrease in the entropy of activation is expected (1*a*).

Further evidence for the biradical character of the transition state is obtained by comparing the activation barriers for the thermal isomerization of the series: **2**, *trans*-1,2-diphenylcyclopropane (**6**), 1-phenylcyclopropane-2-*d* (**5***d*), and cyclopropane-1,2-$d_2$ (**7**) (11). The differences in the activation energies reflect the relative σ-bond strengths. The bond strengths should parallel the extent of spin delocalization in the resulting radicals (i.e. transition state). A reasonable measure of spin delocalization can be obtained from spin density determinations for suitable model radicals. The α-hydrogen hyperfine coupling constant from the electron spin resonance spectrum is roughly proportional to the spin density at the carbon centre, and hence to the spin delocalization (12). The appropriate hydrocarbon radicals which adequately represent the transition state must also have at least one α-hydrogen. The series of model radicals with their corresponding spin densities are shown along with the activation energies for the cyclopropane thermal isomerization (Table 5). A plot of the activation energy versus the spin densities in the transition states (Fig. 2) reveals a good correlation ($r$ = 0.994). We have now confirmed the biradical character of the transition state in both **1** and **2**.

The difference in thermodynamic stability of these *cis* and *trans* isomers (Table 3) is small, less than 2.0 kJ mol$^{-1}$. Two factors (at least) influence the relative stability. Stabilization of the *trans* relative to the *cis* isomer may simply be the result of dipole–dipole interactions with the solvent. The difference in thermodynamic stability will increase as the difference in dipole moments between the

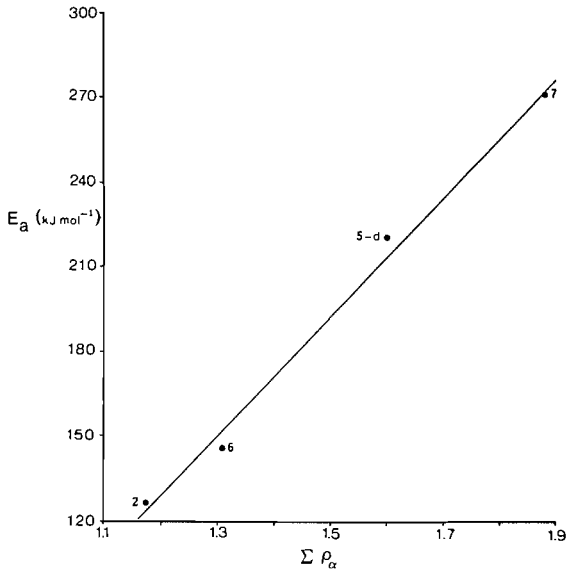


FIG. 2. Graph of activation energy ($E_a$) for cyclopropanes versus the estimated spin density ($\Sigma\rho_\alpha$) of the 1,3-biradical.

two isomers increases (1*a*). Intramolecular donor–acceptor interactions will also influence the relative stability of the two isomers. Electron-withdrawing substituents will lower the energy of the LUMO (i.e. lower the reduction potential) whereas electron-donating substituents will raise the energy of the HOMO (i.e., lower the oxidation potential). The difference in thermodynamic stability of the isomeric pairs will increase as the difference in redox potentials ($E^{ox}_{donor} - E^{red}_{acceptor}$) decreases. Evidence for intramolecular donor–acceptor interactions in similarly substituted cyclopropanes has been reported (8).

Although dipole–dipole interactions with the solvent can be used to rationalize the relative magnitudes of the equilibrium constants for **2***c*, *g*, and *l*, they do not predict the relative stability of *cis* and *trans* **2***j*. On the other hand, if intramolecular donor–acceptor interactions were solely responsi-

Can. J. Chem. Downloaded from www.nrcresearchpress.com by 210.87.254.105 on 09/06/12
For personal use only.

Can. J. Chem. Downloaded from www.nrcresearchpress.com by 210.87.254.105 on 09/06/12
For personal use only.

ble in determining $K_e$, then the equilibrium constant for **2***l* would be expected to be less than that for **2***g*. It is clear that both factors have an influence on the *cis–trans* equilibrium; it is difficult to assess the extent to which each is involved.

## Experimental

The $^1$Hmr and $^{13}$Cmr spectra were recorded on either a Varian T-60 or CFT-20 nmr spectrometer and are reported in parts per million (ppm) downfield from TMS. Infrared spectra were recorded on an air-purged Perkin–Elmer 180 grating infrared spectrometer and are reported in wavenumbers (calibrated against the 1601.8 $cm^{-1}$ absorption of polystyrene). Ultraviolet–visible absorption spectra were recorded on a Cary–Varian 219 absorption spectrometer and are reported in nanometers followed by the molar extinction coefficient. Elemental analyses were performed by Chemialytics, Inc. or Canadian Microanalytics, Inc., and agreed to within 0.3% of the calculated values. The melting points (uncorrected) were obtained on an Sybron Corporation Thermolyne melting point apparatus.

Bath temperatures for the thermal isomerization were maintained using a Fisher Proportional Temperature Control, and did not vary more than 0.5° during any particular run. The temperature was determined using a platinum resistance thermometer (Hewlett–Packard 2802A). Analyses of the cyclopropane mixtures were performed using a Tracor high performance liquid chromatograph which consists of a Tracor 995 isochromatographic pump, Model 970 variable wavelength absorbance detector, a Rheodyne model 7120 loop injection valve (20 μL volume), and a Hewlett–Packard model 7123A strip chart recorder, in conjunction with a Whatman Partisil PXS 10/25 analytical column. The hplc solvents were hexanes (Fisher reagent, distilled) and methylene chloride (Fisher reagent, distilled from phosphorous pentoxide). Peak areas were determined by cutting and weighing or multiplying height by half-width. The apparent mole fractions of the *cis* isomers (obtained by dividing the areas of the peak due to the *cis* isomer by the sum of the areas of both peaks) were converted to true mole fractions with working curves, which were simply plots of apparent vs. true mole fractions constructed with ten accurately weighed samples of "pure" *cis* and *trans* isomers.

The 1,1,2,2-tetraarylcyclopropanes were prepared by the addition of a diarylcarbene to a corresponding 1,1-diarylethylene in benzene. The diarylcarbenes were generated by the photolysis of the corresponding diaryldiazomethanes through a sodium nitrite filter. To reduce the formation of tetraarylazines, the diaryldiazomethanes were added to the olefin solutions in ten equal aliquots, allowing the colour to disappear between additions. The preparation of the diaryldiazomethanes and diarylolefins from the corresponding benzophenones has been described previously (3, 4). The tetraarylcyclopropanes were isolated by medium pressure chromatography or flash chromatography (13) and purified by recrystallization. The yields were generally greater than 60% except for **2***e* which was only 27%. The preparation of 1,1,2,2-tetraphenylcyclopropane has been reported previously (14). Details of the preparation, separation, purification, and characterization of each of the *para*-substituted derivatives are described below.

*1-(4-Methoxyphenyl)-1,2,2-triphenylcyclopropane (*2b*)*

Diphenyldiazomethane (0.9 g, 0.0046 mol) in 10 mL of benzene was added to 1-(4-methoxyphenyl)-1-phenylethylene (1.0 g, 0.0048 mol) in 20 mL of benzene (*vide supra*). After the photolysis was complete, the solvent was evaporated and the reaction mixture separated by medium pressure chromatography (silica gel, hexanes – methylene chloride gradient). The product was recrystallized three times from chloroform–methanol to give colourless plates (mp 145–146°C). Infrared (KBr): 3050 (m), 2839 (w), 1608 (m), 1512 (s), 1290 (m), 1246 (s), 1172 (s), 1028 (s), 798 (m), 699 (s); uv $\lambda_{max}$ (ethanol): 237 (20 000); $^1$Hmr $CDCl_3$) δ: 2.46 (d, 1H, $J$ = 0.1 Hz), 2.50 (d, 1H, $J$ = 0.1 Hz), 3.69 (s, 3H), 6.80 (m, 4H), 7.05 (m, 15H). *Anal.* calcd. for $C_{28}H_{24}O$: C 89.32, H 6.43; found: C89.50, H 6.38.

*1,2-Di(4-methoxyphenyl)-1,2-diphenylcyclopropane (*2c*)*

(4-Methoxyphenyl)phenyldiazomethane (1.5 g, 0.0067 mol) in 10 mL of benzene was added to 1-(4-methoxyphenyl)-1-phenylethylene (1.5 g, 0.0071 mol) in 20 mL of benzene (*vide supra*). After the photolysis was complete, the solvent was evaporated and the reaction mixture was separated by medium pressure chromatography (silica gel, hexanes – methylene chloride gradient). Rechromatographing the mixture of the *cis* and *trans* isomers (silica gel, hexanes – methylene chloride gradient) afforded pure samples of each. The *cis*-1,2-di(4-methoxyphenyl)-1,2-diphenylcyclopropane (*cis* **2***c*) was recrystallized from chloroform–ethanol to give colourless prisms (mp 139–141°C). Infrared (KBr): 3040 (w), 2833 (w), 1608 (m), 1510 (s), 1495 (m), 1447 (m), 1245 (s), 1033 (m), 826 (m), 697; uv $\lambda_{max}$ (ethanol): 236 (17 000); $^1$Hmr ($CDCl_3$) δ: 2.40 (d, 1H, $J$ = 5 Hz), 2.46 (d, 1H, $J$ = 5 Hz), 3.69 (s, 6H), 6.80 (m, 8H), 7.02 (m, 10H). *Anal.* calcd. for $C_{29}H_{26}O_2$: C 85.68, H 6.45; found: C 85.69, H 6.56.

The *trans*-1,2-di(4-methoxyphenyl)-1,2-diphenylcyclopropane (*trans* **1***c*) was recrystallized from chloroform–ethanol to give colourless prisms (mp 205–206°C). Infrared (KBr): 3030 (w), 2830 (m), 1606 (s), 1509 (s), 1457 (m), 1289 (m), 1241 (s), 1031 (s), 831 (m), 692 (m); uv $\lambda_{max}$ (ethanol): 235 (17 000); $^1$Hmr ($CDCl_3$) δ: 2.44 (s, 2H), 3.68 (s, 6H), 6.78 (m, 8H), 7.04 (m, 10H). *Anal.* calcd. for $C_{29}H_{26}O_2$: C 85.68, H 6.45; found: C 85.48, H 6.30.

*1,1-Di(4-methoxyphenyl)-2,2-diphenylcyclopropane (*2d*)*

Diphenyldiazomethane (1.2 g, 0.0062 mol) in 10 mL of benzene was added to 1,1-di(4-methoxyphenyl)ethylene (1.5 g, 0.0063 mol) in 20 mL of benzene (*vide supra*). The solvent was then evaporated and the reaction mixture separated by column chromatography (neutral alumina, hexane–benzene gradient). The product was recrystallized from chloroform–ethanol to give colourless prisms (mp 107–108°C). Infrared (KBr): 3030 (w), 2836 (w), 1608 (m), 1510 (s), 1290 (m), 1247 (s), 1179 (m), 1036 (m), 823 (m), 695 (m); uv $\lambda_{max}$ (ethanol): 236 (22 000); $^1$Hmr ($CDCl_3$) δ: 2.45 (s, 2H), 3.70 (s, 6H), 6.80 (m, 8H), 7.08 (m, 10H). *Anal.* calcd. for $C_{29}H_{26}O_2$: C 85.68, H 6.45; found: C 85.81, H 6.29.

*1,1,2,2-Tetra(4-methoxyphenyl)cyclopropane (*2e*)*

Di(4-methoxyphenyl)diazomethane (1.0 g, 0.004 mol) in 10 mL of benzene was added to 1,1-di(4-methoxyphenyl)ethylene (2.0 g, 0.008 mol) in 20 mL of benzene (*vide supra*). The solvent was then evaporated and the reaction mixture separated by flash chromatography (silica gel, methylene chloride). The product contained a trace amount of a fluorescent impurity which could be removed only by careful chromatography of the product and collecting the last few fractions as the compound eluted (basic alumina, hexane – methylene chloride gradient). The product was recrystallized from chloroform–hexanes to give colourless needles (mp 215.5–216°C). Infrared (KBr): 3030 (w), 2832 (m), 1605 (s), 1507 (s), 1461 (m), 1290 (m), 1241 (s), 1105 (m), 1031 (s), 837 (m), 748 (m); uv $\lambda_{max}$ (ethanol): 233 (32 000); $^1$Hmr ($CDCl_3$) δ: 2.34 (s, 2H), 3.70 (s, 12H), 6.74 (m, 16H). *Anal.* calcd. for $C_{31}H_{30}O_4$: C 79.83, H 6.45; found: C 79.81, H 6.37.

*1-(4-Cyanophenyl)-1,1,2-triphenylcyclopropane (*2f*)*

4-Cyanophenylphenyldiazomethane (1.0 g, 0.0046 mol) in 10 mL of benzene was added to 1,1-diphenylethylene (1.0 g, 0.0056 mol) in 20 mL of benzene (*vide supra*). The solvent was

Can. J. Chem. Downloaded from www.nrcresearchpress.com by 210.87.254.105 on 09/06/12
For personal use only.

then evaporated and the reaction mixture separated by medium pressure chromatography (silica gel, hexane – methylene chloride gradient). The product obtained was recrystallized from chloroform–ethanol to give colourless plates (mp 175–176°C). Infrared (KBr): 3058 (m), 2228 (s), 1603 (s), 1492 (s), 1448 (s), 832 (m), 749 (m), 697 (s), 633 (m); uv $\lambda_{max}$ (ethanol): 243 (20 000), 260 (17 000); $^1$Hmr ($CDCl_3$) δ: 2.56 (d, 1H, $J$ = 6 Hz), 2.65 (d, 1H, $J$ = 6 Hz), 7.30 (m, 19H). *Anal.* calcd. for $C_{28}H_{21}N$: C 90.53, H 5.70; found: C 90.66, H 5.50.

*1,2-Di(4-cyanophenyl)-1,2-diphenylcyclopropane (2g)*

4-Cyanophenylphenyldiazomethane (0.20 g, 0.0009 mol) in 5 mL of benzene was added to 1-(4-cyanophenyl)-1-phenylethylene (0.20 g, 0.001 mol) in 5 mL of benzene (*vide supra*). The solvent was then evaporated and the reaction mixture separated by medium pressure chromatography (silica gel, hexanes – methylene chloride gradient). The *cis* isomer was recrystallized from chloroform–ethanol to give colourless needles (mp 201–202°C). Infrared (KBr): 3060 (w), 2227 (s), 1605 (s), 1496 (s), 1449 (m), 1400 (w), 1008 (m), 833 (m), 761 (m), 695 (s), 628 (m); uv $\lambda_{max}$ (ethanol): 241 (27 000), 255 (22 000); $^1$Hmr ($CDCl_3$) δ: 2.57 (d, 1H, $J$ = 6 Hz), 2.71 (d, 1H, $J$ = 6 Hz), 7.10 (m, 10H) 7.32 (m, 8H). *Anal.* calcd. for $C_{29}H_{20}N_2$: C 87.85, H 5.08; found: C 87.72, H 5.01.

The *trans* isomer was recrystallized from chloroform–ethanol to give colourless plates (mp 106–109°C). Infrared (KBr): 3060 (w), 2227 (s), 1606 (s), 1501 (m), 1444 (w), 1400 (w), 1008 (w), 849 (m), 701 (s), 675 (m), 621 (m); uv $\lambda_{max}$ (ethanol): 241 (27 000), 255 (20 000); $^1$Hmr ($CDCl_3$) δ: 2.65 (s, 2H), 7.15 (m, 10H), 7.22 (m, 8H). *Anal.* calcd. for $C_{29}H_{20}N_2$: C 87.85, H 5.08; found: C 87.69, H 4.99.

*1,1-Di(4-cyanophenyl)-2,2-diphenylcyclopropane (2h)*

Di(4-cyanophenyl)diazomethane (1.3 g, 0.0053 mol) in 10 mL of benzene was added to 1,1-diphenylethylene (1.0 g, 0.0056 mol) in 20 mL of benzene (*vide supra*). The solvent was then evaporated and the reaction mixture separated by column chromatography (neutral alumina, benzene). The produce was recrystallized from chloroform–ethanol to give colourless needles (mp 217–219°C). Infrared (KBr): 2222 (s), 1600 (s), 1495 (m), 1448 (m), 1398 (w), 828 (m), 738 (m), 705 (m), 569 (m); uv $\lambda_{max}$ (ethanol): 243 (26 000), 260 (20 000); $^1$Hmr ($CDCl_3$) δ: 2.64 (s, 2H), 7.10 (m, 10H), 7.26 (m, 8H). *Anal.* calcd. for $C_{29}H_{20}N_2$: C 87.85, H 5.08; found: C 87.96, H 5.28.

*1,1,2,2-Tetra(4-cyanophenyl)cyclopropane (2i)*

Di(4-cyanophenyl)diazomethane (0.5 g, 0.0020 mol) in 10 mL of benzene was added to 1,1-di(4-cyanophenyl)ethylene (0.5 g, 0.0022 mol) in 10 mL of benzene (*vide supra*). The solvent mixture was separated by medium pressure chromatography (silica gel, hexane – methylene chloride gradient). The yellow solid was recrystallized three times from chloroform–hexanes to give colourless plates (mp 233–234.5°C). Infrared (KBr): 3060 (w), 2227 (s), 1605 (s), 1502 (s), 1448 (w), 1405 (m), 1178 (w), 1005 (w), 851 (w), 752 (m), 630 (w); uv $\lambda_{max}$ (ethanol): 243 (56 000), 260 (38 000); $^1$Hmr ($CDCl_3$); δ: 2.68 (s, 2H), 7.20 (m, 16H). *Anal.* calcd. for $C_{31}H_{18}N_4$: C 83.41, H 4.04, N 12.56; found: C 83.11, H 3.82, N 12.51.

*1-(4-Cyanophenyl)-2-(4-methoxyphenyl)-1,2-diphenylcyclopropane (2j)*

4-Methoxyphenylphenyldiazomethane (0.5 g, 0.0022 mol) in 10 mL of benzene was added to 1-(4-cyanophenyl)-1-phenylethylene (0.5, 0.0024 mol) in 10 mL (*vide supra*). The solvent was then evaporated and the mixture separated by medium pressure chromatography (silica gel, hexanes – methylene chloride gradient). Rechromatographing the mixture of the *cis* and *trans* isomers afforded pure samples of each. The *cis* isomer was recrystallized from ethanol to give colourless prisms (mp 158–159°C). Infrared (KBr): 3050 (w), 2833 (w), 2222 (m), 1607 (m), 1512 (s), 1449 (m), 1405 (w), 1247 (s), 1178 (m), 1035 (m), 1005 (w), 832 (m), 700 (s); uv $\lambda_{max}$ (ethanol): 235 (24 000); $^1$Hmr ($CDCl_3$) δ: 2.47 (d, 1H, $J$ = 6 Hz), 2.57 (d, 1H, $J$ = 6 Hz), 3.64 (s, 3H), 7.0 (m, 18H); $^1$Hmr ($C_6D_6$) δ: 1.95 (d, 1H, $J$ = 6 Hz), 2.25 (d, 1H, $J$ = 6 Hz), 3.22 (s, 3H), 6.72 (m, 18H). *Exact Mol. Wt.* calcd.: 401.177955; found: 401.179314.

The *trans* isomer was recrystallized from ethanol to give colourless needles (mp 134–135.5°C). Infrared (KBr): 3050 (w), 2833 (w), 2222 (m), 1603 (m), 1509 (s), 1422 (m), 1403 (w), 1244 (s), 1180 (m), 1030 (m), 1001 (w), 837 (m), 698 (s); uv $\lambda_{max}$ (ethanol): 234 (25 000), 271 (13 000); $^1$Hmr ($CDCl_3$) δ: 2.53 (s, 2H), 3.69 (s, 3H), 6.77 (m, 4H), 7.10 (m, 14H); $^1$Hmr ($C_6D_6$) δ: 2.00 (d, 1H, $J$ = 7 Hz), 2.26 (d, 1H, $J$ = 7 Hz), 3.17 (s, 3H), 6.72 (m, 18H). *Exact Mol. Wt.* calcd.: 401.177955; found: 401.178917.

Crystals of *trans* **2j**, for the X-ray determination, were prepared by slow recrystallization from ethanol–chloroform.

*1-(4-Cyanophenyl)-1-(4-methoxyphenyl)-2,2-diphenylcyclopropane (2k)*

4-Cyano-4′-methoxydiphenyldiazomethane (1.5 g, 0.006 mol) in 10 mL of benzene was added to 1,1-diphenylethylene (2.1 g, 0.0117 mol) in 20 mL of benzene (*vide supra*). The solvent was then evaporated and the reaction mixture separated by chromatography (neutral alumina, hexane–benzene, 1:3). The product was recrystallized from methanol to give colourless prisms (mp 191–192°C). Infrared (KBr): 3040 (w), 2840 (w), 2227 (s), 1608 (s), 1513 (s), 1450 (m), 1398 (w), 1252 (s), 1182 (m), 1031 (m), 1000 (w), 836 (m), 703 (s); uv $\lambda_{max}$ (ethanol): 236 (21 000), 242 (18 000); $^1$Hmr ($CDCl_3$) δ: 2.53 (s, 2H), 3.64 (s, 3H), 7.01 (m, 18H). *Exact Mol. Wt.* calcd.: 401.177955; found: 401.178519.

*1,2-Di(4-cyanophenyl)-1,2-di(4-methoxyphenyl)cyclopropane (2l)*

4-Cyano-4′-methoxydiphenyldiazomethane (0.8 g, 0.0032 mol) in 10 mL of benzene was added to 1-(4-cyanophenyl)-1-(4-methoxyphenyl)ethylene (0.9 g, 0.0038 mol) in 20 mL of benzene (*vide supra*). The solvent was then evaporated and the reaction mixture separated by column chromatography (silica gel, hexanes–benzene gradient) to give a mixture of the *cis* and *trans* isomers. The two isomers were separated by medium pressure chromatography (silica gel, hexanes–benzene gradient). The *cis* isomer was recrystallized from chloroform–ethanol to give colourless needles (mp 157–158°C). Infrared (KBr): 2840 (w), 2230 (s), 1610 (s), 1516 (s), 1300 (m), 1250 (s), 1187 (m), 1136 (m), 850 (m), 753 (m), 596 (m); uv $\lambda_{max}$ (ethanol): 231 (52 000), 267 (32 000); $^1$Hmr ($CDCl_3$) δ: 2.43 (d, 1H, $J$ = 7 Hz), 2.66 (d, 1H, $J$ = 7 Hz), 3.70 (s, 6H), 7.00 (m, 16H). *Anal.* calcd. for $C_{31}H_{24}N_2O_2$: C 81.55, H 5.33; found: C 81.71, H 5.27.

The *trans* isomer was recrystallized from chloroform–ethanol to give colourless prisms (mp 95–96°C). Infrared (KBr): 2840 (w), 2228 (m), 1610 (s), 1513 (s), 1298 (m), 1250 (s), 1181 (m), 937 (m), 852 (m), 757 (w), 591 (w); uv $\lambda_{max}$ (ethanol): 233 (39 000), 262 (35 000); $^1$Hmr ($CDCl_3$) δ: 2.58 (s, 2H), 3.75 (s, 6H), 7.00 (m, 16H). *Anal.* calcd. for $C_{31}H_{24}N_2O_2$: C 81.55, H 5.33; found: C 81.38, H 5.31.

*1,1,-Di(4-cyanophenyl)-2,2-di(4-methoxyphenyl)cyclopropane (2m)*

Di(4-cyanophenyl)diazomethane (1.2 g, 0.0049 mol) in 10 mL of benzene was added to 1,1-di(4-methoxyphenyl)ethylene (1.2 g, 0.005 mol) in 20 mL of benzene (*vide supra*). The solvent was then evaporated and the reaction mixture separated by column chromatography (neutral alumina, benzene). The product was recrystallized from chloroform–ethanol to give colourless needles (mp 203–204°C). Infrared (KBr): 2840 (w),

2230 (s), 1608 (s), 1510 (s), 1452 (s), 1290 (m), 1250 (s), 1112 (w), 1028 (s), 850 (m), 756 (m); uv $\lambda_{max}$ (ethanol): 233 (37 000), 270 (14 000); $^1$Hmr ($CDCl_3$) δ: 2.53 (s, 2H), 3.71 (s, 6H), 7.00 (m, 16H). *Anal.* calcd. for $C_{31}H_{24}N_2O_2$: C 81.55, H 5.33; found: C 81.24, H 5.39.

*Thermal isomerization of* 2c, g, j, l: *kinetics*

Samples tubes were prepared from 5 or 7 mm Pyrex tubing which had been rinsed once with concentrated nitric acid, thrice with distilled water, soaked in 5% aqueous sodium hydroxide (1 h), rinsed again (three times) with distilled water, and then dried in an oven. Samples (in benzene) were degassed (three freeze–pump–thaw cycles) and sealed. Five tubes were then placed simultaneously in a preset insulated kinetic bath. The rates of approach to thermal equilibrium were studied over a 20° temperature range near 120°C. The temperature of the bath did not fall by more than 0.5° when the samples were introduced and recovered to its original value within 1.5 minutes. Samples were removed after specific time intervals and quenched immediately in an ice bath, opened, and analysed by hplc. The rate constants for thermal isomerization ($k_{c\rightarrow t} + k_{t\rightarrow c}$) and the equilibrium compositions were averages of two runs starting with both isomers.

The rate constants were determined by linear regression analysis of the mole fraction vs. time data (assuming first order kinetics), using the minitab II program (15). Arrhenius parameters were determined by the temperature dependence of the rate constants for thermal isomerization using a linear least-squares program.

## Acknowledgements

This work was supported by a grant from the Natural Sciences and Engineering Research Council of Canada (including a scholarship to D.D.M.W.). D.R.A. is grateful for a Fellowship from the John Simon Guggenheim Foundation. We gratefully acknowledge the contribution of Dr. T. S. Cameron for the X-ray analysis. Some of the preliminary preparations were carried out by Nancy Davies as part of her Honours B.Sc. thesis.

1. (*a*) W. J. LEIGH and D. R. ARNOLD. Can. J. Chem. **59**, 609 (1981); (*b*) W. J. LEIGH and D. R. ARNOLD. Can. J. Chem. **59**, 3601 (1981).
2. (*a*) D. R. ARNOLD and M. YOSHIDA. J. Chem. Soc. Chem. Commun. 1203 (1981); (*b*) R. W. R. HUMPHREYS and D. R. ARNOLD. J. Chem. Soc. Chem. Commun. 793 (1979).
3. (*a*) R. W. R. HUMPHREYS and D. R. ARNOLD. Can. J. Chem. **55**, 2286 (1977); (*b*) R. W. R. HUMPHREYS and D. R. ARNOLD. Can. J. Chem. **57**, 2652 (1979).
4. C. R. H. ALLEN and S. CONVERSE. Org. Synth. **VI**, 226 (1941).
5. R. A. MOSS. Acc. Chem. Res. **13**, 58 (1980).
6. (*a*) O. A. SUBBATIN, A. S. KOZMIN, YU. K. GRISHIN, N. M. SERGEYEV, and I. G. BOLESOV. Org. Magn. Reson. **4**, 53 (1972); (*b*) W. F. REYNOLDS and R. H. KOHLER. Tetrahedron Lett. 4671 (1976); (*c*) N. INAMOTO, S. MASUDA, K. TOKUMARU, K. TORI, M. YOSHIDA, and Y. YOSHIMURA. Tetrahedron Lett. 3707 (1976); (*d*) N. INAMOTO, S. MASUDA, K. TORI, and Y. YOSHIMURA. Tetrahedron Lett. 737 (1977); (*e*) N. INAMOTO, S. MASUDA, W. NAKANISHI, and Y. IDEDA. Chem. Lett. 759 (1977).
7. T. A. WITTSTRUCK and E. N. TRACHTENBERG. J. Am. Chem. Soc. **89**, 3810 (1967).
8. V. MANCINI, P. PASSINI, and S. SANTINI. J. Chem. Soc. Perkin Trans. II, 463 (1980).
9. (*a*) J. E. HUHEEY. J. Phys. Chem. **70**, 2086 (1966); (*b*) **69**, 3285 (1965).
10. L. M. JACKMAN and S. STERNBELL. Applications of N.M.R. spectroscopy in organic chemistry. Pergamon Press, New York. 1969. p. 67.
11. J. A. BENSON. Annu. Rev. Phys. Chem. **28**, 111 (1977).
12. J. E. WURTZ and J. R. BOLTON. Electron spin resonance. McGraw-Hill Inc., New York. 1972. Chapt. 6.
13. W. C. STILL, M. KAHN, and A. MITRA. J. Org. Chem. **43**, 2923 (1978).
14. J. E. HODGKINS and M. P. HUGHES. J. Org. Chem. **27**, 4187 (1962).
15. T. A. RYAN, JR., B. L. JOINER, and B. F. RYAN. Minitab student handbook. Duxbury Press, N. Scituate, MA. 1976.
16. K. H. HELLWEGE (*Editor*). Landolf–Börnstein Handbook. Vol. 9. Part b. Organic C-centered radicals. Springer Verlag, Berlin. 1977.
17. J. A. BERSON, L. D. PEDERSON, and B. K. CARPENTER. J. Am. Chem. Soc. **98**, 122 (1976).
18. R. J. CRAWFORD and T. R. LYNCH. Can. J. Chem. **46**, 1457 (1968).

Can. J. Chem. Downloaded from www.nrcresearchpress.com by 210.87.254.105 on 09/06/12
For personal use only.

# Kinetics and mechanism of barium tungstate crystal growth from sodium tungstate melts in platinum crucibles

BIMALENDU NARAYAN ROY[1] AND MANJU RANI ROY

*Department of Chemistry, University of Science and Technology, Kumasi, Ghana*

Received May 12, 1980

BIMALENDU NARAYAN ROY and MANJU RANI ROY. Can. J. Chem. **60**, 2321 (1982).

Kinetics and mechanism of barium tungstate crystal growth from sodium tungstate melts in platinum crucibles were investigated by DTA at crystallization temperatures $T_0$ = 800 to 1000°C by continuous cooling at rates $R_T$ = 0.67 to 3.37°C min$^{-1}$. During an induction period ($\bar{t}$) small crystallites ($\bar{l}$ = 0.003 to 0.03 cm) developed in the solution but the main growth occurred only after sufficient excess solute concentrations ($\Delta\bar{C}$) developed at the end of $\bar{t}$. For crystallizations <80%, the average crystal lengths ($l_\tau$) varied with the growth time ($\tau$) according to $l_\tau^2 = (\bar{l})^2 + 4k_{D_l}M\Delta\bar{C}$, $k_{D_l}$ being the diffusion rate constant and $M$ the metal salt molecular weight. The last 20% growth was rate-controlled only by the development rate of excess solute concentration.

BIMALENDU NARAYAN ROY et MANJU RANI ROY. Can. J. Chem. **60**, 2321 (1982).

Faisant appel à l'ATD, on a étudié la cinétique et le mécanisme de la croissance de cristaux de tungstate de baryum à partir de masse fondue de tungstate de sodium présents dans des creusets de platine; les températures de cristallisation s'étalent de $T_0$ = 800 à 1000°C et le taux de refroidissement continue varie de $R_T$ = 0,67 à 3,37°C min$^{-1}$. Au cours de la période d'induction ($\bar{t}$) des petits cristaux se développent dans la solution mais la croissance principale ne se produit que lorsqu'un excès suffisant de la concentration du soluté ($\Delta\bar{C}$) se manifeste à la fin de $\bar{t}$. Pour des cristallisations <80%, la longueur moyenne des cristaux ($l_\tau$) varie avec le temps de croissance selon l'équation $l_\tau^2 = (\bar{l})^2 + 4k_{D_l}M\Delta\bar{C}$ où $k_{D_l}$ est la constante de vitesse de diffusion et $M$ la masse molaire du sel métallique. Les derniers 20% de la croissance se font à une vitesse qui est contrôlée que par le taux d'évolution de la concentration du soluté en excès.

[Traduit par le journal]

## Introduction

In recent years crystallization kinetics of a large number of inorganic salts have been reported (1–10). In any crystallization from aqueous solutions or melts, the growth process may occur practically immediately after the onset of cooling or the system may exhibit induction periods of different lengths during which only the excess solute concentration develops without any significant growth — the actual growth occurs only after the induction period. In both cases, the growth mechanism may be identical but the kinetic relations will differ depending upon the length of induction periods.

For a diffusion-controlled crystal growth exhibiting induction periods, the rate of the main growth of the "major" side of the main crystal face at any growth time $\tau$ after the induction period ($\bar{t}$) would be expressed (11)

$$[1] \qquad dl_\tau/d\tau = \frac{2(\mathrm{Sh})DM\phi(\Delta C_{sol})_\tau}{l_\tau}(\rho_{sol}/\rho)$$

where Sh is the Sherwood function; $D$ is the diffusion coefficient of the metal salt cations; $M$ is the molecular weight of the solute; $\phi$ is the overall permeability factor; $\tau$ ($=t-\bar{t}$) is the actual growth time; $t$ is the total crystallization time; $l_\tau$ is the crystal length at $\tau$; $(\Delta C_{sol})_\tau$ is the residual excess solute concentration at $\tau$; and $\rho$ and $\rho_{sol}$ are the densities of the crystal and solution respectively. When the natural convection in an unstirred solution is poor, the dimensionless Sherwood function approximately equals 2 and then eq. [1] becomes (11)

$$[2] \qquad dl_\tau/d\tau = \frac{4DM\phi(\Delta C_{sol})_\tau}{l_\tau}(\rho_{sol}/\rho)$$

$$[3] \qquad = \frac{2k_{D_l}M(\Delta C_{sol})_\tau}{l_\tau}$$

where $k_{D_l} = 2D\phi(\rho_{sol}/\rho)$ is the rate constant for diffusion-controlled growth of the "wider" crystal face.

Generally, in crystallizations from melts, the excess solute concentration at any $\tau$ would be

$$[4] \qquad (\Delta C_{sol})_\tau = (\Delta C_\tau - W_\tau/M)$$

where $\Delta C_\tau$ is the overall excess solute concentration up to $\tau$ and $W_\tau$ is the crystal weight deposited at different growth time $\tau$. This equation may be written as

$$[5] \qquad (\Delta C_{sol})_\tau = (\Delta\bar{C} + R_c\tau - \beta l_\tau^3)$$

where $\Delta\bar{C}$ is the excess solute concentration up to $\bar{t}$; $R_c$ is the development rate of excess solute concentration; $N$ is the crystal number at any

[1]Present address: 47 Arlesford Road, London SW9 9JS, U.K.

0008-4042/82/182321-04$01.00/0

©1982 National Research Council of Canada/Conseil national de recherches du Canada

Can. J. Chem. Downloaded from www.nrcresearchpress.com by 210.87.254.6 on 09/06/12
For personal use only.

Can. J. Chem. Downloaded from www.nrcresearchpress.com by 210.87.254.6 on 09/06/12
For personal use only.

crystallization time $t$; $f_s$ is a shape factor; and $\beta$ ($= N\rho f_s/M$) is a function of the crystal number. Combining eqs. [3] and [5]

$$[6] \quad dl_\tau/d\tau = 2k_{D_l}M(\Delta\bar{C} + R_c\tau - \beta l_\tau^3)/l_\tau$$

Integrating, one gets

$$[7] \quad l_\tau^2 = (\bar{l})^2 + A\tau + B\tau^2$$

where $\bar{l}$ is the maximum crystal length up to the end of $\bar{\imath}$, and for any $T_0$ and $R_T$, $A$ and $B$ are constants given by

$$A = 4k_{D_l}M\Delta\bar{C} - 4k_{D_l}M\beta\bar{l}^3$$
$$B = 2k_{D_l}MR_c$$

If $(\Delta C_{sol})_\tau \simeq \Delta\bar{C}$, eq. [3] becomes

$$[8] \quad dl_\tau/d\tau = 2k_{D_l}M\Delta\bar{C}/l_\tau$$

Integrating, one gets

$$[9] \quad l_\tau^2 = (\bar{l})^2 + A'\tau$$

where $A'$ ($= 4k_{D_l}M\Delta\bar{C}$) is a function of $\Delta\bar{C}$ and constant for any $T_0$ and $R_T$.

## Experimental

Barium tungstate was prepared *in situ* in sodium tungstate melts from equimolecular mixtures of the metal carbonate and tungsten trioxide. The saturated solutions were prepared at temperatures slightly higher than the initial crystallization temperature by heating for several hours inside a "Carbolite" electric furnace (Carbolite Co. Ltd., Sheffield, U.K.). These solutions were then cooled down rapidly to room temperature and the solidified melt was ground well and dried at 100°C for 24 h to remove any moisture absorbed during grinding. The requisite amount of this sample was then taken in a small platinum crucible inside a differential thermal analyser (No. 990, E.I. du Pont de Nemours & Co., Wilmington, DE, U.S.A.) and the temperature was gradually raised to slightly higher than the crystallization temperature $T_0$ at a rate of 20°/min. It was held constant at that temperature for sufficient time to ensure complete melting. Then the crystallization was carried out by gradually reducing the temperature from $T_0$ (=800 to 1000°C) down to below 300°C at cooling rates $R_T$ = 40, 120, and 200°C per h according to a pre-assigned automatic cooling programme. The temperatures were recorded automatically on the chart. The DTA curves were traced on standard millimeter graph papers.

From the DTA curves, the eutectic temperature ($T_e$) was determined as the initial melting temperature of the mixtures of metal tungstate and sodium tungstate. The degree of crystallization ($\alpha_t$) at different crystallization time ($t$) was calculated using $\alpha_t = A_t/A_{total}$, where $A_t$ is the area under the thermogram at any time $t$ and $A_{total}$ is the total area under the same thermogram. From these $\alpha_t$ values the length ($l_t$) of barium tungstate crystals at any time was estimated using $\alpha_t = (l_t/\bar{l}_t)^3$, where $l_t$ is the final crystal length. $l_t$ values were measured by optical microscopy from separate crystallization runs in the "Carbolite" electric furnace mentioned above (12).

The rates ($R_c$) of development of excess solute concentration were estimated from the product $aR_T$, where $a = dC/dT$, $C$ being the concentration. Induction periods ($\bar{\imath}$) were determined by extrapolation of the linear parts of the $l_t$ vs. $t$ plots back to the $t$-axis; the induction temperatures ($\bar{T}$) were then given by $\bar{T} = T_0 - R_T\bar{\imath}$. The actual growth time ($\tau$) and the overall excess solute concentration ($\Delta C_\tau$) at different $\tau$ were evaluated respectively from $\tau = t - \bar{\imath}$ and $\Delta C_\tau = C_0 - C_\tau$, where $C_0$ is the initial concentration and $C_\tau$ the concentration at $\tau$. The residual excess solute concentrations, $(\Delta C_{sol})_\tau$, were evaluated from eq. [4], and $W_t/M$ and the final overall excess solute concentrations, $\Delta C_f$, were respectively given by

$$W_\tau/M = N\rho f_s l_\tau^3$$

and

$$\Delta C_f = (C_0 - C_{eu})$$

where $C_{eu}$ is the solubility at the eutectic temperature ($T_{eu}$).

## Results

### *Development of supersaturation*

#### *Overall excess solute concentrations, residual excess solute concentrations, and total crystal weights*

The overall excess solute concentrations ($\Delta C_t$) increased linearly with cooling time $t$ and attained the maximum value, $\Delta C_f$, at the eutectic temperature. The total crystal weights $W_t/M$ increased significantly only after the induction periods. Some typical results for $\Delta C_t$ and $W_t/M$ are shown in Figs. 1 and 2. The amount of excess solute concentration developed at any $t$ and also the final amount was higher than those for barium tungstate crystallization under identical conditions from sodium tungstate melts in alumina crucibles (12).

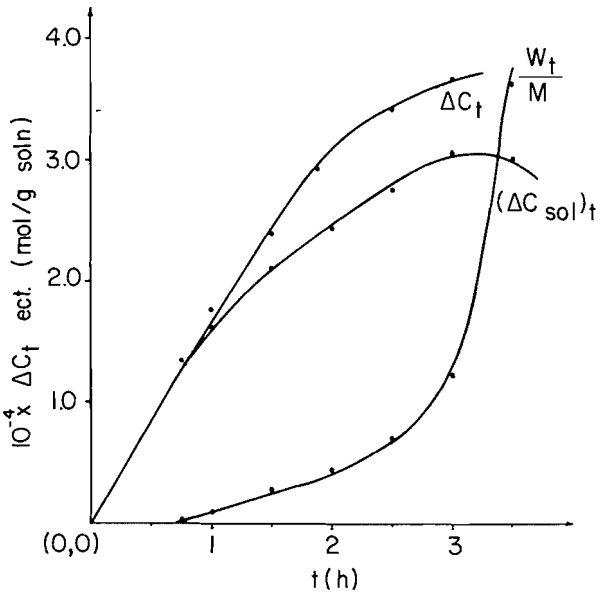


FIG. 1. Crystallization of barium tungstate from sodium tungstate melts at $T_0$ = 900°C and $R_T$ = 40°C/h. Overall excess solute concentrations ($\Delta C_t$), residual excess solute concentrations, $(\Delta C_{sol})_t$, and total crystal weights at different times ($W_t/M$ has no dimensions).

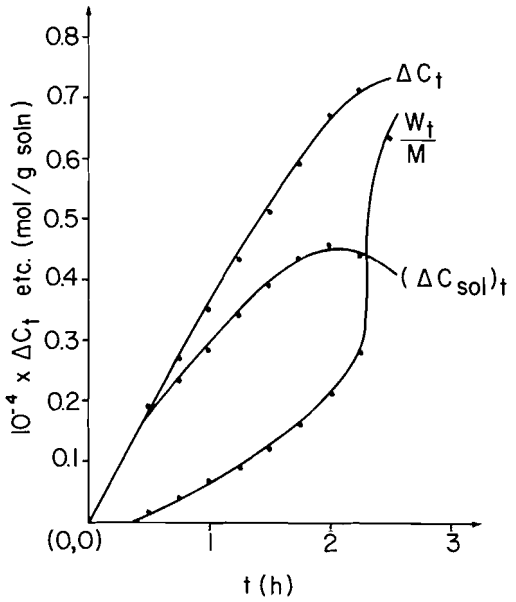


FIG. 2. Crystallization of barium tungstate from sodium tungstate melts at $T_0$ = 1000°C and $R_T$ = 120°C/h. Overall excess solute concentrations ($\Delta C_t$), residual excess solute concentrations ($\Delta C_{sol}$)$_t$, and total crystal weights at different times ($W_t/M$ has no dimensions).

The $\Delta C_t$ and $W_t/M$ values show that at the early stages the amount of residual excess solute concentrations was high. Total crystal weights were very low at the early stages; however, these weights increased with decreasing temperatures up to the time $t^*$ (over 75% crystallization), when all the excess solute deposited on the growing crystals and probably no further growth occurred. This was also observed in the case of barium tungstate crystallization from sodium tungstate melts in alumina crucibles (12).

Very little (or perhaps none at all) material deposited on the early nuclei until the excess solute concentrations in the solution attained some value $\Delta\bar{C}$ at temperature $\bar{T}$. As the crystallization proceeded, the residual excess solute concentrations in the solution at any $t$ deviated more and more from $\Delta C_t$, gradually reached the final value, and then sharply dropped to very low values at $t^*$.

*Critical time ($\bar{t}$), critical temperature ($\bar{T}$), and critical excess solute concentration ($\Delta\bar{C}$)*

Unlike the crystallization of barium tungstate from sodium tungstate melts in alumina crucibles (12), in this case short to medium induction periods were observed, which were ostensibly modified by the cooling rates but there was no direct relationship between $R_T$ and $\bar{t}$. During the induction periods, heterogeneous nuclei slowly formed onto the metal platinate particles within the solutions and probably very small crystallites grew on these nuclei up to the end of $\bar{t}$. Probably the growth kinetics of these crystallites were rate-controlled by a sluggish secondary mononuclear process (13), which was not the case in the crystallization of the same system in alumina crucibles (12).

*Kinetics of crystal growth after the induction periods*

It is well known that crystallization at high supersaturation is expected to be diffusion-limited. Also, the growth rate of metal salt crystals in unstirred low permeability solutions is generally controlled by the diffusion rate of metal salt ions into the growing crystal surfaces. As stated earlier, during the induction period probably very small crystallites grew on the early nuclei up to $\bar{t}$. Since there was no significant growth occurring during the induction period, sufficient amount of excess solute concentration accumulated at the end of $\bar{t}$ and then the main crystal growth occurred. The average crystal lengths ($l_\tau$) at any growth time $\tau$ after the induction periods were evaluated from the $l_t$ versus $t$ plots; $l_\tau^2$ values were then plotted against $\tau$ (Figs. 3–5). These plots were linear according to eq. [9] up to $l_\tau \simeq 0.48 l_f$; these linear relationships indicated that the growth process was probably diffusion rate controlled.

The $A'$ values were estimated for different crystallizations (Table 1). These values generally

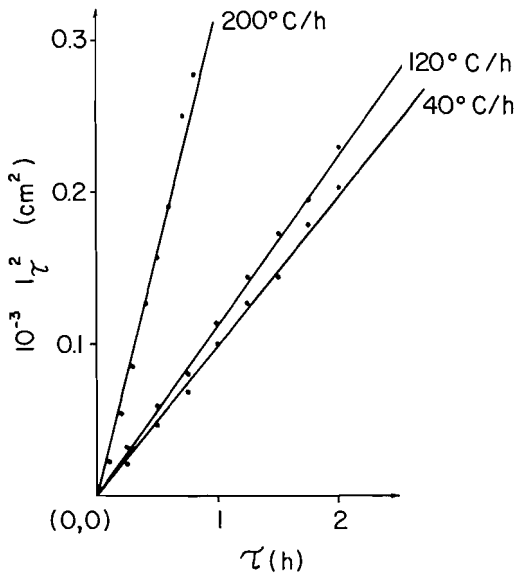


FIG. 3. Crystallization of barium tungstate from sodium tungstate melts at $T_0$ = 800°C; square of crystal lengths ($l_\tau^2$) at different growth times ($\tau$).

Can. J. Chem. Downloaded from www.nrcresearchpress.com by 210.87.254.6 on 09/06/12
For personal use only.

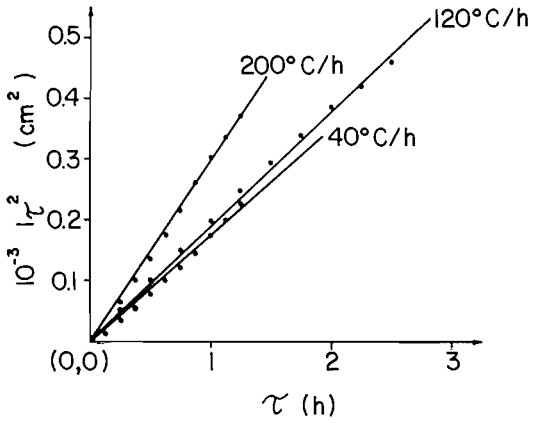


FIG. 4. Crystallization of barium tungstate from sodium tungstate melts at $T_0$ = 900°C; square of crystal lengths ($l_\tau^2$) at different growth times ($\tau$).

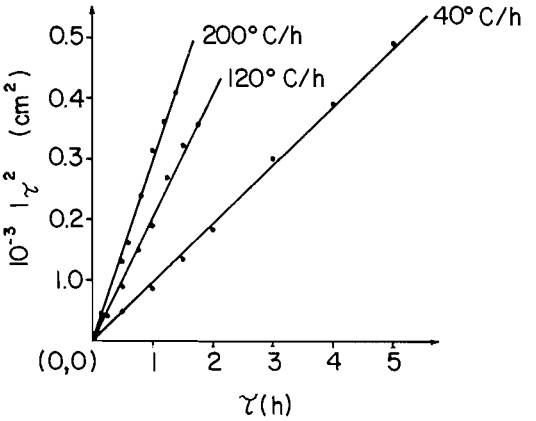


FIG. 5. Crystallization of barium tungstate from sodium tungstate melts at $T_0$ = 1000°C; square of crystal lengths ($l_\tau^2$) at different growth times ($\tau$).

increased as $T_0$ and $R_T$ increased but there was no direct correlation.

*The final growth*

It is assumed that at growth times $\tau > \tau^*$ (over 75% crystallization) some fresh solute continued to separate out from the solution by further cooling but this was probably immediately used up by deposition on the already developed large crystals. Consequently, the residual excess solute concentrations were very low and the growth rates became dependent only on the development of further excess solute concentration effected by the decrease in temperature. For this,

$$[10] \quad l_\tau^3 = (l^*)^3 + b(\tau - \tau^*)$$

where $b$ (= $R_c/\beta$) is a constant. Then at $\tau = \tau^*$, $l_\tau = l^*$. This was observed experimentally.

TABLE 1. Kinetics and mechanism of barium tungstate crystal growth from sodium tungstate melts in platinum crucibles

| $R_T$ (°C/h) | $T_0$ (°C) | $R_c$ (g/g-sol h) | $\bar{t}$ (h) | $\bar{T}$ (°C) | $\Delta\bar{C}$ (g/g sol) | $A'$ (cm$^2$/h) |
|---|---|---|---|---|---|---|
| 40 | 800 | 0.041 | 0.50 | 780 | 0.0026 | 1.4 |
| | 900 | | 1.0 | 860 | 0.0510 | 1.0 |
| | 1000 | | 1.5 | 940 | 0.0869 | 0.99 |
| 120 | 800 | 0.123 | 0.50 | 740 | 0.0201 | 1.5 |
| | 900 | | 0.25 | 870 | 0.0385 | 1.3 |
| | 1000 | | 0.25 | 970 | 0.0439 | 1.1 |
| 200 | 800 | 0.205 | 0.25 | 750 | 0.0176 | 4.0 |
| | 900 | | 0.25 | 850 | 0.0585 | 1.5 |
| | 1000 | | 0.25 | 950 | 0.0739 | 2.7 |

1. A. E. NIELSEN. Acta Chem. Scand. **13**, 784 (1957).
2. A. E. NIELSEN. Acta Chem. Scand. **14**, 1654 (1960).
3. G. H. NANCOLLAS. Trans. Faraday Soc. **57**, 2272 (1961).
4. G. H. NANCOLLAS. Trans. Faraday Soc. **59**, 753 (1963).
5. G. H. NANCOLLAS. J. Cryst. Growth, **3**, 335 (1968).
6. G. H. NANCOLLAS. J. Phys. Chem. **73**, 1735 (1969).
7. A. PACKTER and B. N. ROY. J. Cryst. Growth, **18**, 86 (1973).
8. A. PACKTER and B. N. ROY. Krist. Tech. **9**, 1361 (1974).
9. A. PACKTER and B. N. ROY. Krist. Tech. **10**, 385 (1975).
10. B. N. ROY and S. APPALASAMI. J. Am. Ceram. Soc. **61**, 38 (1978).
11. R. E. TREYBAL. Mass transfer operations. McGraw-Hill, New York. 1968. Chapt. 3.
12. B. N. ROY and V. K. HANDA. J. Cryst. Growth, **47**, 577 (1979).
13. A. E. NIELSEN. Kinetics of precipitation. Pergamon Press, Oxford. 1964. Chapt. 3.

Can. J. Chem. Downloaded from www.nrcresearchpress.com by 210.87.254.6 on 09/06/12
For personal use only.

# Alkylation of benzene by alkyl cations. Stability of the *tert*-butyl benzenium ion

D. K. SEN SHARMA, S. IKUTA,[1] AND P. KEBARLE[2]

*Chemistry Department, University of Alberta, Edmonton, Alta., Canada T6G 2G2*

Received March 4, 1982

D. K. SEN SHARMA, S. IKUTA, and P. KEBARLE. Can. J. Chem. **60**, 2325 (1982).

The kinetics and equilibria of the gas phase reaction [1] *tert*-$C_4H_9^+ + C_6H_6 =$ *tert*-$C_4H_9C_6H_6^+$ were studied with a high ion source pressure pulsed electron beam mass spectrometer. Equilibria [1] could be observed in the temperature range 285–325 K. van't Hoff plots of the equilibrium constants led to $\Delta H_1^0 = -22 \pm 2$ kcal mol$^{-1}$ and $\Delta S_1^0 = -49 \pm 5$ cal K$^{-1}$ mol$^{-1}$. The rate constants at 305 K were $k_{1f} = 1.5 \times 10^{-28}$ molecules$^{-2}$ cm$^6$ s$^{-1}$ and $k_{1r} = 2.9 \times 10^{-19}$ molecules$^{-1}$ cm$^3$ s$^{-1}$. *tert*-$C_4H_9C_6H_6^+$ dissociates easily via [lr] not only because of the low dissociation energy ($-\Delta H_1^0$) but also because of the unusually favorable entropy ($-\Delta S_1^0$). The occurrence of transalkylation reactions: *tert*-$C_4H_9C_6H_6^+$ + alkylbenzene = *tert*-$C_4H_9$ alkylbenzene$^+$ + benzene, was discovered in the present work.

D. K. SEN SHARMA, S. IKUTA et P. KEBARLE. Can. J. Chem. **60**, 2325 (1982).

On a étudié la cinétique et l'équilibre de la réaction en phase gazeuse [1] *tert*-$C_4H_9^+ + C_6H_6 =$ *tert*-$C_4H_9C_6H_6^+$ en faisant appel à un spectromètre de masse à faisceau d'électrons pulsés et ayant une source d'ions à haute pression. Les équilibres [1] peuvent être observés dans l'intervalle de température de 285–326 K. Les courbes de van't Hoff des constantes d'équilibre conduisent à $\Delta H_1^0 = 22 \pm 2$ kcal mol$^{-1}$ et à $\Delta S_1^0 = -49 \pm 5$ cal K$^{-1}$ mol$^{-1}$. Les constantes de vitesse à 305 K sont: $k_{1f} = 1{,}5 \times 10^{-28}$ molécules$^{-2}$ cm$^3$ s$^{-1}$ et $k_{1r} = 2{,}9 \times 10^{19}$ molécules$^{-1}$ cm$^3$ s$^{-1}$. L'ion *tert*-$C_4H_9C_6H_6^+$ se dissocie facilement via [lr] non seulement parce que l'énergie de dissociation est faible ($-\Delta H_1^0$] mais également par suite d'une entropie exceptionnellement favorable ($-\Delta S_1^0$). Dans cette étude, on a découvert la manifestation des réactions de transalkylation: *tert*-$C_4H_9C_6H_6^+$ + alkylbenzène = *tert*-$C_4H_9$ alkylbenzène$^+$ + benzène.

[Traduit par le journal]

## Introduction

The alkylation of benzene and other aromatic hydrocarbons by the electrophilic attack of alkyl cation intermediates is a classical condensed phase reaction. It is of interest in a very wide area. Thus it has played an important part in the development of the theory of carbonium ions in physical organic chemistry (1, 2) and, on the other end of the spectrum, it is an important industrial reaction for the production of alkyl benzenes. In the gas phase, the reactions are of analytical importance in chemical ionization mass spectrometry (3). Thus the often used reagent gases methane, propane, and isobutane produce $C_2H_5^+$, iso-$C_3H_7^+$, and *tert*-$C_4H_9^+$ respectively, as reagent ions. These become involved in alkylation reactions when the unknown is benzene or some other aromatic compound.

The present work describes results obtained from measurement of the kinetics and equilibria of the gas phase reaction [1] with a high pressure mass spectrometer. Reaction [1] represents an association of a carbenium ion, i.e. a Lewis acid with a $\pi$ Lewis base. Association reactions involving various alkyl cations and Lewis bases like $H_2O$, CO, RCl have been described in previous publications from this laboratory (4).

We believe that the present results are at least of partial interest to all areas mentioned above. They do represent also an addition to gas phase ion thermochemistry (5, 6).

$$[1] \quad \textit{tert}\text{-}C_4H_9^+ + C_6H_6 \underset{lr}{\overset{lf}{\rightleftarrows}} \textit{tert}\text{-}C_4H_9{\cdot}C_6H_6^+$$

## Experimental

The measurements were made with the pulsed electron beam high ion source pressure mass spectrometer used in earlier work (4–6). Pulsing of the electron beam permits time resolved detection of the ions. The temperature of the ion source is controlled by means of heaters embedded in the ion source block. The usual procedure of flowing the gas mixture in and out of the ion source was employed. In the absence of such flow an enrichment of the heavier neutral components in the ion source is expected because of the effusive loss of gas through the ion source slits.

In a reaction mixture containing methane as major gas (3 to 4 Torr) and known low pressures of isobutane and benzene where $p$ (isobutane) $\gg$ $p$ (benzene), a sequence of reactions occurs. The dominant ionization is of methane and the final ions in methane are $CH_5^+$ and $C_2H_5^+$. In the presence of isobutane, reactions [2] and [3] convert $CH_5^+$ and $C_2H_5^+$ to $C_4H_9^+$, which in turn reacts with benzene via the desired reaction [1].

$$[2] \quad CH_5^+ + \text{iso-}C_4H_{10} = CH_4 + C_4H_9^+ + H_2$$

$$[3] \quad C_2H_5^+ + \text{iso-}C_4H_{10} = C_2H_6 + C_4H_9^+$$

At suitably high temperatures, reaction [1] becomes reversible which allows the determination of equilibrium [1].

[1]Visiting scientist. Permanent address: Department of Chemistry, Tokyo Metropolitan University, Fukasawa, Setagaya-ku, Tokyo 158, Japan.

[2]Author to whom correspondence may be addressed.

0008-4042/82/182325-07$01.00/0

©1982 National Research Council of Canada/Conseil national de recherches du Canada

Can. J. Chem. Downloaded from www.nrcresearchpress.com by 210.87.254.6 on 09/06/12
For personal use only.

Can. J. Chem. Downloaded from www.nrcresearchpress.com by 210.87.254.6 on 09/06/12
For personal use only.

The ion–time dependence in a typical experiment leading to equilibrium is shown in Fig. 1. The equilibrium constants $K_1$ and their temperature dependence are displayed in Figs. 2 and 3. These results will be discussed in the next section. Here we wish to describe some observations which relate to the choice of concentrations used in the experiments. The data of Figs. 1–3 were obtained with methane 3 Torr, isobutane 1 Torr, and benzene in the 1 to 10 mTorr range. Initial experiments with much lower isobutane concentrations (e.g., isobutane 100 to 30 mTorr, benzene ~5 mTorr) led to anomalous results. A certain residual amount of $C_4H_9C_6H_6^+$ at equilibrium was observed to persist to much higher temperatures than could be expected from Fig. 3. For example, about 10% $C_4H_9C_6H_6^+$ was still observed at 152°C. The corresponding $C_5H_9^+$ was 50%, which leads to an equilibrium constant "$K_1$" = 25 ($Torr^{-1}$) ($p$(benzene) = 8 mTorr). The $K_1$ predicted from Fig. 3 for the same temperature is about four orders of magnitude smaller. Evidence cited below indicates that the residual $C_4H_9C_6H_6^+$ is not *tert*-butyl benzenium but the more stable isobutyl or *sec*-butyl benzenium, formed by the addition of the corresponding isomeric butyl cation to benzene.

Experiments at high temperature and low isobutane pressures showed that the residual $C_4H_9C_6H_6^+$ increased with benzene pressure but only up to a certain limiting concentration (~30%). Increase of the isobutane pressure led to a decrease of the residual butyl benzenium. Pressures above ~0.6 Torr isobutane caused the complete disappearance of the high temperature residual ion and these conditions led also to the normal equilibrium behavior at low temperatures (Figs. 1–3).

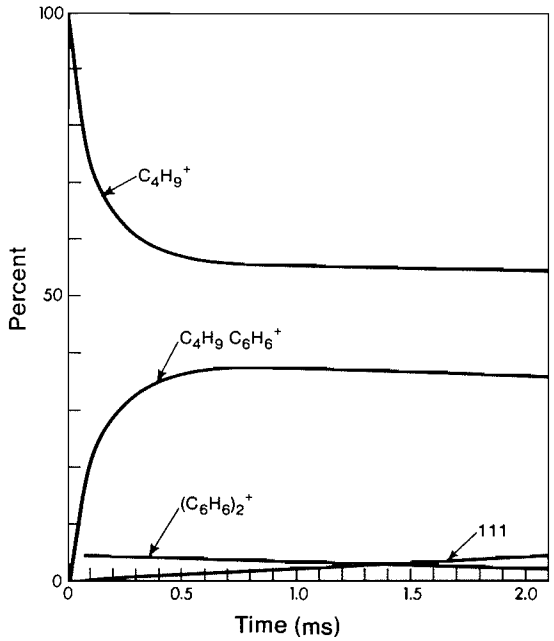


FIG. 1. Kinetics and equilibrium of reaction [1], $C_4H_9^+ + C_6H_6 = C_4H_9C_6H_6^+$. Reaction mixture employed: $CH_4$ 3 Torr, isobutane 1 Torr, benzene 4 mTorr, temperature 32°C. Rapid ion–molecule reactions in major gases methane and isobutane produce $C_4H_9^+$ as practically the only ion. $C_4H_9^+$ adds to benzene; however, reaction is reversible and reaches equilibrium after about 0.5 ms. Equilibrium constant $K_1$ = 170 $Torr^{-1}$ from data in this figure. Approximate rate constants for the forward and reverse direction of the reaction can also be obtained from this figure.

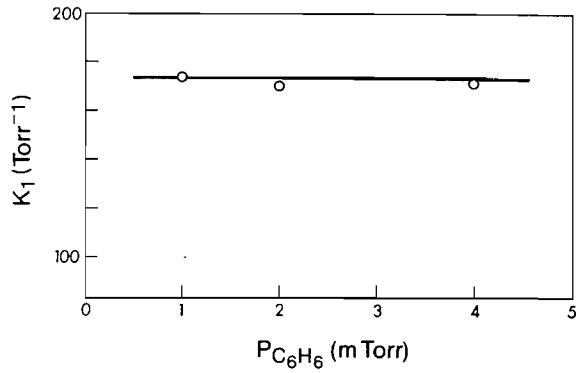


FIG. 2. Invariance of equilibrium constant $K_1$ with pressure of benzene. Temperature 32°C.

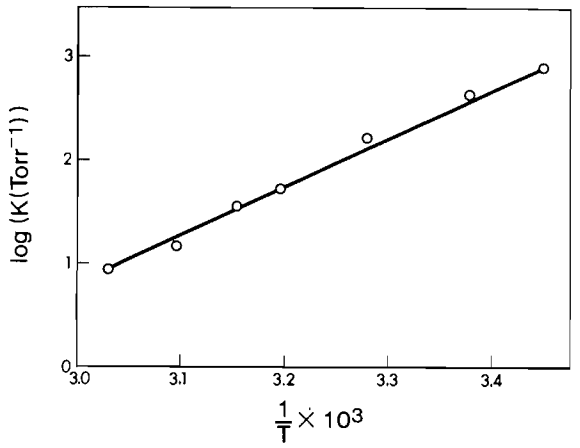


FIG. 3. van't Hoff plot of equilibrium constant $K_1$ obtained from equilibria measurements as illustrated in Fig. 1. Slope and intercept lead to $\Delta H_1^0 = -22 \pm 2$ kcal $mol^{-1}$, $\Delta S_1^0 = 49 \pm 5$ cal $K^{-1}$ $mol^{-1}$ given in Table 1.

Reactions [2] and [3] can produce not only *tert*-$C_4H_9^+$ but also another butyl isomer, x-$C_4H_9^+$. This isomer can either add to benzene giving the stable butyl benzenium by reaction [4] or be converted to *tert*-$C_4H_9^+$ by the hydride abstraction [5], reaction [5] being favored by a high isobutane to benzene ratio.

[4] $\text{x-}C_4H_9^+ + C_6H_6 = \text{x-}C_4H_9C_6H_6^+$

[5] $\text{x-}C_4H_9^+ + \text{iso-}C_4H_8 = \text{x-}C_4H_{10} + \textit{tert}\text{-}C_4H_9^+$

Experiments with $(CH_3)_3CD$ in methane showed that both $CH_5^+$ and $C_2H_5^+$ produced $C_4H_9^+$ *and* $C_4H_8D^+$. The $C_4H_8D^+/C_4H_9^+$ ratio observed for ethyl was approximately 2. The $C_4H_8D^+$ must be, at least initially, of the isobutyl structure. Evidence in the literature (9) suggests that the isobutyl cation is unstable (9*a*); however, the production of the unstable isobutyl was by electron impact (9*b*) and not the milder hydride abstraction occurring in the present work. The present work does not provide any evidence on the nature of the x-$C_4H_9^+$ except that it leads to an adduct that is more stable than *tert*-$C_4H_9C_6H_6^+$. *sec*-$C_4H_9^+$ will form a sufficiently stable benzenium ion to fit our experimental conditions. Thus, we observed that the *sec*-$C_3H_7C_6H_6^+$ ion, formed by the addition of *sec*-$C_3H_7^+$ to benzene, was stable at the elevated temperatures (150°C) at which the x-$C_4H_9C_6H_6^+$ was observed.

TABLE 1. Thermochemical data[a] and approximate rate constants

| Reaction | $-\Delta H^0$ | $-\Delta S^0$ |
|---|---|---|
| [1] *tert*-$C_4H_9^+ + C_6H_6 = tert$-$C_4H_9 \cdot C_6H_6^+$ | $22\pm2^b$ | $49\pm5^b$ |
| | $21.0\pm1^c$ | $46\pm5^d$ |
| iso-$C_3H_7^+ + C_6H_6 =$ iso-$C_3H_7C_6H_6^+$ | $33.8\pm1^e$ | $34\pm2^e$ |
| $C_2H_5^+ + C_6H_6 = C_2H_5C_6H_6^+$ | $46.5\pm1^f$ | $31.5\pm2^f$ |
| | Rate constant[g] | |
| [1] *tert*-$C_4H_9^+ + C_6H_6 = tert$-$C_4H_9 \cdot C_6H_6^+$ | $k_{1f} = 1.5 \times 10^{-28}$ molecules$^{-2}$ cm$^6$ s$^{-1}$ | |
| | $k_{1r} = 2.9 \times 10^{-14}$ molecules$^{-1}$ cm$^3$ s$^{-1}$ | |
| [14] *tert*-$C_4H_9C_6H_6 + CH_3C_6H_5 = tert$-$C_4H_9 \cdot CH_3C_6H_5^+ + C_6H_6$ | $k_{14} \approx 10^{-11}$ molecules$^{-1}$ cm$^3$ s$^{-1}$ | |

[a] Enthalpies in kcal/mol, entropies in cal mol$^{-1}$ K$^{-1}$ at 300 K, standard state 1 atm.
[b] Present experimental work from van't Hoff plot in Fig. 3. Errors are estimated.
[c] Evaluated from eq. [7] $\Delta PA = 1.5$ kcal/mol from McIver and co-workers (10, 11); $\Delta H_f^?$: *tert*-butylbenzene = −7; benzene +19.8; isobutene −4.3 kcal/mol (13).
[d] Estimated (statistical thermodynamics) see text.
[e] From $\Delta H^0_{PT} = -10.1$ kcal/mol, $\Delta G^0_{PT} = -10.5$ kcal/mol (10–12); $\Delta H_f^?$: $C_3H_6$ = 4.9 kcal/mol; isopropylbenzene = 0.9 kcal/mol; $\Delta G_f^?$: $C_3H_6$ = 15 kcal/mol; isopropylbenzene = 32.7 kcal/mol (13, 14).
[f] From $\Delta H^0_{PT} = -21.7$ kcal/mol, $\Delta G^0_{PT} = -21.3$ kcal/mol, based on $\Delta H_f^?$ ($C_2H_5^+$) = 216 kcal/mol (10, 17); $\Delta H_f^?$ (ethylbenzene) = 7.1 kcal/mol, $\Delta G_f^?$ (ethylbenzene) = 31.2 kcal/mol (13, 14).
[g] Rate constants at 32°C. The rate constant $k_{1f}$ was assumed to be third order while $k_{1r}$ was assumed to be second order.

A mixture of methane (3 Torr) and isobutane (1 Torr) was used in the equilibria [1] determinations, rather than neat isobutane at 4 Torr, because an unknown trace impurity (probably $C_4H_8$) in the isobutane led to production of ions of mass 113 and 111. These were noticeable at long reaction times in runs undertaken below room temperature. Mass 113 is probably the $C_4H_9 \cdot C_4H_8^+$ while mass 111 results from dehydrogenation of mass 113.

## Results and discussion

A typical experimental result is shown in Fig. 1. The reaction mixture produces *tert*-$C_4H_9^+$ as essentially the only ion some microseconds after the electron pulse.[3] In the presence of a small concentration of benzene, reaction [1] is seen to occur. The reaction reaches equilibrium after

$$[1] \quad C_4H_9^+ + C_6H_6 \underset{lr}{\overset{lf}{\rightleftarrows}} C_4H_9C_6H_6^+$$

about 0.7 ms. Runs with higher benzene concentration led to a shift of the equilibrium to the right as required by the equilibrium expression [6]. The ion intensity ratio from

$$[6] \quad K_1 = \frac{P(C_4H_9C_6H_6)^+}{P(C_4H_9^+)\,P(C_6H_6)}$$

runs as in Fig. 1, in the steady region, at long reaction times, was substituted into equation [6]. An example of the invariance of $K_1$ with changing benzene pressure is shown in Fig. 2. The results in Fig. 1 illustrate the clean reaction conditions that can be achieved by proper choice of the reaction mixture. The ions of interest, $C_4H_9^+$ and $C_4H_9C_6H_6^+$, represent almost 95% of the total ions observed during most of the reaction time. The reactions leading to $C_4H_9^+$ in the selected reaction mixture are described in the experimental section.

Raising the ion source temperature shifted the equilibrium to the left as expected for an exothermic reaction like [1]. The equilibrium constants $K_1$ determined at different temperatures are shown in the van't Hoff plot Fig. 3. The thermodynamic data $\Delta H_1^0$, $\Delta G_1^0$, and $\Delta S_1^0$ obtained from the plot are given in Table 1. These results can be compared with calculated values obtained through eq. [7] and literature thermochemical data (10–14).

$$[7] \quad \Delta H_1 = \Delta H_{PT} - \Delta H_f^0(\text{iso-}C_4H_8) + \Delta H_f^0(C_4H_9C_6H_5) - \Delta H_f^0(C_6H_6)$$

$$[8] \quad C_4H_9^+ + C_4H_9C_6H_5 = \text{iso-}C_4H_8 + C_4H_9C_6H_6^+$$
$$\Delta H_8^0 = \Delta H_{PT}^0 = PA(\text{iso-}C_4H_8) - PA(C_4H_9C_6H_5)$$

$\Delta H_{PT}^0$ corresponds to the enthalpy for the proton transfer shown in eq. [8]. Analogous equations can be written also for $\Delta G_1^0$ and $\Delta S_1^0$. The proton affinity of butylbenzene has been determined from proton transfer equilibria by McIver and co-workers (10). The proton affinity of isobutene also has been determined by proton transfer equilibria (7, 8, 11, 12). Since only the proton affinity difference is required in eq. [7], one needs only the relative proton affinities, i.e., there is no need to use an absolute PA scale. Heats of formation for the neutrals are also available (13). The $\Delta H^0 = -22$ kcal/mol obtained from the van't Hoff plot is seen to be in relatively good agreement with the value of −21 kcal/mol obtained via eq. [7].

Immediately after the butylation, the proton may

[3] Since all subsequent discussion deals with *tert*-$C_4H_9$, the prefix *tert* will be omitted for brevity in all the subsequent text and formulas.

Can. J. Chem. Downloaded from www.nrcresearchpress.com by 210.87.254.6 on 09/06/12
For personal use only.

Can. J. Chem. Downloaded from www.nrcresearchpress.com by 210.87.254.6 on 09/06/12
For personal use only.

be expected to be in position 1, relative to the butyl group. The relative energies for different positions of the proton on the benzene ring should be similar to those in protonated toluene, for which Hehre and co-workers (15) have made STO-3G calculations. They found the following relative values 1(0); 2(−6.2); 3(−1.7); 4(−8.2), the numbers in brackets being the energies in kcal/mol. The proton affinity (10) of butylbenzene obtained from proton transfer equilibria should relate to the most stable position 4. The (approximate) agreement between $\Delta H_1$ from the equilibria [1] and the calculated $\Delta H_1$ from eq. [7] indicates that the proton in equilibria [1] was in the 2 or 4 position. One may expect considerable energy barrier(s) for the migration of the proton from the 1 to the 2 (and 4) position. The exothermicity of the butyl addition (proton in position 1) which should be around 12–15 kcal/mol is the only source that could provide the energy for the migration. Thus, we assume that the barriers are less than ~15 kcal/mol and the energy is provided by chemical activation.

Approximate rate constants $k_{1f}$ and $k_{1r}$ can be determined from runs like that shown in Fig. 1. These are shown in Table 1. It was assumed that the reaction is third order in the forward and second order in the reverse direction. The $k_{1f} \approx 10^{-28}$ cm$^6$ molecules$^{-2}$ s$^{-1}$ is very small when compared to other third order association reactions involving polyatomic reactants and exothermicities in the 20 kcal/mol range. The low rate constant, however, is not so surprising when one considers that the primary product of [1f] contains the proton in position 1 and thus has a considerably lower exothermicity than 20 kcal/mol. Furthermore, the formation of the adduct is connected with unusually unfavorable entropy, as will be shown below.

Table 1 gives enthalpy changes for the alkylation of benzene by the isopropyl and ethyl cation. These were calculated from equations analogous to [7] and corresponding thermochemical data. As expected, a rapid increase of exothermicity is observed for the series $C_4H_9^+$, *sec*-$C_3H_7^+$, $C_2H_5^+$.

It is possible to calculate the entropy change of the alkylation reactions with an equation analogous to [7] but involving the corresponding entropy terms. The $\Delta S$ changes for the proton transfer reactions are small and are generally estimated from the rotational symmetry numbers. The entropies for the neutrals were taken from Stull *et al.* (14). The calculated entropies for iso-$C_3H_7^+$ and $C_2H_5^+$ alkylation are shown in Table 1. Unfortunately a value for $S^0(C_4H_9 \cdot C_6H_5)$ is not available, so that $\Delta S_1^0$ could not be evaluated from eq. [7]. An estimate of $\Delta S_1^0$ can be made on the basis of equations for translational, rotational, and vibrational entropies from statistical mechanics. The translational and external rotation changes are easily evaluated and amount to $\Delta S^0_{tr} = -36.7$ and $\Delta S^0_{ext\ rot} = -15.2$. (All entropy values in cal K$^{-1}$ mol$^{-1}$.) Space models indicate that the internal rotation of the butyl group relative to $C_6H_6$ in $C_4H_9C_6H_6^+$ may be restricted to a torsional oscillation. The same is true for the internal rotations of the methyl groups. Taking this into account, one obtains a $\Delta S^0_{int\ rot} \approx -1.5$. The total $-\Delta S_1^0$, neglecting all vibrations, is 53.4. This value represents a maximum value for $-\Delta S_1^0$. Several soft vibrations created in the adduct $C_4H_9C_6H_6^+$ will reduce $-\Delta S_1^0$ by some 5–8 units, i.e. to the neighbourhood of 46 cal K$^{-1}$ mol$^{-1}$. This is the estimated value given in Table 1.

The (absolute) entropy changes for the alkylation of benzene are seen to increase rapidly in the order $C_2H_5^+$, *sec*-$C_3H_7^+$, $C_4H_9^+$. The $-\Delta S^0$ value for butyl is unusually large, the largest we have ever measured. The entropy changes for many association reactions fall around 25 cal/degree mol. This is particularly true for clustering reactions, i.e. ion–solvent molecule association (7). The large entropy loss in reaction [1] must be attributed to the relatively large mass and large moments of inertia of both benzene and $C_4H_9^+$ and to the very restricted motions of the butyl group in the $C_4H_9C_6H_6^+$ ion. The very adverse entropy change for reaction [1] contributes significantly to the lack of stability of the $C_4H_9C_6H_6^+$ which was seen to thermally decompose (see Figs. 1 and 3) already below room temperature. Species with a dissociation energy of 22 kcal/mol ($-\Delta H_1$) and more normal entropies remain stable to much higher temperatures.

In superacid solution Olah *et al.* (1*c*) have observed, by $^1$Hmr, that the protonated butylbenzene is stable at −78°C. However, "warming of the solution leads to immediate cleavage of the butyl group" i.e. the reverse of reaction [1]. From this description, it appears that the cleavage is considerably more facile in solution than in the gas phase. This difference probably is largely due to solvation effects, in particular the better solvation of the butyl cation when compared to the butyl benzenium ion.

The facile decomposition of $C_4H_9C_6H_6^+$ is obviously responsible for protolysis being the almost exclusive reaction in the mass spectral chemical ionization of butylbenzene (3) with strong Brönsted acids like $CH_5^+$ and $C_2H_5^+$. But even after the most gentle protonation, thermal decomposition by [1r] will occur at the 100°C temperature commonly used in C.I. ion sources. McIver and

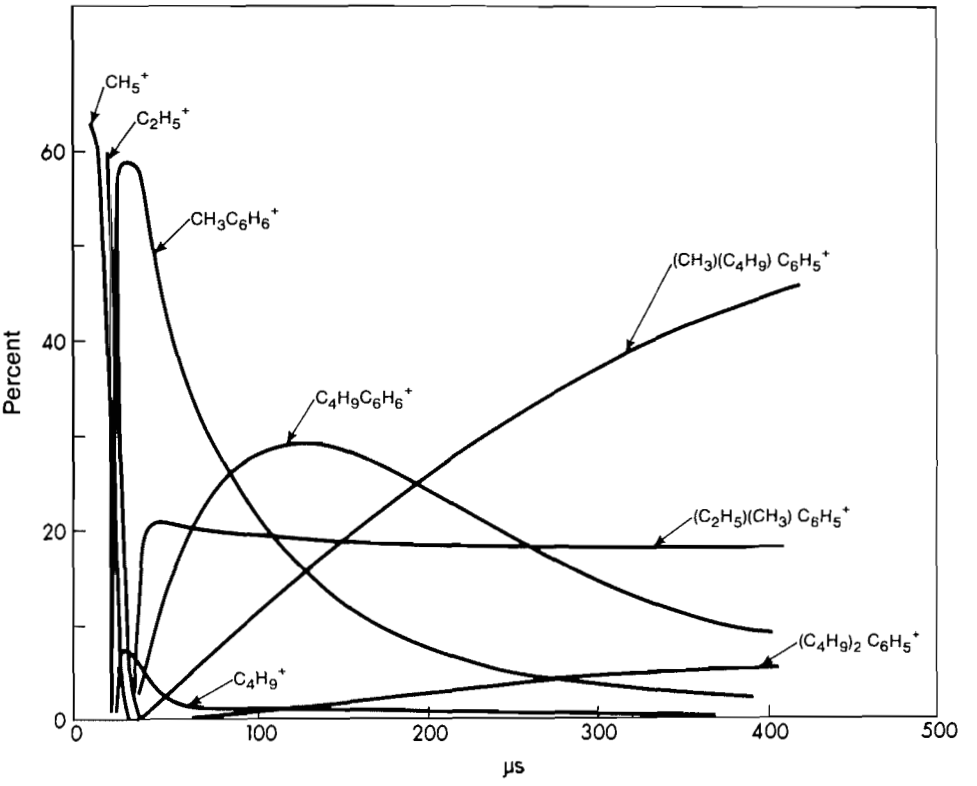


FIG. 4. Time dependence of major ions observed for reaction mixture: $CH_4$ 1.6 Torr, *tert*-butylbenzene 0.7 mTorr. Strongly exothermic protonation of butylbenzene by $CH_5^+$ and $C_2H_5^+$ leads almost exclusively to protolysis: $(C_4H_9C_6H_6^+)^* \longrightarrow C_4H_9^+ + C_6H_6$. The butyl ion produced by the above reaction alkylates the butylbenzene by reaction [10], $C_4H_9^+ + C_4H_9C_6H_5 = (C_4H_9)_2C_6H_5^+$. The doubly butylated benzenium ion is more stable than the monobutylated ion, i.e. $K_{10} \gg K_1$.

co-workers (10) were able to measure proton transfer equilibria involving butylbenzene only because, at the low pressures used in the ICR apparatus, the thermal activation required for [lr] is very much slower than the proton transfer reactions.

Some experiments were made in order to determine the fate of $C_4H_9C_6H_6^+$ produced by protonation of butylbenzene. The time dependence of the ions observed in two such experiments is shown in Figs. 4 and 5. A mixture of methane (1.6 Torr) with traces of butylbenzene (0.7 mTorr) was used in Fig. 4.

The proton transfer from the methane ions $CH_5^+$ and $C_2H_5^+$ is strongly exothermic and results in almost complete protolysis of the butylbenzene. The $C_4H_9^+$ created by the protolysis is seen

$$[9]\quad CH_5^+(\text{or } C_2H_5^+) + C_4H_9C_6H_5 = [C_4H_9C_6H_6^+]^* + CH_4\,(\text{or } C_2H_4)$$

$$[C_4H_9C_6H_6^+]^* \longrightarrow C_4H_9^+ + C_6H_6$$

to alkylate the butylbenzene in reaction [10] which is analogous to [1]. In comparing Figs. 1 and 4, which are for experiments at the same

$$[10]\quad C_4H_9^+ + C_4H_9C_6H_5 = (C_4H_9)_2C_6H_5^+$$

temperature, it becomes immediately obvious that the equilibrium constant $K_{10}$ is much larger than $K_1$, i.e. $K_1 \approx \geq 1.7 \times 10^2$ while $K_{10} \geq 3 \times 10^4$ ($Torr^{-1}$). This is an expected result. It has long been known, from condensed media experiments, that the stability of benzenium ions (cyclohexadienyl cations) increases as the number of alkyl substituents is increased (1, 2). This is due to the greater stabilization of the charge in the benzenium ions by the multiple alkyl substituents. A well-known consequence of this effect is the reduced synthetic utility of Friedel–Crafts alkylations, i.e. the difficulty in stopping the reaction at the single alkylation stage. The product of reaction [10] is most likely the most stable isomer, i.e. the *meta* dibutylbenzenium shown in structure **I**.

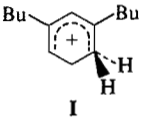


**I**

Not all of the protonated butylbenzene formed by reaction [9] suffers immediate dissociation; a small

Can. J. Chem. Downloaded from www.nrcresearchpress.com by 210.87.254.6 on 09/06/12
For personal use only.

Can. J. Chem. Downloaded from www.nrcresearchpress.com by 210.87.254.6 on 09/06/12
For personal use only.

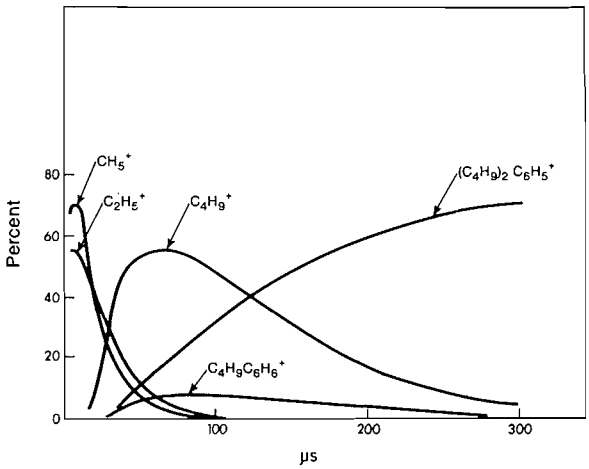


FIG. 5. Time dependence of major ions observed with reaction mixture: $CH_4$ 1 Torr, toluene 10 mTorr, *tert*-butylbenzene 0.5 mTorr. $CH_5^+$ and $C_2H_5^+$ rapidly protonate toluene. The protonated toluene proton transfers to butylbenzene [11] $CH_3C_6H_6^+ + C_4H_9C_6H_5 = CH_3C_6H_5 + C_4H_9C_6H_6^+$. Reaction [11] comes near equilibrium for longer reaction times. Some of the $C_4H_9C_6H_6^+$ decomposes to $C_4H_9^+$ by [lr]. The final major product $(CH_3)(C_4H_9)C_6H_5^+$ is formed by the addition of $C_4H_9^+$ to toluene [12] and also by the direct reaction [14], $C_4H_9C_6H_6^+ + CH_3C_6H_5 = (C_4H_9)(CH_3)C_6H_5^+ + C_6H_6$.

fraction becomes thermalized (see Fig. 4) and then gradually disappears by reactions [lr] and [15] to be discussed below.

The ion–time profiles shown in Fig. 5 were obtained with a gas mixture of the major gas methane (1 Torr) with toluene (10 mTorr) and butylbenzene (0.5 mTorr). For these conditions, proton transfer from $CH_5^+$ and $C_2H_5^+$ to toluene is rapid. The protonated toluene proton transfers to the butylbenzene by reaction [11]. Since the proton affinities of

[11] $CH_3C_6H_6^+ + C_4H_9C_6H_5 = CH_3C_6H_5 + C_4H_9C_6H_6^+$

toluene and butylbenzene are close, reaction [11] reaches equilibrium after $\sim 100\,\mu s$. This is demonstrated by the essentially constant ratio $[C_4H_9C_6H_6^+]/[CH_3C_6H_6^+] \approx 3$ at longer reaction times. This ratio taken together with the concentration ratio of the neutrals, [toluene]/[butylbenzene] = 20, leads to $K_{11} \approx 60$ and $\Delta G^0_{11} = -2.5$ kcal/mol in good agreement with McIver's (10) value of $-2.3$ kcal/mol. The butylbenzenium ion formed via (11) disappears gradually and is replaced by the two ions $(CH_3)(C_4H_9)C_6H_5^+$ and $(C_4H_9)_2C_6H_5^+$. These products can be created by reactions [12] and [13], the association of $C_4H_9^+$ with toluene and butylbenzene. The butyl$^+$ is formed by the thermal

[12] $C_4H_9^+ + CH_3C_6H_5 = C_4H_9CH_3C_6H_5^+$

[13] $C_4H_9^+ + C_4H_9C_6H_5 = (C_4H_9)_2C_6H_5^+$

decomposition of the $C_4H_9C_6H_6^+$, i.e. reaction [lr]. Reactions [lr], [12], and [13] undoubtedly occur, evidence for this is the small, near steady state concentration of $C_4H_9^+$ observed in Fig. 5 over the whole duration of the $C_4H_9C_6H_6^+$ ion. This is consistent with $C_4H_9^+$ being produced by [lr] and disappearing by [12] and [13]. (A "burst" of $C_4H_9^+$ at short reaction times is due to protolysis of butylbenzene by $CH_5^+$ and $C_2H_5^+$.) Comparing the rate of $C_4H_9C_6H_6^+$ disappearance with the expected rate due to reaction [lr] (the rate constant $k_{lr}$ was determined from Fig. 1) one finds that the observed rate in Fig. 5 and other similar runs is much faster. Furthermore this rate was found to increase as the concentration of toluene and butylbenzene was increased. This is very strong evidence that reactions [14] and [15] are also occurring. The rate constants $k_{14}$ and $k_{15}$ could be estimated to be around

[14] $C_4H_9C_6H_6^+ + CH_3C_6H_5 = C_4H_9CH_3C_6H_5^+ + C_6H_6$

[15] $C_4H_9C_6H_6^+ + tert\text{-}C_4H_9C_6H_5 = (C_3H_9)_2C_6H_5^+ + C_6H_6$

$k_{14} \approx k_{15} \approx 10^{-11}$ molecules$^{-1}$ cm$^3$ s$^{-1}$ which is two orders of magnitude lower than the orbiting collision rates. Reactions [14] and [15] probably proceed via the intermediate shown in structure **II** (for toluene). While the positive charge in **II** is formally on the benzene ring, in actual fact a considerable fraction of the charge will be also on the butyl group. After all, in the dissociation [lr] all the charge ends up on the butyl group. Thus, one can visualize the butyl group involved in an electrophilic attack as in **II**. Reactions [14] and [15] via the complex **II** probably have no counterpart in solution where solvent assistance of the dissociation [lr] favors very much the route [lr] followed by alkylations [12] and [13]. Also, solvation of the $C_4H_9C_6H_6^+$ ion probably reduces the electrophilicity of the $C_4H_9$ group and thus its tendency to form an activated complex like **II**. Reactions [14], [15], and the intermediate **II** are somewhat analogous to the alkylation reactions of benzenes by alkyl chloronium ions observed in solution and recently also in the gas phase (16) (see structure **III**). The gas

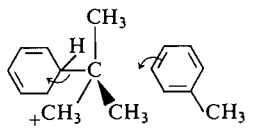


**II**

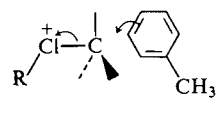


**III**

phase chloronium ion reactions were found to proceed with rate constants much lower than the orbiting rates (16); i.e., the alkylations by butyl benzenium (**II**) and alkylchloronium (**III**) are both relatively slow reactions.

1. (*a*) G. A. OLAH and M. W. MEYER. *In* Friedel–Crafts and related reactions. Vol. 1. Interscience, New York. 1963. p. 646ff; (*b*) G. A. OLAH. Carbocations and electrophilic reactions. John Wiley & Sons, New York, 1973; (*c*) G. A. OLAH, R. H. SCHLOSSBERG, R. D. PORTER, Y. K. MO, D. P. KELLY, and G. D. MATESCU. J. Am. Chem. Soc. **94**, 2034 (1972).
2. W. v.E. DOERING, M. SAUNDERS, J. H. BOYNTON, H. W. EARHART, E. F. WADLEY, W. R. EDWARDS, and G. LABER. Tetrahedron **4**, 178 (1958).
3. F. H. FIELD. Chemical ionization mass spectrometry. *In* Advances in mass spectrometry. *Edited by* E. Kendric. Institute of Petroleum, London. 1968. pp. 657, 658.
4. K. HIRAOKA and P. KEBARLE. J. Am. Chem. Soc. **99**, 360 (1977).
5. K. HIRAOKA and P. KEBARLE. J. Am. Chem. Soc. **99**, 366 (1977).
6. D. K. SEN SHARMA and P. KEBARLE. J. Am. Chem. Soc. **100**, 5826 (1978).
7. P. KEBARLE. Ann. Rev. Phys. Chem. **28**, 445 (1977).
8. M. T. BOWERS (*Editor*). Gas phase ion chemistry. Academic Press, New York. 1979.
9. (*a*) W. J. HEHRE. *In* Applications of electronic structure theory. *Edited by* H. F. Schaefer III. Plenum Press, New York. 1977. p. 301; (*b*) D. M. SHOLD and P. AUSLOOS. J. Am. Chem. Soc. **100**, 7915 (1978); S. G. LIAS, D. M. SHOLD, and P. AUSLOOS. J. Am. Chem. Soc. **102**, 2541 (1980).
10. W. J. HEHRE, R. T. MCIVER, J. A. POPLE, and P. v.R. SCHLEYER. J. Am. Chem. Soc. **96**, 7162 (1974).
11. J. F. WOLF, R. H. STALEY, I. KOPPEL, M. TAAGEPERA, R. T. MCIVER, J. L. BEAUCHAMP, and R. W. TAFT. J. Am. Chem. Soc. **99**, 5417 (1977).
12. R. YAMDAGNI and P. KEBARLE. J. Am. Chem. Soc. **98**, 1320 (1976); Y. K. LAU, Gas phase basicities and proton affinities. Ph.D. thesis, University of Alberta, 1979.
13. J. D. COX and G. PILCHER. Thermochemistry of organic and organometallic compounds. Academic Press, New York. 1970.
14. D. R. STULL, E. F. WESTRUM, JR., and G. C. SINKE. The chemical thermodynamics of organic compounds. John Wiley & Sons, New York. 1969.
15. J. L. DEVLIN III, J. F. WOLF, R. W. TAFT, and W. J. HEHRE. J. Am. Chem. Soc. **98**, 1990 (1976).
16. D. K. SEN SHARMA and P. KEBARLE. J. Am. Chem. Soc. **104**, 19 (1982).
17. J. C. TRAEGER and R. G. MCLOUGHLIN. J. Am. Chem. Soc. **103**, 3647 (1981).

Can. J. Chem. Downloaded from www.nrcresearchpress.com by 210.87.254.6 on 09/06/12
For personal use only.

# Electronic spectroscopy of aromatic Schiff bases. V. Specific interactions involved between some typical benzylideneaniline molecules and small polar molecules

MICHEL BELLETETE[1] AND GILLES DUROCHER

*Département de Chimie, Université de Montréal, C.P. 6210, Succ. A, Montréal (Qué.), Canada H3C 3V1*

Received February 18, 1982

MICHEL BELLETETE and GILLES DUROCHER. Can. J. Chem. **60**, 2332 (1982).

Fluorescence quantum yields ($\phi_F$), theoretical first-singlet radiative decay constants ($k_F^{(u)}$), and first-singlet non-radiative decay constants ($k_{nr}$) of some benzylideneanilines (BA) dissolved in methylcyclohexane have been obtained. High values of $k_{nr}$ are interpreted by the twisting of the molecules around the azomethine bond (C=N) in the first singlet excited state. The absorption spectra of some BA's have also been obtained in methylcyclohexane with various added amounts of polar molecules. BA's with strong electron-donor and/or strong electron-acceptor substituents in the *para* positions give rise to the formation of ground state complexes with small polar molecules. The stoichiometry of the complex is one BA molecule for two polar solvent molecules; when ethanol is used as a polar solvent, it is further involved in hydrogen bonding formation. The fluorescence spectra of 4-dimethylaminobenzylidene-4'-nitroaniline have been obtained in methylcyclohexane with various added amounts of polar species. The results are interpreted by the formation of exciplexes with polar compound. The Lippert–Mataga theory and the more generalized Kawski theory failed to explain the solute–solvent interactions disussed in this paper.

MICHEL BELLETETE et GILLES DUROCHER. Can. J. Chem. **60**, 2332 (1982).

Les rendements de fluorescence ($\phi_F$), les constantes de désactivation radiative théoriques de l'état premier singulet excité ($k_F^{(u)}$) et les constantes de désactivation non-radiatives de l'état premier singulet excité ($k_{nr}$) de certaines molécules de benzylidèneaniline (BA) dissoutes dans le méthylcyclohexane ont été obtenus. Les valeurs élevées de $k_{nr}$ obtenues sont expliquées par la torsion des molécules autour du lien azométhine (C=N) dans l'état premier singulet excité. Les spectres d'absorption de certaines molécules de benzylidèneaniline ont été mesurés dans le méthylcyclohexane avec différentes quantités ajoutées de molécules polaires. Les BA possédant des substituants électro-accepteurs puissants en position Y et/ou des substituants électro-donneurs en position X forment des complexes à l'état fondamental avec les molécules polaires. La stoïchiométrie de ces complexes est une molécule de BA pour deux molécules de solvant polaire; les complexes formés par l'éthanol impliquent la formation d'une liaison hydrogène. Les spectres de fluorescence de la molécule de diméthylamino-4 benzylidène nitro-4'-aniline ont été obtenus dans le méthylcyclohexane pour des additions successives de molécules polaires. Les résultats obtenus sont expliqués en termes d'interactions spécifiques à l'état excité (exciplexe). La théorie de Lippert-Mataga et la théorie plus généralisée de Kawski ne peuvent expliquer les interactions soluté–solvant discutées dans cet article.

## Introduction

The absorption spectroscopy of the *para*-substituted benzylideneanilines (BA) has been studied in recent years and for a review of the literature we refer the readers to parts I and II of this series of papers (1, 2). For band system II of some BA's, assigned to a charge transfer transition, very large excited state dipole moments have been obtained by using the Lippert–Mataga theory describing the solute–solvent interactions (2). On the other hand, the emission spectroscopy of these molecules was unexplored (3–6). Recently, we have shown the existence of luminescence from some BA's (7–9). The purpose of this paper is two-fold: first we want to study the photophysics of some of these BA's and secondly, we want to investigate the possibility of specific interactions taking place between BA's and polar solvents in their ground and/or excited states. The molecules studied here are the following using the same notations as described in an earlier paper (2).

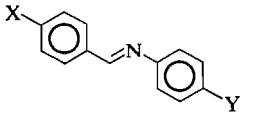


| Compound | X | Y |
|---|---|---|
| **1** | H | H |
| **2** | $OCH_3$ | H |
| **3** | H | $NO_2$ |
| **4** | $OCH_3$ | $OCH_3$ |
| **5** | $OCH_3$ | $NO_2$ |
| **6** | $N(CH_3)_2$ | $NO_2$ |
| **7** | H | $OCH_3$ |
| **8** | $NO_2$ | H |
| **9** | $NO_2$ | $OCH_3$ |
| **13** | $NO_2$ | $NO_2$ |

## Experimental part

The BA's were synthesized and purified as described previously (1, 2). Methylcyclohexane, diethyl ether, acetonitrile, dimethylformamide, and ethanol were purified as described elsewhere (2); *n*-butylbromide (Eastman Kodak) was distilled twice and kept in the dark. Absorption spectra at room temperature have been recorded on Cary-14 and on B & L Spectronic-505 spectrophotometers. The areas under the absorption curves for the calculation of the $k_F^{(u)}$ values were

[1]Predoctoral fellow, now Research Associate at the "Institut de Génie des Matériaux" in Montreal.

0008-4042/82/182332-08$01.00/0

©1982 National Research Council of Canada/Conseil national de recherches du Canada

Can. J. Chem. Downloaded from www.nrcresearchpress.com by 210.87.254.105 on 09/06/12
For personal use only.

Can. J. Chem. Downloaded from www.nrcresearchpress.com by 210.87.254.105 on 09/06/12
For personal use only.

determined by using a program adapted on the "Data General Nova 3/12" minicomputer.

Absorption spectra at several temperatures and fluorescence spectra at room temperature were obtained on a Spex "Fluorolog" instrument model 1902, using a 450 W xenon-arc source. The temperature was varied with a "Polyscience Corporation" model 90 circulator bath using a mixture of water – ethylene glycol as the circulating fluid and connected to the 4-cell sample holder. The temperature (0°C to 60°C) of the samples was measured directly with a thermometer placed in a reference cell (±0.5°C). The fluorescence quantum yields were obtained relative to those of the 3H-indoles (10). Concentrations were varied from 2 to 5 × $10^{-5}$ mol $L^{-1}$ in the absorption and fluorescence studies.

## Results and discussion

### *I. Photophysics of some* p-*substituted BA's in a non-polar solvent*

The absorption spectra of the BA's studied here have been obtained at room temperature in cyclohexane and were published in part I of this series of papers (1). Fluorescence was detected only for molecules **2**, **4**, **6**, and **7**. The fluorescence spectra of these molecules at room temperature in methylcyclohexane are shown in Fig. 1. The intensity has been normalized. The absorption and fluorescence spectra do not show any vibrational structure and do not give rise to good mirror-image relationship as the absorption spectra from ref. 1 are wider than the fluorescence spectra in each case.

The fluorescence quantum yields of molecules **2**, **4**, **6**, and **7** have been measured. For the other molecules, $\phi_F$ was less than 0.0001, the experimental sensitivity limit of our instrumentation. Very small $\phi_F$ values were obtained for all molecules as shown in Table 1. The theoretical first singlet radiative decay constants ($k_F^{(t)}$) have been calculated using the approximate Forster relation (11) since the Strickler and Berg approach (12) necessitates the use of the fluorescence spectra which are not available for many of the molecules studied. The Forster relation is strictly valid only when fluorescence and absorption give good mirror image relationship. This is not the case for the BA molecules studied here and the $k_F^{(t)}$ calculations are thus only approximate and may vary by a factor of 2 as we have shown by application of the Strickler and Berg approach to the fluorescing molecules. Nevertheless, it is interesting to note that the variation in the $k_F^{(t)}$ values of these molecules follows (roughly) the variation in their ground state dipole moments (2).

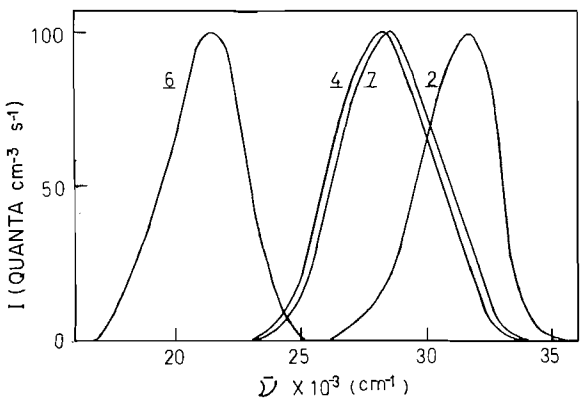


FIG. 1. Fluorescence spectra of molecules **2**, **4**, **6**, and **7** at room temperature in methylcyclohexane. All spectra have been normalized.

Obviously the non-radiative decay constant ($k_{nr}$) is the key parameter as far as the photophysical behaviour of the BA is concerned. Even if it seemed necessary that molecules which emit fluorescence possess a $k_F^{(t)}$ value higher than 3.0 × $10^8$ $s^{-1}$, it is not the only prerequisite since molecules **5** and **9** have shown no fluorescence emission (limit of detection of our apparatus). Such high non-radiative decay constants are difficult to assign to intersystem crossing from $S_1$ to $T_1$ since these rates from singlet $\pi\pi^*$ states vary normally between $10^6$ and $10^8$ $s^{-1}$ (ref. 11, p. 178). Moreover, very weak phosphorescence has been observed in low temperature matrices in only two of these molecules (8). Since the BA's are not rigid in their ground electronic states (1), the first excited singlet state is likely to be deactivated by the twisting of the molecules around the azomethine bond (C=N). This would explain the high values of $k_{nr}$ for all the BA molecules. Recently, Yoshida and Kobayashi have shown that various substituted *N*-benzylideneanilines are converted into their photo *Z*(*cis*) isomers upon irradiation by a high pressure mercury lamp (31). This photochemical behaviour has been correlated to that of stilbene derivatives.

On the other hand, Pinasias *et al.* have shown that the fluorescence quantum yields of *p*-substituted stilbenes increase by decreasing the temperature (13). The temperature-dependent process was attributed to twisting of the molecular parts around the ethylenic bond rather than to internal conversion. Moreover, Fisher *et al.* obtained the same results and gave the same interpretation for non-planar stilbene derivatives (14). Unfortunately, due to the fact that these highly polar BA's are only slightly soluble in non-polar solvents, dimerization of these BA's rapidly occurs in lowering the temperature and the free BA fluorescence is then rapidly quenched. On the other hand, the Stokes shifts ($\bar{\nu}_A - \bar{\nu}_F$) are rather small for molecules **2**, **4**, and **7** but nearly double for molecule **6**, so it might

Can. J. Chem. Downloaded from www.nrcresearchpress.com by 210.87.254.105 on 09/06/12
For personal use only.

TABLE 1. Photophysical properties of some *p*-substituted benzylideneaniline molecules in methylcyclohexane at room temperature

| Molecules | X | Y | $\bar{\nu}_A - \bar{\nu}_F$ ($cm^{-1}$) | $k_F^{(1)} \times 10^{-8}$ ($s^{-1}$) | $\phi_F$ | $k_{nr} \times 10^{-12}$ ($s^{-1}$) |
|---|---|---|---|---|---|---|
| **6** | $N(CH_3)_2$ | $NO_2$ | 4800 | 7.4 | 0.0014 | 0.53 |
| **5** | $OCH_3$ | $NO_2$ | — | 5.8 | <0.0001 | >6 |
| **2** | $OCH_3$ | H | 2200 | 3.0 | 0.0010 | 0.30 |
| **3** | H | $NO_2$ | — | 1.9 | <0.0001 | >2 |
| **1** | H | H | — | 1.9 | <0.0001 | >2 |
| **7** | H | $OCH_3$ | 2700 | 3.6 | 0.0001 | 4 |
| **8** | $NO_2$ | H | — | 1.3 | <0.0001 | >1 |
| **9** | $NO_2$ | $OCH_3$ | — | 3.3 | <0.0001 | >3 |
| **4** | $OCH_3$ | $OCH_3$ | 2200 | 5.2 | 0.0001 | 5 |
| **13** | $NO_2$ | $NO_2$ | — | 1.4 | <0.0001 | >1 |

be that the twisted internal charge transfer excited state involving the dimethylamino group in this molecule also plays a certain role in stabilizing the relaxed $S_1$ state before the fluorescence can occur (27, 28). Finally the 3H-indoles (planar analogs of the BA's), which are more rigid in their ground states and where the twisting of the molecules around the C=N double bond is avoided, show $k_{nr}$ values lower by four orders of magnitude in some cases compared to the BA's (10).

Furthermore, it is quite clear from Table 1 that the non-radiative decay constants of all the substituted BA's are higher by about one order of magnitude than that of stilbene (14) and tetraphenylethylene (29). This suggests that the excited state torsional motions are playing a more active role in the former molecules.

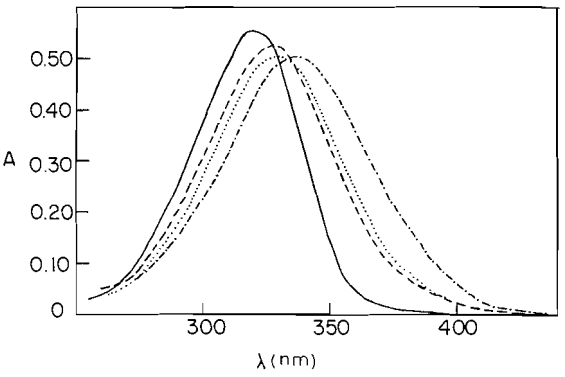


FIG. 2. Absorption spectra of 4-methoxybenzylidene-4'-nitroaniline (**5**) at room temperature in methylcyclohexane with various amounts of ethanol added (— 0.0 *M*, --- 0.188 *M*, ··· 0.273 *M*, ·····- 0.568 *M*).

*II. Ground state specific interactions (complexation)*

The absorption spectra of all the BA molecules studied here have been obtained at room temperature in methylcyclohexane with various added amounts of polar molecules like ethanol and acetonitrile. Some molecules clearly show ground state complexation with polar solvents.

*Molecule 5*

The absorption spectra of 4-methoxybenzylidene-4'-nitroaniline (**5**) have been obtained in methylcyclohexane at room temperature with various added amounts of polar molecules: ethanol ($\mu$ = 1.67 D), *n*-butylbromide ($\mu$ = 2.1 D), and acetonitrile ($\mu$ = 3.35 D). These three series of spectra show two important features: a large red shift of the absorption wavelength and the presence of an isosbestic point only at small concentrations of the polar molecules added as illustrated for the case of ethanol in Fig. 2. We have applied the Lippert–Mataga theory (2, 15, 16) to the solvent shifts and linear correlations have been obtained for the three solvents. However, the values of excited state dipole moment calculated using the different slopes were over 60 D for *n*-butylbromide and over 100 D for ethanol and acetonitrile. This proves that the solvent shifts are too large to be explained by generalized solute–solvent interactions and, furthermore, the existence of an isosbestic point in the spectra suggests that molecule **5** form a ground state complex with small polar molecules. We have also analyzed our solvent-induced frequency shifts according to the more general formula derived by Kawski (17) because, in these equations, the cavity is assumed to be an ellipsoid instead of a sphere, which is somewhat more realistic for the BA's. Linear correlations have also been obtained for the cases of ethanol and *n*-butylbromide as shown in Fig. 3. It is thus rather hazardous to use such plots (Lippert–Mataga and Kawski theories) in the calculation of excited state dipole moments without any meaningful look at all possible interactions involved.

In order to study the nature of the interactions involved in these complexes and specifically to investigate the possibility of hydrogen bonding

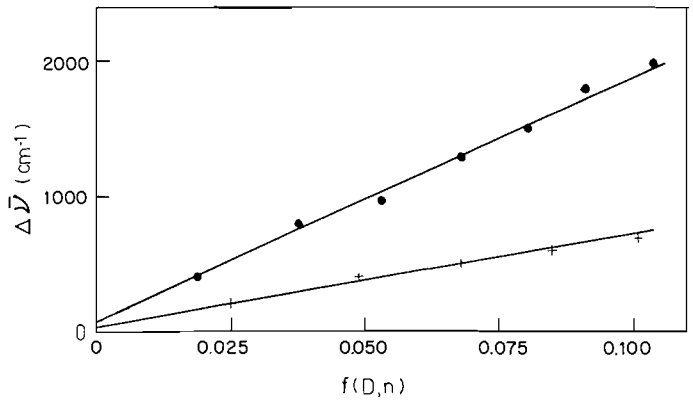


FIG. 3. Absorption solvent shifts for 4-methoxybenzylidene-4′-nitroaniline (5) (● ethanol, + *n*-butylbromide)

$$[24]\quad f(D, n) = \left(\frac{2n^2 + 1}{n^2 + 2}\right)^2 \cdot \left(\frac{D - 1}{2D + 1} - \frac{n^2 - 1}{2n^2 + 1}\right)$$

where $D$ is the dielectric constant and $n$ is the refractive index of the medium.

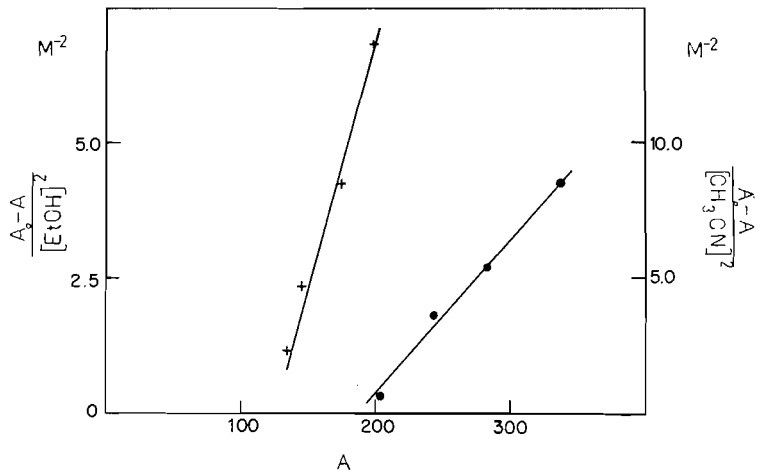


FIG. 4. Plots of $(A_0 - A)/[B]^2$ against $A$ for 4-methoxybenzylidene-4′-nitroaniline (5) in methylcyclohexane at 283 K. (The absorption wavelengths used were 300 nm for ethanol (●) and 290 nm for acetonitrile (+).)

between molecule **5** and ethanol, we recorded the absorption spectra with various amounts of ethanol and acetonitrile added at several temperatures and calculated the ground state equilibrium constant of the complex at each temperature using the following relation (18):

$$[1]\quad K[B]^n = \frac{A_0 - A}{A - A_F}$$

where $K$ is the ground state equilibrium constant, [B] is the concentration of polar molecules, $A_0$ is the absorbance at a particular wavelength in the absence of polar molecules, $A_F$ is the absorbance when all the molecules are complexed in the mixed solvent system, and $A$ is the absorbance of the sample in the presence of varying concentrations of polar molecules. Plots of $(A_0 - A)/[B]^n$ against $A$ have a slope of $K$, the equilibrium constant of the complex. Good linear correlations have been obtained only for $n = 2$, which is the number of polar molecules involved in the complex, giving rise to a stoichiometry of one molecule of **5** for 2 molecules of polar solvent. Figure 4 shows such correlations for ethanol and acetonitrile at 283 K and Table 2 gives the values of $K$ at several temperatures for ethanol and acetonitrile. Linear plots like those shown in Fig. 4 and with the same slope have been obtained by using absorption wavelengths between 290 nm and 315 nm for ethanol and between 280 nm and 300 nm for acetonitrile. The following ther-

Can. J. Chem. Downloaded from www.nrcresearchpress.com by 210.87.254.105 on 09/06/12
For personal use only.

Can. J. Chem. Downloaded from www.nrcresearchpress.com by 210.87.254.105 on 09/06/12
For personal use only.

TABLE 2. Thermodynamic parameters of the ground state molecular complexes of molecule **5**

| Ethanol | | | | Acetonitrile | | | |
|---|---|---|---|---|---|---|---|
| $T$ (K) | $K$ ($M^{-2}$) | $\Delta H^0$ (kJ mol$^{-1}$) | $\Delta S^0$ (J mol$^{-1}$ K$^{-1}$) | $T$ (K) | $K$ ($M^{-2}$) | $\Delta H^0$ (kJ mol$^{-1}$) | $\Delta S^0$ (J mol$^{-1}$ K$^{-1}$) |
| 273 | 43.5 | | | 284 | 179 | | |
| 283 | 26 | | | 294 | 145 | | |
| | | $-43\pm3$ | $-120\pm10$ | | | $-15\pm1$ | $-9\pm1$ |
| 297 | 11 | | | 306 | 102 | | |
| 306 | 6.6 | | | 329 | 74.6 | | |

modynamic relation was used to calculate the enthalpy and the entropy of the complexes:

$$[2] \quad \log K = -\frac{\Delta H^0}{2.303R}\frac{1}{T} + \frac{\Delta S^0}{2.303R}$$

Plots of log $K$ against $1/T$ give slopes of $-\Delta H^0/2.303R$ and an intercept $\Delta S^0/2.303R$. Such plots are shown in Fig. 5 and the values of $\Delta H^0$ and $\Delta S^0$ for ethanol and acetonitrile are given in Table 2.

It is worth pointing out that $\Delta H^0$ is much larger for the complex involving ethanol even if acetonitrile is much more polar than ethanol. This higher energy of formation of the complex in ethanol is responsible for its red-shifted electronic absorption in ethanol compared to acetonitrile. In the literature we find $\Delta H$ values between 1 kJ mol$^{-1}$ and about 18 kJ mol$^{-1}$ for complexes stabilized by dipolar interactions and from 8 kJ mol$^{-1}$ to 40 kJ mol$^{-1}$ for complexes involving hydrogen bonding interactions (19). We then propose that acetonitrile is involved in a complex mainly stabilized by dipole–dipole interactions. For the case of ethanol, dipolar interactions may also contribute to the binding in the complex but hydrogen bonding formation is certainly the most important factor involved in the formation of this kind of complex.

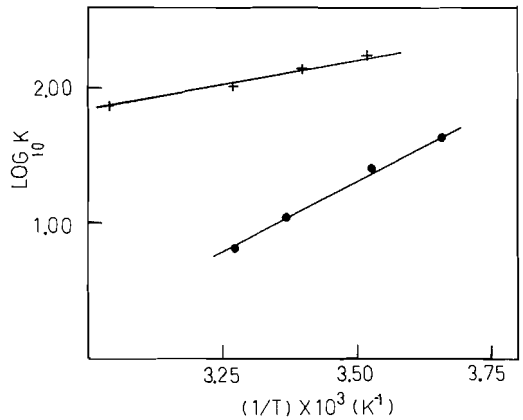


FIG. 5. Plots of log $K$ against $1/T$ for 4-methoxybenzylidene-4′-nitroaniline in methylcyclohexane (● ethanol, + acetonitrile).

Moreover, the entropy change is higher for the complex involving ethanol; this can be explained by the fact that complexes involving hydrogen bond interactions are much more ordered relative to those stabilized by dipolar interactions.

Thermodynamics alone cannot differentiate the sites of the complexation, but recently Lumry *et al.* (20) suggested that indole compounds possess two sites for complexation and that alcohols can serve as proton donor and also electron donor in the interactions with these type of compounds. Scheuer-Lamalle made some theoretical *ab initio* calculations of the electronic density on the substituted phenylimines (R′—CH=N—$C_6H_4$—R) and on the substituted benzaldimine molecules (R′—$C_6H_4$—CH=N—R) (21). She showed that for the phenylimines, the electronic charge on the nitrogen atom of the azomethine bond is practically independent of the substituents R and R′. On the other hand, benzaldimines, where R′ is an electron-donor substituent and R is an electron-acceptor substituent, show a net increase in the electronic charge on the nitrogen atom. By analogy, BA molecules where X is an electron-donor substituent and Y is an electron-acceptor substituent are expected to show the same behavior as that of the benzaldimines. These BA's thus have a negative nitrogen atom with one highly accessible electron lone pair and different positive sites on carbon atoms. Two sites of complexation are therefore also possible in BA's possessing electron-donor substituents in X position and electron-acceptor substituents in Y position. For complexes involving ethanol one molecule is certainly bound at the nitrogen site by hydrogen bonding interaction and the other molecule might be bound elsewhere in the BA by dipolar interactions. For complexes involving acetonitrile, the polar molecules are probably linked at the same positions as for ethanol but this time only dipolar interactions are involved in the stabilization of the complexes.

*Molecule* **6**

The absorption spectra of 4-dimethylamino-benzylidene-4′-nitroaniline (**6**) have been obtained in

Can. J. Chem. Downloaded from www.nrcresearchpress.com by 210.87.254.105 on 09/06/12
For personal use only.

methylcyclohexane at room temperature with various added amounts of ethanol and *n*-butylbromide. Acetonitrile was not used due to the lack of miscibility with methylcyclohexane, less than 2%, which is not enough to observe significant changes in the absorption spectra. Figure 6 shows the case of ethanol and as for molecule **5**, an isosbestic point appeared this time at 385 nm which emphasizes the formation of a ground state complex. The equilibrium constant of the complexes have been calculated using eq. [1] and values of $K = 1.00 \pm 0.20\,M^{-2}$ and $K = 1.5 \pm 0.5\,M^{-2}$ have been obtained for the cases of ethanol and *n*-butylbromide, respectively. The stoichiometry of the complexes is one molecule of **6** for two molecules of polar solvent. By analogy with molecule **5**, the ground state complex is probably stabilized by dipolar interactions for *n*-butylbromide and by hydrogen bonding formation for ethanol. We have applied the Lippert–Mataga (2, 15, 16) and the Kawski (17) relations for the solvent shifts and this time no linear correlation has been obtained for either solvent.

*Molecule 3*

The absorption spectra of benzylidene-4′-nitroaniline have been obtained in methylcyclohexane at room temperature with different added amounts of ethanol and are illustrated on Fig. 7. It is clear there is ground state complexation and $K = 1.0 \pm 0.2\,M^{-2}$. Linear Lippert–Mataga and Kawski correlations have been obtained for the solvent shifts.

All the other BA's studied didn't seem to show any obvious specific interactions with ethanol in their ground electronic state. So only BA's with strong electron-acceptor substituents in the Y position and/or electron-donor substituents in the X position give rise to the formation of ground state

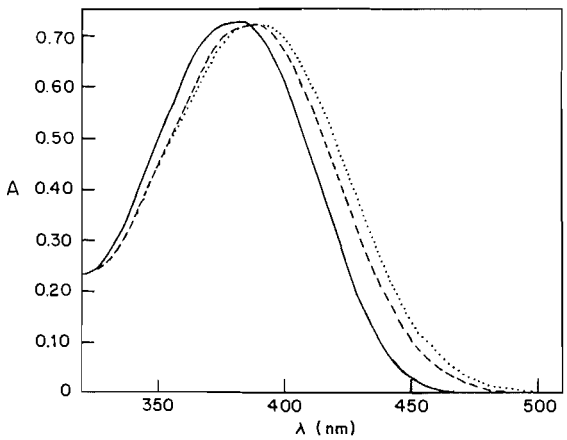


FIG. 6. Absorption spectra of 4-dimethylaminobenzylidene-4′-nitroaniline (**6**) at room temperature in methylcyclohexane with various amounts of ethanol added (— 0.0 *M*, --- 2.02 *M*, ··· 3.24 *M*).

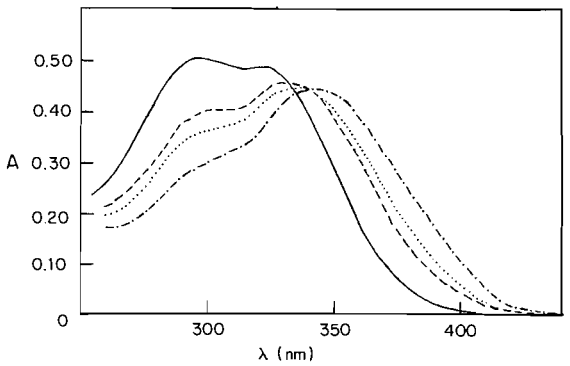


FIG. 7. Absorption spectra of benzylidene-4′-nitroaniline (**3**) at room temperature in methylcyclohexane with various amounts of ethanol added (— 0 *M*, --- 1.07 *M*, ··· 1.56 *M*, ·-·-·- 3.24 *M*).

complexes with small polar molecules. These molecules are likely not to be planar (2) in their ground states; for example, Kobayashi *et al.* (22) using CNDO/S CI calculations have shown that benzylidene-4′-nitroaniline is considerably twisted in its ground state. On the other hand, 4-nitrobenzylidene-4′-methoxyaniline, which is nearly planar (23), shows no evidence of ground state specific interactions. The planarity of the BA's does not seem to be a criterion as far as ground state complexation is concerned. The important factor seems to be the electron density at the different sites of the BA molecules; molecules with strong electron density on the N atom and electronic attraction centers at various C atoms form ground state complexes with small polar molecules. Due to the fact that a high electron density on the nitrogen atom of the azomethine bond favors the distortion of the phenylimine group (loss of planarity of the whole molecule) these BA's probably behave like bichromophores with their own interaction sites.

We have thus shown that the Lippert–Mataga and the more generalized Kawski theories sometimes give linear correlations for the solvent shifts even if ground state complexes exist. Thus these kinds of correlation cannot be used as criteria for the presence or absence of specific interactions with a particular polar solvent. For this reason, some of the excited state dipole moments of polar molecules published in the literature are to be used with caution, since ground state complexation with polar solvents might possibly occur.

### *III. Do any excited state specific interactions exist between BA's and polar solvents?*

Lippert calculated an excited state dipole moment for molecule **6** using absorption and fluorescence maxima in many solvents of different dielectric constants (3). He obtained a roughly linear correlation between $\bar{\nu}_A - \bar{\nu}_F$ and $f(D, n)$ (even if as

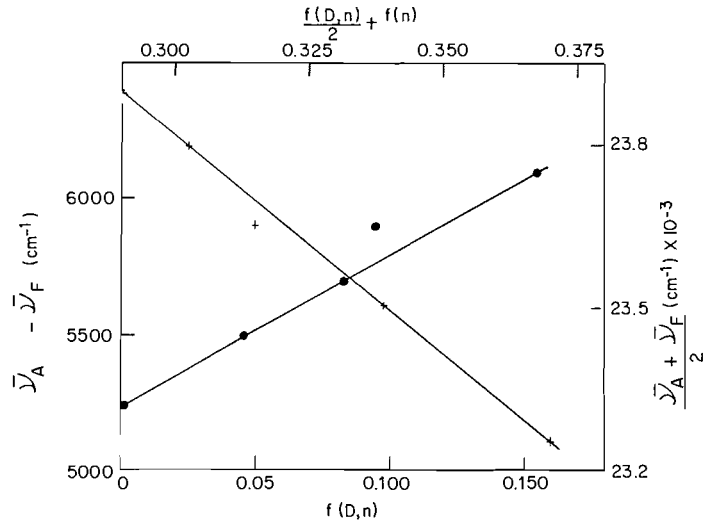


FIG. 8. Plots of $\bar{\nu}_A - \bar{\nu}_F$ vs. $f(D,n)$ (●) and $(\bar{\nu}_A + \bar{\nu}_F)/2$ vs. $f(D,n)/2 + f(n)$ (+) for the solvent shifts of 4-dimethylaminobenzylidene-4′-nitroaniline (**6**) in methylcyclohexane with various amounts of acetonitrile added.

[17, 24] $$f(D, n) = \frac{2n^2 + 1}{n^2 + 2} \cdot \left(\frac{D - 1}{D + 2} - \frac{n^2 - 1}{n^2 + 2}\right)$$

$$f(n) = \frac{3\,(n^4 - 1)}{2\,(n^2 + 2)^2}$$

where $D$ is the dielectric constant and $n$ is the refractive index of the medium.

we have shown above, some of the polar solvents used give rise to ground state complexation) and he obtained an excited state dipole moment of 38 D. To find out if specific interactions in the excited state exist, fluorescence spectra of molecule **6** have been measured at room temperature in methylcyclohexane with different added amounts of diethyl ether, *n*-butylbromide, dimethylformamide (DMF), acetonitrile, and ethanol. The Lippert–Mataga plots using absorption and fluorescence data (2, 15, 16) for the solvent shifts have been made and linear correlations have been obtained only for the cases of DMF and acetonitrile (8). The more generalized Kawski theory (17), using the absorption and fluorescence maxima, was also applied as used by Chama and Viallet (24) for the indole derivatives. Linear correlations were also obtained. Figure 8 shows the case of acetonitrile using the two main expressions given by Chama and Viallet (24).

In each case, the fluorescence intensity of molecule **6** first increases with increasing amounts of polar solvent to reach a maximum and then decreases with further addition of polar molecules. Moreover, the fluorescence is completely extinguished in pure acetonitrile and DMF. This is a behavior typical of exciplex formation followed by exciplex fluorescence quenching when the solvent polarity increases (25). Similar results have been obtained for the equivalent planar analog (3H-indole) where the fluorescence quantum yield and singlet lifetime are much larger and consequently allow us to interpret them in terms of exciplex formation with polar solvents (26). Finally, we have reported in an earlier paper (9) that the fluorescence of some benzylideneanilines (BA's), including molecule **6** and some 3H-indole molecules, shows a blue shift in EPA at 77 K compared to the same solutions at room temperature. At the time we interpreted these results in terms of an emission taking its origin from a non-completely relaxed Franck–Condon excited state due to the rigidity of the medium. However, EPA contains 16.6% of ethanol which we know now is undergoing ground state specific interactions with these solute molecules. At 77 K ground state complexes are favored and exciplexes are not likely to occur compared to the room temperature behavior. This would also explain the blue shift observed in EPA in going from room temperature to 77 K. If the excited ground state complex was responsible for the fluorescence, one would expect a red shift in going from room to lower temperatures. Moreover, the fluorescence intensity of molecule **6** dissolved in methylcyclohexane which contains 1% of DMF decreases exponentially with the reverse of the temperature between 180 K and 220 K. It was impossible to work at temperatures lower than 180 K due to dimerization of the solute molecules. For temperatures higher than 220 K the fluores-

Can. J. Chem. Downloaded from www.nrcresearchpress.com by 210.87.254.105 on 09/06/12
For personal use only.

Can. J. Chem. Downloaded from www.nrcresearchpress.com by 210.87.254.105 on 09/06/12
For personal use only.

cence intensity reaches a saturation. This is also a typical fluorescence emission behaviour for an exciplex (30).

For all these reasons we think that molecule **6** forms exciplexes with polar molecules. In pure polar solvents with high dipole moments like acetonitrile and DMF, the exciplex is completely deactivated so that no fluorescence emissions are detected in these pure solvents.

For the other BA's, the fluorescence was too weak and it was then impossible to do the same kind of experiments. However, we can anticipate that BA's for which the first singlet excited state is charge transfer in nature (electron-donor in X and/or electron-acceptor in Y) will undergo exciplex formation with small polar molecules. Finally we have shown that the Lippert–Mataga and Kawski relations using absorption and fluorescence data may give linear correlations even though specific interactions exist in the ground and excited states.

## Conclusion

BA's show high values of first-singlet non-radiative decay constants ($k_{nr}$) which are interpreted by the twisting of the molecules around the azomethine bond (C=N) in the first-singlet excited state. BA's with strong electron-acceptor substituents in the Y position and/or strong electron-donor substituents in the X position give rise to specific interactions in the ground and/or excited states. This has been rationalized in terms of a highly distorted equilibrium geometry in the ground states of these molecules (a bichromophoric molecular type). Ethanol gives rise to hydrogen bonding formation with BA's and aprotic polar solvents give rise to complexes stabilized by dipolar interactions. Linear solvent shift plots from either the Lippert–Mataga theory or the more generalized Kawski theory are not criteria from which one can conclude that no specific interactions exist between the solute ground and/or excited states and the solvent molecules. Consequently these plots should be used with caution in order to obtain excited state dipole moments without any investigations on the interactions involved with each particular polar solvent used.

## Acknowledgements

This work has been supported by the Natural Sciences and Engineering Research Council of Canada and by the "Ministère de l'Education du Québec, FCAC". One of us (M.B.) acknowledges both organizations for research scholarships during his graduate research studies and also the "Université de Montréal" for a graduate scholarship.

1. B. Scheuer-Lamalle and G. Durocher. Can. J. Spectrosc. **21**, 165 (1976).
2. M. Belletete, B. Scheuer-Lamalle, L. Baril, and G. Durocher. Can. J. Spectrosc. **22**, 31 (1977).
3. E. Lippert. Z. Electrochem. **61**, 962 (1957).
4. O. A. Osipov, Y. A. Zdanov, M. I. Knyazhanskii, V. I. Minkin, A. G. Gavnovskii, and J. D. Sadekov. Russ. J. Phys. Chem. **41**, 322 (1967).
5. E. B. Agracheva and V. F. Gachkovskii. Zh. Obshch. Khim. **40**, 191 (1970).
6. N. A. Vasilenko, R. N. Nurmukhametov, and A. N. Pravednikov. Dokl. Phys. Chem. **223**, 1098 (1975).
7. M. Belletete. Master Thesis, Université de Montréal. 1977.
8. M. Belletete and G. Durocher. Can. J. Chem. **57**, 2539 (1979).
9. M. Belletete and G. Durocher. Can. J. Spectrosc. **24**, 87 (1979).
10. M. Belletete and G. Durocher. Can. J. Chem. To be published.
11. J. B. Birks. Photophysics of aromatic molecules. Wiley Interscience, New York. 1970. p. 88.
12. S. J. Strickler and R. A. Berg. J. Chem. Phys. **37**, 814 (1962).
13. M. N. Pinasias and D. Schultefrohlinde. Ber. Bunsenges Phys. Chem. **79**, 662 (1975).
14. G. Fischer and G. Seger. J. Chem. Soc. Perkin Trans. 2, **14**, 1569 (1975).
15. E. Lippert. Z. Naturforsch. **10**a, 541 (1955).
16. N. Mataga, Y. Kaifu, and M. Koizumi. Bull. Chem. Soc. Jpn. **28**, 690 (1955); **29**, 465 (1956).
17. A. Kawski. Acta Phys. Polonica, **29**, 507 (1966).
18. B. Skalski, D. M. Rayner, and A. G. Szabo. Chem. Phys. Lett. **70**, 587 (1980).
19. R. Forster (*Editor*). Molecular association. Vol. 2. Academic Press. 1979. p. 200; G. C. Pimentel and A. L. McClellan. The hydrogen bond. W. H. Freeman and Company, San Francisco and London. 1960.
20. M. V. Hershberger, R. Lumry, and R. Verrall. Photochem. Photobiol. **33**, 609 (1981).
21. B. Scheuer-Lamalle. Doctorate Thesis, Université Catholique de Louvain. 1976.
22. P. Akaba, K. Tokumaru, and T. Kobayashi. Bull. Chem. Soc. Jpn. **53**, 1993 (1980).
23. P. Skrabal, J. Steiger, and H. Zollinger. Helv. Chim. Acta, **58**, 800 (1975).
24. A. Chama and P. C. Viallet. C. R. Acad. Sci. Ser. C, **270**, 1901 (1970).
25. E. A. Chandross. The exciplex. *Edited by* M. Gordon and W. R. Ware. Academic Press. 1975. p. 187.
26. M. Belletete and G. Durocher. Can. J. Chem. To be published.
27. Z. R. Grabowski, K. Rotkiewicz, W. Rubaszewska, and E. Kirmor-Kaminska. Acta Phys. Pol. A**54**, 767 (1978).
28. G. Wermuth, W. Rettig, and E. Lippert. Ber. Bunsenges. Phys. Chem. **85**, 64 (1981); A. A. Ayuk, W. Rettig, and E. Lippert. Ber. Bunsenges. Phys. Chem. **85**, 553 (1981).
29. P. F. Barbara, S. D. Rand, and P. M. Rentzepis. J. Am. Chem. Soc. **103**, 2156 (1981).
30. E. L. Wehry (*Editor*). Modern fluorescence spectroscopy 2. Plenum Press, New York and London. 1976. pp. 370, 371.
31. M. Yoshida and M. Kobayashi. Bull. Chem. Soc. Jpn. **54**, 2395 (1981).

# Electron spin resonance study of $SO_2$ and CO on CuO–alumina

K. C. KHULBE AND R. S. MANN

*Department of Chemical Engineering, University of Ottawa, Ottawa, Ont., Canada K1N 9B4*

Received May 6, 1981[1]

K. C. KHULBE and R. S. MANN. Can. J. Chem. **60**, 2340 (1982).

The intensity of the $Cu^{2+}$ esr signal increased significantly on the addition of CO or $SO_2$, especially with $SO_2$, at room temperature to the preheated (at 400°C) and evacuated CuO–alumina catalyst. When the CO or $SO_2$ treated sample was evacuated at room temperature, the shape and intensity of the $Cu^{2+}$ esr line returned to their original values. The intensity of the $Cu^{2+}$ esr line decreased, but not to zero, on heating CuO–alumina either with CO or $SO_2$. In the case of $SO_2$, a new line appeared for the $SO_2^-$ ion which was not affected on evacuation. It seems that the $SO_2^-$ do not take part in the reduction of $SO_2$ with CO over the CuO–alumina catalyst.

K. C. KHULBE et R. S. MANN. Can. J. Chem. **60**, 2340 (1982).

L'intensité du signal de rpe de $Cu^{2+}$ augmente de façon significative, spécialement avec le $SO_2$, lors de l'addition de CO ou de $SO_2$ à température ambiante sur un catalyseur CuO–alumine préchauffé (à 400°C) sous vide. L'intensité et la forme du signal de rpe du $Cu^{2+}$ reviennent à leur valeur originale quand les échantillons traités au CO ou au $SO_2$ sont placés sous vide. L'intensité de la bande de rpe du $Cu^{2+}$ diminue, mais ne va pas jusqu'à zéro lorsqu'on chauffe le CuO–alumine soit avec de CO ou du $SO_2$. Dans le cas du $SO_2$, il apparaît une nouvelle ligne correspondant à l'ion $SO_2^-$ que le vide n'affecte pas. Il semble que l'ion $SO_2^-$ ne participe pas dans la réduction du $SO_2$ avec le CO sur un catalyseur de CuO–alumine.

[Traduit par le journal]

## Introduction

It was observed that CuO–alumina catalysts have an excellent efficiency for the formation of elemental sulfur when $SO_2$ was reduced with CO (1–3). The mechanism for this type of reaction can be studied by following the radical formation during adsorption of CO and $SO_2$ on the surface using an esr technique.

The nature of CO adsorption on a solid surface has been studied extensively in the last several years, primarily by infrared methods. Cordischi *et al.* (4) have discussed the formation of $C_2O_2^-$ radicals following adsorption of CO on MgO. Lunsford *et al.* (5, 6) and Khulbe and Mann (7) studied the formation of paramagnetic species during adsorption of $SO_2$ on several solids. However, no such effects are reported for CO or $SO_2$ adsorbed on CuO–alumina.

The preparation of the catalyst and techniques for the esr studies are described elsewhere (8). $SO_2$ and CO, each 99.5% pure, were supplied by Linde and Matheson respectively.

Figure 1(a) shows the esr spectra obtained for the 5% CuO–alumina catalyst at room temperature after it was evacuated and heated at 400°C for 4 hours. The spectrum is assigned to $Cu^{2+}$ ions. It is well known that although nearly all copper ions in the CuO–alumina system contribute to the magnetic susceptibility, only 2% contribute to the esr signals (9). It also has been reported that in the CuO–alumina system, depending on the composition and thermal treatment, copper complexes with $Cu^{3+}$, $Cu^{2+}$, and $Cu^+$ are formed (10) and $Cu^{2+}$ ion complexes are grouped into clusters on the support surface (11). When CO (200 Torr) was added at room temperature to the evacuated and previously heated CuO–alumina system, the shape of the line due to $Cu^{2+}$ ion changed. The intensity of the line almost doubled. It could be possible that CO adsorption modifies Cu–Cu interactions and thereby increases the fraction of total $Cu^{2+}$ seen by esr. However, other possibilities cannot be discarded. On evacuation of the sample for 5 minutes at room temperature, the shape and intensity of the $Cu^{2+}$ esr line returned to their original values.

On heating the CuO–alumina in the presence of CO (200 Torr) at 400°C for 2 minutes, the colour of the catalyst changed from green to grey. The intensity of the $Cu^{2+}$ ion signal decreased slightly after the addition. On heating for a further 2 hours, the catalyst colour changed to pitch black from grey and the concentration of $Cu^{2+}$ ions decreased. On prolonged heating with CO for 24 h at 400°C the esr spectrum of $Cu^{2+}$ remained. However, it is reported that when Cu–zeolite was heated in CO, the $Cu^{2+}$ signals decreased and finally disappeared (12). It is possible that while one particular type of $Cu^{2+}$ reacts with CO at high temperature (~400°C) another type does not. On evacuating the remaining CO, no change was observed in the $Cu^{2+}$ spectra.

When $SO_2$ was added to the CO–CuO–alumina

[1]Revision received June 2, 1982.

0008-4042/82/182340-02$01.00/0

©1982 National Research Council of Canada/Conseil national de recherches du Canada

Can. J. Chem. Downloaded from www.nrcresearchpress.com by 210.87.254.105 on 09/06/12
For personal use only.

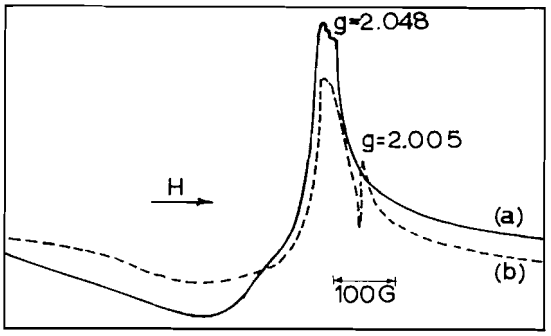


FIG. 1. (a) Electron spin resonance spectrum of $Cu^{2+}$ on the CuO–alumina catalyst; (b) spectrum obtained after the catalyst was exposed to $SO_2$ and heated at 400°C for 2 hours.

system at room temperature, the intensity of the $Cu^{2+}$ line increased slightly. On heating this system at 400°C for 10 min, the concentration of $Cu^{2+}$ ions decreased slightly and a new line at $g = 2.005$ appeared (Fig. 1(b)). This new line is attributed to $SO_2^{-\cdot}$ radical ions (6). The colour of the catalyst changed from black to yellowish black when heated for 24 h at 400°C. The yellowish colour may be due to the formation of elemental sulfur on reduction of $SO_2$ with CO (adsorbed CO which could not be removed from the surface). However, the $Cu^{2+}$ ion spectrum remained the same and the line at $g = 2.005$ increased sharply. On treating this system again with CO, though no effect was observed on the $Cu^{2+}$ ion spectrum, the line at $g = 2.005$ increased slightly. It seems that the $Cu^{2+}$ ions which contribute to the esr spectra do not take part in the CO + $SO_2$ reactions, though $SO_2$ reacts with CO in the presence of Cu ions and forms $SO_2^{-\cdot}$ radical ions on the surface, and elemental sulfur.

In another set of experiments with $SO_2$ was added at room temperature to a fresh CuO–alumina catalyst, previously evacuated at 400°C, the concentration of $Cu^{2+}$ increased markedly as shown by the esr spectra. This increase was greater than that which occurred when CO was added to the fresh catalyst under similar conditions. After evacuation at room temperature, the spectrum of the $Cu^{2+}$ ions reverted to its original shape and intensity. On heating (for 2 min at 400°C) $SO_2$–CuO–alumina ($SO_2$ evacuated at room temperature before heating) the intensity of the $Cu^{2+}$ ion spectrum decreased and the line for $SO_2^{-\cdot}$ at $g = 2.005$ (Fig. 1(b)) appeared. On prolonged heating (~14 h, 400°C), the concentration of $Cu^{2+}$ ions further decreased but not to zero. No change in the esr spectrum of the sample was observed after evacuation.

When CO was added to the evacuated $SO_2^{-\cdot}$–CuO–alumina system ($SO_2$ plus CuO–alumina heated at 400°C for 2 minutes), the intensity of the $Cu^{2+}$ line further decreased slightly. However, when this was heated at 400°C for 5 minutes, the intensity of the $SO_2^{-\cdot}$ signal ($g = 2.005$) increased markedly, though the concentration of $Cu^{2+}$ ions decreased further. On prolonged heating for 14 h at 400°C, the intensity of the $SO_2$ line increased and the concentration of $Cu^{2+}$ ions further decreased, but again not to zero. The colour of the catalyst changed from green to black with a yellowish tinge probably due to elemental sulfur.

Thus it seems that a particular type of $Cu^{2+}$ ions which contributes to the esr signal is not affected when treated with CO or $SO_2$, and that $SO_2^{-\cdot}$ ions do not take part in the reduction of $SO_2$ with CO.

1. V. N. GOETZ, A. SOOD, and J. R. KITTRELL. Ind. Eng. Chem. Prod. Res. Dev. **13**, 110 (1974).
2. C. W. QUINLAN, V. C. OKAY, and J. R. KITTRELL. Ind. Eng. Chem. Process Des. Dev. **12**, 107 (1973).
3. S. KASAOKA, H. TSUMAKI, and T. KOCHIHARA. Nippon Kagaku Kaishi, **2**, 413 (1973).
4. D. CORDISCHI, V. INDOVINA, and M. OCCHIUZZI. J. Chem. Soc. Faraday Trans. **76**, 1147 (1980).
5. J. H. LUNSFORD and J. P. JAYNE. J. Chem. Phys. **44**, 1492 (1966).
6. K. V. S. RAO and J. J. LUNSFORD. J. Phys. Chem. **78**, 649 (1974).
7. K. C. KHULBE and R. S. MANN. J. Catal. **51**, 364 (1978).
8. R. S. MANN and K. C. KHULBE. J. Catal. **42**, 115 (1976).
9. H. LUMBECK and J. VOITLANDER. J. Catal. **13**, 117 (1969).
10. E. S. SVENTSITSKII, V. N. VOROB'EV, and G. SH. TALIPOU. Kinet. Katal. **18**, 201 (1977).
11. K. C. KHULBE, A. MANOOGIAN, R. S. MANN, and P. D. GROVER. J. Catal. **56**, 290 (1979).
12. J. TURKEVICH, Y. ONO, and J. SONIA. J. Catal. **25**, 44 (1972).

Can. J. Chem. Downloaded from www.nrcresearchpress.com by 210.87.254.105 on 09/06/12
For personal use only.

# Composition effects on optical absorption spectra of solvated electrons in alcohol/water mixed solvents[1]

AH-DONG LEU, KAMAL N. JHA, AND GORDON R. FREEMAN

*Chemistry Department, University of Alberta, Edmonton, Alta., Canada T6G 2G2*

Received March 30, 1981

AH-DONG LEU, KAMAL N. JHA, and GORDON R. FREEMAN. Can. J. Chem. **60**, 2342 (1982).

Addition of a few percent of water to an alcohol has a relatively large effect on the shape of the optical absorption spectrum of solvated electrons in the liquid. This occurs whether the optical absorption energy in the pure alcohol is greater or smaller than that in water. Addition of up to 10 mol% of water causes $E_{Amax}$ in methanol and primary alcohols to decrease, while it increases in secondary and tertiary alcohols. At around 10 mol% water in primary alcohols $E_{Amax}$ passes through a minimum and increases again at higher water concentrations, reaching a plateau at about 30 mol% and remaining constant up to about 95 mol% water; over the last part of the composition range to pure water $E_{Amax}$ decreases slightly. The behavior in secondary and tertiary alcohols containing >30 mol% water is similar to that in primary alcohols. The width of the band at half height $W_{1/2}$ is divided at $E_{Amax}$ into "red side" and "blue side" portions $W_r$ and $W_b$, respectively. In methanol and in primary and secondary alcohols, addition of up to 30 mol% of water greatly reduces $W_b$ but has relatively little effect on $W_r$. At >30 mol% water $W_b$ and $W_r$ are similar to those in pure water. In tertiary butyl alcohol the band width is similar to that in pure water, so addition of water to the alcohol makes little change in the band width. The water/alcohol composition effects on the $e_s^-$ absorption band parameters are attributed to changes in solvent structure. This is especially evidenced by the minimum in $E_{Amax}$ at 10 mol% water in a primary alcohol. The changes in band asymmetry $W_b/W_r$ indicate that the types of electronic transition on the low and high energy sides of the band are different.

AH-DONG LEU, KAMAL N. JHA et GORDON R. FREEMAN. Can. J. Chem. **60**, 2342 (1982).

L'addition d'un faible pourcentage d'eau à un alcool a un large effet relatif sur la forme du spectre d'absorption optique des électrons solvatés dans le liquide. Ceci se produit si l'énergie d'absorption optique dans l'alcool pur est supérieure ou inférieure à celle dans l'eau. L'addition de quantité allant jusqu'à 10 mol% d'eau provoque une diminution de $E_{Amax}$ dans le méthanol et les alcools primaires, alors qu'il augmente dans les alcools secondaires et tertiaires. A environ 10 mol% d'eau dans les alcools primaires, $E_{Amax}$ passe par un minimum et augmente de nouveau avec des augmentations de concentrations en eau pour atteindre un plateau à environ 30 mol% alors qu'il demeure constant jusqu'à environ 95 mol% d'eau; à partir de là et jusqu'à l'eau pure, $E_{Amax}$ diminue légèrement. Le comportement, dans les alcools secondaires et tertiaires contenant >30 mol% d'eau, est semblable à celui dans les alcools primaires. La largeur de la bande à mi-hauteur $W_{1/2}$ est divisée à $E_{Amax}$ en deux parties: les "côté rouge" et "côté bleu" dénommés respectivement $W_r$ et $W_b$. Dans le méthanol et dans les alcools primaires et secondaires, l'addition de quantités allant jusqu'à 30 mol% d'eau réduit fortement $W_b$ mais a peu d'effet sur $W_r$. A 30 mol% d'eau, $W_b$ et $W_r$ sont identiques à ceux observés dans de l'eau pure. Dans l'alcool butylique tertiaire, la largeur de la bande est semblable à celle observée dans l'eau pure; l'addition d'eau à l'alcool ne provoque donc que peu de changement dans la largeur de la bande. On attribue les effets de la composition eau/alcool, sur les paramètres de bande d'absorption des $e_s^-$, à des variations de structure du solvant. Ceci est spécialement mix en évidence par le minimum de $E_{Amax}$ à 10 mol% d'eau dans un alcool primaire. Les variations dans l'asymétrie de la bande $W_b/W_r$ indiquent que les types de transition électronique du côté de faible et de forte énergie de la bande sont différentes.

[Traduit par le journal]

## Introduction

The energy levels of solvated electrons, as reflected in the energy of the optical absorption maximum $E_{Amax}$, are determined more by details of the liquid structure than by the dielectric constant or the molecular dipole moment (1, 2). The breadth $W_{1/2}$ and asymmetry $W_b/W_r$ of the optical absorption band are strongly related to the molecular structure of the solvent, but less emphasis had been placed on these band properties until recently. More information is needed about the dependence of the width and asymmetry on solvent structure.

The theoretical interpretation of the optical absorption spectrum requires a quantum statistical mechanical model that includes details of the liquid structure. Simons and co-workers have formulated the problem (3, 4), appropriately introducing the effects of fluctuations in solvent properties at an early stage of the model. Ultimately it was not possible to use realistic structure properties in the calculations. For example, the orientational disorder and the optical and electrical anisotropies of the molecules had to be neglected, and multibody interactions were still handled as sums of pair interactions (3, 4). Although much work remains to be done, an approach similar to that of Simons seems to be most promising for the next major advances in solvated electron theory.

The utility of developing a model by beginning with detailed observed spectral properties has been emphasized (5). The foundation of the model is therefore a relatively complete empirical description of the behavior of electrons in liquids. The present article deals with effects on the optical

[1]Assisted financially by the Natural Sciences and Engineering Research Council of Canada.

0008-4042/82/182342-09$01.00/0

©1982 National Research Council of Canada/Conseil national de recherches du Canada

Can. J. Chem. Downloaded from www.nrcresearchpress.com by 210.87.254.6 on 09/06/12
For personal use only.

Can. J. Chem. Downloaded from www.nrcresearchpress.com by 210.87.254.6 on 09/06/12
For personal use only.

absorption spectrum caused by mixing different hydroxylic solvents.

The absorption spectrum of solvated electrons in a binary solvent exhibits a single absorption band with a maximum at an energy $E_{Amax}$ that is intermediate to the values of $E_{Amax}$ in the pure components (6–20). In a mixed solvent such as an alkane and an alcohol the electrons are selectively solvated by the alcohol (10–16). Similarly, in mixtures of amines and alcohols (15), or an ether with an alcohol or water (17–20), the electrons are selectively solvated by the more polar solvent. The degree of selective solvation is assessed by the relative position of $E_{Amax}$ between those for electrons in the pure components, compared to the composition of the solvent. In a mixture of an amine and water (4) or ammonia and water (8, 9, 17), $E_{Amax}$ is slightly dominated by water. In solutions of an alcohol and water, earlier studies (6, 7) were not detailed enough to portray possible structural or selective solvation effects.

## Experimental

*Materials*

The methanol was Spectrophotometric Reagent Grade from Baker Chemical Co.; ethanol was Absolute Reagent Grade from U.S. Industrial Chemical Co.; 1-propanol, Certified Grade, Matheson, Coleman and Bell Co.; 2-propanol, Spectrophotometric Grade, Aldrich Chemical Co.; 1-butanol and 2-methyl-1-propanol (*i*-butyl alcohol) were Spectranalyzed Grade, Fisher Scientific Co.; 2-butanol and 2-methyl-2-propanol (*t*-butyl alcohol) were Analytical Reagent Grade, BDH Chemical Co.

Ethanol was used without further purification (21). Other alcohols and water were further purified as reported earlier from this laboratory (22, 23).

*Apparatus and techniques*

The optical system, irradiation facilities (22–24), and sample preparation (25) were described elsewhere. A Spectrosil cell of 1.0 cm optical path length was used for spectral measurements with 1.0 μs pulses of 1.8 MeV electrons ($9 \times 10^{16}$ eV/g) in the uv, visible, and ir regions. Appropriate Corning glass filters (26, 27) were placed in front of the optical cell and the monochromator. The dose per pulse was measured with 5 m*M* KCNS solution saturated with oxygen, using $G\varepsilon_{max} = 21\,000$ ($e_s^-$/100 eV *M* cm) at 478 nm (28). The irradiation temperature was 298.0 ± 0.5 K.

The solvated electron spectra were corrected for the decay during the pulse (24). The spectra at wavelengths < 400 nm were also corrected for absorbance due to radicals (24). This correction involved the assumptions that the net decay of radicals over the period of $t_{1/2}$ for $e_s^-$ was negligible, and that the decay of $e_s^-$ leads to negligible net formation of radicals. The second assumption probably leaves a residual error that causes the plotted absorbances to be low at $\lambda \lesssim 320$ nm, or $E \gtrsim 3.9$ eV, due to the formation of $R_2\dot{C}OH$ and $R_2\dot{C}O_s^-$, where R can be either H or an alkyl group (see spectra in section 4 of ref. 29).

## Results

*Alcohol/water solution*

The addition of water to an alcohol shifts the optical absorption energies of solvated electrons in a manner that depends on the nature of the alcohol. The energies at $E_{Amax}$ for electrons in water mixtures with methanol, ethanol, 1-propanol, 2-propanol, and 2-methyl-2-propanol are shown in Fig. 1. The behavior of these curves and those for the other alcohols studied may be summarized as follows. (*i*) For methanol, $E_{Amax}$ decreases gradually as mol% water increases to 30, then is approximately constant until 80%, then decreases again. (*ii*) For the primary alcohols (ethanol, 1-propanol, 1-butanol, and 2-methyl-1-propanol), $E_{Amax}$ decreases rapidly to a minimum at around 10 mol% water, then increases until ~30 mol% water, is approximately constant between 30 and 95 mol%, then decreases slightly to the value in pure water. (*iii*) For the secondary (2-propanol and 2-butanol) and tertiary (2-methyl-2-propanol) alcohols, $E_{Amax}$ is at its lowest for pure alcohol. It increases as mol% water increases to 50, then drifts gently upwards until 95 mol% is reached, then decreases slightly to the pure water value. In the region of 0 to ~30 mol% water, however, the

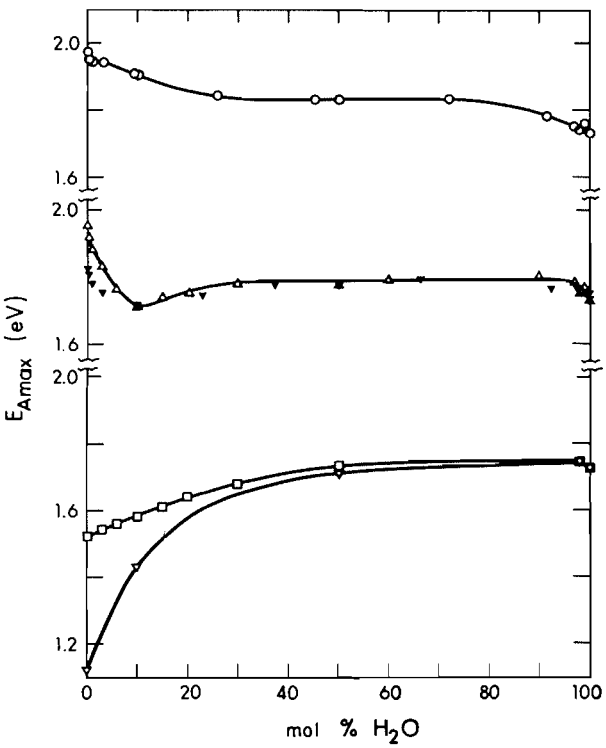


FIG. 1. Composition dependence of $E_{Amax}$ for alcohol/water mixtures at 298 K. ○, methanol; ▼, ethanol; △, 1-propanol; □, 2-propanol; ▽, 2-methyl-2-propanol. Shapes for other primary and secondary alcohols are similar to those for △ and □, respectively.

Can. J. Chem. Downloaded from www.nrcresearchpress.com by 210.87.254.6 on 09/06/12
For personal use only.

TABLE 1. Parameters of solvated electron spectra in alcohol/water at 298 K

| ROH | Mol% water | $E_{Amax}$ (eV) | $W_{1/2}$ (eV) | $\frac{W_{1/2}}{E_{Amax}}$ | $W_r$ (eV) | $W_b$ (eV) | $\frac{W_b}{W_r}$ |
|---|---|---|---|---|---|---|---|
| Methanol | 0 | 1.97 | 1.43 | 0.73 | 0.49 | 0.94 | 1.92 |
| | 10 | 1.90 | 1.26 | 0.66 | 0.45 | 0.81 | 1.80 |
| | 50 | 1.83 | 0.90 | 0.49 | 0.37 | 0.53 | 1.43 |
| | 98 | 1.74 | 0.87 | 0.50 | 0.36 | 0.51 | 1.42 |
| Ethanol | 0 | 1.82 | 1.59 | 0.87 | 0.51 | 1.08 | 2.12 |
| | 10 | 1.71 | 1.19 | 0.70 | 0.45 | 0.74 | 1.64 |
| | 50 | 1.77 | 0.91 | 0.51 | 0.37 | 0.54 | 1.46 |
| | 98 | 1.75 | 0.88 | 0.50 | 0.36 | 0.52 | 1.44 |
| 1-Propanol | 0 | 1.95 | 1.63 | 0.84 | 0.52 | 1.11 | 2.13 |
| | 10 | 1.71 | 1.24 | 0.73 | 0.46 | 0.78 | 1.70 |
| | 50 | 1.77 | 0.92 | 0.52 | 0.38 | 0.54 | 1.42 |
| | 98 | 1.75 | 0.87 | 0.50 | 0.37 | 0.50 | 1.35 |
| 2-Propanol | 0 | 1.52 | 1.45 | 0.95 | 0.44 | 1.01 | 2.30 |
| | 10 | 1.58 | 1.00 | 0.63 | 0.40 | 0.60 | 1.50 |
| | 50 | 1.73 | 0.91 | 0.53 | 0.37 | 0.54 | 1.46 |
| | 98 | 1.75 | 0.86 | 0.49 | 0.36 | 0.50 | 1.39 |
| 1-Butanol | 0 | 1.98 | 1.57 | 0.79 | 0.53 | 1.04 | 1.96 |
| | 10 | 1.73 | 1.23 | 0.71 | 0.45 | 0.78 | 1.73 |
| | 50 | 1.79 | 0.88 | 0.49 | 0.36 | 0.52 | 1.44 |
| | 98 | 1.74 | 0.88 | 0.51 | 0.36 | 0.52 | 1.44 |
| 2-Methyl-1-propanol | 0 | 1.97 | 1.61 | 0.82 | 0.57 | 1.04 | 1.82 |
| | 10 | 1.73 | 1.18 | 0.68 | 0.43 | 0.75 | 1.74 |
| | 50 | 1.78 | 0.89 | 0.50 | 0.36 | 0.53 | 1.47 |
| | 98 | 1.75 | 0.86 | 0.49 | 0.35 | 0.51 | 1.46 |
| 2-Butanol | 0 | 1.59 | 1.57 | 0.99 | 0.47 | 1.10 | 2.34 |
| | 10 | 1.64 | 1.03 | 0.63 | 0.43 | 0.60 | 1.40 |
| | 50 | 1.76 | 0.89 | 0.51 | 0.36 | 0.53 | 1.47 |
| | 98 | 1.75 | 0.86 | 0.49 | 0.35 | 0.51 | 1.46 |
| 2-Methyl-2-propanol | 0 | 1.12 | 0.95 | 0.85 | 0.30 | 0.65 | 2.19 |
| | 10 | 1.43 | 0.91 | 0.64 | 0.36 | 0.55 | 1.53 |
| | 50 | 1.71 | 0.89 | 0.52 | 0.37 | 0.52 | 1.41 |
| | 98 | 1.75 | 0.88 | 0.50 | 0.36 | 0.52 | 1.44 |
| Water | 100 | 1.73 | 0.85 | 0.49 | 0.36 | 0.49 | 1.36 |

increase is more pronounced for tertiary than for secondary alcohols.

All the curves showed relatively rapid change between 0 and 10 mol% water, were essentially horizontal between 30 and 80 mol%, and had a negative slope between about 97 and 100 mol% water. For this reason the representative concentrations chosen to study solutions of the other alcohols were 10, 50, and 98 mol% water.

Aqueous solutions of eight $C_1$ to $C_4$ alcohols having different carbon skeletons were studied to find the effect of molecular structure. The spectrum parameters are listed in Table 1.

*Composition effect upon spectrum shape*

Representative spectra obtained for solvated electrons in methanol/water solutions are shown in Fig. 2. Plots of the spectrum parameters against composition are shown in Fig. 3. The optical absorption spectra for solvated electrons in alcohol/water solutions are skewed towards high energy. The skew decreases as mol% water increases.

The relation of $W_{1/2}$ (band width at half-height) to composition is shown in Fig. 4. For all the alcohols except 2-methyl-2-propanol, $W_{1/2}$ decreases relatively rapidly as mol% water increases to a certain point, then decreases gradually or levels off for the remainder of the curve. (*i*) For methanol and the primary alcohols, most of the decrease occurs up to 50 mol% water. (*ii*) For secondary alcohols, most of the decrease occurs up to 10 mol% water. (*iii*) For the tertiary alcohol, $W_{1/2}$ varies approximately linearly with composition, because the value is only slightly different in water than in the pure alcohol.

The behavior of $W_b$ (the part of $W_{1/2}$ on the blue side of absorption maximum) and of $W_r$ (the part on the red side) as a function of composition is shown in Fig. 5. The sharp decrease in $W_{1/2}$ is largely due

Can. J. Chem. Downloaded from www.nrcresearchpress.com by 210.87.254.6 on 09/06/12
For personal use only.

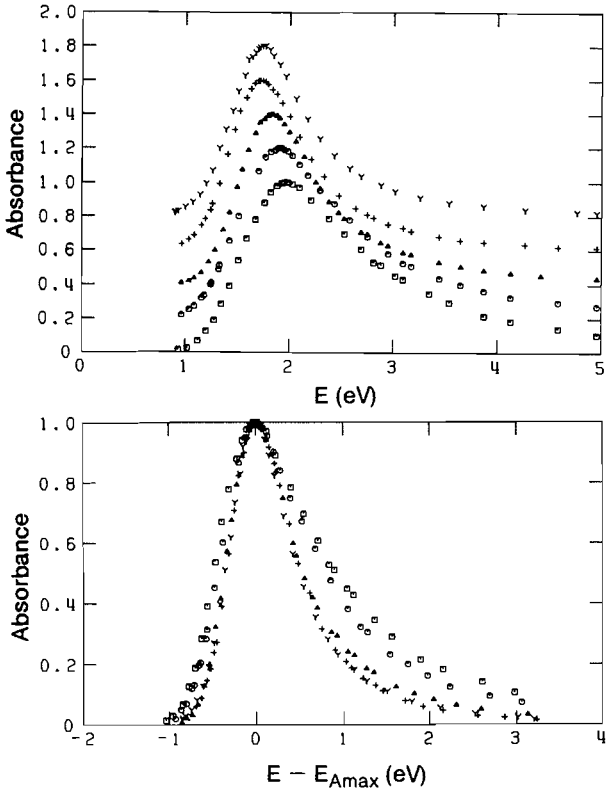


FIG. 2. Optical absorption spectrum of solvated electrons in methanol/water at 298 K and various compositions. Mol% water: □, 0; ○, 10; △, 50; +, 98; Y, 100. *A*. Successive spectra are displaced vertically by 0.2 units. *B*. The spectra are normalized at $E_{Amax}$.

to the decrease of $W_b$; $W_r$ decreases only slightly as mol% water increases.

## Discussion

*Composition dependence of* $E_{Amax}$

The variations of $E_{Amax}$ with composition for methyl, ethyl, 2 isomers of propyl, and 4 isomers of butyl alcohol are summarized in Fig. 6. This figure shows non-ideal behavior in mixing alcohols with water. The overall composition dependence of $E_{Amax}$ can be divided into three categories, one for methyl, another for primary, and a third for secondary and tertiary alcohols. The addition of 3 mol% of any of the alcohols to water causes $E_{Amax}$ to increase slightly (Fig. 6).

The changes of $E_{Amax}$ indicate that the depth of the trap for the excess electron is changed, which we attribute qualitatively to changes in solution structure. Changes in solution structure are also indicated by the nonideal behavior of viscosities (30, 31) and excess enthalpies of mixing (32, 33).

*(i) Pure solvents*

The values of $E_{Amax}$ for electrons in alcohols or

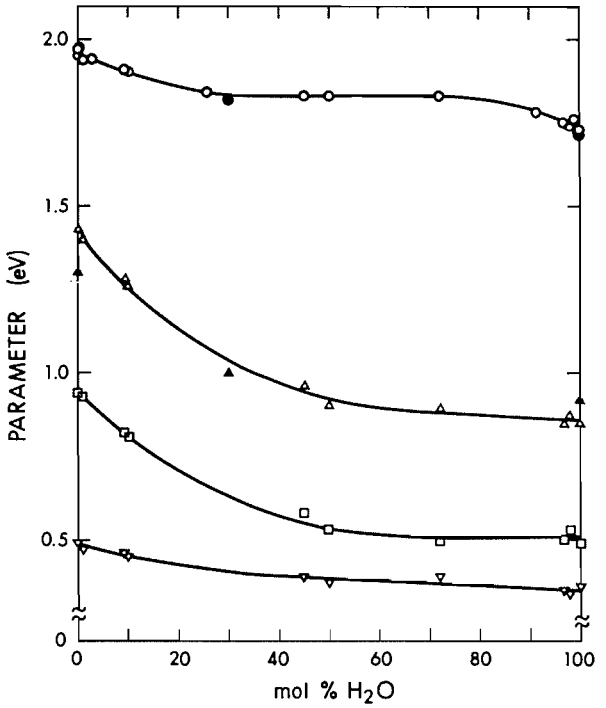


FIG. 3. Composition dependence of spectrum parameters in methanol/water. ○, $E_{Amax}$; △, $W_{1/2}$; □, $W_b$; ▽, $W_r$. ●, ▲ ref. 6.

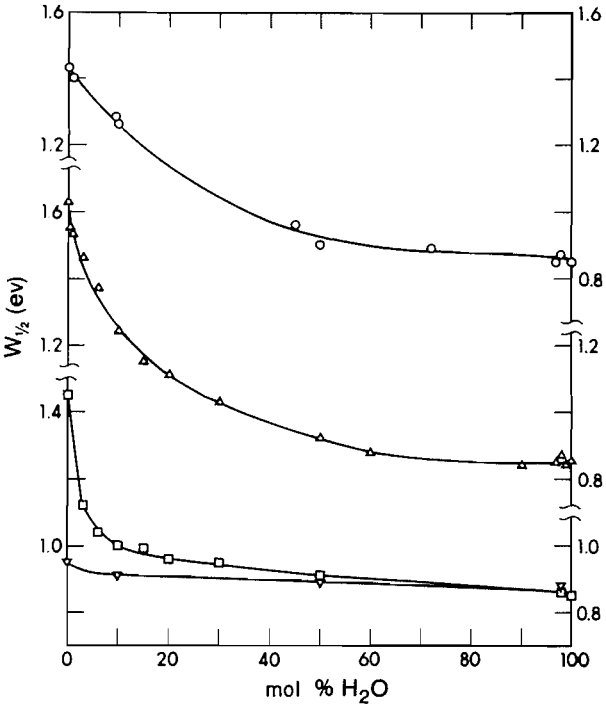


FIG. 4. Composition dependence of $W_{1/2}$ for alcohol/water mixtures at 298 K. ○, methanol; △, 1-propanol; □, 2-propanol; ▽, 2-methyl-2-propanol. Shapes for other primary and secondary alcohols are similar to those for △ and □, respectively.

Can. J. Chem. Downloaded from www.nrcresearchpress.com by 210.87.254.6 on 09/06/12
For personal use only.

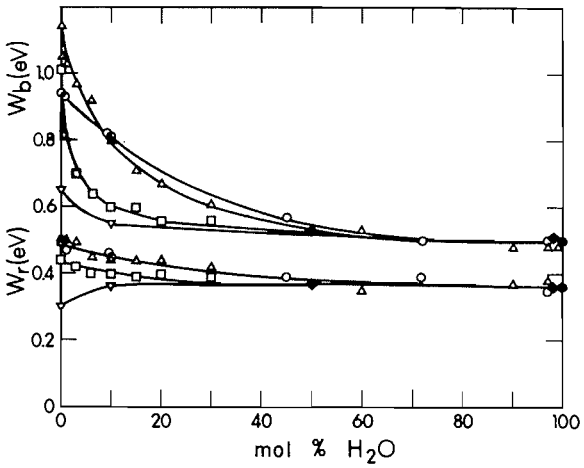


FIG. 5. Composition dependence of $W_b$ and $W_r$ for alcohol/water mixtures at 298 K. ○, methanol; △, 1-propanol; □, 2-propanol; ▽, 2-methyl-2-propanol; ●, water. ◆, average of the similar values for the four compounds. Shapes for other primary and secondary alcohols are similar to those for △ and □, respectively.

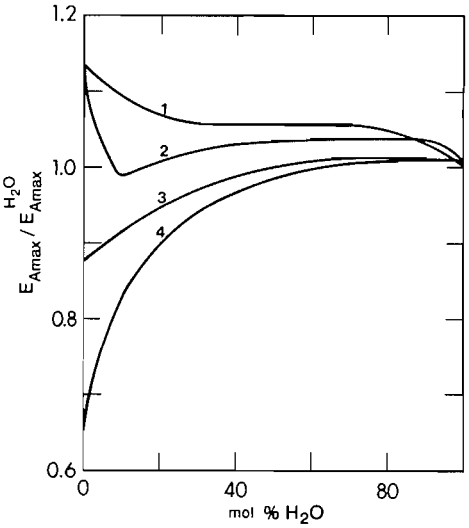


FIG. 6. Composition dependence of $E_{Amax}/E^{H_2O}_{Amax}$ for alcohol/water mixtures at 298 K: *1*, methanol; *2*, 1-propanol; *3*, 2-propanol; *4*, 2-methyl-2-propanol. Shapes for other primary and secondary alcohols are similar to those for *2* and *3*, respectively.

water are in the following order: methanol ≳ primary alcohol > water > secondary alcohol > tertiary alcohol (Table 1). This indicates that the depths of the traps are in the same order. More extensive alkylation of the carbon connected to the —OH inhibits favorable orientation of the alcohol molecules around the electron, presumably because a greater disruption of the normal liquid structure would be required. Branching of the alkyl

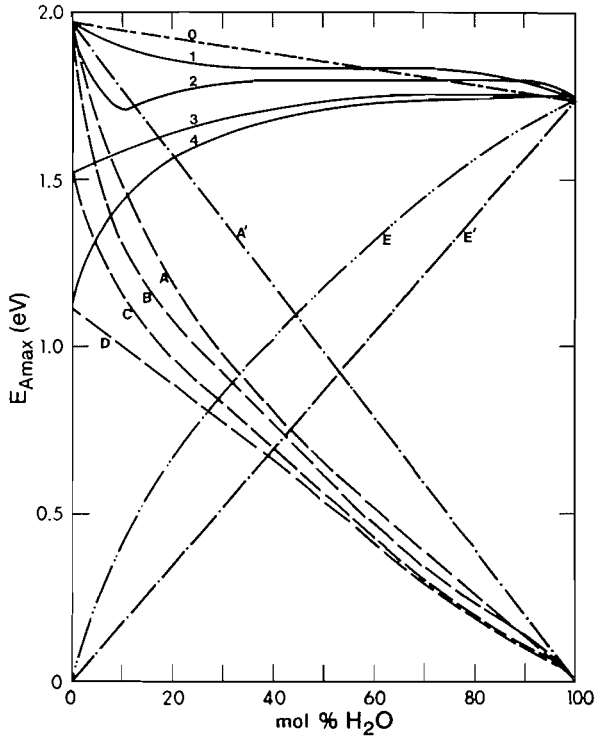


FIG. 7. Approximate resolution of $E_{Amax}$/composition curves. 298 K. Experimental: *1*, methanol; *2*, 1-propanol; *3*, 2-propanol; *4*, 2-methyl-2-propanol. Ideal solution line for methanol/water, *O*; ideal methanol component, *A'*; ideal water component, *E'*. *A*, *B*, *C*, *D*, and *E* are approximate actual component curves for the alcohols and water (see text). Shapes for other primary and secondary alcohols are similar to those of *2* and *3*, *B* and *C*, respectively.

chain at any position other than the carbon to which the —OH is attached makes little difference to the $e_{solv}^-$ optical spectrum. For example, the values of ($E_{Amax}$, $W_r$, $W_b$) in the branched 2-methyl-1-propanol (1.97, 0.57, 1.04) are similar to those in the unbranched 1-butanol (1.98, 0.53, 1.04), while the values in the branched 2-methyl-2-propanol are much lower (1.12, 0.30, 0.65). The large influence of the endgroup, which for alcohols is —C(—)—OH, on $E_{Amax}$ had been pointed out earlier (1) and was implicit in the relatively small dependence of $E_{Amax}$ on chain length for *n*-alkanols (13).

*(ii) Low and intermediate % water regions*

The complex shape of the curve for primary alcohols in Fig. 6 can be interpreted in terms of two tendencies, one to decrease $E_{Amax}$ and the other to increase it. These can then be applied to the solutions of the other alcohols.

Considering first the methanol and 1-propanol

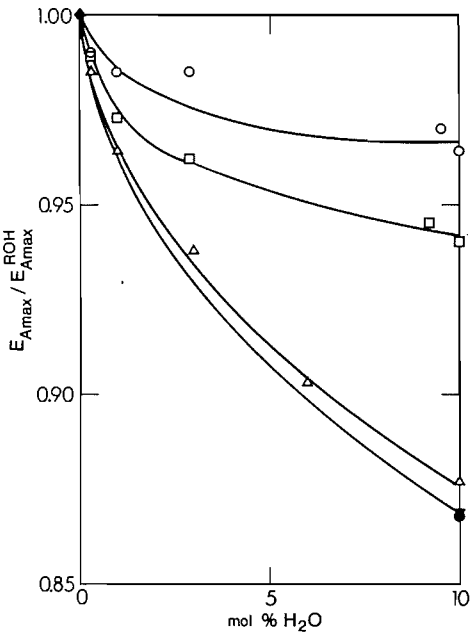


FIG. 8. Composition dependence of $E_{Amax}$ in primary alcohols at low water concentrations, normalized to the value in pure alcohol. 298 K. ○, methanol; □, ethanol; △, 1-propanol; ▽, 1-butanol; ●, 2-methyl-1-propanol; ◆, pure ROH.

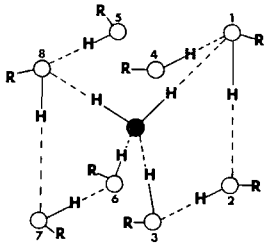

FIG. 9. Possible structure of ~10 mol% water/alcohol solution. ●, oxygen atom in water molecule; ○, oxygen atom in alcohol.

curves *1* and *2* in Fig. 7, ideal solution lines *O*, *A'*, and *E'* were drawn for reference. The observed behavior is distinctly nonideal. The similarity of the shape of curve *2* at >10% water to that of curves *3* and *4* indicates that the behavior of water is similar in all the alcohols. Water makes a greater than proportionate contribution to electron solvation, so curve *E'* should be shifted to about *E*. Curves *A* and *B* are then obtained by subtracting *E* from *1* and *2*, respectively. The alcohols make a less than proportionate contribution to electron solvation in the mixed solvents.

Although curve *E* is probably not the same from one alcohol to another, the general behavior is similar. Curves *C* and *D* were obtained by subtracting *E* from *3* and *4*, for 2-propanol and 2-methyl-2-propanol, respectively. For methanol curve *E* probably lies closer to *E'* than shown in Fig. 7, and for 2-methyl-2-propanol *E* probably lies farther away than shown. Curves *A* and *D* would then be respectively less and more concave than shown in Fig. 7.

Curves *A* to *E* in Fig. 7 indicate that the extra electrons favor sites that contain, or are influenced by, a water molecule. The relative flatness of curves *1* to *4* between about 30 and 90 mol% water indicates that the favored site does not change much over this concentration range. The site is apparently only slightly modified from one in pure water.

The relative amount of disturbance to the electron site caused by adding a small amount of water to a primary alcohol is related to the alkyl chain length. The ratio ($E_{Amax}/E^{ROH}_{Amax}$) decreases progressively more rapidly in the order methanol < ethanol < 1-propanol < 1-butanol ≈ 2-methyl-1-propanol (Fig. 8). It is not possible to say whether the main effect of water is to raise the ground state or to lower the energy of the excited state.

The minimum in $E_{Amax}$ at 10 mol% water in ethanol is observable in the data of Arai and Sauer (6), but they apparently attributed it to experimental scatter. This behavior in the primary alcohol/water solutions indicates that a particular structure exists in the 10% water solutions. If we interpret the minimum as a minimum in the strength of interaction between the excess electron and the solvent OH groups, one may speculate about water-nucleated hydrogen bonded structures such as the one in Fig. 9. This structure is based on considerations of ring polymer (34), octahedral (35), tetrahedral (36), and body centered cubic (37–39) models. Two tetramers of alcohol may be linked through one water molecule (Fig. 9), and the water molecule is occluded by eight alcohol molecules. The stacking together of these structures would be sensitive to the size and shape of the alkyl group, which is consistent with the spectral observations.

*(iii) Small amount of alcohol in water*

The addition of ~3% of any alcohol to water causes $E_{Amax}$ to increase slightly (Fig. 6). The addition of a small amount of a nonelectrolyte to water alters the liquid structure in a way that affects the viscosity (ref. 40, quoted in ref. 32, p. 67) and partial molar volume (41). The addition of a few mol% of ethanol to water increases the partial molar volume of water, and may therefore be considered to enhance the degree of order in the

Can. J. Chem. Downloaded from www.nrcresearchpress.com by 210.87.254.6 on 09/06/12
For personal use only.

Can. J. Chem. Downloaded from www.nrcresearchpress.com by 210.87.254.6 on 09/06/12
For personal use only.

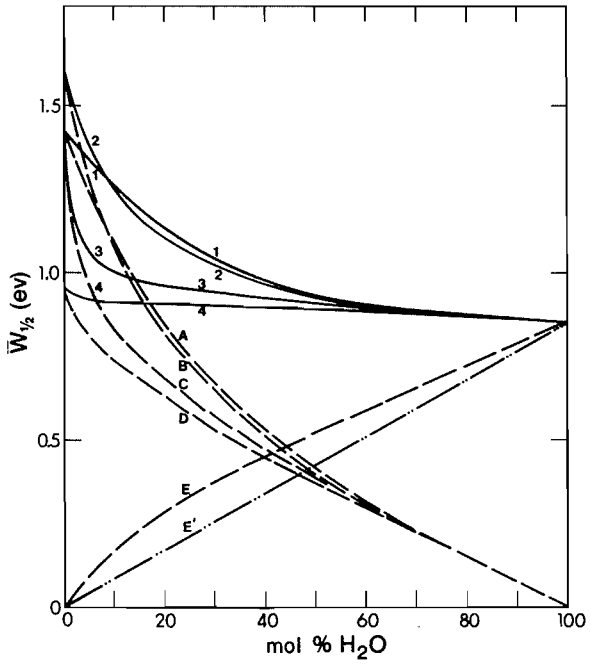


FIG. 10. Approximate resolution of $W_{1/2}$/composition curves. The labelling is the same as in Fig. 7, except that ideal lines *O* and *A'* are omitted. Shapes for other primary and secondary alcohols are similar to those of *2* and *3*, *B* and *C*, respectively.

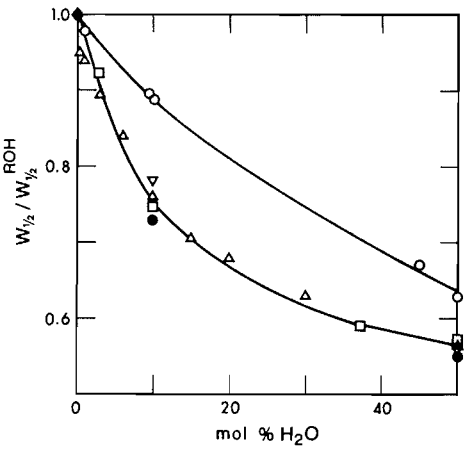


FIG. 11. Composition dependence of $W_{1/2}$ in primary alcohols at low water concentrations, normalized to the value in pure alcohol. The symbols are the same as in Fig. 8.

water structure (lattice-like hydrogen bonded structure). The addition of a few percent of 2-methyl-2-propanol to water also enhances the water structure, but neutron scattering measurements indicate that the structure bears no resemblance to ice (42); in the same system the value of $E_{Amax}$ for the first absorption peak of iodide ions increases over that in pure water (43), similar

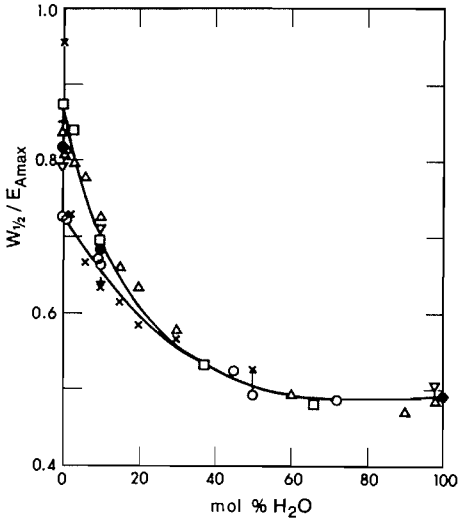


FIG. 12. Composition dependence of $W_{1/2}/E_{Amax}$. The symbols are the same as in Fig. 8 except that here ◆ represents pure water, plus: ×, 2-propanol; +, 2-methyl-2-propanol. At 50 and 98 mol% water the two extreme values of the ratio are shown; the values for the other five alcohols are scattered randomly between these extremes.

to the behavior of solvated electrons. In both cases the slight increase of $E_{Amax}$ is attributed to a small change of solvent structure in the electron or anion site, although it is not yet possible to give details of the change.

*Composition dependence of* $W_{1/2}$

The value of $W_{1/2}$ decreases with increasing water concentration (Fig. 4). Most of the decrease occurs upon the addition of the first 30 mol%. The exception is 2-methyl-2-propanol, in which the value of $W_{1/2}$ is similar to that in water. The sharpness of decrease in $W_{1/2}$ during the addition of the first 10 mol% water to the various alcohols is in the order secondary > primary > methanol > tertiary.

The $W_{1/2}$ curves reflect selective solvation of the electrons by water, as did $E_{Amax}$. By analogy with Fig. 7, the $W_{1/2}$ curves were tentatively divided into alcohol and water contributions (Fig. 10). The water contribution is something like *E*. The alcohol contributions *A* to *D* were approximated by subtracting *E* from the experimental curves *1* to *4*, respectively. Curve *E* for methanol probably lies closer to *E'*, while for 2-methyl-2-propanol *E* probably bulges farther away from *E'* than shown. The behavior is similar to that of $E_{Amax}$. However, the relative amount of disturbance to $W_{1/2}$ caused by adding water to ethanol is similar to that for the longer chain primary alcohols (Fig. 11), whereas for $E_{Amax}$ the behavior in ethanol was closer to that in methanol (Fig. 8).

Can. J. Chem. Downloaded from www.nrcresearchpress.com by 210.87.254.6 on 09/06/12
For personal use only.

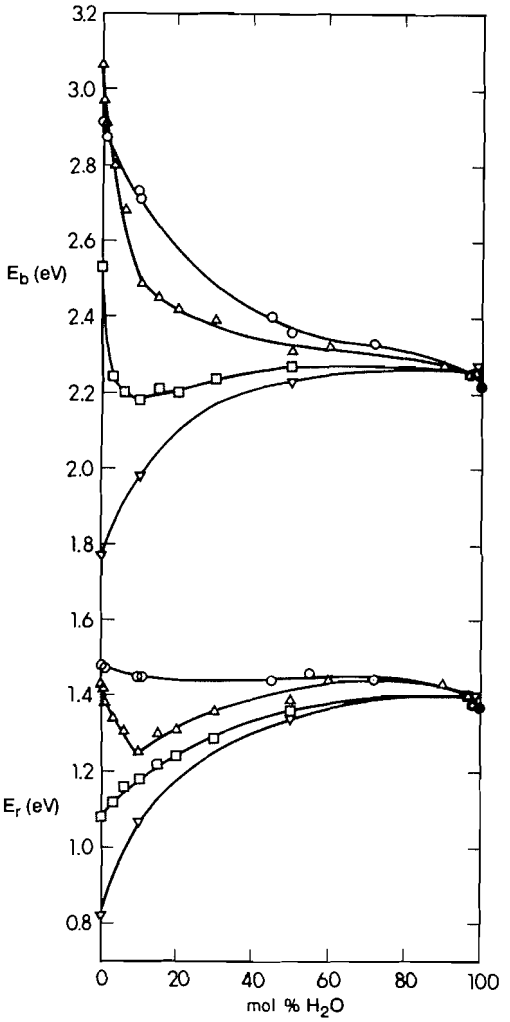


FIG. 13. Composition dependence of $E_r$ and $E_b$. ○, methanol; △, 1-propanol; □, 2-propanol; ▽, 2-methyl-2-propanol; ●, pure water. Shapes for other primary and secondary alcohols are similar to those of △ and □, respectively.

Upon addition of water the ratio $W_{1/2}/E_{Amax}$ decreases most rapidly for 2-propanol and least rapidly for methanol (Fig. 12). The values are the same within the experimental uncertainty for all the alcohols containing ≥ 30 mol% water.

The conclusion is that the band width is more readily disturbed by the addition of water to an alcohol than is $E_{Amax}$.

*Composition dependence of* $W_r$, $W_b$, $E_r$, *and* $E_b$

The shifts of the energies $E_r$ and $E_b$ on the respective red and blue sides of the absorption band at $0.5A_{max}$ are diagnostic of the spectral changes that occur when solvents are mixed. The values of $E_r$ and $E_b$ are related to those of other parameters by eqs. [1]–[3].

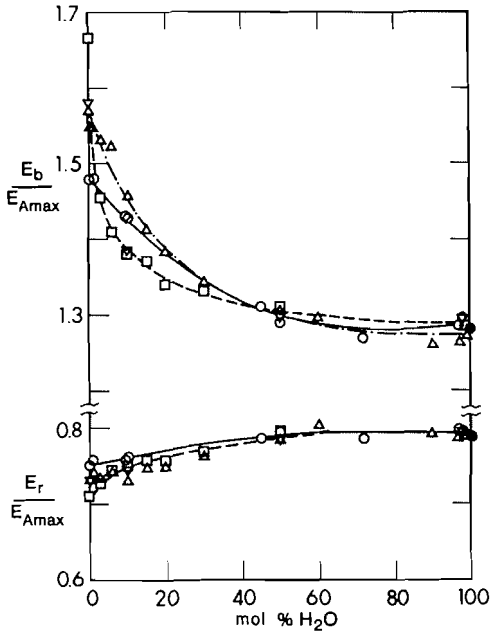


FIG. 14. Composition dependence of the ratios $E_r/E_{Amax}$ and $E_b/E_{Amax}$. The labelling is the same as in Fig. 13.

$$[1] \quad W_{1/2} = W_r + W_b = E_b - E_r$$

$$[2] \quad W_r = E_{Amax} - E_r$$

$$[3] \quad W_b = E_b - E_{Amax}$$

The uncertainties in $E_r$ and $E_b$ are ±0.01 eV, while those in $E_{Amax}$ and $W_{1/2}$ are ±0.02 eV.

The composition dependence of $W_{1/2}$ is generated mainly through $W_b$ (Fig. 5). This supports the interpretation that the low and high energy sides of the absorption band are determined by different processes (22). The low energy side is attributed to a bound–bound transition. The high energy tail presumably represents bound–continuum transitions. The greater width of the alcohol bands, relative to their values of $E_{Amax}$, may be due to a second, bound excited state. The second excited state might be associated with the relatively low scattering power of the alkyl groups, and easily upset by the presence of water.

The value of $E_b$ changes in quite a different manner from that of $E_r$ when water is added to methyl, a primary, or a secondary alcohol (Fig. 13). On going from methanol to water $E_b$ decreases by 0.7 eV while $E_r$ decreases by only 0.1 eV. In the 1-propanol solutions $E_r$ has a minimum at 10 mol% water. The behavior of $E_r$ is similar to that of $E_{Amax}$ for all the alcohol/water solutions. By contrast $E_b$ does not possess a minimum in the primary alcohol solutions, but does in those of 2-propanol (Fig. 13). In the 2-methyl-2-propanol solutions $E_r$ and $E_b$

behave similarly; both increase rapidly with increasing water content up to about 50 mol%, then change little up to about 95%, then decrease slightly to the values in pure water.

When the values of $E_r$ are normalized to those of $E_{Amax}$, the curves for the different types of alcohol cluster together (Fig. 14). The ratio $E_r/E_{Amax}$ *increases* by 5% (methanol) to 12% (2-propanol) between zero and 50 mol% water, then remains constant up to pure water. By contrast the ratio $E_b/E_{Amax}$ *decreases* by 15% (methanol) to 27% (2-propanol), then remains essentially constant up to pure water. This behavior indicates that above 30 mol% water the solvated electrons reside in sites that have characteristics only slightly different from those in pure water.

*Deductions from the water effects*

(*1*) The types of electronic transition are different on the low and high energy sides of the band.

(*2*) The greater breadth of the band in alcohols than in water has more to do with differences in the excited states than with differences in the ground states. These differences are greatly reduced by the addition of ~10 mol% of water to the alcohol.

(*3*) The liquid structure has a dominating effect on the optical absorption energies. The structure effect is clearly evident in the minimum of $E_{Amax}$ at 10 mol% of water in primary alcohol/water mixtures.

**Acknowledgements**

Thanks are due to the staff of the Radiation Research Center for aid with the electronics. Discussions with F.-Y. Jou are also acknowledged.

1. G. R. FREEMAN. J. Phys. Chem. **77**, 7 (1973).
2. F.-Y. JOU and G. R. FREEMAN. Can. J. Chem. **60**, 0000 (1982).
3. J. MCHALE and J. SIMONS. J. Chem. Phys. **67**, 389 (1977).
4. A. BANERJEE and J. SIMONS. J. Chem. Phys. **68**, 415 (1978).
5. (*a*) A. M. BRODSKY and A. V. TSAREVSKY. Soviet Phys. JETP, **43**, 111 (1976); (*b*) M. G. DEBACKER, J. N. DECARPIGNY, and M. LANNOO. J. Phys. Chem. **81**, 159 (1977); (*c*) I. CARMICHAEL. Chem. Phys. Lett. **56**, 339 (1978).
6. S. ARAI and M. C. SAUER, JR. J. Chem. Phys. **44**, 2297 (1966).
7. B. G. ERSHOV and A. K. PIKAEV. Rad. Res. Rev. **2**, 1 (1969).
8. J. L. DYE, M. G. DEBACKER, and L. M. DORFMAN. J. Chem. Phys. **52**, 6251 (1970).
9. R. OLINGER and U. SCHINDEWOLF. Ber. Bunsenges. Phys. Chem. **75**, 693 (1971).
10. L. B. MAGNUSSON, J. T. RICHARDS, and J. K. THOMAS. Int. J. Rad. Phys. Chem. **3**, 295 (1971).
11. B. J. BROWN, N. T. BARKER, and D. F. SANGSTER. J. Phys. Chem. **75**, 3639 (1971).
12. G. R. FREEMAN. J. Phys. Chem. **76**, 944 (1972).
13. R. R. HENTZ and G. A. KENNEY-WALLACE. J. Phys. Chem. **78**, 514 (1974).
14. J. R. BRANDON and R. F. FIRESTONE. J. Phys. Chem. **78**, 792 (1974).
15. T. ITO, N. UJIKAWA, and K. FUEKI. J. Phys. Chem. **79**, 2479 (1975).
16. J. H. BAXENDALE and P. H. G. SHARPE. Chem. Phys. Lett. **41**, 440 (1976).
17. L. M. DORFMAN, F.-Y. JOU, and R. WAGEMAN. Ber. Bunsenges. Phys. Chem. **75**, 681 (1971).
18. L. M. DORFMAN and F.-Y. JOU. *In* Electrons in fluids. *Edited by* J. Jortner and N. R. Kestner. Springer-Verlag, New York. 1973. p. 447.
19. F.-Y. JOU and L. M. DORFMAN. J. Chem. Phys. **58**, 4715 (1973).
20. F. S. DAINTON and R. J. WHEWELL. J. Chem. Soc. Chem. Commun. 493 (1974).
21. S. M. S. AKHTAR and G. R. FREEMAN. J. Phys. Chem. **75**, 2756 (1971).
22. F.-Y. JOU and G. R. FREEMAN. J. Phys. Chem. **81**, 909 (1977).
23. F.-Y. JOU and G. R. FREEMAN. J. Phys. Chem. **83**, 2383 (1979).
24. F.-Y. JOU and G. R. FREEMAN. Can. J. Chem. **54**, 3693 (1976).
25. K. N. JHA, G. L. BOLTON, and G. R. FREEMAN. J. Phys. Chem. **76**, 3876 (1972).
26. F.-Y. JOU and G. R. FREEMAN. Can. J. Chem. **57**, 591 (1979).
27. F.-Y. JOU and G. R. FREEMAN. J. Phys. Chem. **83**, 261 (1979).
28. G. L. BOLTON, K. N. JHA, and G. R. FREEMAN. Can. J. Chem. **54**, 1497 (1976).
29. G. R. FREEMAN. Radiation chemistry of ethanol. NSRDS-NBS 48, U.S. Dept. of Commerce, Washington, D.C. 1974.
30. J. TIMMERMANS. Physico-chemical constants of binary systems. Vol. 4. Interscience, New York. 1960. pp. 163–236.
31. J. A. RIDDICK and W. B. BUNGER. Techniques of chemistry. Vol. II. Organic solvents, physical properties and methods of purification. 3rd ed. Wiley Interscience, New York. 1970. p. 145.
32. F. FRANKS. Physico-chemical processes in mixed aqueous solvents. Elsevier Publishers, New York. 1967. p. 54.
33. C. H. CHIEN, R. A. GREENKORN, and K. C. CHAO. AIChE Journal, **27**, 303 (1981).
34. L. PAULING. The nature of the chemical bond. 3rd ed. Cornell University Press, New York. 1960. p. 473.
35. C. L. V. P. VAN ECK, H. MENDEL, and W. BOAG. Faraday Soc. Discuss. **24**, 200 (1957).
36. L. PAULING. *In* Hydrogen bonding. *Edited by* D. Hadzi. Pergamon Press, London. 1959. p. 1.
37. G. M. BELL. J. Phys. C., Solid State Phys. **5**, 889 (1972).
38. O. WERES and S. A. RICE. J. Am. Chem. Soc. **94**, 8983 (1972).
39. J. W. PERRAM. *In* The hydrogen bond. Vol. 1. *Edited by* P. Schuster, G. Zundel, and C. Sandorfy. North Holland Publishers, Amsterdam-Oxford, 1976. Chapt. 7. p. 358.
40. R. L. KAY. Private communication.
41. W. J. MOORE. Physical chemistry. 3rd ed. Prentice-Hall, Englewood Cliffs, NJ. 1962. p. 122.
42. F. FRANKS, J. RAVENHILL, P. A. EGELSTAFF, and D. I. PAGE. Proc. R. Soc. A**319**, 189 (1970).
43. M. J. BLANDAMER, M. F. FOX, M. C. R. SYMONS, K. J. WOOD, and M. J. WOOTTEN. Trans. Faraday Soc. **64**, 3210 (1968).

Can. J. Chem. Downloaded from www.nrcresearchpress.com by 210.87.254.6 on 09/06/12
For personal use only.

# Complexes of propyl mercury thiocyanates with cobalt, nickel, and zinc thiocyanate

P. P. SINGH AND V. P. SINGH

*Chemistry Department, M.L.K. College, Balrampur-271201 (U.P.), India*

Received November 27, 1981

P. P. SINGH and V. P. SINGH. Can. J. Chem. **60**, 2351 (1982).

RHgSCN (R = *n*-$C_3H_7$, *iso*-$C_3H_7$) react with $M(NCS)_2$ (M = Co(II), Ni(II), Zn(II)) to form compounds of general formula $(SCN)_2M(NCSHgR)_2$. Conductance measurements and infrared and electronic spectral studies indicate that M and mercury atoms are linked by bridging thiocyanate groups. Cobalt and zinc are tetrahedrally coordinated, whereas nickel is octahedral. With the exception of zinc analogs, these compounds form complexes with Lewis bases. Pyridine and nicotinamide form adducts of general formula $L_2(SCN)_2M(NCSHgR)_2$, while 2,2′-bipyridine and 1,10-phenanthroline form cationic–anionic complexes of formula $[M(L—L)_3][RHg(SCN)_2]_2$.

P. P. SINGH et V. P. SINGH. Can. J. Chem. **60**, 2351 (1982).

Le composé RHgSCN (R = *n*-$C_3H_7$, *iso*-$C_3H_7$) réagit avec $M(NCS)_2$ (M = Co(II), Ni(II), Zn(II)) en donnant des composés de formule générale $(SCN)_2M(NCSHgR)_2$. Les mesures de conductivité et les études des spectres infrarouges et électroniques indiquent que les atomes de M et de mercure sont liés par des groupes thiocyanates en position de pont. Le cobalt et le zinc sont coordonnés de manière tétraédrique tandis que le nickel est octaédrique. Ces composés, à l'exception des analogues contenant le zinc, forment des complexes avec les bases de Lewis. La pyridine et la nicotinamide forment des adduits de formule générale $L_2(SCN)_2M(NCSHgR)_2$ tandis que la bipyridine-2,2′ et la phénanthroline-1,10 forment des complexes cationiques–anioniques de formule $[M(L—L)_3][RHg(SCN)_2]_2$.

[Traduit par le journal]

Can. J. Chem. Downloaded from www.nrcresearchpress.com by 210.87.254.40 on 09/06/12
For personal use only.

## Introduction

Recently (1) we have reported a new class of mixed metal compounds of the type $(SCN)_2M(NCSHgR)_2$ (M = Co(II), Ni(II) and R = phenyl) and their complexes. In order to determine the effect of change of phenyl group by *n*-propyl or isopropyl group on the mode of thiocyanate bonding, we report here the synthesis and characterization of another series of thiocyanates and their complexes.

## Experimental

*Materials and manipulations*

Reagent grade solvents were purified before use. *n*-$C_3H_7HgCl$ and *iso*-$C_3H_7HgCl$ were prepared using Grignard reagents. The chlorides were converted into thiocyanate by stirring an acetone solution of *n*-$C_3H_7HgCl$ with an acetone solution of KNCS in a 1:1 molar ratio. The precipitated KCl was filtered off and the filtrate was concentrated by evaporation under reduced pressure. On addition of water to the concentrate the thiocyanate was precipitated, filtered, washed with water, recrystallized from ethanol, and dried in vacuum. The isopropyl analog was similarly prepared.

*Anal.* calcd. for *n*-$C_3H_7HgSCN$: C 11.96, H 2.32, S 10.63, Hg 66.61, N 4.65; found: C 11.25, H 2.10, S 10.50, Hg 65.85, N 4.45, mp 95°C; yield 65%; ir (Nujol): 2165 (ν(CN)), 760 (ν(CS)), 430 $cm^{-1}$ (δ(NCS)).

*Anal.* calcd. for *iso*-$C_3H_7HgSCN$: C 11.96, H 2.32, S 10.63, Hg 66.61, N 4.65; found: C 11.30, H 2.15, S 10.55, Hg 65.95, N 4.25, mp 85°C; yield 65%; ir (Nujol): 2140 (ν(CN)), 750 (ν(CS)), 420 $cm^{-1}$ (δ(NCS)).

*Preparation of complexes $(SCN)_2M(NCSHgR)_2$ (M = Co(II), Ni(II), Zn(II); R = n-$C_3H_7$, iso-$C_3H_7$)*

*$(SCN)_2Co(NCSHgR)$*

1.75 g of $Co(NCS)_2$ (1 mmol) and 6.02 g of *n*-$C_3H_7HgSCN$ (2 mmol) were dissolved in 50 mL of ethanol and 100 mL of ethyl acetate, respectively. The solutions were mixed together and stirred for 20 h. The resulting blue precipitate was filtered, washed with ethanol, and dried in vacuum. The isopropyl analog was similarly prepared. The *n*-propyl derivative has mp 125°C and isopropyl has mp 140°C.

*$(SCN)_2Ni(NCSHgR)_2$*

A solution of 1.75 g of $Ni(NCS)_2$ (1 mmol) in 25 mL of methanol was mixed with a solution of 6.02 g (2 mmol) of *n*-$C_3H_7HgSCN$ in 100 mL of acetone, and the mixture was stirred for 24 h. The resulting grey precipitate was filtered, washed with acetone, and dried in a vacuum. The isopropyl analog was similarly prepared. The compounds were recrystallized from acetone. The *n*-propyl derivative melts at 155°C with decomposition and the isopropyl derivative melts at 165°C with decomposition.

*$(SCN)_2Zn(NCSHgR)_2$*

1.81 g of $Zn(NCS)_2$ (1 mmol) and 6.02 g of *n*-$C_3H_7HgSCN$ (2 mmol) were dissolved in 50 mL of ethanol and 100 mL of acetone, respectively. The solutions were mixed together and stirred for 20 h. The resulting white precipitate was filtered, washed with acetone, and dried in vacuum. The isopropyl analog was similarly prepared. Compounds were recrystallized from acetone. The *n*-propyl derivative has melting point 135°C and the isopropyl derivative has melting point 150°C.

*Preparation of adducts $L_2(SCN)_2M(NCSHgR)_2$ (L = pyridine, nicotinamide) and cationic–anionic complexes $[M(L—L)_3][RHg(SCN)_2]_2$ (L—L = 2,2′-bipyridine, 1,10-phenanthroline; M = Co(II), Ni(II))*

The complexes were prepared by mixing in stoichiometric ratios a suspension of the $(SCN)_2M(NCSHgR)_2$ in ethanol with a solution of the ligand in the same solvent and stirring the mixture for 24 h. Pink cobalt complexes and green nickel complexes were formed; they were filtered, washed with ethanol, and dried in vacuum. Complexes with pyridine and nicotinamide were recrystallized from acetone and 2,2′-bipyridine complexes

0008-4042/82/182351-04$01.00/0

©1982 National Research Council of Canada/Conseil national de recherches du Canada

Can. J. Chem. Downloaded from www.nrcresearchpress.com by 210.87.254.40 on 09/06/12
For personal use only.

were recrystallized from a mixture of ethanol and dimethylsulphoxide.

Alternatively, pyridine complexes were prepared by the following method. $Co(NCS)_2.2py$ was first prepared, recrystallized, and characterized. $Co(NCS)_2.2py$ (3.32 g) was dissolved in 100 mL of ethanol and mixed with 100 mL of an ethanol solution containing 6.02 g of $n$-$C_3H_7HgSCN$ and stirred. A pink compound was formed, filtered, washed with ethanol, recrystallized from acetone, and dried in vacuum. The isopropyl analog was similarly prepared.

Attempts to isolate adducts of oxygen donors such as tetrahydrofuran, dimethylsulphoxide, and dioxane were unsuccessful presumably because of their instability at room temperature.

The adducts and cationic–anionic complexes which have been prepared are: $(py)_2(SCN)_2Co(NCSHg\ n\text{-}C_3H_7)_2$, $(py)_2(SCN)_2Co(NCSHg\ iso\text{-}C_3H_7)_2$, $(py)_2(SCN)_2Ni(NCSHg\ n\text{-}C_3H_7)_2$, $(py)_2(SCN)_2Ni(NCSHg\ iso\text{-}C_3H_7)_2$, $(nia)_2(SCN)_2Co(NCSHg\ n\text{-}C_3H_7)_2$, $(nia)_2(SCN)_2Co(NCSHg\ iso\text{-}C_3H_7)_2$, $(nia)_2(SCN)_2Ni(NCSHg\ n\text{-}C_3H_7)_2$, $(nia)_2(SCN)_2Ni(NCSHg\ iso\text{-}C_3H_7)_2$, $[Co(bipy)_3][(NCS)_2Hg\ n\text{-}C_3H_7]_2$, $[Co(bipy)_3][(NCS)_2Hg\ iso\text{-}C_3H_7]_2$, $[Ni(phen)_3][(NCS)_2Hg\ n\text{-}C_3H_7]_2$, and $[Ni(phen)_3][(NCS)_2Hg\ iso\text{-}C_3H_7]_2$.

Analyses of the complexes and various physical measurements were made as described earlier (1). The analytical, infrared spectral (50–2500 $cm^{-1}$) and electronic spectral data are available from the Depository of Unpublished Data.[1]

## Results and discussion

*$(SCN)_2M(NCSHgR)_2$ ($M$ = Co(II), Ni(II), Zn(II); $R$ = n-$C_3H_7$, iso-$C_3H_7$)*

The unit cell of RHgSCN may be centrosymmetric (2) having the following molecular units.

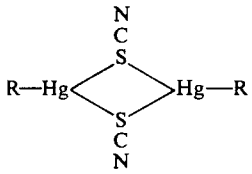


The solid phase infrared spectrum of $n$-$C_3H_7HgSCN$ shows bands at 2165 (ν(CN)), 760 (ν(CS)), 430 (δ(NCS)), 540 (ν(HgC)), and 220 $cm^{-1}$ (ν(HgS)). The position of (CN) and (CS) bands is considerably changed when spectrum is recorded in methanol. ν(CN) is observed at 2130 $cm^{-1}$ and ν(CS) at 690 $cm^{-1}$. This indicates that bridging through sulphur of thiocyanate in $n$-$C_3H_7HgSCN$ is absent in solution.

The analytical results of the complexes indicate that one molecule of $M(NCS)_2$ reacts with two molecules of RHgSCN to form a complex of general formula $(SCN)_2M(NCSHgR)_2$. On complex formation two bands at 2175 and 2080 $cm^{-1}$ appear for ν(CN), 790 and 680 $cm^{-1}$ for ν(CS), 460 and 435 $cm^{-1}$ for δ(NCS), and 212 and 205 $cm^{-1}$ for ν(Hg—SCN), and one band at 520 $cm^{-1}$ for ν(HgC). These changes indicate that the thiocyanate of RHgSCN becomes bridging on complex formation. A band in the ν(CN) region at 2080 $cm^{-1}$ is also observed in all complexes. This can be attributed to N-bonded thiocyanate arising from M—NCS and can be supported by analogy with the corresponding bands reported for $M(NCS)_2.2L$ (3). The position of ν(MN) and ν(CN) bands in $M(NCS)_2$ are not altered on complex formation.

The electronic spectra of $(NCS)_2Co(NCSHgR)_2$ show the presence of two intense bands due to $d$–$d$ transitions in the region 16550 $cm^{-1}$ and 7880 $cm^{-1}$. The position of these bands in solid and solution phase spectra remains the same, showing that there is no solvolysis. The bands in the region 16550 $cm^{-1}$ are assigned to $^4A_2 \rightarrow {}^4T_1(P)$ ($\nu_3$) and in the region 7880 $cm^{-1}$ to $^4A_2 \rightarrow {}^4T_1$ (F) ($\nu_2$). The $Dq$ values as calculated from $\nu_2$ and $\nu_3$ band positions (4) are in the range 454–459 $cm^{-1}$. Magnetic moment values are in the range 4.5–4.6 BM. These results confirm that cobalt has tetrahedral geometry. A $T_d$ local symmetry should produce one ir-active band for ν(MN), which is consistent with the observed number.

The electronic spectra of $(SCN)_2Ni(NCSHgR)_2$ show absorption bands in the region 27780 $cm^{-1}$, 16390 $cm^{-1}$, and 10150 $cm^{-1}$ which may be assigned to the transitions $^3A_{2g} \rightarrow {}^3T_{1g}$ (P) ($\nu_3$), $^3A_{2g} \rightarrow {}^3T_{1g}$ (F) ($\nu_2$), and $^3A_{2g} \rightarrow {}^3T_{2g}$ (F) ($\nu_1$), respectively. The position and assignments of these bands and magnetic moment values (2.90 BM) indicate that Ni(II) acquires octahedral geometry probably by coordinating thiocyanate groups of other molecules (5).

The $Dq$ values of $n$-propyl complexes of both cobalt and nickel are higher than the $Dq$ values of their corresponding isopropyl analogs. This shows that $n$-$C_3H_7HgSCN$ is a stronger base than $iso$-$C_3H_7HgSCN$. On the basis of $Dq$ values of $(SCN)_2Ni(NCSHgR)_2$ they can be placed in the spectrochemical series (1, 6): DMSO < $CH_3OH$ < DMF < $iso$-$C_3H_7NH_2$ < $n$-$C_3H_7NH_2$ < $C_6H_5HgSCN$ < $iso$-$C_3H_7HgSCN$ < $n$-$C_3H_7HgSCN$ < NCS < $NH_3$ < en < Dipy

*Adducts $L_2(SCN)_2M(NCSHgR)_2$ ($M$ = Co(II), Ni(II); $L$ = py, nia)*

The coordination number of cobalt in $(SCN)_2Co(NCSHgR)_2$ is four rather than its maximum six, hence the complexes have the capacity to form adducts with pyridine and nicotinamide. The nickel counterparts also form similar adducts by replacing with ligands the weak thiocyanate bridges in the

[1]Copies of the tables are available, at nominal charge, from the Depository of Unpublished Data, CISTI, National Research Council of Canada, Ottawa, Ont., Canada K1A 0S2.

Can. J. Chem. Downloaded from www.nrcresearchpress.com by 210.87.254.40 on 09/06/12
For personal use only.

octahedral coordination sphere. Zinc analogs, however, decompose into their respective components on reaction with these Lewis bases.

Pyridine or nicotinamide reacts with $(SCN)_2Co(NCSHgR)_2$ to form pink adducts. They are non-conducting (55–63 $cm^{-1}$ mhos/mol) in dimethylformamide (7), and are partly dissociated in dimethylsulphoxide solution. On heating in vacuum pyridine is given off and the parent blue complexes $(SCN)_2Co(NCSHgR)_2$ are obtained. This shows that pyridine is linked to cobalt, changing its tetrahedral geometry to octahedral. Electronic spectra of $L_2(SCN)_2Co(NCSHgR)_2$ give three *d–d* transition bands in the range 20880–21100 $cm^{-1}$, 16300–16700 $cm^{-1}$, and 8700–8900 $cm^{-1}$ assignable to $^4T_{1g} \rightarrow {}^4T_{1g}$ (P) ($\nu_3$), $^4T_{1g} \rightarrow {}^4A_{2g}$ ($\nu_2$), and $^4T_{1g} \rightarrow {}^4T_{2g}$ ($\nu_1$) transitions, respectively. The $\mu_{eff}$ values are in the range 5.10–5.20 BM. The infrared spectra of the complexes show a negative shift in ν(Co—NCS) on adduct formation. These observations also support octahedral coordination geometry around cobalt (8). The $L_2(SCN)_2Ni(NCSHgR)_2$ adducts are also non-conducting in dimethylformamide and partly dissociated in dimethylsulphoxide solution. The pyridine in this case in not given off on heating in vacuum. Electronic spectra indicate the presence of three bands in the range 27000–29800 $cm^{-1}$, 16500–17500 $cm^{-1}$, and 10000–10800 $cm^{-1}$ assigned to $^3A_{2g} \rightarrow {}^3A_{1g}$ (P) ($\nu_3$), $^3A_{2g} \rightarrow {}^3T_{1g}$ (F) ($\nu_2$), and $^3A_{2g} \rightarrow {}^3T_{2g}$ (F) ($\nu_1$) transitions, respectively. The $\mu_{eff}$ values are in the range 2.95–3.15 BM. These results support an octahedral geometry around nickel.

Two bands at 2175 and 2081 $cm^{-1}$ for ν(CN), 790 and 680 $cm^{-1}$ for ν(CS), and 435 and 460 $cm^{-1}$ for δ(NCS) are observed in $(SCN)_2Co(NCSHgR)_2$. On adduct formation the position of the 2175 $cm^{-1}$ band is changed to about 2140 $cm^{-1}$, whereas the positions of the other bands remain unaltered. The negative shift in the band at 2175 $cm^{-1}$ is consistent with the change of tetrahedral coordination geometry around cobalt to octahedral on adduct formation. In addition to this, new bands at 280 $cm^{-1}$ and 125 $cm^{-1}$ which are assigned to ν(ML) and δ(L—M—L) are also observed. There is little or no change in ν(CN) in the case of $(SCN)_2Ni(NCSHgR)_2$ because nickel has octahedral coordination geometry in the complexes and adducts as well.

The proposed coordination of ligand is further supported by the fact that the organomercury compounds show little tendency to increase their coordination number (9), thus the pyridine or nicotinamide is preferentially coordinated to M. Far infrared spectra also do not show any absorption due to Hg—L bond stretching.

*Cationic–anionic complexes $[M(L—L)_3][RHg(SCN)_2]_2$ (M = Co(II), Ni(II); L—L = 2,2′-bipyridine, 1,10-phenanthroline)*

The molar conductance values of 2,2′-bipyridine and 1,10-phenanthroline complexes (122–140 $cm^{-1}$ mhos/mol) in dimethylformamide indicate that they are 1:2 electrolytes. The electronic spectra of cobalt complexes are consistent with octahedral stereochemistry, showing three bands in the range 21000–21100 $cm^{-1}$, 16400–16530 $cm^{-1}$, and 8770–8880 $cm^{-1}$ assigned to $^4T_{1g} \rightarrow {}^4T_{1g}$ (P) ($\nu_3$), $^4T_{1g} \rightarrow {}^4A_{2g}$ ($\nu_2$), and $^4T_{1g} \rightarrow {}^4T_{2g}$ ($\nu_1$) transitions, respectively. The $\mu_{eff}$ values (5.21–5.25 BM) also support the octahedral environment.

The electronic spectra of nickel complexes also indicate three bands in the range 29760–29850 $cm^{-1}$, 17480–17540 $cm^{-1}$, and 10150–10860 $cm^{-1}$ assigned to $^3A_{2g} \rightarrow {}^3A_{2g}$ ($\nu_3$), $^3A_{2g} \rightarrow {}^3T_{1g}$ ($\nu_2$), and $^3A_{2g} \rightarrow {}^3T_{2g}$ ($\nu_1$) transitions, respectively. The positions of these bands and $\mu_{eff}$ values (3.10–3.15 BM) support the octahedral environment around nickel. The infrared spectra of these complexes show two bands for ν(CN), ν(CS), δ(NCS), ν(Hg—SCN) and one band for ν(HgC). These bands are present at about 2060 and 2080 $cm^{-1}$, 705 and 710 $cm^{-1}$, 450 and 440 $cm^{-1}$, 205 and 215 $cm^{-1}$ and at 520 $cm^{-1}$, respectively. The positions of these bands indicate the linkage of thiocyanate through the S-end (10) and their number supports the presence of $[RHg(SCN)_2]^-$ having $C_{2v}$ symmetry. On the basis of these observations it can be presumed that the cation $[M(L—L)_3]^{2+}$ consists of a metal ion duly coordinated with three molecules of 2,2′-bipyridine or 1,10-phenanthroline and the anion consists of a tricoordinated mercury $[RHg(SCN)_2]^-$. Only one band is observed at about 265 $cm^{-1}$, assigned to ν(ML) (11), which supports $O_h$ symmetry for the cation.

Comparisons with $(SCN)_2M(NCSHgPh)_2$, where M = Co(II) and Ni(II), reveal (*1*) the alkyl mercury thiocyanates acquire a higher position in the spectrochemical series than the phenyl mercury thiocyanate, (*2*) $(SCN)_2M(NCSHgPh)_2$ form comparatively stable complexes with oxygen donors such as dimethylsulphoxide and tetrahydrofuran whereas the alkyl analogs form very unstable complexes, and (*3*) Ni(II) in the case of propyl complexes has an octahedral configuration $[Ni(L—L)_3]^{2+}$, whereas in the phenyl complexes it has a square planar configuration $[Ni(L—L)_2]^{2+}$.

**Acknowledgement**

The authors gratefully acknowledge financial support from UGC, New Delhi, and instrumentation facilities from R.S.I.C., Indian Institute of Technology, Madras and Chemistry Department B.H.U., Varanasi. The considerable help of one of the referees is also gratefully acknowledged.

1. P. P. SINGH, S. KUMAR, and M. P. REDDY. Inorg. Chem. **20**, 2711 (1981).
2. R. P. J. COONEY and J. R. HALL. Aust. J. Chem. **22**, 2117 (1969).
3. M. A. PORAI-KOSHITS. Kristallografiya, **4**, 239 (1959).
4. Y. TANABE and S. SUGANO. J. Phys. Soc. Jpn. **9**, 753 (1954).
5. D. FORSTER and D. M. L. GOODGAME. Inorg. Chem. **4**, 715 (1965).
6. A. B. P. LEVER. Inorganic electronic spectroscopy. Elsevier, New York. 1968. p. 336.
7. K. H. SHAW and G. J. SUTTON. Aust. J. Chem. **22**, 1841 (1969).
8. R. J. H. CLARK and C. S. WILLIAMS. Spectrochim. Acta, **22**, 1081 (1966).
9. G. SCHWARZENBACH and M. SCHELLENBERG. Helv. Chem. Acta, **48**, 28 (1965).
10. R. MAKHIJA, L. PAZDERNIK, and R. RIVEST. Can. J. Chem. **51**, 438 (1973).
11. R. G. INSKEEP. J. Inorg. Nucl. Chem. **24**, 763 (1962).

Can. J. Chem. Downloaded from www.nrcresearchpress.com by 210.87.254.40 on 09/06/12
For personal use only.

# Réactivité nucléophile des cyclanones: influence de la stéréochimie *cis/trans* en série bicyclique

C. AGAMI ET T. RIZK

*Laboratoire de Chimie Organique (ERA 127), Université Pierre et Marie Curie, Tour 45, 4 Place Jussieu, 75005 Paris, France*

ET

R. DURAND ET P. GENESTE[1]

*Laboratoire de Chimie Organique Physique Appliquée (ERA 954), École Nationale Supérieure de Chimie de Montpellier, 8, rue École Normale, 34075 Montpellier Cédex, France*

Reçu le 12 février 1982

C. AGAMI, T. RIZK, R. DURAND et P. GENESTE. Can. J. Chem. **60**, 2355 (1982).

La réactivité comparée d'un certain nombre de couples d'isomères *cis/trans* de cétones bicycliques en série décalone-1 et décalone-2 (décalone-2 *trans* et *cis*; méthyl-10 décalone-2 *trans* et *cis*; méthyl-9 décalone-1 *trans* et *cis*; diméthyl-3,10 décalone-2 *trans*) sont étudiés dans le cas de l'addition nucléophile en milieu acide de l'hydroxylamine. Les résultats obtenus aussi bien sur les constantes de vitesse d'addition neutre ou acido catalysée font apparaître une réactivité toujours légèrement supérieure en faveur de l'isomère *trans* (× 2, 4). Ce résultat en accord avec l'hypothèse d'une attaque préférentielle équatoriale du nucléophile est dû aux facteurs conformationnels liés à l'existence dans l'isomère *cis* d'un équilibre stéroïde ⇌ non stéroïde.

C. AGAMI, T. RIZK, R. DURAND, and P. GENESTE. Can. J. Chem. **60**, 2355 (1982).

The relative reactivities of a number of *cis/trans* pairs of bicyclic ketones in the 1- and 2-decalone series (2-decalone; 10-methyl-2-decalone; 9-methyl-1-decalone; and 3,10-dimethyl-2-decalone) have been studied for the nucleophilic addition of hydroxylamine in acidic medium. The results obtained as well as the rate constants for neutral or acid catalysed addition always reveal a slight preference for the *trans*-isomer (× 2.4). This result agrees with the proposal that preferential equatorial attack of a nucleophile is caused by conformational factors related to a steroid ⇌ non-steroid conformation equilibrium in the *cis*-isomers.

[Journal translation]

Can. J. Chem. Downloaded from www.nrcresearchpress.com by 210.87.254.105 on 09/06/12
For personal use only.

## Introduction

Quelques travaux épars dans la littérature (1–6) rapportent des résultats principalement qualitatifs sur les différences de réactivités entre des composés bicycliques isomères *cis/trans*. Ces résultats sont souvent contradictoires, ce qui est probablement dû à la diversité des réactions examinées. Une étude cinétique de la réactivité comparée de couples de cétones bicycliques *cis* et *trans* en série décalone-1 et décalone-2 envers l'hydroxylamine a paru intéressante afin d'obtenir des indications sur l'influence des facteurs conformationnels intervenant dans ces différents isomères.

## Résultats et discussion

La réaction d'oximation a un mécanisme relativement complexe (7–10); elle se fait en deux étapes successives équilibrées tour à tour limitantes selon le pH du milieu. En milieu acide, l'étape d'addition de $NH_2OH$ sur la fonction carbonyle est lente et de plus, soumise à une catalyse acide spécifique. Ce n'est donc que dans ces conditions expérimentales bien précises (9, 10) que l'on peut mesurer correctement les constantes de vitesse $k_0$ et $k_{H^+}$ (Tableau 1) correspondant aux étapes d'addition neutre et acido catalysées.

Nous avons vérifié qu'il existait une bonne corrélation linéaire entre log $k_0$ et log $k_{H^+}$ pour les neuf cyclanones étudiées. La pente de la droite de régression obtenue est voisine de l'unité (pente = 0,86; coefficient de corrélation 0,97). Ce résultat indique que les effets de structure opèrent de la même façon sur $k_0$ et $k_{H^+}$; que les conclusions que l'on peut déduire pour rendre compte des variations de $k_0$ s'appliqueront donc également à celles de $k_{H^+}$.

L'examen du tableau de résultats fait apparaître une grande différence de réactivité entre la *trans* décalone-1 **6** et son dérivé méthylé **7** ($k_0^6/k_0^7 = 18{,}8$ soit $\Delta G = 7230$ J).

La présence d'un groupe méthyle en position axiale α conduit donc à un ralentissement important qui est du même ordre de grandeur que l'énergie conformationnelle habituellement affectée à ce substituant. Ce résultat confirme l'hypothèse d'une attaque équatoriale avec une structure d'état de

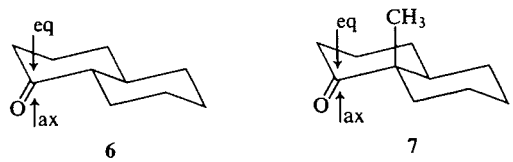


**6** **7**

FIG. 1

[1]Auteur à qui toute correspondance doit être adressée.

0008-4042/82/182355-03$01.00/0

©1982 National Research Council of Canada/Conseil national de recherches du Canada

TABLEAU 1. Constantes de vitesse d'addition de l'hydroxylamine par la voie neutre $k_0$ ou acido catalysée $k_{H^+}$*

| Composé | | $k_0 10^{-3}$ L mole$^{-1}$s$^{-1}$ | $k_{H^+} 10^{-3}$ L mol$^{-2}$s$^{-1}$ | $k_{0\ trans}/k_{0\ cis}$ | *Réference* |
|---|---|---|---|---|---|
| **1** | | 9,0 | 20,5 | | 10 |
| **2** | 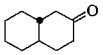 | 7,3 | 21,8 | 2,3 | |
| **3** | 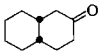 | 3,1 | 8,3 | | |
| **4** | 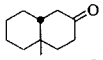 | 5,7 | 15,2 | 2,5 | |
| **5** | 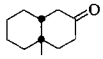 | 2,3 | 7,1 | | |
| **6** | | 6,0 | 15,2 | | 10 |
| **7** | | 0,32 | 0,92 | 2,3 | |
| **8** | | 0,14 | 0,42 | | |
| **9** | 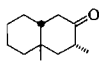 | 0,96 | 2,1 | | |

*Toutes ces mesures ont été effectuées dans l'eau à 25,0 ± 0,1°C et à force ionique constante $\mu$ = 1,0 mol/L; l'erreur sur $k_0$ ou $k_{H^+}$ est inférieure à 2%.

transition qui ressemble au réactif, ce qui paraît désormais parfaitement admis sans que l'on puisse toutefois en donner une explication satisfaisante (11).

Les résultats font apparaître également pour les trois couples de cétones *cis* et *trans* étudiés **2–3**, **4–5** et **7–8** une réactivité supérieure et sensiblement constante de la forme *trans* respectivement égale à 2,3, 2,5 et 2,3.

Puisque dans le cas de l'addition de l'hydroxylamine sur les cétones l'état de transition ressemble aux réactifs, l'application stricte du principe de Curtin–Hammett entraîne que ce sont uniquement les intéractions stériques dans les différents états de transition des deux formes *cis* et *trans* qui doivent être prises en considération.

Ainsi, dans le cas des décalones-2 **2** et **3**, l'examen des différentes structures montre que parmi les trois structures *cis* stéroïde, *cis* non stéroïde et *trans*, vis à vis d'une attaque par la face équatoriale, deux d'entre elles, la non stéroïde et la *trans*, présentent le même encombrement alors que la structure stéroïde probablement minoritaire (12) est la plus encombrée puisqu'elle possède un substituant axial en $\gamma$.

Dans le cas des décalones-1 *cis* et *trans*, **7** et **8**, les trois structures présentent sensiblement le même encombrement vis à vis d'une attaque équatoriale dû au substituant axial en $\alpha$. Un effet identique se retrouve dans le cas des deux décalones-2 **4** et **5** possédant un méthyle angulaire.

Ces identités d'empêchement stérique sur les trois structures conduisent donc aux réactivités analogues observées. La réactivité légèrement plus importante de la forme *trans* est probablement due au fait que les formes *cis* existent en équilibre conformationnel sur la position duquel malheureusement existent beaucoup de résultats expérimentaux discordants.

Enfin, la comparaison des réactivités de **9** et **4** permet de mettre en évidence une différence due à la présence d'un groupe méthyle équatorial en $\alpha$ du groupe carbonyle voisine de 6. Ce ralentissement est probablement du aux effets stériques de torsion par éclipsage partiel de la liaison carbone–oxygène avec le groupement méthyle en équatorial (8).

Ces résultats montrent donc que la faible différence de réactivité entre les composés bicycliques isomères *cis*/*trans* peut parfaitement s'expliquer sur de simples bases conformationnelles. Ainsi que le prévoyait Johnson (1) dès 1943: "the causes of the differences in reactivity must be subtle" à propos de la réactivité comparée des décalones **7** et **8** envers la semi-carbazone.

## Partie expérimentale

A. *Obtention des substrats*

Les décalones sont préparées selon des modes opératoires déjà décrits: décalone-2 *trans* **2** et *cis* **3** (13), méthyl-10

Can. J. Chem. Downloaded from www.nrcresearchpress.com by 210.87.254.105 on 09/06/12
For personal use only.

décalone-2 *trans* **4** (14) et *cis* **5** (15), méthyl-9 décalone-1 *trans* **7** (16) et *cis* **8** (17), diméthyl-3,10 décalone-2 *trans* **9** (18).

Les cétones obtenues sont purifiées par chromatographie sur colonne de gel de silice. L'analyse par chromatographie en phase vapeur (Carbowax 20M) montre que leur pureté est dans chaque cas supérieure à 98%.

B. *Mesures cinétiques*

Les réactions d'oximation sont suivies par spectrophotometrie uv (Gilford 250) en mesurant l'augmentation de la densité optique due à l'apparition des oximes (220 nm) à 25,0 ± 0,1°C. L'eau est utilisée comme solvant, la force ionique maintenue constante $\mu$ = 1,0 mol/L pour les différentes acidités. Les concentrations en cétone et en chlorhydrate d'hydroxylamine sont respectivement de $2,5 \times 10^{-4} M$ et $0,5 M$, différentes concentrations en acide sont étudiées pour chaque cétone afin de déterminer $k_0$ et $k_{H^+}$ [HCl] = $0,5 M$ ($h_0 = 0,609$) et [HCl] = $0,05 M$ ($h_0 = 0,05$). Le mode de détermination de $k_0$ et $k_{H^+}$ a été décrit précédement (9).


1. W. S. Johnson, J. Am. Chem. Soc., **65**, 1317 (1943).
2. G. Lamaty et J. Jullien. Tetrahedron Lett. 1023 (1964).
3. W. Oppolzer, C. Fehr et J. Warneke. Helv. Chem. Acta, **60**, 48 (1977).
4. W. Oppolzer et M. Petrzilka. Helv. Chem. Acta, **61**, 2755 (1978).
5. M. Galberi, P. H. Lewis, S. Middleton et L. E. Stock. Aust. J. Chem. **33**, 101 (1980).
6. C. Agami, M. Fadlallah, C. Puchot et T. Rizk. Tetrahedron. 1982. Sous presse.
7. W. P. Jencks. J. Am. Chem. Soc. **81**, 475 (1959).
8. P. Geneste, G. Lamaty et J. P. Roque. Tetrahedron Lett. 5007 (1971); 5011 (1971); 5015 (1971); Tetrahedron, **27**, 5561 (1980).
9. G. Lamaty, A. Natat, A. Petitjean, J. P. Roque, P. Geneste et B. Schlick. Recl. Trav. Chim. Pays-Bas, **95**, 54 (1976).
10. G. Lamaty, A. Natat, A. Petitjean et J. P. Roque. Recl. Trav. Chim. Pays-Bas, **95**, 93 (1976); **98**, 400 (1979).
11. A. J. Cieplak. J. Am. Chem. Soc. **103**, 4540 (1981).
12. M. Hanack. *Dans* Conformation theory. Academic Press, New York. 1965. p. 201.
13. R. L. Augustine. J. Org. Chem. **23**, 1853 (1958).
14. A. Casadevall, E. Casadevall et M. Lasperas. Bull. Soc. Chim. Fr. 4506 (1968).
15. R. L. Augustine. J. Org. Chem. **28**, 152 (1963).
16. C. Agami, M. Fadlallah et J. Levisalles. Tetrahedron, **37**, 909 (1981).
17. G. Bauduin et Y. Pietrasanta. Tetrahedron, **29**, 4225 (1973).
18. C. Agami, J. Levisalles et B. Lo Civero. Tetrahedron, **35**, 961 (1969).


Can. J. Chem. Downloaded from www.nrcresearchpress.com by 210.87.254.105 on 09/06/12
For personal use only.

# Stereospecific and practical syntheses of both *meso*-cyclopentane-1,2,3-tricarboxylic acids

PELAYO CAMPS[1] AND CARLOS JAIME

*Departamento de Química Orgánica, Facultad de Ciencias, Universidad Autónoma de Barcelona, Bellaterra, Barcelona, Spain*

Received January 13, 1982

PELAYO CAMPS and CARLOS JAIME. Can. J. Chem. **60**, 2358 (1982).

A stereospecific synthesis of both *meso*-cyclopentane-1,2,3-tricarboxylic acids, by using the 1,3-dimethoxytrimethylene bridge as two latent carboxyl groups, is described. A practical synthesis of these acids is also described.

PELAYO CAMPS et CARLOS JAIME. Can. J. Chem. **60**, 2358 (1982).

On décrit une synthèse stéréospécifique des deux acides *méso*-cyclopentanetricarboxyliques-1,2,3 qui utilise le pont diméthoxy-1,3 triméthylène comme groupes carboxyles latents. On décrit également une synthèse pratique de ces acides.

[Traduit par le journal]

Can. J. Chem. Downloaded from www.nrcresearchpress.com by 210.87.254.42 on 09/06/12
For personal use only.

We have recently described the use of the 1,3-dimethoxytrimethylene bridge as two latent carboxyl groups (1). We describe in this communication the use of this latent functionality for the stereospecific synthesis of (1*R*,2*s*,3*S*)-cyclopentane-1,2,3-tricarboxylic acid, **1***a*, and (1*R*,2*r*,3*S*)-cyclopentane-1,2,3-tricarboxylic acid, **2***a*. To the best of our knowledge only one *meso*-cyclopentane-1,2,3-tricarboxylic acid, mp 169–170°C, has so far been described (2). It was obtained by heating the racemic form with acetic anhydride at 150°C, but its configuration was not assigned.

The starting product in our stereospecific synthesis was a mixture of stereoisomers of 2,4-dimethoxy-8-methylenebicyclo[3.2.1]octane, **3**, prepared in two steps from cyclopentanone in 34% overall yield (1, 3) (Scheme 1). Hydroboration of **3** followed by alkaline hydrogen peroxide oxidation gave a crude mixture of (2,4-dimethoxybicyclo[3.2.1]oct-8-yl)methanol, **4**, which was separated by low pressure column chromatography using silica gel (230–400 mesh) (4) as support to give **4***b* (67% yield) and **4***a* (14.9% yield).

The configuration of **4***b* was easily assigned because of the presence of two methoxyl absorptions in the $^1$H nmr spectrum and the observation of an intramolecular hydrogen bond in the ir spectrum. By decoupling experiments carried out on the $^1$H nmr spectrum of **4***a* in the presence of 0.39 equivalents of Eu(fod)$_3$ we obtained the following coupling constant values: $J_{1',8'} = 4.3$ Hz, $J_{2',3'\ endo} = 10.6$ Hz, $J_{2',3'\ exo} = 6.0$ Hz, and $J_{1,8'} = 8.0$ Hz (see Table 1). Assuming a chair conformation for the cyclohexane ring of **4***a* (5), the $J_{2',3'\ exo}$ and $J_{2',3'\ endo}$ values agreed with equatorial methoxyl groups, which, on the other hand, agreed with the stereoisomeric composition of the starting compound (1, 3, 5). The *syn*-stereochemistry[2] of the hydroxymethyl group in **4***a* was established on the basis of the $J_{1',8'}$ value. Table 1 collects coupling constant values in related systems (6–8). As can be seen from Table 1, the *syn*-stereochemistry of the substituent at C8 or C9 is systematically associated with a significant value of $J_{1,8}$ and $J_{5,8}$ in bicyclo[3.2.1]octane systems or $J_{1,9}$ in bicyclo[4.2.1]nonane systems, while the *anti*-stereochemistry is associated with a very small value of $J_{1,8}$ and $J_{5,8}$ or $J_{1,9}$.

Knowing the *syn*-stereochemistry of the hydroxymethyl group in **4***a* and **4***b*, the stereoisomeric mixture **4** was oxidized with Jones reagent to give *syn*-2,4-dimethoxybicyclo[3.2.1]octane-8-carboxylic acid, **5**, as a stereoisomeric mixture in 89% yield. The preparation of *anti*-2,4-dimethoxybicyclo[3.2.1]octane-8-carboxylic acid from **5** required the epimerization at C8. For convenience, the study of the epimerization reaction was carried out on **5***b*, prepared in 93% yield by Jones oxidation of **4***b*. Reaction of **5***b* with ethereal diazomethane gave the corresponding methyl ester **6***b*. Several attempts to epimerize **6***b* by using catalytic amounts of sodium methoxide or potassium *tert*-butoxide were fruitless. Refluxing **6***b* with 4–5 equivalents of potassium *tert*-butoxide in *tert*-butyl alcohol for 60 h, the acid **7***b* was obtained in 71.6% yield. Esterification of **7***b* with ethereal diazometh-

[1]Author to whom correspondence may be addressed. Present address, Departamento de Química Orgánica, Facultad de Ciencias Químicas San Sebastian, Universidad del País Vasco, Alza, San Sebastian, Spain.

[2]The terms *syn* and *anti* in 8-substituted bicyclo[3.2.1]octane and 9-substituted bicyclo[4.2.1]nonane derivatives refer in this context to the relation between the substituent at C8 or C9 and the larger ring to which it is attached, as it is used in refs. 7 and 8.

0008-4042/82/182358-07$01.00/0

©1982 National Research Council of Canada/Conseil national de recherches du Canada

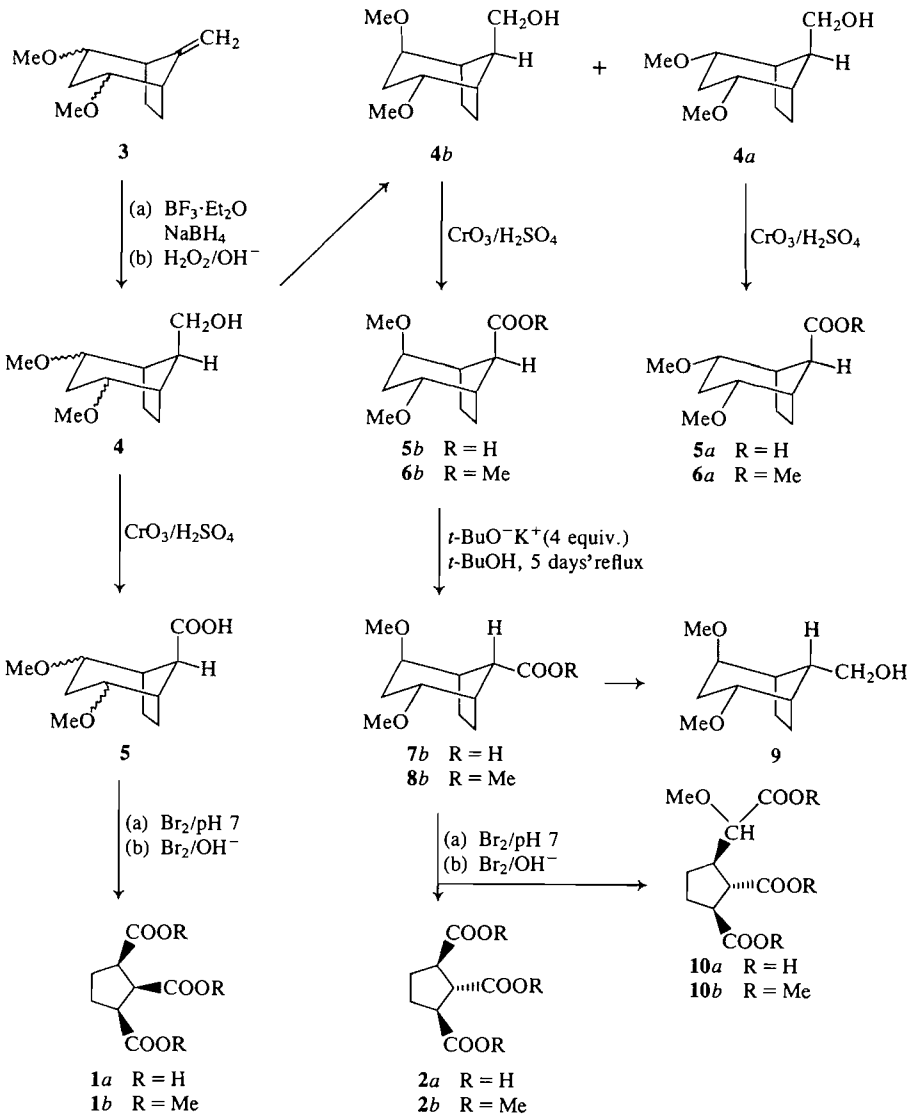


SCHEME 1

ane gave the corresponding methyl ester **8***b*, different from **6***b* (glc). Moreover, $LiAlH_4$ reduction of **8***b* gave the alcohol **9**, in which the *anti* stereochemistry of the hydroxymethyl group is clearly defined by the absence of intramolecular hydrogen bond (ir) and the small value of the coupling constants $J_{1',8'}$ and $J_{5',8'}$ (see Table 1).

It is noteworthy that the acid **7***b* and not its methyl ester **8***b* was the product obtained in the epimerization of **6***b*. The hydrolysis must take place after the epimerization of **6***b* because otherwise epimerization would not easily occur, and probably it implies breaking of the methyl–oxygen bond by nucleophilic attack of the *tert*-butoxide ion on the methyl of the ester function. Alternatively, as suggested by a referee, hydrolysis of a ketene intermediate would lead directly to the acid **7***b*.

We also prepared the ester **6***a*, by Jones oxidation of **4***a* and esterification of the corresponding acid **5***a* with ethereal diazomethane, but we did not attempt its epimerization, because we considered it more simple to carry out the final step of the sequence of Scheme 1 on **7***b*.

The bromine oxidation of the stereoisomeric mixture **5** gave, after esterification of the reaction

Can. J. Chem. Downloaded from www.nrcresearchpress.com by 210.87.254.42 on 09/06/12
For personal use only.

TABLE 1. Diagnostic coupling constants in 8-substituted bicyclo[3.2.1]octane and 9-substituted bicyclo[4.2.1]nonane derivatives

| | | |
|---|---|---|
| 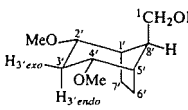 | 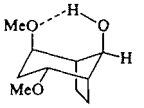 | 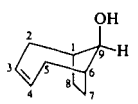 |
| 4a $J_{1',8'} = 4.3$ Hz[a] | $J_{1,8} \sim J_{5,8} = 4$ Hz (ref. 6) | $J_{1,9} = 7$ Hz (ref. 7) |
| | | 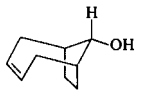 |
| | | $J_{1,9} = 0$ Hz (ref. 7) |
| 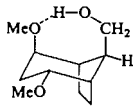 | 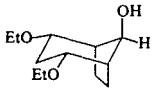 | 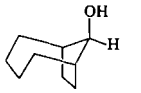 |
| 4b $J_{1',8'} \sim J_{5',8'} = 4$ Hz[b] | $J_{1,8} = 5$ Hz (ref. 6) | $J_{1,9} = 7$ Hz (ref. 8) |
| 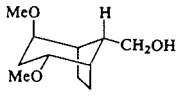 | 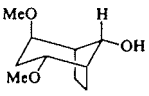 | 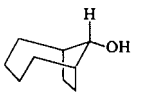 |
| 9 $J_{1',8'} \sim J_{5',8'} = 0$ Hz[a] | $J_{1,8} \sim J_{5,8} = 0$ Hz (ref. 6) | $J_{1,9} = 0$ Hz (ref. 8) |

[a]Value obtained from the $^1$H nmr spectrum in the presence of 0.39 equivalents of Eu(fod)$_3$.
[b]Approximate value obtained from the width of the H8′ absorption with simultaneous irradiation of the H1 protons.

product with ethereal diazomethane and chromatography, trimethyl (1*R*,2*s*,3*S*)-cyclopentane-1,2,3-tricarboxylate, **1***b*, in 18.7% yield. In the same way, bromine oxidation of **7***b* gave a crude product which, by crystallization from a small volume of 3 *N* HCl, afforded a solid, mp 169–171°C, that was characterized as *c*-3-(1-methoxyhydroxycarbonylmethyl)-*r*-1,*t*-2-cyclopentanedicarboxylic acid, **10***a* (21.5% yield). The mother liquors, esterified with ethereal diazomethane and chromatographed, gave trimethyl (1*R*,2*r*,3*S*)-cyclopentane-1,2,3-tricarboxylate, **2***b* (11.1% yield), plus dimethyl *c*-3-(1-methoxymethoxycarbonylmethyl)-*r*-1,*t*-2-cyclopentanedicarboxylate, **10***b* (7% yield).

The proposed structure for **10***a* and **10***b* comes from the spectroscopic and analytical data and mechanistic considerations. Thus, **10***b* showed in its $^1$H nmr spectrum three ester and one ether methoxyls at δ 3.75, 3.72, 3.70, and 3.43, respectively. There was also a doublet absorption ($J$ = 4 Hz) at δ 3.90 corresponding to one proton. The elemental analysis agreed for $C_{13}H_{20}O_7$. These facts pointed to a methyl α-methoxy-α-cyclopentylacetate substituted with two methoxycarbonyl groups in the cyclopentyl ring. The relative position of these substituents and the configuration were assigned on mechanistic grounds. Scheme 2 shows how **10***a* might have been formed.

In the fragmentation step the reaction might have followed a different course than we had observed on other substrates (1) (see Scheme 2). However, this fragmentation–elimination reaction requires the bonds to be broken (C3—C4 and C2—O) to adopt an antiperiplanar arrangement with respect to the C2—C3 bond, difficult to attain if the configuration at C2 is that shown.

No isomerization of **1***a* or **2***a* under the bromine oxidation conditions was expected. The 200 MHz $^1$H nmr spectra of **1***b* and **2***b* confirmed the expected configurations. Both spectra showed symmetrical absorptions for the annular protons as required by *meso*-compounds. The spectrum of **1***b* showed two clearly defined methoxyl absorptions, while only one was observed for **2***b*. The absorption corresponding to the C2 proton appeared in both cases as a triplet, shifted 0.1 ppm downfield for **2***b* with respect to **1***b* due to the shielding of the *cis*-methoxycarbonyl groups at C1 and C3. The most significant difference in both spectra corresponded to the methylene protons that appeared as two complex absorptions at δ 2.3 and 2.0 for **1***b* and as a complex one at δ 2.0 for **2***b*. A greater chemical shift difference must be expected for the methylene protons of **1***b* than for those of **2***b*. Similarly, the 50 MHz $^{13}$C nmr spectra of **1***b* and **2***b* confirmed the assigned configurations. The carbonyl absorptions of **1***b* appeared shifted 1.38 and 1.46 ppm upfield with respect to the corresponding absorptions of **2***b*, due to a greater γ-effect between the methoxycarbonyl groups in **1***b*. Moreover, the methylene carbons (C4 and C5) of **1***b* appeared shifted 3.76 ppm upfield with respect to the corresponding absorption of **2***b*. Assuming the $C_s$ envelope conformations of **1***b* and **2***b* to be the most stable (9), a greater γ-effect for the methylene carbons must be expected in **1***b* because of the axial methoxycarbonyl group at C2 (10).

Hydrolysis of **1***b* by reaction with dilute aqueous HCl gave (1*R*,2*s*,3*S*)-cyclopentane-1,2,3-tricarboxylic acid, **1***a*, in 97% yield, which after two crystallizations from 3 *N* HCl melted at 169–170°C. Esterification of a sample of **1***a* with ethereal diazomethane gave back **1***b*, showing that no isomerization had taken place during hydrolysis. In the same way, **2***b* was hydrolyzed to **2***a* in 95% yield, which after two crystallizations from 3 *N* HCl melted at 183–185°C. Esterification of a sample of **2***a* with ethereal diazomethane gave back **2***b*.

The melting point of **1***a* agrees with that of the described *meso*-cyclopentane-1,2,3-tricarboxylic acid. Since it is obtained under equilibration conditions by refluxing the racemic form with acetic anhydride, we expected it to be **2***a*, which

Can. J. Chem. Downloaded from www.nrcresearchpress.com by 210.87.254.42 on 09/06/12
For personal use only.

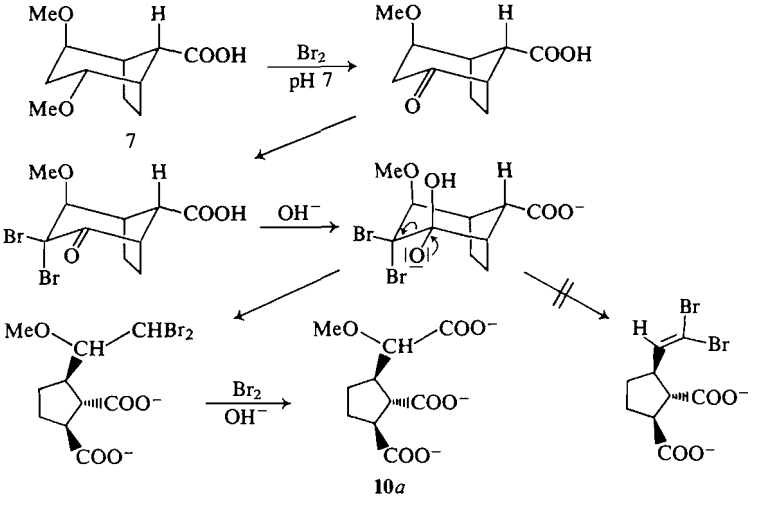

SCHEME 2

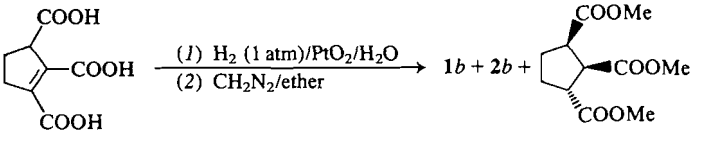

SCHEME 3

must be the thermodynamically more stable. However, it must not be the relative stabilities of these acids, but those of the species present in the reaction medium, that determine the preferred formation of one of them.

Compounds **1***b* and **2***b* were also prepared in a straightforward manner by hydrogenation (11) of the known cyclopentene-1,2,3-tricarboxylic acid (12), **11**, followed by esterification with ethereal diazomethane and column chromatography (Scheme 3).

As can be seen from Table 2, the best stereoselectivity in the hydrogenation of **11** was obtained by using Pt as catalyst. Moreover, a large proportion of **2***b* was always obtained. This product must arise from the hydrogenation of a product of double bond isomerization of **11**. Column chromatography of a mixture of **1***b*, **2***b*, and **12** (from a hydrogenation of **11** using Pt as catalyst) using silica gel as support and hexane–ether mixtures as eluent gave pure **1***b* (52% yield from **11**) and **2***b* (containing 6% **12** (nmr)) (11% yield from **11**). By reaction of a mixture of **1***b*, **2***b*, and **12** (from a Pd/C hydrogenation of **11**) with sodium methoxide in methanol, a 3:1 mixture of **2***b*/**12** was obtained, in agreement with the expected relative stabilities of the trimethyl cyclopentane-1,2,3-tricarboxylates.

Thus the use of the 1,3-dimethoxytrimethylene bridge as two latent carboxyl groups has allowed us to carry out a low yield, but stereospecific, synthesis of the acids **1***a* and **2***a* which, on the other hand, have been easily prepared stereoselectively from **11**.

TABLE 2. Ratios of stereoisomeric trimethyl cyclopentane-1,2,3-tricarboxylates obtained by hydrogenation of **11** in water at atmospheric pressure using different catalysts, followed by reaction with ethereal diazomethane

| Catalyst | 1*b* | 2*b* | 12 |
|---|---|---|---|
| 10% Pd/C | 44 | 42 | 14 |
| 5% Rd/C | 67 | 20 | 13 |
| Pt | 78 | 20 | Traces |

## Experimental

Infrared spectra were recorded on a Perkin–Elmer spectrometer model 720, mass spectra on a Hewlett–Packard spectrometer model 5930A. The $^1$H nmr spectra, unless otherwise stated, were taken at 60 MHz on a Perkin–Elmer R-12A spectrometer, while 200 MHz $^1$H spectra and 50 MHz $^{13}$C spectra were recorded on a Varian XL 200. Chemical shifts are given in ppm relative to internal TMS (δ scale). Melting points were determined on a Kofler hot-stage and are corrected.

Can. J. Chem. Downloaded from www.nrcresearchpress.com by 210.87.254.42 on 09/06/12
For personal use only.

Can. J. Chem. Downloaded from www.nrcresearchpress.com by 210.87.254.42 on 09/06/12
For personal use only.

syn-*(2,4-Dimethoxybicyclo[3.2.1]oct-8-yl)methanol, 4*

Into a three-necked 100 mL flask fitted with reflux condenser, addition funnel, thermometer, Ar atmosphere, and magnetic stirrer, 2.363 g of **3** (13 mmol) in 16 mL anhydrous DME and 0.182 g $NaBH_4$ (4.8 mmol) were introduced. The flask was immersed in a water bath at 20°C and 0.75 mL of boron trifluoride-etherate (6 mmol) in 5 mL anhydrous DME were slowly added (15 min) with stirring, keeping the temperature of the reaction mixture below 25°C. After 1 h stirring, the flask was immersed in an ice bath and 15 mL water and 15 mL aqueous 3 *N* NaOH were introduced. Then 6 mL of 30% $H_2O_2$ was slowly added and the mixture was stirred at room temperature for 1 h. In order to keep the reaction medium alkaline during the addition of $H_2O_2$, 1 mL more of aqueous 3 *N* NaOH was added. Water (25 mL) was added and the solution extracted with $CH_2Cl_2$ (4 × 20 mL). By removing the solvents at reduced pressure from the dried extracts (anhydrous $Na_2SO_4$), 2.364 g of crude product was obtained. The water phase was continuously extracted with ether for 24 h to give 0.236 g more of crude product, total 2.600 g. This crude product on chromatography through 50 g silica gel (230–400 mesh) (4) gave the following fractions: 0.150 g starting product (0.82 mmol) (hexane – ethyl acetate 98:2), 1.743 g of **4***b* (8.71 mmol), 0.073 g of a mixture of **4***b* and **4***a* (0.37 mmol), and 0.389 g of **4***a* (1.94 mmol) (ethyl acetate) (90.4% yield of **4***a* + **4***b* from reacted **3**). Boiling point of **4***a* and **4***b*, 185–190°C (oven)/15 Torr.

*Spectral and analytical data of [(1RS,2RS,4RS,5SR,8SR)-2,4-dimethoxybicyclo[3.2.1]oct-8-yl]methanol, 4*b

Infrared ($CHCl_3$), ν: 3650 and 3450 $cm^{-1}$. The relative intensities remained unchanged on dilution; $^1H$ nmr ($CDCl_3$), δ: 1.1–2.2 (broad, 7H), 2.2–2.5 (broad, 3H, part of this absorption changed on dilution), 3.2–3.8 (complex absorption), 3.33(s), 3.31(s) (total 8H), 3.95 (d, $J$ = 8 Hz, 2H); ms: 200($M^+$, 2), 181(4), 168($M^+$ – MeOH, 100), 150(29), 136(76), 101(MeO—$\overset{+}{C}$H—CH=CH—OMe, 76), 79(59), 71(MeO—$\overset{+}{C}$H—CH=$CH_2$, 76). *Anal.* calcd. for $C_{11}H_{20}O_3$: C 65.97, H 10.07; found: C 65.69, H 10.18.

*Spectral and analytical data of [(1R,2S,4R,5S,8s)-2,4-dimethoxybicyclo[3.2.1]oct-8-yl]methanol, 4*a

Infrared ($CHCl_3$), ν: 3650 and 3450 $cm^{-1}$. The relative intensities of these absorptions varied on dilution; $^1H$ nmr ($CDCl_3$), δ: 1.0–2.5 (broad), 1.85 (s, changed on dilution) (total 10 H), 3.2–3.7 (complex absorption), 3.30(s) (total 8H), 3.8(d, $J$ = 8 Hz, 2H); ms: 200($M^+$, 2), 181(6), 168($M^+$ – MeOH, 42), 151(25), 150(24), 136(25), 101(MeO—$\overset{+}{C}$H—CH=CH—OMe, 100), 71(MeO—$\overset{+}{C}$H—CH=$CH_2$, 59). *Anal.* calcd. for $C_{11}H_{20}O_3$: C 65.97, H 10.07; found: C 65.74, H 10.10.

*(1RS,2RS,4RS,5SR,8SR)-2,4-Dimethoxybicyclo[3.2.1]octane-8-carboxylic acid, 5*b

To a solution of 0.816 g of **4***b* (4.08 mmol) in 20 mL acetone, 2.2 mL of Jones reagent was slowly added and the mixture magnetically stirred at room temperature for 16 h. The solvent was removed at reduced pressure, water (20 mL) was added, and the mixture extracted with ether (7 × 15 mL). The ether extracts were dried over anhydrous $Na_2SO_4$ and the solvent removed at reduced pressure to give 0.815 g of **5***b* as a white solid, mp 106–109°C (ether–hexane) (3.81 mmol, 93% yield); ir($CHCl_3$), ν: 3700–2400(m), 1710(s) $cm^{-1}$; $^1H$ nmr ($CDCl_3$), δ: 1.1–2.3 (broad, 6H), 2.4–3.1 (broad, 3H), 3.2–4.4 (complex absorption), 3.30(s), 3.33(s) (total 8H), 9.07(broad, 1H); ms: 196($M^+$ – $H_2O$, 3), 182(11), 152(11), 101(MeO—$\overset{+}{C}$H—CH=CH—OMe, 100), 71(MeO—$\overset{+}{C}$H—CH=$CH_2$, 54). *Anal.* calcd. for $C_{11}H_{18}O_4$: C 61.66, H 8.74; found: C 61.58, H 8.54.

*(1R,2S,4R,5S,8s)-2,4-Dimethoxybicyclo[3.2.1]octane-8-carboxylic acid, 5*a

Compound **5***a* was prepared as described for **5***b*. From 0.147 g of **4***a* (0.73 mmol), 0.123 g of **5***a* (0.57 mmol, 78% yield) as a white solid, mp 159–163°C, was obtained; ir($CHCl_3$), ν: 3700–2400(s), 1700(s) $cm^{-1}$; $^1H$ nmr ($CDCl_3$), δ: 1.0–2.5 (broad, 6H), 2.5–3.0 (broad, 3H), 3.30–3.85 (complex absorption), 3.35(s) (total, 8H), 9.5 (broad, 1H); ms: 214($M^+$, 2), 199(1), 196(2), 182(13), 101(MeO—$\overset{+}{C}$H—CH=CH—OMe, 100), 71(MeO—$\overset{+}{C}$H—CH=$CH_2$, 54). *Anal.* calcd. for $C_{11}H_{18}O_4$: C 61.66, H 8.47; found: C 61.90, H 8.57.

syn-*2,4-Dimethoxybicyclo[3.2.1]octane-8-carboxylic acid, 5*

The stereoisomeric mixture **5** was prepared as described for **5***b*. From 0.824 g of **4** (4.12 mmol), 0.783 g of **5** (3.65 mmol, 89% yield) was obtained.

*Methyl (1RS,2RS,4RS,5SR,8SR)-2,4-dimethoxybicyclo[3.2.1]-octane-8-carboxylate, 6*b

An ethereal solution of diazomethane was added to 0.815 g of **5***b* (3.81 mmol) until the yellow color persisted. Then the solvent was removed at reduced pressure to give 0.802 g of **6***b* (3.52 mmol, 92% yield) as a liquid, bp 135–140°C (oven)/18 Torr; ir($CCl_4$), ν: 1740(s) $cm^{-1}$; $^1H$ nmr ($CDCl_3$), δ: 1.0–2.2 (broad, 6H), 2.2–3.0 (broad, 3H), 3.0–3.5 (complex absorption), 3.14(s), 3.22(s) (total 7H), 3.53 (s, 3H), 3.97 (ddd, $J$ = 2 Hz, $J'$ = 7 Hz, and $J''$ = 11 Hz); ms: 228($M^+$, 1), 213(1), 196($M^+$ – MeOH, 81), 181(22), 168(16), 153(22), 137(52), 136($M^+$ – MeOH – $HCO_2Me$, 100), 108($C_6H_5$—$OMe^+$, 56), 101(MeO—$\overset{+}{C}$H—CH=CH—OMe, 72), 71(MeO—$\overset{+}{C}$H—CH=$CH_2$, 61). *Anal.* calcd. for $C_{12}H_{20}O_4$: C 63.14, H 8.83; found: C 63.39, H 8.84.

*Methyl (1R,2S,4R,5S,8s)-2,4-dimethoxybicyclo[3.2.1]octane-8-carboxylate, 6*a

Compound **6***a* was prepared as described for **6***b*. From 0.070 g of **5***a* (0.33 mmol), 0.070 g of distilled **6***a* (0.31 mmol, 94% yield), bp 148–152°C (oven)/16 Torr, was obtained; ir($CCl_4$), ν: 1735(s) $cm^{-1}$; $^1H$ nmr ($CDCl_3$), δ: 0.8–2.4 (broad, 7H), 2.57 (broad, 2H), 3.2–3.7 (complex absorption), 3.28(s), 3.68(s) (total 11H); ms: 228($M^+$, 3), 213(3), 197(9), 196(33), 181(9), 168(7), 165(16), 164(12), 149(13), 137(41), 136(17), 101(MeO—$\overset{+}{C}$H—CH=CH—OMe, 100), 71(MeO—$\overset{+}{C}$H—CH=$CH_2$, 55). *Anal.* calcd. for $C_{12}H_{20}O_4$: C 63.14, H 8.83; found: C 63.00, H 8.90.

*(1RS,2RS,4RS,5SR,8RS)-2,4-Dimethoxybicyclo[3.2.1]octane-8-carboxylic acid, 7*b

In a 50 mL flask fitted with a reflux condenser with a $CaCl_2$ tube, 25 mL anhydrous *tert*-butyl alcohol and 1.360 g potassium (34.9 mmol) were introduced. After all potassium had reacted and the solution reached room temperature, 1.833 g of **6***b* (8.04 mmol) in 5 mL anhydrous *tert*-butyl alcohol was added and the solution heated under reflux for 60 h. After cooling, 175 mL water was added and the mixture extracted with $CH_2Cl_2$ (5 × 20 mL). The extracts were washed with water (2 × 5 mL) and dried over anhydrous $Na_2SO_4$ to give, after removing the solvent at reduced pressure, 0.188 g of an unidentified product. The aqueous phase was acidified with concentrated HCl and extracted with ether (5 × 50 mL). The ether extracts were dried over anhydrous $Na_2SO_4$ and the solvent removed at reduced pressure to give 1.232 g of **7***b* (5.76 mmol, 71.6% yield) as an oil that solidified on standing, mp 98–101°C (ethyl acetate – hexane); ir(KBr), ν: 3700–3200(s), 1720(s) $cm^{-1}$; $^1H$ nmr ($CDCl_3$), δ: 1.0–2.2 (broad, 6H), 2.6–2.9 (broad, 3H), 3.2–3.6 (broad), 3.27(s) (total, 8H), 11.1 (broad, 1H); ms: 196($M^+$ – $H_2O$, 0.5), 183(0.5), 103(MeO—$\overset{+}{C}$H—$CH_2$—$CH_2$—OMe, 13),

Can. J. Chem. Downloaded from www.nrcresearchpress.com by 210.87.254.42 on 09/06/12
For personal use only.

101(MeO—$\overset{+}{C}$H—CH=CH—OMe, 30), 71(MeO—$\overset{+}{C}$H—CH=$CH_2$, 100). *Anal.* calcd. for $C_{11}H_{18}O_4$: C 61.66, H 8.47; found: C 61.61, H 8.46.

*Methyl (1*RS,*2*RS,*4*RS,*5*SR,*8*RS*)-2,4-dimethoxybicyclo[3.2.1]-octane-8-carboxylate, 8*b

Compound **8***b* was obtained quantitatively from **7***b* as described for **6***b*, bp 135–140°C (oven)/16 Torr; ir($CCl_4$), v: 1730(s) $cm^{-1}$; $^1H$ nmr ($CDCl_3$), δ: 1.0–2.6 (broad, 6H), 2.6–2.9 (broad, 3H), 3.2–4.0 (broad), 3.30(s), 3.66(s) (total, 11H); ms: 213($M^+$ – Me, 1), 197(2), 196(7), 137(5), 105(5), 101(MeO—$\overset{+}{C}$H—CH=CH—OMe, 22), 71(MeO—$\overset{+}{C}$H—CH=$CH_2$, 100). *Anal.* calcd. for $C_{12}H_{20}O_4$: C 63.14, H 8.83; found: C 63.42, H 9.09.

*[(1*RS,*2*RS,*4*RS,*5*SR,*8*RS*)-2,4-Dimethoxybicyclo[3.2.1]oct-8-yl]methanol, 9*

In a 10 mL flask protected from moisture ($CaCl_2$ tube), 0.069 g $LiAlH_4$ (1.8 mmol), 3 mL ether, and 0.148 g of **8***b* (0.65 mmol) were introduced and the mixture was magnetically stirred at room temperature for 30 min. Wet ether (10 mL) was added and then 10 mL aqueous 0.1 *N* HCl. The ethereal phase was decanted and the aqueous one extracted with ether. By removing the solvent at reduced pressure from the dried ether extracts (anhydrous $Na_2SO_4$), 0.125 g of crude product was obtained. This product was chromatographed through 10 g silica gel (230–400 mesh) (4) to give 0.018 g of starting product (0.08 mmol), eluting with hexane – ethyl acetate 4:1, and 0.075 g of pure **9** (0.37 mmol, 66% yield from unrecovered **8***b*), eluting with hexane – ethyl acetate 1:1. Infrared ($CCl_4$), v: 3660 and 3450 $cm^{-1}$. The relative intensities varied on dilution; $^1H$ nmr ($CDCl_3$), δ: 0.9–2.5 (broad, 10H) (part of this absorption at δ 2.3 varied on dilution), 3.1–3.5 (complex absorption), 3.22(s), 3.38(d, $J$ = 8 Hz) (total 10H); ms: 168($M^+$ – MeOH, 6), 150(1), 138(2), 137(3), 136(2), 110(8), 103(MeO—$\overset{+}{C}$H—$CH_2$—$CH_2$—OMe, 37), 101(MeO—$\overset{+}{C}$H—CH=CH—OMe, 22), 91(15), 71(MeO—$\overset{+}{C}$H—CH=$CH_2$, 100). *Anal.* calcd. for $C_{11}H_{20}O_3$: C 65.97, H 10.07; found: C 65.84, H 10.44.

*Bromine oxidation of 5: trimethyl (1*R,*2*s,*3*S*)-cyclopentane-1,2,3-tricarboxylate, 1*b

In a 50 mL flask, 0.343 g of **5** (1.6 mmol), 32 mL of buffer solution of pH 7 (containing 10.4 mmol of $PO_4H_2^-$ and 13.4 mmol of $PO_4H^{2-}$), and 0.68 mL of bromine (13.2 mmol) were introduced. The flask was stoppered and the mixture magnetically stirred at room temperature for 68 h. Sodium hydroxide (3.92 g, 98 mmol) and 0.4 mL bromine (7.8 mmol) were introduced and stirring continued for 24 h more. The excess bromine was destroyed with solid $Na_2SO_3$, and the solution made acidic by addition of a mixture of ice and concentrated HCl. The solution was continuously extracted with ether for 13 days. The ether was removed at reduced pressure to give 0.330 g of a viscous crude that was treated with excess ethereal diazomethane. The solution was concentrated at reduced pressure and the residue distilled to give 0.245 g of a mixture (glc), bp 165–170°C (oven)/17 Torr. This mixture was chromatographed through 10 g silica gel (230–400 mesh) (4) to give, among other fractions, 0.072 g of **1***b* (0.3 mmol, 18.7% yield), eluting with hexane – ethyl acetate 4:1, bp 165–170°C (oven)/17 Torr; ir (film), v: 1730(s) $cm^{-1}$; 200 MHz $^1H$ nmr ($CDCl_3$), δ: 1.91–2.09 (complex m, 2H), 2.24–2.43 (complex m, 2H), 2.98–3.11 (complex m, 2H), 3.46(t, $J$ = 7 Hz, 1H), 3.65(s, 3H), 3.67(s, 6H); 50 MHz $^{13}C$ nmr ($CDCl_3$), δ: 25.66(C4 and C5), 47.46(C1 and C3), 49.20(C2), 51.89(C2—COO*Me*), 51.93(C1—COO*Me* and C3—COO*Me*), 172.30(C2—*C*OOMe), 172.80 (C1—*C*OOMe and C3—*C*OOMe); ms: 244($M^+$, 1), 213(63), 212(36), 184(12), 180(3), 153(43), 152($M^+$ – MeOH – HCOOMe, 90), 125(100), 124($M^+$ – 2HCOOMe, 100), 93(70). *Anal.* calcd. for $C_{11}H_{16}O_6$: C 54.05, H 6.60; found: C 54.16, H 6.68.

*Bromine oxidation of 7*b

In a 100 mL flask, 1.055 g of **7***b* (4.93 mmol), 56 mL of buffer solution of pH 7 (containing 1.67 mmol of $PO_4H_2^-$ and 2.00 mmol of $PO_4H^{2-}$), and 2.02 mL of bromine (39.5 mmol) were introduced. The flask was stoppered and the mixture magnetically stirred at room temperature for 63 h. Sodium hydroxide (18.96 g, 0.474 mol) and 0.63 mL of bromine (12.3 mmol) were added, and stirring continued for 24 h more. The excess bromine was destroyed with solid $Na_2SO_3$, the solution made acidic by addition of a mixture of ice and concentrated HCl, and extracted continuously with ether for 19 h. The ether was removed at reduced pressure to give 0.720 g of a viscous product that was dissolved in 1 mL of aqueous 3 *N* HCl. From this solution 0.261 g of a solid, mp 169–171°C, that was characterized as **10***a* (1.06 mmol, 21.5% yield), was obtained. The solvent was removed from the mother liquors at reduced pressure, and the residue was esterified with ethereal diazomethane to give, after removing the ether, 0.373 g of a liquid that was chromatographed through 20 g silica gel, eluting with hexane–ether 7:3, to give 0.134 g of **2***b* (0.55 mmol, 11.1% yield) and 0.085 g of **10***b* (0.34 mmol, 7% yield).

*Spectral and analytical data of* c-*3-(1-methoxyhydroxy-carbonylmethyl)*-r-*1*,t-*2-cyclopentanedicarboxylic acid, 10*a

Infrared (KBr), v: 3700–2300(s), 1700(s) $cm^{-1}$; $^1H$ nmr (acetone-$d_6$), δ: 1.5–2.2 (broad, 4H), 2.4–2.9 (broad, 1H), 3.15 (complex absorption, 2H), 3.40 (s, 3H), 3.97 (d, $J$ = 4 Hz, 1H), 8.65 (broad, 3H); ms: 229($M^+$ – OH, 1.4), 228(0.5), 215(0.6), 201(13), 183(29), 156(11), 155(32), 123(14), 111(18), 95(13), 79(19), 67(32), 45(100). *Anal.* calcd. for $C_{10}H_{14}O_7$: C 48.78, H 5.73; found: C 48.25, H 5.68.

*Spectral and analytical data of dimethyl* c-*3-(1-methoxy-methoxycarbonylmethyl)*-r-*1*-t-*2-cyclopentanedi-carboxylate, 10*b

Infrared (film), v: 1730(s) $cm^{-1}$; $^1H$ nmr ($CDCl_3$), δ: 1.6–2.2 (broad, 4H), 2.4–2.9 (broad, 1H), 3.0–3.3 (complex absorption, 2H), 3.43(s, 3H), 3.70(s), 3.72(s), 3.75(s), 3.90(d, $J$ = 4 Hz) (total 10H); ms: 288($M^+$, 0.1), 256(1.3), 229(42), 213(8), 197(7), 169 ($M^+$ – HCOOMe – COOMe, 100), 109(34), 59(46). *Anal.* calcd. for $C_{13}H_{20}O_7$: C 54.16, H 6.99; found: C 54.26, H 6.88.

*Spectral and analytical data of trimethyl (1*R,*2*r,*3*S*)-cyclo-pentane-1,2,3-tricarboxylate, 2*b

Infrared (film), v: 1730(s) $cm^{-1}$; 200 MHz $^1H$ nmr ($CDCl_3$), δ: 1.97–2.09 (complex m, 4H), 3.05–3.20 (complex m, 2H), 3.56(t, $J$ = 8.7 Hz, 1H), 3.71(s, 9H); 50 MHz $^{13}C$ nmr ($CDCl_3$), δ: 29.42(C4 and C5), 47.40(C1 and C3), 50.07(C2), 52.16(C1—COO*Me* and C3—COO*Me*), 52.33(C2—COO*Me*), 173.76(C2—*C*OOMe), 174.18(C1—*C*OOMe and C3—*C*OOMe); ms: 245(0.4), 244($M^+$, 0.3), 213(37), 212(19), 185(14), 184(13), 180(8), 153(47), 152($M^+$ – HCOOMe – MeOH, 100), 125(90), 124($M^+$ – 2HCOOMe, 56), 93(50), 59(80). *Anal.* calcd. for $C_{11}H_{16}O_6$: C 54.09, H 6.60; found: C 54.09, H 6.66.

*(1*R,*2*s,*3*S*)-Cyclopentane-1,2,3-tricarboxylic acid, 1*a

A mixture of 0.492 g of **1***b* (2 mmol), 5 mL water, and 5 drops of concentrated HCl was refluxed for 19 h. The volatile products were removed at reduced pressure to give 0.398 g of **1***a* (1.94 mmol, 97% yield). Crystallized twice from a small volume of aqueous 3 *N* HCl, melted at 169–170°C. Infrared (KBr), v: 3600–2800(s), 1720(s), 1680(s) $cm^{-1}$; ms: 185($M^+$ – OH, 0.2), 167(0.6), 140(2), 112($M^+$ – 2COOH, 22), 67($C_5H_7^+$, 100). *Anal.* calcd. for $C_8H_{16}O_6$: C 47.53, H 4.98; found: C 47.58, H 4.96. A

sample of **1***a* was esterified with ethereal diazomethane, giving back pure **1***b* (glc).

*(1*R,2r,3S)-*Cyclopentane-1,2,3-tricarboxylic acid,* **2**a

Compound **2***a* was obtained from **2***b* in 95% yield, as described for **1***a*. Crystallized twice from a small volume of aqueous 3 *N* HCl, melted at 183–185°C. Compound **2***a* was more difficult to crystallize from 3 *N* HCl than **1***a*. Infrared (KBr), v: 3600–2400(s), 1690(s) $cm^{-1}$; ms: 185($M^+$ – OH, 2), 184(0.8), 167(2), 166(5), 156(6), 140(12), 139(15), 138($M^+$ – HCOOH – $H_2O$, 84), 112(56), 111(44), 110($M^+$ – 2HCOOH, 76), 67($C_5H_7^+$, 100). *Anal.* calcd. for $C_8H_{16}O_6$: C 47.53, H 4.98; found: C 47.51, H 4.98. A sample of **2***a* was esterified with ethereal diazomethane, giving back pure **2***b* (glc).

*Trimethyl (1*R,2s,3S)- *and (1*R,2r,3S)-*cyclopentane-1,2,3-tricarboxylate from 1-cyclopentene-1,2,3-tricarboxylic acid (12),* ***11***

A solution of 3.421 g of **11** (17.1 mmol) in 20 mL water was hydrogenated at atmospheric pressure using 0.600 g $PtO_2$ as catalyst (11). The catalyst was filtered and the residue washed with water (3 × 3 mL). The water was removed from the filtrate at reduced pressure to give 3.056 g of a viscous liquid that was esterified with ethereal diazomethane. By removing the ether, 3.191 g of a crude product was obtained, which was characterized (glc) as a 4:1 mixture of **1***b* and **2***b*, traces of **12** not being excluded. This crude product was chromatographed through 130 g silica gel using hexane–ether mixtures as eluent. The following fractions were obtained: 0.426 g of **2***b* contaminated with 6% **12** (nmr) (hexane–ether 7:3), 0.154 g of mixture of stereoisomers (hexane–ether 7:3), and 2.164 g of pure **1***b* (hexane–ether 6:4).

*Equilibration of a stereoisomeric mixture of trimethyl cyclopentane-1,2,3-tricarboxylate by reaction with sodium methoxide*

A mixture of **1***b*, **2***b*, and racemic trimethyl cyclopentane-1,2,3-tricarboxylate, **12** (1 g from a hydrogenation of **11** with 10% Pd/C and esterification with ethereal diazomethane), 0.246 g of anhydrous sodium methoxide, and 25 mL of anhydrous methanol was heated under reflux for 36 h. The mixture was neutralized with concentrated HCl, the volatile products removed at reduced pressure, and the residue treated with $CHCl_3$. By removing the chloroform at reduced pressure, 0.882 g of a mixture of **2***b* and **12** in the ratio 3:1 (nmr) was obtained.

## Acknowledgements

A fellowship from the "Ministerio de Educación y Ciencia" to C. Jaime is gratefully acknowledged. We gratefully thank M. Guerra from the Instituto de Química Bio-orgánica (Barcelona, Spain) for elemental analysis, Dr. F. Sánchez-Ferrando from the Autónoma University of Barcelona for running the 200 MHz $^1H$ and 50 MHz $^{13}C$ nmr spectra, and Mr. C. Segura for preparing compound **11**.

1. P. Camps and C. Jaime. Can. J. Chem. **59**, 2848 (1981).
2. Beilstein. Handbuch der Organischen Chemie. II, **9**, 703 (1949).
3. P. Camps and C. Jaime. Tetrahedron, **36**, 393 (1980).
4. W. C. Still, M. Kahn, and A. Mitra. J. Org. Chem. **43**, 2923 (1978).
5. P. Camps and C. Jaime. Org. Magn. Reson. **14**, 177 (1980).
6. M. Figueredo. Tesina de Licenciatura, Autónoma University of Barcelona (1979).
7. R. S. Brown and R. W. Marcinko. J. Am. Chem. Soc. **99**, 6500 (1977).
8. A. Diaz and J. Fulcher. J. Am. Chem. Soc. **96**, 7954 (1974).
9. E. L. Eliel. Stereochemistry of carbon compounds. McGraw–Hill Book Co. Inc., New York. 1962. pp. 248–252.
10. G. C. Levy and G. L. Nelson. Carbon-13 nuclear magnetic resonance for organic chemists. Wiley–Interscience, New York. 1972. pp. 44–48.
11. S. N. Balasubrahmanyam and M. Balasubramanian. Tetrahedron, **29**, 683 (1973).
12. R. E. Wesigard, Jr., R. K. Rusell, and L. A. Paquette. J. Am. Chem. Soc. **96**, 7474 (1974).

Can. J. Chem. Downloaded from www.nrcresearchpress.com by 210.87.254.42 on 09/06/12
For personal use only.

# Towards a general scheme for estimating the heats of formation of organic ions in the gas phase. Part II. The effect of substitution at charge-bearing sites

JOHN L. HOLMES AND F. P. LOSSING

*Chemistry Department, University of Ottawa, Ottawa, Ont., Canada K1N 9B4*

Received May 6, 1982

JOHN L. HOLMES and F. P. LOSSING. Can. J. Chem. **60**, 2365 (1982).

The effects on ionic heats of formation of the multiple substitution of $-CH_3$, -OH, or $-OCH_3$ groups, in place of H atoms, are described. It is shown that for all three substituents, good linear correlations exist between $\Delta H_f$(ion) and the logarithm of the number of atoms in the ion (i.e. a quantity proportional to ionic size). The changes in $\Delta H_f$(ion) resulting from successive substitutions at a charge-bearing atom or π-system essentially depend only upon the specific nucleophilic character of the group and the size of the resultant ion. Examples are given of the utility of these correlations in estimating new ionic heats of formation.

JOHN L. HOLMES et F. P. LOSSING. Can. J. Chem. **60**, 2365 (1982).

On décrit les effets des chaleurs ioniques de formation lorsqu'on substitue à des atomes d'hydrogène les groupes $CH_3$, OH, ou $OCH_3$. On montre que, pour chacun des trois substituants, il existe de bonnes corrélations linéaires entre le $\Delta H_f$(ion) et le logarithme du nombre d'atomes dans l'ion (i.e. une quantité proportionnelle à la taille de l'ion). Les variations du $\Delta H_f$(ion) qui résultent des substitutions successives au niveau de l'atome porteur de la charge ou du système π, dépend en majeure partie du caractère nucléophile spécifique du groupe et de la taille de l'ion résultant. On donne des exemples de l'utilité de ces corrélations pour l'évaluation de nouvelles enthalpies ioniques de formation.

[Traduit par le journal]

## Introduction

In Part I of the work (1) we described a method for calculating the heats of formation, $\Delta H_f$, of organic radical cations belonging to homologous series. The generic equation for this method has the form $\Delta H_f(\text{ion}) = A - Bn + C/n$, where $n$ is the number of atoms in the ion and $A$, $B$, and $C$ are constants for the series. The latter were derived from experimental data for members of the unbranched homologous series. When a generic equation for a series has been derived, correction terms for chain-branching effects and double-bond position, etc., can be established. Although the method is empirical, the form of the equation properly reflects the fact that $\Delta H_f$(ion) is the sum of the $\Delta H_f$ of the neutral molecule and its ionization energy (IE). The $A - Bn$ part of the equation is analogous to the thermochemical additivity system of Benson *et al.* (2), which accurately reproduces the linear decrease in $\Delta H_f$(neutral) with increasing homologue size. The IE, however, is not linear in molecular size, but falls at a decreasing rate. Figure 1 shows the decrease in $\Delta H_f$(neutral), ionization energy, and $\Delta H_f$(ion) as a function of molecular size, which here is simply represented by the total

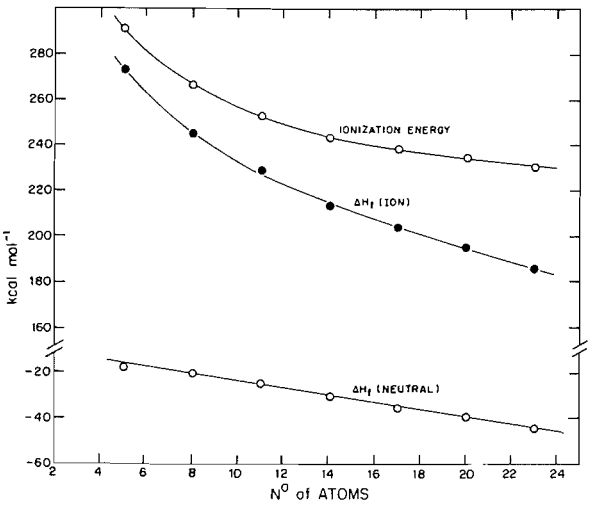


FIG. 1. Ionization energies, heats of formation of neutrals and ions for *n*-alkanes.

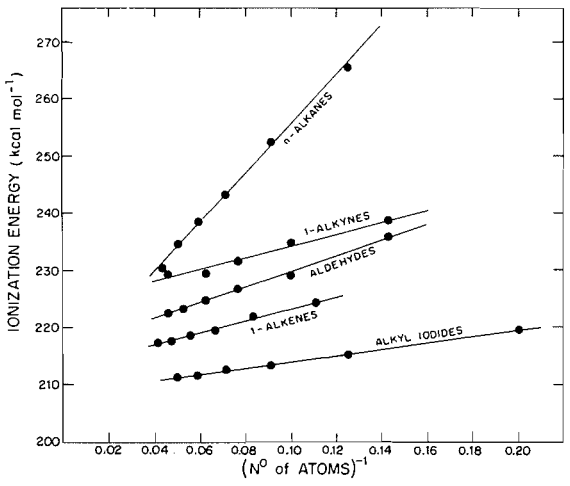


FIG. 2. Ionization energies of linear-homologous molecules vs. (number of atoms)$^{-1}$.

0008-4042/82/182365-07$01.00/0

©1982 National Research Council of Canada/Conseil national de recherches du Canada

Can. J. Chem. Downloaded from www.nrcresearchpress.com by 210.87.254.42 on 09/06/12
For personal use only.

Can. J. Chem. Downloaded from www.nrcresearchpress.com by 210.87.254.42 on 09/06/12
For personal use only.

TABLE 1. Relative stabilization of radicals and ions (kcal mol$^{-1}$)

| Structure | $\Delta H_f(R^\cdot)$ | $D$(R—H) | Relative stability | $\Delta H_f(R^+)$ | $D(R^+—H^-)$ [a] | Relative stability |
|---|---|---|---|---|---|---|
| $H.CH_2—H$ | 34 (4) | 104 | 0 | 261 (4) | 313 | 0 |
| $H_3C.CH_2—H$ | 28 (5) | 100 | 4 | 216 (4, 6) | 271 | 42 |
| $HO.CH_2—H$ | −6.2 (7) | 96 | 8 | 169 (8) | 252 | 61 |
| $CH_3O.CH_2—H$ | −1.3 (7) | 94 | 10 | 157 (8) | 235 | 78 |
| $H_2N.CH_2—H$ | 36 (9) | 94 | 10 | 178 (10) | 218 | 95 |
| $N\equiv C.CH_2—H$ | 51 (11) | 88 | 16 | 286[b] | 305 | 8 |
| $H_2C=CH.CH_2—H$ | 39 (14) | 86 | 18 | 226 (15) | 256 | 57 |

[a] $\Delta H_f[H]^- = 34.7$ kcal mol$^{-1}$.
[b] From AE $m/z$ 40 from $CH_3CN$ = 14.01 (12), and $\Delta H_f[CH_3CN]$ − 15.4 kcal mol$^{-1}$ (13).

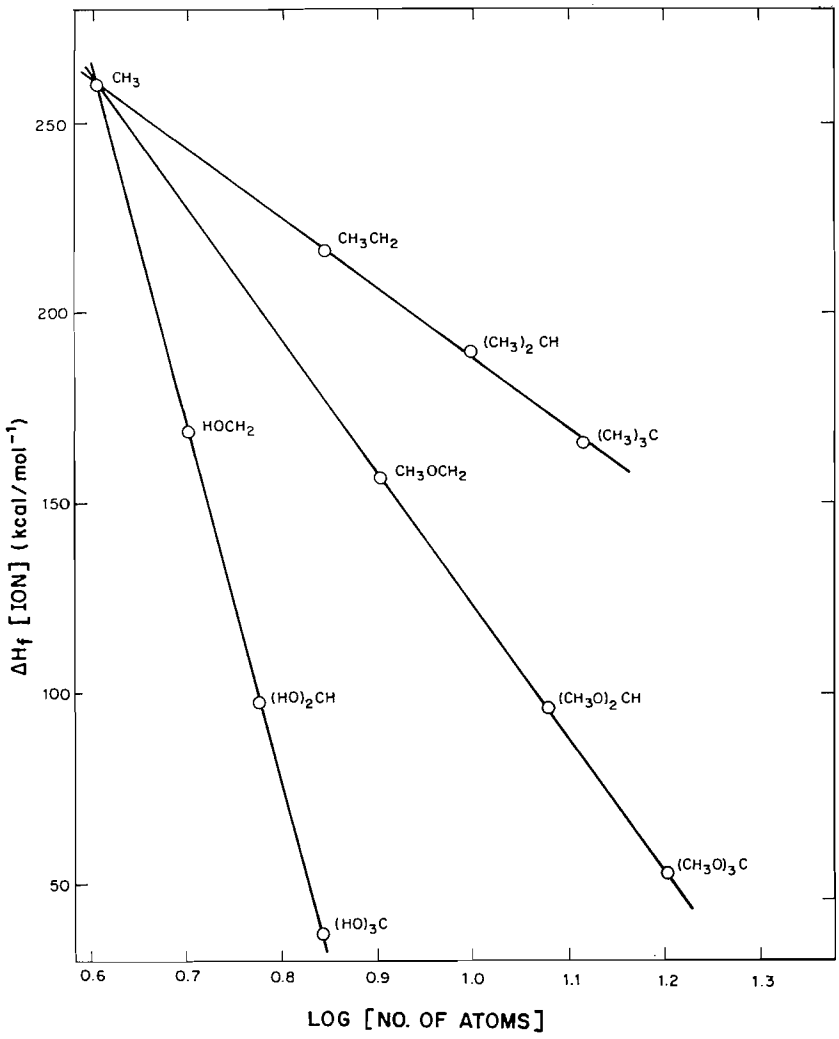


FIG. 3. $\Delta H_f$(ion) for successive substitution of -$CH_3$, -$OCH_3$, and -OH in $CH_3^+$ vs. log (no. atoms).

number of atoms in the ion. The data in Fig. 1 are for the *n*-alkanes, but other unbranched homologous series produce similar graphs. Figure 2 shows that the ionization energies of the members of linear homologous series decrease in an almost linear manner with the reciprocal of the number of atoms. It is evident therefore that the $\Delta H_f$ values for an homologous series of ions ($\Delta H_f$(ion) = $\Delta H_f$(neutral) + IE) can be closely reproduced by an equation of the form $\Delta H_f(\text{ion}) = A - Bn + C/n$. The inclusion of the appropriate correction terms for isomers, e.g. chain-branching, double-bond

Can. J. Chem. Downloaded from www.nrcresearchpress.com by 210.87.254.42 on 09/06/12
For personal use only.

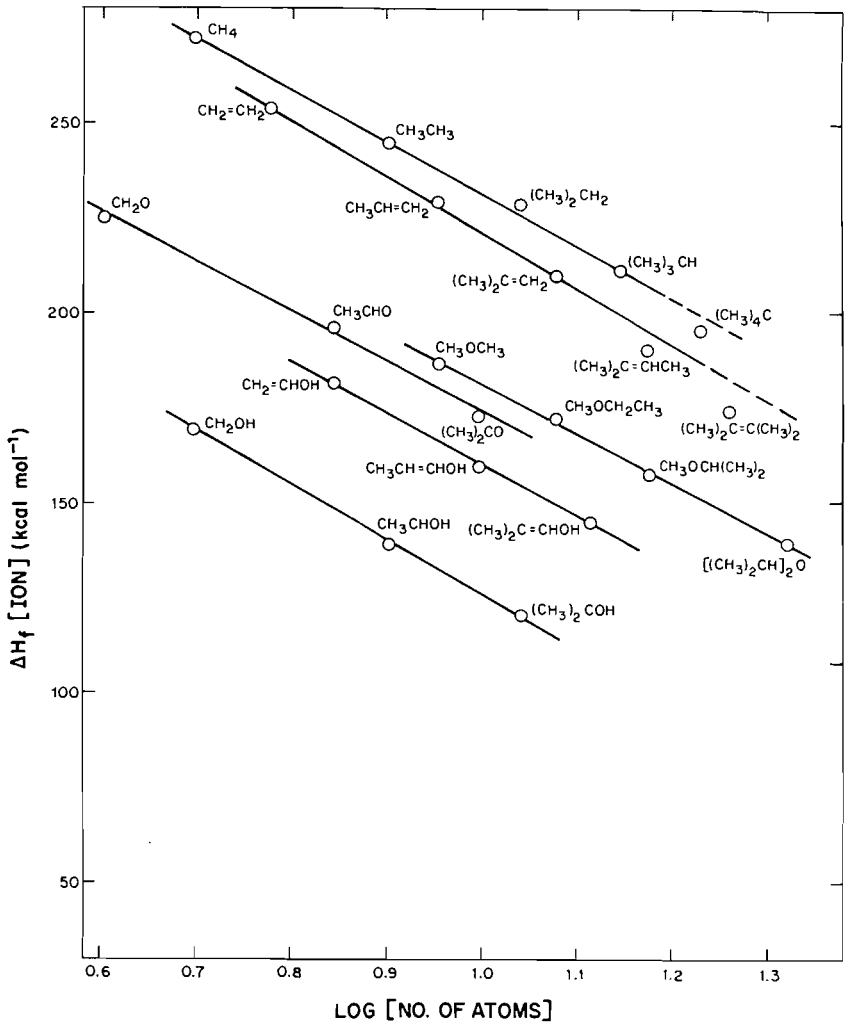


FIG. 4. $\Delta H_f$(ion) for successive substitution of -$CH_3$ at charge bearing sites in odd and even electron ions vs. log (no. atoms).

position, etc., permitted the fitting of almost all the calculated $\Delta H_f$ values to the experimental data to within $\pm 1$ kcal mol$^{-1}$ (1).

Although this method successfully reproduces the heats of formation of homologous radical cations, there are many ions of interest which cannot be described as members of homologous series, but which are nevertheless related structurally. For example, the even electron ions: $CH_3^+$, $CH_3\overset{+}{C}H_2$, $(CH_3)_2\overset{+}{C}H$, $(CH_3)_3\overset{+}{C}$, and the molecular ions of benzene, toluene, dimethyl benzene, trimethyl benzene, etc., are two such families of related ions. Here, a functional group, -$CH_3$, is successively substituted around, in the former case, a common charged site, and in the latter, a $\pi$-system bearing a delocalized charge. For such series the effect of substitution on $\Delta H_f$(ion) is conveniently and simply illustrated by plotting $\Delta H_f$(ion) against the logarithm of the number of atoms (i.e. molecular size). For many series of this kind, as shown in the present work, excellent straight-line relationships are found. Although this type of plot is also successful for the lower members of true homologous series, for higher homologues (above $C_8$) the experimental points fall increasingly below the line. The use of the generic equation avoids this error. The deviation occurs because for the higher homologues the ionization energies fall progressively more slowly, and the successive decreases in $\Delta H_f$(ion) become dominated by the *linear* decrease in $\Delta H_f$(neutral). The present work is concerned with the ionic stabilizing effects (represented here by reductions in $\Delta H_f$(ion)) of the multiple-substitution of -$CH_3$, -OH,

Can. J. Chem. Downloaded from www.nrcresearchpress.com by 210.87.254.42 on 09/06/12
For personal use only.

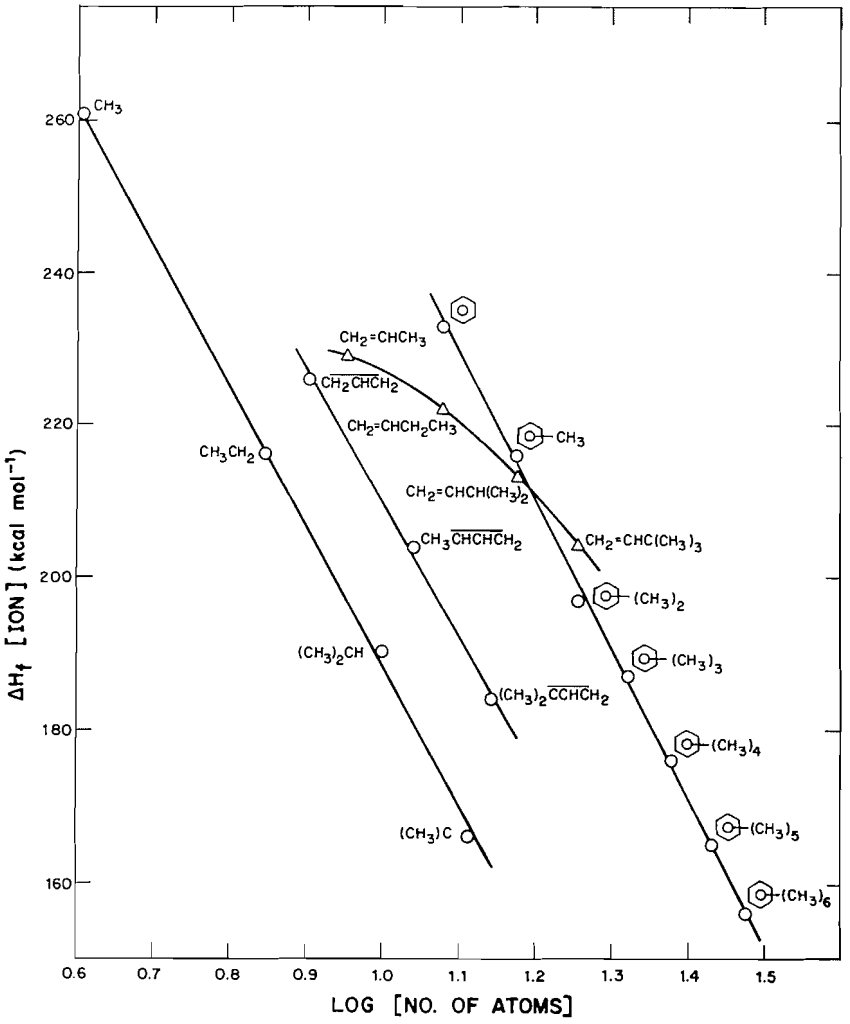


FIG. 5. $\Delta H_f$(ion) for successive substitution of -$CH_3$ at localized and delocalized charge sites (○) and at a site remote from the charge (△) vs. log (no. atoms).

and -$OCH_3$ groups around a common charge-bearing carbon atom or a variety of π-systems. The third type of series, in which the functional group is substituted at a formally uncharged site, will be discussed in a forthcoming publication.

## Experimental

The values of the heats of formation of ions used in this work are given in the Appendix. Most of these were taken from the recent literature, but some were measured in this laboratory by ionization or dissociative ionization of appropriate compounds by impact of a monoenergetic electron beam (3). The $\Delta H_f$(ion) values so obtained are briefly discussed in the Appendix.

## Discussion

The effects of substituent groups on the thermodynamic stability of organic ions has been the subject of intensive investigation for many years, particularly by studies of the relative rates of solvolytic reactions in the liquid phase. It is difficult directly to relate this enormous body of data to gas-phase ionic heats of formation because of solvation and other effects. However, the principal effects of substituent groups are well-understood in terms of the lowering of the energy of the incipient carbonium ion centre by charge delocalization. Substituent groups vary widely in their ability to provide such stabilization; their effects appear to involve both the effect of size and of specific nucleophilic character. These stabilizing effects can quantitatively be compared for radicals via the bond dissociation energies $D(RCH_2—H)$; for even-electron ions, the corresponding quantity in the charged species is the hydride ion affinity or heterolytic bond dissociation energy (HBDE), $D(R\overset{+}{C}H_2—H^-)$. As can be seen from Table 1, the stabilizing effects of various groups on a neutral $CH_3$ centre are greatly different from their effects

Can. J. Chem. Downloaded from www.nrcresearchpress.com by 210.87.254.42 on 09/06/12
For personal use only.

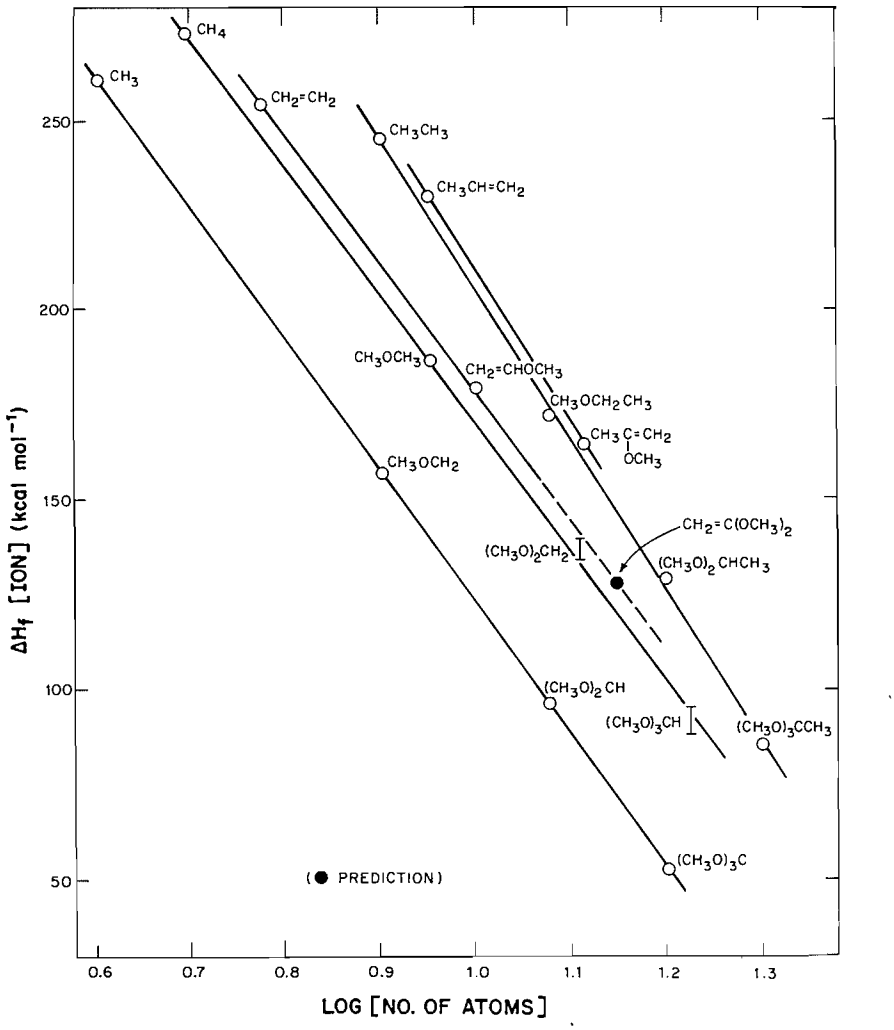


FIG. 6. $\Delta H_f$(ion) for successive substitution of -$OCH_3$ at charge bearing sites in odd and even electron ions vs. log (no. atoms).

on a *charged* centre. It is immediately evident that stabilizing effects are very much greater in ions than in neutrals. The interesting exception in Table 1 is -CN substitution, in which the ion is destabilized relative to the neutral radical. The relation between these effects and ionic abundances in mass spectra has been discussed qualitatively by many authors (see, for example, ref. 16) in terms of the familiar concepts of physical-organic chemistry.

In order to correlate the stabilizing effects of multiple-substitution for both odd- and even-electron ions, it is more convenient to use changes in $\Delta H_f$(ion) along such series, rather than HBDE comparisons. Our purpose here is to illustrate a method for estimating an unknown $\Delta H_f$(ion) from known members of its multiple-substitution series, rather than to make numerical comparisons of the stabilizing power of various substituent groups. As well as their predictive utility for missing members, these correlations can indicate a possible error in $\Delta H_f$ for a given member, or an incorrect structure assignment based on observations other than a $\Delta H_f$.

Figures 3 to 7 are plots of $\Delta H_f$(ion) versus the logarithm of the total number of atoms for members of multiple-substitution series. To facilitate comparison of different groups Figs. 3 to 6 are drawn on the same scale. Figure 3 shows the effect on ionic heat of formation of successive substitution of -$CH_3$, -$OCH_3$, and -OH in $CH_3^+$; data for all members are available (see Appendix). Good straight-line plots are obtained for each substituent. The OH-substitution line is steeper than that for -$OCH_3$, but it should be emphasized that this shows that -OH is the more effective stabilizing group *per atom*. Thus, when correlating ionic heats of formation, the *size* of the substituent group is an

Can. J. Chem. Downloaded from www.nrcresearchpress.com by 210.87.254.42 on 09/06/12
For personal use only.

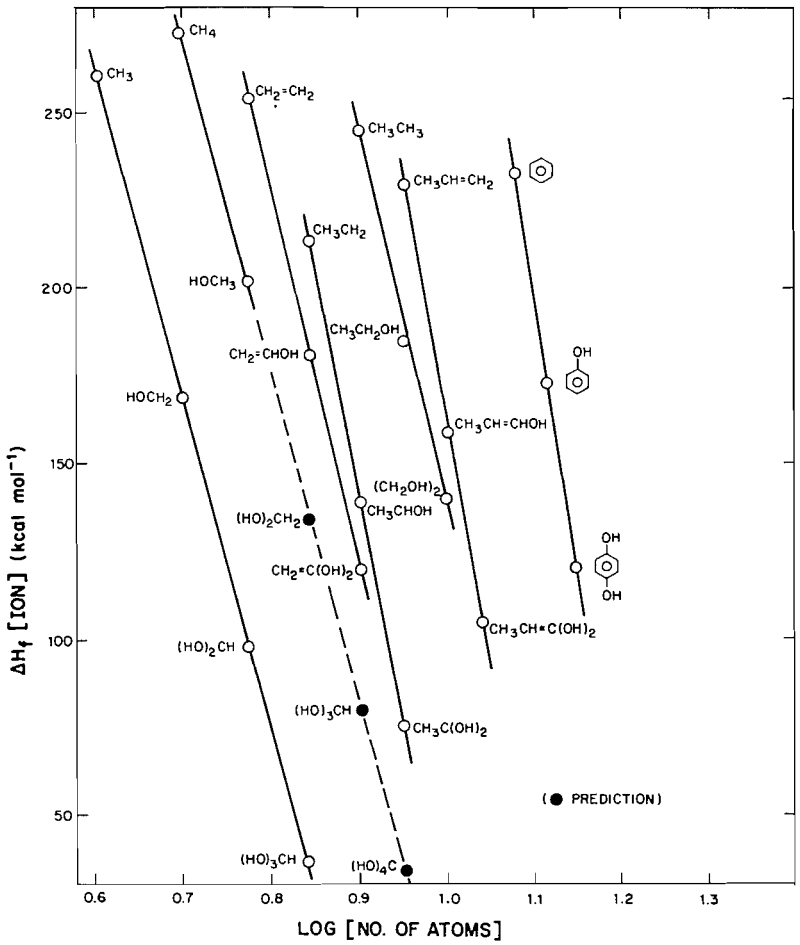


FIG. 7. $\Delta H_f$(ion) for successive substitution of -OH at charge bearing sites in odd and even electron ions vs. log (no. atoms).

important parameter, as well as its specific nucleophilic character.

Figure 4 shows six series for multiple substitution of $-CH_3$ at charge bearing sites in odd- and even-electron cations. Although, as mentioned above, the log plot begins to fail for the higher members of some series, it is evident that the slopes of the lines are closely similar. Thus to a first approximation $-CH_3$ substitution in a series produces an effect which is *only* dependent upon the *size* of the resultant ion.

In Fig. 5, the effect of $-CH_3$ substitution on $\Delta H_f$(ion) is illustrated for four multiple-substitution series. For three of these, the substitution is at either a charged carbon atom, or in contact with a charge-delocalized $\pi$-system, and the $\Delta H_f$(ion) values lie on good straight lines of approximately equal slope. In the fourth series (indicated by triangles in Fig. 5) the substitution is at a site *remote* from the charge, which here is localized in the double bond; the substitution of $-CH_3$ has in this case only a relatively small effect, the greater part of which arises from the changes in $\Delta H_f$(neutral). It is clear that for such remote substitutions, the present method will not give satisfactory estimates of $\Delta H_f$(ion).

Figure 6 similarly displays the effect of multiple-substitution of $-OCH_3$ for five series. One series has a missing member $[CH_2{=}C(OCH_3)_2]^{+\cdot}$, whose $\Delta H_f$(ion) can be predicted from the graph to be $\sim$ 127 kcal mol$^{-1}$.

In Fig. 7 the effect of successive substitution of -OH is illustrated for seven series of ions. The slopes of the lines are not quite identical but, nevertheless, the points are colinear for each series, permitting prediction of $\Delta H_f$-values. For instance, based on the line through the two available points for the series $CH_4$, $CH_3OH$, etc., one can predict that the heats of formation of the remaining members of this series, the as yet unknown ions $[(HO)_2CH_2]^{+\cdot}$, $[(HO)_3CH]^{+\cdot}$, and $[(HO)_4C]^{+\cdot}$, are approximately 134, 80, and 34 kcal mol$^{-1}$ respectively.

**Acknowledgements**

J.H. thanks the Natural Sciences and Engineer-

ing Research Council of Canada for financial support. The authors also thank M. Fingas for his assistance and continuing interest in this work.

1. J. L. Holmes, M. Fingas, and F. P. Lossing. Can. J. Chem. **59**, 80 (1981).
2. S. W. Benson, F. R. Cruikshank, D. M. Golden, G. R. Haugen, H. E. O'Neal, A. S. Rodgers, R. Shaw, and R. Walsh. Chem. Rev. **69**, 279 (1969); S. W. Benson. Thermochemical kinetics. 2nd ed. John Wiley and Sons, New York. 1976.
3. K. Maeda, G. P. Semeluk, and F. P. Lossing. Int. J. Mass Spectrom. Ion Phys. **1**, 395 (1968); F. P. Lossing and J. C. Traeger. Int. J. Mass Spectrom. Ion Phys. **19**, 9 (1976).
4. J. C. Traeger and R. G. McLoughlin. J. Am. Chem. Soc. **103**, 3647 (1981).
5. A. L. Castellhano and D. Griller. J. Am. Chem. Soc. **104**, 3655 (1982).
6. H. M. Rosenstock, R. Buff, M. A. A. Ferreira, S. G. Lias, A. C. Parr, R. L. Stockbauer, and J. L. Holmes. J. Am. Chem. Soc. **104**, 2337 (1982).
7. D. M. Golden and S. W. Benson. Chem. Rev. **69**, 125 (1969).
8. F. P. Lossing. J. Am. Chem. Soc. **99**, 7526 (1977).
9. D. Griller and F. P. Lossing. J. Am. Chem. Soc. **103**, 1586 (1981).
10. F. P. Lossing, Yai-Tai Lam, and A. Maccoll. Can. J. Chem. **59**, 2228 (1981).
11. S. W. Benson and H. E. O'Neal. Kinetic data on gas phase unimolecular reactions. NSRDS–NBS **21** (1970).
12. V. H. Dibeler and S. K. Liston. J. Chem. Phys. **48**, 4765 (1968).
13. J. B. Pedley and J. Rylance. Sussex – N.P.L. computer analyzed thermochemical data: organic and organometallic compounds. Univ. Sussex (1977).
14. M. Rossi, K. D. King, and D. M. Golden. J. Am. Chem. Soc. **101**, 1223 (1979).
15. H. M. Rosenstock, K. Draxl, B. W. Steiner, and J. T. Herron. J. Phys. Chem. Ref. Data Suppl. **6**, No. 1 (1977).
16. F. W. McLafferty. Anal. Chem. **31**, 477 (1959); H. Budzikiewicz, C. Djerassi, and D. H. Williams. Mass spectrometry of organic compounds. Holden–Day Inc. 1967.
17. J. L. Holmes, F. P. Lossing, and J. K. Terlouw. J. Phys. Chem. **80**, 2860 (1976).
18. J. L. Holmes and F. P. Lossing. J. Am. Chem. Soc. **102**, 1591 (1980).
19. V. K. Potapov, I. E. Kardash, and V. V. Sorokin. Khim. Vys. Energ. **6**, 392 (1972).
20. F. A. Houle and J. L. Beauchamp. J. Am. Chem. Soc. **101**, 4067 (1979).
21. R. Yamdagni and P. Kebarle. J. Am. Chem. Soc. **98**, 1320 (1976).

## Appendix: ionic heats of formation (kcal mol$^{-1}$)

Unless given below, all $\Delta H_f$ values are from ref. 15 and are $\Delta H_{f298}$ corrected, where appropriate, from $\Delta H_{f0}$.

Odd electron ions

| Species | $\Delta H_f$ | | Species | $\Delta H_f$ | |
|---|---|---|---|---|---|
| $(CH_3)_2C{=}CH_2$ | 209 | (1) | $CH_2{=}CHOCH_3$ | 179 | (18) |
| $(CH_3)_2C{=}CHCH_3$ | 190 | (1) | $CH_3OCH_2CH_3$ | 172 | (1) |
| $(CH_3)_2C{=}C(CH_3)_2$ | 174 | (1) | $CH_3OCH(CH_3)_2$ | 157 | (1) |
| $HOCH_2CH_2OH$ | 142 | [a] | $CH_2(OCH_3)_2$ | ~137 | [b] |
| $(CH_3)_2CO$ | 172 | (1) | $CH(OCH_3)_3$ | 90–95 | [c] |
| $CH_2{=}CHOH$ | 181 | (17) | $CH_3C(OCH_3)_3$ | ~86 | [d] |
| $CH_2{=}C(OH)_2$ | 120 | (18) | $C_6H_4(OH)_2$ | 120 | [e] |
| $CH_3CH{=}C(OH)_2$ | 105 | (18) | $CH_2{=}C(OCH_3)CH_3$ | 164 | [f] |

[a] $\Delta H_f[HOCH_2CH_2OH] = -92.6$ kcal mol$^{-1}$ (13), and IE (this work) = 10.16 eV.
[b] $\Delta H_f[CH_2(OCH_3)_2] = -83.2$ kcal mol$^{-1}$ (13) and IE ~ 9.5 eV(est.).
[c] $\Delta H_f[CH(OCH_3)_3] = -130.2$ kcal mol$^{-1}$ (13) and IE ~ 9.5 eV(est.).
[d] $\Delta H_f[CH_3C(OCH_3)_3] = -137$ kcal mol$^{-1}$ from additivity (2) and IE (this work) = 9.65 eV.
[e] $\Delta H_f$[1,4-dihydroxy benzene] = −63.4 kcal mol$^{-1}$ (13) and IE = 7.95 eV(19).
[f] From IE this work = 8.64 eV, $\Delta H_f[CH_2{=}C(OCH_3)CH_3] = -34.9$ kcal mol$^{-1}$ by additivity (2).

Even electron ions

| Species | $\Delta H_f$ | | Species | $\Delta H_f$ | |
|---|---|---|---|---|---|
| $CH_3$ | 261 | (4) | $CH_3C(OH)_2$ | 75 | [h] |
| $CH_3CH_2$ | 216 | (4, 6) | $CH_3CHOH$ | 139 | (8) |
| $(CH_3)_3CH$ | 191 | (4, 6) | $(CH_3)_2COH$ | 120 | (8) |
| $(CH_3)_3C$ | 166 | (4, 6, 20) | $CH_3OCH_2$ | 157 | (8) |
| $CH_2OH$ | 168 | (8) | $(CH_3O)_2CH$ | 97 | [i] |
| $CH(OH)_2$ | 98 | [g] | $(CH_3O)_3C$ | 53 | [j] |
| $C(OH)_3$ | 37 | [k] | | | |

[g] From proton affinity PA [HCOOH] = 178 kcal mol$^{-1}$ (21).
[h] From PA [$CH_3COOH$] = 187 kcal mol$^{-1}$ (21).
[i] From AE (this work) $m/z$ 75 $[C_3H_7O_2]^+$ from $CH_3CH(OCH_3)_2 = 9.74$ eV; $\Delta H_f[CH_3CH(OCH_3)_2] = -93.1$ kcal mol$^{-1}$ (13).
[j] From AE (this work) $m/z$ 105 $([C_4H_9O_3]^+$ from $(CH_3O)_3CCH_3 = 9.86$ eV and from $(CH_3O)_3CH = 10.22$ eV. $\Delta H_f[(CH_3O)_3CCH_3] = -141$ kcal mol$^{-1}$ and $\Delta H_f[(CH_3O)_3CH] = -130.2$ kcal mol$^{-1}$ (13).
[k] From AE (this work) $m/z$ 63 $[CH_3O_3]^+ = 11.72$ eV from diethyl carbonate; neutral fragments $C_2H_4$ and $CH_2{=}\dot{C}H$ ($\Delta H_f = 68$ kcal mol$^{-1}$ (11)).

Can. J. Chem. Downloaded from www.nrcresearchpress.com by 210.87.254.42 on 09/06/12
For personal use only.

# Characterization of aspen exploded wood lignin

R. H. MARCHESSAULT,[1] SUZANNE COULOMBE, AND HIROMICHI MORIKAWA
*Department of Chemistry, University of Montreal, C.P. 6128, Montreal, P.Q., Canada*

AND

DANIELLE ROBERT[2]
*Laboratoires de Chimie, Département de Recherche Fondamentale, Centre d'Etudes Nucléaires, 85X-38041, Grenoble Cedex, France*

Received December 22, 1981

R. H. MARCHESSAULT, SUZANNE COULOMBE, HIROMICHI MORIKAWA, and DANIELLE ROBERT. Can. J. Chem. **60**, 2372 (1982).

Exploded wood lignin (EXWL) was extracted from moist steam hydrolysed aspen (*Populus tremuloides*) wood using methanol. The lignin was examined by elemental analysis, gel permeation chromatography, infrared spectroscopy, proton and $^{13}C$ nmr. The observed nmr spectra were compared with those of aspen milled wood lignin (MWL). Typical composition of the material is $C_9H_{9.2}O_{2.7}(OCH_3)_{1.1}$. Assignment of all the signals in the nmr spectrum led to the conclusion that the explosion process causes cleavage of the β-aryl-ether bond. The weight average molecular weight was found to be 1700–1900 and the polydispersity 2.6. The finely divided exploded wood was soluble in 90% methanol/water mixtures to well beyond 20% by weight at room temperature.

R. H. MARCHESSAULT, SUZANNE COULOMBE, HIROMICHI MORIKAWA et DANIELLE ROBERT. Can. J. Chem. **60**, 2372 (1982).

Utilisant le méthanol, on a extrait la lignine de bois éclaté (LBE) de bois de peuplier (*Populis tremuloides*) hydrolysé par de la vapeur humide. On a étudié la lignine en faisant appel à l'analyse élémentaire, à la chromatographie par permation sur gel, à la spectroscopie infrarouge et rmn du proton et du $^{13}C$. On a comparé les spectres de rmn observés à ceux de la lignine du bois moulu de peuplier (LBM). La composition typique du produit est: $C_9H_{9,2}O_{2,7}(OCH_3)_{1,1}$. L'identification de tous les signaux du spectre de rmn conduit à conclure que le processus d'explosion provoque une rupture de la liaison éther en β du groupe aryle. Le poids moléculaire moyen est de 1700–1900 et la polydispersité est de 2,6. Le bois explosé finement divisé est soluble dans des mélanges à 90% méthanol/eau jusqu'à des concentrations allant au-delà de 20% en poids à la température ambiante.

[Traduit par le journal]

## Introduction

A new class of lignin material is appearing in the published literature at this time (1–3). The principal characteristics of these "emerging lignins" are: (*i*) extensive solubility in simple organic solvents and (*ii*) average molecular weights corresponding to oligomeric size molecules. By contrast, lignins from waste pulping liquors have been subjected to extensive exposure to base or acid and as a result may have undergone repolymerization (3) and chemical transformation. Certainly the sulphonic acid groups of the familiar lignosulfonates are known to result from the action of pulping reagents.

Milled wood lignin (MWL) is recognized as an isolated lignin which most closely resembles the true native lignin. The reported (4) molecular weight of 11 000 for the material extracted in dioxane or other neutral solvents and its characteristic nmr spectrum will be used as a reference material in this study.

It is important to note that lignin does not have a regular repeating unit. Nevertheless it is possible to characterize hardwood lignins by the fact that 65% of the interunit linkages are of the aryl-ether type (5). In general it is reported to be a non-linear macromolecule (4, 5). Basic differences between softwood and hardwood lignins relate to the presence of syringyl and guaiacyl groups in hardwoods while softwood lignin has only guaiacyl. Furthermore, in softwood lignins only 45% of the interunit bonds are of the β-aryl-either type.

In this study we will review characterization of organic solvent soluble lignin obtained by explosion of aspen wood (1, 2), which will be referred to as EXWL. The explosion process (6) is a steam hydrolysis at high temperature (220–240°C) and at 600 psi of wood materials followed by mechanical shock and quench to room temperature and atmospheric pressure. Due to the natural acidity of wood, the reaction takes place at acid pH. The process destructures and comminutes the wood tissue and rapidly terminates the chemical reactions underway. The product of this explosive hydrolysis is a finely divided cellulose which retains its intrinsic crystallinity but has been destructured in terms of wood morphology (1). The material is dark brown with a consistency of potting

[1]Present address: Xerox Research Centre of Canada, 2480 Dunwin Drive, Mississauga, Ont., Canada.

[2]Associated with Université Scientifique et Médicale de Grenoble, France.

0008-4042/82/182372-11$01.00/0

©1982 National Research Council of Canada/Conseil national de recherches du Canada

Can. J. Chem. Downloaded from www.nrcresearchpress.com by 210.87.254.42 on 09/06/12
For personal use only.

TABLE 1. Comparison of ultraviolet absorption data between aspen exploded wood lignin and milled wood lignins

| | Absorption coefficient ($E\%_{cm}$) | | | | |
|---|---|---|---|---|---|
| | 238 nm | 260 nm | 280 nm | 305 nm | 350 nm |
| Aspen EXWL | 253 | 171 | 173 | 126 | 71 |
| Hardwood MWL[a] | — | 87–137 | 118–142 | 60–73 | 17–23 |
| Softwood MWL[b] | — | 142–164 | 177–202 | 90–138 | 33.6–51.0 |

[a]Reference 8.
[b]Reference 9.

Can. J. Chem. Downloaded from www.nrcresearchpress.com by 210.87.254.42 on 09/06/12
For personal use only.

soil with about 50% moisture. The various experiments which will be described below are based on a fractionation of the explosion product according to a published scheme (2) which involves: (*a*) water extraction to remove the hemicelluloses and some water soluble lignin; (*b*) alcohol extraction of lignin from the moist residue leaving celulose contaminated with a few percent of lignin and some hemicellulose.

## Experimental

*Lignin samples*

The aspen (*Populus tremuloides*) EXWL sample was prepared by methanol extraction of the moist (50% $H_2O$) exploded wood followed by fractional precipitation with distilled water and drying in air (1, 2). The EXWL was provided by E. A. DeLong of 15 Milne Crescent, Kanata, Ontario, Canada; the explosion process and fractionation follow a preferred description disclosed by him (6): "500–700 psi and 200–238°C (in particular 234°C) achieved in less than 60 s (preferably 45 s)".

*Ultraviolet and infrared spectroscopy*

Ultraviolet spectra of EXWL were recorded at a concentration of 0.0027% in methanol on a "Unicam SP 1700". Infrared spectra were recorded on a Beckman IR 4250 using the KBr disk method.

*Nuclear magnetic resonance spectroscopy*

$^1H$ nmr spectra were recorded at 250 MHz on a CAMECA spectrometer.

$^{13}C$ nmr spectra were recorded at 62.9 MHz on a BRUKER WM250 spectrometer using the FT mode. The protons were broad band decoupled. In both cases the samples were examined at a concentration of 14.5% in DMSO-$d_6$ and the spectra were recorded at a temperature of 333 K. All chemical shifts ($\delta$) are downfield from TMS.

*Intrinsic viscosity*

The intrinsic viscosities of EXWL were determined using an Ubbelohde viscometer. Measurements were made at 25°C at concentrations of 1.1% to 4.7% in methanol, acetone, and pyridine.

*Elemental analyses*

Lignin samples were analysed for C, H, O, and methoxyl content by Schwarzkopf Microanalytical Laboratory, Inc., New York, NY.

*Gel permeation chromatography*

Gel permeation chromatography was carried out using equipment made by Toyo-Soda (TS). The sample was dissolved in tetrahydrofuran at a concentration of 0.525%. Fractionation was achieved by using a combined column polystyrene gel (TSKG4000H8 + G2000H8 or G2500H8X2; Toyo-Soda, Tokyo, Japan) packed in a stainless steel tube (7.5 mm id × 120 cm long) and a sample flow-rate of 1.0 to 1.1 mL at room temperature. The eluant was monitored by differential refractometry (TSKRI-8) and light scattering (TSKLS0-8).

## Results

*Chemical composition of EXWL*

Based on elemental analysis (2), the typical composition of aspen EXWL is $C_9H_{9.2}O_{2.7}(OCH_3)_{1.1}$. Recently, Chua and Wayman (3) have reported aspen MWL of the composition of $C_9H_{8.70}O_{3.05}(OCH_3)_{1.47}$. This indicates that EXWL is a "modified" lignin and characteristically has a low methoxyl content.

The ultraviolet absorption spectrum of aspen EXWL has been reported previously (2). The spectrum is characteristic of phenolic compounds but the absorption maximum is observed at a higher wavelength (238 nm) than is reported for aspen lignin (6, 7). Table 1 lists the absorption coefficient ($E\%_{cm}$) of EXWL at various wavelengths. This table also contains the results of MWL of hardwoods and softwoods reported by Sarkanen *et al.* (8, 9). The absorption coefficient of EXWL is considerably higher than that of hardwood MWL throughout the region of 260 nm to 350 nm and higher or comparable to softwood MWL. The lower absorption coefficient of hardwood MWL at 280 nm, as compared to softwood MWL, is attributed to the presence of syringyl groups in the former lignin (9, 10). In hardwoods, lignins show a high absorption coefficient (maximum values in hardwood MWL in Table 1), which is attributed to the *p*-hydroxybenzoate groups in the lignins (13).

Typical infrared spectra of aspen EXWL are shown in Fig. 1. The spectra showed characteristic "lignin bands", e.g. at 1600 $cm^{-1}$ and 1510 $cm^{-1}$ which are due to aromatic groups (2). Depending on the explosion conditions the spectra showed a difference in the 1700–1750 $cm^{-1}$ region (see

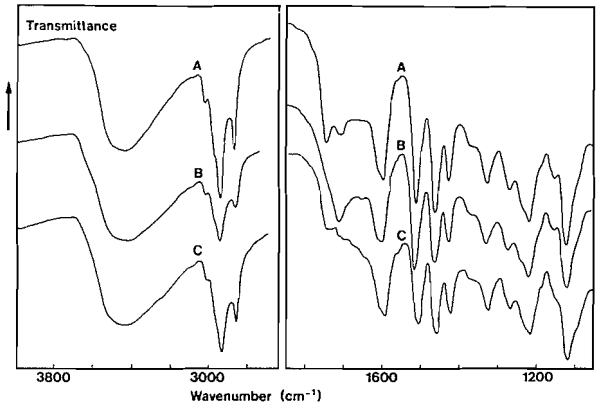


FIG. 1. Infrared spectra of aspen exploded wood lignins before (*A*, *B*) and after (*C*) saponification.

Fig. 1). In one case (spectrum *A*) two bands at 1710 $cm^{-1}$ and 1745 $cm^{-1}$ were observed while the latter band was very weak or not observed in the other (*B*). These bands are assigned to unconjugated carbonyl groups (11, 12). Saponification of EXWL with 0.1 *N* NaOH for 24 h at room temperature decreased the intensities of these bands but significant absorptions remained at these frequencies (*C*). This indicates the presence of unconjugated ketone and/or aldehyde groups as well as carboxyl ester groups in aspen EXWL. In the spectra of lignin preparations including MWL and solvolysis lignins, the bands observed at 1710–1750 $cm^{-1}$ are attributed to unconjugated carboxyl ester groups (6, 13) or unconjugated aliphatic or β-ketone groups (12, 14–18). It should be noted that in the reported lignin spectra the bands due to conjugated carbonyl groups are observed at 1660–1670 $cm^{-1}$ whereas only background absorption was detected in this region of the spectrum of EXWL.

The relative intensities of the unconjugated carbonyl bands in aspen EXWL were higher (about two times) than in the aspen MWL (6, 13). Based on differential infrared spectra of lignins in woods and pulps, Bolker (15, 19) has shown that unconjugated β-ketone groups in isolated lignins are formed during solvolytic isolation. Recently, Lora and Wayman (20) have shown that heating of aspen MWL at low pH increased the absorption intensity of the infrared band attributable to unconjugated β-keto and carboxylic acid groups in the lignin. Thus the results suggest that the explosion process causes some bond-breakage or bond rearrangement resulting in increased carbonyl groups in the lignin fraction.

The proton nmr spectra of MWL and EXWL from aspen are shown in Fig. 2 and assignments are made in Table 2. Comparison of the spectra shows the presence of typical lignin resonances (4, 21–24), e.g. signals *6* and *10*, respectively, are due to protons of methoxyl and aromatic groups. It is noteworthy that a weak, but distinct peak at 5.3 ppm is observable in EXWL, supporting the idea that phenyl coumaran structures are still present in this lignin (22, 26). The addition of $CF_3COOD$ shifted the hydroxyl protons (signal *5*) downfield (21, 25) whereas previously they resonated at 3.4 ppm. There are, nevertheless, important differences in the two spectra: (*i*) signals of saturated aliphatic side chain protons between 0.9 and 2.2 ppm are more intense in EXWL than in MWL which suggests that the side chains in $C_9$ units are saturated or reduced in EXWL; and (*ii*) signals between 4.2 and 5 ppm corresponding to H-α, H-β, and H-γ attached to carbons involved in aryl-ether bonds or hydroxyl bonds become very weak in EXWL. This suggests that β-O—4 linkages have been split and comparison of the $^{13}C$ spectra (see below) strongly supports this interpretation.

The $^{13}C$ nmr spectra of aspen MWL and EXWL are shown in Fig. 3. The assignment of the peaks in the spectra (Table 3) was made based on comparison with the results of lignin model compounds and native lignins reported by Nimz (5), Ludemann and Nimz (27), and Gagnaire and Robert (28). The nomenclature used in this study (Fig. 4) is the same as that used by previous authors (5).

*Carbonyl and carboxyl carbons*

Signal *2*, at 191.7 ppm, is strong in the EXWL spectrum but is very weak in the MWL spectrum, it can be assigned to α-carbon aldehyde groups in syringyl structure; this assignment is in keeping with the relatively greater intensity of signal *16* in EXWL. There are no carbonyl signals in EXWL spectrum towards 200 ppm which could be assigned to unconjugated ketone groups although the infrared spectrum indicates the presence of such groups. Signals *3*, *4*, and *5* between 160 and 169.5 ppm correspond to carboxylic carbons (as in esters) and they are particularly important in MWL but they are absent in EXWL.

*Aromatic carbons*

The major differences between the two spectra concern: (*i*) signal *6*, typical of C-3/C-5 carbons in etherified syringyl units, is definitely less intense in EXWL than in MWL; (*ii*) signal *8*, assigned to C-3

Can. J. Chem. Downloaded from www.nrcresearchpress.com by 210.87.254.42 on 09/06/12
For personal use only.

Can. J. Chem. Downloaded from www.nrcresearchpress.com by 210.87.254.42 on 09/06/12
For personal use only.

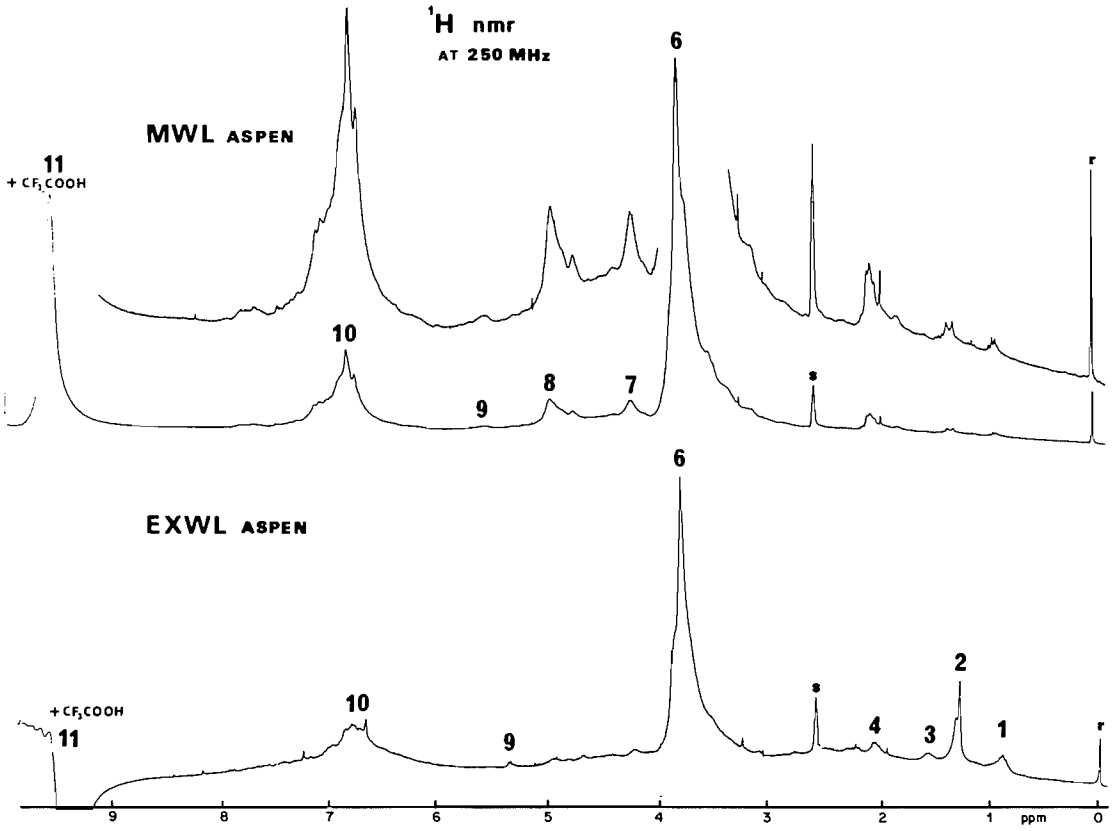


FIG. 2. Proton nmr spectra of MWL lignin and exploded wood lignin from *Populus tremula*. S; solvent (DMSO-$d_6$). Signal *5* shifted downfield in both spectra by addition of $CF_3COOD$. The chemical shifts are in ppm downfield from internal TMS.

TABLE 2. Assignment of $^1$H nmr spectra of aspen milled wood lignin (MWL) and exploded wood lignin EXWL. Chemical shifts are given in ppm downfield from TMS

| Signal | EXWL | MWL | Assignments |
|---|---|---|---|
| *1* | 0.9 | 0.9 | Methyl } protons in aliphatic saturated structures |
| *2* | 1.2 | 1.2 | Methylene } |
| *3* | 1.5 | — | Methylene } |
| *4* | 2.0–2.2 | 2.2 | Methyl or methylene protons adjacent to double bond or carbonyl group |
| *5* | 3.4 shifted to 9.5 | 3.4 shifted to 9.5 | Hydroxyl protons (strongly affected by treatment with $D_2O$) |
| *6* | 3.8 | 3.8 | Methoxyl protons |
| *7* | 4.2 | 4.2 | H-γ in β-O—4 structure |
| *8* | 4.9 | 5.0 | H-γ in β-O—4 structure |
| *9* | 5.3 | 5.3 | H-α in phenyl coumaran structure |
| *10* | 6.4–7.0 | 6.4–7.0 | Aromatic protons |
| *11* | 9.5 | 9.5 | Hydroxyl protons shifted by exchange with $CF_3COOD$ |

Can. J. Chem. Downloaded from www.nrcresearchpress.com by 210.87.254.42 on 09/06/12
For personal use only.

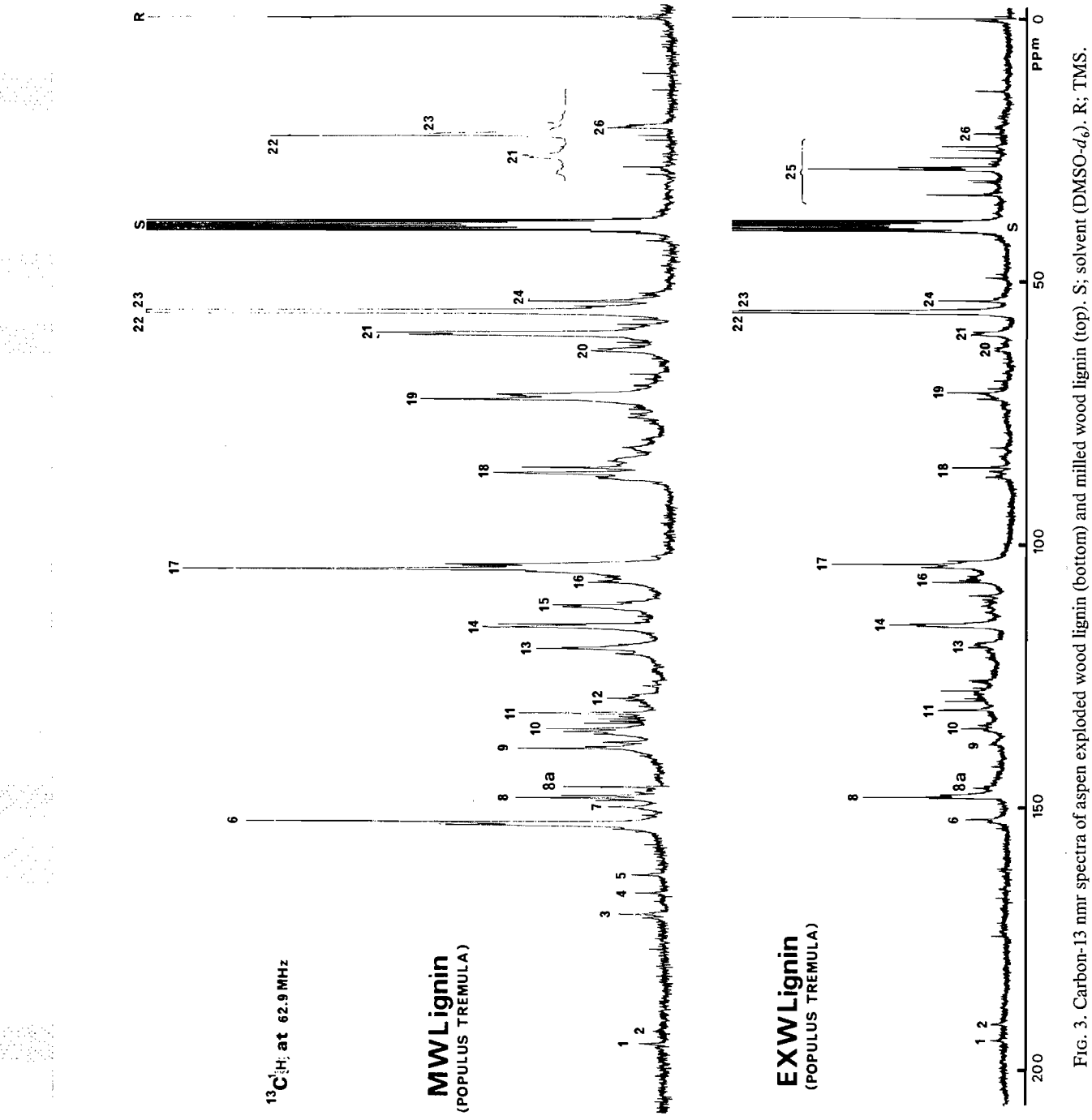


FIG. 3. Carbon-13 nmr spectra of aspen exploded wood lignin (bottom) and milled wood lignin (top). S; solvent (DMSO-$d_6$). R; TMS.

Can. J. Chem. Downloaded from www.nrcresearchpress.com by 210.87.254.42 on 09/06/12
For personal use only.





TABLE 3. Assignment of $^{13}C$ nmr spectra of aspen milled wood lignin (MWL) and exploded wood lignin (EXWL) shown in Fig. 3

| Signal | δ ppm EXWL | Intensity | MWL | Intensity | Assignments |
|---|---|---|---|---|---|
| *1* | 193.8 | w | 194 | w | γ-C(=O)H in cinnamaldehyde |
| *2* | 191.7 | m | 191.6 | vw | α-C(=O)H |
| *3* | — | — | 169.5 | w | α- or β- or γ-C(=O)OR |
| *4* | — | — | 165.3 | w | α- or β- or γ-C(=O)OR |
| *5* | | vw | 160.1 | w | *p*-Hydroxybenzoate groups |
| *6* | 152.3 | m | 152.3 | vs | C-3/C-5 in syringyl, etherified |
| *7* | — | — | 149.2 | w | C-4 in guaïacyl, etherified |
| *8* | 147.9 | s | 147.4 | m | C-3 in guaïacyl and C-3/C-5 in syringyl, non-etherified |
| *8a* | 145.2 | w | 145.2 | m | C-3 in guaïacyl etherified |
| *9* | 137.7 | vw | 137.9 | m | C-1/C-4 in syringyl, non-etherified |
| *10* | 134.7 | m | 134.5 | m | C-1 in guaïacyl etherified, C-4 in pinoresinol and β-1 unit |
| *11* | 131.4 | m | 131.3 | m | C-β in cinnamaldehyde |
| *12* | | broad | 128.4 | w | C-2/C-6 in *p*-hydroxyphenyl units |
| *13* | 119.4 | vw | 119.3 | m | C-6 in guaïacyl etherified |
| *14* | 115.1 | s | 114.9 | m | C-5 in guaïacyl, non-etherified, and C-3/C-5 in *p*-hydroxyphenyl unit |
| *15* | 110.9 | vw | 111.1 | m | C-2 in guaïacyl, etherified |
| *16* | 107 | m | 107 | w | C-2/C-6 in syringyl with α-C(=O)H |
| *17* | 104 | s | 104 | s | C-2/C-6 in syringyl, etherified or not |
| *18* | 85.9 | w | 86.3 | s | C-β in β-O—4 units |
| *19* | 71.3 | w | 71.6 | s | C-α in β-O—4 units |
| *20* | 62.6 | w | 62.6 | w | C-γ and C-β in β-1 dilignol; C-γ in phenylcoumaran |
| *21* | 59.9 | w | 59.8 | s | C-γ in β-O—4 units |
| *22* | 56 | vs | 55 | vs | —$OCH_3$ in syringyl units |
| *23* | 55.6 | vs | 55.5 | vs | —$OCH_3$ in guaïacyl units |
| *24* | 53.6 | m | 53.6 | m | C-β in pinoresinol and phenyl coumaran units |
| *25* | 21–33.6 | m | — | — | Saturated aliphatic side chains carbons |
| *26* | 21 | w | 21 | vw | Saturated aliphatic side chains carbons |

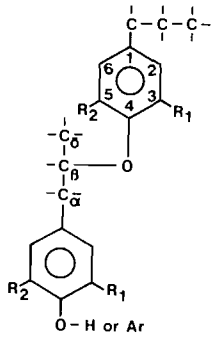


FIG. 4. The β-aryl-ether type (β-O—4) linkage in lignin (ref. 5). Guaiacyl unit: $R_1 = OCH_3$, $R_2 = H$; syringyl unit: $R_1 = R_2 = OCH_3$.

in non-etherified guaiacyl units and C-3/C-5 in non-etherified syringyl, is more intense in EXWL than in MWL; and (*iii*) signal *7*, assigned to C-4 in etherified guaiacyl units, disappears in the EXWL spectrum.

These observations indicate that EXWL is characteristically de-etherified as compared to MWL. This fact is confirmed in the EXWL spectrum by the near disappearance of signals *13* and *15*. On the other hand, signal *14* is relatively more intense in EXWL than in MWL which supports the idea that in addition to an increase of non-etherified units there is an increase of *p*-hydroxyphenyl units. This is confirmed by the somewhat lower methoxyl content for EXWL compared to MWL (cf. below).

*Aliphatic carbons*

Compared to MWL, signals *18*, *19*, and *21* in the EXWL spectrum are significantly weaker. Since these are assignable to C-β, C-α, and C-γ carbons of the propane side chains when β-O—4 linkages are present, the de-etherification must occur at the β-O—4 linkage as a result of the explosion process. This is a reasonable consequence of the predominance of α- and β-aryl-ether linkages (5) and their reported weakness of such linkages in lignin solvolysis studies (5, 29). It has also been reported (30) that the thermal stability of alkyl–aryl linkages is less in hardwoods than in softwoods which is in keeping with the lack of success of the explosion process with gymnosperms.

Methoxyl signals: the resolution of the spectrum allows observation of two distinct signals, *22* and *23*, which are assigned respectively to $—OCH_3$ syringyl and $—OCH_3$ guaiacyl groups; the chemical shifts of these signals and their multiplicity (quartets) support these assignments. An approximate quantitative estimation of the ratio $G_{OCH_3}/S_{OCH_3}$ yields 0.40 and 0.33 for MWL and EXWL, respectively, which suggests that slightly more guaiacyl moieties than syringyl are affected by the explosion process.

Finally, the peaks between 21 and 33 ppm which are due to aliphatic carbons are stronger in the EXWL spectrum than in that of MWL. Signal *26* corresponds to a $—CH_3$ group. This indicates the presence of a saturated propane side chain in EXWL which agrees with the proton nmr results as described above.

*Explosion temperature and chemical composition*

One of the important variables in the explosion process is the maximum temperature prior to pressure release ("explosion temperature"). Because of the short processing period it is not possible to achieve a true equilibrium state, hence pressure was set as rapidly as possible (~630 psi) while time was varied in a sequence of runs which probed the effect of explosion temperature. In no case was the total time more than 60 s. A series of lignin samples derived from exploded wood which had been prepared at different explosion temperatures was examined. These lignins were subjected to elemental and methoxyl analysis. The results of these analyses are shown in Figs. 5 and 6.

The most striking feature of the data is the sharp inflection in the curves at about 235°C. Since the process literature (6) states that 234°C is an optimum temperature for achieving desirable properties such as lignin solubilization and enzyme accessibility of the cellulose (2), the inflection point

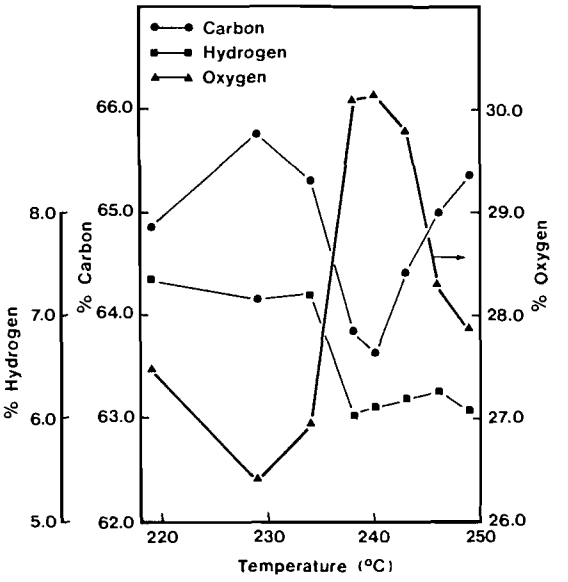


FIG. 5. Carbon, hydrogen, and oxygen content of aspen exploded wood lignin plotted against "explosion temperature".

Can. J. Chem. Downloaded from www.nrcresearchpress.com by 210.87.254.42 on 09/06/12
For personal use only.

Can. J. Chem. Downloaded from www.nrcresearchpress.com by 210.87.254.42 on 09/06/12
For personal use only.

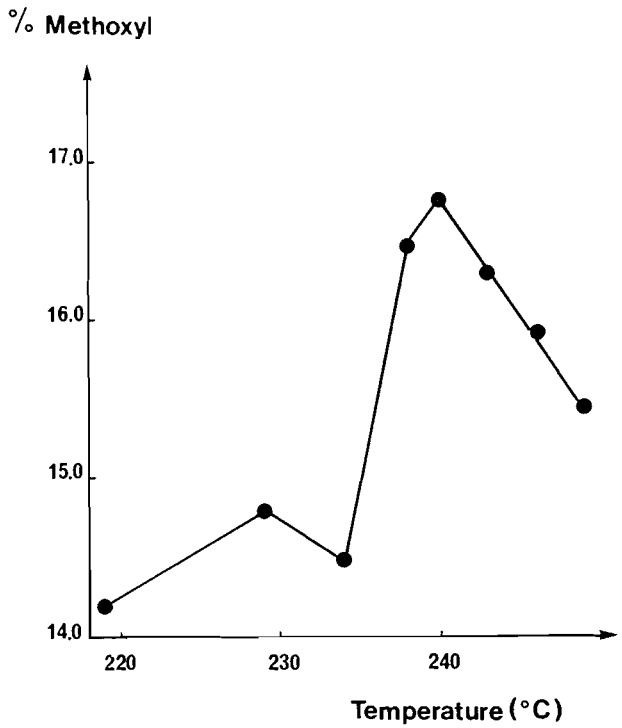


FIG. 6. Methoxyl content of aspen exploded wood lignin plotted against "explosion temperature".

probably has significance in terms of the combined chemical and morphological changes which are taking place. The variation in properties, however, reflects the variation in composition of the extracted lignin and no attempt is made to interpret these results since the total lignin in each sample was not analysed.

*Molecular weight distribution*

Based on the vapor phase method, the number-average molecular weight, $M_n$, of aspen EXWL was found to be 700 g/mol which roughly corresponds to four phenylpropane units (2).

The intrinsic viscosity, [η], values of EXWL in different solvents are listed in Table 4. In general these values are lower than those obtained for aspen autohydrolysis lignins (3) or other lignin preparations (31). The Huggins constant, $k'$ (see Table 4), and the intrinsic viscosities indicate that the "better solvent" for EXWL is in the order: pyridine > methanol > acetone.

A typical gel permeation chromatogram of EXWL is shown in Fig. 7 where the eluant was monitored by differential refractometry (RI) and light scattering (LS). The chromatogram can be divided into five fractions. Table 5 lists molecular

TABLE 4. Intrinsic viscosity, [η], of aspen exploded wood lignin expressed in dL/g; $k'$ is the Huggins constant

| Solvent | [η] | $k'$ |
|---|---|---|
| Methanol | 0.036 | 1.1 |
| Acetone | 0.036 | 1.9 |
| Pyridine | 0.048 | 0.8 |

weight ($M$) ranges (using polystyrene standards) of EXWL obtained by two different column systems. It is clear that about one-third of EXWL is "high" molecular weight ($M$ = 1300–7000) and about two-thirds have molecular weight less than 1300. From these data, the weight-average molecular weight, $M_w$, of EXWL was found to be 1700–1900 and thus the polydispersity, $M_w/M_n$, is 2.4 to 2.7. These molecular weight results and polydispersity estimates are much lower than observed for autohydrolysis lignins (3) or lignosulfonates (32) but similar to the values obtained for kraft lignins (33, 34).

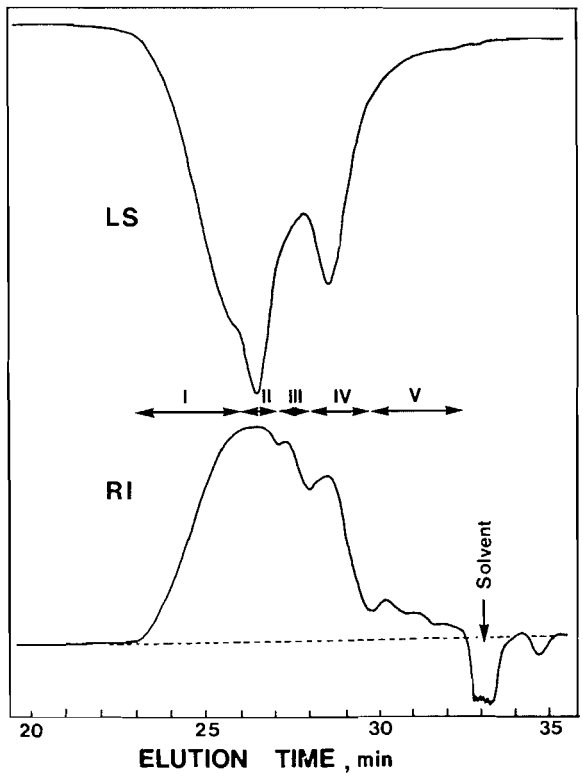


FIG. 7. Gel permeation chromatogram of aspen exploded wood lignin. The combined column (TSKG4000H8 + G2000H8) was used. Elution volume = 1.1 mL × elution time. See text for detail.

TABLE 5. Molecular weight range of aspen exploded wood lignin

| Fraction No. | Relative amount, % | $\bar{M}$ range |
|---|---|---|
| *TSKG4000H8 + G2000H8 column* | | |
| I | 28.9 | 7000–1300 |
| II | 28.7 | 1300–700 |
| III | 15.8 | 700–500 |
| IV | 20.0 | 500–250 |
| V | 6.6 | 250–150 |
| *TSKG2500 column (×2)* | | |
| I | 41.9 | 7000–800 |
| II | 13.4 | 800–600 |
| III | 20.2 | 600–250 |
| IV | 19.1 | 250–200 |
| V | 5.4 | 200–150 |

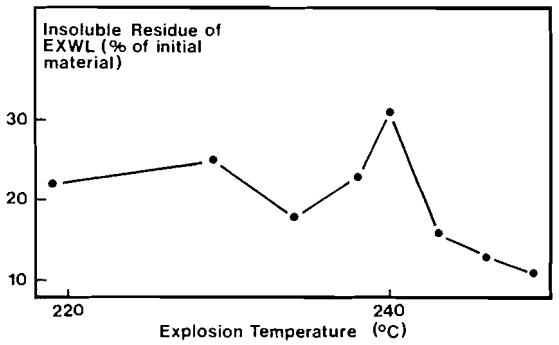


FIG. 9. Insoluble residue of aspen exploded wood lignin in 100% methanol plotted against "explosion temperature". The final concentration of lignin was about 1% and other conditions are as in Fig. 8.

*Solubility of EXWL*

The sample (0.05 to 1.0 g) was added to 5 mL of methanol containing 10% of water and allowed to stand for 24 h at room temperature with occasional stirring, after which the solution was warmed (at 40°C for 15 min) and then filtered. The concentration of the lignin in the solution was estimated from the amount of insoluble residue. From Fig. 8 it is clear that EXWL is dissolved almost linearly up to the concentration of 20% which was the maximum studied.

It should be noted that although the lignin preparations used here were obtained by extraction with methanol followed by precipitation and drying (see Experimental Section), they were found not completely soluble in 100% methanol (Fig. 9). This suggests some effect of drying on the lignin solubility and stresses the importance of water in methanol for achieving full solubility.

During the course of this work the solubility of EXWL in *N*-methylmorpholine *N*-oxide (MMNO), a new solvent for cellulosic materials (35, 36) was tested. The patent literature (36) vaguely specifies MMNO as a solvent for lignin as well as cellulose. A periodate lignin (kindly provided by D. A. I. Goring of the Pulp and Paper Research Institute of Canada) when tested by us was found to be insoluble in the MMNO monohydrate (Eastman Kodak). However, EXWL was soluble at least to 5% by weight in this solvent. Furthermore the exploded wood itself is also soluble in the same solvent and from this solution a thin film could be coagulated in $H_2O$. This film showed the typical characteristics of regenerated cellulose by infrared spectroscopy and X-ray analysis methods (37).

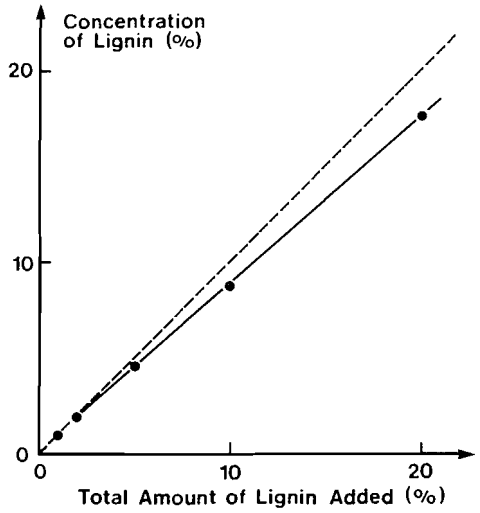


FIG. 8. Solubility of aspen exploded wood lignin in 90% methanol (see text).

## Discussion

The results of this study serve to show how critical reactor variables such as explosion temperature are likely to influence the chemical composition of lignin from the explosion process. Nevertheless the basic structure remains lignin and the compositional changes are of a quantitative nature only. This is important for those who plan biomass strategies especially in terms of chemical uses of lignin. In addition to the chemical composition variation, one can surely expect some changes in molecular weight and polydispersity as a function of explosion temperature. It is noteworthy that the polydispersity of the molecular weight of EXWL is less than reported for autohydrolysis lignin (3). This is not unexpected because the

Can. J. Chem. Downloaded from www.nrcresearchpress.com by 210.87.254.42 on 09/06/12
For personal use only.

Can. J. Chem. Downloaded from www.nrcresearchpress.com by 210.87.254.42 on 09/06/12
For personal use only.

explosion reaction is likely to have been more homogeneous with less opportunity for repolymerization.

From comparative evaluation of the $^{13}C$ spectra for MWL and EXWL it has been possible to conclude that cleavage of the β-O—4 ether bonds has been extensive in the latter material. This will have the effect of increasing the hydrocarbon nature of the carbon chain attached to syringyl and guaiacyl units. At the same time, the concentration of phenolic hydroxyl groups is increased, hence the amphiphilic character of the lignin is heightened. This fact, along with the expected increase in solubility as the molecular weight is lowered (also due to β-O—4 bond cleavage), accounts for the unusual alcohol solubility of EXWL. This property alone could allow numerous applications for this lignin which have not been possible to consider with less soluble product. For example, usage of lignins as copolymerization oligomers is ideal when all starting reactants are soluble.

EXWL can be considered a typical biomass lignin, i.e., it is easily separable from the wood mass following a simple pretreatment of the wood. This pretreatment must unlock the nascent clasp between lignin and cellulose without major loss of their chemical identity. Pretreatment processes to create a "chemicals from wood" economy often depend on a subsequent microbiological transformation of carbohydrate polymers. To achieve high carbohydrate accessibility by enzymes in lignocellulosics the removal of lignin has generally been necessary (38). One of the properties of exploded wood is a remarkable increase in enzyme accessibility (1) of the carbohydrate fraction as a result of the pretreatment. Given the results of this study, it is clear that enzymatic accessibility of cellulose is due to destructuring of the composite relation of lignin matrix and fiber. More important still, the hydrolytic cleavage and high temperature induce a coalescence of the lignin into micron-size domains (1), leaving an accessible cellulose surface. With major restructuring of its topology, the lignin of exploded wood no longer blocks the access of enzymes to the inner cellulose surface of woody fibers (1, 39). Similarly, the substrate has enhanced accessibility to other reagents because the intimate cellulose/lignin interface has been largely eliminated.

## Acknowledgements

The authors acknowledge important assistance from Toshihiko Hanai and Jean St. Pierre of the Chemistry Department, University of Montreal. One of us (D.R.) is indebted to Professor D. Gagnaire, Director of the CNRS Institute, C.E.R.M.A.V., and to Dr. H. Chanzy of the Institute for stimulating encouragement in the development of this study. The work was supported by an NSERC thematic grant, by financial support from NRC's IRAP, and by the Ministère de l'Education du Québec. One of us (R.H.M.) profited from stimulating discussions and helpful criticism from S. Malhotra of Xerox Research Centre of Canada. Finally, we thank the Centre Grenoblois de Résonance Magnétique for providing the nmr facilities.

1. R. H. MARCHESSAULT and J. ST-PIERRE. Proceedings of CHEMRAWN Conference, Toronto, Canada, July, 1978. *Edited by* G. R. Brown and L. E. St. Pierre. Pergamon Press, New York. 1980. pp. 613–625.
2. R. H. MARCHESSAULT, S. COULOMBE, T. HANAI, and H. MORIKAWA. Pulp Pap. Mag. Can. Trans. **6**, TR52-TR56 (1980).
3. M. G. S. CHUA and M. WAYMAN. Can. J. Chem. **57**, 1141 (1979).
4. K. V. SARKANEN and C. H. LUDWIG. Lignins: occurrence, formation, structure and reactions. Wiley-Interscience. 1971.
5. N. NIMZ. Angew. Chem. **86**, 336 (1974); Angew. Chem. Internat. Ed. **13**, 313 (1974).
6. E. A. DELONG. Can. Pat. 1,096,374. 1981.
7. I. A. PEARL and L. R. BUSCHE. TAPPI, **43**, 961 (1961); **43**, 970 (1961).
8. K. V. SARKANEN, H.-M. CHANG, and G. G. ALLAN. TAPPI, **50**, 583 (1967).
9. K. V. SARKANEN, H.-M. CHANG, and G. G. ALLAN. TAPPI, **50**, 587 (1967).
10. O. GOLDSCHMID. *In* Lignins. *Edited by* K. V. Sarkanen and C. H. Ludwig. Wiley-Interscience. 1971. Chapt. 6.
11. H. L. HERGERT. *In* Lignins. *Edited by* K. V. Sarkanen and C. H. Ludwig. Wiley-Interscience. 1971. Chapt. 7.
12. H. P. NAVEAU. Can. J. Chem. **46**, 1893 (1968).
13. D. C. C. SMITH. J. Chem. Soc. 2347 (1955).
14. H. L. HERGERT. J. Org. Chem. **25**, 405 (1960).
15. H. I. BOLKER. Nature, **197**, 489 (1963).
16. D. F. ARSENEAU and J. M. PEPPER. Pulp Pap. Mag. Can. **66**, T415 (1965).
17. A. J. MICHELL, A. J. WATSON, and H. G. HIGGINS. TAPPI, **48**, 520 (1965).
18. J. MARTON, E. ADLER, and K. I. PERSSON. Acta Chem. Scand. **15**, 384 (1961).
19. H. I. BOLKER and N. TERASHIMA. Lignin structure and reactions. Adv. Chem. Ser., No. 59. *Edited by* R. F. Gould. Am. Chem. Soc. Washington. 1966. pp. 110–124.
20. J. H. LORA and M. WAYMAN. TAPPI, **61**, 48 (1978).
21. D. E. BLAND and S. STERNHELL. Nature, **196**, 985 (1962).
22. K. LUNDQUIST and T. OLSOON. Acta Chem. Scand. **1331**, 788 (1977).
23. D. E. BLAND and S. STERNHELL. Aust. J. Chem. **18**, 401 (1965).
24. D. GAGNAIRE, D. ROBERT, M. VIGNON, and PH. VOTTERO. Eur. Polym. J. **7**, 965 (1971).
25. H. M. FALES and A. V. ROBERTSON. Tetrahedron Lett. No. 3, 111 (1962).
26. L. SUTY and E. GALIS. Cellulose Chem. Technol. **6**, 485 (1972).

27. H.-D. LUDEMANN and H. NIMZ. Makromol. Chem. **175**, 2401 (1974); **175**, 2409 (1974).
28. D. GAGNAIRE and D. ROBERT. Makromol. Chem. **178**, 1477 (1977).
29. A. F. A. WALLIS. *In* Lignins: occurrence, formation, structure and reactions. Wiley-Interscience. 1971. p. 345.
30. G. DOMBURG, G. ROSSINSKAYA, and V. SERGEEVA. Chem. Abstr. **87**, 86539P (1977).
31. D. A. I. GORING. *In* Lignins: occurrence, formation, structure and reactions. Wiley-Interscience. 1971. p. 695.
32. V. F. FELICETTA, A. AHOLA, and J. L. MCCARTHY. J. Am. Chem. Soc. **78**, 1899 (1956).
33. J. MARTON and T. MARTON. TAPPI, **47**, 471 (1964).
34. M. WAYMAN and J. I. OBIAGA. Can. J. Chem. **52**, 2102 (1974).
35. H. CHANZY, M. DUBE, and R. H. MARCHESSAULT. J. Polym. Sci., Polym. Lett. Ed. **17**, 219 (1979).
36. D. L. JOHNSON. Br. Pat. No. 1,144,048 (1969).
37. J. ST.-PIERRE and R. H. MARCHESSAULT. Unpublished results.
38. J. E. STONE, A. M. SCALLAN, E. DONEFER, and E. AHLGREN. *In* Celluloses and their applications. Adv. Chem. Ser. Am. Chem. Soc. Washington, DC. 1969. pp. 210–238.
39. L. JURASEK. Dev. Ind. Microbiol. **10**, 177 (1979).

Can. J. Chem. Downloaded from www.nrcresearchpress.com by 210.87.254.42 on 09/06/12
For personal use only.

# Synthèse dans la série des cyclopropanes. Vers le bis-nor-4,5 sarkomycine

ONEIL PELLETIER ET KRZYSZTOF JANKOWSKI
*Département de chimie, Université de Moncton, Moncton, N.-B., Canada E1A 3E9*

Reçu le 15 mai 1981[1]

ONEIL PELLETIER et KRZYSZTOF JANKOWSKI. Can. J. Chem. **60**, 2383 (1982).
Trois synthèses des cyclopropanes en utilisant des carbènes et une par la réaction de Wittig modifiée sont discutées.

ONEIL PELLETIER and KRZYSZTOF JANKOWSKI. Can. J. Chem. **60**, 2383 (1982).
Three cyclopropane syntheses via carbene addition and one via a modified Wittig reaction are discussed.

Can. J. Chem. Downloaded from www.nrcresearchpress.com by 210.87.254.42 on 09/06/12
For personal use only.

## Introduction

L'activité anticancéreuse de la sarkomycine (**1**, l'acide méthylène-2 oxo-3 cyclopentanoïque) est reliée à la présence de trois groupements vicinaux: carbonyle, méthylène exocyclique et carboxyle. Nous avons synthétisé cet antibiotique (1) ainsi que son analogue cyclohexanique (2). Le bis-nor-4,5 sarkomycine, (**2**, l'acide méthylène-2 oxo-3 cyclopropanoïque) est le plus petit cycle qui puisse porter ces trois fonctions. Ce composé peut être obtenu, en principe, par l'addition des carbènes ou des carbènoïdes aux oléfines convenablement substituées.

La liaison double exocyclique du produit **2** peut en principe être obtenue par isomérisation de la liaison double endocyclique du produit **3** avec des bases fortes par analogie en système cyclopentanique et cyclohexanique par exemple (3). Ceci permet donc d'envisager les trois synthèses suivantes: (*i*) l'addition du chlorométhylcarbène (**4**) à l'acétale du dicyano-2,2 cétène (**5**); (*ii*) l'addition du dichlorocarbène (**7**) au butyne-2 oate d'éthyle (**6**); (*iii*) l'addition du chlorocarbométhoxycarbène (**8**) au diéthoxy-1,1 propène (**9**); et une quatrième, la réaction de Wittig modifiée, semblable aux trois précédentes dans un contexte carbènique de ce travail entre (*iv*) l'époxy-2,3 butenoate d'éthyle (**10**) et le triphényldichlorométhyle phosphate (Schéma 1).

Les produits obtenus dans les quatre réactions devraient pouvoir être transformés par l'hydrolyse de CN, la décarboxylation du diacide geminal, le déblocage de la fonction acétale ou cétale, l'hydrolyse du système dichloro geminal, l'élimination de HCl, l'hydrolyse de l'ester et finalement l'isomérisation *endo–exo* de la liaison double en produit **2**.

## Résultats et discussion

Les carbènes s'additionnent très bien aux alcènes (4), cependant leur addition aux alcynes, possèdant un caractère moins nucléophile, s'effectue avec plus de difficulté. De plus, la nucléophilie des carbènes varie en fonction de leur substitution. Ainsi la réactivité d'une espèce carbènique avec l'accepteur de ce carbène dépend de la compatibilité (affinité) électronique respective. Les facteurs stériques imposent davantage de restrictions à cette réactivité, cependant, compte tenu des objectifs synthétiques, ce facteur devient important seulement dans le cas du produit **5**.

La protection de la fonction carbonyle dans la synthèse du produit **2** (ou **3**) par la route carbènique est nécessaire à cause de l'addition possible du carbène au carbonyle et pour protéger les cyclopropanones obtenues contre les réactions de la décarbonylation (5),polymérisation, etc. Dans les synthèses proposées, nous protégeons les fonctions carbonyles par des groupements dihalogéminaux ou par cétalisation.

### *(i) L'addition du chlorométhylcarbène (4) à l'acétale du dicyano-2,2 cétène (5)*

Cette route est complètement inefficace. Le produit **4** formé *in situ* ne réagit pas avec **5** mais donne exclusivement les produits de la polymérisation et d'homologation. Nous avons fait varier la température de la réaction de −50 à 25°C et le rapport de **4**/**5** de 10:1 à 40:1 sans succès. D'ailleurs, la réaction entre **4** et du tétracyano-1,1,2,2 éthylène, ne donne pas non plus le produit d'addition désiré. Cependant le produit **5** réagit avec le dichloro méthyllithium en donnant l'acétal du dicyano-1,1 chloro-2 cyclopropanone (**13**) avec un faible rendement de 2%. Le produit envisagé originalement, l'acétal du dicyano-1,1 chloro-2 méthyle-2 cyclopropanone (**14**), demeure cependant inaccessible à partir du produit **13** à

[1]Révision reçue le 14 mai 1982.

0008-4042/82/182383-04$01.00/0
©1982 National Research Council of Canada/Conseil national de recherches du Canada

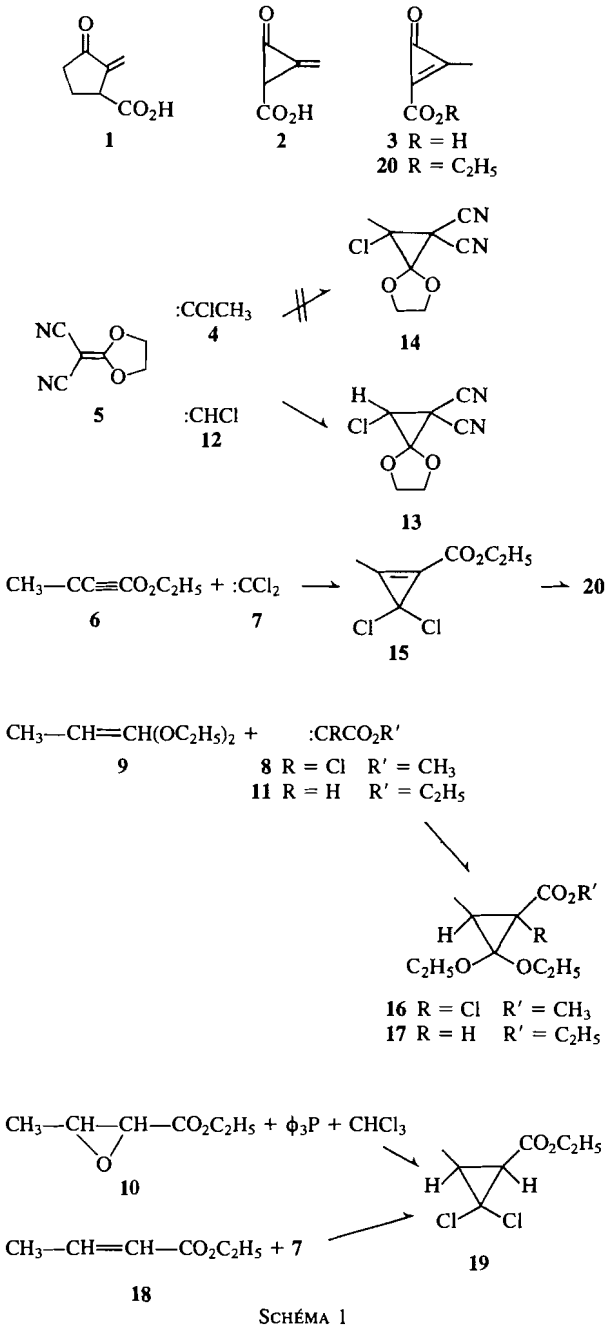


SCHÉMA 1

cause de l'incompatibilité du carbènoïde et de l'oléfine.

*(ii) L'addition du dichlorocarbène (7) au butyne-2 oate d'éthyle (6)*

Le butyne-2 oate d'éthyle (**6**), synthétisé d'après la méthode de Denny et Ross (6), réagit avec le dichlorocarbène **7** en formant l'ester éthylique de l'acide méthyl-2 dichloro-3,3 cyclopropanoïque (**15**) (rendement 15%). La formation du produit **15** n'est pas observée quand on remplace l'acétate de sodium par une solution de phényl bromodichlorométhyl mercure en présence de mailles moléculaires.

L'hydrolyse du produit **15** mène à l'ester éthylique de l'acide méthyl-2 oxo-3 cyclopropènoique (**20**) avec un rendement de 40%. Les produits majeurs des réactions de cette série sont des polymères. Les composés **15** et **20** montrent les signaux de groupement méthyl-2 dans le spectre de rmn à 2.18 et 0.92 respectivement. La présence du groupement *gem*-dichloro déplace le signal de l'ester de 3.66 à 4.22 ppm.

*(iii) L'addition du chlorocarbométhoxycarbène (8) au diéthoxy-1,1 propène (9)*

Ce carbène, préparé à partir du phényl dichlorocarbométhoxyméthyl mercure, offre la voie la plus prometteuse pour la préparation du système de bis-nor-4,5 sarkomycine. Les rendements de l'addition dans ce cas, ainsi que pour l'addition du carboéthoxycarbène à la même oléfine, sont de l'ordre de 40%. Il est donc évident que l'oléfine **9** possède un caractère nucléophile assez prononcé résultant de l'effet électrodonneur des groupements —$OC_2H_5$. Cependant la molécule **16** résiste à la deshydrohalogénation en vue d'obtenir le produit **20** avec des différentes bases utilisées. Tel est le cas aussi bien avant qu'après le déblocage de la fonction cétonique (polymères).

La même oléfine **9** réagit bien avec le carbométhoxycarbène (**11**) généré à partir du diazoacétate d'éthyle en donnant le produit modèle, l'ester éthylique de l'acide méthyl-2 diethoxy-3,3 cyclopropanoïque (**17**).

*(iv) La réaction de Wittig modifiée*

L'époxy-2,3 butanoate d'éthyle (**10**) réagit lentement avec la triphénylphosphine et le chloroforme en présence du *tert*-butanolate de potassium en formant l'ester éthylique de l'acide méthyl-2 dichloro-3,3 cyclopropanoïque (**19**). Cette réaction est une variante de la réaction de Wittig: la réaction classique mène à la formation des oléfines, cependant, l'époxyde soumis au traitement du réactif de Wittig donne le cyclopropane. Le rendement de cette réaction est de l'ordre de 50%. Le même produit, **19**, a été synthétisé par l'addition du dichlorocarbène au butène-2 oate d'éthyle (**18**). Il est à noter que l'utilisation de trichloroacétate de sodium est une source de carbène plus efficace que le phénylbromodichlorométhyl mercure. Le produit **19** traité en milieu acide donne immédiatement le produit **18** avec une perte de monoxyde de carbone.

Can. J. Chem. Downloaded from www.nrcresearchpress.com by 210.87.254.42 on 09/06/12
For personal use only.

Can. J. Chem. Downloaded from www.nrcresearchpress.com by 210.87.254.42 on 09/06/12
For personal use only.

Nous avons examiné la voie la plus simple menant à la formation du produit **3** en utilisant des carbènes. Le choix des carbènes nous semble être un facteur primordial dans la synthèse des dérivés cyclopropaniques. En plus de leur utilité indiscutable dans la synthèse des cycles à trois membres, ils montrent un certain degré de sélectivité envers l'adduit compte tenu des facteurs stériques et électroniques de ce dernier. La conversion du produit **3** en **2** qui demeure un point incertain de la synthèse fera l'objet d'une publication subséquante.

## Partie expérimentale

Les solvants ont été purifiés d'après les méthodes généralement utilisées.

Les spectres ir ont été obtenus avec un spectrophotomètre Perkin–Elmer, modèle 467, soit comme film sur plaques de NaCl soit en solution avec une cellule NaCl (données en $cm^{-1}$).

Les spectres rmn ont été enregistrés avec des appareils Varian T-60 et HR-220. Les déplacements chimiques, δ, sont exprimés en ppm (référence interne TMS) et les constantes de couplages vicinales, $J$, en Hz. Les lettres s, d, t, q et m signifient respectivement singulet, doublet, triplet, quadruplet et multiplet.

Les spectres de masse (sm) (70 eV, 250°C) ont été enregistrés à l'aide des spectromètres de masse Perkin–Elmer RMU-6D et Dupont CEC-21-491 munis d'une sonde à température variable (60–350°C).

La chromatographie sur colonne fut effectuée avec de l'alumine comme absorbant.

Le produit **5** fut synthétisé d'après la recette de Dickinson et Melby (11) (rmn: 4.84); le butyne-2 oate d'éthyle (**6**) d'après Denny et Ross (6) et Gaugh et Trippett (8) (rmn ($CDCl_3$): 2.03, (s, 3H, $CH_3$), 4.20 (q, $J$ = 7.6; 2H, $CH_2$—$CH_3$) et 1.30 (t, 3H, $CH_2$—$CH_3$, $J_{CH_2,CH_3}$ = 7.6)); le diéthoxy-1,1 propène (**9**) d'après le procédé de Walters et McElvain (9) (rmn ($CDCl_4$): 3.48 (q, 1H, $J$ = 6, C*H*), 1.53 (d, 3H, CH—$CH_3$), 3.65 (q, 2H, $CH_2$—$CH_3$) et 1.26 (t, 3H, $CH_2$—$CH_3$)) et l'époxy-2,3 butanoate d'éthyle (**10**) fut acheté chez Aldrich. Les carbènes **4**, **7** et **8** ont été synthétisés *in situ* d'après les méthodes décrites dans la littérature (4). La réaction de Wittig modifiée est modelée sur le procédé de Denny *et al.* (10).

Les nouveaux produits synthétisés **13**, **16**, **17**, **19** et **20** donnent une analyse élémentaire (C, H) satisfaisante. Ces analyses ont été effectuées sur l'appareil Beckman 915A du Département de génie de l'Université de Moncton (7).

Les chromatogrammes en phase vapeur (cpv) ont été enregistrés sur l'appareil Perkin–Elmer 990 en utilisant des colonnes: A 3% OV-1 sur Carbowax 80–120 (3 pi × 1/8 po) et B 3% SE-30 sur Chromosorb 80 (3 pi × 1/8 po).

*Acétal du dicyano-1,1 chloro-2 cyclopropanone (13)*

Dans un ballon à trois cols de 500 mL muni d'un agitateur magnétique, sous une atmosphère d'azote préséchée, fut ajouté du méthyllithium (0.1 mol) et du chlorure de méthylène anhydre (50 mL). Tout en refroidissant le mélange à environ −10°C (glace/NaCl), une solution de l'acétal du dicyano-2,2 cétène (**5**, 0.02 mol) en chlorure de méthylène anhydre fut ajoutée sur une période d'une demi-heure. La solution fut agité davantage pendant 20 h à la température ambiante.

Le mélange réactionnel fut filtré, lavé deux fois avec de l'eau distillée (25 mL), séché au sulfate de magnésium (20 g) et distillé sous pression réduite. Le produit **13** fut distillé à 90°C/0.07 Torr. Rendement.: 2%; ir: 2280, 1070, 720, 2950; rmn: 3.75 (s, 1H, C*H*Cl), 4.53 (s, 4H, $CH_2$); sm *m/z* (I%): 184 ($M^+$, 17), 186 ($M^+$ + 2, 7), 72 (100), 71 (61), 136 (50), 153 (32), 182 (13). *Anal.* calc. pour $C_7H_5O_2N_2Cl$: C 45.52, H 2.73; trouvée: C 45.23, H 2.2%

*Ester éthylique de l'acide méthyl-2 dichloro-3,3 cyclopropènoïque (15)*

Le butyne-2 oate d'éthyle (**6**, 0.03 mol) fut ajouté à une solution de diglyme (3.3 mL) en tétrachloroéthylène (13.0 mL) dans un ballon de 50 mL. Le mélange fut agité et chauffé à une température de 115°C. Ensuite, la quantité de 5.2 g de trichloroacétate de sodium (0.03 mol) fut ajoutée au mélange pendant une demi-heure. Le mélange fut maintenu à une température de 115°C pendant une demi-heure.

La solution fut refroidie, filtrée, et lavée avec de l'éthanol (100 mL, 95%). Le résidu, distillé sous pression réduite, a donné un produit **15**, 33–38°C/1.7 Torr. Rendement: 15%; ir: 760, 1700, 1900; cpv: $R_t$ 1.7 min (col. A); rmn: 2.18 (s, 3H, $CH_3$—C), 3.66 (q, $J$ = 7.2, 2H, $CH_2$—$CH_3$), 1.18 (q, 2H, $CH_2$—$CH_3$); sm *m/z* (I%): 194 ($M^+$, 33), 196 ($M^+$ + 2, 21), 198 ($M^+$ + 4, 5), 112 (100), 149 (37), 166 (21), 151 (20).

*Ester éthylique de l'acide méthyl-2 oxo-3 cyclopropènoïque (20)*

En suivant le procédé utilisé dans la synthèse de **15**, avec le butyne-2 oate d'éthyle, le mélange réactionnel fut chauffé à 125°C pendant 24 h, puis agité avec 100 mL d'eau dans une température ambiente.

La solution fut filtrée, lavée avec de l'eau distillée (25 mL) et de l'acide chlorohydrique (25 mL, 10%) et extrait avec du benzène (50 mL). Les extraits furent séchés avec le sulfate de magnésium anhydre (8.0 g), filtrés, et le solvant évaporé sous vide pour donner le produit **20** (p. eb. 42–45°/0.4 Torr). Rendement: 42%; ir: 1700, 1810, 1950; cpv: $R_t$ 4.1 min (col. A); rmn: 0.92 (s, 3H, $CH_3$), 4.22 (q, $J$ = 7, 2H, $CH_2$, $CH_3$), 1.30 (t, 3H, $CH_2$—$CH_3$); sm *m/z* (I%): 140 ($M^+$, 17), 112 (100), 95 (68), 94 (62), 43 (47), 67 (32). *Anal.* calc. pour $C_7H_8O_3$: C 60.00, H 5.71; trouvée: C 59.75, H 5.6%.

*Ester éthylique de l'acide méthyl-2 diéthoxy-3,3 cyclopropanoïque (17)*

L'acétal **9** (0.025 mol) fut introduit dans un ballon de 200 mL à trois cols contenant du cyclohexane (15 mL) et du sulfate de cuivre (0.4 g). Une solution de diazoacétate d'éthyle (0.10 mol) dans du cyclohexane (75 mL) fut ajoutée au mélange avec l'agitation vigoureuse, goutte à goutte. Le mélange réactionnel fut laissé au reflux pendant deux heures. Le mélange fut filtré, séché au sulfate de magnésium anhydre (5 g) et concentré sous vide.

Le mélange réactionnel fut distillé sous pression réduite. Le produit **17**, distillé à 140°C/0.4 Torr. Rendement: 44%; cpv: $R_t$ 6.2 min (col. B); rmn: 1.32 (d, 3H, $J_{CH_3CH}$ = 9.0, $CH_3$—CH), 1.22 (m, $J_{CH,CH}$ = 2.0, 1H, $CH_3$—C*H*), 2.78 (d, 1H, C*H*—CO), 4.13 (q, $J$ = 7.0, 4H, O$CH_2$—$CH_3$), 1.26 (t, 6H, O$CH_2$—$CH_3$), 3.54 (q, $J$ = 7.0, 2H, COO$CH_2$—$CH_3$), 1.18 (t, 3H, COO$CH_2$—$CH_3$); sm *m/z* (I%): 216 ($M^+$, 7), 161 (100), 188 (63), 187 (41), 170 (27), 142 (21). *Anal.* calc. pour $C_{11}H_{20}O_4$: C 61.11, H 9.33; trouvée: C 60.88, H 9.15.

*Ester méthylique de l'acide chloro-1 méthyl-2 diéthoxy-3,3 cyclopropanoïque (16)*

Le phényl (dichlorocarbométhoxyméthyl) mercure (0.02 mol) fut ajouté à un mélange de diéthoxy-1,1 propène (**9**, 0.03 mol) et de chlorobenzène (25 mL) dans un ballon à trois cols (muni d'un agitateur, d'un thermomètre ainsi que d'une entrée et d'une sortie d'azote séchée à l'hydroxyde de sodium). Le mélange réactionnel fut chauffé à reflux (135°C) pendant sept jours. Le produit **16** distille à 29°C/0.75 Torr. Rendement: 41%; cpv: $R_t$

3.0 min (col. A); rmn: 1.37 (d, $J = 4.0$, 3H, $CH_3$—CH), 2.22 (q, 1H, $CH_3$—CH), 3.40 (s, 3H, $OCH_3$), 4.18 (q, $J = 7.0$, 4H, $COOCH_3$—$CH_3$), 1.23 (t, 6H, $COOCH_2$—$CH_3$); sm *m/z* (I%): 236 ($M^+$, 17), 238 ($M^+ + 2$, 6), 93 (100), 200 (42), 181 (37), 205 (17). *Anal.* calc. pour $C_{10}H_{17}O_4Cl$: C 50.85, H 7.24; trouvée: C 50.65, H 7.0.

*Ester éthylique de l'acide méthyl-2 dichloro-3,3 cyclopropanoïque (**19**)*

*Méthode A*

Le triphénylphosphine (0.20 mol) fut ajouté au *tert*-butanolate de potassium (0.20 mol) et du heptane (250 mL) dans un ballon d'un litre. Le mélange fut refroidi dans un bain de glace et fut agité vigoreusement avec une agitation magnétique. Une solution comprenant du chloroforme (0.20 mol) dans du heptane (200 mL) fut ajoutée au mélange sur une période de 30 min. Le mélange réactionnel fut concentré sous vide à un volume d'environ 100 mL.

L'époxy-2,3 butanoate d'éthyle (**10**, 0.20 mol) fut ajouté au mélange réactionnel concentré et fut chauffé à 65°C pendant trois heures. Le mélange réactionnel fut distillé sous pression réduite. Le produit **19** distille à 28–29°C/0.15 Torr. Rendement: 53%; ir: 740, 1740; cpv: $R_t$ 4.4 (col. A); rmn: 1.38 (m, $J = 5.0$, $J = 1.2$, 3H, CH—$CH_3$), 3.18 (m, $J = 2.0$, 1H, $CH$—$CH_3$), 3.15 (m, 1H, $CH$—CO), 1.3 (t, 3H, $CH_2$—$CH_3$); sm *m/z* (I%): 196 ($M^+$, 31), 198 ($M^+ + 2$, 24), 200 ($M^+ + 4$, 6), 114 (100), 123 (43), 160 (40), 151 (21). *Anal.* calc. pour $C_7H_{10}O_2Cl_2$: C 42.64, H 5.12; trouvée: C 42.45, H 5.00. Analyse de Cl (tritrage $AgNO_3$) calc.: Cl 36.05; trouvée: Cl 35.1.

*Méthode B*

Le butène-2 oate d'éthyle (**18**, 0.035 mol) fut ajouté en solution de 30 mL du glyme au trichloroacétate de sodium (0.067 mol). Le mélange fut chauffé à reflux jusqu'à ce que l'évolution de $CO_2$ cesse. Le mélange réactionnel fut filtré et concentré sous vide puis distillé.

La spectrométrie de masse à température variable du mélange réactionnel a permis l'analyse détaillée des fractions obtenues par la distillation fractionnée. Le produit **19** distille à 40°C/0.3 Torr. Rendement: 17%.

## Remerciements

Nous désirons remercier le Conseil de Recherches de l'Université de Moncton pour l'appui financier accordé à ce travail et au Dr W. D. Jamieson (Conseil national de recherches du Canada, Atlantic Regional Laboratories, Halifax, N.-E.) pour l'enregistrement des spectres de masse des dérivés polychlorés avec la sonde à température variable (STCID). L'aide technique de MM. R. Coulombe, C. Vautour et R. Volpé est grandement appréciée.

1. K. Jankowski. Tetrahedron Lett. **20**, 1733 (1971).
2. K. Jankowski et L. Allain. Brevet canadien, 1018185, le 27 septembre 1977.
3. M. Vidal, M. Vincens et P. Arnaud. Bull. Soc. Chim. Fr. 4543 (1969); 665 (1972).
4. W. Kirmse. Carbene chemistry. Academic Press, New York, NY. 1971.
5. R. Breslow et M. Oda. J. Am. Chem. Soc. **94**, 4787 (1972).
6. D. B. Denny et S. J. Ross. J. Org. Chem. **27**, 998 (1962).
7. O. Pelletier. Thèse de maîtrise, Université de Moncton. 1976.
8. S. T. D. Gaugh et S. Trippett. J. Chem. Soc. 2333 (1962).
9. P. M. Walters et S. M. McElvain. J. Am. Chem. Soc. **62**: 1482 (1940).
10. D. B. Denny, J. J. Viel et M. J. Boskin. J. Am. Chem. Soc. **84**, 3944 (1962).
11. C. L. Dickinson et L. R. Melby. Org. Synth. Collect. Vol. **IV**, 276 (1968).

Can. J. Chem. Downloaded from www.nrcresearchpress.com by 210.87.254.42 on 09/06/12
For personal use only.

# Assay of metallochromic dyes by weight titration with copper(II) using a copper(II) ion-selective electrode

B. KRATOCHVIL AND CARMELITA MAITRA

*Department of Chemistry, University of Alberta, Edmonton, Alta., Canada T6G 2G2*

Received June 2, 1982

B. KRATOCHVIL and CARMELITA MAITRA. Can. J. Chem. **60**, 2387 (1982).

Twelve analytically useful chelating dyes were assayed by potentiometric titrations with copper(II). A copper ion-selective electrode served as end-point indicator. Use of a gravimetric titration system allowed microtitrations to be performed with relative standard deviations of the order of a percent.

B. KRATOCHVIL et CARMELITA MAITRA. Can. J. Chem. **60**, 2387 (1982).

Faisant appel à des titrations potentiométriques avec le cuivre(II), on a essayé douze colorants chélatants utiles en analyse. On a utilisé une électrode sélective pour les ions cuivriques comme indicateur de fin de réaction. L'utilisation d'un système de titrage gravimétrique permet de réaliser des microtitrages avec des déviations standard relatives de l'ordre de 1%.

[Traduit par le journal]

Can. J. Chem. Downloaded from www.nrcresearchpress.com by 210.87.254.40 on 09/06/12
For personal use only.

Metallochromic dyes are widely used in chemical analysis. They serve as equivalence-point indicators in complexation titrimetry, as ligands forming species suitable for spectrophotometric or fluorimetric determinations of metal ions and anions, and as active components in liquid-membrane electrodes (1–4). For some applications knowledge of the purity of the dyes is necessary. Dye purity is important, for example, when measuring acid dissociation constants and metal stability constants (5–7), or when applying techniques such as the ion-increment method for the spectrophotometric measurement of free metal ion concentrations (8). In many other applications, such as indicators for titrations or as ligands for trace metal analysis by spectrophotometry, purity is not critical. Because removal of impurities is often difficult and tedious, their presence is tolerated wherever possible. Therefore most commercially available metallochromic dyes used in analysis contain moderate to high levels of both organic and inorganic impurities. Purification when done usually involves a combination of precipitation, column chromatography, or solvent extraction operations, and may require several days.

Present methods for the quantitative assay of metallochromic dyes include spectrophotometry (ref. 2, pp. 22–75, refs. 9, 10), chromatography (7, 12), and complexation, acid–base, and ion-pair extraction titrations. None of the available methods provide the speed, convenience, and precision desirable for routine analyses. Accordingly, we report here a procedure in which a standard solution of copper(II) is titrated with a solution of the dye under assay. A copper ion-selective electrode (ISE) is used to follow the titration. Most metallochromic dyes form stable complexes with copper(II), and the copper ISE provides a convenient, well-documented method of equivalence-point detection (10, 13, 14). The titrations were performed gravimetrically with small volumes of dilute solutions because of solubility limitations, and in some instances because only limited quantities of purified dye were available.

## Experimental

*Apparatus*

An Orion Model 94-29A cupric ion membrane elecrode was used as the indicating electrode. Measurements of pH were made with a Fisher glass electrode (Cat. #13-639-3). Potentials of the copper(II) and glass electrodes were measured relative to a Fisher Saturated Calomel Electrode (Cat. #13-639-52) with a Fisher Accumet Model 520 Digital pH/ion meter. The titrant was delivered from a 150-mL polypropylene bottle through a 1.6-mm id Tygon tube attached to a nipple near the base of the bottle. In operation, the bottle is placed on a Mettler Model PL-200 top-loading balance and the tube anchored to the balance housing 10 to 15 cm from the nipple with a small weight. The balance, the pH/ion meter and the valve (General Valve Corp., Part No. 2-26-900) controlling the addition of titrant, were interfaced[1] with a PDP 11/03 (Digital Equipment Corp.) minicomputer. Data readouts consisted of balance readings, weight increments of titrant delivered, corresponding electrode potential readings for each weight increment, and point-by-point titration slopes ($\Delta mV/\Delta g$).

Titrations were done in 200-mL polypropylene (Nalge Co., N.Y.) plastic beakers.

*Reagents and solutions*

The dyes were from various sources: Calmagite (CMG) (Fluka); Tiron, Xylenol Orange (XO), and Hydroxy Naphthol Blue (HNB) (Fisher Scientific Co., Fair Lawn, NJ); SNAZOXS,

[1]B. Kratochvil and J. Nolan. Unpublished research.

0008-4042/82/182387-05$01.00/0

©1982 National Research Council of Canada/Conseil national de recherches du Canada

Can. J. Chem. Downloaded from www.nrcresearchpress.com by 210.87.254.40 on 09/06/12
For personal use only.

Methylthymol Blue (MTB), and Eriochrome Blue SE (EBSE) (J. T. Baker Chem. Co., Phillipsburg, NJ); Alizarin Complexone (AC) and Eriochrome Black T (EBT) (Aldrich Chem. Co., Milwaukee, WI); and 1(2-Pyridylazo)-2-naphthol (*o*-PAN) (Eastman Organic Chemicals, Rochester, NY).

Titrant solutions were prepared (assuming 100% purity) to a weight molarity of about $2 \times 10^{-6}$ mol per g of solution. All dyes were analyzed as received except for CMG, which was analyzed both as received and after purification by a previously described method (9).

Stock copper(II) standard solutions were prepared by dissolving AR grade copper shot (Fisher Scientific Co., Fair Lawn, NJ) in a minimum amount of concentrated $HNO_3$. After dissolution and dilution with distilled $H_2O$, the weight of the final solution was obtained to determine the weight molarity, usually about $2.5 \times 10^{-5}$ mol Cu per g of solution.

All other reagents ($NH_4NO_3$, $NH_3$, $HNO_3$, $LiNO_3$, $CH_3CN$, and ethanol) were analytical reagent grade. Distilled water was used for all dilutions unless specified otherwise.

*Procedure*

From 0.1 to 0.25 g portions of stock copper solution (2 to $6 \times 10^{-6}$ mol) were weighed into separate beakers by difference from a Teflon-tipped glass syringe. Precisely 10 mL of 1 *M* $NH_3$ – 1 *M* $NH_4NO_3$ were added and the solution diluted to a total volume of about 100 mL. The pH of the final solution was approximately 9.3. The reference and copper indicating electrodes were inserted into the solution and the sample titrated with the dye solution. The solution was stirred magnetically throughout the titration.

Parameters for the titration, including rate of titrant delivery, equilibration time between addition of titrant increments and reading of potential, frequency of reading, allowable precision for potential and balance readouts, and end-of-titration potentials, were set using a program[1] written in FORTRAN. The actual titration was controlled by a second program,[1] also in FORTRAN. The point of greatest slope ($\Delta mV/\Delta g$) was selected as the end point for each titration.

Indicators which were not readily soluble in water (EBT, EBSE, AC, HNB) were dissolved in dilute (0.01 *M*) $NH_3$–$NH_4NO_3$ buffer. *o*-PAN, because of its insolubility in both $H_2O$ and $NH_3$–$NH_4NO_3$ buffer, was dissolved in 70:30 ethanol–$H_2O$ or $CH_3CN$–$H_2O$. For these titrations, the copper sample solutions and a salt bridge of 0.1 *M* $LiNO_3$ for the SCE were made up in the same solvent composition as used for the dye.

All titrations were done in a constant temperature room at an ambient temperature of 23.5°C.

## Results and discussion

Results of the titrations are shown in Table 1. The acid dissociation constants and the stability constants for Cu(II)–indicator complex formation have been included for ready reference in the discussion. Purities ranged from 36 to 93% except for HNB, which was only available crystallized onto sodium chloride for direct addition as a solid to titration solutions. The percentage of HNB in the sample was so low that several grams of sample were required to carry out the titration within the acceptable titrant weight range (perferably 1 to 10 g) (33). This resulted in a solution containing about 10% NaCl, in which the dye was insoluble. Addition of a small amount of $NH_3$–$NH_4NO_3$ buffer (~0.01 *M* final concentration) effected dissolution.

The sharpness of the titration end points determined the precision of the results. Examples of titration plots are shown in Fig. 1. Titrations with sharp end points included the *o*,*o*′-dihydroxyazo dyes: CMG, EBT, HNB, EBBR, and EBSE. All gave satisfactory precision. EBT and EBBR form 1:1 complexes with copper(II) with fairly high (16, 19, 22) stability constants. Combining ratios and stability constants for the other *o*,*o*′-dihydroxyazo dyes with copper(II) have not been reported, although all are known to form 1:1 complexes of moderate stability with $Ca^{2+}$ and $Mg^{2+}$ (15, 19, 21). The complexation equilibrium of AC with copper(II) does not appear to have been studied. XO and MTB have been reported to form $Cu_2In$, CuIn (1, 5, 29), and CuHIn (5) complexes. A recent study (27), however, reported for MTB the formation of $CuH_2In$ and $CuIn_2$ complexes but not $Cu_2In$. In our results, a plot of potential against weight of titrant did not show a second inflection even though the titrations were carried more than 100% past the 1:1 inflection point with both XO and MTB. The first inflections were drawn out for both, however. SNAZOXS and Tiron have been reported (20, 31) to form both CuIn and $CuIn_2$ complexes. A tendency to form a second weak complex with copper may be the cause of the drawn out end points and low precision observed for SNAZOXS and Tiron, and may have contributed to the poor end points for MTB and XO.

The titration of *o*-PAN in the mixed solvents proceeded as for the aqueous titrations. The precision was, however, poorer than that of the aqueous titrations of the *o*,*o*′-dihydroxyazo dyes. Coetzee and Istone (34) observed that the copper ISE malfunctioned in 100% acetonitrile as solvent but gave calibration plots similar to the aqueous system in mixtures of methanol, ethanol, 2-propanol, dimethylsulfoxide, propylene carbonate, or ethylene glycol with water. Rechnitz and Kenny (35), on the other hand, found the behavior of the electrode in acetonitrile to be similar to that in methanol.

As indicated in Table 1, SNAZOXS and Tiron were assayed at two concentrations. Increased precision was observed for both dyes at higher concentrations. Results at the two levels agreed well for SNAZOXS; agreement was less good with Tiron, but within experimental uncertainties for both. The higher precision at higher concentrations can be attributed to sharper end points for both dyes. Agreement between the two concentrations indicates the absence of bias in end-point selection at low concentrations.

All the plots of potential against weight of dye titrant obtained in this study were asymmetric. This has generally been observed (ref. 33, pp.

Can. J. Chem. Downloaded from www.nrcresearchpress.com by 210.87.254.40 on 09/06/12
For personal use only.

TABLE 1. Results of potentiometric titrations of selected metallochromic indicators with copper(II)[a]

| Indicator | $pK_{H_nIn}$[b] | log $K_{cond}$ CuIn[c] | % Purity[d] | % RSD |
|---|---|---|---|---|
| 1. Calmagite (CMG)<br>1-(2-Hydroxy-5-methyl-phenylazo)-2-naphthol-4-sulfonic acid | $H_2In$ = 8.1,<br>HIn = 12.4 (15);<br>$H_2In$ = 7.9,<br>HIn = 12.3 (9) | | 64.4[e]<br>100.0[f] | 0.2<br>0.7 |
| 2. Eriochrome Blue Black R (EBBR)<br>1-(2-Hydroxy-1-naphthylazo)-2-naphthol-4-sulfonic acid | $H_3In$ = 1.0 (16, 18),<br>$H_2In$ = 7.3 (16, 17, 18),<br>HIn = 13.5 | 21.2 (18) | 36.8 | 0.4 |
| 3. Hydroxy Naphthol Blue[g] (HNB)<br>1-(2-Hydroxy-4-sulfo-1-naphthylazo)-2-hydroxy-naphthalene 3,6-disulfonic acid | $H_2In$ = 6.44,<br>HIn = 12.93 (19) | | 0.168 | 0.9 |
| 4. SNAZOXS<br>7-(4-Sulfo-1-naphthylazo)-8-hydroxyquinoline-5-sulfonic acid | $H_2In$ = 3.0,<br>HIn = 7.0 (20) | CuIn = 10.4,<br>$CuIn_2$ = 9.0 (20) | 39 | 3 |
| 5. Eriochrome Blue SE[g] (EBSE)<br>2-(5-Chloro-2-hydroxy-phenylazo)-1,8-dihydroxy-naphthalene-3,6-disulfonic acid | $H_3In$ = 8.0,<br>$H_2In$ = 10.5,<br>HIn = 11.9 (21) | | 52.5 | 0.8 |
| 6. Eriochrome Black T[g] (EBT)<br>1-(1-Hydroxy-2-naphthylazo)-6-nitro-2-naphthol-4-sulfonic acid | $H_3In$ = 3.9,<br>$H_2In$ = 6.4,<br>HIn = 11.5 (16) | 21.98 (22)<br>21.45 (23) | 50 | 1<br>19 |
| 7. 1-(2-Pyridylazo)-2-naphthol (*o*-PAN) | $H_2In$ = 2.9,<br>HIn = 11.2 (24) | 16.0 (25)<br>16.6 (24)<br>12.6 (24) | <br>93[h]<br>90[i] | <br>3<br>4 |
| 8. Methyl Thymol Blue (MTB)<br>3,3′-Bis-[*N*,*N*′-di(carboxy-methyl)-amino methyl]-thymolsulfophthalein | $H_4In$ = 4.5,<br>$H_3In$ = 7.2,<br>$H_2In$ = 11.2,<br>HIn = 13.4 (26) | $K_{Cu(H_2In)}$ = 31.7 (27) | 54[j] | 2 |
| 9. Xylenol Orange (XO)<br>3,3′-Bis-[*N*,*N*′-di(carboxy-methyl)-amino methyl]-o-cresol sulfonphthalein | $H_6In$ = −1.2,<br>$H_5In$ = 2.6,<br>$H_4In$ = 3.2,<br>$H_3In$ = 6.4,<br>$H_2In$ = 10.4,<br>HIn = 12.3 (28) | $K_{CuH_nIn}$ = 7.18,[k]<br>$K_{Cu_2H_nIn}$ = 5.01[k] (29) | 61.9[j] | 0.4 |
| 10. Alizarin Complexone[g] (AC)<br>3-[Di(carboxymethyl)amino-methyl]-1,2-dihydroxyanthra-quinone | $H_4In$ = 2.57,<br>$H_3In$ = 5.53,<br>$H_2In$ = 5.53,<br>HIn = 12.19 (30) | | 85 | 1 |
| 11. Tiron<br>1,2-Dihydroxybenzene-3,5-disulfonic acid | $H_2In$ = 7.54,<br>HIn = 12.26 (31) | log $K_1$ = 13.93,<br>log $K_2$ = 11.17 (31) | 92 | 3 |
| 12. Thorin<br>2-(2-Hydroxy-3,6-disulfo-1-naphthylazo)-benzenearsonic acid | $H_3In$ = 3.7,<br>$H_2In$ = 8.3,<br>HIn = 11.8 (32) | | | |

[a] Titrations performed in 0.10 *M* $NH_3$–$NH_4NO_3$ buffer, pH 9.3, unless specified otherwise.
[b] Acid ionization constant of the indicated form of the indicator; charges omitted for simplicity.
[c] Logarithm of conditional stability constant of the Cu(II)–indicator complex, where available.
[d] Average of four determinations except for unpurified CMG, HNB, XO, and Tiron (three determinations each) and *o*-PAN in 70:30 $CH_3CN$:$H_2O$ (five determinations). All percentages calculated on basis of a 1:1 copper(II)–indicator complex unless otherwise specified.
[e] Fluka CMG.
[f] Purified according to method described in ref. 9.
[g] Dissolved in 0.01 *M* $NH_3$–$NH_4NO_3$ buffer.
[h] Titrations performed in 70:30 EtOH–$H_2O$ mixture.
[i] Titrations performed in 70:30 $CH_3CN$–$H_2O$ mixture.
[j] Percentage calculated on the basis of a 1:2 In–Cu complex.
[k] Conditional constant determined at pH = 7.0.

Can. J. Chem. Downloaded from www.nrcresearchpress.com by 210.87.254.40 on 09/06/12
For personal use only.

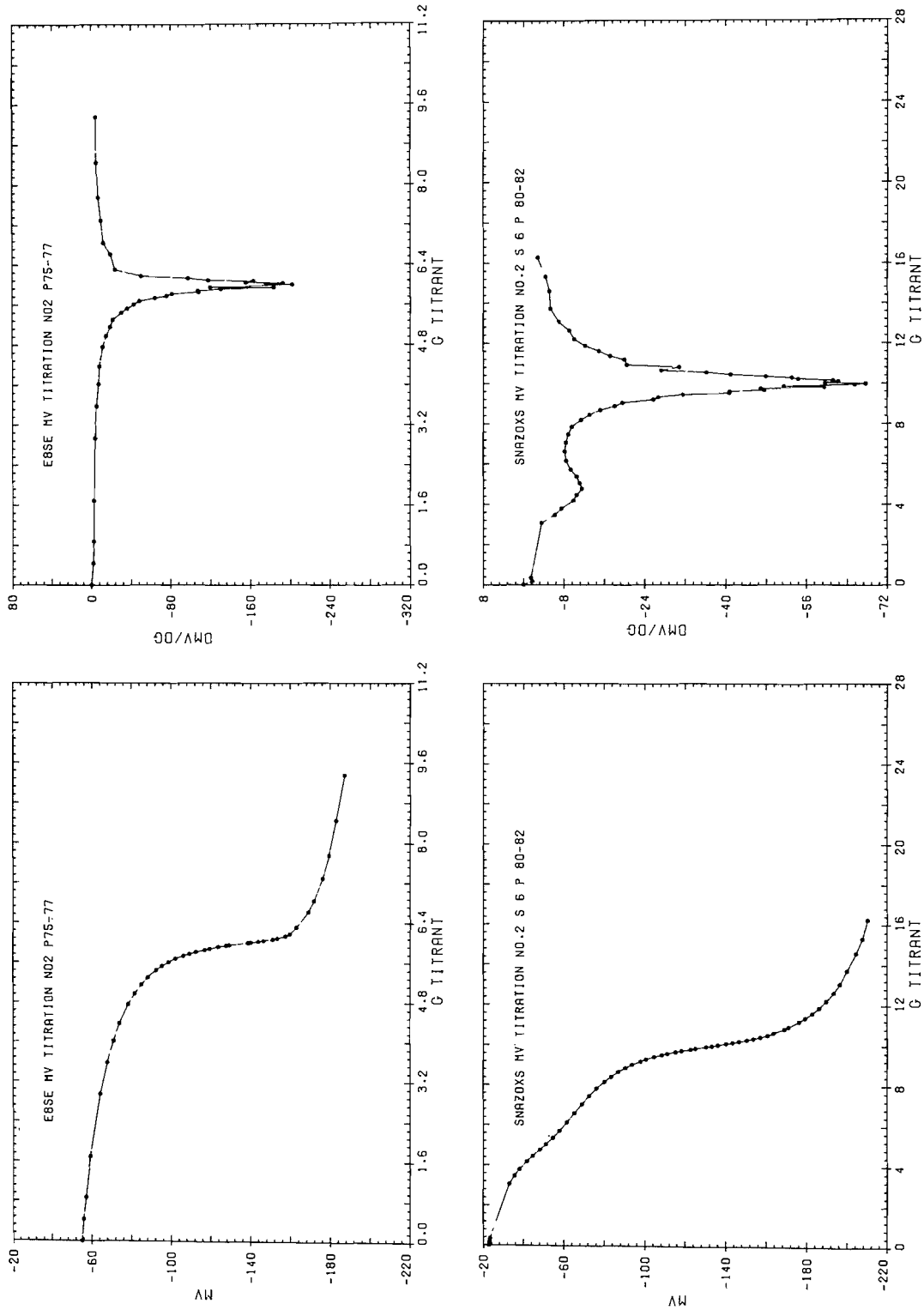


FIG. 1. Conventional and first-derivative plots of titration of copper(II) with approximately $10^{-3}$ weight molar solutions of (top) Eriochrome Blue SE and (bottom) SNAZOXS.

Can. J. Chem. Downloaded from www.nrcresearchpress.com by 210.87.254.40 on 09/06/12
For personal use only.

128–131, ref. 37) for complexometric titrations with ISE indication. Asymmetry in this type of titration with the copper ISE has been attributed to oxygen sensitivity of the copper electrode (38). In general, it has also been observed (37, 39, 40) that in titrations exhibiting asymmetric curves the equivalence point does not coincide with the inflection point, which could introduce systematic errors (ref. 33, pp. 128–131, ref. 37) if the peak in the first derivative plot were taken as the equivalence point. The error has generally been computed (11, 36, 37, 39, 40) to increase with an increase in the concentration of interfering ions, with a decrease in sample ion concentration (leading to non-Nernstian response), with an increase in dilution, and with a decrease in the completeness of the main reaction (low $K_{ML}$) (11, 37, 39, 40).

In this study, we selected as the end point that point corresponding to the highest slope ($\Delta mV/\Delta g$). We found this method to be the least subjective and the most reproducible. The magnitude of the error introduced by this approach could not be assessed for the commercial dyes owing to the unknown nature of the impurities present. However, the results obtained for purified CMG agreed within experimental error with previous analyses by two other methods (9). Accordingly, the method of end-point selection used here does not appear to introduce systematic error.

## Conclusions

The assay of chelating dyes by potentiometric titration with copper(II) has several advantages. One is that copper(II) reacts in a clean, stoichiometric way with most indicator ligands, forming 1:1 complexes with the dihydroxyazo dyes, and 2:1 copper-to-ligand complexes with sulfonephthaleins possessing two iminodiacetate groups attached to the phthalein unit. Another is that colored impurities which do not form complexes but would affect spectrophotometric measurements, such as unreacted starting material or coupled products not possessing chelating capability, do not interfere. A third is that the procedure is rapid and simple, so that it lends itself readily to monitoring of commercial lots of indicators, and to assessing various purification methods. Also, the titration may be performed in aqueous, nonaqueous, or mixed solvents. The method is well suited to automated weight titrations of milligram amounts of material.

1. B. Budesinsky. Chelates in analytical chemistry. Vol. 1. *Edited by* A. J. Barnard, Jr. and H. A. Flaschka. Marcel Dekker, New York. 1969. pp. 15–44.
2. K. Burger. Organic reagents in metal analysis. Pergamon, Sydney. 1973.
3. F. W. Czech and T. P. Hyrchyshyn. Automation in analytical chemistry, Technicon Symposia, 1967, Vol. 1. Mediad, New York. 1968. pp. 273–278.
4. J. Senkyr and J. Petr. Conference on ion-selective electrodes — Budapest, 1977. *Edited by* E. Pungor and I. Buzas. Elsevier, Amsterdam. 1978. p. 559.
5. C. N. Reilley and R. W. Schmid. Anal. Chem. **31**, 887 (1959).
6. S. Nakada, M. Yamada, T. Ito, and M. Fujimoto. Bull. Chem. Soc. Jpn. **50**, 1887 (1977).
7. S. Nakada, M. Yamada, T. Ito, and M. Fujimoto. Bull. Chem. Soc. Jpn. **53**, 3365 (1980).
8. R. B. Fulton and B. Kratochvil. Anal. Chem. **52**, 546 (1980).
9. B. Kratochvil, J. Nolan, F. Cantwell, and R. Fulton. Can. J. Chem. **59**, 2539 (1981).
10. V. Michaylova and N. Kouleva. Talanta, **20**, 453 (1973).
11. T. Anfalt and D. Jagner. Anal. Chem. **45**, 2412 (1973).
12. K. Venkataraman. The chemistry of synthetic dyes. Vol. II. Academic Press, New York. 1952. Chapt. XLII. pp. 1304–1352.
13. J. W. Ross, Jr. and M. S. Frant. Anal. Chem. **51**, 1900 (1969).
14. V. K. Olson, J. D. Carr, J. D. Hargens, and R. Ken Force. Anal. Chem. **48**, 1228 (1976).
15. F. Lindstrom and H. Diehl. Anal. Chem. **32**, 1123 (1960).
16. G. Schwarzenbach and W. Biederman. Helv. Chim. Acta, **31**, 678 (1948).
17. G. P. Hildebrand and C. N. Reilley. Anal. Chem. **29**, 258 (1957).
18. D. W. Rogers, D. A. Aikens, and C. N. Reilley. J. Phys. Chem. **66**, 1582 (1962).
19. A. Itoh and K. Ueno. Analyst, **95**, 583 (1970).
20. L. Meites. Handbook of analytical chemistry. McGraw-Hill, New York. 1963. pp. 3–105.
21. J. S. Brush. Anal. Chem. **33**, 798 (1961).
22. M. Kodama and A. Ebine. Bull. Chem. Soc. Jpn. **40**, 1857 (1967).
23. F. De Oliveira Magalhaes. Cad. Omega, **31**, 175 (1979); Chem. Abstr. 94: 21220.
24. D. Betteridge, Q. Fernando, and H. Freiser. Anal. Chem. **35**, 294 (1963).
25. B. F. Pease and M. B. W. Williams. Anal. Chem. **31**, 1044 (1959).
26. J. Korbl and B. Kakac. Coll. Czech. Chem. Commun. **23**, 889 (1958).
27. B. Karadakov, A. Aleksieva, and D. Venkova. God. Vissh. Khim.-Technol. Inst., Sofia **23**, 265 (1977); Chem. Abstr. 90: 114408.
28. B. Rehak and J. Korbl. Coll. Czech. Chem. Commun. **25**, 797 (1960).
29. K. Ogura, K. Seneo, S. Murakami, and T. Yosino. J. Inorg. Nucl. Chem. **42**, 1165 (1980).
30. F. Ingman, personal communication with E. Wanninen, 1967, cited by E. Wanninen. E. Bishop (*Editor*). Indicators. Pergamon Press, Sydney. 1972. p. 361.
31. Y. Murakami, K. Nakamura, and M. Tokunaga. Bull. Chem. Soc. Jpn. **36**, 669 (1963).
32. D. W. Margerum, C. H. Byrd, S. A. Reed, and C. V. Banks. Anal. Chem. **25**, 1219 (1953).
33. K. Cammann. Working with ion-selective electrodes. Springer-Verlag, Berlin. 1979. p. 131.
34. J. F. Coetzee and W. K. Istone. Anal. Chem. **52**, 53 (1980).
35. G. A. Rechnitz and N. C. Kenny. Anal. Lett. **2**, 395 (1969).
36. R. J. Baczuk and R. J. Dubois. Anal. Chem. **40**, 685 (1968).
37. P. W. Carr. Anal. Chem. **44**, 452 (1972).
38. L. Sucha and M. Suchanek. Anal. Lett. **3**, 613 (1970).
39. F. A. Schultz. Anal. Chem. **43**, 502 (1971).
40. F. A. Schultz. Anal. Chem. **43**, 1523 (1971).

# The crystal structure of 4,7-oxido-7-methyl-7-hydroxymethyl-2,2,6,6-tetramethylpiperidin-1-oxyl[1]

M. CYGLER[2]

*Division of Biological Sciences, National Research Council of Canada, Ottawa, Ont., Canada K1A 0R6*

Received March 11, 1982

M. CYGLER. Can. J. Chem. **60**, 2392 (1982).

4,7-Oxido-7-methyl-7-hydroxymethyl-2,2,6,6-tetramethylpiperidin-1-oxyl, $C_{12}H_{22}NO_3$, crystallizes in the monoclinic space group $P2_1/m$ with unit cell dimensions $a$ = 8.041(1), $b$ = 13.348(1), $c$ = 5.945(1) Å, $\beta$ = 95.90(1)°, $Z$ = 2. Intensity data were measured on a diffractometer and the structure solved by direct methods. The least-squares refinement converged at $R$ = 0.039 for 1304 reflections. Two enantiomeric molecules, differing in the position of the OH group, occupy the same site in the asymmetric unit (each with a probability of 0.5) giving rise to a disorder of the hydroxyl group. The piperidine ring adopts the usual chair conformation, with C—C—C—C torsion angles being intermediate between those observed for C(4) mono- and for bisubstituted nitroxypiperidine derivatives. The N—O bond is 1.282(2) Å long, and it makes an angle of 18.5(2)° with the CNC plane. Molecules are connected by O—H...O hydrogen bonds. The influence of the degree of substitution at C(4) on ring geometry is discussed.

M. CYGLER. Can. J. Chem. **60**, 2392 (1982).

L'oxydo-4,7 méthyl-7 hydroxyméthyl-7 tétraméthyl-2,2,6,6 pipéridineoxyl-1, $C_{12}H_{22}NO_3$, cristallise dans le groupe d'espace monoclinique $P2_1/m$ avec des dimensions de maille de: $a$ = 8,041(1), $b$ = 13,348(1), $c$ = 5,945(1) Å, $\beta$ = 95,90(1)°, $Z$ = 2. On a mesuré les données d'intensité à l'aide d'un diffractomètre, on a résolu la structure par des méthodes directes et on l'a affiné par la méthode des moindres carrés jusqu'à une valeur conventionnelle de $R$ = 0,039 pour 1304 réflexions. Deux molécules énantiomères qui diffèrent par la position du groupe OH occupent le même site dans l'unité asymétrique (chacune ayant une probabilité de 0,5) provoquant une augmentation du désordre du groupe hydroxyle. Le cycle pipéridine adopte la conformation chaise habituelle, avec des angles de torsion C—C—C—C intermédaires entre ceux observés pour des dérivés de nitroxypipéridine mono et bisubstitués en position C-4. La liaison N—O est longue 1,282(2) Å et forme un angle de 18,5(2)° avec le plan CNC. Les molécules sont reliées par des liaisons hydrogènes O—H...O. On discute de l'influence du degré de substitution en position C-4 sur la géométrie du cycle.

[Traduit par le journal]

## Introduction

Nitroxy radicals incorporated in the piperidine ring form stable radicals when shielded by bulky groups at adjacent ring carbon atoms. Conformations of various 2,2,6,6-tetramethylpiperidin-1-oxyl derivatives with different substituents at C(4) have been investigated by the X-ray diffraction method (1–15). The piperidine rings exhibited, with two exceptions, a chair conformation flattened at the nitrogen and distorted to varying extents by interactions of axial substituents. The two exceptions are 2,2,6,6-tetramethylpiperidin-4-one-1-oxyl (13, 14), which adopts a twist conformation in the crystal, and a derivative of 2,2,6,6-tetramethyl-5-methylenepiperidin-4-one-1-oxy with C(3) spiro connected to a system of fused rings (15), where a half-chair conformation was adopted. In the latter compound, two adjacent, $sp^2$ hybridized C atoms are largely responsible for such a conformation. The former molecule may be regarded as an analogue of cyclohexan-1,4-dione, which has also been shown to adopt a twist conformation in the solid state (16). Rozantsev, on the basis of measured dipole moments of 2,2,6,6-tetramethylpiperidin-4-one-1-oxyl, concluded that this molecule has a twist conformation in solution as well (17). Interestingly, however, the results of electron diffraction experiments performed in the gas phase were most consistent with that molecule adopting a chair form (18). It is evident that the carbonyl group greatly lowers the energy difference between chair and twist conformations. On the other hand, a hydroxyimine group bonded to C(4) does not destabilize the chair conformation to the same extent. It was shown that 2,2,6,6-tetramethyl-4-hydroxyimino-piperidin-1-oxyl (19) adopts a chair conformation in the crystal.

A series of 2,2,6,6-tetramethylpiperidine derivatives **1** with an exocyclic double bond at C(4) has recently been synthesized (20). Their imino groups were converted to nitroxy radicals by the standard procedure of oxidation with hydrogen peroxide in the presence of a catalyst (21).

During the oxidation of **1***a* the double bond also was oxidized, giving **2** (the title compound, mp 95.5–96.5°C). In other derivatives the double bond

[1]NRCC No. 20385.

[2]Present address: Department of Biochemistry, University of Alberta, Edmonton, Alta., Canada T6G 2H7. Permanent address: Department of Crystallography, Institute of Chemistry, University of Łódź, Nowotki 18, 91-416 Łódź, Poland.

0008-4042/82/182392-06$01.00/0

©1982 National Research Council of Canada/Conseil national de recherches du Canada

Can. J. Chem. Downloaded from www.nrcresearchpress.com by 210.87.254.40 on 09/06/12
For personal use only.

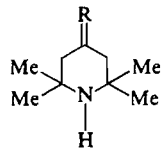


1

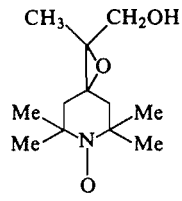


2

*a*: R = $CHCH_2OH$
*b*: R = $C(CH_3)CH_2OH$
*c*: R = $CHC(CH_3)_2OH$
*d*: R = $C(CH_3)C(CH_3)_2OH$

was retained, but the resulting compounds are liquids at room temperature. We have proceeded with the X-ray analysis of **2** in order to investigate the influence of the epoxide moiety on the conformation of the piperidine ring.

## Experimental

Crystal data are as follows:

$C_{12}H_{22}NO_3$ fw = 228.3

Monoclinic, $P2_1/m$, $a = 8.041(1)$, $b = 13.348(1)$, $c = 5.945(1)$ Å, $\beta = 95.90(1)°$, $V = 634.7$ Å$^3$, $Z = 2$, $d_x = 1.195$ g cm$^{-3}$, $\lambda(CuK_\alpha) = 1.54178$ Å, $\mu(CuK_\alpha) = 7.0$ cm$^{-1}$.

Dark red prisms were crystallized from a mixture of benzene and dimethyl sulfoxide. The data were collected at room temperature on an Enraf-Nonius CAD-4 diffractometer, using Ni-filtered $CuK_\alpha$ radiation and a crystal of dimensions 0.49 × 0.32 × 0.12 mm. An $\omega/2\theta$ scan technique was employed for reflections with $\theta$ angles in the range 1–76°. The scan width was $\Delta\omega = (0.7 + 0.2 \tan\theta)°$ and it was extended by 25% on either side for background counts. The aperture was $(2.5 + 0.5 \tan\theta)$ mm wide and 4 mm high. The maximum scan time was 120 s. The intensities of three standard reflections, monitored every 100 min, varied ±2% during the data collection and were used for appropriate scaling of intensities. Three other reflections were used as orientation controls and were measured every 60 reflections. The measured intensities were corrected for Lorentz and polarization factors but not for absorption.

Out of the total of 1382 independent reflections there were 1304 with $I > 1.5\,\sigma(I)$. The systematic absences observed on precession photographs indicated space group $P2_1$ or $P2_1/m$. Because the molecule lacks mirror symmetry and the unit cell contains only two molecules, the space group $P2_1$ was assumed to be correct despite the clearly centrosymmetric statistics of the normalized structure factors. Direct methods (MULTAN (22)) were applied in that space group and the solution with the highest figure of merit revealed an acceptable model. It possessed a plane of symmetry passing through N(1) and C(4), perpendicular to the *y*-axis, with two possible positions for a hydroxyl group on either side of the mirror plane. Accordingly, the space group assignment was changed to $P2_1/m$ and the hydroxyl O atom was refined with an occupancy factor of one-half. The block-diagonal least-squares refinement with isotropic and then anisotropic temperature factors reduced the *R* index to 0.100. A difference map revealed all the H atoms except that of the hydroxyl group. Two further cycles of refinement ($R = 0.047$) followed by another difference map permitted the location of the missing H atom. The final agreement indices are $R = 0.039$ and $R_w = 0.043$ for 1304 reflections. The weighting scheme used in the last few cycles was $w^{-1/2} = 12.0/|F_o|$ for $|F_o| > 12$, otherwise $w^{-1/2} = 1.0$. The mean and maximum shifts/esd for all atoms in the last least-squares cycle were 0.06 and 0.46, respectively. The scattering factor curves were taken from ref. 23.

All calculations were carried out with the NRC crystallographic computing programs by Ahmed, Hall, Pippy, and Huber (24). The final coordinates are listed in Table 1. Lists of anisotropic temperature parameters and of observed and calculated structure factors are available.[3]

TABLE 1. Final fractional coordinates with esd's in parentheses (× $10^4$, for H × $10^3$) and isotropic temperature factors

| Atom | *X* | *Y* | *Z* | *B*(*E*) |
|---|---|---|---|---|
| O(1) | 4355(2) | 2500 | 6841(2) | 4.2(0.1) |
| N(1) | 3022(2) | 2500 | 5455(2) | 2.9(0.1) |
| C(2) | 2500(1) | 3486(1) | 4440(2) | 2.8(0.1) |
| C(21) | 3671(2) | 3767(1) | 2661(2) | 3.9(0.1) |
| C(22) | 2632(2) | 4264(1) | 6332(2) | 3.9(0.1) |
| C(3) | 673(1) | 3427(1) | 3411(2) | 3.0(0.1) |
| C(4) | 247(2) | 2500 | 2026(3) | 2.6(0.1) |
| C(7) | −1091(2) | 2500 | 116(3) | 3.0(0.1) |
| C(8) | −2031(2) | 3448(1) | −589(2) | 4.2(0.1) |
| O(2) | 661(1) | 2500 | −296(2) | 3.0(0.1) |
| O(3) | −2555(2) | 3427(2) | −2917(3) | 4.7(0.1) |
| H(211) | 350(2) | 334(1) | 124(2) | 4.9(0.4) |
| H(212) | 345(2) | 445(1) | 214(3) | 5.5(0.4) |
| H(213) | 485(2) | 373(1) | 338(2) | 4.9(0.3) |
| H(221) | 195(2) | 407(1) | 760(3) | 5.6(0.4) |
| H(222) | 221(2) | 490(1) | 565(3) | 5.3(0.4) |
| H(223) | 376(2) | 433(1) | 704(3) | 5.2(0.4) |
| H(31) | −6(2) | 343(1) | 472(2) | 3.9(0.3) |
| H(32) | 45(2) | 404(1) | 250(2) | 3.6(0.3) |
| H(81) | −303(2) | 350(1) | 26(3) | 5.9(0.4) |
| H(82) | −134(2) | 403(1) | −31(2) | 5.3(0.4) |
| H(3) | −326(5) | 325(3) | −297(6) | 7.2(1.0) |

## Results and discussion

The title compound, obtained by a nonstereospecific reaction, is racemic. Usually enantiomeric molecules are related by crystallographic symmetry or they occupy two distinct positions in the asymmetric unit. The enantiomeric molecules in the present structure differ only by the position of the terminal hydroxyl group. This group is involved in hydrogen bonding in the crystal. However, the geometry of that bond and other intermolecular contacts of the hydroxyl group are the same for both enantiomers. Consequently each enantiomeric molecule can occupy any particular site. The O(3) atom can thus be found with equal probability on either side of the molecule in the average unit cell, giving rise to the observed mirror

[3]These tables may be obtained, at a nominal charge, from the Depository of Unpublished Data, CISTI, National Research Council of Canada, Ottawa, Ont., Canada K1A 0S2.

Can. J. Chem. Downloaded from www.nrcresearchpress.com by 210.87.254.40 on 09/06/12
For personal use only.

Can. J. Chem. Downloaded from www.nrcresearchpress.com by 210.87.254.40 on 09/06/12
For personal use only.

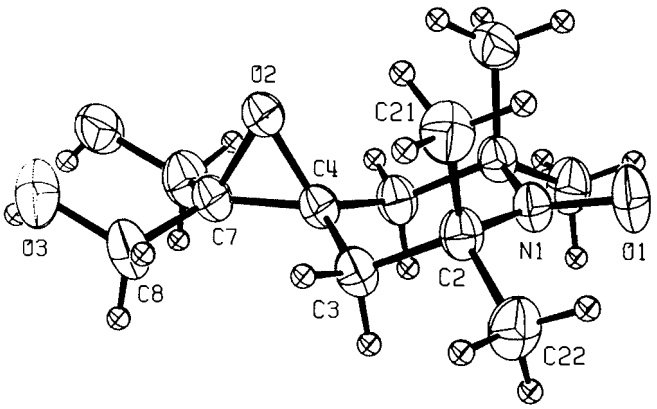


FIG. 1. View of the molecule with the numbering scheme. Both sites for the O(3) atom with occupancy factors 0.5 are shown.

symmetry. A somewhat similar case was described by Krishna Murthy and Vijayan (25), where two conformers, differing by a 180° rotation of a non-symmetrically substituted phenyl ring, occupied the same general position with partial occupancies, leading to a more symmetrical image of the molecule. In that case, however, van der Waals interactions were significantly different for the two conformers, leading to unequal occupancies (0.35 and 0.65).

*Piperidine ring*

A view of the molecule together with the numbering scheme is shown in Fig. 1. Bond lengths, valence, and torsion angles are shown in Fig. 2. The C—H distances, which are not given in Fig. 2, are in the range of 0.96(1) to 1.02(1) Å with the mean value of 0.99(2) Å. The piperidine ring adopts its usual chair conformation, flattened at the nitrogen atom. The O(2) atom of the epoxide ring is in an axial position in relation to the piperidine ring.

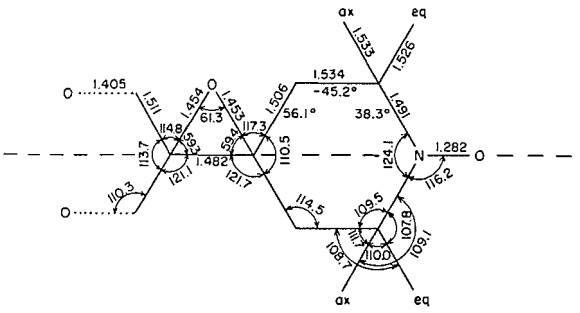


FIG. 2. Bond lengths (Å), valence, and torsion angles (deg). Estimated standard deviations are in the range: 0.002–0.003 Å for bonds; 0.08–0.14° for angles and 0.3° for torsion angles. The dashed line marks schematically the plane of symmetry of the molecule.

In Table 2, a compilation of some geometrical features of various 2,2,6,6-tetramethylpiperidin-1-oxyl derivatives is presented.

It may be stated that the ring becomes less puckered near the C(4) with increasing substitution at C(4). That effect is especially apparent for bisubstituted rings where the C—C—C—C ($\tau_3$) torsion angle is 8° smaller than in mono- and 10° smaller than in unsubstituted derivatives. The N—C—C—C ($\tau_2$) torsion angle also decreases as substitution at C(4) increases; the changes are, however, smaller than for $\tau_3$. No such correlation was observed for torsion angles around the N—C bonds. The C—N—C—C ($\tau_1$) torsion angle varies over a wide range and the average values for bi-, mono-, and unsubstituted derivatives are close.

The distance of 3.382(2) Å between the axial methyl groups is among the shortest found in this series of derivatives. The distance between the O(2) atom of the epoxide ring and the axial methyl groups is 3.307(2) Å, only slightly longer than contacts between the axial substituents in 4-ethynyl-4-hydroxy-2,2,6,6-tetramethylpiperidin-1-oxyl (—C≡...$C_{ax}$ = 2.283(4) Å (12)). Such a distance is attained in the present molecule by increased puckering at C(4). The C—C—C—C ($\tau_3$) torsion angle is between those observed for mono- and bisubstituted rings. The C—N—C—C ($\tau_1$) torsion angle has a larger value than observed in most other compounds; however, similar values have been observed (see Table 2). The endocyclic angles at methylene groups (114.5(1)°) are between those found in mono- and bisubstituted derivatives, e.g., 113.1(5)° in 2,2,6,6-tetramethylpiperidin-4-ol-1-oxyl (5), 113.0(3)° in carbonic acid di(4-hydroxy-2,2,6,6-tetramethylpiperidin-1-oxyl) ester (7) and 117.3(2)° in 4-ethynyl-4-hydroxy-2,2,6,6-tetramethylpiperidin-1-oxyl (12).

TABLE 2. Comparison of some geometrical features of various piperidin-1-oxyl derivatives[a]

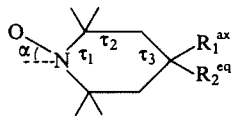


| $R_1$ | $R_2$ | $\tau_1$ | $\tau_2$ | $\tau_3$ | N—O | α | C—N—C | $C_{ax}...C_{ax}$ | References |
|---|---|---|---|---|---|---|---|---|---|
| —H | —H | 32.8 | 45.7 | 61.5 | 1.295 | 19.4 | 125.5 | 3.492 | 2 |
| —H | —H | 33.8 | 47.0 | 63.9 | 1.278 | 17.1 | 123.2 | 3.325 | 3 |
| —H[b] | —H | 41.3 | 47.0 | 64.4 | 1.19 | 5.8 | 128.9 | 3.29 | 4 |
| —H | —OH | 30.1 | 44.8 | 62.4 | 1.290 | 15.8 | 125.2 | 3.390 | 5 |
| —H | $(—CH_2^-)_4R$ | 40.5 | 47.8 | 58.4 | 1.304 | 19.7 | 124.4 | 3.385 | 6 |
| —H | —COOR | 33.4 | 44.3 | 61.5 | 1.286 | 18.1 | 126.5 | 3.462 | 7 |
| —H | —COOR | 33.8 | 46.1 | 61.7 | 1.291 | 19.7 | 125.6 | 3.527 | 7 |
| —H | $—N(CH_3)_2HC_2R$ | 33.7 | 49.0 | 67.5 | 1.285 | 17.6 | 123.2 | 3.541 | 8 |
| —H | $—OC(O)CH_2R$ | 39.3 | 46.3 | 59.9 | 1.251 | 19.1 | 125.2 | 3.390 | 9 |
| —H | $—N(CH_2)CuR$ | 34.6 | 42.1 | 57.0 | 1.32 | 21.2 | 129.6 | 3.38 | 10 |
| —H | $—N(CH_2)CuR$ | 29.9 | 44.6 | 62.8 | 1.30 | 20.5 | 127.5 | 3.60 | 10 |
| —OH | $(—CH_2^-)_4R$ | 34.9 | 44.2 | 54.6 | 1.31 | 19.0 | 126.3 | 3.51 | 11 |
| —C≡ | —OH | 35.9 | 43.6 | 52.7 | 1.281 | 19.6 | 124.7 | 3.479 | 12 |
| | $CH_3$ $CH_2OH$ | 38.3 | 45.2 | 56.1 | 1.282 | 18.5 | 124.1 | 3.382 | This paper |
| Average | | | | | | | | | |
| Unsubstituted | | 36.0(4.6) | 46.6(8) | 63.3(1.3) | | | | | |
| Monosubstituted | | 34.4(3.8) | 45.6(2.2) | 61.4(3.2) | | | | | |
| Bisubstituted | | 35.4(7) | 43.9(4) | 53.7(1.3) | | | | | |

[a]α is the angle between the N—O bond and the CNC plane; $\tau_1$, $\tau_2$, and $\tau_3$ are endocyclic torsion angles in the piperidine ring.
[b]N⁺=O rather than N—O.

*Nitroxy group*

The geometry of the nitroxy group is normal (see Table 2); the N—O distance of 1.282(2) Å and the C—N—C angle of 124.1(1)° are within the range observed in other compounds. The C—N(O)—C group is not planar: the N—O bond forms an angle of 18.5(2)° with the CNC plane.

In a previous study (26) we pointed out that the $C_{ax}$—C—N and $C_{eq}$—C—C endocyclic angles reflect the bulkiness and position of the substituent at the N atom. The angles reported for 2,2,6,6-tetramethylpiperidin-1-oxyl derivatives, 109.0 and 108.9° respectively, agree well with those observed here (Fig. 2).

*Epoxide ring*

The epoxide ring, as found in this structure, is symmetrical, with both C—O bonds and both C—C angles being equal within experimental error. The exocyclic C—C—C angles are significantly larger than the O—C—C angles. While the former are very similar at both C(4) and C(7) (~121.4°), the latter are smaller at the terminal $CH_2OH$ group (114.8(1)°) than at the junction with the piperidine ring (117.3(1)°) due to the interaction of O(2) with the axial methyl groups.

Comparisons of the geometries of epoxide rings were previously made by Brisse *et al.* (27) and Foces-Foces *et al.* (28), and were based on 11 and 14 crystal structures, respectively. We have extended the analysis, using the Cambridge Crystallographic Database (29) and restricting ourselves to determinations with *R* factors less than 0.08 and esd's for C—C bond lengths less than 0.006 Å. The analysed set contained 170 epoxide fragments.[4] Table 3 presents some results of that comparison. The bond lengths and angles in the ring vary over quite a broad range. Mean values

TABLE 3. Summary of the epoxide ring geometry based on 170 structural fragments

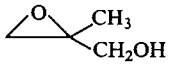


| | C—O (Å) | C—C (Å) | C—O—C (deg) | C—C—O (deg) | Area (Å²) |
|---|---|---|---|---|---|
| Min | 1.401 | 1.427 | 58.5 | 57.1 | 0.883 |
| Max | 1.482 | 1.521 | 63.6 | 62.4 | 0.952 |
| Mean | 1.447 | 1.466 | 60.9 | 59.6 | 0.915 |
| σ | 0.016 | 0.018 | 0.8 | 0.7 | 0.014 |
| σ/mean | 0.011 | 0.012 | 0.013 | 0.013 | 0.015 |

[4]The list of references is part of deposited material.

Can. J. Chem. Downloaded from www.nrcresearchpress.com by 210.87.254.40 on 09/06/12
For personal use only.

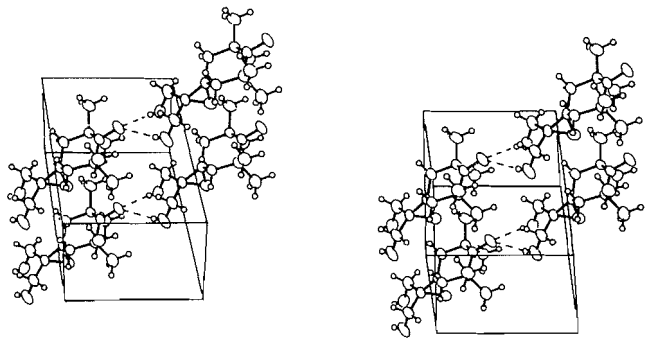

FIG. 3. Stereoview of the molecular packing. Molecules related by two-fold screw axis are omitted for better clarity of the drawing. Hydrogen bonds are marked with dashed lines.

obtained here do not differ significantly from those reported previously.

It was found that a fusion of an epoxide ring with a 5-membered ring or other strained system causes lengthening of the C—C bond (usually above 1.485 Å). Similar lengthening is also caused by $\pi$-donor substituents (e.g., phenyl or —C≡N) to the ring (30).

In the case of a double bond which is one bond away from the epoxide ring, the distal C—O bond in the ring tended to be shorter than the proximal one. A similar effect for a cyclopropane ring was analysed by Allen (31) from structural data. In the epoxide moiety that effect is, however, less pronounced. Out of 38 fragments in the analysed data set with a neighbouring C=O or —C=C— group, 19 showed significant shortening of distal C—O bonds, 11 showed no significant difference, and 8 showed significant lengthening of distal C—O.

*Molecular packing*

The molecules of the title compound are connected by hydrogen bonds between the hydroxyl group and nitroxyl oxygen into chains along the [101] direction (Fig. 3). The geometry of that bond is as follows: O(1)...O(3) = 2.766(3) Å, O(3)—H = 0.61(1) Å, H...O(1) = 2.16(1) Å, O(3)—H...O(1) = 174(4)°. The molecules are packed in such a way that the epoxide ring O(2) points toward the free space between equatorial methyl groups of a neighbouring molecule. The distance between O(2) and the closest H atoms of these methyl groups is 2.70(1) Å and the O(2)...N distance is 3.312(2) Å. The shortest intermolecular contact is between O(3) and the axial H atom at C(3) (2.56(2) Å). All H...H contacts are above 2.57 Å and those of other atoms are above 3.5 Å.

**Acknowledgement**

The author would like to thank Mr. G. Grabowski for supplying him with the crystals.

1. J. LAJZEROWICZ-BONNETEAU. *In* Spin labelling. Theory and applications. *Edited by* L. J. Berliner. Academic Press, New York. 1976, and references cited therein.
2. D. BORDEAUX, J. LAJZEROWICZ-BONNETEAU, R. BRIERE, H. LEMAIRE, and A. RASSAT. Org. Magn. Reson. **5**, 47 (1973).
3. P. MURRAY-RUST. Acta Crystallogr. B**30**, 1368 (1974).
4. L. O. ATOVMYAN, V. A. GOLUBEV, N. I. GOLOVINA, and G. A. KLITSKAYA. Zh. Strukt. Khim. **16**, 92 (1975).
5. L. J. BERLINER. Acta Crystallogr. B**26**, 1198 (1970).
6. R. P. SHIBAEVA and L. P. ROZENBERG. Zh. Strukt. Khim. **15**, 948 (1974).
7. R. P. SHIBAEVA, R. M. LOBKOVSKAYA, and L. P. ROZENBERG. Zh. Struct. Khim. **17**, 876 (1976).
8. A. T. MCPHAIL, M. B. ABOU-DONIA, and G. M. ROSEN. Mol. Pharmacol. **12**, 590 (1976).
9. A. CAPIOMONT. Acta Crystallogr. B**28**, 2298 (1972).
10. L. O. ATOVMYAN, H. I. GOLOBINA, G. A. KLITSKAYA, A. A. MEZHIDOV, A. V. ZVARIKINA, V. B. STRYUKOV, and D. N. FEDUTIN. Zh. Strukt. Khim. **16**, 624 (1975).
11. L. D. ARUTYUNYAN and R. P. SHIBAEVA. Dokl. Akad. Nauk. SSSR, **215**, 881 (1974).
12. M. CYGLER. Acta Crystallogr. B**35**, 195 (1979).
13. R. P. SHIBAEVA, L. D. ATOVMYAN, M. G. NEIGAUZ, L. A. NOVAKOVSKAYA, and S. L. GINZBURG. Zh. Struct. Khim. **13**, 887 (1972).
14. D. BORDEAUX and J. LAJZEROWICZ. Acta Crystallogr. B**30**, 790 (1974).
15. R. P. SHIBAEVA, R. M. LOBKOVSKAYA, A. O. SHAPIRO, and E. G. ROZANTSEV. Zh. Struct. Khim. **18**, 1060 (1977).
16. P. GROTH and O. HASSEL. Acta Chem. Scand. **18**, 923 (1964).
17. E. G. ROZANTSEV. Free nitroxyl radicals. Plenum, New York. 1970.
18. P. ANDERSEN, E. E. ASTRUP, P. S. FREDERICHSEN, and K. F. NAKKEN. Acta Chem. Scand. A**28**, 675 (1974).
19. D. BORDEAUX and J. LAJZEROWICZ. Acta Crystallogr. B**33**, 1837 (1977).
20. G. GRABOWSKI and R. SKOWROŃSKI. Polish J. Chem. **54**, 1887 (1980).
21. G. GRABOWSKI. Private communication.

Can. J. Chem. Downloaded from www.nrcresearchpress.com by 210.87.254.40 on 09/06/12
For personal use only.

22. P. MAIN, S. E. HALL. L. LESSINGER, G. GERMAIN, J. P. DECLERCQ, and M. M. WOOLFSON (1978). MULTAN. A system of computer programs for the automatic solution of crystal structures from X-ray diffraction data. Univs. of York, England and Louvain, Belgium.
23. International tables for X-ray crystallography. Vol. IV. Kynoch Press, Birmingham. 1974.
24. F. R. AHMED, S. R. HALL, M. E. PIPPY, and C. P. HUBER. J. Appl. Crystallogr. **6**, 309 (1973).
25. H. M. KRISHNA MURTHY and M. VIJAYAN. Acta Crystallogr. B**37**, 1102 (1981).
26. M. CYGLER, T. MARKOWICZ, J. SKOLIMOWSKI, and J. SKOWROŃSKI. J. Mol. Struct. **68**, 161 (1980).
27. F. BRISSE, G. JUST, and F. BLANK. Acta Crystallogr. B**34**, 557 (1978).
28. C. FOCES-FOCES, F. H. CANO, and S. GARCIA-BLANCO. Acta Crystallogr. B**33**, 3521 (1977).
29. (*a*) O. KENNARD, D. WATSON, F. ALLEN, W. MOTHERWELL, W. TOWN, and J. RODGERS. Chem. Brit. **11**, 213 (1975); (*b*) F. H. ALLEN, S. BELLARD, M. D. BRICE, B. A. CARTWRIGHT, A. DOUBLEDAY, H. HIGGS, T. HUMMELINK, B. G. HUMMELINK-PETERS, O. KENNARD, W. D. S. MOTHERWELL, J. R. RODGERS, and D. G. WATSON. Acta Crystallogr. B**35**, 2331 (1979).
30. (*a*) D. A. MATTHEWS, J. SWANSON, M. H. MUELLER, and G. D. STUCKY. J. Am. Chem. Soc. **93**, 5945 (1971); (*b*) M. WILSON, F. MATHIS, R. BURGADA, J. JAUD, and J. GALY. Acta Crystallogr. B**34**, 2772 (1978).
31. (*a*) F. H. ALLEN. Acta Crystallogr. B**36**, 81 (1980); (*b*) F. H. ALLEN. Abstracts p. C198, XII IUCr. Congress, 16–25 August 1981, Ottawa.

Can. J. Chem. Downloaded from www.nrcresearchpress.com by 210.87.254.40 on 09/06/12
For personal use only.

# Détermination de propriétés diélectriques de substances polaires: conditions d'applicabilité de l'équation d'Omini

LÉO DEGRÈVE, PAULO ROBERTO BROSSI PELISSARI ET MARIA MARCIA MURTA

*Faculdade de Filosofia, Ciências e Letras de Ribeirão Preto, Universidade de São Paulo, 14100 Ribeirão Preto, São Paulo, Brésil*

Reçu le 5 janvier 1982

LÉO DEGRÈVE, PAULO ROBERTO BROSSI PELISSARI et MARIA MARCIA MURTA. Can. J. Chem. **60**, 2398 (1982).

Une équation qui permet de déterminer le moment dipolaire et la polarisabilité de substances polaires à partir de la mesure de la constante diélectrique de solutions de cette substance avec des solvants apolaires est testée avec différentes paires solvant–soluté. Les résultats indiquent que cette équation fournit de bonnes valeurs du moment dipolaire et de la polarisabilité si le solvant est choisi convenablement.

LÉO DEGRÈVE, PAULO ROBERTO BROSSI PELISSARI, and MARIA MARCIA MURTA. Can. J. Chem. **60**, 2398 (1982).

An equation which allows for the determination of the dipole moment and polarizability of polar substances via the dielectric constant of solutions of the substance in nonpolar solvents is tested using different solute–solvent pairs. The results indicate that this equation provides good values of the dipole moment and of the polarizability if the solvent is correctly chosen.

[Journal translation]

Can. J. Chem. Downloaded from www.nrcresearchpress.com by 210.87.254.5 on 09/06/12
For personal use only.

## Introduction

La détermination du moment dipolaire et de la polarisabilité de molécules est un problème assez ancien quand cette détermination peut être réalisée seulement en solution (voir, par exemple, réf. 2). Les difficultés qui apparaissent dans ces déterminations sont de divers types mais pour l'expérimentateur un problème crucial est celui de savoir quelle est la confiance qu'il peut prêter aux résultats. D'autre part, la simplicité de la manipulation expérimentale est importante aussi. Pour cela, nous nous proposons de tester et d'analyser les conditions d'applicabilité d'une équation publiée par M. Omini (1) qui permet de calculer le moment dipolaire et la polarisabilité d'une substance polaire à partir de la mesure de la constante diélectrique de solutions de diverses concentrations de cette substance avec un solvant apolaire.

Pour tester l'équation d'Omini, la constante diélectrique de mélanges binaires de quatre solvants apolaires et quatre solutés polaires a été mesurée en fonction de la concentration et en fonction de la température. Les moments dipolaires et les polarisabilités ont été calculés et analysés en les comparant aux résultats obtenus par d'autres méthodes afin de déterminer les meilleures conditions d'applicabilité de la théorie d'Omini.

## Partie expérimentale

Comme substances de travail, nous avons utilisé le tétrachlorure de carbone, le benzène, l'hexane normal, l'heptane normal, le chloroforme, le chlorobenzène, le 1-chloro-*n*-pentane et le 2-chloro-2 méthylpropane. Ces substances ont été purifiées suivant les techniques indiquées pour des mesures de propriétés diélectriques (3). La pureté de ces substances a été vérifiée par au moins deux des techniques suivantes: détermination de l'indice de réfraction, de la température d'ébullition, de la constante diélectrique, de la teneur d'eau ou par la spectroscopie infrarouge.

Les constantes diélectriques de solutions de fractions molaires du soluté polaire allant de 0 à 0,5 ont été mesurées à diverses températures entre 25 et 40°C. Les solutions ont été préparées par pesage et les titres molaires calculés directement à partir des masses des substances. Deux cellules de capacitance ont été employées: la première construite d'acier inoxydable et Teflon, la deuxième de laiton, sur lequel une couche d'or a été déposée électrolytiquement, et Teflon. La température a été mesurée hors de la cellule et ensuite une correction a été introduite à partir de la mesure de la température interne des cellules au moyen d'un thermocouple dont la mesure à son tour a été comparée avec celle d'un thermomètre de mercure standardisé. L'erreur finale des mesures de température est ainsi estimée comme étant $\pm 0{,}1°$. Les capacitances ont été mesurée avec un pont de capacitance Général Radio 1620A. De cette manière la précision des résultats expérimentaux est de l'ordre de 0,04%.

## Résultats

Afin de faciliter l'utilisation des résultats expérimentaux, nous avons mis ceux-ci sous la forme:

$$[1]\quad \varepsilon = (a_1 + a_2 f_2 + a_3 f_2^2 + a_4 f_2^3) \times t + b_1 + b_2 f_2 + b_3 f_2^2 + b_4 f_2^3$$

où les coefficients $a_1, \ldots, b_4$ sont obtenus par régression à partir des données expérimentales et $t$ est la température centigrade.

Les tableaux 1 et 2 réunissent les valeurs des $a$ et des $b$ obtenues. Dans le tableau 3, on trouve les

0008-4042/82/182398-05$01.00/0

©1982 National Research Council of Canada/Conseil national de recherches du Canada

Can. J. Chem. Downloaded from www.nrcresearchpress.com by 210.87.254.5 on 09/06/12
For personal use only.

TABLEAU 1. Valeurs des coefficients $a$ ($K^{-1}$) de l'équation [1]

| Solution* | $-10^3 \cdot a_1$ | $-10^3 \cdot a_2$ | $-10^2 \cdot a_3$ | $10^2 \cdot a_4$ |
|---|---|---|---|---|
| a/A | 1,749 | 8,607 | 1,316 | 1,552 |
| a/B | 1,838 | 12,101 | 10,883 | 0,891 |
| a/C | 1,790 | 21,191 | 0,452 | 1,091 |
| a/D | 1,846 | 33,096 | 2,235 | 18,498 |
| b/A | 1,655 | 12,907 | −1,627 | −2,038 |
| b/C | 1,495 | 32,611 | −5,677 | −7,387 |
| b/D | 1,604 | 40,746 | −6,339 | −13,598 |
| c/A | 1,679 | 0,574 | 3,687 | 4,044 |
| c/B | 1,578 | 0,658 | 5,193 | 6,915 |
| c/C | 1,606 | 8,080 | 2,275 | 1,273 |
| c/D | 1,730 | −2,221 | 28,937 | 98,059 |
| d/A | 1,352 | 3,215 | 1,140 | 0,561 |
| d/B | 1,391 | 1,978 | 2,804 | 2,251 |
| d/C | 1,319 | 11,775 | 7,740 | −0,438 |
| d/D | 1,365 | 8,150 | 8,111 | 14,034 |

*Le symbole a représente le tétrachlorure de carbone, b le benzène, c l'hexane normal, d l'heptane normal, A le chloroforme, B le chlorobenzène, C le 1-chloro-*n*-pentane et D le 2-chloro-2 méthylpropane.

TABLEAU 2. Valeurs des coefficients $b$ de l'équation [1]

| Solution* | $b_1$ | $b_2$ | $b_3$ | $b_4$ |
|---|---|---|---|---|
| a/A | 2,2669 | 1,8600 | 0,6401 | 0,3129 |
| a/B | 2,2738 | 3,4097 | 0,8902 | −0,6233 |
| a/C | 2,2720 | 5,0314 | 0,1343 | −0,7777 |
| a/D | 2,2747 | 6,6700 | 1,1924 | −2,9432 |
| b/A | 2,3153 | 2,1571 | −0,5451 | 1,1860 |
| b/C | 2,3156 | 6,0266 | −3,3993 | 3,3399 |
| b/D | 2,3127 | 7,7613 | −6,7446 | 16,0420 |
| c/A | 1,9374 | 1,0744 | 2,1328 | −0,8405 |
| c/B | 1,9322 | 2,3394 | 2,7496 | −1,8908 |
| c/C | 1,9326 | 3,4970 | 1,4821 | 0,3193 |
| c/D | 1,9391 | 3,5853 | 12,4237 | −32,0205 |
| d/A | 1,9479 | 1,1811 | 0,6727 | 1,0496 |
| d/B | 1,9486 | 2,1899 | 1,5777 | 0,1257 |
| d/C | 1,9447 | 3,3997 | −0,5606 | 4,4319 |
| d/D | 1,9475 | 3,0789 | 19,8365 | −69,4218 |

*La signification des symboles est donnée dans le tableau 1.

TABLEAU 3. Moyenne des constantes diélectriques à 0°C et de leur coefficients thermiques, pour quatre solvants

| | $b_1$† | $b_1$‡ | $-10^3 \cdot a_1$§ | $-10^3 \cdot a_1$‡ |
|---|---|---|---|---|
| a* | 2,272±0,004 | 2,278 | 1,81±0,05 | 2 |
| b* | 2,315±0,002 | 2,324 | 1,58±0,08 | 2 |
| c* | 1,934±0,002 | 1,921 | 1,65±0,07 | 1,55 |
| d* | 1,947±0,002 | | 1,36±0,03 | |

*Pour la signification du symbole, voir tableau 1.
†Voir tableau 2.
‡Référence 4.
§Voir tableau 1.

valeurs moyennes des constantes diélectriques à 0°C et leurs coefficients de température pour les solvants apolaires purs. Les tableaux 1 et 2 permettent de reproduire les données expérimentales avec un écart maximum de 0,01%. Le tableau 3 montre que la concordance entre nos résultats et les résultats publiés est bonne.

Pour appliquer l'équation d'Omini (1), les tableaux 1 et 2 ont été utilisés pour calculer les constantes diélectriques des solutions à 25,0, 30,0, 35,0 et 40,0°C pour sept fractions molaires distribuées régulièrement de 0,07 à 0,49 et pour $f_2 = 0$. La densité des solutions a été calculée par la relation: $\rho = f_1\rho_1 + f_2\rho_2$. Les données utilisées dans ce cas sont réunies dans le tableau 4. Etant donné que des différences entre les résultats pour les diverses températures ont été observées (par exemple, le moment dipolaire du chlorobenzène calculé à partir de la constante diélectrique de solutions de tétrachlorure de carbone a été calculé aux quatre températures comme étant de 1,80, 1,81, 1,83 et 1,84 $D$), nous avons introduit leur écart moyen dans le tableau récapitulatif des résultats, tableau 5.

TABLEAU 4. Densité, coefficient de température de la densité, polarisabilité et moment dipolaire des substances utilisées

| | Densité à 25°C[a] ($g\,cm^{-3}$) | Coefficient de température de la densité[a] ($g\,cm^{-3}\,K^{-1}$) | Polarisabilité ($10^{-23}\,cm^3\,mol^{-1}$) | Moment dipolaire ($D$[g]) |
|---|---|---|---|---|
| a* | 1,58439 | 0,00212 | 1,1194[b] | |
| b* | 0,8737 | 0,00104 | 1,063[c] | |
| c* | 0,65481 | 0,00089 | 1,244[d] | |
| d* | 0,67951 | 0,00084 | 1,424[d] | |
| A* | 1,47988 | 0,001857 | 0,860[e] | 1,04[f] |
| B* | 1,1009 | 0,00216 | 1,289[e] | 1,75[f] |
| C* | 0,8769 | 0,00098 | 1,232[d] | 2,15[a] |
| D* | 0,8361 | 0,00182 | 1,038[d] | 2,15[a] |

*Pour la signification des symboles, voir tableau 1.
[a]Référence 3.
[b]Référence 1.
[c]Calculé à partir de l'équation de Clausius–Mossotti.
[d]Référence 5.
[e]Référence 6.
[f]Référence 7.
[g]$1\,D \equiv 3{,}335640 \times 10^{-30}$ C m.

TABLEAU 5. Moments dipolaires et polarisabilité des solutés polaires et leurs différences, en pourcents, en relation aux données du tableau 4 (la signification des symboles est donnée dans le tableau 1)

| Soluté | Solution | $\mu$ ($D$*) | $\Delta\mu$ (%) | $10^{23}\cdot\alpha$ ($cm^3\,mol^{-1}$) | $\Delta\alpha$ (%) |
|---|---|---|---|---|---|
| A | a/A | 0,80 ±0,02 | −23,1 | 1,56 | 39,4 |
| A | b/A | 0,94 ±0,01 | −9,2 | 1,35±0,01 | 57,0 |
| A | c/A | 1,73 ±0,04 | 66,4 | 2,91±0,02 | 238,0 |
| A | d/A | 1,84 ±0,02 | 77,0 | 3,00 | 249,0 |
| B | a/B | 1,82 ±0,02 | 4,0 | 1,26±0,02 | −2,6 |
| B | b/B | 1,785† | 2,0 | 1,315† | 2,0 |
| B | c/B | 0,61 ±0,04 | −65,0 | 2,59±0,03 | 101,0 |
| B | d/B | 0,623±0,009 | −64,4 | 2,50±0,01 | 94,0 |
| C | a/C | 2,17 ±0,02 | 5,9 | 1,38±0,03 | 12,0 |
| C | b/C | 2,26 ±0,03 | 10,2 | 1,38±0,05 | 12,0 |
| C | c/C | 1,59 ±0,02 | −22,4 | 2,51±0,04 | 104,0 |
| C | d/C | 0,82 ±0,04 | −60,0 | 3,39±0,01 | 175,0 |
| D | a/D | 2,0 ±0,2 | −7,0 | 2,5 ±0,3 | 139,0 |
| D | b/D | 1,57 ±0,01 | −27,0 | 3,03±0,01 | 192,0 |
| D | c/D | 0,88 ±0,02 | −59,1 | 3,90±0,02 | 376,0 |
| D | d/D | 1,26 ±0,04 | −41,4 | 3,41±0,04 | 229,0 |

*1 $D \equiv 3{,}335640 \times 10^{-30}$ C m.
†Référence 1.

## Discussion

Afin de faciliter l'analyse des résultats, les substances choisies comme tests ont des formes géométriques différentes, à savoir: globulaire, annulaire et en chaîne flexible. De cette manière, on peut espérer pouvoir séparer les effets spécifiques dûs à la géométrie des molécules, c'est-à-dire finalement dûs à la structure interne des solutions, des effets dûs à la méthode en soi.

L'analyse des résultats du tableau 5 montre immédiatement que les écarts entre les valeurs de $\mu$ et $\alpha_2$ calculées et publiés sont intolérables quand les solvants utilisés sont l'hexane ou l'heptane. Cela semble indiquer que la conformation des molécules de solvant joue un rôle extrêmement important dans la qualité des résultats et confirme que ce type de solvant doit être évité. Les résultats relatifs au chloroforme doivent être regardés avec une certaine réserve puisqu'il existe la possibilité de formation de complexes (8). Cependant le moment dipolaire du chloroforme déterminé à partir de la constante diélectrique de solutions de benzène se trouve dans une limite d'erreur raisonnable ce qui pourrait indiquer qu'aucun complexe ne se forme. Mais l'erreur de la polarisabilité est beaucoup trop grande. Les mêmes observations peuvent être faites au sujet du chlorure de butyle tertiaire.

En règle générale, l'erreur sur le moment dipolaire est beaucoup plus petite que l'erreur sur la polarisabilité. Cela peut s'expliquer par le fait que le moment dipolaire apparait, en réalité, au carré ce qui rapproche fortement les erreurs sur $\alpha_2$ et sur $\mu^2$. D'autre part, il n'existe aucune évidence de ce que le traîtement d'Omini surestime soit $\alpha_2$, soit $\mu$ au détriment de l'autre facteur puisque les erreurs sur $\alpha_2$, et sur $\mu$ sont aussi bien du même signe que de signes opposés. Cependant, il est bon de noter que seulement dans un cas l'erreur sur la polarisabilité est négative.

Les différences entre les résultats obtenus aux diverses températures ne sont pas significatives puisqu'elles sont de 0,28% par degré, en moyenne. Si on considère encore que quand la température augmente, les résultats calculés peuvent aussi bien augmenter que diminuer, on peut conclure qu'il s'agit de variations qui dépendent plus des erreurs expérimentales et de la technique de calcul que de la méthode en soi.

Quand la méthode d'Omini est utilisée en même temps que des méthodes computationnelles de recherche de l'écart minimum, $\sigma^2$, il faut prendre garde au fait que dans certains cas il apparaît un minimum secondaire comme le montre la figure 1 pour le mélange chloroforme/tétrachlorure de carbone.

La théorie d'Omini est rigoureusement exacte quand les indices de réfraction à longueur d'onde infinie sont égaux pour le solvant et pour le soluté (1). Afin de vérifier indirectement cette affirmation, on peut comparer la différence, en pourcentage, entre la polarisabilité du solvant et celle du soluté avec l'erreur, en pourcentage, commise sur l'évaluation du moment dipolaire (cette erreur est donnée dans le tableau 5). Cette comparaison est faite par la figure 2. Les droites relatives au

Can. J. Chem. Downloaded from www.nrcresearchpress.com by 210.87.254.5 on 09/06/12
For personal use only.

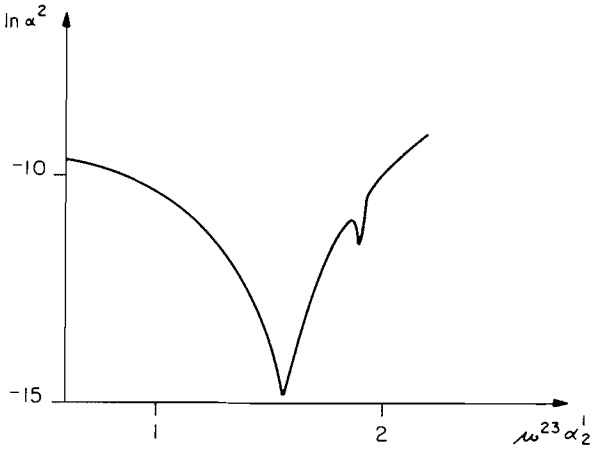


FIG. 1. Logarithme de l'écart quadratique en fonction des valeurs d'essai de la polarisabilité du soluté.

1-chloropentane et au 2-chloro-2 méthylpropane s'écartent de l'origine des axes, où l'erreur est nulle, probablement à cause des erreurs expérimentales. La droite du chlorobenzène s'écarte trop de l'erreur nulle pour qu'il n'y ait pas un autre facteur déterminant; il faut remarquer que les points où $\Delta\mu \approx 65\%$ sont ceux relatifs aux solutions d'hexane et d'heptane ce qui signifie que l'effet de la polarisabilité ne doit pas être considéré seul mais en même temps que les effets dûs aux configurations moléculaires, donc en même temps que les effets entropiques. Les coefficients angulaires de ces trois droites sont très voisins: leur moyenne est de $-0{,}36 \pm 0{,}04$ et la conséquence est qu'une différence de seulement 3% entre les polarisabilité du solvant et du soluté induit une erreur de 10% sur le moment dipolaire. Donc le coefficient angulaire de ces droites est une propriété intrinsèque de la méthode d'Omini appliquée dans des conditions qui ne sont pas exactement celles prévues dans son élaboration. Quant à l'ordonnée à l'origine, elle doit probablement dépendre de la conformation des molécules plus étroitement que le coefficient angulaire. Le coefficient angulaire de la droite du chloroforme est positif, donc de signe opposé aux trois autres. Cependant il faut remarquer que les deux points où $\Delta\mu = 77$ et 66%, qui provoquent la variation du signe, sont ceux où les solvants sont des chaînes flexibles. Cela confirmerait encore une fois que l'hexane et l'heptane ne sont pas des solvants adéquats. L'inversion du signe du coefficient angulaire est peut-être aussi un signal de l'existence de complexe.

Donc il semble que les affirmations d'Omini sur les polarisabilités se confirment puisque les résultats sont meilleurs quand celles-ci sont proches. Cependant la théorie d'Omini ne considère pas un facteur très important, à savoir la forme des molécules qui semble jouer un rôle très important dans la qualité des résultats comme le montre le tableau 6 obtenu à partir de deux méthodes qui tiennent compte de la forme non sphérique des molécules du soluté (6, 7). La constante diélectrique dépend, entre autres facteurs, de la distribution relative des molécules (9) de manière que l'influence de la forme des molécules sur la façon qu'elles ont de se situer dans l'espace (en moyenne) et donc sur leurs interactions est grande. Les variations conséquentes de la constante diélectrique influencent directement la qualité des résultats. Si on compare ce raisonnement avec une hypothèse fondamentale de la théorie d'Onsager (1, 2) qui est de situer un dipôle ponctuel au centre d'une cavité sphérique plongée

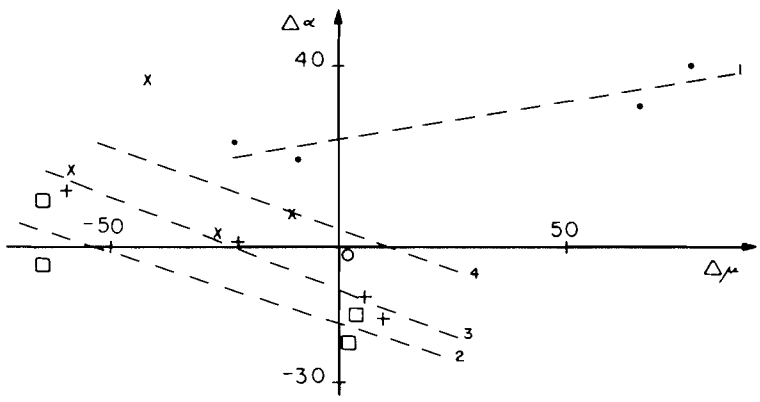


FIG. 2. Pourcentage de le différence depolarisabilité entre le solvant et le soluté en fonction du pourcentage d'erreur donné par la méthode d'Omini. Les droites n° 1, 2, 3 et 4 sont les droites de régression correspondant au chloroforme (●), chlorobenzène (□), 1-chloro-*n*-pentane (+) et 2-chloro-2 méthylpropane (×).

Can. J. Chem. Downloaded from www.nrcresearchpress.com by 210.87.254.5 on 09/06/12
For personal use only.

TABLEAU 6. Moments dipolaires calculés suivant les tableaux 1 et 2 et la référence 7 et polarisabilités corrigées (6). La signification des symbôles est donnée dans le tableau 1

| Soluté | Solution | $\mu$ ($D$*) | $10^{23} \cdot \alpha$ (cm$^3$ mol$^{-1}$) |
|---|---|---|---|
| A | a/A | 1,12 | 1,53 |
| A | b/A | 1,62 | 1,32 |
| A | c/A | 1,03 | 2,85 |
| A | d/A | 1,17 | 2,94 |
| B | a/B | 1,63 | 1,17 |
| B | b/B | | 1,22 |
| B | c/B | 1,65 | 2,40 |
| B | d/B | 1,70 | 2,32 |

*1 $D \equiv 3{,}335640 \times 10^{-30}$ C m.

dans un milieu diélectrique continu, on peut vérifier que le milieu sera "plus continu" si la forme des molécules permet un empilement très régulier ce qui est obtenu seulement avec des molécules de grande symétrie (9). Donc les solvants comme le tétrachlorure de carbone et le benzène doivent fournir les meilleurs résultats et les solvants en chaîne ouverte de mauvais résultats: cela est parfaitement confirmé par les résultats du tableau 5.

## Conclusion

La méthode d'Omini est d'application simple et donne de bons résultats pour estimer le moment dipolaire et la polarisabilité des substances polaires à partir seulement de mesures de la constante diélectrique de solutions. De manière générale, elle ne doit pas être appliquée avec des solvants dont la conformation moléculaire peut varier beaucoup et le solvant doit être choisi de manière à ce que sa polarisabilité soit proche de celle du soluté. Dans ces cas, les résultats seront entâchés d'erreurs de l'ordre de 10% au maximum.

## Remerciements

Nous remercions la Fundação de Amparo à Pesquisa do Estado de São Paulo et le Conselho Nacional de Desenvolvimento Científico e Tecnologico pour leur appui financier.

1. M. OMINI. J. Chem. Phys. **59**, 6478 (1973).
2. C. J. F. BÖTTCHER. Theory of electric polarisation. Elsevier, Amsterdam. Vol. 1, 1973; Vol. 2, 1978.
3. J. A. RIDDICK et W. B. BUNGER. Organic solvents. Wiley–Interscience, New York. 1970.
4. R. C. WEAST (*Editeur*). Handbook of chemistry and physics. 55$^e$ éd. CRC Press, Cleveland. 1974.
5. J. D. HIRSCHFELDER, C. F. CURTISS et R. B. BIRD. Molecular theory of gases and liquids. J. Wiley, New York. 1967.
6. A. K. BURNHAM et T. D. GIERKE. J. Chem. Phys. **73**, 4822 (1981).
7. A. B. MYERS et B. B. BIRGE. J. Chem. Phys. **74**, 3514 (1981).
8. R. D. GREEN. Hydrogen bonding by CH group. MacMillan, London. 1974.
9. L. DEGRÈVE. Mol. Phys. **40**, 837 (1980).

## ADDITIONS AND CORRECTIONS/AJOUTS ET CORRECTIONS

Vol. 59, 1981

**Boris Glavincevski and Sydney K. Brownstein.** Complexing and exchange of boron, aluminum, and gallium chlorides with some Lewis bases.

Page 3012. In the last line of the second experimental paragraph, "26,060,416" should be "26,056,780 (lit $26.057 \times 10^6$)$^2$".

Vol. 60, 1982

**John A. Stone, Dena E. Splinter, and Soon Yau Kong.** A comparison of the relative binding energies of $H^+$ and $NO^+$ to aromatic and haloaromatic bases by high pressure mass spectrometry.

Page 910. The second sentence after reaction [5] on the left hand column of p. 914 should read "$PA(C_6H_5F) - PA(C_6H_6) = +1.4$ kcal mol$^{-1}$ and $PA(C_6H_5Cl) - PA(C_6H_6) = +0.7$ kcal mol$^{-1}$."

**Thomas Birchall, Ronald D. Myers, Jack Passmore, W. A. Shantha Nandana, and George Sutherland.** An iodine-127 Mössbauer study of some chalcogen cations of iodine.

Page 1264. Equation [3] on p. 1265 should read:

$$^{127}\delta_{KI} = 3.74h_s - 0.61h_p - 0.12$$

Can. J. Chem. Downloaded from www.nrcresearchpress.com by 210.87.254.5 on 09/06/12
For personal use only.

# BEST — A new program for rigorous calculation of equilibrium parameters of complex multicomponent systems

RAMUNAS J. MOTEKAITIS AND ARTHUR E. MARTELL[1]

*Department of Chemistry, Texas A&M University, College Station, TX 77843, U.S.A.*

Received March 9, 1982

RAMUNAS J. MOTEKAITIS and ARTHUR E. MARTELL. Can. J. Chem. **60**, 2403 (1982).

The FORTRAN program BEST for the refinement of stability constants from potentiometric data measured on complex systems containing any number of interacting components is described. The core algorithm consists of computation by successive approximations of the pH values at each equilibrium point from an initial set of stability constants based on the equilibrium model. Each approximation results in adjustment of the equilibrium constants being refined in order to improve the fit between the calculated and observed pH values for all the data taken for the system under investigation. Novel features of the algorithm include total generality, minimization of errors with respect to pH, and the avoidance of customary classification labels such as "metal ion", "ligand", "hydroxides", "proton", etc. Several examples of applications to real systems are provided to illustrate the versatility of the program.

RAMUNAS J. MOTEKAITIS et ARTHUR E. MARTELL. Can. J. Chem. **60**, 2403 (1982).

On décrit le programme Fortran BEST, utilisé pour l'amélioration des constantes de stabilité obtenues à partir de données potentiométriques mesurées dans des systèmes complexes contenant des quantités variables de composants qui interagisent. L'algoarithme de base consiste en calculs par approximations successives des valeurs du pH à chaque point d'équilibre et un ensemble initial de constantes de stabilité d'un modèle d'équilibre. Chaque approximation provenant d'un ajustement des constantes d'équilibre est amélioré dans le but de faciliter l'insertion entre les valeurs de pH calculées et observées pour toutes les données relevées pour le système étudié. Les caractéristiques nouvelles de l'algoarithme comprennent une généralité totale, la minimisation des erreurs par rapport au pH et la suppression de la classification habituelle des marqueurs tels "ion métallique", "ligand A", "hydroxydes", "proton", etc. On fournit plusieurs exemples d'applications à des systèmes réels pour illustrer la versatilité du programme.

## Introduction

In a break with the traditional approaches described in the literature, a novel algorithm was recently reported (1) for the determination of any number of overlapping protonation constants from potentiometric titration data wherein the function being minimized is the sum of the squares of the differences between calculated and observed pH values. The main advantage of this new approach stems from the correct statistical treatment in which the mass balance quantities including the volume of titrant added are treated as known parameters while the pH represents the measured dependent variable that reflects the unique set of equilibrium protonation constants that most accurately describe the system. Therefore, minimization of the $\Sigma(pH_{calc} - pH_{obs})^2$ function does not only make chemical sense, but is the mathematically correct choice.

Several recent reviews have appeared which deal both specifically as well as comparatively with the various numerical and analytical methods and programs used in computer calculations of chemical equilibria and stability constants. The comprehensive reviews of Gans (2), Gaizer (3) and the survey by Leggett (4) discuss both popularly used programs and other approaches which had been employed in the determination of stability constants from potentiometric and other data. The common element among all programs surveyed is the choice of minimization of the calculated differences in one or more mass balance terms $T_M$, $T_L$, $T_H$, $T_{OH}$, $\bar{n}$, $v_{titrant}$. A second feature of most published programs is the specific identification and classification of the reacting components into categories such as "metal", "ligand", "proton", and "hydroxide". Legett (5) pointed out that general complexes of formulation $M_mH_j(OH)_kL_n$ are treated by the computer as coming from components M, L, H, $H_2O$ whose concentrations are constrained by the mass balance equations [1]–[3] and the equilibrium constant [4]. Different symbols are employed for each interacting component.

$$[1] \quad C_M = [M] + \Sigma m[M_mH_j(OH)_kL_n]$$

$$[2] \quad C_L = [L] + \Sigma n[M_mH_j(OH)_kL_n]$$

$$[3] \quad C_H = [H] - [OH] + \Sigma j[M_mH_jL_n] - \Sigma k[M_m(OH)_kL_n]$$

$$[4] \quad \beta_{mjkn} = \frac{[M_mH_j(OH)_kL_n][H]^k}{[M]^m[H]^j[H_2O]^k[L]^n}$$

It appears then that there are two drawbacks to the standard strategies employed in the computa-

[1]To whom all correspondence should be addressed.

0008-4042/82/192403-07$01.00/0

©1982 National Research Council of Canada/Conseil national de recherches du Canada

Can. J. Chem. Downloaded from www.nrcresearchpress.com by 210.87.254.42 on 09/06/12
For personal use only.

Can. J. Chem. Downloaded from www.nrcresearchpress.com by 210.87.254.42 on 09/06/12
For personal use only.

tion of equilibrium constants: the choice (other than pH) of the variable being minimized and the usage of cumbersome notation labels which preclude straightforward generalization of the computation problem toward more complicated systems. The program BEST described in this work was written with the object in mind of eliminating these two drawbacks. BEST computes the equilibrium pH value at each equilibrium point and refines the chosen equilibrium constants accordingly, thus minimizing the discrepancies between the calculated and experimentally observed values of pH. The analytical mass balance algorithm depends entirely on the species stoichiometry entered in the input data and does not make a special *a priori* distinction between "metal", "ligand", "hydroxide", and "proton" components. In BEST, the explicit equations [1]–[3] have been replaced by a perfectly general and therefore mathematically more tractable mass balance equation [5] which states that the analytical concentration of a given component is always balanced by its distribution in all the equilibrating species, defined in eq. [6]. The sum of each component is taken over all of the species present, while the product of each species in [6] is taken over the range of all of the components.

$$[5] \quad T_{\text{component}} = \Sigma\gamma[\text{species}]$$

$$[6] \quad [\text{species}] = \beta\prod[\text{component}]^{\gamma}$$

## Mathematical background for program BEST

### *A. Solution of the equilibrium*

For a monophasic solution of $NC$ components and $NS$ species, the generalized mass balance equations in each component of concentration $T_{C_j}$ is

$$[7] \quad T_{C_j} = \sum_{i=1}^{NS} \gamma_{j,i}[S]_i$$

where

$$[8] \quad [S]_i = \beta_i \prod_{k=1}^{NC} [C]_k^{\gamma}{}_{k,i}$$

and $\gamma_{n,j}$ is the stoichiometric coefficient of component $n$ in species $i$, $[S]_i$ is the concentration of species $S_i$, and $\beta_i$ is the overall formation constant for species $i$ from its components C. The set of simultaneous equations [7] is solved most efficiently at each titration point by the Newton–Raphson method (6) by defining the set of $NC$ functions $F_j$ [9] such that $F_j \rightarrow 0$ when the correct concentration of the free components is obtained. The necessary Jacobian $NC \times NC$ determinant [10] is constructed through partial differentiation with respect to each component concentration, $C_j$. Likewise, $NC$ substitution determinants $D_j$ must be evaluated for the iterative process. For example $D_2$ is shown in eq. [11].

$$[9] \quad F_j = \sum_{i=1}^{NC} \gamma_{j,i}[S]_i - T_{C_j}$$

$$[10] \quad D = \begin{vmatrix} \frac{\delta F_1}{\delta C_1} & \frac{\delta F_1}{\delta C_2} & \cdots & \frac{\delta F_1}{\delta C_{NC}} \\ \vdots & \vdots & & \vdots \\ \frac{\delta F_{NC}}{\delta C_1} & \frac{\delta F_{NC}}{\delta C_2} & \cdots & \frac{\delta F_{NC}}{\delta C_{NC}} \end{vmatrix}$$

$$[11] \quad D_2 = \begin{vmatrix} \frac{\delta F_1}{\delta C_1} & F_1 & \cdots & \frac{\delta F_1}{\delta C_{NC}} \\ \vdots & \vdots & & \vdots \\ \frac{\delta F_{NC}}{\delta C_1} & F_{NC} & \cdots & \frac{\delta F_{NC}}{\delta C_{NC}} \end{vmatrix}$$

An initial estimate of the component concentration is refined by the Newton–Raphson method for simultaneous equations with the recursion formula [12]

$$[12] \quad C_j = C_j(\text{previous value}) - D_j/D$$

By convention it was chosen that $C_{NC}$ (when $j = NC$) represents the free hydrogen ion concentration.

### *B. Refinement of equilibrium constants*

The refinement of the basis set of stability constants each representing a species present is accomplished in the following series of steps.

(*1*) For the basis set solve the mass balance equations [7] using eqs. [12] as outlined above.

(*2*) Convert $C_{NC}$ to pH ($-\log C_{NC}$) at each equilibrium point. In effect this is a calculated pH curve.

(*3*) Perturb a small fraction of the basis set by an increment and repeat step *2*.

(*4*) Compare the effect of step *3* with regard to improvement of the fit to the experimental curve and repeat step *3* in the appropriate direction to affect further improvement.

(*5*) Repeat *4* and *3* until refinement of the basis set cannot be further improved.

## Discussion

The main advantage of program BEST is that it provides an easily accessible vehicle for the computation of pH values at each titration point in systems of any complexity. For example the binucleating ligand PXBDE (7) was studied in the

TABLE 1. Computation of pH values with program BEST* for the system PXBDE, EN, $Co^{2+}$, and $O_2$

| Species | Volume base | $a$† | $pH_{obs}$ | $pH_{calcd}$ | Difference |
|---|---|---|---|---|---|
| **1** | 0.000 | 0.000 | 2.577 | 2.563 | 0.014 |
| **2** | 0.200 | 0.140 | 2.634 | 2.631 | 0.003 |
| **3** | 0.400 | 0.280 | 2.717 | 2.710 | 0.007 |
| **4** | 0.600 | 0.421 | 2.812 | 2.807 | 0.005 |
| **5** | 0.800 | 0.561 | 2.932 | 2.929 | 0.003 |
| **6** | 1.000 | 0.701 | 3.092 | 3.099 | −0.007 |
| 7 | 1.200 | 0.841 | 3.346 | 3.377 | −0.031 |
| **8** | 1.400 | 0.982 | 4.233 | 4.293 | −0.060 |
| **9** | 1.800 | 1.262 | 6.162 | 6.192 | −0.030 |
| **10** | 2.000 | 1.402 | 6.265 | 6.277 | −0.012 |
| **11** | 2.200 | 1.543 | 6.322 | 6.328 | −0.006 |
| **12** | 2.450 | 1.718 | 6.373 | 6.374 | −0.001 |
| **13** | 2.700 | 1.893 | 6.413 | 6.411 | 0.002 |
| **14** | 2.950 | 2.069 | 6.448 | 6.444 | 0.004 |
| **15** | 3.200 | 2.244 | 6.482 | 6.476 | 0.006 |
| **16** | 3.400 | 2.384 | 6.502 | 6.500 | 0.002 |
| **17** | 3.600 | 2.524 | 6.529 | 6.524 | 0.005 |
| **18** | 3.800 | 2.665 | 6.553 | 6.549 | 0.004 |
| **19** | 4.000 | 2.805 | 6.576 | 6.573 | 0.003 |
| **20** | 4.200 | 2.945 | 6.600 | 6.599 | 0.001 |
| **21** | 4.400 | 3.085 | 6.627 | 6.625 | 0.002 |
| **22** | 4.600 | 3.226 | 6.654 | 6.652 | 0.002 |
| **23** | 4.800 | 3.366 | 6.681 | 6.681 | −0.000 |
| **24** | 5.000 | 3.506 | 6.711 | 6.712 | −0.001 |
| **25** | 5.200 | 3.646 | 6.748 | 6.746 | 0.002 |
| **26** | 5.400 | 3.787 | 6.785 | 6.782 | 0.003 |
| **27** | 5.600 | 3.927 | 6.824 | 6.822 | 0.002 |
| **28** | 5.800 | 4.067 | 6.862 | 6.868 | −0.006 |
| **29** | 6.000 | 4.207 | 6.917 | 6.920 | −0.003 |
| **30** | 6.200 | 4.348 | 6.975 | 6.982 | −0.007 |
| **31** | 6.400 | 4.488 | 7.048 | 7.059 | −0.011 |
| **32** | 6.650 | 4.663 | 7.169 | 7.193 | −0.024 |
| **33** | 6.900 | 4.839 | 7.367 | 7.433 | −0.066 |
| **34** | 7.130 | 5.000 | 8.927 | 9.009 | −0.082 |

$\sigma(pH)$ fit = 0.02339

*The larger deviations near $a = 1$ and $a = 5$ are characteristic of the steeply sloping parts (inflection regions) of the potentiometric equilibrium curves.
†$a$ = moles base added per mole of metal ion present.

presence of added ethylenediamine (EN), or glycine, cobalt(II), and oxygen (8).

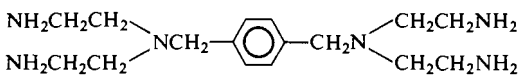

Tetrakis(2-aminoethyl)-α,α′-diamino-*p*-xylene (PXBDE)

Table 1 shows the results of the calculations on this complex system defined by the experimental parameters and the set of overall stability constants for the species shown in Table 2. The five components defining this system are Co(II), ethylenediamine, PXBDE, protons, and oxygen. Because the experiment was run under 1 atm of oxygen, that particular component was not listed per se, but its interaction is implied in species **24**. Species **23** is the unoxygenated binuclear mixed ligand complex while species **24** is the same species with a dioxygen bridge between the two cobalt centers. The input stability constant data had been obtained from separate experiments while only the stability constant of species **24** is determined in the calculation illustrated here. Species **2** is the hydrolysis constant for Co(II) and was taken from Smith and Martell (9). The protonation constants for ethylenediamine **4**, **5**, and PXBDE **7**, **8**, **9**, **10**, **11**, **12** were determined using program PKAS (1). The stability constants **13**, **14**, **15** between EN and Co(II) were determined using BEST anaerobically from titration under nitrogen. Species **16**, **17**, **18** were computed with BEST for 1:1 PXBDE:Co(II) equilibrium mixtures while **21** was determined for 1:2 PXBDE:Co(II) experiments also with BEST. Finally, in a series of experiments the mixed ligand species **22** and **23** were determined using BEST. These prior determinations are necessary in order

Can. J. Chem. Downloaded from www.nrcresearchpress.com by 210.87.254.42 on 09/06/12
For personal use only.

Can. J. Chem. Downloaded from www.nrcresearchpress.com by 210.87.254.42 on 09/06/12
For personal use only.

TABLE 2. Computer output of program BEST showing parameters for the computation of results in Table 1

| | |
|---|---|
| Initial volume | 50.0000 |
| Normality of base | 0.1053 |
| Added acid volume | 0.0000 |
| Added acid concentration | 0.0000 |
| $pH_{corr}$ | 0.0000 |
| Number of data | 34 |
| Components: | |
| 1 Co(II) | 0.15012 mmol |
| 2 EN | 0.15005 mmol |
| 3 PXBDE | 0.07501 mmol |
| 4 $H^+$ | 0.75015 mmol |

| | | Species | | | |
|---|---|---|---|---|---|
| Species | log β | Co(II) | EN | PXBDE | $H^+$ |
| **1** | 0.0000 | 1 | 0 | 0 | 0 |
| **2** | −9.5900 | 1 | 0 | 0 | −1 |
| **3** | 0.0000 | 0 | 1 | 0 | 0 |
| **4** | 9.8900 | 0 | 1 | 0 | 1 |
| **5** | 16.9700 | 0 | 1 | 0 | 2 |
| **6** | 0.0000 | 0 | 0 | 1 | 0 |
| **7** | 10.0600 | 0 | 0 | 1 | 1 |
| **8** | 19.7700 | 0 | 0 | 1 | 2 |
| **9** | 28.8800 | 0 | 0 | 1 | 3 |
| **10** | 37.4500 | 0 | 0 | 1 | 4 |
| **11** | 39.3000 | 0 | 0 | 1 | 5 |
| **12** | 40.5800 | 0 | 0 | 1 | 6 |
| **13** | 5.3800 | 1 | 1 | 0 | 0 |
| **14** | 10.2400 | 1 | 2 | 0 | 0 |
| **15** | 13.8000 | 1 | 3 | 0 | 0 |
| **16** | 9.3900 | 1 | 0 | 1 | 0 |
| **17** | 18.8770 | 1 | 0 | 1 | 1 |
| **18** | 26.6070 | 1 | 0 | 1 | 2 |
| **19** | 0.0000 | 0 | 0 | 0 | 1 |
| **20** | −13.7950 | 0 | 0 | 0 | −1 |
| **21** | 14.5800 | 2 | 0 | 1 | 0 |
| **22** | 19.1000 | 2 | 1 | 1 | 0 |
| **23** | 23.4000 | 2 | 2 | 1 | 0 |
| **24** | 30.1100 | 2 | 2 | 1 | 0 |

to compute the desired oxygenation equilibrium constant **24**.

It is to be noted that the differences in the last column of Table 1 are very small and that there appears to be some deviation near $a$ values of about 1 and 5. The reason for these deviations is related to slight misbalance in the acid–base stoichiometry, for which small deviations are amplified many-fold in the regions of high slope. The standard deviation for overall fit is 0.023 log units. This, taken together with the excellent fit ($\ll 0.01$ pH) in the buffer regions, is indicative of a good equilibrium description of a very complex system. We believe that such refinement heretofore without any approximation was not possible for accurate determination of oxygenation constants.

Table 3 illustrates the added option that BEST offers: a complete species distribution for all of the titration points. The particular example shows point **27** at $a = 3.9$. The second column lists the actual concentration while the third column lists the percent with respect to the first component, Co(II).

Because of the generalized nature of the mass balance equation [7], program BEST may handle much more complex systems, such as those containing several ligands and many metal ions. Such equilibrium studies would be of interest for complex biological systems in proving out the predictions of multicomponent systems derived from separate studies of the components involved.

Furthermore, in these laboratories, BEST was applied to a determination of a Schiff base equilibrium shown in reaction [13], where α-aminoisobutyric acid forms a Schiff base with pyridoxal phosphate. This system was tractable because BEST does not require formal identification of components as "metal ions" or "ligands". As usual, the input parameters shown in Table 4 were used to obtain the very good fit $\sigma = 0.037$ shown in Table 5. It is to be noted that the experiment was performed on an initial volume of 3.00 mL of solution in a micro titration apparatus. In Table 4 the difference between **9** and **8** (11.88) represents the log protonation constant of the totally deprotonated Schiff base, while **10–9** and **11–10** (7.02 and 5.90) represent the next two protonation steps. This is the first report of a potentiometric determination of Schiff base equilibrium constants.

[13]

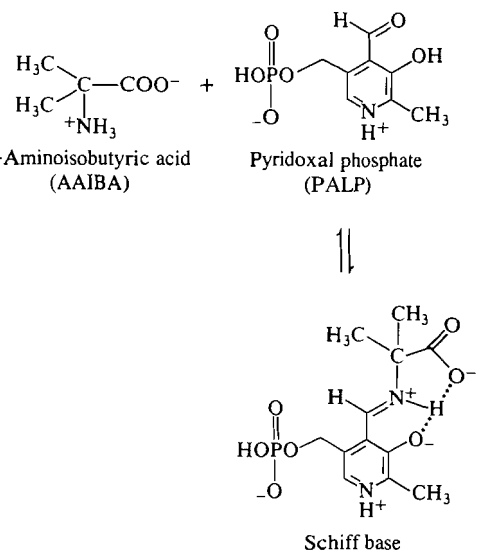


Other applications of BEST have been tested on a variety of gallium(III) complexes with multidentate ligands such as tetraethylenepentaamineheptaacetic acid (TPHA) (10), the study of

Can. J. Chem. Downloaded from www.nrcresearchpress.com by 210.87.254.42 on 09/06/12
For personal use only.

TABLE 3. Sample optimized output for the 27th equilibrium point*

| log β | Actual species concentration | Percentage of total PXBDE | Species | | | |
|---|---|---|---|---|---|---|
| | | | Co(II) | EN | PXBDE | $H^+$ |
| 0.000 | 7.048E-04 | 26.10 | 1 | 0 | 0 | 0 |
| −9.590 | 1.204E-06 | 0.04 | 1 | 0 | 0 | −1 |
| 0.000 | 2.619E-07 | 0.01 | 0 | 1 | 0 | 0 |
| 9.890 | 3.060E-04 | 11.33 | 0 | 1 | 0 | 1 |
| 16.970 | 5.537E-04 | 20.51 | 0 | 1 | 0 | 2 |
| 0.000 | 2.042E-14 | 0.00 | 0 | 0 | 1 | 0 |
| 10.060 | 3.528E-11 | 0.00 | 0 | 0 | 1 | 1 |
| 19.770 | 2.723E-08 | 0.00 | 0 | 0 | 1 | 2 |
| 28.880 | 5.280E-06 | 0.20 | 0 | 0 | 1 | 3 |
| 37.450 | 2.953E-04 | 10.94 | 0 | 0 | 1 | 4 |
| 39.300 | 3.146E-09 | 0.00 | 0 | 0 | 1 | 5 |
| 40.580 | 9.022E-15 | 0.00 | 0 | 0 | 1 | 6 |
| 5.380 | 4.428E-05 | 1.64 | 1 | 1 | 0 | 0 |
| 10.240 | 8.402E-07 | 0.03 | 1 | 2 | 0 | 0 |
| 13.800 | 7.990E-10 | 0.00 | 1 | 3 | 0 | 0 |
| 9.390 | 3.533E-08 | 0.00 | 1 | 0 | 1 | 0 |
| 18.877 | 1.632E-05 | 0.60 | 1 | 0 | 1 | 1 |
| 26.607 | 1.319E-04 | 4.88 | 1 | 0 | 1 | 2 |
| 0.000 | 1.505E-07 | 0.01 | 0 | 0 | 0 | 1 |
| −13.795 | 1.065E-07 | 0.00 | 0 | 0 | 0 | −1 |
| 14.580 | 3.856E-06 | 0.14 | 2 | 0 | 1 | 0 |
| 19.100 | 3.345E-08 | 0.00 | 2 | 1 | 1 | 0 |
| 23.400 | 1.748E-10 | 0.00 | 2 | 2 | 1 | 0 |
| 30.110 | 8.964E-04 | 33.20 | 2 | 2 | 1 | 0 |

| *I* | *VB* | *A* | pH | $pH_{calcd}$ | Diff |
|---|---|---|---|---|---|
| 27 | 5.600 | 3.927 | 6.824 | 6.822 | 0.002 |

*One iteration, $Q$ = 0.82E-05 is a convergence factor.

TABLE 4. Data from a system containing two organic substances capable of forming Schiff bases (reaction [13])

| | |
|---|---|
| Initial volume | 3.0000 |
| Normality of base | 2.0010 |
| Added acid volume | 0.0000 |
| Added acid concentration | 0.0000 |
| $pH_{corr}$ | 0.0000 |
| Number of data | 22 |
| Components: | |
| 1 AAIBA | 0.68250 mmol |
| 2 PALP | 0.74540 mmol |
| 3 HYDROGEN | 2.91870 mmol |

| Species | log β | Species | | |
|---|---|---|---|---|
| | | AAIBA | PALP | $H^+$ |
| **1** | 0.0000 | 1 | 0 | 0 |
| **2** | 10.1950 | 1 | 0 | 1 |
| **3** | 12.7280 | 1 | 0 | 2 |
| **4** | 0.0000 | 0 | 1 | 0 |
| **5** | 7.9800 | 0 | 1 | 1 |
| **6** | 13.6300 | 0 | 1 | 2 |
| **7** | 17.1800 | 0 | 1 | 3 |
| **8** | .1000 | 1 | 1 | 0 |
| **9** | 11.9800 | 1 | 1 | 1 |
| **10** | 19.0000 | 1 | 1 | 2 |
| **11** | 24.9000 | 1 | 1 | 3 |
| **12** | 0.0000 | 0 | 0 | 1 |
| **13** | −13.8800 | 0 | 0 | −1 |

mixed dinuclear complexes of 1,4,7,13,16,19-hexaaza-10,22-dioxacyclotetracosane (BISDIEN) (11), and the mono and dinuclear Fe(III) complexes with 1,4-bis(2′,5′,5′-tricarboxymethyl-2′,5′-diazapentyl)benzene (PXED3A) (12), a bispentadentate ligand. The latter ligand–metal system possesses up to 25 species. The titrations themselves involve more than 100 data points. The most interesting finding is an intramolecularly bound oxide bridge in the dinegative species $Fe_2LO^{2-}$.

Two additional features of BEST deserve mention. The entire algorithm is written in single precision arithmetic, a fact which accounts for more rapid execution relative to the customary double precision routines found in older literature. Also, BEST computes the complete species distribution consistent with the current data base.

Figure 1 is a species distribution diagram of the Schiff base system described in Table 4. The computation was performed utilizing the same mathematical algorithm as found in BEST. In order to obtain this diagram, the pH was varied incrementally and the various quantities were calculated at each pH increment. However, both here and in the original refinement of the equilibrium constants, it was not necessary to invoke artificial approximations of any kind. Currently, program

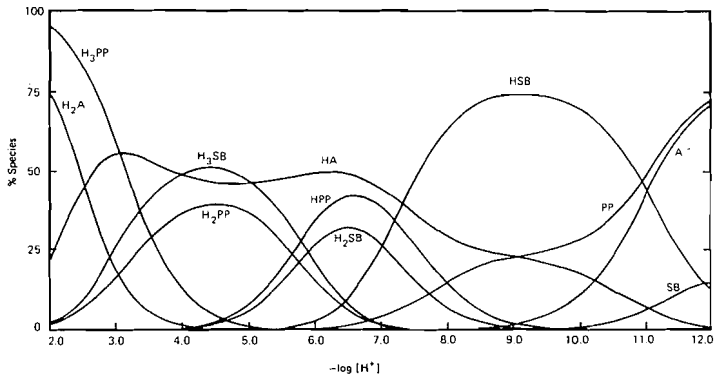


FIG. 1. Species distribution as a function of pH plotted with the stability constants for the pyridoxal phosphate-α-aminoisobutyric acid – Schiff base system. Conditions are the same as those of Table 4. SB = Schiff base, A = amino acid, PP = pyridoxal phosphate.

TABLE 5. Results from refinement of data on the pyridoxal-α-aminoisobutyric acid — Schiff base equilibrium from pH 4.8 to pH 12

| Species | Volume base | $a$† | $pH_{obs}$ | $pH_{calcd}$ | Difference |
|---|---|---|---|---|---|
| 1 | 0.400 | 1.173 | 4.838 | 4.812 | 0.026 |
| 2 | 0.450 | 1.319 | 5.182 | 5.204 | −0.022 |
| 3 | 0.500 | 1.466 | 5.460 | 5.476 | −0.016 |
| 4 | 0.551 | 1.615 | 5.707 | 5.706 | 0.001 |
| 5 | 0.600 | 1.759 | 5.930 | 5.911 | 0.019 |
| 6 | 0.650 | 1.906 | 6.148 | 6.123 | 0.025 |
| 7 | 0.700 | 2.052 | 6.361 | 6.349 | 0.012 |
| 8 | 0.750 | 2.199 | 6.587 | 6.590 | −0.003 |
| 9 | 0.800 | 2.345 | 6.816 | 6.836 | −0.020 |
| 10 | 0.850 | 2.492 | 7.063 | 7.076 | −0.013 |
| 11 | 0.900 | 2.639 | 7.310 | 7.310 | 0.000 |
| 12 | 0.950 | 2.785 | 7.575 | 7.550 | 0.025 |
| 13 | 1.000 | 2.932 | 7.870 | 7.817 | 0.053 |
| 14 | 1.050 | 3.078 | 8.250 | 8.158 | 0.092 |
| 15 | 1.100 | 3.225 | 8.841 | 8.771 | 0.070 |
| 16 | 1.160 | 3.401 | 9.933 | 10.015 | −0.082 |
| 17 | 1.200 | 3.518 | 10.361 | 10.398 | −0.037 |
| 18 | 1.250 | 3.665 | 10.742 | 10.743 | −0.001 |
| 19 | 1.300 | 3.811 | 11.045 | 11.039 | 0.006 |
| 20 | 1.350 | 3.958 | 11.347 | 11.328 | 0.019 |
| 21 | 1.400 | 4.105 | 11.644 | 11.643 | 0.001 |
| 22 | 1.450 | 4.251 | 11.994 | 11.995 | −0.001 |

$\sigma(pH) = 0.03683$

†$a$ = moles base added per mole of AAIBA present.

BEST is DIMENSIONed for 7 components and 121 data points. Higher DIMENSIONing is limited only by the memory available on the MICROMATION Z64 microcomputer employed in the recent work carried out in this laboratory. This microcomputer is equipped with 64K RAM utilizing the Z-80A microprocessor and dual 8″ floppy disks with Chromemco software. Currently, adaptation of program BEST to the VAX-11/780 have improved computer run times by a factor of ~200.

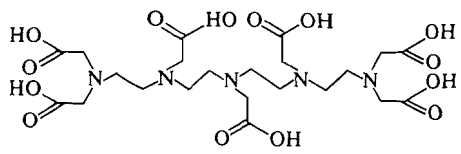

TPHA

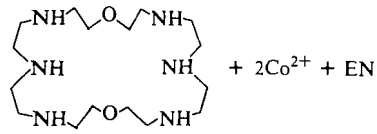


BISDIEN

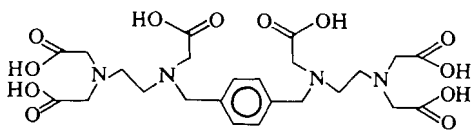

PXED3A

## Program availability

The complete listing for BEST IN FORTRAN IV, including a sample input file with appropriate directions, is available from the Depository of Unpublished Data, CISTI, National Research Council of Canada, Ottawa, Ont., Canada K1A 0S2.

## Acknowledgement

This work was supported by a grant No. A-259 from The Robert A. Welch Foundation.

1. R. J. MOTEKAITIS and A. E. MARTELL. Can. J. Chem. **60**, 168 (1982).
2. P. GANS. Coord. Chem. Rev. **19**, 99 (1976).
3. F. GAIZER. Coord. Chem. Rev. **27**, 195 (1979).
4. D. J. LEGGETT. Am. Lab. **14**, 29 (1982).
5. D. J. LEGGETT. Talanta, **24**, 535 (1977).

Can. J. Chem. Downloaded from www.nrcresearchpress.com by 210.87.254.42 on 09/06/12
For personal use only.

6. H. MARGENAU and R. M. MURPHY. The mathematics of physics and chemistry. Van Nostrand Co., Inc., New York. 1943. p. 476.
7. C. Y. NG, R. J. MOTEKAITIS, and A. E. MARTELL. Inorg. Chem. **11**, 2982 (1979).
8. C. Y. NG, A. E. MARTELL, and R. J. MOTEKAITIS. J. Coord. Chem. **9**, 255 (1979).
9. R. M. SMITH and A. E. MARTELL. Critical stability constants. Vol. 4. Plenum Publishing Corporation, New York. 1976; First Supplement, Vol. 5, in press.
10. R. J. MOTEKAITIS and A. E. MARTELL. Inorg. Chem. **19**, 1646 (1980).
11. R. J. MOTEKAITIS, A. E. MARTELL, J. M. LEHN, and E. WATANABE. Inorg. Chem. To be published.
12. C. Y. NG, R. J. MOTEKAITIS, and A. E. MARTELL. Inorg. Chem. To be published.

Can. J. Chem. Downloaded from www.nrcresearchpress.com by 210.87.254.42 on 09/06/12
For personal use only.

# Rearrangement studies with $^{14}C$. XLVII. The decomposition of chain labeled or ring labeled trianisylvinylphenyltriazene

CHOI CHUCK LEE AND CRAIG A. OBAFEMI

*Department of Chemistry and Chemical Engineering, University of Saskatchewan, Saskatoon, Sask., Canada S7N 0W0*

Received April 1, 1982

CHOI CHUCK LEE and CRAIG A. OBAFEMI. Can. J. Chem. **60**, 2410 (1982).

Simultaneous reactions were carried out on the decomposition of the chain labeled trianisyl[2-$^{14}C$]vinylphenyltriazene (**1**-NNNHPh-2-$^{14}C$) and the ring labeled 1,2-dianisyl-2-*p*-[$^{14}C$]methoxyphenylvinylphenyltriazene (**1**-NNNHPh-2-methoxy-$^{14}C$) in HOAc, HOAc–NaOAc, or $CF_3CH_2OH$–$HClO_4$. In HOAc, the presence of increasing amounts of NaOAc resulted in decreasing extents of isotopic scrambling arising from 1,2-anisyl shifts in the trianisylvinyl cation, in agreement with previous observations. For decompositions in the less nucleophilic TFE, complete equilibration was observed, giving rise to 50.0% and 33.3% scramblings, respectively, for the chain and ring labels. When the data were expressed as % rearrangement, with the assumption that 100% rearrangement would correspond to 50.0% or 33.3% scrambling, respectively, for the chain or ring label, for each experiment under a given set of conditions, the % rearrangement was found to be equal in the chain and in the ring label. These results are discussed in conjunction with earlier data from the acetolysis of doubly labeled 1,2-dianisyl-2-*p*-[$^{14}C$]methoxyphenyl[2-$^{13}C$]vinyl bromide (**1**-Br-2-$^{13}C$-2-methoxy-$^{14}C$) which gave, depending on experimental conditions, either equal or unequal values for the % rearrangement in the chain and in the ring label.

CHOI CHUCK LEE et CRAIG A. OBAFEMI. Can. J. Chem. **60**, 2410 (1982).

On a effectué des réactions de décompositions simultanées dans le AcOH, le AcOH–AcONa ou le $CF_3CH_2OH$–$HClO_4$ du trianisyl [2-$^{14}C$] vinylphényltriazène (**1**-NNNHPh-2-$^{14}C$) marqué dans la chaîne et du dianisyl-1,2 *p*-[$^{14}C$] méthoxyphényl-2 vinylphényltriazène (**1**-NNNHPh-2-méthoxy-$^{14}C$) marqué sur le cycle. Dans le AcOH, la présence de quantités croissantes de AcONa provoque une diminution du taux de mélange isotopique provenant de glissements 1,2 des anisyles du cation trianisylvinyle; ceci est en accord avec des observations antérieures. Dans le cas des décompositions dans le TFE qui est moins nucléophile, on a observé une équilibration complète donnant lieu à des taux de mélanges respectivs de 50% et de 33% pour les composés avec une chaîne ou un cycle marqué. Quand on exprime les données en % de transposition, en se basant sur le fait qu'une transposition à 100% correspond à un mélange de 50,0% ou de 33,3% suivant que le marqueur est sur la chaîne ou sur le cycle, on trouve pour chaque expérience conduite dans un ensemble de conditions données que le % de transposition est le même que le marqueur soit dans la chaîne ou dans le cycle. On discute des ces résultats en fonction des données antérieures provenant de l'acétolyse du bromure de dianisyl-1,2 *p*[$^{14}C$] méthoxyphényl-2 [2-$^{13}C$] vinyle doublement marqué qui donne, suivant les conditions expérimentales, soit des valeurs égales ou inégales du % de transposition suivant que le marqueur est dans la chaîne ou dans le cycle.

[Traduit par le journal]

The acid catalyzed decomposition of triarylvinylphenyltriazene as a method of generating the triarylvinyl cation, presumably via the triarylvinyldiazonium ion, was first reported by Jones and Miller (1). Rearrangements arising from 1,2-aryl shifts across the double bond in the triarylvinyl cation were also observed by these workers. For example, the decomposition in HOAc of 1-phenyl-2,2-di-*p*-tolylvinylphenyltriazene gave 80% of the unrearranged 1-phenyl-2,2-di-*p*-tolylvinyl acetate and 20% of the rearranged 2-phenyl-1,2-di-*p*-tolylvinyl acetate and this rearrangement was completely suppressed by the presence of 10 molar equivalents of added KOAc (1). These findings were interpreted as being consistent with the formation of the free 1-phenyl-2,2-di-*p*-tolylvinyl cation which could undergo 1,2-tolyl shift to give the more stable 2-phenyl-1,2-di-*p*-tolylvinyl cation. The presence of the added more nucleophilic acetate ion would favor product formation from the unrearranged cation, thus decreasing or suppressing the extent of 1,2-shifts to give rearrangement. Similarly, isotopic scramblings arising from 1,2-aryl shifts in triarylvinyl cations derived from the decomposition in HOAc of trianisyl[2-$^{14}C$]vinylphenyltriazene or *cis*- and *trans*-1,2-dianisyl-2-phenyl[2-$^{14}C$]vinylphenyltriazenes have been reported from this laboratory (2, 3). In these studies, it was found that the presence of added NaOAc also decreased the extent of scrambling, in support of the formation of free triarylvinyl cations. Extensive studies on rearrangements of vinyl cations, largely generated from solvolyses, have also been carried out and the results have been summarized in recent reviews (4, 5).

Recently we have investigated the extents of isotopic scrambling in the acetolysis of trianisylvinyl bromide doubly labeled at C-2 with $^{13}C$ and at the methoxy carbon of one of the C-2 anisyl groups with $^{14}C$ (1,2-dianisyl-2-*p*-[$^{14}C$]methoxyphenyl[2-$^{13}C$]vinyl bromide, **1**-Br-2-$^{13}C$-2-methoxy-$^{14}C$). Since the scramblings for the $^{13}C$ and $^{14}C$ labels were measured by two independent methods, namely, $^{13}C$ nmr and $^{14}C$ radioactivity, it was found

0008-4042/82/192410-05$01.00/0

©1982 National Research Council of Canada/Conseil national de recherches du Canada

Can. J. Chem. Downloaded from www.nrcresearchpress.com by 210.87.254.42 on 09/06/12
For personal use only.

Can. J. Chem. Downloaded from www.nrcresearchpress.com by 210.87.254.42 on 09/06/12
For personal use only.

in preliminary trials that the scrambling results from reactions with 1-Br-2-$^{13}$C-2-methoxy-$^{14}$C were essentially the same as those from similar reactions with a 1:1 mixture of singly labeled trianisyl[2-$^{13}$C]vinyl bromide (1-Br-2-$^{13}$C) and 1,2-dianisyl-2-*p*-[$^{14}$C]methoxyphenylvinyl bromide (1-Br-2-methoxy-$^{14}$C) (6). When the acetolysis of 1-Br-2-$^{13}$C-2-methoxy-$^{14}$C was carried out in the presence of low concentrations of added salts, the "% rearrangements" for the chain label and the ring label were unexpectedly found to be unequal. On the other hand, in the presence of high salt concentrations, the % rearrangements for the chain and ring labels were equal, and it was suggested that ion-pairs and free ions, respectively, might be involved in the acetolysis of 1-Br-2-$^{13}$C-2-methoxy-$^{14}$C in the presence of low and high concentrations of added salts (6). Since the decomposition of vinylphenyltriazenes would proceed via the free vinyl cation, in the present work, simultaneous experiments were carried out with the chain labeled trianisyl[2-$^{14}$C]vinylphenyltriazene (1-NNNHPh-2-$^{14}$C) and the ring labeled 1,2-dianisyl-2-*p*-[$^{14}$C]methoxyphenylvinylphenyltriazene (1-NNNHPh-2-methoxy-$^{14}$C) in order to provide scrambling data for comparison with those obtained from the acetolysis of 1-Br-2-$^{13}$C-2-methoxy-$^{14}$C.

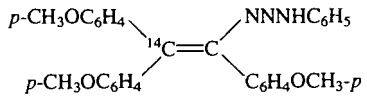


1-NNNHPh-2-$^{14}$C

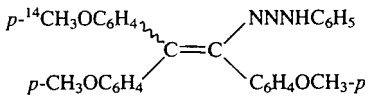


1-NNNHPh-2-methoxy-$^{14}$C

The preparation of 1-NNNHPh-2-$^{14}$C was effected from the reaction of 1-Br-2-$^{14}$C with phenyl azide as previously described (2). Similarly, 1-NNNHPh-2-methoxy-$^{14}$C was obtained from the reaction of 1-Br-2-methoxy-$^{14}$C (6) with phenyl azide. The decomposition of these triazenes was carried out in HOAc, in HOAc containing different amounts of NaOAc, or in 2,2,2-trifluoroethanol (TFE) containing 0.1% $HClO_4$. The products of these decomposition reactions were the isotopically scrambled trianisylvinyl acetates, 1-OAc-1,2-$^{14}$C and 1-OAc-1,2-methoxy-$^{14}$C, or the trianisylvinyl trifluoroethyl ethers, 1-$OCH_2CF_3$-1,2-$^{14}$C and 1-$OCH_2CF_3$-1,2-methoxy-$^{14}$C. Ozonolysis of these products gave rise to dianisyl[$^{14}$C]ketone (2-$^{14}$C) (7), and the difference in the $^{14}$C activities between the product and 2-$^{14}$C gave the extent of scrambling of the label from C-2 to C-1. The results are summarized in Tables 1 and 2.

In the previous study on the decomposition of 1-NNNHPh-2-$^{14}$C in HOAc (2), scramblings of 37.8 and 38.4% were observed in duplicate runs, and the present results from Expts. 1 and 2, Table 1, are in complete agreement with the earlier data. In the earlier work (2), the presence of 1.7 molar equivalents of added NaOAc decreased the scramblings in these duplicate runs to 17.0 and 16.6%, again in agreement with the effects of added NaOAc in the results given in Table 1. A similar trend of decreasing extents of scrambling with increasing amounts of added NaOAc was also observed with the ring labeled substrate 1-NNNHPh-2-methoxy-$^{14}$C (Table 2) and such effects could be interpreted as indicating that the decomposition of trianisylvinylphenyltriazene gave rise to the dissociated "free" trianisylvinyl cation (2). When the decomposition of 1-NNNHPh-2-$^{14}$C or 1-NNNHPh-2-methoxy-$^{14}$C was carried out in TFE, a solvent of lower nucleophilicity (9), a longer lifetime for the trianisylvinyl cation would be possible and thus more extensive 1,2-anisyl shifts could occur resulting in a complete scrambling of 50.0% or 33.3%, respectively, in the decomposition of 1-NNNHPh-2-$^{14}$C or 1-NNNHPh-2-methoxy-$^{14}$C.

Since the maximum extent of scrambling from complete equilibration of the isotopic labels would be 50.0% or 33.3%, respectively, for the chain labeled trianisyl[2-$^{14}$C]vinyl cation or the ring labeled 1,2-dianisyl-2-*p*-[$^{14}$C]methoxyphenylvinyl cation (eqs. [1] and [2]), the scrambling data have been

[1] 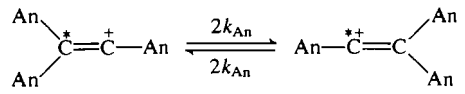


50.0% 50.0%

[2] 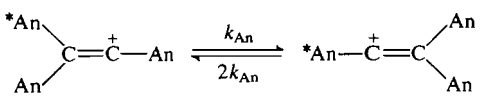


66.7% 33.3%

expressed as "% rearrangement" based on the assumption that 100% rearrangement corresponds to the maximum scrambling of 50.0% or 33.3% (10). Thus the observed % scrambling could be converted to % rearrangement by multiplication with a

TABLE 1. Data from the decomposition of trianisyl[2-$^{14}$C]vinylphenyltriazene (1-NNNHPh-2-$^{14}$C)

| Expt. | [Triazene] (m$M$) | Reaction medium | Specific activity ($10^{-5}$ dpm/mmol) Product[a] Run 1 | Product[a] Run 2 | Product[a] Run 3 | $An_2CO$[b] Run 1 | $An_2CO$[b] Run 2 | $An_2CO$[b] Run 3 | Scrambling from C-2 to C-1 (%) Run 1 | Run 2 | Run 3 |
|---|---|---|---|---|---|---|---|---|---|---|---|
| 1 | 15 | HOAc | 8.46 | 7.76 | 9.15[c] | 5.27 | 4.82 | 5.68 | 37.7 | 37.9 | 37.9 |
| 2 | 144 | HOAc | 9.49 | 12.65 | 7.86[c] | 5.90 | 7.89 | 4.88 | 37.8 | 37.6 | 37.9 |
| 3 | 144 | HOAc – 144 m$M$ NaOAc | 9.84 | 7.65 | 7.89[c] | 7.80 | 6.05 | 6.23 | 20.7 | 20.9 | 21.0 |
| 4 | 144 | HOAc – 288 m$M$ NaOAc | 7.04 | 6.93 | | 5.95 | 5.84 | | 15.5 | 15.7 | |
| 5 | 144 | HOAc – 1440 m$M$ NaOAc | 6.74 | 6.98 | | 6.45 | 6.68 | | 4.3 | 4.3 | |
| 6 | 15 | $CF_3CH_2OH$ – 0.1% $HClO_4$ | 5.98 | 8.20 | | 2.98 | 4.10 | | 50.2 | 50.0 | |
| 7 | 144 | $CF_3CH_2OH$ – 0.1% $HClO_4$ | 8.50 | 6.77 | | 4.26 | 3.38 | | 49.9 | 50.1 | |

[a] The product from the reactions in the HOAc or $CF_3CH_2OH$ medium was the scrambled trianisylvinyl acetate, 1-OAc-1,2-$^{14}$C, or trianisylvinyl trifluoroethyl ether, 1-$OCH_2CF_3$-1,2-$^{14}$C, respectively.
[b] Assayed as the oxime.
[c] Instead of ozonolysis, the trianisylvinyl acetate product was converted by $LiAlH_4$ treatment to 1,2,2-trianisylethanol followed by $KMnO_4$ oxidation to $An_2CO$ (2, 8).

TABLE 2. Data from the decomposition of 1,2-dianisyl-2-$p$-[$^{14}$C]methoxyphenylvinylphenyltriazene (1-NNNHPh-2-methoxy-$^{14}$C)

| Expt. | [Triazene] (m$M$) | Reaction medium | Specific activity ($10^{-5}$ dpm/mmol) Product[a] Run 1 | Product[a] Run 2 | Product[a] Run 3 | $An_2CO$[b] Run 1 | $An_2CO$[b] Run 2 | $An_2CO$[b] Run 3 | Scrambling from C-2 to C-1 (%) Run 1 | Run 2 | Run 3 |
|---|---|---|---|---|---|---|---|---|---|---|---|
| 1 | 15 | HOAc | 5.02 | 4.94 | 4.61[c] | 3.75 | 3.70 | 3.45 | 25.3 | 25.1 | 25.2 |
| 2 | 144 | HOAc | 3.07 | 3.33 | 4.11[c] | 2.29 | 2.49 | 3.07 | 25.4 | 25.2 | 25.3 |
| 3 | 144 | HOAc – 144 m$M$ NaOAc | 3.96 | 3.89 | 5.75[c] | 3.41 | 3.33 | 4.93 | 13.9 | 14.4 | 14.3 |
| 4 | 144 | HOAc – 288 m$M$ NaOAc | 6.89 | 4.49 | | 6.17 | 4.02 | | 10.4 | 10.5 | |
| 5 | 144 | HOAc – 1440 m$M$ NaOAc | 3.05 | 3.00 | | 2.96 | 2.91 | | 3.0 | 3.0 | |
| 6 | 15 | $CF_3CH_2OH$ – 0.1% $HClO_4$ | 4.06 | 3.98 | | 2.71 | 2.65 | | 33.3 | 33.4 | |
| 7 | 144 | $CF_3CH_2OH$ – 0.1% $HClO_4$ | 3.09 | 2.75 | | 2.06 | 1.83 | | 33.3 | 33.5 | |

[a] The product from reaction in the HOAc or $CF_3CH_2OH$ medium was the scrambled trianisylvinyl acetate, 1-OAc-1,2-methoxy-$^{14}$C, or trianisylvinyl trifluoroethyl ether, 1-$OCH_2CF_3$-1,2-methoxy-$^{14}$C, respectively.
[b] Assayed as the oxime.
[c] Instead of ozonolysis, the trianisylvinyl acetate product was converted by $LiAlH_4$ treatment to 1,2,2-trianisylethanol followed by $KMnO_4$ oxidation to give $An_2CO$ (2, 8).

factor of 2 or 3, respectively, for the chain or ring label.

In the earlier work on the acetolysis of 1-Br-2-$^{13}$C-2-methoxy-$^{14}$C (6), when the reaction was carried out in the presence of high concentrations of added salts (e.g. 15 m$M$ substrate with 450 m$M$ NaOAc or 300 m$M$ NaOAc and 300 m$M$ $Et_4NBr$), the "% rearrangement" for the $^{13}$C chain label and for the $^{14}$C ring label from a given experiment were found to be equal, indicating a complete equilibration of the labels in the molecules that have undergone rearrangement. On the other hand, for experiments carried out with lower concentrations of added salt, the equality of the "% rearrangement" for the chain and ring labels was not observed and it was suggested (6) that under such conditions some of the 1,2-anisyl shifts could have occurred in the ion-pair stage. The presence of the counterion would give rise to a front side hindrance, resulting in an incomplete equilibration of the labels. When ionization could proceed further to the dissociated "free" ions in the more polar medium with high concentrations of added salts, the 1,2-shifts would not be hindered by any counterion and complete equilibration was attained.

Given in Table 3 are the mean scrambling data

Can. J. Chem. Downloaded from www.nrcresearchpress.com by 210.87.254.42 on 09/06/12
For personal use only.

Can. J. Chem. Downloaded from www.nrcresearchpress.com by 210.87.254.42 on 09/06/12
For personal use only.

TABLE 3. Mean values of the observed % scrambling expressed as % rearrangement for the chain labeled 1-NNNHPh-2-$^{14}$C and for the ring labeled 1-NNNHPh-2-methoxy-$^{14}$C

| | % Scrambling[a] | | % Rearrangement[b] | |
|---|---|---|---|---|
| Expt. | Chain label | Ring label | Chain label | Ring label |
| 1 | 37.8 | 25.2 | 75.6 | 75.6 |
| 2 | 37.8 | 25.3 | 75.6 | 75.9 |
| 3 | 20.9 | 14.2 | 41.8 | 42.6 |
| 4 | 15.6 | 10.5 | 31.2 | 31.5 |
| 5 | 4.3 | 3.0 | 8.6 | 9.0 |
| 6 | 50.1 | 33.3 | 100 | 100 |
| 7 | 50.0 | 33.4 | 100 | 100 |

[a] Mean values from Tables 1 and 2.
[b] Assuming that 100% rearrangement corresponds to 50.0% or 33.3% scrambling, respectively, for the chain or ring label.

from the decomposition of the chain labeled 1-NNNHPh-2-$^{14}$C or the ring labeled 1-NNNHPh-2-methoxy-$^{14}$C expressed as % rearrangement. It is readily seen that the % rearrangement is the same for the chain labeled or ring labeled substrate. In Expts. 1 and 2, for example, almost 76% of the trianisylvinyl cation has undergone rearrangement with complete equilibration of the labels, while the remaining 24% was captured by solvent without rearrangement. For the reactions in HOAc with the presence of increasing amounts of the more nucleophilic acetate ion (Expts. 3–5), the portion of trianisylvinyl cation that was captured without rearrangement was increased, thus decreasing the net extent of rearrangement. In that portion of the trianisylvinyl cation in which 1,2-anisyl shifts took place, complete equilibration of the labels was achieved since triazene decomposition gave rise to the free cation in which 1,2-shifts could occur without hindrance by the presence of a counterion. These results thus may be regarded as giving support to the previous conclusion (6) that in the acetolysis of 1-Br-2-$^{13}$C-2-methoxy-$^{14}$C, conditions which gave rise to equal values for the % rearrangement in the chain label and in the ring label would involve scrambling in the free cation, while conditions which gave unequal % rearrangement for the chain and ring labels likely involved some scrambling in the ion-pair stage.

Recently, Ikeda *et al.* (11) have investigated the process of 1,2-anisyl shifts in solvolytic reactions with 2,2-dianisyl-1-phenylvinyl bromide specifically labeled with *p*-[$^2H_3$]$CH_3O$ (methoxy-$d_3$) in the *cis* or *trans*-anisyl group. A slight preference was found for the migration of the anisyl group *trans* to the bromine in reactions with HOAc–NaOAc, HOAc–AgOAc, or TFE-2,6-lutidine. It was proposed that this preference for migration of the *trans*-anisyl group was due to the intervention of ion-pairs in the rearrangement process, with the leaving group as the counterion hindering the migration of the anisyl group *cis* to the bromine. This mechanism is essentially the same as that suggested by us in accounting for the unequal % rearrangement found for the chain and ring labels in the acetolysis of 1-Br-2-$^{13}$C-2-methoxy-$^{14}$C under conditions of low concentrations of added salts (6).

## Experimental

*Trianisyl[2-$^{14}$C]vinylphenyltriazene (1-NNNHPh-2-$^{14}$C) and 1,2-dianisyl-2-p-[$^{14}$C]methoxyphenylvinylphenyltriazene (1-NNNHPh-2-methoxy-$^{14}$C)*

The chain labeled 1-NNNHPh-2-$^{14}$C was prepared from 1-Br-2-$^{14}$C and phenyl azide as previously described (2). The ring labeled 1-NNNHPh-2-methoxy-$^{14}$C was obtained from a similar phenyl azide reaction with 1,2-dianisyl-2-*p*-[$^{14}$C]methoxyphenylvinyl bromide (1-Br-2-methoxy-$^{14}$C), the latter being obtained starting from desoxyanisoin and *p*-[$^{14}$C]methoxyphenylmagnesium bromide, again as previously described (6).

*Decomposition of triazene and degradation of the reaction product*

The decomposition of 1-NNNHPh-2-$^{14}$C or 1-NNNHPh-2-methoxy-$^{14}$C in HOAc or HOAc–NaOAc was carried out essentially as described by Lee and Ko (2). Typically, 670 mg (1.44 mmol) of 1-NNNHPh-2-$^{14}$C or 1-NNNHPh-2-methoxy-$^{14}$C and 118 mg (1.44 mmol) of NaOAc in 10 mL of glacial HOAc was stirred at room temperature for 10 min (Expt. 3). The resulting material was worked up as previously described (2) to give the product, trianisyl[1,2-$^{14}$C]vinyl acetate (1-OAc-1,2-$^{14}$C) which was either subjected directly to ozonolysis to give dianisyl-[$^{14}$C]ketone (2-$^{14}$C) (7) or converted by $LiAlH_4$ treatment to 1,2,2-trianisyl[1,2-$^{14}$C]ethanol followed by $KMnO_4$ oxidation to give 2-$^{14}$C.

For the decomposition in TFE–$HClO_4$, typically 69.8 mg (0.15 mmol) of 1-NNNHPh-2-$^{14}$C or 1-NNNHPh-2-methoxy-$^{14}$C was dissolved in 10 mL of TFE containing 0.01 mL of $HClO_4$ (Expt. 6). Evolution of $N_2$ occurred immediately. The mixture was stirred at room temperature for 10 min and then poured into $H_2O$. After extraction with ether, the extract was washed with $H_2O$, dried over $MgSO_4$, and upon removal of the ether 60 mg (90%) of crude product was obtained as an oil. Its nmr spectrum was the same as that of an authentic sample of trianisylvinyl 2,2,2-trifluoroethyl ether (1-$OCH_2CF_3$). The labeled product, 1-$OCH_2CF_3$-1,2-$^{14}$C, was diluted with authentic 1-$OCH_2CF_3$ and then degraded by ozonolysis (7) to give 2-$^{14}$C.

Authentic 1-$OCH_2CF_3$ was prepared from heating a solution of 2.0 g (4.7 mmol) of 1-Br and 1.5 g (14 mmol) of 2,6-lutidine in 40 mL of TFE in a sealed tube at 120°C for 12 h. The resulting material was worked up as described above in the decomposition of triazene in TFE to give an oily product which was repeatedly crystallized from EtOH–$H_2O$, yielding 1.6 g (77%) of pure 1-$OCH_2CF_3$, mp 103–104°C; $^1$H nmr δ($CDCl_3$): 3.70, 3.76, 3.82 (3s, $CH_3O$), 3.91 (q, $CH_2$), 6.5–7.1 (m, arom.). *Anal.* calcd. for $C_{25}H_{23}O_4F_3$: C 67.56, H 5.22; found: C 67.26, H 5.30.

## Acknowledgement

The financial support given by the Natural Sciences and Engineering Research Council of Canada is sincerely acknowledged.

1. W. M. JONES and F. W. MILLER. J. Am. Chem. Soc. **89**, 1960 (1967).
2. C. C. LEE and E. C. F. KO. Can. J. Chem. **54**, 3041 (1976).

3. C. C. LEE and C. A. OBAFEMI. Can. J. Chem. **59**, 1636 (1981).
4. P. J. STANG, Z. RAPPOPORT, M. HANACK, and L. R. SUBRAMANIAN. Vinyl cations. Academic Press, New York. 1979. Chapt. 6 and 7.
5. C. C. LEE. *In* Isotopes in organic chemistry. Vol. 5. Isotopes in cationic reactions. *Edited by* E. Buncel and C. C. Lee. Elsevier Scientific Publishing Co., Amsterdam. 1980. pp. 1–44.
6. C. C. LEE, C. A. OBAFEMI, J. W. QUAIL, and Z. RAPPOPORT. Can. J. Chem. **59**, 2342 (1981).
7. C. C. LEE, U. WEBER, and C. A. OBAFEMI. Can. J. Chem. **57**, 1384 (1979).
8. C. C. LEE, A. J. CESSNA, B. A. DAVIS, and M. OKA. Can. J. Chem. **52**, 2679 (1974).
9. F. L. SCHADT, T. W. BENTLEY, and P. v. R. SCHLEYER. J. Am. Chem. Soc. **98**, 7667 (1976).
10. Y. HOUMINER, E. NOY, and Z. RAPPOPORT. J. Am. Chem. Soc. **98**, 5632 (1976).
11. T. IKEDA, S. KOBAYASHI, H. TANIGUCHI, and Z. RAPPOPORT. J. Am. Chem. Soc. In press.

Can. J. Chem. Downloaded from www.nrcresearchpress.com by 210.87.254.42 on 09/06/12
For personal use only.

# Preparation and crystal and molecular structure of ($\eta^3$-octamethylcyclotetraphosphazane-*P,P,P*)tricarbonylmolybdenum(0), [$\eta^3$-$(CH_3PNCH_3)_4$]Mo$(CO)_3$

KEITH D. GALLICANO, NORMAN L. PADDOCK, STEVEN J. RETTIG, AND JAMES TROTTER

*Department of Chemistry, University of British Columbia, 2036 Main Mall, Vancouver, B.C., Canada V6T 1Y6*

Received March 9, 1982

KEITH D. GALLICANO, NORMAN L. PADDOCK, STEVEN J. RETTIG, and JAMES TROTTER. Can. J. Chem. **60**, 2415 (1982).

The synthesis and physical properties of the phosphazane complex [$\eta^3$-$(CH_3PNCH_3)_4$]Mo$(CO)_3$ are reported. Crystals of ($\eta^3$-octamethylcyclotetraphosphazane-*P,P,P*)tricarbonylmolybdenum(0) are monoclinic, $a$ = 8.6898(9), $b$ = 16.0987(8), $c$ = 14.1156(17) Å, $\beta$ = 98.321(6)°, $Z$ = 4, space group $Cc$. The structure was solved by Patterson and Fourier syntheses and was refined by full-matrix least-squares procedures to $R$ = 0.020 and $R_w$ = 0.024 for 2286 reflections with $I \geq 3\sigma(I)$. The molybdenum atom is coordinated to three phosphorus atoms of the $(MePNMe)_4$ ligand and to three carbonyl ligands in a distorted octahedral geometry. The molecule has approximate mirror symmetry in the solid state. Important bond lengths (corrected for libration) are: Mo—P = 2.537(1), 2.467(1), and 2.513(1), Mo—C = 1.971(4), 2.002(4), and 1.978(4), mean P—N = 1.704(8) for coordinated P, 1.735(7) Å for uncoordinated P. The structural evidence indicates that the phosphazane is a weaker donor to Mo$(CO)_3$ than to three sulphur atoms, and that coordination withdraws electron density from the fourth phosphorus atom. The complex is fluxional in solution.

KEITH D. GALLICANO, NORMAN L. PADDOCK, STEVEN J. RETTIG et JAMES TROTTER. Can. J. Chem. **60**, 2415 (1982).

On rapporte la synthèse et les propriétés physiques du complexe de phosphazane: [$\eta^3$-$(CH_3PNCH_3)_4$] Mo$(CO)_3$. Les cristaux de ($\eta^3$-octaméthylcyclotétraphosphazane-*P,P,P*)tricarbonylmolybolène(0) sont monocliniques et appartiennent au groupe d'espace $Cc$ avec $a$ = 8,6898(9), $b$ = 16,0987(8), $c$ = 14,1156(17) Å, $\beta$ = 98,321(6)°, $Z$ = 4. On a résolu la structure par les synthèses de Patterson et de Fourier et on l'a affiné par la méthode des moindres carrés (matrice complète) jusqu'à des valeurs de $R$ = 0,020 et de $R_w$ = 0,024 pour 2286 réflexions avec $I \geq 3\sigma(I)$. L'atome de molybolène est coordonné à trois atomes de phosphore du ligand (MePNMe) et à trois ligands carbonyle selon une géométrie octaédrique déformée. La molécule est approximativement symétrique à l'état solide. Les angles importants de liaison (corrigés pour la libration sont: Mo—P = 2,537(1), 2,467(1) et 2,513(1), Mo—C = 1,971(4), 2,002(4) et 1,978(4), angle moyen P—N = 1,704(8) pour le P coordonné et 1,735(7) Å pour le phosphore non coordonné. Les preuves structurales indiquent que le phosphazane est un plus faible donneur envers le Mo$(CO)_3$ qu'envers les trois atomes de soufre et que la coordination enlève la densité électronique du quatrième atome de phosphore. Le complexe est fluxionnaire en solution.

[Traduit par le journal]

## Introduction

The phosphazane $(MePNMe)_4$, **1**, was earlier prepared from methyldichlorophosphine and heptamethyldisilazane, and its crystal and molecular structure determined (1). Its reactions with sulphur to give $(MePNMe)_4S_3$ (2) and with acetylenic diesters (3) have been investigated; in both reactions, the phosphorus atoms are the donors. We have prepared the complex [$\eta^3$-$(CH_3PNCH_3)_4$]Mo$(CO)_3$, and have determined its crystal and molecular structure.

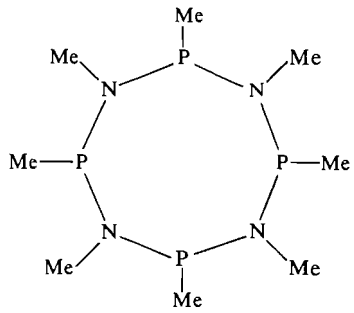

**1**

## Experimental

Molybdenum hexacarbonyl (0.178 g, 0.67 mmol) was added to **1** (0.202 g, 0.67 mmol) in 20 mL toluene at 70°C. The solution was stirred at this temperature under dry nitrogen for 18 h (higher temperatures cause decomposition), during which time a pale yellow solid precipitated. The product was filtered off, washed with toluene, and crystallized from acetonitrile as pale yellow blocks (0.080 g, 25%) of [$\eta^3$-$(CH_3PNCH_3)_4$]Mo$(CO)_3$, **2**. *Anal.* calcd. for $C_{11}H_{24}MoN_4O_3P_4$: C 27.5, H 5.0, N 11.7; found: C 27.2, H 5.2, N 11.6. **2** decomposed above 300°C, after turning brown at 180°C. Its mass spectrum (70 eV) showed the molecular ion and the stepwise loss of three carbonyl groups. $^1$H nmr parameters ($CDCl_3$, internal $Me_4Si$): $\delta(PCH_3)$ = 1.63, $\delta(NCH_3)$ = 2.88 (see Discussion). Infrared bands (Nujol mull): $\nu_{CO}$ = 1928 and 1828, 1817 cm$^{-1}$. Shoulder absorptions at 1854 and 1781 cm$^{-1}$ are attributed to solid state interactions.

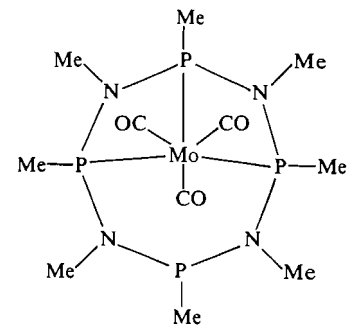

**2**

0008-4042/82/192415-05$01.00/0

©1982 National Research Council of Canada/Conseil national de recherches du Canada

Can. J. Chem. Downloaded from www.nrcresearchpress.com by 210.87.254.6 on 09/06/12
For personal use only.

Can. J. Chem. Downloaded from www.nrcresearchpress.com by 210.87.254.6 on 09/06/12
For personal use only.

*X-ray crystallographic analysis of* $[\eta^3\text{-}(CH_3PNCH_3)_4]Mo(CO)_3$

A crystal ca. 0.080 × 0.225 × 0.325 mm in size was mounted in a general orientation. Unit-cell parameters were refined by least-squares on 2 sin θ/λ values for 25 reflections measured on a diffractometer with Mo Kα$_1$ radiation (λ = 0.70930 Å). Crystal data at 22°C are:

$C_{11}H_{24}MoN_4O_3P_4$ fw = 480.18

Monoclinic, $a = 8.6898(9)$, $b = 16.0987(8)$, $c = 14.1156(17)$ Å, β = 98.321(6)°, $V = 1953.9(3)$ Å$^3$, $Z = 4$, $\rho_c = 1.632$ g cm$^{-3}$, $F(000) = 976$, μ(Mo Kα) = 9.11 cm$^{-1}$. Absent reflections: $hkl$, $h + k \neq 2n$ and $h0l$, $l \neq 2n$, space group $Cc$ ($C_s^4$, No. 9) from structure analysis.

Intensities were measured with graphite-monochromated Mo Kα radiation (λ = 0.71073 Å) on an Enraf-Nonius CAD4-F diffractometer. An ω–2θ scan at 1.01–10.06° min$^{-1}$ over a range of (0.75 + 0.35 tan θ) degrees in ω (extended by 25% on both sides for background measurement) was employed. Data were measured to 2θ = 60°. The intensities of three check reflections, measured every 3600 s throughout the data collection, remained constant to within ±3.7%. After data reduction, an absorption correction was applied using the Gaussian integration method (4, 5). Transmission factors ranged from 0.876 to 0.933 for 96 sampling points. Of the 2846 independent reflections measured, 2286 (80.3%) had intensities greater than $3\sigma(I)$ above background where $\sigma^2(I) = S + 2B + (0.04(S - B))^2$ with $S$ = scan count and $B$ = background count.

The systematic absences allow space groups $C2/c$ or $Cc$, the latter being indicated by the $E$-statistics, the Patterson function and by the number of molecules in the unit-cell. The positions of the Mo and P atoms were determined from the Patterson function and those of the remaining non-hydrogen atoms from a subsequent difference map. After full-matrix least-squares refinement of the non-hydrogen atoms with anisotropic thermal parameters to $R = 0.028$, a difference map gave the positions of all 24 hydrogen atoms which were refined with isotropic thermal parameters in subsequent least-squares cycles. The scattering factors of ref. 6 were used for non-hydrogen atoms and those of ref. 7 for hydrogen atoms. Anomalous scattering factors from ref. 8 were used for the Mo and P atoms. The weighting scheme, $w = 1/\sigma^2(F)$ where $\sigma^2(F)$ is derived from the previously defined $\sigma^2(I)$ gave uniform average values of $w(|F_o| - |F_c|)^2$ over ranges of $|F_o|$ and was employed in the final stages of refinement. Convergence was reached at $R = 0.020$ and $R_w = 0.024$ for 2286 reflections with $I \geq 3\sigma(I)$. For all 2846 reflections $R = 0.037$ and $R_w = 0.024$. The function minimized was $\Sigma w(|F_o| - |F_c|)^2$, $R = \Sigma||F_o| - |F_c||/\Sigma|F_o|$ and $R_w = (\Sigma w(|F_o| - |F_c|)^2/\Sigma w|F_o|^2)^{1/2}$.

On the final cycle of refinement the mean and maximum parameter shifts corresponded to 0.10 and 1.02σ respectively. The mean error in an observation of unit weight was 1.122. A final difference map showed maximum fluctuations of ±0.90 e Å$^{-3}$ near Mo and less than ±0.2 e Å$^{-3}$ away from the Mo and P atoms. The final positional and thermal parameters appear in Tables 1 and 2[1] respectively. Hydrogen atom coordinates and thermal parameters (Table 1*b*) have been deposited. Measured and calculated structure factors have been placed in the Depository of Unpublished Data.[1]

The ellipsoids of thermal motion for the non-hydrogen atoms are shown in Fig. 1. The thermal motion has been analysed in terms of the rigid-body modes of translation, libration, and screw motion (9). The rms standard error in the temperature factors $\sigma U_{ij}$ (derived from the least-squares analysis) is 0.0017 Å$^2$. Analysis of all 23 non-hydrogen atoms gave rms $\Delta U_{ij}$ = 0.0081 Å$^2$ and indicated independent motion of the carbonyl oxygen and methyl carbon atoms. The 12 remaining core atoms were then analysed giving rms $\Delta U_{ij}$ = 0.0023 Å$^2$ and physically reasonable rigid-body parameters. The appropriate bond distances have been corrected for libration (10), using shape parameters $q^2$ of 0.08 for all atoms involved. Corrected bond lengths appear in Table 3 along with the uncorrected values; corrected bond angles do not differ by more than 1σ from the uncorrected values given in Table 4. Intra-annular torsion angles defining the conformations of phosphazane and chelate rings are listed in Table 5. Bond lengths and angles involving hydrogen and a complete listing of torsion angles (Tables 6–8) are included as supplementary material.

TABLE 1. Final positional (fractional × 10$^4$, Mo and P × 10$^5$) and equivalent isotropic thermal parameters ($U \times 10^3$ Å$^2$) with estimated standard deviations in parentheses

| Atom | $x$ | $y$ | $z$ | $U_{eq}$ |
|---|---|---|---|---|
| Mo | 20000 | 31517( 1) | 20000 | 24 |
| P(1) | −4537(10) | 23030( 5) | 15622( 6) | 26 |
| P(2) | 22435(10) | 19388( 5) | 9682( 6) | 26 |
| P(3) | 30776( 9) | 18657( 5) | 28577( 6) | 25 |
| P(4) | 1718(10) | 18800( 6) | 35361( 6) | 28 |
| O(1) | 5350( 4) | 3899( 3) | 2250( 4) | 82 |
| O(2) | 1005( 5) | 4265( 2) | 3644( 3) | 62 |
| O(3) | 1073( 5) | 4532( 2) | 461( 2) | 58 |
| N(1) | 317( 4) | 1703( 2) | 748( 2) | 32 |
| N(2) | 3169( 3) | 1311( 2) | 1836( 2) | 29 |
| N(3) | 1930( 3) | 1363( 2) | 3538( 2) | 30 |
| N(4) | −948( 3) | 1681( 2) | 2448( 2) | 30 |
| C(1) | 4110( 5) | 3625( 2) | 2163( 3) | 40 |
| C(2) | 1390( 5) | 3859( 2) | 3050( 3) | 35 |
| C(3) | 1361( 5) | 4021( 2) | 1035( 3) | 36 |
| C(4) | −2320( 5) | 2624( 4) | 916( 4) | 50 |
| C(5) | 3001( 5) | 1623( 3) | −107( 3) | 43 |
| C(6) | 5014( 4) | 1756( 3) | 3520( 3) | 42 |
| C(7) | −762( 5) | 1199( 3) | 4330( 4) | 44 |
| C(8) | −420( 7) | 1027( 4) | 150( 4) | 57 |
| C(9) | 3484( 7) | 417( 3) | 1761( 4) | 52 |
| C(10) | 2257( 5) | 515( 3) | 3900( 4) | 45 |
| C(11) | −1793( 6) | 897( 3) | 2207( 4) | 48 |

## Results and discussion

The $^1$H nmr spectrum of **2** shows that the molecule is fluxional in solution on the nmr time scale, the mean $PCH_3$ and $NCH_3$ signals, relative to those of **1**, being shifted upfield and downfield by 0.22 and 0.07 ppm respectively. $J_{PCH_3}$ is too small to be measured. The $(N)CH_3$ spectrum appears to be a doublet superimposed on a triplet, and was simulated by assuming equal coupling constants (3.2 Hz) to both pairs of phosphorus atoms. The carbonyl stretching frequencies are similar to, but slightly lower than, those of the $A_1$, $E$ bands (1949, 1835 cm$^{-1}$) in $(Ph_3P)_3Mo(CO)_3$ (11), consistent with some strengthening of the donor function of phosphorus by electron release from nitrogen.

There are no intermolecular contacts less than the sum of van der Waals radii in the crystal of **2**, so

[1]The structure factor table, Table 2 (anisotropic thermal parameters) and other material mentioned in the text are available, at a nominal charge, from the Depository of Unpublished Data, CISTI, National Research Council of Canada, Ottawa, Canada K1A 0S2.

Can. J. Chem. Downloaded from www.nrcresearchpress.com by 210.87.254.6 on 09/06/12
For personal use only.

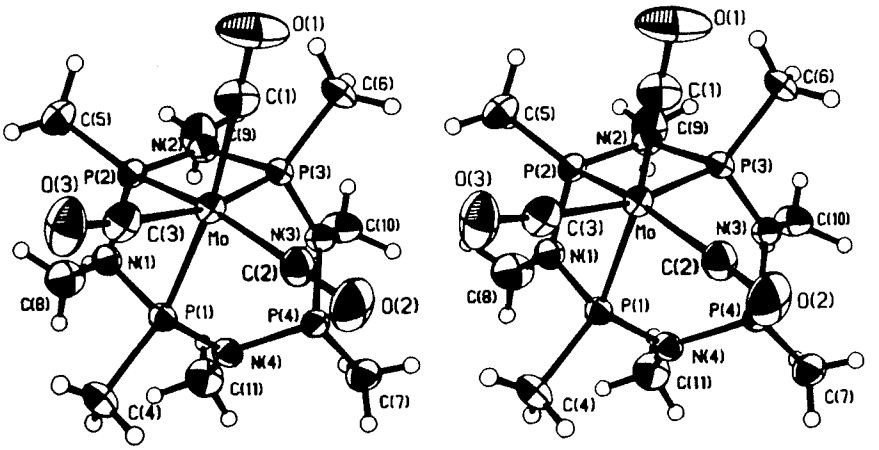


FIG. 1. Stereoscopic view of ($\eta^3$-octamethylcyclotetraphosphazane-*P*,*P*,*P*)tricarbonylmolybdenum(0); 50% probability thermal ellipsoids are shown for the non-hydrogen atoms. Hydrogen atoms have been assigned artificially small thermal parameters for the sake of clarity.

TABLE 3. Bond lengths (Å) with estimated standard deviations in parentheses

| | Length | | | Length | |
|---|---|---|---|---|---|
| Bond | Uncorr. | Corr. | Bond | Uncorr. | Corr. |
| Mo —P(1) | 2.5326(9) | 2.537 | P(3) —N(3) | 1.688(3) | 1.690 |
| Mo —P(2) | 2.4633(8) | 2.467 | P(3) —C(6) | 1.812(4) | 1.813 |
| Mo —P(3) | 2.5101(9) | 2.513 | P(4) —N(3) | 1.740(3) | 1.742 |
| Mo —C(1) | 1.968(4) | 1.971 | P(4) —N(4) | 1.725(3) | 1.728 |
| Mo —C(2) | 2.000(4) | 2.002 | P(4) —C(7) | 1.838(4) | 1.838 |
| Mo —C(3) | 1.975(4) | 1.978 | O(1)—C(1) | 1.155(5) | 1.155 |
| P(1)—N(1) | 1.709(3) | 1.712 | O(2)—C(2) | 1.151(5) | 1.151 |
| P(1)—N(4) | 1.704(3) | 1.706 | O(3)—C(3) | 1.157(5) | 1.157 |
| P(1)—C(4) | 1.817(4) | 1.818 | N(1)—C(8) | 1.467(5) | 1.467 |
| P(2)—N(1) | 1.701(3) | 1.704 | N(2)—C(9) | 1.473(5) | 1.474 |
| P(2)—N(2) | 1.697(3) | 1.699 | N(3)—C(10) | 1.471(5) | 1.471 |
| P(2)—C(5) | 1.812(4) | 1.813 | N(4)—C(11) | 1.476(5) | 1.476 |
| P(3)—N(2) | 1.708(3) | 1.710 | | | |

that the molecule may be considered in isolation. A stereoscopic view of it is shown in Fig. 1. The Mo atom is coordinated by three phosphorus atoms of the $(MePNMe)_4$ ligand and by three carbonyl ligands in a distorted octahedral geometry. Although the molecule has no strict crystallographic symmetry, it is nearly symmetrical about a plane through P(2)MoP(4), and, for the discussion, corresponding dimensions are averaged. In the complex, the crown conformation of the ligand is retained; the changes in its geometry caused by complex formation are discussed below.

In the ligand **1** (1), the configuration of the nitrogen atom is almost planar, the sum of the angles there being 357.1°, whereas the phosphorus atom is pyramidal, the sum of angles being 309.5°. The P—N bond, at 1.722(2) Å, is 0.05 Å shorter than would be expected for a single bond (12). The deficit, though smaller than in phosphazenes (0.09–0.16 Å) (13), represents significant $\pi$-bonding, arising from the acceptor properties of tervalent phosphorus. Such bonding is also found in non-cyclic molecules; in 1,1-bis(diphenylphosphino)-2,2-dimethylhydrazine, the sum of the angles at N(1) is 359.9(2)°, and the mean P—N bond length is 1.715(14) Å (14),[2] and in a diphenylphosphino-amino-substituted phosphetidine a short exocyclic P—N bond (1.691(11) Å) is associated with near planarity (359°) of the atoms attached to nitrogen (15).

Tri-coordination to molybdenum in **2** forms one six-membered and two four-membered rings, with

[2]Here and elsewhere in this report mean values refer to weighted means with rms deviations from the mean in parentheses.

Can. J. Chem. Downloaded from www.nrcresearchpress.com by 210.87.254.6 on 09/06/12
For personal use only.

TABLE 4. Bond angles (deg) with estimated standard deviations in parentheses

| Bonds | Angle (deg) | Bonds | Angle (deg) |
|---|---|---|---|
| P(1)—Mo—P(2) | 64.49(3) | N(2)—P(2)—C(5) | 104.2(2) |
| P(1)—Mo—P(3) | 85.12(3) | Mo—P(3)—N(2) | 94.77(10) |
| P(1)—Mo—C(1) | 167.06(12) | Mo—P(3)—N(3) | 117.40(10) |
| P(1)—Mo—C(2) | 100.60(12) | Mo—P(3)—C(6) | 125.7(2) |
| P(1)—Mo—C(3) | 94.08(12) | N(2)—P(3)—N(3) | 109.48(15) |
| P(2)—Mo—P(3) | 64.75(3) | N(2)—P(3)—C(6) | 103.4(2) |
| P(2)—Mo—C(1) | 102.57(12) | N(3)—P(3)—C(6) | 103.9(2) |
| P(2)—Mo—C(2) | 160.72(12) | N(3)—P(4)—N(4) | 107.13(15) |
| P(2)—Mo—C(3) | 101.16(11) | N(3)—P(4)—C(7) | 100.3(2) |
| P(3)—Mo—C(1) | 89.25(12) | N(4)—P(4)—C(7) | 101.0(2) |
| P(3)—Mo—C(2) | 103.44(11) | P(1)—N(1)—P(2) | 102.9(2) |
| P(3)—Mo—C(3) | 164.75(11) | P(1)—N(1)—C(8) | 128.7(3) |
| C(1)—Mo—C(2) | 92.0(2) | P(2)—N(1)—C(8) | 127.3(3) |
| C(1)—Mo—C(3) | 88.3(2) | P(2)—N(2)—P(3) | 102.91(15) |
| C(2)—Mo—C(3) | 91.68(15) | P(2)—N(2)—C(9) | 127.2(3) |
| Mo—P(1)—N(1) | 94.07(11) | P(3)—N(2)—C(9) | 127.1(3) |
| Mo—P(1)—N(4) | 115.50(11) | P(3)—N(3)—P(4) | 111.1(2) |
| Mo—P(1)—C(4) | 128.9(2) | P(3)—N(3)—C(10) | 122.9(3) |
| N(1)—P(1)—N(4) | 109.02(15) | P(4)—N(3)—C(10) | 124.8(3) |
| N(1)—P(1)—C(4) | 103.4(2) | P(1)—N(4)—P(4) | 112.0(2) |
| N(4)—P(1)—C(4) | 103.6(2) | P(1)—N(4)—C(11) | 120.2(3) |
| Mo—P(2)—N(1) | 96.78(11) | P(4)—N(4)—C(11) | 124.2(3) |
| Mo—P(2)—N(2) | 96.74(10) | Mo—C(1)—O(1) | 179.4(4) |
| Mo—P(2)—C(5) | 142.18(15) | Mo—C(2)—O(2) | 178.5(4) |
| N(1)—P(2)—N(2) | 110.5(2) | Mo—C(3)—O(3) | 176.1(4) |
| N(1)—P(2)—C(5) | 104.6(2) | | |

TABLE 5. Intra-annular torsion angles (deg) standard deviations in parentheses

| Atoms | Angle (deg) |
|---|---|
| N(4)—P(1)—N(1)—P(2) | −107.1(2) |
| N(2)—P(2)—N(1)—P(1) | 87.8(2) |
| N(1)—P(2)—N(2)—P(3) | −91.7(2) |
| N(3)—P(3)—N(2)—P(2) | 113.3(2) |
| N(2)—P(3)—N(3)—P(4) | −108.3(2) |
| N(4)—P(4)—N(3)—P(3) | 75.7(2) |
| N(3)—P(4)—N(4)—P(1) | −80.7(2) |
| N(1)—P(1)—N(4)—P(4) | 113.9(2) |
| P(3)—Mo—P(1)—N(4) | 40.34(12) |
| Mo—P(1)—N(4)—P(4) | 9.6(2) |
| N(3)—P(4)—N(4)—P(1) | −80.7(2) |
| N(4)—P(4)—N(3)—P(3) | 75.7(2) |
| Mo—P(3)—N(3)—P(4) | −1.9(2) |
| P(1)—Mo—P(3)—N(3) | −44.89(13) |
| P(2)—Mo—P(1)—N(1) | −8.68(11) |
| Mo—P(1)—N(1)—P(2) | 11.68(15) |
| Mo—P(2)—N(1)—P(1) | −12.07(15) |
| P(1)—Mo—P(2)—N(1) | 8.77(11) |
| P(3)—Mo—P(2)—N(2) | −5.95(10) |
| Mo—P(2)—N(2)—P(3) | 8.13(14) |
| Mo—P(3)—N(2)—P(2) | −7.95(10) |
| P(2)—Mo—P(3)—N(2) | 5.89(10) |

some corresponding ring strain. The six-membered ring has a distorted boat conformation. Four-membered rings have also been found in the $Fe(CO)_3$ complex of a phosphetidine (16); in **2** they are both non-planar, that containing P(3) being somewhat more so than the other (see Table 5). The mean ring angle at N(1), N(2) (102.9(1)°) is 8.9° less than in **1**. Since this change is unaccompanied by changes in the lengths of the N—C bonds, the σ-hybrids at nitrogen do not lie along the bond directions, and the molecule must be regarded as strained at these points; the method of ref. 13 cannot be used for the assessment of π-contractions.[3] By the same argument, there is no indication of ring strain at the phosphorus atoms in **2**. The difference between the mean lengths of the P—C bonds to P(1), P(2), and P(3) (1.815(3) Å) and to P(4) (1.838(4) Å) is exactly that expected from the difference in N—P—C angle: mean 104.0(6)° at P(1), P(2), and P(3), 100.7(4)° at P(4). On the assumption of *s*/*p* hybridization, we can then calculate the composition and the direction of the lone pair orbital at each phosphorus atom.

Figure 2, calculated from the geometry around the phosphorus atoms, shows that the increased *p*-electron density in the P—Mo regions is attained partly at the expense of P(4) (in agreement with the reduced nucleophilicity found experimentally and spectroscopically at P(4) in the trisulphide (2)), and partly by an increased *s*-component in the ring

[3]As a comparison, the ring in $(MeNPMe)_4S_3$ is apparently unstrained. The especially large bond angles at N(2), N(3) (128.3(2), 129.9(2)°) are associated, through increased *p*-character of the exocyclic bonds, with the longest N—C bonds (1.497(6), 1.511(6) Å).

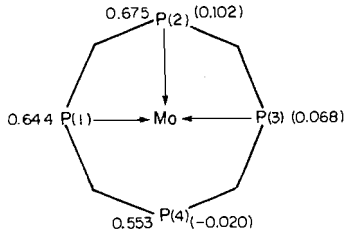


FIG. 2. Fractional $p$-electron density in the lone pair orbitals at phosphorus. Difference from density in the free ligand in parentheses.

bonds. This result is consistent with a reduction of the mean P—N bond length from 1.722(2) Å in **1** to 1.711(17) Å in **2**, a slight increase in the strengths of the bonds meeting at P(1), P(2), and P(3) (mean P—N = 1.704(8) Å) being achieved partly at the expense of P(4)—N (mean 1.735(7) Å). A similar but slightly larger effect is found in the trisulphide $(MePNMe)_4S_3$ (2), in which the ring bonds to the coordinated phosphorus atoms (means 1.688(13) Å) are shorter than those to the fourth atom (mean 1.740(9) Å). Whether assessed by bond angles or bond lengths, the electronic shifts induced by the $S_3$ and $Mo(CO)_3$ groups are qualitatively of the same type, sulphur being the stronger acceptor.

Some differences between the two structures are a consequence of the particular geometry of the $Mo(CO)_3$ group. Its coordination to the phosphazane framework necessarily introduces angular strain, discussed above for the angles at nitrogen, if normal bond lengths are to be preserved in the four-membered rings. Distortion at phosphorus is of another sort, the P—Mo bond directions deviating from the calculated lone pair directions by 23.6° at P(1) and P(3), and by 34.3° at P(2). The P—Mo—P angles are small (64.49(3), 85.12(3), and 64.75(3)°), but there may be no strain here. Certainly, there are other examples of small angles, such as P—Mo—P = 65.6(2)° in $(EtP)_5Mo(CO)_4$ (17) and 64.8(2)° in $(Ph_2PNEtPPh_2)Mo(CO)_4$ (18), and in $(Ph_2PNEtPPhNEtPPh_2)Mo(CO)_3$, **3** (19), the coordination geometry of the tridentate ligand is almost identical with that in **2**, even though the ligand is acyclic, the P—Mo—P angles being 65.0(1), 94.0(1), and 65.3(1)°.

The surprising feature of the structure of **2** is that P(2)—Mo (2.467(1) Å) is significantly shorter than P(1)—Mo, P(3)—Mo (mean 2.525(12) Å), opposite to the situation in **3** where the central P—Mo bond (2.527(4) Å) is significantly longer than the other two (mean 2.451(26) Å). This feature of **2** is consistent with the calculated $p$-electron densities and with the Mo—C distances, that to C(2) being significantly longer (2.002(4) Å) than those to C(1), C(3) (mean Mo—C = 1.975(4) Å), but there seems no obvious explanation. The difference does not appear to be caused by the electronic structure of the phosphazane since all three P=S bonds in the trisulphide are equal. It may simply be that elongation of the P(2)—Mo bond would increase the misalignment of the bond and lone pair directions, thereby reducing the P—Mo—P angle unacceptably, but a compromise of this type which strengthens a bond is unusual.

## Acknowledgments

We thank the Natural Sciences and Engineering Research Council of Canada for financial support and the University of British Columbia Computing Centre for assistance.

1. W. ZEISS, W. SCHWARZ, and H. HESS. Angew. Chem. Int. Ed. Engl. **16**, 407 (1977).
2. W. ZEISS, W. SCHWARZ, and H. HESS. Z. Naturforsch. **35b**, 959 (1980).
3. W. ZEISS and H. HENJE. Chem. Ber. **111**, 1655 (1978).
4. P. COPPENS, L. LEISEROWITZ, and D. RABINOVICH. Acta Crystallogr. **18**, 1035 (1965).
5. W. R. BUSING and H. A. LEVY. Acta Crystallogr. **22**, 457 (1967).
6. D. T. CROMER and J. B. MANN. Acta Crystallogr. Sect. A, **24**, 321 (1968).
7. R. F. STEWART, E. R. DAVIDSON, and W. T. SIMPSON. J. Chem. Phys. **42**, 3175 (1965).
8. D. T. CROMER and D. LIBERMAN. J. Chem. Phys. **53**, 1891 (1970).
9. V. SCHOMAKER and K. N. TRUEBLOOD. Acta Crystallogr. Sect. B, **24**, 63 (1968).
10. D. W. J. CRUICKSHANK. Acta Crystallogr. **9**, 747 (1956); **9**, 754 (1956); **14**, 896 (1961).
11. E. W. ABEL, M. A. BENNETT, and G. WILKINSON. J. Chem. Soc. 2533 (1959).
12. D. W. J. CRUICKSHANK. Acta Crystallogr. **17**, 671 (1964).
13. D. P. CRAIG and N. L. PADDOCK. *In* Non-benzenoid aromatics. Vol. 2. Academic Press, New York. 1971. p. 273.
14. J. B. FAUGHT. Can. J. Chem. **54**, 738 (1976).
15. D. A. HARVEY, R. KEAT, A. N. KEITH, K. W. MUIR, and D. S. RYCROFT. Inorg. Chim. Acta, **34**, L201 (1979).
16. L. S. JENKINS and G. R. WILLEY. J. Chem. Soc. Dalton Trans. 777 (1979).
17. M. A. BUSH and P. WOODWARD. J. Chem. Soc. Sect. A, 1221 (1968).
18. D. S. PAYNE, J. A. A. MOKUOLO, and J. C. SPEAKMAN. J. Chem. Soc. Chem. Commun. 599 (1965).
19. K. K. CHEUNG, T. F. LAI, and S. Y. LAM. J. Chem. Soc. Sect. A, 3345 (1970).

Can. J. Chem. Downloaded from www.nrcresearchpress.com by 210.87.254.6 on 09/06/12
For personal use only.

# The mechanism of sulphide oxidation by *Mortierella isabellina* NRRL 1757

HERBERT L. HOLLAND[1] AND IAN M. CARTER
*Department of Chemistry, Brock University, St. Catharines, Ont., Canada L2S 3A1*

Received March 26, 1982

HERBERT L. HOLLAND and IAN M. CARTER. Can. J. Chem. **60**, 2420 (1982).

A series of aryl substituted phenyl and benzyl methyl sulphides has been oxidized to the corresponding sulphoxides by *Mortierella isabellina* NRRL 1757. The oxygen atom introduced during this enzymic oxidation is derived from the atmosphere and not from water. The rates of oxidation have been determined by uv analysis, and correlated with the Hammett $p$. sigma constants for the phenyl methyl sulphide series. The value of $\rho = -0.67$ so obtained is interpreted in terms of a mechanism of oxidation at sulphur involving an electrophilic attack on the sulphide sulphur by the enzymic activated iron–oxygen complex, followed by conversion of the resulting sulphur cation to sulphoxide.

HERBERT L. HOLLAND et IAN M. CARTER. Can. J. Chem. **60**, 2420 (1982).

On a oxydé une série de méthylthio-benzènes et -phénylméthanes substitués en sulphoxydes correspondants à l'aide de la *Mortierella isabellina* NRRL 1757. L'atome d'oxygène introduit lors de cette oxydation enzymatique provient de l'atmosphère et non de l'eau. On a déterminé les vitesses d'oxydation par l'analyse uv et on les a relié aux constantes sigma $p$ de Hammett, dans le cas des méthylthiobenzènes. On interprète la valeur de $\rho = -0{,}67$ ainsi obtenue en fonction d'un mécanisme d'oxydation au niveau du soufre impliquant une attaque électrophile sur le soufre du sulfure par un complexe fer-oxygène activé enzymatiquement, suivi de la transformation sur cation soufré résultant en sulphoxyde.

[Traduit par le journal]

The enzymic oxidation of sulphides to sulphoxides and sulphones can be efficiently carried out by enzymes from mammalian (1–3) or microbial (4–6) sources. Early work in this area (4–6) was concerned largely with the stereospecificity of sulphoxide formation and metabolism by fungi, whereas more recent work (2, 3, 7, 8) has centered on an investigation of the mechanism of the oxidative reaction when carried out by enzymes from mammalian sources.

May *et al.* (7) found that dopamine β-hydroxlase, a copper-containing mono-oxygenase, can perform sulphoxidation of aryl substituted phenyl alkyl sulphides (eq. [1]), and that with this enzyme the reaction proceeds at rates which indicate a ρ value of −3.6 in the conventional Hammett plot. This value differs considerably from that shown by the same enzyme for β hydroxylation of substituted dopamine derivatives (eq. [2]), where a value of −0.4 was reported (7). These values were interpreted by May *et al.* (7) in terms of a mechanism of enzymic sulphoxidation similar to that of hydrogen peroxide oxidation of sulphides, where a ρ value of −1.13 was observed (9). The large difference in ρ values (−3.6 vs. −1.13) was not commented upon. However, the enzymic ρ value was obtained using only halo substituted and unsubstituted thioanisole, and because of the small range of σ values concerned should be regarded as an approximate value. The mechanistic proposal of May (Scheme 1) involves nucleophilic attack by

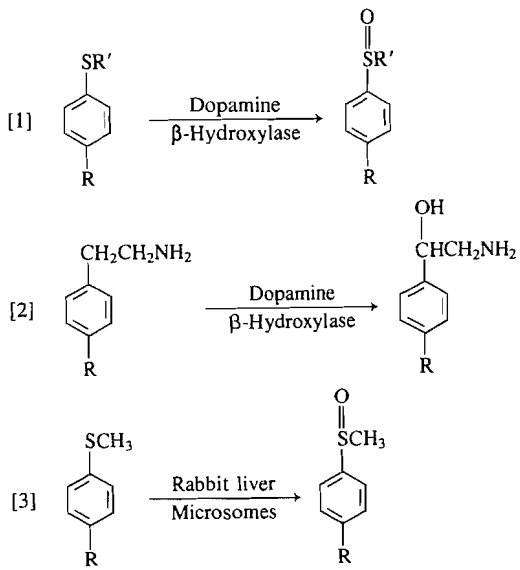


sulphur at an electron deficient activated oxygen intermediate. Hydroxylation, on the other hand, is proposed to proceed via neutral radical intermediates which would necessitate little charge separation in the transition state, a state of affairs consistent with the observed values.

In a parallel investigation, Oae and co-workers (2, 3, 8) have studied the sulphoxidation of substituted phenyl methyl sulphides by a cytochrome P-450 dependent enzyme preparation from rabbit liver (eq. [3]). Their kinetic data gave a $\rho^+$ value of −0.16; the low magnitude of this result, together with the results of model reactions with

[1]Author to whom correspondence may be addressed.

0008-4042/82/192420-06$01.00/0
©1982 National Research Council of Canada/Conseil national de recherches du Canada

Can. J. Chem. Downloaded from www.nrcresearchpress.com by 210.87.254.42 on 09/06/12
For personal use only.

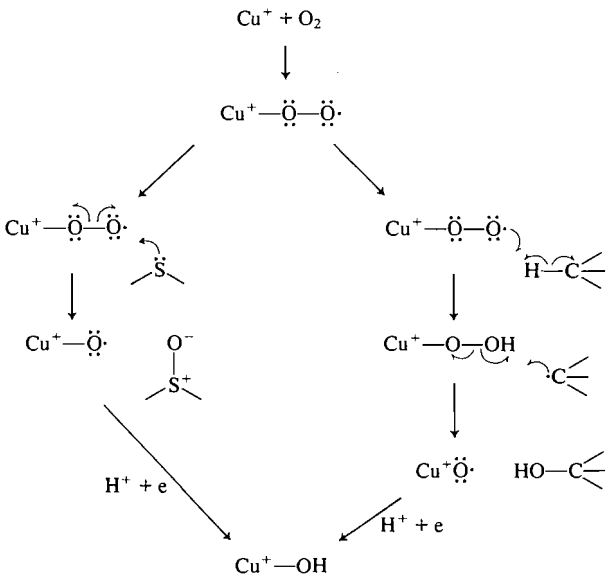

SCHEME 1. Proposed mechanism for sulphoxidation and hydroxylation by dopamine β-hydroxylase (7).

hydroxyl radical generating systems (10–12) and a study of the one-electron oxidation potentials of sulphides, led to the mechanistic proposal shown in Scheme 2, in which the rate determining step involves an activated iron–oxygen species. The correlation coefficients obtained in both the above studies are presented in Table 2.

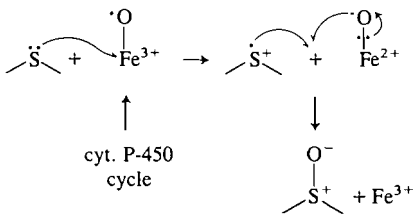

SCHEME 2. Proposed mechanism for sulphoxidation by rabbit liver microsomes (2, 3).

In the present study, we have investigated the sulphoxidation of a series of substituted methyl phenyl (**2**) and benzyl methyl (**4**) sulphides by the fungus *Mortierella isabellina* NRRL 1757 (eq. [4]). This fungus was chosen because it oxidizes sulphides of type **2** and **4** to the corresponding sulphoxides **3** and **5** in high yield and without any detectable further oxidation to sulphone (6); the formation of sulphone occurs to a greater or lesser extent with most of the other fungi reported to perform this reaction (13).

By performing incubations in $^{18}O$ labelled water and air (see Experimental) we have demonstrated that the enzyme catalysing the sulphoxidation of **2***a* shows one of the major characteristic properties of mono-oxygenases, in that the oxygen entering the substrate is derived directly from the atmosphere and not from the aqueous medium. However, other cofactor requirements for this reaction have not been investigated.

The rates of oxidation of sulphides **2** and **4** were determined by monitoring the release of sulphoxides **3** and **5** into the aqueous medium by ultraviolet spectral analysis. The uv data on which these analyses were based, together with the rates so obtained, are presented in Table 1. The following control experiments were performed. Firstly, a culture of fungus grown in the absence of sulphide was monitored over a 36 h period for the production of uv absorbing compounds which might interfere with the analysis: none were found. Secondly, calibration mixtures of sulphide **2***a* and sulphoxide **3***a* of varying composition were made up, and confirmed that the uv method gave reliable estimates of sulphoxide concentration. Thirdly,

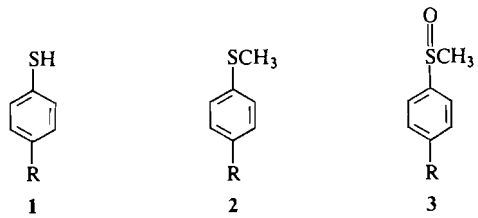

**1–3** *a* R = H
*b* R = $CH_3$
*c* R = $C_2H_5$
*d* R = F
*e* R = Cl
*f* R = Br
*g* R = $NO_2$
*h* R = $OCH_3$

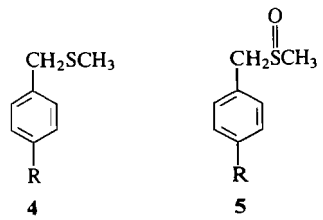

**4, 5** *a* R = H
*b* R = $CH_3$
*c* R = $NO_2$

confirmation of sulphoxide formation was obtained in all cases by both the isolation and characterization of sulphoxide from the incubation medium, and by comparison of the uv trace obtained at the termination of the kinetic runs with that of an authentic sample of sulphoxide. In no case was any

Can. J. Chem. Downloaded from www.nrcresearchpress.com by 210.87.254.42 on 09/06/12
For personal use only.

Can. J. Chem. Downloaded from www.nrcresearchpress.com by 210.87.254.42 on 09/06/12
For personal use only.

TABLE 1. Ultraviolet spectral data of sulphides **2** and **4** and sulphoxides **3** and **5**, and rate constants $K$ for the production of sulphoxides **3** and **5**

| Compound | $\lambda_{max}$ (nm) | log ε (nm) | $K$ (mol s$^{-1}$) | log $k/k_H$ |
|---|---|---|---|---|
| 2*a* | 254 | 4.0(254), 3.57(237) | | |
| 2*b* | 255 | 4.05(255), 3.65(236) | | |
| 2*c* | 257 | 4.04(257), 3.69(235) | | |
| 2*d* | 249 | 3.86(249), 3.51(230) | | |
| 2*e* | 260 | 4.16(260), 3.71(242) | | |
| 2*f* | 262 | 4.21(262), 3.79(243) | | |
| 2*g* | 340 | 4.10(340), 3.61(248) | | |
| 2*h* | 257 | 3.92(257), 3.78(243) | | |
| 4*a* | 247 | 2.89(247), 2.61(260) | | |
| 4*b* | 220 | 3.24(220), 2.79(232) | | |
| 4*c* | 267 | 3.92(267), 3.79(278) | | |
| 3*a* | 237 | 3.66(237), 3.35(254) | $1.37\pm0.05 \times 10^{-8}$ | 0 |
| 3*b* | 236 | 3.58(236), 3.30(255) | $6.1\pm0.1 \times 10^{-9}$ | −0.35 |
| 3*c* | 235 | 3.78(235), 3.27(257) | $6.5\pm0.1 \times 10^{-9}$ | −0.32 |
| 3*d* | 230 | 3.53(230), 3.27(249) | $1.20\pm0.05 \times 10^{-8}$ | −0.06 |
| 3*e* | 242 | 3.72(242), 3.27(260) | $1.0\pm0.05 \times 10^{-8}$ | −0.14 |
| 3*f* | 243 | 4.0(243), 3.50(262) | $3.2\pm0.1 \times 10^{-9}$ | −0.63 |
| 3*g* | 248 | 4.03(248), 2.71(340) | $3.9\pm0.1 \times 10^{-9}$ | −0.56 |
| 3*h* | 243 | 4.02(243), 3.59(257) | $1.9\pm0.1 \times 10^{-8}$ | +0.14 |
| 5*a* | 260 (sh) | 2.40(260), 2.50(247) | $2.2\pm0.2 \times 10^{-8}$ | |
| 5*b* | 232 | 3.83(232), 3.83(220) | $2.1\pm0.2 \times 10^{-8}$ | |
| 5*c* | 278 | 3.94(278), 3.94(267) | $2.1\pm0.2 \times 10^{-8}$ | |

evidence obtained for the formation of a uv absorbing compound other than the sulphoxide.

The complexity of biological reactions, especially in systems involving membrane bound enzymes and very poorly soluble substrates, as is the case in the present study, often makes the interpretation of correlation analyses such as ρ values extremely complex. In an attempt to demonstrate that the variation in rate of sulphoxide production reported herein can be directly correlated to the rate of sulphide oxidation, we have studied the oxidation of the corresponding benzyl methyl sulphides **4** by *M. isabellina*.

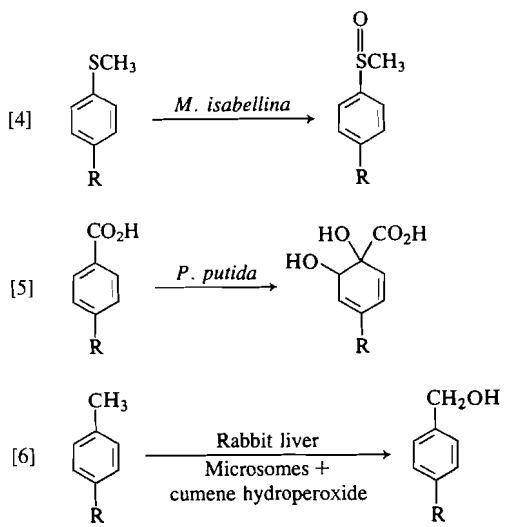


The common rate observed for the oxidation of the different benzyl sulphides **4***a*–**4***c* confirms that the variation in rate observed in the case of the phenyl sulphides **2** is probably attributable to the electronic effect of the *para* substitutent, and not to the difference in size and/or polar nature of the groups concerned. The assumption that the rate of release of sulphoxide into the aqueous medium can be correlated with the rate of oxidation at sulphur, and is not attributable to other factors (such as membrane transport or cofactor oxidation), is based on the following arguments.

Firstly, although the rate determining step in enzymic sulphoxidation is unknown, in cytochrome P-450 dependent mono-oxygenase reactions the rate determining step is the decomposition of the cytochrome P-450 oxygen–substrate complex to products (14); and secondly, externally added sulphoxide is not taken up by the fungal mycelia, suggesting that the degree of association between sulphoxide and cell membrane is low. We therefore conclude that sulphoxide, on its release from the active site, is rapidly passed through the cell wall into the aqueous medium. This conclusion is supported by control experiments in which extraction of both the medium and fungal mycelia at various times after addition of sulphide indicates that sulphoxide is present only in the medium, and that little if any sulphoxide remains in the mycelia.

The Hammett plot obtained for sulphoxidation of the phenyl methyl sulphides **2** is presented in Fig. 1. With the exception of data for **2***b* (R = $CH_3$), **2***c*

TABLE 2. Hammett ρ values obtained for oxidation at sulphur and hydroxylation at carbon

| Transformation | Oxidation at | Oxidizing species | ρ | Reference |
|---|---|---|---|---|
| eq. [1] | S | Dopamine β-hydroxylase | −3.6 | 7 |
| eq. [3] | S | Rabbit liver microsomes | −0.16* | 2 |
| eq. [4] | S | *M. isabellina* | −0.67 | Present work |
| eq. [7] | S | Rabbit liver microsomes | −0.2* | 37 |
| eq. [2] | C | Dopamine β-hydroxylase | −0.4 | 7 |
| eq. [5] | C | *Pseudomonas putida*† | −1.14 | 15 |
| eq. [6] | C | Rabbit liver microsomes/ cumene hydroperoxide | −1.6 | 16 |

*$\rho^+$ value.
†Source of a dioxygenase enzyme.

(R = $C_2H_5$), and **2***f* (R = Br), the points fall on a straight line with a value of −0.67 ($r$ = 0.994). The rates observed in our work, unlike those obtained by Oae and co-workers (2), do not correlate well with $\sigma^+$ values. The deviation of the rates for alkyl substituted sulphide oxidation from this value may reflect a change in the rate limiting step of the reaction, or a degree of hydrophobic interaction between substrate and fungal membrane not present for the other substrates involved. However, this phenomenon is not apparent for the oxidation of the corresponding benzyl sulphide. A comparison of this value with other ρ values for enzymic oxidation at sulphur (2, 3, 7, 8, 37) and carbon (7, 15, 16) is presented in Table 2. The reactions concerned are outlined in eqs. [1]–[7]. With the exception of eq. [1], all the enzymic processes have been proposed, on the basis of a low negative ρ value, to involve a mechanism in which there is not a high degree of electron demand

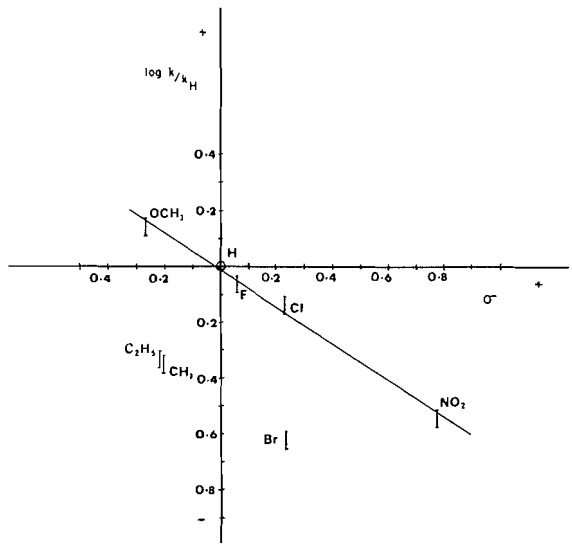


FIG. 1. The Hammett plot for sulphoxidation of phenyl methyl sulphides **2**.

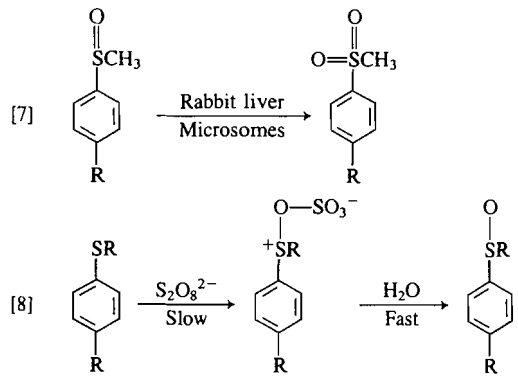


Reference 39

on the substrate in the transition state. In the case of hydroxylation at saturated carbon, a carbon radical intermediate has been proposed (16) (Scheme 3), whereas in the case of oxidation at sulphur, a radical cation species is the proposed intermediate (Scheme 2).

The ρ value of −0.67 obtained in the present study differs appreciably from those obtained using peroxide oxidants ($H_2O_2$, −1.13 (9), isoalloxazine hydroperoxide, −1.67 (38)), and that reported by May *et al.* (7) for dopamine β hydroxylase, −3.6 (but *vide supra* and ref. 38). However, it is close to the value reported by Srinivasan *et al.* (39) for oxidation by potassium persulphate (ρ = −0.87, $\rho^+$ = −0.56), in which the slow step is electrophilic attack at sulphide sulphur by the persulphate ion to form an intermediate sulphur cation (eq. [8]), and

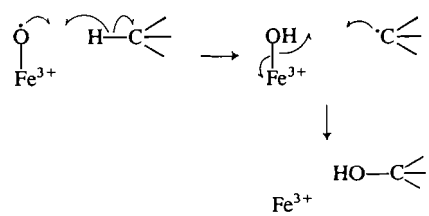


SCHEME 3. Proposed mechanism for hydroxylation at saturated carbon involving radical intermediates (16).

Can. J. Chem. Downloaded from www.nrcresearchpress.com by 210.87.254.42 on 09/06/12
For personal use only.

Can. J. Chem. Downloaded from www.nrcresearchpress.com by 210.87.254.42 on 09/06/12
For personal use only.

also the value observed for the oxidation of sulphoxides to sulphones by *m*-chloroperoxybenzoic acid (−0.54) (24). Our data therefore do not strongly support the one-electron oxidation route proposed for the corresponding mammalian enzymic reaction (2, 3, 37) (Scheme 2), but indicate a transition state in which there is greater electron demand on sulphur. This is consistent with an electrophilic attack by the activated iron–oxygen enzymic complex on sulphur, analogous to that shown in eq. [8].

The relevance of the sulphur oxidation mechanism to the mechanism of hydroxylation at saturated carbon remains to be established, however. The values of ρ obtained for the latter reaction (Table 2) may not reflect the value for a normal cytochrome P-450 dependent mono-oxygenase. Equation [2] involves a copper dependent enzyme, eq. [4] refers to a dioxygenase, and eq. [6] involves the use of cumene hydroperoxide rather than oxygen as the ultimate oxidizing species. It is therefore apparent that definitive data for the carbon hydroxylation reaction are needed so that a more meaningful comparison with sulphur oxidation can be made.

## Experimental

*Apparatus, materials, and methods*

Melting points were determined on a Kofler heating stage and are uncorrected. Infrared spectra were recorded with a Perkin–Elmer 237B spectrometer, and ultraviolet spectra with a Hitachi Perkin–Elmer 124 or Cary 14 spectrophotometer. Proton nmr spectra were obtained at 60 MHz with a Varian A-60 or Bruker WP-60, using $CDCl_3$ as solvent and TMS as internal standard, and $^{13}C$ nmr at 15.18 MHz with a Bruker WP-60, using $CDCl_3$ as solvent and TMS as internal standard. Mass spectra were obtained with an AEI MS 30 interfaced to a Kratos DS 55 data system: isotopic composition was determined by repeated data accumulation over the relevant ion region and application of the appropriate corrections for natural abundances; values are accurate to ± 0.5%. Column chromatography was performed on silica gel (60–200 mesh), and thin layer chromatography on Merck silica gel 60 F-254 (0–2 mm).

*Mortierella isabellina* NRRL 1757 was maintained on slopes composed of 4% malt agar.

*Preparation of substrates*

*p*-Toluenethiol (**1***b*), *p*-fluorobenzenethiol (**1***d*), *p*-chlorobenzenethiol (**1***e*), *p*-bromobenzenethiol (**1***f*), *p*-nitrobenzenethiol (**1***g*), thioanisole (**2***a*), and benzyl methyl sulfide (**4***a*) were commercial samples.

p-*Ethylbenzenethiol* (**1***c*) *and* p-*methoxybenzenethiol* (**1***h*)

These were prepared from the corresponding phenol by the method of Newman and Karnes (17), and gave satisfactory analytical (bp and spectral) data.

*Substituted thioanisoles;* **2**b–**2**h

These were made by alkylation of the corresponding thiophenols **1***b*–**1***h* by the method of Clark and Miller (18) and possessed physical properties similar to those reported (19, 20).

*Substituted phenyl methyl sulphoxides;* **3**a–**3**h

These were prepared from the corresponding sulphides **2** using sodium metaperiodate as oxidant (21), and exhibited spectral and physical properties consistent with those reported (22–27).

*Substituted benzyl methyl sulphides;* **4**b, **4**c

Compound **4***b* was prepared by reaction of the corresponding substituted benzyl chloride with methanethiol using the procedure described (28), and gave satisfactory analytical data (29, 30). *p*-Nitrobenzyl methyl sulphide (**4***c*) (31) was prepared from *p*-nitrobenzyl mercaptan (32) by alkylation with methyl iodide (18).

*Substituted benzyl methyl sulphoxides;* **5**a–**5**c

These were prepared from the corresponding sulphides **4** using sodium metaperiodate as oxidant (21), and exhibited spectral and physical properties consistent with those reported (29, 33, 34).

*Incubations with* Mortierella isabellina *NRRL 1757*

The fungus was grown in a medium composed of glucose (40 g), soybean meal (5 g), yeast extract (5 g), sodium chloride (5 g), and dibasic potassium phosphate (5 g) per litre of distilled water (35). One-litre Erlenmeyer flasks containing 150 mL of the above medium were sterilized, allowed to cool, and then inoculated from a growing slope of *M. isabellina*. The flasks were then placed on a 1 in. rotary shaker (150 rpm) at 25°C for 3 days. After this time, the fungus was removed by filtration and resuspended in distilled water (130 mL in each 1-L Erlenmeyer flask). For preparative studies, sulphide (100 mg in 1.15 mL ethanol) was added to each flask and incubation continued as above for 24–36 h. After this time, the fungus was removed by filtration and the filtrate extracted with chloroform. The extract was dried and evaporated, and then subjected to tlc and spectral analysis. Incubations of sulphides **2** and **4** gave the corresponding sulphoxides **3** and **5** as the only identifiable products.

*Measurement of kinetic data*

For kinetic studies, the mycelia from two flasks were combined and resuspended in 130 mL of distilled water in a single 1-L Erlenmeyer flask. Sulphide (100 mg in 1.15 mL ethanol) was added to each flask at time zero, and the flask returned to the rotary shaker at 25°C. Samples (1 mL) were removed by filtration at various time intervals, and diluted to 25 mL with spectroscopic grade methanol. This solution was then used for uv spectral analysis. The relative proportions of sulphide and sulphoxide were determined by the standard technique of two-component analysis (36), using the wavelengths and extinction coefficients listed in Table 1. The increase in sulphoxide concentration with time gave the rate constants reported for release of sulphoxide into the medium.

*Incubation in* $^{18}O$*-labelled water*

Fungus from one 1-L flask, grown as described above, was placed into 100 mL of $H_2{}^{18}O$ (1.5% enriched) in a 500 mL Erlenmeyer flask, and methyl phenyl sulphide (**2***a*) (100 mg) in ethanol (1 mL) added to the flask. The sulphoxide **3***a* isolated after a 36 h incubation was examined by mass spectrometry and found to contain no higher level of $^{18}O$ then a sample produced in a comparable experiment using unlabelled water.

*Incubation under an* $^{18}O$ *labelled atmosphere*

Fungus from one 1-L flask, grown as described above, was placed in a side arm attached to 500 mL Erlenmeyer flask. The main body of the flask contained 100 mL water and 100 mg methyl phenyl sulphide (**2***a*). Degassing was carried out by alternate freezing, pumping, and thawing. The flask was then filled with an $^{18}O$ enriched atmosphere (nominally 90% $^{18}O$), and sealed. The fungus was added from the side arm, and the sulphoxide **3***a* isolated after a 36 h incubation examined by mass spectrometry: isotopic content, $^{18}O$, 80%; $^{16}O$, 20%.

## Acknowledgements

Financial support was provided by the Natural Sciences and Engineering Research Council of Canada. We are grateful to T. Jones for help in obtaining spectra.

1. S. W. May and R. S. Phillips. J. Am. Chem. Soc. **102**, 5981 (1980).
2. Y. Watanabe, T. Iyanagi, and S. Oae. Tetrahedron Lett. **21**, 3685 (1980).
3. Y. Watanabe, T. Numata, T. Iyanagi, and S. Oae. Bull. Chem. Soc. Jpn. **54**, 1163 (1981).
4. B. J. Auret, D. R. Boyd, H. B. Henbest, and S. Ross. J. Chem. Soc. C, 2371 (1968).
5. B. J. Auret, D. R. Boyd, H. B. Henbest, C. G. Watson, K. Balenovic, V. Polak, V. Johanides, and S. Divjak. Phytochemistry, **13**, 64 (1974).
6. E. Abushanab, D. Reed, F. Suzuki, and C. J. Sih. Tetrahedron Lett. 3415 (1978).
7. S. W. May, R. S. Phillips, P. W. Mueller, and H. H. Herman. J. Biol. Chem. **256**, 8470 (1981).
8. Y. Watanabe, T. Iyanagi, and S. Oae. Tetrahedron Lett. **23**, 533 (1982).
9. G. Modena and L. Mariola. Gazz. Chim. Ital. **87**, 1306 (1957).
10. G. C. Gilbert, J. P. Larkin, and R. O. C. Norman. J. Chem. Soc. Perkin Trans. II, 1748 (1973).
11. M. Bonifacic, H. Möckel, D. Bahnemann, and K. D. Asmus. J. Chem. Soc. Perkin Trans. II, 675 (1975).
12. W. Bose, E. Longfelder, M. Saran, C. Fuchs, and C. Michel. Biochem. Biophys. Res. Commun. **70**, 81 (1976).
13. K. Kieslich. Microbial transformations of non-steroid cyclic compounds. G. Thieme, Stuttgart. 1976. p. 606.
14. Y. Ishimura. *In* cytochrome P-450. *Edited by* R. Sato and T. Omura. Academic Press, New York, NY. 1978. p. 221.
15. W. Reineke and H-J. Knackmuss. Biochim. Biophys. Acta, **542**, 415 (1978).
16. R. C. Blake and M. J. Coon. J. Biol. Chem. **256**, 12127 (1981).
17. M. S. Newman and H. A. Karnes. Org. Synth. **51**, 139 (1966).
18. J. H. Clark and J. M. Miller. J. Am. Chem. Soc. **99**, 498 (1977).
19. G. Jeminet and A. Kergomard. Bull. Soc. Chim. Fr. **9**, 3233 (1967); P. Cagniant. C. R. Acad. Sci. **226**, 1133 (1948).
20. G. W. Buchanan, C. Reyes-Zamora, and D. E. Clark. Can. J. Chem. **52**, 3895 (1974).
21. N. J. Leonard and C. R. Johnson. J. Org. Chem. **27**, 282 (1962).
22. D. Barnard, J. M. Fabian, and H. P. Kock. J. Chem. Soc. 2442 (1949).
23. G. Liandri, A. Mangini, and R. Passerini. J. Chem. Soc. 1386 (1957).
24. A. Cerniani and G. Modena. Gazz. Chim. Ital. **89**, 843 (1959).
25. R. S. Cooke and G. S. Hammond. J. Am. Chem. Soc. **92**, 2739 (1970).
26. R. W. Taft, E. Price, I. R. Fox, I. C. Lewis, K. K. Andersen, and G. T. Davis. J. Am. Chem. Soc. **85**, 3146 (1963).
27. G. Grandi, L. Benedetti, R. Andreoli, and G. G. Battistuzzi. J. Electroanal. Chem. Interfacial Electrochem. **54**, 221 (1974).
28. D. Landini and F. Rolla. Synthesis, 565 (1974).
29. I. D. Entwistle, R. A. W. Johnstone, and B. J. Millard. J. Chem. Soc. C, 302 (1967).
30. R. Mayer, S. Scheithauer, and D. Kunz. Chem. Ber. **99**, 1393 (1966).
31. H. Hellman and D. Eberle. Ann. **662**, 188 (1963).
32. K. Ari. Japan Pat. No. 69 25,763 (30 Oct. 1969); Chem. Abstr. **72**, 43135b (1970).
33. R. R. Fraser, Gurudata, R. N. Renaud, C. Reyes-Zamora, and R. B. Swingle. Can. J. Chem. **47**, 2767 (1969).
34. S. Wolfe and P. M. Kazmaier. Can. J. Chem. **57**, 2388 (1979).
35. J. Rosazza, P. Foss, M. Lemberger, and C. J. Sih. J. Pharm. Sci. **63**, 544 (1974).
36. D. M. Peters, J. M. Hayes, and G. M. Hieftje. A brief introduction to modern chemical analysis. W. B. Saunders, Philadelphia. 1976. p. 427.
37. Y. Watanabe, T. Iyanagi, and S. Oae. Tetrahedron Lett. **23**, 533 (1982).
38. A. Miller. Tetrahedron Lett. **23**, 753 (1982).
39. C. Srinivasan, P. Kuthalingam, and N. Arumugam. Can. J. Chem. **56**, 3043 (1978).

Can. J. Chem. Downloaded from www.nrcresearchpress.com by 210.87.254.42 on 09/06/12
For personal use only.

# Dihydropyridines in synthesis and biosynthesis. V.[1,2] Synthesis of pyridocarbazole alkaloids: olivacine and (±)-guatambuine

JAMES P. KUTNEY, MASAKI NODA, NORMAN G. LEWIS, BEATRICE MONTEIRO, DANUTA MOSTOWICZ, AND BRIAN R. WORTH

*Department of Chemistry, University of British Columbia, 2036 Main Mall, University Campus, Vancouver, B.C., Canada V6T 1Y6*

Received March 15, 1982

JAMES P. KUTNEY, MASAKI NODA, NORMAN G. LEWIS, BEATRICE MONTEIRO, DANUTA MOSTOWICZ, and BRIAN R. WORTH. Can. J. Chem. **60**, 2426 (1982).

A synthetic route to the pyridocarbazole alkaloids, olivacine and guatambuine is described. The crucial step in the synthesis utilizes tricarbonylchromium(0) complexes of a suitable dihydropyridine system and illustrates the application of such complexes for the preparation of such alkaloids.

JAMES P. KUTNEY, MASAKI NODA, NORMAN G. LEWIS, BEATRICE MONTEIRO, DANUTA MOSTOWICZ et BRIAN R. WORTH. Can. J. Chem. **60**, 2426 (1982).

On décrit une voie d'accès aux alcaloides pyridocarbazole, olivacine et guatambuine. L'étape fondamentale de la synthèse utilise les complexes tricarbonylchrome(0) d'un système dihydropyridine convenable et illustre l'application de ces complexes à la préparation de tels alcaloides.

[Traduit par le journal]

The pyridocarbazole alkaloids, including olivacine (**1**) and guatambuine (**2**), have received considerable interest due to their promising antitumor activity (3–5). The total synthesis of representatives of this family of alkaloids has been the subject of numerous studies (6–21). Several of the synthetic approaches reported employed cyclization of pyridyl-substituted indoles to generate the linear pyridocarbazole skeleton. However, the yields obtained have generally been low.

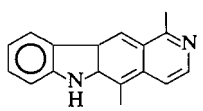

**1**

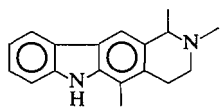

**2**

Our interest in the stabilization and use of very reactive dihydropyridine systems led us to investigate the utility of tricarbonylchromium(0) complexes (e.g. **8**) in the synthesis of natural products (22, 23). Here we envisaged the complex **8** to provide a nucleophilic center at the indole-3 position, for appropriate substitution employing a one-carbon electrophile, and subsequent cyclization to the pyridocarbazole skeleton utilizing the masked enamine (dihydropyridine) unit (Scheme 1).

Condensation of 1-benzenesulphonylindole (**4**), readily derived from indole (**3**), with 4-acetylpyridine gave **5** which was readily hydrolyzed to **6** (19, 24). Iodomethylation of **6** provided the corresponding pyridinium salt **7** in high yield. Reduction of **7** with sodium borohydride and protection of the resulting dihydropyridine, in the usual manner (22), afforded the tricarbonylchromium(0) complex **8** as red crystals in 56% overall yield. High resolution $^1$Hmr revealed two sets of resonances, indicating the product as a mixture of two diastereoisomers in the ratio of 2:1 (see Experimental). As expected, in the major isomer the methyl group (δ 1.44) on the chiral center is in the more stable configuration, that is, on the opposite side of the bulky tricarbonylchromium group. These methyl protons (δ 1.88) of the other epimer being affected significantly by the deshielding property of the tricarbonylchromium group resonated as substantially lower field.

Reaction of complex **8** with the Vilsmeier reagent, prepared from DMF and $POCl_3$, formed an intermediate which on direct treatment with pyridine afforded a mixture of yellow products **12** and **13** in high yield. Considerable efforts were expended in attempting to separate this mixture by various chromatographic methods. Eventually a portion was separated by careful silica gel column chromatography to give sufficient material for characterization of the two compounds. The less polar minor compound was assigned the structure **13** based on its spectral properties (C4-H, broad doublet at δ 8.22, $J$ = 8 Hz; C1-H, singlet at δ 9.14). Clearly structure **14** must possess two doublets for the corresponding C3- and C4-vinyl protons. The major product **12** was isolated as the phosphate salt. Formation of **12** from **8** can be rationalized according to Scheme 1 (viz. **8** → **9** → **10** → **11**). The

[1]For Part IV, see ref. 1.

[2]For a preliminary report of this work see ref. 2.

0008-4042/82/192426-05$01.00/0

©1982 National Research Council of Canada/Conseil national de recherches du Canada

Can. J. Chem. Downloaded from www.nrcresearchpress.com by 210.87.254.105 on 09/06/12
For personal use only.

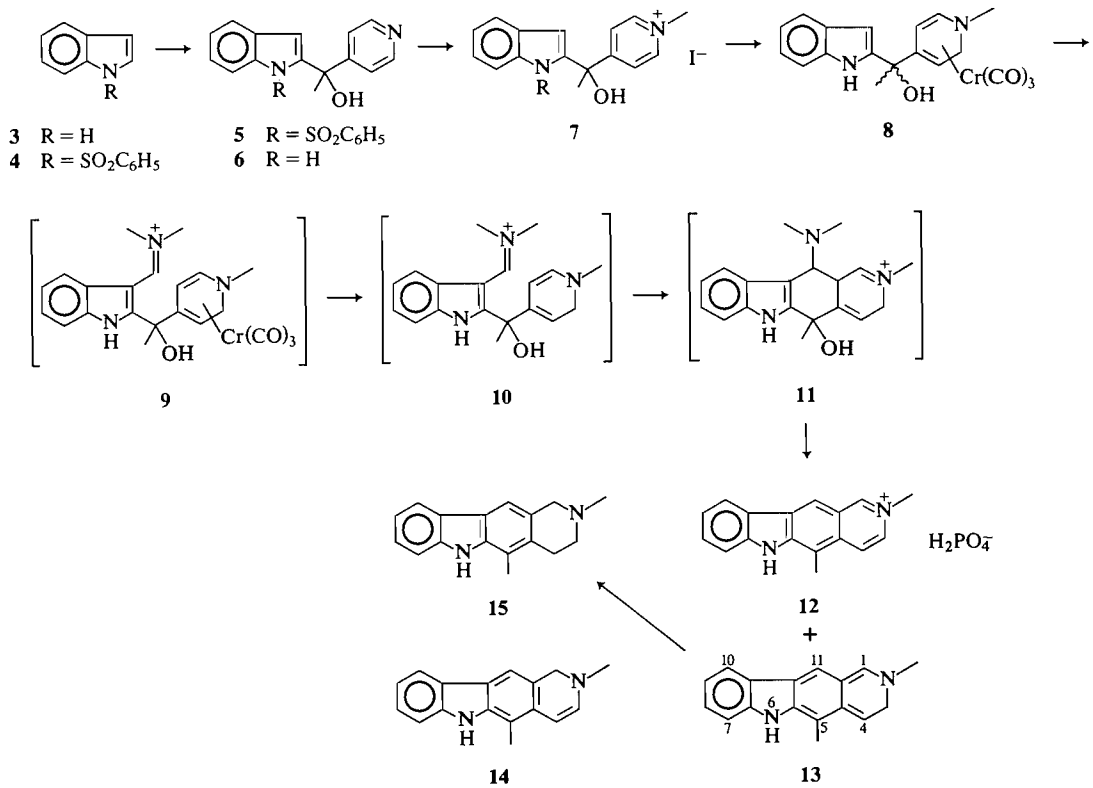


SCHEME 1

reduction product **13**, also isolated in this mixture, can be rationalized via a reductive process involving the dihydropyridine system generated from the complex **8**. However, direct evidence for this process is lacking. Reduction of the mixture **12** and **13** with sodium borohydride resulted in a single product 1-desmethylguatambuine (**15**) (89% yield from **8**). Similar reduction of a small sample of pure **13** also gave **15** as the product, thus supporting the structural assignment for **13**.

With the pyridocarbazole skeleton constructed (compounds **12** and **13**), subsequent elaboration of these intermediates to complete the syntheses of olivacine (**1**) and (±)-guatambuine (**2**) was achieved as shown in Scheme 2. Dehydrogenation of the mixture of **12** and **13** using Pd/C at 300°C afforded a mixture of unconverted **12** and the pyridine derivative **16**. The latter was easily separated from **12** which was also readily demethylated to **16** using triphenylphosphine in DMF or HMPA.

Reaction of **16** with methyllithium in dry THF and subsequent oxidation of the dihydropyridine intermediate with iodine provided olivacine (**1**) in 54% yield. Iodomethylation of **1** followed by reduction with sodium borohydride afforded (±)-guatambuine (**2**). Further confirmation of **1** and **2** was established by thin layer chromatography comparison with authentic samples.

These studies have provided a further demonstration of the utility of chromium tricarbonyl complexing in the stabilization of highly reactive dihydropyridine systems. This reactive dienamine generated *in situ* at an appropriate stage in the synthesis affords an interesting and efficient preparation of pyridocarbazole alkaloids.

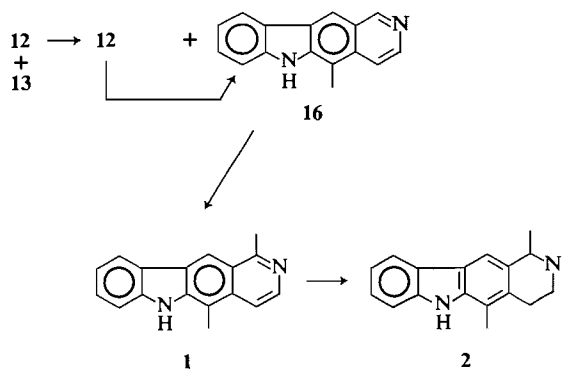


SCHEME 2

Can. J. Chem. Downloaded from www.nrcresearchpress.com by 210.87.254.105 on 09/06/12
For personal use only.

Can. J. Chem. Downloaded from www.nrcresearchpress.com by 210.87.254.105 on 09/06/12
For personal use only.

## Experimental

Melting points were determined on a Kofler block and are uncorrected. Ultraviolet (uv) spectra were recorded on a Cary 15 spectrophotometer in methanol solution. The wavelengths of absorption maxima are reported in nanometers (nm) with log ε in parentheses. Infrared (ir) spectra were measured on a Perkin–Elmer model 710 or 457 spectrophotometer as KBr disc. The absorption maxima are reported in wavenumbers ($cm^{-1}$), calibrated with respect to the absorption band of polystyrene at 1601 $cm^{-1}$. Proton magnetic resonance ($^1$Hmr) spectra were recorded on either a Varian HA- or XL-100 or a 270 MHz spectrometer with TMS as internal standard. The integrated peak areas, signal multiplicities, and proton assignments are given in parentheses. Low resolution mass spectra (ms) were determined on either an AEI MS-902 or an Atlas CH-4B spectrometer. High resolution mass spectra were measured on an AEI MS-902 instrument. Microanalyses were carried out by Mr. P. Borda of the Microanalytical Laboratory, University of British Columbia. Column chromatography utilized Merck silica gel 60 (70–230 mesh). Preparative and thin layer chromatography utilized Merck silica gel $GF_{254}$. As a matter of routine, all reagents and solvents were recrystallized or distilled before use.

*1-Benzenesulfonylindole (4)*

Potassium hydride (54 g, 22.1% (0.29 mol)) was added to a solution of anhydrous THF (150 mL) and HMPA (40 mL) at 0°C. To this mixture was added indole (23.4 g (0.2 mol)) in anhydrous THF (50 mL) over 30 min under nitrogen, which was then warmed to room temperature for 1 h. The mixture was cooled to 0°C and benzenesulfonyl chloride (41 g (0.23 mol)) was added dropwise. The mixture was stirred at room temperature for 20 h and poured into water and extracted with $CH_2Cl_2$. The organic extract was dried ($Na_2SO_4$) and concentrated. The precipitate was filtered to give **4** (35.5 g, 68%). Recrystallization of the product from $CH_2Cl_2$–hexane gave colourless needles, mp 78°C (lit. (23) mp 77.5–79°C).

*1-(1-Benzenesulfonyl indole-2-yl)-1-(4-pyridyl)-ethanol (5)*

*tert*-Butyllithium (40 mL (1.85 *M*), 75 mmol) was added dropwise to benzenesulfonylindole (**4**) (12.8 g, 50 mmol) in dry THF (270 mL) under nitrogen at 0°C. The reaction mixture was stirred at room temperature for 2 h, cooled to 0°C, and 4-acetylpyridine (13 mL, 118 mmol) was added dropwise. The resulting yellowish suspension was stirred overnight at room temperature and poured into water (200 mL) and extracted with $CH_2Cl_2$. The organic extracts were washed with water, dried ($Na_2SO_4$), and evaporated to give colourless crystals. The crystals were filtered and washed with acetone to give **5** (8.5 g, 48%). From the mother liquor crude **5** (2.5 g) was obtained. Recrystallization from acetone–$CHCl_3$ gave pure **5** (2.0 g, 17%), total yield 65%, mp 228–229°C (from $CHCl_3$) (lit. (23) mp. 229–230°C).

*Indole-2-yl-1-(4-pyridyl)-ethanol (6)*

The alcohol **5** (3 g, 7.96 mmol) was added to a 2 *M* methanol sodium hydroxide solution (500 mL) and heated for 4 h, cooled, and extracted with ether (600 mL). The organic extract was evaporated and recrystallized from $CHCl_3$ to give **6** (1.36 g, 72%), mp 218–221°C (lit. (23) mp 221°C); ir $\nu_{max}$: 3400, 3290, 1600; uv $\lambda_{max}$: 283 (3.86), 274 (3.92), 256 (3.95), 253 (3.92), 211 (4.53); $^1$Hmr (DMSO-$d_6$) δ: 1.88 (3H, s), 6.18 (1H, s, OH), 6.31 (1H, d, $J$ = 2 Hz, C3′-H), 7.40–6.80 (4H, m, ArH), 7.46 (2H, d, $J$ = 6 Hz, C3-H, C5-H), 8.49 (2H, d, $J$ = 6 Hz, C2-H, C6-H), 10.92 (1H, s, N*H*); ms *m/e*: 238 ($M^+$), 220, 205, 160. High resolution mass determination, calcd. for $C_{15}H_{14}N_2O$: 238.1106; found: 238.1123. *Anal.* calcd. for $C_{15}H_{14}N_2O$: C 75.63, H 5.88, N 11.76; found: C 75.55, H 5.70, N 11.95.

*Indole-2-yl-1-(4-pyridylmethiodide)-ethanol (7)*

The alcohol **6** (390 mg) was added to a solution of ethyl acetate (30 mL) and $CH_3I$ (2 mL). The suspension was heated at 50°C for 5 h. The resulting precipitate was removed by suction filtration to afford an amorphous powder **7** (554 mg, 89%), ir $\nu_{max}$: 3285, 1640; uv $\lambda_{max}$: 287 (3.63), 277 (3.85), 262 (4.06), 257 (4.07), 217 (4.70); $^1$Hmr (DMSO-$d_6$) δ: 1.98 (3H, s), 4.26 (3H, s, N—$CH_3$), 6.44 (1H, s, C3′-H), 6.72 (1H, s, O*H*), 7.56–6.82 (4H, m, ArH), 8.17 (2H, d, $J$ = 6.8 Hz, C3-H, C5-H), 8.93 (2H, d, $J$ = 6.8 Hz, C2-H, C6-H).

*The complexes 8*

$NaBH_4$ (5%) in ether (40 mL) and 2 *N* NaOH (15 mL) was added to the pyridinium salt **7** (570 mg, 1.5 mmol) in MeOH (15 mL) under nitrogen at 0°C. The two phase system was stirred vigorously for 50 min at 0°C. The aqueous layer was removed, and then the ether layer was washed briefly with 2 *N* NaOH (5 mL) and dried with anhydrous $Na_2SO_4$, $K_2CO_3$, and a small amount of KOH for 1 h at 0°C. The dried ether solution was added under nitrogen to a solution of trisacetonitriletricarbonyl chromium (1.5 equiv.) in dry ether at 0°C and the mixture was stirred for 3 h. The resulting red solution was filtered through previously degassed Florisil (20 g) with degassed dichloromethane under a nitrogen atmosphere to afford **8** as a mixture of diastereomers in the ratio of 2:1. Recrystallization of the red mixture with ether and petroleum ether (30–60°C) under nitrogen gave red needles (390 mg, 56%, mp 65–67°C (dec.)), which contained one mole equiv. of ether (by $^1$Hmr spectroscopy and microanalysis), ir $\nu_{max}$: 1941, 1866, 1821 $cm^{-1}$; uv ($Et_2O$)$\lambda_{max}$: 400 (3.61), 289 (3.87), 281 (3.93), 266 (3.96), 219 (4.53); $^1$Hmr ($C_6C_6$) δ: 1.14 (6H, t, $J$ = 7 Hz, methyl of ether) 1.30 (3H × 1/3, N—C*H*$_3$), 1.34 (3H × 2/3, N—C*H*$_3$), 1.44 (3H × 2/3, C*H*$_3$), 1.88 (3H × 1/3, C*H*$_3$), 1.99 (1H × 1/3, C6-H, bd, $J$ = 10 Hz), 2.09 (1H × 2/3, C6-H, bd, $J$ = 10 Hz), 2.56 (1H × 1/3, C6-H, bd, $J$ = 10 Hz), 2.68 (1H × 2/3, C6-H, bd, $J$ = 10 Hz), 2.62 (1H, OH, bs), 3.15 (1H, C5-H, bs), 3.31 (4H, q, $J$ = 7 Hz, methylene of ether), 4.34 (1H × 1/3, C2-H, bd, $J$ = 5 Hz), 4.45 (1H × 2/3, C2-H, bd, $J$ = 5 Hz), 5.61 (1H × 1/3, C3-H, dd, $J$ = 5 Hz, $J$ = 2 Hz), 5.84 (1H × 2/3, C3-H, dd, $J$ = 5 Hz, $J$ = 2 Hz), 6.14 (1H × 2/3, C3′-H, d, $J$ = 2 Hz), 6.38 (1H × 1/3, C3′-H, d, $J$ = 2 Hz), 7.25–7.35 (3H, C5′,6′,7′-H, m), 7.64–7.78 (1H, C4′-H, m), 8.28–8.56 (N*H*, bs); ms *m/e*: 390 ($M^+$), 376, 372, 362, 334, 320, 306, 288, 237 (100%). High resolution molecular weight determination, calcd. for $C_{19}H_{18}N_2O_4Cr$: 390.0701; found: 390.0704. *Anal.* calcd. for $C_{19}H_{18}N_2O_4Cr.C_4H_{10}O$: C 59.48, H 6.03, N 6.03; found: C 59.50, H 6.13, N 5.93.

*Formation of 12 and 13*

Vilsmeier reagent prepared from DMF (0.4 mL, 5.1 mmol), $POCl_3$ (0.24 mL, 2.6 mmol), and $CH_2Cl_2$ (0.32 mL) was added dropwise to a $CH_2Cl_2$ (5 mL) solution of the complex **8** (948 mg, 2.4 mmol) at −5°C under nitrogen. The mixture was stirred at 0°C for 2 h and then at room temperature for 20 min. After evaporation of the solvent, the residues were dissolved in pyridine (30 mL), and heated at 50–55°C for 5 h. Pyridine was removed and the resulting residue was purified by silica gel (30 g) column chromatography with $CH_2Cl_2$–MeOH (10:1) as eluant to afford a yellow mixture of **12** and **13** (727 mg, 91%, in ratio of ca. 7:3 by $^1$Hmr spectroscopy). This mixture was not readily resolved by various chromatographic methods. Eventually a portion (200 mg) was applied on a silica-gel column (30 g) and eluted carefully with $CH_2Cl_2$–MeOH (10:1). The less polar fractions contained mainly **13** which on recrystallization from ethyl acetate – MeOH gave **13** as yellow needles (40 mg), mp 312–315°C (dec.); ir $\nu_{max}$: 3127, 1660, 1620, 1604, 1595; uv $\lambda_{max}$: 378 (4.05), 312 (4.02), 304 (3.97), 282 (4.34), 235 (4.10); $^1$Hmr (DMSO-$d_6$) δ: 2.55 (3H, s, C*H*$_3$), 3.73 (3H, s, —NC*H*$_3$), 4.02 (2H, C2-H, bt, $J$ = 8 Hz), 7.2–7.8 (4H, C7, 10 – H, m), 8.22 (1H,

Can. J. Chem. Downloaded from www.nrcresearchpress.com by 210.87.254.105 on 09/06/12
For personal use only.

C4-H, d, $J$ = 8 Hz), 8.5 (1H, C11-H, s), 9.14 (1H, C1-H, s), 12.22 (1H, bs, N*H*); ms *m/e*: 250 ($M^+$ +2), 249 ($M^+$ + 1, 100%), 248 ($M^+$), 247, 246, 232, 231, 207, 206, 204. High resolution molecular weight determination, calcd. for $C_{17}H_{16}N_2$: 248.1315; found: 248.1299. More polar fractions containing **12** were combined and concentrated to give the product as yellow needles (140 mg) (from EtOAc–MeOH), mp 297–300°C (dec.); ir $\nu_{max}$: 3150, 1643, 1625, 1610, 1582; uv $\lambda_{max}$: 234 (4.59), 245 (4.51), 280 (4.56), 298 (4.88), 350 (3.89); $^1$Hmr (DMSO-$d_6$) δ: 2.94 (3H, s), 4.46 (3H, s), 7.39 (1H, t, $J$ = 7.5 Hz, C9-H), 7.7–7.8 (2H, m, C 7 & 8 – H), 8.4–8.6 (3H, m, C3 & 4-H, C10-H), 9.11 (1H, s, C11-H), 9.93 (1H, s, C1-H), 12.32 (1H, N*H*). *Anal.* calcd. for $C_{17}H_{15}N_2.H_2PO_4.H_2O$: C 56.36, H 5.29, N 7.73; found: C 56.76, H 5.07, N 7.59.

*Dehydrogenation of a mixture of **12** and **13***

A mixture of **12** and **13** (0.2 g) was mixed with 20% Pd/C (0.2 g) and heated under nitrogen at 300–320°C for 30 min. The black solid was extracted with hot MeOH and the solvent evaporated. The residues were separated by silica gel column chromatography with $CH_2Cl_2$–MeOH as eluant. Elution with $CH_2Cl_2$–MeOH (10:1) afforded **16** (19 mg, 9.5% from complex **8**) as colourless prisms, mp 270–276°C (dec.) ($CH_2Cl_2$–pet. ether) (lit. (16) mp 290–292°C (dec.)); ir $\nu_{max}$: 3120, 1632, 1618, 1595; uv $\lambda_{max}$: 222 (4.41), 236 (4.30), 263 (4.60), 272 (4.73), 282 (4.84), 293 (4.85), 325 (3.74); $^1$Hmr ($CDCl_3$) δ: 2.82 (3H, s), 7.90 (1H, d, $J$ = 6 Hz, C4-H), 8.26 (1H, d, $J$ = 7 Hz, C11-H), 8.54 (1H, d, $J$ = 6 Hz, C3-H), 8.59 (s, C11-H), 9.44 (s, C1-H), 8.2–8.3 (1H, bs, N*H*); ms *m/e*: 232 ($M^+$ 100%), 231, 229, 204, 203. High resolution molecular weight determination, calcd. for $C_{16}H_{12}N_2$: 232.1001; found: 232.0992. *Anal.* calcd. for $C_{16}H_{12}N_2$: C 82.73, H 5.21, N 12.06; found: C 82.40, H 5.11, N 12.31.

Elution with $CH_2Cl_2$–MeOH (5:1) provided unreacted **12** (130 mg).

*Demethylation of **12***

The salt **12** (50 mg) and triphenylphosphine (46 mg, 0.176 mmol) were dissolved in DMF (5 mL) and refluxed under nitrogen for 86 h. After evaporation of solvent, the mixture was separated by silica gel column chromatography to give **16** (18 mg, 54%) and unreacted **12** (23 mg, 46%).

Alternatively, **12** (50 mg) and triphenyl phosphine (46 mg) were dissolved in HMPA (2 mL) and heated under nitrogen at 185–190°C for 5 h. The solvent was removed under reduced pressure and the residue separated by silica gel column chromatography to give the crude product **16** which was suspended in water and then extracted with ether. Evaporation of the ether extracts gave pure **16** (15 mg, 45%).

*N-Methyl-5-methyl-1,2,3,4-tetrahydro-6H-pyrido[4,3-b]carbazole (**15**)*

$NaBH_4$ (excess) was added to a MeOH solution (1 mL) of the mixture of **12** and **13** (10 mg) at 0°C and stirred for 1 h. After evaporation of solvent the residue was taken up in water and extracted with $CH_2Cl_2$. Concentration of the organic extracts gave **15** (7.5 mg, 89% from complex **8**), mp 205–207°C (from ether); ir $\nu_{max}$: 3320, 1613; uv $\lambda_{max}$: 232 (4.62), 238 (4.71), 248 (4.56), 259 (4.40), 287 (4.11), 297 (4.32), 326 (3.66), 340 (3.53); $^1$Hmr (DMSO-$d_6$) δ: 2.52 (3H, s), 2.69 (2H, bs, C3-H), 2.89 (2H, bs, C3-H), 3.17 (1H, s, C1-H), 3.41 (1H, s, C1-H), 3.65 (3H, bs, N—C*H*$_3$), 7.09 (1H, t, $J$ = 7.5 Hz, C9-H), 7.33 (1H, t, $J$ = 7.5 Hz, C8-H), 7.44 (1H, d, $J$ = 8.5 Hz, C7-H), 7.60 (1H, s, C11-H), 7.98 (1H, d, $J$ = 8.5 Hz, C10-H), 10.90 (1H, bs, N*H*); ms *m/e*: 250 ($M^+$), 249 (100%), 233, 207, 191. High resolution molecular weight determination, calcd. for $C_{17}H_{18}N_2$: 250.1471; found: 250.1449. *Anal.* calcd. for $C_{17}H_{18}N_2$: C 80.92, H 7.19, N 11.10; found: C 81.28, H 7.17, N 11.19.

Reduction of **13** (5 mg) with $NaBH_4$ (8 mg) under similar conditions also resulted in a single product **15** (3 mg) with physical properties identical to those above.

*1-Methyl-5-methyl-6H-pyrido[4,3-b]carbazole, olivacine (**1**)*

$CH_3Li$ solution (1 *M*, 0.75 mL) was added to a solution of **16** (35 mg) in dry THF (2 mL) at 0°C under nitrogen. The mixture was stirred at room temperature for 30 min and then refluxed for another 1 h. MeOH was added to quench excess $CH_3Li$ and then $I_2$ (38 mg) was added. After stirring of the mixture for 30 min, the solvent was removed and the residue triturated with water. The product was collected and purified by silica gel column chromatography to give **1** (20 mg, 54%) as yellow prisms (from ether), mp 303–306°C (dec.) (lit. (5) mp 318–326°C (dec.)); ir $\nu_{max}$: 3120, 1635, 1615, 1600; uv $\lambda_{max}$: 218 (4.39), 235 (4.31), 265 (4.49), 273 (4.63), 283 (4.78), 289 (4.77), 303 (4.17), 324 (3.55); $^1$Hmr ($CDCl_3$) δ: 2.82 (3H, s), 3.13 (3H, s), 7.79 (1H, C4-H, d, $J$ = 6 Hz), 8.28 (1H, C10-H, d, $J$ = 7 Hz), 8.3–8.2 (1H, bs, N*H*), 8.42 (1H, C3-H, d, $J$ = 6 Hz), 8.78 (1H, s, C11-H); ms *m/e*: 247, 246 ($M^+$ 100%), 245, 231, 217, 204. High resolution molecular weight determination, calcd. for $C_{17}H_{14}N_2$: 246.1158; found: 246.1156. *Anal.* calcd. for $C_{17}H_{14}N_2.2/3\ H_2O$: C 79.07, H 5.94, N 10.85; found: C 79.38, H 6.20, N 10.13.

*1-Methyl-5-methyl-N-methyl-1,2,3,4-tetrahydropyrido[4,3-b]carbazole, (+)-gutambuine (**2**)*

Olivacine (**1**, 22 mg) and $CH_3I$ (excess) in MeOH (2 mL) were heated at 50°C for 5 h and then evaporated to dryness. The residue was dissolved in MeOH (3 mL) and $NaBH_4$ (excess) was added at 0°C and stirred for 1 h. After removal of solvent, the residue was quenched with water and extracted with $CH_2Cl_2$. The combined organic extract was purified by preparative tlc to give **2** (9 mg, 40%) as colourless needles, mp 247–250°C (from ether) (lit. (9) mp 249–252°C); ir $\nu_{max}$: 3120, 1616; uv $\lambda_{max}$: 216 (4.26), 232 (4.34), 277 (4.42), 247 (4.30), 258 (4.16), 285 (3.86), 296 (4.06), 325 (3.50), 348 (3.42); $^1$Hmr ($CDCl_3$) δ: 1.56 (3H, d, $J$ = 6 Hz), 2.40 (3H, s), 2.54 (3H, s), 3.88 (1H, q, C1-H), 7.74 (1H, s, C11-H), 8.05 (1H, d, $J$ = 8 Hz, C10-H), 7.80 (1H, bs, NH); ms *m/e*: 264 ($M^+$), 263, 249 (100%), 247. High resolution molecular weight determination, calcd. for $C_{18}H_{20}N_2$: 264.1628; found: 264.1617. *Anal.* calcd. for $C_{18}H_{20}N_2$: C 81.78, H 7.63, N 10.60; found: C81.25, H 7.52, N 10.96.

## Acknowledgements

Financial aid from the Natural Sciences and Engineering Research Council of Canada is gratefully acknowledged. We are grateful to Dr. Lewis S. L. Choi for helpful discussions and assistance.

1. J. P. KUTNEY, Y. KARTON, N. KAWAMURA, and B. R. WORTH. Can. J. Chem. **60**, 1269 (1982).
2. J. P. KUTNEY, M. NODA, N. G. LEWIS, B. MONTEIRO, D. MOSTOWICZ, and B. R. WORTH. Heterocycles, **16**, 1469 (1981).
3. A. AHOND, A. CAVE, T. A. CONNORS, L. K. DALTON, N. DAT-XUONG, M. HAYAT, F. LE GOFFIC, A. GOUYETTE, M. M. JANOT, C. KAN-FAN, G. MATHE, J. LE MEN, J. MIET, J. POISSON, P. POTIER, and T. SEVENET. Biomedicine, **21**, 101 (1974).
4. E. M. ACTA, O. P. CREWS, L. GOODMAN, and C. W. MOSHER. J. Med. Chem. **9**, 237 (1966).
5. N. DAT-XUONG, C. GOSS, C. PAOLETTI, and J. B. LE PECQ. C. R. Acad. Sci. **277**, 2289 (1973).
6. J. SCHMUTZ and H. WITTWER. Helv. Chim. Acta, **43**, 793 (1960).
7. M. SAINSBURY. Synthesis, 437 (1977).

8. D. S. GRIERSON and J. P. KUTNEY. Heterocycles, **3**, 171 (1975).
9. T. KAMETANI, Y. ICHIKAWA, T. SUZUKI, and K. FUKUMOTO. Heterocycles, **3**, 401 (1975); J. Chem. Soc. Perkin Trans. I, 2102 (1975).
10. R. BESSELIEVRE and H. P. HUSSON. Tetrahedron Lett. **22**, 1873 (1976).
11. F. A. HOCHSTEIN, G. A. IACOBUCCI, and R. B. WOODWARD. J. Am. Chem. Soc. **81**, 4434 (1959).
12. P. A. CRANWELL and J. E. SAXTON. J. Chem. Soc. 3482 (1966).
13. T. R. GOVINDACHARI, S. RAJAPPA, and V. SUDARSANAM. Indian J. Chem. **1**, 247 (1963).
14. R. N. STILLWELL. Ph.D. Thesis, Harvard University, 1964.
15. L. K. DALTON, S. DEMERAC, B. C. ELMES, J. W. LODER, J. M. SWAN, and T. TEITEI. Aust. J. Chem. **20**, 2715 (1967).
16. K. N. KILMINSTER and M. SAINSBURY. J. Chem. Soc. Perkin Trans. I, 2264 (1972).
17. A. AHOND, F. LE GOFFIC, and A. GOUYETTE. Tetrahedron, **29**, 3357 (1973).
18. N. M. HASAN and A. P. KOZIKOWSKI. J. Org. Chem. **42**, 2039 (1977).
19. R. BESSELIEVRE, C. THAL, H. P. HUSSON, and P. POTIER. J. Chem. Soc. Chem. Commun. **90** (1975).
20. S. J. MARTINEZ and J. A. JOULE. J. Chem. Soc. Chem. Commun. 818 (1976).
21. T. NAITO, N. IIDA, and I. NINOMIYA. J. Chem. Soc. Chem. Commun. 44 (1981).
22. J. P. KUTNEY, R. A. BADGER, W. R. CULLEN, R. GREENHOUSE, M. NODA, V. E. RIDAURA-SANZ, Y. H. SO, A. ZANAROTTI, and B. R. WORTH. Can. J. Chem. **57**, 300 (1979).
23. J. P. KUTNEY, T. C. W. MAK, D. MOSTOWICZ, J. TROTTER, and B. R. WORTH. Heterocycles, **12**, 1517 (1979).
24. H. F. RUSSELL and R. J. SUNDBERG. J. Org. Chem. **38**, 3324 (1973).

Can. J. Chem. Downloaded from www.nrcresearchpress.com by 210.87.254.105 on 09/06/12
For personal use only.

# Experimental chemical shift correlation maps from heteronuclear two-dimensional nuclear magnetic resonance spectroscopy. II: Carbon-13 and proton chemical shifts of α-D-glucopyranose oligomers[1]

GARETH A. MORRIS[2] AND LAURANCE D. HALL

*Department of Chemistry, University of British Columbia, Vancouver, B.C., Canada V6T 1W5*

Received July 11, 1980[3]

Can. J. Chem. Downloaded from www.nrcresearchpress.com by 210.87.254.42 on 09/06/12
For personal use only.

GARETH A. MORRIS and LAURANCE D. HALL. Can. J. Chem. **60**, 2431 (1982).

Double Fourier transform ("2D") nmr methods allow the simultaneous measurement of proton and carbon-13 chemical shifts for each directly bonded carbon–proton pair in a molecule. As well as greatly increasing the number of different resonances that may be distinguished in the spectra of complex systems, the measurement of correlated proton and carbon-13 shifts allows the otherwise inaccessible proton shifts to be determined, and facilitates the assignment of conventional proton and carbon-13 spectra. Results are presented for glucose, maltose, maltotriose, α-cyclodextrin, β-cyclodextrin, and dextran T-10; reassignments are proposed for the carbon-13 spectra of maltose and maltotriose.

GARETH A. MORRIS et LAURANCE D. HALL. Can. J. Chem. **60**, 2431 (1982).

Les méthodes de la rmn faisant appel à une transformation double de Fourier ("2D") permettent de mesurer simultanément les déplacements chimiques du proton et du carbone-13 pour chaque liaison directe carbone–proton d'une molécule. Tout en permettant d'augmenter considérablement le nombre de résonances différentes que l'on peut distinguer dans les spectres des systèmes complexes, la mesure des déplacements chimiques du proton et du carbone-13 liés permet de déterminer les déplacements chimiques autrement inaccessibles du proton et facilite l'identification des spectres conventionnels du proton et du carbone-13. On présente les résultats relatifs au glucose, au maltose, au maltotriose, à l'α-cyclodextrine, à la β-cyclodextrine et au dextran T-10. On propose une identification nouvelle des spectres du carbone-13 du maltose et du maltatriose.

[Traduit par le journal]

## Introduction

The proton nmr spectra of carbohydrates in aqueous solution are always complex, and generally the only resonances that may be assigned easily are those of the anomeric protons, shifted to low field by the combined effects of two neighbouring oxygen atoms. Under favourable conditions, the use of homonuclear double resonance techniques at high magnetic fields can yield reasonably complete assignments of the proton spectra of mono- and disaccharides, but such experiments are extremely time-consuming and are difficult to extend to larger oligosaccharides. In contrast, the proton decoupled carbon-13 spectra of even the most complex natural polysaccharides are well dispersed, the problem being to assign the individual resonances thus resolved.

The purpose of this paper, and of the preceding paper in this series (1),[4] is to illustrate some of the possibilities of the heteronuclear double Fourier transform ("2D") nmr experiments that have been developed in the past few years (2, 3). The particular technique that has been explored is 2D chemical shift correlation (3, 4), which allows the proton chemical shifts of all protons directly bonded to carbon-13 to be determined in a single double Fourier transform experiment. It is possible to determine such information from series of coherent off-resonance decoupling experiments (5–9), but this method is usually slow, difficult, and limited in accuracy. Under favourable conditions, a series of selective decoupling experiments might be expected to require about two orders of magnitude more time for data collection than a normal decoupled spectrum, and ought to yield a limiting accuracy on proton chemical shift values of about ± 0.1 ppm. In contrast, the 2D nmr experiments to be described require about ten times as long for data acquisition as a normal fully decoupled carbon-13 spectrum, and can give proton shifts that are accurate to better than 0.01 ppm.

In 2D nmr a set of free induction decays $\mathbf{S}(t_2)$ is acquired using a pulse sequence containing a variable delay $t_1$, which is incremented for successive decays until a complete matrix $\mathbf{S}(t_1, t_2)$ has been built up. This matrix describes the behaviour of the total nuclear signal as a function both of the time $t_2$ after excitation, and as a function of the delay $t_1$ within the exciting pulse sequence. When this matrix is subjected to a double Fourier transformation, once with respect to $t_2$ and once with

[1]For paper I in this series see ref. 1.

[2]Present address: Department of Chemistry, University of Manchester, Oxford Road, Manchester M13 9PL, England.

[3]Revision received May 25, 1982.

[4]Dr. A. DeBruyn has kindly pointed out a misprint in Table I of this paper: the C-4 proton chemical shift for α-D-galactopyranose should be 3.98 rather than 3.78 ppm.

0008-4042/82/192431-11$01.00/0

©1982 National Research Council of Canada/Conseil national de recherches du Canada

Can. J. Chem. Downloaded from www.nrcresearchpress.com by 210.87.254.42 on 09/06/12
For personal use only.

respect to $t_1$, the result is a two-dimensional spectrum $S(f_1, f_2)$ which describes signal strength as a function of two independent frequencies $f_1$ and $f_2$. Signals are dispersed along the $f_2$ axis according to their resonant frequency during acquisition of the free induction decays, and are dispersed in $f_1$ according to their apparent frequency of oscillation during the delays $t_1$. The pulse sequence is chosen so as to give each of the resonances in a system different frequencies during the two periods $t_1$ and $t_2$, so that their signals are dispersed differently in the two domains of the two-dimensional spectrum. The $f_2$ domain reflects signal behaviour during "real time", but since it is only the nuclear signal at the *end* of the delay $t_1$ which governs the form of the 2D spectrum and not the signals's behaviour *during* $t_1$, signal dispersion in $f_1$ can be made to depend on characteristic frequencies of a spin system that are not measurable from normal spectra. The general techniques and background of 2D nmr and many of the pulse sequences used are described in refs. 2 and 3.

The pulse sequence used for obtaining heteronuclear chemical shift correlation 2D spectra is shown in Fig. 1. Its purpose is to generate decoupled carbon-13 free induction decays in which each carbon signal has been modulated as a function of $t_1$ by the chemical shift frequency of any proton to which it is directly bonded. After double Fourier transformation of the matrix of free induction decays acquired using this pulse sequence, a 2D spectrum is obtained in which one signal appears for each directly bonded carbon–proton pair in a molecule. The $f_1$ and $f_2$ coordinates of these signals are simply the displacement of the proton chemical shift from the proton transmitter frequency and the displacement of the carbon-13 chemical shift from the carbon-13 transmitter respectively, so that for each decoupled carbon-13 signal the chemical shift of any proton bound to that carbon can be determined by simple inspection of the 2D spectrum. Since only one signal appears for each CH group, the dispersion as a function of both the proton and the carbon-13 chemical shift means that a great increase in resolving power is obtained over the conventional spectra of carbon-13 or protons. The mode of action of the pulse sequence of Fig. 1 is discussed in detail in ref. 1, which draws heavily on the work of Ernst and co-workers (10, 11) and of Bodenhausen, Freeman, and co-workers (3, 13–15).

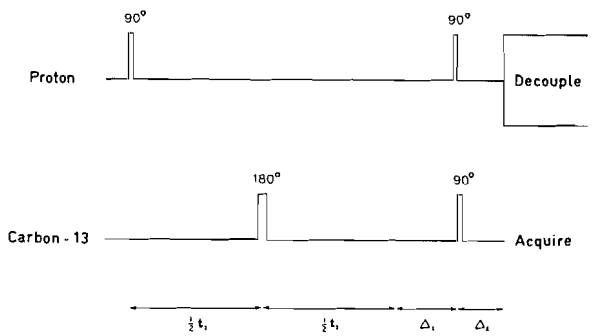


FIG. 1. Pulse sequence used for obtaining heteronuclear chemical shift correlation 2D spectra. For the experiments described $\Delta_1$ was 3 ms and $\Delta_2$ was 2.2 ms.

## Experimental

The instrument used in the work to be described was a home-built superconducting spectrometer operating at 270 MHz for protons and 67.9 MHz for carbon-13, based on a Bruker/Nicolet TT-23 console and an Oxford Instruments 6.3 T solenoid. Experiments were controlled and data processed with the standard NTCFT software package of a Nicolet 1180/293A' data system, equipped with a Diablo magnetic disc of 1.15 megabyte storage capacity. Time domain matrices $S(t_1, t_2)$ of 128 × 1024 or 2048 points were used, with spectral widths in the $f_1$ and $f_2$ domains of 1000 and 3500 Hz respectively.

Glucose (Fisher), maltose and maltotriose (Aldrich), and α-cyclodextrin (Eastman) were used as 10% solutions in $D_2O$ (Merck, Sharp and Dohme), two or three drops of *p*-dioxane (Fisher) in 3 mL of sample being used as internal reference for the proton and carbon-13 chemical shifts. β-cyclodextrin (Corn Products Co.) was used as a saturated solution in $D_2O$ at the experimental temperature of 22 ± 2°C. Dextran T-10 (Pharmacia) was used as a 10% solution in $D_2O$, with dioxane as internal reference; EDTA (ethylenediaminetetracetic acid sodium salt, G. Frederick Smith, approx. 10 mg in 3 mL) was added to scavenge paramagnetic ions which otherwise prevented resolution of the nonanomeric carbon-13 resonances. The chemical shifts of dioxane were taken as 3.76 ppm from internal TSP for protons, and 67.40 ppm from external TMS for carbon-13. Decoupled carbon-13 spectra for these samples required between 2 and 15 min for data acquisition, while the data for the 2D spectra took between 30 and 120 min to collect. A more detailed description of the experimental methods used is given in ref. 1.

## Results

The experimental chemical shift correlation 2D spectrum for α-cyclodextrin (**4**) is shown in Fig. 2. As expected, one peak appears for each CH group; in the methylene groups of dioxane and cyclodextrin C-6 both methylene protons have the same shift. The full stacked plot is time consuming to produce, and fails to make best use of the digitized information available, so for each correlation signal the appropriate cross-section through the $f_1$ domain has been obtained with enhanced digital resolution by zero-filling the appropriate interferogram prior to Fourier transformation. Since these traces summarize the information required from the 2D experiment, results from the series of compounds studied are presented in Figs. 3 to 7 as sets of $f_1$ traces, one for each carbon-13 signal in the 2D correlation spectrum.

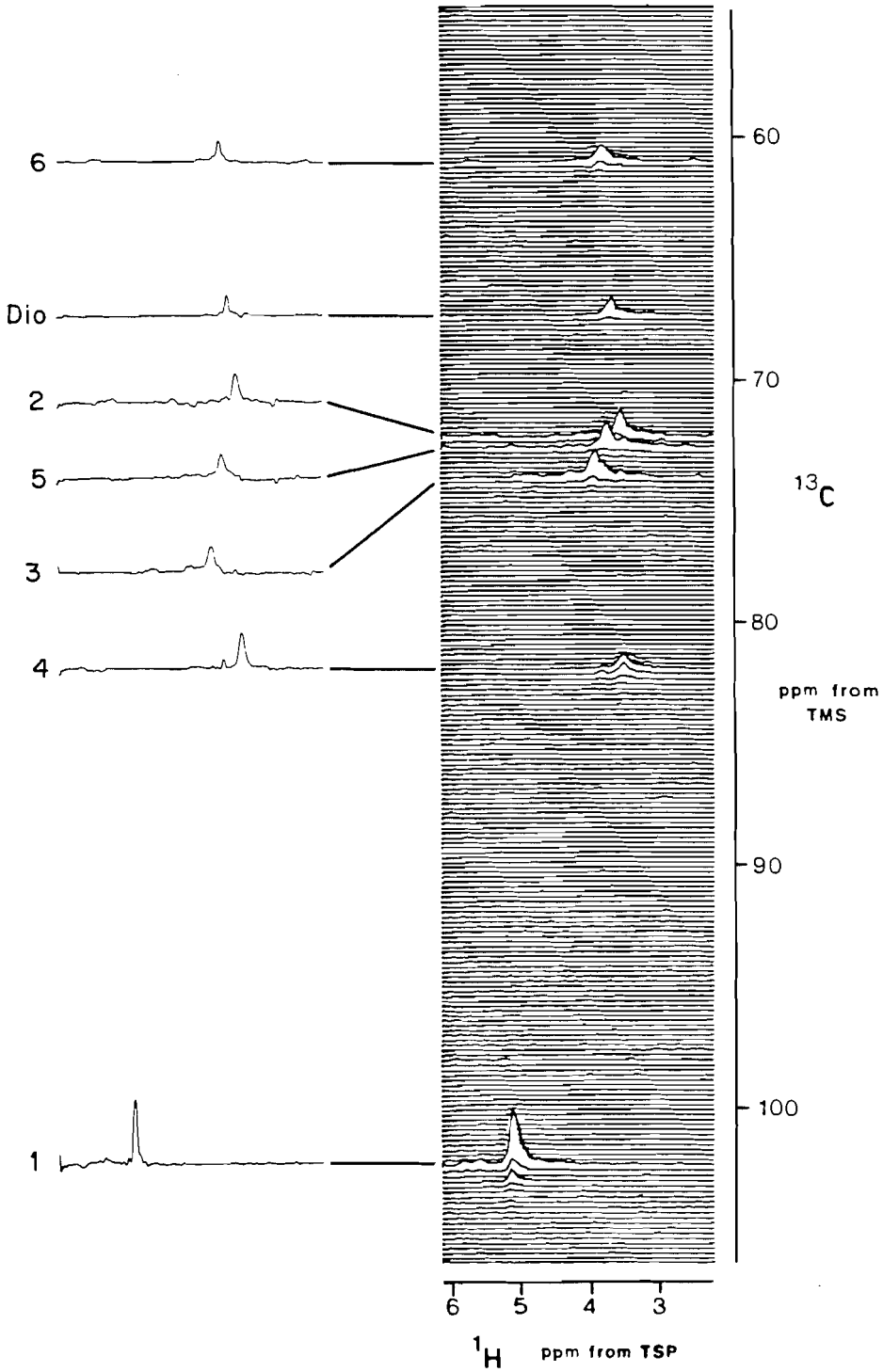


FIG. 2. Stacked plot of a chemical shift correlation 2D spectrum of α-cyclodextrin in $D_2O$, showing signal strength as a function of carbon-13 chemical shift (vertical or $f_2$ axis) and of proton chemical shift (horizontal or $f_1$ axis). Traces bearing signals have been recalculated using zero-filling to improve digital resolution, and are displayed to the left of the full 2D spectrum.

Can. J. Chem. Downloaded from www.nrcresearchpress.com by 210.87.254.42 on 09/06/12
For personal use only.

Can. J. Chem. Downloaded from www.nrcresearchpress.com by 210.87.254.42 on 09/06/12
For personal use only.

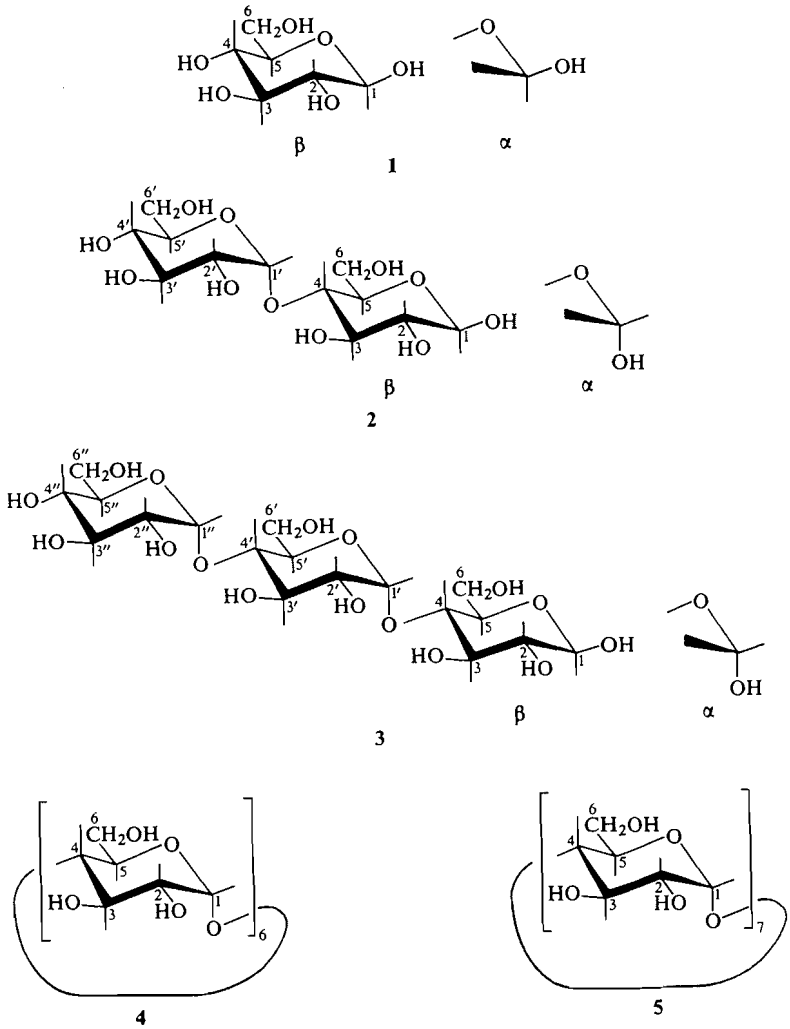


The proton and carbon-13 chemical shifts measured from the one- and two-dimensional spectra are listed in Table 1, together with the estimated standard deviations of the values given. Carbon-13 shifts were measured from the proton decoupled conventional spectrum, and proton shifts from cross-sections through the 2D spectrum. In the latter case interferograms were zero-filled three times before transformation (1); since the proton multiplet structure in $f_1$ is normally symmetrical about the proton chemical shift frequency, this procedure, coupled with parabolic interpolation to find the peak maximum, leads to a real improvement in the precision of measurement of the proton shift. Poor signal-to-noise ratio, overlap, and some types of strong coupling can degrade the accuracy of results, as indicated in Table 1. The sample of β-cyclodextrin (**5**) showed unusually wide carbon-13 lines, possibly due to contamination with paramagnetic ions, while the α-cyclodextrin spectra (Fig. 2) show the presence of a small amount of the β form. The traces shown in Figs. 3 to 7 are mostly presented in phase sensitive form, since this gives optimum precision, but, where carbon-13 signals overlap, the presence of strongly frequency-dependent phase shifts can necessitate the use of absolute-value display.

The assignments of the cyclodextrins and dextran T-10 in Table 1 are based on carbon-13 shifts reported by Colson, *et al.* (16), while those for glucose (**1**) follow Pfeffer *et al.* (17) and Dwek and co-workers (18). Several assignments have been proposed for maltose (**2**) and maltotriose (**3**) (16, 19, 20), but the experimental results obtained suggest a minor adjustment to the assignment of maltose, and a fairly radical reinterpretation of the

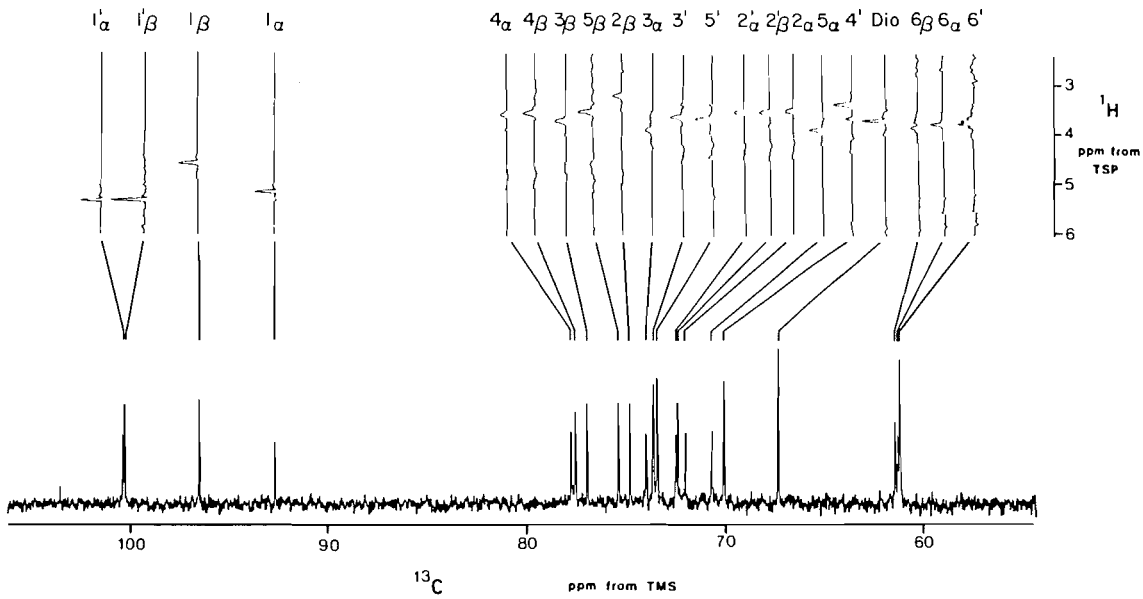


FIG. 3. Figures 3–7 show the experimental results for compounds **2** to **5** and for dextran T-10. The proton decoupled carbon-13 spectrum is shown horizontally, with traces through the $f_1$ domain of the 2D spectrum for each protonated carbon resonance shown displayed vertically. Figure 3 shows the experimental results for D-maltose (**2**).

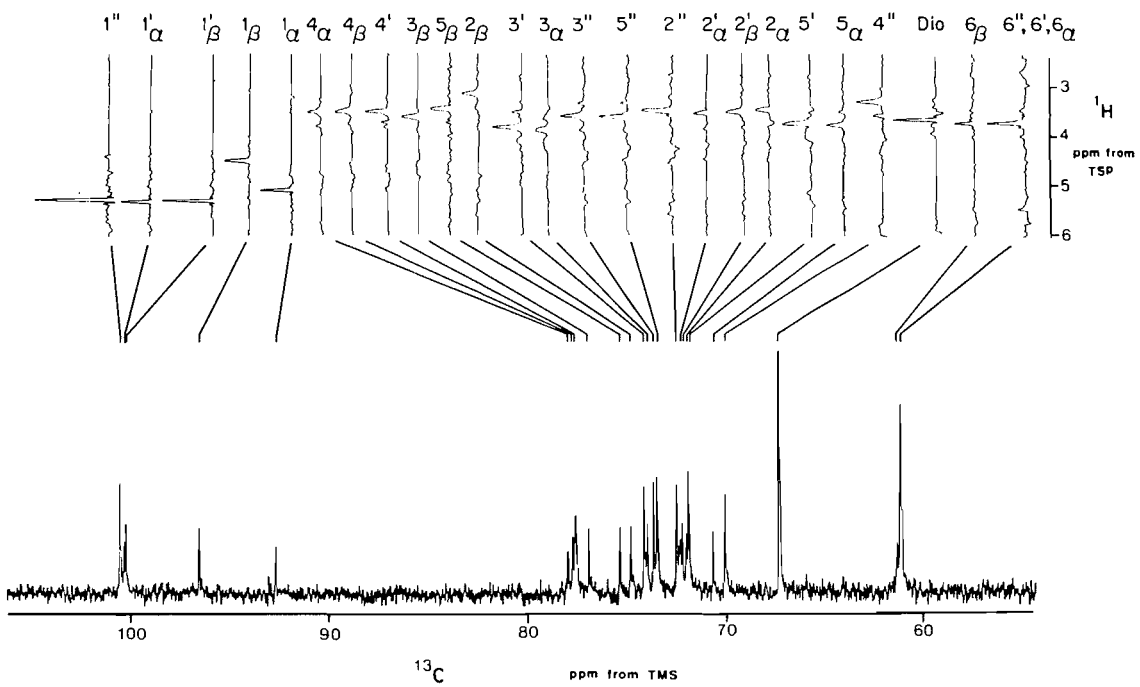


FIG. 4. Experimental results for D-maltotriose (**3**).

Can. J. Chem. Downloaded from www.nrcresearchpress.com by 210.87.254.42 on 09/06/12
For personal use only.

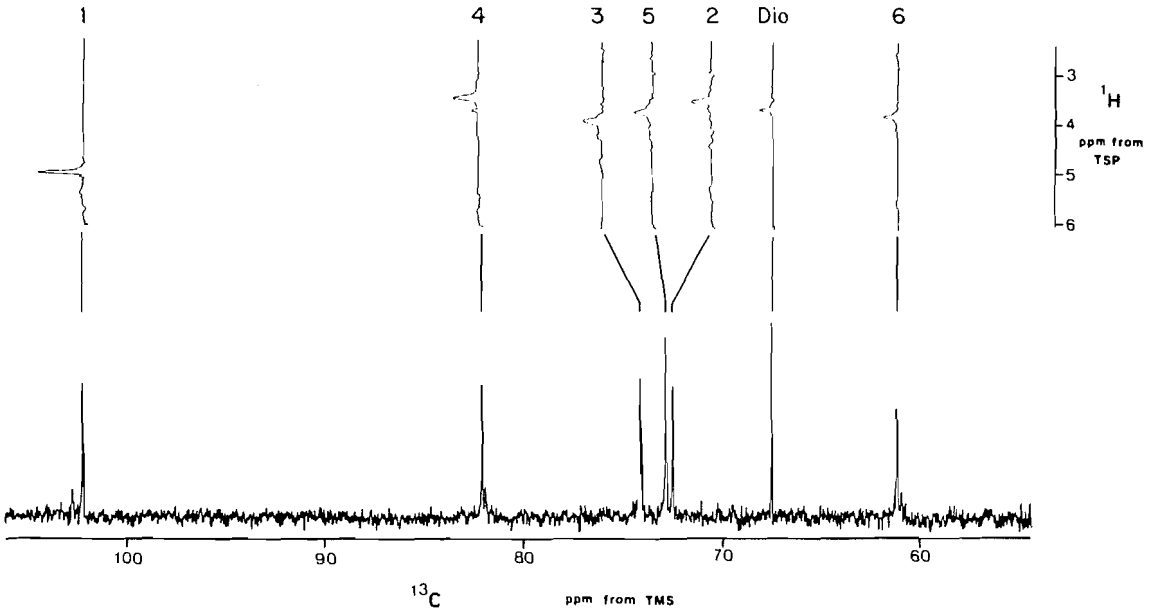


FIG. 5. Experimental results for α-cyclodextrin (**4**).

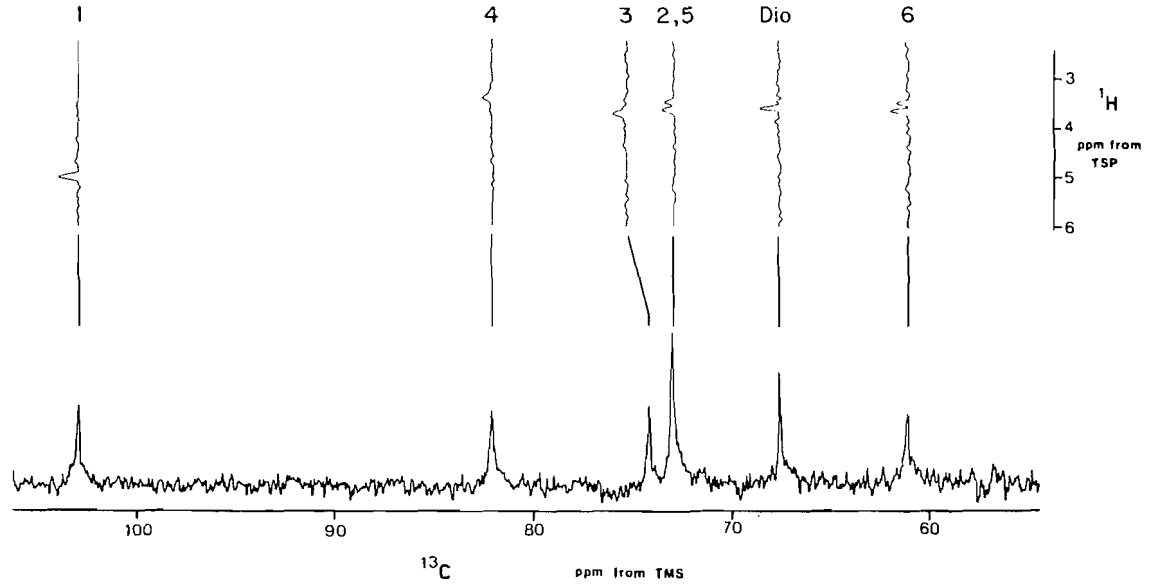


FIG. 6. Experimental results for β-cyclodextrin (**5**).

spectrum of maltotriose.[5] The correlated proton and carbon-13 shifts measured for maltose are, with the minor exception of a reversal of α and β C-6 carbon signals, consistent with all the assignments of Colson *et al.* (16) except those of the 2′ and 5′ resonances. Their assignment implies a reversal of the proton shifts of these two sites compared to those of α-glucose, in contradiction to the partial assignment of the maltose proton spectrum carried out using proton continuous wave INDOR at 300 MHz by DeBruyn *et al.* (21). The exchange of the C-2′ and C-5′ assignments is borne out by the splitting of the reassigned C-2′ carbon-13 resonance due to the anomeric equilibrium at the

[5]During the preparation of this paper Heyraud *et al.* (Biopolymers, **18**, 167 (1979)) have published carbon-13 assignments for maltose and maltotriose identical to those derived here; we thank a referee for drawing this paper to our attention.

Can. J. Chem. Downloaded from www.nrcresearchpress.com by 210.87.254.42 on 09/06/12
For personal use only.

Can. J. Chem. Downloaded from www.nrcresearchpress.com by 210.87.254.42 on 09/06/12
For personal use only.

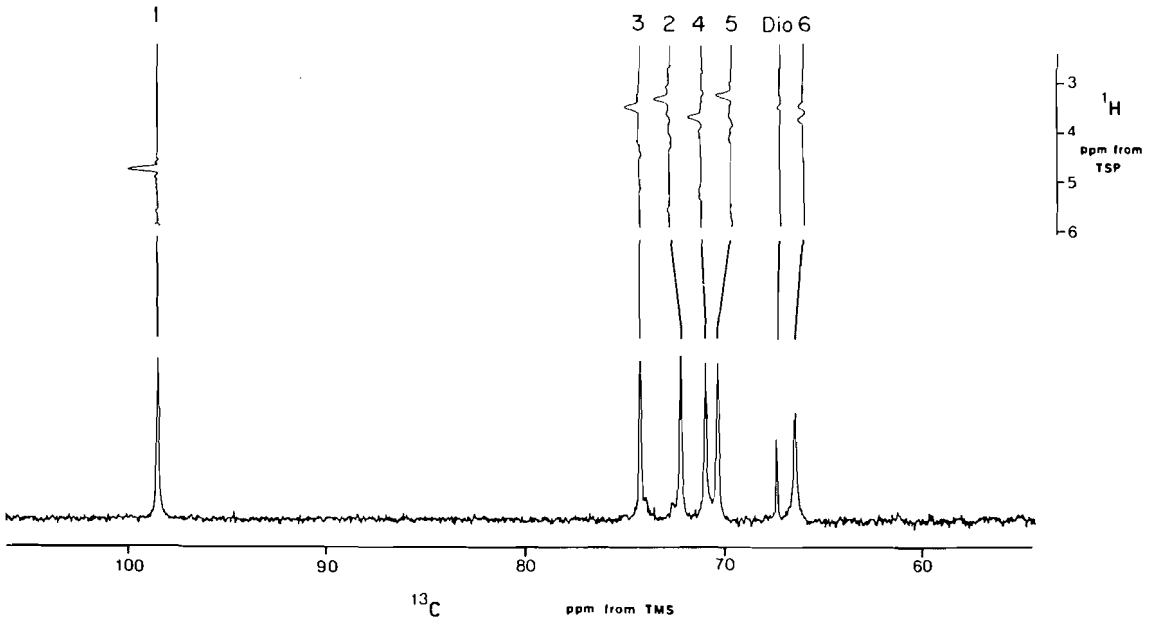


FIG. 7. Experimental results for dextran T-10.

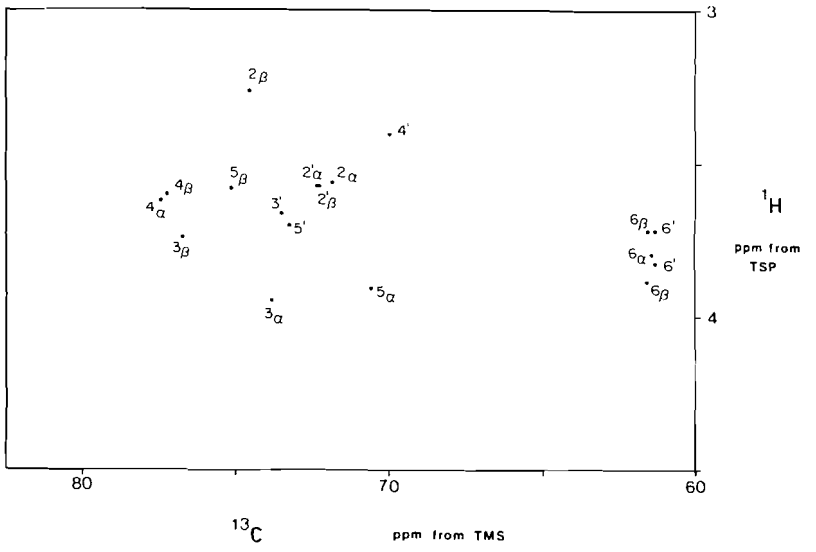


FIG. 8. Chemical shift correlation map for maltose (2).

reducing terminus of maltose, and is also consistent with approximate measurements of the carbon-13 deuterium induced isotope shifts for this system, made by the method of Pfeffer *et al.* (17).

The assignment of the carbon-13 spectrum of maltotriose is a particularly difficult problem to attack by conventional means, and affords a nice illustration of the advantages of using correlated proton and carbon-13 chemical shifts. Correlated shift data are most easily assessed when presented in the form of a shift map such as Fig. 8, for the proton and carbon-13 chemical shifts of maltose. The correlated shifts of maltose may be used as models for those of maltotriose, since the shifts of the reducing rings of maltose and maltotriose should be quite similar, as should those of the nonreducing termini of the two systems. Comparison between Fig. 8 and Fig. 9, the map for

Can. J. Chem. Downloaded from www.nrcresearchpress.com by 210.87.254.42 on 09/06/12
For personal use only.

TABLE 1. Carbon-13 and proton chemical shifts for **1** to **5**[a]

| | Carbon-13 ppm from external TMS | | | | | | Proton ppm from internal TSP | | | | | |
|---|---|---|---|---|---|---|---|---|---|---|---|---|
| | 1 | 2 | 3 | 4 | 5 | 6 | 1 | 2 | 3 | 4 | 5 | 6 |
| D-Glucose (1) | | | | | | | | | | | | |
| α-Glucopyranose | 92.89 | 72.28 | 73.58 | 70.44 | 72.24 | 61.40 | 5.24 | 3.52[b] | 3.71 | 3.40 | 3.82[b] | 3.83,3.69[b] |
| β-Glucopyranose | 96.71 | 74.94 | 76.74 | 70.40 | 76.56 | 61.57 | 4.64 | 3.25 | 3.46 | 3.40 | 3.47 | 3.86[b] |
| Maltose (2) | | | | | | | | | | | | |
| Glucopyranosyl | 100.47,100.38[c] | 72.58,72.49[c] | 73.68 | 70.15 | 73.49 | 61.32 | 5.39,5.40[c] | 3.59,3.59[c] | 3.68 | 3.42 | 3.72 | 3.85,3.74[b] |
| α-Glucopyranose | 92.71 | 72.11 | 74.05 | 77.75 | 70.77 | 61.41 | 5.23 | 3.58 | 3.97 | 3.64 | 3.93 | 3.82 |
| β-Glucopyranose | 96.59 | 74.82 | 77.02 | 77.53 | 75.38 | 61.56 | 4.65 | 3.20 | 3.76 | 3.62 | 3.60 | 3.74,3.91[c] |
| Maltotriose (3) | | | | | | | | | | | | |
| Terminal glucopyranosyl | 100.61 | 72.57 | 73.70 | 70.15 | 73.52 | 61.31 | 5.39 | 3.58 | 3.67 | 3.42 | 3.71 | 3.84 |
| Middle glucopyranosyl | 100.40,100.31[c] | 72.41,72.31[c] | 74.16 | 77.64 | 72.01 | 61.31 | 5.39,5.39[c] | 3.65,3.63[c] | 3.95 | 3.65 | 3.85 | 3.84 |
| α-Glucopyranose | 92.76 | 72.12 | 74.01 | 77.96 | 70.76 | 61.31 | 5.23 | 3.58 | 3.97 | 3.64 | 3.91 | 3.84 |
| β-Glucopyranose | 96.61 | 74.80 | 76.98 | 77.79 | 75.36 | 61.51 | 4.65 | 3.27 | 3.76 | 3.64 | 3.59 | 3.73,3.89[b] |
| α-Cyclodextrin (4) | 102.23 | 72.44 | 74.06 | 82.05 | 72.80 | 61.13 | 5.05 | 3.62 | 3.99 | 3.57 | 3.83 | 3.89 |
| β-Cyclodextrin (5) | 102.81[b] | 72.85[b] | 74.05[b] | 81.95[b] | 72.85[b] | 61.01[b] | 5.09 | 3.64 | 3.88 | 3.59 | 3.78 | 3.90 |
| Dextran T-10 (6) | 98.51 | 72.21 | 74.22 | 70.99 | 70.33 | 66.34 | 4.98 | 3.57 | 3.71 | 3.93 | 3.51 | 3.72,4.00 |

[a]Estimated standard deviation on shift values 0.01 ppm unless otherwise noted.
[b]Estimated standard deviation 0.02 ppm.
[c]α, β respectively.

maltotriose, confirms that the effects of interposing a third α-glucose ring between the nonreducing and the reducing termini are indeed sufficiently small that all of these resonances may be assigned by comparison. This leaves the problem of the central ring of maltotriose, in which the resonances have been perturbed by the formation of glycosidic linkages on both sides of the ring.

The effects of the formation of an α linkage on α-glucose may be deduced by comparison between the shifts of α-glucose and those of the nonreducing ring of maltose, and the effects of adding a glycosidic linkage to C-4 of α-glucose may be found from comparison with the α form of the reducing ring of maltose. To a first approximation these two sets of effects will be additive, so that the expected positions of the correlated shifts of the central ring resonances in Fig. 9 may be predicted by taking the vector sum of the α-glucose – maltose glucosyl and α-glucose – α-maltose glucose shift displacements, as illustrated in Fig. 10. The predicted shifts are more than accurate enough to complete the assignment of the maltotriose carbon-13 and proton resonances, the small deviations observed being attributable to the effects of conformation and concentration dependence.

In order to assess the viability of 2D shift correlation methods for polysaccharide systems, experiments were carried out on dextran T-10, a partially hydrolysed dextran linked predominantly $1\xrightarrow{\alpha}6$, with a mean molecular weight of about 10000. Even at room temperature, linewidths were sufficiently narrow for accurate proton and carbon-13 chemical shifts to be obtained, as can be seen from Fig. 7, provided that EDTA was added to prevent paramagnetic ions from binding to the dextran and broadening all the resonances. These results suggest that at higher sample temperatures it should be possible to study a wide range of polysaccharide systems by 2D shift correlation, with its attendant advantages of improved resolution and greater specificity for characterizing linkages and branching points.

As an illustration of the advantages of chemical shift correlation for the assignment of proton spectra, Fig. 11 a–c shows 270 MHz proton spectra of a 10% solution of maltotriose in $D_2O$. The inserts a and b show a 1 ppm region of the spectrum, with and without resolution enhancement, containing the 24 nonanomeric proton resonances. The assigned chemical shifts measured from the experimental data of Fig. 4 are given below trace b; few other methods are available for making such assignments.

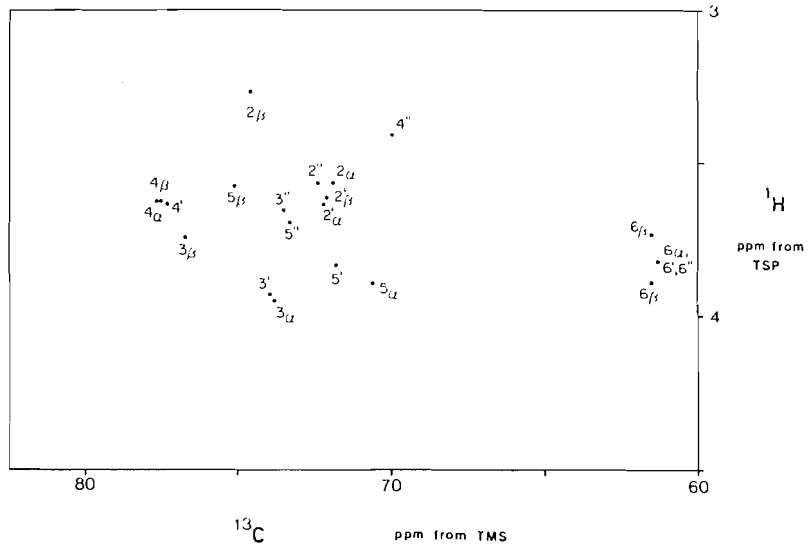


FIG. 9. Chemical shift correlation map for maltotriose (**3**).

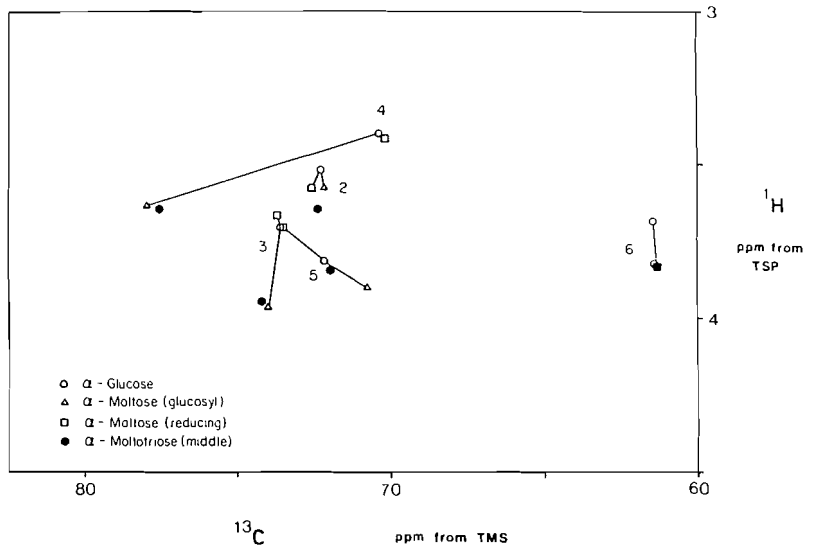


FIG. 10. Chemical shift correlation map for the α-glucose unit in free glucose, maltose, and maltotriose, showing the effect of glycosidic linkage formation.

## Discussion

The results reported here illustrate the utility of heteronuclear two-dimensional nmr spectroscopy in studying a range of typical carbohydrate systems. Proton chemical shifts have been reported for several systems which are very difficult to study by conventional proton nmr methods owing to the great complexity of their spectra, and in the case of maltotriose a new technique for the reliable assignment of complex carbon-13 spectra, particularly well suited to the assignment of oligomer spectra, has been illustrated. The advantages of heteronuclear 2D nmr methods in studying the structure of spectra are common to many other applications of 2D nmr: greatly improved resolution of signals, correlation of different nmr parameters, and measurement of parameters unobtainable by conventional methods. Chemical shift correlation by 2D nmr is a particularly attractive experiment since it is only about a factor of three less

Can. J. Chem. Downloaded from www.nrcresearchpress.com by 210.87.254.42 on 09/06/12
For personal use only.

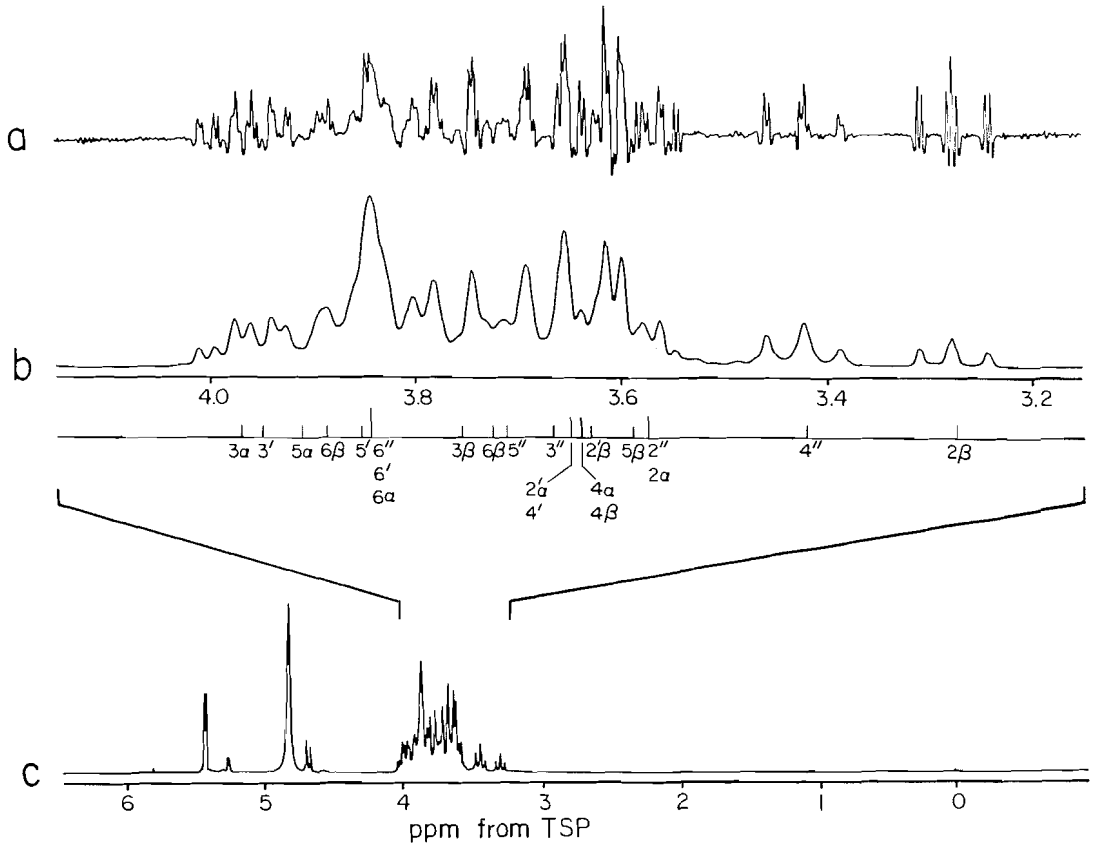


FIG. 11. 270 MHz proton spectra of a 10% solution of maltotriose in $D_2O$, showing (a) and (b) a 1 ppm section with and without resolution enhancement by "double exponential" multiplication of the form $\exp(+at)\exp(-bt^2)$, and (c) the full proton spectrum. Assignments shown under trace (b) indicate the chemical shifts for the 24 nonanomeric protons whose resonances fall in the expanded region, obtained for the experimental results of Fig. 5.

sensitive than normal decoupled carbon-13 nmr, as the carbon-13 signals observed actually originate with the stronger proton polarization, and the rate at which the pulse sequence of Fig. 1 may be repeated is governed not by the carbon-13 but by the proton spin-lattice relaxation time $T_1$. Thus a shift correlation experiment may be carried out in only a fraction of the time needed for a measurement of $T_1$, or for obtaining a set of coherently off-resonance decoupled carbon-13 spectra. The experiments described above were all carried out using instrumentation similar to many commercially available spectrometers; no modification of the software supplied with the computer system was necessary. The small price paid in increased complexity of the nmr experiment is more than offset by the advantages outlined above, which both facilitate the interpretation of nmr experiments on relatively simple systems and increase considerably the size and complexity of molecule that can be made to yield detailed proton and carbon-13 assignments.

## Acknowledgments

This work was supported by operating grants (A1905 to L.D.H.) from the Natural Sciences and Engineering Research Council of Canada and by an Izaak Walton Killam Postdoctoral Fellowship to G.A.M. Components for the spectrometer used were purchased with funds provided by the Chemistry Department and by the President's Emergency Research Equipment Fund, both of U.B.C. The expert assistance of Tom Markus in the construction of the spectrometer was warmly appreciated. A preprint of reference 15 was kindly supplied by Dr. G. Bodenhausen.

1. G. A. MORRIS and L. D. HALL. J. Am. Chem. Soc. **103**, 4703 (1981).
2. W. P. AUE, E. BARTHOLDI, and R. R. ERNST. J. Chem. Phys. **64**, 2229 (1976).
3. R. FREEMAN and G. A. MORRIS. Bull. Magn. Reson. **1**, 5 (1979).
4. R. FREEMAN and G. A. MORRIS. J. Chem. Soc. Chem. Commun. 684 (1978).
5. R. FREEMAN and H. D. W. HILL. J. Chem. Phys. **54**, 3367 (1971).

Can. J. Chem. Downloaded from www.nrcresearchpress.com by 210.87.254.42 on 09/06/12
For personal use only.

6. M. TANABE, T. HAMASAKI, D. THOMAS, and L. F. JOHNSON. J. Am. Chem. Soc. **93**, 273 (1971).
7. B. BIRDSALL, N. J. M. BIRDSALL, and J. FEENEY. J. Chem. Soc. Chem. Commun. 316 (1972).
8. J. C. MACDONALD and M. MAZUREK. J. Magn. Reson. **28**, 181 (1977).
9. F. W. WEHRLI and T. WIRTHLIN. Interpretation of carbon-13 NMR spectra. Heyden, London. 1976.
10. A. A. MAUDSLEY, A. KUMAR, and R. R. ERNST. J. Magn. Reson. **28**, 436 (1977).
11. A. A. MAUDSLEY and R. R. ERNST. Chem. Phys. Lett. **50**, 368 (1977).
12. G. BODENHAUSEN and R. FREEMAN. J. Magn. Reson. **28**, 471 (1977).
13. G. BODENHAUSEN and R. FREEMAN. J. Am. Chem. Soc. **100**, 320 (1978).
14. G. BODENHAUSEN and P. H. BOLTON. J. Am. Chem. Soc. **101**, 1080 (1979).
15. G. BODENHAUSEN and P. H. BOLTON. J. Magn. Reson. **39**, 399 (1980).
16. P. COLSON, H. J. JENNINGS, and I. C. P. SMITH. J. Am. Chem. Soc. **96**, 8081 (1974); P. COLSON, K. N. SLESSOR, H. J. JENNINGS, and I. C. P. SMITH. Can. J. Chem. **53**, 1032 (1975).
17. P. E. PFEFFER, K. M. VALENTINE, and F. W. PARRISH. J. Am. Chem. Soc. **101**, 1265 (1979).
18. S. J. PERKINS, L. N. JOHNSON, D. C. PHILLIPS, and R. A. DWEK. Carbohydr. Res. **59**, 19 (1977).
19. D. E. DORMAN and J. D. ROBERTS. J. Am. Chem. Soc. **93**, 4463 (1971).
20. T. USUI, N. YAMAOKA, K. MATSUDA, K. TUZIMARA, H. SUGIYAMA, and S. SETO. J. Chem. Soc. Perkin Trans. I, 2425 (1973).
21. A. DEBRUYN, M. ANTEUNIS, and G. VERHEGGE. Bull. Soc. Chim. Belg. **84**, 721 (1975).

Can. J. Chem. Downloaded from www.nrcresearchpress.com by 210.87.254.42 on 09/06/12
For personal use only.

# One-electron photooxidation of carbazole in the presence of carbon tetrachloride. Part II. Carbon tetrachloride as a reaction medium. Use of ammonia after irradiation and during irradiation

BOGUMIL ZELENT[1] AND GILLES DUROCHER

*Département de Chimie, Université de Montréal, C.P. 6210, Succ. A, Montréal (Qué.), Canada H3C 3V1*

Received March 11, 1982

BOGUMIL ZELENT and GILLES DUROCHER. Can. J. Chem. **60**, 2442 (1982).

In part I of this series of papers we proposed the mechanism of electron transfer as the primary photochemical reaction in the carbazole – carbon tetrachloride system along with a secondary photochemical reaction initiated by transformations of the radical cation of carbazole in the solvent cage resulting in intermediates:

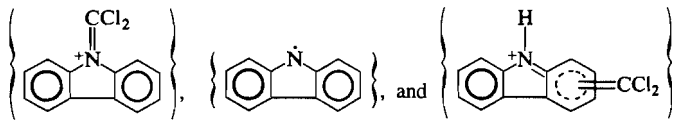

α β $\gamma_i$($i$ = 1, 2, 3, or 4)

In this paper we discuss the influence of ammonia, used *after* and *during* irradiation, on the mechanism of secondary transformation and the formation of thermodynamically stable products in the system studied. Such compounds as *N*-cyanocarbazole, 1-cyanocarbazole, and 3-cyanocarbazole have been formed as the main products during neutralization of the photolyte solution by ammonia gas. The mechanism of formation of these compounds has been explained by the chemical reaction of ammonia with cations α and $\gamma_i$. If ammonia is present in the solution of carbazole in $CCl_4$ during irradiation, such products as *N*,*N*′-dicarbazyl and *N*-cyanocarbazole are mainly formed along with 3-(*N*-carbazyl)carbazole, 3,9-di-(*N*-carbazyl)carbazole, and *N*-cyano-3-(*N*-carbazyl)carbazole. In such a case, reactions of radicals β are the determining factors in the secondary photochemical transformations. Radicals β are formed by the reaction involving ammonia with radical cations of carbazole. All the results in this paper have been discussed taking under consideration the influence of the reaction media on the mechanism of photochemical transformation of carbazole.

BOGUMIL ZELENT et GILLES DUROCHER. Can. J. Chem. **60**, 2442 (1982).

Dans la première partie de cette série d'articles nous avons suggéré que le mécanisme photochimique primaire lors de la réaction du carbazole et du tétrachlorure de carbone en était un de transfert électronique. La réaction photochimique secondaire consiste en la transformation du radical cation du carbazole dans la cage du solvant pour donner les intermédiaires suivants:

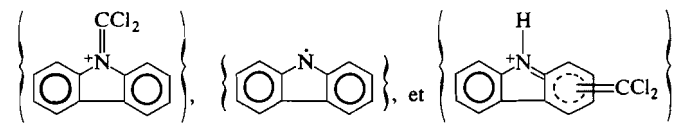

α β $\gamma_i$($i$ = 1, 2, 3, ou 4)

Dans cet article, nous discuterons de l'influence de l'ammoniac utilisé *après* et *avant* l'irradiation, sur le mécanisme secondaire de transformation et de formation de photoproduits thermodynamiquement stables. Lorsque l'ammoniac est ajouté après l'irradiation, le cyano-*N* carbazole, le cyano-1 carbazole et le cyano-3 carbazole ont été surtout obtenus. Ce résultat s'explique par la réaction de l'ammoniac avec les cations α et $\gamma_i$. Si au contraire, l'ammoniac est présent dans la solution du carbazole dans le $CCl_4$ au cours de l'irradiation, les produits suivants sont obtenus avec un bon rendement: dicarbazyl-*N*,*N*′ et cyano-*N* carbazole. Les produits suivants sont également obtenus: (carbazyl-*N*)-3 carbazole, di-(carbazyl-*N*)-3,9 carbazole et cyano-*N*(carbazyl-*N*)-3 carbazole. Les radicaux β sont alors impliqués dans la transformation photochimique. Ces radicaux β sont produits suite à la réaction de l'ammoniac avec les radicaux cations du carbazole. Tous les résultats sont discutés en tenant compte de l'influence du milieu réactionnel sur le mécanisme de la transformation photochimique du carbazole.

## Introduction

Among various halocarbons, carbon tetrachloride is most frequently used as a fluorescence quencher of different aromatic molecules (1–8). Studies of the mechanism of fluorescence quenching by halocarbons focused the attention of researchers upon the possibilities of photochemical reaction in the electron donor molecule – $CCl_4$ system. Therefore $CCl_4$ became used as the medi-

[1]On leave from the Department of Chemistry, University of Gdańsk, 80-952 Gdańsk, Poland.

0008-4042/82/192442-09$01.00/0

©1982 National Research Council of Canada/Conseil national de recherches du Canada

Can. J. Chem. Downloaded from www.nrcresearchpress.com by 210.87.254.40 on 09/06/12
For personal use only.

TABLE 1. Photochemical reaction products of carbazole in the presence of $CCl_4$

| No. | Compound | Reaction medium | |
|---|---|---|---|
| | | $CCl_4(NH_3)$ | $CCl_4$–$NH_3$ |
| **C** | Carbazole | s† | s |
| **1** | Hexachloroethane | b | b |
| **2** | *N*-Trichloroethylenecarbazole | b | |
| **3** | 1-Chlorocarbazole | b | b |
| **22** | 3-Chlorocarbazole | b | b |
| **23** | N,N'-Dicarbazyl | | a |
| **24** | 3,9-Di-(*N*-carbazyl)carbazole | | b |
| **25** | *N*-Cyanocarbazole | a | a |
| **26** | *N*-Cyano-3-(*N*-carbazyl)carbazole* | | b |
| **27** | 3-(*N*-Carbazyl)carbazole | | b |
| **28** | 1-Cyanocarbazole | a | b |
| **29** | 3-Cyanocarbazole | a | b |

*New compound.
†Abbreviations: a, main product of the reaction studied (chemical yields between 5 and 20%); b, minor product of the reaction studied (chemical yields below 5%); s, remaining substrate.

um or as the active component of the medium for photochemical reaction of many potential electron donors (8–16). Such studies not only strongly supported the electron transfer mechanism used to explain the fluorescence quenching but also depicted new possibilities of the application of an electron acceptor like $CCl_4$ in photochemical synthesis.

Because of its significant electron affinity (4), $CCl_4$ forms weak CT complexes with numerous electron donor molecules in their electronic ground state (2, 8, 13, 17–20). The excited states of aromatic molecules are therefore expected to be involved in charge transfer interactions with $CCl_4$ through exciplex formation. Low energy of the C—Cl bond in $CCl_4$ (21) and also the low activation energy of the dissociative process of electron attachment (22) promote the chemical activity of carbon tetrachloride. Therefore the electronic excitation of the electron donor molecule in the presence of $CCl_4$ is accompanied by the process of electron transfer to the $CCl_4$ molecule according to the scheme

$$e^- (\text{donor}) + CCl_4 \rightarrow \dot{C}Cl_3 + Cl^-$$

which is the primary photochemical process initiating complex reactions.

Among aromatic amines known as typical electron donors, carbazole turned out to be an interesting subject of studies of the photophysical and photochemical properties in the presence of halocarbon molecules. The carbazole–$CCl_4$ system in the electronic donor ground state did not show any significant interaction of electron donor–acceptor type. Nevertheless, such interactions appear in the first electronic excited singlet state of the carbazole molecule. This has been supported by studies on the photophysical properties of the carbazole–$CCl_4$ system in various media (1), as well as by the fact that fluorescence quenching of carbazole by $CCl_4$ is accompanied by a photochemical reaction (14). The proposed mechanism of the photochemical transformations in the carbazole–$CCl_4$ system has been discussed in detail in part I of this series of papers (15). This paper is a continuation of the discussion of the photochemical reactions involved in the carbazole–$CCl_4$ system, considering this time the influence of ammonia on the formation of the thermodynamically stable products after irradiation as well as the influence of ammonia on the mechanism and products during irradiation.

## Results and discussion

Irradiation of solutions of carbazole in carbon tetrachloride gives rise to the formation of both stable products such as hexachloroethane (**1**), *N*-trichloroethylenecarbazole (**2**), 1-chlorocarbazole (**3**), and 3-chlorocarbazole (**22**), as well as reactive transient photoproducts stable only in the $CCl_4$ medium. When, after irradiation of carbazole in $CCl_4$, the photolysis solution was saturated with ammonia gas to neutralize the formation of hydrogen chloride, the reactive products underwent transformation to the corresponding cyano derivatives of carbazole. It turned out that *N*-cyanocarbazole (**25**), 1-cyanocarbazole (**28**), and 3-cyanocarbazole (**29**) are the main products formed from these transformations (first column in Table 1). We have also performed the irradiation of carbazole solution in $CCl_4$ saturated with ammonia gas. In this case *N*,*N*'-dicarbazyl (**23**) and **25** are the main products of the reaction. We have also identified

Can. J. Chem. Downloaded from www.nrcresearchpress.com by 210.87.254.40 on 09/06/12
For personal use only.

Can. J. Chem. Downloaded from www.nrcresearchpress.com by 210.87.254.40 on 09/06/12
For personal use only.

the following compounds: 3,9-di-(*N*-carbazyl)carbazole (**24**), *N*-cyano-3-(*N*-carbazyl)carbazole (**26**), and 3-(*N*-carbazyl)carbazole (**27**) in addition to products **1**, **3**, **22**, **28**, and **29** (second column in Table 1).

All the isolated and identified products, using ammonia after and during irradiation, support the carbazole radical cation transformation mechanism that we proposed in part I (15).

These results, along with the known electron acceptor properties of $CCl_4$ as well as the photophysical properties of aromatic electron donor – $CCl_4$ systems (1–4), strongly support the mechanism of the primary photochemical reaction in the carbazole–$CCl_4$ system according to the following:

[1] $C + h\nu \rightarrow {}^1C^*$

[2] ${}^1C^* + CCl_4 \rightarrow {}^1(C^{\delta+}\cdots CCl_4{}^{\delta-})^*_{solv}$

[3] ${}^1(C^{\delta+}\cdots CCl_4{}^{\delta-})^*_{solv} \rightarrow [C^{+\cdot}\ Cl^-\ \dot{C}Cl_3]_{solv}$

The electron transfer from the electronically excited carbazole molecule to the $CCl_4$ molecule in the excited CT complex (eq. [3]) gives rise to chemical transformation in the system studied. The radical cation of carbazole, chloride ion, and trichloromethyl radical are the primary products of the photochemical reaction.

The secondary reactions in the solvent cage are illustrated by the following scheme:

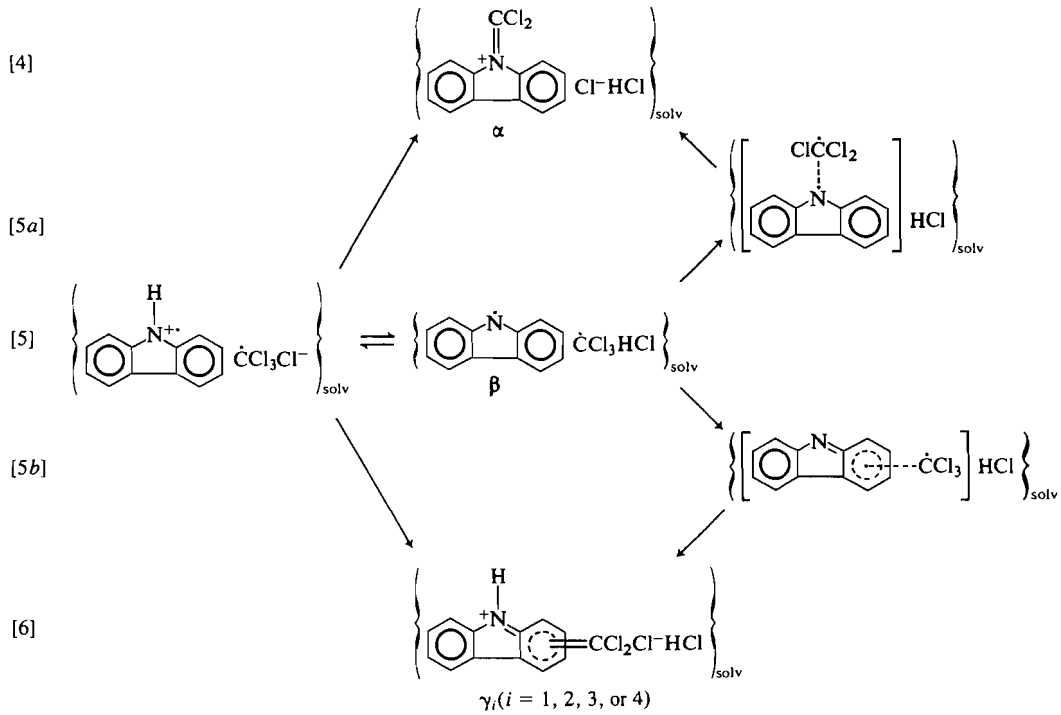


SCHEME 1

The possibilities of transformations of the carbazole radical cation are conditioned by the presence of trichloromethyl radical and chloride ion in the solvent cage. The reaction of the radical cation of carbazole with the trichloromethyl radical can occur with the participation of the nitrogen as well as the ring leading to the formation of the transient ionic products α and $\gamma_i$ (mainly with $i = 1$ or 3). The transformations of the radical cation of carbazole in the solvent cage are accompanied by the formation of thermodynamically stable molecules of hydrogen chloride (eqs. [4] and [6]). On the other hand, the radical cation of carbazole in the presence of chloride ion in the solvent cage can also split off a proton, transforming itself into the radical β. Reaction [5] is reversible (23, 24) because the N—H and H—Cl bond energies are about the same (~431 kJ $mol^{-1}$) (25). So, in the presence of HCl in the solvent cage, radical β can undergo inverse transformation to the carbazole radical cation or can react with the trichloromethyl radical. The reaction of radical β with radical $CCl_3$ can lead to cation α (eq. [5*a*]) as well as to cation $\gamma_i$ (eq. [5*b*]). In each of these reactions chloride ion is being split off.

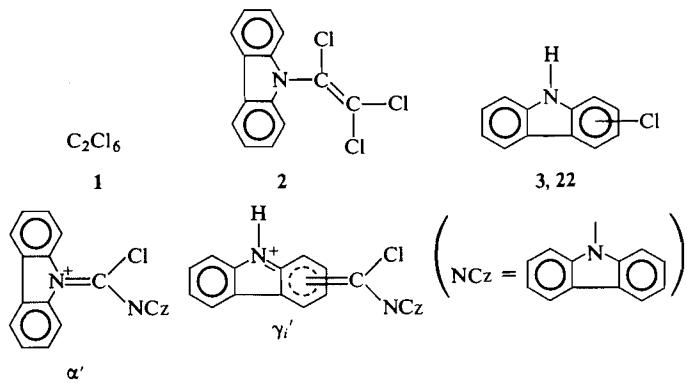


Apart from the reactions in the solvent cage discussed above, both the radical cation of carbazole and the trichloromethyl radical, as well as intermediate products α, β, and $\gamma_i$, participate in the secondary reactions outside the solvent cage. This has been depicted by the nature of the photochemical compounds obtained, such as **1**, **2**, **3**, and **22**, as well as compounds α′ and $\gamma_i$′ which are of intermediate character. The formation mechanism of these products has been proposed and discussed previously (15) and we do not intend to go into further details here.

Acidic reaction media do not favour the formation of *N*,*N*′-dicarbazyl. The lack of this product can be interpreted by the low concentration of radicals β caused by the shift of the equilibrium of reaction [5] towards the radical cation of carbazole and by reactions [5*a*] and [5*b*].

Photochemically generated trichloromethyl radicals initiate chain reactions in the solution according to the scheme:

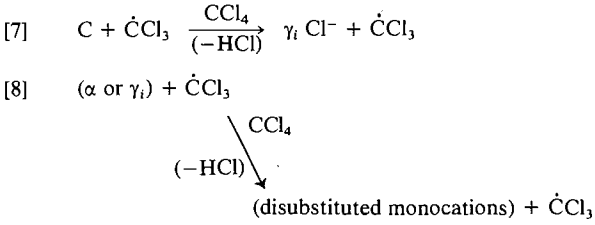


Significant photochemical activity of carbazole solution in $CCl_4$ can be explained by reactions [3] and [7]. Reaction [8] acts as a source of disubstituted monocations in the solution studied.

*Use of $NH_3$ after irradiation*

After saturation of the photolysis solution by ammonia gas, products such as **25**, **28**, and **29** appeared in addition to ammonium chloride among the other compounds of the reaction. This points to the fact that reactive transient products, stable in the $CCl_4$ medium, easily undergo reaction in the presence of ammonia to the corresponding cyano derivatives of carbazole. Therefore the formation of products **25**, **28**, and **29** can be presented by the following ammonolysis mechanism of intermediates α and $\gamma_i$:

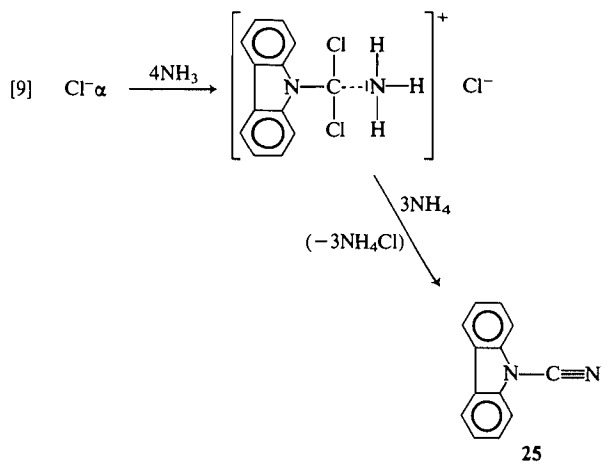


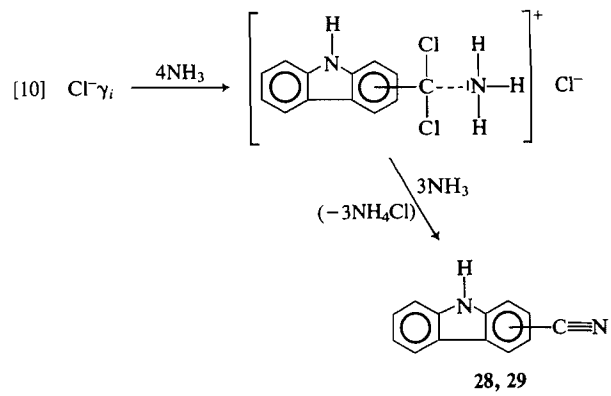


Reactions [9] and [10] are the main sources of these products. In a similar way, intermediates α′ and $\gamma_i$′ might undergo reaction in the presence of ammonia resulting in the corresponding (carboimino-*N*-carbazyl)carbazoles. These, in turn, can undergo rearrangement to cyano derivatives of carbazole.

Can. J. Chem. Downloaded from www.nrcresearchpress.com by 210.87.254.40 on 09/06/12
For personal use only.

We propose the following scheme for these reactions:

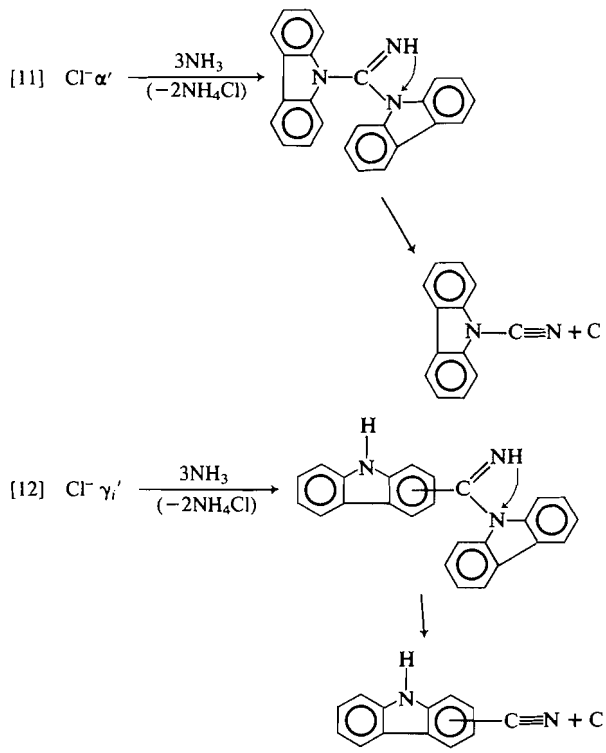


The presence of ammonia in excess, acting as a good scavenger of HCl in the reaction medium, favours the course of reactions [9] to [12].

Decomposition of (carboimino-*N*-carbazyl)carbazoles to carbazole and cyano derivatives of carbazole in reactions [11] and [12] requires a certain activation energy. Therefore, at room temperature, it can take place only partially in the photolyte solution. This reaction occurs mainly on the surface of silica gel during chromatographic separation of products.

When nonactivated silica gel, containing the adsorbed water on its surface, was used, we found (carbo-*N*-carbazyl)carbazoles in the separation fractions. This confirms the presence of (carboimino-*N*-carbazyl)carbazoles in the mixture of products chromatographically analysed. The formation of (carbo-*N*-carbazyl)carbazoles in this case can only be explained by hydrolysis of (carboimino-*N*-carbazyl)carbazoles. Similar reactions have been discussed in the literature (26). We failed to isolate (carboimino-*N*-carbazyl)carbazoles because of the chemical properties mentioned above. The formation mechanism and the chemical properties of these compounds require extended studies.

If the irradiated solution of carbazole in $CCl_4$ is saturated with ammonia gas the main reaction products are as follows: *N*-cyanocarbazole, 1-cyanocarbazole, and 3-cyanocarbazole. It is an indication of the fact that positions 1, 3, 6, 8 and 9(N) are likely to be favoured in the transformations of both the radical cation of carbazole and the carbazyl radical β in the solvent cage. The same principle of transformation for the radical cation of carbazole has been observed in the studies of electrochemical oxidation of carbazole (27). Similarly, the photolysis products of *N*-acetyl carbazole, being formed as a result of the reactions of carbazyl and acetyl radicals in the solvent cage (28), as well as the thermal rearrangement products of *N*,*N*′-dicarbazyl (29), strongly support the mechanism discussed for the reactions between the pair of radicals β and $CCl_3$. These experimentally observed chemical properties of the radical cation of carbazole as well as of radical β are in good agreement with theoretical estimations of the electron charge density in the carbazole molecule (27, 30) and in the carbazyl radical (28).

As we have shown before (15), the radical cation of carbazole can also undergo chemical transformations through positions 2 and 4 but with much less probability than through positions 1 and 3. It is presumably the reason for the low yields of 2-cyanocarbazole and 4-cyanocarbazole in the reaction medium studied. We failed to isolate these products in an amount sufficient for unambiguous identification. Similarly, because of the low yields, we did not manage to isolate dicyano derivatives of carbazole which can be formed as the result of ammonolysis of disubstituted monocations.

*Use of $NH_3$ during irradiation*

The course of photochemical transformations in the carbazole–$CCl_4$ system, discussed above, is radically changed in the presence of ammonia. This is indicated by the qualitative and quantitative composition changes of the photochemical reaction products. The products obtained (see Table 1) show the participation of the radicals β in the secondary reactions. Thus, it may be suggested that the reaction medium favours the formation of the radicals β. Therefore, the active role of ammonia in the reaction medium could be explained by the removal of hydrogen chloride from the reaction medium and also by interaction with the radical cation of carbazole out of the cage according to the following scheme:

Can. J. Chem. Downloaded from www.nrcresearchpress.com by 210.87.254.40 on 09/06/12
For personal use only.

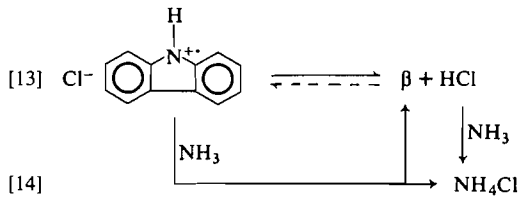


SCHEME 2

Scheme 2 explains the mechanism of formation of the radicals β in the reaction medium. Active interaction between ammonia and radical cations of aromatic amines is well known in the literature (10, 11, 31, 32). The results in these papers show that such interaction usually leads to the transformation of radical cations of aromatic amines to the corresponding radicals.

The reactions involving the recombination of radicals β explain explicitly the formation mechanism of such products as **23** and **27**:

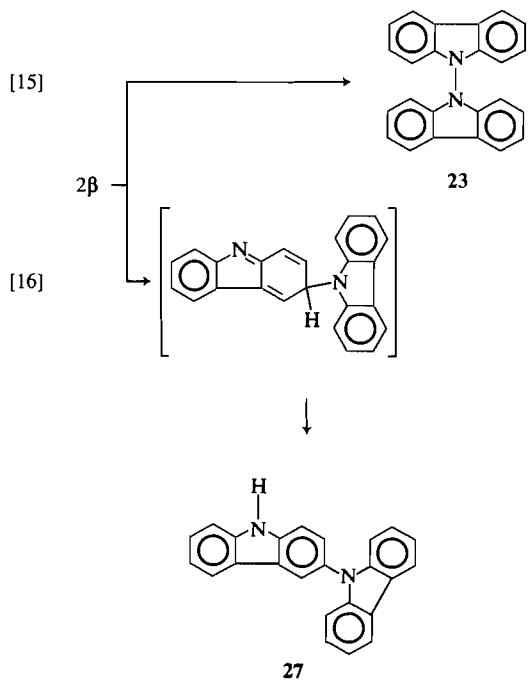


The interaction between radicals β and the carbazole molecule in the presence of hydrogen acceptor may also lead to the formation of product **27** according to reaction [17].

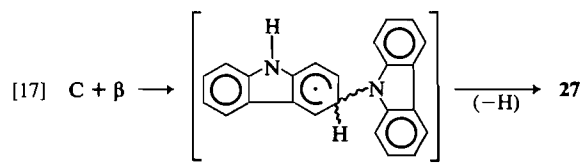


Because the medium favors radical reactions, products **23** and **27** partially undergo further transformation. This is indicated by the formation of product **24** according to reactions [18] and [19].

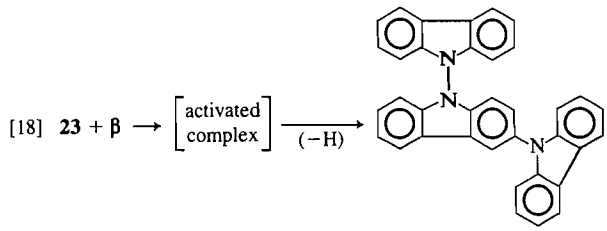


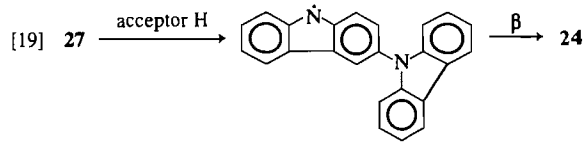


Radicals 3-(*N*-carbazyl)carbazyl appearing in reaction [19] can undergo not only the recombination reaction with radicals β forming trimer **24** but they can recombine with each other resulting in the tetramer 3,3′-di(*N*-carbazyl)-*N*,*N*′-dicarbazyl (33). In the reaction medium studied, radicals 3-(*N*-carbazyl)carbazyl, in the presence of trichloromethyl radicals, can also be the precursor of product **26** according to reaction [20].

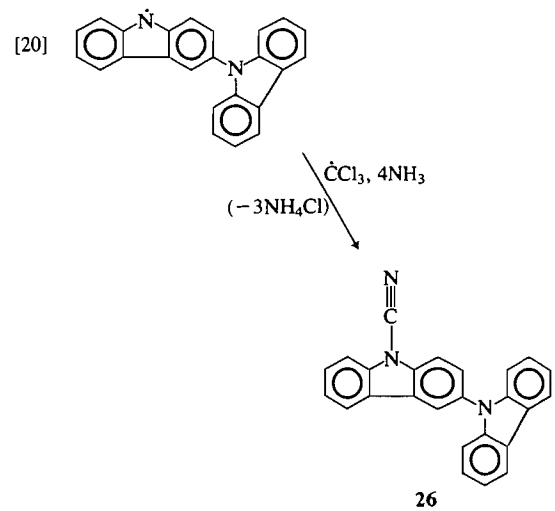


Another possible formation mechanism of **26** can be described by reaction of radical β with *N*-cyanocarbazole:

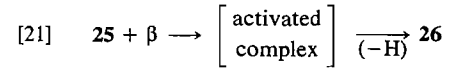


Can. J. Chem. Downloaded from www.nrcresearchpress.com by 210.87.254.40 on 09/06/12
For personal use only.

Can. J. Chem. Downloaded from www.nrcresearchpress.com by 210.87.254.40 on 09/06/12
For personal use only.

Intermediate radical products as well as $CCl_4$ can be hydrogen acceptors in reactions [15]–[19] and [21].

Reactions [15]–[21] indicate the role played by radical β in the formation mechanism of products **23**, **27**, **24**, and **26**. Reactions involving radicals β have been thoroughly studied previously (33). Products **23**, **27**, and **24** are also formed during the chemical oxidation of carbazole with nickel peroxide (34). Thus, some analogies can be observed between photochemical and chemical oxidation of carbazole.

The products presented above along with results described in refs. 33 and 34 indicate that the production of radicals β is always accompanied by the formation of polycarbazoles according to the simplified scheme:

$$\beta \xrightarrow{\beta} (\text{dimers}) \xrightarrow[(-H)]{\beta} (\text{trimers}) \xrightarrow[(-H)]{\beta} \cdots$$

Furthermore these products prove also that radicals β outside the solvent cage take part in the reactions mainly at positions 3 and 9.

Intermediates α and $\gamma_i$ are also formed in the reaction medium studied; they are indicated by the formation of products **25**, **28**, and **29** described by reactions [9] and [10]. Products **28** and **29** are formed with low yields, while **25** as well as **23** are the main products of the discussed photochemical transformation of carbazole.

These studies of the photochemical reaction products lead to the assumption that the probability of transformation of the carbazole radical cation to form the intermediates α and $\gamma_i$ (eqs. [4] and [6] in the presence of ammonia decreases in favour of the formation of radical β (eq. [5]).

The significant yields of products **23** and **25** are connected with the high concentration of β radicals in the reaction medium. Product **23** is formed in reaction [15], while the formation of **25** can be explained by reaction [5*a*] which occurs mainly outside the solvent cage.

All the results discussed in parts I and II will serve as an excellent background for our future spectroscopic and quantitative studies of photochemical reactions in the carbazole–$CCl_4$ system.

## Experimental

*Apparatus*

The $^1$H nmr spectra have been measured with a Bruker WH-90 spectrometer operating at 90 MHz. Chemical shift values are given in a δ scale with respect to TMS as an internal standard. Infrared spectra were recorded on a Perkin–Elmer 710B infrared spectrophotometer and mass spectra were taken with a AE1 MS902 mass spectrometer.

*Materials*

Carbazole was an Eastman Organic Chemical and was used without any further purification. Carbon tetrachloride from American Chemicals was a Spectrograde quality and it was purified as described previously (15). Petroleum ether (boiling range 30–75°C) and benzene were distilled before use.

*General procedure*

Carbazole solution (0.005 *M*) in carbon tetrachloride was deoxygenated with oxygen-free argon and irradiated in a Pyrex Hanovia immersion-well reactor for 1 hour with an Hanovia 679A36 450 W medium-pressure mercury lamp. After irradiation, the solution of photolyte was saturated with ammonia gas, so that hydrogen chloride generated during the reaction was neutralized. Following that, the solution of photolyte was concentrated.

Irradiation of carbazole solution (0.005 *M*, 1 h) in carbon tetrachloride was also carried out in the presence of $NH_3$. A slow stream of ammonia gas was bubbled through the solution before and during irradiation. Hydrogen chloride generated during the photochemical reaction was thus removed from the reaction medium. When irradiation was finished, the solution of photolyte was concentrated.

The photochemical products were then analysed by tlc detected by uv (using Eastman–Kodak tlc plates, silica gel 13181) and separated by column chromatography. The columns were packed with silica gel (Kieselgel 60, Merck, particle size 0.040–0.063 mm). Developing systems consisted of petroleum ether (low boiling fraction) and ethyl ether or benzene. The developed distance on tlc plates was kept at 10 cm. Identified products, on the basis of their $^1$H nmr, ir, and mass spectra, have been listed in Table 1 and their $R_f$ values on tlc plates with silica gel are listed in Table 2.

*Spectral characteristics of the photochemical products*

*Hexachloroethane* (**1**): single crystals. The compound was identified as described previously (15).

N-*Trichloroethylenecarbazole* (**2**): crystalline solid and *1-chlorocarbazole* (**3**): crystalline solid. These compounds were identified as described previously (14, 15).

*3-Chlorocarbazole* (**22**): crystalline solid; ir (film) $\tilde{\nu}_{max}$: 3390 (vs, N—H), 1610 (w), 1590 (w), 1560 (w), 1460 (m), 1440 (s), 1430 (s), 1320 (m), 1280 (w), 1260 (m), 1230 (w), 1210 (vw), 1190 (w), 1095 (w), 1055 (m), 1040 (w), 1010 (vw), 990 (w), 915 (m), 865 (s), 800 (vs), 735 (s), 710 (s) cm$^{-1}$; $^1$H nmr (acetone-$d_6$) δ: 7.09–7.58 (m, 5H, arom), 8.11–8.22 (m, 2H, arom), 10.52 (s, br, 1H, N—H); ($CDCl_3$): 7.10–7.50 (m, 5H, arom), 7.90–8.15 (m, 2H, arom and 1H, N—H); mass spectrum (70 eV) (mol. wt. for $C_{12}H_8NCl$: 201.66), *m/e*: 203 ($M^+$, 30), 201 ($M^+$, 100), 167 (6), 166 (37), 165 (6), 164 (9), 140 (10), 139 (13).

N,N′-*Dicarbazyl* (**23**); crystalline solid. The compound was identified as described previously (14).

*3,9-Di-(*N*-carbazyl)carbazole* (**24**): crystalline solid; ir (film) $\tilde{\nu}_{max}$: 1615 (m), 1595 (m), 1575 (w), 1490 (s), 1475 (s), 1450 (vs), 1320 (m), 1305 (s), 1265 (m), 1225 (vs), 1160 (w), 1145 (w), 1105 (w), 1015 (m), 1000 (w), 990 (w), 960 (vw), 920 (w), 910 (w), 870 (vw), 840 (vw), 800 (m), 740 (vs), 715 (s) cm$^{-1}$; $^1$H nmr ($CDCl_3$) δ: 6.93–7.18 and 7.18–7.55 (2 complex m, 17H, arom), 8.10–8.29 (m, 5H, arom), 8.36 (d, $J$ = 1.5 Hz, 1H, arom); mass spectrum (70 eV) (mol. wt. for $C_{36}H_{23}N_3$: 497.60), *m/e*: 497 ($M^+$, 12), 332 (43), 331 (100), 330 (22), 329 (20), 167 (75), 166 (58), 165 (25), 140 (42), 139 (27).

N-*Cyanocarbazole* (**25**): crystalline solid. The compound was identified as described previously (14).

N-*Cyano-3-(*N*-carbazyl)carbazole* (**26**): crystalline solid; ir (film) $\tilde{\nu}_{max}$: 2220 (vs, C≡N), 1610 (w), 1580 (m), 1565 (w), 1485 (vs), 1470 (s), 1445 (vs), 1350 (w), 1320 (s), 1300 (s), 1260 (w),

Can. J. Chem. Downloaded from www.nrcresearchpress.com by 210.87.254.40 on 09/06/12
For personal use only.

TABLE 2. $R_f$ values of the photoproducts in the carbazole–$CCl_4$ system

| | Developing system (v/v) | | | |
|---|---|---|---|---|
| | Petroleum ether – ethyl ether | | | |
| No.* | 100:1 | 10:1 | 2:1 | Benzene |
| C | 0.05 | 0.22 | 0.57 | 0.76 |
| **2** | 0.74 | 0.82 | 0.86 | 0.91 |
| **3** | 0.23 | 0.53 | 0.77 | 0.84 |
| **22** | 0.04 | 0.14 | 0.40 | 0.73 |
| **23** | 0.54 | 0.77 | 0.84 | 0.91 |
| **24** | 0.32 | 0.68 | 0.82 | 0.90 |
| **25** | 0.22 | 0.57 | 0.78 | 0.77 |
| **26** | 0.09 | 0.41 | 0.75 | 0.79 |
| **27** | | 0.06 | 0.28 | 0.72 |
| **28** | | 0.08 | 0.44 | 0.27 |
| **29** | | 0.02 | 0.14 | 0.24 |

*Notation of compounds is the same as in Table 1.

1220 (s), 1150 (w), 1135 (w), 1100 (w), 900 (w), 860 (vw), 830 (vw), 795 (m), 735 (vs), 710 (s), $cm^{-1}$; $^1H$ nmr ($CDCl_3$) δ: 7.17–8.22 (complex m, 15H, arom); mass spectrum (70 eV) (mol. wt. for $C_{25}H_{15}N_3$: 357.42), *m/e*: 357 ($M^+$, 100), 330 (11), 165 (30), 138 (8).

*3-(*N*-Carbazyl)carbazole* (**27**): crystalline solid; ir (film) $\tilde{\nu}_{max}$: 3385 (vs, N—H), 1610 (w), 1580 (m), 1560 (w), 1490 (vs), 1470 (s), 1455 (vs), 1445 (vs), 1360 (vw), 1320 (s), 1305 (s), 1260 (m), 1225 (vs), 1145 (m), 1130 (m), 1095 (vw), 1000 (w), 990 (w), 900 (m), 860 (vw), 825 (w), 795 (m), 740 (vs), 710 (s), $cm^{-1}$; $^1H$ nmr ($CDCl_3$) δ: 7.16–7.67 (m, 11H, arom), 7.95–8.30 (m, 4H, arom and 1H, N—H); (acetone-$d_6$): 7.18–7.87 (m, 11H, arom), 8.13–8.40 (m, 4H, arom), ~10.72 (broad band, 1H, N—H); mass spectrum (70 eV) (mol. wt. for $C_{24}H_{16}N_2$: 332.41), *m/e*: 332 ($M^+$, 100), 166 (34), 165 (27), 139 (12).

*1-Cyanocarbazole* (**28**): crystalline solid; ir (Nujol film) $\tilde{\nu}_{max}$: 3300 (s, N—H), 2200 (s, C≡N), 1615 (vw), 1595 (m), 1570 (vw), 1490 (w), 1425 (m), 1325 (w), 1315 (m), 1265 (w), 1235 (m), 1220 (w), 1205 (w), 1105 (w), 780 (w), 725 (s), 710 (s) $cm^{-1}$; $^1H$ nmr (acetone-$d_6$) δ: 7.19–7.83 (complex m, 5H, arom), 8.16, 8.24 and 8.40, 8.48 (2d, 2H, arom), 11.13 (s, br, 1H, N—H); ($CDCl_3$): 7.18–7.74 (complex m, 5H, arom), 8.04, 8.12 and 8.22, 8.30 (2d, 2H, arom), 8.97 (s, 1H, N—H); mass spectrum (70 eV) (mol. wt. for $C_{13}H_8N_2$: 192.22), *m/e*: 192 ($M^+$, 100), 191 (7.1), 165 (7.8), 164 (14.2), 138 (4.2), 96 (8.5).

*3-Cyanocarbazole* (**29**): crystalline solid; ir (Nujol film) $\tilde{\nu}_{max}$: 3275 (s, N—H), 2200 (s, C≡N), 1615 (w), 1590 (s), 1570 (vw), 1480 (w), 1395 (w), 1325 (w), 1315 (m), 1275 (w), 1230 (s), 1205 (w), 1190 (m), 1110 (w), 885 (m), 800 (s), 755 (w), 735 (m), 720 (s) $cm^{-1}$; $^1H$ nmr (acetone-$d_6$) δ: 7.19–7.69 (m, 5H, arom), 8.20, 8.29 (d, 1H, arom), 8.58 (s, 1H, arom), 10.92 (s, br, 1H, N—H); ($CDCl_3$): 7.24–7.73 (m, 5H, arom), 8.04, 8.13 (d, 1H, arom), 8.38 (s, 1H, arom), ~8.48 (s, 1H, N—H); mass spectrum (70 eV) (mol. wt. for $C_{13}H_8N_2$: 192.22), *m/e*: 192 ($M^+$, 100), 191 (11.3), 165 (13.4), 164 (17.4), 138 (7.1), 96 (15.6).

## Conclusions

Use of ammonia *after* irradiation of the carbazole solution in $CCl_4$ leads to the appearance of *N*-, 1-, and 3-cyanocarbazoles as the main products in the reaction mixture. The formation of these products indicates that chemical reaction take place between ammonia and intermediates α and $\gamma_i$. This strongly supports the proposed mechanism of transformations of the radical cation of carbazole.

When ammonia was used *during* irradiation of the carbazole solution in $CCl_4$ we obtained *N*,*N*'-dicarbazyl and *N*-cyanocarbazole as the main products in addition to 3-(*N*-carbazyl)carbazole, 3,9-di-(*N*-carbazyl)carbazole, and *N*-cyano-3-(*N*-carbazyl) carbazole. The formation of these products is closely connected with the reactions of radicals β. Radicals β along with intermediates α and $\gamma_i$ also serve as a proof for the presence of radical cations of carbazole in the photochemical reaction medium.

All the intermediate products of the photochemical reaction in the carbazole–$CCl_4$ system indicate that the primary photochemical process is the electron transfer from the singlet excited molecule of carbazole to the $CCl_4$ molecule in the excited CT complex, $^1(C^{\delta+}\cdots CCl_4{}^{\delta-})^*$. Furthermore, transformation of the primary photochemical reaction products depends not only on their particular type, but also on the nature of the reaction media used.

## Acknowledgements

The authors would like to thank the Natural Sciences and Engineering Research Council of Canada and the "Ministère de l'Education du Québec" for financial assistance.

1. A. AHMAD and G. DUROCHER. Can. J. Spectrosc. **26**, 19 (1981); Photochem. Photobiol. **34**, 573 (1981).
2. A. NAMIKI, N. NAKASHIMA, and K. YOSHIHARA. J. Chem. Phys. **71**, 925 (1979).
3. J. KLEIN, V. P. PLAZANET, and G. LAUSTRIAT. J. Chim. Phys. **67**, 302 (1970); J. KLEIN and G. LAUSTRIAT. J. Chim. Phys. **67**, 310 (1970).
4. D. SAPERSTEIN and E. LEVIN. J. Chem. Phys. **62**, 3560 (1975).
5. W. R. WARE and C. LEWIS. J. Chem. Phys. **57**, 3546 (1972); C. LEWIS and W. R. WARE. Chem. Phys. Lett. **15**, 290 (1972).
6. T. TAKAHASHI, K. KIKUCHI, and H. KOKUBUN. J. Photochem. **14**, 67 (1980).
7. W. C. MEYER. J. Phys. Chem. **74**, 2118 (1970); **74**, 2122 (1970); **74**, 2127 (1970).
8. T. LATOWSKI and E. SIKORSKA. Rocz. Chem. **42**, 1063 (1968).
9. T. LATOWSKI and B. ZELENT. Rocz. Chem. **48**, 831 (1974); **51**, 1883 (1977).
10. T. LATOWSKI and B. ZELENT. J. Org. Chem. **44**, 3559 (1979).
11. K. WYRZYKOWSKA, M. GRODOWSKI, K. WEISS, and T. LATOWSKI. Photochem. Photobiol. **28**, 311 (1978).
12. T. IWASAKI, T. SAWADA, M. OKUYAMA, and H. KAMADA. J. Phys. Chem. **82**, 371 (1978); Photogr. Sci. Eng. **22**, 312 (1978).
13. W. J. LAUTENBERGER, E. N. JONES, and J. G. MILLER. J. Am. Chem. Soc. **90**, 1110 (1968); C. J. BIASELLE and J. G.

MILLER. J. Am. Chem. Soc. **96**, 3813 (1974); S. A. MARKARIAN and H. FISHER. J. Chem. Soc. Chem. Commun. 1055 (1979).
14. B. ZELENT and G. DUROCHER. J. Org. Chem. **46**, 1496 (1981).
15. B. ZELENT and G. DUROCHER. Can. J. Chem. **60**, 945 (1982).
16. F. A. CARROLL and D. G. WHITTEN. J. Phys. Chem. **80**, 2046 (1976).
17. R. FOSTER. Organic charge-transfer complexes. Academic Press, New York. 1969. p. 278.
18. M. TAMRES and R. L. STRONG. Molecular association. Vol. 2. *Edited by* R. Foster. Academic Press, New York. 1979. p. 332.
19. K. M. C. DAVIS and M. F. FARMER. J. Chem. Soc. (B), 28 (1967); 859 (1968).
20. T. KUROI, Y. GONDO, M. KUWABARA, R. SHIMADA, and Y. KANDA. Bull. Chem. Soc. Jpn. **54**, 2243 (1981).
21. J. R. BEWS and CH. GLIDEWELL. J. Mol. Struct. **71**, 287 (1981).
22. J. A. AYOLA, W. E. WENTWORTH, and E. C. M. CHEN. J. Phys. Chem. **85**, 3989 (1981); H.-U. SCHEUNEMANN, E. ILLENBERGER, and H. BAUMGÄRTEL. Ber. Bunsenges. Phys. Chem. **84**, 580 (1980).
23. E. J. LAND. Prog. React. Kinet. **3**, 371 (1965).
24. A. LEDWITH and M. SAMBHI. J. Chem. Soc. Chem. Commun. 64 (1965).
25. S. L. MUROV. Handbook of photochemistry. Marcel Dekker, Inc., New York. 1973.
26. D. G. NEILSON. The chemistry of amidines and imidates. *Edited by* S. Patai. John Wiley and Sons, New York. 1975. p. 385.
27. J. F. AMBROSE and R. F. NELSON. J. Electrochem. Soc. **115**: 1159 (1968); J. F. AMBROSE, L. L. CARPENTER, and R. F. NELSON. J. Electrochem. Soc. **122**, 876 (1975).
28. H. SHIZUKA, M. KATO, T. OCHIAI, K. MATSUI, and T. MORITA. Bull. Chem. Soc. Jpn. **43**, 67 (1970).
29. V. DAVE. Can. J. Chem. **50**, 3397 (1972).
30. I. FISCHER-HJALMARS and M. SUNDBORN. Acta Chem. Scand. **22**, 607 (1968).
31. T. LATOWSKI and B. ZELENT. Rocz. Chem. **51**, 1405 (1977).
32. E. ZADOR, J. M. WARMAN, L. H. LUTHJENS, and A. HUMMEL. J. Chem. Soc. Faraday Trans. I, **70**, 227 (1974).
33. W. A. WATERS and J. E. WHITE. J. Chem. Soc. (C), 740 (1968).
34. J. SUGITA. Nippon Kagaku Zasshi, **88**, 659 (1967); Chem. Abstr. **69**, 10319z (1968).

Can. J. Chem. Downloaded from www.nrcresearchpress.com by 210.87.254.40 on 09/06/12
For personal use only.

# Magnetic non-equivalence of fluorine atoms of a trifluoromethyl group

MOHSIN A. KHAN,[1] DONALD F. TAVARES,[2] AND ARVI RAUK
*Department of Chemistry, University of Calgary, Calgary, Alta., Canada T2N 1N4*

Received March 19, 1982

MOHSIN A. KHAN, DONALD F. TAVARES, and ARVI RAUK. Can. J. Chem. **60**, 2451 (1982).

The three fluorine atoms of *N,N*-dialkyl amide and chloride derivatives of 2-methoxy-2-phenyl-3,3,3-trifluoropropanoic acid are magnetically nonequivalent below −60°C and exhibit a clear ABC coupling pattern from which chemical shifts and geminal coupling constants are readily derived. The chemical shifts span a range of about 10 ppm and the geminal coupling constants average about 110 Hz. A five bond coupling of about 5 Hz is observed between the hydrogens of the methoxy group and one of the nonequivalent fluorine atoms of the trifluoromethyl group. Barriers to the hindered rotation about the single bond to the trifluoromethyl group are in the range 36–46 kJ/mol.

MOHSIN A. KHAN, DONALD F. TAVARES et ARVI RAUK. Can. J. Chem. **60**, 2451 (1982).

Les trois atomes de fluor du *N,N*-dialkylamide et du chlorure provenant de l'acide méthoxy-2 phényl-2 trifluoro-3,3,3 propanoique sont magnétiquement non équivalents en dessous de −60°C et présentent un modèle clair de couplage ABC duquel on déduit facilement les déplacements chimiques et les constantes de couplage géminal. Les déplacements chimiques s'étalent sur un intervalle de 10 ppm environ et les constantes de couplage géminal sont en moyenne de 110 Hz environ. On observe un couplage à travers 5 liaisons de 5 Hz environ entre les hydrogènes du groupe méthoxy et l'un des atomes de fluor non équivalent du groupe trifluorométhyle. Les barrières à la rotation encombrée autour de la liaison simple du groupe trifluorométhyle sont de l'ordre de 36 à 46 kJ/mol.

[Traduit par le journal]

Can. J. Chem. Downloaded from www.nrcresearchpress.com by 210.87.254.5 on 09/06/12
For personal use only.

## Introduction

Fluorine nmr is an important technique in structural determination because of the extreme range (~800 ppm) of chemical shifts that are observed. $^{19}F$ chemical shifts and coupling constants have been used extensively to derive conformational and configurational information, much of it, however, in compounds in which the fluorine atoms are attached to rigid ring systems. In conformationally mobile systems, some information is lost due to averaging over structures, a consequence of the relatively long time scales of nmr experiments. Frequently, however, specific information may be obtained at temperatures at which conformation or group exchanges are slow on the nmr time scale.

The nmr spectral measurements of diastereomeric ester and amide derivatives of 2-methoxy-2-phenyl-3,3,3-trifluoropropanoic acid **1** have been routinely used for the determination of absolute configurations and optical purities of chiral alcohols and amines, after the pioneering work of Mosher and co-workers (1, 2). The esters, **3**, and amides of primary amines, **4** ($R^1$ = H), each display a single sharp fluorine resonance and mixtures of configurationally diastereomeric compounds often have separated signals for the $-CF_3$ groups, rendering assessment of relative abundances by integration facile. The conformational (or geometric) diastereoisomerism of which each of **3** and **4** ($R^1$ = H) is capable, namely (*Z*)-**3** ⇄ (*E*)-**3** and (*Z*)-**4** ⇄ (*E*)-**4**, is not evident in the ambient temperature nmr spectrum. Either the rate of interconversion is sufficiently rapid to average the signals of the geometric diastereomers or the equilibrium favours one of the isomers to the virtual exclusion of the other.

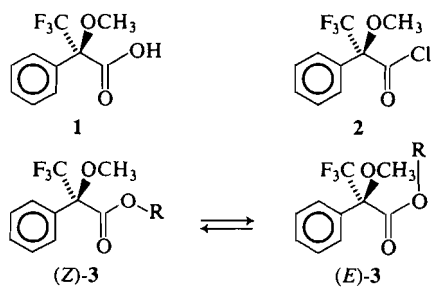


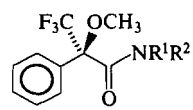


**4**

The former is unlikely, since it is known that rotation about the carbon–nitrogen bond of amides, including amides from primary amines (3), is hindered by a barrier of about 67–92 kJ/mol (3, 4). The corresponding barriers in esters are probably somewhat lower. For simple acetates and formates, barriers in the range 42–55 kJ/mol have been obtained by *ab initio* computations (5). Acyclic esters exist preferentially in the *Z*-conforma-

[1]Present address: Department of Chemistry, University of Karachi, Karachi-32, Pakistan.

[2]Author to whom correspondence may be addressed.

0008-4042/82/192451-05$01.00/0

©1982 National Research Council of Canada/Conseil national de recherches du Canada

Can. J. Chem. Downloaded from www.nrcresearchpress.com by 210.87.254.5 on 09/06/12
For personal use only.

tion, (*Z*)-**3** (6, 7) which is at least 7.6 kJ/mol (the value for *tert*-butyl formate (7)) more stable than the *E*-conformer. *Ab initio* computations have yielded values in the range 17–35 kJ/mol in favour of the *Z*-form, e.g. (*Z*)-**3**, over the *E*-form, e.g. (*E*)-**3**, for methyl formate and methyl acetate (5, 8, 9). For amides of primary amines, the situation is similar. The carbon–nitrogen backbone in proteins has the *Z*-configuration, and simple acyclic *N*-monoalkyl amides also adopt the *Z*-conformation to the virtual exclusion of the other except in the case of formamides (10). For more complex *N*-monoalkyl amides, and for *N*,*N*-dialkyl amides, it is generally agreed that minimization of steric repulsions is the single most important factor which leads to a preference of one conformation over the other (11, 12) and this should be the case for **4** also.

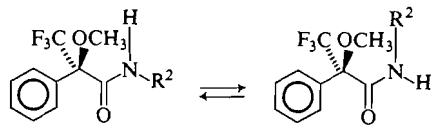

(*Z*)-**4** ($R^1$ = H) (*E*)-**4** ($R^1$ = H)

Amides of chiral secondary amines, e.g. **4** ($R^1 \neq R^2 \neq$ H), present complications for the determination of absolute configurations or optical purities which arise from the fact that, in general, pairs of geometric diastereomers as well as configurational diastereomers are evident in the $^1$H nmr spectrum (13, 14), at ambient temperature. Indeed, the room temperature $^{19}$F nmr spectrum of amide **5**, pre-

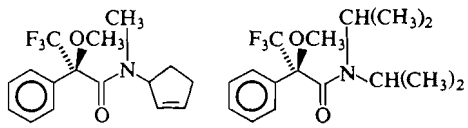

**5** **7**

pared in connection with another study, shows two broad, unequal, overlapping absorptions. While multiple absorptions in the $^{19}$F nmr spectrum were expected, the breadth of the lines was not. We present below the analysis of several derivatives of **1**, namely **2**, **6**–**8**, in which nmr spectral changes are attributed to unusually high barriers to hindered rotation about the carbon–carbon single bond to the trifluoromethyl group.

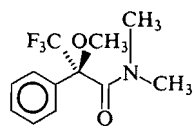

**6**

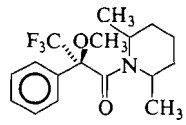

**8**

## Experimental

*Materials*

Dimethylamine, diisopropylamine, and 2,6-dimethylpiperidine were commercial reagent grade, and were redistilled before use and their purity checked by glc (Porapak Q). The 2,6-dimethylpiperidine (Aldrich Chemical Co.) is the *cis*- or (*R*,*S*)-isomer as verified by $^{13}$C nmr spectroscopy (14). No trace of the *trans*- or (*d*,*l*)-isomer is detectable in the ambient temperature $^{13}$C spectrum.

*2-Methoxy-2-phenyl-3,3,3-trifluoropropanoyl chloride* (**2**)
(α-Methoxy-α-trifluoromethylphenylacetyl chloride)

Racemic and (+)-α-methoxy-α-trifluoromethylphenylacetic acids (Aldrich Chemical Co.) were converted to the corresponding acid chlorides by a modification of the published procedure (1) using a catalytic amount of dimethylformamide (15).

*Preparation of (±) and (+)-2-methoxy-2-phenyl-3,3,3-trifluoropropanamides*

(a). The amides of ammonia (**4**, $R^1 = R^2$ = H) and dimethylamine (**6**) were prepared according to the general procedure of Mosher (1) and were characterized by $^1$H nmr spectroscopy. Samples were diluted with the appropriate solvent for the $^{19}$F nmr spectroscopy experiments.

(b). The amides of diisopropylamine (**7**) and 2,6-dimethylpiperidine (**8**) required heating with the acid chloride for 3 h (reflux) followed by standing at room temperature for 18–20 h. The amides were characterized by $^1$H nmr and samples were diluted with the appropriate solvent for the $^{19}$F nmr experiments.

*Nuclear magnetic resonance experiments*

The $^{19}$F nmr spectra were recorded at 188.1 MHz on a Varian XL-200 spectrometer, equipped with a variable temperature controller (accurate to ±1°C). All spectra were referenced against TFA (trifluoroacetic acid) in $CDCl_3$ and converted to the ∂ scale (16) using the conversion factor: $\partial = \partial_{TFA} - 76.1$ ppm. For the temperature range +60°C to −65°C, $CDCl_3$ was used as the solvent; for the range −60°C to −128°C, $CFCl_3$ was used as the solvent and the instrument was run unlocked, using the same machine frequencies employed in the locked spectra and assuming no field drift.

## Results and discussion

### *Low temperature $^{19}$F nmr spectrum and parameters of the trifluoromethyl group*

The temperature dependence of the $^{19}$F nmr spectrum of **6** is typical of that of the other compounds and is shown in Fig. 1. At 22°C there is a single, somewhat broadened, resonance at δ = −71.3 ppm. Upon lowering the sample temperature, the signal broadens considerably and disappears at about −50°C, the coalescence temperature in both $CDCl_3$ and $CFCl_3$. At lower temperatures ($CFCl_3$) the signal reappears and sharpens into an ABC coupling pattern at −100°C. The observations must be due to hindered rotation about the C—$CF_3$

Can. J. Chem. Downloaded from www.nrcresearchpress.com by 210.87.254.5 on 09/06/12
For personal use only.

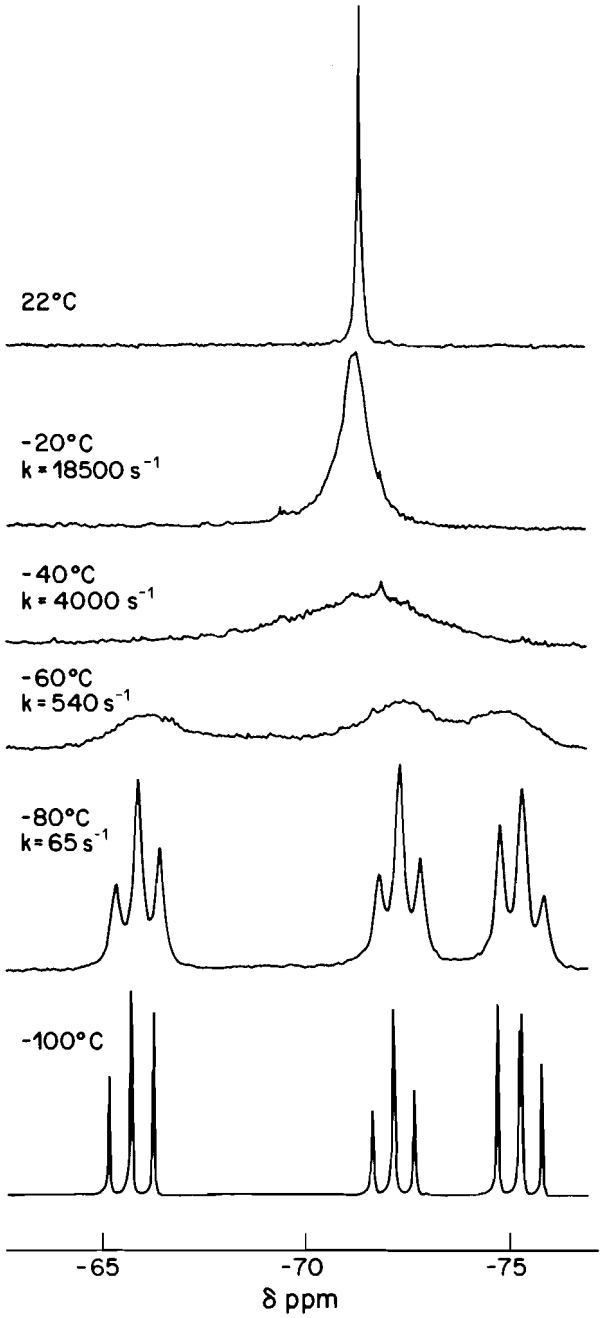


FIG. 1. The $^{19}F$ nmr spectra of **6** in the temperature range 23°C to −100°C. Rate constants were determined by lineshape fitting using DNMR3 (ref. 22). The spectra at the two lowest temperatures were recorded in $CFCl_3$, the rest in $CDCl_3$.

bond. The $^{19}F$ nmr spectral data of **6**, as well as **2**, **7**, and **8**, are given in Table 1. We refer to the individual fluorine resonances as $F_A$, $F_B$, and $F_C$ where $F_A$ is at highest frequency and $F_C$ at the lowest.

The nmr spectral data of all of the compounds of Table 1 have the following features in common. The $^1H$ nmr shows a five bond coupling, $^5J_{HF} = 2$ Hz, between the $CF_3$ group and the protons of the methoxy group. The long range coupling is highly stereospecific since only the middle fluorine ($F_B$) resonance displays broadening due to the (unresolved) coupling in the $^{19}F$ spectrum when $CF_3$ rotation is slow on the nmr time scale. In the case of **7**, the low temperature proton spectrum was recorded down to −80°C. The signal of the methoxy protons, initially a quartet, $^5J_{HF} = 1.9$ Hz, undergoes coalescence and then sharpens into a doublet, $^5J_{HF_B} = 4.7$ Hz. Since $(^5J_{HF_A} + {}^5J_{HF_B} + {}^5J_{HF_C})/3 = 1.9$ Hz, neither $^5J_{HF_A}$ nor $^5J_{HF_C}$ can exceed 1 Hz, thus confirming the stereospecificity of the long-range coupling to a single fluorine atom.

The average $CF_3$ chemical shift of all of the compounds is $-70.2 \pm 0.5$ ppm at low temperature. The narrowness of the observed range suggests that the local electronic and magnetic environment of the $CF_3$ group is similar in all cases. The median chemical shift difference $\langle \delta F_A - \delta F_C \rangle$ is 10.3 ppm ± 1.2 ppm. All of the observed geminal coupling constants $^2J_{FF}$ are in the range $111 \pm 8$ Hz. For each compound the same pattern is observed, namely $J_{AC} > J_{AB} > J_{BC}$.

Individual fluorine resonances arising from restricted rotation about a single bond to a trifluoromethyl group have been previously reported, first in 2,2,3,3-tetrachloro-1,1,1,4,4,4-hexafluorobutane (17) and then other halo alkanes (18, 19) and in several trifluoromethyl substituted phosphoranes (20, 21). The chemical shifts and coupling constants reported in Table 1 for derivatives of **1** are similar to those previously observed in the perhaloalkanes, although in the latter compounds, the chemical shift differences between the individual fluorine atoms of the $CF_3$ group are somewhat larger, 12–16 ppm (17–19).

*Barriers to the hindered rotation*

From the limiting values of chemical shifts and coupling constants, given in Table 1, and the temperature dependence of the lineshapes of the $^{19}F$ signals (e.g. **6**, Fig. 1), activation parameters were obtained for **2**, **6**, and **7** using the computer programme DNMR3 (22*a*) for rate constants. In each case, satisfactorily straight lines were obtained in a plot of $\ln(k/T)$ vs. $1/T$.

$$[1] \quad k = \left(\frac{k_B}{h} T\right) e^{-(\Delta H^{\ddagger} - T\Delta S^{\ddagger})/RT}$$

$\Delta H^{\ddagger}$ and $\Delta S^{\ddagger}$ were obtained from the "least squares" lines. Free energies of activation, $\Delta G^{\ddagger}$,

TABLE 1. $^{19}F$ nuclear magnetic resonance parameters and $CF_3$ rotation barriers for derivatives of **1**

| Compound | Chemical shifts (ppm)[a] | | | Coupling constants (Hz) | | | $T_c$(°C) | Activation parameters | | |
|---|---|---|---|---|---|---|---|---|---|---|
| | $\partial F_A$ | $\partial F_B$ | $\partial F_C$ | $J_{AB}$ | $J_{AC}$ | $J_{BC}$ | | $\Delta G^{\ddagger}$ kJ/mol | $\Delta H^{\ddagger}$ kJ/mol | $\Delta S^{\ddagger}$ J/mol-deg |
| **2**[b] | −65.97 | −70.33 | −75.12 | 112.5 | 113.9 | 109.4 | −90 | 33.0 ±0.1[f] | 34.2±1.3[f] | 6.3±7.4[f] |
| **6**[c] | −66.09 | −72.26 | −75.67 | 108.9 | 117.1 | 106.1 | −50 | 40.46±0.01[g] | 35.8±0.5[g] | −21.0±2.4[g] |
| **7** | −64.95 | −71.64 | −74.68 | 107.8 | 118.1 | 106.4 | −10 | 47.25±0.04[h] | 44.1±0.5[h] | −11.8±2.2[h] |
| **8***a*[e] | −65.00 | −71.96 | −75.09 | 109.6 | 113.4 | 107.8 | −20 | 46[i] | | |
| **8***b*[e] | −63.92 | −70.20 | −75.43 | 107.5 | 118.3 | 104.9 | | | | |

[a]Values ($\partial$) are cited relative to $CFCl_3$ (16). The relative values are accurate to the level of significance shown.
[b]In $CFCl_3$ at −128°C.
[c]In $CFCl_3$ at −100°C.
[d]In $CDCl_3$ at −63.5°C.
[e]Relative abundance **8***a*/**8***b* = 2.0, in $CDCl_3$ at −63°C. These correspond to the geometric isomers which arise from rotation about the amide C(O)—N bond.
[f]Temperatures (°C) and rate constants ($s^{-1}$): −60, 45 000; −80, 4900; −100, 225; −110, 92; −115, 37; −120, 16.5.
[g]Temperatures (°C) and rate constants ($s^{-1}$): 0, 60 000; −20, 18 500; −40, 4000; −60, 540; −65, 390; −80, 65.
[h]Temperatures (°C) and rate constants ($s^{-1}$): 21, 20 000; 0, 5200; −20, 1020; −40, 142; −50, 56; −55, 27.
[i]Estimated using the Eyring equation (see text), $k_c \approx 1700\ s^{-1}$.

were obtained at the coalescence temperature $T_c$, using eq. [2]. Errors were estimated using eq. [3], following Binsch and Kessler (22*b*).

$$[2]\quad \Delta G^{\ddagger} = \Delta H^{\ddagger} - T_c \Delta S^{\ddagger}$$

$$[3]\quad \sigma(\Delta G^{\ddagger}) \approx |\sigma(\Delta H^{\ddagger}) - T\sigma(\Delta S^{\ddagger})|$$

The results are given in Table 1. For **8**, lineshape analysis could not be used because the low temperature $^{19}F$ spectra are complicated due to the presence of geometric (rotational) diastereomers. These occur as a consequence of rotation about the C(O)—N bond. The free energy of activation for **8** was estimated from the Eyring equation (eq. [4]), where an approximate rate constant, $k_c$, at the coalescence temperature, $T_c$,

$$[4]\quad k_c = \left(\frac{k_B}{h} T_c\right) e^{-\Delta G^{\ddagger}/RT_c}$$

was obtained using DNMR3 and average limiting chemical shifts taken from Table 1. The values so obtained for **8** are: $\Delta G^{\ddagger} = 46$ kJ/mol, $T_c = -20$°C, $k_c = 1700\ s^{-1}$.

Barriers to hindered rotation about C—C single bonds have been the subject of several reviews (3, 23). Barriers to rotation about bonds of the $sp^3$–$sp^3$ type range from 11.7 kJ/mol (for ethane) to values as high as 140 kJ/mol, generally increasing with the size of the substituents. Barriers to rotation about bonds terminating in the $CF_3$ group are generally in the range 16–35 kJ/mol (17) (16.4 kJ/mol for $CF_3CF_3$) (24). Values obtained in the present study (Table 1) are somewhat higher than the norm but consistent with the high coalescence temperatures observed, and reflect the severe steric crowding of the substituents at the chiral centre. Indeed it is very difficult to prepare a spacefilling model of any of the compounds **2**–**8**.

*Stereochemistry of the individual fluorine resonances*

It would be of interest to assign the individual fluorine resonances in the chiral environment of the derivatives of **1**. Although an unambiguous assignment cannot be made at this time, several facts are consistent with the assignment shown in structure **9**, where $F_A$ is at highest frequency and X is Cl or a

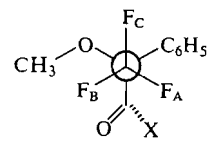


**9**

—$NR^1R^2$ group. In each of the compounds listed in Table 1, the individual fluorine atoms of the trifluoromethyl group are separated by about 10 ppm. $^{19}F$ chemical shifts have been related to the covalency of the bonding to fluorine and to the anisotropy of the charge distribution of the fluorine atom. A shift to low field (deshielding) due to the paramagnetic contribution is greatest in covalently bonded fluorine and is zero in the spherically symmetric $F^-$ ion (25). Although explicit calculation of the chemical shifts of fluorines in systems such as **1**–**8** is beyond our present capabilities, in order to obtain a measure of the amount of covalent character of the bonds to the three fluorine atoms, we have performed extensive geometry optimization by the MNDO method (26) on one of the conformers of **6**, shown below, which we judged from construction of spacefilling models most likely to correspond to the global minimum. Beginning with $\theta_1 = 0°$ and $\theta_2 = -60°$, and optimizing a total of 34 independent structural parameters (bond lengths, bond angles, and dihedral angles (only the internal geometry of the three methyl groups and

Can. J. Chem. Downloaded from www.nrcresearchpress.com by 210.87.254.5 on 09/06/12
For personal use only.

the phenyl ring were constrained to standard values), the structure relaxed to $\theta_1 = 1°$ ($CF_3$ groups eclipsed to carbonyl group) and $\theta_2 = -50°$. The calculated anisotropies (27), $L(X)$, of the three fluorine atoms and bond orders (27), $B(C,F)$, of the bond to the fluorine atom can be used as indicators of covalent character. The calculated quantities for the three fluorine atoms (structure **9**) are $L(F_A) = 0.3458$, $L(F_B) = 0.3425$, $L(F_C) = 0.3404$, $B(C,F_A) = 0.9347$, $B(C,F_B) = 0.9289$, and $B(C,F_C) = 0.9253$. Although the differences in anisotropy and bond order appear to be small, direct application of the observed (25) correspondence between chemical shift and covalency yields the result that $F_A$ should be at highest frequency and $F_C$ at lowest.

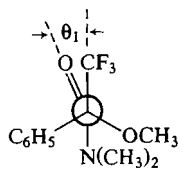


*6a*

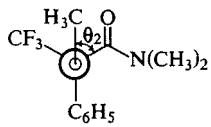


*6b*

The above result is consistent with the assignment of $F_B$ as the fluorine atom which is coupled to the protons of the methoxy group. The computations show the closest contact to be between $F_B$ and the methyl group, $r(F_B—CH_3O) = 2.50$ Å, compared to $r(F_A—CH_3) = 4.24$ Å and $r(F_C—CH_3O) = 3.18$ Å. The observed 5-bond F—H coupling is reminiscent of the stereospecific 5-bond F—F coupling reported by Weigert and Roberts (17), which was ascribed to "through space" or "direct" coupling, a mechanism which has substantial experimental support (28, 29). Although Weigert has urged restraint in the correlation of structure with "through space" coupling constants (19), the observed couplings $^5J_{F_B—H} = 4.3$ Hz in **6**, $^5J_{F_B—H} = 4.7$ Hz in **7** are very nearly those expected for $r(F_B—H) = 2.5$ Å using Myhre's curve which relates $J_{HF}$ to $r(F—H)$ (29).

## Acknowledgments

We thank the Natural Sciences and Engineering Research Council of Canada for financial support of this work. We also thank R. Yamdagni for determining the nmr spectra and T. S. Sorensen for many useful discussions.

1. J. A. Dale, D. L. Dull, and H. S. Mosher. J. Org. Chem. **34**, 2543 (1969).
2. G. R. Sullivan, J. A. Dale, and H. S. Mosher. J. Org. Chem. **38**, 2143 (1973).
3. H. Kessler. Angew. Chem. Int. Ed. Engl. **9**, 219 (1970).
4. (*a*) M. T. Rogers and J. C. Woodbrey. J. Phys. Chem. **66**, 540 (1962); (*b*) A. Greenville Wittaker and S. Siegel. J. Chem. Phys. **43**, 1575 (1965); (*c*) F. Conti and W. von Philipsborn. Helv. Chim. Acta, **50**, 603 (1967); (*d*) A. Montaudo, P. Maravigna, S. Caccamese, and V. Librando. J. Org. Chem. **39**, 2806 (1974).
5. I. G. John and L. Radom. J. Mol. Struct. **36**, 133 (1977).
6. (*a*) R. F. Curl, Jr. J. Chem. Phys. **30**, 1529 (1959); (*b*) M. Simonetta and S. Cakra. *In* The chemistry of carboxylic acids and esters. *Edited by* S. Patai. Wiley Interscience, New York, NY. 1962. pp. 1–52; (*c*) G. I. L. Jones and N. L. Owen. J. Mol. Struct. **18**, 1 (1973); (*d*) S. W. Charles, G. I. L. Jones, N. L. Owen, S. J. Cyvin, and B. N. Cyvin. J. Mol. Struct. **16**, 225 (1973); (*e*) N. S. True and R. K. Bohn. J. Mol. Struct. **36**, 173 (1977).
7. Y. Omura, J. Corset, and P. Bonnet. J. Mol. Struct. **66**, 93 (1980).
8. G. I. L. Jones, D. G. Lister, N. L. Owen, M. C. L. Gerry, and P. Palmieri. J. Mol. Spectrosc. **60**, 348 (1976).
9. D. G. Lister, N. L. Owen, and P. Palmieri. J. Mol. Struct. **31**, 411 (1976).
10. L. A. LaPlanche and M. T. Rogers. J. Am. Chem. Soc. **86**, 337 (1964).
11. L. A. LaPlanche and M. T. Rogers. J. Am. Chem. Soc. **85**, 3728 (1963).
12. A. J. R. Bourn, D. G. Gillies, and E. W. Randall. Tetrahedron, **22**, 1825 (1966).
13. (*a*) J. Jacobus and T. B. Jones. J. Am. Chem. Soc. **92**, 4583 (1970); (*b*) W. L. Nelson and T. R. Burke, Jr. J. Org. Chem. **43**, 3641 (1978).
14. D. Wendisch, H. Feltkamp, and U. Scheidegger. Org. Magn. Reson. **5**, 129 (1972).
15. Y. Egawa, M. Suzuki, and T. Okuda. Chem. Pharm. Bull. **11**, 589 (1963).
16. Manual of recommended practices in spectroscopy – terms, symbols, conventions and references relating to nuclear magnetic resonance spectroscopy. E386-6GT, ASTM publication, 1969.
17. F. J. Weigert and J. D. Roberts. J. Am. Chem. Soc. **90**, 3577 (1968).
18. F. J. Weigert, M. B. Winstead, J. I. Garrels, and J. D. Roberts. J. Am. Chem. Soc. **92**, 7359 (1970).
19. F. J. Weigert and W. Mahler. J. Am. Chem. Soc. **94**, 5314 (1972).
20. R. G. Cavell and K. I. The. Inorg. Chem. **17**, 355 (1978).
21. K. I. The and R. G. Cavell. Inorg. Chem. **16**, 1463 (1977).
22. (*a*) D. A. Kleier and G. Binsch. QCPE, **11**, 165 (1970); (*b*) G. Binsch and H. Kessler. Angew. Chem. Int. Ed. Engl. **19**, 411 (1980).
23. (*a*) J. Dale. Tetrahedron, **22**, 3373 (1966); (*b*) E. Wyn-Jones and R. A. Pethrick. Top. Stereochem. **5**, 205 (1970); (*c*) M. Oki. Angew. Chem. Int. Ed. Engl. **15**, 87 (1976).
24. (*a*) P. N. Brier. J. Mol. Struct. **6**, 23 (1970); (*b*) D. F. Eggers, Jr., R. C. Lord, and C. W. Wickstrom. J. Mol. Spectrosc. **59**, 63 (1976).
25. (*a*) H. S. Gutowsky and C. J. Hoffman. J. Chem. Phys. **19**, 1259 (1951); (*b*) A. Saika and C. P. Slichter. J. Chem. Phys. **22**, 26 (1954).
26. W. Thiel. QCPE, **11**, 353 (1978).
27. D. R. Armstrong, P. G. Perkins, and J. J. P. Stewart. J. Chem. Soc. Dalton Trans. 838 (1973).
28. E. Abushanab. J. Am. Chem. Soc. **93**, 6532 (1971).
29. P. C. Myhre, J. W. Edwards, and J. D. Kruger. J. Am. Chem. Soc. **88**, 2459 (1966).

Can. J. Chem. Downloaded from www.nrcresearchpress.com by 210.87.254.5 on 09/06/12
For personal use only.

# The solubilization of potassium permanganate by polyethylene glycols

DONALD G. LEE AND HASAN KARAMAN

*Department of Chemistry, The University of Regina, Regina, Sask., Canada S4S 0A2*

Received March 9, 1982

DONALD G. LEE and HASAN KARAMAN. Can. J. Chem. **60**, 2456 (1982).

The abilities of various cyclic and acyclic polyethers to solubilize potassium permanganate in organic solvents have been compared. In general, the cyclic compounds (crown ethers) are more effective than acyclic polyethers of comparable molecular weights. Each mole of 18-crown-6 is capable of solubilizing one mole of potassium permanganate in most solvents whereas the corresponding linear polymer, dimethyloctaethylene glycol, is much less effective, particularly in solvents of low polarity. Very long chain polymers are capable of complexing more than one mole of potassium ion per mole of polyether and thus bringing more than one mole of potassium permanganate into solution. A comparison with other studies on acyclic polyethylene glycols suggests that these structures would be helical with the oxygen complexed potassium ions inside and the permanganate anions arranged along the exterior.

DONALD G. LEE et HASAN KARAMAN. Can. J. Chem. **60**, 2456 (1982).

On a comparé les propriétés qu'ont divers polyéthers cycliques ou acycliques de solubiliser le permanganate de potassium dans des solvants organiques. En général, les composés cycliques (éthers couronnes) sont plus efficaces que les polyéthers acycliques de poids moléculaires comparables. Chaque mole d'éther-18 couronne-6 est capable de solubiliser une mole de permanganate de potassium dans la plupart des solvants alors que le polymère linéaire correspondant, le diméthyloctaéthylèneglycol, est beaucoup moins efficace, particulièrement dans les solvants de faible polarité. Les très longues chaînes de polymères peuvent complexer plus d'une mole d'ion potassium par mole de polyéther et solubilisent de ce fait plus d'une mole de permanganate de potassium. La comparaison avec d'autres études sur les polyéthylèneglycols acycliques suggère que ces structures peuvent être en hélice; les ions potassium, complexés par l'oxygène, sont à l'intérieur et les anions permanganates disposés à l'extérieur.

[Traduit par le journal]

## Introduction

The complexation of metal cations by polyethers is a well established method for solubilizing ionic reagents in organic solvents (1). Both cyclic (2) and acyclic (3) polyethylene glycols have been used to dissolve ionic reagents in organic solvents. The dissolved ionic reagents can then be used in a variety of chemical reactions (4).

Several synthetic procedures that utilize permanganate dissolved in organic solvents with the aid of polyethers have been reported (5) and in an attempt to optimize these procedures, as well as to obtain a better understanding of the fundamental principles involved, we have undertaken a quantitative study of the phase distributions of potassium permanganate in the presence of cyclic and acyclic polyethers.

## Experimental

*Materials*

The crown ethers were obtained from the Aldrich Chemical Co., the methoxypolyethylene glycols from Union Carbide Ltd., dimethyloctaethylene glycol from Prof. Herbert Lehmkuhl, and the trimethylsilanepolyethylene glycols from Dr. Gerd Rossmey. The solvents used were Fisher, spectro grade. Finely powdered potassium permanganate was obtained from the Carus Chemical Company.

*Extinction coefficients*

Since we intended to use its absorption spectrum to determine the concentration of permanganate in several solvents, it was first necessary to obtain extinction coefficients in each solvent.

TABLE 1. Extinction coefficients for permanganate in various solvents

| Solvent | 514 nm | 526 nm |
|---|---|---|
| Dichloromethane | 1720±30 | 2570±20 |
| Chloroform | 1710±30 | — |
| Benzene | 1750±40 | 2410±50 |
| Water | 1750±30 | 2410±40 |

In order to do this a solution of benzyltriethylammonium chloride ($1.60 \times 10^{-2}$ *M*) was prepared in the solvent under consideration and an aliquot (5 mL) was used to extract smaller volumes (0.2, 0.4, 0.6, 0.8, and 1.0 mL) of $1.65 \times 10^{-3}$ *M* aqueous potassium permanganate. (Benzyltriethylammonium chloride is a very efficient phase transfer agent for $KMnO_4$ and it was observed to be completely extracted from the aqueous solutions under these conditions.) The absorbances were then measured at two points (514 and 526 nm) and extinction coefficients obtained from the slopes of absorbance vs. concentration plots. This procedure was repeated at least three times for each solvent and the extinction coefficient for aqueous permanganate solutions was calculated similarly. The results are summarized in Table 1.

As the data indicate, extinction coefficients are the same in all of the solvents within the limits of experimental uncertainty. All measurements were subsequently made at 514 nm where the extinction coefficient was assumed to be 1740 L $mol^{-1}$ $cm^{-1}$. It was noted, however, that identical results were obtained in several cases where measurements were also made at 526 nm.

*Distribution ratios*

Distribution ratios relating to the ability of polyethers to bring solid $KMnO_4$ into solution were determined in the following manner. Initially, solid powdered potassium permanganate was extracted with solutions of polyethers and the number of moles of $KMnO_4$ which dissolved was determined spectrophotomet-

0008-4042/82/192456-04$01.00/0

©1982 National Research Council of Canada/Conseil national de recherches du Canada

Can. J. Chem. Downloaded from www.nrcresearchpress.com by 210.87.254.5 on 09/06/12
For personal use only.

Can. J. Chem. Downloaded from www.nrcresearchpress.com by 210.87.254.5 on 09/06/12
For personal use only.

rically. The ratio of the number of moles of permanganate which had dissolved to the number of moles of polyether initially present ($[MnO_4^-]_{org}/[Polyether]_{initial}$) was designated by the symbol $K_R$. Under these conditions it may be assumed that permanganate exists in the organic solvents as an ion pair tightly associated with polyether complexed potassium ions (6).

In a typical experiment, five solutions containing different concentrations of polyether were prepared in a particular solvent and aliquots (5 mL) of each solution were added to test tubes containing an excess (0.1 g) of finely powdered potassium permanganate. After equilibrium had been established (vigorous shaking) the excess solid potassium permanganate was removed by centrifuging and the clear supernatant transferred to a cuvette. Absorbances at 514 nm were measured using a Unicam 500 SP spectrophotometer equipped with a thermostated cell compartment and $K_R$ values were obtained from plots of permanganate concentration vs. the initial concentration of polyether. A typical plot has been reproduced in Fig. 1.

## Results and discussion

The distribution ratios obtained when methylene chloride was used as the solvent have been collected in Table 2. An examination of the $K_R$ values reveals at least one surprising result; the longer chain polyethers are capable of solubilizing more than one mole of $KMnO_4$, with the longest polymers being capable of bringing an average of almost six moles of permanganate into solution. The quantity $n/K_R$ indicates the number of oxyethylene units required to solubilize one mole of $KMnO_4$. This value is lowest for the macrocyclic ethers, 18-crown-6 and dibenzo-18-crown-6, presumably because complexation constants are greater with preformed rings (7). It is apparent from the $K_R$ values that each of these crown ethers is capable of complexing one mole of potassium ion; however, two moles of 15-crown-5 are required per mole of $K^+$, suggesting that this complex exists as a sandwich with the cation situated between a pair of crowns (8, 9).

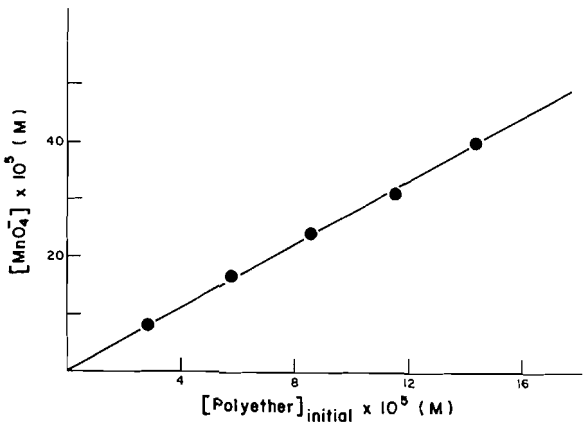


FIG. 1. A typical plot for the estimation of $K_R$ values. The system illustrated is $CH_3(OCH_2CH_2)_{44.7}OH$ in methylene chloride.

TABLE 2. Distribution ratios in methylene chloride[a]

| Polyether | $K_R$ | $n/K_R$[b] |
|---|---|---|
| 15-Crown-5 | 0.56±0.01 | 10 |
| 18-Crown-6 | 0.99±0.01 | 6 |
| Dibenzo-18-crown-6 | 0.95±0.02 | 6 |
| $(CH_3)_3Si(OCH_2CH_2)_{7.3}OSi(CH_3)_3$ | 0.67±0.02 | 11 |
| $CH_3(OCH_2CH_2)_8OCH_3$ | 0.81±0.01 | 10 |
| $(CH_3)_3Si(OCH_2CH_2)_{11.4}OSi(CH_3)_3$ | 0.92±0.02 | 12 |
| $CH_3(OCH_2CH_2)_{11.8}OH$ | 1.02±0.02 | 12 |
| $CH_3(OCH_2CH_2)_{16.3}OH$ | 1.40±0.01 | 12 |
| $CH_3(OCH_2CH_2)_{44.7}OH$ | 2.91±0.15 | 15 |
| $CH_3(OCH_2CH_2)_{113}OH$ | 5.84±0.04 | 19 |

[a]At 25°C.
[b]$n$ = the average number of oxyethylene units.

Complexes of more than one mole of cation per mole of polyether are not unknown. For example, binuclear S-shaped complexes of KSCN with acyclic polyethers have been prepared and studied crystallographically (10). However, we are not aware of previously reported examples where as many as six cations were complexed by a single polyether.

Crystallographic studies have established that polyethylene glycols exist in the solid state as distorted helices containing about seven oxygens per loop (11). Consequently it is to be expected, when these compounds complex a salt in an organic solvent, that the oxygens would fold inward around the positive ion and the methylenes would form a nonpolar sheath projecting into the solvent (1). Since a crown with six oxygens is capable of complexing a potassium ion it might be expected that each loop of the helix could also accommodate one cation. However, if cations were situated within the cavity of the helix there would be a certain amount of electrical repulsion which would discourage the location of ions on adjacent loops. As a consequence it may be seen that as the number of cations per mole of polyether increases the number of oxyethylene units required per cation also increases.

It is apparent from a consideration of the data in Table 2 that the most important characteristic of the acyclic polyethers is the length of the chain and not the nature of the terminal "caps" (12), (see Fig. 2).

The ratios obtained when chloroform was used as the solvent are similar to those obtained with methylene chloride for the crowns but somewhat smaller for the acyclic polyethers. The latter may be due to the lower polarity of chloroform (13) which would increase the energy required to

TABLE 3. Distribution ratios ($K_R$) in various solvents[a]

| Polyether | Methylene chloride | Chloroform | Toluene |
|---|---|---|---|
| 18-Crown-6 | 0.99 | 1.03 | 1.03 |
| Dibenzo-18-crown-6 | 0.95 | 0.83 | 0.77 |
| $(CH_3)_3Si(OCH_2CH_2)_{7.3}OSi(CH_3)_3$ | 0.67 | 0.25 | 0.080 |
| $CH_3(OCH_2CH_2)_8OCH_3$ | 0.81 | 0.14 | 0.075 |
| $(CH_3)_3Si(OCH_2CH_2)_{11.4}OSi(CH_3)_3$ | 0.92 | 0.23 | 0.26 |
| $CH_3(OCH_2CH_2)_{11.8}OH$ | 1.02 | 0.42 | 0.51 |
| $CH_3(OCH_2CH_2)_{16.3}OH$ | 1.40 | 0.60 | 0.72 |
| $CH_3(OCH_2CH_2)_{44.7}OH$ | 2.91 | 1.56 | 0 |
| $CH(OCH_2CH_2)_{113}OH$ | 5.84 | 4.30 | 0 |

[a]At 25°C.

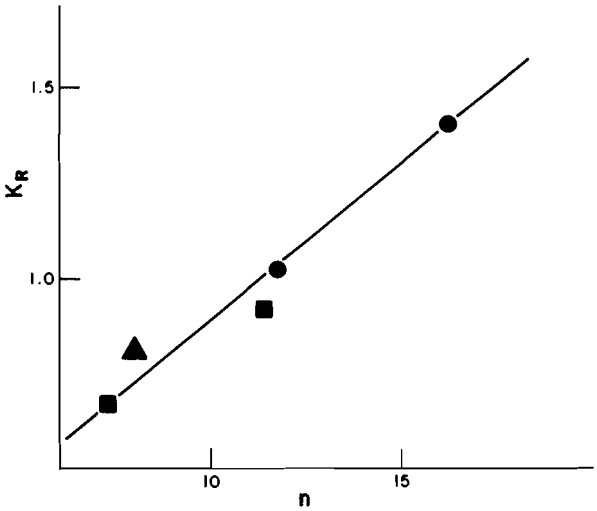


FIG. 2. Plot of $K_R$ against the number of oxyethylene units in the chain. ▲, $CH_3(OCH_2CH_2)_nOCH$; ●, $CH_3(OCH_2CH_2)_nOH$; ■, $(CH_3)_3Si(OCH_2CH_2)_nOSi(CH_3)_3$.

solubilize an ion pair. This is further emphasized by the data in Table 3 from which it is clearly evident that the acyclic polyether complexes are more sensitive to changes in solvent polarity than are the crowns. The ability of dibenzo-18-crown-6 to function in solvents of low polarity (as compared to 18-crown-6) is somewhat decreased, possibly because the aromatic rings lend rigidity to the crown and withdraw electrons from the oxygens, thus decreasing its capability of complexing the potassium ions (14).

Although the effects of solvent changes on the magnitude of binding constants in homogeneous systems have been studied (15), the effects on phase changes of the type described here have been given less attention. However, when Brandstrom (6) studied the distribution of tetrabutylammonium salts between water and several organic solvents, he found that the smaller anions such as chloride were more easily extracted into chloroform than methylene chloride, but for ions in which the charge to mass ratio was small the reverse was true. For example, the salts of larger anions such as perchlorate and trinitrophenolate were more soluble in methylene chloride. The behavior of permanganate in the present study thus appears to be similar to that exhibited by other anions which can delocalize the negative charge over several oxygens.

Finally, it may be noted that these results lead to certain conclusions that have practical application to the oxidation of organic compounds in nonaqueous solvents. (*i*) The acyclic polyethers can be used as effectively to solubilize $KMnO_4$ as the more expensive crowns, provided that their lower efficiency is compensated for by use of longer chains. (*ii*) The concentration of permanganate in solution can be controlled by selection of an acyclic polyether of the appropriate length. A rough estimate of the concentrations to be expected can be obtained from interpolation of the data in Tables 2 and 3. (*iii*) Of the solvents studied, the use of methylene chloride resulted in the highest concentrations of potassium permanganate. The acyclic polyethers were all found to be completely incapable of solubilizing $KMnO_4$ in nonpolar solvents such as carbon tetrachloride or pentane.

**Acknowledgements**

The authors are grateful for financial support from the Natural Sciences and Engineering Research Council of Canada, Imperial Oil Limited, and the Carus Chemical Company.

1. N. S. POONIA and A. V. BAJAJ. Chem. Rev. **79**, 389 (1979).
2. F. DEJONG and D. N. REINHOUDT. Adv. Phys. Org. Chem. **17**, 279 (1980).
3. F. VOGTLE and E. WEBER. Angew. Chem. Int. Ed. Engl. **18**, 753 (1979).
4. S. YANAGIDA, K. TAKAHASHI, and M. OKAHARA. Bull. Chem. Soc. Jpn. **50**, 1386 (1977); **51**, 1294 (1978); R. A. BARTSCH, P. N. JURI, and M. A. MILLA. Tetrahedron Lett.

Can. J. Chem. Downloaded from www.nrcresearchpress.com by 210.87.254.5 on 09/06/12
For personal use only.

2499 (1979); R. A. BARTSCH and I. W. YANG. Tetrahedron Lett. 2503 (1979); V. TAKAKI and J. SMID. J. Am. Chem. Soc. **96**, 2588 (1974).
5. D. G. LEE and V. S. CHANG. J. Org. Chem. **43**, 1532 (1978); D. G. LEE. *In* Oxidation in organic chemistry, Part D. *Edited by* W. S. Trahanvosky. Academic Press, New York. 1982. p. 147.
6. A. BRANDSTROM. Adv. Phys. Org. Chem. **15**, 267 (1977).
7. J. M. TIMKO, S. S. MOORE, D. M. WALBA, P. C. HIBERTY, and D. J. CRAM. J. Am. Chem. Soc. **99**, 4207 (1977).
8. R. M. IZATT, R. E. TERRY, D. P. NELSON, Y. CHAN, D. J. EATOUGH, J. S. BRADSHAW, L. D. HANSEN, and J. J. CHRISTENSEN. J. Am. Chem. Soc. **98**, 7626 (1976).
9. P. R. MALLINSON and M. R. TRUTER. J. Chem. Soc. Perkin Trans. II, 1818 (1972).
10. G. WEBER and W. SAENGER. Angew. Chem. Int. Ed. Engl. **18**, 227 (1979); F. VOGTLE and V. HEIMANN. Chem. Ber. **111**, 2757 (1978).
11. Y. TAKAHASHI and H. TADOKORO. Macromolecules, **6**, 672 (1973); H. TADOKORO, Y. CHATANI, T. YOSHIHARA, S. TAHARA, and S. MURAHASHI. Makromol. Chem. **73**, 109 (1964).
12. B. TUMMLER, G. MAASS, F. VOGTLE, H. SIEGER, U. HEIMANN, and E. WEBER. J. Am. Chem. Soc. **101**, 2588 (1979).
13. M. J. KAMLET, J. L. ABBOUD, and R. W. TAFT. J. Am. Chem. Soc. **99**, 6027 (1977).
14. J. D. LAMB, R. M. IZATT, J. J. CHRISTENSEN, and D. J. EATOUGH. *In* Coordination chemistry of macrocyclic compounds. *Edited by* G. A. Melson. Plenum, New York. 1979. p. 145.
15. D. M. DISHONG and G. W. GOKEL. J. Org. Chem. **47**, 147 (1982).

Can. J. Chem. Downloaded from www.nrcresearchpress.com by 210.87.254.5 on 09/06/12
For personal use only.

# Kinetics of the intermolecular exchange reaction $Cp_3U^{III}$–$Cp_3U^{IV}Cl$

M. BURTON, G. FOLCHER,[1] H. MARQUET-ELLIS, AND P. RIGNY
*Département de Physico-chimie, LRMCI(LA331), CEN-Saclay, 91191 Gif-sur-Yvette, France*
AND
C. GIANNOTTI
*C.N.R.S., Institut de Chimie des Substances Naturelles, 91190 Gif-sur-Yvette, France*

Received March 25, 1982

M. BURTON, G. FOLCHER, H. MARQUET-ELLIS, P. RIGNY, and C. GIANNOTTI. Can. J. Chem. **60**, 2460 (1982).

The intermolecular exchange of cyclopentadienyl groups in the system $UCp_3$–$UCp_3Cl$ in THF solution between 170–300 K was investigated by $^1H$ nmr. The kinetic results show a bimolecular mechanism and suggest an electron transfer via the chlorine atom. This first example of a symmetrical exchange in the $U^{III}$–$U^{IV}$ system illustrates the lability of actinide organometallic compounds.

M. BURTON, G. FOLCHER, H. MARQUET-ELLIS, P. RIGNY et C. GIANNOTTI. Can. J. Chem. **60**, 2460 (1982).

L'échange intermoléculaire des groupes cyclopentadienyl dans le système $Cp_3U$–$Cp_3UCl$ en solution THF, entre 170 et 300 K a été étudié par rmn du proton. Les résultats cinétiques montrent qu'il s'agit d'un mécanisme bimoléculaire et suggère un transfert d'électron par l'intermédiaire d'un atome de chlore. Ce premier exemple d'échange symétrique $U^{III}$–$U^{IV}$ illustre la labilité de coordinence des composés organométalliques des actinides.

The study of exchange reactions provides particularly useful information in understanding the reactivity of organometallic complexes. In the specific case of uranium organometallics of the type $(C_5H_5)_3UX$ their relative inertness (1–3) is generally explained by saturation of the coordination sphere caused by three $\pi$ bonding $C_5H_5$ groups and a monodentate ligand, e.g. halogen or alkyl.

During previous work on the reduction of $U^{IV}$ cyclopentadienyls (5, 6) we noticed in the $^1H$ nmr the appearance of two reduced species well characterized by their optical and nmr spectra.

These two species have already been identified by Kanellakopulos *et al.* as $UCp_3$ and $UCp_3$.THF (4). We assigned the nmr data according to the published optical spectra. The reaction between $UCp_3$, which is most likely a dimer, and the adduct $UCp_3$.THF is not clearly understood. Nevertheless the observed optical spectrum of the product, which gives a singlet at 20 ppm, is very similar to $UCp_3$.THF. Here we present the unexpected behaviour of $UCp_3$.THF in the presence of $Cp_3UCl$, namely an exchange between the two molecules in THF solution at ambient temperature.

## Experimental

$UCp_3Cl$, $UCp_3CH_3$, and $UCp_3(iPr)$ were prepared and photolyzed according to the published procedure (6). In a typical experiment an equimolar quantity of $UCp_3Cl$ and $UCp_3CH_3$ in THF ($10^{-2}$ *M*) was photolyzed in an nmr tube. During irradiation the nmr signals for $UCp_3CH_3$ diminished while the signal for $UCp_3Cl$ was displaced upfield. A less easy method has also been employed in order to confirm the results: a careful reduction of $Cp_3UCl$ by $LiAlH_4$ in THF is achieved, the reaction followed by nmr to minimize the excess of reductant. The solution is filtered and the solvent removed; the resulting solid, vacuum dried, can be used to make THF solutions. The main disadvantage of this method is that the solid $Cp_3U$ (THF), which is not a well cristallized compound, does not dissolve entirely in THF at room temperature (as, for instance, reported in ref. 4).

In both cases, the relative concentration of $Cp_3U$THF and $Cp_3UCl$ was obtained by integration of the exchange peak and from the relationship $\nu - \nu_B = P_A(\nu_A - \nu_B)$ where $\nu$ represents the resonance frequency and $P$ the populations of the species in exchange. The nmr spectra were run on a Varian NV14 equipped with a variable temperature accessory. One resonance of THF was chosen as internal lock.

## Results and discussion

Figure 1 summarizes the behaviour of the Cp signal as a function of temperature between −16 and −76°C. It reveals a rapid exchange on the nmr timescale of Cp groups between $Cp_3U$ Cl and $Cp_3U$ from ambient temperature down to −50°C, and slow at less than −70°C. This exchange can be represented thus:

$$(A)\ Cp^*\ CP_2U\ Cl + (B)\ Cp_3U \rightleftharpoons Cp_3U\ Cl + Cp^*\ Cp_2U$$

remembering that species A and B have uranium in the IV and III oxidation states respectively.

The mechanism of this exchange can be understood by considering the parameters involved. Firstly, the reaction order can be found by plotting (Fig. 2) the line width at half height of the exchange peak as a function of the relative concentrations of the two species.

Two cases are considered.

(*a*) First order, $dA/dt = dB/dt = k_1A$

(*b*) Second order, $dA/dt = dB/dt = k_2\,A.B$

[1]Author to whom correspondence may be addressed.

0008-4042/82/192460-03$01.00/0
©1982 National Research Council of Canada/Conseil national de recherches du Canada

Can. J. Chem. Downloaded from www.nrcresearchpress.com by 210.87.254.6 on 09/06/12
For personal use only.

Can. J. Chem. Downloaded from www.nrcresearchpress.com by 210.87.254.6 on 09/06/12
For personal use only.

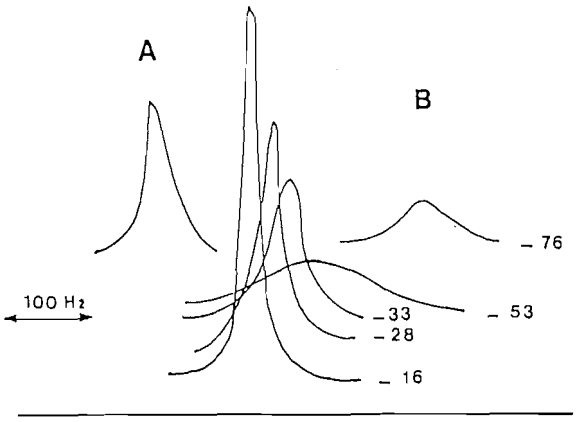


FIG. 1. The $^1H$ nmr spectra at 60 MHz of Cp in $Cp_3U$–$Cp_3U$ Cl system in THF. Temperature dependence.

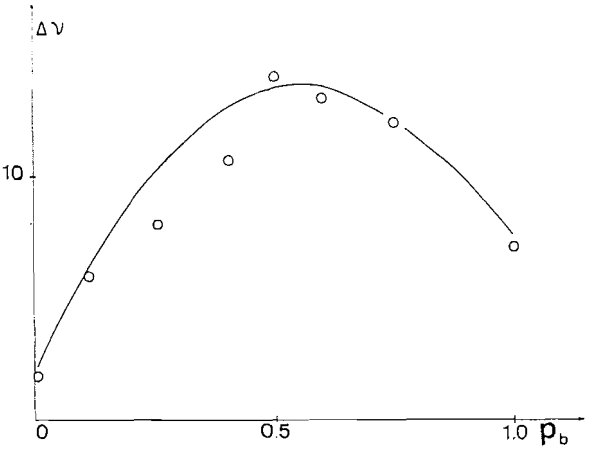


FIG. 2. Experimental (○) line width vs. $[UCp_3]/[UCp_3] + [UCp_3Cl]$. Solid line fits eq. [3] at room temperature.

In both cases $1/\tau = 1/\tau_A + 1/\tau_B$

Under rapid exchange conditions $2\pi\tau\Delta\nu \ll 1$. We can therefore employ the following expression (7)

$$[1] \quad \Delta = P_A \Delta_A^0 + P_B \Delta_B^0 + 4\pi^2 (\Delta\nu)^2 P_A P_B \tau$$

where $\Delta$ is the width at half height, $\Delta^0$ indicates the pure species in the absence of exchange, $\Delta\nu$ the difference in the resonance frequency between A and B, and $P_A$ and $P_B$ the respective populations of species A and B.

With first order kinetics,

$$[2] \quad \Delta = (1 - P_A)\Delta_B + P_A \Delta_A + P_A \frac{(1 - P_A)^2}{k_1} \times 4\pi^2 \Delta\nu^2$$

Assuming a second order reaction

$$[3] \quad \Delta = (1 - P_A)\Delta_B + P_A \Delta_A + P_A \frac{(1 - P_A)}{k_2 C} \times 4\pi^2 \Delta\nu^2$$

where $C$ is the total concentration of A and B.

Figure 2 is in good agreement with the expression depicting 2nd order kinetics. $\Delta_B$ is taken to be 7 Hz, the value for pure $UCp_3$, $\Delta_A$ is around 2 Hz and rapidly becomes negligible. $k_2 C$ is calculated to be $3.4 \times 10^5\ s^{-1}$.

The exchange is therefore second order with a rate constant of approximately $3 \times 10^6\ s^{-1}\ mol^{-1}$ at room temperature. The study as a function of temperature is shown in Figs. 1 and 3.

Figure 1 presents the behaviour of the exchange peak both in the region of rapid exchange (i.e. $2\pi\tau\Delta\nu \ll 1$) between −16 and −53°C and in the region of slow exchange (i.e. $2\pi\tau\Delta\nu \gg 1$) at temperatures below −76°C.

In the example chosen the populations $P_A$ and $P_B$ were equal to 0.4 and 0.6 respectively giving $1/\tau = 1/\tau_A + 1/\tau_B \sim 2.5/\tau_B$.

The formula [1] permits the calculation of $\Delta$ as a function of the temperature down to −50°C ($\Delta\nu$ is temperature variable but can be determined from the displacements of pure A and B in the same temperature range).

Thus for slow exchange we obtain $1/\tau_B = \pi(\Delta - \Delta^0)$ in which $\Delta^0$ represents the width in the absence of exchange and is negligible compared with $\Delta$.

Figure 3 demonstrates the linear variation in $\Delta$ as a function of $1/T$ from which the activation energy is calculated as 7.6 kcal $mol^{-1}$. Thus $\tau_B$ varies from 0.6 ms to 6 ms between −16°C and −50°C. The

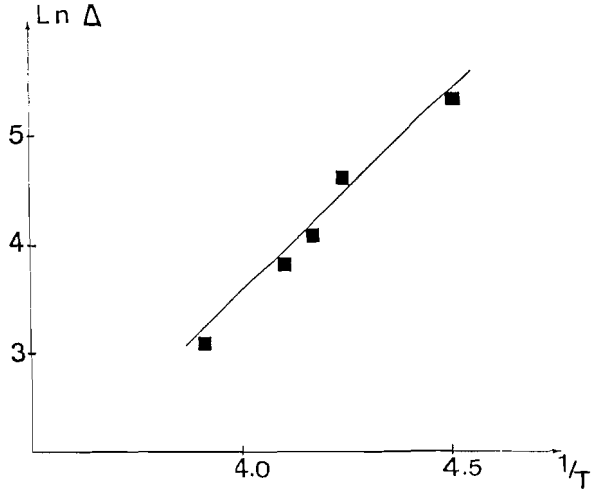


FIG. 3. Arrhenius plot of the line width of the Cp signal between −10 and −50°C.

values determined from the case of slow exchange are in good agreement with those calculated from rapid exchange. These values are less precise because the broad peaks observed do not fit exactly into a Lorentzian analysis. A more complete calculation would thus be necessary to determine better values of $\tau$.

From these measurements at slow exchange we have been able to deduce values for the bimolecular exchange constants $k_2$ ($k_2 = 1/2.5\,\tau\,[A]$) of $7 \times 10^4$ $s^{-1}\,mol^{-1}$ at $-16°C$, $7 \times 10^3$ $s^{-1}\,mol^{-1}$ at $-50°C$, and 50 $s^{-1}\,mol^{-1}$ at $-80°C$.

Two conclusions can be drawn from these results. It is the first example of symmetrical exchange demonstrated for $U^{3+}$ and the rate found is much greater than those encountered in other similar exchanges, in transition metal complexes for instance (8).

This rate must be interpreted in term of specificity of the uranium (or 5 f block elements) in an electron transfer mechanism and can be connected with the interesting properties of this ion as a reducing agent (9, 10). The molecular mechanism of this reaction suggests the presence of a complex $Cp_3U\text{-}Cl\ldots UCp_3(THF)$. In the bimetallic complex, the $Cl^-$ can be transferred from one uranium to the other.

Such a transfer achieves the electron exchange between the two uraniums and will give, on the Cp nmr spectrum, the measured broadening. A similar type of electron transfer by halogen bridge is known for several metal ion couples i.e. $Co^{3+}/Cu^{2+}$, $Fe^{3+}/Eu^{2+}$ (8); the assumed bimolecular complex is expected to be favoured by the facile enhancement of coordination number of the actinides. Thus $Cp_3U(THF)$ can easily give an adduct with $Cl^-$. On the other hand, it is well established (11, 12) in the case of β dicetonates that these complexes with high coordinance number are very labile; in this case it is assumed that the intermediate can undergo a very rapid decomposition.


1. B. KANELLAKOPULOS and K. W. BAGNALL. MPT Int. Rev. Sci. Ser. 1, **7**, 299 (1972).
2. P. J. FAGAN, J. M. MANRIQUEZ, and T. J. MARKS. Organometallics of the f elements. *Edited by* T. J. Marks and R. D. Fischer. D. Reidel, Dordrecht. 1979. p. 113.
3. T. J. MARKS, A. M. SEYAM, and J. R. KOLB. J. Am. Chem. Soc. **95**, 5529 (1973).
4. B. KANELLAKOPULOS, E. D. FISCHER, E. DORNBERGER, and F. BAUMGARTNER. J. Organometal. Chem. **24**, 507 (1970).
5. G. FOLCHER and H. MARQUET-ELLIS. J. Organometal. Chem. **131**, 257 (1977).
6. E. KLAHNE, C. GIANNOTTI, H. MARQUET-ELLIS, G. FOLCHER, and R. D. FISCHER. J. Organometal. Chem. **201**, 397 (1980).
7. J. A. POPLE, W. G. SCHNEIDER, and H. J. BERNSTEIN. High resolution NMR. McGraw-Hill, New York. 1979. p. 818.
8. R. D. CANNON. Electron transfer reactions. Butterworths, London. 1980. p. 257.
9. R. T. WANG and H. H. ESPENSON. J. Am. Chem. Soc. **93**, 380 (1971).
10. A. EKSTROM, A. B. MCLAREN, and L. E. SMYTHE. Inorg. Chem. **16**, 1032 (1973).
11. G. FOLCHER, J. PARIS, P. PLURIEN, P. RIGNY, and E. SOULIE. Chem. Commun. 3 (1974).
12. G. FOLCHER, C. KIENER, P. RIGNY, and J. VIRLET. Chem. Phys. Lett. **60**, 135 (1978).


Can. J. Chem. Downloaded from www.nrcresearchpress.com by 210.87.254.6 on 09/06/12
For personal use only.

# Simulation of edge effects in electroanalytical experiments by orthogonal collocation. Part 2. Theory for cyclic voltammetry

BERND SPEISER AND STANLEY PONS[1]

*Department of Chemistry, University of Alberta, Edmonton, Alta., Canada T6G 2G2*

Received February 23, 1982

BERND SPEISER and STANLEY PONS. Can. J. Chem. **60**, 2463 (1982).

We showed in this paper the use of two-dimensional collocation to spatially discretize partial differential equations describing a model of cyclic voltammetric experiments under the influence of edge effects. The formal similarity of discretized equations for even very complicated mechanisms has been demonstrated by considering the oxidation scheme of phenol **I**. This similarity simplifies the writing and testing of computer programs used to calculate numerical simulation results. In fact, a change in mechanism normally only requires the exchange of a few FORTRAN statements while the main body of the program is untouched. We see this as one of the great advantages of our method which outweighs the difficulties encountered while assessing the features and behavior of a new type of a model, as this two-dimensional one. A thorough discussion of the numerical results for cyclic voltammetry simulations is given in part 4.

BERND SPEISER et STANLEY PONS. Can. J. Chem. **60**, 2463 (1982).

Nous montrons dans cette publication l'application d'une collocation bidimensionnelle aux équations différentielles partielles discontinues spatialement, décrivant un modèle d'expériences en voltamétrie cyclique sous l'influence des effets d'angle. On démontre la similitude formelle des équations discontinues, même dans le cas de mécanismes très compliqués, en considérant le mécanisme d'oxydation du phénol I. Cette similitude simplifie le développement et la vérification des programmes d'ordinateurs utilisés pour calculer les résultats de simulations numériques. En fait, un changement de mécanisme ne requiert normalement qu'un changement de quelques énoncés du langage Fortran tandis que le programme principal demeure inchangé. Nous percevons ceci comme un des grands avantages de notre méthode qui fait ressortir les difficultés rencontrées lorsqu'on détermine les caractéristiques et le comportement d'un nouveau type de modèle comme celui à deux dimensions. Dans la 4e partie de ce travail, on présente une discussion complète des résultats numériques des simulations en voltamétrie cyclique.

[Traduit par le journal]

## Introduction

We have used orthogonal collocation not only for the solution of linear diffusion problems but also for simulation of two-dimensional models (1, 2). Thus, it is possible to simulate edge effects on electroanalytical experiments using this fast and flexible numerical technique.

Cyclic voltammetry is one of the most commonly used electroanalytical methods and it might be of considerable interest to calculate the effects caused by edge diffusion on the $i/E$-curves. Lines and Parker (3) have observed an increase of $\Delta E_p$ when using microelectrodes and attributed this to edge effects, a conclusion which was confirmed by theoretical calculations by Heinze (4). Speiser and Rieker (5) found dramatic changes in cyclic voltammograms of 2,6-di-*tert*-butyl-4[4-dimethylaminophenyl]-phenol **I** in unbuffered, neutral acetonitrile when decreasing the electrode area from 0.29 $cm^2$ to 0.0022 $cm^2$. These experiments have also been explained in terms of edge diffusion. Up to now, however, it was not possible to simulate the complex mechanism describing the oxidation of **I** under the conditions of a finite circular disc electrode.

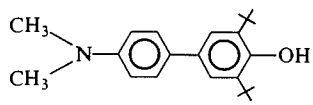


**I**

This paper expands the theory of two-dimensional orthogonal collocation to cyclic voltammetry and mechanisms as complex as the oxidation of **I**. It will only deal with the mathematics of the method, while a complete numerical analysis showing the usefulness of the derived equations will be given in part 4. This partition has been used because the analysis (which has to be done to validate the new two-dimensional collocation method) requires the discussion of many parameters. We point out, however, that this has to be done only once, while extension to more complicated mechanisms is obvious. Also, research on a comparison of the experimental results with **I** and numerical simulations is under way.

[1]To whom all correspondence should be addressed.

0008-4042/82/192463-14$01.00/0

©1982 National Research Council of Canada/Conseil national de recherches du Canada

Can. J. Chem. Downloaded from www.nrcresearchpress.com by 210.87.254.6 on 09/06/12
For personal use only.

Can. J. Chem. Downloaded from www.nrcresearchpress.com by 210.87.254.6 on 09/06/12
For personal use only.

## Initial and boundary conditions

The initial and boundary conditions have been given by Nicholson and Shain (6) and used by Speiser and Rieker (7) in the context of orthogonal collocation for linear diffusion. Pons (8) simulated cyclic voltammograms under spherical diffusion conditions using orthogonal collocation.

For simulation of edge effects we employ our two-dimensional model of a finite, circular electrode of radius $r_0$ imbedded into an insulator body (1). The radius of the insulator may go to infinity.

We assume an EC mechanism:

[1] $$A \underset{+ne^{\ominus}}{\overset{-ne^{\ominus}}{\rightleftharpoons}} B \quad E^0, n$$

[2] $$B \rightarrow C \qquad k$$

where the diffusion controlled electron transfer is described by the formal potential, $E^0$, and the number of transferred electrons, $n$. The chemical step [2] proceeds with a rate constant $k$.

Fick's second law for the substrate A takes the form

[3] $$\frac{\partial c_A}{\partial t} = D\left[\frac{\partial^2 c_A}{\partial x^2} + \frac{1}{r}\frac{\partial c_A}{\partial r} + \frac{\partial^2 c_A}{\partial r^2}\right]$$

where $t$ is time and $x$ and $r$ are the distance coordinate perpendicular to the electrode and the radial coordinate respectively. The total diffusion is expressed as superimposition of a linear and a cylindrical term.

For species B and C eqs. [4] and [5] hold:

[4] $$\frac{\partial c_B}{\partial t} = D\left[\frac{\partial^2 c_B}{\partial x^2} + \frac{1}{r}\frac{\partial c_B}{\partial r} + \frac{\partial^2 c_B}{\partial r^2}\right] - kc_B$$

[5] $$\frac{\partial c_C}{\partial t} = D\left[\frac{\partial^2 c_C}{\partial x^2} + \frac{1}{r}\frac{\partial c_C}{\partial r} + \frac{\partial^2 c_C}{\partial r^2}\right] + kc_B$$

For convenience the diffusion coefficient of all species is set equal to $D$.

We assume that A is the only species present in the solution at the beginning of the experiment, its concentration being $c_A^0$. Thus, the initial conditions are

$t = 0,\ x \geq 0,\ r \geq 0$:

[6] $$c_A(x,r,0) = c_A^0$$

[7] $$c_B(x,r,0) = c_C(x,r,0) = 0$$

At a distance far from the electrode no concentration changes take place during the experiment. This yields the boundary conditions at $x \rightarrow \infty$ and $r \rightarrow \infty$

$t > 0,\ x \rightarrow \infty,\ r \geq 0$:

[8] $$c_A(\infty,r,t) \rightarrow c_A^0$$

[9] $$c_B(\infty,r,t) = c_C(\infty,r,t) = 0$$

$t > 0,\ x \geq 0,\ r \rightarrow \infty$:

[10] $$c_A(x,\infty,t) \rightarrow c_A^0$$

[11] $$c_B(x,\infty,t) = c_C(x,\infty,t) = 0$$

At the electrode surface the concentrations of A and B are given by [12] and [13], while [14] holds for species C:

$t > 0,\ x = 0,\ 0 \leq r \leq r_0$:

[12] $$\left(\frac{\partial c_A}{\partial x}\right)_{x=0} = -\left(\frac{\partial c_B}{\partial x}\right)_{x=0}$$

$$[13] \quad \frac{c_A(0,r,t)}{c_B(0,r,t)} = \exp\left[\frac{nF}{RT}(E^0 - E)\right] = \theta_{A/B} S_\lambda(t)$$

$$[14] \quad \left(\frac{\partial c_C}{\partial x}\right)_{x=0} = 0$$

Equation [13] reflects the special features of cyclic voltammetry if

$$[15] \quad \theta_{A/B} = \exp\left[\frac{nF}{RT}(E^0 - E_{start})\right]$$

and

$$[16] \quad S_\lambda(t) = \begin{cases} \exp[2(m-1)at_\lambda - at] & \text{for } 2(m-1)t_\lambda \le t \le (2m-1)t_\lambda \\ \exp[at - 2m\,at_\lambda] & \text{for } (2m-1)t_\lambda \le t \le 2m\,t_\lambda \end{cases} \qquad m = 1,2,\ldots$$

Here $F$, $R$, and $T$ have their usual meaning, $E_{start}$ is the starting potential of the scan, $t$ the time when the scan is reversed, $m$ the number of the present scan. A cycle consists of two scans. Finally $a$ is given by

$$[17] \quad a = \frac{nF}{RT} v$$

where $v$ is the scan rate, $dE/dt$.

There is no redox reaction at the insulator and hence no flux through this surface. Thus

$t > 0$, $x = 0$, $r > r_0$:

$$[18] \quad \left(\frac{\partial c_A}{\partial x}\right)_{x=0} = \left(\frac{\partial c_B}{\partial x}\right)_{x=0} = \left(\frac{\partial c_C}{\partial x}\right)_{x=0} = 0$$

At $r = 0$ there must be no flux in $r$-direction because our model is symmetric around $r = 0$:

$t > 0$, $x \ge 0$, $r = 0$:

$$[19] \quad \left(\frac{\partial c_A}{\partial r}\right)_{r=0} = \left(\frac{\partial c_B}{\partial r}\right)_{r=0} = \left(\frac{\partial c_C}{\partial r}\right)_{r=0} = 0$$

It is convenient (1) to divide the space in the $r$-direction into two parts, inside and outside of $r_0$. The concentration may be described by $c_1$ and $c_2$, respectively. The two concentration functions have to fulfill the conditions [20] and [21] at $r = r_0$ for all species.

$t > 0$, $x \ge 0$, $r = r_0$:

$$[20] \quad c_1(x,r_0,t) = c_2(x,r_0,t)$$

$$[21] \quad \left(\frac{\partial c_1}{\partial r}\right)_{r=r_0} = \left(\frac{\partial c_2}{\partial r}\right)_{r=r_0}$$

**Transformation to a dimensionless problem**

Equations [3]–[21] are transformed into a dimensionless problem by

$$[22] \quad X = x/L$$

$$[23] \quad c^*_{A1} = c_{A1}/c^0_A$$

$$[24] \quad c^*_{A2} = c_{A2}/c^0_A$$

$$[25] \quad c^*_{B1} = c_{B1}/c^0_A$$

$$[26] \quad c^*_{B2} = c_{B2}/c^0_A$$

$$[27] \quad c^*_{C1} = c_{C1}/c^0_A$$

$$[28] \quad c^*_{C2} = c_{C2}/c^0_A$$

Can. J. Chem. Downloaded from www.nrcresearchpress.com by 210.87.254.6 on 09/06/12
For personal use only.

[29a] $R = r/r_0 \qquad \text{for } 0 \leq r \leq r_0$

[29b] $R = (r - r_0)/(M - r_0) \qquad \text{for } r \geq r_0$

[30] $T' = at$

[31] $\alpha = kD/r_0^2$

Here $X$ is a dimensionless distance perpendicular to the electrode, $L$ is a distance from the electrode defined such that diffusion effects are negligible at all times, the $c^*$'s are dimensionless concentrations, $R$ and $R'$ are dimensionless coordinates in $r$-direction for the inner and outer functions respectively, while $M$ is defined as $L$ except it is a radial distance from the center of the electrode. The symbols $T'$ and $\alpha$ denote the dimensionless simulation time and rate constant respectively.

Thus, we get the dimensionless differential equations:

[32] $$\frac{\partial c^*_{A1}}{\partial T'} = \beta \frac{\partial^2 c^*_{A1}}{\partial X^2} + \frac{\beta'}{R}\frac{\partial c^*_{A1}}{\partial R} + \beta' \frac{\partial^2 c^*_{A1}}{\partial R^2}$$

[33] $$\frac{\partial c^*_{B1}}{\partial T'} = \beta \frac{\partial^2 c^*_{B1}}{\partial X^2} + \frac{\beta'}{R}\frac{\partial c^*_{B1}}{\partial R} + \beta' \frac{\partial^2 c^*_{B1}}{\partial R^2} - \alpha c^*_{B1}$$

[34] $$\frac{\partial c^*_{C1}}{\partial T'} = \beta \frac{\partial^2 c^*_{C1}}{\partial X^2} + \frac{\beta'}{R}\frac{\partial c^*_{C1}}{\partial R} + \beta' \frac{\partial^2 c^*_{C1}}{\partial R^2} + \alpha c^*_{B1}$$

[35] $$\frac{\partial c^*_{A2}}{\partial T'} = \beta \frac{\partial^2 c^*_{A2}}{\partial X^2} + \frac{\sqrt{\beta'}\,\beta''}{\sqrt{\beta''} + \sqrt{\beta'}R'}\frac{\partial c^*_{A2}}{\partial R'} + \beta'' \frac{\partial^2 c^*_{A2}}{\partial R'^2}$$

[36] $$\frac{\partial c^*_{B2}}{\partial T'} = \beta \frac{\partial^2 c^*_{B2}}{\partial X^2} + \frac{\sqrt{\beta'}\,\beta''}{\sqrt{\beta''} + \sqrt{\beta'}R'}\frac{\partial c^*_{B2}}{\partial R'} + \beta'' \frac{\partial^2 c^*_{B2}}{\partial R'^2} - \alpha c^*_{B2}$$

[37] $$\frac{\partial c^*_{C2}}{\partial T'} = \beta \frac{\partial^2 c^*_{C2}}{\partial X^2} + \frac{\sqrt{\beta'}\,\beta''}{\sqrt{\beta''} + \sqrt{\beta'}R'}\frac{\partial c^*_{C2}}{\partial R'} + \beta'' \frac{\partial^2 c^*_{C2}}{\partial R'^2} + \alpha c^*_{B2}$$

where $\beta$ is given by

[38] $\beta = D/aL^2$

$\beta'$ contains only experimental parameters

[39] $\beta' = D/ar_0^2$

and

[40] $\beta'' = D/a(M - r_0)^2$

As in the case of the chronoamperometric simulations (1) we have two dimensionless parameters, here $\beta$ and $\beta''$. The parameter $\beta'$ is given by experimental parameters and thus the simulations will depend on $\beta'$ as, e.g., on $\alpha$.

The transformed initial and boundary conditions are given by

$T' = 0,\ 0 \leq X \leq 1,\ 0 \leq R \leq 1,\ 0 \leq R' \leq 1$:

[41] $c^*_{A1}(X,R,0) = c^*_{A2}(X,R',0) = 1$

[42] $c^*_{B1}(X,R,0) = c^*_{B2}(X,R',0) = c^*_{C1}(X,R,0) = c^*_{C2}(X,R',0) = 0$

$T' > 0,\ X = 1,\ 0 \leq R \leq 1$:

[43] $c^*_{A1}(1,R,T') = 1$

[44] $c^*_{B1}(1,R,T') = c^*_{C1}(1,R,T') = 0$

$T' > 0,\ X = 1,\ 0 \leq R' \leq 1$:

[45] $c^*_{A2}(1,R',T') = 1$

Can. J. Chem. Downloaded from www.nrcresearchpress.com by 210.87.254.6 on 09/06/12
For personal use only.

Can. J. Chem. Downloaded from www.nrcresearchpress.com by 210.87.254.6 on 09/06/12
For personal use only.

[46] $c^*_{B2}(1,R',T') = c^*_{C2}(1,R',T') = 0$

$T' > 0$, $0 \leq X \leq 1$, $R' = 1$:

[47] $c^*_{A2}(X,1,T') = 1$

[48] $c^*_{B2}(X,1,T') = c^*_{C2}(X,1,T') = 0$

$T' > 0$, $X = 0$, $0 \leq R \leq 1$:

[49] $$\left(\frac{\partial c^*_{A1}}{\partial X}\right)_{X=0} = -\left(\frac{\partial c^*_{B1}}{\partial X}\right)_{X=0}$$

[50] $$\frac{c^*_{B1}(0,R,T')}{c^*_{A1}(0,R,T')} = \theta_{A/B} S_\lambda(T')$$

with

[51] $$S_\lambda(T') = \begin{cases} \exp\,[2(m-1)T'_\lambda - T'] \\ \exp\,[T' - 2mT'_\lambda] \end{cases} \qquad m = 1,2,\ldots$$

where

[52] $T'_\lambda = at_\lambda$

[53] $$\left(\frac{\partial c^*_{C1}}{\partial X}\right)_{X=0} = 0$$

$T' > 0$, $X = 0$, $0 < R' \leq 1$:

[54] $$\left(\frac{\partial c^*_{A2}}{\partial X}\right)_{X=0} = \left(\frac{\partial c^*_{B2}}{\partial X}\right)_{X=0} = \left(\frac{\partial c^*_{C2}}{\partial X}\right)_{X=0} = 0$$

$T' > 0$, $0 \leq X \leq 1$, $R = 0$:

[55] $$\left(\frac{\partial c^*_{A1}}{\partial R}\right)_{R=0} = \left(\frac{\partial c^*_{B1}}{\partial R}\right)_{R=0} = \left(\frac{\partial c^*_{C1}}{\partial R}\right)_{R=0} = 0$$

$T' > 0$, $0 \leq X \leq 1$, $R = 1$ ($R' = 0$):

[56] $c^*_{A1}(X,1,T') = c^*_{A2}(X,0,T')$

[57] $c^*_{B1}(X,1,T') = c^*_{B2}(X,0,T')$

[58] $c^*_{C1}(X,1,T') = c^*_{C2}(X,0,T')$

[59] $$\left(\frac{\partial c^*_{A1}}{\partial R}\right)_{R=1} = \sqrt{\frac{\beta''}{\beta'}}\left(\frac{\partial c^*_{A2}}{\partial R'}\right)_{R'=0}$$

[60] $$\left(\frac{\partial c^*_{B1}}{\partial R}\right)_{R=1} = \sqrt{\frac{\beta''}{\beta'}}\left(\frac{\partial c^*_{B2}}{\partial R'}\right)_{R'=0}$$

[61] $$\left(\frac{\partial c^*_{C1}}{\partial R}\right)_{R=1} = \sqrt{\frac{\beta''}{\beta'}}\left(\frac{\partial c^*_{C2}}{\partial R'}\right)_{R'=0}$$

## Application of two-dimensional collocation

As in the case of chronoamperometry (1), we have to solve the system of second order partial differential equations [32]–[37] under the conditions [41]–[61] to get the dimensionless concentrations of species A, B, and C as functions of $X$, $R$ ($R'$), and $T'$. We use the two-dimensional collocation method outlined in part 1 of this series (1) to discretize eqs. [32]–[37] with respect to the grid of collocation points $(X_i, R_k)$ in the $X/R$-space.

We have shown (1) that the first and second derivatives of the concentration with respect to $x$ and $r$

Can. J. Chem. Downloaded from www.nrcresearchpress.com by 210.87.254.6 on 09/06/12
For personal use only.

respectively at a collocation point $(x_i, r_k)$ may be expressed as

$$[62] \quad \left(\frac{\partial c}{\partial x}\right)_{x_i,r_k} = \sum_{j=1}^{N_x+2} A_{i,j}c(x_j,r_k,t)$$

$$[63] \quad \left(\frac{\partial^2 c}{\partial x^2}\right)_{x_i,r_k} = \sum_{j=1}^{N_x+2} B_{i,j}c(x_j,r_k,t)$$

$$[64] \quad \left(\frac{\partial c}{\partial r}\right)_{x_i,r_k} = \sum_{l=1}^{N_r+2} C_{l,k}c(x_i,r_l,t)$$

$$[65] \quad \left(\frac{\partial^2 c}{\partial r^2}\right)_{x_i,r_k} = \sum_{l=1}^{N_r+2} D_{l,k}c(x_i,r_l,t)$$

where $N_x$ and $N_r$ are the numbers of interior collocation points (chosen as the roots of an orthogonal polynomial (9)) in the $x$- and $r$-direction, respectively, and $A_{i,j}$, $B_{i,j}$, $C_{l,k}$, and $D_{l,k}$ are elements of matrices. The numerical values of those elements depend only on the degree and kind of the polynomial chosen for collocation (10). Thus, if the matrix elements have once been calculated they may be used for any problem. The degree of the polynomial used depends on the desired accuracy of the simulation.

Using eqs. [62]–[65] we may discretize the partial differential equations [32]–[37] in terms of the concentrations at the collocation points. If we introduce the boundary conditions [43]–[48] we arrive at eqs. [66]–[71].

$$[66] \quad \left.\frac{dc^*_{A1}}{dT'}\right|_{X_i,R_k} = \beta\left\{B_{i,1}c^*_{A1}(0,R_k,T') + B_{i,N_x+2} + \sum_{j=2}^{N_x+1} B_{i,j}c^*_{A1}(X_j,R_k,T')\right\} + \beta'\left\{E_{1,k}c^*_{A1}(X_i,0,T') + E_{N_R+2,k}c^*_{A1}(X_i,1,T') + \sum_{l=2}^{N_R+1} E_{l,k}c^*_{A1}(X_i,R_l,T')\right\}$$

$$[67] \quad \left.\frac{dc^*_{B1}}{dT'}\right|_{X_i,R_k} = \beta\left\{B_{i,1}c^*_{B1}(0,R_k,T') + \sum_{j=2}^{N_x+1} B_{i,j}c^*_{B1}(X_j,R_k,T')\right\} + \beta'\left\{E_{1,k}c^*_{B1}(X_i,0,T') + E_{N_R+2,k}c^*_{B1}(X_i,1,T') + \sum_{l=2}^{N_R+1} E_{l,k}c^*_{B1}(X_i,R_l,T')\right\} - \alpha c^*_{B1}$$

$$[68] \quad \left.\frac{dc^*_{C1}}{dT'}\right|_{X_i,R_k} = \beta\left\{B_{i,1}c^*_{C1}(0,R_k,T') + \sum_{j=2}^{N_x+1} B_{i,j}c^*_{C1}(X_j,R_k,T')\right\} + \beta'\left\{E_{1,k}c^*_{C1}(X_i,0,T') + E_{N_R+2,k}c^*_{C1}(X_i,1,T') + \sum_{l=2}^{N_R+1} E_{l,k}c^*_{C1}(X_i,R_l,T')\right\} + \alpha c^*_{B1}$$

$$[69] \quad \left.\frac{dc^*_{A2}}{dT'}\right|_{X_i,R_k} = \beta\left\{B_{i,1}c^*_{A2}(0,R'_k,T') + B_{i,N_{R'}+2} + \sum_{j=2}^{N_{R'}+1} B_{i,j}c^*_{A2}(X_j,R'_k,T')\right\} + \beta''\left\{F'_{1,k}c^*_{A2}(X_i,0,T') + F'_{N_{R'}+2,k} + \sum_{l=2}^{N_{R'}+1} F'_{l,k}c^*_{A2}(X_i,R'_l,T')\right\}$$

$$[70] \quad \left.\frac{dc^*_{B2}}{dT'}\right|_{X_i,R_k} = \beta\left\{B_{i,1}c^*_{B2}(0,R'_k,T') + \sum_{j=2}^{N_x+1} B_{i,j}c^*_{B2}(X_j,R'_k,T')\right\} + \beta''\left\{F'_{1,k}c^*_{B2}(X_i,0,T') + \sum_{l=2}^{N_{R'}+1} F'_{l,k}c^*_{B2}(X_i,R'_l,T')\right\} - \alpha c^*_{B2}$$

$$[71] \quad \left.\frac{dc^*_{C2}}{dT'}\right|_{X_i,R_k} = \beta\left\{B_{i,1}c^*_{C2}(0,R'_k,T') + \sum_{j=2}^{N_x+1} B_{i,j}c^*_{C2}(X_j,R'_k,T')\right\} + \beta''\left\{F'_{1,k}c^*_{C2}(X_i,0,T') + \sum_{l=2}^{N_{R'}+1} F'_{l,k}c^*_{C2}(X_i,R'_l,T')\right\} + \alpha c^*_{B2}$$

with

$$[72] \qquad E_{l,k} = \frac{C_{l,k} + R_k D_{l,k}}{R_k}$$

and

$$[73] \qquad F'_{l,k} = \frac{\sqrt{\beta'}}{\sqrt{\beta''} + \sqrt{\beta'}\, R'_k}\, C'_{l,k} + D'_{l,k}$$

Primed matrix elements correspond to the outer discretization function. As in the case of chronoamperometry we have to substitute implicit equations for the unknown concentrations at the boundaries. The calculation of the $c^*_1(X_i,0,T')$, $c^*_1(X_i,1,T')$, $c^*_2(X_i,0,T')$, $c^*_1(0,R_k,T')$, and $c^*_2(0,R'_k,T')$ is essentially the same as for chronoamperometric simulations and we refer to part 1 of this series (1) for the derivations. They are (1):

$$[74] \qquad c^*_{A1}(X_i,0,T') = -\frac{1}{G_1}\left\{\sum_{l=2}^{N_R+1} G_l c^*_{A1}(X_i,R_l,T') + \sum_{l=2}^{N_{R'}+1} C_{N_R+2,1} C'_{l,1} c^*_{A2}(X_i,R'_l,T') + C_{N_R+2,1} C'_{N_R+2,1}\right\}$$

$$[75] \qquad c^*_{B1}(X_i,0,T') = -\frac{1}{G_1}\left\{\sum_{l=2}^{N_R+1} G_l c^*_{B1}(X_i,R_l,T') + \sum_{l=2}^{N_{R'}+1} C_{N_R+2,1} C'_{l,1} c^*_{B2}(X_i,R'_l,T')\right\}$$

$$[76] \qquad c^*_{C1}(X_i,0,T') = -\frac{1}{G_1}\left\{\sum_{l=2}^{N_R+1} G_l c^*_{C1}(X_i,R_l,T') + \sum_{l=2}^{N_{R'}+1} C_{N_R+2,1} C_{l,1} c^*_{C2}(X_i,R'_l,T')\right\}$$

$$[77] \qquad c^*_{A1}(X_i,1,T') = c^*_{A2}(X_i,0,T') = \frac{1}{G_1}\left\{\sum_{l=2}^{N_R+1} H_l c^*_{A1}(X_i,R_l,T') + \sum_{l=2}^{N_{R'}+1} C_{1,1} C'_{l,1} c^*_{A2}(X_i,R'_l,T') + C_{1,1} C'_{N_R+2,1}\right\}$$

$$[78] \qquad c^*_{B1}(X_i,1,T') = c^*_{B2}(X_i,0,T') = \frac{1}{G_1}\left\{\sum_{l=2}^{N_R+1} H_l c^*_{B1}(X_i,R_l,T') + \sum_{l=2}^{N_{R'}+1} C_{1,1} C'_{l,1} c^*_{B2}(X_i,R'_l,T')\right\}$$

$$[79] \qquad c^*_{C1}(X_i,1,T') = c^*_{C2}(X_i,0,T') = \frac{1}{G_1}\left\{\sum_{l=2}^{N_R+1} H_l c^*_{C1}(X_i,R_l,T') + \sum_{l=2}^{N_{R'}+1} C_{1,1} C'_{l,1} c^*_{C2}(X_i,R'_l,T')\right\}$$

$$[80] \qquad c^*_{C1}(0,R_k,T') = -\frac{1}{A_{1,1}} \sum_{j=2}^{N_x+1} A_{1,j} c^*_{C1}(X_j,R_k,T')$$

$$[81] \qquad c^*_{A2}(0,R'_k,T') = -\frac{1}{A_{1,1}}\left\{A_{1,N_x+2} + \sum_{j=2}^{N_x+1} A_{1,j} c^*_{A2}(X_j,R'_k,T')\right\}$$

$$[82] \qquad c^*_{B2}(0,R'_k,T') = -\frac{1}{A_{1,1}} \sum_{j=2}^{N_x+1} A_{1,j} c^*_{B2}(X_j,R'_k,T')$$

$$[83] \qquad c^*_{C2}(0,R'_k,T') = -\frac{1}{A_{1,1}} \sum_{j=2}^{N_x+1} A_{1,j} c^*_{C2}(X_j,R'_k,T')$$

with

$$[84] \qquad G_l = (C_{N_R+2,N_R+2} - C'_{1,1}) C_{l,1} - C_{l,N_R+2} C_{N_R+2,1}$$

and

$$[85] \qquad H_l = C_{1,N_R+2} C_{l,1} - C_{1,1} C_{l,N_R+2}$$

Can. J. Chem. Downloaded from www.nrcresearchpress.com by 210.87.254.6 on 09/06/12
For personal use only.

Can. J. Chem. Downloaded from www.nrcresearchpress.com by 210.87.254.6 on 09/06/12
For personal use only.

The values of $c^*_{A1}(0,R_k,T')$ and $c^*_{B1}(0,R_k,T')$ may be calculated from eqs. [49] and [50], yielding

$$[86]\qquad c^*_{A1}(0,R_k,T') = -\frac{\theta_{A/B}S_\lambda(T')}{A_{1,1}[1+\theta_{A/B}S_\lambda(T')]}\left\{A_{1,N_x+2}+\sum_{j=2}^{N_x+1}A_{1,j}[c^*_{A1}(X_j,R_k,T')+c^*_{B1}(X_j,R_k,T')]\right\}$$

and

$$[87]\qquad c^*_{B1}(0,R_k,T') = -\frac{1}{A_{1,1}[1+\theta_{A/B}S_\lambda(T')]}\left\{A_{1,N_x+2}+\sum_{j=2}^{N_x+1}A_{1,j}[c^*_{A1}(X_j,R_k,T')+c^*_{B1}(X_j,R_k,T')]\right\}$$

Now we may substitute [74]–[87] into eqs. [66]–[71] which gives us finally the discretized equations describing the time dependence of the concentration of all three species A, B, and C at the collocation points.

From [66] it follows, using [74], [77], and [86],

$$[88]\qquad \left.\frac{dc^*_{A1}}{dT'}\right|_{X_i,R_k} = \beta\left\{-\frac{B_{i,1}\theta_{A/B}S_\lambda(T')}{A_{1,1}[1+\theta_{A/B}S_\lambda(T')]}\left[A_{1,N_x+2}+\sum_{j=2}^{N_x+1}A_{1,j}[c^*_{A1}(X_j,R_k,T')+c^*_{B1}(X_j,R_k,T')]\right]+B_{i,N_x+2}+\sum_{j=2}^{N_x+1}B_{i,j}c^*_{A1}(X_j,R_k,T')\right.$$
$$\left.+\frac{\beta'}{G_1}\left\{I_{1,k}C'_{N_R+2,1}+\sum_{l=2}^{N_R+1}[J_{l,k}(C'_{1,1}-C_{N_R+2,N_R+2})-I_{1,k}C_{l,N_R+2}-I_{l,k}C_{1,N_R+2}]c^*_{A1}(X_i,R_l,T')+\sum_{l=2}^{N_{R'}+1}I_{1,k}C'_{l,1}c^*_{A2}(X_i,R'_l,T')\right\}\right.$$

where

$$[89]\qquad I_{l,k} = E_{N_R+2,k}C_{l,1} - E_{l,k}C_{N_R+2,1}$$

and

$$[90]\qquad J_{l,k} = E_{1,k}C_{l,1} - E_{l,k}C_{1,1}$$

If we combine [67] with [75], [78], and [87], we get

$$[91]\qquad \left.\frac{dc^*_{B1}}{dT'}\right|_{X_i,R_k} = \beta\left\{-\frac{B_{i,1}}{A_{1,1}[1+\theta_{A/B}S_\lambda(T')]}\left[A_{1,N_x+2}+\sum_{j=2}^{N_x+1}A_{1,j}[c^*_{A1}(X_j,R_k,T')+c^*_{B1}(X_j,R_k,T')]\right]\right.$$
$$\left.+\sum_{j=2}^{N_x+1}B_{i,j}c^*_{B1}(X_j,R_k,T')\right\}+\frac{\beta'}{G_1}\left\{\sum_{l=2}^{N_R+1}[J_{l,k}(C'_{1,1}-C_{N_R+2,N_R+2})-I_{1,k}C_{l,N_R+2}\right.$$
$$\left.-I_{l,k}C_{1,N_R+2}]c^*_{B1}(X_i,R_l,T')+\sum_{l=2}^{N_{R'}+1}I_{1,k}C'_{l,1}c^*_{B2}(X_i,R'_l,T')\right\}-\alpha c^*_{B1}$$

similarly [68] gives, with [76], [79], and [80],

$$[92]\qquad \left.\frac{dc^*_{C1}}{dT'}\right|_{X_i,R_k} = \frac{\beta}{A_{1,1}}\sum_{j=2}^{N_x+1}K_{i,j}c^*_{C1}(X_j,R_k,T')$$
$$+\frac{\beta'}{G_1}\left\{\sum_{l=2}^{N_R+1}[J_{l,k}(C'_{1,1}-C_{N_R+2,N_R+2})-I_{1,k}C_{l,N_R+2}-I_{l,k}C_{1,N_R+2}]c^*_{C1}(X_i,R_l,T')\right.$$
$$\left.+\sum_{l=2}^{N_{R'}+1}I_{1,k}C'_{l,1}c^*_{C2}(X_i,R'_l,T')\right\}+\alpha c^*_{B1}$$

For the outer function describing the concentration of species A it holds from [69], [77], and [81]

$$[93]\qquad \left.\frac{dc^*_{A2}}{dT'}\right|_{X_i,R'_k} = \frac{\beta}{A_{1,1}}\left\{K_{i,N_x+2}+\sum_{j=2}^{N_x+1}K_{i,j}c^*_{A2}(X_j,R'_k,T')\right\}$$
$$+\frac{\beta''}{G_1}\left\{L'_{N_{R'}+2,k}+\sum_{l=2}^{N_R+1}F'_{1,k}H_l c^*_{A1}(X_i,R_l,T')+\sum_{l=2}^{N_{R'}+1}L'_{l,k}c^*_{A2}(X_i,R'_l,T')\right\}$$

Equations [70], [78], and [82] combine to give

$$[94]\quad \left.\frac{dc^*_{B2}}{dT'}\right|_{X_i,R'_k} = \frac{\beta}{A_{1,1}}\sum_{j=2}^{N_x+1} K_{i,j}c^*_{B2}(X_j,R'_k,T') + \frac{\beta''}{G_1}\left\{\sum_{l=2}^{N_R+1} F'_{1,k}H_l c^*_{B1}(X_i,R_l,T') + \sum_{l=2}^{N_{R'}+1} L'_{l,k}c^*_{B2}(X_i,R'_l,T')\right\} - \alpha c^*_{B2}$$

Finally [71], [79], and [83] yield

$$[95]\quad \left.\frac{dc^*_{C2}}{dT'}\right|_{X_i,R'_k} = \frac{\beta}{A_{1,1}}\sum_{j=2}^{N_x+1} K_{i,j}c^*_{C2}(X_j,R'_k,T') + \frac{\beta''}{G_1}\left\{\sum_{l=2}^{N_R+1} F'_{1,k}H_l c^*_{C1}(X_i,R_l,T') + \sum_{l=2}^{N_{R'}+1} L'_{l,k}c^*_{C2}(X_i,R'_l,T')\right\} + \alpha c^*_{B2}$$

where we used

$$[96]\quad K_{i,j} = B_{i,j}A_{1,1} - B_{i,1}A_{1,j}$$

and

$$[97]\quad L'_{l,k} = F'_{l,k}G_1 + C_{1,1}C'_{l,1}F'_{1,k}$$

Thus, the system of six second order partial differential equations [32]–[37] has been converted into a set of $3N_x(N_R + N_{R'})$ simultaneous ordinary differential equations, [88] and [91]–[95]. After integrating this set we get the concentrations of species A, B, and C at the collocation points $(X_i,R_k)$ and $(X_i,R'_k)$ as a function of the simulation time $T'$.

One of the distinctive features of the orthogonal collocation approach can be seen from a comparison of eqs. [88] and [91]–[95]. Those formulae are very similar from a structural point of view. Furthermore, compared to the expressions describing the model of a chronoamperometric experiment (1), there are only few changes in the inner functions, while the outer functions are the same both for the models of cyclic voltammetry and chronoamperometry.

### Calculation of the current

Also, the calculation of the current is fully analogous to that performed for the chronoamperometric model. Again we have to integrate the flux over the part between 0 and $r_0$ on the $r$-axis

$$[98]\quad i = nFD\int_0^{r_0} 2\pi r\left(\frac{\partial c_A}{\partial x}\right)_{x=0} dr$$

Transforming the right hand side of eq. [98] into a dimensionless form we get

$$[99]\quad i = nFAc^0_A\sqrt{Da\pi}\sqrt{\frac{\beta}{\pi}}\,2\int_0^1 R\left(\frac{\partial c^*_{A1}}{\partial X}\right)_{X=0} dR$$

or, using Nicholson and Shain's current function (6),

$$[100]\quad \chi = \frac{i}{nFAc^0_A\sqrt{Da\pi}} = 2\sqrt{\frac{\beta}{\pi}}\int_0^1 R\left(\frac{\partial c^*_{A1}}{\partial X}\right)_{X=0} dR$$

The integration may be performed exactly by a quadrature method (ref. 9, p. 134), for we know the derivative $(\partial c^*_{A1}/\partial X)_{X=0}$ at all collocation points:

$$[101]\quad \chi = 2\sqrt{\frac{\beta}{\pi}}\sum_{l=1}^{N_R+2} Q_l R_l \frac{1}{1+\theta_{A/B}S_\lambda(T')} \times\left[A_{1,N_x+2} + \sum_{j=2}^{N_x+1} A_{1,j}c^*_{A1}(X_j,R_l,T') - \theta_{A/B}S_\lambda(T')\sum_{j=2}^{N_x+1} A_{1,j}c^*_{B1}(X_j,R_l,T')\right]$$

where the elements of the vector $\boldsymbol{Q}$ depend only on the degree and kind of the trial function in $r$-direction.

Can. J. Chem. Downloaded from www.nrcresearchpress.com by 210.87.254.6 on 09/06/12
For personal use only.

Can. J. Chem. Downloaded from www.nrcresearchpress.com by 210.87.254.6 on 09/06/12
For personal use only.

### Model mechanism for oxidation of I

It has been shown (11, 12) that the oxidation of **I** (denoted as A) may be described by an ECE-type mechanism, where protons released after the oxidation step are picked up by unoxidized phenol molecules giving the protonated form of **I**, $HA^{\oplus}$. The latter is oxidized at more positive potentials releasing two protons during reaction. The end product of both reactions is the stable phenoxenium cation, E, which is most probably formed from the neutral phenoxy radical, C, in a homogeneous redox reaction between C and the primary radical cation B (12). The intermediate D was not characterized further. The observation of changes in voltammograms of **I** with electrode size has been attributed to the protonation reaction $A \rightarrow HA^{\oplus}$ which causes a phenol-free layer in front of the electrode (5). The time after which phenol again reaches the electrode surface is decreased if more substrate diffuses into this layer due to edge effects.

$$A \underset{+e^{\ominus}}{\overset{-e^{\ominus}}{\rightleftharpoons}} B \qquad E^0_{A/B},\ n_1 = 1$$

$$B \longrightarrow H^{\oplus} + C \qquad k_1$$

$$H^{\oplus} + A \longrightarrow HA^{\oplus} \qquad k_2$$

$$HA^{\oplus} \underset{+e^{\ominus}}{\overset{-e^{\ominus}}{\rightleftharpoons}} D \qquad E^0_{HA^{\oplus}/D},\ n_2 = 1$$

$$D \longrightarrow 2H^{\oplus} + C \qquad k_3$$

$$B + C \rightleftharpoons A + E \qquad K_4 \gg 1,\ k_4/k_{-4} = K_4$$

$$C \underset{+e^{\ominus}}{\overset{-e^{\ominus}}{\rightleftharpoons}} E \qquad E^0_{C/E},\ n_3 = 1$$

With our two-dimensional simulation model it is now possible to include the effects of a finite disc into the calculations. This may also serve as a further example for the application of orthogonal collocation to electroanalytical problems. In this paper we show the derivation of the expressions for $dc^*/dT'$ for the species involved, while the comparison with experimental results will be reported in part 4 of this series.

The kinetic diffusion equations for the above model mechanism in dimensionless form are

[102] $$\frac{\partial c^*_{A1}}{\partial T'} = \beta \frac{\partial^2 c^*_{A1}}{\partial X^2} + \frac{\beta'}{R}\frac{\partial c^*_{A1}}{\partial R} + \beta' \frac{\partial^2 c^*_{A1}}{\partial R^2} - \alpha_2 c^*_{H^{\oplus}1} c^*_{A1} - \alpha_{-4} c^*_{A1} c^*_{E1} + \alpha_4 c^*_{B1} c^*_{C1}$$

[103] $$\frac{\partial c^*_{B1}}{\partial T'} = \beta \frac{\partial^2 c^*_{B1}}{\partial X^2} + \frac{\beta'}{R}\frac{\partial c^*_{B1}}{\partial R} + \beta' \frac{\partial^2 c^*_{B1}}{\partial R^2} - \alpha_1 c^*_{B1} - \alpha_4 c^*_{B1} c^*_{C1} + \alpha_{-4} c^*_{A1} c^*_{E1}$$

[104] $$\frac{\partial c^*_{C1}}{\partial T'} = \beta \frac{\partial^2 c^*_{C1}}{\partial X^2} + \frac{\beta'}{R}\frac{\partial c^*_{C1}}{\partial R} + \beta' \frac{\partial^2 c^*_{C1}}{\partial R^2} + \alpha_1 c^*_{B1} + \alpha_3 c^*_{D1} - \alpha_4 c^*_{B1} c^*_{C1} + \alpha_{-4} c^*_{A1} c^*_{E1}$$

[105] $$\frac{\partial c^*_{H^{\oplus}1}}{\partial T'} = \beta \frac{\partial^2 c^*_{H^{\oplus}1}}{\partial X^2} + \frac{\beta'}{R}\frac{\partial c^*_{H^{\oplus}1}}{\partial R} + \beta' \frac{\partial^2 c^*_{H^{\oplus}1}}{\partial R^2} + \alpha_1 c^*_{B1} + 2\alpha_3 c^*_{D1} - \alpha_2 c^*_{A1} c^*_{H^{\oplus}1}$$

[106] $$\frac{\partial c^*_{HA^{\oplus}1}}{\partial T'} = \beta \frac{\partial^2 c^*_{HA^{\oplus}1}}{\partial X^2} + \frac{\beta'}{R}\frac{\partial c^*_{HA^{\oplus}1}}{\partial R} + \beta' \frac{\partial^2 c^*_{HA^{\oplus}1}}{\partial R^2} + \alpha_2 c^*_{A1} c^*_{H^{\oplus}1}$$

[107] $$\frac{\partial c^*_{D1}}{\partial T'} = \beta \frac{\partial^2 c^*_{D1}}{\partial X^2} + \frac{\beta'}{R}\frac{\partial c^*_{D1}}{\partial R} + \beta' \frac{\partial^2 c^*_{D1}}{\partial R^2} - \alpha_3 c^*_{D1}$$

[108] $$\frac{\partial c^*_{E1}}{\partial T'} = \beta \frac{\partial^2 c^*_{E1}}{\partial X^2} + \frac{\beta'}{R}\frac{\partial c^*_{E1}}{\partial R} + \beta' \frac{\partial^2 c^*_{E1}}{\partial R^2} + \alpha_4 c^*_{B1} c^*_{C1} - \alpha_{-4} c^*_{A1} c^*_{E1}$$

[109] $$\frac{\partial c^*_{A2}}{\partial T'} = \beta \frac{\partial^2 c^*_{A2}}{\partial X^2} + \frac{\beta'' \sqrt{\beta'}}{\sqrt{\beta''} + \sqrt{\beta' R'}}\frac{\partial c^*_{A2}}{\partial R'} + \beta'' \frac{\partial^2 c^*_{A2}}{\partial R'^2} - \alpha_2 c^*_{H^{\oplus}2} c^*_{A2} - \alpha_{-4} c^*_{A2} c^*_{E2} + \alpha_4 c^*_{B2} c^*_{C2}$$

[110] $$\frac{\partial c^*_{B2}}{\partial T'} = \beta \frac{\partial^2 c^*_{B2}}{\partial X^2} + \frac{\beta'' \sqrt{\beta'}}{\sqrt{\beta''} + \sqrt{\beta' R'}}\frac{\partial c^*_{B2}}{\partial R'} + \beta'' \frac{\partial^2 c^*_{B2}}{\partial R'^2} - \alpha_1 c^*_{B2} - \alpha_4 c^*_{B2} c^*_{C2} + \alpha_{-4} c^*_{A2} c^*_{E2}$$

Can. J. Chem. Downloaded from www.nrcresearchpress.com by 210.87.254.6 on 09/06/12
For personal use only.

[111] $$\frac{\partial c^*_{C2}}{\partial T'} = \beta \frac{\partial^2 c^*_{C2}}{\partial X^2} + \frac{\beta'' \sqrt{\beta'}}{\sqrt{\beta''} + \sqrt{\beta'} R'} \frac{\partial c^*_{C2}}{\partial R'} + \beta'' \frac{\partial^2 c^*_{C2}}{\partial R'^2} + \alpha_1 c^*_{B2} + \alpha_3 c^*_{D2} - \alpha_4 c^*_{B2} c^*_{C2} + \alpha_{-4} c^*_{A2} c^*_{E2}$$

[112] $$\frac{\partial c^*_{H\oplus_2}}{\partial T'} = \beta \frac{\partial^2 c^*_{H\oplus_2}}{\partial X^2} + \frac{\beta'' \sqrt{\beta'}}{\sqrt{\beta''} + \sqrt{\beta'} R'} \frac{\partial c^*_{H\oplus_2}}{\partial R'} + \beta'' \frac{\partial^2 c^*_{H\oplus_2}}{\partial R'^2} + \alpha_1 c^*_{B2} + 2\alpha_3 c^*_{D2} - \alpha_2 c^*_{A2} c^*_{H\oplus_2}$$

[113] $$\frac{\partial c^*_{HA\oplus_2}}{\partial T'} = \beta \frac{\partial^2 c^*_{HA\oplus_2}}{\partial X^2} + \frac{\beta'' \sqrt{\beta'}}{\sqrt{\beta''} + \sqrt{\beta'} R'} \frac{\partial c^*_{HA\oplus_2}}{\partial R'} + \beta'' \frac{\partial^2 c^*_{HA\oplus_2}}{\partial R'^2} + \alpha_2 c^*_{A2} c^*_{H\oplus_2}$$

[114] $$\frac{\partial c^*_{D2}}{\partial T'} = \beta \frac{\partial^2 c^*_{D2}}{\partial X^2} + \frac{\beta'' \sqrt{\beta'}}{\sqrt{\beta''} + \sqrt{\beta'} R'} \frac{\partial c^*_{D2}}{\partial R'} + \beta'' \frac{\partial^2 c^*_{D2}}{\partial R'^2} - \alpha_3 c^*_{D2}$$

[115] $$\frac{\partial c^*_{E2}}{\partial T'} = \beta \frac{\partial^2 c^*_{E2}}{\partial X^2} + \frac{\beta'' \sqrt{\beta'}}{\sqrt{\beta''} + \sqrt{\beta'} R'} \frac{\partial c^*_{E2}}{\partial R'} + \beta'' \frac{\partial^2 c^*_{E2}}{\partial R'^2} + \alpha_4 c^*_{B2} c^*_{C2} - \alpha_{-4} c^*_{A2} c^*_{E2}$$

where

[116] $$\alpha_j = k_j/a, \qquad j = 1, 3$$

[117] $$\alpha_2 = k_2 c^0_A/a$$

and

[118*a*] $$\alpha_4 = k_4 c^0_A/a$$

[118*b*] $$\alpha_{-4} = k_{-4} c^0_A/a$$

In addition to the initial conditions [41] and [42] we assume

$T' = 0, 0 \leq X \leq 1, 0 \leq R \leq 1, 0 \leq R' \leq 1$:

[119] $$c^*_{H\oplus_1}(X,R,0) = c^*_{H\oplus_2}(X,R',0) = c^*_{HA\oplus_1}(X,R,0) = c^*_{HA\oplus_2}(X,R',0) = c^*_{D1}(X,R,0) = c^*_{D2}(X,R',0) = c^*_{E1}(X,R,0) = c^*_{E2}(X,R',0) = 0$$

The boundary conditions now include

$T' > 0, X = 1, 0 \leq R \leq 1$:

[120] $$c^*_{H\oplus_1}(1,R,T') = c^*_{HA\oplus_1}(1,R,T') = c^*_{D1}(1,R,T') = c^*_{E1}(1,R,T') = 0$$

$T' > 0, X = 1, 0 \leq R' \leq 1$:

[121] $$c^*_{H\oplus_2}(1,R',T') = c^*_{HA\oplus_2}(1,R',T') = c^*_{D2}(1,R',T') = c^*_{E2}(1,R',T') = 0$$

$T' > 0, 0 \leq X \leq 1, R' = 1$:

[122] $$c^*_{H\oplus_2}(X,1,T') = c^*_{HA\oplus_2}(X,1,T') = c^*_{D2}(X,1,T') = c^*_{E2}(X,1,T') = 0$$

$T' > 0, X = 0, 0 \leq R \leq 1$:

[123] $$\left(\frac{\partial c^*_{HA\oplus_1}}{\partial X}\right)_{X=0} = -\left(\frac{\partial c^*_{D1}}{\partial X}\right)_{X=0}$$

[124] $$\frac{c^*_{HA\oplus_1}(0,R,T')}{c^*_{D1}(0,R,T')} = \theta_{HA\oplus/D} S_\lambda(T')$$

(where $\theta_{HA\oplus/D}$ is defined in analogy to $\theta_{A/B}$)

[125] $$\left(\frac{\partial c^*_{H\oplus_1}}{\partial X}\right)_{X=0} = 0$$

[126] $$\left(\frac{\partial c^*_{C1}}{\partial X}\right)_{X=0} = -\left(\frac{\partial c^*_{E1}}{\partial X}\right)_{X=0}$$

Can. J. Chem. Downloaded from www.nrcresearchpress.com by 210.87.254.6 on 09/06/12
For personal use only.

[127] $$\frac{c^*_{C1}(0,R,T')}{c^*_{E1}(0,R,T')} = \theta_{C/E}S_\lambda(T')$$

$T' > 0$, $X = 0$, $0 < R' \leq 1$:

[128] $$\left(\frac{\partial c^*_{H\oplus 2}}{\partial X}\right)_{X=0} = \left(\frac{\partial c^*_{HA\oplus 2}}{\partial X}\right)_{X=0} = \left(\frac{\partial c^*_{D2}}{\partial X}\right)_{X=0} = \left(\frac{\partial c^*_{E2}}{\partial X}\right)_{X=0} = 0$$

$T' > 0$, $X \geq 0$, $R = 1$ ($R' = 0$):

[129] $$c^*_{H\oplus 2}(X,0,T') = c^*_{H\oplus 1}(X,1,T')$$

[130] $$c^*_{HA\oplus 2}(X,0,T') = c^*_{HA\oplus 1}(X,1,T')$$

[131] $$c^*_{D2}(X,0,T') = c^*_{D1}(X,1,T')$$

[132] $$c^*_{E2}(X,0,T') = c^*_{E1}(X,1,T')$$

[133] $$\left(\frac{\partial c^*_{H\oplus 1}}{\partial R}\right)_{R=1} = \sqrt{\frac{\beta''}{\beta'}}\left(\frac{\partial c^*_{H\oplus 2}}{\partial R'}\right)_{R'=0}$$

[134] $$\left(\frac{\partial c^*_{HA\oplus 1}}{\partial R}\right)_{R=1} = \sqrt{\frac{\beta''}{\beta'}}\left(\frac{\partial c^*_{HA\oplus 2}}{\partial R'}\right)_{R'=0}$$

[135] $$\left(\frac{\partial c^*_{D1}}{\partial R}\right)_{R=1} = \sqrt{\frac{\beta''}{\beta'}}\left(\frac{\partial c^*_{D2}}{\partial R'}\right)_{R'=0}$$

[136] $$\left(\frac{\partial c^*_{E1}}{\partial R}\right)_{R=1} = \sqrt{\frac{\beta''}{\beta'}}\left(\frac{\partial c^*_{E2}}{\partial R'}\right)_{R'=0}$$

$T' > 0$, $X \geq 0$, $R = 0$:

[137] $$\left(\frac{\partial c^*_{H\oplus 1}}{\partial R}\right)_{R=0} = \left(\frac{\partial c^*_{HA\oplus 1}}{\partial R}\right)_{R=0} = \left(\frac{\partial c^*_{D1}}{\partial R}\right)_{R=0} = \left(\frac{\partial c^*_{E1}}{\partial R}\right)_{R=0} = 0$$

Now, the set of equations [102]–[115] in connection with the initial conditions [41], [42], and [119] and the boundary conditions [43]–[50], [54]–[61], and [120]–[137] has to be solved.

After proceeding in the same manner as for the EC mechanism we arrive at

[138] $$\left.\frac{dc^*_{A1}}{dT'}\right|_{X_i,R_k} = \text{RHS [88]} - \alpha_2 c^*_{H\oplus 1}c^*_{A1} - \alpha_{-4}c^*_{A1}c^*_{E1} + \alpha_4 c^*_{B1}c^*_{C1}$$

[139] $$\left.\frac{dc^*_{B1}}{dT'}\right|_{X_i,R_k} = \{\text{RHS [91] without kinetic term}\} - \alpha_1 c^*_{B1} - \alpha_4 c^*_{B1}c^*_{C1} + \alpha_{-4}c^*_{A1}c^*_{E1}$$

[140] $$\left.\frac{dc^*_{C1}}{dT'}\right|_{X_i,R_k} = \beta\left\{-\frac{B_{i,1}\theta_{C/E}S_\lambda(T')}{A_{1,1}[1+\theta_{C/E}S_\lambda(T')]}\sum_{j=2}^{N_x+1}A_{1,j}[c^*_{C1}(X_j,R_k,T') + c^*_{E1}(X_j,R_k,T')] + \sum_{j=2}^{N_x+1}B_{i,j}c^*_{C1}(X_j,R_k,T')\right\} + \frac{\beta'}{G_1}\left\{\sum_{l=2}^{N_R+1}[J_{l,k}(C'_{1,1} - C_{N_R+2,N_R+2}) - I_{1,k}C_{l,N_R+2} - I_{l,k}C_{1,N_R+2}]c^*_{C1}(X_i,R_l,T') + \sum_{l=2}^{N_{R'}+1}I_{1,k}C'_{l,1}c^*_{C2}(X_i,R'_l,T')\right\} + \alpha_1 c^*_{B1} + \alpha_3 c^*_{D1} - \alpha_4 c^*_{B1}c^*_{C1} + \alpha_{-4}c^*_{A1}c^*_{E1}$$

[141] $$\left.\frac{dc^*_{H\oplus 1}}{dT'}\right|_{X_i,R_k} = \{\text{RHS [92] without kinetic term and } c^*_{H\oplus 1} \text{ substituted for } c^*_{C1}\} + \alpha_1 c^*_{B1} + 2\alpha_3 c^*_{D1} - \alpha_2 c^*_{A1}c^*_{H\oplus 1}$$

[142] $$\left.\frac{dc^*_{HA\oplus_1}}{dT'}\right|_{X_i,R_k} = \{\text{RHS [140] without kinetic terms and } c^*_{HA\oplus_1} \text{ substituted for } c^*_{C1},\ c^*_{D1} \text{ substituted for } c^*_E \text{ and } \theta_{HA\oplus/D} \text{ substituted for } \theta_{C/E}\} + \alpha_2 c^*_{A1} c^*_{H\oplus_1}$$

[143] $$\left.\frac{dc^*_{D1}}{dT'}\right|_{X_i,R_k} = \{\text{RHS [91] without kinetic term and } c^*_{D1} \text{ substituted for } c^*_{B1},\ c^*_{HA\oplus_1} \text{ substituted for } c^*_A \text{ and } \theta_{HA\oplus/D} \text{ substituted for } \theta_{A/B}\} - \alpha_3 c^*_{D1}$$

[144] $$\left.\frac{dc^*_{E1}}{dT'}\right|_{X_i,R_k} = \{\text{RHS [91] without kinetic term and } c^*_{E1} \text{ substituted for } c^*_{B1},\ c^*_{C1} \text{ substituted for } c^*_{A1} \text{ and } \theta_{C/E} \text{ substituted for } \theta_{A/B}\} + \alpha_4 c^*_{B1} c^*_{C1} - \alpha_{-4} c^*_{A1} c^*_{E1}$$

[145] $$\left.\frac{dc^*_{A2}}{dT'}\right|_{X_i,R'_k} = \text{RHS [93]} - \alpha_2 c^*_{H\oplus_2} c^*_{A2} - \alpha_{-4} c^*_{A2} c^*_{E2} + \alpha_4 c^*_{B2} c^*_{C2}$$

[146] $$\left.\frac{dc^*_{B2}}{dT'}\right|_{X_i,R'_k} = \{\text{RHS [94] without kinetic term}\} - \alpha_1 c^*_{B2} - \alpha_4 c^*_{B2} c^*_{C2} + \alpha_{-4} c^*_{A2} c^*_{E2}$$

[147] $$\left.\frac{dc^*_{C2}}{dT'}\right|_{X_i,R'_k} = \{\text{RHS [95] without kinetic term}\} + \alpha_1 c^*_{B2} + \alpha_3 c^*_{D2} - \alpha_4 c^*_{B2} c^*_{C2} + \alpha_{-4} c^*_{A2} c^*_{E2}$$

[148] $$\left.\frac{dc^*_{H\oplus_2}}{dT'}\right|_{X_i,R'_k} = \{\text{RHS [95] without kinetic term and } c^*_{H\oplus_2} \text{ substituted for } c^*_{C2}\} + \alpha_1 c^*_{B2} + 2\alpha_3 c^*_{D2} - \alpha_2 c^*_{A2} c^*_{H\oplus_2}$$

[149] $$\left.\frac{dc^*_{HA\oplus_2}}{dT'}\right|_{X_i,R'_k} = \{\text{RHS [95] without kinetic term and } c^*_{HA\oplus_2} \text{ substituted for } c^*_{C2}\} + \alpha_2 c^*_{A2} c^*_{HA\oplus_2}$$

[150] $$\left.\frac{dc^*_{D2}}{dT'}\right|_{X_i,R'_k} = \{\text{RHS [95] without kinetic term and } c^*_{D2} \text{ substituted for } c^*_{C2}\} - \alpha_3 c^*_{D2}$$

[151] $$\left.\frac{dc^*_{E2}}{dT'}\right|_{X_i,R'_k} = \{\text{RHS [95] without kinetic term and } c^*_{E2} \text{ substituted for } c^*_{C2}\} + \alpha_4 c^*_{B2} c^*_{C2} - \alpha_{-4} c^*_{A2} c^*_{E2}$$

Again, the close resemblance of all expressions may be noted. The current function in this model is determined by the fluxes of A, $HA^\oplus$, and C to the electrode

[152] $$\chi = 2\sqrt{\frac{\beta}{\pi}}\int_0^1 R\left[\left(\frac{\partial c^*_{A1}}{\partial X}\right)_{X=0} + \left(\frac{\partial c^*_{HA\oplus_1}}{\partial X}\right)_{X=0} + \left(\frac{\partial c^*_{C1}}{\partial X}\right)_{X=0}\right] dR$$

$$= 2\sqrt{\frac{\beta}{\pi}}\sum_{l=1}^{N_R+2} Q_l R_l \left[\frac{1}{1+\theta_{A/B}S_\lambda(T')}\left\{A_{1,N_x+2} + \sum_{j=2}^{N_x+1} A_{1,j} c^*_{A1}(X_j,R_k,T') - \theta_{A/B}S_\lambda(T')\sum_{j=2}^{N_x+1} A_{1,j} c^*_{B1}(X_j,R_l,T')\right\} + \frac{n_2}{n_1}\frac{1}{1+\theta_{HA\oplus/D}S_\lambda(T')}\right.$$

$$\times\left\{\sum_{j=2}^{N_x+1} A_{1,j} c^*_{HA\oplus_1}(X_j,R_k,T') - \theta_{HA\oplus/D}S_\lambda(T')\sum_{j=2}^{N_x+1} A_{1,j} c^*_D(X_j,R_k,T')\right\}$$

$$\left. + \frac{n_3}{n_1}\frac{1}{1+\theta_{C/E}S_\lambda(T')}\left\{\sum_{j=2}^{N_x+1} A_{1,j} c^*_{C1}(X_j,R_k,T') - \theta_{C/E}S_\lambda(T')\sum_{j=2}^{N_x+1} A_{1,j} c^*_E(X_j,R_k,T')\right\}\right]$$

**Acknowledgement**

We thank the Office of Naval Research, Washington, D.C., for support of this work.

Can. J. Chem. Downloaded from www.nrcresearchpress.com by 210.87.254.6 on 09/06/12
For personal use only.

1. B. SPEISER and S. PONS. Can. J. Chem. **60**, 1352 (1982).
2. B. SPEISER and S. PONS. In preparation.
3. R. LINES and V. D. PARKER. Acta Chem. Scand. B**31**, 369 (1977).
4. J. HEINZE. Private communication.
5. B. SPEISER and A. RIEKER. Electrochim. Acta, **23**, 983 (1978).
6. R. S. NICHOLSON and I. SHAIN. Anal. Chem. **36**, 706 (1964).
7. B. SPEISER and A. RIEKER. J. Electroanal. Chem. **102**, 373 (1979).
8. S. PONS. Can. J. Chem. **59**, 1538 (1981).
9. J. VILLADSEN and M. L. MICHELSEN. Solution of differential equation models by polynomial approximation. Prentice Hall, Englewood Cliffs. 1978.
10. L. F. WHITING and P. W. CARR. J. Electroanal. Chem. **81**, 1 (1977).
11. B. SPEISER and A. RIEKER. J. Electroanal. Chem. **102**, 373 (1979).
12. B. SPEISER and A. RIEKER. J. Electroanal. Chem. **110**, 231 (1980).

Can. J. Chem. Downloaded from www.nrcresearchpress.com by 210.87.254.6 on 09/06/12
For personal use only.

# Structure and bonding of mononuclear and homobinuclear chelates of some divalent metal ions with the ligand 1,8-dihydroxyanthraquinone

CONSTANTINOS A. TSIPIS[1] AND EVANGELOS G. BAKALBASSIS
*Laboratory of Inorganic Chemistry, University of Thessaloniki, Thessaloniki, Greece*
AND
VASSILIOS P. PAPAGEORGIOU AND MARIA N. BAKOLA-CHRISTIANOPOULOU
*Department of Chemical Engineering, College of Engineering, University of Thessaloniki, Thessaloniki, Greece*
Received January 29, 1982

CONSTANTINOS A. TSIPIS, EVANGELOS G. BAKALBASSIS, VASSILIOS P. PAPAGEORGIOU, and MARIA N. BAKOLA-CHRISTIANOPOULOU. Can. J. Chem. **60**, 2477 (1982).

The chelating ability of 1,8-dihydroxyanthraquinone with the divalent metal ions Cu(II), Ni(II), Mn(II), and Zn(II) has been studied. The Cu(II) and Ni(II) metal ions gave both mononuclear and homobinuclear chelates, while Mn(II) and Zn(II) gave only the mononuclear chelates. It is therefore evident that 1,8-dihydroxyanthraquinone can coordinate to the divalent metal ions either through its monoanionic form as a chelating bidentate ligand or through its dianionic form as a chelating tridentate ligand. In the homobinuclear chelates each metal ion is bonded to two terminal oxygen atoms and shares two bridging oxygen atoms with the other metal ion. Most of the chelates were found to contain also molecules of water either as coordinated and/or as crystalline water. The mononuclear and homobinuclear chelates of Cu(II) and Ni(II) gave, on reaction with pyridine, adducts which are also discussed. The structure and bonding of these chelates are discussed in relation to their spectroscopic and magnetic data.

CONSTANTINOS A. TSIPIS, EVANGELOS G. BAKALBASSIS, VASSILIOS P. PAPAGEORGIOU et MARIA N. BAKOLA-CHRISTIANOPOULOU. Can. J. Chem. **60**, 2477 (1982).

On a étudié la propriété de la dihydroxy-1,8 anthraquinone de former des chélates avec les ions des métaux bivalents tels le Cu(II), le Ni(II), le Mn(II) et le Zn(II). Les ions Cu(II) et Ni(II) donnent à la fois des chélates mononucléaires et homobinucléaires, tandis que le Mn(II) et le Zn(II) donnent uniquement des chélates mononucléaires. Il est par conséquent évident que la dihydroxy-1,8 anthraquinone peut coordonner les ions des métaux divalents, soit sous sa forme monoanionique, comme un ligand chélatant bidentate, soit sous sa forme dianionique comme un ligand chélatant tridentate. Dans les chélates homobinucléaires, chaque ion métallique se lie à deux atomes d'oxygène terminaux et partage deux atomes d'oxygène en position de pont avec l'autre ion métallique. On a trouvé que la plupart des chélates contiennent également des molécules d'eau, soit sous forme coordonnée ou sous forme cristalline. On discute également des adduits provenant de la réaction des chélates mononucléaires et homobinucléaires du Cu(II) et du Ni(II) avec la pyridine. On discute de la structure et de la liaison de ces chélates en se basant sur les données spectroscopiques et magnétiques.

[Traduit par le journal]

## Introduction

Quinones and their substituted derivatives have long been known to possess numerous chemically and biologically significant properties (1–3). It is not surprising then that these compounds have attracted considerable experimental and theoretical interest which has stimulated basic and applied research in several areas. Thus, quinones and their derivatives, either synthetic or naturally occurring, have been extensively utilized as acid–base indicators, pigments, and drugs. Also, they have found important applications in electrochemistry, analytical chemistry, and coordination chemistry. In the field of biology the interest has been focused on their antimicrobial and anti-tumor activity and some drugs based on quinones are now in use.

Since in most of the above applications of quinones and their derivatives their chelating ability plays an important role, the study of their metal chelates would be of great value in understanding mechanisms of their chemical and biological function. In fact, in the last few years a number of papers concerning the synthesis, characterization, thermal stability, and biological function of some metal chelates of hydroxybenzoquinones, hydroxynaphthoquinones, and hydroxyanthraquinones have been published (4–16). As far as we know, only one paper concerning the study of the chelating ability of 1,8-dihydroxyanthraquinone (chrysazin) with some divalent metal ions has been published (14). However, in this paper no details on the structure and bonding of the chelates are given, since the authors' interest was focused on the relation of the chelating ability of the ligand with its tumor-promoting activity.

This work is part of an effort to develop a better understanding of the structure and bonding of mononuclear and homobinuclear chelates of 1,8-dihydroxyanthraquinone (1,8-DHAQ) with some divalent metal ions, as well as to study their

[1]To whom all correspondence should be addressed.

0008-4042/82/192477-07$01.00/0
©1982 National Research Council of Canada/Conseil national de recherches du Canada

Can. J. Chem. Downloaded from www.nrcresearchpress.com by 210.87.254.42 on 09/06/12
For personal use only.

Can. J. Chem. Downloaded from www.nrcresearchpress.com by 210.87.254.42 on 09/06/12
For personal use only.

ability to form adducts with nitrogeneous bases. This study is of considerable importance, from a biological point of view, since DNA contains nitrogen donor atoms and hence it could interact in a similar way with the metal chelates under investigation.

## Experimental

*Physical measurements*

Infrared spectra were recorded, in the region of 4000–250 $cm^{-1}$, on a Perkin-Elmer 467 spectrophotometer using KBr discs or Nujol mulls. Electronic spectra were obtained on a Perkin-Elmer Hitachi 200 spectrophotometer and on a Cary 17D spectrophotometer, using both freshly prepared solutions in DMF and Nujol mulls. Magnetic susceptibility measurements were done by the Faraday technique at different magnetic field strengths using $Hg[Co(SCN)_4]$ as the calibrant. Diamagnetic corrections were made using Pascal's constants. Carbon, hydrogen, and nitrogen were determined using a Perkin-Elmer 240 Elemental Analyzer.

*Starting materials*

All solvents were of reagent grade and were used without further purification in synthetic work. The 1,8-DHAQ ligand was obtained commercially from Sarsyntex and used without further purification.

*Preparation of the complexes*

*$Cu(C_{14}H_7O_4)_2$ (I), $Cu(C_{14}H_7O_4)_2(OH_2)_2$ (II)*: 0.96 g (4 mmol) of 1,8-DHAQ were dissolved in 200 mL of absolute ethanol and the solution was warmed to boiling and then was filtered while warm. To this warm light orange solution 20 mL of an ethanolic solution containing 0.4 g (2.0 mmol) of $Cu(CH_3COO)_2 \cdot H_2O$ were added slowly under continuous magnetic stirring. During the mixing of the two solutions, a brown–red solid precipitated. The mixture was left stirring at room temperature for 1 h and then was kept in a refrigerator overnight before filtering. The precipitate was washed several times with small portions of ethanol, acetone, and finally with diethyl ether until the washings were colourless and was dried in a vacuum desiccator over $P_2O_5$. It must be noted that compound II is isolated when we use an aqueous solution of $Cu(CH_3COO)_2 \cdot H_2O$.

*$Cu(C_{14}H_7O_4)_2(Py)(OH_2)$ (III)*: 0.3 g (0.55 mmol) of the bis-(1,8-dihydroxyanthraquinonato)copper(II) complex were dissolved in a mixture of 10 mL dimethylformamide and 10 mL pyridine under heating and the resulting solution was filtered while warm. The filtrate, after cooling, was diluted by gradual addition of 10 mL of distilled water and a red–brown precipitate formed. The precipitate was filtered off, washed several times with small portions of acetone and diethyl ether, and dried in a vacuum desiccator over $P_2O_5$.

*$Cu_2(C_{14}H_6O_4)_2$ (IV)*: to a boiling ethanolic solution of 0.88 g (4.4 mmol) of $Cu(CH_3COO)_2 \cdot H_2O$ in 40 mL of absolute ethanol, a hot solution of 0.96 g (4.0 mmol) of 1,8-DHAQ in 200 mL of absolute ethanol was added slowly under continuous magnetic stirring. During the mixing of the two solutions, a red–brown solid precipitated. The mixture was boiled for 10 min more and then it was left stirring for 1 h at room temperature. The precipitate was isolated by filtration, washed several times with small portions of ethanol, acetone, and finally with diethyl ether, and dried in a vacuum desiccator over $P_2O_5$.

*$Cu_2(C_{14}H_6O_4)_2(Py)(OH_2)$ (V)*: 0.3 g (0.48 mmol) of the bis-(1,8-dihydroxyanthraquinonato)dicopper(II) complex was dissolved in a mixture of 15 mL dimethylformamide and 30 mL pyridine under heating. A brown–violet precipitate was formed and was isolated by filtration, washed with diethyl ether, and dried in a vacuum desiccator over $P_2O_5$.

*$Zn(C_{14}H_7O_4)_2$ (VI), $Mn(C_{14}H_7O_4)_2(OH_2)_2$ (VII), $Ni(C_{14}H_7O_4)_2(OH_2)_2$ (VIII)*: these compounds were obtained using a similar procedure. In all cases the hydrated metal acetates dissolved in the appropriate amount of ethanol were used as starting materials. The metal-to-ligand ratio used was 1:2. In cases where no precipitate appears immediately on mixing of the two solutions, the mixtures were left for longer periods or refluxed for about 4 h.

*$[Ni_2(C_{14}H_6O_4)_2(OH_2)_4] \cdot 2H_2O$ (IX), $[Ni_2(C_{14}H_6O_4)_2Py_2(OH_2)_2] \cdot 2H_2O$ (X)*: the dinickel complex was prepared according to the method used for the preparation of the dicopper complex. For the preparation of its 1:2 adduct with pyridine the following procedure was followed: 0.3 g (0.4 mmol) of the dinickel complex was dissolved in 30 mL of boiling pyridine and any undissolved material was removed by filtration. The filtrate was diluted with 200 mL of diethyl ether and was left in a refrigerator for 3 days. The dark violet precipitate formed was filtered, washed several times with small portions of diethyl ether, and dried under vacuum.

## Results and discussion

For the planar molecule of 1,8-DHAQ (symmetry group $C_{2v}$), which contains three oxygen donor atoms, one could expect coordination with divalent metal ions according to the following ways:

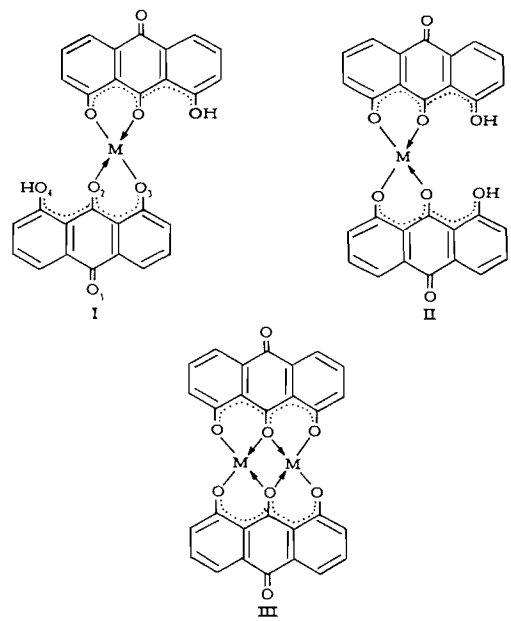


SCHEME 1. 1,8-DHAQ chelates of divalent metal ions.

In the isomeric structures **I** and **II** the 1,8-DHAQ acts, through its monoanionic form, as a chelating bidentate ligand forming with the metal ion a six-membered ring which is expected to be stabilized by a considerable delocalization of the $\pi$-electron density. In structure **III** the 1,8-DHAQ

TABLE 1. Analytical* and some physical data

| | Compound | Yield (%) | Color | %C | %N | %H |
|---|---|---|---|---|---|---|
| I, | $Cu(C_{14}H_7O_4)_2$ | 90 | Brown–red | 62.46 (62.05) | | 2.65 (2.60) |
| II, | $Cu(C_{14}H_7O_4)_2(OH_2)_2$ | 85 | Brown–red | 58.25 (58.18) | | 2.96 (3.14) |
| III, | $Cu(C_{14}H_7O_4)_2(Py)(OH_2)$ | 94 | Red–brown | 62.25 (62.02) | 2.12 (2.19) | 3.23 (3.31) |
| IV, | $Cu_2(C_{14}H_6O_4)_2$ | 98 | Red–brown | 55.27 (55.73) | | 2.13 (2.00) |
| V, | $Cu_2(C_{14}H_6O_4)_2(Py)(OH_2)$ | 44 | Brown–violet | 57.69 (58.07) | 2.10 (2.05) | 2.54 (2.51) |
| VI, | $Zn(C_{14}H_7O_4)_2$ | 43 | Red–brown | 61.82 (61.82) | | 2.70 (2.59) |
| VII, | $Mn(C_{14}H_7O_4)_2(OH_2)_2$ | 44 | Brown | 59.22 (59.06) | | 3.29 (3.18) |
| VIII, | $Ni(C_{14}H_7O_4)_2(OH_2)_2$ | 70 | Red–brown | 58.62 (58.67) | | 3.18 (3.17) |
| IX, | $Ni_2[(C_{14}H_6O_4)_2(OH_2)_4]\cdot 2H_2O$ | 82 | Violet–red | 47.61 (47.46) | | 3.04 (2.83) |
| X, | $Ni_2[(C_{14}H_6O_4)_2Py_2(OH_2)_2]\cdot 2H_2O$ | 37 | dark-violet | 55.14 (55.38) | 3.63 (3.40) | 3.45 (3.67) |

*Figures in parentheses are the calculated values.

acts, through its dianionic form, as a chelating tridentate ligand forming binuclear metal chelates, which can be either homo- or heterobinuclear. In these chelates each metal ion is bonded to two terminal oxygen atoms and shares two bridging oxygen atoms with the other metal ion.

With the foregoing aspects in mind we could not understand why Van Duuren *et al.* (14) were able to isolate only the 1:2 metal-to-ligand chelates, although the authors, using Job's method, showed that 1,8-DHAQ gave 1:1 metal-to-ligand chelates. By varying the reaction conditions for the formation of the chelates we were able to isolate, in addition to the 1:2 chelates, homobinuclear chelates in the case of Cu(II) and Ni(II) metal ions, while Zn(II) and Mn(II) gave only the 1:2 chelates. The structures of these homobinuclear chelates as well as of their adducts with pyridine in relation to their spectroscopic and magnetic data will be discussed in the present paper. Also in the paper are included some known 1:2 mononuclear chelates, since no details on the structure and bonding of these chelates are given in the literature (14).

The analytical data for the compounds studied, their colours and yields are shown in Table 1. All compounds were fine powders or microcrystalline materials, stable in air, and do not melt up to 300°C. They were insoluble in most of the common organic solvents and water, but were soluble in DMF and DMSO and slightly soluble in methylene chloride. Most of the isolated compounds contain also molecules of water either as coordinated and/or as crystalline water. By heating the chelates at 50°C under vacuum (2 mm Hg) over $P_2O_5$ we found that only the chelates $Ni_2(C_{14}H_6O_4)_2(H_2O)_6$ and $Ni_2(C_{14}H_6O_4)_2(Py)_2(H_2O)_4$ showed weight changes. The weight changes observed correspond to the loss of two water molecules per molecule of each of the above chelates. Hence, two molecules of water are present as crystalline water in these chelates.

*Infrared spectra*

The most relevant absorption bands in the ir spectra of the studied compounds and their tentative assignments are shown in Table 2. Band assignments were based on the comparison method by considering the ir spectra of the chelates with different structures, as well as of the free ligand and its parent compound, anthraquinone. All the compounds showed a number of intense bands in the region 1200–1700 $cm^{-1}$, which are due to normal modes of vibration of the ligand affected by its coordination and hence are of great importance for the elucidation of its coordination mode. Parts of the ir spectra of some representative chelates are shown in Fig. 1.

The stretching frequency of the uncoordinated carbonyl group of the ligand is not affected by the coordination and its frequency $\nu(C\cdots O)_1$ is similar to that of the free ligand and its parent compound, anthraquinone (1690 $cm^{-1}$). In contrast, the coordinated carbonyl group, as well as the hydrogen bonded carbonyl of 1,8-DHAQ, gave absorption bands $\nu(C\cdots O)_2$ at lower frequencies relative to that of the uncoordinated carbonyl group. The difference $\nu(C\cdots O)_1 - \nu(C\cdots O)_2$, which amounts to some 60–90 $cm^{-1}$, depends slightly on the nature of the central atom and the type of the chelate. For the central atoms studied the difference decreases in the order: Cu > Zn > Ni > Mn > H and is higher in binuclear than in mononuclear chelates. All these observations could be easily explained on the basis of the expected structures **I** or **II** for the mononuclear chelates and structure **III** for the binuclear ones. The substitution of the hydrogen atom by the central metal ion results in higher shifting, because the metal ions are better electron density acceptors

Can. J. Chem. Downloaded from www.nrcresearchpress.com by 210.87.254.42 on 09/06/12
For personal use only.

TABLE 2. Relevant ir frequencies ($cm^{-1}$) of some 1,8-dihydroxyanthraquinone chelates of divalent metal ions and their assignments

| Compound | $\nu(C\cdots O)_1$ | $\nu(C\cdots O)_2$ | $\nu(C\cdots O)_3$ | $\nu(C\cdots O)_4$ | $\nu_{sym}(M—O)$ | $\nu_{asym}(M—O)$ |
|---|---|---|---|---|---|---|
| $C_{14}H_8O_4$ | 1690 m | 1640 vs | 1217 s | 1217 s | — | — |
| **I** | 1686 m | 1622 vs | 1234 m | 1211 s | 539 w | 315 w |
| **II** | 1686 m | 1625 vs | 1238 m | 1212 vs | 542 w | 318 w |
| **III** | 1682 m | 1626 vs | 1238 m | 1212 vs | 540 w | 315 w |
| **IV** | 1682 m | 1602 vs | 1219 vs | 1219 vs | 550 w | 355 w |
| **V** | 1682 m | 1608 vs | 1202 vs | 1202 vs | 548 w | 359 w |
| **VI** | 1684 m | 1625 vs | 1203 vs | 1203 vs | 510 w | 350 w |
| | | | | | | 332 w |
| **VII** | 1684 m | 1629 vs | 1225 s | 1210 vs | 480 w | 327 w |
| **VIII** | 1686 m | 1629 vs | 1238 vs | 1212 vs | 530 w | 335 w |
| **IX** | 1678 m | 1610 vs | 1200 vs | 1200 vs | 538 w | 358 w |
| **X** | 1680 m | 1610 vs | 1208 vs | 1208 vs | 528 w | 355 w |

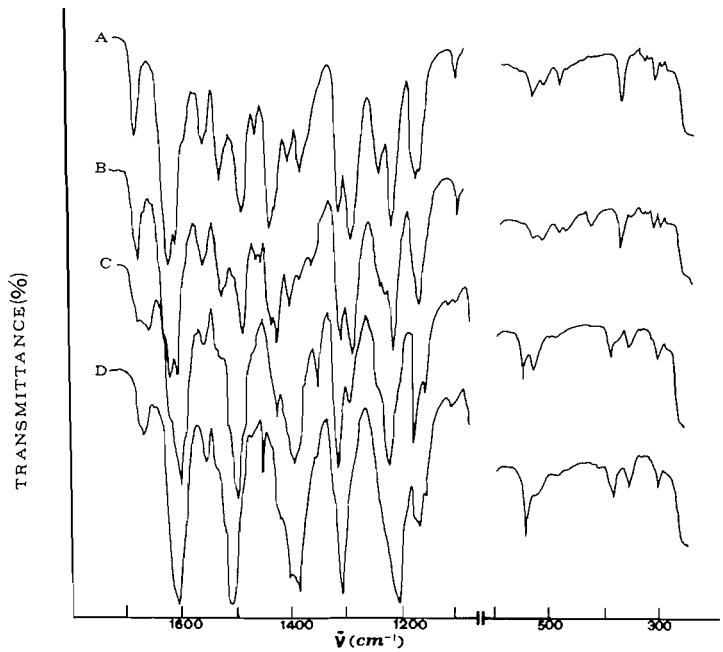


FIG. 1. Part of the ir spectra (KBr discs) of some representative mononuclear and homobinuclear chelates of 1,8-dihydroxyanthraquinone: *A*, $Cu(C_{14}H_7O_4)_2$; *B*, $Cu(C_{14}H_7O_4)_2(Py)(OH_2)$; *C*, $Cu_2(C_{14}H_6O_4)_2$; *D*, $Cu_2(C_{14}H_6O_4)_2(Py)(OH_2)$.

than the hydrogen atom. The lowering of the metal ion's ability to accept electron density from the ligand by its coordination with pyridine in the adducts is also reflected from the lower values of the $\nu(C\cdots O)_1 - \nu(C\cdots O)_2$ differences.

Special attention should be paid to the region 1200–1250 $cm^{-1}$ in the ir spectra of the studied chelates, since some bands related to the bonding mode of the ligand occur in this region. It is well known (17–19) that in hydroxyanthraquinones the $\nu(C\cdots O)$ band occurs in the region 1200–1250 $cm^{-1}$. The position of this band indicates that the C—O bond has a fractional double bond character. The chelates in question gave the band due to $\nu(C\cdots O)_3$ and $\nu(C\cdots O)_4$ (for numbering see structure I) in the same region. If we assign this band to $\nu(C\cdots O)$ we would expect the band to show the following characteristics. For the mononuclear chelates, where the electron density distribution into the chelate ring containing the metal ion differs from that of the chelate rings containing the hydrogen bonds, two bands due to $\nu(C\cdots O)$ stretching must be observed [$\nu(C\cdots O)_3 \neq \nu(C\cdots O)_4$]. In contrast, for the homobinuclear chelates, where the electron density distribution into all the chelate rings formed is the same, only one band would be expected [$\nu(C\cdots O)_3 = \nu(C\cdots O)_4$].

Of interest and considerable importance is also

Can. J. Chem. Downloaded from www.nrcresearchpress.com by 210.87.254.42 on 09/06/12
For personal use only.

TABLE 3. Electronic spectral data of 1,8-DHAQ chelates with bivalent metal ions in DMF solutions*

| Compound | Band II | Band III | Band IV |
|---|---|---|---|
| **I** | 24.21 sh† (4.22)‡ 23.47 (4.25) 22.22 (4.18) | 19.60 (3.27) 18.51 sh (3.26) 17.09 sh (3.10) | |
| **II** | 23.98 sh (4.19) 23.41 (4.22) 22.62 (4.16) | 19.37 (3.52) 18.62 (3.53) 17.09 sh (3.26) | |
| **III** | 24.09 sh (4.34) 23.36 (4.38) 22.57 (4.31) | 19.60 sh (3.74) 18.72 (3.78) 17.51 sh (3.70) | |
| **IV** | 24.27 sh (3.79) 23.42 (3.82) 22.47 (3.75) | 19.49 (3.28) 18.41 sh (3.26) 17.09 sh (3.19) | |
| **V** | 24.09 sh (4.77) 23.36 (4.80) 22.52 sh (4.74) | 19.41 (4.21) 18.51 (4.23) 17.39 sh (4.18) | |
| **VI** | 23.80 sh (4.92) 23.25 (4.94) 22.42 sh (4.87) | | |
| **VII** | 24.03 sh (4.69) 23.31 (4.72) 22.57 (4.65) | 18.79 (4.02) 17.63 sh (3.98) | |
| **VIII** | 24.09 sh (4.12) 23.36 (4.15) 22.83 sh (4.12) | 19.88 sh (3.72) 18.69 (3.81) 17.54 sh (3.73) | 10.20 sh (1.47) 8.89 (1.88) |
| **IX** | 24.33 sh (4.48) 23.41 (4.51) 22.22 sh (4.46) | 19.41 sh (4.42) 18.51 (4.46) | 10.36 (1.95) 8.77 (1.55) |
| **X** | 23.80 sh (4.11) 23.41 (4.12) 22.37 sh (4.07) | 19.53 (4.04) 18.62 (4.08) 16.86 sh (3.82) | 10.12 (1.99) 9.16 (1.68) |

*The spectra were also obtained in solid state (Nujol mulls) and in some cases in $CH_2Cl_2$ or EtOH solutions in order to investigate the region of 30–50 kK of the spectra. In this region the Band I exists.
†sh = shoulder.
‡Figures in parentheses are the values of log $\varepsilon_{mol}$.

the region 300–700 $cm^{-1}$ of the ir spectra of the chelates under consideration. This region contains several absorptions with medium or weak intensities. Some of them are typical absorptions of the free ligand while the rest, which are sensitive to the central metal ion and the structure of the chelates, are attributed to the normal modes of vibration of the $MO_4$ and $M_2O_6$ moieties of the chelates. In order to make a reasonable assignment of these bands we used the comparison method. Thus, we have compared the ir spectra of the studied compounds with those of the corresponding acetylacetonate complexes, for which the absorption bands have been fully characterized on the basis of theoretical treatment (20–23). A similar pattern for the absorption bands in the region 300–700 $cm^{-1}$ for both classes of compounds has been observed, the only difference being the shifts of the bands. Such a shift must be expected on the basis of the different electron donor and acceptor abilities of the 1,8-DHAQ and the acetylacetonato ligands.

The number and the form of the bands due to M—O stretching for the 1:2 chelates are similar to those of the corresponding 1:2 metal acetylacetonates. Hence, since the 1:2 metal acetylacetonates have $D_{2h}$ symmetry we can conclude that our 1:2 chelates adopt structure **I** which also has $D_{2h}$ symmetry. On the basis of $D_{2h}$ symmetry we can assign the band in the region 450–550 $cm^{-1}$ to $\nu_{sym}$(M—O) stretching vibration (symmetry species $B_{1u}$) and the band in the region 310–360 $cm^{-1}$ to $\nu_{asym}$(M—O) stretching vibration (symmetry species $B_{2u}$). The third ir-active vibration (symmetry species $B_{3u}$) occurs at a lower frequency (below 300 $cm^{-1}$) and could not be observed in the present study. Both $\nu_{sym}$(M—O) and $\nu_{asym}$(M—O) bands of the chelates studied here are shifted to higher frequencies relative to the corresponding bands of the analogous acetylacetonates. This observation could be explained on the basis of the enhanced $\pi$-electron density delocalization into the chelate rings of the chelates under consideration over that in the metal acetylacetonates. The $\nu_{sym}$(M—O) and $\nu_{asym}$(M—O) are sensitive to the nature of the central metal ion. For the $\nu_{sym}$(M—O) band the following order of decreasing frequencies has been observed: Cu > Ni > Zn > Mn. This sequence is in accordance with the sequence observed for the stability constants of the chelates of these divalent metal ions with analogous oxygen donor ligands (20).

The only chelate which gave a different pattern for the $\nu$(M—O) bands was that of zinc(II). This is no doubt due to the ability of zinc(II) to adopt a tetrahedral and not a square planar geometry.

*Electronic spectra*

The positions of the band maxima and of discernible shoulders, as well as their log $\varepsilon_{mol}$ values, are given in Table 3.

In the region 30–50 kK a composite band (band I) occurs, which exhibits a maximum at about 40 kK and a shoulder at about 35 kK. Band I is not included in Table 3, as it was masked by the absorption of the solvent, but it was observed in the solid state spectra and in some cases in $CH_2Cl_2$ or EtOH solutions as well.

In the region 20–25 kK another intense multicomponent band (band II) occurs, which exhibits a main peak at about 23.0–23.5 kK and two shoulders, one on each side of the main peak, as well. Both bands I and II are attributed to intraligand transitions, which are the characteristic benzenoid and quinoid ET transitions of the ligand (24, 25).

In the region 15–25 kK an intense envelope type band (band III) occurs, which is absent in the spectra of the free ligand and the zinc(II) chelate as well. Band III is sensitive to the nature of the

Can. J. Chem. Downloaded from www.nrcresearchpress.com by 210.87.254.42 on 09/06/12
For personal use only.

TABLE 4. Magnetic susceptibility data of the homobinuclear chelates at room temperature and different magnetic field strengths

| Compound | $\mu_{eff}$, BM | | |
|---|---|---|---|
| | 4.000 G | 8.000 G | 11.700 G |
| **IV**, $Cu_2(C_{14}H_6O_4)_2$ | 0.97 | 0.81 | 0.80 |
| **V**, $Cu_2(C_{14}H_6O_4)_2(Py)(OH_2)$ | 1.04 | 0.97 | 0.97 |
| $Ni_2(C_{14}H_6O_4)(OH_2)_4$ | 2.40 | 2.29 | 2.25 |
| **IX**, $[Ni_2(C_{14}H_6O_4)(OH_2)_4]\cdot 2H_2O$ | 2.50 | 2.39 | 2.40 |
| **X**, $[Ni_2(C_{14}H_6O_4)_2(Py)_2(OH_2)_2]\cdot 2H_2O$ | 2.56 | 2.48 | 2.45 |

central atom and the type of the chelate and has an intensity very close to the intensity of CT transitions. Hence we can assign band III to CT transitions which could be either of the L → M or L ← M type. The absence of band III in the spectrum of the zinc(II) chelate indicates that this band must be of the L → M type. If band III is an L → M CT band one could expect a shifting of the band (the main peak of band III is at 18–19 kK) to higher energies as the electron density on the central atom increases. In fact, this is the case for the chelates studied.

Finally, in the region 5–15 kK only the nickel(II) chelates exhibit a weak and broad absorption band (band IV). Band IV is characteristic of octahedral nickel(II) complexes and is attributed to the $^3T_{2g} \leftarrow {}^3A_{2g}$ electronic transition. For the tetragonally distorted complexes band IV splits into two well separated bands which are attributed to $^3B_{2g} \leftarrow {}^3B_{1g}$ and $^3E_g \leftarrow {}^3B_{1g}$ (26). The observed splitting of the band IV in the spectra of the nickel(II) chelates studied supports their distorted octahedral geometry. The 10 *Dq* values obtained are about 9.0 kK, very close to those of the octahedral nickel(II) complexes with oxygen donor ligands. The other two expected *d–d* transitions ($^3A_{2g} \leftarrow {}^3B_{1g}$, $^3E_g \leftarrow {}^3B_{1g}$) for the distorted octahedral nickel(II) complexes are obscured by the intense CT transitions and could not be observed. The same is also true for the expected *d–d* transitions ($^2A_g \leftarrow {}^2B_{1g}$; $^2B_{2g}$, $^2B_{3g} \leftarrow {}^2B_{1g}$) of the Cu(II) chelates of $D_{2h}$ symmetry (27–29).

It must be noticed that, after heating the homobinuclear nickel(II) chelates to remove the crystalline water, no spectral changes were observed. This fact indicates the existence of the same nickel chromophores before and after heating and hence the two molecules of water were present as crystalline water.

*Magnetic data*

The room temperature magnetic moments of the mononuclear chelates **I**, **II**, **III**, **VI**, **VII**, and **VIII** ($\mu_{eff}$ = 1.93, 2.10, 2.21, 0.00, 6.03, and 3.29 BM, respectively) are normal and in accordance with the proposed structures of the chelates (30). However, the room temperature magnetic data of the homobinuclear chelates obtained at different magnetic field strengths (Table 4) reflect a considerable spin–spin interaction between the unpaired electrons on the adjacent metal ions. The low magnetic moments observed both at low and high field strengths are indicative of the operation of antiferromagnetism in these compounds. On the other hand, the slight increase of the magnetic moments as the magnetic field strength decreases is indicative of the operation of ferromagnetism as well. Thus, the magnetic exchange phenomenon observed in the studied homobinuclear chelates is analogous to that observed in the case of other binuclear Cu(II) and Ni(II) chelates (31–35) and could be explained on the basis of the same mechanism. However, it must be noted that in the homobinuclear chelates studied, the magnetic data indicate a more favorable magnetic exchange which is dominated by antiferromagnetism than in the previously studied chelates (32–36). This could be expected on the basis of the better-developed π system on the 1,8-DHAQ ligand than in the 1,3,5-triketonato ligand.

Finally, it is worthwhile mentioning that the pyridine adducts gave high magnetic moments which in some cases were subnormal. The same was also observed previously (36) in the case of quinoline and isoquinoline adducts of the $Cu(acac)_2$ chelates.

1. R. A. MORTON. Biochemistry of quinones. *Edited by* R. A. Morton. Academic Press, New York. 1965.
2. R. H. THOMSON. Naturally occurring quinones. Academic Press, New York. 1971.
3. S. PATAI. The chemistry of the quinoid compounds, Part 2. *Edited by* S. Patai. John Wiley, London. 1974.
4. R. S. BOTTEI and P. L. GERACE. J. Inorg. Nucl. Chem. **23**, 245 (1961).
5. R. S. BOTTEI and D. QUANE. J. Inorg. Nucl. Chem. **26**, 1919 (1964).
6. R. S. BOTTEI and C. P. MCEACHERN. J. Inorg. Nucl. Chem. **32**, 2653 (1970).

Can. J. Chem. Downloaded from www.nrcresearchpress.com by 210.87.254.42 on 09/06/12
For personal use only.

7. R. SUEMITSU. Doshisha Daigaku Rikogaku Hokoku, 153 (1965): Chem. Abstr. **63**, 15737*f* (1965).
8. R. N. AIZENBERG, I. M. REIBEL, A. YA. SYCHEV, R. S. AIZENBERG, F. F. KAZANTSEV, and F. R. SHCHERBANOVSKAYA. Tr. Kishiner. Sel. Khoz. Inst. **72**, 79 (1971): Chem. Abstr. **78**, 90562*x* (1973).
9. A. M. TALATI and V. N. MISTRY. Labdev, Part A, **10**, 141 (1972): Chem. Abstr. **80**, 33372c (1972).
10. A. DUFRENSE, C. G. DE LIMA, J. KNUDSEN, and J. E. MOREIRA. J. Inorg. Nucl. Chem. **35**, 789 (1973).
11. H. DWAIN COBLE and H. F. HOLTZCLAW, JR. J. Inorg. Nucl. Chem. **36**, 1049 (1974).
12. S. B. PADHYE, C. R. JOSHI, and B. A. KULKARNI. J. Inorg. Nucl. Chem. **39**, 1289 (1977).
13. P. H. MERRELL. Inorg. Chim. Acta, **32**, 99 (1979).
14. D. L. VAN DUUREN, A. SEGAL, S. S. TSENG, G. M. RUSCH, G. LOEWENGART, U. MATÉ, D. ROTH, A. SMITH, and S. MELCHIONNE. J. Med. Chem. **21**, 26 (1978).
15. B. E. ZAITSEV, N. P. VASILÉVA, and B. N. IVANOV-EMIN. Russ. J. Inorg. Chem. **16**, 502 (1971).
16. B. BOGDANOVIĆ and M. YUS. Angew. Chem. **91**, 681 (1979).
17. R. M. ISSA, Y. Z. AHMED, and A. H. ZEWAIL. Egypt. J. Chem. **15**, 1 (1972).
18. M. ST. C. FLETT. J. Chem. Soc. 1441 (1948).
19. D. HADZI and N. E. SHEPPARED. J. Am. Chem. Soc. **73**, 5460 (1950).
20. K. NAKAMOTO, P. J. MCCARTHY, and A. E. MARTELL. Nature, **183**, 459 (1959).
21. K. NAKAMOTO and A. E. MARTELL. J. Chem. Phys. **32**, 588 (1960).
22. K. NAKAMOTO, P. J. MCCARTHY, and A. E. MARTELL. J. Am. Chem. Soc. **83**, 1272 (1961).
23. M. MIKAMI, I. NAKAGAWA, and T. SHIMANOUCHI. Spectrochim. Acta, **23**A, 1037 (1967).
24. I. SINGH, R. T. OGATA, R. E. MOORE, C. W. J. CHANG, and P. J. SCHEUER. Tetrahedron, **24**, 6053 (1968).
25. R. M. ISSA, M. S. EL-EZAHY, and A. H. ZEWALL. Z. Phys. Chem. **244**, 155 (1970).
26. A. B. P. LEVER. Coord. Chem. Rev. **3**, 119 (1968).
27. K. SONE. J. Am. Chem. Soc. **75**, 5207 (1953).
28. R. L. BELFORD, M. CALVIN, and G. BELFORD. J. Chem. Phys. **26**, 1165 (1957).
29. R. L. BELFORD and J. W. CARMICHAEL, JR. J. Chem. Phys. **46**, 4515 (1967).
30. B. N. FIGGIS and J. LEWIS. Progress in inorganic chemistry. Vol. 6. *Edited by* F. A. Cotton. 1967. p. 37.
31. W. E. HATFIELD and J. C. MORRISON. Inorg. Chem. **5**, 1390 (1966).
32. W. E. HATFIELD and F. L. BUNGER. Inorg. Chem. **5**, 1161 (1966).
33. W. E. HATFIELD, C. S. FOUNTAIN, and R. WHYMAN. Inorg. Chem. **5**, 1855 (1966).
34. A. P. GINSBERG, R. L. MARTIN, and R. C. SHERWOOD. Inorg. Chem. 7, 932 (1968).
35. D. P. MURTHA and R. L. LINTVEDT. Inorg. Chem. **9**, 1532 (1970).
36. R. J. CASEY and W. R. WALKER. J. Inorg. Nucl. Chem. **29**, 1301 (1967).


Can. J. Chem. Downloaded from www.nrcresearchpress.com by 210.87.254.42 on 09/06/12
For personal use only.

# Correlations between spectroscopic properties of aromatic molecules and fragmentation rates of their metastable molecular ions in a mass spectrometer

ROBERT K. BOYD AND BORI SHUSHAN

*Guelph-Waterloo Centre for Graduate Work in Chemistry (Guelph Campus), University of Guelph, Guelph, Ont., Canada N1G 2W1*

Received August 10, 1981[1]

ROBERT K. BOYD and BORI SHUSHAN. Can. J. Chem. **60**, 2484 (1982).

Unexpected correlations have been found between spectroscopic (uv and nmr) properties of some aromatic systems (specifically polycyclic aromatic hydrocarbons and chlorinated biphenyls) and fragmentation rates of the corresponding metastable molecular ions in a field-free region of a mass spectrometer. The meaning of these empirical correlations is explored via the quasi-equilibrium theory of mass spectra. For the case of the polycyclic aromatic hydrocarbons for which more complete ancillary data are available, a reasonably self-consistent account of the correlations can be obtained via the ionisation energy as the crucial parameter. The case of the chlorinated biphenyls is less clear, due to a lack of subsidiary data. However, the best explanation available appears to involve a systematic shift in the energy deposition function with increasing steric interaction around the biphenyl linkage.

ROBERT K. BOYD et BORI SHUSHAN. Can. J. Chem. **60**, 2484 (1982).

On a trouvé des corrélations inattendues entre les propriétés spectroscopiques (uv et rmn) de quelques systèmes aromatiques (hydrocarbures aromatiques polycycliques et chlorobiphényles spécifiquement) et les vitesses de fragmentation des ions moléculaires métastables correspondants dans la région de libre champ d'un spectromètre de masse. On explore la signification de ces corrélations empiriques via la théorie de quasi équilibre des spectres de masse. Dans le cas des hydrocarbures aromatiques polycycliques, pour lesquels on dispose de données accessoires complètes, on peut obtenir une interprétation raisonnablement valable des corrélations par l'intermédiaire de l'énergie d'ionisation comme paramètre fondamental. Le cas des chlorobiphényles est moins clair, à cause du manque de données secondaires. Cependant, la meilleure explication disponible semble impliquer un glissement systématique dans la fonction d'énergie de précipitation avec une augmentation de l'interaction stérique autour de la liaison biphényle.

[Traduit par le journal]

## Introduction

In some recent work (1), devoted to exploiting the diagnostic capabilities of metastable ion studies in differentiating between isomeric chlorinated biphenyls (PCBs), a correlation was observed between the fragmentation intensities and the number of chlorine substituents *ortho* to the biphenyl linkage. This correlation, which had been noticed before (2) in the conventional mass spectra of these compounds, was attributed (2) to relief of steric strain in the molecular ions following expulsion of one or more chlorine atoms. In an attempt to improve upon this correlation, a parameter more sensitive to steric strain was sought. The so-called A-band of biphenyls (3) in the ultraviolet is attributed (3) to a transition to an excited state involving delocalisation over two quinonoid rings via a double-bond linkage. This view will be discussed more fully below, but clearly bulky *ortho* substituents will restrict the degree of attainable coplanarity, and thus affect the transition energy. An unexpectedly significant correlation was found (1) between the energy of the A-band transition for chlorinated biphenyls and the (M − 2Cl)/(M − Cl) intensity ratio in the metastable spectra (*B*/*E* linked scan for molecular ion as parent ion).

The original intent of seeking such correlations was to provide some partially predictive scheme to assist in cross-checking structures of chlorinated biphenyls other than the 31 standards (mono- through tetra-chloro substitution) which were available (1). However, the correlation thus found (1) was clearly of more fundamental significance. Accordingly, we have continued investigations of such correlations, and have extended them to include similar data obtained previously (4, 5) for polycyclic aromatic hydrocarbons (PAH). The latter correlations appear to be susceptible to a more satisfactory interpretation than those found for the PCBs.

## I. Polycyclic aromatic hydrocarbons

### *(a) Experimental results*

The raw data to be used here and the mass spectrometric techniques used to obtain them have been described previously (4, 5). The fragment ion intensities are those obtained for metastable molecular ions which fragmented in the first field-free region of a conventional double-focussing mass spectrometer. They were obtained as peak heights observed in linked scans at constant *B*/*E*, and thus correspond to the heights of the full metastable peaks (6).

[1]Revision received June 18, 1982.

0008-4042/82/192484-16$01.00/0

©1982 National Research Council of Canada/Conseil national de recherches du Canada

Can. J. Chem. Downloaded from www.nrcresearchpress.com by 210.87.254.105 on 09/06/12
For personal use only.

Can. J. Chem. Downloaded from www.nrcresearchpress.com by 210.87.254.105 on 09/06/12
For personal use only.

The fragmentation reactions of molecular ions of PAH, which are of lowest appearance energy, correspond to loss of one and two hydrogen atoms. (The higher energy fragmentation reactions (5) do not show significant correlations.) The $(M - H)^+$ and $(M - 2H)^{+\cdot}$ intensities from metastable molecular ions *do* separately correlate fairly well with the transition energy of the so-called *p*-band (7) of the neutral PAH in the ultraviolet. This transition connects the $^1A$ ground state to the excited state designated $^1L_a$ in the free electron model of Platt (8). However, a slightly better correlation was found between the sum of the intensities $[(M - H)^+ + (M - 2H)^{+\cdot}]$ (normalised to the main-beam molecular ion intensity) and the *p*-band energy. This correlation for the 17 alternant aromatic hydrocarbons studied (5) is shown as Fig. 1. The two non-alternant hydrocarbons studied (5) (fluorene and fluoranthene) did not appear to fit the general trend, and have been omitted from Fig. 1. In Table 1 are listed the 17 alternant hydrocarbons studied (5), together with their molecular formulae and (0–0) *p*-band transition energies taken from Birks' monograph (9).

Before attempting any interpretation of Fig. 1, some background information will be useful. Previously (5), evidence was presented suggesting that the expulsion of hydrogen atoms from these PAH molecular ions is a stepwise process:

$$M^{+\cdot} \rightarrow (M - H)^+ + H^\cdot \rightarrow (M - 2H)^{+\cdot} + 2H^\cdot$$

It seems improbable (5) that loss of molecular hydrogen occurs in a single step. Thus, the $[M - H)^+ + (M - 2H)^{+\cdot}]$ may reasonably be regarded as a measure of the total intensity, on the timescale of the "metastable window" (see below), in the lowest energy reaction channel available to the PAH molecular ions.

The left hand curve in Fig. 1 correlates the data for the linear acenes plus perylene and benzoperylenes; the correlation coefficient for this set was found to be 0.96. The remaining compounds are correlated by the right hand curve of Fig. 1, with a correlation coefficient of 0.91. Both *cata*-condensed and *peri*-condensed PAH appear in both sets, so that this particular distinction appears to be of no significance in this regard.

*(b) Phenomenological identification of parameters underlying observed correlation*

The question to be faced concerns the connection between energy differences between *stationary* electronic states of neutral PAH molecules, on the one hand, and fragmentation *rates* of the corresponding molecular ions, on the other. In order to investigate this question, it is necessary to refer to some theory of fragmentation rate constants. Recently (10) Lorquet published a review of theories of unimolecular dissociation, particularly as applied to ions under collision-free conditions. It is not necessary to attempt here a summary of this scholarly perspective (10) in order to justify the present use of statistical theories of unimolecular fragmentation. Modern justifications of such theories, in particular of the so-called "energy randomisation" postulate underlying the use of a microcanonical rate constant $k(\varepsilon)$, are somewhat different (10) from those offered by the originators (11, 12). The most widely used statistical theory (Rice–Ramsperger–Kassel–Marcus or RRKM theory (11), alternatively quasi-equilibrium theory or QET (12)) leads to the following general expression for the microcanonical rate constant:

$$k(\varepsilon) = \left(\frac{\sigma}{h}\right) \frac{G^*(\varepsilon - \varepsilon_0)}{N(\varepsilon)}$$

where $\sigma$ is a symmetry factor, $N(\varepsilon)$ is the density of states, at internal energy $\varepsilon$, of the reactant, and $G(\varepsilon)$ is the integral of $N(\varepsilon)$ over the range $\varepsilon = 0$ to $\varepsilon$. The asterisk denotes a property of the transition state, i.e. to a system with one (usually vibrational)

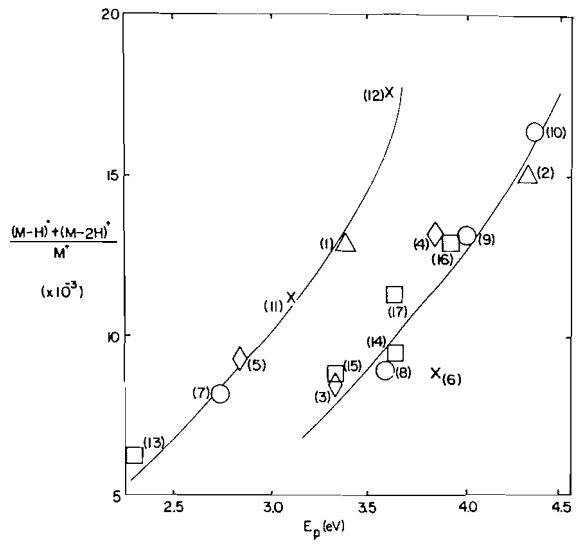


FIG. 1. Correlation of metastable ion fragmentation intensities ((M − 1) + (M − 2) peak heights in B/E linked scan spectra), with *p*-band energies for alternant hydrocarbons. Solid curves are least-squares fits, and the numbers designate the compounds (see Table 1). $E_p$ values are (0–0) energies (9). Isomeric series: △, $C_{14}H_{10}$; ◇, $C_{20}H_{12}$; ○, $C_{18}H_{12}$; □, $C_{22}H_{14}$; ×, single isomers. Numbers on symbols refer to code in Table 1.

Can. J. Chem. Downloaded from www.nrcresearchpress.com by 210.87.254.105 on 09/06/12
For personal use only.

TABLE 1. Alternant hydrocarbons whose metastable ion spectra were obtained

| Compound name | Formula | Code[a] | Code of Birks[b] | $p$-Band energy (eV)[c] | $10^3 \times [(M - H)^+ + (M - 2H)^{+\cdot}]/(M^{+\cdot})$[a] | IE (eV)[d] |
|---|---|---|---|---|---|---|
| Anthracene | $C_{14}H_{10}$ | 1 | 3.1 | 3.31 | 12.9 | 7.41 |
| Phenanthrene | $C_{14}H_{10}$ | 2 | 3.2 | 4.24 | 15.0 | 7.86 |
| 3,4-Benzopyrene (benzo[*a*]pyrene) | $C_{20}H_{12}$ | 3 | 5.3 | 3.22 | 8.5 | 7.12 |
| 1,2-Benzopyrene (benzo[*e*]pyrene) | $C_{20}H_{12}$ | 4 | 5.2 | 3.73 | 13.2 | 7.41 |
| Perylene | $C_{20}H_{12}$ | 5 | 5.1 | 2.85 | 9.2 | 6.97 |
| Pyrene | $C_{16}H_{10}$ | 6 | 4.1 | 3.71 | 8.4 | 7.41 |
| Tetracene | $C_{18}H_{12}$ | 7 | 4.2 | 2.63 | 8.2 | 6.97 |
| 1,2-Benzanthracene (tetraphene) | $C_{18}H_{12}$ | 8 | 4.3 | 3.46 | 8.9 | 7.41 |
| Chrysene | $C_{18}H_{12}$ | 9 | 4.4 | 3.89 | 13.1 | 7.59 |
| Triphenylene | $C_{18}H_{12}$ | 10 | 4.6 | 4.36 | 16.4 | 7.88 |
| 1,12-Benzoperylene (benzo[*g*,*h*,*i*]perylene) | $C_{22}H_{12}$ | 11 | 6.2 | 3.20 | 11.6 | 7.15 |
| Coronene | $C_{24}H_{12}$ | 12 | 7.1 | 3.51 | 18.6 | 7.29 |
| Pentacene | $C_{22}H_{14}$ | 13 | 5.4 | 2.12 | 6.2 | 6.61 |
| 1,2,5,6-Dibenzanthracene | $C_{22}H_{14}$ | 14 | 5.7 | 3.55 | 9.5 | 7.38 |
| 3,4-Benzotetraphene | $C_{22}H_{14}$ | 15 | 5.13 | 3.40 | 8.8 | 7.20 |
| Picene | $C_{22}H_{14}$ | 16 | 5.9 | 3.82 | 12.9 | 7.52 |
| 1,2,3,4-Dibenzanthracene | $C_{22}H_{14}$ | 17 | 5.6 | 3.55 | 11.3 | 7.39 |

[a]Reference 5.
[b]Table 1.1, ref. 9, includes structural formulae.
[c]Table 5.4, ref. 9. Values quoted are for (0–0) transition.
[d]References 17 to 21.

degree of freedom removed. $\varepsilon_0$ is the critical energy for dissociation.

Quantitative evaluation of this expression requires detailed knowledge of the internal modes of both reactant and transition state. This would present a formidable problem for the reactants of interest in the present work. For qualitative purposes, it is common practice (13, 14) to use an oversimplified model involving $s$ degenerate classical, harmonic oscillators of frequency v; the RRKM expression then reduces to:

$$[1] \quad k(\varepsilon) = \nu\left(1 - \frac{\varepsilon_0}{\varepsilon}\right)^{s-1}$$

In the following discussion eq. [1] will be used. The qualitative conclusions thus reached can be re-expressed in terms of the full RRKM expression, but the arguments then become extremely wordy as a consequence of lack of specific knowledge of the internal mode properties underlying the quantities $N$ and $G^*$. (The parameters v and $s$ define $N$ and $G^*$ in this simplest conceivable model.) It will prove more convenient to transform to an energy scale $E$, measured relative to the zero-point energy of the neutral molecule:

$$[2] \quad E = \varepsilon + IE_a$$

where $IE_a$ is the adiabatic (0–0) ionisation energy. Then, eqs. [1] and [2] give:

$$[3] \quad k(E) = \nu[(E - AE_a)/(E - IE_a)]^{s-1}$$

where $AE_a$ is the adiabatic appearance energy for the product ion, i.e. the appearance energy without any kinetic shift contribution.

Now if the times $t_1$, $t_2$, $t_3$, $t_4$ represent, respectively, the ion-source residence time, the time of entry into the field-free region, the time of leaving the field-free region, and the time of arrival at the detector, it is straightforward to show that:

$$[4] \quad (M^+_{obs}/M^+_{tot}) = A\int_{IE_a}^{\infty} P(E)\exp[-k(E)t_4]dE$$

$$[5] \quad (F^+_{IS}/M^+_{tot}) = B\int_{IE_a}^{\infty} P(E)\{1 - \exp[-k(E)t_1]\}dE$$

$$[6] \quad (m^*/M^+_{tot}) = (F^+_{MS}/M^+_{tot}) = C\int_{IE_a}^{\infty} P(E)\{\exp[-k(E)t_3] - \exp[-k(E)t_2]\}dE$$

In eqs. [4]–[6], the various $F^+$ and $M^+$ are ion fluxes of product (fragment) ions and molecular (parent) ions, respectively. $M^+_{tot}$ is the total flux of molecular ions produced, while $M^+_{obs}$ is the flux which survives to the detector, and is measured as the molecular ion intensity in the conventional

Can. J. Chem. Downloaded from www.nrcresearchpress.com by 210.87.254.105 on 09/06/12
For personal use only.

mass spectrum. $F^+_{IS}$ is the flux of fragment ions produced within the ion source, and $F^+_{MS}$ that produced from metastable $M^+_{ions}$ within the field-free region, yielding an observed peak intensity m*. $A$, $B$, and $C$ are instrumental parameters which include such effects as ion transmission efficiency, detector response, use of peak heights instead of peak areas to measure intensities, etc. $P(E)$ is the normalised internal energy distribution function of the $M^+$ ions at the instant of creation; as such, it has non-zero values for $E > IE_a$, while $k(E)$ has non-zero values only for $E > AE_a$, in the absence of quantum effects. The lower limit of integration, in eqs. [5] and [6], could thus equally well be $AE_a$. The ordinate of Fig. 1 corresponds to $(m^*/M^+_{obs})$, i.e. to (eq. [6]/eq. [4]).

Strictly, all of $A$, $B$, $C$, $t_2$, $t_3$, $t_4$ are functions of the masses of the various ions. It does not seem conceivable that any of these parameters could be responsible for the regularities observed in Fig. 1, particularly in view of the differences observed between PAH isomers. Thus, the quantities $P(E)$, $\nu$, $s$, $IE_a$, and $AE_a$ remain for consideration. Two different quantities must be selected from these five to account for Fig. 1. The first, conveniently labelled parameter $X$, must correlate with $E_p$ to account for the smooth trends observed. The second (parameter $Y$) must account for the split into two clearly separated families of PAH (Fig. 1). Parameter $X$ will be sought first.

The quantities $P(E)$ and $\nu$ will now be considered as candidates for parameter $X$. Some indication of their potential in this regard can be obtained from a consideration of the conventional mass spectra (ion-source reactions), which are known (15) to be practically identical for isomeric PAH. Because of the relatively short residence time within the ion source, $F^+_{IS}$ must arise predominantly from fragmentations of molecular ions with large amounts of internal energy. If $E$ is large enough, $k(E)$ given by eq. [3] approaches the value $\nu$. With this approximation, eq. [5] becomes:

$$[7a] \quad (F^+_{IS}/M^+_{tot}) \approx B[1 - \exp(-\nu t_1)] \int_{EA_a + \bar{E}_{IS}}^{\infty} P(E)dE$$

$$[7b] \quad (F^+_{IS}/M^+_{obs}) = (B/A)\,(\exp \nu t_4)\,[1 - \exp(-\nu t_1)]$$

where $\bar{E}_{IS}$ is the average (assumed large) kinetic shift for molecular ions fragmenting in the ion source. Thus, the observed invariance of both $(F^+_{IS}/M^+_{tot})$ and $(F^+_{IS}/M^+_{obs})$ within an isomeric series of PAH would seem to imply that both $\nu$ and the integral in eq. [7a] are essentially constant. Strictly, the expression for $M^+_{obs}$ (eq. [4]) should account for *all* reactions of $M^+$; however, in the case of PAH, the loss of H atoms is easily the major fragmentation channel and the essentially qualitative conclusions to be drawn would not be affected by such a correction. Thus, these considerations provide some justification for discarding both $\nu$ and at least the high-energy tail of $P(E)$ as candidates for parameter $X$. It is also difficult to provide theoretical reasons to account for a simple correlation of either $\nu$ or $P(E)$ with $E_p$.

The parameter $s$ (eq. [3]) is somewhat nebulous (13, 14), but is generally between 30–50% of the total number of vibrational modes in the fragmenting ion; near the fragmentation threshold, this fraction can drop to about 20%. Unfortunately, it does not seem possible to deduce much phenomenological evidence for or against the suitability of $s$ as a candidate for parameter $X$. Again, it would be difficult to understand theoretically why an "effective number of oscillators" should correlate simply with $E_p$, particularly within an isomeric series.

The remaining possibilities for parameter $X$ are $AE_a$ and $IE_a$. The manner in which these quantities affect $k(E)$ and its convolution with $P(E)$ is illustrated qualitatively for the present case in Fig. 2. (This figure, and associated discussion, have been modified from a more general discussion given previously (13).) Nothing is known of the form of $P(E)$ (13, 14), and the only assumption made here is that $P(E)$ falls off to small values for both very large and very small values of $(E - IE_a)$. Then, since it is known (15) that the molecular ion $M^+_{obs}$ constitutes most of the ion current $M^+_{tot}$ (60% in the least favourable case listed (15)), the relative dispositions of the $P(E)$ and $k(E)$ curves in Fig. 2 must be such that $M^+_{obs}$ (= $M^+_0$ + $M^+_E$ in Fig. 2) accounts for the majority of the area under the $P(E)$ curve, as shown. The value of IE determines the general position along the $E$ axis of the $P(E)$ curve, while AE determines that of the $k(E)$ curve. Thus, it is clear from Fig. 2 that an increase in m* (i.e. $F^+_{MS}$, eq. [6]) can result from either a decrease in $AE_a$ or from an increase in $IE_a$. The only assumption required in reaching this conclusion was that concerning the very general form of $P(E)$; the requirement that $M^+_{obs}$ constitute the majority of $M^+_{tot}$ is derived from experimental observation (15).

Unfortunately, very little experimental information is available concerning the appearance energies of fragment ions of PAH. Some early data (16) for several PAH included only phenanthrene of those studied here (Table 1). Some additional AE values for $C_{18}H_{12}$ isomers were obtained more recently (5). All of these data (5, 16) were obtained

Can. J. Chem. Downloaded from www.nrcresearchpress.com by 210.87.254.105 on 09/06/12
For personal use only.

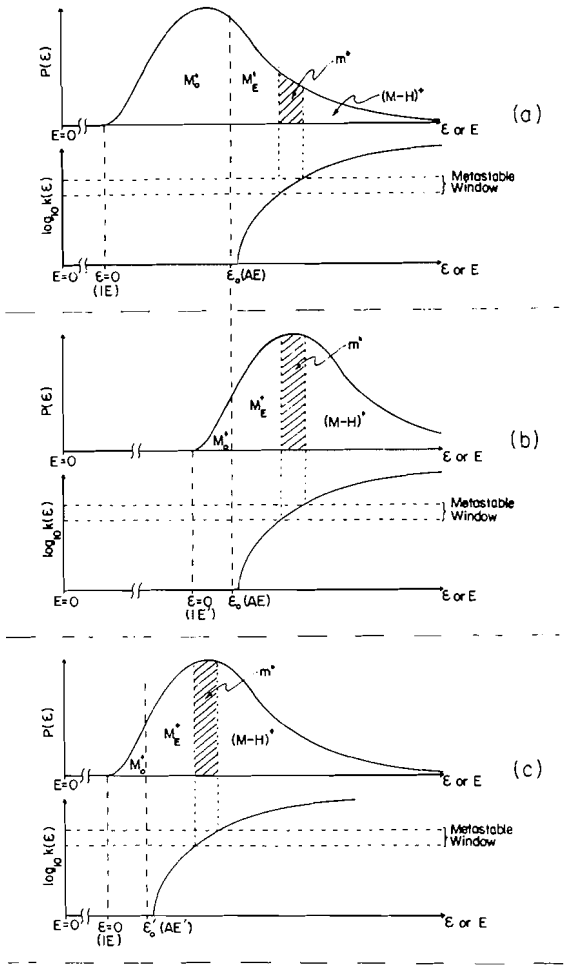


FIG. 2. Qualitative indication, of effects of changing ionization energy IE and appearance energy AE, on metastable peak intensity $m^*$. Internal energy deposition function $P(\varepsilon)$ is assumed to be a fixed function of $\varepsilon = (E - \mathrm{IE})$, while $k(\varepsilon)$ is given by eq. [3]. $M^+_0$, molecular ions with internal energy below reaction threshold; $M^+_E$, molecular ions with insufficient energy to react on instrumental timescale; m*, molecular ions with internal energies, and thus lifetimes, appropriate to fragmentation within the field-free region (metastable window); $(M - H)^+$, fragment ions formed within the ion source. (*a*) Low IE, high AE; (*b*) high IE, high AE; (*c*) low IE, low AE.

using unfiltered electron beams in conventional mass spectrometers, and are thus of low reliability. Nevertheless, the data thus obtained (5) for the appearance energies of $(M - H)^+$ fragments from $C_{18}H_{12}$ isomers are informative: tetracene, 14.5 eV; chrysene, 15.1 eV; triphenylene, 15.4 eV; 1,2-benzanthracene, 15.3 eV. (The last value was measured but not reported previously (5).) Thus, within this limited set of data, AE does *not* correlate with $E_p$ (Table 1). Probably the only significant difference observed within these AE values is that between the value for tetracene and the rest. Thus, this admittedly meagre evidence does suggest that $AE_a$ is probably not parameter $X$, but may correspond to parameter $Y$ which accounts for the separation of the acene series (plus perylene and the benzperylenes) from the other PAH studied (Fig. 1). This tentative proposal clearly requires further experimental test.

By elimination, then, $IE_a$ remains as the only candidate for parameter $X$. Accurate values of $IE_a$ have been obtained by Schmidt for a large number of PAH, using photoelectron spectroscopy (17–21). It was shown (20), for *cata*-condensed PAH only, that the lowest ionisation energies correlated well with $E_p$ values. The latter were estimated mostly from solution spectra taken at room temperature, with some empirical corrections applied for solvent shifts. In the present work the values of $E_p$ used were those corrected to the 0–0 transition by Birks (9); these values appear to be generally lower by about 0.1 eV than those used by Schmidt (17–21). The IE values obtained by Schmidt (17–21) are also 0–0 values ($IE_a$ values) since the first band in the photoelectron spectra generally showed well-resolved vibrational structure with a spacing (1300 $cm^{-1}$) very close to that observed in the *p*-bands. Figure 3 shows the correlation between the values of $IE_a$ and Birks' values (9) for the 0–0 *p*-band transition energies for the 17 PAH studied in the present work. This correlation,

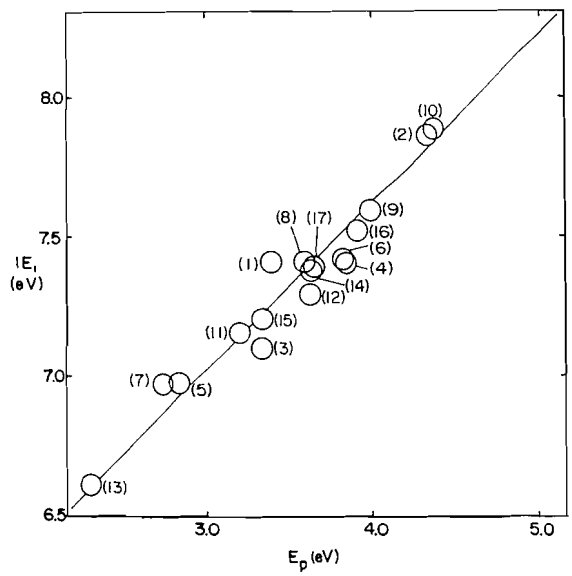


FIG. 3. Plot of ionisation energies for alternant PAH (data from photoelectron spectroscopy (17–21)) vs. *p*-band energies (9). Both are (0–0) transition energies. Solid line is least-squares fit (eq. [8]), and numbers designate the compounds (Table 1).

Can. J. Chem. Downloaded from www.nrcresearchpress.com by 210.87.254.105 on 09/06/12
For personal use only.

which refers to both *cata*- and *peri*-condensed PAH, may be expressed as:

[8] $IE_a/eV = 5.42(\pm 0.08) + 0.55(\pm 0.04)E_p$

The standard deviation is ±0.12 eV; correlation coefficient 0.96.

As emphasised previously (20), the quality of this and similar correlations is remarkable in view of the range of structural types of PAH, the varying degrees of non-planarity, etc. There is thus little doubt, in the present context, that $IE_a$ may be identified as parameter $X$, i.e. that parameter responsible for the correlation of metastable ion fragmentation rates with $E_p$. Identification of parameter $Y$, responsible for the split into two distinct families (Fig. 1), is much less certain though the data available do support the idea that $AE_a$ (eq. [3]) may be thus identified.

*(c) Theoretical considerations*

Since our original correlation between $E_p$ and metastable ion fragmentation intensities (Fig. 1) has now been reduced to one between $E_p$ and $IE_a$ (Fig. 3), some attempt must now be made to understand the latter. Simple Hückel theory of the π-electron system gives, for alternant PAH:

[9] $IE_i = -\alpha + m_i\beta$

[10] $E_i(HO,LU) = 2m_i\beta$

In eqs. [9] and [10], α and β have their usual significance in Hückel theory, and $m_i$ is the constant characteristic of the particular $(PAH)_i$. $IE_i$ is the ionisation energy corresponding to removal of an electron from the highest occupied Hückel MO. $E_i(HO,LU)$ denotes the energy for an electronic transition between the highest occupied and lowest unoccupied molecular orbitals. Then, eqs. [9] and [10] predict:

[11] $IE = -\alpha + 0.5E_p$

provided that the experimental IE and $E_p$ values may be identified with the theoretical quantities described above.

Simple Hückel theory thus correctly predicts the linear correlation between IE and $E_p$. The experimentally determined slope (eq. [8]) is reasonably close to that predicted (eq. [11]). Schmidt (20) showed that inclusion of electron repulsion effects in the spirit of self-consistent field theory, but without configuration interaction, sufficed to bring theoretical and experimental slopes into much better agreement. Presumably, when electron repulsion is included, the energies of the relevant configurations differ sufficiently to reduce the CI correction to a second-order effect (20). However, Schmidt (20) did not discuss the intercept which should correspond to the Coulomb integral (−α) for carbon. This quantity is *not* simply interpretable as the ionisation energy of an electron in the $p_z$ orbital of an isolated $sp^2$-hybridised carbon atom, but rather (22) as the mean of this ionisation energy and the corresponding electron affinity. The recommended values (22) of these latter parameters lead to a value of −5.7 eV for α, and thus to a theoretically predicted intercept of 5.7 eV for eq. [8]. The experimental value is thus slightly lower than that predicted by simple theory. However, the calculations of Schmidt (20) show that corrections for electron repulsion would act in the correct direction to also reduce this discrepancy. Thus, simple π-electron theory accounts remarkably well, on a semi-quantitative level, for the correlation between IE and $E_p$ (Fig. 3) and thus also in a more qualitative fashion for the relation (Fig. 1) between $E_p$ and the metastable ion fragmentation intensity.

There is nonetheless one conceptual problem remaining. This concerns the fact that Hückel theory considers the π-electron wavefunctions to be orthogonal to the wavefunctions describing the σ-framework. That is, the excess energy deposited in the π-electron system by the ionisation event cannot, according to the Hückel theory, be transferred to the σ-framework which is involved in the fragmentation reactions (fission of C—H bonds). However, this violation of a principal tenet of quasi-equilibrium theory (12) and other statistical theories of unimolecular reaction rates arises only if the simple Hückel theory is taken too seriously. For example, the (solution) electron spin resonance (esr) spectroscopy of the same PAH radical cations of interest here show hyperfine splittings due to the σ-bonded protons. The magnitudes of these hyperfine splittings can be well correlated (23) with spin densities (which usually (24) parallel "unpaired electron densities") calculated from the Hückel theory of the π-electrons. The accepted mechanism underlying the McConnel relationship (24) involves spin polarisation, which is unlikely to provide a means of transforming sizeable amounts of π-electronic energy to vibrational energy of the σ-framework. Nonetheless, the esr phenomenon does show that the Hückel theory can be extremely useful in correlating phenomena which apparently contradict the theory's primary postulate concerning orthogonality of the π and σ wavefunctions.

The question remains as to whether a theoretical approach less pragmatic than the Hückel theory might not provide additional insights. A successful approach to π electron energies has been devel-

TABLE 2. Resonance energies calculated by method of Herndon (30)

| Molecule (M) | RE(M), eV | | RE($M^{+\cdot}$), eV | |
|---|---|---|---|---|
| | Present | Ref. 30 | Present | Ref. 30 |
| Tetracene | 1.907 | 1.907 | 5.989 | 5.989 |
| Picene | 3.039 | 3.039 | 6.984 | 6.984 |
| 1,2,5,6-Dibenzanthracene | 2.945 | — | 6.942 | — |
| 3,4-Benzotetraphene | 2.842 | — | 6.886 | — |
| 1,2,3,4-Dibenzanthracene | 3.039 | — | 6.960 | — |

oped by Dewar and collaborators (22, 25), using a Pople-type SCF-MO method with allowance for σ-bond compression energies. A remarkably simple recipe, which reproduces the PAH resonance energies given by Dewar's method, has been devised by Herndon (26–29). This ingenious procedure, which involves only a simple count of Kekulé valence-bond structures, reproduces the resonance energies from SCF-MO calculations of Dewar (22, 25) to within an average deviation of ±0.04 eV, via the algorithm (29):

$$[12] \quad RE(M) = 1.185 \ln [CSC(M)]$$

where RE(M) is the resonance energy of the PAH molecule M, and CSC(M) is the "corrected structure count" of the Kekulé structures for M, as described by Herndon (26–29).

The interest in resonance energies, in the present context, arises from a suggestion, due originally to Franklin (16). An observed trend of increase in appearance energy for $(M - H)^+$ fragments for six PAH, with increasing resonance energy of the parent molecule, was interpreted in terms of the loss of a hydrogen atom from $M^{+\cdot}$ being accompanied by the opening of at least one aromatic ring (16). This suggestion was re-examined more recently (5) in terms of metastable-ion fragmentation intensities. Based only on the series of PAH compounds of formula $C_{18}H_{12}$ (Table 1), for which experimental resonance energies were available, it was concluded (5) that the metastable-ion intensities were consistent with loss of one H atom *not* destroying the aromatic system (i.e. the opposite conclusion to that of Franklin (16)), but that losses of 2H of $CH_3$ and of $C_2H_2$ *do* appear to disrupt the aromatic structure of the molecular ion; the latter two reactions *must* do so, of course. The availability of reliable theoretical values of resonance energy should permit some additional understanding of this particular point. More recently (30), Herndon has extended his procedure to the molecular ions (radical cations $M^{+\cdot}$) of PAH, and showed that the experimental ionisation energies could be reproduced to within ±0.16 eV by the simple formula:

$$[13] \quad [IE(M)1eV = 11.277 + RE(M) - 1.044 \ln [CSC(M^{+\cdot})]$$

The last term in eq. [13] was assumed by Herndon (30) to correspond to $RE(M^{+\cdot})$; this assumption is examined below, but for now will be assumed to be valid. Herndon (30) has calculated resonance energies, for both M and $M^{+\cdot}$, for most of the PAH studied here. Table 2 gives additional results obtained in the present investigation, including calculations undertaken for comparison with the original work (30).

Thus, it is now possible to test the proposed role of resonance energy, in controlling the energetics and rates of fragmentation reactions of metastable ions of PAH, in a more meaningful way. Unfortunately the results are disappointing. Figure 4 shows the best correlation found, that between the $(M - H)^+$ intensity (from metastable $M^{+\cdot}$) and $RE(M^{+\cdot})$. The data separate (Fig. 4) into isomeric series; all attempts to place these data on a common basis, by

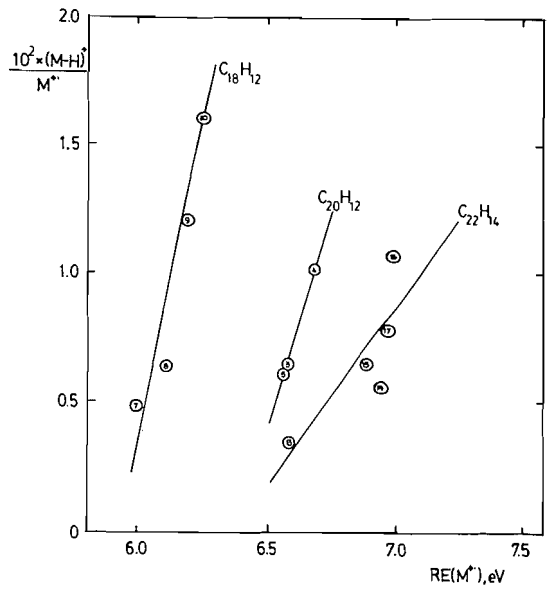


FIG. 4. Correlation between $(M^{+\cdot} \rightarrow (M - H)^+)$ metastable peak intensities (peak heights, *B*/*E*-linked scans) and resonance energies of $M^{+\cdot}$.

Can. J. Chem. Downloaded from www.nrcresearchpress.com by 210.87.254.105 on 09/06/12
For personal use only.

Can. J. Chem. Downloaded from www.nrcresearchpress.com by 210.87.254.105 on 09/06/12
For personal use only.

normalising RE($M^{+\cdot}$) to the number of $\pi$ electrons, or to the number of carbon–carbon bonds, or aromatic rings etc., produced scatter plots. More surprisingly, the data for $(M - CH_3)^+$ and $(M - C_2H_2)^{+\cdot}$ did not correlate at all with RE($M^{+\cdot}$), with the exception of the rather poor correlations for the $C_{18}H_{12}$ isomeric series shown previously (5). In view of our ignorance of the structures of these fragment ions, it is not possible to investigate *differences* in resonance energies between reactants ($M^{+\cdot}$) and products (e.g. $(M - C_2H_2)^{+\cdot}$) as a more suitable correlating parameter. The significance of the correlations shown in Fig. 4 is not clear, particularly in view of the correlations (of similar quality) with parameters reflecting steric strain (4, 5).

Finally, in this section, we wish to comment briefly on the physical interpretation of the remarkable empirical relation eq. [13]. The value of the constant term (11.277 eV) led Herndon (30) to propose that the ionisation energy of M is simply the *p*-ionisation energy of the $(sp^3;V_4)$ valence state of carbon (11.42 eV (31) or 11.30 eV (32), according to two different estimates), plus the resonance energy of M minus the resonance energy of $M^{+\cdot}$. This picture is not sensibly altered if the $\pi$-ionisation energy of a (tr tr tr $\pi$) valence state of carbon (11.19 eV (32)) is taken for comparison; this latter valence state seems intuitively more applicable to the present purpose than does the $(sp^3;V_4)$ valence state. In this notation, tr denotes a trigonal $sp^2$ hybrid orbital. In any event, a simple energy diagram (Fig. 5) connecting the various states involved shows that if Herndon's interpretation (30) is correct, there must exist some close correlations between various other parameters which are either purely fortuitous or result from relationships existing at a level more fundamental than that of the present discussion.

In fact, there appears to be no need to invoke valence states of C and $C^+$ at all. The ground-state ionisation energy of a carbon atom is 11.264 eV (33), very close to Herndon's (3) least-squares parameter (11.277 eV, eq. [13]); further, the localised bond energies used to define the reference state against which resonance energy is measured invariably involve formation of bonds from ground-state atoms. The localised bond energies used here are *not* the conventional energies of double and single carbon–carbon bonds, but rather the values derived by Dewar (25) for linear conjugated polyenes. These localised bond energies are additive, the $\pi$-contributions to the "single" bonds being absorbed into the empirical bond energies (34). Such "classical" polyenes are thus non-resonating, having only one single unexcited resonance structure, i.e. CSC(M) = 1, in Herndon's notation (26–30). From Fig. 5:

$$[14]\quad \mathrm{IE\ (eV)} = 11.264 + [\mathrm{LBE(M)} - \mathrm{LBE}(M^{+\cdot})] + \mathrm{RE(M)} - \mathrm{RE}(M^{+\cdot})$$

$$[15]\quad 1.044 \ln [\mathrm{CSC}(M^{+\cdot})] = \mathrm{RE}(M^{+\cdot}) - [\mathrm{LBE(M)} - \mathrm{LBE}(M^{+\cdot})]$$

The effect of the difference in localised bond energies (LBE) can presumably be accounted for within the parametrisation of eq. [13], and must presumably track the value of RE($M^{+\cdot}$) at least approximately.

Since eqs. [8] and [13] both hold, a linear relationship must hold between $E_p$(M) and ln [CSC($M^{+\cdot}$)]. Rather than plotting the data according to the combination of eqs. [8] and [13], a relationship analogous to that described by eq. [13] for IE was sought for $E_p$. The excited $\pi^*$ state reached in the transition characterised by $E_p$ is believed to be reasonably well described as a quinonoid structure, e.g. that in biphenyl as investigated theoretically by Hofmann (35). The number of Kekulé structures, for such an excited state, should be very close to half the number of structures for the corresponding radical cation and is exactly so for some of the simpler cases investigated by direct counting. Figure 6 shows [$E_p$(M) − RE(M)] plotted against ln [CSC(M*)], for the 17 PAH studied in the mass spectrometer (5) plus such diverse PAH as benzene, naphthalene, azulene, biphenyl, biphenylene, fluoranthene, and ovalene; also included in Fig. 6 are data for the linear conjugated polyenes containing one to six double bonds inclusive. It is important to note that the $E_p$ values used were those corresponding to the *maxima* in the absorption bands, *not* the 0–0 transition energies. The latter do not correlate well. For example, the 0–0 transition energy for the appropriate $\pi$–$\pi^*$ transition in ethylene ($S_0 \rightarrow S_1$) is about 4.7 eV, compared with about 7.6 eV at the band maximum (36), while this correction is only 0.1–0.2 eV at most for the larger PAH (9) which remain essentially planar in the excited state. A least-squares fit to the data in Fig. 6 gives:

$$[16]\quad E_p\ (\mathrm{eV}) = 7.01(\pm 0.92) + \mathrm{RE(M)} - 1.107(\pm 0.045) \ln [\mathrm{CSC(M^*)}]$$

(standard error = ±0.45 eV; correlation coefficient = −0.94).

This correlation is not as good as that obtained by Herndon (30) for the corresponding ionisation energies (eq. [13]). Nonetheless, the wide range of

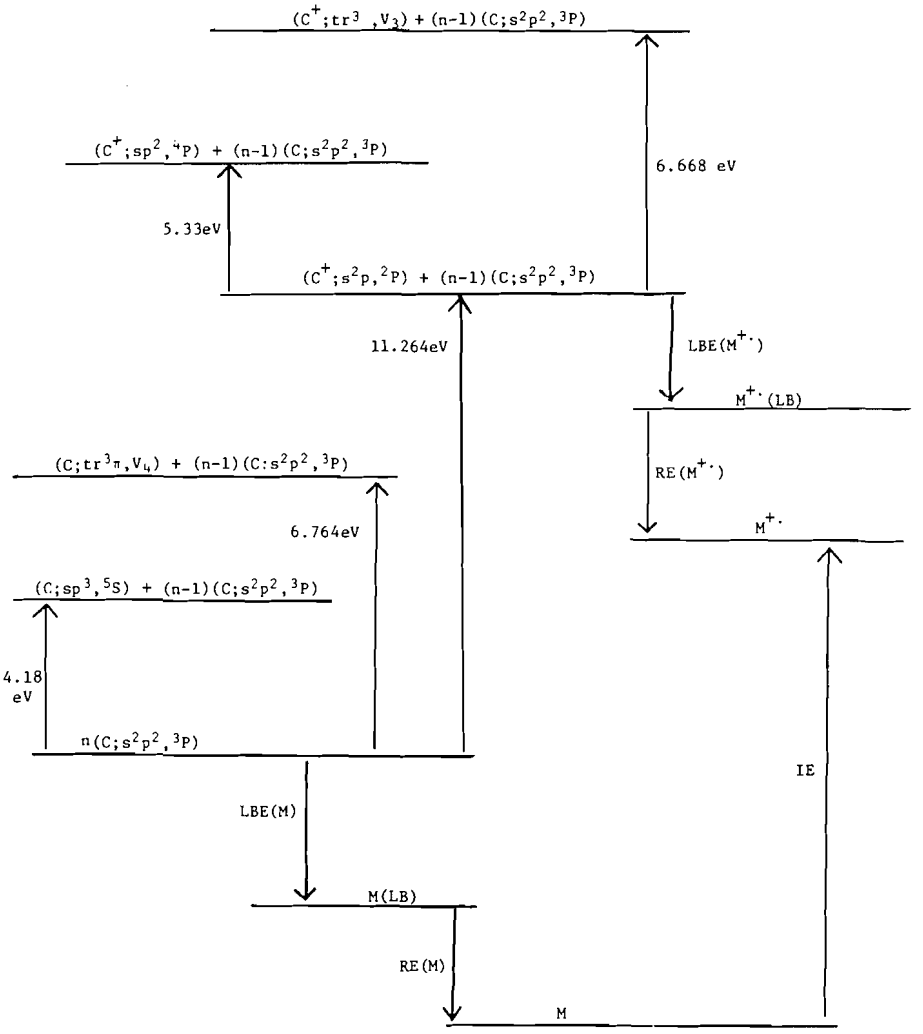


FIG. 5. Energy diagram (not to scale) showing relations between relevant states of C and of $C^+$, for a PAH molecule containing $n$ carbon atoms. (Hydrogen atoms omitted for clarity.) Energy differences between spectroscopically observed states from ref. 33; energies of valence states from ref. 32. Localised bond energies (LBE) for neutral M are values of Dewar (25) for conjugated linear polyenes, and resonance energies (RE) are defined relative to this reference state (see text). (Notation (tr) used for valence state description refers to trigonal $sp^2$ hybrid.)

acyclic and aromatic hydrocarbons (ethylene to ovalene) thus correlated seems remarkable. The use of vertical (band maximum) rather than adiabatic (0–0) transition energies is difficult to justify. A somewhat similar dilemma has been discussed previously (37). At least, eq. [16] permits an estimate of $E_p$ to be made for compounds (e.g. hexacene) which are photo-labile. Figure 1 then gives some indication of predicted metastable ion intensities.

## II. Polychlorinated biphenyls

*(a) Experimental results*

In the case of biphenyls, the absorption band in the ultraviolet, which corresponds ($^1L_a$ excited state) to the $p$-band in fused-ring PAH, is often referred to as the A-band (3). The separate correlations, with the band maximum $\lambda_A$, of $(M - Cl)^+/M^{+\cdot}$ and $(M - 2Cl)^{+\cdot}/M^{+\cdot}$ intensity ratios (metastable transitions, peak heights in linked scans at constant $B/E$ (1)) are shown in Figs. 7 and 8 (note the logarithmic scale in Fig. 7). The raw data have been described previously (1). In both cases, the data for the 3,3′- and 4,4′-dichlorobiphenyls fall well below the best (least-squares) polynomial fit to the data. However, when the $(M - Cl)^+/(M - 2Cl)^{+\cdot}$ ratio is statistically corrected, the overall correlation is greatly improved (Fig. 9). (A tetrachlorobiphenyl is statistically more likely to lose one Cl than is a dichlorobiphenyl, by a factor of 2,

Can. J. Chem. Downloaded from www.nrcresearchpress.com by 210.87.254.105 on 09/06/12
For personal use only.

Can. J. Chem. Downloaded from www.nrcresearchpress.com by 210.87.254.105 on 09/06/12
For personal use only.

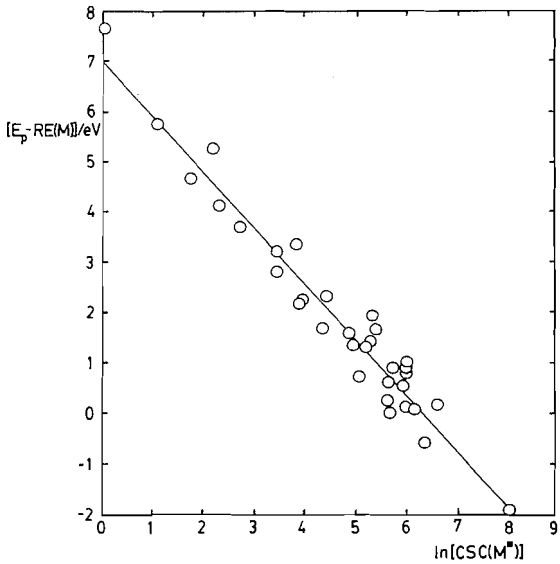


FIG. 6. Plot of ($E_p$ – RE) vs. ln [CSC(M*)], for a series of PAH (lower right of graph) and conjugated linear polyenes (upper left of graph). $E_p$ values correspond to band maxima (3, 9) (vertical transitions). Full line is least-squares fit (eq. [16]).

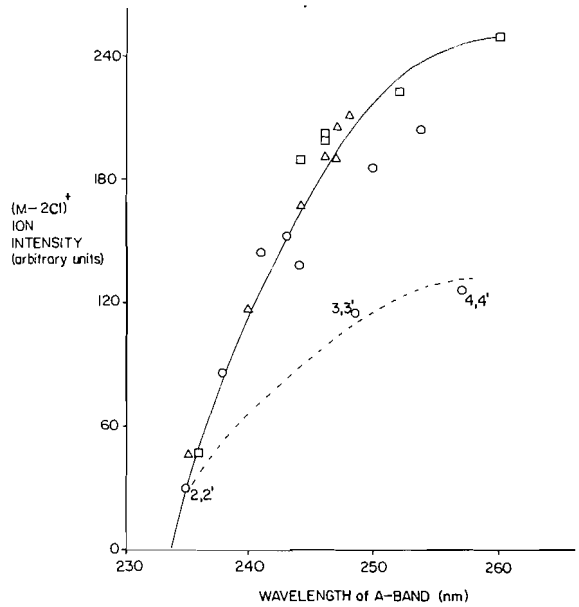


FIG. 8. Correlation of metastable peak heights (normalised to molecular ion = $10^5$), corresponding to $M^{+\cdot} \rightarrow (M - 2Cl)^{+\cdot}$, with $\lambda_A$. Symbols as in Fig. 7.

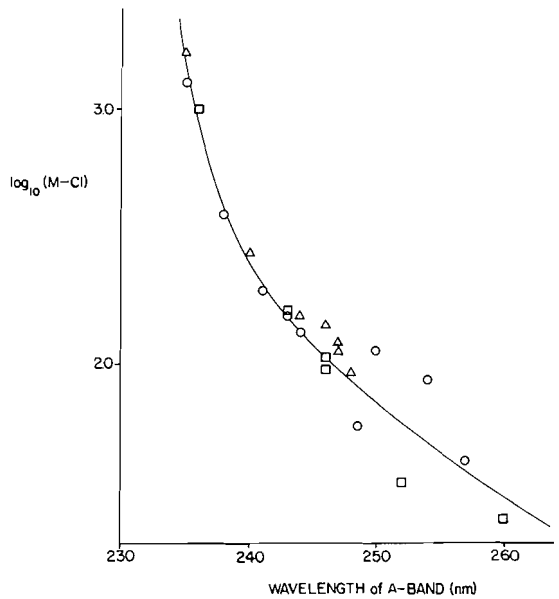


FIG. 7. Correlation of metastable peak heights (normalised to molecular ion = $10^5$), corresponding to $M^{+\cdot} \rightarrow (M - Cl)^+$ for PCB molecular ions, with $\lambda_A$. Circles, dichlorobiphenyls; triangles, trichlorobiphenyls; squares, tetrachlorobiphenyls.

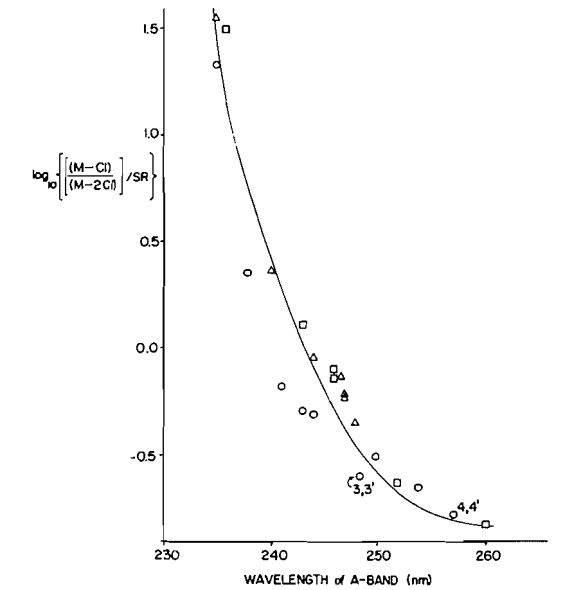


FIG. 9. Logarithmic plot of intensity ratio $(M - Cl)^+/(M - 2Cl)^{+\cdot}$ for metastable ion fragmentations, versus $\lambda_A$. SR is the ratio predicted on the basis of simple statistics (see text).

while the corresponding ratio for loss of two Cl is 6; the statistically predicted ratios (SR in Fig. 9) were calculated this way (1).) Figure 9 is similar to a correlation published previously (1), but plotted on a logarithmic scale in order to spread the data points. It is important to note that the following tetrachlorobiphenyl isomers are omitted from Figs. 7–9, due to the impossibility (1) of observing their A-band maxima: 2,2′,6,6′; 2,2′,5,6′; 2,2′,5,5′; 2,2′,4,5′; 2,2′,3,5′; 2,2′,3,3′. All of these contain three or four chlorine substituents *ortho* to the biphenyl linkage, or else contain two *ortho* chlorines plus at least one *meta* chlorine substituent to

Can. J. Chem. Downloaded from www.nrcresearchpress.com by 210.87.254.105 on 09/06/12
For personal use only.

buttress the steric interaction. (In contrast, the 2,2′,4,4′-isomer gives a reasonably well-defined A-band (1).)

Recently (38), values of kinetic energy release have been measured from metastable peak widths, for expulsion of chlorine from molecular ions of PCBs. In the present work, only the $M^{+\cdot} \rightarrow (M - Cl)^+$ reactions were studied in this way. The technique used was a scan of accelerating voltage (39) yielding a series of peaks corresponding to reactions giving $(M - Cl)^+$ fragment ions containing $^{35}Cl$ only. For all PCBs containing two or more chlorine atoms, there are two such reactions, viz. loss of $^{35}Cl$ from molecular ions containing $^{35}Cl$ only, and loss of $^{37}Cl$ from molecular ions containing just one $^{37}Cl$ atom. The corresponding peaks are not well resolved from one another; an example is shown in Fig. 10. However, by assuming the peaks to be Gaussian (a reasonable approximation in the present case), it was possible to show that the low-energy half of the major peak (loss of $^{35}Cl$) is only marginally perturbed by the minor component. The correction to the major peak height was only about 5% in the case of tetrachlorobiphenyls (the worst case), while that to the half-height was negligible. Thus, by measuring the half-width at half-height, on the low-energy side of the major peak, and applying a small correction, reasonably reliable values of kinetic energy release were obtainable for these first field-free region reactions. The results obtained are shown in Table 3, together with results obtained previously (38). The latter were obtained (38) by a different technique which does not require the correction described above; the discrepancies will be discussed below. In agreement with previous findings (38), some of the peaks had a small foot on one side, corresponding to reactions leading to fragment ions of the selected mass via loss of a neutral fragment of approximate mass 30. This interference was completely absent in about half of the compounds studied, and may be due to some impurity.

Finally, $^{13}C$ nuclear magnetic resonance spectra were obtained for some of the compounds studied. The motivation for this work lay in previous findings (40) that deviations of chemical shifts, from values predicted from additivity relations, correlate with the degree of steric hindrance to free rotation about the biphenyl linkage. It was hoped that this data would provide more subtle information, concerning the lack of planarity in the ground-state molecule, than does the A-band maximum. The spectra were obtained on a Bruker WM250 Fourier transform spectrometer at 62.83 MHz, using full noise proton decoupling, at a temperature of 309 K. The samples were dissolved in chloroform-$d_1$, and chemical shifts were assigned relative to the central resonance of the chloroform-$d_1$ triplet as 77.30 ppm. The results obtained for four PCBs not previously investigated (40) are

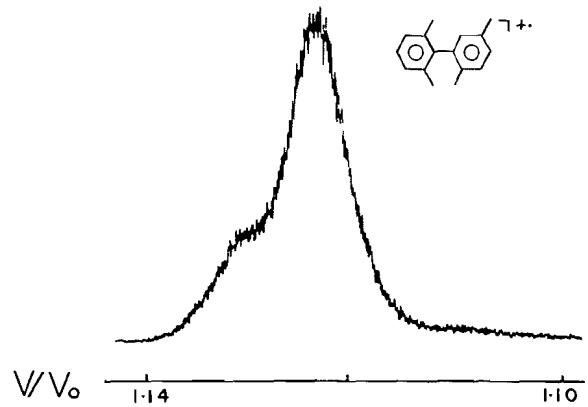


FIG. 10. Metastable peak obtained by a scan of accelerating voltage $V$, with magnet set to transmit $(M - Cl)^+$ fragment ions ($^{35}Cl$ only) from 2,2′,5,6′-tetrachlorobiphenyl.

TABLE 3. Kinetic energy release $T$ (meV) in metastable decompositions of molecular ions of PCBs, to give $(M - Cl)^+$ fragment ions (all $^{35}Cl$ isotopes). Calculated from full width at half-maximum

| | $T$ | |
|---|---|---|
| Chlorine substitution | Present work[a] | Literature[b] |
| 2,2′ | 34±2 | 26 |
| 3,3′ | 62±5 | 53 |
| 4,4′ | 50±3 | 38 |
| 2,3 | 60±2 | |
| 2,4 | 43±5 | |
| 2,6 | 63±2 | |
| 3,4 | 90±3 | |
| 3,5 | 69±2 | |
| 2,2′,5 | 36±3 | |
| 2,3′,5 | 67±7 | |
| 2,4′,5 | 58±5 | |
| 2,3,4 | 85±5 | |
| 2,4,5 | 63±3 | |
| 2,4,6 | 69±3 | |
| 3,3′,5,5′ | 50±2 | 76 |
| 3,3′,4,4′ | 54±2 | 100 |
| 2,2′,6,6′ | 55±3 | 30 |
| 2,2′,5,5′ | 51±4 | |
| 2,2′,4,4′ | 63±4 | |
| 2,2′,3,3′ | 38±3 | |
| 2,2′,5,6′ | 45±4 | |
| 2,2′,3,5′ | 50±3 | |
| 2,3,3′,4′ | 45±2 | |
| 2,3′,4′,5 | 47±2 | |

[a]Averages of 3 scans, with standard deviations; first field-free region metastables (accelerating voltage scan), VG7070F mass spectrometer. Correction applied for contribution from reaction of molecular ion containing one $^{37}Cl$, to give $(M - {}^{37}Cl)^+$.
[b]Reference 38; second field-free region metastables (electric sector voltage scans), VG ZAB-2F reverse geometry mass spectrometer.

Can. J. Chem. Downloaded from www.nrcresearchpress.com by 210.87.254.105 on 09/06/12
For personal use only.

shown in Table 4, together with values predicted from additivity relationships given previously (40). The assignments shown in Table 4 were made on the basis of relative values of observed chemical shifts compared with the calculated values, and on the basis of relative intensities where appropriate. Thus, for example, in 2,3-dichlorobiphenyl, C2 is the quaternary carbon furthest from a proton, and should thus correspond to the weakest signal observed. This is in accord with the chemical shift assignment.

*(b) Phenomenological interpretation of observed correlation*

Unfortunately, in the case of the PCBs, there is no information available concerning ionisation and appearance energies. The origins of the observed correlations (Figs. 7–9) are thus obscure, and the following discussion correspondingly more speculative than in the PAH case.

*(c) Theoretical considerations*

It is *not* assumed, in what follows, that the ionisation energy is the crucial parameter which correlates with both the molecular $^1L_a$ transition energies and the fragmentation rates of molecular ions of PCBs. In the PCB case, the phenomenon appears to be associated with steric interactions near the biphenyl linkage, and the best guess as to the key parameter turns out to be the internal energy distribution, $P(E)$.

It is possible to obtain some insight into this problem from the work of Wagner and Scheve (41), who constructed a potential energy diagram which accounted semi-quantitatively for the effects of *ortho*-chlorine substitution on singlet–triplet transitions of biphenyl. Based upon absorption and emission spectra, and their quenching characteristics, as well as on electron paramagnetic resonance spectra of the excited triplets, it was concluded (41) that the electronically excited state is planar, in contrast with the twisted ground-state equilibrium configuration for the gaseous molecule. Figure 11 has been drawn as a qualitative extension of the ideas of Wagner and Scheve (41) to include the molecular ion. The large increases in absorption transition energies, with increased *ortho* substitution, are due (41) to large increases in ground-state twisting and to the steep slopes of the excited state curves at larger values of the inter-ring dihedral angle. For present purposes, it is necessary to assume that the potential energy curve for the electronic ground state of the molecular ion is qualitatively similar to that for the relevant neutral excited state, as indicated in Fig. 11; this assumption is now discussed further.

TABLE 4. $^{13}C$ shieldings (δ, ppm) of chlorinated biphenyls (values calculated from additivity relations (40) in parentheses)

| Chlorine substitution | δ | | | | | | | | | | | |
|---|---|---|---|---|---|---|---|---|---|---|---|---|
| | C-1 | C-2 | C-3 | C-4 | C-5 | C-6 | C-1′ | C-2′ | C-3′ | C-4′ | C-5′ | C-6′ |
| 2,3 | 143.29 | 131.54 | 133.97 | 129.78 | 129.72 | 128.23 | 139.67 | 128.43 | 129.57 | 127.39 | 129.57 | 128.43 |
| | (140.05) | (132.31) | (136.30) | (127.76) | (127.34) | (127.20) | (137.92) | (127.19) | (128.77) | (126.79) | (128.77) | (127.19) |
| 2,4 | 138.65 | 133.61 | 132.33 | 134.00 | 127.84 | 129.99 | 139.46 | 128.42 | 129.59 | 128.15 | 129.59 | 128.42 |
| | (136.83) | (132.86) | (130.85) | (133.81) | (126.32) | (130.45) | (138.28) | (127.12) | (128.81) | (127.22) | (128.81) | (127.12) |
| 3,5 | 144.56 | 125.93 | 135.62 | 128.73 | 135.62 | 125.93 | 138.87 | 127.33 | 129.30 | 127.43 | 129.30 | 127.33 |
| | (143.70) | (125.27) | (134.92) | (126.49) | (134.92) | (125.27) | (136.94) | (126.25) | (128.21) | (126.49) | (128.21) | (126.25) |
| 2,3′,4′,5 | 138.24 | 131.04 | 131.49 | 129.52 | 132.80 | 131.46 | 139.84 | 130.49 | 133.20 | 132.88 | 131.12 | 128.91 |
| | (136.75) | (129.14) | (131.83) | (127.81) | (131.73) | (129.33) | (137.80) | (128.86) | (134.30) | (132.46) | (129.07) | (126.26) |

Can. J. Chem. Downloaded from www.nrcresearchpress.com by 210.87.254.105 on 09/06/12
For personal use only.

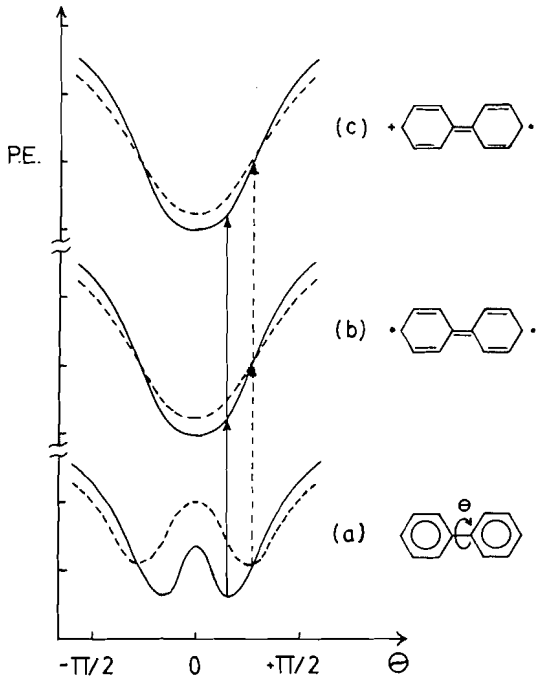


FIG. 11. Postulated form of potential energy, as a function of dihedral angle θ between the rings, for biphenyl (drawn after work of Wagner and Scheve (40)). Solid curves are for a biphenyl with little steric interaction around the biphenyl linkage, and dashed curves are for a case with appreciable interaction. (*a*) Curves for ground-state neutral molecules; (*b*) curves for $^1L_a$ excited states of neutral molecules; (*c*) curves for molecular ions.

The nature of the molecular orbitals in biphenyl have been investigated by Imamura and Hofmann (35), using a self-consistent field approach (π-electrons only). For a biphenyl molecule constrained to planarity, the molecular orbitals may be classified according to specified (35) symmetry properties with respect to two planes, one containing the long biphenyl axis and one perpendicular to it. A correlation diagram was constructed (35) to connect the levels of a planar biphenyl molecule with those of a molecule in which the planes of the rings are at 90° to one another. The four possible symmetries which arise for energy levels of planar biphenyl, along with their associated tendencies with respect to planarity or twisting, are: SA (tends to induce twisting), AS or AA (energy essentially independent of twist angle), and SS (tends to induce coplanarity of rings). The highest occupied level in ground-state biphenyl is SA, while the lowest unoccupied level is SS. While this description strictly applies to only planar biphenyl, the correlation diagram (35) indicates that at the equilibrium twist angle of about 40°, the highest occupied and lowest unoccupied levels do indeed correlate with these levels of the planar molecule.

The lowest excited state ($^1L_a$ in Platt's notation (9)) is due to the SA → SS excitation, and should thus (see above) induce a greater degree of planarity in the excited state. Calculations (35) indicate that the planar quinonoid valence bond structure for the excited state, shown in Fig. 11, is a reasonable description. For example, the calculated π bond order for the biphenyl bond is 0.26 in the ground state and 0.48 in the excited state (35). The molecular ion was not discussed (35), but removal of one electron from the highest occupied level (SA in planar biphenyl) should reduce the tendency towards twisting, though possibly to a lesser extent than in the neutral excited state in which the electron is excited to the SS level. However, an INDO/1 calculation (42) for planar geometry (all valence electrons included) has confirmed the essential conclusions (35) for the neutral ground state, and supports the planar quinonoid structure, with largely localised charge and spin densities, for the molecular ion as indicated in Fig. 11. For example, the π-bond order of the biphenyl bond is calculated (42) to be 0.49 in the molecular ion, while the spin densities at the *para* carbons are +0.45, close to theoretical maximum values. A more complete study of the geometries of neutral and ionised biphenyl is being undertaken (42), but these preliminary results do provide some support for the qualitative features of Fig. 11.

Thus the increasing degree of fragmentation of metastable molecular ions of PCBs, with increasing extent of chlorine substitution *ortho* to the biphenyl linkage, may be interpreted (Fig. 11) in terms of increasing the average twist angle in the ground state. This probably involves increasing both the twist angle at which a potential energy minimum occurs, and also increasing the barrier to internal rotation so that the potential minima represent increasingly preferred orientations. The present intent, in studying the $^{13}C$ nmr spectra of these compounds, was to obtain some insight into these rotational barriers. However, mere deviations from chemical shifts predicted from additivity relations (see ref. 40 and Table 4) were found to give very poor correlations with any of the other parameters, even for C-1 and C-1′, which are known (40) to display the largest of such deviations. In fact, the best available information on rotational barriers in PCBs, from nmr studies, appears to come from temperature dependences (40) of proton chemical shifts over the range 160 K to 340 K. These data (40) indicate rotational barriers of about 4–16 kJ $mol^{-1}$ for PCBs with no *ortho* substituents,

Can. J. Chem. Downloaded from www.nrcresearchpress.com by 210.87.254.105 on 09/06/12
For personal use only.

and of about 35 kJ $mol^{-1}$ or less for PCBs with at least one *ortho* substituent on each ring (40). PCBs with chlorine substituents on all four *ortho* positions displayed (40) no temperature dependence of proton chemical shift, and in the experimental temperature range (40) in solution are probably effectively locked into one conformation. If these solution data are transferable to the situation in the ion source (isolated molecules at ca. 500 K), they are of the correct magnitude to support the above proposal that increasing the degree of *ortho* substitution increases the internal rotational barrier, and thus the equilibrium fraction of molecules at or near the potential minima. Together with the postulated steeply sloping potential curves for the molecular ions (Fig. 11), this accounts, via appropriate change in $P(E)$, for the increased tendency to fragmentation actually observed for the metastable molecular ions of PCBs. (It should also be added that chlorine substitution on benzene is known (43) to split and shift the lowest band in the photoelectron spectra, so the complete picture is more complex.)

However, the correlations observed for the PCBs (Figs. 7–9) are more subtle than this, since the $(M - 2Cl)^{+\cdot}$ intensities *decrease* with increasing resistance to internal rotation, as indicated by the uv transition energy. The (generally more intense) $(M - Cl)^+$ fragment *does* increase in intensity, but some attempt seems necessary to examine the $(M - 2Cl)^+/(M - Cl)^{+\cdot}$ intensity ratio (Fig. 9). The study of kinetic energy release (Table 3) was undertaken as an extension of earlier work (38) aimed at elucidating the relationship between the mechanisms leading to these two fragment ions.

Comparison (Table 3) of $T$ values for the symmetrically substituted dichlorobiphenyls shows that the present values are generally higher than, but parallel reasonably well, values obtained previously (38). This is in accord with expectations based on the conclusion (38) that $T$ is here dominated by contributions from the kinetic shift $\varepsilon^{\neq}$. The present experiments involved appreciably shorter ion lifetimes, and thus presumably higher average energies for the fragmenting ions, than did the previous work (38). Much more disconcerting are the values obtained here for 3,3′,5,5′- and 3,3′,4,4′-tetrachlorobiphenyls. The MIKES technique used previously (38) is inherently more reliable than that available in the present work, but uncertainties in the correction applied (see above) are far too small to account for the observed discrepancies (Table 3). It was feared that we may have confused tetrachlorobiphenyl isomers while running the experiments, and obtained a different sample of the 3,3′,4,4′-isomer from an independent source. (We are indebted to Dr. N. J. Bunce for this sample.) The results obtained using this second sample were indistinguishable from those obtained using the commercial sample (Table 3). We thus cannot account for these discrepancies. (Discrepancies of a factor of about 3 have been observed previously (44) between $T$ values obtained for fragmentations occurring in the second field-free region of a ZAB-2F instrument, and values for first field-free-region reactions (45).) However, the present results do cast further doubt on the tentative categorisation into classes with and without multiple *meta*-chlorine substituents (38). Thus, the present data do *not* support the suggestion (38) that PCBs with several *meta*-chlorine substituents are necessarily associated with larger $T$ values. Indeed, there appears to be little useful information in Table 3. This is a disappointingly negative conclusion, but seems inescapable.

In fact, the most clearcut conclusions reached in the previous study (38) were based upon thermochemical arguments. In particular, to account for the observation that the $(M - Cl)^+$ fragment is generally (but not invariably (1, 46)) less intense than the $(M - 2Cl)^{+\cdot}$ fragment in fragmentations of metastable molecular ions of PCBs, while the situation is reversed for conventional mass spectra, it was necessary (38) to postulate two distinct mechanisms for formation of $(M - 2Cl)^{+\cdot}$ ions. One of these mechanisms must be a low-energy process which does *not* compete with formation of $(M - Cl)^+$ ions, while the other is a higher energy process (38). The simplest mechanism consistent with the available information appears to be the following:

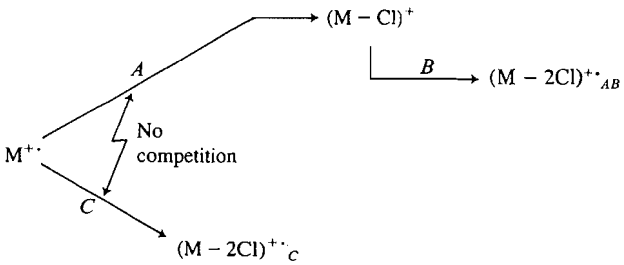


Only those molecular ions with large amounts of internal energy (primarily those fragmenting in the ion source) will produce $(M - Cl)^+$ ions with sufficient energy to proceed via process $B$ to give $(M - 2Cl)^{+\cdot}_{AB}$ ions. These fragment ions need not have the same structure as those formed in the low-energy path $C$. The postulated situation is summarised in Fig. 12, where it is assumed that increase in steric interaction near the biphenyl

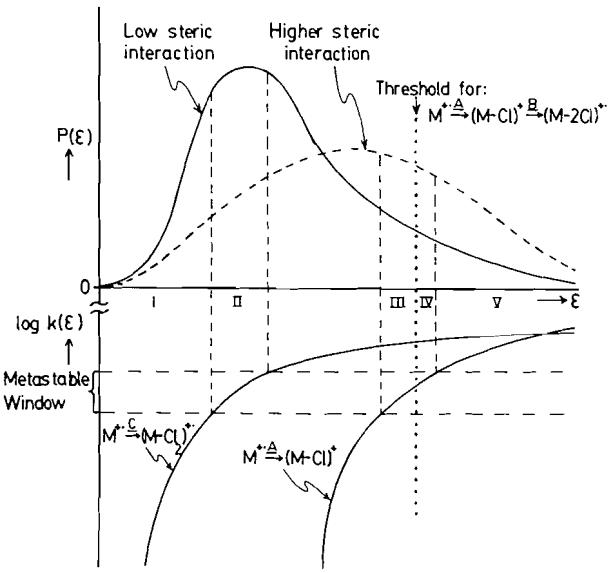


FIG. 12. Schematic illustration of effect of steric effects due to chlorine substitution *ortho* to biphenyl linkage of PCBs. The internal energy distributions $P(\varepsilon)$ are assumed normalised. Reactions *A* and *C* are assumed to not compete. A specified $k(\varepsilon)$ value is assumed, for simplicity, to define one unique ion lifetime (see also Fig. 2). Regions *I–V* denote the following: *I*, molecular ions; *II*, metastable ions giving $(M - 2Cl)^{+\cdot}{}_{C}$; *III*, metastable ions giving $(M - Cl)^{+}$; *IV*, metastable ions giving $(M - 2Cl)^{+\cdot}{}_{AB}$; *V*, ions fragmenting in ion source.

linkage shifts the $P(\varepsilon)$ distributions to higher energies, as discussed with reference to Fig. 11, but does not markedly alter the nature of the rate constants $k(\varepsilon)$. This is almost certainly an oversimplification, but no information on $k(\varepsilon)$ is available.

For simplicity, only one $P(\varepsilon)$ curve has been drawn for each of a "high" and "low" degree of steric interaction. (In fact, if processes *A* and *C* do not compete, there should be two $P(\varepsilon)$ curves for each case.) To account for the *decrease* in $(M - 2Cl)^{+\cdot}{}_{C}$ with increase in steric interaction (decrease in $\lambda_A$, Fig. 8), Region II (Fig. 12) must be on the low-energy side of the crossover point of the two $P(\varepsilon)$ curves. For similar reasons (Fig. 7), Region III must be to the high-energy side of this point. The $k(\varepsilon)$ curve for process *C* must be at lower energy, as described previously (38), and must therefore not compete directly with process *A*. Since at least some PCBs exhibit process *B* in metastable ion spectra (38, 46), the threshold for this process must be close to the region appropriate to process *A* for metastable ions.

Figure 12 represents an extension of earlier ideas (38), now including the observations summarised in Figs. 7 and 8 in the light of the discussion of Fig. 11. It is not yet clear, however, how to account for the remarkable success of Fig. 9 in correlating the $(M - 2Cl)^{+\cdot}/(M - Cl)^{+}$ ratio. Comparisons of ionisation efficiency curves for $M^{+\cdot}$, $(M - Cl)^{+}$, and $(M - 2Cl)^{+\cdot}$ with those for metastable transitions connecting these species could be informative. None of the above addresses itself, in any case, to more detailed mechanistic questions such as the extent of chlorine atom scrambling (46–48), or the involvement of 5-membered ring chloronium ion intermediates (2).

## Conclusions

The present work represents an attempt to understand some unexpected correlations found to exist between spectroscopic (uv) properties of neutral molecules and unimolecular fragmentation rates of their radical cations in the mass spectrometer. The work is necessarily speculative in part, but it has been possible to account for the existence, if not the precise form, of the correlations in the context of modern theories of physical organic chemistry. In the case of the fused-ring polycyclic aromatic hydrocarbons (PAH), it is clear that the crucial parameter which links the optical absorption energy to the ion fragmentation rate is the ionisation energy. The separation of the PAH correlation into two distinct well-defined families may tentatively be ascribed to a difference, in appearance energies for the ion fragments, between the linear acenes (plus two other species) and all the other PAHs studied. These conclusions appear to be consistent with modern theories of the π-electron systems in aromatic hydrocarbons.

In the case of the polychlorobiphenyls (PCBs), the conclusions reached are more tentative due to a lack of subsidiary information. However, it is possible to account for the existence of the correlations by analogy with the known photochemistry and photophysics of PCBs. The crucial feature here is the relative geometries of the ground and excited states; the ground state of the molecular ion of a PCB is expected to have a geometry similar to that of the neutral excited state involved in the photochemistry, and this has been confirmed by an INDO/1 calculation in the present work. These geometry differences manifest themselves in parallel trends in both the uv absorption energy and in the energy deposition function for the molecular ion.

The general conclusion is that these empirical correlations, which at first seemed to us sufficiently strange and unexpected as to be probably spurious coincidences, can be satisfactorily accommodated within accepted ideas of physical organic chemistry and unimolecular fragmentation theory.

Can. J. Chem. Downloaded from www.nrcresearchpress.com by 210.87.254.105 on 09/06/12
For personal use only.

Can. J. Chem. Downloaded from www.nrcresearchpress.com by 210.87.254.105 on 09/06/12
For personal use only.

## Acknowledgements

We are indebted to Dr. H. O. Pritchard for valuable discussions on valence states, to Dr. N. J. Bunce for the PCB sample, to Dr. M. C. Zerner for the INDO/1 calculations, to Mr. A. Quesnel for assistance in obtaining the metastable peak shapes, and to Dr. C. Rodgers, Bruker Spectrospin (Canada) Ltd., for the $^{13}C$ nmr spectra. We also acknowledge the generous help of Dr. M. Bursey and Dr. R. Hass in investigating the discrepancies in the values of kinetic energy release for the PCBs. This work was supported by the Natural Sciences and Engineering Research Council of Canada.

1. B. Shushan, N. J. Bunce, R. K. Boyd, and C. T. Corke. Biomed. Mass Spectrom. In press.
2. L. A. Levy and E. O. Oswald. Biomed. Mass Spectrom. **3**, 88 (1976).
3. H. Suzuki. Electronic absorption spectra and geometry of organic molecules. Academic Press, New York. 1967. Chapt. 12.
4. B. Shushan, S. H. Safe, and R. K. Boyd. Anal. Chem. **51**, 156 (1979).
5. B. Shushan and R. K. Boyd. Org. Mass Spectrom. **15**, 445 (1980).
6. R. K. Boyd and J. H. Beynon. Org. Mass Spectrom. **12**, 163 (1977).
7. E. Clar. Polycyclic hydrocarbons. Vol. 1. Academic Press, New York. 1964. Chapt. 7.
8. J. R. Platt. J. Chem. Phys. **17**, 484 (1949).
9. J. B. Birks. Photophysics of aromatic molecules. Wiley-Interscience, London. 1970.
10. J. C. Lorquet. Org. Mass Spectrom. **16**, 469 (1981).
11. R. A. Marcus. J. Chem. Phys. **20**, 359 (1952).
12. H. M. Rosenstock, M. B. Wallenstein, A. L. Wahrhaftig, and H. Eyring. Proc. Nat. Acad. Sci. U.S.A. **38**, 667 (1952).
13. D. H. Williams and I. Howe. Principles of organic mass spectrometry. McGraw-Hill. 1972.
14. K. Levsen. Fundamental aspects of organic mass spectrometry. Verlag Chemie. 1973.
15. E. Stenhagen, S. Abrahamsson, and F. W. McLafferty. Registry of mass spectral data. Wiley. 1974.
16. P. Natalis and J. L. Franklin. J. Phys. Chem. **69**, 2935 (1965).
17. E. Clar and W. Schmidt. Tetrahedron, **31**, 2263 (1975).
18. E. Clar and W. Schmidt. Tetrahedron, **32**, 2563 (1976).
19. S. Obenland and W. Schmidt. J. Am. Chem. Soc. **94**, 6633 (1975).
20. W. Schmidt. J. Chem. Phys. **66**, 828 (1977).
21. E. Clar and W. Schmidt. Tetrahedron, **35**, 1027 (1979).
22. M. J. S. Dewar. The molecular orbital theory of organic chemistry. McGraw-Hill. 1969. pp. 379–380.
23. (*a*) J. R. Bolton. *In* Radical ions. *Edited by* E. T. Kaiser and L. Kevan. Interscience, New York. 1968. Chapt. 1; (*b*) G. Vincow. *In* Radical ions. *Edited by* E. T. Kaiser and L. Kevan. Interscience, New York. 1968. Chapt. 4.
24. H. M. McConnell. J. Chem. Phys. **24**, 632 (1956); J. Chem. Phys. **28**, 1188 (1958).
25. M. J. S. Dewar and C. de Llano. J. Am. Chem. Soc. **91**, 789 (1969).
26. W. C. Herndon. J. Am. Chem. Soc. **95**, 2404 (1973).
27. W. C. Herndon and M. L. Ellzey, Jr. J. Am. Chem. Soc. **96**, 6631 (1974).
28. W. C. Herndon. Thermochim. Acta, **8**, 225 (1974).
29. R. Swinborne-Sheldrake, W. C. Herndon, and I. Gutman. Tetrahedron Lett. **10**, 755 (1975).
30. W. C. Herndon. J. Am. Chem. Soc. **98**, 887 (1976).
31. H. O. Pritchard and H. A. Skinner. Chem. Rev. **55**, 745 (1955).
32. J. Hinze and H. H. Jaffé. J. Am. Chem. Soc. **84**, 540 (1962).
33. C. E. Moore. Atomic energy levels as derived from the analyses of optical spectra. Vol. I, NSRDS-NBS 35, National Bureau of Standards. 1971.
34. M. J. S. Dewar and G. J. Gleicher. J. Am. Chem. Soc. **87**, 692 (1965).
35. A. Imamura and R. Hofmann. J. Am. Chem. Soc. **90**, 5379 (1968).
36. A. J. Merer and R. S. Mulliken. Chem. Rev. **69**, 639 (1969).
37. J. Ridley and M. Zerner. Theoret. Chim. Acta, **32**, 111 (1973).
38. J. R. Hass, M. M. Bursey, L. A. Levy, and D. J. Harvan. Org. Mass Spectrom. **14**, 319 (1979).
39. R. G. Cooks, J. H. Beynon, R. M. Caprioli, and G. R. Lester. Metastable ions. Elsevier. 1973.
40. N. K. Wilson. J. Am. Chem. Soc. **97**, 3573 (1975).
41. P. J. Wagner and B. J. Scheve. J. Am. Chem. Soc. **99**, 2888 (1977).
42. M. C. Zerner. Private communication.
43. A. D. Baker, D. P. May, and D. W. Turner. J. Chem. Soc. 22 (1968).
44. J. Grotemeyer and H.-F. Grützmacher. *In* Current topics in mass spectrometry and chemical kinetics. *Edited by* J. H. Beynon and M. L. McGlashan. Heyden. 1982. p. 29.
45. B. J. Stapleton, R. D. Bowen, and D. H. Williams. J. Chem. Soc. Perkin Trans. II, 1219 (1979).
46. S. Safe, O. Hutzinger, and W. D. Jamieson. Org. Mass Spectrom. **7**, 169 (1973).
47. S. Safe and O. Hutzinger. Chem. Commun. 446 (1971).
48. S. Safe and O. Hutzinger. J. Chem. Soc. Perkin I, 686 (1972).

# Isotope effects in nucleophilic substitution reactions. IV. The effect of changing a substituent at the α carbon on the structure of $S_N2$ transition states

KENNETH CHARLES WESTAWAY AND ZBIGNIEW WASZCZYLO
*Chemistry Department, Laurentian University, Sudbury, Ont., Canada P3E 2C6*

Received July 28, 1981[1]

KENNETH CHARLES WESTAWAY and ZBIGNIEW WASZCZYLO. Can. J. Chem. **60**, 2500 (1982).

Kinetic studies, secondary α-deuterium kinetic isotope effects, primary chlorine kinetic isotope effects (1), Hammett ρ values determined by changing the substituent in the nucleophile, and activation parameters have been used to determine the detailed (relative) structures of the transition states for the $S_N2$ reactions between *para*-substituted benzyl chlorides and thiophenoxide ion. A rationale for the U-shaped Hammett ρ plots observed when *para*-substituted benzyl compounds react with negatively charged nucleophiles is also presented.

KENNETH CHARLES WESTAWAY et ZBIGNIEW WASZCZYLO. Can. J. Chem. **60**, 2500 (1982).

On a utilisé des études cinétiques, des données relatives aux effets isotopiques cinétiques secondaires du deutérium en α et aux effets isotopiques cinétiques primaires du chlore (1), des valeurs ρ de Hammett déterminés en changeant les substituants du nucléophile et des paramètres d'activation pour déterminer les structures détaillées (relatives) des états de transition des réactions $S_N2$ entre les chlorures de benzyles substitués en position *para* et l'ion thiophénate. On présente également une explication raisonnable pour la forme en U des courbes de ρ de Hammett observées lorsque les composés benzyliques substitués en position *para* réagissent avec les nucléophiles chargés négativement.

[Traduit par le journal]

## Introduction

Determining the effect of substituents on the structure of $S_N2$ transition states has been of interest for several years (1–6). Several different techniques, such as kinetic studies (2, 3), solvent effects (4), thermodynamic properties (4, 7), and kinetic isotope effects (1, 5, 6, 8–10), have been used in an attempt to determine how substituents affect transition state structure. In spite of these efforts, the influence of substituents is not understood. The major reason for this is that the structures of the transition states have not been determined in enough detail to indicate how the substituents alter all of the transition state bonds. In a recent study of substituent effects on $S_N2$ transition states, Westaway and Ali (6) showed that detailed transition state structures can be obtained from a combination of primary leaving group kinetic isotope effects, secondary α-deuterium kinetic isotope effects, and Hammett ρ values. The same criterion and others have been applied to the $S_N2$ reactions between *para*-substituted benzyl chlorides and thiophenoxide ion to determine how substituents at the α carbon affect the structure of an $S_N2$ transition state.

This series of reactions was studied for another reason. The reactions between *para*-substituted benzyl compounds and negatively charged nucleophiles invariably give curved (U-shaped) Hammett ρ plots with the minimum at the unsubstituted compound, i.e., the substrates, with electron donating substituents such as methoxy and methyl or electron withdrawing substituents such as chloro and nitro, react faster than the unsubstituted compound (2). This behaviour is observed regardless of the structure of the substrate, the leaving group, the solvent, or the nucleophile (11–18), i.e., it is a general phenomenon that is associated with the change in substituent. Although several explanations have been suggested for this unusual behaviour, the reason for the curvature in the Hammett plot is not known. The detailed knowledge of the $S_N2$ transition states for this series of reactions has allowed the authors to provide a rationale for the curved Hammett ρ plots that are observed for the reactions between negatively charged nucleophiles and *para*-substituted benzyl compounds.

## Results and discussion

Both of the objectives of this study, i.e., to determine (*i*) what changes occur in the structure of an $S_N2$ transition state when a substituent at the α carbon is altered, and (*ii*) why U-shaped Hammett plots are observed in the $S_N2$ reactions of benzyl compounds with negatively charged nucleophiles, were achieved by measuring the secondary α-deuterium kinetic isotope effects, the Hammett ρ values obtained by changing the substituent in the nucleophile, and the activation parameters for the reactions between *para*-substituted thiophenoxide ions and *para*-substituted benzyl chlorides in 0.250

[1]Revision received June 3, 1982.

0008-4042/82/192500-21$01.00/0
©1982 National Research Council of Canada/Conseil national de recherches du Canada

Can. J. Chem. Downloaded from www.nrcresearchpress.com by 210.87.254.40 on 09/06/12
For personal use only.

TABLE 1. Rate constants for the reactions of *para*-substituted thiophenoxide ions with *para*-substituted benzyl chlorides in 0.250 *M* lithium methoxide in methanol

| Temperature °C | Substituent Y[b] | *para*-Substituent Z[a] | | | |
|---|---|---|---|---|---|
| | | $CH_3O$ | $CH_3$ | H | Cl |
| −9.3 | $CH_3O$ | | | 0.3234±0.0005[c] | |
| 0 | $CH_3O$ | 1.548±0.017[c] | 1.413±0.006 | 1.149±0.014 | 1.130±0.009 |
| 20 | $CH_3O$ | | | 120.0[d] | |
| 0 | $CH_3$ | | | 0.2728±0.0009 | |
| 20 | $CH_3$ | 3.285±0.006 | 2.776±0.012 | 2.211±0.011 | 1.984±0.032 |
| 30 | $CH_3$ | | | 5.990±0.004 | |
| 0 | H | | | 0.1743±0.0009 | |
| 20 | H | 2.053±0.015 | 1.867±0.012 | 1.427±0.021 | 1.176±0.004 |
| 30 | H | | | 4.236±0.005 | |
| 0 | Cl | | | 0.3534±0.0015 | |
| 20 | Cl | 4.641±0.027 | 3.840±0.003 | 2.728±0.017 | 2.038±0.021 |
| 30 | Cl | | | 8.182±0.001 | |
| 0 | $NO_2$ | 2.469±0.011 | 1.754±0.030 | 1.300±0.011 | 0.718±0.005 |
| 20 | $NO_2$ | 14.90±0.06 | 12.51±0.05 | 7.684±0.043 | 5.088±0.049 |
| 30 | $NO_2$ | | | 18.190±0.029 | |

[a] The *para*-substituent on the nucleophile (see eq. [1]).
[b] The *para*-substituent on the substrate (see eq. [1]).
[c] Standard deviation calculated for the rate constants from between 4 and 7 kinetic runs.
[d] Measured by Grimsrud (1). This rate constant was only used because all other rate constants at 20°C were within experimental error of those reported by Grimsrud.

molar lithium methoxide in methanol at 20°C, eq. [1].

[1] 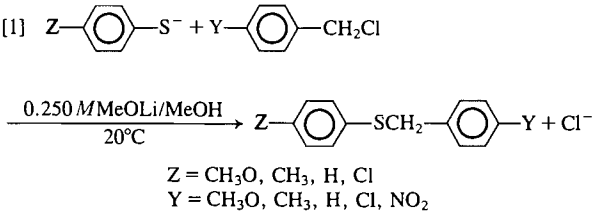


Z = $CH_3O$, $CH_3$, H, Cl
Y = $CH_3O$, $CH_3$, H, Cl, $NO_2$

*Kinetic studies*

The reactions between *para*-substituted thiophenoxide ions and *para*-substituted benzyl chlorides in 0.250 *M* lithium methoxide in methanol were followed by measuring the increase in the absorbance in a Beckman D.U. spectrophotometer. The second order rate constants measured at 0°C, 20°C, and 30°C are given in Table 1. The rate constants measured by the uv technique are in excellent agreement with those determined by Grimsrud (1) using a titrimetric method. With one exception (Y = $CH_3O$), the kinetic studies at 20°C produced good second order plots and gas chromatographic analyses of the reaction mixtures showed that the reactions were clean.

In the *para*-methoxybenzyl chloride reactions, however, slightly curved kinetic plots were observed at 20°C. The analysis of the products of the reaction revealed that a competing solvolysis of the substrate occurred, eq. [2]. A gas chromatographic analysis of the products from several different reactions showed that the solvolysis product, *para*-methoxybenzylmethyl ether, could be reduced to three percent of the product when the reaction was carried out at 0°C with a fivefold excess of the thiophenoxide ion, Table 2. Gas chromatographic analyses of reaction products from the reactions of *p*-methoxythiophenoxide ion and of *p*-chlorothiophenoxide ion with *p*-methoxybenzyl chloride also showed that the solvolysis product was reduced to 3 ± 1% of the product when the reactions were carried out at 0°C with a fivefold excess of thiophenoxide ion.

The amount of the solvolytic product in the *para*-methylthiophenoxide ion – *para*-methoxy-

[2] 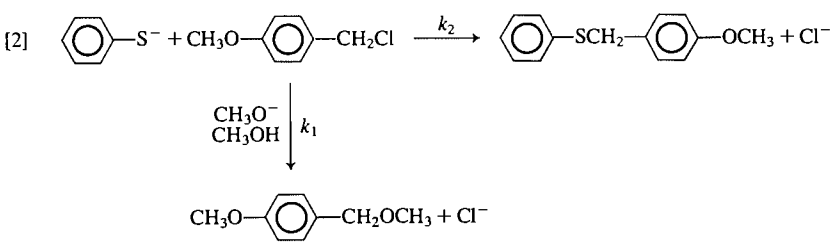


Can. J. Chem. Downloaded from www.nrcresearchpress.com by 210.87.254.40 on 09/06/12
For personal use only.

Can. J. Chem. Downloaded from www.nrcresearchpress.com by 210.87.254.40 on 09/06/12
For personal use only.

TABLE 2. The effect of temperature and concentration on the product distribution in the reactions between thiophenoxide ion and *para*-methoxybenzyl chloride

| Temperature (°C) | Concentration of $C_6H_5S^-$ (mol/L) | Concentration of $CH_3OC_6H_4CH_2Cl$ (mol/L) | Percent solvolysis[a] |
|---|---|---|---|
| 30 | $6.42 \times 10^{-3}$ | $2.00 \times 10^{-3}$ | 30±1 |
| 20 | $6.58 \times 10^{-3}$ | $2.09 \times 10^{-3}$ | 23±1 |
| 0 | $6.49 \times 10^{-3}$ | $2.04 \times 10^{-3}$ | 11±1 |
| 0 | $2.12 \times 10^{-2}$ | $3.89 \times 10^{-3}$ | 3±1 |

[a] These results are from 3 or 4 different analyses.

benzyl chloride reaction could not be determined gas chromatographically because the $S_N2$ product could not be separated from the 4,4′-ditolyldisulfide (the oxidation product of the unreacted *para*-methylthiophenoxide ion) which formed during the work-up of the product. Although the product could not be analyzed accurately, the area of the gas chromatographic peak associated with the solvolytic product was comparable to those observed in the reactions with the other nucleophiles. In addition, calculations of the product composition based on the measured second order rate constant and the first order rate constant ($k_1 = 8 \times 10^{-6}\ s^{-1}$, determined from a computer analysis of the other reactions) indicated that 2.8% of the product would be *para*-methoxybenzylmethyl ether.

These conditions were recognized as satisfactory for kinetic studies since an error in the experimentally determined secondary α-deuterium kinetic isotope effect and the Hammett ρ values caused by the small amount of solvolysis would be too small to be detected. Thus, the kinetic isotope effects, Hammett ρ values, and activation parameters measured for the series of reactions between the *para*-substituted thiophenoxide ions and *para*-substituted benzyl chlorides are clearly those associated with the $S_N$ reaction shown in eq. [1]. This ensures that any conclusions based on these results will be pertinent to the reactions under investigation.

*Proof of mechanism*

The kinetic studies, Table 1, provide strong evidence that the $S_N$ reactions between *para*-substituted thiophenoxide ions and *para*-substituted benzyl chlorides are $S_N2$ processes. The carbocation $S_N$ mechanisms such as the $S_N1$ ($S_N1$ Lim) mechanism ($k_1$ slow) and the other mechanisms where the $k_2$ or the $k_3$ step is the slow step of the reaction, eq. [3], can be ruled out because all of the reactions display clean second order kinetics and are first order in the substrate and in the nucleophile. This indicates that the nucleophile is involved in the transition state of the rate-determining step of the reaction. An additional indication that the S---$C_\alpha$ bond is forming in the transition state of these reactions is provided by the small Hammett ρ values found for all of the reactions in this study, Table 3. The Hammett ρ value for the protonation reactions of *para*-substituted thiophenoxide ions in methanol at 20°C is −1.99 (2). Thus, the magnitude of the ρ value should be approximately −2.0 for any reaction where the charge on sulfur has been totally destroyed in the transition state of the rate-determining step of the reaction. The small negative Hammett ρ values measured for the benzyl chloride reactions indicate that the change in charge on the sulfur atom is far from complete (S—$C_\alpha$ bond formation is only partially complete) in the transition state of the rate-determining step of these reactions. Obviously, this eliminates a carbocation mechanism where the $k_1$, the $k_2$, or the $k_3$ step is rate determining.

[3] $$RCl \underset{k_{-1}}{\overset{k_1}{\rightleftharpoons}} R^+Cl^- \underset{k_{-2}}{\overset{k_2}{\rightleftharpoons}} R^+\|Cl^- \underset{k_{-3}}{\overset{k_3}{\rightleftharpoons}} R^+ + Cl^-$$
$$\begin{array}{ccc} ArS^- \downarrow k_4 & ArS^- \downarrow k_5 & ArS^- \downarrow k_6 \\ RSAr & RSAr & RSAr \end{array}$$

The $S_N2C^+$ type mechanism (with $k_4$ and/or $k_5$ and/or $k_6$ slow, eq. [3]) can also be eliminated. These mechanisms involve a fast, reversible rupture of the C—Cl bond followed by a rate-

TABLE 3. Hammett ρ values[a] for substitution on the nucleophile in the reactions between *para*-substituted thiophenoxide ions and *para*-substituted benzyl chlorides at 20°C

| Substituent (Y)[b] | ρ | Correlation coefficient |
|---|---|---|
| $CH_3O$ | −0.283[c]±0.026[d] | 0.920 |
| $CH_3$ | −0.434±0.026 | 0.964 |
| H | −0.500±0.015 | 0.991 |
| Cl | −0.720±0.018 | 0.994 |
| $NO_2$ | −0.961±0.002 | 0.995 |
| $NO_2$ | −1.035[c]±0.022 | 0.996 |

[a] The individual rate constants are given in Table 1.
[b] Substituent on the benzyl chloride.
[c] At 0°C.
[d] Standard deviation.

Can. J. Chem. Downloaded from www.nrcresearchpress.com by 210.87.254.40 on 09/06/12
For personal use only.

determining step in which the ion pair or the carbocation reacts with the nucleophile. A mechanism in which the C—Cl bond ruptured in a fast and reversible step would display a small *equilibrium* chlorine isotope effect. Two different investigators have concluded that an equilibrium chlorine isotope effect would be 1.0037 and 1.0057 (19, 20). The much larger chlorine kinetic isotope effects of 1.00983 ± 0.00029 found by Grimsrud (1) for the reactions of thiophenoxide ion with *para*-substituted benzyl chlorides in the solvent system and at the temperature used in this investigation, show that the C—Cl bond is also breaking in the rate-determining step and not prior to it. These isotope effects clearly rule out all of the $S_N2C^+$ mechanisms.

In conclusion, the large chlorine kinetic isotope effects, small Hammett ρ values, and good second order kinetics exclude all of the carbocation $S_N$ mechanisms and indicate that all of the reactions between the *para*-substituted thiophenoxide ions and *para*-substituted benzyl chlorides proceed via an $S_N2$ mechanism.[2] Thus, this system of reactions can be used to determine how different substituents at the α carbon affect the structure of the $S_N2$ transition state and to determine why U-shaped Hammett ρ plots are observed for these $S_N2$ reactions.

### Determination of transition state structures

In describing how changes in the *para* substituent affect the transition state structure for this series of $S_N2$ reactions, it is necessary to determine how these structural changes affect the bonding between the α carbon and the leaving group (chloride ion), the α carbon and the incoming nucleophile (sulfur of the thiophenoxide ion), as well as any changes in bonding between the α carbon and the benzene ring.

*Chlorine kinetic isotope effects*

One widely used method of determining the length of the α-carbon – leaving group bond in the transition state is to measure the leaving group heavy atom kinetic isotope effect. In one study, Grimsrud measured the leaving group chlorine kinetic isotope effects for the reactions of interest, i.e., the $S_N2$ reactions between thiophenoxide ion and *para*-substituted benzyl chlorides in 0.250 molar lithium methoxide in methanol at 20°C (1). The chlorine kinetic isotope effects were useful in this study because they indicated how the α-carbon – chlorine transition state bond was affected by a change in the *para*-substituent on the benzene ring. The chlorine kinetic isotope effects measured by Grimsrud are given in Table 4.

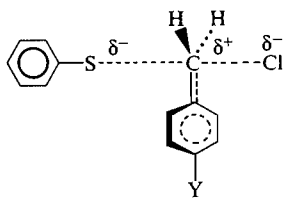


Although the standard deviation on the average kinetic isotope effect for this series of reactions exceeds the error ascribed to the individual kinetic isotope effects, the differences in the isotope effect caused by a change in the *para*-substituent are small and random. The simplest explanation is that the chlorine kinetic isotope effects are the same, or virtually the same, for all of the $S_N2$ transition states.

The interpretation of the effectively constant chlorine isotope effects observed for this series of reactions is not simple, however. Extensive theoretical calculations by Saunders (21) and Sims *et al.* (22) have shown that the magnitude of the leaving group chlorine isotope effect increases as the amount of C---Cl bond rupture increases (the bond order decreases) in the transition state of the rate-determining step. Thus, a larger chlorine isotope effect would indicate a longer C---Cl bond in the transition state of an $S_N2$ reaction. The almost constant chlorine isotope effects observed by Grimsrud suggest, therefore, that the C---Cl transition state bond length is not changed significantly when the *para*-substituent on the benzene ring is altered, i.e., that the C---Cl transition state bond has the same, or nearly the same, length for all the substituents.

TABLE 4. Chlorine kinetic isotope effects for the $S_N2$ reactions of thiophenoxide ion with *para*-substituted benzyl chlorides in 0.250 *M* lithium methoxide in methanol at 20°C

| *para*-Substituent "Y" | $k^{35}/k^{37}$[a] |
|---|---|
| $CH_3O$ | 1.01012 |
| $CH_3$ | 1.00963 |
| H | 1.00976 |
| Cl | 1.01013 |
| $NO_2$ | 1.00950 |
| | Average = 1.00983±0.00029[b] |

[a]The error on the individual kinetic isotope effects is ±0.00015.
[b]Standard deviation for the average kinetic isotope effect.

[2]It is worth noting that the second order kinetics, the small Hammett ρ value of −0.961, the small secondary α-deuterium kinetic isotope effect of 1.039, and the large chlorine kinetic isotope effect of 1.00950 clearly show that the *para*-nitrobenzyl chloride does not react via an electron transfer mechanism.

Can. J. Chem. Downloaded from www.nrcresearchpress.com by 210.87.254.40 on 09/06/12
For personal use only.

Although this explanation of the effectively constant isotope effects is the most obvious and straightforward, it is known that several other factors, in addition to the carbon–chlorine transition state bond order, affect the magnitude of a chlorine leaving group kinetic isotope effect. Theoretical calculations (28) indicate that (*i*) the force constant of the reacting (C—Cl) ground state bond, (*ii*) the nucleophile – α carbon transition state bond order, (*iii*) the amount of conjugation (π bond order) between the benzene ring and the α carbon in the transition state, (*iv*) changes in the reaction coordinate motion, i.e., from displacement by the nucleophile to displacement by the aryl group, and (*v*) solvation of the developing chloride ion all affect the magnitude of the isotope effect.

Although these effects influence the magnitude of the chlorine leaving group kinetic isotope effects in $S_N2$ reactions, fairly sophisticated calculations show that they are small with respect to the effect of a change in the C—Cl transition state bond order (28). For example, (*i*) the vibrational frequency of the C—Cl ground state bond decreases gradually from 680 $cm^{-1}$ in *para*-methoxybenzyl chloride to 625 $cm^{-1}$ for the *para*-nitrobenzyl chloride.[3] This means that the chlorine isotope effect would be slightly larger (the theoretical maximum isotope effect only changes by 0.0009 over the series) in the *para*-methoxybenzyl chloride reaction (29) (*vide infra*); (*ii*) a decrease in the nucleophile – α carbon transition state bond order leads to a slight decrease in the chlorine isotope effect (28). For example, decreasing the nucleophile – α carbon bond order from 1.00 to 0.40 only decreases the isotope effect by 0.001. Thus, a slightly smaller chlorine isotope effect would be expected for the *para*-methoxybenzyl chloride reaction (*vide infra*); (*iii*) increasing the amount of conjugation in the transition state causes a very slight increase in the isotope effect. For example, changing from 0% to 100% conjugation in a very loose transition state increases the isotope effect by less than 0.001 (28). Since the change in transition state π bond order is fairly small for all of the reactions in this series (*vide infra*), the changes in conjugation would have an extremely small effect on the isotope effect. A slightly larger isotope effect would be expected in the *para*-methoxybenzyl chloride reaction, however; (*iv*) changing the reaction coordinate motion from displacement by the nucleophile to displacement by the aryl group increases the isotope effect. In fact, increasing the contribution of displacement by the aryl group from 40% to 70% of the reaction coordinate motion can increase the isotope effect by as much as 0.001. In fact, this effect would be very small in this reaction series because very large changes in the reaction coordinate motion have almost no effect on the magnitude of the isotope effect when the C—Cl bond order is small in the transition state (28) (*vide infra*); (*v*) the solvation effect, i.e., the change in the solvation energy of the developing chloride ion, is thought to have the greatest effect on the magnitude of a chlorine kinetic isotope effect. If this were important, decreases in the C—Cl transition state bond order would not lead to a larger isotope effect. This would occur because the increased vibrational energy from the hydrogen bonding between the solvent, methanol, and the developing chloride ion would compensate for the loss of bonding in extending the C---Cl transition state bond. This means that the total bonding to the chloride ion and thus the magnitude of the isotope effect would not change when the C---Cl bond is more completely ruptured in the transition state. This idea, which was originally suggested by Thornton (23), has been substantiated by theoretical calculations by Sims and co-workers (24, 25). Sims' calculations show that strong solvation of the developing chloride ion in the transition state not only lowers the magnitude of the chlorine isotope effect, but also suggests that the chlorine kinetic isotope effect may be levelled in reactions with large amounts of C---Cl bond rupture in the transition state.

This levelling effect, although theoretically possible, seems unlikely in light of experimental results which show that very large *leaving group* chlorine kinetic isotope effects do not change significantly even with drastic changes in solvent, i.e., in cases where large changes in the solvation of the chloride ion would be expected. For example, changing the solvent from DMF where there is no hydrogen bonding to 97% aqueous methanol where hydrogen bonding should be important, only changes the chlorine isotope effects by an average of 0.0012 ± 0.0003 in the $S_N2$ reactions of *para*-substituted benzyl chlorides with 4-nitrophenoxide ion, 4-cyanophenoxide ion, or with azide ion (25). Moreover, changing the non-hydrogen bonding solvents, DMF or DMSO, to methanol in the $S_N2$ reaction between *n*-butyl chloride and thiophenoxide ion only changes the chlorine isotope effect by between 0.0002 and 0.0003 (20), i.e., by slightly more than the experimental error in the individual isotope effect. If the transition state structure of these reactions is not altered by a change in solvent as Westaway suggests (27), solvation by hydrogen bonding has a very small effect on the magnitude of the chlorine isotope effect even in reactions where

[3]J. W. Taylor, University of Wisconsin. Private communication.

Can. J. Chem. Downloaded from www.nrcresearchpress.com by 210.87.254.40 on 09/06/12
For personal use only.

the C---Cl bond is mainly broken in the transition state and hydrogen bonding to the developing chloride ion would be expected to be important. These results suggest that hydrogen bonding to solvent does not influence the chlorine isotope effect in C---Cl bond breaking reactions significantly and it seems unlikely therefore, that the constant isotope effects are the effect of levelling, i.e., of changes in the solvation of the developing chloride ion.

Thus, although the magnitude of chlorine leaving group kinetic isotope effects can be affected by changes in the nucleophile – α carbon and benzene ring – α carbon (π) transition state bond orders, changes in the reaction coordinate motion, and changes in solvation of the developing chloride ion, theoretical calculations by Brubaker (28), and the solvent effects on *leaving group* chlorine kinetic isotope effects indicate that these effects are small with respect to those resulting from changes in the $C_\alpha$—Cl transition state bond order. Moreover, three of the five effects (*i*, *iv*, and *v*) should have an extremely small influence on the magnitudes of the isotope effects for this series of reactions and the other two effects (*ii* and *iii*) work in opposite directions. This means that the magnitude of the chlorine leaving group isotope effect is almost completely determined by the $C_\alpha$---Cl transition state bond order.

Finally, the chlorine leaving group kinetic isotope effects in other $S_N2$ reactions of *para*-substituted benzyl chlorides decrease when a more electron withdrawing substituent is placed on the benzene ring (*vide infra*). This shows that these isotope effects can respond to changes in transition state structure in $S_N2$ reactions. Thus, the constant chlorine isotope effects in the *para*-substituted benzyl chloride – thiophenoxide ion $S_N2$ reactions must indicate that the $C_\alpha$—Cl transition state bond order is not sensitive to changes in substituent and the best explanation of the effectively constant chlorine isotope effects found in the *para*-substituted benzyl chloride – thiophenoxide ion reaction series is that the $C_\alpha$—Cl bond is equally broken in all of the transition states of these reactions.

Finally, it is worth noting that the chlorine isotope effects are large. They are approximately 88% of the theoretical maximum chlorine isotope effect (29) and indicate that the $C_\alpha$---Cl transition state bonds are very long for all the *para*-substituted benzyl chlorides.

*Secondary α-deuterium kinetic isotope effects*

Once the substituent effect on the $C_\alpha$---Cl transition state bond had been determined, it was necessary to determine how the S---C transition state bond changes when the substituent on the benzyl chloride is altered. Westaway and Ali have recently shown that the magnitude of the secondary α-deuterium kinetic isotope effect can be related to the nucleophile – leaving group transition state distance in a closely related series of reactions (6). This is possible because the magnitude of secondary α-deuterium kinetic isotope effects in $S_N2$ reactions is primarily determined by the differences in the energy of the $C_\alpha$—H(D) out-of-plane bending vibrations in the initial and transition states (31, 34, 35). Since the point of structural change is four bonds away from the $C_\alpha$—H(D) bond, the frequencies of the $C_\alpha$—H(D) out-of-plane bending vibrations are the same (1450 ± 5 $cm^{-1}$) for all the *para*-substituted benzyl chlorides used in this study. This means that the differences in the transition state out-of-plane bending vibrations determine the magnitude of these isotope effects. The effect of transition state structure on the magnitude of the secondary α-deuterium kinetic isotope effect can be illustrated using eq. [4].

$$[4] \quad (k_H/k_D) = \exp \tfrac{1}{2}\left[\sum^{3n-6} \Delta u_i - \sum^{3n-7} \Delta u_i^{\ddagger}\right]$$

where $\frac{1}{2}\Delta u_i = \frac{1}{2}(u_{i_H} - u_{i_D})$ is the zero-point energy difference in the initial state and $\frac{1}{2}\Delta u_i^{\ddagger}$ is the corresponding difference in the transition state. The

$$\sum^{3n-6} \Delta u_i$$

term is the same for all of the reactants and thus a smaller secondary α-deuterium kinetic isotope effect would be observed when the

$$\sum^{3n-7} \Delta u^{\ddagger}$$

term is larger, i.e., when the steric crowding around the α carbon is greater in the transition state, the vibrational energy and zero-point energy difference for the $C_\alpha$—H(D) out-of-plane bending vibration are greater. Obviously, decreasing either or both of the S--$C_\alpha$ and $C_\alpha$---Cl bond lengths (the total S---Cl distance) in the transition state would increase the steric crowding around the α carbon and decrease the magnitude of the isotope effect. Thus, the magnitude of the isotope effect is related to the S---Cl distance in the transition states of these reactions, (refs. 6, 28, 36 and Fig. 1). Since the constant chlorine kinetic isotope effects indicate that the $C_\alpha$---Cl transition state bond length is the same for all the reactions, any change in the magnitude of the secondary α-deuterium kinetic isotope effect results from a change in the S---C transition state bond length. The secondary α-

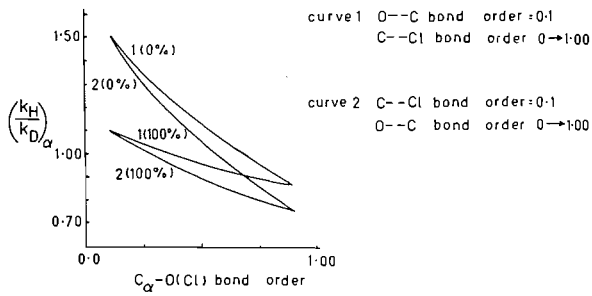


FIG. 1. The effect of conjugation between the α carbon and the benzene ring on the α carbon on the magnitude of the secondary α-deuterium kinetic isotope effect in the $S_N2$ reaction between alkoxide ion and benzyl chloride (28). The percent $C_\alpha$=Ar conjugation in the transition state is given in brackets for each curve.

deuterium kinetic isotope effects were measured for this series of reactions to determine how the S--$C_\alpha$ bond lengths changed when the structure of the substrate was altered.

The secondary α-deuterium isotope effects in the reactions between thiophenoxide ion and *para*-substituted benzyl chlorides were determined by a comparative technique, i.e., by reacting the undeuterated and deuterated[4] benzyl chlorides with thiophenoxide ion under identical conditions in separate experiments. The average rate constant for each was determined from between four and seven kinetic runs. Finally, since the secondary α-deuterium kinetic isotope effects in the reactions between thiophenoxide ion and *para*-methoxybenzyl chloride could only be measured at or below 0°C, the isotope effects for the *para*-methyl and unsubstituted benzyl chlorides were measured at 0° and 30°C to determine the temperature dependence of the isotope effect so that the magnitude of the isotope effect for the *para*-methoxybenzyl chloride reaction could be estimated at 20°C. The rate constants and isotope effects are given in Table 5.

An examination of the results in Table 5 shows that the magnitude of the isotope effect decreases as a more electron withdrawing substituent is placed on the benzene ring on the α carbon. This means that the S--Cl (nucleophile – leaving group) distance is shorter when a more electron withdrawing group is present in the substrate. Since the chlorine isotope effects show that the $C_\alpha$--Cl bond lengths are the same in all of the transition states, the S--$C_\alpha$ bond must be shorter in the transition state when a more electron withdrawing substituent is present on the benzene ring.

The only exception to this trend is found with the *para*-methoxybenzyl chloride reaction. The secondary α-deuterium kinetic isotope effects for the *para*-methyl and *para*-methoxybenzyl chloride reactions at 0°C are the same. Thus, the magnitude of the isotope effect for the *para*-methoxybenzyl chloride reaction at 20°C should be identical to the isotope effect for the *para*-methylbenzyl chloride reaction at 20°C., i.e., approximately 1.10 per $CD_2$ group or 1.05 per α-D. This means that the S--Cl distance and therefore, the S--$C_\alpha$ distance are equal in the two transition states in spite of the fact that the methoxy substituent is more electron donating than the methyl group. The chlorine and secondary α-deuterium kinetic isotope effects and the relative transition state structures suggested by these isotope effects are shown in Table 6.

The identical lengths of the S---$C_\alpha$ transition state bond for the reactions where the *para*-substituent is methoxy and methyl is difficult to explain because the more electron donating methoxy substituent would be expected to lead to a transition state with a longer S---$C_\alpha$ bond. This apparent inconsistency could be explained if the magnitude of the α-deuterium isotope effects were inversely related to the amount of $C_\alpha$=Ar conjugation in the transition state. One might expect this relationship would hold because an increase in conjugation means that the $C_\alpha$=Ar transition state bond order ($n^{\ddagger}_{C=Ar}$) is increased and thus the vibrational energy (force constant) for this bond would be greater. The $C_\alpha$—H out-of-plane bending force constants depend on the total bond order to the α carbon (25) and thus the

$$\sum^{3n-7} \Delta u_i^{\ddagger}$$

term (eq. [4]) would be larger and a smaller secondary α-deuterium isotope effect would be observed. In fact, theoretical calculations by Brubaker (28) on the $S_N2$ reactions between alkoxide ions and *para*-substituted benzyl chlorides suggest that this relationship should exist. Brubaker's calculations show that the magnitude of the isotope effect is smaller when conjugation with the aryl group on the α carbon is larger, i.e., when $n^{\ddagger}_{C=Ar}$ is greater, Fig. 1. The effect of increased conjugation is greater for looser transition states. For example, the isotope effect is reduced from 1.50 to 1.10 when the conjugation is increased from 0 to 100% for the loose transition state with $n^{\ddagger}_{C-Cl} + n^{\ddagger}_{C-O} = 0.2$, whereas a much smaller decrease from 0.89 to 0.77 is observed when the conjugation is increased from

[4]Nuclear magnetic resonance spectroscopy indicated that each deuterated benzyl chloride was 99% deuterated at the α carbon. A mass spectrometric analysis at low ionizing voltage indicated that the benzyl chlorides were between 98.6 and 99.1% deuterated (between 97.2 and 98.2% dideuterated) at the α carbon.

Can. J. Chem. Downloaded from www.nrcresearchpress.com by 210.87.254.40 on 09/06/12
For personal use only.

TABLE 5. Rate constants and secondary α-deuterium isotope effects in the reactions between thiophenoxide ion and *para*-substituted benzyl chlorides at 0°C, 20°C, and 30°C

| *para*-Substituent and temperature | $k_H \times 10^2$ (L/mol s) | $k_D \times 10^2$ (L/mol s) | $(k_H/k_D)_\alpha$ | $(k_H/k_D)_\alpha^{1/2}$ |
|---|---|---|---|---|
| $CH_3O$ (0°C) | 1.149±0.014[a] | 1.020±0.017[a] | 1.126±0.023[b] | 1.061 |
| $CH_3$ (0°C) | 0.2728±0.0009 | 0.2422±0.0018 | 1.125±0.009 | 1.061 |
| (20°C) | 2.211±0.011 | 2.017±0.025 | 1.096±0.015 | 1.047 |
| (30°C) | 5.990±0.004 | 5.485±0.004 | 1.092±0.001 | 1.045 |
| H (0°C) | 0.1743±0.0009 | 0.1576±0.0015 | 1.092±0.012 | 1.045 |
| (20°C) | 1.427±0.021 | 1.351±0.014 | 1.056±0.019 | 1.028 |
| Cl (20°C) | 2.728±0.017 | 2.607±0.039 | 1.046±0.017 | 1.023 |
| $NO_2$ (20°C) | 7.684±0.043 | 7.395±0.039 | 1.039±0.008 | 1.019 |

[a]Standard deviation.
[b]The standard error in the individual isotope effects is $1/k_D[(\Delta k_H)^2 + (k_H/k_D)^2 \times (\Delta k_D)^2]^{1/2}$ where $\Delta k_H$ and $\Delta k_D$ are the standard deviations for the rate constants for the undeuterated and deuterated substrates, respectively (30).

0 to 100% in a tight transition state with $n^{\ddagger}_{C-Cl} + n^{\ddagger}_{C-O} = 0.8$. These results indicate that looser transition states with greater conjugation could have secondary α-deuterium kinetic isotope effects comparable to or even smaller than those observed for tighter transition states where little or no conjugation is present.[5] Obviously, conjugation should be more important with the more electron donating *p*-$CH_3O$ substituent than the *p*-$CH_3$ substituent. When this factor is taken into consideration, it seems highly probable that the S---$C_\alpha$ transition state bond is longer for the transition state where the *para*-substituent is methoxy. If this argument is correct, the S---C bond becomes shorter as a more electron withdrawing substituent is added to the benzene ring for all transition states.

[5]One of the referees pointed out that the secondary α-deuterium kinetic isotope effects for various solvolysis reactions of 1-(*para*-methoxyphenyl)ethyl chloride and 1-phenylethyl chloride were identical. If an increase in conjugation decreases the magnitude of the isotope effect as is suggested, one would expect that the isotope effects for the 1-(*para*-methoxyphenyl)ethyl chloride solvolysis should be smaller than the isotope effects found for the unsubstituted substrate in the same reactions because conjugation should be more important in the 1-phenylethyl series where a carbocation intermediate is produced than in the benzyl series of $S_N2$ reactions.

The referee believes that the constant secondary α-deuterium kinetic isotope effects in the 1-phenylethyl series cast doubt on the proposed explanation. However, it appears that the constant α-deuterium isotope effects in the 1-phenylethyl series are unusual because the secondary β-deuterium kinetic isotope effects for these same reactions change markedly when the substituent is changed. Since these changes in the β-deuterium isotope effect are attributed to changes in mechanism and/or transition state structure, it is difficult to understand why the α-deuterium isotope effects in the 1-phenylethyl series are not altered by a change in substituent. We are unable to explain the very different trends in the secondary α-deuterium kinetic isotope effects for the carbonium ion solvolyses of the 1-(*para*-substituted phenyl)ethyl chlorides and the $S_N2$ reactions of the *para*-substituted benzyl chlorides.

*Hammett ρ values*

Although the relative lengths of most of the S---$C_\alpha$ transition state bonds can be given with some certainty, the difference between the S---$C_\alpha$ transition state bonds in the reactions of *para*-methoxy and *para*-methylbenzyl chlorides is based on an experimentally untested theory and there is no positive experimental proof that the S---$C_\alpha$ bond is indeed longer in the case where the *para*-substituent is methoxy. As a result, it was important to show that the S---$C_\alpha$ transition state bond actually becomes longer when the more electron donating methoxy substituent is added to the benzene ring. Westaway and Ali (6) have recently shown that the length of the nucleophile – α-carbon transition state bond in an $S_N2$ reaction can be determined by measuring the Hammett ρ values associated with changing the *para*-substituent on the nucleophile. The charge density on the sulfur atom of the nucleophile is obviously substrate independent and thus the variation in the Hammett ρ value must be the result of a different charge density on the sulfur atom in the transition state. The sulfur atom would experience only a small decrease in negative charge density in going to a transition state with a long S---$C_\alpha$ bond and thus the ρ value should be small and negative. If the nucleophile – α-carbon transition state bond is short (strong) on the other hand, only a small amount of negative charge would be on the sulfur atom of the nucleophile in the transition state. As a result, the change in charge on the sulfur atom in going from the thiophenoxide ion to the transition state is large and a large negative ρ value would be observed. Thus, a larger (more negative) ρ value indicates that the S---$C_\alpha$ bond is shorter in the transition state.

This technique was applied to the reactions of each of the substrates used in this study in order to confirm that the S---$C_\alpha$ bond shortens when more electron withdrawing substituents are present in

Can. J. Chem. Downloaded from www.nrcresearchpress.com by 210.87.254.40 on 09/06/12
For personal use only.

TABLE 6. The effect of a substituent change at the α carbon on the transition state structure of an $S_N2$ reaction

| *para*-Substituent "Y" | $k^{35}/k^{37}$ | Relative C---Cl distance | $(k_H/k_D)_\alpha$ 20°C | Relative S-----Cl distance | Relative transition state structure |
|---|---|---|---|---|---|
| $CH_3O$ | 1.01012 | C-----Cl | 1.096[a] | S----------Cl | S-------C-----Cl |
| $CH_3$ | 1.00963 | C-----Cl | 1.096 | S----------Cl | S-------C-----Cl |
| H | 1.00976 | C-----Cl | 1.056 | S---------Cl | S-----C-----Cl |
| Cl | 1.01013 | C-----Cl | 1.046 | S---------Cl | S----C-----Cl |
| $NO_2$ | 1.00950 | C-----Cl | 1.039 | S--------Cl | S---C-----Cl |

[a]Estimated from the data presented in Table 5.

the substrate. The *para*-substituent "Z" on the thiophenoxide ion was changed from $CH_3O$ to $CH_3$ to H and to Cl and the rate constant for the reaction of every nucleophile was measured with each of the substrates (Table 1). The Hammett ρ values and the correlation coefficients for each substrate are given in Table 3.

Unfortunately, the ρ value for the *para*-methoxybenzyl chloride reactions had to be determined from the rate constants at 0°C and estimated at 20°C. This was done by measuring the temperature dependence of the ρ value for the *para*-nitrobenzyl chloride reactions. This reaction series was chosen because the *para*-nitrobenzyl chloride had the largest ρ value and would therefore, be expected to show the greatest temperature dependence. The results in Table 3 show that the Hammett ρ value for the *para*-nitrobenzyl chloride reaction increases by eight percent when the temperature is reduced by 20°C. Assuming the same temperature dependence, the Hammett ρ value for the *para*-methoxybenzyl chloride reaction at 20°C would be −0.26.

The results in Table 3 show that the Hammett ρ value becomes more negative whenever a more electron withdrawing substituent is placed on the substrate. This indicates that the S---$C_\alpha$ transition state bond is shorter when a more electron withdrawing substituent is on the substrate. Thus, these results support the changes in the S---$C_\alpha$ transition state bond indicated by the variation in the secondary α-deuterium kinetic isotope effects. It is worth noting that the magnitude of the Hammett ρ value is much larger for the *para*-methylbenzyl chloride reaction than for the *para*-methoxybenzyl chloride reaction. This substantiates that the S---$C_\alpha$ bond is much longer in the latter transition state and confirms that the S--$C_\alpha$ bond shortens in all of the transition states when a more electron withdrawing substituent is placed on the benzene ring on the α carbon. This supports Brubaker's suggestion that the equal secondary α-deuterium isotope effects for the two reactions are due to a greater $C_\alpha$=--Ar bond order (conjugation) in the transition state of the *para*-methoxybenzyl chloride reaction.

Finally, it is interesting to try to provide a rationale for the above results, i.e., to explain why the S---C transition state bond becomes shorter whereas the C---Cl bond remains unchanged as a more electron withdrawing substituent is added to the benzene ring. One explanation is that the C---Cl bond is equally broken in all the transition states because the free energy required to displace the same leaving group is the same for each reaction. The change in the S---$C_\alpha$ bond could be qualitatively explained by assuming that the nucleophilic push required to rupture the C—Cl bond comes from a combination of electron density supplied by the nucleophile and electron density from the benzene ring bonded to the α carbon. When a strongly electron donating substituent is present on the benzene ring, the benzene ring supplies most of the electron density that is needed to push out the leaving group. In this case, little electron density is needed from the nucleophile and the nucleophile – α-carbon transition state bond is long. When an electron withdrawing substituent is on the benzene ring, little or no electron density will be provided by the benzene ring and most of the electron density required to rupture the C—Cl bond comes from the nucleophile. As a result, the nucleophile – α-carbon (S---$C_\alpha$) bond is much shorter in the transition state.

*Conjugation between the α carbon and the benzene ring*

Two different factors suggest that resonance between the α carbon and the benzene ring plays an important role in determining the structure of the transition states in the $S_N2$ reactions between thiophenoxide ion and *para*-substituted benzyl chlorides. Because the Hammett ρ value observed for the *para*-methoxybenzyl chloride reaction is smaller than the ρ value for the *para*-methylbenzyl chloride reaction, the S---$C_\alpha$ transition state bond is longer in the former reaction. Yet, identical secon-

Can. J. Chem. Downloaded from www.nrcresearchpress.com by 210.87.254.40 on 09/06/12
For personal use only.

Can. J. Chem. Downloaded from www.nrcresearchpress.com by 210.87.254.40 on 09/06/12
For personal use only.

dary α-deuterium isotope effects, which suggest that the S--$C_\alpha$ bonds are equally long in the two transition states, are observed for these two reactions. The identical isotope effects can be rationalized if $C_\alpha$=--Ar conjugation is greater in the *para*-methoxybenzyl chloride transition state. In addition, a consideration of the changes that occurred in the S---$C_\alpha$ and $C_\alpha$---Cl transition state bonds, when the substituent is altered, led to the suggestion that electron density from the nucleophile and electron density from the aryl group on the α carbon work in a complementary fashion in displacing the chloride ion. If these ideas are correct, $C_\alpha$=--Ar bonding plays a major role in determining transition state structure. It was important, therefore, to demonstrate that $C_\alpha$=--Ar conjugation has a major influence on the transition state structures of these $S_N2$ reactions.

Young and Jencks (37) recently showed that a modified Yukawa–Tsuno expression, eq. [5]:

$$[5] \quad \log (k/k_0) = \rho\sigma^n + \rho^r(\sigma^+ - \sigma^n)$$

can be used to determine the relative importance of polar and resonance effects in $S_N2$ reactions. The constants ρ and $\rho^r$ represent the sensitivity of the reaction to polar and resonance effects, respectively. The $\sigma^+$ substituent constant describes the interaction of the substituent with a carbonium ion, $\sigma^n$ represents the polar effect of the substituent (38), and $(\sigma^+ - \sigma^n)$ represents the ability of the substituent to donate electrons by resonance. The resonance effect of the substituent $(\sigma^+ - \sigma^n)$ decreases in the order methoxy > methyl > chloro. $(\sigma^+ - \sigma^n)$ is zero for the hydrogen and nitro substituents that do not donate electrons through resonance.

Equation [5] correlates the substituent effects on the reaction rates with the polar ($\rho\sigma^n$) and resonance ($\rho^r(\sigma^+ - \sigma^n)$) effects of the substituents. If resonance between the α carbon and the benzene ring is important in this reaction series, $\rho^r$ should be large. In fact, if the resonance effect is more important than the polar effect, $\rho^r$ will be larger than ρ. In the reaction series studied, the H and $NO_2$ substituents do not have a resonance effect and the Yukawa–Tsuno equation reduces to the simple Hammett equation for polar effects, eq. [6], for these two substituents.

$$[6] \quad \log (k/k_0) = \rho\sigma^n$$

A plot of log $k/k_0$ versus $\sigma^n$ for the *para*-hydrogen and *para*-nitro substituted benzyl chloride reactions at 20°C gives a line of slope = 0.94. When the other substituents are placed on the Hammett $\rho\sigma^n$ diagram, Fig. 2, the points corresponding to the

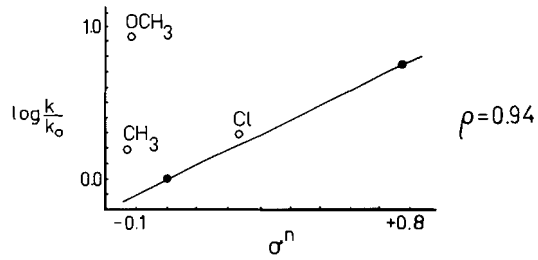


FIG. 2. Deviation of the rate constant for the *para*-methoxy, *para*-methyl, and *para*-chlorobenzyl chlorides from the log $(k/k_0) = 0.94\,\sigma^n$ plot.

*p*-$CH_3O$,[6] the *p*-$CH_3$, and the *p*-Cl benzyl chlorides show positive deviations from the ρ = 0.94 line. It is worth noting that the resonance effect (Δ log $k/k_0$) is much greater for *p*-$CH_3O$ (1.029) than for *p*-$CH_3$ (0.311) in agreement with the conclusion reached from the studies of the secondary α-deuterium isotope effects. The small deviation from the $0.94.\sigma^n$ line for the *p*-Cl substituent (0.058) is consistent with the overriding polar effect of this substituent. These deviations, which represent the resonance contribution of the substituents, can be evaluated from eq. [7].

$$[7] \quad \Delta \log (k/k_0) = \log (k/k_0) - 0.94\,\sigma^n = \rho^r(\sigma^+ - \sigma^n)$$

In fact, the slope of the Δ log $(k/k_0)$ versus $(\sigma^+ - \sigma^n)$ plot is $\rho^r = -1.67$. The standard deviation is ±0.08 and the correlation coefficient is 0.988.

The importance of the resonance effect is indicated by the relative sensitivity of the reaction series to the resonance and polar effects of the substituents. The larger absolute value of $\rho^r$, i.e., $|\rho^r/\rho| = |1.67/0.94| = 1.78$, indicates that the resonance effect is large in the reactions between thiophenoxide ions and *para*-substituted benzyl chlorides. This confirms that resonance ($C_\alpha$=--Ar bonding) is important in these reactions.

Once the values of ρ and $\rho^r$ had been determined, the Yukawa–Tsuno plot could be drawn, curve a, Fig. 3. The good linearity and high correlation coefficient of 0.985 illustrates that the Yukawa–Tsuno equation can be successfully applied to the data measured for this series of reactions. More important, however, is the information this treatment provides about the importance of conjugation between the α carbon and the aryl group.

Although the $\rho^r$ value was determined by using the three substituents with a significant electron

[6]The rate constant of 0.12 L/mol-s at 20°C reported by Grimsrud (1) was used because all of Grimsrud's other rate constants at 20°C were within experimental error of those determined in this work.

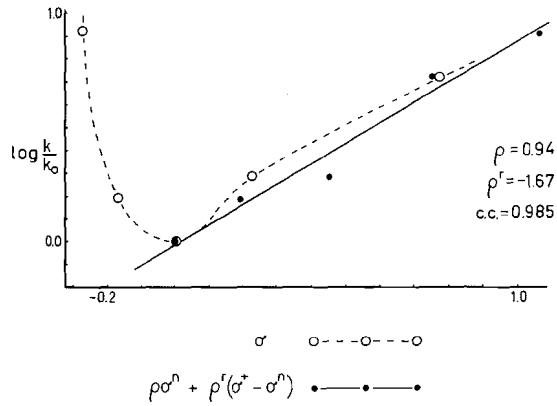


FIG. 3. The Yukawa–Tsuno plot (solid circles and line, curve a) and the Hammett plot (open circles and dotted line, curve b) for the $S_N2$ reactions between *para*-substituted benzyl chlorides and thiophenoxide ions at 20°C.

donating resonance effect, the large value of $\rho^r = -1.67$ suggests that conjugation is important in all of the transition states, i.e., even when the *para*-substituent "Y" is hydrogen and nitro. The nitro substituent is much more electron withdrawing than hydrogen, however, and the $C_\alpha$=Ar bond order would be expected to be much smaller in the *para*-nitrobenzyl chloride transition state than in the transition state where the substituent "Y" is hydrogen. This conclusion is supported by the work of Fuchs and Carlton (39) who studied the reactions of *para*-substituted benzyl chlorides and 3-nitro 4-substituted benzyl chlorides with thiosulfate ion in 60% aqueous acetone at 30°C and with water in 50% aqueous ethanol at 60°C. Application of the Yukawa–Tsuno equation to their data shows that the introduction of the 3-nitro group reduces the $\rho^r$ value from −3.99 to −0.96 for the reactions with thiosulfate ion and from −11.21 to −2.43 for the solvolysis reactions in aqueous ethanol. The large decrease in $\rho^r$ shows that the resonance with the α carbon (the $C_\alpha$=Ar transition state bond order) decreases when a more electron withdrawing substituent is added to the benzene ring of the substrate. However, $\rho^r$ is still finite for the 3-nitro 4-substituted benzyl chlorides and thus $C_\alpha$=Ar conjugation would be expected in all of the transition states investigated in this study.

The enthalpies of activation were determined for these reactions to (*i*) confirm that conjugation between the α carbon and the benzene ring was important in all of the transition states, and (*ii*) because these values could be used to demonstrate how the C=Ar bond length (conjugation) was related to the nucleophile – α-carbon bond lengths in these transition states. This approach requires two reasonable assumptions. The first assumption is that the enthalpy of activation ($\Delta H^\ddagger$) can be expressed in terms of an enthalpy of activation for each of the bonds that are made (the $C_\alpha$—S and the π bond between the α carbon and the benzene ring) or broken (the $C_\alpha$—Cl bond) in the transition state, eq. [8].

$$[8] \quad \Delta H^\ddagger = -\Delta H^\ddagger_{C=Ar} - \Delta H^\ddagger_{S-C} + \Delta H^\ddagger_{C-Cl}$$

The first two terms in eq. [8] are negative because the bond forming reactions reduce the magnitude of $\Delta H^\ddagger$. The second assumption is that the individual $\Delta H^\ddagger$ terms can be estimated using eq. [9].

$$[9] \quad \Delta H^\ddagger = \text{B.D.E.}\ (n^\ddagger - n_R)$$

where B.D.E. is the bond dissociation energy and $n^\ddagger$ and $n_R$ are the bond orders in the transition state and the reactant, respectively. Substituting the appropriate B.D.E. for the reacting bonds (69 kcal/mol for the C—Cl bond in benzyl chloride (40, 41), 59 kcal/mol for the benzyl C—S bond in benzylmethyl sulfide (41), and 63 kcal/mol for the π bond (42)) and $n_R$ values (1.00 for the C—Cl bond and 0.00 for the C—S and π bonds) in eq. [8] and rearranging gives eq. [10].

$$[10] \quad n^\ddagger_{C=Ar} = \frac{-\Delta H^\ddagger + 69(n^\ddagger_{C-Cl} - 1.0) - 59n^\ddagger_{S-C}}{63}$$

This means that $n^\ddagger_{C=Ar}$, the bond order of the π bond between the α carbon and the benzene ring in the transition state, could be estimated if values of $n^\ddagger_{C-Cl}$ and $n^\ddagger_{S-C}$ were known.

Although the exact values of $n^\ddagger_{C-Cl}$ and $n^\ddagger_{S-C}$ cannot be determined, they can be *estimated* from the magnitudes of the chlorine kinetic isotope effects and the Hammett ρ values observed for these reactions. Dividing the average chlorine isotope effect of 1.00983 ± 0.00029 by the theoretical maximum chlorine isotope effect of 1.0111 at 20°C indicates that the $C_\alpha$---Cl bond rupture is approximately 88% complete[7] (the $C_\alpha$---Cl bond order is approximately 0.12) in all of the transition states (29).

The $n^\ddagger_{S-C}$ for each reaction was *estimated* by dividing the Hammett ρ values obtained when the substituent on the nucleophile was changed (Table 3) by −1.99, the Hammett ρ value for the protonation of *para*-substituted thiophenoxide ions in methanol at 20°C (2). While the −1.99 is only an approximation for the ρ value that would be observed when the negative charge on sulfur is com-

[7]It is realized that this is a crude method of estimating the $C_\alpha$---Cl bond order. The theoretical maximum was calculated using the average $C_\alpha$—Cl stretching frequency of 650 $cm^{-1}$.

Can. J. Chem. Downloaded from www.nrcresearchpress.com by 210.87.254.40 on 09/06/12
For personal use only.

TABLE 7. Enthalpies and entropies of activation and the $C_\alpha$---Cl, S---$C_\alpha$, and $C_\alpha$=Ar transition state bond orders for the reactions between thiophenoxide ion and *para*-substituted benzyl chlorides

| *para*-Substituent "Y" | $\Delta H^{\neq}$(kcal/mol) | $\Delta S^{\neq}$(cal/mol K) | $n^{\neq}_{C-Cl}$ | $n^{\neq}_{S-C}$ | $n^{\neq}_{C=Ar}$ |
|---|---|---|---|---|---|
| $CH_3O$ | 18.37±0.11[a] | −0.03 | 0.12 | 0.13 | 0.55 |
| $CH_3$ | 16.33±0.11 | −10.33 | 0.12 | 0.22 | 0.50 |
| H | 16.81±0.30 | −9.50 | 0.12 | 0.25 | 0.46 |
| Cl | 16.51±0.38 | −9.21 | 0.12 | 0.36 | 0.36 |
| $NO_2$ | 13.85±0.13 | −16.31 | 0.12 | 0.48 | 0.29 |

[a]Standard deviation/($[1/T_{max}] - [1/T_{min}]$).

pletely destroyed in the transition state of a C—S bond forming reaction, the authors believe it is a good approximation because the charge on the sulfur atom is completely destroyed in the equilibrium and the substrates, solvent, and temperature are identical to those used in measuring the ρ values for the $S_N2$ reactions.

The enthalpy ($\Delta H^{\neq}$) and entropy ($\Delta S^{\neq}$) of activation for all but one of these reactions were determined from the rate constants measured at 0°C, 20°C, and 30°C, Table 1. The $\Delta H^{\neq}$ and $\Delta S^{\neq}$ for the *para*-methoxybenzyl chloride reaction, on the other hand, were determined from the rate constants measured at −9.3°C, 0°C, and Grimsrud's rate constant at 20°C,[8] Table 1. The activation parameters and the calculated $n^{\neq}_{C-Cl}$, $n^{\neq}_{S-Cl}$, and $n^{\neq}_{C=Ar}$ are given in Table 7.

Although the bond orders in Table 7 are based on crude estimates and are only approximate, they illustrate two important features of these $S_N2$ transition states. First, all of the $n^{\neq}_{C=Ar}$ (π bond orders) are large. For example, the estimated $n^{\neq}_{C=Ar}$ is still 0.29 even in the transition state with the strongly electron withdrawing nitro substituent. This demonstrates that resonance between the benzene ring and the α carbon is important in all of these transition states and confirms the conclusion based on the use of the modified Yukawa–Tsuno equation.

The second observation is even more important, however. The linearity (the correlation coefficient is 0.994) of the $n^{\neq}_{C=Ar}$ versus $n^{\neq}_{S-C}$ plot, Fig. 4, demonstrates that $n^{\neq}_{C=Ar}$ varies inversely with $n^{\neq}_{S-C}$. This supports the qualitative relationship between the transition states that was suggested above, i.e., that electron density provided by the conjugation *and* the nucleophile are involved in displacing the leaving group and that the S--$C_\alpha$ transition state bond becomes shorter when a more electron withdrawing substituent is placed on the benzene ring and the conjugation decreases. This inverse relationship between the S---$C_\alpha$ and the $C_\alpha$=Ar bond orders means that the transition state structure is determined by the amount of $C_\alpha$=Ar conjugation in the transition state. This, in turn, suggests that the amount of conjugation should be related to the individual properties of each substituent. If this is true, the conjugation from the benzene ring should be related to the ρ value of the substituent on the benzene ring of the substrate. In fact, a good linear relationship is observed. A plot of $n^{\neq}_{C=Ar}$ versus the σ value of the *para*-substituent on the benzene ring has a correlation coefficient of 0.967, Fig. 5. This indicates that the resonance contribution of the benzene ring does vary as the

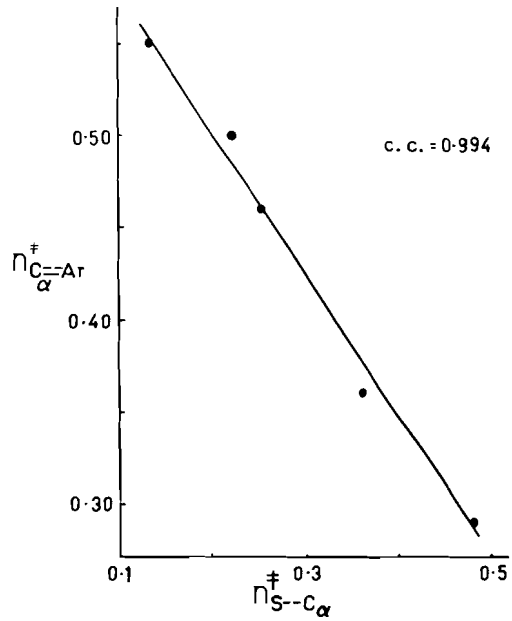


FIG. 4. The $C_\alpha$=Ar transition state π bond order (conjugation) versus the S---$C_\alpha$ transition state bond order for the $S_N2$ reactions between thiophenoxide ion and *para*-substituted benzyl chlorides.

[8]Grimsrud's rate constant at 20°C was only used because all other rate constants at 20°C were within experimental error of those reported by Grimsrud. The small error in $\Delta H^{\neq}$ for this compound (Table 7) also indicates that Grimsrud's rate constant was accurate.

Can. J. Chem. Downloaded from www.nrcresearchpress.com by 210.87.254.40 on 09/06/12
For personal use only.

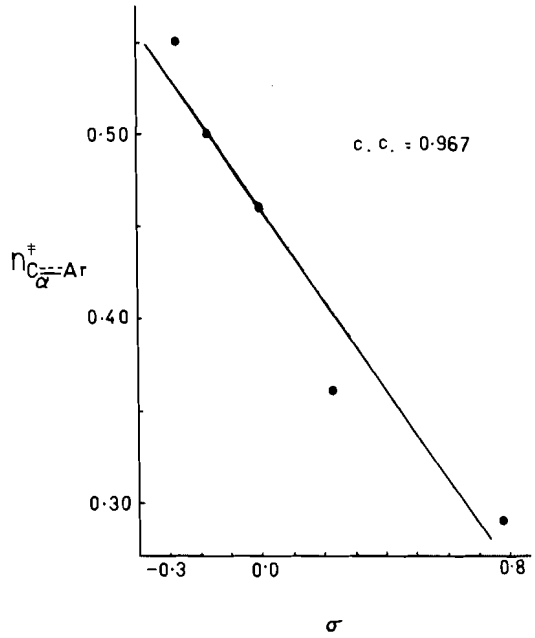


FIG. 5. A plot of the $C_\alpha$---Ar transition state π bond order versus the σ constant of the *para*-substituent "Y" in the reaction between *para*-substituted benzyl chlorides and thiophenoxide ions.

electron donating ability of the substituent. This in turn determines the S---$C_\alpha$ transition state bond order.

Combining the constant $C_\alpha$---Cl bond lengths with the shortening S---$C_\alpha$ bonds and the diminishing $C_\alpha$---Ar bond order, as the substituent on the substrate becomes more electron withdrawing, leads to detailed qualitative descriptions of the transition state structures in the reactions between thiophenoxide ion and *para*-substituted benzyl chlorides, Fig. 6. The plane of the benzene ring will be perpendicular to the S--$C_\alpha$--Cl axis so that the π electrons of the benzene ring can overlap with the partially filled orbitals on the α carbon. Finally, it is worth noting that the Hammett ρ values for the reactions of all the substrates are very small with respect to the −1.99 observed in the equilibrium reaction where the negative charge on the sulfur atom is completely destroyed (2). This indicates that the S--C transition state bonds are long in all cases. Since the chlorine (leaving group) isotope effects are large for all of the reactions, the C---Cl transition state bonds are also long. This means that all of the transition states are loose, i.e., are of the decreased total bonding (DTB) type.

### The effect of bond strength on transition state structure

The transition state structures in Fig. 6 show that the introduction of a more electron withdrawing substituent to the substrate shortens the nucleophile – α-carbon bond and reduces the conjugation between the α carbon and the benzene ring but does not alter the α-carbon – leaving group bond in the transition state. Having established the changes in the transition state structure, it was important to compare these results with those found for other similar reactions.

With one exception (49), the secondary α-deuterium kinetic isotope effects reported for the $S_N2$ reactions of several other benzyl substrates (5, 45–48) are smaller when a more electron withdrawing substituent is on the benzene ring. Moreover, this trend seems to be independent of the nucleophile and the solvent. Unfortunately, the smaller isotope effects found when a more electron withdrawing substituent is present only mean that the transition state is tighter, i.e., the nucleophile – leaving group distance is shorter, and there is no indication whether (*i*) the nucleophile – α-carbon bond, (*ii*) the α-carbon – leaving group bond, or (*iii*) both of these bonds are affected by the change in substituent. Thus, although our results agree with those found by other workers, these isotope effects do not give enough information so that one can determine whether the changes found in the benzyl chloride – thiophenoxide ion transition state structures are common to all reactions of benzyl substrates.

An examination of the chlorine kinetic isotope effects found for other $S_N2$ reactions of *para*-substituted benzyl chlorides showed that the chlorine isotope effects were independent of the *para*-substituent for some reactions but were substituent dependent in others. Obviously, the simple explanation presented above does not explain the changes in the transition state structure for all $S_N2$ reactions. For example, if one considers the reverse of the reactions studied, i.e., the displacement of thiophenoxide ion from benzylphenyl sulfide by chloride ion, the principle of microscopic reversibility states that the C---S bond (the α-carbon – leaving group bond) will shorten and that the Cl---C bond (the nucleophile – α-carbon bond) will remain unchanged when a more electron withdrawing substituent is on the benzene ring. This is opposite to the results given above, i.e., where the α-carbon – leaving group bond remained constant and the nucleophile – α-carbon bond shortened. Since the principle of microscopic reversibility must hold, another factor must play an important role in determining the changes in transition state structure. A consideration of this problem led to the conclusion that the relative bond strengths of the nucleophile – α-carbon and α-carbon – leaving group bonds are important in

Can. J. Chem. Downloaded from www.nrcresearchpress.com by 210.87.254.40 on 09/06/12
For personal use only.

Can. J. Chem. Downloaded from www.nrcresearchpress.com by 210.87.254.40 on 09/06/12
For personal use only.

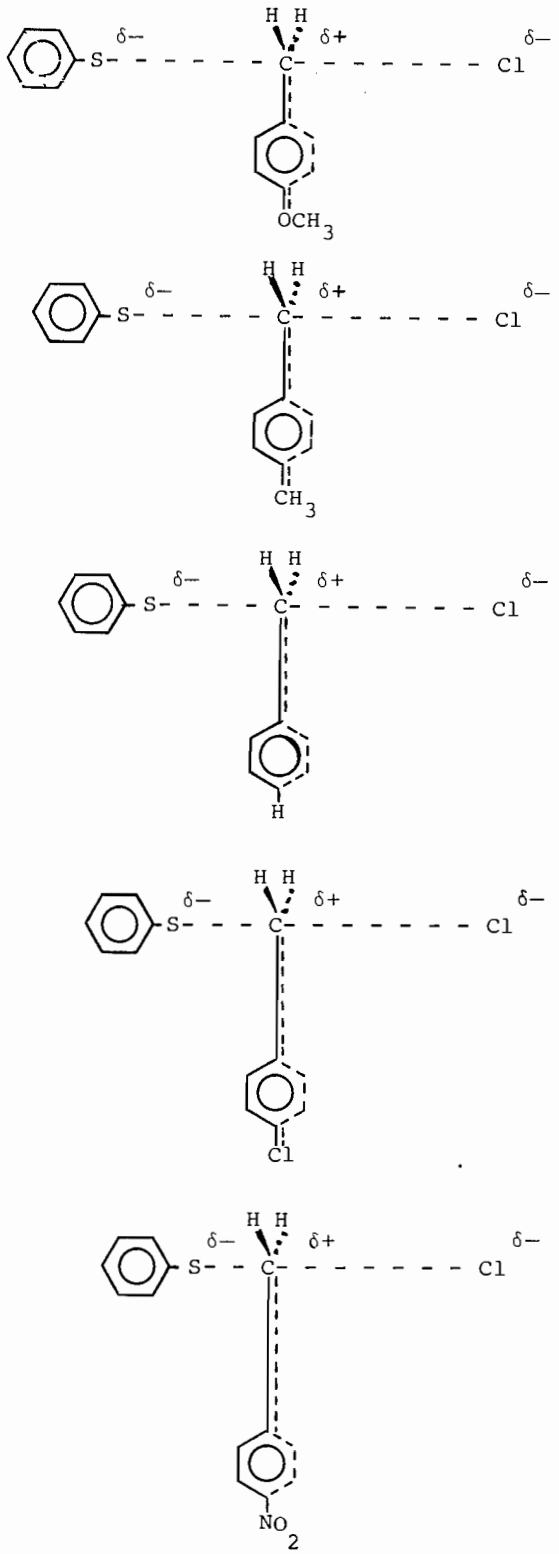


FIG. 6. The effect of changing the *para*-substituent on the transition state structure of the $S_N2$ reactions between thiophenoxide ion and *para*-substituted benzyl chlorides.

determining which reacting bond will be altered by a change in substituent. In fact, it is proposed that a change in the substituent on the α carbon will affect the length of the weaker reacting bond but will have considerably less or no effect on the stronger reacting bond in an $S_N2$ transition state. An examination of the chlorine isotope effects for other reactions supports this suggestion.

Reppond (26) studied the reactions of *para*-substituted benzyl chlorides with various nucleophiles in DMF and in 97% aqueous methanol and found that changing the substituent from *p*-$CH_3$ to *p*-$NO_2$ led to a significant decrease in the chlorine isotope effect, i.e., it decreased by 0.0013 in both solvents when the nucleophiles were *para*-cyano or *para*-nitrophenoxide ions. Constant chlorine isotope effects were observed in both solvents, however, when the nucleophile was azide ion. This is consistent with the above proposal because the C—Cl bond is weaker than the O—C bond, but stronger than the $N_3$—C bond (40). Grimsrud and Taylor (43) also found that the chlorine isotope effect decreased by 0.0012 as the substituent on the benzene ring was changed from *p*-$OCH_3$ to *p*-$NO_2$ in the reactions between *para*-substituted benzyl chlorides and phenoxide ion in methanol. Again, the weaker C—Cl bond changed when the substituent on the α carbon was altered. In addition, Hill and Fry (44) found that the chlorine isotope effect decreased by 0.0021 when the substituent on benzyl chloride was changed from *p*-$CH_3O$ to *p*-$NO_2$ for the reactions with cyanide ion and thiosulfate ion but remained constant for the solvolysis reactions in 80% aqueous dioxane. These results are expected because the NC—$C_\alpha$ and O—$C_\alpha$ bonds are stronger than the C—Cl bond, whereas the new $H_2\overset{+}{O}$—$C_\alpha$ bond is weaker than the $C_\alpha$—Cl bond (41). Grimsrud (1) also found constant chlorine isotope effects in the reactions of *para*-substituted benzyl chlorides with iodide ion, *n*-butylthiolate, and thiophenoxide ion. This also is consistent with the bond-strength hypothesis because both the I—C and the S—C bonds are weaker than the C—Cl bond. The one exception to this rule is the reaction series between *para*-substituted benzyl chlorides and methoxide ion in methanol, where essentially constant chlorine isotope effects are observed (1). This may be due to the fact that the attacking nucleophile is methanol. If this occurred, the new $CH_3$—$\overset{+}{O}$(H)—$C_\alpha$ bond would be the weakest bond in the transition state and the C—Cl transition state bond, and thus the chlorine isotope effects, should not be affected by a change in substituent.

In fact, all but one set of results are consistent

Can. J. Chem. Downloaded from www.nrcresearchpress.com by 210.87.254.40 on 09/06/12
For personal use only.

with the bond strength postulate. Thus it is proposed that adding a more electron withdrawing substituent to the benzene ring of the substrate will lead to a transition state where the weakest reacting bond is shorter, the conjugation between the benzene ring and the α carbon is reduced, and the stronger reacting bond has not been altered significantly.

### Comparison of the experimental results and theoretical predictions

Once the actual transition state structures had been determined, the effect of changing a substituent at the α carbon could be compared with the theoretical predictions based on Thornton's reacting bond rule (50) and More O'Ferrall's energy surface (6, 51). According to Thornton's rule, the overall effect of a $S_N2$ reaction is comprised of the substituent effect on the perpendicular and the parallel vibrations of the transition state. For the perpendicular effect, introducing a more electron withdrawing substituent to the α carbon should lead to a tighter transition state with shorter S--C and C--Cl bonds. A more electron withdrawing substituent makes an increase in the parallel vibration easier for the S--C bond but more difficult for the C--Cl bond and no change in structure is predicted. Thus the overall effect is to shorten the S--C and C--Cl transition state bonds. This is obviously in discord with the experimental results because the C--Cl bond length is substituent independent. However, Thornton predicts that the parallel effect can be important when the two reacting bonds have different strengths. In these cases, Thornton states that the parallel effect will be determined from the substituent effect on the stronger reacting bond. Since the S—$C_\alpha$ bond is weaker (59 kcal/mol) than the $C_\alpha$—Cl bond (69 kcal/mol), the substituent effect on the parallel vibration will be determined from its effect on the $C_\alpha$---Cl bond. Since a more electron withdrawing substituent will make the C---Cl bond more difficult to stretch, shorter S--C and longer C--Cl transition state bonds are predicted. If the substituent effects on the perpendicular and parallel vibrations are equal, adding a more electron withdrawing substituent should lead to the changes in transition state structure that are observed experimentally, i.e., the transition state should have a shorter S---$C_\alpha$ and an unchanged $C_\alpha$---Cl bond. Although the experimental results are consistent with an equal parallel and perpendicular effect, this explanation seems surprising because the bond strengths only differ by 10 kcal/mol.

It is interesting that this approach also leads to the observed behaviour if one considers an $S_N2$ reaction where the nucleophile – α-carbon bond is stronger than the α-carbon – leaving group bond, e.g., the reaction between phenoxide ion and benzyl chloride. In this case, the parallel effect would be determined by the nucleophile – α-carbon (C—O) bond, i.e., adding a more electron withdrawing substituent would lead to a transition state with a longer nucleophile – α-carbon bond and a shorter α-carbon – leaving group bond. If the parallel and perpendicular effects are equally important, the overall effect would be little or no change in the nucleophile – α-carbon bond and a decrease in the α-carbon – leaving group bond length. In fact, the decreasing chlorine (leaving group) isotope effects found by Reppond (26) and Grimsrud and Taylor (43) in the $S_N2$ reactions between benzyl chlorides and phenoxide ions are consistent with this prediction.

Finally, it is worth noting that this is the only way that the experimental results and the predictions based on Thornton's reacting bond rule can be compatible. This suggests that the force constants of the two bonds and the parallel effect are more important in these $S_N2$ reactions than Thornton and the others predicted.

The More O'Ferrall method of predicting the substituent effect on the transition state structure is based on considering the substituent effect on the energy of the reactants, products, and two hypothetical intermediates: a carbonium ion and a pentavalent carbanion, Fig. 7. The upper curve represents the reaction coordinate for the *para*-nitrobenzyl chloride reaction and the lower curve is the reaction coordinate for the *para*-methoxybenzyl chloride reaction. The transition states for both these reactions are depicted by "b" and "a" respectively. All other transition states lie on the line connecting "a" and "b". This is required because the constant chlorine isotope effects indicate that the $C_\alpha$---Cl bond length (bond order) is the same for all transition states. The points "a" and "b" are drawn so that the $S_\alpha$---C transition state bond orders correspond to those estimated from the Hammett ρ values. This implies that the transition states are all product-like, i.e., they lie above the diagonal joining the two hypothetical intermediates, and are of the DTB type, i.e., they lie below the diagonal connecting the reactants and products.

The substituent effect on the transition state structure is determined by considering the substituent effect on the energies of both intermediates (a perpendicular effect) and the reactants and products (a parallel effect). The overall substituent

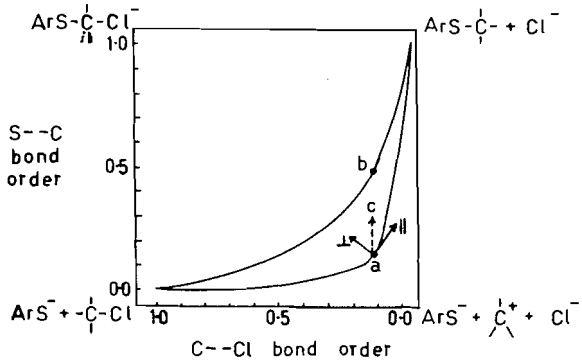


FIG. 7. The More O'Ferrall energy surface for the reactions between thiophenoxide ion and *para*-substituted benzyl chlorides.

effect is given by the resultant of the perpendicular and the parallel effect. Both the perpendicular and the parallel effect can be determined from the substituent effect on the transition state of the *para*-methoxybenzyl chloride reaction. A more electron withdrawing substituent at the α carbon will destabilize the carbonium ion (raise the bottom right corner) but stabilize the negatively charged adduct (lower the top left corner) thus creating a perpendicular shift (⊥) toward the adduct. The parallel effect is determined from the substituent effect on the vibrational frequencies of the C—Cl and S—C bonds in the reactants and products. Changing the substituent on benzyl chloride from $CH_3O$ to $NO_2$ leads to a decrease in the frequency of the C—Cl bond from 680 $cm^{-1}$ to 625 $cm^{-1}$. Thus, a more electron withdrawing substituent at the α carbon weakens the C—Cl bond, increases the energy of the reactant molecule, and raises the bottom left corner of the energy surface. The sulfur – benzyl carbon bond is weaker than the C—Cl bond and thus the same change in substituent ought to have a greater effect on the energy of the S—C bond and of the product molecule. Since the substituent effect should be in the same direction for the S—C and C—Cl bonds, a more electron withdrawing substituent would be expected to increase the energy of the product more than the energy of the reactant, i.e., the upper right corner will be raised more than the lower left corner. As a result, a more electron withdrawing substituent creates a parallel shift (||) toward the product. The unchanged C---Cl bond length and a shorter S---C bond that is actually observed experimentally (arrow c) is only predicted if the parallel effect is at least as large as the perpendicular effect. Again, the unusual importance of the parallel effect in this series of reactions is required if one is to obtain the experimental results. The authors are unable to rationalize the importance of the parallel effect in this series of reactions.

In conclusion, both Thornton's rule and More O'Ferrall's energy surface method can only predict the substituent effect at the α carbon if the parallel effect is equal to or greater than the perpendicular effect. The results of this study indicate that these theories will have to be modified, perhaps by considering the effect of the strengths of the nucleophile – α-carbon and α-carbon – leaving group bonds and/or the changing conjugation with the benzene ring on the α carbon, before they will be able to predict the substituent effects in $S_N2$ reactions correctly. As presently constituted, the theories do not predict (*i*) the importance of the parallel effect in these $S_N2$ reactions, (*ii*) the substituent effects found in this study nor those found in another detailed study of $S_N2$ transition states (6), nor (*iii*) the different substituent effects on the chlorine isotope effects in the $S_N2$ reactions of benzyl substrates.

## Curved Hammett plots

When *para*-substituted benzyl substrates react with negatively charged nucleophiles, U-shaped Hammett plots are always obtained (2, 16, 18, 39, 52–55). The observation that the minimum in these Hammett plots invariably occurs in the vicinity of the unsubstituted substrate regardless of the leaving group (18), the nucleophile (2), or the solvent (17), indicates that the U-shaped plots are a result of the properties of the substituent on the substrate. The Hammett plot obtained from the rate constants of the reactions between the negatively charged nucleophile, thiophenoxide ion, and *para*-substituted benzyl chlorides at 20°C is normal, i.e., it is U-shaped with a minimum when the *para*-substituent is hydrogen, Fig. 3, curve b.

The curvature of the Hammett plots has been attributed to three factors: (*i*) a change from an $S_N2$ to a carbonium ion $S_N$ mechanism as electron withdrawing substituents are changed to electron donating substituents (16, 56, 57); (*ii*) a change in transition state structure, i.e., a change in the relative importance of bond breaking and bond making in the transition state (2, 18, 53, 54); and (*iii*) a variable resonance effect of the substituents (58). All three explanations for the U-shaped Hammett plots will be considered in the light of the experimental results to determine which of these factors is responsible for the curvature.

Although a change in mechanism from a carbonium ion $S_N$ mechanism to an $S_N2$ mechanism has occurred in some reactions where curved Hammett plots have been found, it is not the explanation for

Can. J. Chem. Downloaded from www.nrcresearchpress.com by 210.87.254.40 on 09/06/12
For personal use only.

Can. J. Chem. Downloaded from www.nrcresearchpress.com by 210.87.254.40 on 09/06/12
For personal use only.

the curved Hammett plot in the reactions between thiophenoxide ion and *para*-substituted benzyl chlorides. The second order kinetics and small Hammett ρ values show that the S--C bond formation occurs in the transition state of the rate-determining step of the reaction. The large chlorine isotope effects demonstrate that the C---Cl bond is also breaking in the transition state of the rate-determining step. Since the S---C bond formation and the C---Cl bond rupture both occur in the slow step of the reaction, all of these reactions occur by an $S_N2$ mechanism. As a result, the curved Hammett plot observed for these reactions cannot be caused by a change in mechanism.

The curvature of the Hammett plots has also been attributed to changes in the relative amounts of bond formation and bond rupture in the transition state. The rationale for curvature follows. If the S---$C_\alpha$ bond order exceeds the $C_\alpha$---Cl bond order in the transition state (a product-like transition state), the α carbon will be less positively charged in the transition state than it was in the initial state. The reaction will be accelerated by electron withdrawing substituents and a positive ρ value (the slope of the log $(k/k_0)$ versus σ curve is positive) would be observed. For the reactant-like transition states, on the other hand, the α carbon will be more positively charged in the transition state because the electron density lost from the α carbon when the $C_\alpha$---Cl bond is weakened is not fully replaced by the partial formation of the S---$C_\alpha$ bond. In this case, the reaction will be accelerated by electron donating substituents and a negative ρ value (slope) would be observed. Thus, the Hammett plot should have a negative slope (ρ value) when electron donating substituents are present and the transition states are reactant-like, and a positive slope and product-like transition states when the substituents are electron withdrawing.

Three pieces of evidence suggest that this is not the explanation for the curved Hammett plot. First, the Hammett ρ values for substitution in the thiophenoxide ion suggest that the S---$C_\alpha$ bond orders range from approximately 0.13 to 0.48, Table 7, while the chlorine isotope effects indicate that the $C_\alpha$---Cl bond order is approximately 0.12 in all the transition states. Thus, the S---$C_\alpha$ bond order is greater than the $C_\alpha$---Cl bond order for all the substituents and all of the transition states are product-like. Obviously, the curved Hammett plot cannot be a result of changing from a reactant-like to a product-like transition state.

This conclusion is supported by an analysis of the enthalpies of activation. Even if one assumes that the S--$C_\alpha$ and $C_\alpha$---Cl transition state bond orders based on the Hammett ρ values and the chlorine isotope effects are wrong, and that the transition state does change from reactant-like when the *para*-substituents are $CH_3O$ and $CH_3$ to product-like when the substituents are Cl and $NO_2$, there would be a gradual increase in the total bonding to the α carbon as a more electron withdrawing substituent was added to the substrate. This gradual increase in bonding should lead to a gradual decrease in $\Delta H^{\ddagger}$ and, in fact, this is observed, Table 7. However, the changes that occur in the rate constants when the substituents are varied, i.e., the cause of the curvature in the Hammett plot, do not parallel the changes in the enthalpy of activation. Since the curved Hammett plot does not correlate with the enthalpies of activation which reflect the increase in the relative importance of bond making over bond breaking, it must be concluded that the curved Hammett plot is not a result of the changes in the relative importance of bond formation and bond rupture in the transition state.

Finally, if the curved Hammett plots were a result of changing the transition state structure from reactant-like to product-like, the position of the minimum in the Hammett plot should shift away from the reaction where the *para*-substituent is hydrogen when different nucleophiles, different leaving groups, and/or different solvents are used, i.e., since changes in the nucleophile, leaving group, or solvent would alter the structure of the transition state, the change from a reactant-like to a product-like transition state (the minimum) should occur when substituents other than hydrogen are present. Since the minimum in the U-shaped Hammett plots invariably occurs when the substituent is hydrogen, a change from reactant-like to product-like transition states cannot be the cause of the curvature in the Hammett plots.

The remaining possibility is that the curved Hammett plot is a result of a variation in the resonance effect. Young and Jencks (58) have demonstrated that the curved Hammett plot observed in the reversible reactions of bisulfate ion with *para*-substituted acetophenones can be attributed to a changing balance between the resonance and polar effects for different substituents. By using the modified Yukawa–Tsuno equation, the authors separated the polar and resonance effects of each substituent and evaluated the contribution of these effects to the reaction rate, e.g., the electron donating substituents ($p$-$CH_3O$, $p$-$CH_3$) stabilize the transition state mainly through a resonance

Can. J. Chem. Downloaded from www.nrcresearchpress.com by 210.87.254.40 on 09/06/12
For personal use only.

effect whereas electron withdrawing substituents, such as $p$-$NO_2$, stabilize the transition state through a polar effect. An analysis of the results obtained in the benzyl chloride – thiophenoxide ion reaction show that the variable resonance effect of the substituents is responsible for the curvature in the Hammett plots. A good linear correlation between the rate constants and the resonance and polar contributions of the substituents was obtained when the modified Yukawa–Tsuno equation was applied to the rate constants obtained in this study, Fig. 3a. This confirmed that the curved Hammett plot observed in this reaction series is also a result of the resonance stabilization of the transition state by electron donating substituents on the benzene ring, and not of a change in mechanism or the relative importance of bond making and bond breaking in the transition state.

This explanation for the curvature is attractive for other reasons.

(*i*) When the modified Yukawa–Tsuno equation was applied to many $S_N2$ reactions of benzyl substrates with negatively charged nucleophiles, a good linear relationship was found (2, 39, 54). Thus, this explanation of the curved Hammett plots is general, i.e., it explains why curved Hammett plots are observed regardless of the nucleophile, the solvent, or the leaving group.

(*ii*) It relates the curvature of the Hammett plot to the individual properties of the substituents, i.e., it explains why the change in the slope is invariably around $p$-H. In the reactions of benzyl substrates with negatively charged nucleophiles, the upward curvature of the Hammett plot for electron withdrawing substituents occurs because transition states are stabilized by electron withdrawal through the polar effect. The α carbon in these reactions is less positively charged in the transition state than in the substrate because the decrease in the charge density on the α carbon that occurs when the C---Cl bond is weakened is more than compensated by charge density from the formation of the nucleophile – α-carbon bond.

The transition states with electron donating substituents are stabilized by a large resonance effect between the substituent and the benzene ring. In these cases, the electron density donated by resonance reduces the positive charge on the α carbon and stabilizes the transition state. As a result, these compounds react faster than the unsubstituted substrate and a U-shaped Hammett plot is observed. Since the change between electron donating (a strong resonance effect) and electron withdrawing substituents (a strong polar effect) occurs at hydrogen, this is where the minimum occurs in the Hammett plots.

(*iii*) It explains why linear Hammett plots are observed in $S_N2$ reactions where the resonance effect is absent (59, 60).

## Conclusions

The results of this study have shown that adding a more electron withdrawing substituent to the benzene ring in the $S_N2$ reactions between *para*-substituted benzyl chlorides and thiophenoxide ion leads to a transition state with a shorter S--$C_\alpha$ bond, less conjugation between the benzene ring and the α carbon, and virtually no change in the $C_\alpha$---Cl bond. The magnitude of the isotope effects and Hammett ρ values also suggest that the transition states are loose, and product-like.

The results of this and other studies have led the authors to conclude that the strengths of the nucleophile – α-carbon and α-carbon – leaving group bonds play an important role in determining substituent effects on transition state structure. The results suggest that the weaker reacting bond will be shortened and the conjugation reduced but that there will be little or no change in the stronger reacting bond in an $S_N2$ transition state when a more electron withdrawing group is added to the benzene ring of a benzyl compound.

A comparison of the results and the substituent effects predicted by Thornton's reacting bond rule and the More O'Ferrall energy surface method suggests that the parallel effect is of equal or greater importance than the perpendicular effect. This had not been predicted by these theories and it appears that this factor, as well as the strengths of the reacting bonds and the effect of conjugation with the α carbon, will have to be considered before these theories can predict the substituent effects in $S_N2$ transition states correctly.

These studies also suggest that the magnitude of the secondary α-deuterium kinetic isotope effect is significantly lower when conjugation between the aryl group and the α carbon is more important in the transition state. This means one must be careful in using the magnitude of these isotope effects to determine transition state structure in reactions where conjugation with the α carbon is possible.

Finally, this study has shown that the U-shaped Hammett plots observed when negatively charged nucleophiles react with benzyl compounds in $S_N2$ reactions are caused by a variation in the importance of resonance and polar effects of the substituents and not by a change in mechanism or the

Can. J. Chem. Downloaded from www.nrcresearchpress.com by 210.87.254.40 on 09/06/12
For personal use only.

relative importance of bond formation and bond cleavage in the transition state.

## Experimental

*Preparation of materials*

All but one of the undeuterated *para*-substituted benzyl chlorides were commercially available. Each substrate was further purified by vacuum distillation or by recrystallization. The *para*-methoxybenzyl chloride was synthesized by treating an etherial solution of *para*-methoxybenzyl alcohol with concentrated hydrochloric acid (61). The pure product was unstable. As a result, it was stored in dry diethyl ether and distilled under reduced pressure immediately before use. All the deuterated benzyl chlorides, except the *para*-nitrobenzyl chloride, were synthesized by reducing the *para*-substituted methyl benzoates to the alcohols with lithium aluminum deuteride (62). The *para*-methyl and *para*-chlorobenzyl-1,1-$d_2$ alcohols were converted into the chloride with $PCl_5$ (63). The *para*-methoxybenzyl-1,1-$d_2$ alcohol was treated with concentrated hydrochloric acid in ether (61). Benzyl-1,1-$d_2$ chloride was prepared by treating benzyl-1,1-$d_2$ alcohol with Lucas reagent (62). The *p*-nitrobenzyl-1,1-$d_2$ chloride was prepared by nitrating benzyl-1,1-$d_2$ chloride with nitric acid in the presence of acetic anhydride (64).

Twenty grams of fuming nitric acid ($d$ = 1.5) was added slowly with stirring to 30 g of freshly distilled acetic anhydride at 5°C. The temperature of the solution was allowed to rise to 20°C and 5.0 g (0.04 mol) of benzyl-1,1-$d_2$ chloride was added dropwise. The temperature was kept at 20°C during the addition by adjusting the rate of addition and cooling. After all the benzyl-1,1-$d_2$ chloride had been added, the reaction mixture was stirred 8 h at room temperature and then poured onto 100 g of ice. The organic layer was separated and the aqueous layer was extracted with three 50-mL portions of ether. The ether extracts were combined with the organic layer, washed ten times with water, and then dried overnight with anhydrous magnesium sulfate. After the ether had been removed on the rotary evaporator, a distillation yielded 5.84 g of *para*-nitrobenzyl-1,1-$d_2$ chloride (bp 93–97°C at 1 Torr). The product was recrystallized once from methanol and twice from *n*-hexane to give 2.0 g (29%) of *para*-nitrobenzyl-1,1-$d_2$ chloride, mp 72.5–73.5°C. A mass spectrometric analysis at low ionizing voltage showed that the product was 97.2% dideuterated (98.6% deuterated) at the α carbon. The mass spectrometric analysis indicated that all the *para*-substituted benzyl chlorides were between 98.8 and 99.1% deuterated (97.6 to 98.2% dideuterated at the one position) (*vide infra*).

All of the *para*-substituted benzenethiols used in this study were purchased from Aldrich Chemical Company and purified by vacuum distillation. The *p*-Cl and *p*-$CH_3$ benzenethiols were further purified by recrystallization from petroleum ether (bp 60–80°C). The physical properties were in agreement with the literature values. The purified thiols were stored under nitrogen and used within one month.

*Kinetic measurements*

In a typical reaction "extra-dry" nitrogen was bubbled through a mixture of 2 g sodium methoxide and 1.5 L of anhydrous methanol for 0.5 h and then the methanol was distilled under a stream of "extra-dry" nitrogen. Approximately one liter of freshly distilled methanol was transferred into a glove bag. The paraffin oil was removed from approximately 2.7 g of lithium pellets (BDH) by immersing them in petroleum ether. The clean lithium was then transferred to a beaker containing petroleum ether and placed in the glove bag. The glove bag was sealed and purged twice with nitrogen. The oxide layer was removed from the lithium by swirling it in methanol until its surface became lustrous. The purified metal was slowly added to 800 mL of methanol. After the solution had cooled for one hour, two 10-mL samples were removed for titration. The lithium methoxide solution was transferred to a calibrated one-liter Erlenmeyer flask and stoppered tightly. The glove bag was opened and the two 10-mL samples titrated with 0.500 $N$ hydrochloric acid. Finally, sufficient methanol to make the final solution 0.250 $M$ in lithium methoxide was added to the lithium methoxide solution under a nitrogen atmosphere in the glove bag.

Once the correct concentration of lithium methoxide had been obtained, the glove bag was refilled with "extra-dry" nitrogen and a stirring bar and 75 mL of the 0.250 $M$ lithium methoxide solution were introduced into several reaction flasks. All the reaction flasks were stoppered, sealed with parafilm, and stored until they were used in a kinetic run. All the solutions were used within three weeks.

The kinetic runs were carried out in constant temperature baths maintained at 20.00 ± 0.02°C and 30.00 ± 0.02°C. The reactions at 0°C were carried out in a distilled water – ice bath. In a typical reaction, the reaction flask containing the 0.250 $M$ lithium methoxide – methanol solution was allowed to equilibrate at least one hour and then the parafilm seal was removed from the flask and a weighted amount of the nucleophile was introduced under a stream of "extra-dry" nitrogen. The liquid benzenethiols (*p*-H and *p*-$CH_3O$ benzenethiol) were accurately weighed in a gas-tight syringe stoppered with a rubber septum. The syringe and the septum were reweighed after the benzenethiol had been injected into the reaction flask. The weight difference gave the weight of the benzenethiol. The solid benzenethiols (*p*-methyl and *p*-chlorobenzenethiol) were weighed in a small glass vial. The glass vial containing the benzenethiol was simply dropped into the reaction vessel. When the nucleophile had dissolved in the solvent, a weighed amount of the substrate was added under a stream of "extra-dry" nitrogen and the electric timer was activated. The reaction flask was quickly stoppered with a greased adaptor fitted with a serum cap that was shielded from the methanol vapours by a piece of parafilm. The liquid benzyl chlorides (Y = H, $CH_3$, and $CH_3O$) were accurately weighed in a syringe fitted with a rubber septum. The *p*-chlorobenzyl chloride was melted in warm water and then weighed using the same technique. The solid *p*-nitrobenzyl chloride was accurately weighed and then dissolved in 1 mL of anhydrous methanol (distilled under nitrogen) in a small vial. The vial containing this solution was dropped into the reaction vessel. In the *p*-nitrobenzyl chloride reactions 0.253 $M$ lithium methoxide solution was used so that the final solution was 0.250 $M$ in lithium methoxide. Usually, fifteen 2-mL samples were withdrawn from the flask with a 2.5-mL Hamilton gas-tight syringe fitted with a 6 inch needle. The reaction was quenched by injecting each sample into a 25-mL volumetric flask containing approximately 15 mL of 95% ethanol and 4 mL of 0.2–0.3 $N$ sulfuric acid in ethanol. After every sample, "extra-dry" nitrogen was injected into the reaction flask to assure positive pressure inside the vessel and to prevent oxidation of the nucleophile (65). The samples were analyzed on a single-beam Beckman D.U. uv spectrophotometer. After the last sample had been taken, the reaction was left in the bath for ten half-lives, i.e., taken to completion, and then the infinity samples were analyzed.

In the reactions of the *para*-methyl, *para*-hydrogen, and *para*-chlorobenzyl chlorides at 0°C, the reaction flask was removed from the bath and left at room temperature so that these reactions would go to completion in a reasonably short

Can. J. Chem. Downloaded from www.nrcresearchpress.com by 210.87.254.40 on 09/06/12
For personal use only.

time. After ten half-lives at room temperature, the reaction mixture was equilibrated for one hour at 0°C and then the infinity samples were taken.

At least 4 infinity samples were anlyzed for each reaction. The standard deviation for the average infinity absorbance ($A_\infty$) was generally ±0.002. The initial absorbance ($A_0$) was obtained by extrapolating an absorbance versus time plot to the $t = 0$. The maximum possible error of 0.005 in the $A_0$ value did not affect the value of the rate constant.

The nucleophile/substrate ratio was between 1.2 and 2.0 in all of the reactions involving the *p*-$CH_3$, *p*-Cl, and *p*-$NO_2$ benzyl chlorides and the concentrations of the nucleophile and the substrate were adjusted so that the half-life of the reaction was between 40 and 60 min for all of the reactions carried out at 20°C and 30°C and most of the reactions at 0°C. For some of the reactions at 0°C, however, the half-life was longer because the benzylphenyl sulfides were only sparingly soluble in the solvent at 0°C and low concentrations of the substrate had to be used so that the reaction mixtures were homogeneous.

The wavelength and dilution techniques used in studying the reactions were chosen so that two criteria were satisfied, i.e., so that (*i*) the change in absorbance during the reaction was a maximum, and (*ii*) the absorbance at infinity was below 0.80. With one exception, the wavelengths used in this study were between 255 and 270 nm although all of the reactions could have been followed at 265 nm. The reactions between *para*-nitrobenzyl chloride and thiophenoxide ions were monitored at 320 nm.

The second order rate constant was determined from the slope of the linear least-squares line of the log $[c_1 - x]/[c_2 - x]$ versus $t$ plot. $c_1$ is the initial concentration of the thiophenoxide ion and $c_2$ is the initial concentration of the substrate. $x$, the concentration of the substrate (product formed) in "$t$" seconds, is given by $x = c_2\,([A_t - A_0]/[A_\infty - A_0])$ where $A_0$ is the absorbance at $t = 0$, $A_t$ is the absorbance at time "$t$", and $A_\infty$ is the average absorbance at $t$ = infinity. If any kinetic point was more than twice the standard deviation from the least-squares line, the point was rejected and the calculations were repeated. Usually none of the points were rejected. The plots, which extended to between 50 and 80% of completion, were linear and had correlation coefficients greater than 0.999. The average rate constants were obtained from between 4 and 7 kinetic runs.

*Product analysis*

All but one of the *para*-substituted benzyl chlorides reacted with *para*-substituted thiophenoxide ions to give quantitative yields of the appropriate benzylphenyl sulfide in a clean $S_N2$ reaction (1). The $S_N2$ reaction between *para*-methoxybenzyl chloride and *para*-substituted thiophenoxide ions, however, was accompanied by a pseudo first order (solvolysis) reaction giving *para*-methoxybenzylmethyl ether. The percent ether in the product was determined in a gas chromatographic analysis performed on a Varian 3700 gas chromatograph fitted with a flame ionization detector and CDS 111 digital integrator. The injector and detector temperatures were maintained at 220°C and 300°C respectively. The $S_N2$ and solvolysis products in a 10 μL sample were separated by temperature programming an 8 ft × ⅛ in. column of 3% SE-30 on 100/200 mesh gas Chrom Q operating at a flow rate of 7.5 mL/min. The separation was achieved by maintaining the temperature at 100°C for 16 min and then increasing the temperature to 190°C at 80°C/min. The gas chromatograms from the reactions of *para*-methoxybenzyl chloride and *p*-$CH_3O$, *p*-H, and *p*-Cl substituted thiophenoxide ions at 0°C exhibited a very small peak at 13.3 min representing 3 ± 1 percent of the product, followed by 2 large peaks. The minor product in all cases was the *para*-methoxybenzylmethyl ether. The two large peaks were found to be the $S_N2$ product of the reaction and the oxidation product of the *para*-substituted thiophenoxide ion which formed during the work-up (65). The identity of all of the compounds was confirmed by comparing the retention times with authentic samples of each compound (66).

*Deuterium analysis*

The deuterium content of the deuterated *para*-substituted benzyl chlorides was determined in a mass spectrometric analysis at low ionizing voltage. In a typical analysis, the ionizing voltage was reduced until the $M - 1$ peak in the mass spectrum of the undeuterated benzyl chloride disappeared. The average ratio of the heights of the M+1/M peaks for the undeuterated benzyl chloride ($a/b$ in eq. [15]) was obtained by measuring the heights of the M and M+1 peaks from at least twelve different scans of the undeuterated benzyl chloride. The relative amounts of the monodeuterated ($d_1$) and dideuterated ($d_2$) benzyl chloride in the deuterated substrates were determined using the equation

$$[15] \quad H_{M^+} = d_2 + \left(\frac{a}{b}\right) d_1$$

$H_{M^+}$ is the height of the molecular ion peak for the deuterated compound and $d_1$ is equal to the height of the $M - 1$ peak (the molecular ion peak for the monodeuterated compound). The percentage dideuterated benzyl chloride in each deuterated substrate was calculated from at least twelve different scans. These analyses showed that the deuterated *para*-substituted benzyl chlorides were between 97.2 and 98.2 percent dideuterated at the one position. The remaining material was monodeuterated, i.e., no peaks were observed at the *m/e* for the molecular ion of the undeuterated compound.

## Acknowledgements

The authors wish to thank Laurentian University and the Natural Sciences and Engineering Research Council of Canada for the financial support required to complete this study.

1. E. P. Grimsrud. Ph.D. Dissertation, University of Wisconsin, Madison, WI. 1971.
2. R. F. Hudson and G. Klopman. J. Chem. Soc. 1062 (1962).
3. F. P. Ballistreri, E. Maccarone, and A. Mamo. J. Org. Chem. **41**, 3364 (1976).
4. E. C. F. Ko and A. J. Parker. J. Am. Chem. Soc. **90**, 6447 (1968).
5. K. M. Koshy and R. E. Robertson. J. Am. Chem. Soc. **96**, 914 (1974).
6. K. C. Westaway and S. F. Ali. Can. J. Chem. **57**, 1354 (1979).
7. K. M. Koshy, R. E. Robertson, G. S. Dyson, and S. Singh. Can. J. Chem. **54**, 3614 (1976).
8. H. Yamataka and T. Ando. J. Am. Chem. Soc. **101**, 266 (1979).
9. M. P. Friedberger and E. R. Thornton. J. Am. Chem. Soc. **98**, 2861 (1976).
10. J. F. Willey and J. W. Taylor. J. Am. Chem. Soc. **102**, 2387 (1980).
11. C. Beguin and J. J. Delpuech. Bull. Soc. Chim. Fr. 378 (1969).
12. K. Bowden and R. S. Cook. J. Chem. Soc. B, 1529 (1968).
13. C. G. Swain, W. D. Burrows, and B. J. Schowen. J. Org. Chem. **33**, 2534 (1968).

Can. J. Chem. Downloaded from www.nrcresearchpress.com by 210.87.254.40 on 09/06/12
For personal use only.

14. G. KLOPMAN and R. F. HUDSON. Helv. Chim. Acta, **44**, 1914 (1961).
15. E. C. F. KO and K. T. LEFFEK. Can. J. Chem. **48**, 1865 (1970).
16. A. R. STEIN. Tetrahedron Lett. 4145 (1974).
17. R. FUCHS and A. NISBET. J. Am. Chem. Soc. **81**, 2371 (1959).
18. T. THORSTENSON, R. ELIASON, and J. SONGSTAD. Acta Chem. Scand. Ser. A, **31**, 276 (1977).
19. H. F. KOCH and D. B. DAHLBERG. J. Am. Chem. Soc. **102**, 6102 (1980).
20. D. G. GRACZYK, J. W. TAYLOR, and C. R. TURNQUIST. J. Am. Chem. Soc. **100**, 7333 (1978).
21. W. H. SAUNDERS, JR. Chem. Scr. **8**, 27 (1975).
22. L. B. SIMS, A. FRY, L. R. NETHERTON, J. C. WILSON, K. D. REPPOND, and W. S. CROOK. J. Am. Chem. Soc. **94**, 1364 (1972).
23. E. R. THORNTON. Solvolysis mechanisms. Ronald Press, New York. 1964. pp. 199–206.
24. L. B. SIMS, G. W. BURTON, and D. M. BRUBAKER. 173rd American Chemical Society National Meeting, New Orleans, LA. March, 1977.
25. G. W. BURTON, L. B. SIMS, J. C. WILSON, and A. FRY. J. Am. Chem. Soc. **99**, 3371 (1977).
26. K. D. REPPOND. Ph.D. Dissertation, University of Arkansas, Fayetteville, AR. 1974.
27. K. C. WESTAWAY. Can. J. Chem. **56**, 2691 (1978).
28. D. M. BRUBAKER. Ph.D. Dissertation, University of Arkansas, Fayetteville, AR. 1978.
29. L. MELANDER. Isotope effects on reaction rates. Ronald Press, New York. 1960. p. 20.
30. T. B. CRUMPLER and J. H. YOE. Chemical computations and errors. J. Wiley and Sons, Inc., New York. 1940. p. 178.
31. V. J. SHINER, JR. Isotope effects in chemical reactions. A.C.S. Monograph 166. *Edited by* C. J. Collins and M. S. Newman. Van Nostrand Reinhold, New York. 1971. pp. 104–136.
32. E. C. F. KO and K. T. LEFFEK. Can. J. Chem. **49**, 129 (1971).
33. H. HUMSKI, V. SENDIGAREVIC, and V. J. SHINER, JR. J. Am. Chem. Soc. **96**, 6187 (1974).
34. V. J. SHINER, JR., M. W. RAPP, E. A. HALEVI, and M. WOLFSBERG. J. Am. Chem. Soc. **90**, 7171 (1968).
35. J. BRON. Can. J. Chem. **52**, 903 (1974).
36. C. H. GRAY, J. K. COWARD, K. B. SCHOWEN, and R. L. SCHOWEN. J. Am. Chem. Soc. **101**, 4351 (1979).
37. P. R. YOUNG and W. P. JENCKS. J. Am. Chem. Soc. **101**, 3288 (1979).
38. J. HINE. Physical organic chemistry. 2nd ed. McGraw Hill Book Co., New York. 1962. pp. 87–90.
39. R. FUCHS and D. M. CARLTON. J. Org. Chem. **27**, 1520 (1962).
40. R. C. WEAST (*Editor*). Handbook of chemistry and physics. 60th ed. Chemical Rubber Company Press, Boca Raton, FL. 1980. pp. 231–241.
41. K. B. WIBERG. Physical organic chemistry. J. Wiley and Sons, New York. 1964. p. 242.
42. R. O. C. NORMAN. Principles of organic synthesis. Methuen and Co. Ltd., London. 1972. p. 53.
43. E. P. GRIMSRUD and J. W. TAYLOR. J. Am. Chem. Soc. **92**, 739 (1970).
44. J. W. HILL and A. FRY. J. Am. Chem. Soc. **84**, 2763 (1962).
45. K. M. KOSHY, R. E. ROBERTSON, and W. M. J. STRACHAN. Can. J. Chem. **51**, 2959 (1973).
46. A. V. WILLI, C. K. HO, and A. GHANBARPOUR. J. Org. Chem. **37**, 1185 (1972).
47. V. J. SHINER, JR., M. RAPP, and H. R. PINNICK, JR. J. Am. Chem. Soc. **92**, 232 (1970).
48. V. P. VITULLO, J. GRABOWSKI, and S. SRIDHARAN. J. Am. Chem. Soc. **102**, 6463 (1980).
49. V. F. RAAEN, T. JUHLKE, F. J. BROWN, and C. J. COLLINS. J. Am. Chem. Soc. **96**, 5928 (1974).
50. E. R. THORNTON. J. Am. Chem. Soc. **89**, 2915 (1967).
51. J. M. HARRIS, S. G. SHAFER, J. R. MOFFATT, and A. R. BECKER. J. Am. Chem. Soc. **101**, 3295 (1979).
52. J. O. SHRECK. J. Chem. Educ. **2**, 103 (1971).
53. C. G. SWAIN and W. P. LANGSDORF, JR. J. Am. Chem. Soc. **73**, 2813 (1951).
54. K. BOWDEN and R. S. COOK. J. Chem. Soc. B, 1529 (1968).
55. E. C. F. KO and K. T. LEFFEK. Can. J. Chem. **50**, 1297 (1972).
56. C. D. JOHNSON. The Hammett equation. Cambridge University Press. 1973. p. 50.
57. H. ARONOVITCH and A. PROSS. Tetrahedron Lett. 2729 (1977).
58. P. R. YOUNG and W. P. JENCKS. J. Am. Chem. Soc. **101**, 3288 (1979).
59. H. D. HOLTZ and L. M. STOCK. J. Am. Chem. Soc. **87**, 2404 (1965).
60. G. BADDELEY and G. M. BENNETT. J. Chem. Soc. 1819 (1935).
61. R. QUELET and J. ALLARD. Bull. Soc. Chim. Fr. **4**, 1468 (1937).
62. K. C. WESTAWAY and A. N. BOURNS. Can. J. Chem. **50**, 2332 (1972).
63. W. GERRARD. J. Chem. Soc. 741 (1946).
64. C. K. INGOLD and E. H. INGOLD. J. Chem. Soc. 2249 (1928).
65. G. CAPOZZI and G. MODENA. The chemistry of the thiol group. Part 2. *Edited by* S. Patai. J. Wiley and Sons, Interscience. 1974. p. 806.
66. Z. WASZCZYLO. M.Sc. Thesis, Laurentian University, Sudbury, Ont. 1981.

Can. J. Chem. Downloaded from www.nrcresearchpress.com by 210.87.254.42 on 09/06/12
For personal use only.

COMMUNICATION

# Novel prostaglandin $E_2$ derivatives from $PGA_2$

GUSTAVO GARCIA, YVONNE GRILLASCA, AND JOAQUIN TAMARIS
*Facultad de Quimica, Universidad Nacional Autonoma de Mexico*

ANDREW GREENE
*Université Scientifique et Médicale, Grenoble, France*

AND

PIERRE CRABBÉ[1]
*Department of Chemistry, University of Missouri, Columbia, MO 65211, U.S.A.*

Received April 21, 1982

GUSTAVO GARCIA, YVONNE GRILLASCA, JOAQUIN TAMARIS, ANDREW GREENE, and PIERRE CRABBÉ. Can. J. Chem. **60**, 2521 (1982).

An original approach for the synthesis from $PGA_2$ of C-10 substituted $PGE_2$ analogues is reported. A remarkable regio- and cyclo-selective Baeyer–Villiger reaction is described.

GUSTAVO GARCIA, YVONNE GRILLASCA, JOAQUIN TAMARIS, ANDREW GREENE et PIERRE CRABBÉ. Can. J. Chem. **60**, 2521 (1982).

On décrit la synthèse de nouvelles prostaglandines substituées en position 10 par une méthode originale. On rapporte une remarquable réaction d'oxydation de Baeyer–Villiger, qui est simultanément régio-, cyclo- et stéréosélective.

A number of modified prostaglandins have recently been obtained from naturally occurring $PGA_2$ (**1***a*) through chemical (1) and photochemical (2) transformations. In this communication a photochemical preparation from $PGA_2$ of new C-10 derivatives of $PGE_2$ not easily accessible by other routes is described.

Initial pilot reactions were performed with 15*R* $PGA_2$[2] from the marine corals *Plexaura homomalla*. Having established the appropriate reaction conditions, the sequence was applied to $PGA_2$ methyl ester with the 15*S* configuration.[3] $PGA_2$ methyl ester (**1***b*) in methylene chloride containing excess vinyl acetate, at −78°C under nitrogen, was irradiated with a Hanau TQ150 high pressure ultraviolet lamp equipped with a Pyrex filter. A mixture of stereoisomeric cycloadducts (**2***a*) ($[\alpha]_D$ +31° ($CHCl_3$); $\nu_{max}$ (neat): 3450, 1740 $cm^{-1}$, δ (in $CCl_4$, using TMS as a standard): 0.89 (t, 20-Me), 1.93 and 1.97 (s, OAc), 3.6 (s, $CO_2Me$), ca. 5.1–6.3 (m, vinylic H)) was obtained in 87% yield. There is ample precedent for the photochemical cycloaddition to the $\Delta^{10}$-double bond of $PGA_2$ under these conditions (2). No significant amount of any positional isomer, i.e., C-10′-acetoxy derivative, was found (3).

For the subsequent transformations of the cyclobutane ring, the C-15 hydroxyl group had to be appropriately protected. The *tert*-butyldimethylsilyl ether **2***b* ($\nu_{max}$ (neat): 1740 $cm^{-1}$; δ ($CCl_4$): 0.89 (20-Me, 15-*t*-Bu), 1.93 and 1.97 (s, OAc), 3.59 (s, $CO_2Me$), 4.00 (m, $\overset{|}{C}H—O—$), 5.15–5.67 (m, vinylic H); ms *m/e*: 548 ($M^+$), 517 ($M^+ - OMe$), 419 ($M^+ - t$-Bu)), obtained in quantitative yield from the isomeric mixture **2***a* by the usual procedure, proved to be the best of the several protecting groups examined. An essentially identical mixture (**2***b*) was obtained when the *tert*-butyldimethylsilyl ether **1***c*, readily prepared from **1***b*, was irradiated in the presence of vinyl acetate.

Hydrolysis of the C-11′ acetate of compound **2***b* with potassium carbonate in aqueous methanol for 30 min at 20°C gave selectively the corresponding alcohol **2***c*: $[\alpha]_D$ +19° ($CHCl_3$); $\nu_{max}$ (neat): 3450, 1740, 1600 $cm^{-1}$; δ ($CCl_4$): 0.88 (20-Me, 15-*t*-Bu), 3.7 (s, $CO_2Me$), 5.53 (m, *cis* vinylic H), 5.63 (m, *trans* vinylic H). Oxidation of the C-11′-hydroxyl group in **2***c* with pyridinium dichromate in dry methylene chloride (4) afforded the C-10,11 isomeric diketo derivatives in 76% yield: $[\alpha]_D$ −6° ($CHCl_3$); $\nu_{max}$ (neat): 1790, 1740–1735 $cm^{-1}$; δ

[1]Author to whom correspondence may be addressed.

[2]15*R* $PGA_2$ was obtained from the coral collected along the coast of Yucatan peninsula (Mexico).

[3]15*S* $PGA_2$ was collected along the coast of Cuba.

0008-4042/82/192521-03$01.00/0

©1982 National Research Council of Canada/Conseil national de recherches du Canada

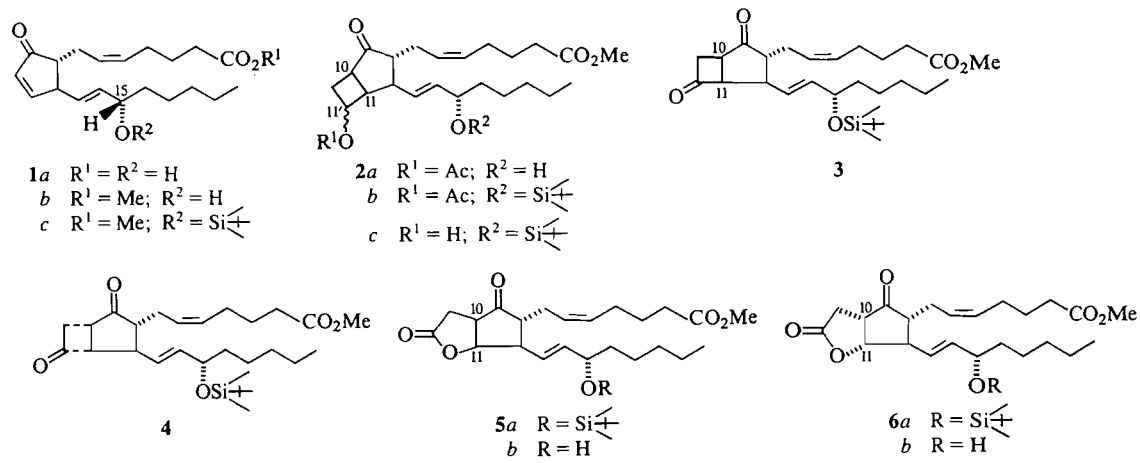


(CCl$_4$): 0.88 (20-Me, 15-*t*-Bu), 3.58 (s, $CO_2Me$), 4.03 (m, CHO—), 5.46 (m, *cis* vinylic H), 5.63 (m, *trans* vinylic H). Preparative tlc separation on silicagel (hexane–AcOEt, 3:1) of these stereoisomers provided 40% of the diketo derivative (**3**) and 60% of its α-isomer (**4**). Individual treatment of the diketones **3** and **4** with 2 equiv. of 30% hydrogen peroxide in aqueous acetic acid (5) at 0°C furnished the corresponding keto lactones **5***a* and **6***a* respectively in ca. 90% yield. A noteworthy feature of the Baeyer–Villiger reaction of these diketones is the apparently complete regio- (and cyclo-) selectivity observed.

The structure and stereochemistry of these bicyclic prostanoid lactones were established on the basis of their spectroscopic and chiroptical properties. The less polar isomer **6***a* displayed: $[\alpha]_D$ −12° ($CHCl_3$); $\nu_{max}$ (neat): 1790, 1740–1735 cm$^{-1}$; δ ($CDCl_3$): 0.89 (20-Me, *t*-Bu), 3.66 (s, $CO_2Me$), 4.2 (m, 15βH), 5.43 (m, *cis* vinylic H), 5.76 (m, *trans* vinylic H); ms *m/e*: 520 ($M^+$). The more polar lactone isomer **5***a* exhibited: $[\alpha]_D$ +2° ($CHCl_3$); $\nu_{max}$ (neat): 1790, 1740–1735 cm$^{-1}$; δ ($CDCl_3$): 0.92 (20-Me, *t*-Bu), 3.66 (s, $CO_2Me$), 4.2 (m, 15βH), 5.43 (m, *cis* vinylic H), 5.76 (m, *trans* vinylic H); ms *m/e*: 520 ($M^+$).

The salient feature of the nmr spectra is the signal associated with the C-11 proton. While in the lactone derivative **5***a* the C-11α proton appears at 5.03 ppm as a pseudo-triplet ($J$ = 4.5 Hz), in the lactone isomer **6***a* the 11β proton appears as a doublet of doublets at ca. 4.9 ppm with coupling constants $J_{H_{10,11}}$ = 5 Hz and $J_{H_{11,12}}$ = 8 Hz, thus supporting the γ-lactone stereochemical assignment.

The hydrolysis of both ethers **5***a* and **6***a* could be achieved directly in the acid medium at the end of the Baeyer–Villiger reaction, simply by diluting with water and leaving at room temperature for 2 h. The less polar α-lactone derivative **6***b* presented $\nu_{max}$ (neat): 3450, 1780, 1740 cm$^{-1}$; δ ($CDCl_3$): 0.89 (t, 20-Me), 3.66 (s, $CO_2Me$), 4.1 (m, 15βH), 5.4 (m, *cis* vinylic H), 5.73 (m, *trans* vinylic H); ms *m/e*: 406 ($M^+$). The more polar isomeric lactone **5***b* exhibited: $\nu_{max}$ (neat): 3450, 1780, 1740 cm$^{-1}$; δ ($CDCl_3$): 0.89 (t, 20-Me), 3.66 (s, $CO_2Me$), 4.13 (m, 15βH), 5.4 (m, *cis* vinylic H), 5.75 (m, *trans* vinylic H); ms *m/e*: 406 ($M^+$).

These stereochemical assignments were further supported by the CD curves. The C-10,11β lactone derivative **5***a* displayed an intense negative Cotton effect in the 300 nm region ($[\theta]_{292}$ −12350) (dioxane). Its C-10,11α stereoisomer **6***a* showed a weak negative Cotton effect CD curve in the same region ($[\theta]_{299}$ −4450) (dioxane). Similarly, the 15-alcohol of the β-isomer **5***b* exhibited a much stronger negative CD curve ($[\theta]_{302}$ −8555) (dioxane) than its α-counterpart **6***b* ($[\theta]_{294}$ −4245) (dioxane). These findings are in agreement with previous studies which have shown that C-10,11β cyclo-prostanoids display an intense negative Cotton effect in the 300 nm region (2).

Compound **6***b* is a $PGE_2$ derivative in which formally a C-10 acetic acid chain is cyclized with the C-11α hydroxyl. It is of interest to note that a recent report (6) mentions a Baeyer–Villiger oxidation of a similar system to yield the expected keto-lactone, along with the corresponding carboxymethyl enone resulting from lactone cleavage. Work in progress involves the conversion of $PGA_2$ to other PGE derivatives using this simple photochemical approach.

Can. J. Chem. Downloaded from www.nrcresearchpress.com by 210.87.254.42 on 09/06/12
For personal use only.

**Acknowledgements**

We wish to thank Mr. Antonio Padilla, Laboratorio Antonio Munoz, Ministerio de Salud Publica, La Habana, Cuba, for a sample of $PGA_2$ used in this study. We are indebted to Professor Albert Burgstahler, The University of Kansas, for the CD curves.

1. C. V. GRUDZINSKAS and M. J. WEISS. Tetrahedron Lett. 141 (1973); A. GUZMAN and P. CRABBÉ. Chem. Ind. 635 (1973); A. GUZMAN, M. VERA, and P. CRABBÉ. Prostaglandins, **8**, 85 (1974).
2. P. CRABBÉ, G. A. GARCIA, and C. RIUS. Tetrahedron Lett. 2951 (1972); J. Chem. Soc. Perkin Trans. I, 810 (1973); P. CRABBÉ, E. VELARDE, and G. A. GARCIA. J. Chem. Soc. Chem. Commun. 480 (1973); P. VOGEL and P. CRABBÉ. Helv. Chim. Acta, **56**, 557 (1973); G. A. GARCIA, L. A. MALDONADO, and P. CRABBÉ. *In* Prostaglandin research. *Edited by* P. Crabbé. Academic Press, New York. 1977. Chapt. 7. p. 269.
3. E. J. COREY, J. D. BASS, R. LE MAHIEU, and R. B. MITRA. J. Am. Chem. Soc. **86**, 5570 (1964).
4. E. J. COREY and G. SCHMIDT. Tetrahedron Lett. 399 (1979).
5. E. J. COREY and T. RAVINDRANATHAN. Tetrahedron Lett. 4753 (1971); P. A. GRIECO. J. Org. Chem. **37**, 2363 (1972); M. J. BAGDANAWICZ, T. AMBELANG, and B. M. TROST. Tetrahedron Lett. 923 (1973).
6. HSING-JANG LIU and P. CHI-LIN YAO. Can. J. Chem. **55**, 822 (1977).

Can. J. Chem. Downloaded from www.nrcresearchpress.com by 210.87.254.42 on 09/06/12
For personal use only.

# Formation and decomposition of radical anions. A theoretical study

HUGO VILLAR AND EDUARDO A. CASTRO[1]

*INIFTA, Sección Química Teórica, Sucursal 4 – Casilla de Correo 16, La Plata 1900, Argentina*

AND

ROBERTO A. ROSSI

*Departamento de Química Orgánica, Facultad de Ciencias Químicas, Universidad Nacional de Córdoba, 5000 Córdoba, Argentina*

Received August 26, 1981[2]

HUGO VILLAR, EDUARDO A. CASTRO, and ROBERTO A. ROSSI. Can. J. Chem. **60**, 2525 (1982).

A theoretical study of the reaction coordinate for the coupling of phenyl radical with methyl anion, chloride and fluoride ions to yield the corresponding radical anion is carried out. In this process, σ and σ* MO's associated to the new bond are formed. The σ* MO is the lowest lying of the system for the radical anion formed in the coupling with chloride ion. With methyl anion and fluoride ion, σ and σ* MO's are also formed, but before they reach the equilibrium distance of the radical anion intermediate, the π* MO equals its energy with the incipient σ*, and from there on to the equilibrium distance, the odd electron stays in the π* MO.

HUGO VILLAR, EDUARDO A. CASTRO et ROBERTO A. ROSSI. Can. J. Chem. **60**, 2525 (1982).

On a réalisé une étude théorique des coordonnées de la réaction de couplage du radical phényle avec l'anion méthyle, les ions chlorure et fluorure qui conduit à l'anion radicalaire correspondant. Dans ce processus, il se forme des OM σ et σ* associés à la nouvelle liaison. L'orbitale moléculaire σ* est la plus basse orbitale liante du système d'anion radicalaire formé lors du couplage avec l'ion chlorure. Dans le cas de l'anion méthyle et de l'ion fluorure, il se forme également des OM σ et σ* mais avant qu'elles n'atteignent la distance d'équilibre de l'anion radicalaire intermédiaire, l'énergie de l'OM π* naissante devient égale à celle de l'OM σ* naissante et à partir de ce point jusqu'à la distance d'équilibre, l'électron célibataire demeure dans l'OM π*.

[Traduit par le journal]

## I. Introduction

During the last few years there has been a growing interest towards the chemical study of radical anions (1–4), because of their remarkable importance in organic electrochemistry and monomolecular nucleophilic substitution reactions. It is a well known fact that when radical anions of aromatic systems are attached to a nucleofugal group, they decompose to yield an aromatic radical and an anion corresponding to the nucleofugal group (5). The occurrence of such a reaction (6) as well as the decomposition rate depend to a great extent on the nature of the aromatic substrate, the presence of another substituent, and the position of the leaving group with respect to the substituents (2, 7).

Many experimental results indicate that during dissociation, the odd electron is transferred from a π* MO to a σ* MO (9, 10). This explanation would be an acceptable one when the σ* MO is associated to the nucleofugal – aromatic substrate bond, and that such a bond would be unstable. On the contrary, when the odd electron is located in a π* MO, the unstableness would spread over the whole molecule in general, and in a few cases, located on a particular bond (10). Consequently, the stable form of the radical anion could be assigned when the odd electron is in a π* MO, and its decomposition would take place by way of a transition to a σ* MO (11, 12). The coupling process (8) must correspond to an identical coordinate reaction as that of the decomposition (owing to the microscopic reversibility principle). Up to now, radical anions have been studied from a theoretical point of view by means of Hückel-like methods combined with PMO analysis (10). Then, as a natural following step, we deem appropriate to apply a somewhat more elaborate method which allows us to obtain a point-by-point information about the reaction coordinate, for elucidating the reasons responsible for the behavior of radical anions with respect to their relative stability as well as the correlation of their decomposition rates.

The purpose of this paper is to report the calculations of the reaction coordinate by INDO and CNDO/2 methods, for the coupling of phenyl radical with methyl, fluoride, and chloride anions. Theoretical results are then discussed in a comparative way with available experimental data.

## II. Calculation procedure

The molecular orbital calculations were made by the INDO method (13, 14) for toluene and fluorobenzene radical anions, while for chlorobenzene

[1]To whom all correspondence should be addressed.

[2]Revision received January 4, 1982.

0008-4042/82/202525-03$01.00/0

©1982 National Research Council of Canada/Conseil national de recherches du Canada

Can. J. Chem. Downloaded from www.nrcresearchpress.com by 210.87.254.105 on 09/06/12
For personal use only.

Can. J. Chem. Downloaded from www.nrcresearchpress.com by 210.87.254.105 on 09/06/12
For personal use only.

radical anion the CNDO/2 method was chosen because of computer space limitations. We started the analysis of the reaction coordinate for $(Ph—CH_3)^{-\cdot}$ by determining the minimum total energy for each one of the reactants, i.e. $Ph^{\cdot}$ and $CH_3^-$. For the methyl anion we found an equilibrium distance $d_{C—H} = 1.130$ Å and a planar conformation. The equilibrium distances for $Ph^{\cdot}$ were determined by keeping up the $C_2$ symmetry axis. The values obtained are (see Fig. 1) $a = 1.370$ Å; $b = 1.405$ Å; $c = 1.380$ Å; and $d_{C—H} = 1.080$ Å. The reaction coordinate was simulated starting from the equilibrium values for the isolated species at an infinite distance. Then, from a value of 8 Å for the distance $d_{Ph^{\cdot}—CH_3}$ a linear variation of the angle HCH of the $CH_3$ group with $d_{C—C}$ was made up to reach the equilibrium distances in the radical anion. We give the potential curve in Fig. 2. We can see that the variation is regular, so we believe that the chosen mimicked reaction coordinate is a reasonable one. Figure 3 shows the energy of the frontier orbitals as functions of the reaction coordinate. For the radical anions $(Ph—F)^{-\cdot}$ and $(Ph—Cl)^{-\cdot}$ we simulated the reaction coordinate in a similar fashion, and potential curves (not reported here) are equivalent to that shown in Fig. 2. The energy of frontier orbitals as a function of the C—X distance for $(Ph—F)^{-\cdot}$ and $(Ph—Cl)^{-\cdot}$ are displayed in Figs. 4 and 5.

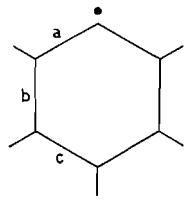


FIG. 1. Geometric parameters for phenyl radical.

## III. Analysis of results and discussion

These results demonstrate quantitatively that in the process of coupling of an aryl radical with a nucleophile, σ and σ* MO's are formed. As the reactants approach each other, σ decreases and σ* increases their energies, and two different situations can be found. If σ* is the lowest antibonding MO, such as in the coupling of $Ph^{\cdot}$ and $Cl^-$, the radical anion will be unstable and it can revert to the starting molecule. On the other hand, in the coupling of $Ph^{\cdot}$ with methyl anion or fluoride ion, σ and σ* MO's are also formed, but before reaching the equilibrium distances of the radical anions, the π* MO equals its energy with the incipient σ* MO, and from there on, σ* is always higher in energy than the π* MO, so that the radical anion formed is

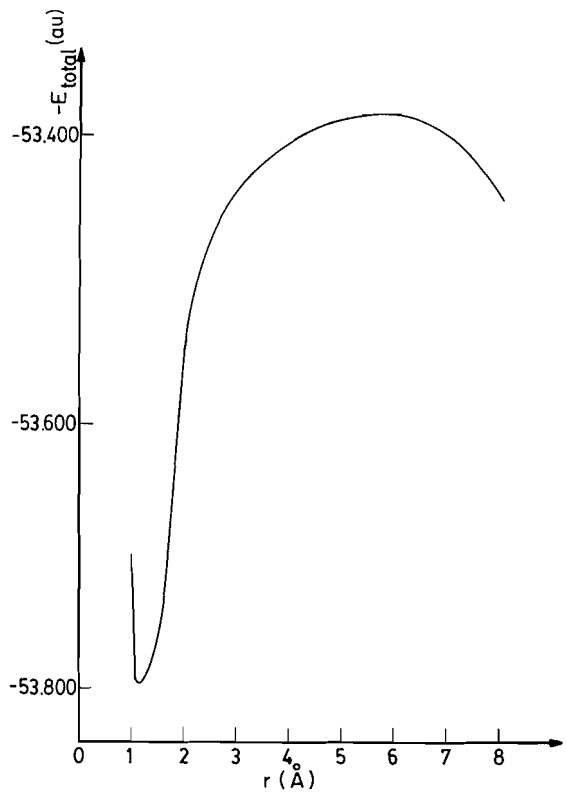


FIG. 2. Total energy curve for the $(Ph—CH_3)^{-\cdot}$ system as a function of the reaction coordinate.

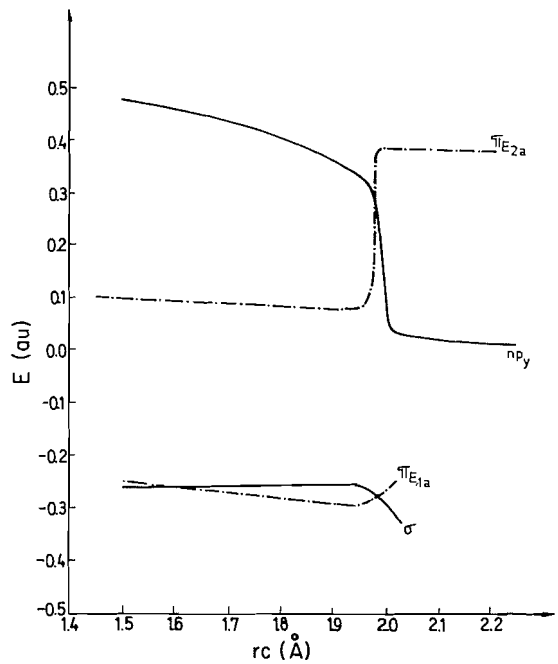


FIG. 3. Variation of the frontier orbital energies as a function of the reaction coordinate for the $(Ph—CH_3)^{-\cdot}$ system.

Can. J. Chem. Downloaded from www.nrcresearchpress.com by 210.87.254.105 on 09/06/12
For personal use only.

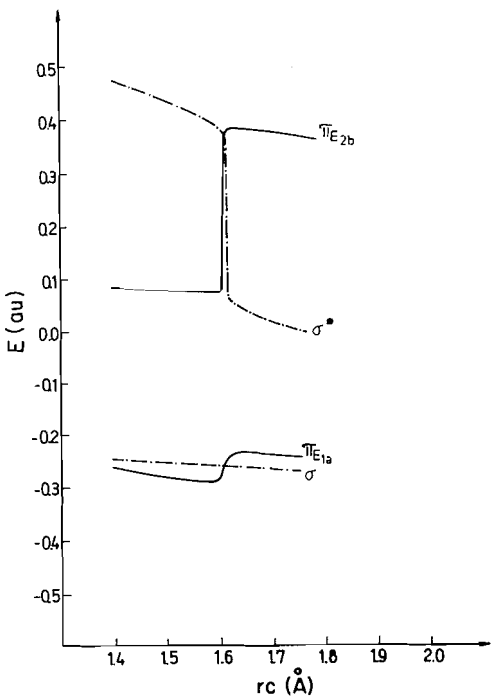


FIG. 4. Variation of the frontier orbital energies along the reaction coordinate for the $(Ph—F)^{-\cdot}$ system.

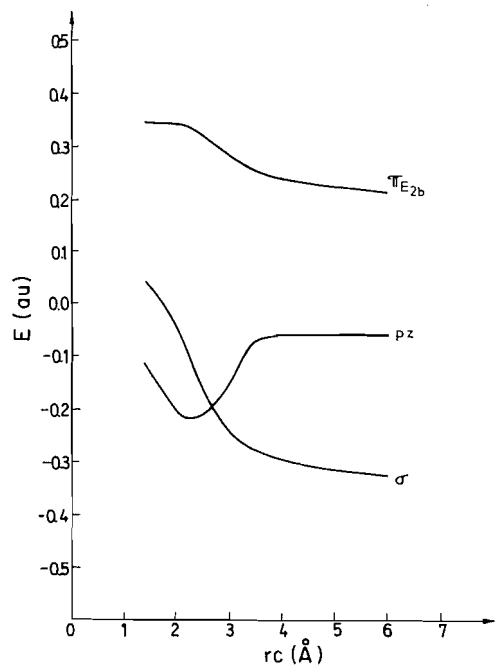


FIG. 5. Variation of the frontier orbital energies as a function of the reaction coordinate for the $(Ph—Cl)^{-\cdot}$ system.

a $\pi^*$ one. However, there is a difference between these two radical anions. Toluene radical anion does not decompose into reactants, but fluorobenzene radical does (5). From Figs. 3 and 4 we can see that the distance of the orbital crossing is farther from equilibrium in toluene than in the fluorobenzene radical anion. What eventually happens is that by internal conversion, the odd electron is transferred from the $\pi^*$ MO to the $\sigma^*$ MO, and this process is more probable the shorter the orbital crossing distance from the equilibrium. Vibrations of the radical anion provide the transfer mechanism between these orthogonal orbitals. That is to say, vibrations lower the symmetry momentarily and allows the states to mix (12). These results are in agreement with those found in $S_{RN}1$ reactions. Carbanionic nucleophiles couple with aryl radicals in a very efficient way, but coupling reaction with halide ions is not known, although the reverse reaction (5) is well known. The relative energies of the $\sigma^*$ and $\pi^*$ MO's in the coupling process in the $S_{RN}1$ mechanism are important not only with the halide ions, but also with nucleophiles derived from Te (15), As (16), and Sb (17), in which reversible coupling with aryl radicals leads to the scrambling of aryl rings. These results were ascribed to the low lying $\sigma^*$ MO's of the carbon–nucleophile bond formed (10).

1. E. T. KAISER and L. KEVAN. Radical ions. Interscience, New York. 1968; N. L. HOLY and J. D. MARCUM. Angew. Chem. Internat. Ed. Engl. **10**, 115 (1971); M. SZWARC. Prog. Phys. Org. Chem. **6**, 323 (1968); M. SZWARC. Carbanions, living polymers and electron transfer processes. Interscience, New York. 1968.
2. L. NADJO and J. M. SAVEANT. J. Electroanal. Chem. **30**, 41 (1971); J. GRIMSHAW and J. TROCHA-GRIMSHAW. J. Electroanal. Chem. **56**, 443 (1974); K. ALWAIR and J. GRIMSHAW. J. Chem. Soc. Perkin II, 1811 (1973).
3. E. J. HART and M. ANBAR. The hydrated electron. Wiley, New York. 1979.
4. L. M. DORFMAN. Acc. Chem. Res. **3**, 224 (1970).
5. R. A. ROSSI and J. F. BUNNETT. J. Am. Chem. Soc. **96**, 112 (1974).
6. J. G. LAWLESS and M. D. HAWLEY. J. Electroanal. Chem. **21**, 365 (1969); R. P. VAN DUYNE and C. N. REILLEY. Anal. Chem. **44**, 158 (1971); R. F. NELSON, A. K. CARPENTER, and E. T. SEO. J. Electroanal. Soc. **120**, 206 (1973).
7. G. J. GORES, C. E. KOEPPED, and D. E. BARTAK. J. Org. Chem. **44**, 380 (1979).
8. J. F. BUNNETT. Acc. Chem. Res. **11**, 413 (1978).
9. H. RIEDERER, J. HÜTTERMANN, and M. C. R. SYMONS. J. Chem. Soc. Chem. Commun. 313 (1978).
10. R. A. ROSSI. J. Chem. Educ. In press.
11. M. C. R. SYMONS. Pure Appl. Chem. **53**, 223 (1981).
12. R. G. PEARSON. Symmetry rules for chemical reactions. Wiley, New York. 1976. Chapt. 5. p. 440.
13. J. A. POPLE and D. L. BEVERIDGE. Approximate molecular orbital theory. McGraw-Hill, New York. 1970.
14. P. A. DOBOSCH. Quant. Chem. Prog. Exchange No. 141 (1971), Indiana University.
15. A. B. PIERINI and R. A. ROSSI. J. Org. Chem. **44**, 4667 (1979).
16. R. A. ROSSI, R. A. ALONSO, and S. M. PALACIOS. J. Org. Chem. **46**, 2489 (1981).
17. R. A. ALONSO and R. A. ROSSI. J. Org. Chem. **47**, 77 (1982).

# Fittig bislactones in cyclopentenone synthesis: short synthesis of methylenomycin B

GEORGE M. STRUNZ AND G. SANKAR LAL

*Maritimes Forest Research Centre, Canadian Forestry Service, Department of the Environment, P.O. Box 4000, Fredericton, N.B., Canada E3B 5P7*

Received May 18, 1982

GEORGE M. STRUNZ and G. SANKAR LAL. Can. J. Chem. **60**, 2528 (1982).

Treatment of the Fittig bislactone, 3-(1,1-dihydroxypropyl)glutaric acid di-γ-lactone, with methyllithium, followed by alkali, afforded 5-carboxymethyl-2,3-dimethylcyclopent-2-en-1-one. This compound on decarboxylation with lead tetraacetate afforded the antibiotic methylenomycin B.

GEORGE M. STRUNZ et G. SANKAR LAL. Can. J. Chem. **60**, 2528 (1982).

Le bislactone de Fittig, le di-γ-lactone de l'acide glutarique 3-(1,1-dihydroxypropyl), réagit avec le méthyllithium suivi par l'alkali pour fournir carboxyméthyl-5-diméthyl-2,3-cyclopentèn-2-one-1. La décarboxylation oxidative de ce composé par le tétraacétate de plomb fournit l'antibiotique méthylenomycine B.

Can. J. Chem. Downloaded from www.nrcresearchpress.com by 210.87.254.105 on 09/06/12
For personal use only.

The formation of bislactones of structure **1** by acylative decarboxylation of tricarballylic acid through the action of acid anhydrides was reported by Rudolf Fittig more than eighty years ago (1).[1] The reaction, which appears to be formally analogous to the more familiar Dakin–West reaction discovered later (2, 3), has been usefully exploited in natural product synthesis (4). Borohydride reduction under alkaline conditions of a Fittig bislactone (**1**, R = $C_8H_{17}$) gave *trans*-tetrahydro-2-octyl-5-oxo-3-furanacetic acid, a key intermediate in the synthesis of *dl*-avenaciolide by Parker and Johnson (4).

The arrangement of functionality in the bislactones is such that, for reaction with appropriate carbanion species, they might be regarded as masked enol lactones possessing a protected acetic acid side chain. These compounds could thus be potential precursors of 1,4-diketones, hence of substituted cyclopentenones, cf. refs. 5–7.

In this paper we report the realization of such a cyclopentenone synthesis, and its application in a short synthesis of the antibiotic methylenomycin B (8, 9), previously synthesized by Jernow *et al.* (9).[2]

Rather surprisingly, the reaction of propionic anhydride with tricarballylic acid did not give satisfactory yields of the required precursor **1** (R = $C_2H_5$) under conditions where acetic anhydride readily afforded the lower homologous bislactone, cf. refs. 3, 4. The desired conversion could, however, be effected in acceptable yield (53%) with catalysis by pyridine.

Treatment of **1** (R = $C_2H_5$) with slightly more than one equivalent of methyllithium gave a salt, which in principle can exist as an equilibrium mixture containing any or all of the species **2***a*–*c*. Without isolation, this intermediate was treated with aqueous ethanolic sodium hydroxide solution, affording, after chromatographic purification, the cyclized product **3**. The yield for the methyllithium reaction is profoundly influenced by the selection of an appropriate solvent system: it appears to be desirable to find a solvent from which the lithium salt **2** will separate as a fine powdery precipitate. In the present case the reaction was conducted in a 1:3 tetrahydrofuran–toluene mixture at −78°C. The overall yield of pure **3** obtained from **1** (R = $C_2H_5$) was 50%.

While a number of routes are conceivable for effecting the final conversion of **3** to **4** (e.g. Hunsdiecker, Curtius, and related reactions), the procedure developed independently by Rao and co-workers (10) and Ho and Wong (11) for preparing α-methylene lactones offered the most direct approach. This method is based on the Kochi oxidative decarboxylation of acids by lead tetraacetate in the presence of cupric acetate (12). Since the decarboxylation is believed to involve free radical as well as carbonium ion intermediates (12), its applicability in the present instance was not assured in view of the known propensity of methylenomycin B to spontaneous polymerization (8, 9). In the event, however, brief treatment of **3** with lead tetraacetate in refluxing benzene containing pyridine and a catalytic amount of cupric acetate gave, after chromatographic purification, the desired product **4** in 31% yield.

[1]Fittig employed the sodium salt of tricarballylic acid (1), but later investigators found that better yields of bislactones were obtained when the free acid was used (3), particularly if the reaction flask was previously washed with a strongly alkaline detergent (4).

[2]Since submission of this manuscript, reports of two other syntheses of methylenomycin B have been published (13, 14).

0008-4042/82/202528-03$01.00/0

©1982 National Research Council of Canada/Conseil national de recherches du Canada

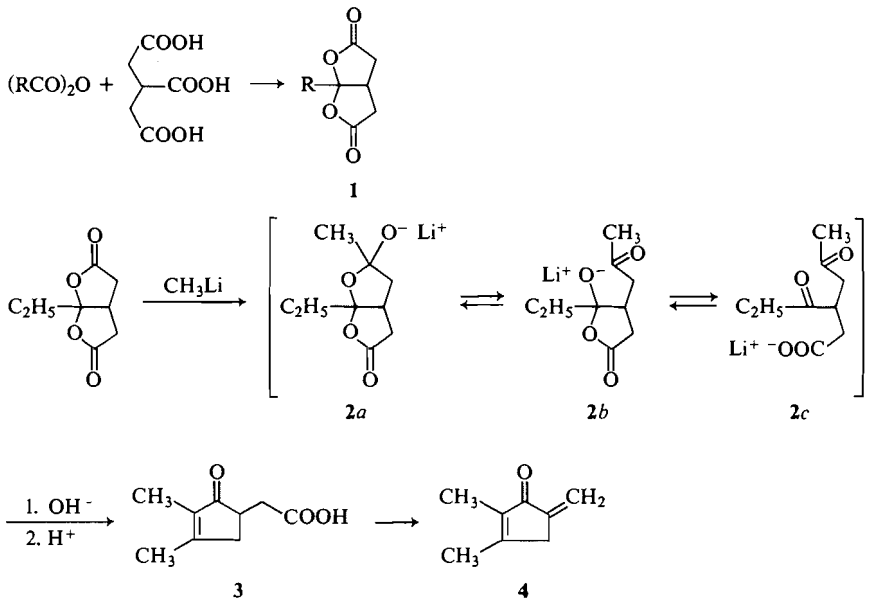

Comparison of the spectroscopic characteristics of the product with published data (8, 9)[3] confirmed its identity with methylenomycin B. Like the earlier investigators (8, 9) we have also had to contend with the spontaneous polymerization of **4** during subsequent manipulations.

Further studies on the reaction of Fittig bislactones with organometallic reagents are in progress to investigate the scope of the reaction in cyclopentenone synthesis.

## Experimental

Melting points were determined on a hot-stage apparatus and are uncorrected. Infrared and ultraviolet spectra were recorded on Beckman Acculab 2 and DK-2A spectrophotometers respectively. Nuclear magnetic resonance spectra were run on a Varian T-60 instrument. Mass spectra were obtained with an Hitachi Perkin–Elmer RMU-6D mass spectrometer. High resolution mass spectra were provided by Mr. A. I. Budd, University of Alberta. Microanalyses were performed by Spang Microanalytical Laboratory, Eagle Harbor, MI.

*3-(1,1-Dihydroxypropyl)glutaric acid di-γ-lactone (1, R = $C_2H_5$)*

Tricarballylic acid (2.0 g, 11.4 mmol) was added to refluxing propionic anhydride (20 mL, distilled before use) containing pyridine (0.2 mL). The solution was heated under reflux, and carbon dioxide evolution was periodically monitored by the precipitation of carbonate from a solution of barium hydroxide. The initial, quite vigorous, evolution of carbon dioxide moderated after about 1 h, but it had still not ceased after 4.5 h when the reaction was terminated by distillation of the volatile material. The residue was dissolved in acetone and treated with activated charcoal. After removal of the charcoal by filtration, evaporation of the solvent *in vacuo* yielded a pale brown residue which crystallized on standing. Recrystallization from toluene afforded almost colorless crystals of **1** (R = $C_2H_5$) (1.03 g, 53%), mp 65–66°C; ir ($CHCl_3$): 1800 $cm^{-1}$; nmr ($CDCl_3$) δ: 1.07 (3H, t, $J$ = 7 Hz), 2.06 (2H, q, $J$ = 7 Hz), 2.26–3.26 (5H, m); mass spectrum *m/e* (relative intensity) (ion) *inter alia*: 171.0642 (0.18) $(C_8H_{11}O_4)^+$, $(MH^+)$, 141.0186(38) $(C_6H_5O_4)^+$, 126.0682(6) $(C_7H_{10}O_2)^+$, 113.0241(15) $(C_5H_5O_3)^+$, 99.0081(22) $(C_4H_3O_3)^+$, 98.0732(62) $(C_6H_{10}O)^+$, 69.0344(7) $(C_4H_5O)^+$, 57.0365(100) $(C_3H_5O)^+$, 55.0204(31) $(C_3H_3O)^+$. *Anal.* calcd. for $C_8H_{10}O_4$: C 56.46, H 5.93; found: C 56.32, H 5.89.

*5-Carboxymethyl-2,3-dimethylcyclopent-2-en-1-one (3)*

A 100 mL three-necked round bottom flask equipped with a reflux condenser and a nitrogen inlet tube, a pressure equalizing dropping funnel, and a rubber septum stopper was charged with the bislactone **1** (R = $C_2H_5$) (2.0 g, 11.8 mmol). Anhydrous tetrahydrofuran (10 mL) was added through the dropping funnel under a nitrogen atmosphere, and when the bislactone was in solution, toluene (30 mL) was added. The flask was immersed in a Dry Ice – acetone bath, then an ether solution of methyllithium (containing 13.0 mmol) was added by syringe with magnetic stirring during 30 min, resulting in the separation of a fine precipitate. When the addition was complete the solvent was removed by distillation under reduced pressure. The residual lithium salt was heated at reflux under a nitrogen atmosphere for 16 h with a solution containing sodium hydroxide (2.4 g, 60 mmol) in water (20 mL) and ethanol (20 mL). After the alkali treatment, most of the ethanol was removed under reduced pressure, and the solution was adjusted with 50% hydrochloric acid to pH 2 and extracted with ether (5 × 30 mL). The ether solution was extracted with saturated sodium bicarbonate solution (5 × 25 mL). The aqueous phase was then made acidic by addition of 50% hydrochloric acid and extracted with ether (5 × 30 mL). After washing with water and drying over magnesium sulfate, the solvent was removed *in vacuo* to give a pale brown residue which crystallized on standing. The product was purified by chromatography on silica gel preparative layer plates (solvent system, acetone–toluene 1:3). In this manner the acid **3**

[3]We thank Dr. Jane Jernow, Hoffmann-La Roche Inc., Nutley, New Jersey for supplying us with the infrared spectrum of methylenomycin B.

Can. J. Chem. Downloaded from www.nrcresearchpress.com by 210.87.254.105 on 09/06/12
For personal use only.

(990 mg, 50% from bislactone) was obtained as white crystals, mp 89–95°C; ir ($CHCl_3$): 3700–2400 (br), 1715–1700, 1650 $cm^{-1}$; uv $\lambda_{max}$ (EtOH): 234 nm (ε 11 300); nmr ($CDCl_3$) δ: 1.72 (3H, br s), 2.07 (3H, br s), 2.20–3.05 (5H + impurity, m), 9.42 (1H, br s); mass spectrum *m/e* (relative intensity) (ion) *inter alia*: 168.0785(77) $(C_9H_{12}O_3)^{\ddagger}$, (M‡), 151.0733(10) $(C_9H_{11}O_2)^+$, 150.0681(59) $(C_9H_{10}O_2)^{\ddagger}$, 124.0854(11) $(C_8H_{12}O)^{\ddagger}$, 123.0807(94) $(C_8H_{11}O)^+$, 122.0733(100) $(C_8H_{10}O)^{\ddagger}$, 109.0648(28) $(C_7H_9O)^+$, 108.0574(56) $(C_7H_8O)^{\ddagger}$, 107.0499(39) $(C_7H_7O)^+$, 95.0856(21) $(C_7H_{11})^+$, 94.0782(31) $(C_7H_{10})^{\ddagger}$, 93.0704(10) $(C_7H_9)^+$, 81.0705 (21) $(C_6H_9)^+$, 80.0624(27) $(C_6H_8)^{\ddagger}$, 79.0553(59) $(C_6H_7)^+$, 67.0555(24) $(C_5H_7)^+$, 55.0565(17) $(C_4H_7)^+$.

A sample was sublimed (65°C/ca. 0.2 Torr) for analysis: mp 94–97°C. *Anal.* calcd. for $C_9H_{12}O_3$: C 64.27, H 7.19; found: C 64.31, H 7.18.

*2,3-Dimethyl-5-methylenecyclopent-2-en-1-one: methylenomycin B (4)*

A 50 mL two-necked round bottom flask fitted with a reflux condenser, a nitrogen inlet, and a glass stopper was charged with the acid **3** (250 mg, 1.49 mmol), lead tetraacetate (1.120 g, 2.53 mmol), cupric acetate monohydrate (70 mg, 0.35 mmol), and pyridine (0.05 mL, 49.1 mg, 0.62 mmol). The system was purged with nitrogen and dry benzene (12.0 mL) was added. The mixture was stirred at 22°C for 30 min and was then heated under reflux for 25 min, after which it was poured into cold water (100 mL). The benzene layer was separated and the aqueous phase was extracted with methylene chloride (4 × 25 mL). The combined extracts were concentrated *in vacuo* to about 2 mL and applied to silica gel preparative layer plates for purification of the product (solvent system, toluene–ethyl acetate 5:95). In this manner **4** (56.8 mg, 31%) was obtained as a colorless oil, identified as methylenomycin B by comparison of spectra with published data (8, 9).[3] Infrared (neat film): 1690, 1660, 1625 $cm^{-1}$; uv $\lambda_{max}$ (EtOH) nm (ε): 241 (5800), 263 (sh 4200); nmr ($CDCl_3$) δ: 1.81 (br s, $CH_3$), 2.11 (br s, $CH_3$) 3.13 (br s, $—CH_2—$), 5.36, 6.07 (broad singlets, olefinic $CH_2$); all signals showing splitting due to coupling; mass spectrum *m/e* 122 (M‡).

While solutions of the product **4** in chloroform or methylene chloride could be stored for moderate periods (several days) in the refrigerator, removal of solvent resulted in polymerization; the resulting colorless material could not be redissolved in the same solvents. Jernow *et al.* (9) have observed that methylenomycin B forms a stable complex with 30% hydrogen peroxide solution, from which it may be recovered unchanged by solvent extraction. This provides an excellent means of storing methylenomycin B for longer periods.

## Acknowledgments

We thank M. Mario Ebacher, undergraduate cooperative program participant from l'Université de Sherbrooke, for technical assistance in part of this work.

1. R. Fittig. Justus Liebigs Ann. Chem. **314**, 1 (1901).
2. H. D. Dakin and R. West. J. Biol. Chem. **78**, 91 (1928); **78**, 745 (1928); **78**, 757 (1928).
3. A. Lawson. J. Chem. Soc. 144 (1957).
4. W. L. Parker and F. Johnson. J. Org. Chem. **38**, 2489 (1973).
5. G. I. Fujimoto. J. Am. Chem. Soc. **73**, 1856 (1951); B. Belleau. J. Am. Chem. Soc. **73**, 5441 (1951).
6. C. A. Henrick, E. Böhme, J. A. Edwards, and J. H. Fried. J. Am. Chem. Soc. **90**, 5926 (1968).
7. J. C. Canévet and F. Sharrard. Tetrahedron Lett. **23**, 181 (1982).
8. T. Haneishi, N. Kitahara, Y. Takiguchi, M. Arai, and S. Sugawara. J. Antibiot. **27**, 386 (1974); T. Haneishi, A. Terahara, M. Arai, T. Hata, and C. Tamura. J. Antibiot. **27**, 393 (1974).
9. J. Jernow, W. Tautz, P. Rosen, and T. H. Williams. J. Org. Chem. **44**, 4212 (1979).
10. K. J. Divakar, P. P. Sane, and A. S. Rao. Tetrahedron Lett. 399 (1974).
11. T. L. Ho and C. M. Wong. Synth. Commun. **4**, 133 (1974).
12. J. D. Bacha and J. K. Kochi. Tetrahedron, **24**, 2215 (1968).
13. Y. Takahashi, H. Kosugi, and H. Uda. J. Chem. Soc. Chem. Commun. 496 (1982).
14. M. Mikołajczyk, S. Grzejszczak, and P. Łyżwa. Tetrahedron Lett. **23**, 2237 (1982).

Can. J. Chem. Downloaded from www.nrcresearchpress.com by 210.87.254.105 on 09/06/12
For personal use only.

# Synthesis of some *N*- and *S*-glycosides of D-galactose bearing hydrazinocarbonyl and diazomethylcarbonyl functions in the aglycon

GILLES DUPUIS AND BENOÎT LECLAIR

*Département de Biochimie, Université de Sherbrooke, Sherbrooke (Qué.), Canada J1H 5N4*

Received March 12, 1982

GILLES DUPUIS and BENOÎT LECLAIR. Can. J. Chem. **60**, 2531 (1982).

We describe the synthesis of *N*- and *S*-glycosides derived from D-galactopyranose in which the aglycon bears certain reactive groups. In a first series, the anomeric carbon is linked to an amino group that is acylated by a functionalized succinic acid chain. The terminal group of the aglycon moiety is a hydrazide function which can be converted by ultraviolet light irradiation into an azide and a nitrene. Alternatively, the terminal group is a diazoketone function which can be converted into a carbene, by ultraviolet light irradiation. A second series comprises glycosides of 1-thio-β-D-galactopyranose. The aglycon consists of a 6-carbon chain with a carboxylic end group. The latter has been converted into a hydrazide and diazoketone function. We show that the diazo group of the diazoketones (compounds **5** and **12**) is susceptible to decomposition by ultraviolet irradiation, being nearly quantitatively decomposed after 3 minutes. These compounds add to a growing list of hexose derivatives which can be used in the field of photoaffinity-labeling of the sugar binding sites of certain lectins and of hexose transport systems, or to prepare modified proteins or ligands for affinity chromatography.

GILLES DUPUIS et BENOÎT LECLAIR. Can. J. Chem. **60**, 2531 (1982).

Nous décrivons la synthèse de *N*- et *S*-glucosides dérivés du D-galactopyranose chez lesquels la portion aglycone porte certains groupements réactifs. Dans la première série de dérivés, le carbone anomérique est lié à un groupement aminé qui est acylé par un acide succinique fonctionnalisé. D'une part, la partie terminale de la portion aglycone est une fonction hydrazide qui peut être convertie en azide et en nitrène, après irradiation par la lumière ultraviolette. D'autre part, le groupement terminal de l'aglycone est une diazocétone qui peut être convertie en un dérivé carbène, par irradiation sous lumière ultraviolette. Dans la deuxième série de dérivés, nous avons préparé des glycosides du 1-thio-β-D-galactopyranose. La portion aglycone est une chaîne de six unités de carbone se terminant par un groupement carboxyle. Ce dernier a été converti en hydrazide ou en diazocétone. Nous montrons que le groupement cétodiazo des composés **5** et **12** est décomposé par irradiation ultraviolette. Trois minutes d'irradiation suffisent à décomposer les produits. Les composés décrits ici s'ajoutent à la liste de dérivés d'hexoses déjà décrits dans la littérature, lesquels peuvent être utilisés comme photo-marqueurs, du site de fixation de glucides chez des lectines et dans le système de transport des hexoses ou pour préparer des protéines modifiées ou des colonnes d'affinité ayant des glucides comme affinants.

## Introduction

The method of affinity-labeling has achieved success for determination of the nature of the amino acid residues located in the environment of the "active site" of biologically active proteins such as enzymes, antibodies, and others (1–3). This method is based on the synthesis of suitable reactive derivatives of the natural ligand or of molecules structurally related to it. The choice of derivatives is dictated by several factors such as reactivity, specificity of labeling, and stability in the medium used for reaction.

The design of affinity-labeling reagents has been extended to light-sensitive reagents (photoaffinity-labeling). This approach was pioneered by Westheimer and his group in their study of the active site of chymotrypsin (4). These workers used a diazo derivative which yielded a highly reactive nitrene after irradiation by light (5, 6).

Other types of derivatives have also been prepared. The ones used mainly are diazo and chloromethyl ketone derivatives or other activated forms of the carbonyl function (7, 8).

The choice of ligand is dictated by the properties of the protein to be modified. For instance in the case of lectins, a class of proteins which can specifically recognize monosaccharides or polysaccharidic structures (9, 10), synthesis of labeling probes would involve preparation of suitably modified glycosides. From a synthetic standpoint, the synthesis of monosaccharide derivatives appears to be the simplest route for affinity-labeling of lectins.

We have selected D-galactose as a model hexose and report the synthesis of derivatives wherein the anomeric carbon bears an aminoacyl chain or a *S*-alkyl chain. The compounds possess a hydrazide group which should be easily transformable into the corresponding azide (11) and nitrene groups (12), or a diazoketone function which can be transformed into the corresponding carbene, by ultraviolet irradiation (13).

## Results and discussion

### *Synthesis of 1-amino-β-D-galactopyranosides*

β-D-Galactopyranosylamine **2** (14) was *N*-acylated to give the methyl succinamido derivative **3**. This was done in a manner similar to the one described by Gordon *et al.* (15) for the synthesis of the ε-aminocaproyl derivative of β-D-galactopy-

0008-4042/82/202531-06$01.00/0

©1982 National Research Council of Canada/Conseil national de recherches du Canada

Can. J. Chem. Downloaded from www.nrcresearchpress.com by 210.87.254.42 on 09/06/12
For personal use only.

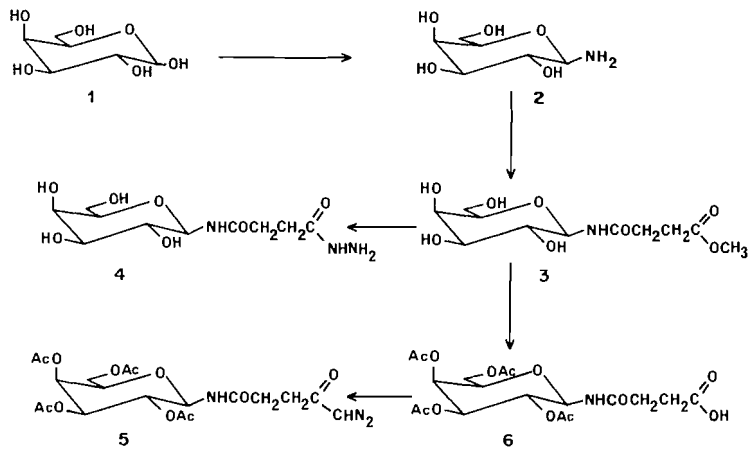

SCHEME 1

ranosylamine. Briefly, the mixed anhydride prepared from monomethyl succinate and isobutyl chloroformate constituted the necessary acylating agent which was allowed to react with compound **2** suspended in DMF.[1] Compound **3** was obtained crystalline in 70% yield. Attempts to prepare the analogous derivative of α-D-galactopyranosylamine failed. Treatment of compound **3** for two hours with hydrazine in refluxing methanol afforded a nearly quantitative yield of the crystalline hydrazide **4**.

In order to prepare the free acid from compound **3**, the latter was saponified by treatment with a methanolic solution of KOH, under reflux, for a brief period of time. Under these conditions, the methyl ester group was quantitatively cleaved, as evidenced by $^1$Hmr and ir spectra, whereas the amide bond remained intact. The oily compound was peracetylated with acetic anhydride in pyridine to afford compound **6**.

Several methods have been used to introduce the diazoketone function. These include conversion of the free acid into an acyl halide (16–20) and subsequent reaction with diazomethane or reaction of a mixed anhydride with diazomethane (21). We selected the mixed anhydride method because of simplicity of its application to **6**. The triethylammonium salt of **6** was treated with isobutyl chloroformate, and the ensuing mixed anhydride was mixed with an ether solution of freshly prepared diazomethane. Stirring the mixture at room temperature (overnight) gave only a low yield of conversion of the anhydride, as evidenced by the strong ir band at 1760 cm$^{-1}$. The mixture was therefore gently heated under reflux for 18 h, in the dark. An ir spectrum revealed complete disappearance of the 1760 cm$^{-1}$ absorption band and appearance of the characteristic diazo band at 2200 cm$^{-1}$ and a band at 1640 cm$^{-1}$ for the diazo ketone structure. These spectral features suggested a successful conversion of **6** into **5**.

The light sensitivity of diazo derivative **5** was investigated by irradiation of the compound with an ultraviolet lamp. The disappearance of the band at 254 nm was followed spectrophotometrically. A fifty percent decrease in optical density was observed after less than one minute, and nearly quantitative decomposition occurred after 3 minutes of irradiation.

*Synthesis of 1-thio-β-D-galactopyranosides*

Alkyl 1-thioaldopyranosides containing an amino, imido ester, aldehyde, or ester group at the terminal position of the aglycon have previously been reported (22–26). These compounds can be prepared by *S*-alkylation of 1-thioglycoses or by reaction of ethyleneimine with 1-thioaldose derivatives. Because of the demonstrated facility of the first approach (23), this method was selected in the present study.

A series of 1-thio-β-D-galactopyranose derivatives was generated by introduction of a medium size alkyl chain of six carbon units bearing the appropriate reactive functions. The starting material was 2,3,4,6-tetra-*O*-galactopyranosyl bromide (27) which was allowed to react with thiourea, as described by Bonner and Kahn (28). The ensuing crystalline hydrobromide salt **7** was quantitatively reduced to 2,3,4,6-tetra-*O*-acetyl-1-thio-β-D-galactopyranose **8** by treatment with sodium bisulfite at alkaline pH (29). The potassium thiolate of **8** was allowed to react with methyl 6-bromohexanoate, as

[1]Abbreviations used: DMF, *N*,*N*-dimethylformamide; $^1$Hmr, proton magnetic resonance; ir, infrared; THF, tetrahydrofuran; m, multiplet; t, triplet; s, singlet.

Can. J. Chem. Downloaded from www.nrcresearchpress.com by 210.87.254.42 on 09/06/12
For personal use only.

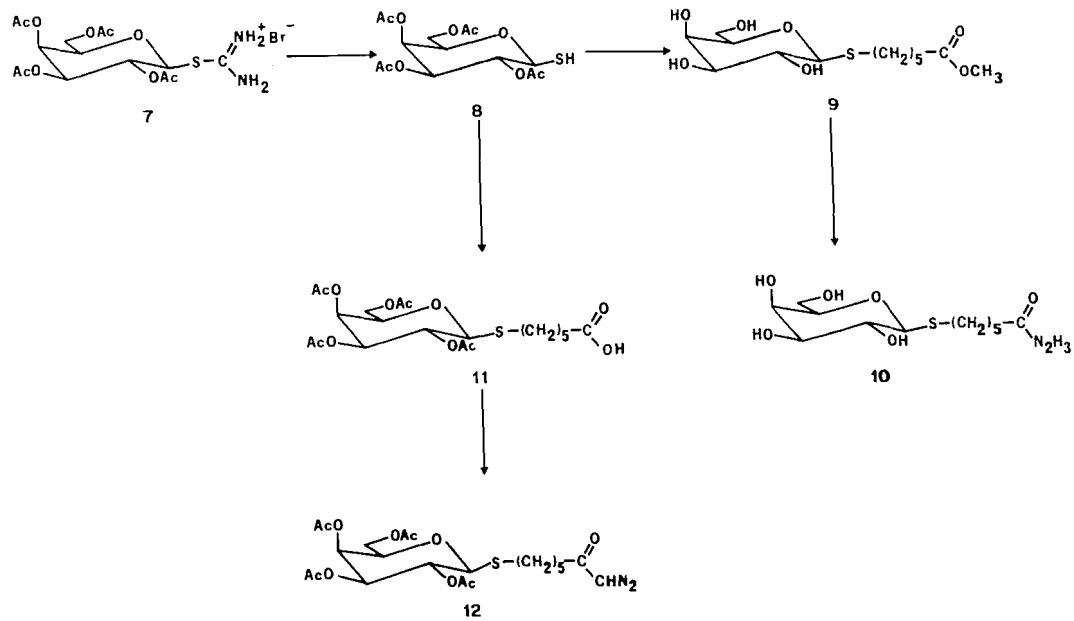

SCHEME 2

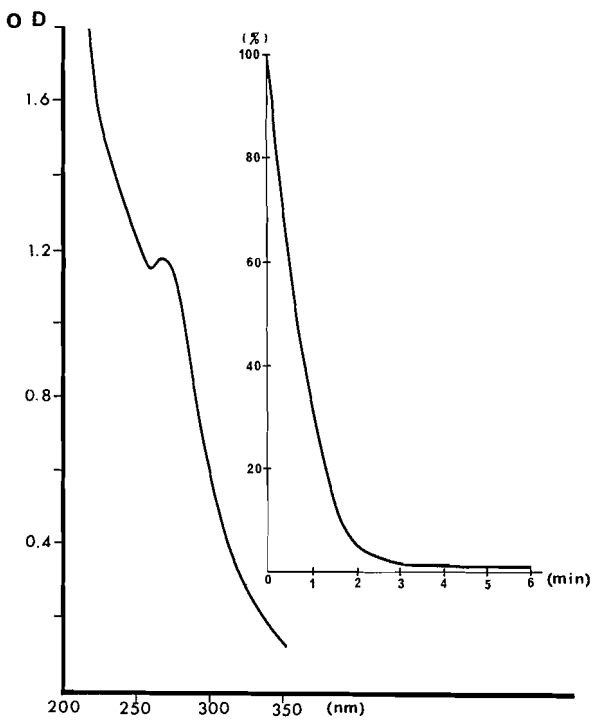


FIG. 1. Ultraviolet spectrum of 1-diazo-7-(2,3,4,6-tetra-*O*-acetyl-β-D-galactopyranosylthio)-2-heptanone (**12**) in ethanol. OD is the optical density. *N*-(2,3,4,6-Tetra-*O*-acetyl-β-D-galactopyranosyl)-5-diazo-4-oxopentanamide **5** had a spectrum identical to that of **12**. The insert shows the remaining proportion (%) of compound **12** as a function of time (min) of irradiation with a polychromatic ultraviolet lamp. The quantity of remaining compound was determined at 254 nm. The decomposition of compound **5** gave a similar curve.

described (25), and the oily product was deacetylated with sodium methoxide in methanol, to give the crystalline thioglycoside **9**. Reaction of **9** with hydrazine in refluxing methanol gave the crystalline hydrazine **10** (30).

The diazo ketone **12** was obtained in two steps from the peracetylated thiogalactose **8**. First, the free acid intermediate **11** was prepared by reaction of the potassium salt of compound **8** with potassium 6-bromohexanoate, followed by acidification. Compound **11** was then converted into the desired diazo derivative **12** by allowing the mixed anhydride prepared from **11** and isobutyl chloroformate to react with an excess of ethereal diazomethane, under reflux. The diazo derivative **12** was decomposed by ultraviolet irradiation as shown in Fig. 1. The kinetic course of decomposition was identical to that of compound **5**.

## Conclusions

Compounds prepared in this study should prove to be useful for affinity-labeling of lectins possessing a specificity for galactose such as those obtained from jequirity beans, peanuts, osage oranges, castor beans, and from *Bandeiraea simplicifolia* (10). It may be pointed out that the hydrazides **4** and **10** can probably be converted into the corresponding azides (11) affording the possibility of generating nitrenes, by irradiation (12). Furthermore, diazo derivatives such as compounds **5** and **12** should yield highly reactive carbenes, after irradiation (13), but they can also be

Can. J. Chem. Downloaded from www.nrcresearchpress.com by 210.87.254.42 on 09/06/12
For personal use only.

Can. J. Chem. Downloaded from www.nrcresearchpress.com by 210.87.254.42 on 09/06/12
For personal use only.

transformed into halomethyl ketone derivatives by treatment with HBr or HCl (31). This transformation provides an additional tool for affinity-labeling studies. It is to be noted that compounds **5** and **12** are peracylated glycosides; however, the acetyl groups can be removed by treatment with sodium methoxide/methanol, without affecting the diazo function.

Sugar derivatives such as those described here can be used in biological systems apart from the study of the nature of lectin sugar binding sites. These may include the study of sugar transport systems in prokaryote and eukaryote cells (32, 33), the nature of the components involved in galactose-induced "puffing" of *Drosophila* giant chromosomes (34), etc. In addition, they represent further agents which can be used to prepare affinity columns (15, 35–37), to modify proteins by reaction with alkyl glycosides (11, 30, 38, 39), and to study cell adhesion to glycoside-modified solid surfaces and proteins (40).

## Experimental

D-Galactose was obtained from Sigma Chemical Co. (St. Louis, MO); other reagents were from Aldrich Chemical Co. (Milwaukee, WI) or from Fisher Scientific Co. or Canlab (Montreal).

All evaporations were performed under reduced pressure at 20–45°C, with a rotary evaporator. Melting points were determined in capillary tubes on a Tottoli apparatus (Brinkman Instruments, Rexdale, Ontario) and are not corrected. Thin layer chromatography was performed on silica gel G-coated glass plates. Plates were developed in the following system (v/v): I, chloroform – acetic acid – water (6:7:1); II, methanol–chloroform (1:1); III, acetone – petroleum ether 65–110°C (9:1); IV, benzene – ethyl acetate (5:1). Compounds were revealed by spraying the plates with dilute sulfuric acid followed by heating. Optical rotations were determined by Galbraith Laboratories (Knoxville, TN). The $^1$Hmr spectra were recorded on a Varian T-60 spectrometer; chemical shifts are presented in parts per million (δ) with reference to tetramethylsilane as internal standard. Infrared spectra were determined with a Perkin–Elmer spectrometer, model 457. Ultraviolet spectra were recorded on a Cary model 118 instrument.

*N-(β-D-Galactopyranosyl)-3-methoxycarbonylpropanamide (3)*

In a three-neck flask protected from moisture, monomethyl succinate (3.96 g; 30 mmol) was dissolved in DMF (50 mL), triethylamine (4.16 mL; 30 mmol) was added, and the solution was cooled at −5°C. Isobutyl chloroformate (3.94 mL; 30 mmol) was then added slowly, under stirring. The mixture was stirred for 20 min at −5°C, and then filtered, by suction, into a chilled (−5°C) flask containing a suspension of β-D-galactopyranosylamine ($R_f^I$, 0.21; mp 138°C (lit. (14) m.p. 137–138°C) (4.50 g; 25 mmol) in DMF (250 mL). The reaction mixture was stirred for 30 min at −5°C. It was then placed in an ice bath and stirred for 16 h at ambient temperature without removal of the bath. The solvent was evaporated and the oily product was crystallized from 1-butanol. Yield, 5.1 g (70%); mp 167°C; $R_f^I$, 0.33; $[\alpha]_D^{20}$ +11.3° (*c* 1, $H_2O$); $^1$Hmr ($D_2O$): 2.65 s (4H, $2CH_2$), 3.60 s (3H, $CO_2$—$CH_3$). *Anal.* calcd. for $C_{11}H_{19}NO_8$ (293.2): C 45.05, H 6.53, N 4.78; found: C 44.69, H 6.24, N 5.08.

*N-(β-D-Galactopyranosyl)-3-hydrazinocarbonylpropanamide (4)*

Compound **3** (0.5 g, 1.7 mmol) was dissolved in anhydrous methanol (3 mL) and absolute hydrazine (0.2 mL; 6.1 mmol) was added. The solution was heated under reflux for two hours. Cooling afforded crystals which were recrystallized from methanol. Yield, 0.48 g (95%); mp 236°C (dec.); $R_f^I$ 0.14; $[\alpha]_D^{20}$ = +7.8° (*c* 1, $H_2O$). *Anal.* calcd. for $C_{10}H_{19}N_3O_7$ (293.3): C 40.95, H 6.53, N 14.33; found: C 40.92, H 6.53, N 14.12.

*N-(2,3,4,6-Tetra-O-acetyl-β-D-galactopyranosyl)-3-carboxypropanamide (6)*

Compound **3** (1 g; 3.4 mmol) was dissolved in absolute methanol (5 mL) and a solution of KOH (2 g; 35 mmol) in anhydrous methanol (10 mL) was added. The mixture was heated under reflux for 8–10 min, cooled, acidified to pH 2.5 with 1 *N* HCl, and evaporated to dryness. Two successive evaporations of added methanol gave an oily residue which was dissolved in freshly distilled pyridine (5 mL), and acetic anhydride (5 mL) was added. The mixture was left at room temperature for 6 h. The suspension was filtered and the solvents were evaporated. Two successive evaporations of added methanol afforded a viscous material which was purified on a silicic acid column (2 × 30 cm) and equilibrated with chloroform. The desired product was eluted with 5% methanol in chloroform. The product was precipitated from chloroform by the addition of ether. Yield, 1.1 g (70%); mp 118–120°C; $R_f^{II}$ 0.3; $[\alpha]_D^{20}$ +27.8° (*c* 1, $CHCl_3$); $^1$Hmr ($CDCl_3$): 2.05 m (12 H, 4 $CH_3$—*CO*), 2.60 m (4H, 2 $CH_2$), 4.10 m (3H, $CHCH_2$—*OAc*), 5.20 m (3H, 3 CH—*OAc*), 11.50 s (1H, $CO_2H$). *Anal.* calcd. for $C_{18}H_{25}NO_{12}$ (447.39): C 48.32, H 5.63, N 3.13; found: C 48.56, H 5.66, N 3.44.

*N-(2,3,4,6-Tetra-O-acetyl-β-D-galactopyranosyl-5-diazo-4-oxopentanamide (5)*

Compound **6** (1.8 g; 4 mmol) was dissolved in a 4:1 mixture of THF/DMF (10 mL), the temperature was lowered to −5°C, and triethylamine (0.57 mL; 4 mmol) was added. Isobutyl chloroformate (0.53 mL; 4 mmol) was then added dropwise to the stirred mixture which was filtered after 15 min. the filtrate was transferred to a solution of diazomethane in ether (alcohol-free) (70 mL) contained in a polished-glass flask (Aldrich). The reaction mixture was protected from light and gently heated under reflux for 18 h. The solvent was evaporated and a slightly colored, oily residue was obtained. The ir spectrum showed the presence of the diazo function (2200 $cm^{-1}$), and of the carbonyl group of the acetyl (1740 $cm^{-1}$) and diazoketone (1640 $cm^{-1}$) functions, indicating that compound **5** was formed.

*S-(2,3,4,6-Tetra-O-acetyl-β-D-galactopyranosyl)-pseudothiouronium bromide (7)*

2,3,4,6-Tetra-*O*-acetyl-α-D-galactopyranosylbromide, mp, 88°C (lit. (27) mp 84–85°C) (13.2 g; 32 mmol), was dissolved in acetone (13 mL) and recrystallized thiourea (2.7 g; 35 mmol) was added. The mixture was boiled under reflux for 15 min and then allowed to cool. The crystals of **7** were filtered off and recrystallized from acetone and from 2-propanol. Yield, 12.9 g (83%); mp 172°C (lit. (22) mp 171–171.5°C); $R_f^{III}$, 0.24.

*5-(Methoxycarbonyl)pentyl-1-thio-β-D-galactopyranoside (9)*

2,3,4,6-Tetra-*O*-acetyl-1-thio-β-D-galactopyranose **8** was obtained by reduction of **7** according to the procedure of Černý *et al.* (29). The thio sugar (1.5 g; 4.12 mmol) was dissolved in acetone (20 mL) and an aqueous solution of $K_2CO_3$ (0.57 g; 4.12 mmol) was added. After 30 s the mixture was lyophilyzed. The rest of the procedure was done in a manner similar to that of Connolly *et al.* (25). The dry potassium salt of **8** was suspended in DMF (25 mL) and methyl 6-bromohexanoate (prepared from 6-bromohexanoic acid and etheral diazomethane) (0.8 g; 4

Can. J. Chem. Downloaded from www.nrcresearchpress.com by 210.87.254.42 on 09/06/12
For personal use only.

mmol) in DMF (5 mL) was added. The reaction mixture was stirred for 2 h at room temperature. The precipitate was removed by filtration and the solvent evaporated. The residue was dissolved in chloroform and the solution was washed with water. The organic phase was dried and evaporated. The product was an oil, as previously reported (25). For deacetylation, the product was dissolved in anhydrous methanol (5 mL) and 0.5 mL of 0.43 *M* $NaOCH_3$ in methanol was added. The mixture was stored in the dark for 18 h, at room temperature, then neutralized to pH 7.0 with *N* HCl and evaporated to dryness. The solid was dissolved in boiling ethyl acetate and the filtered solution deposited cyrstals on cooling. Yield, 0.67 g (50%, based on compound **8**); mp 96°C; $R_f^1$ 0.66; $[\alpha]_D^{20}$ −24.1° (*c* 1, $H_2O$); $^1$Hmr ($D_2O$): 1.50 m (6H, inner methylene groups of aglycon), 2.35 t (2H, $CH_2$—$CO_2CH_3$), 2.65 t (2H, $CH_2$—*S*), 3.55 m (7H, pyranosic protons), 3.60 s (3H, $CO_2$—$CH_3$). *Anal.* calcd. for $C_{13}H_{24}SO_7$ (324.4): C 48.13, H 7.46; found: C 48.42, H 7.36.

*6-(β-D-Galactopyranosylthio)hexanoic acid hydrazide (10)*

A solution of compound **9** (0.5 g; 1.54 mmol) in anhydrous methanol (3 mL) containing absolute hydrazine (0.2 mL; 6.1 mmol) was heated under reflux for 2 h and evaporated. Compound **10** was crystallized from ethanol. Yield, 460 mg (92%); mp 180°C (lit. (30) mp 182–183°C); $R_f$ 0.31; $[\alpha]_D^{20}$ − 26.7° (*c* 1, $H_2O$). *Anal.* calcd. for $C_{12}H_{24}N_2O_6S$ (324.4): C 44.43, H 7.46, N 8.64; found: C 44.32, H 7.36, N 8.44.

*1-Diazo-7-(2,3,4,6-tetra-O-acetyl-β-D-galactopyranosylthio)-2-heptanone (12)*

The carboxylic acid **11** was prepared from the potassium salt of **8** in a manner similar to that of compound **9**. Thus, the potassium salt of **8** (1.5 g; 4.1 mmol) was allowed to react with the potassium salt of 6-bromohexanoic acid (0.8 g; 4.1 mmol) in acetone–water (1:1 v/v, 20 mL). The mixture was stirred for two hours at room temperature, then acidified to pH 3 with *N* HCl and extracted with chloroform. The oil obtained after evaporation was purified on a silicic acid column (2 × 30 cm) equilibrated with chloroform. The desired compound **11**, an oil, was eluted with chloroform. Yield, 1.4 g (70%); $R_f^V$ 0.20; $[\alpha]_D^{20}$ − 8.6° (*c*, 1, $CHCl_3$); $^1$Hmr ($CDCl_3$): 1.50 m (6H, inner methylene groups of aglycon), 2.05 four s (12H, $4CO_2CH_3$), 2.30 t (2H, $CH_2$—$CO_2H$), 2.70 t (2H, *S*—$CH_2$), 4.00 s (2H, $CH_2$—*OAc*), 5.10 m (3H, CH—*OAc*), 11.20 s (1H, $CO_2H$).

A mixture of compound **11** (1.72 g; 3.6 mmol) and triethylamine (0.5 mL: 3.6 mmol) in THF (9 mL) was cooled to −5°C, and isobutyl chloroformate (0.47 mL; 3.6 mmol) was added in portions, with stirring. After 15 min, the mixture was filtered and added to an ethanol-free ether solution of diazomethane (24.5 mmol), in a "Vitro" flask (Aldrich). The reaction mixture was gently boiled under reflux for 18 h in the dark. Evaporation of the solvents gave **12** as an oil; ir (neat): 2100 (CH=N=N), 1640 (ketonic CO), and 1745 (ester CO); $^1$Hmr ($CDCl_3$): 1.60 m (6H, inner methylene groups of the aglycon), 2.10 four s (12H, 4 $CO_2$—$CH_3$), 2.50 t (2H, $CH_2$—*COCHN*$_2$), 2.89 t (2H, *S*—$CH_2$), 3.40 s (1H, $CHN_2$), 4.10 s (2H, $CH_2$—*OAc*), 5.20 m (CH—OAC).

*Deacetylation of compound 12*

Compound **12** (40 mg; 0.085 mmol) was dissolved in a minimum amount of anhydrous methanol and $NaOCH_3$ (0.010 mmol) in anhydrous methanol (25 μL) was added. The solution was stored in the dark for 8 h at room temperature, carefully neutralized to pH 4.5 with dilute acetic acid, and evaporated. The syrupy residue was dissolved in a small volume of anhydrous methanol and the suspension was centrifuged. Evaporation of the organic layer afforded an oily product which showed (ir) the characteristic bands of the diazo (2100) and the ketonic carbonyls (1640). In addition, the ultraviolet spectrum showed the characteristic maximum of absorption at 254 nm.

*Ultraviolet spectra and kinetics of decomposition of compounds 5 and 12*

The ultraviolet spectra of compounds **5** and **12** in ethanol (Fig. 1) showed an absorption maximum at 254 nm. Each compound was irradiated with an ultraviolet lamp ("Mineral light" UVSL 25, Ultraviolet Products, Inc., San Gabriel, CA) placed at 10 cm from the solutions. Spectra were recorded at various intervals, and the percentage of untransformed compound is plotted as a function of time of irradiation (Fig. 1). After 1 min of irradiation, approximately 70% of compounds **5** and **12** were decomposed. Complete photolysis was observed after 3 min of irradiation.

## Acknowledgements

The authors are indebted to the Medical Research Council of Canada for financial support (grant MT 6343) and to the Université de Sherbrooke for a "Subvention Institutionnelle à la Recherche Libre".

1. S. J. Singer. Adv. Protein Chem. **22**, 1 (1967).
2. D. Givol. Int. Rev. Biochem. Defence and Recognition II B, **23**, 71 (1979).
3. D. S. Sigman and G. Mooser. Annu. Rev. Biochem. **44**, 889 (1975).
4. J. Shafer, P. Baronowsky, R. Laursen, F. Finn, and F. H. Westheimer. J. Biol. Chem. **241**, 421 (1966).
5. H. Bayley and J. R. Knowles. Methods Enzymol. **46**, 69 (1977).
6. V. Chowdhry and F. H. Westheimer. Annu. Rev. Biochem. **48**, 293 (1979).
7. H. Nakayama and Y. Kanaoka. FEBS Lett. **37**, 200 (1973).
8. C. A. Converse and F. F. Richards. Biochemistry, **8**, 4431 (1969).
9. H. Lis and N. Sharon. Annu. Rev. Biochem. **42**, 541 (1973).
10. I. J. Godlstein and C. E. Hayes. Adv. Carbohydr. Chem. Biochem. **35**, 127 (1978).
11. R. U. Lemieux, D. A. Barker, and D. R. Bundle. Can. J. Biochem. **55**, 507 (1977).
12. W. Lwowski. Angew. Chem. Int. Ed. Engl. **6**, 897 (1967).
13. W. Kirmse. Carbene chemistry. Academic Press, New York. 1964.
14. R. Barker, C.-K. Chiang, I. P. Trayer, and R. L. Hill. Methods Enzymol. **34B**, 317 (1974).
15. J. A. Gordon, S. Blumberg, H. Lis, and N. Sharon. FEBS Lett. **24**, 193 (1972).
16. W. Reid and H. Mengler. Fortschr. Chem. Forsch. **5**, 1 (1965).
17. F. Weygand and H. J. Bestmann. Newer Prep. Methods Org. Chem. **3**, 451 (1964).
18. H. O. House and C. J. Blankley. J. Org. Chem. **33**, 53 (1968).
19. E. Shaw, M. Mares-Guia, and W. Cohen. Biochemistry, **4**, 2219 (1965).
20. D. P. Bloxham, R. A. Chalkley, S. J. Coghlin, and W. Salam. Biochem. J. **175**, 999 (1978).
21. C. G. Rasool, S. Nicolaidis, and M. Akhtar. Biochem. J. **157**, 675 (1976).
22. S. Chipowsky and Y. C. Lee. Carbohydr. Res. **31**, 339 (1973).

23. R. T. LEE and Y. C. LEE. Carbohydr. Res. **77**, 149 (1979).
24. Y. C. LEE, C. P. STOWELL, and M. J. KRANTZ. Biochemistry, **15**, 3956 (1976).
25. D. T. CONNOLLY, S. ROSEMAN, and Y. C. LEE. Carbohydr. Res. **87**, 227 (1980).
26. R. T. LEE and Y. C. LEE. Carbohydr. Res. **34**, 151 (1974).
27. W. T. HASKINS, R. M. HANN, and C. S. HUDSON. J. Am. Chem. Soc. **64**, 1852 (1942).
28. W. A. BONNER and J. E. KAHN. J. Am. Chem. Soc. **73**, 2241 (1951).
29. M. ČERNÝ, J. STANĚK, and J. PACÁK. Monatsh. **94**, 290 (1963).
30. K. KAWAGUCHI, M. KUHLENSCHMIDT, S. ROSEMAN, and Y. C. LEE. J. Biol. Chem. **256**, 2230 (1981).
31. C. SCHOELLMANN and E. SHAW. Biochemistry, **2**, 252 (1963).
32. H. R. KABACK. Annu. Rev. Biochem. **39**, 561 (1970).
33. M. HOSANG, E. M. GIBBS, D. F. DIEDRICH, and G. SEMENZA. FEBS Lett. **130**, 244 (1981).
34. W. BEERMANN. Chromosoma, **41**, 297 (1973).
35. K. FILKA, J. ČOUPEK, and J. KOCOUREK. Biochim. Biophys. Acta, **539**, 518 (1978).
36. J. PIPKOVA, V. HOREJSI, and J. KOCOUREK. Biochim. Biophys. Acta, **541**, 515 (1978).
37. H. LIS, R. LOTAN, and N. SHARON. Ann. NY Acad. Sci. **234**, 232 (1974).
38. R. T. LEE and Y. C. LEE. Biochemistry, **19**, 156 (1980).
39. D. H. BUSS and I. J. GOLDSTEIN. J. Chem. Soc. C, 1457 (1968).
40. P. H. WEIGEL, R. L. SCHNAAR, M. S. KUHLENSCHMIDT, E. SCHMELL, R. T. LEE, Y. C. LEE, and S. ROSEMAN. J. Biol. Chem. **254**, 10830 (1979).

Can. J. Chem. Downloaded from www.nrcresearchpress.com by 210.87.254.42 on 09/06/12
For personal use only.

# The gas-phase thermal decomposition of cyclobutanol[1]

R. A. BACK

*Division of Chemistry, National Research Council of Canada, Ottawa, Ont., Canada K1A 0R6*

Received October 6, 1981[2]

R. A. BACK. Can. J. Chem. **60**, 2537 (1982).

The thermal decomposition of cyclobutanol has been studied in the gas phase in a static system at pressures from 3–6 Torr and temperatures from 250 to 450°C. The major products observed were ethylene and acetaldehyde, while *n*-butyraldehyde was a minor product. First-order rate constants based on ethylene formation in a Pyrex vessel conditioned by carbon deposition gave Arrhenius parameters of $A = 2.14\ (\pm 0.2) \times 10^{14}\ s^{-1}$ and $E = 57.3\ (\pm 1)$ kcal/mol. Under the same conditions, the ratio *n*-butyraldehyde/ethylene increased with decreasing temperature, corresponding to an activation energy of about 50 kcal/mol for butyraldehyde formation and a frequency factor about $10^4$ times lower than that for ethylene production. In an untreated Pyrex vessel the decomposition showed strong surface catalysis with much lower activation energies for both processes. It is suggested that both ethylene and *n*-butyraldehyde are formed from a common $\dot{C}H_2CH_2CH_2\dot{C}HOH$ biradical by cleavage and by hydrogen transfer through a 6-membered cyclic transition state respectively. The thermal decomposition is thus the reverse of the Type II and II′ processes observed in the photolysis of *n*-butyraldehyde.

R. A. BACK. Can. J. Chem. **60**, 2537 (1982).

On a étudié la décomposition thermique du cyclobutanol en phase gazeuse dans un système statique à des pressions variant de 3 à 6 Torr et à des températures allant de 250 à 450°C. Les produits majoritaires observés sont l'éthylène et l'acétaldéhyde tandis que le butyraldehyde est le produit secondaire. Les constantes de vitesse d'ordre un, évaluées à partir de la formation d'éthylène dans un récipient en pyrex traité au noir de charbon, permettent de déterminer les paramètres d'Arrhénius $A = 2{,}14\ (\pm 0{,}2) \times 10^{14}\ s^{-1}$ et $E = 57{,}3\ (\pm 1)$ kcal/mol. Dans les mêmes conditions, le rapport *n*-butyraldehyde/éthylène augmente lorsque la température diminue; ceci correspond à une énergie d'activation d'environ 50 kcal/mol pour le butyraldehyde.

[Traduit par le journal]

## Introduction

The thermal decompositions of cyclobutane and its derivatives have been very extensively studied (1). Simple unimolecular decomposition into two ethylene molecules (or substituted ethylenes) is the usual mode of decomposition, generally believed to proceed through a biradical intermediate formed by ring opening:

[1] $\square \longrightarrow -CH_2CH_2CH_2CH_2- \rightarrow 2C_2H_4$

In a few systems, alternative reactions of the biradical (other than isomerization) can compete with reaction [1]. In cyclobutanone, for example, minor products are cyclopropane and CO, although it is not clear whether they are formed from the same biradical which decomposes to yield ethylene and ketene, the main products, or by a totally different pathway (2). A better example is isopropenylcyclobutane, which forms 1-methylcyclohexene with a yield almost 80% of the normal fragmentation products by ring closure of an allylic resonance structure of the biradical (1, 3). A third and especially interesting example is the decomposition of *cis*-1,2-dimethylcyclobutanol. A brief account by Feit (4) reports two pairs of decomposition channels at 381°C, each pair proceeding through a common biradical and yielding not only the substituted ethylenes expected from fragmentation, but also the hexanone isomers formed by transfer of the O—H hydrogen through a cyclic six-membered transition state. The latter process is exactly the reverse of the biradical formation step postulated in the Norrish type II photochemical decomposition of these same ketones, and the fragmentation products are those observed in the latter processes in the gas phase (4). In the photolysis of the appropriate aldehydes and ketones (5, 6) isomeric cyclobutanols are produced, and it is clear that these photolyses and the thermal decomposition of the cyclobutanols are intimately related, and warrant further investigation.

No comparable studies of the thermal decomposition of cyclobutanol itself have been reported in the open literature, although a Ph.D. thesis on the subject was submitted to the University of Rochester in 1967 by P. M. Stacey, from the laboratory of the late W. D. Walters (7). Fragmentation to ethylene and acetaldehyde was the main decomposition path, and Arrhenius parameters based on carefully calibrated $\Delta p$ measurements were reported for the temperature range 405–445°C. *n*-Butyraldehyde was also observed to be a very minor product, but was not measured systematically. The present paper describes a more thorough study of the thermal decomposition, with measure-

[1]NRCC No. 20497.

[2]Revision received May 7, 1982.

0008-4042/82/202537-05$01.00/0

©1982 National Research Council of Canada/Conseil national de recherches du Canada

Can. J. Chem. Downloaded from www.nrcresearchpress.com by 210.87.254.42 on 09/06/12
For personal use only.

ment of both product channels based on product analysis and covering a much wider range of temperature.

## Experimental

The decomposition was studied in a conventional static system, using a cylindrical Pyrex vessel about 3 cm in diameter and 10 cm long, with rounded ends, of about 55 $cm^3$ volume, mounted in a tube furnace controlled to ±0.5°C. In the first series of experiments no special treatment was given to the surface of the reaction vessel. In the second series, a light carbon coating was deposited on the surface by the pyrolysis of about 100 Torr of isobutene for 10 h at 450°C. To test for surface effects a similar vessel was used, packed with lengths of 5 mm od Pyrex tubing which increased the surface/volume ratio by a factor of 3. The reaction vessels were attached through a metal valve to a grease-free vacuum line. Pressure was measured by a quartz spiral gauge or a mercury manometer, and because the vacuum line was at ambient temperature, pressures of cyclobutanol were limited by its vapor pressure. The reaction was started by admitting the cyclobutanol vapor to the hot reaction vessel and terminated by opening the valve leading through a cold trap (77 K) to a Toepler pump. The entire sample, reagent and condensible and noncondensible products, was then transferred by Toepler pump to the pickup of a gas chromatograph for analysis. One of two columns was usually employed, either 6 m of Durapak phenylisocyanate on Porasil-C for hydrocarbon analysis, or 3 m of squalane on Celite for analysis of aldehydes and ketones, and duplicate experiments were made to obtain complete product analysis.

Cyclobutanol of stated purity 99+% was purchased from Aldrich Chemical Co. and used after rigorous degassing and simple trap-to-trap distillation. Very small amounts of ethylene and several other hydrocarbons remained, and traces of acetaldehyde and butyraldehyde were present. These impurities were all also products of the pyrolysis and small corrections were made to measured product yields.

## Results and discussion

*Reaction products*

The major products of the decomposition under all conditions were ethylene and acetaldehyde, as found by Stacey (7). Vinyl alcohol would be expected from the simple decomposition analogous to reaction [1], but would not have been directly detected in the present experiments as it would have been strongly retained on the columns employed. In the untreated vessel ethylene and acetaldehyde were observed in approximately equal amounts except at the lowest temperature (250°C) where acetaldehyde was about 80% of the ethylene. In the conditioned vessel acetaldehyde was consistently less than the ethylene, ranging from 65 to 85%. Very recently it has been shown by mass spectrometry that vinyl alcohol is a major primary product of the pyrolysis of cyclobutanol vapor in a quartz tube at 950°C and about 1 mTorr pressure (8). The stability of vinyl alcohol has been a subject of some controversy, the isomerization being apparently very surface sensitive. It seems probable that vinyl alcohol was formed initially in the present experiments but mostly isomerized to acetaldehyde before analysis, more efficiently in the untreated vessel than in the conditioned one. Careful analysis on a β,β′-phenylnaphthylamine column showed that ethylene oxide, another possible isomer of vinyl alcohol, was not a product.

The only other product of any importance was *n*-butyraldehyde, which ranged in yield in the untreated vessel from about 15% of the ethylene at 250°C to about 4% at 450°C, and was rather less in the conditioned vessel.

Other minor products were $CH_4$ (0.2–0.9%), $C_2H_6$ (~0.1%), propylene (0.3–2.5%), butadiene (1.5–3.2%), and cyclobutanone (1–5%); yields in parentheses are ranges of initial values in the untreated vessel, relative to ethylene, between 250 and 450°C. Yields in the conditioned vessel were much less.

*Kinetics of the decomposition*

Production of ethylene and butyraldehyde can be described by two parallel first-order unimolecular reactions,

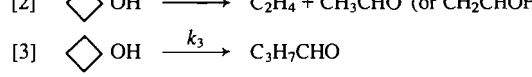


Rate constants based on yields of $C_2H_4$ and $C_3H_7$-CHO were independent of conversion up to about 10% and independent of pressure over the relatively narrow range of pressures employed (3–6 Torr). (A series of experiments in sealed untreated Pyrex tubes of ~10 $cm^3$ volume at higher pressures (~110 Torr) gave product yields and rate constants similar to those in the untreated fixed vessel.) At higher temperatures and higher conversions secondary decomposition of the aldehydes set in and yields of minor products increased.

Rates of decomposition were very much faster in the untreated reaction vessel, and less temperature dependent. Arrhenius plots of $k_2$, based on ethylene formation, are shown in Fig. 1. The Arrhenius parameters in the untreated vessel ($E$ = 32 kcal/mol, $A = 10^7$ $s^{-1}$) are much too low for a homogeneous reaction and the decomposition is obviously occurring on the surface. Values for the carbon-coated vessel of $E = 57.3 \pm 1$ kcal/mol and $A = 2.14\ (\pm 0.2) \times 10^{14}$ $s^{-1}$ on the other hand, are compatible with those observed for other homogeneous cyclobutane decompositions; the reduction in $E$ by about 5 kcal/mol from that for the parent cyclobutane seems reasonable for hydroxyl substitution. Experiments in a packed, conditioned reaction vessel with S/V increased by about a factor of 3 showed no significant change (Fig. 1) and

Can. J. Chem. Downloaded from www.nrcresearchpress.com by 210.87.254.42 on 09/06/12
For personal use only.

Can. J. Chem. Downloaded from www.nrcresearchpress.com by 210.87.254.42 on 09/06/12
For personal use only.

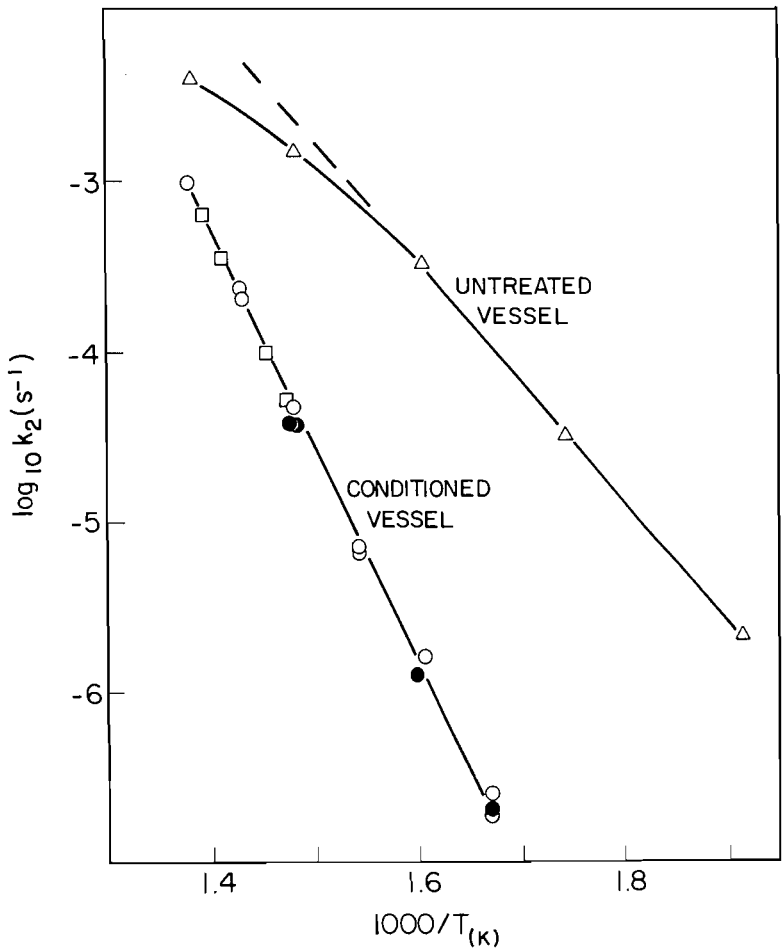


FIG. 1. Arrhenius plot of first-order rate constant $k_2$ for the thermal decomposition of cyclobutanol based on formation of $C_2H_4$. Stacey's data (Table XIV, ref. 7) = □.

it appears that the decomposition in the carbon-coated vessel was almost entirely homogeneous. Although alcohols are notoriously surface sensitive, the magnitude of the surface effect in cyclobutanol seems unusually large, with the rate of decomposition at 600 K almost 600 times faster in the clean vessel than in the carbon-coated one. Stacey (7) also found a large surface effect in the decomposition, which could be eliminated by seasoning the vessel by repeated prolonged pyrolysis of cyclobutanol or olefins. In such a seasoned vessel, Arrhenius parameters of $E = 60.1$ kcal/mol and $A = 1.28 \times 10^{15}$ s$^{-1}$ were obtained, independent of surface/volume ratio. While these values are substantially higher than ours, the actual rate constants on which they are based (plotted in Fig. 1) are in excellent agreement with the present data. Low Arrhenius parameters are generally suspect, since a variety of systematic errors (residual surface reaction, for example) tend in that direction. On the other hand, Stacy's data cover a narrow temperature range and depend on $\Delta p$ measurements at fairly high conversions, and on balance, our present Arrhenius parameters are probably more reliable.

Figure 2 shows Arrhenius plots of the product ratio $C_3H_7CHO/C_2H_4$ (i.e., $k_3/k_2$) for the treated and untreated reaction vessels; the ratio increases with decreasing temperature and is consistently higher and less temperature-dependent in the latter.

*Mechanism of the reaction*

The present observations point to a mechanism analogous to that suggested for 1,2-dimethylcyclobutane (4), shown in Fig. 3, which also shows the energetics of the decomposition. If the isomerization of the biradical is assumed to proceed with little or no activation energy, as seems probable,

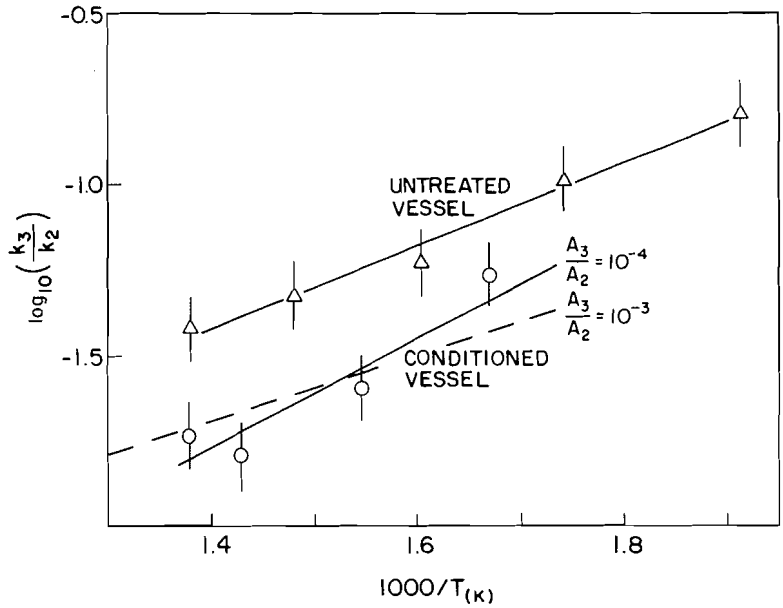


FIG. 2. Arrhenius plot of $k_3/k_2$, based on relative yields of *n*-butyraldehyde and ethylene.

the value of $E_2 - E_3 = 7.3$ derived from Fig. 2 for the conditioned vessel can be approximately equated to the activation energy for the decomposition of the biradical; from the value of $E_2 = 57.3$, the heat of formation of the biradical from cyclobutanol then becomes 50 (all energies in kcal/mol). These values are in reasonable accord with those calculated for similar systems by Benson *et al.* (1), making allowance for the effect of OH substitution. The value of $A_2/A_3 = \sim 10^4$ is at least 10 times larger than can reasonably be predicted from simple estimates of entropies of activation. The dashed line in Fig. 2 has been drawn to give $A_2/A_3 = 10^3$, and results in $E_2 - E_3 = 4.3$ kcal/mol. This seems a rather low activation energy for dissociation of the biradical, and perhaps a small barrier of 2 or 3 kcal/mol to the formation of the transition state for reaction [3], leaving 6 or 7 kcal/mol for dissociation, would be a happier solution. It is unfortunate that the low yields of *n*-butyraldehyde, its secondary decomposition, and possible surface effects, make the measurements of $k_2/k_3$ rather uncertain. The present system is a somewhat unusual example of a two-channel system in which the high-energy channel, reaction [2], predominates despite its higher energy requirements, because of a favourable frequency factor.

Feit (4) reported a ratio of methylbutylketone/propylene of about 8% for the decomposition of 1,2-dimethylcyclobutanol at 381°C; this is more than three times the analogous $C_3H_7CHO/C_2H_4$ ratio at the same temperature in the conditioned vessel in the present experiments. No temperature dependence of this ratio was reported and surface conditions were not specified, although the activation energy of 58 kcal/mol, based on disappearance of the cyclobutanol, was close to that found in the present study; the frequency factor was about 5 times larger.

Dehydration, a major mode of decomposition of some alcohols (9), does not seem to be important with cyclobutanol. The expected product, cyclobutene, would have been unstable at the temperatures of the decomposition, isomerizing to butadiene. The latter was a product in the untreated vessel, rising from 1.5% of the $C_2H_4$ at 250°C to 3.3% at 450°C; it was barely measurable in the conditioned vessel, less than 0.5% at the highest temperature. The other minor products, $CH_4$, $C_2H_6$, $C_3H_6$, and cyclobutanone were also almost negligible in the conditioned vessel. Their larger production in the untreated vessel probably came from free-radical reactions initiated at the surface; there was also a marked secondary formation of these products, probably from the decomposition of acetaldehyde and butyraldehyde.

The photolysis of *n*-butyraldehyde has been thoroughly studied, both in the gas phase and in solution, in a number of laboratories, most recently by Berces and co-workers (10). It was shown that both singlet and triplet excited states were precursors of ethylene, the type II photolysis product, and cyclobutanol, with both products presumed to arise from the $\dot{C}H_2CH_2CH_2\dot{C}HOH$ biradical

Can. J. Chem. Downloaded from www.nrcresearchpress.com by 210.87.254.42 on 09/06/12
For personal use only.

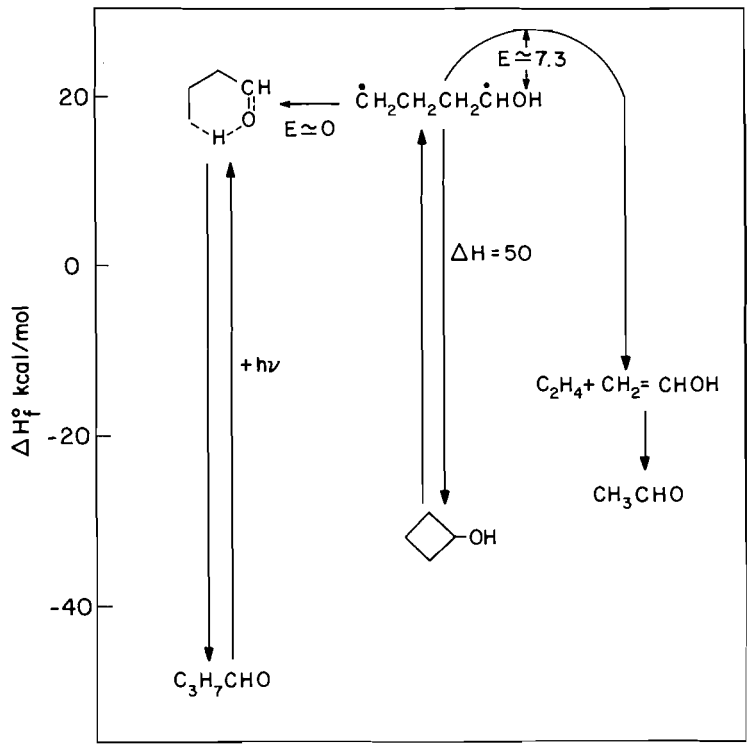


FIG. 3. Mechanism and energetics of the thermal decomposition of cyclobutanol.

formed by hydrogen transfer through a six-membered transition state (Fig. 3). The quantum yields of these products changed relatively little in going from the gas to the liquid phase, indicating that the biradical was formed directly from the excited singlet or triplet states rather than through a vibrationally excited ground state, and that vibrational excitation of the excited states was also not an important factor. In isooctane solution, the ratio $C_2H_4$/cyclobutanol (i.e., cleavage/ring closure) was 4.33, independent of temperature, while in the gas phase at 100 Torr the same ratio was 6.8 at room temperature. The difference between the gas phase and the solution, and a temperature dependence in the gas phase value, were attributed to a change in the singlet/triplet ratio, with the singlet yielding ethylene preferentially. The present study yields no information about ring closure in the cyclobutanol biradical, but Feit (4) in the thermal decomposition of *cis*-1,2-dimethylcyclobutanol at 381°C found appreciable *cis–trans* isomerization, indicating ring closure at a rate about one-third that of the cleavage to form propylene, i.e., cleavage/ring closure = 3.33. Making allowance for possible effects of methyl substitution, this value is close enough to those observed in the photolysis of *n*-butyraldehyde to support the contention that similar biradicals are intermediates in both systems.

1. S. W. BENSON and H. E. O'NEAL. Kinetic data on gas phase unimolecular reactions. NSRDS-NBS 21, Washington. 1970.
2. A. T. BLADES. Can. J. Chem. **47**, 615 (1969); T. H. McGEE and A. SCHLEIFER. J. Phys. Chem. **76**, 963 (1972); **77**, 1317 (1973); A. T. BLADES and S. SANDHU. J. Phys. Chem. **77**, 1316 (1973).
3. R. J. ELLIS and H. M. FREY. Trans. Faraday Soc. **59**, 2076 (1963).
4. E. D. FEIT. Tetrahedron Lett. 1475 (1970).
5. N. C. YANG, S. P. ELLIOT, and B. KIM. J. Am. Chem. Soc. **91**, 7551 (1969).
6. J. D. COYLE. J. Chem. Soc. B, 2254 (1971).
7. P. M. STACEY. Ph.D. Thesis. University of Rochester, Rochester, NY. 1968; Diss. Abstr. B. **29**, 1632 (1968).
8. F. P. LOSSING. Private communication.
9. H. KNOZINGER. The chemistry of the hydroxyl group. Part 2. *Edited by* S. Patai. Wiley, Interscience. New York. 1971. p. 641.
10. S. FÖRGETEG, T. BÉRCES and S. DÓBÉ. Int. J. Chem. Kinet. **11**, 219 (1979); S. FÖGETEG and T. BÉRCES. Int. J. Chem. Kinet. **11**, 239 (1979).

Can. J. Chem. Downloaded from www.nrcresearchpress.com by 210.87.254.42 on 09/06/12
For personal use only.

# Pressure and fluence dependence in the decomposition of cyclobutanone vapor by a pulsed $CO_2$ laser[1]

R. A. BACK

*Division of Chemistry, National Research Council of Canada, Ottawa, Ont., Canada K1A 0R6*

Received November 6, 1981[2]

R. A. BACK. Can. J. Chem. **60**, 2542 (1982).

A re-examination of the decomposition of cyclobutanone vapor by a pulsed $CO_2$ laser over a range of pressure and fluence has shown that the apparent disagreement in previous measurements of the pressure dependence of the $C_3H_6/C_2H_4$ product ratio can be explained by differences in absorbed energy density. At low pressures of cyclobutanone, the energy of the decomposing molecules is apparently higher at low fluence than at high fluence, and an explanation is suggested in terms of a variation in the relative proportions of "collision-modified" and "collision-free" reactions with changing pressure and absorbed energy density.

R. A. BACK. Can. J. Chem. **60**, 2542 (1982).

Une nouvelle étude de la décomposition de la cyclobutanone en phase vapeur par un laser déclenché à impulsion de $CO_2$, à diverses pressions et à divers fluence a montré que le désaccord apparent rapporté antérieurement relativement à l'effet de la pression sur le rapport de produit $C_3H_6/C_2H_4$ peut s'expliquer par des différences de densité d'énergie absorbée. A de faibles pressions de cyclobutanone, l'énergie des molécules en décomposition est apparemment plus élevée à faible fluence qu'à grand fluence; on suggère une explication en fonction de la variation des proportions relatives des réactions "modifiées par les collisions" et "sans collision" suivant la pression et la densité d'énergie absorbée.

[Traduit par le journal]

## Introduction

In the last several years, four reports from four different laboratories have described studies of the decomposition of cyclobutanone vapor induced by a pulsed $CO_2$ laser (1–4). While in all these studies decomposition was observed to follow the same two channels as seen in the thermal decomposition,

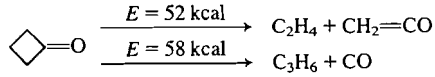


the ratio of these two channels and its dependence on cyclobutanone pressure varied considerably. In particular, Back and Back (1) found that $C_3H_6/C_2H_4$ increased sharply as the pressure was reduced below 2 Torr, while the three other groups (2–4) found that it decreased. This result was surprising, since conditions and procedures were roughly similar in these systems; we have therefore made further studies of the decomposition in an attempt to resolve these differences.

## Experimental

The reaction vessel was a brass cylinder 2 cm in diameter and 0.5 cm long, fitted with plane NaCl windows at each end. The laser beam was stopped down to give a diameter between 1.2 and 0.8 cm centered in the vessel. Two side tubes and valves permitted evacuation, filling with reagent, and direct pickup of total product and reagent for gc analysis. Source of reagent, gas handling, and analysis were otherwise as described previously (1). The laser was a Lumonics TEA laser similar to that described previously (1). It was used partially focussed with a 2 m f.l. Ge lens placed 60, 80, or 105 cm from the centre of the cell, thus giving slightly converging beams with three different incident fluences of about 1.6, 2.2, and 3.5 J/cm$^2$. The laser was tuned to the P(20) line in the 9.6 micron band (1046.9 cm$^{-1}$), the same frequency used in our previous study (1). (As correctly pointed out by Starov *et al.* (4) this frequency was erroneously reported as 1059 cm$^{-1}$ in ref. 1.)

## Results and discussion

The products were those observed previously, $C_2H_4$, cyclopropane, and propylene, the latter only significant at low pressure; ketene was not measured. In Fig. 1 is plotted the ratio $C_3H_6/C_2H_4$, where $C_3H_6$ is the sum of the cyclopropane and propylene, for the three fluences employed, together with curves representing the previous measurements. (The data of Starov *et al.* (4) are not shown, but lie close to those of Harrison *et al.* (2). Data from focussed beams reported previously from several laboratories (1–4) are also not shown and are not considered in the present discussion; the extreme conditions at the focus in these experiments (100% decomposition, high fluence and temperature, high probability of secondary reactions) we feel are not conducive to quantitative interpretation.)

It is evident that the present data effectively bridge the gap between the previously discordant results. Thus at the high fluence, the product ratio decreases with decreasing pressure, as observed by Harrison *et al.* (2), Koda and co-workers (3), and Starov *et al.* (4), while at the medium and low fluences the ratio turns upwards at low pressure in

[1]NRCC No. 20498.

[2]Revision received April 29, 1982.

0008-4042/82/202542-04$01.00/0

©1982 National Research Council of Canada/Conseil national de recherches du Canada

Can. J. Chem. Downloaded from www.nrcresearchpress.com by 210.87.254.6 on 09/06/12
For personal use only.

Can. J. Chem. Downloaded from www.nrcresearchpress.com by 210.87.254.6 on 09/06/12
For personal use only.

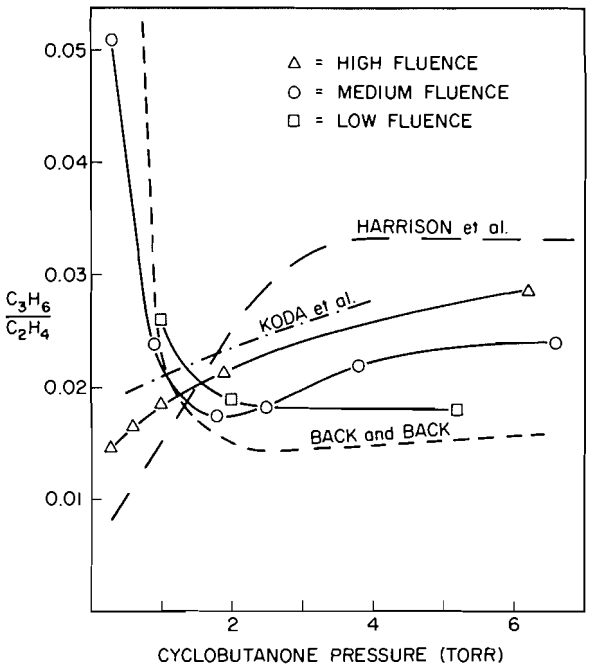


FIG. 1. Variation of the $C_3H_6/C_2H_4$ ratio with cyclobutanone pressure from the present study (points shown) and refs. 1–3 (curves only). $C_3H_6$ = cyclopropane + propylene.

agreement with previous measurements in this laboratory (1). There seems general agreement (1–4) that the product ratio at pressures above a few Torr measures simply the effective temperature of the decomposing cyclobutanone gas, which in turn reflects the absorbed energy density per pulse (J/cm³). If on this basis the 6 sets of data in Fig. 1 are placed in relative order of absorbed energy density,[3] there is seen to be a consistent systematic change in the pressure dependence of the $C_3H_6/C_2H_4$ ratio with changing absorbed energy density.

It appears that two opposing effects are superimposed, one causing a decrease in the product ratio as the pressure is decreased, the other causing an increase. At high fluence the former predominates, and at low fluence the latter; in our medium-fluence data both effects are evident, a decrease in the ratio down to about 2 Torr, and a sharp increase at lower pressures. If the $C_3H_6/C_2H_4$ ratio reflects the energy content of the decomposing cyclobutanone molecules, it must be concluded that at pressures below about 1 Torr, this energy content varies *inversely* with absorbed fluence.

Support for this conclusion also comes from the yields of propylene observed. It was first suggested by Blades (5) that propylene is formed in the cyclobutanone pyrolysis from the small fraction of cyclopropane molecules formed with sufficient vibrational excitation (> 65 kcal/mol) to isomerize, and which do so before they are deactivated by collision. Calculations by Koda *et al.* (3) based on the RRKM theory suggest that propylene is formed the same way in the laser-induced decomposition. In Fig. 2 are shown values of the ratio propylene/(propylene + cyclopropane) from the present experiments together with some previous data (1) not published before. From a value around 1 or 2% at high pressure, the ratio turns up sharply at low pressure at all fluences, but the lower the fluence, the greater the increase and the higher the pressure at which it begins. At 0.3 Torr, 75% of the cyclopropane isomerized to propylene at the medium fluence, while at the high fluence only 9% isomerized. The observations of Koda *et al.* (3) and Harrison *et al.* (2) that propylene was negligible at all pressures with the unfocussed laser are

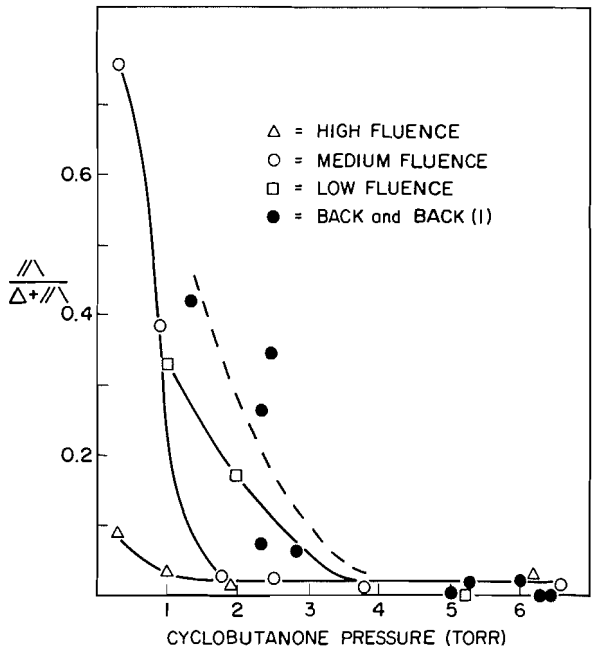


FIG. 2. Variation in the propylene/(total $C_3H_6$) ratio with cyclobutanone pressure from present work and ref. 1.

[3]Absorbed energy density, not incident fluence, is the critical parameter, not easily estimated in the absence of accurate absorption measurements and well-defined beam geometries. From the high-pressure $C_3H_6/C_2H_4$ ratios in Fig. 1, absorbed energy density was clearly much higher in ref. 2 than in ref. 1, although reported incident fluence was higher in the latter. The difference in this case is in the much stronger absorption of the 1073 $cm^{-1}$ radiation used by Harrison *et al.* compared to that of the 1046.9 $cm^{-1}$ radiation used in ref. 1 and the present study.

compatible with the data in Fig. 2, taking into account their higher absorbed energy densities. While there is some scatter in the data in Fig. 2, since absolute yields of propylene are small, they again suggest strongly that the energy content of the cyclopropane formed, and hence of the decomposing cyclobutanone molecules, varied inversely with fluence at low pressures.

In seeking an explanation of this somewhat paradoxical conclusion, it should be noted that the probability of decomposition depended very strongly on fluence at all pressures (Fig. 3). Thus for pressures of 1 Torr or lower, at low fluence, very few molecules decomposed per pulse, but apparently did so with very high energies; at high fluence many more decomposed but at much lower average energy. A tentative explanation can be suggested if the decomposition is treated as the sum of two processes. The first, which can be called the collision-modified process, is a complex dynamic competition involving interaction with the radiation field, collisional energy redistribution, decomposition, and cooling by expansion and conduction, such as has been modelled, for example, by Steel and co-workers (4). The second is a collision-free process, the decomposition of that small fraction of molecules that by statistical chance are directly pumped by the laser radiation to levels above the dissociation energy and dissociate before suffering appreciable energy loss by collision. At high pressure, only the first process is important, and it approximates in the limit to a thermal decomposition; the effective temperature, and hence the $C_3H_6/C_2H_4$ ratio, is roughly independent of pressure. As the pressure is decreased below a few Torr, the probability of decomposition via the first process decreases, for a variety of reasons, and as this is still the dominant process, the total probability of decomposition also decreases (Fig. 3). The average energy and hence the $C_3H_6/C_2H_4$ ratio for molecules decomposing by the first process also decreases, as predicted by Steel *et al.* (4). Probability of decomposition by the second process, on the other hand, increases with decreasing pressure as the time between collisions becomes longer and at some point this will become a significant fraction of the total decomposition. Because the rate of decomposition of an excited molecule increases sharply with its excess energy above the decomposition threshold, the collision-free process will be heavily weighted towards highly excited molecules which have a higher probability of decomposing before collision, and the effective "temperature" of decomposition and hence the $C_3H_6/C_2H_4$ ratio will be much higher

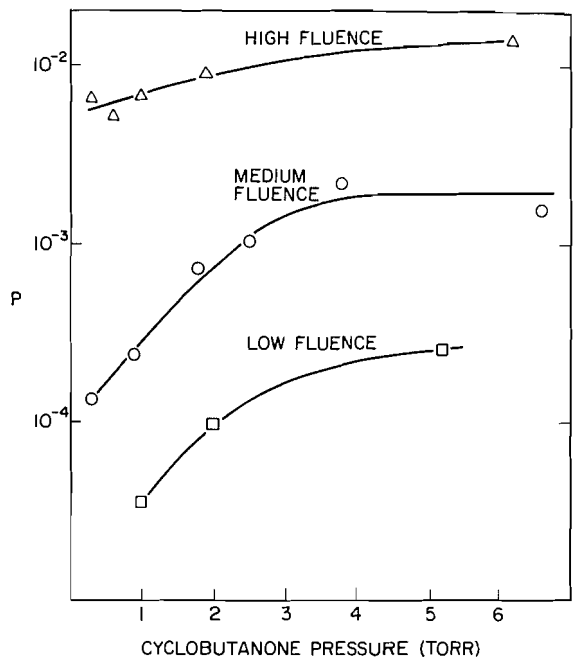


FIG. 3. Probability $P$ of decomposition of a molecule in the irradiated zone in a single pulse, as a function of cyclobutanone pressure.

than in the collision-modified process. We suggest therefore that the increase in this product ratio with decreasing pressure at low fluence (Fig. 1) may arise from an increasing proportion of collision-free decomposition sufficient to overcome the downward trend in the effective temperature of the collision-modified process. If now the probability of decomposition via the collision-modified process falls off less rapidly with decreasing pressure at high fluence than at low fluence (which appears to be borne out by the variation in the overall probability of decomposition shown in Fig. 3), then the collision-free decomposition becomes important at progressively lower pressures as the fluence is increased. In the experiments described in refs. 2–4 and at the highest fluence used in the present work, this has not yet occurred at the lowest pressure employed and the product ratio is still decreasing. In the very low pressure limit when the decomposition becomes completely collision-free, the $C_3H_6/C_2H_4$ ratio must of course revert again to a normal (i.e., direct) dependence on fluence, as dictated by common sense and any reasonable modelling of the system. As this limit is approached the ratio at low fluence will fall as the weighting in favour of the more highly excited molecules disappears; the high-fluence ratio may or may not actually increase, depending on factors affecting

Can. J. Chem. Downloaded from www.nrcresearchpress.com by 210.87.254.6 on 09/06/12
For personal use only.

the pumping efficiency at low pressure, but the high-fluence and low-fluence curves must cross again before reaching the low-pressure limit.

In conclusion, the present study has demonstrated that previous experimental disagreement about the pressure dependence of the $C_3H_6/C_2H_4$ ratio in the laser-induced decomposition of cyclobutanone is real, but can be reconciled in terms of a complex dependence on absorbed energy density. A tentative mechanistic explanation is offered which appears to account reasonably well for most of the experimental observations, including the overall probability of decomposition and the variation of the $C_3H_6/C_2H_4$ and the propylene/cyclopropane ratios.

**Acknowledgements**

The author wishes to thank M. H. Back and C. Steel for helpful discussions.

1. M. H. Back and R. A. Back. Can. J. Chem. **57**, 1511 (1979).
2. R. G. Harrison, H. L. Hawkins, R. M. Leo, and P. John. Chem. Phys. Lett. **70**, 555 (1980).
3. S. Koda, Y. Ohnuma, T. Ohkawa, and S. Tsuchiya. Bull. Chem. Soc. Jpn. **53**, 3447 (1980).
4. V. Starov, N. Selamoglu, and C. Steel. J. Phys. Chem. **85**, 320 (1981).
5. A. T. Blades. Can. J. Chem. **47**, 615 (1969).

Can. J. Chem. Downloaded from www.nrcresearchpress.com by 210.87.254.6 on 09/06/12
For personal use only.

# Stereochemical studies. XI. Equilibria between δ-hydroxy-acids and δ-lactones in aqueous tetrahydrofuran. Relative stabilities of isomeric δ-lactones

JOHN T. EDWARD, ELLEN COOKE, AND THEMISTOCLES C. PARADELLIS
*Department of Chemistry, McGill University, Montreal, P.Q., Canada H3A 2K6*

Received September 1, 1981[1]

JOHN T. EDWARD, ELLEN COOKE, and THEMISTOCLES C. PARADELLIS. Can. J. Chem. **60**, 2546 (1982).

The equilibrium constants $K'$ for the hydrolysis of 13 δ-lactones to hydroxy-acids in 54% (mol/mol) aqueous tetrahydrofuran at 25°C have been determined. The equilibrium constants for the isomerization of the five δ-lactones into their epimers, and for the isomerization of their hydroxy-acids into their epimers, have been calculated by the methods of conformational analysis. These calculated values are consistent with the experimental values of $K'$. Addition of methyl groups to a hydroxy-acid decreases $K'$ (the Thorpe–Ingold effect).

JOHN T. EDWARD, ELLEN COOKE et THEMISTOCLES C. PARADELLIS. Can. J. Chem. **60**, 2546 (1982).

On a déterminé les constantes d'équilibre $K'$ pour l'hydrolyse de 13 δ-lactones en 54% (mol/mol) tetrahydrofuran aqueux. Egalement on a calculé les constantes d'équilibre pour l'épimerisation de cinq δ-lactones, et pour l'épimerisation de cinq hydroxy-acides correspondantes, par les méthodes de l'analyse conformationelle. Les valeurs calculés sont cohérents avec les valeurs de $K'$. L'addition d'un groupement méthyl à un hydroxy-acide a pour résultat une diminution en $K'$ (l'effet Thorpe–Ingold).

## Introduction

The relative stabilities of two isomers such as *cis* and *trans*-decalin may be established by their direct equilibration over a suitable catalyst (1). In 50% sulfuric acid *trans*-1-oxa-2-oxohydrindane is converted completely into its *cis* epimer (2), and consequently we hoped to epimerize δ-lactones in hot formic acid. Some epimerization is indeed observed, but it is masked by the more extensive decomposition of the δ- into γ-lactones (3). Consequently, in the present paper we attempt to determine the relative stabilities of epimeric δ-lactones by an indirect method. A consideration of the thermodynamic cycle of Scheme 1 shows that the free energy change $\Delta G^0$ for the isomerization of a *trans* to a *cis* lactone is given by:

[1] $$\Delta G^0 = \Delta G_1^0 + \Delta G_2^0 - \Delta G_3^0$$

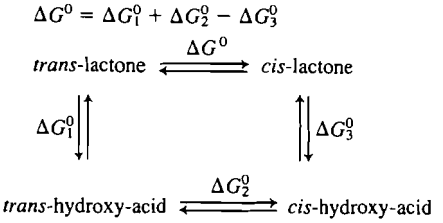


SCHEME 1

We have determined $\Delta G_1^0$ and $\Delta G_3^0$ for the equilibration of *trans* (**3**, **5**, **8**, **12** in Scheme 2) and *cis* lactones (**4**, **6**, **7**, **9**, **13**) with their hydroxy-acids in 54% (mol/mol) aqueous tetrahydrofuran, a solvent chosen because it dissolved all the lactones under study. Unfortunately, we were unable to find conditions under which the epimeric hydroxy-acids could be epimerized in this solvent, and so we have been forced to compute $\Delta G_2^0$ by the methods of conformational analysis. A few other δ-lactones (**1**, **2**, **10**, **11**) which did not belong to an epimeric pair were available, and their equilibration with their corresponding hydroxy-acids was also studied.

## Experimental

*Materials*

The lactones were prepared according to the literature (references in Scheme 2). The purity of the solid lactones was evident from satisfactory melting points. The purity of several liquid and low-melting solid lactones was checked by hydrolyzing them with a known excess of 0.100 *N* sodium hydroxide solution for 23 h, then back-titrating with 0.100 *N* hydrochloric acid solution. The purity was always found to be higher than 97%, which was judged adequate for our purposes.

Distilled water was redistilled in an all-glass apparatus, and passed through a deionizing resin immediately before use. Reagent-grade tetrahydrofuran from freshly-opened bottles was used; it was found that results were unchanged if the tetrahydrofuran was dried over calcium hydride and then passed through an alumina column.

*Experimental procedure*

The equilibration mixtures were prepared by weight, using a five-figure electric balance, to contain 0.050–0.100 *M* lactone, 0.010 *M* hydrochloric acid, tetrahydrofuran, and water. Aliquots (5–10 mL) were transferred to ampoules which were stoppered, cooled in ethanol – Dry Ice, sealed, and placed in a constant temperature bath at 25.0 ± 0.1°C. Samples of the solvent mixture (without lactone) were made up and sealed in ampoules to serve as blanks. After a week[2] the ampoules were opened, and aliquots (1.00–2.00 mL) were pipetted into 13 mL of water or 80% (v/v) tetrahydrofuran (depending on the solubility of the lactone) at 10°C and titrated with 0.100 *M*

[1]Revision received May 21, 1982.

[2]Equilibrium was generally reached in 1–2 days. Analyses after 2 weeks and 4 weeks gave the same results as after one week.

0008-4042/82/202546-08$01.00/0
©1982 National Research Council of Canada/Conseil national de recherches du Canada

Can. J. Chem. Downloaded from www.nrcresearchpress.com by 210.87.254.6 on 09/06/12
For personal use only.

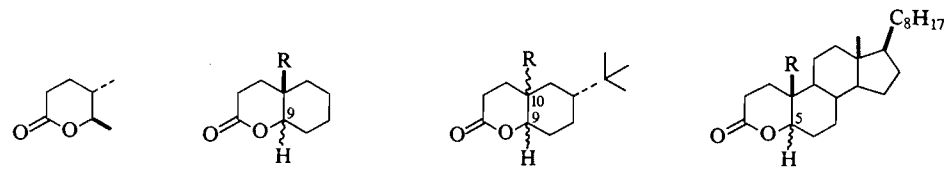

**1**(4)

**2**(3)

**3** (R = H; 9α) (5)
**4** (R = H; 9β) (4)
**5** (R = Me; 9α) (6)
**6** (R = Me; 9β) (7)

**7** (R = H; 9α, 10α) (4)
**8** (R = H; 9α, 10β) (3)
**9** (R = H; 9β, 10β) (3)
**10** (R = Me; 9α, 10α) (4)

**11** (R = H; 5α) (8)
**12** (R = Me; 5α) (9)
**13** (R = Me; 5β) (9)

SCHEME 2

aqueous sodium hydroxide at 10°C under $CO_2$-free $N_2$, using a Sargent–Welch Model DR pH meter 530000 and combination electrode 530070-10. Separate experiments showed that under these conditions there was no appreciable hydrolysis of lactone to hydroxy-acid during titration. The precision of the titration procedure was estimated to be ±0.20%, and the accuracy ±0.50%, from experiments in which potassium acid phthalate solutions were sealed into ampoules, placed in the constant temperature bath, and then removed and titrated as above.

All equilibrations were done at least in duplicate, with two or three aliquots being titrated per sample.

## Results and discussion

*Determination of* $\Delta G_1^0$ *and* $\Delta G_3^0$

For the equilibrium

$$\text{Lactone (L)} + H_2O \rightleftarrows \text{Hydroxy-acid (HA)}$$

the equilibrium constant $K$ is given by

$$[2] \quad K = \frac{a_{HA}}{a_L a_{H_2O}} = \frac{c_{HA}}{c_L} \cdot \frac{\gamma_{HA}}{\gamma_L a_{H_2O}}$$

where $a$ stands for activity, $c$ for concentration, and $\gamma$ for activity coefficient. Because the concentration of water in the aqueous tetrahydrofuran solvent was in large excess of the concentration of lactone, it remained effectively constant during the equilibration reaction. Furthermore, if we make infinite dilution in 54% (*m*/*m*) aqueous tetrahydrofuran the standard state for the lactone and hydroxy-acid, $\gamma_{HA} \approx 1$ and $\gamma_L \approx 1$ for the low concentrations in our experiments, so that we can define an equilibrium constant $K'$ ($\equiv K a_{H_2O}$)

$$[3] \quad K' = c_{HA}/c_L$$

The experimental values of $K'$ are given in Table 1. The lactone **4** was available as the pure isomer, but **3** was available only in a 65:35 mixture of **3**/**4** (as established by nmr), and so the experimental errors for the values of $K'$ and of $\Delta G^0$ ($\equiv -RT \ln K'$) reported for **3** in Table 1 may be larger than for the other lactones. The same is true for the values reported for **5**, which was available only as a 83:17 mixture of **5**/**6**.

The smaller $K'$, the greater the tendency of the hydroxy-acid to cyclize. A scrutiny of the values of $K'$ in Table 1 shows that this tendency is enhanced by the addition of a methyl group (compare **1** and **2**; **3** and **5**; **4** and **6**; **7** and **10**; **11** and **12**), an example of the Thorpe–Ingold effect (10, 11*a*). However, the cyclization tendency is enhanced much more by fusion of the steroidal BCD ring system to the lactone ring: compare **11** and **8**.

*Calculation of* $\Delta G_2^0$ *for the isomerization of the hydroxy-acids*

The free energy differences between epimeric hydroxy-acids were calculated by conventional methods, assuming the following differences in enthalpy $\Delta H^0$ between axial and equatorial orientations.

1. Hydroxyl group, 0.9 kcal/mol.[3] A skew $CH_2\cdots OH$ or $CH_3\cdots OH$ interaction was assigned half this value, 0.45 kcal/mol.
2. Methyl, 1.8 kcal/mol (11*b*).
3. $CH_2CH_2CO_2H$, 2.1 kcal/mol.

Entropy differences were calculated on the assumption that the hydroxyl or $CH_2R$ group in an equatorial position has three rotational conformations, and hence an entropy of rotation of $R \ln 3$, and in the axial position only two conformations,[4]

[3]This can be only an educated guess, because thermodynamic studies of the equilibrium: axial-OH ⇄ equatorial-OH, have not been carried out in THF–$H_2O$, and the equilibrium is solvent-sensitive (12). However, it is a plausible value, lying between the value of 0.83 kcal/mol for the aprotic but polar solvent, 1,2-dimethoxyethane, and 1.09 kcal/mol for the protic 2-propanol (12).

[4]Eliel and Gilbert (12) have discussed the question of the population of rotational conformations (two "OH-outside", one "OH-inside") of axial hydroxyl, and advance evidence (persuasive but not definitive) that in nonpolar solvents each conformation may be equally populated. However, they also point out that the axial hydroxyl hydrogen can probably not bond readily to an acceptor solvent molecule from the "OH-inside" conformations, so that this conformation would be highly disfavored in the aqueous–organic solvent used in the present study.

Can. J. Chem. Downloaded from www.nrcresearchpress.com by 210.87.254.6 on 09/06/12
For personal use only.

Can. J. Chem. Downloaded from www.nrcresearchpress.com by 210.87.254.6 on 09/06/12
For personal use only.

TABLE 1. Thermodynamic parameters for δ-lactone – hydroxy-acid equilibria in 54% (*m*/*m*) aqueous tetrahydrofuran at 25°C

| Lactone | %Hydroxy-acid at equilibrium | $K'$ | $\Delta G^0$ (kcal/mol) |
|---|---|---|---|
| *trans*-γ,δ-Dimethyl-δ-valerolactone **1** | 41.5±0.2 | 0.71 | 0.20 |
| γ,γ,δ-Trimethyl-δ-valerolactone **2** | 22.0±0.1 | 0.28 | 0.75 |
| *trans*-1-Oxadecal-2-one **3** | 47.2±1.2[a] | 0.89 | 0.07 |
| *cis*-1-Oxadecal-2-one **4** | 57.1±0.2 | 1.3 | −0.17 |
| *trans*-10-Methyl-1-oxadecal-2-one **5** | 43.9±0.9[b] | 0.78 | 0.15 |
| *cis*-10-Methyl-1-oxadecal-2-one **6** | 16.8±0.2 | 0.20 | 0.95 |
| 6α-*tert*-Butyl-1-oxa-9α,10α-decal-2-one **7** | 64.5±0.7 | 1.8 | −0.35 |
| 6α-*tert*-Butyl-1-oxa-9α-10β-decal-2-one **8** | 44.1±0.2 | 0.79 | 0.14 |
| 6α-*tert*-Butyl-1-oxa-9β,10β-decal-2-one **9** | 57.9±0.25 | 1.4 | −0.19 |
| 6α-*tert*-Butyl-10α-methyl-1-oxa-9α-decal-2-one **10** | 40.0±0.2 | 0.67 | 0.24 |
| 4-Oxa-5α-estran-3-one **11** | 10.6±0.2 | 0.12 | 1.26 |
| 4-Oxa-5α-cholestan-3-one **12** | 9.0±0.1 | 0.099 | 1.37 |
| 4-Oxa-5β-cholestan-3-one **13** | 4.2±0.2 | 0.044 | 1.85 |

[a]A mixture of 65% **3** and 35% **4** (by nmr) had 50.7±0.2% hydroxy-acid at equilibrium; from the measurements with **4** (next line in table), 20.0±0.1% of this hydroxy-acid came from **4**, and hence 30.7±0.2% from **3**, whence the fraction of **3** hydrolysed to hydroxy-acid at equilibrium is 0.307/(0.65 − 0.307) = 0.472.
[b]Calculated in similar fashion after finding a mixture of 83% of **5** and 17% of **6** had 39.3±0.1% hydroxy-acid at equilibrium.

and hence has an entropy of rotation of $R \ln 2$ (13). At 25°C this effect will cause the OH or $CH_2R$ group in the equatorial position to be favored entropically by $RT(\ln 3 - \ln 2) = 0.24$ kcal/mol over the same group in the axial position.

The ring systems of the hydroxy-acids (HA), **7**-HA, **8**-HA, **9**-HA, **12**-HA, and **13**-HA formed by hydrolysis of lactones **7**, **8**, **9**, **12**, and **13**, can exist in essentially only one conformation, shown in Scheme 3, and hence calculation of the free energy differences between epimers of these hydroxy-acids is relatively straightforward. The enthalpic ($\Delta H^0$) and entropic ($T\Delta S^0$) contributions to the free energy differences between the epimers are listed in Table 2. From these values the free energies $\Delta G_2^0$ of the epimerization reactions were calculated, and are also given in the table.

The computation of the free energy differences between the epimeric acids **14** and **15** (R = H) (Scheme 4), formed by opening the lactones **3** and **4**, is more difficult, because each ring system can exist in two conformations. Consequently, to obtain the free energy change for the epimerization:

TABLE 2. Thermodynamic parameters (in kcal/mol) for hydroxy-acids corresponding to lactones **7**, **8**, **9**, **12**, and **13**, and free energies of epimerization $\Delta G_2^0$

| | $\Delta H^0$ | | | | |
|---|---|---|---|---|---|
| Hydroxy-acid | $CH_2R$ | OH | $T\Delta S^0$ | $\Delta G^0$ | $\Delta G_2^0$ |
| **8**-HA | — | 0.45 | 0.24 | 0.21 | 0 |
| **9**-HA | — | 1.35 | 0 | 1.35 | 1.14[a] |
| **7**-HA | 2.1 | 0.45 | 0 | 2.55 | 2.34[b] |
| **12**-HA | — | 0.90 | 0.24 | 0.66 | 0 |
| **13**-HA | — | 1.35 | 0 | 1.35 | 0.69[c] |

[a]For **8**-HA ⇄ **9**-HA, given by $\Delta G^0$ (**9**-HA) − $\Delta G^0$ (**8**-HA).
[b]For **8**-HA ⇄ **7**-HA, given by $\Delta G^0$ (**7**-HA) − $\Delta G^0$ (**8**-HA).
[c]For **12**-HA ⇄ **13**-HA, given by $\Delta G^0$ (**13**-HA) − $\Delta G^0$ (**12**-HA).

**14** (R = H) ⇄ **15** (R = H), it is necessary first to calculate and take account of the mol fractions of the conformers **14***a* (R = H) and **14***b* (R = H), making up **14** (R = H), and of the mol fractions of the conformers **15***a* (R = H) and **15***b* (R = H), making up **15** (R = H). These mol fractions depend on the free energy differences $\Delta\Delta G^0$ between the two conformations (11*c*). Values of $\Delta G^0$ for each conformation were obtained by summing up the

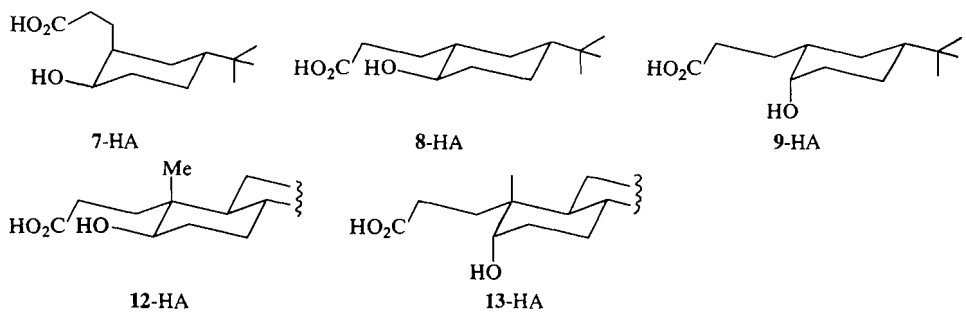


SCHEME 3

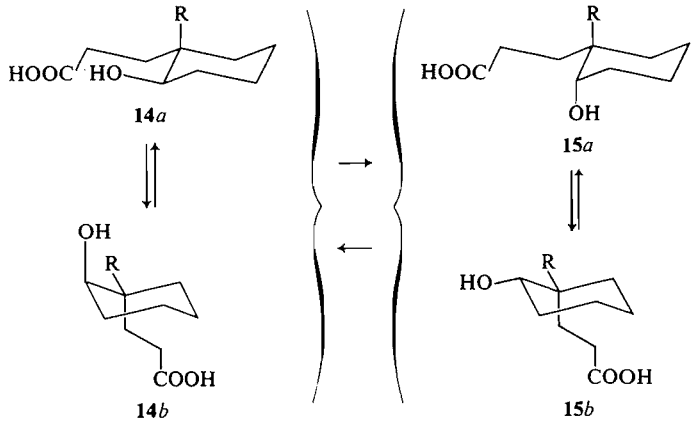


SCHEME 4

different enthalpic and entropic contributions. These are given in Table 3, as well as the $\Delta\Delta G^0$ values derived from their differences, and thence the mol fractions $x_i$ of each conformation.

We may now consider the free energy change for the reaction: **14** (R = H) ⇄ **15** (R = H). Since more than 99% of **14** (R = H) exists in the conformation **14***a*, both the enthalpy and the entropy (i.e. the free energy) of **14** will be close to that of **14***a*, given in Table 3. The 0.6% of **14** present as the conformation **14***b* will raise the enthalpy and decrease the entropy very slightly, raising the free energy according to the equation (11*d*):

[4] $\Delta G^0 = \Sigma x_i \Delta G^0_i$

However, this very small increase in free energy coming from the presence of a trace of **14***b* (R = H) is counterbalanced by the decrease in free energy coming from the entropy of mixing $\Delta S^0_m$ (11*d*), given by the equation:

[5] $\Delta S^0_m = R \Sigma x_i \ln x_i$

The free energy change due to $\Delta S^0_m$ at 25°C is given in Table 4. The free energy of the epimeric hydroxy-acid **15** (R = H) also lies between those of its constituent conformers **15***a* (R = H) and **15***b* (R = H) (given in Table 3), but now it is favoured (with respect to **14** (R = H)) by a greater entropy of mixing (see Table 4). Summing up the various contributions listed in Table 4, we see that a free energy difference $\Delta G^0_2$ of 1.07 kcal/mol favours **14** (R = H) over its epimer **15** (R = H).

The free energy difference between **14** (R = Me) and **15** (R = Me), which also exist as mixtures of conformers, was calculated in similar fashion (see Tables 3 and 4).

*Relative stabilities of epimeric lactones:* $\Delta G^0$

With $\Delta G^0_1$ and $\Delta G^0_3$ from Table 1 and $\Delta G^0_2$ from Tables 2 and 4, it is possible to calculate $\Delta G^0$ for the hypothetical *trans* ⇄ *cis* lactone epimerization using eq. [1]. The values thus obtained are given in Table 5.

These values accord moderately well with the values $\Delta G^0_{calc}$ for the hypothetical epimerization reaction calculated by the usual rules of conforma-

TABLE 3. Thermodynamic parameters (in kcal/mol) and mol fractions $x_i$ for different conformations of hydroxy-acids **14** and **15** (R = H and Me)

| | | $\Delta H^0$ | | | | | | | |
|---|---|---|---|---|---|---|---|---|---|
| Acid | R | Me | $CH_2R$ | OH | Total | $T\Delta S^{0a}$ | $\Delta G^0_i$ | $\Delta\Delta G^0$ | $x_i$ |
| **14***a* | H | — | — | 0.45 | 0.45 | 0.48 | −0.03 | 3.0 | 0.994 |
| **14***b* | H | — | 2.1 | 0.90 | 3.0 | 0 | 3.0 | | 0.006 |
| **15***a* | H | — | — | 1.35 | 1.35 | 0.24 | 1.11 | 1.2 | 0.883 |
| **15***b* | H | — | 2.1 | 0.45 | 2.55 | 0.24 | 2.31 | | 0.117 |
| **14***a* | Me | 1.8 | — | 0.90 | 2.7 | 0.48 | 2.22 | 1.2 | 0.883 |
| **14***b* | Me | — | 2.1 | 1.35 | 3.45 | 0 | 3.45 | | 0.117 |
| **15***a* | Me | 1.8 | — | 1.35 | 3.15 | 0.24 | 2.91 | −0.15 | 0.437 |
| **15***b* | Me | — | 2.1 | 0.90 | 3.0 | 0.24 | 2.76 | | 0.563 |

[a] Differences in entropy-of-mixing due to differences in numbers of OH and CHR rotational conformers.

Can. J. Chem. Downloaded from www.nrcresearchpress.com by 210.87.254.6 on 09/06/12
For personal use only.

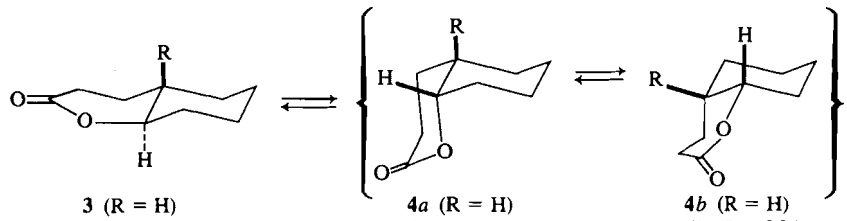

**3** (R = H)
**5** (R = Me)

**4***a* (R = H)
**6***a* (R = Me)

**4***b* (R = H)
**6***b* (R = Me)

SCHEME 5

TABLE 4. Free energies (in kcal/mol) of epimeric hydroxy-acids **14** and **15** (R = H and Me), and thence free energies of epimerization $\Delta G_2^0$

| Acid | R | $\Sigma x_i \Delta G^0_i$ | $RT\Sigma x_i \ln x_i$ | $\Delta G^0$ | $\Delta G_2^0$ |
|---|---|---|---|---|---|
| **14** | H | −0.01 | 0.02 | −0.03 | 1.07[a] |
| **15** | H | 1.25 | 0.21 | 1.04 | |
| **14** | Me | 2.36 | 0.21 | 2.15 | 0.27[b] |
| **15** | Me | 2.83 | 0.41 | 2.42 | |

[a]For **14** (R = H) ⇄ **15** (R = H).
[b]For **14** (R = Me) ⇄ **15** (R = Me).

TABLE 5. Free energy differences $\Delta G^0$ (in kcal/mol) of epimeric δ-lactones

| Reaction | $\Delta G^0$ from [1] | $\Delta G^0_{calc}$ |
|---|---|---|
| **3** ⇄ **4** | 1.3 | 1.4 |
| **5** ⇄ **6** | −0.5 | 0.05 |
| **8** ⇄ **9** | 1.4 | 1.5 |
| **8** ⇄ **7** | 2.8 | 2.5 |
| **12** ⇄ **13** | 0.2 | 0.3 |

tional analysis. To obtain $\Delta G^0_{calc}$ we calculate first $\Delta H^0$, and then $T\Delta S^0$, as follows.

We assume that all the lactone rings of **1** – **13** are in the half-chair conformation, with the ester linkage and the atoms attached to it coplanar or nearly so (14). We then count the number of skew interactions in each compound (or in each conformation, as in the case of **4** and **6** (Scheme 5), which can exist in two conformations *a* and *b*) and compute $\Delta H^0$ for each compound (Table 7) or each conformation (Table 6), assuming the following skew interaction enthalpies (in kcal/mol): C···C, 0.9; CO···C, 0.7 (11*e*, 15); O···C, 0.3.

In the case of the conformationally-mobile compounds **4** and **6**, $\Delta H^0$ lies somewhere between the values for each separate conformation, depending on the mol fractions $x_1$ and $x_2$ (11*d*):

$$[6] \quad \Delta H^0 = x_1 \Delta H_1^0 + x_2 \Delta H_2^0$$

The mol fractions in turn are determined by $\Delta H_1^0$ (it being assumed that the entropies of the various conformations are identical), and are given in Table 6 along with the values of $\Delta H^0$ calculated from eq. [6].

The differences $\Delta\Delta H^0$ between the enthalpies $\Delta H^0$ of the epimeric lactones are given in Table 7. These parallel (roughly!) the summed values $\Sigma\sigma$ of the $^{13}C$ chemical shifts, the latter being given in Table 8. For epimeric cyclohexane derivatives, Perlin and Koch (16) have shown that the net shielding of $^{13}C$ nuclei is higher in the more strained epimer. Thus a comparison of the summed values of the $^{13}C$ chemical shifts ($\Sigma\sigma$) of *cis* and *trans* 1,2-, 1,3-, and 1,4-dimethylcyclohexanes, where the enthalpy difference is 1.8 kcal/mol, showed differences $\Delta\Sigma\sigma$ of 26–30 ppm, $\Sigma\sigma$ being smaller in the more strained compound.[5] A similar comparison for epimeric cyclohexanols, where $\Delta\Delta H^0 \approx 0.9$ kcal/mol, showed $\Delta\Sigma\sigma \approx 16$ ppm. The similar relation shown between $\Delta\Sigma\sigma$ and our computed $\Delta\Delta H^0$ values increases our confidence in the latter.

Assuming no differences in entropy between epimers, the values of $\Delta G^0_{calc}$ for **8** ⇄ **9**, **8** ⇄ **7**, and **12** ⇄ **13** in Table 5 are obtained from the $\Delta\Delta H^0$ values of Table 7. However, the epimers **4** and **6** are stabilized by entropy of mixing (given by eq. [5]); this contribution is given in Table 6. The $\Delta G^0_{calc}$ values for **3** ⇄ **4** and **5** ⇄ **6** in Table 5 are obtained by subtracting the $T\Delta S^0$ values of Table 6 from the $\Delta\Delta H^0$ values of Table 7.

Considering the many approximations made, the agreement between $\Delta G^0$ and $\Delta G^0_{calc}$ in Table 5 is reasonably satisfactory except for the equilibrium **5** ⇄ **6**. The poor agreement in this case may have two reasons: (a) the $\Delta G_1^0$ value for **5** was obtained from the experimental value for a mixture of epimeric lactones **5**/**6** and from $\Delta G_3^0$ of **6**, and could suffer from cumulative experimental errors; (b) $\Delta G_2^0$ for the equilibration of the hydroxy-acids **14** (R = Me) and **15** (R = Me) (Scheme 4) could be seriously in error because of the abnormal behaviour of 1,1,2-trisubstituted cyclohexanes. Mursakulov *et al.* (17) showed that in equilibrations of such compounds the equatorial conformer is favoured to

[5]This is for shift values relative to TMS. Perlin and Koch measured shifts upfield from benzene, and under these circumstances their rule states that $\Sigma\sigma$ is *larger* for the more strained isomer.

Can. J. Chem. Downloaded from www.nrcresearchpress.com by 210.87.254.6 on 09/06/12
For personal use only.

Can. J. Chem. Downloaded from www.nrcresearchpress.com by 210.87.254.6 on 09/06/12
For personal use only.

TABLE 6. Thermodynamic parameters of conformationally-mobile lactones **4** and **6**, based on the mol ratios $x$ of conformers at 25°C

| | $\Delta H^0$ (kcal/mol) | | | | | | |
|---|---|---|---|---|---|---|---|
| Conformer | C···C | CO···C | O···C | Total | $x$ | $\Delta H^{0a}$ (kcal/mol) | $T\Delta S^{0b}$ (kcal/mol) |
| **4***a* | 0.9 | — | 0.6 | 1.5 | 0.84 | 1.66 | 0.26 |
| **4***b* | 1.8 | 0.7 | — | 2.5 | 0.16 | | |
| **6***a* | 2.7 | — | 0.6 | 3.3 | 0.66 | 3.44 | 0.38 |
| **6***b* | 2.7 | 0.7 | 0.3 | 3.7 | 0.34 | | |

[a] Calculated from [6].
[b] Calculated from [5].

TABLE 7. Enthalpies and summed $^{13}C$ nmr shifts ($\Sigma\sigma$, in ppm) of lactones

| | $\Delta H^0$ (kcal/mol) | | | | | | |
|---|---|---|---|---|---|---|---|
| Lactone | C···C | CO···C | O···C | Total | $\Delta\Delta H^0$ (kcal/mol) | $\Sigma\sigma$ | $\Delta\Sigma\sigma$ |
| **3** | — | — | — | 0 | 1.66 | 457 | 21 |
| **4** | | | | 1.66[a] | | 436 | |
| **5** | 2.7 | — | 0.3 | 3.0 | 0.44 | 480 | 9 |
| **6** | | | | 3.44[a] | | 471 | |
| **8** | — | — | — | 0 | 1.5 | 539 | 23 |
| **9** | 0.9 | — | 0.6 | 1.5 | | 516 | |
| **8** | — | — | — | 0 | 2.5 | 539 | 29 |
| **7** | 1.8 | 0.7 | — | 2.5 | | 510 | |
| **12** | 0.9[b] | — | 0.3 | 1.2 | 0.3 | | |
| **13** | 0.9[b] | — | 0.6 | 1.5 | | | |

[a] From Table 6.
[b] Excluding axial interaction of 10-Me group with B- and C-rings.

a greater extent than would be predicted from first principles: that one of the skew repulsions of the equatorial conformer "somehow disappears". A tentative explanation was advanced, in which the axial group repelled the geminal equatorial group to an extent that the skew equatorial–equatorial interaction of the vicinal equatorial groups was reduced to zero. Applied to the equilibrium **14** (R = Me) ⇄ **15** (R = Me), this effect would reduce $\Delta H^0$ of both **14***a* (R = Me) and **15***b* (R = Me) by 0.45 kcal/mol. The effect of this, carried through the various calculations outlined above, would be to raise $\Delta G_2^0$ from 0.29 kcal/mol (Table 4) to 0.49 kcal/mol, and to increase $\Delta G^0$ for **5** ⇄ **6** from −0.5 kcal/mol to −0.3 kcal/mol, somewhat closer to the $\Delta G^0_{calc}$ of 0.05 kcal/mol (Table 5).[6]

The agreement between $\Delta G^0$ and $\Delta G^0_{calc}$ in Table 5 is as good as could be expected, in view of the fact that possible entropy contributions due to vibration, solvation, etc., have been ignored, and that a simple additive scheme has been used for computing enthalpy contributions. Obviously a more detailed study of the effect of changing solvent, temperature, etc., is required.

*The Thorpe–Ingold effect*

We have found experimentally that the change from R = H to R = Me in the hydroxy-acid **16** makes the formation of the lactone **12** easier than the formation of lactone **11** by 0.11 kcal/mol (see Table 1). The newly-introduced methyl group destabilizes both **16** (R = Me) and **12** by the introduction (*inter alia*) of an additional O···C skew interaction. However, it will be noted that, accepting our values for the HO···C (0.45) and the lactone O···C (0.3 kcal/mol) skew interactions[7] given above, the destabilization of **16** (R = Me) should be more serious than the destabilization of **12** by 0.15 kcal/mol. This would explain the experimental result, and may be *one* of the factors operating to bring about the Thorpe–Ingold effect. However, the explanation of the greater stabiliza-

[6] We are indebted to a referee for pointing out ref. 17, and the above argument based on it. The referee notes that a similar argument would raise $\Delta G_2^0$ of **12**-HA ⇄ **13**-HA, and thence $\Delta G^0$ of **12** ⇄ **13** (Table 5), but it seems likely that the distortions possible in a 1,1,2-trisubstituted cyclohexane which lead to the "disappearance" of one skew interaction in the equatorial conformer are not possible in the more rigid hydroxy-acid **12**-HA.

[7] In hydroxylic solvents it is reasonable that the HO···C skew interaction have a greater enthalpy than the ester-O···C interaction because of the greater solvation of the hydroxyl group.

TABLE 8. $^{13}C$ Chemical shifts of isomeric δ-lactones

| Lactone | C | δ $^{13}C^a$ | Lactone | C | δ $^{13}C^a$ | Lactone | C | δ $^{13}C^a$ | Lactone | C | δ $^{13}C^a$ |
|---|---|---|---|---|---|---|---|---|---|---|---|
| **3**[b,c] | 2 | 170.5 | **4**[b] | 2 | 171.3 | **5**[b,d] | 2 | 170.5 | **6**[b] | 2 | 170.5 |
| | | 82.1 | | 9 | 77.4 | | 9 | 87.1 | | 9 | 82.9 |
| | | 34.5 | | | 32.8 | | | 38.0 | | | 33.0 |
| | | 32.8 | | | 30.4 | | | 35.1 | | | 31.8 |
| | | 31.2 | | | 27.1 | | | 33.3 | | | 31.4 |
| | | 29.8 | | | 27.1 | | | 27.6 | | | 28.0 |
| | | 26.5 | | | 24.5 | | | 27.4 | | | 26.8 |
| | | 25.4 | | | 24.5 | | | 24.3 | | | 24.3 |
| | | 24.2 | | | 20.6 | | | 21.1 | | | 21.1 |
| | | | | | | | 11 | 15.3 | | 11 | 21.1 |
| | | Sum 457 | | | Sum 436 | | | Sum 480 | | | Sum 471 |
| **8**[e] | 2 | 169.6 | **9**[e] | 2 | 170.6 | **7**[e] | 2 | 168.2 | | | |
| | 9 | 80.0 | | 9 | 75.6 | | 9 | 79.5 | | | |
| | | 46.9 | | | 46.9 | | | 40.0 | | | |
| | | 38.4 | | | 33.0 | | | 32.0 | | | |
| | | 32.3 | | | 31.9 | | | 31.0 | | | |
| | | 31.8 | | | 30.7 | | | 29.7 | | | |
| | | 31.8 | | | 27.8 | | | 29.5 | | | |
| | | 29.5 | | *t*-Bu | 27.2 | | | 28.5 | | | |
| | *t*-Bu | 27.4 | | | 26.4 | | *t*-Bu | 26.7 | | | |
| | | 26.4 | | | 25.0 | | | 24.8 | | | |
| | | 24.7 | | | 20.5 | | | 20.3 | | | |
| | | Sum 539 | | | Sum 516 | | | Sum 510 | | | |

[a] Chemical shifts (ppm) are relative to TMS.
[b] Neat liquid.
[c] From spectrum of mixture of **3**/**4** by subtracting peaks due to **4**.
[d] From spectrum of mixture of **5**/**6** by subtracting peaks due to **6**.
[e] In benzene.

tion of **2**, as compared with **1**, requires a consideration of many other factors, and is more difficult because of the greater numbers of conformations available both to the lactones and to the hydroxy-acids. This and other cases will be discussed later.

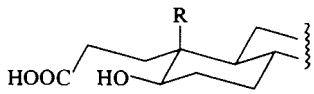


**16**

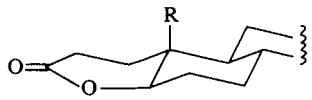


**11** (R = H)
**12** (R = Me)

## Acknowledgments

We are grateful to Prof. A. S. Perlin and Dr. H. Koch for discussion and advice, and to a referee whose helpful comments have led to the rewriting of several sections of the paper. We thank the National Research Council of Canada for financial support. J. T. E. acknowledges assistance from the National Research Council of Canada – Le Centre National de la Recherche Scientifique de France Scientific Cooperation Program, and thanks Prof. R. Schaal, La CNRS 161, Paris, in whose laboratory the first draft of this paper was written, for his hospitality and interest.

1. N. L. ALLINGER and J. L. COKE. J. Am. Chem. Soc. **81**, 4080 (1959).
2. J. KLEIN. J. Am. Chem. Soc. **81**, 3611 (1959).
3. J. T. EDWARD, E. COOKE, and T. C. PARADELLIS. Can. J. Chem. **59**, 597 (1981).
4. E. COOKE, T. C. PARADELLIS, and J. T. EDWARD. Can. J. Chem. **60**, 29 (1982).
5. H. O. HOUSE, H. BADAD, R. B. TOOTHILL, and A. W. NOLTES. J. Org. Chem. **27**, 4141 (1962).
6. H. O. HOUSE and M. SCHELLENBAUM. J. Org. Chem. **28**, 34 (1963).
7. J. T. EDWARD and J. M. FERLAND. Can. J. Chem. **44**, 1317 (1966).
8. J. T. EDWARD and J. M. FERLAND. Can. J. Chem. **44**, 1299 (1966).
9. J. T. EDWARD and P. F. MORAND. Can. J. Chem. **38**, 1325 (1960).
10. O. H. WHEELER and E. E. G. DE RODRIQUEZ. J. Org. Chem. **29**, 1227 (1964).

Can. J. Chem. Downloaded from www.nrcresearchpress.com by 210.87.254.6 on 09/06/12
For personal use only.

11. E. L. ELIEL, N. L. ALLINGER, S. J. ANGYAL, and G. A. MORRISON. Conformational analysis. John Wiley, New York. 1965; (*a*) p. 191; (*b*) p. 53; (*c*) p. 11; (*d*) pp. 23–24; (*e*) p. 441.
12. E. L. ELIEL and E. C. GILBERT. J. Am. Chem. Soc. **91**, 5487 (1969).
13. H. S. AARON, C. P. FERGUSON, and C. P. RADER. J. Am. Chem. Soc. **89**, 1431 (1967); A. KOLBE. Tetrahedron, **29**, 3019 (1973).
14. A. M. MATHIESON. Tetrahedron Lett. 81 (1963); G. KARTHA and D. J. HAAS. J. Am. Chem. Soc. **86**, 3630 (1964); K. K. CHEUNG, K. H. OVERTON, and G. A. SIM. Chem. Commun. 634 (1965); T. PHILIP, R. L. COOK, T. B. MALLOY, N. L. ALLINGER, S. CHANG, and Y. YUN. J. Am. Chem. Soc. **103**, 2151 (1981).
15. J. T. EDWARD, P. G. FARRELL, and F. SHAHIDI. Can. J. Chem. **57**, 2585 (1979).
16. A. S. PERLIN and H. J. KOCH. Can. J. Chem. **48**, 2639 (1970).
17. I. G. MURSAKULOV, E. A. RAMAZANOV, M. M. GUSEINOV, N. S. ZEFIROV, V. V. SAMOSHIN, and E. L. ELIEL. Tetrahedron, **36**, 1885 (1980).

Can. J. Chem. Downloaded from www.nrcresearchpress.com by 210.87.254.6 on 09/06/12
For personal use only.

# Complexes formés par addition d'éthers-couronnes aux énolates de $Na^+$ et $K^+$ de l'acétylacétate d'éthyle: structures cristallines et système d'équilibres en solution dans le THF et le DMSO

C. CAMBILLAU[1] ET G. BRAM[2]

*Groupe de Recherche 12, C.N.R.S., B.P. 28, 94320 Thiais, France*

J. CORSET

*Laboratoire de Spectroscopie Infrarouge et Raman, C.N.R.S., B.P. 28, 94320 Thiais, France*

ET

C. RICHE

*Institut de Chimie des Substances Naturelles, C.N.R.S., 91190 Gif-sur-Yvette, France*

Reçu le 17 décembre 1981[3]

C. CAMBILLAU, G. BRAM, J. CORSET et C. RICHE. Can. J. Chem. **60**, 2554 (1982).

La structure cristalline du complexe énolate de sodium de l'acétylacétate d'éthyle (AAE) – 15-couronne-5 ($E^-Na^+$–15C5) est décrite et comparée à celle précédemment publiée du complexe $E^-K^+$–18C6. Il s'agit dans les deux cas de paires d'ions de contact complexées extérieurement par la couronne. $Na^+$ sort du plan moyen de la couronne de 1,05 Å. La structure de ces complexes est conservée en solution dans le THF. Les résultats obtenus concernant l'addition de couronnes (C) aux énolates $E^-M^+$ en solution dans le THF (ir et cinétique) ou le DMSO (ir et conductimétrie) sont interprétés dans le cadre d'un système de quatre équilibres entre les quatre espèces ioniques: $E^-M^+$, $E^-||M^+$, $E^-M^+$–C et $E^-||M^+$ – C. Certaines valeurs de ces constantes d'équilibre ont été déterminées. À partir d'un certain excès de couronne, les deux espèces $E^-M^+$–C et $E^-||M^+$ – C restent seules en présence. La position de cet équilibre au plateau dépend fortement du solvant et du couple cation couronne. Certains résultats antérieurs dans la littérature, concernant l'alkylation des énolates de l'AAE sont rediscutés en fonction de cet équilibre au plateau.

C. CAMBILLAU, G. BRAM, J. CORSET, and C. RICHE. Can. J. Chem. **60**, 2554 (1982).

The crystal structure of the ethylacetoacetate (EAA) sodium enolate – 15 crown 5 complex ($E^-Na^+$–15C5) is described and compared with the $E^-K^+$–18C6 structure already published. Both entities are contact ion pairs externally complexed by the crown. The $Na^+$ cation is out of the mean plane of the crown (1,05 Å). The structure of both complexes is retained in THF solution. The effects observed upon addition of crowns to $E^-M^+$ enolates in THF solution (ir and kinetics) or DMSO solution (ir and conductivity) are discussed on the basis of an equilibrium between four ionic species: $E^-M^+$, $E^-||M^+$, $E^-M^+$–C, and $E^-||M^+$ – C. Some values of equilibrium constants have been determined. Of special interest is the simultaneous presence of the two species $E^-M^+$–C and $E^-||M^+$ – C when crown ether is added in excess. The position of the plateau equilibrium between these two species depends on the nature of the solvent, the cation, and the crown. Some previous results in the literature about alkylation of EAA enolates are rediscussed in relation to this plateau equilibrium.

Depuis une dizaine d'années, le chimiste organicien dispose de deux grandes classes de complexants macrocycliques des cations afin d'"activer" les anions: les éthers-couronnes monocycliques (1) et les cryptands bicycliques (2). L'effet de l'addition de cryptands à des sels alcalins semble à présent bien documenté: le cation est encapsulé[4] par le cryptand et toute interaction directe anion–cation disparaît (3, 4);[5] il s'ensuit une réactivité accrue de l'anion, comparable à celle de l'ion libre.

C'est le résultat que nous avons observé pour les solutions d'énolate de $K^+$ de l'AAE dans le THF ou le DMSO lors d'addition de cryptand (2,2,2) (5). L'addition de couronnes à des solutions de sels alcalins peut conduire à des structures et distributions d'espèces en solution fort différentes selon les cas (6, 7). En effet, la solvatation du cation dans le plan laisse alors subsister deux sites d'interaction possibles. Parmi les facteurs intervenant sur la structure des espèces, citons par exemple la polarité du milieu, les tailles respectives du cation et de la couronne, etc. ... Dans cet article, nous nous proposons de rationnaliser les phénomènes résultant de l'addition de couronnes à des solutions de sels alcalins. A cette fin, nous utiliserons comme substrats les énolates de $Na^+$ et $K^+$ de l'AAE ($E^-Na^+$, $E^-K^+$) complexés par les 15-couronne-5 (15C5) et 18-couronne-6 (18C6). Nous avons déjà montré dans un article précédent (5) que l'espèce très prédominante résultant de la complexation de $E^-K^+$ par la 8C6 dans le THF est une paire d'ions où le cation est complexé extérieurement par la

[1]Auteur à qui toute correspondance doit être adressée: G.R.12, C.N.R.S., B.P.28, 94320 Thiais, France.

[2]Adresse actuelle: Laboratoire des Réactions Sélectives sur Supports, Université de Paris-Sud, Bât. 410, 91405 Orsay Cedex, France.

[3]Révision reçue le 8 juin 1982.

[4]Le cation n'est pas entièrement encapsulé lorsque son rayon est très supérieur à celui de la cavité du cryptand (8). Nous avons d'autre part mis en évidence un autre comportement "anormal" apparu lors de la complexation du sel de $Li^+$ de l'AAE par le cryptand (2,1,1): la formation d'ion triple (9).

[5]Selon la polarité du solvant, les espèces alors formées seront des paires d'ions lâches ou des ions dissociés.

0008-4042/82/202554-12$01.00/0

©1982 National Research Council of Canada/Conseil national de recherches du Canada

Can. J. Chem. Downloaded from www.nrcresearchpress.com by 210.87.254.5 on 09/06/12
For personal use only.

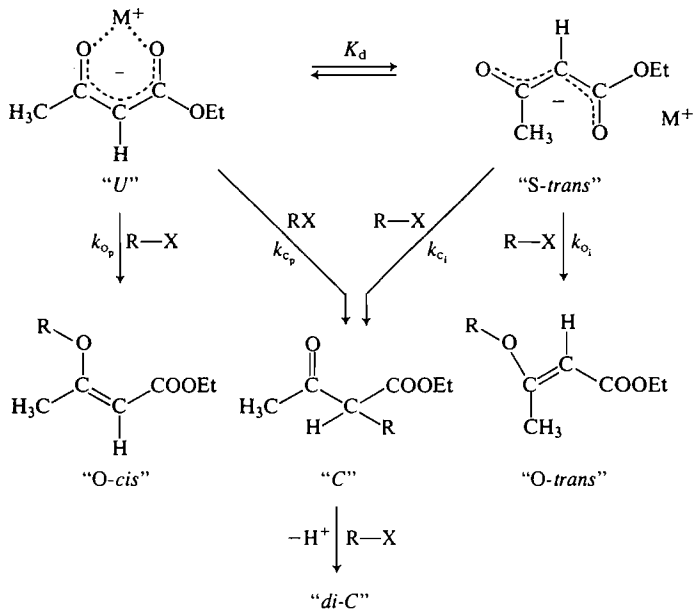


SCHÉMA 1

couronne. La O-alkylation de cette espèce de structure en *U* ne devrait conduire qu'à un éther d'énol *cis* (4). En effet, l'obtention d'éther d'énol *cis* et *trans* dans les produits d'alkylation d'énolates de composés β-dicarbonylés (tels ceux de l'AAE) a été interprétée (11, 12) en invoquant une relation directe entre la structure des éthers d'énol et celle en *U* ou *W* des deux entités réactives: la paire d'ions chélate (*U*) et l'anion dissocié ou relâché que nous avons montré être de conformation *S-trans* (13).

Dans ce cadre, nous avons expliqué la présence abondante d'éther d'énol *trans* observée dans l'alkylation de $E^-K^+$ + 18C6 (5) en postulant un équilibre entre deux espèces complexées par la couronne: l'une serait la paire d'ions à cation couronnée en *U*, l'autre, de structure *S-trans* (13), existerait en faible quantité mais sa forte réactivité se traduisait par la présence d'éther d'énol *trans*. Cette deuxième espèce pourrait être, par exemple, une paire d'ions séparée par le solvant. Smid a montré l'existence d'un tel équilibre dans le cas de sels de fluorényl (6, 7). Nous présenterons dans une première partie la structure déterminée par diffraction des rayons X du complexe $E^-Na^+$–15C5 en la comparant à celle, déjà publiée, de $E^-K^+$–18C6 (14, 5). Nous utiliserons la conductrimétrie et la spectroscopie infrarouge dans le DMSO, solvant particulièrement dissociant, pour étudier l'état d'association de nos substrats. Dans le THF, solvant associant pour nos sels, nous compléterons l'étude ir par des résultats issus de mesures cinétiques interprétées grâce à un modèle (présenté en annexe). Nous discuterons enfin, en nous appuyant sur nos résultats, certaines conclusions erronées dans la littérature.

## I. Résultats

### *1. Structure cristalline du complexe $E^-Na^+$–15C5; comparaison avec celle de $E^-K^+$–18C6*

#### *(a) Structure générale des composés*

La structure du composé $E^-Na^+$–15C5 (Figs. 1 et 2) est celle d'une entité énolate (cation couronne) isolée dans la maille. Ce résultat confirme la structure du complexe $E^-K^+$–18C6 (14, 5) premier exemple de structure d'énolate alcalin non polymérique (15, 16). Le cation est lié d'un côté à l'anion énolate et de l'autre à la couronne ce qui permet de définir ces composés comme des paires d'ions de contact complexées extérieurement par la couronne. Dans les deux composés le cation sort du plan moyen de la couronne de 1,05 Å ($Na^+$) et 0,90 Å ($K^+$). Les distances atomes d'oxygène de l'énolate–cation (Fig. 2, Tableau 1) augmentant du sodium au potassium d'une valeur égale à la différence des rayons ioniques de ces cations. Le rayon que l'on peut calculer pour ces atomes d'oxygène chargés de l'énolate est très proche du rayon de van der Waals covalent de cet atome (1,34 et 1,36 Å pour 1,40 Å (19)). On en déduit que l'énolate est en contact de van der Waals avec son cation.

Can. J. Chem. Downloaded from www.nrcresearchpress.com by 210.87.254.5 on 09/06/12
For personal use only.

Can. J. Chem. Downloaded from www.nrcresearchpress.com by 210.87.254.5 on 09/06/12
For personal use only.

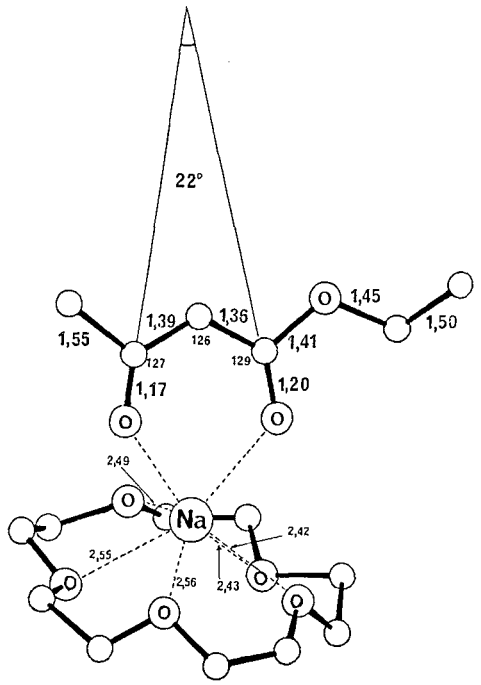


FIG. 1. Angles (degrés) et distances (Å) dans les complexes $E^-Na^+$–15C5 et $E^-K^+$–18C6.

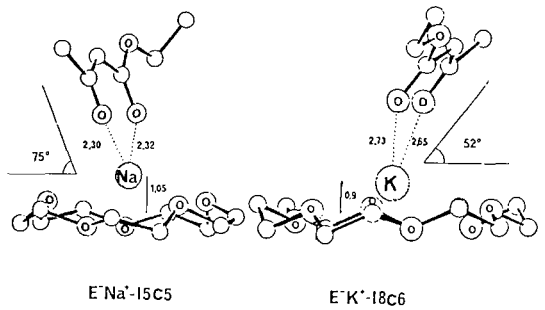


FIG. 2. Vue selon le plan moyen des couronnes, des complexes $E^-Na^+$–15C5 et $E^-K^+$–18C6 (distances en Å).

Les distances moyennes entre les oxygènes de la couronne et le cation augmentent avec le rayon ionique, du sodium (2,49 Å) au potassium (2,92 Å). Celles-ci sont supérieures de 0,1 à 0,2 Å à celles observées dans d'autres complexes où le cation est situé dans le plan de la couronne, $SCN^-K^+$–18C6 (2,80 Å) (17), $TsO^-K^+$–18C6 (2,81 Å) (18), et à celle de $I^-Na^+$ – Benzo-15C5, $H_2O$ (2,39 Å), complexe dans lequel le cation ne sort du plan de la couronne que de 0,15 Å (10). Il résulte de ceci que les oxygènes de la couronne et le cation ne sont plus au contact de van der Waals (Tableau 1). De plus, l'écart entre la valeur mesurée de la distance $O_{couronne}$—$M^+$ et la valeur calculée $r(M^+) + r(O)$,

TABLEAU 1. Distances ou rayon de van der Waals (Å) observés dans les complexes ENa–15C5 et EK–18C6

| | $Na^+$ | $K^+$ | $d(K^+ - Na^+)$ |
|---|---|---|---|
| $r_c(M^+)^a$ | 0,97 | 1,33 | 0,36 |
| $d(O_E^-M^+)^b$ | 2,31 | 2,69 | 0,38 |
| $r(O_E^-)$ | 1,34 | 1,36 | 0,02 |
| $d(O_CM^+)^c$ | 2,49 | 2,92 | 0,43 |
| $r(O_C)$ | 1,52 | 1,59 | 0,07 |

[a]Rayon ionique (19).
[b]$O_E^-$: oxygènes des énolates.
[c]$O_C$: oxygènes de la couronne.

passe de 0,12 Å pour $Na^+$ à 0,19 Å pour $K^+$ (Tableau 1). Les oxygènes de la 18C6 sont donc plus éloignée de $K^+$ que ceux de la 15C5 ne le sont de $Na^+$ du point de vue des sphères de van der Waals. Les conditions de stabilité stérique maximale de la couronne sont bien respectées dans le complexe $E^-K^+$–18C6 ou dans le complexe $SCN^-$-$K^+$–18C6 (17). En effet, le motif —C—O—C—C— est bien plan, et l'angle de rotation entre ce motif et les liaisons adjacentes est de 60°, ce qui assure aux hydrogènes une position décalée. Par contre, la 15C5 de par son manque de symétrie présente pour ces angles des écarts notables par rapport aux valeurs idéales: en particulier quatre atomes d'hydrogène sont éclipsés dans un motif $C_2H_4$ (17°) (Schéma 2).[6]

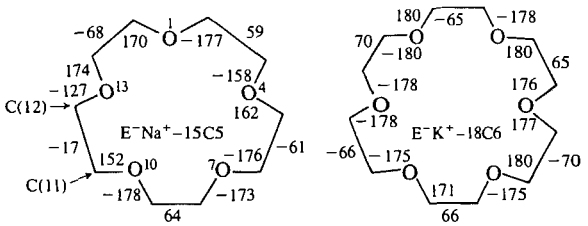


SCHÉMA 2 (Angles dièdres en degrés)

### *(b) Structure des anions énolates dans ces complexes*

Les longueurs et les angles des liaisons des énolates sont proches dans les deux complexes (Fig. 1). Il est remarquable que, malgré la dissymétrie générale de l'anion énolate de l'AAE, le motif $C_3O_2^-$ ait une symétrie presque $C_{2v}$ dans le complexe EK–18C6 et encore assez voisine de $C_{2v}$ dans le complexe ENa–15C5. La planéité de l'énolate dans le complexe EK–18C6 est rigoureuse, mais dans le complexe ENa–15C5, l'énolate présente deux déviations à cette planéité. L'une vient de la

[6]On observe dans la structure cristalline une forte agitation thermique au niveau de l'atome C(12). Ceci peut en fait correspondre à un désordre dynamique ou statique dû aux interactions défavorables dans la 15C5.

Can. J. Chem. Downloaded from www.nrcresearchpress.com by 210.87.254.5 on 09/06/12
For personal use only.

conformation *gauche* du groupement éthyle dont l'angle de torsion est de 38 degrés, l'autre met en jeu le motif $C_3O_2^-$: l'angle entre ses deux moitiés est, en effet, de 7 degrés.

*2. Étude en milieu dissociant (DMSO)*

*(a) Énolates seuls*

En préalable à toute addition de couronne, nous avons examiné l'état initial des solutions de ENa et EK dans le DMSO. À cette fin, nous avons utilisé deux méthodes: le titrage conductimétrique par le cryptand (cf. Annexe et réf. 20) pour déterminer les coefficients de dissociation $\alpha$, et la spectroscopie infrarouge afin d'identifier les espèces en équilibre.

*Conductrimétrie*

La Figure 3 présente des courbes de titrage conductimétrique obtenues en ajoutant le cryptand (2,2,2) à des solutions de $\phi_4$BNa, $\phi_4$BK, ENa et EK dans le DMSO. Les cations de ces quatre sels sont complexés quantitativement par le cryptand puisqu'un plateau est atteint dès un équivalent de cryptand ajouté. À ce plateau, les conductivités des sels de $Na^+$ sont les mêmes que celles des sels de $K^+$, aux incertitudes de mesure prés. Ceci indique que les cations de ces sels entièrement dissociés ($Na^+$–(2,2,2)) et ($K^+$–(2,2,2)) ont une même mobilité. On peut alors calculer les valeurs de $\alpha$ pour ENa et EK 0,1 *M* dans le DMSO (cf. Annexe). On trouve respectivement $\alpha = 0{,}15$ et $\alpha = 0{,}45$.

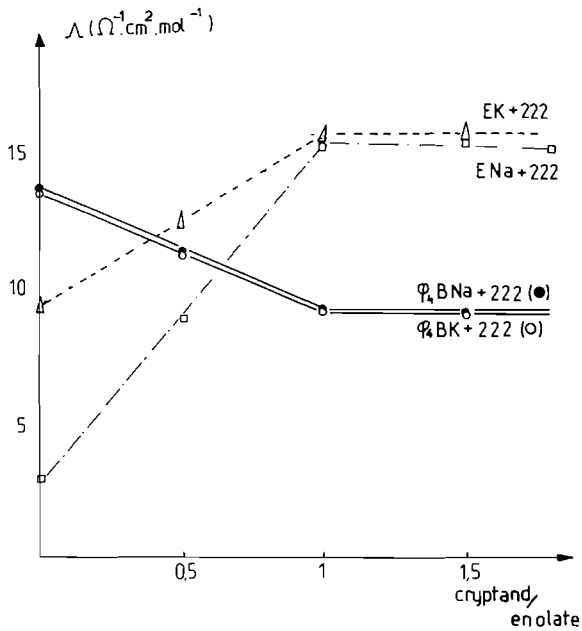


FIG. 3. Conductivités mesurées à 25°C pour des solutions 0,1 *M* dans le DMSO, de tétraphénylborates et d'énolates de $Na^+$ et $K^+$, seuls ou en présence de cryptands.

*Spectroscopie infrarouge*

Les spectres ir de ENa, EK et $E^-(K^+(2,2,2))$ en solution dans le DMSO sont présentés dans la Fig. 4. Les absorptions de $E^-(K^+(2,2,2))$ caractéristiques de l'énolate libre (5) à 1525 et 1637 $cm^{-1}$ se retrouvent en épaules dans le spectre de $E^-K^+$; par contre, seule la première est visible en très faible épaulement dans le spectre de $E^-Na^+$, ce qui corrobore le résultat conductrimétrique. Les bandes à 1474, 1514 et 1656 $cm^{-1}$ communes à $E^-Na^+$ et $E^-K^+$ appartiennent au cycle chélate $C_3O_2^-M^+$ des paires d'ions (5).

Les solutions de $E^-M^+$ dans le DMSO contiennent donc deux espèces en équilibre: la paire d'ions chélaté en *U*, et l'énolate dissocié:

$$E^-M^+, s \underset{}{\overset{K_d}{\rightleftharpoons}} E^- + M^+, s$$

avec

$$K_d(E^-Na^+) < K_d(E^-K^+)$$

*(b) Effet de l'addition de couronnes*

Nous avons mesuré la conductivité de solutions 0,1 *M* dans le DMSO de ENa, EK, $\phi_4$BNa et $\phi_4$BK lors de l'addition de 15C5 et 18C6 par la méthode précédemment décrite. Nous observons dans la Fig. 5 que les courbes conductrimétriques $\Lambda =$

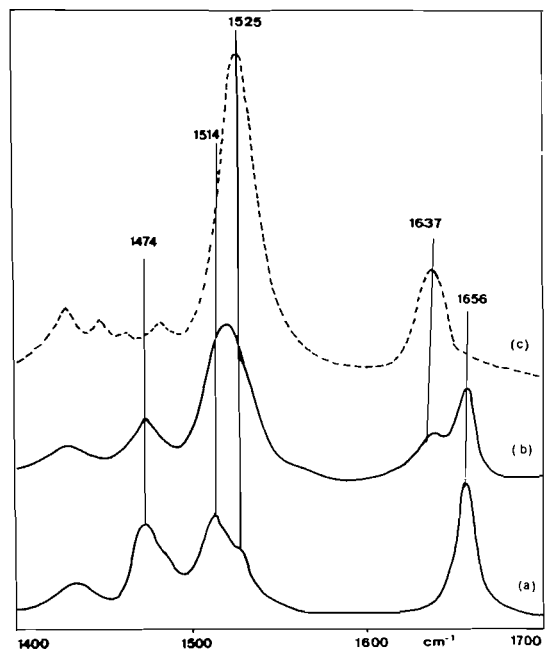


FIG. 4. Spectres infrarouges dans la zone 1500–1700 $cm^{-1}$ de $E^-Na^+$, $E^-K^+$, et $E^-(K^+(2,2,2))$ dans le DMSO. (a) $E^-Na^+$ 0,12 *M*; $1 \times c = 6{,}4 \times 10^{-7}$ mol $cm^{-2}$; (b) $E^-K^+$ 0,1 *M*; $1 \times c = 5{,}4 \times 10^{-7}$ mol $cm^{-2}$; (c) $E^-(K^+(2,2,2))$ 0,1 *M*; $1 \times c = 5{,}4 \times 10^{-7}$ mol $cm^{-2}$.

Can. J. Chem. Downloaded from www.nrcresearchpress.com by 210.87.254.5 on 09/06/12
For personal use only.

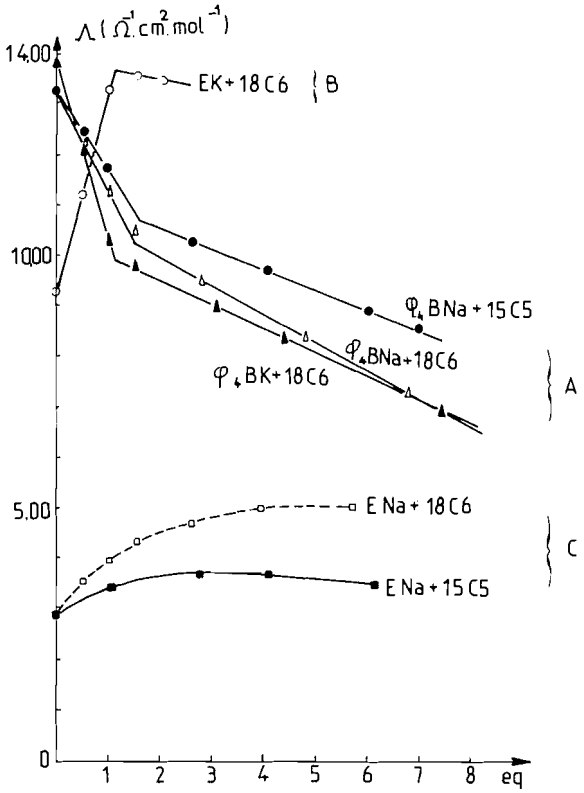


FIG. 5. Conductivités mesurées à 25°C, pour des solutions 0,1 *M* dans le DMSO, de tetraphénylborates et d'énolates de $Na^+$ et de $K^+$, en présence de 18C6 et de 15C5.

$f$(eq.) de $\phi_4B^-M^+$ sont décrites par 2 segments de droites successifs (courbe A). Un premier où la conductivité décroit rapidement ce qui traduit la diminution de mobilité du cation complexé. Un deuxième de pente plus faible rend compte d'une dilution et d'un accroissement de viscosité de la solution pour l'addition de quantités importantes de couronnes. L'abscisse de leur intersection indique le nombre d'équivalents de couronne nécessaires pour déplacer l'équilibre de complexation, sensiblement un équivalent; la valeur de la conductivité $\Lambda_1$ en ce point est celle des ions dissociés $\phi_4B^-$ et $M^+C$. Ces valeurs sont caractéristiques de la mobilité des cations complexés et suivent la séquence: $\lambda(Na^+–15C5) > \lambda(Na^+–18C6) > \lambda(K–18C6) > \lambda(K–(2,2,2))$ en accord avec les tailles de ces entités (Tableau 2). L'addition de 18C6 à une solution de EK dans le DMSO provoque d'abord une forte augmentation de la conductivité (courbe B). Puis, à partir de 1, 1 équivalent de couronne, la conductivité diminue légèrement pour les mêmes raisons citées précédemment. La conductivité $\Lambda_1$ correspondant au déplacement des équilibres de complexation du cation est *inférieure à celle de*

TABLEAU 2. Conductivités mesurées (en $\Omega^{-1}$ cm$^2$ mol$^{-1}$) pour des solutions 0,1 *M* dans le DMSO de tétraphénylborates et d'énolates de Na et de K en présence de couronnes. Rappel des valeurs en présence de cryptand (2,2,2) ($T^{re}$ = 25°C)

| Sel | (0,1 *M*) | C | Équiv. | Valeur limite |
|---|---|---|---|---|
| EK | 9,30 | 18C6 | 1,1 | 13,70 |
| $\phi_4$BK | 13,80 | 18C6 | 1,1 | 9,90 |
| EK | 9,30 | (2,2,2) | 1 | 15,30 |
| $\phi_4$BK | 13,70 | (2,2,2) | 1 | 9,15 |
| ENa | 2,90 | 15C5 | 1,1 | 3,40[a] |
| ENa | 2,90 | 18C6 | 1 | 3,95[a] |
| $\phi_4$BNa | 13,30 | 15C5 | 1,6 | 10,70 |
| $\phi_4$BNa | 13,30 | 18C6 | 1,5 | 10,25 |

[a]Cette valeur ne correspond pas à un plateau.

*$E^-(K^+–(2,2,2))$* (cf. Tableau 2) contrairement à ce que l'on attendrait pour un composé totalement dissocié puisque nous avons vu plus haut que $\lambda(K^+–18C6) > \lambda(K^+–(2,2,2))$. Cette valeur de $\Lambda_1$ traduit donc une *dissociation incomplète* de la paire d'ions au plateau. Le calcul (cf. Annexe) rend compte d'une dissociation de 85% de EK–18C6. L'énolate de sodium, beaucoup plus faiblement dissocié que EK présente un comportement fort différent. Nous voyons sur la Fig. 5 que l'addition du 15C5 ou de 18C6 ne provoque que de faibles augmentations de conductivités (courbes C). Il est intéressant de voir que la conductivité de ENa en présence de 18C6 est plus élevée que celle en présence de 15C5, pour une même quantité de couronne ajoutée. *La 18C6 est donc plus efficace que la 15C5 pour dissocier l'énolate de sodium.*

*Infrarouge*

L'addition de 0,5 à 1,1 équivalents de 18C6 à une solution de EK 0,12 *M* dans le DMSO provoque une augmentation des absorptions de l'ion libre (5) à 1637 et 1524 cm$^{-1}$ (Fig. 6), et une diminution de celles à 1656, 1473, 1214 cm$^{-1}$. Une addition supplémentaire de couronne ne modifie pas le spectre. Les équilibres de complexation sont donc totalement déplacés par addition de 1,1 équivalent de couronne, ce qui est en accord avec les résultats conductimétriques. Nous attribuons sur le spectre correspondant au plateau les absorptions à 1656, 1473, 1214 cm$^{-1}$, à l'espèce non dissociée $E^-K^+$–18C6 dans laquelle l'énolate chélate encore $K^+$ (5). La décomposition graphique des bandes à 1656 et 1637 cm$^{-1}$ du spectre au plateau, et la comparaison avec celle mesurée à 1637 cm$^{-1}$ pour $E^-(K^+(2,2,2))$ en solution dans le DMSO nous donne une valeur approchée du coefficient de dissociation de 0,80 proche de la valeur obtenue par dosage conductimétrique. La dissociation de ENa en présence de 18C6 (Fig. 6) est beaucoup plus faible que celle de EK. Nous trouvons les bandes de la paire d'ions à

Can. J. Chem. Downloaded from www.nrcresearchpress.com by 210.87.254.5 on 09/06/12
For personal use only.

1654, 1514, 1487 (ep), 1475, 1220 $cm^{-1}$. Les absorptions de l'énolate dissocié sont visibles en épaules à environ 1636 et 1524 $cm^{-1}$. Entre 2 et 11 équivalents de 18C6 ajoutés, le renversement d'intensité des épaules à 1524 et 1514 $cm^{-1}$ indique nettement une dissociation croissante de l'énolate; celle-ci reste faible, comme le confirme la courbe de dosage conductrimétrique. La 15C5, comme nous l'avons déjà remarqué lors de l'étude conductimétrique, est moins efficace que la 18C6 pour dissocier ENa. Les épaules à 1524 et 1636 $cm^{-1}$ sont très peu marquées, et la concentration en ion libre reste faible même en présence de six équivalents de couronne. (Ce spectre, très proche de celui de ENa, n'est pas présenté ici.)

L'existence de *deux espèces au plateau*, l'une associée, l'autre dissociée, mises en évidence tant en conductimétrie que par ir implique l'existence de l'équilibre **IV**:

$$\textbf{IV} \quad E^-M^+\text{–C,s} \overset{K_4}{\rightleftharpoons} E^- + M^+\text{–C,s}$$

En effet, cet équilibre est insensible à l'addition de couronne en excès:

$$K_4 = \frac{(E^-)(M^+\text{–C})}{(E^-M^+\text{–C})}$$

De plus, l'existence des équilibres **I** et **IV** implique celle des équilibres **II** et **III**, la complexation du cation pouvant en effet passer par la paire d'ions ou par le cation libre. Le modèle ci-dessous, à quatre équilibres, rend bien compte de nos résultats.

$$\begin{array}{ccc} E^-K^+, \text{DMSO} & \overset{K_1\,(\textbf{I})}{\rightleftharpoons} & E^- + K^+, \text{DMSO} \\ + & & + \\ 18C6 & & 18C6 \\ \Big\downarrow\Big\uparrow K_2 \;(\textbf{II}) & & K_3\;(\textbf{III})\Big\downarrow\Big\uparrow \\ E^-K^+\text{–18C6, DMSO} & \underset{(\textbf{IV})}{\overset{K_4}{\rightleftharpoons}} & E^- + K^+\text{–18C6, DMSO} \end{array}$$

### 3. *Études en milieu associant (THF)*

*Infrarouge*

Le spectre de $E^-Na^+$ en solution 0,1 *M* dans le THF présente de nombreuses bandes et épaules dans la région de 1400–1700 $cm^{-1}$ (Fig. 7). Un résultat analogue a été trouvé pour le spectre de $E^-K^+$ dans le THF (5). Il a été interprété par l'existence de deux espèces en équilibre: la paire d'ions solvatée et la paire d'ions faisant partie d'aggrégats. Cette conclusion peut être étendue à ENa dans le THF. Lors de l'addition de 15C5 ou de 18C6, le spectre se simplifie. Pour quatre équivalents de 15C5 et 12 de 18C6, on n'obtient plus que

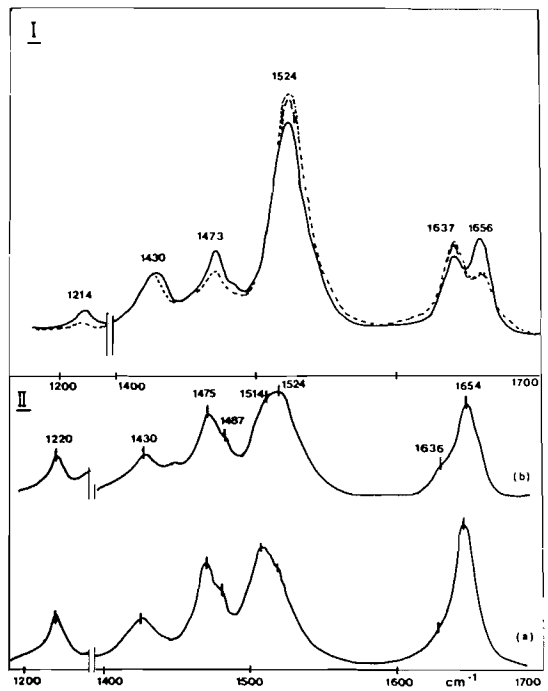


FIG. 6. I. Spectres d'absorptions ir de $E^-K^+$ en solution 0,12 *M* dans le DMSO-$d_6$, en présence de 0,5 (———), 1,1 (– – –) et 2,3 (---) équivalents de 18C6 ($1 \times c = 6{,}4 \times 10^{-7}$ mol $cm^{-2}$). II. Spectres d'absorptions ir de $E^-Na^+$ en solution 0,11 *M* dans le DMSO-$d_6$, en présence de (a) deux et (b) 11 équivalents de 18C6 ($1 \times c = 5{,}9 \times 10^{-7}$ mol $cm^{-2}$).

trois bandes caractéristiques du cycle chélate ($\nu_s$CO, $\nu_a$CC, $\nu_a$CO) à 1657, 1518 et 1472–1476 $cm^{-1}$. Les fréquences de ces absorptions sont proches de celles de ENa–15C5 cristallin que l'on trouve à 1663, 1525 et 1466 $cm^{-1}$. Comme dans le cas de $E^-K^+$ + 18C6, l'espèce existant au plateau est bien la paire d'ions couronnée. Rappelons que 2 équivalents de 18C6 sont nécessaires pour atteindre le plateau ir avec EK (5). Ainsi, l'ordre des affinités est:

$$\text{ENa} + 18C6 < \text{ENa} + 15C5 < \text{EK} + 18C6$$

*Cinétique d'alkylation*

La Figure 8 présente les résultats de l'alkylation par EtI de $E^-K^+$ en présence de 18C6 et de $E^-Na^+$ en présence des 15C5 et 18C6. À partir d'un certain nombre d'équivalents de couronne ajoutés, les constantes de vitesse ne varient plus: le plateau cinétique est donc atteint. Les constantes de vitesse d'alkylation au plateau ne dépendent pas de la couronne utilisée mais seulement du cation lié à l'énolate. Par contre, le nombre d'équivalents de couronne nécessaires pour atteindre le plateau dépend à la fois du cation et de la couronne étudiés (Fig. 8). Ainsi, il faut 1,5 à 2 équivalents de 18C6

Can. J. Chem. Downloaded from www.nrcresearchpress.com by 210.87.254.5 on 09/06/12
For personal use only.

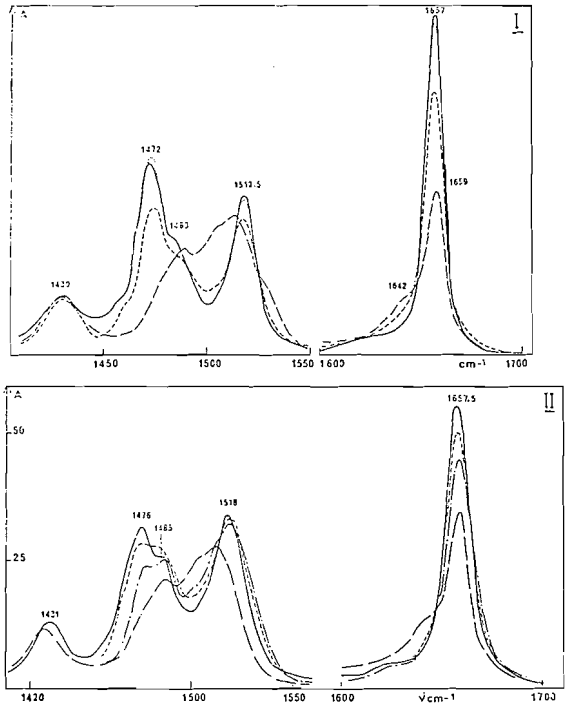


FIG. 7. Spectres d'absorptions ir de $E^-Na^+$ en solution dans le THF. I. En présence de 15C5. C/E = 0 (---); 1 (---); 5 (———); 10 (···). 1 × $c$: 5,4 × $10^{-7}$ mol $cm^{-2}$. II. En présence de 18C6. C/E: 0 (---); 2(—·—); 4 (---) et 12 (———). 1 × $c$: 5,4 × $10^{-7}$ mol $cm^{-2}$.

pour déplacer l'équilibre de complexation de EK, et respectivement 4 et 12 équivalents pour déplacer totalement les équilibres de complexation de ENa par les 15C5 et 18C6. Ces nombres d'équivalents nécessaires sont donc une mesure de l'affinité des différentes couronnes pour les paires d'ions $E^-M^+$. Ils recoupent bien les résultats infrarouge.

Nous avons en outre mesuré les constantes de vitesse d'alkylation par EtBr de EK et ENa en présence de 18C6 et de ENa en présence de 15C5 dans les conditions du plateau cinétique (Tableau 3). Comme dans le cas de l'alkylation par EtI, la valeur des constantes cinétiques au plateau ne dépend que du cation de l'énolate, et non de la couronne qui le complexe. Des quantités appréciables d'éthers d'énols apparaissent dans l'alkylation par EtBr de EK et ENa en présence de 18C6. L'isomère prépondérant est l'éther d'énol O-*trans*. Alors que les constantes cinétiques de ENa complexé par la 18C6 et la 15C5 sont très proches, la quantité d'éthers d'énols obtenue par alkylation du premier complexe est supérieure à celle obtenue pour le second. Dans le cadre du modèle représenté par l'équilibre **IV**, la connaissance de la constante globale d'alkylation $k_t$ et du pourcentage d'éthers d'énol O-*trans* permet d'obtenir la valeur de la constante de vitesse apparente de formation de l'éther d'énol *trans*: $k$ (O-*trans*). Si nous admettons que $E^-(K^+(2,2,2))$ est un bon modèle de l'espèce relâchée (ou dissociée) $E^-$, ($M^+$–C), α est donné par le rapport:

$$\alpha = \frac{k(\text{O-}trans)}{k_0(E^-(K^+ - (2,2,2))}$$

Les résultats du calcul de α (selon l'annexe 2) sont présentés dans le Tableau 4. Nous voyons que pour $E^-K^+$–18C6, α est de l'ordre de 0,3–0,5%. La valeur de α pour ENa–18C6 est supérieure à celle de ENa–15C5. Les valeurs, toutes inférieures à 1% expliquent que l'espèce dissociée (ou relâchée) ne puisse être détectée par spectroscopie ir.

## II. Discussion et conclusion

Nous discuterons nos résultats dans le cadre du modèle à quatre équilibres:

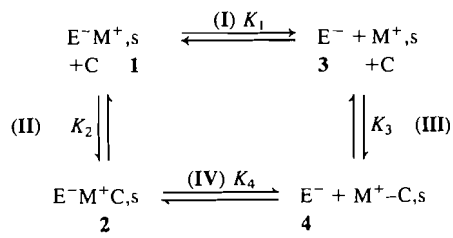


Dans le THF, les courbes d'accession au plateau ir et cinétique résultent principalement du déplacement de l'équilibre **II** vers la paire d'ions couronnée **2**. Nous excluons en effet le passage par les équilibres **I**, **III**, **IV** pour un système aussi associé que $E^-M^+$ dans le THF. La "rapidité" d'obtention du plateau cinétique ou ir traduit alors l'affinité de la couronne pour le cation chélaté selon la séquence:

THF $K_2(\text{ENa} + 18\text{C6}) < K_2(\text{ENa} + 15\text{C5}) < K_2(\text{EK} + 18\text{C6})$

Au plateau, les résultats cinétiques nous permettent de préciser que l'on est en fait en présence d'un équilibre (**IV**) entre paire d'ions couronnée et énolate relâché, cette dernière espèce, peu abondante, étant invisible par ir. Un modèle de calcul permet de trouver: $K_4$ (ENa + 15C5) < $K_4$ (ENa + 18C6) < $K_4$ (EK + 18C6).

Dans le DMSO, l'équilibre **I** est déjà appréciable initialement (on trouve **1** et **3**). Ceci implique que la complexation par la couronne doit pouvoir passer *à la fois* par les chemins **II** et **III**. Ainsi, aucune information ne peut a priori être recueillie sur les valeurs relatives de $K_2$ dans ce solvant. Cependant,

Can. J. Chem. Downloaded from www.nrcresearchpress.com by 210.87.254.5 on 09/06/12
For personal use only.

TABLEAU 3. Résultats (orientations et vitesses) concernant l'alkylation par EtBr à 25°C de solutions 0,02 *M* dans le THF d'énolates de $Na^+$ et de $K^+$ seuls on en présence de complexants (EtBr: 0,02–0,03 M)

| Énolate | $k_t$ ($M^{-1}$ min$^{-1}$) | %O | O-*trans* / O-total (× 100) | %O-*cis* | %O-*trans* | %C | %di-C |
|---|---|---|---|---|---|---|---|
| ENa | | 2,4 | 9 | 2,2 | 0,2 | 96,2 | 1,4 |
| EK | | 5,3 | 51 | 2,6 | 2,7 | 92,2 | 2,5 |
| ENa–15C5 | 0,020 | 1,4 | 29 | 1 ∓0,2 | 0,4∓0,1 | 96,6∓1 | 2 ∓0,6 |
| ENa–18C6 | 0,019 | 7,5 | 93 | 0,5∓0,15 | 7 ∓0,4 | 84 ∓0,8 | 8,6∓1,1 |
| EK–18C6 | 0,16 | 12,1 | 90 | 1,2∓0,4 | 10,9∓1,1 | 79 ∓0,8 | 8,9∓1,8 |
| E(K(2,2,2)) | 7,9 | 43 | 100 | 0 | 43 | 48 | 9 |

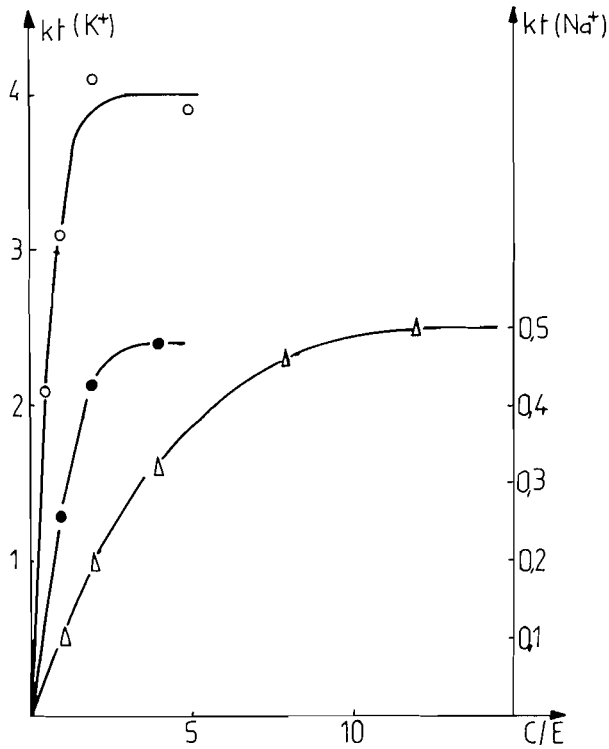


FIG. 8. Courbes $k_t = f$ (couronne/énolate) obtenues dans l'alkylation par EtI à 25°C dans le THF, de $E^-K^+$ 0,02 *M* en présence de 18C6 (○) et de $E^-Na^+$ 0,02 *M* en présence de 15C5 (●) ou de 18C6 (△). ($k_t$: $M^{-1}$ min$^{-1}$).

la complexation de EK aboutit à un plateau ir et conductimétrique qui traduit l'équilibre **IV** et permet d'accéder à $K_4$.

Les quatre constantes d'équilibre sont liées par la relation:

$$K_4 = K_1(K_3/K_2)$$

Comme dans ce cas $K_4 > K_1$ (Tableau 5), il découle que $K_3 > K_2$.

Ainsi l'affinité de la 18C6 pour $K^+$ solvaté est plus grande que pour $K^+$ dans la paire d'ions. Ceci peut être expliqué par une répulsion entre les oxygènes chargés de l'énolate et ceux de la couronne. Ce résultat était d'ailleurs attendu pour le cation $K^+$. A l'inverse, certains résultats de Smid (6, 7) montrent la grande difficulté pour une couronne à arracher $Na^+$ (libre) à sa sphère de solvant polaire (oxétane); elle choisit dans ce cas la complexation d'une paire d'ions de contact (anion = fluorényl) plus facile à désolvater. En est-il de même pour $E^-Na^+$?

Malheureusement les plateaux conductimétriques n'ont pu être obtenus pour $E^-Na^+$. Nous avons constaté simplement qu'à concentration identique en couronne, la dissociation de $E^-Na^+$ est plus forte avec la 18C6 qu'avec la 15C5. Sans les valeurs des constantes $K_4$, nous ne pouvons comparer la complexation par la 18C6 et la 15C5 de la paire d'ions et du cation libre.

Cependant, il serait intéressant de connaître *les valeurs relatives* de $K_4$ (ENa + 15C5) et $K_4$ (ENa + 18C6) dans le DMSO. Pour cela, deux assomptions sont nécessaires; nous admettrons: (*i*) que $K_2$ (ENa + C) dans le DMSO a les mêmes valeurs relatives que dans le THF, puisqu'il s'agit dans les deux cas de la complexation d'une paire d'ions de contact et que le rôle du solvant est moins important dans ce cas que dans celui de l'ion libre; (*ii*) que $K_3$ ($Na^+$–15C5) < $K_3$ ($Na^+$–18C6) comme il a déjà été observé dans des milieux dissociants ($H_2O$ ou MeOH) (2).

On obtient alors: $K_3$ (ENa + 15C5) < $K_3$ (ENa + 18C6) et $K_2$ (ENa + 15C5) > $K_2$ (ENa + 18C6) d'où $(K_3/K_2)$ (ENa + 15C5) ≪ $(K_3/K_2)$ (ENa + 18C6). Comme $K_3/K_2 = K_4/K_1$ et que $K_1$ est le même pour les 2 systèmes, $K_4$ (ENa + 15C5) ≪ $K_4$ (ENa + 18C6).

De ce fait, *la même séquence de* $K_4$ *est trouvée dans le THF et le DMSO:*

THF et DMSO:

$$K_4(\text{ENa} + 15\text{C5}) < K_4(\text{ENa} + 18\text{C6}) < K_4(\text{EK} + 18\text{C6})$$

Nous regroupons dans le Tableau 5 les valeurs

TABLEAU 4. Valeurs calculées à partir des résultats cinétiques, des coefficients de dissociation des complexes ENa–15C5, ENa–18C6 et EK–18C6 en solution 0,02 *M* dans le THF

| | ENa–15C5 | | | ENa–18C6 | | | EK–18C6 | | |
|---|---|---|---|---|---|---|---|---|---|
| | $k_{O_{tr}}$ | $k_{O_i}$ | $\alpha(\times 1000)$ | $k_{O_{tr}}$ | $k_{O_i}$ | $\alpha(\times 1000)$ | $k_{O_{tr}}$ | $k_{O_i}$ | $\alpha(\times 1000)$ |
| Et I | — | — | — | — | — | — | 0,1 | 31 | 3,2 |
| Et Br | $8 \times 10^{-5}$ | 3,4 | 0,023 | $1,3 \times 10^{-3}$ | 3,4 | 0,38 | 0,017 | 3,4 | 5 |

des constantes (ou leurs grandeurs relatives) des équilibres **I**, **II** et **IV** dans le THF ou le DMSO.

La moins grande affinité apparente de la 15C5 pour ENa par rapport à celle de la 18C6 pour EK peut être expliquée par les résultats cristallographiques: la 15C5 ne peut, en effet, assumer une structure décalée régulière. La faible affinité de la 18C6 pour ENa peut s'expliquer par la perte de la structure régulière de la 18C6 d'une part, et certainement par le fait que, d'autre part, $Na^+$ et la couronne ne sont pas en contact de van der Waals. Remarquons enfin l'inversion de l'ordre des constantes $K_2$ et $K_4$ pour $E^-Na^+$:

$$K_2(E^-Na^+ + 15C5) > K_2(E^-Na^+ + 18C6)$$

$$K_4(E^-Na^+ + 15C5) < K_4(E^-Na^+ + 18C6)$$

Une telle inversion a été observée par Smid (6) pour le fluorényl–sodium.

Elle pourrait être expliquée par une intervention du solvant au niveau du complexe cation–couronne. Cette intervention serait moins nécessaire à la stabilisation du complexe $E^-Na^+$–C qu'à celle du complexe $Na^+$–C. La meilleure accessibilité du solvant au cation $Na^+$ via les sites apicaux de la 18C6 expliquerait alors ces résultats.[7]

L'ensemble de nos résultats montre avec quelle prudence l'effet de l'addition de couronnes doit être analysé avant de tirer des conclusions. Ils contredisent en effet les interprétations que Reutov et coll. ont émises dans une séries d'articles (21–23) consacrés à l'étude du même système que le nôtre.

D'une part, ces auteurs ont invoqué un équilibre en paires d'ions *de contact S-cis* et *W* pour expliquer l'obtention d'éther d'énols *cis* et *trans* à partir de $E^-M^+$ dans le dioxanne (21), ce qui est totalement contredit par nos résultats.

D'autre part, ils ont interprété l'existence d'un plateau cinétique lors de l'addition de 18C6 à $E^-M^+$ dans le DMF (22) ou dans d'autres solvants plus ou moins dissociants (23), par la *formation exclusive* des ions dissociés. Ainsi, les constantes cinétiques obtenues devaient être celles de l'ion dissocié plus ou moins solvaté. En fait, des constantes mesurées sont des constantes apparentes $\alpha \cdot k_i$ ($k_i$ = constante de l'ion libre) dépendant à la fois de la position de l'équilibre **IV** et de la réactivité de l'ion libre.

## III. Partie expérimentale

*1. Matières premières*

(a) La préparation des énolates ainsi que la purification des solvants des réactifs alkylants et des couronnes ont été décrits précédemment (5, 12).

*2. Mesures cinétiques*

Les techniques de mesures cinétique ainsi que leur traitement ont été décrits précédemment (5, 12). Il en est de même pour les dosages de produits d'alkylation effectués par cpg ou $^1$H-rmn.

*3. Structure cristalline de $E^-Na^+$–15C5*

L'addition de couronne 15C5 à une solution concentrée ($c$ = 0,2 *M*) d'énolate de sodium dans le THF conduit à l'apparition d'un précipité cristallisé en aiguilles fines. Un cristal de dimensions 0,5 × 0,3 × 0,2 mm obtenu par recristallisation dans le benzène (saturation 0,4 *M*) a été scellé dans un tube en verre de Lindeman.

*Données cristallographiques*

$C_6H_9O_3^-$, $C_{10}H_{20}O_5$, $Na^+$ $M = 372$

Orthorhombique, groupe spatial $P2_12_12_1$, $a$ = 9,150 (2), $b$ = 13,127 (3), $c$ = 16,566 (3) Å; $V$ = 1989,8 Å$^3$, $\rho_c$ = 1,3; $Z$ = 4, $\lambda$ = 1,5418 Å (Cu K monochromateur au graphite).

L'enregistrement des données de diffraction a été réalisé sur un diffractomètre Philips PW 1100 avec la radiation $K_\alpha$ du cuivre. Les intensités des trois réflexions de référence, mesurées toutes les 120 minutes, décroissaient avec le temps d'une manière isotrope (maximum 5%). Un facteur de décomposition a été calculé à partir des valeurs de ces intensités. Cette correction de décomposition, fonction du temps a été approchée par un polynome d'ordre quatre en utilisant la méthode des

[7]Un des rapporteurs suggère que le complexe ($Na^+$–18C6) adopte une conformation dans laquelle la 18C6 est repliée, comme dans le complexe ($H_2O$, $SCN^-Na^+$–18C6) (27). Un des deux sites apicaux serait alors solvaté par un oxygène de la couronne repliée, l'autre par le solvant. Cette conformation plus favorable au sens des contacts de van der Waals doit comporter cependant de fortes interactions répulsives dans la couronne, et si elle peut être préférée dans le cristal, rien ne permet d'affirmer qu'elle existe dans un solvant aussi basique que le DMSO. Nous ne pouvons donc trancher entre les deux structures suivantes du complexe $Na^+$– 18C6 en solution.

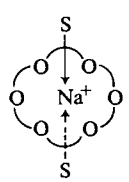


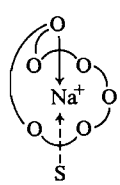


Can. J. Chem. Downloaded from www.nrcresearchpress.com by 210.87.254.5 on 09/06/12
For personal use only.

TABLEAU 5. Constantes d'équilibres concernant ENa et EK dans le THF ou le DMSO, selon le modèle à quatre équilibres

| | | |
|---|---|---|
| $K_1$ | THF | ENa < EK |
| | DMSO | ENa = $2{,}6 \times 10^{-3}$ EK = $37 \times 10^{-3}$ |
| $K_2$ | THF | ENa + 18C6 < ENa + 15C5 < EK + 18C6 |
| | DMSO | ? |
| $K_3$ | THF ou DMSO | ? |
| $K_4$ | THF | ENa + 15C5 : $10^{-11}$ ENa + 18C6 : $3 \times 10^{-9}$ EK + 18C6 : $3 \times 10^{-7}$ |
| | DMSO | ENa + 15C5 < ENa + 18C6 < EK + 18C6 : 0,32 |
| | $K_d = \frac{\alpha^2 \cdot C}{1-\alpha}$ | |

TABLEAU 6. Coordonnées atomiques ($\times 10^4$) et coefficient d'agitation thermique isotrope équivalent (Å$^2$)

| Atom | $X$ | $Y$ | $Z$ | "$B$" |
|---|---|---|---|---|
| O ( 1) | 3468 ( 9) | 4750 ( 7) | 5427 ( 5) | 8,4 |
| C ( 2) | 3417 (14) | 5580 (11) | 5994 (11) | 9,1 |
| C ( 3) | 2726 (13) | 5257 (12) | 6764 (12) | 10,3 |
| O ( 4) | 3573 ( 9) | 4483 ( 8) | 7040 ( 5) | 8,6 |
| C ( 5) | 2813 (16) | 3808 (16) | 7606 (10) | 11,2 |
| C ( 6) | 3620 (24) | 2873 (16) | 7653 (10) | 13,1 |
| O ( 7) | 3639 ( 9) | 2431 ( 8) | 6892 ( 6) | 8,1 |
| C ( 8) | 4344 (16) | 1421 (14) | 6849 (12) | 11,2 |
| C ( 9) | 4403 (20) | 1166 (14) | 5995 (16) | 12,5 |
| O (10) | 5215 (10) | 1802 ( 7) | 5616 ( 7) | 8,1 |
| C (11) | 5046 (15) | 1600 (13) | 4820 (12) | 13,0 |
| C (12) | 5256 (22) | 2418 (13) | 4338 ( 7) | 19,5 |
| O (13) | 5233 ( 9) | 3362 ( 7) | 4632 ( 5) | 8,6 |
| C (14) | 4331 (18) | 3918 (18) | 4238 ( 8) | 13,2 |
| C (15) | 4202 (13) | 5002 (12) | 4656 ( 8) | 10,1 |
| O (16) | 7005 ( 7) | 3190 ( 5) | 7078 ( 4) | 6,6 |
| C (17) | 8630 (14) | 3346 ( 8) | 8147 ( 6) | 9,2 |
| C (18) | 7884 (10) | 3728 ( 8) | 7365 ( 5) | 4,8 |
| C (19) | 8416 (10) | 4638 ( 8) | 7049 ( 6) | 5,0 |
| C (20) | 7977 (10) | 5077 ( 7) | 6346 ( 6) | 4,2 |
| O (21) | 6990 ( 7) | 4839 ( 5) | 5902 ( 4) | 5,7 |
| O (22) | 8810 ( 7) | 5942 ( 5) | 6126 ( 4) | 6,8 |
| C (23) | 8442 (14) | 6471 ( 8) | 5384 ( 7) | 8,4 |
| C (24) | 9827 (12) | 6809 ( 8) | 4978 ( 6) | 7,7 |
| Na ( ) | 5307 ( 3) | 3541 ( 3) | 6093 ( 2) | 4,6 |

moindres carrés. Sur un total de 1738 réflexions mesurées ($\theta < 68°$), 1038 répondant au critère $I > 3\sigma(I)$ (calculé à partir des erreurs statistiques de comptage) ont été considérées comme observées et utilisées lors de l'affinement des coordonnées de la structure.

La structure a été résolue par les méthodes directes à l'aide du programme MULTAN (24). Les coordonnées et les coefficients d'agitation thermique ont été affinés par la méthode des moindres carrés en minimisant l'expression $\Sigma w (|F_o| - |F_c|)^2$ où $w = 1/\sigma^2(F_o)$. Les atomes d'hydrogène ont été introduits dans les calculs de facteurs de structure en position idéale ($d_{C-H} = 1{,}0$ Å, $B_H = B_C$). Ceux du groupe méthyle C (17) ont été localisés sur une série de Fourier différence. Le facteur résiduel en fin d'affinement était de $R_w = 0{,}086$. Les facteurs de diffusion atomique ont été extraits des réfs. 25 (C, O, Na$^+$) et 26 pour H. Les coordonnées atomiques sont rassemblées dans le Tableau 6. On notera la forte agitation thermique générale qui se traduit par des valeurs élevées des $B$ équivalents (Tableau 6). Ceux-ci étant respectivement de: 4,6 (Na$^+$), 6,5 (énolate), 8,1 (oxygène de 15C5) et 12,3 (carbone de 15C5).[8]

*4. Enregistrement des spectres infrarouges*

Les spectres infrarouges sont enregistrés sur les spectrophotomètres Beckmann IR 12 et Perkin–Elmer 180. La résolution choisie est de 1 cm$^{-1}$. La précision des mesures est de $\mp$ 1 cm$^{-1}$. Les cuves utilisées pour les spectres de solutions sont en $CaF_2$, d'épaisseur allant de 8,5 à 2000 μ. Les spectres de solutions présentés ont été linéarisés.

*5. Étude conductimétrique*

Nous avons réalisé cette étude sur un conductivimètre Philips PW 9501/01 équipé d'une cellule de mesure PR 9512/00 possédant une constante de 0,685 cm$^{-1}$. La fréquence utilisée (2000 Hz) permet des mesures dans la gamme de 100 à 100000 $\times$ $10^{-6}\,\Omega^{-1}\,cm^{-1}$. La compensation de température est choisie et manuelle. Les solutions sont placées dans un récipient rodé sur lequel vient s'adapter l'électrode. Après 10 min de thermostatisation à 25°C (bain Haake uniterm R 21, $T^{re} \mp 0{,}05$°C), la valeur affichée de la constante de cellule est vérifiée, puis la valeur de la conductivité de la solution est lue.


1. H. K. FRENSDORFF. J. Am. Chem. Soc. **93**, 600 (1971).
2. J. M. LEHN. Acc. Chem. Res. **11**, 49 (1978).
3. Y. M. CAHEN et A. I. POPOV. J. Solution Chem. **4**, 599 (1975).
4. J. L. DYE. Angew. Chem. Int. Ed. Engl. **18**, 587 (1979).
5. C. CAMBILLAU, G. BRAM, J. CORSET, C. RICHE et C. PASCARD-BILLY. Tetrahedron, **34**, 2675 (1978).
6. J. SMID. Angew. Chem. Int. Ed. Engl. **11**, 112 (1972).
7. J. SMID. Intra-Sci. Chem. Rep. **7**, 75 (1973).
8. (*a*) J. L. DYE, C. W. ANDREWS et J. M. CERASO. J. Phys. Chem. **79**, 3076, 1975; (*b*) E. MEI, A. I. POPOV et J. L. DYE. J. Am. Chem. Soc. **99**, 6532 (1977).
9. C. CAMBILLAU, G. BRAM, J. CORSET et C. RICHE. Nouv. J. Chim. **3**, 9 (1979); C. CAMBILLAU et M. OUREVITCH. J. Chem. Soc. Chem. Commun. 996 (1981).
10. M. A. BUSH et M. R. TRUTER. J. Chem. Soc. Perkin Trans. II, 345 (1972).
11. A. L. KURTS, A. MACIAS, I. P. BELETSKAYA et O. A. REUTOV. Dokl. Akad. Nauk SSSR, **197**, 310 (1971) (traduction anglaise).


[8]Les facteurs d'agitation thermique des atomes non hydrogène, les coordonnées des atomes d'hydrogène et les facteurs de structure observés et calculés ont été déposés dans les données supplémentaires, et peuvent être obtenues à un prix nominal, en s'adressant au Dépôt de données non publiées, ICIST, Conseil national du recherches du Canada, Ottawa, Ont., Canada K1A 0S2.

Can. J. Chem. Downloaded from www.nrcresearchpress.com by 210.87.254.5 on 09/06/12
For personal use only.

12. (*a*) G. BRAM, F. GUIBE et P. SARTHOU. Tetrahedron Lett. 4905 (1971); (*b*) F. GUIBE, P. SARTHOU et G. BRAM. Tetrahedron, **30**, 3139 (1974).
13. C. CAMBILLAU et F. GUIBE. Can. J. Chem. **60**, 634 (1982).
14. C. RICHE, C. PASCARD-BILLY, C. CAMBILLAU et G. BRAM. J. Chem. Soc. Chem. Commun. 183 (1977).
15. F. A. SHRODER et H. P. WEBER. Acta Crystallogr. Sect. B, **31**, 1745 (1975).
16. D. E. FENTON, C. NAVE et M. R. TRUTER. J. Chem. Soc. Dalton Trans. 2198 (1973).
17. J. D. DUNITZ, M. DOBLER, P. SEILER et R. D. PHIZACKERLEY. Acta Crystallogr. Sect. B, **30**, 2733 (1974).
18. P. GROTH. Acta Chem. Scand. **25**, 3189 (1971).
19. L. PAULING. *Dans* The nature of the chemical bond. 3e éd. Cornell. 1960.
20. J. P. COLLMAN, R. G. FINKE, J. N. CAWS et J. I. BRAUMAN. J. Am. Chem. Soc. **99**, 2515 (1977).
21. A. L. KURTS, S. M. SAKEMBAEVA, I. P. BELETSKAYA et O. A. REUTOV. Zh. Org. Khim. **10**, 1588 (1974) (traduction anglaise).
22. A. L. KURTS, S. M. SAKEMBAEVA, I. P. BELETSKAYA et O. A. REUTOV. Zh. Org. Khim. **9**, 1579 (1973) (traduction anglaise).
23. A. L. KURTS, S. M. SAKEMBAEVA, I. P. BELETSKAYA et O. A. REUTOV. Vestn. Mosk. Univ. Khim. **28**, 58 (1973) (traduction anglaise).
24. P. MAIN, M. M. WOOLFSON, M. M. LESSINGER, G. GERMAIN et J. P. DECERCQ. MULTAN 74, a system of computer programs for the automatic solution of crystal structures from X-ray diffraction data. Univ. of York (England) and Louvain (Belgium). 1974.
25. P. A. DOYLE et P. S. TURNER. Acta Crystallogr. Sect. A, **24**, 390 (1968).
26. R. F. STEWART, E. R. DAVIDSON et W. T. SIMPSON. J. Chem. Phys. **42**, 3175 (1965).
27. M. DOBLER, J. D. DUNITZ et P. SEILER. Acta Crystallogr. Sect. B, **30**, 2741 (1974).

## Annexes

*1. Annexe conductimétrique. Dosage conductimétrique à l'aide du cryptand (2,2,2)*

Cette technique présentée initialement par Collman *et al.* (20) a été modifiée et discutée plus en détail dans un de nos articles précédents. Nous en rappelons l'essentiel (13).

Il est admis en première approximation que la mobilité des ions est indépendante de la concentration en espèces ioniques dans le milieu. Les conductivités équivalentes $\Lambda_i$ du tétraphénylborate de $K^+$ et de l'énolate de $K^+$ étudié en l'absence de cryptand sont alors donnés par les relations

$$[1] \quad \Lambda_{i,EK} = \alpha(\lambda_{E^-} + \lambda_{K^+})$$

$$[2] \quad \Lambda_{i,\phi_4BK} = \alpha(\lambda_{\phi_4B^-} + \lambda_{K^+})$$

$\alpha$ désignant le coefficient de dissociation de l'énolate et $\lambda$ les conductivités ioniques équivalents des ions.

En présence de cryptand, l'énolate est totalement dissocié et les conductivités équivalentes au plateau sont égales à:

$$[3] \quad \Lambda_{pl,EK} = \lambda_{E^-} + \lambda_{K^+\,crypté}$$

$$[4] \quad \Lambda_{pl,\phi_4BK} = \lambda_{\phi_4B^-} + \lambda_{K^+\,crypté}$$

Des équations [1]–[4] on tire la relation [5] utilisée pour la détermination approchée du coefficient de dissociation des énolates:

$$[5] \quad \alpha_{approx.} = \frac{\Lambda_{i,EK}}{\Lambda_{pl,EK} + \Lambda_{i,\phi_4BK} - \Lambda_{pl,\phi_4BK}}$$

La même méthode a été appliquée dans le cas du titrage conductimétrique par les couronnes.

Dans le cas de $E^-K^+ + 18C6$ on a:

$$\Lambda_{11} = \lambda_{\phi_4B^-} + \lambda_{(K^+-18C6)} = 9{,}9\,\Omega^{-1}\,cm^2\,mol^{-1}$$

$$\Lambda_{12} = \lambda_{\phi_4B^-} + \lambda_{(K^+(2,2,2))} = 9{,}15\,\Omega^{-1}\,cm^2\,mol^{-1}$$

$$\Lambda_{13} = \lambda_{E^-} + \lambda_{(K^+(2,2,2))} = 15{,}3\,\Omega^{-1}\,cm^2\,mol^{-1}$$

$$\Lambda_{13} - \Lambda_{12} + \Lambda_{11} = \lambda_{E^-} + \lambda_{K^+-18C6} = 16{,}05\,\Omega^{-1}cm^2\,mol^{-1}$$

$$\Lambda_{1(E^-K^+ + 18C6)} = \alpha(\lambda_{E^-} + \lambda_{K^+-18C6}) = 13{,}7\,\Omega^{-1}\,cm^2\,mol^{-1}$$

$$\alpha = \frac{\Lambda_{1(E^-K^+ + 18C6)}}{\lambda_{E^-} + \lambda_{K^+-18C6}} = \frac{13{,}7}{16{,}05} = 0{,}85$$

*2. Annexe cinétique. À l'aide d'un modèle dissociatif: calcul de* $\alpha$

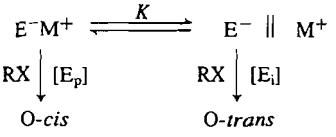


*Observés:* $k_t$, % O-*cis*, % O-*trans*
$k_{O_c}$ et $k_{O_t}$ déterminés.

$$[6] \quad \frac{dO_c}{dt} = k_{O_c} \cdot [E_t] \cdot [RX]$$

$$[7] \quad \frac{dOt}{dt} = k_{O_t} \cdot [E_t] \cdot [RX]$$

$k_{O_c}$ et $k_{O_t}$ sont des constantes apparentes mesurées expérimentalement.

Les constantes *vraies* font intervenir les concentrations en $E_p$ et $E_i$. Nous les nommerons $k_{O_p}$ et $k_{O_i}$:

$$[8] \quad \frac{dO_p}{dt} = k_{O_p} \cdot [E_p] \cdot [RX]$$

$$[9] \quad \frac{dO_i}{dt} = k_{O_i} \cdot [E_i] \cdot [RX]$$

$$[10] \quad k_{O_c} \cdot [E_t] = k_{O_p} \cdot [E_p] \qquad [6] \text{ et } [8]$$

$$[11] \quad k_{O_t} \cdot [E_t] = k_{O_i} \cdot [E_i] \qquad [7] \text{ et } [9]$$

Can. J. Chem. Downloaded from www.nrcresearchpress.com by 210.87.254.5 on 09/06/12
For personal use only.

Or, le coefficient de dissociation $\alpha$ est tel que:

$$\alpha = [E_i]/[E_t] \quad \text{et} \quad 1-\alpha = [E_p]/[E_t]$$

d'où:

[12] $k_{O_c} = k_{O_p} \cdot ([E_p]/[E_t]) = k_{O_p} \cdot (1-\alpha)$

[13] $k_{O_t} = k_{O_i} \cdot ([E_i]/[E_t]) = k_{O_i}$

[14] $$\frac{O_c}{O_t} = \frac{k_{O_c}}{k_{O_t}} = \frac{(1-\alpha)}{\alpha} \cdot \frac{k_{O_p}}{k_{O_t}} \quad [12]/[13]$$

Or,

$$\frac{dO_c}{dt} + \frac{dO_t}{dt} = k_{O_c} \cdot [E_t] \cdot [RX] + k_{O_t} \cdot [E_t] \cdot [RX]$$
$$= k_{O_p} \cdot [E_p] \cdot [RX] + k_{O_i} \cdot [E_i] \cdot [RX]$$

[15] $k_{O_c} + k_{O_t} = k_{O_p} \cdot (1-\alpha) + k_{O_i}$

On obtient donc un système linéaire de deux équations à trois inconnues: $k_{O_p}$, $k_{O_i}$, et $\alpha$.

$$\frac{k_{O_c}}{k_{O_t}} = \frac{1-\alpha}{\alpha} \cdot \frac{k_{O_p}}{k_{O_i}}$$

$$k_{O_c} + k_{O_t} = k_{O_p}(1-\alpha) + k_{O_i}$$

En faisant l'hypothèse que:
$k_{O_i} \approx k_O$ ($E^-(K^+,2,2,2)$), on obtient un système de deux équations:

$$\alpha = \frac{k_{O_t}}{k_{O_i}} = \frac{k_{O_t}}{k_O(EK,2,2,2)}$$

avec

$$k_{O_t} = k_t \cdot \frac{\text{O total}}{\text{pr. total}} \cdot \frac{\text{O-}trans}{\text{pr. total}}$$

et $k_O(E^-(K^+(2,2,2)))$ étant déterminé expérimentalement par ailleurs (5).

Can. J. Chem. Downloaded from www.nrcresearchpress.com by 210.87.254.5 on 09/06/12
For personal use only.

# Absolute rate constants for hydrocarbon autoxidation. 32. On the self-reaction of 1,1-diphenylethylperoxyl in solution[1]

J. A. HOWARD, J. H. B. CHENIER, AND T. YAMADA[2]

*Division of Chemistry, National Research Council of Canada, Ottawa, Ont., Canada, K1A 0R9*

Received May 6, 1982

J. A. HOWARD, J. H. B. CHENIER, and T. YAMADA. Can. J. Chem. **60**, 2566 (1982).

The major products of the self-reaction of 1,1-diphenylethylperoxyl have been determined from product studies of the autoxidation of 1,1-diphenylethane, induced decomposition of 1,1-diphenylethyl hydroperoxide, and decomposition of 2,2,3,3-tetraphenylbutane under an atmosphere of oxygen. Overall self-reaction is a complex free-radical process involving the intermediacy of 1,1-diphenylethoxyl and 1-phenyl-1-phenoxyethoxyl which undergo H-atom abstraction, β-scission and, in the case of the former radical, rearrangement. Hydroperoxide decomposition under an atmosphere of $^{36}O_2$ has shown that 1,1-diphenylethylperoxyl undergoes β-scission faster than α-cumylperoxyl at 303 K in solution. The values of the rate constants for self-reaction of $Ph_2C(Me)O_2\cdot$ relative to those for *tert*-butylperoxyl are, however, not affected by this reaction. Furthermore they are not affected to any appreciable extent by the efficiency with which $Ph_2C(Me)O\cdot$, formed in nonterminating self-reactions, escape from the solvent cage. They are influenced principally by the first-order rate of decomposition of $Ph_2C(Me)OOOOC(Me)Ph_2$.

J. A. HOWARD, J. H. B. CHENIER et T. YAMADA. Can. J. Chem. **60**, 2566 (1982).

On a déterminé les produits principaux de l'auto-réaction du diphényl-1,1 éthylperoxyle à partir d'études des produits provenant de l'auto-oxydation du diphényl-1,1 éthane, de la décomposition induite du diphényl-1,1 éthylhydroperoxyde et de la décomposition du tétraphényl-2,2,3,3 butane sous atmosphère d'oxygène. L'auto-réaction globale est un processus par radical libre complexe impliquant comme intermédiaire le diphényl-1,1 éthoxyle et le phényl-1 phénoxy-1 éthoxyle qui subissent une perte d'hydrogène, une scission β et, dans le cas du premier radical, une transformation. La décomposition de l'hydroperoxyde sous atmosphère de $^{36}O_2$ révèle que le diphényl-1,1 éthylperoxyle subit une scission β plus rapidement que l'α cumylperoxyle à 303 K en solution. Les valeurs de constantes de vitesse d'auto-réaction du $Ph_2C(Me)O_2\cdot$ par rapport à celles du *tert*-butylperoxyle ne sont pas, cependant, affectées par cette réaction. De plus elles ne sont pas affectées de façon appréciable par l'efficacité avec laquelle le $Ph_2C(MeO)\cdot$, formé lors d'auto-réactions intermédiaires, s'échappe de la cage du solvant. Elles sont principalement influencées par la vitesse de décomposition d'ordre un du $Ph_2C(Me)OOOOC(Me)Ph_2$.

[Traduit par le journal]

## Introduction

It has recently been re-established (1) that rates of self-reaction of α-cumylperoxyl in solution are second-order with respect to the radical concentration at 303 K and that, although β-scission of this radical (reaction [1]) occurs at this temperature, the steady-state concentration of cumyl is too low to influence the magnitude of the *overall* termination rate constant, $2k_t$, for autoxidation of cumene and the rate constant for self-reaction to give di-α-cumyl peroxide, $2k'_t$.

[1] $PhCMe_2O_2\cdot \rightleftarrows Ph\dot{C}Me_2 + O_2$

The related 1,1-diphenylethylperoxyl also decays with second-order kinetics in solution at 303 K and the values of $2k_t$ and $2k'_t$ for this radical are *both* approximately ten times larger than the corresponding rate constants for α-cumylperoxyl (2).

Recently Nangia and Benson (3) re-examined the kinetics and mechanisms for self-reactions of tertiary alkylperoxyls and concluded that the large values observed for the termination rate constants for α-cumylperoxyl and 1,1-diphenylethylperoxyl relative to the value for *tert*-butylperoxyl are the result of rather low efficiencies of cage escape for the more bulky α-cumyloxyl and 1,1-diphenylethoxyl relative to the high efficiency of cage escape for *tert*-butoxyl.

[2]

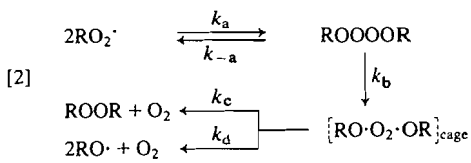


Thus they suggest that values of the rate constant ratio $k_c/k_d$ for R = $PhCMe_2$ and $Ph_2CMe$ are larger than $k_c/k_d$ for R = *t*-Bu. However, we found experimentally (1) that there is little or no difference in the values of this ratio for $PhCMe_2O_2\cdot$ and *t*-$BuO_2\cdot$ and that the differences in the magnitudes of $2k_t$ and $2k'_t$ for these two tertiary alkylperoxyls are due primarily to differences in the magnitude of the unimolecular rate constant for tetroxide decomposition, $k_b$.

Nangia and Benson (3) also concluded, from thermochemical calculations based on reasonable values of $\Delta H^0_f$ and $\Delta S^0_f$, that although β-scission of $PhCMe_2O_2\cdot$ is not important at ambient tempera-

[1]Issued as NRCC No. 20482.

[2]NRCC Research Associate 1979–1981.

0008-4042/82/202566-07$01.00/0

©1982 National Research Council of Canada/Conseil national de recherches du Canada

Can. J. Chem. Downloaded from www.nrcresearchpress.com by 210.87.254.105 on 09/06/12
For personal use only.

Can. J. Chem. Downloaded from www.nrcresearchpress.com by 210.87.254.105 on 09/06/12
For personal use only.

tures under normal experimental conditions it can become important for $Ph_2CMeO_2\cdot$ at oxygen concentrations $< 10^{-3}\,M$. This is because of the difference in the stabilization energies of $PhC\dot{M}e_2$ and $Ph_2C\dot{M}e$ (3) and $\Delta H_f^0$ for $Ph_2C\dot{M}e$ was calculated to be about a factor of 12 times larger than $\Delta H_f^0$ for $PhC\dot{M}e_2$.

The present paper reports the results of a series of experiments similar to those reported previously for α-cumylperoxyl (1) designed to rationalize the difference in the kinetics for the second-order mutual reaction of α-cumylperoxyl and 1,1-diphenylethylperoxyl in solution and to estimate the importance of β-scission of 1,1-diphenylethylperoxyl at ambient temperatures, reaction [3], and the possible involvement of the reaction of 1,1-diphenylethylperoxyl with 1,1-diphenylethyl, reaction [4], in the overall chain termination process for autoxidation of 1,1-diphenylethane.

[3] $Ph_2C(Me)O_2\cdot \rightleftarrows Ph_2C\dot{M}e + O_2$

[4] $Ph_2C(Me)O_2\cdot + Ph_2C\dot{M}e \rightarrow Ph_2C(Me)OOC(Me)Ph_2$

In addition, this work also provides some quantitative information on the relative rates of H-atom abstraction and β-scission of 1,1-diphenylethoxyl and 1-phenyl-1-phenoxylethoxyl in solution at 303 K, radicals which are formed by nonterminating interactions of $Ph_2C(Me)O_2\cdot$.

## Experimental

*Materials*

1,1-Diphenylethane was prepared by reduction of 1,1-diphenylethylene (Aldrich) and purified by preparative gas–liquid chromatography. 1,1-Diphenylethyl hydroperoxide was prepared from 1,1-diphenylethanol and 30% $H_2O_2$ (4). 1,1-Diphenylethyl peroxide was prepared from 1,1-diphenylethyl hydroperoxide by the procedure of Bassey *et al.* (5). *o*-Benzoquinone was prepared by oxidation of catechol with lead oxide. No attempt was made to purify this compound and it contained a decomposition product as a major impurity. 2,2-Diphenyloxirane was prepared from 1,1-diphenylethylene via 1,1-diphenyl-2-bromoethanol (6). 1-Phenyl-1-phenoxyethyl hydroperoxide was prepared by autoxidation of phenyl α-methylbenzyl ether in the presence of *tert*-butyl hydroperoxide at 30°C. The hydroperoxide was not separated from the reaction mixture and it was concluded that the major product peak in the liquid phase chromatogram was the hydroperoxide. Phenyl benzoate was prepared from benzoyl chloride and phenol. 2,2,3,3-Tetraphenylbutane and di-*tert*-butyl hyponitrite had been prepared previously in our laboratory (1). Phenol, acetophenone, benzophenone, and 1,1-diphenylethanol were commercially available and were purified by standard methods. $^{36}O_2$ (99.1 at.%) was obtained from Merck, Sharpe and Dohme Canada Ltd.

*Product studies*

Oxidation and decomposition products were identified by a combination of gc–ms and hplc techniques as described previously (1). Yields of most of the oxygenated products were determined by reverse-phase hplc and were accurate to ~ ±10%. We did, however, experience difficulty measuring yields of 2,2-diphenyloxirane because it was produced in rather low yields and had a tendency to decompose during analysis.

## Results

*Products of autoxidation of 1,1-diphenylethane*

The major products of the di-*tert*-butyl hyponitrite initiated autoxidation of 1,1-diphenylethane at 303 K are 1,1-diphenylethyl hydroperoxide, 1,1-diphenylethanol, acetophenone, phenol, benzoquinones, 1,1-diphenylethyl peroxide, phenyl benzoate, and benzophenone and are consistent with the elementary reactions given in Scheme 1. The yields of these oxygenated products, formed under different experimental conditions, are given in Tables 1 and 2, and their total yield accounted for > 90% of the oxygen absorbed. 1-Phenyl-1-phenoxyethyl hydroperoxide and the unsymmetric peroxide, $Ph_2C(Me)OOC(Me)(OPh)Ph$, were not identified.

Autoxidation of 1,1-diphenylethane initially decelerates as oxygen is absorbed, probably because the steady-state concentration of chain-carrying peroxyls decreases because of reaction with the phenol produced in reaction [19]. Yields of $Ph_2C(Me)OOH$ were, therefore, lower than calculated from the oxidizability of $Ph_2CMeH$, $k_p/(2k_t)^{\frac{1}{2}} = 1.1 \times 10^{-3}\,M^{-\frac{1}{2}}\,s^{-\frac{1}{2}}$ (2), the average calculated rate of chain initiation, $R_i$, and the total reaction time.

*p*-Benzoquinone was positively identified as a reaction product while *o*-benzoquinone was not present in final reaction mixtures. There was, however, evidence for a decomposition product of the *ortho* isomer, suggesting that it was formed but was not stable under the reaction conditions. The

TABLE 1. Products from thermally initiated autoxidation of 1,1-diphenylethane (5.48 *M*) at 303 K

| $P_{O_2}$(atm) | 0.4 | 1 | 10.3 |
|---|---|---|---|
| Reaction time (h) | 168 | 23 | 168 |
| Product | Yield (m*M*) | | |
| $[BON_2OB]_0$[a] | 14.4 | 38.7 | 14.4 |
| $p$-$C_6H_4O_2$ | 0.8 | 0.7 | 2.1 |
| PhOH | 3.7 | 0.4 | 9.5 |
| PhC(O)Me | 5.4 | 1.6 | 14 |
| $Ph_2C(Me)OH$ | 10.2 | 4 | 12.5 |
| $Ph_2C(Me)OOH$ | 480 | 130 | 560 |
| $Ph_2C{=}O$ | 3 | 0.14 | 2.75 |
| 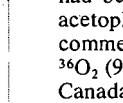 | ←——— | Trace | ———→ |
| PhC(O)OPh[b] | — | — | — |
| $(Ph_2C(Me)O)_2$ | 5.5 | 1.6 | 7.6 |

[a]Initial concentration.
[b]Not measured because of interference from $BON_2OB$.

Can. J. Chem. Downloaded from www.nrcresearchpress.com by 210.87.254.105 on 09/06/12
For personal use only.

*Initiation*:

[5] Production of free-radicals

*Propagation*:

[6] $Ph_2\dot{C}Me + O_2 \rightarrow Ph_2C(Me)O_2\cdot$

[7] $Ph_2C(Me)O_2\cdot + Ph_2CHMe \rightarrow Ph_2C(Me)OOH + Ph_2\dot{C}Me$

*Termination*:

[8] $2Ph_2C(Me)O_2\cdot \rightleftarrows Ph_2C(Me)OOOO(Me)CPh_2$

[9] $Ph_2C(Me)OOOO(Me)CPh_2 \rightarrow [Ph_2C(Me)\dot{O} + O_2 + \dot{O}(Me)CPh_2]_{cage}$

[10] $[Ph_2C(Me)\dot{O} + O_2 + \dot{O}(Me)CPh_2]_{cage} \xrightarrow{a} Ph_2C(Me)OO(Me)CPh_2$; $\xrightarrow{b} 2Ph_2C(Me)\dot{O} + O_2$

[11] $Ph_2C(Me)\dot{O} + Ph_2CHMe \rightarrow Ph_2C(Me)OH + Ph_2\dot{C}Me$

[12] $Ph_2C(Me)\dot{O} \rightarrow Ph_2C{=}O + Me$

[13] $Ph_2C(Me)\dot{O} \rightarrow PhC(Me)(\dot{O})Ph$

[14] $PhC(\dot{Me})OPh + O_2 \rightarrow PhC(Me)(OPh)CO_2\cdot$

[15] $PhC(Me)(OPh)CO_2\cdot + Ph_2CHMe \rightarrow PhC(Me)(OPh)COOH + Ph_2\dot{C}Me$

[16] $PhC(Me)(OPh)CO_2\cdot + Ph_2C(Me)O_2\cdot \rightleftarrows PhC(Me)(OPh)COOOOC(Me)Ph_2$

[17] $PhC(Me)(OPh)COOOOC(Me)Ph_2 \rightarrow PhC(Me)(OPh)COOC(Me)Ph_2$; $\rightarrow PhC(Me)(OPh)\dot{C}O + Ph_2C(Me)\dot{O} + O_2$

[18] $PhC(Me)(OPh)\dot{C}O + Ph_2CHMe \rightarrow PhC(Me)(OPh)COH + Ph_2\dot{C}Me$

[19] $PhC(Me)(OPh)COH \rightarrow PhC(O)Me + PhOH$

[20] $PhC(Me)(OPh)\dot{C}O \rightarrow PhC(O)OPh + Me$

SCHEME 1

production of benzoquinones can be accounted for by reaction of phenol with peroxyls, reactions [21] and [22]. Yields of *p*-benzoquinone plus phenol were very similar to yields of acetophenone, indicating that *o*-benzoquinone was not formed in appreciable amounts. Interestingly, the yield of *p*-benzoquinone relative to the yield of phenol fell as the reaction proceeded, probably because

TABLE 2. Product yields as a function of time for thermally initiated autoxidation of 1,1-diphenylethane (5.48 *M*) at 303 K[a]

| Reaction time (h) | 71 | 97 | 191 | 266 | 412 |
|---|---|---|---|---|---|
| Product | | | Yield (m*M*) | | |
| $\Delta[BON_2OB]$ | 16.8 | 20.4 | 27.7 | 30 | 31.6 |
| $p$-$C_6H_4O_2$ | 1.75 | 2.0 | 3.4 | 3.7 | 3.1 |
| PhOH | 1.4 | 1.7 | 4.6 | 8.5 | 15 |
| PhC(O)Me | 1.6 | 2.2 | 6.5 | 15 | 36 |
| $Ph_2C(Me)OH$ | 4.2 | 5.5 | 9.2 | 9.7 | 7 |
| $Ph_2C(Me)OOH$ | 230 | 380 | 700 | 840 | 900 |
| $Ph_2C{=}O$ | 0.375 | 0.54 | 0.8 | 1.25 | 2 |
|  | — | — | — | [b] | [b] |
| PhC(O)OPh | — | — | — | [b] | [b] |
| $(Ph_2C(Me)O)_2$ | 3.65 | 4.2 | 10.5 | 16 | 34.5 |

[a] $P_{O_2}$ = 1 atm, $[BON_2OB]_0$ = 32 m*M*.
[b] Trace amounts of these products were formed.

phenoxyls reacted with $Ph_2C(Me)OOH$ to regenerate phenol, rather than with $Ph_2C(Me)O_2\cdot$ to give quinone.

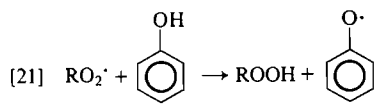


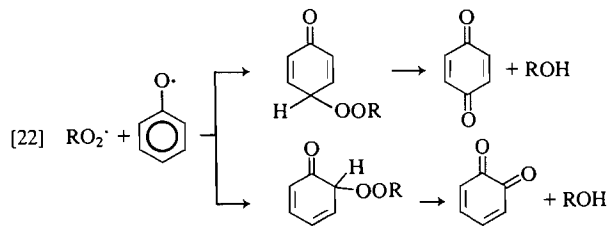


Relative yields of products originating from $Ph_2C(Me)\dot{O}$ which escape the solvent cage, reaction [10*b*], to yields of 1,1-diphenylethyl peroxide formed in reaction [10*a*] are 2–4 which gives a rate constant ratio, $k_{10b}/k_{10a}$ of 1–2. From this ratio we can calculate that $Ph_2C(Me)\dot{O}$ are produced with an efficiency of 50–67% by decomposition of di-1,1-diphenylethyl tetroxide which is slightly less than the efficiency of 83–94% obtained for production of α-cumyloxyl by decomposition of di-α-cumyl tetroxide (1).

Yields of 1,1-diphenylethanol, acetophenone, phenyl benzoate, and benzophenone indicate that 1,1-diphenylethoxyl undergoes H-atom abstraction, β-scission, and rearrangement to give 1-phenyl-1-phenoxylethoxyl (reaction [13]) and that this latter radical undergoes H-atom abstraction and β-scission. The relative importance of these reactions can, however, not be assessed because the concentration of $Ph_2C(Me)OOH$, a reactive H-atom donating product, increases during autoxidation.

A further conclusion that can be drawn from the data in Table 1 is that relative yields of 1,1-diphenylethyl hydroperoxide to 1,1-diphenylethyl peroxide do not depend to any appreciable extent on the pressure of oxygen above the liquid in the range 0.4–10.3 atm. This implies that β-scission of $Ph_2C(Me)O_2\cdot$, reaction [3], is not sufficiently important to influence the chain length because if it did the ratio of hydroperoxide to peroxide would be reduced by a decrease in the oxygen pressure.

2,2-Diphenyloxirane is formed in trace amounts, probably by alkoxyl radical attack on the methyl group of 1,1-diphenylethyl hydroperoxide (see later) produced by extensive autoxidation.

*Induced decomposition of 1,1-diphenylethyl hydroperoxide under an atmosphere of* $^{36}O_2$

The yields of the major reaction products formed by induced decomposition of $Ph_2C(Me)OOH$ with thermally generated *tert*-butoxyls, reaction [23], in $CH_3CN$ and $C_6H_5Cl$ are given in Table 3.

[23] $t\text{-BuO}\cdot + Ph_2C(Me)OOH \rightarrow t\text{-BuOH} + Ph_2C(Me)O_2\cdot$

We were not able to estimate final concentrations of $Ph_2C(Me)OOH$ because PhC(Me)(OPh)OOH, a possible reaction product, could not be distinguished from $Ph_2C(Me)OOH$ by hplc analysis. It would, however, appear, from the high yields of $Ph_2C(Me)OH$ produced after reduction with $Ph_3P$, that a substantial concentration of $Ph_2C(Me)OOH$ was not decomposed by the same concentration of *tert*-butyl hyponitrite as was required to completely decompose $PhC(Me)_2OOH$. This suggests that the chain length for the induced decomposition of $Ph_2CMeOOH$ is less than that for $PhCMe_2OOH$. A reduction in the *overall* chain length could result from reaction of $Ph_2C(Me)O_2\cdot$ with phenol produced in the decomposition. That is, reaction

Can. J. Chem. Downloaded from www.nrcresearchpress.com by 210.87.254.105 on 09/06/12
For personal use only.

Can. J. Chem. Downloaded from www.nrcresearchpress.com by 210.87.254.105 on 09/06/12
For personal use only.

TABLE 3. Product yields from induced decomposition of $Ph_2C(Me)OOH$ at 303 K

| Solvent | $CH_3CN$ | | PhCl |
|---|---|---|---|
| Reaction time (day) | 14 | 30 | 19 |
| Product | Yield (m$M$) | | |
| $[Ph_2C(Me)OOH]_0$ | 220 | 220 | 205 |
| $\Delta[BON_2OB]$ | 28 | 29 | 31 |
| $p$-$C_6H_4O_2$ | 2.7 | 4.0 | 4.2 |
| PhOH | 4.2 | 9 | 1.35 |
| PhC(O)Me | 8.0 | 17 | 8.6 |
| $Ph_2C(Me)OH$ | 7.0 | 12 | [a] |
| ROOH[b] | 160 | 250 | 210 |
| $Ph_2C{=}O$ | 0.6 | 1.1 | 0.95 |
| | | Trace | |
| PhC(O)OPh | 2.8 | 3.1 | 0.9 |
| $(Ph_2C(Me)O)_2$ | 1.0 | 2.0 | 3.5 |

[a]Not detected because of interference from chlorobenzene.
[b]Total hydroperoxide remaining.

TABLE 4. Product yields from induced decomposition of $Ph_2CMeOOH$ in chlorobenzene under an atmosphere of $^{36}O_2$ at 303 K

| Product | Yield (m$M$) |
|---|---|
| $Ph_2C(Me)OH$[a,b] | 43 |
| $Ph_2C(Me)^{18}OH$ | 307 |
| PhOH | 2.6 |
| $Ph^{18}OH$ | 18.5 |
| PhC(O)Me | 9.7 |
| $PhC(^{18}O)Me$ | 30.2 |
| | (1.0) |
|  | (7.14) |

[a]Alcohol produced in the reaction and by reduction of excess $Ph_2C(Me)OOH$.
[b]It should be noted that the relative yields of this product are much more accurate than the absolute yields.
[c]Relative yields.

[21] competes with reaction [10$a$] as the major chain termination process.

The reaction products are consistent with the elementary reactions [5] to [20] except for 2,2-diphenyloxirane which is probably produced by alkoxyl attack at the methyl group of the hydroperoxide followed by an intramolecular $S_H2$ reaction by the carbon centred radical on the peroxide function.

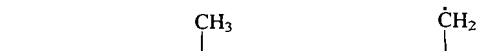

[24] $RO\cdot + (C_6H_5)_2C(CH_3)COOH \rightarrow ROH + (C_6H_5)_2C(\dot{C}H_2)COOH$

[25] $(C_6H_5)_2C(\dot{C}H_2)COOH \rightarrow (C_6H_5)_2C(O)CH_2 + HO\cdot$

Analogous reactions probably account for the trace of 2-methyl-2-phenyloxirane produced by $t$-BuO· induced decomposition of $PhCMe_2OOH$ (1).

The relative yields of 1,1-diphenylethyl peroxide and *all* the products derived from $Ph_2C(Me)O\cdot$ which escape the solvent cage give $k_{10b}/k_{10a} \sim 8$–9, implying that $Ph_2C(Me)O\cdot$ are produced with a efficiency of ~ 90% by decomposition of 1,1-diphenylethyl tetroxide, a slightly larger value than that calculated from product yields of $Ph_2C(Me)H$ autoxidation.

When this reaction was conducted under an atmosphere of $^{36}O_2$ the gaseous oxygen at the end of the experiment contained 10% $^{32}O_2$, and $^{18}O$ enriched 1,1-diphenylethanol, acetophenone, phenol, and 2,2-diphenyloxirane were formed in the yields given in Table 4. A comparison of the yields of these compounds with the yields of the unenriched products reveals that $Ph_2C(Me)OH$, PhOH, and  were enriched to the extent of 88% whereas PhC(O)Me was only enriched to 75%. When these results are compared with the yields of $^{18}O$ enriched $PhCMe_2OH$ (1.25%) and PhC(O)Me (7–6%) produced from self-reaction of $PhCMe_2O_2\cdot$ under an atmosphere of $^{36}O_2$ (1) it is clear that $Ph_2C(Me)O_2\cdot$ undergoes β-scission faster than $PhCMe_2O_2\cdot$, a result which is consistent with the relative stabilization energies of $Ph_2\dot{C}Me$ and $Ph\dot{C}Me_2$ (3).

We have previously shown that the rate constant for β scission of a peroxyl ($k_\beta$) in the presence of its hydroperoxide, under an atmosphere of $^{36}O_2$, can very approximately be estimated from the expression

$$k_\beta = \frac{k_{dis}[R^{18}O^{18}O\cdot]\,[ROOH]}{[RO_2\cdot]}$$

In the present case R = $Ph_2CMe$, $k_\beta = k_3$ and $k_{dis}$, the rate constant for reaction of $Ph_2C(Me)O_2\cdot$ with $Ph_2C(Me)OOH$, can be assumed to be 570 $M^{-1}$ s$^{-1}$ at 303 K (7).

The average ratio of $^{18}O$ enriched product to normal product (excluding acetophenone) is 7.1, ignoring the small amount of $^{32}O_2$ evolved in the reaction. This ratio, in conjunction with an average hydroperoxide concentration of 0.425 $M$, gives $k_3 \sim 1700$ s$^{-1}$ which is ca. 3 orders of magnitude larger than the value of the rate constant for β-scission of $PhCMe_2O_2\cdot$. Again if we assume that $k_{-3} = 10^{9.5}$ $M^{-1}$ s$^{-1}$, the equilibrium constant for reaction [3] can be estimated to be $\sim 10^{6.3}$ $M^{-1}$.

Can. J. Chem. Downloaded from www.nrcresearchpress.com by 210.87.254.105 on 09/06/12
For personal use only.

The steady-state concentration of $Ph_2\dot{C}Me$ at 1 atm of $O_2$ ($10^{-2}$ *M*) is, therefore, ca. $10^{-4.3}$[$Ph_2C(Me)O_2\cdot$] and if $k_4$ is $10^8$ $M^{-1}$ $s^{-1}$ (1) the rate of reaction [4] can be calculated to be $\sim 10^{3.7}$ $M^{-1}$ $s^{-1}$ which is negligible compared to the values of $2k_t = 1.35 \times 10^5$ $M^{-1}$ $s^{-1}$ and $2k_t' = 6.4 \times 10^4$ $M^{-1}$ $s^{-1}$ for $Ph_2C(Me)O_2\cdot$ at 303 K (2). However, as Nangia and Benson (3) have suggested, the rate of reaction [4] at 0.1 atm of $O_2$ is comparable to the rate of self-reaction of $Ph_2C(Me)O_2$.

The insignificance of reaction [4] at 303 K was confirmed by the observation that rates of autoxidation of cumene containing $Ph_2C(Me)OOH$ (0.38 *M*), i.e., under conditions where $Ph_2C(Me)O_2\cdot$ was the principal rate controlling chain carrying peroxyl, were independent of the oxygen pressure from 50 to 740 Torr.

*Products of 2,2,3,3-tetraphenylbutane decomposition in the presence of oxygen*

In order to investigate more fully the products of the self-reaction of $Ph_2C(Me)O_2\cdot$, $Ph_2\dot{C}Me$ was generated under an atmosphere of $O_2$ in $CH_3CN$ at 303 K by thermolysis of 2,2,3,3-tetraphenylbutane (TPB). Decomposition of TPB is a first-order process with a rate constant of $2.1 \times 10^{-6}$ $s^{-1}$ at 303 K and radicals are produced with an efficiency of 100%. An 18 m*M* solution absorbed oxygen with a rate of $9.5 \times 10^{-8}$ $M$ $s^{-1}$ which was close to the rate of production of $Ph_2\dot{C}Me$. Aliquots were taken periodically from the reaction and subjected to analysis by high performance liquid chromatography. The major reaction products and their yields after 23, 52.5, 73, and 95 h of reaction are given in Table 5 and are consistent with the elementary reactions [5]–[20] for the self-reaction of $Ph_2C(Me)O_2\cdot$ plus reaction of $Ph_2C(Me)O_2\cdot$ with a H-atom donor such as $CH_3CN$ or a reaction product such as phenol to give 1,1-diphenylethyl hydroperoxide. Di(1,1-diphenylethyl) peroxide was not observed because it had the same retention time as TPB under our analytical conditions.

TABLE 5. Products from thermal decomposition of 2,2,3,3-tetraphenylbutane in the presence of oxygen in $CH_3CN$ at 303 K

| Reaction time (h) | 23 | 52.5 | 75 | 95 |
|---|---|---|---|---|
| Products | Yield (m*M*) | | | |
| ΔTPB | 1.93 | 5.9 | 7.8 | 9.2 |
| *p*-$C_6H_4O_2$ | 0.66 | 1.3 | 1.4 | 1.5 (1.4)[a] |
| PhOH | 0.05 | 0.19 | 0.24 | 0.28 (.32) |
| PhC(O)Me | 1.65 | 3.75 | 4.0 | 4.3 (4.5) |
| $Ph_2C(Me)OH$ | 0.8 | 1.9 | 2 | 2.1 (2.1) |
| $Ph_2C(Me)OOH$ | 0.77 | 2.0 | 2.4 | 3.0 (3.2) |
| $Ph_2C{=}O$ | 0.095 | 0.23 | 0.25 | 0.28 (0.26) |
| PhC(O)OPh | 1.45 | 2.8 | 2.9 | 3.2 (2.8) |

[a]The yields in parentheses are for a decomposition that was only analysed after 95 h.

The low yield of benzophenone indicates that $Ph_2C(Me)O\cdot$ undergoes β-scission reaction [12], as well as H-atom abstraction [11] and rearrangement [13], but the rate of β-scission is relatively slow. Thus, the relative yields of 1,1-diphenylethanol and benzophenone give $k_{11}[RH]/k_{12} = 4.4$ and if $CH_3CN$ is the sole H-atom donor, RH = 19.14 *M* and $k_{11}/k_{12} = 0.23$. Unfortunately the absolute value of $k_{12}$ cannot be calculated because absolute rate constants for reaction of alkoxyls with $CH_3CN$ are not known. We did, however, find that cumyloxyl, produced by thermolysis of di-α-cumyl hyponitrite in $CH_3CN$, gave a ratio of α-cumyl alcohol to acetophenone = 0.2. This indicates, somewhat surprisingly, that $PhCMe_2O\cdot$ undergoes β-scission ~20 times faster than $Ph_2CMeO\cdot$.

As expected from reaction [19], the yield of phenol plus *p*-benzoquinone was approximately equal to the yield of acetophenone. The benzoquinone yield was, however, about ten times larger than the phenol yield, indicating substantial oxidation of phenol by peroxyls.

The relative yields of acetophenone and phenyl benzoate suggest that $k_{18}[RH]/k_{20} = 0.68$ and, if $CH_3CN$ is the H-atom donor, $k_{18}/k_{20} = 0.0355$. Thus $PhCMe(OPh)O\cdot$ undergoes β-scission ~ 6.5 times more readily than $Ph_2C(Me)O\cdot$.

## Conclusions

We can conclude from this study of the self-reactions of 1,1-diphenylethylperoxyl in solution that the reaction products are consistent with a complex series of free-radical reactions which involve the intermediacy of 1,1-diphenylethoxyl and 1-phenyl-1-phenoxylethoxyl. The former radical undergoes H-atom abstraction, β-scission, and rearrangement while the latter radical undergoes β-scission and H-atom abstraction.

The relative product yields agree with the products obtained from thermolysis of 2,2,6,6-tetramethyl-4-oxo-1-(1,1-diphenylethoxy) piperidine (8) and are more reliable than our earlier product studies of 2,2,3,3-tetraphenylbutane oxidation (9) and induced decomposition of 1,1-diphenylethyl hydroperoxide (10). This reflects the superiority of hplc over glc for the analysis of autoxidation products.

$Ph_2C(Me)O_2\cdot$ undergoes β-scission in solution at 303 K with a rate constant of ~1700 $s^{-1}$, compared with a value of ~2 $s^{-1}$ for $PhCMe_2O_2\cdot$, suggesting that there is ~4 kcal $mol^{-1}$ difference in the stabilization energies of $Ph_2\dot{C}Me$ and $Ph\dot{C}Me_2$. The

steady-state concentration of $Ph_2\dot{C}Me$ during autoxidation of $Ph_2CMeH$ is, however, not large enough to influence the overall termination rate constant at ambient temperatures.

$Ph_2C(Me)O\cdot$, produced by decomposition of 1,1-diphenylethyl tetroxide, escape the solvent cage with an efficiency > 50%, indicating that the nature of the alkyl moiety (R = *t*-Bu, $PhCMe_2$, $Ph_2CMe$) has very little influence on this efficiency. We can, therefore, conclude that differences in termination rate constants for *t*-$BuO_2\cdot$, $PhCMeO_2\cdot$, and $Ph_2CMeO_2\cdot$ are principally due to differences in the stability of the appropriate tetroxides towards irreversible homolysis. It should, however, be noted that phenol is a product of the autoxidation of 1,1-diphenylethane, and its rapid chain terminating reaction with chain carrying peroxyls could influence the *overall* termination rate constant after autoxidation has been in progress.

1. J. A. HOWARD, J. E. BENNETT, and G. BRUNTON. Can. J. Chem. **59**, 2253 (1981).
2. J. A. HOWARD. Adv. Free Radical Chem. **4**, 49 (1972).
3. P. S. NANGIA and S. W. BENSON. Int. J. Chem. Kinet. **12**, 29 (1980).
4. D. E. BESSING, C. A. MATUSAK, and W. E. MCEWAN. J. Am. Chem. Soc. **86**, 3824 (1964).
5. M. BASSEY, E. BUNCEL, and A. G. DAVIES. J. Chem. Soc. 2550 (1955).
6. S. J. CRISTOL, J. R. DOUGLASS, and J. S. MEEK. J. Am. Chem. Soc. **73**, 816 (1951).
7. J. H. B. CHENIER and J. A. HOWARD. Can. J. Chem. **53**, 623 (1975).
8. J. A. HOWARD and J. C. TAIT. J. Org. Chem. **43**, 4279 (1978).
9. J. A. HOWARD and J. H. B. CHENIER. Can. J. Chem. **54**, 382 (1976).
10. J. A. HOWARD and K. U. INGOLD. Can. J. Chem. **47**, 3797 (1969).

Can. J. Chem. Downloaded from www.nrcresearchpress.com by 210.87.254.105 on 09/06/12
For personal use only.

# Correlation of alkane solubilities in water with connectivity index

JOHN T. EDWARD

*Department of Chemistry, McGill University, 801 Sherbrooke St. West, Montreal, P.Q., Canada H3A 2K6*

Received February 10, 1982

JOHN T. EDWARD. Can. J. Chem. **60**, 2573 (1982).

The solubility of alkanes in water has been shown previously to be correlated both with the surface area of the molecular cavity containing the molecule in water, and the first-order connectivity index $^1\chi$ of the alkane; it is now shown that both the surface area and $^1\chi$ are dependent on the number of methyl, methylene, methine, and quaternary carbon groups in the alkane, modified by the degree of folding of the chain (as measured by $Z_g$).

JOHN T. EDWARD. Can. J. Chem. **60**, 2573 (1982).

On a montré antérieurement qu'on pouvait relier la solubilité des alcanes dans l'eau à la fois à la surface de la cavité moléculaire contenant la molécule dans l'eau et à l'indice de conductivité d'ordre un $^1\chi$ de l'alcane. Nous montrons maintenant que $^1\chi$ dépendent du nombre de méthyle, de méthylène, de méthine et des groupes de carbone quaternaire de l'alcane, modifiés par le degré d'enroulement de la chaîne (tel que mesuré par $Z_g$).

[Traduit par le journal]

Hansch (1) showed that the biological activities of a series of related compounds were sometimes partially, and sometimes totally, a function of the partition coefficients $P$ of the compounds between water and *n*-octanol. (Since to a good approximation $\log P$ is a linear function of $\log S$, where $S$ is the solubility of the compounds in water (2), this is equivalent to saying that in such cases the biological activity is partially or totally a function of $S$.) Hansch (1) produced a plausible model to explain such behaviour: the rate or the extent to which a compound passes through various lipoidal barriers to arrive at the target site in the organism varies with $P$. In some cases the biological activity also depends on the reactivity of the compound at the target site, and hence on a two-parameter equation involving Hammett or Taft's substituent constant $\sigma$ as well as $P$.

In an alternative approach Kier, Hall, and their colleagues (3–5) related biological activities (and many physical properties) of organic compounds to one or more connectivity indices $^m\chi_t$ (of order $m$ and type $t$). Connectivity indices depend on the topology of the molecule, and are briefly explained below; their physical significance has been unclear. For many activities and properties even the first-order connectivity index $^1\chi$ sufficed for a reasonable correlation.

The success of two radically different approaches suggests some underlying connection between them. In the present paper it is shown that for the particular case of alkanes, both the solubility $S$ in water and $^1\chi$ depend on the number of methyl, methylene, methine, and quaternary carbon atoms, modified slightly by the degree of chain folding as measured by the "*gauche* number" $Z_g$ (6, 7). (A similar argument was developed, but less completely, on the relation between $^m\chi_t$ and molecular volumes and heats of vaporization of alkanes (8); it seemed worthwhile to carry out the same exercise for $S$ (and by inference $P$) because of the central importance of $P$ in explanations of biological activity.)

## Relation of solubilities of alkanes to molecular cavity surface areas

The solubilities of alkanes in water decrease as the molecules become larger, because of the greater energy required to form a cavity for the molecule in the cohesive solvent (9–15), but there has been disagreement in the past as to whether this energy is proportional to the volume or the surface area of the cavity.[1] It is now generally agreed (11–14, 16) that the energy (and thence $\ln 1/S$) are correlated better with the surface area of the cavity,[2] but there has been less agreement on the

[1]The various ways in which the surface area and volume of a molecule may be defined have been discussed by Pearlman (16) in a penetrating and valuable review. For a homologous series of compounds the volume and surface area are linearly related.

[2]Counter to this consensus, Hansch and his colleagues (10) have recently claimed to find a better correlation between $\log P$ (and by inference $\log (1/S)$ (2)) and the molecular volume of hydrocarbons and apolar molecules. They obtained molecular volumes from the volume of water displaced by Corey–Pauling–Koltun (CPK) models of the molecules wrapped in flexible polyethylene. CPK models (17), like most space-filling models (18), seriously underestimate the van der Waals radius of hydrogen in order to allow models of slightly congested molecules to be made. This results in unrealistic volumes for most organic molecules, since hydrogen accounts for such a large proportion of their volume (73% in the case of propane: see Fig. 1).

0008-4042/82/202573-06$01.00/0

©1982 National Research Council of Canada/Conseil national de recherches du Canada

Can. J. Chem. Downloaded from www.nrcresearchpress.com by 210.87.254.40 on 09/06/12
For personal use only.

Can. J. Chem. Downloaded from www.nrcresearchpress.com by 210.87.254.40 on 09/06/12
For personal use only.

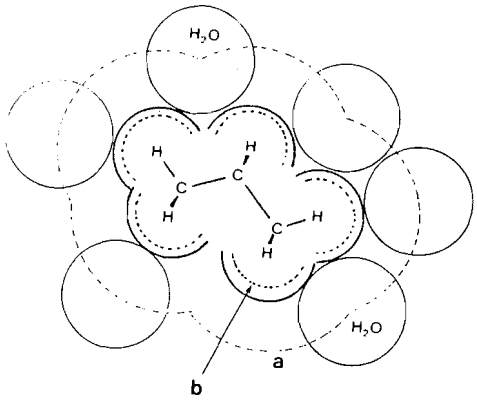


FIG. 1. Scale drawing of propane surrounded by water molecules, represented as spheres of radius 1.5 Å. Cavity surface according to (*a*) Hermann (ref. 12); (*b*) Leo, Hansch, and Jow (ref. 10).

best measurement of the cavity area.[3] It would now seem that the most plausible and successful model is that of Hermann (12). He defines the cavity surface area $A$ of a molecule in water as the area of the surface traced out by the centre of a water molecule (radius $r_w$ assumed to be 1.5 Å) rolling over the van der Waals surface (19) of the molecule. This is illustrated in Fig. 1 for propane. The solubilities of straight- and branched-chain and of cyclic alkanes are then found to correlate well with $A$ according to

$$[1] \quad kT \ln S = -b_0 A - C_0$$

where $b_0$ and $C_0$ are constants at a given temperature. This equation accounts for the fact that a branched-chain alkane, which has a lower $A$ but the same van der Waals volume and van der Waals surface area as its straight-chain isomer, has a greater solubility.

The cavity surface areas $A$ for 23 alkanes in their most extended conformation, calculated according to Hermann by a computer program with input information of bond lengths, bond angles, van der Waals radii of the atoms, and $r_w = 1.5$ Å for water, are given in Table 1.

Approximately the same values of $A$ are obtained by the equation

$$[2] \quad A = A_0 + \sum n_i A_i + \sum n_k S_k$$

where $A_0$ (= 115 Å$^2$) is a constant for all molecules (analogous to the constant covolume required in additive schemes for molecular volumes (7, 8)), $A_i$ is the surface increment from group $i$ (methyl, methylene, methine, or quaternary carbon), $n_i$ is the number of such groups, $S_k$ is the effect on the surface area of structural feature $k$, and $n_k$ is the number (integral or fractional) of such features. The values of the $A$ and $S$ parameters are given in Table 2, and were obtained by least-squares fitting of Hermann's values of $A$ to [2]. The data are sufficient to determine a unique value for $A_s$, but not for other values of $A_i$; $A_0 = 115$ Å$^2$ was chosen to keep $A_p$, $A_t$, and $A_q$ all positive.

The values of $A$ calculated by [2] and given in Table 1 take account of the fact that branched-alkanes, even in their most extended conformation, necessarily include one or more *gauche* arrangements. Thus the calculated value of $A$ for 2-methylbutane (2-MeC$_4$) is for conformation **1***a* (or equally its enantiomer **1***b*) having one *gauche* arrangement

**1***a* **1***b* **1***c*

($z_g = 1$: see ref. 7). In fact, in solution at 25°C these conformations are in equilibrium with a smaller amount of the conformation **1***c* ($z_g = 2$), so that the weighted-average *gauche* number $Z_g$ ($\equiv \sum x_i z_{g(i)}$, where $x_i$ is the mole fraction of conformation $i$ and $z_{g(i)}$ the number of *gauche* arrangements in it) of 2-methylbutane is 1.13 (19). This value of $Z_g$ (= $n_g$ in the symbolism of [2]) must be used in [2] to give the surface area of the cavity containing the average, as opposed to the maximally-extended molecule; the former surface area must then be used in [1].

The coiling of a molecule, as indicated by its $Z_g$, and even more cyclization of the molecule, reduce the area in contact with solvent water molecules. This is shown by the negative $S$ parameters in Table 2. Similar negative parameters (with magnitudes in the same relative order) are required in additive schemes of molecular volumes (21). The plot of log $S$ against $A$, as calculated by [2], is given in Fig. 2*B*, and shows how well the experimental data support [1]. (This is essentially the same as Fig. 2 in ref. 11, except that in this paper $A$ values were computed *ab initio* and not derived from [2].)

### Relation of solubilities of alkanes to first-order connectivity index $^1\chi$

Kier, Hall, and Murray (22) related the solubilities of alkanes to the changing topology of the molecules. The molecule is regarded as a graph, the atoms forming the vertices and the bonds the edges of the graph. Hydrogen atoms are suppressed, so that the five alkanes, ethane, propane, *n*-butane,

[3]Hansch *et al.* (9) equate the cavity surface area to the molecular surface area as calculated according to Bondi (19). Such a calculation yields identical cavity areas for straight- and branched-chain alkanes, and for this and other reasons is inadequate.

Can. J. Chem. Downloaded from www.nrcresearchpress.com by 210.87.254.40 on 09/06/12
For personal use only.

TABLE 1. Connectivity index $^1\chi$ and cavity surface area parameters (in Å$^2$) for alkanes in water

| Alkane | $^1\chi$ | $(A_0 + \sum n_i A_i)$ | $\sum n_k S_k$[a] | $A$ (eq. [7])[a] | $A$ (Hermann)[a, b] |
|---|---|---|---|---|---|
| $C_2$ | 1.000 | 191.6 | 0 | 191.6 | 191.52 |
| $C_3$ | 1.414 | 223.5 | 0 | 223.5 | 223.35 |
| $C_4$ | 1.914 | 255.4 | 0 | 255.4 | 255.15 |
| 2-$MeC_3$ | 1.732 | 248.5 | 0 | 248.5 | 249.10 |
| $C_5$ | 2.414 | 287.3 | 0 | 287.3 | 286.97 |
| 2-$MeC_4$ | 2.270 | 280.4 | −6.2 | 274.2 | 274.58 |
| 2,2-$Me_2C_3$ | 2.000 | 270.1 | 0 | 270.1 | 270.14 |
| $C_6$ | 2.914 | 319.2 | 0 | 319.2 | 319[c] |
| 2-$MeC_5$ | 2.770 | 312.3 | −6.2 | 306.1 | 306.41 |
| 3-$MeC_5$ | 2.808 | 312.3 | −12.4 | 299.9 | 300.08 |
| 2,2-$Me_2C_4$ | 2.561 | 302.0 | −12.4 | 289.6 | 290.76 |
| $C_7$ | 3.414 | 351.1 | 0 | 351.1 | 351[c] |
| 2,4-$Me_2C_5$ | 3.126 | 337.3 | −12.4 | 324.9 | 324.71 |
| $C_8$ | 3.914 | 383.0 | 0 | 383.0 | 383[c] |
| 2,2,4-$Me_3C_5$ | 3.416 | 358.9 | −18.6 | 340.3 | 338.93 |
| 2,2,5-$Me_3C_6$ | 3.916 | 390.8 | −18.6 | 372.3 | 373.01 |
| *cyc*-$C_5$[d] | 2.500 | 274.5 | −17.9 | 256.6 | 255.40 |
| *cyc*-$C_6$ | 3.000 | 306.4 | −26.8 | 279.6 | 279.10 |
| Me-*cyc*-$C_5$ | 2.893 | 299.5 | −17.9 | 281.6 | 282.70 |
| *cyc*-$C_7$ | 3.500 | 338.3 | −36.4 | 301.9 | 301.94 |
| Me-*cyc*-$C_6$ | 3.394 | 331.4 | −26.8 | 304.6 | 304.85 |
| *cyc*-$C_8$ | 4.000 | 370.2 | −47.6 | 322.6 | 322.58 |
| *cis*-1,2-$Me_2$-*cyc*-$C_6$ | 3.805 | 356.4 | −39.2 | 317.2 | 315.50 |

[a]For the most fully extended conformation.
[b]Values from ref. 12, except footnote *c*.
[c]Values from ref. 20.
[d]Cyclopentane.

TABLE 2. Contributions (in Å$^2$) to cavity surface area from group increments $A$ and structural features $S$ of alkanes

| Group | $A$ | Structural feature | $S$ |
|---|---|---|---|
| —$CH_3$ | 38.3 | *Gauche* | −6.2 |
| >$CH_2$ | 31.9 | 5-Membered ring | −17.9 |
| >CH— | 18.6 | 6-Membered ring | −26.8 |
| >C< | 1.9 | 7-Membered ring | −36.4 |
| | | 8-Membered ring | −47.6 |

isobutane, and neopentane, are represented as shown in Scheme 1. Such graphs may be decomposed into subgraphs of differing orders $m$: zero order, consisting of single vertices; first-order, consisting of an edge joining two vertices; second-order, consisting of two edges linking three vertices; and so on.

The simple connectivity value $\delta_i$ of a vertex $i$ is the number of other vertices to which it is joined. Values of $\delta_i$ for the vertices of the five alkanes of Scheme 1 are shown in the scheme above the graphs. Kier and Hall (3) (following earlier work of Randic (23)) have defined connectivity indices $^m\chi$ based on the $\delta_i$ values of all the $n$ subgraphs of order $m$ into which a graph can be decomposed. The first-order connectivity index $^1\chi$ is defined by

$$[3] \qquad {}^1\chi = \sum_{s=1}^{n} (\delta_i \delta_j)_s^{-1/2}$$

where $s$ identifies a first-order subgraph (an edge), $\delta_i$ and $\delta_j$ are the connectivity values at each end of an edge, and $n$ is the number of edges in the graph. In Scheme 1 the $(\delta_i \delta_j)_s^{-1/2}$ values are shown beside each edge for the five alkanes, and below are shown the $^1\chi$ values obtained by their summation.

Kier, Hall, and Murray (22) found that the solubilities of 18 alkanes in water follow fairly well the relation

$$[4] \qquad \ln S = -1.505 - 2.533\,{}^1\chi$$

(correlation coefficient $r = 0.958$; standard deviation $s = 0.511$). Considering the ease of calculating $^1\chi$ for any known structure, the success of [4], and of a large number of other equations relating physical properties to one or more $^m\chi_t$ values (3), must be considered quite striking. However, the agreement of the experimental data with [4] is distinctly inferior to its agreement with [1], as shown by a comparison of Fig. 2*A* with Fig. 2*B*. Furthermore, [1] is derived from thermodynamic theory, while [4] is an empirical relationship. Kier (5) says: "It is a tough challenge, looking for physical

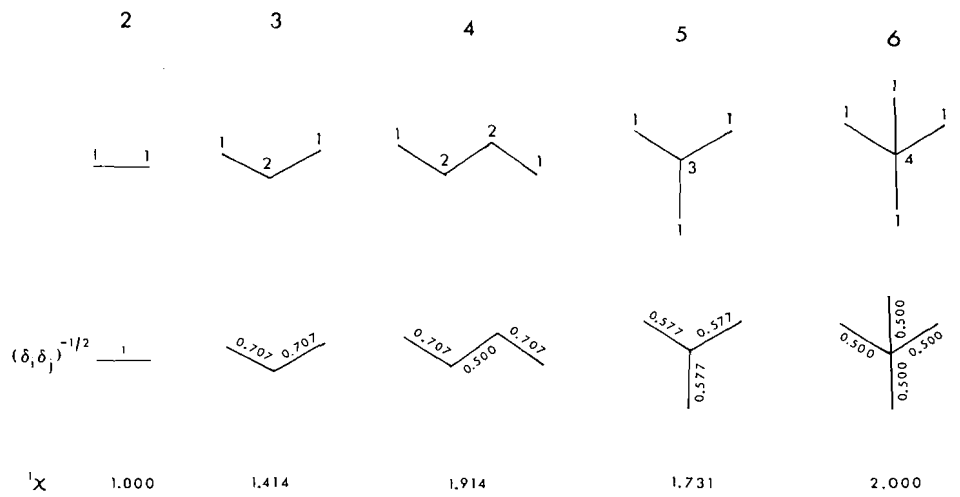


SCHEME 1. Graphs of the alkanes ethane **2**, propane **3**, *n*-butane **4**, *iso*butane **5**, and neopentane **6**. Valencies $\delta_i$ of each vertex shown. On line below, $(\delta_i\delta_j)^{-1/2}$ values of each first-order subgraph (edge) shown; and on bottom line $^1\chi$ values obtained by summation of $(\delta_i\delta_j)^{-1/2}$ terms.

meaning . . . [in] the connectivity indexes''. It was suggested earlier (8) that in an alkane $^1\chi$ is determined by the number and type of carbon atoms (methyl, methylene, methine, and quaternary carbon), modified by chain coiling; i.e. by precisely the factors determining the area of the cavity surface according to [2]. We now examine this suggestion in more detail.

## Relation of $^1\chi$ to numbers and types of carbon atoms and to structural features in alkane molecules

We first look at the sixteen non-cyclic alkanes of Table 1. These are made up of straight-chain compounds, alkanes having a methyl branch at position 2 or 3, alkanes having a *gem*-dimethyl group at position 2, and some mixed types.

Consider first propane and the higher *n*-alkanes. From an examination of **4** → **7** in Scheme 2, it is apparent that each additional $CH_2$ (secondary or *s*) increases $^1\chi$ of an *n*-alkane by 0.500. Subtracting 0.500 from $^1\chi$ (1.414) of propane leaves 0.914 for the two $CH_3$ (primary or *p*) groups, or 0.457 for each $CH_3$. Consequently, for propane and higher *n*-alkanes (and for cyclic alkanes, but not for ethane):

$$[5] \quad {}^1\chi = 0.457n_p + 0.500n_s$$

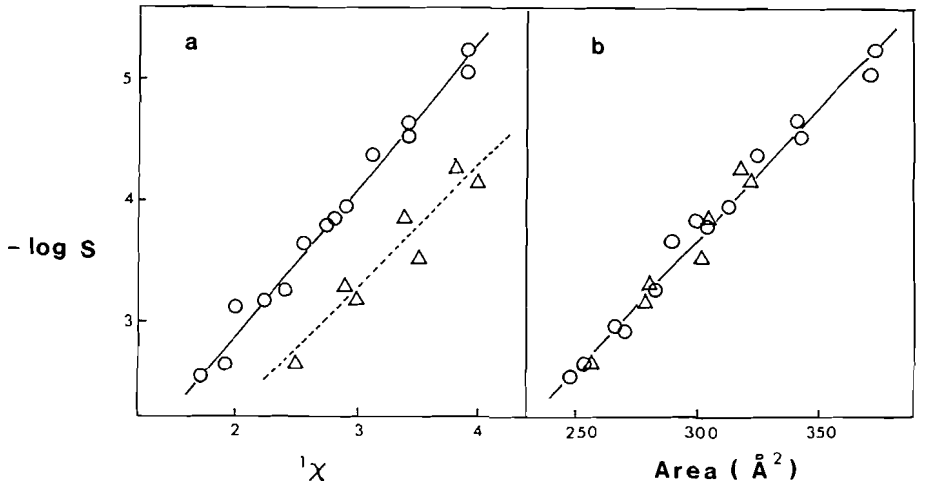


FIG. 2. Relation of molal solubility *S* to (*a*) connectivity index $^1\chi$, and (*b*) cavity surface area according to [2]. Symbols: ○, acyclic; △, cyclic alkanes.

Can. J. Chem. Downloaded from www.nrcresearchpress.com by 210.87.254.40 on 09/06/12
For personal use only.

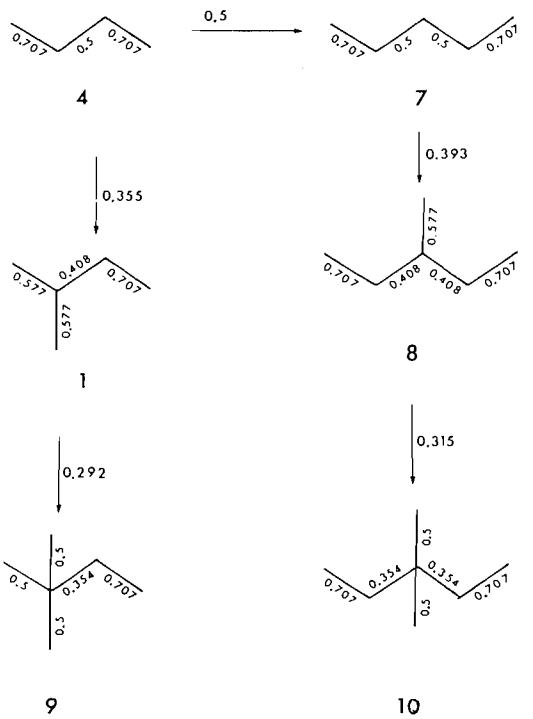


SCHEME 2. Increases in $^1\chi$ shown beside arrows, as carbon atoms are successively added to *n*-butane. Values of $(\delta_i\delta_j)^{-1/2}$ for each edge shown on graphs; $^1\chi$ values obtained by summation of $(\delta_i\delta_j)^{-1/2}$ terms.

(an equation advanced without proof previously (8)).

Looking now at **4** → **1** in Scheme 2, we see that adding a methyl group (*p*) at position 2 (and necessarily converting one $CH_2$ group (*s*) to CH (tertiary or *t*)) leads to an additional $(\delta_i\delta_j)^{-1/2}$ contribution to $^1\chi$ of 0.577 from the new bond, partially offset by diminutions in $(\delta_i\delta_j)^{-1/2}$ contributions from bonds 1,2 and 2,3, so that the overall change $\Delta^1\chi$ on going from **4** → **1** is 0.355. In terms of group contributions, the change may be represented by $p + t - s = 0.355$. Retaining $p = 0.457$ and $s = 0.500$, we obtain $t = 0.398$, so that for 2-methylbutane and higher homologues having a 2-methyl group

[6] $$^1\chi = 0.457n_p + 0.500n_s + 0.398n_t$$

Addition of a methyl group to the 3-position of **7** to give **8** results in $\Delta^1\chi = 0.393$, whence it may be shown, by arguments similar to those above, that for **8** and higher homologues having a methyl branch on a carbon atom at least two bonds away from the end of the chain (and for cyclic alkanes with a methyl branch)

[7] $$^1\chi = 0.457n_p + 0.500n_s + 0.436n_t$$

For 2,2-dimethylbutane (**9**) and higher homologues having a geminal 2,2-dimethyl group, similar arguments lead to

[8] $$^1\chi = 0.457n_p + 0.500n_s + 0.233n_q$$

and for 3,3-dimethylpentane (**10**) and higher homologues and for *gem*-dimethyl cyclic compounds to:

[9] $$^1\chi = 0.457n_p + 0.500n_s + 0.294n_q$$

These equations manifestly lack generality; other equations would be required for more highly branched compounds. However, they serve to demonstrate, for the limited number of classes of compounds considered above, that $^1\chi$ is determined by the number, suitably weighted, of $CH_3$, $CH_2$, and CH groups and of quaternary carbon atoms in an alkane, modified by connectivity differences (differences in site of branching).[4] Furthermore, the weighting of $CH_2$, CH, and quaternary carbon atoms (but not of $CH_3$) in [5]–[9], is in the same order as the weighting of the $A_i$ values of these groups in Table 2. Nevertheless, the diversity of structural types of alkanes in Table 1 is greater than that covered in [5]–[9], so that it is perhaps surprising that $(A_0 + \sum n_iA_i)$ for the 23 alkanes of Table 1 is roughly proportional to $^1\chi$. This is shown in Fig. 3*A*. Straight- and branched-chain alkanes lie close to one straight line, and cyclic alkanes close to another.

The structural features term $\sum n_kS_k$ of [2] (for the time-averaged molecule, not the artificially extended one whose $\sum n_kS_k$ values are given in Table 1) is also related to $^1\chi$. This is shown in Fig. 3*B*. *n*-Alkanes lie accurately on one straight line, cyclic compounds cluster about another one, the diverse branched compounds are scattered but show a general trend to increasing $\sum n_kS_k$ with increasing $^1\chi$. Overall, a fair correlation is found between $^1\chi$ and *A* (as calculated from [2]) as shown in Fig. 3*C*. It can be seen that non-cyclic alkanes lie about one straight line, cyclic alkanes about another.[5] Consequently, to the extent that $\log S$ is determined by *A*, as required by [1], we can expect $-\log S$ plotted against $^1\chi$ to lie on one of two straight lines: one for acyclic, one for cyclic alkanes. This we have already observed in Fig. 2*A*.

[4]It is possible that higher order $^m\chi$ functions are also determined by the number and weightings of various types of carbon atoms, but this remains to be demonstrated.

[5]Randic (23) has already pointed out a linear relationship between Hermann's cavity surface area and a "branching index" (which later became $^1\chi$), without discussing its molecular basis, and without pointing out the divergent behaviour of cyclic and acyclic alkanes.

Can. J. Chem. Downloaded from www.nrcresearchpress.com by 210.87.254.40 on 09/06/12
For personal use only.

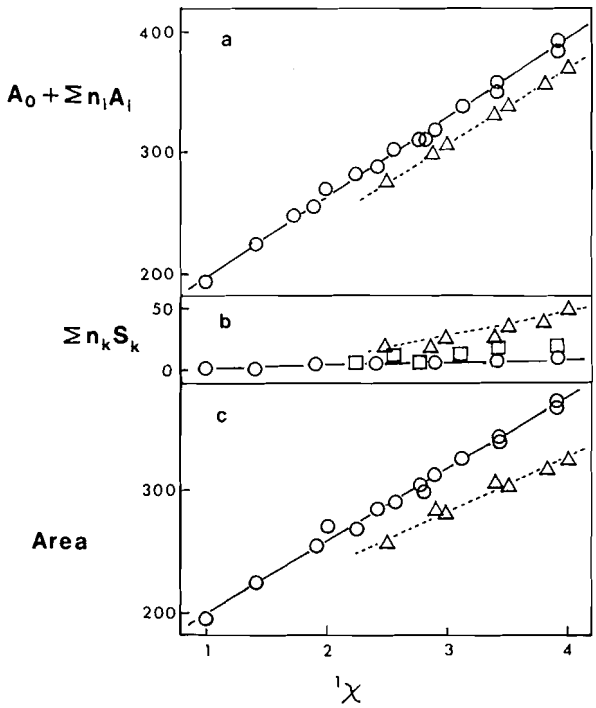


FIG. 3. Relation of cavity surface area terms of [2], and of total area (all in Å²), to first-order connectivity index $^1\chi$. In *a*, *b*, and *c*: △, cyclic alkanes. In *a* and *c*: ○, acyclic alkanes. In *b*: ○ *n*-alkanes; □, branched acyclic alkanes.

In summary, we can say that the solubility in water of alkanes (straight, branched, and cyclic) is related roughly to the first-order connectivity index $^1\chi$ because both are determined by the number and types of carbon atoms and the extent of chain coiling or cyclization. Heats of vaporization (which may be considered rough measures of molecular cohesiveness) and molecular volumes (measures of molecular bulk) are related to $^1\chi$ (and higher order $^m\chi_t$ values) for the same reasons (8). These are properties of central importance. Cramer (24) has shown by factor analysis that a large number of the properties of liquid compounds (activity coefficient, molar refractivity, boiling point, molar volume, magnetic susceptibility, dielectric constant, surface tension, viscosity, etc.) are linear functions of two orthogonal parameters (*B* and *C*) which he identifies with the "bulk" and "cohesiveness" of the individual molecules. To the extent that the latter parameters are linearly related to $^1\chi$ (or to mixtures of $^1\chi$ and other $^m\chi_t$ values), the various properties enumerated above should also be related to $^1\chi$. This may serve to adumbrate possible molecular explanations for the very large number of correlations discovered by Kier, Hall, and their collaborators (3), although this cannot be more than an article of faith until the molecular basis of the higher order connectivity indices is known.[6]


## Acknowledgment

The financial support of the Natural Sciences and Engineering Research Council of Canada is gratefully acknowledged.



1. C. HANSCH. Acc. Chem. Res. **2**, 232 (1969).
2. C. HANSCH, J. E. QUINLAN, and G. L. LAWRENCE. J. Org. Chem. **33**, 347 (1968).
3. L. B. KIER and L. H. HALL. Molecular connectivity in chemistry and drug research. Academic Press, New York. 1976.
4. L. B. KIER and L. H. HALL. J. Pharm. Sci. **70**, 583 (1981).
5. L. B. KIER. *In* Physical chemical properties of drugs. *Edited by* S. H. Yalkowsky, A. A. Sinkula, and S. C. Valvani. Marcel Dekker, New York. 1980. pp. 277–319.
6. G. MANN. Tetrahedron, **23**, 3375 (1967); G. MANN, M. MÜHLSTÄDT, J. BRABAND, and E. DÖRING. Tetrahedron, **23**, 3393 (1967).
7. J. T. EDWARD, P. G. FARRELL, and F. SHAHIDI. J. Phys. Chem. **82**, 2310 (1978); J. T. EDWARD, P. G. FARRELL, and F. SHAHIDI. J. Phys. Chem. **83**, 419 (1979).
8. J. T. EDWARD. Can. J. Chem. **60**, 480 (1982).
9. W. P. JENCKS. Catalysis in chemistry and enzymology. McGraw-Hill, New York. 1969. p. 418.
10. A. LEO, C. HANSCH, and P. Y. C. JOW. J. Med. Chem. **19**, 611 (1976).
11. O. SINANOGLU. Molecular associations in biology. *Edited by* B. Pullman. Academic Press, New York. 1967. p. 427.
12. R. B. HERMANN. J. Phys. Chem. **76**, 2754 (1972).
13. M. J. HARRIS, T. HIGUCHI, and J. H. RYTTING. J. Phys. Chem. **77**, 2694 (1973).
14. G. L. AMIDON, S. H. YALKOWSKY, and S. LEUNG. J. Pharm. Sci. **63**, 3225 (1974).
15. C. MCAULIFFE. J. Phys. Chem. **70**, 1267 (1966).
16. R. S. PEARLMAN. *In* Physical chemical properties of drugs. *Edited by* S. H. Yalkowsky, A. A. Sinkula, and S. C. Valvani. Marcel Dekker, New York. 1980. pp. 321–347.
17. W. L. KOLTUN. Biopolymers, **3**, 665 (1965).
18. G. S. HARTLEY and C. ROBINSON. Trans. Faraday Soc. **48**, 847 (1952); C. ROBINSON and E. J. AMBROSE. Trans. Faraday Soc. **48**, 854 (1952).
19. A. BONDI. J. Phys. Chem. **68**, 441 (1964).
20. G. L. AMIDON, S. H. YALKOWSKY, and S. LEUNG. J. Pharm. Sci. **63**, 1858 (1974).
21. J. T. EDWARD, P. G. FARRELL, and F. SHAHIDI. Can. J. Chem. **57**, 2892 (1979).
22. L. B. KIER, L. H. HALL, and W. J. MURRAY. J. Pharm. Sci. **64**, 1974 (1975).
23. M. RANDIC. J. Am. Chem. Soc. **97**, 6609 (1975).
24. R. D. CRAMER. J. Am. Chem. Soc. **102**, 1837 (1980); **102**, 1894 (1980).


[6]In this article attention has been deliberately restricted to alkanes, because their conformational behaviour is uncomplicated. These compounds can be described solely by $^m\chi_t$ functions derived from simple numerical adjacency values δ of the carbon atoms. For compounds containing heteroatoms Kier and Hall (3) have developed valence molecular connectivity indices $^m\chi^v$, derived in similar fashion from valence delta $\delta^v$ values, which are based on the count of valence electrons participating in σ, π, and lone-pair orbitals in the atom, exclusive of bonds to hydrogen. Better correlations are often obtained using $^m\chi^v$ rather than $^m\chi$. At present a molecular explanation of these correlations seems remote.

Can. J. Chem. Downloaded from www.nrcresearchpress.com by 210.87.254.40 on 09/06/12
For personal use only.

# The direct electrochemical synthesis of neutral and anionic complexes of thorium(IV)

N. KUMAR AND DENNIS G. TUCK[1]

*Department of Chemistry, University of Windsor, Windsor, Ont., Canada N9B 3P4*

Received April 23, 1982

N. KUMAR and DENNIS G. TUCK. Can. J. Chem. **60**, 2579 (1982).

The electrochemical oxidation of thorium into solutions of halogen ($X_2$; X = Cl, Br) in acetonitrile yields the adducts $ThX_4.4CH_3CN$ in good yield. With solutions of $X_2 + R_4NX$, the products are $(R_4N)_2ThX_6$. Neutral chelate complexes such as $Th(acac)_4$ (acac = 2,4-pentanedionate) can also be prepared in a one-step synthesis from the metal, but cationic complexes could not be obtained by electrochemical methods.

N. KUMAR et DENNIS G. TUCK. Can. J. Chem. **60**, 2579 (1982).

L'oxydation électrochimique du thorium dans des solutions d'acétonitrile contenant des halogènes ($X_2$; X = Cl, Br) conduit à des adduits du type $ThX_4.4CH_3CN$ avec un bon rendement. Avec des solutions de $X_2 + R_4NX$, on obtient des produits du type $(R_4N)_2ThX_6$. On peut également préparer des chélates complexes neutres, tel $Th(acac)_4$ (acac = pentane dionate-2,4), en une seule étape à partir du métal, mais on n'a pas pu obtenir les complexes cationiques par des méthodes électrochimiques.

[Traduit par le journal]

## Introduction

The coordination chemistry of thorium, like that of other actinide elements, still reveals some surprising lacunae, despite the actual or potential industrial importance of these elements. The general chemistry of thorium is described in various reviews and standard texts (1–4), but few papers have appeared on the coordination chemistry in recent years, and these for the most part concerned with neutral or anionic derivatives of thorium tetrachloride or tetrabromide.

We now report work on the direct electrochemical oxidation of thorium metal into solutions of chlorine or bromine in acetonitrile. These experiments represent a natural extension of previous direct electrochemical syntheses of the neutral halides of various main group and transition metals (5–10). Solution phases of $X_2 + R_4NX$ yield salts of $ThX_6^{2-}$ anions (X = Cl, Br). We have also successfully snythesised $Th(acac)_4$ and similar compounds, again following earlier work (10), but attempts to prepare cationic complexes (11) were unsuccessful.

## Experimental

*Materials*

Thorium (Alfa Inorganics) was supplied as a rod and sliced into discs ca. 8 mm diameter and 1 mm thick. Acetonitrile (BDH Ltd.) was dried over phosphorus pentoxide and distilled under nitrogen before use. Neutral ligands and tetraalkylammonium halides were dried for 3–4 h at 105°C before use. Other reagents were used as supplied.

*Analysis and spectroscopy*

Thorium was determined by dissolving the complex and titrating the resultant solution at pH 2.1 against EDTA, using Alizarin S as indicator (12). Halogen analysis was by the Volhard technique. Microanalysis on selected compounds was carried out by Guelph Chemical Laboratories Ltd.

Infrared spectra were recorded on a Perkin-Elmer IR-18 instrument, and were used both to identify metal–halogen vibrations and to confirm the presence of neutral ligands or tetraalkylammonium cations.

*Electrochemical methods*

The electrochemical syntheses followed methods described in earlier publications (6–9). The solution phase, typically 50 mL in volume, was contained in a 100 mL tall-form beaker; the cathode was a platinum foil (1 × 1 cm) while a disc of thorium suspended on a platinum wire formed the anode. All preparations were carried out under an atmosphere of dry nitrogen. Details of the experimental conditions are given in Tables 1 and 2 and in the paragraphs below.

*Preparation of $ThX_4.4CH_3CN$ (X = Cl, Br)*

The final product of the electrochemical oxidation of thorium into bromine (2–4 g) in 50 mL acetonitrile was a solution of $ThBr_4$. Addition of diethyl ether led to the precipitation of $ThBr_4.4CH_3CN$ which was collected, washed with ether, and dried *in vacuo* at room temperature. The corresponding $ThCl_4.4CH_3CN$ was obtained with an electrolyte phase of acetonitrile containing dissolved chlorine, which was bubbled through the solution with nitrogen gas as a diluent (8). This adduct is insoluble in the reaction mixture and is simply collected, washed, and dried at the end of the experiment.

The compounds were identified by thorium and halogen analysis (Table 3), and by infrared spectroscopy. The $\nu(C\equiv N)$ mode of the ligand is found at 2280 $cm^{-1}$ in both species (c.f. 2273, 2278 $cm^{-1}$ reported by Bagnall *et al.* (13)); $\nu(M—Cl)$ is at 248 $cm^{-1}$, and $\nu(Th—Br)$ at 180 $cm^{-1}$ (c.f. 256 and 188 $cm^{-1}$, ref. 13).

The uncomplexed halides can be easily obtained by heating the acetonitrile adducts *in vacuo*, following the procedures of Bagnall *et al.* (13).

*Neutral adducts of $ThCl_4$ and $ThBr_4$*

Acetonitrile can be displaced from the tetrahalide complex by other ligands, so that the electrochemical synthesis also provides a route to other neutral adducts. In both systems, excess halogen remaining after the electrolysis was first removed by bubbling dry nitrogen through the solution for approximately 30 min.

In the case of $ThCl_4.4CH_3CN$, the suspension in acetonitrile

[1]To whom all correspondence should be addressed.

0008-4042/82/202579-04$01.00/0

©1982 National Research Council of Canada/Conseil national de recherches du Canada

Can. J. Chem. Downloaded from www.nrcresearchpress.com by 210.87.254.105 on 09/06/12
For personal use only.

TABLE 1. Experimental conditions for electrochemical preparations of neutral and anionic halide complexes of thorium

| Product | $CH_3CN$ vol (mL) | Mass of halogen (g) | Mass of $R_4NX$ (g) | Initial Voltage (V) | Initial Current (mA) | Time of electrolysis (h) | Mass of metal dissolved (g) | % Yield of product |
|---|---|---|---|---|---|---|---|---|
| $ThCl_4.4CH_3CN$ | 50 | — | —[a] | 25 | 25 | 5 | 1.00 | 97 |
| $ThBr_4.4CH_3CN$ | 40 | 4.0 | —[a] | 8 | 50 | 3 | 0.6 | 91 |
| $[Et_4N]_2ThCl_6$ | 50 | — | 1.5 | 4 | 50 | 4 | 0.8 | 55 |
| $[Me_4N]_2ThBr_6$ | 50 | 4 | 1.5 | 5 | 50 | 5 | 0.6 | 62 |

[a]15 mg of $Et_4NClO_4$ added in these experiments.

TABLE 2. Experimental conditions for electrochemical preparation of chelate complexes of thorium

| Product[a] HL | Vol acetone (mL) | Wt/vol HL (g/mL) | Initial Voltage (V) | Initial Current (mA) | Time of electrolysis (h) | Th dissolved (g) | % Yield of product |
|---|---|---|---|---|---|---|---|
| $Th(acac)_4$ | 40 | 4 | 45 | 50 | 4.5 | 0.36 | 72 |
| $Th(tfha)_4$ | 50 | 2.5 | 30 | 40 | 5.0 | 0.32 | 77 |
| $Th(oxine)_4$ | 50 | 1.8 | 45 | 20 | 4.0 | 0.15 | 53 |

[a]acac = 2,4-pentanedionate; tfha = 1,1,1-trifluoromethyl-heptane-2,5-dionate; oxine = 8-hydroxyquinolinate.

TABLE 3. Analytical results and yields for thorium complexes

| Product[a] | Colour | Yield[b] (%) | Thorium (%) Found | Thorium (%) Calcd. | Halogen (%) Found | Halogen (%) Calcd. |
|---|---|---|---|---|---|---|
| $ThCl_4.4CH_3CN$ | Colourless | [c] | 43.7 | 43.1 | 27.2 | 26.4 |
| $ThBr_4.4CH_3CN$ | Colourless | [c] | 32.2 | 32.4 | 44.6 | 44.6 |
| $(Et_4N)_2ThCl_6$ | Colourless | [c] | 32.0 | 32.9 | 29.5 | 30.1 |
| $(Me_4N)_2ThBr_6$ | Colourless | [c] | 27.2 | 27.0 | 55.3 | 55.8 |
| $ThCl_4.5dmso$ | Colourless | 64 | 30.3 | 30.4 | 17.8 | 18.6 |
| $ThCl_4.3Ph_3PO$ | Colourless | 71 | 18.6 | 19.2 | [d] | |
| $ThCl_4.2bipy$ | Colourless | 73 | 33.9 | 33.8 | 20.0 | 20.6 |
| $ThCl_4.phen$ | Colourless | 80 | 41.7 | 41.9 | 25.0 | 25.6 |
| $ThBr_4.6dmso$ | Colourless | 64 | 21.8 | 22.7 | 30.9 | 31.3 |
| $ThBr_4.3Ph_3PO$ | Pale yellow | 63 | 16.1 | 16.7 | [e] | |
| $ThBr_4.2bipy$ | Colourless | 78 | 26.7 | 26.9 | 37.2 | 37.0 |
| $ThBr_4.2phen$ | Colourless | 88 | 25.3 | 25.5 | 33.8 | 35.0 |
| $Th(acac)_4$ | Colourless[f] | 72 | 37.1 | 36.9 | [g] | |
| $Th(tfha)_4$ | Colourless | 77 | 22.0 | 22.9 | | |
| $Th(oxine)_4$ | Yellow | 53 | 28.2 | 28.7 | | |

[a]dmso = dimethylsulphoxide; bipy = 2,2'-bipyridine; phen = 1,10-phenanthroline; acac = 2,4-pentanedionate; tfha = 1,1,1-trifluoromethyl-2,4-heptanedionate; oxine = 8-hydroxyquinolate.
[b]Based on metal dissolved electrochemically.
[c]See Table 1.
[d]Found: C 47.8, H 3.4; calcd: C 46.8, H 3.2.
[e]Found: C 51.0, H 3.7; calcd: C 52.8, H 3.7.
[f]Melting point 170°C.
[g]Found: C 38.2, H 4.4; calcd: C 38.2, H 4.5.

was stirred with the appropriate ligand in excess for 1 h at room temperature. For $ThBr_4.4CH_3CN$, the solution in acetonitrile obtained from the electrolysis was used, after removing excess halogen. The products were then collected, washed, and dried in the usual way.

*Preparation of $ThX_6^{2-}$ salts (X = Cl, Br)*

In keeping with previous work (14), the electrochemical oxidation of thorium into acetonitrile solutions containing $R_4NX$ and $X_2$ (see Table 1) proceeded smoothly. At the end of the electrolysis, excess halogen was removed as described above, and the solution cooled to 0°C. In the case of X = Cl, R = Et, this caused precipitation of the salt $(Et_4N)_2ThCl_6$ which was collected, washed with diethyl ether, and dried *in vacuo*. For X = Br, R = Me, it was necessary to reduce the volume of the solution phase by ca. 25%, after which cooling produced crystals of $(Me_4N)ThBr_6$ which were collected, washed, and dried.

*Preparation of neutral chelate complexes*

The electrolyte phase for these syntheses consisted of an acetone solution of the appropriate parent acid (Table 2). After electrolysis, the solution was filtered in order to eliminate traces of solid impurity, and the solvent removed *in vacuo*. The resultant residue was dissolved in toluene and reprecipitated by the addition of petroleum ether; the final product was collected and dried *in vacuo*.

In addition to the known compounds $Th(acac)_4$ (acac =

Can. J. Chem. Downloaded from www.nrcresearchpress.com by 210.87.254.105 on 09/06/12
For personal use only.

Can. J. Chem. Downloaded from www.nrcresearchpress.com by 210.87.254.105 on 09/06/12
For personal use only.

2,4-pentanedionate) and $Th(oxine)_4$ (oxine = 8-hydroxyquinolate), we also obtained $Th(tfha)_4$ (tfha = 1,1,1-trifluoroheptane-2,5-dionate). An attempt to prepare a salicylaldehyde derivative by this route was unsuccessful.

The $^1H$ nmr of $Th(acac)_4$ showed resonances at 1.17 ($CH_3$) and 4.67 (CH) ppm from TMS, in the intensity ratio 6:1, as required for a β-diketonate complex.

## Results and discussion

*Adducts of neutral halides*

The electrochemical synthesis of $ThX_4.4CH_3CN$ (X = Cl, Br) represents a convenient, rapid, and simple route to these compounds. The methods reported in the literature (3, 4) involve high temperature reactions to give $ThX_4$, which is then converted to the acetonitrile complex. The acetonitrile adducts, which are the primary products of the electrochemical synthesis, can be easily converted to other adducts as described above, or heated *in vacuo* to remove acetonitrile (13), and this latter sequence offers a simple pathway to the tetrachloride and tetrabromide. These systems have many parallels with earlier work on the preparation of acetonitrile and other adducts of the tetrahalides of titanium, zirconium, and hafnium (7).

It is worth noting here that the electrochemical oxidation of thorium into acetonitrile solutions of iodine gives rise to thorium(II) compounds (15). Such differences between iodine and the lighter halogens in stabilising low oxidation states have been noted previously in the case of copper (8) and indium (5).

The thorium(IV) adducts prepared electrochemically are for the most part identical in composition and spectral properties with those reported by earlier authors (13, 16, 17). Any discussion of the differences which do exist is beyond the scope of the present work.

*Anionic halogeno complexes*

The electrochemical oxidation of a metal into an non-aqueous solution of $R_4NX + X_2$ represents a simple one-step route to the tetraalkylammonium salts of $MX_n^{m-}$ anions (14), and we can now add thorium to the list of main group and transition metal elements for which this has been demonstrated. The salts $(Et_4N)_2ThCl_6$ and $(Me_4N)_2ThBr_6$ were obtained in good yield from the metal and in good crystalline form. Both compounds have been reported previously by Brown (18), who reacted $ThX_4$ (or $ThX_4.4CH_3CN$) with the appropriate tetraalkylammonium halide in boiling acetonitrile. The advantages of the electrochemical method are that it is a one-step reaction, starting from the metal, and that the thermal preparation of the tetrahalide is avoided.

*β-Diketonate and related complexes*

Following earlier work on the electrochemical preparation of $M(acac)_{2,3}$ species (10), and more recent studies of a range of similar cadmium complexes (19), we have investigated the direct synthesis of analogous thorium compounds. Both $Th(acac)_4$ and the related derivative of $CF_3CO-CH_2COC_3H_7$ were easily obtained in good yield by a route which appears simpler than those previously reported (20, 21), in that the number of steps is reduced. The corresponding oxinato complex $Th(oxine)_4$ was also obtained without the extra molecule of 8-hydroxyquinoline which is complexed to the thorium oxinate as the product of other syntheses of this compound, and which must be removed by pyrolysis (22).

*Cationic complexes*

In a previous publication (11), we described simple one-step syntheses of cationic complexes of a number of metallic elements with $CH_3CN$ or dimethylsulphoxide, using a mixture of the ligand with concentrated aqueous $HBF_4$ as the electrolyte; the products are then typically obtained as the salts $[ML_6](BF_4)_n$ (L = $CH_3CN$, dmso). Attempts to apply this method to the synthesis of the corresponding thorium species were unsuccessful. The anode rapidly became coated with a layer of white material, which effectively prevented further reaction. We believe that this material is a thorium fluoride species, formed by decomposition of the $BF_4^-$ anion at the electrode surface

[1] $BF_4^- \rightarrow BF_4^{\cdot} + e$

[2] $BF_4^{\cdot} \rightarrow BF_3 + F^{\cdot}$

[3] $nF^{\cdot} + Th \rightarrow ThF_n$

*Electrochemical efficiency*

As in previous work, we have measured the electrochemical yield ($E_F$), defined as moles of metal dissolved per Faraday of electricity. Such experiments are typically carried out at a constant current of 20 mA over 2 h.

For the $CH_3CN/X_2$ systems, we find $E_F = 0.27$ mol $F^{-1}$ for X = Cl, and 0.26 for X = Br. These values correspond to the anodic process

[4] $Th + 4X^- \rightarrow ThX_4 + 4e$

and are exactly in keeping with the products obtained from the acetonitrile solution, namely, the adducts of $ThCl_4$ and $ThBr_4$. Moreover, these $E_F$ values are equal within experimental error to those required for Faradaic behaviour, in sharp contrast to the results for other $M/X_2$ electrochemical systems (6–9) for which the values of $E_F$ were in the

range 1–10 mol $F^{-1}$. The reasons for these differences are not obvious at this point.

For the experiments involving β-diketonate or oxinate, the $E_F$ values were found to be

Th/Hacac $E_F = 0.18$ mol $F^{-1}$
Th/Htfha $E_F = 0.19$ mol $F^{-1}$
Th/Hoxine $E_F = 0.22$ mol $F^{-1}$

close to the value of 0.25 mol $F^{-1}$ required for an anode reaction such as

[5] $Th + 4acac^- \rightarrow Th(acac)_4 + 4e$

which implies the Faradaic behaviour found in other metal/β-diketonate electrolytic oxidations (10). As in such experiments, the formation of gas ($H_2$) at the cathode was noted. The rather low values of $E_F$ may imply a resistance of thorium metal to the oxidation reaction [5], with some anions being discharged without causing oxidation of the metal.

*General*

The electrochemical oxidation of thorium provides a simple room temperature reaction for the direct synthesis of a variety of thorium(IV) compounds in good yield (Table 3). We conclude that the electrochemical synthesis of thorium compounds could replace many of the earlier methods on the grounds of simplicity and convenience.

**Acknowledgement**

This work was supported by an Operating Grant (to D.G.T.) under the Strategic Grant Programme of the Natural Sciences and Engineering Research Council of Canada.

1. P. Pascal. Nouveau Traité de Chimie Minérale. Vol. 9. Masson, Paris. 1963.
2. K. W. Bagnall. Coord. Chem. Rev. **2**, 146 (1967).
3. D. Brown. MTP international review of science. Inorg. Chem. Ser. 1. Vol. 7. *Edited by* K. W. Bagnall. Butterworths, London. 1972. p. 87.
4. D. Brown. Comprehensive inorganic chemstry. Vol. 5. *Edited by* A. F. Trotman-Dickenson. Pergamon Press, Oxford. 1973. p. 151.
5. J. J. Habeeb and D. G. Tuck. Chem. Commun. 808 (1975).
6. J. J. Habeeb, L. Neilson, and D. G. Tuck. Can. J. Chem. **55**, 2631 (1977).
7. J. J. Habeeb, F. F. Said, and D. G. Tuck. Can. J. Chem. **55**, 3882 (1977).
8. J. J. Habeeb, L. Neilson, and D. G. Tuck. Inorg. Chem. **17**, 306 (1978).
9. J. J. Habeeb, F. F. Said, and D. G. Tuck. J. Chem. Soc. Dalton Trans. 1161 (1980).
10. J. J. Habeeb, D. G. Tuck, and F. H. Walters. J. Coord. Chem. **8**, 27 (1978).
11. J. J. Habeeb, F. F. Said, and D. G. Tuck. J. Chem. Soc. Dalton Trans. 118 (1981).
12. J. J. Fritz and J. J. Ford. Anal. Chem. **25**, 1640 (1953).
13. K. W. Bagnall, D. Brown, and P. J. Jones. J. Chem. Soc. A, 1763 (1966).
14. J. J. Habeeb, L. Neilson, and D. G. Tuck. Synth. React. Inorg. Metal-org. Chem. **6**, 105 (1976).
15. N. Kumar and D. G. Tuck. Unpublished results.
16. K. W. Bagnall, D. Brown, D. H. Holah, and F. Lux. J. Chem. Soc. A, 465 (1968).
17. B. C. Smith and M. A. Wassef. J. Chem. Soc. A, 1817 (1968).
18. D. Brown. J. Chem. Soc. A, 766 (1966).
19. L. Bustos and D. G. Tuck. Unpublished results.
20. M. Biltz. Annalen, **331**, 334 (1904).
21. T. Yoshimura, C. Miyake, and S. Imoto. Bull. Chem. Soc. Jpn. **46**, 2096 (1973).
22. T. Moeller and M. V. Ramaniah. J. Am. Chem. Soc. **75**, 3946 (1953).

Can. J. Chem. Downloaded from www.nrcresearchpress.com by 210.87.254.105 on 09/06/12
For personal use only.

# Copper complexes of polyfunctional phthalazines. Mononuclear and polynuclear derivatives

DOROTHY V. BAUTISTA, JOHN C. DEWAN, AND LAURENCE K. THOMPSON[1]

*Department of Chemistry, Memorial University of Newfoundland, St. John's, Nfld., Canada A1B 3X7*

Received March 8, 1982

DOROTHY V. BAUTISTA, JOHN C. DEWAN, and LAURENCE K. THOMPSON. Can. J. Chem. **60**, 2583 (1982).

Mononuclear, binuclear, and trinuclear copper(II) complexes of the tetradentate ligands 1,4-di(2′-pyridyl) aminophthalazine (PAP) and 1,4-di(4′-methyl-2′-pyridyl) aminophthalazine (PAP4Me) and binuclear complexes of the tetradentate ligand 1,4-di(6′-methyl-2′-pyridyl) aminophthalazine (PAP6Me) are reported. In a series of binuclear carboxylate derivatives carboxylate bridges exist between copper centres in all cases and in some cases oxygen bridges (hydroxide or methoxide) are indicated. In all other polynuclear derivatives hydroxide bridges are anticipated on the basis of analytical, spectral, and magnetic data. The ligands exist as anionic groups in some binuclear carboxylate derivatives while in the other polynuclear systems neutral ligands are found. In reactions in aqueous solution protonated mononuclear derivatives are obtained for both PAP and PAP4Me in cases where solutions of the metal salts are inherently acidic, followed by polynuclear, neutral ligand complexes which form when the pH increases. Mononuclear protonated complexes are not obtained with PAP6Me, where steric factors may prevent the formation of such derivatives. Low magnetic moments (1.1–1.5 BM) are observed for most hydroxy bridged complexes while even lower values (<0.70 BM) are observed for two binuclear complexes of PAP6Me, indicating the possibility of strong antiferromagnetic exchange between metal centres. A preliminary X-ray investigation of the complex $[Cu_2(PAP4Me)(OH)(NO_3)_2(H_2O)_2]NO_3$ indicates a triple bridged binuclear structure including a bidentate nitrate bridge and a hydroxide bridge with an oxygen bridge angle of 115.2°.

DOROTHY V. BAUTISTA, JOHN C. DEWAN et LAURENCE K. THOMPSON. Can. J. Chem. **60**, 2583 (1982).

On a préparé les complexes mono-, bi- et trinucléaires du cuivre(II) des ligands tétradentates di(pyridyl 2′)-1,4 aminophtalazine (PAP) et di-(méthyl-4′ pyridyl-2′)-1,4 aminophtalazine (PAP4Me) et les complexes binucléaires du ligand tétradentate di(méthyl-6′ pyridyl-2′)-1,4 aminophtalazine (PAP6Me). Dans une série de dérivés carboxylates binucléaires, il existe dans tous les cas des ponts carboxylates entre les centres cuivre et, dans certains cas, on trouve des ponts oxygènes (hydroxyde ou méthylate). En se basant sur des données analytiques, spectrales et magnétiques, on prévoit qu'il existera des ponts hydroxydes dans tous les autres dérivés polynucléaires. Les ligands existent sous forme de groupes anioniques dans certains carboxylates binucléaires tandis que, dans d'autres systèmes polynucléaires, on trouve des ligands neutres. Lorsque les solutions de sels métalliques sont intrinsèquement acides, on obtient des dérivés mononucléaires protonés avec le PAP et le PAP4Me en solution aqueuses et des complexes polynucléaires de ligands neutres lorsque le pH augmente. On n'obtient pas de complexes mononucléaires protonés avec le PAP6Me alors que des facteurs stériques empêchent la formation de tels dérivés. On a observé de faibles moments magnétiques (1.1–1.5 BM) pour la plupart des complexes ayant un pont hydroxyde tandis qu'on observe des valeurs plus faibles (< 0.70 BM) pour deux complexes binucléaires du PAP6Me; ceci indique qu'il existe une possibilité d'un fort échange antiferromagnétique entre les centres métalliques. Une étude préliminaire du complexe $[Cu_2(PAP4Me)(OH)(NO_3)_2(H_2O)_2]NO_3$ par cristallographie de rayons X indique une structure binucléaire triplement pontée incluant un pont nitrate bidentate et un pont hydroxyde avec un angle du pont oxygène de 115,2°.

[Traduit par le journal]

## Introduction

Binucleating ligands containing just nitrogen donor atoms have received some attention in recent years and have been based largely on substituted "diazine" type units. Polyfunctional ligands derived from hydrazine (1–3), pyrazole (4–8), pyridazine (4, 9–11), and phthalazine (4, 9, 11, 12–19) form transition metal complexes in which the metals are brought into close proximity because of the presence of the $N_2$, diazine, fragments in these systems. Antiferromagnetic exchange between the adjacent metal centres has been demonstrated in some of these complexes (4, 11, 13, 15, 16, 18) and catecholase activity has been shown with binuclear copper complexes of the binucleating ligand 1,4-di(2′-pyridyl) aminophthalazine (PAP) (Fig. 1). In a recent paper (21) binuclear copper complexes of the ligand 3,6-bis(2′-pyridyl) pyridazine are described and an X-ray structure of the chloro-derivative reveals a double bridge involving the pyridazine $N_2$ and a hydroxide. Binuclear complexes involving macrocyclic, nitrogen-containing ligands have also been synthesized (14, 22).

PAP has been shown to bind preferentially to two metal centres forming binuclear complexes with copper, cobalt, nickel, and zinc salts (13, 15, 16, 18, 19). Antiferromagnetic exchange exists between the metal centres in cobalt, nickel, and copper complexes of PAP (13, 15, 16, 18). PAP appears to be quite sensitive to protonation, even in mildly acidic solution, and as a result of the inherent acidity of aqueous and alcoholic solutions of certain commercially available metal salts, protonated

[1]To whom all correspondence should be addressed.

0008-4042/82/202583-11$01.00/0

©1982 National Research Council of Canada/Conseil national de recherches du Canada

Can. J. Chem. Downloaded from www.nrcresearchpress.com by 210.87.254.5 on 09/06/12
For personal use only.

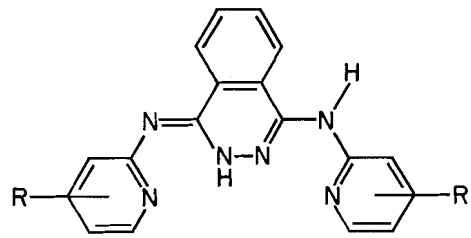

FIG. 1. PAP (R = H), PAP4Me (R = 4 methyl), PAP6Me (R = 6 methyl).

mononuclear (1:2) complexes are obtained as initial products, in certain reactions, followed by binuclear or polynuclear derivatives containing neutral ligand (18, 19).

In this paper we describe some copper complexes of PAP, which have not been previously reported, and some copper complexes of two closely related pyridyl phthalazines: 1,4-di(4′-methyl-2′-pyridyl) aminophthalazine (PAP4Me) and 1,4-di(6′-methyl-2′-pyridyl) aminophthalazine (PAP6Me). These ligands are previously unreported. Protonated mononuclear, neutral ligand binuclear and polynuclear complexes are obtained for PAP4Me, these systems bearing a close resemblance to counterparts with PAP itself, while for PAP6Me only binuclear complexes are obtained. The absence of any protonated mononuclear (1:2) complexes of the pyridyl phthalazine involving a methyl substituent in the 6-position on the pyridine ring is no doubt due to steric constraints imposed by such groups. However, in keeping with the general ability of PAP type ligands to act as weak bases, protonated ligand salts are produced in certain reactions involving PAP6Me. Preliminary X-ray structural details of the complex $[Cu_2(PAP\text{-}4Me)(OH)(NO_3)_2(H_2O)_2]NO_3$ are also reported.

## Experimental

Electronic spectra were recorded with a Cary 17 spectrometer and infrared spectra with a Perkin-Elmer Model 283 spectrometer. Magnetic susceptibilities were obtained at room temperature by the Faraday method using a Cahn Model #7600 Faraday Magnetic Susceptibility system, coupled to a Cahn gram electrobalance. Nuclear magnetic resonance spectra were run as solutions in deuterochloroform using a Bruker WP80 spectrometer and mass spectra were run using a Hitachi-Perkin Elmer RMU-6E with the direct insertion probe. Microanalyses were carried out by Canadian Microanalytical Service, Vancouver (C, H, N). Metal analyses were determined by atomic absorption with a Varian Techtron AA-5, after digestion of the samples in concentrated $HNO_3$ or aqua regia.

*Ligands*

PAP was prepared as described previously (13) but can also be prepared conveniently by the following procedure.

*1,4-Di(4′-methyl-2′-pyridyl) aminophthalazine (PAP4Me)*

1,3-Di(4′-methyl-2′-pyridyl) iminoisoindoline was prepared by fusing phthalonitrile (12.8 g, 0.100 mol) and 2-amino-4-methylpyridine (21.6 g, 0.200 mol) and maintaining a temperature of 220°C until ammonia evolution ceased (approximately 12 h). Extraction of the solid, which formed on cooling, into ethanol gave yellow crystals on recrystallization (yield = 24.2 g; 75%) (mp 164°C) (lit. 165–166°C, ref. 22).

The isoindoline (15.0 g, 0.050 mol) was dissolved in methanol (400 mL) under reflux, 85% hydrazine hydrate (8.0 mL) added, and the mixture refluxed for 15 h, or until ammonia evolution had essentially ceased. Filtration and reduction in volume led to the formation of a yellow crystalline product, which was recrystallized from ethanol (yield = 13.2 g, 84%) and dried at 80°C under vacuum for 3 h (mp 178°C). *Anal.* calcd. for $C_{20}H_{18}N_6$: C 70.2, H 5.26, N 24.6; found: C 70.2, H 5.45, N 24.3. Mass spectrum, major mass peaks (*m/e* (relative intensity)) 342 (100) P, 327 (10), 235 (23), 222 (25), 93 (68), 92 (95); $^1$H nmr ($CDCl_3$) (σ(relative intensity)) 2.33 (45) (singlet, $CH_3$), 6.68 (15) (doublet, pyridine $H_5$), 7.10 (7) (singlet, pyridine $H_3$), 7.7 (36) (multiplet, 1NH, *o*-phenylene $H_\beta$, pyridine $H_6$), 8.1 (15) (multiplet, *o*-phenylene $H_\alpha$), 8.75 (7) (broad singlet, 1NH). The observation of two different types of NH indicates that the ligand exists in chloroform solution in the tautomeric form illustrated in Fig. 1. Also the absence of a symmetric set of resonances attributable to a symmetrically disubstituted benzene ring indicates the presence of a tautomeric form of the ligand in which the phthalazine moiety is not bisected by a mirror plane. In the infrared spectrum two bands attributable to NH stretch are observed at 3270 and 3200 cm$^{-1}$, again supporting two different NH groups.

*1,4-Di(6′-methyl-2′-pyridyl) aminophthalazine (PAP6Me)*

PAP6Me was prepared in the same way as PAP4Me and obtained as a yellow crystalline solid which was recrystallized from ethanol and dried at 80°C, under vacuum, for 3 h (yield isoindoline = 41%; yield phthalazine = 83%) (mp 158–161°C). *Anal.* calcd. for $C_{20}H_{18}N_6$: C 70.2, H 5.26, N 24.6; found: C 69.9, H 5.37, N 24.3. Mass spectrum, major mass peaks (*m/e* (relative intensity)) 342 (100) P, 235 (24), 93 (84), 92 (90); $^1$H nmr ($CDCl_3$) (σ(relative intensity)) 2.52 (30) (singlet, methyl), 6.76 (10) (doublet, pyridine $H_5$), 7.52 (10) (doublet, pyridine $H_3$), approximately 7.8 (30) (poorly defined multiplet, *o*-phenylene $H_\alpha$, $H_\beta$, pyridine $H_4$), 8.75 (5) (NH). The NH resonance is very broad and an estimate of its integrated intensity suggests only one proton. Location of the second NH proton was unsuccessful, but it may be buried beneath the rather broad envelope of resonances in the range 6.7–8.05. The indication of two different types of NH suggests that the ligand exists in chloroform in the tautomeric form shown in Fig. 1. Also, unlike the isoindoline, whose nmr spectrum clearly shows an AA′BB′ splitting pattern associated with a symmetrically *o*-disubstituted benzene ring, the phthalazine shows an asymmetric set of resonances due to the fused benzene ring protons, indicating an unsymmetrical ligand involving two different types of NH. In the mull infrared spectrum a sharp, single absorption at 3400 cm$^{-1}$ suggests the possibility of just one type of NH in the solid state and a symmetrical tautomer probably involving hydrogen atoms bound to just the exocyclic nitrogen atoms.

*Copper complexes*

*$[Cu(PAPH)_2(NO_3)_2](NO_3)_2.0.5H_2O$ (I), $[Cu_3(PAP)_2(OH)_2(NO_3)_2](NO_3)_2.4H_2O$ (II)*

PAP (1.00 g; 3.18 mmol) was added to a solution of $Cu(NO_3)_2.3H_2O$ (0.770 g; 3.19 mmol) dissolved in water (200 mL) and the mixture refluxed for 2 h. The resulting green solution was filtered and allowed to stand at room temperature in a loosely covered beaker. Buff-coloured crystals (**I**) were obtained and after several days this product was filtered off, washed with ethanol and ether, and dried under vacuum and the mother

Can. J. Chem. Downloaded from www.nrcresearchpress.com by 210.87.254.5 on 09/06/12
For personal use only.

Can. J. Chem. Downloaded from www.nrcresearchpress.com by 210.87.254.5 on 09/06/12
For personal use only.

liquor allowed to evaporate further. A second crop of buff crystals was obtained and the process repeated. A third crop of crystals contained I plus a green crystalline product (II) and finally green crystals (II) were obtained as the sole product in the fourth crop. The green product was recrystallized from water, washed with ethanol and ether, and dried under vacuum.

Pairs of products, including in each case a protonated mononuclear derivative and a polynuclear neutral ligand derivative, were obtained in a similar fashion from the reaction of $Cu(ClO_4)_2.6H_2O$ (**III**, buff; **IV**, green) with PAP in methanol or water and reactions of $Cu(NO_3)_2.3H_2O$ (**XV**, buff–yellow; **XVI**, blue), $Cu(ClO_4)_2.6H_2O$ (**XVII**, green–yellow; **XVIII**, green), and $Cu(BF_4)_2.6H_2O$ (**XIX**, green–yellow; **XX**, green) with PAP4Me in aqueous solution. In certain cases recrystallization of a product was effected from methanol and solvate molecules are found in the complex.

*$[Cu_2(PAP)$(p-tolylSCH$_2$COO)$_4].1.5H_2O$ (IX)*

$CuCO_3.Cu(OH)_2.H_2O$ (0.800 g; 3.35 mmol) and *p*-tolylthioacetic acid (2.34 g; 12.7 mmol) were added to methanol (150 mL) and the mixture refluxed for 15 min. PAP (1.00 g; 3.18 mmol) was added and the mixture refluxed for 1 h and the resulting green solution filtered. Reduction in volume of the solution did not produce a product and so the solvent was completely removed and the resulting green solid extracted with $MeOH/CHCl_3$ (50/50). On standing a green powder was formed, which was filtered, washed with ether, and dried under vacuum.

The other copper thio- and sulfoxy-carboxylate complexes (**V–VIII**, **X**, **XI**) were prepared similarly using stoichiometric amounts of copper carbonate and the appropriate carboxylic acid and obtained as green solids.

*$[Cu_2(PAP4Me)(OH)Cl_3].H_2O$ (XII)*

PAP4Me (1.00 g; 2.92 mmol) was added to a solution of $CuCl_2.2H_2O$ (3.23 g; 18.9 mmol) dissolved in water (100 mL) and the mixture refluxed for 1 h. A green precipitate formed which was filtered, washed with water, recrystallized from water, and dried under vacuum at room temperature.

The corresponding bromo-complex (**XIII**) and the copper chloride and copper bromide complexes of PAP6Me (**XXI**, **XXII**) were prepared similarly and obtained as green crystalline solids.

*$[Cu_2(PAP4Me)(CH_3COO)_2(OH)].H_2O$ (XIV)*

PAP4Me (1.00 g; 2.92 mmol) was added to a solution of cupric acetate (1.17 g; 2.96 mmol) dissolved in ethanol (300 mL) and the mixture refluxed for 45 min. The volume of the resulting green solution was reduced to approximately 100 mL and allowed to stand. A powdery khaki-green product was obtained which was recrystallized from methanol to give a khaki-green solid. The product was filtered off, washed with methanol and ether, and dried under vacuum at room temperature.

The copper acetate complex of PAP6Me (**XXIII**) was prepared similarly and obtained as a khaki-green powder.

*$[Cu_2(PAP6Me)(OH)(NO_3)_2]NO_3$ (XXIV)*

PAP6Me (0.500 g; 1.46 mmol) was dissolved under reflux in ethanol (100 mL). $Cu(NO_3)_2.3H_2O$ (0.688 g; 2.92 mmol) was dissolved in a mixture of ethanol (10 mL) and water (5 mL) and the solution added to the solution of the ligand. The resulting dark green solution was refluxed for 1 h and allowed to stand. A dark green product formed which was filtered, washed with ethanol and ether, and recrystallized from methanol.

*$[PAP6MeH_2](ClO_4)_2$ (XXV), $[Cu_2(PAP6Me)(OH)(H_2O)_2](ClO_4)_3.0.5H_2O$ (XXVI)*

PAP6Me (0.500 g; 1.46 mmol) was dissolved under reflux in ethanol (20 mL) and the solution added to a solution of $Cu(ClO_4)_2.6H_2O$ (1.08 g; 2.92 mmol) dissolved in water (30 mL). The resulting dark green solution was refluxed for 15 min and cooled. A light yellow powder formed (0.26 g) which was filtered off (**XXV**), washed with ethanol, and dried under vacuum. Reduction in volume of the mother liquor produced a dark green solid (0.48 g) which was filtered off (**XXVI**), washed with ethanol, and dried under vacuum.

Satisfactory analytical data have been obtained for these complexes and are reported in Table 1, which has been placed in the Depository of Unpublished Data.[2]

## Results and discussion

The new ligands described in this paper (PAP-4Me, PAP6Me; Fig. 1) are analogues of the parent pyridyl phthalazine (PAP) in which methyl groups have been introduced at the 4- and 6-positions of the pyridine ring. They are all prepared by a common synthetic route in which ring expansion of the isoindoline precursor is effected simply by reaction with hydrazine hydrate. The synthetic route to the isoindoline precursors involves the direct reaction of phthalonitrile and the appropriate 2-aminopyridine at high temperatures for periods of up to 12 h followed by extraction into ethanol. This direct fusion method, which we have used routinely for a number of years, provides good yields of the disubstituted isoindolines and is a more efficient procedure than previously reported syntheses involving phthalonitrile (23, 24) and 1,3-diiminoisoindoline (25) as starting materials. The synthesis of the 5-methyl isoindoline by this route was recently reported by Addison and coworkers (26).

### *Characterization of the complexes*

Previously reported copper complexes of PAP have included binuclear systems involving two metals bound to the same ligand (13) and mononuclear derivatives in which two bidentate ligands are bound to the same metal (19). Polynuclear derivatives involving three copper centres and a binuclear derivative involving two metals bound simultaneously to two tetradentate ligands have also been reported (19). In a series of binuclear copper carboxylate derivatives of PAP the $pK_a$ of the corresponding carboxylic acid determined whether or not the ligand was neutral or anionic. For acids whose $pK_a$ is greater than 3.8 complexes of the type $[Cu_2(PAP–H)(RCOO)_3]$ (PAP–H indicates anionic PAP involving loss of a proton) are formed, whereas for acids whose $pK_a$ is less than 3.8 complexes of the type $[Cu_2(PAP)(RCOO)_4]$, involving neutral ligand, are formed (13).

In an attempt to involve sulphur centres in the coordination sphere of the metal in binuclear systems of this sort, carboxylate complexes involv-

[2]A photocopy may be obtained at a nominal charge, upon request, from the Depository of Unpublished Data, CISTI, National Research Council of Canada, Ottawa, Ont., Canada K1A 0S2.

Can. J. Chem. Downloaded from www.nrcresearchpress.com by 210.87.254.5 on 09/06/12
For personal use only.

ing sulphur-containing carboxylic acids were synthesized. Instead of isolating the copper carboxylate itself the binuclear carboxylate complexes (**V–XI**) were synthesized by reacting ligand, copper carbonate, and the appropriate acid in a suitable solvent. Both 1:2:3 and 1:2:4 stoichiometries (ligand:metal:carboxylic acid) were used in synthesizing these compounds. However, two distinct compounds were obtained only in the case of phenylthioacetic acid and since a neutral ligand is indicated for **V**, in which three carboxylate groups are found, the remaining anionic charge can exist as either methoxide or hydroxide. The absence of any infrared absorption associated with OH suggests the former assignment. For the remaining systems only one compound formed regardless of the chosen stoichiometry.

The $pK_a$ values of the thio- and sulfoxyacetic acids fall in the range 2.6–3.5 and if the previous criterion for the type of complex formed were to apply then only derivatives of the type $[Cu_2(PAP)(RCOO)_4]$ or those involving neutral ligand should be formed. Neutral ligand derivatives are confirmed for all the carboxylate complexes in the solid state, with the possible exception of **VII**, by the presence of at least one charge transfer band at 27000 $cm^{-1}$ or higher (13). Although compound **VII** has a solid state charge transfer band at 27500 $cm^{-1}$, analytical and other data suggest an anionic derivative.

Previous studies have shown that the presence of an infrared band above 1000 $cm^{-1}$, associated with the ring breathing mode of the pyridine ring in PAP, indicates the coordination of this group to the metal centres (13). Absorptions in the range 1017–1025 $cm^{-1}$ (Table 2) for compounds **V–IX** indicate the involvement of the pyridine rings in coordination and suggest that PAP behaves as a tetradentate ligand. Similar absorptions could not be observed for compounds **X**, **XI** because of interfering bands associated with the sulfoxy groups.

Infrared absorptions found in the solid state in the range 1626–1345 $cm^{-1}$ for all the carboxylate complexes can be associated with both terminal and bridging carboxylate groups (13). Typically two absorptions occur around 1600 $cm^{-1}$, the one at higher energy being associated with the antisymmetric vibration of a terminal carboxylate while the lower energy absorption is associated with the antisymmetric mode of a bridging carboxylate. Other carboxylate bands occurring around 1400 $cm^{-1}$ are assigned to symmetric vibrations associated with both bridging and terminal carboxylates, although distinction between these bands is difficult. A comparison of the solid state spectra in this region with those obtained in chloroform solution (Table 2) indicates the possible disproportionation of certain species in solution. For compounds **VI** and **IX**, which contain four carboxylate groups, a new carboxylate band appears around 1700 $cm^{-1}$, which is not observed in the solid state (**VIII** was not soluble enough in chloroform to be studied), while the other carboxylate absorptions remain approximately the same. Since absorptions of this sort around 1700 $cm^{-1}$ can be associated with the free carboxylic acid itself it is suggested that these neutral tetracarboxylate derivatives dissociate via loss of one molecule of the appropriate carboxylic acid to form tricarboxylates, containing anionic ligand, in solution. This is supported by the observation of only one charge transfer absorption around 24000 $cm^{-1}$ associated with anionic PAP. There was no infrared evidence to indicate the involvement of the sulfur or sulfoxy groups in coordination to the metal centres in these complexes.

The solid state electronic spectra of the carboxylate complexes (Table 3) are in general characterized by a major absorption in the range 14500–16400 $cm^{-1}$ accompanied in many cases by a low energy shoulder. The spectra are very similar to those reported previously for related tri- and tetracarboxylate derivatives which were assigned square pyramidal coordination geometries (13). In the solid state charge transfer bands are observed in all cases at 27000 $cm^{-1}$ or above, signalling the presence of neutral ligand. These data can be rationalized reasonably in all cases except compound **VII** where analytical results indicate three carboxylate functions and the absence of a hydroxide group, thus suggesting an anionic ligand. Certainly in solution in chloroform this species appears to contain anionic ligand.

Magnetic moments, measured at room temperature (Table 3), appear normal for compounds **VI**, **VIII**, and **IX**, being in excess of the spin only value for copper(II), and indicate that any antiferromagnetic exchange between the metal centres is small. Efficient bridge exchange groups, e.g. oxygen centres, are therefore considered to be absent in these systems (27–29). Considerably reduced room temperature moments are observed for compounds **V**, **X**, and **XI** in keeping with the proposal that in addition to having phthalazine and carboxylate bridges the copper centres are also bridged by oxygen groups, viz. a methoxide in **V** and hydroxides in **X** and **XI**. For compound **VII**, a slightly reduced room temperature moment signals weaker exchange and the absence of an oxygen bridge. Proposed structures for the carboxylate complexes are given in Fig. 2. Compound **VII** may be a four-coordinate derivative but could also be five-

TABLE 2. Infrared data ($cm^{-1}$)

| | Compound | νCN | Other |
|---|---|---|---|
| **I**, | $[Cu(PAPH)_2(NO_3)_2](NO_3)_2.0.5H_2O$ | 1619, 1625, 1635, 1664 | 1748, 1759, 1765 ($\nu_1 + \nu_4$, $NO_3^-$)<br>996, 1014(pyr) |
| **II**, | $[Cu_3(PAP)_2(OH)_2(NO_3)_2](NO_3)_2.4H_2O$ | 1610, 1640 | 1764, 1756, 1749 ($\nu_1 + \nu_4$, $NO_3^-$)<br>3400(OH, $H_2O$), 3280(NH), 1002, 1021(pyr) |
| **III**, | $[Cu(PAPH)_2](ClO_4)_4.0.5H_2O$ | 1628, 1631, 1655 | 1110($ClO_4^-$), 3380(NH)<br>1007(pyr) |
| **IV**, | $[Cu_3(PAP)_2(OH)_2(MeOH)_2](ClO_4)_4$ | 1618, 1637 | 1065, 1100 ($ClO_4^-$)<br>3340(NH), 3525(OH, MeOH) |
| **V**, | $[Cu_2(PAP)(PhSCH_2COO)_3(OMe)].H_2O$ | 1617, 1641 | 1025(pyr), 1400, 1585, 1604($RCOO^-$), 3300(NH)<br>[a] 1365(sh), 1400(sh), 1600, 1615(sh)($RCOO^-$) |
| **VI**, | $[Cu_2(PAP)(PhSCH_2COO)_4].H_2O$ | 1614, 1640(sh) | 1025(pyr), 1355(sh), 1398, 1593, 1626($RCOO^-$), 3300(NH), 3400, 3470($H_2O$)<br>[a] 1365, 1400(sh), 1595, 1610, 1700($RCOO^-$) |
| **VII**, | $[Cu_2(PAP)(o\text{-tolylSCH}_2COO)_3]$ | 1640 | 1018(pyr), 1400(sh), 1594, 1616($RCOO^-$)<br>[a] 1400(sh), 1594, 1615($RCOO^-$) |
| **VIII**, | $[Cu_2(PAP)(m\text{-tolylSCH}_2COO)_4]$ | 1633 | 1017(pyr), 1356, 1396, 1586, 1607($RCOO^-$) |
| **IX**, | $[Cu_2(PAP)(p\text{-tolylSCH}_2COO)_4].1.5H_2O$ | 1640 | 1018(pyr), 1367, 1405(sh), 1591, 1615($RCOO^-$)<br>[a] 1400(sh), 1595, 1605, 1725($RCOO^-$) |
| **X**, | $[Cu_2(PAP)(OH)(PhS(O)CH_2COO)_3]$ | 1640(sh) | 1345(sh), 1410(sh), 1592, 1615($RCOO^-$)<br>[a] 1352, 1590(sh), 1617($RCOO^-$) |
| **XI**, | $[Cu_2(PAP)(OH)(p\text{-tolylS(O)CH}_2COO)_3].H_2O$ | 1640(sh) | 1395(sh), 1400(sh), 1590, 1612<br>[a] 1400(sh), 1590(sh), 1620 |
| **XII**, | $[Cu_2(PAP4Me)(OH)Cl_3].H_2O$ | 1618, 1643 | 3360(NH), 3560(OH)<br>321(Cu—Cl) |
| **XIII**, | $[Cu_2(PAP4Me)(OH)Br_3]$ | 1620, 1640 | 3350, 3460(NH), 3610(OH)<br>230(Cu—Br) |
| **XIV**, | $[Cu_2(PAP4Me)(OH)(CH_3COO)_2(H_2O)]$ | 1644 | 1360, 1404(sh), 1590, 1629($RCOO^-$), 3300(NH)<br>[a] 1360, 1400(sh), 1593, 1628($RCOO^-$) |
| **XV**, | $[Cu(PAP4MeH)_2](NO_3)_4$ | 1621, 1635, 1655, 1660(sh) | 1755 ($\nu_1 + \nu_4$, $NO_3^-$), 3280(NH) |
| **XVI**, | $[Cu_2(PAP4Me)(OH)(H_2O)_2(NO_3)_2]NO_3$ | 1626, 1645 | 1751, 1753, 1766, 1784 ($\nu_1 + \nu_4$, $NO_3^-$), 3300(NH), 3500($H_2O$), 3580(OH), 290(Cu—O) |
| **XVII**, | $[Cu(PAP4MeH)_2](ClO_4)_4.2MeOH$ | 1620, 1637, 1640 | 1060, 1100($ClO_4^-$), 3330(NH), 3580(MeOH) |
| **XVIII**, | $[Cu_3(PAP4Me)_2(OH)_2(H_2O)_2](ClO_4)_4.MeOH$ | 1622, 1645 | 1065, 1100($ClO_4^-$), 3330(NH), 3590($H_2O$), 3650(OH) |
| **XIX**, | $[Cu(PAP4MeH)_2](BF_4)_4.H_2O$ | 1620, 1640, 1662 | 1060($BF_4^-$), 3360(NH), 3560(sh), 3620($H_2O$) |
| **XX**, | $[Cu_3(PAP4Me)(OH)_2(H_2O)_2](BF_4)_4$ | 1630(sh), 1643 | 1060($BF_4^-$), 3320(NH), 3550($H_2O$), 3600(OH) |
| **XXI**, | $[Cu_2(PAP6Me)(OH)Cl_3].2H_2O$ | 1612, 1630 | 3380(NH), 3450, 3520($H_2O$), 3620(OH)<br>286, 301(Cu—Cl) |
| **XXII**, | $[Cu_2(PAP6Me)(OH)Br_3]$ | 1612, 1624 | 3400(NH), 3620(OH)<br>255, 277(Cu—Br) |
| **XXIII**, | $[Cu_2(PAP6Me)(CH_3COO)_3].0.5H_2O$ | 1612, 1633 | 1404, 1585($RCOO^-$), 3290(NH), 3410($H_2O$)<br>305(sh), 320(Cu—O)<br>[a] 1360, 1380, 1575, 1720 |
| **XXIV**, | $[Cu_2(PAP6Me)(OH)(NO_3)_2]NO_3$ | 1614, 1633 | 1724, 1750, 1757 ($\nu_1 + \nu_4$, $NO_3^-$), 3320(NH), 3480(OH), 285, 305(Cu—O) |
| **XXV**, | $[PAP6MeH_2](ClO_4)_2$ | 1618, 1622, 1645(sh), 1650, 1660(sh) | 1080($ClO_4^-$), 3320(NH) |
| **XXVI**, | $[Cu_2(PAP6Me)(OH)(H_2O)_2](ClO_4)_3.0.5H_2O$ | 1615, 1632 | 1070, 1095($ClO_4^-$), 3350(NH), 3430, 3500(sh)($H_2O$), 3680(OH)<br>265(Cu—O) |

[a] Solution in chloroform.

Can. J. Chem. Downloaded from www.nrcresearchpress.com by 210.87.254.5 on 09/06/12
For personal use only.

TABLE 3. Electronic spectra ($cm^{-1}$) (log ε) and magnetic moments

| Compound | | *d–d* | CT | μ $(BM)_{Cu}$ (room temperatur |
|---|---|---|---|---|
| **I**, $[Cu(PAPH)_2(NO_3)_2](NO_3)_2.0.5H_2O$ | [a] | [15700]18200 | 27800 | 1.90 |
| **II**, $[Cu_3(PAP)_2(OH)_2(NO_3)_2](NO_3)_2.4H_2O$ | [a] | [11700], [14800]16900 | 27400 | 1.32 |
| **III**, $[Cu(PAPH)_2](ClO_4)_4.0.5H_2O$ | [a] | [13300][15600] | 28500 | 1.80 |
| **IV**, $[Cu_3(PAP)_2(OH)_2(MeOH)_2](ClO_4)_4$ | [a] | [10500][14800]16700 | 28200 | 1.43 |
| **V**, $[Cu_2(PAP)(PhSCH_2COO)_3(OMe)].H_2O$ | [a] | [10800]14800 | 28900 | 1.30 |
| | [f] | [10900](1.94)14500(2.31) | 24600(4.25) | |
| **VI**, $[Cu_2(PAP)(PhSCH_2COO)_4].H_2O$ | [a] | 15900 | 28900 | 1.85 |
| | [f] | [10900](2.05)14300(2.32) | 24450(4.20) | |
| **VII**, $[Cu_2(PAP)(o\text{-tolylSCH}_2COO)_3]$ | [a] | [10800]15400 | [24400]27500 | 1.62 |
| | [f] | 14900(2.26) | 24600(4.18)25600(4.17) | |
| **VIII**, $[Cu_2(PAP)(m\text{-tolylSCH}_2COO)_4]$ | [a] | [13900]16400 | 28200 | 1.83 |
| **IX**, $[Cu_2(PAP)(p\text{-tolylSCH}_2COO)_4].1.5H_2O$ | [a] | 14500 | 28600 | 1.78 |
| | [f] | [10900](2.01)14900(2.34) | 24500(4.23) | |
| **X**, $[Cu_2(PAP)(OH)(PhS(O)CH_2COO)_3]$ | [a] | 15200 | [24000][27300] | 1.50 |
| | [f] | 14900(2.20) | 24600(4.04)26900(4.07) | |
| **XI**, $[Cu_2(PAP)(OH)(p\text{-tolylS(O)CH}_2COO)_3].H_2O$ | [a] | [11000]14900 | [24400]27000 | 1.32 |
| | [f] | 15000(2.19) | 24600(4.02)27400(4.10) | |
| **XII**, $[Cu_2(PAP4Me)(OH)Cl_3].H_2O$ | [a] | [13200]15900 | 29400 | 1.43 |
| **XIII**, $[Cu_2(PAP4Me)(OH)Br_3]$ | [a] | 16100 | 28200 | 1.20 |
| | [b] | 10600(1.53)15800(1.83) | 29400(3.25) | |
| **XIV**, $[Cu_2(PAP4Me)(OH)(CH_3COO)_2(H_2O)]$ | [a] | 17400 | 24700 | 1.42 |
| | [c] | [17600](1.93) | 25400(2.98) | |
| **XV**, $[Cu(PAP4MeH)_2](NO_3)_4$ | [a] | [14800]18200 | 28600 | 2.10 |
| | [c] | | 28100(4.44) | |
| **XVI**, $[Cu_2(PAP4Me)(OH)(H_2O)_2(NO_3)_2]NO_3$ | [a] | 16300 | 28200 | 1.12 |
| | [c] | 16500(1.96) | 29600(3.14) | |
| **XVII**, $[Cu(PAP4MeH)_2](ClO_4)_4.2MeOH$ | [a] | [14700][18300]23800 | 28600 | 1.90 |
| | [c] | | 28900(4.49) | |
| **XVIII**, $[Cu_3(PAP4Me)_2(OH)_2(H_2O)_2](ClO_4)_4.MeOH$ | [a] | [10600][14800]16900 | [28600] | 1.54 |
| | [b] | [11000][14000]16100 | 27000(4.14) | |
| **XIX**, $[Cu(PAP4MeH)_2](BF_4)_4.H_2O$ | [a] | [17100] | 28200 | 1.90 |
| | | | 28700(4.45) | |
| **XX**, $[Cu_3(PAP4Me)(OH)_2(H_2O)_2](BF_4)_4$ | [a] | [10500][14600]16500 | 29000 | 1.31 |
| | [b] | [10500](1.84)[14000](2.12) 15600(2.14) | 29300(4.56) | |
| **XXI**, $[Cu_2(PAP6Me)(OH)Cl_3].2H_2O$ | [a] | 14800 | 27800 | 0.68 |
| | [b] | 14800 | 28900 | |
| **XXII**, $[Cu_2(PAP6Me)(OH)Br_3]$ | [a] | 17200 | [27800] | 0.66 |
| | [b] | | 29100(4.14) | |
| **XXIII**, $[Cu_2(PAP6Me)(CH_3COO)_3].0.5H_2O$ | [a] | [16000] | 23800 | 1.60 |
| | [c] | 17200(2.37) | 24700(4.19) | |
| **XXIV**, $[Cu_2(PAP6Me)(OH)(NO_3)_2]NO_3$ | [a] | 16400 | [28600] | 1.20 |
| | [b] | 14500(2.11) | 29100(4.14) | |
| **XXV**, $[PAP6MeH_2](ClO_4)_2$ | [a] | | [26700]27800 | |
| **XXVI**, $[Cu_2(PAP6Me)(OH)(H_2O)_2](ClO_4)_3.0.5H_2O$ | [a] | [14000]16700 | [28900] | 1.30 |
| | [c] | 16500(2.12) | [25300] | |

[a]Mull transmittance.
[b]Solution spectra in water.
[c]Solution spectra in methanol.
[d]Solution spectra in nitromethane.
[e]Solution spectra in ethanol.
[f]Solution spectra in chloroform.

Can. J. Chem. Downloaded from www.nrcresearchpress.com by 210.87.254.5 on 09/06/12
For personal use only.

Can. J. Chem. Downloaded from www.nrcresearchpress.com by 210.87.254.5 on 09/06/12
For personal use only.

coordinate via intermolecular association involving the terminal carboxylates as was observed previously (13).

In a previous paper (19) we reported the formation of two different complexes from the reaction of copper tetrafluoroborate and PAP in aqueous solution: a mononuclear derivative, $[Cu(PAPH)_2(H_2O)_2](BF_4)_4$, containing protonated bidentate ligand, and a polynuclear, neutral ligand derivative which was formulated as a trinuclear system, $[Cu_3(PAP)_2(OH)_2](BF_4)(BF_3OH)_3.5H_2O$. The ease with which PAP became protonated, even in weakly acidic solutions, was shown to be the reason why such a mixture of compounds was formed. Surprisingly a similar situation arose in the reactions between copper nitrate and copper perchlorate with PAP (approximately 0.1 *M* solutions of copper nitrate and copper perchlorate have pH values of 3.7 each).

Buff-coloured protonated derivatives (**I**, **III**) were obtained as initial products from the reactions of copper nitrate and copper perchlorate with PAP in aqueous solution. The presence of up to four CN stretching vibrations in the infrared (Table 2) can be attributed to the presence of protonated PAP (19). The observtion of three nitrate combination bands (30) can be interpreted in terms of the presence of both ionic and monodentate nitrate and in keeping with the electronic spectrum (Table 3), it seems reasonable to assume a tetragonally distorted six-coordinate structure for **I** involving two axially bound monodentate nitrate groups and two in-plane bidentate protonated PAP ligands. The perchlorate derivative (**III**) appears to have an analogous square planar structure without the involvement of any axial ligand. Magnetic moments for these compounds are typical of mononuclear copper derivatives.

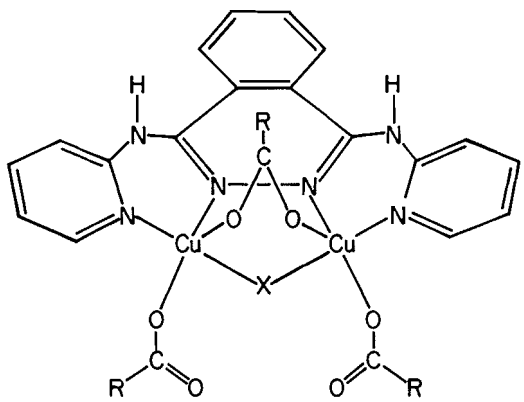


FIG. 2. Proposed structures for **V** (X = OMe), **X**, **XI** (X = OH), **VI**, **VIII**, **IX** (X = RCOO).

Additional green products (**II**, **IV**) are also obtained from both reaction mixtures, which do not contain protonated ligand. Two CN bands are observed in the infrared in each case, typical of neutral PAP. Nitrate combination bands indicate the presence of both ionic and monodentate nitrate in **II**, while for **IV** the $\nu_3$ perchlorate vibration, although it is slightly split, probably indicates ionic perchlorate. Pyridine ring breathing absorptions are observed for **II** in excess of 1000 $cm^{-1}$, indicative of the presence of tetradentate PAP (13), while for **IV** such absorptions are hidden by the perchlorate band. Elemental analyses suggest a metal-to-ligand ratio of 3:2 for **II** and **IV**, which requires the presence of two hydroxy groups to complete a charge balance. Rather broad infrared absorptions at 3400 $cm^{-1}$ (**II**) and 3525 $cm^{-1}$ (**IV**) are associated with water (**II**) and methanol (**IV**) and bridging hydroxy groups, probably involved in hydrogen bonding.

The electronic spectra of **II** and **IV** are very similar in the solid state involving three major absorptions and resemble very closely the spectrum of $[Cu_3(PAP)_2(OH)_2](BF_4)(BF_3OH)_3.5H_2O$ (19), suggesting a similar species. In general the binuclear copper complexes of PAP involve five-coordinate copper centres and only one major *d–d* band is observed in this region of the spectrum (13). The three prominent absorptions observed for **II** and **IV** therefore suggest the possible presence of more than one different stereochemistry for the copper centres in these systems. A reasonable suggestion for the structures of **II** and **IV** is illustrated in Fig. 3 in which two tetradentate ligands are bound simultaneously to three copper centres in a trinuclear arrangement. The central copper is six-coordinate being bound to the other two copper centres via phthalazine and hydroxy bridges. The outer two copper atoms are probably four-coordinate, the fourth coordination site being occupied by monodentate nitrates in **II** and methanol molecules in **IV**. Such a system can be rationalized spectroscopically by assuming that the highest energy *d–d* component can be associated with the two distorted square planar copper centres and that the two lower energy components can be asso-

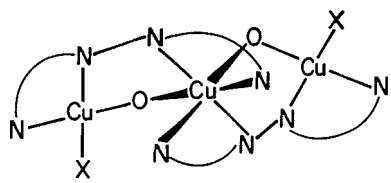


FIG. 3. Proposed structures for the cation in **II** (X = $NO_3$), **IV** (X = MeOH), **XVIII** and **XX** (X = $H_2O$).

Can. J. Chem. Downloaded from www.nrcresearchpress.com by 210.87.254.5 on 09/06/12
For personal use only.

ciated with a *cis*-$N_4O_2$ six-coordinate copper centre. Magnetic moments per copper centre for **II** and **IV** are quite low, indicating significant spin exchange, which would again support the presence of hydroxy bridges between the copper centres.

PAP4Me, which involves methyl substituents at the 4-position on the pyridine ring, forms similar copper complexes to those of PAP. This is perhaps not so surprising since substituents at the 4-position would not be expected to exert any unusual electronic or steric effects. Compounds **XII** and **XIII** are analogous to the PAP counterparts with hydroxy and halogeno bridges between the copper centres and reduced room temperature moments indicative of antiferromagnetic exchange (13, 31) (Fig. 2; X = OH, RCOO = halide). However, the moments are somewhat lower than those of the PAP analogues (Cl, $\mu$ = 1.60 BM; Br, $\mu$ = 1.66 BM) (13) which may indicate some structural modification at the binuclear centre in the systems.

The acetate complex **XIV** contains two acetate groups, according to elemental analysis, and has a low energy charge transfer absorption (13) indicative of the presence of anionic ligand (it is assumed that PAP and its simple methylated analogues will exhibit similar $\pi$–$\pi^*$ absorptions). In keeping with these data a hydroxy bridge is also implicated and although there is weak infrared evidence for the presence of such a group the low magnetic moment does indicate such a bridge. The high energy single *d*–*d* absorption (Table 3), present both in the solid state and solution, is consistent with a five-coordinate derivative. In the infrared, absorptions are observed both in the solid state and in chloroform solution consistent with the presence of both bridging and terminal carboxylate groups. A rather broad weak absorption around 3500 $cm^{-1}$ is associated with the hydroxide bridge and water molecule. Considering all the data a reasonable structure would involve a terminal carboxylate on one copper centre, a carboxylate and a hydroxide bridge, and a water molecule bound to the other copper centre (Fig. 2, X = OH, one terminal carboxylate replaced by $H_2O$). The formation of a hydroxy derivative in this case is seen as a result of the presence of water in the ethanol used to prepare the complex.

As in the case of PAP, two nitrate complexes are obtained. **XV** is clearly a protonated, mononuclear derivative which has a pseudo square planar structure according to both infrared and electronic spectral data. The presence of only one nitrate combination band at 1755 $cm^{-1}$ signifies the presence of ionic nitrate only. The blue neutral ligand species **XVI** appears to be a binuclear derivative, unlike its PAP counterpart. Infrared data suggest a hydroxy bridged species involving coordinated water and the complex absorption in the combination ($\nu_1 + \nu_4$) nitrate region suggests more than one type of nitrate group. The bands at 1751 and 1766 $cm^{-1}$ can be associated with monodentate nitrate and the band at 1753 $cm^{-1}$ with ionic nitrate. However, the high energy band at 1784 $cm^{-1}$ may be associated with a bridging bidentate nitrate (30).

Preliminary X-ray studies on this system (32) confirm the binuclear structure (Fig. 4) (Table 4) involving tetradentate PAP4Me, a hydroxide bridge, and a bidentate nitrate bridge. A second nitrate group is bound to Cu(2) with a bond length to O(2) of 2.034 Å. The interatomic distance Cu(2)—O(14) of 2.738 Å may indicate the nitrate group to be a weakly bound unsymmetrical bidentate chelating ligand giving rise to a distorted six-coordinate tetragonal structure around Cu(2). In a review of metal nitrate bonding (33) it is suggested that the nitrate group may be considered bidentate if the difference in the two closest metal–oxygen distances does not exceed 0.7 Å. The coordination geometry around Cu(1) can be considered to be tetragonal, six-coordinate with a long axial bond to O(16) of a water molecule. Of particular significance in the structure is the large bridge angle at O(1) (115.2°) and the metal–metal separation (3.138 Å). Full details of this structure will be published elsewhere.

We have recently examined the structure and magnetism of a series of complexes, $[Cu_2(PAP)(OH)X_3]$ (X = Cl, Br, $IO_3$) (34), and find that the binuclear centre can be tuned by varying the non-hydroxy bridge. The Cu—O—Cu bridge angle

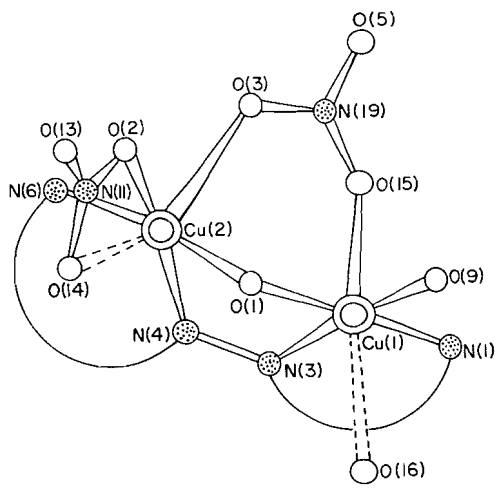


FIG. 4. X-ray structure for the cation in $[Cu_2(PAP4Me)(OH)(NO_3)_2(H_2O)_2]NO_3$.N(1)N(3)N(4)N(6) represents the ligand PAP4Me; O(9)$H_2O$, O(16)$H_2O$ ($R$ = 0.035).

TABLE 4. Selected bond lengths and bond angles for $[Cu_2(PAP-4Me)(OH)(H_2O)_2(NO_3)_2]NO_3$ ($R$ = 0.035)

| Bond | Length (Å) | Bonds | Angle (deg) |
|---|---|---|---|
| Cu(1)—N(1) | 1.951 | Cu(1)—O(1)—Cu(2) | 115.2 |
| Cu(1)—N(3) | 2.022 | O(15)—Cu(1)—O(16) | 169.2 |
| Cu(1)—O(1) | 1.857 | O(1)—Cu(1)—N(1) | 174.3 |
| Cu(1)—O(9) | 2.009 | N(3)—Cu(1)—O(9) | 173.5 |
| Cu(1)—O(15) | 2.428 | O(15)—Cu(1)—O(1) | 95.5 |
| Cu(1)—O(16) | 2.617 | O(3)—Cu(2)—O(14) | 129.8 |
| Cu(1)—Cu(2) | 3.138 | O(2)—Cu(2)—N(4) | 168.8 |
| | | N(6)—Cu(2)—O(1) | 171.3 |
| | | O(3)—Cu(2)—O(1) | 94.8 |
| Cu(2)—N(4) | 2.042 | | |
| Cu(2)—N(6) | 1.965 | | |
| Cu(2)—O(1) | 1.858 | | |
| Cu(2)—O(2) | 2.034 | | |
| Cu(2)—O(3) | 2.330 | | |
| Cu(2)—O(14) | 2.738 | | |

is increased from 100° to 114° on replacing a chlorine bridge by an iodate bridge and the exchange integral increases from $-2J$ = 201 to $-2J$ = 335 $cm^{-1}$. Room temperature moments for these two systems are 1.66 BM (Cl) and 1.39 BM ($IO_3$). The low room temperature moment (1.12 BM) observed for **XVI** is consistent with the larger oxygen bridge angle for this nitrate bridged system and suggests the possibility of enhanced antiferromagnetic exchange.

The reaction of copper perchlorate and tetrafluoroborate with PAP4Me parallels the same reactions involving PAP. In both cases protonated, mononuclear derivatives, **XVII**, **XIX**, are produced which have pseudo-square planar structures involving bidentate, protonated PAP4Me. Also polynuclear derivatives, **XVIII** and **XX**, are obtained as final products in these reactions, which are analogues of **II** and **IV**, and are assumed to have the same basic structure (Fig. 3) but involving coordinated water at the four-coordinate copper centres.

Normal magnetic moments are observed for **XVII** and **XIX**, as would be expected for mononuclear derivatives, while the reduced moments observed for **XVIII** and **XX** are indicative of polynuclear species involving antiferromagnetic exchange. Three major absorptions are observed in the mull transmittance spectra of **XVIII** and **XX**, which can be associated with two different copper stereochemistries. Infrared data confirm the presence of protonated ligand in the mononuclear complexes **XVII** and **XIX** by the appearance of more than two νCN bands while for the polynuclear systems just two such bands are observed.

The introduction of a methyl group in the four position of the pyridine ring does not appear to have caused any major differences between the coordination chemistry of PAP and PAP4Me other than perhaps the formation of a binuclear nitrate complex with PAP4Me. However, a 6-methyl substituted ligand, in which the methyl group would be in a much better position to sterically influence the binuclear centre, might produce different complexes or analogues in which the dimensions of the binuclear centre might change.

Dark green binuclear products are obtained with copper chloride and bromide with PAP6Me (**XXI**, **XXII**) which appear to be analogues of the corresponding PAP and PAP4Me derivatives. Infrared absorptions observed at 3620 $cm^{-1}$ in both cases are indicative of the presence of a hydroxy bridge and other bands in the range 250–300 $cm^{-1}$ can be attributed to copper–halogen bonds. One major visible absorption is observed in each case which can be attributed to five-coordinate copper(II). On the surface these two compounds appear to have structures similar to their PAP and PAP4Me analogues (Fig. 2; X = OH, RCOO = halogen). However, the very low room temperature magnetic moments indicate the likelihood of enhanced magnetic exchange in these systems which can be seen as a result of the 6-methyl groups exerting a steric effect which forces the pyridine rings away from the binuclear centre thus increasing the metal–metal separation and the oxygen bridge angle. However, we await structural data and variable temperature magnetic studies to confirm this.

The copper acetate complex of PAP6Me (**XXIII**) appears to be similar to the acetate complex of PAP itself. A low energy charge transfer band (Table 3) indicates the presence of anionic ligand both in the solid state and in solution, while a single visible absorption, observed in the solid state spectrum at 16000 $cm^{-1}$, is consistent with a five-coordinate derivative. In methanol solution the $d$–$d$ absorption is observed at 17200 $cm^{-1}$, 1200 $cm^{-1}$ higher than in the solid state, suggesting the possibility of a change in stereochemistry. Carboxylate bands are observed in the infrared in the solid state (Nujol mull) at 1404 and 1585 $cm^{-1}$ which can be associated with the antisymmetric and symmetric vibrations of a bridging acetate. It was not possible to identify bands associated with terminally bound carboxylates. In chloroform solution four carboxylate bands can be picked out. Bands at 1575 and 1380 $cm^{-1}$ are associated with bridging carboxylate while the band at 1360 $cm^{-1}$ is assigned to the symmetric stretch of a terminal carboxylate. The band at 1700 $cm^{-1}$, which is absent in the mull spectrum, must be due to the "missing" antisymmetric stretch of a terminally bound carboxylate.

Can. J. Chem. Downloaded from www.nrcresearchpress.com by 210.87.254.5 on 09/06/12
For personal use only.

Can. J. Chem. Downloaded from www.nrcresearchpress.com by 210.87.254.5 on 09/06/12
For personal use only.

As with $Cu_2PAP(CH_3COO)_3$ (13), a loose intermolecular association is proposed between two terminal carboxylates on one binuclear complex with copper atoms on a neighbouring complex leading to a reduction in the antisymmetric frequency of the terminal carboxyl groups. This band is presumably hidden among the CN vibrations associated with the ligand itself in the solid state spectrum. The proposed intermolecular association would lead to a five-coordinate structure in the solid state (Fig. 5) but in solution, where the intermolecular association is broken, a four-coordinate system should exist. The observation of a *d–d* band in methanol at 17200 $cm^{-1}$ is certainly consistent with a four-coordinate system in which the stereochemistry at the copper centres is distorted square planar.

The binuclear nitrate complex (**XXIV**) is obtained from the reaction between copper nitrate and PAP6Me in aqueous ethanol. An infrared absorption at 3480 $cm^{-1}$ can be associated with a hydroxide bridge while nitrate combination bands are indicative of two types of nitrate (30). The absorption at 1750 $cm^{-1}$ indicates an ionic nitrate while absorptions at 1724 and 1757 $cm^{-1}$ suggest the presence of bidentate nitrate. The absence of a high energy nitrate combination band, indicative of the presence of a nitrate bridge, suggests a different structure for this complex than was observed for **XVI**. The *d–d* absorption in the solid state at 16400 $cm^{-1}$ can be associated with five-coordinate copper(II) and a five-coordinate binuclear structure is suggested in the solid state involving a hydroxy bridge and two bidentate nitrate groups (Fig. 6). The low magnetic moment of 1.20 BM suggests significant exchange and supports the proposed double bridged structure. In aqueous solution a much lower energy *d–d* absorption is observed, suggesting the formation of a solvated derivative.

In the reaction between copper perchlorate and PAP6Me in aqueous ethanol two products are

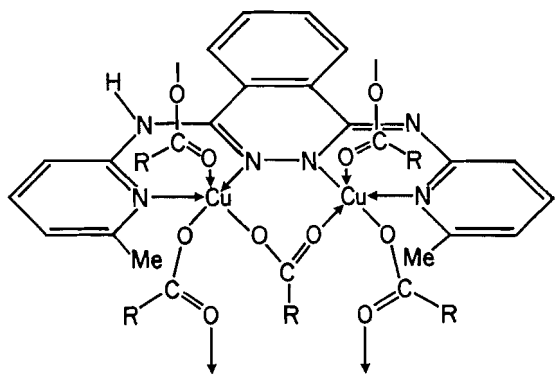


FIG. 5. Proposed structure for **XXIII**.

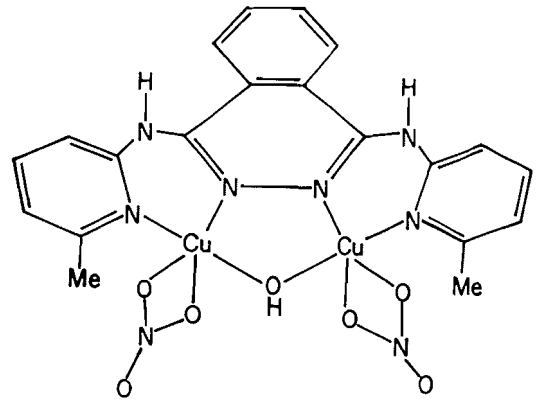


FIG. 6. Proposed structure for **XXIV**.

formed. Initially a yellow solid (**XXV**) is obtained followed by a green product (**XXVI**) on reduction of the volume of the mother liquor. **XXV** exhibits five infrared bands associated with CN stretch in the ligand and indicates the presence of protonated PAP6Me. This compound contains no metal and appears to be a diperchlorate salt in which the ligand is protonated at two sites (presumably both pyridine nitrogen atoms) (19). The formation of a salt of this type is a departure from the trend we have seen with the other systems in which, when the ligand acted as a base, mononuclear protonated complexes were formed. In the case of PAP6Me, however, the 6-methyl groups on the pyridine rings may exert enough of a steric influence that to form a mononuclear bis-bidentate ligand complex is not possible. Models suggest that this is so.

The green copper perchlorate complex (**XXVI**) is a binuclear derivative involving a hydroxide bridge and coordinated water. There is little evidence to suggest the involvement of perchlorate in the copper coordination sphere unless the slight splitting of the $\nu_3$ vibration is considered to be significant. In a recent paper Lippard and co-workers report the structure of a binuclear copper perchlorate complex of a binucleating macrocyclic ligand (35). In addition to a hydroxide bridge, a weakly bound bridging bidentate perchlorate group was also found to be present (Cu—O(perchlorate) ~ 2.6 Å). However, no infrared data were reported for the perchlorate group in this complex. Perhaps a rather weak splitting of $\nu_3$ would be expected in this case. The *d–d* absorption at 16700 $cm^{-1}$ (**XXVI**) is consistent with a four-coordinate system involving one coordinated water molecule per copper centre and a hydroxide bridge (Fig. 6; $NO_3$ replaced by $H_2O$) but the possibility of a five-coordinate derivative should not be ruled out.

Binuclear copper complexes involving antifer-

Can. J. Chem. Downloaded from www.nrcresearchpress.com by 210.87.254.5 on 09/06/12
For personal use only.

romagnetic exchange between metal centres are potential models for the binuclear oxygen-breathing protein hemocyanin and copper-containing oxidase enzymes, e.g. tyrosinase, laccase. Magnetic measurements on protein extracts indicate strong antiferromagnetic exchange between the copper(II) centres in Rhus vernicifera laccase ($-2J \geq 1000$ $cm^{-1}$) (36) and in oxyhemocyanin (Megathura crenulata; $-2J \geq 1250$ $cm^{-1}$) (37). Strong antiferromagnetic exchange is observed in binuclear copper systems involving single hydroxy bridges (29, 35, 38) and exchange increases with bridge angle (29, 34). An oxygen bridge from, e.g., tyrosine has been suggested as a super-exchange medium for both oxyhemocyanin (39) and enzymes containing Type III copper centres (35, 38) and other donor groups around the copper centres are thought to include histidine (38). With these properties in mind we see our complexes as potential models for such centres and are embarked on a program to investigate detailed magnetic and structural characteristics of some of our systems. We anticipate that varying the bridge groups between the copper centres and creating steric factors on the coordinated pyridine groups will alter the dimensions of the binuclear centre and vary the magnetic exchange.

The catecholase activity of the complex $[Cu_2(PAP)(OH)Cl_3]$ has already been demonstrated (20). Preliminary results indicate that this system also catalytically oxidizes ascorbic acid and that the complex $[Cu_2(PAP6Me)(OH)Cl_3]$ is also catecholase active. Reports on these studies will be published elsewhere.

**Acknowledgement**

We thank the Natural Sciences and Engineering Research Council of Canada for financial support for this study.

1. W. J. Stratton and D. H. Busch. J. Am. Chem. Soc. **82**, 4834 (1960).
2. W. J. Stratton and P. J. Ogren. Inorg. Chem. **9**, 2588 (1970).
3. W. J. Stratton. Inorg. Chem. **9**, 517 (1970).
4. P. W. Ball and A. B. Blake. J. Chem. Soc. A, 1415 (1969).
5. J. Powell and A. Kuksis. Can. J. Chem. **57**, 2986 (1979).
6. K. S. Chong, S. J. Rettig, A. Storr, and J. Trotter. Can. J. Chem. **57**, 3090 (1979).
7. K. S. Chong, S. J. Rettig, A. Storr, and J. Trotter. Can. J. Chem. **57**, 3099 (1979).
8. K. S. Chong, S. J. Rettig, A. Storr, and J. Trotter. Can. J. Chem. **57**, 3119 (1979).
9. J. E. Andrew, P. W. Ball, and A. B. Blake. Chem. Commun. 143 (1969).
10. L. G. Kuz'mina, N. G. Bokii, Yu. T. Struchkov, A. V. Arutyunyan, L. Y. Rybin, and M. I. Rybinskaya. J. Struct. Chem. **12**, 801 (1971).
11. P. W. Ball and A. B. Blake. J. Chem. Soc. Dalton, 852 (1974).
12. J. E. Andrew and A. B. Blake. J. Chem. Soc. A, 1408 (1969).
13. L. K. Thompson, V. T. Chacko, J. A. Elvidge, A. B. P. Lever, and R. V. Parish. Can. J. Chem. **47**, 4141 (1969).
14. W. Rosen. Inorg. Chem. **10**, 1832 (1971).
15. A. B. P. Lever, L. K. Thompson, and W. M. Reiff. Inorg. Chem. **11**, 104 (1972).
16. A. B. P. Lever, L. K. Thompson, and W. M. Reiff. Inorg. Chem. **11**, 2292 (1972).
17. D. A. Sullivan and G. J. Palenik. Inorg. Chem. **16**, 1127 (1977).
18. J. A. Doull and L. K. Thompson. Can. J. Chem. **58**, 221 (1980).
19. J. C. Dewan and L. K. Thompson. Can. J. Chem. **60**, 121 (1982).
20. A. B. P. Lever, B. S. Ramaswamy, and S. R. Pickens. Inorg. Chim. Acta, **46**, L59 (1980).
21. M. Ghedini, G. De Munno, G. Denti, A. M. Manotti Lanfredi, and A. Tiripicchio. Inorg. Chim. Acta, **57**, 87 (1982).
22. R. W. Stotz and R. C. Stoufer. Chem. Commun. 1682 (1970).
23. W. O. Siegl. J. Org. Chem. **42**, 1872 (1977).
24. P. F. Clark, J. A. Elvidge, and R. P. Linstead. J. Chem. Soc. 3593 (1953).
25. J. A. Elvidge and R. P. Linstead. J. Chem. Soc. 5000 (1952).
26. A. W. Addison and P. J. Burke. J. Heterocyclic Chem. **18**, 803 (1981).
27. D. J. Hodgson. Prog. Inorg. Chem. **19**, 173 (1975).
28. Van H. Crawford, H. W. Richardson, J. R. Wasson, D. J. Hodgson, and W. E. Hatfield. Inorg. Chem. **15**, 2107 (1976).
29. M. S. Haddad and D. N. Hendrickson. Inorg. Chim. Acta, **28**, L121 (1978).
30. A. B. P. Lever, E. Mantovani, and R. S. Ramaswamy. Can. J. Chem. **49**, 1957 (1971).
31. G. Marongiu and E. C. Lingafelter. Acta Crystallogr. B, **38**, 620 (1982).
32. A. W. Hanson. Personal communication.
33. C. E. Addison, N. Logan, S. C. Wallwork, and C. D. Garner. Q. Rev. Chem. Soc. **25**, 289 (1971).
34. L. K. Thompson and A. W. Hanson. To be published.
35. P. K. Coughlin and S. J. Lippard. J. Am. Chem. Soc. **103**, 3228 (1981).
36. D. M. Dooley, R. A. Scott, J. Ellinghaus, E. I. Solomon, and H. B. Gray. Proc. Natl. Acad. Sci. USA, **75**, 3019 (1978).
37. E. I. Solomon, D. M. Dooley, R. H. Wang, H. B. Gray, M. Cerdonio, F. Mogno, and G. L. Romani. J. Am. Chem. Soc. **98**, 1029 (1976).
38. P. L. Burk, J. A. Osborn, M-T Youinou, Y. Agnus, R. Louis, and R. Weiss. J. Am. Chem. Soc. **103**, 1273 (1981).
39. A. R. Amundsen, J. Whelan, and B. Bosnich. J. Am. Chem. Soc. **99**, 6730 (1977).

# An experimental study of the reactivity and relative basicity of the methoxide anion in the gas phase at room temperature, and their perturbation by methanol solvation

GERVASE I. MACKAY, ASIT B. RAKSHIT, AND DIETHARD K. BOHME

*Department of Chemistry and Centre for Research in Experimental Space Science, York University, Downsview, Ont., Canada M3J 1P3*

Received January 19, 1982

GERVASE I. MACKAY, ASIT B. RAKSHIT, and DIETHARD K. BOHME. Can. J. Chem. **60**, 2594 (1982).

Flowing afterglow measurements at 296 ± 2 K are reported which explore three aspects of the gas-phase acid–base chemistry of the methoxide anion. Firstly, the intrinsic reactivity of this ion has been determined from measurements of rate constants for solvent-free proton-transfer reactions with molecules more acidic than methanol including $CH_2{=}C{=}CH_2$, $C_6H_5CH_3$, $C_2H_5OH$, $C_2H_2$, $CH_3CN$, $CH_3COCH_3$, $CH_3CHO$, $CH_3NO_2$, and HCN. Secondly, equilibrium constant measurements have been performed for solvent-free proton-transfer reactions which provide a gas-phase scale of acidities for these molecules relative to the acidity of methanol. Finally, rate constants were measured for the reactions of these acids with methoxide ions solvated with up to three molecules of methanol. The results establish trends in reactivity as a function of step-wise solvation when relative acidity is preserved and when a reversal occurs in the relative acidity upon solvation.

GERVASE I. MACKAY, ASIT B. RAKSHIT et DIETHARD K. BOHME. Can. J. Chem. **60**, 2594 (1982).

On rapporte les mesures d'écoulement après incandescence à 296 ± 2 K qui explorent trois aspects de la chimie acide–base en phase gazeuse de l'anion méthanolate. Premièrement, on a déterminé la réactivité intrinsèque de cet ion à partir des mesures des constantes de vitesse de réactions de transfert de proton libre du solvant avec les molécules plus acides que le méthanol incluant: $CH_2{=}C{=}CH_2$, $C_6H_5CH_3$, $C_2H_5OH$, $C_2H_2$, $CH_3COCH_3$, $CH_3CHO$, $CH_3NO_2$ et HCN. Deuxièment, on a mesuré la constante d'équilibre des réactions de transfert de proton libre du solvant qui fournissent une échelle d'acidité en phase gazeuse de ces molécules par rapport à l'acidité du méthanol. Finalement, on a mesuré les constantes de vitesse des réactions de ces acides avec les ions méthanolates solvatés par un maximum de trois molécules de méthanol. Les résultats établissent les tendances de réactivité en fonction d'une solvatation par étape lorsque l'acidité relative est préservée et quand il se produit une inversion dans l'acidité relative lors de la solvatation.

[Traduit par le journal]

## Introduction

Recent studies of gas-phase reactions of anions which have solution analogues have provided, for the first time, a direct quantitative measure of the *intrinsic* stability and reactivity of anions found in solution and an assessment of the absolute influence of solvation on these quantities. For example, gas-phase measurements of rate and equilibrium constants for solvent-free acid–base reactions of type [1]

[1] $B^- + AH \rightleftharpoons A^- + BH$

and solvated acid–base reactions of type [2]

[2] $B^-.S_n + AH \rightleftharpoons A^-.S_n + BH$

have provided both a measure of the absolute intrinsic reactivity and relative intrinsic basicity of anions as well as an indication of their perturbation by step-wise solvation. This has been illustrated by results obtained recently in our laboratory using the flowing afterglow technique for reactions of the hydroxide ion, an important base in solution (1, 2). Here we report an extension of our studies to the acid–base chemistry of the methoxide ion. Three aspects of this chemistry have been explored. Firstly, the intrinsic reactivity of the methoxide ion has been determined from measurements of rate constants for solvent-free proton-transfer reactions with molecules more acidic than methanol in the gas phase. Secondly, equilibrium constant measurements have been carried out for solvent-free proton-transfer reactions to provide a gas-phase scale of acidities of acids relative to the acidity of methanol. Finally, experiments were performed with methoxide ions solvated with up to three added methanol molecules which provide insight into the perturbation of the intrinsic reactivity and basicity of the methoxide ions by step-wise methanol solvation. The reagent acids were chosen to cover a range in overall energetics sufficient to establish the pattern of this perturbation which appeared to emerge from these studies.

## Experimental

The experiments were performed in a flowing plasma mass spectrometer (flowing afterglow) system. Details of the instrument together with the method of operation and data analysis have been elaborated elsewhere (3, 4). The anions were produced in a flowing plasma either by electron impact or by secondary ionization or ion–molecule reactions and were permitted to thermalize by collisions with a helium or hydrogen buffer gas to the ambient room temperature of 296 ± 2 K prior to entering the reaction region. The plasma was generated with ionizing electrons having energies in the range 35–70 eV. The filament emission of the electron gun was maintained at a fixed

0008-4042/82/202594-12$01.00/0

©1982 National Research Council of Canada/Conseil national de recherches du Canada

Can. J. Chem. Downloaded from www.nrcresearchpress.com by 210.87.254.105 on 09/06/12
For personal use only.

Can. J. Chem. Downloaded from www.nrcresearchpress.com by 210.87.254.105 on 09/06/12
For personal use only.

TABLE 1. Rate and equilibrium constants measured for proton-transfer reactions of solvent-free anions at 296 ± 2 K

| Reaction | $k^a$ | $K^b$ |
|---|---|---|
| $CH_3O^- + H_2CCCH_2 \rightarrow H_2CCCH^- + CH_3OH$ | 0.87±0.35 | 1.4±0.3 |
| $CH_3O^- + C_6H_5CH_3 \rightarrow C_6H_5CH_2^- + CH_3OH$ | 1.5±0.5 | 1.4±0.3 |
| $CH_3O^- + C_2H_5OH \rightarrow C_2H_5O^- + CH_3OH$ | 3.3±1.0 | |
| $CH_3O^- + C_2H_2 \rightarrow C_2H^- + CH_3OH$ | 1.6±0.4 | (2.7±0.7) × $10^3$ |
| $CH_3O^- + CH_3CN \rightarrow CH_2CN^- + CH_3OH$ | 3.5±0.9 | ≥ 1 × $10^4$ |
| $CH_3O^- + CH_3COCH_3 \rightarrow CH_3COCH_2^- + CH_3OH$ | 2.3±0.6 | ≥ 1 × $10^4$ |
| $CH_3O^- + CH_3CHO \rightarrow {}^-CH_2CHO + CH_3OH$ | 2.0±0.6 | ≥ 1 × $10^4$ |
| $CH_3O^- + CH_3NO_2 \rightarrow CH_2NO_2^- + CH_3OH$ | 3.1±0.8 | ≥ 1 × $10^4$ |
| $CH_3O^- + HCN \rightarrow CN^- + CH_3OH$ | 3.3±0.8 | ≥ 1 × $10^4$ |
| $H_2CCCH^- + C_2H_2 \rightarrow C_2H^- + H_2CCCH_2$ | 0.70±0.18 | (2.1±0.5) × $10^3$ |
| $C_2H_5O^- + C_2H_2 \rightarrow C_2H^- + C_2H_5OH$ | 1.4±0.4 | 17±4 |
| $(CH_3)_2CHO^- + C_2H_2 \rightarrow C_2H^- + (CH_3)_2CHOH$ | ≥0.1 | 1.2±0.3 |
| $C_2H^- + CH_3CN \rightarrow CH_2CN^- + C_2H_2$ | 1.5±0.4 | (3.0±0.7) × $10^2$ |
| $CH_2CN^- + CH_3COCH_3 \rightarrow CH_3COCH_2^- + CH_3CN$ | 0.30±0.09 | ≥ 5 × $10^2$ |

[a]The measured forward rate constant along with the estimated uncertainty in units of $10^{-9}$ cm$^3$ molecule$^{-1}$ s$^{-1}$.
[b]The value of $K$ represents the weighted mean together with its standard error of measurements including one or more of $k_f/k_r$ and $K_{ratio}$ in one or both directions of reaction.

TABLE 2. Rate constants[a] measured for reactions of solvated methoxide ions with acids, AH, in the gas phase at 296 ± 2 K

| AH | $CH_3O^-.CH_3OH$ | $CH_3O^-.(CH_3OH)_2$ | $CH_3O^-.(CH_3OH)_3$ |
|---|---|---|---|
| $H_2CCCH_2$ | ≤ 0.001 | ≤ 0.001 | ≤ 0.001 |
| $CH_3CCH$ | ≤ 0.001 | | |
| $C_6H_5CH_3$ | ≤ 0.001 | | |
| $C_2H_5OH$ | 2.9±1.0 | 1.2±0.4 | ≥ 0.2 |
| $C_2H_2$ | ≤ 0.001 | | |
| $CH_3CN$ | ≤ 0.001 | ≤ 0.002 | ≤ 0.002 |
| $CH_3COCH_3$ | 1.7±0.4 | ≤ 0.002 | ≤ 0.002 |
| $CH_3CHO$ | 1.5±0.6 | ≤ 0.01 | ≤ 0.01 |
| $CH_3NO_2$ | 2.3±0.7 | 1.9±0.6 | 1.3±0.5 |
| HCN | 3.2±1.0 | 3.1±1.0 | 3.0±1.1 |

[a]Rate constants and their estimated accuracies are given in units of $10^{-9}$ cm$^3$ molecule$^{-1}$ s$^{-1}$.

value in the range 0.5 to 1.5 mA. The ions present in the plasma were sampled through a small orifice mounted at the tip of a nose cone situated at the end of the reaction region and mass analysed with a quadrupole mass spectrometer. The observed variation in the ion signals as a function of neutral reagent addition provided the raw data from which the rate and equilibrium constants were determined. As has been the case in our previous studies, the buffer, source, and reagent gases or vapours were all of high purity.

Methoxide ions were generated by passing $CH_3OH$ into a He or $H_2$ buffer gas upstream of the filament at total pressures of ca. 0.4 Torr. The ions were solvated by reactions of type [3].

[3] $$CH_3O^-.(CH_3OH)_n + CH_3OH + He(H_2) \rightarrow CH_3O^-.(CH_3OH)_{n+1} + He(H_2)$$

The partial pressure of methanol was varied from ca. 0.005 to 2 mTorr in order to change the initial relative population of the cluster ions $CH_3O^-.(CH_3OH)_n$; $n$ was observed to take on values between 0 and 3 at the operating conditions of the experiments reported here. In deriving rate constants from the observed decays of $CH_3O^-.(CH_3OH)_n$, account was taken of the initial decay which could arise due to the depletion of the precursor ion $CH_3O^-.(CH_3OH)_{n-1}$. The magnitude of this depletion could be assessed in those studies in which the daughter ion $CH_3O^-.(CH_3OH)_n$ did not react with the added neutral reagent.

## Results

The rate and equilibrium constants measured in this study for acid–base reactions of types [1] and [2] are summarized in Tables 1 and 2. The sources of uncertainty have been described previously (3, 4). The following section provides a more detailed account of the measurements. They are presented in order of increasing acidity of the reagent acid.

### $H_2CCCH_2$

$CH_3O^-$ was established in both He and $H_2$ carrier gases at low methanol flows and moderately low pressures to avoid significant depletion of $CH_3O^-$ by clustering. Under these conditions the dominant source and sink of $CH_3O^-$ in the reaction region upon the addition of allene was the reversible reaction:

[4] $$CH_3O^- + H_2CCCH_2 \rightleftharpoons H_2CCCH^- + CH_3OH$$

Can. J. Chem. Downloaded from www.nrcresearchpress.com by 210.87.254.105 on 09/06/12
For personal use only.

We have reported elsewhere that the deprotonation of allene in this fashion is expected to establish the allenyl anion without subsequent 1,3-hydrogen migration to form the isomeric $CH_3—C{\equiv}C^-$ structure (5). A minor product (< 1%) of unknown origin was observed at $m/e = 38 (C_3H_2^-?)$ but it was sufficiently small to be ignored in the equilibrium analysis. The experiments provided values for $k_4 = (8.7 \pm 3.5) \times 10^{-10}$ cm$^3$ molecule$^{-1}$ s$^{-1}$, $k_4/k_{-4} = 1.36 \pm 0.41$ and $K_4 = 1.40 \pm 0.42$. The $CH_3O^-.CH_3OH$ in the reaction region did not react with allene, $k \leq 1 \times 10^{-12}$ cm$^3$ molecule$^{-1}$ s$^{-1}$. An extended analysis of the data confirmed that its presence did not prevent the determination of a reliable value for the true equilibrium constant of reaction [4]. Doubly and triply solvated methoxide ions were established at higher flows of methanol and these also did not react with allene.

One investigation was carried out in an attempt to determine the equilibrium constant for reaction [4] from the reverse direction. The $H_2CCCH^-$ ions were produced by proton transfer to $OH^-$ prior to the reaction region. At low additions of methanol the $CH_3O^-$ signal was observed to increase rapidly with an accompanying decline in the $H_2CCCH^-$ signal, indicating that proton transfer to $H_2CCCH^-$ from methanol is rapid and the major loss process for $H_2CCCH^-$ in the reaction region. The $CH_3O^-$ was observed to decline at large additions of methanol as a result of clustering. It was possible to fit the variations in the $H_2CCCH^-$ and $CH_3O^-$ signals using an extended analysis by incorporating the value for $k_4/k_{-4} = 1.36$ obtained from the forward study and a value of $k = 9.3 \times 10^{-27}$ cm$^6$ molecule$^{-2}$ s$^{-1}$ for the three-body rate constant of clustering determined from the decay of the $CH_3O^-$ signal at large methanol additions. This result provides additional confidence in the value of the equilibrium constant determined from the study in the forward direction.

The proton-transfer equilibrium

[5] $H_2CCCH^- + C_2H_2 \rightleftharpoons C_2H^- + H_2CCCH_2$

was investigated with the addition of acetylene into a He (or $H_2$) – $H_2CCCH_2$ – $H_2O$ plasma in which $H_2CCCH^-$ is produced initially by proton transfer from allene to $OH^-$ or directly by electron impact on allene. Small but negligible amounts of an ion at $m/e = 38$ were again observed to be produced. Analysis of the observed decay of the $H_2CCCH^-$ ion provided values for $k_5 = (7.0 \pm 1.8) \times 10^{-10}$ cm$^3$ molecule$^{-1}$ s$^{-1}$ and $k_5/k_{-5} = (2.1 \pm 0.6) \times 10^3$. The ion signal ratio plots at high additions of $C_2H_2$ provided a value for $K_5 = (2.3 \pm 0.8) \times 10^3$. The flow of allene was varied from $2.17 \times 10^{17}$ to $2.4 \times 10^{19}$ molecules s$^{-1}$. No attempt was made to investigate this equilibrium from the reverse direction due to the large value of the equilibrium constant.

### $CH_3CCH$

Figure 1 shows the variation of the dominant negative ions resulting from the addition of propyne into a He–$CH_3OH$ plasma in which $CH_3O^-$ is initially a dominant negative ion. $C_3H_3^-$ is rapidly produced by the reaction

[6] $CH_3O^- + CH_3CCH \rightarrow C_3H_3^- + CH_3OH$

and it reacts further with propyne to produce $C_2H^-$, presumably by the nucleophilic-displacement reaction:

[7] $C_3H_3^- + CH_3CCH \rightarrow C_2H^- + C_4H_6$

Some production of $C_2H^-$ from the direct displacement by $CH_3O^-$ could not be excluded. The impurity ion $Cl^-$ and the cluster ion $CH_3O^-.CH_3OH$ are seen to be insensitive to the addition of propyne.

The deprotonation of propyne in reaction [6] may proceed either at the methyl or acetylenyl positions. The former will lead to an anion which rearranges to the allenyl anion (5):

[8] $^-CH_2—C{\equiv}CH \rightarrow CH_2{=}C{=}CH^-$

Further rearrangement to the more stable $CH_3—C{\equiv}C^-$ anion by 1,3-hydrogen migration involves a large activation barrier (6). Separate measurements have shown that deprotonation of propyne by $OH^-$ occurs predominantly at the methyl position so that most of the $C_3H_3^-$ produced in reaction [6] can be expected to be of the allenyl form. This implies that the reaction which introduces the observed curvature in the decay of $CH_3O^-$ is likely to be:

[9] $C_3H_3^- + CH_3OH \rightarrow CH_3O^- + CH_2{=}C{=}CH_2$

rather than the true reverse to reaction [6] which would regenerate propyne.

Reaction [7] was investigated separately in experiments in which $C_3H_3^-$ was produced from either allene or propyne by deprotonation with $OH^-$ (5). The measured rate constant was observed to be insensitive to the history of $C_3H_3^-$ and to have a value of $(8.0 \pm 2.0) \times 10^{-11}$ cm$^3$ molecule$^{-1}$ s$^{-1}$.

### $C_6H_5CH_3$

The study of reaction [10] was straightforward.

[10] $CH_3O^- + C_6H_5CH_3 \rightleftharpoons C_6H_5CH_2^- + CH_3OH$

Proton transfer was the only observed product channel proceeding with a rate constant of $(1.5 \pm 0.5) \times 10^{-9}$ cm$^3$ molecule$^{-1}$ s$^{-1}$. The cluster ion $CH_3O^-.CH_3OH$ was observed not to react rapidly with toluene, $k \leq 10^{-12}$ cm$^3$ molecule$^{-1}$ s$^{-1}$. No

Can. J. Chem. Downloaded from www.nrcresearchpress.com by 210.87.254.105 on 09/06/12
For personal use only.

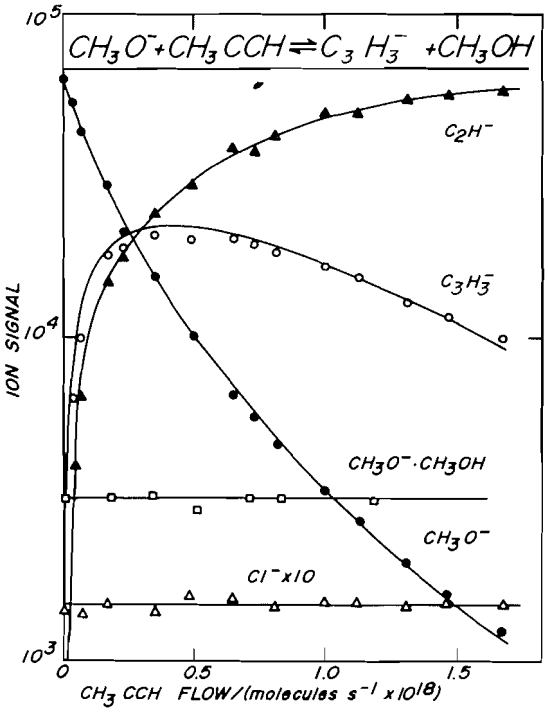


FIG. 1. The variation in dominant negative ions observed upon the addition of propyne into a He–$CH_3OH$ plasma in which $CH_3O^-$ is initially a dominant negative ion. $T = 296$ K, $P = 0.354$ Torr, $\bar{v} = 7.7 \times 10^3$ cm $s^{-1}$, $L = 59$ cm, and the $CH_3OH$ flow is $2.0 \times 10^{17}$ molecules $s^{-1}$.

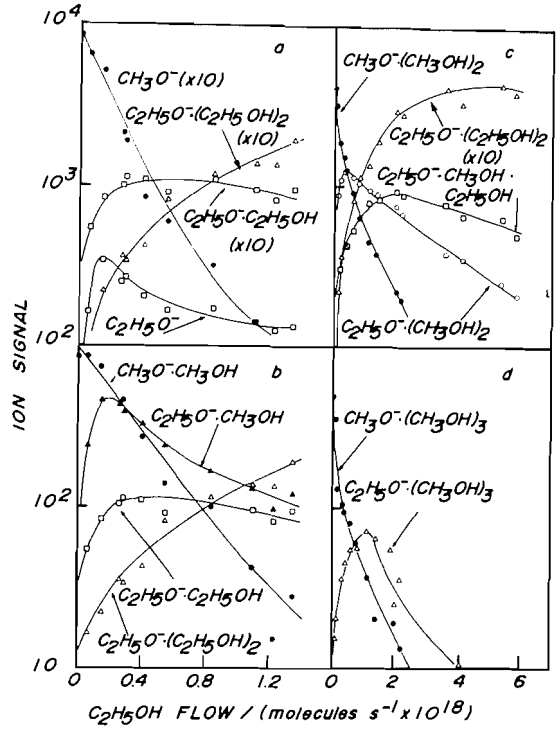


FIG. 2. A split view of observations recorded for the reactions of $CH_3O^-.(CH_3OH)_n$ with ethanol. The buffer gas is He. $T = 295$ K, $P = 0.333$ Torr, $\bar{v} = 8.1 \times 10^3$ cm $s^{-1}$, $L = 46$ cm, and the methanol flow is approximately $6 \times 10^{19}$ molecules $s^{-1}$.

evidence was found for competing and/or secondary reactions involving $C_6H_5CH_2^-$. Analysis of the observed $CH_3O^-$ decays under conditions approaching equilibrium provided a value for $k_{10}/k_{-10} = 1.4 \pm 0.5$ which is in exact agreement with the value for $K_{10} = 1.4 \pm 0.5$ obtained from ratio plot analyses under equilibrium conditions. Equilibrium was also approached from the reverse direction for which $C_6H_5CH_2^-$ was produced from the proton transfer between $OH^-$ and toluene. The decay of this ion at low methanol flows provided a value for $k_{10}/k_{-10} = 1.3 \pm 0.6$ while the equilibrium ion ratio led to a value for $K_{10} = 1.2 \pm 0.5$.

*$C_2H_5OH$*

The decays in the ion signals corresponding to $CH_3O^-$ and the solvated ions $CH_3O^-.CH_3OH$, $CH_3O^-.(CH_3OH)_2$, and $CH_3O^-.(CH_3OH)_3$ observed upon the addition of ethanol into a He–$CH_3OH$ plasma are shown in Fig. 2. Analysis of the data indicated that all of these ions react rapidly with ethanol in solvated acid–base reactions of type [11] with rate constants of $(3.3 \pm 1.0)$, $(2.9 \pm 1.0)$, $(1.2 \pm 0.4)$, and $(>0.2) \times 10^{-9}$ $cm^3$ $molecule^{-1}$ $s^{-1}$, respectively. The product ions $C_2H_5O^-.(CH_3OH)_n$ at $n = 0$ to 3 were observed to rise and then fall in concentration indicating further rapid reactions with ethanol. Evidently solvent exchange or "switching" reactions of type [12] were occurring. Both $C_2H_5O^-.C_2H_5OH$ and $C_2H_5O^-.CH_3OH.C_2H_5OH$ were observed to rise concomitant to the fall of the corresponding $C_2H_5O^-.(CH_3OH)_n$ species. $C_2H_5O^-.CH_3OH.C_2H_5OH$ was observed to displace still another methanol molecule according to reaction [13].

[11] $CH_3O^-.(CH_3OH)_n + C_2H_5OH \rightarrow C_2H_5O^-.(CH_3OH)_n + CH_3OH$

[12] $C_2H_5O^-.(CH_3OH)_n + C_2H_5OH \rightarrow C_2H_5O^-.(CH_3OH)_{n-1}.C_2H_5OH + CH_3OH$

[13] $C_2H_5O^-.CH_3OH.C_2H_5OH + C_2H_5OH \rightarrow C_2H_5O^-.(C_2H_5OH)_2 + CH_3OH$

Finally, the profiles in Fig. 2 also provide evidence for the occurrence of ethanol addition reactions of type [14] for $n = 0$ and 1. Taken together, the solvated proton-transfer reactions of type [11] appear to indicate sequences of solvent switching

[14] $C_2H_5O^-.(C_2H_5OH)_n + C_2H_5OH + He \rightarrow C_2H_5O^-.(C_2H_5OH)_{n+1} + He$

Can. J. Chem. Downloaded from www.nrcresearchpress.com by 210.87.254.105 on 09/06/12
For personal use only.

and solvent addition reactions which combine to ultimately establish the ethoxide ion solvated exclusively by ethanol.

While the unsolvated proton-transfer reaction between $CH_3O^-$ and $C_2H_5OH$ did not appear to attain equilibrium under our operating conditions, an analysis of the dependence on ethanol flow of the solvated product to reactant ion ratios for reactions of type [11] for $n = 1$, 2, and 3 did indicate regimes of methanol and ethanol flow for which equilibrium appeared to be established. Figure 3 shows the attainment of equilibrium for the solvated proton-transfer reaction [15] as well as the

[15] $CH_3O^-.CH_3OH + C_2H_5OH \rightleftharpoons C_2H_5O^-.CH_3OH + CH_3OH$

ensuing solvent-switching reaction [16]. The linearity observed in the ion ratio plots for these

[16] $C_2H_5O^-.CH_3OH + C_2H_5OH \rightleftharpoons C_2H_5O^-.C_2H_5OH + CH_3OH$

two reactions provided values for $K$ of 7.6 ± 2.7 and 2.0 ± 1.0, respectively. For the higher solvated proton-transfer reactions of type [11] with $n = 2$ and 3, an analysis of the data indicated values for the equilibrium constants of approximately 4 and 1, respectively.

An unsuccessful attempt was made to approach equilibrium for the unsolvated proton-transfer reaction from its reverse direction by adding methanol into a He–$C_2H_5OH$ plasma in which $C_2H_5O^-$ was initially a dominant negative ion. However, equilibrium was again observed to be established for reactions [15] and [16]. The equilibrium constants deduced from the corresponding ratio plots were in good agreement with those derived from the forward study having values of 7.8 ± 3.9 and 2.5 ± 0.9, respectively.

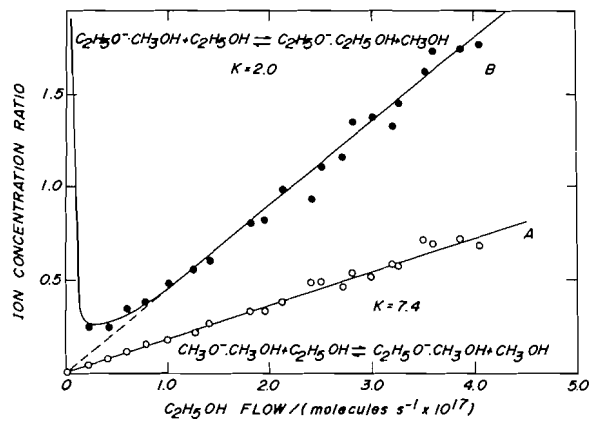


FIG. 3. The variation in ion concentration ratios observed upon the addition of ethanol into a He–$CH_3OH$ plasma. $T$ = 295 K, $P$ = 0.354 Torr, $\bar{v} = 8.4 \times 10^3$ cm $s^{-1}$, $L$ = 85 cm, and the flow of methanol is $4.09 \times 10^{17}$ molecules $s^{-1}$. Curve $A$: the ion concentration ratio $[C_2H_5O^-.CH_3OH]/[CH_3O^-.CH_3OH]$ divided by 10. Curve $B$: the ion concentration ratio $[C_2H_5O^-.C_2H_5OH]/[C_2H_5O^-.CH_3OH]$. The initial curvature arises from the production of $C_2H_5O^-.CH_3OH$ in the reaction region.

## $C_2H_2$

We have observed the proton-transfer reaction of $CH_3O^-$ with acetylene previously; it proceeded rapidly with a rate constant of $(1.6 \pm 0.4) \times 10^{-9}$ $cm^3$ $molecule^{-1}$ $s^{-1}$ (7) which was reproduced in the present studies. At the methanol flows used in the present experiments sufficient back reaction was introduced to allow the evaluation of the equilibrium constant for reaction [17] both from the ratios of ion and neutral concentrations at

[17] $CH_3O^- + C_2H_2 \rightleftharpoons C_2H^- + CH_3OH$

equilibrium and from the ratio of rate constants derived from the decay of $CH_3O^-$ and they were in good agreement. The values obtained were $(2.6 \pm 1.2) \times 10^3$ and $(2.7 \pm 1.1) \times 10^3$, respectively. Figure 4 shows data which provide a measure of the ratio of rate constants. The solvated species

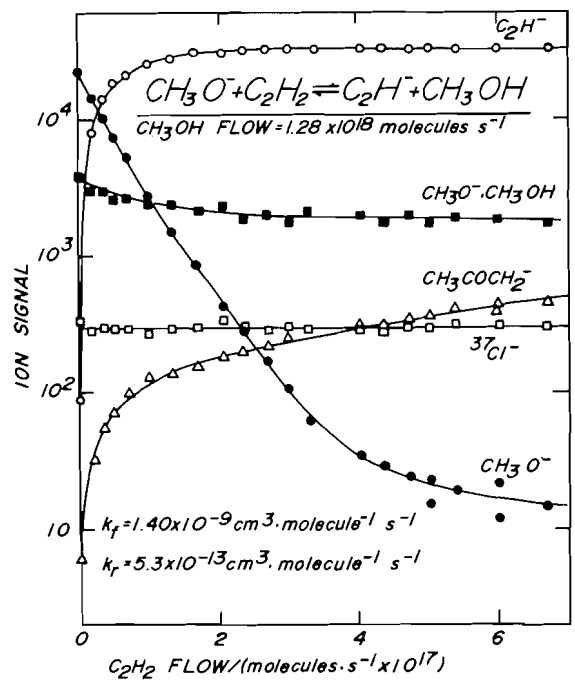


FIG. 4. The variation in dominant negative ions recorded upon the addition of acetylene into a He–$CH_3OH$ plasma in which $CH_3O^-$ is initially a dominant negative ion. The solid line through the $CH_3O^-$ decay represents a computer fit to the data with the values of the rate constants indicated. The initial decay in the $CH_3O^-.CH_3OH$ arises from the depletion of the $CH_3O^-$ source ion. $T$ = 298 K, $P$ = 0.317 Torr, $\bar{v} = 7.7 \times 10^3$ cm $s^{-1}$, and $L$ = 84 cm.

Can. J. Chem. Downloaded from www.nrcresearchpress.com by 210.87.254.105 on 09/06/12
For personal use only.

$CH_3O^-.CH_3OH$ which was also observed to be present in the reaction region, failed to react with a measurable rate, $k \leq 1 \times 10^{-12}$ cm$^3$ molecule$^{-1}$ s$^{-1}$.

The reaction of the ethoxide anion

[18] $C_2H_5O^- + C_2H_2 \rightleftharpoons C_2H^- + C_2H_5OH$

could also be driven into equilibrium under quite similar operating conditions. Again there was good agreement between the ratio of rate constants, $k_{18}/k_{-18} = 17.0 \pm 6.8$ and the equilibrium constant derived from equilibrium concentrations, $K_{18} = 16.4 \pm 6.6$. The forward rate constant was determined to be $(1.4 \pm 0.4) \times 10^{-9}$ cm$^3$ molecule$^{-1}$ s$^{-1}$. One experiment was carried out in which $C_2H^-$ was produced in a $He/CH_4$ plasma in the absence of $C_2H_2$. The rate constant for the reverse reaction, $k_{-18} = 1.0 \times 10^{-10}$ cm$^3$ molecule$^{-1}$ s$^{-1}$, could then be evaluated directly from the slope of the $C_2H^-$ decay using Analysis A (3). This value, when coupled with the rate constant obtained from the forward study, provided a value for $k_{18}/k_{-18} = 14 \pm 8$. The cluster ion $C_2H_5O^-.C_2H_5OH$ became the dominant primary ion in the reaction region already at relatively low flows, $2 \times 10^{17}$ molecules s$^{-1}$. It was also observed not to react with $C_2H_2$, $k \leq 1 \times 10^{-12}$ cm$^3$ molecule$^{-1}$ s$^{-1}$.

With $(CH_3)_2CHO^-$ equilibrium was established already at the smallest measurable additions of $C_2H_2$. This precluded the determination of unique values for the forward and reverse rate constants for reaction [19].

[19] $(CH_3)_2CHO^- + C_2H_2 \rightleftharpoons C_2H^- + (CH_3)_2CHOH$

The measurements did, however, provide values for the ratio of rate constants $k_{19}/k_{-19} = 1.16 \pm 0.41$ and the equilibrium constant derived from equilibrium concentrations $K_{19} = 1.13 \pm 0.45$.

*$CH_3CN$*

We have reported previously that reaction [20]

[20] $CH_3O^- + CH_3CN \rightarrow CH_2CN^- + CH_3OH$

proceeds very rapidly with a rate constant at room temperature of $(3.5 \pm 0.9) \times 10^{-9}$ cm$^3$ molecule$^{-1}$ s$^{-1}$ without any significant displacement to form $CN^-$ (8). Furthermore, the reaction could not be driven to equilibrium under our operating conditions. Consequently attempts were made to establish equilibrium for the less exoergic proton-transfer reaction [21]. Both He and $H_2$ were used as

[21] $C_2H^- + CH_3CN \rightleftharpoons CH_2CN^- + C_2H_2$

buffer gases and the $C_2H^-$ was produced either by electron impact on acetylene at ca. 40 eV or via the rapid proton transfer from $C_2H_2$ to $OH^-$ (9). Figure 5 shows a representative variation of dominant negative ions recorded upon the addition of

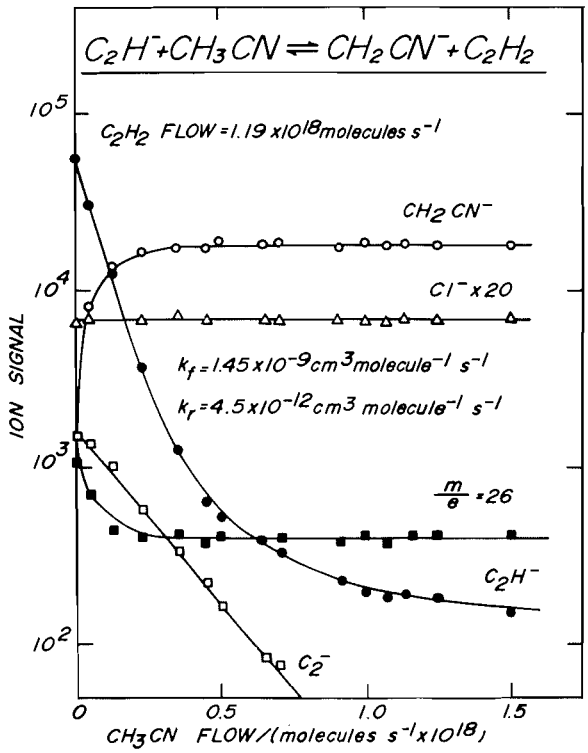


FIG. 5. The variation in dominant negative ions recorded upon the addition of $CH_3CN$ into a $He-C_2H_2$ plasma in which $C_2H^-$ is initially a dominant negative ion. The solid line through the $C_2H^-$ decay is a computer fit with the values of the rate constants indicated. $T = 295$ K, $P = 0.365$ Torr, $\bar{v} = 8.3 \times 10^3$ cm s$^{-1}$, and $L = 60$ cm.

acetonitrile into a $He-C_2H_2$ plasma in which $C_2H^-$ was initially a major ion. The majority of the $C_2H^-$ decay and accompanying increase in the $CH_2CN^-$ signal can be attributed to the proton-transfer reaction [21]. The initial decay in the mass 26 signal is due to the reaction of the $^{13}C^{12}CH^-$ isotope. The failure of the mass 26 ion signal to rise sets an upper limit of 0.5% to the production of $CN^-$ by nucleophilic displacement. The mass discrimination plots in all experiments exhibited excellent linearity over a range in $CH_3CN$ flow which was varied by over a factor of 200 and the mass discrimination factor was found to be independent of the $CH_3CN$ concentration and reaction length which had values of 59 and 85 cm. The application of our standard analyses to the curved $C_2H^-$ decays and the ratio plots led to values for the ratio of rate constants and the equilibrium constant, respectively, which agreed within the uncertainty of the measurements: $k_{21} = (1.5 \pm 0.4) \times 10^{-9}$ and $k_{-21} = (4.8 \pm 1.7) \times 10^{-12}$ cm$^3$ molecule$^{-1}$ s$^{-1}$, $k_{21}/k_{-21} = (3.1 \pm 0.9) \times 10^2$, and $K_{21} = (3.0 \pm 1.2) \times 10^2$. The weighted mean of the values for $k_{21}/k_{-21}$ and $K_{21}$

Can. J. Chem. Downloaded from www.nrcresearchpress.com by 210.87.254.105 on 09/06/12
For personal use only.

provides a best estimate of the true value for the equilibrium constant of $3.0 \times 10^2$ with a standard error of $\pm 0.7 \times 10^2$ for reaction [21].

The solvated cluster ions $CH_3O^-.(CH_3OH)_n$ with $n = 1$, 2, and 3 were observed not to react rapidly with $CH_3CN$, $k \leq 2 \times 10^{-12}$ cm$^3$ molecule$^{-1}$ s$^{-1}$. Apparently a reversal in the relative acidity of $CH_3OH$ and $CH_3CN$ occurs already at the addition of one solvent methanol molecule.

*$CH_3COCH_3$*

Figure 6 shows data which reveal the transition in kinetics with the stepwise solvation of $CH_3O^-$ with methanol in reactions of type [22].

[22] $CH_3O^-.(CH_3OH)_n + CH_3COCH_3 \rightarrow CH_3COCH_2^-.(CH_3OH)_n + CH_3OH$

The unsolvated methoxide ion reacts rapidly with a rate constant determined to be $(2.3 \pm 0.6) \times 10^{-9}$ cm$^3$ molecule$^{-1}$ s$^{-1}$ but does not approach equilibrium. However, equilibrium was nearly achieved for the reaction of the singly solvated ion for which a slightly smaller rate constant of $(1.7 \pm 0.4) \times 10^{-9}$ cm$^3$ molecule$^{-1}$ s$^{-1}$ was obtained, while the doubly and triply solvated species failed to react, $k < 2 \times 10^{-12}$ cm$^3$ molecule$^{-1}$ s$^{-1}$.

Since equilibrium could not be established for the solvent-free reaction of the methoxide ion with acetone, an attempt was made to approach an equilibrium in a proton-transfer reaction with the much less basic anion $CH_2CN^-$. The only product ion formed at low additions of acetone into a He–$CH_3CN$ plasma in which $CH_2CN^-$ was established by proton-transfer from $CH_3CN$ to $OH^-$ was $CH_3COCH_2^-$ so that the decay of $CH_2CN^-$ could be attributed to the proton-transfer reaction [23]. At large acetone additions the cluster-

[23] $CH_2CN^- + CH_3COCH_3 \rightarrow CH_3COCH_2^- + CH_3CN$

ing reaction [24] proceeded towards equilibrium. The product to reactant ion concentration ratio at

[24] $CH_3COCH_2^- + CH_3COCH_3 + He \rightleftharpoons CH_3COCH_2^-.CH_3COCH_3 + He$

equilibrium provided a value of $(1.5 \pm 0.5) \times 10^6$ (standard state = 1 atm) for the equilibrium constant of reaction [24]. A small amount of $CH_2CN^-.CH_3CN$ present initially was rapidly depleted by the solvated proton-transfer reaction [25].

[25] $CH_2CN^-.CH_3CN + CH_3COCH_3 \rightleftharpoons CH_3COCH_2^-.CH_3CN + CH_3CN$

An extended analysis of the data provided only a lower limit to the equilibrium constant for reaction [23] of 500. The initial decay of $CH_2CN^-$ provided a

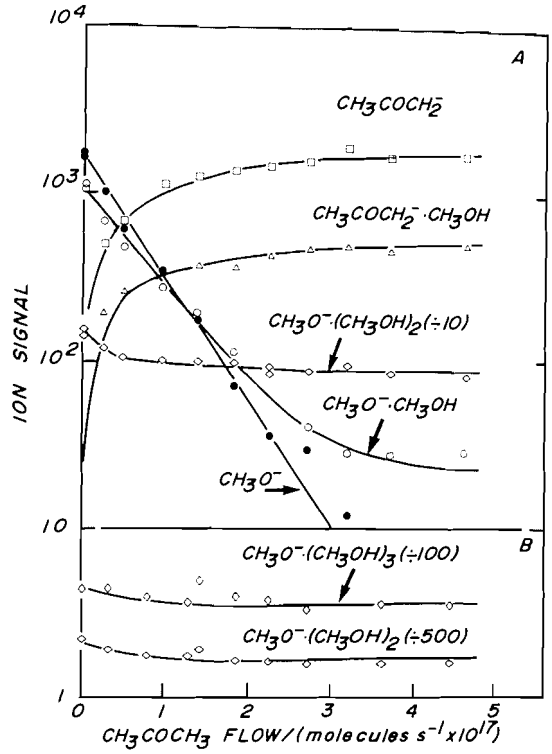


FIG. 6. Observations recorded for the reactions of $CH_3O^-.(CH_3OH)_n$ with acetone in a He buffer at a low flow ($A$: $\sim 5 \times 10^{17}$ molecules s$^{-1}$) and a high flow ($B$: $\sim 2 \times 10^{19}$ molecules s$^{-1}$) of methanol. $T = 295$ K, $P = 0.323$ Torr, $\bar{v} = 8 \times 10^3$ cm s$^{-1}$, and $L = 46$ cm.

forward rate constant for reaction [23] of $(3.0 \pm 0.9) \times 10^{-10}$ cm$^3$ molecule$^{-1}$ s$^{-1}$.

An attempt was also made to establish equilibrium for reaction [23] from the reverse direction. It was evident that $CH_3COCH_2^-$ does not react rapidly with $CH_3CN$ either by proton transfer or by $CN^-$ displacement: no significant increase was observed for the $m/e = 40$ and 26 ion signals. The cluster ion $CH_3COCH_2^-.CH_3CN$ was formed instead by the association reaction [26] for which the ion ratio plot at large flows of $CH_3CN$ indicated an equilibrium constant of $(1.0 \pm 0.5) \times$

[26] $CH_3COCH_2^- + CH_3CN + He \rightleftharpoons CH_3COCH_2^-.CH_3CN + He$

$10^7$ (standard state = 1 atm). Also the solvent-switching reaction [27] appeared to achieve

[27] $CH_3COCH_2^-.CH_3COCH_3 + CH_3CN \rightleftharpoons CH_3COCH_2^-.CH_3CN + CH_3COCH_3$

equilibrium with an equilibrium constant of $4 \pm 3$.

*$CH_3CHO$*

The solvent-free and singly-solvated methoxide

Can. J. Chem. Downloaded from www.nrcresearchpress.com by 210.87.254.105 on 09/06/12
For personal use only.

ion were observed to react rapidly with acetaldehyde with rate constants of (2.0 ± 0.6) and (1.5 ± 0.6) × $10^{-9}$ $cm^3$ $molecule^{-1}$ $s^{-1}$. Both $^-CH_2CHO$ and $^-CH_2CHO.CH_3OH$ were observed as product ions in amounts which balanced the initial $CH_3O^-$ and $CH_3O^-.CH_3OH$ signals, respectively, in accordance with reaction [28].

[28] $CH_3O^-.(CH_3OH)_n + CH_3CHO \rightarrow {}^-CH_2CHO.(CH_3OH)_n + CH_3OH$

The reactions with $n = 2$ and 3 appeared not to proceed rapidly, $k < 1 \times 10^{-11}$ $cm^3$ $molecule^{-1}$ $s^{-1}$, and there was no significant production of $^-CH_2CHO.(CH_3OH)_n$ with $n = 2$ and 3. The $^-CH_2CHO$ reacted further, presumably to form the adduct $^-CH_2CHO.CH_3CHO$ which was observed to appear at larger additions of $CH_3CHO$ into the reaction region. The $^-CH_2CHO.CH_3OH$ appeared to react further by the solvent-switching reaction [29].

[29] $^-CH_2CHO.CH_3OH + CH_3CHO \rightarrow {}^-CH_2CHO.CH_2CHO + CH_3OH$

*$CH_3NO_2$*

The solvent free $CH_3O^-$ and the solvated $CH_3O^-.(CH_3OH)_n$ ions with $n = 1$ to 3 were all observed to react rapidly with nitromethane in reactions of type [30] with rate constants of (3.1 ± 0.8), (2.3 ± 0.7), (1.9 ± 0.6), and (1.3 ± 0.5) × $10^{-9}$

[30] $CH_3O^-.(CH_3OH)_n + CH_3NO_2 \rightarrow CH_2NO_2^-.(CH_3OH)_m + (n - m + 1)CH_3OH$

$cm^3$ $molecule^{-1}$ $s^{-1}$, respectively. We have reported previously a rate constant of (3.2 ± 0.8) × $10^{-9}$ $cm^3$ $molecule^{-1}$ $s^{-1}$ for the solvent-free reaction (10). All of the corresponding solvated product ions were observed to be produced, albeit $CH_2NO_2^-.(CH_3OH)_3$ appeared in only trace amounts. Also the product ion profiles provided evidence for the exchange of solvent in reactions of type [31] for $n = 1$ and 2, and the addition of

[31] $CH_2NO_2^-.(CH_3OH)_n + CH_3NO_2 \rightarrow CH_2NO_2^-.CH_3NO_2 + CH_3OH$

$CH_3NO_2$ to $CH_2NO_2^-$ according to reaction [32]. At the operating conditions of these experiments

[32] $CH_2NO_2^- + CH_3NO_2 + He \rightarrow CH_2NO_2^-.CH_3NO_2 + He$

there was no indication of the establishment of equilibrium in any of the reactions of type [30].

*HCN*

Figure 7 reveals the influence of methanol solvation on the reaction of methoxide ion with HCN. Rapid reactions of type [33] were observed

[33] $CH_3O^-.(CH_3OH)_n + HCN \rightarrow CN^-.(CH_3OH)_m + (n - m + 1)CH_3OH$

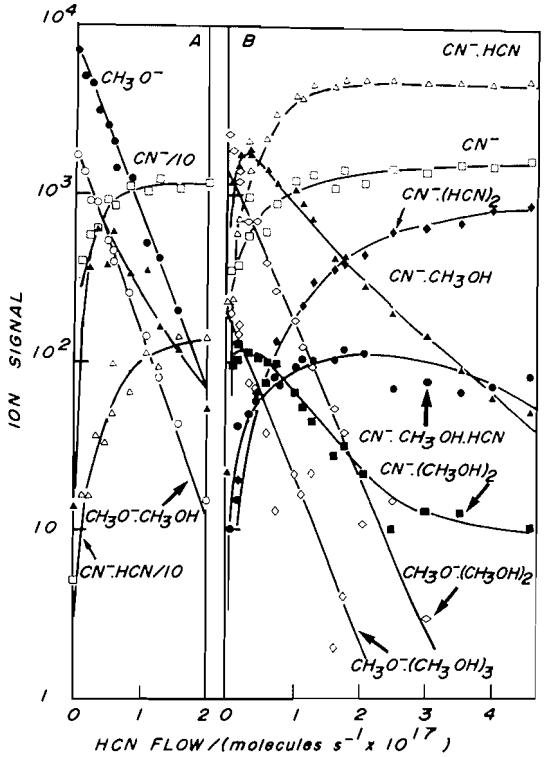


FIG. 7. A split view of observations recorded for the reactions of $CH_3O^-.(CH_3OH)_n$ with hydrogen cyanide at a low flow (*A*: ~1 × $10^{19}$ molecules $s^{-1}$) and a high flow (*B*: ~4 × $10^{19}$ molecules $s^{-1}$) of methanol. The buffer gas is He. $T = 296$ K, $P = 0.343$ Torr, $\bar{v} = 8.1 \times 10^3$ cm $s^{-1}$, and $L = 46$ cm.

for all of the $CH_3O^-.(CH_3OH)_n$ ions with the rate constants for $n = 0$, 1, 2, and 3 having values of (3.3 ± 0.8), (3.2 ± 1.0), (3.1 ± 1.0), and (3.0 ± 1.1) × $10^{-9}$ $cm^3$ $molecule^{-1}$ $s^{-1}$, respectively. The product ion profiles indicated further rapid solvent switching reactions of type [34] for $n = 1$ and 2 for

[34] $CN^-.(CH_3OH)_n + HCN \rightarrow CN^-.(CH_3OH)_{n-1}.HCN + CH_3OH$

which rate constants of (1.5 ± 0.5) and (1.4 ± 0.5) × $10^{-9}$ $cm^3$ $molecule^{-1}$ $s^{-1}$ were deduced. The reaction for $n = 2$ appeared to approach equilibrium (with an equilibrium constant > 1 × $10^3$) and was followed by further solvent exchange according to reaction [35] to completely eliminate $CH_3OH$ from the solvation shell of $CN^-$.

[35] $CN^-.CH_3OH.HCN + HCN \rightarrow CN^-.(HCN)_2 + CH_3OH$

## Discussion

*A. Intrinsic kinetics*

The room-temperature rate constants measured in this study for the reactions of solvent-free methoxide anions and several other unsolvated

Can. J. Chem. Downloaded from www.nrcresearchpress.com by 210.87.254.105 on 09/06/12
For personal use only.

anions are summarized in Table 1. Protonation of the methoxide ion was observed to proceed rapidly in all cases with rate constants exceeding $8 \times 10^{-10}$ $cm^3$ $molecule^{-1}$ $s^{-1}$. The corresponding efficiencies determined from the ratios of the measured rate constant to the collision rate constant calculated using the AADO theory (11) all exceed 60%. The slowest and least efficient (10%) reaction measured was that between $CH_2CN^-$ and acetone which involves the protonation of a charge-delocalized anion.

Few other measurements are available for comparison. A rate constant of $6.58 \times 10^{-10}$ $cm^3$ $molecule^{-1}$ $s^{-1}$, which is about one-half of our room-temperature value, has been reported for the reaction of $CH_3O^-$ with toluene involving reagent ions with a laboratory energy of ca. 0.3 eV in a tandem spectrometer (12). An ion cyclotron resonance (ICR) measurement of the rate constant for this reaction resulted in a value of only $(2.0 \pm 0.2) \times 10^{-10}$ $cm^3$ $molecule^{-1}$ $s^{-1}$ (13) which is about seven times smaller than our value. Better agreement with the ICR results is obtained for the reaction of $CH_3O^-$ with ethanol for which the ICR measurements yielded $(1.2 \pm 0.3) \times 10^{-9}$ $cm^3$ $molecule^{-1}$ $s^{-1}$ (13).

Several new association reactions were identified in this study. Of particular note are reaction [24] and the analogous reaction with acetaldehyde. The clustering reactions may also be written as aldol-type condensations as in reaction [36]. Self-condensation reactions of this type are well

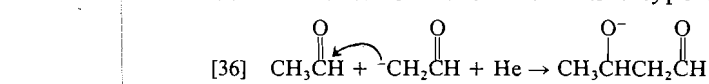

[36] $CH_3\overset{O}{\overset{\|}{C}}H + {}^-CH_2\overset{O}{\overset{\|}{C}}H + He \rightarrow CH_3\overset{O^-}{\overset{|}{C}}HCH_2\overset{O}{\overset{\|}{C}}H + He$

known in solution where they proceed readily in the presence of aqueous base.

### *B. Intrinsic energetics*

#### *Equilibrium constants*

The room-temperature equilibrium constants for the solvent-free proton-transfer reactions measured in this study and which provide the basis of the gas-phase scale of acidities derived below are also included in Table 1. The equilibrium constants for the three reactions of alkoxide ions with $C_2H_2$ supersede those reported a decade ago by Bohme and co-workers (14) in their first attempt to quantify differences in gas-phase acidities of organic compounds. These earlier flowing afterglow measurements, which relied on an inferior method for the measurement of concentrations of alcohol vapours, provided equilibrium constants of $3 \times 10$, $1 \times 10$, and 1 for the reactions of $CH_3O^-$, $C_2H_5O^-$, and $(CH_3)_2CHO^-$, respectively. They are to be compared with the current values of $(2.7 \pm 0.7) \times 10^3$, $17 \pm 4$, and $1.2 \pm 0.3$. With the exception of the results for the $CH_3O^-$ reaction, the agreement is within the experimental uncertainties of the two sets of measurements. The early results (15) for the reactions of $CH_3O^-$ with the allene and toluene, which provided limiting values for $K$ of $\lesssim 0.5$ and $\lesssim 1$ respectively, are also superseded by the present measurements, which yielded a value for $K$ of $1.4 \pm 0.3$ for both of these reactions.

Table 3 provides a comparison of our present and some earlier flowing afterglow results with those obtained by McIver and his colleagues with the pulsed-ICR mass spectrometer which operates at considerably different conditions of total pressure and reagent ion history, and a neutral gas and ion temperature which has been estimated to be 320 K (16). The agreement with the most recent ICR results reduced to apply at a temperature of 298 K (16) is within a factor of 2 in the majority of cases.

#### *Absolute and relative gas-phase acidities*

Bartmess and co-workers have recommended an absolute gas-phase acidity for methanol of 372.6 kcal $mol^{-1}$ (16) based on a standard enthalpy change and standard entropy change for the deprotonation of methanol of 379.2 kcal $mol^{-1}$ and 22.0 cal $mol^{-1}$ $K^{-1}$, respectively. In the same paper these authors have shown that the standard enthalpy change which can be derived from the best available values for $EA(CH_3O)$, $D(CH_3O—H)$, and IP(H) has an average value of 381.2 kcal $mol^{-1}$. We have adopted this latter value for the standard enthalpy change and recommend an absolute gas-phase acidity for methanol of $374.6 \pm 2$ kcal $mol^{-1}$. This value has been used as a reference for the assignment of the absolute gas-phase acidities indicated in Table 4 which also includes the differences in gas-phase acidity determined from the equilibrium constants measured with the flowing afterglow technique.

### *C. Influence of solvation on intrinsic kinetics and energetics*

Under our experimental operating conditions methanol solvent is added as a vapour in trace amounts (< 1%) to a flowing plasma of helium or hydrogen at low total presures (ca. 0.3 Torr). The reagent base, $B^- = CH_3O^-$, is produced by the ionization of methanol and allowed to build up a solvation shell upstream by successive methanol addition reactions to form ions of the type $CH_3O^-.(CH_3OH)_n$. These solvated ions then participate in reactions with the added acid, AH, as they enter the reaction region downstream. An ensuing solvated proton-transfer reaction of type

Can. J. Chem. Downloaded from www.nrcresearchpress.com by 210.87.254.105 on 09/06/12
For personal use only.

TABLE 3. A comparison of values for equilibrium constants determined using the flowing afterglow (FA) technique with values determined using the ICR technique

| Reaction | $K$(FA)[a] | $K$(ICR)[a,b] |
|---|---|---|
| $CH_3O^- + C_6H_5CH_3 \rightleftharpoons C_6H_5CH_2^- + CH_3OH$ | *1.4±0.3* | *1.7* |
| $CH_3O^- + C_2H_5OH \rightleftharpoons C_2H_5O^- + CH_3OH$ | $(1.6\pm0.7)\times10^2$ [2] | *1.9 × 10², (23±2)* |
| $CH_3O^- + C_2H_2 \rightleftharpoons C_2H^- + CH_3OH$ | *(2.7±0.7) × 10³* | $1.1\times10^4$ [2], $((2.9\pm1.2)\times10^2$ [3]) |
| $C_2H_5O^- + C_2H_2 \rightleftharpoons C_2H^- + C_2H_5OH$ | *17±4* | *58* (12±2 [2]) |
| $(CH_3)_2CHO^- + C_2H_2 \rightleftharpoons C_2H^- + (CH_3)_2CHOH$ | *1.2±0.3* | *1.2* (1.3±0.1 [2]) |
| $C_2H^- + CH_3CN \rightleftharpoons CH_2CN^- + C_2H_2$ | *(3.0±0.7) × 10²* | 96 [3] |
| $CH_2CN^- + CH_3COCH_3 \rightleftharpoons CH_3COCH_2^- + CH_3CN$ | *≥ 5 × 10²* | $2.2\times10^2$ [2] |
| $CH_3S^- + CH_3NO_2 \rightleftharpoons CH_2NO_2^- + CH_3SH$ | *1.9±0.3*[c] | *3.3* |
| $SH^- + HCN \rightleftharpoons CN^- + H_2S$ | *1.6±2*[d] | *6.4, 9.5±1.5*[e] |
| $CH_3O^-.CH_3OH + C_2H_5OH \rightleftharpoons C_2H_5O^-.CH_3OH + CH_3OH$ | *7.7±2.2* | *7.5±2*[f] |
| $C_2H_5O^-.CH_3OH + C_2H_5OH \rightleftharpoons C_2H_5O^-.C_2H_5OH + CH_3OH$ | *2.3±0.6* | *2±0.5*[f] |

[a]A value is in italics if the equilibrium has been studied directly. The other values were obtained by combining the results of equilibrium measurements for two or more reactions, the actual number of reactions is given in brackets.
[b]Values of $K$ derived from the values of $\delta\Delta G^0$ (reduced to 298 K) reported by Bartmess, Scott, and McIver in ref. 16 (Fig. 3) unless indicated otherwise. The values in parentheses are those reported earlier by McIver and Miller in ref. 17.
[c]Reference 10.
[d]Reference 18.
[e]Reference 19.
[f]Reference 20.

TABLE 4. Relative and absolute gas-phase acidities at 298 K, ΔGA and GA(AH) in kcal mol$^{-1}$, based on flowing afterglow measurements. The values in parentheses are those recommended by Bartmess, Scott, and McIver on the basis of pulsed-ICR mass spectrometer measurements (16)

| GA(AH) | AH | ΔGA |
|---|---|---|
| (345.8) | HCN | |
| | | 1.6±0.1 (1.3) |
| (347.1) | $H_2S$ | |
| (352.0) | $CH_3NO_2$ | |
| | | 0.4±0.1 (0.7) |
| (352.7) | $CH_3SH$ | |
| ≤362.8 (361.6) | $CH_3COCH_3$ | |
| | | >3.7 (2.8) |
| 366.5 (364.4) | $CH_3CN$ | |
| | | 3.4±0.2 (2.8) |
| 369.9 (367.2) | $C_2H_2$ | |
| | | 0.11±0.15 (0.3) |
| 370.0 (367.5) | $(CH_3)_2CHO$ | |
| | | 1.7±0.2 (2.3) |
| 371.6 (369.5) | $C_2H_5OH$ | |
| | | 4.5±0.2 (5.1) |
| 374.4 (372.3) | $C_6H_5CH_3$, $CH_2{=}C{=}CH_2$ | |
| | | 0.20±0.13 (0.3) |
| 374.6 (372.6) | $CH_3OH$ | |
| | | 4.7±0.2 (5.4) |

[2] may then establish the newly solvated species $A^-.(CH_3OH)_n$. In the time available in the reaction region these species in turn may optimize their stability by exchanging the methanol molecules in the solvation shell for the acid molecules, AH, or simply by adding the latter. Figure 8 shows a general scheme of the sequential solvated-ion chemistry which is implied by our measurements.

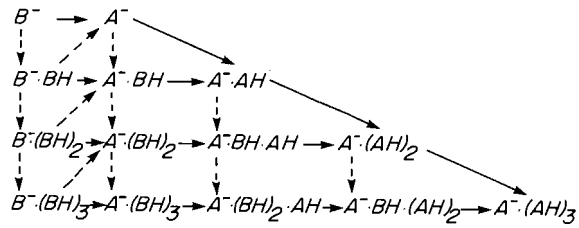


FIG. 8. A general scheme representative of the possible solvated ion chemistry proceeding under flowing afterglow conditions. The solid horizontal arrows represent solvated acid–base or solvent exchange reactions with AH. The solid diagonal arrows represent solvent addition reactions with AH. The dashed vertical arrows represent possible solvent addition reactions with BH. The dashed diagonol arrows represent possible solvated acid–base reactions with a concomitant "boiling off" of solvent BH.

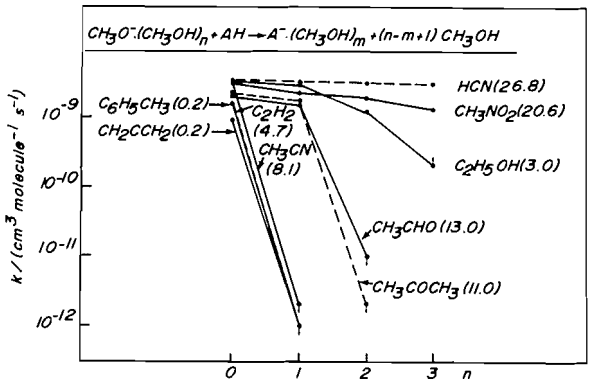


FIG. 9. Observed variations in the rate constants for the reactions of solvated methoxide ions with acids AH as a function of step-wise solvation. The values indicated in parentheses correspond to the relative intrinsic acidities of the acids AH and $CH_3OH$, i.e. $-\Delta G^0$ (in kcal $mol^{-1}$) for the solvent-free reactions at 298 K.

The chemical sequence indicated may be interrupted at any level of solvation depending on the nature of the added acid.

The rate constants obtained for the solvated proton-transfer reactions of the species $CH_3O^-.(CH_3OH)_2$ with the acids added in this study are summarized in Table 2 and presented graphically in Fig. 9. Solvation of $CH_3O^-$ is seen to lead to two extreme types of behaviour: (*a*) The addition of only one methanol molecule to the methoxide ion essentially closes the reactions of this ion with allene, toluene, acetylene, and methylcyanide. The rate constant is observed to drop dramatically by more than a factor of $\sim 10^3$ from an initial value of ca. $10^{-9}$ $cm^3$ $molecule^{-1}$ $s^{-1}$. (*b*) For the reactions of ethanol, nitromethane, and hydrogen cyanide the addition of three molecules of methanol does not reduce the rate by more than a factor of $\sim 10$. The reactions with acetone and acetaldehyde show an intermediate behaviour in that the sharp drop in rate is delayed until the addition of two molecules of methanol to the methoxide ion.

The remarkable divergence of the rate constants observed in this study can be accounted for by a consideration of the degree of stabilization of the reactant and product ions by solvation and their influence on overall reaction energetics. The rate of proton transfer can be expected to remain high upon solvation if the reaction remains exoergic. Conversely, a sharp drop in the rate can be anticipated if solvation renders the reaction endoergic. The solvent-free reactions are all exoergic: they span a range in $-\Delta G^0$, i.e. relative intrinsic acidity, from 0.2 to 26.8 kcal $mol^{-1}$. The free energy of solvation of $CH_3O^-$, which can be deduced to be approximately 17 kcal $mol^{-1}$ for the addition of the first methanol molecule (1), will act to decrease the reaction exoergicities and can lead to changes in the sign of $\Delta G^0$, i.e. reversals in relative acidity, and therefore reversals in the preferred direction of reaction unless it is offset by the solvation energy of the conjugate base produced. In other words, exoergicity will be preserved if the free energy of solvation of the conjugate base produced is comparable to or greater than the corresponding free energy of solvation of $CH_3O^-$ or if a lower free energy of solvation of the product base is offset by the exoergicity of the unsolvated reaction.

The carbanions produced by the deprotonation of allene and toluene, the two acids in this study with an intrinsic acidity almost identical to that of methanol, are expected to have free energies of solvation insufficient to compensate for the high solvation energy of $CH_3O^-$. The sharp drop in the rate of deprotonation observed upon the addition of just one molecule of solvent can therefore be interpreted as a manifestation of a reversal in the relative acidity of these two carbon acids and methanol. A similar situation seems to apply to the formation of $C_2H^-.CH_3OH$ and $CH_2CN^-.CH_3OH$ although the solvent-free reactions are somewhat more exoergic. Again a reversal in relative acidity appears to result after the addition of just one methanol molecule.

For the deprotonation of acetone and acetaldehyde by $CH_3O^-$ reversals also appear to occur but they are delayed by one additional molecule of solvent: the sharp decline in rate occurs at $n = 2$. In these cases the exoergicities of the solvent-free reactions are within 6 kcal $mol^{-1}$ of compensating for the high free energy of solvation of $CH_3O^-$. Also some of the negative charge on the anions produced from these two carbon acids is

Can. J. Chem. Downloaded from www.nrcresearchpress.com by 210.87.254.105 on 09/06/12
For personal use only.

transferred to the oxygen which may result in some enhancement in the stability of the solvated species.

No reversals are observed for the deprotonation of nitromethane, hydrogen cyanide, and ethanol: reaction [2] remains rapid up to the addition of three methanol molecules to $CH_3O^-$. The intrinsic acidity of ethanol, an oxygen acid, is relatively close to that of methanol but in this case the order of acidity is preserved by the strong solvation of $C_2H_5O^-$. The intrinsic acidities of nitromethane and hydrogen cyanide are sufficiently high to offset the weaker anion–methanol interactions expected for $CH_2NO_2^-$ and $CN^-$. In fact, reactions of type [37] for AH = HCN or $CH_3NO_2$ in which some of

$$[37]\quad CH_3O^-.(CH_3OH)_n + AH \rightarrow A^-.(CH_3OH)_m + (n - m + 1)CH_3OH$$

the methanol is "boiled off" are exoergic at least for $n = 1$ and $m = 0$. Indeed the product spectra observed for these two reactions appear to be "shifted" in favour of lower degrees of solvation of $A^-$.

The clear pattern which has emerged from the trends in the rates of the acid–base reactions of the solvated methoxide ions which have been determined in this study and their dependence on the overall energetics of reaction is likely to be representative of the transition from the gas-phase to the solution in the rates of exothermic acid–base reactions generally and provides a vivid confirmation of expectations based on solution measurements.

**Acknowledgement**

We thank the Natural Sciences and Engineering Research Council for financial support. Also we thank one of the referees for drawing our attention to the possibility of aldol-type condensations for several of the association reactions observed in this study.

1. G. I. MACKAY and D. K. BOHME. J. Am. Chem. Soc. **100**, 327 (1978).
2. S. D. TANNER, G. I. MACKAY, and D. K. BOHME. Can. J. Chem. **59**, 1615 (1981).
3. D. K. BOHME, R. S. HEMSWORTH, H. W. RUNDLE, and H. I. SCHIFF. J. Chem. Phys. **58**, 3504 (1973).
4. G. I. MACKAY, R. S. HEMSWORTH, and D. K. BOHME. Can. J. Chem. **54**, 1624 (1976).
5. G. I. MACKAY and D. K. BOHME. Org. Mass. Spectrom. **15**, 593 (1980).
6. A. C. HOPKINSON. *In* The chemistry of functional groups. The chemistry of the carbon–carbon double bond. *Edited by* S. Patai. John Wiley and Sons, Toronto. 1978. Chapt. 4, p. 85.
7. G. I. MACKAY, K. TANAKA, and D. K. BOHME. Int. J. Mass Spectrom. Ion Phys. **24**, 125 (1977).
8. G. I. MACKAY, L. D. BETOWSKI, J. D. PAYZANT, H. I. SCHIFF, and D. K. BOHME. J. Phys. Chem. **80**, 2919 (1976).
9. D. K. BOHME, G. I. MACKAY, H. I. SCHIFF, and R. S. HEMSWORTH. J. Chem. Phys. **61**, 2175 (1974).
10. G. I. MACKAY and D. K. BOHME. Int. J. Mass Spectrom. Ion Phys. **26**, 327 (1978).
11. T. SU, E. C. F. SU, and M. T. BOWERS. J. Chem. Phys. **69**, 2243 (1978).
12. C. LIFSHITZ, R. L. C. WU, and T. O. TIERNAN. J. Am. Chem. Soc. **100**, 2040 (1978).
13. J. I. BRAUMAN, C. A. LIEDER, and M. J. WHITE. J. Am. Chem. Soc. **95**, 927 (1973).
14. D. K. BOHME, E. LEE-RUFF, and L. B. YOUNG. J. Am. Chem. Soc. **93**, 4608 (1971).
15. D. K. BOHME, E. LEE-RUFF, and L. B. YOUNG. J. Am. Chem. Soc. **94**, 5153 (1972).
16. J. E. BARTMESS, J. A. SCOTT, and R. T. MCIVER. J. Am. Chem. Soc. **101**, 6046 (1979).
17. R. T. MCIVER and J. S. MILLER. J. Am. Chem. Soc. **96**, 4323 (1974).
18. D. BETOWSKI, G. I. MACKAY, J. PAYZANT, and D. K. BOHME. Can. J. Chem. **53**, 2365 (1975).
19. R. T. MCIVER, JR. and J. R. EYLER. J. Am. Chem. Soc. **93**, 6334 (1971).
20. R. T. MCIVER, JR., J. A. SCOTT, and J. M. RIVEROS. J. Am. Chem. Soc. **95**, 2706 (1973).

Can. J. Chem. Downloaded from www.nrcresearchpress.com by 210.87.254.105 on 09/06/12
For personal use only.

# Theoretical prediction of protein antigenic determinants from amino acid sequences

SERAFIN FRAGA
*Department of Chemistry, University of Alberta, Edmonton, Alta., Canada T2G 2G2*
Received April 21, 1982

SERAFIN FRAGA. Can. J. Chem. **60**, 2606 (1982).

The locations of the antigenic determinants in a protein are predicted from its amino acid sequence by a modified Hopp–Woods method, proposed in this work, using both hydrophilicity and recognition factors. The amino acid – amino acid interaction energies, from which the recognition factors have been defined, have been evaluated by a semiempirical method, developed at this laboratory, using $1/R$ expansions parameterized on the basis of the results from accurate SCF calculations. The present procedure, which eliminates most of the uncertainties in the original Hopp–Woods method, leads to a very satisfactory prediction of the antigenic determinants.

SERAFIN FRAGA. Can. J. Chem. **60**, 2606 (1982).

On peut prévoir les sites des déterminants antigéniques d'une protéine à partir de la séquence d'acides aminés en faisant appel à une méthode modifiée de Hopp–Woods proposée dans ce travail et qui utilise à la fois l'hydrophilicité et les facteurs de reconnaissance. Utilisant une méthode semi-empirique mise au point dans ce laboratoire, qui fait appel aux expansions $1/R$ et en se basant sur les résultats obtenus à partir de calculs de champs auto-cohérants précis, on a évalué les énergies d'interaction entre acides aminés à partir desquelles on a défini les facteurs de reconnaissance. Le procédé actuel, qui élimine la plupart des incertitudes de la méthode originale de Hopp–Woods, conduit à une prévision très satisfaisante des déterminants antigéniques.
[Traduit par le journal]

## Introduction

The experimental prediction of protein antigenic determinants may be carried out either by synthesis of peptidic fragments (to be tested later for immunological activity) or by study of the influence of amino acid substitution in homologous series of proteins. Unfortunately both methods are time-consuming and difficult and therefore it is of considerable interest to develop a theoretical procedure for such a prediction, in which case the experimental work could be greatly reduced.

Hopp and Woods (1) have recently proposed one such method, based on a possible correlation with the hydrophilicity of the amino acids. This method, which only requires a knowledge of the amino acid sequence, leads always to the correct prediction of at least one antigenic determinant.

The reason, however, that this method may fail, usually predicting too large a number of regions with antigenic activity, may be found in the fact that the hydrophilicity, although an important factor, is probably not the only one. In particular, it would seem that the interaction between amino acids might also play a certain role.

The purpose of this work is then to investigate the possibility of modifying the Hopp–Woods method by consideration of the amino acid interactions.

## Preliminary work

The information required for the method proposed in this work consists of the amino acid sequence for the protein under study, the hydrophilicity factors for the individual amino acids, and the recognition factors corresponding to the interaction between individual amino acids.

The amino acid sequence for the protein under study will be available from experimental work and the hydrophilicity factors to be used are those of Levitt (2), as modified by Hopp and Woods (1).

The energies for the interaction between amino acids have been evaluated for this work using a recent formulation developed at this laboratory (3), based on $1/R$ expansions parameterized on the basis of the results of accurate self-consistent field calculations. The actual calculations involve a search of the minima in the configuration space by a steepest-descent procedure.

The calculations have been carried out for all the amino acids of interest and Table 1 collects the interaction energies corresponding to the most stable association of any two amino acids. For the purposes of this work, the recognition factor for a given amino acid has been defined as the average of the stabilization energies (in absolute value) of all the associations in which it is involved. The corresponding values are given in Table 2.

## Methodology

The procedure involves the determination of the hydrophilicity, recognition, and global profiles for the protein under study.

The determination of the hydrophilicity profile, using a modified Hopp–Woods procedure, in-

0008-4042/82/202606-05$01.00/0
©1982 National Research Council of Canada/Conseil national de recherches du Canada

Can. J. Chem. Downloaded from www.nrcresearchpress.com by 210.87.254.105 on 09/06/12
For personal use only.

Can. J. Chem. Downloaded from www.nrcresearchpress.com by 210.87.254.105 on 09/06/12
For personal use only.

volves the following steps: (*a*) The set of six consecutive amino acid residues, at positions $i-2, i-1, i; i+1, i+2, i+3$ in the sequence of the protein, is considered to constitute the hexapeptide $h_i$. (*b*) Each hexapeptide in the protein is ascribed a hydrophilicity factor equal to the average of the hydrophilicity factors of its constituent residues. (*c*) The *i*-th amino acid residue is then ascribed a hydrophilicity factor equal to the average of the values corresponding to the hexapeptides $h_{i-1}$ and $h_i$. ($h_0$ is ascribed the value 0 and the values for $h_1$ and $h_2$ are obtained using four and five amino acids, respectively; the same considerations apply to the tail of the protein.) (*d*) The hydrophilicity factors obtained in this way are plotted vs. the sequence position, yielding the hydrophilicity profile of the protein.

The recognition profile is obtained in a similar fashion, using the recognition factors instead of the hydrophilicity factors, and the global profile is then defined by multiplication of the hydrophilicity and recognition factors corresponding to each sequence position in the protein.

For simplicity in their inspection, in the hydrophilicity and global profiles only the positive values are plotted. All the curves are smoothed by interpolation.

## Discussion of the results

Within the framework of the Hopp–Woods procedure, a region for which a peak is observed in the hydrophilicity profile is predicted to correspond (or to be adjacent) to an antigenic determinant. The argument is that the regions with high hydrophilicity will most probably appear on the surface of the protein, once it has adopted its tertiary structure.

The tertiary structure, however, will be stabilized not only by the interactions of the amino acid residues with the solvent but also by the interactions between residues in different regions of the peptidic chain. The final result will depend, therefore, on the relative values of all such interactions in each case and a complete *a priori* prediction is not possible unless a complete quantum-mechanical calculation is performed, with consideration of the aqueous environment.

An alternative may be found, however, for a theoretical prediction of antigenic determinants under the assumption that the amino acid – amino acid interactions are more important than the hydrophilicity in determining the tertiary structure, although a positive hydrophilicity is still a prerequisite for the corresponding region to appear on the surface of the protein (and perhaps be associ-

TABLE 1. Interaction energies (in kJ) of the most stable amino acid – amino acid associations[a]

| | ala | arg | asn | asp | cys | glu | gln | gly | his | hyp | ile | leu | lys | met | phe | pro | ser | thr | trp | tyr | val |
|---|---|---|---|---|---|---|---|---|---|---|---|---|---|---|---|---|---|---|---|---|---|
| ala | 60 | | | | | | | | | | | | | | | | | | | | |
| arg | 79 | 94 | | | | | | | | | | | | | | | | | | | |
| asn | 94 | 101 | 97 | | | | | | | | | | | | | | | | | | |
| asp | 84 | 95 | 93 | 87 | | | | | | | | | | | | | | | | | |
| cys | 90 | 99 | 97 | 88 | 84 | | | | | | | | | | | | | | | | |
| glu | 77 | 91 | 88 | 88 | 98 | 94 | | | | | | | | | | | | | | | |
| gln | 63 | 81 | 92 | 63 | 74 | 63 | 77 | | | | | | | | | | | | | | |
| gly | 85 | 92 | 98 | 56 | 92 | 92 | 62 | 88 | | | | | | | | | | | | | |
| his | 74 | 96 | 82 | 77 | 83 | 82 | 64 | 72 | 87 | | | | | | | | | | | | |
| hyp | 77 | 107 | 91 | 77 | 92 | 74 | 88 | 83 | 89 | 83 | | | | | | | | | | | |
| ile | 64 | 97 | 104 | 93 | 89 | 90 | 77 | 86 | 86 | 117 | 91 | | | | | | | | | | |
| leu | 73 | 84 | 99 | 80 | 89 | 93 | 75 | 81 | 100 | 72 | 68 | 78 | | | | | | | | | |
| lys | 85 | 90 | 94 | 85 | 81 | 72 | 80 | 82 | 69 | 111 | 71 | 74 | 81 | | | | | | | | |
| met | 71 | 86 | 77 | 82 | 75 | 87 | 80 | 79 | 74 | 71 | 71 | 79 | 80 | 88 | | | | | | | |
| phe | 62 | 104 | 83 | 81 | 79 | 87 | 80 | 90 | 71 | 84 | 72 | 66 | 78 | 69 | 69 | | | | | | |
| pro | 67 | 106 | 100 | 75 | 94 | 99 | 95 | 90 | 85 | 90 | 100 | 92 | 90 | 85 | 74 | 90 | | | | | |
| ser | 89 | 113 | 112 | 87 | 101 | 110 | 84 | 91 | 92 | 104 | 108 | 106 | 108 | 105 | 111 | 112 | 137 | | | | |
| thr | 100 | 97 | 92 | 99 | 107 | 87 | 75 | 68 | 98 | 88 | 99 | 94 | 97 | 77 | 84 | 102 | 115 | 93 | | | |
| trp | 95 | 94 | 93 | 81 | 89 | 87 | 113 | 110 | 121 | 134 | 109 | 94 | 115 | 85 | 87 | 103 | 146 | 103 | 120 | | |
| tyr | 75 | 82 | 79 | 70 | 89 | 69 | 76 | 79 | 81 | 83 | 85 | 80 | 84 | 81 | 82 | 90 | 122 | 88 | 93 | 94 | |
| val | 78 | 97 | 106 | 66 | 84 | 93 | 83 | 90 | 90 | 81 | 73 | 97 | 89 | 85 | 87 | 79 | 103 | 94 | 116 | 94 | 86 |

[a]All values in this table are negative.

Can. J. Chem. Downloaded from www.nrcresearchpress.com by 210.87.254.105 on 09/06/12
For personal use only.

TABLE 2. Amino acid recognition factors[a]

| Amino acid | Recognition factor | Amino acid | Recognition factor |
|---|---|---|---|
| ala | 78 | leu | 85 |
| arg | 95 | lys | 87 |
| asn | 94 | met | 80 |
| asp | 81 | phe | 81 |
| cys | 89 | pro | 91 |
| glu | 87 | ser | 107 |
| gln | 78 | thr | 93 |
| gly | 84 | trp | 104 |
| his | 84 | tyr | 84 |
| hyp | 90 | val | 89 |
| ile | 88 | | |

[a]The larger the recognition factor, the more easily is the amino acid recognized by any other.

ated with antigenic activity). The basic rules that have been developed (and found to be appropriate) are as follows: (*a*) The highest peak in the hydrophilicity profile will be assumed, as shown by Hopp and Woods (1), to correspond or to be immediately adjacent to an antigenic determinant. (*b*) The regions with negative hydrophilicity will never correspond to regions of antigenic activity. (*c*) The regions with positive hydrophilicity and high recognition will be assumed to lack antigenic activity. (*d*) Only those regions with positive hydrophilicity and low recognition will be assumed to correspond (or to be adjacent) to antigenic determinants.

In practice, the application of these rules is best carried out through a comparison of the hydrophilicity and global profiles. First, in the hydrophilicity profile the regions of positive hydrophilicity are ordered according to the decreasing magnitude of the highest peak within each region and then an equivalent ordering is performed in the global profile. A comparison of the two sets of ordering indices will then yield the required information: a region of high recognition (which is therefore to be discarded) will be characterized by a lower ordering index in the global than in the hydrophilicity profile. Among those regions whose ordering indices have remained the same or have increased, those which show an increase in the magnitude of their highest peaks (relative to the peak of the region of highest hydrophilicity) in the global profile by comparison to what it is in the hydrophilicity profile will alse be discarded. (Independently of recognition considerations, all the regions not including at least six residues will also be discarded.)

These rules have been tested for bovine basic myelin protein, hen egg-white lysozyme, sperm whale myoglobin, and tobacco mosaic virus protein. For simplicity in the discussion, the designations "waste" and "success" have been introduced: the waste of a prediction defines that fraction of experimental work that will be wasted when confirming the prediction, so that a waste of 0% indicates that all the predicted determinants possess activity; the success rate, on the other hand, gives the percentage ratio of the number of correctly predicted determinants over the number of known determinants.

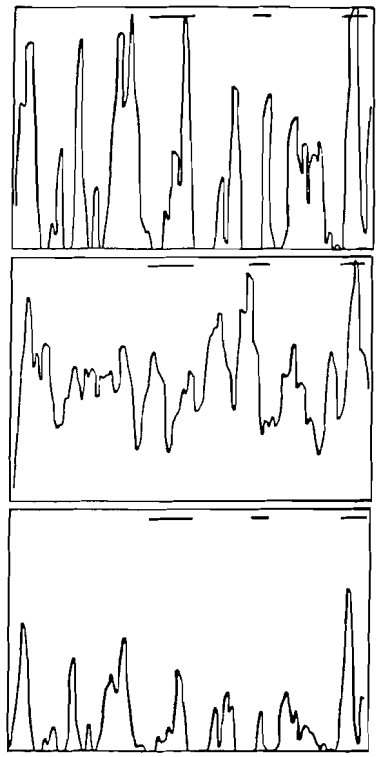

FIG. 1. Hydrophilicity (top), recognition (middle), and global (bottom) profiles for bovine basic protein. The horizontal lines at the top of each profile mark the positions of the known antigenic determinants.

The discussion (in which the regions with negligible hydrophilicity are not included) is as follows:

*(a) Bovine basic myelin protein (Fig. 1)*

It consists of 169 residues, with 4 sequential determinants (Eylar (4), Westall and Thompson (5)) at positions 64–73, 74–85, 113–121, and 153–166; for the discussion here, the first two determinants (which are adjacent) will be taken as one.

There are 10 regions of positive hydrophilicity and 7 determinants are predicted, corresponding to regions *2* (residues 17–23), *3* (residues 28–35), *5* (residues 43–64), *6* (residues 70–84), *7* (residues 95–107), *8* (residues 118–123), and *10* (residues 155–169), for a prediction with 57% waste and 100% success.

Can. J. Chem. Downloaded from www.nrcresearchpress.com by 210.87.254.105 on 09/06/12
For personal use only.

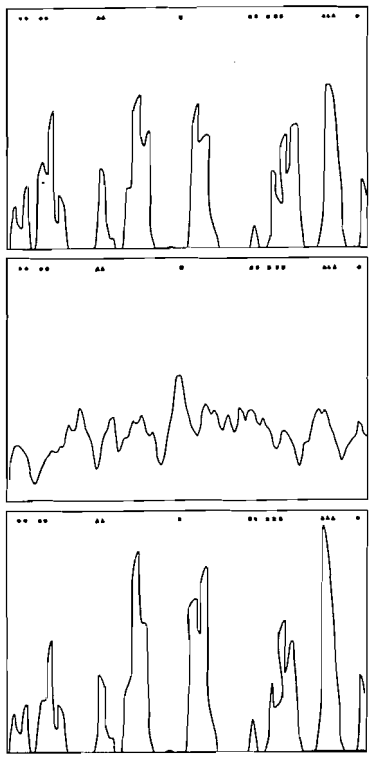

FIG. 2. Hydrophilicity (top), recognition (middle), and global (bottom) profiles for hen egg-white lysozyme. The symbols at the top of each profile mark the positions of the known antigenic determinants.

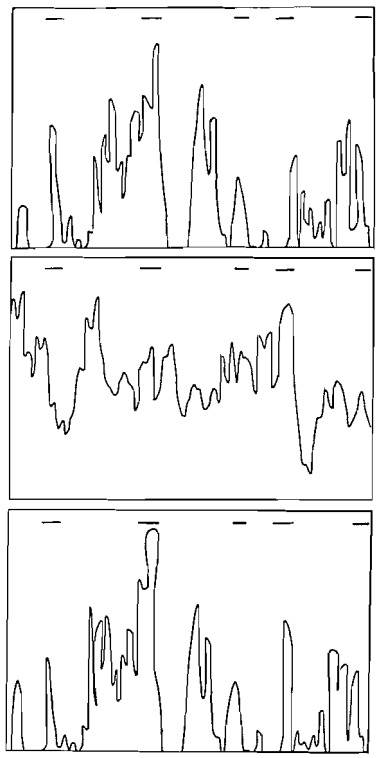

FIG. 3. Hydrophilicity (top), recognition (middle), and global (bottom) profiles for sperm whale myoglobin. The horizontal lines at the top of each profile mark the positions of the known antigenic determinants.

*(b) Hen egg-white lysozyme (Fig. 2)*

It consists of 129 residues, with 3 conformational determinants (Atassi and Habeeb (6), Atassi and Lee (7)) involving the residues (5, 7, 13, 14, and 125), (33, 34, 113, 114, and 116), and (62, 87, 89, 93, 96, 97), respectively.

There are 9 regions of positive hydrophilicity and 4 determinants are predicted, corresponding to regions *1* (residues 1–8), *2* (residues 11–21), *3* (residues 32–38), and *8* (residues 111–120), which correspond to the main components of the first two known determinants. This is a prediction with 0% waste and 67% success.

*(c) Sperm whale myoglobin (Fig. 3)*

It consists of 153 residues, with 5 sequential determinants (Atassi (8, 9)) at positions 15–22, 56–62, 94–99, 113–119, and 145–151.

There are 9 regions of positive hydrophilicity and 6 determinants are predicted, corresponding to regions *2* (residues 16–26), *3* (residues 32–65), *4* (residues 75–90), *5* (residues 93–103), *8* (residues 123–135), and *9* (residues 137–150), for a prediction with 33% waste and 80% success.

*(d) Tobacco mosaic virus protein (Fig. 4)*

It consists of 158 residues, with 3 sequential determinants (Anderer (10), Benjamini (11), and Milton and van Regenmortel (12)) at positions 62–68, 108–113, and 153–158.

There are 10 regions of positive hydrophilicity and 2 determinants are predicted, corresponding to regions *6* (residues 61–71) and *8* (residues 103–118), for a prediction with 0% waste and 67% success.

## Conclusions

The theoretical prediction of protein antigenic determinants should be based on calculations with consideration of the tertiary structure and the aqueous environment.

The results presented in this work indicate, however, that a simplified model, with consideration of both hydrophilic and recognition factors, constitutes a rather attractive alternative, because of its simplicity and high rate of success.

Although the above rules have been developed in a semi-empirical fashion, they may be easily rationalized by a semi-quantitative argument, taking

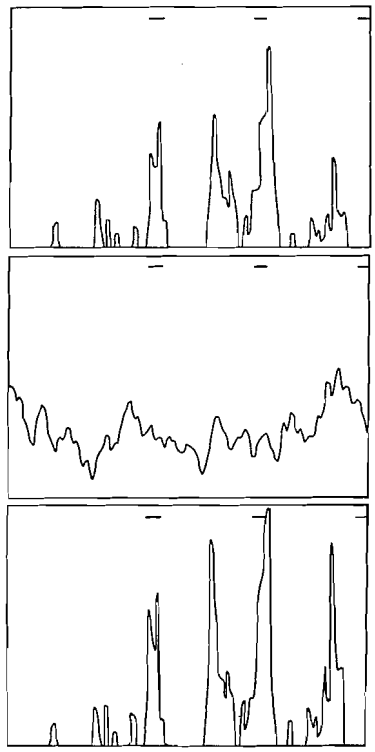

FIG. 4. Hydrophilicity (top), recognition (middle), and global (bottom) profiles for tobacco mosaic virus protein. The horizontal lines at the top of each profile mark the positions of the known antigenic determinants.

into account that the greater the recognition factor the more stable the association with another amino acid is.

As seen from Table 2, all amino acids have appreciable recognition factors and consequently it is understandable that those regions with low hydrophilicity will tend to arrange themselves within the interior of the protein, as this arrangement will lead to a more stable conformation. In fact, this consideration applies to all the regions with a high recognition, independently of their hydrophilicity so that only those regions of (relative) low recognition and high hydrophilicity remain as the likely candidates to appear on the surface of the protein.

As it is the case with any semi-empirical method, the usefulness of the present procedure should be based on its success rate and from that point of view it seems to constitute a powerful tool for the prediction of antigenic determinants.

The main limitation of this work arises from the neglect of conformational considerations, except as approximated through the use of recognition factors, and therefore it must be emphasized that conformational determinants cannot be predicted as such (i.e., the fact that several predicted sequential determinants may constitute part of a single conformational determinant will not be known from the results obtained).

It is expected, however, that recognition profiles may be of use in the prediction of some conformational characteristics (such as the existence of sharp bends) and this point will be examined in future work, as well as the influence of the aqueous environment.

1. T. P. HOPP and K. R. WOODS. Proc. Natl. Acad. Sci. (U.S.) **76**, 3824 (1981).
2. M. LEVITT. J. Mol. Biol. **104**, 59 (1976).
3. S. FRAGA. J. Comput. Chem. In press.
4. E. H. EYLAR. Adv. Exp. Med. Biol. **98**, 259 (1977).
5. F. C. WESTALL and M. THOMPSON. Immunochemistry, **15**, 189 (1978).
6. M. Z. ATASSI and A. F. S. A. HABEEB. *In* Immunochemistry of proteins. Vol. 2. *Edited by* M. Z. Atassi. Plenum Press, New York. 1977. p. 177.
7. M. Z. ATASSI and C. L. LEE. Biochem. J. **171**, 429 (1978).
8. M. Z. ATASSI. Immunochemistry, **12**, 423 (1975).
9. M. A. ATASSI. *In* Immunochemistry of proteins. Vol. 2. *Edited by* M. Z. Atassi. Plenum Press, New York. 1977. p. 77.
10. F. A. ANDERER. Z. Naturforsch. **18b**, 1010 (1963).
11. E. BENJAMINI. *In* Immunochemistry of proteins. Vol. 2. *Edited by* M. Z. Atassi. Plenum Press, New York. 1977. p. 265.
12. R. C. DE L. MILTON and M. H. V. VAN REGENMORTEL. Mol. Immunol. **16**, 179 (1979).

Can. J. Chem. Downloaded from www.nrcresearchpress.com by 210.87.254.105 on 09/06/12
For personal use only.

# Internal barriers to rotation in 2,6-difluoroisopropyl and 2,6-difluoroethylbenzenes. Overlap of dynamic nuclear magnetic resonance (DNMR) and the *J* method

TED SCHAEFER, RICHARD P. VEREGIN, REINO LAATIKAINEN, RUDY SEBASTIAN, KIRK MARAT, AND JAMES L. CHARLTON

*Department of Chemistry, University of Manitoba, Winnipeg, Man., Canada R3T 2N2*

Received April 15, 1982

Can. J. Chem. Downloaded from www.nrcresearchpress.com by 210.87.254.5 on 09/06/12
For personal use only.

TED SCHAEFER, RICHARD P. VEREGIN, REINO LAATIKAINEN, RUDY SEBASTIAN, KIRK MARAT, and JAMES L. CHARLTON. Can. J. Chem. **60**, 2611 (1982).

The temperature-dependent $^{19}F$ nmr spectra of 2,6-difluoroisopropylbenzene yield $\Delta G^{\ddagger}_{155}$, $\Delta H^{\ddagger}$, and $\Delta S^{\ddagger}$ as 6.93 (5) kcal/mol, 6.1(1) kcal/mol, and −5.0 (8) cal/mol K, respectively, for the internal rotation of the isopropyl group about the $sp^2$–$sp^3$ carbon–carbon bond. The long-range spin–spin coupling constant over six bonds, $^6J_p^{H,CH}$, combined with the *J* method gives a twofold internal potential barrier of 5.0 ± 1.6 kcal/mol at 305 K. Although in this barrier range the *J* method suffers from large errors, the two methods yield comparable values for the barrier height. The lineshape method is inapplicable to 2,6-difluoroethylbenzene. The *J* method finds the preferred conformation and a twofold barrier of 6.0 ± 2 kcal/mol, again in a barrier region where this method is inaccurate. Relative to hydrogen, the fluorine substituents cause substantial increases in the barriers to internal rotation. Signs of the stereospecific couplings, $^4J_o^{F,CH}$, are determined.

TED SCHAEFER, RICHARD P. VEREGIN, REINO LAATIKAINEN, RUDY SEBASTIAN, KIRK MARAT et JAMES L. CHARLTON. Can. J. Chem. **60**, 2611 (1982).

La mesure de spectres de rmn du $^{19}F$ en fonction de la température du difluoro-2,6 isopropylbenzène permet d'obtenir les valeurs des $\Delta G^{\ddagger}_{155}$, $\Delta H^{\ddagger}$ et $\Delta S^{\ddagger}$ qui sont respectivement de 6,93 (5) kcal/mol, 6,1(1) kcal/mol et −5,08(8) cal/mol K pour la rotation interne du groupe isopropyle autour de la liaison carbone–carbone $sp^2$–$sp^3$. La constante de couplage à longue distance à travers six liaisons $^6J_p^{H,CH}$, combinée à la méthode *J* donne une barrière de potentiel interne binaire de 5,0 ± 1,6 kcal/mol à 305 K. Bien que dans cet ordre de grandeur, pour la barrière, la méthode *J* comporte de grandes erreurs, les deux méthodes donnent des valeurs comparables pour la hauteur de la barrière. La méthode de la forme des lignes ne peut s'appliquer dans le cas du difluoro-2,6 éthylbenzène. La méthode *J* permet d'établir la conformation préintégrée et une barrière binaire de 6,0 ± 2 kcal/mol; il s'agit encore d'une région de la barrière où cette méthode n'est pas précise. Par rapport à l'hydrogène, les substituants fluor provoquent une augmentation substantielle des barrières internes à la rotation. On a déterminé des signes de couplages stéréospécifiques $^4J_o^{F,CH}$.

[Traduit par le journal]

## Introduction

According to the *J* method (1) the twofold barrier to rotation about the $sp^2$–$sp^3$ bond in isopropylbenzene is 1.95 ± 0.2 kcal/mol (1 cal ≡ 4.184 *J*). This method depends on the $\sin^2\theta$ dependence of $^6J_p^{H,CH}$ in **1** (X = H). A quantum mechanical hindered rotor model allows the calculation of the expectation value of $\sin^2\theta$ as a function of temperature, barrier, and reduced moment of inertia. Measurements of $^6J$ implies a value of $\langle\sin^2\theta\rangle$ according to $^6J = {}^6J_{90}\langle\sin^2\theta\rangle$, where $^6J_{90}$ is the magnitude of $^6J$ when the α C—H bond rotates out of the benzene plane by 90°.

When X = $CH_3$, the classical DNMR method and molecular mechanics calculations agree that the barrier is twofold (2) and much larger than in **1** (X = H). Lineshape analysis of the temperature-dependent $^1H$ nmr specra yields a free energy of activation, $\Delta G^{\ddagger}_{238}$, of 12.8 kcal/mol for the hindered rotation of the isopropyl fragment.

The DNMR method (3,4) depends on the dephasing of magnetization caused by the internal rotation. When the internal rotation rate increases

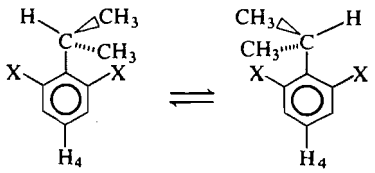


**1** **1**

sufficiently the dephasing process becomes more difficult to follow by DNMR. In consequence, very low barriers have not been measured by this technique, the lowest value being a $\Delta G^{\ddagger}_{93}$ of 4.2 kcal/mol (5). The *J* method suffers from an opposite disadvantage. As the barrier increases, the observed $^6J$ becomes less sensitive to $V_2$, particularly above about 3 kcal/mol.

It is desirable to apply both methods to the same barrier. When properly used, the lineshape method gives accurate $\Delta H^{\ddagger}$ and $\Delta S^{\ddagger}$ parameters (6). The J method has a different theoretical basis, has a relatively limited applicability at present, and yields a barrier parameter whose relationship to $\Delta G^{\ddagger}$ and its components is not immediately clear. If

0008-4042/82/202611-06$01.00/0

©1982 National Research Council of Canada/Conseil national de recherches du Canada

Can. J. Chem. Downloaded from www.nrcresearchpress.com by 210.87.254.5 on 09/06/12
For personal use only.

these two methods[1] were to yield compatible barrier parameters for the same process, the result might be taken as a severe test of the $J$ method.

Accordingly, the chosen molecule is one in which $^6J_p^{H,CH}$ is most sensitive to $V_2$. In **1** (X = F), $\langle \sin^2\theta \rangle$ varies between 0.5 and zero as $V_2$ increases from zero to infinity, respectively. Because fluorine is relatively small, there is the possibility that both $V_2$ and $\Delta G^{\ddagger}$ are measurable. Of course, the components of $\Delta G^{\ddagger}$ are also needed, implying measurements over a range of temperatures.

While the J method is not as general as DNMR in its applicability, it does have one significant advantage, exemplified by **2**. If X = H in **2**, the $J$ method shows that the preferred conformation, **2***a*, is the

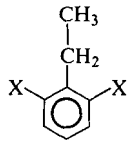

**2**

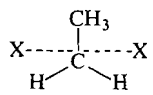

**2***a*

one in which the methyl group lies in a plane perpendicular to the benzene ring ($\theta = 30°$ in $\sin^2\theta$). Hence DNMR is in principle inapplicable because there exists no Larmor frequency indicator of the internal reorientation rate.[2] By way of contrast, the $J$ method yields a $V_2$ of 1.2 ± 0.2 kcal/mol for rotation about the $sp^2$–$sp^3$ bond, in good agreement with a recent thermodynamic conclusion (1, 9).

In this paper **1** (X = F) and **2** (X = F) are investigated, the former by the two methods and the latter by the $J$ method. The results provide a comparison of the two methods and data on fluorine as a steric inhibitor of internal rotation of alkyl groups on a benzene ring.

## Experimental

*Synthesis*

Compound **1** (X = F) was prepared from 2,6-difluorobenzoic acid (Aldrich) via the methyl benzoate and treatment of the latter with methyl magnesium iodide in ether to give the alcohol. The alcohol was converted to the α-methylstyrene derivative with toluene-*p*-sulfonic acid. The alkene was hydrogenated in ethanol and extracted and purified by distillation to give **1** (X = F). Detials of the exact procedure are given in ref. 10.

Compound **2** (X = F) was prepared from 2,6-difluoroacetophenone (Maybridge) by a modification of the Wolff–Kishner method exactly as described in ref. 11. It was also synthesized by the palladium-catalyzed coupling (12) of tetramethyltin and 2,6-difluorobenzyl bromide (Maybridge). However, when using tetrakis(triphenylphosphine) palladium(0) as a catalyst as prescribed on p. 4996 of ref. 12, the characteristic blackening occurred only after some weeks.

*Samples*

All samples were prepared in 5 mm od diameter nmr tubes. They were degassed by the freeze–pump–thaw procedure, using as many as seven cycles, and were flame-sealed. For **1** (X = F) they included a 5 mol% solution in acetone-$d_6$ with a drop of $C_6F_6$, a 5 mol% solution in $CS_2$ with 4 mol% of tetramethylsilane, a 5 mol% solution in 1:1 v/v acetone-$d_6$ and isopentane, and an approximately 5 mol% solution in 1:1 v/v $CD_2Cl_2$ and isopentane. For **2** (X = F), a 2 mol% solution in $CCl_4$ containing 25% by volume of $C_6D_{12}$ and a 15 vol% solution in $CCl_4$ with 5 vol% TMS were prepared.

*Spectral measurements*

For **1** (X = F), the $^1$H nmr spectrum (acetone-$d_6$) at 90.020 MHz (centerband) was acquired in the FT mode on a WH-90 Bruker spectrometer in the manner described recently (13). A sweep width of 760 Hz and three separate experiments gave peak frequencies with an average deviation of 0.015 Hz. The $^{19}$F nmr spectra were obtained in a similar way at 84.670 MHz, except that the methyl protons were selectively decoupled, using a sweep width of 200 Hz. Average peak frequency variations were about 0.002 Hz. Multiple resonance $^1$H nmr experiments (14) utilized the $CS_2$ solution and an HA100 spectrometer in the frequency sweep mode.

Such experiments were also done for **2** (X = F) with the 15 vol% solution in $CCl_4$ on the HA100. The $^1$H nmr spectrum of **2** (X = F) in a 2 mol% solution in $CCl_4$–$C_6D_{12}$ was recorded on the WH-90 in the FT mode and gave linewidths of about 0.12 Hz. All these measurements were made at probe temperatures of 305 ± 1 K.

The variable temperature measurements of the $^{19}$F resonance of **1** (X = F) employed broadband decoupling of the protons on the WH-90 and frequency ranges of 500 to 1000 Hz. The temperature controller (B-VT-1000) was calibrated with a thermocouple in a dummy nmr tube and its dial readings agreed with the thermocouple to within ± 1 K. In order to reach 140 K the nitrogen gas stream was precooled by passing it through a copper coil immersed in liquid nitrogen before it reached the usual heat exchanger.

## Results and discussion

*Spectral analyses*

These employed the computer programs LAME (15, 16), MAOCON (17), NUMARIT (18), and DAVINS (19). The fully-coupled, 12-spin $^1$H nmr spectrum of **1** (X = F) at 305 K was analyzed to give the results in Table 1. The $^{19}$F nmr spectrum (methyl protons decoupled) was analyzed as part of a 6-spin system (Table 1). The double resonance experiments (14) designed to determine the signs of $^4J_o^{F,CH_\alpha}$ and $^5J_o^{F,CH_3}$ could be confirmed by partial simulations of the ensuing spectra with the computer program DOR (20). The magnitude of $^6J_p^{H,CH}$ was estimated from the partially resolved doublets in the H-4 region at 100 MHz together with a simulation of overlapping lorentzians with linewidths at half-height of 0.13 Hz, the width characteristic of single peaks in the H-3 region. An analysis of the digitized ring proton region of the

[1] Spin-lattice relaxation measurements also provide information on intramolecular reorientation processes. The barriers provided by this method are somewhat model dependent. A recent review (7) gives a thorough discussion of the strengths and pitfalls of this approach; for example, when applied to intrinsically small barriers.

[2] This restriction can sometimes be lifted by the use of liquid crystals as solvents (8), although their use has a number of disadvantages in DNMR studies. In particular, **1** and **2** have spin systems too large for this purpose.

TABLE 1. The $^1H$ and $^{19}F$ nmr spectral parameters for **1** (X = F) at 305 K and 90.020 MHz (centerband) and 84.670 MHz

| Parameter[a] | Value | Parameter | Value | |
|---|---|---|---|---|
| $\nu_F$ | 4131.8[b] | $^4J_o^{F,CH}$ | −0.603(4)[d] | −0.599(13)[e] |
| $\nu_{(CH_3)}$ | 119.064(2)[c] | $^5J_o^{F,CH}$ | +0.956(3)[g] | — |
| $\nu_{(CH)}$ | 303.319(3) | $^5J_m^{H,CH}$ | 0.292(3) | — |
| $\nu_3$ | 622.041(2) | $^6J_p^{H,CH}$ | (−)0.080±0.020[h] | (−)0.098(7)[i] |
| $\nu_4$ | 650.281(2) | Peaks observed ($^1H$) | | 100 |
| $^3J_{(CH,CH_3)}$ | 7.098(2) | Transitions assigned ($^1H$) | | 1089 |
| $^3J_{23}$ | 10.416(4) | Transitions calculated ($^1H$) | | 1777 |
| $^3J_{34}$ | 8.380(2) | Peaks observed ($^{19}F$) | | 24 |
| $^4J_{35}$ | 1.147(6) | Transitions assigned ($^{19}F$) | | 36 |
| $^4J_{26}$ | 6.339(17)[f] | rms deviation ($^1H$) | | 0.033 |
| $^4J_{24}$ | 6.383(3) | rms deviation ($^{19}F$) | | 0.033 |
| $^4J_{25}$ | −1.311(4) | | | |

[a]For a 5.2 mol% solution in acetone-$d_6$, containing a small amount of $C_6F_6$.
[b]In Hz to low field of $C_6F_6$.
[c]From a NUMARIT analysis (18), standard deviations in the last one or two significant figures being given in parentheses.
[d]From NUMARIT (18).
[e]From LAME (15, 16), sign determined by tickling experiments at 100 MHz.
[f]From LAME (15, 16) with $CH_3$ protons decoupled.
[g]Sign is positive.
[h]Determined at 100 MHz as described in text.
[i]From a DAVINS (19) analysis of the ring proton peaks; 969 points of the 2048 points in range 685.0 to 595.0 Hz were iterated on (27 iterations at an average of 8.9 s of cpu time per iteration), using information from the NUMARIT runs.

TABLE 2. The $^1H$ nmr spectral parameters for **2** (X = F) at 305 K and 90.020 MHz (centerband)

| Parameter[a] | Value | | Parameter | Value | |
|---|---|---|---|---|---|
| $\nu_{(CH_3)}$ | 108.450(4)[b] | —[c] | $^4J_{24}$ | 6.369(2)[b] | 6.370(1)[c] |
| $\nu_{(CH_2)}$ | 241.745(2) | — | $^5J_{25}$ | −1.308(5) | −1.305(2) |
| $\nu_{3,5}$ | 608.093(2) | 608.095(1) | $^4J_o^{F,CH_2}$ | 1.288(1)[d] | — |
| $\nu_4$ | 633.544(2) | 633.540(1) | $^5J_o^{F,CH_3}$ | ±0.301(3)[e] | — |
| $^3J_{34}$ | 8.348(1) | 8.352(1) | $^5J_m^{H,CH_2}$ | 0.363(2) | 0.364(1) |
| $^3J_{(CH_2,CH_3)}$ | 7.543(2) | — | $^6J_p^{H,CH_2}$ | −0.335(2) | −0.341(2) |
| $^3J_{23}$ | 8.970(5) | 8.964(2) | rms deviation | $0.013_5$ | 0.008 |
| $^4J_{35}$ | 1.129(7) | 1.120(4) | Peaks assigned | 159 | 145 |
| $^4J_{26}$ | 7.584(6) | 7.584(2) | | | |

[a]2 mol% solution in $CCl_4$, containing 25 v/v% $C_6D_{12}$.
[b]Analyzed with NUMARIT (18); standard deviations being approximated from the error vectors.
[c]Analyzed with MAOCON (17).
[d]Sign determined by multiple resonance at 100 MHz and a 15 mol% solution in $CCl_4$.
[e]Sign determination was unsuccessful.

spectrum obtained at 90 MHz (transferred from the Nicolet 1180 on the Bruker instrument to the Amdahl 470/V7 system via a telephone line) by the program Davins (19) gave another estimate of $^6J_p^{H,CH}$ (Table 1).

The $^1H$ nmr spectrum of **2** (X = F) was first partially analyzed as a 7-spin system (ignoring the methyl protons) with Maocon. This was followed by a 10-spin analysis with Numarit, with the results given in Table 2. Figure 1 displays the calculated and observed spectra of the methylene protons.

*Variable temperature pre-exchange lifetimes*

Pre-exchange lifetimes were extracted from the exchange-broadened proton-decoupled $^{19}F$ nmr spectra of **1** (X = F) by methods used in this laboratory for many years (21–27). The many possibilities of error in such extractions (6), particularly for two-site exchange between components of the doublet, have been thoroughly discussed and will not be repeated here. The detailed procedure can be found in ref. 10.

In brief, at 140 K the doublet separation is 290 Hz, but the doublets are already somewhat broadened by the rate process. The linewidth of internal $C_6F_6$ peaks was used as the linewidth expected in the absence of the rate process in **1**. The spectrum could be simulated as a function of the lifetime and of the chemical shift difference for a negligible rate of exchange. Above coalescence, which occurs very near 156 K, it was deemed correct to use a constant limiting internal chemical shift with a reference linewidth given by $C_6F_6$ and only one unknown parameter, the pre-exchange lifetime, $\tau$. In this way a temperature range of 60 K could be achieved, rather smaller than desired. Viscosity and/or solubility problems precluded measurements below 140 K, while at temperatures

Can. J. Chem. Downloaded from www.nrcresearchpress.com by 210.87.254.5 on 09/06/12
For personal use only.

Can. J. Chem. Downloaded from www.nrcresearchpress.com by 210.87.254.5 on 09/06/12
For personal use only.

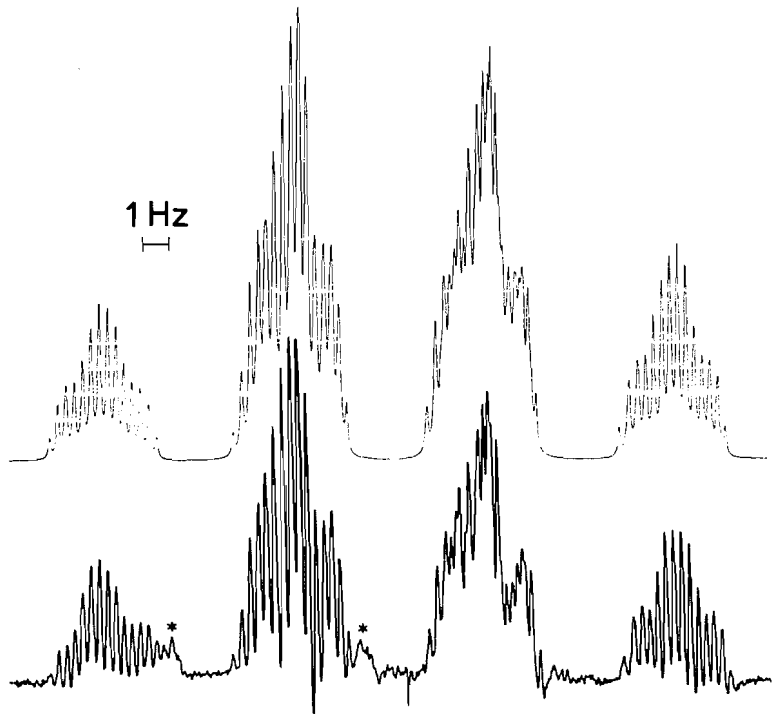


FIG. 1. The observed and calculated methylene proton $^1H$ nmr spectra at 90 MHz of a 2 mol% solution of 2,6-difluoroethylbenzene in a 25% v/v $C_6D_{12}/CCl_4$ solution at 305 K. The calculated spectrum has a linewidth at half-height of 0.12 Hz. Because the methylene protons form part of a 10-spin system and are coupled to all the other 8 spins, each peak in the spectrum contains many transitions. Impurity bands are indicated by asterisks. The many repeated spacings are ca. 0.3 Hz in magnitude.

above 200 K the exchange broadening was judged as too small for reliable work.

Observed spectra were compared with calculated lineshapes from a Versatic plotter, whose scale was ca. 25 × 60 cm and had been tested and adjusted for uniformity. Particular attention was paid to comparisons at 0.25, 0.50, and 0.75 of the maximum peak heights. In this way $\tau$ values, ranging from $1.46(4) \times 10^{-2}$ s at 140 K to $1.25(10) \times 10^{-5}$ s at 200 K, could be extracted.

Although one is dealing with a simple doublet, the Larmor frequency difference is substantial and some degree of accuracy in $\tau$ is attainable. Furthermore, different solvents give the same $\tau$ values to within experimental error. For example, at 180 K one has $\tau$ as $9.1(5) \times 10^{-5}$ s in the acetone–isopentane solvent and as $9.9(9) \times 10^{-5}$ s in the acetone solution.

*Activation parameters for* **1** *(X = F)*

These were extracted in the normal way. A plot of $\ln(1/\tau T)$ versus $1/T$ is shown in Fig. 2. An error propagation treatment, using the computer program ACTPAR (6), gave $\Delta G^{\ddagger}_{155}$ as 6.93(5) kcal/mol (within a degree or two of coalescence), $\Delta H^{\ddagger}$ as 6.1(1) kcal/mol, $\Delta S^{\ddagger}$ as −5.0(8) cal/mol K, $E_a$ = 6.5(1) kcal/mol, and $\log A = 11.9(2)$. A transmission coefficient of unity was assumed for the activated state. Another error analysis (24, 28) of $\Delta S^{\ddagger}$ gave 0.5 cal/mol K as its uncertainty. If the standard deviations are multiplied by two, one has $\Delta H^{\ddagger} = 6.1(2)$ kcal/mol and $\Delta S^{\ddagger} = -5.0(1.6)$ cal/mol K.

The negative value of $\Delta S^{\ddagger}$ may be compared with negative values of $\Delta S^{\ddagger}$ for a series of α,α-dihalo-2,6-dihalobenzenes and related compounds (21–27, 29, 30). The average value of $\Delta S^{\ddagger}$ for twelve sets of measurements is −3.9 cal/mol K. Considering that in the transition state the isopropyl group could lose more degrees of freedom than a $CHX_2$ (X = halogen), the present number of − 5 cal/mol deg is acceptable. $E_a$ and $\Delta H^{\ddagger}$ differ by about RT over the temperature range used for **1** (X = F).

*The twofold barrier,* $V_2$*, by the* J *method for* **1** *(X = F)*

The values of $^6J_p^{H,CH}$ obtained by the two approaches (Table 1) suggest $-0.08_9 \pm 0.03_0$ Hz. Utilization of $-1.20 \pm 0.02$ Hz for $^6J_{90}^{H,CH}$ (1) gives $\langle \sin^2 \theta \rangle$ as $0.07_4 \pm 0.02_6$. Figure 3 emphasizes the insensitivity of $\langle \sin^2 \theta \rangle$ to $V_2$ in this range of $V_2$ (the curve becomes much steeper for lower $V_2$). One

Can. J. Chem. Downloaded from www.nrcresearchpress.com by 210.87.254.5 on 09/06/12
For personal use only.

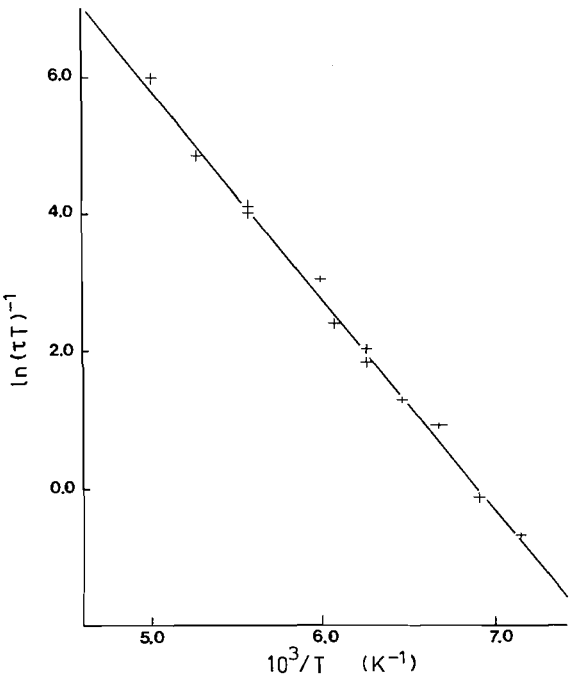


FIG. 2. A plot of $\ln(1/\tau T)$ versus $1/T$ for the internal rotation about the $sp^2$–$sp^3$ carbon–carbon bond in 2,6-difluoroisopropylbenzene between 140 and 200 K. The correlation coefficient is 0.998. An error propagation analysis yields $\Delta H^{\ddagger}$ as 6.1(1) kcal/mol and $\Delta S^{\ddagger}$ as −5.0(8) cal/mol K. $\Delta G^{\ddagger}_{155}$ is 6.93(5) kcal/mol, very near coalescence. Duplicate determinations of $\tau$ at the same temperature in the diagram employed different solvents.

has $V_2$ as 5.0 ± 1.6 kcal/mol, where the uncertainty is simply estimated from the projections of $\langle \sin^2 \theta \rangle$ onto the curve in Fig. 3.

$V_2$ is represented in the $J$ method by $0.5\ V_2(1 - \cos 2\theta)$. The hindered rotor calculations give the zero-point torsional energy of the ground state as 0.07 kcal/mol. The identification $\Delta H^{\ddagger} = V_2 + \Delta ZP$, where ΔZP is the zero-point energy of the transition state minus the zero-point energy of the ground state, allows an estimate of ΔZP as ca. 0.1 kcal/mol. To within experimental error, then, the two methods give the same barrier to internal rotation in **1** (X = F). Note that, *if* $\Delta S^{\ddagger}$ *were zero*, then $V_2$ would not agree with the subsequently *implied* $\Delta G^{\ddagger} = \Delta H^{\ddagger} =$ 6.9 kcal/mol.

This attempted overlap of the two methods has not been completely successful. By their very nature, the two methods must be somewhat inaccurate in the region of overlap. In the present instance, DNMR is more accurate than the $J$ method. The latter assumes a twofold cosine barrier and a hindered rotor model, the former an activated process. Molecular mechanics calculations on the isopropyl group confirm a twofold rotational barrier (2).

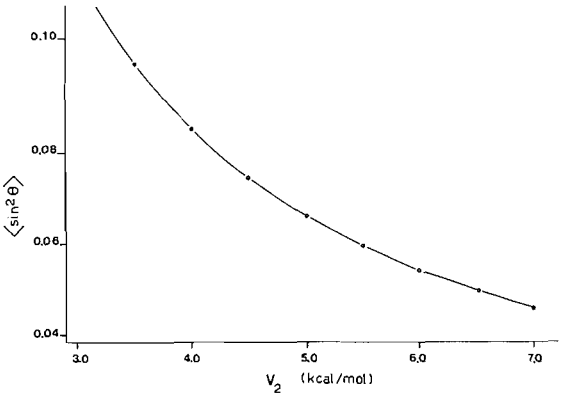


FIG. 3. Part of a plot of $\langle \sin^2 \theta \rangle$ versus $V_2$ for the rotation of the isopropyl group in 2,6-difluoroisopropylbenzene at 305 K. The hindered rotor model used a value of $0.9 \times 10^{-38}$ gm cm² for the reduced moment of inertia. The value of $\langle \sin^2 \theta \rangle$ is insensitive to this parameter. The basis set consisted of 51 free rotor functions. $\langle \sin^2 \theta \rangle$ varies between 0.5 for $V_2 = 0$ and 0.0 for $V_2 = \infty$ and is very insensitive to $V_2$ in the region depicted in this figure. The details of the calculations leading to figures such as this one can be found in ref. 1.

$V_2$ in isopropylbenzene is only 2 kcal/mol, so that two *ortho* fluorine substituents cause a substantial increase in the barrier. It is of interest whether a similar increase occurs in ethylbenzene on fluorine substitution.

### $V_2$ *in* **2** *(X = F) by the* J *method*

$^6J_p^{H,CH}$ is −0.338(12) Hz assuming an error equal to twice the difference between the values from the two analyses in Table 2. Taking $^6J_{90}$ as −1.22 ± 0.02 Hz (1) implies $\langle \sin^2 \theta \rangle$ as 0.277 ± 0.015. A reduced moment of inertia of $0.5 \times 10^{-38}$ gm cm², a basis set of 51 free rotor functions, and a $T$ of 305 K gives a tabulation[3] of $\langle \sin^2 \theta \rangle$ as a function of $V_2$. Again, because **2***a* is the preferred conformer, $\langle \sin^2 \theta \rangle$ approaches 0.25 in the high barrier limit and a large error in the derived value of $V_2$ is once more inevitable for the present molecule. One finds $V_2$ as 6.0 ± 2.0 kcal/mol.

Parenthetically one may note that $^6J_p^{H,CH_3}$ in 2,6-difluorotoluene[4] is −0.62 Hz, the same as in toluene (31), so that the $^6J_{90}$ employed above is correct (1). Further, the present result for $V_2$ in **2** (X = F) implies that $^6J_p^{H,CH}$ in **2** (X = Cl) lies very close to $0.25 \times {}^6J_{90}$ or −0.30 Hz. The observed value is −0.29 ± 0.02 Hz (32).

*If* the errors in the large $V_2$ values are disregarded, *then* the results in this paper suggest that the increase in the barrier on going from X = H to X = F in **1** and **2** is larger for the latter. The

[3]The values of $\langle \sin^2 \theta \rangle$ are rather insensitive to the reduced moment of inertia at this temperature.

[4]Unpublished work in this laboratory.

transitional conformation in **2** has a $CH_3$ group eclipsing the *ortho* C—F bond, while for **1** the high energy conformer has the α C—H bond at 90° to the benzene plane and therefore the two $CH_3$ groups lie in planes at 30° to the benzene plane. A molecular mechanics calculation would be very useful for these two molecules.

Whether the barriers in these molecules are entirely steric is not certain. One might, for example, speculate about the rotational angle dependence of hyperconjugative interactions of the C—H and C—C bonds in the sidechain with the π electrons of the ring. For a recent study of, and extensive literature references to, steric interactions and intramolecular rate processes see ref. 33.[5]

*Other long-range couplings*

Of particular interest are $^4J_o^{F,CH}$ and $^5J_o^{F,CH_3}$ in Tables 1 and 2. Their signs and magnitudes confirm an inadequacy in the INDO MO FPT computations for $^4J_o^{F,CH_3}$ in 2-fluorotoluene (35). The inadequacy may well arise from an improper account of the direct coupling mechanism. Synthesis of the requisite additional compounds is in hand and may allow an empirical delineation of the rotational angle dependence of $^4J_o^{F,CH}$ and of $^5J_o^{F,CH_3}$.

## Conclusions

For 2,6-difluoroisopropylbenzene the *J* method and DNMR appear to agree in their assessment of the internal barrier to rotation about the $sp^2$–$sp^3$ carbon–carbon bond. Therefore it can be said, tentatively in view of experimental and conceptual difficulties, that nmr spectroscopy as distinct from nmr relaxation methods can be used to measure barriers to internal rearrangements which range from near zero (*J* method) to as large as 30 kcal/mol (DNMR).

## Acknowledgements

We are grateful to Professor G. Binsch for a listing of the computer program ACTPAR. This work was supported by the Natural Sciences and Engineering Research Council of Canada. R.L. thanks the Research Council for the Natural Sciences of the Academy of Finland for support.

1. W. J. E. Parr and T. Schaefer. Acc. Chem. Res. **13**, 400 (1980).
2. A. Mannschreck and L. Ernst. Chem. Ber. **104**, 228 (1971).
3. H. S. Gutowsky and A. Saika. J. Chem. Phys. **21**, 1688 (1953).
4. L. M. Jackman and F. A. Cotton (*Editors*). Dynamic nuclear magnetic resonance spectroscopy. Academic Press, New York. 1975.
5. F. A. L. Anet and I. Yavari. J. Am. Chem. Soc. **99**, 6752 (1977).
6. G. Binsch and H. Kessler. Angew. Chem. Int. Ed. Engl. **19**, 411 (1980).
7. J. B. Lambert, R. J. Nienhuis, and J. W. Keepers. Angew. Chem. Int. Ed. Engl. **20**, 487 (1981).
8. Z. Luz, R. Naor, and E. Meirovitch. J. Chem. Phys. **74**, 6621 (1981).
9. A. Miller and D. W. Scott. J. Chem. Phys. **68**, 1317 (1978).
10. R. P. Veregin. M.Sc. thesis. University of Manitoba. 1982.
11. A. Vogel. Textbook of practical organic chemistry. 4th ed. Longman Group Limited, London. 1978. pp. 600–606.
12. D. Milstein and J. K. Stille. J. Am. Chem. Soc. **101**, 4992 (1979).
13. T. Schaefer and R. Sebastian. J. Magn. Reson. **41**, 395 (1980).
14. R. Freeman and W. A. Anderson. J. Chem. Phys. **37**, 2053 (1962).
15. S. Castellano and A. A. Bothner-By. J. Chem. Phys. **41**, 3863 (1964).
16. C. W. Haigh. Ann. Rep. NMR Spectrosc. **4**, 311 (1971).
17. R. Laatikainen. J. Magn. Reson. **27**, 169 (1977); Ph.D. thesis, University of Jyväskylä, Finland. 1979.
18. A. R. Quirt and J. S. Martin. J. Magn. Reson. **5**, 318 (1971); J. S. Martin, A. R. Quirt, and K. F. Worvill. The nmr program library, Daresbury Laboratory, Daresbury, U.K.
19. D. S. Stephenson and G. Binsch. J. Magn. Reson. **37**, 395 (1980); Quantum chemistry program exchange, **13**, 378 (1979).
20. G. Govil and D. H. Whiffen. Mol. Phys. **12**, 449 (1967).
21. B. J. Fuhr, B. W. Goodwin, M. H. Hutton, and T. Schaefer. Can. J. Chem. **48**, 1558 (1970).
22. B. H. Barber and T. Schaefer. Can. J. Chem. **49**, 789 (1971).
23. M. A. H. Stewart, T. Schaefer, H. M. Hutton, and C. M. Wong. Can. J. Chem. **49**, 1085 (1971).
24. J. Peeling, B. W. Goodwin, T. Schaefer, and C. M. Wong. Can. J. Chem. **49**, 1489 (1971).
25. J. Peeling, B. W. Goodwin, T. Schaefer, and J. B. Rowbotham. Can. J. Chem. **51**, 2110 (1973).
26. J. Peeling, J. B. Rowbotham, L. Ernst, and T. Schaefer. Can. J. Chem. **52**, 2414 (1974).
27. H. M. Hutton, W. E. Hiebert, and V. Mark. Can. J. Chem. **56**, 1261 (1978).
28. L. L. Schaleger and F. A. Long. Adv. Phys. Org. Chem. **1**, 1 (1963).
29. H. Gyulai, B. J. Fuhr, H. M. Hutton, and T. Schaefer. Can. J. Chem. **48**, 3877 (1970).
30. J. Peeling, T. Schaefer, and C. M. Wong. Can. J. Chem. **48**, 2839 (1970).
31. M. P. Williamson, R. Kostelnik, and S. M. Castellano. J. Chem. Phys. **49**, 2218 (1968).
32. A. F. Janzen and T. Schaefer. Can. J. Chem. **49**, 1818 (1971).
33. G. Bott, L. D. Field, and S. Sternhell. J. Am. Chem. Soc. **102**, 5618 (1980).
34. B. Nilsson, P. Martinson, K. Olsson, and R. E. Carter. J. Am. Chem. Soc. **96**, 3190 (1974).
35. R. E. Wasylishen and M. Barfield. J. Am. Chem. Soc. **97**, 4545 (1975).

[5] $\Delta G^{\ddagger}$ for the rotation of a neopentyl moiety past an ortho C—F bond is a ca. 4 kcal/mol higher than for rotation past an *ortho* C—H bond in 1,3,5-trineopentyl benzenes (34).

Can. J. Chem. Downloaded from www.nrcresearchpress.com by 210.87.254.5 on 09/06/12
For personal use only.

# Homonuclear one- and two-dimensional nuclear Overhauser effect experiments and spin-echo correlated spectroscopy. Application to prostaglandin $E_1$ and 6-keto-prostaglandin $E_1$[1]

GEORGE KOTOVYCH AND GERDY H. M. AARTS
*Department of Chemistry, University of Alberta, Edmonton, Alta., Canada T6G 2G2*

Received February 11, 1982

GEORGE KOTOVYCH and GERDY H. M. AARTS. Can. J. Chem. **60**, 2617 (1982).

Nuclear Overhauser effect one-dimensional and two-dimensional nuclear magnetic resonance experiments are reported for prostaglandin $E_1$. The two-dimensional nuclear Overhauser effect measurements are combined with spin-echo correlated spectroscopy in order to assign the complete high-field proton magnetic resonance spectrum of 6-keto-prostaglandin $E_1$. The advantages of these two-dimensional techniques are illustrated in these studies. It is also observed that the 6-keto-prostaglandin $E_1$ H-10α proton is substituted more readily by deuterium than are the other protons α to the keto groups.

GEORGE KOTOVYCH et GERDY H. M. AARTS. Can. J. Chem. **60**, 2617 (1982).

On rapporte des expériences en rmn sur l'effet Overhauser nucléaire à une et à deux dimensions pour la prostaglandine $E_1$. Les mesures de l'effet Overhauser nucléaire sont combinées avec la spectroscopie spin-écho de corrélation dans le but d'identifier le spectre complet de résonance magnétique du proton à haut champ de la céto-6 prostaglandine $E_1$. On illustre dans ces études les avantages de ces techniques à deux dimensions. On a également observé que le proton H-10α de la prostaglandine $E_1$ est substitué plus facilement par le deutérium que les autres protons en α des groupes cétoniques.

[Traduit par le journal]

Prostacyclin (Prostaglandin $I_2$, $PGI_2$) is the most potent inhibitor of platelet aggregation and a potent vasodilator (1, 2). It is unstable and rapidly hydrolyses to 6-keto-prostaglandin $F_{1\alpha}$. The metabolism of $PGI_2$ or 6-keto-prostaglandin $F_{1\alpha}$ by 9-hydroxy-prostaglandin dehydrogenase in human platelets leads to a more stable substance, 6-keto-prostaglandin $E_1$ (6-keto-$PGE_1$) (3) with similar biological activity to $PGI_2$ (4, 5). In our continuing studies of the structure–activity relationships of $PGI_2$ and its derivatives, we found it very difficult to analyze the complete proton magnetic resonance spectrum of 6-keto-$PGE_1$. Even at 400 MHz, due to the overlap of the multiplets in the high-field region, standard decoupling and one-dimensional nuclear Overhauser effect (nOe) measurements could not be used to assign all of the proton resonances. The complete assignment was possible by means of the combined two-dimensional nOe measurements and spin-echo correlated spectroscopy (SECSY).

The selective proton–proton one-dimensional (1D) nOe experiments have been extensively applied in the study of molecular structure and conformation (6–9). This experiment requires the measurement of the intensity change of a proton resonance upon saturating another proton. Two-dimensional nOe experiments have recently been developed for the investigation of cross-relaxation and chemical exchange processes (10–15). The advantages of this technique over the one-dimensional nOe experiment are (a) the simultaneous measurement of all the nOe's between closely-spaced protons in a molecule, and (b) the elimination of problems associated with the irradiation of multiplets that occur in crowded spectral regions, or that are partially resolved. In the present study, both advantages are illustrated.

The 2D nOe measurements have been combined with 2D correlated spectroscopy measurements (16, 17). The latter experiment represents a powerful technique for studying *J*-coupling connectivities (18–22). Combining these experiments yields valuable information on the nOe connectivities, as

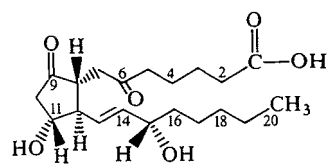


6-Keto-$PGE_1$

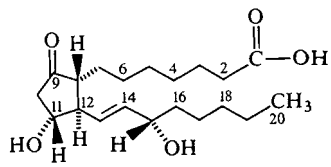


$PGE_1$

[1]Paper No. 9 in a series of high-field nmr studies on the prostaglandins and vitamins. For paper No. 8, see ref. 31.

0008-4042/82/202617-08$01.00/0
©1982 National Research Council of Canada/Conseil national de recherches du Canada

Can. J. Chem. Downloaded from www.nrcresearchpress.com by 210.87.254.5 on 09/06/12
For personal use only.

TABLE 1. Results of proton–proton 1D nOe difference and 2D nOe experiments performed on $PGE_1$ in $CD_3OD$ solution at 295 K

| Observed nOe's | | | |
|---|---|---|---|
| (A) 1D nOe Experiments[a] Irradiated protons From | To | (B) 2D nOe Experiment[c] From | To |
| 2 | 3,4 | 2 | 3, 4 |
| | | 3 | 2, 4 |
| | | 4 | 3 |
| 8 | 7,7*(w),[b] 13, 14 | 8 | 13, 14(c.s.), 12 |
| 8, 10α | 10β, 11, 12 | | |
| | | 10α | 10β, 11 |
| 10β | 10α, 11 | 10β | 10α, 11 |
| 11 | 8,[b] 10β, 12(w) | 11 | 10α,[d] 10β, 12(c.s.) |
| 11, 15 | 13, 14 | 11, 15 | 13, 14 |
| 15 | 16, 16*(w),[b] 17(w)[b] | | |
| 12 | 8, 10α,[b] 11, 13, 14 | 12 | 8, 11(c.s.) 13, 14 |
| 13, 14 | 8, 11, 12, 15 | 13, 14 | 8(c.s.), 11, 12, 15 |
| | | 19 | 20 |
| 20 | 19 | 20 | 19 |

[a]The H-8 and H-10α overlapping multiplets were simultaneously irradiated, as were the overlapping H-11 and H-15 multiplets. The observed nOe's were assigned to individual irradiated protons whenever possible on the basis of a molecular model. 1D nOe experiments were carried out on the multiplet at 1.2 to 1.7 ppm but the results are difficult to interpret due to the many overlapping proton resonances. The decoupling power levels were chosen in such a manner as to minimize the perturbation of neighboring multiplets.
[b]No nOe observed in the 2D experiment; w represents a weak 1D nOe.
[c]Weak 2D nOe's observed on expanded contour plots, or observed by taking cross sections parallel to the $F_1$ axis, are labelled c.s. $\tau_M = 0.5$ s.
[d]No nOe observed in the 1D experiment.

well as on the *J*-coupling connectivities for the molecule under study. In the present study, spin-echo correlated spectroscopy (SECSY) and the 2D nOe measurements have been combined to assign completely the high-field proton magnetic resonance spectrum of 6-keto-$PGE_1$. In addition, the nOe's obtained for prostaglandin $E_1$ ($PGE_1$) using both the 1D and 2D techniques are compared.

## Experimental

Prostaglandin $E_1$ was a gift from Dr. J. E. Pike, and 6-keto-$PGE_1$ was a gift from Dr. R. A. Johnson and Mr. Frank H. Lincoln of the Upjohn Company in Kalamazoo, MI, U.S.A. The nmr measurements were carried out on 0.06 *M* prostaglandin solutions in $CD_3OD$ (99.6%) (Merck, Sharp and Dohme). The $CD_3OD$ was vacuum distilled. Solutions of 6-keto-$PGE_1$ (0.06 *M*) were also prepared in phosphate buffer (0.20 *M* and 0.40 *M*) in $D_2O$ at a pH of 7.0 (uncorrected meter reading). All of the samples were degassed using the freeze–pump–thaw technique. Details of the sample preparation have been reported previously (23).

The nmr experiments were carried out in the Fourier transform mode using the Bruker WH-400/ DS nmr spectrometer and the Aspect 2000 data system. The chemical shifts are reported with respect to internal TMS. The one-dimensional measurements were obtained using 32K data points with a resolution of 0.244 Hz/pt or, in several cases, 0.305 Hz/pt. The resolution for the two dimensional nmr experiments was 2.05 Hz/pt in both dimensions, $F_1 = 525$, $F_2 = 2100$, using 512 and 2048 data points, respectively.

The one-dimensional nOe difference experiments were performed following standard procedures (23, 24). The two-dimensional nmr measurements were carried out using the Bruker software package (25). The 2D nOe experiment employs a sequence of three 90° pulses (90°–$t_1/2$ – 90°–$t_m$ – 90° – $t_1/2$-FID). The mixing time, $t_m$, is of central importance in measuring 2D nOe's. During this period, cross relaxation leads to exchange of magnetization between neighboring protons. The present experiments were carried out at several values of $t_m$ and the cross peaks were reproducible (15). The evolution time is $t_1$. The SECSY experiment employs two 90° pulses in the sequence (90°–$t_1/2$ – 90°–$t_1/2$-FID). The delay time $t_1/2$ after the last pulse allows both experiments to be represented in the same manner.

## Results

The results of the 1D nOe experiments for $PGE_1$ are presented in Table 1A. A contour plot of the 2D nOe experiment is presented in Fig. 1, and the data are summarized in Table 1B. The $PGE_1$ proton multiplets were assigned on the basis of standard decoupling, inversion recovery, and the 1D nOe experiments. In Fig. 1, the cross peaks are connected by the straight lines. Exchange of magnetization between any two protons, due to dipole–dipole interactions, is manifested by these cross peaks which indicate the presence of nOe's between the protons thus connected. For $PGE_1$ a wide range of $\tau_M$ values was used, from 0.1 s to 1.4 s. Extensive data handling procedures were used for the 2D nOe data to confirm the presence of weak cross peaks. These include taking cross sections parallel to the $F_1$ axis, and expanding the contour plots.

The results of the SECSY experiments performed on $PGE_1$ are shown in Fig. 2. Only the high-field region is shown as it illustrates the manner in which multiplets can be readily observed in regions of the spectrum where there is extensive multiplet overlap. The cross peaks in the SECSY experiment arise from proton–proton *J* connectiv-

Can. J. Chem. Downloaded from www.nrcresearchpress.com by 210.87.254.5 on 09/06/12
For personal use only.

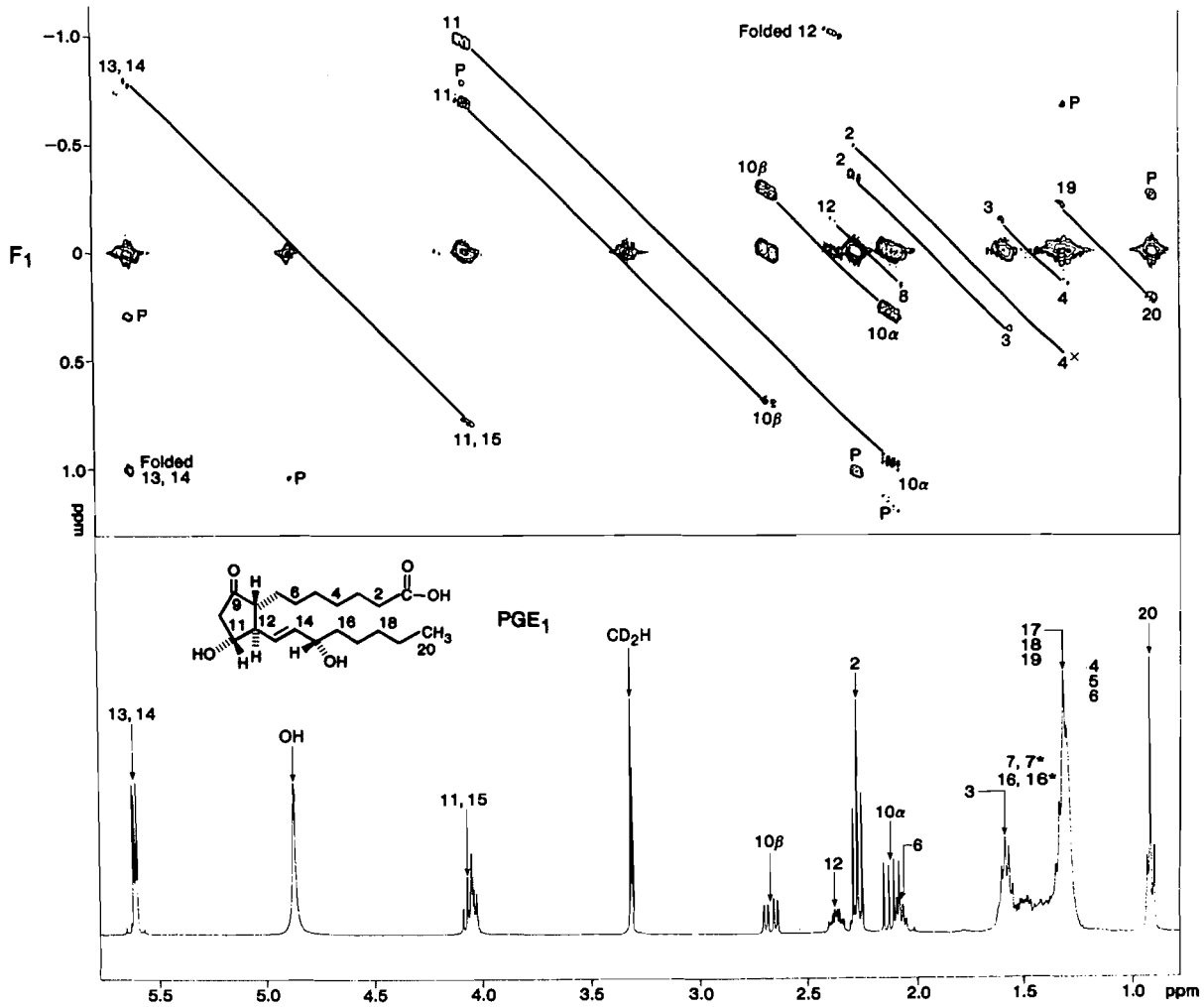


FIG. 1. *Top*. Contour plot of the proton–proton 2D nOe experiment for $PGE_1$ in $CD_3OD$ (0.06 *M*). The strong peaks on the horizontal axis passing through $F_1 = 0$ correspond to a 1D spectrum. The cross peaks are labelled and are connected with the solid lines, indicating nOe's between the nuclei whose resonances have the same chemical shift difference on the horizontal and vertical axes. Phantom peaks are labelled P (refs. 32 and 33). The × refers to the weak contour that was observed but not plotted. The $\tau_M$ was 0.5 s, 32 transients were accumulated and the total observation time was 21.4 h. The delay time between pulse sequences was 7.5 s. The FID's were multiplied by a sine bell function before Fourier transformation. The smaller spectral width along the vertical axis accounts for the folded contours. *Bottom*. The normal Fourier transform 1D spectrum obtained for $PGE_1$.

ities. The contour plot of the 2D nOe experiment for 6-keto-$PGE_1$ is combined with the contour plot for the SECSY experiment in Fig. 3. The top half of the contour plot (Fig. 3A) is for the 2D nOe experiment, while the bottom half (Fig. 3B) is for the SECSY experiment. At least two values of $t_m$ were used for the 2D nOe experiments. The cross peaks for both the 2D nOe and the SECSY experiments are labelled in Fig. 3 and are connected by the straight lines. In this way, protons which experience both the nOe and the *J* connectivities are connected. In Figs. 1–3 the straight lines intersect the horizontal axis at an angle of 135°.

For the 2D nOe experiments, as most of the nOe's are between *J*-coupled protons, transfer of magnetization by zero-quantum transitions cannot be excluded under the experimental conditions used (15, 26–28), which include phase cycling to eliminate multiple quantum transitions. Hence *J* cross peaks may also appear in the spectrum. For a quantitative interpretation of the 2D nOe data, the *J* cross peaks must be separated from the 2D nOe cross peaks. In view of the excellent agreement between the 1D nOe and the 2D nOe data for $PGE_1$, the qualitative interpretation of the 2D nOe data is valid.

Can. J. Chem. Downloaded from www.nrcresearchpress.com by 210.87.254.5 on 09/06/12
For personal use only.

Can. J. Chem. Downloaded from www.nrcresearchpress.com by 210.87.254.5 on 09/06/12
For personal use only.

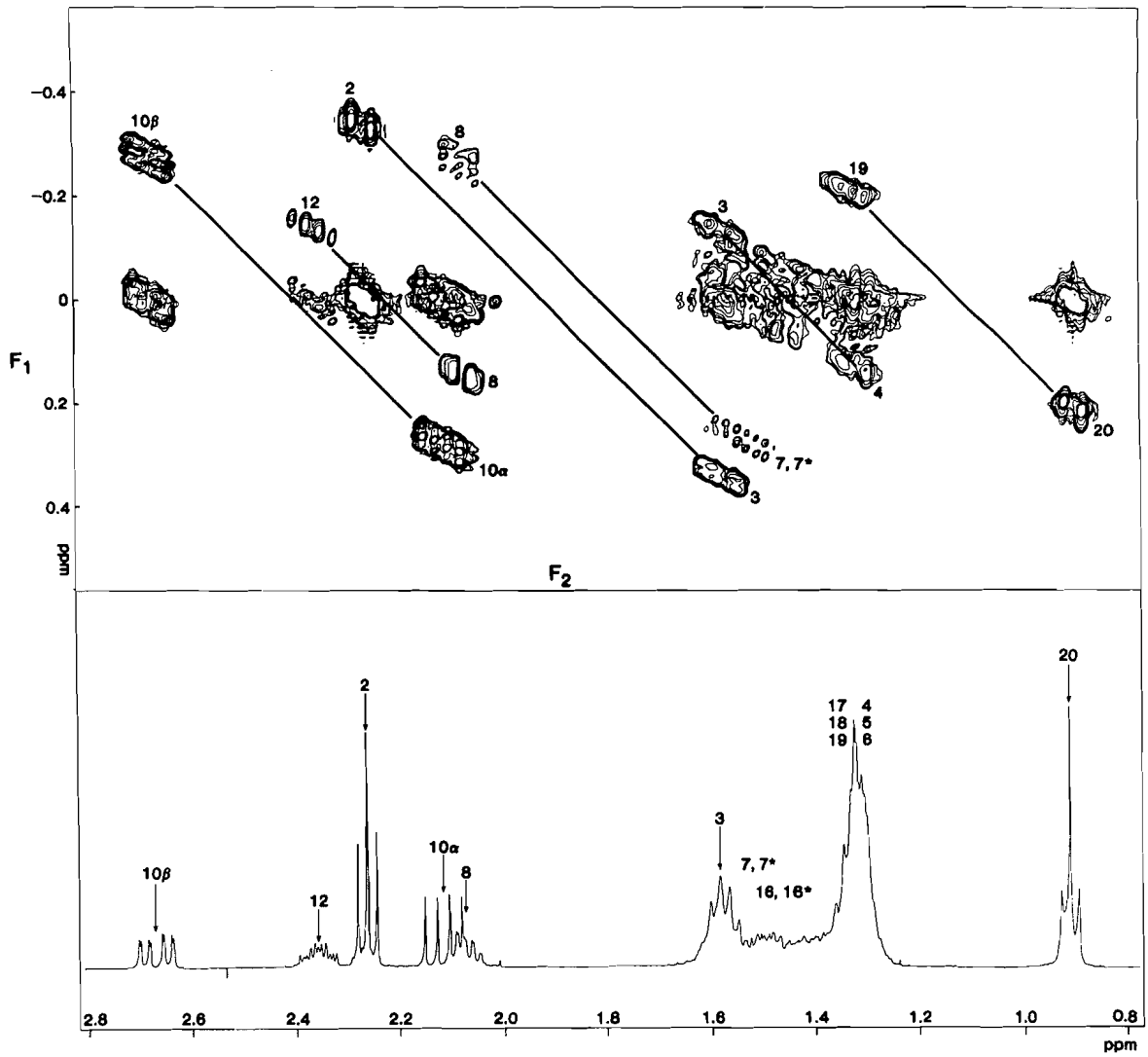


FIG. 2. *Top*. The contour plot for the SECSY experiment for $PGE_1$ in $CD_3OD$ (0.06 *M*). Only the high-field region is shown. The cross peaks are labelled and are connected by the straight lines. *Bottom*. The normal Fourier transform 1D spectrum obtained for $PGE_1$. Note the long-range H-10β to H-8 coupling constant.

The results of the nmr experiments carried out as a function of time on 6-keto-$PGE_1$ in 0.20 *M* phosphate buffer in $D_2O$ (pH 7.0) are shown in Fig. 4. By integrating these spectra, it is observed that after 28 hours the H-10α protons are substituted by deuterium to an extent of about 66%. In the same period of time, the total H-10β and H-7,7* multiplet decreases in intensity by one third of a proton, as does the H-5, H-8, and H-12 multiplet. After an extended period of time, further nmr measurements showed that protons H-10β and H-8 are also replaced by deuterium. Hence H-10α is substituted by deuterium more readily than are the other protons α to the keto groups.

The chemical shifts and coupling constants for $PGE_1$ and 6-keto-$PGE_1$ were calculated to first order with an accuracy of about ±0.010 ppm and ±0.20 Hz, respectively. These data are reported in Table 2 for the methanol solutions together with the coupling constants for 6-keto-$PGE_1$ in buffer solutions. Good agreement is observed between the coupling constants for both molecules in the methanol solutions, indicating similar conformations of the five-membered rings. The coupling constants for $PGE_1$ compare with those previously observed for $PGE_2$ in $CDCl_3$ (29).

## Discussion

The 1D nOe measurements have been extensively applied in our studies of prostacyclin (9),

Can. J. Chem. Downloaded from www.nrcresearchpress.com by 210.87.254.5 on 09/06/12
For personal use only.

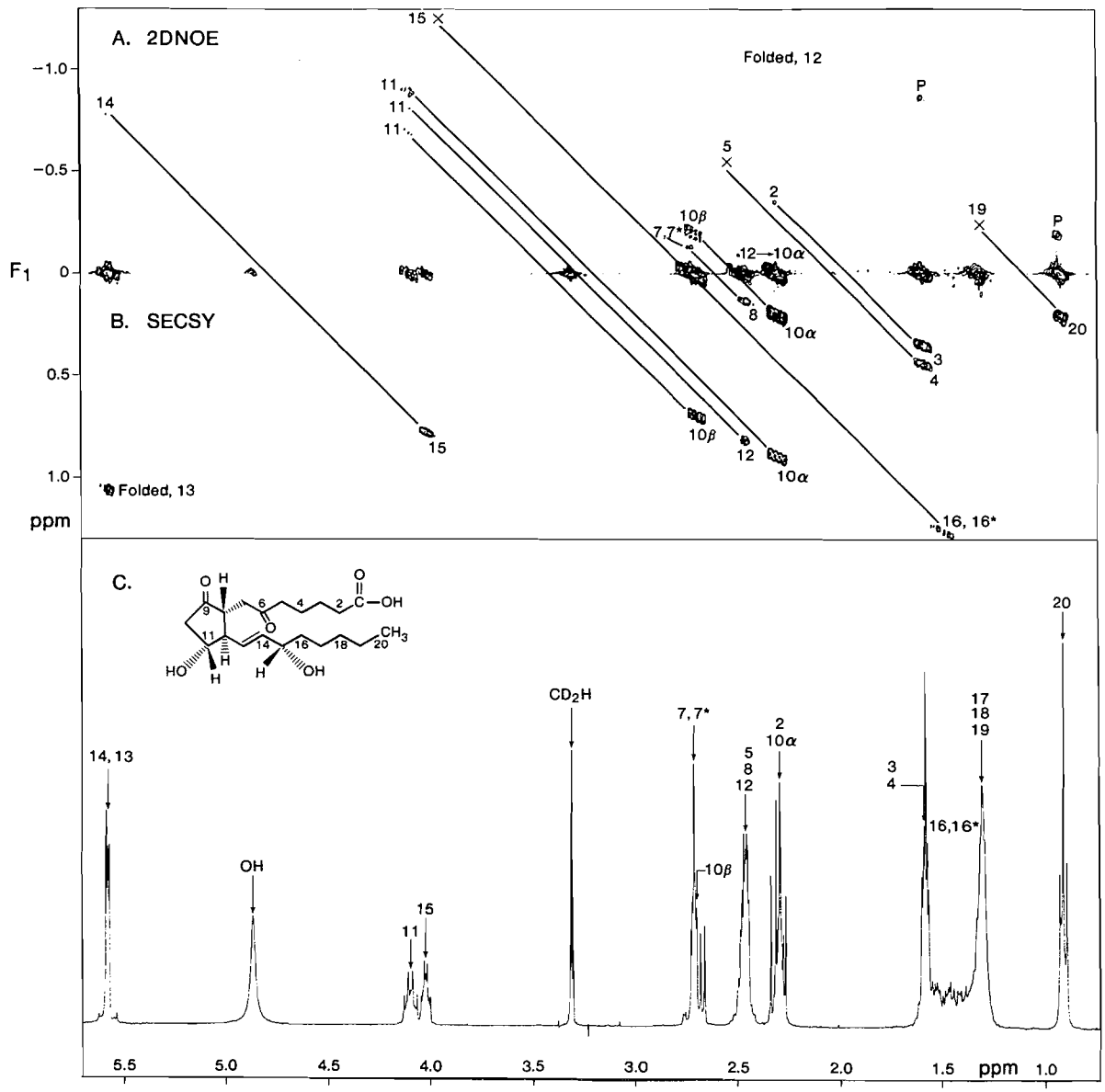


FIG. 3. The combined contour plot of the proton–proton 2D nOe experiment (2A) and the SECSY experiment (2B) for 6-keto-$PGE_1$. The cross peaks for both the 2D nOe and the SECSY experiments are labelled and are connected by the straight lines. Phantom peaks are labelled with a P. The × refers to contours that were observed but not plotted. For the 2D nOe experiment, $t_m$ equals 0.35 s. 32 transients were accumulated and the delay time between pulse sequences was 7.5 s. The FID's were multiplied by a sine bell function before Fourier transformation. The normal Fourier transform 1D spectrum obtained for 6-keto-$PGE_1$ is shown in C. The line assignments are indicated in the figure.

(6*R*)-prostaglandin $I_1$ (23), prostaglandin $E_2$ (29), (6*S*)-prostaglandin $I_1$ (30), and carboprostacyclin (31). These studies have now been extended to the 2D nOe experiment. A comparison of the data for $PGE_1$ in Table 1 shows the advantages of the 2D nOe experiment. The nOe from H-8 to H-12 is clearly visible, as is the nOe from H-10α to H-10β and H-11. On the other hand, in the 1D nOe experiment, both the H-8 and the H-10α protons must be simultaneously irradiated due to the overlapping multiplets. Then some of the observed nOe's can obviously be assigned to H-8 only, based on molecular model distances. However, the nOe's to H-10β, H-11, and H-12 are more difficult to assign. This was accomplished using the 2D nOe experiment. Finally, all of the observed nOe's in

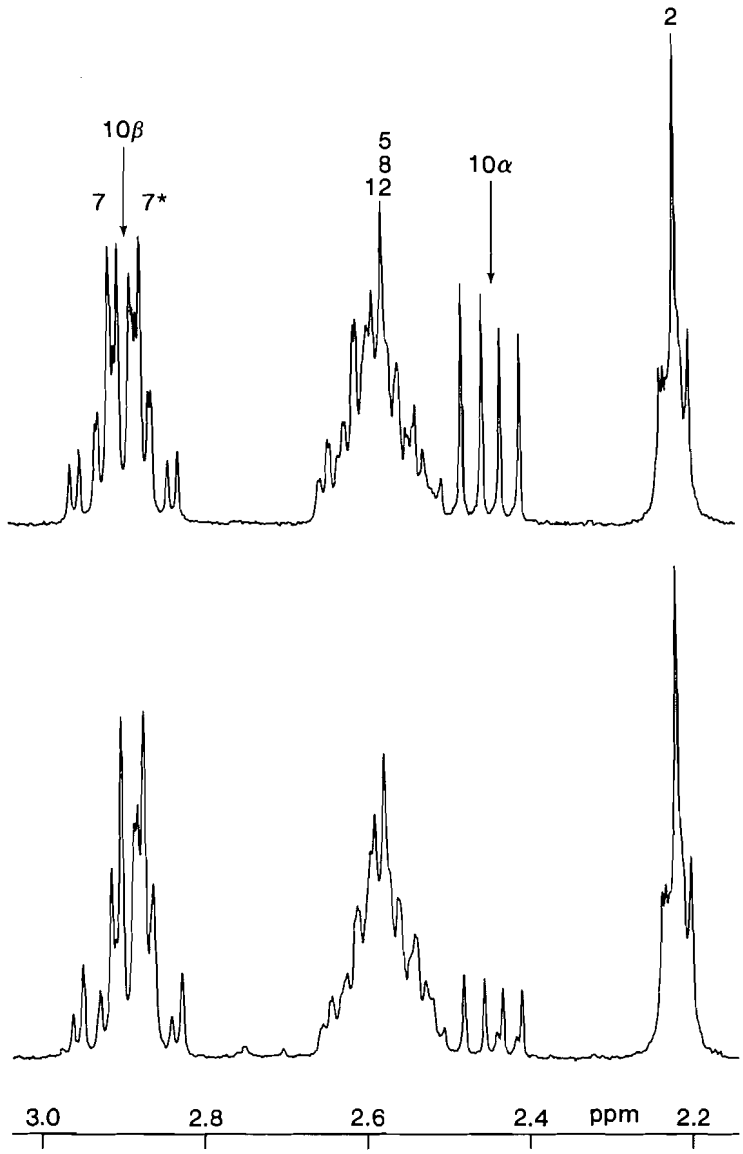


FIG. 4. Top spectrum: high-field region of the normal 1D spectrum observed for 6-keto-$PGE_1$ in phosphate buffer (0.20 *M*, pH 7.0) in $D_2O$. Bottom spectrum was obtained 28 h later.

the 2D experiment were obtained simultaneously, whereas seven experiments were required to obtain the 1D nOe data (in about the same time).

The SECSY experiment allows the determination of proton–proton *J*-connectivities. The great utility of this experiment is seen in Fig. 2. For example, the multiplet corresponding to the H-7,7* proton, which is coupled to H-8, is clearly evident in the top spectrum, whereas it would be impossible to observe this multiplet in the normal spectrum shown in the bottom of Fig. 2 due to the extensive multiplet overlap.

In view of the binding studies planned for 6-keto-$PGE_1$, a complete assignment of the proton magnetic resonance spectrum was required. This spectrum is shown in Fig. 3C for $CD_3OD$ solutions. A difficulty arises in the assignment of the proton resonances due to the extensive multiplet overlap in the high field region. Protons H-7, H-7*, H-5, and H-8 are difficult to assign by applying standard decoupling and 1D nOe techniques. In phosphate buffer, at a pH of 7.0, only the H-2 and H-10α proton multiplets no longer overlap and are thus simplified (Fig. 4). It was also observed that the

Can. J. Chem. Downloaded from www.nrcresearchpress.com by 210.87.254.5 on 09/06/12
For personal use only.

TABLE 2. Proton chemical shifts (with respect to TMS) and coupling constants for $PGE_1$ and 6-keto-$PGE_1$[a] in $CO_3OD$

| Proton | $PGE_1$ (0.06 *M*) | | 6-Keto-$PGE_1$ (0.06 *M*) | |
|---|---|---|---|---|
| | Chemical shift (ppm) | Coupling constants (Hz) | Chemical shift (ppm) | Coupling constants (Hz) |
| 2 | 2.26 | $J(2—3) = 7.4$ | 2.28[b] | $J(2—3) = \sim 6.8$[b] |
| 3 | 1.58[c] | $J(3—4) = 7.3$[c] | 1.58[b] | |
| 4 | 1.31[b] | | 1.58[b] | |
| 5 | 1.3 | | ~2.47[b] | |
| 6 | 1.3[b] | | — | |
| 7, 7* | 1.51,[b] 1.59[b] | | 2.70 | $J(7—7^*) = (18.61)$ |
| 8 | 2.07[c] | $J(7—8)$ } $= 5.7$[c]<br>$J(7^*—8)$ }<br>$J(8—10\beta) = 1.35$[c]<br>$J(8—12) = 12.0$[c] | 2.45 | $J(8—10\beta) = (1.3)$ |
| 10α | 2.12 | $J(10\alpha—10\beta) = 18.3$ | 2.29[b] | $J(10\alpha—10\beta) = 18.25$[b] (18.7) |
| | | $J(10\alpha—11) = 9.3$ | | $J(10\alpha—11) = 9.6$[b] (9.7) |
| 10β | 2.67 | $J(10\beta—11) = 7.3$ | 2.69[b] | $J(10\beta—11) = 7.5$[b] (8.9) |
| 11 | 4.05[b] | $J(11—12) = 8.6$[b] | 4.09 | $J(11—12) = 9.0$ (7.7) |
| 12 | 2.36 | | 2.45 | |
| 13, 14 | 5.61 | | 5.58 | |
| 15 | 4.04[b] | | 4.02 | |
| 16, 16* | 1.47,[b] 1.56[b] | | ~1.5 | |
| 17, 18, 19 | 1.32 | | 1.32 | |
| 20 | 0.91 | $J(19—20) = 7.0$ | 0.91 | $J(19—20) = 7.0$ |

[a]The coupling constants in brackets, for 6-keto-$PGE_1$, are for the buffer solutions.
[b]Value obtained from 1D-nOe difference spectra.
[c]Value obtained from inversion recovery spectra.

H-10α proton was replaced by deuterium more readily than are the other protons α to the keto groups. However, the question of assigning the above-mentioned protons still remained.

The 2D nOe experiment combined with the SECSY experiment allowed this assignment to be carried out. The results of these two experiments, combined in one contour plot, are shown in Figs. 3A and 3B. Protons which experience both the nOe and the *J*-connectivity are connected by the straight lines. As seen from the figure, all of the expected nOe and *J* connectivities are present, for example, between H-10β and H-10α. In addition, separate contours are observed for H-7,7*, which can be distinguished from the H-10β contours. A connectivity is then established between H-7,7* and H-8 (at 2.45 ppm). The H-5 multiplet is also assigned a chemical shift of 2.45 ppm because a *J*-connectivity is observed from H-4 to H-5. Finally, the expected nOe between H-12 and H-10α is observed. Molecular models indicate that these two latter protons are in close spatial proximity. However, there is no coupling between H-12 and H-10α. Hence the combined 2D nOe and SECSY experiments lead to the assignment of H-5, H-7,7*, and H-8 and hence to the complete assignment of the 6-keto-$PGE_1$ spectrum as shown in Fig. 3C.

In summary, it can be readily seen that the combined 2D nOe and the spin-echo correlated spectroscopy (SECSY) experiments have proven to be of great value in the analysis of complex spectra.

**Acknowledgements**

The authors wish to acknowledge Dr. J. E. Pike, Dr. R. A. Johnson, and Mr. H. Lincoln for the gifts of the prostaglandins, valuable discussions with Dr. A. D. Bain, Dr. S. Brownstein, Dr. H.-J. Liu, and Dr. T. T. Nakashima, and the Natural Sciences and Engineering Research Council of Canada, the Alberta Heart Foundation, and the University of Alberta for generous financial assistance.

1. S. MONCADA, R. GRYGLEWSKI, S. BUNTING, and J. R. VANE. Nature (London), **263**, 663 (1976).
2. S. MONCADA and J. R. VANE. *In* Advances in prostaglandin and thromboxane research. Vol. 6. *Edited by* B. Samuelsson, P. W. Ramwell, and R. Paoletti. Raven Press, New York. 1980.
3. P. Y.-K. WONG, W. H. LEE, P. H.-W. CHAO, R. F. REISS, and J. C. MCGIFF. J. Biol. Chem. **255**, 9021 (1980).
4. P. Y.-K. WONG, J. C. MCGIFF, F. F. SUN, and W. H. LEE. Eur. J. Pharmacol. **60**, 245 (1979).
5. C. P. QUILLEY, P. Y.-K. WONG, and J. C. MCGIFF. Eur. J. Pharmacol. **57**, 273 (1979).
6. J. H. NOGGLE and R. E. SCHIRMER. The nuclear Overhauser effect. Chemical applications. Academic Press, New York. 1971.

Can. J. Chem. Downloaded from www.nrcresearchpress.com by 210.87.254.5 on 09/06/12
For personal use only.

7. R. A. BELL and J. K. SAUNDERS. Can. J. Chem. **48**, 1114 (1970).
8. J. D. GLICKSON, S. L. GORDON, T. P. PITNER, D. G. AGRESTI, and R. WALTER. Biochemistry, **15**, 5721 (1976).
9. G. KOTOVYCH, G. H. M. AARTS, T. T. NAKASHIMA, and G. BIGAM. Can. J. Chem. **58**, 974 (1980).
10. J. JEENER, B. H. MEIER, P. BACHMANN, and R. R. ERNST. J. Chem. Phys. **71**, 4546 (1979).
11. B. H. MEIER and R. R. ERNST. J. Am. Chem. Soc. **101**, 6441 (1979).
12. S. MACURA and R. R. ERNST. Mol. Phys. **41**, 95 (1980).
13. A. KUMAR, R. R. ERNST, and K. WÜTHRICH. Biochem. Biophys. Res. Commun. **95**, 1 (1980).
14. C. BÖSCH, A. KUMAR, R. BAUMANN, R. R. ERNST, and K. WÜTHRICH. J. Magn. Reson. **42**, 159 (1981).
15. A. KUMAR, G. WAGNER, R. R. ERNST, and K. WÜTHRICH. J. Am. Chem. Soc. **103**, 3654 (1981).
16. A. KUMAR, G. WAGNER, R. R. ERNST, and K. WÜTHRICH. Biochem. Biophys. Res. Commun. **96**, 1156 (1980).
17. G. WAGNER, A. KUMAR, and K. WÜTHRICH. Eur. J. Biochem. **114**, 375 (1981).
18. W. P. AUE, E. BARTHOLDI, and R. R. ERNST. J. Chem. Phys. **64**, 2229 (1976).
19. K. NAGAYAMA, K. WÜTHRICH, and R. R. ERNST. Biochem. Biophys. Res. Commun. **90**, 305 (1979).
20. K. NAGAYAMA, A. KUMAR, K. WÜTHRICH, and R. R. ERNST. J. Magn. Reson. **40**, 321 (1980).
21. A. D. BAIN, R. A. BELL, J. R. EVERETT, and D. W. HUGHES. J. Chem. Soc. Chem. Commun. 256 (1980).
22. A. D. BAIN, J. BORNAIS, and S. BROWNSTEIN. Can. J. Chem. **59**, 723 (1981).
23. G. KOTOVYCH and G. H. M. AARTS. Can. J. Chem. **58**, 2649 (1980).
24. R. RICHARZ and K. WÜTHRICH. J. Magn. Reson. **30**, 147 (1978).
25. G. BALIMANN. The details of the program are included in the manual entitled "FT NMR 2D-PROGRAM" version No. 801010. Bruker Spectrospin. Nov. 1980.
26. S. MACURA, Y. HUANG, G. SUTER, and R. R. ERNST. J. Magn. Reson. **43**, 259 (1981).
27. S. MACURA, K. WÜTHRICH, and R. R. ERNST. J. Magn. Reson. **46**, 269 (1982).
28. S. MACURA, K. WÜTHRICH, and R. R. ERNST. J. Magn. Reson. **47**, 351 (1982).
29. G. KOTOVYCH, G. H. M. AARTS, and G. BIGAM. Can. J. Chem. **58**, 1577 (1980).
30. G. KOTOVYCH, G. H. M. AARTS, and T. T. NAKASHIMA. Can. J. Chem. **59**, 1449 (1981).
31. G. KOTOVYCH and G. H. M. AARTS. Org. Magn. Reson. **18**, 77 (1982).
32. G. BODENHAUSEN, R. FREEMAN, R. NIEDERMEYER, and D. L. TURNER. J. Magn. Reson. **26**, 133 (1977).
33. A. D. BAIN, R. A. BELL, J. R. EVERETT, and D. W. HUGHES. Can. J. Chem. **58**, 1947 (1980).


Can. J. Chem. Downloaded from www.nrcresearchpress.com by 210.87.254.5 on 09/06/12
For personal use only.

# Kinetics and mechanisms of the oxidation of a nickel(II) oxime complex by cobalt(III) aquo ions in acidic aqueous media. Formation of a Ni(IV) complex

D. H. MACARTNEY[1] AND A. MCAULEY[2]

*Department of Chemistry, University of Victoria, Victoria, B.C., Canada V8W 2Y2*

Received March 23, 1982

D. H. MACARTNEY and A. MCAULEY. Can. J. Chem. **60**, 2625 (1982).

The kinetics of the oxidation of a nickel(II) oxime complex to the corresponding nickel(IV) species by aquo cobalt(III) has been investigated in aqueous $CF_3SO_3H$ at various acidities (0.063–0.263 *M*) and temperatures (10.5–30.6°C). The inverse dependence of the rate constants on $[H^+]$ is attributed to a reaction pathway

$$CoOH^{2+} + Ni(II)(H_2L)^{2+} \xrightarrow{k_2} Co(II) + Ni(III)(H_2L)^{3+}$$

with $k_2 = 1.75 \times 10^4\ M^{-1}\ s^{-1}$, $\Delta H^{\ddagger} = 6.2 \pm 0.5$ kcal mol$^{-1}$, $\Delta S^{\ddagger} = -29.6 \pm 8.0$ cal deg mol$^{-1}$ ($K_h = 2 \times 10^{-3}\ M$ for the hydrolysis constant for cobalt(III)). The self-exchange parameter for the $Ni^{II}/Ni^{III}$-oxime couple ($k_{11} = 2.3 \times 10^3\ M^{-1}\ s^{-1}$, $\Delta G^{*} = 10.4$ kcal mol$^{-1}$) has been estimated from Marcus theory correlations. Comparisons are made between this value and the parameters determined for the Ni(II)/(III) tetra-aza macrocycle complexes.

D. H. MACARTNEY et A. MCAULEY. Can. J. Chem. **60**, 2625 (1982).

On a étudié la cinétique de l'oxydation du complexe de l'oxime de nickel(II) en nickel(IV) correspondant par le cobalt(III) aqueux, dans du $CF_3SO_3H$ aqueux à différentes acidités (0,063–0,263 *M*) et à différentes températures (10,5–30,6°C). On attribue au mécanisme réactionnel ci-dessous, l'influence inverse de $[H^+]$ sur la constante de vitesse

$$CoOH^{2+} + Ni(II)(H_2L)^{2+} \xrightarrow{k_2} Co(II) + Ni(III)(H_2L)^{3+}$$

avec $k_2 = 1{,}75 \times 10^4\ M^{-1}\ s^{-1}$, $\Delta H^{\ddagger} = 6{,}2 \pm 0{,}5$ kcal mol$^{-1}$, $\Delta S^{\ddagger} = -29{,}6 \pm 8{,}0$ cal deg mol$^{-1}$ ($K_h = 2 \times 10^{-3}$ pour la constante d'hydrolyse du cobalt(III)). On a évalué le paramètre d'auto-échange du couple $Ni^{II}/Ni^{III}$-oxime ($k_{11} = 2{,}3 \times 10^3\ M^{-1}\ s^{-1}$, $\Delta G^{*} = 10{,}4$ kcal mol$^{-1}$) à partir des corrélations de la théorie de Marcus. On a comparé ces valeurs entre elles et on déterminé les paramètres des complexes tétraazamacrocycles de Ni(II)/(III).

[Traduit par le journal]

## Introduction

There has been considerable recent interest in the formation of complexes of nickel in oxidation states higher than +2 (1–4). Attention has been paid principally to the use of tetra-aza macrocycles as ligands stabilising the ter-valent state. In these systems, there is evidence for the unpaired electron in the low-spin $d^7$ ion occupying a $d_z^2$ orbital since hyperfine interactions with axial ligands have been confirmed by esr studies (4, 5). There are, however, fewer complexes reported for the nickel(IV) state. Compounds containing di-oxime ligands have been prepared and studied (3, 6–8). Generally, a hexadentate ligand of the type **I** (3,14-dimethyl-4,7,10,13-tetraazahexadeca-3,13-diene-2,12-dione dioxime, $H_2L$) has been employed since pseudo-octahedral geometry is observed to be maintained in the $NiN_6$ complexes of nickel(II), (III), and (IV). The preparation of the Ni(IV) oxime by oxidation of the nickel(II) species has been carried out both electrochemically ($E^0(Ni^{IV}/Ni^{II}) = 0.95$ V) (8) or chemically with nitric acid (7). A similar chemical oxidation with $Ni(HL_1)^{2+}$ (where $HL_1$ represents the tridentate ligand 2-(2-aminoethyl)imino-3-butanone oxime) results in the Ni(IV) species $Ni(L_1)_2^{2+}$ which has been characterised by a crystal structure (9). Aqueous solutions of nickel(IV) complexes are stable for relatively long periods (weeks at 5°C) and, in keeping with the low-spin $d^6$ configuration, are of sufficient optical stability to be resolved (10).

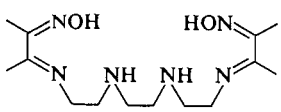


**I**

In this paper, the kinetics and mechanism of the oxidation of $Ni(II)H_2L^{2+}$ by $Co(III)_{aq}$ are discussed. Since there is no change in the inner-sphere geometry of the reductant during the course of reaction, an outer-sphere mechanism is postulated. There has been increased use recently of the Marcus theory (11–14) to describe cross correlations of rate constants with free energy changes and also to derive self-exchange rates for reactants. We have used an approach of this type to attempt to

[1]Present address: Department of Chemistry, Brookhaven National Laboratories, Upton, Long Island, New York.

[2]To whom all correspondence should be addressed.

0008-4042/82/202625-04$01.00/0

©1982 National Research Council of Canada/Conseil national de recherches du Canada

Can. J. Chem. Downloaded from www.nrcresearchpress.com by 210.87.254.40 on 09/06/12
For personal use only.

Can. J. Chem. Downloaded from www.nrcresearchpress.com by 210.87.254.40 on 09/06/12
For personal use only.

determine the rate of electron transfer for the Ni(II)/Ni(III) oxime couple.

## Experimental

*Reagents*

The oxime ligand, $H_2L$, was prepared by the condensation of butanedione monoxime with triethylenetetramine in ether. The nickel(II) oxime complex, $[Ni(H_2L)](ClO_4)_2$, was prepared by the addition of the ligand $H_2L$ to a methanol solution of $Ni(ClO_4)_2.6H_2O$ (7). The product was recrystallized from water and dried over $CaCl_2$. Analysis of the complex (Canadian Microanalytical Service) was satisfactory; observed (calculated) C 29.71 (29.49), H 5.02 (4.91), N 14.75 (14.70).

Solutions of hexaquocobalt(III) were prepared by the anodic oxidation of cobaltous perchlorate in perchloric acid (~5 *M*). The electrolysis was carried out near 0°C at a platinum electrode with $O_2$-free nitrogen passing through the solution. The stock solutions were analysed spectrophotometrically for Co(III) at 605 nm ($\varepsilon = 35.3\ M^{-1}\ cm^{-1}$) (15).

Owing to the insolubility of the nickel(II) oxime in perchlorate media, the kinetic studies were carried out in trifluoromethanesulphonic acid (Aldrich). The ionic strength of the reactant solutions was maintained at 0.50 *M* using lithium trifluoromethanesulphonate prepared by neutralising $CF_3SO_3H$ with lithium carbonate.

*Kinetic experiments*

The kinetic studies were made using a stopped-flow apparatus described previously (16). Thermostatting was maintained to within ±0.05°C in the temperature range 10.5–30.6°C. The reactions were followed by monitoring the formation of the nickel(IV) oxime product at 500 nm. All measurements were made under pseudo-first-order conditions of excess nickel(II) oxime concentrations. Plots of ln $(A_\infty - A_t)$ against time, derived from the absorbance data collected by a PCM-12 mini-computer, were linear for at least 3 half-lives. Rate constants were evaluated using a least-squares analysis of the slopes.

## Results

The visible spectrum of the products ($\lambda_{max}$ at 500 nm and 430 nm) of the oxidation of the nickel(II) oxime complex, $Ni(H_2L)^{2+}$, by $Co^{3+}$ in acidic aqueous media is consistent with the formation of a nickel(IV) species, $NiL^{2+}$ (7). The stoichiometry of the overall reaction

[1] $2Co^{3+} + Ni^{II}(H_2L)^{2+} \rightarrow 2Co^{2+} + Ni^{IV}L^{2+} + 2H^+$

was confirmed by a spectrophotometric titration ($\lambda$ = 500 nm) of 2.07 ± 0.10 mol of $Co^{3+}$ reacting per mol of the nickel oxime.

The observed rate constants exhibited a first-order dependence on the concentration of $Ni(H_2L)^{2+}$ as shown in Fig. 1. The second-order rate constants measured over the acid concentration range 0.063–0.263 *M* at five temperatures (10.5–30.6°C) are listed in Table 1. The rate constants were found to increase with decreasing hydrogen ion concentration. This inverse dependence is attributed to the hydrolysis of the $Co^{3+}$ ion ($pK_h = 2.7$) (15) rather than to a deprotonation of the oxime ligand in the $Ni(H_2L)^{2+}$ complex ($pK_1 = 5.9$, $pK_2 = 7.8$) at higher pH (7).

The rate law observed for the appearance of

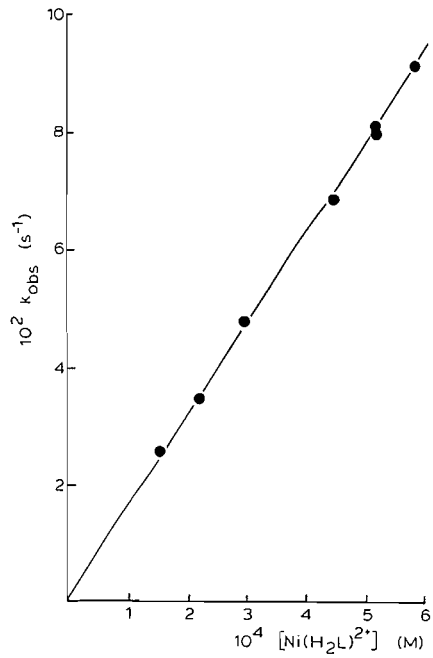


FIG. 1. The dependence of $k_{obs}$ on $Ni(H_2L)^{2+}$ in the reaction with $Co^{3+}$ at 25°C, $[H^+] = 0.236\ M$ ($CF_3SO_3H$).

TABLE 1. Second order rate constants for the reaction of Co(III)aq with $Ni(II)(H_2L)^{2+}$ at various $[H^+]$ and temperatures, $I = 0.5\ M$ ($LiCF_3SO_3$)

| $10 \times k_{obs}$ ($s^{-1}$) | $10^4 \times$ Ni(II) ($M$) | $k_0$ ($M^{-1}\ s^{-1}$) |
|---|---|---|
| $T$ = 25.0 °C, $[H^+] = 0.263\ M$ | | |
| 0.255 | 1.48 | 147 |
| 0.341 | 2.22 | 154 |
| 0.476 | 2.96 | 161 |
| 0.685 | 4.46 | 154 |
| 0.797 | 5.26 | 152 |
| 0.908 | 5.94 | 153 |

| $T$ (°C) | $k_0$ ($M^{-1}\ s^{-1}$) when $[H^+]/M$ = 0.236 | 0.213 | 0.163 | 0.113 | 0.063 |
|---|---|---|---|---|---|
| 10.5 | 46.2±0.6 | 50.2±1.0[a] | 63.1 | 87.6 | 140 |
| 16.5 | 63.0 | 77.0 | 103±0.7 | 141±1.3 | 250±3 |
| 20.8 | 90.7 | 112 ±1 | 149 | 200 | 366±5 |
| 25.0 | 154 ±3 | 176 | 238 | 337 | 551±4[b] |
| 30.6 | 254 | 297 | 362±10 | 560±5 | 956±8 |

[a] $[H^+] = 0.221\ M$.
[b] $[H^+] = 0.065\ M$.

$Ni(IV)L^{2+}$ may be expressed in the form

[2] $d[Ni(IV)L^{2+}]/dt = (a/[H^+])[Ni(II)H_2L^{2+}]_t[Co(III)]_t$

Plots of the derived second order rate constant, $k_0$, against $[H^+]^{-1}$, shown in Fig. 2, were linear at the various temperatures investigated. Within the limits of error, using a least-squares analysis, no systematic variation of intercept with temperature

Can. J. Chem. Downloaded from www.nrcresearchpress.com by 210.87.254.40 on 09/06/12
For personal use only.

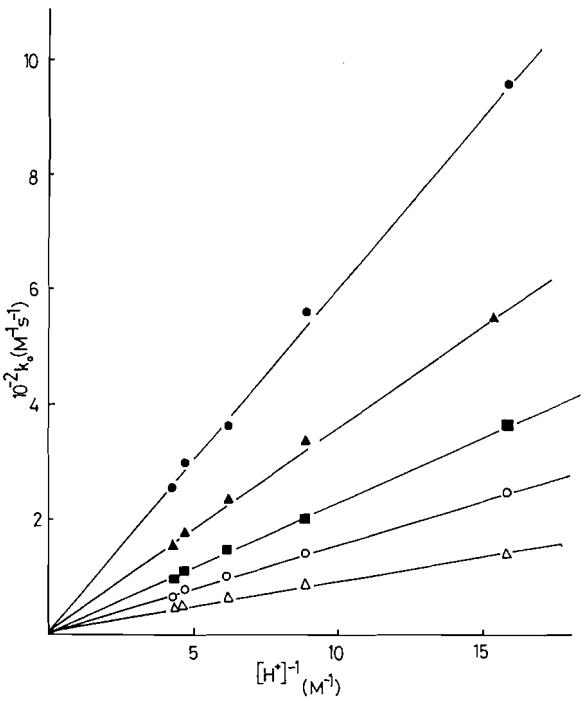


FIG. 2. A plot of $k_0$ against $1/[H^+]$ for the reaction of $Ni(H_2L)^{2+}$ with $Co^{3+}$ at several temperatures. △, $T$ = 10.5°C; ○, $T$ = 16.5°C; □, $T$ = 20.8°C; ▲, $T$ = 25.0°C; ●, $T$ = 30.6°C.

was noted, in general one standard deviation being greater than the intercept values obtained.

## Discussion

The observed rate laws may be derived from the following mechanistic scheme:

[3] $Co(H_2O)_6^{3+} \overset{K_h}{\rightleftharpoons} Co(H_2O)_5(OH)^{2+} + H^+$

[4] $Co^{3+} + Ni(II)H_2L^{2+} \xrightarrow{k_1} Co(II) + Ni(III)(H_2L)^{3+}$

[5] $Co(OH)^{2+} + Ni(II)H_2L^{2+} \xrightarrow{k_2} Co(II) + Ni(III)(H_2L)^{3+}$

[6] $Co(III) + Ni(III)L^{+} \xrightarrow{fast} Co(II) + Ni(IV)L^{2+}$

The rate law for the rate-determining one-electron oxidation may thus be written as

$$[7] \quad d[Ni(IV)L^{2+}]/dt = \frac{(k_1[H^+] + k_2K_h)}{([H^+] + K_h)} \times [Ni(II)]_t[Co(III)]_t$$

Under the conditions of study, $K_h$ (= $2 \times 10^{-3}$ $M$) < $[H^+]$ and since the intercept $k_1 < 10\ M^{-1}\ s^{-1}$ (Fig. 2), eq. [7] reduces to the form

$$[8] \quad d[Ni(IV)L^{2+}]/dt = \frac{k_2K_h}{[H^+]} [Ni(II)]_t[Co(III)]_t$$

where (eq. [2]) $a = k_2K_h$. The individual rate constants, $k_2$ (Table 2), have been derived using $K_h = 2 \times 10^{-3}$ $M$ (15) at 25°C while the dissociation constants at other temperatures were calculated using activation parameters (15, 17) associated with [3]; $\Delta H = 10 \pm 2$ kcal mol$^{-1}$ and $\Delta S = 21 \pm 8$ cal deg mol$^{-1}$. Specific rate constants were determined from a least-squares fit of the data in eq. [8] and are listed together with the corresponding activation parameters in Table 2.

The rate-determining step proposed is the one-electron oxidation (eq. [5]) to the nickel(III) species, $(Ni(III)H_2L)^{3+}$. From a knowledge of the proton equilibria for the nickel(II) complex (7) it is evident that only the fully protonated form is present under the conditions of the reaction. In the case of the nickel(III) ion, there is evidence (18) that in solutions of $[H^+] \sim 1.0\ M$ the species present is $Ni(III)HL^{2+}$. Above pH ~ 4 (p$K$ = 3.91) the deprotonated complex $Ni(III)L^+$ begins to predominate. In the present system, it is proposed that after electron transfer there is rapid dissociation to form $Ni(III)HL^{2+}$ (and possibly $Ni(III)L^+$). We have measured the acid-independent $Ni(IV)L^{2+}/Ni(III)L^+$ potential in *p*-toluenesulphonic acid media ($E^0$ = 0.64 V) and a rapid second oxidation to the nickel(IV) product is expected on the basis of the free energy changes involved.

It is of interest to note that in the corresponding oxidation of $Ni(cyclam)^{2+}$ (cyclam = 1,4,8,11-tetraazacyclotetradecane) (1) the sole reactive species is $CoOH^{2+}$. A hydroxide-mediated electron transfer within a specifically oriented outer-sphere precursor complex of $CoOH^{2+}$ and the square planar nickel(II) cyclam species has been suggested as an explanation.

The Marcus theory (11) for outer-sphere electron transfer reactions relates the free energy parameters for a cross-reaction ($\Delta G_{12}^0$, $\Delta G_{12}^*$) to the component self-exchange reactions ($\Delta G_{11}^*$, $\Delta G_{22}^*$). The relationship may be expressed in the form (19)

$$[9] \quad \Delta G_{12}^* = w + \lambda_{12}/4 + \Delta G_{12}^0/2 + (\Delta G_{12}^0)^2/4\lambda_{12}$$

TABLE 2. Specific rate constants and activation parameters* for the oxidation of $Ni(II)(H_2L)^{2+}$ by $CoOH^{2+}$

| $T$ (°C) | $k_2K_h$ ($s^{-1}$) | $10^{-4}k_2$ ($M^{-1}\ s^{-1}$) |
|---|---|---|
| 10.5 | 8.2±0.3 | 1.08 |
| 16.5 | 15.7±0.5 | 1.43 |
| 20.8 | 23.0±0.7 | 1.59 |
| 25.0 | 35.6±1.4 | 1.96 |
| 30.6 | 60 ±2.5 | 2.41 |

*$\Delta H_2^{\neq} = 6.2 \pm 0.9$ kcal mol$^{-1}$, $\Delta S_2^{\neq} = -30 \pm 8$ kcal mol$^{-1}$.

Can. J. Chem. Downloaded from www.nrcresearchpress.com by 210.87.254.40 on 09/06/12
For personal use only.

where $\lambda_{12} = 2(\Delta G_{11}^* + \Delta G_{22}^*)$, and $w$ is a parameter encompassing the work term associated with each of the free energy contributions. The work terms are usually small at an ionic strength $> 0.5\,M$ and, with reactants of the same charge type, tend to cancel each other out. Estimates for other reaction systems such as [5] may be derived using the expression (20)

$$w = 4.24 z_1 z_2 / r(1 + 0.329\, I^{1/2} r)$$

where $r$ is the distance of closest approach of the centres. Crystal data are not yet available for the nickel(II) oxime under study but bond lengths are available for a closely related complex (9), *bis*-2-(2-aminoethyl)imino-3-butanoneoximato nickel(II) which contains Ni—N, —oxime, —amine, and —imine groups and where the distorted octahedral geometry around the metal centre is retained on oxidation to Ni(IV). In the derivation of work terms the value of $r$ used was 10 Å. The activation free energy for the $CoOH^{2+/+}$ exchange has been measured previously (21) ($\Delta G_{22}^* = 11.2$ kcal mol$^{-1}$) and the reduction potential of $CoOH^{2+}$ may be estimated from that of the $Co^{3+}/Co^{2+}{}_{aq}$ couple (1.86 ± 0.02 V) (15) and the hydrolysis constants for the $Co^{3+}$ (p$K$ = 2.74) (15) and $Co^{2+}$ (p$K$ = 9.6) (22) aquo ions ($E^0{}_{CoOH^{2+/+}} = 1.44$ V).

Evidence favouring an outer-sphere reaction of $CoOH^{2+}$ with nickel(II)($H_2L$) may be presented by application of the cross reaction. Using the reaction of Ni(II)$(H_2L)^{2+}$ with Ru(bipy)$_3{}^{3+}$ in 1.0 $M$ *p*-toluenesulphonate medium, we have estimated (23) a value of 1.23 V for the reduction potential of the $Ni(H_2L)^{3+/2+}$ couple. From the resulting free energy change ($\Delta G^0 = -4.84$) for the $CoOH^{2+}$/$Ni(II)H_2L^{2+}$ system, a value of $\Delta G_{11}^* = 10.4 \pm 0.7$ kcal mol$^{-1}$ ($k_{11} = 2.4 \pm 1.6 \times 10^3\, M^{-1}\, s^{-1}$) may be obtained. A preliminary study of the oxidation of $Ni(II)H_2L^{2+}$ by a series of iron(III)–polypyridine complexes (23) yields a self-exchange parameter of $\sim 3 \times 10^3\, M^{-1}\, s^{-1}$. The exchange rate is also very similar to those derived recently by Lappin (18) for similar species. Using Co(phen)$_3{}^{2+}$ as reductant, he has derived $k_{11}$ values of $10^3\, M^{-1}\, s^{-1}$ and $2 \times 10^3\, M^{-1}\, s^{-1}$, respectively, for the Ni(HL)$^{2+/+}$ and $NiL^{+/0}$ exchanges. The Ni(II)/(III) oxime self-exchange parameters are close to those for the Ni(II)/(III) cyclam complexes ($1 \pm 0.3 \times 10^3\, M^{-1}\, s^{-1}$) (24). The oxime species retain an octahedral configuration in both oxidation states whereas a change from square-planar $Ni(II)L^{2+}$ to octahedral $NiL(OH_2)_2{}^{3+}$ occurs when L is a tetraaza macrocycle. The similarity in the self-exchange parameters suggests that there is only a small reorganisation energy associated with the change in geometry. There is also evidence that a square-planar–octahedral equilibrium (25) exists for these macrocycles and it may be that the axially solvated forms react in these outer sphere processes. Further kinetic studies on nickel(II) complexes with other cyclic and non-cyclic ligands will be helpful in examining the effects of ring size and geometry on the thermodynamics of electron exchange in these ions.

## Acknowledgements

We are indebted to the Natural Sciences and Engineering Council of Canada for support. D. H. M. thanks the University of Victoria for the award of a Graduate Fellowship. We also acknowledge with thanks details of unpublished data provided by Dr. Graham Lappin.

1. J. C. Brodovitch and A. McAuley. Inorg. Chem. **20**, 1667 (1981).
2. J. M. T. Raycheba and D. W. Margerum. Inorg. Chem. **20**, 1441 (1981).
3. A. G. Lappin, M. C. M. Laranjeira, and L. Youda-Owei. J. Chem. Soc. Dalton Trans. 721 (1981).
4. A. Bencini, L. Fabbrizzi, and A. Poggi. Inorg. Chem. **20**, 2544 (1981).
5. R. I. Haines and A. McAuley. Coord. Chem. Rev. **39**, 77 (1981).
6. K. Nag and A. Chakravorty. Coord. Chem. Rev. **33**, 87 (1980).
7. J. G. Mohanty, R. P. Singh, and A. Chakravorty. Inorg. Chem. **14**, 2178 (1975).
8. J. G. Mohanty and A. Chakravorty. Inorg. Chem. **15**, 2912 (1976).
9. H. Saarinen, J. Korvenranta, and E. Nasakkala. Acta Chem. Scand. A**34**, 443 (1980).
10. P. J. Heaney, A. G. Lappin, R. D. Peacock, and B. Stewart. J. Chem. Soc. Chem. Commun. 769 (1980).
11. R. A. Marcus. Ann. Rev. Phys. Chem. **15**, 155 (1964).
12. M. A. Ratner and R. D. Levine. J. Am. Chem. Soc. **102**, 4898 (1980).
13. M. J. Weaver and E. L. Yee. Inorg. Chem. **19**, 1936 (1980).
14. C. O. Adestinewo and A. Adegite. Inorg. Chem. **18**, 3597 (1979).
15. G. Davies and B. Warnqvist. Coord. Chem. Rev. **5**, 349 (1970).
16. K. J. Ellis and A. McAuley. J. Chem. Soc. Dalton Trans. 1533 (1973).
17. L. H. Sutcliffe and J. R. Weber. Trans. Faraday Soc. **52**, 1225 (1956).
18. A. G. Lappin. Private communication.
19. R. G. Wilkins. Study of kinetics and mechanism of reactions of transition metal complexes. Allyn and Bacon, Boston. 1974. p. 279.
20. G. M. Brown and N. Sutin. J. Am. Chem. Soc. **101**, 883 (1979).
21. H. S. Habib and J. P. Hunt. J. Am. Chem. Soc. **88**, 1668 (1966).
22. A. G. Sykes. Kinetics of inorganic reactions. Pergamon Press, Oxford. 1966. p. 280.
23. D. H. Macartney and A. McAuley. To be published.
24. D. H. Macartney, T. Oswald, and A. McAuley. J. Chem. Soc. Chem. Commun. 274 (1982).
25. A. Anichini, L. Fabbrizzi, P. Paoletti, and R. M. Clay. Inorg. Chim. Acta, **24**, L21 (1977).

# The reaction of active nitrogen with fluoroethylenes

WILLIAM E. JONES AND MAHMOODA G. AHMED
*Department of Chemistry, Dalhousie University, Halifax, N.S., Canada B3H 4J3*

Received April 13, 1982

WILLIAM E. JONES and MAHMOODA G. AHMED. Can. J. Chem. **60**, 2629 (1982).

The reactions of active nitrogen with the fluoroethylenes $C_2H_3F$, 1,1-$C_2H_2F_2$, $C_2HF_3$, and $C_2F_4$ have been investigated in a conventional flow system using a mass spectrometer to detect products and intermediate species. Addition of various gases (H, $H_2$, $NH_3$, $CH_4$, $N_2O$, $N_2(A^3\Sigma_u^+)$, and F) to the reacting mixtures provides evidence that both H and F atoms play significant roles in the reaction mechanisms, while $N_2A^3\Sigma_u^+$ does not. A brief discussion of possible mechanisms is presented.

WILLIAM E. JONES et MAHMOODA G. AHMED. Can. J. Chem. **60**, 2629 (1982).

On a étudié les réactions de l'azote actif avec les fluoroéthylènes $C_2H_3F$, $C_2H_2F_2$-1,1, $C_2HF_3$ et $C_2F_4$, dans un système à écoulement conventionnel et en utilisant un spectromètre de masse pour détecter les produits et les espèces intermédiaires. L'addition de différents gaz (H, $H_2$, $NH_3$, $CH_4$, $N_2O$, $N_2(A^3\Sigma_u^+)$ et F) au mélange réactionnel fournit la preuve que les deux atomes H et F jouent un rôle important dans le mécanisme réactionnel tandis que $N_2A^3\Sigma_u^+$ n'apporte aucune contribution. On discute brièvement des mécanismes possibles.

[Traduit par le journal]

## Introduction

The reactions of active nitrogen with hydrocarbons have been investigated by many workers. In particular, the reaction with ethylene has been studied extensively and several mechanisms have been suggested (1–5). In contrast, reports on the reactions of active nitrogen with fluoro-substituted ethylenes are scanty and there are considerable uncertainties about the mechanism of these reactions.

In an earlier study on the reaction of active nitrogen with perfluorinated olefins (6), a mechanism analogous to the early mechanism was proposed for the active nitrogen – hydrocarbon system (1). A bimolecular addition of a nitrogen atom to the fluorocarbon was suggested to be the initial step, which in the case of the tetrafluoroethylene reaction would be written as in [1].

$$[1] \quad N + C_2F_4 \rightarrow (C_2F_4N) \begin{cases} \rightarrow F_2CN + CF_2 \\ \rightarrow FCN + CF_3 \end{cases}$$

However, it is now believed that the mechanism of the hydrocarbon – active nitrogen reaction is not as simple as was suggested by Winkler and coworkers (1). Rather the reactions are considerably complicated by the involvement of hydrogen atoms and hydrocarbon radicals (2–5). More recently, Safrany and Jaster (4) proposed that the reaction of olefin with active nitrogen is initiated by hydrogen atoms rather than nitrogen atoms. This initiation step is alleged to produce alkyl radicals which are ultimately attacked by the N atoms. In light of this mechanism, one might suggest that hydrogen or fluorine atoms play a similar role in the reaction of fluoroethylene molecules with active nitrogen. Alternatively, it might be suggested in agreement with Merchand and Stringat (7), who studied the reaction with tetrafluoroethylene ($C_2F_4$), that the reaction is initiated by excited molecular nitrogen $N_2(A^3\Sigma_u^+)$. Involvement of excited state molecular nitrogen was also suggested by Johnson and Fontijn (8) in the final chemiexcitation step producing emission from the same reaction. This paper describes our attempts to determine whether either or both of the above possibilities are important.

## Experimental

Active nitrogen was produced in a conventional fast flow system by a 2450 MHz electrodeless discharge sustained by a 100 W Kiva MPG-2 generator. Hydrogen or fluorine atoms were also produced by 2450 MHz radiation from a Burdick MW/200 generator. Both nitrogen and hydrogen (or fluorine) gases could be activated simultaneously in separate discharge regions and introduced to the reaction flow tube. Typical flow conditions were: $N_2$, $1.2 \times 10^{-4}$ mol $s^{-1}$; $H_2$, $4.5 \times 10^{-5}$ mol $s^{-1}$; $F_2$ (1% in He), $1.5 \times 10^{-7}$ mol $s^{-1}$. The concentration of atomic nitrogen was measured by NO titration. The total pressure in the reaction tube was 0.95 Torr. The pressure in the mass spectrometer was approximately $2 \times 10^{-5}$ Torr. An ionization voltage of 23 eV was used to produce the ions.

The reaction tube was constructed from a 75 cm long 20 mm od Pyrex tube. The tube contained 9 multiperforated gas inlets spaced at various intervals along the tube. A portion of the reaction mixture passed directly into a T.O.F. mass spectrometer ionization chamber through a line of sight double pinhole system. The flow system, pinhole region, mass spectrometer, and data acquisition system are described in detail elsewhere (9).

Molecular nitrogen and hydrogen were obtained from Linde. Vinyl fluoride, 1,1-difluoroethylene, trifluoroethylene, methane, nitric oxide, and ammonia were supplied by Matheson. Nitrous oxide was a product of Canadian Liquid Air Limited. Tetrafluoroethylene was prepared by thermal decomposition of tetrafluoroethylene polymer boiling chips. All condensible

0008-4042/82/202629-05$01.00/0
©1982 National Research Council of Canada/Conseil national de recherches du Canada

Can. J. Chem. Downloaded from www.nrcresearchpress.com by 210.87.254.5 on 09/06/12
For personal use only.

Can. J. Chem. Downloaded from www.nrcresearchpress.com by 210.87.254.5 on 09/06/12
For personal use only.

TABLE 1. Mass peaks attributable to products of the reaction of active nitrogen with fluoroethylenes and possible positive ions[d]

| m/z | $CH_2$=CHF | $CH_2$=$CF_2$ | CHF=$CF_2$ | $CF_2$=$CF_2$ |
|---|---|---|---|---|
| 15 | $[CH_3, NH]^b$ | | | |
| 16 | $[CH_4, NH_2]^b$ | | | |
| 17 | $NH_3{}^b$ | $NH_3{}^b$ | $NH_3{}^c$ | |
| 20 | $HF^b$ | $HF^b$ | $HF^b$ | |
| 26 | $[C_2H_2, CN]^b$ | $[C_2H_2, CN]^b$ | | |
| 27 | $HCN^a$ | $HCN^a$ | $HCN^a$ | |
| 31 | $CF^c$ | | | |
| 33 | $[NF, CH_2F]^c$ | | | |
| 39 | $CHCN^b$ | | | |
| 40 | $CH_2CN^b$ | | | |
| 41 | $CH_3CN^a$ | | | |
| 45 | | $FCN^b$ | $FCN^a$ | $FCN^a$ |
| 50 | | $CF_2{}^b$ | $CF_2{}^a$ | $CF_2{}^a$ |
| 51 | $[C_2HCN, CHF_2]^c$ | | | |
| 52 | $[C_2N_2, NF_2]^c$ | $[C_2N_2, NF_2]^c$ | $[C_2N_2, NF_2]^b$ | $[C_2N_2, NF_2]^b$ |
| 57 | $H_5C_2N_2{}^c$ | | | |
| 58 | $H_6C_2N_2{}^c$ | | | |
| 64 | $C_2H_2F_2{}^b$ | | $C_2H_2F_2{}^c$ | |
| 69 | | $CF_3{}^c$ | $CF_3{}^a$ | $CF_3{}^a$ |
| 70 | | | $CF_3H^c$ | |
| 71 | $NF_3{}^b$ | | | |
| 88 | | $CF_4{}^b$ | $CF_4{}^b$ | |
| 100 | | | $C_2F_4{}^b$ | |
| 114 | | | | $C_2F_4N^b$ |
| 119 | | | | $C_2F_5{}^b$ |

[a]Major product peak.
[b]Minor product peak.
[c]Very small product peak.
[d][] Indicates several possible ions to account for the peak.

gases were purified by bulb-to-bulb distillation until no impurities could be detected mass spectrometrically. Nitrogen was purified by passing it through hot copper turnings and a liquid nitrogen trap.

## Results and discussion

Addition of fluoroethylene to active nitrogen produced a luminescent reaction flame about 10–15 cm in length. With $C_2H_3F$ and 1,1-$C_2H_2F_2$ the flame was greenish white, while with $C_2HF_3$ and $C_2F_4$ it was orange yellow. The *m/z* values of those positive ions attributable to products of the reactions are presented in Table 1.

Similar to the hydrocarbon – active nitrogen reactions a major product of the reaction of active nitrogen with $C_2H_3F$, 1,1-$C_2H_2F_2$, and $C_2HF_3$ was HCN (*m/z* 27). As the number of fluorine atoms in the ethylene molecule increase a decrease is observed in the relative amount of HCN produced and the peaks at *m/z* 50 ($CF_2{}^+$) and *m/z* 69 ($CF_3{}^+$) become progressively more important. If the fluoroethylene – active nitrogen reaction is truly analogous to the hydrocarbon – active nitrogen reaction, we might expect to obtain significant amounts of FCN as a product. A mass peak at *m/z* 45 in the reaction of 1,1-$C_2H_2F_2$, $C_2HF_3$, and $C_2F_4$ with active nitrogen probably corresponds to FCN. However, the relatively small amount of FCN produced could be due to its decomposition or its involvement in further reactions such as the formation of polymer. In the $C_2H_3F$ reaction, the *m/z* 45 peak is a major fragmentation peak of $C_2H_3F$ itself, which thus precludes the detection of FCN. For each of the fluorocarbons studied polymer was formed on the wall of the reaction tube as was found to be the case in earlier studies (6).

The reactions of active nitrogen with the fluoroethylenes are quite complex. The type and number of products formed, and the uncertainty about the initiation step make a quantitative study difficult. In an attempt to decide whether excited molecular nitrogen or species other than those present in active nitrogen played a significant role, we introduced a number of additives (H, $H_2$, F, $NH_3$, $N_2O$, $CH_4$, $N_2(A^3\Sigma_u^+)$) into the reacting mixtures. An indication of the effects of these additives on various product peaks is given in Figs. 1 to 3.

### *Effect of hydrogen atoms*

On addition of H atoms, the reaction of $C_2H_3F$ with active nitrogen was greatly enhanced, as evidenced by a sharp decrease in the length and increase in the intensity of the reaction flame. A

Can. J. Chem. Downloaded from www.nrcresearchpress.com by 210.87.254.5 on 09/06/12
For personal use only.

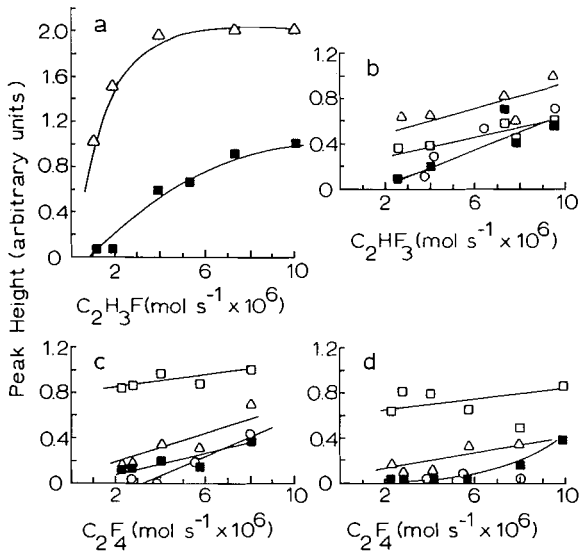


FIG. 1. Variation of major product mass peaks. (*a*) $HCN^+$ in $C_2H_3F$ reaction, (*b*) $HCN^+$ in $C_2HF_3$ reaction, (*c*) $CF_2^+$ in $C_2F_4$ reaction, (*d*) $CF_3^+$ in $C_2F_4$ reaction. □, Active nitrogen with fluoroethylene. ■, Addition of $H_2$ to reaction. △, Addition of H (in $H_2$) to reaction. ○, Addition of $NH_3$ to reaction.

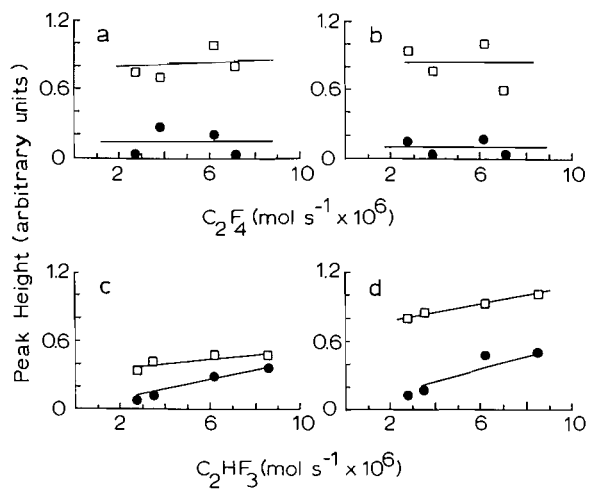


FIG. 2. Variation of major product mass peaks. (*a*) $CF_2^+$ in $C_2F_4$ reaction, (*b*) $CF_3^+$ in $C_2F_4$ reaction, (*c*) $FCN^+$ in $C_2HF_3$ reaction, (*d*) $CF_2^+$ in $C_2HF_3$ reaction. □, Active nitrogen with fluoroethylene. ●, Addition of $CH_4$ to reaction.

large decrease was also observed in the $N^+$ (from N) mass spectral peak, while a large increase was observed in the product peaks corresponding to $HCN^+$, $HF^+$, $CH_3^+$, $CH_4^+$, and $CH_3CN^+$. An example of this increase is given for the major product peak $HCN^+$ in Fig. 1*a*. A similar although not as pronounced effect was observed when H atoms were added to the 1,1-$C_2H_2F_2$ and $C_2HF_3$

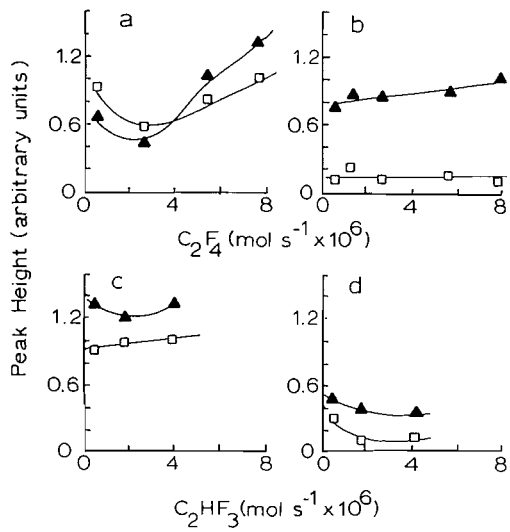


FIG. 3. Variation of major product mass peaks. (*a*) $CF_2^+$ in $C_2F_4$ reaction, (*b*) $CF_3^+$ in $C_2F_4$ reaction, (*c*) $CF_2^+$ in $C_2HF_3$ reaction, (*d*) $CF_3^+$ in $C_2HF_3$ reaction. □, Active nitrogen with fluoroethylene. ▲, Addition of F atoms to reaction.

reactions with active nitrogen. Figure 1*b* presents the effect on the $HCN^+$ peak for $C_2HF_3$.

In contrast to the above behaviour, product formation in the $C_2F_4$ – active nitrogen reaction was inhibited by the addition of H atoms. This inhibition may be on account of the presence of $H_2$ (see below) since the H atoms were present in an excess of molecular hydrogen. Results are shown for the two major product peaks, $CF_2^+$ and $CF_3^+$ in Fig. 1*c*, *d*.

*Effect of molecular hydrogen*

The addition of molecular hydrogen to the reaction of $C_2F_4$ with active nitrogen resulted in almost complete quenching of the reaction as evidenced by extinction of the reaction flame and decrease in product yields particularly at low flow rates of $C_2F_4$ (Fig. 1*b*, *c*). Although the reaction was quenched, the formation of small amounts of HF was noted on addition of $H_2$. Addition of $H_2$ to the $C_2HF_3$ reaction decreased product yields significantly at low $C_2HF_3$ flow rates, but had little effect at high $C_2HF_3$ flow rates (Fig. 1*b*). Addition of $H_2$ to 1,1-$C_2H_2F_2$ and $C_2H_3F$ appeared to have little effect on the reaction.

*Effect of ammonia and methane*

As with $H_2$, ammonia (Figs. 1*b*, *c*) and methane (Fig. 2*a*) essentially quenched the reaction of active nitrogen with $C_2F_4$, but did produce small amounts of HF. Ammonia (Fig. 1*d*) and methane (Fig. 2*b*) also severely inhibited the reaction with $C_2HF_3$. The reaction with 1,1-$C_2H_2F_2$ and $C_2H_3F$

Can. J. Chem. Downloaded from www.nrcresearchpress.com by 210.87.254.5 on 09/06/12
For personal use only.

was not significantly affected by the addition of ammonia or methane.

*Effect of fluorine atoms*

The effect of fluorine atoms on the major product peaks of the reactions with $C_2F_4$ and $C_2HF_3$ are indicated in Fig. 3. When added to the $C_2F_4$ reaction, a very significant increase in the $CF_3^+$ product peak was observed (Fig. 3*b*), while the $CF_2^+$ product peak underwent a slight decrease at low $C_2F_4$ flow, and a slight increase at increased $C_2F_4$ flow. A shorter and brighter reaction flame was also noted on the addition of fluorine atoms. In the $C_2HF_3$ reaction a small increase in both the $CF_2^+$ and $CF_3^+$ peaks was observed.

*Effect of nitrous oxide*

The addition of $N_2O$ had very little effect on these reactions. No new detectable products were found nor did $N_2O$ quench the reactions as might have been expected if excited molecular nitrogen ($A^3\Sigma_u^+$) was an important initiating species.

*Addition of $N_2(A^3\Sigma_u^+)$*

Excited molecular nitrogen $N_2(A^3\Sigma_u^+)$ was produced from metastable Ar as described by Meyer *et al.* (10) and admitted to the $C_2F_4$ and $C_2HF_3$ active nitrogen reaction mixtures. This addition did not appear to affect either the reaction flame characteristics, or the type or amount of products formed.

Contrary to earlier suggestions (7, 8), it seems from the above observations that the effect of excited molecular nitrogen $N_2(A^3\Sigma_u^+)$ is minimal in initiating the reaction of active nitrogen with $C_2F_4$ or $C_2HF_3$. Both $NH_3$ and $N_2O$ are known to be efficient quenchers of $N_2(A^3\Sigma_u^+)$ (11). The large effect on the reaction by $NH_3$ seems to be contradictory to the observation of no effect by $N_2O$. This contradiction may be explained if fluorine atoms are considered to be an important species in these reactions. $NH_3$ reacts very rapidly with F atoms (12) while the reaction of F with $N_2O$ is very slow (12).

Additional evidence that F atoms play a role in these reactions is shown by the inhibiting effect of H and/or $H_2$, $H_2$, and $CH_4$ (all of which react rapidly, $k > 10^{13}$ cm$^3$ mol$^{-1}$ s$^{-1}$, with F (12)) on the reaction with $C_2F_4$ and to a lesser extent on the reaction with $C_2HF_3$ and by the formation of HF or increased amounts of HF with these additions. Further, the addition of F atoms to the reactions with $C_2F_4$ and $C_2HF_3$ enhanced the reaction.

This conclusion, that F atoms play an important role in the $C_2F_4$ and $C_2HF_3$ – active nitrogen reactions, is complementary to the earlier suggestions (2–5) that H atoms play a significant role in hydrocarbon – active nitrogen reactions. With some hesitation, it may be suggested that F atoms are the initiating species in these reactions much as H atoms have been suggested as the initiating species for hydrocarbon – active nitrogen reactions (4).

We can only speculate on the initiation step. If F atoms are the initiating species for the $C_2F_4$ reaction they must result from either reaction [2*a*] or [2*b*],

[2*a*] $N + N + C_2F_4 \rightarrow N_2 + C_2F_3 + F$ $\quad \Delta H = -427$ kJ mol$^{-1}$

[2*b*] $N_2^* + C_2F_4 \rightarrow N_2 + C_2F_3 + F$

where $N_2^*$ indicates some excited species of $N_2$ other than the $A$ state.[1] Alternatively, since the C=C bond is the weakest in $C_2F_4$ the initiation by N or $N_2^*$ might produce $CF_2$ radicals as in [3*a*] or [3*b*],

[3*a*] $N + N + C_2F_4 \rightarrow 2CF_2 + N_2$ $\quad \Delta H = -586$ kJ mol$^{-1}$

[3*b*] $N_2^* + C_2F_4 \rightarrow 2CF_2 + N_2$

followed by rapid reaction of atomic nitrogen with the $CF_2$ radicals.

Attack of the F atom on the fluorocarbon would produce an excited radical [4] which may directly dissociate

[4] $F + C_2F_4 \rightarrow [C_2F_5]^* \rightarrow CF_2 + CF_3$

or react with N atoms as in [5]

[5] $C_2F_5 + N \rightarrow F_2CN + CF_3$

These reactions will be followed by a series of rapid reactions involving the radicals and N or F atoms as in [6] to [11]. Such reactions can explain the rapid and complete reaction of nitrogen at very low concentrations of $C_2F_4$.

[6] $CF_3 + N \rightarrow F_2CN + F$ $\quad \Delta H = -69$ kJ mol$^{-1}$

[7] $CF_2 + N \rightarrow F_2CN$ $\quad \Delta H = -479$ kJ mol$^{-1}$

[8] $CF_2 + N \rightarrow FCN + F$ $\quad \Delta H = -258$ kJ mol$^{-1}$

[9] $CF_2 + F \rightarrow CF_3$ $\quad \Delta H = -410$ kJ mol$^{-1}$

[10] $F_2CN + N \rightarrow FCN + NF$ $\quad \Delta H = -90$ kJ mol$^{-1}$

[11] $NF + N \rightarrow N_2 + F$ $\quad \Delta H = -630$ kJ mol$^{-1}$

The rates of addition of H atoms to fluoroethylenes are known to be fast (13, 14), while the abstraction of an H or F atom by H are reported to

[1]Values of $\Delta H_f^0$ used in the calculation of heats of reaction were obtained from the National Bureau of Standards, Circular No. 26, except for: FCN, $-13 \pm 42$ kJ mol$^{-1}$ (ref. 15); $H_2CN$, $-180$ kJ mol$^{-1}$ (ref. 4); $F_2CN$, $-155$ kJ mol$^{-1}$; $C_2H_4F$, $-180$ kJ mol$^{-1}$; HFCN, $+47$ kJ mol$^{-1}$ (all calculated using MNDO, ref. 16).

be less likely processes (14). From the present observation that addition of H atoms greatly enhances the reactions $C_2H_3F$, 1,1-$C_2H_2F_2$, and $C_3HF_3$ with active nitrogen we suggest that hydrogen addition reactions initiate these reactions in the same way as proposed for hydrocarbon reactions (4). A set of possible reactions can thus be proposed for the hydrogen-containing fluorocarbons as shown in reactions [12] to [20].

[12] $C_2H_3F + H \rightarrow C_2H_4F$ $\Delta H = -280$ kJ mol$^{-1}$

[13] $C_2H_4F + N \rightarrow H_2CN + CH_2F$ $\Delta H = -139$ kJ mol$^{-1}$

[14] $\rightarrow HFCN + CH_3$ $\Delta H = -105$ kJ mol$^{-1}$

[15] $CH_3 + N \rightarrow H_2CN + H$ $\Delta H = -212$ kJ mol$^{-1}$

[16] $H_2CN + N \rightarrow HCN + NH$ $\Delta H = -197$ kJ mol$^{-1}$

[17] $CH_2F + N \rightarrow HFCN + H$ $\Delta H = -178$ kJ mol$^{-1}$

[18] $HFCN + N \rightarrow NH + FCN$ $\Delta H = -200$ kJ mol$^{-1}$

[19] $\rightarrow NF + HCN$ $\Delta H = -154$ kJ mol$^{-1}$

[20] $NH + N \rightarrow N_2 + H$ $\Delta H = -584$ kJ mol$^{-1}$

Similar sets of reactions could be proposed for 1,1-$C_2H_2F_2$ and $C_2HF_3$.

However, it is likely that both H atoms and F atoms play significant roles in the reaction of $C_2HF_3$ and to a lesser extent in the reaction of 1,1-$C_2H_2F_2$. In these reactions a mechanism would have to combine appropriate reactions from the H and F atom mechanisms.

## Acknowledgements

We acknowledge financial assistance from the Faculty of Graduate Studies at Dalhousie for a scholarship to M.G.A., and from the Natural Sciences and Engineering Research Council of Canada for operating and equipment grants to W.E.J.

1. A. N. Wright and C. A. Winkler. Active nitrogen. Academic Press. 1968.
2. J. T. Herron. J. Phys. Chem. **69**, 2736 (1965).
3. J. T. Herron and R. E. Huie. J. Phys. Chem. **72**, 2538 (1968).
4. D. R. Safrany and W. Jaster. J. Phys. Chem. **72**, 518 (1968).
5. S. Takahashi and S. Miyazaki. Bull. Chem. Soc. Jpn. **50**(6), 1627 (1977).
6. N. Madhavan and W. E. Jones. Can. J. Chem. **46**, 3483 (1968).
7. J. Merchand and R. Stringat. C. R. Acad. Sci., Paris, t. **263** B, 1254 (1968).
8. S. E. Johnson and A. Fontijn. Chem. Phys. Lett. **23**, 252 (1973).
9. L. Ramaley, K. Ling, D. Burkholder, M. Ieki, and W. E. Jones. Chem. Biomed. Environ. Instru. **9**(4), 335 (1979).
10. J. A. Meyer, D. H. Klosterboer, and D. W. Setser. J. Chem. Phys. **55**, 2084 (1971).
11. J. A. Meyer, D. W. Setser, and W. G. Clark. J. Phys. Chem. **76**, 1 (1972).
12. W. E. Jones and E. G. Skolnik. Chem. Rev. **76**, 563 (1976).
13. L. Teng. Ph.D. Thesis, Dalhousie University. 1972.
14. R. D. Penzhorn and H. L. Sandoval. J. Phys. Chem. **74**, 2065 (1970).
15. S. W. Benson. Thermochemical kinetics. John Wiley and Sons, New York. 1968. p. 198.
16. W. Thiel. MNDO molecular orbital calculations. QCPE 353.

Can. J. Chem. Downloaded from www.nrcresearchpress.com by 210.87.254.5 on 09/06/12
For personal use only.

# Isomérie *Z*–*E* des spirochromènes oxa- et thiazolidiniques-1,3 à deux atomes de carbone asymétriques. Comparaison avec les spirochromènes oxa- et thiaziniques-1,3 homologues

MICHEL MAGUET, YVES POIRIER ET ROBERT GUGLIELMETTI

*Laboratoire de synthèse organique, LA C.N.R.S. 322, Université de Bretagne Occidentale, Faculté des Sciences et Techniques, 6, Avenue V. Le Gorgeu, 29283 Brest Cedex, France*

Reçu le 4 février 1982

MICHEL MAGUET, YVES POIRIER et ROBERT GUGLIELMETTI. Can. J. Chem. **60**, 2635 (1982).

La synthèse de spirochromènes oxa- et thiazolidiniques-1,3 à deux atomes de carbone asymétriques en α de l'oxygène ou du soufre conduit généralement à un mélange de deux diastéréoisomères où la configuration *Z* prédomine. L'examen de modèles de Dreiding et l'application de l'équation de Karplus permettent une résolution satisfaisante de ce problème. Par contre, un seul isomère existe en séries tétrahydro-2,4,5,6 oxa- ou thiazinique-1,3 homologues. L'étude de la géométrie du cycle azoté prouve alors que la configuration peut être *Z* ou *E* selon que l'un des atomes de carbone asymétriques est en α ou en β de l'oxygène ou du soufre.

MICHEL MAGUET, YVES POIRIER, and ROBERT GUGLIELMETTI. Can. J. Chem. **60**, 2635 (1982).

The synthesis of oxa- and thiazolidine-1,3 spirochromenes with two asymmetric carbon atoms in an α position to oxygen or sulphur leads generally to a mixture of two diastereoisomers for which the *Z* configuration is predominant. Examination of Dreiding models and application of the Karplus equation allow a good solution of this problem. On the other hand, only one isomer exists in the 2,4,5,6-tetrahydro oxa- or thiazine-1,3 homolog compounds. The study of the geometry of the aza ring proves then that the configuration may be *Z* or *E* according to whether one of the asymmetric carbon atoms is in an α or β position to oxygen or sulphur.

## Introduction

L'un des aspects les plus originaux de la synthèse des spirochromènes oxa- et thiazolidiniques-1,3 **1** et **2** est l'obtention de deux diastéréoisomères *E* et *Z* quand ces composés présentent deux atomes de carbone asymétriques en α de l'atome d'oxygène ou de soufre (1, 2). Leur structure est la suivante:

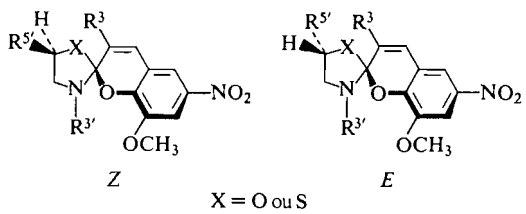


Gruda *et al.* (3, 4) ont déjà signalé à propos de spirochromènes indoliniques asymétriquement substitués en position 3′ que l'étude de la cinétique de l'isomérisation *Z*–*E* est possible par la rmn $^1$H. C'est là une différence essentielle avec nos résultats. Nous avons constaté que les rapports **1***E*/**1***Z* et **2***E*/**2***Z* sont selon cette technique indépendants du temps et de la nature du solvant utilisé pour la réalisation du spectre. La séparation des deux diastéréoisomères – possible en série indolinique (4) – n'était pas notre motivation principale.[1] En effet, les spectres de rmn $^1$H à 250 MHz des mélanges *Z*/*E* sont suffisamment explicites pour permettre une approche de la géométrie des cycles oxa- et thiazolidiniques par le biais de l'équation de Karplus. Le même travail a été conduit dans le cas des spirochromènes tétrahydro oxa- et thiaziniques-1,3 de formules générales **3** et **4** pour lesquels on ne rencontre qu'un seul diastéréoisomère. Le présent mémoire concerne les deux points suivants.

1. L'identification du diastéréoisomère majoritaire.

2. L'approche de la stéréochimie des cycles azotés des composés **1**–**4**.

La résolution de ces deux problèmes est particulièrement intéressante. Nous avons montré en effet que la géométrie des photomérocyanines colorées produites par irradiation ultraviolette des spirochromènes dépend de la géométrie de ces derniers (5, 6). Il en résulte des répercussions au niveau des propriétés spectroscopiques et des applications potentielles de ces composés.

[1]La séparation des diastéréoisomères dans les séries oxazolidinique et thiazolidinique – irréalisable par cristallisation fractionnée – peut être envisagée grâce à la chromatographie liquide sous pression. L'ampleur des difficultés rencontrées ne nous a pas incité à développer nos recherches par cette technique.

0008-4042/82/212635-09$01.00/0

©1982 National Research Council of Canada/Conseil national de recherches du Canada

Can. J. Chem. Downloaded from www.nrcresearchpress.com by 210.87.254.105 on 09/06/12
For personal use only.

Can. J. Chem. Downloaded from www.nrcresearchpress.com by 210.87.254.105 on 09/06/12
For personal use only.

## Résultats et discussion

### I. *Spirochromènes oxa- et thiazolidiniques-1,3 1 et 2*

#### I.1 *Identification du diastéréoisomère majoritaire*

Les spirochromènes suivants ont été étudiés:

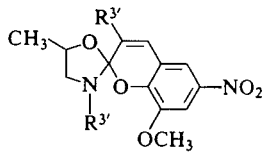

1

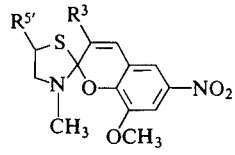

2

**1***a* $R^{3'} = CH_3$; $R^3 = C_2H_5$ **2***a* $R^{5'} = R^3 = CH_3$
**1***b* $R^{3'} = CH_3$; $R^3 = C_6H_5$ **2***b* $R^{5'} = CH_3$; $R^3 = OCH_3$
**1***c* $R^{3'} = CH_3$; $R^3 = OC_2H_5$ **2***c* $R^{5'} = t\text{-}C_4H_9$; $R^3 = CH_3$
**1***d* $R^{3'} = i\text{-}C_3H_7$; $R^3 = CH_3$ **2***d* $R^{5'} = t\text{-}C_4H_9$; $R^3 = i\text{-}C_3H_7$
**2***e* $R^{5'} = C_6H_5$; $R^3 = CH_3$
**2***f* $R^{5'} = OCH_3$; $R^3 = CH_3$

Les spectres de rmn $^1H$ ont été réalisés à 250 MHz et dans le deutériochloroforme (température de la sonde 20°C). Les figures 1 et 2 démontrent l'existence de deux diastéréoisomères pour les spirochromènes **1***a* et **2***a*. Les données les plus remarquables concernant les composés **1***a*–**1***d* et **2***a*–**2***f* sont groupées dans les Tableaux 1 et 2. Nous y indiquons les pourcentages des deux diastéréoisomères que nous désignons par *Min.* (minoritaire) et par *Maj.* (majoritaire). Le Tableau 2 montre que la proportion de *Maj.* va en augmentant (de 55 à 75%) avec l'encombrement soit de la position 5′ (spirochromènes **2***a*, **2***c* et **2***e*), soit des positions 3 et 5′ (spirochromène **2***d*). La détermination de la nature *Z* ou *E* du diastéréoisomère *Maj.* nécessite l'étude du dernier acte de la synthèse des spirochromènes, celui où la mérocyanine intermédiaire se referme selon le mécanisme généralement admis (7). On ne connaît pas la géométrie de cette entité fugace, mais il est vraisemblable que la partie azahétérocyclique se rapproche de celle des sels quaternaires par ses conformations possibles (8).

Sur cette base, nous avons réalisé un modèle de Dreiding de la mérocyanine **2**′*c* précurseur du spirochromène **2***c* (fig. 3).

Il est logique d'admettre que le groupement *tert*-butyle adopte une situation pseudo-équatoriale. S'il en était autrement, l'encombrement stérique serait tel, que la refermeture ne pourrait se faire que d'un seul côté, d'où formation d'un seul diastéréoisomère. Or, dans le cas où le groupement *tert*-butyle est pseudo-équatorial la refermeture conduisant à l'isomère *E* sera défavorisée par une gêne due à l'hydrogène pseudo-axial $H^{5''}$. Aucune gêne de ce type ne se rencontre dans une refermeture donnant le diastéréoisomère *Z*. Celui-ci sera donc majoritaire dans le cas du spirochromène **2***c*. Le raisonnement est identique pour **2***d* et **2***e*.

Le substituant $R^{5'}$ n'intervient donc dans la formation des deux diastéréoisomères que de manière indirecte. Lorsque $R^{5'} = CH_3$, la possibilité d'avoir ce substituant en situation pseudo-axiale n'est plus négligeable. La proportion de diastéréoisomère minoritaire *E* va augmenter dans les séries oxa- et thiazolidiniques (composés **1***a*–**1***d*, **2***a* et **2***b*). Le cas du spirochromène thiazolidinique **2***f* est particulier en raison de la formation d'un seul diastéréoisomère. Le calcul selon l'équation de Karplus montre que le substituant $R^{5'} = OCH_3$ est pseudo-axial dans ce composé (cf. Tableau 4). Le diastéréoisomère *E* se formera seul (cf. fig. 4).

#### I.2 *Approche de la stéréochimie des cycles oxa- et thiazolidiniques*

*I.2.1* Nous avons appliqué les travaux de Elguero et Fruchier (9) à la détermination de l'angle de torsion du fragment éthanique dans les spirochromènes **1** et **2**. On fait appel pour celà aux deux méthodes classiques basées sur l'équation de Karplus et où intervient soit la différence soit le rapport des constantes de couplage vicinal *cis* et *trans*. Ce mode de calcul permet de déterminer, outre l'angle de torsion $\phi$, la population $x_A$ du conformère avec $R^{5'}$ pseudo-axial (on fait abstraction dans l'équilibre ci-dessous de la partie chroménique des composés **1** et **2**).

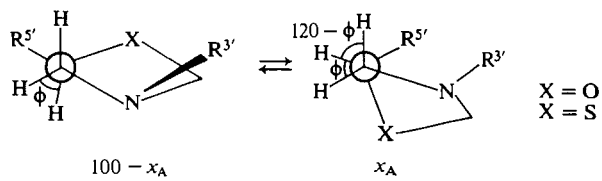

$100 - x_A$ $x_A$ X = O X = S

On admet que l'angle de pliage des deux conformères est le même. Ceci est faux car le conformère le plus encombré sera moins plié que l'autre. Néanmoins, il est intéressant de connaître les conséquences d'une telle hypothèse.

*I.2.2* La conduite des calculs selon la réf. 9 réclame la résolution des points suivants.

L'analyse du cas des spirochromènes oxa- et thiazolidiniques non substitués en 4′, 4″ et en 5′, 5″. Nous avons choisi pour cela les deux composés ci-dessous:

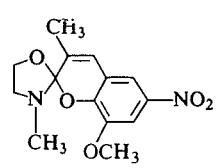

**1***e*

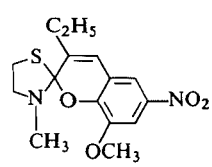

**2***g*

Can. J. Chem. Downloaded from www.nrcresearchpress.com by 210.87.254.105 on 09/06/12
For personal use only.

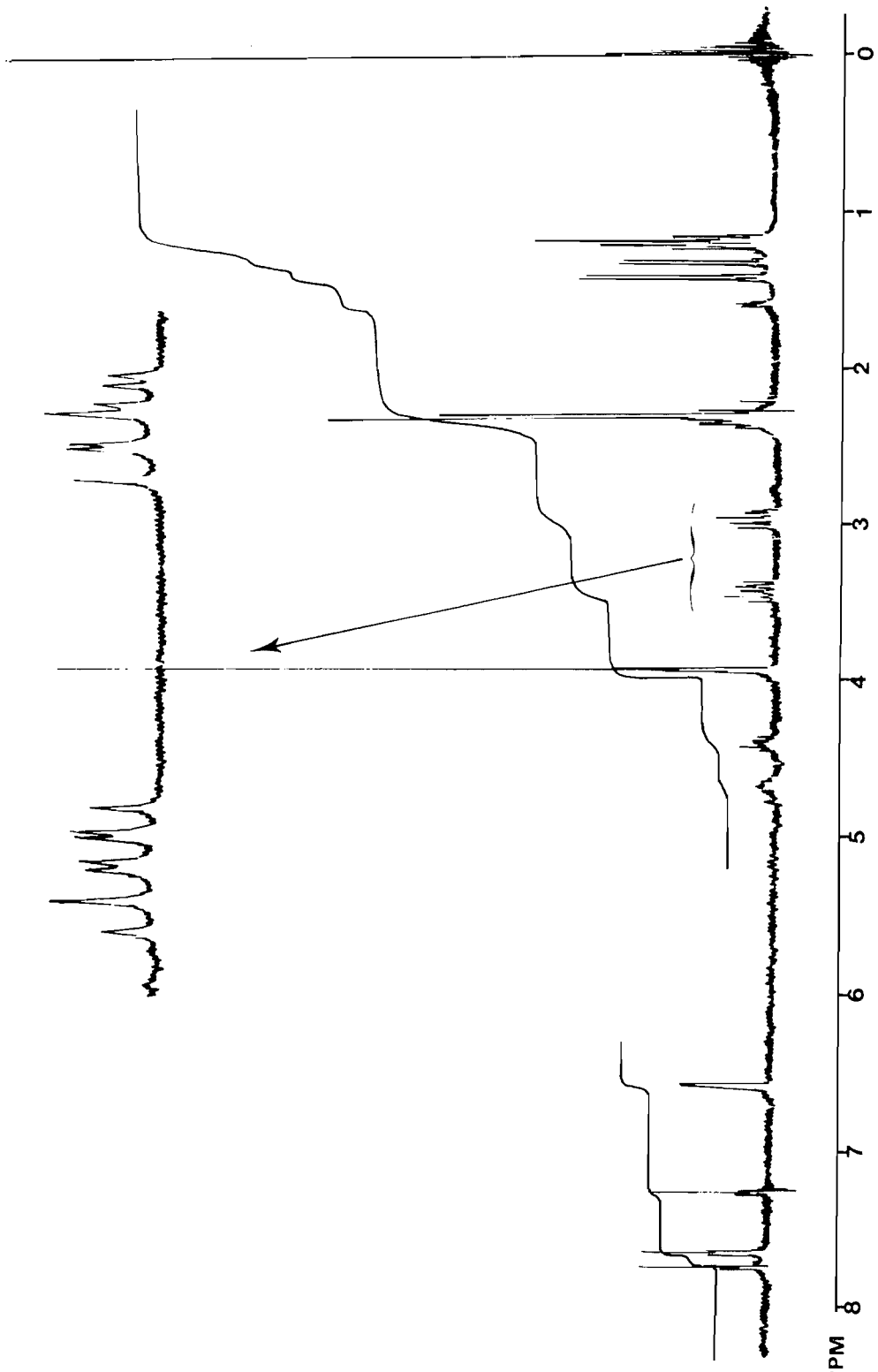


FIG. 1. Mise en évidence par la rmn $^1H$ à 250 MHz (solvant $CDCl_3$) de l'existence de deux diastéréoisomères pour le spirochromène **1***a*.

Can. J. Chem. Downloaded from www.nrcresearchpress.com by 210.87.254.105 on 09/06/12
For personal use only.

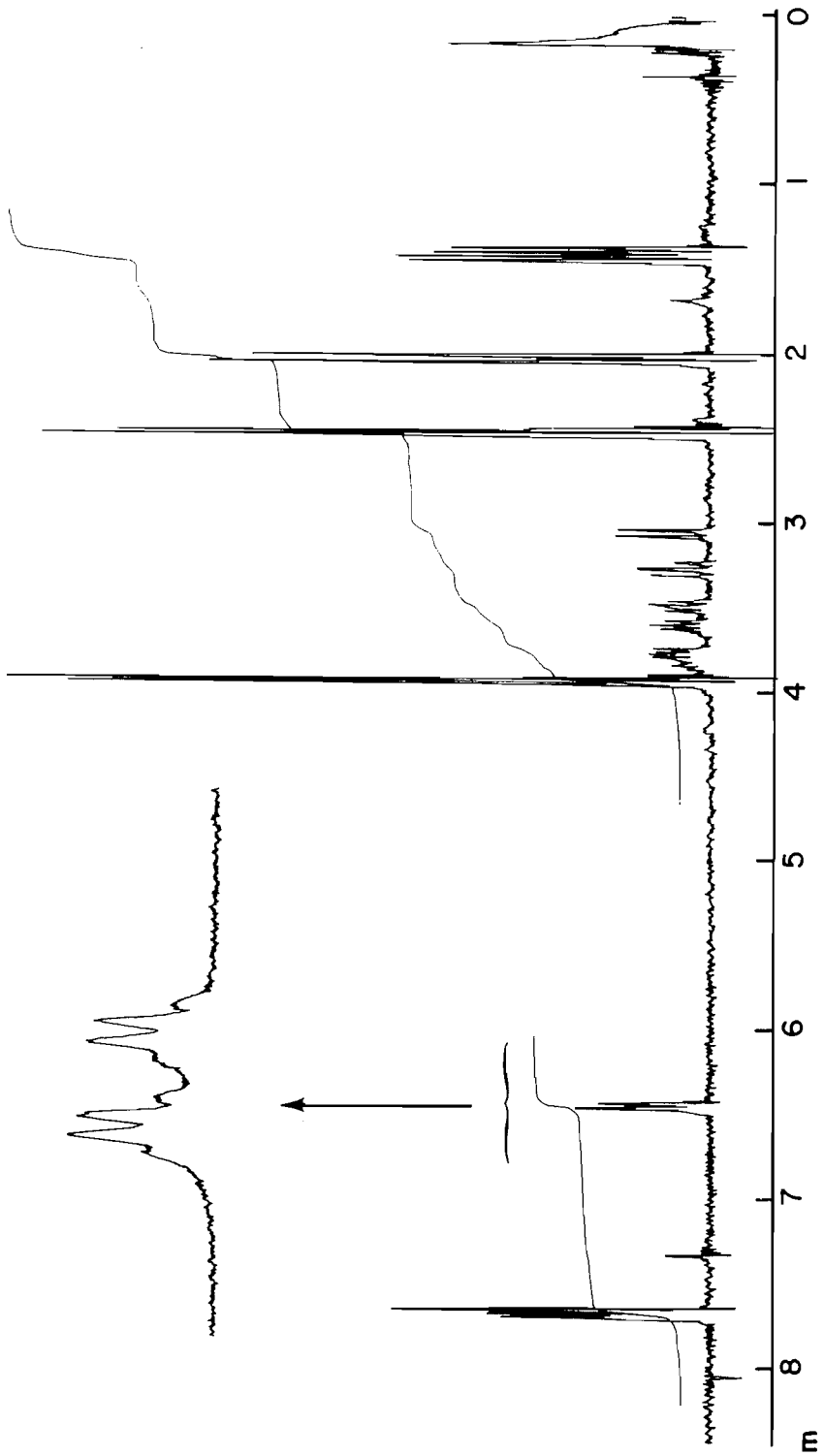


FIG. 2. Mise en évidence par la rmn $^1H$ à 250 MHz (solvant $CDCl_3$) de l'existence de deux diastéréoisomères pour le spirochromène **2***a*.

TABLEAU 1. Spectrométrie de rmn $^1H$ (réalisée à 250 MHz)[a] des spirochromènes oxazolidiniques-1,3 **1**

| Composés | "Nature" du diastéréoisomère | $R^{3'}$ | $CH_2$ en 4′ et 4″ | $CH_3$ en 5′ | H en α de l'atome d'oxygène | H éthylénique |
|---|---|---|---|---|---|---|
| | *Min.* (40%) | 2,27 3H s | 2,92 1H d de d ($J$ = 7,5 – $J$ = 2,5)<br>3,37 1H d de d ($J$ = 7,5 – $J$ = 6,3) | 1,31 d ($J$ = 6,3) | 4,66 m | 6,58 t ($J$ = 1,5) |
| **1***a* | *Maj.* (60%) | 2,29 3H s | 2,98 1H d de d ($J$ = 8,5 – $J$ = 7,5)<br>3,44 1H t ($J$ = 8,5) | 1,39 d ($J$ = 6,3) | 4,39 m | 6,56 t ($J$ = 1,5) |
| | *Min.* (32%) | 2,25 3H | 2,98 1H d de d ($J$ = 7,5 – $J$ = 3)<br>3,52 1H t ($J$ = 7,5) | 1,31 d ($J$ = 6) | 4,77 m | 6,92 s |
| **1***b* | *Maj.* (68%) | s + épaulement | 3,08 1H t ($J$ = 8)<br>3,44 1H t ($J$ = 8) | 1,47 d ($J$ = 6) | 4,53 m | 6,93 s |
| | *Min.* (45%) | 2,45 3H s | 2,93 1H d de d ($J$ = 7,5 – $J$ = 5,8)<br>3,43 1H d de d ($J$ = 7,5 – $J$ = 6,5) | 1,31 d ($J$ = 6,3) | 4,66 m | 5,88 s |
| **1***c* | *Maj.* (55%) | 2,42 3H s | 3,00 1H t ($J$ = 8)<br>3,48 1H d de d ($J$ = 8 – $J$ = 6) | 1,43 d ($J$ = 6,3) | 4,46 m | 5,90 s |
| | *Min.* (≤50%) | 1,06 6H d ($J$ = 6)<br>2,94 – 3,12 1H m | 2,85 1H d de d ($J$ = 7,5 – $J$ = 3,5)<br>3,32 1H d de d ($J$ = 7,5 – $J$ = 6,5) | 1,31 d ($J$ = 6) | 4,72 m | 6,58 q ($J$ = 1,5) |
| **1***d* | *Maj.* (≥50%) | 1,08 6H d ($J$ = 6)<br>2,94–3,12 1H m | 2,94–3,12 1H m<br>3,59 1H t ($J$ = 7,5) | 1,44 d ($J$ = 6) | 4,38 m | 6,55 q ($J$ = 1,5) |

[a]δ en ppm/TMS, multiplicité, $J$(Hz), solvant $CDCl_3$ s: singulet, d: doublet, d de d: doublet de doublets, t: triplet, q: quadruplet, m: multiplet, *Min.*: minoritaire *Maj.*: majoritaire.

Les spectres de rmn $^1H$ ont été réalisés à 250 MHz dans le deutériochloroforme. Celui du spirochromène **1***e* est du type ABMX et celui du spirochromène **2***g* du type ABCD.

L'analyse du système ABCD est possible en faisant appel aux paramètres de la littérature. Nous avons choisi ceux déterminés par Wilson et Bazzone (10) pour la *tert*-butyl-2 thiazolidine-1,3. La simulation permet un premier affinage des données. L'itération au moyen du programme LAOCOON GP1 conduit aux valeurs du Tableau 3.

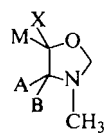


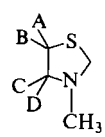


Pour le système ABMX, certains paramètres sont accessibles en analysant la partie MX. On procède encore par simulation et par itération. Les paramètres de rmn sont indiqués dans le Tableau 3.

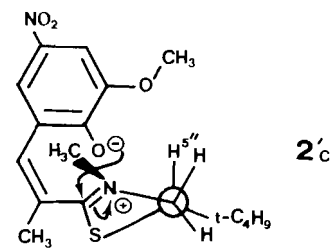


**2′c**

FIG. 3. Mise en évidence de la gêne stérique défavorisant une refermeture en diastéréoisomère *E* pour le spirochromène **2***c*.

Can. J. Chem. Downloaded from www.nrcresearchpress.com by 210.87.254.105 on 09/06/12
For personal use only.

TABLEAU 2. Spectrométrie de rmn $^1H$ (réalisée à 250 MHz)[a] des spirochromènes thiazolidiniques-1,3 **2**

| Composés | "Nature" du diastéréoisomère | $NCH_3$ | $R^{4'}$ et $R^{4''}$ | $R^{5'}$ | H en α de l'atome de soufre | H éthylénique |
|---|---|---|---|---|---|---|
| **2***a* | *Min.* (45%) | 2,45 s | 3,27 1H Partie X d'un $ABM_3X$<br>3,75 1H Partie B d'un $ABM_3X$<br>$J_{BX} = 9,2$<br>$J_{AX} = 10,2$<br>$J_{AB} = 6 - J_{MX} = J_{BM} = 0$ | 1,39 3H d ($J = 6,5$) Partie M d'un $ABM_3X$ | 3,80 m Partie A d'un $ABM_3X$ | 6,40 q ($J = 1,4$) |
| | *Maj.* (55%) | 2,47 s | 3,05 1H Partie X d'un $ABM_3X$<br>3,48 1H Partie B d'un $ABM_3X$<br>$J_{BX} = 9,2$<br>$J_{AX} = 0,7$<br>$J_{AB} = 6,4$<br>$J_{MX} = J_{BM} = 0$ | 1,43 3H d ($J = 6,7$) Partie m d'un $ABM_3X$ | 3,59 m Partie A d'un $ABM_3X$ | 6,43 q ($J = 1,4$) |
| **2***b* | *Min.* (40%) | 2,56 s | 3,16 1H d de d ($J = 8,5$ et $J = 1,5$)<br>3,65 – sous les $OCH_3$ 1H m | 1,44 3H d ($J = 7$) | 3,65 – sous les $OCH_3$ | 5,80 s + |
| | *Maj.* (60%) | 2,54 s | 3,28 1H t ($J = 9,5$)<br>3,62 1H d de d ($J = 9,5 - J = 6,8$) | 1,42 3H d ($J = 6,5$) | m | épaulement |
| **2***c* | *Min.* (25%) | 2,42 s | 3,28–3,64 Partie AB d'un ABX – m | 0,94 9H s | 3,72 Partie X d'un ABX $\lvert J_{AX} + J_{BX}\rvert = 17,5$ | 6,38 q ($J = 1,5$) |
| | *Maj.* (75%) | 2,45 s | | 0,96 9H s | 3,58 Partie X d'un ABX $\lvert J_{AX} + J_{BX}\rvert = 17,5$ | 6,36 q ($J = 1,5$) |
| **2***d*[b] | *Min.* (20%) | 2,40 s | 3,25–3,85 2H m | 0,96 9H s | Dans le massif $R^{4'} = R^{4''} = H$ | 6,47 s élargi |
| | *Maj.* (80%) | 2,42 s | | 0,98 9H s | | 6,44 s élargi |
| **2***e* | *Min.* (32%) | 2,54 s | 3,53 1H d ($J = 10$ et $J = 0$)<br>3,62–3,80 1H m | 7,2–7,72 m | 4,63 d ($J = 7$ et $J = 0$) | 6,43 q ($J = 1,5$) |
| | *Maj.* (68%) | 2,52s | 3,68 1H Partie AB<br>3,73 1H d'un ABX ($J_{AB} = 10$) | | 4,85 Partie X d'un ABX $\lvert J_{AX} + J_{BX}\rvert = 17,5$ | 6,44 q ($J = 1,5$) |
| **2***f* | Un seul diastéréoisomère décelable | 2,52 s | 3,5 1H d ($J = 10,5$ et $J = 0$)<br>3,79 1H d de d ($J = 10,5$ et $J = 4$) | 3,33 3H s | 5,20 d ($J = 4$ et $J = 0$) | 6,45 q ($J = 1,5$) |

[a]δ en ppm/TMS, multiplicité, $J$(Hz), solvant $CDCl_3$ s: singulet, d: doublet, d de d: doublet de doublets, t: triplet, q: quadruplet, m: multiplet, *Min.*: minoritaire *Maj.*: majoritaire.

[b]Spectre réalisé à 100 MHz sur un appareil JEOL JNM FX 100.

Dans les deux cas, on a vérifié la validité de ces paramètres en comparant les spectres expérimentaux à 100 MHz avec ceux calculés à partir des données de l'itération.

En accord avec les travaux de Devillers *et al.* (11) sur quelques oxazolidines-1,3, on choisit pour le composé **1***e*:

$$J_{trans} = \frac{J_{AM} + J_{BX}}{2} = 5,96\,\text{Hz};$$

$$J_{cis} = \frac{J_{AX} + J_{BM}}{2} = 7,60\,\text{HZ}$$

Can. J. Chem. Downloaded from www.nrcresearchpress.com by 210.87.254.105 on 09/06/12
For personal use only.

TABLEAU 3. Déplacements chimiques et constantes de couplage pour les spirochromènes **1***e* et **2***g* (solvant $CDCL_3$), δ en ppm/TMS, *J* en Hz

| Composé | $\delta_X$ | $\delta_M$ | $\delta_A$ | $\delta_B$ | $J_{AB}$ | $J_{AM}$ | $J_{AX}$ | $J_{BM}$ | $J_{BX}$ | $J_{MX}$ | Erreur RMS |
|---|---|---|---|---|---|---|---|---|---|---|---|
| **1***e* | 4,33 | 4,04 | 3,35 | 3,28 | −7,56 | 9,93 | 8,12 | 7,08 | 1,99 | −7,45 | 0,231 |

| Composé | $\delta_A$ | $\delta_B$ | $\delta_C$ | $\delta_D$ | $J_{AB}$ | $J_{AC}$ | $J_{AD}$ | $J_{BC}$ | $J_{BD}$ | $J_{CD}$ | Erreur RMS |
|---|---|---|---|---|---|---|---|---|---|---|---|
| **2***g* | 3,58 | 3,46 | 3,18 | 3,05 | −9,2 | 11,39 | 6,22 | 6,99 | 0,92 | −9,59 | 0,124 |

TABLEAU 4. Détermination de l'angle ϕ et de la population $x_A$ du conformère pseudo-axial dans les spirochromènes oxazolidiniques **1** et thiazolidiniques **2** (*J* en Hz; *Min.*: minoritaire; *Maj.*: majoritaire)

| Spirochromènes | "Nature" du diastéréoisomère | $J_{cis}^{exp}$ | $J_{trans}^{exp}$ | Méthode des différences ϕ(°) | Méthode des différences $x_A$(%) | Méthode des rapports ϕ(°) | Méthode des rapports $x_A$(%) |
|---|---|---|---|---|---|---|---|
| **1***e* | — | 7,60 | 5,96 | 35 | 50 | 38 | 50 |
| **1***a* | *Min.* | 6,3 | 2,5 | 39 | 86 | 41 | 78 |
| | *Maj.* | 8,5 | 7,5 | 22 | ~0 | 30 | 22 |
| **1***b* | *Min.* | 7,5 | 3 | 30 | 75 | 35 | 69 |
| | *Maj.* | 8 | 8 | 26 | ~0 | 33 | 22 |
| **1***c* | *Min.* | 6,5 | 5,8 | 37 | 44 | 40 | 49 |
| | *Maj.* | 6 | 8 | 41 | 21 | 42 | 32 |
| **1***d* | *Min.* | 6,5 | 3,5 | 37 | 73 | 40 | 69 |
| **2***g* | — | 6,15 | 6,60 | 45 | 50 | 44 | 50 |
| **2***b* | *Maj.* | 6,8 | 9,5 | 36 | ~0 | 38 | 13 |
| **2***e* | *Min.* | 7 | 0 | 35 | 118 | 38 | 98 |
| **2***f* | — | 4 | 0 | 52 | 125 | 51 | 108 |

De même, selon la réf. 10, on prend pour **2***g*:

$$J_{trans} = \frac{J_{AD} + J_{BC}}{2} = 6{,}60\,\text{Hz};$$

$$J_{cis} = \frac{J_{AC} + J_{BD}}{2} = 6{,}15\,\text{HZ}$$

Le passage spirochromène non substitué – spirochromène $R^{5'}$ – substitué grâce aux incréments de structure relatifs à $R^{5'}$. Nous avons utilisé ceux déterminés par Abraham et Pachler (12).

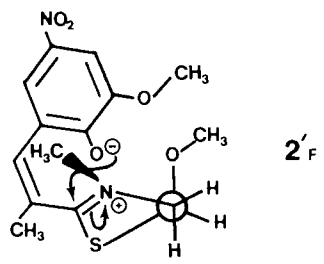


FIG. 4. Mise en évidence de la gêne stérique défavorisant une refermeture en diastéréoisomère *Z* pour le spirochromène **2***f*.

La détermination de $J_{cis}$ et de $J_{trans}$ pour les spirochromènes **1***a*–**1***d* et **2***b*, **2***e*, **2***f*. En accord avec les conclusions de divers auteurs (9, 13–15), nous avons admis qu'un substituant alkyle ou phényle blinde le proton vicinal en situation *cis* et le déblinde en situation *trans*. Nous avons vérifié l'exactitude de cette règle en étudiant des spirochromènes **1** et **2** à cycles oxa- et thiazolidiniques *cis* et *trans* diméthylés en positions 4′, 5′ (8).

*I.2.3* Le Tableau 4 présente les résultats concernant les spirochromènes **1** et **2** dont les spectres de rmn $^1H$ se sont révélés totalement exploitables. On peut relever les points suivants: (*i*) l'accord entre les deux méthodes (rapports et différences) est excellent; (*ii*) les deux conformations de l'hétérocycle azoté sont énergétiquement équivalentes dans le cas des composés non substitués **1***e* et **2***g* ($x_A = 50\%$); (*iii*) le diastéréoisomère *Maj.* présente toujours le substituant $R^{5'}$ = alkyle ou aryle en situation pseudo-équatoriale ($x_A \sim 0$). La règle contraire s'applique au diastéréoisomère *Min.* Ceci confirme notre attribution d'une géométrie *Z* pour le *Maj.* Le groupement $R^{5'} = OCH_3$ du spirochromène thiazolidinique **2***f* occupe un site pseudo-

Can. J. Chem. Downloaded from www.nrcresearchpress.com by 210.87.254.105 on 09/06/12
For personal use only.

axial ($x_A \sim 100\%$). C'est là une confirmation de la formation du seul diastéréoisomère *E* (cf. Paragraphe I.1); (*iv*) en raison du caractère approximatif de notre calcul, (on relève en effet des valeurs de $x_A$ supérieures à 100%), il est difficile de se prononcer quant aux angles $\phi$ de plissement des deux diastéréoisomères. Néanmoins, la tendance qui se dégage du Tableau 4 corrobore les conclusions tirées de l'examen des modèles de Dreiding pour l'identification des géométries *Z* ou *E*.

II. *Spirochromènes tétrahydro oxa- et thiaziniques-1,3, 3 et 4*

Les spirochromènes **3** et **4** suivants ont été étudiés:

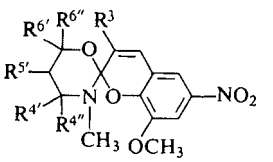

**3**

**3***a* $R^{4'} = R^{4''} = R^{6'} = CH_3$; $R^{5'} = R^{6''} = H$, $R^3 = C_6H_5$

**3***b* $R^{4'} = R^{4''} = H$; $R^{5'} = R^{6'} = R^{6''} = R^3 = CH_3$

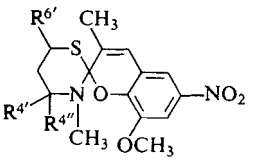

**4**

**4***a* $R^{4'} = R^{4''} = R^{6'} = CH_3$

**4***b* $R^{4'} = R^{4''} = H$; $R^{6'} = CH_3$

Le Tableau 5 regroupe les aspects les plus intéressants des spectres de rmn $^1H$ réalisés à 250 MHz et dans le deutériochloroforme (température de la sonde 20°C). Les quatre spirochromènes étudiés présentent un seul diastéréoisomère quelle que soit la position de l'un des atomes de carbone asymétriques par rapport à l'atome d'oxygène ou de soufre (en α: **3***a*, **4***a*, **4***b* ou en β: **3***b*). Nous avons déterminé la géométrie des cycles oxaziniques et thiaziniques afin d'interpréter ce fait qui différencie les séries à cinq chaînons **1** et **2** de celles à six **3** et **4**.

II.1 *Détermination de l'angle $\phi$ de torsion du cycle*

Les angles dièdres des protons vicinaux *gauches* sont calculés par application de la formule de Forrest et d'une équation de Karplus (16, 17). On trouve $\phi ae = \phi = 66°$ (**3***a*), 60° (**3***b*), 69° (**4***a*). La géométrie des cycles oxaziniques et thiaziniques s'écarte un peu de la forme chaise. On peut penser que l'inversion de cycle ne peut se réaliser par suite d'interactions de non-liaison prohibitives dans un conformère. Ainsi pour le spirochromène **4***a*, par exemple:

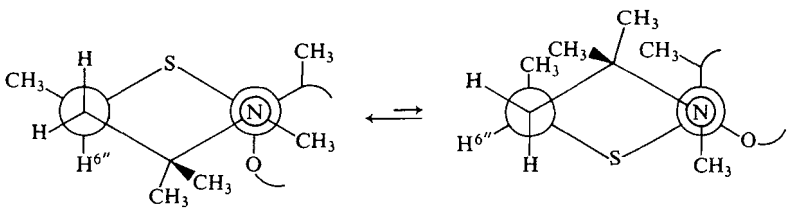

*C* ⟷ *C'*

La chaise *C'*, et, d'une manière plus générale, l'un des conformères possibles, sera toujours défavorisé en raison des interactions entre le substituant $R^3$ ($R^3 = CH_3$ pour **4***a*) et les substituants axiaux en positions 4', 4'' et 6', 6''. Par ailleurs, un conformère tel que *C'* avec le $CH_3$ en 6' axial peut être éliminé également au vu des constantes de couplage entre $H^{6''}$ et les autres protons. L'oxygène du cycle chroménique sera toujours axial et la chaise sera toujours du type *C*.

Le Tableau 5 indique que le proton équatorial est toujours le plus blindé que l'on considère les positions 4' et 4'' ou les positions 5' et 5'' dans les composés **3***a*, **3***b* et **4***b*. Ce fait n'est pas exceptionnel pour cette dernière position. Booth et Lemieux (18) le signalent à propos de tétrahydro oxazines. Ils l'attribuent à une relation 1,3 entre l'atome d'oxygène et l'atome de carbone portant les hydrogènes. Samitov *et al.* (19) concluent de même pour la diméthyl-3,4 phényl-6 tétrahydro-2,4,5,6 oxazine-1,3. Par contre, pour les autres positions, la règle est que le proton axial résonne à champ plus fort que l'équatorial. L'exception qui se rencontre ici pour la position 4', 4'' a été également signalée par Kazantsev *et al.* (20) au sujet de la triméthyl-3,5,6 phényl-6 tétrahydro-2,4,5,6 oxazine-1,3. Dans tous les cas, les auteurs admettent une conformation chaise.

II.2 *Identification du seul diastéréoisomère formé en séries oxazinique **3** et thiazinique **4***

On prendra le cas du spirochromène **3***b* pour exemple. Deux diastéréoisomères sont possibles:

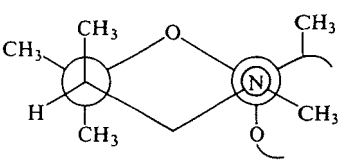

*E*

Can. J. Chem. Downloaded from www.nrcresearchpress.com by 210.87.254.105 on 09/06/12
For personal use only.

TABLEAU 5. Spectrométrie de rmn $^1H$ (réalisée à 250 MHz)[a] de quelques spirochromènes oxaziniques-1,3 **3** et thiaziniques-1,3 **4**

| Composés | $NCH_3$ | $R^{4'}$ | $R^{4''}$ | $R^{5'}$ | $R^{5''}$ | $R^{6'}$ | $R^{6''}$ |
|---|---|---|---|---|---|---|---|
| **3***a* | | | | 1,67 H B } Partie AB<br>1,60 H A } d'un $ABM_3X$ | | | 4,52 H ax.<br>Partie X |
| | | 1,12 | 3H s | A ax $J_{AB} = -13$ | | 1,18 3H | d'un $ABM_3X$ |
| | 2,13 | | | B éq $J_{AX} = 12,2$ | | d ($J = 6,3$) | |
| | s | 1,49 | 3H s | $J_{BX} = 1,35$ | | | m |
| | | | | $J_{AM} = J_{BM} = 0$ | | | |
| **3***b* | | 2,59 $H^{4'}$ éq. d de d | | 0,89 3H | 1 proton ax | 1,14 | 3H s |
| | | $J_{H^{4'}-H^{4''}} = -11,5$ | | | | | |
| | 2,28 | $J_{H^{4'}-H^{5'}} = 4,2$ | | d ($J = 7$) | sous $R^3 = CH_3$ | 1,27 | 3H s |
| | s | 3,04 $H^{4''}$ ax t | | | | | |
| | | $J_{H^{4''}-H^{5'}} = 11,5$ | | | | | |
| **4***a* | | | | 1,73 H B } Partie AB | | | 1H ax. partie |
| | | 1,28 | 3H s | 1,86 H A } d'un $ABM_3X$ | | 1,12 3H d | X d'un $ABM_3X$ |
| | 2,53 | | | A éq $J_{AB} = -13$ | | ($J = 6,5$) | 3,46 m |
| | | 1,46 | 3H s | $J_{AX} = 1,85$ | | | |
| | s | | | B ax $J_{BX} = 12,7$ | | | |
| | | | | $J_{AM} = J_{BM} = 0$ | | | |
| **4***b* | | 2,89 $H^{4'}$ éq. d de t | | 1,69 – 1,90 1H m | | | 1H dans le |
| | 2,45 | $J_{H^{4'}-H^{4''}} = -12,5$ | | 1H sous le $CH_3$ | | 1,14 3H d | massif |
| | s | $J_{H^{4'}-H^{5'}} = J_{H^{4'}-H^{5''}} = 3,5$ | | éthylénique | | ($J = 6,8$) | 3,23–3,46 |
| | | 3,23–3,46 $H^{4''}$ ax. m | | | | | |

[a]δ en ppm/TMS, multiplicité, $J$(Hz); solvant $CDCl_3$; s: singulet; d: doublet; d de d: doublet de doublets; d de t: doublet de triplets; m: massif; ax: axial; eq.: équatorial.

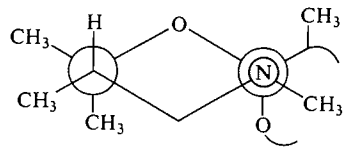


*Z*

On élimine les autres conformères en accord avec les conclusions du paragraphe II.1.

La rmn $^1H$ indique que le substituant $R^{5'} = CH_3$ est équatorial (Tableau 5). Le diastéréoisomère *Z* est donc le seul à se former. Les spirochromènes **3***a*, **4***a* et **4***b* auront par contre la configuration *E*.

## Partie expérimentale

Les spirochromènes **1–4** sont des composés nouveaux dont nous avons déjà relaté la synthèse et les caractéristiques physiques de façon détaillée (1, 2, 21, 22). Les spectres de rmn $^1H$ à 250 MHz ont été enregistrés sur un appareil Cameca.

## Remerciements

Nous remercions vivement Mme le Professeur M. L. Martin (Faculté des Sciences de Nantes) pour ses conseils et son amicale collaboration à l'analyse des spectres ABCD et ABMX. Mme Mabon a réalisé les itérations (programme LAOCOON GP1). Nous remercions aussi Mlle J. Berger (Université d'Aix-Marseille III) pour la réalisation des spectres et Mrs. J. Elguero et A. Fruchier pour l'envoi du tableau permettant le calcul des angles de torsion en séries à cinq chaînons.

1. M. MAGUET, Y. POIRIER et R. GUGLIELMETTI. Bull. Soc. Chim. Fr. 550 (1978).
2. M. MAGUET et R. GUGLIELMETTI. Bull. Soc. Chim. Fr. 539 (1978).
3. I. GRUDA et R. M. LEBLANC. Can. J. Chem. **54**, 576 (1976).
4. I. GRUDA, R. M. LEBLANC et J. SOCHANSKI. Can. J. Chem. **56**, 1296 (1978).
5. M. MAGUET, F. GARNIER et R. GUGLIELMETTI. J. Chem. Res. S, 145 (1982); M, 1522 (1982).
6. M. MAGUET, F. GARNIER et R. GUGLIELMETTI. Nouv. J. Chim. **6**, 207 (1982).
7. R. GUGLIELMETTI et J. METZGER. Bull. Soc. Chim. Fr. 2824 (1967).
8. M. MAGUET. Thèse de Doctorat ès-Sciences, Brest (1980).
9. J. ELGUERO et A. FRUCHIER. An. Quim. **70**, 141 (1974).
10. G. E. WILSON JR. et T. J. BAZZONE. J. Am. Chem. Soc. **96**, 1465 (1974).
11. J. DEVILLERS, DAO HUY GIAO et J. NAVECH. C. R. Acad. Sci. Sér. C, **277**, 1067 (1973).
12. R. J. ABRAHAM et K. G. R. PACHLER. Mol. Phys. **7**, 165 (1964).
13. R. A. WOHL. J. Org. Chem. **38**, 3099 (1973).
14. R. A. WOHL et J. CANNIE. J. Org. Chem. **38**, 1787 (1973).
15. R. A. WOHL et D. F. HEADLEY. J. Org. Chem. **37**, 4401 (1972).
16. T. P. FORREST. Org. Magn. Reson. **6**, 355 (1974).
17. T. P. FORREST. J. Am. Chem. Soc. **97**, 2628 (1975).
18. H. BOOTH et R. U. LEMIEUX. Can. J. Chem. **49**, 777 (1971).
19. YU. YU. SAMITOV, O. I. ZHUK, B. V. UNKOVSKIJ, I. P. BOJKO et YU. F. MALINA. Zh. Org. Khim. **9**, 201 (1973).
20. YU. E. KAZANTSEV, I. P. BOJKO, YU. F. MALINA, O. I. ZHUK, YU. YU. SAMITOV et B. V. UNKOVSKIJ. Zh. Org. Khim. **9**, 2597 (1973).
21. M. MAGUET, Y. POIRIER et R. GUGLIELMETTI. Bull. Soc. Chim. Fr. 561 (1978).
22. M. MAGUET, Y. POIRIER et R. GUGLIELMETTI. Bull. Soc. Chim. Fr. 568 (1978).

Can. J. Chem. Downloaded from www.nrcresearchpress.com by 210.87.254.105 on 09/06/12
For personal use only.

# Analyse par résonance magnétique nucléaire $^{13}C$ de la stabilité relative des spirochromènes et des mérocyanines dérivant du méthoxy-3 nitro-5 salicylaldéhyde

MICHEL MAGUET, MICHEL LE BACCON, YVES POIRIER ET ROBERT GUGLIELMETTI

*Laboratoire de synthèse organique, LA C.N.R.S. 322, Université de Bretagne Occidentale, Faculté des Sciences et Techniques, 6, Avenue Le Gorgeu, 29283 Brest Cedex, France*

Reçu le 3 mars 1982

MICHEL MAGUET, MICHEL LE BACCON, YVES POIRIER et ROBERT GUGLIELMETTI. Can. J. Chem. **60**, 2644 (1982).

Les sels d'hétérocycloimmonium réagissent avec le méthoxy-3 nitro-5 salicylaldéhyde pour donner en général des spirochromènes ou des mérocyanines. Seuls ces derniers composés se forment en séries thiazolinique et benzimidazolinique. Le greffage d'une chaîne paraffinique sur les mérocyanines permet leur étude en rmn $^{13}C$. La confrontation de leurs spectres avec ceux des sels d'hétérocycloimmonium met en évidence une hyperconjugaison stabilisatrice en séries thiazolinique et benzimidazolinique. La série benzoxazolinique apparaît comme une série charnière : les stabilités des spirochromènes et des mérocyanines y sont voisines. On peut ainsi déterminer la valeur limite du déplacement chimique de l'atome de carbone concerné par la spiroannellation des mérocyanines.

MICHEL MAGUET, MICHEL LE BACCON, YVES POIRIER, and ROBERT GUGLIELMETTI. Can. J. Chem. **60**, 2644 (1982).

Heterocycloimmonium salts generally react with 3-methoxy 5-nitro salicylaldehyde to give spirochromenes or merocyanines. Only the latter compounds are obtained in the thiazolinic and the benzimidazolinic series. The linking of a paraffinic ring to the merocyanines allows their $^{13}C$ nmr study. The comparison of their spectra with those of heterocycloimmonium salts stresses a hyperconjugative effect in the thiazolinic and the benzimidazolinic series. The benzoxazolinic series appears to be in an intermediate position : the thermodynamic stabilities of spirochromenes and merocyanines are quite similar. The limiting value of the chemical shift of the carbon atom involved in the spiroannellation of merocyanines, can be approximately determined.

## Introduction

L'action des sels d'hétérocycloimmonium sur le méthoxy-3 nitro-5 salicylaldéhyde[1] peut être schématisée par l'équation suivante :

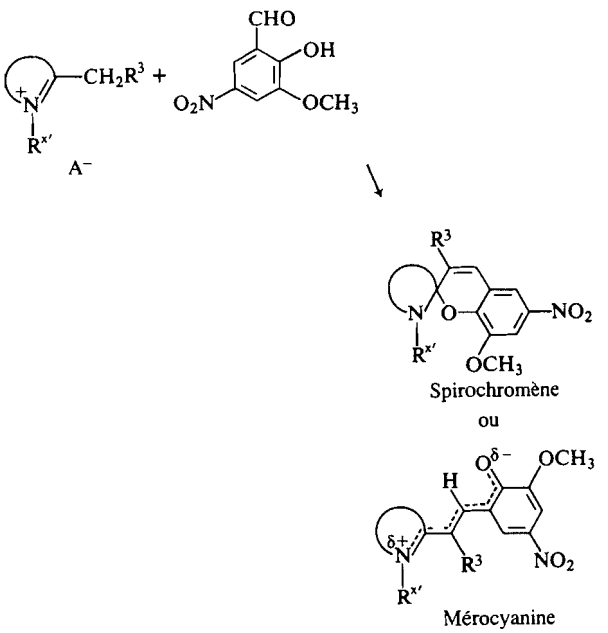


Les données de la littérature jointes aux résultats du laboratoire permettent de dégager trois cas possibles. Il peut y avoir : (*1*) formation de spirochromènes quel que soit $R^3$ et en particulier $R^3$ = H. C'est le cas des séries indolinique (1), pipéridinique et thiazinique-1,4 (2) ; (*2*) formation de spirochromènes pour $R^3 \geq CH_3$. Si $R^3$ = H, on isole une mérocyanine permanente. C'est le cas des séries benzothiazolinique (3,4) benzoxazolinique (5), oxa- et thiazolidinique-1,3, oxa- et thiazinique-1,3 (6–9) ; et (*3*) formation systématique d'une mérocyanine permanente quel que soit $R^3$ en séries thiazolinique (5) et benzimidazolinique (10).

On peut rencontrer des cas limites. Le comportement des mérocyanines benzoxazoliniques **1***a* et **1***b* en est un exemple.

Le spectre de rmn $^1H$ de **1***a* en solution dans le deutériochloroforme (fig. 1) et le spectre uv–visible de **1***b* en solution dans le toluène (fig. 2) montrent une refermeture de ces mérocyanines en spirochromènes. La généralisation des travaux de Veksler *et al.* (11) et de Zakhs *et al.* (12) par Sinkin *et al.* (13) conduit à la conclusion qu'un sel de méthyl-2

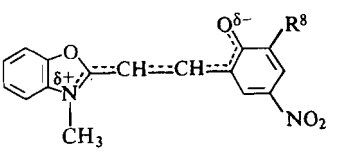


**1***a* $R^8 = CH_2OC_{16}H_{33}$
**1***b* $R^8 = OCH_3$

[1]Le méthoxy-3 nitro-5 salicylaldéhyde est très couramment utilisé dans ce genre de synthèse car il peut conduire à des spirochromènes dotés d'excellentes propriétés photochromiques et donc très intéressants au niveau des applications potentielles.

0008-4042/82/212644-10$01.00/0

©1982 National Research Council of Canada/Conseil national de recherches du Canada

Can. J. Chem. Downloaded from www.nrcresearchpress.com by 210.87.254.5 on 09/06/12
For personal use only.

Can. J. Chem. Downloaded from www.nrcresearchpress.com by 210.87.254.5 on 09/06/12
For personal use only.

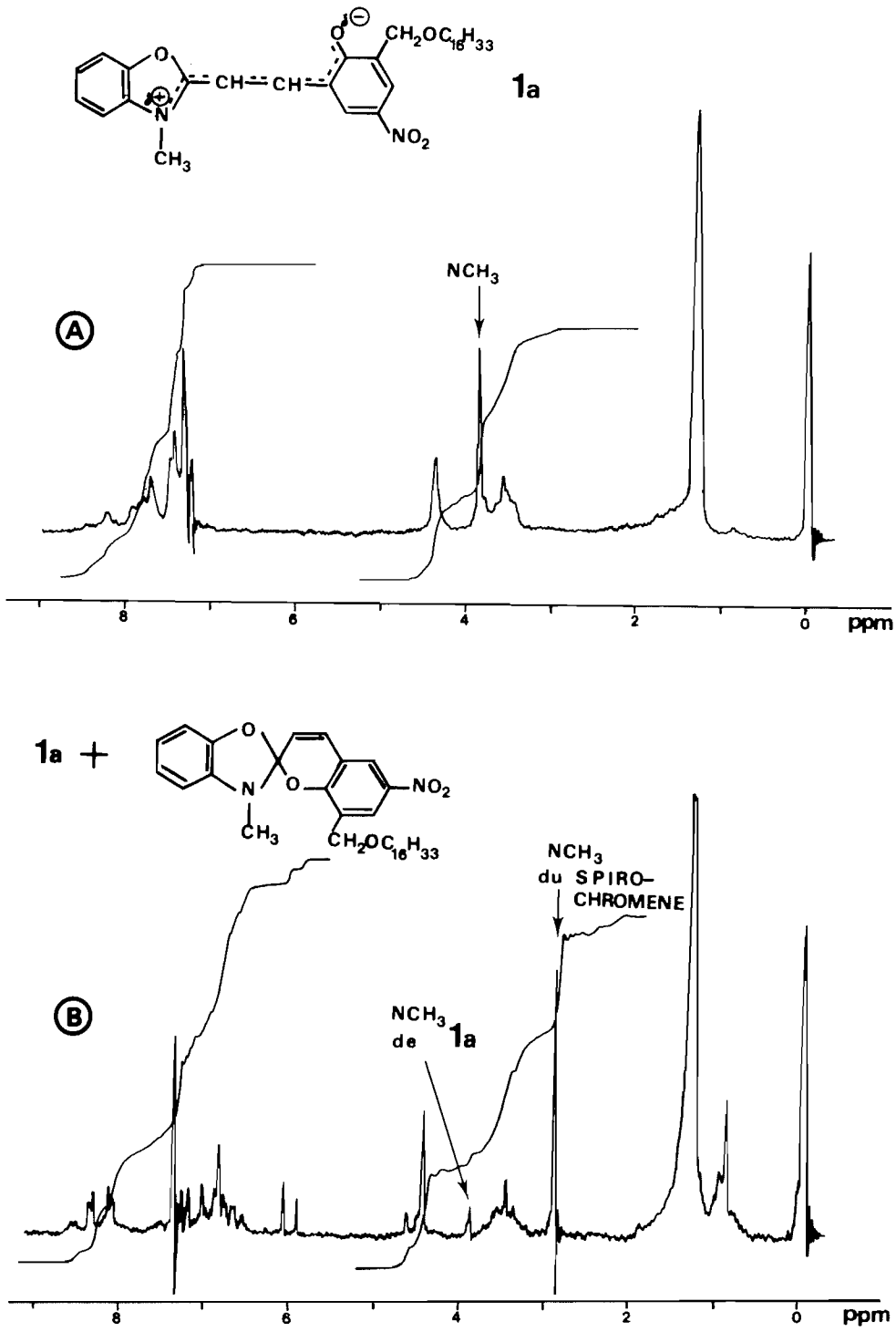


FIG. 1. Evolution du spectre de rmn $^1H$ de la mérocyanine 1*b* en solution dans $CDCl_3$. Spectre A: $t = 0$; spectre B: $t = 24$ h.

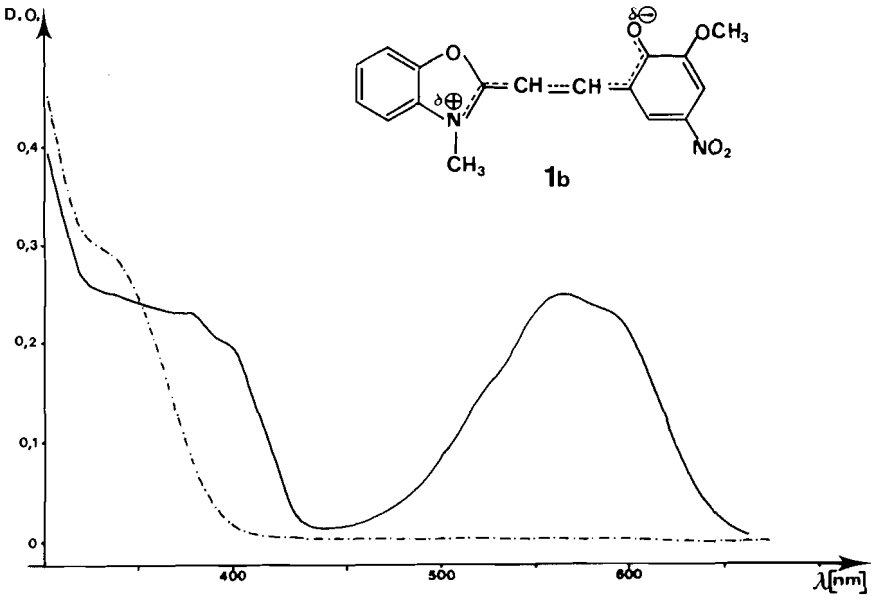


FIG. 2. Evolution du spectre uv–visible de la mérocyanine *1b* en solution dans le toluène (concentration inconnue en raison de la très faible solubilité). ——— Immédiatement après la mise en solution. —.—.—.— Après 24 h à l'obscurité (on peut revenir à l'état initial par irradiation uv).

benzoxazolium ne peut donner de spirochromènes. Il y a là une contradiction avec nos résultats expérimentaux. Le problème de la stabilité relative des spirochromènes et des mérocyanines obtenus à partir du méthoxy-3 nitro-5 salicylaldéhyde se trouve ainsi posé. La rmn $^{13}C$ nous a semblé une méthode de choix pour parvenir à sa résolution, la refermeture d'une mérocyanine intéressant l'atome de carbone en α de l'atome d'azote.

La logique veut donc que l'on étudie en premier lieu les mérocyanines permanentes synthétisables dans la plupart des séries (les séries indolinique, pipéridinique et thiazinique-1,4 exceptées). La très faible solubilité de ce type de composé dérivant du méthoxy-3 nitro-5 salicylaldéhyde (e.g., la mérocyanine *1b*) est une difficulté insurmontable pour une étude en rmn $^{13}C$. Celle-ci est rendue possible par le greffage d'une chaîne paraffinique ($R^8$ = $CH_2OC_{16}H_{33}$). Les mérocyanines étudiées présentent la structure suivante :[2,3]

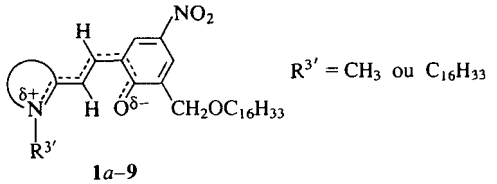


*1a–9*

[2]La numérotation des atomes de carbone dans ces mérocyanines ne correspond pas à la nomenclature officielle. Nous l'avons adoptée par souci de simplification.

[3]La justification de cette structure est donnée dans la partie expérimentale (paragraphe II.3).

Le remplacement du substituant $R^8 = OCH_3$ par le substituant $R^8 = CH_2OC_{16}H_{33}$ ne modifie pas les propriétés des mérocyanines (cf. figs. 1 et 2). Les composés ***1a–9*** sont donc des modèles acceptables pour notre travail.

## Résultats et discussion

### I. *Résonance magnétique nucléaire $^{13}C$ des mérocyanines permanentes 1a–9($R^3$ = H)*

Les spectres de rmn $^{13}C$ ont été réalisés dans le deutériochloroforme à la température ambiante. Le Tableau 1 regroupe les déplacements chimiques de la partie azahétérocyclique. Le Tableau 2 concerne la chaîne diméthinique et la partie phénolate. L'identification des carbones est facilitée par la comparaison des divers spectres, par l'intervention d'effets d'incréments connus (14) et par des résultats acquis au laboratoire (15, 16). Les atomes de carbone 3 et 4 du pont diméthinique ont été repérés grâce à des découplages sélectifs réalisés sur les mérocyanines **5**, **7** et **8**. On a pu ainsi établir que le proton éthylénique situé à champ fort est porté par le carbone sortant à champ faible et inversement. Ce résultat est en accord avec la structure proposée ci-dessus pour les mérocyanines ***1a–9*** et avec les données de la littérature (16). On retrouve également deux faits bien connus : l'alternance des densités électroniques sur le pont diméthinique (16, 17) et le déplacement chimique du carbone 8a (178 à 180 ppm, Tableau 2), bien plus proche de celui d'un atome de carbone de type

Can. J. Chem. Downloaded from www.nrcresearchpress.com by 210.87.254.5 on 09/06/12
For personal use only.

Can. J. Chem. Downloaded from www.nrcresearchpress.com by 210.87.254.5 on 09/06/12
For personal use only.

TABLEAU 1. Spectrométrie[a] de rmn $^{13}C$ de quelques mérocyanines de formule

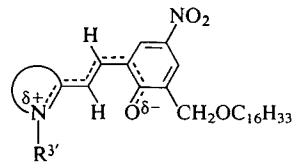

| Noyau azahétérocyclique | 2′ | 3′a ou 1′a+3′a | 4′ | 4′a | 4′b | 5′ | 6′ | 6′a | 7′ | 7′a |
|---|---|---|---|---|---|---|---|---|---|---|
| 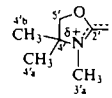 2 | *169,1*<br>169,8 | *31,8*<br>32,9 | *66,2*<br>65,2 | *23,8*<br>24,0 | | *80,8*<br>80,2 | — | — | — | — |
| 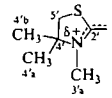 3 | 179,3 | 32,5 | 73,5 | 24,2 | | 40,1 | — | — | — | — |
| 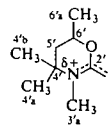 4 | *167,7*<br>168,1 | 33,5 | 57,9 | 26,2 | 27,5 | 42,9 | 71,8 | 20,1 | — | — |
| 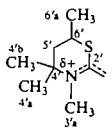 5 | *176,8*<br>176,6 | *31,8*<br>31,8 | *63,2*<br>61,8 | *26,3*<br>26,2 | *27,5*<br>28,1 | *44,7*<br>45,5 | *37,9*<br>37,7 | *20,2*<br>19,9 | — | — |
| | | | | | | | | | | 127,9 |
| 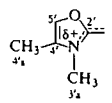 6 | *162,8*<br>163,0 | 30,9 | 129,9 | 7,4 | — | 134,7 | — | — | — | — |
| 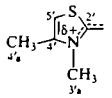 7 | *172,0*<br>172,5 | 35,9 | 143,8 | 14,5 | — | 111,8 | — | — | — | — |
| 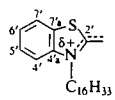 8 | 172,3 | — | 114,3 | 140,9 | — | 128,9 | 127,1 | — | 122,9 | 126,5 |
| 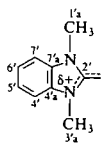 9 | *151,1*<br>150,7 | 32,8 | 111,4 | 131,0 | — | 126,5 | 126,5 | — | 114,4 | 131,0 |

[a]δ $^{13}C$ des carbones de la partie hétérocyclique azotée. Solvant : $CDCl_3$. Enregistrement à 20°C. Solvant : DMSO-$d_6$. Enregistrement à 70°C (chiffres en italique).

phénolate que de celui d'un atome de carbone de type quinonique.

Hormis ces constatations classiques, on ne peut dégager des Tableaux 1 et 2 aucun argument étayant le fait que seules des mérocyanines sont stables dans les séries oxazolinique, thiazolinique et benzimidazolinique quel que soit $R^3$. Le seul déplacement chimique variant de façon significative est celui du carbone 2,2′ susceptible d'être le siège de la spiroannellation. La différence des valeurs entre la série oxazolinique (composé **6** ; δ = 163 ppm) et la série oxazinique (composé **4** ; δ =

Can. J. Chem. Downloaded from www.nrcresearchpress.com by 210.87.254.5 on 09/06/12
For personal use only.

TABLEAU 2. Spectrométrie[a] de rmn $^{13}C$ de quelques mérocyanines de formule

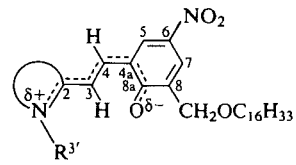

| Mérocyanines | 2 | 3 | 4 | 4a | 5 | 6 | 7 | 8 | 8a |
|---|---|---|---|---|---|---|---|---|---|
| **2** | *169,1* | *98,5* | *152,8* | *119,6* | *131,2*[b] | *130,8*[b] | *125,0* | *132,6*[b] | *178,5* |
| | 169,8 | 96,7 | 155,4 | 119,4 | 133,3[b] | 132,3[b] | 125,1 | 133,3[b] | 179,6 |
| **3** | 179,3 | 107,1 | 156,8 | 119,9 | 133,1[b] | 133,7[b] | 125,7 | 133,1[b] | 180,1 |
| **4** | *167,7* | | | | | | | | |
| | 168,1 | 103,3 | 153,6 | 119,5 | 133,4[b] | 132,7[b] | 125,1 | 131,9[b] | 179,5 |
| **5** | *176,8* | *115,1* | *147,9* | *120,2* | *130,6*[b] | *130,8*[b] | *124,7* | *132,1*[b] | *178,2* |
| | 176,6 | 113,6 | 150,8 | 119,7 | 132,0[b] | 132,9[b] | 124,8 | 132,9[b] | 179,5 |
| **6** | *162,8* | | | | | | | | |
| | 163,0 | 98,0 | 149,3 | 119,4 | 131,1[b] | 132,3[b] | 124,9 | 134,7[b] | 179,0 |
| 7 | *172,0* | | | | | | | | |
| | 172,5 | 108,4 | 147,6 | 120,1 | 131,4[b] | 132,3[b] | 125,4 | 131,9[b] | 178,9 |
| **8** | 172,3 | 106,2 | 152,1 | 119,9 | 132,3[b] | 133,2[b] | 125,7 | 132,7[b] | 180,0 |
| **9** | *151,1* | | | | | | | | |
| | 150,7 | 101,0 | 148,8 | 119,4 | 130,3 | 132,0 | 125,1 | 132,0 | 178,4 |

[a]$\delta$ $^{13}C$ des carbones de la chaine diméthinique et de la partie phénolate. Solvant : $CDCl_3$. (enregistrement à 20°C). Solvant : DMSO-$d_6$ : chiffres en italique (enregistrement à 70°C.
[b]Déplacements chimiques voisins : possibilité de permutation.

168,1 ppm) va dans le sens des constatations expérimentales. On peut y joindre la série benzimidazolinique (composé **9** ; $\delta$ = 150,7 ppm). Par contre, la série benzothiazolinique (composé **8** ; $\delta$ = 172,3 ppm) donne des spirochromènes contrairement à la série thiazolinique (composé **7** ; $\delta$ = 172,5 ppm). Ainsi la mérocyanine **10** ne peut se refermer bien que $\delta$C-2′ = 173,5 ppm (solvant $CDCl_3$).

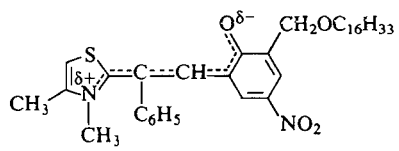

**10**

Il est certain que l'étude de la mérocyanine **1***a* aurait pu être fructueuse. Malheureusement, la faible solubilité de ce composé et le fait qu'il évolue dans le temps (cf. figure 1) excluent la possibilité de déterminer $\delta$C-2′.

Les composés **1***a*–**9** ne sont donc pas des modèles suffisants pour prévoir la stabilité relative des spirochromènes et des mérocyanines au sein de chaque série. Nous avons alors choisi d'étudier les sels hétérocycliques qui conduisent à ces composé.

## II. *Résonance magnétique nucléaire $^{13}C$ de sels d'hétérocycloimmonium*

Nous avons groupé dans le Tableau 3 les spectres de rmn $^{13}C$ de divers sels quaternaires méthylés en 2 et à partir desquels on obtient uniquement des mérocyanines permanentes. Le Tableau 4 présente les déplacements chimiques du carbone 2 (ou 3 pour la série thiazinique-1,4) de sels pouvant conduire les uns à des spirochromènes, les autres à des mérocyanines. Le solvant choisi est le DMSO-$d_6$, certains sels étant peu solubles dans $CDCl_3$. On peut dégager les points suivants.

(*a*) Les sels méthylés en 2 (ou en 3) fournissent des formes fermées stables quand on a $\delta$C-2 (ou -3) > 191 ppm. Ceci se rencontre en séries thiazinique-1,4, pipéridinique et indolinique (composés **20**, **21**, **22**). On peut estimer importante la localisation de la charge positive sur le carbone siège de la refermeture.

(*b*) Quand pour un sel méthylé en 2, on a $\delta$ C-2 < 191 ppm, le seul composé à se former est une mérocyanine. C'est le cas des séries oxa- et thiazolidinique, oxa- et thiazinique-1,3, benzothiazolinique et benzimidazolinique (composés **11**–**14**, **26** et **27**).

(*c*) Les sels **18** et **19** (Tableau 4) substitués en -2 par un groupement éthyle présentent une valeur $\delta$C-2 < 191 ppm (187,3 ppm pour **19** et 174,3 ppm pour **18**). Ils conduiront néanmoins à des spirochromènes en raison du facteur stérique apporté par $R^3 = CH_3$.

(*d*) On relève pour les sels de thiazolium **23** et **24** des valeurs de $\delta$ C-2 égales à 177,3 et 179,3 ppm respectivement (Tableau 4), c'est-à-dire des chif-

TABLEAU 3. Spectrométrie[a] de rmn $^{13}C$ de sels d'hétérocycloimmonium conduisant à des mérocyanines permanentes

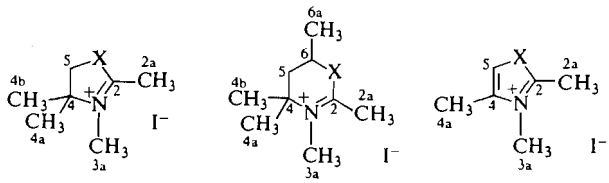

| Composés | Carbones | | | | | | | | |
|---|---|---|---|---|---|---|---|---|---|
| | 2 | 2a | 3a | 4 | 4a | 4b | 5 | 6 | 6a |
| 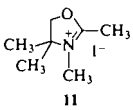 **11** | 175,2 | 15,7 | 30,2 | 67,2 | 24,2 | | 82,2 | — | — |
| 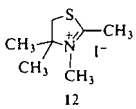 **12** | 187,9 | 20,1 | 35,1 | 76,6 | 24,4 | | 42,8 | — | — |
| 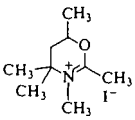 **13** | 173,5 | 22,5 | 35,4 | 59,4 | 25,8 | 26,2 | 40,9 | 74,4 | 20,3 |
| 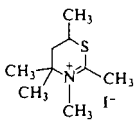 **14** | 182,3 | 27,4 | 33,9 | 64,0 | 24,9 | 27,1 | 43,0 | 39,3 | 20,1 |
| 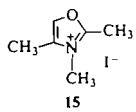 **15** | 165,4 | 8,06 | 33,3 | 131,9 | 13,9 | — | 138,2 | — | — |
| 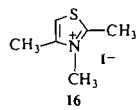 **16** | 171,2 | 16,6 | 36,9 | 145,8 | 13,9 | — | 117,1 | — | — |

[a] $\delta^{13}C$ en ppm/TMS. Solvant: DMSO-$d_6$.

fres supérieurs à celui (174,3 ppm) enregistré pour l'iodure d'oxazinium **18**. Or les tosylates **23** et **24** ne donnent que des mérocyanines permanentes telles que **10** (5). L'effet stérique compensateur de $R^3$ n'est plus suffisant dans ce cas. Pour interpréter ceci, il faut déterminer les déplacements chimiques des carbones 4 et 5 du cycle thiazolique. Ces valeurs sont accessibles grâce au découplage total, au découplage par faible bruit et à l'effet Overhauser (Tableau 4).

Le parallèle entre nos résultats et ceux de Faure *et al.*(18, 19) est mis en relief par le Tableau 5. L'atome de carbone 4 est toujours blindé quand on passe du thiazole au cation thiazolium. C'est le contraire pour le carbone 5. En accord avec les auteurs précédents, on peut envisager une important délocalisation de la charge positive sur l'ensemble de la molécule. Ceci rejoint les conclusions de Haake et Miller (20) selon lesquels la charge positive est répartie sur l'azote et surtout sur le soufre. Une forme sulfonium est la meilleure représentation de l'ion thiazolium.

Plus concrètement, Aldrich *et al.* (21) ont établi que dans l'ion triméthyl-3,4,5 thiazolium-1,3 l'atome de soufre porte une charge $q = 0{,}453$, alors que l'atome de carbone 2 est quasiment neutre ($q = 0{,}106$).

La comparaison des déplacements chimiques du carbone 2 (ou 2′) dans les Tableaux 1 et 3 ne peut être effectuée rigoureusement que s'ils se rappor-

Can. J. Chem. Downloaded from www.nrcresearchpress.com by 210.87.254.5 on 09/06/12
For personal use only.

TABLEAU 4. δEC des carbones[a] 2 (ou 3), 4 et 5 dans des sels d'hétérocycloimmonium alkylés en -2 ou en -3 conduisant à (a) des spirochromènes ; (b) des mérocyanines permanentes

| (a) | Composés | δC-2 | (b) | Composés | δC-2 | δC-4 | δC-5 |
|---|---|---|---|---|---|---|---|
| | 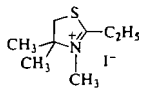 **17** | 193,4 | | 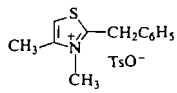 **23** | 177,3 | 146,3 | 118,5 |
| | 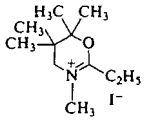 **18** | 174,3 | | 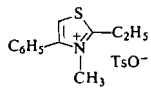 **24** | 179,3 | 149,2 | 120,2 |
| | 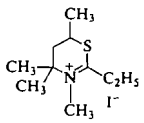 **19** | 187,3 | | 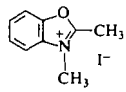 **25** | 170,7 | | |
| | 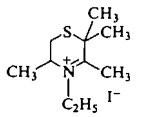 **20** | 191,3 | | 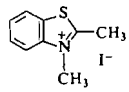 **26** | 177,1 | | |
| | 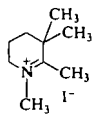 **21** | 195,2 | | 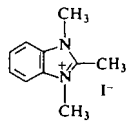 **27** | 153,1 | | |
| | 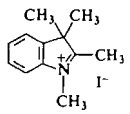 **22** | 196,5 | | | | | |

[a]δ$^{13}$C en ppm/TMS. Solvant: DMSO-$d_6$.

tent à des composés étudiés dans la même solvant. Nous avons examiné les spectres de rmn $^{13}$C des mérocyanines **2–9** dans le DMSO-$d_6$. La plupart de ces composés y sont peu solubles et l'enregistrement doit être réalisé à 70°C. Les résultats, quoique fragmentaires, montrent que le passage du sel (Tableau 3) à la mérocyanine (Tableau 1) s'accompagne d'un blindage du C-2 de 5,5 à 6,1 ppm en séries oxazolidinique, oxa- et thiazinique-1,3. Par contre, en séries oxazolinique et thiazolinique le déplacement chimique du C-2 dans le sel est voisin de celui du C-2′ dans la mérocyanine (0,8 ppm de différence pour **7**, 2,6 ppm pour **6**). Ainsi, la forme sulfonium mise en évidence pour les sels de thiazolium est envisageable pour les mérocyanines qui en dérivent. De plus, l'important blindage de C-5′ dans la mérocyanine **7** (111,8 ppm contre 117,1 ppm pour le sel **16**) est en faveur d'une hyperconjugaison du groupement méthyle. Cette résonance accrue pourrait stabiliser fortement les mérocyanines **7** (de même que **6**) et interdire leur refermeture en spirochromènes malgré un effet stérique favorable de $R^3$ = alkyle ou aryle. Une hyperconjugaison serait également envisageable dans les spirochromènes mais resterait limitée à la partie azahétérocyclique. Par contre, dans les mérocyanines, elle peut être étendue à l'ensemble de la molécule.

(*e*) La conclusion précédente s'applique à la série benzimidazolinique. En effet, le blindage de C-2 (δ = 153,1 ppm) dans l'iodure de benzimidazolium **27** peut s'expliquer par une dispersion de la charge positive sur les hydrogènes des groupements méthyle. Ceci a été avancé en série imidazolinique (21). Cette notion doit être étendue à la mérocyanine **9** (Tableau 3 ; δ C-2′ = 151,1 ppm) d'où une importante stabilisation.

(*f*) La valeur de δC-2 = 170,7 ppm (Tableau 4) pour l'iodure de benzoxazolium **25** apparaît comme

Can. J. Chem. Downloaded from www.nrcresearchpress.com by 210.87.254.5 on 09/06/12
For personal use only.

Can. J. Chem. Downloaded from www.nrcresearchpress.com by 210.87.254.5 on 09/06/12
For personal use only.

TABLEAU 5. Déplacements chimiques des C-4 et C-5 de quelques thiazoles et ions derivés (Solvant DMSO-$d_6$)

| Composés ou ions | δC-4 | δC-5 |
|---|---|---|
| Phényl-4 thiazole[a] | 155,3 | 114,0 |
| Cation phényl-4 thiazolium[a] | 153,3 | 116,9 |
| Diméthyl-2,4 thiazole | 152,5 | 114,1 |
| **16** | 145,8 | 117,1 |
| Ethyl-2 phényl-4 thiazole[a] | 154,0 | 112,5 |
| **24** | 149,2 | 120,2 |
| Benzyl-2 méthyl-4 thiazole | 152,6 | 114,6 |
| **23** | 146,3 | 118,5 |

[a]Résultats de Faure *et al.* (18).

TABLEAU 6. Caractéristiques des sels d'hétérocycloimmonium

| Sel | Synthèse de la base (référence) | *F*(°C) |
|---|---|---|
| **15** | (23, 24) | 262[a] |
| **16** | (25) | 267[a] |
| **20** | (26) | Solide pâteux |
| **21** | (27) | Solide pâteux |
| **22** | Commercial | 262[a] |
| **23** | (28) | 131 |
| **24** | (29) | 109[a] |
| **25** | (30) | 216 |
| **26** | (31) | 238 |
| **27** | (32) | 252 |

[a]Fin d'une plage de fusion de plusieurs degrés.

une valeur limite en dessous de laquelle un sel quaternaire ne conduira jamais quel que soit $R^3$ à un spirochromène stable en réagissant avec le méthoxy-3 nitro-5 salicylaldéhyde. Les mérocyanines **1***a* et **1***b* obtenues à partir de l'iodure **25** évoluent en solution (cf. figs. 1 et 2) vers des spirochromènes qui se décomposent quand on essaie de les isoler.

(*g*) De même que Kleinpeter et Borsdorf (22) nous avons classé l'acidité des hydrogènes du groupement méthyle en 2 pour les sels quaternaires des Tableaux 3 et 4. L'ordre est établi en fonction du déplacement chimique du carbone 2. Il est le suivant, par ordre décroissant d'acidité : cation indolinium > cation pipéridinium > cation thiazinium-1,4 > cation thiazolinium > cation thiazinium-1,3 > cation benzothiazolium > cation oxazolinium > cation oxazinium > cation thiazolium > cation benzoxazolium > cation oxazolium > cation benzimidazolium.

Il n'est pas étonnant de trouver dans les plus acides les cations ne possédant pas d'hétéroatomes en α du carbone 2. La délocalisation de la charge positive est moindre, comme cela a été constaté en série dihydroisoquinoléinium (12).

## Partie expérimentale

I. *Synthèse des sels*[4] *d'hétérocycloimmonium* ***11–27***

La synthèse des sels **11–14** et **17–19** a déjà été décrite (6–9). Nous avons appliqué le même mode opératoire à la préparation des autres iodures.

Les tosylates **23** et **24** sont obtenus en chauffant pendant 3 à 4 heures à 140°C, un mélange équi-moléculaire de thiazole et de tosylate de méthyle. Les sels sont alors isolés selon la technique employée pour les iodures. Les rendements sont quantitatifs. Ce sont des composés hygroscopiques à conserver au dessicateur. Les nouveaux sels sont rassemblés dans le Tableau 6 avec les références concernant la préparation des bases.

II. *Synthèse des mérocyanines* ***1–10***

II.1 *Synthèse du n-hexadécyloxyméthyl-3 nitro-5 salicylaldéhyde*

On ajoute à 0,1 mol (26,4 g) de n-hexadécylate de sodium en suspension dans 100 $cm^3$ de benzène, 0,1 mol (21,5 g) de chlorométhyl-3 nitro-5 salicylaldéhyde (33) dissoute dans le même volume de benzène. Le milieu réactionnel devient limpide assez rapidement. On chauffe alors au reflux pendant une heure. On filtre et concentre à sec. Le résidu repris par du benzène est chromatographié sur de l'alumine à 10% d'eau. L'élution avec un mélange benzène–éther de pétrole (70:30) fournit l'aldéhyde attendu. On le purifie par cristallisation dans le cyclohexane. C'est un solide beige fondant à 72°C. Le rendement ne dépasse pas 30%.

II.2 *Mérocyanines* ***2–10***

On dissout un mélange équimoléculaire de n-hexadécyloxyméthyl-3 nitro-5 salicylaldéhyde et de sel quaternaire dans le minimum d'éthanol anhydre. On rajoute la quantité stoechiométrique de pipéridine et on abandonne pendant 48 h à l'obscurité et à la température ambiante. On filtre le solide qui a précipité et on le sèche sous vide (on peut laver les mérocyanines **6**, **7** et **10** avec un peu d'éthanol. Eviter de le faire dans les autres séries en raison d'une solubilité importante).

II.3 *Mérocyanines* ***1****a et* ***1****b*

On opère dans du benzène anhydre à la température ambiante (avec le méthoxy-3 nitro-5 salicylaldéhyde (34) pour **1***b*). Après 48 h on recueille le solide formé. On le sèche, le lave avec de l'eau distillée puis de l'éthanol. On sèche à nouveau et on ne purifie pas davantage les mérocyanines **1***a* et **1***b*. La mérocyanine **1***b* est un solide brun vert, $F$ = 194°C ; Rdt : 36%.

Le Tableau 7 regroupe les mérocyanines préparées autres que **1***b*. Elles ne sont pas purifiables par cristallisation. Leur structure est confirmée par la spectroscopie de masse et par la rmn $^1H$ dans le deutériochloroforme. Quelques exemples de cette dernière (voir les formules, Tableau 1) sont présentés ci-dessous (δ en ppm, $J$ en Hz).

**3** : 0,87 (t mal résolu, 3H, chaîne paraffininque), 1,27 (s, chaîne paraffinique), 1,53 (s, $2CH_3$ géminés), 3,26 (s, $^+NCH_3$), 3,32 (s, $CH_2$ en α du soufre), 3,26–3,91 (m, 2H chaîne paraffinique), 4,46 (s, $CH_2$—$OC_{16}H_{33}$), 7,41 (d, *H4*, $J$ = 14), 8,12 (d, *H3*, J = 15), 7,92 (s, *H5* + *H7*).

**4** : 0,87 (t mal résolu, 3H, chaîne paraffinique), 1,28 (s, chaîne paraffinique), 1,48 et 1,52 (2s, $2CH_3$ géminés), 1,57 (d, $CH_3$ en α de l'oxygène, $J$ = 6), 1,80–2,20 (m, $CH_2$ en β de l'oxygène), 3,27

[4]Le sel nécessaire à l'élaboration de la mérocyanine **8** est obtenu en traitant le méthyl-2 benzothiazole par le tosylate de n-hexadécyle pendant 60 h en tube scellé à 140°C. Purification classique $F$ = 140°C. Rdt : 77%.

Can. J. Chem. Downloaded from www.nrcresearchpress.com by 210.87.254.5 on 09/06/12
For personal use only.

TABLEAU 7. Caractéristiques physiques des mérocyanines **1***a*–**10**

| Mérocyanines | *m/e* | Aspect | *F*(°C)[a] | Rdt (%) |
|---|---|---|---|---|
| **1***a* | 551 ($M^{\ddagger}+1$) | Poudre rouge brique | 141[b] | 39 |
| **2** | 530 ($M^{\ddagger}$) | Aiguilles rouges | 114[b] | 53 |
| **3** | — | Cristaux rouge foncé | 89 | 19 |
| **4** | 558 ($M^{\ddagger}$) | Aiguilles orangées | 150 | 47 |
| **5** | 575 ($M^{\ddagger}+1$) | Aiguilles rouge mordoré | 131 | 59 |
| **6** | 515 ($M^{\ddagger}+1$) | Cristaux rouge vif | 199 | 33 |
| **7** | 531 ($M^{\ddagger}+1$) | Cristaux rouge sombre | 231 | 69 |
| **8** | 777 ($M^{\ddagger}+1$) | Cristaux rouge mordoré | 190 | 43 |
| **9** | 564 ($M^{\ddagger}+1$) | Poudre vermillon | >260 | 88 |
| **10** | — | Cristaux rouge brique | 92[b] | 51 |

[a]Points de fusion déterminés au microscope Reichert à platine chauffante.
[b]Température repérant la fin d'une plage de fusion de quelques degrés.

(s, $^{+}NCH_3$), 3,55 (t, $OCH_2$—$C_{15}H_{31}$, $J = 6$), 4,20–4,70 (m, H en α de l'oxygène), 4,52 (s, $CH_2$—$OC_{16}H_{33}$), 7,64 (d, *H4*, $J = 14$), 8,07 (d, *H3*, $J = 14$), 8,02 (s, *H5* + *H7*).

**7** : 0,87 (t mal résolu, 3H, chaîne paraffinique), 1,29 (s, chaîne paraffinique), 2,37 (d, $CH_3$ éthylénique, $J = 1,5$), 3,40–3,80 (m, 2H, chaîne paraffinique), 3,72 (s, $^{+}NCH_3$), 4,48 (s, $CH_2$ $OC_{16}H_{33}$), 6,77 (q, H éthylénique, $J = 1,5$), 7.23 (d, H4, $J = 15$), 8,57 (d, *H3*, $J = 15$), 7,78 (d, *H7*, $J = 3$), 7,90 (d, *H5*, $J = 3$).

On relève une configuration *trans* au niveau du pont diméthinique. Le déblindage de *H3* est attributé à la proximité spatiale de l'oxygène phénolate (5, 16). Ceci est généralisable à toutes les mérocyanines **1***a*–**10**.

III. *Résonance magnétique nucléaire du carbone 13*

Les enregistrements en rmn $^{13}C$ des mérocyanines ont été réalisés sur un spectromètre JEOL de type FX 60 équipé d'un calculateur (JEC 980B) de 24 K.

Nous avons enregistré pour chaque composé, un spectre en découplage total (largeur d'impulsion 3 à 8 μs ; temps de répétition 1,2 s ou 1,5 s ; largeur spectrale = 4000 Hz ; nombre d'impulsions 1000 à 50 000) et un spectre en découplage par bruit de faible puissance (51 dB).

Les spectres des sels quaternaires et de la mérocyanine **10** ont été enregistrés sur un spectromètre JNM FX 100 équipé d'un calculateur de 32 K. Le découplage par faible bruit est réalisé par découplage total à 10 kHz de la fréquence de résonance du proton. La largeur spectrale est de 6250 Hz soit 250 ppm.

IV. *Spectres ultraviolet et visible*

L'évolution du spectre uv–visible de la mérocyanine benzoxazolinique **1***b* a été suivie sur un appareil Cary 219.

V. *Spectre de masse*

Les spectres de masse des mérocyanines ont été réalisés sur un appareil Nermag R 1010. La technique de l'impact électronique a été appliquée aux composés **2** et **4**. L'énergie des électrons est de 70 eV et la programmation de température va de 35 à 350°C à raison de 1,5°C par seconde. Les autres mérocyanines ne donnant pas d'ions moléculaires significatifs par impact électronique ont été analysées en désorption chimique. Le gaz réactant est l'ammoniac et la programmation du filament va de 0 à 300 mA à raison de 1,5 mA par seconde.

## Remerciements

Nous remercions vivement Mr. D. Picart (Laboratoire de Biochimie Faculté de Médecine, 22, rue C. Desmoulins, Brest, France) pour la réalisation et l'analyse des spectres de masse des mérocyanines.

1. A. HINNEN, C. AUDIC et R. GAUTRON. Bull. Soc. Chim. Fr. 2066 (1968).
2. G. PETILLON. Thèse de 3ème cycle, Brest (1979).
3. A. SAMAT. Thèse de Doctorat ès-Sciences, Brest (1976).
4. R. GUGLIELMETTI et J. METZGER. Bull. Soc. Chim. Fr. 2824 (1967).
5. M. MAGUET. Thèse de Doctorat ès-Sciences, Brest (1980).
6. M. MAGUET, Y. POIRIER et R. GUGLIELMETTI. Bull. Soc. Chim. Fr. 550 (1978).
7. M. MAGUET et R. GUGLIELMETTI. Bull. Soc. Chim. Fr. 539 (1978).
8. M. MAGUET, Y. POIRIER et R. GUGLIELMETTI. Bull. Soc. Chim. Fr. 561 (1978).
9. M. MAGUET, Y. POIRIER et R. GUGLIELMETTI. Bull. Soc. Chim. Fr. 568 (1978).
10. J. C. LE DUC. Thèse de 3ème. cycle. Brest (1975).
11. K. V. VEKSLER, E. R. ZAKHS, V. M. TREIGER et L. S. EFROS. Khim. Geterosikl. Soedin. 447 (1971).
12. E. R. ZAKHS, E. B. BASHUT-SKAYA et L. S. EFROS. Khim Geterotsikl. Soedin. 818 (1976).
13. B. JA. SINKIN, V. I. MINKIN et L. E. NIVOROZHKIN. Khim. Geterotsikl. Soedin. 1180 (1978).
14. J. B. STOTHERS. Carbon-13 nmr spectroscopy. *Edité par* A. T. Blomquist et H. Wasserman. Academic Press, New York et London. 1972.
15. M. LE BACCON. Thèse de Doctorat ès-Sciences, Brest (1978).

16. J. P. J. BESSE, A. M. SAMAT, J. Y. LE GALL, A. J. LE BEUZE et R. J. GUGLIELMETTI. Org. Magn. Reson. **11**, 493 (1978).
17. A. M. SAMAT, R. J. GUGLIELMETTI et G. J. MARTIN. Org. Magn. Reson. **8**,62 (1976).
18. R. FAURE, A. ASSAF, E. J. VINCENT et J. P. AUNE. J. Chim. Phys. **75**, 727 (1978).
19. R. FAURE, J. P. GALY, E. J. VINCENT et J. ELGUERO. Can. J. Chem. **56**, 46 (1978).
20. P. HAAKE et W. B. MILLER. J. Am. Chem. Soc. **85**, 4044 (1963).
21. H. S. ALDRICH, W. L. ALWORTH et N. R. CLEMENT. J. Am. Chem. Soc. **100**, 2362 (1978).
22. E. KLEINPETER et R. BORSDORF. J. Prakt. Chem. **315**, 765 (1973).
23. A. SCHUFTAN. Ber. **28**, 3070 (1895).
24. Société Nationale des Pétroles d'Aquitaine, brevet allemand, N° 1915232 (1969).
25. A. HANTZSCH. Ann. Chem. **250**, 265 (1889).
26. F. ASINGER, H. DIEM et W. SCHÄFER. Monatsh. Chem. **95** 1335 (1964).
27. M. LARCHEVEQUE, A. DEBAL et T. CUVIGNY. Bull. Soc. Chim. Fr. 1710 (1974).
28. H. ERLENMEYER, H. BAUMANN et E. SORKIN. Helv. Chim. Acta, **31**, 1978 (1948).
29. F. ASINGER, M. THIEL et L. SCHRÖDER. Ann. Chem. **610**, 49 (1957).
30. J. RONDON, R. GUGLIELMETTI et J. METZGER. Bull. Soc. Chim. Fr. 2581 (1971).
31. R. GUGLIELMETTI, E. PRETELLI et J. METZGER. Bull. Soc. Chim. Fr. 2812 (1967).
32. J. PINNOW. **32**, 1669 (1889).
33. L. D. TAYLOR et B. DAVIS. J. Org. Chem. **28**, 1713 (1963).
34. W. DAVIES. J. Chem. Soc. **123**, 1575 (1923).

Can. J. Chem. Downloaded from www.nrcresearchpress.com by 210.87.254.5 on 09/06/12
For personal use only.

# Nickel atom – ligand reactions: evidence for an unstable $\eta^3$-benzylnickel species from mixed-ligand cocondensations with nickel atoms[1]

J. Stephen Hartman[2] and Eric C. Kelusky

*Department of Chemistry, Brock University, St. Catharines, Ont., Canada L2S 3A1*

Received January 15, 1982

J. Stephen Hartman and Eric C. Kelusky. Can. J. Chem. **60**, 2654 (1982).

Detailed studies of nickel atom – benzyl halide cocondensation reactions, with and without a second organic ligand, have been carried out. Benzyl halides (X = Cl, Br) when cocondensed with nickel atoms at −196°C give no isolable organonickel product but only bibenzyl and nickel(II) halide, indicative of an initial unstable benzylnickel compound. Allyl chloride/benzyl chloride mixtures do not give the stable $\eta^3$-allylnickel chloride, but instead a highly-unstable sublimable yellow solid which apparently is the $\eta^3$-benzylnickel chloride dimer. All of this work indicates complexities in the initial metal atom interactions with the ligands. A further case is reported in which the presence of aluminosilicate insulating wool drastically changes the products obtained.

J. Stephen Hartman et Eric C. Kelusky. Can. J. Chem. **60**, 2654 (1982).

On a étudié en détail les réactions de cocondensation de l'atome de nickel avec l'halogénure benzyle en présence ou en l'absence d'un deuxième ligand organique. La cocondensation des halogénures de benzyle (X = Cl, Br) avec les atomes de nickel à −196°C ne permet pas de d'isoler des produits organonickels mais uniquement du bibenzyle et des halogénures de nickel(II) qui révèlent la formation initiale d'un composé benzylnickel instable. Les mélanges des chlorures d'allyle et de benzyle ne donnent pas le chlorure stable de $\eta^3$-allylnickel, mais conduisent de préférence à un solide jaune très instable, qui se sublime, et qui est apparemment un dimère de chlorure de $\eta^3$-benzylnickel. Tout ce travail indique la complexité des interactions initiales de l'atome métallique avec les ligands. On rapporte un autre cas où la présence d'une laine isolante alumino-silicate modifie profondément la nature des produits obtenus.

[Traduit par le journal]

## Introduction

In the last ten years metal atom – ligand cocondensation reactions have become an important synthetic technique (1–6). In an early study, allyl halides cocondensed with nickel atoms were shown to give the $\eta^3$-allylnickel halide dimers **I** (X = Cl, Br) in good yield (7). Palladium analogues of **I** can be prepared similarly (5), and benzyl chloride cocondensed with palladium has been shown to give the $\eta^3$-benzylpalladium chloride dimer **II** (8). Conventional synthetic techniques have been used to obtain $\eta^1$-benzylnickel chlorides stabilized with a variety of other ligands (9, 10).

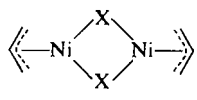


**I**

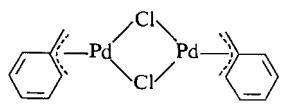


**II**

We now report studies of mixed-ligand cocondensations with nickel, carried out with hopes of preparing the nickel analogue of **II** and nickel complexes containing both $\eta^3$-allyl and $\eta^3$-benzyl ligands. We find that the presence of allyl chloride facilitates formation of a benzylnickel species, not obtainable by cocondensing pure benzyl halide with nickel. We report here our studies of the formation of the highly-unstable benzylnickel species, and of related systems.

## Experimental

*Metal atom reactions*

The metal atom reactor was of a standard type (2, 4, 11), involving generation of metal atoms in an electrically-heated tungsten crucible (Sylvania Emissive Products) and cocondensation with the substrate on the walls of the reaction vessel, cooled with a liquid nitrogen bath. The apparatus is very similar to that of Fig. 3 of ref. 11. A highly detailed description of the procedure is given in ref. 11.

*Nickel with allyl bromide (7)*

Cocondensation of nickel (1.005 g) with 8.0 mL of allyl bromide at −196°C, followed by pumping off excess allyl bromide and sublimation of the red product at 70°C, gave **I** (X = Br, 1.47 g, 24%). The mass spectrum included clusters at *m/e* 360 (51) $[(C_3H_5)NiBr]_2^+$, 319 (16) $(C_3H_5)Ni_2Br_2^+$, 278 (25) $Ni_2Br_2^+$, 140 (100) $C_6H_{10}Ni^+$, 99 (88) $C_3H_5Ni^+$.

*Nickel with allyl chloride (7)*

Cocondensation of nickel (1.02 g) with 8.0 mL of allyl chloride at −196°C, followed by pumping off excess allyl chloride and sublimation of the red–brown product at 70°C, gave **I** (X = Cl; 1.12 g, 23.6%). The mass spectrum included clusters at *m/e* 272 $[(C_3H_5)NiCl]_2^+$, 231 $(C_3H_5)Ni_2Cl_2^+$, 190 $Ni_2Cl_2^+$, 99 $NiC_6H_{10}^+$.

*Nickel with benzyl chloride*

Nickel (0.953 g) was cocondensed with 25 mL of benzyl chloride at −196°C to give a deep red matrix. On warming the matrix colour disappeared. Excess benzyl chloride was pumped off and extraction with chloroform gave 0.52 g of bibenzyl (17.9%). $^1$H nmr: δ 2.93 (2H, s), δ 7.25 (5H, s). $^{13}$C nmr: 141.8,

[1]Presented in part at the 63rd Chemical Institute of Canada Conference, Ottawa, Ontario, June 8–11, 1980.

[2]To whom all correspondence should be addressed.

0008-4042/82/212654-07$01.00/0

©1982 National Research Council of Canada/Conseil national de recherches du Canada

Can. J. Chem. Downloaded from www.nrcresearchpress.com by 210.87.254.6 on 09/06/12
For personal use only.

TABLE 1. Minor products from allyl chloride/benzyl chloride/nickel cocondensation, as determined by gas chromatography/mass spectroscopy[a]

| Product | Mass spectral data |
|---|---|
| 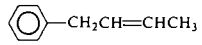 | 132(46), 117(100), 91(61), 77, 65, 51[b] |
| 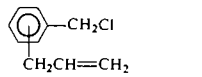 | 168(0.6), 166(1.6), 131(2), 127(12), 125(27), 117(11), 91(100), 77(7), 65(16), 51(11) |
| 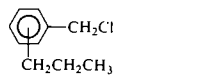 | 170(1.4), 168(4.7), 133(5), 127(6.7), 125(16), 91(100), 77(6), 65(14), 51(9) |
| 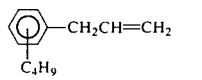 | 174(3), 145(4), 131(23), 117(23), 91(100), 77(9), 65(15), 51(8) |

[a]GC/MS did not fully resolve all species. As a result all mass abundances are not reported.
[b]Literature values: 132(46), 117(100), 91(55), 77(14), 65(23), 51(26) (ref. 27).

128.5, 128.4, 125.9, and 37.9 ppm. Mass spectrum: *m/e* 182 (16), 104 (3), 91 (100), 65 (11), 51 (5), 39 (7).

Addition of 5 mL $Et_3P$ to the cocondensate at −196°C, followed by warming, gave bibenzyl and a red solid identified as $(Et_3P)_2NiCl_2$ by its mass spectrum: *m/e* 366 (trace) $NiCl_2(PEt_3)_2^+$, 331 (trace) $NiCl(PEt_3)_2^+$, 153 (12) $ClPEt_3^+$, 118 (100) $PEt_3^+$, 89 (45) $PEt_2^+$, 60 (31) $PEt^+$; $^1H$ nmr: 1.4 (3H, m), 1.7 (2H, m). The $^1H$ nmr of the crude mixture showed that the products were present in equimolar quantities.

*Aggregation or complexation of bibenzyl*

Whereas pure bibenzyl (mp 52°C) is easily sublimable under our workup conditions, the matrices obtained from nickel atom cocondensations involving benzyl halides gave a brown involatile solid which did not melt or sublime even at 70°C under high vacuum, and from which we recovered large quantities of bibenzyl by extraction with chloroform. An aggregation or complex of bibenzyl with nickel halide and/or with finely divided metallic nickel is indicated.

*Nickel with benzyl bromide*

Nickel (0.515 g) was cocondensed with 25 mL of benzyl bromide at −196°C to give a deep red matrix. The colour disappeared on warming. The excess benzyl bromide was pumped off; bibenzyl was recovered and identified by its $^1H$ nmr and mass spectrum, as above.

Addition of 5 mL $Et_3P$ to the cocondensate at −196°C, followed by warming, gave bibenzyl and a red solid identified as $(Et_3P)_2NiBr_2$ by its mass spectrum: *m/e* 454 (trace) $NiBr_2(PEt_3)_2^+$, 375 (trace) $NiBr(PEt_3)_2^+$, 197 (18.6) $BrPEt_3^+$, 118 (100) $PEt_3^+$, 89 (42) $PEt_2^+$, 60 (31) $PEt^+$. The $^1H$ nmr of the crude mixture showed that the bibenzyl and $NiBr_2(PEt_3)_2$ were present in equimolar amounts.

*Nickel with equimolar allyl chloride/benzyl chloride*

Cocondensation of nickel (0.955 g) with 25 mL of an equimolar mixture of allyl chloride and benzyl chloride at −196°C, followed by warming and pumping off the unreacted allyl and benzyl chloride, gave a highly air-sensitive yellow solid which was sublimed to a cold finger at 65°C. This decomposed slowly at ambient temperature to give bibenzyl, nickel chloride, and nickel metal, and could not be obtained in a pure form. (Bibenzyl and nickel(II) chloride do not sublime from our reaction mixtures and hence could only arise as decomposition products.) Repeated attempts to obtain the mass spectrum of the yellow solid under a variety of conditions gave only bibenzyl (parent ion: *m/e* 182). A gas chromatogram of a chloroform solution of the yellow solid on a 3% FE 30 on CHROM W column showed only bibenzyl (calibrated with a known sample). GC/MS analysis of the residue in the reaction vessel after sublimation, using a column with 3% 56 30/CHROM W/SPECIAL GC, showed predominantly bibenzyl and several other organic species which were present in yields of less than 0.5% (Table 1).

Trapping with 5 mL $Et_3P$ at −196°C yielded 0.495 g of bibenzyl and 1.039 g of $(Et_3P)_2NiCl_2$, both of which were identified by $^1H$ nmr and mass spectra, as above. Trapping with 10 mL triisobutylphosphine at −196°C yielded bibenzyl and red $(i\text{-}Bu_3P)_2NiCl_2$ in equimolar amounts, as determined by comparison of $^1H$ nmr integrals of the crude mixture. The $(i\text{-}Bu_3P)_2NiCl_2$ (26%) was identified by its $^{13}C$ nmr: 25.3 ppm (β-C), 25.6 (γ-C), 31.1 (α-C, d of d), and by its uv/visible spectrum (bands at 500, 402, 268, 251 mμ; known sample: 502, 406, 269, 247 mμ).

*Nickel with equimolar allyl chloride/benzyl bromide*

Cocondensation of nickel (1.33 g) with 25 mL of an equimolar mixture of allyl chloride and benzyl bromide at −196°C, followed by warming and pumping off the unreacted organic substrate, yielded two sublimable products: a yellow solid (subl. 65°C) and a red solid (subl. 70°C). The latter, identified from its mass spectrum as the $\eta^3$-allylnickel chloride dimer **I**, had $^{13}C$ nmr peaks at 56.0 and 105.4 ppm.

Addition of $Et_3P$ to a solution of the yellow solid in chloroform gave, in addition to metallic nickel, bibenzyl and $(Et_3P)_2NiBr_2$ as identified by the mass spectrum (*m/e* 454 (trace), 375 (trace), 197 . . . as above, for the nickel complex; *m/e* 182 (18), 104 (5), 91 (100), 65 (10), and 51 (7) for bibenzyl). The $^1H$ nmr of the crude mixture showed that the products were present in equimolar quantities.

The yellow solid could not be completely freed of **I** by sublimation; its $^{13}C$ spectrum showed the 56.0 and 105.4 ppm peaks of **I**, as well as bibenzyl peaks at 37.8, 125.9, 128.3, 128.4, and 141.7 ppm. Peaks assigned to the yellow solid occur at 41.4, 72.0, 126.6, 127.8, 130.6, and 132.2 ppm. These disappear with time as the bibenzyl peaks grow, and all peaks become broad due to the formation of paramagnetic nickel(II) bromide.

*Nickel with equimolar allyl bromide/benzyl bromide*

Cocondensation of nickel (1.102 g) with 25 mL of an equimolar mixture of allyl bromide and benzyl bromide at −196°C, followed by warming and pumping off the unreacted organic

Can. J. Chem. Downloaded from www.nrcresearchpress.com by 210.87.254.6 on 09/06/12
For personal use only.

Can. J. Chem. Downloaded from www.nrcresearchpress.com by 210.87.254.6 on 09/06/12
For personal use only.

substrate, yielded a red solid (subl. 70°C) identified as the allylnickel bromide dimer, but no sublimable yellow solid. The remainder of the product in the reaction vessel, in addition to nickel metal, was identified as bibenzyl and nickel bromide, in approximately equimolar quantities.

*Palladium with equimolar allyl chloride/benzyl chloride*

Cocondensation of palladium (0.852 g) with 25 mL of an equimolar mixture of allyl chloride and benzyl chloride at −196°C, followed by pumping off the unreacted organic substrate, yielded 0.184 g (6.3%) of the $\eta^3$-allylpalladium chloride dimer **II**, as identified by its mass spectrum (parent ion cluster at *m/e* 368) and $^1$H nmr (δ 3.03 (2H, d), 4.10 (2H, d), 5.40 (1H, m)). Also observed were very weak clusters at *m/e* 468 $(benzylPdCl)_2^+$ and 377 $(benzylPd_2Cl_2)^+$ and bibenzyl peaks (*m/e* 182, 91). Thus both $\eta^3$-allyl- and $\eta^3$-benzylpalladium chloride dimers form, but no peak could be detected at *m/e* 418 which would correspond to the parent ion of an analogous mixed allyl, benzylpalladium chloride compound.

*Nickel with benzyl halides, using Kaowool crucible insulation*

*(i) Nickel with benzyl chloride*

Cocondensation of nickel (0.86 g) with 26 g of benzyl chloride at −196°C in the presence of Kaowool crucible insulation gave a matrix which, when allowed to warm to ambient temperature, melted down the sides of the vessel and began to bubble, with evolution of hydrogen chloride (ir bands at 2875 cm$^{-1}$). After all volatiles were pumped off, 24.3 g of product was collected that was insoluble in all solvents used (pentane, chloroform, acetone, dimethylsulfoxide, acetonitrile). However, the addition of $Et_3P$ to the finely ground solid gave 1.42 g of $(Et_3P)_2NiCl_2$ (26.5% based on nickel; identified by mass spectrum and $^1$H nmr as above) and 23.8 g of insoluble white solid. This was identified by its mass spectrum as a mixture of polybenzylic species: *m/e* 632 (0.5), 542 (1), 452 (1.4), 362 (3), 272 (8), 181 (23), 179 (38), 91 (100). On slowly heating the mass spectrometer inlet the same peaks were present and also new peaks at higher mass appeared (*m/e* 722, 812, 902, and 992). These became larger as the inlet temperature was increased. These results, together with a fragmentation pattern indicative of a monosubstituted aromatic ring, suggest structures **III** ($n$ = 1–9).

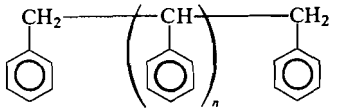

**III**

Metastable scanning techniques (12, 13) confirm that the polybenzylic mass spectral peaks arise from separate species in the ionization chamber of the mass spectrometer rather than being fragments of a higher-mass parent ion. For a suspected parent ion, a $V$ scan (12) will determine whether it is itself a daughter of some higher-mass ion, while a $V^2/E$ scan (13) will determine its daughter ions. While the results (Table 2) require that the polybenzyls **III** are present in the mass spectrometer source, we cannot exclude the presence of less volatile higher polymers, or that the observed fragments might be formed in the source from the breakdown of a higher polymer.

*(ii) Nickel with benzyl bromide*

Cocondensation of nickel (0.52 g) with 25 mL of benzyl bromide at −196°C in the presence of Kaowool crucible insulation gave a red matrix. On warming to ambient temperature the red colour disappeared and hydrogen bromide was given off (ir bands at 2560 cm$^{-1}$). By workup methods similar to those used in the analogous benzyl chloride system, 3.46 g of polybenzylic product were obtained. Mass spectrum: *m/e* 632 (1), 542 (3), 452 (6), 362 (6), 361 (6), 272 (1), 271 (15), 182 (28), 181 (99), 91 (100).

TABLE 2. Metastable scanning techniques applied to suspected parent ions in the mass spectrum of a polybenzyl product

| Suspected parent ion *m/e* values | Parent ions (by $V$ scan) | Daughter ions (by $V^2/E$ scan)[a] |
|---|---|---|
| 632 | | 529, 438, 422, 406, 332, 317 |
| 542 | 635±5 | 374, 361, 283, 270 |
| 452 | None | 360, 283, 270, 256 |
| 362 | None | 270, 193, 181, 180 |
| 272 | 357±6 | 193, 180 |
| 181 | 276±5<br>366±6<br>459±6<br>549±6 | |
| 179 | 187±5<br>195±5<br>272±4<br>364±4<br>455±5 | |
| 91 | 267±7<br>354±8 | |

[a]Errors are ±2 *m/e* units.

*(iii) Nickel with equimolar allyl bromide/benzyl bromide*

Cocondensation of nickel (0.62 g) with 25 mL of an equimolar allyl bromide/benzyl bromide mixture at −196°C in the presence of Kaowool crucible insulation gave an initial red matrix which on warming yielded hydrogen bromide and 2.17 g of a solid. Major peaks of the mass spectrum of the solid (Table 3) show that this is primarily a polybenzyl but that an allyl group or a bromine can become incorporated.

*Instrumentation*

Mass spectra were obtained on an AEI MS30 double beam spectrometer operating at 70 eV for most compounds, but at 19 eV for some of the less stable compounds. GC/MS runs were performed on a column with 3% 56 30/CHROM W/SPECIAL GC.

$V$ scans and $V^2/E$ scans, the two metastable scanning techniques used in this study, were carried out with the KRATOS metastable scan unit. Both follow decompositions in the field-free region between the ionization chamber and the electrostatic analyser of the MS-30 mass spectrometer. In the $V$ scan, the spectrometer is tuned to a peak of known mass (daughter ion $m_2^+$). The electrostatic analyser is held constant and the accelerating voltage $V$ is increased linearly. This gives the precursor or parent ions $m_1^+$ which give rise to that daughter ion (12). In the $V^2/E$ scan, the spectrometer is tuned to a peak of known mass; the electrostatic analyser voltage is then increased linearly while simultaneously $V$ is increased proportionally to the square of the electrostatic analyser voltage. This gives a spectrum which shows the peak the instrument was tuned to, and the daughter ions which arise from it (13).

Nuclear magnetic resonance spectra were recorded on a Bruker WP-60 Fourier Transform nmr spectrometer operating at 60 MHz ($^1$H) and at 15.08 MHz ($^{13}$C). $^{13}$C spectra were obtained using a 3759 Hz sweep width and 1.089 second acquisition time for an 8K FID. Thirty-degree pulses were used, with the Phase Alternating Pulse Sequence, and 5 W of proton noise decoupling were applied. Proton spectra were obtained with a 750 Hz sweep width and a 5.5 s acquisition time.

TABLE 3. Major mass spectral peaks of the polymeric nickel/allyl bromide/benzyl bromide/Kaowool reaction product

| | Composition: number of structural units incorporated | | |
|---|---|---|---|
| *m/e* | Benzyl | Allyl | Bromine |
| 182 | 2 | 0 | 0 |
| 222 | 2 | 1 | 0 |
| 260/262 | 2 | 0 | 1 |
| 222 | 3 | 0 | 0 |
| 312 | 3 | 1 | 0 |
| 362 | 4 | 0 | 0 |
| 402 | 4 | 1 | 0 |

*Materials*

Nickel pellets (99.95% purity) and palladium sponge (99.5% purity) were obtained from A. D. Mackay Limited. The allyl and benzyl halides (Aldrich) were used without further purification, although purity was checked by GC/MS. Toluene was purified by shaking with cold sulfuric acid, followed by washing with water, drying over phosphorus pentoxide, and distilling, with the first and last cuts being rejected. Chloroform was purified by predrying over calcium chloride and distilling from phosphorus pentoxide, the first and last cuts being rejected, and stored in the dark.

## Results and discussion

*(i) Single-ligand systems*

The cocondensation of benzyl chloride or benzyl bromide with nickel at −196°C gives an initial red matrix, similar to that observed in other arene–metal cocondensations (14) and interpreted as π-arene–metal complex formation, but on warming only bibenzyl and nickel(II) halide can be recovered. The presence of bibenzyl is consistent with the formation of an unstable benzylnickel complex. Trapping experiments, in which triethylphosphine is added to the initial matrix at −196°C in the hope of stabilizing an initially-formed organometallic linkage by incorporation of a phosphine ligand, give only bibenzyl and $(Et_3P)_2NiX_2$ (X = Cl, Br) on warming.

Similar cocondensations of a benzyl halide with nickel, but with the crucible surrounded by aluminosilicate insulating wool (Kaowool, available from Morganite Ceramic Fibers, Neston, England, is a stable high-temperature ceramic fiber with no organic binder, consisting principally of $Al_2O_3 \cdot 2SiO_2$), give on warming a mixture of nickel(II) halide, hydrogen halide, and polybenzyl species containing from three to at least nine benzyl units, as determined by mass spectroscopy. Covering of the insulation by brass foil gives only bibenzyl and nickel(II) halide, as in the absence of insulation. Klabunde and co-workers have recently reported similar major effects of crucible insulation on product distribution and yields in the synthesis of the $\eta^3$-benzylpalladium chloride dimer, **II**, and have demonstrated that pyrolysis reactions on the greatly increased surface area, when insulation is present, result in the production of organic free radicals from the substrate (14). Similar free radical processes are implicated here, although the products are different, i.e., polymer rather than the bibenzyl and toluene that were Klabunde's principal products. Hence crucible insulation was dispensed with in the mixed-ligand studies described below, despite the greater thermal losses involved.

The cocondensation of allyl chloride or bromide with nickel, with or without Kaowool insulation, gives the $\eta^3$-allylnickel halide dimers **I** in good yield, as reported by Piper and Timms (7).

*(ii) Mixed-ligand systems*

An equimolar mixture of allyl chloride and benzyl chloride, cocondensed with nickel atoms, does not give **I** but instead a hitherto-unreported yellow sublimable solid that decomposes very readily to bibenzyl, nickel(II) chloride, and nickel. Absence of decomposition products derivable from allyl chloride shows that the allyl group is not incorporated in the sublimable species. Addition of trialkylphosphines ($Et_3P$, $i$-$Bu_3P$) to the −196°C matrix yields equimolar amounts of bibenzyl and $(R_3P)_2NiCl_2$ but no other products.

An equimolar mixture of allyl bromide and benzyl bromide, cocondensed with nickel atoms, gives only the products which can be formed in the separate unmixed-ligand experiments, i.e., **I** (X = Br), bibenzyl, and nickel(II) bromide.

An intermediate mixed-ligand system, allyl chloride and benzyl bromide, when cocondensed with nickel gives two sublimable solids which can be separated by fractional sublimation: red **I** (X = Cl), and a yellow material which decomposes readily to give bibenzyl and nickel(II) bromide, and appears to be the bromine analogue of the sole product of the allyl chloride/benzyl chloride/nickel system. Addition of $Et_3P$ to a solution of this compound gives bibenzyl and $(Et_3P)_2NiBr_2$, identified by its mass spectrum.

Cocondensation of palladium atoms with an equimolar mixture of allyl chloride and benzyl chloride, followed by extraction with toluene, gives a yellow product identified as mainly $\eta^3$-allylpalladium chloride dimer from its mass spectrum. The mass spectrum also shows very weak clusters corresponding to the $\eta^3$-benzylpalladium chloride dimer **II** but none corresponding to a mixed allyl/benzylnickel chloride dimer.

*(iii) Structure of the unstable benzylnickel species*

Decomposition of the product of the allyl chloride/benzyl halide/nickel cocondensation reaction,

Can. J. Chem. Downloaded from www.nrcresearchpress.com by 210.87.254.6 on 09/06/12
For personal use only.

TABLE 4. $^{13}C$ chemical shifts of **IV** and some model compounds[a]

| Compound | Carbon C-1 | C-2 | C-3 | C-4 to C-7 | Reference |
|---|---|---|---|---|---|
| 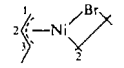 | 49.6 | 105.6 | 71.2 | | 17 |
| 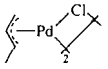 | 58.3 | 111.4 | 81.4 | | 18 |
| 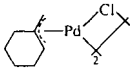 | 58.2 | 126.0 | 68.8 | | 18 |
| 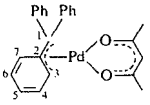 | 73.3 | 116.0 | 102.3[b] | 133.1[c], 127.9[d], 102.3[b] | 19 |
| 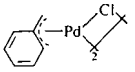 | 42.1 | 125–133 | 107.0 | 125–133 | 20 |
| 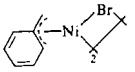 | 41.4 | 126–132 | 72.0 | 126–132 | This work |

[a]ppm to low field of internal tetramethylsilane.
[b]Averaged signal of C-3 and C-7 due to fluxional behaviour.
[c]Averaged signal of C-4 and C-6.
[d]C-5.

to give bibenzyl and nickel(II) halide in a 1:1 molar ratio as well as nickel metal but no other products, suggests structure **IV** (X = Cl, Br) analogous to **I** and **II**. Trapping experiments are consistent with this. However, the volatility of the product, greater than that of the allylnickel chloride dimer is anomalous and suggests that **IV** may vaporize as a monomer. Dissociation to the highly unstable monomer would be consistent with its extreme reactivity.

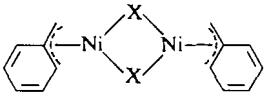

**IV**

Compound **II**, the palladium analogue of our proposed structure **IV**, also gives bibenzyl as a final product when reacted with $Et_3P$, but in the palladium case stepwise addition allows the isolation of an $\eta^1$-benzylnickel complex (15). An analogous but less stable $\eta^1$-benzylnickel complex is a likely intermediate in the reaction of **IV** with phosphines. Palladium species of this type tend to be much more stable than their nickel analogues (16).

Attempts to obtain mass spectra of **IV** showed only the presence of bibenzyl. A $^{13}C$ nmr spectrum was obtained on a deuterochloroform solution of **IV** (X = Br) but decomposition had already commenced and peaks attributable to bibenzyl were already larger than those of the unstable species. The peaks assigned to the unstable compound diminish on standing at ambient temperature, with corresponding growth of the bibenzyl peaks. The chemical shifts are reasonably consistent with those of other, similar $\eta^3$-allylmetal compounds (17–20) (Table 4). A complete assignment is difficult since peaks in the 125–133 ppm region are obscured by additional resonances, including the bibenzyl decomposition product. The peaks at 41.4 and 72.0 ppm are fully consistent with allylic bonding to nickel (21), and are difficult to account for in any other way.

The only previously-reported $\eta^3$-benzylnickel compounds appear to be **VI**. Compound **V** (X = Cl, Br) has been prepared by ethylene displacement from $(Ph_3P)_3Ni(C_2H_4)$ by benzyl halides (22). An $\eta^1 \rightleftharpoons \eta^3$ equilibrium in solution, with displacement of $Ph_3P$, was proposed on the basis of cryoscopic and $^1H$ nmr studies. These authors obtain decomposition products analogous to ours from their solutions (bibenzyl, $Ph_3P$, $(Ph_3P)_2NiX_2$, and nickel) but their complexes are considerably more stable. As in our work, no nickel-containing fragments were detected in the mass spectrum.

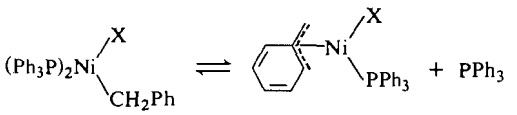

**V** **VI**

Can. J. Chem. Downloaded from www.nrcresearchpress.com by 210.87.254.6 on 09/06/12
For personal use only.

Can. J. Chem. Downloaded from www.nrcresearchpress.com by 210.87.254.6 on 09/06/12
For personal use only.

*(iv) Rationalization of product distributions*

In metal atom – ligand cocondensations the interaction of metal atom and substrate first occurs on the freshly-formed cocondensation surface. The substrate and metal atoms are still mobile and the metal atoms are highly reactive, and in favourable cases a bond can form between metal atom and substrate. The initial organometallic species may then undergo further reactions, either at the cocondensation temperature or during warmup, to give the isolable products. Mobilities within the cocondensation matrix are important, especially when intermolecular reactions such as dimerization must occur, and are greatly affected by changes in attractive forces among the large excess of substrate molecules forming the matrix. Hence products and yields can be greatly changed by minor modifications to the matrix that affect mobility. For example, the use of *n*-hexane as substrate diluent in place of *n*-pentane when trimethylphosphine is cocondensed with iron atoms drastically decreases the yield of $HFe(CH_2PMe_2)(PMe_3)_3$ (1, 23), and the differing internal attraction of *n*-pentane and *n*-hexane, typified by their 35° difference in melting points, can explain this. Recent studies by Ozin and co-workers involving metal atom condensations in polymer matrices at temperatures much higher than −196°C have confirmed the importance of mobility effects (24). Aggregation of metal atoms to form colloidal metal can become predominant when mobility is either too low or too high, leaving a narrow temperature (i.e., mobility) range which favours desired products.

On the assumption that substrate melting points are indicative of mobilities in low-temperature matrices, our pattern of reactivities can be rationalized. The allyl halides have the lowest melting points of our organic substrates (allyl chloride, −134.5°C; allyl bromide, −119.4°C; benzyl chloride, −39°C; benzyl bromide, −3°C; acrylonitrile, −83.5°C). Hence the allyl halides form matrices of the highest mobility, favouring the formation of $\eta^3$-allynickel halide dimers by monomer diffusion. Benzyl halide matrices should be far less mobile, and the intitial monomeric benzylnickel halide probably decomposes before it can diffuse to form the less unstable dimer. Allyl halide/benzyl halide matrices should have intermediate mobilities, and dimerization of benzylnickel halide monomer is more likely to win out over monomer decomposition. Even here, a close balance of the two processes is apparently involved; the absence of **IV** from the allyl bromide/nickel bromide cocondensations might be the result of significantly lower mobility in this matrix, in accord with the higher melting points of the bromides compared to the analogous chlorides.

The absence of **I** from the allyl chloride/benzyl chloride cocondensation product might result from preferential formation of **VII** rather than **VIII** in the initial metal atom – ligand interaction. **VIII** is

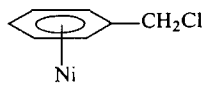


**VII**

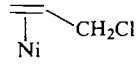


**VIII**

known from the work of Ozin and Powers (25) and is stable up to −153°C. **VII** is the nickel analogue of the initial benzyl chloride – palladium species proposed by Klabunde *et al.* (8, 15). Once **VII** forms in preference to **VIII**, intramolecular rearrangement followed by dimerization would give **IV**, as in the analogous palladium system (8, 15):

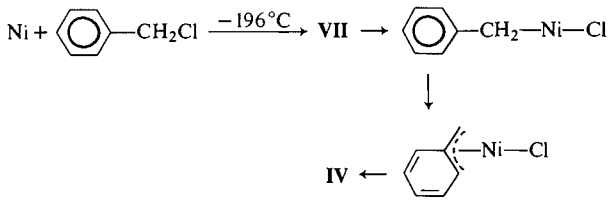


Some **VIII** should form as well at −196°C, and a mixed $\eta^3$-allyl-$\eta^3$-benzylnickel halide dimer would be expected. No such species has been detected, but GC/MS analysis of the cocondensation residue, after sublimation of the volatile product, does show several organic species in addition to bibenzyl, all of which incorporate both allyl and benzyl fragments (Table 1). All of these products can be rationalized in terms of reactions of ligands in a mixed allylbenzylnickel compound.

A similar effect in inhibiting the formation of **I** has been observed in allyl bromide/acrylonitrile/nickel cocondensations. Neither **I**, nor the polymer obtained in acrylonitrile/nickel cocondensations, is obtained but instead a highly-unstable species which, from its decomposition products, appears to be a nickel complex containing both allyl and acrylonitrile groups (26). Metal atom cocondensation reactions with mixed ligands may hold many surprises even in cases in which the corresponding single-ligand reactions are well known.

**Acknowledgements**

We thank the Natural Sciences and Engineering Research Council of Canada for financial support and for the award of a Scholarship (to E.C.K.). We are indebted to Professor M. J. McGlinchey of McMaster University for helpful discussions, to Mr. T. R. B. Jones and Professor J. M. Miller for

helpful discussions and assistance with the mass spectrometer and nmr instrumentation, and to Professor K. J. Klabunde of Kansas State University for providing a $^{13}C$ nmr spectrum of compound **II**.

1. P. L. TIMMS and T. W. TURNEY. Adv. Organomet. Chem. **15**, 52 (1977).
2. J. R. BLACKBOROW and D. YOUNG. Metal vapour synthesis in organometallic chemistry. Springer-Verlag, Berlin. 1979.
3. K. J. KLABUNDE. *In* Reactive intermediates. Vol. I. *Edited by* R. A. Abramovich. Plenum Press, New York and London. 1980. Chapt. 2.
4. M. MOSKOVITS and G. A. OZIN (*Editors*). Cryochemistry. Wiley Interscience, New York. 1976.
5. K. J. KLABUNDE. Acc. Chem. Res. **8**, 343 (1975).
6. P. L. TIMMS. Adv. Inorg. Chem. Radiochem. **14**, 121 (1972).
7. M. PIPER and P. L. TIMMS. J. Chem. Soc. Chem. Commun. 52 (1972).
8. J. S. ROBERTS and K. J. KLABUNDE. J. Organomet. Chem. **85**, C13 (1975).
9. K. JACOB, E. PIETZNER, S. VASTAG, and K.-H. THIELE. Z. Anorg. Allgem. Chem. **432**, 187 (1977).
10. K. JACOB, K.-H. THIELE, C. GEYER, and G. WELDE. Z. Anorg. Allgem. Chem. **462**, 177 (1980).
11. D. F. SHRIVER (Editor-in-chief). Inorganic syntheses. Vol. XIX. John Wiley and Sons, New York. 1979. Chapt. 2, pp. 59–69.
12. R. G. COOKS, J. H. BEYNON, R. M. CAPRIOLI, and G. R. LESTER. Metastable ions. Elsevier, Amsterdam. 1973. Chapt. 3.
13. A. F. WESTON, K. R. JENNINGS, S. EVANS, and R. M. ELLIOTT. Int. J. Mass Spectrom. Ion Phys. **20**, 317 (1976); D. L. KEMP, R. G. COOKS, and J. H. BEYNON. Int. J. Mass Spectrom. Ion Phys. **21**, 93 (1976).
14. K. L. KLABUNDE, T. GROSHENS, H. F. EFNER, and M. KRAMER. J. Organomet. Chem. **157**, 91 (1978).
15. J. S. ROBERTS and K. J. KLABUNDE. J. Am. Chem. Soc. **99**, 2509 (1977).
16. K. J. KLABUNDE. Angew. Chem. Int. Ed. Engl. **14**, 287 (1975).
17. L. A. CHURLYAEVA, M. I. LOBACH, G. P. KONDRATERKOV, and V. A. KORMER. J. Organomet. Chem. **39**, C23 (1972).
18. Y. SENDA, H. SUDA, J. ISHIYAMA, S. IMAIZUMI, A. KASAHARA, T. IZUMI, and T. KATO. Bull. Chem. Soc. Jpn. **50**, 1608 (1977).
19. B. E. MANN, A. KEASEY, A. SONADA, and P. M. MAITLIS. J. Chem. Soc. Dalton Trans. 338 (1979).
20. K. J. KLABUNDE. Private communication.
21. P. W. JOLLY and R. MYNOTT. Adv. Organomet. Chem. **19**, 257 (1981).
22. E. BARTSCH, E. DINJUS, R. FISCHER, and E. UHLIG. Z. Anorg. Allgem. Chem. **433**, 5 (1977).
23. P. L. TIMMS. Angew. Chem. Int. Ed. Engl. **14**, 273 (1975).
24. C. G. FRANCIS, H. HUBER, and G. A. OZIN. Inorg. Chem. **19**, 219 (1980); G. A. OZIN, C. G. FRANCIS, H. X. HUBER, and L. F. NAZAR. Inorg. Chem. **20**, 3635 (1981).
25. G. A. OZIN and W. J. POWERS. Inorg. Chem. **17**, 2836 (1978).
26. J. S. HARTMAN and E. C. KELUSKY. Unpublished work.
27. Eight peak index of mass spectra. 2nd ed. Mass Spectrometry Data Centre, Reading, U.K. 1974.

Can. J. Chem. Downloaded from www.nrcresearchpress.com by 210.87.254.6 on 09/06/12
For personal use only.

# The lycoctonine family of alkaloids: a stereochemical revision[1]

O. E. EDWARDS

*Division of Chemistry, National Research Council of Canada, 100 Sussex Drive, Ottawa, Ont., Canada K1A 0R6*

AND

M. PRZYBYLSKA

*Division of Biological Sciences,, National Research Council of Canada, 100 Sussex Drive, Ottawa, Ont., Canada K1A 0R6*

Received April 6, 1982

O. E. EDWARDS and M. PRZYBYLSKA. Can. J. Chem. **60**, 2661 (1982).

A redetermination of the structure of des(oxymethylene)lycoctonine hydriodide has shown that a wrong choice had been made between the real and false mirror image peaks for the atoms of the 1-methoxyl group in the original pseudosymmetric Fourier synthesis. It has been demonstrated that lycoctonine samples from many sources are identical, and that no rearrangement took place in forming des(oxymethylene)lycoctonine. Hence all alkaloids that have been related to lycoctonine have a 1α-methoxyl group.

O. E. EDWARDS et M. PRZYBYLSKA. Can. J. Chem. **60**, 2661 (1982).

Une nouvelle détermination de la structure de l'iodhydrate du des(oxyméthylène) lycoctonine montre qu'on s'est trompé dans le choix des pics des images réelles et fausses dans un miroir des atomes du groupe méthoxy-1 dans la synthèse originale pseudosymétrique de Fourier. On démontre que les échantillons de lycoctonine, provenant de diverses sources, sont identiques et qu'il n'y a pas de transposition lors de la formation du des(oxyméthylène) lycoctonine. Ainsi tous les alcaloïdes qu'on a relié à la lycoctonine ont un groupe méthoxy en position 1 de configuration α.

[Traduit par le journal]

Can. J. Chem. Downloaded from www.nrcresearchpress.com by 210.87.254.105 on 09/06/12
For personal use only.

The skeleton, configuration of functional groups, and absolute stereochemistry of the diterpenoid alkaloid lycoctonine were determined by X-ray analysis of a simple derivative, des(oxymethylene)-lycoctonine hydriodide (1, 2). Subsequent chemical correlations resulted in assignment of structure and stereochemistry to the Delphinium alkaloids browniine (3), delpheline (4), and deltaline (5) and to the Aconite alkaloid chasmanine (6). This also provided the first direct chemical link between the two groups of alkaloids.

Total synthesis of chasmanine (7) and an X-ray structural analysis on its 14-*O*-benzoate hydrochloride (8) have since established beyond doubt that the C-1 configuration assigned to chasmanine in the above-mentioned work (6) was wrong, making it appear that the browniine–chasmanine correlation was in error. However, new X-ray analyses in our laboratories on lycoctonine transformation products (9, 10) have indicated that the error lay in the originally assigned configuration at C-1 in lycoctonine, and that all the alkaloids that have been related to lycoctonine, chasmanine, or browniine have 1α- methoxyl groups.[2]

## Results and discussion

In reexamining the question of the early assignment of configuration (1, 2) it seemed important to us to ensure that only one "lycoctonine" existed, i.e. that a stereoisomer had not been chosen for the X-ray analysis and that the alkaloids from the varied sources were identical. This has been done in part by comparison of X-ray powder patterns (12) and of other physical properties in our study of the alkaloids of *Inula royleana* (13). We now extend this with comparison of $^1$H nmr and $^{13}$C nmr spectra and X-ray powder patterns of the alkaloid and some of its transformation products from the early work in the 1950's and later work. Thus lycoctonine samples and derivatives from *D. consolida* L. (14), *D. brownii* Rydb. (*D. glaucum* S. Watts) (15), *D. elatum* L. (16), *D. ajacis* L. (now *Consolida ambigua* L.) (17), *D. barbeyi* Huth (18), and *Inula royleana* D. C. Prod. (13) were shown to be identical.

A second concern was whether the preparation of des(oxymethylene)lycoctonine proceeded without any stereochemical change. The gentle, nearly neutral conditions of the permanganate oxidation of lycoctonine, giving in part des(oxymethylene)-lycoctonam seemed unlikely to have epimerized C-1. Decarboxylation of lycoctonamic acid at 200°C gave the same compound (19*a*). But the more drastic lithium aluminum hydride reduction of des(oxymethylene)lycoctonam (refluxing dioxane) was more suspect. However, reoxidation of the resulting des(oxymethylene)lycoctonine gave a good yield of des(oxymethylene)lycoctonam iden-

[1]Issued as NRCC No. 20499.

[2]This revision was first announced in print in ref. 11.

0008-4042/82/212661-07$01.00/0

©1982 National Research Council of Canada/Conseil national de recherches du Canada

Can. J. Chem. Downloaded from www.nrcresearchpress.com by 210.87.254.105 on 09/06/12
For personal use only.

tical with material obtained directly from lycoctonine.[3]

Clearly then, the anomaly lay in the original X-ray analysis of (+)-des(oxymethylene)lycoctonine hydriodide monohydrate (1, 2). The reexamination of this early determination was therefore undertaken. A crystal of the original sample was used to remeasure the data on a Nonius CAD-4 diffractometer with Ni-filtered Cu radiation. The unit-cell dimensions were corrected to: $a = 12.758(1)$, $b = 9.415(1)$, $c = 10.990(1)$ Å and $\beta = 97.81(1)°$. Out of 2644 measured reflections with $\theta \leq 70°$, 2012 were above threshold of $2\sigma(I_{net})$. The $\omega - 2\theta$ scanning method was used.

The space group is $P2_1$ and the structure had been solved by the heavy atom technique. The $x$ and $z$ coordinates of the iodine atom were derived from a Patterson projection. Its $y$ coordinate was assumed to be 0.250 and a three-dimensional Fourier synthesis was carried out using the phases based on the iodine contributions. This procedure imparted the symmetry of the centrosymmetric space group $P2_1/m$ by producing planes of symmetry at $y = 1/4$ and 3/4. The atomic peaks were therefore doubled and the choice between the real $(x, y, z)$ and the false mirror image peaks $(x, \frac{1}{2} - y, z)$ had been made on the basis of the examination of bond lengths and angles. In those days the computing facilities were rather poor and the refinement of the atomic coordinates thus derived had been limited to $F_o - F_c$ syntheses of the $h0l$, $0kl$, and $hk0$ zones, followed by the calculation of the $hkl$ structure factors. The $R$ index for 2162 observed reflections measured visually from Weissenberg films was 0.24.

The C(1) atom[4] had been situated close to the false plane of symmetry at $y = \frac{1}{4}$ in the original Fourier synthesis and the orientation of the ring A was such that the two symmetry related sets of peaks for O(1) and C(20) represented the α- and β-configurations of the 1-methoxy group. It appeared therefore that a wrong set of peaks was chosen for the real atoms in the interpretation of that synthesis. This was first tested by calculating structure factors, using new X-ray data, for observed reflections for two models: one with the previously published coordinates with 1-methoxyl in the β configuration and the other with the $y$ coordinates of C(1), O(1), and C(20) changed from 0.224, 0.080, and 0.039 to 0.276, 0.420, and 0.461, respectively. The $B$ value for all atoms in both cases was taken as 4.5 Å$^2$. The difference between the $R$ values was small (0.187 and 0.181, respectively), but it indicated that the second model with the 1α-methoxyl may be the correct one.

A difference synthesis carried out on the basis of structure factors, which had no contributions of 1-methoxy atoms, showed two weak peaks for each of the two configurations. Those for the α-configuration were, however, about 50% higher in intensity than those for β. Having adjusted the thermal parameters for different atoms and placed the 1-methoxy group in the α-configuration, the structure was refined by block-diagonal least-squares, minimizing $\Sigma w(|F_o| - |F_c|)^2$ with $w = 1/\{1 + [(|F_o| - 10)/15]^4\}$.

The refinement converged to $R = 0.085$ and $R_w = 0.098$. A difference map carried out close to the end of refinement showed residual density of only 0.4e Å$^{-3}$ at the positions for atoms of the methoxy group in both configurations. It was possible to locate all hydrogen atoms from difference syntheses except those of the disordered C(20) methyl group. The non-hydrogen atoms were refined anisotropically, but the parameters of the H atoms were fixed.

The atomic parameters are presented in Tables 1 and 2 and the bond lengths and the valency angles in Fig. 1. The $x$ and $z$ coordinates agree within 0.08 Å with the values published earlier, however, the $y$ coordinates show considerable differences, particularly for C(1), C(2), C(3), and O(7), as their refinement by two-dimensional difference maps had been seriously hampered by overlapping. The bond lengths for O(1)—C(1), C(4)—C(5), C(8)—C(9), and C(15)—C(16) have improved considerably and C(1)—C(11) increased from 1.50 to 1.57 Å.

The torsion angles are given in Fig. 1c. They are similar to those found in other aconitine and lycoctonine type alkaloids in which the boat form of the ring A is stabilized by the intramolecular hydrogen bonding (20–25). The projection of the structure is shown in Fig. 2, in which all the hydrogen-bonding parameters are presented. The molecule of water plays an important part in linking together neighbouring alkaloid molecules and the anion. The H ... I distances of 3.12 and 3.27 Å are only slightly shorter than the sum of the van der Waals radii of 3.35 Å. All other intermolecular contacts are normal.

To prove that this refined structure is the correct one, the effect on the refinement of changing of the 1-methoxy configuration back to β was studied. The H(11) atom was removed. The final $R$ values

[3]Variation in melting point range suggested that an isomer (*N*-acetyl?) was present in varying minor amounts in des(oxymethylene)lycoctonam but this was not evident in the nmr spectra.

[4]The numbering system corresponds to the generally accepted one for the $C_{19}$ diterpenoid alkaloids (19*b*), as is shown in **1**.

Can. J. Chem. Downloaded from www.nrcresearchpress.com by 210.87.254.105 on 09/06/12
For personal use only.

TABLE 1. Final coordinates (and their e.s.d's) of the non-hydrogen atoms (× $10^4$).

$$B_{eq} = \frac{8\pi^2}{3} \sum_i \sum_j U_{ij} a_i^* a_j^* \mathbf{a}_i . \mathbf{a}_j$$

| Atom | $x$ | $y$ | $z$ | $B_{eq}$ (Å$^2$) |
|---|---|---|---|---|
| I | 2245(1) | 2500 | 615(1) | 5.0 |
| N | 8421(8) | 4438(10) | 1765(9) | 2.7 |
| O(1) | 6461(7) | 4061(11) | 668(9) | 4.0 |
| O(2) | 9462(6) | 41(9) | 3091(7) | 2.8 |
| O(3) | 9631(5) | 3399(9) | 4016(7) | 2.8 |
| O(4) | 9056(6) | 1050(9) | 5265(7) | 2.8 |
| O(5) | 6888(7) | 159(11) | 5841(8) | 3.5 |
| O(6) | 6189(6) | 3492(12) | 6089(9) | 3.7 |
| O(7) | 8321(8) | 7813(12) | 6278(13) | 5.6 |
| C(1) | 6600(8) | 2531(21) | 643(9) | 3.0 |
| C(2) | 6930(10) | 1994(20) | −553(11) | 4.3 |
| C(3) | 8031(10) | 2506(31) | −750(9) | 4.5 |
| C(4) | 8859(9) | 2367(18) | 425(9) | 2.9 |
| C(5) | 8430(9) | 1398(12) | 1385(10) | 2.5 |
| C(6) | 9270(9) | 1382(11) | 2528(10) | 2.3 |
| C(7) | 8840(6) | 2468(15) | 3430(7) | 1.8 |
| C(8) | 8274(8) | 1733(12) | 4424(10) | 2.1 |
| C(9) | 7438(8) | 654(13) | 3821(11) | 2.4 |
| C(10) | 6828(8) | 1177(12) | 2592(10) | 2.4 |
| C(11) | 7440(8) | 2144(10) | 1771(9) | 2.0 |
| C(12) | 5847(9) | 2006(15) | 2971(11) | 3.1 |
| C(13) | 5956(8) | 1931(15) | 4369(12) | 3.0 |
| C(14) | 6519(8) | 496(12) | 4608(10) | 2.3 |
| C(15) | 7798(8) | 2847(11) | 5253(10) | 2.4 |
| C(16) | 6623(8) | 3148(14) | 5009(10) | 2.7 |
| C(17) | 7992(7) | 3324(10) | 2572(9) | 1.8 |
| C(19) | 9186(10) | 3822(13) | 989(11) | 3.0 |
| C(20) | 5488(13) | 4566(22) | 50(16) | 5.3 |
| C(21) | 10118(9) | −828(16) | 2461(13) | 3.8 |
| C(22) | 6064(11) | −124(19) | 6545(13) | 4.0 |
| C(23) | 6612(13) | 4783(23) | 6615(15) | 5.1 |
| C(24) | 8891(11) | 5759(12) | 2408(13) | 3.5 |
| C(25) | 8124(19) | 6493(18) | 3109(22) | 6.7 |

TABLE 2. Fractional coordinates of H atoms (× $10^3$) and isotropic temperature factors. The first five atoms are attached to N and O atoms as shown in Fig. 2. The numbering of the parent C atom can be derived from the remaining atoms by omitting the last digit

| Atom | $x$ | $y$ | $z$ | $B$(Å$^2$) |
|---|---|---|---|---|
| H(1) | 785 | 474 | 121 | 3.2 |
| H(3) | 1032 | 333 | 388 | 3.9 |
| H(4) | 953 | 71 | 462 | 3.2 |
| H(71) | 753 | 812 | 631 | 6.0 |
| H(72) | 860 | 818 | 691 | 6.0 |
| H(11) | 572 | 215 | 63 | 3.5 |
| H(21) | 640 | 222 | −128 | 5.0 |
| H(22) | 689 | 82 | −53 | 5.0 |
| H(31) | 799 | 371 | −94 | 5.0 |
| H(32) | 834 | 206 | −150 | 5.0 |
| H(41) | 967 | 206 | 39 | 4.4 |
| H(51) | 841 | 49 | 139 | 3.9 |
| H(61) | 996 | 174 | 235 | 3.2 |
| H(91) | 798 | −30 | 387 | 3.6 |
| H(101) | 660 | 24 | 204 | 3.0 |
| H(121) | 511 | 149 | 259 | 3.5 |
| H(122) | 583 | 308 | 266 | 3.5 |
| H(131) | 519 | 190 | 467 | 3.5 |
| H(141) | 600 | −32 | 426 | 3.5 |
| H(151) | 797 | 248 | 618 | 3.5 |
| H(152) | 821 | 383 | 516 | 3.5 |
| H(161) | 651 | 406 | 441 | 3.5 |
| H(171) | 743 | 383 | 310 | 2.5 |
| H(191) | 988 | 384 | 144 | 4.0 |
| H(192) | 928 | 453 | 24 | 4.0 |
| H(211) | 966 | −122 | 160 | 5.0 |
| H(212) | 1085 | −67 | 250 | 5.0 |
| H(213) | 1036 | −180 | 289 | 5.0 |
| H(221) | 635 | −25 | 738 | 5.0 |
| H(222) | 564 | −109 | 620 | 5.0 |
| H(223) | 551 | 77 | 645 | 5.0 |
| H(231) | 742 | 457 | 665 | 6.0 |
| H(232) | 639 | 568 | 605 | 6.0 |
| H(233) | 638 | 492 | 754 | 6.0 |
| H(241) | 955 | 577 | 287 | 4.5 |
| H(242) | 884 | 623 | 161 | 4.5 |
| H(251) | 842 | 744 | 355 | 6.0 |
| H(252) | 735 | 658 | 250 | 6.0 |
| H(253) | 790 | 584 | 384 | 6.0 |

became appreciably higher ($R$ = 0.099 and $R_w$ = 0.123) and the bond lengths showed in general larger differences from the values obtained for the skeleton from more accurate X-ray determinations. The intermolecular contacts were satisfactory, but the O(1) ... H(22) and O(1) ... H(101) distances became unacceptably short. In addition, the final difference map showed peaks at positions for O(1) and C(20) in the α-configuration of ~2.0 and ~1.5e Å$^{-3}$, respectively.

In spite of the low accuracy of this redetermination, we can conclude that the β-configuration of the 1-methoxy group in the original analysis was wrong and that it is definitely α. This study has also shown that it would have been difficult to establish unambiguously the C(1) configuration in this derivative without recourse to better data and modern methods of refinement.

Thus lycoctonine has the structure and stereochemistry shown in **2** and browniine is represented by **3**. In a recent communication (26) Pelletier and co-workers have confirmed this revised stereochemistry by relating lycoctonine, browniine, delphatine, and delsoline through their methyl

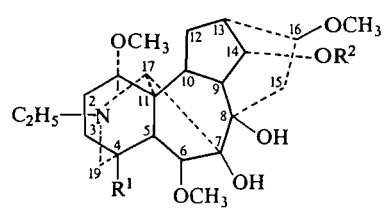


**1** $R^1 = H$ $R^2 = CH_3$
**2** $R^1 = CH_2OH$ $R^2 = CH_3$
**3** $R^1 = CH_2OCH_3$ $R^2 = H$

Can. J. Chem. Downloaded from www.nrcresearchpress.com by 210.87.254.105 on 09/06/12
For personal use only.

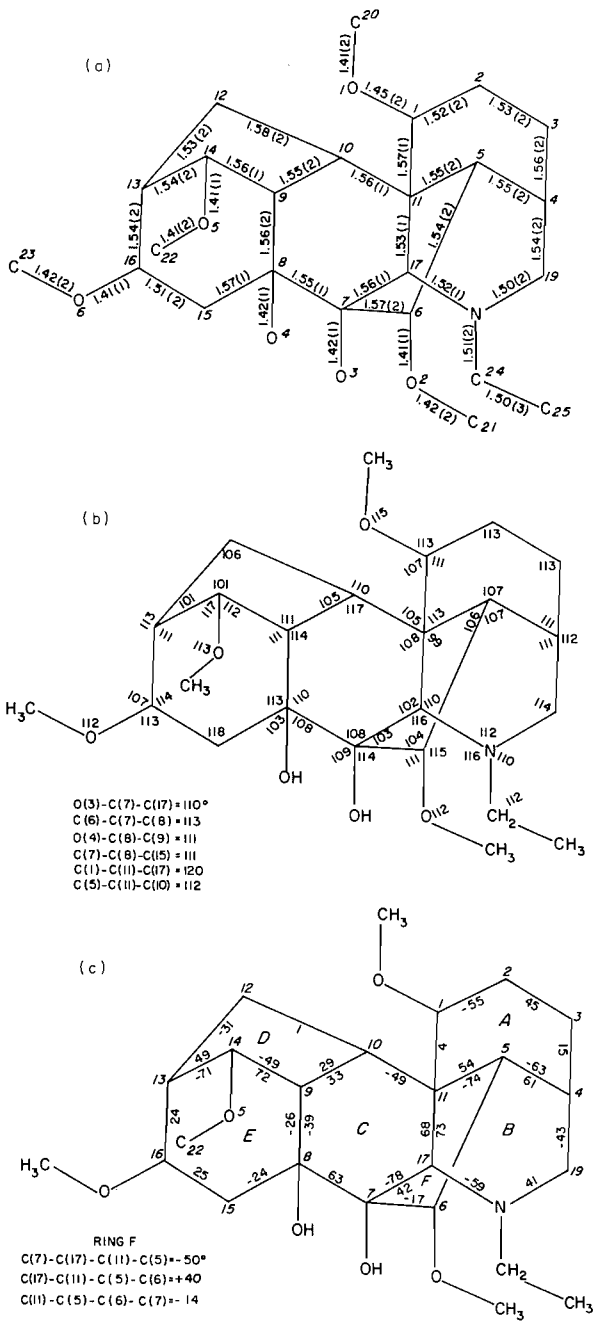


FIG. 1. (*a*) Bond lengths (Å) with their e.s.d.'s. (*b*) Valency angles (°); e.s.d.'s are 0.8 to 1.1° with the exception of those at C(2), C(3), and C(24) which are 1.3, 1.4, and 1.2°, respectively. (*c*) Torsion angles (°); e.s.d.'s are 0.5 to 0.9°.

ethers. Since delsoline has a 1α-hydroxyl group (27), the alkaloids with a 1-methoxyl group also have a 1α configuration.

Alkaloids which had been chemically correlated with lycoctonine, browniine, or delpheline, and which hence also require revision of their C-1 stereochemistry, are 14-*O*-acetylbrowniine (15*b*, 28), 14-*O*-acetyldelectine (29), *N*-acetyldelectine (30), ajacine (31), anthranoyllycoctonine (14, 15, 18, 32), 14-*O*-benzoylbrowniine (33), 14-dehydrobrowniine (33, 34), delbiterine (33), delectine (35), delectinine (35), delphatine (26, 28*b*, 36), deltaline (5, 37), dictyocarpine (38), elatine (37), lycaconitine (37, 39), methyllycaconitine (13, 37, 40), septentriodine (41), and tricornine (42).

A number of bases with 1-methoxyl groups have had their configurations assigned on the basis of their $^{13}C$ nmr spectra. Thus ajacusine (43), ajadine (43), and ambiguine (44) have chemical shifts for C-1 similar to lycoctonine and browniine (85 ± 2 ppm), while delcaroline (45) has a similar C-1 chemical shift to those of dictyocarpine and deltaline (79 ± 1 ppm), alkaloids with a 1α-hydroxyl group. However, no spectra seem to be available for 1β-methoxy alkaloids, so the assignments are open to question.

Since it should be possible to prepare methyl ethers of 1-epidelsoline (46), 1-epidelphisine (23), delphirine (47), and talatizidine (48), one should be able to ascertain whether a useful $^{13}C$ nmr shift difference exists between the epimers in both the lycoctonine and aconine series of alkaloids.

Other lycoctonine-type bases: delcorine (49), dehydrodelcorine (49), delcoridine (50), 6-deoxydelcorine (51), and ilidine (52) have been assigned 1α-methoxyl groups by interpretation of their mass spectra. The criterion was that 1-oxygenated bases with α configuration had low (less than 6%) ratios of the $M - 15$ to the $M - 31$ peaks while those with the β configuration had higher ratios (20–30%) (53). Since the examples used for the latter were lycoctonine and browniine, which are now shown to have 1α-methoxyl groups, this criterion is invalid. However, the apparent chemical correlation of delcorine with delphatine (26) seems to establish the correctness of these assignments.[5]

The revised configuration at C-1 vindicates the browniine–chasmanine correlation (6), which has often been questioned. The C-1 configurations of alkaloids which have been chemically related to chasmanine have already been corrected (54). New esters of browniine and dictyocarpinine have recently been isolated, but the corrected stereochemistry has been presented in ref. 55.

Two complex lycoctonine esters, avadharidine (56) and delsemine (57), are artifacts arising from ammonolysis of lycaconitine and methyllycaconitine, respectively, during isolation. Similarly, sep-

[5]This correlation has, to the best of our knowledge, not been documented.

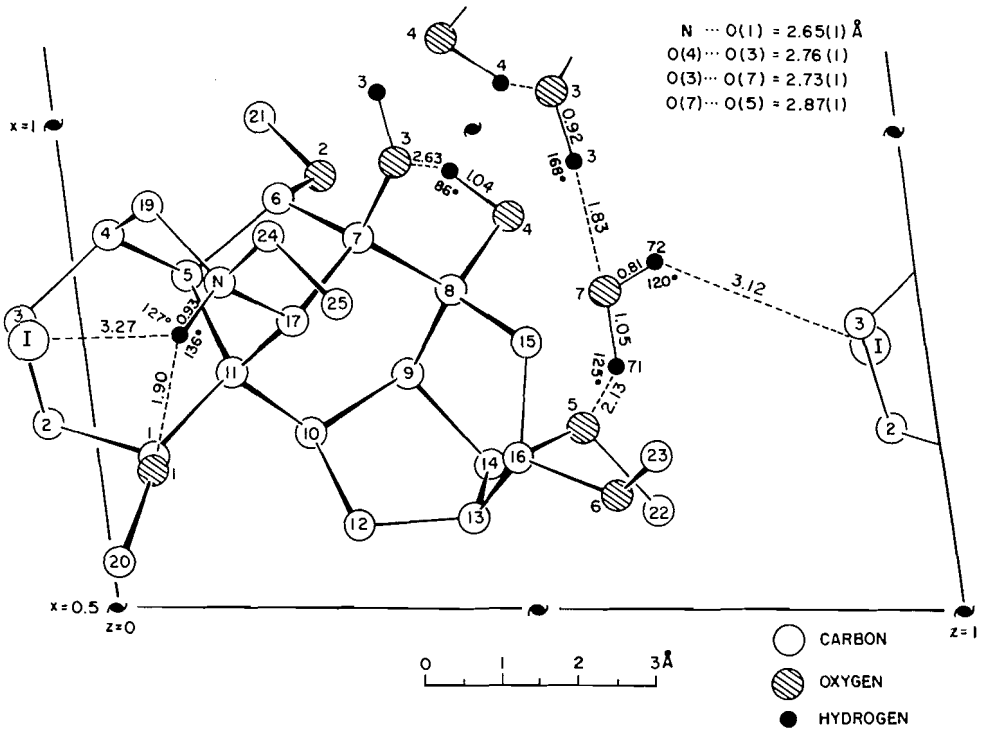


FIG. 2. A projection of the structure along the *b* axis. The hydrogen bonds are shown by broken lines.

tentrionidine (cashmiradelphine) (41, 58) and septentrionine probably are artifacts of methanolysis of lycaconitine and 8-*O*-methyllycaconitine, respectively.

## Experimental

Thin layer and preparative thin layer chromatography was done on silica gel plates with fluorescent indicator. Infrared spectra were obtained on a Perkin–Elmer Model grating spectrometer, $^1$H nmr spectra on a Varian EM 360 spectrometer, and $^{13}$C nmr spectra on a Brucker WP 80 spectrometer.

*Lycoctonine hydrate*

Early samples from Delphinium species (14, 15) and from *Inula royleana* (13) had identical $^1$H nmr spectra. In $C_6D_6$ (ca. 50 mg in 0.4 mL) it gave signals at δ 4.06 (1H, s), 3.87 (1H, s), 3.54 (1H, s), 3.32 (3H, s), 3.24 (3H, s), 3.16 (3H, s), 3.06 (3H, s), 1.17 (3H, t, $J$ = 7 Hz). In $CDCl_3$ the signals were at δ 4.04 (1H, s) 3.82 (1H, s), 3.42 (3H, s), 3.38 (3H, s), 3.32 (3H, s), 3.24 (3H, s), and 1.02 (3H, t, $J$ = 7 Hz).

Its $^{13}$C nmr spectrum in $C_6D_6$ had signals at δ 90.7, 88.5, 84.3, 84.0, 82.7, 77.6, 67.6, 64.9, 57.9, 57.7, 56.2, 55.7, 52.8, 51.1, 49.8, 48.9, 46.1, 43.3, 38.6, 38.0, 33.7, 31.7, 28.8, 26.1, 14.1 (25 carbons).

*Des(oxymethylene)lycoctonam*

Samples from permanganate oxidation of lycoctonine from *D. brownii* and *D. consolida* (19) were purified by preparative tlc on silica plates using 10% methanol in chloroform for development. They crystallized from ether as radiating clusters (pincushions) of rods, as isolated rods, or as prisms. The forms were interchangeable on recrystallization from acetone–ether. Some samples melted below 150°C, resolidified, sintered around 171°C, and melted completely by 181°C. The majority sintered at 171°C and melted by 180°C. Samples of prisms from early work on lycoctonine from Delphinium species (19) had mp 178–180.5°C. Similar prisms prepared from methyl lycaconitine from *Inula royleana* (13) had mp 179–181°C. The mixture mp of the two was 177–180°C.

The $^1$H nmr spectra of all samples of des(oxymethylene)lycoctonam in deuteriochloroform were identical. Because of the sensitivity of several chemical shifts to concentration, the spectra in deuteriobenzene were more difficult to reproduce exactly. The $^{13}$C nmr spectra of the different samples were identical as were the X-ray powder patterns of the same crystal forms.

$^1$H nmr ($CDCl_3$): a partially concealed multiplet near δ 4 (1H), 3.90 (1H, s, OH), 3.57 (1H, s), 3.42 (3H, s), 3.37 (3H, s), 3.20 (3H, s), 1.10 (3H, t, $J$ = 7 Hz); $^1$H nmr ($C_6D_6$): 4.34 (1H, m), 3.82 (1H, s), 3.58 (1H, s), 3.36 (3H, s), 3.10 (3H, s), 2.84 (3H, s), 2.78 (3H, s), 1.25 (3H, t, $J$ = 7 Hz); $^{13}$C nmr ($CDCl_3$): 170.3(s), 95.3(d), 85.9(s), 83.4(d), 82.0(d), 81.4(d), 76.4(s), 62.6(d), 58.8 (q), 57.5(q), 56.0(q), 55.2(q), 47.7(d), 47.1(d), 46.7(s), 44.8(d), 43.0(t), 42.7(d), 37.5(d), 32.8(t), 28.3(t), 25.0(t), 24.1(t), 11.8(q) (24 signals).

*Des(oxymethylene)lycoctonine*

A sample of methyllycaconitine from *Inula royleana* (13) was hydrolysed to give lycoctonine. This was oxidized to obtain des(oxymethylene)lycoctonam which was reduced to des(oxymethylene)lycoctonine (19*a*). The hydriodide of the base had mp 173°C and proved identical (mixture mp, $^1$H nmr spectrum, and X-ray powder patterns) with an old sample prepared from Delphinium sources (14, 15). The perchlorate of the base formed clusters of rectangular plates from methanol – ethyl acetate. This melted or sintered around 136°C, resolidified, and melted at 178–180°C. A dried sample gave only the higher mp. An old sample from lycoctonine from Delphinium species (14) had mp 181–183°C. The mixture mp was 180–181°C. The $^1$H nmr

Can. J. Chem. Downloaded from www.nrcresearchpress.com by 210.87.254.105 on 09/06/12
For personal use only.

Can. J. Chem. Downloaded from www.nrcresearchpress.com by 210.87.254.105 on 09/06/12
For personal use only.

spectra of the dried salts were identical as were their X-ray powder patterns.

The base gave a $^1$H nmr spectrum in $C_6D_6$ with signals at δ 3.92 (1H, s), 3.75 (1H, s), 3.50 (1H, s), 3.44 (3H, s), 3.16 (3H, s), 3.08 (3H, s), 2.94 (3H, s), 2.70 (1H, s), 1.17 (3H, t, $J$ = 7 Hz). Its perchlorate in $D_2O$–DSS solution gave $^1$H nmr signals at δ 3.9 (1H, s), 3.37 (3H, s), 3.35 (9H, s) and 1.25 (3H, t, $J$ = 7 Hz).

*Oxidation of des(oxymethylene)lycoctonine*

A solution of des(oxymethylene)lycoctonine (135 mg) was dissolved in 4 mL of acetone containing 0.5 mL of water and 0.05 mL of acetic acid. Powdered potassium permanganate was added in small portions with stirring, until an excess persisted for 30 min. The suspension was filtered, then the filtrate evaporated to small volume on a rotating evaporator. The residue was taken up in methylene chloride. After washing with aqueous sodium carbonate, then drying and distilling, the solution gave 145 mg of neutral product. This crystallized from ether–hexane giving 119 mg of crude des(oxymethylene)lycoctonam, which was purified on silica gel plates using 10% methanol in chloroform for development. The substance from the main zone (101 mg) crystallized as rods from acetone–hexane, mp 169–178°C. On recrystallization from the same solvent it formed clusters of rectangular prisms, mp 169–180°C, mixture mp with the product from permanganate oxidation of lycoctonine, 169–180°C. The $^1$H and $^{13}$C nmr spectra of the samples were identical.

## Acknowledgements

We thank Drs. W. B. Cook, R. C. Cookson, A. Chatterjee, K. L. Handa, and T. M. Sharp for reference samples of alkaloids and Dr. D. G. Garratt and Mr. R. Kolt for $^{13}$C nmr spectra.

1. M. Przybylska and L. Marion. Can. J. Chem. **34**, 185 (1956).
2. M. Przybylska. Acta Crystallogr. **14**, 424 (1961).
3. M. H. Benn, M. A. M. Cameron, and O. E. Edwards. Can. J. Chem. **41**, 477 (1963).
4. O. E. Edwards, L. Marion, and K. H. Palmer. Can. J. Chem. **36**, 1097 (1958); R. C. Cookson and M. E. Trevett. J. Chem. Soc. 984 (1958); 2689 (1958).
5. M. Carmack, J. P. Ferris, J. Harvey, Jr., P. L. Magat, E. W. Martin, and D. W. Mayo. J. Am. Chem. Soc. **80**, 497 (1958).
6. O. E. Edwards, L. Fonzes, and L. Marion. Can. J. Chem. **44**, 583 (1966).
7. T. Y. R. Tsai, C. S. J. Tsai, W. W. Sy, M. N. Shanbhag, W. C. Liu, S. F. Lee, and K. Wiesner. Heterocycles, **7**, 217 (1977).
8. W. H. De Camp and S. W. Pelletier. Acta. Crystallogr. Sect. B, **33**, 722 (1977).
9. M. Cygler, M. Przybylska, and O. E. Edwards. Acta Crystallogr. Sect. B, **38**, 429 (1982).
10. M. Cygler, M. Przybylska, and O. E. Edwards. Acta Crystallogr. Sect. B, **38**, 1500 (1982).
11. O. E. Edwards. Can. J. Chem. **59**, 3039 (1981).
12. W. H. Barnes and M. Przybylska. Can. J. Chem. **31**, 511 (1953).
13. O. E. Edwards and M. N. Rodger. Can. J. Chem. **37**, 1187 (1959).
14. L. Marion and O. E. Edwards. J. Am. Chem. Soc. **69**, 2010 (1947).
15. (*a*) L. Marion and R. H. F. Manske. Can. J. Res. B, **24**, 1 (1946); (*b*) V. N. Aiyar, M. H. Benn, Y. Y. Huang, J. M. Jacyno, and A. J. Jones. Phytochem. **17**, 1453 (1978).
16. J. A. Goodson. J. Chem. Soc. 139 (1943).
17. S. W. Pelletier, R. S. Sawhney, H. K. Desai, and N. V. Mody. J. Nat. Prod. **43**, 395 (1980).
18. W. B. Cook and O. A. Beath. J. Am. Chem. Soc. **74**, 1411 (1958).
19. (*a*) O. E. Edwards and L. Marion. Can. J. Chem. **30**, 627 (1952); (*b*) O. E. Edwards. *In* The alkaloids. Vol. 1. *Edited by* J. E. Saxton. Specialist Periodical Reports, The Chemical Society, London. 1971. Chapt. 16.
20. G. I. Birnbaum. Acta Crystallogr. Sect. B, **26**, 755 (1970).
21. K. A. Kerr and P. W. Codding. Acta Crystallogr. Sect. B, **38**, 1237 (1982).
22. P. W. Codding and K. A. Kerr. Acta Crystallogr. Sect. B, **37**, 379 (1981).
23. S. W. Pelletier, Z. Djarmati, S. Lajšić, and W. H. De Camp. J. Am. Chem. Soc. **98**, 2617 (1976).
24. W. H. De Camp and S. W. Pelletier. Acta Crystallogr. Sect. B, **33**, 722 (1977).
25. S. W. Pelletier, W. H. De Camp, D. L. Herald, Jr., and S. W. Page. Acta Crystallogr. Sect. B, **33**, 716 (1977).
26. S. W. Pelletier, N. V. Mody, K. I. Varughese, J. A. Maddry, and H. K. Desai. J. Am. Chem. Soc. **103**, 6536 (1981).
27. F. Sparatore, R. Greenhalgh, and L. Marion. Tetrahedron, **4**, 157 (1958).
28. (*a*) V. G. Kazlekhin, V. A. Tel'nov, M. S. Yunusov, and S. U. Yunusov. Khim. Prir. Soedin. 869 (1977); (*b*) S. W. Pelletier, N. V. Mody, R. S. Sawhney, and J. Bhattacharyya. Heterocycles, **7**, 327 (1977).
29. B. T. Salimov, M. S. Yunusov, and S. Yu. Yunusov. Khim. Prir. Soedin. 716 (1977).
30. B. T. Salimov, M. S. Yunusov, and S. Yu. Yunusov. Khim. Prir. Soedin. 128 (1977).
31. J. A. Goodson. J. Chem. Soc. 108 (1944).
32. S. K. Talapatra and A. Chatterjee. J. Ind. Chem. Soc. **36**, 437 (1959).
33. B. T. Salimov, M. S. Yunusov, and S. Yu. Yunusov. Khim. Prir. Soedin. 106 (1978).
34. M. H. Benn. Can. J. Chem. **44**, 1 (1966).
35. B. T. Salimov, M. S. Yunusov, S. Yu. Yunusov, and A. S. Narzullaev. Khim. Prir. Soedin. 665 (1975); B. T. Salimov, N. D. Abdullaev, M. S. Yunusov, and S. Yu. Yunusov. Khim. Prir. Soedin. 235 (1978).
36. M. S. Yunusov and S. Yu. Yunusov. Khim. Prir. Soedin. 334 (1970).
37. A. D. Kuzovkov and F. T. Platanova. Zh. Obshch. Khim. **29**, 2782 (1959).
38. A. S. Narzullaev, M. S. Yunusov, and S. Yu. Yunusov. Khim. Prir. Soedin. **9**, 443 (1973).
39. S. Sakai, N. Shinma, S. Hasegawa, and T. Okamoto. Yakugaku Zasshi, **98**, 1376 (1978); V. A. Tel'nov, N. M. Golubev, and M. S. Yunusov. Khim. Prir. Soedin. 675 (1976).
40. R. C. Cookson, J. E. Page, and M. E. Trevett. J. Chem. Soc. 4028 (1954); A. Khalique, S. Papadopoulos, I. Wright, and Z. Valenta. Chem. Ind. (London), 513 (1959); V. N. Aiyar, M. H. Benn, T. Hanna, J. Jacyno, S. H. Roth, and J. L. Wilkens. Experientia, **35**, 1367 (1979).
41. S. W. Pelletier, R. S. Sawhney, and A. J. Aasen. Heterocycles, **12**, 377 (1979).
42. S. W. Pelletier and J. Bhattacharyya. Phytochem. **16**, 1464 (1977).
43. S. W. Pelletier and R. S. Sawhney. Heterocycles, **9**, 463 (1978).
44. S. W. Pelletier, R. S. Sawhney, and N. V. Mody. Heterocycles, **9**, 1241 (1978).

45. S. W. PELLETIER, N. V. MODY, and R. C. DESAI. Heterocycles, **16**, 747 (1981).
46. V. SKARIC and L. MARION. Can. J. Chem. **38**, 2433 (1960).
47. S. W. PELLETIER and J. BHATTACHARYYA. Tetrahedron Lett. 4679 (1976).
48. S. W. PELLETIER, L. H. KEITH, and P. C. PARASARATHY. J. Am. Chem. Soc. **89**, 4146 (1967).
49. A. S. NARZULLAEV, M. S. YUNUSOV, and S. YU. YUNUSOV. Khim. Prir. Soedin. 497 (1973).
50. M. G. ZHAMIERASHVILI, V. A. TEL'NOV, M. S. YUNUSOV, and S. YU. Yunusov. Khim. Prir. Soedin. 663 (1980).
51. A. S. NARZULLAEV, M. S. YUNUSOV, and S. YU. YUNUSOV. Khim. Prir. Soedin. 412 (1974).
52. M. G. ZHAMIERASHVILI, V. A. TEL'NOV, M. S. YUNUSOV, and S. YU. Yunusov. Khim. Prir. Soedin. 836 (1977).
53. M. S. YUNUSOV, YA. V. RASHKES, and S. YU. YUNUSOV. Khim. Prir. Soedin. 85 (1972); M. S. YUNUSOV, YA. V. RASHKES, V. A. TEL'NOV, and S. YU. YUNUSOV. Khim. Prir. Soedin. 515 (1969).
54. S. W. PELLETIER, Z. DJARMATI, and S. LAJŠIĆ. J. Am. Chem. Soc. **96**, 7817 (1974).
55. S. W. PELLETIER, O. D. DAILEY, N. V. MODY, and J. D. OLSEN. J. Org. Chem. **46**, 3284 (1981).
56. A. D. KUZOVKOV and P. S. MASSAGETOV. Zh. Obshch. Khim. **25**, 178 (1955).
57. S. W. PELLETIER and J. BHATTACHARYYA. Tetrahedron Lett. 2735 (1977).
58. M. SHAMMA, P. CHINNASANY, G. A. MIANA, A. KHAN, M. BASHIP, M. SALAZAR, P. PATIL, and J. L. BEAL. J. Nat. Prod. **42**, 615 (1979).

Can. J. Chem. Downloaded from www.nrcresearchpress.com by 210.87.254.105 on 09/06/12
For personal use only.

# Étude de la réactivité des thiényldiazines: nitration et résonance magnétique nucléaire de $^{13}C$ dans $H_2SO_4$ concentré

JEAN BOURGUIGNON, STELLA CHAPELLE, PIERRE GRANGER ET GUY QUEGUINER[1]

*Laboratoire de Chimie Organique Hétérocyclique, Institut National Supérieur de Chimie Industrielle de Rouen, Faculté des Sciences et des Techniques de Rouen, 76130 Mont Saint Aignan, France*

Reçu le 23 février 1982

JEAN BOURGUIGNON, STELLA CHAPELLE, PIERRE GRANGER et GUY QUEGUINER. Can. J. Chem. **60**, 2668 (1982).

La réactivité des thiényldiazines **1** à **7** a été étudiée par l'intermédiaire de la réaction de nitration. Dans le but d'établir une relation entre la réactivité et la structure électronique de ces composés, nous avons enregistré et interprété leurs spectres de rmn $^{13}C$ dans $CDCl_3$ et dans $H_2SO_4$ concentré.

Les renseignements fournis par les spectres $^{13}C$ ont par ailleurs permis d'expliquer les réactivités relatives observées lors de réactions de concurrence entre les thiényldiazines **1** et **2**, **2** et **7**, **2** et **4**, **2** et **6**.

Cette méthode constitue une approche rarement utilisée pour étudier une substitution électrophile aromatique d'une molécule dans son milieu réactionnel.

JEAN BOURGUIGNON, STELLA CHAPELLE, PIERRE GRANGER, and GUY QUEGUINER. Can. J. Chem. **60**, 2668 (1982).

The reactivity of the thienyl diazines **1** to **7** has been studied by means of the nitration reaction. In order to examine any relationship between the reactivity and the electronic structure of these compounds, we have recorded their $^{13}C$ nmr spectra in $CDCl_3$ and in concentrated sulfuric acid.

The $^{13}C$ results are correlated to relative reactivities observed during competitive reactions between the thienyl diazines **1** and **2**, **2** and **7**, **2** and **4**, **2** and **6**.

This method is a rarely-used approach for the study of electrophilic substitution of a molecule in the reaction mixture.

Les systèmes bihétérocycliques constitués d'un cycle riche en électrons, le thiophène et d'un cycle pauvre en électrons ont particulièrement retenu l'attention des chercheurs depuis quelques années. La combinaison d'un cycle π-excédentaire et d'un cycle π- déficitaire se traduit, bien évidemment par une modification des propriétés respectives des deux cycles. C'est ainsi que Kauffmann *et al.* (1) ont réalisé une intéressante comparaison des réactivités électrophiles et nucléophiles de divers systèmes hétérocycliques assemblés.

Un certain nombre de réactions électrophiles ont été réalisées avec succès dans le cas d'autres systèmes bihétérocycliques constitués d'un thiophène et d'une diazine assemblés ou accolés, notamment par Gronowitz, Robba et coll. (2).

Les résultats décrits dans la littérature font apparaître que la réaction de nitration constitue un excellent modèle pour étudier et comparer la réactivité des systèmes bihétérocycliques assemblés ou accolés. C'est ce qui nous a conduit à l'appliquer à l'étude de la réactivité de thiényldiazines (3), de thiénodiazines (4) et de la (thiényl-2)-2 thiéno[2,3-*d*]pyrimidine (5). Ce dernier composé présente d'ailleurs la particularité d'être constitué d'un cycle diazinique à la fois assemblé et accolé à un cycle thiophénique.

Il est connu que la rmn de $^{13}C$ permet assez souvent d'obtenir des renseignements sur la densité électronique des systèmes π hétérocycliques en particulier. On admet souvent que le déplacement chimique d'un carbone donné est directement lié à la densité électronique à son niveau (6). C'est pourquoi nous avons décidé d'utiliser cette méthode pour compléter la discussion des résultats obtenus lors de la nitration des thiényldiazines **1** à **7**. Nous avons pour notre part enregistré les spectres de rmn de $^{13}C$ des composés étudiés tout d'abord dans $CDCl_3$ puis dans $H_2SO_4$ concentré. Dans ce dernier cas, les molécules étudiées se trouvent dans leur milieu réactionnel. Ceci constitue une approche utilisée pour la première fois, à notre connaissance, de la

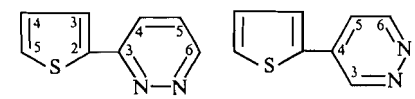

**1** **2**

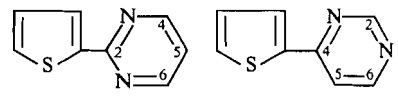

**3** **4**

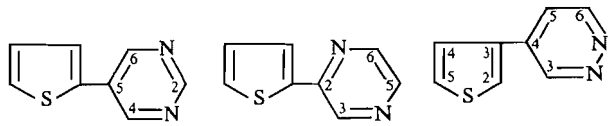

**5** **6** **7**

[1]Auteur à qui correspondance doit être adressée.

0008-4042/82/212668-07$01.00/0

©1982 National Research Council of Canada/Conseil national de recherches du Canada

Can. J. Chem. Downloaded from www.nrcresearchpress.com by 210.87.254.40 on 09/06/12
For personal use only.

TABLEAU 1. Pourcentage d'isomères obtenus lors de la nitration des (thiényl-2)diazines

| Thiényl diazine | % Dérivé nitré en 4 | % Dérivé nitré en 5 | Référence |
|---|---|---|---|
| **1** | 31 | 69 | 3*c* |
| **2** | 27 | 73 | 3*c* |
| **3** | 65 | 35 | 2*e*[a] |
| **4** | 40 | 60 | 2*a* |
| **5** | 25 | 75 | 3*a* |
| **6** | 33 | 66 | 3*a* |

[a]Gronowitz et Liljefors (2*b*) annoncent respectivement 47 et 53% alors que Morel et coll. (2*e*) annoncent 65 et 35%. Ces dernières valeurs ont été confirmées par nous-mêmes.

structure d'un système hétérocyclique soumis à une substitution électrophile aromatique dans l'acide sulfurique.

## I. Nitration des (thiényl-2)diazines

### 1. Résultats

La nitration se fait avec un excellent rendement et fournit un mélange en proportions variables du dérivé nitré en 4 et du dérivé nitré en 5 sur le cycle thiophénique (Tableau 1). L'obtention de ces deux isomères résulte de la compétition entre l'effet électroattracteur de la diazine protonée (3*c*), orienteur en *méta* (sommet 4) et la réactivité élevée de la position α du thiophène (sommet 5).

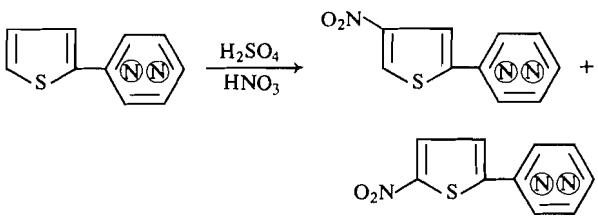


*Spectres de résonance magnétique nucléaire de* $^{13}C$

*(a) Spectres dans le deutériochloroforme*

L'attribution des divers signaux des carbones des composés étudiés **1** à **6** rassemblés, dans le Tableau 2 a été effectuée selon les données de la littérature ci-dessous: (*i*) utilisation des déplacements chimiques des cycles thiophénique et diazinique et des constantes de couplage $^1J$(C—H) relevées dans la littérature (7) qui permettent, entre autre, la distinction des carbones en α et en β du soufre; (*ii*) utilisation des constantes de couplage à longue distance $J$(C—H) et du découplage sélectif pour lever certaines ambiguïtés.

Dans le cas du composé **1**, l'attribution de déplacement chimique du carbone 5 pyridazinique à 126,6 ppm est basée sur le fait que $^2J_{C_5-H_4} \simeq 0$ et $^2J_{C_5-H_6} \simeq 5$ Hz (7*b*) conduisant à l'observation d'un doublet alors que le carbone 3 thiophénique à 126,4 ppm se présente sous forme d'un massif complexe à cause des valeurs de $^2J_{C_3-H_4}$ et $^2J_{C_3-H_5}$ de l'ordre de 5 et 8 Hz (7*a*).

Les carbones 3 et 4 du cycle thiophénique des composés **3**, **4** et **5** ont été différenciés par leurs $J$ longue distance qui conduisent à des largeurs de raie différentes. De plus dans le cas du composé **5**, nous avons vérifié l'attribution en effectuant un découplage sélectif: l'irradiation de H4 (δ = 7,16 ppm en rmn de $^1$H) permet d'observer un découplage total de la raie à 128,4 ppm alors que la raie à 125,3 ppm n'est que partiellement découplée et donne une constante de couplage résiduelle de 12 Hz ($\delta H_3$ = 7,42 ppm).

L'attribution des déplacements chimiques des carbones 3 et 5 du cycle pyrazinique du composé **6** a été effectuée par analogie avec les valeurs relevées pour la phényl pyrazine (7*e*).

Dans le cas du composé **7**, l'attribution des signaux correspondants aux carbones 2 et 5 du cycle thiophénique pourraît être inversée. Notre attribution est effectuée par analogie avec les résultats de la littérature (7*a*).

Les valeurs des déplacements chimiques des (thiényl-2)diazines dans $CDCl_3$ indiquées dans le Tableau 2 révèlent qu'il n'existe pas de différences importantes pour un carbone thiophénique donné lorsque l'on passe d'un composé à un autre. On note par exemple les écarts ci-dessous pour les déplacements chimiques des carbones 4 et 5 (choisis car ce sont les positions de nitration): carbone 5: de 127,3 à 130,2 ppm; carbone 4: de 127,6 à 128,5 ppm.

Ces écarts trop faibles ne nous permettent pas de comparer valablement la réactivité des thiényldiazines que nous avons soumises à la nitration. Cette réaction s'effectuant en milieu acide sulfurique concentré, nous avons alors décidé d'enregistrer les spectres des produits étudiés dans ce même milieu. On peut penser, en effet, que l'étude des spectres de $^{13}$C des (thiényl-2)diazines dans leur milieu réactionnel a plus de chances de fournir des renseignements intéressants concernant leur réactivité.

Can. J. Chem. Downloaded from www.nrcresearchpress.com by 210.87.254.40 on 09/06/12
For personal use only.

Can. J. Chem. Downloaded from www.nrcresearchpress.com by 210.87.254.40 on 09/06/12
For personal use only.





TABLEAU 2. Spectres de $^{13}C$ des thiényldiazines dans $CDCl_3$, $J$ constante de couplage à une liaison

| | Carbones thiophéniques | | | | | | | | Carbones diaziniques | | | | | | | | | |
|---|---|---|---|---|---|---|---|---|---|---|---|---|---|---|---|---|---|---|
| Compose | δC2 | $J$ | δC3 | $J$ | δC4 | $J$ | δC5 | $J$ | δC2 | $J$ | δC3 | $J$ | δC4 | $J$ | δC5 | $J$ | δC6 | $J$ |
| **1** | 140,1 | — | 126,4 | 169 | 127,6 | 170 | 128,8 | 185,5<br>7,7<br>et 8 | — | — | 154,6 | — | 121,9 | 168<br>6 et 6 | 126,6 | 166 | 149,7 | 187 |
| **2** | 136,6 | — | 126,6 | 166,2<br>7 et 6 | 128,5 | 170 | 128,5 | 185 | — | — | 151 | 182 | 131,6 | — | 120,4 | 166,2<br>10,5<br>et 1 | 147,6 | 182 |
| **3** | 143,3 | — | 128,7 | 168<br>6 et 10 | 128,0 | 168<br>5 et 5 | 129,6 | 185,5 | 161,3 | — | — | — | 156,8 | 183<br>7,5 | 118 | 166,5<br>7 et 7 | 156,8 | 183<br>7,5 |
| **4** | 141,8 | — | 127,5 | 170 | 128,4 | 171 | 130,2 | 186<br>8 | 159,1 | 204<br>12 | — | — | 158,6 | — | 114,9 | 167<br>8 | 157,1 | 182<br>9 |
| **5** | 136,2 | — | 125,3 | 167,2<br>6 et 9 | 128,5 | 169,5<br>3,5<br>et 3,5 | 127,3 | 187,5<br>7,5 et<br>10,5 | 156,7 | 205,5<br>10,5<br>et 10,5 | — | — | 153,2 | 181,5<br>3 et<br>9,75 | 129 | — | 153,2 | 181,5<br>3 et<br>9,75 |
| **6** | 141,4 | — | 125,5 | 176<br>10 | 128,2 | 176<br>10 | 129 | 196<br>8 et 10 | 148,7 | — | 143,2 | 184 | — | — | 140,1 | 184 | 141,9 | 184<br>10 et<br>10 |
| **7** | 124,7 | 182<br>7,7<br>et 6 | — | — | 124,6 | 168 | 127,5 | 189<br>6 et 5 | — | — | 151 | 182 | — | — | 121,6 | 168 | 148,6 | 182<br>4,4 et<br>4,4 |

TABLEAU 3. Spectres de $^{13}C$ des thiényldiazines dans $H_2SO_4$

| | Carbones thiophéniques | | | | | | | | Carbones diaziniques | | | | | | | | | |
|---|---|---|---|---|---|---|---|---|---|---|---|---|---|---|---|---|---|---|
| Composé | δC2 | $J$ | δC3 | $J$ | δC4 | $J$ | δC5 | $J$ | δC2 | $J$ | δC3 | $J$ | δC4 | $J$ | δC5 | $J$ | δC6 | $J$ |
| **1** | [a] | — | 137,4 | — | 133,9 | — | 139,5 | — | — | — | — | — | 127 | — | 136,8 | — | 150,3 | — |
| **2** | 146,4 | — | 137,9 | 180 | 133,9 | 177<br>3,75 | 141,8 | 198 | — | — | 148,6 | 195 | 135,7 | — | 128 | 180<br>3 | 151 | 192<br>4,5 |
| **3** | 123,3 | — | 143,7 | 174<br>6 et 9 | 134,4 | 180 | 150,5 | 192<br>9,4 et<br>9,4 | 151,1 | — | — | — | 159,7 | 204 | 120,6 | 195 | 159,7 | 204 |
| **4** | [a] | — | 145,3 | 172,5<br>9 et<br>5,25 | 136,1 | 180<br>5 | 148,7 | 202,5<br>6 | 151,4 | 225<br>7 | — | — | 156,7 | — | 121,9 | 184,5<br>4,5 | 156 | 192<br>7 et 11 |
| **5** | [a] | — | 135,1 | 168<br>10,5<br>et 6 | 132,3 | 174<br>4,5<br>et 4,5 | 139,3 | 198<br>12 et 7 | 144,7 | 210<br>13,5<br>et 7,5 | — | — | 152,1 | 201<br>5,2 et<br>5,2 | [a] | — | 152,1 | 201<br>5,2 et<br>5,2 |
| **6** | 127,3 | — | 133 | 180 | 130,8 | 180 | 139,7 | 200 | 146,9 | — | 146,9 | 196 | — | — | 139,7 | 192 | 142,8 | 208 |
| **7**[b] | 135,4 | 193,5 | 145,2 | — | 128,3 | 181 | 130,9 | 192 | — | — | 147,7 | 199 | ? | — | 126,1 | 174 | 150,5 | 195 |

[a]Les valeurs de δ ou de $J$ n'ont pu être relevées en raison de la complexité du spectre ou de certaines difficultés d'enregistrement (cas du composé 1).
[b]$J$ relevés à −20°C.

Can. J. Chem. Downloaded from www.nrcresearchpress.com by 210.87.254.40 on 09/06/12
For personal use only.

*(b) Spectres dans $H_2SO_4$*

Une étude préalable en rmn de $^1H$ nous a montré que certains composés étudiés se sulfonaient rapidement. C'est ainsi que nous avons rencontré de grandes difficultés pour enregistrer le spectre de $^{13}C$ du composé **1** (voir partie expérimentale).

D'une manière générale, l'interprétation des spectres des divers composés dans l'acide sulfurique a été déduite de l'examen des constantes de couplage et surtout de l'examen des variations de déplacements chimiques, en tenant compte des résultats obtenus par Pugmire et Grant (8) sur la mono ou la diprotonation des diazines. Les signaux sont fins, les déplacements chimiques sont mesurés sans ambiguïté (il ne se forme pas de produit sulfoné, il peut y avoir échange rapide entre les espèces monoprotonée ou diprotonée).

L'ensemble des résultats en milieu sulfurique concentré est présenté dans le Tableau 3. De ceux-ci on constate que: (*i*) les carbones du cycle pyrimidinique ont des déplacements chimiques très voisins de ceux observés pour le mono ou le dicathion pyrimidinium (8), et (*ii*) les carbones du cycle thiophénique ont des déplacements chimiques très comparables à ceux du cycle thiophénique dans le bithiényl-2,2′ protoné en milieu superacide (9). Les forts déblindages des carbones 3 et 5 sont attribués à la présence d'une charge positive sur les sommets correspondants dans les formules limites ci-dessous:

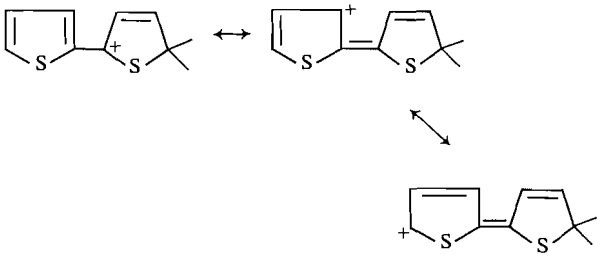

L'interprétation du spectre du composé **4** dans l'acide sulfurique pose un problème au niveau du carbone 5 du cycle thiophénique et du carbone 6 du cycle pyrimidinique. Si l'on s'en tient aux constantes de couplage observées, il semblerait (par analogie avec le composé **3**) que les déplacements chimiques de ces deux carbones seraient respectivement de 156 ppm et 148,7 ppm. Cette dernière valeur représente alors un blindage trop important du carbone pyrimidinique par rapport à son déplacement chimique dans $CDCl_3$ (8,4 ppm) au lieu de 1 à 2 ppm observés par Pugmire et Grant (8). C'est pourquoi nous avons finalement choisi l'interprétation indiquée dans le Tableau 3.

## 2. Discussion

La nitration des (thiényl-2)diazines **1** à **6** fournit un mélange de (nitro-4 et -5 thiényl-2)diazines avec, en général, un pourcentage plus élevé de l'isomère en 5. Or si on examine les déplacements chimiques des carbones correspondants dans $H_2SO_4$, on constate que le carbone 5 est toujours plus déblindé que le carbone 4. On a d'ailleurs l'ordre suivant $\delta C_4 < \delta C_3 < \delta C_5$. Cette situation est la conséquence de l'effet électroattracteur de la diazine qui s'exerce essentiellement sur les sommets 3 et 5.

Il n'apparaît donc pas de corrélation directe entre la réactivité préférentielle en 5 et le déplacement chimique du carbone correspondant.

Cependant la nitration fournit de 27% à 65% de dérivé nitré en 4 (voir Tableau 1).

L'obtention de ces dérivés nitrés est la conséquence de l'effet exercé par le cycle diazinique protoné orienteur en *méta*, qui entre en concurrence avec la réactivité élevée de la position α du cycle thiophénique.

Si on examine la différence des déplacements chimiques entre les carbones 5 et 4 du cycle thiophénique des diverses thiényldiazines (en solution dans $H_2SO_4$) et les pourcentages de (nitro-4 thiényl-2)diazines obtenus, on observe qu'il y a une bonne corrélation entre ces deux grandeurs.

Seul le composé **1** se trouve légèrement en dehors du classement proposé, mais il faut rappeler les difficultés rencontrés pour enregistrer son spectre dans l'acide sulfurique.

On peut estimer que plus l'écart des déplacements chimiques entre les deux sommets est élevé plus la réactivité en 5 est défavorisée par rapport à la réactivité en 4.

On peut donc penser qu'il est possible dans

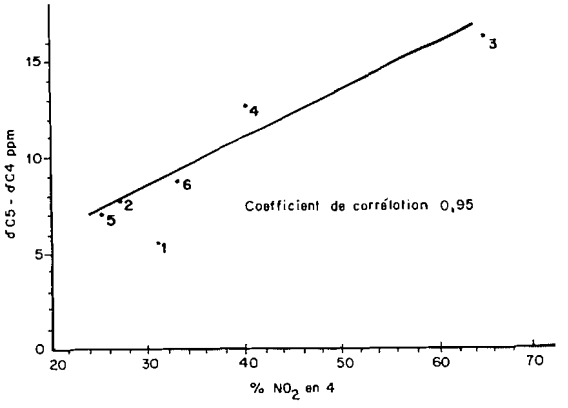


FIG. 1. δC5 – δC4 en fonction du % de dérivé nitré en 4 des (thiényl-2)diazines **1** à **6**.

Can. J. Chem. Downloaded from www.nrcresearchpress.com by 210.87.254.40 on 09/06/12
For personal use only.

TABLEAU 4. Réactions de concurrence entre les thiényldiazines

| Diazines de départ | Nitration de chaque diazine (%) | Rendement global[a] | |
|---|---|---|---|
| 1 + 2 | 50% 1 et 50% 2 | 91% | Position d'assemblage sur la pyridazine |
| 2 + 7 | 30% 2 et 70% 7 | 82% | Position d'assemblage sur le thiophène |
| 2 + 4 | 75% 2 et 25% 4 | 93,5% | Nature de la diazine |
| 2 + 6 | 60% 2 et 40% 6 | 86% | Nature de la diazine |

[a]Rendement global: voir partie expérimentale pour sa détermination.

certains cas de prévoir les réactivités relatives des sommets α et β de cycles thiophéniques diversement substitués en 2 à partir des différences de déplacement chimique de ces deux sommets α et β en milieu acide.

## II. Réaction de concurrences entre les thiényldiazines

Les résultats que nous venons d'exposer concernant la nitration des thiényldiazines nous ont permis de préciser l'influence des ions diazinium sur la nitration du cycle thiophénique. Les renseignements ainsi obtenus peuvent être utilement complétés par une étude de la réactivité relative de ces systèmes bihétérocycliques opposés dans des réactions de concurrence selon la méthode utilisée par Kauffmann *et al.* pour étudier les réactivités relatives de nombreux composés biaryliques (1).

Nous avons réalisé trois type de réactions de concurrence: (*i*) entre la (thiényl-2)-3 pyridazine (**1**) et la (thiényl-2)-4 pyridazine (**2**) dans lesquelles la pyridazine est assemblée par son sommet 3 ou 4 au cycle thiophénique; (*ii*) entre la (thiényl-2)-4 pyridazine (**2**) et la (thiényl-3)-4 pyridazine (**7**) dans le but d'apprécier l'influence de la pyridazine selon qu'elle est assemblée par le sommet 2 ou 3 du thiophène; (*iii*) entre la (thiényl-2)-4 pyridazine (**2**) d'une part et la (thiényl-2)-4 pyrimidine (**4**) ou la (thienyl-2)pyrazine (**6**) d'autre part dans le but d'apprécier cette fois le rôle de la diazine liée au thiophène.

### 1. Résultats

Le choix de ces réactions de concurrence s'est trouvé imposé par la possibilité de déterminer la composition des mélanges réactionnels par rmn de $^1H$. Il est, en particulier, nécessaire de choisir des isomères dont l'un au moins est facilement repérable en rmn par la présence d'un pic caractéristique dans une région donnée du spectre. La même propriété doit se retrouver pour l'un au moins des dérivés nitrés. Ces considérations nous ont conduit à utiliser la (thiényl-2)-4 pyridazine (**2**) comme partenaire privilégié dans les différentes nitrations compétitives mises en oeuvre.

Par ailleurs, pour que le bilan de la réaction de concurrence ait une signification il faut que la nitration des thiényldiazines mises ainsi en compétition se fasse individuellement avec un excellent rendement. C'est le cas de toutes les réactions étudiées (voir Tableau 1) et aussi de la nitration de la (thiényl-3)-4 pyridazine (**7**) qui fournit le dérivé nitré en 5 sur le cycle thiophénique avec un rendement de 89% (3*c*).

Les résultats sont rassemblés dans le Tableau 4.

### 2. Discussion

Les résultats des réactions de concurrence permettent de compléter la discussion sur la réactivité des thiényldiazines en utilisant notamment les renseignements fournis par les spectres de rmn de $^{13}C$ dans $H_2SO_4$.

(*a*) Les groupes pyridazinyl-3 ou pyridazinyl-4 protonés exercent des effets identiques sur la réactivité du thiophène. Cela signifie que l'importance de l'effet électroattracteur de l'ion pyridazinium est indépendante de sa position d'assemblage au cycle thiophénique. Les déplacements chimiques, très voisins en rmn de $^{13}C$ des carbones thiophéniques des composés **1** et **2** dans l'acide sulfurique sont en accord avec ce résultat.

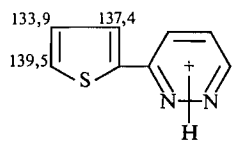


1

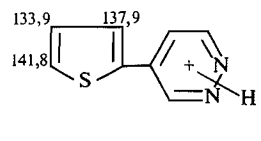


2

(*b*) On note que le groupe pyridazinyl-4 désactive plus le thiophène quand il lui est relié par le sommet 2 plutôt que par le sommet 3. Ce comportement avait déjà été mis en évidence par Gronowitz et Liljefors (2*b*) lors de l'étude de la nitration des (thiényl-2 et -3)-2 pyrimidines. Ce résultat apparaît normal si on examine les facteurs qui influencent

Can. J. Chem. Downloaded from www.nrcresearchpress.com by 210.87.254.40 on 09/06/12
For personal use only.

les réactivités du sommet 2 de la (thiényl-2)-4 pyridazine et du sommet 5 de la (thiényl-3)-4 pyridazine.

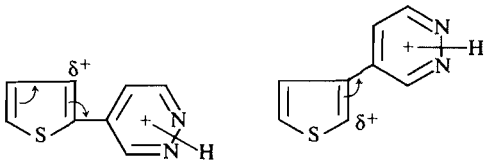

2 7

Les formules limites les plus significatives sont celles représentées ci-dessus où apparaissent des charges (ou des fractions de charges) dues au effets -M ou -I exercés par le cycle pyridazinique sur les sommets 3 et 5 du composé **2** et sur le sommet 2 du composé **7**. On constate que le cycle pyridazinique assemblé en 2 au cycle thiophénique entraîne une déficience électronique sur le sommet 5, ce qui diminue bien sûr la réactivité de ce sommet vis-à-vis d'un réactif électrophile. A l'inverse, le groupe pyridazinyle assemblé en 3 au cycle thiophénique appauvrit surtout le sommet 2 en électrons et exerce peu d'effet sur le sommet 5 où a lieu l'attaque. Là encore, l'étude des spectres de $^{13}C$ dans l'acide sulfurique confirme le résultat observé. En effet, si on examine le déblindage subit par un carbone donné des composés **2** et **7** dans l'acide sulfurique par rapport à son déplacement chimique dans $CDCl_3$ on a les valeurs suivantes (tirées des Tableaux 2 et 3).

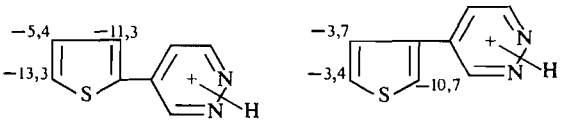

2 7

On constate que globalement, les carbones thiophéniques du composé **2** sont plus déblindés que ceux du composé **7** ce qui traduit bien une désactivation plus importante exercée par la pyridazine dans le premier composé par rapport au second. On peut ajouter que le déblindage nettement plus faible du carbone 5 du composé **7** par rapport aux carbones 4 et 5 du composé **2** correspond lui aussi à une plus grande réactivité de ce sommet.

(*c*) En ce qui concerne l'influence de la nature de la diazine assemblée au cycle thiophénique, on observe que le groupe pyrimidyl-4 exerce un effet désactivant plus élevé que celui du groupe pyridazinyl-4, cependant que le groupe pyrazinyl-2 possède un effet intermédiaire. Ces résultats peuvent s'expliquer si on considère que l'effet le plus important semble être celui exercé par le nombre et la proximité des liaisons iminium conjuguées avec le thiophène (3*c*).

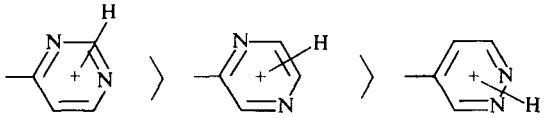

On peut remarquer qu'il existe une corrélation entre ce classement et celui établi lors de la comparaison des pourcentages de dérivé nitré en 4 obtenus dans la nitration des (thiényl-2)diazines (Tableau 1). Rappelons que ce classement est en accord avec l'examen des spectres de rmn de $^{13}C$ des composés étudiés en milieu acide.

D'une manière générale, on peut noter que les résultats obtenus peuvent s'expliquer en faisant intervenir les effets électroniques. On peut ajouter que les renseignements fournis par les spectres de rmn de $^{13}C$ dans l'acide sulfurique peuvent être corrélés avec les réactivités de ces thiényldiazines. Il faut cependant remarquer qu'il n'existe pas de relation directe entre le déplacement chimique d'un carbone du cycle thiophénique dans $CDCl_3$ et la position de nitration sur ce cycle.

Ces méthodes (étude des produits de la nitration et examen des spectres de $^{13}C$ dans le milieu réactionnel) fournissent une image précise de l'effet désactivant exercé par les ions diazinium et de la réactivité des thiényldiazines.

## Partie expérimentale

*1. Enregistrement des spectres de résonance magnétique nucléaire $^{13}C$*

Les spectres $^{13}C$ dans $CDCl_3$ ont été enregistrés sur un Spectromètre WP 80 à transformée de Fourier à 20,11 MHz à 28°C. La référence interne utilisée est le pic central du deutérochloroforme pris à 76,91 ppm. Les spectres en solution dans l'acide sulfurique ont été obtenus sur un WH 90C multinoyaux à 22,63 MHz et 28°C. Le lock utilisé était un capillaire de benzène à température ordinaire et d'acétone à basse température. La référence a été prise par rapport au pic central du $C_6D_6$ du capillaire (127,96 ppm) ou de l'acétone-$d_6$ (29,22 ppm) sans correction de susceptibilité magnétique.

*Composé 1 dans $H_2SO_4$*: nous avons enregistré le spectre normal cinq minutes après la mise en solution dans $H_2SO_4$ concentré, alors qu'il y a déjà une quantité importante de produit sulfoné. Une heure plus tard on constate que l'échantillon est uniquement constitué de produit sulfoné (en 5 sur le cycle thiophénique). Par différence on peut repérer dans le spectre enregistré après cinq minutes les signaux correspondants au produit **1** dans le milieu réactionnel. Cependant, les valeurs relevées ne sont pas comparables à celles relevées pour les autres composés, car le milieu n'est pas le même (absence de produit sulfoné dans les autres cas). C'est pourquoi nous n'avons pas envisagé le comportement du produit **1** dans la discussion.

*2. Nitration des thiényldiazines*

Les réactifs de départ ont été préparés selon les méthodes

décrites dans le littérature (2*a*, 2*e*, 3*a*, 3*c*). La nitration a été effectuée dans les conditions indiquées précédemment (3*c*).

*3. Réactions de concurrence*

Le réactif utilisé lors des réactions de nitration est préparé de la même manière pour les essais de concurrence (3*c*) Le mode opératoire utilisé pour effectuer les quatre réactions de concurrence est identique et peut se résumer ainsi.

Les deux thiényldiazines mises en compétition sont dissoutes dans l'acide sulfurique concentré à 0°C. Puis sous agitation et en maintenant à 0°C, on ajoute la quantité stoechiométrique du réactif nitrant pour nitrer un seul constituant.

Après une durée de réaction de trois heures, le milieu réactionnel est intégralement versé sur de la glace pilée, puis neutralisé à pH 7 par de l'ammoniaque concentrée. Le précipité obtenu est filtré, lavé soigneusement, séché puis pesé. Ce précipité contient en général des produits nitrés issus de la réaction, le filtrat contenant surtout les thiényldiazines n'ayant pas réagi. Il est extrait au chloroforme. Cet extrait soigneusement lavé est débarrassé du solvant sous pression réduite, puis pesé. Cela permet de faire le bilan global de la réaction qui nous renseigne sur la validité de l'essai effectué.

Le spectre de rmn des diverses fractions récupérées permet de déterminer leur composition. Le rendement global est calculé à partir des rendements en produits nitrés obtenus et en produits de départ récupérés.


1. T. KAUFFMANN, J. KÖNIG, D. KÖRBER, H. LEXY, H. J. STREITBERGER, A. M. VAHRENHORST et A. WOLTERMANN. Tetrahedron Lett. 389 (1977).
2. (*a*) S. GRONOWITZ et J. BÖLER. Ark. Kemi, **28**, 587 (1968); (*b*) S. GRONOWITZ et S. LILJEFORS. Acta Chem. Scand. Ser. B, **31**, 771 (1977); (*c*) S. GRONOWITZ et E. SANDBERG. Ark. Kemi, **32**, 269 (1970); (*d*) M. ROBBA, J. M. LECOMTE et M. CUGNON DE SEVRICOURT. Tetrahedron, **27**, 487 (1971); (*e*) J. PANKIEWICZ, B. DECROIX et J. MOREL. C.R. Acad. Sci. Ser. C, **281**, 39 (1975).
3. (*a*) J. BOURGUIGNON, J. M. BOUCLY, J. C. CLINET et G. QUEGUINER. C. R. Acad. Sci. Ser. C, **281**, 1019 (1975); (*b*) S. GRONOWITZ et S. LILJEFORS. Chem. Scr. **13**, 39 (1978/79); (*c*) J. BOURGUIGNON, C. BECUE et G. QUEGUINER. J. Chem. Res. (*S*) 104 (1981), (*M*) 1401 (1981).
4. J. BOURGUIGNON, M. LEMARCHAND et G. QUEGUINER. J. Heterocycl. Chem. **17**, 1019 (1980).
5. J. BOURGUIGNON, M. MOREAU, G. QUEGUINER et P. PASTOUR. Bull. Soc. Chim. Fr. 676 (1977).
6. (*a*) E. BREITMAIER et W. VOELTER. $^{13}C$ nmr spectroscopy. 2nd éd. Verlag Chemie. 1978. p. 69; (*b*) J. B. STOTHERS. Carbon-13 nmr spectroscopy. Academic Press, New York. 1972; (*c*) G. DANA, O. CONVERT, J. P. GIRAULT et E. MULLER. Can. J. Chem. **54**, 1827 (1976).
7. (*a*) S. GRONOWITZ, I. JOHNSON et A. B. HÖRNFELQ. Chem. Scr. 7, 76 (1975); (*b*) F. J. WEIBERT, J. HUSAR et J. D. ROBERTS. J. Org. Chem. **38**, 1313 (1973); (*c*) C. J. TURNER et G. W. H. CHEESEMAN. Org. Magn. Reson. **8**, 357 (1976); (*d*) J. RIAUD, M. T. CHENON et N. LUMBROSO-BADER. Org. Magn. Reson. **9**, 572 (1977); (*e*) M. MATSUO, S. MATSUMOTO, T. KURIHARA, V. AKITA, T. WATANABE et A. OHTA. Org. Magn. Reson. **13**, 172 (1980).
8. R. J. PUGMIRE et D. M. GRANT. J. Am. Chem. Soc. **90**, 697 (1968).
9. D. A. FORSYTH et D. E. VOGEL. J. Org. Chem. **44**, 3917 (1979).


Can. J. Chem. Downloaded from www.nrcresearchpress.com by 210.87.254.40 on 09/06/12
For personal use only.

# Secondary metabolites from the red alga *Laurencia intricata*: halogenated enynes[1]

JOHN H. CARDELLINA II,[2] STEPHEN B. HORSLEY,[3] JON CLARDY, S. R. LEFTOW, AND JERROLD MEINWALD

*Department of Chemistry, Cornell University, Ithaca, NY 14853, U.S.A.*

Received December 23, 1981

JOHN H. CARDELLINA II, STEPHEN B. HORSLEY, JON CLARDY, S. R. LEFTOW, and JERROLD MEINWALD. Can. J. Chem. **60**, 2675 (1982).

Extracts of the red alga *Laurencia intricata*, collected in Bermuda, have yielded two new halogenated C-15 enynes, bermudenynol and its acetate. Spectroscopic evidence for the assignment of structures **1***a* and **1***b* to these compounds is presented. X-ray analysis verified the proposed structures and established their stereochemistry.

JOHN H. CARDELLINA II, STEPHEN B. HORSLEY, JON CLARDY, S. R. LEFTOW et JERROLD MEINWALD. Can. J. Chem. **60**, 2675 (1982).

Des extraits de l'algue rouge *Laurencia intricata*, recueillis aux Bermudes, ont permis d'isoler deux nouveaux enzymes de type ényne halogénés en position C-15, soit le bermudenynol et son acétate. On présente les preuves spectroscopiques qui appuient les structures **1***a* et **1***b* proposées. L'analyse par rayons X confirme ces structures et établi leur stéréochimie.

[Traduit par le journal]

## Introduction

Red algae of the genus *Laurencia* are prolific sources of an unusual series of halogenated secondary metabolites characterized by a straight chain, fifteen-carbon skeleton which incorporates a terminal, conjugated enyne functionality (1). While it has been apparent for some time that these compounds are sequestered by certain mollusks (*Aplysia* spp.) which graze on *Laurencia*, it was demonstrated only recently that the C-15 enynes can serve as potent feeding deterrents to potential predators of these mollusks (2). In our continuing investigation of compounds which play a role in the chemical ecology of marine organisms, we have isolated two new halogenated C-15 enynes from specimens of *Laurencia intricata* collected in Bermuda.

## Discussion

Successive chromatography of the acetone extracts of the alga on Florisil and Sephadex LH-20 yielded bermudenynol, **1***a*, a crystalline major metabolite (6.9% of the extract). Infrared absorptions at 3265 and 2095 (very weak) $cm^{-1}$ and the ultraviolet absorption spectrum indicated the presence of the terminal conjugated enyne moiety; this assignment was further substantiated by the $^1H$ and $^{13}C$ nmr spectra (see Tables 1 and 2). Mass spectral studies revealed a weak molecular ion cluster at *m/e* 380; both the isotopic abundances and fragment ion masses revealed the presence of one bromine and two chlorine atoms in bermudenynol, leading to a likely molecular formula of $C_{15}H_{19}BrCl_2O_2$. The presence of fifteen carbon and nineteen hydrogen atoms was confirmed by $^{13}C$ nmr analysis. Moreover, the presence of two alkynyl and four alkenyl carbons in the $^{13}C$ nmr spectrum required a monocyclic structure for **1***a*.

Extensive $^1H$ nmr decoupling experiments led us to partial structure **A** (X = heteroatom) for

TABLE 1. $^1H$ nuclear magnetic resonance spectra of bermudenynol and bermudenynyl acetate[a]

| Position | Bermudenynol | Bermudenynyl acetate |
|---|---|---|
| 1 | 3.17, d, $J$ = 1.5 | 3.20, d, $J$ = 2 |
| 3 | 5.41, dd, $J$ = 10.5, 1.5 | 5.53, dd, $J$ = 10.5, 2 |
| 4 | 6.20, t, $J$ = 10.5 | 5.88, t, $J$ = 10.5 |
| 5 | 5.58, dd, $J$ = 10.5, 2 | 5.27, dd, $J$ = 10.5, 3 |
| 6 | 3.36, m | 4.88, dd, $J$ = 7.5, 3 |
| 7 | 3.36, m | 3.65, m |
| 8 | 1.90–2.65, m | 1.70–2.30, m |
| 9 | 5.97, dd, $J$ = 9, 7 | 5.92, t, $J$ = 9 |
| 11a | 3.43, dd, $J$ = −15, 4 | 3.40, dd, $J$ = −15, 4 |
| 11b | 2.84, dd, $J$ = −15, 5 | 2.80, dd, $J$ = −15, 5 |
| 12 | 4.05, ddd, $J$ = 11, 5, 4 | 4.03, m |
| 13 | 3.62, dt, $J$ = 11, 3.5 | 3.65, m |
| 14 | 1.95, dq, $J$ = 7, 3.5 | 1.70–2.30, m |
| 15 | 0.98, t, $J$ = 7 | 0.99, t, $J$ = 7.5 |

[a]Spectra recorded at 90 MHz in $CCl_4$; chemical shifts in δ units, TMS = 0.

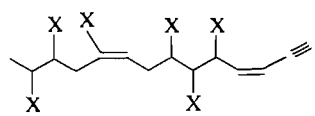


**A** x = heteroatom

[1]Contribution #848 from the Bermuda Biological Station.

[2]Address correspondence to this author at: Department of Chemistry, Montana State University, Bozeman, Montana 59717.

[3]Visiting fellow on leave from the U.S.D.A., Forest Service, Northeastern Forest Experiment Station, Warren, PA 16365.

0008-4042/82/212675-03$01.00/0

©1982 National Research Council of Canada/Conseil national de recherches du Canada

Can. J. Chem. Downloaded from www.nrcresearchpress.com by 210.87.254.6 on 09/06/12
For personal use only.

Can. J. Chem. Downloaded from www.nrcresearchpress.com by 210.87.254.6 on 09/06/12
For personal use only.

TABLE 2. $^{13}C$ nuclear magnetic resonance spectra of bermudenynol and poiteol[a]

| Carbon | Bermudenynol | Poiteol[b] |
|---|---|---|
| 1 | 85.7 | 84.4 |
| 2 | 78.7 | 79.4 |
| 3 | 110.6 | 111.3 |
| 4 | 141.6 | 142.2 |
| 5 | 60.4 | 61.0 |
| 6 | 74.1 | 75.6 |
| 7 | 82.9 | 86.4 |
| 8 | 30.8 | 33.6 |
| 9 | 127.0 | 52.7 |
| 10 | 132.5 | 53.5 |
| 11 | 41.1 | Obscured by solvent |
| 12 | 50.0 | 50.7 |
| 13 | 80.2 | 80.6 |
| 14 | 25.6 | 27.0 |
| 15 | 6.8 | 7.3 |

[a]Spectra recorded at 20 MHz in acetone-$d_6$; chemical shifts in $\delta$ units, TMS = 0.
[b]See ref. 3.

bermudenynol. The mass spectral fragmentation data indicated that one chlorine atom was allylic to the enyne functionality (loss of 99 daltons; $C_5H_4Cl$), and that the other was probably bound to an olefinic carbon atom, since it was retained in most fragment ions and lost only late in the fragmentation scheme.

Acetylation of bermudenynol proved to be facile; a monoacetate was obtained, thereby confirming the presence of an unhindered hydroxyl (3520 $cm^{-1}$) group in **1***a*. The $^1H$ nmr spectrum of this acetate was superimposable on that of a minor constituent of the *L. intricata* extract isolated from a less polar fraction. The semisynthetic and natural acetates also behaved identically ($R_f$ values and $H_2SO_4$ charring characteristics) in two tlc systems. Detailed analysis of $^1H$ nmr decoupling experiments conducted with this compound placed the acetate group at C-6 and allowed assignment of structure **1***b* to the acetate and **1***a* to bermudenynol.

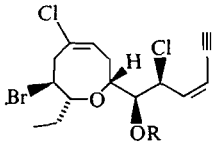


**1** *a* R = H
*b* R = $COCH_3$

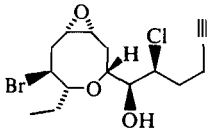


**2**

Placement of the bromine substituent at C-12 was supported by the similarity of the chemical shifts observed for the C-12 protons in **1***a* and **1***b* with that of the C-12 methine in poiteol, **2** (3). Since the decoupling experiments had placed the acetate/hydroxyl moieties at C-6, an ether linkage from C-7 to C-13 was required. In fact, comparison of the $^{13}C$ nmr spectra of **1***a* and **2** (see Table 2) revealed excellent correspondence of the carbon resonances, with the exception of those of C-8 through C-11, where the differences in functionality obviously warrant spectral differences. These similarities suggest the same relative stereochemistry of the chiral centers at C-5, C-6, C-7, C-12, and C-13 in **1***a*, **1***b*, and **2**. It is likely that there is a close biosynthetic relationship between bermudenynol and poiteol, since nucleophilic chloride ion attack on the epoxide ring at C-10 in **2**, followed by protonation of the resulting alkoxide ion and dehydration, would give **1***a*.

To verify the proposed stereochemistry, a needle-shaped crystal of bermudenynol of dimensions 0.15 × 0.15 × 0.40 mm was selected for single-crystal X-ray analysis. Preliminary X-ray photographs showed monoclinic symmetry and accurate cell constants, determined from a least-squares fit of fifteen moderate 2$\theta$-values, were $a$ = 10.52(5), $b$ = 5.57(3), and $c$ = 15.80(6) Å and $\beta$ = 108.97°. Systematic extinctions (0$k$0 absent if $k$ = 2 + 1) and the known chirality were uniquely accommodated by the space group $P2_1$ and the density indicated one molecule of $C_{15}H_{19}BrCl_2O_2$ formed the asymmetric unit. All unique diffraction maxima with $2\theta \leq 46°$ were collected on a fully automated four-circle diffractometer using graphite monochromated MoK$\alpha$ (0.710069 Å) radiation and a variable speed $\omega$-scan technique. Of the 1452 reflections surveyed, 1306 (90%) were judged observed [$|F_o| \geq 3\sigma(F_o)$].

The structure was solved by conventional heavy atom techniques. A three-dimensional Patterson synthesis was deconvoluted to determine the bromine and chlorine positions (for major crystallographic programs employed, see ref. 4). The remaining nonhydrogen atoms were located on successive $F_o$-synthesis. Full-matrix least-squares refinement with anisotropic temperature factors for the nonhydrogen atoms, isotropic hydrogens, and anomolous dispersion corrections have converged to a residual of 0.104 for the structure shown and 0.106 for the enantiomer.

Figure 1 shows a computer generated perspective drawing of the final X-ray model of **1***a*. Hydrogen atoms are omitted for clarity. Bond distances and angles agree well with generally accepted values and there were no unusually short intermolecular contacts. The configurations at the five chiral centers are 5($R$*), 6($R$*), 7($R$*), 12($S$*), and 13($R$*) and the double bond of the enyne functionality has a *cis* or *Z* configuration.[4]

[4]Tables of fractional coordinates, thermal parameters, bond distances, bond angles, and observed and calculated structure factors are available, at a nominal charge, from the Depository of Unpublished Data, CISTI, National Research Council of Canada, Ottawa, Ont., Canada K1A 0S2.

Can. J. Chem. Downloaded from www.nrcresearchpress.com by 210.87.254.6 on 09/06/12
For personal use only.

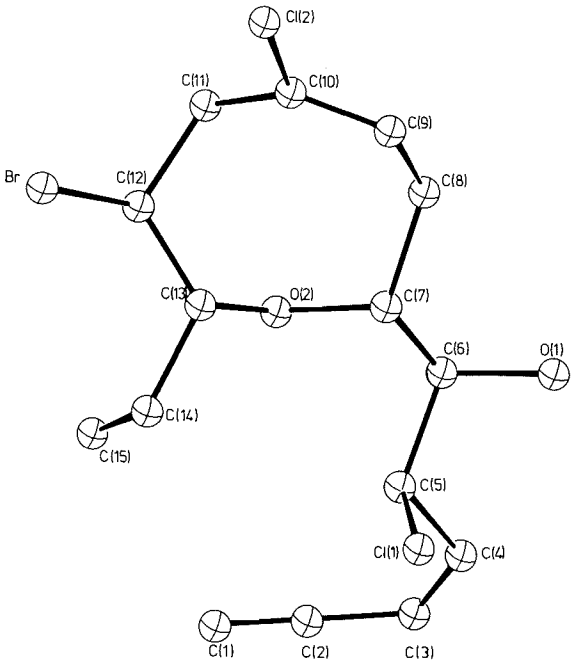


FIG. 1. Computer-generated perspective view of bermudenynol (1*a*). Hydrogens are omitted for clarity.

## Experimental

Infrared spectra were recorded on a Perkin–Elmer Model 257 grating infrared spectrophotometer, ultraviolet spectra on a Beckman DB-G spectrophotometer, and optical rotations on a Perkin–Elmer Model 141 polarimeter. Mass spectra were obtained on an Associated Electronic Industries MS-902 mass spectrometer operated at 70 eV. The $^1$H nmr spectra were obtained on a Varian EM-390 spectrometer; $^{13}$C nmr spectra were obtained on a Varian CFT-20 spectrometer; chemical shifts are reported in ppm (δ units) downfield from tetramethylsilane as an internal standard.

*Isolation of bermudenynol*

Specimens of *Laurencia intricata* were collected at depths of one to three feet in Castle Harbour, Bermuda in October 1979, and preserved in acetone prior to analysis. The acetone extracts were decanted and concentrated under reduced pressure. The residual aqueous phase was extracted with $CH_2Cl_2$ to yield a dark green syrup (4.5 g) which was chromatographed on Florisil. Fourteen fractions were collected from the Florisil column (136 g) by elution with mixtures of hexane, ethyl acetate, and methanol of gradually increasing polarity. Sephadex LH-20 gel filtration (2.5 × 191 cm, eluted with $CH_2Cl_2$–MeOH, 1:1) of 407 mg of fraction 4 gave 310 mg of a colorless oil which crystallized on standing. Recrystallization from hexane gave prisms of bermudenynol, 1*a*, mp 80–81°C; $[\alpha]_D^{25}$ +187° (*c* 0.756, $CHCl_3$); uv $\lambda_{max}$ (cyclohexane): 220 nm (ε = 19 600); ir ($CS_2$) $\nu_{max}$: 3520, 3265, 3015, 2940, 2890, 2840, 2095, 1639, 1371, 1238, 1080, 1059, 1023, 970, 935, 888, 851, 815, 750 cm$^{-1}$; CI ms *m/e* (rel. int.): 383(M + 3, 16), 381(M + 1, 13), 347(33), 345(27), 303(41), 301(16), 285(4), 283(13), 281(10), 267(33), 265(M − HBr, HCl, 100), 253(12), 251(10), 229(47), 203(8), 201(7), 197(18), 195(11), 189(10), 187(15), 185(46), 173(25), 171(70), 165(16), 159(9), 157(11), 155(35), 145(13), 143(47), 129(12), 127(13), 107(51), 95(39), 59(22); $^1$H and $^{13}$C nmr data are presented in Tables 1 and 2, respectively.

*Acetylation of 1*a

Acetic anhydride, 0.4 mL, was added to a solution of 25.2 mg of bermudenynol, 1*a*, in pyridine (0.8 mL). The mixture was allowed to stand at room temperature for 8 h, at which time the solvent and excess reagents were removed *in vacuo*, yielding a light brown gum. Gel filtration through Sephadex LH-20 (2 × 100 cm, eluted with $CH_2Cl_2$–MeOH, 1:1) to give 27.6 mg (99%) of a colorless oil, 1*b*; for $^1$H nmr, see Table 1.

*Isolation of bermudenynol acetate*

Fraction 2 from the Florisil chromatography of the crude extract was rechromatographed on silica gel; elution with hexane–$Et_2O$ (9:1) gave 1*b*, 18 mg, a colorless oil, identical by $^1$H nmr (Table 1) and tlc with the acetate prepared from 1*a*.

## Acknowledgments

We thank Mr. Francis Connor for assistance in the field work and Dr. John Schwede for identifying the alga. The field work was supported by H. B. Wilkinson and Continental Corporation Fellowships (to J.H.C.) from the Bermuda Biological Station. Partial support of this work by the U.S.D.A., Forest Service, Northeastern Forest Experiment Station (for S.B.H., Visiting Fellow) and by the Schering Corporation is gratefully acknowledged.

1. R. E. MOORE. *In* Marine natural products: chemical and biological perspectives. Vol. 1. *Edited by* P. J. Scheuer. Academic Press, New York. 1978. Chapt. 2.
2. R. B. KINNEL, R. K. DIETER, J. MEINWALD, D. VAN ENGEN, J. CLARDY, T. EISNER, M. O. STALLARD, and W. FENICAL. Proc. Natl. Acad. Sci. U.S.A. **76**, 3576 (1979).
3. B. M. HOWARD, G. R. SCHULTE, W. FENICAL, B. SOLHEIM, and J. CLARDY. Tetrahedron. **36**, 1747 (1980).
4. MULTAN: G. GERMAIN, P. MAIN and M. M. WOOLFSON. Acta Crystallogr., Sect, B**26**, 274 (1970); M. M. WOOLFSON. Acta Crystallogr. Sect, A**33**, 219 (1977); ORFLS (locally modified version): W. R. BUISING, K. O. MARTIN and H. A. LVEY. Oak Ridge National Laboratory Report ORNL-TM-305; ORFFE: W. A. BUSING and H. A. LEVY, Oak Ridge National Laboratory Publication ORNL-59-12-3; ORTEP: C. K. JOHNSON, Oak Ridge National Laboratory Report ORNL-TM-3794.

# A convenient entry into the rhoeadan skeleton. Total synthesis of (±)-*cis*-alpinigenine[1]

IJAZ AHMAD AND VICTOR SNIECKUS

*Guelph–Waterloo Centre for Graduate Work in Chemistry, Department of Chemistry, University of Waterloo, Waterloo, Ont., Canada N2L 3G1*

Received April 1, 1982

IJAZ AHMAD and VICTOR SNIECKUS. Can. J. Chem. **60**, 2678 (1982).

Condensation of 4-bromoisochroman-3-one (**8***a*) with *N*-methyl-3,4-dimethoxy-β-phenethylamine (**7**) provides the aminolactone **9***a* which by diisobutylaluminum hydride reduction followed by polyphosphoric acid mediated cyclization gives the tetracyclic product **10***a*, thus constituting a convergent, short entry into the rhoeadan alkaloid skeleton. Chromium trioxide oxidation of **10***a* affords a low yield of the corresponding lactone **11***a*. A parallel series of reactions starting from 7,8-dimethoxy-4-bromoisochroman-3-one (**8***b*), prepared either via Baeyer–Villiger oxidation of 4,5-dimethoxy-2-indanone (**14**) or, more conveniently, via benzeneboronic acid assisted condensation of 3-hydroxy-4-methoxyphenylacetic acid (**18**) with formaldehyde, yields 7,8,12,13-tetramethoxy-3-methylrhoeadan (**10***b*). Oxidation of compound **10***b* with chromium trioxide gives the corresponding lactone **11***b* also in low yield. Since **11***b* has been previously converted into (±)-*cis*-alpinigenine (**11***c*) and (±)-*cis*-alpinine (**11***d*), this work constitutes total syntheses of these alkaloids.

IJAZ AHMAD et VICTOR SNIECKUS. Can. J. Chem. **60**, 2678 (1982).

La condensation de la bromo-4 isochromanone-3 (**8***a*) sur la *N*-méthyldiméthoxy-3,4 β-phénéthylamine (**7**) conduit à l'aminolactone (**9***a*) qui, par réduction par l'hydrure de diisobutylaluminium suivie d'une cyclisation en présence d'acide polyphosphorique, donne le produit tétracyclique **10***a*. Ceci constitue une voie d'accès convergente et courte au squelette de l'alcaloide rhoéadane. L'oxydation du composé **10***a* par le trioxyde de chrome conduit, avec un faible rendement, à la lactone correspondante, **11***a*. Une série parallèle de réactions partant de la diméthoxy-7,8 bromo-4 isochromanone-3 (**8***a*), préparée soit par une oxydation de Baeyer–Villiger de la diméthoxy-4,5 indanone-2 (**14**) soit plus facilement par condensation de l'acide hydroxy-3 méthoxy-4 phénylacétique (**18**) sur le formaldéhyde en présence d'acide benzèneboronique, conduit au tétraméthoxy-7,8,12,13 méthyl-3 rhoéadane (**10***b*). L'oxydation du composé **10***b* par le trioxyde de chrome donne la lactone correspondante **11***b* également avec un faible rendement. Depuis que le composé **11***b*, a été transformé antérieurement en (±)-alpinigénine *cis* (**11***c*) et en (±)-alpinine *cis* (**11***d*), ce travail constitue une synthèse totale de ces alcaloides.

[Traduit par le journal]

The Rhoeadine–Papaverrubine class of alkaloids (**1**) (1) is comprised of about 30 bases elaborated almost exclusively within the *Papaver* genus (2, 3). Its major distinguishing structural feature, exhibited only by three other alkaloid types (*Cephalotaxus* group (**2**) (4), stepinonine, a bisbenzylisoquinoline (**3**) (5), and the recently discovered chilenine (**4**) (6)), is the benzazepine skeleton (rings A/B in **1**). This and other inherent structural and stereochemical points of interest as well as the discovery of potentially useful biological activity (1, 7) have provided the predictable stimulus for synthetic effort (1, 2, 8). Most routes (Table 1, refs. 9–13) are initiated from or proceed via intermediates of other classes of benzylisoquinoline alkaloids. The most economic route to rhoeadans reported to date employs phthalideisoquinoline alkaloids as starting materials (10). This route is rendered attractive by the recent availability of improved syntheses of the latter class of alkaloids (2, 14). An attractive synthetic method for the rhoeadan skeleton starting from *N*-benzyl-3,4-dihydroisoquinolinium salts has been developed by Shamma and Töke (12). However, this strategy appears not to have been applied to synthesis of the alkaloids themselves, owing perhaps to the lack of

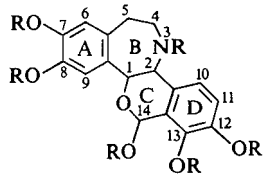


**1**

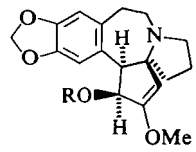


**2**

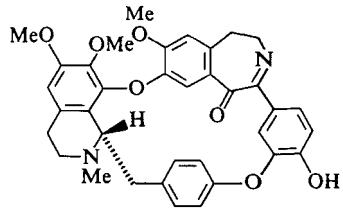


**3**

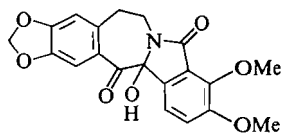


**4**

[1]Abstracted in part from the thesis of I.A. submitted in partial fulfillment for the Ph.D. degree, University of Waterloo, 1975.

0008-4042/82/212678-09$01.00/0

©1982 National Research Council of Canada/Conseil national de recherches du Canada

Can. J. Chem. Downloaded from www.nrcresearchpress.com by 210.87.254.42 on 09/06/12
For personal use only.

TABLE 1. Synthesis of rhoeadan alkaloids

| Precursor alkaloid type | Number of steps | Overall yield | Ref. |
|---|---|---|---|
| Spirobenzylisoquinoline[a] | 8 | ~1% | 9 |
| Phthalideisoquinoline | 5 | 24% | 10 |
| Protoberberine[b] | 5 | 11% | 11 |
| *N*-Benzyl-3,4-dihydroisoquinolinium salt[c] | 6 | 45% | 12 |
| Protoberberine[d] | 8 | 7% | 13 |

[a]Based on a β-phenethylamine starting material.
[b]A synthetic substance was used as starting material.
[c]Synthesis of the rhoeadan ring skeleton only was achieved.
[d]Converted into a relay benz[*d*]indeno[1,2-*b*]azepine system which was also available by total synthesis and had been transformed into a rhoeadan alkaloid.

convenient routes to contiguously substituted C/D ring precursors, a situation which has been recently rectified (15). Herein we report a new efficient and convergent entry into the rhoeadan ring system and its application to the synthesis of the (±)-*cis*-alpinigenine (**11***c*) (11, 16).

Several precedents notwithstanding (8), the amide lactone **6**, readily available from the condensation of the aminoisochroman-3-one **5** with 3,4-dimethoxyphenylacetyl chloride, could not be cyclized to a benzazepine derivative under a variety of Friedel–Crafts conditions. The aminolactone **9***a*, prepared in high yield by condensation of the *N*-methyl-β-phenethylamine **7** with 4-bromoisochroman-3-one (**8***a*) (available via Baeyer–Villiger reaction of 2-indanone) (Scheme 1), likewise failed to cyclize or suffered extensive decomposition under Lewis acid catalyzed conditions.[2] In the expectation of increasing reactivity, compound **9***a* was partially reduced with diisobutylaluminum hydride (Dibal) to give the aminolactol **9***b* in high yield. When **9***b* was exposed to neat polyphosphoric acid at 35°C, the desired rhoeadan derivative **10***a* was obtained (13% overall yield from indene).[3] The nmr and ms data of **10***a* were consistent with the tetracyclic structure showing close similarity to those observed for the rhoeadan alkaloids (1). Furthermore, the C-1 and C-2 proton doublets at δ 4.72 and 3.72 respectively showed a coupling constant, $J_{1,2}$ = 2.5 Hz, consistent with a *cis*-B/C ring juncture as expected on the basis of an α-oxo carbonium ion intermediate leading to the thermodynamically more stable stereochemistry (16).

The application of the above model study to the synthesis of the rhoeadan alkaloid, *cis*-alpinigenine (**11***c*), required (a) a search for methods to effect oxidative functionalization at C-14 and (*b*) the

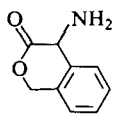


5

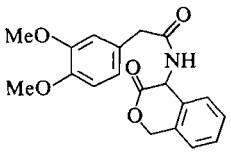


6

development of a route for the dimethoxyisochroman-3-one **8***b*. In order to achieve the first goal, a number of oxidations (e.g., acetoxylation using peroxyesters/$Cu^+$ (17), hydroxylation using $Ce^{+4}$ (18), *t*-BuOK/*t*-BuOH/$O_2$/DMSO (19), Triton B/pyridine/$O_2$ (20))[4] were carried out on the model compound **10***a* with uniformly unsuccessful results. Finally, oxidation using $CrO_3$ in acetic acid (21) gave a mixture of at least six products from which the lactone **11***a* was isolated in ~10% yield by preparative thick-layer chromatography. The conversion of rhoeadan lactones analogous to **11***a* into the corresponding alkaloids (**1**), including *cis*-alpinigenine (**11***c*), is well documented (10, 13*a*). In view of this and in the hope that greater

[2]Attempts to obtain a potentially more attractive intermediate **i** by condensation of **7** with 4-bromoisochroman-1,3-dione gave instead **ii** which formed the basis of a general synthesis of phthalideisoquinoline alkaloids (ref. 14).

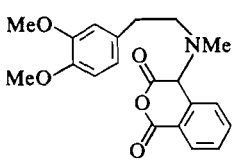


i

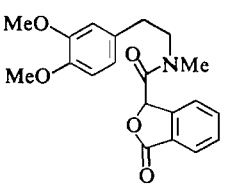


ii

[3]A number of other Lewis acid catalysts (e.g. $POCl_3$, $BF_3$·$Et_2O$, HCl) failed to yield **10***a*. Concentrated sulfuric acid furnished the indenobenzazepine **iii** in low yield (see Experimental).

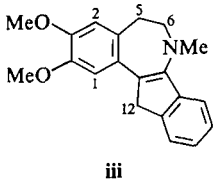


iii

[4]These reactions are described in the Ph.D. thesis of I.A.

Can. J. Chem. Downloaded from www.nrcresearchpress.com by 210.87.254.42 on 09/06/12
For personal use only.

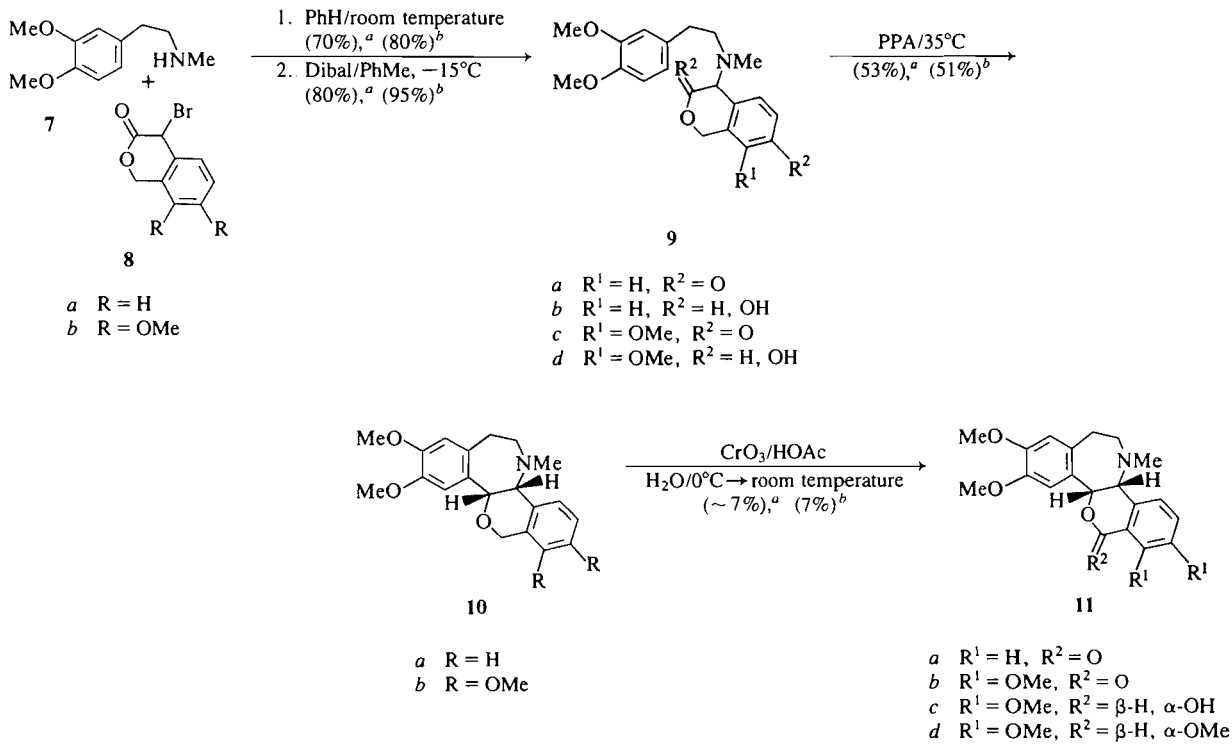


SCHEME 1

[a]Yields for **8***a* series.
[b]Yields for **8***b* series.

C-14 oxidative regioselectivity would be achieved in **10***b* as a result of the presence of activating ring D methoxy groups, the second task, that of synthesizing the isochroman-3-one **8***b* component required for *cis*-alpinigenine, was undertaken.

The construction of 7,8-dimethoxyisochroman-3-one (**8***b*) was achieved by alternative classical and modern methodologies (Scheme 2). In the classical approach, 2,3-dimethoxyphenylpropionic acid (**12**), prepared from 2,3-dimethoxybenzaldehyde by Knoevenagel technology, was subjected to Friedel–Crafts cyclization using polyphosphoric acid to give the 1-indanone **13** in high yield. Ketone transposition to the 2-indanone **14** was effected uneventfully by a four-step sequence. Baeyer–Villiger oxidation with *m*-chloroperbenzoic acid gave a mixture of two isochromanones **15** and **16** which could not be separated by preparative tlc using multiple development and a variety of solvent systems. Examination of the integrated nmr spectrum of this mixture and comparison with authentic **15** synthesized by an alternative route (see Experimental) established that the isomers **15** and **16** were present in a 60:40 ratio in the mixture.[5] The lack of regioselectivity in the formation of **15** and **16** is perhaps expected on the basis of the similar electronic factors and lack of steric constraints operating in the Baeyer–Villiger rearrangement of the intermediate resulting from **14**.[6]

Bromination of the mixture of isochromanones **15**, **16** with one equivalent of bromine gave two major products, **17** and **8***b*, in a 1.3:1 ratio which were easily separated by taking advantage of their solubility differences in ether. Based on the 60:40 ratio of the starting isochromanones **15** and **16**, the

[5]This synthesis of **15** and **16** was first executed in 1972 by C. F. Tahk and K. R. Cuppet at Kent State University in independent synthetic work aimed at the rhoeadan alkaloids which was abruptly terminated. We are grateful to Drs. Tahk and Cuppet for allowing us to develop and use this route and for providing assistance, experimental details, spectra and samples, and for many stimulating discussions.

[6]In contrast, and as expected, Baeyer–Villiger reaction of 5,6-dimethoxy-2-indanone yields 6,7-dimethoxyisochroman-3-one, a useful intermediate for the synthesis of berberine alkaloids (22).

Can. J. Chem. Downloaded from www.nrcresearchpress.com by 210.87.254.42 on 09/06/12
For personal use only.

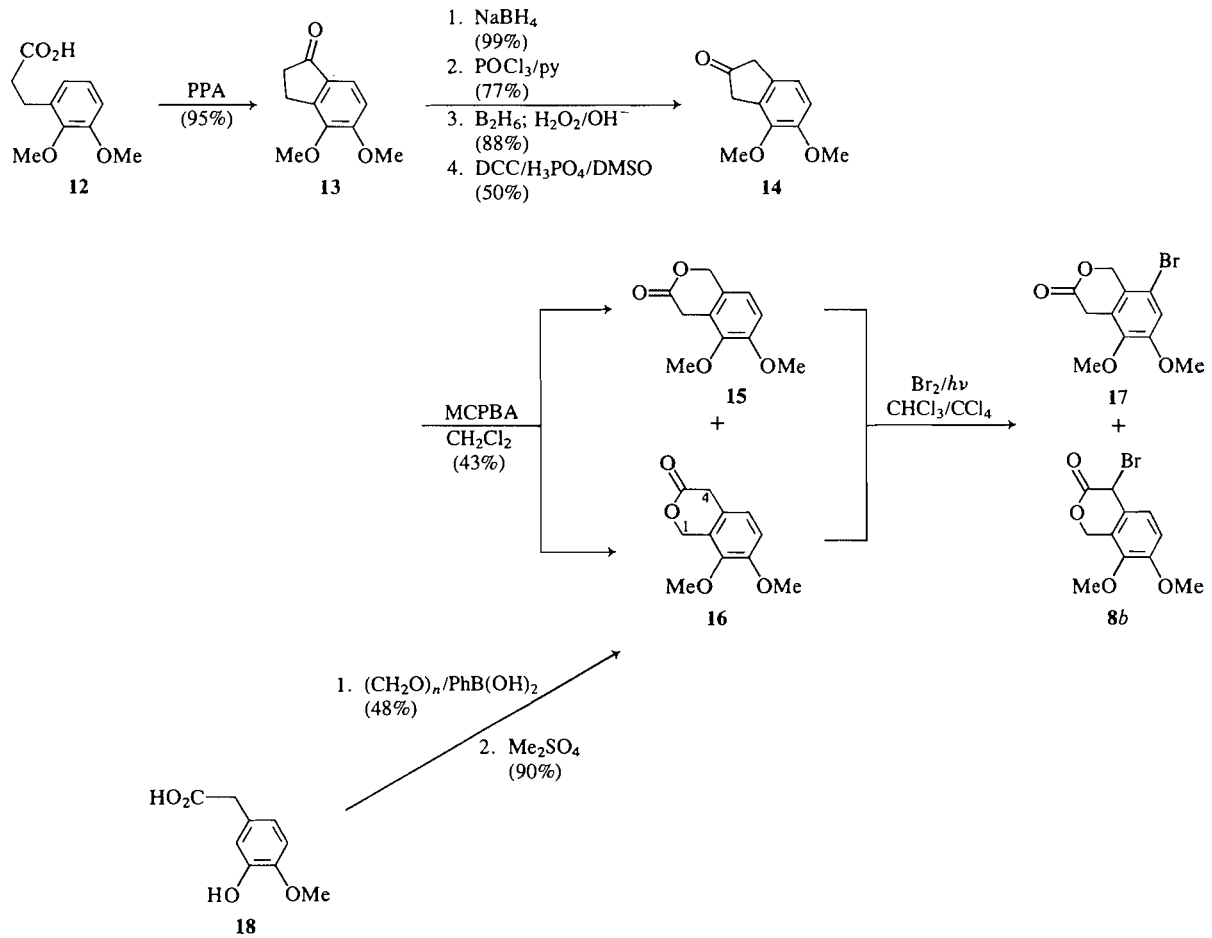


SCHEME 2

calculated yield of **8***b* from **14** is 14%. Their structures were assigned by nmr and ms data, in particular, comparison of such spectra for **8***b* with the model compound **8***a* (see Experimental). The formation of **17** may reflect steric interference to free radical C-4 bromination.

During the course of this work, Nagata and co-workers reported on the direct preparation of the required isochromanone **8***b* in 83% yield by treatment of homoisovanillic acid (**18**) with paraformaldehyde in the presence of benzeneboronic acid followed by conventional methylation (23). This interesting regiospecific introduction of a one-carbon unit, contrasting with normal electrophilic substitution behavior of such systems,[7] most likely involves the intermediacy of a phenoxyboronic acid which coordinates formaldehyde, thereby transferring it into the 2-position of the aromatic ring.[8,9] Unfortunately, in our hands, the reaction of **18** with paraformaldehyde gave 8-hydroxy-7-methoxyisochroman-3-one only in a reproducible 48% yield.[10] Nevertheless, this short route afforded the key intermediate **16** in gram quantities in 25% overall yield (based on commercially available isovanillin), thus showing considerable

[7]For example, the HCl-mediated reaction of 3,4-dimethoxyphenylacetic acid with formaldehyde provides 6,7-dimethoxyisochroman-3-one in 84% yield (24). See also ref. 23*b*.

[8]Intermediate boron heterocycles have been isolated in many cases (23*b*).

[9]Such *ortho*-transfer reactions via prior heteroatom to catalyst coordination have opened new strategies for regiospecific synthesis of polysubstituted aromatics (25).

[10]The yields are critically dependent on the manner of addition of paraformaldehyde and benzeneboronic acid and on the efficiency of water removal from the reaction mixture. Our yields were achieved using a Dean–Stark trap and not the special water separator employed by Nagata *et al.* (23). We are indebted to Drs. W. Nagata and K. Okada for correspondence and a photograph of the water separator and to Dr. M. T. Thomas for carrying out the experiments.

Can. J. Chem. Downloaded from www.nrcresearchpress.com by 210.87.254.42 on 09/06/12
For personal use only.

Can. J. Chem. Downloaded from www.nrcresearchpress.com by 210.87.254.42 on 09/06/12
For personal use only.

advantage in convenience and efficiency over the Baeyer–Villiger approach described above.[11,12]

The condensation of the bromoisochromanone **8***b* with two equivalents of the β-phenethylamine **7** produced the aminolactone **9***c* in high yield. Dibal reduction led smoothly and in quantitative yield to lactol **9***d* which upon treatment with PPA at steam bath temperatures produced the tetramethoxyrhoeadan **10***b*. Unfortunately, chromium trioxide oxidation of **10***b* gave a complex mixture of products from which 14-oxy-*cis*-alpinigenine (**11***c*) was isolated in low yield by preparative tlc. The identity of **11***b* was established by comparison (mp, mixture mp, tlc, ir, nmr, ms) with an authentic sample prepared by an alternative route also at the University of Waterloo (13*a*).[13] Since **11***b* has been previously converted into *cis*-alpinigenine (**11***c*) and *cis*-alpinine (**11***d*) in high yields (13*a*), our work completes total syntheses of these alkaloids.

The utility of this synthesis for the preparation of rhoeadan alkaloids is undermined by the low yield in the final oxidation step, **10***a*, **10***b* → **11***a*, **11***b*. However, it represents a convenient entry into the rhoeadan ring system (**10***a* in 13%, **10***b* in 7% overall yields) from readily available precursors. The synthesis of **10***b* is made attractive by the efficient preparation of the isochromanone **16** (23, 30).

## Experimental

Microanalyses were performed by A. G. Gygli, Toronto, Ontario. Melting points were measured on a Fisher–Johns apparatus and are uncorrected. Infrared spectra were determined on a Beckmann IR-10 spectrophotometer. The nmr spectra were obtained with a Varian T-60 spectrometer using TMS as internal standard in $CDCl_3$ solution unless otherwise stated. Mass spectra (ms) were recorded on a A.E.I. MS-30 double beam, double-focussing instrument; peaks with *m/e* > 100 and % rel. intensity > 20 only are given. Silica gel 60 (70–230 mesh) and aluminum oxide (neutral, activity 1) from Brinkmann, Canada and Florisil (60–100 mesh) from Fisher Scientific were used for column chromatography; silica gel GF-254 (type 60) and aluminum oxide G (type E) obtained from Brinkmann, Canada were employed for thick-layer chromatography. The phrase standard work-up means extraction with either $CH_2Cl_2$ of $CHCl_3$ followed by drying over $Na_2SO_4$, filtration, and evaporation to dryness *in vacuo*.

*4-Aminoisochroman-3-one (5)*

Indan-2-one (31) was converted into *isochroman-3-one* by a literature method (32), mp 81–83°C (lit. (33) mp 80.6–81°C), ir and nmr identical with those reported (33).

A solution of isochroman-3-one (6.0 g, 40 mmol) and *n*-butyl nitrite (6.2 g, 60 mmol) in a mixture of anhydrous THF (28 mL) and ether (16 mL) was added dropwise to an ice-cold, stirred solution of sodium ethoxide (from sodium metal, 1.04 g, 45 mmol) in a mixture of anhydrous ethanol (15 mL) and ether (20 mL) maintained under nitrogen. The red mixture was stirred at ice-bath temperature for 8 h, treated with water (50 mL), and the resulting solution was washed with ether (80 mL). After acidification (concentrated HCl), the aqueous layer deposited, in 20 h, colourless needles of *4-hydroxyiminoisochroman-3-one* (2.5 g) which were collected by filtration. The filtrate was concentrated *in vacuo* and extracted with chloroform to yield an additional 0.3 g of product (total yield, 39%), mp 191–193°C (EtOH–$CHCl_3$); ir (KBr) $\nu_{max}$: 3460, 1738, 1620 $cm^{-1}$; nmr δ: 5.44 (s, 2H), 7.42–7.65 (m, 4H); ms *m/e* (% rel. intensity): 177 (25, $M^+$), 133 (37), 132 (46), 117 (70), 116 (80), 105 (31), 104 (100), 103 (30), 102 (20). *Anal.* calcd. for $C_9H_7O_3N$: C 61.02, H 3.98, N 7.91; found: C 60.97, H 3.88, N 7.84.

Hydrogenation of 4-hydroxyimino-isochroman-3-one (0.25 g, 1.4 mmol) over platinum oxide in glacial acetic acid (8 mL) at 50 psi and room temperature followed by neutralization ($NH_4OH$) and standard work-up gave a colorless oil which was dissolved in dry ether and subjected to a stream of dry HCl gas. The resulting precipitate was collected and dried under reduced pressure to give 0.26 g (93%) of *4-amino-isochroman-3-one hydrochloride*, mp 154–158°C; ir (KBr) $\nu_{max}$: 3450 (br), 2880 (br), 1762 $cm^{-1}$, which was used without further purification.

N-*4-(Isochroman-3-one)-2-(3,'4'-dimethoxyphenyl)-acetamide (6)*

A solution of 3,4-dimethoxyphenylacetyl chloride (34) (0.215 g, 1 mmol) in THF (0.8 mL) was added dropwise to a stirred mixture of 4-amino-isochroman-3-one hydrochloride (0.20 g, 1 mmol) and a few drops of a saturated solution of aqueous $NaHCO_3$ in THF (3 mL). The mixture was stirred for 15 min and treated successively with ether (15 mL) and water (10 mL). The resulting colorless precipitate was recrystallized from aqueous EtOH to give 0.28 g (82%) of compound **6**, mp 155–156.5°C; ir (KBr) $\nu_{max}$: 1740, 1642 $cm^{-1}$; nmr δ: 3.80 (s, 2H), 3.93, 3.96 (2 × s, 6H), 5.20–5.83 (m, 3H), 6.4 (br s, 1H, $D_2O$ exch.), 7.0 (br s, 3H), 7.35 (br s, 4H); ms *m/e* (% rel. intensity): 341 (4, $M^+$), 178 (68), 163 (28), 152 (44), 151 (100), 137 (20), 119 (42), 118 (20), 117 (26), 107 (33), 106 (23). *Anal.* calcd. for $C_{19}H_{19}NO_5$: C 66.86, H 5.61, N 4.10; found: C 67.02, H 5.68, N 4.09.

*4-Bromoisochroman-3-one (8a)*

A solution of isochroman-3-one (7.41 g, 50 mmol) in a mixture of spectral grade chloroform (15 mL) and carbon tetrachloride (15 mL) was placed in a two-necked flask fitted with a condenser and a dropping funnel whose lower end was drawn into a

[11]Among the other approaches attempted to achieve the synthesis of **16**, the irradiation of **iv**, X = Br or Cl (26), the acid-catalyzed reaction of **iv** and **v** (27), and the benzylic metalation and carbonation of **vi**, X = $NEt_2$, R = Me (28) resulted either in recovery of starting material, partial degradation, or decomposition. In addition, the selective oxidation of the non-benzylic alcohol function of **vi**, X = OH, R = $CH_2CH_2OH$ (29) could not be achieved (footnote 4 and S. O. de Silva and M. T. Thomas, unpublished results, University of Waterloo).

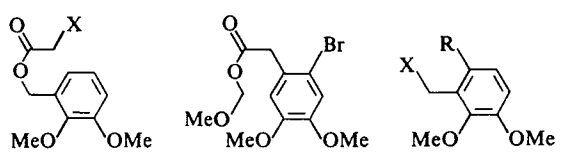


**iv** **v** **vi**

[12]Recently, **16** has been prepared in high yield via **vi**, X = $NMe_2$, R = $CH_2OH$ obtained by successive metalation (*n*-BuLi) and formaldehyde treatment of **vi**, X = $NMe_2$, R = H (30).

[13]We are grateful to Professor R. Rodrigo and Dr. K. Orito for an authentic sample of **11***b* and pertinent spectral data.

Can. J. Chem. Downloaded from www.nrcresearchpress.com by 210.87.254.42 on 09/06/12
For personal use only.

capillary. The solution was brought to reflux with an unfrosted lamp (200 W, General Electric) positioned 15–20 cm from the flask. Bromine (8 g, 50 mmol) in carbon tetrachloride (10 mL) was slowly introduced. Instant decoloration of bromine was observed. The mixture was further refluxed for 1 h, cooled, diluted with chloroform (30 mL), and washed with successive portions of 5% aqueous sodium bicarbonate solution (20 mL) and water (20 mL). Standard work-up gave 8.4 g of a yellow oil which was purified by column chromatography (Florisil, $CHCl_3$–PhH, 65:35 eluent) to give 7 g (79%) of compound **8***a* as a pale yellow oil, bp 116–117°C/0.3 Torr. Treatment with decolorizing carbon followed by crystallization from ether gave **8***a* as colorless crystals, mp 58.5–59.5°C; ir ($CHCl_3$) $\nu_{max}$: 1740 $cm^{-1}$; nmr δ: 5.25, 5.72 (2 × d, 2H, $J$ = 14 Hz), 5.50 (s, 1H), 7.40 (s, 4H); ms *m/e* (% rel. intensity): 228, 226 (17, $M^+$), 147 (100), 119 (58), 118 (20), 103 (32). *Anal.* calcd. for $C_9H_7BrO_2$: C 47.60, H 3.10; found: C 47.81, H 3.10.

*4-(*N*-Methyl)-β-3′,4′-dimethoxyphenylethylamino)-isochroman-3-one (***9***a)*

A solution of 4-bromoisochroman-3-one (**8***a*) (1.77 g, 10 mmol) in anhydrous benzene (14 mL) was added dropwise under nitrogen to a stirred solution of *N*-methyl-β-3,4-dimethoxyphenethylamine (**7**) (14) (3.91 g, 20 mmol) in dry benzene (20 mL). The mixture was stirred at room temperature for 2 h. The precipitated hydrobromide of **7** was collected by filtration and the filtrate was diluted with benzene (50 mL) and washed with successive portions of 50% aqueous sodium bicarbonate solution (20 mL) and water (20 mL). Standard work-up gave an oil which was purified by column chromatography (silica gel, $CHCl_3$–MeOH, 300:1 eluent) to afford 2.4 g (70%) of compound **9***a* as a colorless thick oil, ir ($CHCl_3$) $\nu_{max}$: 1745 $cm^{-1}$; nmr δ: 2.46 (s, 3H), 2.87 (br s, 4H), 3.78 (s, 6H), 4.31 (s, 1H), 5.03, 5.33 (2 × d, 2H, $J$ = 14 Hz), 6.76 (s, 3H), 7.20–7.50 (m, 4H); ms *m/e* (% rel. intensity); 341 (0.5, $M^+$), 190 (100), 147 (31), 119 (28). *Anal.* calcd. for $C_{20}H_{23}NO_4$: C 70.36, H 6.79, N 4.10; found: C 70.49, H 6.66, N 4.00.

*4-(*N*-Methyl-β-3′,4′-dimethoxyphenylethylamino)-isochroman-3-ol (***9***b)*

A solution of diisobutylaluminum hydride (Alfa Products) (3 mL, 20% *n*-hexane solution) in dry toluene (5 mL) was added dropwise to a stirred solution of compound **9***a* (0.15 g, 0.4 mmol) in toluene (20 mL) at −15°C (ice–salt bath) under nitrogen. The mixture was stirred for 1 h and treated successively with a 2 *M* solution of isopropyl alcohol in toluene (5 mL) and water (0.2 mL). The mixture was stirred at room temperature for 2 h, chloroform (15 mL) and anhydrous sodium sulfate (0.75 g) were added, and the whole was subjected to filtration. The filtrate was concentrated under reduced pressure to give crude material which was purified by column chromatography (silica gel, $CHCl_3$–MeOH, 98:2 eluent) to furnish 120 mg (80%) of compound **9***b* as a colourless oil; ir ($CHCl_3$) $\nu_{max}$: 3270 (br) $cm^{-1}$; nmr δ: 2.31 (s, 3H, $NCH_3$), 2.67–3.15 (m, 4H, $—CH_2CH_2$), 3.60 (d, 1H, $J$ = 3 Hz, C-4 H), 3.82, 3.87 (2 × s, 6H, 2 × $OCH_3$), 4.80 (s, 2H, C-1 H), 4.83 (d, 1H, $J$ = 3 Hz, C-3 H), 5.40 (br s, 1H, OH, $D_2O$ exch.) 6.80 (s, 3H, A ring H), 7.08–7.50 (m, 4H, D ring H); ms *m/e* (% rel. intensity): 343 (< 0.5, $M^+$) 192 (100), 174 (25), 165 (27), 152 (25), 151 (35), 149 (25), 133 (27), 131 (25), 121 (35), 119 (34), 103 (28). *Anal.* calcd. for $C_{20}H_{25}NO_4$: C 69.96, H 7.34, N 4.08; found: C 70.07, H 7.24, N 4.23.

*7,8-Dimethoxy-3-methylrhoeadan (***10***a)*

A mixture of compound **9***b* (1.0 g, 2.9 mmol) and polyphosphoric acid (15 g) (35) was mechanically stirred at 35°C for 24 h. The resulting reddish brown syrup was poured into a stirred ice–water mixture (40 g), basified with ammonium hydroxide, and subjected to standard work-up to give 0.70 g of crude material. Preparative tlc separation (aluminum oxide, activity 1, $CHCl_3$ eluent) followed by recrystallization from chloroform–ethanol afforded 0.5 g (53%) of compound **10***a*, mp 158.5–159°C; nmr δ: 2.38 (s, 3H, $NCH_3$), 2.60–3.50 (m, 4H, $—CH_2CH_2$), 3.72 (d, 1H, $J$ = 2.5 Hz, C-2 H), 3.88, 3.90 (2 × s, 6H, 2 × $OCH_3$), 4.72 (d, 1H, $J$ = 2.5 Hz, C-1 H), 4.97, 5.30 (2 × d, 2H, $J$ = 14 Hz, C-14 H), 6.73, 6.86 (2 × s, 2H, A ring H), 7.10–7.50 (m, 4H, D ring H); ms *m/e* (% rel. intensity): 325 (54, $M^+$), 296 (57), 206 (100), 193 (39), 164 (25), 146 (30). *Anal.* calcd. for $C_{20}H_{23}NO_3$: C 72.82, H 7.12, N 4.30; found: C 72.42, H 7.08, N 4.33.

*7,8-Dimethoxy-3-methylrhoeadan-14-one (***11***a)*

A solution of chromium trioxide (0.8 g) in a mixture of water (1 mL) and glacial acetic acid (4 mL) was added dropwise to an ice-cold, stirred solution of compound **10***a* (1 g, 3.1 mmol) in glacial acetic acid (20 mL). The mixture was stirred at ice-bath temperatures for 15 min, at room temperature for 30 min, treated with an equal volume of water, and extracted with chloroform (6 × 50 mL). The organic extract was washed successively with 5% aqueous sodium bicarbonate solution (30 mL) and water (30 mL) and subjected to standard work-up to give a brown syrup which was resolved into six fractions by preparative tlc (silica gel, $CHCl_3$–MeOH, 100:8). One of the high $R_f$ fractions gave 73 mg (7%) of compound **11***a* as a colourless solid, mp 203–205°C; ir (KBr) $\nu_{max}$: 1718 $cm^{-1}$; nmr δ: 2.21 (s, 3H, $NCH_3$), 2.40–3.40 (m, 4H, $—CH_2CH_2$), 3.51 (d, 1H, $J$ = 2 Hz, C-2 H), 3.82, 3.90 (2 × s, 6H, 2 × $OCH_3$), 5.38 (d, 1H, $J$ = 2 Hz, C-1 H), 6.72, 6.77 (2 × s, 2H, A ring H), 7.40–8.40 (m, 4H, D ring H); ms *m/e* (% rel. intensity): 339 (10, $M^+$), 206 (100), 193 (33) 146 (34). *Anal.* calcd. for $C_{20}H_{21}NO_4$: C 70.37, H 6.24, N 4.13; found: C 70.11, H 6.30, N 4.19.

*5,6,7,12-Tetrahydro-7-methyl-2,3-dimethoxybenz[*d*]indeno-[1,2-*b*]azepine (iii)*

A solution of compound **9***b* (300 mg, 0.8 mmol) in concentrated sulfuric acid (1 mL) was stirred in an ice–water bath for 20 min, treated with ice-water (5 g), and neutralized with ammonium hydroxide solution. Standard work-up gave an oil which was resolved by preparative tlc (silica gel, $CHCl_3$–MeOH, 100:1.5) into three major components one of which ($R_f$ ~0.75) yielded 72 mg (27%) of a colorless oil, nmr δ: 2.90–3.35 (m, 4H, C-5, C-6 H), 3.02 (s, 3H, $NCH_3$), 3.84 (s, 2H, C-12 H), 3.89, 3.95 (2 × s, 6H, 2 × $OCH_3$), 6.74, 7.14 (2 × s, 2H, A ring H), 7.20–7.60 (m, 4H, D ring H); ms *m/e*: 307 ($M^+$). The nmr spectrum was very similar to spectra of analogous more highly substituted benz[*d*]indeno[1,2-*b*]azepine derivatives (9, 13*a*, 36). The instability of compound **iii** precluded its further characterization.

*3-(2,3-Dimethoxyphenyl)propionic acid (***12***)*

Hydrogenation of 2,3-dimethoxycinnamic acid (21.17 g, 102 mmol) (37) over 10% Pd/C (0.164 g) in glacial acetic acid (270 mL) at 65°C and 30 psi gave a solid which upon recrystallization from pentane–cyclohexane afforded 20.15 g (94%) of compound **12**, mp 64–66°C (lit. (38) mp 69–70°C); ir ($CHCl_3$) $\nu_{max}$: 1705 $cm^{-1}$; nmr δ: 2.78 (m, 4H), 3.81 (s, 6H), 6.80 (m, 3H).

*4,5-Dimethoxyindan-1-one (***13***)*

A mixture of compound **12** (11.56 g, 55 mmol) and freshly prepared (35) polyphosphoric acid (100 g) was stirred mechanically at steam bath temperatures for 10 min. The dark red mixture was poured into a stirred ice–water mixture (360 g) and extracted with methylene chloride (4 × 60 mL). The organic extract was washed successively with 10% aqueous sodium bicarbonate (ca. 50 mL) and water (50 mL), and subjected to standard work-up to give 10 g (95%) of compound **13** as a colourless solid, mp 74–76°C (lit. (39) mp 74°C); ir (KBr) $\nu_{max}$:

Can. J. Chem. Downloaded from www.nrcresearchpress.com by 210.87.254.42 on 09/06/12
For personal use only.

1705 $cm^{-1}$; nmr δ: 2.62–3.10 (m, 4H), 3.95 (s, 3H), 3.98 (s, 3H), 7.04 (d, 1H, $J$ = 9 Hz), 7.55 (d, 1H, $J$ = 9 Hz).

This reaction was previously effected in low yield using $P_2O_5$ (38).

*4,5-Dimethoxyindan-1-ol*

Powdered sodium borohydride (2.27 g, 60 mmol) was added in portions to a stirred solution of compound **13** (10 g, 52 mmol) in ethanol (65 mL). The mixture was stirred for 30 min, refluxed for 20 min, diluted with water (300 mL), and extracted with methylene chloride (3 × 100 mL). Standard work-up afforded 10 g (99%) of 6,7-dimethoxyindan-1-ol, mp 91–92°C; ir (KBr) $\nu_{max}$: 3300 $cm^{-1}$; nmr δ: 1.9 (br s, 1H, $D_2O$ exch.), 1.95–3.20 (m, 4H), 5.15 (t, 1H, $J$ = 6.5 Hz), 6.76, 7.06 (2 × d, 2H, $J$ = 9 Hz) which was used in the next reaction without further purification.

*6,7-Dimethoxyindene*

Freshly distilled phosphorus oxychloride (25 g, 163 mmol) was added dropwise to a stirred, ice-cold solution of 4,5-dimethoxyindan-1-ol (10 g, 52 mmol), in anhydrous pyridine (75 mL). The solution was allowed to stand for 45 min, refluxed for 35 min, cooled, and poured slowly into a stirred ice–water mixture (400 mL). 6 *N* Hydrochloric acid (80 mL) was added and the whole was extracted with methylene chloride (5 × 50 mL). Standard work-up followed by steam distillation and extraction of the distillate with methylene chloride gave 7 g (77%) of 6,7-dimethoxyindene as a colourless oil, bp 88–93°C/0.55–0.9 Torr; ir (neat) $\nu_{max}$: 1613 $cm^{-1}$; nmr δ: 3.10–3.50 (m, 2H), 3.85, 3.95 (2 × s, 6H), 6.20–7.30 (m, 4H). *Anal.* calcd. for $C_{11}H_{12}O_2$: C 74.98, H 6.86; found: C 74.89, H 6.83.

*4,5-Dimethoxyindan-2-ol*

Under a dry nitrogen atmosphere, a solution of 6,7-dimethoxyindene (6.86 g, 39 mmol) in anhydrous THF (15 mL) was added dropwise to a magnetically stirred 1 *M* solution of diborane in THF (Aldrich) (19.5 mL, 19.5 mmol) at a rate so as to keep the temperature below 30°C. The resulting solution was stirred 2 h and treated successively with water (0.5 mL), 3 *N* aqueous sodium hydroxide (13.6 mL), and 30% hydrogen peroxide (4.8 mL, 47 mmol) during which time the temperature of the mixture was maintained below 35°C. The reaction mixture was stirred for 16 h, diluted with ether (25 mL), and treated with saturated solid sodium chloride. Standard work-up followed by distillation afforded 6.68 g (88%) of 4,5-dimethoxyindan-2-ol, bp 116–122°C/0.1 Torr; mp 54–56°C; ir (KBr) $\nu_{max}$: 3497 $cm^{-1}$; nmr δ: 2.24 (s, 1H, $D_2O$ exch.), 2.50–3.40 (m, 4H), 3.84 (s, 6H), 4.40–4.80 (m, 1H), 6.73, 6.93 (2 × d, 2H, $J$ = 9 Hz). *Anal.* calcd. for $C_{11}H_{14}O_3$: C 68.02, H 7.27; found: C 68.19, H 7.35.

*4,5-Dimethoxyindan-2-one (14)*

To a stirred solution of 4,5-dimethoxyindan-2-ol (6.6 g, 36 mmol) and dicyclohexylcarbodiimide (22.25 g, 108 mmol) in a mixture of benzene (100 mL) and dry dimethyl sulfoxide (10 mL), was added 0.7 mL of a 5 *M* solution of orthophosphoric acid in dry dimethyl sulfoxide. The mixture was stirred under nitrogen for 20 h and the resulting precipitate was collected by filtration and washed with benzene (75 mL). The combined filtrate was treated with 5% aqueous sodium bicarbonate solution (100 mL) and the mixture was stirred for 1 h. Standard work-up gave a brown oil which was dissolved in absolute ethanol (30 mL) and the resulting solution was cooled to −20°C to deposit 3.7 g of brown crystalline solid. Recrystallization from absolute ethanol gave 3.43 g (50%) of compound **14** as pale yellow needles, mp 91.5–93°C; ir ($CHCl_3$) $\nu_{max}$: 1746 $cm^{-1}$; nmr δ: 3.47 (s, 4H), 3.83 (s, 6H), 6.82, 7.0 (2 × d, 2H, $J$ = 9 Hz). *Anal.* calcd. for $C_{11}H_{12}O_3$: C 68.73, H 6.29; found: C 68.77, H 6.20.

*5,6-Dimethoxyisochroman-3-one (15) and 7,8-dimethoxyisochroman-3-one (16) by Baeyer–Villiger reaction*

A solution of compound **14** (5 g, 26 mmol) and *m*-chloroperbenzoic acid (8.2 g, 40.4 mmol) in chloroform (100 mL) was stirred with the exclusion of air for 2 days. The resulting precipitate was collected by filtration and the filtrate was concentrated *in vacuo* to give 9.0 g of solid which was redissolved in chloroform (150 mL) and shaken with 5% aqueous sodium bicarbonate solution (100 mL) until gas evolution ceased. Standard work-up gave 5.5 g of a light brown solid which upon two recrystallizations from ether–pentane at −20°C provided 2.31 g (43%) of a mixture of the isomeric compounds **15** and **16**, mp 40–45°C; ir (KBr) $\nu_{max}$: 1752 $cm^{-1}$; nmr δ: 3.65 (s, 0.6 H), 3.77 (s, 1.4 H), 3.87, 3.90 (2 × s, 6H), 5.26 (s, 1.4 H), 5.44 (s, 0.6 H), 6.90 (s, 2H); ms *m/e*: 208 ($M^+$). *Anal.* calcd. for $C_{11}H_{12}O_4$: C 63.45, H 5.81; found: C 63.56, H 5.84.

Comparison of the integrated nmr spectrum of the mixture of **15** and **16** with that of pure **15**, synthesized independently as described below, allowed the assignments of the resonances at δ 3.65 (s, —$CH_2CO$), 3.87 (s, $OCH_3$), 5.26 (s, —$CH_2O$) to compound **16**. Therefore the mixture consists of a 60:40 ratio of the isomeric isochroman-3-ones **15** and **16**.

Since attempts to separate this mixture by fractional crystallization and repeated tlc on silica gel and alumina using a variety of solvent systems failed, it was subjected to bromination as described below.

*5,6-Dimethoxyisochroman-3-one (15)*

2,3-Dimethoxybenzaldehyde was converted into 2,3-dimethoxyphenylacetic acid by the following reactions and intermediates: (*1*). $NaBH_4$/EtOH/room temperature/20 h → 2,3-dimethoxybenzyl alcohol (99%), mp 49–51°C (lit. (38) mp 46–48°C); (*2*). $SOCl_2$/PhH/ɲ/1.5 h → 2,3-dimethoxybenzyl chloride (99%), used without purification; (*3*). NaCN/$H_2O$ (40) → 2,3-dimethoxybenzyl cyanide (85%), used without purification; (*4*). 20% aqueous KOH/ɲ/4 h → 2,3-dimethoxyphenylacetic acid (87%), mp 80–82°C (lit. (41) mp 84°C).

A mixture of this compound (1.5 g, 7.6 mmol), concentrated hydrochloric acid (2 mL), glacial acetic acid (3.5 mL), and 30% aqueous formalin solution (0.8 g, 8 mmol) was heated at steam bath temperatures for 2 h. Water (15 mL) was added and the mixture was extracted with chloroform (3 × 40 mL). Standard work-up gave 1.2 g of a thick oil which was resolved by preparative tlc (silica gel, $CHCl_3$–MeOH, 100:1) into the following: *band 1* ($R_f$ = 0.4): 5,6-dimethoxyisochroman-3-one (**15**), 0.12 g (7.5%), mp 153–155°C; ir ($CHCl_3$) $\nu_{max}$: 1740 $cm^{-1}$; nmr δ: 3.78 (s, 2H, —$CH_2$), 3.88, 3.90 (2 × s, 6H, 2 × $OCH_3$), 5.24 (s, 2H, —$CH_2CO$), 6.83, 7.0 (2 × d, 2H, $J$ = 8 Hz, aromatic H); ms *m/e* (% rel. intensity): 208 (7, $M^+$), 193 (71), 164 (100). *Anal.* calcd. for $C_{11}H_{12}O_4$: C 63.45, H 5.81; found: C 63.30, H 5.83; *band 2*: ($R_f$ = 0.1): 5,6-dimethoxy-8-methylenehydroxyisochroman-3-one, 0.6 g (38%), mp 110–112°C; ir ($CHCl_3$) $\nu_{max}$: 3620, 1740 $cm^{-1}$; nmr δ: 2.10 (br s, 1H, OH, $D_2O$ exch.), 3.70 (s, 2H, —$CH_2O$), 3.80, 3.87 (2 × s, 6H, 2 × $OCH_3$), 4.64 (s, 2H, —$CH_2OH$), 5.33 (s, 2H, —$CH_2CO$), 6.87 (s, 1H, aromatic H); ms *m/e* (% rel. intensity): 238 (100, $M^+$), 220 (46), 192 (21), 179 (24), 177 (31), 123 (29). *Anal.* calcd. for $C_{12}H_{14}O_5$: C 60.50, H 5.92; found: C 60.32, H 5.90.

*4-Bromo-7,8-dimethoxyisochroman-3-one (8b) and 5,6-dimethoxy-8-bromoisochroman-3-one (17)*

A mixture of the dimethoxyisochroman-3-ones **15** and **16** (1.04 g, 5 mmol) was brominated according to the procedure used for the preparation of **8***a*. Evaporation to dryness followed by treatment of the residue with ether (5 mL) gave compound **17**, mp 170–172°C; ir (KBr) $\nu_{max}$: 1704 $cm^{-1}$; nmr δ: 3.86, 3.90 (2 × s, 6H), 3.97 (s, 2H), 4.70 (s, 2H), 7.14 (s, 1H). *Anal.* calcd. for $C_{11}H_{11}BrO_4$: C 46.01, H 3.86; found: C 45.80, H 3.90.

The above filtrate was evaporated *in vacuo* at room temperature to give a pale yellow oil which upon column chromatography (silica gel, $CHCl_3$ eluent) yielded 0.55 g (38%) of compound **8***b* as a colourless oil which crystallized upon refrigera-

Can. J. Chem. Downloaded from www.nrcresearchpress.com by 210.87.254.42 on 09/06/12
For personal use only.

tion, mp 122–123°C; ir (KBr) $\nu_{max}$: 1750 $cm^{-1}$; nmr δ: 3.88, 3.98 (2 × s, 6H, 2 × $OCH_3$), 5.15, 5.60 (2 × d, 2H, $J$ = 14 Hz, C-1 H), 5.80 (s, 1H, C-4 H), 6.98 (s, 2H, aromatic H); ms *m/e* (% rel. intensity): 288, 286 (7, $M^+$), 208 (26), 207 (100), 179 (31), 151 (31). *Anal.* calcd. for $C_{11}H_{11}BrO_4$: C 46.01, H 3.86; found: C 45.84, H 4.01.

*7,8-Dimethoxyisochroman-3-one (**16**) from homoisovanillic acid (**18**)*

The Nagata procedure (23) was adapted. A mixture of homoisovanillic acid (**18**) (42) (1.82 g, 10 mmol), benzeneboronic acid (2.0 g), and benzene (100 mL) was stirred and refluxed with azeotropic removal of water (Dean–Stark trap) for 1 h. Paraformaldehyde (1.0 g) was added and the reflux was continued as before for a total of 9 h during which time paraformaldehyde (2 g) was added at 2 h intervals. Next day reflux was resumed using a new condenser after addition of benzeneboronic acid (1 g). Paraformaldehyde was added as before. After 28 h of reaction extending over 4 days, benzene was removed *in vacuo*, water (30 mL) was added to the oily residue, and the mixture was heated at 90–100°C for 1.5 h. The solid which formed was collected by filtration without cooling the mixture and was dissolved in methylene chloride. The organic extract was washed with water, dried ($Na_2SO_4$), and evaporated to dryness to yield 0.939 g (48%) of *8-hydroxy-7-methoxyisochroman-3-one*, mp 180–183°C (lit. (23*a*) mp 183–185°C). Methylation according to Nagata and co-workers (23*a*) gave compound **18** in 90% yield, mp 97–99°C (lit. (23*a*) mp 98–100°C).

*4-(N-Methyl-β-3′,4′-dimethoxyphenylethylamino)-7,8-dimethoxyisochroman-3-one (**9**c)*

The condensation of compound **8***b* (0.29 g, 1 mmol) with *N*-methyl-3,4-dimethoxy-β-phenethylamine (**7**) (0.39 g, 2 mmol), carried out according to the procedure described for the preparation of **9***a*, gave a yellow oil which was chromatographed (silica gel, $CHCl_3$–EtOAc, 2:1 eluent) to give 0.35 g (88%) of compound **9***c* as a colourless oil, ir ($CHCl_3$) $\nu_{max}$: 1740 $cm^{-1}$; nmr δ: 2.33 (s, 3H), 2.72 (br s, 4H), 3.81, 3.83, 3.87 (3 × s, 12H), 4.48 (s, 1H), 4.80, 5.55 (2 × d, 2H, $J$ = 14 Hz), 6.60–6.73 (m, 3H), 6.90 (s, 2H); ms *m/e* (% rel. intensity): 401 (0.5, $M^+$), 250 (80), 207 (100), 179 (20), 151 (21). *Anal.* calcd. for $C_{22}H_{27}NO_6$: C 65.82, H 6.78, N 3.49; found: C 65.64, H 6.71, N 3.45.

*4-(N-Methyl-β-3′,4′-dimethoxyphenylethylamino)-7,8-dimethoxyisochroman-3-ol (**9**d)*

Dibal reduction of compound **9***c* (0.35 g, 0.87 mmol) according to the procedure used to obtain compound **9***b* gave 0.30 g (99%) of oily product which was chromatographed (silica gel, $CHCl_3$–MeOH, 100:2.5 eluent) to give the lactol **9***d* as a colorless oil, ir ($CHCl_3$) $\nu_{max}$: 3300 $cm^{-1}$; nmr δ: 2.33 (s, 3H, $NCH_3$), 2.70–3.10 (m, 4H, $—CH_2CH_2$), 3.71 (d, 1H, $J$ = 3 Hz, C-4 H), 3.81, 3.85, 3.87, 3.90 (4 × s, 12H, 4 × $OCH_3$), 4.70 (d, 1H, $J$ = 3 Hz, C-3 H), 4.76 (s, 2H, C-1 H), 5.60 (br s, 1H, OH, $D_2O$ exch.), 6.60–7.0 (m, 4H, aromatic H), 7.2 (s, 1H, aromatic H); ms *m/e* (% rel. intensity): 403 (< 0.5, $M^+$), 252 (100), 209 (68), 181 (53), 179 (21), 165 (23), 152 (27). *Anal.* calcd. for $C_{22}H_{29}NO_6$: C 65.49, H 7.24, N 3.47; found: C 65.58, H 7.39, N 3.45.

*7,8,12,13-Tetramethoxy-3-methylrhoeadan (**10**b)*

A mixture of the lactol **9***d* (0.35 g, 0.86 mmol) and polyphosphoric acid (10 g) was mechanically stirred and heated at steam bath temperatures for 3.5 h. Standard work-up (see preparation of **10***a*) followed by preparative tlc (alumina, $CHCl_3$ eluent) gave 0.17 g (51%) of compound **10***b* as a colorless oil which crystallized, mp 164–166°C; ir ($CHCl_3$) $\nu_{max}$: 1605 $cm^{-1}$; nmr δ: 2.33 (s, 3H, $NCH_3$), 2.60–3.60 (m, 4H, $—CH_2CH_2$), 3.86 (br s, 12H, 4 × $OCH_3$), 4.04 (d, 1H, $J$ = 2 Hz, C-2 H), 4.50 (d, 1H, $J$ = 2 Hz, C-1 H), 4.87, 5.30 (2 × d, 2H, $J$ = 14 Hz, C-14 H), 6.72, 6.80 and 6.88 (3 × s, 4H, aromatic H); ms *m/e* (% rel. intensity): 385 (47, $M^+$), 370 (25), 357 (31), 356 (98), 354 (41), 343 (28), 342 (100), 326 (20), 207 (22), 206 (100), 204 (22), 194 (22), 193 (56), 192 (59), 191 (31), 190 (22), 179 (28), 178 (47), 177 (22), 176 (28), 165 (37), 164 (44), 163 (36), 162 (25), 161 (25), 151 (34), 150 (34), 149 (34), 148 (34), 147 (22), 135 (28), 134 (31), 133 (22), 121 (31), 119 (22), 118 (25), 107 (25), 103 (22). *Anal.* calcd. for $C_{20}H_{27}NO_5$: C 68.52, H 7.06, N 3.63; found: C 68.31, H 7.20, N 3.52.

*7,8,12,13-Tetramethoxy-3-methylrhoeadan-14-one (14-oxo-cis-alpinigenine) (**11**b)*

The procedure for the oxidation of compound **10***a* to **11***a* was closely followed. From the rhoeadan **10***b* (0.5 g, 1.29 mmol) there was obtained 0.48 g of a crude material which was subjected to preparative tlc (silica gel, $CHCl_3$–MeOH, 100:2 eluent) and was thereby resolved into eight bands, one of which ($R_f$ ~0.6) yielded 35 mg (7%) of compound **11***b*, mp 194–196°C (lit. (13*a*) mp 195–196°C), whose tlc, mixture mp, ir, and ms were shown to be identical with a sample of synthetic material kindly provided by Professor Rodrigo and Dr. Orito (13*a*).

## Acknowledgements

We are grateful to Dr. M. T. Thomas for the alternative synthesis of **16** and P. L. McBroom and C. Chun for preparation of starting materials. The financial support of the Natural Sciences and Engineering Research Council of Canada and Bristol Laboratories, Syracuse, N.Y. is gratefully acknowledged.

1. M. Shamma. The isoquinoline alkaloids. Academic Press, New York. 1972. p. 399.
2. M. Shamma and J. L. Moniot. Isoquinoline alkaloids research, 1972–1977. Plenum Press, New York. 1978. p. 337.
3. F. Stermitz. Recent Adv. Phytochem. **1**, 161 (1968).
4. J. A. Finlay. Int. Rev. Sci. Org. Chem. Ser. 2, **9**, 23 (1976).
5. T. Ibuka, T. Konoshima, and Y. Inubushi. Chem. Pharm. Bull. Jpn. **23**, 114 (1975); **23**, 133 (1975).
6. V. Fajaro, V. Elango, B. K. Cassels, and M. Shamma. Tetrahedron Lett. 39 (1982).
7. S. Kasparek. Adv. Heterocycl. Chem. **17**, 45 (1974).
8. T. Kametani and K. Fukomoto. Heterocycles, **3**, 931 (1975).
9. H. Irie, S. Tani, and H. Yamane. J. Chem. Soc. Perkin Trans. I, 2986 (1972).
10. (*a*) W. Kloetzer, S. Teitel, and A. Brossi. Helv. Chim. Acta, **55**, 228 (1972); (*b*) W. Kloetzer, S. Teitel, J. Blout, and A. Brossi. Monatsh. Chem. **103**, 435 (1972); (*c*) R. Hohlbrugger and W. Kloetzer. Chem. Ber. **112**, 849 (1979).
11. S. Prabhakar, A. M. Lobo, M. R. Tavares, and I. M. C. Oliveira. J. Chem. Soc. Perkin Trans. I, 1273 (1981).
12. M. Shamma and L. Töke. Tetrahedron, **31**, 1991 (1975).
13. (*a*) K. Orito, R. H. Manske, and R. Rodrigo. J. Am. Chem. Soc. **96**, 1944 (1974); (*b*) B. Nalliah, R. H. Manske, and R. Rodrigo. Tetrahedron Lett. 2853 (1974).
14. S. O. de Silva, I. Ahmad, and V. Snieckus. Can. J. Chem. **57**, 1598 (1979).
15. S. O. de Silva, J. N. Reed, and V. Snieckus. Tetrahedron Lett. 5099 (1978).
16. H. Ronsch, A. Guggisberg, M. Hesse, and H. Schmid. Helv. Chim. Acta, **60**, 2402 (1977).
17. D. J. Rawlinson and G. Sosnovsky. Synthesis, 1 (1972); 567 (1973).
18. V. K. Grover and Y. K. Gupta. Aust. J. Chem. **23**, 757

(1970); D. M. PIATAK and L. S. EICHMEIER. J. Chem. Soc. Chem. Commun. 772 (1971).
19. J. GUTZWILLER and M. USKOKOVIC. J. Am. Chem. Soc. **100**, 576 (1978).
20. Y. SPRINZAK. J. Am. Chem. Soc. **80**, 5449 (1958).
21. J. N. SRIVASTAVA and D. N. CHAUDHURY. J. Org. Chem. **27**, 4337 (1962).
22. A. CHATTERJEE and S. GHOSH. Synthesis, 818 (1981).
23. (*a*) W. NAGATA, H. ITAZAKI, K. OKADA, T. WAKABAYASHI, K. SHIBATA, and N. TOKUTAKE. Chem. Pharm. Bull. Jpn. **23**, 2867 (1975); (*b*) W. NAGATA, K. OKADA, and T. AOKI. Synthesis, 365 (1979).
24. J. FINKLESTEIN and A. BROSSI. J. Heterocycl. Chem. **4**, 315 (1967).
25. G. CASIRAGHI, G. CASNATI, G. PUGLIA, G. SARTORI, and G. TERENGHI. J. Chem. Soc. Perkin Trans I, 1862 (1980); T. TOYODA, K. SASAKURA, and T. SUGASAWA. J. Org. Chem. **46**, 189 (1981), and references cited therein.
26. M. IKEDA, K.-I. HIRAO, Y. OKUNO, and O. YONEMITSU. Tetrahedron Lett. 1181 (1974).
27. T. A. BRYSON. Synth. Commun. **3**, 173 (1973).
28. R. L. VAUX, F. N. JONES, and C. F. HAUSER. J. Org. Chem. **29**, 1387 (1964).
29. S.-I. MURAHASHI, K.-I. ITO, T. NAOTA, and Y. MAEDA. Tetrahedron Lett. 5327 (1981).
30. N. S. NARASIMHAN, R. S. MALI, and B. S. KULKARNI. Tetrahedron Lett. 2797 (1981).
31. J. E. HORAN and R. W. SCHIESSLER. Org. Synth. Coll. Vol. V, 647 (1973).
32. G. A. SWAN. J. Chem. Soc. 1720 (1949).
33. J. H. MARKGRAF and S. J. BASTA. Synth. Commun. **2**, 139 (1972).
34. M. S. GIBSON, G. W. PRENTON, and J. M. WALTHEW. J. Chem. Soc. C, 2234 (1970).
35. A. J. BIRCH, R. JAEGER, and R. ROBINSON. J. Chem. Soc. 582 (1945).
36. T. KAMETAMI, M. S. PREMILA, S. HIRATA, H. SETO, H. NEMOTO, and K. FUKUMOTO. Can. J. Chem. **53**, 3824 (1975).
37. J. KOO, M. S. FISHER, G. N. WALKER, and J. BLAKE. Org. Synth. Coll. Vol. IV, 327 (1963).
38. W. H. PERKIN, JR. and R. ROBINSON. J. Chem. Soc. **105**, 2376 (1914).
39. J. W. HUFFMAN and C. E. OPLIGER. J. Org. Chem. **36**, 111 (1971).
40. R. ADAMS and A. F. THAL. Org. Synth. Coll. Vol. I, 107 (1932).
41. G. TSATSAS. Ann. Pharm. Fr. **7**, 733 (1949); Chem. Abstr. **44**, 5370d (1950).
42. R. GREWE and H. FISCHER. Chem. Ber. **96**, 1520 (1963); K. C. RICE and A. BROSSI. J. Org. Chem. **45**, 592 (1980).

Can. J. Chem. Downloaded from www.nrcresearchpress.com by 210.87.254.42 on 09/06/12
For personal use only.

# Troponoid. V.[1] Crystallographic studies on AY-27110 — a dopamine agonist of the troponylpiperazine series[2]

FARID RAMADAN AHMED

*Division of Biological Sciences, National Research Council of Canada, Ottawa, Ont., Canada K1A 0R6*

AND

JEHAN BAGLI

*Ayerst Research Laboratories, 1025 Boulevard Laurentien, Saint Laurent (Montréal), Qué., Canada H4R 1J6*

Received May 29, 1982

FARID RAMADAN AHMED and JEHAN BAGLI. Can. J. Chem. **60**, 2687 (1982).

The crystal structure and absolute configuration of a *p*-bromobenzoyl derivative, **2**, of the (−)2-[4-[2-hydroxy-2-(3′,4′-dimethylphenyl)ethyl]-1-piperazinyl]-2,4,6-cycloheptatrien-1-one, **3***a* (AY-27110), which is a dopamine agonist, have been determined by an X-ray analysis. Crystals of $C_{28}H_{29}BrN_2O_5$, fw = 553.47, are monoclinic $P2_1$, $a$ = 12.553(2), $b$ = 6.359(1), $c$ = 17.575(3) Å, β = 108.32(1)°, $V$ = 1331.81 Å$^3$, $Z$ = 2, $\rho_c$ = 1.380, $\rho_o$ = 1.384 g cm$^{-3}$. For 2155 observed reflexions, the final $R$ is 0.036 and $R(w)$ is 0.039. The chirality of this enantiomer is shown to be $S(-)$, based on 18 reflexions with significant differences in the intensities of the corresponding Friedel pairs. The piperazine ring has a distorted chair form that is flattened at the N atom nearest the cycloheptatriene ring as for the psychoactive agents loxapine and amoxapine.

FARID RAMADAN AHMED et JEHAN BAGLI. Can. J. Chem. **60**, 2687 (1982).

On a déterminé par analyse aux rayons X la structure cristalline et la configuration absolue d'un dérivé *p*-bromobenzoyle (**2**) de la (−)[(hydroxy-2(diméthyl-3′,4′ phényl)-2 éthyl)-4 pipérazinyl-1]-2 cycloheptatriène-2,4,6 one-1 (**3***a*) (AY-27110) qui est un antagoniste de la dopamine. Les cristaux de $C_{28}H_{29}BrN_2O_5$, pm = 553,47, sont monocliniques et appartiennent au groupe d'espace $P2_1$ avec $a$ = 12,553(2), $b$ = 6,359(1), $c$ = 17,575(3) Å, β = 108,32(1)°, $V$ = 1331,81 Å$^3$, $Z$ = 2, $\rho_c$ = 1,380, $\rho_o$ = 1,384 g cm$^{-3}$. On a résolu la structure et on l'a ajusté jusqu'à des valeurs conventionnelles de $R$ = 0,036 et de $R(w)$ = 0,039 pour 2155 réflexions observées. On montre que la chiralité de cet énantiomère est $S(-)$ à partir 18 réflexions avec des différences d'intensité significatives des paires de Friedel correspondantes. Le cycle pipérazine a une forme chaise déformée qui est applatie au niveau de l'atome de N le plus près du cycloheptatriène comme dans le cas de la loxapine et l'amoxapine; des agents psychoactifs.

[Traduit par le journal]

## Introduction

Central dopaminergic mechanisms are known to be impaired in Parkinson's disease (2). Bromocriptine (CB-154), a dopamine agonist, has recently been reported to alleviate these symptoms (3). However, bromocriptine, an ergot derivative, affects not only the dopaminergic system but also other neuronal systems; its effect therefore is not specific. One of the objectives of our synthesis program was to discover a non-ergot dopamine agonist which is more specific than bromocriptine.

We have recently synthesized a series of troponylpiperazine derivatives (4), some of which demonstrated dopamine agonist activity (5). Compound **1** (2-[4-[2-hydroxy-2-(3′,4′-dimethoxyphenyl)ethyl]-1-piperazinyl]-2,4,6-cycloheptatrien-1-one) emerged as the compound of choice for further biological investigation. It was resolved into its optical enantiomers **3***a* (AY-27,110) and **3***b* using ditoluyl tartaric acids. It was found that the biological activity (5) was associated with the (−) enantiomer **3***a*. It was therefore of interest to establish the absolute configuration of the carbon atom β to the N-4 of the piperazine ring (see formula **1**). For this purpose compound **3***a* was converted to its *p*-

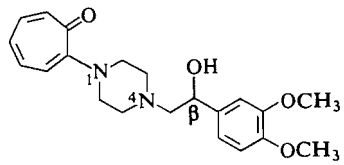

**1**

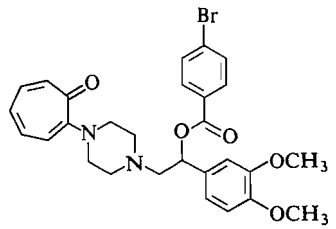

**2**

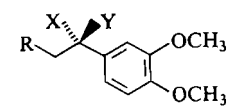

R = troponylpiperazine

**3***a*, $S(-)$, X = H, Y = OH

**3***b*, $R(+)$, X = OH, Y = H

[1]For parts I–IV, see ref. 1.

[2]NRCC No. 20519.

0008-4042/82/212687-05$01.00/0

©1982 National Research Council of Canada/Conseil national de recherches du Canada

Can. J. Chem. Downloaded from www.nrcresearchpress.com by 210.87.254.6 on 09/06/12
For personal use only.

Can. J. Chem. Downloaded from www.nrcresearchpress.com by 210.87.254.6 on 09/06/12
For personal use only.

bromobenzoyl derivative **2** and subjected to X-ray studies.

## Experimental

*Preparation of 4-bromobenzoic acid, 1-(3,4-dimethoxyphenyl)-2-[4-(7-oxo-1,3,5-cycloheptatrien-1-yl)-1-piperazinyl]ethyl ester (2)*

Triethylamine (0.218 g, or 0.3 mL, 1.8 equiv.) was added to a solution of alcohol **3***a* (0.444 g, 1 equiv.) in methylene chloride (4 mL); then 4-bromobenzoyl chloride (0.473 g, 1.8 equiv.) was added. The mixture was stirred for 3.5 h at room temperature, diluted with chloroform, washed with water, dried, and the solvent was removed. The residue was filtered through silica gel (50 g) and the product eluted with ethyl acetate. The product thus obtained was recrystallized twice from chloroform–ether to yield pure product (0.33 g, 69.8%) mp 129–133°C. *Anal.* calcd. for $C_{28}H_{29}BrN_2O_5$ (553.47): C 60.76, H 5.28, N 5.06; found: C 60.46, H 5.23, N 5.10. Infrared ($CHCl_3$) 1715, 1560 $cm^{-1}$, nmr ($CDCl_3$), δ7.55–7.9 (4H, m, arom.), 6.8 (8H, m, arom.), 6.1 (1H, m, C*H*—O), 3.85–3.8 (6H, 2 × s, C*H*$_3$—O), 3.2 (4H, m, C*H*$_2$—N), 2.75 (6H, m, C*H*$_2$—N), ms: *m/e* 554/552 $(M)^+$,

352 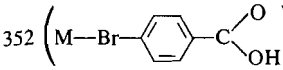 , 185/183 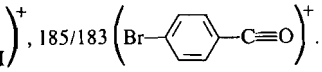 .

*X-ray crystallographic analyses*

*(−) 4-Bromobenzoic acid, 1-(3,4-dimethoxyphenyl)-2-[4-(7-oxo-1,3,5-cycloheptatrien-1-yl)-1-piperazinyl]ethyl ester*

$C_{28}H_{29}BrN_2O_5$ fw = 553.47

Monoclinic, $P2_1$, $a$ = 12.553(2), $b$ = 6.359(1), $c$ = 17.575(3) Å, β = 108.32(1)°, $V$ = 1331.81 Å$^3$, $Z$ = 2, $\rho_c$ = 1.380, $\rho_o$ = 1.384 g $cm^{-3}$, $F(000)$ = 572, μ(Cu) = 24.25 $cm^{-1}$.

Measurements were carried out on an Enraf-Nonius CAD-4F diffractometer with Ni-filtered Cu radiation ($\lambda(K\alpha_1)$ = 1.54056, $\lambda(K\alpha_2)$ = 1.54439 Å) on a prismatic crystal, 0.09 × 0.11 × 0.40 mm, mounted with its length along the φ axis. The cell parameters were based on 15 well-centered reflexions, θ = 30–40°, and the indexing was for a right-handed set of unit-cell axes. The intensity data were measured by ω–2θ scans for ω ranges of (0.8 + 0.14 tan θ), extended by 25% at each end for the backgrounds, at scan speeds of 0.64 to 2.51° $min^{-1}$ in ω. A total of 2991 reflexions in the $hkl$ and $\bar{h}kl$ octants with θ = 0–75° were measured, and of these 2153 were considered observed at the 2σ($I$) level. Three standard reflexions, scanned after every hour of exposure time, showed small random variations within ±1.5% of their mean values. The net intensities were corrected for Lorentz and polarization effects, and for absorption by the Gaussian integration method (6) assuming a 4 × 4 × 6 point grid. The range of the absorption corrections to the intensities was 1.20–1.51. Similarly, the Friedel pairs of $hkl$ and $\bar{h}kl$ with θ = 0–20° were scanned and treated in the same way. The discrepancy index for the structure amplitudes of the 50 $h0l$ and $\bar{h}0\bar{l}$ Friedel pairs which have no imaginary components was only 0.014.

Structure determination was by the heavy-atom method. After refinement of the non-hydrogen atomic parameters to $R$ = 0.064 for the observed reflexions, the H atoms were located from a difference map and included in the refinement with isotropic $B$ values. When $R$ was reduced to 0.046, the effect of the anomalous dispersion of Br was tried for the two possible enantiomorphs. The corresponding $R$ indexes, after one cycle of refinement for each, were 0.0434 and 0.0422, indicating a correct determination of the absolute configuration at the 0.5% level (the Hamilton ratio $\mathcal{R}_{1,1726,0.005}$ = 1.0024 while the experimental $R$ ratio = 1.028 and $R_w$ ratio = 1.030). Also, all the 18 Friedel pairs listed in Table 1 which showed the most significant anomalous dispersion effect consistently favoured one enantiomorph. Further refinement of the parameters for the correct enantiomorph produced the values listed in Tables 2 and 3,[3] for which $R$ = 0.036 and $R(w)$ = 0.039.[3] The refinement was by block-diagonal least-squares on $\Sigma w(F_o - F_c)^2$ with $w^{-1} = 1 + [(|F_o| - p_2)/p_1]^2$, $p_1$ = 30 and $p_2$ = 15 in the last three cycles (to make $\Sigma w(F_o - F_c)^2$ independent of $|F_o|$). The unobserved reflexions were excluded, as were (2̄04) and (2̄67) which showed relatively high discrepancies. The scattering factor curves were from ref. 7 and the computer programs were those of ref. 8. In the final cycle, the mean parameter shift was 0.2σ (maximum = 1.2σ) and $[\Sigma w(\Delta F)^2/(m - n)]^{1/2}$ = 0.6. The final difference map contained random electron densities between −0.25 and 0.19 e Å$^{-3}$.

TABLE 1. Friedel pairs (θ = 0–20°) with the most significant anomalous dispersion effect

| $hkl$ | $I(hkl)$ | $I(\bar{h}\bar{k}\bar{l})$ | $\frac{I(hkl)}{I(\bar{h}\bar{k}\bar{l})}$ | $\left[\frac{F_c(hkl)}{F_c(\bar{h}\bar{k}\bar{l})}\right]^2$ |
|---|---|---|---|---|
| 111 | 32025 | 29213 | 1.10 | 1.05 |
| −111 | 442 | 779 | 0.57 | 0.68 |
| 112 | 11070 | 10254 | 1.08 | 1.04 |
| −122 | 966 | 1040 | 0.93 | 0.92 |
| −113 | 11258 | 9938 | 1.13 | 1.11 |
| −123 | 1618 | 1430 | 1.13 | 1.09 |
| 211 | 15810 | 14998 | 1.05 | 1.04 |
| −213 | 8434 | 7668 | 1.10 | 1.06 |
| −215 | 2140 | 2684 | 0.80 | 0.89 |
| 311 | 808 | 674 | 1.20 | 1.15 |
| −311 | 8371 | 7563 | 1.11 | 1.06 |
| −312 | 4043 | 4417 | 0.92 | 0.92 |
| 322 | 1470 | 1207 | 1.22 | 1.07 |
| −314 | 9133 | 9988 | 0.91 | 0.95 |
| 411 | 235 | 346 | 0.68 | 0.75 |
| 412 | 1946 | 2208 | 0.88 | 0.91 |
| −412 | 1652 | 1499 | 1.10 | 1.07 |
| −514 | 1612 | 1763 | 0.91 | 0.92 |

## Results and discussion

A perspective view of the molecular structure showing the absolute configuration as determined from this X-ray analysis is presented in Fig. 1. The chirality at C(15), according to the Cahn–Ingold–Prelog system of notation (9), with the priority sequence HO > $CH_2NH_2$ > $C_6H_5$ > H is *S*(−) as shown in **3***a*. The arbitrarily-selected atomic numbering system and the bond lengths, not corrected for thermal vibration, are presented in Fig. 2. The valence angles and some selected torsion angles are given in Fig. 3 and Table 4, respectively.

The geometry of the piperazinyl ring in this compound is very similar to that of the corresponding rings in the psychoactive agents loxapine and

[3]The structure factor table and anisotropic thermal parameters of the non-hydrogen atoms are available, at a nominal charge, from the Depository of Unpublished Data, CISTI, National Research Council of Canada, Ottawa, Ont., Canada K1A 0S2.

Can. J. Chem. Downloaded from www.nrcresearchpress.com by 210.87.254.6 on 09/06/12
For personal use only.

TABLE 2. Fractional coordinates ($\times 10^4$; $\times 10^5$ for Br) and the equivalent isotropic temperature factors (Å$^2$) for the heavier atoms ($B_{eq} = \frac{8}{3}\pi^2 \Sigma_i \Sigma_j U_{ij}\, a_i^*\, a_j^*\, \mathbf{a}_i \cdot \mathbf{a}_j$)

| Atom | $x$ | $y$ | $z$ | $B_{eq}$ |
|---|---|---|---|---|
| Br | 71559(5) | −50000 | −4692(4) | 9.22(2) |
| C(1) | 8693(4) | −7999(8) | 5857(3) | 4.8(1) |
| C(2) | 9745(5) | −8684(10) | 6419(3) | 6.4(2) |
| C(3) | 10759(5) | −7805(12) | 6709(3) | 6.9(2) |
| C(4) | 11138(4) | −5851(10) | 6539(3) | 5.8(2) |
| C(5) | 10538(4) | −4440(10) | 6030(3) | 5.3(2) |
| C(6) | 9406(4) | −4525(8) | 5540(3) | 4.7(1) |
| C(7) | 8573(4) | −5978(7) | 5428(2) | 4.0(1) |
| N(8) | 7502(3) | −5512(6) | 4927(2) | 4.5(1) |
| C(9) | 7195(4) | −3342(8) | 4707(3) | 5.3(2) |
| C(10) | 5944(4) | −3118(9) | 4448(3) | 5.7(2) |
| N(11) | 5429(3) | −4427(7) | 3747(2) | 4.2(1) |
| C(12) | 5698(4) | −6626(8) | 3978(3) | 4.7(1) |
| C(13) | 6950(4) | −6955(9) | 4257(3) | 4.9(1) |
| C(14) | 4218(3) | −4040(9) | 3397(3) | 4.7(1) |
| C(15) | 4033(3) | −2120(8) | 2865(2) | 4.1(1) |
| C(16) | 2827(3) | −1450(8) | 2524(2) | 3.9(1) |
| C(17) | 2072(3) | −2614(8) | 1914(3) | 4.0(1) |
| C(18) | 963(3) | −1991(8) | 1588(2) | 4.1(1) |
| C(19) | 602(3) | −168(9) | 1872(2) | 4.3(1) |
| C(20) | 1341(4) | 947(8) | 2485(3) | 4.9(1) |
| C(21) | 2449(3) | 313(9) | 2800(2) | 4.7(1) |
| C(22) | 5400(3) | −1700(9) | 2189(3) | 4.5(1) |
| C(23) | 5819(3) | −2600(9) | 1556(3) | 4.6(1) |
| C(24) | 5405(4) | −4428(10) | 1145(3) | 5.9(2) |
| C(25) | 5805(4) | −5129(11) | 541(3) | 6.6(2) |
| C(26) | 6636(4) | −4040(11) | 374(3) | 6.0(2) |
| C(27) | 7078(4) | −2275(13) | 778(3) | 7.4(2) |
| C(28) | 6668(4) | −1565(11) | 1375(3) | 6.3(2) |
| C(29) | 560(4) | −4616(11) | 573(3) | 6.0(2) |
| C(30) | −904(4) | 2271(10) | 1744(3) | 6.0(2) |
| O(1) | 7859(3) | −9153(6) | 5753(2) | 6.2(1) |
| O(2) | 180(2) | −3009(6) | 987(2) | 5.0(1) |
| O(3) | −501(2) | 377(6) | 1501(2) | 5.4(1) |
| O(4) | 4465(2) | −2635(5) | 2211(2) | 4.4(1) |
| O(5) | 5878(3) | −331(7) | 2637(2) | 7.0(1) |

TABLE 3. Fractional coordinates ($\times 10^3$) and isotropic temperature factors (Å$^2$) for the H atoms

| Atom | $x$ | $y$ | $z$ | $B_{iso}$ |
|---|---|---|---|---|
| H(2) | 955(4) | −1023(10) | 665(3) | 7.5(13) |
| H(3) | 1133(4) | −869(9) | 705(3) | 6.9(14) |
| H(4) | 1196(5) | −557(13) | 685(4) | 11.5(20) |
| H(5) | 1095(4) | −303(9) | 593(3) | 6.5(12) |
| H(6) | 925(3) | −337(8) | 522(2) | 5.1(11) |
| H(9,1) | 747(4) | −278(9) | 520(3) | 6.9(13) |
| H(9,2) | 752(3) | −300(8) | 427(2) | 5.3(11) |
| H(10,1) | 556(4) | −321(11) | 489(3) | 8.6(17) |
| H(10,2) | 577(5) | −175(11) | 423(3) | 9.9(17) |
| H(12,1) | 544(3) | −714(8) | 442(2) | 5.0(11) |
| H(12,2) | 528(3) | −736(8) | 349(2) | 5.3(10) |
| H(13,1) | 717(3) | −846(7) | 446(2) | 4.2(09) |
| H(13,2) | 721(3) | −673(7) | 378(2) | 4.9(10) |
| H(14,1) | 386(3) | −383(8) | 384(3) | 6.2(11) |
| H(14,2) | 391(3) | −527(8) | 306(2) | 4.9(10) |
| H(15) | 441(3) | −91(7) | 314(2) | 4.0(10) |
| H(17) | 233(3) | −395(7) | 173(2) | 4.5(10) |
| H(20) | 110(4) | 216(9) | 266(3) | 7.1(13) |
| H(21) | 294(3) | 107(6) | 323(2) | 3.6(09) |
| H(24) | 485(4) | −508(11) | 125(3) | 7.8(13) |
| H(25) | 550(4) | −636(10) | 28(3) | 9.0(17) |
| H(27) | 757(4) | −174(9) | 67(3) | 7.5(14) |
| H(28) | 690(4) | −51(10) | 166(3) | 8.5(15) |
| H(29,1) | 117(3) | −402(7) | 40(2) | 4.4(09) |
| H(29,2) | 92(4) | −574(9) | 97(3) | 6.9(13) |
| H(29,3) | −8(5) | −480(12) | 18(3) | 8.8(15) |
| H(30,1) | −43(4) | 327(9) | 165(3) | 6.3(12) |
| H(30,2) | −85(4) | 212(10) | 242(3) | 8.6(15) |
| H(30,3) | −163(4) | 236(10) | 142(3) | 7.9(15) |

amoxapine (10). It has a distorted chair form with its four C atoms slightly non-planar ($\chi^2 = 27.3$, deviations from mean plane ±0.013(5) Å). N(8) and N(11) lie on opposite sides at significantly different distances (−0.642(3) and 0.708(4) Å, respectively) from the mean plane of the C atoms. While the endocyclic angles are approximately tetrahedral, 108.0(4)–111.0(4)°, the exocyclic angles are well above tetrahedral values with the angles of 119.3(4) and 119.7(4)° at N(8) considerably larger than those of 112.5(4) and 113.2(4)° at N(11). The flattening of the ring at N(8) was interpreted for loxapine and amoxapine (10) as indicative of some electron delocalization into the bond corresponding to N(8)–C(7), although its length in those structures, as in the present work, was 1.388 Å, i.e. within the range expected for C($sp^2$)—N($sp^3$) bonds (11). The other C—N bonds have a mean length of 1.466(11) Å in the present structure and 1.462(8) Å in the other two structures.

The cycloheptatriene ring is nearly planar, with $\chi^2 = 31.6$ for the seven C atoms. However, excluding C(1), the other six C atoms are coplanar ($\chi^2 = 1.8$) while C(1) is off that plane by −0.036(5) Å, resulting in a slight bend of 2.8(5)° between the plane C(2)—C(1)—C(7) and that of the six atoms. O(1) lies at 0.034(4) Å from the C(2)—C(1)—C(7)

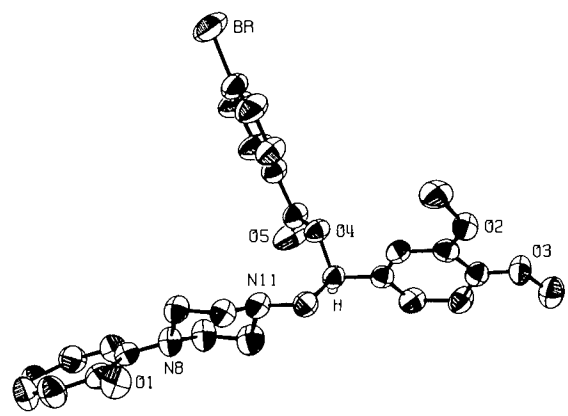


FIG. 1. A perspective view of the molecular structure showing its absolute configuration.

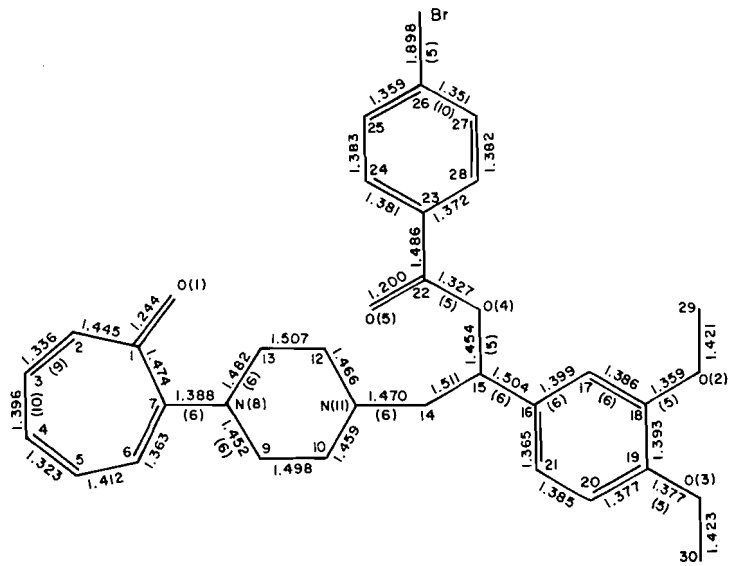


FIG. 2. Bond lengths (Å). The estimated standard deviations are 0.007–0.008 Å except for those given in parentheses.

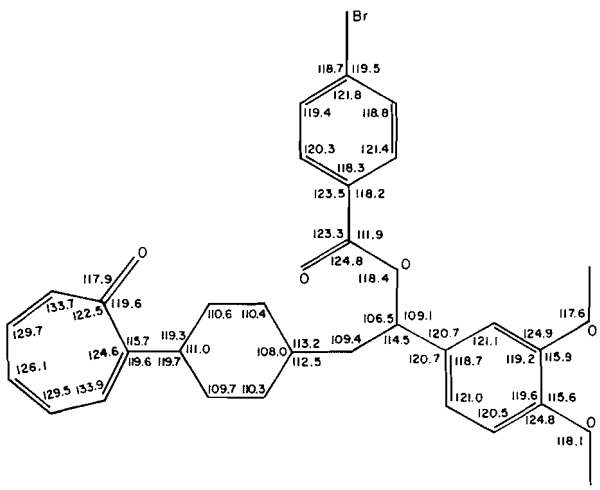


FIG. 3. Valence angles (deg). The estimated standard deviations are 0.4–0.6°.

TABLE 4. Selected torsion angles

| Atoms | Torsion angle (deg) |
|---|---|
| N(11)—C(14)—C(15)—C(16) | −175.1(4) |
| N(11)—C(14)—C(15)—O(4) | 64.1(4) |
| C(15)—O(4)—C(22)—O(5) | −5.9(7) |
| C(15)—O(4)—C(22)—C(23) | 172.1(4) |
| C(17)—C(18)—O(2)—C(29) | −10.9(6) |
| C(19)—C(18)—O(2)—C(29) | 167.7(4) |
| C(20)—C(19)—O(3)—C(30) | 2.5(7) |
| C(18)—C(19)—O(3)—C(30) | −177.5(4) |
| C(14)—C(15)—O(4)—C(22) | −109.4(4) |
| C(16)—C(15)—O(4)—C(22) | 126.5(4) |

plane. The three C=C double bonds have a mean value 1.341 Å which is comparable to the average value (12) of 1.337(6) Å.

The C atoms of the *p*-bromobenzoic group are coplanar ($\chi^2 = 15.3$) with deviations within ±0.013 Å, but the substituents Br and C(22) are at distances 0.059(2) and 0.052(5) Å from the plane of the ring. The Br—C(26) distance of 1.898(5) Å is comparable to the value 1.902(10) Å for *p*-bromobenzoic acid (13).

The remaining aromatic ring C(16) to C(21) is planar ($\chi^2 = 15.2$) with the substituents C(15), O(2), and O(3) in the plane of the ring. The two methyl groups C(29) and C(30) lie on the same side of the ring plane but at unequal distances of 0.260(6) and 0.123(6) Å, respectively. This imbalance is reflected in the corresponding torsion angles in Table 4. The average C—C length in the two aromatic rings is 1.378(14) Å and the average C—H length is 0.97(8) Å. The molecules are separated by normal van der Waals contacts.

In summary, the above assigns the chirality of β-C-atom of **2** as *S*. In turn the chirality of that carbon in AY-27110 follows. The biological activity thus resides with the *S*(−) enantiomer.


## Acknowledgements

The assistance of Mrs. M. E. Pippy with the computations and of Dr. C. P. Huber with ORTEP is gratefully acknowledged.



1. Part I: J. BAGLI and M. ST.-JACQUES. Can. J. Chem. **56**, 578 (1978); Part II: J. BAGLI, T. BOGRI, B. PALAMETA, and M. ST.-JACQUES. Can. J. Chem. **57**, 1949 (1979); Part III: J.


Can. J. Chem. Downloaded from www.nrcresearchpress.com by 210.87.254.6 on 09/06/12
For personal use only.

BAGLI, T. BOGRI, B. PALAMETA, R. MARTEL, H. ROBINSON, T. PUGSLEY, and W. LIPPMANN. J. Med. Chem. **22**, 1186 (1979); Part IV: D. MENARD, M. ST.-JACQUES, and J. BAGLI. Can. J. Chem. **60**, 231 (1982).
2. J. R. BIANCHINE, G. M. SHAW, J. E. GREENWALD, and S. M. DANDALIDES. Fed. Proc. Fed. Am. Soc. Exp. Biol. **37**, 2434 (1978).
3. A. RASCOL, B. GUIVAUD, J. L. MONTASTNIC, J. DAVID, and M. CLAVET. J. Neurol. Neurosurg. Psychiatry, **42**, 143 (1979).
4. J. BAGLI, T. BOGRI, K. VOITH, T. PUGSLEY, and W. LIPPMANN. J. Med. Chem. To be published.
5. J. BAGLI and K. VOITH. J. Med. Chem. To be published.
6. W. R. BUSING and H. A. LEVY. Acta Crystallogr. **10**, 180 (1957).
7. (*a*) International tables for X-ray crystallography. Vol. IV. Kynoch Press, Birmingham. 1974; (*b*) R. F. STEWART, E. R. DAVIDSON, and W. T. SIMPSON. J. Chem. Phys. **42**, 3175 (1965).
8. F. R. AHMED, S. R. HALL, M. E. PIPPY, and C. P. HUBER. J. Appl. Crystallogr. **6**, 309 (1973).
9. R. S. CAHN, C. K. INGOLD, and V. PRELOG. Experientia, **12**, 81 (1956); J. JACQUES, C. GROS, and S. BOURCIER. *In* Stereochemistry, fundamentals and methods. Vol. 4. *Edited by* H. B. Kagan. 1977. p. 116.
10. D. B. COSULICH and F. M. LOVELL. Acta Crystallogr. Sect. B**33**, 1147 (1977).
11. D. R. LIDE. Tetrahedron, **17**, 125 (1962).
12. O. KENNARD, D. G. WATSON, F. H. ALLEN, N. W. ISAACS, W. D. S. MOTHERWELL, R. C. PETTERSON, and W. G. TOWN (*Editors*). Molecular structures and dimensions. Vol. A1. Utrecht. 1972.
13. K. OHKURA, S. KASHINO, and M. HAISA. Bull. Chem. Soc. Jpn. **45**, 2651 (1972).

Can. J. Chem. Downloaded from www.nrcresearchpress.com by 210.87.254.6 on 09/06/12
For personal use only.

# The thermal and photochemical decomposition of *cis*-1,2-cyclobutanedicarboxylic anhydride in the vapour phase[1]

R. A. BACK AND J. M. PARSONS

*Division of Chemistry, National Research Council of Canada, Ottawa, Ont., Canada K1A 0R6*

Received May 6, 1982

R. A. BACK and J. M. PARSONS. Can. J. Chem. **60**, 2692 (1982).

The thermal decomposition of *cis*-1,2-cyclobutanedicarboxylic anhydride (CBA) has been studied in a static system in the range 625–725 K. The major process observed was a homogeneous unimolecular decomposition to form ethylene and maleic anhydride, with first-order rate parameters $A = 1.14(\pm 0.1) \times 10^{14}$ s$^{-1}$ and $E = 55.1 \pm 1$ kcal/mol. A very minor decomposition channel yielding butadiene, $CO_2$, and CO was also observed, with $A = 8.4(\pm 0.1) \times 10^{14}$ s$^{-1}$ and $E = 67.5 \pm 1$ kcal/mol.

The decomposition induced by a pulsed $CO_2$ laser was also studied briefly; the same two decomposition channels were observed and their dependence on fluence and pressure examined.

The ultraviolet photolysis of CBA was also investigated between 210 and 365 nm. In addition to the products found in the thermal reaction, cyclobutene was also a major product, and product ratios were measured as a function of wavelength and added $CO_2$. Mechanisms in the three systems are discussed and compared.

R. A. BACK et J. M. PARSONS. Can. J. Chem. **60**, 2692 (1982).

On a étudié la décomposition thermique de l'anhydride cyclobutanedicarboxylique-1,2 *cis* (ACB) dans un système statique avec un intervalle de température allant de 625 à 725 K. Le processus principal observé est une décomposition unimoléculaire homogène qui conduit à l'éthylène et à l'anhydride maléique, avec des paramètres de vitesse d'ordre un de $A = 1{,}14(\pm 0{,}1) \times 10^{14}$ s$^{-1}$ et de $E = 55{,}1 \pm 1$ kcal/mol. On a également observé une voie très secondaire de décomposition qui conduit au butadiène, au $CO_2$ et au CO avec $A = 8{,}4(\pm 0{,}1) \times 10^{14}$ s$^{-1}$ et $E = 67{,}5$ kcal/mol.

On a également étudié brièvement la décomposition induite par un laser à impulsion de $CO_2$. On a observé les deux modes de décomposition et on a examiné l'effet de la fluence et de la pression sur ces voies de décomposition.

On a également étudié la photolyse dans l'ultraviolet du (ACB) entre 210 et 365 nm. En plus des produits trouvés dans la réaction thermique, le cyclobutane est également un produit principal et on mesure les rapports des produits en fonction de la longueur d'onde et du $CO_2$ ajouté. On discute et on compare les mécanismes de ces trois systèmes.

[Traduit par le journal]

## Introduction

There have been few quantitative studies of the thermal decomposition of cyclic anhydrides of dicarboxylic acids, and except for a brief survey of a few mercury-photosensitized reactions (1), their gas-phase photochemistry has also been neglected. In a recent investigation of maleic anhydride in this laboratory (2), it was concluded that both the thermal and photochemical decomposition in the gas phase followed a simple concerted unimolecular path,

[1] Maleic anhydride $\rightarrow C_2H_2 + CO_2 + CO$

with $E = 60.9$ kcal/mol and $A = 2.14 \times 10^{14}$ s$^{-1}$ for the thermal process. With *cis*-1,2-cyclobutanedicarboxylic anhydride (hereafter CBA), the analogous decomposition would yield cyclobutene, but there is also the possibility of a second reaction path, cleavage of the cyclobutane ring. Simple two-channel unimolecular decompositions can be useful probes of energy distributions in thermal and photochemical reactions (3, 4). The present paper describes the thermal decomposition of CBA, a brief study of the decomposition induced by a pulsed $CO_2$ laser, and the photochemical decomposition in the ultraviolet region. Some of the results have been briefly presented elsewhere (3).

[1]NRCC No. 20545.

## Experimental

The pyrolysis and uv photolysis were studied in simple static systems using apparatus and methods employed earlier with maleic anhydride (2). The uv light source was a Hg–Xe 1000 W lamp fitted with a monochromator. The infrared laser experiments were done in a cylindrical Pyrex vessel, 10 cm long and 4 cm in diameter, fitted with NaCl windows at each end. Radiation of 9.20 μm from a Lumonics pulsed $CO_2$ TEA laser (4) was used unfocussed at a fluence of ~ 0.7 J/cm$^2$, or passed through a 2 m f. l. Ge lens placed 1 m from the reaction cell to give a slightly converging beam with a fluence in the reaction cell about 4 times higher. The reaction cell in all experiments was heated to 125°C to permit an adequate vapor pressure of CBA. CBA was obtained from Aldrich with a stated purity of 96% with the parent acid the main impurity; since the latter is much less volatile than the anhydride, the purity of the vapor used in our experiments was probably better than 99%. No other impurities could be detected by gas chromatography.

## Results and discussion

### *The thermal decomposition*

The only important primary product volatile at room temperature was ethylene, presumably formed by cleavage of the cyclobutane ring:

0008-4042/82/212692-05$01.00/0

©1982 National Research Council of Canada/Conseil national de recherches du Canada

Can. J. Chem. Downloaded from www.nrcresearchpress.com by 210.87.254.40 on 09/06/12
For personal use only.

[2] 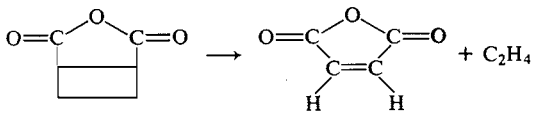

Maleic anhydride was not positively identified as a product, but formation of $C_2H_2$, $CO_2$, and CO as secondary products as the reaction progressed was good evidence for its formation (2).

The only other primary hydrocarbon product found in significant amounts was 1,3-butadiene, which varied from about 0.15 to 0.03% of the ethylene. Comparable yields of CO and $CO_2$ were also observed, and there seems little doubt that these products come from cleavage of the anhydride ring:

[3] 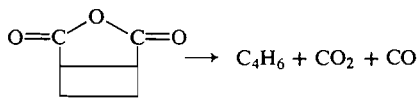

It is not clear whether cyclobutene is an intermediate, as its thermal isomerization to butadiene is fast enough at the reaction temperatures to preclude its detection (5).

Figure 1 shows Arrhenius plots of $k_2$, the first-order rate constant based on $C_2H_4$ formation, and $k_3/k_2$, given by $C_4H_6/C_2H_4$. No significant variation with pressure was observed within the rather narrow range of pressure employed (2–7 Torr), nor when the surface/volume ratio was increased by a factor of 9 in a packed vessel. Reactions [2] and [3] thus appear to be occurring as homogeneous unimolecular reactions, and Arrhenius parameters of $A_2 = 1.14\ (\pm 0.1) \times 10^{14}\ s^{-1}$, $E_2 = 55.1 \pm 1$ kcal/mol, $A_3 = 8.40\ (\pm 0.1) \times 10^{14}\ s^{-1}$, and $E_3 = 67.5 \pm 1$ kcal/mol can be estimated from the plots in Fig. 1.

Reaction [2] is appreciably slower, with a lower $A$ factor and higher $E$ than the analogous decompositions (5) of cyclobutanecarboxaldehyde ($A = 2.7 \times 10^{14}$, $E = 53.3$) and of cyclobutylmethyl ketone ($A = 3.4 \times 10^{14}$, $E = 54.5$), both of which have carbonyl groups adjacent to the cyclobutane ring. This may reflect constraints on the resonance stabilization of the biradical imposed by the presence of the anhydride ring.

The activation energy of reaction [3] is 6.6 kcal/mol higher than that for the analogous decomposition of maleic anhydride; this is somewhat surprising since reaction [3] is only 14.1 kcal/mol endothermic[2] (to yield cyclobutene) compared with

[2]Based on $\Delta H_f^0$ for maleic anhydride of −96.8 kcal/mol and $\Delta H_f^0$ for CBA of −98.6 (based on additivity relations), both in the vapour phase (6, 7).

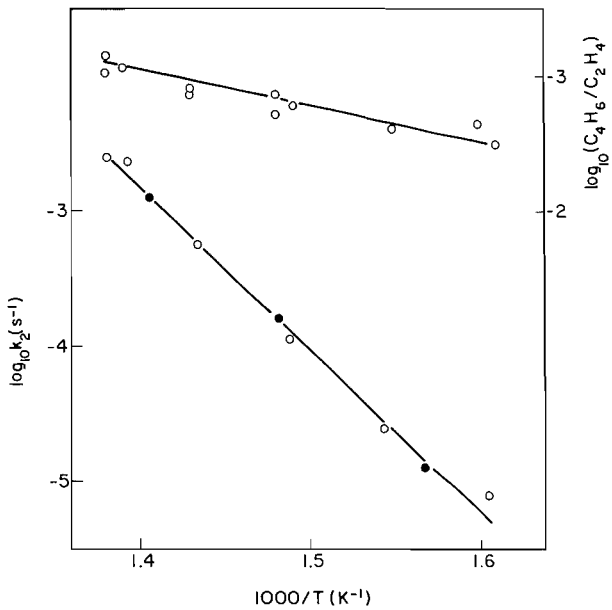


FIG. 1. Arrhenius plots for $k_2$ (bottom) and $k_3/k_2$ (top) for the thermal decomposition of CBA. Solid points are for packed reaction vessel.

an endothermicity of 30.5 for reaction [1]. The higher activation energy is partially compensated by a higher frequency factor, about 4 times larger than for maleic anhydride. The energy required to open the almost strain-free anhydride ring (5) may be estimated as at least 75 kcal/mol, indicating that reaction [3], like reaction [1], probably proceeds by a concerted rather than a biradical mechanism, although the frequency factor is somewhat high. The rather high barrier to reaction may reflect the considerable distortion needed in the transition state for optimum incipient $\pi$ bond formation in the cyclobutene product, which would require the two rings to lie normal to one another and the H atoms in the plane of the cyclobutane ring. Much less distortion would be required in the analogous decomposition of maleic anhydride.

The activation energy of reaction [2], and the $A$-factor, are compatible with a biradical process, but as with other cyclobutane derivatives, in the absence of firm evidence one way or the other, a concerted mechanism cannot be ruled out.

*The infrared multiphoton decomposition*

Products were the same as in the thermal reaction, with relatively more butadiene, between 0.1 and 1% of the ethylene. The extent of decomposition, expressed as a probability of decomposition in a single pulse of a molecule in the laser beam, is

Can. J. Chem. Downloaded from www.nrcresearchpress.com by 210.87.254.40 on 09/06/12
For personal use only.

Can. J. Chem. Downloaded from www.nrcresearchpress.com by 210.87.254.40 on 09/06/12
For personal use only.

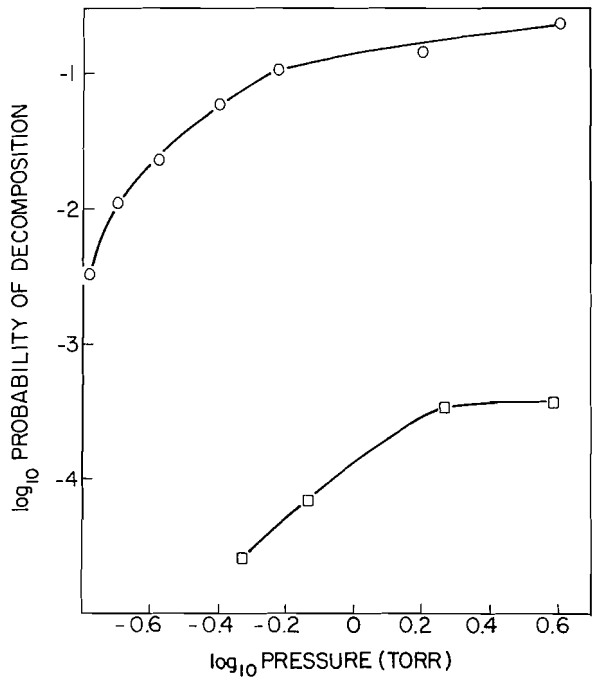


FIG. 2. log–log plot of the probability of decomposition during a single laser pulse vs. the pressure of CBA. □, unfocussed beam; ○, converging beam with fluence increased by a factor of 4.

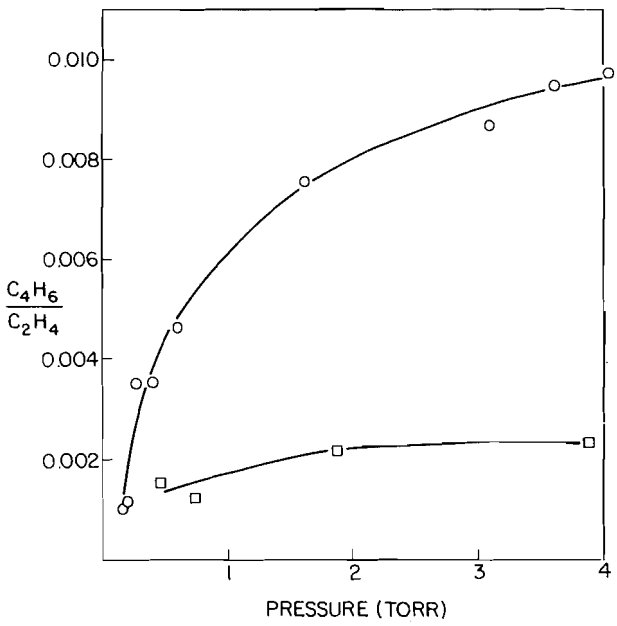


FIG. 3. Product ratio vs. pressure of CBA in the $CO_2$ laser induced decomposition. □, unfocussed beam; ○, converging beam with fluence increased by a factor of 4.

shown in Fig. 2 in a log–log plot as a function of pressure for the two fluences employed. A strong (~ 5th-power) dependence on fluence is evident, and at both fluences the probability of decomposition fell off sharply with decreasing pressure. Figure 3 shows the variation with pressure of the ratio $C_4H_6/C_2H_4$ for the same experiments. The ratio at the highest pressures corresponds to effective "temperatures" of decomposition of 945 and 778 K at the high and low fluences respectively. At both fluences the $C_4H_6/C_2H_4$ ratio falls markedly with decreasing pressure, the decrease being more pronounced at the higher fluence. These trends are similar to those observed recently in the decomposition of cyclobutanone (8) and probably have similar causes; the small yields of $C_4H_6$ make the measurements too inaccurate to extend to the lower fluences and lower pressures required to see whether the similarity in the two systems is significant.

*Photolysis in the ultraviolet*

Figure 4 shows the absorption spectrum of CBA vapor measured at 3.02 Torr at 145°C in a cell 3.7 m long. The observed absorption almost certainly arises from a $\pi^* \leftarrow n$ transition. By analogy with the maleic anhydride spectrum (2) the broad absorption with $\varepsilon_{max} = 60$ at 230 nm and the very weak

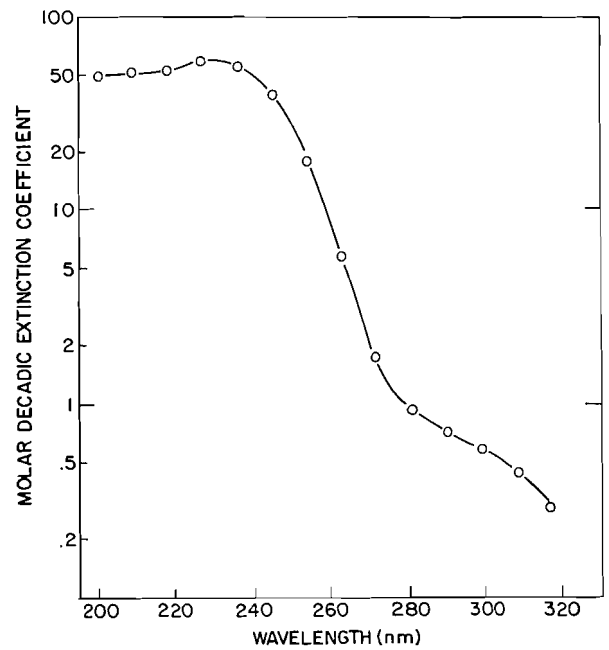


FIG. 4. Ultraviolet absorption spectrum of CBA vapor, measured at 3.02 Torr and 145°C, in units of $cm^{-1}\ M^{-1}$.

shoulder around 300 nm might be assigned to the $\pi^* \leftarrow n^+$ and $\pi^* \leftarrow n^-$ transitions respectively. However, the separation of 1.33 eV is much larger than might be expected from the photoelectric spectrum of succinic anhydride which shows a

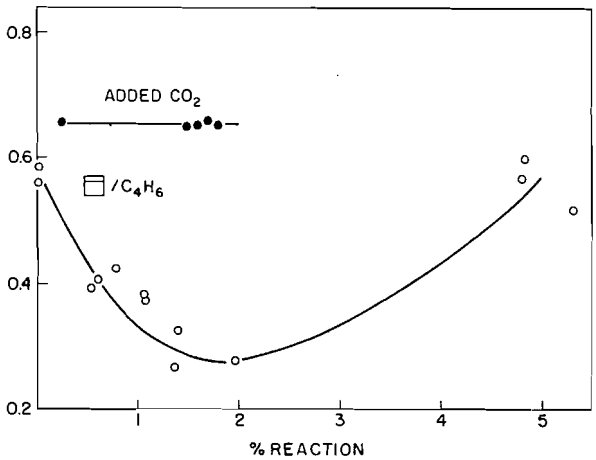


FIG. 5. Variation in product ratio with % reaction in the photolysis of CBA at 240 nm. Solid points are with added $CO_2$ at pressures of 10–100 Torr.

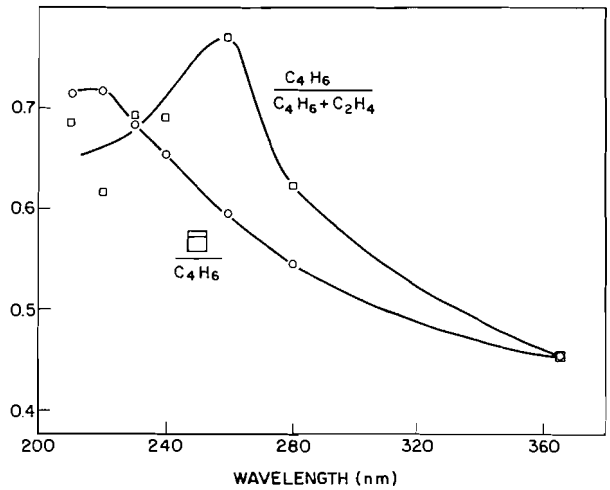


FIG. 6. Product ratios vs. wavelength in the photolysis of CBA with added $CO_2$.

splitting of 0.81 eV, and it is difficult to see why the transition at 300 nm should be so much weaker. No structure was evident anywhere in the spectrum.

Ethylene and butadiene again were products of the photodecomposition, and cyclobutene was also observed. The $C_4$ hydrocarbons were relatively much more important than in the thermal reaction, with the ratio (total $C_4H_6$)/$C_2H_4$ ranging from 0.4 to 3.0, where total $C_4H_6$ = 1,3-butadiene + cyclobutene. The yield of $C_2H_4$ was a linear function of photolysis time up to at least 5% conversion, but cyclobutene and butadiene have an unusual dependence on time (or % reaction) shown in Fig. 5 for the photolysis at 240 nm. The ratio cyclobutene/(total $C_4H_6$) fell sharply from a value of about 0.6 at the shortest photolysis time (7 s), reached a minimum of about 0.3 after 1 or 2% reaction, and finally rose again to about its initial value. The ratio (total $C_4H_6$)/(total $C_4H_6$ + $C_2H_4$) showed a much smaller change; it appeared to rise slightly, then fall again, over the same range of photolysis times. Similar behaviour was observed at other wavelengths. The cause of these effects is obscure;[3] it was discovered, however, that they essentially disappeared on the addition of $CO_2$ at pressures between 10 and 100 Torr.

[3]To explain the observations, there must be a rapid secondary isomerization of cyclobutene to butadiene (which is then reversed at longer photolysis times) and which is eliminated by the addition of $CO_2$. Gas phase thermal isomerization is too slow at 125°C; a surface process might be invoked if it could be inhibited by $CO_2$ adsorption on active sites. An isomerization of cyclobutene photosensitized by the maleic anhydride product building up in the system, which at 240 nm absorbs light much more strongly than CBA, and which could be quenched by $CO_2$, is another possibility. It was not thought useful to pursue these effects further in the present study.

For the photolysis at 240 nm under these conditions, values of cyclobutene/(total $C_4H_6$) = 0.65 and (total $C_4H_6$)/(total $C_4H_6$ + $C_2H_4$) = 0.69 were obtained, independent of $CO_2$ pressure, CBA pressure, and photolysis time. Similar measurements were made at other wavelengths from 210 to 366 nm, and the product ratios obtained are shown in Fig. 6.

The lack of pressure dependence of the product ratios in Fig. 6, and of the yield of decomposition, points to a short-lived excited state that decomposes before much stabilization by collision. Since there is no reason to expect an excited $\pi^* \leftarrow$ n state of a carbonyl compound to be dissociative itself, there must be fast internal conversion to high vibrational levels of the ground state which then rapidly dissociates.

The ratio (total $C_4H_6$)/(total $C_4H_6$ + $C_2H_4$) increases with increasing photon energy (Fig. 6) reaching a maximum of about 0.76 at 260 nm, then declines slightly. The frequency factors for reactions [2] and [3] in the thermal reaction would predict a maximum value of 0.88 for this ratio at infinite temperature. The observed values are probably compatable with a statistical decomposition of a highly excited ground-state molecule, the photon energy at 260 nm of 110 kcal/mol corresponding to excess energies of 55 and 42 kcal/mol for reactions [2] and [3] respectively. The slight decline in the product ratios at shorter wavelengths might suggest a different decomposition mechanism, favoring reaction [2], for photolysis in the $\pi^* \leftarrow \pi$ transition which probably begins to underlie the $\pi^* \leftarrow$ n transition at these wavelengths (Fig. 4).

Can. J. Chem. Downloaded from www.nrcresearchpress.com by 210.87.254.40 on 09/06/12
For personal use only.

The ratio cyclobutene/(total $C_4H_6$) does *not* correspond to an equilibrium between cyclobutene and butadiene since at infinite temperature a maximum value of only 0.14 is predicted from the equilibrium constant at infinite temperature (5). It thus appears that cyclobutene is a primary product of a decomposition analogous to that of maleic anhydride. It also appears that butadiene is *not* formed by subsequent decomposition of vibrationally excited cyclobutene, since some pressure dependence would then have been expected, and a decrease in cyclobutene relative to butadiene with decreasing wavelength; it seems more probable that the two hydrocarbons are primary products of parallel unimolecular reactions. These may be the same reactions which occurred in the thermal decomposition, in which a concerted mechanism was favored on energetic grounds, and in which it was impossible to say whether butadiene, or cyclobutene, or both, were primary products, since any cyclobutene formed would have isomerized thermally to butadiene before analysis. The higher energy available in the photolysis, however, would permit biradical formation by opening of the anhydride ring, with subsequent decomposition to CO, $CO_2$, and cyclobutene or butadiene, and such a biradical mechanism may well be operative.

1. I. S. KRULL and D. R. ARNOLD. Tetrahedron Lett. **50**, 4349 (1969).
2. R. A. BACK and J. M. PARSONS. Can. J. Chem. **59**, 1342 (1981).
3. R. A. BACK. J. Photochem. **17**, 233 (1981).
4. M. H. BACK and R. A. BACK. Can. J. Chem. **57**, 1511 (1979).
5. S. W. BENSON and H. E. O'NEAL. Kinetic data on gas phase unimolecular reactions. NSRDS-NBS 21, Washington, DC. 1970.
6. Handbook of chemistry and physics. 62nd ed. CRC Press Inc. Boca Raton, Florida. 1981–1982. Heats of combustion, vaporization and fusion of organic compounds.
7. R. C. WILHOIT and D. SHIAO. J. Chem. Eng. Data, **9**, 595 (1964).
8. R. A. BACK. Can. J. Chem. **60**, 2542 (1982).

Can. J. Chem. Downloaded from www.nrcresearchpress.com by 210.87.254.40 on 09/06/12
For personal use only.

# Limiting activity coefficients in dilute solutions of nonelectrolytes. I. Determination for polar–nonpolar binary mixtures by a novel apparatus, and a solubility-parameter treatment of results

ETELA MILANOVÁ AND GENILLE C. B. CAVE

*Department of Chemistry, McGill University, Montreal, P.Q., Canada H3A 2K6*

Received January 26, 1982

ETELA MILANOVÁ and GENILLE C. B. CAVE. Can. J. Chem. **60**, 2697 (1982).

The activity coefficients of several solutes in dilute binary solutions of nonelectrolytes were determined at 20°C from vapor–liquid equilibria in a novel static equilibration apparatus, by gas-chromatographic analysis of the equilibrium vapor phase. The solutes were nitromethane, nitroethane, 1-nitropropane, 2-nitropropane, acetonitrile, propionitrile, ethyl acetate, and *n*-butyl acetate in *n*-heptane and in benzene as solvents, and also carbon tetrachloride as solute in each of the above-listed polar compounds as the solvent.

The modifications by Weimer and Prausnitz and by Blanks and Prausnitz to the Scatchard–Hildebrand equation in order to accommodate binary mixtures containing a polar component were tested by using the values found in the present work for the limiting activity coefficients of these solutes. In addition, it was found that the ratio of the dipole – induced dipole interaction parameter for polar solutes in the two nonpolar solvents was nearly constant.

Three methods for evaluating the dispersion contribution to the solubility parameter of a polar compound were considered.

ETELA MILANOVÁ et GENILLE C. B. CAVE. Can. J. Chem. **60**, 2697 (1982).

Utilisant un nouvel appareil d'équilibration statique faisant appel à l'analyse par chromatographie en phase gazeuse, des phases vapeur à l'équilibre, on a déterminé les coefficients d'activité de plusieurs solutés dans des solutions binaires diluées de nonélectrolytes à 20°C. Les solutés sont le nitrométhane, le nitroéthane, le nitro-1 propane, le nitro-2 propane, l'acétonitrile, le propionitrile, l'acétate d'éthyle et l'acétate de *n*-butyle dans le *n*-heptane et dans le benzène comme solvants. Le tétrachlorure de carbone a été utilisé également comme soluté dans les composés polaires mentionnés ci-dessus considérés comme solvants.

Utilisant les valeurs trouvées dans ce travail comme coefficients limites d'activité de ces solvants, on a vérifié les modifications de Weimer et Prausnitz ainsi que celles de Blancks et Prausnitz apportées à l'équation de Scatchard–Hildebrand dans le but d'accomoder les mélanges binaires contenant un composant polaire. De plus on a trouvé que le rapport du paramètre d'interaction dipôle – dipôle induit pour les solutés polaires dans les deux solvants non polaires est presque constant. On a considéré trois méthodes d'évaluation de la contribution de la dispersion au paramètre de solubilité d'un composé polaire.

[Traduit par le journal]

## Introduction

Limiting activity coefficients for liquid nonelectrolyte systems are useful in analytical chemistry and in engineering design and practices. In addition, these values for judiciously chosen binary mixtures permit further testing of already proposed empirical and theoretical concepts or solution models for simple systems, or their extension or modification to accommodate new data.

The present study has two purposes. First, activity coefficients of several solutes in dilute binary solutions of nonelectrolytes were measured from vapor–liquid equilibria at 20°C for several polar–nonpolar systems, and the limiting activity coefficients obtained by extrapolation. For these measurements, a novel apparatus was designed for use with a gas chromatograph having a flame-ionization detector, which made possible the accurate measurement of vapor concentrations down to much more dilute solutions than by conventional methods. As a result, the extrapolation to infinite dilution was short. Second, the values found for the limiting activity coefficients were used to test two correlations involving a dipole – induced dipole interaction parameter ($\psi_{12}$), reported by Prausnitz and co-workers (1, 2). In addition, the ratio of these parameters for each of several polar solutes in two nonpolar solvents is examined.

An extensive literature exists on experimental methods for obtaining the data necessary to calculate activity coefficients for liquid binary systems of nonelectrolytes. The two principal classes of method have been the use of equilibrium stills, and the measurement of the specific retention volume of the solute in a gas-chromatographic column coated with the solvent, which must be relatively nonvolatile. Equilibrium stills include distillation, circulation, dew- and bubble-point, static and flow types. Hála *et al.* (3) have reviewed single-stage devices and list their advantages and disadvantages. Isothermal distillation is the classical method (4), but it may be subject to serious errors (5). Circulation stills may introduce uncertainty as to whether the measured temperature and compositions are for equilibrium conditions. In addition, most data obtained from stills are for liquid concentrations relatively far from infinite

0008-4042/82/212697-10$01.00/0

©1982 National Research Council of Canada/Conseil national de recherches du Canada

Can. J. Chem. Downloaded from www.nrcresearchpress.com by 210.87.254.105 on 09/06/12
For personal use only.

Can. J. Chem. Downloaded from www.nrcresearchpress.com by 210.87.254.105 on 09/06/12
For personal use only.

dilution. The pressure (or temperature) vs. composition curves then have curvatures that are too ill-defined to permit calculation, from the slopes, of reliable values for activity coefficients at infinite dilution. The design of a static distillation apparatus is somewhat complex, and sample withdrawal can cause difficulties.

In a simple static apparatus containing the solution, a sample of the equilibrium vapor for analysis is removed either by a syringe (6, 7), or by running mercury into the vessel and collecting the displaced vapor. In all cases it is assumed that equilibrium is not disturbed by the sample withdrawal. Wichterle and Boubliková (8) avoided that uncertainty by fusing an ungreased double-loop stopcock to the neck of the equilibration vessel. One loop comprized part of the vapor space over the solution; the other carried the carrier gas of a gas chromatograph. By a 180° turn of the stopcock the equilibrium vapor was swept into the gas chromatograph for analysis. However, this design has not been widely used, possibly because the fabrication of a greaseless stopcock leakproof at carrier-gas pressures is difficult, and the stopcock is likely to require periodic and time-consuming maintenance.

In view of the difficulties or uncertainties with published apparatus designs, and the need to measure very low concentrations of a vapor component in order to obtain limiting activity coefficients, a new design was conceived and constructed for the present work. It consisted of a static equilibrium cell capped by a rotatable head. This head was fitted with three calibrated vapor-sampling loops that could be sequentially filled with equilibrium vapor over the solution, then switched directly into the carrier-gas stream of a gas chromatograph. This design made possible repetitive measurements of the concentrations of components present in a true sample of the equilibrium vapor over a multicomponent liquid mixture, as does that of Wichterle and Boubliková (8).

Limiting activity coefficients (hereafter abbreviated $\gamma_2^\infty$ for the solute) were found in the present work for nitromethane, nitroethane, 1-nitropropane, 2-nitropropane, acetonitrile, propionitrile, ethyl acetate, and *n*-butyl acetate in *n*-heptane and in benzene as solvents, and also for carbon tetrachloride in each of the above-listed polar compounds as solvents.

## Experimental

*Gas chromatograph*

A Pye gas chromatograph, Series 104 with two exchangeable detector heads, was used. Helium was the carrier gas for the thermal-conductivity detector, and nitrogen for the flame-ionization detector. Packed columns 1/4-in. or 1/8-in. o.d. and lengths 2–5 ft were used in a temperature-controlled oven compartment, with separate temperature control for the sample-injection port. The chromatograms were recorded with a Sargent SR one-millivolt recorder, and the peak areas were measured with an attached disc-area integrator (Model 204, Disc Instruments, Inc.).

*Static liquid–vapor equilibration apparatus*

The liquid–vapor equilibration apparatus was designed to have a gas-chromatographic sampling loop of accurately known volume as an integral part of the vapor space above the liquid. Thus, the apparatus permitted the direct measurement by gas chromatography of the concentrations of minor components in a sample of the equilibrium vapor over a liquid mixture.

The apparatus consisted of a glass cell (Fig. 1) capped by a novel vapor-sampling valve (Fig. 2). Constructional details are reported elsewhere (9*a*). Briefly, the cell and valve could be connected together by a leak-free coupling, the components of which consisted of a threaded brass coupling, a silicone-greased Viton O-ring, and a thin circular Teflon washer. The lower face *F* of the valve (component *A* in Fig. 2*a*) was machined to leave a circular V-projection (*L*) which bit into the Teflon washer to ensure the gas-tight fit between valve and cell.

The valve is shown as sectional drawings in Fig. 2; *a* and *b* are in elevation 60° apart, and *c* is in plan. Components included an inverted cup (*A*) of stainless steel fixed to a disc (*I*) of Rulon, and an upper rotatable disc (*B*) of stainless steel. These components could be tightened to an appropriate tension by disc springs and a locknut on spindle *N*. Of the six 1/4-in. holes drilled vertically from the upper surface of *A* only one diagonal pair was drilled completely through *A*, to provide access to the glass cell. The other four holes were sunk only to corresponding horizontal holes in *A*. Stainless steel tubing welded to each of these horizontal holes, and fitted with a Swagelock nut and ferrule (*H*, Fig. 2*a*), provided for connections to carrier gas and vacuum.

Six holes through Rulon disc *I* and disc *B* were aligned with those in cup *A*. A calibrated sampling loop of carefully cleaned copper tubing was silver-welded into each diagonal pair of holes in *B*.

*Materials*

All chemicals were further purified by conventional methods that are described elsewhere (9*b*). Except for benzene, which was purified by fractional crystallization, the final purification step was fractional distillation under nitrogen, with the middle third being kept. Each product was then stored over molecular sieves 3A in a brown bottle. Care was taken to ensure dry products. The water content of the stored acetone was 0.007%.

Quantitative gas-chromatographic analysis of the final products indicated that the nitro compounds were 99.5 mol% pure with homologs as the major impurities, *n*-hexane was 99.5 mol% and *n*-heptane 99.8 mol% with aliphatic hydrocarbons the major impurities, and the others were 99.9 mol% or better. Densities at 21°C agreed well with literature values (10).

*Procedure*

Procedural details are reported elsewhere (9*c*). Briefly, a 30–50 mL sample of the liquid for study, prepared by weight in the case of mixtures, was placed in the glass cell. An aliquot was reserved for calibration purposes. After attaching the valve, with one of its sampling loops an integral part of the vapor space, the liquid was frozen and the apparatus evacuated. After thawing, the cell was immersed up to nut *A* (Fig. 1) in a water thermostat at 20.00 ± 0.05°C, with the room temperature at 24 ± 1°C. The sample was stirred continuously by a Teflon-coated

Can. J. Chem. Downloaded from www.nrcresearchpress.com by 210.87.254.105 on 09/06/12
For personal use only.

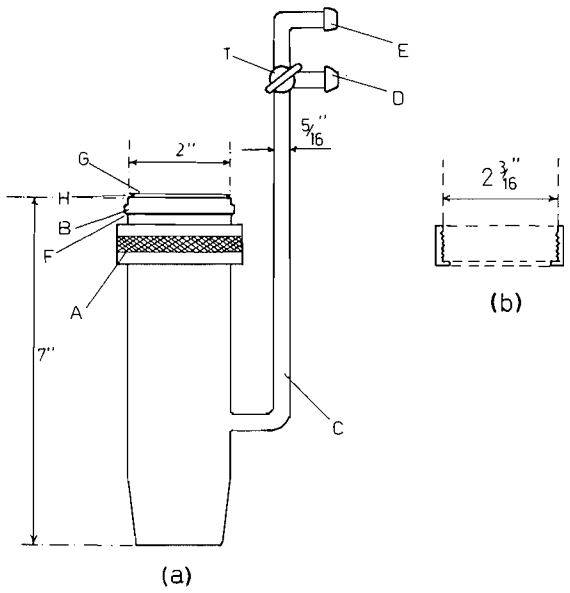


FIG. 1. Schematic diagram of the glass equilibration cell (*a*), and a cut-away view of the brass nut (*b*): *A*, brass nut with inner thread; *B*, glass collar; *C*, side arm; *D* and *E*, outlet tubes with semi-ball joints; *F*, Viton O-ring; *G*, Teflon washer with projection; *H*, T three-way glass stopcock with a "T" plug.

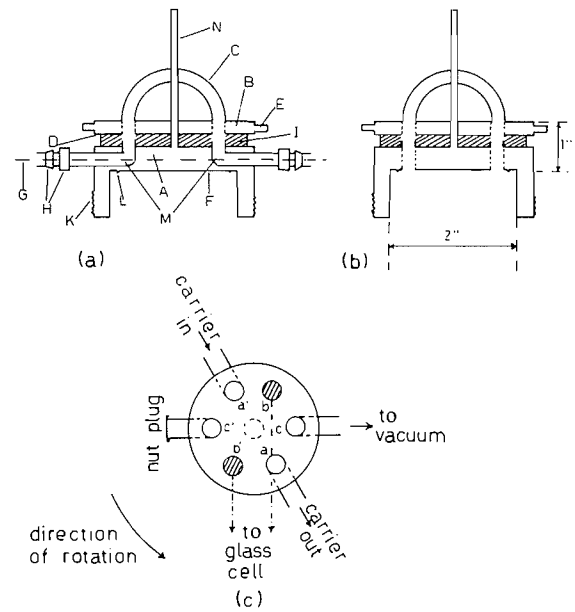


FIG. 2. Gas-chromatographic sampling valve; (*a*), cross-section through "inject" or "by-pass" positions; (*b*), cross-section through "fill" position; (*c*), functional positions of the three sampling loops: *A*, inverted stainless steel cylindrical cup with lower face *F* and narrow *V* projection *L*; *B*, stainless steel disc with flat face *D* and pins *H* for a lever; *I*, Rulon disc; *K*, male thread on cup *A* to engage brass nut in Fig. 1; *G*, depth of four holes in cup *A* (see text); *M*, horizontal holes in *A*; *H*, Swagelock female nut and fitting ferrule; *C*, gas-sampling loop; *N*, spindle.

TABLE 1. Calibration of the sampling loops by two independent methods

| Loop No. | Mean volumes and standard deviations* From water calibration (mL) | From vapor calibration (mL) |
|---|---|---|
| 1 | 1.857±0.0074 | 1.870±0.0085 |
| 2 | 2.088±0.0029 | 2.113±0.0167 |
| 3 | 2.536±0.0042 | 2.534±0.0109 |

*$n = 3$.

magnetic bar. Liquid–vapor equilibrium was established within 30 min.

The equilibrium vapor in the sampling loop *bb'* (Fig. 2*c*) was then swept into the gas chromatograph by rotating disc *B* (Fig. 2) anticlockwise by 60°. Simultaneously, evacuated loop *cc'* became the sampling loop for another vapor sample. In practice, several repetitive samples were taken, with the first one usually being rejected.

Between repetitive vapor samples, calibration standards in the form of measured volumes of the reserved part of the liquid sample were injected into the gas chromatograph via a separate injection port, by a 10-μL Hamilton syringe (No. 710N). This syringe was found to deliver correct to 1%, by a spectrophotometric determination of the benzene it dispensed into *n*-heptane diluted to volume. Further, the measured vapor concentrations over several pure liquids agreed with literature values when the calibration curve used was prepared from liquid samples injected with this syringe.

*Calibration of the three sampling loops*

Prior to the copper loops being welded to the base of disc *B* (Fig. 2*a*) their volumes were measured by weighing them empty, then filled with water. A very small increment in the effective sample volume occurred because the weld was not flush with the face of disc *B*, but it was calculated and added to the loop volume. The corrected volumes are in column 2 of Table 1.

A second, preferred method was to measure the equilibrium vapor concentrations over four pure solvents — benzene, *n*-hexane, carbon tetrachloride, and acetone — by using the above-described equilibration apparatus and procedure, and a thermal conductivity cell as the glc detector. The pure liquids were injected for the calibration graphs. From these data and the known second virial coefficients (11) and reported values (10) of the vapor pressures of the pure liquids at 20°C, the volume of each loop was calculated from the equation of state, with due allowance for the thermal expansion of the equilibrium vapor from 20°C in the cell to the ambient temperature (about 24°C) in the loop. The mean values are in column 3 of Table 1. They agree well with those in column 2, which is evidence of the absence of any significant deficiency in the proposed apparatus and procedure.

*Reliability of the equilibration apparatus and procedure*

The reliability of the apparatus and procedure was confirmed by vapor-concentration measurements of both components of the benzene–*n*-hexane system over the entire concentration range, by using a thermal conductivity detector. From these data the activity coefficients of both liquid components at 20°C were calculated as described below, with the pure liquid component being taken as the standard state. Our results are in Table 2. They are compared in Fig. 3 with those at 25°C of Smith and Robinson (12) and with those at 24.98°C of Jain *et al.* (13). As further proof of agreement of all these data, an

TABLE 2. Rational activity coefficients ($\gamma$) of each component in the systems *n*-hexane–benzene and acetone–benzene, at 20°C*

| Mole fraction of *n*-hexane | $\gamma$ | | Mole fraction of acetone | $\gamma$ | |
|---|---|---|---|---|---|
| | *n*-Hexane | Benzene | | Acetone | Benzene |
| 0.0496 | 1.991 | 1.007 | 0.0804 | 1.480 | 1.012 |
| 0.0654 | 1.872 | 1.006 | 0.0834 | 1.441 | 1.024 |
| 0.1058 | 1.778 | 1.013 | 0.0847 | 1.448 | 1.001 |
| 0.1906 | 1.542 | 1.030 | 0.1414 | 1.345 | 1.024 |
| 0.3091 | 1.340 | 1.099 | 0.1641 | 1.318 | 1.021 |
| 0.4337 | 1.187 | 1.181 | 0.2968 | 1.192 | 1.060 |
| 0.5628 | 1.105 | 1.291 | 0.3773 | 1.150 | 1.075 |
| 0.6946 | 1.036 | 1.371 | 0.4772 | 1.104 | 1.134 |
| 0.8394 | 1.014 | 1.543 | 0.5497 | 1.063 | 1.163 |
| 0.9032 | 1.011 | 1.595 | 0.5548 | 1.060 | — |
| 0.9301 | 1.007 | 1.629 | 0.6998 | 1.021 | 1.248 |
| | | | 0.7826 | 1.011 | 1.350 |
| | | | 0.8073 | 1.004 | 1.333 |

*Each tabulated value of $\gamma$ is the grand mean computed by permitted pooling of the means for the three sample loops. For each loop there were 2–3 replicates of sample and of pure liquid. Variances were computed with higher terms being neglected. Homogeneity of these variances allowed pooling, to give 0.014 as the pooled standard deviation of each grand mean.

area-consistency test was carried out as devised by Redlich and Kister and by Herington and described by Ellis (14).

Further evidence of the method's reliability was our value of 1.15 ± 0.01 for the limiting activity coefficient of carbon tetrachloride in benzene at 20°C; a flame-ionization detector was used for the necessary measurements in very dilute solutions. This value compares favorably with 1.12 found for 40°C when Ellis and Jonah (15) applied an extrapolation procedure to the data of Scatchard *et al.* (16). Only a small temperature dependence of this limiting activity coefficient is expected in view of the low positive enthalpy of mixing.

Vapor concentrations of both components of the acetone–benzene system were also measured over the entire concentration range, and the activity coefficients of both liquid components at 20°C calculated as described below. Our results are in Table 2. They agree well with those of Brown and Smith (17) who used a circulation still under isothermal conditions, but not with those of Campbell *et al.* (18) and Litvinov (19), who obtained decidedly higher results by using bubble saturators. Brown and Smith (20) reported a value of 38 cal mol$^{-1}$ for the enthalpy of mixing of an equimolar mixture of acetone and benzene. Therefore, the temperature differences 20°C, 25°C, 45°C could not account for those higher values.

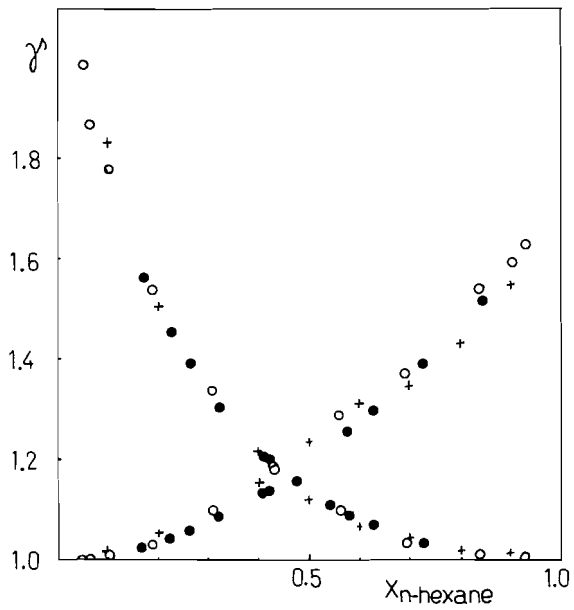


FIG. 3. Activity coefficients ($\gamma$) of *n*-hexane and benzene in their binary mixtures as a function of the mole fraction ($x$) of *n*-hexane; ○, this work (20°C); +, Smith and Robinson (12) (25°C); ●, Jain, Gupta, and Lark (13) (24.98°C).

## Results

Limiting activity coefficients were evaluated from equilibrium vapor concentrations over dilute solutions of the polar solutes in *n*-heptane and in benzene as solvents, and for carbon tetrachloride as solute in each of the polar compounds as solvents. Generally, the range of solute concentrations was 0.001–0.01 mole fraction. The standard state of the solute was the pure liquid at 20°C.

The activity coefficients of the solutes were calculated first without correction for nonideality of the vapor phase, from the usual relationship $\gamma_2 = C_2/x_2C_{02}$. Here $C_2$ is the molar concentration of solute in the equilibrium vapor over the binary solution, obtained from the moles in the known volume of the gas-chromatographic sampling loop; $x_2$ is the known mole fraction of the solute in the equilibrium binary liquid, a correction having been made to the known initial mole fraction, for loss of solute to the vapor phase; and $C_{02}$ is the molar concentration of solute in the equilibrium vapor over the pure liquid solute, obtained also from the gas-chromatographic analysis of the equilibrium vapor of pure solute.

Since replicates both of the binary solution and

Can. J. Chem. Downloaded from www.nrcresearchpress.com by 210.87.254.105 on 09/06/12
For personal use only.

TABLE 3. Limiting activity coefficients of some polar solutes in *n*-heptane and in benzene at 20°C

| Solute | In *n*-heptane | | In benzene | | $-B_{22}$‡ $\left(\frac{mL}{mol} \times 10^{-3}\right)$ |
|---|---|---|---|---|---|
| | Mean value* | sd† | Mean value* | sd† | |
| Nitromethane | 48.19 | 0.89 | 3.570 | 0.083 | 4.35 |
| Nitroethane | 25.37 | 0.48 | 2.238 | 0.034 | 5.50 |
| 1-Nitropropane | 16.13 | 0.21 | 1.964 | 0.041 | 5.90 |
| 2-Nitropropane | 12.73 | 0.22 | 1.719 | 0.027 | 5.10 |
| Acetonitrile | 41.22 | 0.50 | 3.307 | 0.013 | 6.70 |
| Propionitrile | 23.76 | 0.38 | 2.261 | 0.018 | 7.40 |
| Ethyl acetate | 3.671 | 0.031 | 1.143 | 0.019 | 2.49 |
| *n*-Butyl acetate | 2.808 | 0.028 | ≈1.04 | | 3.70 |

*Corrected for vapor imperfections.
†sd means standard deviation, obtained from the "Linfit" computations based on 5 to 7 points in each case.
‡$B_{11}$ for *n*-heptane = −2750, for benzene = −1506 mL mol$^{-1}$. $B_{22}$ for nitromethane, acetonitrile, and ethyl acetate are measured values (11), for the other four solutes they are our estimates.

the calibrating solution were always run, mean values and standard deviations could be computed for each activity coefficient by making use of the well-known relationship for the propagation of errors. Then for each binary mixture the mean activity coefficient and its standard deviation were plotted as a function of mole function $x_2$ of solute. In each case the linearity of the graph was visually evident over the mole fraction range 0.001–0.01 used. Further, over this concentration range the standard deviations were homogeneous. Then for each graph a straight line was fitted by using a subroutine "Linfit" with an unweighted mode. Therefrom, the values of the intercepts $\gamma_2^\infty$ at $x_2 = 0$ and their standard deviations were found. More specific details of the full statistical treatment and also all the basic data are given elsewhere (9).

Each value of $\gamma_2^\infty$ was then corrected for imperfections in the equilibrium vapor phases, as follows. Corrected activity coefficients ($\gamma_2^\infty$) were computed for each binary system by using [1].

$$[1] \quad \ln \gamma_2 = \ln \frac{C_2}{x_2 C_{02}} + 2B_{22}(C_2 - C_{02}) + 2B_{12}C_1$$

where $C_1$ is the solvent concentration in the vapor; $B_{22}$ and $B_{12}$ are the second virial coefficients for pure solute and the mixture respectively. The value of $B_{12}$ was approximated by using the formula $B_{12} = \frac{1}{2}(B_{11} + B_{22})$.

For the calculation, the first term on the right-hand side of [1] was the uncorrected value of $\gamma_2^\infty$, $C_2$ in the $B_{22}$ term was zero, and $C_1$ in the $B_{12}$ term was the vapor concentration above pure solvent. These corrected values of $\gamma_2^\infty$ and their standard deviations are entered in Tables 3 and 4. Most of the corrections amounted to about 1% of the uncorrected values.

The values given by Dymond and Smith (11) were used for $B_{22}$, and are in column 6 of Table 3. For nitroethane, 1-nitropropane, 2-nitropropane, propionitrile, and *n*-butyl acetate literature values were unavailable. They were estimated from an original empirical relationship which was found to apply to some 25 polar and nonpolar liquids tried. Details are reported elsewhere (9*d*). Briefly, when known virial coefficients at 340 K of several homologous series of both polar and nonpolar liquids were plotted against their molar energies of vaporization at their boiling points a family of curves was obtained, one for each homologous series. Values of $B_{22}$ for the above-noted five components were then read from the appropriate curves. To convert them to 298 K, an extrapolation procedure was used based on the general pattern of the known temperature-dependence of several homologous series of polar compounds.

TABLE 4. Limiting activity coefficients of carbon tetrachloride in several polar solvents at 20°C

| Solvent | Mean value* | sd† |
|---|---|---|
| Nitromethane | 9.591 | 0.054 |
| Nitroethane | 3.350 | 0.023 |
| 1-Nitropropane | 2.250 | 0.024 |
| 2-Nitropropane | 2.106 | 0.013 |
| Acetonitrile | 6.605 | 0.045 |
| Propionitrile | 2.896 | 0.020 |
| Ethyl acetate | 1.274 | 0.008 |
| *n*-Butyl acetate | 0.943 | 0.019 |

*Corrected for vapor imperfections.
†See Table 3. $B_{11}$ for carbon tetrachloride = −1603 mL mol$^{-1}$.

## Discussion of results

The Scatchard–Hildebrand equation for the energy of mixing for a binary nonpolar solution is

$$[2] \quad \Delta E = \phi_1\phi_2 (x_1V_1 + x_2V_2) (c_{11} + c_{22} - 2c_{12})$$

Can. J. Chem. Downloaded from www.nrcresearchpress.com by 210.87.254.105 on 09/06/12
For personal use only.

TABLE 5. Values of $k$ in the Weimer–Prausnitz correlation $\psi_{12} = k\,{}^{p}\delta_1{}^2$ *

| Solute(s) | Solvent(s) | $k$ | Source |
|---|---|---|---|
| Polar | $n$-Heptane | 0.250 | This work (Fig. 4) |
| Polar | Benzene | 0.452 | This work (Fig. 4) |
| $CCl_4$ | Polar | 0.437 | This work (Fig. 5) |
| Polar | Octadecane | 0.251 | Ref. 21 |
| Polar | Benzyl diphenyl | 0.433 | Ref. 21 |
| Saturated hydrocarbons | Polar | 0.396 | Ref. 1 |
| 1-Pentene | Polar | 0.415 | Ref. 1 |
| Benzene | Polar | 0.450 | Ref. 1 |

*Subscript 1 denotes solvent.

where $\phi$ is the volume fraction, $x$ the mole fraction, and $V$ the molar volume of each component. The terms $c_{11}$ and $c_{22}$ may be obtained from the solubility parameters $\delta_1$ and $\delta_2$ respectively of the pure components, and $c_{12}$ is equated to $(c_{11}c_{22})^{1/2}$.

In order to accommodate polar–nonpolar binary mixtures, [2] is usually extended as follows: (*i*) $c_{11}$ for the polar component is split into polar and nonpolar contributions

$$[3] \quad c_{11} = {}^{p}\delta_1{}^2 + {}^{d}\delta_1{}^2$$

and, (*ii*) the solute–solvent interaction parameter $c_{12}$ is split into a dispersion contribution and a contribution which represents the dipole – induced dipole interactions between the polar–nonpolar pairs in the mixture. Superscripts d and p denote dispersion and polar interactions or contributions, respectively.

For the solute–solvent interaction parameter $c_{12}$, Prausnitz and co-workers (1, 2) wrote $c_{12} = {}^{d}\delta_1{}^{d}\delta_2 + \psi_{12}$, where ${}^{d}\delta_1{}^{d}\delta_2$ is the geometric-mean term customarily used for the dispersion contribution and $\psi_{12}$ is what they called the apparent induction energy density parameter. These modifications led them to

$$[4] \quad RT \ln \gamma_2{}^{\infty} = V_2[({}^{d}\delta_1 - {}^{d}\delta_2)^2 + {}^{p}\delta_1{}^2 - 2\psi_{12}] + RT\left[\ln \frac{V_2}{V_1} + 1 - \frac{V_2}{V_1}\right]$$

where their last term is the Flory–Huggins entropy term which takes into account the differences in $V_1$ and $V_2$, the molar volumes of the two components.

Weimer and Prausnitz (1) plotted function $L$, namely,

$$RT \ln \gamma_2{}^{\infty} - V_2({}^{d}\delta_1 - {}^{d}\delta_2)^2 - RT\left[\ln \frac{V_2}{V_1} + 1 - \frac{V_2}{V_1}\right] \text{ vs. } V_2{}^{p}\delta_1{}^2$$

separately for seven saturated hydrocarbons, for 1-pentene, and for benzene as the nonpolar solutes (subscript 2) in a variety of polar solvents that spanned a wide range of $V_2{}^{p}\delta_1{}^2$ values, and over a wide temperature range. For each of the three types of solute (i.e. saturated, unsaturated, aromatic) the plot was linear and through the origin, and gave the correlation $\psi_{12} = k\,{}^{p}\delta_1{}^2$. Their values of $k$ depended only on the type of solute, and are in Table 5. The deviations of their values of ln $\gamma_2{}^{\infty}$ were in general within 10%.

We tried similar plots for our values of $\gamma_2{}^{\infty}$ listed in Tables 3 and 4, with the values for ${}^{d}\delta$, ${}^{p}\delta$, and $V$ being taken from ref. 1. Our plots of $L$ vs. $V_2{}^{p}\delta_2{}^2$ for the polar solutes in the nonpolar solvents $n$-heptane and benzene are in Fig. 4, and of $L$ vs. $V_2{}^{p}\delta_1{}^2$ for carbon tetrachloride in the polar solvents are in Fig. 5. Clearly, the broken lines through the origin are poor fits to our data, particularly in view of the relatively high precision of our $\gamma_2{}^{\infty}$ values as exemplified by their low standard deviations. In fact, better fits — but still not acceptable ones — were obtained by lines not passing through the origin. However, for comparative purposes values for $k$ were calculated for these broken lines through the origin in Figs. 4 and 5. They are entered in Table 5.

The binary systems in Fig. 5 belong to the same category as those of Weimer and Prausnitz (1), namely, a given nonpolar solute infinitely dilute in polar solvents. The binary systems in Fig. 4, on the contrary, consist of polar solutes infinitely dilute in a given nonpolar solvent, as did systems studied by Harris and Prausnitz (21). Weimer and Prausnitz clearly demonstrated a correlation between $\psi_{12}$ and ${}^{p}\delta_1$ for their systems, where subscript 1 denotes polar solvent. To conform with their method of treating the data, we necessarily tested our systems in Fig. 4 for correlation between $\psi_{12}$ and ${}^{p}\delta_2$, where subscript 2 denotes polar solute; Harris and Prausnitz did the same with their systems.

Much less scatter for our data was obtained when the values of $\psi_{12}$ were calculated by using the data in Tables 3 and 4 with [4], and then plotted against ${}^{p}\delta_2\delta_1$ for Table 3, and ${}^{p}\delta_1\delta_2$ for Table 4 (subscript 1 denotes the solvent). These plots are in Fig. 6.

Can. J. Chem. Downloaded from www.nrcresearchpress.com by 210.87.254.105 on 09/06/12
For personal use only.

Can. J. Chem. Downloaded from www.nrcresearchpress.com by 210.87.254.105 on 09/06/12
For personal use only.

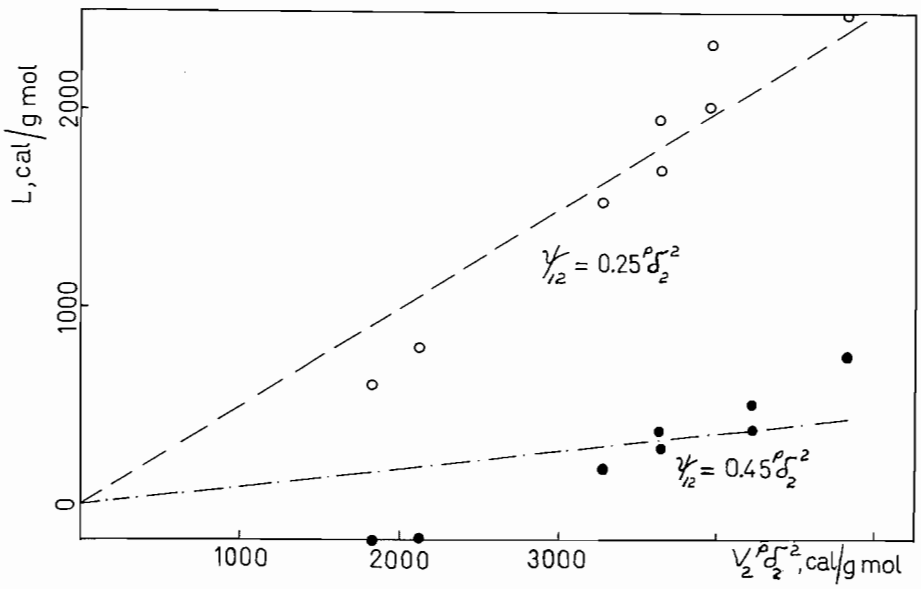


FIG. 4. Plots of $L$ ($= V_2{}^p\delta_2{}^2 - 2V_2\psi_{12}$) versus $V_2{}^p\delta_2{}^2$ for eight polar solutes (2) in *n*-heptane (○) and in benzene (●).

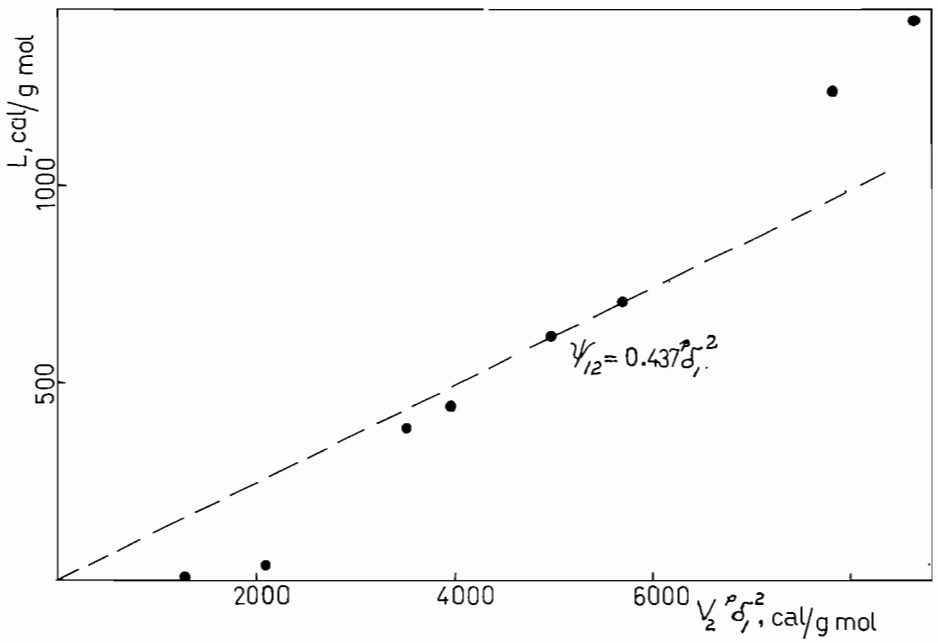


FIG. 5. Plots of $L$ ($= V_2{}^p\delta_1{}^2 - 2V_2\psi_{12}$) versus $V_2{}^p\delta_1{}^2$ for carbon tetrachloride (2) in eight polar solvents (1).

Blanks and Prausnitz (2) had proposed this $\psi_{12}$ vs. $\delta_1{}^p\delta_2$ relationship for their data on polymers.

It is clear from [4] that reliable values for $\psi_{12}$ require reliable values of ${}^d\delta_1$ and ${}^d\delta_2$. This matter was considered in the present work.

Kirchnerová and Cave (22) showed empirically that plots of $\delta$ vs. refractivity ($R$) for several homologous series of hydrocarbons gave straight lines over the range of compounds chosen, one line for each homologous series. These plots have been used (9) for estimating the polar (${}^p\delta$) and nonpolar (${}^d\delta$) contributions to the solubility parameters of polar liquids. Keller *et al.* (23) have also advocated the use of the correlation between ${}^d\delta$ and the Lorenz–Lorenz refractive-index function.

In the present work, plots of $\delta$ vs. $R$ were made

TABLE 6. Dispersion contributions to the solubility parameters of polar liquids at 25°C as calculated by three methods

| Liquid | $\delta_{total}$ (cal$^{1/2}$ cm$^{-3/2}$) | $^{d}\delta$ (cal$^{1/2}$ cm$^{-3/2}$) | | |
|---|---|---|---|---|
| | | London | Slater–Kirkwood | Homomorph plots* |
| Nitromethane | 12.59 | 7.32 | 7.89 | 8.08 |
| Nitroethane | 11.41 | 7.48 | 7.92 | 8.04 |
| 1-Nitropropane | 10.46 | 7.62 | 7.98 | 8.06 |
| 2-Nitropropane | 10.12 | 7.35 | 7.88 | 7.95 |
| Acetonitrile | 11.79 | 6.84 | 7.00 | 8.03 |
| Propionitrile | 10.65 | 7.14 | 7.28 | 7.97 |
| Ethyl acetate | 8.90 | 7.08 | 7.43 | 7.58 |
| *n*-Butyl acetate | 8.61 | 7.37 | 7.76 | 7.74 |

*All homomorph-plot values except those of the esters are reported in ref. 1; those of the esters were calculated by the present writers, using the method in ref. 1.

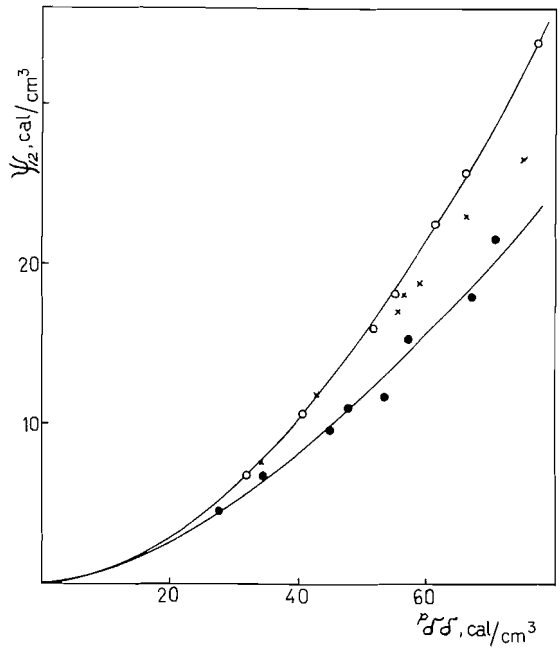


FIG. 6. Plots of the induction energy-density parameter $\psi_{12}$ versus $^{p}\delta\delta$, namely $^{p}\delta_2\delta_1$ for polar solutes ($^{p}\delta_2$) in *n*-heptane (●) and in benzene (×), and $^{p}\delta_1\delta_2$ for carbon tetrachloride ($\delta_2$) in the polar solvents (○).

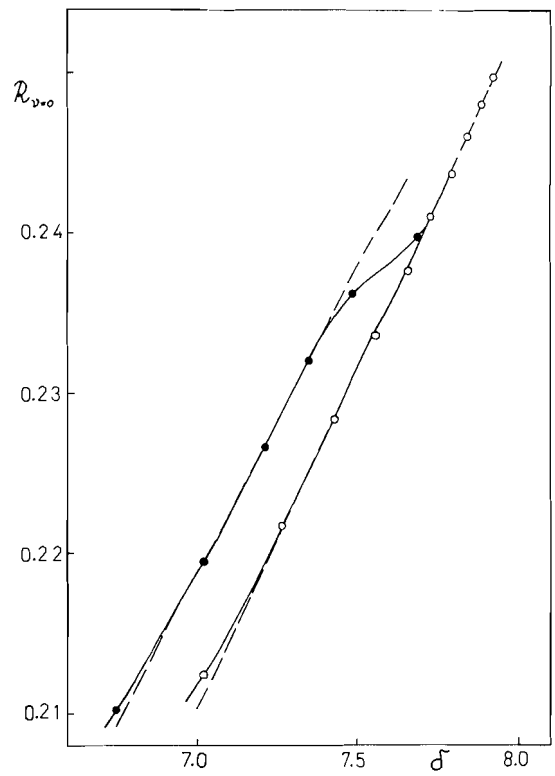


FIG. 7. Solubility parameter (δ) vs. refractivity (*R*) at zero frequency, for *n*-alkanes $C_4H_{10}$ to $C_{14}H_{30}$ (○), and 2-methyl alkanes $C_4H_{10}$ to $C_{10}H_{22}$ (●).

for *n*-alkanes and 2-methyl alkanes, over a wider range for each series than Kirchnerová and Cave had used, namely from $C_4H_{10}$ to $C_{14}H_{30}$ for the *n*-alkanes, and $C_4H_{10}$ to $C_{10}H_{22}$ for the 2-methyl alkanes. The data necessary for δ were from standard sources (24), and the values of *R* were calculated for zero frequency from bond polarizabilities (25). These plots are shown in Fig. 7. Both plots show curvature at the lower ends, and while the *n*-alkane curve then continues as a straight line, the 2-methyl alkane curve shows a limited linear region followed by a previously unreported sigmoid shape which then appears to merge with the *n*-alkane curve.

The solubility parameter may be expressed as a function of the energy of pair-interactions. The London equation for the potential energy of a pair of nonpolar molecules *in vacuo* leads to δ as a function of refractivity, *R*. Alternatively, the Slater–Kirkwood equation (26) leads to δ as a

Can. J. Chem. Downloaded from www.nrcresearchpress.com by 210.87.254.105 on 09/06/12
For personal use only.

TABLE 7. Values of $c_{12}$ in [2], $\psi_{12}$ in [4], and the ratios of $\psi_{12}$ in benzene to their values in *n*-heptane for eight polar solutes at infinite dilution in benzene and *n*-heptane at 20°C

| Solute | $\delta_{293.2}$ (cal$^{1/2}$ cm$^{-3/2}$) | $^{d}\delta_{293.2}$ (cal$^{1/2}$ cm$^{-3/2}$) | $V_{293.2}$ (cm$^3$ mol$^{-1}$) | $c_{12}$ (cal cm$^{-3}$) | | $\psi_{12}$ (cal cm$^{-3}$) | | $\psi_{12}$ (benzene) |
|---|---|---|---|---|---|---|---|---|
| | | | | *n*-Heptane | Benzene | *n*-Heptane | Benzene | $\psi_{12}$ (*n*-heptane) |
| Nitromethane | 12.68 | 7.94 | 53.63 | 85.38 | 115.49 | 25.91 | 42.20 | 1.32 |
| Nitroethane | 11.49 | 7.98 | 71.45 | 80.04 | 105.23 | 20.27 | 31.58 | 1.27 |
| 1-Nitropropane | 10.53 | 8.03 | 88.97 | 74.04 | 95.83 | 13.89 | 21.71 | 1.30 |
| 2-Nitropropane | 10.20 | 7.93 | 90.14 | 71.52 | 92.87 | 12.13 | 19.67 | 1.32 |
| Acetonitrile | 11.88 | 7.07 | 52.48 | 75.84 | 105.87 | 22.89 | 40.62 | 1.44 |
| Propionitrile | 10.72 | 7.34 | 70.45 | 71.53 | 96.58 | 16.55 | 28.83 | 1.42 |
| Ethyl acetate | 8.99 | 7.49 | 97.83 | 64.37 | 82.59 | 8.27 | 13.46 | 1.32 |
| *n*-Butyl acetate | 8.69 | 7.82 | 131.79 | 63.51 | 80.06 | 4.94 | 7.88 | 1.30 |
| | | | | | | | | Mean = 1.34 |
| | | | | | | | | $s_x$ = 0.061 |
| Solvent | | | | | | | | |
| *n*-Heptane | 7.49 | | 146.55 | | | | | |
| Benzene | 9.23 | | 88.87 | | | | | |

function of $R^{3/4}n^{1/4}/V^{1/4}$, where $n$ is the number of valence electrons in the molecule. Plots of $\delta$ vs. $R^{3/4}n^{1/4}/V^{1/4}$ for the same set of *n*-alkanes and the same set of 2-methyl alkanes as were used for Fig. 7 showed shapes that were similar to those in Fig. 7, with the 2-methyl alkane curve finally merging at $C_{11}H_{24}$ with that of the *n*-alkane curve which, as in Fig. 7, was linear except at the lower end.

The values of $^{d}\delta$ for the polar solutes studied in the present work were read both from the $R$ vs. $\delta$ calibration curve, and the $R^{3/4}n^{1/4}/V^{1/4}$ vs. $\delta$ curve, and are entered in columns 3 and 4 respectively of Table 6. The values of $R$ were required at zero frequency, and were calculated from bond polarizabilities (25) except in the case of the nitro compounds. For each of them, the value of $R$ at zero frequency was calculated (27) from the refractive indices at three different frequencies. Column 5 of Table 6 gives for comparison the values of $^{d}\delta$ calculated from homomorph plots.

In the present work, when values of $^{d}\delta$ were needed they were taken from plots of $R^{3/4}n^{1/4}/V^{1/4}$ vs. $\delta$, except where otherwise noted.

By using the values of $\gamma_2^{\infty}$ in Table 3, the corresponding values of $c_{12}$ were found from [2], and those of $\psi_{12}$ from [4]. The results are in Table 7. For these calculations, values of $\delta$ at 20°C were used, and are in Table 7. They were calculated from enthalpies of vaporization at 25°C (10) and the molar heat contents of liquid and of ideal vapor. Values for $^{d}\delta$ at 20°C are also entered in Table 7. They were estimated by the method described above for the $^{d}\delta$ values in column 4 of Table 6, except that the calibration curves were for 20°C.

Of particular interest is the ratio for each polar solute of its value of $\psi_{12}$ in *n*-heptane to its value in benzene. These ratios are in column 9 of Table 7. The standard deviation is only 0.061 for the eight solutes.

The near-constancy of this ratio shows some promise of being a way to estimate from limited data the limiting activity coefficients of polar solutes in nonpolar solvents. Thus, if the limiting activity coefficient of a polar solute is known in one nonpolar solvent, it may be practical to estimate with acceptable accuracy its value in another nonpolar solvent, provided the ratio of the $\psi_{12}$ values has already been found for the two solvents. To establish the degree of generality of this empirical rule for the ratios, more solvents are currently being studied in this laboratory.

The decreases in the value of $\psi_{12}$ for a given homologous series illustrated to a very limited degree in Table 7 appear to be systematic, and suggest a generality; but the decrements per $CH_2$ group are too irregular in the table to warrant quantification at present.

## Acknowledgments

We are grateful to Mr. A. Kluck of McGill University for the fabrication of the sampling valve, to Dr. S. Afrashtehfar for assistance in some of the computations for Table 3, and to the National Research Council of Canada for financial assistance.

1. R. F. WEIMER and J. M. PRAUSNITZ. Hydrocarbon Process. **44** (9), 237 (1965).
2. R. F. BLANKS and J. M. PRAUSNITZ. I & EC, Fundamentals, **3**, 2 (1964).
3. E. HÁLA, J. PICK, V. FRIED, and D. VILÍM. Vapor–liquid equilibria. Pergamon Press, Oxford. 1967.
4. H. V. REGNAULT. Anal. Chim. **15**, 129 (1848).

Can. J. Chem. Downloaded from www.nrcresearchpress.com by 210.87.254.105 on 09/06/12
For personal use only.

5. J. N. PEARCE and N. D. SNOW. J. Phys. Chem. **31**, 231 (1927).
6. G. MAFFIOLO and J. VIDAL. Bull. Soc. Chim. Fr. No. 8, 2810 (1971).
7. J. KLOPSTOCK and M. ROZINSKI. J. Chromatogr. **50** (3), 504 (1970).
8. I. WICHTERLE and L. BOUBLIKOVÁ. I & EC, Fundamentals, **8**, 585 (1969).
9. E. MILANOVÁ. Ph.D. Thesis. McGill University, Montreal, P.Q. 1975: (*a*) pp. 45–52; (*b*) pp. 70–75; (*c*) pp. 55–58, 75–78; (*d*) pp. 82–87.
10. J. A. RIDDICH and W. B. BUNGER. *In* Techniques of chemistry. Vol. II. Organic solvents. 3rd ed. *Edited by* A. Weisberger. Wiley-Interscience. 1970.
11. J. H. DYMOND and E. B. SMITH. The virial coefficients of gases. Clarendon Press, Oxford. 1969.
12. V. C. SMITH and L. J. ROBINSON. J. Chem. Eng. Data, **15** (3), 391 (1970).
13. D. V. S. JAIN, V. K. GUPTA, and B. S. LARK. Ind. J. Chem. **8**, 815 (1970).
14. S. R. M. ELLIS. Rev. Ser. **6**, 289 (1969).
15. S. R. M. ELLIS and D. A. JONAH. Chem. Eng. Sci. **17**, 971 (1962).
16. G. SCATCHARD, S. E. WOOD, and J. M. MOCHEL. J. Am. Chem. Soc. **62**, 712 (1940).
17. I. BROWN and P. SMITH. Austr. J. Chem. **10**, 423 (1957).
18. A. N. CAMPBELL, E. M. KARTZMARK, and R. M. CHATTERJEE. Can. J. Chem. **44**, 1183 (1966).
19. N. D. LITVINOV. Zh. fiz. khim. **14**, 782 (1940).
20. I. BROWN and P. SMITH. Austr. J. Chem. **10**, 417 (1957).
21. H. G. HARRIS and J. M. PRAUSNITZ. J. Chromatogr. Sci. **7**, 685 (1969).
22. J. KIRCHNEROVÁ and G. C. B. CAVE. Can. J. Chem. **54**, 3909 (1976).
23. R. A. KELLER, B. L. KARGER, and L. R. SYNDER. *In* Gas chromatography. 1970 Proc. 8th Int. Symp. *Edited by* R. Stock and S. G. Perry. The Institute of Petroleum, London. 1971. p. 125.
24. American Petroleum Institute. Selected values of physical and thermodynamic properties of hydrocarbons and related compounds. Project 44. Carnegie Press, Pittsburgh. 1953. Plus Supplements.
25. E. A. MOELWYN-HUGHES. Physical chemistry. MacMillan, New York. 1964.
26. J. C. SLATER and J. G. KIRKWOOD. Phys. Rev. **37**, 682 (1931).
27. C. P. SMYTH. Dielectric behavior and structure. McGraw-Hill, New York. 1955. pp. 405, 406.

Can. J. Chem. Downloaded from www.nrcresearchpress.com by 210.87.254.105 on 09/06/12
For personal use only.

# Méthode générale d'obtention des α-céto esters β-fluorés

ALI OURARI, ROGER CONDOM ET ROGER GUEDJ

*Laboratoire de Chimie Structurale Organique, Université de Nice, Parc Valrose, 06034 Nice Cédex, France*

Reçu le 24 mars 1982

ALI OURARI, ROGER CONDOM et ROGER GUEDJ. Can. J. Chem. **60**, 2707 (1982).

Une méthode générale de préparation des alkyl-3 (ou aryl) fluoro-3 oxo-2 esters est décrite. Les esters glycidiques sont ouverts par le mélange HF–pyridine (70% poids/poids) puis oxydés par le réactif de Jones; les dérivés correspondants des esters fluoropyruviques sont obtenus avec de bons rendements.

ALI OURARI, ROGER CONDOM, and ROGER GUEDJ. Can. J. Chem. **60**, 2707 (1982).

A general method of synthesis of 3-alkyl (or aryl) 3-fluoro 2-oxo esters is described. The opening of glycidic esters with HF–pyridine (70% w/w), followed by oxidation with Jones reagent, give the corresponding derivatives of fluoropyruvic esters in good yields.

La synthèse des fluoropyruvates a été très peu étudiée, les travaux réalisés dans ce domaine concernent l'obtention de l'acide fluoropyruvique (1) et l'α-oxo-β-fluorohexanoate d'éthyle (2). Récemment, Tsushima et coll. (3, 14) ont signalé que l'action du fluor élémentaire sur les α-céto esters donne les fluoropyruvates correspondants.

Les méthodes décrites ci-dessus ne peuvent être appliquées que pour des cas particuliers; par exemple, l'acide fluoropyruvique est obtenu à partir de l'oxalo fluoroacétate et l'α-oxo β-fluoro-hexanoate d'éthyle à partir de l'ester α-fluoro glycidique correspondant:

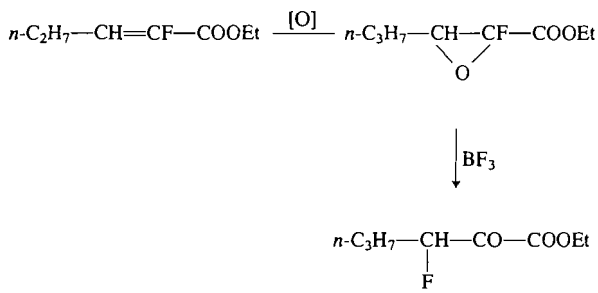

Cette méthode n'a pas pu être étendue aux dérivés aromatiques par le fait que l'ester acrylique α-fluoré ne s'époxyde pas.

C'est la raison pour laquelle, compte tenu de l'intérêt présenté par les propriétés biologiques des pyruvates notamment dans le domaine des antibiotiques (13), nous avons mis au point une méthode de synthèse simple et générale permettant l'accès à des α-céto esters β-fluorés diversement substitués. Le schéma réactionnel est le suivant:

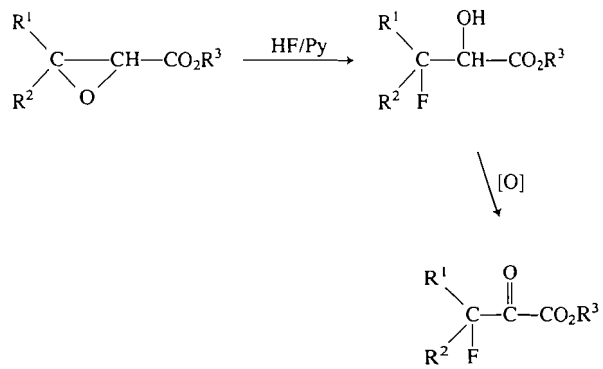

où $R^1$ = H, alkyle, aryle; $R^2$ = alkyle, aryle; $R^3$ = $C_2H_5$ ou $CH(CH_3)_2$.

## Partie expérimentale

Les époxydes sont obtenus par condensation du composé carbonylé sur le chloroacétate d'éthyle au moyen du *tert*-butylate de potassium (4) en quantités stoechiométriques (5). L'ester glycidique (**10***a*) a été synthétisé en utilisant l'isopropylate de potassium. L'ester glycidique ainsi obtenu (0,04 mol) est dissous dans 10 mL de $CH_2Cl_2$, puis 20 mL d'acide fluorhydrique en solution dans la pyridine (70% w/w) sont ajoutés à 5°C environ. Après distillation, le fluoroalcool (0,02 mol) est dissous dans 200 mL d'acétone. La solution est agitée magnétiquement et 210 mL du réactif de Jones sont ajoutés goutte à goutte, la température étant maintenue vers 5°C. Le mélange est abandonné pendant une nuit, puis traité. Le céto ester obtenu est distillé sous pression réduite.

## Résultats

A. Les esters glycidiques **1***a* (6), **2***a* (7), **3***a* (8), **4***a*, **5***a*, **6***a*, **11***a*, **12***a* (9), **8***a* (10), **9***a* (6) de départ sont conformes à ceux décrits dans la littérature. Composé **10***a*: rendement 25%, p.Eb: 86°C/28 Torr; rmn $^1H$ δ: 3,16 (Hα et Hβ, 2H, m); 0,98

0008-4042/82/212707-04$01.00/0

©1982 National Research Council of Canada/Conseil national de recherches du Canada

Can. J. Chem. Downloaded from www.nrcresearchpress.com by 210.87.254.105 on 09/06/12
For personal use only.

Can. J. Chem. Downloaded from www.nrcresearchpress.com by 210.87.254.105 on 09/06/12
For personal use only.

TABLEAU 1. Intermédiaires de synthèse, points d'ébullition et caractérisation infra-rouge des α-céto esters β-fluorés

| Composé n° | *a* | *b* | *c* | Rdt % | p.Eb. °C/Torr | Infrarouge ν cm$^{-1}$ |
|---|---|---|---|---|---|---|
| **1** | 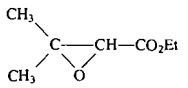 | 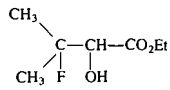 | 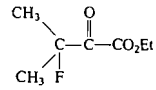 | 58 | $61_{18}$ | 1751<br>1727 |
| **2** | 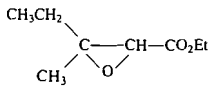 | 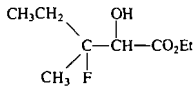 | 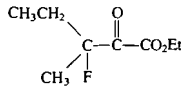 | 85 | $70_{18}$ | 1748<br>1727 |
| **3** | 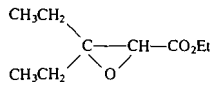 | 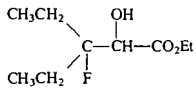 | 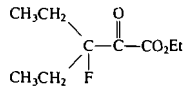 | 87 | $85_{16}$ | 1751<br>1724 |
| **4** | 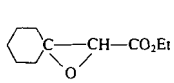 | 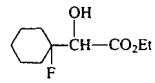 | 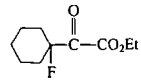 | 66 | $113_{18}$ | 1748<br>1727 |
| **5** | 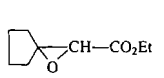 | 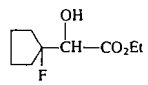 | 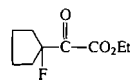 | 64 | $98_{18}$ | 1745<br>1724 |
| **6** | 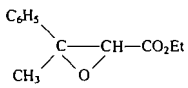 | 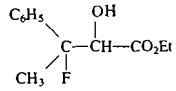 | 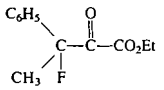 | 80 | $109_{2.0}$ | 1751<br>1730 |
| **7** | 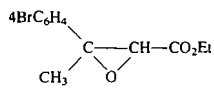 | 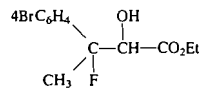 | 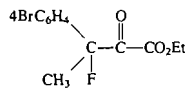 | 82 | $135_{1.5}$ | 1751<br>1733 |
| **8** | 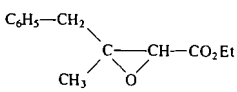 | 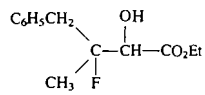 | 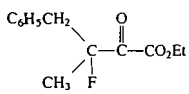 | 86 | $123_{2.0}$ | 1748<br>1724 |
| **9** | 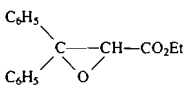 | 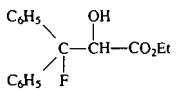 | 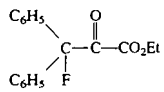 | 62 | $147_{1.5}$ | 1745<br>1727 |
| **10** | 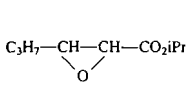 | 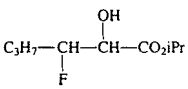 | 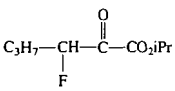 | 69 | $94_{18}$ | 1751<br>1721 |
| **11** | 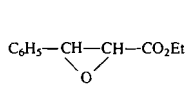 | 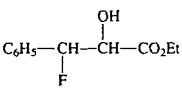 | 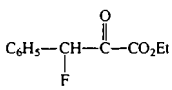 | 76 | $114_{2.5}$ | 1724<br>1695 |
| **12** | 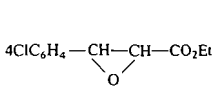 | 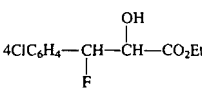 | 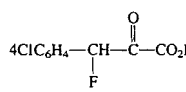 | 75 | $130_{2.0}$ | 1751<br>1727 |

($CH_3(CH_2)_2$, 3H, t, $^3J$ = 7,0 Hz); 5,10 ($(CH_3)_2CH$, 1H, m); 1,28 ($(CH_3)_2CH$, 6H, d, $J$ = 6,4 Hz) ppm. Composé **7***a*: rendement 71%, p.Eb: 126°C/0,8 Torr (mélange *cis–trans*); rmn $^1$H *cis* δ: 0,97 ($CH_3CH_2$, 3H, t, $J$ = 7,0 Hz); 3,66 (Hα, 1H, s); 3,94 ($CH_3CH_2$, 2H, q); 7,37 (4 Br-$C_6H_4$, 4H, m); *trans* δ: 1,32 ($CH_3CH_2$, 3H, t, $J$ = 7,0 Hz); 3,40 (Hα, 1H, s); 4,30 ($CH_3CH_2$, 2H, q); 7,37 (4 Br-$C_6H_4$, 4H, m) ppm.

B. Certaines fluorhydrines **4***b*, **5***b*, **6***b* et **11***b*, **12***b* (9, 11) sont déjà décrites. Les caractéristiques des fluorhydrines nouvelles sont les suivantes. Composé **1***b*: rendement 76%, p.Eb.: 80°C/18 Torr; ir$\bar{\nu}_{OH}$ = 3460; $\bar{\nu}_{CO}$ = 1709 cm$^{-1}$; rmn $^1$H δ: 1,32 ($CH_3CH_2$, 3H, t, $J$ = 7,0 Hz); 1,39 ($CH_3$, 3H, d, $J_{CH_3\text{-}C\text{-}F}$ = 21,7 Hz); 1,44 ($CH_3$, 3H, d, $J_{CH_3\text{-}C\text{-}F}$ = 21,7 Hz); 3,45 (OH, 1H, s); 4,29 ($CH_3CH_2$, 2H, q); 4,10 (Hα, 1H, d, $J_{H\text{-}C\text{-}C\text{-}F}$ = 15,8 Hz) ppm; rmn $^{19}$F ϕ: 149,8 ppm; heptuplet dédoublé. Composé **2***b*: rendement 78%, p.Eb. 88°C/16 Torr; ir$\bar{\nu}_{OH}$ = 3460 cm$^{-1}$; $\bar{\nu}_{CO}$ = 1704 cm$^{-1}$; rmn $^1$H (mélange *érythro* + *thréo*) δ: 0,97 ($CH_3CH_2O$, 3H, t, $J$ = 7,5 Hz); 1,00

TABLEAU 2. Caractéristiques spectrales – masse et résonance magnétique nucléaire – des α-céto esters β-fluorés

| Composé n° | *m/e* | Résonance magnétique nucléaire $^1H$ (δ) et $^{19}F$ (ϕ) |
|---|---|---|
| **1***c* | 162<br>61 | δ: 1,37 ($CH_3CH_2$, 3H, t, $J$ = 7,0 Hz); 1,64 (2 $CH_3$, 6H, d, $J_{F-CH_3}$ = 21,4 Hz); 4,37 ($CH_3$—$CH_2$, 2H, q) ppm<br>ϕ: 152,0 ppm; heptuplet; $^3J_{FH}$ = 21,3 Hz |
| **2***c* | 176<br>75 | δ: 0,98 ($CH_3$—$CH_2$—C, 3H, t, $J$ = 7,3 Hz); 1,37 ($CH_3$—$CH_2O$, 3H, t, $J$ = 7,0 Hz); 1,58 ($CH_3$, 3H, d, $J_{FH}$ = 21,7 Hz); 4,37 ($CH_3CH_2O$, 2H, q) ppm<br>ϕ: 161,9 ppm; multiplet; $J_{F-CH_3}$ = 21,3 Hz, $J_{F-CH_2}$ = 18,3 Hz |
| **3***c* | 190<br>69 | δ: 0,96 (2 $CH_3$—$CH_2C$, 6H, t, $J$ = 7,5 Hz); 1,37 ($CH_3CH_2O$, 3H, t, $J$ = 7,0 Hz); 4,36 ($CH_3$—$CH_2O$, 2H, q) ppm<br>ϕ: 171,8 ppm; multiplet; $^3J_{FH}$ = 18,0 Hz |
| **4***c* | 202<br>81 | δ: 1,36 ($CH_3CH_2$, 3H, t, $J$ = 7,0 Hz); 1,39–2,15 (-$(CH_2)_5$-, multiplet); 4,32 ($CH_3CH_2$, 4H, q) ppm<br>ϕ: 171,8 ppm; multiplet; $^3J_{FH}$ = 18,0 Hz |
| **5***c* | 188<br>87 | δ: 1,36 ($CH_3CH_2$, 3H, t, $J$ = 7,0 Hz); 1,50–2,28 (-$(CH_2)_4$-, m); 4,35 ($CH_3CH_2$, 2H, q) ppm<br>ϕ: 154,0 ppm; multiplet |
| **6***c* | 224<br>123 | δ: 1,30 ($CH_3CH_2$, 3H, t, $J$ = 7,0 Hz); 1,93 ($CH_3$, 3H, d, $J_{FCCCH_3}$ = 22,8 Hz); 4,27 ($CH_3$—$CH_2$, 2H, q); 7,40 ($C_6H_5$, 5H, m) ppm<br>ϕ: 157,2 ppm; quadruplet; $J_{F-CCCH_3}$ = 21,3 Hz |
| **7***c* | 302/304<br>201/203 | δ: 1,30 ($CH_3CH_2$, 3H, t, $J$ = 7,0 Hz); 1,85 ($CH_3$, 3H, d, $J_{FCCCH_3}$ = 22,0 Hz); 4,26 ($CH_3CH_2$, 2H, q); 7,90 (4Br-$C_6H_4$, 4H, m) ppm<br>ϕ: 157,9; quadruplet; $J_{FCCCH_3}$ = 21,3 Hz |
| **8***c* | — | δ: 1,29 ($CH_3$—$CH_2$, 3H, t, $J$ = 7,0 Hz); 1,54 ($CH_3$, 3H, d, $J_{FCCCH_3}$ = 21,7 Hz); 3,17 ($C_6H_5$—$CH$, 1H, d, $J_{F-CC-H}$ = 25,2 Hz); 3,30 ($C_6H_5$—$CH$, 1H, d, $J_{F-CC-H}$ = 25,2 Hz)<br>ϕ: 158,0 ppm; multiplet; $J_{FCCH_3}$ = 21,3 Hz, $J_{F-C-CH_2}$ = 24,4 Hz |
| **9***c* | — | δ: 1,28 ($CH_3$—$CH_2$, 3H, t, $J$ = 7,0 Hz); 4,67 ($CH_3$—$CH_2$, 2H, q); 7,39 (2$C_6H_5$, 10H, m) ppm<br>ϕ: 146,6 ppm; singulet |
| **10***c* | 208* | δ: 0,98 ($CH_3$-, 3H, t); 1,36 (($CH_3$)$_2$CH, 6H, d, $J$ = 6,4 Hz); 5,14 (($CH_3$)$_2$CH, 1H, m); 5,31 (H, 1H, multiplet dédoublé, $J_{FH}$ = 48,0 Hz) ppm<br>ϕ: 199,0 ppm; $^2J_{FH}$ = 48,8 Hz, $^3J_{F-H}$ = 24,4 Hz |
| **11***c* | 210<br>109 | δ: 1,24 ($CH_3CH_2$, 3H, t, $J$ = 7,0 Hz); 4,23 ($CH_3CH_2$, 2H, q); 6,27 (H, 1H, d, $J_{F-H}$ = 47,2 Hz); 7,41 ($C_6H_5$, 5H, m) ppm<br>ϕ: 183,9 ppm; doublet; $^2J_{FH}$ = 47,7 Hz |
| **12***c* | 244/246<br>143/145 | δ: 1,29 ($CH_3CH_2$, 3H, t, $J$ = 7,0 Hz); 4,27 ($CH_3CH_2$, 2H, q); 6,40 (H, 1H, d, $^2J_{F-H}$ = 45,7 Hz); 7,40 ($C_6H_4$, 4H, m) ppm<br>ϕ: 184,7 ppm; doublet; $^2J_{FH}$ = 48,8 Hz |

*Ce spectre a été obtenu par ionisation chimique ($M^+$ et $NH_4$). Les autres spectres ont été obtenus par impact électronique.

($CH_3CH_2O$, 3H, t, $J$ = 7,5 Hz); 1,33 ($CH_3CH_2^-$, 3H, t, $J$ = 7,0 Hz); 1,39 ($CH_3$, 3H, d, $J_{F-CC-CH_3}$ = 22,0 Hz); 1,74 ($CH_3$, 3H, d, $J_{F-CC-CH_3}$ = 22,0 Hz); 4,13 (Hα, 1H, d, $J_{F-CC-H}$ = 13,5 Hz); 4,16 (Hα, 1H, d, $J_{H-CC-F}$ = 17,6 Hz); 4,30 ($CH_3CH_2O$, 2H, q, $J$ = 7,0 Hz) ppm; rmn $^{19}F$ ϕ: 158,4 et 158,7 ppm après irradiation des multiplets. Composé **3***b*: rendement 80%, p.Eb. 101°C/18 Torr; ir $\bar{\nu}_{OH}$ = 3460 $cm^{-1}$; $\bar{\nu}_{CO}$ = 1704 $cm^{-1}$; rmn $^1H$ δ: 0,93 ($CH_3CH_2C$, 3H, t, $J$ = 7,0 Hz); 0,97 ($CH_3CH_2C$, 3H, t, $J$ = 7,0 Hz); 1,30 ($CH_3CH_2O$, 3H, t, $J$ = 7,3 Hz); 3,12 (OH, 1H, s); 4,20 (Hα, 1H, d, $^3J_{FH}$ = 15,8 Hz); 4,30 ($CH_3CH_2O$, 2H, q, $J$ = 7,3 Hz) ppm; rmn $^{19}F$ ϕ: 166,0 ppm (multiplet). Composé **7***b*: rendement 95%, F = 66–67°C (diéthyloxyde – éther de pétrole); ir $\bar{\nu}_{OH}$ = 3460 $cm^{-1}$; $\bar{\nu}_{CO}$ = 1712 $cm^{-1}$; rmn $^1H$ (mélange *érythro* + *thréo*) δ: 1,01 ($CH_3CH_2$, 3H, t, $J$ = 7,0 Hz); 1,21 ($CH_3CH_2$, 3H, t, $J$ = 7,0 Hz); 1,74 ($CH_3$, 3H, d, $J_{CH_3-CC-F}$ = 23,2 Hz); 1,77 ($CH_3$, 3H, d, $J_{CH_3-CC-F}$ = 23,2 Hz); 3,31 (OH, 1H, s); 4,08 ($CH_3CH_2$, 2H, q); 4,16 ($CH_3CH_2$, 2H, q); 4,29 (Hα, 1H, d, $J_{H-CC-F}$ = 15,0 Hz); 4,35 (Hα, 1H, d, $J_{H-CC-F}$ = 19,6 Hz); 7,36 (4 Br-$C_6H_4$, 4H, m) ppm; rmn $^{19}F$ ϕ: 157,0 et 161,6 ppm (doublet de quadruplets). Composé **8***b*: rendement 50%, p.Eb. 130°C/2 Torr; ir $\bar{\nu}_{OH}$ = 3460 $cm^{-1}$; $\bar{\nu}_{CO}$ = 1704 $cm^{-1}$; rmn $^1H$ (mélange *érythro* + *thréo*) δ: 1,27 ($CH_3$, 3H, d, $J_{F-CC-CH_3}$ = 22,7 Hz); 1,30 ($CH_3CH_2$, 3H, t, $J$ = 7,0 Hz); 1,31 ($CH_3$, 3H, d, $J_{F-CC-CH_3}$ = 22,0 Hz); 3,26 (OH, 1H, s); 4,06 (Hα, 1H, d, $J_{F-CC-H}$ = 10,5 Hz); 4,08 (Hα, 1H, d, $J_{F-CC-H}$ = 17,5 Hz); 4,26 ($CH_3CH_2$, 2H, q, $J$ = 7,0 Hz); 7,27 ($C_6H_5$, 5H, m) ppm; rmn $^{19}F$ ϕ = 155,8 et 156,8 ppm après irradiation (multiplets). Composé **9***b*: rendement 76%, F = 81–82°C (diéthyloxyde); ir $\bar{\nu}_{OH}$ = 3460 $cm^{-1}$; $\bar{\nu}_{CO}$ = 1712 $cm^{-1}$; rmn $^1H$ δ: 0,95 ($CH_3CH_2$, 3H, t); 3,40 (OH, 1H, s); 3,96 ($CH_3CH_2$, 2H, q, $J$ = 7,0 Hz); 4,86 (Hα, 1H, d, $J_{F-CC-H}$ = 18,0 Hz); 7,29 (2 $C_6H_5$, 10H, m) ppm; rmn $^{19}F$ ϕ = 159,0 (doublet) ppm. Composé **10***b*: rendement 84%, p.Eb.

Can. J. Chem. Downloaded from www.nrcresearchpress.com by 210.87.254.105 on 09/06/12
For personal use only.

105°C/28 Torr; ir $\bar{\nu}_{OH}$ = 3460 $cm^{-1}$; $\bar{\nu}_{CO}$ = 1709 $cm^{-1}$; rmn $^1H$ (mélange *érythro* + *thréo*) δ: 0,95 ($CH_3$—$(CH_2)_2$, 3H, t, $J$ = 7,0 Hz); 1,29 ($(CH_3)_2CH$, 6H, d, $J$ = 6,4 Hz); 1,31 ($(CH_3)_2CH$, 6H, d, $J$ = 6,4 Hz); 2,94 (OH, 1H, s); 4,26 (Hα, 1H, dd, $J_{F\text{-}CC\text{-}F}$ = 18,6 Hz, $^3J_{HH}$ = 3,3 Hz); 5,17 ($(CH_3)_2CH$, 1H, m) ppm; rmn $^{19}F$ φ: 191,7 et 196,5 ppm (multiplets).

C. Les caractéristiques des fluoropyruvates ont été rassemblées dans les tableaux 1 et 2. Remarques: Les spectres ir correspondent aux produits attendus (bande CO large 1718–1730 $cm^{-1}$). Le pourcentage en produit ènolisable est très faible (non décelé en rmn $^1H$) et en accord avec les résultats obtenus par Bergmann (12).

Les spectres rmn du proton ont été enregistrés dans $CDCl_3$ (TMS réf. interne), ceux du fluor ont été effectués dans le même solvant, la référence interne étant $CFCl_3$. Ces spectres ont été réalisés sur Brucker Spectrospin 100 MHz, les déplacements chimiques sont exprimés en ppm et les constantes de couplage en Hz.

En ce qui concerne la spectrométrie de masse: les fragments donnés dans les tableaux sont respectivement l'ion moléculaire et le pic de base. Le pic M + 1 est observé dans tous les cas et la perte de HF s'effectue à partir de l'ion moléculaire et du pic de base.


1. I. Blank, J. Mager et E. D. Bergmann. J. Chem. Soc. 2190 (1955).
2. E. Elkik et M. Leblanc. Bull. Soc. Chim. Fr. **3**, 870 (1971).
3. T. Tsushima, J. Nishikawa, T. Sato et H. Tanida. Tetrahedron Lett. 3593 (1980).
4. E. W. Bachelor et R. K. Bansal. J. Org. Chem. 3600 (1969).
5. M. B. Castro, J. Villieras et N. Ferracutti. C.R. Acad. Sci. Paris, Sér. C, **268**, 1403 (1969).
6. A. Rutkowski et H. Dajew. Ber. **64**, 693 (1931).
7. R. P. Linstead et M. S. Mann. J. Chem. Soc. 2070 (1930).
8. L. Claisen. Ber. **338**, 690 (1905).
9. A. I. Ayi, M. Remli, R. Condom et R. Guedj. J. Fluorine Chem. **17**, 565 (1981).
10. G. Darzens. C.R. Acad. Sci. Paris, **139**, 1214 (1904).
11. J. Jullien et R. Gardaix. Bull. Soc. Chim. Fr. **3**, 2721 (1969).
12. E. Bergmann. Bull. Soc. Chim. Fr. **4**, 2676 (1965).
13. P. Bey. Sci. Tech. Pharm. **4**, 171 (1978).
14. T. Tsushima, K. Kahada, T. Tsuji et S. Misaki. J. Org. Chem. **47**, 1107 (1982).


Can. J. Chem. Downloaded from www.nrcresearchpress.com by 210.87.254.105 on 09/06/12
For personal use only.

# Oxidation of 1,1-disubstituted hydrazines with benzeneseleninic acid and selenium dioxide. Facile preparation of tetrazenes

THOMAS G. BACK[1] AND RUSSELL G. KERR

*Department of Chemistry, University of Calgary, Calgary, Alta., Canada T2N 1N4*

Received March 15, 1982

THOMAS G. BACK and RUSSELL G. KERR. Can. J. Chem. **60**, 2711 (1982).

Various 1,1-disubstituted hydrazines were oxidized with benzeneseleninic acid in methanol, generally producing the corresponding tetrazenes in high yield. Studies of the by-products of the reaction, of the effects of protic vs. aprotic solvents, and trapping experiments suggest that *N*-aminonitrenes are unlikely intermediates in this oxidation. An alternative mechanism involving a Pummerer-like reaction of seleninamides derived from the hydrazines is proposed. Tetrazene formation fails when the hydrazine precursor contains an aryl or *p*-toluenesulfonyl substituent, or when it is highly hindered. Selenium dioxide may be employed as the oxidant instead of the seleninic acid, but is generally less efficacious in achieving high tetrazene yields.

THOMAS G. BACK et RUSSELL G. KERR. Can. J. Chem. **60**, 2711 (1982).

Une variété de hydrazines 1,1-disubstituées a été oxydée par l'acide benzèneséléninique et, en général, de bons rendements des tétrazènes correspondants ont été obtenus. Les études des sous-produits de ces réactions, les effets des solvants protiques et aprotiques, ainsi que le résultat d'une expérience de trappage suggèrent que les *N*-aminonitrénes sont des intermédiaires improbables dans cette oxydation. Un méchanisme alternatif est proposé, dans lequel un séléninamide dérivé de l'hydrazine de départ subit une réaction de Pummerer. La formation des tétrazènes ne réussit pas quand l'hydrazine contient un substituant aryle ou *p*-toluènesulfonyle et également quand l'hydrazine est très encombrée. Le dioxyde de sélénium peut être employé comme agent d'oxydation au lieu de l'acide séléninique, mais la formation des tétrazènes correspondants est généralement moins efficace.

A number of reagents have been employed in the oxidations of 1,1-disubstituted hydrazines **1** to tetrazenes (diaminodiazenes) **2**. Examples include oxides of lead (1, 2), mercury (3–5) and manganese (6), halogens (3, 4), potassium bromate (4), iodate (4) and permanganate (7), lead tetraacetate (8), quinone (2, 9), and *tert*-butyl hypochlorite (10).

Recent studies have shown that benzeneseleninic acid (3) and anhydride (**4**) are efficient oxidants of various hydrazines and hydrazo derivatives (11–13). As an extension of this work, we were prompted to examine the similar oxidation of 1,1-disubstituted hydrazines with **3**. Preliminary results indicated that the transformation of compounds **1** to their corresponding tetrazenes **2** could be smoothly achieved in this manner (14). It is the intent of the present article to further delineate the scope and limitations of this method and to comment on its mechanism. We also describe for the first time several experiments in which selenium dioxide was employed as the oxidant.

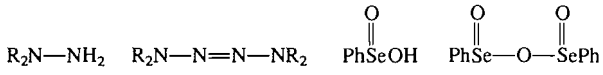

**1** **2** **3** **4**

## Results and discussion

The oxidation of hydrazines **1***a*–**1***g* with benzeneseleninic acid **3** in methanol provides tetrazenes **2***a*–**2***g* as the principal products, generally in high yield (see Table 1, entries 1, 6, 10–12, 14, and 16). In most cases the reactions are vigorous and enhanced tetrazene yields were obtained by performing the oxidations at −10°C and by the prompt work-up of the products. The separation of the tetrazenes from diphenyl diselenide and other by-products was readily achieved by preparative tlc. In the case of the relatively insoluble tetrazenes **2***e*–**2***g*, the products crystallized directly from the reaction mixture. This procedure therefore provides a convenient method for the conversion of a variety of 1,1-disubstituted hydrazines to tetrazenes.

Further experiments revealed that a high concentration of both reactants is necessary for optimum results. Entries 2 and 3 in the table reveal that considerable reductions in product yields occurred when either the hydrazine or the seleninic acid was introduced by slow addition. The use of water as solvent instead of methanol in the preparation of **2***a* resulted in only a small reduction in yield (entry 4) while aprotic solvents such as chloroform or diglyme afforded significantly lower yields of **2***b* (entries 7 and 8). Hydrazines **1***f* and **1***g* were oxidized as their sulfates (entries 14–16); an attempt to react the free base of **1***g* with seleninic acid **3** resulted in the recovery of starting material. The low reactivity of the latter compound is in part attributed to its poor solubility in methanol, and may to a large extent be circumvented by employment of the sulfate salt.

[1]Author to whom correspondence should be addressed.

0008-4042/82/212711-08$01.00/0

©1982 National Research Council of Canada/Conseil national de recherches du Canada

Can. J. Chem. Downloaded from www.nrcresearchpress.com by 210.87.254.42 on 09/06/12
For personal use only.

TABLE 1. Preparation of tetrazenes

| Entry | Hydrazine **1**, $R_2N$ | Oxidant | Yield of **2** (%)[a] | Conditions[b] |
|---|---|---|---|---|
| 1 | **1***a*  | **3** | 74 | Standard |
| 2 | **1***a* | **3** | 39 | Slow addition of **3** |
| 3 | **1***a* | **3** | 7 | Slow addition of **1***a* |
| 4 | **1***a* | **3** | 60 | $H_2O$ solvent, RT |
| 5 | **1***a* | $SeO_2$ | 73 | Standard |
| 6 | **1***b*  | **3** | 78 | Standard |
| 7 | **1***b* | **3** | 40 | $CHCl_3$ solvent |
| 8 | **1***b* | **3** | 43 | Diglyme solvent, RT |
| 9 | **1***b* | $SeO_2$ | 32 | Standard |
| 10 | **1***c*  | **3** | 75 | Standard |
| 11 | **1***d* $Me_2N$ | **3** | 28[c] | Standard |
| 12 | **1***e* $(PhCH_2)_2N$ | **3** | 75 | Standard |
| 13 | **1***e* | $SeO_2$ | 39[d] | RT |
| 14 | **1***f*[e]  | **3** | 96 | Standard |
| 15 | **1***f*[e] | $SeO_2$ | Trace | RT |
| 16 | **1***g*[e]  | **3** | 86 | RT |

[a]Isolated yield unless otherwise noted.
[b]Standard conditions are described in the experimental section. Any deviations with respect to the mode of addition, solvent, or temperature are indicated in the table. RT = room temperature.
[c]Determined by uv.
[d]Isolated as a mixture with hydrazone **8**; yield determined by integration of the nmr spectrum.
[e]Employed as the sulfate salt.

The use of selenium dioxide in lieu of seleninic acid **3** (entries 5, 9, 13, and 15) was found to give capricious results. For example, *N*-aminopiperidine (**1***a*) gave comparable yields of **2***a* with the two oxidants, while the similar morpholine derivative **1***b* afforded a much lower yield of **2***b* with selenium dioxide. Furthermore, the latter oxidant provided a poor yield of tetrazene **2***e* from **1***e* and failed to react significantly with hydrazine **1***f* even after a longer than normal reaction time at room temperature instead of at −10°C. The use of selenium dioxide also results in the formation of finely divided red selenium as a by-product, which poses additional difficulties during work-up. Consequently, the use of the dioxide in place of seleninic acid **3** is generally not recommended.

Compelling evidence exists for the formation of intermediate *N*-aminonitrenes (1,1-diazenes) **5** in the oxidations of 1,1-disubstituted hydrazines with certain other reagents such as lead tetraacetate (15). Trapping experiments employing olefins (16, 17) or sulfoxides (16, 18) have resulted in the formation of high yields of *N*-aminoaziridines and sulfoximines, respectively. In the case of the highly hindered and persistent *N*-(2,2,6,6-tetramethylpiperidyl)nitrene (**6**), direct characterization by spectroscopic methods was achieved at low temperatures (19–21). Tetrazene formation may result from the further reaction of the aminonitrenes with their precursor hydrazines to produce tetrazanes **7**, which in turn are further oxidized to the final products. In several instances, the tetrazanes have been successfully isolated (22). The direct dimerization of aminonitrenes appears

Can. J. Chem. Downloaded from www.nrcresearchpress.com by 210.87.254.42 on 09/06/12
For personal use only.

Can. J. Chem. Downloaded from www.nrcresearchpress.com by 210.87.254.42 on 09/06/12
For personal use only.

to be a less common source of tetrazenes, but evidence for such a process has been provided for the dimerization of **6** to tetrazene **2***h* (20). These processes are illustrated in Scheme 1.

Several of our results indicate that a different mechanism is involved in the present oxidations of hydrazines **1** with **3**. First, the fragmentation of *N*-(dibenzylamino)nitrene to bibenzyl and nitrogen is known to compete favourably with tetrazene formation, frequently providing the major product (6, 9, 10, 23, 24). In contrast, the oxidation of **1***e* with **3** affords no significant amount of bibenzyl, producing instead the tetrazene **2***e* (75%) and hydrazone **8** (22%) as the principal products. Furthermore, aminonitrenes bearing α-hydrogens are capable of tautomerization to the dipolar species **9** (24, 25), a process which is favoured in protic solvents (24). Under such conditions, *N*-piperidino and *N*-morpholinonitrenes are reported to produce cyclic dimers **10**, to the nearly complete exclusion of the corresponding tetrazenes (24). Again, these results contrast with the present system wherein higher yields of tetrazenes **2***a* and **2***b* were produced in protic solvents such as methanol or water than in aprotic solvents such as chloroform or diglyme (see Table 1, entries 1, 4, and 6–8). The trapping of *N*-phthalimidonitrene with dimethyl sulfoxide during the oxidation of **1***g* with **3** was also studied. The sulfoximine **11** had previously been obtained in 74% yield when hydrazine **1***g* was treated with lead tetraacetate in dimethyl sulfoxide (18). However, the present

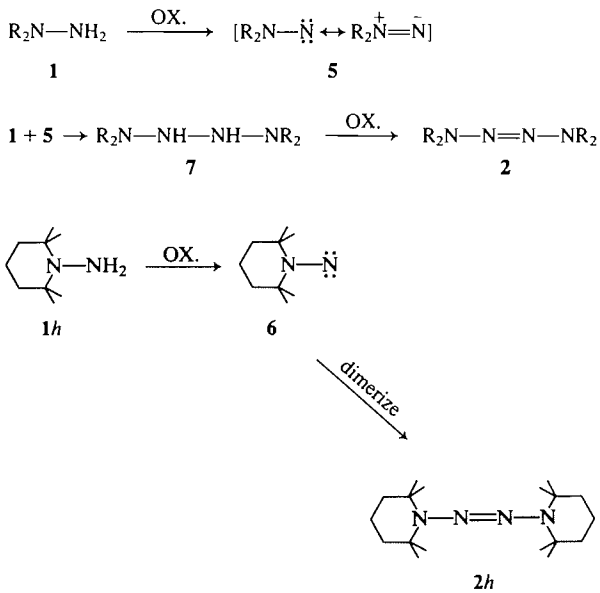


SCHEME 1

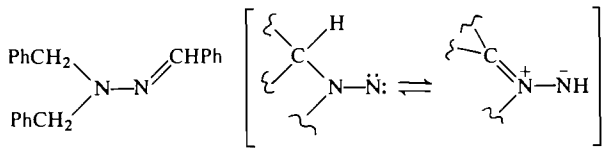


8 9

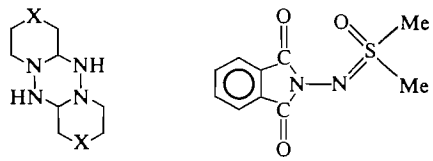


10 X = $CH_2$ or O 11

reaction with **3** afforded the far lower yield of 18% of adduct **11**. These experiments suggest that pathways other than those displayed in Scheme 1 occur in the present oxidations, and that aminonitrene intermediates do not account for a substantial portion of the products obtained.[2]

An attempt was also made to detect the formation of aminonitrene **6** in the oxidation of hydrazine **1***h* with **3**. Since intermediate **6** is known to be stable at −78°C and to possess a deep purple colour (21), its direct observation should be possible if it is produced in the present oxidation at similar temperatures. Unfortunately, the highly hindered parent hydrazine **1***h* failed to react with the seleninic acid below −5°C. At higher temperatures, nitrogen evolution occurred, accompanied by decomposition to a complex mixture of unidentified products. Conclusions regarding the intermediacy of aminonitrene **6** in the present oxidation of **1***h* are therefore precluded.

A plausible mechanism for tetrazene formation which circumvents the need for aminonitrene intermediates is shown in path a of Scheme 2. Seleninylation of **1** with **3** produces seleninamide **12**, resulting in a Pummerer-type reaction catalyzed by the seleninic acid. The Pummerer intermediate **14**

[2]A referee has commented that the evidence for aminonitrene intermediates is not compelling for all reported cases where 1,1-disubstituted hydrazines are oxidized to tetrazenes. We agree that the mechanisms of such oxidations may not be identical in all situations. However, solid evidence for the formation of aminonitrenes has been demonstrated in many of the oxidations cited above, and such species are widely accepted as being common intermediates in these processes. We therefore feel that it is not unreasonable to attribute the observed differences between our results and those in the literature to the fact that the latter reactions involve aminonitrenes as their authors suggest, whereas ours do not.

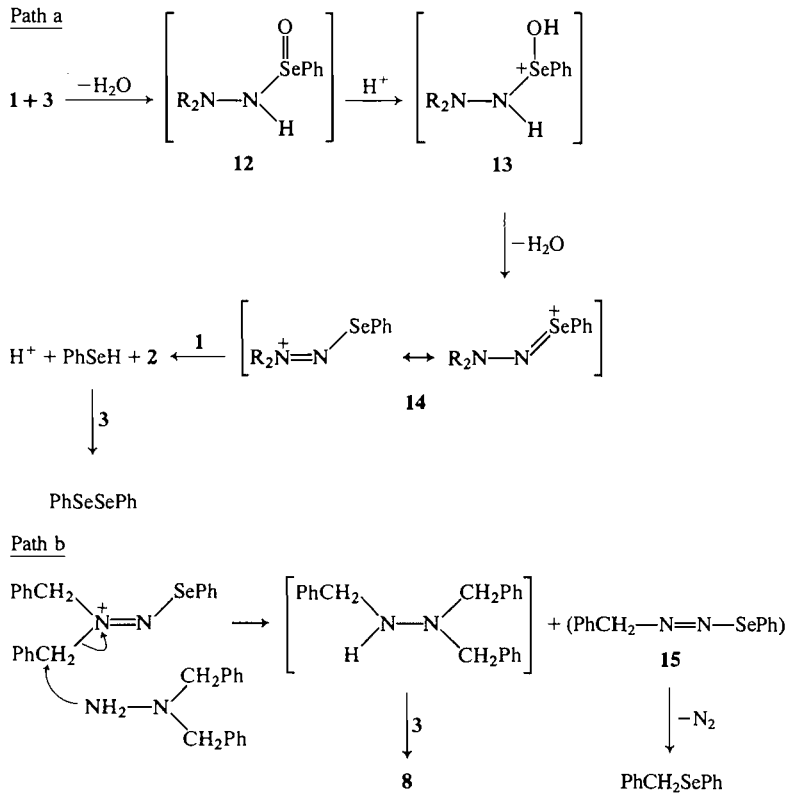


SCHEME 2

is thus generated via species **13**.[3] The further reaction of **14** with hydrazine **1** then affords the product tetrazene with concomitant formation of benzeneselenol, which is readily oxidized to diphenyl diselenide by the seleninic acid. Related Pummerer reactions of selenoxides have been previously reported (26–32) and seleninic acid **3** is known to be an effective catalyst in these processes (26, 27). The use of polar solvents such as methanol or water may facilitate these transformations by solvation of the ionic intermediates shown in the above scheme. The formation of hydrazone **8** in the oxidation of *N*,*N*-dibenzylhydrazine **1***e* is also consistent with the Pummerer reaction in Scheme 2. The Pummerer intermediate **14** may undergo attack by hydrazine **1***e* at one of the benzylic positions instead of at the *N'*-nitrogen atom (path b), resulting in the formation of tribenzylhydrazine and diazene **15**. Further oxidation of the hydrazine by **3** leads to the observed product **8**, while nitrogen extrusion from **15** provides benzyl phenyl selenide, a small amount of which was also isolated from the reaction mixture. Additional support for these steps derives from literature precedents. The formation of **8** from tribenzylhydrazine closely resembles the oxidation of certain amines with the related oxidants benzeneseleninyl chloride (33) and anhydride **4** (34) to produce imine intermediates. Also, nitrogen extrusions from aryl or acyl analogues of **15** have previously been postulated to account for the observed formation of aryl phenyl selenides and selenoesters in the oxidations of arylhydrazines or hydrazides with **3** (11). The transformations depicted in Scheme 2 are therefore entirely consistent with both the present and previous observations.

[3]The conversion of **12** to **14** could also be achieved by seleninylation rather than protonation of the seleninamide oxygen atom by **3**, resulting in the formation of intermediate **i** in lieu of **13**. Similarly, oxidations performed with methanolic selenium dioxide (dimethyl selenite) could proceed via intermediates **ii** or **iii**.

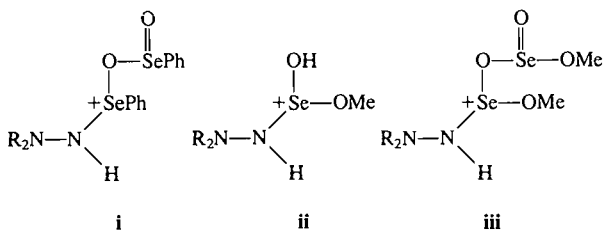


Can. J. Chem. Downloaded from www.nrcresearchpress.com by 210.87.254.42 on 09/06/12
For personal use only.

Can. J. Chem. Downloaded from www.nrcresearchpress.com by 210.87.254.42 on 09/06/12
For personal use only.

We also report that certain 1,1-disubstituted hydrazines undergo anomalous oxidations with seleninic acid **3**. Thus, *N*-methyl-*N*-phenylhydrazine (**1***i*) afforded a complex mixture which provided *N*-methyl-*p*-(phenylseleno)aniline (**16**) as the only recognizable component. Similarly, the oxidation of *N*,*N*-diphenylhydrazine (**1***j*) produced a mixture containing at least ten components, whose identification was not attempted. It therefore appears that this method is unsuitable for the preparation of tetrazenes bearing aryl substituents.

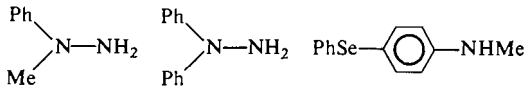


**1***i* **1***j* **16**

The oxidation of *N*-benzyl-*N*-*p*-toluenesulfonylhydrazine (**1***k*) with **3** also proved to be anomalous. When the reaction was performed in chloroform, the principal products were the sulfone **17**, the sulfinate ester **18**, and the selenosulfonate **19**, isolated in yields of 38%, 25%, and 30% respectively, along with diphenyl diselenide. These results suggest that the ambident *p*-toluenesulfinate anion is formed as an intermediate and undergoes either *S*- or *O*-benzylation, or selenenylation to afford the respective products **17**–**19**. Scheme 3 illustrates a possible mechanism in which the elimination of *p*-toluenesulfinic acid from the initially formed intermediate **20** (analogous to **12** in Scheme 2) simultaneously generates the putative benzylating species **21**. The alkylation of the sulfinate anion with the latter (or with benzyldiazonium ion derived from its decomposition) affords the observed products **17** and **18** as well as benzeneselenenic acid (**22**). Any sulfinic acid which escapes benzylation can react with the selenenic acid to furnish the selenosulfonate **19**. A similar reaction has been previously employed by Gancarz and Kice (35) to prepare this selenosulfonate from its corresponding sulfinic acid. The known disproportionation (36, 37) of unreacted selenenic acid accounts for the formation of diphenyl diselenide. A small amount of benzyl phenyl selenide was also produced. Finally, additional evidence for the presence of an electrophilic benzylating agent such as **21** (or the related diazonium species) derives from an analogous experiment performed in methanol. In this case, the nucleophilic solvent effectively competes with the sulfinic acid to produce benzyl methyl ether in 70% yield. The previous benzylation of the sulfinic acid is thus suppressed and it is free to react instead with selenenic acid **22**. Consequently, an enhanced

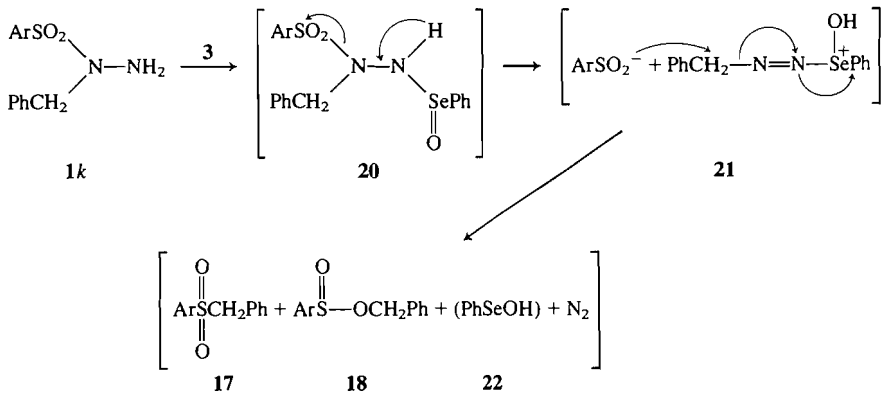


**1***k* **20** **21**

**17** **18** **22**

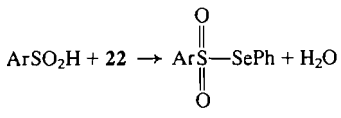


**19**

SCHEME 3[a]

[a]Ar = *p*-tolyl.

Can. J. Chem. Downloaded from www.nrcresearchpress.com by 210.87.254.42 on 09/06/12
For personal use only.

yield of 71% of selenosulfonate **19** is obtained under these conditions.[4]

It is evident that the oxidation of 1,1-disubstituted hydrazines with benzeneseleninic acid, and less reliably with selenium dioxide, provides facile access to a variety of tetrazenes. Anomalous results are expected in those cases where the hydrazine contains aryl substituents, leaving groups such as the sulfonyl moiety, or where it is highly hindered.

## Experimental

*General*

Melting points were determined on an A. H. Thomas hot stage apparatus. Ultraviolet and ir spectra were recorded on a Varian–Cary 219 and a Perkin–Elmer 467 spectrometer, respectively. The nmr spectra were obtained on a Hitachi Perkin–Elmer R24B instrument at 60 MHz or on a Varian XL-200 spectrometer at 200 MHz. All nmr spectra were taken in $CDCl_3$ solution and are reported in ppm (δ) downfield from TMS as the internal standard. Mass spectra were recorded on a Varian MAT CH5 instrument. Elemental analyses were obtained by Mr. L. Malek. Preparative tlc was performed on Analtech 20 × 20 cm glass plates coated with 1 mm of silica gel GF. The gc analyses were carried out on a Varian 3700 instrument equipped with a flame ionization detector and a Varian CDS-111 electronic integrator. Stainless steel columns (1.8 m × 0.3 cm) packed with 10% OV-101 on Chromosorb WHP were used. Benzeneseleninic acid was either purchased from the Aldrich Chemical Co. or prepared from the nitric acid oxidation of diphenyl diselenide according to the method of Barton *et al.* (38). In the latter case, the initially formed nitrate salt was neutralized *in situ* with aqueous NaOH and reprecipitated with concentrated HCl. Literature methods were employed in the preparation of hydrazines **1***e* (39), **1***h* (3), and **1***k* (40). All other reagents were obtained from commercial sources. Diphenyl diselenide was produced in all of the hydrazine oxidations involving **3**, but was only isolated in a few representative examples.

*Preparation of Tetrazenes (see Table 1)*

N,N′-*Bis(piperidino)diazene* (**2**a)

*Under standard conditions*

A solution of *N*-aminopiperidine (**1***a*) (100 mg, 1.00 mmol) in 3 mL of MeOH was cooled to −10°C. Seleninic acid **3** (189 mg, 1.00 mmol) was added in a single portion and the solution rapidly turned yellow from the formation of diphenyl diselenide. After 5–10 min, the reaction mixture was allowed to warm to room temperature and the solvent was promptly removed *in vacuo*. The residue was separated by preparative tlc (20% EtOAc–hexane) to afford 72 mg (74%) of **2***a*; mp 42–43°C (lit. (6) mp 44°C) from EtOH–$H_2O$; identified by its ir and uv spectra (6); mass spectrum, *m/e* 196 ($M^+$).

*By slow addition*

When the seleninic acid in 5 mL of MeOH was added over 40 min (by a mechanically driven syringe pump) to the hydrazine in 3 mL of MeOH at −10°C and worked up as above, the yield of **2***a* was 38 mg (39%). Similarly, slow addition of **1***a* to **3** afforded 7 mg (7%) of **2***a*.

*In $H_2O$*

The reactants were stirred 2 h in 5 mL of $H_2O$ at room temperature. The solution was then extracted with 3 × 5 mL of $CHCl_3$, the combined organic layers were dried ($MgSO_4$) and chromatographed in the usual manner to provide 59 mg (60%) of **2***a*. Gas chromatographic analysis prior to work-up revealed no detectable *N*-nitrosopiperidine.

*With $SeO_2$ as oxidant*

A solution of $SeO_2$ (111 mg, 1.00 mmol) in 1 mL of MeOH was added in one portion to hydrazine **1***a* in 2 mL of MeOH at −10°C. A red precipitate (selenium) rapidly formed. After 5–10 min, the reaction mixture was evaporated to dryness *in vacuo*, triturated with $CHCl_3$, filtered through Celite, and chromatographed in the usual manner. The yield of **2***a* was 72 mg (73%).

N,N′-*Bis(morpholino)diazene* (**2**b)

*Under standard conditions*

*N*-Aminomorpholine (**1***b*) (102 mg, 1.00 mmol) was oxidized with **3** (189 mg, 1.00 mmol) as in the case of **1***a*. Preparative tlc (40% EtOAc – hexane) afforded 78 mg (78%) of **2***b*; mp 153–155°C (lit. (6) mp 157°C) from MeOH; identified by its ir and uv spectra (6); mass spectrum, *m/e* 200 ($M^+$). A more mobile component provided 88 mg of diphenyl diselenide, identified by comparison with an authentic sample (mp, tlc). Attempts to crystallize **2***b* directly from the reaction mixture resulted in contamination with diphenyl diselenide.

*In aprotic solvents*

When the above reaction was repeated in chloroform at −10°C or in diglyme at room temperature, the yield of **2***b* was 40% and 43% respectively.

*With $SeO_2$ as oxidant*

Hydrazine **1***b* (102 mg, 1.00 mmol) was oxidized with $SeO_2$ (111 mg, 1.00 mmol) as described for **1***a*. The yield of **2***b* was 32 mg (32%).

N,N′-*Bis(2,6-dimethylpiperidino)diazene* (**2**c)

*N*-Amino-2,6-dimethylpiperidine (**1***c*) (128 mg, 1.00 mmol) was oxidized with **3** (189 mg, 1.00 mmol) under the standard conditions described for **1***a*. Preparative tlc (25% EtOAc – hexane) afforded 95 mg (75%) of **2***c*, which solidified upon cooling; mp 36–40°C (lit. (5) mp 44–45°C); uv (MeCN), $\lambda_{max}$: 249 nm (ε 9800), 284 nm (sh, ε 2500); ir (film): 1455, 1370, 1320, 1282, 1212, 1110, 1054 $cm^{-1}$; Raman spectrum, 1445 $cm^{-1}$ (N=N); nmr (200 MHz) δ: 3.52 (m, 4H, CH), 1.85–1.4 (complex, 12H, $CH_2$), 1.05 (d, $J$ = 6.6 Hz, 12H, $CH_3$); mass spectrum, *m/e* 252 ($M^+$).

N,N′-*Bis(dimethylamino)diazene* (**2**d)

*N*,*N*-Dimethylhydrazine (**1***d*) (60 mg, 1.00 mmol) was oxidized with **3** (95 mg, 0.50 mmol) under the standard conditions described for **1***a*. Volatile material was distilled, first at 20 Torr then at 0.05 Torr pressure, into a cold trap maintained at −78°C. Ultraviolet analysis of the distillate (lit. (25) uv (MeOH) $\lambda_{max}$: 277 nm, log ε 3.92) indicated the presence of 16 mg

[4]The formation of **19** in methanol solution could also arise from the diazene **v**, in turn derived from the methanolysis of **iv**. However, the formation of **17** and **18** in chloroform solution would be difficult to rationalize from species **iv**. A free radical mechanism for the oxidation of **1***k* cannot be entirely ruled out, but again would not readily explain the formation of benzyl methyl ether in methanol solution.

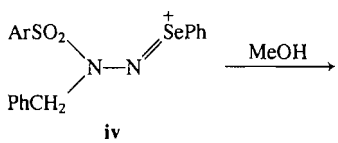


**iv**

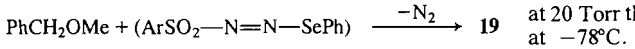


**v**

Can. J. Chem. Downloaded from www.nrcresearchpress.com by 210.87.254.42 on 09/06/12
For personal use only.

(28%) of **2***d*. A slightly lower yield was obtained when an equimolar amount of **3** was employed.

N,N′-*Bis(dibenzylamino)diazene (2*e)

*Under standard conditions*

*N,N*-Dibenzylhydrazine (**1***e*) (212 mg, 1.00 mmol) was oxidized with **3** (189 mg, 1.00 mmol) as in the case of **1***a*. A white, crystalline precipitate formed within several seconds and was filtered after 10 min to afford 158 mg (75%) of **2***e*; mp 95–98°C (lit. (9) mp 95–96°C); uv (MeOH) $\lambda_{max}$: 287 nm (ε 12 000); ir ($CHCl_3$): 1607, 1497, 1457, 1352, 957, 700 $cm^{-1}$; nmr (60 MHz) δ: 7.12 s, 20H, Ph), 4.30 (s, 8H, $CH_2$); mass spectrum, *m/e* 420 ($M^+$). The filtrate was concentrated and separated by preparative tlc (50% $C_6H_6$ – hexane) to give 33 mg (22%) of hydrazone **8**, mp 81–82°C (from MeOH), identical (mp, ir, nmr) to an authentic sample prepared from **1***e* and benzaldehyde. A more mobile band was rechromatographed (20% $CCl_4$ – hexane) to afford 100 mg of diphenyl diselenide and 6 mg of benzyl phenyl selenide, identified by its nmr and mass spectra.

*With $SeO_2$ as oxidant*

Hydrazine **1***e* (106 mg, 0.50 mmol) and $SeO_2$ (56 mg, 0.50 mmol) were stirred in 3 mL of MeOH at room temperature. A red precipitate (selenium) gradually appeared. After 10 min, the solution was worked up as in the case of **1***a*. Preparative tlc (50% $C_6H_6$ – hexane) afforded 77 mg of an unseparated mixture of **2***e* and **8**, whose respective yields of 39% and 47% were determined from the integrated intensities of their nmr signals.

trans-*3,3′-Bis(2-oxazolidinonyl)diazene (2*f)

*Under standard conditions*

3-Amino-2-oxazolidinone sulfate (**1***f*) (100 mg, 0.50 mmol) was oxidized with **3** (95 mg, 0.50 mmol) as in the case of **1***a*. The reaction mixture was allowed to warm to room temperature and an insoluble white solid was filtered to afford 48 mg (96%) of **2***f*; mp 295–300°C dec. (lit. (4) mp 298–299°C); identified by its uv and ir spectra (4).

*With $SeO_2$ as oxidant*

When $SeO_2$ was employed instead of **3** in the above procedure, the filtered solid consisted of starting material **1***f* contaminated by a trace of tetrazene **2***f* (detected by tlc) even after a reaction time of 43 h at room temperature.

trans-N,N′-*Bis(phthalimido)diazene (2*g)

*N*-Aminophthalimide (**1***g*) (162 mg, 1.00 mmol), seleninic acid **3** (189 mg, 1.00 mmol), and sulfuric acid (98 mg, 1.00 mmol) were stirred 45 min in 3 mL of MeOH at room temperature. An insoluble white solid was then filtered to afford 137 mg (86%) of **2***g*; mp 295°C dec. (lit. (8) mp 294–299°C dec.); identified by its ir and mass spectra (8). When the experiment was performed without sulfuric acid, only unreacted **1***g* was recovered.

*Trapping of* N-*phthalimidonitrene from 1*g *and 3 with DMSO*

Hydrazine **1***g* (81 mg, 0.50 mmol) and seleninic acid **3** (95 mg, 0.50 mmol) were stirred in 1 mL of dry DMSO at room temperature. After 10 min, DMSO was removed from the yellow solution *in vacuo* and the residue was separated by preparative tlc (10% MeOH – $CHCl_3$) to provide, in decreasing order of mobility, 74 mg of diphenyl diselenide, 11 mg (15%) of phthalimide, identical to an authentic sample (mp, tlc, ir), and 21 mg (18%) of *S,S*-dimethyl-*N*-phthalimidosulfoximine (**11**); mp 208–210°C (lit. (18) mp 208–210°C); nmr (60 MHz) δ: 7.75 (m, 4H, aromatic), 3.28 (s, 6H, $CH_3$), with ir and mass spectra as reported in the literature (18). More polar components were poorly separated and were not further investigated.

*Oxidation of* N-*amino-2,2,6,6-tetramethylpiperidine (1*h) *with 3*

Hydrazine **1***h* (70 mg, 0.45 mmol) and seleninic acid **3** (85 mg, 0.45 mmol) were added to 5 mL of MeOH at −70°C. No reaction was evident and the mixture was slowly permitted to warm to room temperature. At ca. −5°C, a yellow colour appeared and gas evolution commenced, becoming increasingly vigorous as warming continued. No significant amount of tetrazene **2***h* could be isolated from the mixture. When the reaction was repeated in $CDCl_3$ solution at room temperature, copious gas evolution occurred and the nmr spectrum of the remaining solution revealed a complex mixture of products.

*Oxidation of* N-*methyl*-N-*phenylhydrazine (1*i) *and* N,N-*diphenylhydrazine (1*j) *with 3*

Hydrazine **1***i* (122 mg, 1.00 mmol) was oxidized with **3** (189 mg, 1.00 mmol) under the standard conditions described for **1***a*. Separation by preparative tlc (20% EtOAc – hexane) afforded 75 mg (29%) of *N*-methyl-*p*-phenylselenoaniline (**16**) as an oil, identical to an authentic sample (*vide infra*) in all respects, as well as a large number of unidentified products. The similar oxidation of **1***j* produced an extremely complex mixture containing at least ten components (tlc), which was not further investigated.

N-*Methyl*-p-*phenylselenoaniline (16)*

Freshly redistilled *N*-methylaniline (107 mg, 1.00 mmol) and benzeneselenenyl chloride (191.5 mg, 1.00 mmol) were stirred 3 min in 3 mL of MeOH at room temperature. The reaction mixture was evaporated *in vacuo* and separated as in the preceding procedure to provide 73 mg (28%) of **16**; ir (film): 3425, 1595, 1577, 1500, 1475, 1435, 1318, 1290, 1260, 1180, 1019, 810, 730, 685 $cm^{-1}$; nmr (200 MHz) δ: 7.44 (d, $J$ = 8.5 Hz, 2H, $C_6H_4$), 7.35–7.10 (m, 5H, Ph), 6.55 (d, $J$ = 8.5 Hz, 2H, $C_6H_4$), 3.86 (br s, exchanged, 1H, NH), 2.84 (s, 3H, $CH_3$); mass spectrum, *m/e* 263 ($M^+$, $^{80}Se$), 261 ($M^+$, $^{78}Se$). *Anal.* calcd. for $C_{13}H_{13}NSe$: C 59.54, H 5.01, N 5.34; found: C 59.51, H 5.02, N 5.36.

*Oxidation of* N-*benzyl*-N-p-*toluenesulfonylhydrazine (1*k) *with 3*

*In $CHCl_3$*

Hydrazine **1***k* (138 mg, 0.50 mmol) and seleninic acid **3** (95 mg, 0.50 mmol) were stirred 10 min in 5 mL of $CHCl_3$ at room temperature. A vigorous reaction with gas evolution was observed. The reaction mixture was concentrated *in vacuo* and separated by preparative tlc (20% EtOAc – hexane) to afford three main components. The top band provided 30 mg of a yellow oil consisting of diphenyl diselenide and benzyl phenyl selenide in a molar ratio of 57:43 (yield of selenide: 9%), as determined by integration of the nmr spectrum of the mixture. The identities of these two products was confirmed by gc – mass spectral analysis. The second band was further separated by preparative tlc ($CH_2Cl_2$) to give 46 mg (30%) of selenosulfonate **19**, identical to an authentic sample (12) (mp, ir, nmr), and 31 mg (25%) of benzyl *p*-toluenesulfinate (**18**) obtained as an oil (lit. (41) mp 22–24°C); ir (film): 1596, 1499, 1455, 1132 $cm^{-1}$; nmr spectrum as reported in the literature (42). The bottom component afforded 47 mg (38%) of sulfone **17**, mp 140–144°C (lit. (43) mp 144–145°C), identified by its ir and nmr spectra (44).

*In MeOH*

The above reaction was repeated in 5 mL of MeOH. The solution slowly turned clear and yellow. An internal standard (*p*-xylene) was added after 45 min at room temperature and gc analysis revealed the presence of 43 mg (70%) of benzyl methyl ether, further identified by gc – mass spectrometry. The mixture was then separated by preparative tlc ($CH_2Cl_2$) to afford 16 mg of diphenyl diselenide containing a trace of benzyl phenyl selenide, 111 mg (71%) of selenosulfonate **19**, and 25 mg (20%) of sulfinate ester **18**.

## Acknowledgements

We thank the Natural Sciences and Engineering

Research Council of Canada for financial support and Dr. R. A. Kydd for the Raman spectrum of compound **2***c*.


1. D.-H. BAE and H. J. SHINE. J. Org. Chem. **45**, 4448 (1980).
2. S. F. NELSEN and D. H. HEATH. J. Am. Chem. Soc. **91**, 6452 (1969).
3. J. R. ROBERTS and K. U. INGOLD. J. Am. Chem. Soc. **95**, 3228 (1973).
4. P. S. FORGIONE, G. S. SPRAGUE, and H. J. TROFFKIN. J. Am. Chem. Soc. **88**, 1079 (1966).
5. C. G. OVERBERGER, L. C. PALMER, B. S. MARKS, and N. R. BYRD. J. Am. Chem. Soc. **77**, 4100 (1955).
6. I. BHATNAGAR and M. V. GEORGE. J. Org. Chem. **33**, 2407 (1968).
7. G. S. HAMMOND, B. SEIDEL, and R. E. PINCOCK. J. Org. Chem. **28**, 3275 (1963).
8. D. W. JONES. J. Chem. Soc. Perkin Trans. I, 1150 (1976).
9. R. L. HINMAN and K. L. HAMM. J. Am. Chem. Soc. **81**, 3294 (1959).
10. C. G. OVERBERGER and B. S. MARKS. J. Am. Chem. Soc. **77**, 4104 (1955).
11. T. G. BACK, S. COLLINS, and R. G. KERR. J. Org. Chem. **46**, 1564 (1981).
12. T. G. BACK and S. COLLINS. Tetrahedron Lett. 2213 (1980).
13. D. H. R. BARTON, D. J. LESTER, and S. V. LEY. J. Chem. Soc. Perkin Trans. I, 1212 (1980).
14. T. G. BACK. J. Chem. Soc. Chem. Commun. 530 (1981).
15. T. L. GILCHRIST and C. W. REES. *In* Carbenes, nitrenes and arynes. Studies in modern chemistry. Thomas Nelson and Sons, London. 1969. pp. 36–40.
16. D. J. ANDERSON, T. L. GILCHRIST, D. C. HORWELL, and C. W. REES. Chem. Commun. 146 (1969).
17. R. S. ATKINSON and C. W. REES. Chem. Commun. 1230 (1967).
18. D. J. ANDERSON, D. C. HORWELL, E. STANTON, T. L. GILCHRIST, and C. W. REES. J. Chem. Soc. Perkin Trans. I, 1317 (1972).
19. P. B. DERVAN, M. E. SQUILLACOTE, P. M. LAHTI, A. P. SYLWESTER, and J. D. ROBERTS. J. Am. Chem. Soc. **103**, 1120 (1981).
20. W. D. HINSBERG III and P. B. DERVAN. J. Am. Chem. Soc. **101**, 6142 (1979).
21. W. D. HINSBERG III and P. B. DERVAN. J. Am. Chem. Soc. **100**, 1608 (1978).
22. D. J. ANDERSON, T. L. GILCHRIST, and C. W. REES. Chem. Commun. 800 (1971).
23. M. BUSCH and B. WEISS. Ber. **33**, 2701 (1900).
24. D. M. LEMAL and T. W. RAVE. J. Am. Chem. Soc. **87**, 393 (1965).
25. D. M. LEMAL, F. MENGER, and E. COATS. J. Am. Chem. Soc. **86**, 2395 (1964).
26. T. G. BACK, N. IBRAHIM, and D. J. MCPHEE. J. Org. Chem. In press.
27. T. G. BACK and N. IBRAHIM. Tetrahedron Lett. 4931 (1979).
28. B. E. NORCROSS, J. M. LANSINGER and R. L. MARTIN. J. Org. Chem. **42**, 369 (1977).
29. H. J. REICH and S. K. SHAH. J. Org. Chem. **42**, 1773 (1977).
30. K. B. SHARPLESS and K. M. GORDON. J. Am. Chem. Soc. **98**, 300 (1976).
31. H. J. REICH, J. M. RENGA, and I. L. REICH. J. Am. Chem. Soc. **97**, 5434 (1975).
32. Y. OKAMOTO, K. L. CHELLAPPA, and R. HOMSANY. J. Org. Chem. **38**, 3172 (1973).
33. M. R. CZARNY. Synth. Commun. **6**, 285 (1976).
34. M. R. CZARNY. J. Chem. Soc. Chem. Commun. 81 (1976).
35. R. A. GANCARZ and J. L. KICE. J. Org. Chem. **46**, 4899 (1981).
36. T. HORI and K. B. SHARPLESS. J. Org. Chem. **43**, 1689 (1978).
37. H. J. REICH, S. WOLLOWITZ, J. E. TREND, F. CHOW, and D. F. WENDELBORN. J. Org. Chem. **43**, 1697 (1978).
38. D. H. R. BARTON, S. V. LEY, P. D. MAGNUS, and M. N. ROSENFELD. J. Chem. Soc. Perkin Trans. I, 567 (1977).
39. M. J. S. DEWAR and W. B. JENNINGS. J. Am. Chem. Soc. **95**, 1562 (1973).
40. C. S. ROONEY, E. J. CRAGOE, JR., C. C. PORTER, and J. M. SPRAGUE. J. Med. Chem. Chim. Ther. **5**, 155 (1962).
41. A. H. WRAGG, J. S. MCFADYEN, and T. S. STEVENS. J. Chem. Soc. 3603 (1958).
42. J. W. WILT and W. J. WAGNER. Chem. Ind. 1389 (1964).
43. R. C. WEAST (*Editor*). CRC handbook of chemistry and physics. 58th ed. CRC Press, Cleveland. 1977. p. C-506.
44. W. W. SIMONS (*Editor*). The Sadtler handbook of infrared spectra and The Sadtler handbook of proton nmr spectra. Sadtler–Heyden, Philadelphia. 1978.


Can. J. Chem. Downloaded from www.nrcresearchpress.com by 210.87.254.42 on 09/06/12
For personal use only.

# Le photocatalyseur $MoO_3/SiO_2$: activité et structure

ARNAUD MAHAY ET SERGE KALIAGUINE
*Département de génie chimique. Université Laval, Québec (Qué.), Canada G1K 7P4*
ET
PIERRE C. ROBERGE
*Département de chimie, Université Laval, Québec (Qué.), Canada G1K 7P4*

Reçu le 15 avril 1982

ARNAUD MAHAY, SERGE KALIAGUINE et PIERRE C. ROBERGE. Can. J. Chem. **60**, 2719 (1982).

On a étudié l'activité d'un photocatalyseur $MoO_3/SiO_2$, constitué par un dépôt de molybdène sur de la silice, dans la réaction d'oxydation photocatalytique du cyclohexane par l'oxygène. Les résultats comparés à ceux du catalyseur $V_2O_5/SiO_2$ étudié précédemment, mettent en évidence un comportement du même type, notamment une recristallisation importante des espèces isolées photocatalytiquement actives, à la surface du catalyseur pendant la réaction. Ceci est confirmé par une analyse par spectroscopie de réflectance diffuse de la surface des catalyseurs avant et après réaction. L'ensemble de ces deux types de résultats fait apparaître deux types d'espèces superficielles: des cations $Mo^{+6}$ en coordination tétraédrique, actifs, isolés et fixes au cours de la réaction, et des cations $Mo^{+6}$ en coordination octaédrique liés sous forme d'espèces polymériques de surface, pouvant migrer dans les conditions de la réaction. Cette migration mène à une fixation et une agglomération de ces espèces octaédriques et à la possibilité de créer des ponts Mo—O—Mo entre une espèce tétraédrique et une octaédrique. Du fait de cette incorporation, la majorité des espèces tétraédriques conserve sa coordination mais perd son activité photocatalytique.

ARNAUD MAHAY, SERGE KALIAGUINE, and PIERRE C. ROBERGE. Can. J. Chem. **60**, 2719 (1982).

The activity of molybdenum oxide supported on silica gel ($MoO_3/SiO_2$) for the photocatalytic oxidation of cyclohexane has been investigated. A comparison of results with those obtained in a previous investigation with $V_2O_5/SiO_2$ indicates a similar behaviour, namely recrystallization involving photocatalytically active isolated species on the surface during the reaction. This has been confirmed by diffuse reflectance spectroscopic analysis of the catalysts before and after the reaction. From the two series of experimental results it can be concluded that two kinds of surface species exist: (1) $Mo^{+6}$ cations in tetrahedral coordination, isolated and fixed on the surface, are active in photocatalysis; (2) $Mo^{+6}$ cations in octahedral coordination, under the form of polymeric surface species, able to migrate in the conditions of the photocatalytic reaction. This migration leads to the fixation and agglomeration of these octahedral species and to the possible creation of Mo—O—Mo bridges between a tetrahedral and an octahedral species. In that case, the majority of the tetrahedral species does not change its coordination but loses its photocatalytic activity.

Can. J. Chem. Downloaded from www.nrcresearchpress.com by 210.87.254.5 on 09/06/12
For personal use only.

## Introduction

La photocatalyse hétérogène des réactions d'oxydation par l'oxygène en phase gazeuse a fait l'objet, au cours des dix dernières années, d'une importante activité de recherche. Certains ont mis à profit les conditions particulièrement douces de ces réactions (température et pression ambiantes) pour contrôler la sélectivité des oxydations partielles de différents hydrocarbures (1, 2). D'autres ont vu dans ces phénomènes une des étapes des cycles d'oxydoréduction impliquant le rayonnement et donc susceptibles d'être mis à profit pour le stockage chimique de l'énergie lumineuse (3–5). D'autres enfin étudient ces phénomènes pour les informations qu'ils fournissent sur la nature de la surface des solides photocatalyseurs (6, 7). Ces informations sont d'intérêt non seulement pour l'utilisation de ces catalyseurs en photocatalyse, mais également pour la compréhension de leur action en catalyse thermique classique.

Les objectifs du travail présenté ici, appartiennent à cette troisième catégorie. Nous nous sommes en effet intéressés aux dépôts d'oxydes de métaux de transition sur des supports isolants inertes tels que la silice. Ces catalyseurs ont le double avantage de présenter d'une part une grande surface exposée à la lumière, et d'autre part de permettre une grande dispersion de l'oxyde déposé ce qui permet des concentrations importantes de sites cationiques isolés les uns des autres à la surface du support.

Selon Kazansky et coll. (8), l'absorption du rayonnement ultraviolet et d'une partie du rayonnement visible par ce type de site mène à la formation d'un état de transfert de charge:

$$[1] \quad M^{n+} - O^{2-} + h\nu \rightleftarrows [M^{(n-1)+} \ldots O^-]^*$$

L'espèce activée $O^-$ s'est révélée très réactive, même à basse température.

Dans les travaux antérieurs de notre laboratoire, l'attention s'est portée sur des catalyseurs de ce type, susceptibles d'absorber dans la partie visible du spectre, à savoir le pentoxyde de vanadium déposé sur gel de silice ($V_2O_5/SiO_2$) (9) et le pentoxyde de tantale déposé sur gel de silice ($Ta_2O_5/SiO_2$) (10). Dans ce qui suit, nous présen-

0008-4042/82/212719-06$01.00/0
©1982 National Research Council of Canada/Conseil national de recherches du Canada

Can. J. Chem. Downloaded from www.nrcresearchpress.com by 210.87.254.5 on 09/06/12
For personal use only.

tons une étude sur les propriétés photocatalytiques du trioxyde de molybdène déposé sur gel de silice ($MoO_3/SiO_2$). Parallèlement nous avons effectué une étude des catalyseurs utilisés, par spectroscopie de réflectance diffuse uv–visible, qui dans le cas des dépôts d'oxyde de molybdène, fournit des informations relativement précises (11) sur l'état de coordination des cations molybdène à la surface du dépôt.

## Procédures expérimentales

*Préparation des catalyseurs*

Les catalyseurs ont été préparés par imprégnation d'un gel de silice par une solution aqueuse de paramolybdate d'ammonium (pH de 5 à 6), suivi d'un séchage à 120°C et d'une calcination dans l'air pendant une nuit à 500°C. L'imprégnation a été faite par la méthode dite de remplissage du volume total des pores pour laquelle le volume de la solution ne doit pas excéder celui des pores.

Le paramolybdate d'ammonium $[(NH_4)_6(Mo_7O_{24})4H_2O]$ est un produit de pureté garantie (Anachemia AC 630) dont les principales impuretés cationiques sont le plomb (0,001%) et le magnésium (0,02%). Le support est une silice commerciale (Fisher S662) garantie pure à 99,9%, de granulométrie 60 à 200 mesh et de surface spécifique voisine de 450 $m^2/g$.

La concentration du molybdène dans les différents catalyseurs, exprimée en pourcentage pondéral de molybdène a varié de 0,1 à 2%.

*Mesure de l'activité photocatalytique*

L'étude de l'activité photocatalytique a porté sur l'oxydation en phase gazeuse, du cyclohexane par l'oxygène. Le montage expérimental utilisé à cette fin a déjà été décrit dans une publication antérieure (12, 13). Il comporte un tube réacteur vertical en quartz, à la paroi intérieure duquel le catalyseur est disposé sous forme d'une couche de 2 mm d'épaisseur. Ce réacteur contient environ 50 g de catalyseur et la surface éclairée de cette couche est d'environ 350 $cm^2$. Il est entouré double enveloppe de quartz dans laquelle circule de l'eau distillée à température contrôlée. L'ensemble est placé au foyer d'un réflecteur elliptique en aluminium poli, l'autre foyer étant occupé par une lampe tubulaire au mercure à moyenne pression (Hanovia SS78 A16) d'une puissance nominale de 2 kW et émettant effectivement 700 W dans l'ultraviolet.

Les réactifs gazeux sont alimentés par le haut et un dispositif comportant un tube de céramique poreuse permet d'effectuer un soutirage continu sur toute la hauteur de la colonne. La sortie du réacteur est reliée à un chromatographe en phase gazeuse (F et M modèle 720) par une ligne en acier inoxydable et une vanne d'échantillonnage chauffées.

L'alimentation gazeuse est obtenue en faisant circuler un débit d'oxygène dans un saturateur à température contrôlée, contenant le cyclohexane. Le cyclohexane (Fisher C-552 ou Anachemia AC-2717-5) était d'une pureté minimale 99%. L'oxygène (Linde high purity) de pureté garantie 99,6% était débarrassé de traces d'eau et de dioxyde de carbone par passage sur une colonne de Driérite et une colonne d'Ascarite.

Tous les essais rapportés ici ont été obtenus dans des conditions dites standards, déjà utilisées dans les études antérieures (7, 9, 10). Ces conditions sont: un débit d'oxygène pur mesuré avant la saturation de 35 $cm^3/min$ ramené à TPN, une température de saturation de 35°C, ce qui assure une pression partielle de cyclohexane dans l'alimentation de 20,2 kPa, une température du réacteur de 60°C.

*Essais de réflectance diffuse*

Ces essais ont été effectués à l'aide d'un spectrophotomètre Bausch et Lomb Spectronic 505 muni d'une sphère intégrante et permettant des mesures dans le domaine spectral allant de 220 à 600 nm. Les échantillons étaient constitués de mélanges très homogènes de poudre de MgO (Fisher M 51) et de catalyseur en proportion pondérale de 50%, comprimés sous une force de 90 000 N, en pastilles de 38 mm de diamètre. La référence était une pastille de MgO et de gel de silice préparée dans les mêmes conditions.

De tels essais ont été effectués avec des catalyseurs fraîchement préparés ainsi qu'avec des catalyseurs ayant été utilisés plusieurs jours dans le réacteur. Dans ce dernier cas les échantillons ont été recalcinés dans l'air à 500°C pendant plusieurs heures avant la préparation de la pastille.

## Résultats expérimentaux et discussion

*Activité photocatalytique*

Dans les conditions standards décrites ci-dessus les produits observés de l'oxydation de cyclohexane sont le $CO_2$ et l'eau. Certains produits de l'oxydation partielle tels la cyclohexanone, l'éthanal et le propanal ne sont obtenus qu'à l'état de traces. En conséquence, nous avons choisi de repérer l'activité photocatalytique par la mesure du pourcentage molaire de $CO_2$ dans les gaz quittant le réacteur. Selon la teneur en molybdène du catalyseur, deux comportements ont été observés pour les variations de l'activité photocatalytique en fonction du temps de réaction. Pour les catalyseurs comportant un pourcentage de molybdène supérieur ou égal à 0,5%, on a obtenu un comportement dit de *type A* représenté à la figure 1. Après une période initiale où le pourcentage de $CO_2$ augmente très rapidement, un maximum est atteint et l'activité photocatalytique rediminue lentement pendant une période de plusieurs jours avant d'atteindre une valeur stationnaire. Dans ce cas le catalyseur prend rapidement une couleur verte. Pour les plus faibles valeurs de la teneur en molybdène on obtient le comportement dit de *type B*, représenté à la figure 2. L'activité photocatalytique augmente continuellement avec le temps jusqu'à atteindre une valeur stationnaire. Dans ce cas le catalyseur ne se colore que très légèrement, en raison de la faible concentration superficielle des espèces hydratées. La figure 3 donne les variations du pourcentage de $CO_2$ correspondant à l'activité stationnaire, en fonction de la teneur en molybdène du catalyseur. On voit que cette activité limite passe par un maximum pour une valeur du pourcentage en molybdène voisine de 0,75%.

Le passage d'un comportement de type B à un comportement de type A pour une valeur faible de la teneur en cations, ainsi que le changement du sens de la variation de l'activité stationnaire avec la concentration superficielle des cations, ont été

Can. J. Chem. Downloaded from www.nrcresearchpress.com by 210.87.254.5 on 09/06/12
For personal use only.

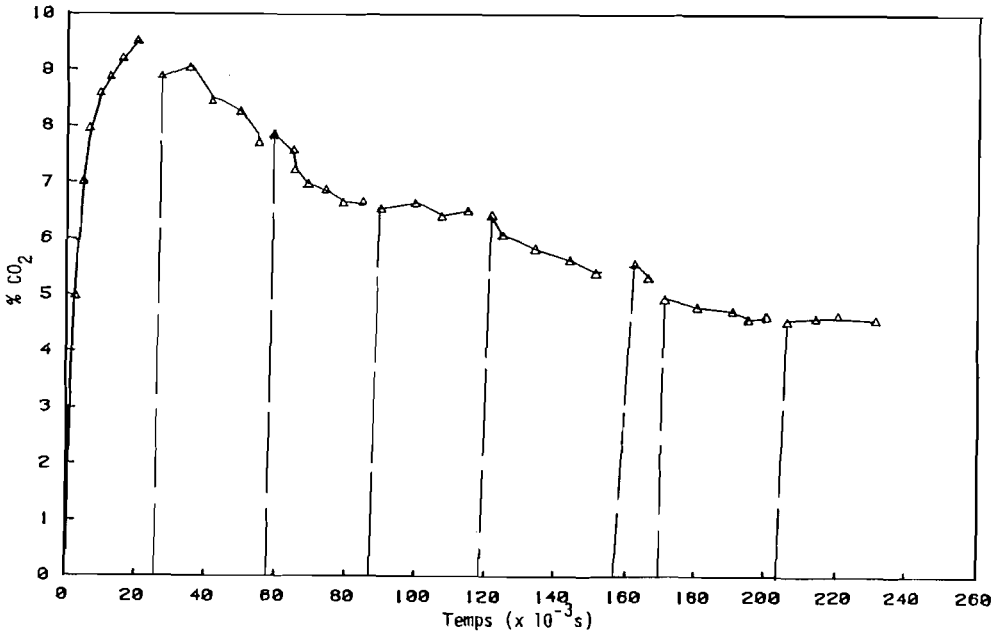


FIG. 1. Evolution de l'activité avec le temps pour le catalyseur de teneur 1% en molybdène (comportement de type A).

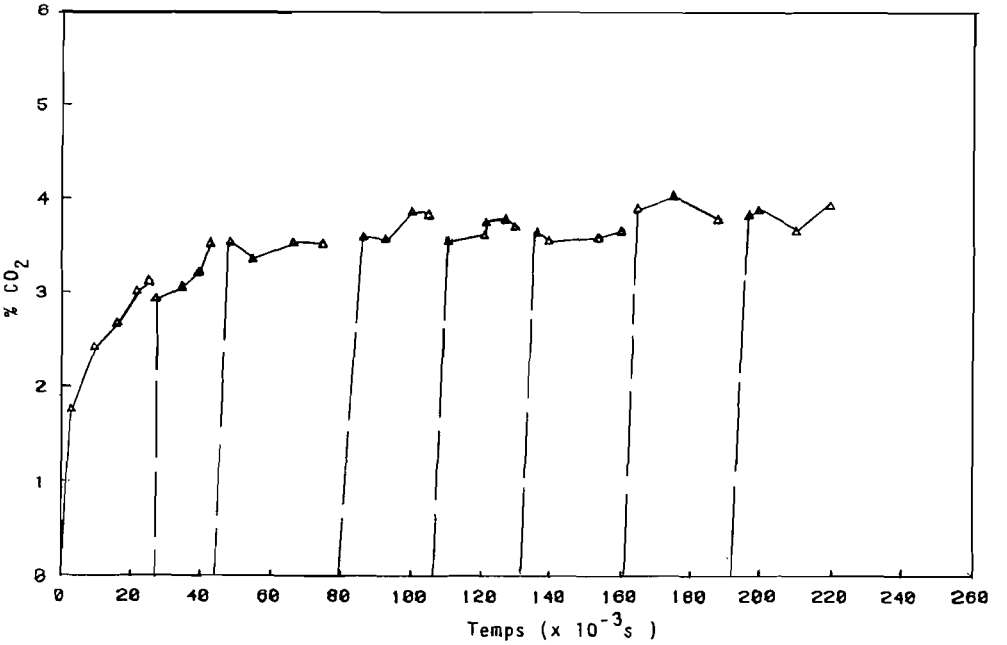


FIG. 2. Evolution de l'activité avec le temps pour le catalyseur de teneur 0,1% en molybdène (comportement de type B).

également observés avec le système $V_2O_5/SiO_2$ (9, 7). On peut donc interpréter les évolutions observées aux figures 1, 2 et 3 de la même façon que dans le cas de $V_2O_5/SiO_2$.

Les augmentations initiales d'activités aux figures 1 et 2 (mise à part la première demi-heure qui correspond à la mise en régime thermique de la lampe) sont associées à l'hydratation progressive des sites actifs. Comme l'ont montré Gristkov *et al.* (8), dans le cas de $V_2O_5/SiO_2$, l'hydratation du site

Can. J. Chem. Downloaded from www.nrcresearchpress.com by 210.87.254.5 on 09/06/12
For personal use only.

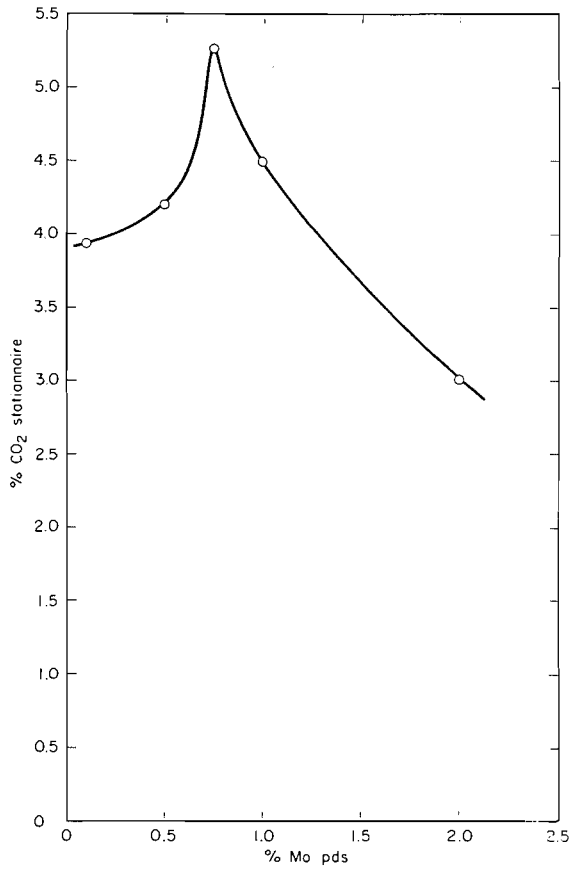


FIG. 3. Variation de l'activité stationnaire avec la teneur en molybdène.

déplace le seuil d'absorption de l'espèce active vers le rouge. L'augmentation d'activité serait alors liée à celle du nombre des photons absorbés par le site cationique, la source lumineuse utilisée étant polychromatique.

La diminution d'activité observée ensuite à la figure 1, est associée à une certaine mobilité des cations superficiels $Mo^{+6}$ dans les conditions de la réaction photocatalytique. Cette mobilité a pour effet une diminution de la dispersion des cations, qui forment des espèces oxymolybdiques polymériques bidimensionnelles et éventuellement des microcristaux superficiels de $MoO_3$. Si on admet que le site actif est un cation $Mo^{+6}$ isolé:

[2] 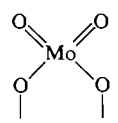


cette recristallisation provoque une diminution du nombre des sites actifs sur la surface. Plus la concentration totale en molybdène est élevée, plus cette diminution devrait être importante, ce qui correspond bien aux résultats de la figure 3. Par ailleurs, nous avons vérifié que la diminution d'activité était bien irréversible: un catalyseur d'une teneur de 1% en molybdène ayant été utilisé pendant plusieurs jours et ayant donc atteint son activité stationnaire a été calciné à 500°C pendant quelques heures et réintroduit dans le réacteur. On n'observe alors pas le comportement de type A, mais bien celui de type B. En d'autres mots, le comportement de type B correspondrait à un système où les espèces molybdiques superficielles n'auraient pas de mobilité. Il est donc logique dans ce cas de trouver un tel comportement pour les très faibles teneurs en molybdène (figure 2). En effet, lors de l'imprégnation les ions métalliques ont tendance à s'adsorber préférentiellement sur les sites du support donnant lieu à l'interaction la plus forte. Les espèces produites sur ces sites pendant la calcination seraient donc également les moins mobiles.

Le phénomène de recristallisation invoqué ici serait à rapprocher de celui décrit par Callahan *et al.* (14) dans le cas du traitement hydrothermique de $MoO_3$ déposé sur un gel de silice. La croissance des cristaux superficiels de $MoO_3$ lors de ce traitement est expliquée par l'existence d'un complexe de surface mobile du type acide silicomolybdique.

*Spectres de réflectance diffuse*

Les spectres de réflectance diffuse obtenus avec nos catalyseurs comportent deux pics d'absorption respectivement aux longueurs d'onde voisines de 265 et 330 nm. Selon la littérature (11) ces pics correspondent à des espèces Mo(VI) respectivement en coordination d'oxygène tétraédrique pour le pic à 265 nm, et octaédrique pour celui à 330 nm. Ces assertions ont été vérifiées en déterminant les spectres du molybdate de sodium $Na_2MoO_4$ (Mo(VI) en coordination tétraédrique) et du paramolybdate d'ammonium et de l'oxyde pur $MoO_3$ (Mo(VI) principalement en coordination octaédrique). Ces spectres sont présentés à la figure 4.

La figure 5 donne les spectres obtenus, avec les catalyseurs fraîchement préparés. Le pic des espèces tétraèdriques déjà important pour une teneur en molybdène de 0,1% croît jusqu'à 0,75% et demeure stable aux teneurs supérieures. Par contre, le pic des espèces octaédriques quasi nul pour la teneur 0,1% croît de façon continue pour toutes les autres valeurs de la teneur en molybdène.

Si l'on rapproche ces résultats de ceux de la figure 3, on constate que l'activité catalytique est corrélée avec la hauteur du pic des espèces tétraédriques pour les trois teneurs les plus faibles. Au

Can. J. Chem. Downloaded from www.nrcresearchpress.com by 210.87.254.5 on 09/06/12
For personal use only.

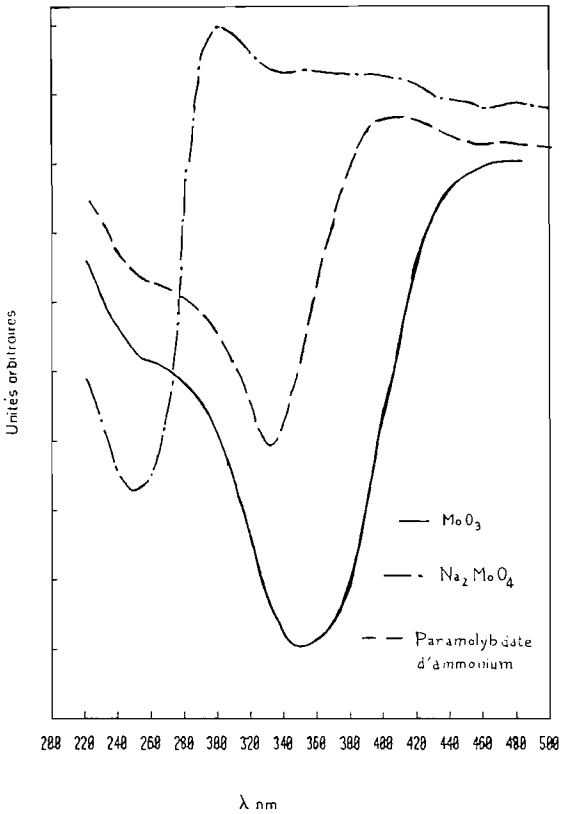


FIG. 4. Spectres de réflectance diffuse des composés purs de référence.

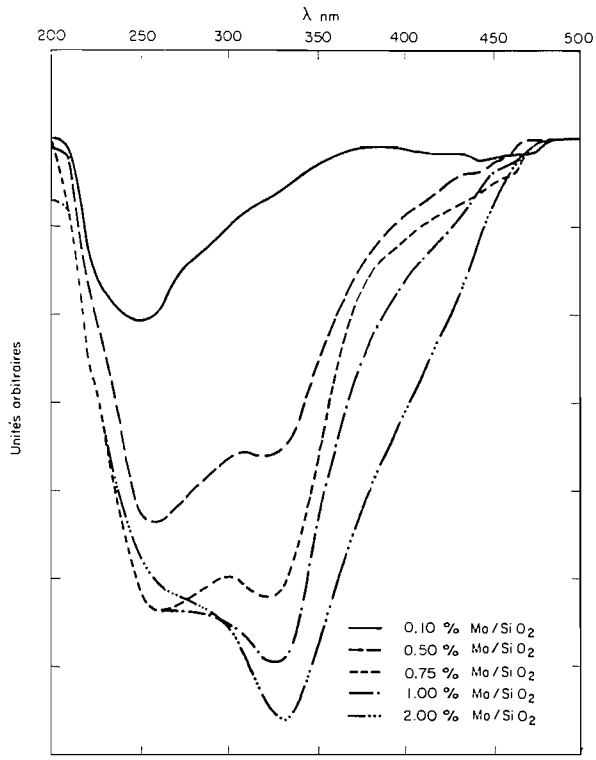


FIG. 5. Spectres de réflectance diffuse des catalyseurs avant réaction.

delà de 0,75% de molybdène, l'activité décroît alors que le pic des espèces octaédriques augmente. Il semble donc que les espèces octaédriques ne contribuent pas à l'activité photocatalytique. Ceci est en accord avec la vision selon laquelle seules les espèces isolées sont actives (8), puisque les espèces octaédriques sont des espèces oxymolybdiques polymériques, qui ne peuvent exister isolées.

Cependant, il est clair d'après la figure 5, que l'activité photocatalytique n'est plus corrélée avec la hauteur du pic tétraédrique pour les teneurs en molybdène supérieures à 0,75%. En effet, l'intensité du pic ne varie plus alors que l'activité diminue. Nous pensons que ces résultats signifient qu'il faut distinguer deux sortes d'espèces oxymolybdiques en coordination tétraédrique: une première espèce du type [2] est isolée sur la surface et active en photocatalyse, alors que la seconde est liée par au moins un pont Mo—O—Mo à d'autres espèces oxymolybdiques et perd de ce fait son activité photocatalytique.

On peut expliquer cette perte d'activité de la façon suivante: lorsque l'espèce $M^{n+}$ de l'équation [1] est liée à d'autres cations de même nature par des ponts M—O—M, les charges produites par l'absorption du rayonnement sont délocalisées sur l'ensemble polymérique. Par conséquent, l'état de transfert de charge produit par la réaction [1] a une durée de vie beaucoup plus courte, qui ne serait alors plus suffisante pour que le $O^-$ formé ait le temps de réagir avec le cyclohexane.

Nous avons également déterminé les spectres de réflectance diffuse de catalyseur ayant été utilisés dans les conditions standards pendant un temps suffisamment long pour que l'activité stationnaire soit atteinte. Après une nouvelle calcination nous avons obtenu les spectres présentés à la figure 6. La comparaison entre les résultats des figures 5 et 6 est présentée au tableau 1, qui donne les valeurs mesurées des rapports des hauteurs des pics des espèces tétraédrique et octaédrique $H_T/H_O$. Ce tableau montre que la valeur du rapport $H_T/H_O$ diminue au cours de l'utilisation du catalyseur. Pour la teneur de 0,1% en molybdène, ce rapport ne peut être déterminé avec suffisamment de précision en raison de la très petite valeur de $H_O$ dans ce cas. Ces résultats pourraient impliquer que la recristallisation produite dans les conditions de la réaction photocatalytique, s'accompagne d'un changement

Can. J. Chem. Downloaded from www.nrcresearchpress.com by 210.87.254.5 on 09/06/12
For personal use only.

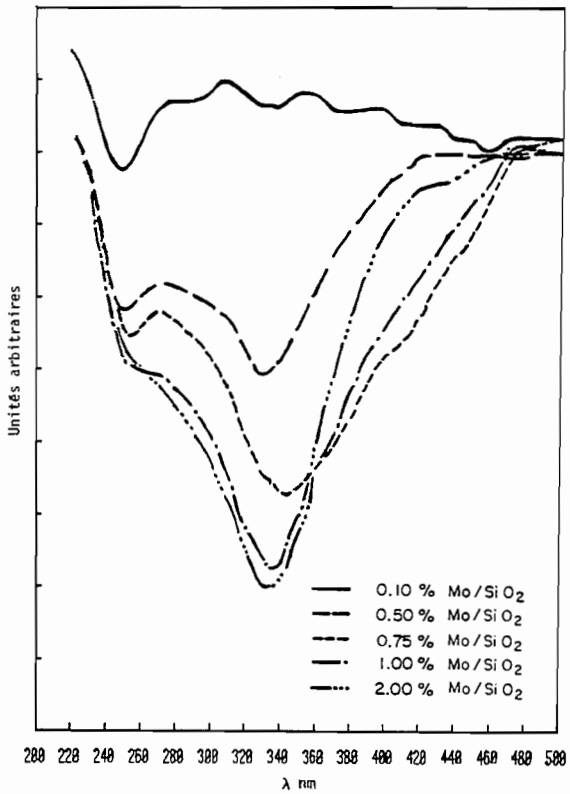


FIG. 6. Spectres de réflectance diffuse des catalyseurs après réaction.

TABLEAU 1. Valeurs des rapports $H_T/H_0$ avant et après réaction

| % pds Mo | $H_T/H_0$ catalyseur fraîchement préparé | $H_T/H_0$ catalyseur utilisé |
|---|---|---|
| 0,5 | 1,2 | 0,94 |
| 0,75 | 1,0 | 0,71 |
| 1,0 | 0,9 | 0,70 |
| 2,0 | 0,8 | 0,63 |

de coordination pour un certain nombre d'espèces tétraédriques. On ne peut toutefois exclure que la réorganisation de surface des espèces octaédriques n'entraîne une augmentation de leur absorptivité en raison d'une délocalisation électronique accrue.

## Conclusion

On peut donner une interprétation unique et cohérente des variations avec le temps de réaction et avec la teneur en molybdène, de l'activité photocatalytique d'une part, et des spectres de réflectance diffuse des dépôts $MoO_3/SiO_2$ d'autre part. Selon cette interprétation, la méthode de préparation et de prétraitement du catalyseur produit sur la surface des espèces oxymolybdiques où le molybdène peut être en coordination tétraédrique ou octaédrique. Les espèces ainsi produites sont de deux types: (1) des espèces en forte interaction avec la silice, seules formées aux plus faibles teneurs en molybdène et où le cation $Mo^{+6}$ en coordination tétraédrique est isolé et actif en photocatalyse; (2) des espèces polymériques plus faiblement liées au réseau de la silice où les cations $Mo^{+6}$ sont essentiellement en coordination octaédrique. Ces espèces ne sont pas actives en photocatalyse, mais elles possèdent une certaine mobilité dans les conditions de la réaction photocatalytique. Dans ces conditions elles peuvent alors se fixer aux espèces isolées qui perdent alors leur activité, certaines d'entre elles pouvant également changer de coordination.

1. M. FORMENTI et S. J. TEICHNER. Specialist Periodical Report, Catalysis. Vol. 2. The Chemical Society, London. 1978. p. 87.
2. M. N. MOZZANEGA, J. M. HERRMANN et P. PICHAT. Tetrahedron Lett. **34**, 2965 (1977).
3. K. I. ZAMAREV et V. N. PARMON. Catal. Rev.-Sci. Eng. **22**, 261 (1980).
4. T. KAWAÏ et T. SAKATA. Paper No. B-38. 7th International Congress on Catalysis, Tokyo. June 30–July 4th, 1980.
5. A. J. BARD et B. KRAEUTLER. J. Am. Chem. Soc. **100**, 2239 (1978).
6. A. M. PERSHIN, B. N. SHELIMOV et V. B. KAZANSKY. J. Catal. **64**, 426 (1980).
7. S. KALIAGUINE, A. MAHAY et P. C. ROBERGE. Proc. 2nd World Congress of Chemical Engineering. Vol. 3. Montréal. 1981. p. 272.
8. A. M. GRITSKOV, V. A. SHVETS et V. B. KAZANSKY. Kinet. Katal. **14**, 1062 (1973).
9. D. L. NGUYEN, P. C. ROBERGE et S. KALIAGUINE. Can. J. Chem. Eng. **57**, 288 (1979).
10. S. KALIAGUINE, M. GNAKOURY et P. C. ROBERGE. Can. J. Chem. Eng. **59**, 710 (1981).
11. H. PRALIAUD. J. Less Com. Met. **54**, 387 (1977).
12. P. WITIER, L. ESTAQUE, P. C. ROBERGE et S. KALIAGUINE. Can. J. Chem. Eng. **55**, 352 (1978).
13. A. MAHAY. Thèse M.Sc., Département de génie chimique, Université Laval, Canada. 1982.
14. J. L. CALLAHAN, R. H. PETRUCCI et C. A. BROWN. J. Colloid Sci. **15**, 418 (1960).

# Solvent effects on the nitrogen and β-hydrogen hyperfine splitting constants of aminoxyl radicals obtained in spin trapping experiments

EDWARD G. JANZEN, GREGORY A. COULTER, UWE M. OEHLER, AND JOHN P. BERGSMA

*Guelph–Waterloo Centre for Graduate Work in Chemistry, Department of Chemistry, University of Guelph, Guelph, Ont., Canada N1G 2W1*

Received April 12, 1982

EDWARD G. JANZEN, GREGORY A. COULTER, UWE M. OEHLER, and JOHN P. BERGSMA. Can. J. Chem. **60**, 2725 (1982).

The nitrogen and β-hydrogen hyperfine splitting constants (hfsc) for phenyl, 4-nitrophenyl, 4-pyridyl, benzoyl, and trichloromethyl spin adducts of α-phenyl *tert*-butyl nitrone (PBN) as well as for the *tert*-butoxyl adduct of 5,5-dimethylpyrroline-*N*-oxide (DMPO) have been obtained as a function of solvent (30 solvents). A useful linear relationship between the β-H hfsc and the N-hfsc of each aminoxyl is found except for the benzoyl adduct of PBN. Some speculations regarding the structural significance of these correlations is presented.

EDWARD G. JANZEN, GREGORY A. COULTER, UWE M. OEHLER et JOHN P. BERGSMA. Can. J. Chem. **60**, 2725 (1982).

On a déterminé, en fonction de solvant (30 solvants), les constantes de couplage hyperfin (cch) de l'azote et de l'hydrogène en β des adduits de spin des phényle, nitro-4 phényle, pyridyle-4, benzoyle et trichlorométhyle de l'α-phényl *tert*-butylnitrone (PBN) ainsi que l'adduit du *tert*-butylate de la *N*-oxyde de la diméthyl-5,5 pyrroline (ODMP). On a trouvé une relation linéaire utile entre les cch du H en β et la cch du N qui s'applique à chaque aminoxyle à l'exception de l'adduit du benzoyle de BPN. On présente quelques hypothèses relatives à la signification structurale de ces corrélations.

[Traduit par le journal]

## Introduction

It is well known that nigrogen hyperfine splitting constants ($a_N$ or N-hfsc's) for dialkyl and alicyclic aminoxyl radicals increase with increase in solvent polarity (1–5)[1]. This solvent effect is attributed to the increased importance of resonance structure **2** with increase in solvent polarity:

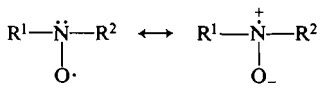

**1** **2**

That the spin density on the nitrogen atom does indeed increase with increase in solvent polarity is shown by the fact that *both* the hydrogen and the nitrogen hfsc's increase with increase in solvent polarity in the case of *tert*-butyl aminoxyl (5):

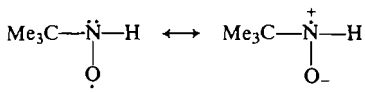

**3** **4**

Knauer and Napier (7) searched for the best correlation between $a_N$ and common solvent polarity parameters using the stable aminoxyls **5**, **6**, and **7**:

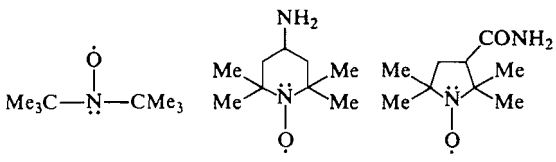

**5** **6** **7**

[1]It should be noted that this trend does not hold for *tert*-butoxy *tert*-butyl aminoxyl radical (6).

The best fit was obtained when the following parameters were used: Dimroth and Reichardt's $E_{t(30)}$ values (8), Kosower's *Z*-values (9), or Berson's Ω values (10). Since $E_{t(30)}$ values are available for more solvents (Knauer and Napier used 31 solvents), this parameter is most convenient for the purpose of this study. It should be noted that plots of $a_N$ for one aminoyxl vs. $a_N$ for another in the same solvents gave excellent correlations.

It is of interest and of some importance to investigate the nature of the solvent effect on both the nitrogen and β-hydrogen hfsc in aminoxyl radicals formed in spin trapping reactions:

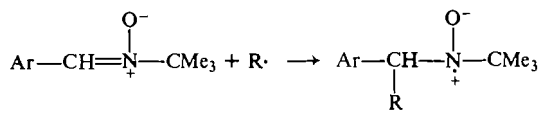

**8**

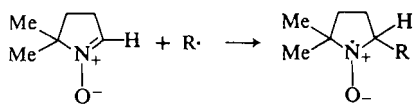

DMPO **9**

This is because assignment of the spin adduct spectrum is usually based on producing the same aminoxyl by an alternate route. Often this alternate route involves use of a different solvent and recognition of the influence of solvent on both the N- and β-H hfsc is of utmost importance. It would be most useful if a correlation between the β-H and N-hfsc was available for each spin adduct so that the values in any solvent could be predicted given that information about these parameters in some

0008-4042/82/212725-09$01.00/0

©1982 National Research Council of Canada/Conseil national de recherches du Canada

Can. J. Chem. Downloaded from www.nrcresearchpress.com by 210.87.254.40 on 09/06/12
For personal use only.

Can. J. Chem. Downloaded from www.nrcresearchpress.com by 210.87.254.40 on 09/06/12
For personal use only.

other solvent was at hand. To collect all this data seems like an impossible task. It would be better to investigate a few adducts in detail and search for some rules to use as a guide in predicting the hfsc's of some other spin adduct as a function of solvent.

In a review of spectra assigned to the hydroxy and hydroperoxy adducts of phenyl *tert*-butyl nitrone (PBN) it was found that the points on a plot of $a_\beta^H$ vs. $a_N$ appeared to fall on two lines (11): $a_\beta^H = 0.604a_N - 6.53$ and $a_\beta^H = 1.26a_N - 15.7$. These were assigned to the hydroxy and hydroperoxy adducts respectively.[2] The good agreement was taken as supporting evidence for the assignment of the spectra obtained in different solvents. In this paper the question is turned around: if spectra of known spin adducts are obtained in different solvents, will the β-H hfsc bear a linear relationship with the N-hfsc of each adduct and will the slope of this plot have any relation to the nature of the radical trapped?

Since the kinetic stability of spin adducts varies considerably, only very persistent examples can be studied. Also, since many solvents are themselves good hydrogen atom donors, the *in situ* method of producing spin adducts can not be used for all solvents. At this time results for only five spin adducts have been obtained: the phenyl adduct of PBN (**10**), the phenyl adduct of α-(4-pyridyl)-*tert*-butyl nitrone (4-PyBN) (**11**), the 4-nitrophenyl adduct of PBN (**12**), the trichloromethyl adduct of PBN (**13**), the benzoyl adduct of PBN (**14**), and the *tert*-butoxyl adduct of 5,5-dimethylpyrroline-*N*-oxide (DMPO) (**15**):

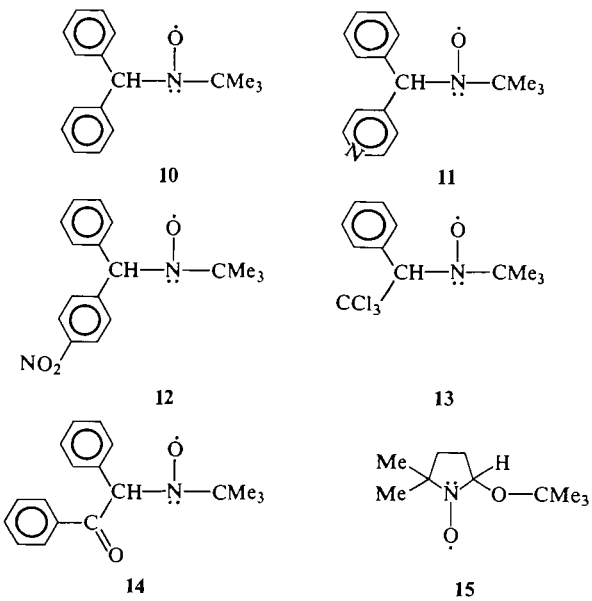


Three of these radicals (**10–12**) have groups with the same steric requirements but with slightly different polarity while two others differ in both steric requirements and polarity of one group (**13** and **14**). Most of the 31 solvents selected by Knauer and Napier (7) have been used in this study.

## Experimental

Solutions of the spin trap and radical source were either warmed for about 10 min at 45°C or photolyzed at room temperature for up to 30 min (only for **13**). The resulting solution was evaporated at room temperature to yield a solid residue. This residue was taken up in enough solvent to produce a 0.05 *M* solution (based on initial trap concentration). The solution was transferred to a degassing chamber connected to an esr flat cell (17). After outgassing with a nitrogen stream for 15 mins the solution was introduced into a flat cell without exposing the contents to the atmosphere. The specific methods used were: **10** from PBN plus phenyl radical (from commercially available phenylazotriphenylmethane (PAT)); **11** from 4-PyBN (18) plus phenyl radical from PAT; **12** from PBN plus 4-nitrophenyl from 4-nitrophenylazotriphenylmethane;[3] **13** from PBN plus trichloromethyl radical from photolysis of either $CCl_4$ or $CBrCl_3$ in the appropriate halocarbon (19); **14** from PBN and benzoyl radical (from benzaldehyde plus *tert*-butoxyl radical from thermal decomposition of di-*tert*-butyl peroxyoxalate); and **15** from DMPO plus *tert*-butoxyl radicals, also from di-*tert*-butylperoxyoxalate decomposition in benzene.

The spectra were obtained with a Varian E-104 epr spectrometer. The recorder was calibrated using Fremy's salt in aqueous alkaline solution ($a_N$ = 13.09 G) (20). The separation of the peaks of the spectrum was measured as many times as

[2]Data from three new references and one previously omitted are given below:

$C_6H_5CH(OH)N(O^\cdot)CMe_3$

| $a_N$ | $a_\beta^H$ (Calc'd) | (Exp'tl) | Error | Reference |
|---|---|---|---|---|
| 15.9 | 3.04 | 3.0 | 0.0 | 12 |
| 15.45 | 2.77 | 2.80 | −0.03 | 13 |
| 15.40 | 2.74 | 2.75 | +0.01 | 13 |
| 15.2 | 2.62 | 2.8 | −0.2 | 14 |
| 15.2 | 2.62 | 3.0 | −0.4 | 15 |

$C_6H_5CH(OOH)N(O^\cdot)CMe_3$

| $a_N$ | $a_\beta^H$ (Calc'd) | (Exp'tl) | Error | Reference |
|---|---|---|---|---|
| 14.25 | 2.28 | 2.23 | +0.05 | 16 |
| 14.80 | 2.95 | 2.38 | +0.57 | 13 |
| 14.80 | 2.95 | 2.50 | +0.45 | 13 |

Since in the original publication (11) the average error cited for these correlations was ±0.05 for the hydroxy adduct (7 examples – largest deviation ±0.09) and ±0.13 for the hydroperoxy adduct (8 examples – largest deviation +0.20), the large differences in values calculated for the assigned spectra in refs. 14 and 15 (hydroxy adduct) and 15 (hydroperoxy adduct) places some doubt on these measurements and/or assignments.

[3]We are grateful to Prof. W. A. Pryor for providing us with a sample of 4-nitrophenylazotriphenylmethane.

FIG. 1. The esr spectrum of the phenyl radical adduct to 4-PyBN (**11**) in (A) benzene, (B) water.

possible ($a_N$ eight times, $a_\beta^H$ six times, using both maxima and minima of the first derivative presentation) and an average value recorded. Solubility difficulties prevented values from being obtained for **11** in hexane and **12**, **13**, and **14** in water.

## Results and discussion

### *PBN spin adducts: nitrogen hyperfine splitting constants*

The esr spectra obtained from **11** and **15** in benzene and in water are shown in Figs. 1 and 2. The effect of increasing solvent polarity is clearly seen in the increase in both the triplet and doublet spacings. The β-H and N-hfsc's obtained in 30 solvents for **10–13** are listed in Table 1.

The plot of $a_N$ vs. $E_{t(30)}$ for **10** is shown in Fig. 3. Although there is some scatter, a good straight line correlation with solvent polarity is found ($r^2$ = 0.958, slope = 0.047). In order to test whether the hydrogen-bonding solvents are the major source of the scatter, the plot was calculated without these solvents. No substantial improvement is found in the case of **10** ($r^2$ = 0.950, slope 0.034). The slope is slightly smaller due to the value for water which lies substantially above the line of best fit for the plot including all solvents. Knauer and Napier (7) made similar observations (i.e. the slope decreased when the H-bonding solvents were omitted for 2 out of 3 examples).

Not shown in a figure is the fact that $a_N$ for **10** varies with solvent polarity in just the same way as does $a_N$ for **5**, i.e. a plot of $a_N$ for **10** vs. $a_N$ for **5** is linear and a good correlation is found: $a_N(\mathbf{5}) = 1.068\, a_N(\mathbf{10}) + 0.030$; $r^2 = 0.985$.

The plots of $a_N$ vs. $E_{t(30)}$ for **11–13** are similar to Fig. 3. The slopes and correlation coefficients are given in Table 2. It is clear that the correlations are reasonable in most cases. The slope decreases in the order **10** > **11** > **12** > **13** and is smaller if the H-bonding solvents are omitted (except for **13** (Fig. 4) where the slope is equal).[4]

The plot of $a_N$ for the benzoyl adduct, **14**, vs. $E_{t(30)}$ is shown in Fig. 5 ($r^2$ = 0.928). Not as many solvents could be utilized (17 solvents). The slope is quite small (0.025) and is similar to that found for the trichloromethyl adduct.

In summary it appears that for most $C_6H_5$-CHRN(O·)$CMe_3$ aminoxyls the N-hfsc's obtained

[4]It is interesting to note that the value for chloroform (spectro Grade) for **10**, **11**, and **12**, but not for **13**, is also too high for the straight-line correlation; Prof. J. J. Lindberg has suggested H-bonding as the reason for this deviation.

Can. J. Chem. Downloaded from www.nrcresearchpress.com by 210.87.254.40 on 09/06/12
For personal use only.

FIG. 2. The esr spectrum of the *tert*-butoxyl radical adduct to DMPO (**15**) in (A) benzene, (B) water.

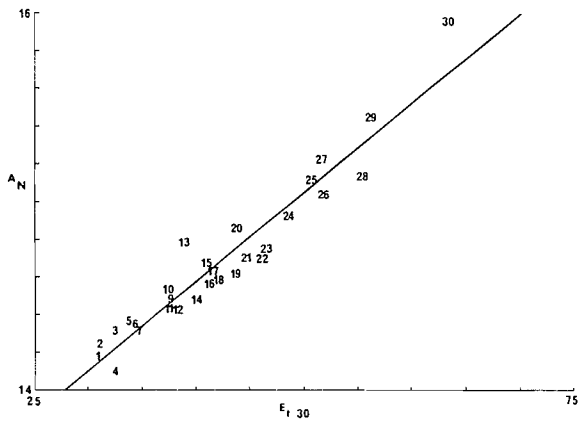


FIG. 3. Plot of $a_N$ vs. $E_{t(30)}$ for phenyl radical spin adduct to PBN (**10**).

are quite well correlated with a solvent parameter such as $E_{t(30)}$. Furthermore as the electronegativity of R increases, $a_N$ *and* the slope of $a_N$ vs. $E_{t(30)}$ decreases. The former means that the contribution of **2** decreases as the R groups become more electronegative. Since the slopes also decrease with increase in electronegativity of R, the polarization of the β-bond attached to the electronegative group must also increase and cause further destabilization of **17** as the polarity of the solvent increases:

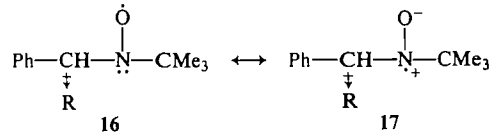


**16** **17**

On the basis of the slopes of $a_N$ vs. $E_{t(30)}$ the electronegativity of R follows the sequence: phenyl < 4-pyridyl ≃ 4-nitrophenyl < benzoyl ≃ trichloromethyl. This order is quite reasonable if based on the expected electronegativities of these groups.

### β-*Hydrogen hyperfine splitting constants*

A plot of the β-H hfsc's vs. $E_{t(30)}$ for **10** is shown in Fig. 6. The correlation is quite reasonable ($r^2$ = 0.953). Again the point for water falls considerably above the line of best fit.

Since $a_N$ has been shown to correlate with $E_{t(30)}$ for all PBN spin adducts studied (**10–14**) it should be possible to eliminate this polarity parameter and use the N-hfsc's directly since, for a given aminoxyl radical, $a_N$ can be considered a polarity parameter itself. The plot of the β-H hfsc's vs. $a_N$ for **10** in 30 solvents is shown in Fig. 7. The fit to a linear correlation is quite good: $r^2$ = 0.978.

Can. J. Chem. Downloaded from www.nrcresearchpress.com by 210.87.254.40 on 09/06/12
For personal use only.

Can. J. Chem. Downloaded from www.nrcresearchpress.com by 210.87.254.40 on 09/06/12
For personal use only.

TABLE 1. Hyperfine splitting constants of PBN spin adducts[a]

| Solvent | $E_{t(30)}$[b] | 10 | | 11 | | 12 | | 13 | | 14 | |
|---|---|---|---|---|---|---|---|---|---|---|---|
| | | $a_N$ | $a_\beta^H$ | $a_N$ | $a_\beta^H$ | $a_N$ | $a_\beta^H$ | $a_N$ | $a_\beta^H$ | $a_N$ | $a_\beta^H$ |
| 1. n-Hexane | 30.9 | 14.18 | 2.07 | — | — | 14.12 | 1.94 | 13.83 | 1.61 | — | — |
| 2. Cyclohexane | 31.2 | 14.25 | 2.00 | 14.06 | 1.77 | 14.13 | 1.90 | 13.79 | 1.61 | 14.17 | 4.55 |
| 3. Carbon tetrachloride | 32.5 | 14.32 | 2.20 | 14.17 | 1.89 | 14.21 | 2.09 | 13.85 | 1.60 | 14.20 | 4.45 |
| 4. Carbon disulfide | 32.6 | 14.10 | 2.06 | 14.11 | 1.91 | 14.19 | 1.94 | 13.90 | 1.68 | — | — |
| 5. Toluene | 33.9 | 14.36 | 2.19 | 14.22 | 1.92 | 14.25 | 2.08 | 13.91 | 1.65 | 14.27 | 4.56 |
| 6. Benzene | 34.5 | 14.34 | 2.24 | 14.25 | 1.99 | 14.29 | 2.13 | 14.00 | 1.68 | 14.23 | 4.52 |
| 7. Diethyl ether | 34.6 | 14.33 | 2.17 | 14.22 | 1.95 | 14.22 | 2.13 | 13.95 | 1.68 | — | — |
| 8. 1,4-Dioxane | 36.0 | 14.44 | 2.31 | 14.33 | 2.03 | 14.32 | 2.19 | 13.99 | 1.68 | — | — |
| 9. Tetrahydrofuran | 37.4 | 14.43 | 2.21 | 14.27 | 1.96 | 14.32 | 2.16 | 14.00 | 1.71 | 14.34 | 4.50 |
| 10. Chlorobenzene | 37.5 | 14.53 | 2.44 | 14.31 | 2.06 | 14.33 | 2.20 | 13.93 | 1.77 | 14.34 | 4.58 |
| 11. Bromobenzene | 37.5 | 14.48 | 2.34 | 14.32 | 2.05 | 14.35 | 2.23 | 13.99 | 1.70 | — | — |
| 12. 1,2-Dimethoxyethane | 38.2 | 14.42 | 2.35 | 14.34 | 2.00 | 14.38 | 2.21 | 14.00 | 1.74 | 14.26 | 4.58 |
| 13. Chloroform | 39.1 | 14.79 | 2.61 | 14.58 | 2.26 | 14.51 | 2.39 | 14.04 | 1.81 | 14.60 | 4.44 |
| 14. Pyridine | 40.2 | 14.47 | 2.41 | 14.44 | 2.17 | 14.45 | 2.32 | 14.06 | 1.85 | — | — |
| 15. Methylene chloride | 41.1 | 14.68 | 2.58 | 14.52 | 2.24 | 14.52 | 2.42 | 14.19 | 1.81 | — | — |
| 16. Acetophenone | 41.3 | 14.56 | 2.46 | 14.44 | 2.14 | 14.45 | 2.32 | 14.06 | 1.84 | 14.40 | 4.65 |
| 17. 1,2-Dichloroethane | 41.9 | 14.63 | 2.69 | 14.45 | 2.24 | 14.48 | 2.37 | 14.13 | 1.85 | — | — |
| 18. Acetone | 42.2 | 14.58 | 2.50 | 14.43 | 2.27 | 14.48 | 2.39 | 14.15 | 1.81 | 14.38 | 4.76 |
| 19. Dimethylformamide | 43.8 | 14.62 | 2.53 | 14.48 | 2.25 | 14.50 | 2.43 | 14.14 | 1.87 | — | — |
| 20. *tert*-Butyl alcohol | 43.9 | 14.86 | 2.85 | 14.63 | 2.44 | 14.60 | 2.50 | 14.19 | 1.90 | 14.58 | 4.75 |
| 21. Dimethyl sulfoxide | 45.0 | 14.70 | 2.60 | 14.61 | 2.37 | 14.58 | 2.51 | 14.16 | 1.87 | 14.50 | 4.72 |
| 22. Acetonitrile | 46.0 | 14.70 | 2.74 | 14.55 | 2.36 | 14.60 | 2.55 | 14.25 | 1.87 | 14.53 | 4.74 |
| 23. Nitromethane | 46.3 | 14.75 | 2.72 | 14.59 | 2.40 | 14.64 | 2.58 | 14.22 | 1.94 | 14.55 | 4.71 |
| 24. Isopropyl alcohol | 48.6 | 14.92 | 2.98 | 14.65 | 2.45 | 14.73 | 2.63 | 14.27 | 1.93 | 14.67 | 4.70 |
| 25. Benzyl alcohol | 50.8 | 15.12 | 2.88 | 14.81 | 2.45 | 14.84 | 2.68 | 14.39 | 2.00 | — | — |
| 26. Acetic acid | 51.9 | 15.22 | 3.12 | 14.66 | 2.37 | 14.89 | 2.74 | [c] | [c] | 14.83 | 4.72 |
| 27. Ethyl alcohol | 51.9 | 15.03 | 2.99 | 14.71 | 2.45 | 14.82 | 2.70 | 14.34 | 2.06 | 14.74 | 4.60 |
| 28. Methyl alcohol | 55.5 | 15.13 | 3.12 | 14.83 | 2.58 | 14.94 | 2.86 | 14.42 | 2.12 | — | — |
| 29. Ethylene glycol | 56.3 | 15.45 | 3.22 | 14.81 | 2.58 | 15.09 | 2.97 | 14.51 | 2.19 | — | — |
| 30. Water | 63.1 | 15.96 | 4.21 | 15.73 | 3.57 | [c] | [c] | [c] | [c] | — | — |

[a]All hfsc's measured in gauss ± 0.05.
[b]Values in kcal/mol.
[c]Spin adduct insoluble; no spectrum obtained.

TABLE 2. Slope and correlation coefficient data of plots $a_N$ vs. $E_{t(30)}$ for PBN spin adducts in all solvents, and with hydrogen bonding solvents removed

| Spin adduct | Slope | $r^2$, Correlation coefficient | Solvents |
|---|---|---|---|
| **10** | 0.047 | 0.958 | 30 solvents |
| **10** | 0.034 | 0.950 | No H-bonding solvents[a] |
| **11** | 0.036 | 0.921 | 29 solvents |
| **11** | 0.032 | 0.976 | No H-bonding solvents[a] |
| **12** | 0.034 | 0.988 | 29 solvents |
| **12** | 0.031 | 0.991 | No H-bonding solvents[a] |
| **13** | 0.022 | 0.869 | 28 solvents |
| **13** | 0.022 | 0.966 | No H-bonding solvents[a] |
| **14** | 0.025 | 0.928 | 17 solvents |

[a]The values for *tert*-butyl alcohol, isopropyl alcohol, benzyl alcohol, acetic acid, ethyl alcohol, methyl alcohol, ethylene glycol, and water were omitted.

The plots of the β-H hfsc's vs. $a_N$ for **11** and **12** are similar to Fig. 7. The plot of $a_\beta^H$ vs. $a_N$ for **13** is shown in Fig. 8 because of the continuing interest in the biomedical field in detecting, by spin trapping, trichloromethyl radicals from the metabolism of perhalocarbons (e.g. carbon tetrachloride (21). The correlation coefficients for the plots for **11–13** are given in Table 3.

For the benzoyl adduct, **14**, the plot of the β-H hfsc's vs. $a_N$ is severely scattered as shown in Fig. 9. Since the plot of $a_N$ vs. $E_{t(30)}$ gives a satisfactory correlation with all solvents (Fig. 5), the problem must rest with the solvent effect on the β-H hfsc. When the H-bonding solvents are removed, a fair correlation is obtained ($r^2 = 0.844$). The slope is smaller than for the trichloromethyl adduct (slope = 0.655) but has less meaning with the fewer usable solvents (17 solvents).

In summary it appears that plots of the β-H hfsc vs. $a_N$ from spin adduct spectra of aminoxyl radicals are linear for nonpolar groups or with polar groups substituted at positions far away from the nitrogen–oxygen function. If the polar group is near to this function, e.g. in the β-position, the nature of the substituent is important. Thus trichloromethyl is well-behaved while benzoyl is not. In the latter case the β-H hfsc never realizes its full potential of about 5 gauss as predicted from the

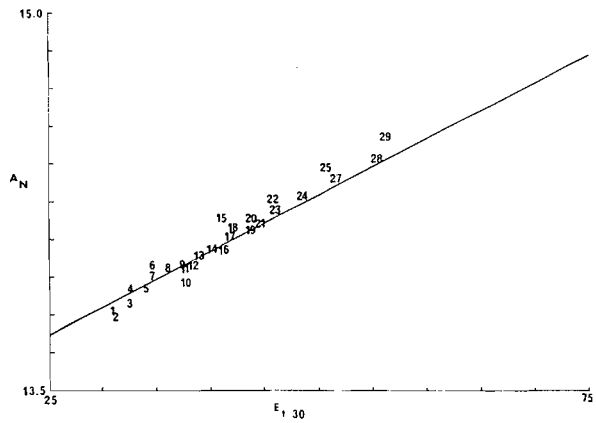


FIG. 4. Plot of $a_N$ vs. $E_{t(30)}$ for the trichloromethyl radical spin adduct to PBN (**13**).

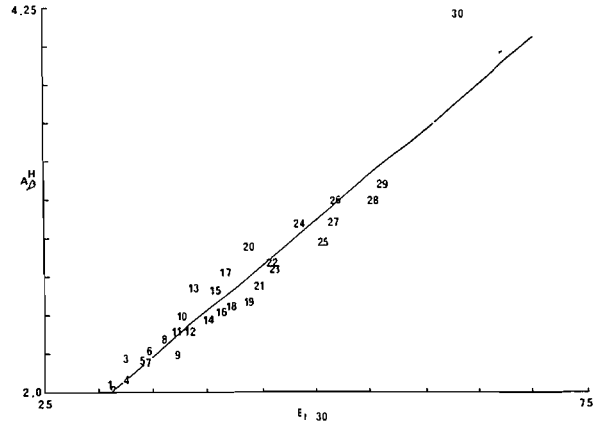


FIG. 6. Plot of $a_\beta^H$ vs. $E_{t(30)}$ for the phenyl radical spin adduct to PBN (**10**).

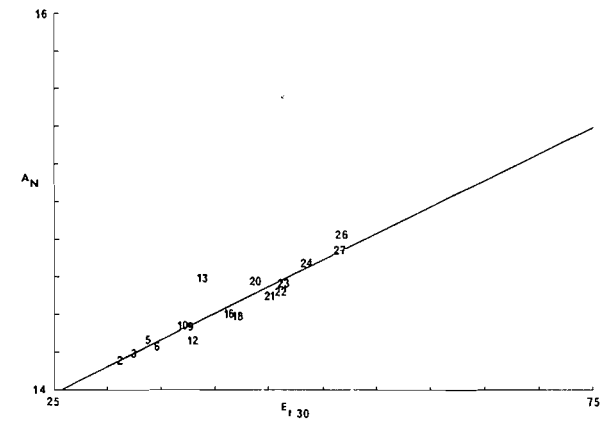


FIG. 5. Plot of $a_N$ vs. $E_{t(30)}$ for the benzoyl radical spin adduct to PBN (**14**).

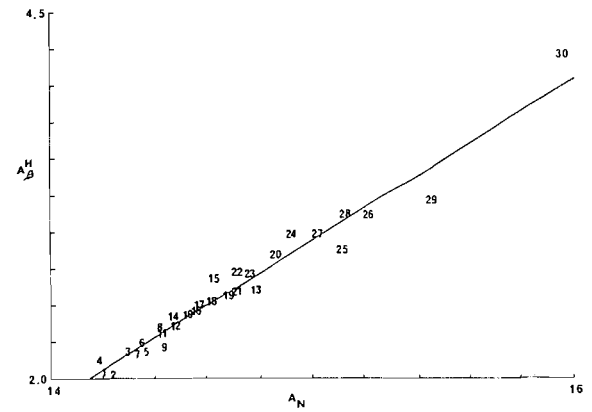


FIG. 7. Plot of $a_\beta^H$ vs. $a_N$ for the phenyl radical spin adduct to PBN (**10**).

influence of solvent polarity on $a_N$. One can speculate and attribute this to a change in the dihedral angle of the C—H bond caused by a change in conformation as a result of hydrogen-bonding. The degree to which the values for the β-H hfsc's fall off the line correlating the values in the non-hydrogen-bonding solvents is inversely proportional to the bulk of the organic group: *tert*-butyl alcohol < isopropyl alcohol < ethanol. The nature of the H-bonding solvent effect on the benzoyl adduct is not known. Perhaps H-bonding to the carbonyl of the benzoyl group and to the aminoxyl function occurs in a special way (intramolecular?), such that the dihedral angle is increased, thereby off-setting the effect of an increase in spin density on the nitrogen atom of the aminoxyl function.

The equations for the linear correlations between $a_\beta^H$ and $a_N$ for PBN spin adducts are as follows:

for **10** $a_\beta^H = 1.11\ a_N - 13.69$

**11** $a_\beta^H = 1.06\ a_N - 13.08$

**12** $a_\beta^H = 1.08\ a_N - 13.24$

**13** $a_\beta^H = 0.796\ a_N - 9.40$

**14** $a_\beta^H = 0.655\ a_N - 4.79$

(no H-bonding solvents)

*DMPO spin adducts*

It was of interest to see what the solvent effect would be on a DMPO spin adduct. However, since spin adducts of cyclic traps are less persistent than those of PBN, only the *tert*-butoxyl adduct of DMPO (**15**) has been studied at this time.

Solvent polarity has a dramatic effect on the spectrum of **15** (Fig. 2). This is almost entirely due to the large increase in β-H hfsc with increase in solvent polarity since the slope of the plot of $a_N$ vs. $E_{t(30)}$ is not unusual (slope = 0.054, $r^2 = 0.945$, Fig.

Can. J. Chem. Downloaded from www.nrcresearchpress.com by 210.87.254.40 on 09/06/12
For personal use only.

Can. J. Chem. Downloaded from www.nrcresearchpress.com by 210.87.254.40 on 09/06/12
For personal use only.

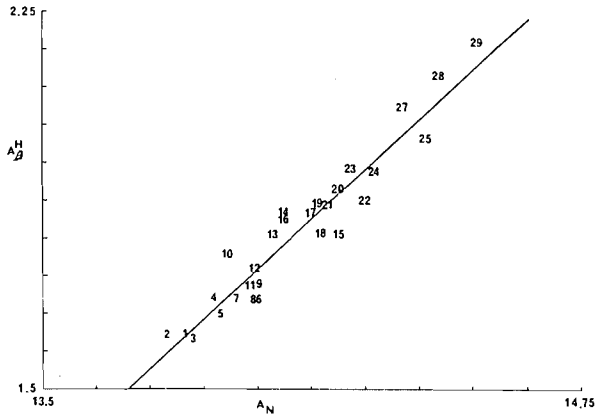


FIG. 8. Plot of $a_\beta^H$ vs. $a_N$ for the trichloromethyl radical spin adduct to PBN (**13**).

TABLE 3. Slope and correlation coefficient data of plots $a_\beta^H$ vs. $a_N$ for PBN spin adducts in all solvents, and with hydrogen bonding solvents removed

| Spin adduct | Slope | $r^2$, correlation coefficient | Solvents, figure |
|---|---|---|---|
| **10** | 1.11 | 0.978 | 30 solvents |
| **11** | 1.06 | 0.989 | 29 solvents |
| **12** | 1.08 | 0.988 | 29 solvents, Fig. 8 |
| **13** | 0.796 | 0.959 | 28 solvents, Fig. 9 |
| **14** | 0.275 | 0.507 | 17 solvents, Fig. 10 |
| **14** | 0.655 | 0.844 | No H-bonding solvents[a] |

[a]The values for *tert*-butyl alcohol, isopropyl alcohol, acetic acid, and ethyl alcohol were omitted.

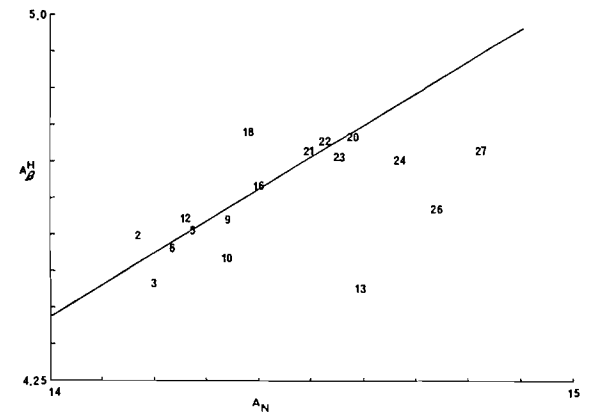


FIG. 9. Plot of $a_\beta^H$ vs. $a_N$ for the benzoyl radical spin adduct to PBN (**14**). The line is the least squares trace omitting H-bonding solvents (i.e. 20, 24, 26, 27).

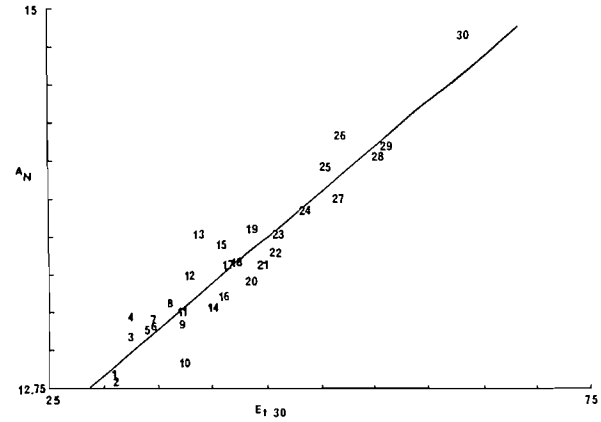


FIG. 10. Plot of $a_N$ vs. $E_{t(30)}$ for the *tert*-butoxyl radical spin adduct to DMPO (**15**).

TABLE 4. Hyperfine splitting constants for *tert*-butoxyl adduct of DMPO[a]

| Solvent | $E_{t(30)}$[b] | $a_N$ | $a_\beta^H$ | $a_\gamma^H$ |
|---|---|---|---|---|
| 1. n-Hexane | 30.9 | 12.84 | 6.19 | 2.15 |
| 2. Cyclohexane | 31.2 | 12.77 | 6.13 | 2.13 |
| 3. Carbon tetrachloride | 32.5 | 13.06 | 7.22 | 2.04 |
| 4. Carbon disulfide | 32.6 | 13.16 | 7.48 | 2.01 |
| 5. Toluene | 33.9 | 13.10 | 7.48 | 1.97 |
| 6. Benzene | 34.5 | 13.12 | 7.87 | 1.90 |
| 7. Diethyl ether | 34.6 | 13.16 | 7.10 | 1.94 |
| 8. 1,4-Dioxane | 36.0 | 13.26 | 8.13 | 1.87 |
| 9. Tetrahydrofuran | 37.4 | 13.13 | 7.87 | 1.87 |
| 10. Chlorobenzene | 37.5 | 12.90 | 8.13 | 1.78 |
| 11. Bromobenzene | 37.5 | 13.22 | 8.45 | 1.81 |
| 12. 1,2-Dimethoxyethane | 38.2 | 13.42 | 8.32 | 1.65 |
| 13. Chloroform | 39.1 | 13.67 | 9.71 | 1.61 |
| 14. Pyridine | 40.2 | 13.22 | 9.55 | 1.61 |
| 15. Methylene chloride | 41.1 | 13.61 | 10.00 | 1.55 |
| 16. Acetophenone | 41.3 | 13.29 | 9.16 | 1.68 |
| 17. 1,2-Dichloroethane | 41.9 | 13.48 | 9.68 | 1.64 |
| 18. Acetone | 42.2 | 13.48 | 9.22 | 1.61 |
| 19. Dimethylformamide | 43.8 | 13.38 | 9.80 | 1.52 |
| 20. *tert*-Butyl alcohol | 43.9 | 13.70 | 8.40 | 1.88 |
| 21. Dimethyl sulfoxide | 45.0 | 13.48 | 10.32 | 1.48 |
| 22. Acetonitrile | 46.0 | 13.54 | 10.71 | 1.35 |
| 23. Nitromethane | 46.3 | 13.67 | 11.09 | 1.29 |
| 24. Isopropyl alcohol | 48.6 | 13.80 | 9.09 | 1.77 |
| 25. Benzyl alcohol | 50.8 | 14.06 | 10.67 | 1.45 |
| 26. Acetic acid | 51.9 | 14.25 | 10.71 | 1.52 |
| 27. Ethyl alcohol | 51.9 | 13.87 | 9.93 | 1.68 |
| 28. Methyl alcohol | 55.5 | 14.13 | 11.29 | 1.30 |
| 29. Ethylene glycol | 56.3 | 14.19 | 12.26 | 1.23 |
| 30. Water | 63.1 | 14.84 | 16.03 | — |

[a]All hfsc's measured in gauss ± 0.05.
[b]Values in kcal/mol.

10). Another interesting feature is the change in γ-H hfsc with polarity of solvent (Table 4). While the β-H hfsc's increase with increase in solvent polarity the γ-H hfsc's decrease as the solvent polarity increases (Fig. 11). The linear correlations are as follows: $r^2 = 0.916$, slope = 3.96 for $a_\beta^H$ vs. $a_N$; $r^2 = 0.767$, slope = −0.484 for $a_\gamma^H$ vs. $a_N$.

It seems remarkable that while the slope of the β-H hfsc vs. $a_N$ is positive, the slope of the γ-H hfsc vs. $a_N$ is negative. This result can be explained in

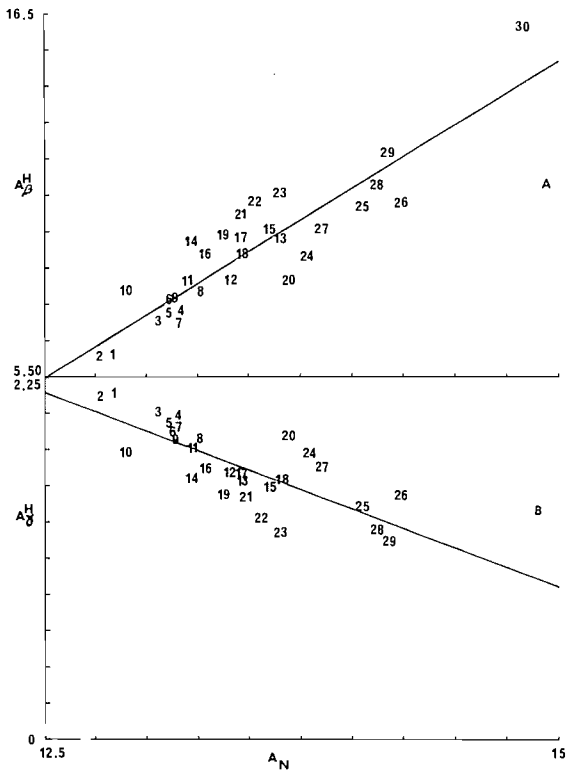


FIG. 11. Plot of (A) $a_\beta^H$ vs. $a_N$, (B) $a_\gamma^H$ vs. $a_N$ for the *tert*-butoxyl radical spin adduct to DMPO (**15**).

terms of a solvent dependent change in the dihedral angle of the β-hydrogen caused by twisting of the α-carbon so that the W-plan to the γ-hydrogen attached to the β-carbon is altered. The reason for this could be the attempt by the 5-membered ring to twist so that the N—O and C—O dipoles in **15** are opposed to the greatest possible extent. In polar solvents the aminoxyl dipole is solvated and the dipole–dipole interaction between the two functions is diminished. The ring relaxes to a more planar configuration where the dihedral angle to the β-H is smaller. Since spin transmission to the γ-hydrogen is best for twisted ring structures (22), the γ-H hfsc would be expected to be largest in nonpolar solvents and decrease as the ring becomes more planar in more polar solvents.

The equations for the best lines of fit in Fig. 11 are as follows:

$$a_\beta^H = 3.96\, a_N - 44.2$$
$$a_\gamma^H = 0.484\, a_N - 8.21$$

*Equations for the plots of the* β*-H hfsc's vs.* $a_N$

The observation that the β-hydrogen hyperfine splitting constants depend on $a_N$ for a number of aminoxyl radicals seems to point to the Heller–McConnell equation (23):

$$a_\beta^H = (B_0 + B\cos^2\theta)\rho_N$$

where $B_0 = a_\beta^H$ when $\theta = 90°$, $B$ = the hyperconjugative proportionality constant, $\theta$ = the dihedral angle between the C—H bond and the $p$-orbital on nitrogen, and $\rho_N$ = spin density on nitrogen. If $a_N$ is proportional to $\rho_N$, and $B_0$, B, and $\theta$ are all constant, as a function of solvent, a linear equation would result:

$$a_\beta^H = Ca_N$$

However, a plot of this equation should go through zero. The observed plots do not. Instead the lines take on the form:

$$a_\beta = Ca_N + C'$$

In practice $C'$ is large and negative indicating a large negative β-H hfsc remains when $a_N$ is zero. This might perhaps make sense if the aminoxyl function is nonplanar and slight changes in *both* the spin density and the configuration about nitrogen occur with change in polarity of the solvent. This point will be addressed in a future paper. In any event the Heller–McConnell equation was not meant to take nonplanarity factors at the radical center into account.

## Conclusions

Linear relationships between the two parameters ($a_\beta^H$, $a_N$) for PBN and DMPO spin adducts provide a useful tool in coupling constant prediction. By obtaining spin adduct coupling constants in only a few solvents, the hfsc's ($a_\beta^H$ and $a_N$) may be found in any other solvent from the calculated slope. Further work in this area is underway.

## Acknowledgements

Support from the Natural Sciences and Engineering Research Council of Canada is gratefully acknowledged. Also one of us (E.G.J.) is very grateful to the Oklahoma Medical Research Foundation for an invitation to spend two months (November–December, 1981) in their laboratories where this paper was written.

1. K. UMEMOTO, Y. DEGUCHI, and H. TAKAKI. Bull. Chem. Soc. Jpn. **36**, 560 (1963); K. MUKAI, H. NISHIGUCHI, K. ISHIZU, Y. DEGUCHI, and H. TAKAKI. Bull. Chem. Soc. Jpn. **40**, 2731 (1967).
2. H. LEMAIRE and A. RASSAT. J. Chim. Phys. Phys.-Chim. Biol. **61**, 1580 (1964); R. BRIERE, H. LEMAIRE, and A. RASSAT. Tetrahedron Lett. 1775 (1964); R. BRIER, H. LEMAIRE, and A. RASSAT. Bull. Soc. Chim. Fr. **11**, 3273 (1965).
3. A. L. BUCHACHENKO and O. P. SUKHANOVA. Zh. Strukt. Khim. **6**, 32 (1965).

Can. J. Chem. Downloaded from www.nrcresearchpress.com by 210.87.254.40 on 09/06/12
For personal use only.

4. T. KAWAMURA, S. MATSUNAMI, and T. YONEZAWA. Bull. Chem. Soc. Jpn. **40**, 1111 (1967).
5. TH. A. J. W. WAJER, A. MACKOR, and TH. J. DEBOER. Tetrahedron, **25**, 175 (1969); O. KIKUCHI and K. SOMENO. Bull. Chem. Soc. Jpn. **40**, 2549 (1967).
6. E. G. JANZEN and G. A. COULTER. Tetrahedron Lett. **22**, 615 (1981).
7. B. R. KNAUER and J. J. NAPIER. J. Am. Chem. Soc. **98**, 4395 (1976).
8. K. DIMROTH, C. REICHARDT, T. SIEPMANN, and F. BOHLMANN. Justus Liebigs Ann. Chem. **661**, 1 (1963).
9. E. M. KOSOWER. J. Am. Chem. Soc. **80**, 3253 (1958).
10. A. BERSON, Z. HAMLET, and W. A. MUELLER. J. Am. Chem. Soc. **84**, 297 (1962).
11. E. G. JANZEN, D. E. NUTTER, JR., E. R. DAVIS, B. J. BLACKBURN, J. L. POYER, and P. B. MCCAY. Can. J. Chem. **56**, 2237 (1978).
12. J. W. LOWN, H-H. CHEN, S-K. SIM, and J. A. PLAMBECK. Bioorg. Chem. **8**, 17 (1979).
13. C. D. JAEGER and A. J. BARD. J. Phys. Chem. **83**, 3146 (1979).
14. J. L. ROBERTS, M. M. MORRISON, and D. T. SAWYER. J. Am. Chem. Soc. **100**, 329 (1978).
15. F. P. SARGENT and E. M. GARDY. Can. J. Chem. **53**, 3128 (1975).
16. N. OHTO, E. NIKI, and Y. KAMIYA. J. Chem. Soc. Perkin Trans. II, 1770 (1977).
17. G. A. RUSSELL, E. G. JANZEN, and E. T. STROM. J. Am. Chem. Soc. **86**, 1807, (1964).
18. E. G. JANZEN, R. L. DUDLEY, and R. V. SHETTY. J. Am. Chem. Soc. **101**, 243 (1979).
19. E. G. JANZEN, D. E. NUTTER, JR., E. R. DAVIS, H. J. STRONKS, J. L. POYER, P. B. MCCAY, and H. N. BLOUNT. Can. J. Chem. **58**, 1596 (1980).
20. J. B. HOWELL and D. C. MCAIN. J. Phys. Chem. **73**, 4405 (1969).
21. J. L. POYER, R. A. FLOYD, P. B. MCCAY, E. G. JANZEN, and E. R. DAVIS. Biochim. Biophys. Acta, **539**, 402 (1978); E. K. LAI, P. B. MCCAY, T. NAGUCHI, and K-L FONG. Biochem. Pharmacol. **28**, 2231 (1979); J. L. POYER, P. B. MCCAY, E. K. LAI, E. G. JANZEN, and E. R. DAVIS. Biochem. Biophys. Res. Commun. **94**, 1154 (1980).
22. F. W. KING. Chem. Rev. **76**, 157 (1976).
23. C. HELLER and H. M. MCCONNELL. J. Chem. Phys. **32**, 1535 (1960).

Can. J. Chem. Downloaded from www.nrcresearchpress.com by 210.87.254.40 on 09/06/12
For personal use only.

# The effect of an external electric field on the photochemistry of *x*-phthalocyanine particles in heptane

JOHN R. HARBOUR AND SANDRA L. ISSLER

*Xerox Research Centre of Canada, 2480 Dunwin Drive, Mississauga, Ont., Canada L5L 1J9*

Received December 14, 1981[1]

JOHN R. HARBOUR and SANDRA L. ISSLER. Can. J. Chem. **60**, 2734 (1982).

A system is described which allows for the determination of the photo-efficiency of pigment particles in low dielectric solvents as a function of electric field. The charge carriers in this system are both molecular and particulate and the photo-induced current is a function of dissolved oxygen concentration. The maximum quantum efficiency was determined to be 23% at high electric field ($2 \times 10^5$ V/cm) and low light intensity for *x*-phthalocyanine particles in heptane. Initial efforts at spin trapping in this system reveal the synergistic generation of a nitroxone and alkylperoxy spin adduct of α-phenyl *N*-*t*-butyl nitrone. Both of these adducts are, however, neutral and it is demonstrated that this system is not well suited for the detection of trapped ionic radicals.

JOHN R. HARBOUR et SANDRA L. ISSLER. Can. J. Chem. **60**, 2734 (1982).

On décrit un système qui permet de déterminer la photo-efficacité de particules de pigment dans des solvants de faible constantes diélectriques en fonction du champ électrique. Les porteurs de charge dans ce système sont à la fois moléculaires et particulaires et le courant photo-induit est fonction de la concentration en oxygène dissous. On a déterminé que l'efficacité quantique maximum est égale à 23% à champ électrique fort ($2 \times 10^5$ V/cm) et à faible intensité de lumière pour des particules de *x*-phtalocyanine dans l'heptane. Nos efforts initiaux dans le but de capter des spin dans ce système révèlent qu'il y a formation synergistique d'un adduit de spin nitronone et alkylperoxy de l'α-phényl *N*-*t*-butylnitrone. Ces deux adduits sont, cependant, neutres et on démontre que ce système ne convient pas très bien à la détection des radicaux ioniques piégés.

[Traduit par le journal]

## Introduction

The photochemistry of pigment dispersions has been rather extensively investigated, particularly in regard to solar energy utilization (SEU) (1–4). Pigment dispersions also form the basis of a novel imaging technique referred to as photoactive pigment electrography (PAPE) (5). In both of these systems it is essential that the inherent quantum efficiency for hole/electron generation, as well as the efficiency of the subsequent interfacial charge transfer, be relatively high. The overall efficiency ($\Phi_{overall}$) can be considerably enhanced if the process is carried out in an electric field, *E*. This can be accomplished by application of an external *E* or creation of an internal *E* through formation of e.g., a Schottky barrier. Hence, in both SEU and PAPE systems it is of importance to know the *E* dependence of the overall efficiency as well as the molecular events which give rise to this dependence.

Hartmann and Schmidlin (6) and Hartmann and Noolandi (7) have reported results of photo-induced charge transfer as a function of *E* at phthalocyanine ($H_2Pc$) liquid interfaces using vacuum-sublimed thin films. Similar experiments have been reported by Tang *et al.* (8) with chlorophyll a (Chl a) films. In their study, which is closest experimentally to ours, microcrystals of Chl a were electro-deposited from non-polar solvents onto a transparent electrode which was biased negatively (implying that the microcrystals were positively charged). However, molecular Chl a was present in the solution during their experiments. The identity of the pigment particles has also been maintained in studies by Popovic (9) in which the particles were dispersed in a non-conducting polymer matrix sandwiched between two electrodes, one of which was transparent. The efficiency of charge separation as a function of *E* was determined for $H_2Pc$ pigments using this technique.

Loutfy and Sharp (10, 11) also used particle dispersions ($H_2Pc$ in polymer) overcoated with a partially transparent metal electrode which creates a Schottky barrier to determine $\Phi_{overall}$ for $H_2Pc$ pigments. This photovoltaic solar cell measures efficiency of pigment particles as a function of internal *E* (12).

It is of importance in the characterization of pigments to measure $\Phi_{overall}$ without significantly altering the properties of the particles. Only one of the above-mentioned studies measures the photo-efficiency of the pigment particles in a liquid phase (8). Since the PAPE process occurs in an insulating solvent, it is important to measure the efficiency as a function of *E* (5), under conditions as close as possible to the actual system. This paper reports on our initial efforts at creating an experimental set-up which allows one to monitor the photo-efficiency of pigments initially in dispersion as a function of *E*. In order to gain a better understanding of the

[1]Revision received June 30, 1982.

0008-4042/82/212734-06$01.00/0

©1982 National Research Council of Canada/Conseil national de recherches du Canada

Can. J. Chem. Downloaded from www.nrcresearchpress.com by 210.87.254.105 on 09/06/12
For personal use only.

Can. J. Chem. Downloaded from www.nrcresearchpress.com by 210.87.254.105 on 09/06/12
For personal use only.

molecular events, we have applied the technique of spin trapping (13, 14) to these systems.

## Experimental

The sample cell used for this study was designed by Novotny (15). Briefly, it was comprised of two indium oxide coated glass plates (NESATRON) separated by a flat ring of Teflon. Spacers of 250 and 500 μ were used and the interior diameter of the Teflon ring was 3.8 cm. The top electrode had two ground glass ports through which the dispersion could be added or emptied and closed to the atmosphere. This electrode-spacer system was placed between two flat metal rings and the system was sealed by tightening screws with a torque wrench to a reproducible pressure.

The sample cell was placed in series with a $10^5$ Ω resistor and a 0 to 3000 V Fluke 415B High Voltage Power Supply. The current was monitored by measuring the voltage generated across the $10^5$ Ω resistor with a Philips model PM3234 storage scope.

The light source consisted of a 300 W Quartzline projection lamp controlled by a variable transformer. The lamp was located 4 cm above the cell and air cooled. A broad band interference filter (710 nm) was generally employed for the determination of photo-induced currents (PIC's) and light-generated esr signals. However, equivalent results were obtained for the PIC's with a narrow band, 620 nm interference filter. For the determination of quantum efficiency, a narrow band (± 10 nm) interference filter (620 nm) was used and the light intensity was measured using an Alphametrics Model dc 1010 radiometer with a Model P1100S Silicon light probe.

Electron spin resonance spectra were recorded on a Varian E-12 ESR spectrometer. A 0.4% by wt. $x$-$H_2Pc$ in heptane mixture was dispersed by ultrasonic irradiation and placed immediately in the electroded cell. An $E$ was applied to plate out the pigment particles and then the solvent was removed and replaced with a 0.3 $M$ PBN solution ($\lambda_{max}$ = 285 nm) in heptane. This technique does not alter the magnitude of the PIC and prevents ultrasonic irradiation of the spin trap solution which can result in spin adduct formation (16). The voltage (3000 V over 250 nm) was first switched on to determine the dark current and then the light (60 V) was turned on for 10 s before both voltage and light were switched off. The solution was immediately removed, nitrogen purged, and transferred to an aqueous esr tube for measurement. The entire process, including the recording of the spectrum, took between 2 and 3 min.

$x$-Phthalocyanine ($x$-$H_2Pc$) was prepared by the method of Byrne and Kury (17). Heptane (Burdick and Jackson, distilled in glass), 5,5-dimethyl-1-pyrroline-1-oxide, DMPO (Aldrich), and α-phenyl N-$t$-butyl nitrone, PBN (spin trap producers) were used as received. The soluble tetra-*tert*-butyl phthalocyanine ($t$-b-$H_2Pc$) was a gift from James Duff, Xerox Research Centre of Canada.

## Results and discussion

### *I. Photoconductivity measurements*

A typical current/time plot as a function of illumination for $x$-$H_2Pc$ particles dispersed in heptane is shown in Fig. 1. The magnitude of the increase reflects the efficiency of the overall charge generation and transfer. This efficiency is essentially independent of pigment loading over the range shown in Table 1. Hence the wt% of pigment loading was selected to fall in this non-critical

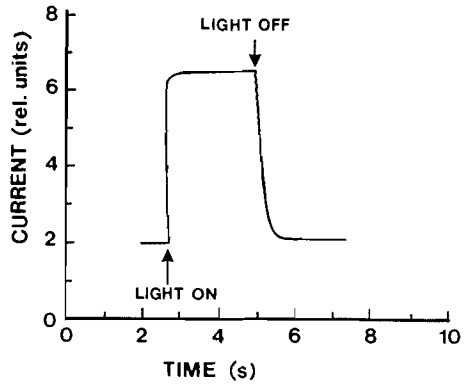


FIG. 1. Typical result for the PIC as a function of time for an $x$-$H_2Pc$ dispersion in heptane.

region (0.1 → 0.4%) where one need not worry about a PIC dependence on pigment concentration. There was no difference in PIC for either a negative or positive polarity of the top electrode. The implications of this result are discussed below.

Figure 2 shows the efficiency (PIC) as a function of $E$. This superlinear dependence is similar qualitatively to the work of Hartmann and Noolandi (7) but different from Tang *et al.* (8), who show a saturation with $E$. Changing the thickness from 250 nm to 500 nm gave the same PIC for an equivalent $E$. This demonstrates that the efficiency of the overall process is not limited by charge transfer from one electrode to the other. $\Phi_{overall}$ (at $3 \times 10^4$ V/cm) decreased with increasing light intensity as shown in Fig. 3. $\Phi_{overall}$ continued to decrease at higher light intensities. At $5 \times 10^{16}$ photons/s, $\Phi_{overall}$ dropped to 0.027 and at the highest intensity ($1.3 \times 10^{17}$ photons/s) $\Phi_{overall}$ was equal to 0.017.

The application of an $E$ in the dark brought about the electrophoretic migration of these particles to both electrodes. This implies that the dispersion originally had particles with both positive and negative surface charge. Removal of the liquid after this deposition gave a colourless solvent, indicating that essentially all of the particles plated out (phthalocyanine is totally insoluble in heptane). Hence the photoconductivity occurs from particles which are adsorbed onto the $In_2O_3$ surface.

The PIC must have some of its origin from the migration of particles between electrodes. Support for this comes from an experiment in which the cell, after application of an $E$ in the dark, is disassembled and then reassembled after one of the electrodes had been cleaned. This PIC for this new cell was very low initially but with time increased significantly. Concurrent with this increase was the

TABLE 1. PIC results for the study of concentration dependence

| | PIC (A) | | | |
|---|---|---|---|---|
| Applied $E$ (V/cm) | 0.1 wt% | 0.2 wt% | 0.4 wt% | 2.0 wt% |
| $1 \times 10^4$ | $2.1 \times 10^{-7}$ | $2.1 \times 10^{-7}$ | $2.0 \times 10^{-7}$ | — |
| $2 \times 10^4$ | $2.3 \times 10^{-6}$ | $2.2 \times 10^{-6}$ | $2.0 \times 10^{-6}$ | — |
| $3 \times 10^4$ | $7.2 \times 10^{-6}$ | $7.3 \times 10^{-6}$ | $7.2 \times 10^{-6}$ | $5.2 \times 10^{-6}$ |
| $4 \times 10^4$ | $1.7 \times 10^{-5}$ | $1.7 \times 10^{-5}$ | $1.7 \times 10^{-5}$ | $1.5 \times 10^{-5}$ |

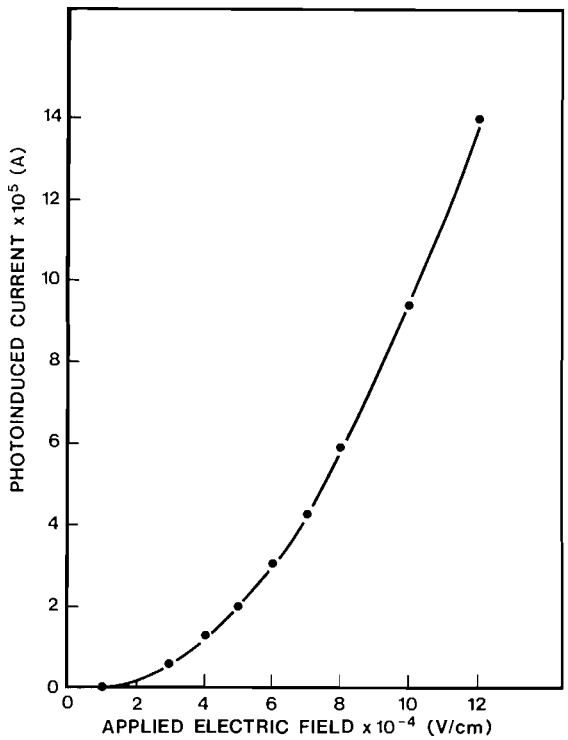


FIG. 2. PIC dependence on $E$ for an $x$-$H_2Pc$ dispersion in heptane (4 mg/mL) using a 250 μ spacer.

observation that the "cleaned" electrode was now covered with $x$-$H_2Pc$ particles. This not only demonstrates that the charged $x$-$H_2Pc$ particles do migrate across the cell, it also shows that maximum PIC's are only observed when both electrodes are coated. These results can be described by the following mechanism for particle migration assuming that the top electrode is positive.

$$[1]\quad (x\text{-}H_2Pc)^0_{anode} \xrightarrow{nh\nu} ne^- + (x\text{-}H_2Pc)^{n+}_{anode}$$

$$[2]\quad (x\text{-}H_2Pc)^{n+}_{anode} \rightarrow (x\text{-}H_2Pc)^{n+}_{cathode}$$

$$[3]\quad ne^- + (x\text{-}H_2Pc)^{n+}_{cathode} \rightarrow (x\text{-}H_2Pc)^0_{cathode}$$

Light absorbed by the $x$-$H_2Pc$ particles creates electron/hole pairs which is followed by charge injection into the $In_2O_3$ (reaction [1]). The holes ($nh^+$) remaining on the $x$-$H_2Pc$ particles cause the particle to become positively charged and it is then electrophoretically driven to the cathode (reaction [2]). The injected electrons essentially reduce the positively charged particles as shown in reaction [3]. Those particles which are adsorbed on the cathode can also absorb light and subsequently inject holes (rather than electrons) and produce current in a manner analogous to that expressed by reactions [1]–[3]. This mechanism is consistent with the fact that equivalent PIC's are observed regardless of the polarity of the top electrode and with the fact that a migration of particles within the cell is observed.

The PIC also has a contribution from ionic carriers. This would certainly be expected from the results of prior work (6–8) in which all the current was associated with ionic, soluble carriers. In our system this was confirmed by several different experiments. Purging the dispersion with $N_2$ prior to filling the cell had a significant effect on the PIC (Fig. 4) compared to both the air-saturated and $O_2$-saturated systems. In fact, the PIC showed an ~50% increase in going from $N_2$- to $O_2$-purged systems. Detection of $O_2^-$ during the photolysis of $x$-$H_2Pc$ dispersions (18, 19) suggests that $O_2^-$ may be a possible ionic carrier in this system, consistent with the oxygen effect on PIC. Finally, soluble $t$-b-$H_2Pc$, when dissolved and placed within the cell also exhibited PIC's but to a much lesser extent. Nevertheless, in this system, the only possible charge carriers are soluble ions and therefore the observation of a PIC is consistent with an ionic component to the PIC.

The $\Phi_{overall}$ for this process (Fig. 3) is shown to be 0.011 at low light intensity and an $E$ of $3 \times 10^4$ V/cm. Figure 2 shows that at the highest $E$ used ($2 \times 10^5$ V/cm), $\Phi$ is increased by a factor of ~21. This factor of 21 is surprisingly not a function of the light intensity. For light intensities of $5 \times 10^{13}$, $6 \times 10^{15}$, and $4 \times 10^{16}$ photons/cm$^2$ s, a constant value for the ratio of $\Phi_{overall}$ at $3 \times 10^4$ V/cm and $1.2 \times 10^5$ V/cm was obtained. Therefore an extrapolated value of $\Phi_{overall} = 0.23$ is achieved for maximum efficiency. (This does not take into account the increase that would be expected if the sample were $O_2$ purged). This can be contrasted to a $\Phi_{overall} \simeq 0.01$ for chlorophyll (8); $5 \times 10^{-4}$ for $H_2Pc$ films at 2

Can. J. Chem. Downloaded from www.nrcresearchpress.com by 210.87.254.105 on 09/06/12
For personal use only.

Can. J. Chem. Downloaded from www.nrcresearchpress.com by 210.87.254.105 on 09/06/12
For personal use only.

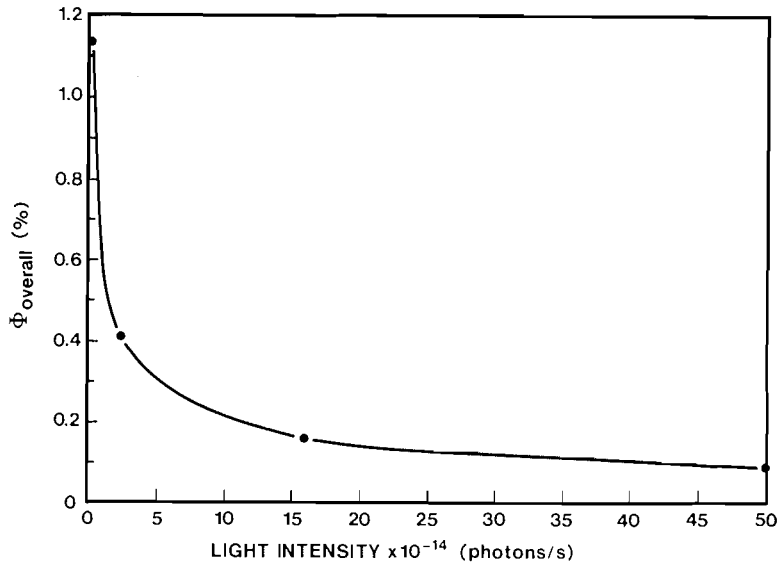


FIG. 3. The dependence of $\Phi_{overall}$ on light intensity for an $x$-$H_2Pc$ dispersion in heptane (2 mg/mL).

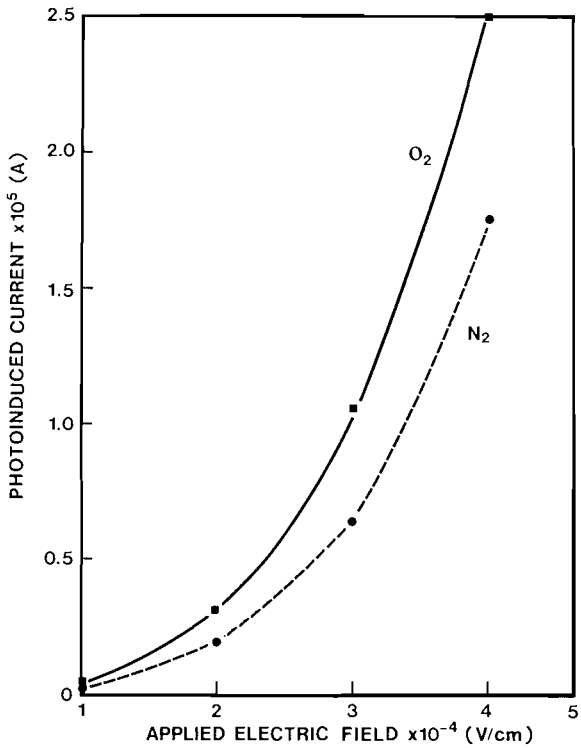


FIG. 4. The PIC as a function of $E$ for a $N_2$-purged dispersion (○) and an $O_2$-purged (□) $x$-$H_2Pc$ in heptane dispersion (2 mg/mL).

$\times$ $10^5$ V/cm (6) and $7 \times 10^{-3}$ for $H_2Pc$ films at $6 \times 10^5$ V/cm (7). This result implies that the particles of $x$-$H_2Pc$ are far more photoactive than films of $H_2Pc$ and/or that this system, which allows for particle migration, increases the efficiency by inclusion of particle charge carriers to the overall PIC's. This experimental set-up, in any event, provides for a determination of the $\Phi_{overall}$ for pigment particles which have potential for use in PAPE systems. The allowance for particle migration mimics the real PAPE system and therefore provides a more realistic determination of pigment performance under reproducible conditions in a closed cell.

*II. Spin trapping*

It is of interest to determine the nature of the molecular intermediates involved during these electric-field-enhanced photochemical reactions. Previously, spin trapping has been employed in the study of pigment dispersions in the absence of an external $E$ (14, 18, 20). These studies were successful in the detection of radical intermediates including $O_2^-$, $\cdot OH$, and $\cdot CO_2^-$ upon photolysis of pigment dispersions. We, therefore, introduced spin traps within this system in an effort to detect short-lived radical intermediates. The application of spin traps for a study of electrode reactions has been previously demonstrated (21, 22).

With PBN ($\sim 10^{-2}$ $M$) present in the $x$-$H_2Pc$ dispersion, PIC's were obtained which were only slightly less than the PIC's measured without PBN. This result suggests that PBN is acting essentially as an inert component of the system. Electron spin resonance observation of this solution after a 10 s application of an $E$ revealed that very little spin adduct formation occurred (Fig. 5*a*). Similar results were obtained upon photolysis of this dispersion in the absence of an $E$ (Fig. 5*b*). However,

Can. J. Chem. Downloaded from www.nrcresearchpress.com by 210.87.254.105 on 09/06/12
For personal use only.

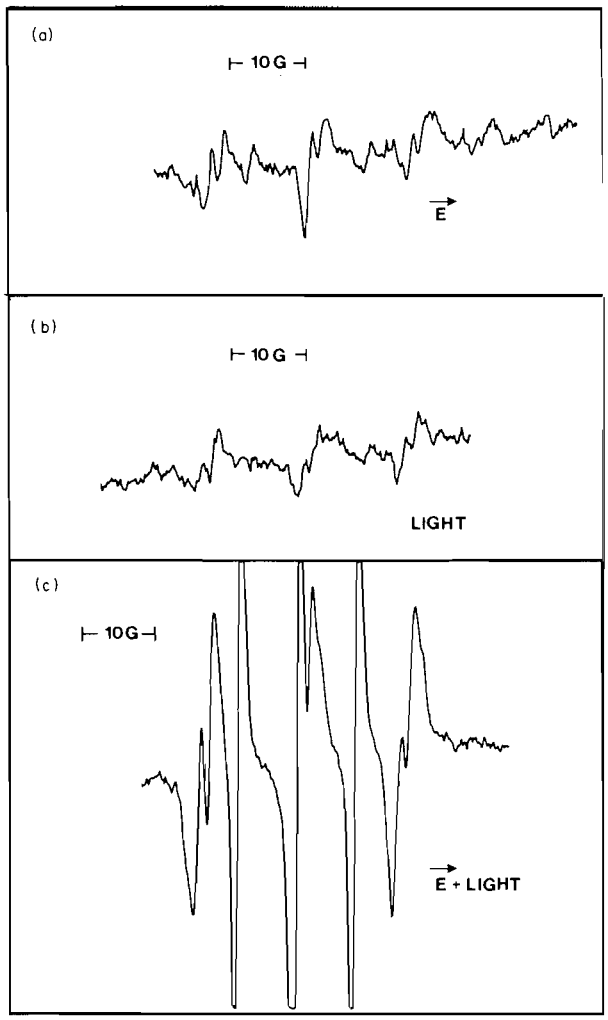


FIG. 5. The esr spectra obtained from a saturated PBN solution of heptane added to the cell after plating out of the $x$-$H_2Pc$ particles. (*a*) $E$ only ($1.2 \times 10^5$ V/cm), (*b*) light only, and (*c*) $E$ ($1.2 \times 10^5$ V/cm) and light. Spectrometer settings were equivalent for these three cases: 1.6 G, modulation amplitude; 15 mW, microwave power; 0.3 s, time constant; $1.25 \times 10^4$, receiver gain; 2 min, scan time. The solutions were $N_2$ purged before transfer to the esr cell to enhance sensitivity.

with both $E$ and illumination for a 10 s period, the esr signal shown in Fig. 5*c* resulted. This spectrum is a superposition of at least three separate nitroxide spectra. The 3 line spectrum with $a^N = 7.9$ most likely arises from a nitroxone (22).

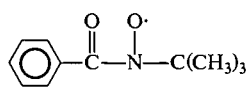

The second major component with $a^N = 13.4$ G and $a^H = 1.5$ is typical of alkylperoxy adducts (23, 24). Apparent as shoulders on this spectrum is a third component of unknown splittings. Nevertheless, one can deduce that both $a^N$ and $a^H$ are larger than those of the alkyl peroxy adducts. Under some circumstances, temporary shorting of the electrodes at these high electric fields was observed as a spike in the oscilloscope trace. In these cases significant quantities of the alkylperoxy radical adducts were generated (Fig. 6). This was reproducible and points out the necessity of monitoring the PIC's of samples being analyzed by esr.

The cooperative effect of both light and $E$ in producing radicals is clear evidence of a synergistic process. Nevertheless, the origin of the adducts is not obvious. PBN could be oxidized to the nitroxone in this process to yield the neutral spin adduct. The alkylperoxy adduct may result from the reaction of $O_2$ with an alkyl radical generated during the electrical breakdown of the cell. In the case of no apparent shorting, the light induces a high current which could create a partial shorting resulting in the generation of the same radical adduct. The third radical adduct is unknown. The important thing to note is that both major radical adducts are neutral. This would, in fact, be the expected result since charged spin adducts would be driven by the electric field (usually with electrophoretic mobilities of $\sim 1 \times 10^{-4}$ cm$^2$/V s) to the electrode surface. It is known that radical adducts readily undergo redox reactions and would therefore react at the electrode to yield either a diamagnetic product or another nitroxide. Since the cell thickness is 250 $\mu$, a charged radical adduct would exist at an $E = 2 \times 10^5$ V/cm for $\tau \simeq 1$ ms. This millisecond lifetime severely limits the steady-state concentration of radical adducts generated from the trapping of charged radicals. On the other hand, the neutral radicals will tend to accumulate over the 10 s illumination period. Hence photogenerated $O_2^-$ radicals which might be expected as at least one of the ionic carriers (19) were not observed in the trapping experiments.

Several experiments were attempted with DMPO in spite of the fact that problems were encountered when DMPO was present. The PIC's were significantly reduced and an agglomeration of pigment particles on the Nesatron surface was observed. When the esr experiments were attempted, an adduct was generated with $a^N = 13.2$ G and $a^H = 9.9$ G (a three-line nitroxide ($a^N = 13.5$ G) was present in the dark). This unknown adduct (which could result from a peroxy radical) was generated with either light and/or $E$.

## Conclusions

A system has been presented which permits the determination of the electric field dependence of

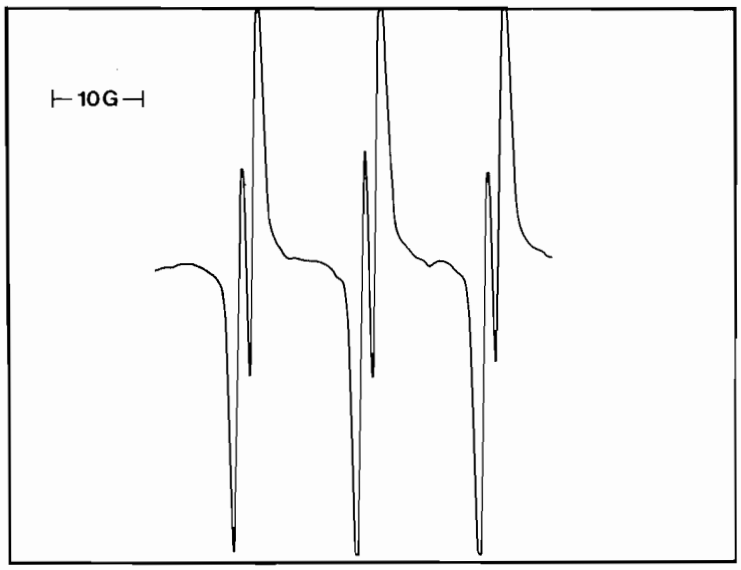


FIG. 6. Electron spin resonance signal obtained when shorting of the cell occurred. Same settings as in Fig. 5 except receiver gain was reduced to $1.25 \times 10^3$.

photochemical charge exchange of pigment particles. This is especially important for the evaluation of particles in which their identity can be maintained. An example of an application is determination of the change in photochemistry as a result of surface modification for SEU. The technique is particularly adapted for screening potential pigments in PAPE imaging systems and for noting the effect of added compounds. Both molecular and particulate charge carriers contribute to the PIC and $O_2$ is shown to enhance the effect. Spin trapping experiments reveal a synergism of *E* and light in the production of neutral spin adducts. Both an alkylperoxyl and a nitroxone were identified. "Shorting" of the cell generates the alkylperoxyl radical. It is shown that ionic radicals trapped by PBN which create charged spin adducts can not be effectively detected with this system.

**Acknowledgements**

We thank Vladimer J. Novotny for providing the cell for these experiments, James R. Bolton and the University of Western Ontario for use of the esr facilities, Michael A. Hopper for discussions concerning the experimental set-up, James M. Duff for the gift of tetra-*tert*-butylphthalocyanine, and Michael L. Hair for his continued support of this work.

1. T. R. RUBIN, J. G. CALVERT, G. T. RANKIN, and W. MACNEVEN. J. Am. Chem. Soc. **75**, 2850 (1953).
2. T. FREUND and W. P. GOMES. Catal. Rev. **3**, 1 (1969).
3. J. R. HARBOUR and M. L. HAIR. J. Phys. Chem. **81**, 1791 (1977).
4. A. J. BARD. J. Photochem. **10**, 59 (1979).
5. J. W. WEIGL. Angew. Chem. Int. Ed. Engl. **16**, 374 (1977).
6. G. C. HARTMANN and F. W. SCHMIDLIN. J. Appl. Phys. **46**, 266 (1975).
7. G. C. HARTMANN and J. NOOLANDI. J. Chem. Phys. **66**, 3498 (1977).
8. C. W. TANG, F. DOUGLAS, and A. C. ALBRECHT. J. Phys. Chem. **79**, 2723 (1975).
9. Z. D. POPOVIC. To be published.
10. R. O. LOUTFY and J. H. SHARP. J. Chem. Phys. **71**, 1211 (1979).
11. R. O. LOUTFY, J. H. SHARP, C. K. HSIAO, and R. HO. J. Appl. Phys. **52**, 5218 (1981).
12. Z. D. POPOVIC and R. O. LOUTFY. J. Appl. Phys. To be published.
13. E. G. JANZEN. Acc. Chem. Res. **4**, 31 (1971).
14. J. R. HARBOUR and M. L. HAIR. J. Phys. Chem. **83**, 652 (1979).
15. V. NOVOTNY and M. L. HAIR. J. Colloid. Interface Sci. **71**, 273 (1979).
16. J. R. HARBOUR. Unpublished results.
17. J. F. BYRNE and P. F. KURY. U.S. Patent 3357989 (1967).
18. J. R. HARBOUR and M. L. HAIR. J. Phys. Chem. **82**, 1397 (1978).
19. J. R. HARBOUR, M. L. HAIR, and S. L. ISSLER. Can. J. Chem. **60**, 1523 (1982).
20. C. D. JAEGER and A. J. BARD. J. Phys. Chem. **83**, 3146 (1979).
21. A. J. BARD, J. C. GILBERT, and R. D. GOODIN. J. Am. Chem. Soc. **96**, 620 (1974).
22. T. H. WALTER, E. E. BANCROFT, G. L. MCINTIRE, E. R. DAVIS, L. M. GIERASCH, H. N. BLOUNT, H. J. STRONKS, and E. G. JANZEN. Can. J. Chem. In press.
23. M. V. MERRITT and R. A. JOHNSON. J. Am. Chem. Soc. **99**, 3713 (1977).
24. E. G. JANZEN, D. E. NUTTER, E. R. DAVIS, B. J. BLACKBURN, J. L. POYER, and P. B. MCCAY. Can. J. Chem. **56**, 2237 (1978).

Can. J. Chem. Downloaded from www.nrcresearchpress.com by 210.87.254.105 on 09/06/12
For personal use only.

# A theoretical study on the *cis/trans*-isomerization of azodioxymethane

TSUTOMU MINATO, SHINICHI YAMABE,[1] AND HISAKAZU ODA

*Department of Chemistry, Nara University of Education, Takabatake-cho, Nara 630, Japan*

Received May 5, 1982

TSUTOMU MINATO, SHINICHI YAMABE, and HISAKAZU ODA. Can. J. Chem. **60**, 2740 (1982).

The state correlation diagram for the *cis/trans*-isomerization of azodioxymethane is presented. The direct interconversion through N—N twisting is found to be symmetry-forbidden in a thermal reaction, whereas it is symmetry-allowed photochemically. In the thermal reaction, the fragmentation of the *cis* form into two nitrosomethanes and their recombination to the *trans* form take place via the symmetry-allowed "from step to step" mechanism. The potential energy is calculated by the *ab initio* MO method of a 4-31G basis set and a solvent effect is found to be indispensable in reproducing the energetics of these reactions.

TSUTOMU MINATO, SHINICHI YAMABE et HISAKAZU ODA. Can. J. Chem. **60**, 2740 (1982).

On présente le diagramme de corrélation d'état de l'isomérisation *cis/trans* de l'azodioxyméthane. On a trouvé que l'interconversion directe par l'intermédiaire d'une torsion de la liaison —N—N est interdite par raison de symétrie dans une réaction thermique, tandis qu'elle est permise photochimiquement. Dans une réaction thermique, la fragmentation de la forme *cis* en deux nitrosométhanes ainsi que leur combinaison en forme *trans* se fait par un mécanisme "étape par étape" qui est symétriquement permis. On a calculé l'énergie potentielle par la méthode *ab initio* des OM d'un ensemble de base 4-31G et on a trouvé un effet de solvant indispensable pour la reproduction des effets énergétiques de ces réactions.

[Traduit par le journal]

## I. Introduction

Aliphatic nitroso compounds, R—N=O, where R is a primary or secondary alkyl group, are known to stay almost exclusively in dimeric form in solution. From experimental studies, thermodynamical and kinetic parameters for the dimerization of nitrosoalkanes have been obtained (1). Cross-over and trapping experiments have shown that the *cis/trans*-isomerization of the dimer does not proceed by rotation around the N—N bond but via free monomers (2). So far, few theoretical studies have been made on the mechanism of isomerization. Hoffmann, with use of the extended Hueckel MO method (3), pointed out that HNO (parent molecule of nitrosomethane) dimerizes to a *trans* product in the "bent-out-of-plane path", one of the non-least-motion paths. Heiberg examined the least-motion path with the rigorous CI (4). However, it is not yet known why the direct isomerization by route (I) shown in Fig. 1 is unfavorable. It is also of interest to examine how the reaction proceeds via monomers ((II)-1 → (II)-2 in the figure).

In the present work, these reaction paths are systematically investigated with the aid of the state correlation diagram (5). This is useful in minimizing the effort in searching for the potential surface. Based on the outline of the reaction coordinate given by the diagram, we trace the minimum-energy path of the "symmetry-allowed" process with the *ab initio* MO method. In view of the potential energy and the electronic structure of the dimer and monomer, their stability and reactivity are discussed.

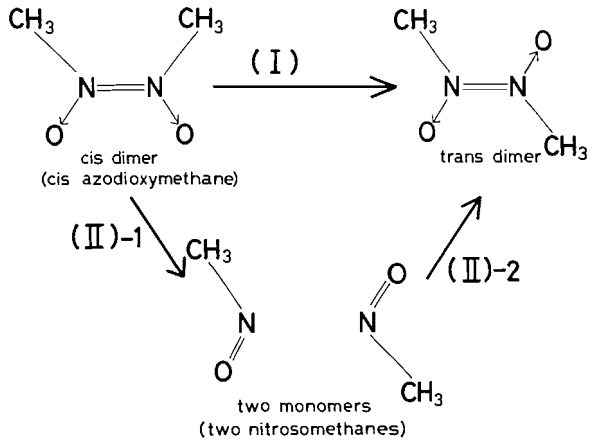


FIG. 1. Two routes (I) and (II) for the *cis/trans* interconversion of azodioxymethane.

## II. Procedure

The electron distribution is computed with RHF MO of a 4-31G valence-double-ζ basis set internal to the GAUSSIAN 70 program (6). The equilibrium geometry of the monomer and two dimers is optimized. In Fig. 2, the obtained geometries are displayed together with the Mulliken atom population and the dipole moment. The crystal structures give a 0.09 Å difference in the N—N bond length between *cis* and *trans* forms (7). The present calculation reproduces this trend, although it is somewhat smaller (0.03 Å). The N—O bonds in dimers are longer than that of the monomer. This

[1]To whom all correspondence should be addressed.

0008-4042/82/212740-09$01.00/0

©1982 National Research Council of Canada/Conseil national de recherches du Canada

Can. J. Chem. Downloaded from www.nrcresearchpress.com by 210.87.254.5 on 09/06/12
For personal use only.

Can. J. Chem. Downloaded from www.nrcresearchpress.com by 210.87.254.5 on 09/06/12
For personal use only.

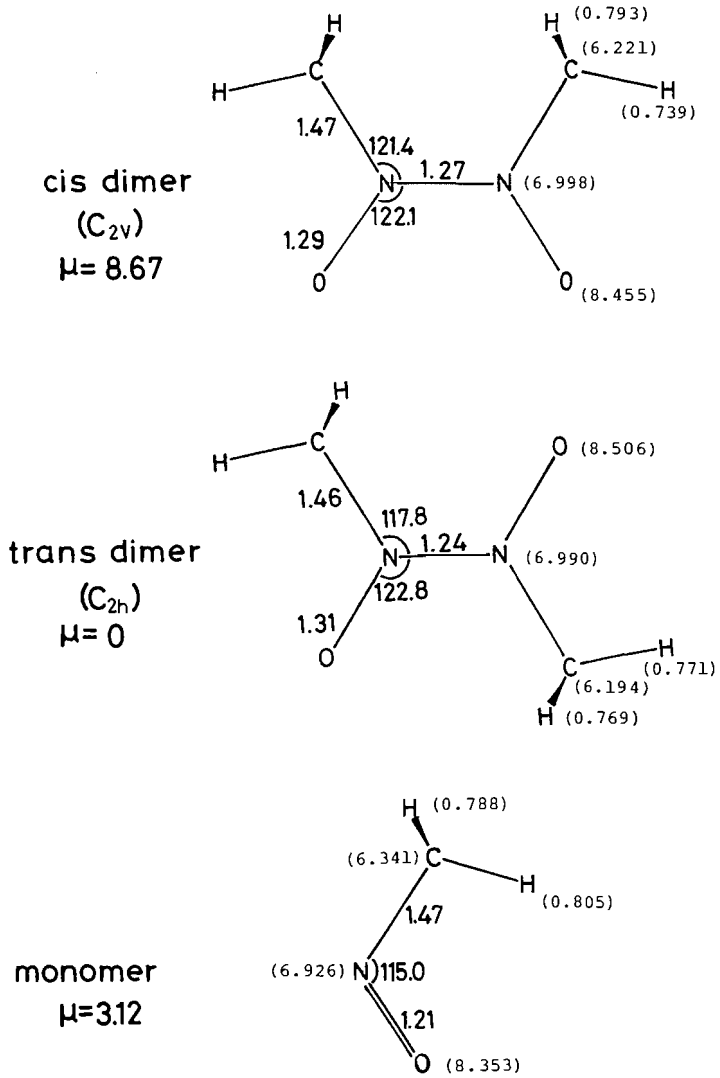


FIG. 2. The structures of *cis* and *trans* dimers and the monomer optimized with the 4-31G basis set. The bond distance and the angle are in Å and in degree, respectively. The numbers in parentheses are Mulliken atom populations. μ is the dipole moment in debye unit.

means that those bonds lose their double-bond character in dimers. It is noticed that the *cis* dimer has a remarkably larger dipole moment than the *trans* dimer and the monomer.

MO's obtained for the optimized geometries are assigned to symmetry orbitals according to the point group ($C_{2v}$ or $C_{2h}$) for the least-motion (i.e, the highest-symmetry) path. In view of the MO levels, the correlation diagram for the low-lying excited states as well as for the ground state may be drawn. When the least-motion path is found to be symmetry-forbidden in any state of interest, a non-least-motion path should be introduced. This corresponds to the relaxation of the symmetry imposed on the reacting system. For the relaxed (lowered) symmetry, it is judged whether the forbiddeness remains or not. Once the diagram gives the allowed path (i.e., the restriction by the orbital symmetry is removed), the minimum-energy path along the symmetry-allowed direction may be traced.

### III. Qualitative description of reaction paths

In Table 1, we show a schedule of examining individual correlation diagrams for the three routes in Fig. 1. In Fig. 3, route (I) of the direct *cis* → *trans*

TABLE 1. List of various state correlation diagrams for point groups imposed on the path of the isomerization in the ground state

| Route No. | Reaction | Highest symmetry | Relaxed symmetry | Figure | Judgement |
|---|---|---|---|---|---|
| (I) | *cis* dimer → *trans* dimer | $C_2$ | | Fig. 4 | Forbidden |
| (II)-1 | *cis* dimer → two monomers | $C_{2v}$ | | Fig. 5 | Forbidden |
| | | | $C_s$ | Fig. 6(*a*) | Forbidden |
| | | | $C_s'$ | Fig. 6(*b*) | Forbidden |
| | | | $C_2$ | Fig. 6(*c*) | Allowed |
| (II)-2 | two monomers → *trans* dimer | $C_{2h}$ | | Fig. 7 | Forbidden |
| | | | $C_s$ | Fig. 8(*a*) | Forbidden |
| | | | $C_2$ | Fig. 8(*b*) | Forbidden |
| | | | $i$ | Fig. 8(*c*) | Allowed |

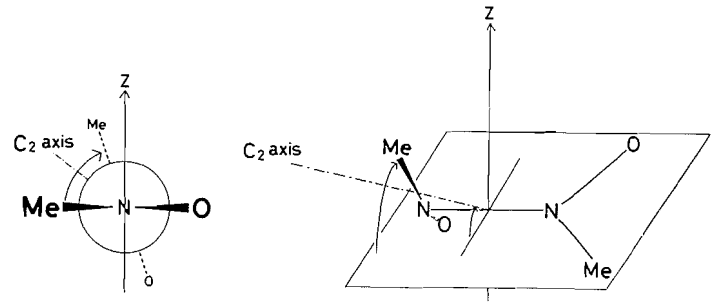


FIG. 3. The direct twisting mechanism of *cis* → *trans* isomerization of the dimer.

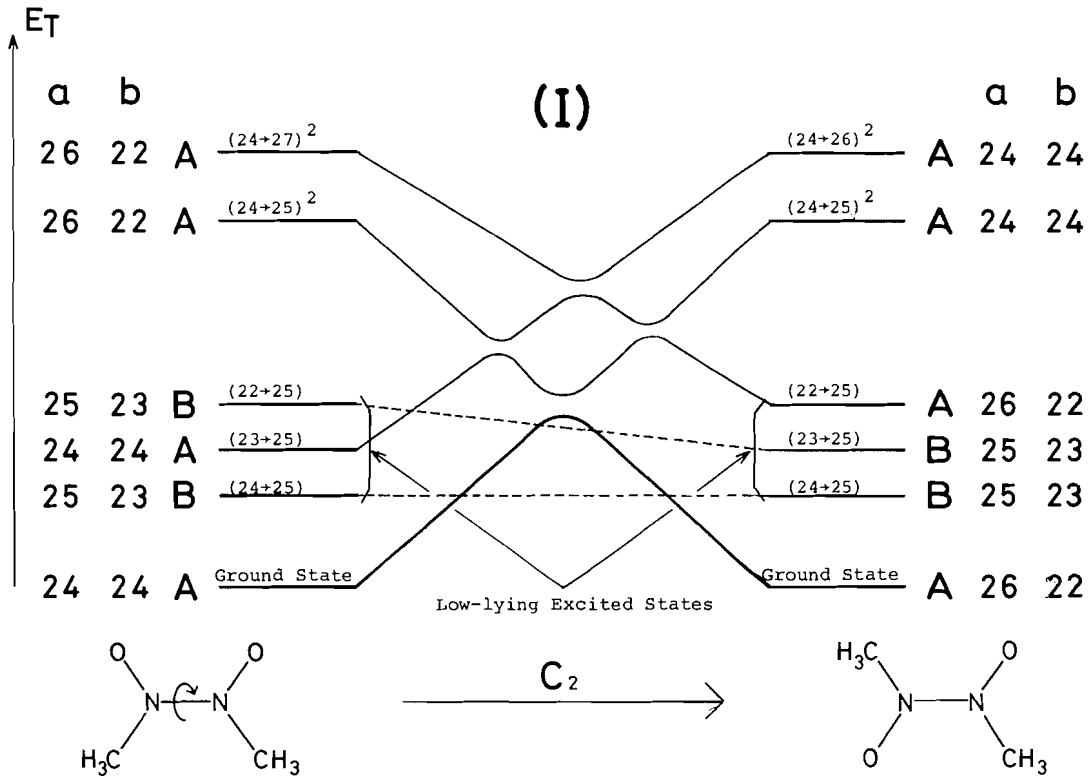


FIG. 4. The state correlation diagram of the direct *cis* → *trans* isomerization. In both edges of the figure, 48 electrons of the dimer are assigned to two symmetry orbitals (*a* and *b*). (24 → 25) is, for instance, an electron excitation mode to generate the main configuration of an excited state relative to the ground-state configuration. $E_T$ is the total energy of each state.

Can. J. Chem. Downloaded from www.nrcresearchpress.com by 210.87.254.5 on 09/06/12
For personal use only.

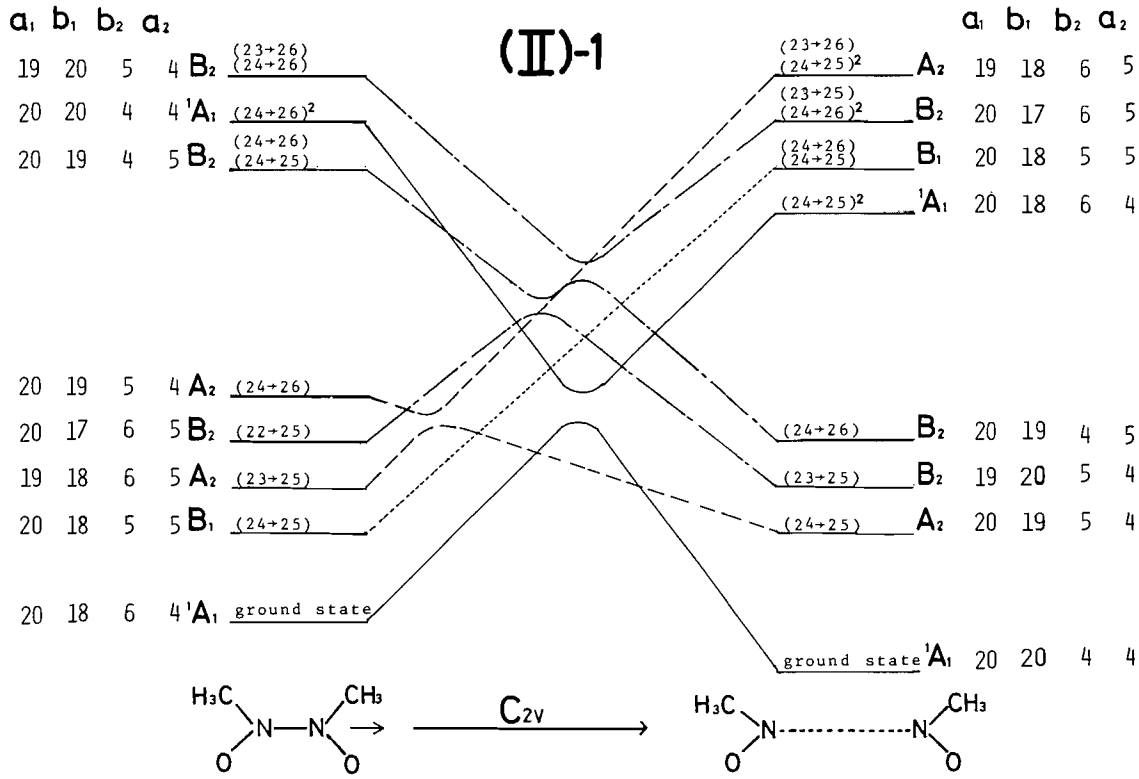


FIG. 5. The state correlation diagram of the fragmentation of the *cis* dimer to two monomers along the $C_{2v}$ path.

interconversion is exhibited. The $C_2$ axis rotating with one nitroso group is maintained. In Fig. 4, the state correlation diagram for this route is shown. It immediately demonstrates that the $C_2$ path is symmetry-forbidden with the energy barrier of the avoided crossing in the ground state. Therefore, the thermal *cis*/*trans* interconversion is evidently unfavorable. In view of this result, we move on to route (II). For the fragmentation of the *cis* dimer, (II)-1, the least-motion path retains the $C_{2v}$ symmetry. In Fig. 5, the correlation diagram is shown, which again indicates symmetry-forbiddeness for the thermal dissociation. In Fig. 6, three diagrams for the relaxation of the $C_{2v}$ symmetry are given. Among the three, only the $C_2$ path in Fig. 6(*c*) becomes symmetry-allowed. This switch is represented by the removal of the energy barrier of the avoided crossing of two curves. The bold line for state A with $a = 24$ and $b = 24$ electrons indicates the symmetry-allowed process. Another ($C_{2v} \rightarrow C_2$) distortion made by the twisting elimination (shown later in Fig. 9) is also found to bring about the symmetry-allowed path. Thus the decomposition of the *cis* dimer takes place along the $C_2$ pathway.

For the recombination of two monomers to form the *trans* dimer, (II)-2, the least-motion path keeps the $C_{2h}$ symmetry. In Fig. 7, the correlation diagram is drawn, and thermal association is symmetry-forbidden. To seek the symmetry-allowed path, three ways of distortion are introduced in Fig. 8. Among them, a course retaining the inversion operation i becomes symmetry-allowed for the ground state in Fig. 8(*c*).

Reviewing the analysis of route (II) in terms of a state correlation diagram, we may summarize the ground-state mechanism qualitatively by Fig. 9. For both (II)-1 and (II)-2, the "from step to step of stairs" dissociation ($C_2$) and recombination (i) are symmetrically favorable. However, for (II)-1, it should be energetically judged which $C_2$ path is better (expressed by "?").

The state correlation diagrams give information on not only the thermal reaction but also the photochemical reaction. Figure 4 shows that the direct isomerization which is symmetry-forbidden in the ground state is symmetry-allowed in the lowest excited state (B). That is, the direct interconversion is predicted to take place photochemically. As for route (II) in the photochemical reaction, the $C_s'$ fragmentation in Fig. 6(*b*) and the $C_2$ recombination in Fig. 8(*b*) are likely.

Can. J. Chem. Downloaded from www.nrcresearchpress.com by 210.87.254.5 on 09/06/12
For personal use only.

Can. J. Chem. Downloaded from www.nrcresearchpress.com by 210.87.254.5 on 09/06/12
For personal use only.

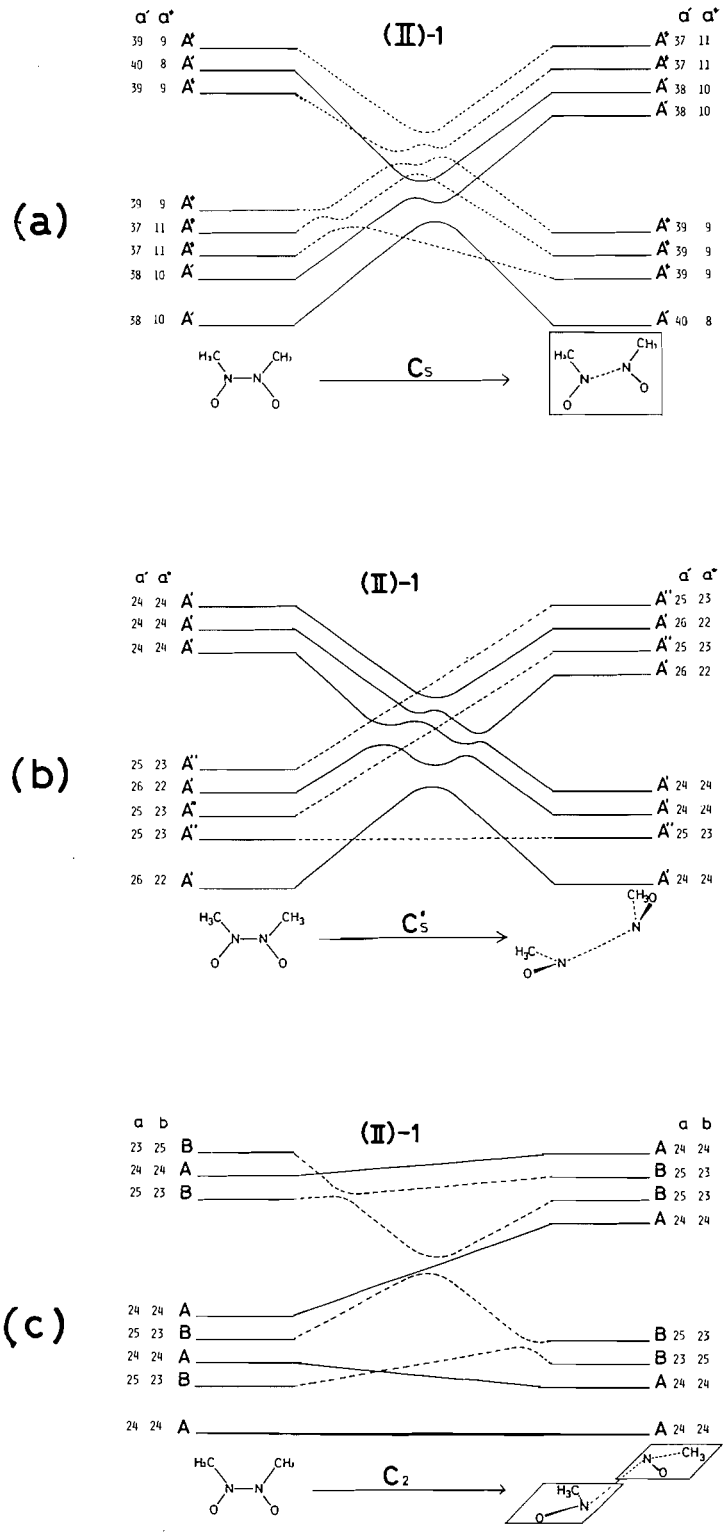


FIG. 6. The state correlation diagram along three symmetry-relaxed paths.

Can. J. Chem. Downloaded from www.nrcresearchpress.com by 210.87.254.5 on 09/06/12
For personal use only.

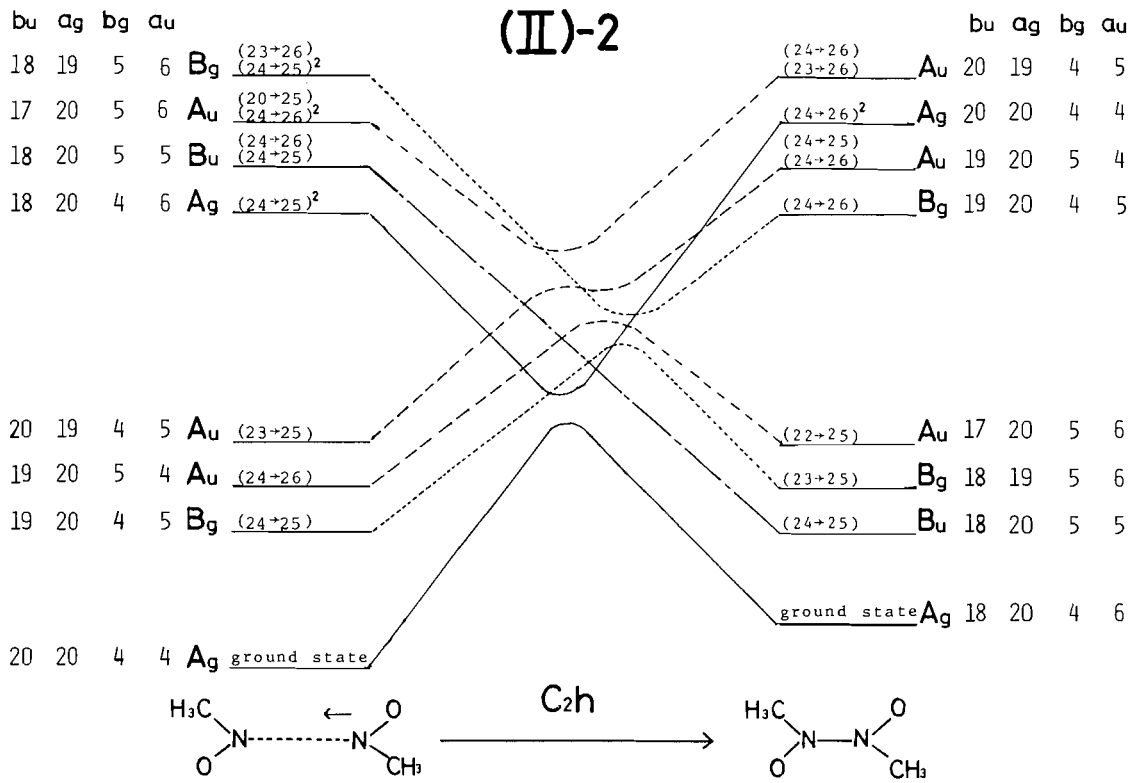


FIG. 7. The state correlation diagram of the recombination of two monomers to the *trans* dimer along the $C_{2h}$ path.

## IV. Results and discussion

For (II)-1, the changes of $E_T$'s along two different paths (? in Fig. 9) are compared. The calculated result shows that the "from step to step" separation is more preferable than the twisting scission. In Fig. 10, a snapshot of the two routes (II)-1 and (II)-2 is exhibited. According to Heiberg's result (4), the energy ascent of the symmetry forbiddeness is sharp at $R \cong 1.7$ Å, which is avoided in our figure by the drastic bent-out-of-plane motion. At $R \leqq 1.4$ Å, the planar structures ($C_{2v}$ for (II)-1 and $C_{2h}$ for (II)-2) are retained.

In Fig. 11, two energy profiles for the path of Fig. 10 are exhibited. One is "without solvation" which is obtained by the standard SCF calculation. The other is "with solvation" and consists of an energy correction through two types of solvent effect. Such a correction is necessary in view of the experimental data. For the "without solvation" case, the structural stability is in the order of

*trans* dimer > two monomers > *cis* dimer

which is in contrast to the experimental order (2)

*trans* dimer > *cis* dimer > two monomers

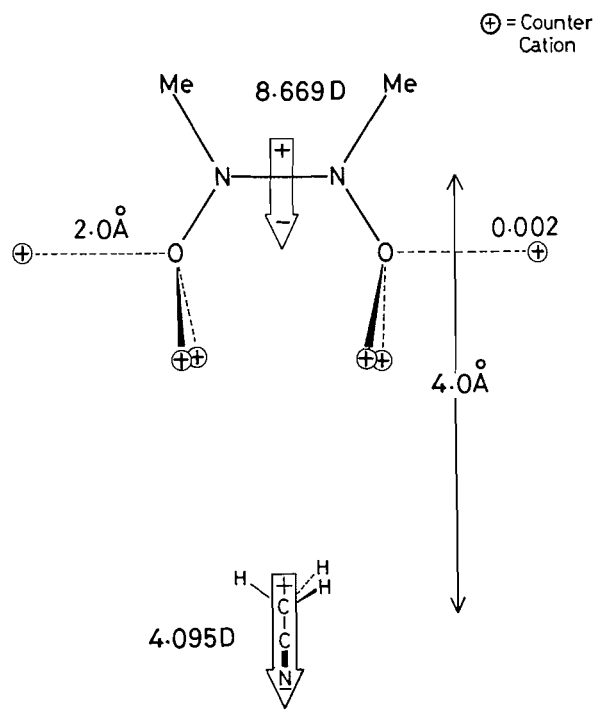

Can. J. Chem. Downloaded from www.nrcresearchpress.com by 210.87.254.5 on 09/06/12
For personal use only.

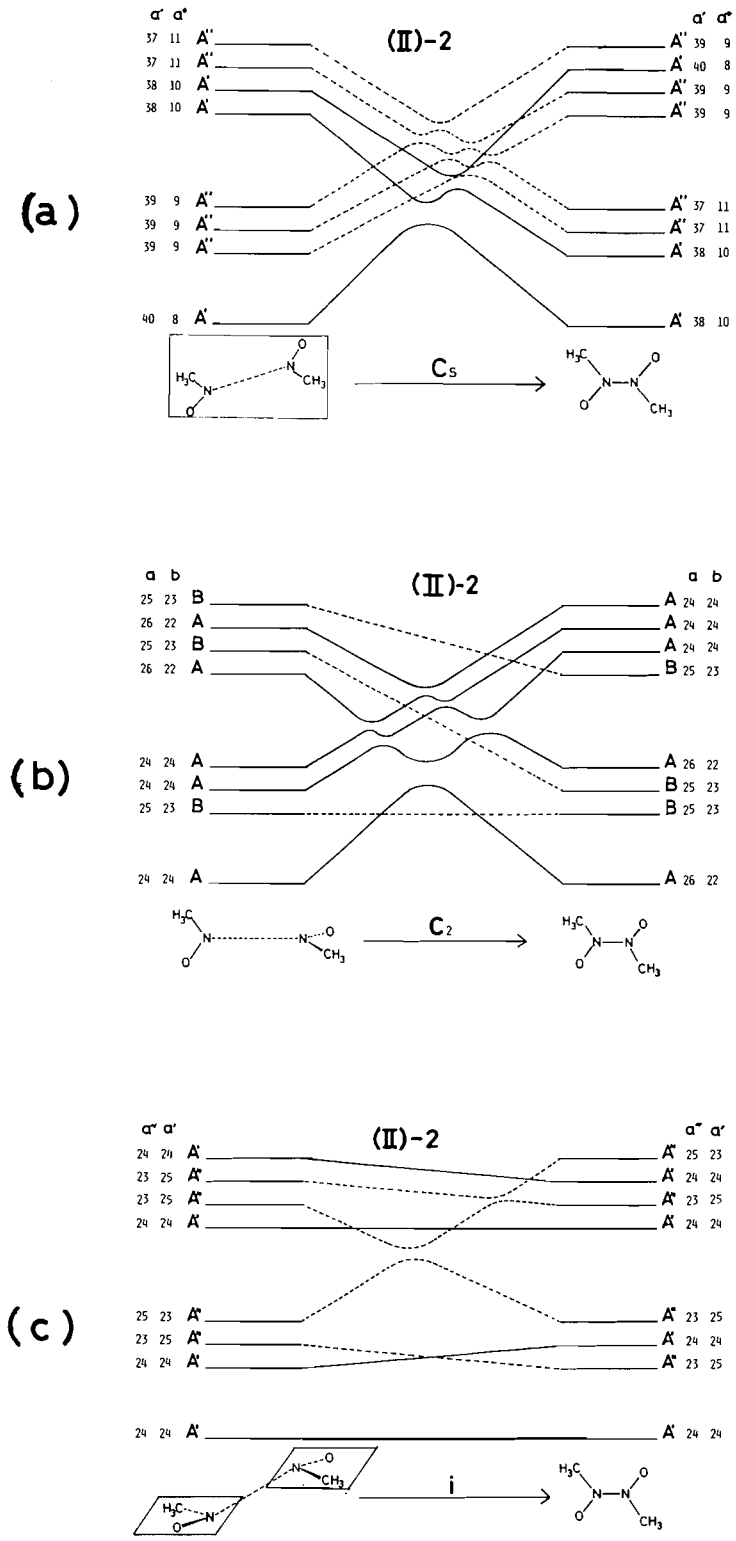


FIG. 8. The state correlation diagram along three symmetry-relaxed paths.

Can. J. Chem. Downloaded from www.nrcresearchpress.com by 210.87.254.5 on 09/06/12
For personal use only.

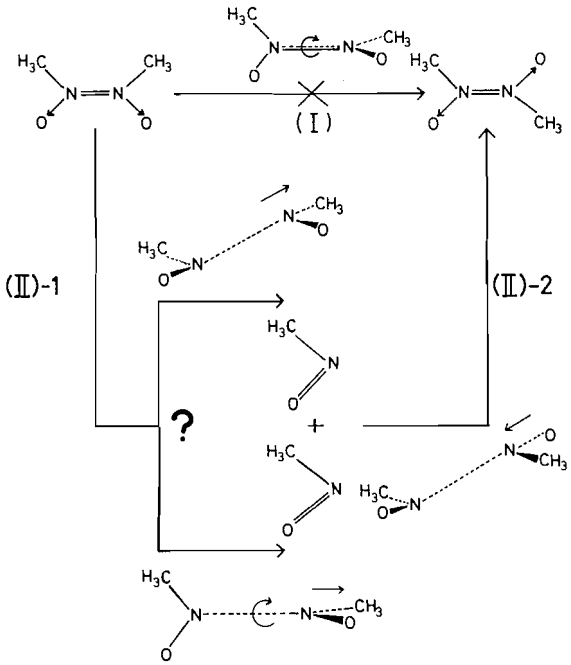


FIG. 9. Summary of the consideration on the reaction paths in the ground state based on the state correlation diagrams.

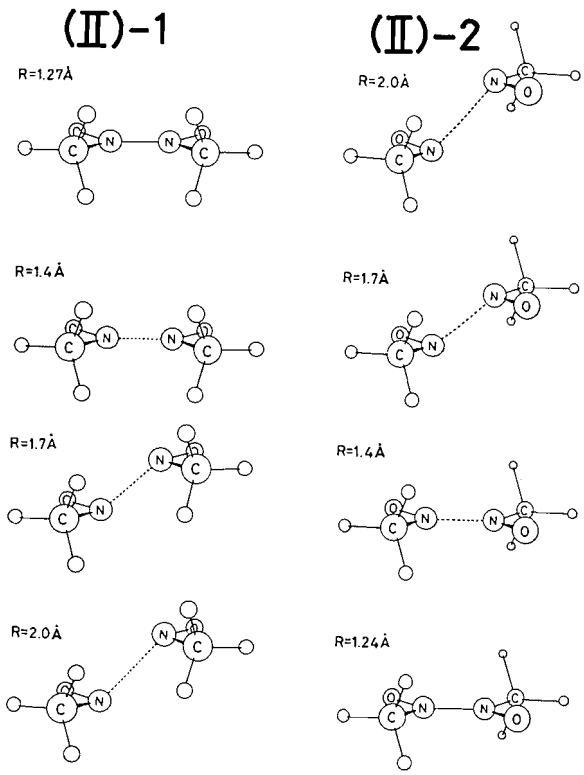


FIG. 10. The snapshots of the fragmentation of the *cis* dimer ($C_2$) and the recombination of two monomers (i). $R$ is the distance between two N atoms. Empty circles are hydrogen atoms.

This apparent discrepancy is easily solved by considering the solvent (acetonitrile) effect. This polar solvent molecule should interact with the electron-rich oxygen atom of the dimer. In general, a molecule with an electron-rich atom is stabilized significantly by the Coulombic field presented by the surrounding cationic site (methyl group) of acetonitrile. Indeed, a tentative calculation, including counter cations with their effective charge = +0.002 for two dimers and the monomer, has switched the order of stability to[2]

*trans* dimer > *cis* dimer > two monomers

Another disagreement is found in the comparison of the activation energies ($E_a$'s) of (II)-2 and the reverse route of (II)-1, route (II)-1′. Experimental analysis has suggested that $E_a$[(II)-2] is larger than $E_a$[(II)-1′] (2), whereas "without solvation" gives the opposite result. This indicates that another solvent effect should be considered. The structural difference of the two dimers is reflected in the values of the dipole moment ($\mu$) shown in Fig. 2. $\mu_{\text{acetonitrile}}$ is calculated to be 4.10 D (exptl. = 3.92 D). Since $\mu_{cis\ \text{dimer}}$ (= 8.67 D) is very large, the permanent dipole–dipole interaction as well as the Coulombic effect may not be neglected.

Acetonitrile molecules distant from the *cis* dimer (~ 4 Å) operate as an origin of the dipolar field to result in the stabilization ($E_\mu$) through this interaction. A test calculation which makes use of the model in the figure above gives $E_\mu = -15$ kcal/mol.[3] This is a serious correction to the potential energy of (II)-1, whereas that of (II)-2 is not affected at all by this interaction since $\mu_{trans\ \text{dimer}} = 0$. The potential energies of "with solvation" shown in Fig. 11 include the Coulombic and the dipole–dipole interactions and they reproduce well the experimentally suggested energy changes (2). The energy profiles with solvation and without solva-

[2]The positive point charges are located in the direction of an $sp^3$ hybrid orbital on the oxygen atoms of the dimers and the monomer. This location apparently overestimates the Coulombic stabilization of the *cis* dimer, because each oxygen is attracted not only by the positive charges close to it but also by those of the nearby oxygen. However, $E_T$'s without and with the charges are −337.1047 → −337.2045 au for the *cis* dimer and −337.1359 → −337.2375 au for the *trans* dimer, which indicates that the net stabilization of the former dimer is estimated to be almost the same as that of the latter. Alternative locations of the point charges were also tested, and were found to give a similar equality. Thus, the present way of placing the point charges toward each oxygen atom does not bias the result in favor of the *cis* form.

[3]$E_\mu$ is estimated by the following equation.

$$E_\mu = -2(\mu_{\text{acetonitrile}})^2 \cdot (\mu_{cis\ \text{dimer}})^2/(3L^6 \cdot kT) \quad (T = 298\ \text{K})$$

$k$ is Boltzmann's constant, $L$ is the distance between two dipole moments and is taken here to be 4.0 Å.

Can. J. Chem. Downloaded from www.nrcresearchpress.com by 210.87.254.5 on 09/06/12
For personal use only.

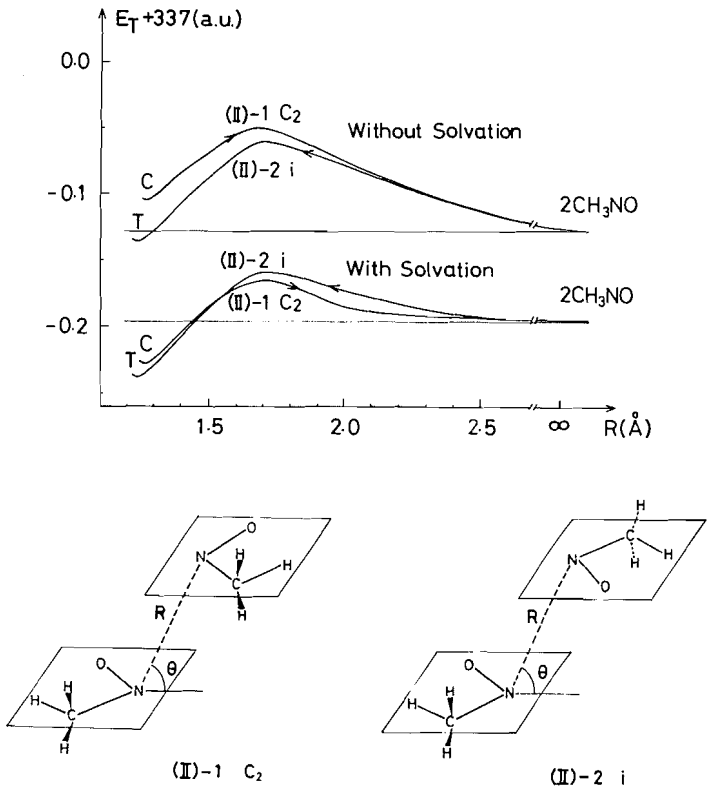


FIG. 11. The energy profile of *cis/trans* isomerization of the dimer in the ground state. C and T denote *cis* and *trans* dimers, respectively.

tion show that the fragmentation and recombination have maxima in $E_T$ at $R = 1.7$ Å. In other words, the transition states of both reactions are located there. Heiberg's result gives a sharp energy ascent at $R \simeq 1.7$ Å by the symmetry-forbiddeness (4). This ascent is removed by the bent-out-of-plane motion. The interaction between two monomers is small at $R > 2.0$ Å, as the flat energy profiles show.

## V. Concluding remarks

In this work, the *cis/trans* isomerization of azodioxymethane has been discussed in terms of the state correlation diagrams and *ab initio* calculations have been made to follow the paths. The diagrams show that direct *cis/trans* isomerization is thermally unfavorable, whereas it is a symmetry-allowed photochemical route. The thermal isomerization takes place via the fragmentation of the *cis* dimer into monomers and their recombination to the *trans* dimer. Their reaction paths are represented by the "from step to step" mechanism. Thus, the diagram may be used as a guide to seek the reaction path.

The energies in the gas phase, "without solvation", are calculated to be entirely different from the experimental ones. The consideration of a solvent effect gives a good correlation between theoretical and experimental data. The importance of this effect in the reaction is due to the large polarity of the *cis* dimer and the solvent molecule.

## Acknowledgment

The authors thank Institute for Molecular Science for allotment of the CPU time of the HITAC M-200H computer.

1. (*a*) B. G. GOWENLOCK and W. LÜTTKE. Q. Rev. **12**, 321 (1958); (*b*) W. LÜTTKE and V. SCHABACKER. Ann. **687**, 236 (1965); (*c*) J. P. FREEMAN. J. Org. Chem. **28**, 2508 (1963); (*d*) G. COLLIN, R. HÖHN, H. G. HAUTHAL, H. HÜBNER, W. PRITZKOW, W. ROLLE, H. SCHAEFER, and M. WAHREN. Ann. **702**, 55 (1967).
2. TH. A. J. W. WAJER and TH. J. DEBOER. Rec. Trav. Chim. **91**, 565 (1972).
3. R. HOFFMANN, R. GLEITER, and F. B. MALLORY. J. Am. Chem. Soc. **92**, 1460 (1970).
4. A. B. HEIBERG. Chem. Phys. **43**, 415 (1979).
5. S. YAMABE, T. MINATO, and Y. OSAMURA. Int. J. Quant. Chem. **18**, 243 (1980).
6. W. J. HEHRE, W. A. LATHAN, R. DITCHFIELD, M. D. NEWTON, and J. A. POPLE. Program #236, QCPE, Indiana University, Bloomington, IN, USA. 1973.
7. M. VAN MEERSSCHE and G. GERMAIN. Bull. Soc. Chim. Belges. **68**, 244 (1959).

# Kinetics of the oxidation of ethane and 1-butene over manganese oxide supported on carbon fibres

CRAIG FAIRBRIDGE[1] AND JAMES R. MACCALLUM

*Department of Chemistry, The University of St. Andrews, St. Andrews, Fife, Scotland, KY16 9ST*

AND

ROBERT A. ROSS

*Alcan International Limited, Kingston Laboratories, Box 8400, Kingston, Ont., Canada K7L 4Z4*

Received May 3, 1982

CRAIG FAIRBRIDGE, JAMES R. MACCALLUM, and ROBERT A. ROSS. Can. J. Chem. **60**, 2749 (1982).

The oxygen/ethane and oxygen/1-butene reactions have been investigated in a continuous flow system at atmospheric pressure over a manganese oxide/carbon fibre catalyst. The products of reaction were carbon dioxide and water. Apparent activation energies were $108 \pm 4$ kJ mol$^{-1}$ for the former reaction from 673 to 573 K, and $81 \pm 4$ kJ mol$^{-1}$ for the latter from 573 to 473 K. Kinetic data for both reactions were best described by the rate equation:

$$r = \frac{kap_{O_2}^{0.5}\, bp_{HC}^{0.5}(p_{O_2}\, p_{HC})}{(1 + ap_{O_2}^{0.5} + bp_{HC}^{0.5})^2}$$

The surface mechanism may be complex and it is proposed that reactants interact as adsorbed species each of which is adsorbed on two surface sites. Both oxygen and the hydrocarbon gas appear to be directly involved in further steps. Scanning electron microscopy, X-ray photoelectron spectroscopy, and low temperature krypton adsorption were used to assess the catalyst structure.

CRAIG FAIRBRIDGE, JAMES R. MACCALLUM et ROBERT A. ROSS. Can. J. Chem. **60**, 2749 (1982).

Les réactions oxygène/éthane et oxygène/1-butene sont étudiées à pression atmosphérique dans un systeme à débit continu sur un catalyseur oxyde de manganèse/fibre de carbone. Les produits de la réaction sont le dioxyde de carbone et l'eau. Les énergies d'activation apparentes sont $108 \pm 4$ kJ mol$^{-1}$ pour la premiere réaction (673 à 573 K) et $81 \pm 4$ kJ mol$^{-1}$ pour la deuxieme réaction (573 à 473 K). Les données cinétiques pour les deux réactions sont bien décrites par l'équation suivante:

$$r = \frac{kap_{O_2}^{0.5}\, bp_{HC}^{0.5}(p_{O_2}\, p_{HC})}{(1 + ap_{O_2}^{0.5} + bp_{HC}^{0.5})^2}$$

Les mécanismes des réactions de surface peuvent être assez complexes; il est proposé une accumulation des réactifs dans une couche adsorbée. Chaque réactif est probablement adsorbé en deux sites différents sur la surface. L'oxygene et l'hydrocarbure semblent être directement impliqués dans des réactions ultérieures. La microscopie à balayage électronique, la spectroscopie photoélectronique à rayons-X, et l'adsorption de krypton à faible température sont utilisées pour déterminer la structure du catalyseur.

## Introduction

A number of key heterogeneous catalytic reactions have been examined over manganese oxides in recent years (1–4); including directly related work on the oxidation of ethane on manganese(III) oxide by nitric oxide (5), and by oxygen (6). These oxides were finely-divided, pure materials with no support or carrier, in contrast to the present investigation where high purity carbon fibres have been adapted for use as support media for manganese oxide in a study of the catalytic oxidation reactions of both ethane and 1-butene.

Catalysts consisting of metals on activated carbon supports have been used in many reactions including $NO_x$ reduction (7, 8) and hydrocarbon oxidation (9) but the application of carbon fibres as catalyst supports has received relatively little attention. Carbon filaments alloyed with transition metals such as nickel, cobalt, chromium, and manganese have been used as catalysts for the dehydration of secondary alcohols (10), while a platinum/carbon fibre catalyst was described in connection with hydrocarbon conversion reactions (11). Because of their mechanical strength, thermal stability, flame and chemical resistance, carbon fibres could prove to be applicable as supports with long service life (12), particularly in the hydrocarbon conversion field (11).

## Experimental

*Apparatus and procedure*

Helium was used as the carrier gas in the quartz reactor flow system (13) and in the Hewlett-Packard Research Chromatograph, Model 5754B. A thermal conductivity bridge and stainless steel analytical columns, 305 × 0.32 cm od packed with Poropak Q, were used to analyze for oxygen, carbon dioxide, ethane, 1-butene, and water. The column oven was temperature programmed with a 3 min post-injection interval at 333 K, followed by a 60 K min$^{-1}$ increase to 408 K, whereupon the temperature was maintained for 8 min prior to recycling.

[1]Present address: Energy Research Laboratories, CANMET, Energy, Mines and Resources, Canada, 555 Booth Street, Ottawa, Ont., Canada K1A 0G1.

0008-4042/82/212749-06$01.00/0

©1982 National Research Council of Canada/Conseil national de recherches du Canada

Can. J. Chem. Downloaded from www.nrcresearchpress.com by 210.87.254.42 on 09/06/12
For personal use only.

Can. J. Chem. Downloaded from www.nrcresearchpress.com by 210.87.254.42 on 09/06/12
For personal use only.

Reaction rate measurements were conducted at a total flow rate of 350 mL $min^{-1}$ (NTP) on 1 g catalyst samples, conditions which indicated that gas phase diffusion as well as heat and mass transfer effects were minimal (14). The experimental reaction rate, equated to the rate of carbon dioxide production, was recorded after steady catalyst activity had been achieved at <8% hydrocarbon conversion. The only products observed by gas chromatography were those expected from complete hydrocarbon oxidation, namely, carbon dioxide and water.

Catalyst surface areas measured by low temperature krypton adsorption (BET; 77 K; $\sigma$ = 19.5 Å$^2$) were reproducible to $\pm$0.2 $m^2$ $g^{-1}$. Surface structures were examined by a scanning electron microscope, Cambridge Stereoscan 600, and by an X-ray photoelectron spectroscope, Vacuum Generator ESCA-3.

*Materials*

"Modmor" high modulus reinforcing carbon fibre, Type III S, was supplied by Morganite Modmor Limited. Fibres, in 10 cm lengths, were sprayed with a 50% w/w aqueous solution of manganese(II) nitrate (BDH Chemicals Limited) and dried with a hot air gun at temperatures up to 573 K. The fibres were sprayed and dried in 10 cycles and chemical analysis (15) indicated 9.5% w/w manganese on the carbon after treatment in nitrogen at 773 K for 2 h. The fibre surface area increased from 1.8 to 3.8 $m^2$ $g^{-1}$ as a result.

Ethane (99.0%), 1-butene (99.0%), and oxygen (99.99%) were supplied by Matheson of Canada Limited. Carbon dioxide (99.5%) and helium (99.995%) were obtained from Canadian Liquid Air Limited. Water used in the gas saturators was distilled, de-ionized, and degassed prior to use.

## Results

*Reaction rate order measurements*

Rate orders were determined at 623 and 523 K, respectively, for the oxygen/ethane and the oxygen/1-butene catalytic reactions.

*Oxygen/ethane*

When the catalyst was exposed to 2.63 kPa oxygen and 2.62 kPa ethane at 673 K, the initial rate of carbon dioxide formation was very high, possibly due to partial oxidation of the carbon fibres. The rate of product formation decreased quickly to a steady level in 3 h and remained constant thereafter for at least 48 h. The surface area of catalysts treated in this way was 6.9 $m^2$ $g^{-1}$.

A reaction rate order of 0.3 with respect to oxygen partial pressure was determined at 623 K, Fig. 1, by altering the partial pressure from 0.31 to 14.15 kPa. The partial pressure of ethane was maintained at 2.57 kPa for these experiments.

With the partial pressure of oxygen held constant at 2.47 kPa, the partial pressure of ethane was adjusted from 0.69 to 10.05 kPa. The rate order with respect to ethane concentration was 0.4 as determined from the linear plot of ln (rate) versus ln (partial pressure), Fig. 1.

Variations in the carbon dioxide partial pressure from 0.67 to 6.44 kPa had no effect on the rate of reaction with oxygen and ethane partial pressures maintained at 2.68 and 2.74 kPa, respectively.

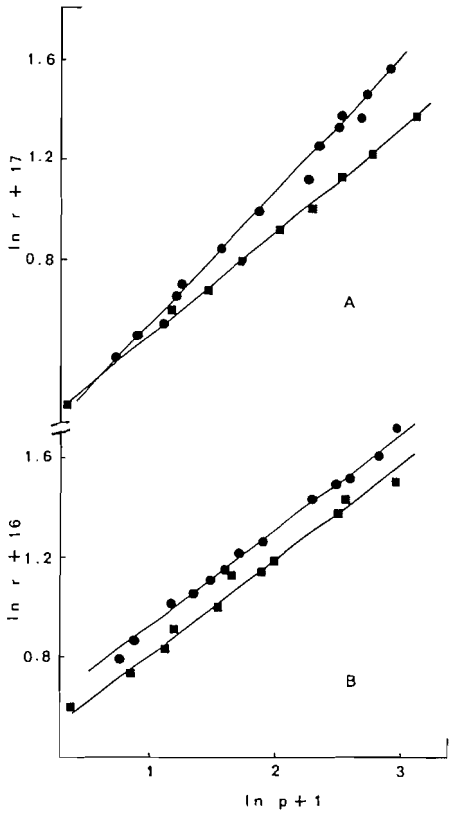


FIG. 1. The effects of component partial pressures (oxygen, ■; hydrocarbon, ●) on the reaction rate of the oxygen/ethane (*A*) and the oxygen/1-butene (*B*) reactions over manganese oxide/carbon fibre catalysts.

Therefore, the rate order was zero with respect to carbon dioxide.

Oxygen and ethane partial pressures were held at 2.63 and 2.71 kPa, respectively, while the partial pressure of water vapour was altered from 0.06 to 2.11 kPa. A zero rate order with respect to water vapour partial pressure was determined.

The experimental rate of the oxygen/ethane reaction at 623 K over the manganese oxide/carbon fibre catalyst was therefore expressed by:

$$[1] \quad r = k p_{O_2}^{0.3} p_{C_2H_6}^{0.4}$$

*Oxygen/1-butene*

Upon exposure of the catalyst to the reaction mixture, 2.69 kPa oxygen and 3.04 kPa 1-butene, a significant amount of carbon dioxide was initially liberated at 573 K. This was related to a measure of oxidation of the carbon fibres. The rate of production decreased over 24 h to a value which remained constant for at least 24 h. The catalyst surface area after this treatment was 11.1 $m^2$ $g^{-1}$.

The partial pressure of 1-butene was altered from

Can. J. Chem. Downloaded from www.nrcresearchpress.com by 210.87.254.42 on 09/06/12
For personal use only.

TABLE 1. The effect of temperature on reaction rate constants

| Oxygen/ethane | | Oxygen/1-butene | |
|---|---|---|---|
| Temperature (K) | $k \times 10^{-5}$ ($mol^{0.3}\ L^{-0.3}\ m^{-2}\ s^{-1}$) | Temperature (K) | $k \times 10^{-5}$ $mol^{0.2}\ L^{-0.2}\ m^{-2}\ s^{-1}$ |
| 673 | 26.0 | 573 | 95.3 |
| 663 | 20.5 | 563 | 66.2 |
| 653 | 13.4 | 553 | 48.8 |
| 643 | 9.55 | 543 | 36.1 |
| 633 | 7.07 | 533 | 27.3 |
| 623 | 5.16 | 523 | 18.7 |
| 613 | 3.61 | 513 | 13.4 |
| 603 | 2.48 | 503 | 9.34 |
| 593 | 1.91 | 493 | 5.71 |
| 583 | 1.31 | 483 | 4.08 |
| 573 | 0.922 | 473 | 2.46 |

0.82 to 7.15 kPa and a rate order of 0.4 was obtained while the oxygen partial pressure was held at 2.46 kPa, Fig. 1.

With 1-butene partial pressure maintained at 2.68 kPa, the oxygen pressure was adjusted from 0.32 to 7.36 kPa. The rate order derived from these results was 0.4 with respect to the partial pressure of oxygen.

The partial pressures of oxygen and 1-butene were maintained at 2.61 and 2.69 kPa, respectively, and the effects of a variation from 0.50 to 9.31 kPa in carbon dioxide partial pressure were observed. The results gave a rate order of zero with respect to carbon dioxide partial pressure.

Experiments were also carried out in which the partial pressure of water vapour was adjusted from 0.09 to 2.50 kPa in the reaction mixture of 2.57 kPa oxygen and 2.81 kPa 1-butene and a zero rate order dependence on water vapour partial pressure was determined.

The experimental rate of reaction was therefore given by:

$$[2] \quad r = k p_{O_2}^{0.4} p_{C_4H_8}^{0.4}$$

*Temperature effects*

*Oxygen/ethane*

After catalyst pretreatment with 2.63 kPa oxygen and 2.76 kPa ethane at 673 K for 4 h, rate constants were calculated from the integrated form of eq. [1] at 10 K intervals from 673 K to 573 K, Table 1. The data, when plotted in the Arrhenius fashion, Fig. 2, produced an apparent activation energy of $108 \pm 4$ kJ $mol^{-1}$ and a pre-exponential factor of $5.42 \times 10^4$ $mol^{0.3}\ L^{-0.3}\ m^{-2}\ s^{-1}$.

*Oxygen/1-butene*

The catalyst was treated at 573 K with 2.47 kPa oxygen and 2.71 kPa 1-butene for 24 h prior to kinetic studies. Rate constants, Table 1, were calculated from eq. [2] from 573 to 473 K. An apparent activation energy of $81 \pm 4$ kJ $mol^{-1}$ and a pre-exponential factor of $2.16 \times 10^4$ $mol^{0.2}\ L^{-0.2}\ m^{-2}\ s^{-1}$ resulted from the Arrhenius plot, Fig. 2.

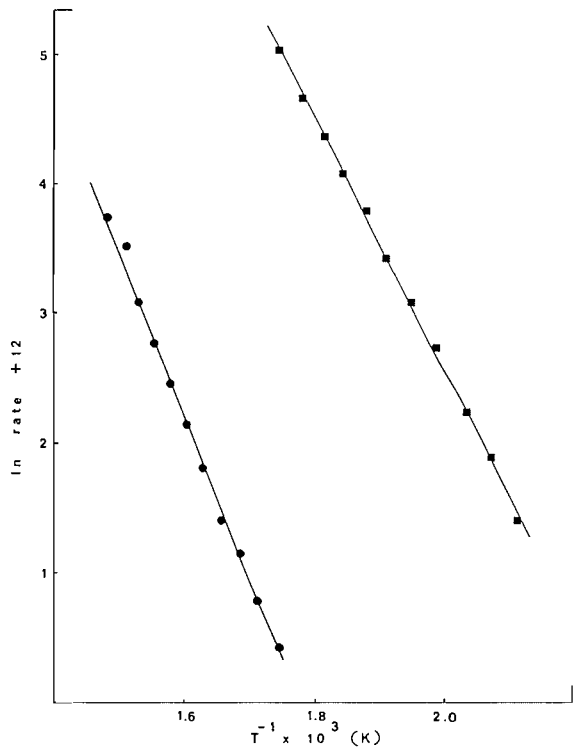


FIG. 2. Arrhenius plots for the oxygen/ethane (●) and oxygen/1-butene (■) reactions over manganese oxide/carbon fibre catalysts.

*Scanning electron microscopy*

The scanning electron micrographs, Fig. 3, show the effects of the oxygen/1-butene reaction at 573 K on the "Modmor" fibre supported catalyst. It

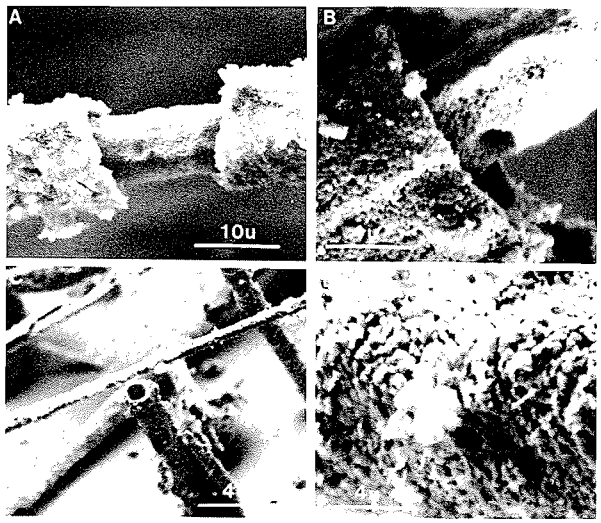


FIG. 3. Scanning electron micrographs of manganese oxide/carbon fibre catalyst after the oxygen/1-butene reaction at 573 K.

appears that the outer sheath and central core of the carbon fibre remain intact, while the radial continuum (16) has been oxidized, Fig. 3*A* and *B*. In many cases, the ends of the fibres seem hollow, Fig. 3*C*, and the fibre surface rough and pitted, Fig. 3*D*. The outer sheath of some fibres may have peeled away.

The manganese oxide particles appeared to be well dispersed on the fibre surface. Their texture resembled that observed for manganese(III) oxide catalysts in similar studies (5). The structure of the manganese oxide/carbon fibre catalyst after the oxygen/ethane reaction at 623 K was very similar to that shown in Fig. 3.

*X-ray photoelectron spectroscopy*

X-ray photoelectron spectra were obtained using Al $K_\alpha$ radiation and a 50 eV electron analyzer pass energy. Spectra were corrected for charging by reference to the C(1*s*) line at 285.0 eV. CHN analysis of pure "Modmor" gave weight percentages of 92.7 carbon, 1.5 hydrogen, 5.8 nitrogen, and 1.5 oxygen (by difference), while XPS indicated surface atomic percentages of 78 carbon, 3 nitrogen, 14 oxygen, 1 sodium, 3 sulphur, and 1 calcium. The presence of the surface impurities sodium, sulphur, and calcium indicated by XPS are difficult to rationalize and it should be noted that neither sulphur nor calcium was detected on the manganese oxide/carbon fibre catalyst after reaction.

Atomic percentages determined after the oxygen/ethane reaction at 623 K were 53 carbon, 33 oxygen, 10 manganese, and 4 sodium. After catalysis of the oxygen/1-butene reaction at 523 K, the catalyst surface contained 48% carbon, 36% oxygen, 11% manganese, and 5% sodium. The O(1*s*) spectra gave a binding energy of 529.0 eV on all samples; the Mn($2p_{3/2}$), a binding energy of 641.0 eV; the Na(1*s*), 1071 eV; and the N(1*s*) spectra on pure "Modmor" gave 400.5 eV.

The oxygen binding energy is close to that expected in metal oxides and significantly less than that usually characteristic of molecular oxygen. Although it is difficult to distinguish between manganese(II) and manganese(III) oxide by XPS alone, the spectra resemble those obtained with manganese(III) oxide catalysts (6) when both XRD and chemical analysis confirmed that the oxide was present as manganese(III) oxide in all bulk samples. If it is assumed that all manganese is associated as $Mn_2O_3$ then this accounts for approximately 15% oxygen and leaves remaining the amount of oxygen found on the original fibre surface. In terms of weight percentages, there is 30% manganese on the surface of the fibres, compared with 9.5% based on chemical analysis. This implies that the manganese is concentrated near the surface as was observed by scanning electron microscopy.

## Discussion

The interpretation of kinetic data by the application of the extended Langmuir–Hinshelwood theory to describe possible surface mechanisms has been discussed (17–19) and the limitations inherent in methods of deriving mechanistic schemes from the correlation of statistical relationships with surface reaction models have been well analyzed (20–23). The approach is applied to the present results as a useful guide to the possible nature of the surface interactions especially when considered in conjunction with the surface analysis data.

Computer analysis of the oxygen and hydrocarbon rate order results gave only one kinetic expression of a Langmuir–Hinshelwood type which could accommodate the data. It was the same for both oxygen/ethane and oxygen/1-butene reactions:

$$[3] \quad r = \frac{kap_{O_2}^{0.5} bp_{HC}^{0.5} (p_{O_2} p_{HC})}{(1 + ap_{O_2}^{0.5} + bp_{HC}^{0.5})^2}$$

where $p_{HC}$ represents appropriately the partial pressure of ethane or 1-butene, while $a$ and $b$ are adsorption coefficients. Plots of $p^{0.5}$ against $(p^{1.5}/r)^{0.5}$ were linear, Fig. 4.

The form of eq. [3] suggests that oxygen and hydrocarbon interact initially as two adsorbed species, each adsorbed possibly on two surface sites as indicated by the square root relationships of partial pressure (24). The $(p_{O_2} p_{HC})$ term indicates

Can. J. Chem. Downloaded from www.nrcresearchpress.com by 210.87.254.42 on 09/06/12
For personal use only.

Can. J. Chem. Downloaded from www.nrcresearchpress.com by 210.87.254.42 on 09/06/12
For personal use only.

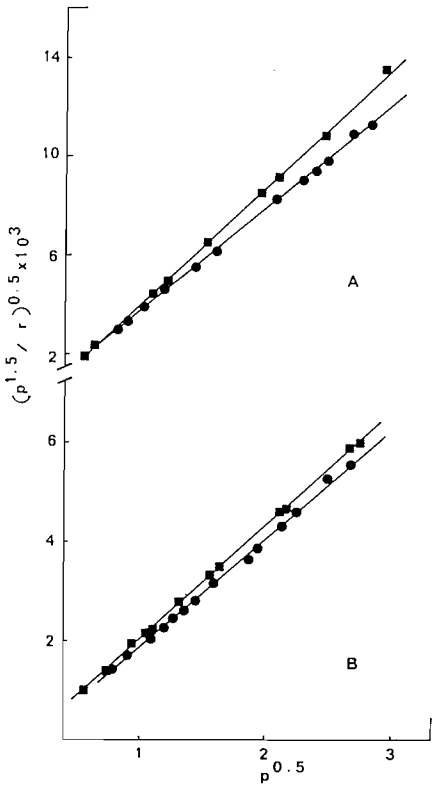


FIG. 4. Reduced plots corresponding to the Langmuir–Hinshelwood expression [3] for oxygen, ■, and hydrocarbon, ●, rate orders in the oxygen/ethane (*A*) and oxygen/1-butene (*B*) reactions over manganese oxide/carbon fibre catalysts.

that both oxygen and hydrocarbon interact in further steps within the complex overall reaction.

Evidence presented by Thomas (25) concerning ethane oxidation over nickel(II) oxide suggests that ethane was adsorbed prior to surface reaction with preadsorbed oxygen. Chemisorption of ethane was thought to involve C—H bond rupture. Yu Yao and Kummer (26) described the rate-determining step in the oxidation of ethane on nickel(II) oxide as involving the formation of a $C_2H_{5(ads)}$ species. This was believed to arise through the adsorption of ethane as $C_2H_5$ or by the interaction of adsorbed oxygen with gas phase or adsorbed ethane with attack at the C—H bond. In the absence of specific evidence regarding the adsorbed intermediates and based upon a Langmuir–Hinshelwood kinetic interpretation, a plausible surface reaction scheme for the oxygen/ethane reaction may be formulated:

[4] $C_2H_6 + 2S = C_2H_{6(ads)}$

[5] $O_2 + [\ ] + C_2H_{6(ads)} \rightarrow C_2H_{5(ads)} + [OOH]$

[6] $C_2H_6 + S + [OOH] \rightarrow C_2H_{5(ads)} + [O] + H_2O$

with additional reactions summarized by:

[7] $2C_2H_{5(ads)} + [O] + 6O_2 \rightarrow 4CO_2 + 5H_2O + [\ ] + 4S$

where S represents a surface site and [ ], a surface anion vacancy.

The square root relationships with respect to ethane and oxygen are rationalized in steps [4] and [5] respectively. Reaction [5] represents the adsorption of oxygen and interaction with adsorbed ethane to produce a surface $C_2H_5$ species. An additional reaction involving ethane is described by step [6] which represents dissociative adsorption. The additional and complex reactions involving oxygen are summarized in [7].

Rate constants derived for the oxygen/ethane reaction over unsupported manganese(III) oxide (6) were approximately sixteen times greater than those found in the present study under similar conditions from 573 to 593 K. The apparent activation energy determined in the earlier work, 130 kJ $mol^{-1}$, was somewhat higher than that here, 108 kJ $mol^{-1}$. Similarly, the pre-exponential factor for the reaction over unsupported manganese(III) oxide was higher, $9.72 \times 10^7$, than that obtained with the supported oxide, $5.42 \times 10^4$. Reaction rate orders with respect to oxygen and ethane were 0.5 and 0.6, respectively, for the oxygen/ethane reaction over manganese(III) oxide at 573 K, and 0.3 and 0.4 for the reaction over the present supported catalyst at 623 K. Comparison of the values for apparent activation energies and pre-exponential factors obtained for ethane oxidation over the two preparations of manganese oxide catalysts shows an isokinetic effect similar in extent to that analyzed for a number of hydrocarbon oxidation reactions over metallic oxides (27). A simple explanation of this would be that the catalytic rate of the oxygen/ethane reaction over unsupported manganese(III) oxide is higher because there are more active sites per unit area for catalysis. It appears also that the adsorption of each reactant may require two surface sites on the supported catalyst, and one only on the unsupported manganese(III) oxide (6).

A similar reaction scheme may be applicable to the oxygen/1-butene reaction:

[8] $C_4H_8 + 2S = C_4H_{8(ads)}$

[9] $O_2 + [\ ] + C_4H_{8(ads)} \rightarrow C_4H_{7(ads)} + [OOH]$

[10] $C_4H_8 + S + [OOH] \rightarrow C_4H_{7(ads)} + [O] + H_2O$

[11] $2C_4H_{7(ads)} + 11O_2 + [O] \rightarrow 8CO_2 + 7H_2O + [\ ] + 4S$

The square root relationships in eq. [3] with respect to 1-butene and oxygen are rationalized in steps [8] and [9], while the influence of the $(p_{O_2}p_{C_4H_8})$ term is apparent from [11] which represents the total

Can. J. Chem. Downloaded from www.nrcresearchpress.com by 210.87.254.42 on 09/06/12
For personal use only.

stoichiometry of a number of reactions that have not been identified separately. The overall stoichiometry for both the oxygen/ethane and oxygen/1-butene reactions corresponds to that expected for complete hydrocarbon oxidation.

The value obtained for the apparent activation energy in the oxygen/1-butene reaction in the present study was only slightly lower than that determined over unsupported manganese(III) oxide (28), 81 as opposed to 88 kJ $mol^{-1}$. The pre-exponential factor was $2.16 \times 10^4$ for catalysis on the supported oxide and $2.94 \times 10^5$ for unsupported manganese(III) oxide. The activation energy corresponds closely to that found for the complete oxidation of ethane on both palladium (29) and nickel(II) oxide (26), and to that for the oxidation of propane over manganese(IV) oxide (30). Other comparable results may be noted elsewhere including ethylene or benzene oxidation over supported manganese(III) oxide which gave activation energies of 57 kJ $mol^{-1}$ (31) while ethylene oxidation on copper(II) oxide yielded values from 84 to 113 kJ $mol^{-1}$ (32).

The rate-determining step in these reactions may involve C—H bond rupture as has been postulated previously for the oxygen/ethane reaction over various catalysts (6, 25, 26). The present investigation has indicated that carbon fibres may be used as catalyst supports in deep oxidation reactions. Further studies of various impregnation techniques should be carried out with the aim of producing a higher surface area fibre support which is able to maintain mechanical strength and physical properties.

## Acknowledgements

We are pleased to thank Imperial Oil Limited, Sarnia for financial support, Mr. A. MacKenzie, Lakehead University, for SEM analysis, and Dr. D. Creber and Mr. R. Lazier, Alcan International Limited, for XPS analysis.

1. E. F. McCaffrey, D. G. Klissurski, and R. A. Ross. J. Catal. **26**, 380 (1972); Can. J. Chem. **49**, 3778 (1971).
2. B. W. Krupay and R. A. Ross. Can. J. Chem. **51**, 3520 (1973).
3. B. W. Krupay and R. A. Ross. J. Catal. **39**, 369 (1975).
4. B. W. Krupay and R. A. Ross. Can. J. Chem. **56**, 10 (1978).
5. R. A. Ross and C. Fairbridge. Can. J. Chem. **59**, 2232 (1981).
6. C. Fairbridge and R. A. Ross. Can. J. Chem. **60**, 893 (1982).
7. G. H. Meguerian, A. L. Hensley, Jr., and E. P. Steigelmans, Fr. 2,072,561 (cl. B01J, C01B, F01n), 29 Oct. 1971, US Appl. 800,850, 28 Nov. 1969.
8. N. Ninomiga, H. Nishino, T. Aibe, and K. Itoga. Ger. Offen. 2,433,076 (Cl. B01D), 06 Feb. 1975, Japan Appl. 73,78,980, 12 Jul. 1973.
9. K. Fujimoto and T. Kunugi. Proc. Int. Cong. Catal., 5th. *Edited by* J. W. Hightower. North-Holland, Amsterdam. Paper No. 28 (1973).
10. I. N. Ermolenko, A. M. Safonova, R. I. Bel'skaya, G. K. Berezovik, and Ya. M. Paushkin. Vesti. Akad. Nauk Belorus. SSSR, Ser. Khim. Nauk, **6**, 20 (1974).
11. T. G. Olfer'eva, O. V. Bragin, I. N. Ermolenko, and A. M. Safonova. Kinet. Katal. **18**, 933 (1977).
12. A. Kuroda, H. Aizawa, Y. Masubuchi, G. Ishihara, S. Matsuhisa, and S. Taira. Japan. Kokai. 75, 33, 187 (Cl. 13aG02, 13aG01), 31 Jul. 1973, Appl. 73, 83,608, 26 Jul. 1973.
13. D. V. Fikis, W. J. Murphy, and R. A. Ross. Can. J. Chem. **56**, 2530 (1978).
14. C. N. Satterfield. Mass transfer in heterogeneous catalysis. M.I.T. Press. 1970.
15. A. I. Vogel. A textbook of inorganic analysis. Longmans, Green and Co., London. 1962. p. 434.
16. F. R. Barnet and M. K. Norr. US NTIS AD Rep. 1974, No. 784415/2 GA.
17. O. A. Hougen and K. M. Watson. Ind. Eng. Chem. **35**, 529 (1943).
18. K. H. Yang and O. A. Hougen. Chem. Eng. Prog. **46**, 146 (1950).
19. O. A. Hougen and K. M. Watson. Chemical process principles. Part III. Wiley, New York and London. 1966.
20. M. Boudart. AICHE J. **18**, 465 (1972).
21. M. Zdrazil. J. Catal. **31**, 313 (1973).
22. S. W. Weller. Chemical reaction engineering reviews. *Edited by* H. M. Hulbert. Am. Chem. Soc., Washington, DC. 1975.
23. L. Beranek. Catal. Rev. Sci. Eng. **16**, 1 (1977).
24. P. H. Emmett (*Editor*). Catalysis. Vol. V. Reinhold, New York. 1954.
25. W. J. Thomas. Trans. Faraday Soc. **53**, 1124 (1957); Trans. Faraday Soc. **55**, 624 (1959).
26. Y-F. Yu Yao and J. T. Kummer. J. Catal. **28**, 124 (1973).
27. A. K. Galwey. Adv. Catal. **26**, 247 (1977).
28. C. Fairbridge. Ph.D. Thesis. The University of St. Andrews, St. Andrews, Scotland. 1981.
29. C. F. Cullis and T. G. Nevell. Proc. R. Soc. London A, **349**, 523 (1976).
30. O. S. Zanevskaya, V. Ya.Vol'fson, and O. T. Chugaeva, Kinet. Katal. **10**, 8 (1973).
31. B. Dmuchovsky, M. C. Freerks, and F. B. Zienty. J. Catal. **4**, 577 (1965).
32. E. P. Koutsoukas and K. Nobe. Ind. Eng. Chem., Prod. Res. Devel. **4**, 425 (1965).

# Osmotic and activity coefficients of triorganophosphates in *n*-octane[1]

NORMAN H. SAGERT AND DANNY W. P. LAU

*Research Chemistry Branch, Atomic Energy of Canada Limited, Whiteshell Nuclear Research Establishment, Pinawa, Man., Canada R0E 1L0*

Received April 19, 1982

NORMAN H. SAGERT and DANNY W. P. LAU. Can. J. Chem. **60**, 2755 (1982).

Vapor pressure osmometry was used to measure osmotic coefficients for tributylphosphate (TBP), tricresylphosphate (TCP), and triethylhexylphosphate (TEHP) in *n*-octane at 30, 40, 50, and 60°C and at molalities up to 0.3 mol/kg. Activity coefficients and excess thermodynamic properties (unsymmetrical definition) were calculated from these osmotic coefficients. At 30°C, the excess Gibbs free energies for 0.1 mol of solute in 1.0 kg *n*-octane were −42 J, −66 J, and −20 J for TBP, TCP, and TEHP, respectively. The more ideal behavior of the TEHP–octane system is attributed to the increasing importance of hydrocarbon–hydrocarbon interactions as the chain length is increased. The excess enthalpies for 0.1 mol of solute in 1.0 kg of solvent were −100 J, −300 J, and −150 J for TBP, TCP, and TEHP, respectively. Thus, association of these solutes arises primarily from entropic effects.

Our data could generally be accommodated adequately by postulating association of monomers into dimers. The exception was TCP at lower temperatures, where more complex models were required.

NORMAN H. SAGERT et DANNY W. P. LAU. Can. J. Chem. **60**, 2755 (1982).

On a utilisé l'osmométrie de la pression de vapeur pour mesurer les coefficients d'osmose des phosphates de tributyle (TBP), de tricrésyle (TCP) et de triéthylhexyle (TEHP) dans le *n*-octane à 30, 40, 50 et 60°C et à des molalités allant jusqu'à 0,3 mol/kg. A partir de ces coefficients d'osmose, on a calculé les coefficients d'activité et les propriétés thermodynamiques en excès (définition non symétrique). A 30°C, les énergies libres de Gibbs en excès pour 0,1 mol de soluté dans 1,0 kg de *n*-octane sont de −42 J, −66 J et −20 J respectivement pour le TBP, le TCP et le TEHP. On attribue le comportement plus idéal du système TEHP–octane à l'importance croissante des interactions hydrocarbure–hydrocarbure avec l'allongement de la chaîne. Les enthalpies en excès pour 0,1 mol de soluté dans 1,0 kg de solvant sont de −100 J, −300 J et −150 J respectivement pour le TBP, le TCP et le TEHP. Ainsi l'association de ces solutés provient principalement des effets d'entropie.

Nos données peuvent généralement s'accomoder de façon adéquate en postulant une association de monomères dans les dimères. Le TCP fait exception à de basses températures où des modèles plus complexes sont nécessaires.

[Traduit par le journal]

## Introduction

The neutral organic phosphates, particularly tributylphosphate (TBP), are used in many solvent extraction processes. In the nuclear industry, such processes are widely used for the reprocessing of irradiated nuclear fuel (1). We have begun a program to study interfacial properties relevant to these solvent extraction systems (2, 3), and thus, we need to know activity coefficients for organic phosphates in various hydrocarbon and aqueous media. The purpose of this work is to measure activity coefficients of three triorganophosphates, TBP, tricresylphosphate (TCP), and triethylhexylphosphate (TEHP), in *n*-octane. Osmotic coefficients of triorganophosphates have been measured previously (4–7), usually at high solute molality. However, data at lower solute molalities were needed for our surface studies. Also, data at lower molalities are useful in determining activities at higher molalities, since the osmotic coefficients must be integrated from zero to the given molality in order to obtain the activity coefficient at that molality.

## Experimental

Osmotic coefficients were measured at 30, 40, 50, and 60°C using a Corona/Wescan Model 232A vapor pressure osmometer. In this apparatus, the steady-state temperature difference is measured between a drop of pure solvent (*n*-octane) and a drop of solution, both drops being maintained in a chamber saturated with pure solvent vapor (8, 9). Thermistors are used as temperature sensors, and the difference in the voltage developed across the two thermistors, $\Delta V$, is measured at a constant bridge current. The operation of this particular instrument is described in detail by Burge (10). To extend the range of the technique to higher solute molalities, solutions whose osmotic coefficients were known were used as both reference solution and vapor-saturating solution. The $\Delta V$'s were obtained relative to these reference solutions (11).

At each of the four temperatures employed, the instrument was calibrated using solutions of *n*-hexadecane in *n*-octane as standards (11). The voltage difference, $\Delta V$, was divided by the *n*-hexadecane molality, $m$, and $\Delta V/m$ was plotted as a function of $m$. Since these solutions are close to ideal (12), straight lines were obtained with small slopes. The value of $\Delta V/m$, extrapolated to zero molality, was taken as the reference value $(\Delta V/m)_r$.

In addition to the measurements in *n*-octane, some measurements of osmotic coefficients were made for TBP in *n*-hexane at 25°C to allow comparison with literature values (4). The calibration procedures were similar to those described above.

The source and purification of TBP have been described (2). TCP was obtained from Applied Sciences Laboratories, TEHP from Chem Service, and *n*-hexadecane was Matheson, Coleman and Bell spectrograde. These solutes were used as received.

[1]Issued as AECL No. 7587.

0008-4042/82/222755-05$01.00/0

©1982 National Research Council of Canada/Conseil national de recherches du Canada

Can. J. Chem. Downloaded from www.nrcresearchpress.com by 210.87.254.40 on 09/06/12
For personal use only.

Can. J. Chem. Downloaded from www.nrcresearchpress.com by 210.87.254.40 on 09/06/12
For personal use only.

*n*-Octane was obtained from Humphries Chemical Co. (99+%) and was distilled in glass. It was dried over molecular sieves before use. *n*-Hexane was from Caledon Chemical Co. It was also distilled in glass and dried. Solutions were made up by volume, and molalities were calculated from measured densities.

## Results and discussion

Osmotic coefficients, $\phi$, for the solutions of triorganophosphates were calculated from eq. [1] (8, 9):

$$[1] \quad \phi = \left(\frac{\Delta V}{m}\right) \Big/ \left(\frac{\Delta V}{m}\right)_r$$

This equation assumes that the practical molal osmotic coefficient, $\phi$, for the reference condition, *n*-hexadecane in *n*-octane extrapolated to infinite dilution, is 1.000. Some typical results[2] for TBP, TEHP, and TCP at 30°C are shown in Fig. 1. Although osmotic coefficients are given to four significant figures to avoid compounding calculation errors, they are accurate only to 0.5% at best. Attempts were made to fit polynomials to the data but, because of the scatter, the fits had inflexions and thus were not satisfactory. Hence the practical molal osmotic coefficients were fitted using a simple rational function, eq. [2].

$$[2] \quad \phi = \frac{1 + A_1 m}{1 + A_2 m}$$

Table 1 lists the constants obtained from such fits using a non-linear least-squares fitting routine based on the algorithm of Brown and Dennis (13) (Chalk River Nuclear Laboratories Program MLSQQ). The errors reported in Table 1 are the standard deviations of the parameters. The solid lines in Fig. 1 were obtained from the constants listed in Table 1. From eq. [2], it is apparent that this equation predicts that practical molal osmotic coefficients will vary linearly with molality for very dilute solutions, i.e., $d\phi/dm \rightarrow A_1 - A_2$ as $m \rightarrow 0$. Thus, this rational function predicts the same limiting behavior as the more conventional polynomial fit (8, 9).

The molal activity coefficients of the solute, $\gamma_2$, were calculated using Bjerrum's relation (14), eq. [3], where $\gamma_2$ is that activity coefficient which approaches 1.0 at zero solute molality.

$$[3] \quad d[(1 - \phi)m] + m \, d \ln \gamma_2 = 0$$

When the Bjerrum expression is combined with eq. [2], an expression for the activity coefficient, eq. [4], is obtained.

[2]All the measured osmotic coefficients are available, at a nominal charge, from the Depository of Unpublished Data, CISTI, National Research Council of Canada, Ottawa, Ont., Canada K1A 0S2.

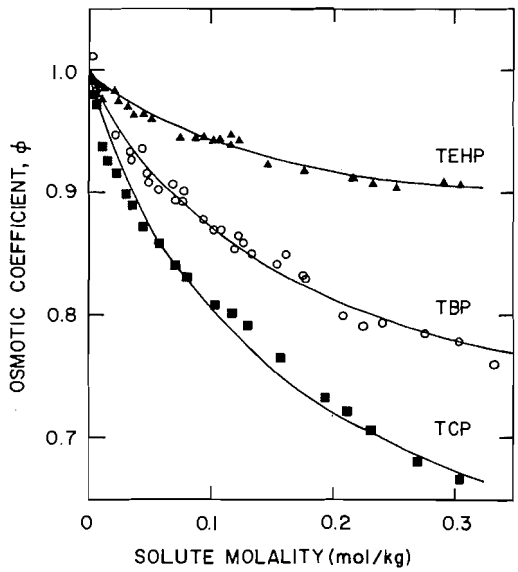


FIG. 1. Osmotic coefficients for TBP (○), TEHP (▲), and TCP (■) at 30°C plotted against solute molality. The lines are fitted using eq. [2] and the constants of Table 2.

$$[4] \quad \ln \gamma_2 = \frac{A_1 - A_2}{A_2}\left[\left\{\ln (1 + A_2 m)\right\} + \left\{\frac{A_2 m}{1 + A_2 m}\right\}\right]$$

If desired, solvent activity can be calculated using eq. [5] (8).

$$[5] \quad \ln X_1 f_1 = -\frac{m M_1 \phi}{1000}$$

where $X_1$ is the mole fraction, $f_1$ the mole fraction activity coefficient, and $M_1$ is the molecular weight of the solvent.

One framework for discussing activity coefficients is in terms of the total excess thermodynamic functions: the total excess Gibbs free energy, $G^{ex}$, the total excess enthalpy, $H^{ex}$, and the total excess entropy, $S^{ex}$, per kg of solvent (15). Expressions for these quantities, applicable for the dilute solutions used here, are given by eqs. [6], [7], and [8] (15).

$$[6] \quad G^{ex} = mRT(1 - \phi + \ln \gamma_2)$$

$$[7] \quad H^{ex} = \partial(G^{ex}/T)/\partial(1/T)$$

$$[8] \quad TS^{ex} = H^{ex} - G^{ex}$$

Total excess Gibbs free energies, $G^{ex}$, calculated from the fitted lines shown in Fig. 1, are given in Fig. 2. The TEHP–*n*-octane system is the most ideal of the three, giving the least negative values of $G^{ex}$; the TBP–*n*-octane system is intermediate, and the TCP–*n*-octane system is the least ideal, with the most negative values of $G^{ex}$. The standard states used here are such that deviations from

TABLE 1. Constants of eq. [2] for osmotic coefficients of triorganophosphates in *n*-octane

| Solute | $T$ (°C) | No. of points | $A_1$ (kg/mol) | $A_2$ (kg/mol) | $10^3$ Residual sum of deviations squared |
|---|---|---|---|---|---|
| TBP | 30 | 32 | 4.04±0.47 | 6.12±0.56 | 2.49 |
| | 40 | 42 | 8.97±1.21 | 11.91±1.42 | 7.37 |
| | 50 | 29 | 6.50±1.25 | 8.28±1.41 | 3.38 |
| | 60 | 28 | 8.62±1.54 | 10.63±1.72 | 3.48 |
| TEHP | 30 | 29 | 6.34±0.83 | 7.39±0.90 | 0.73 |
| | 40 | 28 | 13.49±2.35 | 15.07±2.52 | 1.48 |
| | 50 | 30 | 1.15±0.80 | 1.40±0.84 | 1.05 |
| | 60 | 35 | 9.94±3.05 | 10.59±3.16 | 1.79 |
| TCP | 30 | 23 | 3.46±0.60 | 6.74±0.83 | 5.59 |
| | 40 | 18 | 1.74±0.61 | 3.82±0.80 | 5.79 |
| | 50 | 28 | 1.74±0.30 | 3.59±0.39 | 2.96 |
| | 60 | 26 | 1.72±0.25 | 3.34±0.31 | 1.07 |
| TBP (in *n*-hexane) | 15 | 17 | 2.73±1.55 | 4.16±1.77 | 3.39 |
| | 25 | 20 | 1.08±0.90 | 1.72±0.97 | 1.26 |

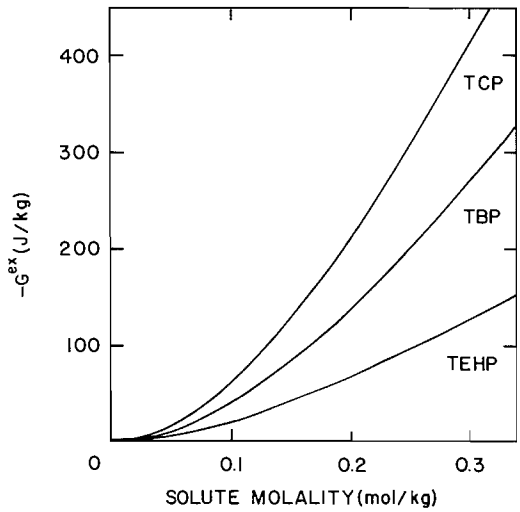


FIG. 2. Total excess Gibbs free energies for TCP, TBP, and TEHP at 30°C calculated from the fitted lines in Fig. 1.

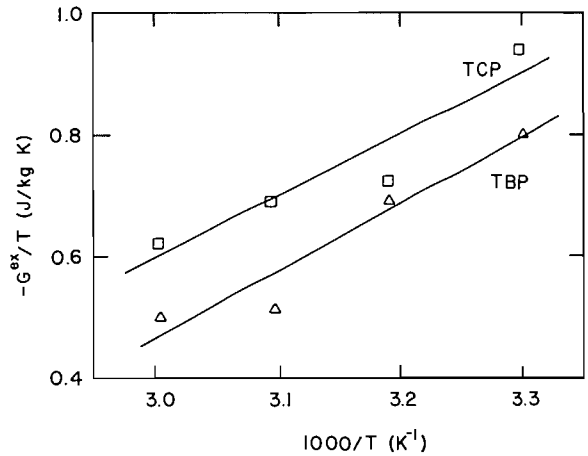


FIG. 3. Determination of total excess enthalpies using a plot suggested by eq. [7]. The results shown are for TCP (□) and TBP (△), both at 0.25 mol/kg.

ideality are essentially a measure of solute–solute interactions. Thus solute–solute interactions in *n*-octane are in the order TEHP < TBP < TCP. Apelblat (7) has also found that TEHP forms more ideal solutions in hydrocarbons than does TBP. He feels that self-association of the phosphate groups is balanced by thermal–athermal effects resulting from steric hindrance caused by the side chains of the hydrocarbon group, and that hydrocarbon–hydrocarbon interactions will become more important as the hydrocarbon chain length increases. Apparently, with TCP, solute–solute interactions are greater than with TBP. These interactions probably arise from interactions of the phosphate group with the π-bonding system of the cresyl groups. Such interactions have been postulated previously between TBP and benzene (16, 17). Direct dipole–dipole interactions are probably no larger than for TBP since the dipole moment for tritolylphosphate is smaller than that for TBP, at least in carbon tetrachloride (18).

Figure 3 shows the total excess Gibbs free energies for TBP and TCP, measured at different temperatures, plotted in the form suggested by eq. [7] so as to obtain the total excess enthalpy. These enthalpies were not determined very accurately because the temperature variation of $\phi$ was not large compared to the experimental error. Our estimates of the total excess Gibbs free energies, enthalpies, and entropies at 30°C are shown in Table 2. In all cases, the total excess enthalpies are much more negative than the total excess Gibbs free energies. Thus, a balance between entropic processes and enthalpic processes appears to control the deviations from ideality in these systems.

Can. J. Chem. Downloaded from www.nrcresearchpress.com by 210.87.254.40 on 09/06/12
For personal use only.

Can. J. Chem. Downloaded from www.nrcresearchpress.com by 210.87.254.40 on 09/06/12
For personal use only.

TABLE 2. Total excess thermodynamic functions for triorganophosphates in *n*-octane at 30°C

| Solute | Molality (mol/kg) | $G^{ex}$ (J/kg) | $H^{ex}$ (J/kg) | $S^{ex}$ (J/(K kg)) |
|---|---|---|---|---|
| TBP | 0.10 | −42.2 | −100 | −0.2 |
| | 0.25 | −243 | −1100 | −2.8 |
| TEHP | 0.10 | −20.3 | −150 | −0.4 |
| | 0.25 | −93.9 | −650 | −1.8 |
| TCP | 0.10 | −66.0 | −300 | −0.8 |
| | 0.25 | −287 | −1000 | −2.4 |

The use of Bjerrum's relationship implies that the standard states used are those of unit activity coefficient for an infinitely dilute solution of the solute in *n*-octane. This is the standard state commonly used for electrolyte solutions, as distinct from the standard state of unit activity for the pure component usually used for non-electrolyte solutions (19). Thus, our activity coefficients measure deviations from the proportionality of activity to mole fraction (or molality for dilute solutions) of solute, i.e., from Henry's law. However, they do not give any information about the Henry's law constants themselves. It is necessary to know the Henry's law constants to convert from the activity coefficients measured here to those normally reported for non-electrolyte solutions (19). Generally these constants are not available for the systems considered here. However, Rozen *et al.* (4) have measured activity coefficients for TBP in *n*-hexane at 25°C by the solvent vapor-pressure method. They were not able to consider solutions more dilute than 0.05 mole fraction (0.58 molal), but were able to deduce an activity of 4.36 for TBP when infinitely dilute in *n*-hexane, based on a standard state of unit activity for pure liquid TBP. Using this value, our activity coefficients for TBP in *n*-hexane can be compared with those of Rozen *et al.* (4), and such a comparison is shown in Fig. 4. Our results help to close the gap between zero molality and the values of Rozen *et al.*, and show reasonable agreement with them.

An entirely different way of treating the observed non-idealities is to assume that they are entirely accounted for by agglomeration of solute molecules and that the individual species behave in a totally ideal way. A number of different treatments are possible. One such treatment is to assume that agglomeration stops with the formation of dimers (20). For the systems studied here, this assumption is not unreasonable, as the chief solute–solute interaction is expected to be dipole–dipole attraction (4, 21, 22). Agglomeration into dimers leads to eq. [9] (19).

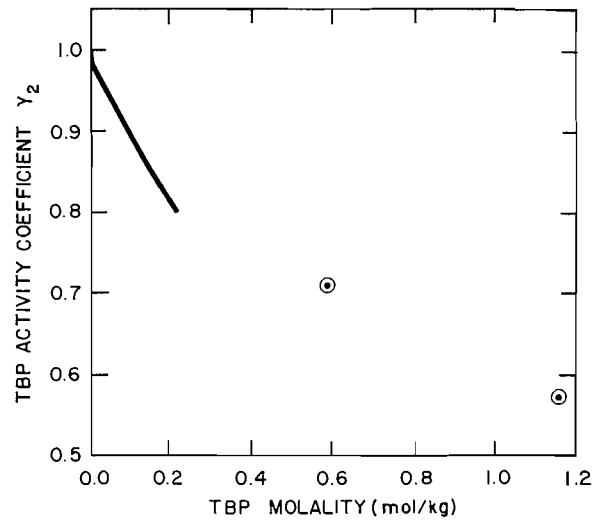


FIG. 4. Activity coefficients for TBP in *n*-hexane at 25°C. The solid line represents our fitted data and the circles (⊙) are calculated from the data of Rozen *et al.* (4).

$$[9] \quad \frac{1}{\phi} = 1 + K_2 \frac{(2\phi - 1)^2 m}{\phi}$$

where $K_2$ is the equilibrium constant for dimerization. Good fits of the experimented data for TBP and TEHP were obtained, and the dimerization constants are shown in Fig. 5 as a function of reciprocal temperature. These dimerization constants and the association constants given below are probably good to ±10%. The values for TBP dimerization constants compare well with the value of 2.9 in hexane (23) and 2.6 and 2.5 in dodecane and cyclohexane (24), all at 22°C, as measured by Petkoviç. The slopes of the lines in Fig. 5 correspond to standard enthalpies of dimerization of −27.5 and −28.4 kJ/mol for TBP and TEHP, respectively. For TCP, the monomer–dimer model did not fit the data at the lower temperatures, although it did give reasonable fits at 50 and 60°C ($r$ = 0.93 and 0.97, respectively). The two valid dimerization constants are shown in Fig. 5.

Another frequently used model (8) is that of a monomer forming a multimer by some scheme. One of these schemes is step-wise addition with equal equilibrium constants for the addition of each monomer unit. For this, eq. [10] holds (8, 19),

$$[10] \quad \frac{1}{\phi} = 1 + K_n \phi m$$

where $K_n$ is the equilibrium constant for the addition of each monomer unit. The fits of data are acceptable, although, for TBP in particular, intercepts were larger than with eq. [9]. The values of

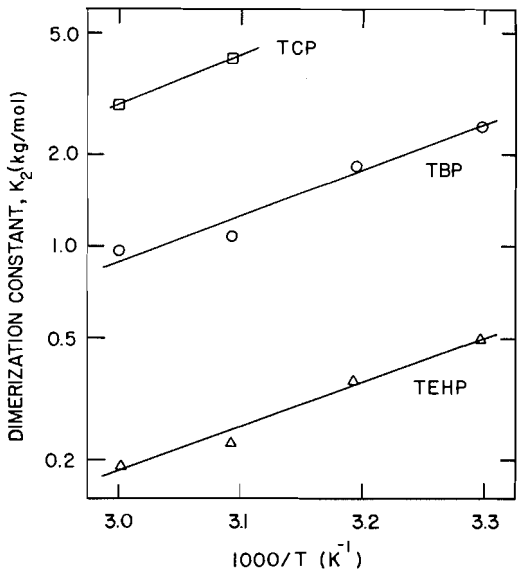


FIG. 5. Dimerization constants calculated from fits to eq. [9] for TCP (□), TBP (○), and TEHP (△), plotted against the reciprocal of the absolute temperature.

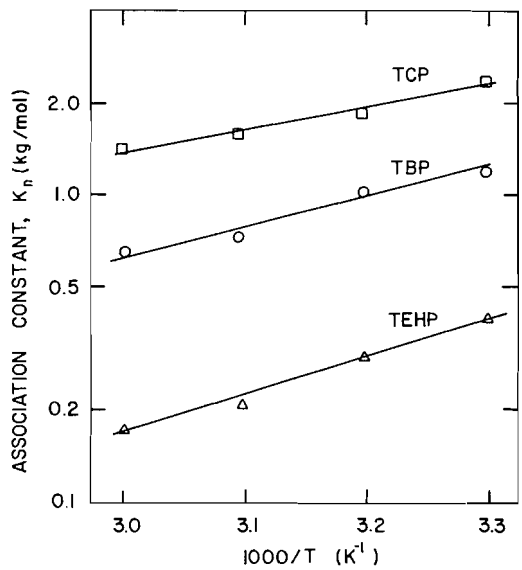


FIG. 6. Step-wise association constants calculated from fits to eq. [10] for TCP (□), TBP (○), and TEHP (△) plotted against the reciprocal of the absolute temperature.

$K_n$ are plotted in Fig. 6 as a function of reciprocal temperature. The standard enthalpies for addition of monomer segments are −13.9, −17.5, and −24.0 kJ/mol for TCP, TBP, and TEHP, respectively.

More complex treatments of association data are available (25), but they are probably not warranted for our data. Our data fit best a monomer–dimer association model for TBP and TEHP, and for TCP at higher temperatures. Thus, they give support to such a model. This is gratifying since there is evidence in the literature that neutral organic phosphates do not form aggregates higher than dimers (4, 21, 22). However, our data clearly do not support a monomer–dimer model for TCP at lower temperatures, and some form of extended aggregation is postulated.

**Acknowledgements**

We thank our colleagues at the Whiteshell Nuclear Research Establishment, and in particular R. J. Lemire, J. Paquette, and M. J. Quinn, for aid and advice.

1. Y. MARCUS and A. S. KERTES. Ion exchange and solvent extraction of metal complexes. John Wiley, New York. 1969. p. 650.
2. N. H. SAGERT, W. LEE, and M. J. QUINN. Can. J. Chem. **57**, 1218 (1979).
3. N. H. SAGERT and W. LEE. Can. J. Chem. **58**, 2789 (1980).
4. A. M. ROZEN, L. P. KHORKHORINA, V. G. YURKIN, and N. M. NOVIKOVA. Dokl. Akad. Nauk SSSR, **153**, 1387 (1963).
5. A. APELBLAT. Chem. Script. **10**, 67 (1976).
6. A. APELBLAT. J. Inorg. Nucl. Chem. **40**, 1783 (1978).
7. A. APELBLAT. J. Inorg. Nucl. Chem. **42**, 411 (1980).
8. C. KLOFUTAR and S. PALJK. J. Chem. Soc. Faraday I, **75**, 825 (1979).
9. A. S. KERTES and G. MARKOVITS. J. Phys. Chem. **72**, 4202 (1968).
10. D. E. BURGE. J. Appl. Polymer Sci. **24**, 293 (1979).
11. R. AVEYARD, B. J. BRISCOE, and J. CHAPMAN. J. Colloid Interface Sci. **44**, 282 (1973).
12. J. H. HILDEBRAND and R. L. SCOTT. The solubility of nonelectrolytes. 3rd ed. Dover Publications, New York. 1964. p. 111.
13. K. M. BROWN and J. E. DENNIS, JR. Numer. Math, **18**, 289 (1972).
14. E. A. GUGGENHEIN and R. H. STOKES. Equilibrium properties of aqueous solutions of single strong electrolytes. Pergamon Press, Oxford. 1969. p. 13.
15. R. H. STOKES. *In* Activity coefficients in electrolyte solutions. Vol. 1. *Edited by* R. M. Pytkowicz. CRC Press, Boca Raton, Florida. 1979. pp. 24–26.
16. N. H. SAGERT, W. LEE, and M. J. QUINN. Can. J. Chem. **69**, 1244 (1982).
17. S. SIEKIERSKI. J. Inorg. Nucl. Chem. **24**, 205 (1962).
18. D. M. PETKOVIĆ, B. A. KEZELE, and D. R. RAJIC. J. Phys. Chem. **77**, 922 (1973).
19. G. N. LEWIS and M. RANDALL. Thermodynamics. McGraw-Hill, New York. 1961. pp. 245–255.
20. P. O. P. TS'O, I. S. MELVIN, and A. C. OLSON. J. Am. Chem. Soc. **85**, 1289 (1963).
21. A. M. ROZEN, V. G. YURKIN, T. I. RUDENKO, and M. YA ZEL'VENSKII. Radiokhimiya, **15**, 411 (1973).
22. A. S. KERTES. *In* Recent advances in liquid–liquid extraction. *Edited by* C. Hanson. Pergamon Press, New York. 1971. pp. 38–40.
23. D. M. PETKOVIĆ. *In* Solvent extraction chemistry. *Edited by* D. Dyrssen, J. O. Liljenzin, and J. Rydberg. North Holland, Amsterdam. 1967. pp. 305–308.
24. D. M. PETKOVIĆ. J. Inorg. Nucl. Chem. **30**, 603 (1968).
25. J. ROBESON, B. W. FOSTER, S. N. ROSENTHAL, E. T. ADAMS, JR., and E. J. FENDLER. J. Phys. Chem. **85**, 1254 (1981).

Can. J. Chem. Downloaded from www.nrcresearchpress.com by 210.87.254.40 on 09/06/12
For personal use only.

# Synthesis and Diels–Alder reactions of (*E*)-6,6-dimethoxy-3-hexen-2-one

PETER YATES AND STEPHEN PAUL DOUGLAS
*Lash Miller Chemical Laboratories, University of Toronto, Toronto, Ont., Canada M5S 1A1*

Received February 2, 1982

PETER YATES and STEPHEN PAUL DOUGLAS. Can. J. Chem. **60**, 2760 (1982).

Treatment of 3,3-dimethoxypropanal (**2**) with (acetylmethylene)triphenylphosphorane (**4**) gives (*E*)-6,6-dimethoxy-3-hexen-2-one (**5**). Reaction of **5** with cyclopentadiene, 1,3-cyclohexadiene, anthracene, and 1,3-diphenylisobenzofuran gives Diels–Alder adducts, which on hydrolysis are converted to the corresponding keto aldehydes. Attempts to effect intramolecular aldol condensation of the latter were unsuccessful. Hydrolysis of the *exo*-acetyl adduct from 1,3-diphenylisobenzofuran with aqueous formic acid gives 4-acetyl-2,3,3a,4,5,9b-hexahydro-5,9b-diphenylnaphtho[1,2-*b*]furan-2,5-diol, via aldehyde formation and hydrolytic cleavage of the ether bridge. The adducts from cyclopentadiene under anhydrous acid conditions give 3-acetyl-9-methoxytetracyclo[4.3.0.0$^{2,4}$.0$^{3,7}$]nonane (**27**).

PETER YATES et STEPHEN PAUL DOUGLAS. Can. J. Chem. **60**, 2760 (1982).

Le diméthoxy-3,3 propanal (**2**) réagit avec l'(acétylméthylène) triphénylphosphorane (**4**) en donnant la (*E*)-diméthoxy-6,6 hexène-3 one-2 (**5**). Le composé **5** réagit avec le cyclopentadiène, le cyclohexadiène-1,3, l'anthracène et le diphényl-1,3 isobenzofuranne en donnant des adduits de Diels Alder qui, par hydrolyse, donnent les céto aldéhydes correspondants. On a essayé vainement de réaliser une condensation aldolique intramoléculaire avec ces cétoaldéhydes. L'hydrolyse de l'adduit *exo*-acétyl provenant du diphényl-1,3 isobenzofuranne, avec l'acide formique aqueux, donne l'acétyl-4 hexahydro-2,3,3a,4,5,9b diphényl-5,9b naptho[1,2-*b*]furannediol-2,5 par l'intermédiaire de la formation de l'aldéhyde et du clivage, par hydrolyse, du pont éther. Les adduits provenant du cyclopentadiène dans un milieu acide anhydre donnent l'acétyl-3 méthoxy-9 tétracyclo[4.3.0.0$^{2,4}$.0$^{3,7}$]nonane (**27**).

[Traduit par le journal]

Shakespeare said of Cleopatra "Age cannot wither her, nor custom stale Her infinite variety." The same could be said of the Diels–Alder reaction. In recent years the scope of this reaction has been greatly expanded by the utilization of a large variety of dienes and dienophiles. We report here on the synthesis and Diels–Alder reactions of the dienophile 6,6-dimethoxy-3-hexen-2-one. We have shown that this can serve, via hydrolysis of its Diels–Alder adducts, as an equivalent of the dienophile 3-hexene-2,6-dione, but we have not been successful in effecting the intramolecular aldol condensation of the keto aldehydes resulting from such hydrolyses, which would have permitted its use as an equivalent of the dienophile 2,5-cyclohexadienone.

Base-catalyzed addition of two equivalents of methanol to propiolaldehyde (**1**) (1) gave β,β-dimethoxypropionaldehyde (**2**) (2), containing 10% of β-methoxyacrolein (**3**) as shown by $^1$H nmr spectroscopy. This mixture was treated with (acetylmethylene)triphenylphosphorane (**4**) to give 6,6-dimethoxy-3-hexen-2-one (**5**) (Scheme 1). No effort was devoted to removal of **3** from the original mixture since it was anticipated that it would be unreactive in a Wittig reaction with **4** because of electron donation to the aldehyde group by the methoxyl group. This was indeed found to be the case in that only the enone **5** was formed in the reaction of the mixture of compounds **2** and **3** with the Wittig reagent **4** and that **3** (2) alone failed to react with **4**.

The ir spectrum of **5** showed a strong band at 5.95 μm and a medium band at 6.12 μm in accord with the presence of an α,β-unsaturated ketonic system; a strong band at 10.25 μm suggested that the product has the *trans* (*E*) configuration as in **5** (3). In its $^1$H nmr spectrum the olefinic proton signals appear as a doublet at δ 6.02 ($J$ = 15 Hz) and a doublet of triplets at δ 6.63 ppm ($J$ = 15 and 7.5 Hz); the magnitude of the larger coupling constant established that the product has the *trans* (*E*) configuration. The uv spectrum of **5** ($\lambda_{max}$ (pentane) 216 nm (ε 9500), 321 nm (ε 35)) is in accord with the presence of a monosubstituted α,β-unsaturated ketonic function. In its $^{13}$C nmr spectrum the α and β ethylenic carbon signals occur at δ 133.6 and 142.3 ppm, respectively (cf. the corresponding signals in 3-buten-2-one at δ 138.5 and 129.3 ppm).

Reaction of **5** with a large excess of cyclopentadiene at 100–110°C in the absence of solvent for three days gave a 55:45 mixture of the stereoisomeric Diels–Alder adducts **6** and **7** (Scheme 2) in almost quantitative yield. Individual assignments of structure to the *endo* and *exo* isomers[1] were made from their $^1$H nmr spectra on the basis of decoupling experiments and the following earlier

[1]The designations *endo* and *exo* are made with reference to the acetyl group.

0008-4042/82/222760-06$01.00/0
©1982 National Research Council of Canada/Conseil national de recherches du Canada

Can. J. Chem. Downloaded from www.nrcresearchpress.com by 210.87.254.5 on 09/06/12
For personal use only.

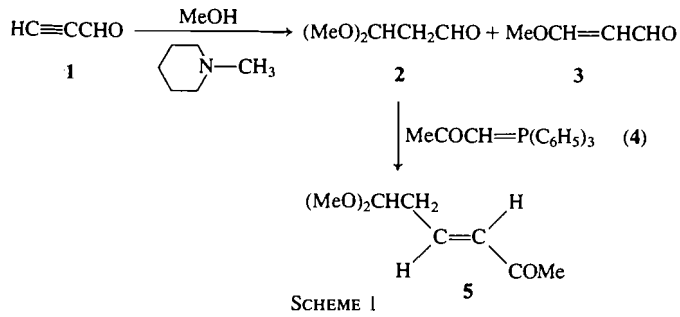


SCHEME 1

observations regarding the spectra of bicyclo-[2.2.1]heptenes: (*i*) signals of *exo* protons and the protons of *exo* substituents appear downfield relative to those of the corresponding *endo* protons (4) and (*ii*) electron-withdrawing *endo* substituents deshield the bridgehead (5) and often shield the olefinic protons nearest to them (6). Thus under the reaction conditions used there is a slight preference for formation of the *endo* adduct. It is probable that under these conditions the reaction is under kinetic control (7) and the modest stereoselectivity is analogous to that observed in the cases of other simple α,β-unsaturated carbonyl compounds under such circumstances (7, 8). Hydrolysis of **6** with 1.2 *N* hydrochloric acid in tetrahydrofuran gave the keto aldehyde **8** (Scheme 2) whose ir spectrum showed strong bands at 5.81 and 5.85 μm.

Reaction of **5** with 1,3-cyclohexadiene at 100–120°C yielded the adducts **9** and **10** (Scheme 2). The individual stereochemical assignments are again based on their $^1$H nmr spectra, since bicyclo[2.2.2]-octenes have been observed to exhibit the same downfield shift of the signals of *exo* relative to *endo* protons as in the case of bicyclo[2.2.1]heptenes (4, 6). Again the *endo* isomer was formed in slight preponderance. Hydrolysis of this isomer gave the keto aldehyde **11**, whose ir spectrum showed strong bands at 5.80 and 5.85 μm.

Cycloaddition of **5** to anthracene was best effected with an excess of the dienophile at 150°C (reaction did not occur at 120°C). Adduct **12** (Scheme 3) was thus obtained in 77% yield (based on anthracene). This product was hydrolyzed to the keto aldehyde **13**.

The Diels–Alder reaction of **5** with 1,3-diphenylisobenzofuran was carried out in boiling benzene. After 3 days, reaction was complete to give a mixture of the *exo* (**14**) and *endo* (**15**) adducts in a 4:1 ratio (Scheme 4). Individual assignments of stereochemistry were made on the basis of a comparison of the $^1$H nmr spectra of the adducts, since it has previously been shown that in systems of this type *endo* protons again are shielded relative to *exo* protons (9, 10). The carbonyl-stretching

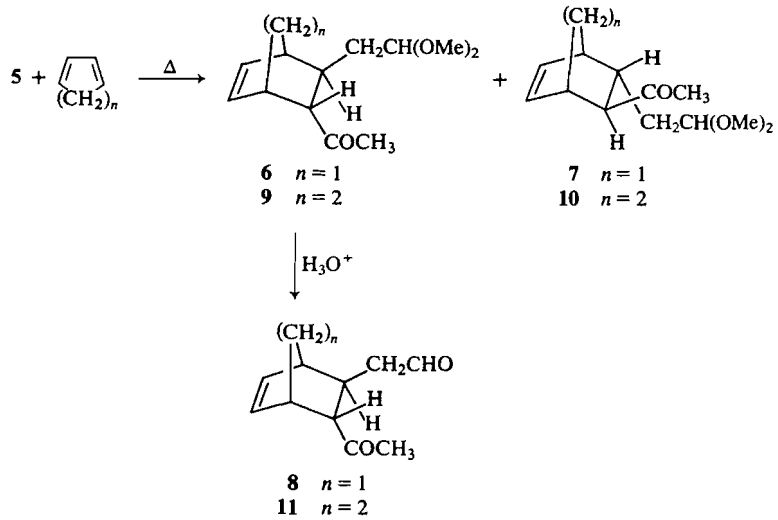


SCHEME 2

Can. J. Chem. Downloaded from www.nrcresearchpress.com by 210.87.254.5 on 09/06/12
For personal use only.

Can. J. Chem. Downloaded from www.nrcresearchpress.com by 210.87.254.5 on 09/06/12
For personal use only.

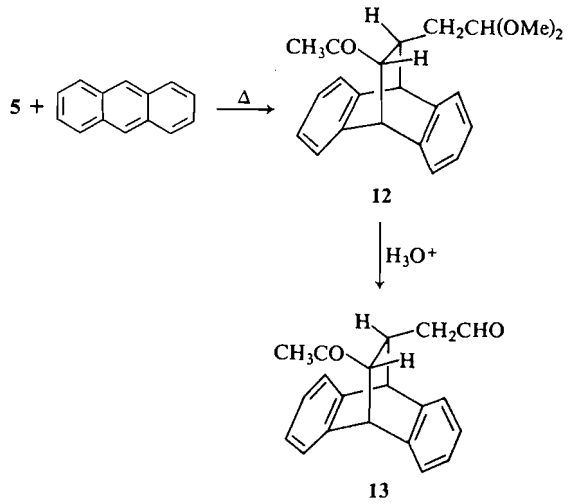


SCHEME 3

bands in the ir spectra of **14** and **15** occur at unusually long wavelength (5.92 μm); this may be the result of interaction of the carbonyl group with a methoxyl group or the phenyl substituent at the adjacent bridgehead position. Hydrolysis of **14** with 1.2 *N* hydrochloric acid in tetrahydrofuran gave the expected keto aldehyde **16**, but the reaction was capricious; in some runs the product underwent further reaction and in others hydrolysis was incomplete. Treatment with aqueous 90% formic acid (11) led to hydrolysis of both the acetal and ether bridge functions, giving hemiacetal **17** in high yield. In the $^1$H spectrum of **17** the large coupling constant ($J$ = 12 Hz) between H-4 and H-3a is attributable to a *trans* diaxial relationship between these protons, and the further coupling of H-3a with only one of the H-3 protons can be interpreted in terms of the preferred conformation of the hemiacetal ring. As in the case of **15** the carbonyl-stretching band in the ir spectrum of **17** occurs at an unusually long wavelength (5.95 μm): here the major contributing factor is probably hydrogen-bonding of the carbonyl group with the adjacent hydroxyl group. Such hydrogen bonding is also evidenced by the relatively low field position (δ 4.63) of the signal of the tertiary hydroxyl proton in the $^1$H nmr spectrum of **17**.

It was hoped that the keto aldehydes of type **8** could be induced to undergo intramolecular aldol condensation to give cyclohexenones of type **18**, products that are formally derived from Diels–Alder reactions of 2,5-cyclohexadienone. An analogous condensation was observed by Johns (12) on treatment of the keto aldehyde **19** with alcoholic potassium hydroxide. It was recognized that compounds of type **8** differ from **19** in having a *trans* rather than a *cis* relationship between the acetyl and acetaldehyde groups, and although Valenta and co-workers (13) have observed the aldol condensation in basic medium of the *trans* isomer **20** to give a cycloheptenone, there appears to have been no report of the closure of a six-membered ring in the *trans* series. It was considered that under the basic (or acidic) conditions of the aldol reaction equilibration of the *trans* compounds of type **8** would occur with their *cis* isomers via epimerization at the carbon atom bearing the acetyl group and that these isomers would then undergo the aldol reaction. However, no simple aldol condensation products could be detected when compounds of type **8** were subjected to a variety of basic conditions analogous to those used in the cases of **19** and **20** (12, 13) and related cases (14); only starting

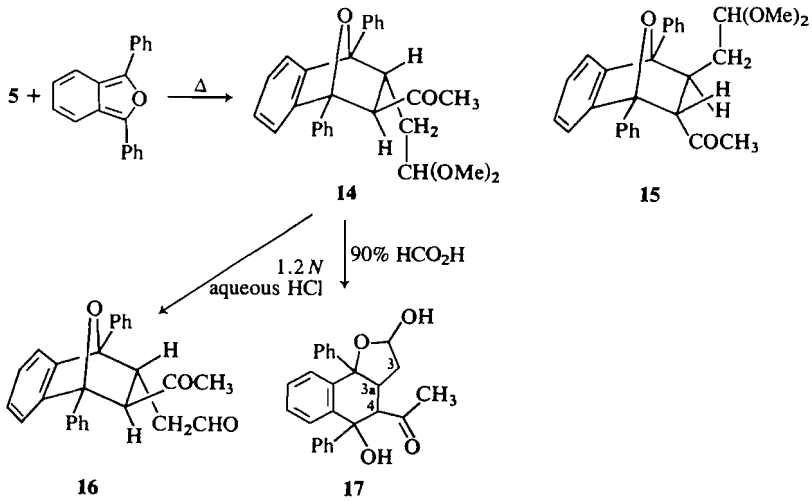


SCHEME 4

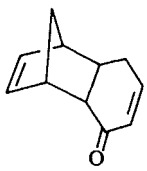

18

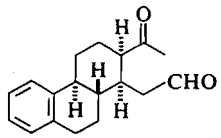

19

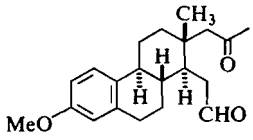

20

material or polymeric products were isolated in each case. Attempts at acid-catalyzed cyclization (15) were also of no avail.

In case these results were due to the failure of the keto aldehydes of type **8** to undergo equilibration with their *cis* isomers, a preliminary investigation was made of the direct synthesis of such an isomer. Ultraviolet irradiation of **5** in benzene gave a ~ 1:1 mixture of **5** and its *cis* isomer, **21**, as shown by its $^1$H nmr spectrum. Reaction of this mixture with cyclopentadiene followed by hydrolysis gave a mixture whose $^1$H nmr spectrum indicated that it consisted of the *cis* isomers **22** and **23** together with

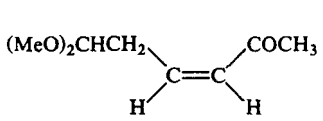

21

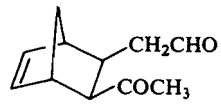

22

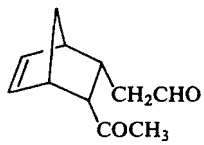

23

**8** and the other *trans* keto aldehyde. However, treatment of this mixture under several of the aldol conditions referred to above resulted only in the epimerization of the *cis* to the *trans* keto aldehydes.

In case the failure of the cyclization reactions was associated with the presence of the ethylenic double bond in compounds of type **8**, compounds **6** and **9** were hydrogenated and hydrolyzed to give **24** and **25**, respectively. But again aldol condensation could not be effected.

An attempt was also made to effect cyclization of a mixture of the keto acetals **6** and **7** under acidic conditions to give a product of type **26**. However, treatment of the mixture with *p*-toluenesulfonic acid in benzene gave compound **27** and a product that is tentatively assigned structure **28**, together with polymeric products (Scheme 5). The $^1$H nmr spectra of **27** and **28** showed that each retained a single methoxyl group. The ir spectrum of **27** showed a carbonyl-stretching band at 5.90 μm, indicating conjugation of the acetyl group with an ethylenic double bond or cyclopropyl group. That the latter is the case was established by the $^{13}$C nmr spectrum of **27**, which showed no olefinic carbon signals. Compounds **27** and **28** are considered to

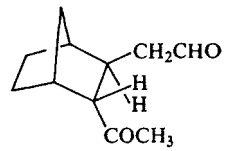

24

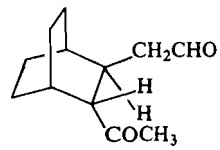

25

arise from the *exo* keto acetal **7** by the routes shown in Scheme 5.

## Experimental

Melting points were determined with a Thomas–Hoover capillary melting point apparatus, and are uncorrected. Infrared spectra were taken in $CHCl_3$ solution; band intensities are strong, unless designated as medium (m) or weak (w). Proton and carbon-13 nuclear magnetic resonance ($^1$H and $^{13}$C nmr) spectra were taken in $CDCl_3$ solution. Unless otherwise stated, solutions in organic solvents were dried over anhydrous $MgSO_4$ and concentrated by means of a Buchi "Rotovapor ⟨R⟩" rotary evaporator.

*(E)-6,6-Dimethoxy-3-hexen-2-one (5)*

Propargyl alcohol was oxidized to propiolaldehyde (**1**) with chromic acid (1) in 45% yield; bp 58–60°C (lit. (1) bp 59–61°C); ir $\lambda_{max}$: 3.53 (w), 4.78 (w), 5.96 μm; $^1$H nmr δ: 9.17 (s, 1H), 3.58 (s, 1H). Base-catalyzed addition of two molar equivalents of methanol to the aldehyde (2) gave β,β-dimethoxypropionaldehyde (**2**) in 80% yield; ir $\lambda_{max}$: 3.59 (w), 5.82 μm; $^1$H nmr δ: 2.70 (m, 2H), 3.40 (s, 6H), 4.83 (t, $J$ = 5 Hz, 1H), 9.73 (t, $J$ = 2 Hz, 1H). The crude product, which contained 10% of β-methoxyacrolein (**3**) (2) as shown by $^1$H nmr spectroscopy, was used without further purification.

A solution of aldehyde **2** (23.76 g, 201 mmol) and (acetylmethylene)triphenylphosphorane (**4**) (16) (64.1 g, 201 mmol) in anhydrous tetrahydrofuran (250 mL) was boiled under reflux for 5 days under a constant positive pressure of nitrogen. The solution was concentrated and the precipitated triphenylphosphine oxide was separated by suction filtration and washed with cold benzene. The combined filtrate and washings were concentrated, the concentrate was cooled to −78°C, and a second crop of triphenylphosphine oxide was removed. Concentration of the filtrate followed by flash distillation (100°C, 0.05 Torr) of the residue gave **5** as a colorless liquid (26.44 g, 83%), bp 51–53°C (0.05 Torr); ir $\lambda_{max}$: 5.93, 6.12 (m), 7.35 (w) μm; uv $\lambda_{max}$ (ε) (pentane): 216 (9 500), 321 (35) nm; $^1$H nmr δ: 2.22 (s, 3H), 2.53 (m, 2H), 3.37 (s, 6H), 4.43 (t, $J$ = 6 Hz, 1H), 6.02 (d, $J$ = 15 Hz, 1H), 6.68 (dt, $J$ = 7.5 Hz, 15 Hz, 1H); $^{13}$C nmr δ: 26.8 (q), 36.2 (t), 53.2 (q), 103.1 (d), 133.6 (d), 142.3 (d), 198.05 (s). *Anal.* calcd. for $C_8H_{14}O_3$: C 60.74, H 8.92; found: C 60.49, H 8.87.

Can. J. Chem. Downloaded from www.nrcresearchpress.com by 210.87.254.5 on 09/06/12
For personal use only.

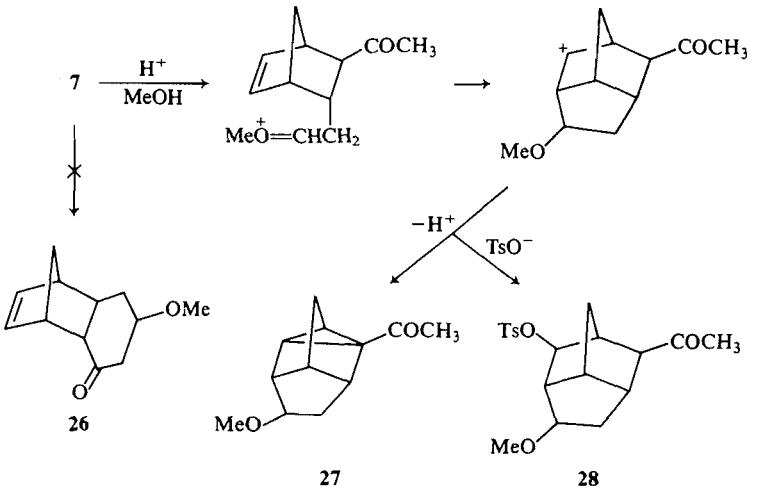


SCHEME 5

*Diels–Alder reaction of 5 with cyclopentadiene. Formation of* endo-*5-acetyl*-exo-*6-(2,2-dimethoxyethyl)bicyclo[2.2.1]-hept-2-ene (6) and* exo-*5-acetyl*-endo-*6-(2,2-dimethoxy-ethyl)bicyclo[2.2.1]hept-2-ene (7)*

Compound **5** (1.00 g, 6.32 mmol) and 1,3-cyclopentadiene (6.6 g, 100 mmol) were placed in a Carius tube (15 × 20 × 250 mm) and the tube was cooled (−196°C), sealed, and heated for 3 days at 110–120°C. The tube was cooled and opened and the contents were subjected to high vacuum pumping (0.01 Torr) at room temperature to remove most of the dimerized diene. Chromatography (silica gel, 7:3 hexane and ethyl acetate) afforded adducts **6** and **7** (total 1.37 g, 97%); the *endo*-acetyl isomer **6** had the longer retention time and comprised 57% of the mixture. Compound **7**: ir $\lambda_{max}$: 5.86 μm; $^1$H nmr δ: 1.50 (m, 2H), 1.85 (m, 2H), 2.05 (m, 1H), 2.10 (s, 3H), 2.60 (m, 2H), 3.16 (m, 1H), 3.27 (s, 3H), 3.30 (s, 3H), 4.35 (t, $J$ = 5 Hz, 1H), 5.83 (m, 1H), 6.20 (m, 1H). Compound **6**: ir $\lambda_{max}$: 5.86 μm; $^1$H nmr δ: 1.42 (m, 2H), 1.55 (m, 2H), 2.02 (m, 1H), 2.23 (s, 3H), 2.50 (m, 1H), 2.88 (m, 2H), 3.30 (s, 6H), 4.31 (t, $J$ = 5 Hz, 1H), 6.18 (m, 2H); $^{13}$C nmr δ: 28.4 (q), 36.6 (d), 38.2 (t), 45.9 (d), 46.4 (t), 47.2 (d), 52.3 (q), 59.3 (d), 103.9 (d), 131.6 (d), 137.9 (d), 207.5 (s). *Anal.* calcd. for $C_{13}H_{20}O_3$: C 69.61, H 8.98; found: C 69.25, H 8.89.

*Diels–Alder reaction of 5 with 1,3-cyclohexadiene. Formation of* endo-*5-acetyl*-exo-*6-(2,2-dimethoxyethyl)bicyclo-[2.2.2]oct-2-ene (9) and* exo-*5-acetyl*-endo-*6-(2,2-dimethoxyethyl)bicyclo[2.2.2]oct-2-ene (10)*

Compound **5** (1.00 g, 6.32 mmol) and 1,3-cyclohexadiene (6.6 g, 100 mmol) were heated in a Carius tube as described above. High vacuum pumping (0.01 Torr) at 35–40°C removed most of the dimerized diene and chromatography (silica gel, 6:4 cyclohexane and ethyl acetate) of the residue afforded the *endo* and *exo* stereoisomers **9** and **10** (1.02 g, 68%); the *endo* acetyl adduct (60% of the mixture) had the longer retention time. Compound **10**: ir $\lambda_{max}$: 5.85 μm; $^1$H nmr δ: 1.05–1.09 (m, 7H), 1.9–2.5 (m, 3H), 2.19 (s, 3H), 3.22 (s, 6H), 4.25 (t, $J$ = 5 Hz, 1H), 6.00 (m, 2H). Compound **9**: ir $\lambda_{max}$: 5.85 μm; $^1$H nmr δ: 1.05–1.09 (m, 7H), 1.9–2.5 (m, 2H), 2.12 (s, 3H), 2.78 (m, 1H), 3.23 (s, 3H), 3.28 (s, 3H), 4.29 (t, $J$ = 5 Hz, 1H), 6.14 (m, 2H); $^{13}$C nmr δ: 18.4 (t), 26.4 (t), 28.3 (q), 33.2 (d), 34.5 (d), 37.7 (t), 52.6 (q), 53.1 (q), 58.8 (d), 104.4 (d), 129.9 (d), 136.6 (d), 209.3 (s). *Anal.* calcd. for $C_{14}H_{22}O_3$: C 70.56, H 9.30; found: C 70.76, H 9.21.

*Diels–Alder reaction of 5 with anthracene. Formation of* trans-*7-acetyl-8-(2,2-dimethoxyethyl)dibenzobicyclo-[2.2.2]octadiene (12)*

Compound **5** (1.35 g, 8.54 mmol) and anthracene (1.01 g, 5.68 mmol) were heated in a Carius tube at 150°C for 5 days. High vacuum pumping (0.01 Torr) at 50°C followed by elution through a silica gel column (30 × 2 cm) with 70% hexane in ethyl acetate afforded the adduct **12** (1.48 g, 77% based on consumed anthracene) as a viscous oil; ir $\lambda_{max}$: 5.83 μm; $^1$H nmr δ: 1.50 (m, 3H), 2.07 (s, 3H), 2.42 (m, 1H), 3.19 (s, 3H), 3.25 (s, 3H), 4.12 (m, 1H), 4.35 (m, 1H), 4.44 (m, 1H), 7.10 (m, 8H); $^{13}$C nmr δ: 28.5 (q), 37.1 (d), 38.7 (t), 47.4 (d), 49.4 (d), 52.5 (q), 53.1 (q), 60.2 (d), 103.8 (d), 126.3–123.1 (7 signals), 139.2 (s), 141.05 (s), 142.5 (s), 143.8 (s), 207.1 (s). *Anal.* calcd. for $C_{22}H_{24}O_3$: C 78.54, H 7.19; found: C 78.56, H 7.44.

*Diels–Alder reaction of 5 with 1,3-diphenylisobenzofuran. Formation of* exo-*2-acetyl-1,2,3,4-tetrahydro*-endo-*3-(2,2-dimethoxyethyl)-1,4-epoxynaphthalene (14) and* endo-*2-acetyl-1,2,3,4-tetrahydro*-exo-*3-(2,2-dimethoxyethyl)-1,4-epoxynaphthalene (15)*

Compound **5** (1.00 g, 6.32 mmol) and 1,3-diphenylisobenzofuran (1.70 g, 6.30 mmol) were heated in boiling benzene (20 mL) for 72 h. The solvent was removed and the oily residue was crystallized from hexane – ethyl acetate to give the *exo*-acetyl isomer **14** (2.01 g, 74%), mp 103–105°C. The mother liquor contained the *endo*-acetyl isomer **15** together with a small amount of **14**. Compound **15**: ir $\lambda_{max}$: 5.92, 6.23 (w) μm; $^1$H nmr δ: 1.70 (s, 3H), 1.45–2.2 (m, 2H), 2.80 (m, 1H), 3.17 (s, 6H), 3.70 (m, 1H), 4.25 (m, 1H), 7.40 (m, 14H). Compound **14**: ir $\lambda_{max}$: 5.92, 6.23 (w) μm; $^1$H nmr δ: 0.55–1.0 (m, 1H), 1.92 (s, 3H), 1.8–2.2 (m, 1H), 2.85 (d, $J$ = 4.5 Hz, 1H), 3.1–3.4 (m, 1H), 3.25 (s, 6H), 4.2–4.4 (m, 1H), 7.45 (m, 14H); $^{13}$C nmr δ: 27.2 (q), 35.9 (t), 45.6 (d), 53.5 (q), 53.7 (q), 67.7 (d), 89.8 (s), 90.7 (s), 103.6 (d), 118.4 (d), 121.6 (d), 128.6–125.8 (7 signals), 136.2 (s), 136.3 (s), 144.8 (s), 148.2 (s), 209.1 (s). *Anal.* calcd. for $C_{28}H_{28}O_4$: C 78.48, H 6.59; found: C 78.48, H 6.59.

*Hydrolysis of 6, 9, and 12. Formation of the keto aldehydes 8, 11, and 13*

A mixture of the acetal (5 mmol), tetrahydrofuran (5 mL), and 1.2 *N* hydrochloric acid (5 mL) was stirred under nitrogen at

Can. J. Chem. Downloaded from www.nrcresearchpress.com by 210.87.254.5 on 09/06/12
For personal use only.

Can. J. Chem. Downloaded from www.nrcresearchpress.com by 210.87.254.5 on 09/06/12
For personal use only.

room temperature for ca. 10 h. Addition of water (10 mL) followed by extraction with dichloromethane (3 × 5 mL), washing of the extract with aqueous 5% sodium bicarbonate, drying, and removal of the solvent gave the keto aldehydes in quantitative yield.

endo-*6-Acetyl*-exo-*5-(2-oxoethyl)bicyclo[2.2.1]hept-2-ene (8)*: ir $\lambda_{max}$: 3.63 (w), 5.81, 8.85 μm; $^1$H nmr δ: 1.5–7.5 (m, 3H), 2.15 (s, 3H), 2.5–2.8 (m, 4H), 3.21 (m, 1H), 5.85 (dd, $J$ = 3, 6 Hz, 1H), 6.22 (dd, $J$ = 3, 6 Hz, 1H), 9.74 (t, $J$ = 2 Hz, 1H). *Anal.* calcd. for $C_{11}H_{14}O_2$: C 73.13, H 7.92; found: C 73.92, H 8.00.

endo-*6-Acetyl*-exo-*5-(2-oxoethyl)bicyclo[2.2.2]oct-2-ene (11)*: ir $\lambda_{max}$: 3.64 (w), 5.80, 5.85 μm; $^1$H nmr δ: 1.1–1.9 (m, 5H), 2.15 (s, 3H), 2.3–2.6 (m, 4H), 2.85 (m, 1H), 5.9–6.6 (m, 2H), 9.75 (t, $J$ = 2 Hz, 1H). *Anal.* calcd. for $C_{12}H_{16}O_2$: C 74.97, H 8.39; found: C 74.48, H 8.33.

trans-*7-Acetyl-8-(2-oxoethyl)dibenzobicyclo[2.2.2]octadiene (13)*: ir $\lambda_{max}$: 3.64 (w), 5.81, 5.83 (sh) μm; $^1$H nmr δ: 1.23 (m, 1H), 2.15 (s, 3H), 2.20 (m, 3H), 4.16 (d, $J$ = 2 Hz, 1H), 4.44 (d, $J$ = 2 Hz, 1H), 7.12 (m, 8H), 9.64 (t, $J$ = 1 Hz, 1H).

*Treatment of 14 with 90% formic acid. Formation of 4-acetyl-2,3-3a,4,5,9b-hexahydro-5,9b-diphenylnaptho[1,2-b]-furan-2,5-diol (17)*

A solution of **14** (0.250 g, 0.853 mmol) in aqueous 90% formic acid (15 mL) was allowed to stand under nitrogen at room temperature for 2 h. The mixture was diluted with water (20 mL) and extracted with dichloromethane (3 × 5 mL). Crystallization of the oily residue from hexane – ethyl acetate yielded the tricyclic hemiacetal **17** as colorless prisms (0.201 g, 86%), mp 191–192°C; ir $\lambda_{max}$: 2.80 (w), 2.95 (m), 5.95, 6.26 (w) μm; $^1$H nmr δ: 1.4–2.3 (m, 2H), 1.90 (s, 3H), 3.31 (dd, $J$ = 6, 12 Hz, 1H), 3.98 (m, 1H; absent after $D_2O$ treatment), 4.38 (d, $J$ = 12 Hz, 1H), 4.63 (s, 1H; absent after $D_2O$ treatment), 5.75 (dd, $J$ = 3, 5 Hz, 1H; d, $J$ = 5 Hz, after $D_2O$ treatment), 6.6–7.8 (m, 14H); $^{13}$C nmr δ: 34.4 (q), 35.6 (t), 44.3 (d), 58.0 (d), 76.4 (s), 88.4 (s), 98.8 (d), 125.8–147.4 (13 signals), 216.8 (s). *Anal.* calcd. for $C_{26}H_{24}O_4$: C 77.98, H 6.04; found: C 77.72, H 6.05.

*Attempted intramolecular aldol condensation of keto aldehydes 8, 11, and 13*

The conditions tried included treatment with the following reagents under the conditions indicated: aqueous 10% potassium hydroxide in methanol (12) with stirring at room temperature, 40°C, and at reflux; potassium hydroxide in boiling aqueous tetrahydrofuran (13, 14*a*); increasingly concentrated aqueous potassium hydroxide (5, 10, 15, and 20%) in equal volumes of methanol; a catalytic amount of piperidinium acetate in benzene (14*b*) at room temperature; methanolic tetramethylammonium hydroxide at 60°C; an excess of aluminum *tert*-butoxide in boiling benzene (14*c*); a catalytic amount of potassium *tert*-butoxide in boiling *tert*-butyl alcohol; potassium carbonate in boiling methanol (14*d*); a catalytic amount of anhydrous *para*-toluenesulfonic acid in boiling benzene (15*a*); hydrochloric acid, water, and tetrahydrofuran (15*b*) with stirring at room temperature and at reflux.

*Irradiation of (E)-6,6-dimethoxy-3-hexen-2-one (5). Formation of (Z)-6,6-dimethoxy-3-hexen-2-one (21)*

A solution of **5** (0.160 g, 0.010 mol) in benzene (100 mL) was degassed by bubbling nitrogen from a fine capillary tube through the length of a 40 × 5 cm quartz tube for 1 h. The tube was sealed and irradiated in a Rayonet photochemical reactor (330 nm) for 6 h. Benzene was removed and the resulting oil was molecularly distilled to give a ~ 50:50 mixture of **21** and **5** (92%); ir $\lambda_{max}$: 5.93, 6.12 (m), 7.35 (w) μm; $^1$H nmr δ (**21** only): 2.10 (s, 3H), 2.95 (m, 2H), 3.33 (s, 6H), 4.45 (t, $J$ = 6 Hz, 1H), 6.20 (m, 2H).

*Treatment of 6 and 7 with p-toluenesulfonic acid. Formation of 3-acetyl-9-methoxytetracyclo[4.3.0.0$^{2,4}$.0$^{3,7}$]nonane (27)*

A solution of **6** and **7** (0.508 g, 2.26 mmol) and anhydrous *p*-toluenesulfonic acid (0.60 g, 0.31 mmol) in dry benzene (25 mL) was boiled under reflux for 1 h. The solution was diluted with water (10 mL) and extracted with ether (4 × 5 mL) and the organic phase was concentrated, yielding a black oil. This was triturated with a small amount of hexane – ethyl acetate (7:3) which separated insoluble, polymerized material. The solution was concentrated and chromatographed (silica gel, 7:3 hexane and ethyl acetate) and yielded tosylate **28** as an oil (0.1421 g, 18%) and the tetracyclic ketone **27** (0.0925 g, 21%) as a colorless oil which was molecularly distilled at 44.5°C (0.065 Torr). Compound **28**: ir $\lambda_{max}$: 5.86, 6.23 (w) μm; $^1$H nmr δ: 1.2–2.5 (m, 9H), 2.07 (s, 3H), 2.44 (s, 3H), 3.14 (s, 3H), 3.60 (m, 1H), 4.14 (m, 1H), 7.32 (d, $J$ = 8 Hz, 2H), 7.26 (d, $J$ = 8 Hz, 2H); $^{13}$C nmr δ: 21.7, 28.8, 33.5, 40.4, 40.7, 44.0, 45.0, 54.3, 56.8, 59.1, 85.9, 88.1, 127.6, 129.8, 134.2, 144.7, 206.2. Compound **27**: ir $\lambda_{max}$: 5.90, 9.90 (w) μm; $^1$H nmr δ: 1.38 (m, 1H), 1.67 (m, 3H), 1.97 (s, 3H), 2.10 (m, 2H), 2.29 (m, 3H), 3.24 (s, 3H), 3.61 (m, 1H); $^{13}$C nmr δ: 27.0 (q), 27.6 (d), 29.4 (d), 31.1 (t), 35.8 (t), 40.8 (d), 42.0 (d), 48.8 (d), 56.1 (q), 81.7 (d), 206.5 (s). *Anal.* calcd. for $C_{12}H_{16}O_2$: C 74.97, H 8.39; found: C 74.77, H 8.46.

## Acknowledgement

We thank the Natural Sciences and Engineering Research Council of Canada for support of this work.

1. J. C. Sauer. Org. Synth. Coll. Vol. **IV**, 813 (1963).
2. A. P. Skoldinov, A. P. Arendaruk, and G. M. Godzhello. J. Org. Chem. U.S.S.R. **6**, 421 (1970).
3. L. J. Bellamy. The infra-red spectra of complex molecules. 2nd ed. Methuen, London. 1958. pp. 45–49.
4. L. M. Jackman and S. Sternhell. Applications of nuclear magnetic resonance spectroscopy in organic chemistry. 2nd ed. Pergamon, New York. 1969. pp. 230–232.
5. J. C. Davis, Jr. and T. V. Van Auken. J. Am. Chem. Soc. **87**, 3900 (1965).
6. P. Laszlo and P. v. R. Schleyer. J. Am. Chem. Soc. **86**, 1171 (1964).
7. J. R. L. Smith, R. O. C. Norman, and M. R. Stillings. Tetrahedron, **34**, 1381 (1978).
8. H. Wollweber. Diels–Alder–Reaktion. Georg Thieme Verlag, Stuttgart. 1972. p. 14.
9. R. R. Fraser and S. O'Farell. Tetrahedron Lett. 1143 (1962).
10. M. A. Battiste and C. T. Sprouse, Jr. Tetrahedron Lett. 4661 (1970); R. Breslow, G. Ryan, and J. T. Groves. J. Am. Chem. Soc. **92**, 988 (1970).
11. A. Gorgues. Bull. Soc. Chim. Fr. 529 (1974).
12. W. F. Johns. J. Org. Chem. **26**, 4583 (1961).
13. J. Das, R. Kubela, G. A. Macalpine, Z. Stojanac, and Z. Valenta. Can. J. Chem. **57**, 3308 (1979).
14. (*a*) J. Matsuda, S. Murada, and Y. Izumi. J. Org. Chem. **45**, 237 (1980); (*b*) G. Stork, E. E. Van Tamelen, L. J. Friedman, and A. W. Burgstahler. J. Am. Chem. Soc. **75**, 384 (1953); (*c*) B. M. Trost and W. C. Vladuchick. J. Org. Chem. **44**, 148 (1979); (*d*) G. Gormely, Jr., Y. Y. Chan, and J. Fried. J. Org. Chem. **45**, 1447 (1980).
15. (*a*) S. W. Baldwin and J. M. Wilkinson. J. Am. Chem. Soc. **102**, 3634 (1980); (*b*) R. E. Abbott and T. A. Spencer. J. Org. Chem. **45**, 5398 (1980).
16. F. Ramirez and S. Dershowitz. J. Org. Chem. **22**, 41 (1957).

# Hydrocarbon ions in fuel-rich, $CH_4$–$C_2H_2$–$O_2$ flames as a probe for the initiation of soot: interpretation of the ion chemistry

JOHN M. GOODINGS, SCOTT D. TANNER,[1] AND DIETHARD K. BOHME

*York University, Department of Chemistry, 4700 Keele Street, Downsview, Ont., Canada M3J 1P3*

Received March 25, 1982

JOHN M. GOODINGS, SCOTT D. TANNER, and DIETHARD K. BOHME. Can. J. Chem. **60**, 2766 (1982).

The ion chemistry is discussed for fuel-rich, nearly sooting, methane–oxygen flames at atmospheric pressure with added acetylene. Different types of ion–molecule reactions, both positive and negative, which can contribute through chemical ionization (CI) processes are summarized including their dependence on temperature, pressure, and equivalence ratio $\phi$. Extensive data were presented previously involving ion concentration profiles measured with a mass spectrometer as a function of distance along the axis of conical flames. An understanding of the dominant CI processes provides insight into the early chemical stage of soot formation associated with the flame reaction zone. The negative ion profiles show moderately unsaturated hydrocarbon ions upstream formed by proton transfer followed by progressive dehydrogenation; the highly unsaturated, carbonaceous ions observed downstream appear to arise by two- and three-body electron attachment, charge transfer, and H-atom stripping. The negative hydrocarbon ions can all be explained in terms of polyacetylene derivatives. The same build-up of carbonaceous species downstream is evident from the positive ion profiles. A major role is ascribed to proton transfer reactions with lesser contributions from charge transfer and ion–molecule condensation; three-body association is probably insignificant. Experiments with added acetylene indicate extensive fuel pyrolysis early in the reaction zone. There is no evidence that an ionic mechanism is dominant in forming soot precursors compared with neutral condensation reactions. Because of complexities in the positive ion chemistry, the negative ions appear to provide the more straightforward probe of the underlying neutral chemistry.

JOHN M. GOODINGS, SCOTT D. TANNER et DIETHARD K. BOHME. Can. J. Chem. **60**, 2766 (1982).

On discute de la chimie ionique dans les flammes du méthane–oxygène riches en combustible et sur le point de former de la suie, auxquelles on a ajouté de l'acétylène et à la pression atmosphérique. On classifie les différents types de réactions ion–molécule, tant positives que négatives qui peuvent contribuer via des processus d'ionisation chimique (IC) et on inclut également l'effet de la température, de la pression et du rapport d'équivalence $\phi$ sur ces réactions. On a présenté antérieurement de nombreuses données impliquant les profils de concentration des ions mesurés à l'aide d'un spectromètre de masse en fonction de la distance le long de flammes coniques. Une compréhension des processus IC dominant fournit un renseignement au sujet de la première étape de formation de la suie associée à la zone de réaction de flamme. Les profils de l'ion négatif montrent que, près de la flamme, on retrouve des ions d'hydrocarbonés modérement insaturés qui se forment par un transfert de proton suivi d'une déshydrogénation progressive. Les ions carbonés hautement insaturés observés plus loin semblent provenir de liaisons électroniques à deux et trois composantes saturées, de transferts de charge et de l'élimination d'atomes d'hydrogène. On peut expliquer les ions carbonés négatifs en termes de dérivés polyacétyléniques. La même accumulation d'espèces carbonés loin de la flamme peut être mise en évidence à partir des profils des ions positifs. On attribue un rôle prépondérant aux réactions de transfert de proton accompagné de contributions moindres de transferts de charge et de condensations ion–molécule: une association à trois composantes n'est probablement pas importante. Les expériences conduites avec de l'acétylène ajouté indiquent une abondante pyrolyse du carburant se produisant très tôt dans la zone de réaction. Il n'y a pas de preuve d'un mécanisme ionique dominant lors de la formation des précurseurs de suie par comparaison avec les réactions neutres de condensation. A cause de la complexité de la chimie de l'ion positif, les ions négatifs apparaissent comme les meilleures guides pour étudier la chimie neutre sous jacente.

[Traduit par le journal]

## Introduction

In a recent article (1), here designated as paper I, we reported experimental data on the axial distribution of both positive and negative ions monitored directly through the reaction zones of fuel-rich $CH_4$–$C_2H_2$–$O_2$ flames at atmospheric pressure. The natural hydrocarbon ions $C_nH_x^{\pm}$ were studied as a probe of the early chemical stages of soot formation. In that paper, the phenomenological changes in the ion distribution which accompanied changes in the equivalence ratio $\phi$ and temperature were noted. In this report we interpret the previous data from the point of view of the ion–molecule reaction chemistry. It is hoped that an understanding of the kinetics and energetics of the ion–molecule reactions responsible for the observed flame-ion distribution will lead to further insights into the initial chemistry leading to soot.

The types of reactions commonly thought to dominate the ion chemistry of flames have been conveniently classified. Those processes which result in the ionization of neutral flame intermediates include chemi-ionization, thermal ionization, electron attachment, charge transfer, and proton-transfer. The latter four reaction types share the characteristic that the neutral reactant of molecular weight $M$ is converted in most cases to an ion of $m/e = M^{\pm}$, $(M + 1)^+$, or $(M - 1)^-$. As a result, the identification of the neutral precursors from the ion

[1]Present address: Sciex Inc., 55 Glencameron Road, #202, Thornhill, Ont., Canada L3T 1P2.

0008-4042/82/222766-11$01.00/0

©1982 National Research Council of Canada/Conseil national de recherches du Canada

Can. J. Chem. Downloaded from www.nrcresearchpress.com by 210.87.254.5 on 09/06/12
For personal use only.

Can. J. Chem. Downloaded from www.nrcresearchpress.com by 210.87.254.5 on 09/06/12
For personal use only.

spectrum is relatively simple for systems in which these reaction types predominate. More difficult to deconvolute is the spectrum resulting from "ionic polymerization" reactions such as condensation and three-body association.

### Types of ion–molecule reactions relevant to hydrocarbon flame chemistry

A considerable data base on the kinetics of relevant hydrocarbon ion–molecule reactions exists. However, most of the kinetic measurements have been performed at or near room temperature and at low pressure. This section presents an overview of our current understanding of the kinetics of ion–neutral reactions involving hydrocarbon molecules and radicals. To facilitate the application of the data base to flames burning at atmospheric pressure, the dependence of the kinetics of the major reaction types on temperature ($T$) and pressure ($P$) is reviewed.

*1. Chemi-ionization*

Neutral reactions leading to the formation of ions are usually endothermic. Exceptions may arise when the reactants are radicals and electronically-excited molecules, the concentrations of which will show a strong positive $T$-dependence. It is now generally agreed that the major source of natural flame ions is the chemi-ionization reaction (2, 3)

[1] $CH + O \rightarrow CHO^+ + e^-$

Of those chemi-ionization reactions which yield directly a hydrocarbon ion, the most frequently cited are

[2] $CH^* + C_2H_2 \rightarrow C_3H_3^+ + e^-$

[3] $CH^* + C_2H_4 \rightarrow C_3H_5^+ + e^-$

However, these latter sources have been discounted as anything but minor contributors to the total ion density (4). No $P$-dependence is expected for chemi-ionization reactions, except for the possible quenching of excited reactants.

*2. Thermal ionization*

The spontaneous ionization of energetic molecules may be regarded as a quasi-unimolecular Lindemann process

[4$a$] $C_nH_x + M \rightarrow (C_nH_x)^* + M$

[4$b$] $(C_nH_x)^* \rightarrow C_nH_x^+ + e^-$

In the high pressure limit, appropriate for thermal ionization in atmospheric pressure flames, the classical RRK treatment (5) yields an Arrhenius-type unimolecular rate constant

$$k = \nu \exp(-E_a/RT)$$

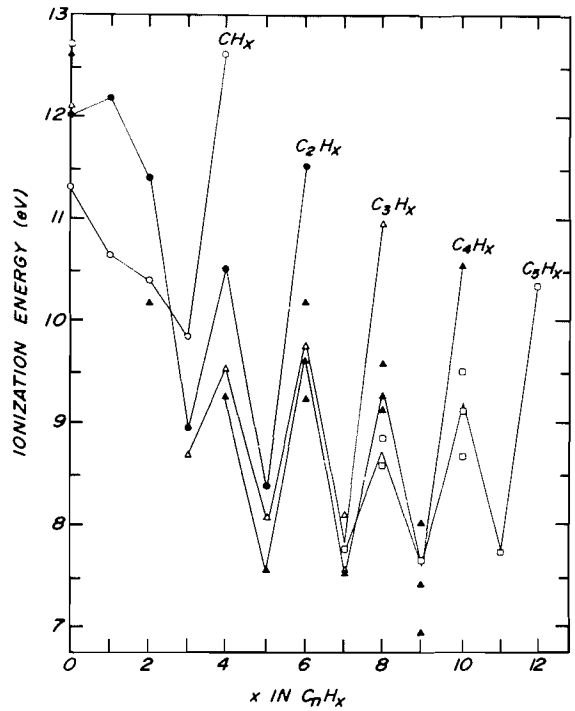


FIG. 1. Ionization energies of aliphatic hydrocarbon radicals and molecules. In cases where data for several isomers are shown, the line is drawn through the arithmetic mean of the ionization energies.

where $\nu$ is typically $10^{13}$ to $10^{15}$ $s^{-1}$ and the activation energy $E_a$ is approximately the ionization energy IE of $C_nH_x$. The IE's of aliphatic $C_nH_x$ radicals and molecules show remarkable trends with the parity of $x$ and magnitude of $n$, as given in Fig. 1. The obvious feature is the alternation of IE with $x$; IE's of odd-$x$ species are roughly 1.5 eV lower than those of similar species with even-$x$. Also, the IE tends to decrease with increasing $n$ (except for $x = 0$). It is assumed that the thermal ionization process is pressure-saturated for an atmospheric pressure flame.

*3. Proton transfer*

These reactions are frequently observed to be simple and fast. Examples include

[5] $HCO^+ + C_2H_2 \rightarrow C_2H_3^+ + CO$

[6] $OH^- + CH_3C_2H \rightarrow C_3H_3^- + H_2O$

for which these were the only reaction channels observed (6, 7), and the rate constants were large, $(1.4 \pm 0.4) \times 10^{-9}$ and $(1.7 \pm 0.3) \times 10^{-9}$ $cm^3$ $molecule^{-1}$ $s^{-1}$, respectively. In fact, the rate constants for proton transfer reactions are generally found to be well-approximated by the AADO

TABLE 1. Proton affinities, $PA^0_{298}$ in kJ mol$^{-1}$, for some hydrocarbon flame species in order of decreasing PA[a]

| Ion | Molecule | PA | Ref. | Ion | Molecule | PA | Ref. |
|---|---|---|---|---|---|---|---|
| $C_5H_7^+$ | Cyclopentadiene | 837 | 9 | $C_4H_3^+$ | Diacetylene | 724 | 10 |
| $CH_3^+$ | $CH_2$ | 828 | 10 | $CH_3O^+$ | Formaldehyde | 715 | 14 |
| $C_4H_7^+$ | Isobutene | 812 | 9 | $C_4H_{11}^+$ | Isobutane | 699 | 9 |
| $C_2H_3O^+$ | Ketene | 807 | 11 | $H_3O^+$ | Water | 692 | 15 |
| $C_7H_9^+$ | Toluene | 787 | 9 | $C_2H_5^+$ | Ethylene | 682 | 15 |
| $C_3H_5^+$ | Allene | 778 | 10 | $C_2H_2^+$ | $C_2H$ | 682 | 10 |
| $C_3H_5^+$ | Methylacetylene | 770 | 10 | $C_2H_3^+$ | Acetylene | 636 | 10 |
| $C_4H_7^+$ | 1-Butene | 766 | 9 | $CH^+$ | Carbon | 628 | 10 |
| $C_4H_7^+$ | *cis*-2-Butene | 757 | 9 | $C_3H_9^+$ | Propane | 619 | 9 |
| $CH_5O^+$ | Methanol | 757 | 12 | $C_2H_6^+$ | Ethyl radical | 602 | 10 |
| $C_4H_7^+$ | *trans*-2-Butene | 753 | 9 | $C_2H_7^+$ | Ethane | 595 | 15 |
| $C_3H_7^+$ | Propene | 753 | 12 | $CHO^+$ | Carbon monoxide | 592 | 16 |
| $C_6H_7^+$ | Benzene | 753 | 9 | $CH_5^+$ | Methane | 546 | 16 |
| $C_5H_9^+$ | Cyclopentene | 745 | 9 | $CHO_2^+$ | Carbon dioxide | 538 | 16 |
| $C_2H^+$ | $C_2$ | 732 | 10, 13 | $CH_4^+$ | Methyl radical | 529 | 10 |
| $CH_2^+$ | CH | 728 | 10 | | | | |

[a]The PA's of some important flame ions containing oxygen are included as benchmarks.

ion–molecule collision theory of Su, Su, and Bowers (8). This theory predicts reactions involving non-polar species to be temperature-independent, while reactions involving very polar species can be expected to approach a $T^{-1/2}$-dependence. It is commonly the case that proton transfer will take place if it is exothermic. The data base of proton affinities for aliphatic hydrocarbons is rather scant; some relevent values that have been reported are listed in Table 1. Occasionally, an exothermic proton transfer process is observed to compete (with varying success) with other reaction channels. Such is the case for the reaction

$$[7]\quad O^- + C_2H_2 \xrightarrow{0.6} e^- + C_2H_2O$$
$$\xrightarrow{0.3} C_2H^- + OH$$
$$\xrightarrow{0.05} HC_2O^- + H$$
$$\xrightarrow{0.05} C_2^- + H_2O$$

which, nonetheless, has the large overall rate constant $(2.0 \pm 0.3) \times 10^{-9}$ cm$^3$ molecule$^{-1}$ s$^{-1}$ (17). Finally, dissociative proton transfer, in which the product ion breaks up in a unimolecular process, is frequently observed in reactions for which the simple proton transfer is sufficiently exothermic, for example (18),

$$[8]\quad CH_5^+ + C_2H_6 \rightarrow C_2H_7^+ + CH_4$$
$$\rightarrow C_2H_5^+ + CH_4 + H_2$$

Since it is expected that the proton affinities of $C_nH_x$ species increase with $n$, more pronounced dissociation of the proton transfer product ion may occur for the larger hydrocarbons. The overall rate constant is not expected to be $P$-dependent. However, the branching ratio may show $P$-dependence depending on the lifetime of the ionic collision complex.

*4. Charge transfer*

The rate constants for many charge transfer reactions involving simple species are also often found to be in good agreement with the predictions of the AADO collision theory. However, in such cases two conditions are usually met: (*a*) the reactants are polyatomics (since the requirement for energy resonance is more easily fulfilled when there is a high density of states); and (*b*) other reaction channels, such as proton transfer and condensation, are not competitive. The latter requirement appears to be more difficult to satisfy for charge transfer reactions involving hydrocarbons; we are not aware of any example in the published literature. Examples of charge transfer to a hydrocarbon proceeding in isolation but involving dissociation are known, however. The thermochemistry which governs these reactions involves the ionization energies of the reactants, and so the data of Fig. 1 apply here as well. The rates of charge transfer reactions, when efficient, are expected to show only a weak $T^{-1/2}$-dependence and no $P$-dependence.

*5. Condensation*

Reactions in which new bonds between heavy atoms (e.g. C, O) are formed are termed condensation reactions. Examples which have been reported may be separated into two classes which are defined by the observed kinetics. The rate constants for condensation reactions which are rapid at room temperature are usually well-approximated by the AADO collision theory. Some of these reactions are slow at room temperature and may be

Can. J. Chem. Downloaded from www.nrcresearchpress.com by 210.87.254.5 on 09/06/12
For personal use only.

TABLE 2. Reactions of positive hydrocarbon ions with methane measured at room temperature

$C_nH_x^+ + CH_4 \longrightarrow C_{n+1}H_{x+1}^+ + H_2 + H$ (*a*)
$\longrightarrow C_{n+1}H_{x+2}^+ + H_2$ (*b*) } Condensation
$\longrightarrow C_{n+1}H_{x+3}^+ + H$ (*c*) }
$\xrightarrow{M} C_{n+1}H_{x+4}^+$ (*d*) (3-body association)
$\longrightarrow C_nH_{x+1}^+ + CH_3$ (*e*) H-transfer
$\longrightarrow C_nH_{x+2}^+ + CH_2$ (*f*) $H_2$-transfer

| $C_nH_x^+$ | (*a*) | (*b*) | (*c*) | (*d*) | (*e*) | (*f*) | $k$ ($\times 10^{-9}$)[a] | Ref. |
|---|---|---|---|---|---|---|---|---|
| $C^+$ | | √ | √ | | | | 1.2 | 19, 20, 21 |
| $CH^+$ | √ | √ | √ | | | | 1.3 | 19, 21 |
| $CH_2^+$ | | √ | √ | | | | 1.2 | 19, 21 |
| $CH_3^+$ | | √ | | | | | 1.2 | 19, 22 |
| $CH_4^+$ | | | | | √ | | 1.5 | 22 |
| $C_2^+$ | √ | √ | √ | | √ | √ | 1.4 | 19 |
| $C_2H^+$ | | √ | √ | √ | √ | | 1.1 | 19 |
| $C_2H_2^+$ | | √ | √ | | | | 1.0 | 19 |
| $C_2H_3^+$ | | √ | | | | | 0.17 | 19, 21 |
| $C_2H_4^+$ | | | | | | | < 0.0001 | 19 |

[a]Rate constants in units of $cm^3$ $molecule^{-1}$ $s^{-1}$.

TABLE 3. Reactions of positive hydrocarbon ions with acetylene measured at room temperature

$C_nH_x^+ + C_2H_2 \longrightarrow C_{n+2}H_x^+ + H_2$ (*g*)
$\longrightarrow C_{n+2}H_{x+1}^+ + H$ (*h*) } Condensation
$\xrightarrow{M} C_nH_x^+ \cdot C_2H_2$ (*i*) } (3-body association)
$\longrightarrow C_{n+1}H_{x-2}^+ + CH_4$ (*j*) }
$\longrightarrow C_2H_3^+ + C_nH_{x-1}$ (*m*) Proton transfer

| $C_nH_x^+$ | (*g*) | (*h*) | (*i*) | (*j*) | (*m*) | $k$ ($\times 10^{-9}$)[a] | $k$ ($\times 10^{-25}$)[b] | Ref. |
|---|---|---|---|---|---|---|---|---|
| $CH^+$ | | | | | √ | 0.8 | | 21 |
| $CH_3^+$ | √ | | | | | 1.2 | | 23 |
| $CH_5^+$ | | | | | √ | 1.56 | | 6 |
| $C_2^+$ | | √ | | | | 3, 2.65 | | 21 |
| $C_2H^+$ | | √ | | | √ | 2.4, 1.47, 2.45, 1.3 | | 21 |
| $C_2H_2^+$ | √ | √ | | | | 1.15, 1.52, 1.22, 0.90, 0.79, 0.33 | | 21 |
| | √ | √ | √ | | | 1.39 | | |
| | √ | √ | √ | | √ | 1.25 | | |
| | √ | √ | | | √ | 1.94, 1.41 | | |
| $C_2H_3^+$ | | | √ | | | | 2.98 ($H_2$) | 24 |
| | | | | | | 0.71, 0.085, 0.31[c] | | 21 |
| $C_2H_5^+$ | | | √ | | | | 1.34 ($H_2$) | 24 |
| | | | | √ | | 0.0075 | | 24 |
| $C_2H_6^+$ | | | | | | 0.10, 1.4[c] | | 21 |

[a]Rate constants in units of $cm^3$ $molecule^{-1}$ $s^{-1}$.
[b]Rate constants in units of $cm^6$ $molecule^{-2}$ $s^{-1}$.
[c]Product ions not given.

expected to show a $T$-dependence which is positive. Many examples are provided in the summaries given in Tables 2 and 3 for reactions of hydrocarbon ions with $CH_4$ and $C_2H_2$, respectively. Reactions of these ions with $H_2$, a major product in fuel-rich flames, are summarized in Table 4. One representative of the first type of condensation reactions is (23)

[9] $CH_3^+ + C_2H_2 \rightarrow C_3H_3^+ + H_2$

which is rapid ($1.2 \times 10^{-9}$ $cm^3$ $molecule^{-1}$ $s^{-1}$) and no other products were observed. By the same token, the reaction (19, 21)

[10] $C_2H_3^+ + CH_4 \rightarrow C_3H_5^+ + H_2$

is slow ($0.17 \times 10^{-9}$ $cm^3$ $molecule^{-1}$ $s^{-1}$) which probably places it in the category of reactions

Can. J. Chem. Downloaded from www.nrcresearchpress.com by 210.87.254.5 on 09/06/12
For personal use only.

TABLE 4. Reactions of positive hydrocarbon ions with hydrogen measured at room temperature unless otherwise noted

$$C_nH_x^+ + H_2 \longrightarrow C_nH_{x+1}^+ + H \quad (n)$$
$$\xrightarrow{M} C_nH_{x+2}^+ \quad (p)$$

| $C_nH_x^+$ | (n) | (p) | $k$ ($\times 10^{-9}$)[a] | $k$ ($\times 10^{-27}$)[b] | Ref. |
|---|---|---|---|---|---|
| $C^+$ | | √ | <0.0005 | 0.021 (He)[c] | 25, 26 |
| $CH^+$ | √ | | 1.2 | | 25 |
| $CH_2^+$ | √ | | 1.6 | | 25 |
| $CH_3^+$ | | √ | | 0.13 (He)[d] | 25 |
| $CH_4^+$ | √ | | 0.033 | | 25 |
| $C_2^+$ | √ | | 1.4 | | 25 |
| $C_2H^+$ | √ | | 1.7 | | 25 |
| $C_2H_2^+$ | √ | √ | 0.010 | 1.2 (He) | 25 |
| $C_2H_3^+$ | | √ | | 0.02 (He) | 25 |
| | | | | 0.015 ($H_2$) | 24 |
| $C_2H_4^+$ | | | <0.00004 | | 25 |
| $C_2H_5^+$ | | | <0.00004 | | 25 |

[a]Rate constants in units of cm³ molecule$^{-1}$ s$^{-1}$.
[b]Rate constants in units of cm⁶ molecule$^{-2}$ s$^{-1}$.
[c]Measured at 90 K.
[d]Measured in the temperature range 225–300 K.

having an activation energy. Condensation reactions are not necessarily limited to positive ions; the somewhat special case of associative detachment may be thought of as negative ion condensation. An example which competes successfully with proton transfer has already been presented in [7] involving the reaction of $O^-$ with acetylene where the condensation product is uncharged (17). Also, room-temperature studies of reactions of $C_2^-$ and $C_2H^-$ with $CH_4$ and $C_2H_2$ (27) failed to reveal any condensation products ($k$'s < $10^{-13}$ cm³ molecule$^{-1}$ s$^{-1}$).

*6. Three-body association*

Ion–molecule clustering reactions are commonly viewed as proceeding via a simple energy transfer mechanism

[11a] $C_2H_3^+ + C_2H_2 \rightarrow (C_2H_3^+ \cdot C_2H_2)^*$

[11b] $(C_2H_3^+ \cdot C_2H_2)^* + M \rightarrow C_2H_3^+ \cdot C_2H_2 + M$

A strongly negative $T^{(1-s)}$-dependence (where $s$ is the number of internal degrees of freedom involved in "sinking" the excess energy) is observed at low pressures (28), changing to a weak $T^{-1/2}$-(AADO)-dependence at pressure saturation (8). A linear $P$-dependence is observed for the unsaturated process. The saturation pressure is decreased for stronger cluster bonds, for more complex intermediates (larger values of $s$), and for lower temperature. Three "types" of cluster ions may be distinguished on the basis of the strength of the association bond. the weakest type is the simple electrostatic bond, such as that for $O_2^+ \cdot N_2$. These bond dissociation energies are typically $\lesssim$ 80 kJ mol$^{-1}$. On the other end of the scale are the strong chemical bonds, such as that observed for $C_2H_3^+ \cdot H_2$ which is indistinguishable from $C_2H_5^+$ derived from the protonation of ethylene (29). Bridging these extremes are the proton-bound intermediates such as $C_2H_3^+ \cdot C_2H_2$ which is a symmetric example.

*7. Electron attachment*

Little experimental work has been done on the $T$-dependence of polyatomic electron attachment reactions. The process is generally believed to take place via a modified Bloch–Bradbury mechanism:

[12a] $C_nH_x + e^- \rightarrow (C_nH_x^-)^*$

[12b] $(C_nH_x^-)^* + M \rightarrow C_nH_x^- + M$

Of the two systems which have been studied in detail, attachment to $O_2$ appears to be well-described by this mechanism, while that to NO is not. This has been explained (30) in terms of the great difference in the lifetimes of the resonant states, $(X^-)^*$; that for $(O_2^-)^*$ is sufficiently long to allow the reaction to be viewed as taking place through two distinct stages, while that for $(NO^-)^*$ is so short that a one-step mechanism must be invoked. However, it may be expected that the energy-transfer (2-step) mechanism is appropriate for the polyatomic $C_nH_x$ hydrocarbons because of the greater number of internal degrees of freedom available to stabilize the intermediate. The kinetics should then be described by the same equations invoked earlier for three-body association reactions. For large molecules having many degrees of freedom, the lifetimes of the intermediates may be long enough to allow the reaction to be characterized as bimolecular (31). Electron affinity (EA) values are known for the $CH_x$ ($x$ = 0–3) species. For higher $C_nH_x$ ($n \geq 2$) species, EA values for the most part are either unknown or uncertain. The stable hydrocarbons have, in general, negative EA's and so electron attachment is an important process only for radical species. It has often been suggested (32) that hydrocarbon anions in flames may result from dissociative attachment reactions. Chief among these is the source proposed for $C_2H^-$

[13] $e^- + C_2H_2 \rightarrow C_2H^- + H$

However, for the thermal electrons of the flames discussed here this reaction is sufficiently endothermic (260 kJ mol$^{-1}$) so as to ensure that its contribution to the observed $C_2H^-$ concentration is minimal. The same conclusion is likely to apply to all stable hydrocarbons. Not enough is known about the energetics of $C_nH_x$ radicals to predict the importance of their dissociative attachment reactions to the negative ionization observed in flames.

*8. Associative detachment*

Competing with the thermal detachment of elec-

Can. J. Chem. Downloaded from www.nrcresearchpress.com by 210.87.254.5 on 09/06/12
For personal use only.

Can. J. Chem. Downloaded from www.nrcresearchpress.com by 210.87.254.5 on 09/06/12
For personal use only.

trons from anions in flames are associative detachment reactions. The relatively large H-atom concentration in hydrocarbon flames facilitates reactions of the type

[14] $C_nH_x^- + H \rightarrow C_nH_{x+1} + e^-$

Most commonly, the product of this reaction is a stable (i.e. non-radical) hydrocarbon molecule. Associative detachment reactions are also expected to be rapid with OH and possibly O. The kinetics may be obtained by applying the principle of detailed balance to dissociative attachment. Since the equilibrium constant may be expected to shift in favor of the reactants ($X^- + H$) as the temperature increases, and the rate constant for dissociative attachment decreases with $T$ (33), the rate constant for associative detachment reactions may be expected to show a slightly negative $T$-dependence. Phelps (33) has argued that for reactions involving a complex which has a short lifetime ($< 10^{-14}$ s) against auto-detaching (such as $O^- + H_2$), the rate constant will be essentially independent of temperature; those having longer auto-detaching lifetimes (such as $O^- + NO$) will demonstrate a weak, approximately $T^{-1/2}$-dependence. Despite the decrease of the rate constant with temperature, the rate of associative detachment reactions in flames may be expected to increase rapidly with temperature in response to the overriding increase in the rate of formation of radicals.

## Discussion

The companion paper I (1) concluded with a summary of the major observations involving positive and negative ion profiles in fuel-rich $CH_4$–$O_2$ flames with, and without, added $C_2H_2$. Much more can be learned about the early chemical stage of soot formation by a detailed consideration of these results in terms of the kinds of ionic reactions given in the previous section which dominate in different regions of these flames: upstream; in the reaction zone proper; and downstream in the burnt gas. This discussion will be presented in accordance with the summary in I; total ionization profiles will be considered first, followed by the behaviour of individual negative ion species, and then positive ion species. Finally, the trends evident in the flame chemistry are discussed as the equivalence ratio $\phi$ is increased at constant temperature towards the sooting point by the addition of acetylene.

### *A. Total ionization profiles*

*Positive ions*

The total positive curves in all flames studied show the usual rapid rise through the reaction zone, peaking just downstream, before tailing away through the burnt gas via electron–ion recombination. At constant $\phi$, the peak magnitude shows a positive temperature dependence $T^\beta$ with $\beta \simeq 2.5$ (Fig. 1(*b*) of I). This strong positive $T$-dependence is reasonable for both kinds of source reactions mentioned in the previous section, namely, chemi-ionization and thermal ionization. If the pair of curves with $T_{ad} = 2401$ and 2488 K for $\phi = 2.22 \pm 0.01$ are normalized at the peak, the rising portions through the reaction zone are the same, and there is no shift in peak position. Accordingly, there is no reason to invoke any source reaction other than the usual chemi-ionization process (2, 3)

[1] $CH + O \rightarrow HCO^+ + e^-$

upstream and through the reaction zone. On the other hand, the rate of recombination in the hotter flame is reduced downstream through the burnt gas. Most of the positive charge in this region is present as $H_3O^+$ ions, whose rate of electron–ion recombination

[15] $H_3O^+ + e^- \rightarrow H + H + OH$

has been variously found to have zero $T$-dependence (34) or a $T^{-1.6}$-dependence (35). The downstream behaviour might be accounted for by the negative $T$-dependence. Alternatively, it may possibly indicate the involvement of an additional source term, namely, thermal ionization of carbonaceous radicals of low ionization energy whose presence is expected downstream in these very fuel-rich flames.

*Negative ions*

The total negative ion profile in all flames studied is double-peaked. It rises upstream in approximate coincidence with the total positive profile and then breaks away to form a primary maximum midway through the reaction zone. The profile shows a valley near the end of the reaction zone, followed by a secondary maximum just downstream. The magnitude of the upstream peak decreases with increasing $\phi$ (negative $\phi$-dependence) and has little $T$-dependence. This upstream maximum arises because of the relative rates for formation and loss of negative ions, the rates being equal at the peak. The formation process is mainly three-body electron attachment, primarily to $O_2$, while the loss processes include thermal detachment and ion–radical associative detachment reactions, primarily with H atoms in these fuel-rich flames (36). The negative $\phi$-dependence at constant temperature is a consequence of the decrease in the concentration of $O_2$ and increase in H atoms. The apparent lack of $T$-dependence was observed for a pair of flames at constant $\phi$ (Fig. 1(*b*) in I); in the hotter flame, the

Can. J. Chem. Downloaded from www.nrcresearchpress.com by 210.87.254.5 on 09/06/12
For personal use only.

positive ions increase while the negative ions remain about the same. This relative decrease in negative ion concentration is in keeping with an enhanced rate for both kinds of loss processes; note that the concentration of H increases at higher temperature. However, little of this upstream behaviour provides much insight into the chemical initiation of soot formation.

In contrast, the secondary maximum downstream shows both a strongly positive $\phi$- and $T$-dependence. Also, the negative ion profile in the richer flame tails out considerably further downstream. As discussed below, this behaviour is consistent with an increase in the rate of production of $C_nH_x^-$ ions from hydrocarbon neutrals, for example polyacetylenes or their radicals, whose concentrations increase rapidly with both $\phi$ and $T$. These species must be intimately involved in the initiation of soot.

*B. Negative ion profiles*

The individual negative ion profile peaks appear in three distinct regions. In the first of these, oxygenated anions are found upstream (e.g. $O^-$, $OH^-$, $O_2^-$, $CH_3O^-$, $O^-\cdot H_2O$, $OH^-\cdot H_2O$, impurity traces of $^{35}Cl^-$ and $^{37}Cl^-$, $C_2HO^-$, $C_2H_3O^-$, $CHO_2^-$, $O_3^-$, etc., in order of increasing mass, and including $^{13}C$, $^{18}O$, and D isotopically substituted species). These ions are formed by charge transfer from primary $O_2^-$ ions and by proton transfer from parent neutrals by strong bases such as $OH^-$ and $O^-$; every profile peaks close to the $OH^-$, $O^-$, and $O_2^-$ peak positions. In fact, all of the anions with $m/e < 80$ amu can be interpreted as oxygenated species (Fig. 5 of I) with the exception of $C_2H^-$ and possibly a trace of $C_2^-$.

In the second region, a number of moderately unsaturated hydrocarbon anions are observed to peak in the valley region of the total negative ion profile (Figs. 1 and 5 of I). All of these can be interpreted as arising by proton transfer from a stable neutral hydrocarbon, viz. $C_2H^-(C_2H_2)$, $C_3H_3^-(C_3H_4)$, $C_3H_5^-(C_3H_6)$, $C_4H^-(C_4H_2)$, $C_4H_3^-(C_4H_4)$, $C_4H_5^-(C_4H_6)$, and $C_5H_5^-(C_5H_6)$

[16] $OH^- + C_nH_x \rightarrow C_nH_{x-1}^- + H_2O$

In each case, a decreasing concentration of the reagent anion $OH^-$ combined with a rising concentration of the reagent neutral might be expected to yield a maximum product ion concentration in the valley region. It is just possible that the prominent signals at 41, 53, and 65 amu represent a series based on deprotonated ketenes $HC(=C)_m=O^-$ with $m = 1$, 2, and 3, respectively. The important point is that at least some of these peaks in the valley region provide clear evidence for the growth of unsaturated hydrocarbon species as the combustion process proceeds.

In the third region, very highly unsaturated $C_nH_x^-$ ions are observed to peak just beyond the reaction zone, completing a picture of progressive dehydrogenation as the flame chemistry develops. The resultant hydrogen made available appears downstream as $H_2O$ and $H_2$. An important point in the negative ion chemistry is the degree to which it is likely to be free from condensation reactions which complicate the positive ion chemistry. Attention has been drawn to this hypothesis earlier in connection with pure $CH_4$–$O_2$ flames (36). It is important because, if valid, the wide variety of negative ions observed argues in favour of a neutral rather than an ionic mechanism for the buildup of carbonaceous species leading to soot formation.

The whole series of highly unsaturated $C_nH_x^-$ ions in the third region arises near the maximum concentration of free electrons at $z = 0.04 \pm 0.02$ mm. The concentrations of the observed ions alternate with the parity of $n$, the even-$n$ species being larger in agreement with the early observations of Green (37). For $n$ even, the most abundant species are the acetylenic anions $C_2H^-$, $C_4H^-$, $C_6H^-$ ..... with $x = 1$. For $n$ odd, the most abundant ions tend to be those with $x = 0$ and 5 such as $C_3^-$, $C_3H_5^-$, $C_5^-$, and $C_5H_5^-$.

The obvious question concerns the identity of the primary negative ions downstream. The $OH^-$ profile has a secondary maximum at this point in the flame (Fig. 7 of I) which could arise in coincidence with the free electron maximum by dissociative or three-body electron attachment

[17] $e^- + H_2O \rightarrow OH^- + H$

[18] $e^- + OH + M \rightarrow OH^- + M$

The relatively high concentrations of $H_2O$ and OH in this region would favour the rates of reactions [17] and [18]. A strong base such as $OH^-$ would promote chemical ionization of carbonaceous neutrals by proton transfer as in reaction [16]. Secondary ions (e.g. $C_n^-$) can be produced by stripping reactions

[19] $C_nH_x^- + H \rightarrow C_nH_{x-1}^- + H_2$

As an alternative to the proton transfer/stripping mechanism, it is probable that some of the $C_nH_x$ neutrals have positive electron affinities such that three-body and even two-body electron attachment processes may be competitive (31, 36). In general, however, the proton transfer-based mechanism is preferred.

In the $C_4H_x^-$ series, small signals corresponding to $x = 3$, 4, and 5 were also observed (Fig. 2(*b*) of I) which could arise by proton abstraction from

Can. J. Chem. Downloaded from www.nrcresearchpress.com by 210.87.254.5 on 09/06/12
For personal use only.

dimethylacetylene followed by H atom stripping. This mechanism is thought to be more likely than hydrogenation of the highly unsaturated species, for example, by the reverse of reaction [19], although the thermochemistry is not known.

Methylpolyacetylenes $C_nH_4$ or the isomeric polyallenes can lead to ionic species with $n$ odd, but impose a limit on $x \leq 4$. In the lower series with $n = 3$ and 5, the ionic concentrations increase with decreasing $x$, and the ions with $x = 4$ are not observed. Presumably the same combination of proton transfer followed by H atom stripping reactions is involved as with $n$ even. However, these parent molecules do not explain the origin of the relatively large signals observed for $n$ odd with $x = 5$. The $C_nH_5^-$ ions are thought to arise by proton abstraction from $C_nH_6$ species derived, for example, by $H_2$ elimination reactions of polyacetylenes with propylene, or methylpolyacetylenes with ethylene.

Note that these schemes provide a probable explanation for the observed intensity alternation with the parity of $n$ (Fig. 2(*a*) in I). Both the $C_nH_4$ and $C_nH_6$ parent neutrals invoked for the ions with $n$ odd are secondary reaction products of the basic polyacetylenes responsible for the larger ion signals observed with $n$ even. For a given $n$, the concentrations of the secondary derivatives would be expected to be less than the concentration of the corresponding primary reagent. The main reason for exploring this negative ion chemistry in some depth is to show that all of it can be based on acetylene. The early chemical stage leading to soot formation appears overwhelmingly to involve neutral condensation (polymerization) reactions of acetylene, the negative ions serving as a probe. Implicit in this discussion has been the notion that a negative chemical ionization process applied to a neutral flame intermediate preserves the identity of that neutral by producing an ion of the same, or nearly the same, mass.

### *C. Positive ion profiles*

The positive hydrocarbon ions $C_nH_x^+$ form a number of series through the flame reaction zone defined by the value of $n$ with $0 \leq x \leq 10$ (Fig. 2(*c*) of I). In each series, the profile peak positions evolve downstream with decreasing values of $x$ amounting to progressive dehydrogenation (Figs. 3 and 4 of I). Also within each series, the peak magnitudes (*a*) tend to be larger for small values of $x$, (*b*) maximize for $x = 3$, and (*c*) show a measure of alternation with the parity of $x$, odd $x$ being larger. Overall, the series are remarkably similar such that the positive ion chemistry appears to be essentially independent of $n$.

To what degree are these positive ions formed by simple CI processes (e.g. proton transfer, charge transfer, etc.) involving large hydrocarbon neutrals? Or, do they merely result from fast, ion–molecule condensation reactions which reveal little about the buildup of carbonaceous precursors to soot formation? Or possibly the ion–molecule condensation reactions are themselves competitive, with implications for an ionic mechanism of soot formation? These are the questions this discussion attempts to answer by considering the kinds of positive ion–molecule reactions likely to be involved, by making use of published data available for individual ion–molecule reactions given in Tables 2–4, and by seeking a correlation with the negative ion data.

#### *Thermal ionization*

This process can be discounted as a significant ion source in ordinary hydrocarbon flames (38). There is no known constituent of sufficient concentration and low enough ionization energy (IE) to yield a reasonable ion density even at equilibrium, and the kinetics are too slow for equilibrium to be approached in the flame reaction zone. Nevertheless, it is worth noting for aliphatic $C_nH_x$ radicals and molecules the trends in IE with $n$ and $x$ given in Fig. 1. The obvious feature is the alternation of IE with $x$; IE's of odd-$x$ species are roughly 1.5 eV lower than those of similar species with even-$x$. This, of course, describes quite well the alternation observed in the positive ion mass spectrum. Also, the IE tends to decrease with increasing $n$ (except for $x = 0$). We have estimated the concentration of $C_4H_5^+$ from thermal ionization of $C_4H_5$ radicals present with a mole fraction of $10^{-5}$ at the adiabatic flame temperature $T_{ad} = 2455$ K for a flame with $\phi = 2.15$. The calculated density of $1 \times 10^8$ ions cm$^{-3}$ agrees very well with the maximum concentration measured for $C_4H_5^+$, based on an estimate of $4 \times 10^{10}$ ions cm$^{-3}$ for the peak of the total positive ionization curve (39). This model can be discounted upstream in the reaction zone where the temperature $< T_{ad}$ because of the strong positive $T$-dependence for thermal ionization. Nevertheless, it may possibly represent a competitive process for hydrocarbonaceous ion formation downstream in the burnt gas. This is the source process mentioned in Section A on total ionization profiles to explain the apparent decrease in the rate of electron–ion recombination observed with increasing $\phi$ and $T$.

#### *Three-body association*

The bond-dissociation energies of electrostatically-bound ion–molecule clusters are expected to increase with increasing dipole moment of the

Can. J. Chem. Downloaded from www.nrcresearchpress.com by 210.87.254.5 on 09/06/12
For personal use only.

neutral. The relatively low dipole moments of the hydrocarbon intermediates, the difficulty in explaining the observed intensity alternation with $x$, and the failure to account for the dehydrogenation series for a given $n$ all argue against any major contribution from three-body association. Certainly in the hot part of the flame, the strong negative $T$-dependence of these reactions renders them unlikely. A somewhat greater contribution might be expected in the cooler domain far upstream except that oxygenated hydrocarbons would be preferred as clustering agents in this region for reasons of higher dipole moment and concentration. Similar considerations apply to three-body association reactions leading to the formation of hydrogen-bonded or chemically-bonded adducts even though their rates may be higher.

*Condensation*

Many of the smaller hydrocarbon ions have been observed to undergo condensation reactions having high rate constants at room temperature with both elements of the fuel, $CH_4$ and $C_2H_2$, as is evident from Tables 2 and 3. A condensation-dominated ion chemistry might explain the positive ion $n$-series to some extent. Complications arise because a number of the hydrocarbon ions can participate in rapid, exothermic, *hydrogenation* reactions even at room temperature as given in Table 4. Molecular hydrogen is available as a reagent since it becomes a major combustion product downstream in these fuel-rich flames. Ion–molecule condensation reactions will be occurring throughout the flame with simultaneous dehydrogenation, e.g. reaction types (*a*), (*b*), (*c*), (*g*), (*h*), and (*j*) given in Tables 2 and 3, although the extrapolation of this data base to flame temperatures and higher-$n$ ions is uncertain. However, the limited room temperature data are of little help in explaining the intensity alternation with $x$. On the other hand, the similarity of the various $n$-series is consistent with ubiquitous condensation reactions involving the same neutral reagents, namely, $CH_4$ and $C_2H_2$.

*Charge transfer*

Charge transfer reactions cannot explain the rapid buildup of hydrocarbon ions of high molecular weight. If charge transfer plays a major role, it presupposes the neutral polymerization of the fuel early in the flame. From Fig. 1, the lower IE's of the $C_nH_x$ neutrals having odd $x$ mean that charge transfer is the best mechanism available to account for the measure of intensity alternation (Fig. 2(*c*) of I) observed within each $n$-series. It is significant that, typically, IE($C_nH_x$, $x$ odd) < IE(HCO) $\simeq$ 8.7 eV < IE($C_nH_x$, $x$ even), such that charge transfer reactions of primary $HCO^+$ ions are exothermic with many odd-$x$ species formed by fuel pyrolysis. These reactions may be fast enough to deplete the $HCO^+$ as rapidly as it is formed, in keeping with the failure to observe significant amounts of $HCO^+$ far upstream where $C_nH_x^+$ ions are prominent. If a charge transfer mechanism is truly dominant, the initial neutral pyrolysis products must undergo sequential dehydrogenation via the *neutral* flame chemistry; the $C_nH_x^+$ series would then evolve by progressive charge transfer to the dehydrogenation intermediates.

*Proton transfer*

The data base of known PA's for $C_nH_x$ species given in Table 1 is insufficient to identify any clear-cut trends with $n$ and $x$, although the PA appears to increase with the degree of unsaturation (increasing C/H ratio). However, a proton transfer mechanism is consistent with the observed intensity alternation with $x$ within each $n$-series. Even-$x$ hydrocarbon neutrals (except for $x = 0$) almost always correspond to stable molecules which will tend to be present in higher steady-state concentrations in the flame, unlike odd-$x$ species which are always free radicals. Obviously, even-$x$ neutrals protonate to form odd-$x$ ions.

If the positive ion chemistry is dominated by proton transfer, it presupposes that the neutral chemistry involves an initial pyrolysis stage with condensation followed by progressive dehydrogenation. The latter is expected to proceed mainly via H atom abstraction in such a fuel-rich flame. The terminal stable member of each $n$-series of neutrals from a point of view of dehydrogenation is a polyacetylene which must await oxidative cleavage or neutral condensation. This may explain the maximum for $x = 3$ obtained in each $n$-series of ions. Also, this chemical scheme (neutral pyrolysis with condensation, ionic proton transfer) provides a consistent basis for the observed similarity of the various $n$-series of ions.

### *D. The influence of $C_2H_2$ added to the $CH_4$ fuel*

The results discussed in Sections B and C pertain to a $CH_4$–$C_2H_2$–$O_2$ flame (17.7% $C_2H_2$) with $\phi$ = 2.47 in which traces of yellow soot luminescence could be seen around the cooler perimeter. However, similar profile data were also measured for a leaner $CH_4$–$O_2$ flame without added $C_2H_2$ having $\phi$ = 2.15 burning at the *same temperature*. When the data from the richer flame are compared with those from the leaner, most of the differences are entirely consistent with decreased C/O and increased C/H ratios (point 6 in the summary of I): unsaturated $C_nH_x^{\pm}$ ion signals increase at the expense of oxygenated ions upstream; the ion profile peaks

Can. J. Chem. Downloaded from www.nrcresearchpress.com by 210.87.254.5 on 09/06/12
For personal use only.

become broader (it was suspected that the reaction zone thickness had increased) and more skewed in the downstream directions (e.g., $C_3H_3^+$ in Fig. 8 of I); positive ions having high $n$ and low $x$ values are enhanced.

In a relatively few isolated cases, profile peak magnitudes in the reaction zone showed a considerable decrease with added $C_2H_2$ (at +15, +49, +61, −17, and −60 amu from Figs. 6 and 7 of I). Some of these are readily understandable in terms of known fast reactions with $C_2H_2$ which have been measured at room temperature; for example

[20] $CH_3^+ + C_2H_2 \rightarrow C_3H_3^+ + H_2$ (23)

[21] $OH^- + C_2H_2 \rightarrow C_2H^- + H_2O$ (6)

Somewhat surprisingly, however, the two sets of profiles obtained for the two flames were remarkably similar as to relative peak heights, positions, and shapes. Evidently the identities of the fuel molecules are essentially lost early in the reaction zone through pyrolysis and decomposition processes. Even the upstream peaks of the $C_2H^-$ and $C_2H_3^+$ profiles (Figs. 7 and 8 of I) which are closely related to acetylene did not respond greatly to the addition of 17.7% of $C_2H_2$. In fact, the significant change at −25 amu was the appearance of an additional shoulder in a position *intermediate* between the upstream and downstream peaks. This shoulder is indicative of $C_2H_2$ synthesis in the reaction zone subsequent to the disappearance of the original $C_2H_2$ fuel. Thus, these results with varying $\phi$ at constant temperature provide additional evidence that the fuel undergoes pyrolysis very early in the flame.

## Conclusions

The total ionization profiles, both positive and negative, in these fuel-rich flames were examined with regard to their $T$-dependence, $\phi$-dependence, profile shape, peak position, and possible source and sink reactions. The positive profiles are consistent with a major chemi-ionization source reaction upstream persisting through the reaction zone, and possibly a minor source term downstream arising from thermal ionization of hydrocarbon radicals of low ionization energy. This latter source term may well become dominant as the flame is made increasingly fuel-rich (40). The behaviour of the negative profiles is consistent with electron attachment to oxygen upstream, and hydrocarbon ion production downstream in the burnt gas based on the presence of carbonaceous neutral species.

Individual negative ion profiles correspond to oxygenated anions upstream. Further downstream in the reaction zone, in a region corresponding to a valley in the total negative ion profile, several profiles show peaks representative of moderately unsaturated hydrocarbon anions. They appear to be formed by proton transfer from stable hydrocarbon neutrals, and are resistant to destruction by associative detachment with H atoms. They are important because they illustrate the growth of unsaturated hydrocarbon species originating in the reaction zone. The progressive dehydrogenation continues downstream in the burnt gas giving rise to highly unsaturated carbonaceous anions which appear to be formed by proton abstraction from corresponding neutrals by $OH^-$ and H atom stripping. An important point is the degree to which negative ions participate in ion–molecule condensation reactions; if minimal, the observations argue for neutral condensation as the mechanism responsible for the buildup of large carbonaceous species leading to soot formation. Note that all of the negative hydrocarbon ions can be explained in terms of polyacetylene derivatives; we favour the idea that methylpolyacetylenes and not allenic derivatives are responsible for the intensity alternation observed for $C_nH_x^-$ ions (lower for $n$ odd).

Individual positive profiles for $C_nH_x^+$ ions have been considered in the light of several kinds of ion–molecule reactions. The relative contributions of the different kinds can be judged to some extent from observations on progressive dehydrogenation downstream, intensity maxima for $x = 3$, $x$ intensity alternation, the great similarity of different $n$ series, and considerations involving magnitudes of measured rate constants, $T$-, $\phi$-, and $P$-dependence, and the dependence of IE on $n$ and $x$ (see Fig. 1). On these bases, we conclude that proton transfer reactions play a major role throughout the flame in the chemical ionization of neutral species and, to a lesser extent, charge transfer. These mechanisms presuppose extensive fuel pyrolysis early in the reaction zone, and a backbone of neutral polymerization chemistry resulting in the formation of large carbonaceous species, the precursors of soot. Ion–molecule condensation reactions must also be occurring but appear to be of lesser importance; perhaps such reactions involving methane are responsible for masking the intensity alternation with $n$ which is a major feature of the negative ion spectrum (see Fig. 2 of I). Thermal ionization will not be competitive in these flames except perhaps for a minor contribution downstream in the burnt gas. Finally, the role of three-body association reactions is probably insignificant in view of the observations and considerations outlined above.

Many of these notions are reinforced by the experiments in which acetylene was added to the methane fuel. In general, the fact that nearly all of

the ion profiles, both positive and negative, are remarkably unaffected by acetylene provides additional evidence for early fuel pyrolysis. As a general conclusion based on these studies of the early chemical stages leading to soot formation, the ion–molecule chemistry might conceivably make some contribution but is not thought to be dominant compared with neutral mechanisms involving polymerization of the fuel. Because of complexities associated with the positive ion chemistry, we believe that the negative ion profiles give the better picture of the chemical growth towards soot formation, the negative ions merely serving as a probe of the underlying neutral chemistry.


1. S. D. TANNER, J. M. GOODINGS, and D. K. BOHME. Can. J. Chem. **59**, 1760 (1981).
2. H. F. CALCOTE. Eighth Symposium (International) on Combustion, Williams and Wilkins, Baltimore, MD. 1962. p. 184.
3. K. N. BASCOMBE, J. A. GREEN, and T. M. SUGDEN. Adv. Mass Spectrom. **2**, 66 (1962).
4. A. FONTIJN. Prog. Reaction Kinet. **6**, 75 (1971).
5. R. E. WESTON and H. A. SCHWARA. Chemical kinetics. Prentice-Hall, Englewood Cliffs, NJ. 1972. p. 130.
6. G. I. MACKAY, K. TANAKA, and D. K. BOHME. Int. J. Mass Spectrom. Ion Phys. **24**, 125 (1977).
7. S. D. TANNER, G. I. MACKAY, and D. K. BOHME. Can. J. Chem. **59**, 1615 (1981).
8. T. SU, E. C. F. SU, and M. T. BOWERS. J. Chem. Phys. **69**, 2243 (1978).
9. R. WALDER and J. L. FRANKLIN. Int. J. Mass Spectrom. Ion Phys. **36**, 85 (1980).
10. H. M. ROSENSTOCK, K. DRAXL, B. W. STEINER, and J. T. HERRON. J. Phys. Chem. Ref. Data, **6**, (1977), Supplement 1.
11. G. B. DEBROU, J. E. FULFORD, E. G. LEWARS, and R. E. MARCH. Int. J. Mass Spectrom. Ion Phys. **26**, 345 (1978).
12. G. I. MACKAY and D. K. BOHME. Int. J. Mass Spectrom. Ion Phys. **26**, 327 (1978).
13. J. B. HOPKINS, D. E. POWERS, and R. E. SMALLEY. J. Chem. Phys. **74**, 6985 (1981).
14. K. TANAKA, G. I. MACKAY, and D. K. BOHME. Can. J. Chem. **56**, 193 (1978).
15. D. K. BOHME and G. I. MACKAY. J. Am. Chem. Soc. **103**, 2173 (1981).
16. D. K. BOHME, G. I. MACKAY, and H. I. SCHIFF. J. Chem. Phys. **73**, 4976 (1980).
17. D. K. BOHME, G. I. MACKAY, H. I. SCHIFF, and R. S. HEMSWORTH. J. Chem. Phys. **61**, 2175 (1974).
18. G. I. MACKAY, H. I. SCHIFF, and D. K. BOHME. Can. J. Chem. **59**, 1771 (1981).
19. N. G. ADAMS and D. SMITH. Chem. Phys. Lett. **47**, 383 (1977).
20. R. S. HEMSWORTH, R. C. BOLDEN, M. J. SHAW, and N. D. TWIDDY. Chem. Phys. Lett. **5**, 237 (1970).
21. L. W. SIECK and S. G. LIAS. J. Phys. Chem. Ref. Data, **5**, 1123 (1976).
22. D. SMITH and N. G. ADAMS. Int. J. Mass Spectrom. Ion Phys. **23**, 123 (1977).
23. D. SMITH and N. G. ADAMS. Chem. Phys. Lett. **54**, 535 (1978).
24. J. A. BURT, J. L. DUNN, M. J. MCEWAN, M. M. SUTTON, A. E. ROCHE, and H. I. SCHIFF. J. Chem. Phys. **52**, 6062 (1970).
25. D. SMITH and N. G. ADAMS. Astrophys. J. **217**, 741 (1977).
26. F. C. FEHSENFELD, D. B. DUNKIN, and E. E. FERGUSON. Astrophys. J. **188**, 43 (1974).
27. H. I. SCHIFF and D. K. BOHME. Int. J. Mass Spectrom. Ion Phys. **16**, 167 (1975).
28. D. SMITH and N. G. ADAMS. Astrophys. J. (Lett.), **220**, L87 (1978).
29. S. D. TANNER, G. I. MACKAY, and D. K. BOHME. Can. J. Chem. **57**, 2350 (1979).
30. G. E. CALEDONIA. Chem. Rev. **75**, 333 (1975).
31. L. G. CHRISTOPHOROU. Atomic and molecular radiation physics. Wiley-Interscience, London. 1971. p. 500.
32. A. N. HAYHURST and D. B. KITTELSON. Combust. Flame, **31**, 37 (1978).
33. A. V. PHELPS. Can. J. Chem. **47**, 1783 (1969).
34. A. N. HAYHURST and N. R. TELFORD. J. Chem. Soc. Faraday Trans. I, **70**, 1999 (1974).
35. R. KELLY and P. J. PADLEY. Trans. Faraday Soc. **66**, 1127 (1970).
36. J. M. GOODINGS, D. K. BOHME, and C.-W. NG. Combust. Flame, **36**, 45 (1979).
37. J. A. GREEN. 26th AGARD Propulsion and Energetics Panel, Pisa, Italy, AGARD Conference Proceedings No. 8. Vol. I. Edited by H. D. Wilsted. 1965. p. 191.
38. H. F. CALCOTE. Combust. Flame, **1**, 385 (1957).
39. J. M. GOODINGS, D. K. BOHME, and C.-W. NG. Combust. Flame, **36**, 27 (1979).
40. J. L. DELFAU, P. MICHAUD, and A. BARASSIN. Combust. Sci. Technol. **20**, 165 (1979).


Can. J. Chem. Downloaded from www.nrcresearchpress.com by 210.87.254.5 on 09/06/12
For personal use only.

# Étude, par spectroscopie de vibration, de deux solvants de la cellulose: La *N*-méthyl morpholine *N*-oxyde et son monohydrate

PHAM THI MAÏ, MARIE-HÉLÈNE HERZOG-CANCE, ANTOINE POTIER ET JACQUELINE POTIER[1]

*Laboratoire des Acides Minéraux, L.A. 79 associé au C.N.R.S., Université des Sciences et Techniques de Languedoc, Place Eugène Bataillon, 34060 Montpellier Cédex, France*

Reçu le 1 avril 1982

PHAM THI MAÏ, MARIE-HÉLÈNE HERZOG-CANCE, ANTOINE POTIER et JACQUELINE POTIER. Can. J. Chem. **60**, 2777 (1982).

Les spectres infrarouge et Raman de la *N*-méthyl morpholine *N*-oxyde et de son monohydrate ont été étudiés entre 4000 et 50 $cm^{-1}$. Pour ces deux composés, classés parmi les meilleurs solvants de la cellulose, il existe seulement le conformère où les groupes NO et $CH_3$ sont respectivement en positions axiale et équatoriale. Sur les spectres Raman de la *N*-méthyl morpholine *N*-oxyde anhydre, l'interaction dipôle–dipôle est caractérisée par une raie intense à 75 $cm^{-1}$.

Les molécules peuvent être divisées en deux parties: une partie hydrophobe ($O(CH_2)_2$) qui ne joue aucun rôle dans la dissolution de la cellulose, et une partie hydrophile qui est capable de stabiliser une chaine de molécules d'eau et révèle l'importance de l'environnement pyramidal des molécules d'eau dans le monohydrate.

PHAM THI MAÏ, MARIE-HÉLÈNE HERZOG-CANCE, ANTOINE POTIER, and JACQUELINE POTIER. Can. J. Chem. **60**, 2777 (1982).

The ir and Raman spectra of *N*-methyl morpholine *N*-oxide and its monohydrate have been investigated in the frequency range 4000–50 $cm^{-1}$. For these two compounds, classified among the best cellulose solvents, there exists only the conformer where NO and $CH_3$ groups are respectively in axial and equatorial positions. For anhydrous *N*-methyl morpholine *N*-oxide, the dipole–dipole interaction is characterized by a strong line at 75 $cm^{-1}$ in the Raman spectra.

The molecules can be divided into two parts: a hydrophobic part ($O(CH_2)_2$) not active in the cellulose dissolution, and a hydrophilic part, which is able to stabilize a chain of water molecules and reveals the importance of the pyramidal environment of water molecules in the monohydrate.

## Introduction

La *N*-méthyl morpholine *N*-oxyde est connue pour son pouvoir solvant vis à vis de la cellulose (1). Une bonne connaissance des interactions entre l'eau et cette base est une première approche de l'étude de ce phénomène complexe. On peut penser que le comportement de la *N*-méthyl morpholine *N*-oxyde (NMMNO) vis à vis des associations par liaisons hydrogène qui existent dans la glace est une image de ce qui se passera dans le milieu complexe cellulose–NMMNO.

L'analyse des spectres de NMMNO et de son monohydrate a été menée en les comparant à ceux de la morpholine et de la *N*-méthyl morpholine (NMM) dans l'état cristallisé. Pour la première, on dispose cependant de l'étude détaillée de Vedal *et al.* (2) qui est une base de départ appréciable, en particulier, au niveau de la détermination des vibrations du cycle; tandis que le passage de la morpholine à NMM permet de préciser les vibrations du groupe $CH_3$. Grâce à la deutération sélective des atomes d'hydrogène du cycle ou de la molécule d'eau pour $NMMNO \cdot H_2O$ il est possible d'attribuer les bandes dues à la molécule d'eau.

Cette analyse spectroscopique est divisée en quatre parties consacrées respectivement aux vibrations du squelette $NC_4O$, à celles des groupes $CH_2$ et $CH_3$,[2] du groupe NO et enfin à celles de la molécule d'eau et des liaisons hydrogène.

## I. Les vibrations du squelette $NC_4O$

Les attributions sont basées non seulement sur le travail de Vedal *et al.* (2) sur la morpholine et la pipéridine mais aussi sur les données des composés hétérocycliques: l'oxyde de pentaméthylène (3), le tellurure d'oxane (4) et le séléniure de pentaméthylène (5).

### *Les vibrations de valence* ν*(CO)*

On remarque que les fréquences relevées dans ce travail sont comparables à celles de Vedal *et al.* (2) de plus, comme ces auteurs, on observe pour $\nu_s(CO)$ deux composantes à 830 et 850 $cm^{-1}$ pour la morpholine liquide; ces deux composantes traduisent l'existence des deux conformères de la morpholine (atome d'hydrogène en position axiale ou équatoriale). Pour le cristal, la présence de quatre raies sur le spectre Raman (Fig. 1) signifie qu'à côté des deux conformères existe aussi un effet de corrélation. Bien que la structure ne soit pas connue, il semble que l'existence des deux types de

[1]Auteur à qui toute correspondance doit être adressée.

[2]La discussion relative aux groupes $CH_2$ et $CH_3$ (10 à 15) acheminée au dépôt des données non publiées n'est pas présentée ici, ainsi que les tableaux récapitulatifs. Ces données peuvent être obtenues à un prix nominal, en s'adressant au Dépôt de données non publiées, ICIST, Conseil national de recherches du Canada, Ottawa, Ont., Canada K1A 0S2.

0008-4042/82/222777-08$01.00/0

©1982 National Research Council of Canada/Conseil national de recherches du Canada

Can. J. Chem. Downloaded from www.nrcresearchpress.com by 210.87.254.6 on 09/06/12
For personal use only.

Can. J. Chem. Downloaded from www.nrcresearchpress.com by 210.87.254.6 on 09/06/12
For personal use only.

conformères dans le cristal soit compatible avec une structure en chaîne où les molécules de morpholine seraient reliées par des liaisons hydrogène N—H...N.

On observe aussi la présence de deux conformères pour NMM, de plus la substitution de l'atome d'hydrogène par le groupe $CH_3$ conduit à des glissements de fréquences plus ou moins importants selon le conformère.

Le comportement de NMMNO et de son monohydrate (Fig. 1) est différent; on ne relève dans l'état cristallisé qu'une seule vibration $\nu_s(CO)$ à 812 $cm^{-1}$, il n'y a donc qu'un seul conformère ce qui est en accord avec les données structurales de Perez et coll. (6) et conformément aux travaux de Cook *et al.* (7), c'est le conformère où le groupe NO est en position axiale et le groupe $CH_3$ équatorial.

On doit remarquer qu'en Raman, le déplacement des fréquences $\nu_s(CO)$ entre NMM et NMMNO est moins important ($\Delta\nu$ = 24 $cm^{-1}$) que celui noté entre la morpholine et NMM ($\Delta\nu$ = 44 $cm^{-1}$), il est pratiquement nul lorsqu'on passe de NMMNO à NMMNO·$H_2O$. Ce fait met en évidence les perturbations provenant de l'introduction du groupe $CH_3$ sur le cycle et *exclut la participation de l'atome d'oxygène endocyclique dans la formation de la liaison hydrogène*. Le déplacement vers les hautes fréquences quand on passe de NMM à NMMNO est surprenant, on s'attendrait plutôt à un effet inverse puisque les électrons de l'atome d'azote sont engagés dans la coordination avec l'atome d'oxygène.

*Les vibrations de valence* $\nu(NC)$

*Pour les vibrations de valence* $\nu(N(CH_2)_2)$, on note la présence de deux vibrations qui correspondent aux deux conformères de la morpholine et de NMM tandis que pour NMMNO et NMMNO·$H_2O$ on ne retrouve bien évidemment que la vibration correspondant au conformère où le groupe $CH_3$ est équatorial (Fig. 2).

Entre la morpholine et NMM, on remarque un abaissement de fréquence pour $\nu(N(CH_2)_2)$ dû au fait que le groupement $CH_3$ se fixe à la place de l'atome d'hydrogène et provoque un alourdissement de l'atome d'azote; lorsqu'on passe à NMMNO et NMMNO·$H_2O$, l'augmentation de fréquence qui apparaît peut s'expliquer si l'on tient compte de la contrainte apportée aux liaisons N—$CH_2$ lors de la fixation de l'atome d'oxygène et aussi de l'interaction dipôle–dipôle très forte qui assure la cohésion de la maille cristalline dans NMMNO tandis que dans le monohydrate, où cette interaction disparaît, comme on le verra lors de l'étude du groupe NO, on remarque alors un abaissement de fréquence.

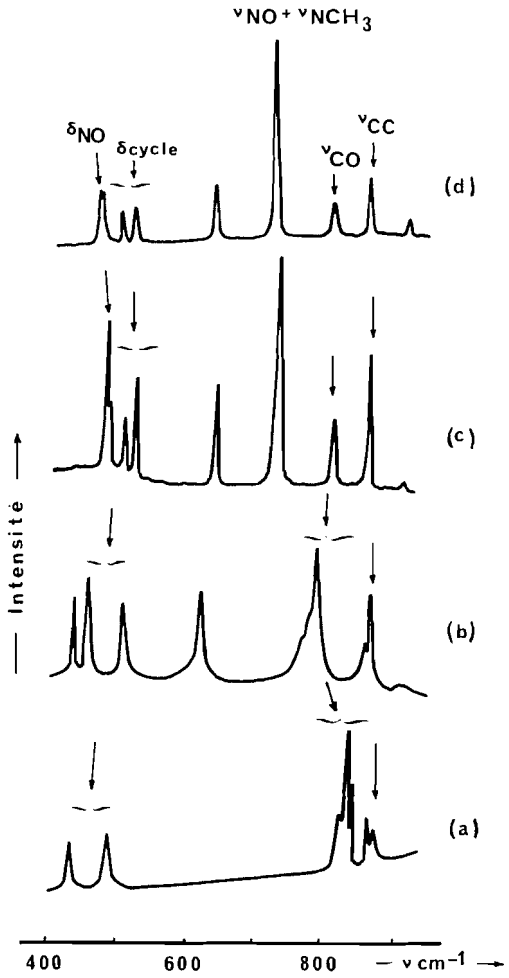


FIG. 1. Spectres Raman de (a) la morpholine, (b) NMM, (c) NMMNO et (d) NMMNO·$H_2O$ entre 400 et 800 $cm^{-1}$.

On doit noter en plus, une variation d'intensité assez remarquable, en effet, sur les spectres Raman de NMMNO la raie à 1070 $cm^{-1}$ est relativement moins intense que celle à 1093 $cm^{-1}$ (Fig. 2) tandis que pour le monohydrate elles sont toutes deux d'intensité moyenne. Il semble que l'on puisse interpréter cette augmentation d'intensité par un effet de cristal: le couplage intermoléculaire entre les deux molécules de l'unité asymérique du monohydrate exaltant l'intensité de $\nu$(CN) à 1070 $cm^{-1}$.

*La vibration de valence* $\nu(N—CH_3)$ apparaît en Raman à 1021, 1109 et 1108 $cm^{-1}$ respectivement pour NMM, NMMNO et NMMNO·$H_2O$ (Fig. 2). Comme pour les vibrations $\nu(N(CH_2)_2)$ la forma-

Can. J. Chem. Downloaded from www.nrcresearchpress.com by 210.87.254.6 on 09/06/12
For personal use only.

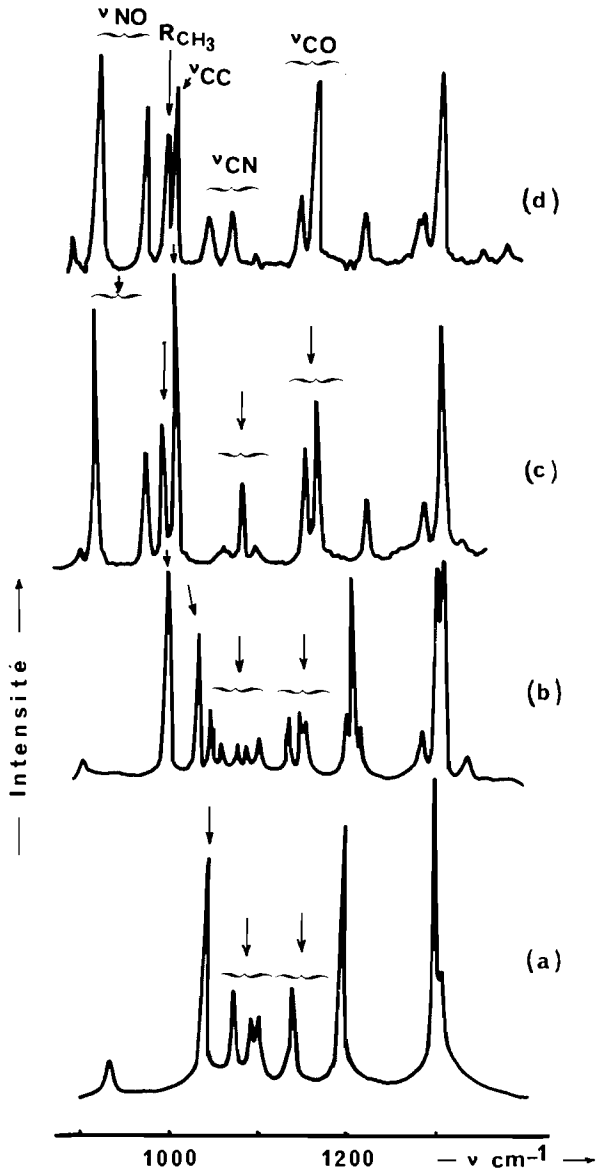


FIG. 2. Spectres Raman de (a) la morpholine, (b) NMM, (c) NMMNO et (d) NMMNO·$H_2O$ entre 900 et 1300 $cm^{-1}$.

tion de la liaison hydrogène tend à diminuer l'influence de l'interaction azote ↔ oxygène.

La figure 3 reproduit les spectres ir des composés étudiés, on y retrouve les fréquences des bandes correspondant aux vibrations ν(CN).

*Domaine entre 300 et 500 $cm^{-1}$*

Comme Vedal *et al.* (2), on observe pour la morpholine les *déformations du cycle* entre 400 et 500 $cm^{-1}$ et à des fréquences voisines pour NMM, NMMNO et NMMNO·$H_2O$.

On attend en outre plusieurs fréquences correspondant *aux déformations δ(N—$CH_3$) et δ(NO)*. Dans la triméthylamine *N*-oxyde (TMANO) où l'édifice moléculaire possède une symétrie $C_{3v}$, Giguere et Chin (8) et Kida (9) ont identifié $\delta_{deg}$ ($N(CH_3)_3$) en infrarouge autour de 380 $cm^{-1}$. On relève pour NMM des vibrations à 350 et 360 $cm^{-1}$ en ir (349, 358 et 366 $cm^{-1}$ en Raman) tout à fait compatibles avec δ(N—$CH_3$). La multiplicité des raies ou bandes est encore attribuable à l'existence de deux conformères. Pour NMMNO et NMMNO·$H_2O$ on retrouve δ(N—$CH_3$) respectivement à 328 et 330–347 $cm^{-1}$ en Raman (330 et 340–350 $cm^{-1}$ en ir).

Le glissement de fréquence entre les spectres de NMM, NMMNO et NMMNO·$H_2O$ traduit l'influence plus ou moins grande de l'atome d'oxygène sur l'atome d'azote.

## II. Les vibrations du groupe NO engagé

*Les vibrations de valence ν(NO)*

A priori on attend une seule vibration de valence pour le groupe NO, cependant, il faut noter que, par suite des couplages entre les différents vibrateurs autour de l'azote, la vibration ν(NO) n'est pas pure et doit contribuer aux vibrations ν(N—$CH_2$), ν(N—$CH_3$) et aux mouvements du cycle.

La comparaison entre les spectres ir et Raman des différents composés (Figs. 2 et 3) révèle l'existence d'un doublet à 927–988 $cm^{-1}$ en ir (932–990 $cm^{-1}$ en Raman) sur les spectres de NMMNO anhydre et 940–990 $cm^{-1}$ en ir (936–990 $cm^{-1}$ en Raman) pour le monohydrate. Lors de la deutériation du cycle, les deux raies se déplacent à 928 et 980 $cm^{-1}$ (avec un rapport isotopique $\rho \simeq 1{,}01$).

L'apparition de ce doublet, comme le triplet signalé par Devinsky *et al.* (16) est surprenante car on attend, a priori, qu'une seule vibration ν(NO). Gallais et coll. (17) lors d'une étude sur les oxydes d'amines tertiaires, a aussi remarqué un doublet à 950–970 $cm^{-1}$ pour ν(NO) des oxydes de triéthanolamine et de diméthylaniline et n'a pas su l'interpréter. En 1963, Kida (9) en étudiant des complexes avec la triméthylamine *N*-oxyde a effectivement observé un doublet pour le chlorhydrate dans l'état solide et une seule bande en solution, il attribue alors le doublet à un effet de couplage.

On pourrait penser que l'interaction dipôle–dipôle permettrait d'expliquer la présence du doublet (à 932 et 990 $cm^{-1}$) pour ν(NO) mais il n'est rien puisque ce doublet est toujours présent dans le monohydrate (à 936 et 990 $cm^{-1}$).

Notons que l'on observe aussi une variation de

Can. J. Chem. Downloaded from www.nrcresearchpress.com by 210.87.254.6 on 09/06/12
For personal use only.

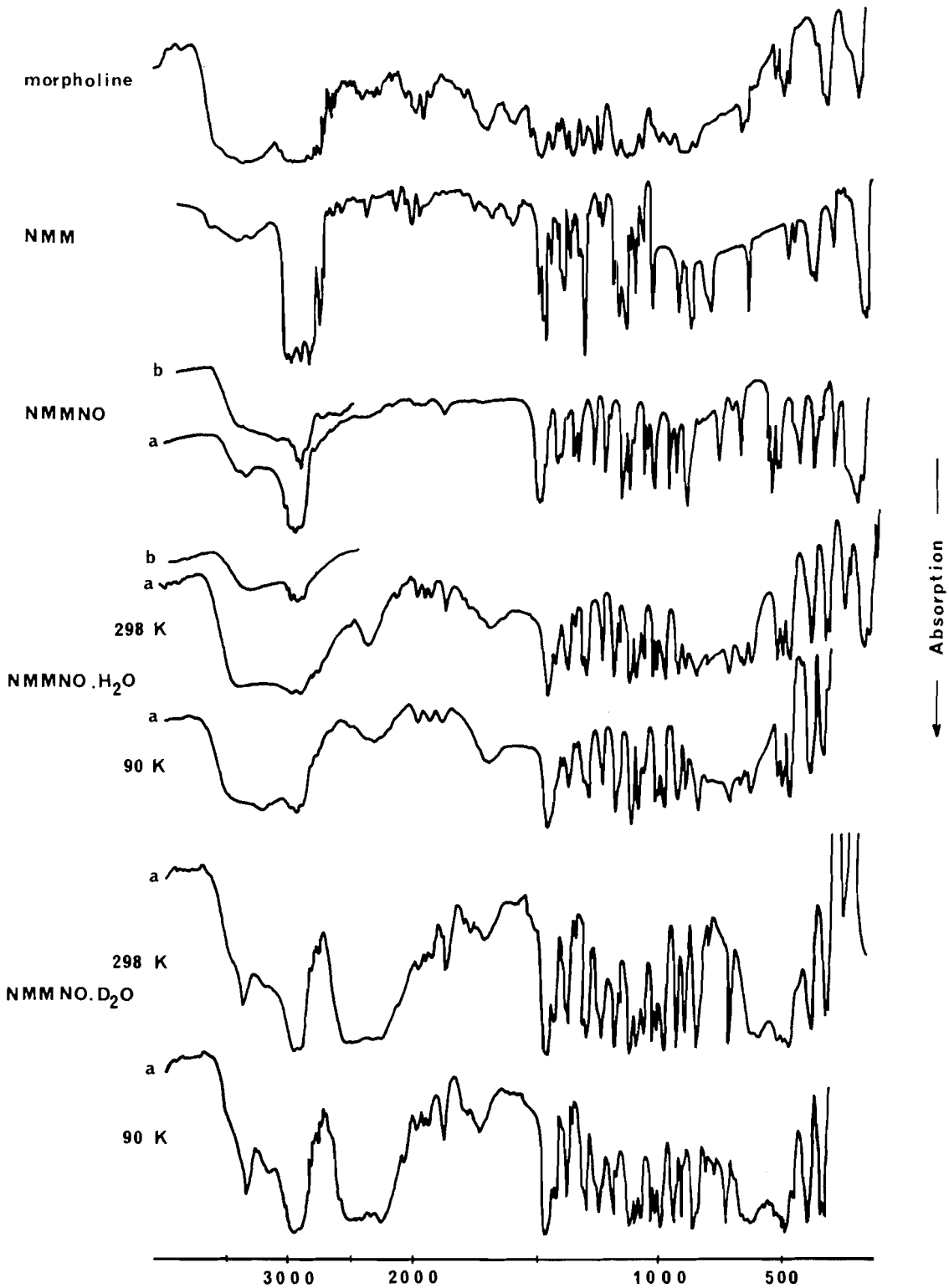


FIG. 3. Spectres ir des différents composés (en suspension (a) dans le Nujol, (b) dans le Fluorolube).

Can. J. Chem. Downloaded from www.nrcresearchpress.com by 210.87.254.6 on 09/06/12
For personal use only.

l'intensité relative des deux raies du doublet lorsque le groupe NO est solvaté par la molécule d'eau. (Ce phénomène a déjà été observé par Devinsky pour les alkyl morpholine *N*-oxyde (16) et par Gallais et coll. pour les oxydes d'amines tertiaires (17). Ceci est compatible avec le changement de symétrie moléculaire, la symétrie $C_s$ dans NMMNO devenant $C_1$ dans le monohydrate.

Il faut souligner un autre fait surprenant: *le raccourcissement de la liaison N—O* lorsqu'on passe de NMMNO à son monohydrate. Ce renforcement de la liaison N—O est inattendu car on s'attendrait plutôt à un allongement de cette liaison lors de la formation de la liaison hydrogène et en même temps à un déplacement de ν(NO) vers les basses fréquences.

Cette évolution peut cependant être expliquée très facilement. Dans NMMNO anhydre, Perez et coll. (6) ont montré que les groupes NO sont orientés de façon antiparallèle et que l'interaction électrostatique assure la cohésion de l'édifice cristallin. C'est la polarité de la liaison NO (18) qui est responsable de cette interaction dipôle–dipôle. Cette interaction, importante, se matérialise par la présence d'une raie intense à 75 $cm^{-1}$ sur le spectre de NMMNO anhydre (raie absente sur le spectre du monohydrate) (Fig. 4). Cette fréquence s'intègre très bien parmi celles relevées par Ghersetti *et al.* (19) pour la pyridine *N*-oxyde et par Jakobsen et Brash (20) pour une série de composés organiques (entre 80 et 50 $cm^{-1}$).

On peut donc penser que la création de liaisons hydrogène dans le monohydrate amène une interaction de force comparable (ou plus faible) que celle due à l'interaction dipôle–dipôle, ce qui permet d'expliquer les évolutions des fréquences des différentes vibrations déjà signalées quand on passe de NMMNO à son monohydrate.

Par ailleurs, les fréquences relevées pour la vibration ν(NO) se classent correctement dans le diagramme $\nu(NO) = f(d(NO))$ présenté sur la figure 5 en fonction des distances $d(NO)$ = 1,391 Å et 1,383 Å trouvées respectivement pour NMMNO anhydre et monohydratée par Perez et coll. (6) lors de l'édude structurale. Ces distances sont proches de celles observées pour la triméthylamine *N*-oxyde (TMANO) (1,41 Å) (18).

Avant de clore ce paragraphe consacré aux vibrations de valence ν(NO), on doit signaler l'apparition d'une nouvelle raie ou bande vers 720 $cm^{-1}$, sur les spectres de NMMNO et NMMNO·$H_2O$. Cette composante n'est pas sans évoquer celles observés par Gambi et Ghersetti (23) pour la pyridine *N*-oxyde et Kida (9) pour la triméthylamine *N*-oxyde. Ces auteurs l'attribuent à la vibration ν(NO) couplée avec les mouvements du cycle et plus particulièrement N—$(CH_2)_2$. Il semble qu'une attribution similaire puisse être fait ici, et ceci d'autant plus que cette composante est sensible à la deutériation du cycle.

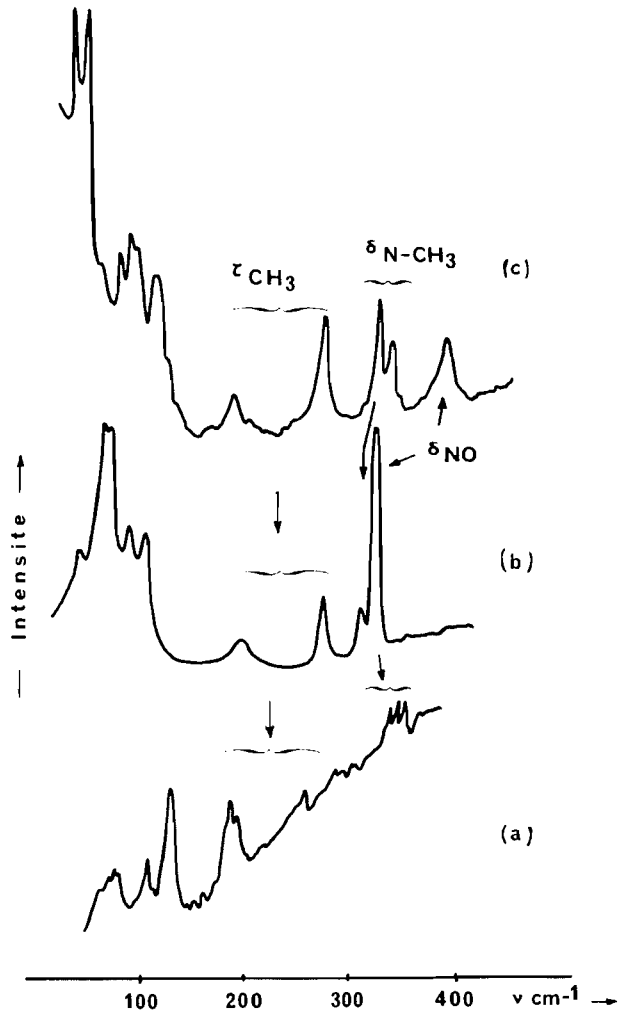


FIG. 4. Spectres Raman entre 100 et 400 $cm^{-1}$: (a) NMM, (b) NMMNO et (c) NMMNO·$H_2O$.

*Les déformations δ(NO)*

On attend deux déformations: une dans le plan, l'autre hors du plan. Ghersetti et coll. les ont observées respectivement pour la pyridine *N*-oxyde (PNO) à 468 et 226 $cm^{-1}$ (23) tandis que pour la quinoline ces auteurs retrouvent la déformation hors du plan à 340 $cm^{-1}$ (25).

La comparaison des spectres de NMMNO et NMMNO·$H_2O$ conduit à proposer pour ces deux mouvements les deux composantes à 478 et 343

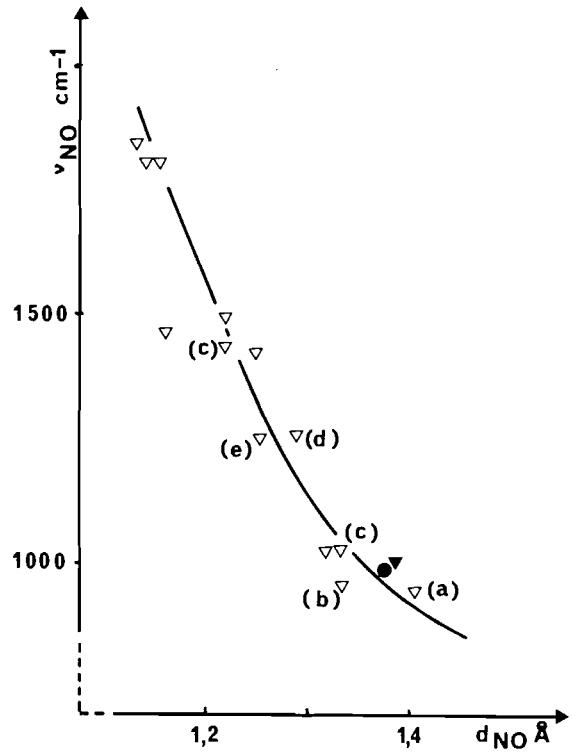


FIG. 5. Variation des fréquences ν(NO) en fonction des longueurs $d$(NO) (●) NMMNO, (▼) NMMNO·$H_2O$ (ce travail et réf. 6); (a) TMANO (18); (b) $[NO_3 \cdot 2HNO_3]^-$ (21); (c) $[NO_3 \cdot HNO_3]^-$ (22); (d) PNO (23) et (e) $H_3O^+NO_3^-$ (24).

cm$^{-1}$ en Raman (480 et 340 en ir) pour NMMNO et pour le monohydrate: 476 et 395 cm$^{-1}$ en Raman (480 et 400 cm$^{-1}$ en ir). Pour ce dernier on observe un léger déplacement de fréquence quand on passe à NMMNO·$H_2O$ (478 et 391 cm$^{-1}$ en Raman et 480 et 390 cm$^{-1}$ en ir) très certainement comme on peut le constater sur la figure 1, il y a couplage entre δ(NO) (487 cm$^{-1}$) et les déformations du cycle qui interviennent dans le même domaine de fréquence.

### III. Les vibrations de la molécule d'eau

Le spectre ir de NMMNO·$H_2O$ (Fig. 3) est complexe. La présence des liaisons hydrogène (6) contribue à la complexité du spectre en provoquant les bandes larges A, B et C (26). Elles sont localisées autour de 3200, 1500 et 800 cm$^{-1}$. On peut être étonné de la faible fréquence de la dernière. Un tel abaissement de fréquence a déjà été observé par Hadzi (26) qui attribue cet effet à l'interaction de la bande C avec une autre bande D existant vers le bas domaine pour les liaisons hydrogène faibles. Nous reviendrons sur la bande C un peu plus loin.

*Les vibrations de valence*

En Raman, on observe une raie large centrée à 3315 cm$^{-1}$ avec un épaulement à 3200 cm$^{-1}$ et en ir un massif large entre 3000 et 3500 cm$^{-1}$ (Fig. 3) (spectres enregistrés à 298 et 90 K en suspension dans le Nujol). Sur un échantillon de faible épaisseur en suspension dans le Fluorolube, on relève une seule bande large à 3350 cm$^{-1}$ tout-à-fait comparable à la raie Raman.

Dans ce domaine de fréquence, il est toujours difficile de faire une attribution sans ambiguité du fait de l'interférence de l'harmonique de $\delta_{OH}$ et des résonances de Fermi. Malheureusement, les difficultés d'obtention de grandes quantité de NMMNO anhydre ont empêché une étude complète à taux de $D_2O$ variable. On a pu, cependant, utiliser le domaine des fréquences $\nu_{OH}$ d'un complexe incomplètement deutérié.

On note que sur le spectre apparait pour $\nu_{OH}$-(OHD) une bande intense à 3340 cm$^{-1}$ avec un épaulement à 3440 cm$^{-1}$ et une bande à 3140 cm$^{-1}$. On pourrait être tenté d'attribuer ces deux bandes aux vibrateurs OH(OHD) impliqués dans les deux liaisons hydrogène (2,72 et 2,82 Å) (6). Cependant ces fréquences correspondent d'aprés la courbe de Novak (27) à des distances O...O de 2,67 et 2,75 Å; un tel écart est difficilement concevable car, il serait un des plus importants parmi les écarts expérimentaux observés.

Il parait plus logique d'attribuer l'épaulement à 3440 cm$^{-1}$ et la bande à 3340 cm$^{-1}$ aux deux vibrateurs OH(OHD) attendus ($d_{O...O}$ = 2,82 et 2,75 Å d'aprés Novak). La bande à 3140 cm$^{-1}$ serait due à la présence d'une combinaison ($\nu_{OH} + \nu_R$) comme Bertie et Whalley (28) l'ont trouvé pour la glace II. Il faut noter que ces fréquences: 3340 et 3440 cm$^{-1}$ pour NMMNO·$H_2O$ sont compatibles avec celles observées par Bertie et Whalley pour les glaces II et V (28). Pour les films de glace, Haas et Hornig (29) et Ford et Falk (30) notent des fréquences plus basses; de même que Bertie et Whalley pour les glaces I et III (31).

*Les vibrations de déformation*

On doit remarquer qu'en ir, la bande large à 1680 cm$^{-1}$ ne peut être attribuée à la base puisque sur le spectre de NMMNO anhydre on n'observe aucune bande entre 1800 et 1600 cm$^{-1}$.

Sur le spectre du produit deutérié apparaît un épaulement à 1250 cm$^{-1}$ absent sur le spectre du complexe hydrogéné; le rapport isotopique de 1,34 est tout-à-fait correct. Un fait similaire est observé en Raman où, entre 1600 et 1800 cm$^{-1}$ apparait un massif large dont le maximum est difficile à locali-

Can. J. Chem. Downloaded from www.nrcresearchpress.com by 210.87.254.6 on 09/06/12
For personal use only.

Can. J. Chem. Downloaded from www.nrcresearchpress.com by 210.87.254.6 on 09/06/12
For personal use only.

ser pour le complexe hydrogéné tandis qu'à 1250 $cm^{-1}$ on relève sur le spectre de l'homologue deutérié un épaulement à la raie à 1237 $cm^{-1}$ attribuable à $\delta(D_2O)$.

Les bandes relevées entre 1800 et 1700 $cm^{-1}$ sur le spectre ir de NMMNO·$D_2O$ semblent attribuables à des combinaisons faisant intervenir $\delta(D_2O)$ et des modes de libration.

*Les librations*

Il reste à localiser les deux librations attendues en ir pour la molécule $H_2O$. Pour la première, sur le spectre ir de l'homologue deutérié on observe à 450 $cm^{-1}$ une bande absente sur le spectre de l'homologue hydrogéné; avec un rapport isotopique de 1,35 on peut penser qu'elle correspond à l'élargissement qui apparaît autour de 610 $cm^{-1}$ sur le spectre du composé hydrogéné.

Ceci permet de rendre compte de la bande à 2300 $cm^{-1}$ qui serait la combinaison classiquement observée: $\delta_{OH_1} + \nu_R$ (1680 + 610 = 2290 $cm^{-1}$); dans le composé deutérié elle glisse à 1700 $cm^{-1}$ (1250 + 450).

L'autre libration est plus délicate à détecter; avec des liaisons hydrogène comparables, Bertie et Whalley (28) obtiennent un spectre ir de la glace II (ou V) qui présente de nombreuses analogies avec celui de NMMNO·$H_2O$. $\nu_{OH(OHD)}$ = 3350 et $\delta_{OH}$ = 1690 $cm^{-1}$ pour la glace, 3340 et 1680 $cm^{-1}$ pour NMMNO·$H_2O$. On note en plus sur leur spectre une bande large centrée vers 800 $cm^{-1}$ que ces auteurs attribuent à une libration. Cette bande est tout-à-fait similaire à celle observée dans ce travail et qui glisse par deutériation, cependant la largeur du massif et la présence des bandes de la base rendent difficile la localisation du maximum avec précision. Bien que 800 $cm^{-1}$ soit une fréquence un peu élevée pour une libration de la molécule $H_2O$ coordinée, il est tentant de proposer cette attribution en se souvenant que l'on a déjà observé une fréquence particulièrement élevée pour $\delta(H_2O)$; ceci doit être relié à l'environnement pyramidal de l'atome d'oxygène.

On a vu que les fréquences observées pour les vibrations de la molécule d'eau sont identiques à celles notées par Bertie et Whalley pour la glace II. D'autre part la structure cristalline du monohydrate de NMMNO a révélé la présence de chaines de molécules d'eau reliées entre elles par des liaisons hydrogène et dans lesquelles l'atome d'oxygène est tricoordiné. Les molécules de NMMNO bloquent la formation de l'environnement tétraédrique de l'atome d'oxygène tel qu'il est rencontré dans la glace et plus particulièrement la glace II (32, 33).

## Conclusion

Dans ce travail, on a pu montrer, par spectroscopie de vibration, que si pour la morpholine et la *N*-méthyl morpholine il existe deux conformères dans la *N*-méthyl morpholine *N*-oxyde et son monohydrate seul subsiste le conformère où les groupes N—O et $CH_3$ sont respectivement en position axiale et équatoriale.

Il a été possible de mettre en évidence, pour NMMNO, l'interaction dipôle–dipôle caractérisée par la raie intense à 75 $cm^{-1}$ sur le spectre Raman. Cette interaction est de force comparable à celle de la pyridine *N*-oxyde et nettement plus important que celle observée par Jakobsen et Brash (20) pour une série de composés organiques.

L'évolution des fréquences ν(OH), δ(OH) et des librations (notamment celle observée à 800 $cm^{-1}$) souligne le rôle de l'environnement pyramidal de la molécule d'eau dans le monohydrate et révèle que NMMNO est apte à stabiliser une chaine de molécules d'eau aussi rigide que le cycle de la glace II. Ceci justifie le choix du monohydrate de NMMNO comme modèle de l'interaction cellulose–NMMNO.

Par ailleurs, la non variation des fréquences de ν(CO) révèle que le groupement $O(CH_2)_2$ est hydrophobe et ne jouera aucun rôle dans la dissolution de la cellulose.

## Annexe expérimentale

*Echantillons*

Les échantillons de *N*-méthyl morpholine *N*-oxyde et son monohydrate nous ont été fournis par l'équipe de Monsieur Chanzy, Maître de Recherches, au Centre de Recherche sur les Macromolécules Végétales (Grenoble, France). Les processus de synthèse sont décrits par Maia *et al.* (6).

NMMNO·$D_2O$ a été préparé au Laboratoire à partir de NMMNO anhydre.

*Appareillage*

Les spectres ir ont été enregistrés sur un spectromètre Perkin–Elmer 180. La cellule à température variable est de type conventionnel (VLT2). Les échantillons sont dispersés dans le Nujol ou le Fluorolube. Les faces utilisées sont en chlorure d'argent ou en iodure de césium.

Les spectres Raman sont enregistrés sur un spectromètre Raman Dilor couplé à un analyseur modulaire multicanaux Tracor (Northern Instrument). Le Laser à Argon ionisé Spectra Physics a une puissance maximale de 1 W sur la raie à 5145 Å. Les échantillons sont dans des tubes de verre Pyrex de 5 mm de diamètre scellés sous vide. Leur refroidissement est assuré par un ensemble cryostat et régulation de température Coderg.

## Remerciements

Nous remercions Monsieur Chanzy, Maître de Recherches au CERMAV (Grenoble, France), son équipe et particulièrement Messieurs Perez et Peguy qui nous ont fournis les échantillons de NMMNO, NMMNO-$d_8$ et NMMNO·$H_2O$ et avec

lesquels nous avons eu des discussions fructueuses.


1. H. CHANZY, M. DUBE et R. H. MARCHESSAULT. J. Polym. Sci. Polym Lett. Ed. **17**, 219 (1979).
2. D. VEDAL, O. H. ELLESTAD, P. KLABOE et G. HAGEN. Spectrochim. Acta Part A, **32**, 877 (1976).
3. D. VEDAL, O. H. ELLESTAD, P. KLABOE et G. HAGEN. Spectrochim. Acta Part A, **31**, 339 (1975).
4. O. H. ELLESTAD, P. KLABOE et G. HAGEN. Spectrochim. Acta Part A, **29**, 1247 (1973).
5. D. VEDAL, O. H. ELLESTAD, P. KLABOE et G. HAGEN. Spectrochim. Acta Part A, **31**, 355 (1975).
6. E. MAIA, A. PEGUY et S. PEREZ. Acta Crystallogr. Sect. B, **37**, 1858 (1981).
7. M. J. COOK, A. R. KATRITZKY et M. MORENO-MANAS. J. Chem. Soc. B, 1330 (1971).
8. P. A. GIGUERE et D. CHIN. Can. J. Chem. **39**, 1214 (1961).
9. S. KIDA. Bull. Chem. Soc. Jpn. **36**, 712 (1973).
10. G. DELLEPIANE et J. OVEREND. Spectrochim. Acta, **22**, 593 (1966).
11. W. C. HARRIS et S. F. BUSH. J. Chem. Phys. **56**, 6147 (1972).
12. J. R. DURIG et W. C. HARRIS. Spectrochim. Acta Part A, **27**, 1955 (1971).
13. S. WEISS et G. E. LEROI. Spectrochim. Acta Part A, **25**, 1759 (1969).
14. W. C. HARRIS et I. W. LEVIN. J. Mol. Spectrosc. **43**, 117 (1972).
15. W. C. HARRIS et I. W. LEVIN. J. Chem. Phys. **54**, 3277 (1971).
16. F. DEVINSKY, I. LACKO, A. NAGY et L. KRASNEC. Chem. Zvesti, **32**, 100 (1978).
17. P. MATHIS-NOEL, R. WOLF et F. GALLAIS. C.R. Acad. Sci. 1873 (1956).
18. Y. KURODA et M. KIMURA. Spectrochim. Acta, **22**, 47 (1966).
19. S. GHERSETTI, S. GIORGIANNI, M. MINARI et G. SPUNTA. Spectrochim. Acta Part A, **29**, 1207 (1973).
20. R. J. JAKOBSEN et J. W. BRASH. J. Am. Chem. Soc. **86**, 3571 (1964).
21. L. DIOP et J. POTIER. J. Mol. Struct. **36**, 191 (1977).
22. L. DIOP. Thèse Montpellier (1976).
23. A. GAMBI et S. GHERSETTI. Spectrosc. Lett. **8**, 627 (1977).
24. M. H. HERZOC-CANCE, J. POTIER, A. POTIER, P. DHAMELINCOURT, B. SOMBRET et F. WALLARD. J. Raman Spectrosc. **7**, n° 6, 303 (1978).
25. S. GHERSETTI, S. GIORGIANNI, M. MINARI et G. SPUNTA. Spectrochim. Acta Part A, **31**, 445 (1975).
26. D. HADZI et N. KOBILAROV. J. Chem. Soc. A, 439 (1966); D. HADZI. Pure Appl. Chem. **11**, 135 (1965), et références incluses.
27. A. NOVAK. Struct. Bonding (Berlin), **18**, 177 (1974).
28. J. E. BERTIE et E. WHALLEY. J. Chem. Phys. **40**, 1646 (1964).
29. C. HAAS et D. F. HORNIG. J. Chem. Phys. **32**, 1763 (1960).
30. T. A. FORD et M. FALK. Can. J. Chem. **46**, 3579 (1968).
31. J. E. BERTIE et E. WHALLEY. J. Chem. Phys. **40**, 1637 (1964).
32. B. KAMB, W. C. HAMILTON, S. J. LAPLACA et A. PRAKASH. J. Chem. Phys. **55**, 4 (1971); B. KAMB. Acta Crystallogr. **17**, 1437 (1964).
33. PHAM THI MAÏ. Thèse Montpellier (1981).


Can. J. Chem. Downloaded from www.nrcresearchpress.com by 210.87.254.6 on 09/06/12
For personal use only.

# Régiosélectivité de l'hydrogénation catalytique de quelques pyrido[2,3-*b*]pyrazines

JEAN-MARIE COSMAO, NOËL COLLIGNON ET GUY QUEGUINER

*Laboratoire de Chimie Organique, Institut National Supérieur de Chimie Industrielle de Rouen, B.P. 8, 76130 Mont Saint-Aignan, France*

Reçu le 24 février 1982

JEAN-MARIE COSMAO, NOËL COLLIGNON et GUY QUEGUINER. Can. J. Chem. **60**, 2785 (1982).

L'hydrogénation catalytique sur charbon palladié de quelques pyrido[2,3-*b*]pyrazines dans l'éthanol conduit à des mélanges de dérivés tétrahydrogénés-1,2,3,4 ou 5,6,7,8 sauf dans deux cas où elle est régiosélective: pour l'hétérocycle non substitué la réduction a lieu sur le cycle pyrazine; pour le dérivé diphénylé en -2,3 elle concerne le cycle pyridinique. Dans l'acide acétique pur, la réduction fournit uniquement les tétrahydro-1,2,3,4 pyrido[2,3-*b*]pyrazines. L'étude particulière de la réduction de la diphényl-2,3 pyrido[2,3-*b*]pyrazine en fonction de l'acidité du solvant et celle de quelques uns de ses dérivés di- et tétrahydrogénés suggère que cette sélectivité peut résulter de l'isomérisation d'espèces intermédiaires partiellement hydrogénées.

JEAN-MARIE COSMAO, NOËL COLLIGNON, and GUY QUEGUINER. Can. J. Chem. **60**, 2785 (1982).

Catalytic hydrogenation on palladium–carbon in ethanol of several pyrido[2,3-*b*]pyrazines leads to mixtures of the 1,2,3,4- and 5,6,7,8-tetrahydro derivatives except in two cases: the reduction of the nonsubstituted heterocycle takes place on the pyrazine ring and, in the case of the 2,3-diphenyl derivative, the pyridine ring is reduced. In pure acetic acid this reduction provides only 1,2,3,4-tetrahydropyrido[2,3-*b*]pyrazines. A study of the reduction of 2,3-diphenylpyrido[2,3-*b*]pyrazine and several di- and tetrahydro derivatives as a function of solvent acidity suggests that the observed selectivity could result from the isomerization of partially hydrogenated intermediates.

[Journal translation]

Poursuivant notre travail sur la réduction de composés hétéroaromatiques polyazotés (1, 2), nous avons plus particulièrement étudié l'hydrogénation catalytique de la pyrido[2,3-*b*]pyrazine **1** et de quatre de ses dérivés substitués sur le noyau pyrazine **2–5**.

Dans les années antérieures et parallèlement à nos travaux, de nombreuses recherches ont été consacrées à la réduction de cet hétérocycle (3). Les réductions par les hydrures complexes d'aluminium (4–6) ou de bore (1, 7, 8), par le chlorure de titane (9) lui ont été appliquées avec succès de même que la réduction électrochimique (10–13) et l'action des organométalliques (5, 14).

Les produits obtenus sont généralement les dérivés tétrahydrogénés-1,2,3,4, sauf dans deux cas (7, 13) où la réduction du noyau pyridine est observée; d'ailleurs, dans ce dernier cas les auteurs obtiennent un mélange de composés réduits sur l'un ou l'autre cycle et montrent que la réduction du cycle pyridine résulte en réalité de l'isomérisation du dérivé dihydrogéné-1,4 en dérivé dihydrogéné-5,8.

Au cours de ces travaux, l'hydrogénation catalytique n'est utilisée que de façon très ponctuelle (6, 13) et n'a fait l'objet d'aucune étude systématique. Nous avons choisi d'utiliser cette méthode pour la réduction des pyrido[2,3-*b*]pyrazines et nous nous sommes particulièrement intéressés à la régiosélectivité de la réaction, dont nous avons montré qu'elle était sous l'étroite dépendance de deux facteurs principaux: la présence de substituants sur le cycle pyrazine d'une part et l'acidité du solvant réactionnel d'autre part.

## Résultats et discussion

Dans ce travail, nous nous sommes limités à l'emploi du catalyseur commercial: charbon palladié à 10%, l'hydrogénation étant conduite à pression atmosphérique et température ambiante, jusqu'à volume d'hydrogène absorbé constant.

### I. *Réduction comparée de quelques pyrido[2,3-*b*]-pyrazines dans l'éthanol ou l'acide acétique*

Dans les conditions opératoires définies ci-dessus, l'hydrogénation catalytique de la pyrido-[2,3-*b*]pyrazine **1** et de ses dérivés: méthyl-3 **2**, diméthyl-2,3 **3**, phényl-3 **4** et diphényl-2,3 **5** conduit exclusivement aux dérivés tétrahydrogénés correspondants *a* ou *b* ou au mélange des deux (schéma 1). Le rendement chimique global est

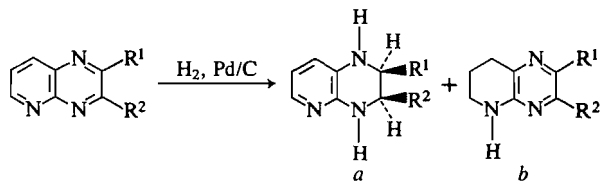


**1**, **1***a* $R^1 = H, R^2 = H$
**2**, **2***a*, **2***b* $R^1 = H, R^2 = CH_3$
**3**, **3***a*, **3***b* $R^1 = CH_3, R^2 = CH_3$
**4**, **4***a*, **4***b* $R^1 = H, R^2 = C_6H_5$
**5**, **5***a*, **5***b* $R^1 = C_6H_5, R^2 = C_6H_5$

SCHÉMA 1

0008-4042/82/222785-07$01.00/0

©1982 National Research Council of Canada/Conseil national de recherches du Canada

Can. J. Chem. Downloaded from www.nrcresearchpress.com by 210.87.254.42 on 09/06/12
For personal use only.

Can. J. Chem. Downloaded from www.nrcresearchpress.com by 210.87.254.42 on 09/06/12
For personal use only.

quantitatif. Lorsqu'ils sont en mélange, les dérivés *a* et *b* sont facilement séparables par chromatographie liquide sur alumine (l'éluant est le chloroforme).

Nous reportons sur le Tableau 1, la composition exprimée en % et déterminée par rmn $^1H$, des mélanges bruts de réduction lorsque le solvant réactionnel est l'éthanol ou l'acide acétique.

1. En milieu éthanolique l'hétérocycle **1** est réduit sélectivement du coté pyrazinique, comme avec les autres systèmes réducteurs.

Pour les dérivés substitués, la présence de groupements volumineux (alkyles ou aryles) sur le cycle pyrazine favorise la réduction du cycle pyridine. Ainsi dans le cas de **5**, obtient-on uniquement la diphényl-2,3 tétrahydro-5,6,7,8 pyrido[2,3-*b*]pyrazine.

Ces résultats sont à comparer à ceux de Braun et coll. (15–18) pour la série de la quinoléine, à ceux de Weitkamp (19) pour le naphtalène et à ceux de Fu *et al.* (20) pour les hydrocarbures aromatiques polycycliques. Dans le cas de la quinoléine, Braun et coll. montrent que la présence de substituants sur le cycle pyridine conduit à des mélanges de produits réduits, les uns sur le cycle pyridine, les autres sur le cycle benzène.

Lors de l'hydrogénation d'alkylnaphtalènes en alkyltétrahydronaphtalènes, Weitkamp obtient aussi un mélange dans lequel le composé majoritaire est réduit sur le cycle non substitué.

Nos résultats en série pyrido[2,3-*b*]pyrazine concordent bien avec ces observations et nous proposons d'expliquer ce comportement par l'existence de deux réactions compétitives conduisant à l'un ou l'autre des dérivés tétrahydrogénés *a* ou *b*. Les vitesses respectives de ces deux réactions dépendraient non seulement de l'encombrement stérique des substituants, mais également de leur effet électronique, ainsi que de la nature du solvant.

2. En milieu acide acétique, par contre, nous obtenons toujours la réduction sélective du noyau pyrazine quels que soient la taille et le nombre des substituants. Un effet analogue a déjà été mis en évidence lors de l'hydrogénation de la quinoléine et de l'isoquinoléine sur oxyde de platine (21–23): en milieu alcoolique la réduction concerne le cycle pyridine de la molécule, alors que dans les milieux très acides ($CF_3COOH$, HCl–MeOH, $H_2SO_4$–$CH_3COOH$) la réduction du cycle benzénique est prépondérante.

Ces résultats nous ont incités à étudier l'influence de l'acidité du solvant dans le cas de la diphényl-2,3 pyrido[2,3-*b*]pyrazine avec laquelle nous observons un effet maximum sur l'orientation de la réduction en passant de l'éthanol à l'acide acétique.

TABLEAU 1. Hydrogénation des pyrido-[2,3-*b*]-pyrazines

| | Solvant | | | |
|---|---|---|---|---|
| | EtOH | | AcOH | |
| Substrat | *a*% | *b*% | *a*% | *b*% |
| **1** | 100 | 0 | —* | — |
| **2** | 40 | 60 | 100 | 0 |
| **3** | 20 | 80 | 100 | 0 |
| **4** | 40† | 60 | 100 | 0 |
| **5** | 0 | 100 | 100 | 0 |

*Dans ce cas les produits de réduction n'ont pu être isolés.
†Litterature (13): **4***a*/**4***b* = 20:80.

## II. *Influence de l'acidité du solvant sur la réduction de la diphényl-2,3 pyrido[2,3-b]pyrazine* **5**

### II-1. *Résultats*

Pour couvrir un large domaine d'acidité, nous avons choisi la série des acides carboxyliques suivants: trifluoroacétique, formique, acétique et propionique. Ces acides sont utilisés à l'état pur comme solvant de réduction. Dans le cas de l'acide acétique nous avons testé également l'effet d'un cosolvant: le benzène. Les résultats sont rassemblés dans le Tableau 2, où nous avons rappelé, à titre de comparaison, le résultat obtenu avec l'éthanol.

Avec les acides trifluoroacétique, formique et acétique, la réaction s'effectue sélectivement sur le cycle pyrazine. Le cas de l'acide propionique est intéressant puisqu'il constitue l'exemple-charnière où les deux réactions de réductions sont compétitives. Enfin l'adjonction (volume à volume) d'un cosolvant neutre comme le benzène à l'acide acétique inverse complétement l'orientation de la réduction par rapport à l'acide pur: ce comportement doit pouvoir être expliqué par la dimérisation bien connue des acides carboxyliques dans le benzène qui diminue fortement leur acidité apparente (24*a*).

En vue d'approfondir le rôle fondamental de l'acidité du solvant sur l'orientation de la réduction de **5**, il nous a paru important d'essayer de préciser d'abord le site de protonation de cet hétérocycle et

TABLEAU 2. Hydrogénation de la diphényl-2,3 pyrido[2,3-*b*]-pyrazine

| Acide | p$K_a$ ($H_2O$) | % **5***a** | % **5***b** |
|---|---|---|---|
| $CF_3COOH$ | 0,23 | 100 | 0 |
| HCOOH | 3,74 | 100 | 0 |
| $CH_3COOH$ | 4,76 | 100 | 0 |
| $CH_3CH_2COOH$ | 4,87 | 55–60 | 35–40 |
| $CH_3COOH$/benzène | — | 0 | 100 |
| EtOH | — | 0 | 100 |

*Les dosages sont effectués sur les spectres rmn $^1H$ des produits bruts de réaction. Les rendements bruts globaux sont quantitatifs.

TABLEAU 3. Différences de déplacement chimique des carbones des pyrido[2,3-*b*]pyrazines **1** et **5** et de la quinoléïne entre les solvants acides et neutres

| Hétérocycle | Solvant | C2 | C3 | C4 | C6 | C7 | C8 |
|---|---|---|---|---|---|---|---|
| 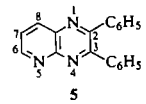 **5** | HCOOH | 4,3 | 4,4 | — | −6,9 | 1 | 10,2 |
| | $CF_3COOH$ | * | * | — | −7,9 | 1 | 10,3 |
| | $CH_3COOH$/benzène | 0 | 0 | — | −1 | 0 | 0,5 |
| 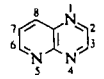 **1** | $CH_3COOD$ | 0,8 | 0,9 | — | 0 | 1 | 0,7 |
| | HCOOH | 2,4 | 2,6 | — | −3,2 | 1,4 | 5,6 |
| | $CF_3COOH$ | 6,6 | 5,4 | — | −5,6 | 2,1 | 11,8 |
| 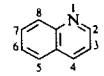 | $CH_3COOD$† | −1,8 | 1,1 | 5,8 | 2,5 | 3,5 | −4,5 |
| | $CF_3COOH$ | −5,8 | 1,2 | 13,1 | 5 | 7,4 | −8,5 |
| | $H_2O$/HCl‡ | −5,5 | 1,6 | 11 | 3,7 | 5,5 | −7,6 |

*Non déterminé.
†$CDCl_3$ (25).
‡Dans ce cas le solvant de référence n'est pas $CDCl_3$, mais le mélange $H_2O$/acétone (26).

de comparer sa basicité à celle de la quinoléine et des pyrido[2,3-*b*]pyrazines. Pour ce travail, nous avons fait appel à deux méthodes complémentaires: la résonance magnétique nucléaire du carbone-13 et la neutralisation par l'acide perchlorique.

II-2. *Analyse des spectres de rmn $^{13}C$*

Pour des raisons de solubilité nous avons limité notre étude rmn $^{13}C$ de l'hétérocycle **5** aux milieux suivants: acide trifluoroacétique, acide formique et mélange acide acétique/benzène. À titre de comparaison nous avons également étudié les spectres de l'hétérocycle **1** et de la quinoléine.

Nous reportons nos résultats (Tableau 3) en donnant, pour chaque carbone analysé, la différence de déplacement chimique $\Delta\delta$ entre la valeur mesurée dans le solvant acide et celle mesurée dans le deutériochloroforme: $\Delta\delta = \delta_{RCOOH} - \delta_{CDCl_3}$ (en ppm).

La quinoléine ($pK_a = 4{,}45$ (27)) étant totalement protonée dans l'acide trifluoroacétique (28), l'analyse des mesures de rmn $^{13}C$ permet de conclure qu'elle l'est incomplétement dans l'acide acétique.

Pour la pyrido[2,3-*b*]pyrazine **1**, les faibles valeurs des $\Delta\delta_i$ dans l'acide acétique conduisent à admettre que cet hétérocycle n'est pratiquement pas protoné dans ce solvant. Par contre, dans l'acide trifluoroacétique les $\Delta\delta_i$ des carbones C6, C7 et C8 de **1** sont très voisins des $\Delta\delta_i$ des carbones C2, C3 et C4 de la quinoléine dans le même solvant: nous en déduisons que **1** est sans doute monoprotoné sur l'azote N5 dans ce solvant. La possibilité d'une seconde protonation (sur N1 ou N4) nous semble à écarter car les $\Delta\delta_i$ des carbones C2 et C3 sont voisins et positifs; de plus, le faible $pK_a$ de **1** = 1,2 (29) n'est pas favorable à une diprotonation.

Les $\Delta\delta_i$ de **1** dans l'acide formique sont intermédiaires entre ceux de l'acide acétique et ceux de l'acide trifluoroacétique: nous postulons, dans ce cas, l'existence d'un équilibre entre la base libre et sa forme monoprotonée sur N5.

En utilisant des arguments analogues pour la diphényl-2,3 pyrido[2,3-*b*]pyrazine **5**, nos conclusions sont les suivantes: dans le mélange acide acétique/benzène (1:1), **5** n'est pas protoné; dans l'acide trifluoroacétique et dans l'acide formique, l'espèce prépondérante est la forme monoprotonée sur N5. Ce résultat tend à prouver que **5** est une base plus forte que **1**. Les mesures dans l'acide acétique pur n'ont pu être faites, mais il est probable, d'après les résultats précédents, que **5** est incomplètement protoné dans ce solvant.

II-3. *Étude de la salification des pyrido[2,3-b]-pyrazines par l'acide perchlorique dans l'acide acétique*

Nous avons tracé les courbes de titrage potentiométrique (24*b*) (différence de potentiel entre l'électrode de verre et l'électrode de référence

Can. J. Chem. Downloaded from www.nrcresearchpress.com by 210.87.254.42 on 09/06/12
For personal use only.

TABLEAU 4. Potentiels de demi-neutralisation

| | Basicité décroissante | | | | | |
|---|---|---|---|---|---|---|
| Hétérocycle | > 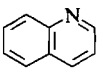 ⋙ 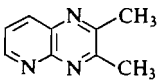 > 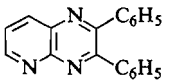 > 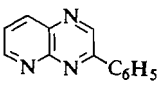 > 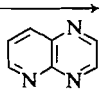 | | | | | |
| | | | **3** | **5** | **4** | **1** |
| $\Delta V_i$ (mV) | −198 | −178 | −118 | −106 | −94 | −60 |

$Hg|Hg_2(CH_3CO_2)_2|LiCH_3CO_2$ saturé$|LiClO_4$ 0,1 *M* dans $CH_3COOH$ anhydre) par l'acide perchlorique, des hétérocycles **1**, **3**, **4**, **5**, de la pyridine et de la quinoléïne. L'allure générale des courbes et la mesure des potentiels de demi-neutralisation nous a permis de classer les molécules étudiées par ordre de basicité décroissante (Tableau 4).

En conclusion, la pyridine et la quinoléïne sont des bases fortes dans l'acide acétique, alors que les pyrido[2,3-*b*]pyrazines **1**, **3**, **4** et **5** sont des bases faibles, donc peu protonées dans ce solvant.

II-4. *Interprétation partielle des résultats*

Les mesures précédentes montrent qu'en solution dans l'acide acétique, la diphényl-2,3 pyrido-[2,3-*b*]pyrazine **5** n'est que partiellement protonée et que la protonation a lieu sur l'azote pyridinique. Les résultats concernant la réduction de **5** dans l'éthanol (ou le mélange acide acétique/benzène) et dans l'acide acétique pur pourraient s'interpréter par le schéma 2.

Dans le premier cas (milieu non protonant) la base libre est hydrogénée sur le cycle le plus riche en électrons (voie A), dans le second cas la concentration en espèces protonées est faible mais si on admet $V_B \gg V_A$, la voie B est prépondérante et le cycle réduit est également le plus riche en électrons. L'hypothèse d'une réduction plus rapide en milieu acide résulte d'un comportement général des hétérocycles azotés (30), mais l'acidité du solvant peut également accélérer l'étape ultérieure de désorption des espèces réduites.

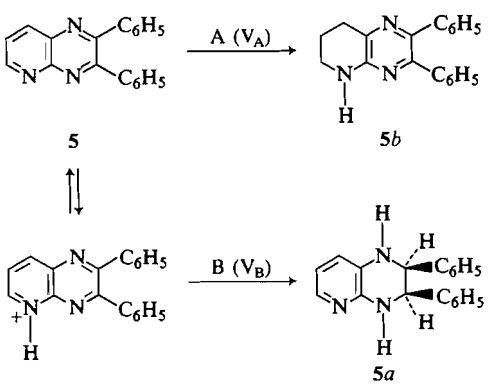

SCHÉMA 2

Cependant, lors de l'hydrogénation sur oxyde de platine du cycle benzénique de la quinoléïne en milieu très acide, Vierhapper et coll. (21, 23, 31) notent que la présence d'une charge positive sur l'azote pyridinique n'est pas le facteur déterminant puisque l'hydrogénation de sels de quinolinium *N*-méthylés conduit aux dérivés tétrahydrogénés-1,2,3,4 dans l'éthanol et aux dérivés réduits sur le cycle benzénique, dans l'acide trifluoroacétique.

Vierhapper (31) suggère alors que l'activation du cycle benzénique pourrait résulter de la formation de complexes π ou σ avec le solvant.

Enfin, le mécanisme peut aussi faire intervenir des espèces intermédiaires partiellement réduites comme dans le cas de la réduction électrochimique (13). À ce propos, dans le cadre particulier de l'hydrogénation de la diphényl-2,3 pyrido[2,3-*b*]-pyrazine, nous nous sommes proposés d'étudier la réduction de quelques formes dihydrogénées de cet hétérocycle dont nous disposions au laboratoire et susceptibles d'être des intermédiaires réactionnels. Nous avons également envisagé les possibilités d'isomérisations des composés tétrahydrogénés-1,2,3,4 et -5,6,7,8.

III. *Hydrogénation des formes partiellement réduites de la diphényl-2,3 pyrido[2,3-*b*]-pyrazine 5*

Le composé **5***b* étant le produit de réduction de **5** dans l'éthanol, il était intéressant de le soumettre aux conditions d'hydrogénation dans l'acide acétique. Au bout de 24 heures (temps suffisant pour observer la réduction complète de **5** en **5***a* dans l'acide acétique), l'analyse du mélange réactionnel montre la présence de **5***a* et de **5***b* dans des proportions équivalentes.

Cet essai montre que la transformation de **5***b* en **5***a* est effective mais lente dans ces conditions. Il est donc peu probable que **5***b* soit un intermédiaire de la réaction **5** → **5***a* puisqu'il n'est pas détecté en fin de réaction (soit environ après 24 h d'hydrogénation).

Inversement, si nous soumettons **5***a* aux conditions de l'hydrogénation dans l'éthanol, nous n'observons aucune isomérisation ni absorption d'hydrogène après 24 h de réaction. Le dérivé **5***b*

Can. J. Chem. Downloaded from www.nrcresearchpress.com by 210.87.254.42 on 09/06/12
For personal use only.

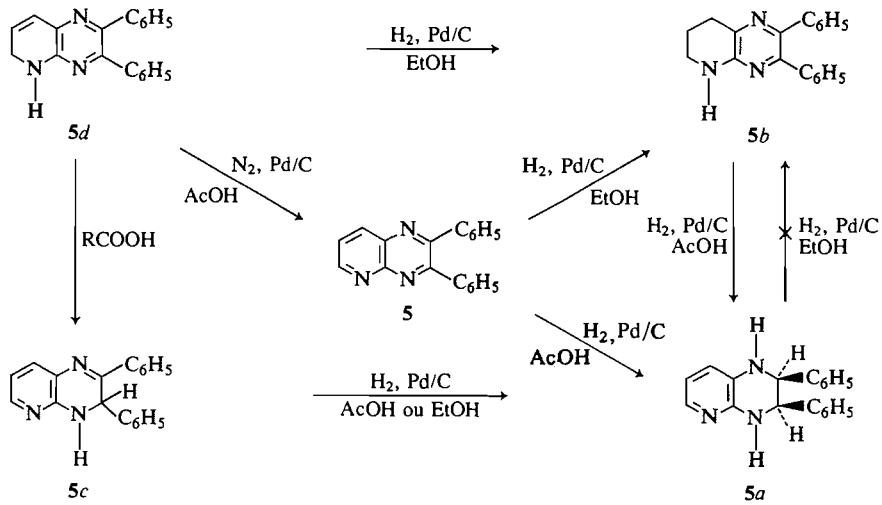

SCHÉMA 3

semble donc plus stable thermodynamiquement que le dérivé **5***a*.

L'hydrogénation de la dihydro-3,4 diphényl-2,3 pyrido[2,3-*b*]pyrazine **5***c* dans l'acide acétique (et aussi dans l'éthanol) conduit à la saturation spécifique du cycle pyrazine.

Le composé **5***c* pourrait donc être intermédiaire dans l'hydrogénation de **5** en milieu acétique. Le résultat obtenu dans l'éthanol montre par contre que **5***c* ne peut être un intermédiaire dans ce cas.

Dans l'acide acétique, l'hydrogénation de la dihydro-5,6 diphényl-2,3 pyrido[2,3-*b*]pyrazine **5***d* conduit à un mélange de **5***a* et **5***b* dans un rapport **5***a*/**5***b* variable avec le temps de purge de l'installation.

Ce résultat curieux, nous a amenés à mettre en évidence les deux phénomènes suivants. (1) À 20°C dans l'acide acétique, en présence du catalyseur, mais en l'absence d'hydrogène, **5***d* s'aromatise très rapidement en **5** en libérant de l'hydrogène. (2) À 20°C dans l'acide acétique, en l'absence de catalyseur et d'hydrogène, **5***d* se transpose en **5***c*. La réaction est complète en 1 heure; à 30°C elle est complète en 5 minutes. Dans l'acide trifluoroacétique, la réaction est pratiquement instantanée.

Ces différentes observations peuvent expliquer le résultat de l'hydrogénation de **5***d* dans l'acide acétique: la transformation **5***d* → **5***b* qui semble normale doit résulter d'une réduction directe sans intermédiaire. Par contre la transformation surprenante à priori **5***d* → **5***a* peut s'interpréter par l'existence des intermédiaires **5***c* et(ou) **5** et la formation de ces intermédiaires peut intervenir pendant la phase préparatoire de l'opération (mise en solution, purge du réacteur), ce qui explique les variations des proportions en produits finaux.

En résumé, pour l'hydrogénation de la diphényl-2,3 pyrido[2,3-*b*]pyrazine **5** dans un acide carboxylique, nous pouvons faire intervenir les chemins réactionnels compétitifs suivants (schéma 3).

Dans l'hypothèse de l'existence des intermédiaires **5***c* et **5***d* ce schéma rend bien compte des résultats reportés sur le tableau 2: dans les acides purs, lorsque l'isomérisation **5***d* → **5***c* est rapide (R = $CF_3$, H et $CH_3$), **5***a* se forme exclusivement, lorsqu'elle est plus lente (R = Et), la transformation **5***d* → **5***b* devient compétitive. Dans l'éthanol et le mélange acide acétique/benzène, cette dernière réaction est prépondérante et **5***b* est le seul produit de réduction isolé.

## Partie expérimentale

Les spectres rmn $^1H$ sont enregistrés à 60 MHz sur le spectromètre Varian T60 du service commun de mesures de physiques de l'I.N.S.C.I.R.; le solvant est le deutériochloroforme ($CDCl_3$) et la référence interne le tétraméthylsilane ($Me_4Si$); les abréviations suivantes sont utilisées: s = singulet, d = doublet, t = triplet, q = quadruplet, sex = sextuplet, mu = multiplet, m = massif. Les spectres rmn $^{13}C$ sont enregistrés à 20,11 MHz sur le spectromètre Brucker WH 90 du centre de mesures physiques de l'Université de Rouen; les échantillons sont en solution dans le deutériochloroforme ($CDCl_3$) ou dans les acides carboxyliques deutériés ou non. Ces solvants servent eux-mêmes de référence interne. Les spectres ir sont tracés sur Beckman Acculab TM (pastille KBr). Les points de fusion sont déterminés sur banc Kofler et ne sont pas corrigés. Les analyses élémentaires (C, H, N Technicon) sont en accord avec les formules brutes à ± 0,3% près.

*Synthèse des pyrido[2,3-b]pyrazines*

Parmi les modes opératoires existants pour la préparation de ce dérivé, nous avons utilisé ceux de Boutte (32) **1**, **2**, Chekir (13) **3**, et Vinot (6, 33) **4** et **5**.

Pour le dérivé méthyl-3 pyrido[2,3-*b*]pyrazine **2**, la position du substituant méthyle est établie sans ambiguité par comparaison des différences des déplacements chimiques rmn $^{13}C$ des

Can. J. Chem. Downloaded from www.nrcresearchpress.com by 210.87.254.42 on 09/06/12
For personal use only.

Can. J. Chem. Downloaded from www.nrcresearchpress.com by 210.87.254.42 on 09/06/12
For personal use only.

carbones des dérivés **1** et **2** (tableau 5) et de ceux de la quinoléine et de la méthyl-2 quinoléine (25) l'effet d'un substituant méthyle sur le déplacement chimique du carbone porteur est de +9 ppm par rapport au carbone de la molécule non substituée.

*Hydrogénations des pyrido[2,3-*b*]pyrazines*

Les hydrogénations sont effectuées dans un appareillage simple de laboratoire à pression et température ambiantes.

*Hydrogénation en milieu alcoolique*

Nous introduisons successivement dans le réacteur d'hydrogénation de 250 mL, une suspension de 300 mg de charbon palladié à 10% dans 25 mL d'éthanol puis $10^{-2}$ mol d'hétérocycle et enfin 25 mL d'éthanol. Le réacteur est purgé par 3 L d'azote puis 3 L d'hydrogène. L'hydrogénation effectuée sous agitation magnétique est poursuivie jusqu'à volume d'hydrogène absorbé constant.

Après 24 h de réaction, le catalyseur est éliminé par filtration sur un lit de Célite 545 de 3 cm d'épaisseur. Le solvant est ensuite évaporé sous pression réduite. Le dosage du produit brut est effectué sur le spectre rmn $^1$H.

*Hydrogénation en milieu acide carboxylique*

Le processus utilisé est le même que pour l'hydrogénation en milieu alcoolique sauf en ce qui concerne le traitement final: le filtrat est refroidi dans la glace puis neutralisé par une solution de soude concentrée. La solution aqueuse obtenue est extraite par trois fois 50 mL de chloroforme et la phase organique est lavée par 10 mL d'une solution de chlorure de sodium saturée, puis séchée sur sulfate de magnésium anhydre et évaporée sous pression réduite.

*Pyrido[2,3-*b*]pyrazine* **1**

L'hydrogénation de **1** en milieu alcoolique conduit avec un rendement quantitatif à un solide jaune pâle la tétrahydro-1,2,3,4 pyrido[2,3-*b*]pyrazine **1***a* (5, 8) pur en rmn. Ce dérivé recristallise de l'éther (Rdt = 75%). Fusion: 128°C; ir ($cm^{-1}$) $CHCl_3$, $\nu_{NH}$: 3430, 2940; rmn $^1$H (ppm): 7,42 (q, H6, $J_{67}$ = 4,5 Hz, $J_{68}$ = 2 Hz), 6,58 (q, H8, $J_{78}$ = 7,5 Hz, $J_{68}$ = 2 Hz), 6,38 (q, H7, $J_{67}$ = 4,5 Hz, $J_{78}$ = 7,5 Hz), 6,0 (m, NH), 4,05 (m, NH); 3,40 (m, 2H2 + 2H3).

*Méthyl-3 pyrido[2,3-*b*]pyrazine* **2**

En milieu alcoolique nous obtenons un mélange (40:60) des dérivés tétrahydrogénés **2***a* et **2***b*. Nous avons séparé 500 mg de ce mélange sur une colonne d'alumine de 30 cm de longueur en éluant au chloroforme, nous avons obtenu 200 mg de chacun de ces composés à l'état pur.

L'hydrogénation en milieu acide acétique conduit uniquement au dérivé **2***a*.

*Méthyl-3 tétrahydro-1,2,3,4 pyrido[2,3-*b*]pyrazine* **2**a

Fusion: 123°C (benzène–héxane); ir ($cm^{-1}$) $\nu_{NH}$: 3370, 3220; rmn $^1$H (ppm): 7,21 (q, H6, $J_{67}$ = 4,5 Hz, $J_{68}$ = 2 Hz), 6,60 (q, H8, $J_{68}$ = 2 Hz, $J_{78}$ = 7,5 Hz), 6,35 (q, H7, $J_{67}$ = 4,5 Hz, $J_{78}$ = 7,5 Hz), 5,4 (m, NH), 2,75–3,85 (m, 2H2 + H3), 1,18 (d, $CH_3$, $J$ = 6 Hz).

*Méthyl-3 tétrahydro-5,6,7,8 pyrido[2,3-*b*]pyrazine* **2**b

Fusion: 99–100°C (héxane); ir ($cm^{-1}$) $\nu_{NH}$: 3250; rmn $^1$H (ppm): 7,57 (s, H2), 5,1 (m, NH), 3,43 (sex, 2 H6, $J$ = 6 Hz, $J_{H6\text{-}NH}$ = 2 Hz), 2,90 (t, 2H8, $J$ = 6 Hz), 2,3 (s, $CH_3$), 2,03 (mu, 2 H7).

*Diméthyl-2,3 pyrido[2,3-*b*]pyrazine* **3**

En milieu alcoolique nous obtenons un mélange (20:80) des dérivés tétrahydrogénés **3***a* et **3***b* que nous avons séparés par chromatographie sur colonne d'alumine (éluant: chloroforme/benzène; Rdt **3***b* = 55%).

En milieu acide acétique nous obtenons sélectivement le dérivé **3***a* (Rdt = 75%).

cis-*Diméthyl-2,3 tétrahydro-1,2,3,4 pyrido[2,3-*b*]pyrazine* **3**a (4, 34, 35)

Fusion: 111,5°C; ir ($cm^{-1}$) $\nu_{NH}$: 3230, 3380; rmn $^1$H (ppm): 7,50 (q, H6, $J_{68}$ = 2 Hz, $J_{67}$ = 4,5 Hz), 6,73 (q, H8, $J_{68}$ = 2 Hz, $J_{78}$ = 8 Hz), 6,43 (q, H7, $J_{67}$ = 4,5 Hz, $J_{78}$ = 8 Hz), 4,9 (m, NH), 3,55 (m, NH + H2 + H3), 1,14 (d, $CH_3$, $J$ = 6 Hz), 1,10 (d, $CH_3$, $J$ = 6 Hz).

*Diméthyl-2,3 tétrahydro-5,6,7,8 pyrido[2,3-*b*]pyrazine* **3**b

Fusion: 114°C; ir ($cm^{-1}$) $\nu_{NH}$: 3260; rmn $^1$H (ppm): 4,9 (m, NH), 3,37 (sex, 2H6, $J$ = 6 Hz, $J_{H6\text{-}NH}$ = 2 Hz), 2,87 (t, 2H8), 2,33 (s, $CH_3$), 2,30 (s, $CH_3$), 2,03 (mu, 2 H7).

*Phényl-3 pyrido[2,3-*b*]pyrazine* **4**

En milieu alcoolique nous obtenons un mélange (35–40:60–65) des dérivés tétrahydrogénés **4***a* et **4***b* dont nous pouvons séparer une proportion importante de **4***a* par recristallisation dans le chloroforme puis par chromatographie sur alumine avec le chloroforme comme éluant, nous obtenons **4***b* (Rdt **4***a* = 25%, Rdt **4***b* = 45%).

Le dérivé **4***a* est obtenu sélectivement par hydrogénation dans l'acide acétique (Rdt = 80%).

*Phényl-3 tétrahydro-1,2,3,4 pyrido[2,3-*b*]pyrazine* **4**a (13)

Fusion: 181°C; ir ($cm^{-1}$) $\nu_{NH}$: 3200, 3360; rmn $^1$H (ppm): 7,33 (m, H6 + $C_6H_5$), 6,70 (q, H8, $J_{68}$ = 2 Hz, $J_{78}$ = 7 Hz), 5,3 (m, NH), 4,65 (q, H3, $J$ = 3,5 Hz, $J$ = 7 Hz), 3,4 (m, NH), 3,35 (m, 2H2).

*Phényl-3 tétrahydro-5,6,7,8 pyrido[2,3-*b*]pyrazine* **4**b (6)

Fusion: 166°C; ir ($cm^{-1}$) $\nu_{NH}$ = 3210; rmn $^1$H (ppm): 8,10 (s, H2), 7,83 (m, 2H($C_6H_5$)), 7,37 (m, 3H($C_6H_5$)), 5,4 (m, NH), 3,33 (sex, 2H6, $J$ = 6 Hz, $J_{H6\text{-}NH}$ = 2 Hz), 2,90 (t, 2H7, $J$ = 6 Hz, 2,03 (mu, 2H8).

*Diphényl-2,3 pyrido[2,3-*b*]pyrazine* **5**

L'hydrogénation catalytique de **5** en solution alcoolique nous permet d'obtenir quantitativement la diphényl-2,3 tétrahydro-5,6,7,8 pyrido[2,3-*b*]pyrazine **5***b* (6) que nous purifions par recristallisation dans l'alcool ou le cyclohexane (Rdt = 80%). Fusion:[1] 185°C; ir ($cm^{-1}$) $\nu_{NH}$: 3250; rmn $^1$H (ppm):[2] 7,25 (m, 10H, $2C_6H_5$), 5,6 (m, NH), 3,27 (sex, 2H6, $J$ = 5,5 Hz, $J_{H6\text{-}NH}$ = 3 Hz), 3,0 (t, 2H8, $J$ = 6 Hz), 2,05 (mu, 2H7).

L'hydrogénation catalytique de **5** dans l'acide acétique conduit à la *cis*-diphényl-2,3 tétrahydro-1,2,3,4 pyrido[2,3-*b*]pyrazine **5***a* (6) que nous pouvons recristalliser dans le mélange alcool–eau (2:3) (Rdt = 75%). Fusion = 206°C; ir ($cm^{-1}$) $\nu_{NH}$: 3240, 3415; rmn $^1$H (ppm): 7,53 (q, H6, $J_{67}$ = 5 Hz, $J_{68}$ = 2 Hz), 6,93 (H8 + $2C_6H_5$), 6,5 (q, H7, $J_{67}$ = 5 Hz, $J_{78}$ = 7,5 Hz), 5,37 (m, NH), 4,77 (m, H2 + H3), 4,03 (m, NH).

*Synthèse des dihydro diphenyl-2,3 pyrido[2,3-*b*]pyrazines* **5**c *et* **5**d[3]

*Diphényl-2,3 dihydro-3,4 pyrido[2,3-*b*]pyrazine* **5**c (15)

À une suspension de **5** (2,7 g, 0,01 mol) dans l'acide acétique glacial (50 mL) refroidi au bain de glace, nous ajoutons en 1 heure, le tétrahydruroborate de potassium (1,62 g, 0,03 mol) par petites portions en maintenant la température entre 0 et 15°C.

[1]L'analyse thermique différentielle de ce produit, montre qu'il y a absorption d'énergie vers 144°C mais que la fusion s'effectue à 185°C.

[2]Nous avons observé une variation importante du déplacement chimique des protons H6 de 3 ppm en solution saturée (70 mg dans 400 mg de solvant) à 3,3 ppm en solution diluée (10 mg dans 400 mg). L'effet sur les protons H8 est pratiquement nul et très faible pour les protons H7 (inférieur à 0,1 ppm).

Ces deux remarques[1,2] nous incitent à penser qu'il doit exister des liaisons hydrogène préférentielles entre ces molécules en solution, ce qui provoque une cristallisation dans un système métastable.

[3]La synthèse de ces dérivés fait partie d'un travail sur la réduction des pyrido[2,3-*b*]pyrazines par les hydrures métalliques qui est actuellement en cours.

TABLEAU 5. Résonance magnétique nucléaire $^{13}C$ ($CDCl_3$)

| | C2 | C3 | C6 | C7 | C8 | C9 | C10 |
|---|---|---|---|---|---|---|---|
| δ | 146,6 | 157,0 | 153,2 | 123,7 | 137,5 | 135,4 | 150,2 |
| $\Delta(\delta_2 - \delta_1)$ | +0,3 | +9 | −1,3 | −2 | −1,3 | −3,2 | −1,4 |
| | C3 | C2 | C8 | C7 | C6 | C10 | C9 |
| $\Delta(\delta_{MeQ} - \delta_Q)$* | +1 | +8,6 | −0,8 | −0,0 | −0,9 | −0,4 | −1,8 |

*Q = quinoléine; MeQ: méthyl-2 quinoléine (25).

Nous laissons 3 heures à température ambiante. Nous hydrolysons par la glace pilée (20 g), puis alcalinisons par une solution de soude concentrée. Le mélange est extrait au chloroforme (3 fois 100 mL). Les phases organiques réunies sont lavées par une solution aqueuse (2 fois 10 mL) saturée de chlorure de sodium puis séchées sur sulfate de magnésium et évaporées sous pression réduite. Le produit obtenu est solubilisé dans le minimum de chloroforme et reprécipité par 10 mL d'éther éthylique. On obtient ainsi 1,8 g (Rdt = 66%) de **5***c* que l'on peut recristalliser dans le méthanol ou un mélange benzène–hexane. Fusion: 205°C; ir ($cm^{-1}$) $\nu_{NH}$: 3210; rmn $^1H$ (ppm): 7,20–8,10 (m, H6 + H8 + $2C_6H_5$), 6,70 (q, H7, $J_{67}$ = 5 Hz, $J_{78}$ = 7,5 Hz), 5,92 (s, H3), 5,75 (m, NH).

*Diphényl-2,3 dihydro-5,6 pyrido[2,3-*b*]pyrazine* **5**d

À une solution de **5** (5,66 g, 0,02 mol) d'acide acétique (5,4 g, 0,09 mol) dans du benzène sec (100 mL), nous ajoutons en maintenant la température inférieure à 10°C, le tétrahydruroborate de potassium (1,62 g, 0,03 mol) par petites portions sous bonne agitation. Nous laissons 2 heures à température ambiante puis portons à 35°C pendant 30 min. Après un traitement analogue au précédent nous isolons 4,2 g (Rdt = 76%) de **5***d* que l'on peut recristalliser dans l'alcool. Fusion: 209°C; ir ($cm^{-1}$) $\nu_{NH}$: 3230; rmn $^1H$ (ppm): 7,23 (m, $2C_6H_5$), 6,47 (sex, H8, $J_{68}$ = 2 Hz, $J_{78}$ = 10 Hz), 6,17 (m, NH), 5,78 (mu, H7, $J_{78}$ = 10 Hz, $J_{67}$ = 4 Hz, $J_{H7\text{-}NH}$ = 2 Hz), 4,0 (mu, 2H6, $J_{67}$ = 4 Hz,[4] $J_{68}$ = 2 Hz[4]).

## Remerciements

Nous tenons à remercier Monsieur le Professeur P. Granger et le Docteur S. Chapelle pour les spectres rmn $^{13}C$ et leur précieux conseils dans ce domaine ainsi que M. et J. P. Salaun pour leur collaboration à l'étude de la protonation des pyrido[2,3-*b*]pyrazines.

1. J. M. COSMAO, N. COLLIGNON et G. QUEGUINER. J. Heterocycl. Chem. **16**, 973 (1979).
2. J. M. COSMAO. Thèse de Docteur-Ingénieur, Université de Rouen, 1.9.81.
3. G. W. H. CHEESEMAN et R. F. COOKSON. Condensed pyrazines. The chemistry of heterocyclic compounds. Vol. 35. Wiley–Interscience, New York. 1979. p. 524.
4. R. C. DESELMS et S. MOSHER. J. Am. Chem. Soc. **82**, 3762 (1960).
5. D. BOUTTE, G. QUEGUINER et P. PASTOUR. C. R. Acad. Sci. Paris Ser. C, **273**, 1529 (1971).
6. N. VINOT et P. MAITTE. Bull. Soc. Chim. Fr. 3100 (1973).
7. D. BOUTTE, G. QUEGUINER et P. PASTOUR. C. R. Acad. Sci. Paris Ser. C, **275**, 1645 (1971).
8. R. C. BUGLE et R. A. OSTERYOUNG. J. Org. Chem. **44**, 1719 (1979).
9. J. ARMAND, K. CHEKIR et J. PINSON. J. Heterocycl. Chem. **17**, 1237 (1980).
10. K. B. WIBERG et T. P. LEWIS. J. Am. Chem. Soc. **92**, 7154 (1970).
11. J. ARMAND, K. CHEKIR, J. PINSON et N. VINOT. C. R. Acad. Sci. Paris Ser. C, **281**, 547 (1975).
12. J. ARMAND, K. CHEKIR, J. PINSON. C. R. Acad. Sci. Paris Ser. C, **284**, 391 (1977).
13. J. ARMAND, K. CHEKIR et J. PINSON. Can. J. Chem. **56**, 1804 (1978).
14. N. VINOT et P. MAITTE. Bull. Soc. Chim. Fr. 251 (1976).
15. J. V. BRAUN, A. PETZOLD et J. SEEMAN. Ber. **55**, 3779 (1922).
16. J. V. BRAUN, W. GMELIN et A. SCHULTHEISS. Ber. **56**, 1338 (1923); **56**, 1347 (1923).
17. J. V. BRAUN, W. GMELIN et A. PETZOLD. Ber. **57**, 382 (1924).
18. J. V. BRAUN et G. LEMKE. Ann. Chem. **478**, 176 (1930).
19. A. W. WEITKAMP. Adv. Catal. **18**, 1 (1968).
20. P. P. FU, H. M. LEE et R. G. HARVEY. J. Org. Chem. **45**, 2797 (1980).
21. F. W. VIERHAPPER et E. L. ELIEL. J. Am. Chem. Soc. **96**, 2256 (1974).
22. J. Z. GINOS. J. Org. Chem. **40**, 1191 (1975).
23. F. W. VIERHAPPER et E. L. ELIEL. J. Org. Chem. **40**, 2729 (1975).
24. G. CHARLOT et B. TREMILLON. Les réactions chimiques dans les solvants et les sels fondus. Gauthier–Villars, Paris. 1968 (*a*) p. 162; (*b*) pp. 213–219.
25. JA-AN SU, E. SIEW, E. V. BROWN et S. L. SMITH. Org. Magn. Reson. **10**, 122 (1977).
26. P. VAN DE WEIJER, H. THIJSSE et D. VAN DER MEER. Org. Magn. Reson. **8**, 187 (1976).
27. G. JONES. Quinolines. The chemistry of heterocyclic compounds. Vol. 32. Wiley–Interscience, New York. 1977.
28. R. PASTOR, J. MUSSO et A. CAMBON. Bull. Soc. Chim. Fr. 3009 (1973).
29. A. ALBERT et G. B. BARLIN. J. Chem. Soc. C, 5737 (1963).
30. M. FREIFELDER. Practical catalytic hydrogenation. Wiley–Interscience, New York. 1971.
31. M. HONEL et F. W. VIERHAPPER. J. Chem. Soc. Perkin Trans. I, 1933 (1980).
32. D. BOUTTE. Thèse de Docteur-Ingénieur, Université de Rouen, 8 juillet 1972.
33. N. VINOT et P. MAITTE. C. R. Acad. Sci. Ser. C, **275**, 681 (1972).
34. R. A. ARCHER et H. S. MOSHER. J. Org. Chem. **32**, 1378 (1967).
35. K. WINTERFELD et M. WILDERSOHN. Arch. Pharm. **303**, 1002 (1970).

[4]Après échange $D_2O$.

Can. J. Chem. Downloaded from www.nrcresearchpress.com by 210.87.254.42 on 09/06/12
For personal use only.

# Solid states structures of 1,4-diacetyl-1,4-dihydroquinoxaline and 1,2-diacetyl-1,2-dihydrobenzo[*c*]cinnoline; two potential antiaromatic heterocyclic compounds

JOSEPH ARMAND

*Laboratoire de Physicochimie des Solutions, Université Pierre et Marie Curie, Bâtiment F, 8 Rue Cuvier, 75230 Paris Cedex 05, France*

AND

MICHÈLE PHILOCHE-LEVISALLES

*Laboratoire de Chimie Systématique, Université Pierre et Marie Curie, Bâtiment F, 8 Rue Cuvier, 75230 Paris Cedex 05, France*

Received January 20, 1982

JOSEPH ARMAND and MICHÈLE PHILOCHE-LEVISALLES. Can. J. Chem. **60**, 2792 (1982).

A crystallographic investigation shows that the 1,4-diacetyl-1,4-dihydroquinoxaline **2** possesses a plane of symmetry perpendicular to the N(1)—N(4) axis and that the 1,4-dihydropyrazine ring exists under a well developed boat conformation. This allows one to reject an azahomoaromatic structure with six delocalized π electrons and a pair of electrons localized on a nitrogen atom. The C(2)=C(3) double bond is localized. **2** shows a *ZZ* conformation and the molecule indicates an angular shape analogous to that of 1,5-dihydroalloxazines.

In the solid state 1,2-diacetyl-1,2-dihydrobenzo[*c*]cinnoline is not planar. The dihedral angle between the two benzenic rings is 19.5°. The N-acetyl groups present an *E,E*-conformation and their stereochemical arrangement prevents the nitrogen pairs from being delocalized toward the neighbouring benzenic groups. This shows that **3** is not an antiaromatic molecule.

JOSEPH ARMAND et MICHÈLE PHILOCHE-LEVISALLES. Can. J. Chem. **60**, 2792 (1982).

On montre par cristallographie que la 1,4-diacetyl-1,4-dihydroquinoxaline **2** présente un plan de symétrie perpendiculaire à l'axe $N_1N_4$ et que le noyau 1,4-dihydropyrazine adopte une forme bateau suffisamment prononcée pour exclure une structure de type azahomoaromatique comprenant un ensemble de 6 électrons π délocalisés et une paire d'électrons localisée sur un atome d'azote. La double liaison C(2)=C(3) est localisée. **2** adopte une conformation *ZZ* et l'ensemble de la molécule a une forme angulaire analogue à celle des 1,5-dihydroalloxazines.

A l'état solide, la 1,2-diacetyl-1,2-dihydrobenzo[*c*]cinnoline n'est pas plane. Les deux noyaux benzéniques présentent entre eux un angle dièdre de 19,5°. Les groupements N-acétylés ont une conformation *E,E*, leur disposition dans l'espace montre que les paires d'électrons libres des atomes d'azote ne sont pas délocalisées vers les noyaux benzéniques voisins. Ces résultats montrent que **3** n'est pas une molécule antiaromatique.

## Introduction

There has been considerable recent interest in the study of potential antiaromatic heterocyclic compounds (1). In the case of N-heterocyclic derivatives, the replacement of two diametrically opposed ethylenic groups in cyclooctatetraene by two >N—R groups leads to 1,4-dihydropyrazine derivatives, while the replacement of two vicinal ethylenic groups leads to 1,2-dihydropyridazine derivatives. These derivatives are potential 8π-electron systems (1) and the examination of their solid state structure allows a precise determination the extent of delocalization of the eight electrons. In a preceding paper we have investigated (2) the structure of 1,4-diacetyl-1,4-dihydro-2,3-diphenylpyrazine **1**. In order to define the influence of benzannelation on the the structure of 1,4-dihydropyrazine ring we have undertaken the structural examination of **2**. Further, to the best of our knowledge, the detailed structure of compounds with a 1,2-dihydropyridazine ring has never been determined; **3** appears as an example of such compounds and its stability is high enough to permit a stereochemical determination.

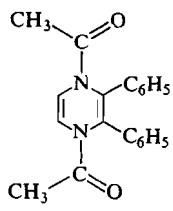

**1**

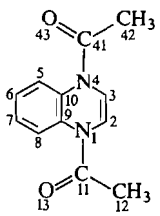

**2**

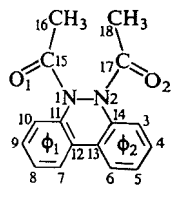

**3**

## Results

### *1. 1,4-Diacetyl-1,4-dihydroquinoxaline 2*

Positional parameters and isotropic thermal parameters are given in Table 1. Table 2 lists bond lengths and Table 3 some selected bond angles. Figures 1 and 2 are ORTEP drawings of the crystal structure of **2**. Tables of observed and calculated

0008-4042/82/222792-05$01.00/0

©1982 National Research Council of Canada/Conseil national de recherches du Canada

Can. J. Chem. Downloaded from www.nrcresearchpress.com by 210.87.254.105 on 09/06/12
For personal use only.

Can. J. Chem. Downloaded from www.nrcresearchpress.com by 210.87.254.105 on 09/06/12
For personal use only.

TABLE 1. Positional parameters (× $10^4$) and isotropic thermal parameters* with esd's in parentheses for 1,4-diacetyl-1,4-dihydroquinoxaline

| Atom | $x$ | $y$ | $z$ | $B_{iso}$ (Å²) |
|---|---|---|---|---|
| O(13) | 4838(1) | 553(1) | 2338(1) | 3.7(1) |
| N(1) | 3361(1) | 1615(1) | 1875(1) | 2.5(1) |
| C(9) | 4057(1) | 2047(1) | 297(1) | 2.3(1) |
| C(2) | 2259(1) | 2072(2) | 2573(2) | 2.8(1) |
| C(8) | 4657(2) | 1592(2) | −1250(2) | 3.1(1) |
| C(11) | 3812(2) | 875(2) | 2808(2) | 2.7(1) |
| C(12) | 2986(2) | 497(2) | 4436(2) | 3.8(1) |
| C(7) | 5280(2) | 2047(2) | −2760(2) | 3.8(1) |
| H(121) | 2839(24) | 910(23) | 5442(24) | |
| H(122) | 3465(22) | 23(28) | 5013(24) | |
| H(123) | 2115(24) | 342(21) | 3907(25) | |
| H(2) | 1535(21) | 1739(20) | 2946(20) | |
| H(7) | 5749(24) | 1732(21) | −3869(25) | |
| H(8) | 4679(19) | 919(21) | −1217(23) | |

*$B_{iso}$ for the non-H atoms is calculated by the expression

$$B_{iso} = \frac{4}{3}\Sigma_i\Sigma_j\beta_{ij}(a_i.a_j)$$

TABLE 2. Bond lengths (Å) (esd's) in 1,4-diacetyl-1,4-dihydroquinoxaline

| Bond | Length |
|---|---|
| N(1) —C(2) | 1.425(3) |
| N(1) —C(9) | 1.437(3) |
| N(1) —C(11) | 1.377(3) |
| C(11) —O(13) | 1.220(3) |
| C(11) —C(12) | 1.500(4) |
| C(2) —C(3) | 1.316(3) |
| C(9) —C(10) | 1.391(3) |
| C(9) —C(8) | 1.391(3) |
| C(8) —C(7) | 1.385(4) |
| C(7) —C(6) | 1.392(4) |
| C(2) —H(2) | 0.94(4) |
| C(7) —H(7) | 1.01(4) |
| C(8) —H(8) | 1.03(4) |
| C(12) —H(121) | 0.93(4) |
| C(12) —H(122) | 0.96(4) |
| C(12) —H(123) | 1.00(4) |

structure factor amplitudes and of temperature factors were put in the Depository of Unpublished Data.[1]

The molecule presents a plane of symmetry perpendicular to the N(1)—N(4) axis, thus the carbon atoms of the 1,4-dihydropyrazine ring are coplanar. The phenyl ring is planar and atoms N(1) and N(4) belong to this plane. The conformation of the 1,4-dihydropyrazine ring corresponds to a boat form displaying a mirror symmetry. If A is the middle of the C(2)—C(9) segment and B the middle of the C(3)—C(10) segment (Fig. 3), it is possible to define the following angles, as in the case of **1** (2): α = 180° − (N(1)AB), β = 180° − (N(4)BA), γ = (AN(1)C(11)), and δ = (BN(4)C(41)). In the case of **2** one finds α = β = 27.9°, γ = δ = 173.4°. As could be expected the atoms N(1), C(11), C(12), O(13) on one side and N(4), C(14), C(42), O(43) on the other side are coplanar. The angles between these planes and the mediating plane of the 1,4-dihydropyrazine ring (N(1)ABN(4) plane) is 80.2°. As shown in Fig. 1 both amide groups present a *Z* conformation. The large values of the angles around N(1) and N(4) imply a substantial $sp^2$ character for the nitrogen atoms. The dihedral angle between the N(1)C(2)C(3)N(4) and N(1)C(9)C(10)N(4) planes is equal to 33.3°.

[1]A complete set of tabular data is available, at a nominal charge, from the Depository of Unpublished Data, CISTI, National Research Council of Canada, Ottawa, Ont., Canada K1A 0S2.

TABLE 3. Selected bond angles (esd's) in 1,4-diacetyl-1,4-dihydroquinoxaline

| Bonds | Angle |
|---|---|
| C(2) —N(1) —C(9) | 114.7(4) |
| C(11) —N(1) —C(2) | 122.4(5) |
| C(11) —N(1) —C(9) | 122.4(4) |
| O(13) —C(11) —N(1) | 121.3(5) |
| O(13) —C(11) —C(12) | 122.1(6) |
| N(1) —C(2) —C(3) | 119.5(5) |
| N(1) —C(9) —C(10) | 117.5(4) |
| C(10) —C(9) —C(8) | 120.2(5) |
| C(9) —C(8) —C(7) | 119.4(5) |
| C(8) —C(7) —C(6) | 120.4(6) |

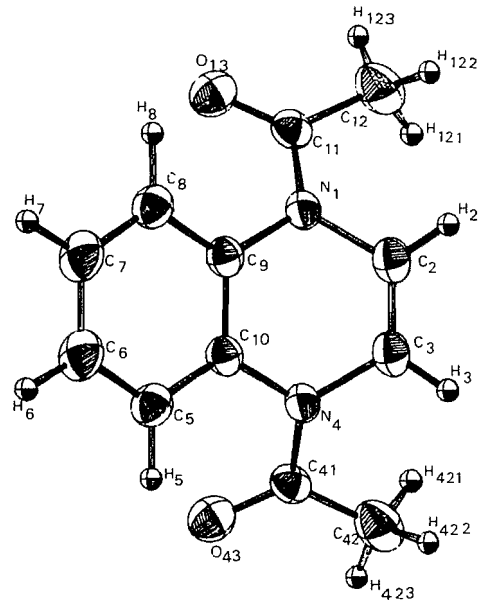


FIG. 1. ORTEP drawing of the crystal structure of **2**.

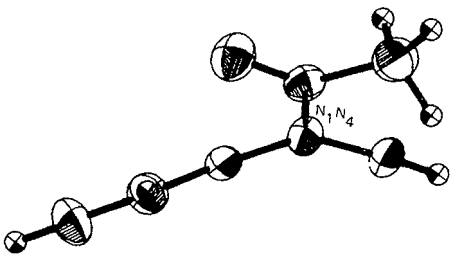


FIG. 2. ORTEP drawing of the crystal structure of **2**: view along the N(1)N(4) axis.

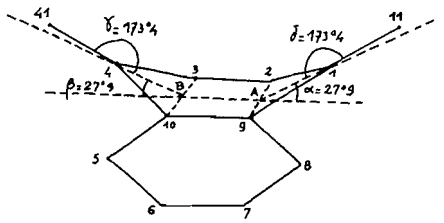


FIG. 3. Angles α, β, γ, and δ within **2**.

### *2. 1,2-Diacetyl-1,2-dihydrobenzo[c]cinnoline* **3**

Positional parameters and isotropic thermal parameters are given in Table 4. Table 5 lists bond lengths and Table 6 some selected bond angles. Figure 4 is an ORTEP drawing of the structure of **3**. Tables of observed and calculated structure factor amplitudes and of temperature factors were lodged with the Depository of Unpublished Data.[1]

The phenyl rings $\phi_1$ and $\phi_2$ are planar. Atoms N(1) and C(13) are in the plane of $\phi_1$ and atoms N(2) and C(12) in the plane of $\phi_2$. The dihedral angle between these two planes is equal to 19.5°; the values of the distances between N(1) and the plane of $\phi_2$ on one hand and between N(2) and the plane of $\phi_1$ on the other hand are respectively 0.8 Å and 0.77 Å. Thus the heterocyclic ring is not planar. The atoms are located in the planes of a dihedra: N(1), C(11), C(12), C(13) in one plane and N(2), C(14), C(13), C(12) in the other plane, the axis C(12)C(13) being at the intersection of the two planes. The atoms N(1), C(15), C(16), O(1) on one side and N(2), C(17), C(18), O(2) on the other side are coplanar. As shown in Fig. 4, both amide groups present an *E* conformation.

## Discussion

In the case of **2** the 1,4-dihydropyrazine ring presents a pronounced boat shape as $\alpha = \beta = 27.9°$. If one considers the axis of the orbital of the nonbonding N(1) pair as being perpendicular to the C(2)C(9)C(11) plane, it is found that this axis makes an angle of 57.9° with the plane C(2)C(3)C(9)C(10). The value of this angle — identical to that existing

TABLE 4. Positional parameters (× $10^4$) and isotropic thermal parameters* with esd's in parentheses in 1,2-diacetyl-1,2-dihydrobenzo[*c*]cinnoline

| Atom | *x* | *y* | *z* | $B_{iso}$ (Å$^2$) |
|---|---|---|---|---|
| N(1) | 742(1) | 2242(2) | 163(1) | 2.6(1) |
| N(2) | 822(1) | 2488(2) | 1149(1) | 2.6(1) |
| O(1) | 187(1) | 2997(2) | −1133(1) | 4.8(1) |
| O(2) | 948(1) | 1545(2) | 2592(1) | 4.4(1) |
| C(3) | 1027(1) | 4568(3) | 2090(2) | 3.2(1) |
| C(4) | 1409(1) | 5729(3) | 2247(2) | 3.8(1) |
| C(5) | 1969(1) | 6038(3) | 1670(2) | 3.8(1) |
| C(6) | 2144(1) | 5168(2) | 932(2) | 3.1(1) |
| C(7) | 2551(1) | 2975(2) | −499(2) | 3.6(1) |
| C(8) | 2648(1) | 2064(3) | −1238(2) | 3.1(1) |
| C(9) | 2119(1) | 1201(3) | −1518(2) | 2.4(1) |
| C(10) | 1485(1) | 1231(2) | −1056(1) | 2.3(1) |
| C(11) | 1394(1) | 2155(2) | −323(1) | 2.4(1) |
| C(12) | 1915(1) | 3039(2) | −25(2) | 2.4(1) |
| C(13) | 1764(1) | 3992(2) | 760(1) | 2.4(1) |
| C(14) | 1205(1) | 3701(2) | 1353(1) | 2.4(1) |
| C(15) | 178(1) | 2856(3) | −282(2) | 3.1(1) |
| C(16) | −424(1) | 3232(3) | 329(2) | 4.4(1) |
| C(17) | 802(1) | 1382(3) | 1758(2) | 3.1(1) |
| C(18) | 580(2) | 43(3) | 1364(2) | 4.5(1) |
| H(3) | 634(13) | 4311(27) | 2498(18) | |
| H(4) | 1308(14) | 6340(31) | 2726(19) | |
| H(5) | 2246(13) | 6946(30) | 1784(21) | |
| H(6) | 2561(14) | 5392(27) | 473(18) | |
| H(7) | 2939(13) | 3685(29) | −315(18) | |
| H(8) | 3085(12) | 2054(28) | −1566(19) | |
| H(9) | 2170(14) | 523(30) | −2022(20) | |
| H(10) | 1108(12) | 580(28) | −1244(17) | |
| H(161) | −293(14) | 4104(30) | 700(19) | |
| H(162) | −556(14) | 2516(30) | 713(20) | |
| H(163) | −799(13) | 3608(32) | −49(20) | |
| H(181) | 850(14) | −241(32) | 852(21) | |
| H(182) | 555(15) | −699(31) | 1808(20) | |
| H(183) | 150(15) | 67(32) | 1081(20) | |

*$B_{iso}$ for the non-H atoms is calculated by the expression

$$B_{iso} = \frac{4}{3}\Sigma_i\Sigma_j\beta_{ij}(a_i.a_j)$$

TABLE 5. Selected bond lengths (Å) (esd's) in 1,2-diacetyl-1,2-dihydrobenzo-[*c*]cinnoline*

| Bond | Length |
|---|---|
| N(1) —N(2) | 1.421(4) |
| N(2) —C(14) | 1.430(4) |
| C(14) —C(13) | 1.396(5) |
| C(13) —C(12) | 1.478(5) |
| C(12) —C(11) | 1.393(5) |
| C(11) —N(1) | 1.440(4) |
| N(1) —C(15) | 1.396(5) |
| C(15) —C(16) | 1.495(6) |
| C(15) —O(1) | 1.209(5) |
| N(2) —C(17) | 1.383(5) |
| C(17) —O(2) | 1.221(5) |
| C(17) —C(18) | 1.489(6) |

*Average C—C distances for the phenyl rings: ϕ(1), 1.390(6); ϕ(2), 1.387(6).

Can. J. Chem. Downloaded from www.nrcresearchpress.com by 210.87.254.105 on 09/06/12
For personal use only.

Can. J. Chem. Downloaded from www.nrcresearchpress.com by 210.87.254.105 on 09/06/12
For personal use only.

TABLE 6. Selected bond angles (esd's) in 1,2-diacetyl-1,2-dihydrobenzo[*c*]-cinnoline*

| Bonds | Angle |
|---|---|
| C(11) —N(1) —N(2) | 112.4(5) |
| N(1) —N(2) —C(14) | 113.2(6) |
| N(2) —C(14) —C(13) | 116.8(7) |
| C(14) —C(13) —C(12) | 118.2(7) |
| C(13) —C(12) —C(11) | 118.5(7) |
| C(12) —C(11) —N(1) | 117.0(7) |
| C(11) —N(1) —C(15) | 119.8(6) |
| N(2) —N(1) —C(15) | 117.0(6) |
| N(1) —C(15) —O(1) | 119.1(8) |
| N(1) —C(15) —C(16) | 117.1(7) |
| N(1) —N(2) —C(17) | 118.2(6) |
| C(14) —N(2) —C(17) | 122.8(7) |
| N(2) —C(17) —C(18) | 117.8(7) |
| N(2) —C(17) —O(2) | 119.3(8) |

*Average C—C—C angles for the phenyl rings: $\phi(1)$, 120°; $\phi(2)$, 120°.

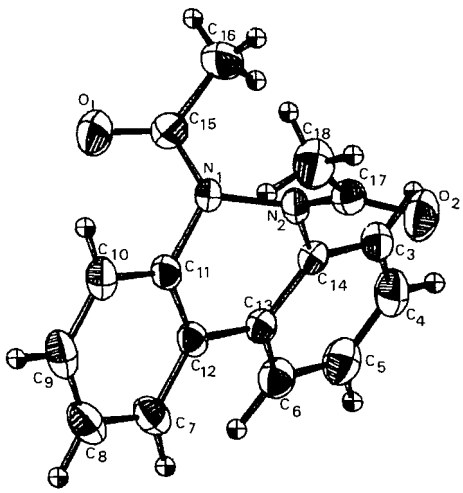


FIG. 4. ORTEP drawing of the crystal structure of **3**.

between the axis of the N(4) lone pair and the plane C(2)C(3)C(9)C(10), as the molecule is symmetrical — does not support the hypothesis of a delocalization of the nonbonding pairs of N(1) and N(4) towards the 1,4-dihydropyrazine ring. This is confirmed by the length of the C(2)C(3) double bond (1.316 Å) which corresponds to a localized double bond. These results show that the molecule is not antiaromatic and rule out the hypothesis of the separation of the eight π electrons into six electrons delocalized on the ring and two electrons on one nitrogen atom. Now, if one compares the structures of **1** and **2** it is observed that **2** presents, in contrast to **1**, a symmetry plane perpendicular to the N(1)N(4) axis (in the case of **1** (2) the values of the angles were $\alpha = 30.9°$, $\beta = 34.5°$, $\gamma = 168.1°$, $\delta = 173.5°$); the bond lengths are quite similar for **1** and **2**. In particular, the length of the C(2)C(3) bond of **2** (1.316 Å) is near that of the C(5)C(6) bond of **1** (1.320 Å). The dihedral angle between the mean N(1)C(2)C(3)N(4) and N(1)C(9)C(10)N(4) planes is 33.3° in the case of **2**; it is smaller than in the case of **1** (38.2°) but it is similar to the value found for some 1,5-dihydroalloxazines (3, 4).

In order for **3** to display an antiaromatic character the two nitrogen lone pairs should be conjugated with the benzenic ring and these two benzenic rings should be conjugated together. The angle of 19.5° measured between these rings shows that the last condition is not fulfilled. Further, as in the case of **2**, the axis of the orbital of the nitrogen lone pair of N(1) must be perpendicular to the N(2)C(11)C(15) plane; this axis makes an angle of 35° with the plane of the benzenic ring $\phi_1$ thus preventing any delocalization of the nonbonding electrons of N(1) towards $\phi_1$. In the case of N(2) the axis of the lone pair makes an angle of 39° with $\phi_2$ which also rules out any delocalization of the nonbonding electrons of N(2) towards $\phi_2$.

All these results show that **3** is not antiaromatic: π conjugation of the cyclic 8π system, and hence electron delocalization, is thwarted by the angular skeleton of the 1,2-dihydropyridazine ring and by the positions of the lone pairs of electrons on nitrogen atoms.

It should be remarked that the two acetyl groups take the *E*,*E*-conformation where the two methyl groups are neighbours. However, there is no steric hindrance as the two acetyl groups are not coplanar, the value of the dihedral angle C(15)N(1)-N(2)C(17) is 61°.

## Experimental

The 1,4-diacetyl-1,4-dihydroquinoxaline and the 1,2-diacetyl-1,2-dihydrobenzo[*c*]cinnoline have been prepared according to ref. 5. The single crystals used in the crystallographic study were obtained by slow evaporation of solutions of **2** and **3** in dimethylformamide.

Crystal data of **2** are as follows:

$C_{12}H_{22}N_2O_2$ fw = 216

Orthorhombic, $a = 10.438(2)$, $b = 15.363(3)$, $c = 6.638(2)$ Å, $V = 1064.5$ Å$^3$, $Z = 4$, $\rho_c = 1.33$ g cm$^{-3}$, $\rho_o = 1.32(2)$ g cm$^{-3}$ (20°C, Mo $K_\alpha$ $\lambda = 0.707$ Å, $\mu = 0.96$ cm$^{-1}$).

Preliminary X-ray photographs showed the following systematic absences: $0kl$, $k + l = 2n + 1$, $hk0$, $h = 2n$; a statistical analysis of the intensity data indicated the centrosymmetric space group *Pnma*. A crystal (0.45 × 0.30 × 0.25 mm) was mounted with the *a* axis parallel to the φ axis of a Philips automated diffractometer equipped with a graphite monochromator. The intensities of all reflections having 2θ less than 50° were measured using the variable ω–2θ scan technique. During the course of the data collection three standard reflections were measured every 54 reflections. A total of 1433 reflections were measured, 909 of which had $I > 4\sigma(I)$. The data were reduced to $|F_o|$ by the routine procedure. Lorentz and polarization but no absorption or extinction corrections were

applied. The scattering factors for neutral atoms were taken from ref. 6. The structure was determined by direct methods (MULTAN) (7) and refined by large block least-squares $\Sigma\omega(F_o - |F_c|)^2 = \min$ with $\omega = 1/\sigma^2$. The refinement with anisotropic thermal parameters on the non-hydrogen atoms converged to $R = 0.092$. At this stage, a difference Fourier map revealing the positions of all the hydrogen atoms was calculated; refinement of their positional parameters was carried out, using the thermal parameters of the corresponding heavy atoms at the end of isotropic refinement. The refinement converged with $R = 0.047$ and $R_w = 0.055$.

Crystal data of **3** are as follows:

$C_{16}H_{14}N_2O_2$ fw = 266

Orthorhombic, $a = 19.350(4)$, $b = 9.797(2)$, $c = 14.110(3)$ Å, $V = 2674.9$ Å$^3$, $Z = 8$, $\rho_c = 1.32$ g cm$^{-3}$, $\rho_o = 1.30(2)$ g cm$^{-3}$ (20°C, Mo $K_\alpha$ $\lambda = 0.707$ Å, $\mu = 0.85$ cm$^{-1}$).

Preliminary X-ray photographs showed the following systematic absences: $0kl$, $k = 2n + 1$; $h0l$, $l = 2n + 1$; $hk0$, $h + k = 2n + 1$; a statistical analysis of the intensity data indicated the centrosymmetric space group *Pbcn*. A crystal (0.50 × 0.20 × 0.35 mm) was mounted with the *a* axis parallel to the $\phi$ axis of a Philips automated diffractometer equipped with a graphite monochromator. The intensities of all reflections having $2\theta$ less than 50° were measured using the variable $\omega$–$2\theta$ scan technique. During the course of the data collection three standard reflections were measured every 54 reflections. A total of 2737 reflections were measured, 1714 of which had $I > 4\sigma(I)$. The data were reduced to $|F_o|$ by the routine procedure. Lorentz and polarization but no absorption or extinction corrections were applied. The scattering factors for neutral atoms were taken from ref. 6. The structure was determined by direct methods (MULTAN) (7) and refined by large block least-squares $\Sigma\omega(F_o - |F_c|)^2 = \min$ with $\omega = 1/\sigma^2$. The refinement with anisotropic thermal parameters on the non-hydrogen atoms converged to $R = 0.087$. At this stage, a difference Fourier map revealing the positions of all the hydrogen atoms was calculated; refinement of their positional parameters was carried out, using the thermal parameters of their corresponding heavy atoms at the end of isotropic refinement. The refinement converged with $R = 0.051$ and $R_w = 0.056$.

In this paper when it is stated that atoms are coplanar, it means that they were found in the same plane within experimental accuracy.

1. R. R. SCHMIDT. Angew. Chem. Internat. Edit. **14**, 581 (1975).
2. J. ARMAND, C. BOIS, M. PHILOCHE-LEVISALLES, M. J. POUET, and M. P. SIMONNIN. Can. J. Chem. **60**, 349 (1982).
3. R. NORRESTAM, P. KIERKEGAARD, B. STENSLAND, and L. TORBJÖRNSSON. J. Chem. Soc. Chem. Commun. 1250 (1969).
4. P. KIERKEGAARD, O. RONNQUIST, and P. E. WERNER. Tetrahedron Lett. 4667 (1969).
5. H. LUND and J. SIMONET. Compt. Rend. Acad. Sci. Ser. C, **277**, 1387 (1973).
6. International tables for X-ray crystallography. Vol. IV. The Kynoch Press, Birmingham, England. 1974.
7. G. GERMAIN, P. MAIN, and M. M. WOOLFSON. Acta Crystallogr. A, **27**, 268 (1971).

Can. J. Chem. Downloaded from www.nrcresearchpress.com by 210.87.254.105 on 09/06/12
For personal use only.

# Electrochemical reduction of quinoxalino[2,3-*b*]quinoxaline

JOSEPH ARMAND AND LINE BOULARES
*Laboratoire de Physicochimie des Solutions, E.N.S.C.P., 11 Rue Pierre et Marie Curie, 75231 Paris Cedex 05, France*

CHRISTIAN BELLEC
*Laboratoire de Chimie des Hétérocycles, Université Pierre et Marie Curie, 4, Place Jussieu, 75230 Paris Cedex 05, France*

AND

JEAN PINSON
*Laboratoire d'Electrochimie, Université Paris VII, 2, Place Jussieu, 75231 Paris Cedex 05, France*

Received May 7, 1982

JOSEPH ARMAND, LINE BOULARES, CHRISTIAN BELLEC, and JEAN PINSON. Can. J. Chem. **60**, 2797 (1982).

The electrochemical reduction of quinoxalino[2,3-*b*]quinoxaline gives fluoflavine (**2**) the structure of which is discussed. The electrochemical reduction of fluoflavine in acidic medium leads to a hexahydroquinoxalino[2,3-*b*]quinoxaline. A reduction mechanism is proposed based on cyclic voltammetry results and preparative electrolysis. The results obtained in the case of quinoxalino[2,3-*b*]quinoxaline are used to rationalize the results obtained in the case of pyrazino[2,3-*b*]pyrazines and pyrazino[2,3-*b*]quinoxalines.

JOSEPH ARMAND, LINE BOULARES, CHRISTIAN BELLEC et JEAN PINSON. Can. J. Chem. **60**, 2797 (1982).

La réduction électrochimique de la quinoxalino[2,3-*b*]quinoxaline fournit la fluoflavine (**2**) dont la structure est discutée. La réduction électrochimique de la fluoflavine en milieu acide fournit une hexahydroquinoxalino[2,3-*b*] quinoxaline. Un mécanisme de réduction utilisant les résultats de la voltammétrie cyclique et des électrolyses préparatives est proposé. La présente étude permet également de rationaliser certains résultats obtenus dans des études antérieures relatives aux pyrazino[2,3-*b*] pyrazines et pyrazino[2,3-*b*] quinoxalines.

Can. J. Chem. Downloaded from www.nrcresearchpress.com by 210.87.254.6 on 09/06/12
For personal use only.

We have been interested for some time in the electrochemical reduction of heterocyclic compounds with two 1,4-nitrogen atoms in a six-membered ring. We now report the electrochemical reduction in protic and aprotic medium of the quinoxalino[2,3-*b*]quinoxaline, **1**. This compound possesses two conjugated

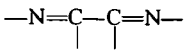

systems and it seemed interesting to investigate how the conjugation of two such systems would influence their electrochemical behaviour. A single electrochemical study of **1** has been published (1); however, its conclusions are erroneous.

As we shall see later on, the electrochemical reduction of the quinoxalino[2,3-*b*]quinoxaline **1** leads to fluoflavine which is a dihydro quinoxalino-[2,3-*b*]quinoxaline. It can also be prepared by condensation of 2,3-dichloroquinoxaline with *o*-phenylene diamine (2). The structure of fluoflavine has remained controversial as some authors assigned a 5,12-dihydro structure **2** (3), while others assigned a 5,11-dihydro structure **2***a* (2). Therefore, we shall first discuss the structure of fluoflavine.

### The structure of fluoflavine

Some of the problems arising in the investigation of the structure of this compound stem from its very low solubility in usual solvents (methanol, acetonitrile, dimethylsulphoxide, dimethylformamide). It can be dissolved in hot acetic acid or in cold trifluoroacetic acid. Our first attempts aimed at obtaining an unambiguous determination of the structure by X-ray crystallography, but we were unable to obtain suitable crystals from $CH_3COOH$ or $CF_3COOH$ solutions. An nmr spectrum recorded in $CF_3COOH$ shows a single AA'BB' pattern for the eight aromatic protons, which gives no indication on the structure of fluoflavine the protons of the benzenic rings being equivalent because of the protonation of the nitrogen atoms and the fast exchange of these protons.

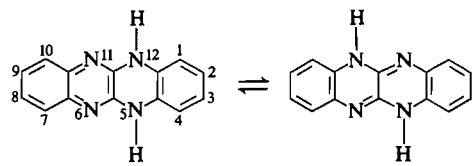

**2** **2***a*

An nmr spectrum of fluoflavine in $Me_2SO$-$d_6$ obtained on a 250 MHz spectrometer after 3000 accumulations shows two aromatic multiplets located respectively at 6.45–6.75 ppm (4H) and 6.90–7.13 ppm (4H) and a broad signal at 9.92 ppm corresponding to the two NH protons. This spectrum rules out the existence of a fast equilibrium

0008-4042/82/222797-07$01.00/0
©1982 National Research Council of Canada/Conseil national de recherches du Canada

between the tautomers **2** and **2***a* because the aromatic protons of the two benzenic rings would be equivalent and the spectrum would consist of a single AA'BB' pattern, the width of which can be estimated to about 0.15 ppm (the aromatic protons of 5,10-dihydro-2,3-dimethyl-pyrazino[2,3-*b*]quinoxaline appear as an AA'BB' pattern with a width of 0.12 ppm). Thus, fluoflavine has either structure **2** or structure **2***a*. Structure **2** should give rise to two separated AA'BB' patterns. The aromatic protons of 1,2,3,4-tetrahydrophenazine **3** appear as a multiplet between 7.50 and 8.10 ppm (4) while that of 5,10-bis-*n*-propyl-5,10-dihydrophenazine **4** appear

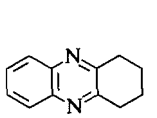

**3**

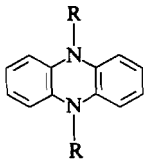

**4** R = *n*-propyl

between 6.06 and 6.70 ppm (5). Thus, the observed spectrum is in agreement with structure **2**, but its poor resolution does not permit the measurement of the characteristics of the two possible AA'BB' patterns. This is why it is not possible to rule out structure **2***a* which could also evidence two multiplets of equal intensity. By heating fluoflavine in acetic anhydride a single diacetyl derivative **25** is obtained. Its 250 MHz nmr spectrum shows two aromatic AA'BB' patterns which proves that **25** is a 5,12-diacetylated derivative. The structure of **25** is confirmed by its electrochemical reduction (vide infra) which gives *N*,*N*'-diacetyl *o*-phenylene diamine. Obtaining a single diacetyl derivative in the 5,12-positions is in agreement with structure **2** but does not allow the exclusion of structure **2***a*; indeed, it is possible that at high temperature the **2***a* → **2** interconversion be faster than the acetylation of **2**.

We have shown previously (8) that the electrochemical reduction of the pyrazino[2,3-*b*]quinoxaline **18** leads to the only 5,10-dihydro derivative **20**, **18** and **20** forming a redox couple (see Scheme 4). As we shall see further the electrochemical reduction of **1** only gives fluoflavine and **1** and fluoflavine also form a redox couple. As **1** and **18** have very similar structures this result favours structure **2** for fluoflavine.

It should also be remarked that the condensation of 2,3-dichloroquinoxaline with 1,2-diamino-4,5-dimethylbenzene gives a solid which by heating in acetic anhydride leads to a mixture of the 5,12-diacetyl-5,12-dihydro derivative **7** and of the 6,11-diacetyl-6,11-dihydro derivative **8**. This result points to the formation of a mixture of the 5,12-dihydro derivative **5** and of a 6,11-dihydro derivative **6** upon condensation. As the influence of the methyl groups on the structure of a dihydroquinoxalino[2,3-*b*]quinoxaline is most likely very small, the structures of **5** and **6** support structure **2** for fluoflavine.

Thus, although there is no formal proof that fluoflavine has structure **2**, the above results show structure **2** as the most likely; thus it will be used in this paper.

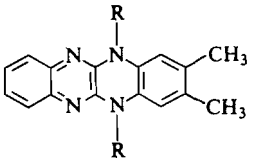

**5**, R = H
**7**, R = $COCH_3$

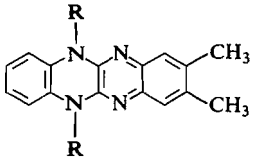

**6**, R = H
**8**, R = $COCH_3$

*Electrochemical reduction of quinoxalino[2,3-b]-quinoxaline*

In aprotic medium ($CH_3CN$) a voltammogram of **1** presents two reversible peaks at $E_1^0 = -0.37$ V and $E_2^0 = -1.05$ V which correspond to the formation of a radical anion and a dianion.

In hydroorganic medium (50/50 v/v water–dimethylformamide) **1** presents a 2F wave which is pH dependent between pH 4 and 12: $E_{1/2}$ (V) = 0.44 − 0.058pH; **1** is unstable in more acidic or more basic media. Between pH 4 and 6, this first wave is followed by a pH-dependent 4F wave: $E_{1/2}$ (V) = −0.75 − 0.068pH; above pH 6 the height of the second wave decreases and disappears at pH > 8.

A preparative electrolysis of **1** on the first plateau gives **2**. The second 4F wave is that of **2**. The electrochemical reduction of **2** in acidic medium where it is slightly more soluble leads to 5,5a,6,11,-11a,12-hexahydroquinoxalino[2,3-*b*]quinoxaline, **9**. When **9** is heated in acetic anhydride, it furnishes a triacetyl derivative **10**. The large value of the $^3J_{5a-11a}$ coupling constant (18 Hz) of **10** points to a *trans* configuration for the hydrogens 5a and 11a. The results are summarized in Scheme 1.

The results of a previous polarographic study of **1** (1) are erroneous as the authors do not mention the first wave of **1** and assign the second wave to **1** instead of **2**. Besides, no preparative electrolysis is described.

Concerning the reduction mechanism, the formation of **2** from **1** is in agreement with what could be expected from the known reduction of compounds with a pyrazine ring. Pyrazines (9), quinoxalines (10), and pyrido[2,3-*b*]pyrazines (11) are first reduced to compounds with a

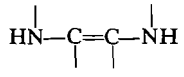

Can. J. Chem. Downloaded from www.nrcresearchpress.com by 210.87.254.6 on 09/06/12
For personal use only.

Can. J. Chem. Downloaded from www.nrcresearchpress.com by 210.87.254.6 on 09/06/12
For personal use only.

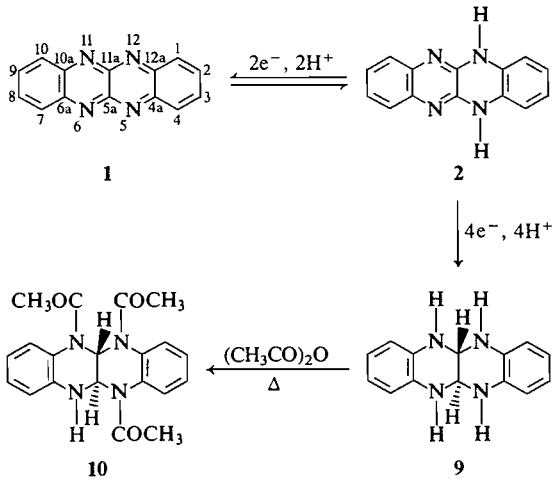

SCHEME 1

structure. The same reaction is observed for the reduction of **1** into **2**. But unlike previous compounds which rearrange to

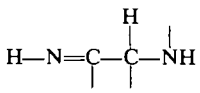

structures the

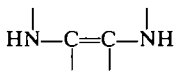

structure of **2** is stable. This is obviously related to the increased number of conjugated cycles.

In the case of **2**, one could expect for the same reasons as above the primary formation of a 5,6,11,12-tetrahydrogenated compound **11** which would rearrange to a 5,5a,6,12-tetrahydrogenated compound **12**, the reduction of which would lead to a hexahydrogenated compound such as **9** (Scheme 3).

Compounds such as **11** with a

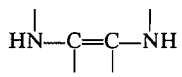

structure are usually characterized by an anodic peak on their voltammogram. The potential of this anodic peak is generally near or identical to that of the cathodic peak of the parent heterocycle (see, e.g., 2-phenylquinoxaline (10), 2,3-diphenylpyrazine (9), diphenylpyrido[3,4-*b*]pyrazine (11)). No anodic peak which could correspond to **11** can be observed on mercury, but on a glassy carbon electrode, an anodic peak $II_a$ appears at $E_{pa}$ = +0.65 V if the cathodic peak of fluoflavine $II_c$ ($E_{pc}$ = −0.93 V) has been scanned before (Fig. 1, $v$ = 0.2 V $s^{-1}$, pH 1, 50% DMF), the reversible couple which appears at $E^0$ = +0.45 V, $I_c/I_a$ being that of fluoflavine itself.

In order to find out the origin of the large positive shift of the anodic peak we investigated the behaviour of 2-morpholinoquinoxaline **13** where the pyrazine ring also bears a nitrogen substituent.

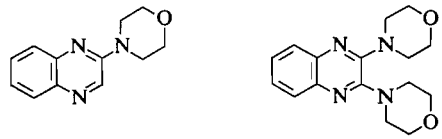

In hydroorganic medium (50/50 v/v methanol–water) **13** presents a 2F cathodic wave (1 < pH < 4.5: $E_{1/2}$ = −0.15 − 0.11 pH and 4.5 < pH < 13: $E_{1/2}$ = −0.39 − 0.061 pH). Its electrolysis in basic medium furnishes the 3,4-dihydro-2-morpholinoquinoxaline and its cyclic voltammetry in basic medium (25% DMF, 0.1 *N* NaOH, $v$ = 20 V $s^{-1}$) shows a cathodic peak at $E_{pc}$ = −1.50 V and an anodic peak at $E_{pa}$ = −0.88 V. Thus in basic media 2-morpholinoquinoxaline presents a voltammetric behaviour similar to the other quinoxalines already investigated. Its reduction is summarized in Scheme 2.

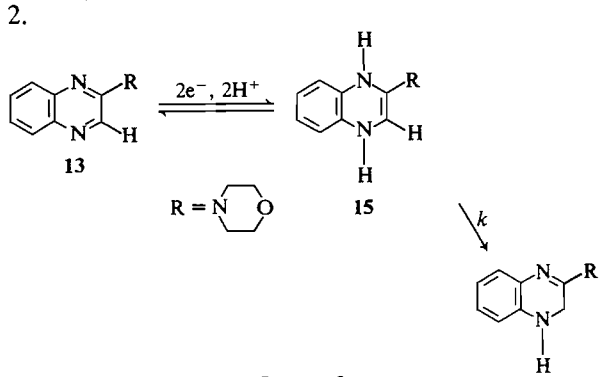

SCHEME 2

In acidic medium under the same conditions as fluoflavine ($v$ = 0.2 V $s^{-1}$, pH = 1, 50% DMF) the cathodic peak of **13** is observed at $E_{pc}$ = −0.50 V and the anodic peak corresponding to the

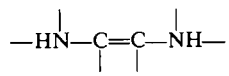

structure **15** appears at $E_{pa}$ = +0.73 V. In the same way 2,3-dimorpholinoquinoxaline **14** gives under the same conditions a cathodic peak at $E_{pc}$ = −0.93 V and an anodic peak at $E_{pa}$ = +0.78 V corresponding to **16**;

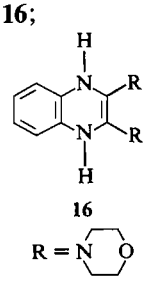

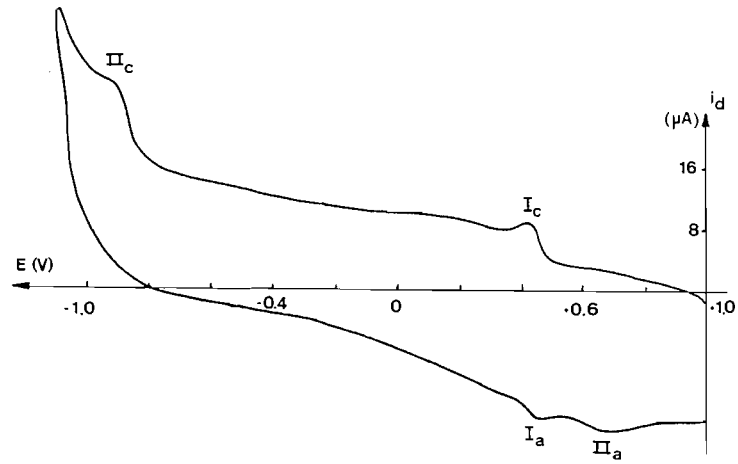


FIG. 1. Voltammogram of fluoflavin **2** at pH 1; 50% DMF; $v = 0.2\,V\,s^{-1}$.

Thus, it appears that in the case of

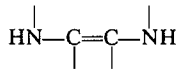

structures substituted by amino groups on the two central atoms their anodic peak is shifted to positive potentials in acidic medium. This can be related to the protonation of the amino substituents. The protonated amino groups are strongly electron-withdrawing making the reoxidation of the

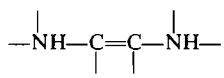

system more difficult. This can also be confirmed with the diacetyl derivative of fluoflavine **25** (Scheme 5) which gives a 2F cathodic peak at $E_{pc} = -0.51\,V$ and an anodic peak at $E_{pa} = -0.31\,V$ ($v = 0.2\,V\,s^{-1}$, pH 1, 50% DMF). Indeed in the case of **25** the two substituted amino groups remain unprotonated.

Scheme 3 can be proposed for the reduction of

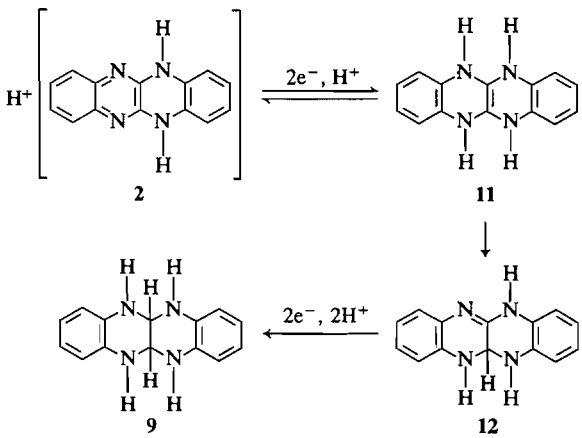


SCHEME 3

fluoflavine. It is not possible to accurately measure the rate of rearrangement of **11** to **12** as the cathodic wave of fluoflavine merges in the background discharge upon increasing the sweep rate, but its order of magnitude can be estimated to about 0.2 $s^{-1}$ from the peaks height.

*Electrochemical reduction of pyrazino[2,3-b]-pyrazines and pyrazino[2,3-b]quinoxalines*

Let us now turn back to the reduction of less conjugated systems such as pyrazino[2,3-*b*]pyrazines **17** and pyrazino[2,3-*b*]quinoxalines **18**. In the

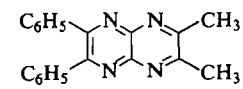

**17**

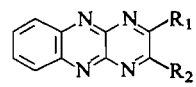

**18**

case of **17** one observes a 2F wave corresponding to the formation of a 1,4- (or 5,8-) dihydroderivative **19**, followed by a 4F wave in acidic medium. In the same way **18** presents a 2F wave corresponding to the formation of a 5,10-dihydroderivative **20** (8) followed by a 4F wave in acidic medium (7). In both cases preparative electrolysis at the level of the second plateau lead to gummy products from which no defined product could be characterized. A cyclic voltammogram of **17** ($v = 0.2\,V\,s^{-1}$, glassy carbon electrode, pH = 4.3, 50% DMF) presents a cathodic peak at $E_{pc} = -0.50\,V$ and an anodic peak at $E_{pa} = -0.26\,V$ corresponding to the **17/19** couple. A second cathodic peak is observed at $-1.16\,V$. If one scans at potentials more negative than this second peak at $v = 50\,V\,s^{-1}$ an anodic peak appears at $+0.59\,V$ which can be assigned to **21** by comparison with the voltammograms of **2**, **13**, and **14**. The same kind of voltammogram is observed in the case of **18** where an anodic peak appears at $+0.63\,V$ ($v = 0.2\,V\,s^{-1}$) if the second cathodic peak has been

Can. J. Chem. Downloaded from www.nrcresearchpress.com by 210.87.254.6 on 09/06/12
For personal use only.

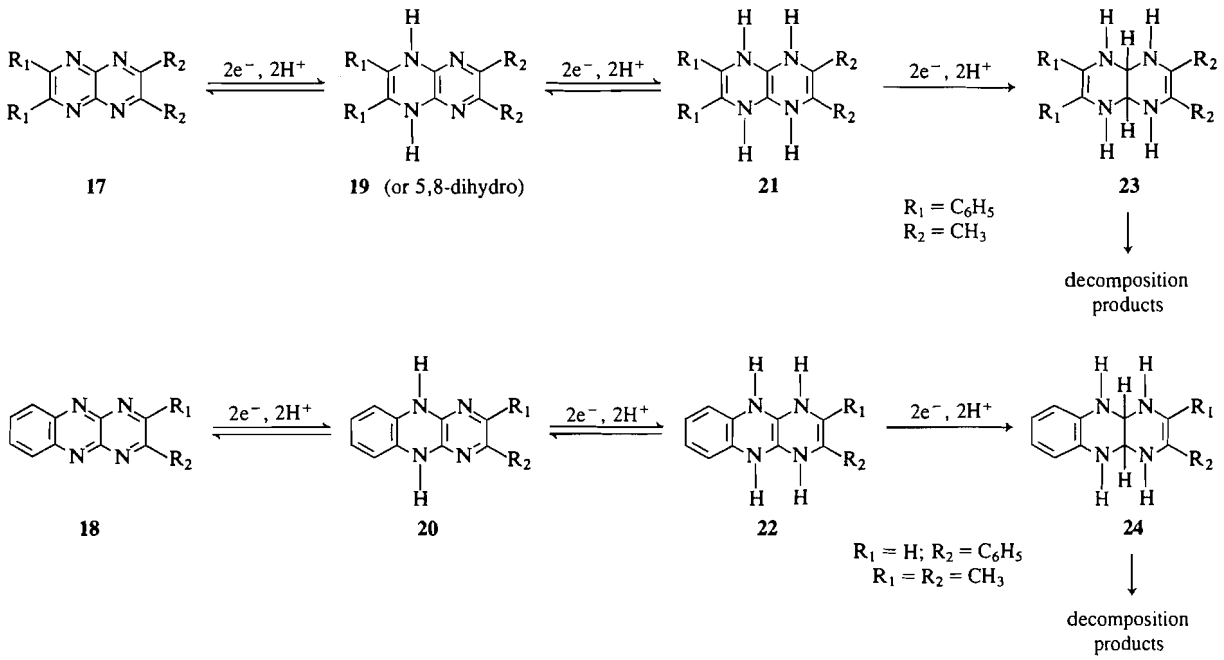


SCHEME 4

scanned beforehand. Scheme 4 can be proposed for the reduction of **17** and **18**. The instability of **23** and **24** is most likely related to their enediamine structure, while **9** which possesses a structure similar to that of *o*-phenylene diamine is stable.

*Electrochemical reduction of 5,12-diacetyl-5,12-dihydroquinoxalino[2,3-*b*]quinoxaline 25*

When heated in acetic anhydride, **2** furnishes **25** which is more soluble than **2** in the usual solvents. In $CH_3CN$, the voltammogram of **25** presents a first monoelectronic cathodic peak at $E_{pc1} = -1.5$ V followed by a bielectronic peak at $E_{pc2} = -2.35$ V (at 0.2 V $s^{-1}$). The first peak corresponds to the formation of the radical anion, while an electrolysis at the level of the second peak mainly gives fluoflavine.

An electrolysis of **25** in $CH_3CN$ in the presence of acetic anhydride gives the 5,6,11,12-tetraacetylated-5,6,11,12-tetrahydro derivative **26***a* (Scheme 5). In the presence of methylchloroformate the 5,6-diacetyl-11,12-dicarbomethoxy-5,6,11,12-tetrahydro derivative **26***b* is obtained. In hydroorganic medium ($CH_3CN$–$H_2O$; 50/50 v/v), **25** shows a 2F polarographic wave which is pH dependent, $E_{1/2}$ (V) = −0.37 − 0.08 pH. An electrolysis of a $10^{-3}$ *M* solution gives an oxidizable compound with a 2F anodic wave at a potential near that of the cathodic wave of **25**. At pH 1.5 this reduction compound gives a product more easily reduced than **25** so that 4F/mol are consumed during the electrolysis. A preparative electrolysis gives a mixture of *N*,*N*′-diacetyl orthophenylenediamine **27** and 1,2,3,4-tetrahydroquinoxaline-2-one **28**. It has been shown previously (12, 13) that the 2,3-dihydroxyquinoxaline **29** leads to **28** by electrochemical reduction, thus the formation of **27** and **28** from **25** should follow the reaction path described in Scheme 5. The primary reduction product responsible for the anodic wave on the voltammogram of **25** would be 5,6-diacetyl-5,6,11,12-tetrahydroquinoxalino[2,3-*b*]quinoxaline **30**, in agreement with a

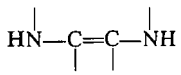

structure described above. The formation of **30** is also supported by the formation of **26** when the reduction is carried out in the presence of acetic anhydride. **30** would be hydrolyzed in acidic medium into **27** and **29**, the latter compound leading to **28**.

## Experimental section

Melting points are uncorrected. $^1$H-nmr spectra were recorded on a Bruker WH 80, a Varian A 60, and a Bruker 250 MHz spectrometer, using tetramethylsilane (TMS) as internal standard. The apparatus and techniques used for the electrochemical studies and pH measurements have been described previously (11). All the potentials are referred to the saturated calomel electrode (sce); the temperature of the solutions was 20°C. The microanalyses were performed by the "Service de Microanalyse-Université Pierre et Marie Curie". The following abbreviations are used in reporting nmr results: s = singlet, d = doublet, t = triplet, q = quadruplet, m = multiplet.

Can. J. Chem. Downloaded from www.nrcresearchpress.com by 210.87.254.6 on 09/06/12
For personal use only.

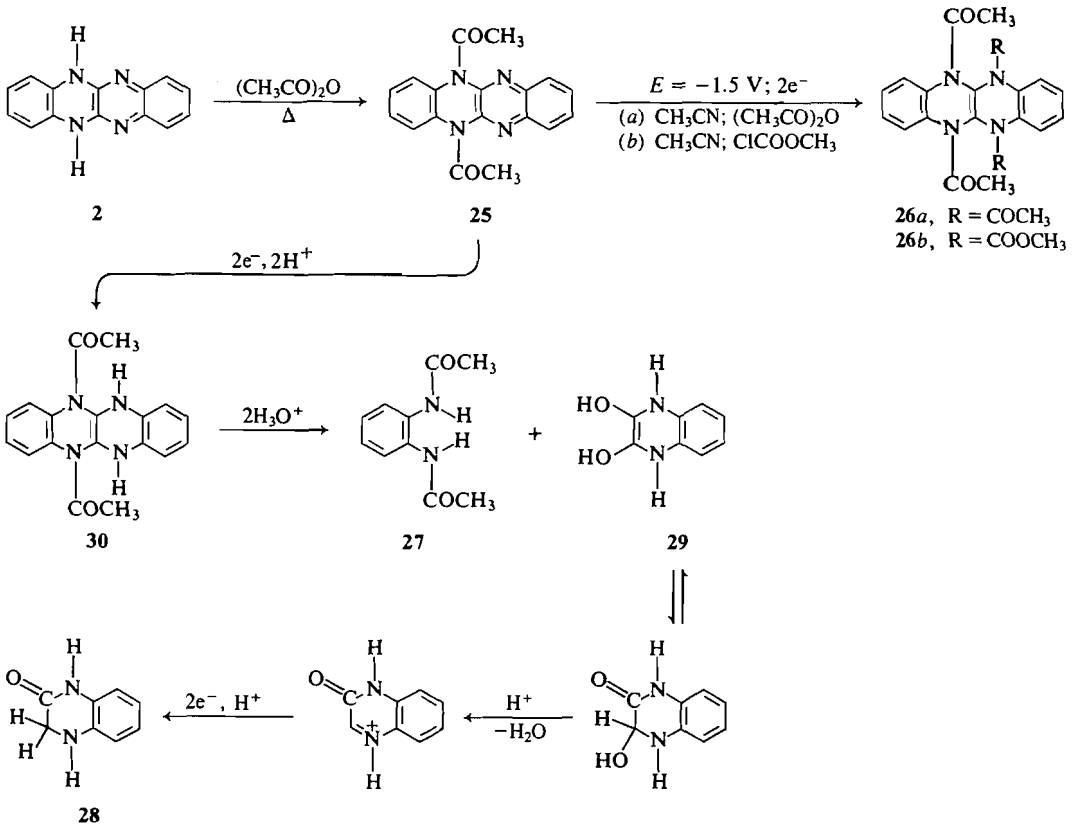


SCHEME 5

*Preparation of 1 and 2*

Quinoxalino[2,3-*b*]quinoxaline **1** was prepared from 5,12-dihydroquinoxalino[2,3-*b*]quinoxaline **2** (fluoflavine) according to ref. 14. Compound **2** was obtained (2) by condensation of *o*-phenylenediamine with 2,3-dichloroquinoxaline.

*5,12-Diacetyl-5,12-dihydroquinoxalino[2,3-*b*]quinoxaline, 25*

A suspension of 500 mg of **2** in 25 mL of acetic anhydride was refluxed for 24 h. Acetic anhydride was evaporated and the residue was crystallized from ethylacetate; 400 mg; mp 202–203°C. $^1$H-nmr ($CDCl_3$, 250 MHz): 5-$CH_3CO$ and 12-$CH_3CO$, s, 2.59 ppm (6H); 1-H, 2-H, 3-H, 4-H, AA'BB' pattern at 7.34 ppm, m (2H) and 7.94 ppm, m (2H); 7-H, 8-H, 9-H, 10-H, AA'BB' pattern at 7.82 ppm, m (2H) and 8.27 ppm, m (2H). *Anal.* calcd. for $C_{18}H_{14}N_4O_2$: C 67.91, H 4.43, N 17.60; found: C 67.85, H 4.51, N 17.56.

*Preparation of 5,12-diacetyl-5,12-dihydro-2,3-dimethylquinoxalino[2,3-*b*]quinoxaline, 7, and 6,11-diacetyl-6,11-dihydro-2,3-dimethylquinoxalino[2,3-*b*]quinoxaline, 8*

A mixture of 5 g of 2,3-dichloroquinoxaline and 6.8 g of 2,3-diamino-5,6-dimethylbenzene in 50 mL of ethyleneglycol was refluxed for 45 min. The cooled reaction mixture was filtered, washed with dimethylformamide and ethanol to give 5.2 g of a yellow–orange solid. This solid (500 mg) was then refluxed in 25 mL of acetic anhydride for 2 h. Acetic anhydride was evaporated and the residue was filtered, washed with water, and dried to give 590 mg of a mixture of **7** and **8** as shown by nmr. Compound **7** is less soluble in ethylacetate than **8**, the two products have been obtained pure after several crystallizations. **7**: mp 210°C, $^1$H-nmr ($CDCl_3$): 2-$CH_3$, 3-$CH_3$, 5-$COCH_3$, 12-$COCH_3$, 2.27 and 2.53 ppm, two s (2 × 3H); 1-H, 4-H, 7.50 ppm, s (2H); 7-H, 8-H, 9-H, 10-H, AA'BB' pattern, 7.60–8.15 ppm, m (4H). *Anal.* calcd. for $C_{20}H_{18}N_4O_2$: C 69.35, H 5.24, N 16.18; found: C 69.29, H 5.28, N 16.22. **8**: mp 215°C; $^1$H-nmr ($CDCl_3$): 2-$CH_3$, 3-$CH_3$, 6-$COCH_3$, 11-$COCH_3$, 2.50 ppm and 2.55 ppm, two s (2 × 3H); 1-H, 4-H, 7.72 ppm, s (2H); 7-H, 8-H, 9-H, 10-H, AA'BB' pattern at 7.23 ppm, m (2H) and 7.84 ppm, m (2H). *Anal.* calcd. for $C_{20}H_{18}N_4O_2$: C 69.35, H 5.24, N 16.18; found: C 69.48, H 5.19, N 16.09.

*Electrolysis of 1 in hydroorganic medium: preparation of 2*

An electrolysis was carried out at pH 6.75 and $E = -0.5$ V (sce). The cathodic compartment contained 100 mg of **1** in 200 mL of solution (dimethylformamide 50%). At the end of the electrolysis (2F per mol) the precipitate in the cell was filtered, washed with water and ethanol, then dried to give 95 mg of 5,12-dihydroquinoxalino[2,3-*b*]quinoxaline **2**.

*Electrolysis of 2 in hydroorganic medium: preparation of 9*

An electrolysis was carried out using 800 mg of **2** partially dissolved in 200 mL of solution (50% $CH_3CN$; 1 *N* $H_2SO_4$) at $E = -0.9$ V. At the end of the electrolysis (4.2 F per mol), acetonitrile was evaporated and the solution was neutralized with 2 *N* NaOH. The solid precipitated was filtered, washed with water, and dried to give 570 mg of 5,5a,6,11,11a,12-hexahydroquinoxalino[2,3-*b*]quinoxaline **9**, mp 270–275°C dec.[1]

[1]The solid state structure and the solution conformations of **9** are presently under investigation. This compound has a structure analogous to 1,4,5,8-tetraazadecalin (TAD) systems which have been the subject of recent sustained interest, see e.g., ref. 6.

Can. J. Chem. Downloaded from www.nrcresearchpress.com by 210.87.254.6 on 09/06/12
For personal use only.

Can. J. Chem. Downloaded from www.nrcresearchpress.com by 210.87.254.6 on 09/06/12
For personal use only.

$^1$H-nmr (DMSO-$d_6$): 5-H, 6-H, 11-H, 12-H, 4.45 ppm, m (2H) and 5.22 ppm, m (2H) exchanged with $D_2O$; 5a-H, 11a-H, 4.57 ppm, s (2H); 1-H, 2-H, 3-H, 4-H, 7-H, 8-H, 9-H, 10-H, 6.5 ppm, m (4H) and AA'BB' pattern centered at 7.32 ppm (4H). *Anal.* calcd. for $C_{14}H_{14}N_4$: C 70.56, H 5.92, N 23.51; found: C 70.64, H 6.01, N 23.35.

*Acetylation of 9: preparation of 10*

A solution of 650 mg of **9** in 5 mL of acetic anhydride was refluxed for 15 h, cooled at 0°C. The solid precipitated was filtered, washed with water, and dried to give 360 mg of 5,6,11-triacetyl-5,5a,6,11,11a,12-hexahydroquinoxalino[2,3-*b*]quinoxaline **10**, mp 222–223°C. $^1$H-nmr ($CDCl_3$): 5-$COCH_3$, 6-$COCH_3$, 11-$COCH_3$, three singlets at 1.90, 2.45, and 2.80 ppm (3 × 3H); 5a-H, 11a-H, two d at 4.56 ppm and 5.98 ppm, $J_{5a-11a}$ = 18 Hz; 1-H, 2-H, 3-H, 4-H, 7-H, 8-H, 9-H, 10-H, m, 7.1–8.4 ppm (8H); 12-H, broad s, 9.87 ppm (1H) exchanged with $D_2O$. *Anal.* calcd. for $C_{20}H_{20}N_4O_3$: C 65.92, H 5.53, N 15.38; found: C 66.07, H 5.56, N 15.30.

*Electrolysis of 25 in acetonitrile*

The cathodic solution contained 60 mL of solvent, 580 mg of **25**, and 6 g of tetrabutylammonium iodide; $E = -2.4$ V. At the end of the electrolysis (2.1F per mol) the solution was poured into 200 mL of water and the solid precipitated was filtered, washed with water, and dried to give 200 mg of **2**.

*Electrolysis of 25 in acetonitrile in the presence of acetic anhydride: preparation of 26*a

The cathodic solution contained 60 mL of solvent, 800 mg of **25**, 8 mL of acetic anhydride, and 6 g of tetrabutylammonium iodide; $E = -1.5$ V. A solid precipitated during the electrolysis. At the end, the precipitate was filtered, washed with water and acetonitrile, and dried to give 200 mg of 5,6,11,12-tetraacetyl-5,6,11,12-tetrahydroquinoxalino[2,3-*b*]quinoxaline ***26a***, mp > 300°C. $^1$H-nmr (TFA): 5-$COCH_3$, 6-$COCH_3$, 11-$COCH_3$, 12-$COCH_3$, s, 2.50 ppm (12H); 1-H, 2-H, 3-H, 4-H, 7-H, 8-H, 9-H, 10-H, m, 7.4–8.0 ppm (8H). *Anal.* calcd. for $C_{22}H_{20}N_4O_4$: C 65.33, H 4.99, N 13.86; found: C 65.26, H 5.04, N 13.97.

*Electrolysis of 25 in acetonitrile in the presence of methylchloroformate: preparation of 26*b

The cathodic solution contained 60 mL of solvent, 800 mg of **25**, and 6 ml of methylchloroformate and 6 g of tetrabutylammonium iodide; $E = -1.5$ V. At the end of the electrolysis ($i < 3$ mA) the catholyte was poured into 250 mL of water. The solid precipitated was filtered, washed with water, and dried to give 690 mg of 5,12-diacetyl-6,11-dicarbomethoxy-5,6,11,12-tetrahydroquinoxalino[2,3-*b*]quinoxaline, ***26b***, mp 294°C. $^1$H-nmr (TFA): 5-$COCH_3$, 12-$COCH_3$, s, 2.50 ppm (6H); 6-$COOCH_3$, 11-$COOCH_3$, s, 4.0 ppm (6H); 1-H, 2-H, 3-H, 4-H, 7-H, 8-H, 9-H, 10-H, m, 7.3–8.0 ppm (8H). *Anal.* calcd. for $C_{22}H_{20}N_4O_6$: C 60.54, H 4.62, N 12.84; found: C 60.61, H 4.64, N 12.93.

*Electrolysis of 25 in hydroorganic medium*

Electrolysis was carried out with 800 mg of **25** in 200 mL of solution (50% $CH_3CN$; 0.1 *N* $H_2SO_4$); $E = -0.7$ V. At the end of the electrolysis (4F per mol) acetonitrile was evaporated. The solution was neutralized with solid $NaHCO_3$ and extracted three times with 60 mL of chloroform. The organic layer was dried with $Na_2SO_4$ and evaporated to give 300 mg of a solid which was shown by nmr to be a mixture of *N*,*N'*-diacetylorthophenylenediamine **27** and 1,2,3,4-tetrahydroquinoxaline-2-one **28**. Compound **27** is soluble in ethyl acetate, contrary to **28**. This allows the separation of products which were both identified with authentic samples: **27** (15) and **28** (16).

*Preparation of 2-morpholinoquinoxaline 13 and 2,3-dimorpholinoquinoxaline 14*

Compound **13** was prepared according to ref. 17. 2,3-Dimorpholinoquinoxaline **14** was obtained by heating 2,3-dichloroquinoxaline (5 g) and morpholine (15 mL) in a stainless steel vessel for 24 h at 140°C. The solid obtained was poured into 200 mL of water, filtered, and crystallized in $CHCl_3/CH_3OH$; 80/20, v/v; 3.6 g, mp 223°C. $^1$H-nmr (TFA): 5-H, 6-H, 7-H, 8-H, AA'BB' pattern at 7.6–8.1 ppm (4H); $CH_2$ of morpholine ring, m at 3.8–4.5 ppm (16H). *Anal.* calcd. for $C_{16}H_{20}N_4O_2$: C 63.98, H 6.71, N 18.65; found: C 64.07, H 6.66, N 18.87.

*Electrolysis of 2-morpholinoquinoxaline 13 in hydroorganic medium*

**13** (560 mg) was dissolved in 100 mL of solution (50% $CH_3OH$, NaOH 0.1 *N*) and electrolyzed at −1.4 V. After consumption of about 2F per mol the methanol was evaporated and the solution was extracted with ether. The ethereal extracts were evaporated. The residual oil was dried over $P_2O_5$ to give 320 mg of an hygroscopic solid: 3,4-dihydro-2-morpholinoquinoxaline, mp = 90°C dec. $^1$H-nmr ($CDCl_3$ + $D_2O$): $CH_2$ of morpholine ring, m, 3.3–3.8 ppm (8H); 3-$CH_2$, s, 3.92 ppm (2H); 5-H, 6-H, 7-H, 8-H, m, 6.4–7.2 ppm (4H). *Anal.* calcd. for $C_{16}H_{22}N_4O_2$: C 63.55, H 7.30, N 18.53; found: C 63.47, H 7.38, N 18.52.

1. P. O. Kosonen and R. Gustafsson. Finn. Chem. Lett. 204 (1977).
2. S. Hunig, D. Scheutzow, H. Schlaf, and H. Quast. Liebig's Ann. **765**, 110 (1972).
3. G. M. Badger and P. J. Nelson. Aust. J. Chem. **16**, 445 (1963).
4. J. Stating, S. Reiffers, and H. Wynberg. Synthesis, 211 (1971).
5. G. F. Bettinetti, S. Maffei, and S. Pietra. Synthesis, 748 (1976).
6. (*a*) B. Fuchs, S. Weinman, U. Shmuelli, A. R. Katritzky, and R. C. Patel. Tetrahedron Lett. **22**, 354 (1981); (*b*) J. Jazwinski and R. A. Kolinski. Tetrahedron Lett. **22**, 1711 (1981).
7. J. Armand, K. Chekir, and J. Pinson. C.R. Acad. Sci. Ser. C, **284**, 391 (1977).
8. J. Armand, L. Boulares, K. Chekir, and Ch. Bellec. Can. J. Chem. **59**, 3237 (1981).
9. J. Armand, K. Chekir, and J. Pinson. Can. J. Chem. **52**, 3971 (1974).
10. J. Pinson and J. Armand. Coll. Czech. Chem. Commun. **36**, 585 (1971).
11. J. Armand, K. Chekir, and J. Pinson. Can. J. Chem. **56**, 1804 (1978).
12. J. Armand, Y. Armand, and L. Boulares. C.R. Acad. Sci. Ser. C, **286**, 17 (1978); Journées d'Electrochimie, Tours, France. (1978).
13. R. Gottlieb and W. Pfleiderer. Chem. Ber. **111**, 1753 (1978).
14. W. Ried and P. Schäfer. Chem. Ber. **103**, 2225 (1970).
15. K. J. Morgan and A. M. Turner. Tetrahedron, **22**, 1175 (1966).
16. J. Ploechl. Chem. Ber. **19**, 6 (1886).
17. G. W. Cheeseman. J. Chem. Soc. 3236 (1957).

# The synthesis of some 11-substituted tetrahydrocannabinol metabolites[1,2]

JOHN W. APSIMON,[3] T. LEE COLLIER, AND MICHAEL D. GUIVER

*The Ottawa-Carleton Institute for Research and Graduate Studies in Chemistry, Carleton Campus, Ottawa, Ont., Canada K1S 5B6*

Received April 14, 1982

JOHN W. APSIMON, T. LEE COLLIER, and MICHAEL D. GUIVER. Can. J. Chem. **60**, 2804 (1982).

9-Bromo-11-oxo-hexahydrocannabinol (**5**) was prepared from the ketocannabinoid **3***b* via the epoxysulfone **4**. The dehydrobromination of the bromoaldehyde **5** could be controlled to give either the thermodynamically more stable $\Delta^8$-aldehyde **2***c*, or the $\Delta^9$-aldehyde **1***c* by an intramolecularly assisted elimination. Reduction of the unsaturated aldehydes gave the allylic alcohol metabolites **2***a* and **1***a*, respectively.

JOHN W. APSIMON, T. LEE COLLIER et MICHAEL D. GUIVER. Can. J. Chem. **60**, 2804 (1982).

On a séparé le bromo-9 oxo-11 hexahydrocannabinol (**5**) à partir du cétocannabinoïde **3***b* via l'époxysulfone **4**. On peut controler la déhydrobromation du bromaldéhyde **5** pour obtenir soit le $\Delta^8$-aldéhyde (**2***c*) thermodynamiquement le plus stable, soit le $\Delta^9$-aldéhyde (**1***c*) par une élimination intramoléculaire assistée. La réduction des aldéhydes insaturés a conduit à l'alcool allylique des métabolites **2***a* et **1***a* respectivement.

[Traduit par le journal]

## Introduction

The potential importance of tetrahydrocannabinol (THC) metabolites in biological investigations has resulted in considerable effort directed towards their synthesis (1). In this paper, we report two synthetic routes to both 11-hydroxy-$\Delta^9$-THC (**1***a*)[4] and 11-hydroxy-$\Delta^8$-THC (**2***a*), the major psychotomimetically active metabolites of $\Delta^9$-THC (**1***b*) and $\Delta^8$-THC (**2***b*), respectively.

Most of the previous syntheses of **1***a* have involved transformations of $\Delta^9$-THC (**1***b*) or $\Delta^{9(11)}$-THC (**3***a*), or condensations of olivetol (**9**) with suitable terpenoid synthons. One attempted synthesis of particular interest relating to our strategy and starting from benzylated 11-nor-9-keto-HHC[5] (**3***b*) failed to provide **1***a* by phenoxide-assisted intramolecular elimination of chloride ion in **3***c*, but instead led to the thermodynamically more stable $\Delta^8$-isomer **2***a* (2). Despite many efforts, a simple efficient synthesis of the metabolite **1***a* has not been accomplished; the highest yielding synthesis at present is 20% of the metabolite from **1***b* reported by Pitt *et al.* (3). Many of the syntheses have so far produced low overall yields, lack of regioselectivity in the introduction of the $\Delta^9$-unsaturation and the oxygen function, and often involve difficult separations. In addition, reactions involving olivetol condensations frequently give rise to abnormal THC by-products (incorrect orientation of the pentyl sidechain).

The problems stem in part from the lability of the $\Delta^9$-unsaturation, traditionally attributed to the steric interactions between H-10 and the phenolic oxygen, and H-10a and the 6α-methyl group. Under acid-catalysis the double bond at $\Delta^9$ rapidly equilibrates to the $\Delta^8$ position, relieving the steric strain of these non-bonded interactions (4). More

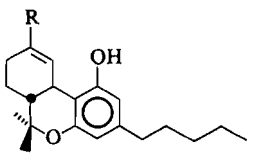

**1***a*, R = $CH_2OH$
*b*, R = $CH_3$
*c*, R = CHO

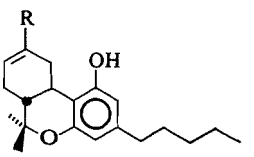

**2***a*, R = $CH_2OH$
*b*, R = $CH_3$
*c*, R = CHO

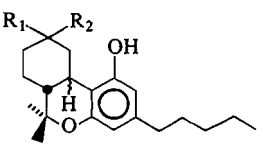

**3***a*, $R_1$, $R_2$ = $CH_2$ *trans*-6a,10a
*b*, $R_1$, $R_2$ = O, *trans*-6a,10a
*c*, $R_1$ = (C=O)N-morpholino, $R_2$ = Cl *trans*-6a, 10a
*d*, $R_1$, $R_2$ = O, *cis*-6a,10a

[1]Taken in part from M.Sc. thesis of Michael Guiver, Carleton University, Ottawa, 1980.

[2]Presented in part at the 63rd Canadian Chemical Conference, Ottawa, 1980.

[3]To whom all correspondence should be addressed.

[4]Two numbering systems for cannabinoids are extensively in use today. One is based on the formal chemical rules for numbering of benzopyran. The second nomenclature has a biogenetic basis, regarding cannabinoids as substituted monoterpenoids. The former system is used in this paper.

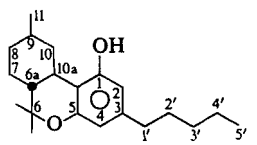

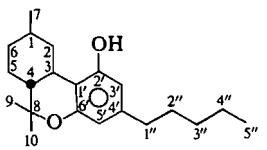

[5]Hexahydrocannabinol.

0008-4042/82/222804-06$01.00/0

©1982 National Research Council of Canada/Conseil national de recherches du Canada

Can. J. Chem. Downloaded from www.nrcresearchpress.com by 210.87.254.5 on 09/06/12
For personal use only.

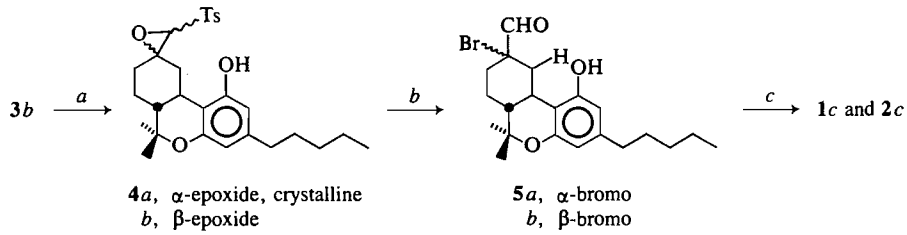


FIG. 1. Synthesis of **1***c* and **2***c*. Reagents: (*a*), $TsCH_2Cl$, phase transfer; (*b*), $MgBr_2$ in $Et_2O$ or THF; (*c*) intramolecular elimination, collidine; thermodynamic elimination, $Li_2CO_3$, LiBr, DMF.

recently, an alternative explanation has been put forward by Dalzell *et al.* based on torsional strain in the THC ring system (5).

In contrast to the above, the synthesis of **2***a* has been beset by fewer problems, since this is the thermodynamically preferred isomer. Two high yield syntheses have been reported up to the present time, both from the same laboratory (6, 7). In the first synthesis, however, a difficult separation is involved.

Our synthetic strategy, outlined in Fig. 1, is based on the dehydrobromination of **5**, obtained from ketone **3***b* via an intermediate epoxysulfone **4**.[6] Under normal dehydrobrominating conditions, the thermodynamically more stable $\Delta^8$ isomer **2***c* is formed. However, under carefully controlled conditions and the judicious choice of base, the $\Delta^9$-unsaturation may be generated by H-10α proton abstraction initiated by the phenoxide anion, giving rise to isomer **1***c* as outlined in structure **6**. Phen-

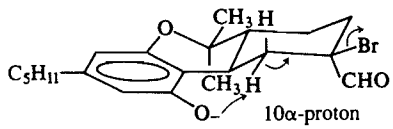


**6**

oxide-assisted intramolecular eliminations of a similar nature have already been successfully demonstrated in the contrathermodynamic conversion of $\Delta^8$-THC (**2***b*) to $\Delta^9$-THC (**1***b*) (8). However, Pitt and co-workers were unable to synthesise the metabolite **1***a* by a similar strategy (2).

## Results and discussion

The starting material, 11-*nor*-9-keto-6a,10a-*trans*-HHC (**3***b*) was prepared using a method developed by Archer and co-workers by condensing olivetol (**9**) with 2-(4-methoxy-1,4-cyclohexadienyl)-2-propanol (**10**) in the presence of stannic

[6]All compounds whose syntheses are described in this work are racemic mixtures; the naturally occurring THC ring junction (−)-(6aR,10aR) is shown only for convenience.

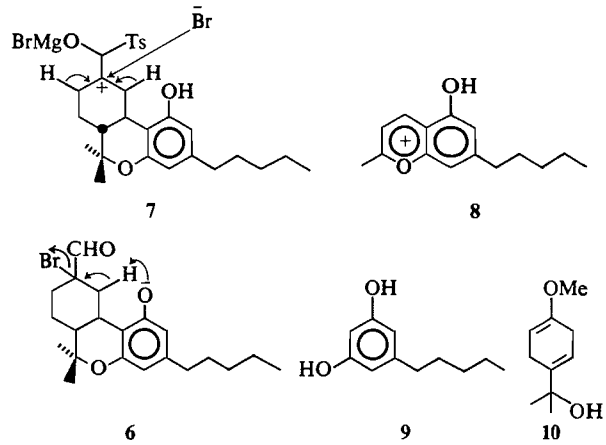


chloride and one molar equivalent of water to give 11-*nor*-9-keto-6a,10a-*cis*-HHC (**3***d*) in 24% yield (9). The acid-catalyzed isomerisation of the *cis*-ketone to the required starting material **3***b* with the *trans*-ring junction was accomplished in 58% yield using $AlCl_3$.

The synthesis of the bromoaldehydes **5** is based on the novel one-carbon homologation developed by Durst and co-workers in which a ketone is converted to an epoxysulfone and then cleaved with $MgBr_2$ in ether or THF to give an α-bromoaldehyde (10). Epoxysulfones may be prepared directly from ketones in high yields by using the phase transfer conditions of Makosza, obviating the isolation of an intermediate chlorohydrin (11). The overall transformation involves nucleophilic attack of the base-generated α-chloro-α-sulfonyl carbanion on the carbonyl group followed by intramolecular displacement of the chloride, to give a Darzens type condensation. Working with simple epoxysulfones, Durst and co-workers obtained bromoaldehydes cleanly and in high yield, demonstrating the value of this mild homologation method.

In this work an isomeric mixture of the unstable epoxides **4** was prepared in high yield under

Can. J. Chem. Downloaded from www.nrcresearchpress.com by 210.87.254.5 on 09/06/12
For personal use only.

Can. J. Chem. Downloaded from www.nrcresearchpress.com by 210.87.254.5 on 09/06/12
For personal use only.

phase-transfer conditions from the ketone **3***b*, chloromethyl-*p*-tolyl sulfone (prepared by a method based on ref. 12)[7] and 50% aqueous NaOH solution using benzyltriethylammonium chloride as the catalyst. The high sensitivity of these epoxides to acid-catalyzed decomposition necessitated using water adjusted to slightly basic pH during the work-up of the reaction.

Analysis of the crude products by thin layer chromatography indicated two major components with similar characteristics. The more polar of the two compounds could be isolated by crystallization and its nmr spectrum was compared with that of the mixture. Only two signals were significantly different between the two isomers in these spectra; the epoxide protons at δ 3.95 (**4***b*) and δ 3.90 (**4***a*) and the aromatic H-2 protons at δ 6.13 (**4***a*) and δ 6.06 (**4***b*). The ratio of the two isomers as determined by the relative integration of the H-2 protons was 43 (**4***a*):57 (**4***b*). The stereochemistry of the epoxides was assumed to be α and β, respectively, based on the ratio and stereochemical inversion about C-9 of the bromoaldehydes **5***a* and *b* formed in the next step of the synthetic sequence.

The Lewis acid cleavage of the epoxysulfones **4** with $MgBr_2$ in ether or THF gave a good yield of bromoaldehydes. The nature of the products formed was determined by the solvent used. In the case of THF, only isomeric bromoaldehydes **5***a* and **5***b* were obtained. In ether, where the reaction occurred more rapidly, one epimer **5***b* as well as unsaturated aldehydes **1***c* and **2***c* were formed. The stereochemistry of the bromoaldehydes was determined by comparison of the nmr spectra of the isomeric mixture **5***a* and **5***b* and the single isomer **5***b*; the latter displays a large difference in the upfield chemical shift of the 6α-methyl group (13).[8] Molecular models demonstrate that in epimer **5***b*, the 6α-methyl group is within the shielding region of the carbonyl group, whereas H-10a lies within the deshielding region. Thus, H-10a is shifted 29 Hz downfield (δ 3.97, broadened doublet, $J_{vic}$ = 13 Hz) and the 6α-methyl group is shifted 18 Hz upfield (δ 0.99) with respect to **5***a*. The ratio of the bromoaldehyde epimers arising from the epoxide cleavage in THF was also 43 (**5***b*):57 (**5***a*) as determined by integration of the aldehyde signals in the proton spectrum. The overall data suggests an $S_N2$ type reaction on epoxide cleavage by bromide ion where inversion about C-9 occurs (i.e. **4***a* → **5***b*, **4***b* → **5***a*).

As mentioned above only the β-bromoaldehyde isomer **5***b* was isolated where ether was used. We originally assumed that the α-bromo isomer, **5***a*, in which there is a 1,2-diaxial arrangement of hydrogen and bromine, spontaneously dehydrobrominates in ether, forming **1***c* and **2***c* while leaving the less-reactive **5***b* unchanged. This does not appear to be the case, however, since epoxide cleavage in THF, followed by replacement of solvent by ether, showed no evidence for unsaturated aldehydes **1***c* and **2***c* after hydrolysis of the complexes. It is therefore suggested that the dehydrobromination process observed during epoxide cleavage in ether proceeds by means of an intermediate such as **7** in which the three fates indicated lead to the observed products. Neutralisation of this carbocationic species from the least hindered β face leads to **5***b*. On the other hand, in the reaction using THF as a solvent, $S_N2$ cleavage of epoxides **4***a* and **4***b* by bromide ion would lead directly to the products observed.

The unstable $\Delta^9$-aldehyde **1***c* (5%) and the $\Delta^8$-aldehyde **2***c* (18%) were separated by careful column chromatography and crystallized. The olefinic proton of **1***c* (δ 7.88) displays an unusually large downfield chemical shift with respect to the olefinic proton of **2***c* (δ 6.88) in the nmr spectrum (3)[9] due to the highly deshielded region in which it resides. In the mass spectrum of **2***c*, which has been studied by Inayama and co-workers (14), the enhanced abundance of the common cannabinoid fragment ion *m/e* 231, **8**, is diagnostic for the $\Delta^8$-unsaturation and arises from a retro-Diels–Ader (RDA) reaction in the isoprenoid ring of the molecule. In contrast, the $\Delta^9$-aldehyde **1***c* displays a very low abundance of this ion. The $\Delta^9$-aldehyde **1***c* has been identified as a metabolite from the incubation products of **1***b* with rat liver microsomes (15). In this case, however, the investigators observed an abundant fragment ion at *m/e* 231 of the derivatised product.

Attempts to synthesise **1***c* by intramolecular displacement of bromide in **5***b* (see **6**) using potassium *t*-amylate or sodium hydride under various conditions led to indefinite results despite their successful use in the synthesis of $\Delta^9$-THC (**1***b*) (8). No evidence of either **1***c* or **2***c* in the reaction products was observed. It is clear from projection **6** that no ideal geometry for elimination exists for **5***a* or **5***b* by an intramolecular pathway. However, use of pyridine as a weak base to remove only the most

[7]The use of the bromo-analogue was found to be unsuitable, when methyl-*p*-tolylsulfone was formed as a by-product.

[8]In 6a,10a-*trans* THC's, the 6α-methyl group appears upfield with respect to the 6β-methyl substituent. See ref. 13 for a detailed nmr study.

[9]Nuclear magnetic resonance and ir spectra of the authentic materials were kindly supplied by Dr. Colin G. Pitt of the Research Triangle Institute, North Carolina, and Dr. Raj K. Razdan of the Sisa Institute for Research, Inc., Massachusetts.

Can. J. Chem. Downloaded from www.nrcresearchpress.com by 210.87.254.5 on 09/06/12
For personal use only.

acidic phenolic proton provided evidence for this process when aldehydes **1***c* and **2***c* were cleanly obtained in the ratio of 15:85 (based on integrating the olefinic proton signals in the nmr spectrum of the mixture). By using the more hindered base, collidine, this ratio was increased to 52:48 and the unsaturated aldehydes were easily separated by column chromatography. Other bases such as 2,6-di-*t*-butyl pyridine and quinoline gave respectively no reaction and predominantly **2***c*.

Heating **5***b* with $Li_2CO_3$ and LiBr in DMF (16) (conditions which presumably exclude phenoxide participation), the 1,2-elimination of HBr proceeded smoothly to provide the $\Delta^8$-aldehyde **2***c* in 90% isolated yield together with a 3% yield of the $\Delta^9$-aldehyde **1***c*.

The aldehydes **1***c* and **2***c* were reduced to the metabolites **1***a* and **2***a* with $LiAlH_4$ in THF. In a preliminary communication from another laboratory, the reduction of **1***c* with $LiAlH_4$ was reported to proceed smoothly, but no conditions were specified (17). In our laboratories, however, various amounts of aromatic impurities in **1***a* were observed in the samples that were reduced under our conditions.

This route represents a facile synthesis of 11-hydroxy-$\Delta^8$-THC (**2***a*) from 11-*nor*-9-keto-HHC (**3***b*) via **5***b* with an overall yield of 64%. This compares favourably in terms of yield to the method reported by Pitt *et al.* (33%) (2) for the preparation of **2***a* from benzylated **3***b*. The overall yield of 11-oxo-$\Delta^9$-THC (**1***a*) via **5***b* was 36.5% based on recovered starting material. This synthetic route has the advantage that THC metabolite aldehydes and acids can also be made available if required. Our continuing work in this area is directed to the efficient regioselective formation of the thermodynamically less stable $\Delta^9$ isomers of various THC metabolites.

## Experimental

Melting points were determined on a Fisher-Johns melting point block and are uncorrected, and the infrared spectra were determined on a Perkin-Elmer 237B grating spectrophotometer. Nuclear magnetic resonance spectra were obtained on Varian Associates Model HA-100 instruments with deuteriochloroform as the solvent and tetramethylsilane as internal standard. Chemical shifts are expressed in the δ scale and the following abbreviations are used in describing the nmr signals: singlet (s), doublet (d), triplet (t), multiplet (m), and broadened (br). Combustion analyses were performed by Spang Microanalytical Laboratories, Eagle Harbour, Michigan and Guelph Chemical Laboratories Ltd., Guelph, Ontario. The mass spectra were determined with an H.P. 5985 G.C.-M.S. Quadrupole instrument at the Health and Welfare Canada operated at an ionising potential of 70 eV.

Pre-coated plates from E. Merck Reagents (silica gel F-254, 0.25 mm layer thickness) were used for thick layer; bands were observed by viewing under a uv source or by heating the plate sprayed with a 1% solution of ceric ammonium nitrate in 50% aqueous sulphuric acid.

Tetrahydrofuran was distilled from $LiAlH_4$ and benzene was distilled from, and stored over, sodium metal. Mallikrodt anhydrous ether was used in the preparation of $MgBr_2$. All other solvents were glass distilled prior to use. The term "work-up" refers to: extraction of the reaction mixture with solvent (× 3), washing the combined extracts with water (× 3) and saturated aqueous sodium chloride, drying of the organic phase with magnesium sulphate, and removal of solvent under reduced pressure. Water used in the work-up of reactions was adjusted to pH 7.2 by the addition of aqueous sodium bicarbonate and monitoring the change with a pH meter.

*11*-nor-*9-Keto-6a,10a*-cis-*HHC* (*3*d)

The *cis*-ketocannabinoid **3***d* was prepared following mainly the procedure of Archer *et al.* (9). To a stirred solution of olivetol **9** (18.025 g, 100 mmol) and **10** (20.188 g, 120 mmol) in dichloromethane (400 mL) and under nitrogen at −15°C was added water (1.8 mL, 100 mmol), followed by the dropwise addition of $SnCl_4$ (26 mL, 222 mmol) over a 2 h period. The mixture was stirred at 0°C for 7 h after which time it was poured into water (500 mL) and extracted several times with ether. The ethereal extracts were washed three times with aqueous NaOH (1 *M*), three times with water, and then dried over $MgSO_4$. After filtering off the solids and removing the solvent, the material was crystallized from hexanes to yield the *cis*-ketocannabinoid **3***d* (7.58 g, 24%) as the major product (ref. 9 reports a 12% yield). Traces of the less polar *trans* **3***b* isomer were observed by tlc analysis (20% EtOAc in benzene). Analytically pure *cis*-ketocannabinoid **3***d* was obtained by H.P.L.C. (Waters Prep System – 500, 40% EtOAc in hexanes) and had the following characteristics: mp 149.5–150.5°C (lit. 149.5–150.5°C (8*a*)); ir (KBr pellet), 3255 $cm^{-1}$ (OH), 1690 $cm^{-1}$ (C=O); nmr δ 0.87 (3H, t, $J$ = 6 Hz, C-5′ $CH_3$), 1.34 (3H, s, C-6α $CH_3$), 1.40 (3H, s, C-6β $CH_3$), 2.42 (2H, m, Ar—$CH_2$), 6.22 (2H, s, H-2 and H-4), 7.38 (1H, s, Ar—OH $D_2O$ exchangeable).

*11*-nor-*9-Keto-6a,10a*-trans-*HHC* (*3*b)

The *trans*-ketocannabinoid **3***b* was prepared mainly by the procedure of Archer *et al.* (9). Aluminum chloride (13.5 g, 100 mmol) was added to a solution of *cis*-ketocannabinoid (9.00 g, 28.4 mmol) in dichloromethane (450 mL). The mixture was stirred for 3 h at room temperature under nitrogen and then additional $AlCl_3$ (7.5 g, 562 mmol) was added and the stirring continued for a further 2 h. After work-up with dichlormethane, the solid was crystallized ($CH_2Cl_2$/hexanes) to give **3***b* as the major product by tlc analysis (20% EtOAc in benzene), with only a trace of the *cis*-isomer (**3***d*) remaining. Selective recrystallization (methanol/water) afforded pure **3***b* (5.22 g, 58%) obtained as the higher melting polymorph: mp 160–163°C (lit. 163–165°C (8*a*)); ir (KBr pellet), 3285 $cm^{-1}$ (OH), 1695 $cm^{-1}$ (C=O); nmr, δ 0.89 (3H, br t, $J$ = 6 Hz, C-5′ $CH_3$), 1.13 (3H, s, C-6α $CH_3$), 1.48 (3H, s, C-6β $CH_3$), 2.46 (2H, br t, $J$ = 8 Hz, Ar—$CH_2$), 4.19 (1H, br d, $J$ = 15 Hz, H-10a), 6.23 (1H, d, $J$ = 2 Hz, H-2), 6.31 (1H, d, $J$ = 2 Hz, H-4), 7.93 (1H, s, Ar—OH $D_2O$ exchangeable).

*9, 11-Epoxy-11-tosyl-6a,10a*-trans-*HHC* (*4*a,b)

Employing the phase transfer conditions of Makosza *et al.* (11), ketocannabinoid **3***b* (316.4 mg, 1.0 mmol), chloromethyl-*p*-tolylsulfone (204.6 mg, 1.0 mmol), and benzyltriethylammonium chloride (50 mg, 0.22 mmol) were dissolved in 8 mL of acetonitrile. 20 mL of aqueous sodium hydroxide (50%) was added and the mixture stirred vigourously under nitrogen in a stoppered flask. After 2 h, the yellow slurry was poured into water (200 mL) and worked up with ether to yield **4** (464.5 mg,

Can. J. Chem. Downloaded from www.nrcresearchpress.com by 210.87.254.5 on 09/06/12
For personal use only.

96%), sufficiently pure (tlc 10% EtOAc in benzene) to use for the next step. The more polar isomer **4***a* was crystallized from ether or hexane and had the following characteristics: mp 124.5–128°C (dec); ir (KBr pellet), 2950 $cm^{-1}$ (OH), 820 $cm^{-1}$ (epoxide); nmr δ 0.88 (3H, br t, $J$ = 6 Hz, C-5′ $CH_3$), 1.09 (3H, s, C-6α $CH_3$), 1.39 (3H, s, C-6β $CH_3$), 2.45 (3H, s, Ts—$CH_3$), 3.90 (1H, s, epoxide-H), 4.09 (1H, br d, $J$ = 14 Hz, H-10a), 5.44 (1H, br s, Ar—OH $D_2O$ exchangeable), 6.13 (1H, br s H-2), 6.22 (1H, br s H-4), 7.36 (2H, d, $J_{AB}$ = 8 Hz, Ts), 7.87 (2H, d, $J_{AB}$ = 8 Hz, Ts); ms, *m/e* (rel. intensity) 484 (2), 329 (29), 328 (37), 286 (12), 285 (12), 272 (38), 231 (34), 193 (55), 91 (100). *Anal.* calcd. for $C_{28}H_{36}O_5S$: S 6.62; found: S 6.44

*9-Bromo-11-oxo-6a,10a*-trans-*HHC* (**5**a,b)

Magnesium bromide was prepared by stirring together magnesium (243 mg, 10 mmol) and 1,2-dibromoethane (0.86 mL, 10 mmol) in dry THF (20 mL) under nitrogen until the reaction was completed. A solution of **4***a*, *b* (370 mg, 0.76 mmol) in THF (20 mL) was added via syringe, and the mixture was stirred for 2 days at room temperature. The mixture was poured into water and worked up with ether. The material was purified by eluting from a thin column of Florisil (15 g, 100–200 mesh, 7% ether in light petroleum ether) to yield **5***a*, *b* (228.5 mg, 73%): ir ($CCl_4$), 3600 $cm^{-1}$ (sharp, free OH), 3475 $cm^{-1}$ (broad, H-bonded OH), 1727 $cm^{-1}$ (C=O); nmr, δ 0.88 (3H, t, $J$ = 6 Hz, C-5′ $CH_3$), 0.99 and 1.17 (3H, s, C-6α $CH_3$), 1.36 and 1.41 (3H, s, C-6β $CH_3$), 2.43 (2H, br t, $J$ = 6 Hz, Ar—$CH_2$), 3.68 and 3.97 (1H, br d, $J$ = 14 Hz and $J$ = 13 Hz, H-10a), 4.85 and 4.98 (1H, br s, Ar—OH $D_2O$ exchangeable), 6.07 and 6.10 (1H, s, H-2), 6.24 (1H, br s, H-4), 9.37 and 9.47 (1H, s, CHO); ms, *m/e* (rel. intensity), 410 (28), 408 (28), 354 (30), 352 (33), 330 (21), 329 (76), 328 (11), 311 (14), 285 (12), 245 (15), 231 (15), 193 (100).

*Reaction of 9,11-epoxy-11-tosyl-6a,10a*-trans-*HHC* (**4**a,b) *with $MgBr_2$ in ether*

Magnesium bromide was prepared by stirring together magnesium (243 mg, 10 mmol) and 1,2-dibromoethane (0.86 mL, 10 mmol) in anhydrous ether (40 mL) under nitrogen until the reaction was completed. A solution of **4***a*, *b* (484 mg, 1.0 mmol) in anhydrous ether (40 mL) was added dropwise to the cooled reagent (0°C) and the stirring was continued for 2 h, after which time the reaction mixture was poured into chilled water (200 mL). After work-up with ether, tlc analysis (10% EtOAc in benzene) indicated three major products: **5***b*, **1***c*, and **2***c*. The less polar compound **5***b* was easily isolated (65%) by elution from a thin column of Florisil (15 g, 100–200 mesh, 7% ether in light petroleum ether). Compounds **1***c* and **2***c* were separated by further careful elution from the column (12% ether in light petroleum ether) in 5% and 18% yields respectively (**1***c* isomerises to **2***c* when left on the column for a period of 12 h or more). Analytical samples of **1***c* and **2***c* were obtained by crystallization (ether/*n*-heptane and hexane respectively).

*9β-Bromo-11-oxo-6a,10a*-trans-*HHC* (**5**b): ir ($CCl_4$), 3600 $cm^{-1}$ (sharp, free OH), 3475 $cm^{-1}$ (broad, bonded OH), 1725 $cm^{-1}$ (C=O); nmr, δ 0.88 (3H, br t, $J$ = 6 Hz, C-5′ $CH_3$), 0.99 (3H, s, C-6α $CH_3$), 1.36 (3H, s, C-6β $CH_3$), 2.43 (2H, br t, $J$ = 7 Hz, Ar—$CH_2$), 3.97 (1H, br d, $J$ = 13 Hz, H-10a), 5.10 (1H, br s, Ar—OH $D_2O$ exchangeable), 6.10 (1H, br s, H-2), 6.24 (1H, br s, H-4), 9.37 (1H, s, CHO); ms, *m/e* (rel. intensity), 410 (13), 408 (13), 354 (17), 352 (16), 330 (28), 329 (91), 328 (12), 311 (21), 285 (13), 245 (22), 231 (17), 193 (100). *Anal.* calcd. for $C_{21}H_{29}O_3Br$: C 61.62, H 7.14, Br 19.52; found: C 61.87, H 7.34, Br 19.34.

*11-Oxo-6a,10a*-trans-Δ⁹-*THC* (**1***c*): mp 77–79.5°C; ir ($CCl_4$), 3600 $cm^{-1}$ (sharp, free OH), 3350 $cm^{-1}$ (broad, bonded OH), 1690 $cm^{-1}$ (C=O); nmr δ 0.88 (3H, br t, $J$ = 6 Hz, C-5′ $CH_3$), 1.15 (3H, s, C-6α $CH_3$), 1.45 (3H, s, C-6β $CH_3$), 2.48 (2H, m, Ar—$CH_2$), 3.51 (1H, br d, $J$ = 15 Hz, H-10a), 5.24 (1H, br s, Ar—OH $D_2O$ exchangeable), 6.16 (1H, br s, H-2), 6.30 (1H, br s, H-4), 7.88 (1H, br s, H-10), 9.45 (1H, s, CHO); ms, *m/e* (rel. intensity), 328 (100), 313 (8), 299 (34), 285 (18), 243 (10), 231 (6), 217 (8), 193 (12). *Anal.* calcd. for $C_{21}H_{28}O_3$: C 76.79, H 8.59; found: C 76.66, H 8.95.

*11-Oxo-6a,10a*-trans-Δ⁸-*THC* (*2c*): mp 119–120.5°C; ir ($CCl_4$), 3610 $cm^{-1}$ (sharp, free OH), 3425 (broad, bonded OH), 1680 $cm^{-1}$ (C=O); nmr δ 0.87 (3H, br t, $J$ = 6 Hz, C-5′ $CH_3$), 1.13 (3H, s, C-6α $CH_3$), 1.41 (3H, s, C-6β $CH_3$), 2.42 (2H, br t, $J$ = 7 Hz, Ar—$CH_2$), 3.92 (1H, br d, $J$ = 18 Hz, H-10α), 6.16 (1H, br s, H-2), 6.22 (1H, br s, H-4), 6.51 (1H, s, Ar—OH $D_2O$ exchangeable), 6.88 (1H, m, H-8), 9.46 (1H, s, CHO); ms (14), *m/e* (rel. intensity), 328 (82), 286 (28), 285 (19), 273 (20), 272 (100), 245 (8), 231 (74), 193 (100). *Anal.* calcd. for $C_{21}H_{28}O_3$: C 76.79, H 8.59; found: C 76.56, H 8.52.

*11-Oxo-6a,10a*-trans-Δ⁸-*THC* (*2c*)

To a solution of the bromoaldehyde **5***b* (204.5 mg, 0.50 mmol) in dimethylformamide (50 mL) was added lithium carbonate (74 mg, 1.0 mmol) and lithium bromide (16) (44 mg, 0.50 mmol). The reaction was heated at 100°C under nitrogen for 6 h, then cooled and poured into 100 mL of water. After work-up with ether and careful chromatography (Florisil 12% ether in light petroleum ether) two products were isolated: Δ⁹-aldehyde **1***c* (5.0 mg 3%) and Δ⁸-aldehyde **2***c* (148.7 mg, 90%). An analytical sample of **2***c* obtained by recrystallization from hexanes had identical spectral characteristics compared with the previously isolated compound: *Anal.* calcd. for $C_{21}H_{28}O_3$: C 76.79, H 8.59; found: C 76.53, H 8.94.

*11-Oxo-*Δ⁹-*THC* (**1***c*) *(impure sample)*: ms, *m/e* (rel. intensity), *346* (28), 328 (100), 313 (10), *311* (27), *309* (24), 299 (59), *290* (19), 285 (27), *257* (22), 243 (18), 231 (13), 217 (18), 193 (36).

*Synthesis of 11-oxo-6a,10a*-trans-Δ⁹-*THC* (**1**c) *from 9β bromo-11-oxo-6a,10a*-trans *HHC* (**5**b)

Collidine[10] (10 mL) was added to a stirred solution of bromoaldehyde (**5***b*) (79.0 mg, 0.19 mmol) in refluxing benzene (25 mL) under argon, in the presence of 4A molecular sieves. The mixture was refluxed for 72 h. Chromatography on Florisil after work-up (elution with 7% ether in light petroleum) provided **5***b* (38.4 mg, 48.6%), **2***c* (15.4 mg, 24.3%), and **1***c* (16.7 mg, 26.3%).

*11-Hydroxy-6a,10a*-trans-Δ⁹-*THC* (*1a*)

Lithium aluminum hydride (3 mg, 0.08 mmol) was added to a solution of the Δ⁹-aldehyde **1***c* (36 mg, 0.11 mmol) in THF (10 mL), and the mixture was stirred under nitrogen at room temperature for 4 h. Saturated ammonium chloride solution was added to the reaction until no more aluminum salts precipitated out, and the supernatant layer was poured off. Repeated washings of the precipitate with ether followed by work-up of the combined organics furnished the impure allylic alcohol **1***a* (36 mg, 99%); the material was partially purified by precipitation from carbon tetrachloride which was difficult to remove entirely: ir ($CCl_4$), 3600 $cm^{-1}$ (sharp, free OH), 3340 $cm^{-1}$ (broad, bonded OH); nmr δ 0.89 (3H, br t, $J$ = 6 Hz, C-5′ $CH_3$), 1.10 (3H, s, C-6α $CH_3$), 1.43 (3H, s, C-6β $CH_3$), 2.43 (2H, br t, $J$ = 7 Hz, Ar—$CH_2$), 3.26 (1H, br d, $J$ = 11 Hz, H-10a), 4.03 (2H, br s, H-11), 6.13 (1H, br s, H-2), 6.25 (1H, br s, H-4), 6.72 (1H, br s, H-10); ms (14); *m/e* (rel. intensity), 330 (19), 312 (8), 300 (22), 299 (100), 297 (18), 269 (7), 231 (13), 217 (11), 193 (13). The spectroscopic data were identical to those of the authentic material.[9]

*11-Hydroxy-6a,10a*-trans-Δ⁸-*THC* (*2a*)

To a solution containing the Δ⁸-aldehyde **2***c* (220 mg, 0.67 mmol) in 30 mL of THF was added lithium aluminum hydride

[10]Collidine was distilled from and stored over NaOH. Benzene was degassed prior to use.

(13 mg, 0.34 mmol). The mixture was stirred under nitrogen for 3 h at room temperature until no more starting material remained. Saturated ammonium chloride was added dropwise until the solution lost its yellow colour and no more aluminum hydrates precipitated out. After the organic layer was poured off, the precipitate was washed repeatedly with ether and the combined extracts were worked-up. Precipitation from carbon tetrachloride (7 mL) afforded the metabolite **2***a* (196 mg, 88%) as a white amorphous solid: ir ($CCl_4$), 3600 $cm^{-1}$ (sharp, free OH), 3340 $cm^{-1}$ (broad, bonded OH); nmr $\delta$ = 0.87 (3H, br t, $J$ = 6 Hz, C-5′ $CH_3$), 1.05 (3H, s, C-6$\alpha$ $CH_3$), 1.35 (3H, s, C-6$\beta$ $CH_3$), 2.41 (2H, br t, $J$ = 7 Hz, Ar—$CH_2$), 3.48 (1H, br d, $J$ = 17 Hz, H-10$\alpha$), 4.04 (2H, br s, H-11), 5.69 (1H, m, H-8), 6.10 (1H, d, $J$ = 1.5 Hz, H-2), 6.23 (1H, d, $J$ = 1.5 Hz, H-4); ms (14), *m/e* (rel. intensity), 330 (55), 312 (13), 297 (15), 274 (26), 270 (13), 269 (29), 257 (18), 256 (18), 246 (11), 245 (11), 231 (100), 214 (18), 193 (59), 174 (30), 173 (12). *Anal.* calcd. for $C_{21}H_{30}O_3$: C 76.32, H 9.15; found: C 76.19, H 9.43 (recrystallization from 10% ether in light petroleum ether is preferable since carbon tetrachloride is difficult to remove completely from purified samples of **2***a*).

## Acknowledgements

We thank the Natural Sciences and Engineering Research Council of Canada and Health and Welfare Canada (NMUD program) for generous financial assistance towards this work. M.D.G. thanks Carleton University for financial assistance.

We thank Raj Capoor of the University of Ottawa for nmr spectra and Dr. G. Nelville and J.-C. Ethier of Health and Welfare Canada for gc/ms determinations. National Health and Welfare Canada kindly provided some samples of 11-*nor*-9-keto-HHC (**3***b*) for preliminary studies.

1. C. R. B. JOYCE and S. H. CURRY (*Editors*). The botany and chemistry of cannabis. J. and A. Churchill, London. 1970. W. D. M. PATON and J. CROWN (*Editors*). Cannabis and its derivatives, Oxford University Press, London. 1972; R. K. RAZDAN. Prog. Org. Chem. **8**, 78 (1973); R. MECHOULAM (*Editor*). Marijuana. Chemistry, pharmacology, metabolism and clinical effects. Academic Press, New York, NY. 1973; R. MECHOULAM, N. K. MCCALLUM, and S. BURSTEIN. Chem. Rev. **76**, 75 (1976); G. G. NAHAS (*Editor*). Marihuana: chemistry, biochemistry and cellular effects, Springer-Verlag, New York, NY. 1976; R. K. RAZDAN. *In* The total synthesis of natural products. Vol. 4. *Edited by* J. W. ApSimon. Wiley-Interscience. 1981. p. 185.
2. C. G. PITT, F. HAUSER, R. L. HAWKS, S. SATHE, and M. E. WALL. J. Am. Chem. Soc. **94**, 8578 (1972).
3. C. G. PITT, M. S. FOWLER, S. SATHE, S. C. SRIVASTAVA, and D. L. WILLIAMS. J. Am. Chem. Soc. **97**, 3798 (1975).
4. D. B. ULISS, R. K. RAZDAN, H. C. DALZELL, and G. R. HANDRICK. Tetrahedron Lett. 4369 (1975); Tetrahedron, **33**, 2055 (1977); Y. GAONI and R. MECHOULAM. J. Am. Chem. Soc. **88**, 5673 (1966).
5. H. C. DALZELL, D. B. ULISS, G. R. HANDRICK, and R. K. RAZDAN. J. Org. Chem. **46**, 949 (1981).
6. R. K. RAZDAN, D. B. ULISS, and H. C. DALZELL. J. Am. Chem. Soc. **95**, 2361 (1973).
7. K. K. WEINHARDT, R. K. RAZDAN, and H. C. DALZELL. Tetrahedron Lett. 4827 (1971).
8. (*a*) K. E. FAHRENHOLTZ, M. LURIE, and R. W. KIERSTEAD. J. Am. Chem. Soc. **89**, 5934 (1967); (*b*) T. PETRZILKA and C. SIKEMEIER. Helv. Chim. Acta, **50**, 2111 (1967).
9. R. A. ARCHER, W. B. BLANCHARD, W. A. DAY, D. W. JOHNSON, E. R. LAVAGNINO, C. W. RYAN, and J. E. BALDWIN. J. Org. Chem. **42**, 2277 (1977); J. W. APSIMON, A. M. HOLMES, and C. I. JOHNSON. Can. J. Chem. **60**, 308 (1982).
10. T. DURST, K-C. TIN, F. DE REINACH-HIRTZBACH, J. M. DECESARE, and M. D. RYAN. Can. J. Chem. **57**, 258 (1979); F. DE REINACH-HIRTZBACH and T. DURST. Tetrahedron Lett. 3677 (1976).
11. A. JOŃCZYK, K. BAŃKO, and M. MAKOSZA. J. Org. Chem. **40**, 266 (1975).
12. W. M. ZIEGLER and R. CONNOR. J. Am. Chem. Soc. **62**, 2596 (1940).
13. R. A. ARCHER, D. B. BOYD, P. V. DEMARCO, I. J. TYMINSKI, and N. L. ALLINGER. J. Am. Chem. Soc. **92**, 5200 (1970).
14. S. INAYAMA, A. SAWA, and E. HOSOYA. Chem. Pharm. Bull. **24**, 2209 (1976).
15. Z. BEN-ZVI and S. BURSTEIN. Res. Commun. Chem. Pathol. Pharmacol. **8**, 223 (1974).
16. L. F. FIESER and M. FIESER (*Editors*). Reagents for organic synthesis. Vol. 1. John Wiley and Sons, Inc., New York. 1967.
17. D. B. ULISS, G. R. HANDRICK, H. C. DALZELL, and R. K. RAZDAN. J. Am. Chem. Soc. **100**, 2929 (1978).

Can. J. Chem. Downloaded from www.nrcresearchpress.com by 210.87.254.5 on 09/06/12
For personal use only.

# The stereochemistry of the enzymic decarboxylation of L-arginine and of L-ornithine[1]

JAMES C. RICHARDS AND IAN D. SPENSER[2]

*Department of Chemistry, McMaster University, Hamilton, Ont., Canada L8S 4M1*

Received May 25, 1982

JAMES C. RICHARDS and IAN D. SPENSER. Can. J. Chem. **60**, 2810 (1982).

The decarboxylation of L-ornithine to yield putrescine, catalyzed by the L-ornithine decarboxylase (EC 4.1.1.17) of *E. coli*, and the decarboxylation of L-arginine to yield agmatine, catalyzed by the L-arginine decarboxylase (EC 4.1.1.19) of *E. coli*, take place with retention of configuration.

JAMES C. RICHARDS et IAN D. SPENSER. Can. J. Chem. **60**, 2810 (1982).

La décarboxylation de la L-ornithine qui est catalysée par la décarboxylase de la L-ornithine (EC.4.1.1.17) de *E. coli* et qui conduit à la putrescine et la décarboxylation de la L-arginine, catalysée par la décarboxylase de la L-arginine (EC.4.1.1.19) de *E. coli* et qui conduit à la agmatine, se font avec rétention de configuration.

[Traduit par le journal]

## Introduction

Enzymes that catalyze the decarboxylation of L-α-amino acids are found in microorganisms, in mammalian tissues, and in plants. These enzymes show high substrate specificity for individual amino acids. The reaction that is catalyzed involves the conversion of a chiral centre within the L-α-amino acid, R—$CH(NH_2)CO_2H$, into a prochiral centre within the corresponding amine R—$CH_2$—$NH_2$. It was demonstrated (1) almost 30 years ago that the reaction mediated by three of these enzymes (EC 4.1.1.25 L-tyrosine decarboxylase, from *Streptococcus faecalis*; EC 4.1.1.18 L-lysine decarboxylase, from *Bacillus cadaveris*; EC 4.1.1.15 L-glutamate decarboxylase, from *Clostridium welchii* and from *Escherichia coli*) takes a stereochemically defined course, but it was not established at that time whether reaction takes place with net retention or with net inversion of configuration. Later, the actual stereochemical course of these reactions was determined.

The conversions of L-tyrosine into tyramine (2), of L-lysine into cadaverine (3), and of L-glutamate into γ-aminobutyric acid (4), each catalyzed by the appropriate enzyme, all take place with net retention of configuration, as shown by means of isotopic labelling with deuterium or tritium. Thus, decarboxylation of L-(i.e., *S*-)-tyrosine in $^2H_2O$ yields *R*-(1-$^2$H)tyramine (2), and of L-glutamate in $^2H_2O$ yields *R*-4-amino(4-$^2$H)butyric acid (4). Similarly, decarboxylation of L-[2-$^3$H]lysine in water generates *S*-[1-$^3$H]cadaverine, whereas L-lysine in tritiated water yields *R*-[1-$^3$H]cadaverine (3). The chirality of the products was determined by kinetic (2), enzymic (3), or chemical (4) correlation with compounds of known stereochemistry.

Net retention in the decarboxylation of L-tyrosine (5), of L-lysine (6, 7), and of L-glutamate (8–10), catalyzed by bacterial enzymes, was later confirmed by independent methods and was found also in reactions catalyzed by enzymes from mammalian sources (5, 8) and by plant systems (5, 6). Net retention has been demonstrated also in the decarboxylation of histidine, catalyzed by bacterial enzymes (EC 4.1.1.22 histidine decarboxylase, from *Lactobacillus* and from *Clostridium welchii*) (11, 12), and of tryptophan, catalyzed by a mammalian enzyme (EC 4.1.1.28 aromatic L-amino acid decarboxylase, from hog kidney) (13).

Very recently a D-amino acid decarboxylase (EC 4.1.1.20 *meso*-α,ε-diaminopimelate decarboxylase, from *Bacillus sphaericus*) has been shown to catalyze an analogous decarboxylation with inversion of configuration (14).

We now add two more L-α-amino acid decarboxylases of bacterial origin to the list of the enzymes that catalyze the decarboxylation of their substrates with net retention of configuration. The two enzymes are L-ornithine decarboxylase (EC 4.1.1.17) which catalyzes the decarboxylation of L-ornithine into putrescine, and L-arginine decarboxylase (EC 4.1.1.19), which mediates the conversion of L-arginine into agmatine (Scheme 4).

## Methods and results

DL-(2-$^2$H)Ornithine (**4**) and L-(2-$^2$H)arginine (**9**) were prepared by the reaction sequences shown in Schemes 1 and 2.

Decarboxylation of the L-component of DL-ornithine in deuterium oxide, and of the L-component of DL-(2-$^2$H)ornithine in water, catalyzed by L-ornithine decarboxylase (L-ornithine carboxylyase, EC 4.1.1.17) (ex *Escherichia coli*, Sigma

[1]A preliminary account of part of this work was presented at the 62nd Canadian Chemical Conference of the Chemical Institute of Canada, Vancouver, B.C., June 1979.

[2]Author to whom correspondence may be addressed.

0008-4042/82/222810-11$01.00/0

©1982 National Research Council of Canada/Conseil national de recherches du Canada

Can. J. Chem. Downloaded from www.nrcresearchpress.com by 210.87.254.6 on 09/06/12
For personal use only.

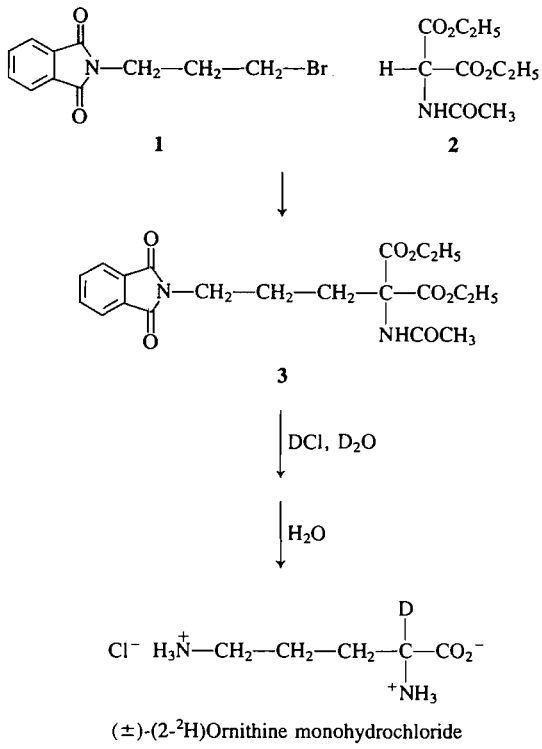


1 2 3 4

SCHEME 1. Synthesis of (±)-(2-$^2$H)ornithine.

Chemical Co.) gave the enantiomers of (1-$^2$H)-putrescine. L-Ornithine (**14**) in deuterium oxide gave (−)-(1-$^2$H)putrescine dihydrochloride (**15**), L-(2-$^2$H)ornithine in water gave (+)-(1-$^2$H)putrescine dihydrochloride. The ORD curves of the two samples are shown in Fig. 1.

The enantiomers of (1-$^2$H)agmatine were obtained similarly from L-arginine, catalyzed by L-arginine decarboxylase (L-argininine carboxylyase, EC 4.1.1.19) (ex *E. coli*, Sigma Chemical Co.). L-Arginine (**16**) in deuterium oxide gave (−)-(1-$^2$H)agmatine sulfate (**10**), L-(2-$^2$H)arginine in water gave (+)-(1-$^2$H)agmatine sulfate. The ORD curves of the enantiomeric (1-$^2$H)agmatine samples are shown in Fig. 2.

Alkaline hydrolysis with sodium hydroxide in ethanol led to quantitative conversion of agmatine into putrescine. (−)-(1-$^2$H)Agmatine sulfate (**10**) yielded (−)-(1-$^2$H)putrescine dihydrochloride (**15**), (+)-(1-$^2$H)agmatine sulfate yielded (+)-(1-$^2$H)-putrescine dihydrochloride. Within experimental error, the ORD curves of the (1-$^2$H)putrescine samples, so obtained, were coincident with those of the samples obtained by decarboxylation (Fig. 1).

The samples of (1-$^2$H)agmatine were converted in 2 steps (Scheme 3) into 4-phthalimidobutyric acid which was converted into the corresponding methyl ester.

The sample of (−)-(1-$^2$H)agmatine sulfate (**10**) gave (−)-4-phthalimido(4-$^2$H)butyric acid (**12**) which, in turn, gave (−)-methyl 4-phthalimido-(4-$^2$H)butyrate (**13**). Conversely, (+)-(1-$^2$H)agmatine sulfate gave (+)-4-phthalimido(4-$^2$H)butyric acid. The ORD curves of the enantiomeric 4-phthalimido(4-$^2$H)butyric acids are shown in Fig. 3.

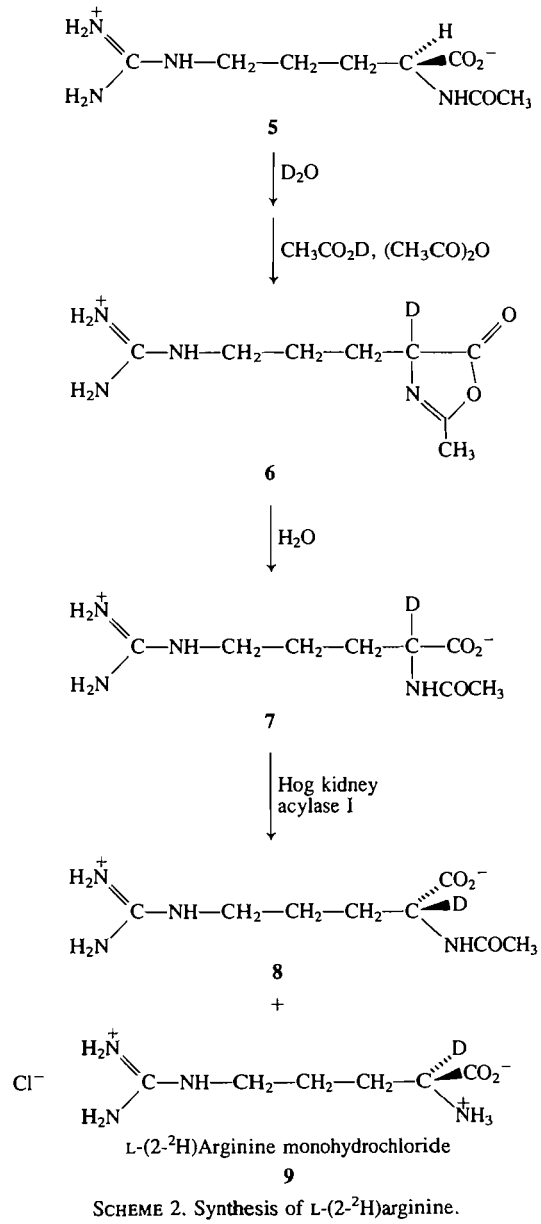


5 6 7 8 9

SCHEME 2. Synthesis of L-(2-$^2$H)arginine.

Can. J. Chem. Downloaded from www.nrcresearchpress.com by 210.87.254.6 on 09/06/12
For personal use only.

Can. J. Chem. Downloaded from www.nrcresearchpress.com by 210.87.254.6 on 09/06/12
For personal use only.

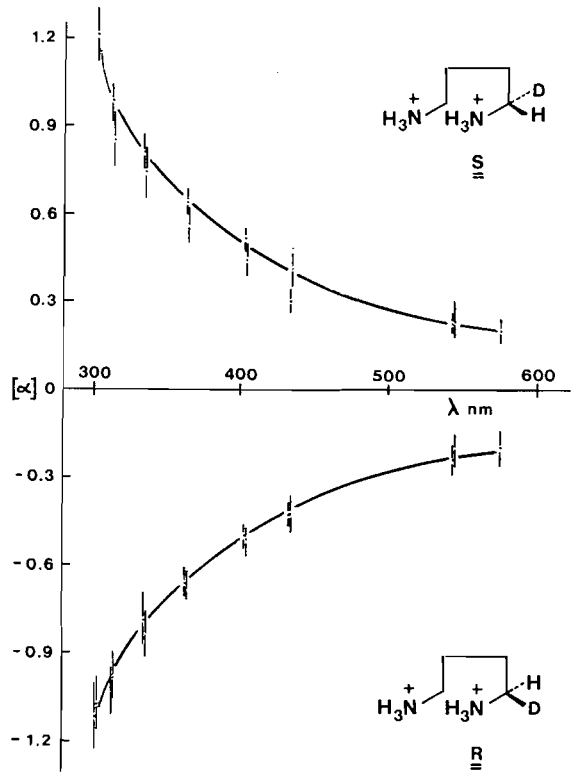


FIG. 1. Optical rotary dispersion (ORD) curves of (+)- and (−)-(1-$^2$H)putrescine dihydrochloride. The samples were prepared by decarboxylation of ornithine (value plotted on the left, for each wave length) and by hydrolysis of agmatine (value on the right).

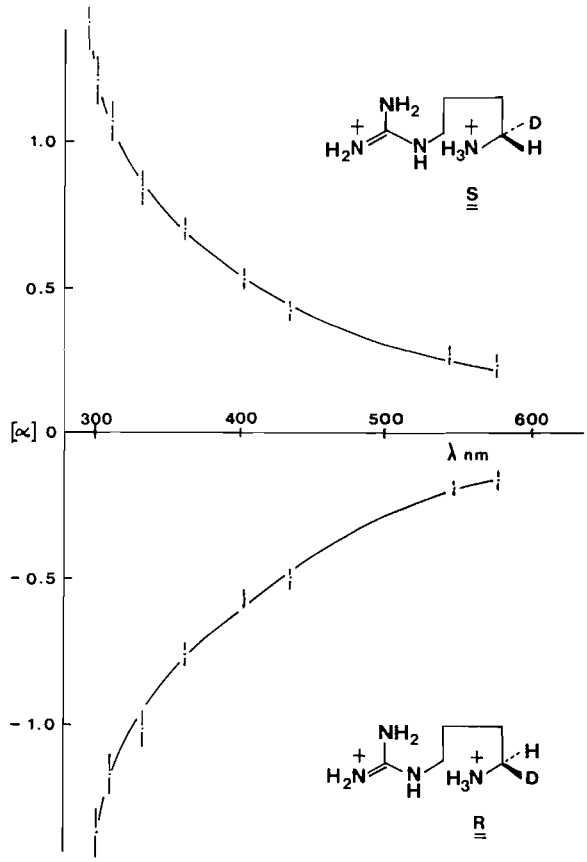


FIG. 2. ORD curves of (+)- and (−)-(1-$^2$H)agmatine sulfate.

An authentic specimen of (−)-methyl *R*-4-phthalimido(4-$^2$H)butyrate was obtained from M. H. O'Leary, University of Wisconsin. This sample had been prepared by methylation of (−)-4-phthalimido(4-$^2$H)butyric acid which had been obtained by decarboxylation in $^2H_2O$ of L-glutamic acid, catalyzed by L-glutamate decarboxylase (L-glutamate carboxylyase, EC 4.1.1.15, *ex E. coli*), and had been shown to have *R*-chirality by direct correlation with an authentic specimen, prepared from chiral (2-$^2$H)glycine by a series of reactions which did not affect the stereochemistry at the chiral centre (4).

The sample of (−)-methyl 4-phthalimido(4-$^2$H)-butyrate (**13**) derived from (−)-(1-$^2$H)agmatine sulfate (**10**) and the sample of (−)-methyl *R*-4-phthalimido(4-$^2$H)butyrate supplied by M. H. O'Leary showed similar, but not coincident, plane negative ORD curves (Fig. 4), and identical mass spectra (Fig. 5).

## Discussion

The stereochemistry of the replacement of the carboxyl group of an α-amino acid by a solvent proton, in the course of the reaction catalyzed by an L-α-amino acid decarboxylase (1, 15), can be determined if the prochiral centre that is generated in the course of the decarboxylation is rendered chiral by isotopic substitution. If the decarboxylation of the amino acid is carried out in the presence of isotopically labelled water ($^3$HOH or $^2H_2O$), one of the enantiomers of the amine will be generated. The other enantiomer arises when a 2-labelled sample ([2-$^3$H]- or (2-$^2$H)-) of the L-α-amino acid undergoes decarboxylation in aqueous solution (3, 5–7, 13, 16, 17).

When tritium is employed as the tracer (3, 5–8, 10, 11, 13, 16) a very small fraction only of the molecules that comprise the labelled starting material ([2-$^3$H]amino acid or $^3$HOH) will carry $^3$H. It follows that only very few of the molecules comprising the product will be labelled, i.e., will be chiral and, in principle, optically active. The optical activity of the resulting product will thus be immeasurably small. Stereochemical analysis of the product is possible by means of enzymes of known stereospecificity.

When deuterium is employed as the marker (4, 9,

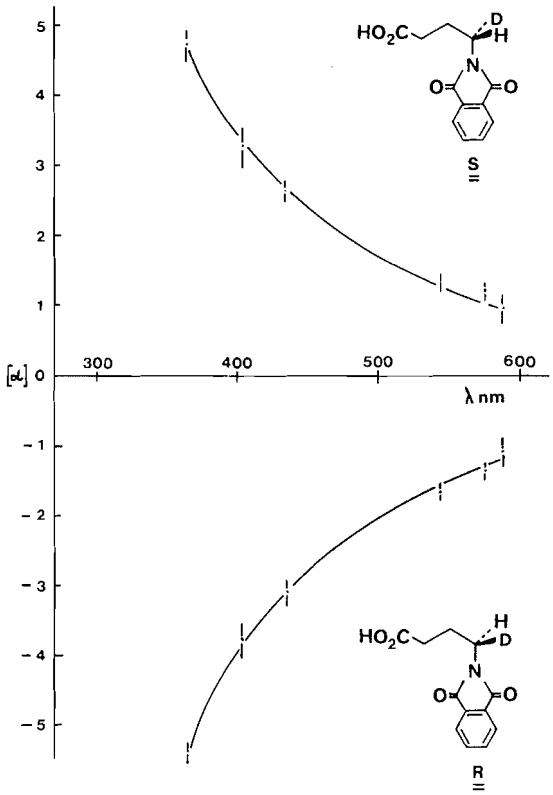


FIG. 3. ORD curves of (+)- and (−)-4-phthalimido(4-$^2$H)butyric acid.

12, 14, 17) starting material can, in principle, be fully deuterated ($^2H_2O$), or fully deuterated at the appropriate position ((2-$^2$H)amino acid). The product will then consist entirely of molecules that are correspondingly deuterated, and is therefore not only chiral but its optical activity will, in all likelihood, be measurable (subject to the sensitivity of the detection instruments). The chirality of the product can then be determined by the classical method of measuring optical activity followed by assignment of configuration by comparison of this activity with that of standards of known configuration (4, 12, 14). Alternatively, nmr methods can be applied (9, 17) in the configurational assignment.

We have determined the stereochemistry of the enzymic decarboxylations of ornithine and arginine by deuterium labelling, followed by adaptation of the classical approach to configurational assignment, measurement of optical activity, and comparison with standards of known stereochemistry.

Samples of the two enantiomeric (1-$^2$H)putrescines were isolated as dihydrochlorides. They were obtained, respectively, by the action of L-ornithine decarboxylase (from *E. coli*) on L-ornithine (**14**) in the presence of $^2H_2O$ (ca. 98 at.% $^2$H), and on the L-component of DL-(2-$^2$H)ornithine. The DL-(2-

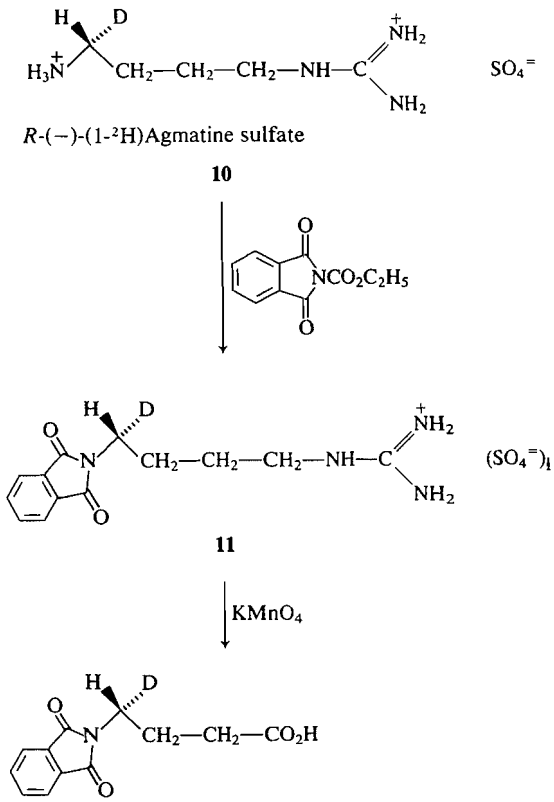


SCHEME 3. Conversion of (1-$^2$H)agmatine into methyl 4-phthalimido(4-$^2$H)butyrate.

$^2$H)ornithine (**4**) was prepared by adaptation of a conventional synthetic route (18) (Scheme 1). The ORD curves of the enantiomeric (1-$^2$H)putrescines are shown in Fig. 1. The sample derived from L-(2-$^2$H)ornithine was (+)-(1-$^2$H)putrescine dihydrochloride, that derived from L-ornithine (**14**) in $^2H_2O$ (Scheme 4) was (−)-(1-$^2$H)putrescine dihydrochloride (**15**).

Similarly, samples of the two enantiomeric (1-$^2$H)agmatines, isolated as sulfates, were obtained by action of L-arginine decarboxylase (from *E. coli*) on L-arginine in the presence of $^2H_2O$, and on L-(2-$^2$H)arginine, respectively. The L-(2-$^2$H)arginine (**9**) was prepared from α-*N*-acetyl-L-arginine

Can. J. Chem. Downloaded from www.nrcresearchpress.com by 210.87.254.6 on 09/06/12
For personal use only.

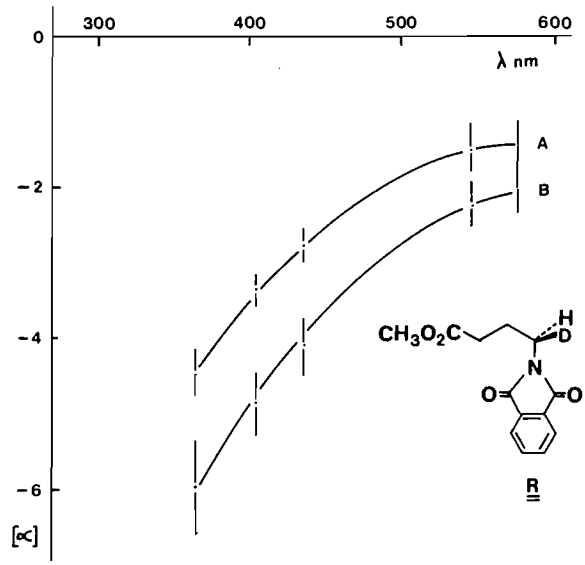


FIG. 4. ORD curves of (−)-methyl 4-phthalimido(4-$^2$H)-butyrate (**13**). Curve A: Sample supplied by M. H. O'Leary. Curve B: Sample obtained from (−)-(1-$^2$H)agmatine sulfate (**10**) (Scheme 3).

(**5**) by exchange (via the oxazolone (**6**)) and stereospecific hydrolysis employing acylase I (19) (Scheme 2). The sample of agmatine sulfate derived from L-(2-$^2$H)arginine was (+)-(1-$^2$H)agmatine sulfate, that derived from L-arginine (**16**) in $^2H_2O$ (Scheme 4) was (−)-(1-$^2$H)agmatine sulfate (**10**).

It was a simple matter to establish the relative configuration of the samples of (1-$^2$H)putrescine and (1-$^2$H)agmatine. Hydrolysis of (−)-(1-$^2$H)-agmatine sulfate (**10**) with ethanolic sodium hydroxide (10% w/v),[3] which maintained the chiral integrity at C-1 but cleaved the guanidino group, gave (−)-(1-$^2$H)putrescine dihydrochloride (**15**) (Scheme 4). Similarly, (+)-(1-$^2$H)agmatine sulfate gave (+)-(1-$^2$H)putrescine dihydrochloride.

It follows that the levorotary samples of (1-$^2$H)-putrescine dihydrochloride and of (1-$^2$H)agmatine sulfate have the same configuration at C-1. Since these two samples were derived from L-ornithine, and from L-arginine, respectively, by decarboxylation in $^2H_2O$, it follows further that the steric course of the decarboxylation of L-ornithine, catalyzed by L-ornithine decarboxylase, is identical with that of the decarboxylation of L-arginine, catalyzed by L-arginine decarboxylase.

[3]Hydrolysis with barium hydroxide solution (20, 21) or with aqueous sodium hydroxide (22), conditions which have been employed to convert L-arginine into L-ornithine (20, 21) and DL-ornithine (22), respectively, did not lead to quantitative conversion of chiral deuterio-agmatine into chiral deuterio-putrescine.

Congruently, the dextrorotary samples of (1-$^2$H)-putrescine dihydrochloride and of (1-$^2$H)agmatine sulfate correspond in configuration at C-1. Each was derived from the corresponding L-(2-$^2$H)amino acid. Thus, the decarboxylations catalyzed by L-ornithine decarboxylase and by L-arginine decarboxylase take the same stereochemical course. Either both reactions proceed with net retention of configuration or they both proceed with net inversion.

This question was settled by a chemical conversion of (−)-(1-$^2$H)agmatine into a product of known chirality by a reaction sequence which did not affect the chiral centre at C-1 (Scheme 3).

(1-$^2$H)Agmatine rather than (1-$^2$H)putrescine was chosen for chemical correlation with a known standard in order to avoid possible complications due to the $C_{2v}$ symmetry of putrescine.

(1-$^2$H)Agmatine was converted into the 1-*N*-phthaloyl derivative (**11**). The primary amino group was thus afforded protection from oxidative attack. The guanidino group was then removed by oxidation with potassium permanganate, yielding 4-phthalimido(4-$^2$H)butyric acid (**12**) whose stereochemical integrity had been maintained. By this reaction sequence (−)-(1-$^2$H)agmatine sulphate (**10**) yielded (−)-4-phthalimido(4-$^2$H)butyric acid (**12**), and (+)-(1-$^2$H)agmatine sulfate gave (+)-4-phthalimido(4-$^2$H)butyric acid.

A sample of (−)-4-phthalimido(4-$^2$H)butyric acid (**12**) was converted into the corresponding methyl ester, (−)-methyl 4-phthalimido(4-$^2$H)butyrate (**13**) (isotopic enrichment (ms) 98.2 ± 0.3 at.% $^2H_1$). This derivative was compared directly with an authentic specimen of (−)-methyl 4-phthalimido-*R*-(4-$^2$H)butyrate (isotopic enrichment 92.5 ± 0.4 at.% $^2H_1$, 4.7 ± 0.4% $^2H_2$), which had been prepared in the laboratory of M. H. O'Leary, University of Wisconsin (4). The absolute configuration of this sample ultimately rests on chemical correlation with that of *R*-(2-$^2$H)glycine (**17**) (4).

The two samples of (−)-methyl 4-phthalimido-(4-$^2$H)butyrate (**13**), that from (−)-(1-$^2$H)agmatine sulfate (**10**) and that supplied by O'Leary, both showed plane negative ORD curves (Fig. 4). They gave identical mass spectra (Fig. 5).

Since (−)-methyl 4-phthalimido(4-$^2$H)butyrate has the *R*-configuration, the (−)-(1-$^2$H)agmatine sulfate from which it was obtained, by a reaction sequence which did not affect the chiral centre, also has the *R*-configuration (see Scheme 3, no change in ligand priorities around the chiral centre).

Since this *R*-(−)-(1-$^2$H)agmatine sulfate had been obtained from L-arginine by decarboxylation in $^2H_2O$, catalyzed by L-arginine decarboxylase

Can. J. Chem. Downloaded from www.nrcresearchpress.com by 210.87.254.6 on 09/06/12
For personal use only.

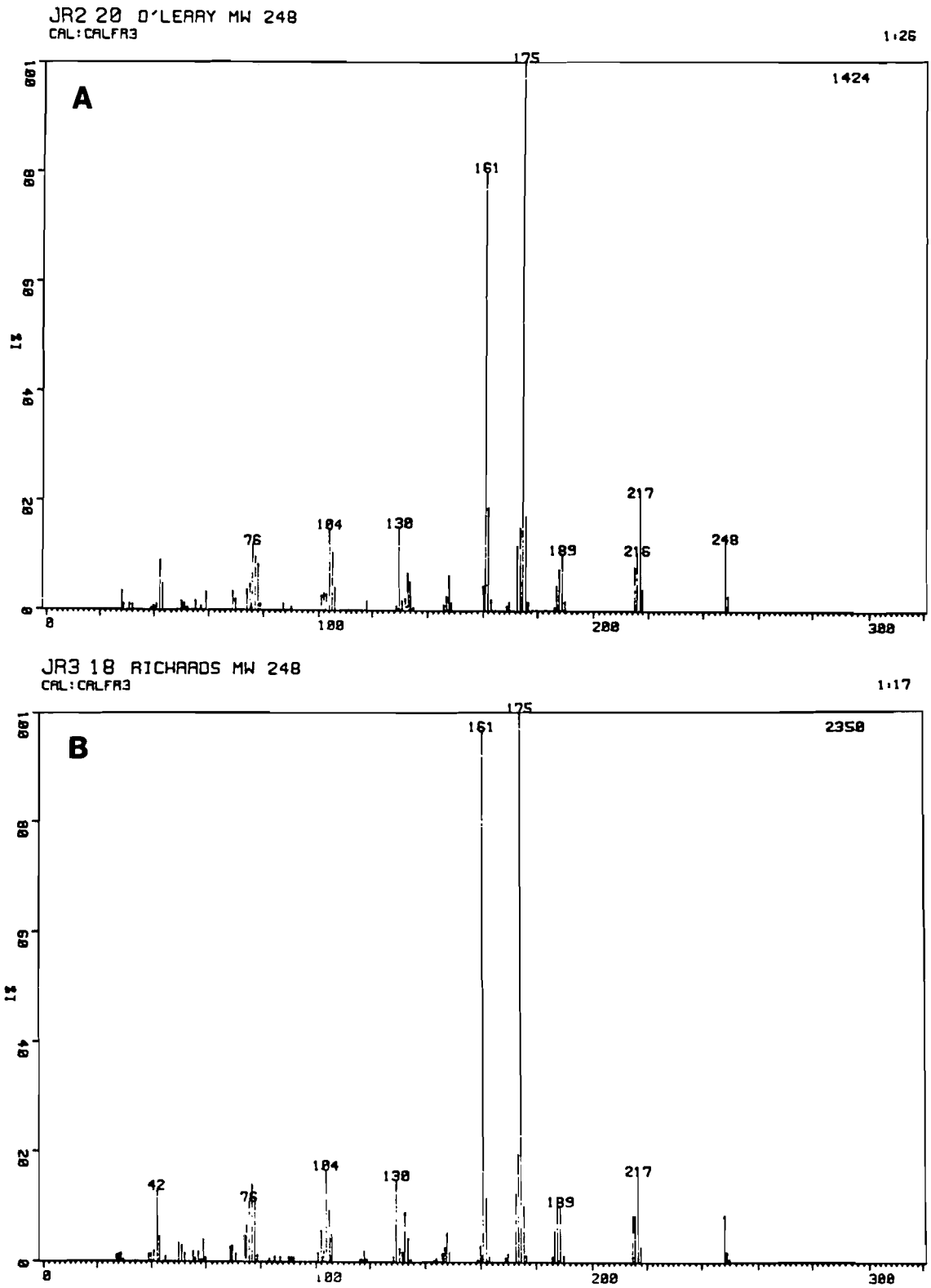


FIG. 5. Mass spectra of (−)-methyl 4-phthalimido(4-$^2$H)butyrate (**13**). Spectrum A: Sample supplied by M. H. O'Leary. Spectrum B: Sample obtained from (−)-(1-$^2$H)agmatine sulfate (**10**) (Scheme 3).

Can. J. Chem. Downloaded from www.nrcresearchpress.com by 210.87.254.6 on 09/06/12
For personal use only.

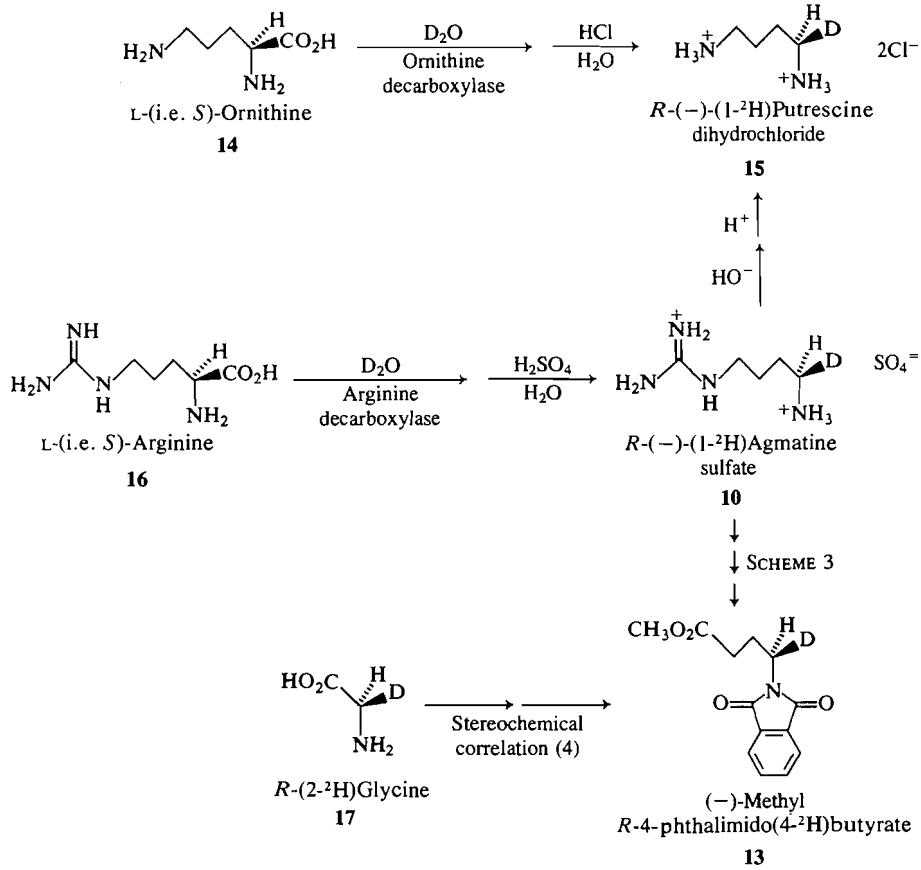


SCHEME 4. Stereochemical interrelationship of L-ornithine, L-arginine, and their conversion and degradation products.

(EC 4.1.1.19, from *E. coli*) (Scheme 4), the reaction catalyzed by this enzyme proceeds with net retention of configuration.

Since *R*-(−)-(1-$^2$H)agmatine sulfate yielded (−)-(1-$^2$H)putrescine dihydrochloride in a reaction which does not affect the chiral centre, this compound is *R*-(−)-(1-$^2$H)putrescine dihydrochloride.

Since the *R*-(−)-(1-$^2$H)putrescine dihydrochloride had been obtained from L-ornithine by decarboxylation in $^2H_2O$, catalyzed by L-ornithine decarboxylase (EC 4.1.1.17, from *E. coli*), the reaction catalyzed by this enzyme proceeds with net retention of configuration.

These configurational relationships are summarized in Scheme 4.

## Experimental

A. *(2-$^2$H)Amino acids*

1. DL-*(2-$^2$H)Ornithine (18)*

*Diethyl 2-acetamido-2-(3-phthalimidopropyl)malonate (3) (23)*

Diethyl acetamidomalonate (**2**) (Aldrich Chemical Co.) (2.16 g) was dissolved in hot dry ethanol[4] in a two-necked round bottom flask, fitted with a reflux condenser, calcium sulfate drying tube, and a pressure equalizing dropping funnel. A solution of sodium ethoxide (250 mg of sodium in 14 mL ethanol) was added and the resulting solution was heated at reflux while *N*-(3-bromopropyl)phthalimide (**1**) (Aldrich Chemical Co.) (2.69 g) in hot ethanol (14 mL) was added dropwise over 10 min. The reaction mixture was refluxed 20 h, and was then cooled to 0°C. Water (35 mL) was added to give the substitution product. Yield 2.85 g, 71%; mp 116–116.5°C (from 95% ethanol) (lit. (23) mp 115–116°C; (25) 111–112°C); $^1$H nmr ($^2HCCl_3$), δ: 1.20 (6H, t, *J* 7.2 Hz), 1.53 (2H, m), 2.00 (3H, s), 2.40 (2H, m), 3.67 (2H, t, *J* 7.2 Hz), 4.23 (4H, q, *J* 7.2 Hz), 6.80 (1H, s), 7.77 (4H, m).

DL-*(2-$^2$H)Ornithine monohydrochloride (4)*

Diethyl 2-acetamido-2-(3-phthalimidopropyl)malonate (**3**) (784 mg) was suspended in a solution of deuterium oxide containing deuterium chloride (38%, w/w in $^2H_2O$, 10 mL) (Merck, Sharp, and Dohme, 99.7 at.% $^2$H) in a small flask fitted with a reflux condenser and calcium sulfate drying tube. The mixture was heated at reflux for 18 h, cooled to 0°C, and diluted with water (10 mL). Phthalic acid, which precipitated, was filtered off and washed with water (2 × 1 mL). The combined filtrate and washings were concentrated to dryness *in vacuo*, and the residue was repeatedly dissolved in water and evaporated to dryness to remove exchangeable deuterium. The residue, crude ornithine dihydrochloride, was dissolved in hot 95% ethanol (8 mL), the solution was cooled to room temperature, filtered, and pyridine (ca. 600 mg) was added. DL-(2-$^2$H)-Ornithine monohydrochloride (398 mg) which precipitated was recrystallized from aqueous ethanol, mp 235–237°C (dec.) (lit. (nondeuteriated) (22) mp 232°C (dec.); (25) 222–224°C (dec.);

[4]Absolute ethanol purified by the Lund–Bjerrum method (24) was used throughout.

Can. J. Chem. Downloaded from www.nrcresearchpress.com by 210.87.254.6 on 09/06/12
For personal use only.

Can. J. Chem. Downloaded from www.nrcresearchpress.com by 210.87.254.6 on 09/06/12
For personal use only.

(18) 215–216°C (dec.)). The $^1$H nmr spectrum ($^2H_2O$) was similar to that of authentic unlabelled material and indicated that this sample was ca. 98% deuterium labelled at C-2; δ: 1.90 (4H, m, H-3, 4), 3.05 (2H, t, *J* 6.8 Hz, H-5), 3.80 (ca. 0.02 H, H-2). The $^2$H nmr spectrum ($H_2O$, 107 *mM*, 200 transients) showed one signal at 3.7 ppm (relative to $^1H^2HO$ at 4.7 ppm).

In another experiment, hydrolysis of **3** (900 mg) gave a sample of DL-(2-$^2$H)ornithine monohydrochloride (**4**) (330 mg) which was ca. 92% $^2$H-labelled in the 2-position as determined by $^1$H nmr.

2. *L-(2-$^2$H)Arginine*

α-N-*Acetyl*-L-*arginine dihydrate (5)*

L-Arginine monohydrochloride (4.24 g) was acetylated with acetic anhydride in aqueous sodium bicarbonate by a published procedure (26), yielding α-acetyl-L-arginine dihydrate (4.10 g, 81%); mp 267–268°C (from water) (lit. (27) (DL) mp 256°C); $^1$H nmr ($^2H_2O$), δ: 1.73 (4H, m, H-3, 4), 2.05 (3H, s, $COCH_3$), 3.23 (2H, t, *J* 6.8 Hz, H-5), 4.20 (1H, d of d, $J_1 \sim 7.8$ Hz, $J_2 \sim 4.8$ Hz, H-2); ORD, $[\alpha]_{289}$ −10.1 ± 0.3°, $[\alpha]_{296}$ −12.3 ± 0.3°, $[\alpha]_{302}$ −14.1 ± 0.3°, $[\alpha]_{312}$ −15.8 ± 0.3°, $[\alpha]_{334}$ −16.6 ± 0.3°, $[\alpha]_{365}$ −16.0 ± 0.3°, $[\alpha]_{405}$ −13.6 ± 0.3°, $[\alpha]_{436}$ −11.9 ± 0.3°, $[\alpha]_{546}$ −7.6 ± 0.2°, $[\alpha]_{577}$ −6.7 ± 0.1°, $[\alpha]_{589}$ −6.3 ± 0.2 (*c* 2% in 1 *N* HCl, 25°C) (lit. (26) $[\alpha]_{589}$ −7.0° (*c* 2% in 1 *N* HCl)).

α-N-*Acetyl*-DL-*(2-$^2$H)arginine dihydrate (7) (cf. ref. 28)*

α-*N*-Acetyl-L-arginine dihydrate (3.9 g) was dissolved in deuterium oxide (5 mL) and the solvent was evaporated *in vacuo*. This process was repeated three times to effect replacement of the exchangeable protons by deuterium. The residue was then recrystallized from deuterium oxide (3 mL) and deuterium oxide of crystallization was removed by drying over phosphorus pentoxide at 75°C for 24 h. The product so obtained, α-acetylarginine, in which all exchangeable protons had been replaced by $^2$H, mp 253–255°C (lit. (nondeuteriated) (28) mp 250°C), was dissolved in deuterioacetic acid (25 mL) which had been prepared in the following way (cf. ref. 29).

A mixture of freshly distilled acetic anhydride (Fisher) (bp 137–138°C, 40 mL) and deuterium oxide (Merck, Sharp and Dohme, 99.7 at.% $^2$H) (8 g) was stirred at room temperature under a stream of dry nitrogen until the solution was homogeneous (ca. 3 h). Distillation under anhydrous conditions gave deuterioacetic acid, $CH_3CO_2{}^2H$, bp 112–114°C. The $^1$H nmr spectrum of a sample of the product indicated that it was ≥ 98% deuterium labelled and contained a trace of acetic anhydride (ca. 1%).

Acetic anhydride (bp 137–138°C, 1.7 mL) was added to the solution of α-*N*-acetylarginine in deuterioacetic acid, and the mixture was heated at reflux under dry nitrogen. After 2 h deuterium oxide (0.4 mL) was added and heating at reflux was continued for 30 min. The solution was cooled to room temperature, acetic acid removed *in vacuo*, and the residue, a yellow oil, was dissolved in water (5 mL). The solution was evaporated, the residue redissolved in water, and the solution again evaporated. The oil was then redissolved in water (5 mL), the pH of the solution was adjusted to pH 8 with concentrated ammonium hydroxide, acetone (1 mL) was added, and the mixture cooled to 0°C. The crystals which formed were filtered off, washed with cold water, and dried *in vacuo* over phosphorus pentoxide. The sample of α-*N*-acetyl-DL-(2-$^2$H)arginine (**7**) dihydrate (3.4 g) so obtained (optically inactive, mp 268–270°C (from water)), was 85–90% deuterium labelled at C-2 ($^1$H nmr). Deuterium was also present in the acetyl group.

*L-(2-$^2$H)Arginine (9) monohydrochloride and α-acetyl-D-(2-$^2$H)arginine (8) dihydrate (cf. refs. 19, 26)*

The pH of a solution of α-*N*-acetyl-DL-(2-$^2$H)arginine dihydrate (3.2 g) in water (140 mL) was adjusted to pH 6.8 with hydrochloric acid (10% w/v). Hog kidney acylase I (Sigma, 6300 U/mg,[5] 8.6 mg) in water (20 mL) was added. The resulting solution was incubated at 36°C in a constant temperature water bath for 23 h. The pH of the enzymic reaction mixture was then adjusted to pH 4.8 with glacial acetic acid, Norite was added, and the mixture filtered through Celite. The clear filtrate was concentrated *in vacuo* (7 mL), and after cooling in a refrigerator for several days, α-*N*-acetyl-D-(2-$^2$H)arginine (**8**) dihydrate, which crystallized, was filtered off and washed with water. Yield 1.4 g, 89%; mp 268–269°C (from water); ORD, $[\alpha]_{289}$ +14.0 ± 0.3°, $[\alpha]_{296}$ +16.9 ± 0.4°, $[\alpha]_{302}$ +18.0 ± 0.4°, $[\alpha]_{312}$ +19.4 ± 0.4°, $[\alpha]_{334}$ +19.6 ± 0.4°, $[\alpha]_{365}$ +17.9 ± 0.4°, $[\alpha]_{405}$ +15.3 ± 0.3°, $[\alpha]_{436}$ +13.2 ± 0.3°, $[\alpha]_{546}$ +8.3 ± 0.2°, $[\alpha]_{577}$ +7.2 ± 0.2°, $[\alpha]_{589}$ +6.8 ± 0.2° (*c* 2.06% in 1 *N* HCl, 25°C) (lit. (26) (nondeuteriated) $[\alpha]_{589}$ +7.0° (*c* 2% in 1 *N* HCl)).

The combined filtrate and washings containing L-(2-$^2$H)arginine (**9**) (10 mL) were diluted with water (25 mL), sodium hydroxide solution (5% w/v) was added to pH 11, and the solution was cooled in an ice bath. Benzaldehyde (1.3 mL) was added and the mixture stirred at 0°C for 2 h. The benzylidine derivative which separated was filtered off and was washed with ethanol and ether. Yield, 1.54 g, 93%; mp 198–199°C (dec.) (lit. (31) mp 206–207°C (dec.)).

The solution of the benzylidine derivative (1.53 g) in aqueous hydrochloric acid (2 *N*, 12 mL) was heated (95°C) 20 min with stirring. After cooling to room temperature, the mixture was extracted with ether (2 × 5 mL) and the ether layers were discarded. The aqueous phase, containing the dihydrochloride of L-(2-$^2$H)arginine, was evaporated *in vacuo*. The residue was dissolved in hot 95% ethanol (5 mL), the solution cooled to room temperature, and filtered. L-(2-$^2$H)Arginine monohydrochloride was precipitated from the filtrate by addition of pyridine (1.2 mL), and was recrystallized from aqueous ethanol. Yield 1.1 g, 91% from the benzylidine derivative; mp 222–223°C (lit. (nondeuteriated) (31) mp 220°C); $^1$H nmr ($^2H_2O$), δ: 1.74 (4H, m, H-3, 4), 3.17 (2H, t, *J* 6.8 Hz, H-5), 3.72 (ca. 0.15 H, H-2, i.e., ca. 85% of $^2$H); ORD, $[\alpha]_{296}$ +94.5 ± 1.9°, $[\alpha]_{302}$ +87.7 ± 1.9°, $[\alpha]_{312}$ +75.6 ± 1.5°, $[\alpha]_{334}$ +58.6 ± 1.2°, $[\alpha]_{365}$ +43.3 ± 0.9°, $[\alpha]_{405}$ +31.4 ± 0.6°, $[\alpha]_{436}$ +25.3 ± 0.5°, $[\alpha]_{546}$ +14.1 ± 0.3°, $[\alpha]_{577}$ +12.4 ± 0.3°, $[\alpha]_{589}$ +11.7 ± 0.2° (*c*, 2.06% in water, 25°C). An authentic sample of unlabelled L-arginine monohydrochloride showed a plane positive ORD spectrum: $[\alpha]_{296}$ +94.0 ± 1.9°, $[\alpha]_{302}$ +87.2 ± 1.7°, $[\alpha]_{312}$ +75.4 ± 1.5°, $[\alpha]_{334}$ +58.6 ± 1.2°, $[\alpha]_{365}$ +43.3 ± 0.9°, $[\alpha]_{405}$ +31.5 ±0.6°, $[\alpha]_{436}$ +25.4 ± 0.5°, $[\alpha]_{546}$ +14.0 ± 0.3°, $[\alpha]_{577}$ +12.4 ± 0.3°, $[\alpha]_{589}$ +11.7 ± 0.2° (*c* 2.07% in water, 25°C) (lit. (28) $[\alpha]_{589}$ +11.30° (*c*, 5.0% in water, 25°C), (31) $[\alpha]_{589}$ +12.2°, +12.3° (*c*, 5.0% in water, 25°C)).

A sample of L-(2-$^2$H)arginine monohydrochloride (67 mg) which was ≥ 92% $^2$H-labelled (by $^1$H nmr) was obtained from α-*N*-acetyl-L-arginine under a similar set of reaction conditions (see above) except that the $^2$H for $^1$H exchange reaction was optimized by following the course of the reaction in perdeuterioacetic acid – acetic anhydride solution by $^1$H nmr.

B. *Decarboxylation of (2-$^2$H)amino acids to (1-$^2$H)amines*

1. *Ornithine*

*Decarboxylation of ornithine, catalysed by L-ornithine decarboxylase (E.C. 4.1.1.17) from* E. coli

(i) *(−)-(1-$^2$H)Putrescine dihydrochloride (15) by decarboxylation of the L-component of unlabelled DL-ornithine in deuterium oxide solution*

Anhydrous sodium carbonate (Analar) (111 mg) was added to a stirred solution of perdeuterioacetic acid (Merck, Sharp, and Dohme, 99.7 at.% $^2$H) in deuterium oxide (Stohler Isotopes, 99.8 at.% $^2$H) (0.2 *M*, 15 mL) under an atmosphere of dry

[5] 1 U will hydrolyse 1 μmol of *N*-acetyl-L-methionine/h at pH 7.0 at 25°C. Hydrolysis of α-*N*-acetyl-L-arginine is ca. 60 times slower (30).

Can. J. Chem. Downloaded from www.nrcresearchpress.com by 210.87.254.6 on 09/06/12
For personal use only.

nitrogen. After stirring for 1 h, DL-ornithine monohydrochloride (Aldrich) (98 mg), which had been stripped of exchangeable protons by repeated solution in $^2H_2O$ and evaporation to dryness (3 times), and L-ornithine decarboxylase (Sigma, 0.06 U/mg)[6] (45 mg) were dissolved in the buffered solution (ca. p$^2$H 5). The enzymic reaction mixture, in a flask fitted with a calcium sulfate drying tube, was agitated at 36°C for 40 h. The enzymic reaction mixture was then acidified with 4 *N* hydrochloric acid, heated on a steam bath for 30 min, and cooled to room temperature. The precipitated enzyme was removed by centrifugation, followed by filtration of the supernatant solution through Celite. The filtrate was lyophilyzed, the residue dissolved in 10% sodium hydroxide (3 mL), and the alkaline solution saturated with sodium chloride. The product was extracted into 1-butanol (4 × 5 mL), the butanol extract was acidified by addition of a solution of hydrogen chloride in butanol, and the solution was then concentrated *in vacuo* (5 mL). (−)-(1-$^2$H)Putrescine dihydrochloride (46 mg) was recrystallized from 95% ethanol; $^1$H nmr ($^2H_2O$), δ: 1.77 (4H, m, H-2,3), 3.06 (ca. 3H, m, H-1,4); CI ms 90 (M + H, 5%), 74 (5), 73 (M − $NH_3$, 100), 72 (2), (CI ms of authentic unlabelled material, 89 (M + H, 5%), 73 (5), 72 (M − $NH_3$, 100), 71 (2)); 99.7 ± 0.3% $^2H_1$ determined by CI ms. The sample showed a plane negative ORD curve. Another sample of (−)-(1-$^2$H)putrescine dihydrochloride obtained as above from L-ornithine monohydrochloride (rather than from DL-) was 98.7 ± 1.2% mono-$^2$H labelled at C-1, determined by CI ms, and gave ORD, $[\alpha]_{302}$ −1.12 ± 0.11°, $[\alpha]_{313}$ −1.03 ± 0.08°, $[\alpha]_{334}$ −0.78 ± 0.09°, $[\alpha]_{365}$ −0.66 ± 0.05°, $[\alpha]_{405}$ −0.50 ± 0.04°, $[\alpha]_{436}$ −0.43 ± 0.04°, $[\alpha]_{546}$ −0.24 ± 0.05°, $[\alpha]_{577}$ −0.20 ± 0.06° (*c* 2.26% in 0.1 *N* HCl, 26°C, uncorrected for incomplete deuteration).

(ii) *(+)-(1-$^2$H)Putrescine dihydrochloride by decarboxylation of the* L-*component of* DL-*(2-$^2$H)ornithine*

A solution of DL-(2-$^2$H)ornithine monohydrochloride (~ 98% $^2$H) (100 mg) and L-ornithine decarboxylase (40 mg) in acetate buffer (0.2 *M*, pH 5.0, 15 mL) was incubated at 36°C for 20 h. After work-up, (+)-(1-$^2$H)putrescine dihydrochloride was obtained and recrystallized from 95% ethanol (yield 45 mg). The $^1$H nmr spectrum ($^2H_2O$) was identical with that of (−)-(1-$^2$H)-putrescine and the sample showed a plane positive ORD curve; CI ms, 90 (M + H, 3%), 74 (5), 73 (M − $NH_3$, 100), 72 (5); 97.2 ± 0.3% $^2H_1$ determined by CI ms.

Another sample of (+)-(1-$^2$H)putrescine dihydrochloride obtained by enzymic decarboxylation of DL-(2-$^2$H)ornithine (ca. 92% $^2$H) was 93.1 ± 0.9% mono-$^2$H labelled at C-1 (determined by CI ms); ORD, $[\alpha]_{302}$ +1.21 ± 0.09°, $[\alpha]_{313}$ +0.98 ± 0.06°, $[\alpha]_{334}$ +0.81 ± 0.06°, $[\alpha]_{365}$ +0.64 ± 0.04°, $[\alpha]_{405}$ +0.51 ± 0.04°, $[\alpha]_{436}$ +0.30 ± 0.03°, $[\alpha]_{546}$ +0.23 ± 0.03°, $[\alpha]_{577}$ +0.20 ± 0.04° (*c* 2.86% in 0.1 *N* HCl, 26°C, uncorrected for incomplete deuteration).

Unreacted D-(2-$^2$H)ornithine was reisolated from the incubation mixture. The alkaline solution remaining after extraction of the (1-$^2$H)putrescine into butanol was neutralized with concentrated hydrochloric acid, and was then applied to a column (25 × 1 cm) of Dowex 50-X8 ($H^+$ form). The column was washed with water (25 mL), hydrochloric acid (2 *N*, 25 mL), and water (25 mL). D-(2-$^2$H)ornithine was eluted with ammonia (1 *M*, 25 mL), and was isolated as the monohydrochloride, as described earlier.

The $^1$H and $^2$H nmr spectra of the sample of D-(2-$^2$H)ornithine monohydrochloride (ca. 92% $^2$H) were identical with those of the DL-(2-$^2$H)ornithine from which it was derived. ORD, $[\alpha]_{265}$ −157.8 ± 7.9°, $[\alpha]_{280}$ −114.8 ± 5.7°, $[\alpha]_{289}$ −98.0 ± 4.9°, $[\alpha]_{296}$ −87.3 ± 4.4°, $[\alpha]_{302}$ −80.7 ± 4.0°, $[\alpha]_{313}$ −69.2 ± 3.5°, $[\alpha]_{334}$ −52.8 ± 2.6°, $[\alpha]_{365}$ −39.3 ± 2.0°, $[\alpha]_{405}$ −29.0 ± 1.5°, $[\alpha]_{436}$ −23.4 ± 1.2°, $[\alpha]_{546}$ −14.4 ± 0.8°, $[\alpha]_{577}$ −12.9 ± 0.7°, $[\alpha]_{589}$ −12.1 ± 0.8°, (*c*. 0.63% in water, 25°C).

An authentic sample of unlabelled L-ornithine (**10**) monohydrochloride gave the following ORD: $[\alpha]_{265}$ + 166.3 ± 3.3°, $[\alpha]_{280}$ +124.9 ± 2.5°, $[\alpha]_{289}$ +107.6 ± 2.2°, $[\alpha]_{296}$ +96.1 ± 1.9°, $[\alpha]_{302}$ +88.9 ± 1.8°, $[\alpha]_{313}$ +78.1 ± 1.6°, $[\alpha]_{334}$ +61.7 ± 1.2°, $[\alpha]_{365}$ +45.1 ± 0.9°, $[\alpha]_{405}$ +32.3 ± 0.7°, $[\alpha]_{436}$ +26.1 ± 0.5°, $[\alpha]_{546}$ +13.6 ± 0.4°, $[\alpha]_{577}$ +11.5 ± 0.3°, $[\alpha]_{589}$ +11.8 ± 0.5°, (*c*, 0.49% in water, 25°C); (lit. (32) $[\alpha]_{589}$ +11.0° (*c*, 5.5% in water, 23°C)).

2. *Arginine*

*Decarboxylation of arginine catalysed by* L-*arginine decarboxylase (E.C. 4.1.1.19) from* E. coli

(i) *(−)-(1-$^2$H)Agmatine sulfate (**10**) by decarboxylation of* L-*arginine (**16**) in deuterium oxide solution*

L-Arginine monohydrochloride (Eastman) (90 mg) was twice dissolved in deuterium oxide and evaporated to dryness to effect replacement of exchangeable protons with deuterium. The amino acid was then dissolved in perdeuterioacetate–$^2H_2O$ buffer (ca. p$^2$H 5.2, 20 mL) to yield a 0.02 *M* solution. The buffer had been prepared from perdeuterioacetic acid (0.2 *M* in $^2H_2O$) and anhydrous sodium carbonate (8.36 mg/mL) (see under Decarboxylation of ornithine). L-Arginine decarboxylase (Sigma; 0.7 U/mg)[7] (43 mg) was added and the resulting solution incubated at 36°C in a flask equipped with a calcium sulfate drying tube. After 30–40 h the incubation mixture was acidified (ca. pH 2) with concentrated hydrochloric acid, treated with Norite, heated on a steam bath for 30 min, and filtered through Celite. The filtrate was evaporated, the residue dried *in vacuo* over sodium hydroxide and then dissolved in 5% sodium hydroxide solution (1–2 mL). The alkaline solution was saturated with sodium chloride and extracted with 1-butanol (4 × 3 mL). Evaporation of the butanol gave an oil which was redissolved in aqueous sulfuric acid (0.1 *M*, ca. 1 mL). After addition of methanol and cooling at 0°C overnight the crystalline sulfate of (−)-(1-$^2$H)agmatine separated and was recrystallized from water–methanol. Yield 72 mg; mp 238–240°C (lit. (nondeuteriated) (33) mp 236–239°C); $^1$H nmr ($^2H_2O$, relative to $^1H^2HO$ at 4.63 ppm), δ: 1.66 (4H, m, H-2,3), 2.95 (ca. 1H, t (br), $J \sim 6.8$ Hz, H-1), 3.18 (2H, m, H-4); ORD, $[\alpha]_{302}$ −1.37 ± 0.08°, $[\alpha]_{313}$ −1.17 ± 0.07°, $[\alpha]_{334}$ −1.01 ± 0.06°, $[\alpha]_{365}$ −0.76 ± 0.04°, $[\alpha]_{405}$ −0.57 ± 0.03°, $[\alpha]_{436}$ −0.50 ± 0.03°, $[\alpha]_{546}$ −0.19 ± 0.02°, $[\alpha]_{579}$ −0.16 ± 0.03° (*c*, 6.52% in water, 25°C, uncorrected for incomplete deuteration); $^2$H nmr ($H_2O$, 180 *mM*, 100 transients) showed one signal at 3.0 ppm apart from that due to natural abundance $^2$H in water (4.7 ppm).

(ii) *(+)-(1-$^2$H)Agmatine sulfate by decarboxylation of* L-*(2-$^2$H)arginine*

A solution of L-(2-$^2$H)arginine monohydrochloride (ca. 92% $^2$H) (0.02 *M*) and L-arginine decarboxylase (0.7 U/mg)[7] (75 mg) in acetate buffer (0.2 *M*, pH 5.2, 35 mL) was incubated at 36°C for 40 h. The reaction mixture was worked up, as described under (i), to give (+)-(1-$^2$H)agmatine sulfate (100 mg). The mp and nmr spectra ($^1$H and $^2$H) were similar to those obtained for (−)-(1-$^2$H)agmatine sulfate. The sample showed a plane positive ORD curve; $[\alpha]_{297}$ +1.42 ± 0.11°, $[\alpha]_{302}$ +1.21 ± 0.08°, $[\alpha]_{313}$ +1.07 ± 0.07°, $[\alpha]_{334}$ +0.84 ± 0.06°, $[\alpha]_{365}$ +0.70 ± 0.04°, $[\alpha]_{405}$ +0.53 ± 0.03°, $[\alpha]_{436}$ +0.42 ± 0.03°, $[\alpha]_{546}$ +0.27 ± 0.03°, $[\alpha]_{577}$ +0.23 ± 0.04° (*c*, 4.18% in water, 25°C, uncorrected for incomplete deuteration).

C. *Conversion of agmatine into putrescine*

1. *Hydrolysis of agmatine to putrescine*

A solution of agmatine sulfate (55 mg) in ethanol–water

[6] 1 U will release 1.0 μmol carbon dioxide from L-ornithine per min at pH 5.0 at 37°C.

[7] 1 U will release 1.0 μmol carbon dioxide from L-arginine per min at pH 5.2 at 37°C.

Can. J. Chem. Downloaded from www.nrcresearchpress.com by 210.87.254.6 on 09/06/12
For personal use only.

(70:30, v/v, 3 mL) containing sodium hydroxide (10%, w/v) was heated at reflux under a nitrogen atmosphere. When the reaction was complete (ca. 20 h) as revealed by paper chromatography (Whatman 3 MM, 1-butanol – acetic acid – pyridine – water 4:1:1:2; visualized with ninhydrin (0.3% w/v, in 1-butanol – acetic acid, 97:3, v/v); agmatine, $R_f$ 0.36; putrescine, $R_f$ 0.27), the reaction mixture was cooled to room temperature and acidified to pH 4 with 10% hydrochloric acid. After evaporation of the solvent the residue was dissolved in sodium hydroxide solution (10% w/v, 3 mL), the solution saturated with sodium chloride and extracted with 1-butanol (3 × 3 mL). The butanol extract was acidified with HCl–butanol and concentrated *in vacuo* (~ 4 mL). Putrescine dihydrochloride which separated was collected and recrystallized from aqueous ethanol. Yield, 33 mg, 87%. The $^1$H nmr spectrum was identical with that of authentic material.

(i) *Conversion of (−)-(1-$^2$H)agmatine sulfate (**10**) into (−)-(1-$^2$H)putrescine dihydrochloride (**15**)*

Hydrolysis of (−)-(1-$^2$H)agmatine sulfate (65 mg), as described for unlabelled material, gave (−)-(1-$^2$H)putrescine dihydrochloride (41 mg) which was twice recrystallized from aqueous ethanol: CI ms, 90 (M + H, 3%), 74 (5), 73 (M − $NH_3$, 100), 72 (2); 99.4 ± 0.4% $^2$H, determined by CI ms; ORD, $[\alpha]_{302}$ −1.07 ± 0.09°, $[\alpha]_{313}$ −0.98 ± 0.08°, $[\alpha]_{334}$ −0.84 ± 0.08°, $[\alpha]_{365}$ −0.67 ± 0.05°, $[\alpha]_{405}$ −0.52 ± 0.05°, $[\alpha]_{436}$ −0.43 ± 0.06°, $[\alpha]_{546}$ −0.21 ± 0.06° (*c*, 1.84% in 0.1 *N* HCl, 26°C, uncorrected for incomplete deuteration).

(ii) *Conversion of (+)-(1-$^2$H)agmatine sulfate into (+)-(1-$^2$H)putrescine dihydrochloride*

Hydrolysis of (+)-(1-$^2$H)agmatine sulfate (40 mg) gave (+)-(1-$^2$H)putrescine dihydrochloride (22 mg) which was twice recrystallized from water: CI ms, 90 (M + H, 5%), 74 (5), 73 (M − $NH_3$, 100) 72 (10); 91.7 ± 0.8% $^2$H, determined by CI ms; ORD, $[\alpha]_{313}$ +0.85 ± 0.09°, $[\alpha]_{334}$ +0.75 ± 0.09°, $[\alpha]_{365}$ +0.56 ± 0.06°, $[\alpha]_{405}$ +0.44 ± 0.05°, $[\alpha]_{436}$ +0.41 ± 0.06°, $[\alpha]_{546}$ +0.24 ± 0.06° (*c*, 1.61% in 0.1 *N* HCl, 26°C, uncorrected for incomplete deuteration).

Paper chromatography (see above) of the samples of (−)- and (+)-(1-$^2$H)putrescine dihydrochloride obtained from Experiments (i) and (ii), above, showed single ninhydrin positive and Sakaguchi (34) negative spots at $R_f$ 0.27. The $^1$H nmr spectra ($^2H_2O$) of both samples were identical with those of (1-$^2$H)-putrescine dihydrochloride obtained from ornithine.

D. *Conversion of agmatine into phthalimidobutyric acid*

1. *4-Phthalimidobutylguanidine sulfate* (cf. **11**)

To a stirred solution containing agmatine sulfate (228 mg, 1 mmol) and sodium bicarbonate (168 mg, 2 mmol) in water (3 mL) was added *N*-carbethoxyphthalimide (Aldrich) (232 mg, 1 mmol) in small portions over 15 min at room temperature. After stirring for 1 h, the reaction mixture was cooled to 0°C and the product, which precipitated, was recrystallized from methanol. Yield 225 mg; mp 213–214°C; $^1$H nmr ($C^2H_3CO_2{}^2H$), δ: 1.70 (4H, m (br), H-2,3), 3.30 (2H, t (br), H-1), 3.84 (2H, t (br), H-4), 7.85 (4H, m, ArH). *Anal.* calcd. for $(C_{13}H_{17}N_4O_2)_2SO_4 2H_2O$: C 47.69, H 5.85, N 17.12, $SO_4^=$ 14.67; found: C 47.65, H 5.98, N 17.09, $SO_4^=$ 14.49%.

2. *4-Phthalimidobutyric acid* (cf. **12**)

A solution of potassium permanganate (0.4 *M*) in 1 *N* sulfuric acid was added in small portions (ca. 0.1 mL) to a stirred suspension of 4-phthalimidobutylguanidine (27 mg) in 1 *N* sulfuric acid (1 mL) at room temperature. Additions of the oxidant were made until the colour of permanganate in the reaction mixture was no longer discharged (ca. 0.5 mL over 1 h). Stirring was continued for 1 h and the reaction mixture was then decolourized with sodium bisulfite. After cooling at 0°C, the product, which precipitated, was extracted into chloroform (3 × 2 mL). The combined extracts were dried over anhydrous sodium sulfate and filtered. Evaporation gave 4-phthalimidobutyric acid (13 mg) as a white solid which was recrystallized three times from water; mp 115–116°C (lit. (35) mp 115–118°C); $^1$H nmr ($^2HCCl_3$), δ: 2.01 (2H, quin., *J* 6.8 Hz, H-3), 2.32 (2H, t, *J* 6.8 Hz, H-2), 3.76 (2H, t, *J* 6.8 Hz, H-4), 7.75 (4H, m, ArH), 10.2 (1H, s (br), $CO_2H$); ms, *m/e*: 233 (M, 4%), 215 (M − $H_2O$, 19), 187 (15), 174 (70), 173 (42), 160 (100), 104 (19), 76 (24). The mp and spectral properties were the same as those of an authentic sample prepared from γ-aminobutyric acid and *N*-carbethoxyphthalimide (4).

3. *Conversion of (1-$^2$H)agmatine into 4-phthalimido(4-$^2$H)-butyric acid*

(i) *N*-Carbethoxyphthalimide (82 mg) was added to a stirred solution of (−)-(1-$^2$H)agmatine sulfate (**10**) (70 mg) in 0.5 *M* sodium bicarbonate (1.5 mL). The resulting mixture was stirred at room temperature for 20 min and then cooled to 0°C. After standing at 0°C for 30 min, the product was collected by filtration, washed with cold water (1 mL), cold ethanol (1 mL), and chloroform (1 mL), and dried *in vacuo* over sodium hydroxide. 4-Phthalimido(4-$^2$H)butylguanidine (**11**) (66 mg), so obtained, was recrystallized from methanol – acetic acid (20:1); mp 210–212°C. The $^1$H nmr spectrum ($C^2H_3CO_2{}^2H$) of the deuteriated sample was similar to that of unlabelled material (see above) except that the signal at 3.84 ppm (H-4) corresponded to ca. 1.05 hydrogen atoms only.

Permanganate oxidation of a sample of the ($^2$H)guanidine derivative (49 mg) in aqueous sulfuric acid (1 *N*), as described for unlabelled material, gave (−)-4-phthalimido(4-$^2$H)butyric acid (**12**) (23 mg) which was recrystallized three times from water; mp 112–114°C; $^1$H nmr ($C^2HCl_3$), δ: 2.05 (2H, q, *J* 6.8 Hz), 2.39 (2H, t, *J* 6.8 Hz), 3.75 (ca. 1H, t, *J* 6.8 Hz), 7.80 (4H, m), 10.2 (1H, s (br)); $^2$H nmr ($CHCl_3$, 30 *mM*, 2172 transients) showed a single signal at 3.74 ppm apart from that due to natural abundance $^2$H in $CHCl_3$ (7.27 ppm); ms, *m/e*: 234 (M, 3%), 216 (M − $H_2O$, 7), 215 (M − $H^2HO$, 9), 188 (8), 187 (6), 175 (41), 174 (30), 173 (17), 161 (100), 160 (5), 104 (16), 76 (22); 97.2 ± 0.2% $^2H_1$, determined by ms; ORD, $[\alpha]_{365}$ −5.39 ± 0.14°, $[\alpha]_{405}$ −3.79 ± 0.22°, $[\alpha]_{436}$ −3.07 ± 0.18°, $[\alpha]_{546}$ −1.64 ± 0.13°, $[\alpha]_{577}$ −1.37 ± 0.14°, $[\alpha]_{589}$ −1.08 ± 0.22° (*c*, 0.91% in methanol, 25°C, uncorrected for incomplete deuteration) (lit. (4) $[\alpha]_{589}$ −1.69°).

A sample of (−)-4-phthalimido(4-$^2$H)butyric acid (**12**) (5 mg) was dissolved in ether (1 ml), a solution of diazomethane in ether (1 mL) (36) was added, and the mixture was allowed to stand overnight. The product, (−)-methyl 4-phthalimido(4-$^2$H)butyrate (**13**) was recrystallized from methanol, mp 87–88°C (lit. (nondeuteriated) (35) mp 89–90°C); ms, *m/e*: 248 (M, 9%), 217 (M − $OCH_3$, 18), 216 (8), 189 (10), 188 (10), 175 (100), 174 (20), 161 (95), 130 (15), 104 (17), 77 (15), 76 (12); 98.2 ± 0.3% $^2H_1$, determined by ms; ORD, $[\alpha]_{365}$ −5.97 ± 0.60°, $[\alpha]_{405}$ −4.84 ± 0.40°, $[\alpha]_{436}$ −4.06 ± 0.30°, $[\alpha]_{546}$ −2.21 ± 0.30°, $[\alpha]_{577}$ −2.02 ± 0.30° (*c*, 0.34% in methanol, 25°C, uncorrected for incomplete deuteration).

An unlabelled sample of methyl 4-phthalimidobutyrate was prepared analogously; mp 87–88°C (from methanol); ms, *m/e*: 247 (M, 13%), 216 (M − $OCH_3$, 19), 215 (17), 188 (9), 187 (11), 174 (100), 173 (23), 160 (79), 130 (11), 104 (14), 77 (12), 76 (6).

An authentic sample of (−)-methyl 4-phthalimido(4-$^2$H)-butyrate (**13**) was supplied by Dr. M. H. O'Leary, University of Wisconsin. This sample had been prepared (4) by methylation of (−)-4-phthalimido(4-$^2$H)butyric acid which had been obtained by decarboxylation in $^2H_2O$ of L-glutamic acid, catalyzed by L-glutamic decarboxylase; mp 88–89°C (from methanol); ms, *m/e*: 248 (M, 13%), 217 (M − $OCH_3$, 21), 216 (10), 189 (10), 188 (8), 175 (100), 174 (15), 161 (80), 130 (15), 104 (15), 77 (10), 76 (12); 92.5 ± 0.4% $^2H_1$, 4.7 ± 0.4% $^2H_2$, determined by ms; ORD,

$[\alpha]_{365}$ −4.45 ± 0.30°, $[\alpha]_{405}$ −3.35 ± 0.20°, $[\alpha]_{436}$ −2.76 ± 0.20°, $[\alpha]_{546}$ −1.48 ± 0.30°, $[\alpha]_{577}$ −1.43 ± 0.30° (*c*, 0.39% in methanol, 25°C, uncorrected for incomplete deuteration).

(ii) A sample of 4-phthalimido(4-$^2$H)butylguanidine (80 mg) obtained by the method described above from (+)-(1-$^2$H)-agmatine sulfate (72 mg) showed mp 213–214°C (from methanol – acetic acid (20:1)) and a $^1$H nmr spectrum in which the signal at 3.84 ppm corresponded to ca. 1.15 hydrogen atoms. Oxidation of part of this sample (60 mg), as described above, gave (+)-4-phthalimido(4-$^2$H)butyric acid (28 mg), mp 112–114°C (3 times from water). The $^1$H ($^2HCCl_3$) and $^2$H ($CHCl_3$, 30 *mM*, 1584 transients) nmr spectra of this material were similar to those obtained for the (−)-(4-$^2$H)phthalimide; ms, *m/e*: 234 (M, 3%), 216 (M − $H_2O$, 8), 215 (M − $H^2HO$, 10), 188 (9), 187 (7), 175 (44), 174 (39), 173 (19), 161 (100), 160 (16), 104 (17), 76 (25); 84.7 ± 0.3% $^2H_1$ determined by ms; ORD, $[\alpha]_{365}$ +4.77 ± 0.27°, $[\alpha]_{405}$ +3.26 ± 0.29°, $[\alpha]_{436}$ +2.62 ± 0.17°, $[\alpha]_{546}$ +1.32 ± 0.11°, $[\alpha]_{577}$ +1.20 ± 0.13°, $[\alpha]_{589}$ +0.96 ± 0.22° (*c*, 0.97% in methanol, 25°C, uncorrected for incomplete deuteration).

E. *Instrumental methods*

*Measurement of optical activity*

Optical rotation was measured by means of a Perkin–Elmer 241 MC polarimeter equipped with a mercury emission lamp, using a 1 dm polarimeter tube. At least 10 readings were taken at each mercury emission line. Mean values and 95% confidence limits are reported.

*The $^1H$ nmr spectra* at 90 MHz were recorded on a Varian EM 390 spectrometer at ambient temperature. Chemical shifts are reported as ppm downfield from DSS or TMS as internal standards, respectively, for samples in $^2H_2O$ or $^2HCCl_3$ solution.

*The $^2H$ nmr spectra* were recorded on a Bruker WH 90 pulsed Fourier transform spectrometer operating at 13.82 MHz at ambient temperature, with broad band proton noise decoupling. Spectra were obtained of samples in aqueous or chloroform solution in 10 mm (od) sample tubes, using $^2H_2O$ as external lock. The signal due to natural abundance $^2$H in $^2$HOH or $^2HCCl_3$ served as internal standard. Chemical shifts are downfield from perdeuteriotetramethylsilane.

*Mass spectra* were determined on a Micromass 7070F double focussing mass spectrometer, operating with electron impact (EI) or chemical ionization (CI), by direct injection of the samples. Methane at $5 \times 10^{-5}$ mm Torr was the reagent gas for CI. The isotopic content in deuterium enriched samples was calculated as described by Biemann (37).

## Acknowledgements

This investigation was supported by a grant from the Natural Sciences and Engineering Research Council of Canada.

We are indebted to Professor Marion H. O'Leary, Department of Chemistry, University of Wisconsin, Madison, WI, for supplying a reference sample of (−)-methyl *R*-4-phthalimido(4-$^2$H)butyrate.

One of us (I.D.S.) thanks the Institut für Organische Chemie der Universität Karlsruhe for a visiting professorship, Professor J. Rétey for the hospitality of his laboratory, and the Deutscher Akademischer Austauschdienst for a stipend.

1. S. Mandeles, R. Koppelman, and M. E. Hanke. J. Biol. Chem. **209**, 327 (1954).
2. B. Belleau and J. Burba. J. Am. Chem. Soc. **82**, 5751 (1960).
3. E. Leistner and I. D. Spenser. J. Chem. Soc. Chem. Commun. 378 (1975).
4. H. Yamada and M. H. O'Leary. Biochemistry, **17**, 669 (1978).
5. A. R. Battersby, E. J. T. Chrystal, and J. Staunton. J. Chem. Soc. Perkin Trans. I, 31 (1980).
6. H. J. Gerdes and L. Leistner. Phytochemistry, **18**, 771 (1979).
7. A. R. Battersby, R. Murphy, and J. Staunton. J. Chem. Soc. Perkin Trans. I, 449 (1982).
8. M. Bouclier, M. J. Jung, and B. Lippert. Eur. J. Biochem. **98**, 363 (1979).
9. E. Santaniello, M. G. Kienle, A. Manzocchi, and E. Bosisio. J. Chem. Soc. Perkin Trans. I, 1677 (1979).
10. A. R. Battersby, J. Staunton, and J. Tippett. J. Chem. Soc. Perkin Trans. I, 455 (1982).
11. A. R. Battersby, M. Nicoletti, J. Staunton, and R. Vleggaar. J. Chem. Soc. Perkin Trans. I, 43 (1980).
12. E. Santaniello, A. Manzocchi, and P. A. Biondi. J. Chem. Soc. Perkin Trans. I, 307 (1981).
13. D. R. Houck and H. G. Floss. J. Nat. Prod. **44**, 760 (1981).
14. Y. Asada, K. Tanizawa, S. Sawada, T. Suzuki, H. Misono, and K. Soda. Biochemistry, **20**, 6881 (1981).
15. J. C. Vederas and H. G. Floss. Acc. Chem. Res. **13**, 455 (1980).
16. E. Leistner and I. D. Spenser. J. Am. Chem. Soc. **95**, 4715 (1973).
17. J. C. Richards and I. D. Spenser. J. Am. Chem. Soc. **100**, 7402 (1978).
18. M. Fields, D. E. Walz, and S. Rothchild. J. Am. Chem. Soc. **73**, 1000 (1951).
19. S. M. Birnbaum and J. P. Greenstein. Arch. Biochem. Biophys. **39**, 108 (1952).
20. W. R. Boon and W. Robson. Biochem. J. **29**, 2684 (1935).
21. D. E. Rivard. Biochem. Prep. **3**, 97 (1953).
22. P. B. Hamilton and R. A. Anderson. Biochem. Prep. **3**, 96 (1953).
23. C.-Y. Yüan, C.-T. Lin, and J.-H. Liu. Hua Hsüeh Hsüeh Pao, **25**, 183 (1959); Chem. Abstr. **54**, 4405c (1960).
24. A. I. Vogel. A text-book of practical organic chemistry. 3rd ed. Longmans, Green & Co., London. 1956. p. 167.
25. V. I. Maimind, O. M. Enisherlova, K. M. Ermolaev, R. G. Vdovina, G. A. Galegov, and M. M. Shemiakin. Zh. Obshch. Khim. **28**, 2223 (1958); J. Gen. Chem. U.S.S.R. (Engl. Transl.) **28**, 2260 (1958).
26. S. M. Birnbaum, M. Winitz, and J. P. Greenstein. Arch. Biochem. Biophys. **60**, 496 (1956).
27. P. J. Fodor, V. E. Price, and J. P. Greenstein. J. Biol. Chem. **178**, 503 (1949).
28. A. A. Plentl and W. T. Kelly. Anal. Biochem. **17**, 397 (1966).
29. A. F. Thomas. Deuterium labelling in organic chemistry. Appleton-Century-Crofts, New York. 1971. p. 11.
30. J. B. Jones and J. F. Beck. *In* Techniques of chemistry. Vol. 10. pt. 1. *Edited by* J. B. Jones, C. J. Sih, and D. Perlman. John Wiley, New York. 1976. p. 206.
31. E. Brand and M. Sandberg. Org. Synth. Coll. Vol. **2**, 49 (1943).
32. A. Hunter. Biochem. J. **33**, 27 (1939).
33. T. A. Smith and F. J. Richards. Biochem. J. **84**, 292 (1962).
34. I. Smith and H. G. Horsefall. *In* Chromatographic and electrophoretic techniques. Vol. 1. 3rd ed. *Edited by* I. Smith. William Heinemann, London. 1969. p. 290.
35. S. Gabriel and J. Colman. Chem. Ber. **41**, 513 (1908).
36. A. I. Vogel. A text-book of practical organic chemistry. 3rd ed. Longmans, Green & Co, London. 1956. p. 971.
37. K. Biemann. Mass spectrometry: organic chemical applications. McGraw Hill, New York. 1962. p. 204.

Can. J. Chem. Downloaded from www.nrcresearchpress.com by 210.87.254.6 on 09/06/12
For personal use only.

# Pyrones. IX.[1] Synthetic approaches to the fungal metabolite phacidin and its derivatives

GERALD ARTHUR POULTON AND TERRY DONALD CYR

*Department of Chemistry, University of Victoria, P.O. Box 1700, Victoria, B.C., Canada V8W 2Y2*

Received April 1, 1982

G. A. POULTON and T. D. CYR. Can. J. Chem. **60**, 2821 (1982).

The synthesis of the antibiotic fungal metabolite phacidin **1** (4-methoxy-6-nonanoyl-2*H*-pyran-2-one-3-carboxaldehyde) and two related compounds is reported. Phacidin has been prepared in four steps from the readily available triacetic acid lactone (4-hydroxy-6-methyl-2*H*-pyran-2-one), while the decarbonylated derivative **2** and the bromo compound **3** have been synthesized utilizing a route based upon the condensation of the dianion of ethyl acetoacetate with a substituted 1,3-dithiane-2-carboxaldehyde.

G. A. POULTON et T. D. CYR. Can. J. Chem. **60**, 2821 (1982).

On rapporte la synthèse d'un métabolite fongique aux propriétés antibiotiques: la phacidine **1** (méthoxy-4 nonanoyl-6 (2*H*)pyranone-2 carboxaldehyde-3) ainsi que deux composés apparentés. La phacidine a été préparée en quatre étapes à partir de la lactone de l'acide triacétique (hydroxy-4 méthyl-2 (2*H*)pyranone-2) facilement accessible, tandis que le dérivé décarbonylé **2** et le composé bromé **3** ont été synthétisés en utilisant une voie basée sur la condensation du dianion de l'acétoacétate d'éthyle avec un dithiane-1,3 carboxaldéhyde-2 substitué.

[Traduit par le journal]

Phacidin **1**, a metabolic product of the canker fungus *Potebniamyces balsamicola* Smerlis var. *boycei* Funk, has been shown to possess potentially useful antifungal activity (1). Elucidation of the structure of this mycotoxin involved an examination of its chemical transformations and the spectra of phacidin and several derivatives, most particularly the decarbonylated compound **2** and the bromo derivative **3** (Scheme 1). Such elucidation was rendered more difficult by the great similarities in spectra between 4-alkoxy-2-pyrones and 2-alkoxy-4-pyrones (2), and final confirmation of structure was only obtained with the completion of the synthesis of phacidin (3). Herewith we report the synthetic routes which were investigated, and the experiments which led to the successful synthesis of **1**, **2**, and **3**.

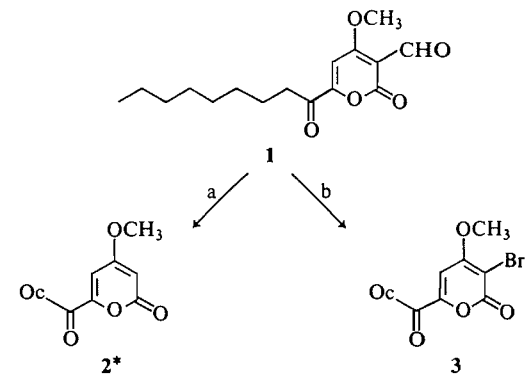


*In this and all subsequent schemes and tables, Oc = *n*-octyl; reagents: a $(Ph_3P)_3RhCl$, $C_6H_6$; b $Br_2$, $H_2O$

SCHEME 1. Preparation of derivatives of phacidin.

Complex pyrones have been synthesized via three different routes: (i) by synthesis of the ring from suitably substituted acyclic precursors, (ii) from carbohydrate derivatives, and (iii) by modification of naturally occurring pyrones. Synthesis of pyrones from carbohydrate derivatives has not normally been a productive route, mainly due to low yields, and has not been used for the preparation of 4-oxy-2-pyrones. A wide variety of routes has been devised leading to these compounds which are based upon the formation of a particular carbon–carbon bond of the pyrone ring. Commonly used routes include the carboxylation of β-diketones (formation of the 2,3-bond) followed by cyclization of the 3,5-diketoacids (4), base catalyzed condensation of two β-ketoesters (forming the 3,4-bond (5)), condensations of ketenes or ketene acetals (3,4-bond (6)), or the condensation of mono- or di-anions of β-ketoesters with acid derivatives or aldehydes (formation of 4,5-bond (7) or 5,6-bond (8), respectively). Elaboration of naturally occurring pyrones into more complex, larger molecules has been achieved through functionalization of ring methyl groups by radical bromination (9), oxidation (10), or anion formation (11), although recent results (12) indicate that deprotonation at C-3 can compete with anion formation at the methyl position.

Our successful synthesis of phacidin was based upon the choice of triacetic acid lactone (4-hydroxy-6-methyl-2*H*-pyran-2-one) **4** as starting material. The key step in the proposed synthesis (see Scheme 2) was the introduction of the formyl group at C-3; accordingly, model studies were carried out with this substrate and its methyl ether (see Table

[1]For Part VIII in this series, see ref. 27.

0008-4042/82/222821-09$01.00/0

©1982 National Research Council of Canada/Conseil national de recherches du Canada

Can. J. Chem. Downloaded from www.nrcresearchpress.com by 210.87.254.42 on 09/06/12
For personal use only.

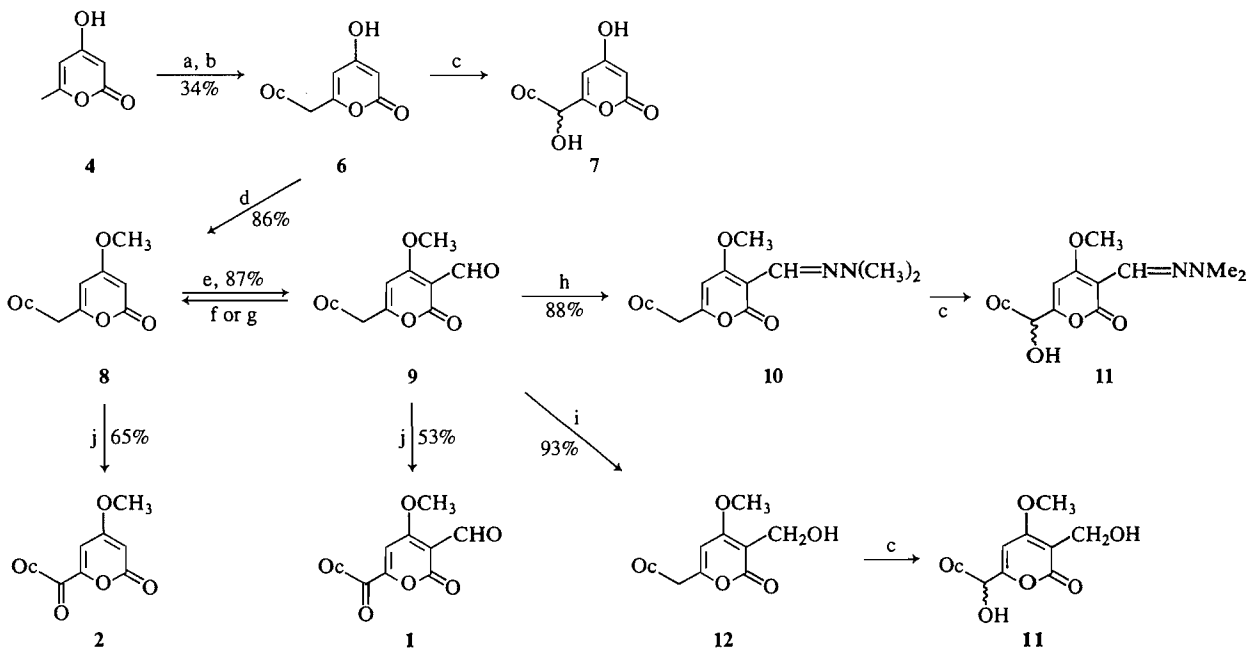


Reagents: a 2BuLi; b OcBr; c LDA, $O_2$; d $(CH_3)_2SO_4$, $K_2CO_3$; e $Cl_2CHOCH_3$, $TiCl_4$; f $HOCH_2CH_2OH$, TsOH, $C_6H_6$; g $(CH_3O)_3CH$, $Ce^{III}$; h $H_2NN(CH_3)_2$, TFA; i $NaBH_4$, $CH_3OH$; j $SeO_2$

SCHEME 2. Synthesis of phacidin 1.

1). After fruitlessly trying a variety of reagents and conditions (13–17), we achieved success using a process which involved treatment of the methoxypyrone with excess dichloromethyl methyl ether, followed by excess anhydrous titanium tetrachloride under a nitrogen atmosphere. The intermediate product was readily hydrolyzed by water at 0°C to produce the aldehyde, 4-methoxy-6-methyl-2*H*-pyran-2-one-3-carboxaldehyde **5** (37%).

With a suitable formylation procedure in hand, triacetic acid lactone **4** was treated with two equivalents of butyllithium, and the dianion thus formed successfully alkylated at carbon with 1-bromooctane, producing 4-hydroxy-6-nonyl-2-pyrone **6** in low yield. That alkylation had proceeded as desired at the methyl group and not at C-3 or the 4-oxygen was evident from the retained signals in the $^1$Hmr spectrum at δ 11.1 (broad, OH) and at δ 6.02 and 5.60 (both doublets, $J = 4.5$ Hz, indicating unsubstituted 3,5-positions) and from the replacement of the 6-methyl signal by a two proton triplet at δ 2.48. An attempt to oxidize the benzylic position of the nonyl side chain via oxygenation of the dianion (19) was unsuccessful; only traces of the desired 4-hydroxy-6-(1′-hydroxynonyl)-2-pyrone **7** were obtained.

In order to improve selectivity and solubility, the methyl ether **8** was prepared by a normal base-promoted methylation (20). Formylation was then effected using the conditions established earlier and the desired 4-methoxy-6-nonyl-2-pyrone-3-carboxaldehyde **9** isolated in high yield. Substitution was confirmed by the disappearance of the C-3 proton resonance at δ 5.48, the collapse of the C-5 resonance to a singlet at δ 6.05, and the presence of the aldehyde resonance at δ 10.14.

Since the aldehyde itself was unlikely to survive an anion oxygenation procedure, attempts were made to protect it by derivatization. Treatment of the aldehyde **9** with ethylene glycol under acid catalysis produced, as the only isolable pyrone product, the deformylated 4-methoxy-6-nonyl-2-pyrone **8** (45%); similar results were obtained when trimethyl or triethyl orthoformate was used. The *N*,*N*-dimethylhydrazone was successfully prepared in high yield, but oxygenation of the anion of **10** gave mainly recovered starting material and decomposition products. Reduction of the formyl group (to the alcohol **12**) followed by oxygenation also gave no reaction or led mainly to decomposition products, indicating that such an oxidative route was unlikely to prove useful. Similar attempts using oxodiperoxymolybdenum (pyridine) (hexamethyl phosphoric triamide) (21) also failed.

Suzuki *et al.* (10) had demonstrated that the 6-methyl group could be successfully oxidized to a carbonyl compound by means of selenium dioxide oxidation. Again using 4-methoxy-6-nonyl-2-py-

Can. J. Chem. Downloaded from www.nrcresearchpress.com by 210.87.254.42 on 09/06/12
For personal use only.

Can. J. Chem. Downloaded from www.nrcresearchpress.com by 210.87.254.42 on 09/06/12
For personal use only.

TABLE 1. Acylation and alkylation of 4-methoxy-6-methyl-2*H*-pyran-2-one and 4-hydroxy-6-methyl-2*H*-pyran-2-one

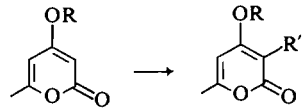

4 5

| Starting material R | Reagents | Conditions: Addition | Conditions: Reaction | Expected product R' | Yield % | Reference |
|---|---|---|---|---|---|---|
| H | $DMF, POCl_3$ | 100°C | 1 h | —CHO | 0 | 13 |
| $CH_3$ | $DMF, POCl_3$ | 100°C | 1 h | —CHO | 0 | 13 |
| H | HCl, CO, TFA | 0°C | 48 h | —CHO | 0 | 14 |
| H | 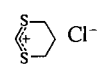 $Cl^-, Et_3N$ | −78°C | rt, 2 h | | 0 | 15 |
| $CH_3$ | 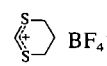 $BF_4^-$, DBU, THF | 0°C | rt, 4 h | | 0 | 15 |
| H | $Me_2NH, HCHO, H_2O$ | rt* | 24 h | $—CH_2NMe_2$ | 0 | 16 |
| H | $ClCH_2OMe$, AcOH | rt | 2 wk | $—CH_2Cl$ | 0 | 17 |
| $CH_3$ | $ClCH_2OMe, TiCl_4$ | rt | 5 h | $—CH_2Cl$ | Trace | 17 |
| H | $Cl_2CHOMe, TiCl_4$ | rt | 0.25 h | —CHO | 0 | 18 |
| $CH_3$ | $Cl_2CHOMe, SnCl_4, CH_2Cl_2$ | −20°C | Reflux 1.5 h | —CHO | 0 | 18 |
| $CH_3$ | $Cl_2CHOMe, ZnCl_2, CDCl_3$ | −20°C | rt, 1 wk | —CHO | 0 | 18 |
| $CH_3$ | $Cl_2CHOMe, SnCl_4, (ClCH_2)_2$ | −20°C | Reflux 2.5 h | —CHO | 0 | 18 |
| $CH_3$ | $Cl_2CHOMe, TiCl_4, CH_2Cl_2$ | rt | 20 h | —CHO | 37 | 18 |

*Abbreviation, rt: room temperature.

TABLE 2. Selenium dioxide oxidation of 4-methoxy-6-nonyl-2-pyrone (**8**) and 4-methoxy-6-nonyl-2-pyrone-3-carboxaldehyde (**9**)

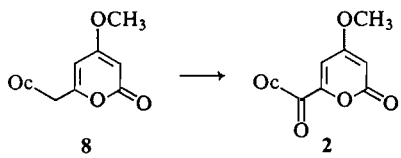

**8** **2**

| Conditions | Time | Products | Ratio |
|---|---|---|---|
| $SeO_2$, dioxane, Δ | 13 h | **24, 2, 8** | 2:5:1 |
| $SeO_2$, EtOH, Py, Δ | 12 h | **8** | |
| $SeO_2$, diglyme, Δ | 0.5 h | **2, 8** | 4:1 |

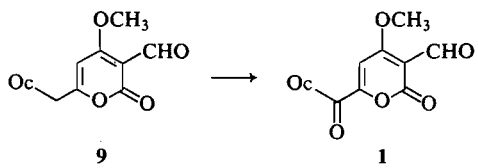

**9** **1**

| Conditions | Time | Products | Ratio | Yield |
|---|---|---|---|---|
| $SeO_2$, diglyme, Δ | 5 min | **9, 1** | 6:1 | 71% |
| $SeO_2$, diglyme, Δ | 30 min | **9, 1** | 3:2 | 34 |
| $SeO_2$, dioxane, Δ | 30 h | **9** + dec. | | |
| $SeO_2$, *m*-xylene, Δ | 30 min | **9, 1** | 3:1 | 82 |

rone **8** as a model compound, conditions were developed which maximized the yield of the desired ketone **2** (see Table 2); freshly sublimed selenium dioxide was found to be essential for the reaction to succeed, as only decomposition ensued when reagent $SeO_2$ was used. Application of similar conditions to the oxidation of the aldehyde **9** (freshly sublimed $SeO_2$ in refluxing *m*-xylene, 30 min) produced a mixture of starting material **9** and phacidin **1** in a ratio of 3:1 (82% recovery). Phacidin was isolated by preparative thin layer chromatography, and the sample thus obtained had identical mp and spectral properties to the natural product.

Use of an alternate route based upon dithiane alkylation (8, 22) allowed us to prepare the derivatives **2** and **3** (see Schemes 3 and 4). 1,3-Dithiane was alkylated under standard conditions yielding 2-octyl-1,3-dithiane (**14**) in 99% yield. Subsequent treatment of **14** with n-butyllithium provided a monoanion which was reacted with dimethylformamide to produce the aldehyde **15** (87%) or with ethyl chloroformate yielding the ester **16** (74%). It was our intention to react the ester with the dianion of ethyl acetoacetate and produce the 4-hydroxy-2-pyrone directly, thus obviating the extra step involved in oxidation of the dihydropyrone; unfortunately, the desired product was not forthcoming

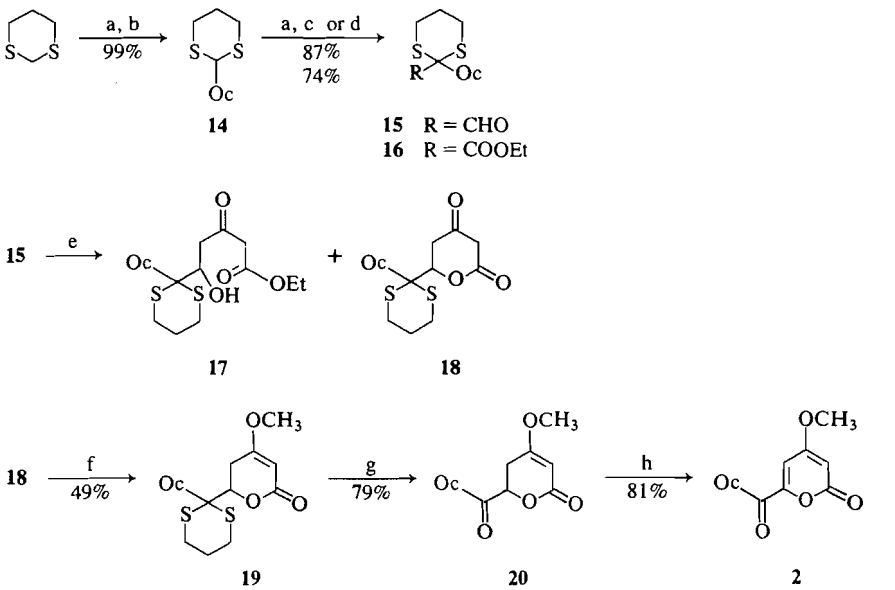


Reagents: a BuLi, THF; b OcBr; c DMF; d EtOOCCl; e $LiCH_2COCHCOOEt\ Na^+$; f NaH, $(CH_3)_2SO_4$; g $HgCl_2$, HgO, EtOH; h NBS, $h\nu$

SCHEME 3. Synthesis of decarbonyl phacidin **2**.

from this reaction. The aldehyde **15** smoothly condensed with the dianion of ethyl acetoacetate producing the desired 5,6-dihydropyrone **18** in 99% yield. When the reaction was carried out on a larger scale, the yield of the cyclized product dropped to 38%, and a second product, the nonlactonized ethyl 5-hydroxy-3-oxo-5-(2-octyl-1,3-dithian-2-yl)-pentanoate **17**, was also isolated. Surprisingly, this hydroxyester could not be subsequently induced to cyclize, either under acid or base conditions. The structure of the desired 5,6-dihydro-4-hydroxy-6-(2-octyl-1,3-dithian-2-yl)-2-pyrone **18** was evident from its molecular ion (*m/z* 344) and fragmentation pattern, the carbonyl stretching peaks at 1760 and 1726 $cm^{-1}$, and the $^1$Hmr spectrum.

The alcohol functionality of **18** was then methylated to produce the 4-methoxy compound **19**, showing $M^+$ at *m/z* 358 (chemical ionization) and $\nu_{CO}$ at 1720 $cm^{-1}$. Since unsaturation in the side chain has previously been shown to aid oxidation of dihydropyrones to pyrones (23), hydrolysis of the dithiane was investigated. Low and variable yields were encountered using the procedure of Seebach and Meyer (8), and therefore the hydrolysis was carried out by adding **19** dropwise to a rapidly stirred, refluxing ethanol slurry of mercuric chloride and mercuric oxide. The ketone **20** (*m/z* 268, $\nu_{CO}$ 1719 $cm^{-1}$) was obtained in 79% yield.

The dehydrogenation of **20** to a pyrone was accomplished by first brominating C-5 under free radical conditions (NBS, $h\nu$), with the subsequent spontaneous dehydrobromination yielding **2**; dehydrobromination was forced to completion simply by removing the HBr formed by bubbling a slow stream of nitrogen through the reaction mixture. The spectral data for the 4-methoxy-6-nonanoyl-2*H*-pyran-2-one **2** thus obtained were in complete accord with those of the decarbonylated compound obtained from the natural product (2).

Phacidin could not be synthesized directly from this product; formylation of **2** under the conditions used previously did not result in ring substitution, but in preparation of the *gem*-dihalide **21**, a not-unexpected transformation (18). Subsequent substitution of the ring in **21** did not ensue, presumably due to the deactivating nature of the dihaloalkyl substituent. A similar formylation attempt on the ethylenedithio derivative **22** also failed, yielding only traces of the desired aldehyde **23** and the deprotected starting material **2**. Reduction of the ketone gave the alcohol **24** which, under the same conditions, produced a complex mixture of products which decomposed extensively during chromatography. Among the products, as identified from their spectra, were the chloro-compound **25**, the chloro-aldehyde **26**, and the dehydrochlorinated aldehyde **27**.

Bromination of 2-pyrones at the 3-position has been demonstrated (24), and we therefore proceeded to the synthesis of bromophacidin **3**. Model experiments with 4-methoxy-6-methyl-2*H*-pyran-2-one **4** confirmed that modest yields of brominated

Can. J. Chem. Downloaded from www.nrcresearchpress.com by 210.87.254.42 on 09/06/12
For personal use only.

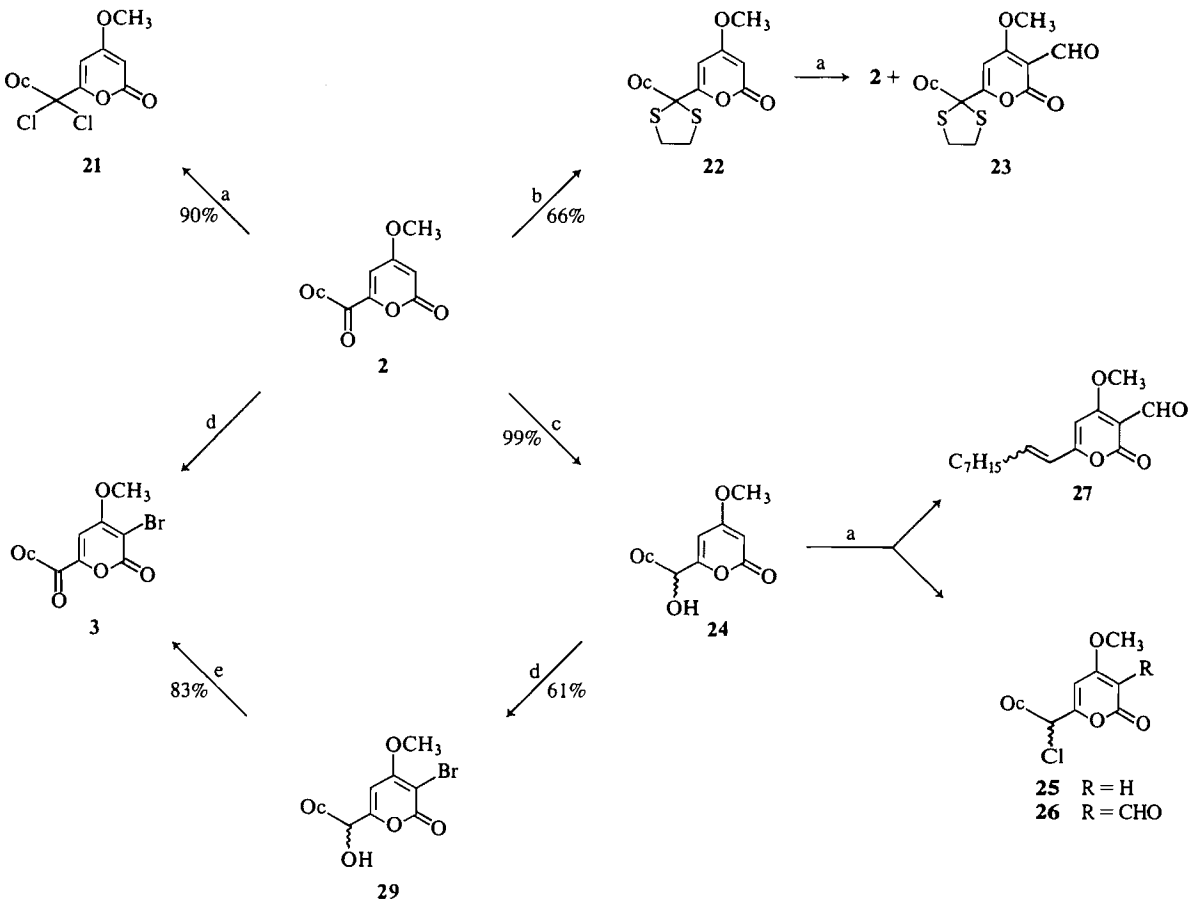


Reagents: a $Cl_2CHOCH_3$, $TiCl_4$; b $HSCH_2CH_2SH$, $BF_3{\cdot}Et_2O$; c $NaBH_4$; d NBS, $I_2$; e $MnO_2$

SCHEME 4. Transformations of 4-methoxy-6-nonanoyl-2-pyrone.

product could be obtained. Thus, bromination of 4-methoxy-6-nonanoyl-2*H*-pyran-2-one, **2**, was attempted using NBS with traces of iodine under conditions similar to those used successfully in the model, but only starting material was isolated, once

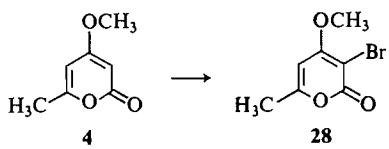


again indicating the deactivated nature of this pyrone ring.

Bromination of the hydroxyalkyl pyrone **24** proceeded smoothly under the same conditions to produce the 3-bromo compound **29** which showed molecular ions at *m/z* 348/346 and $\nu_{CO}$ at 1731 $cm^{-1}$. Bromophacidin **3** was successfully synthesized from this alcohol by a standard manganese dioxide oxidation (83%); the properties of this sample were identical in all respects with those of the material obtained from treatment of the natural product with bromine (2), thus confirming its structure and confirming the unusual bromo-deformylation which took place. Direct replacement of formyl by halogen, although not common, has been reported previously. Markovac and MacDonald (25) have used bromine in acetic acid to transform a 2-formylpyrrole to the bromide, while Canonica *et al.* (26) have used chlorine to effect deformylation in the steroid series.

## Experimental

Nuclear magnetic resonance data were obtained on a Perkin–Elmer R12B (60 MHz) or R32 (90 MHz) instrument (proton) or Nicolet TT-14 (15.1 MHz) instrument (carbon) in $CDCl_3$ solution and are referenced to internal TMS. Electron impact mass spectra (70 eV) were obtained using the Hitachi–Perkin–Elmer RMU-7E, methane chemical ionization mass spectra on the Finnigan 3300, ultraviolet spectra in 95% EtOH on the Beckman SP800, and infrared spectra on the Perkin–Elmer 283 instruments. Thin layer chromatography was performed on Polygram Sil G/UV254 precoated plates (Brinkmann Instrument Inc.), column chromatography on 60–200 mesh silica gel (Davison

Can. J. Chem. Downloaded from www.nrcresearchpress.com by 210.87.254.42 on 09/06/12
For personal use only.

Can. J. Chem. Downloaded from www.nrcresearchpress.com by 210.87.254.42 on 09/06/12
For personal use only.

Instrument Inc.), and preparative thin layer chromatography on MN-Kieselgel G/UV254 (Macherey, Nagel & Co.). Organic solvents were distilled prior to use, and organic solutions dried over anhydrous sodium sulfate. All mp are uncorrected. Bath temperature is reported for low temperature reactions.

*4-Methoxy-6-methyl-2-pyrone-3-carboxaldehyde, 5*

To 4-methoxy-6-methyl-2-pyrone, **4** (0.96g, 0.69 mmol), in dry chloroform (5 mL) was added dichloromethyl methyl ether (0.63 mL, 7.0 mmol), then $TiCl_4$ (0.66 mL, 6.0 mmol) with stirring under nitrogen at 10°C. A red oil formed at the bottom of the flask, and HCl bubbled off the reaction mixture. The reaction was worked up, after stirring 19 h at 20°C, by carefully adding ice water, then extracting the mixture with chloroform. The chloroform extracts were washed ($H_2O$, saturated aqueous NaCl), dried, evaporated, then chromatographed (50% ethyl acetate/pentane) to give 4-methoxy-6-methyl-2-pyrone-3-carboxaldehyde, **5**, 43 mg, 37%; ir (KBr): 3089, 2854, 2761, 1739, 1670, 1637, 1618, 1512, 1472, 1453, 1439, 1418, 1402, 1391, 1372, 1356, 1330, 1231, 1010, 832, 767, 700, 522 $cm^{-1}$; $^1$Hmr δ: 10.15 (1H, s), 6.29 (1H, s), 4.06 (3H, s), 2.36 (3H, s); ms *m/e* (relative intensity): 168 ($M^+$, 30), 153 (5), 140 (66), 139 (22), 125 (19), 111 (36), 110 (100), 95 (46), 93 (13), 69 (41), 53 (27), 43 (91), and 39 (21).

*4-Hydroxy-6-nonyl-2-pyrone, 6*

To triacetic acid lactone, **4** (6.0 g, 47.6 mmol) in THF (100 mL), under dry nitrogen at −78°C, was added n-BuLi (105 mmol). After warming the slurry to 0°C, then stirring for 2 h, n-octyl bromide (8.68 mL, 50 mmol) was added. The clear red solution was stirred at 20°C for 14 h, then ice water (100 mL) was added, and the hexane layer removed. The aqueous layer was extracted with pentane (3 × 50 mL), then acidified to pH 6 with concentrated HCl and extracted with ether (3 × 100 mL). The combined ether extracts were washed ($H_2O$, saturated aqueous NaCl), dried, evaporated, then chromatographed and recrystallized (hexane) to give 4-hydroxy-6-nonyl-2-pyrone **6**, 3.88 g, 34%, mp 78–79°C; ir (NaCl): 2980, 2930, 2860, 1704, 1665, 1634, 1587, 1504, 1479, 1324, 1303, 1267, 1248, 1150, 847 $cm^{-1}$; uv $\lambda_{max}$: 203 (log ε 4.32), 238 (3.86), 282 nm (3.85); $^1$Hmr δ: 11.1 (1H, br s), 6.02 (1H, br d, $J$ = 4.5 Hz), 5.60 (1H, d, $J$ = 4.5 Hz), 2.48 (2H, t, $J$ = 7.0 Hz), 1.8–1.0 (14H, m), 0.88 (3H, t, $J$ = 7.5 Hz); ms *m/e* (relative intensity): 239 (6), 238 ($M^+$, 21), 223 (7), 179 (15), 178 (30), 163 (25), 140 (18), 139 (98), 137 (20), 136 (39), 135 (13), 127 (15), 126 (36), 112 (16), 111 (87), 110 (15), 98 (46), 97 (31), 95 (21), 85 (31), 84 (69), 83 (21), 82 (38), 81 (20), 71 (25), 69 (53), 67 (16), 57 (31), 55 (39), 45 (30), 44 (10), 43 (100), and 41 (36). *Anal.* calcd. for $C_{14}H_{22}O_3$: C 70.55, H 9.30; found: C 70.43, H 9.25.

*Attempted oxygenation of 4-hydroxy-6-nonyl-2-pyrone, 6*

To 4-hydroxy-6-nonyl-2-pyrone, **6** (100 mg, 0.42 mmol), in THF (6 mL) and diisopropylamine (0.10 mL, 0.77 mmol) at −78°C under a nitrogen atmosphere was added n-BuLi (0.48 mL, 0.77 mmol). The solution was warmed to 0°C over 1 h, stirred 1 h, and oxygen admitted via a syringe. After 1 h, the oxygen was flushed out with nitrogen, triethyl phosphite (0.2 mL, 1.24 mmol) added, and the solution stirred 1.5 h. Iced HCl (5%, 10 mL) and ether (10 mL) were added, the aqueous layer extracted with dichloromethane (3 × 15 mL), and the combined organic phases dried and evaporated. Chromatography of the resulting liquid (5% iPrOH/$CH_2Cl_2$) gave a small amount of 4-hydroxy-6-(1′-hydroxynonyl)-2-pyrone **7**; $^1$Hmr δ: 6.26 (1H, br s), 5.55 (1H, br s), 4.90 (1H, m), 2.0–1.15 (12H, m), 0.90 (3H, t, $J$ = 7.5 Hz); ms *m/e* (relative intensity): 254 ($M^+$, 4.5), 178 (3), 155 (9), 135 (11), 111 (25), 83 (37), 65 (33), 58 (26), 45 (100), 44 (37), 43 (54), and 41 (32).

*4-Methoxy-6-nonyl-2-pyrone, 8*

To 4-hydroxy-6-nonyl-2-pyrone, **6** (0.97 g, 4.08 mmol), and anhydrous $K_2CO_3$ (4.15 g, 30 mmol) in 2-butanone (100 mL) was added dimethyl sulphate (0.42 mL, 4.5 mmol). The mixture was refluxed under nitrogen with stirring for 23 h, then cooled, filtered, and evaporated. Chromatography (25% ethyl acetate/pentane), then recrystallization (pentane), gave 4-methoxy-6-nonyl-2-pyrone **8**, 0.91 g, 86%, mp 58–59°C; ir (NaCl): 3076, 2958, 2925, 1853, 1736, 1648, 1565, 1468, 1459, 1447, 1411, 1262, 1240, 1134, 1026, 933, 872, 848, 827, 801, 718 $cm^{-1}$; uv $\lambda_{max}$: 297 nm (log ε 3.99); $^1$Hmr δ: 5.86 (1H, d, $J$ = 2.5 Hz), 5.48 (1H, d, $J$ = 2.5 Hz), 3.87 (3H, s), 2.49 (2H, t, $J$ = 8.1 Hz), 2.0–1.1 (14H, m), 0.90 (3H, br t); ms *m/e* (relative intensity): 253 (5), 252 ($M^+$, 26), 237 (2), 223 (3), 209 (6), 195 (5), 152 (62), 140 (74), 125 (100), 112 (16), 111 (11), 98 (32), 69 (29), 59 (15), and 55 (15). *Anal.* calcd. for $C_{15}H_{24}O_3$: C 71.39, H 9.59; found: C 71.47, H 9.52.

*4-Methoxy-6-nonyl-2-pyrone-3-carboxaldehyde, 9*

To 4-methoxy-6-nonyl-2-pyrone, **8** (0.5 g, 2 mmol), in $Cl_2CHOCH_3$ (5 mL, 55 mmol) at −5°C under nitrogen was added titanium tetrachloride (2.2 mL, 20 mmol). A continuous nitrogen flow was maintained to remove the HCl evolved, and the temperature was allowed to rise from −5° to 15°C over 15 h. Ice was carefully added to the orange product, followed by ether, until the oil had dissolved completely. The ether solution (100 mL) was then washed ($H_2O$, saturated aqueous NaCl), dried, and evaporated to give 4-methoxy-6-nonyl-2-pyrone-3-carboxaldehyde **9**. Recrystallization from cyclohexane gave 0.49 g, 87% of product, mp 66–70°C; ir (NaCl): 3100, 2952, 2920, 2848, 1750, 1727, 1645, 1629, 1525, 1470, 1448, 1434, 1410, 1378, 1340, 1263, 1244, 1220, 1114, 1015, 975, 829, 760 $cm^{-1}$; uv $\lambda_{max}$: 227 (log ε 3.17), 247 (2.76), 322 nm (3.08); $^1$Hmr δ: 10.14 (1H, s), 6.05 (1H, s), 4.01 (3H, s), 2.56 (2H, t, $J$ = 6.0 Hz), 1.9–1.1 (14H, m), 0.88 (3H, br t); ms *m/e* (relative intensity): 281 (26), 280 ($M^+$, 47), 253 (18), 252 (100), 251 (78), 224 (18), 223 (100), 181 (28), 177 (35), 167 (44), 163 (20), 154 (20), 153 (92), 140 (48), 125 (23), 123 (54), 110 (27), 95 (20), 69 (29), 57 (19), 56 (27), and 55 (31). *Anal.* calcd. for $C_{16}H_{24}O_4$: C 68.55, H 8.69; found: C 68.62, H 8.71.

*3-Hydroxymethyl-4-methoxy-6-nonyl-2-pyrone, 12*

To 4-methoxy-6-nonyl-2-pyrone-3-carboxaldehyde, **9** (50 mg, 0.18 mmol), in methanol (3 mL) was added sodium borohydride (20 mg, 0.54 mmol) with stirring at 0°C. After 1 h, a further 20 mg of sodium borohydride was added, and stirring was continued for 1 h. Water was then added, and the resulting solution was extracted with ether (2 × 25 mL). The ether solution was washed (saturated aqueous NaCl), dried, evaporated, and the product recrystallized from pentane/ether to give 3-hydroxymethyl-4-methoxy-6-nonyl-2-pyrone **12**, 47 mg, 93%, mp 63–66°C; ir (NaCl): 3500–3180 (br), 2960, 2925, 2855, 1710, 1685, 1641, 1564, 1483, 1473, 1459, 1423, 1403, 1385, 1358, 1290, 1272, 1263, 1234, 1183, 1082, 1008, 998, 901 $cm^{-1}$; $^1$Hmr δ: 6.05 (1H, s), 4.53 (2H, s), 3.88 (3H, s), 2.49 (2H, t, $J$ = 7.0 Hz), 1.9–1.1 (14H, m), 0.88 (3H, br t); ms *m/e* (relative intensity): 283 (15), 282 ($M^+$, 69), 281 (32), 267 (76), 264 (33), 253 (95), 237 (39), 165 (55), 155 (100), 153 (45), 152 (70), 127 (72), 125 (53), 95 (29), 83 (31), 81 (29), 71 (35), 69 (49), 57 (55), 55 (58), 43 (58), and 41 (53).

*Selenium dioxide oxidation of 4-methoxy-6-nonyl-2-pyrone, 8*

4-Methoxy-6-nonyl-2-pyrone **8** (100 mg, 0.4 mmol) and freshly sublimed selenium dioxide (200 mg, 1.8 mmol) were refluxed in dry bis(2-methoxyethyl) ether (diglyme, 3.5 mL) for 0.5 h under nitrogen with rapid stirring. The solution was then cooled, evaporated, and extracted with ether (20 mL). The ether extract was washed (saturated aqueous $NaHCO_3$, saturated aqueous NaCl), dried, and evaporated. The product was a mixture (90 mg) containing 4-methoxy-6-nonanoyl-2-pyrone, **2**, and 4-

Can. J. Chem. Downloaded from www.nrcresearchpress.com by 210.87.254.42 on 09/06/12
For personal use only.

methoxy-6-nonyl-2-pyrone, **8**, in a ratio of 4:1. The yield of compound **2** was 65%. Spectral data were identical to those reported below.

*4-Methoxy-6-nonanoyl-2-pyrone-3-carboxaldehyde, **1***

4-Methoxy-6-nonyl-2-pyrone-3-carboxaldehyde **9** (30 mg, 0.12 mmol) and freshly sublimed $SeO_2$ (110 mg, 1.0 mmol) in dry *m*-xylene (2 mL) were refluxed for 0.5 h with rapid stirring under nitrogen. The products were isolated from the reaction mixture, as above, to give a mixture of compounds **9** and **1** in a ratio of 3:1, by $^1$Hmr. Preparative thin layer chromatography (50% ethyl acetate/pentane) gave compound **9** (18.3 mg, 61% recovery) and the desired product, compound **1** (6.5 mg, 21%). Compound **1** was recrystallized twice from cyclohexane, yield 53% (based on unrecovered starting material), mp 111–114°C (lit. (2) mp 112–113°C); ir (KBr): 2958, 2930, 1725, 1700, 1689, 1617, 1527, 1519, 1478, 1234 cm$^{-1}$; uv $\lambda_{max}$: 223 (log ε 4.13), 272 (3.28), 342 nm (3.97); $^1$Hmr δ: 10.11 (1H, s), 7.08 (1H, s), 4.13 (3H, s), 2.93 (2H, t, $J$ = 6.8 Hz), 1.9–1.1 (12H, m), 0.90 (3H, br t); ms *m/e* (relative intensity): 294 (M$^+$, 4), 266 (3), 265 (0.5), 238 (1), 154 (12), 153 (100), 141 (6), 125 (12), 123 (4), 71 (11), 69 (15), 57 (17), 55 (16), 43 (16), and 41 (15).

*2-Octyl-1,3-dithiane, **14***

To a dry THF solution (250 mL) of 1,3-dithiane (10 g, 83.4 mmol) at −10 to −15°C under dry nitrogen was added n-BuLi (84 mmol). The temperature was maintained at −15°C for 2 h, then reduced to −78°C and n-octyl bromide (16.1 g, 83.4 mmol) was added. The reaction mixture was maintained at −78°C for 2 h, −20°C for 1 h, 0°C for 1 h, then warmed to 20°C over 15 h. The THF was removed by evaporation, then water (50 mL) added, and the solution extracted with ether (2 × 100 mL). The ether extracts were washed ($H_2O$), dried ($K_2CO_3$), evaporated, then chromatographed (10% dichloromethane/pentane) to give 2-octyl-1,3-dithiane (**14**), 19.07 g, 98.5%; ir (film): 2954, 2855, 1466, 1442, 1415, 1276, 1243, 1181, 909, 867, 778, 720, 681, 660 cm$^{-1}$; $^1$Hmr δ: 4.12 (1H, t, $J$ = 6.5 Hz), 3.0–2.8 (6H, m), 2.3–1.1 (14H, m), 0.90 (3H, t, $J$ = 6 Hz); ms *m/e* (relative intensity): 232 (M$^+$, 33), 157 (17), 132 (4), 119 (100), 106 (6), 73 (7), 55 (11), 45 (15), 43 (39), 41 (44), and 39 (17). *Anal.* calcd. for $C_{12}H_{24}S_2$: C 62.01, H 10.41; found: C 62.04, H 10.62.

*2-Octyl-1,3-dithiane-2-carboxaldehyde, **15***

To 2-octyl-1,3-dithiane **14** (5 g, 21.6 mmol), in dry THF (25 mL) under nitrogen at −15°C, was added n-BuLi (24 mmol). After stirring for 3 h at −15°C, the solution was cooled to −60°C and freshly distilled dimethylformamide (3.47 mL, 45 mmol) was added dropwise. After stirring the solution a further 30 min, water (45 mL) was added and the solution acidified with concentrated HCl. The aqueous phase was extracted with ether (3 × 25 mL) and then the combined organic extracts dried, evaporated, and chromatographed (dichloromethane) to give 2-octyl-1,3-dithiane-2-carboxaldehyde **15**, 4.89 g, 87%; ir (film): 2950, 2930, 2858, 2695, 1720, 1468, 1424, 1279, 908 cm$^{-1}$; $^1$Hmr δ: 9.05 (1H, s), 3.3–1.1 (20H, m), 0.90 (3H, t, $J$ = 6 Hz); ms *m/e* (relative intensity): 260 (M$^+$, 1.5), 233 (9), 232 (16), 231 (100), 145 (2), 119 (2), 107 (3), 81 (2), 75 (2), 73 (2.5), and 55 (3). *Exact Mass* calcd. for $C_{13}H_{24}O_1S_2$: 260.131; found: 260.130.

*2-Ethoxycarbonyl-2-octyl-1,3-dithiane, **16***

To 1,3-dithiane (1 g, 8.34 mmol), in dry THF (25 mL) under nitrogen at −20°C, was added n-BuLi (8.6 mmol). The solution was stirred at −15°C for 2 h, then cooled to −78°C. n-Octyl bromide (1.45 mL, 8.34 mmol) was then added, and the temperature was allowed to rise to −30°C over 2 h, then to 20°C over 1 h. The solution was then cooled to −78°C, n-BuLi added, then warmed to 0°C over 4.5 h. The 2-octyl-2-lithio-1,3-dithiane solution was then added to ethyl chloroformate (0.2 mol) at −78°C over 15 min. The reaction mixture was stirred at −78°C for 12 h, then at 0°C for 1 h. Evaporation followed by chromatography (dichloromethane/pentane) gave 2-ethoxycarbonyl-2-octyl-1,3-dithiane (**16**), 1.72 g, 73%; ir (film): 2982, 2960, 2855, 1725, 1422, 1418, 1315, 1280, 1246, 1224, 1174, 1130, 1094, 1025, 906 cm$^{-1}$; $^1$Hmr δ: 4.35 (2H, q, $J$ = 7.5 Hz), 3.6–1.1 (20H, m), 1.36 (3H, t, $J$ = 7.5 Hz), 0.91 (3H, t, $J$ = 7 Hz); ms *m/e* (relative intensity): 304 (M$^+$, 9), 232 (18), 231 (100), 143 (17), 119 (16), 97 (19), 95 (16.5), 83 (20), 81 (20), 71 (22), 69 (27), 57 (36), 55 (42), 43 (32), and 41 (33). *Exact Mass* calcd. for $C_{15}H_{28}O_2S_2$: 304.158; found: 304.151.

*5,6-Dihydro-4-hydroxy-6-(2-octyl-1,3-dithian-2-yl)-2-pyrone, **18***

(A) To sodium hydride (54% in mineral oil, 1.2 g, 27 mmol), in dry THF (40 mL) under nitrogen at 0°C, was added ethyl acetoacetate (3.16 mL, 25 mmol). After 10 min, n-BuLi (26 mmol) was added, the temperature was maintained for 10 min, then the solution cooled to −78°C. 2-Octyl-1,3-dithiane-2-carboxaldehyde, **15** (385 mg, 14.8 mmol) was then added. After the solution was warmed to 0°C, then stirred for 0.5 h, water (125 mL) was added, and the solution stirred at 20°C for 22 h. The aqueous solution was then extracted with ether (2 × 20 mL), cooled to 0°C, acidified with concentrated HCl, and extracted with dichloromethane. The dichloromethane extracts were dried, then evaporated to give 5,6-dihydro-4-hydroxy-6-(2-octyl-1,3-dithian-2-yl)-2-pyrone, **18**, 5.05 g, 99%, which was filtered through silica gel (10% 2-propanol/dichloromethane), mp 87–90°C; ir (NaCl): 3100, 2955, 2920, 2852, 1760, 1726, 1670, 1610, 1465, 1415, 1360, 1275, 1228, 1190, 1030, 885, 826 cm$^{-1}$; $^1$Hmr δ: 4.96 (1H, dd, $J$ = 10, 5 Hz), 3.6–1.1 (24H, m), 0.87 (3H, br t); ms *m/e* (relative intensity): 344 (M$^+$, 2), 300 (11), 231 (85), 195 (15), 194 (98), 187 (20), 106 (86), 96 (28), 95 (100), 85 (39), 44 (30), and 43 (34). *Anal.* calcd. for $C_{17}H_{28}O_3S_2$: C 59.27, H 8.19; found: C 59.05, H 8.24.

(B) When the above reaction was carried out on a larger scale (120 mmol of the aldehyde **15**) the yield of compound **18** was reduced to 38%, and a second compound was isolated, ethyl 5-hydroxy-3-oxo-5-(2-octyl-1,3-dithian-2-yl)pentanoate, **17**, in 34% yield; ir (film): 3490, 2958, 2929, 2855, 1744, 1715, 1469, 1423, 1410, 1390, 1368, 1220, 1177, 1155, 1095, 1070, 1030, 909 cm$^{-1}$; $^1$Hmr δ: 4.71 (1H, dt, $J$ = 9.0, 2.5 Hz), 4.26 (2H, q, $J$ = 8.5 Hz), 3.58 (2H, s), 3.3–2.4 (7H, m), 2.2–1.2 (19H, m), 0.90 (3H, br t); ms *m/e* (relative intensity): 390 (M$^+$, 0.1), 253 (10), 252 (15), 251 (100), 119 (2), 107 (4), 106 (3), 73 (3), 69 (3), 57 (3), 55 (4), and 43 (5).

*5,6-Dihydro-4-methoxy-6-(2-octyl-1,3-dithian-2-yl)-2-pyrone, **19***

To the 4-hydroxy-2-pyrone **18** (8 g, 23.3 mmol), in dry THF (50 mL) under nitrogen, was added sodium hydride (54% in mineral oil, 1.24 g, 27.9 mmol). After stirring for 0.5 h at −10°C, the solution was cooled to −30°C and dimethyl sulphate (3.8 g, 30 mmol) added. The solution was stirred for 60 h at 20°C, then evaporated. Water was added, and the product extracted with dichloromethane (3 × 50 mL). The organic solution was dried, evaporated, then chromatographed (2-propanol/dichloromethane) to yield the 4-methoxy-2-pyrone **19**, 4.1 g, 49%; ir (film): 2928, 2855, 1720, 1628, 1460, 1444, 1383, 1340, 1280, 1249, 1225, 1195, 1176, 1095, 1080, 1040, 1000, 821 cm$^{-1}$; $^1$Hmr δ: 5.12 (1H, d, $J$ = 2.5 Hz), 4.71 (1H, dd, $J$ = 13, 4.5 Hz), 3.72 (3H, s), 3.5–1.1 (22H, m), 0.88 (3H, br t); ms *m/e* (relative intensity): CI 359 (M + 1, 16), 327 (12), 303 (15), 269 (61), and 231 (100); EI 233 (11), 232 (16), 231 (100), 145 (3), 119 (3), 107 (3), 81 (4), 73 (7), 57 (6), 55 (14), 43 (9), and 41 (20). *Exact Mass* calcd. for $C_{18}H_{30}O_3S_2$: 358.181; found: 358.178.

Can. J. Chem. Downloaded from www.nrcresearchpress.com by 210.87.254.42 on 09/06/12
For personal use only.

*5,6-Dihydro-4-methoxy-6-nonanoyl-2-pyrone, **20***

5,6-Dihydro-4-methoxy-6-(2-octyl-1,3-dithian-2-yl)-2-pyrone, **19** (1.6 g, 4.47 mmol), in 95% ethanol (20 mL) was added dropwise to a rapidly stirring slurry of mercuric chloride (1.46 g, 5.36 mmol) and mercuric oxide (1.16 g, 5.36 mmol) in 95% ethanol at 78°C. After refluxing for 1 h, the solution was cooled, filtered, then HCl (0.05 *M*, 40 mL) was added. The solution was stirred 12 h, then extracted with dichloromethane, dried, evaporated, and chromatographed (7% i-PrOH/$CH_2Cl_2$) to give 5,6-dihydro-4-methoxy-6-nonanoyl-2-pyrone, **20**, 0.95 g, 79%, mp 77–79°C (cyclohexane); ir (NaCl): 2919, 2889, 2848, 1719, 1627, 1471, 1444, 1401, 1291, 1252, 1237, 1128, 1113, 1000, 860 $cm^{-1}$; uv $\lambda_{max}$: 233.4 nm (log ε 3.95); $^1$Hmr δ: 5.27 (1H, s), 4.84 (1H, t, $J$ = 7 Hz), 3.83 (3H, s), 2.79 (2H, t, $J$ = 7 Hz), 2.75 (2H, t, $J$ = 7 Hz), 2.0–1.1 (12H, m), 0.89 (3H, br t); ms *m/e* (relative intensity): 268 ($M^+$, 3), 195 (2), 170 (1), 141 (8), 128 (34), 127 (100), 99 (5), 71 (7), 67 (7), 57 (7.5), 55 (5), 43 (13), and 41 (9). *Exact Mass* calcd. for $C_{15}H_{24}O_4$: 268.172; found: 268.173. *Anal.* calcd.: C 67.14, H 9.01; found: C 66.59, H 9.23.

*4-Methoxy-6-nonanoyl-2-pyrone, **2***

5,6-Dihydro-4-methoxy-6-nonanoyl-2-pyrone **20** (536 mg, 2 mmol) and *N*-bromosuccinimide (NBS, 392 mg, 2.2 mmol) in carbon tetrachloride (50 mL) were refluxed for 1.5 h under nitrogen, while being irradiated with a tungsten lamp (100 W). Additional NBS (39 mg, 0.22 mmol) was then added, and refluxing/irradiation was continued for 1 h. The solution was allowed to stand under nitrogen for 24 h, then nitrogen was bubbled slowly through the solution for 24 h. The $CCl_4$ solution was then washed ($H_2O$, saturated aqueous NaCl), dried, evaporated, and the product recrystallized (95% ethanol) to give 4-methoxy-6-nonanoyl-2-pyrone **2**, 430 mg, 81%, mp 123–124°C (lit. (2) mp 120–121°C); ir (NaCl): 3080, 2942, 2914, 2874, 2850, 1726, 1708, 1637, 1518, 1470, 1464, 1450, 1413, 1400, 1374, 1343, 1272, 1261, 1255, 1170, 1016, 998, 980, 879, 865, 851 $cm^{-1}$; uv $\lambda_{max}$: 220 (log ε 4.11), 254 (3.18), 306 nm (3.60); $^1$Hmr δ: 6.72 (1H, d, $J$ = 2.5 Hz), 5.68 (1H, d, $J$ = 2.5 Hz), 3.83 (3H, s), 2.85 (2H, t, $J$ = 7.5 Hz), 1.9–1.1 (12H, m), 0.87 (3H, br t, $J$ = 7 Hz); ms *m/e* (relative intensity): 266 ($M^+$ 4.5), 238 (3), 168 (3), 128 (2), 127 (6), 126 (7), 125 (100), 69 (4), 59 (5), and 43 (5). *Anal.* calcd. for $C_{15}H_{22}O_4$: C 67.69, H 8.33; found: C 67.61, H 8.37.

*4-Methoxy-6-(1′-hydroxynonyl)-2-pyrone, **24***

To 4-methoxy-6-nonanoyl-2-pyrone **2** (108 mg, 0.406 mmol), in methanol (5 mL) at −5°C, was added sodium borohydride (3.8 mg, 0.4 mmol) in three portions at intervals of 0.5 h. After a total of 2.5 h, water (15 mL) and chloroform (20 mL) were added to the reaction mixture. The chloroform solution was washed (saturated aqueous NaCl), dried, then evaporated and recrystallized (methanol/water) to yield 4-methoxy-6-(1′-hydroxynonyl)-2-pyrone **24**, 101 mg, 99%, mp 40–41°C (aqueous MeOH); ir(NaCl): 3410, 2950, 2928, 2855, 1701, 1647, 1568, 1455, 1411, 1345, 1124, 1031, 810 $cm^{-1}$; $^1$Hmr δ: 6.04 (1H, d, $J$ = 2.4 Hz), 5.36 (1H, d, $J$ = 2.4 Hz), 4.32 (1H, m), 3.76 (3H, s), 3.38 (1H, d, $J$ = 6 Hz, exch. with $D_2O$), 2.3–1.1 (14H, m), 0.88 (3H, t, $J$ = 6 Hz); ms *m/e* (relative intensity): 269 (3), 268 (16), 267 (1), 237 (2), 179 (2), 169 (5), 156 (4), 125 (100), and 69 (42). *Anal.* calcd. for $C_{15}H_{24}O_4$: C 67.14, H 9.02; found: C 66.94, H 8.97.

*3-Bromo-4-methoxy-6-methyl-2-pyrone, **28***

To 4-methoxy-6-methyl-2-pyrone **4** (280 mg, 2.0 mmol), in $CCl_4$ (20 mL), was added NBS (450 mg, 2.5 mmol) and iodine (10 mg). The solution was refluxed for 2 h in the dark, then evaporated, dissolved in dichloromethane (30 mL), washed ($H_2O$, saturated aqueous NaCl), dried, and evaporated to yield 3-bromo-4-methoxy-6-methyl-2-pyrone **28**, 200 mg, 46%, mp 157–157.5°C (lit. (19) mp 155–156°C); $^1$Hmr δ: 6.15 (1H, s), 4.01 (3H, s), 2.29 (3H, s); ms *m/e* (relative intensity): 220 ($M^+$, 82), 218 ($M^+$, 82), 192 (67), 190 (71), 178 (17), 177 (13), 176 (17), 175 (13), 149 (100), 147 (100), 139 (27), 97 (23), 95 (24), 85 (25), 83 (35), 81 (29), 71 (38), 69 (41), and 67 (21). *Anal.* calcd. for $C_7H_7Br_1O_3$: C 38.39, H 3.22; found: C 38.40, H 3.00.

*Attempted bromination of 4-methoxy-6-nonanoyl-2-pyrone, **2***

To compound **2** (54 mg, 0.2 mmol) in $CCl_4$ (7 mL) under nitrogen was added NBS (48 mg, 0.27 mmol) and iodine (2 mg). The reaction mixture was refluxed in the dark for 24 h, then diluted with dichloromethane (15 mL), washed ($H_2O$, saturated aqueous NaCl), dried, then evaporated to yield only starting material by $^1$Hmr and tlc.

*3-Bromo-4-methoxy-6-(1′-hydroxynonyl)-2-pyrone, **29***

4-Methoxy-6-(1′-hydroxynonyl)-2-pyrone **24** (42 mg, 0.16 mmol), NBS (35.6 mg, 0.2 mmol), and iodine (trace) in carbon tetrachloride (20 mL) were refluxed under nitrogen in the dark for 1 h. Dichloromethane (20 mL) was then added and the solution was washed ($H_2O$, saturated aqueous NaCl), dried, evaporated, and chromatographed (50% ethyl acetate/pentane) to yield 3-bromo-4-methoxy-6-(1′-hydroxynonyl)-2-pyrone **29**, 34 mg, 61%, which was recrystallized from pentane, mp 93–94°C; ir (NaCl): 3440, 2960, 2924, 2858, 1731, 1680, 1636, 1523, 1469, 1390, 1324, 1229, 1060 $cm^{-1}$; $^1$Hmr δ: 6.44 (1H, s), 4.6–4.25 (1H, m), 3.98 (3H, s), 3.0–2.7 (1H, m), 2.2–1.0 (14H, m), 0.88 (3H, t, $J$ = 6 Hz); ms *m/e* (relative intensity): 348 ($M^+$, 8.5), 346 ($M^+$, 10), 267 (2), 266 (4), 249 (5), 248 (4), 247 (5), 207 (10), 206 (5), 205 (32), 204 (4), 203 (24), 149 (6), 147 (6), 126 (8), 125 (100), and 41 (36). *Anal.* calcd. for $C_{15}H_{23}Br_1O_4$: C 51.88, H 6.68; found: C 51.96, H 6.61.

*3-Bromo-4-methoxy-6-nonanoyl-2-pyrone, **3***

3-Bromo-4-methoxy-6-(1′-hydroxynonyl)-2-pyrone **29** (20 mg, 0.056 mmol) in benzene (5 mL) was stirred rapidly under nitrogen with activated manganese dioxide (50 mg), for 3 h. Additional manganese dioxide (30 mg) was then added, and the stirring was continued for 18 h. The product was filtered through silica gel (50% ethyl acetate/pentane) to yield 3-bromo-4-methoxy-6-nonanoyl-2-pyrone, **3**, 16 mg, 83%, which was recrystallized from 95% ethanol, mp 78–80°C (lit. (2) mp 79–80°C); ir (KBr): 2949, 2920, 2846, 1733, 1699, 1620, 1510, 1459, 1380, 1305, 1230, 1078, 982, 939, 738 $cm^{-1}$; $^1$Hmr δ: 7.03 (1H, s), 4.07 (3H, s), 2.93 (2H, t, $J$ = 6.5 Hz), 2.0–1.1 (12H, m), 0.88 (3H, br t); ms *m/e* (relative intensity): 346 ($M^+$, 8.5), 344 ($M^+$, 9), 318 (2), 316 (2), 265 (5), 249 (5), 248 (15), 247 (6), 246 (15), 237 (13), 206 (10), 205 (99), 204 (10), 203 (100), 149 (17), 125 (40), 124 (11), 69 (7), 57 (7), 55 (7), 43 (8), and 41 (6).

## Acknowledgements

The authors wish to thank the University of Victoria for continued research support, and to acknowledge the award of the Lewis J. Clark Graduate Fellowship to T. D. Cyr. Some support from the Natural Sciences and Engineering Research Council (NSERC) of Canada is also acknowledged.

1. A. S. Sekhon and A. Funk. J. Antimicrob. Chemother. **3**, 95 (1977).
2. G. A. Poulton, T. D. Cyr, and E. E. McMullan. Can. J. Chem. **57**, 1451 (1979).
3. G. A. Poulton and T. D. Cyr. Can. J. Chem. **58**, 2158 (1980).
4. S. N. Huckin and L. Weiler. J. Am. Chem. Soc. **96**, 1082 (1974); T. M. Harris and J. V. Hay. J. Am. Chem. Soc. **99**, 1631 (1977).

5. J. N. COLLIE. J. Chem. Soc. **59**, 607 (1891).
6. T. KATO, Y. YAMAMOTO, and S. TAKEDA. Chem. Pharm. Bull. **21**, 1047 (1973); K. BALENOVIC. Recl. Trav. Chim. Pays-Bas, **67**, 282 (1948).
7. E. SUZUKI and S. INOUE. Synthesis, 259 (1975).
8. D. SEEBACH and H. MEYER. Angew. Chem. Int. Ed. Engl. **13**, 77 (1974).
9. J. L. BLOOMER, S. M. H. ZAIDI, J. T. STRUPCZEWSKI, C. S. BROSZ, and L. A. GUDZYK. J. Org. Chem. **39**, 3615 (1974).
10. E. SUZUKI, R. HAMAJIMA, and S. INOUE. Synthesis, 192 (1975).
11. J. L. DOUGLAS and T. MONEY. Tetrahedron, **23**, 3545 (1967); R. L. EDWARDS and I. Mir. J. Chem. Soc. C, 411 (1967); M. P. WACHTER and T. M. HARRIS. Tetrahedron, **26**, 1685 (1970).
12. T. A. CARPENTER, P. J. JENNER, F. J. LEEPER, and J. STAUNTON. J. Chem. Soc. Chem. Commun. 1227 (1980).
13. S. R. MOORTY, V. SUNDARAMURTHY, and N. V. S. RAO. Ind. J. Chem. **11**, 854 (1973).
14. L. L. WOODS and P. A. DIX. J. Org. Chem. **26**, 1028 (1961).
15. P. G. GASSMAN and D. R. AMICK. Tetrahedron Lett. 3463 (1974).
16. E. ZIEGLER and E. KIESEWETTER. Monatsh. Chem. **96**, 659 (1965).
17. J. VRKOC and F. SORM. Czech. Patent No. 161,395. 15 Nov. 1975; Chem. Abstr. **85**, 77997t (1976).
18. C. A. BUEHLER and D. E. PEARSON. Survey of organic syntheses. Vol. I. John Wiley and Sons, Inc., New York. 1970. p. 335.
19. W. ADAM and O. CUETO. J. Org. Chem. **42**, 38 (1977).
20. J. D. BU'LOCK and H. G. SMITH. J. Chem. Soc. 502 (1960).
21. E. VEDEJS, D. A. ENGLER, and J. E. TELSCHOW. J. Org. Chem. **43**, 188 (1978).
22. G. M. STRUNZ, C. J. HEISSNER, M. KAKUSHIMA, and M. A. STILLWELL. Can. J. Chem. **52**, 825 (1974).
23. T. REFFSTRUP and P. M. BOLL. Acta Chem. Scand. Ser. B, **30**, 613 (1976).
24. T. M. HARRIS, C. M. HARRIS, and C. K. BRUSH. J. Org. Chem. **35**, 1329 (1970).
25. A. MARKOVAC and S. F. MACDONALD. Can. J. Chem. **43**, 3364 (1965).
26. L. CANONICA, G. JOMMI, F. PELIZZONI, and C. SCHOLASTICO. Gazz. Chim. Ital. **95**, 138 (1965).
27. T. D. CYR and G. A. POULTON. Can. J. Chem. **60**, 133 (1982).

Can. J. Chem. Downloaded from www.nrcresearchpress.com by 210.87.254.42 on 09/06/12
For personal use only.

# Réactivité des *N*-vinylaziridines fonctionnalisées. Synthèse de dérivés des α,β-déhydro α-amino acides

YVONNE GELAS-MIALHE, EVELYNE TOURAUD ET ROGER VESSIERE[1]

*École Nationale Supérieure de Chimie, Université de Clermont-Ferrand, B.P. 45, 63170 Aubiere, France*

Reçu le 31 mars 1982

YVONNE GELAS-MIALHE, EVELYNE TOURAUD et ROGER VESSIERE. Can. J. Chem. **60**, 2830 (1982).

Les cyano-2 et éthoxycarbonyl-2 *N*-vinylaziridines sont préparées par action de cyano-2 et éthoxycarbonyl-2 aziridines *N*-non substituées sur des composés activés, acétyléniques ou éthyléniques β-chlorés. Leur isomérisation sous l'influence d'un agent nucléophile conduit dans la plupart des cas à des α,β-déhydro α-amino esters et nitriles provenant de l'attaque du nucléophile en C-3. Leur thermolyse provoque préférentiellement la rupture de la liaison carbone–carbone du cycle, avec formation des α-vinylamino esters et nitriles.

YVONNE GELAS-MIALHE, EVELYNE TOURAUD, and ROGER VESSIERE. Can. J. Chem. **60**, 2830 (1982).

Secondary 2-cyano- and 2-ethoxycarbonylaziridines react with acetylenic compounds and activated vinylic chlorides to give 2-cyano and 2-ethoxycarbonyl *N*-vinylaziridines. The nucleophile-catalysed isomerization of these compounds generally gives α,β-dehydro α-amino acid derivatives involving nucleophilic attack at C-3. Thermal isomerization, involving predominantly cleavage of the carbon–carbon bond of the ring, forms α-vinylamino esters and nitriles.

Les dérivés aziridiniques constituent les intermédiaires de synthèse d'une très grande variété de systèmes hétérocycliques (1). Ainsi les alkyl-2 ou aryl-2 oxazolines peuvent être obtenues par isomérisation thermique ou nucléophile de *N*-acylaziridines (2–8). Très peu de travaux ont été consacrés aux *N*-vinylaziridines bien que plusieurs méthodes de synthèse de ces composés soient décrites (9–30). Toutefois, plusieurs auteurs (15, 19, 23, 25, 26) ont examiné le comportement vis à vis d'agents nucléophiles de quelques *N*-vinylaziridines non fonctionnalisées sur le cycle; leurs résultats montrent que la réaction peut évoluer soit vers la formation d'un hétérocycle à cinq maillons (15, 19, 23, 25, 26) soit, plus rarement, vers l'obtention de produits d'ouverture du cycle aziridine (19*b*, 23).

Nous avons entrepris une étude plus générale de ces réactions d'isomérisation nucléophile en examinant en particulier le comportement des *N*-vinylaziridines fonctionnalisées, l'introduction d'une fonction activante étant en effet susceptible de modifier considérablement l'évolution des réactions. Nous avons également étudié l'isomérisation thermique de plusieurs composés dont nous avions examiné le réarrangement initié par un nucléophile.

Les *N*-vinylaziridines utilisées pour cette étude ont été préparées par action, sur des dérivés acétyléniques ou éthyléniques β-chlorés, de diverses aziridines secondaires fonctionnalisées (Tableau 1). Ces dernières ont été obtenues par action de l'ammoniac sur des esters, nitriles ou cétones α,β dibromés (Réaction de Cromwell (31), Schéma 1); plusieurs d'entre elles étaient connues et leur configuration,[2] notamment au niveau de l'atome d'azote, déterminée par rmn $^1$H (32, 33). Nous avons déduit la configuration relative des atomes de carbone C-2 et C-3 du cycle de la valeur de la constante de couplage $^3J_{H\text{-}2\text{—}H\text{-}3}$; la position de l'atome d'hydrogène lié à l'atome d'azote a été déterminée à partir de la valeur des couplages $^3J_{H\text{—}N\text{—}C\text{—}H\text{-}2}$ et $^3J_{H\text{—}N\text{—}C\text{—}H\text{-}3}$. Dans le cas du composé **6***S*R**, la mise en évidence du couplage $^3J_{H\text{—}C\text{—}N\text{—}H}$ (cf. partie expérimentale) montre que dans l'intervalle de température 20–60°C, la molécule possède la configuration pour laquelle l'hydrogène lié à l'atome d'azote et la fonction éthoxycarbonyle sont en position *cis*. Nous justifions la stabilité de cet invertomère, comme celle des dérivés **1** et **8** (32, 33), par l'existence d'une liaison hydrogène intramoléculaire:

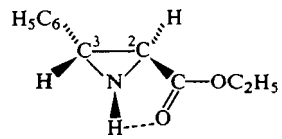


**6***S*R**

Les spectres de rmn du composé **7***R*R** (cf. partie expérimentale) montrent que, entre 20 et 60°C, seul existe l'invertomère pour lequel les trois atomes d'hydrogène sont situés du même côté du plan du

[1]Auteur à qui toute correspondance doit être adressée.

[2]Les termes *S*R** et *R*R** définissent la configuration relative des atomes de carbone C-2 et C-3 du cycle aziridine; comme le montre le schéma, les atomes d'hydrogène liés aux atomes C-2 et C-3 du cycle sont en *trans* par rapport au plan du cycle dans le composé *S*R**; ils sont en *cis* dans le composé *R*R**. Les termes *E* et *Z* précisent la configuration de la double liaison.

0008-4042/82/222830-22$01.00/0

©1982 National Research Council of Canada/Conseil national de recherches du Canada

Can. J. Chem. Downloaded from www.nrcresearchpress.com by 210.87.254.105 on 09/06/12
For personal use only.

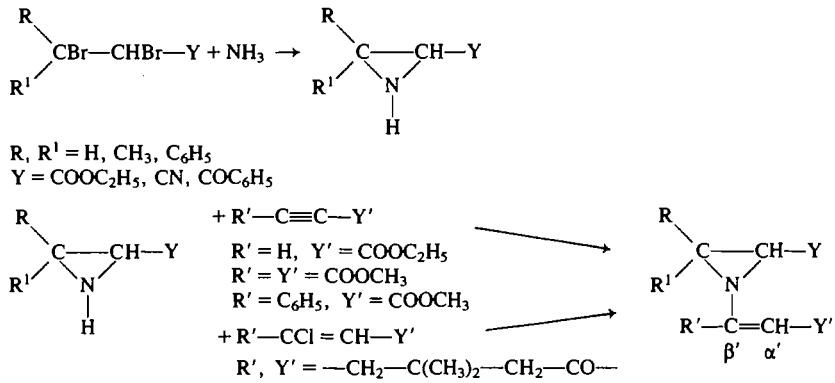


SCHÉMA 1

cycle ce qui correspond à un encombrement minimum de la molécule.

### Synthèse des *N*-vinylaziridines

Les *N*-vinylaziridines **9** à **25** ont été obtenues soit par addition nucléophile soit par substitution nucléophile des aziridines fonctionnalisées **1** à **8** sur des dérivés acétyléniques ou éthyléniques β-chlorés activés par un groupement électroattracteur Y′ (Schéma 1 et Tableau 1).

La stéréochimie[2] de tous ces composés a été établie d'après l'étude de leurs spectres de rmn $^1H$ (cf. partie expérimentale; Tableau 4). En particulier la position relative des substituants fixés sur les atomes de carbone C-2 et C-3 du cycle a été déduite du couplage vicinal $^3J_{H\text{-}2—H\text{-}3}$. Par ailleurs, lorsque R′ = H, la valeur de la constante de couplage $J_{H_{\alpha'}—H_{\beta'}}$ permet de déterminer la configuration de la double liaison. Lorsque R′ représente un groupement méthoxycarbonyle ou phényle, le déplacement chimique de l'atome d'hydrogène $H_{\alpha'}$ permet de préciser la stéréochimie de cette même double liaison.

Les réactions d'addition ont été effectuées soit dans un solvant protique, l'éthanol, elles conduisent alors à un mélange des isomères *E* et *Z*, soit dans un solvant aprotique, elles sont alors très fortement stéréosélectives et correspondent à une *cis* addition de l'amine sur la triple liaison activée. Ces résultats sont en accord avec ceux de la littérature (10, 12, 14, 16).

La réaction de la phényl-3 cyano-2 aziridine **7** avec le propiolate d'éthyle ne conduit pas à une *N*-vinylaziridine; le seul produit isolé a été identifié au pyrrole **26**:

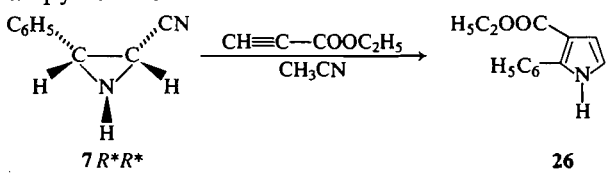


7 *R*R** 26

Il en est de même dans la réaction de la cétone **8** avec le propiolate d'éthyle (expérience No 39). Deux produits ont été isolés et identifiés aux pyrroles **27** et **28**:

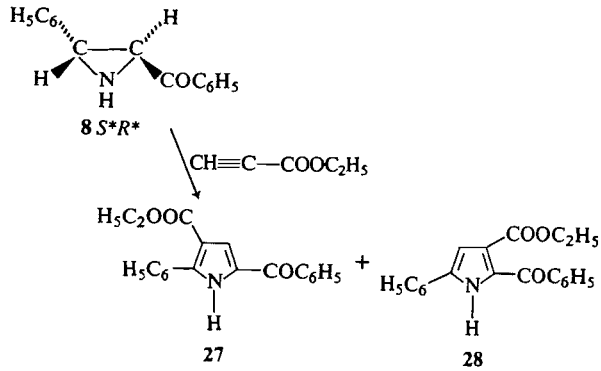


27 28

Ces réactions dont un exemple est décrit dans la littérature (11) font intervenir la cycloaddition dipolaire d'un ylure d'azométhine sur l'acétylénique activé:

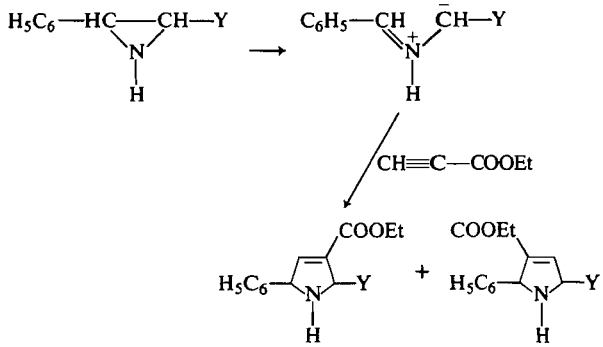


Les pyrrolines-3 ainsi formées conduisent aux pyrroles par déshydrogénation ou élimination de cyanure d'hydrogène.

### Isomérisation nucléophile des *N*-vinylaziridines

Les conditions dans lesquelles les réactions d'isomérisation ont été réalisées et la nature des

Can. J. Chem. Downloaded from www.nrcresearchpress.com by 210.87.254.105 on 09/06/12
For personal use only.

Can. J. Chem. Downloaded from www.nrcresearchpress.com by 210.87.254.105 on 09/06/12
For personal use only.



TABLEAU 1. Synthèse des aziridines

Aziridines secondaires 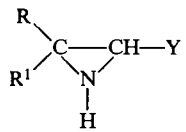

| Exp. No | No | R | R¹ | Y | Stéréochimie[a] | Dérivé acétylénique ou éthylénique β-chloré | Solvant de réaction | No | *N*-vinylaziridines Stéréochimie[a] | Rdt |
|---|---|---|---|---|---|---|---|---|---|---|
| 1 | **1** | H | H | $COOC_2H_5$ | — | $CH{\equiv}C{-}COOC_2H_5$ | DMSO | **9** | *E* | 66% |
| 2 | | H | H | $COOC_2H_5$ | — | $CH{\equiv}C{-}COOC_2H_5$ | $C_2H_5OH$ | | *E*/*Z* = 50:50 | 72% |
| 3 | | H | H | $COOC_2H_5$ | — | $H_3COOC{-}C{\equiv}C{-}COOCH_3$ | DMSO | **10** | *E* | 54% |
| 4 | | H | H | $COOC_2H_5$ | — | $H_3COOC{-}C{\equiv}C{-}COOCH_3$ | $C_2H_5OH$ | | *E*/*Z* = 50:50 | 62% |
| 5 | | H | H | $COOC_2H_5$ | — | $H_5C_6{-}C{\equiv}C{-}COOCH_3$ | DMSO | **11** | *E*/*Z* = 80:20 | 30% |
| 6 | | H | H | $COOC_2H_5$ | — | $H_5C_6{-}C{\equiv}C{-}COOCH_3$ | $C_2H_5OH$ | | *E*/*Z* = 55:45 | 44% |
| 7 | | H | H | $COOC_2H_5$ | — | 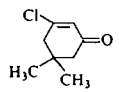 | DMSO | **12** | — | 20% |
| 8 | | H | H | $COOC_2H_5$ | — | | $C_2H_5OH$ | | — | 44% |
| 9 | **2** | H | H | CN | — | $CH{\equiv}C{-}COOC_2H_5$ | DMSO | **13** | *E*/*Z* = 90:10 | 39% |
| 10 | | H | H | CN | — | $CH{\equiv}C{-}COOC_2H_5$ | $CH_3CN$ | | *E*/*Z* = 90:10 | 26% |
| 11 | | H | H | CN | — | $CH{\equiv}C{-}COOC_2H_5$ | $C_2H_5OH$ | | *E*/*Z* = 60:40 | 60% |
| 12 | | H | H | CN | — | $H_3COOC{-}C{\equiv}C{-}COOCH_3$ | DMSO | **14** | *E* | 25% |
| 13 | | H | H | CN | — | $H_3COOC{-}C{\equiv}C{-}COOCH_3$ | $C_2H_5OH$ | | *E*/*Z* = 80:20 | 71% |
| 14 | **3** | $CH_3$ | H | $COOC_2H_5$ | *R*R*/S*R** = 70:30 | $CH{\equiv}C{-}COOC_2H_5$ | DMSO | **15** | *R*R*E/S*R*E* = 80:20 | 57% |
| 15 | | $CH_3$ | H | $COOC_2H_5$ | *R*R*/S*R** = 70:30 | $CH{\equiv}C{-}COOC_2H_5$ | $CH_3CN$ | | *R*R*E/S*R*E* = 80:20 | 80% |
| 16 | | $CH_3$ | H | $COOC_2H_5$ | *R*R*/S*R** = 70:30 | $CH{\equiv}C{-}COOC_2H_5$ | $C_2H_5OH$ | | (*R*R*E*+*R*R*Z*)/(*S*R*E*+ *S*R*Z*) = 80:20 avec *E*/*Z* = 45:55 | 80% |
| 17 | | $CH_3$ | H | $COOC_2H_5$ | *R*R*/S*R** = 70:30 | $H_3COOC{-}C{\equiv}C{-}COOCH_3$ | DMSO | **16** | *R*R*E/S*R*E* = 80:20 | 52% |
| 18 | | $CH_3$ | H | $COOC_2H_5$ | *R*R*/S*R** = 70:30 | $H_3COOC{-}C{\equiv}C{-}COOCH_3$ | $C_2H_5OH$ | | *E*/*Z* = 40:60 | 58% |
| 19 | | $CH_3$ | H | $COOC_2H_5$ | *R*R*/S*R** = 70:30 | $H_5C_6{-}C{\equiv}C{-}COOCH_3$ | DMSO | **17** | *R*R*E*/*R*R*Z* = 70:30 | 30% |
| 20 | | $CH_3$ | H | $COOC_2H_5$ | *R*R*/S*R** = 70:30 | $H_5C_6{-}C{\equiv}C{-}COOCH_3$ | $C_2H_5OH$ | | *R*R*E*/*R*R*Z* = 50:50 | 80% |
| 21 | | $CH_3$ | H | $COOC_2H_5$ | *R*R*/S*R** = 70:30 | 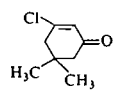 | DMSO | **18** | *R*R** | 25% |
| 22 | | $CH_3$ | H | $COOC_2H_5$ | *R*R*/S*R** = 70:30 | | $C_2H_5OH$ | | *R*R** | 50% |
| 23 | **4** | $CH_3$ | $CH_3$ | $COOC_2H_5$ | — | $CH{\equiv}C{-}COOC_2H_5$ | $C_2H_5OH$ | **19** | *E*/*Z* = 40:60 | 21% |
| 24 | **5** | $CH_3$ | H | CN | *R*R*/S*R** = 50:50 | $CH{\equiv}C{-}COOC_2H_5$ | DMSO | **20** | *R*R*E/S*R*E/R*R*Z/S*R*Z* = 60:30:5:5 | 47% |
| 25 | | $CH_3$ | H | CN | *R*R*/S*R** = 50:50 | $CH{\equiv}C{-}COOC_2H_5$ | $CH_3CN$ | | | 42% |
| 26 | | $CH_3$ | H | CN | *R*R*/S*R** = 50:50 | $CH{\equiv}C{-}COOC_2H_5$ | $C_2H_5OH$ | | *R*R*E/S*R*E/R*R*Z/S*R*Z* = 30:20:25:25 | 90% |

Can. J. Chem. Downloaded from www.nrcresearchpress.com by 210.87.254.105 on 09/06/12
For personal use only.



TABLEAU 1. (*Suite et fin*)

Aziridines secondaires

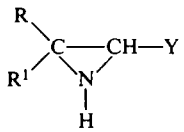

| Exp. No | No | R | R¹ | Y | Stéréochimie[a] | Dérivé acétylénique ou éthylénique β-chloré | Solvant de réaction | *N*-vinylaziridines No | Stéréochimie[a] | Rdt |
|---|---|---|---|---|---|---|---|---|---|---|
| 27 | | $CH_3$ | H | CN | *R*R*/S*R** = 50:50 | $H_3COOC—C\equiv C—COOCH_3$ | DMSO | **21** | *R*R*E/S*R*E* = 70:30 | 22% |
| 28 | | $CH_3$ | H | CN | *R*R*/S*R** = 50:50 | $H_3COOC—C\equiv C—COOCH_3$ | $CH_3CN$ | **21** | *R*R*E/S*R*E/R*R*Z/S*R*Z* = 60:30:5:5 | 63% |
| 29 | | $CH_3$ | H | CN | *R*R*/S*R** = 50:50 | $H_3COOC—C\equiv C—COOCH_3$ | $C_2H_5OH$ | | *R*R*E/S*R*E/R*R*Z/S*R*Z* = 35:20:25:20 | *72%* |
| 30 | **6** | $C_6H_5$ | H | $COOC_2H_5$ | *R*R** | $CH\equiv C—COOC_2H_5$ | DMSO | **22** | *R*R*E/R*R*Z* = 90:10 | 34% |
| 31 | | $C_6H_5$ | H | $COOC_2H_5$ | *R*R** | $CH\equiv C—COOC_2H_5$ | $C_2H_5OH$ | | *R*R*E/R*R*Z* = 40:60 | 48% |
| 32 | | $C_6H_5$ | H | $COOC_2H_5$ | *S*R** | $CH\equiv C—COOC_2H_5$ | $C_2H_5OH$ | | *S*R*Z* | 48% |
| 33 | | $C_6H_5$ | H | $COOC_2H_5$ | *S*R** | $CH\equiv C—COOC_2H_5$ | $CH_3CN$ | | [b] | |
| 34 | | $C_6H_5$ | H | $COOC_2H_5$ | *S*R** | $H_3COOC—C\equiv C—COOCH_3$ | $CH_3CN$ | **23** | *S*R*E* | 61% |
| 35 | | $C_6H_5$ | H | $COOC_2H_5$ | *S*R** | $H_3COOC—C\equiv C—COOCH_3$ | $C_2H_5OH$ | | *S*R*E/S*R*Z* = 10:90 | 69% |
| 36 | **7** | $C_6H_5$ | H | CN | *R*R** | $CH\equiv C—COOC_2H_5$ | $C_2H_5OH$ | **24** | *R*R*Z* | 54% |
| 37 | | $C_6H_5$ | H | CN | *R*R** | $CH\equiv C—COOC_2H_5$ | $CH_3CN$ | | [c] | |
| 38 | | $C_6H_5$ | H | CN | *S*R** | $H_3COOC—C\equiv C—COOCH_3$ | $CH_3CN$ | **25** | *S*R*E* | 17% |
| 39 | **8** | $C_6H_5$ | H | $CO—C_6H_5$ | *S*R** | $CH\equiv C—COOC_2H_5$ | [e] | | [d] | |

[a] *R*R** et *S*R** définissent la stéréochimie au niveau des carbones du cycle, *E* et *Z* au niveau de la double liaison.
[b] Pas de réaction après 15 jours de chauffage.
[c] Le produit isolé est le pyrrole **26**.
[d] Deux pyrroles isomères **27** et **28** sont isolés dans cette réaction.
[e] DMSO (50°C) et xylène à reflux.

Can. J. Chem. Downloaded from www.nrcresearchpress.com by 210.87.254.105 on 09/06/12
For personal use only.



TABLEAU 2. Isomérisation nucléophile des *N*-vinylaziridines

| Exp. No | *N*-vinylaziridines | Conditions expérimentales | Produits d'isomérisation: Dérivés α-aminés α,β-insaturés [a] | Dérivé iodé | Autres produits |
|---|---|---|---|---|---|
| 40 | 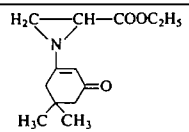 | 4 h reflux DME | 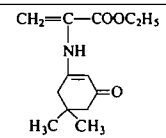 | | |
| | **12** | | **29** | | |
| 41 | 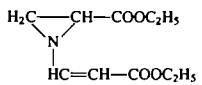 | 5 h reflux DME | 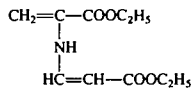 | | |
| | **9*E*** | | **30*Z*** | | |
| 42 | 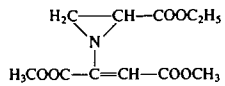 | 1 h reflux DME | 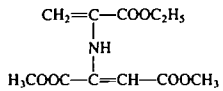 | 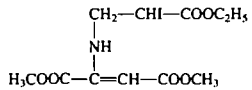 | |
| | **10*E*** | | **31*E*** (55%) | **32*E*** (45%) | |
| 43 | **10*E*** | 18 h temp. ambiante DME | **31*E*** (40%) | **32*E*** (25%) | **10*Z*** (35%) |
| 44 | **10*Z*** | 18 h, temp. ambiante DME | **31*E*** (80%) | **32*E*** (15%) | **10*Z*** (5%) |
| 45 | 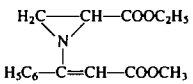 | 8 h reflux DME | 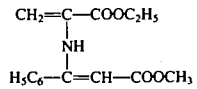 | 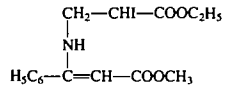 | |
| | **11*E*** + **11*Z*** (50:50) | | **33** (70%) | **34** (30%) | |
| 46 | 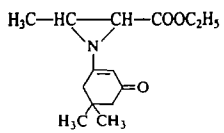 | 18 h reflux DME | 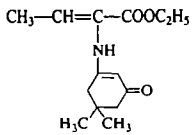 | | |
| | **18*R*R**** | | **35*E*** + **35*Z*** (50:50) 80% | | **18*R*R**** (20%) |

Can. J. Chem. Downloaded from www.nrcresearchpress.com by 210.87.254.105 on 09/06/12
For personal use only.



TABLEAU 2. (*Suite*)

| Exp. No | *N*-vinylaziridines | Conditions expérimentales | Produits d'isomérisation<br>Dérivés α-aminés α,β-insaturés<br> 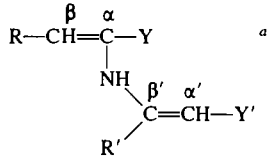 [a] | Dérivé iodé | Autres produits |
|---|---|---|---|---|---|
| 47 | **18***R**R** | 55 h<br>reflux DME | **35***E* + **35***Z* (35:65) | | |
| 48 | **18***R**R** | 90 h[b]<br>reflux $C_6H_6$ | **35***E* + **35***Z* (35:65) 75% | | **18***R**R** (25%) |
| 49 | **18***R**R** | 60 h[c]<br>reflux $CH_3CN$ | **35***Z* (50%) | | **18***R**R** (50%) |
| 50 | 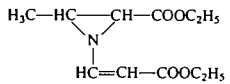 <br>**15***R**R**E* | 45 h<br>reflux DME | 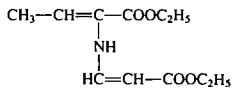 <br>**36***EZ* + **36***ZZ* (50:50) | | |
| 51 | **15***S**R**E* | 45 h<br>reflux DME | **36***EZ* + **36***ZZ* (75:25) | | |
| 52 | 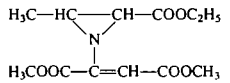 <br>**16***R**R**E* + **16***S**R**E* (80:20) | 24 h<br>reflux DME | 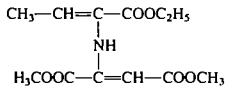 <br>**37***ZE* + **37***EE* (75:25) 75% | | 16*R**R**Z* + **16***S**R**Z* (50:50) 25% |
| 53 | **16***R**R**E* + **16***S**R**Z* (50:50) | 24 h<br>reflux DME | **37***ZE* + **37***EE* (75:25) 75% | | **16***R**R**Z* + **16***S**R**Z* (50:50) 25% |
| 54 | 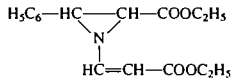 <br>**22***R**R**Z* | 6 h<br>reflux DME | 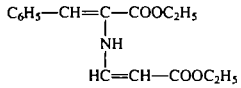 <br>**38***ZZ* | | |
| 55 | 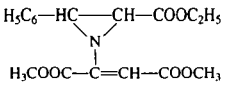 <br>**23***S**R**E* | 6 h<br>reflux DME | | | **23***S**R**E* + **23***S**R**Z* (15:85) |

Can. J. Chem. Downloaded from www.nrcresearchpress.com by 210.87.254.105 on 09/06/12
For personal use only.





TABLEAU 2. (*Suite et fin*)

| Exp. No | *N*-vinylaziridines | Conditions expérimentales | Produits d'isomérisation: Dérivés α-aminés α,β-insaturés[a] | Dérivé iodé | Autres produits |
|---|---|---|---|---|---|
| 56 | 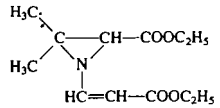 | 24 h reflux DME | | | **19***E* + **19***Z* (80:20) |
| | **19***E* + **19***Z* (40:60) | | | | |
| 57 | 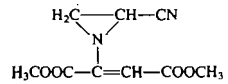 | 2,5 h 40°C DME | | 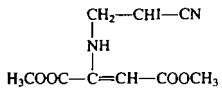 | 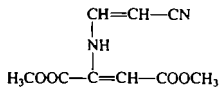 |
| | **14***E* | | | **40***E* (60%) | **39***ZE* + **39***EE* (65:35) (40%) |
| 58 | **14***E* + **14***Z* (70:30) | 6 h 40°C DME | | | **39***ZE* + **39***EE*(65:35) |
| 59 | 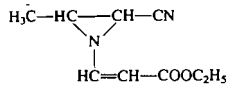 | 6 h 40°C DME | 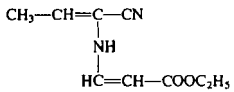 | | |
| | **20***R*R*E* + **20***S*R*E* (75:25) | | **41***ZZ* + **41***EZ* (65:35) | | |
| 60 | 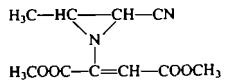 | 6 h 40°C DME | 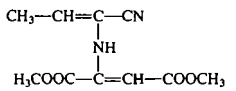 | 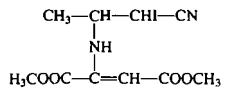 | **21***R*R*Z* (40%) |
| | **21***R*R*E* + **21***S*R*E* (60:40) | | **42** (10%) | **43***E* (50%) | |

[a] La configuration de la liaison $C_\alpha{=}C_\beta$ est définie d'abord, puis celle de la liaison $C_{\alpha'}{=}C_{\beta'}$.
[b] Iodure de tétra *n*-butylammonium.
[c] Thiocyanate de potassium.

Can. J. Chem. Downloaded from www.nrcresearchpress.com by 210.87.254.105 on 09/06/12
For personal use only.

produits obtenus sont précisées dans le Tableau 2. Les composés ont été identifiés principalement par leurs spectres de rmn (cf. partie expérimentale). La structure du dérivé iodé **32** est confirmée par l'analyse élémentaire et par l'obtention, en présence de triéthylamine de l'ester α,β-insaturé β-aminé **44**:

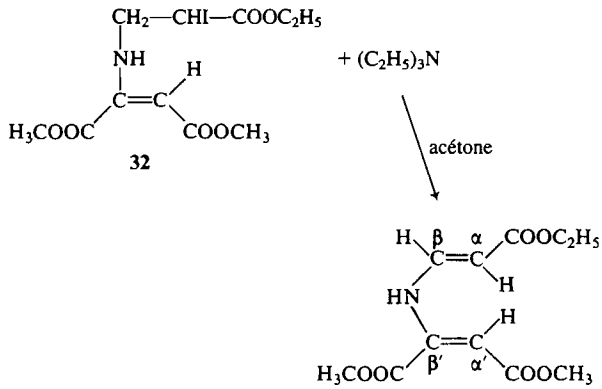


Le composé **43** traité par la triéthylamine en solution dans l'acétone conduit à l'aziridine **21** mélange des isomères *S*R** et *R*R** avec prépondérance de ce dernier:

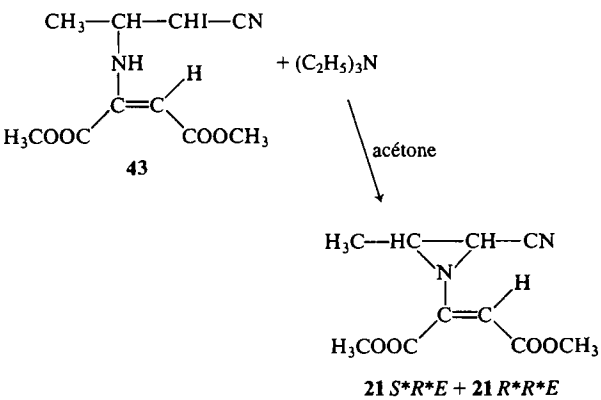


Les résultats observés (Tableau 2) montrent que les vinylaziridines étudiées se réarrangent toujours en formant par ouverture de l'hétérocycle des produits dont la structure s'apparente à celle des divinylamines. La réactivité des aziridines non substituées en position 3 est supérieure à celle des méthyl-3 aziridines; la diméthyl-3,3 aziridine (expérience no 56) n'est pas isomérisée par l'iodure de sodium.

La réaction d'ouverture est généralement régiospécifique, l'attaque de l'ion iodure ayant lieu exclusivement sur l'atome de carbone C-3 (expériences no 40, 41, 46 à 54, 59). Cependant, pour trois aziridines, l'approche du nucléophile sur l'atome de carbone C-3 est compétitive avec une attaque sur l'atome de carbone C-2 porteur de la fonction activante (expériences no 42 à 45, 60). Enfin, dans le cas de la cyano-2 aziridine **14** (expériences no 57 et 58) la réaction est régiospécifique et correspond à une attaque du nucléophile sur l'atome de carbone substitué par la fonction nitrile. En l'absence de résultats cinétiques, il ne nous est pas possible de préciser si l'attaque du nucléophile en position 3 est un processus concerté (mécanisme $S_N2$) ou non concerté (mécanisme $S_N1$). Cette dernière éventualité nous semble cependant peu probable en raison du manque de réactivité de la diméthyl-3,3 aziridine **19** et de la plus faible réactivité des méthyl-3 aziridines par rapport aux composés non substitués en position 3. Un mécanisme "pseudo $S_N2$" faisant intervenir un état de transition à caractère de carbocation peut rendre compte de l'ensemble de nos résultats:

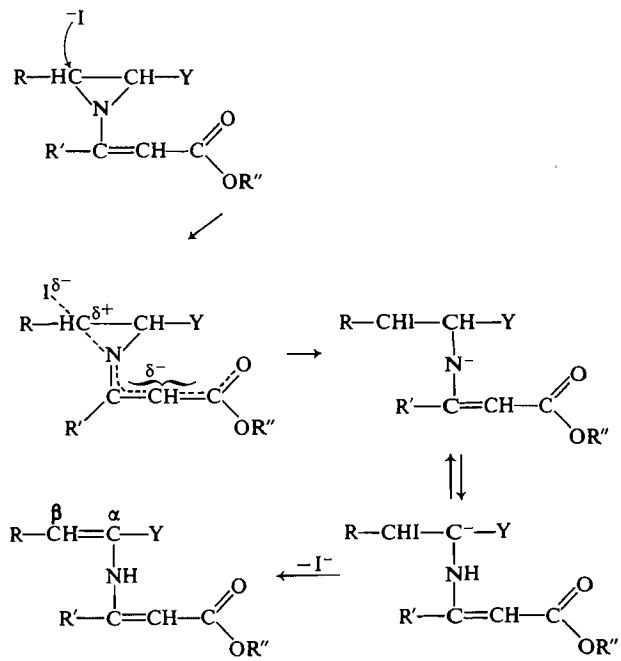


L'intermédiaire β-iodé perd facilement l'anion $I^-$ pour conduire aux dérivés α,β insaturés.

La formation des composés α-iodés β-aminés **32**, **34**, **40** et **43** implique une attaque de l'ion iodure sur l'atome de carbone porteur de la fonction activante. L'attaque ayant lieu sur l'atome de carbone dont le caractère électrophile est le plus marqué, cette réaction doit présenter un caractère $S_N2$ plus accentué que la précédente. L'intermédiaire formé lors de cette réaction étant peu apte à éliminer un ion iodure, sa protonation conduit alors aux composés α-iodés β-aminés:

Can. J. Chem. Downloaded from www.nrcresearchpress.com by 210.87.254.105 on 09/06/12
For personal use only.

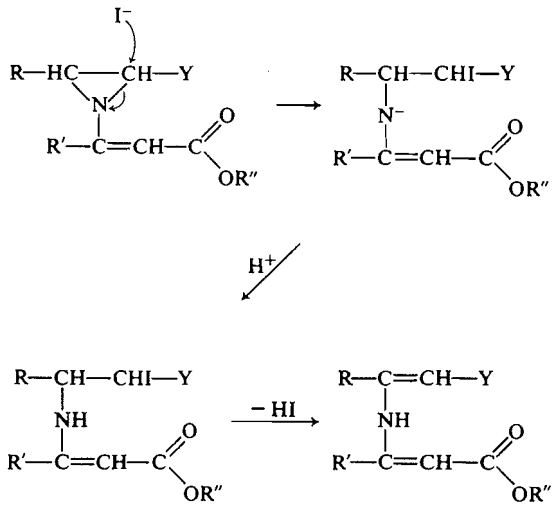

L'élimination à partir du dérivé **40** d'une molécule d'iodure d'hydrogène conduit au β-énaminonitrile **39**.

Par ailleurs, l'examen des résultats du Tableau 2 (expériences no 43, 52, 53, 55, 56, 60) montre que parallèlement à l'ouverture nucléophile du cycle aziridine a lieu une réaction d'isomérisation de la double liaison de l'aziridine. À partir des aziridines **10***E*, **16***E*, **21***E* et **23***E* cette réaction conduit aux aziridines de configuration *Z* (expériences no 43, 52, 53, 55, et 60).

Chez les énamines obtenues, l'isomérisation des deux doubles liaisons intervient également, postérieurement à la formation de ces composés; en effet la double liaison $C_{\alpha'}=C_{\beta'}$ de l'énamine, lorsqu'elle est substituée par une seule fonction ester, adopte toujours la configuration *Z* (expériences no 41, 50, 51, 54, 59), elle prend par contre la configuration *E* lorsqu'elle est substituée par deux groupements méthoxycarbonyle (expériences no 42, 43, 44, 52, 53, 57, 58, 60) et cela, quelle que soit la configuration de la double liaison de l'aziridine. L'isomérisation de la double liaison $C_\alpha=C_\beta$ est mise en évidence par comparaison des expériences no 46 et 47; la quantité d'isomère **35***Z* augmente en effet avec le temps de réaction. L'étude de la configuration de la liaison $C_\alpha=C_\beta$ des énamines ne peut donc être utilisée pour préciser le mécanisme d'ouverture du cycle aziridine.

La plupart des réactions que nous avons étudiées ont été initiées par l'iodure de sodium. Nous avons constaté que la quantité de nucléophile utilisée ne modifie pas l'issue de la réaction, et ceci contrairement à certains résultats (7). Notre étude montre également que le remplacement de l'iodure de sodium par un iodure d'ammonium quaternaire ou par le thiocyanate de potassium ne provoque aucun changement dans l'évolution de la réaction (expériences no 47, 48, 49).

### Isomérisation thermique des *N*-vinylaziridines

Nous avons rassemblé dans le Tableau 3 les conditions expérimentales dans lesquelles ont été réalisées les isomérisations thermiques. Nous y précisons également la nature des produits identifiés.

La formation, à partir des aziridines **16** et **21** des ester et nitrile α,β-insaturés α-aminés **37** et **42** (expériences no 61 et 62) est comparable à l'obtention d'α-benzamido benzalacétophénones à partir de diaroyl-1,2 aziridines (2*e*). Cette réaction implique la rupture de la liaison C-3—N du cycle aziridine; l'hétérolyse de cette liaison est facilitée par la présence sur l'atome d'azote du groupement vinyle activé. L'intermédiaire dipolaire évolue ensuite par migration de proton:

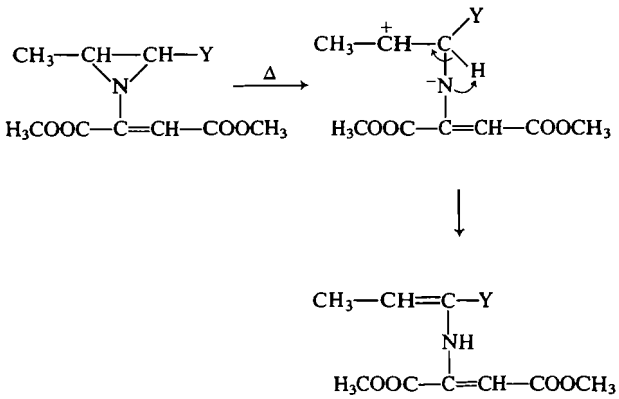

Y = $COOC_2H_5$, CN

La formation, à côté des dérivés α-aminés α,β-insaturés **37** et **42** des composés α-aminés **45** et **46** montre que la rupture de la liaison C-3—N du cycle est en compétition avec celle de la liaison C-2—C-3, cette dernière étant d'ailleurs largement prépondérante. Deux mécanismes peuvent expliquer la formation de ces composés.

(a) *Mécanisme concerté – migration sigmatropique 1,5*

Ce mécanisme est analogue à celui proposé pour l'isomérisation thermique d'acyl-1 alkyl-2 cyclopropanes (34). Nous l'avons également proposé pour rendre compte de l'isomérisation en pyrroles de (*N*-méthylidenealkylamino)-2 aziridines (35). Il fait intervenir un transfert 1,5 d'hydrogène accompagnant la rupture de la liaison C-2—C-3 du cycle aziridine:

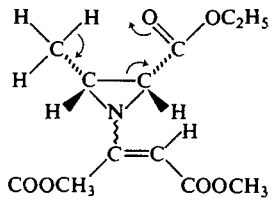

16 *R*R*E*

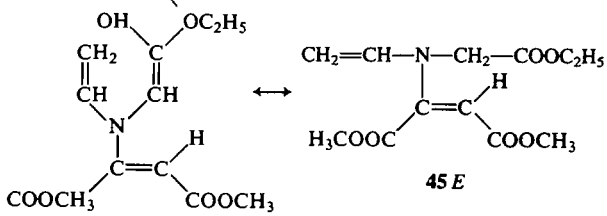

45 *E*

Ce mécanisme permet notamment de justifier le manque de réactivité du composé **21***S*R*Z* (expérience no 63).

(b) *Mécanisme ionique*

Un mécanisme de ce type a été proposé pour interpréter l'isomérisation des méthyl-3 benzoyl-2 alkyl-1 aziridines en pyrroles (36). Il met en jeu une ouverture conrotatoire de l'aziridine en ylure d'azométhine suivie d'une migration intramoléculaire de proton:

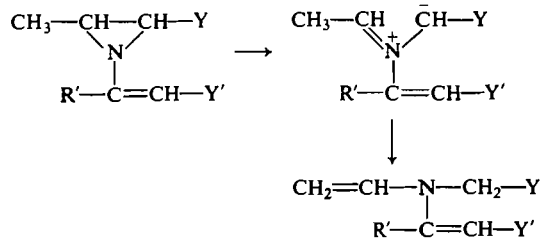

Dans la thermolyse de l'aziridine **18***R*R**, on note la formation, à côté du dérivé **47**, de l'aminoester **48** (expérience no 64). On peut penser, en accord avec d'autres auteurs (37–41) que l'ylure d'azométhine intermédiaire est hydrolysé en aminoalcool; ce dernier se décompose en acétaldéhyde et aminoester:

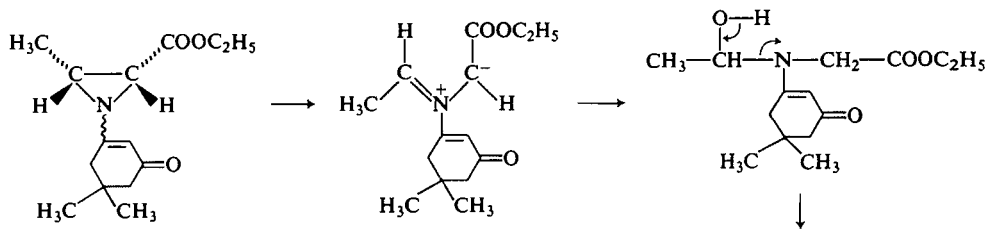

18 *R*R**

48

## Conclusion

Contrairement à ce que l'on pouvait attendre les *N*-vinylaziridines fonctionnalisées ne se réarrangent pas en hétérocycles à cinq atomes.

Leur isomérisation, sous l'influence de réactifs nucléophiles, en dérivés d'acides α-aminés α,β-insaturés constitue une très bonne méthode de préparation de ces composés auxquels il est souvent difficile d'accéder par d'autres voies (42–48). Ces dérivés font pourtant l'objet depuis quelques années d'un regain d'intérêt en raison notamment de la présence de tels enchaînements dans plusieurs antibiotiques polypeptidiques isolés du milieu de culture de microorganismes (42).

Par ailleurs, la plupart des produits d'isomérisation des *N*-vinylaziridines fonctionnalisées constituent des systèmes à 6 électrons π dont le réarrangement thermique ou photochimique que nous étudions actuellement doit conduire à des hétérocyclisations dignes d'intérêt.

## Partie expérimentale

Les spectres de résonance magnétique nucléaire ont été enregistrés à l'aide des appareils Perkin–Elmer R 24 et Varian T 60 pour $^1H$ et JEOL FX 60 pour $^{13}C$, en utilisant le tétraméthylsilane comme référence interne. Les déplacements chimiques sont exprimés en ppm et les constantes de couplage en Hz. Les spectres infrarouge ont été effectués sur un spectrophotomètre Perkin–Elmer 157. Les chromatographies sur colonne ont été

Can. J. Chem. Downloaded from www.nrcresearchpress.com by 210.87.254.105 on 09/06/12
For personal use only.

Can. J. Chem. Downloaded from www.nrcresearchpress.com by 210.87.254.105 on 09/06/12
For personal use only.



TABLEAU 3. Isomérisation thermiques des *N*-vinylaziridines

| Exp. No | *N*-vinylaziridines | Conditions expérimentales | Produits d'isomérisation | | |
|---|---|---|---|---|---|
| | | | Dérivés α-aminé α,β-insaturé | α-Vinylaminoester ou nitrile | Autres produits |
| 61 | 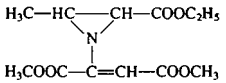 | 2 h 170°C | 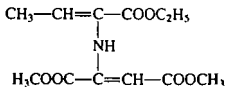 | 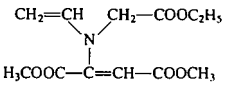 | **16***R*R*E* (30%) |
| | **16***R*R*E* | | **37***ZE* (5%) | **45***E* (65%) | |
| 62 | 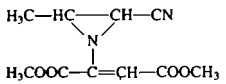 | 1 h 15 170°C | 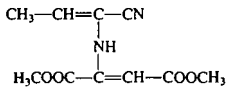 | 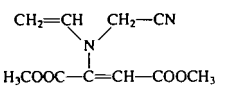 | **21***R*R*Z* + **21***S*R*Z* (30:70) 40% |
| | **21***R*R*E*/**21***S*R*E*/**21***R*R*Z*/ **21***S*R*Z* = 65:5:10:20 | | **42***ZE* + **42***EE* (50:50) 5% | **46***E* (55%) | |
| 63 | **21***S*R*Z* | 1 h 15; 170°C | | | **21***S*R*Z* |
| 64 | 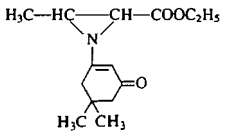 | 1 h 160°C | | 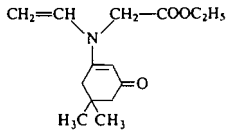 | 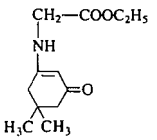 |
| | **18***R*R** | | | **47** (70%) | **48** (30%) |

Can. J. Chem. Downloaded from www.nrcresearchpress.com by 210.87.254.105 on 09/06/12
For personal use only.

réalisées soit sur gel de silice 60 (Merck No 7734) soit à moyenne pression sur Lichoprep SI 60 (colonnes Merck Lobar). Les chromatographies sur plaques à l'échelle préparative ont été réalisées sur gel de silice 60 (plaques Merck 5717).

*Diméthyl-5,5 chloro-3 cyclohexène-2 one*

Préparée selon un procédé décrit (49).

*Préparation des aziridines secondaires*

*Aziridines **1**, **2**, **3** et **5***

Préparées selon Burzin et Enderer (50).

*Ethoxycarbonyl-2 aziridine **1***

Rdt 25%; $Eb_{0,05}$ = 25–30°C (litt. (51) $Eb_{12}$ = 53–55°C); ir ($cm^{-1}$): 3220, 1725; rmn $^1H$($CDCl_3$): 1,30 (t, $COOCH_2CH_3$, $J$ = 7,2), 4,20 (q, $COOCH_2$), 1,15 à 1, 45 (m, N—H), 1,83 (dd, H-3, $J$ = 1,6 (*gem*), $J$ = 5,6 (*cis*)), 1,95 (dd, H-3, $J$ = 1,6 (*gem*), $J$ = 3,0 (*trans*)), 2,48 (dd, H-2, $J$ = 3,0, $J$ = 5,6); rmn $^{13}C$($CDCl_3$): 14,2–61,6–173,0 ($COOCH_2CH_3$), 27,2 (C-3), 28,9 (C-2).

*Cyano-2 aziridine **2***

Rdt 40%; $Eb_{0,01}$ = 32–34°C (litt. (50) $Eb_{0,1}$ = 38–39°C); rmn $^1H$ ($CDCl_3$): 1,60 (s large, N—H), 2,10 (s large, 2H), 2,55 (s large, H-2); rmn $^{13}C$ ($CDCl_3$): 15,3 (C-2), 26,1 (C-3), 120,1 (CN).

*Méthyl-3 éthoxycarbonyl-2 aziridine **3***

Obtenue sous forme d'un mélange des isomères *R*R**(70%) et *S*R**(30%): Rdt 54%; $Eb_{0,1}$ = 32–40°C (litt. (52) $Eb_{12}$ = 70–75°C); ir ($cm^{-1}$): 3335, 3225, 1745, 1730. Les deux isomères sont séparés par distillation sur colonne à bande tournante.

Isomère ***3R*R****: $Eb_{10}$ = 63°C; rmn $^1H$ ($CDCl_3$): 1,30 (t, $COOCH_2CH_3$, $J$ = 7,2), 4,25 (q, $COOCH_2$), 1,05 à 1,45 (m, N—H), 1,25 (d, $CH_3$, $J$ = 5,6), 2,30 (qd, H-3, $J$ = 5,6, $J$ = 5,8 (*cis*)), 2,61 (d, H-2, $J$ = 5,8); rmn $^{13}C$ ($CDCl_3$): 13,1 ($CH_3$), 33,6 (C-3), 34,9 (C-2).

Isomère ***3S*R****: $Eb_{10}$ = 53°C; rmn $^1H$ ($CDCl_3$): 1,35 (t, $COOCH_2CH_3$, $J$ = 7,2) 4,15 (q, $COOCH_2$), 1,25 (d, $CH_3$, $J$ = 5,2), 1,20 à 1,55 (m, N—H), 2,10 à 2,40 (m, 2H, H-2, H-3); rmn $^{13}C$ ($CDCl_3$): 18,1 ($CH_3$), 34,8 (C-2), 36,2 (C-3).

*Méthyl-3 cyano-2 aziridine **5***

Obtenue sous forme d'un mélange des isomères *S*R* (50%) et R*R* (50%) Rdt 52%; $Eb_{0,3}$* = 48–50°C; ir ($cm^{-1}$): 3250, 2210; rmn $^1H$ ($CDCl_3$): 1,25 (d, 1,5H, $J$ = 5,2), 1,35 (d, 1,5H, $J$ = 5,0), 1,58 (s large, N—H), 2,15 à 2,65 (m, H-2, H-3); rmn $^{13}C$ ($CDCl_3$): 17,9 ($CH_3$), 18,0 ($CH_3$), 21,2 (C-2), 21,5 (C-2), 31,3 (C-3), 34,6 (C-3), 118,9 (CN), 119,7 (CN).

*Aziridines **4**, **6** et **7***

À 100 mL de DMSO sec saturé d'ammoniac, on ajoute 0,02 mol de dérivé dibromé. Le mélange réactionnel est laissé sous agitation et sous pression pendant 60 h, puis versé dans de l'eau glacée. On extrait à l'éther; les phases étherées sont lavées à l'eau, séchées sur sulfate de magnésium et concentrées. Les produits obtenus sont alors purifiés par chromatographie sur colonne (éther de pétrole/acétate d'éthyle 70:30).

*Diméthyl-3,3 éthoxycarbonyl-2 aziridine **4***

Préparée par Expert (53); rmn $^1H$ ($CDCl_3$): 1,30 (s, $(CH_3)_2$), 1,80 (s large, N—H), 2,50 (s, H-2); rmn $^{13}C$ ($CDCl_3$): 14,3–61,2–170,9 ($COOCH_2CH_3$), 18,9 ($CH_3$), 26,0 ($CH_3$), 39,7 (C-3), 42,2 (C-2).

*Phényl-3 éthoxycarbonyl-2 aziridine **6***

Le produit brut est un mélange des isomères *R*R** (50%) et *S*R** (50%) qui sont séparés par chromatographie sur colonne (éther de pétrole/acétate d'éthyle 50:50).

Isomère ***6R*R****: Rdt 30%; $F$ = 63°C; ir ($cm^{-1}$): 3600, 1735; rmn $^1H$ ($CDCl_3$): 0,90 (t, $COOCH_2CH_3$, $J$ = 7,0), 3,86 (q, $COOCH_2$), 1,85 (s large, N—H), 2,82 (d, H-2, $J$ = 6,6 (*cis*)), 3,30 (d, H-3, $J$ = 6,6), 7,22 (s, $C_6H_5$); rmn $^{13}C$ ($CDCl_3$): 13,9–61,1–169,1 ($COOC_2H_5$), 37,2 (C-2), 39,9 (C-3), 127,5–128,1–128,4–130,0 ($C_6H_5$).

Isomère ***6S*R****: Rdt 40%; ir ($cm^{-1}$): 3225, 1730; rmn $^1H$ ($CDCl_3$): 1,90 (t large, N—H, $J$ = 7,8 (*trans*) et $J$ = 9,2 (*cis*)), 2,57 (dd, H-2, $J$ = 2,5 (*trans*) et $J$ = 7,8 (*trans*)), 3,25 (dd, H-3, $J$ = 2,5 (*trans*) et $J$ = 9,2 (*cis*)), 7,28 (s, $C_6H_5$), 1,27 (t, $COOCH_2CH_3$, $J$ = 7,0), 4,25 (q, $COOCH_2$); rmn $^{13}C$ ($CDCl_3$): 14,2–61,7–171,6 ($COOC_2H_5$), 39,5 (C-2), 40,3 (C-3), 126,2–127,7–128,4–137,9 ($C_6H_5$).

*Phényl-3 cyano-2 aziridine **7***

Obtenue sous forme d'un mélange des isomères *S*R** (50%) et *R*R** (50%) qui sont séparés par chromatographie sur colonne (éther de pétrole/acétate d'éthyle 70:30).

Isomère ***7R*R****: Rdt 30%; $F$ = 102°C; ir ($cm^{-1}$): 3300, 2250; rmn $^1H$ ($CDCl_3$): 1,60 (t large, N—H, $J$ = 9,2 (*cis*) et $J$ = 9,4 (*cis*)), 2,80 (dd, H-2, $J$ = 6,0 (*cis*) et $J$ = 9,4 (*cis*)), 3,40 (dd, H-3, $J$ = 6,0 (*cis*) et $J$ = 9,2 (*cis*)); rmn $^{13}C$ ($CDCl_3$): 25,1 (C-2), 37,9 (C-3), 117,3 (CN), 126,9–127,9–128,5–134,0 ($C_6H_5$).

Isomère ***7S*R****: Rdt 30%; ir ($cm^{-1}$): 3280, 2230; rmn $^1H$ ($CDCl_3$): 1,82 (s large, N—H), 2,36 (s large, H-2), 3,51 (s large, H-3), 7,22 (s, $C_6H_5$); rmn $^{13}C$ ($CDCl_3$): 24,3 (C-2), 39,9 (C-3), 118,8 (CN), 125,9–128,5–129,8–135,7 ($C_6H_5$).

*Phényl-3 benzoyl-2 aziridine **8***

Préparée selon Weber et Bandlow (54). Rdt 79%; $F$ = 97–98°C (litt. (55) $F$ = 100–102°C); rmn $^1H$ ($CDCl_3$): 2,70 (t large, N—H), 3,20 (dd, H-2, $J$ = 2,4 (*trans*), $J$ = 8,8 (*cis*)), 3,50 (dd, H-3, $J$ = 2,4 (*trans*), $J$ = 6,8 (*trans*)), 7,20 à 7,80 (m, $C_6H_5$); rmn $^{13}C$ ($CDCl_3$): 43,5 (C-2), 44,1 (C-3), 126,4–128,1–128,5–128,7, 129,0–134,0–136,1–138,5 ($C_6H_5$), 196,0 (C=O).

*Synthèse des* N*-vinylaziridines*

*Préparation des dérivés **9**, **10**, **11**, **13** à **17**, **19** à **25***

À une solution de 0,02 mol d'aziridine dans 20 mL de solvant, agitée magnétiquement, on ajoute un équivalent de composé acétylénique. Le mélange réactionnel est chauffé à 40°C (DMSO) ou 60°C (éthanol ou acétonitrile), l'évolution de la réaction étant suivie par chromatographie sur couche mince. En fin de réaction, on évapore le solvant (éthanol ou acétonitrile) ou verse le mélange réactionnel dans une solution aqueuse saturée de NaCl, extrait à l'éther, lave à l'eau, sèche puis concentre (DMSO). Le produit brut est purifié par chromatographie sur colonne (éther de pétrole, acétate d'éthyle). Le pourcentage des isomères formés ainsi que les rendements de toutes les réactions sont précisés dans le Tableau 1. Les spectres de rmn $^1H$ et $^{13}C$ sont donnés dans les Tableaux 4 et 5.

*Dérivé **9**E*: ir ($cm^{-1}$): 1750, 1710, 1635; *Anal.* calc. pour $C_{10}H_{15}NO_4$: C 56,33, H 7,09, N 6,57, O 30,01; trouvé: C 55,71, H 7,08, N 6,40, O 29,27.

*Dérivé **10**Z*: $F$ = 76°C; *Anal.* calc. pour $C_{11}H_{15}NO_6$: C 51,38, H 5,88, N 5,45, O 37,33; trouvé: C 51,54, H 5,82, N 5,39, O 37,39.

*Dérivé **10**E*: ir ($cm^{-1}$): 1750, 1730, 1630; *Anal.* calc. pour $C_{11}H_{15}NO_6$: C51,38, H 5,88, N 5,45, O 37,33; trouvé: C 51,36, H 5,89, N 5,18, O 37,48.

*Dérivé **11***(E + Z): *Anal.* calc. pour $C_{15}H_{17}NO_4$: C 65,45, H 6,18, N 5,09, O 23,27; trouvé: C 65,40, H 6,20, N 5,04, O 23,23.

*Dérivé **13**E*: ir ($cm^{-1}$): 1725, 1640.

*Dérivé **13**Z*: $F$ = 50°C; *Anal.* calc. pour $C_8H_{10}N_2O_2$: C 57,82, H 6,06, N 16,85, O 19,26; trouvé: C 57,92, H 6,07, N 16,47, O 19,57.

*Dérivé **14**E*: ir ($cm^{-1}$): 2250, 1735, 1640; *Anal.* calc. pour $C_9H_{10}N_2O_4$: C 51,43, H 4,80, N 13,33, O 30,45; trouvé: C 51,20, H 4,81, N 13,19, O 30,69.

*Dérivé **15**E* (*15*R*R*E/*15*S*R*E = *80:20*): ir ($cm^{-1}$): 1740,

Can. J. Chem. Downloaded from www.nrcresearchpress.com by 210.87.254.105 on 09/06/12
For personal use only.





TABLEAU 4. Spectres de résonance magnétique nucléaire $^1H$ des *N*-vinylaziridines

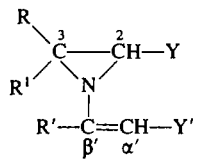


| No | R' | R | R' | Y' | Y | δH-2 | δR' | δR | $\delta H_{\alpha'}$ | δR' | δY' | δY | $J_{H\text{-}2—R'}$ | $J_{H\text{-}2—R}$ | $J_{R'—R}$ | $J_{H_{\alpha'}—R'}$ |
|---|---|---|---|---|---|---|---|---|---|---|---|---|---|---|---|---|
| **9***E* | H | H | H | $COOC_2H_5$ | $COOC_2H_5$ | 2,78 dd | 2,25 m | 2,47 m | 5,42 d | 7,45 d | 1,28 t, 1,30 t, 4,20 q, 4,18 q $J$ = 7,2 | | 6,0 | 2,9 | 1,8 | 13,6 |
| **9***Z* | H | H | H | $COOC_2H_5$ | $COOC_2H_5$ | 2,95 dd | 2,40 dd | 2,58 dd | 5,20 d | 6,60 d | 1,30 t, 1,32 t, 4,25 q, 4,10 q $J$ = 7,6 | | 5,6 | 3,2 | 1,8 | 9,6 |
| **10***E* | H | H | $COOCH_3$ | $COOCH_3$ | $COOC_2H_5$ | 2,90 dd | 2,38 dq | 2,58 dd | 5,45 s | 3,70 s, 3,90 s | | 1,30 t, 4,22 q $J$ = 7,0 | 6,0 | 3,4 | 1,4 | — |
| **10***Z* | H | H | $COOCH_3$ | $COOCH_3$ | $COOC_2H_5$ | 3,10 dd | 2,67 d | 2,57 d | 6,25 s | 3,75 s, 3,83 s | | 1,30 t, 4,23 q $J$ = 7,0 | 6,0 | 3,4 | — | — |
| **11***E* | H | H | $C_6H_5$ | $COOCH_3$ | $COOC_2H_5$ | 2,65 dd | 2,32 dd | 2,55 d | 5,50 s | 7,20 à 7,70 m | 3,52 s | 1,15 t, 4,07 q $J$ = 7,0 | 5,0 | 2,2 | 1,8 | — |
| **11***Z* | H | H | $C_6H_5$ | $COOCH_3$ | $COOC_2H_5$ | 2,92 dd | 2,38 d | 2,60 dd | 5,62 s | 7,38 m | 3,70 s | 1,22 t, 4,15 q $J$ = 7,0 | 6,0 | 3,2 | 1,0 | — |
| **12** | H | H | 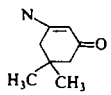 | | $COOC_2H_5$ | 2,78 dd | 2,25 m | 2,55 dd | 5,52 s | | 1,10 s, 2,20 s, 2,30 s | 1,30 t, 4,12 q $J$ = 7,0 | 6,0 | 3,0 | 1,6 | — |
| **13***E* | H | H | H | $COOC_2H_5$ | CN | 2,75 dd | 2,38 dd | 2,52 dd | 5,50 d | 7,39 d | 1,28 t, 4,20 q $J$ = 7,0 | — | 5,6 | 3,0 | 1,2 | 13,6 |
| **13***Z* | H | H | H | $COOC_2H_5$ | CN | 2,98 dd | 2,50 à 2,70 m | | 5,40 d | 6,55 d | 1,30 t, 4,18 q $J$ = 7,0 | — | 5,8 | 3,2 | — | 9,2 |
| **14***E* | H | H | $COOCH_3$ | $COOCH_3$ | CN | 2,93 dd | 2,47 d | 2,65 d | 5,53 s | 3,60 s, 3,87 s | | — | 6,2 | 3,2 | <0,5 | — |
| **14***Z* | H | H | $COOCH_3$ | $COOCH_3$ | CN | 2,70 à 3,00 m | 2,30 à 2,70 m | | 6,31 s | 3,80 s, 3,93 s | | — | — | — | — | — |
| **15***R*R*E* | H | $CH_3$ | H | $COOC_2H_5$ | $COOC_2H_5$ | 2,72 d | 2,40 qd | 1,38 d | 5,39 d | 7,42 d | 1,32 t, 1,28 t, 4,25 q, 4,10 q $J$ = 6,2 et $J$ = 7,0 1,32 t, 1,28 t, | | 6,5 | — | 5,4 | 13,6 |

Can. J. Chem. Downloaded from www.nrcresearchpress.com by 210.87.254.105 on 09/06/12
For personal use only.



TABLEAU 4. (*Suite*)

| No | $R^1$ | R | R′ | Y′ | Y | δH-2 | $\delta R^1$ | δR | $\delta H_{\alpha'}$ | δR′ | δY′ | δY | $J_{H\text{-}2—R^1}$ | $J_{H\text{-}2—R}$ | $J_{R^1—R}$ | $J_{H_{\alpha'}—R'}$ |
|---|---|---|---|---|---|---|---|---|---|---|---|---|---|---|---|---|
| **15***S*R*E* | H | $CH_3$ | H | $COOC_2H_5$ | $COOC_2H_5$ | 2,58 d | 2,75 qd | 1,38 d | 5,40 d | 7,40 d | 4,28 q, 4,18 q $J = 7,0$ | | 3,0 | — | 6,0 | 13,6 |
| **15***R*R*Z* | H | $CH_3$ | H | $COOC_2H_5$ | $COOC_2H_5$ | 2,83 d | 2,58 q | 1,45 d | 5,17 d | 6,52 d | 1,30 t, 1,41 t, 4,15 q, 4,31 q $J = 7,0$ | | 6,2 | — | 6,0 | 9,0 |
| **15***S*R*Z* | H | $CH_3$ | H | $COOC_2H_5$ | $COOC_2H_5$ | 2,60 à 2,80 m | | 1,40 d | 5,21 d | 6,51 d | 1,25 t, 1,30 t, 4,12 q, 4,23 q $J = 7,0$ | | — | — | 5,2 | 9,4 |
| **16***R*R*E* | H | $CH_3$ | $COOCH_3$ | $COOCH_3$ | $COOC_2H_5$ | 2,90 d | 2,60 dq | 1,38 d | 5,40 s | 3,70 s, 3,85 s | | 1,30 t, 4,20 q $J = 7,0$ | 6,2 | — | 6,0 | — |
| **16***S*R*E* | H | $CH_3$ | $COOCH_3$ | $COOCH_3$ | $COOC_2H_5$ | 2,50 à 3,00 m | | 1,38 d | 5,40 s | 3,70 s, 3,85 s | | 1,30 t, 4,18 q $J = 7,0$ | — | — | 6,0 | — |
| **16***R*R*Z* | H | $CH_3$ | $COOCH_3$ | $COOCH_3$ | $COOC_2H_5$ | 2,30 à 2,90 m | | 1,40 d | 6,18 s | 3,75 s, 3,85 s | | 1,30 t, 4,22 q $J = 7,0$ | — | — | 5,2 | — |
| **16***S*R*Z* | H | $CH_3$ | $COOCH_3$ | $COOCH_3$ | $COOC_2H_5$ | 3,20 d | 2,70 dq | 1,50 d | 6,20 s | 3,73 s, 3,83 s | | 1,27 t, 4,20 q $J = 7,0$ | 3,2 | — | 5,6 | — |
| **17***R*R*E* | H | $CH_3$ | $C_6H_5$ | $COOCH_3$ | $COOC_2H_5$ | 2,78 d | 2,50 dq | 1,45 d | 5,58 s | 7,20 à 7,40 m | 3,68 s | 1,30 t, 4,29 q $J = 7,0$ | 6,2 | — | 5,6 | — |
| **17***R*R*Z* | H | $CH_3$ | $C_6H_5$ | $COOCH_3$ | $COOC_2H_5$ | 2,65 d | 2,40 q | 1,43 d | 5,40 s | 7,20 à 7,70 m | 3,52 s | 1,23 t, 4,19 q $J = 7,0$ | 6,7 | — | 5,8 | — |
| **18***R*R** | H | $CH_3$ | | | $COOC_2H_5$ | 2,78 d | 2,48 qd | 1,38 d | 5,48 s | 1,08 s 2,20 s 2,32 s | | 1,32 t, 4,25 q $J = 7,0$ | 6,0 | — | 5,4 | — |
| **19***E* | $CH_3$ | $CH_3$ | H | $COOC_2H_5$ | $COOC_2H_5$ | 2,53 s | | 1,40 s 1,44 s | 5,40 d | 7,40 d | 1,30 t, 1,36 t, 4,15 q, 4,30 q $J = 7,0$ | | — | — | — | 13,5 |
| **19***Z* | $CH_3$ | $CH_3$ | H | $COOC_2H_5$ | $COOC_2H_5$ | 2,65 s | | | 5,23 d | 6,48 d | | | — | — | — | 9,0 |
| **20***R*R*E* | H | $CH_3$ | H | $COOC_2H_5$ | CN | 2,75 d | 2,45 dq | 1,45 d | 5,43 d | 7,35 d | 1,22 t, 4,15 q $J = 7,0$ | — | 6,0 | — | 5,4 | 14,0 |

Can. J. Chem. Downloaded from www.nrcresearchpress.com by 210.87.254.105 on 09/06/12
For personal use only.



TABLEAU 4. (*Suite et fin*)

| No | R' | R | R'' | Y' | Y | δH-2 | δR' | δR | $\delta H_{\alpha'}$ | δR'' | δY' | δY | $J_{H\text{-}2—R'}$ | $J_{H\text{-}2—R}$ | $J_{R'—R}$ | $J_{H_{\alpha'}—R''}$ |
|---|---|---|---|---|---|---|---|---|---|---|---|---|---|---|---|---|
| **20***S*R*E* | H | $CH_3$ | H | $COOC_2H_5$ | CN | 2,30 à 2,90 m | | 1,50 d | 5,52 d | 7,37 d | 1,22 t, 4,15 q $J = 7,0$ | — | — | — | 5,4 | 14,0 |
| **20***R*R*Z* | H | $CH_3$ | H | $COOC_2H_5$ | CN | 2,30 à 2,90 m | | 1,50 d | 5,25 d | 6,43 d | 1,25 t, 4,20 q $J = 7,2$ | — | — | — | 5,4 | 9,0 |
| **20***S*R*Z* | H | $CH_3$ | H | $COOC_2H_5$ | CN | 2,60 à 2,80 m | | 1,45 d | 5,40 d | 6,55 d | 1,28 t, 4,15 q $J = 7,0$ | — | — | — | 5,0 | 9,0 |
| **21***R*R*E* | H | $CH_3$ | $COOCH_3$ | $COOCH_3$ | CN | 2,90 d | 2,65 dq | 1,47 d | 5,48 s | 3,70 s, 3,90 s | | — | 5,4 | — | 5,0 | — |
| **21***S*R*E* | H | $CH_3$ | $COOCH_3$ | $COOCH_3$ | CN | 2,50 à 2,90 m | | 1,35 d | 5,55 s | 3,70 s, 3,90 s | | — | — | — | 5,5 | — |
| **21***R*R*Z* | H | $CH_3$ | $COOCH_3$ | $COOCH_3$ | CN | 2,40 à 3,00 m | | 1,55 d | 6,28 s | 3,80 s, 3,90 s | | — | — | — | 5,4 | — |
| **21***S*R*Z* | H | $CH_3$ | $COOCH_3$ | $COOCH_3$ | CN | 3,05 d | 2,85 dq | 1,49 d | 6,42 s | 3,75 s, 3,85 s | | — | 3,0 | — | 5,2 | — |
| **22***R*R*E* | H | $C_6H_5$ | H | $COOC_2H_5$ | $COOC_2H_5$ | 3,50 m | 3,10 d | 7,33 m | 5,55 d | 7,60 d | 1,25 t, 0,95 t, 4,02 q, 3,92 q $J = 7,0$ | | 6,0 | — | — | 14,0 |
| **22***R*R*Z* | H | $C_6H_5$ | H | $COOC_2H_5$ | $COOC_2H_5$ | 3,55 d | 3,10 d | 7,18 m | 5,22 d | 6,62 d | 1,12 t, 0,89 t, 4,05 q, 3,93 q $J = 7,0$ | | 6,6 | — | — | 9,0 |
| **22***S*R*Z* | H | $C_6H_5$ | H | $COOC_2H_5$ | $COOC_2H_5$ | 3,57 d | 3,32 d | 7,25 m | 5,27 d | 6,55 d | 1,27 t, 4,20 q $J = 7,0$ | | 2,8 | — | — | 9,0 |
| **23***S*R*E* | H | $C_6H_5$ | $COOCH_3$ | $COOCH_3$ | $COOC_2H_5$ | 3,50 à 4,00 m | 3,18 d | 7,10 à 7,50 m | 5,45 s | 3,80 s, 3,64 s | | 1,28 t, 4,24 q $J = 7,0$ | 2,8 | — | — | — |
| **23***S*R*Z* | H | $C_6H_5$ | $COOCH_3$ | $COOCH_3$ | $COOC_2H_5$ | 3,50 à 4,00 m | | 7,10 à 7,50 m | 6,32 s | 3,70 s, 3,50 s | | 1,25 t, 4,15 q $J = 7,0$ | — | — | — | — |
| **24***R*R*Z* | H | $C_6H_5$ | H | $COOC_2H_5$ | CN | 3,55 d | 3,06 d | 7,30 à 7,50 m | 5,35 d | 6,05 d | 1,20 t, 4,15 q $J = 7,2$ | — | 5,6 | — | — | 9,0 |
| **25***S*R*E* | H | $C_6H_5$ | $COOCH_3$ | $COOCH_3$ | CN | 3,60 à 4,00 m | 3,13 d | 7,20 à 7,50 m | 5,61 s | 3,90 s, 3,78 s | | — | 2,8 | — | — | — |

Can. J. Chem. Downloaded from www.nrcresearchpress.com by 210.87.254.105 on 09/06/12
For personal use only.

1710, 1640; *Anal.* calc. pour $C_{11}H_{17}NO_4$: C 58,14, H 7,54, N 6,16, O 28,16; trouvé: C 57,82, H 7,57, N 6,15, O 28,48.

*Dérivé* ***16***E (***16***R*R*E/***16***S*R*E = *80:20)*: ir ($cm^{-1}$): 1740, 1725, 1640.

*Dérivé* ***16***S*R*Z: *Anal.* calc. pour $C_{12}H_{17}NO_6$: C 53,13, H 6,27, N 5,17, O 35,42; trouvé: C 52,65, H 6,41, N 5,07, O 35,41.

*Dérivé* ***17*** (***17***R*R*E/***17***R*R*Z = *50:50)*: ir ($cm^{-1}$): 1750, 1720, 1620; *Anal.* calc. pour $C_{16}H_{19}NO_4$: C 66,41, H 6,63, N 4,84, O 22,12; trouvé: C 65,78, H 6,64, N 4,67, O 22,26.

*Dérivé* ***19*** (***19***E/***19***Z = *40:60)*: ir ($cm^{-1}$): 1730, 1640, 1630.

*Dérivé* ***20*** (***20***R*R*E/***20***S*R*E/***20***R*R*Z/***20***S*R*Z = *60:30:5:5)*: ir ($cm^{-1}$): 2230, 1720, 1635.

*Dérivé* ***21***E (***21***R*R*E/***21***S*R*E = *70:30)*: ir ($cm^{-1}$): 2210, 1740, 1720, 1625; *Anal.* calc. pour $C_{10}H_{12}N_2O_4$: C 53,57, H 5,39, N 12,49, O 28,54; trouvé: C 53,26, H 5,43, N 12,46, O 28,79.

*Dérivé* ***23*** (***23***S*R*E/***23***S*R*Z = *10:90)*: ir ($cm^{-1}$): 1750, 1740, 1720, 1700, 1630, 1620.

*Dérivé* ***24***R*R*Z: ir ($cm^{-1}$): 2200, 1700, 1620.

*Dérivé* ***25***S*R*E: ir ($cm^{-1}$): 2200, 1720, 1680, 1610.

*Préparation des dérivés* ***12*** *et* ***18***

À une solution de 0,02 mol d'aziridine dans 20 mL de solvant on ajoute 0,02 mol de diméthyl-5,5 chloro-3 cyclohexène-2 one et un équivalent de triéthylamine. Le mélange réactionnel maintenu sous agitation magnétique est chauffé à 50°C (DMSO) ou à reflux (éthanol) durant 48 h. Il est traité par une solution aqueuse de chlorure de sodium et extrait trois fois à l'éther. La phase organique est séchée sur sulfate de magnésium puis concentrée.

*Dérivé* ***12***: purifié par chromatographie sur colonne (acétate d'éthyle); ir ($cm^{-1}$): 1730, 1590; *Anal.* calc. pour $C_{13}H_{19}NO_3$: C 65,74, H 8,01, N 5,90, O 20,25; trouvé: C 65,58, H 8,06, N 5,90, O 20,84; rmn $^1H$ ($CDCl_3$): Tableau 4; rmn $^1H$ ($CDCl_3$): Tableau 5.

*Dérivé* ***18R*R****: purifié par chromatographie sur colonne (éther de pétrole/acétate d'éthyle 50:50); ir ($cm^{-1}$): 1755, 1665, 1615; *Anal.* calc. pour $C_{14}H_{21}NO_3$: C 66,91, H 8,42, N 5,57, O 19,10; trouvé: C 66,98, H 8,41, N 5,62, O 18,90; rmn $^1H$ ($CDCl_3$): Tableau 4; rmn $^{13}C$ ($CDCl_3$): Tableau 5.

*Préparation du dérivé* ***26***

À 1,00 g (7 mmol) de phényl-3 cyano-2 aziridine en solution dans 10 mL d'acétonitrile sec, on ajoute 0,68 g (7 mmol) de propiolate d'éthyle. Le mélange réactionnel est porté à reflux durant trois jours. On évapore le solvant puis purifie par chromatographie sur colonne (éther de pétrole/acétate d'éthyle 70:30). On isole le pyrrole **26**: ir ($cm^{-1}$): 3350, 1740, 1710; rmn $^1H$ ($CDCl_3$): 1,20 (t, $COOCH_2CH_3$, $J$ = 7,0), 4,12 (q, $COOCH_2$), 6,65 (spectre AB, 2H, $J$ = 3,2), 7,10 à 7,70 (m, $C_6H_5$), 9,0 (s large, N—H); rmn $^{13}C$ ($CDCl_3$): 14,2q–59,6t–165,2s ($COOC_2H_5$), 112,1d–117,8d (CH=), 128,0–128,4–128,6–129,0 (m, $C_6H_5$), 132,3s–137,0s (=C<).

*Obtention des dérivés* ***27*** *et* ***28***

À 0,01 mol de phényl-3 benzoyl-2 aziridine en solution dans 10 mL de DMSO, on ajoute 0,01 mol de propiolate d'éthyle. Le mélange réactionnel est chauffé à 30°C durant 36 h. On ajoute de l'eau et extrait au benzène. La phase organique est lavée à l'eau, séchée sur sulfate de magnésium et concentrée. On purifie par chromatographie sur colonne (éther de pétrole/acétate d'éthyle 85:15). Deux produits sont isolés et identifiés aux pyrroles **27** et **28**.

Pyrrole **27**: $F$ = 166–167°C; rmn $^1H$ ($CDCl_3$): 1,15 (t, $COOCH_2CH_3$, $J$ = 7,0), 4,15 (q, $COOCH_2$), 7,00 à 8,00 (m, 11H); rmn $^{13}C$ ($CDCl_3$): 14,2q–60,1t–164,1s ($COOCH_2CH_3$), 114,7 (s, C=), 122,7 (d, CH=), 128,1–128,5–129,0–129,2–129,6–130,0–130,6–132,3 (m, $C_6H_5$), 137,5 (s, C=), 143,0 (s, C=), 185,1 (s, C=O).

Pyrrole **28**: rmn $^1H$ ($CDCl_3$): 1,21 (t, $COOCH_2CH_3$, $J$ = 7,0), 4,20 (q, $COOCH_2$), 7,20 à 7,80 (m, 11H); rmn $^{13}C$ ($CDCl_3$): 14,1–59,9–163,9 ($COOCH_2CH_3$), 188,1 (C=O), 117,0, 127,0, 127,4, 128,5, 128,9, 129,2, 129,7, 130,1, 131,2, 131,3, 133,5, 137,2.

*Isomérisation nucléophile des* N*-vinylaziridines*

À 1,00 g de *N*-vinylaziridine en solution dans 50 mL de diméthoxyéthane sec et fraichement distillé, on ajoute un équivalent d'iodure de sodium. Le mélange réactionnel, maintenu sous courant d'azote, est chauffé pendant un temps indiqué dans le Tableau 2. Aprés évaporation du solvant, le résidu est repris par 50 mL de chlorure de méthylène puis lavé à l'eau. Les extraits organiques sont séchés sur sulfate de magnésium puis concentrés. Le produit brut est analysé par rmn $^1H$; sa composition est donnée dans le Tableau 2.

*Isomérisation de l'aziridine* ***12***

Le dérivé **29** est purifié par chromatographie sur colonne (acétate d'éthyle): Rdt 43%; rmn $^1H$ ($CDCl_3$): Tableau 6.

*Isomérisation de l'aziridine* ***9***

Le dérivé **30***Z* est purifié par chromatographie sur colonne (éther de pétrole/acétate d'éthyle 70:30): Rdt 30%; ir ($cm^{-1}$): 3190, 1745, 1650; rmn $^1H$ ($CDCl_3$): Tableau 6.

*Isomérisation de l'aziridine* ***10***

Les composés **10***Z*, **31***E* et **32***E* sont séparés par chromatographie sur colonne (éther de pétrole/acétate d'éthyle 70:30).

**31***E*: Rdt 25%; ir ($cm^{-1}$): 3120, 1750, 1690, 1630; rmn $^1H$ ($CDCl_3$): Tableau 6; rmn $^{13}C$ ($CDCl_3$): Tableau 7.

**32***E*: Rdt 10%; ir ($cm^{-1}$): 3250, 1730, 1610: rmn $^1H$ ($CDCl_3$): 1,25 (t, $COOCH_2CH_3$, $J$ = 7,0), 4,20 (q, $COOCH_2$), 3,70 (m, $CH_2$—N), 3,65 (s, $COOCH_3$), 3,80 (s, $COOCH_3$), 4,50 (dd, CHI, $J$ = 6,0 et $J$ = 7,0), 5,25 (s, =CH), 8,60 (t, N—H, $J$ = 7,0); rmn $^{13}C$ ($CDCl_3$): 13,7q–62,1t ($OCH_2CH_3$), 50,9q ($OCH_3$), 52,8q ($OCH_3$), 163,7–170,0–170,2 (C=O), 19,3 (d, CHI), 49,0 (t, $CH_2$—N), 90,2 (d, =CH), 149,4 (s, N—C=); *Anal.* calc. pour $C_{11}H_{16}NO_6I$: I 32,99; trouvé: I 32,78.

*Synthèse du dérivé* ***44***

À 1 mmol de **32***E* en solution dans 5 mL d'acétone, on ajoute 3 équivalents de triéthylamine. Le mélange réactionnel est laissé à température ambiante durant 16 h. On évapore le solvant et on reprend au chlorure de méthylène. La phase organique est lavée à l'eau, séchée sur sulfate de magnésium puis concentrée. On purifie par chromatographie sur colonne (éther de pétrole/acétate d'éthyle 70:30) et isole le dérivé **44**: Rdt 20%; rmn $^1H$ ($CDCl_3$): 1,25 (t, $COOCH_2CH_3$, $J$ = 7,0), 4,15 (q, $COOCH_2$), 3,75s–3,87s ($COOCH_3$), 5,35 (d, =CH—$COOC_2H_5$, $J$ = 13,0), 5,62 (s, =CH—$COOCH_3$), 8,02 (t, N—CH=, $J$ = 13,0), 10,06 (d, N—H, $J$ = 13,0); rmn $^{13}C$ ($CDCl_3$): 14,4–60,0 ($OC_2H_5$), 51,7–53,3 ($OCH_3$), 162,4–167,6–169,4 (C=O), 96,7 (=CH—$COOC_2H_5$), 99,9 (=CH—$COOCH_3$), 141,5 (N—CH=), 144,1 (N—C=).

*Isomérisation de l'aziridine* ***11***

Les dérivés **33** et **34** sont séparés par chromatographie sur plaques préparatives (éther de pétrole/acétate d'éthyle 85:15). **33**: Rdt 30%; rmn $^1H$ ($CDCl_3$): Tableau 6; rmn $^{13}C$ ($CDCl_3$): Tableau 7. **34**: rmn $^1H$ ($CDCl_3$): 1,30 (t, $COOCH_2CH_3$, $J$ = 7,0), 4,20 (q, $COOCH_2$), 3,65 (s, $COOCH_3$), 4,00 à 4,40 (m, 3H), 4,68 (s, =CH), 7,30 (s, $C_6H_5$), 8,65 (s large, N—H); rmn $^{13}C$ ($CDCl_3$): 13,7–62,1 ($OC_2H_5$), 50,4 ($OCH_3$), 169,9–170,1 (C=O), 19,0 (CHI), 48,5 ($CH_2$—N), 87,9 (=CH—$COOCH_3$), 163,2 (N—CH=).

*Isomérisation de l'aziridine* ***18***R*R*

Le dérivé **35**(*E*+*Z*) est purifié par chromatographie sur plaques préparatives (éther de pétrole/acétate d'éthyle 50:50): Rdt 30%; ir ($cm^{-1}$): 3220, 1725, 1590; rmn $^1H$ ($CDCl_3$): Tableau

Can. J. Chem. Downloaded from www.nrcresearchpress.com by 210.87.254.105 on 09/06/12
For personal use only.



TABLEAU 5. Spectres de résonance magnétique nucléaire $^{13}C$ des *N*-vinylaziridines

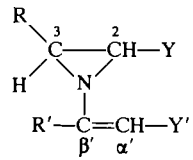

| No | R | R′ | Y′ | Y | δC-2 | δC-3 | $\delta C_{\alpha'}$ | $\delta C_{\beta'}$ | δR | δR′ | δY′ | δY |
|---|---|---|---|---|---|---|---|---|---|---|---|---|
| **9***E* | H | H | $COOC_2H_5$ | $COOC_2H_5$ | 36,4 d | 33,6 t | 107,5 d | 154,6 d | — | — | 14,2 q, 14,3 q, 60,1 t, 60,7 t, 166,9 s, 168,8 s | |
| **9***Z* | H | H | $COOC_2H_5$ | $COOC_2H_5$ | 39,6 d | 35,9 t | 104,5 d | 151,7 d | — | — | 14,2 q, 14,3 q, 59,7 t, 61,5 t, 165,2 s, 169,0 s | |
| **10***E* | H | $COOCH_3$ | $COOCH_3$ | $COOC_2H_5$ | 37,0 | 33,1 | 105,3 | 155,6 | — | 51,7, 52,9, 165,2, 165,7 | | 14,1, 61,8, 168,0 |
| **10***Z* | H | $COOCH_3$ | $COOCH_3$ | $COOC_2H_5$ | 39,5 d | 36,6 t | 108,0 d | 149,5 s | — | 51,5 q, 52,8 q, 165,4 s, 163,7 s | | 14,1 q, 61,5 t, 169,2 s |
| **12** | H | | | $COOC_2H_5$ | 36,1 | 33,2 | 111,7 | 168,4 | — | 28,3, 32,5, 42,4, 50,9, 198,9 | | 14,1, 61,8, 168,5 |
| **13***E* | H | H | $COOC_2H_5$ | CN | 23,2 d | 33,7 t | 109,7 d | 152,2 d | — | — | 14,2 q, 60,4 t, 166,2 s | 116,3 s |
| **13***Z* | H | H | $COOC_2H_5$ | CN | 26,7 d | 36,1 t | 106,6 d | 150,4 d | — | — | 14,2 q, 60,0 t, 164,9 s | 117,4 s |
| **14***E* | H | $COOCH_3$ | $COOCH_3$ | CN | 24,0 | 33,4 | 107,4 | 153,2 | — | 52,0, 53,3, 164,6, 165,2 | | 116,3 |
| **14***Z* | H | $COOCH_3$ | $COOCH_3$ | CN | 27,3 | 36,6 | 110,8 | 148,1 | — | 51,9, 53,2, 164,8, 162,9 | | 117,0 |
| **15**(*R*R** + *S*R**)*E* | $CH_3$ | H | $COOC_2H_5$ | $COOC_2H_5$ | 42,0, 43,1 | 40,9 | 106,6, 106,9 | 152,2, 155,0 | 12,9; 15,1 | — | 14,2, 59,8, 59,9, 166,9, 167,8, | 14,3, 61,3, 61,5 168,3 |
| **16***R*R*E* | $CH_3$ | $COOCH_3$ | $COOCH_3$ | $COOC_2H_5$ | 43,2 d | 41,1 d | 104,5 d | 156,3 s | 13,1 q | 51,7 q, 52,8 q, 165,3 s, 165,7 s | | 14,3 q, 61,5 t, 167,2 s |
| **16***S*R*E* | $CH_3$ | $COOCH_3$ | $COOCH_3$ | $COOC_2H_5$ | 43,0 | 41,3 | 104,7 | 152,6 | 15,3 | | | 14,3, 61,7, 167,5 |

Can. J. Chem. Downloaded from www.nrcresearchpress.com by 210.87.254.105 on 09/06/12
For personal use only.





TABLEAU 5. (*Suite et fin*)

| No | R | R′ | Y′ | Y | δC-2 | δC-3 | $\delta C_{\alpha'}$ | $\delta C_{\beta'}$ | δR | δR′ | δY′ | δY |
|---|---|---|---|---|---|---|---|---|---|---|---|---|
| **16***R*R*Z* | $CH_3$ | $COOCH_3$ | $COOCH_3$ | $COOC_2H_5$ | 45,8 | 43,8 | 108,5 | 150,6 | 12,9 | 51,5, 52,8, 165,0, 163,7 | | 14,4, 61,2, 168,3 |
| **17***R*R*E* | $CH_3$ | $C_6H_5$ | $COOCH_3$ | $COOC_2H_5$ | 46,2 | 43,9 | 101,9 | 165,7 | 13,5 | 126,9, 128,4, 128,6, 128,8, 129,7, 138,4 | 51,0, 164,5 | 14,4, 61,1, 168,7 |
| **18***R*R** | $CH_3$ | | | $COOC_2H_5$ | 41,3 d | 40,2 d | 110,0 d | 167,6 s | 13,3 q | 28,2 q, 28,3 q, 33,1s, 42,0 t, 50,9 t, 198,6 s | | 14,2 q, 61,4 t, 169,1 s |
| **20***S*R*Z* | $CH_3$ | H | $COOC_2H_5$ | CN | 31,5 | 44,9 | 106,9 | 148,4 | 16,6 | — | 14,3, 59,9, 165,1 | 116,3 |
| **20***S*R*E* | $CH_3$ | H | $COOC_2H_5$ | CN | 29,1 | 42,2 | 109,4 | 150,5 | 15,8 | — | 14,2, | |
| **20***R*R*Z* | $CH_3$ | H | $COOC_2H_5$ | CN | 29,6 | 40,0 | 106,1 | 150,0 | 14,8 | — | 60,0, 60,2 | 115,8, |
| **20***R*R*E* | $CH_3$ | H | $COOC_2H_5$ | CN | 32,5 | 42,0 | 108,6 | 152,8 | | — | 164,9, 166,3 | 116,4 |
| **21***S*R*Z* | $CH_3$ | $COOCH_3$ | $COOCH_3$ | CN | 32,3 | 45,5 | 110,4 | 146,9 | 16,8 | 51,7, 53,1, 163,2, 165,2 | | 116,1 |
| **21***R*R*E* | $CH_3$ | $COOCH_3$ | $COOCH_3$ | CN | 29,9 d | 40,4 d | 106,5 d | 153,9 s | | | | 115,5 s |
| **21***S*R*E* | $CH_3$ | $COOCH_3$ | $COOCH_3$ | CN | 29,6 d | 42,0 d | 107,3 d | 150,4 s | 15,0, 15,3, 15,5 | 51,9 q, 53,1 q, 163,2s, 164,6 s, 164,8 s, 165,3 s | | 115,3 s |
| **21***R*R*Z* | $CH_3$ | $COOCH_3$ | $COOCH_3$ | CN | 33,7 d | 42,8 d | 110,0 | 149,0 | | | | 116,6 |
| **23***S*R*Z* | $C_6H_5$ | $COOCH_3$ | $COOCH_3$ | $COOC_2H_5$ | 47,5 | 49,7 | 107,5 | 147,1 | 126,3, 128,1, 128,4, 136,7 | 51,3, 163,9, | 52,7, 165,6 | 14,1, 61,5, 167,7 |
| **24***R*R*Z* | $C_6H_5$ | H | $COOC_2H_5$ | CN | 36,6 | 47,4 | 106,8 | 149,8 | 127,0, 128,6, 129,0, 132,8 | — | 14,2, 60,3, 164,7 | 115,7 |
| **25***S*R*E* | $C_6H_5$ | $COOCH_3$ | $COOCH_3$ | CN | 40,0 | 46,6 | 97,1 | 145,2 | 128,6, 128,8, 129,1, 129,2, 129,7, 132,7 | 51,7, 163,0, | 53,2, 169,4 | 111,9 |

Can. J. Chem. Downloaded from www.nrcresearchpress.com by 210.87.254.105 on 09/06/12
For personal use only.





TABLEAU 6. Spectres de résonance magnétique nucléaire $^1H$ des énamines

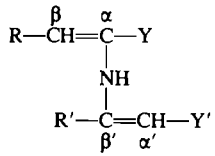

| | | | | | δ (ppm) | | | | | | | J(Hz) | | |
|---|---|---|---|---|---|---|---|---|---|---|---|---|---|---|
| No | R | Y | R′ | Y′ | N—H | R | $H_\beta$ | $H_{\alpha'}$ | R′ | Y′ | Y | $H_{\alpha'}$—R′ | $H_\beta$—R | R′—NH |
| **29** | H | $COOC_2H_5$ | 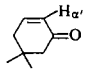 | | 7,02 s. large | 5,42 et 5,93 s. large | s. large | 5,66 s | 1,11 s (6H), 2,18 s (2H), 2,34 s (2H) | | 1,32 t, 4,30 q $J = 7,0$ | — | <0,5 | — |
| **30*Z*** | H | $COOC_2H_5$ | H | $COOC_2H_5$ | 9,92 d. large | 5,02 et 5,42 s. large | s large | 4,95 d | 7,00 dd | | 1,39 t, 1,32 t, 4,36 q, 4,25 q $J = 7,0$ | 9,0 | <0,5 | 13,0 |
| **31*E*** | H | $COOC_2H_5$ | $COOCH_3$ | $COOCH_3$ | 9,95 s. large | 4,92 et 5,60 s. large | s. large | 5,45 s | 3,80 s, 3,73 s | | 1,32 t, 4,25 q $J = 7,0$ | — | <0,5 | — |
| **33** | H | $COOC_2H_5$ | $C_6H_5$ | $COOCH_3$ | 10,00 s. large | 4,12 et 5,30 s. large | s. large | 5,00 s | 7,27 s | 3,74 s | 1,27 t, 4,27 q $J = 7,0$ | — | <0,5 | — |
| **35*E*** | $CH_3$ | $COOC_2H_5$ | 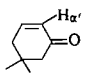 | | 7,25 d. large | 2,10 d | 6,22 q | 4,92 s | 1,07 s (6H), 2,13 s large, 2,30 s large, 2,35 s large | | 1,30 t, 4,18 q, 4,21 q $J = 7,0$ | — | 7,8 | — |
| **35*Z*** | | | | | | 1,75 d | 6,90 q | 5,17 s | | | | — | 7,0 | — |
| **36*EZ*** | $CH_3$ | $COOC_2H_5$ | H | $COOC_2H_5$ | 9,65 d. large | 2,09 d | 5,75 q | 4,72 d | 6,88 dd | 1,27 t, 4,13 q $J = 7,0$ | 1,39 t, 4,29 q | 9,0 | 7,0 | 13,6 |
| **36*ZZ*** | $CH_3$ | $COOC_2H_5$ | H | $COOC_2H_5$ | | 1,87 d | 6,25 q | 4,74 d | 7,00 dd | | | 9,0 | 7,5 | — |
| **37*EE*** | $CH_3$ | $COOC_2H_5$ | $COOCH_3$ | $COOCH_3$ | 9,45 s. large | 2,05 d | 5,95 q | 5,42 s | 3,75 s, 3,85 s | | 1,30 t, 4,20 q, $J = 7,0$ | — | 7,0 | — |
| **37*ZE*** | $CH_3$ | $COOC_2H_5$ | $COOCH_3$ | $COOCH_3$ | | 1,88 d | 6,51 q | 5,58 s | 3,72 s, 3,75 s | | 1,28 t, 4,18 q $J = 7,0$ | — | 7,6 | — |
| **38*ZZ*** | $C_6H_5$ | $COOC_2H_5$ | H | $COOC_2H_5$ | 9,73 d large | 7,20 à 7,60 m | 6,95 s | 4,73 d | 6,80 dd | 1,26 t, 1,39 t, 4,18 q, 4,35 q $J = 7,0$; $J = 7,5$ | | 8,6 | — | 13,0 |
| **41*EZ*** | $CH_3$ | CN | H | $COOC_2H_5$ | 9,60 d large | 2,00 d | 5,80 q | 4,75 d | 6,98 dd | 1,28 t, 4,12 q $J = 7,0$ | — | 8,5 | 7,4 | 12,0 |
| **41*ZZ*** | $CH_3$ | CN | H | $COOC_2H_5$ | 9,90 d large | 1,83 d | 5,58 q | 4,85 d | 7,05 dd | 1,28 t, 4,14 q $J = 7,0$ | — | 9,0 | 7,8 | 13,0 |

TABLEAU 7. Spectres de résonance magnétique nucléaire $^{13}C$ des énamines

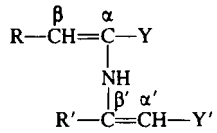

| No | R | Y | R′ | Y′ | δ (ppm) R | R′ | Y′ | Y | $C_\alpha$ | $C_\beta$ | $C_{\alpha'}$ | $C_{\beta'}$ |
|---|---|---|---|---|---|---|---|---|---|---|---|---|
| **31***E* | H | $COOC_2H_5$ | $COOCH_3$ | $COOCH_3$ | — | 51,3–52,7 164,2–163,8 | | 14,1, 61,8, 169,4 | 135,7 | 95,5 | 106,3 | 146,4 |
| **33** | H | $COOC_2H_5$ | $C_6H_5$ | $COOCH_3$ | — | 127,7, 128,6, 129,6, 134,5 | 50,9, 164,4 | 14,1, 61,8, 169,5 | 135,5 | 94,4 | 105,5 | 157,5 |
| **35**(*E*+*Z*) | $CH_3$ | $COOC_2H_5$ | | | 14,4 | 28,3, 32,8, 43,3, 50,3, 197,8 | | 14,2, 61,4, 164,3 | 135,5 135,6 | 99,1, 98,5 | 128,2, 127,3 | 161,6, 161,4 |
| **36***EZ* | $CH_3$ | $COOC_2H_5$ | H | $COOC_2H_5$ | 14,5 | — | 14,2–59,2–61,4 169,0–170,0– | | 130,0 | 86,7 | 116,3 | 142,7 |
| **36***ZZ* | $CH_3$ | $COOC_2H_5$ | H | $COOC_2H_5$ | 13,8 | | 170,3 | 170,6 | 130,9 | 88,0 | 120,3 | 143,7 |
| **37***EE* | $CH_3$ | $COOC_2H_5$ | $COOCH_3$ | $COOCH_3$ | 12,7 | 52,4–51,1 164,0–163,9 | | 14,1, 61,2, 170,5 | 131,0 | 91,3 | 125,0 | 148,3 |
| **37***ZE* | $CH_3$ | $COOC_2H_5$ | $COOCH_3$ | $COOCH_3$ | 13,8 | 52,7–50,8 169,8–164,4 | | 14,1, 61,0, 170,0 | 130,0 | 91,8 | 127,5 | 150,0 |
| **41***EZ* | $CH_3$ | CN | H | $COOC_2H_5$ | 14,6 | 14,4, 59,7 | | 112,7 | 114,1 | 88,6 | 121,4 | 143,4 |
| **41***ZZ* | $CH_3$ | CN | H | $COOC_2H_5$ | 12,0 | 170,2, 170,4 | | | 115,9 | 89,3 | 119,2 | |

6; rmn $^{13}C$ ($CDCl_3$): Tableau 7. Manipulation avec $[CH_3-(CH_2)_3]_4\overset{+}{N}, I^-$: on isole **35**: Rdt 40%. Manipulation avec KSCN: on isole **35***Z*: Rdt 15%.

*Isomérisation de l'aziridine **15***E

Le dérivé **36**(*EZ*+*ZZ*) est purifié par chromatographie sur colonne (hexane/éther 1:1+10% méthanol anhydre +10% acétate d'éthyle): Rdt 40%; rmn $^1H$ ($CDCl_3$): Tableau 6; rmn $^{13}C$ ($CDCl_3$): Tableau 7.

*Isomérisation de l'aziridine **16***

Les produits **16***R*R*Z*, **16***S*R*Z* et **37** sont séparés par chromatographie sur colonne (éther de pétrole/acétate d'éthyle 85:15). **37**(*ZE*+*EE*): Rdt 40%; rmn $^1H$ ($CDCl_3$): Tableau 6; rmn $^{13}C$ ($CDCl_3$): Tableau 7.

*Isomérisation de l'aziridine **22***R*R*Z

Le dérivé **38***ZZ* est purifié par chromatographie sur plaques préparatives (éther de pétrole/acétate d'éthyle 85:15): Rdt 25%; rmn $^1H$ ($CDCl_3$): Tableau 6.

*Isomérisation de l'aziridine **23***S*R*E

Un mélange des isomères *S*R*E* et *S*R*Z* de l'aziridine **23** est isolé par chromatographie sur plaques préparatives (éther de pétrole/acétate d'éthyle 85:15): Rdt 53%.

*Isomérisation de l'aziridine **19***

Un mélange des isomères *E* et *Z* de l'aziridine **19** est isolé par chromatographie sur colonne (éther de pétrole/acétate d'éthyle 70:30): Rdt 30%.

*Isomérisation de l'aziridine **14***E

Les composés **39** et **40** sont séparés par chromatographie sur plaques préparatives (éther de pétrole/acétate d'éthyle 70:30). **39**(*ZE*+*EE*): Rdt 15%; *F* = 84–85°C; ir ($cm^{-1}$): 3220, 3130, 2240, 1750, 1695, 1650; rmn $^1H$ ($CDCl_3$): 3,77s–3,80s–3,90s (6H, $COOCH_3$), 4,47 (d, 0,65H, *J* = 8,0), 4,81 (d, 0,35H, *J* = 13,0), 5,74s–5,79s (1H, =CH), 7,90 (d, 1H, *J* = 8,0), 7,98 (d, 1H, *J* = 13,0), 10,1 (s large, N—H); rmn $^{13}C$ ($CDCl_3$): 51,9–52,1–53,0–53,3–162,2–162,5–168,9–169,4 ($COOCH_3$), 73,4–76,7 (=CH—CN), 98,5–99,0 (=CH—$COOCH_3$), 141,8–142,5 (N—CH=), 144,5–145,5 (N—C=). **40**: rmn $^1H$ ($CDCl_3$): 3,76 (s, $COOCH_3$), 3,85 (s, $COOCH_3$), 3,80 (m, $CH_2$—N), 4,55 (dd, CHI, *J* = 6,5 et *J* = 7,6), 5,45 (s, =CH), 8,60 (t, N—H, *J* = 7,0).

*Isomérisation de l'aziridine **20***E

Le dérivé **41**(*ZZ*+*EZ*) est purifié par chromatographie sur colonne (éther de pétrole/acétate d'éthyle 85:15): Rdt 34%. On isole: **41***ZZ*: *F* = 63°C; rmn $^1H$ ($CDCl_3$): Tableau 6; rmn $^{13}C$ ($CDCl_3$): Tableau 7. **41**(*ZZ*+*EZ*): *F* = 55–60°C; ir ($cm^{-1}$): 3160, 2210, 1670, 1625; rmn $^1H$ ($CDCl_3$): Tableau 6; rmn $^{13}C$ ($CDCl_3$): Tableau 7.

*Isomérisation de l'aziridine **21***E

L'aziridine **21***R*R*Z*, le dérivé **42** et le produit iodé **43** sont séparés par chromatographie sur plaques préparatives (éther de pétrole/acétate d'éthyle 70:30). **21***R*R*Z*: *F* = 82°C; rmn $^1H$ ($CDCl_3$): Tableau 4; rmn $^{13}C$ ($CDCl_3$): Tableau 5. **42**: rmn $^1H$ ($CDCl_3$): Tableau 6. **43**: Rdt 20%; ir ($cm^{-1}$): 3820, 2250, 1750,

Can. J. Chem. Downloaded from www.nrcresearchpress.com by 210.87.254.105 on 09/06/12
For personal use only.

Can. J. Chem. Downloaded from www.nrcresearchpress.com by 210.87.254.105 on 09/06/12
For personal use only.

1650, 1630; rmn $^1$H ($CDCl_3$): 1,45d–1,55d ($CH_3$), 3,72s–3,90s ($COOCH_3$), 3,80 (m, 1H), 4,70 (d, 1H, $J$ = 4,0), 8,20 (dd, N—H); *Anal.* calc. pour $C_{10}H_{13}N_2O_4I$: I 36,08; trouvé: I 35,98.

*Action de la triéthylamine sur le dérivé iodé* ***43***

Une solution de 1 mmol de **43** et de 3 mmol de triéthylamine dans 5 mL d'acétone est agitée pendant 24 h à température ambiante. Aprés évaporation du solvant sous vide, le résidu est purifié par chromatographie sur colonne (éther de pétrole/acétate d'éthyle 85:15). On isole un mélange des isomères *S*R** et *R*R** de l'aziridine **21***E* identifiés par rmn $^1$H.

*Isomérisation thermique des* N*-vinylaziridines*

Un échantillon de 0,2 g de *N*-vinylaziridine pure est chauffé en tube scellé à une température et durant un temps indiqués dans le Tableau 3. Le produit brut est analysé par rmn $^1$H; sa composition est donnée dans le Tableau 3.

*Isomérisation de l'aziridine* ***16***R*R*E

Les composés **45***E*, **16***R*R*E* et **37***ZE* sont séparés par chromatographie sur colonne (benzène/acétate d'éthyle 85:15). **45***E*: Rdt 40%; rmn $^1$H ($CDCl_3$): 1,30 (t, $COOCH_2CH_3$, $J$ = 7,0), 4,23 (q, $COOCH_2$), 3,65s–3,92s ($COOCH_3$), 4,12 (s, N—$CH_2$), [4,40 (2H) et 6,45 (1H) spectre ABX, $CH_2$=CH)] 5,00 (s, =CH—$COOCH_3$); rmn $^{13}$C ($CDCl_3$): 14,1q–61,7t ($OC_2H_5$), 51,2q–53,1q ($OCH_3$), 167,2s–164,9s–166,8s (C=O), 48,4 (t, $CH_2$—N), 92,3 (d, =CH—$COOCH_3$), 94,3 (t, $CH_2$=), 134,5 (d, =CH—N), 150,8 (s, N—C=).

*Isomérisation de l'aziridine* ***21***

Le dérivé **46**, les isomères *S*R** et *R*R** de l'aziridine **21** et le dérivé **42** sont séparés par chromatographie sur colonne (éther de pétrole/acétate d'éthyle 85:15). **46***E*: Rdt 20%; $F$ = 105°C; rmn $^1$H ($CDCl_3$): 3,75s–3,98s ($COOCH_3$), 4,30 (s, N—$CH_2$), [4,50 (1H)–4,70 (1H)–6,38 (1H) (spectre ABX, $CH_2$=CH)], 5,18 (s, =CH—$COOCH_3$), rmn $^{13}$C ($CDCl_3$): 34,8 (t, $CH_2$—N), 51,6q–53,5q–164,2s–166,2s ($COOCH_3$), 95,4 (d, =CH—$COOCH_3$), 95,9 (t, $CH_2$=), 133,3 (d, =CH—N), 149,1 (s, N—C=). **42**: Rdt 10%.

*Isomérisation de l'aziridine* ***18***R*R*

Les dérivés **47** et **48** sont séparés par chromatographie sur colonne (acétate d'éthyle). **47**: Rdt 40%; ir ($cm^{-1}$): 1750, 1630, 1590; rmn $^1$H ($CDCl_3$): 1,12 (s, $(CH_3)_2$), 1,28 (t, $COOCH_2CH_3$, $J$ = 7,0), 4,25 (q, $COOCH_2$), 2,20 (s, 2H), 2,43 (s, 2H), 4,26 (s, N—$CH_2$), [4,30(1H)–4,50(1H)–6,80(1H) spectre ABX, $CH_2$=CH)], 5,30 (s, =CH); rmn $^{13}$C ($CDCl_3$): 14,2q–61,7t–167,7s ($COOC_2H_5$), 28,6 (q, $(CH_3)_2$), 33,2 (s, >C<), 40,8 (t, $CH_2$), 49,8 (t, $CH_2$), 47,9 (t, N—$CH_2$), 94,1 (t, $CH_2$=), 103,1 (d, =CH—CO), 134,2 (d, =CH—N), 159,2 (s, N—C=), 197,8 (s, C=O). **48**: Rdt 40%. $F$ = 85°C; ir ($cm^{-1}$): 3280, 1760, 1660, 1610; rmn $^1$H ($CDCl_3$): 1,10 (s, $(CH_3)_2$), 1,30 (t, $COOCH_2CH_3$, $J$ = 7,0), 4,25 (q, $COOCH_2$), 2,15 (s, $CH_2$), 2,30 (s, $CH_2$), 3,85 (d, N—$CH_2$, spectre AB), 6,10 (t large, N—H); rmn $^{13}$C ($CDCl_3$): 14,1–61,8–169,2 ($COOCH_2CH_3$), 28,3 ($(CH_3)_2$), 32,8 (>C<), 43,1 ($CH_2$), 44,3 (N—$CH_2$), 50,3 ($CH_2$), 96,5 (=CH), 162,4 (N—C=), 197,1 (C=O).


1. H. C. VAN DER PLAS. Ring transformation of heterocycles. Vol. 1. Academic Press, London et New-York. 1973.
2. (*a*) H. W. HEINE, M. E. FETTER et E. M. NICHOLSON. J. Am. Chem. Soc. **81**, 2202 (1959); (*b*) H. W. HEINE, W. G. KENYON et E. M. JOHNSON. J. Am. Chem. Soc. **83**, 2570 (1961); (*c*) H. W. HEINE. Angew. Chem. Int. Ed. Engl. **10**, 528 (1962) (*d*) H. W. HEINE, D. C. KING et L. A. PORTLAND. J. Org. Chem. **31**, 2662 (1966); (*e*) H. W. HEINE et M. S. KAPLAN. J. Org. Chem. **32**, 3069 (1967).
3. (*a*) P. E. FANTA et E. N. WALSH. J. Org. Chem. **30**, 3574 (1965); (*b*) J. Org. Chem. **31**, 59 (1966); (*c*) I. J. BURNSTEIN, P. E. FANTA et B. S. GREEN. J. Org. Chem. **35**, 4084 (1970).
4. R. D. GUTHRIE et D. MURPHY. J. Chem. Soc. 3828 (1965).
5. T. A. FOGLIA, L. M. GREGORY et G. MAERKER. J. Org. Chem. **35**, 3779 (1970).
6. D. HAIDUKEWYCH et A. I. MEYERS. Tetrahedron Lett. 3031 (1972).
7. J. W. LOWN, T. ITOH et N. ONO. Can. J. Chem. **51**, 856 (1973).
8. D. A. TOMALIA, N. D. OJHA et B. P. THILL. J. Org. Chem. **34**, 1400 (1969).
9. I. Y. POSTOVSKII, E. I. GRINBLAT et L. F. TREFILOVA. J. Gen. Chem. USSR, **31**, 363 (1961).
10. J. E. DOLFINI. J. Org. Chem. **30**, 1298 (1965).
11. A. PADWA et L. HAMILTON. Tetrahedron Lett. 4363 (1965).
12. (*a*) W. E. TRUCE et D. G. BRADY. J. Org. Chem. **31**, 3543 (1966); (*b*) W. E. TRUCE et L. D. MARKLEY. J. Org. Chem. **35**, 3275 (1970); (*c*) W. E. TRUCE et D. W. ONKEN. J. Org. Chem. **40**, 3200 (1975).
13. R. HUISGEN, B. GIESE et H. HUBER. Tetrahedron Lett. 1883 (1967).
14. (*a*) E. WINTERFELDT et H. PREUSS. Angew. Chem. Int. Ed. Engl. **4**, 689 (1965); (*b*) Chem. Ber. **99**, 450 (1966); (*c*) E. WINTERFELDT et J. M. NELKE. Chem. Ber. **101**, 2381 (1968).
15. T. SASAKI, T. YOSHIOKA et K. SHOJI. J. Chem. Soc. C, 1086 (1969).
16. J. C. CHALCHAT, F. THERON et R. VESSIERE. Bull. Soc. Chim. Fr. 711 (1970).
17. (*a*) A. NIEDERHAUSER, A. FREY et M. NEUENSCHWANDER. Helv. Chim. Acta, **56**, 944 (1973); (*b*) M. NEUENSCHWANDER et P. BIGLER. Helv. Chim. Acta, **56**, 959 (1973).
18. M. A. CALCAGNO et E. E. SCHWEIZER. J. Org. Chem. **43**, 4207 (1978).
19. (*a*) H. W. WHITLOCK et G. L. SMITH. Tetrahedron Lett. 1389 (1965); (*b*) J. Am. Chem. Soc. **89**, 3600 (1967).
20. W. E. TRUCE et M. L. GORBATY. J. Org. Chem. **35**, 2113 (1970).
21. J. C. CHALCHAT, F. THERON et R. VESSIERE. Bull. Soc. Chim. **12**, 4486 (1970).
22. W. REID et A. H. SCHMIDT. Justus Liebigs Ann. Chem. 1863 (1975).
23. (*a*) G. CASINI, F. CLAUDI, M. GRIFANTINI et S. MARTELLI. J. Heterocycl. Chem. **11**, 377 (1974); (*b*) I. ANTONINI, F. CLAUDI, G. CRISTALLI, M. GRIFANTINI et S. MARTELLI. J. Heterocycl. Chem. **17**, 181 (1980); (*c*) J. Heterocycl. Chem. **18**, 399 (1981).
24. D. A. ARCHER et B. W. SINGER. J. Chem. Soc. Perkin Trans. I, 2484 (1976).
25. A. KUMAR, H. ILA et H. JUNJAPPA. J. Chem. Soc. Chem. Commun. 592 (1976).
26. W. D. RUDORF. Tetrahedron, **36**, 1791 (1980).
27. T. FUKUNAGA. J. Am. Chem. Soc. **94**, 3242 (1972).
28. Y. NOMURA, N. HATANAKA et Y. TAKEUCHI. Chem. Lett. 901 (1976).
29. T. AGAWA, M. ISHIKAWA, M. KOMATSU et Y. OHSHIRO. Chem. Lett. 335 (1980).
30. A. HASSNER, B. A. BELINKA, M. HABER et P. MUNGER. Tetrahedron Lett. 1863 (1981).
31. (*a*) N. H. CROMWELL et H. HOEKSEMA. J. Am. Chem. Soc. **71**, 708 (1949); (*b*) N. H. CROMWELL et G. D. MERCER. J. Am. Chem. Soc. **79**, 3819 (1957).
32. A. LOPEZ. Thèse de Docteur-Ingénieur, Toulouse, 1974.
33. M. ELMEKKI ATTIA. Thèse de Docteur-Ingénieur, Clermont-Ferrand, 1978.
34. R. M. ROBERTS, R. G. LANDOLT, R. N. GREENE et E. W. HEYER. J. Am. Chem. Soc. **89**, 1404 (1967).
35. Y. GELAS-MIALHE, R. HIERLE et R. VESSIERE. J. Heterocycl. Chem. **11**, 347 (1974).

36. A. PADWA, D. DEAN, A. MAZZU et E. VEGA. J. Am. Chem. Soc. **95**, 7168 (1973).
37. Y. GELAS-MIALHE, R. HIERLE et R. VESSIERE. Bull. Soc. Chim. Fr. 709 (1974).
38. P. B. WOLLER et N. H. CROMWELL. J. Heterocycl. Chem. **5**, 579 (1968).
39. J. A. DEYRUP. J. Org. Chem. **34**, 2724 (1969).
40. F. TEXIER et R. CARRIE. Bull. Soc. Chim. Fr. 4119 (1971).
41. J. W. LOWN et M. H. AKTHAR. Can. J. Chem. **50**, 2236 (1972).
42. U. SCHMIDT, J. HAÜSLER, E. ÖHLER et H. POISEL. Progress in the chemistry of organic natural products. Vol. 37. *Edité par* L. Zechmeister, W. Herz, H. Grisebach et G. W. Kirby. Springer-Verlag, Vienne, New York. 1979. pp. 251–327.
43. (*a*) C. SHIN, M. MASAKI et M. OTHA. J. Org. Chem. **32**, 1860 (1967); (*b*) J. E. BALDWIN, S. B. HABER, C. HOSKINS et L. I. KRUSE. J. Org. Chem. **42**, 1239 (1977).
44. (*a*) H. POISEL et U. SCHMIDT. Angew. Chem. Int. Ed. Engl. **15**, 294 (1976); (*b*) H. POISEL et U. SCHMIDT. Chem. Ber. **108**, 2547 (1975); (*c*) A. J. KOLAR et R. K. OLSEN. Synthesis, 457 (1977).
45. C. SHIN, Y. YONEZAWA et J. YOSHIMURA. Chem. Lett. 1095 (1976).
46. Y. OZAKI, T. IWASAKI, H. HORIKAWA, M. MIYOSHI et K. MATSUMOTO. J. Org. Chem. **44**, 391 (1979).
47. J. D. M. HERSCHIED, H. P. H. SCHOLTEN, M. W. TIJHUIS et H. C. J. OTTENHEIJM. J. R. Neth. Chem. Soc. **100**, 73 (1981).
48. T. MORIYA, K. MATSUMOTO et M. MIYOSHI. Synthesis, 915 (1981).
49. R. D. CLARK et C. H. HEATHCOCK. J. Org. Chem. **41**, 636 (1976).
50. K. BURZIN et K. ENDERER. Angew. Chem. Int. Ed. Engl. **11**, 151 (1972).
51. K. D. GUNDERMANN et G. HOLTMANN. Chem. Ber. **91**, 160 (1958).
52. A. FUERST, E. KYBURZ et S. MAJNONI. Chem. Abstr. **59**, 11424b (1963).
53. J. EXPERT. Mémoire CNAM, Clermont-Ferrand, 1980.
54. F. G. WEBER et C. BANDLOW. Z. Chem. **13**, 467 (1973).
55. P. L. SOUTHWICK et D. R. CHRISTMAN. J. Am. Chem. Soc. **74**, 1886 (1952).

Can. J. Chem. Downloaded from www.nrcresearchpress.com by 210.87.254.105 on 09/06/12
For personal use only.

# The crystal structure of benzenediazonium tetrafluoroborate, $C_6H_5N_2^+ \cdot BF_4^-$ [1]

MIROSLAW CYGLER AND MARIA PRZYBYLSKA

*Division of Biological Sciences, National Research Council of Canada, Ottawa, Ont., Canada K1A 0R6*

AND

RICHARD MACLEOD ELOFSON

*Alberta Research Council, 11315-87th Ave., Edmonton, Alta., Canada T6G 2C2*

Received May 6, 1982

MIROSLAW CYGLER, MARIA PRZYBYLSKA, and RICHARD MACLEOD ELOFSON. Can. J. Chem. **60**, 2852 (1982).

Benzenediazonium tetrafluoroborate, $C_6H_5N_2^+ \cdot BF_4^-$, crystallizes in space group $P2_1/a$ with unit cell dimensions $a = 17.347(2)$, $b = 8.396(1)$, $c = 5.685(1)$ Å, $\beta = 92.14(1)°$, $Z = 4$. The structure was solved by direct phasing methods using the program SHELX 76. The parameters were refined by full-matrix least-squares to a final $R = 0.063$ for 1346 observed reflections. The bond lengths and angles agree very well with those of Rømming for benzenediazonium chloride. The C—N and N≡N bond lengths are 1.415(3) and 1.083(3) Å, respectively, and the bonds of the benzene ring do not show any significant differences as they vary from 1.371(5) to 1.383(4) Å. There are three N···F close contacts of ≤ 2.84 Å and the positive charge appears to be shared between the nitrogen atoms.

MIROSLAW CYGLER, MARIA PRZYBYLSKA et RICHARD MACLEOD ELOFSON. Can. J. Chem. **60**, 2852 (1982).

Le tétrafluoroborate de benzènediazonium $C_6H_5N_2^+ \cdot BF_4^-$ cristallise dans le groupe d'espace $P2_1/a$ avec des dimensions de maille de $a = 17,347(2)$, $b = 8,396(1)$, $c = 5,685(1)$ Å, $\beta = 92,14(1)°$, $Z = 4$. On a résolu la structure par la méthode de phase directe utilisant le programme SHELX 76. On a ajusté les paramètres par la méthode des moindres carrés (matrice complète) jusqu'à une valeur finale de $R = 0,063$ pour 1346 réflexions observées. Les longueurs de liaison et les angles s'accordent bien avec ceux de Rømming relatifs au chlorure de benzènediazonium. Les longueurs de liaison C—N et N≡N sont respectivement de 1,415(3) et 1,083(3) Å et les liaisons du cycle benzène ne présentent aucune différence significative puisqu'elles varient de 1,371(5) à 1,383(4) Å. Il y a trois liaisons N···F très rapprochées ≤ 2,84 Å et la charge positive semble être partagée entre les atomes d'azote.

[Traduit par le journal]

## Introduction

The representation of aryl diazonium salts by resonance forms has concerned organic chemists for over one hundred years (1). Discussion has centred on the relative contributions of canonical structures **1**, **2**, and **3**.

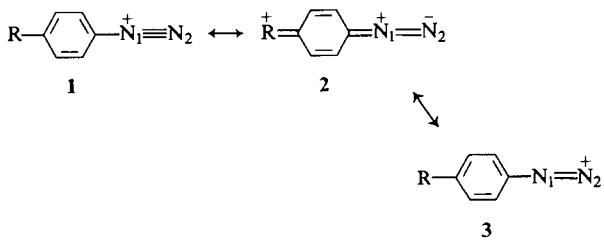

**1** **2** **3**

The dominance of structure **1** for the ground state of benzenediazonium chloride was established by Rømming in 1963 (2, 3). His and subsequent X-ray investigations showed that the C(1)—N(1) bond length corresponds to that of a C—N single bond and N(1)—N(2) to a triple bond. Similar results were obtained for a number of substituted diazonium salts with complex anions. In *p*-benzenebisdiazonium tetrachlorozincate (4) in addition to N≡N and N—C bonds of 1.09(1) and 1.42(1) Å, respectively, there is an appreciable deviation from hexagonal symmetry of the benzene ring showing the "antiquinoid" geometry. There is therefore no evidence in these structures for the contribution of **2**.

Nevertheless Hammett correlations of certain other parameters such as infrared stretching frequencies (5) and redox properties (6) have continued to use $\sigma^+$ constants rather than $\sigma^p$ constants to obtain good results. These procedures suggested that contributions from the form **2** were important to describe the properties of these compounds.

In the original study of Rømming the interaction of the chlorine ion with hydrogen of the aromatic ring was indicated by the short H(2)...Cl distance of only 2.5 Å, one half of an Ångstrom unit less than the sum of the van der Waals radii of these atoms. Also in our laboratory the polarographic half-wave reduction potential of the aryl diazonium chlorides has been found to be up to 500 mV more negative than that of the tetrafluoroborate, which we interpret as evidence of complex formation (7). Since such an interaction could conceivably have altered some structural parameters it was decided to carry out X-ray analyses of some aryl diazonium tetrafluoroborate salts including *p*-diethylamino benzenediazonium tetrafluoroborate as the low accur-

[1]NRCC No. 20552.

0008-4042/82/222852-04$01.00/0

©1982 National Research Council of Canada/Conseil national de recherches du Canada

Can. J. Chem. Downloaded from www.nrcresearchpress.com by 210.87.254.42 on 09/06/12
For personal use only.

Can. J. Chem. Downloaded from www.nrcresearchpress.com by 210.87.254.42 on 09/06/12
For personal use only.

acy study of a related compound (8) gave longer N—N and N—C bond lengths than expected.

## Experimental

Crystal data are as follows:

$C_6H_5N_2^+ \cdot BF_4^-$ fw = 191.9

Monoclinic, $P2_1/a$, $a$ = 17.347(2), $b$ = 8.396(1), $c$ = 5.685(1) Å, $\beta$ = 92.14°(1), $V$ = 827.4 Å$^3$, $Z$ = 4, $D_x$ = 1.54, $D_m$ = 1.53 g cm$^{-3}$ (by flotation in toluene and $CCl_4$ mixture). $F(000)$ = 384, $\mu$ (Cu K$\bar{\alpha}$) = 14.6 cm$^{-1}$.

The data were collected at room temperature with the Nonius CAD-4 procedures. Three prisms, crystallised from acetonitrile, had to be used as they deteriorated on exposure to light and X-rays. Two of them were almost spherical with diameters varying from 0.32 to 0.37 mm and the third one was 0.24 × 0.27 × 0.34 mm. Reflections in the range $1° < \theta \leq 75°$ were measured using the $\omega$–2$\theta$ technique for $\Delta\omega = (1.20 + 0.15 \tan\theta)°$, with a maximum scan time of 150 s. Two reflections were used as intensity monitors every 100 min of exposure time. Their intensities changed slowly during the first 20 to 30 h of exposure to X-rays and much more rapidly on further irradiation of the crystal. Only data collected in that first period were accepted. A decrease in intensity tolerated with each crystal did not exceed 4%.

The three sets of data were merged to produce 1757 unique reflections out of which 1346 (77%) were observed above threshold of $2\sigma(I_{net})$. The net intensities, after scaling, were corrected for Lorentz and polarization effects but not for absorption.

The atomic coordinates were found by direct methods and refined by full-matrix minimization of $\Sigma w(|F_o| - |F_c|)^2$ using the program system SHELX 76 (9).

The weighting function applied was

$$w = 16.64/(\sigma^2|F_o| + 0.00015\,|F_o|^2)$$

where $\sigma(|F_o|)$ is derived from counting statistics.

The H atoms were located on a difference map, carried out when $R$ was 0.09. The atomic scattering factors for C, N, B, and F were taken from International tables for X-ray crystallography (10) and those for H from Stewart, Davidson, and Simpson (11). Refinement with anisotropic thermal parameters for non-hydrogen atoms and isotropic for H atoms reduced $R$ to a final value of 0.063 ($R_w$ = 0.075) for the 1346 observed reflections. The final difference map showed distribution in the range −0.32 to 0.45 e Å$^{-3}$.

Some calculations were carried out with the NRC crystallographic computer programs by Ahmed, Hall, Pippy, and Huber (12).

Final positional and thermal parameters are presented in Table 1.[2]

## Discussion

The bond lengths and angles of both ions are shown in Fig. 1. The angle C(1)—N(1)—N(2) in the present structure is 179.5(3)° and the C—H bond lengths are in the range 0.89 to 1.01(4) Å.

The benzenediazonium ion has an approximate plane of symmetry passing through the N(2), N(1), C(1), and C(4) atoms as is indicated by the similarity of appropriate bonds and angles (see Fig. 1). Table 2 shows the comparison of the averaged geometry of the benzene ring in the present compound and in benzenediazonium chloride (3, 13), where the molecule was situated on a two-fold axis. The bond lengths and angles of the fluoroborate salt agree better with those from the more accurate analysis of benzenediazonium chloride, carried out at −160°C, with the exception of the three averaged bonds of the ring. However, the small differences shown by the bonds of the benzene ring in the tetrafluoroborate salt are not statistically signifi-

TABLE 1. Fractional coordinates with esd's in parentheses (× 10$^4$ for non-hydrogen atoms and × 10$^3$ for H) and isotropic temperature factors × 10$^3$ ($U_{eq} = 1/3(U_{11} + U_{22} + U_{33})$)

| Atom | $x$ | $y$ | $z$ | $U_{eq}$ or $U$(Å$^2$) |
|---|---|---|---|---|
| B | 1709(2) | 2928(4) | 4962(6) | 56(2) |
| F(1) | 1871(1) | 2425(3) | 2729(3) | 87(2) |
| F(2) | 1399(1) | 1640(3) | 6104(4) | 102(2) |
| F(3) | 2384(1) | 3401(4) | 6009(5) | 127(2) |
| F(4) | 1188(1) | 4107(3) | 4822(6) | 126(2) |
| N(1) | 2902(1) | 4627(3) | 442(4) | 54(1) |
| N(2) | 2361(1) | 5266(4) | 517(5) | 74(2) |
| C(1) | 3610(1) | 3796(3) | 323(4) | 48(1) |
| C(2) | 4034(2) | 4070(4) | −1645(5) | 61(2) |
| C(3) | 4728(2) | 3271(4) | −1717(6) | 68(2) |
| C(4) | 4958(2) | 2257(4) | 63(7) | 67(2) |
| C(5) | 4506(2) | 2002(4) | 1977(6) | 66(2) |
| C(6) | 3897(2) | 2278(4) | 2138(5) | 59(2) |
| H(2) | 386(2) | 482(4) | −296(6) | 70(9) |
| H(3) | 504(2) | 345(4) | −316(6) | 75(10) |
| H(4) | 540(2) | 173(5) | 6(6) | 76(10) |
| H(5) | 466(2) | 126(4) | 315(6) | 72(10) |
| H(6) | 374(2) | 263(4) | 326(5) | 52(7) |

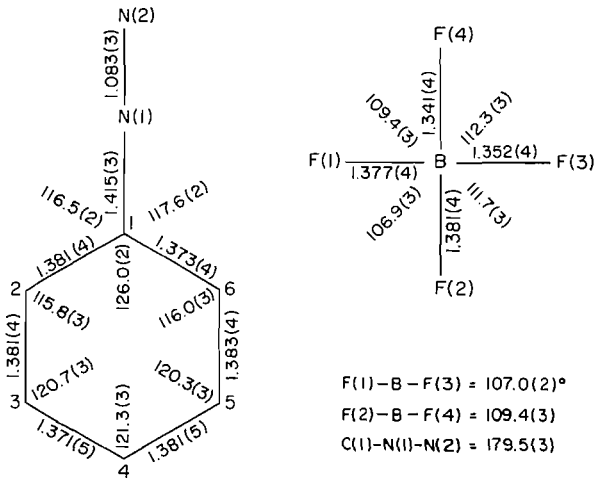


FIG. 1. Bond lengths (Å) and valency angles (deg) in benzenediazonium tetrafluoroborate and their esd's in parentheses.

[2]Tables of observed and calculated structure factors and of temperature factors are available, at a nominal charge, from the Depository of Unpublished Data, CISTI, National Research Council of Canada, Ottawa, Ont., Canada K1A 0S2.

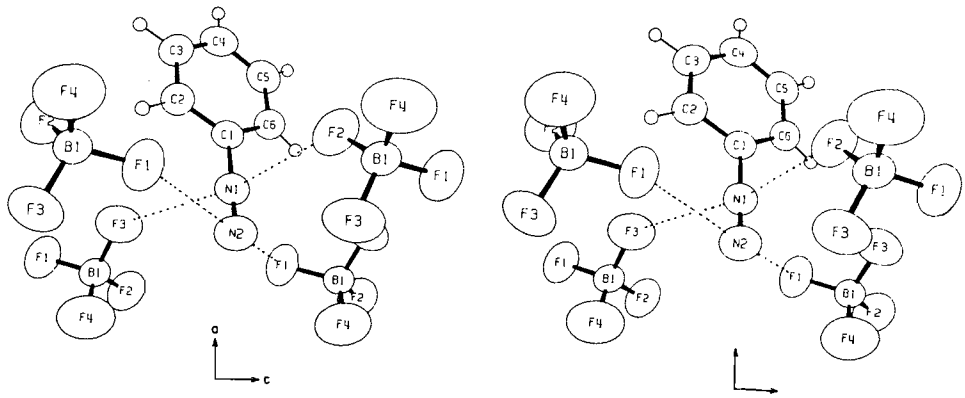


FIG. 2. A stereoscopic view of benzenediazonium cation with surrounding $BF_4^-$ groups. The closest N to F contacts are shown by broken lines.

TABLE 2. Bond lengths and angles in benzenediazonium tetrafluoroborate and in benzenediazonium chloride (esd's in parentheses)

| | Length | | |
|---|---|---|---|
| | | $C_6H_5N_2Cl$† | |
| Bond | $C_6H_5N_2BF_4$* | *a* | *b* |
| N(1)—(N(2) | 1.083(3) Å | 1.097(6) Å | 1.093(2) Å |
| N(1)—C(1) | 1.415(3) | 1.385(9) | 1.410(2) |
| C(1)—C(2) | 1.377(4) | 1.374(8) | 1.396(2) |
| C(2)—C(3) | 1.382(4) | 1.383(10) | 1.392(2) |
| C(3)—C(4) | 1.376(5) | 1.376(8) | 1.395(2) |
| C(1)—C(4) | 2.682(4) | 2.689(8) | |

| | Angle | | |
|---|---|---|---|
| | | $C_6H_5N_2Cl$† | |
| Bonds | $C_6H_5N_2BF_4$* | *a* | *b* |
| C(1)—C(2)—C(3) | 115.9(3) | 117.6(7) | 115.9(2) |
| C(2)—C(3)—C(4) | 120.5(3) | 119.8(7) | 120.6(2) |
| C(3)—C(4)—C(5) | 121.3(3) | 121.7(7) | 121.1(2) |
| C(6)—C(1)—C(2) | 126.0(2) | 124.8(6) | 126.1(2) |

*The averaged values for the symmetry related pairs.
†*a*, ref. 3, data collected at room temperature; *b*, ref. 13, investigation at −160°C.

cant and since they do not appear in the low temperature study of the chloride salt, they may not be real. In both compounds the C(1)···C(4) distance is shorter than in benzene.

The bond lengths and angles reported for benzenediazonium tribromide (14) are also very similar. However, they are not included in Table 2 as, having been derived by two-dimensional methods, they are less accurate.

The endocyclic torsion angles of the benzene ring vary from 0 to 2.1(0.5)° and the ring deviates significantly from planarity ($\chi^2 = 26.6$). The C(2) and C(6) atoms are at 0.010(3) and 0.008(3) Å, respectively, from the plane calculated for the six atoms of the ring, and C(1) with C(4) are on the opposite side with distances of −0.006(2) and −0.005(4) Å. The N(1) and N(2) atoms were found at −0.016(2) and −0.023(3) Å from the plane.

The packing of $BF_4^-$ ions surrounding the benzenediazonium cation is shown in the stereoscopic drawing by ORTEP (15) in Fig. 2. Each nitrogen atom makes four short contacts <3.1 Å with F of each of the four anions. These distances are listed in order of increasing values:

| Atoms | Distance (Å) | Atoms | Distance (Å) |
|---|---|---|---|
| N(1)···F(2) | 2.829(3)* | N(2)···F(1) | 2.841* |
| N(1)···F(3) | 2.837(4)* | N(2)···F(1) | 2.941(4)* |
| N(1)···F(1) | 2.912(3) | N(2)···F(3) | 3.005(4) |
| N(1)···F(1) | 2.996(3) | N(2)···F(2) | 3.056(3) |

The two shortest contacts of each group, marked by asterisks, are depicted in Fig. 2 by broken lines. They include the three contacts which are slightly shorter than the sum of van der Waals radii (2.85 Å).

The close approaches of F to both N atoms indicate that the electron density of the N(1)—N(2) triple bond may be displaced towards the N(1) atom resulting in sharing of the positive charge between the two nitrogen atoms. Similar observations were made concerning the structures of benzenediazonium chloride and benzenediazonium tribromide. It seems therefore that in addition to the main resonance form **1**, shown in "Introduction", the form **3** makes some contribution to the structure of the cation. There is no evidence of **2**.

In benzenediazonium chloride and tribromide derivatives the shortest of the halogen to nitrogen distances are those to the outer nitrogen N(2). In the present structure those to N(1) are the shortest. Since the small differences between N(1)···F and N(2)···F closest contacts depend not only on the charge distribution but also on the geometrical arrangement, it is not possible to derive on their basis which nitrogen is likely to have a greater

Can. J. Chem. Downloaded from www.nrcresearchpress.com by 210.87.254.42 on 09/06/12
For personal use only.

positive charge. It is interesting, however, that the N(1)···F closest approaches agree with the results of the CNDO/2 calculations carried out by Rømming (16) for the diazonium ion and for benzenediazonium surrounded by four negative fluorine ions, as the positive charges on N(1) turned out to be slightly higher (+0.31 and +0.33) than on N(2) (+0.18 and +0.25).

The N···F distances can be correlated with the differences in the B—F bond lengths. Since F(2) makes the closest approach to N of 2.829 Å and F(1) has four close contacts, B—F(2) and B—F(1) are expected to be the longest. They are 1.381(4) and 1.377(4) Å respectively, vs. 1.352(4) Å for B—F(3). F(4)···N(2) is appreciably longer (3.384(4) Å) and accordingly B—F(4) is the shortest of the four bonds (1.341(4) Å).

The closest F···H approaches are F(2)···H(2) = 2.38(3) Å and F(2)···H(3) = 2.42(3) Å. They are slightly shorter than the sum of van der Waals radii of 2.55 Å and they indicate that very weak C—H···F hydrogen bonds may be present. C(2)—H(2) and C(3)—H(3) are 1.01(3) and 1.00(4) Å, respectively, C(2)—H(2)···F(2) = 174.1(2.7)° and C(3)—H(3)···F(2) = 133.6(2.6)°. Since the redox potential of benzenediazonium tetrafluoroborate is normal and virtually identical to that of the perchlorate salt, it must be assumed that the bond lengths of the benzene ring are unaffected by the weak H···F interactions. Even the much stronger H(2)···Cl interactions in benzenediazonium chloride do not seem to have any such effect.


1. H. Zollinger. Azo and diazo chemistry. Interscience, New York. 1961.
2. C. Rømming. Acta Chem. Scand. **13**, 1260 (1959).
3. C. Rømming. Acta Chem. Scand. **17**, 1444 (1963).
4. A. Mostad and C. Rømming. Acta Chem. Scand. **22**, 1259 (1968).
5. Y. Ishino and Y. T. Hirashima. Kagaku tu Kagyo, **52**, 384 (1978).
6. R. M. Elofson and F. F. Gadallah. J. Org. Chem. **34**, 854 (1969).
7. R. M. Elofson and J. K. Laidler. In preparation.
8. Ya. M. Nesterova and M. A. Porai-Koshits. Zh. Strukt. Khim. **12**, 108 (1971).
9. G. M. Sheldrick. SHELX. Program for crystal structure determination. University of Cambridge, England. 1976.
10. International tables for X-ray crystallography. Vol. IV. Kynoch Press, Birmingham. 1974. p. 72.
11. R. F. Stewart, E. R. Davidson, and W. T. Simpson. J. Chem. Phys. **42**, 3175 (1965).
12. F. R. Ahmed, S. R. Hall, M. E. Pippy, and C. P. Huber. NRC crystallographic programs for the IBM/360 system, Accession Nos. 133–147; J. Appl. Crystallogr. **6**, 309 (1973).
13. C. Rømming. The chemistry of the diazonium and diazo groups. *Edited by* S. Patai. J. Wiley and Sons, New York. 1978. p. 98.
14. O. Andresen and C. Rømming. Acta Chem. Scand. **16**, 1882 (1962).
15. C. K. Johnson. ORTEP. Report ORNL-3794, revised. Oak Ridge National Laboratory, Tennessee.
16. C. Rømming. Acta Chem. Scand. **26**, 523 (1972).


Can. J. Chem. Downloaded from www.nrcresearchpress.com by 210.87.254.42 on 09/06/12
For personal use only.

# The photochemistry of $Ru(bpy)_3^{2+}$ in basic medium

JIN-GOU XU[1] AND GERALD B. PORTER[2]

*Department of Chemistry, University of British Columbia, Vancouver, B.C., Canada V6T 1Y6*

Received May 26, 1982

JIN-GOU XU and GERALD B. PORTER. Can. J. Chem. **60**, 2856 (1982).

$Ru(bpy)_3^{2+}$ is photodecomposed in 0.3 *M* NaOH with $\phi = 3.3 \times 10^{-4}$. With methyl viologen also present, electron transfer quenching of the luminescence is accompanied by formation of the one electron reduction product of methyl viologen, $MV^+$. The $Ru(bpy)_3^{3+}$ formed in the corresponding oxidation is rapidly reduced by either $OH^-$ or $MV^+$ to Ru(II).

JIN-GOU XU et GERALD B. PORTER. Can. J. Chem. **60**, 2856 (1982).

Le $Ru(bpy)_3^{2+}$ se décompose photochimiquement dans une solution à 0,3 *M* de NaOH avec $\phi = 3{,}3 \times 10^{-4}$. En présence de viologène de méthyle, l'arrêt de la luminescence par transfert d'électron s'accompagne de la formation d'un produit de réduction à un électron du viologène de méthyle, $MV^+$. Le $Ru(bpy)_3^{3+}$ qui se forme lors de l'oxydation correspondante est rapidement réduit soit par $OH^-$ ou $MV^+$ en Ru(II).

[Traduit par le journal]

There are a number of reports (1–7) on the photodecomposition of solutions containing the complex ion tris(bipyridyl)ruthenium(II), $Ru(bpy)_3^{2+}$, especially in non-aqueous solvents (2, 3, 6, 7). It is stable to light in acetonitrile (8) and at room temperature in 0.1 *M* HCl (1, 2). Decomposition yields are generally small except that, in chlorinated non-polar solvents, Gleria, Minto, Beggiato, and Bortolus (3) found a value of ca. 0.2. The product of photodecomposition is generally a disubstituted derivative, with one bipyridine ligand replaced by two acido ligands, two solvent molecules, or one of each. Watts, Harrington, and Van Houten (5) give evidence for a one-ended bipyridine; however, Durham *et al.* (8) state that it is only an unstable intermediate which reacts in minutes to produce the stable bis complex. In aqueous solution, $Ru(bpy)_3^{2+}$ photodecomposes, with small quantum yield only at pH ≃ 0 at room temperature or in less acid solutions at 60°C.

Okura, Kim-Thuan, and Takeuchi (9) recently described the sensitized photoreduction of methyl viologen (1,1′-dimethyl-4,4′-bipyridinium dichloride) or $MV^{2+}(Cl^-)_2$ by $Ru(bpy)_3^{2+}$ in an anaerobic 0.3 *M* NaOH solution. They established that back reaction of the reduced form of $MV^{2+}$ with the oxidized Ru(III) complex competes with reduction of Ru(III) by hydroxide. Thus, the concentration of the reduced form, $MV^+$, builds up in solution, as evidenced by the blue colour. Okura *et al.* (9) reported that $Ru(bpy)_3^{2+}$ is not used up and that $MV^{2+}$ is slowly regenerated in the dark.

We report here several further aspects of this interesting reaction.

## Experimental

$Ru(bpy)_3Cl_2 \cdot 6H_2O$ was purified by recrystallization from distilled water. Other chemicals were reagent grade and were used without further purification. Lifetimes and quantum yields were measured by techniques we have previously described (10), using a nitrogen laser/detector combination and ferrioxalate actinometry, respectively. Solutions were deoxygenated prior to irradiation by bubbling argon through for 20 min in a Zwickel flask (10). For some experiments, to ensure that air was not leaking into the cuvette, it was placed in a box through which nitrogen was flowed.

The concentrations of $Ru(bpy)_3^{2+}$ and $MV^+$ were monitored at 453 and 620 nm, respectively, in a Cary 11 Spectrophotometer, with intermittent irradiation at 436 nm from a 100 W PEK mercury lamp. The incident intensity was ca. $5 \times 10^{15}$ quanta $s^{-1}$. In experiments using nitrogen flushing around the cuvette, the concentration of $MV^+$ was measured continuously by absorption at 620 nm in situ, with a quartz halogen lamp, a double monochromator, and a photomultiplier. The resulting signal of % transmission was recorded as a function of time.

## Results

The lifetime of the emitting state of $Ru(bpy)_3^{2+}$ was found to be independent of pH in deoxygenated solution: 640 ns in 0.3 *M* NaOH solution versus 650 ns in neutral aqueous solution. Continuous irradiation in deoxygenated 0.3 *M* NaOH results in a small decrease in the maximum absorbance of $Ru(bpy)_3^{2+}$ at 453 nm. The quantum yield for disappearance of the substrate is $3.3 \times 10^{-4}$. Although we have not characterized the product of this reaction, we do not find a spectrum of $Ru(bpy)_2(OH)_2$, of $Ru(bpy)_2(H_2O)_2^{2+}$, or of $Ru(bpy)_2(OH)H_2O^+$ after irradiation (11).

$MV^{2+}$ quenches the emitting state of $Ru(bpy)_3^{2+}$ in a near diffusion-controlled process. We find a linear Stern–Volmer relation between ln τ and $[MV^{2+}]$, with $k_q = 8.8 \times 10^8\ M^{-1}\ s^{-1}$, at $[Ru(bpy)_3^{2+}] = 5.0 \times 10^{-5}\ M$. In 0.3 *M* NaOH solution,

[1]On leave from Xiamen University, Xiamen, Fujian, China.
[2]To whom all correspondence should be addressed.

0008-4042/82/222856-03$01.00/0
©1982 National Research Council of Canada/Conseil national de recherches du Canada

Can. J. Chem. Downloaded from www.nrcresearchpress.com by 210.87.254.105 on 09/06/12
For personal use only.

Can. J. Chem. Downloaded from www.nrcresearchpress.com by 210.87.254.105 on 09/06/12
For personal use only.

the quenching constant is $1.2 \times 10^9 M^{-1} s^{-1}$. Other data with neutral salts added to the solution show that this is just an ionic strength effect on the quenching constant for like-charged donor and acceptor.

On irradiation of a solution containing $1.3 \times 10^{-3} M$ $MV^{2+}$, which is sufficient to half-quench the emitting state of $Ru(bpy)_3^{2+}$, the reduced form of methyl viologen, $MV^+$, is formed with an initial quantum yield of 0.029. The quantum yield decreases gradually with extent of reaction as noted by Okura *et al.* (9). On extended exposure, the concentration of $MV^+$ reaches a constant value.

After irradiation in the dark, $[MV^+]$ decreases rapidly at first and then remains constant when the cell is flushed outside with nitrogen gas. The Zwickel flask technique for deoxygenation with argon leaves the cell with a ground glass joint, which is lightly greased, and two Teflon plug stopcocks. In this cell in air, $MV^+$ decays slowly in the dark, as found by Okura *et al.* (9). When the cell is protected from air leaking in, the initial decay amounts to about 5% of the $MV^+$ present in the solution after irradiation. Subsequent to this, $[MV^+]$ remains constant for more than a day. However, the concentration of $MV^+$ remaining does vary from one run to another, and is in the range of $1–2 \times 10^{-5} M$.

$Ru(bpy)_3^{2+}$ is photodecomposed in solution containing $MV^{2+}$ with approximately the same quantum yield as that in the absence of $MV^{2+}$.

Addition of air after irradiation bleaches the blue colour of $MV^+$ instantly. However, some residual absorption remains from other decomposition products, one of which is tentatively identified as the monomethyl derivative of $MV^{2+}$: 1-methyl-4-(pyridyl)pyridinium chloride (12).

When, in addition to $MV^{2+}$, EDTA is added to the solution ($10^{-3} M$ EDTA, $0.3 M$ NaOH, $5 \times 10^{-5} M$ $Ru(bpy)_3^{2+}$, and $1.3 \times 10^{-3} M$ $MV^{2+}$), the blue colour of $MV^+$ is developed much more rapidly. In the initial stages of the reaction, the quantum yield for formation of $MV^+$ is $0.42 \pm 0.10$. After irradiation is stopped, $[MV^+]$ remains constant unless air is admitted.

## Discussion

The lifetime data show that there is no major interaction of hydroxide to quench the MLCT emitting state of $Ru(bpy)_3^{2+}$. Nevertheless, there is a reaction that leads to a small amount of substrate decomposition. It occurs whether or not $MV^{2+}$ is present, but the quantum yield measurement in the presence of $MV^{2+}$ is subject to too large an uncertainty because of overlapping spectra to decide if the quantum yield decreases in proportion to the quenching of the emitting state.

The formation of $MV^+$ on irradiation of $Ru(bpy)_3^{2+}$ in the presence of $MV^{2+}$ at high pH can be interpreted by reactions [1] to [5]:

[1] $Ru(bpy)_3^{2+} + h\nu \rightarrow {}^*Ru(bpy)_3^{2+}(MLCT)$

[2] ${}^*Ru(bpy)_3^{2+} \rightarrow Ru(bpy)_3^{2+} (+ h\nu)$

[3] ${}^*Ru(bpy)_3^{2+} + MV^{2+} \rightarrow Ru(bpy)_3^{3+} + MV^+$

[4] $Ru(bpy)_3^{3+} + MV^+ \rightarrow Ru(bpy)_3^{2+} + MV^{2+}$

[5] $Ru(bpy)_3^{3+} + OH^- \rightarrow Ru(bpy)_3^{2+} + \ldots.$

Reactions [2] and [3] are well known (13) and account for the quenching of the phosphorescence by $MV^{2+}$. In acid solution, reaction [3] occurs so rapidly that no net reaction can be observed except for the transient absorption in flash photolysis experiments (13) due to $MV^+$ as well as the concomitant bleaching of the absorption of $Ru(bpy)_3^{2+}$ itself. The electron transfer process of reaction [3] seems to be the only bimolecular quenching mode of the emitting MLCT state; energy transfer to $MV^{2+}$ cannot occur as it has no low-lying electronic states available.

At high pH, reaction [4] competes favourably with reaction [3], at least in the initial stages of the irradiation before $MV^+$ builds up. Reaction [4] has been studied by Creutz and Sutin (14) using stopped-flow spectrophotometry. The Ru(II) complex is formed in a first order reaction with, in the pH range near 13:

$$k_{obs} = 148[OH^-] + 138[OH^-]^2 \ s^{-1}$$

at 25°C and $\mu = 1 M$

The reaction products are complex: aside from $Ru(bpy)_3^{2+}$, five other eluents are found in the reacted solution by ion exchange chromatography (14). Molecular oxygen is an important product at pH 10, but amounts to only 2% of the oxidized material at pH 13.6.

Analysis of this mechanism using steady-state concentrations for ${}^*Ru(bpy)_3^{2+}$ and $Ru(bpy)_3^{3+}$ gives:

$$[6] \quad \phi_{MV^+} = \left\{\frac{\alpha k_3[MV^{2+}]}{k_2 + k_3[MV^{2+}]}\right\} \times \left\{\frac{k_5[OH^-]}{k_4[MV^+] + k_5[OH^-]}\right\}$$

in which the second order term in $[OH^-]$ has been absorbed in $k_5$ for simplicity. The factor $\alpha$ is included to recognize the fact that the electron

Can. J. Chem. Downloaded from www.nrcresearchpress.com by 210.87.254.105 on 09/06/12
For personal use only.

transfer may have less than unit efficiency because of "primary recombination" (15), that is, back electron transfer before the donor and acceptor can diffuse apart more than ca. one molecular diameter. According to eq. [6], the quantum yield for $MV^+$ formation decreases as the amount of $MV^+$ increases in accord with the experimental data. With $[MV^+] \simeq 10^{-5}\ M$, and assuming that $k_4 = 1.2 \times 10^9\ M^{-1}\ s^{-1}$, equal to $k_2$, eq. [6] requires that the quantum yield be reduced to less than 1% of its initial value, again consistent with the data found. The initial value of $\phi_{MV^+}$ is 0.029; however, it is likely that the initial buildup of $[MV^+]$ is too fast for our slow response apparatus to follow. Indeed, if the initial quantum yield were appreciably higher than 0.029, inadvertent exposure to stray light would reduce the apparent initial yield.

In order to investigate this point, experiments with added EDTA were carried out. The reaction

[7] $Ru(bpy)_3^{3+} + EDTA \rightarrow Ru(bpy)_3^{2+} + ....$

must be added to the mechanism. Equation [6] becomes

$$[8]\quad \phi_{MV^+} = \left\{\frac{\alpha k_3[MV^{2+}]}{k_2 + k_3[MV^{2+}]}\right\} \times \left\{\frac{k_5[OH^-] + k_7[EDTA]}{k_4[MV^+] + k_5[OH^-] + k_7[EDTA]}\right\}$$

The initial quantum yield is 0.42. Assuming that $k_7$ is also diffusion controlled, eq. [8] indicates that $\phi_{MV^+}$ does not depend on $[MV^+]$, in agreement with experiment. The concentration of $MV^{2+}$ is such as to provide exactly 50% quenching of the emitting state, thus the first term in eq. [8] is $0.5\alpha$. It follows from this value and the experimental quantum yield that $\alpha$ is one, within experimental error, and that the quenching of the luminescence is entirely a result of the electron transfer of reaction [3], without back transfer.

In the experiment without added EDTA, the small apparent initial quantum yield for $MV^+$ formation of 0.029, if caused by a trace of $MV^+$, represents $[MV^+] = 6 \times 10^{-7}\ M$. This is near the lower limit of our detection.

In the post irradiation period, $[MV^+]$ decreases rapidly at first. We suggest that either dioxygen or some other oxidant formed in the reaction of $Ru(bpy)_3^{3+}$ with $OH^-$ in minor amount reacts with $MV^+$. Once this small amount of oxidizing material is consumed, $MV^+$ is stable. With EDTA present, Ru(III) is reduced only by EDTA, other oxidizing materials are not formed, and there is no initial decay of $MV^+$.

**Acknowledgements**

The support of the Natural Sciences and Engineering Council of Canada is gratefully acknowledged. Further support was received (J.-G.X.) from the Government of the Peoples Republic of China and Xiamen University.

1. J. Van Houten and R. J. Watts. J. Am. Chem. Soc. **98**, 4853 (1976).
2. P. E. Hoggard and G. B. Porter. J. Am. Chem. Soc. **100**, 1457 (1978).
3. M. Gleria, F. Minto, G. Beggiato, and D. Bortolus. J. Chem. Soc. Chem. Commun. 285 (1978).
4. J. Van Houten and R. J. Watts. Inorg. Chem. **17**, 3381 (1978).
5. R. J. Watts, J. S. Harrington, and J. Van Houten. Adv. Chem. Ser. Am. Chem. Soc. Washington, D.C. **168**, 57 (1978).
6. K. M. Wallace and P. E. Hoggard. Inorg. Chem. **18**, 2934 (1979).
7. K. M. Wallace and P. E. Hoggard. Inorg. Chem. **19**, 2141 (1980).
8. R. C. Young, J. K. Nagle, and T. J. Meyer. Unpublished work quoted in B. Durham, J. L. Walsh, C. L. Carter, and T. J. Meyer. Inorg. Chem. **19**, 860 (1980).
9. I. Okura, N. KimThuan, and M. Takeuchi. Inorg. Chim. Acta, **53**, L149 (1981); **57**, 257 (1982).
10. G. B. Porter and J. Van Houten. Inorg. Chem. **19**, 2903 (1980).
11. B. Durham, S. R. Wilson, D. J. Hodgson, and T. J. Meyer. J. Am. Chem. Soc. **102**, 600 (1980).
12. J. A. Farrington, A. Ledwith, and M. F. Stam. J. Chem. Soc. Chem. Commun. 259 (1969).
13. C. R. Bock, T. J. Meyer, and D. G. Whitten. J. Am. Chem. Soc. **96**, 4710 (1974).
14. C. Creutz and N. Sutin. Proc. Nat. Acad. USA, **72**, 2858 (1975).
15. R. M. Noyes. J. Am. Chem. Soc. **77**, 2042 (1955).

# Determination of low specific surface areas of minerals and oxides by gas–solid chromatography[1]

PETER R. TREMAINE,[2] ALFRED G. WIKJORD, AND JACQUES C. LEBLANC

*Atomic Energy of Canada Ltd., Whiteshell Nuclear Research Establishment, Pinawa, Man., Canada R0E 1L0*

Received January 15, 1982

PETER R. TREMAINE, ALFRED G. WIKJORD, and JACQUES C. LEBLANC. Can. J. Chem. **60**, 2859 (1982).

Gas–solid chromatography is shown to provide a method for measuring the specific surface area of non-porous particulate mineral or oxide samples in the range 0.005 to 0.5 $m^2 g^{-1}$ with precision as high as ±10%. Mesitylene is a convenient sorbate and was found to occupy an area of 71 ± 5 $Å^2$ per molecule on silicate surfaces, by calibration with glass particles having well defined surface geometries. The rather low values obtained for the *C* parameter, when fitting retention volume data to the BET equation, suggest that the area occupied by mesitylene may be affected by the surface on which it is adsorbed. Hydrocarbon contaminants are a major interference. No specialized instrumentation is required.

PETER R. TREMAINE, ALFRED G. WIKJORD et JACQUES C. LEBLANC. Can. J. Chem. **60**, 2859 (1982).

On montre que la chromatographie solide fournit une méthode de mesurer la surface spécifique de particules non poreuses d'échantillons de minéraux ou d'oxydes de l'ordre de 0,005 à 0,5 $m^2 g^{-1}$ avec une précision pouvant atteindre ±10%. Le mésitylène est un excellent produit de sorption et on a trouvé qu'il occupe une surface de 71 ± 5 $Å^2$ par molécule sur des surfaces de silice en utilisant comme référence les particules de verre ayant des surfaces géométriques bien définies. Les valeurs plutôt faibles obtenues pour le paramètre *C*, lorsqu'on insère les données du volume de rétention dans l'équation BET, suggèrent que l'aire occupée par le mésitylène peut être affectée par la surface sur laquelle il est absorbé. Les contaminants hydrocarbonés constituent la principale interférence. Aucun instrument spécial n'est requis.

[Traduit par le journal]

## Introduction

While instrumentation for determining powder surface areas in excess of 1 $m^2 g^{-1}$ is well developed, there remains a need for simple reliable techniques capable of measuring much lower specific areas. This need is particularly acute for experimentalists studying mineral dissolution kinetics (see, for example, ref. 1) and the sorption of radionuclides by rocks such as granite (2, 3) since particle diameters in excess of 10 μm, i.e. surface areas lower than 0.5 $m^2 g^{-1}$, are often required. Very low surface areas can be measured by static techniques using xenon adsorption (4) and by commercial flow systems using nitrogen or other rare gas adsorption with special cells (5, 6). These methods require dedicated, rather specialized equipment.

The use of inverse gas–solid chromatography (GSC) to measure sorption isotherms on non-porous materials is well established (7–9). The method is appealing because it is fast and uses conventional gas chromatographs, which are readily available. Briefly, the material to be studied is packed into a chromatographic column where it acts as the stationary phase. An organic "probe" molecule is then injected into the inert carrier gas stream. Under the correct conditions (10), the volume of carrier gas required to elute the injection from the column is related to the thermodynamic partition of the probe between the mobile and stationary phases. As a result, the adsorption isotherm can be calculated from the retention volumes and elution peak heights corresponding to injections of different sizes.

Inverse chromatography has been used to measure the surface areas of inorganic salts (11) and polymer fibers (8, 9, 12–14) using large probe molecules near room temperature. Thibault and co-workers (15) measured low specific surface areas of metals using methane as a probe molecule at liquid nitrogen temperatures. The purpose of our study was to investigate the practical lower limit of usefulness of the method when used for determining the surface areas of minerals and oxides, by measuring the sorption of the large organic molecules that are convenient to use near room temperature.

## Experimental methods

A Hewlett Packard 7620 A gas chromatograph equipped with flame ionization detectors and a sub-ambient temperature controller was used. The columns containing the mineral samples were prepared by simply pouring the sample into 0.6 or 1.2 cm id copper tubing, contained at one end by a Swagelok connection fitted with stainless steel mesh. Prior to use the tubing was washed with trichloroethylene and dried under vacuum. The coiled columns were mounted vertically in the chromatograph to minimize the risk of channelling. Temperature was controlled by the air bath of the chromatograph and monitored using calibrated chromel–alumel thermocouples

[1]AECL 7577.

[2]Present address: Oil Sands Research Department, Alberta Research Council, 11315-87 Avenue, Edmonton, Alta., Canada T6G 2C2.

0008-4042/82/222859-04$01.00/0

©1982 National Research Council of Canada/Conseil national de recherches du Canada

Can. J. Chem. Downloaded from www.nrcresearchpress.com by 210.87.254.40 on 09/06/12
For personal use only.

Can. J. Chem. Downloaded from www.nrcresearchpress.com by 210.87.254.40 on 09/06/12
For personal use only.

fixed to the column. Variations along the length of the column were less than 0.3°C. In order to minimize back pressure, the flowrate of the nitrogen carrier gas was maintained near the lower limit of the detector, about 32 $cm^3$ $min^{-1}$ at room temperature, and was determined by a bubble flow meter. Column backpressure was monitored using a mercury manometer.

Sorption isotherms were obtained by making a series of sorbate injections ranging in volume from 10 μL to less than 1 nL and correcting the volume for the pressure drop (8, 10). The carrier gas hold up time in the column was determined by injecting a small amount of methane with the sorbate. Corrected net retention volumes, $V_N$, and sorbate partial pressures, $p$, corresponding to the maxima of elution peaks of different sizes were plotted so that $q$, the surface concentration of adsorbate (mol $g^{-1}$) would be obtained as a function of $p$ by integrating the plot in the usual way (8–10, 12–14).

Glass spheres (Chromatographic Specialities) and glass fibers (Corning) were used to test the method because of their well defined geometries. Their geometric areas were estimated by averaging the diameters of at least 25 spheres or fibers, as measured from electron micrographs, and their surface roughness, defined as the ratio of the area accessible to the sorbate molecule to the geometric area, was assumed to be unity (4). Screened samples of sintered magnetite (1), 60/80 mesh, and fractured labradorite, 40/60 mesh, were used to test the method on more realistic mineral samples. Mesitylene (Polyscience Corp.) and *n*-decane (Aldrich Gold Label) were used as the sorbates without purification.

For comparison with the GSC results using mesitylene and decane, surface areas were also measured by nitrogen physisorption at −195°C using a Quantasorb surface area analyzer (Quantachrome Corp., Syosset, NY). The data were obtained by Particle Data Laboratories Ltd. (in Elmhurst, IL) and the surface areas were calculated from a 5 point BET plot. Immediately prior to measurement, samples were degassed at 110°C for 4 h in a $H_2$ stream of 20 $cm^3$ $min^{-1}$ which flowed through the Quantasorb cell. The reproducibility of the method was adversely affected by small desorption peaks and baseline disturbances due to thermal diffusion in the sample vessel (6).

## Results

Adsorption isotherms obtained from the chromatograph were plotted in the form $p/p_0$ vs. $(p/p_0)/[q(1 - p/p_0)]$, in order to fit the result to the Brunauer–Emmett–Teller expression (16)

$$[1] \quad \frac{p/p_0}{q(1 - p/p_0)} = \frac{1}{q_m C} + \left(\frac{C - 1}{q_m C}\right)\frac{p}{p_0}$$

Here $p_0$ is the vapour pressure of the decane or mesitylene sorbate, taken from the API tables (17), $q_m$ is the monolayer capacity which we wish to obtain, and $C$ is an adjustable parameter. Typical plots are shown in Fig. 1. Values of $q_m$ and $C$ were obtained by least-squares fits of data in the range $0.05 < p/p_0 < 0.35$ to straight lines, as shown in the figure. No evidence of non-linearity was observed in this range. The $C$ values for sorption on magnetite, labradorite, and a few of the glass samples ranged from 4 to 6, typical of hydrocarbon sorption on dry oxygen-rich organic surfaces (12–14) and slightly lower than those obtained for higher surface area minerals by sorption/desorption methods (18). Many of the glass samples yielded the low results ($C$ = 2 to 3) which are expected when organic molecules are adsorbed onto hydrated surfaces (19).

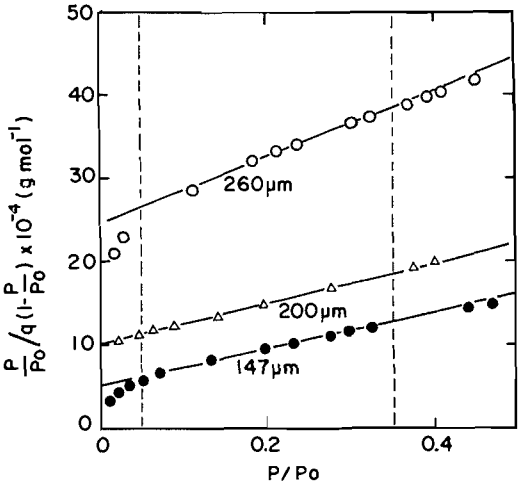


FIG. 1. Typical BET plots obtained from the adsorption of organic sorbates on 260 μm, 200 μm, and 147 μm diameter glass beads at 34.9, 25.2, and 64.7°C, respectively: △, mesitylene; ○, decane. Dashed lines show the limit of linearity assumed for the fit.

Since GSC is a dynamic method, it is important to ensure that the criteria for obtaining an equilibrium sorption isotherm from the peak maxima method are met (10). Sorption effects on the flow rate are minimal for these small injection volumes. The peak maxima throughout any set of injection volumes lay on a common envelope, although some peak rounding occurred, due to the very small retention volumes. Lowering the linear flow rate by increasing the column diameter from 0.6 to 1.2 cm did not affect the values obtained for the specific monolayer coverage within the precision of the data. Likewise, changing the temperature by ±20°C within the range −5 to 80°C and increasing the length of the column from 70 to 180 cm had no measurable effect. The area of the empty column, ≈ 0.03 $m^2$ for a column 70 cm long and 0.6 cm id, was routinely determined by the exact procedures outlined above for columns containing sample. The empty column area was subtracted from that obtained when the sample was present.

During the course of this work, two or three samples were inadvertently contaminated with traces of hydrocarbon from a compressed air line. These yielded anomalously high values of $q_m$ by comparison with duplicate, uncontaminated samples. The contaminants could be apparently removed by heating the column to 200°C, since this

TABLE 1. Comparison of specific surface areas by $N_2$ and mesitylene adsorption

| Sample | Specific surface area/$m^2\ g^{-1}$ | | |
|---|---|---|---|
| | $N_2$ (Quantasorb) | Mesitylene (GSC) | $N_2$ area / GSC area |
| Glass beads (200 μm) | 0.08† | 0.013±0.002 | 6 |
| Sintered magnetite | 0.17±0.10* | 0.033±0.004 | 5 ±2 |
| Labradorite fragments | 0.13±0.06* | 0.08 ±0.01 | 1.6±0.7 |

*Error limits are the spread between duplicate samples. The value reported is the mean.
†One sample only.

invariably produced a large irregular detector response, and subsequent measurements using the same column gave results in agreement with the uncontaminated samples.

The specific surface area of a sample can be calculated from $q_m$ if the area occupied by each mole of sorbate can be determined. We determined this by assuming that the glass bead and fiber samples had no roughness on the scale of the sorbate molecules so that the monolayer capacity could be considered to occupy an area equal to the geometric area of the surface (4). The calibration was done using sorption isotherms from the fiber samples since these had the largest specific surface areas, low back pressure and, hence, yielded the most precise monolayer capacities. The resulting area occupied per mesitylene molecule was 71 ± 5 Å². A comparison of several mesitylene and decane monolayer capacities from the same samples yielded the value 87 ± 5 Å² for decane. The correlation between geometric area and the areas measured using these values is shown in Fig. 2 for several samples of glass beads whose specific areas are much lower than the fiber samples. In all cases, GSC and geometric areas agree to within the statistical scatter.

Dorris and Gray (14) have pointed out that mesitylene is ideal for surface area measurements since it is a disk-like molecule with very limited conformational freedom. Indeed, our value of 71 Å²/molecule is very close to the value of 67 Å²/molecule which is obtained if the mesitylene monolayer can be described by close packed disks of radius 4.5 Å², consistent with the molecular dimensions of mesitylene lying flat. We believe this value is typical of the untreated silica surfaces studied here, but note that it may not be appropriate for other material since the cross sectional area occupied by organic molecules can be strongly affected by the surface on which they are adsorbed (18). For example, our value of 71 Å² is substantially larger than Dorris and Gray's result for mesitylene sorbed on cellulose, 51 Å²/molecule. Recent work by Lowell *et al.* (18) suggests that

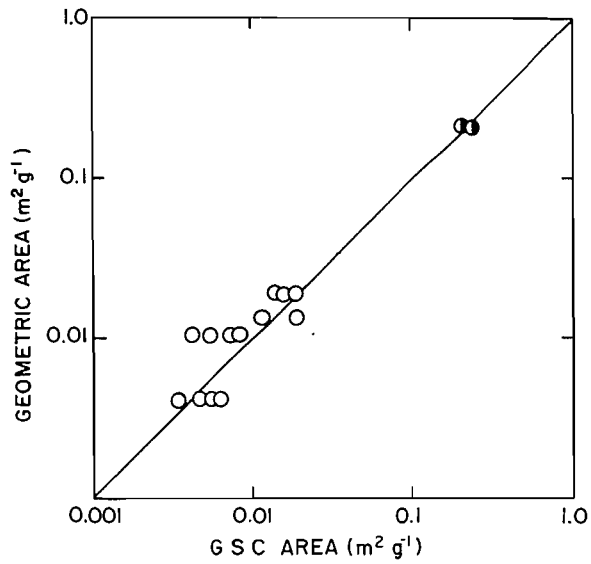


FIG. 2. Correlation between the measured geometric area and the GSC area calculated assuming 71 Å² for the area occupied by mesitylene. ○, glass beads; ◑, glass fibers.

changes in the cross sectional area of molecules on a given material, due to hydration, oxidation or some other change in the surface chemistry, would be accompanied by a marked change in the value of the *C* parameter.

As illustrated by Fig. 2, the precision of the method was about ±10% for specific surface areas above 0.01 $m^2\ g^{-1}$ and ±25% for lower specific areas, probably because the correction for the surface area of the column walls becomes substantial. The effective lower limit appears to be about 0.005 $m^2\ g^{-1}$, while the upper limit is imposed by the increasing column backpressures which accompany decreasing particle size; probably 0.5 $m^2\ g^{-1}$ is a reasonable upper limit for all but fiber samples.

Specific areas obtained by mesitylene adsorption near room temperature and $N_2$ adsorption at −195°C are compared in Table 1. The statistical scatter in the $N_2$ areas is much greater than the precision that can usually be obtained (6), possibly because of the

Can. J. Chem. Downloaded from www.nrcresearchpress.com by 210.87.254.40 on 09/06/12
For personal use only.

small desorption signals and thermal diffusion effects. Nevertheless, the values for all three samples are substantially larger than those from the GSC method using mesitylene as the sorbate. Some of the difference is undoubtedly due to the fact that nitrogen adsorption measures surface roughness on a scale (16 Å$^2$) much smaller than that for mesitylene (71 Å$^2$). Variations in the cross sectional area of the mesitylene between the different materials may also be a factor.

We conclude that gas–solid chromatography with mesitylene as a sorbate provides an accurate method for measuring the monolayer capacities of non-porous minerals whose specific areas lie in the range 0.005 to 0.5 $m^2 g^{-1}$, to a precision as high as $\pm 10\%$. These monolayer capacities provide an accurate measure of relative differences in the specific areas of samples of a given mineral on a scale of about 71 Å$^2$/molecule, providing the $C$ values lie within a narrow range. Absolute specific surface areas are less well defined because of uncertainties in the area occupied by the sorbate molecule. Trace hydrocarbons are the major interference. Because the method requires no specialized equipment and provides the necessary sensitivity, it is attractive as a research tool for characterizing batches of low surface area material to be used in subsequent experiments and for monitoring sample alterations caused by changes in parameters such as temperature or humidity, which can be made without removing the sample from the column. The technique is more time consuming (two or three samples per day) than commercial systems and requires reasonably large samples. These difficulties, coupled with the need to characterize the sorbate area for each mineral, limit its usefulness for more routine work.

**Acknowledgements**

We are indebted to Drs. D. G. Gray, H. W. Habgood, J. Boon, and K. Takamura for their constructive comments on the manuscript.

1. (*a*) P. R. Tremaine and J. C. LeBlanc. J. Solution Chem. **9**, 415 (1980); (*b*) P. V. Balakrishnan. Can. J. Chem. Eng. **55**, 357 (1977); (*c*) J. W. Morse. Am. J. Sci. **274**, 97 (1974).
2. J. F. Relyea and R. J. Serne. Batelle Pacific Northwest Laboratory Report PNL-2872. 1979.
3. S. C. MacLean, D. G. Coles, and H. C. Weed. Lawrence Livermore Laboratory Report UCID-17928.
4. P. Chenebault and A. Schurenkamper. J. Phys. Chem. **69**, 2300 (1965).
5. D. Kourilova and M. Krejci. J. Chromatogr. **65**, 71 (1972).
6. S. Lowell and S. Karp. Anal. Chem. **44**, 1706 (1972).
7. R. J. Laub and R. L. Pecsok. Physicochemical applications of gas chromatography. Wiley-Interscience, NY. 1979. Chapt. 7.
8. D. G. Gray. Prog. Polym. Sci. **5**, 1 (1977).
9. J. M. Braun and J. E. Guillet. Adv. Polym. Sci. **21**, 107 (1976).
10. J. R. Conder. Chromatographia, **7**, 387 (1974).
11. A. Dyer, D. Leigh, and W. E. Sharples. J. Chromatogr. **118**, 319 (1976).
12. U. B. Mohlin and D. G. Gray. J. Colloid Interface Sci. **47**, 747 (1974).
13. P. R. Tremaine and D. G. Gray. J. Chem. Soc. Faraday I, **71**, 2170 (1975).
14. G. M. Dorris and D. G. Gray. J. Colloid Interface Sci. **71**, 93 (1979).
15. S. Thibault, J. Amouroux, and J. Talbot. Bull. Soc. Chim. Fr, 1319 (1968).
16. S. Brunauer, P. H. Emmett, and E. Teller. J. Am. Chem. Soc. **60**, 309 (1938).
17. Selected values of properties of hydrocarbons and other related compounds. American Petroleum Institute Project 44, Thermodynamics Research Center, College Station, Texas. 1974.
18. S. Lowell, J. Shields, G. Charalambous, and J. Manzione. J. Colloid Interface Sci. **86**, 191 (1982).
19. S. Katz and D. G. Gray. J. Colloid Interface Sci. **82**, 339 (1981).

Can. J. Chem. Downloaded from www.nrcresearchpress.com by 210.87.254.40 on 09/06/12
For personal use only.

# Synthèse stéréospecifique de nucléosides pyrimidiques par la méthode de Hilbert–Johnson[1]

CHRISTIAN H. GAGNIEU, ANNIE V. GROUILLER ET HENRI PACHECO

*Service de Chimie Biologique, Bât. 406, INSA, 20, av. Albert Einstein, 69621 Villeurbanne, France*

Reçu le 4 mars 1982

CHRISTIAN H. GAGNIEU, ANNIE V. GROUILLER et HENRI PACHECO. Can. J. Chem. **60**, 2863 (1982).

La condensation de la diméthoxy-2,4-pyrimidine avec les bromoglycosides dérivés des méthyl désoxy-4-pentopyranosides **2–7** et du méthyl tri-*O*-benzoyl-3,5,6-glucofuranose **20** conduit de façon stéréospécifique aux nucléosides **8–13** et **22** de configuration *trans* 1′,2′. La stéréochimie de cette réaction n'est pas influencée par la structure du sucre de départ mais est liée à la présence de l'hydroxyle en C-2. La synthèse de l'époxyde **18**, obtenue par action de NaH sur les bromhydrines **17** dérivées de **7** tend à confirmer l'hypothèse d'une réaction assistée par un intermédiaire de type époxydium à partir de la bromhydrine *trans*. Quant à la bromhydrine *cis*, elle serait soumise à la substitution directe de l'halogène anomérique par la base; l'hypothèse de la formation intermédiaire d'un ion carbonium a pu être écartée puisque les réactions de glycosylation de type $S_N1$ du composé **19** par MeOH ou t-BuOH conduisent de façon préférentielle à des composés de configuration *cis*.

CHRISTIAN H. GAGNIEU, ANNIE V. GROUILLER, and HENRI PACHECO. Can. J. Chem. **60**, 2863 (1982).

Condensation of 2,4-dimethoxy pyrimidine with bromoglucosides derived from methyl 4-deoxypentopyranosides **2–7** and from 3,5,6-tri-*O*-benzoyl glucofuranose, **20**, leads in a stereospecific manner to the nucleosides **8–13** and **22** with the *trans* 1′,2′ configuration. The stereochemistry of this reaction is not influenced by the structure of the starting sugar but rather is directed by the presence of the C-2 hydroxyl group. The synthesis of epoxide **18**, obtained by the action of NaH on the bromohydrine **17**, derived from **7**, supports the intervention of a reaction assisted by an epoxide-like intermediate derived from the *trans*-bromohydrine. On the other hand, the *cis*-bromohydrine undergoes direct substitution of anomeric halogen by base. The possibility of the formation of a carbocation-like intermediate is discounted since $S_N1$ type glycosylation reactions of **19** by MeOH or *t*-BuOH lead preferentially to products with the *cis*-configuration.

[Journal translation]

## Introduction

La synthèse de nucléosides pyrimidiques par la méthode de Hilbert–Johnson (1) utilisant les dialkoxy-2,4-pyrimidines peut être réalisée dans de bonnes conditions à partir d'halogénosucres possédant un hydroxyle libre; en effet, nous avons montré dans un précédent travail qu'une telle réaction pouvait être appliquée à des bromures de désoxy-4-pentopyranosides non protégés en C-3 et substitués en C-2 par des groupements *O*-alkyle ou *O*-acyle (2). Les résultats classiques obtenus au niveau de la stéréospécificité de cette réaction, qui se traduisent par la formation de nucléosides *trans* lorsqu' un groupement participant est présent en C-2 (3) et par l'obtention majoritaire de nucléosides *cis* lorsque ce groupement est non participant (4), nous ont permis de conclure que la stéréochimie de la réaction de glycosylation n'est que peu influencée par la fonction hydroxyle lorsque celle-ci est placée en β de l'halogène anomérique. Il est concevable qu'une telle fonction puisse jouer un rôle plus important dans la synthèse si elle est placée en α de l'halogène, en raison des possibilités de participation directe à la réaction de glycosylation. Quelques rares synthèses de nucléosides à partir d'halogénosucres présentant un hydroxyle libre en C-2 ont été rapportées (5, 6). Ces réactions qui concernaient des bases non naturelles telles que le diméthyl-5,6-benzimidazole ou des alkylpyridines conduisaient de façon prépondérante à des nucléosides *trans* 1′,2′. Il semblait intéressant de rechercher si une telle stéréospécificité pouvait être obtenue avec les méthodes classiques de synthèse des nucléosides (7), appliquées à des bromhydrines anomériques. La méthode de Hilbert–Johnson, avec laquelle l'obtention directe de nucléosides pyrimidiques non totalement protégés est aisée, a été choisie pour réaliser cette étude.

Dans le présent article nous rapportons les résultats obtenus lors de la condensation de la diméthoxy-2,4-pyrimidine (DMP) avec les bromhydrines dérivées des méthylglycosides **2–7**, ainsi que les travaux réalisés pour déterminer la nature de l'influence de l'hydroxyle libre sur la stéréochimie de la réaction.

## Résultats et discussion

Les substituants au niveau du C-3 des méthylglycosides **2–7** (Fig. 1) ont été choisis en fonction de leur nature chimique et de leur encombrement stérique de façon à évaluer, le cas échéant, leur influence sur la réaction de condensation. Les

[1]Travail présenté en partie au 4th International Round Table Nucleoside, Nucleotide and their Biological Applications, 4–6 février 1981, Anvers, Belgique.

0008-4042/82/222863-07$01.00/0

©1982 National Research Council of Canada/Conseil national de recherches du Canada

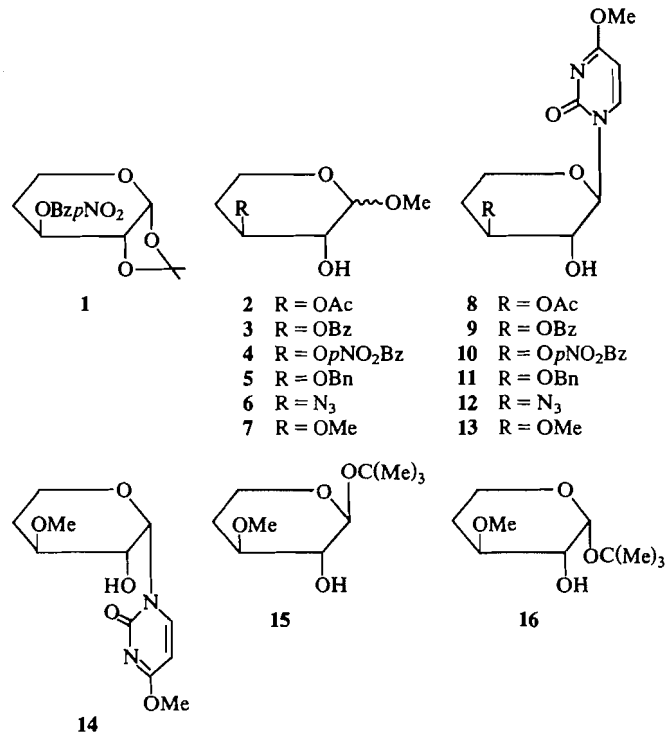


FIG. 1

dérivés acétylé, benzoylé et benzylé **2**, **3** et **5** ont été décrits dans un précédent article (2); le composé **6** présentant un groupement azide en C-3 est également connu (8).

La préparation du méthyl désoxy-4-*O*-*p*-nitrobenzoyl-3-α et β-DL-*thréo*-pentopyranoside **4**[2] a été réalisée par la méthanolyse en milieu acide du désoxy-4-*O*-isopropylidène-1,2-*O*-*p*-nitrobenzoyl-3-β-DL-*thréo*-pentopyranose **1** obtenu par action du chlorure de *p*-nitrobenzoyle en présence de pyridine sur le désoxy-4-*O*-isopropylidène-1,2-β-DL-*thréo*-pentopyranose (9). Le composé **4** a été obtenu sous forme d'un mélange des isomères α et β dans le rapport 4:1. Les méthyl désoxy-4-*O*-méthyl-3-α et β-DL-*thréo*-pentopyranosides **7** ont été obtenus séparément par action d'un excès de méthylate de sodium en solution méthanolique sur les méthyl anhydro-2,3-désoxy-4-α ou β-DL-*érythro*-pentopyranoses (10). L'ouverture de l'époxyde β est régiosélective et conduit exclusivement au composé 7α tandis que l'ouverture de l'époxyde α conduit à un mélange du composé 7β et d'un produit méthylé en C-2 et hydroxylé en C-3, dans le rapport 10:1.

La synthèse des bromoglycosides à partir des composés **2**–**7** s'est révélée aussi délicate que pour les sucres hydroxylés en C-3; le même procédé de bromuration a été utilisé mais pour les produits **5** et **6** la réaction a dû être réalisée à plus basse température (−15°C) pour limiter la débenzylation dans le cas du composé **5** et la dégradation du groupement azide pour le composé **6**. Les réactions de condensation de la DMP avec les bromhydrines obtenues ont été réalisées dans les conditions décrites pour la synthèse des nucléosides hydroxylés en C-3 (2). Les nucléosides sont obtenus très rapidement avec de bons rendements (69–85%).

À partir des méthylglycosides **2**–**6**, seuls les nucléosides de configuration *trans* 1′,2′ **8**–**12** ont été obtenus; la stéréospécificité de la réaction est ici absolue, mais dans le cas du composé méthylé **7**, des traces du nucléoside **14** de configuration *cis* 1′,2′ ont pu être détectées et isolées à côté de l'isomère *trans* **13**. La quantité de nucléoside **14** est très faible et ne représente que 4,5% de la masse totale de nucléoside méthylé obtenue. Ces résultats montrent que la nature et l'encombrement stérique des substituants en C-3 n'ont que peu d'influence sur la stéréochimie de la réaction.

Les différents mécanismes réactionnels susceptibles de conduire à des nucléosides à partir d'halohydrines ont été proposés par Freyne *et al.* (6) et sont similaires à ceux rapportés dans la figure 2.

[2]Les composés **1**–**19** sont racémiques, mais un seul énantiomère (L) est représenté dans les figures.

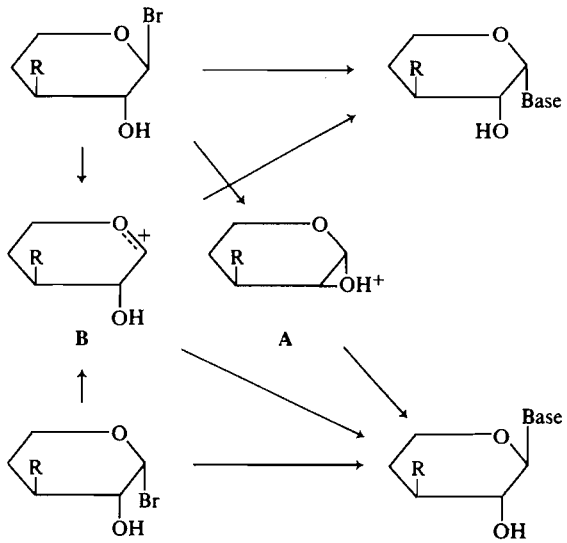


FIG. 2

La stéréospécificité observée dans les réactions de condensation, réalisées à partir de mélanges anomériques de bromures, pourrait être expliquée d'une part par la substitution de type $S_N2$ de l'halogène par la base au niveau de la bromhydrine *cis* 1,2 et d'autre part par l'ouverture en C-1 d'un intermédiaire de type époxydium (**A**) dérivé de la bromhydrine *trans* et provenant de l'attaque nucléophile de l'halogène anomérique par l'hydroxyle en C-2, en présence de la base. Le passage par un ion carbonium intermédiaire de type **B** est également envisageable mais il est vraisemblable que son intervention conduirait à la formation de composés *cis* 1',2' en liaison avec l'encombrement stérique existant au niveau du C-3.

Il était intéressant d'une part de vérifier la possibilité de formation d'un époxyde, et donc d'un ion époxydium, à partir des bromhydrines utilisées, et d'autre part d'évaluer la participation de chacun des mécanismes évoqués, dans le processus réactionnel global.

Les tentatives de synthèse d'époxydes ont été réalisées à partir du méthyl glycoside **7** dont la préparation est aisée et dont le groupement en C-3 est, dans une large mesure, chimiquement inerte. En chimie des sucres, la formation d'un cycle oxirane en C1—C2 peut être réalisée selon la méthode de Yamaguchi et Schuerch (11) par action de *t*-BuOK sur une halohydrine en solution benzénique. Cette méthode appliquée aux bromures dérivés de **7** n'a pas donné l'époxyde **18** attendu mais a conduit à la synthèse du composé **15** de configuration *trans* 1,2 présentant un groupement *tert*-butyloxy en C-1 et à des traces de son isomère **16** de configuration *cis*. La formation de l'époxyde **18** a pu être obtenue par traitement des bromures **17** avec du NaH en suspension dans $CH_2Cl_2$ à −30°C (Fig. 3) mais son isolement n'a pas pu être réalisé en

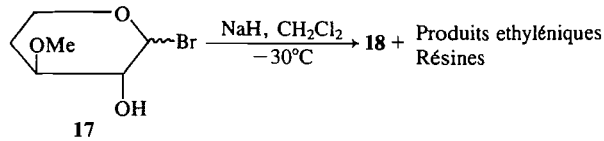


FIG. 3

raison notamment de la très grande complexité du milieu réactionnel qui contient des composés de structure éthylénique et des produits résineux. Il a pu être visualisé en ccm sur des plaques de gel de silice anhydres par révélation avec un réactif spécifique des époxydes[3] (12); sa mobilité dans AcOEt était voisine de celle des bromures.

L'analyse en rmn de ce composé ne pouvait être effectuée directement dans le milieu réactionnel brut, il fallait au préalable, éliminer $CH_2Cl_2$, ce qui a été réalisé par coévaporation avec du benzène-$d_6$. Le spectre obtenu dans ce solvant présentait en particulier 2 doublets étroits ($J \sim 2{,}5$ Hz) à 4,70 et 2,75 ppm pouvant correspondre aux protons H-1 et H-2 d'un composé de type époxyde. Les réactions reportées dans la figure 4, effectuées sur le mélange réactionnel et suivies en rmn, tendent à confirmer cette structure.

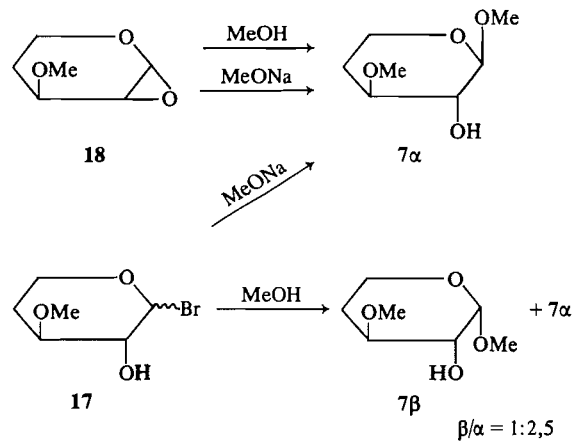


FIG. 4

L'addition de MeONa ou MeOH conduit de façon instantanée à la synthèse exclusive du méthylglycoside 7α dont le spectre rmn est très caractéristique, et à la disparition simultanée des 2 doublets. La stéréospécificité observée dans ces réactions, qui est indépendante de la nucléophilicité des réactifs, est caractéristique de l'ouverture

[3]Pulvérisation d'une solution de rouge de méthyle et de NaI dans du n-butanol suivie d'un chauffage à 140°C.

d'un époxyde. De plus, l'action de MeONa sur les bromhydrines, réalisées dans les mêmes conditions, conduit également au seul composé 7α alors que la réaction avec MeOH qui ne peut pas donner lieu à la formation d'un époxyde intermédiaire, aboutit à un mélange des composés 7α et 7β dans le rapport 2,5:1.

La formation d'un composé de type époxyde dans la réaction des bromhydrines avec une base est donc très probable, mais dans le cas de la condensation avec la DMP il ne peut s'agir que d'une entité activée, de type époxidium, puisque l'intervention d'un proton est nécessaire dans le mécanisme d'ouverture du cycle oxirane par cette base. Il est vraisemblable que la molécule réagissante soit constituée par un complexe entre l'époxyde et la base protonée.

Dans le processus réactionnel global de la condensation de la DMP avec les bromhydrines, l'importance du rôle joué par la formation de l'ion époxydium d'une part et par la substitution directe de l'halogène anomérique d'autre part dépend essentiellement de la proportion des bromhydrines *cis* et *trans* au moment de l'addition de la base. Quant à la participation d'un ion carbonium nous avons pu déduire des réactions reportées dans la figure 5 qu'elle est peu importante.

En effet, dans les réactions de glycosylation du composé **19** (13), réalisées avec MeOH ou *t*-BuOH en présence de résine Dowex $50H^+$, les groupements méthoxyle et *tert*-butoxyle sont introduits préférentiellement en position *cis* par rapport à l'hydroxyle en C-2. Ces réactions qui sont de type $S_N1$ donnent des résultats similaires avec des substrats dont l'encombrement stérique en C-3 est plus important tels que des composés benzoylé ou benzylé.

La synthèse des nucléosides à partir des désoxy-4-pentopyranoses pouvant constituer un cas particulier sur le plan stéréochimique du fait de l'absence de substituant en C-4 et C-5, il était nécessaire de réaliser le même type de réaction à partir de sucres naturels classiques dans lesquels tous les carbones sont substitués. Ainsi nous avons réalisé la condensation de la DMP sur les bromures **21** obtenus par action prolongée de HBr à $-10°C$ dans $CH_2Cl_2$ sur le méthyl tri-*O*-benzoyl-3,5-6-glucofuranose **20** (14). Cette condensation, réalisée selon la technique habituelle, a conduit de façon exclusive au nucléoside **22** de configuration *trans* 1',2' (Fig. 6). Le rendement moyen obtenu (62%) ne dépend pas de la réactivité des bromures mais de la synthèse de ces derniers qui s'accompagne d'une dégradation partielle du sucre de départ.

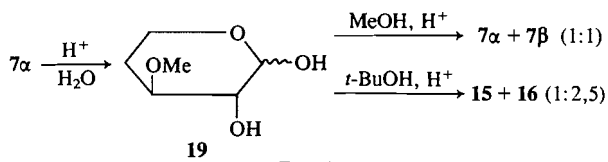


FIG. 5

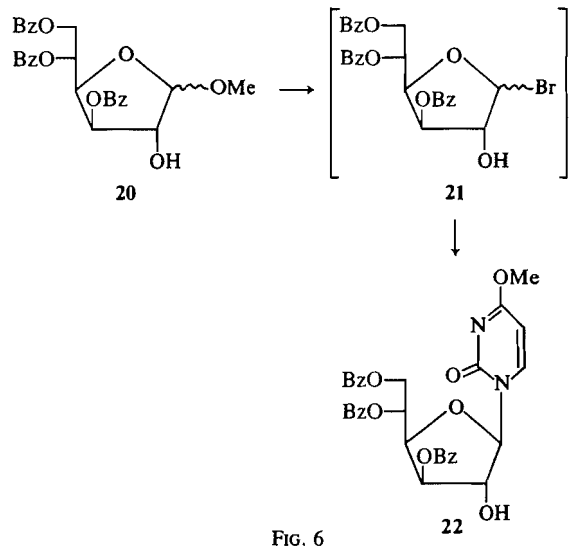


FIG. 6

## Conclusion

La stéréospécificité observée dans les réactions de condensation d'une bromhydrine en C-1, C-2 avec la DMP et qui se traduit par la formation exclusive de nucléoside *trans* 1',2' ne dépendrait pas de la structure du sucre de départ mais essentiellement des possibilités de formation d'un intermédiaire réactionnel de type époxyde liées à la présence du groupement hydroxyle en C-2.

## Partie expérimentale

*Méthodes générales*

Le déroulement des réactions a été suivi en ccm sur gel de silice (Kieselgel 60 $F_{254}$, Merck 5535) et la révélation des chromatogrammes a été réalisée par pulvérisation de réactif phosphomolybdique suivie d'un chauffage à 100°C. Les ccm de l'époxyde **18** ont été réalisées sur plaques de gel de silice préalablement déshydratées à 100°C pendant 2 h, les chromatogrammes ont été révélés par pulvérisation d'une solution contenant 100 mg de rouge de méthyle et 200 mg de NaI dans 20 mL de n-butanol suivie d'un chauffage à 140°C pendant 5 minutes; les époxydes sont révélés en jaune sur fond rouge. La purification des produits a été réalisée par chromatographie liquide sous basse pression, sur gel de silice (Kieselgel 60 $F_{254}$ et 60, Merck 10757 et 9385). Les points de fusion, mesurés sur banc Kofler ne sont pas corrigés. Les indices de réfraction ont été mesurés sur un réfractomètre OPL et les spectres ir ont été enregistrés sur le spectrophotomètre Beckman Acculab-4. Les spectres rmn ont été enregistrés à 60, 80 ou 350 MHz sur les spectromètres Perkin Elmer R 24 B, Brüker WP 80 et Caméca 350. Les déplacements chimiques sont exprimés en ppm, le tetraméthylsilane étant pris comme référence zéro. Lorsque les

spectres ont été enregistrés dans $D_2O$ comme solvant, le *tert*-butanol a été utilisé comme référence pour les déplacements chimiques. Les microanalyses ont été effectuées par le service central de microanalyse du C.N.R.S., division de Lyon.

*Désoxy-4-*O*-isopropylidène-1,2-*O*-*p*-nitrobenzoyl-3-*β-DL-*thréo-pentopyranose (1)*

À une solution de désoxy-4-*O*-isopropylidène-1,2-β-DL-*thréo*-pentopyranose (9) (1 g, 5,75 mmol) dans $CH_2Cl_2$ (20 mL) contenant de la pyridine (3 mL) sont ajoutés à 0°C et sous forte agitation, des cristaux de chlorure de *p*-nitrobenzoyle (1,1 g, 5,93 mmol). Le mélange est agité 1 h à 0°C puis 2 h à température ambiante. On ajoute alors de l'eau (20 mL) et de l'éthanol (1 mL) et on extrait la phase aqueuse obtenue par $CH_2Cl_2$ (2 × 25 mL); la phase organique est lavée par une solution saturée de $NaHCO_3$ (30 mL) puis par de l'eau (30 mL); l'extrait organique est séché sur $Na_2SO_4$ et le solvent est évaporé sous pression réduite pour donner un résidu cristallin qui, par trituration dans de l'ether éthylique (15 mL) fournit 1,4 g (75,5%) de **1** sous forme de cristaux jaunâtres. Les eaux mère de cristallisation sont évaporées et le résidu pâteux obtenu est recristallisé dans le mélange AcOEt–hexane 1:5 pour donner 330 mg supplémentaires de **1**; rendement global: 93%: pf 140°C; $R_f$ 0,75 (AcOEt–hexane, 1:1); $\nu_{max}$ (KBr): 3120, 3090, 3060, 1600 et 720 ($C_6H_4$), 1720 (ester), 1370 et 1380 (isopropylidène) $cm^{-1}$; rmn ($CDCl_3$) δ: 5,50 (m, 1H, $J_{2,3}$ = 3,6 Hz, $J_{3,4'}$ = $J_{3,4}$ = 4,3 Hz, H-3), 5,38 (d, 1H, $J_{1,2}$ = 3,3 Hz, H-1), 4,01 (t, 1H, H-2), 3,90–3,70 (m, 2H, H-5, H-5'), 2,20 (m, 1H, $J_{4,4'}$ = −14,5 Hz, $J_{4',5'}$ = 8,1 Hz, $J_{4',5}$ = 6,3 Hz, H-4'), 1,75 (m, 1H, H-4), 8,24 et 8,16 (2d, 4H, $C_6H_4$), 1,52 et 1,33 (2s, 6H, 2-$CH_3$) *Anal.* calc. pour $C_{15}H_{17}NO_7$: C 55,73, H 5,26, N 4,33; trouvée: C 55,65, H 5,45, N 4,32.

*Méthyl désoxy-4-*O*-p-nitrobenzoyl-3-désoxy-4-α et* β-DL-thréo-*pentopyranoside (4)*

Une solution de **1** (1,15 g, 3,56 mmol) dans MeOH (35 mL) contenant de la résine Dowex 50H$^+$ anhydre (1 g), fraîchement activée par HCl, est chauffée 2 h à 60°C; la résine est alors filtrée et rincée par MeOH bouillant (20 mL). Le filtrat est évaporé et le produit liquide obtenu est purifié sur colonne de gel de silice dans le solvant acétone–hexane 1:2 pour donner une poudre blanche (840 mg, 80%) constituée par un mélange des composés **4α** et **4β** dans le rapport 4:1. Ces 2 composés n'ont pas été séparés: pf 140–144°C; $\nu_{max}$ (KBr): 3520 et 3420 (OH), 3130, 1605 et 710 ($C_6H_4$), 1710 et 1280 (ester) $cm^{-1}$; rmn (DMSO-$d_6$): *composé* **4α**, δ: 4,93 (m, 1H, $J_{2,3}$ = 8,4 Hz, $J_{3,4}$ = 5,1 Hz, $J_{3,4'}$ = 10 Hz, H-3), 4,64 (d, 1H, $J_{1,2}$ = 6,7 Hz, H-1), 5,45 (d, 1H, OH), 3,37 (s, 3H, $OCH_3$), 8,25 et 8,10 (2d, 4H, $C_6H_4$); *Composé* **4β**, δ: 5,00 (m, 1H, H-3), 4,63 (d, 1H, $J_{1,2}$ = 3,4 Hz, H-1), 5,10 (d, 1H, OH), 3,25 (s, 3H, $OCH_3$), 8,25 et 8,10 (2d, 4H, $C_6H_4$). *Anal.* calc. pour $C_{13}H_{15}NO_7$: C 52,53, H 5,05, N 4,71; trouvée: C 52,41, H 5,23, N 4,64.

*Méthyl désoxy-4-*O*-méthyl-3-α ou* β-DL-thréo-*pentopyranosides (7)*

A une solution de MeONa obtenue par dissolution à chaud de sodium (2 g) dans MeOH (40 mL) est ajouté à température ambiante de l'anhydro-2,3-désoxy-4-α ou β-DL-pentopyranose (9) (5,4 g, 41,5 mmol). La solution obtenue est agitée une nuit à 35°C puis neutralisée par HCl 6 *N*. De l'acétate d'éthyle est alors ajouté (40 mL) et les sels sont filtrés puis lavés par AcOEt (10 mL). Le filtrat est évaporé et le résidu aqueux obtenu est extrait par AcOEt (2 × 30 mL). La phase organique est séchée sur $Na_2SO_4$ et évaporée sous pression réduite pour donner un liquide jaunâtre. le composé **7α**, obtenu à partir de l'anhydrosucre β, est purifié par distillation au four à boules à 115–120°C sous 3 Torr, c'est une huile incolore (5,775 g, 86%): $n_D^{20}$ 1,4580; $R_f$ 0,17 (AcOEt–hexane, 2:1); $\nu_{max}$ (film): 3460 (OH), 2850 (OMe) $cm^{-1}$; rmn ($D_2O$) δ: 2,96 (d, 1H, $J_{1,2}$ = 7,2 Hz, H-1), 2,73 (m, 1H, $J_{5,5'}$ = −12 Hz, $J_{5,4'}$ = 5,2 Hz, $J_{5,4}$ = 2,3 Hz, H-5), 2,18 (m, 1H, H-5'), 2,17 (m, 1H, H-3), 1,96 (dd, 1H, $J_{2,3}$ = 10 Hz, H-2), 0,93 (m, 1H, $J_{4,4'}$ = −13 Hz, $J_{4,3}$ = 5 Hz, $J_{4,5'}$ = 2,3 Hz, H-4), 0,27 (m, 1H, $J_{4',5'}$ = 11,5 Hz, $J_{4',3}$ = 10 Hz, H-4'), 2,25 et 2,17 (2 s, 6H, 2-$OCH_3$). *Anal.* calc. pour $C_7H_{14}O_4$: C 51,85, H 8,64; trouvé: C 51,72, H 8,80. Le composé **7β** obtenu à partir de l'anhydrosucre α est purifié par chromatographie sur gel de silice dans le solvant AcOEt–hexane 3:1 pour donner une huile incolore (91%): $n_D^{20}$ 1,4560; $R_f$ 0,37 (AcOEt–hexane, 3:1); $\nu_{max}$ (film): caractéristiques identiques à celles du composé **7α**; rmn ($D_2O$) δ: 3,53 (d, 1H, $J_{1,2}$ = 2,4 Hz, H-1), 2,53 (t, 1H, $J_{2,3}$ = 1,5 Hz, $J_{3,4'}$ = 2 Hz, $J_{3,4}$ = 1,5 Hz, H-3), 2,41 (d, 1H, H-5), 2,31 (m, 1H, H-5'), 2,30–2,18 (1H, H-2), 0,93 (m, 1H, $J_{4,4'}$ = −13,5 Hz, H-4), 0,30 (m, 1H, H-4'), 2,19 et 2,15 (2s, 6H, 2-$OCH_3$). *Anal.* calc. pour $C_7H_{14}O_4$: C 51,85, H 8,64; trouvé: C 51,81, H 8,78.

*Méthode générale de synthèse des nucléosides 8–14*

À une solution de méthylglycoside (10 mmol) dans $CH_2Cl_2$ (60 mL) à 0 ou −15°C est ajoutée une solution de HBr à demi saturation dans $CH_2Cl_2$ à raison de 5 équivalents d'acide par équivalent de sucre. Lorsque les produits de départ ont disparu, la solution est dégazée par un courant d'azote anhydre, hors du bain réfrigérant et jusqu'à réapparition des méthylglycosides (environ 10 min); on ajoute alors en une seule fois du tamis moléculaire 10 Å et on agite jusqu'à disparition totale des vapeurs d'HBr dans le vase à réaction. On procède alors à l'addition de la DMP (2 equiv./equiv. de sucre) et le mélange obtenu est porté à reflux pendant 5 min. le solvant est évaporé et le résidu pâteux est trituré dans MeOH chaud. Les sels sont éliminés par filtration et rinçés par MeOH bouillant (2 × 30 mL). Le filtrat est évaporé à sec et l'huile jaunâtre obtenue est diluée dans le mélange acétone–méthanol 10:1 (10 mL/g de résidu). Le précipité est éliminé par filtration et rincé avec de l'acétone. Le filtrat est évaporé et le concentré réactionnel huileux obtenu est purifié pour donner les nucléosides attendus.

*(O-acétyl-3-désoxy-4-α-*DL-*thréo-pentopyranosyl)-1-méthoxy-4-pyrimidinone-2 (8)*

Synthèse à partir de **2**; la dilution du concentré réactionnel par le mélange acétone–hexane 1,5:1 conduit à la précipitation d'une partie du nucléoside **8** (73%); le reste du nucléoside est obtenu par chromatographie sur gel de silice de la solution de cristallisation, dans le même solvant; rendement global 84%. Les caractéristiques physiques du nucléoside obtenu sont identiques à celles qui ont été précédemment décrites (1).

*(O-benzoyl-3-désoxy-4-α-*DL-*thréo-pentopyranosyl)-1-méthoxy-4-pyrimidinone-2 (9)*

Synthèse à partir du composé **3**; la dilution de l'extrait réactionnel par AcOEt (6 mL/g d'extrait) provoque la précipitation d'une grande partie du nucléoside **9** qui est obtenu pur sous forme d'une poudre blanche. Le reste du nucléoside, dissous dans la solution de cristallisation est isolé par chromatographie sur gel de silice dans AcOEt pur; rendement global 83%: pf 160–170°C; $R_f$ 0,45 (AcOEt); $\nu_{max}$ (KBr): 3370 (OH), 3100, 1600, 705 et 680 ($C_6H_5$), 1715 et 1270 (ester), 1670, 1630, 1545 et 1480 (base) $cm^{-1}$; rmn (DMSO-$d_6$) δ: 5,59 (d, 1H, $J_{1,2}$ = 9,3 Hz, H-1'), 5,10 (m, 1H, $J_{3',2'}$ = 9,3 Hz, $J_{3',4'}$ = 5,8 Hz, $J_{3',4''}$ = 11 Hz, H-3'), 4,08–3,68 (m, 3H, H-2, H-5', H-5''), 2,15 et 1,83 (2m, 2H, H-4' et H-4''), 5,57 (d, 1H, OH), 8,05 et 6,02 (2d, 2H, $J_{5,6}$ = 7,7 Hz, H-6 et H-5), 7,95 et 7,53 (2m, 5H, $C_6H_5$), 3,81 (s, 3H, OMe); *Anal.* calc. pour $C_{17}H_{18}N_2O_6$: C 58,96, H 5,20, N 8,09; trouvée: C 59,01, H 5,21, N 7,95.

*(Désoxy-4-*O*-p-nitrobenzoyl-3-α-*DL-*thréo-pentopyranosyl)-1-méthoxy-4-pyrimidinone-2 (10)*

Synthèse à partir du composé **4**. Le nucléoside est cristallisé à partir des extraits réactionnels par dilution avec le mélange

ether éthylique – éthanol 10:1 (10 mL/g d'extrait). La faible quantité de nucléoside restant dissoute dans la solution de cristallisation est récupérée par chromatographie dans AcOEt; rendement global 79%: pf 263–265°C (déc.); $R_f$ 0,36 (AcOEt); $\nu_{max}$ (KBr): 3410 (OH), 3125, 3090, 1605 et 720 ($C_6H_4$), 1720 et 1295 (ester), 1660, 1635, 1530 et 1490 (base) $cm^{-1}$; rmn (DMSO-$d_6$) δ: 5,60 (d, 1H, $J_{1,2}$ = 9,6 Hz, H-1'), 5,15 (m, 1H, $J_{3',2'}$ = 9 Hz, $J_{3',4'}$ = 5,3 Hz, $J_{3',4''}$ = 10,8 Hz, H-3'), 4,00 (dd, 1H, H-2'), 4,10–3,65 (m, 2H, H-5', H-5''), 2,18 (m, 1H, H-5'), 1,85 (m, 1H, H-5''), 8,33 et 8,15 (2d, 4H, $C_6H_4$), 8,05 et 6,00 (2d, 2H, $J_{5,6}$ = 7,5 Hz, H-6 et H-5), 5,64 (d, 1H, OH), 3,83 (s, 3H, OMe); *Anal.* calc. pour $C_{17}H_{17}N_3O_8$: C 52,17, H 4,35, N 10,74; trouvée: C 52,21, H 4,42, N 10,93.

*(O-benzyl-3-désoxy-4-α-*DL*-thréo-pentopyranosyl)-1-méthoxy-4-pyrimidinone-2 (**11**)*

Synthèse à partir du composé **5**; la dilution de l'extrait réactionnel par le solvant: acétone–hexane 1,5:1 (7 mL/g d'extrait) provoque la précipitation d'une grande partie du nucléoside **11** qui est récoltée par filtration et lavée par le mélange acétone–hexane 2:1. Le reste de nucléoside, contenu dans la solution de cristallisation est récupéré par chromatographie sur colonne de gel de silice dans le solvant acétone–hexane 1,5:1; rendement global: 85%; pf 128°C; $R_f$ 0,32 (acétone–hexane 1,5:1); $\nu_{max}$ (KBr): 3200 (OH), 3050, 3020 et 700 ($C_6H_5$), 1640, 1545 et 1480 (base) $cm^{-1}$; rmn (DMSO-$d_6$) δ: 5,46 (d, 1H, $J_{1',2'}$ = 8,8 Hz, H-1), 4,00–3,30 (m, 4H, H-2', H-3', H-5', H-5''), 2,09 (m, 1H, $J_{4',3'}$ = 9,5 Hz, $J_{4',4''}$ = −12,5 Hz, H-4'), 1,63 (m, 1H, $J_{4'',5'}$ = 5,5 Hz, $J_{4'',5''}$ = 11 Hz, H-4''), 8,00 et 6,00 (2d, 2H, $J_{5,6}$ = 7,3 Hz, H-6 et H-5), 7,30 et 4,66 (2s, 5H et 2H, $C_6H_5$—$CH_2$), 5,40 (d, 1H, OH), 3,83 (s, 3H, OMe); *Anal.* calc. pour $C_{17}H_{20}N_2O_5$: C 61,45, H 6,02, N 8,43; trouvée: C 61,39, H 6,00, N 8,57.

*(Azido-3-didésoxy-3,4-α-*DL*-thréo-pentopyranosyl)-1-méthoxy-4-pyrimidinone-2 (**12**)*

Synthèse à partir du composé **6**; le nucléoside est obtenu pur sous forme d'une laque par chromatographie de l'extrait réactionnel sur colonne de gel de silice dans le solvant acétone–hexane 1,5:1; la trituration de cette laque avec de l'éther éthylique provoque la cristallisation du nucléoside qui est obtenu sous forme d'une poudre blanche; rendement: 69%; pf 208–210°C (déc.); $R_f$ 0,35 (acétone–hexane, 1,5:1); $\nu_{max}$ (KBr): 3200 (OH), 2120 ($N_3$), 1650, 1550 et 1490 (base) $cm^{-1}$; rmn (DMSO-$d_6$) δ: 5,52 (d, 1H, $J_{1',2'}$ = 8,2 Hz, H-1'), 4,00–3,50 (m, 4H, H-2', H-3', H-5', H-5''), 2,00 (m, 1H, $J_{4',4''}$ = −12,5 Hz, H-4'), 1,66 (m, 1H, H-4''), 8,00 et 6,05 (2d, 2H, $J_{5,6}$ = 7,2 Hz, H-6 et H-5), 5,78 (d, 1H, OH), 3,86 (s, 3H, OMe); *Anal.* calc. pour $C_{10}H_{13}N_5O_4$: C 44,94, H 4,87, N 26,22; trouvée: C 45,00, H 4,95, N 26,08.

*(Désoxy-4-O-méthyl-3-α et β-*DL*-thréo-pentopyranosyl)-1-méthoxy-4-pyrimidinone-2 (**13** et **14**)*

Synthèse à partir du composé **7**; l'extrait réactionnel est chromatographié sur colonne de gel de silice dans le solvant acétone–hexane 7:1 pour donner les nucléosides **13** et **14** sous forme de laque. Le composé **13** cristallise par trituration dans l'éther éthylique; rendement global 72% (95,5% de **13** et 4,5% de **14**).

*Composé **13***: pf 162–164°C; $R_f$ 0,44 (acétone–hexane, 7:1); $\nu_{max}$ (KBr): 3260 (OH), 2880 et 2860 (OMe), 1650, 1540 et 1485 (base) $cm^{-1}$; rmn (DMSO-$d_6$) δ: 5,37 (d, 1H, $J_{1',2'}$ = 8,5 Hz, H-1'), 3,50 (m, 1H, H-2'), 4,00–3,30 (m, 3H, H-3', H-5', H-5''), 2,05 (m, 1H, $J_{4',4''}$ = −13 Hz, H-4'), 1,45 (m, 1H, H-4''), 7,95 et 5,95 (2d, 2H, $J_{5,6}$ = 7,4 Hz, H-6 et H-5), 5,25 (d, 1H, OH), 3,81 (s, 3H, OMe base), 3,35 (s, 3H, OMe sucre); *Anal.* calc. pour $C_{11}H_{16}N_2O_5$: C 51,56, H 6,25, N 10,94; trouvée: C 51,42, H 6,21, N 11,11.

*Composé **14***: $R_f$ 0,63 (acétone–hexane, 7:1); $\nu_{max}$ (KBr): caractéristiques identiques à celles du composé **13**; rmn (DMSO-$d_6$) δ: 5,68 (s, 1H, $J_{1',2'} \sim 1$ Hz, H-1), 3,90–3,20 (m, 4H, H-2', H-3', H-5', H-5''), 2.00 (m, 1H, $J_{4',4''}$ = −13 Hz, H-4'), 1,50 (m, 1H, H-4''), 7,83 et 5,97 (2d, 2H, $J_{5,6}$ = 7,3 Hz, H-6 et H-5), 5,33 (d, 1H, OH), 3,85 (s, 3H, OMe base), 3,35 (s, 3H, OMe sucre); *Anal.* calc. pour $C_{11}H_{16}N_2O_5$: C 51,56, H 6,25, N 10,94; trouvée: C 51,83, H 6,39, N 10,77.

*Action de NaH sur les bromhydrines dérivées de **7***

Les solutions neutres de bromhydrines, obtenues comme décrit précédemment, sont filtrées pour éliminer le tamis moléculaire. Le filtrat est refroidi à −30°C puis du NaH est ajouté (4 equiv./equiv. de sucre); la suspension obtenue est agitée à la même température jusqu'à l'arrêt du dégagement gazeux (environ 6 h) puis filtré pour éliminer le NaH en excès et les sels qui ont précipité. La ccm dans AcOEt de la solution obtenue révèle la présence de nombreux produits dont quelques uns sont révélés par une solution aqueuse neutre de $KMnO_4$ et dont un, à $R_f$ 0,15, est révélé par un réactif des époxydes. Ce composé qui disparaît instantanément lors de l'addition de MeOH ou MeONa pour donner le produit 7α serait l'époxyde **18**; rmn ($C_6D_6$) δ: 4,70 (d, 1H, $J_{1,2} \sim 2,5$ Hz, H-1), 2,75 (d, 1H, H-2).

*Réaction de glycosylation du désoxy-4-O-méthyl-3-α et β-*DL*-thréo-pentopyranose (**19**)*

Le composé **19** est obtenu par hydrolyse de **7** dans une solution d'HCl 6 *N* (15 mL/g de sucre) à 80°C pendant 1 heure. La solution est neutralisée par $Na_2CO_3$ et évaporée à sec à 50°C sous pression réduite. Le résidu pâteux obtenu est dilué par MeOH et les sels sont éliminés par filtration. Le filtrat est évaporé pour donner le composé **19** (94%) sous forme d'une huile contenant les 2 isomères α et β dans le rapport 2:1; $R_f$ 0,25–0,15 (AcOEt); $\nu_{max}$ (film): 3400 (OH), 2840 (OMe) $cm^{-1}$; rmn ($D_2O$) δ: 3,93 (d, 1/3H, $J_{1,2}$ = 2,5 Hz, H-1 β), 3,27 (d, 2/3 H, $J_{1,2}$ = 7,4 Hz, H-1 α), 2,23 (s, 3H, OMe α + β), 1,00 (m, 1H, H-4 α + β), 0,40 (m, 1H, H-4' α + β); *Anal.* calc. pour $C_6H_{12}O_4$: C 48,65, H 8,11; trouvée: C 48,60, H 8,35.

Les réactions de glycosylation sont réalisées par chauffage à 80°C pendant 1–2 h du composé **19** (10 mmol) dissous dans MeOH ou t-BuOH (30 mL) en présence de résine Dowex $50H^+$ (1 g). La réaction avec MeOH conduit de façon quantitative aux composés 7α et 7β dans le rapport 1:1. La réaction avec *t*-BuOH, plus lente et incomplète conduit à un mélange des composés **15** et **16** dans le rapport 1:2,5. Ces produits ont été séparés par chromatographie sur colonne de gel de silice dans l'acétate d'éthyle pur.

*tert-Butyl désoxy-4-O-méthyl-3-α et β-*DL*-thréo-pentopyranoside (**15** et **16**)*

Le composé **15** est cristallisé: pf 64–65°C; $R_f$ 0,60 (AcOEt); $\nu_{max}$ (KBr): 3420 (OH), 2880 (OMe) $cm^{-1}$; rmn ($CDCl_3$) δ: 4,33 (d, 1H, $J_{1,2}$ = 7,4 Hz, H-1), 4,00 (m, 1H, $J_{5,5'}$ = −12 Hz, $J_{5,4}$ = 2 Hz, $J_{5,4'}$ = 5,4 Hz, H-5), 3,60–3,15 (m, 3H, H-2, H-3, H-5'), 3,50 (s, 3H, OMe), 2,50 (s, 1H, OH), 2,07 (m, 1H, $J_{4,4'}$ = −12 Hz, H-4), 1,73 (m, 1H, H-4'), 1,33 (s, 9H, 3 $CH_3$); *Anal.* calc. pour $C_{10}H_{20}O_4$: C 58,82, H 9,80; trouvée: C 58,77, H 9,89. le composé **16** est une huile: $R_f$ 0,68 (AcOEt); $\nu_{max}$ (film): caractéristiques identiques à celles du composé **15**: rmn ($CDCl_3$) δ: 5,10 (d, 1H, $J_{1,2}$ = 2,8 Hz, H-1), 3,50 (dd, 1H, $J_{2,3}$ = 3,2 Hz, H-2), 4,00–3,30 (m, 3H, H-3, H-5, H-5'), 3,45 (s, 3H, OMe), 2,10 (m, 1H, $J_{4,4'}$ = −12 Hz, H-4), 1,77 (m, 1H, H-4'), 1,33 (s, 9H, $3CH_3$); *Anal.* calc. pour $C_{10}H_{20}O_4$: C 58,82, H 9,80; trouvée: C 59,05, H 9,74.

*Synthèse du (tri-O-benzoyl-3,5,6-β-*D*-glucofuranosyl)-1-méthoxy-4-pyrimidinone-2 (**22**)*

Une solution de méthyl tri-*O*-benzoyl-3,5-6-α et β-D-gluco-

furanose **20** (5 mmol) dans $CH_2Cl_2$ (25 mL) est saturée à −10°C par du HBr gazeux anhydre. La solution est agitée 5 h à cette température puis est laissée une nuit à 0°C. La réaction n'est pas complète et l'on note, en ccm, la présence de produits de dégradation et d'un spot à $R_f$ 0,28 (AcOEt–hexane, 1:1) correspondant aux bromures **21**. La solution est dégazée à température ambiante par un courant d'azote anhydre jusqu'à disparition des vapeurs d'HBr dans le vase à réaction; du tamis moléculaire 10 Å (5 g) est alors ajouté et la suspension obtenue est agitée pendant 5 min. De la DMP est ajoutée (15 mmol) et le mélange est chauffé 5 min à reflux. La suspension est alors traitée selon la technique habituelle et l'extrait réactionnel est chromatographié sur colonne de gel de silice dans le solvant AcOEt–hexane 3:1 pour donner le nucléoside **22** sous forme d'une poudre blanche: $[\alpha]_D^{23}$ +42° (*c* 0,046, éthanol); pf 134–140°C; $R_f$ 0,40 (AcOEt–hexane, 3:1); $\nu_{max}$ (KBr): 3420 (OH), 3060, 1600, 1590, 700 et 675 ($C_6H_5$), 1720 et 1270–1240 (ester), 1660–1620, 1550 et 1480 (base) $cm^{-1}$; rmn ($CD_3COCD_3$) δ: 6,13 (m, 1H, H-5'), 6,00 (s, 1H, $J_{1',2'} \sim 1$ Hz, H-1'), 5,84 (d, 1H, $J_{OH,2'} = 4$ Hz, OH), 5,66 (d, 1H, $J_{3',4'} = 3$ Hz, H-3'), 5,25–4,75 (m, 3H, H-4', H-6'6"), 4,63 (d, devient singulet par addition de $D_2O$, 1H, $J_{2,3'} \sim 1$ Hz, H-2), 8,45 et 6,03 (2d, 2H, $J_{5,6} = 7,5$ Hz, H-6 et H-5), 7,90 et 7,50 (2m, 15H, $3C_6H_4$), 3,84 (s, 3H, OMe). *Anal.* calc. pour $C_{32}H_{28}N_2O_{10}$: C 64,0, H 4,67, N 4,67; trouvée: C 64,13, H 4,63, N 4,58.

## Remerciements

Nous tenons à remercier le C.N.R.S. (ERA 560) et l'I.N.S.E.R.M. (U 205) de leur aide financière.

1. G. E. Hilbert et T. B. Johnson. J. Am. Chem. Soc. **52**, 4489 (1930).
2. C. H. Gagnieu, A. V. Grouiller et H. Pacheco. Can. J. Chem. **60**, 2238 (1982).
3. J. A. Montgomery et H. J. Thomas. J. Med. Chem. **22**, 1109 (1979); J. A. Montgomery et H. J. Thomas. J. Heterocycl. Chem. **16**, 353 (1979).
4. F. M. Unger, R. Christian et P. Waldstätten. Tetrahedron Lett. 605 (1979); J. A. Montgomery et A. G. Laseter. J. Med. Chem. **17**, 360 (1974); J. Kiburis, A. B. Foster et J. H. Westwood. J. Chem. Soc., Chem. Commun. 44 (1975).
5. M. Haga, R. K. Ness et H. G. Fletcher. J. Org. Chem. **33**, 1810 (1968).
6. E. J. Freyne, E. L. Esmans, J. A. Lepoivre et F. C. Alderweireldt. Carbohydr. Res. **78**, 235 (1980).
7. K. A. Watanabe, D. H. Hollenberg et J. J. Fox. J. Carbohydr. Nucleosides-Nucleotides, **1**, 1 (1974).
8. D. Bouchu, M. Abou-Assali, A. Grouiller, G. Carret et H. Pacheco. Eur. J. Med. Chem. **16**, 43 (1981).
9. C. H. Gagnieu et A. V. Grouiller. Carbohydr. Res. **84**, 61 (1980).
10. C. H. Gagnieu et A. V. Grouiller. J. Chem. Soc. Perkin Trans. I, **82**(4), 1009 (1982).
11. H. Yamaguchi et C. Schuerch. Carbohydr. Res. **81**, 192 (1980).
12. J. G. Buchanan et J. C. P. Schwarz. J. Chem. Soc. 4770 (1962).
13. F. Sweet et R. K. Brown. Can. J. Chem. **46**, 1592 (1968).
14. CIBA Ltd. Brevet Britt. 909,279; oct. 31 1962; Chem. Abst. **60**, 378e (1963).

# Molecular rearrangements. III. Thermal decomposition of some selected thioesters

ABOEL-MAGD A. ABDEL-WAHAB,[1] AHMED M. EL-KHAWAGA, AND MOHAMED T. ISMAIL
*Chemistry Department, Faculty of Science, Assiut University, Assiut, Egypt*

Received February 5, 1982

ABOEL-MAGD A. ABDEL-WAHAB, AHMED M. EL-KHAWAGA, and MOHAMED T. ISMAIL. Can. J. Chem. **60**, 2870 (1982).

Four selected thioesters (**1–4**) were prepared and pyrolyzed in the absence of promoters either alone or in isoquinoline solvent. These esters include benzyl thiobenzoate (**1**), phenyl phenylthioacetate (**2**), benzyl phenylthioacetate (**3**), and phenyl thiobenzoate (**4**). Pyrolysis of **1** gave mainly 2,3,4,5-tetraphenylthiophene in addition to benzene, biphenyl, benzyl thiol, and benzoic acid. Thermal decomposition of **1** under nitrogen gave benzaldehyde, benzil, and only a trace of benzoic acid in addition to the former products. Compound **2** afforded essentially toluene and dibenzyl in addition to benzene, biphenyl, phenyl sulphide, thiophenol, and phenyl acetic acid. Thermolysis of **3** gave toluene and stilbene beside small quantities of benzyl thiol and phenylacetic acid. Finally, thermal decomposition of **4** in isoquinoline gave benzene, biphenyl, phenyl sulphide, thianthrene, thiophenol, benzoic acid, and 1-phenylisoquinoline. $H_2S$ and CO are also produced in all cases. In these rearrangements, the C—S bonds undergo homolytic fission either simultaneously or selectively. No isomer redistribution precedes the coupling reactions. Plausible mechanisms for the above facts are proposed.

ABOEL-MAGD A. ABDEL-WAHAB, AHMED M. EL-KHAWAGA et MOHAMED T. ISMAIL. Can. J. Chem. **60**, 2870 (1982).

On a préparé quatre thioesters (**1–4**) et on les a pyrolysés en l'absence de promoteurs soit à l'état pur ou dans l'isoquinoléine comme solvant. Ces esters comprennent: le thiobenzoate de benzyle (**1**), le phénylthioacétate de phényle (**2**), le phénylthioacétate de benzyle (**3**) et le thiobenzoate de phényle (**4**). La pyrolyse du composé **1** donne principalement le tétraphényl-2,3,4,5 thiophène en plus du benzène, du biphényle, du benzylthiol et de l'acide benzoique. La décomposition thermique du composé **1** sous azote conduit au benzaldéhyde, au benzyle et seulement à une trace d'acide benzoique en plus des premiers produits. Le composé **2** conduit essentiellement au toluène et au bibenzyle en plus du benzène, du biphényle, du sulfure de phényle, du thiophénol et de l'acide phénylacétique. La thermolyse du composé **3** donne le toluène et le stilbène à côté de faibles quantités de benzylthiol et d'acide phénylacétique. Finalement, la décomposition thermique du composé **4** dans l'isoquinoléine donne le benzène, le biphényle, le sulfure de phényle, le thianthrène, le thiophénol, l'acide benzoique et la phényl-1 isoquinoléine. Dans tous les cas, on obtient également du $H_2S$ et du CO. Dans ces transpositions, les liaisons C—S subissent une fission homolytique soit simultanément soit sélectivement. Aucune redistribution d'isomères ne précède les réactions de couplage. On propose un mécanisme plausible qui permet de comprendre les faits mentionnés ci-dessus.

[Traduit par le journal]

## Introduction

The action of Raney nickel on the decomposition of some thioesters was studied elsewhere (1). In the present work, we extended our studies on the thermolysis of sulphur compounds in the absence of promoters (2, 3) to thioesters, and the utility of such esters for the generation of free radicals and the possible fate of these radicals was also examined.

## Results and discussion

The investigated thioesters, benzyl thiobenzoate (**1**), phenyl phenylthioacetate (**2**), benzyl phenylthioacetate (**3**), and phenyl thiobenzoate (**4**), were prepared and pyrolyzed in the absence of promoters. It has been known for over a century that common esters decompose only above 300°C (4). The decomposition of **1** and **3** was found to start only above 220°C and that of **2** and **4** was started above 230°C. However, heating of benzyl thiobenzoate (**1**) at 240°C for 20 h (Expt. 1) gave mainly tetraphenylthiophene (97% yield) in addition to benzene (15%), biphenyl (10%), benzyl thiol (5%), and benzoic acid (30%). Unexpectedly, we could not isolate any trace of tetraphenylthiophene from the pyrolysate of phenyl phenylthioacetate (**2**, Expt. 5) or benzyl phenylthioacetate (**3**, Expt. 7). However, thermolysis of **2** gave mainly toluene (35%) and dibenzyl (45%) in addition to minor amounts of phenyl sulphide (20%), biphenyl (5%), thiophenol (14%), and phenylacetic acid (2%), while toluene (25%) and stilbene (35%) were the major products of the pyrolysis of **4** beside a small amount of benzyl thiol (3%) and phenylacetic acid (2%). Also, thermal decomposition of phenyl thiobenzoate (**4**) in isoquinoline gave benzene (5%), biphenyl (8%), phenyl sulphide, (40%), thianthrene (5%), thiophenol (10%), and benzoic acid (20%) in addition to 1-phenylisoquinoline (3%). Thermolysis of **4** in the absence of isoquinoline (neat) gave complicated products, together with an amount of tarry matter.

A plausible mechanism for the above facts is proposed in Schemes 1–4. According to this mechanism, the rearrangement products seem to be formed through an intermolecular process involving a homolytic fission of C—S linkages (5, 6). The fission may take place either simultaneously (7)

[1]Author to whom correspondence may be addressed.

0008-4042/82/222870-06$01.00/0
©1982 National Research Council of Canada/Conseil national de recherches du Canada

Can. J. Chem. Downloaded from www.nrcresearchpress.com by 210.87.254.6 on 09/06/12
For personal use only.

Can. J. Chem. Downloaded from www.nrcresearchpress.com by 210.87.254.6 on 09/06/12
For personal use only.

with the formation of $R_1^{\cdot}$, CO, S, and $R_2^{\cdot}$ or selectively (8) with the formation of $R-\overset{O}{\overset{\|}{C}}-S^{\cdot}$ and $R_2^{\cdot}$ or $R_1\overset{O}{\overset{\|}{C}}^{\cdot}$ and $R_2S^{\cdot}$ radicals. This, of course, is dependant on the type of $R_1$ and $R_2$.

When **1** is pyrolyzed, the fragmentation may

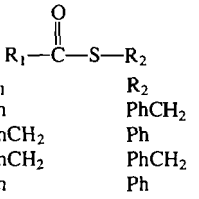

| | $R_1$ | $R_2$ |
|---|---|---|
| **1** | Ph | $PhCH_2$ |
| **2** | $PhCH_2$ | Ph |
| **3** | $PhCH_2$ | $PhCH_2$ |
| **4** | Ph | Ph |

result in the formation of benzyl and thiobenzoate radicals or, most probably, benzyl and benzoyl radicals in addition to sulphur atoms. The thiobenzoate radical tends to lose sulphur, forming benzoyl radical which is amenable to splitting off carbon monoxide (9, 10). However, the formation of tetraphenylthiophene (TPT) in almost quantitative yield substantiates the second probability. The only pathway for the formation of TPT is through dehydrogenation of tetrahydrotetraphenylthiophene formed by interaction of stilbene with sulphur, readily available in the reaction medium. The dehydrogenation of dibenzyl, formed by dimerization of benzyl radicals, gives stilbene (2, 3). The production of hydrogen sulphide gas during pyrolysis indicates that sulphur acts as dehydrogenating agent during the course of the reaction.

It is worthwhile to mention that the formation of one molecule of TPT requires four molecules of **1** and at least two (or three) atoms of sulphur. It is clear from Scheme 1 that the decomposition of four molecules of **1** is accompanied by the generation of four sulphur atoms, which means that the necessary sulphur is available in the reaction medium.

The isolation of benzoic acid in only 30% yield (Expt. 1) shows that most of the benzoyl radicals

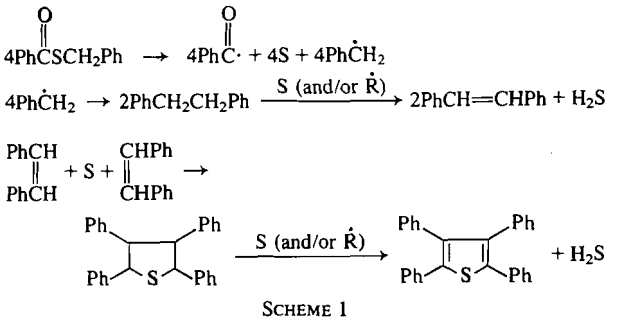

SCHEME 1

split off carbonyl groups as carbon monoxide, and phenyl radicals would be produced during the reaction. Carbon monoxide produced in this manner readily reduced palladium chloride to metallic palladium (1). The phenyl radicals were either dimerized to diphenyl or abstract hydrogen ($H_2$ Abst.) to form benzene. These findings are the same even when pyrolysis was conducted for only 8 h (Expt. 2). It is noteworthy that pyrolysis of **1** under a nitrogen atmosphere (Expt. 3) gave only a trace amount of benzoic acid. This means that the molecular oxygen is responsible for the formation of benzoic acid (11) as shown in Scheme 2. The formation of a trace amount of the acid is not unexpected during the extraction process of the pyrolysates. Furthermore, benzaldehyde and benzil were isolated in addition to the other products isolated in Expt. 1. Interestingly, pyrolysis of **1** in isoquinoline (Expt. 4) gave, in addition to the former products, the intermediates dibenzyl and stilbene, which confirms our suggested mechanism (Scheme 1). The basic extract of Expt. 4 gave 1-phenylisoquinoline and a trace of 1-benzylisoquinoline, confirming the free radical nature of these rearrangements. Furthermore, we believe that the chemisorption of the thioester, or sulphur produced from its decomposition, on the surface of the metallic catalysts or the formation of metal sulphide (10, 12) eliminates sulphur from the reaction medium and gives us a reasonable explanation for the lack of formation of TPT in the experiments of Hauptmann (1).

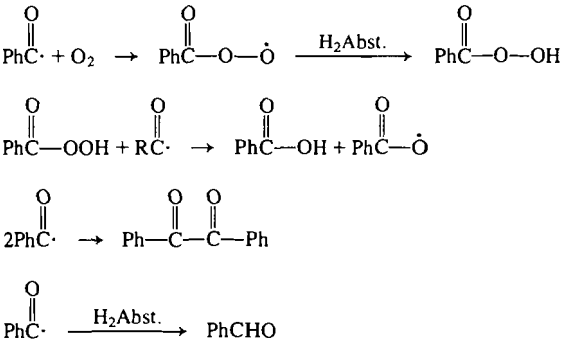

SCHEME 2

On the other hand, the lack of formation of TPT during the pyrolysis of **2** (Expt. 5) may be ascribed to the unavailability of sulphur, as the fission of the Ph—S bond is rather more difficult than that of $PhCH_2-S$ or $C-S$ bonds (8), which indicates a selective C—S bond fission during the thermal decomposition of **2**. Therefore, the benzyl radicals

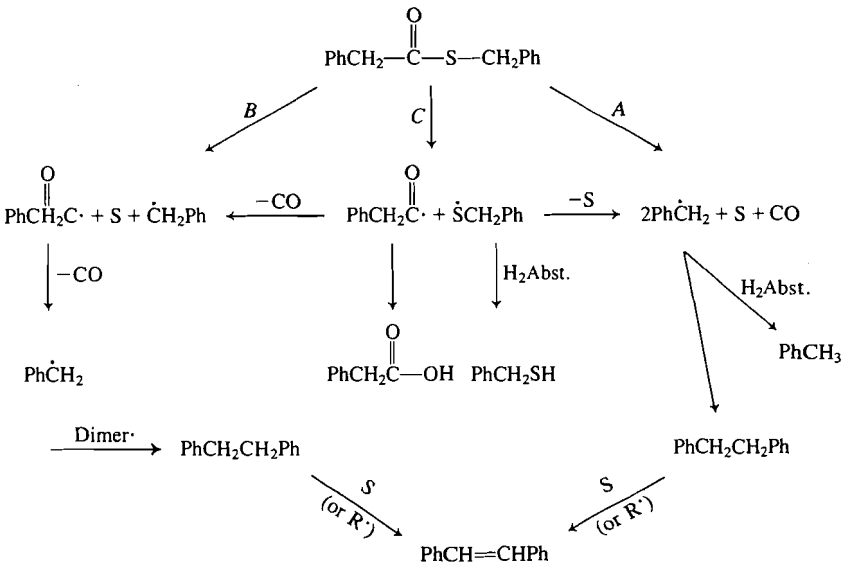


SCHEME 3

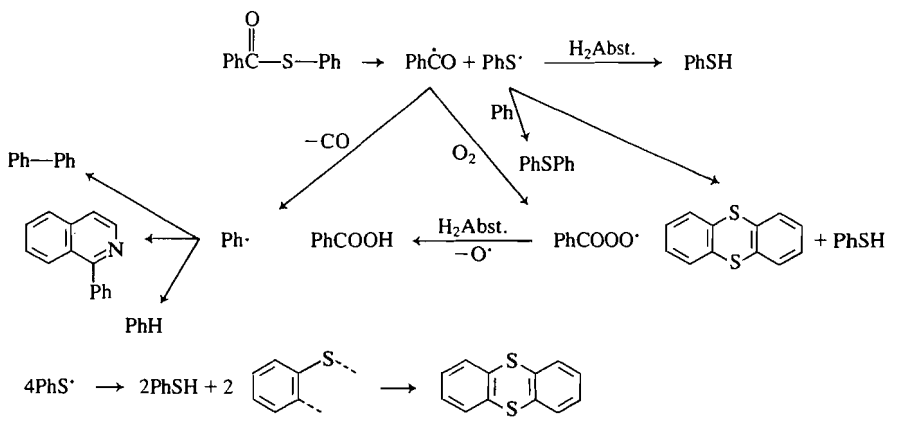


SCHEME 4

formed either directly or from decarbonation of the phenylacetyl radical tend to dimerize to dibenzyl or to abstract hydrogen, forming toluene. The formation of sizeable amounts of dibenzyl indicates a free radical reation (13). The thiophenoxy radical (PhṠ) may abstract hydrogen to thiophenol or undergoes further fragmentation to phenyl radical and sulphur leading to the formation of biphenyl, phenyl sulphide, and benzene. Also, the formation of benzyl phenyl sulphide is not unexpected. However, it undergoes further fragmentation under these conditions (2). As a further confirmation of the role of sulphur in defining the type of products, when benzyl phenylthioacetate (3) was pyrolyzed under the same conditions as previously (Expt. 7), we could not isolate TPT even in trace amounts. Instead, toluene and stilbene were the major products. Of course, all sulphur was consumed in the dehydrogenation of dibenzyl to stilbene. Also, phenylacetic acid was obtained in only 2% yield, which indicates that the decarbonation of the phenylacetyl radical is easier than that of the benzoyl radical (Expts. 1 and 7) and that the benzyl radical may be formed directly. This could be ascribed to the strength of the Ph—C(=O) bond as compared to the PhCH$_2$C(=O) bond and also to the stability of the benzyl radical. Also, the low yield of

Can. J. Chem. Downloaded from www.nrcresearchpress.com by 210.87.254.6 on 09/06/12
For personal use only.

TABLE 1. Thermal decomposition products of thioesters (**1–4**)

| Run | Thioester | Conditions[a] Solvent | Temp. (°C) | Time (h) | Neutral Products Name | % | Acidic and Basic Products Name | % | Neutral Residue (g) |
|---|---|---|---|---|---|---|---|---|---|
| 1 | $PhCOSCH_2Ph$ | — | 240 | 20 | Benzene | 15 | Benzoic acid | 30 | 0.7 |
| | | | | | Biphenyl | 10 | Benzyl thiol | 5 | |
| | | | | | TPT | 97 | | | |
| 2 | $PhCOSCH_2Ph$ | — | 240 | 8 | Benzene | 17 | Benzoic acid | 35 | 0.6 |
| | | | | | Biphenyl | 12 | Benzyl thiol | 6 | |
| | | | | | TPT | 95 | | | |
| 3 | $PhCOSCH_2Ph$[b] | — | 240 | 8 | Benzene | 13 | Benzoic acid | Trace | 0.4 |
| | | | | | Biphenyl | 11 | Benzyl thiol | 6 | |
| | | | | | Benzil | 4 | | | |
| | | | | | Benzaldehyde | 25 | | | |
| | | | | | TPT | 95 | | | |
| 4 | $PhCOSCH_2Ph$ | Isoquinoline | 260 | 20 | Benzene | 18 | Benzoic acid | 31 | 0.6 |
| | | | | | Biphenyl | 10 | Benzyl thiol | 5 | |
| | | | | | Dibenzyl | 2 | 1-Phenylisoquinoline | 2 | |
| | | | | | Stilbene | 19 | 1-Benzylisoquinoline | Trace | |
| | | | | | TPT | 73 | | | |
| 5 | $PhCH_2COSPh$ | — | 240 | 8 | Benzene[c] | 3 | Phenylacetic acid | 2 | 0.7 |
| | | | | | Toluene | 35 | Thiophenol | 14 | |
| | | | | | Biphenyl | 5 | | | |
| | | | | | Dibenzyl | 45 | | | |
| | | | | | Phenyl sulphide | 20 | | | |
| 6 | $PhCH_2COSPh$ | Isoquinoline | 260 | 20 | Benzene[c] | 5 | Phenylacetic acid | 3 | 0.7 |
| | | | | | Toluene | 38 | | | |
| | | | | | Biphenyl | 8 | Thiophenol | 10 | |
| | | | | | Dibenzyl | 40 | | | |
| | | | | | Phenyl sulphide | 15 | 1-Benzylisoquinoline | 2 | |
| 7 | $PhCH_2COSCH_2Ph$ | — | 240 | 8 | Toluene | 25 | Phenylacetic acid | 2 | 0.5 |
| | | | | | Stilbene | 35 | Benzyl thiol | 3 | |
| 8 | $PhCH_2COSCH_2Ph$ sulphur | | 240 | 8 | Toluene[c] | 5 | Phenylacetic acid | 2 | 0.3 |
| | | | | | TPT | 90 | Benzyl thiol | 2 | |
| 9 | $PhCH_2COSCH_2Ph$ | Isoquinoline | 260 | 20 | Toluene | 35 | Phenylacetic acid | 2 | 0.4 |
| | | | | | Stilbene | 30 | Benzyl thiol | 5 | |
| | | | | | | | 1-Benzylisoquinoline | 2 | |
| 10 | PhCOSPh | Isoquinoline | 260 | 20 | Benzene[c] | 5 | Benzoic acid | 20 | 0.6 |
| | | | | | Biphenyl | 8 | Thiophenyl | 10 | |
| | | | | | Phenyl sulphide | 40 | 1-Phenylisoquinoline | 3 | |
| | | | | | Thianthrene | 5 | | | |

[a]The conversion was complete at the end of thermolysis.
[b]This experiment was carried out under nitrogen.
[c]Determined by glc analysis of the crude pyrolysate.

benzyl thiol (3%) indicates that route *C* (Scheme 3) is not predominant. Furthermore, a cross experiment (Expt. 8) was conducted with a mixture of **3** and sulphur under the same conditions. As expected, TPT was isolated in 90% yield, in addition to very small amounts of toluene, benzyl thiol, and phenylacetic acid.

Finally, thermolysis of phenyl thiobenzoate (**4**) at 240°C gave a complicated, black, product mixture, together with an amount of tarry matter. However, thermolysis of **4** in isoquinoline made the decomposition controlled and benzene, biphenyl, thiophenol, phenyl sulphide, thianthrene, thiophenol, benzoic acid, and 1-phenylisoquinoline were isolated.

Most probably, rearrangement of **4** takes place after selective fission of the C—S bonds. The formation of thianthrene is expected on the basis of the disproportionation of thiophenoxy radicals (14). Trapping of phenyl radicals (Expts. 4 and 10) and benzyl radicals (Expts. 2 and 9) by means of isoquinoline offers further evidence for the free radical fission of thioesters. Furthermore, it was noticed that no isomer redistribution precedes the

Can. J. Chem. Downloaded from www.nrcresearchpress.com by 210.87.254.6 on 09/06/12
For personal use only.

Can. J. Chem. Downloaded from www.nrcresearchpress.com by 210.87.254.6 on 09/06/12
For personal use only.

coupling reactions under the reaction conditions used (15).

## Experimental

Melting points were determined on a Kofler melting point apparatus and were uncorrected. Column chromatographic separations were carried out using 100 × 1 cm glass columns packed with neutral alumina using successively petroleum ether (40–60°C), petroleum ether (40–60°C) – petroleum ether (60–80°C) mixtures, petroleum ether (60–80°C), petroleum ether (60–80°C) – benzene mixtures, benzene, benzene–ether mixtures, ether, ether–methanol mixtures, and finally methanol. Thin-layer chromatography was performed using 10 × 3 cm glass plates coated with silica gel. The glc analyses were carried out on a Pye–Unicam apparatus, series 105, using a 5 ft × ¼ in. column packed with SE30 over Chromosorb.

Identification of the products was confirmed using authentic samples, elemental analysis, tlc and/or glc techniques. All molecular rearrangements were carried out in duplicate. Results are given in Table 1.

*Starting materials*

Benzyl thiobenzoate, phenyl phenyl phenylthioacetate, benzyl phenylthioacetate, and phenyl thiobenzoate were prepared as described before (16–18).

It is worthwhile to mention that a number of preliminary experiments were carried out to determine the proper temperature for pyrolysis. However, results showed that the decomposition of **1** and **3** starts only above 220°C and above 230°C for **2** and **4**. Also, it was found that 240°C is the lowest temperature at which the conversion of the thioesters (**1–4**) was complete at the end of pyrolysis.

*General procedure*

The thioester (15 g) was placed in a 50 mL round flask fitted with an efficient reflux condenser (1.5 m length) and heated either alone (Expts. 1, 2, 3, 5, and 7) or in 15 mL isoquinoline solvent (Expts. 4, 6, 9, and 10) using a temperature controlled heating mantle adjusted to the desired temperature. The temperature was measured using a thermometer immersed in the reaction flask. The exit gases were trapped in lead acetate for $H_2S$ and passed over palladium chloride for CO. After decomposition was complete, the pyrolysate was subjected to normal distillation up to 140°C (except in Expt. 3 where the oil bath temperature was raised to 200°C), using a microdistillation system, for separation of low boiling point products such as benzene and/or toluene. Benzene was collected at 75–80°C and its glc analysis showed a single peak at 0.7 min at 90°C, as for an authentic sample, and toluene was collected at 105–110°C and revealed a peak at 1 min at 90°C, comparable with an authentic sample. Benzaldehyde was collected at 175–180°C and showed a peak at 2.8 min at 90°C, as did an authentic sample; mp of 2,4-dinitrophenylhydrazine derivative and mmp 236°C (lit. (19) mp 236°C).

The nondistillable residue was dissolved in ether and the ether solution was extracted with two 10 mL portions of 10% $NaHCO_3$ solution for separation of acids and twice with 10 mL of 5% NaOH solution for separation of thiols. The alkaline extracts were separately neutralized with 2 *N* HCl and the products, acids and thiols, were separated and identified. The acid-free ether solution was resolved either directly by glc and/or column chromatography (Expts. 1, 2, 3, 5, 7, and 9) or separated into neutral and basic products (Expts. 4, 6, 9, and 10) using HCl solution. In Expts. 1, 2, and 3 most of the TPT was separated by filtration as an ether insoluble product and recrystallized from amyl alcohol, mp and mmp 189°C (lit. (20) mp 185°C). The neutral products were eluted from the chromatogram column using the former sequence of eluents. Biphenyl was eluted with petroleum ether (40–60°C), and showed a glc peak at 3.0 min at 140°C, mp and mmp 70°C (lit. (21) mp 71–79°C). Dibenzyl was eluted with petroleum ether (40–60°C) – petroleum ether (60–80°C) mixture (1:2), and showed a single peak at 3.3 min at 140°C, mp and mmp 52°C (lit. (22) mp 52–53°C). Stilbene was eluted with petroleum ether (60–80°C), mp as well as mmp 125°C (lit. (23) mp 124°C). Phenyl sulphide was eluted with petroleum ether (60–80°C) and identified as phenyl sulphone obtained from its oxidation using a $H_2O$ – acetic acid mixture (24), mp and mmp 128°C (lit. (25) mp 128–129°C). Thianthrene was eluted with petroleum ether (60–80°C) – benzene mixture (5:1), mp and mmp 158°C (lit. (26) mp 158–159°C). 2,3,4,5-Tetraphenylthiophene was eluted with petroleum ether (60–80°C) – benzene mixture (1:1), mp and mmp 188°C (lit. (20) mp 185°C). Benzil was eluted with petroleum ether (60–80°C) – benzene mixture (1:2), mp and mmp 96°C (lit. (19) mp 196°C).

The acidic extract was neutralized and the amine fraction was extracted with ether. Ether was evaporated and isoquinoline was distilled at 240°C. The residue was analysed using column chromatography. 1-Phenylisoquinoline (Expts. 4 and 10) was eluted with petroleum ether (60–80°C) – benzene (2:3) mixture, mp and mmp 95°C (petroleum ether (60–80°C), lit. (27) mp 95–96°C); mp of picrates 164°C (ethanol) (lit. (27) mp 165–166°C). 1-Benzylisoquinoline (Expts. 6 and 9) was eluted with petroleum ether (60–80°C) – benzene mixture (1:1), mp and mmp 55°C (lit. (28) mp 56°C); mp of picrates 180°C (lit. (27) mp 182°C). In Expt. 4, the mixture of 1-benzylisoquinoline and 1-phenylisoquinoline was analysed using preparative thin-layer chromatography, $R_f = 0.4$ and 0.6, respectively, and the solvent used was petroleum ether (60–80°C) – benzene mixture (1:1).

*Thermolysis of benzyl phenylthioacetate in the presence of sulphur*

A mixture of benzyl phenylthioacetate (15 g) and sulphur (2 g) was heated for 8 h. The reaction mixture was processed as described before in the general procedure (Expt. 8).

1. H. Hauptmann and B. Wladislaw. J. Am. Chem. Soc. **72**, 710 (1950).
2. A. E. Abdel-Rahman and A. A. Abdel-Wahab. Indian J. Chem. **18** (B), 402 (1979).
3. A. A. Abdel-Wahab and A. E. Abdel-Rahman. Indian J. Chem. **20**(B), 636 (1981).
4. C. H. De Puy and R. W. King. Chem. Rev. **60**, 431 (1960).
5. H. Hauptmann and W. F. Walter. Chem. Rev. **62**, 347 (1962); G. R. Pettit and E. E. Van Tamelon. Org. React. **12**, 356 (1962).
6. W. A. Bonner. J. Am. Chem. Soc. **74**, 1034 (1952).
7. W. Z. Heldt. J. Org. Chem. **30**, 3897 (1965).
8. L. Pauling. The nature of the chemical bond and the nature of molecules and crystals. 3rd ed. George Banta Co., U.S.A. 1960.
9. A. Mailhe and F. Godon. Bull. Soc. Chim. **19**, 449 (1916); A. Mailhe. C. R. Acad. Sci. **180**, 111 (1925).
10. W. A. Waters. The chemistry of free radicals. Oxford University Press. 1946. p. 116.
11. (*a*) H. L. J. Backstrom. Z. Physik. Chem. (Leipzig), **25B**, 99 (1934); (*b*) E. Briner and A. Lardon. Helv. Chim. Acta, **19**, 1062 (1936); (*c*) F. A. Carey and R. J. Sunnberg. Advanced organic chemistry. Part A. A. Plenum Publishing Corporation, New York. 1977. p. 531.
12. H. H. Voge. Catalysis, 407 (1958).
13. L. O. Farng and J. L. Kice. J. Org. Chem. **46**, 2599 (1981).
14. A. Schonberg and A. Mustafa. J. Chem. Soc. 889 (1949).
15. R. M. Noys. J. Chem. Phys. **22**, 1349 (1953); J. Am. Chem. Soc. **77**, 2044 (1955); J. Phys. Chem. **65**, 763 (1961).

16. R. OTTO and R. HIDEN. Ber. **13**, 1285 (1880).
17. K. MIYAKI and S. YAMAGISHI. J. Pharm. Soc. Jpn, **76**, 436 (1956).
18. R. SCHILLER and R. OTTO. Ber. **9**, 1636 (1876).
19. A. I. VOGEL. A text book of practical organic chemistry. 3rd ed. Low and Brydone, London. 1965.
20. E. BERGMAN. J. Chem. Soc. 505 (1936).
21. F. J. GARICK. Trans. Faraday Soc. **23**, 451 (1927).
22. E. C. KLEIDERER and E. C. KORNFELD. J. Org. Chem. **13**, 485 (1948).
23. D. A. BALLARD and W. M. DEHN. J. Am. Chem. Soc. **54**, 3969 (1932).
24. H. GILMAN and H. S. BROADBENT. J. Am. Chem. Soc. **69**, 2053 (1947).
25. H. GILMAN and R. E. FOTHERGILL. J. Am. Chem. Soc. **51**, 3506 (1929).
26. G. DOUGHERTY and P. D. HAMMOND. J. Am. Chem. Soc. **57**, 117 (1935).
27. W. DAVIES, J. F. KEFFORD, and J. S. OSBORNE. J. Chem. Soc. 360 (1939).
28. V. J. PRAUN and J. NELLES. Ber. **70B**, 1767 (1937).

Can. J. Chem. Downloaded from www.nrcresearchpress.com by 210.87.254.6 on 09/06/12
For personal use only.

# Decomposition of PCB's in the radio-frequency glow discharge plasmas of oxygen, hydrogen, and water vapor

K. HIRAOKA,[1] K. AOYAMA, T. NAKAMURA, S. MOCHIZUKI, K. MITSUMORI, AND K. MATSUNAGA

*Faculty of Engineering, Yamanashi University, Takeda-4, Kofu 400, Japan*

Received March 24, 1982

K. HIRAOKA, K. AOYAMA, T. NAKAMURA, S. MOCHIZUKI, K. MITSUMORI, and K. MATSUNAGA. Can. J. Chem. **60**, 2876 (1982).

A study was made on the decomposition of PCB's in a radio-frequency glow discharge plasma. PCB's were completely decomposed in plasmas of a few Torr of oxygen, hydrogen, and water vapor. Gaseous products from PCB's in an oxygen plasma were carbon monoxide, carbon dioxide, water, hydrogen chloride, chlorine, and chlorine dioxide. Hazardous compounds such as phosgene and vinyl chloride were not detected by gc–ms analysis. The total quantity of oxygen flowed past the sample was only about three times the stoichiometric oxygen required for the perfect oxidation of PCB's. In a hydrogen plasma, PCB's gave ethane and isobutane as major gaseous products and several higher hydrocarbons as minor products. Almost all of the chlorine in PCB's was converted to hydrogen chloride. Major products from PCB's in a water vapor plasma were carbon dioxide, carbon monoxide, and hydrogen chloride. No other products were detected. The mechanisms for reactions occurring in plasmas are discussed. The importance of the wall effect for the formation of solid products is discussed.

K. HIRAOKA, K. AOYAMA, T. NAKAMURA, S. MOCHIZUKI, K. MITSUMORI et K. MATSUNAGA. Can. J. Chem. **60**, 2876 (1982).

On a étudié la décomposition du PCB dans un plasma dont l'effluve se situe dans le domaine des fréquences radio. Le PCB se décompose complètement dans des plasmas d'oxygène, d'hydrogène ou de vapeur d'eau sous pression réduite (quelques Torr). Les produits gazeux obtenus dans un plasma d'oxygène sont le monoxyde de carbone, le bioxyde de carbone, l'eau, le chlorure d'hydrogène, le chlore et le bioxyde de chlore. L'analyse par cg–sm n'a pas permis de déceler la présence de produits dangeureux tels le phosgène, et le chlorure de vinyle. La quantité totale d'oxygène qui traverse l'échantillon représente seulement environ le triple de la quantité stochiométrique requise pour réaliser l'oxydation du PCB. Dans un plasma d'hydrogène, le PCB conduit à l'éthane, et à l'isobutane comme produits gazeux principaux et à plusieurs hydrocarbures supérieurs comme produits secondaires. Presque tout le chlore des PCB se transforme en chlorure d'hydrogène. Les produits majoritaires obtenus à partir du PCB dans un plasma d'eau sont le bioxyde de carbone, le monoxyde de carbone et le chlorure d'hydrogène. On n'a pas décelé d'autres produits. On discute des mécanismes des réactions qui se produisent dans les plasmas. On conclut à l'importance de l'effet de paroi lors de la formation de produits solides.

[Traduit par le journal]

Can. J. Chem. Downloaded from www.nrcresearchpress.com by 210.87.254.40 on 09/06/12
For personal use only.

For the decomposition of PCB's, methods using molten salt (1), pyrolysis (2, 3), radiolysis (4–7), photolysis (8), and dechlorination by alkali metal – naphthalene (9) have been reported.

In this study, we attempted to find out whether PCB's could be decomposed in low-temperature glow discharge plasmas. It was found that PCB's were decomposed completely in plasmas of a few Torr pressure of oxygen, hydrogen, and water vapor. In this paper, the results of detailed analyses of decomposition products are given and mechanisms for the decomposition of PCB's in glow discharge plasmas are discussed.

## Experimental

*Samples*

Samples of PCB's were Kanechlor-200 (KC-200) and Kanechlor-500 (KC-500). Their empirical formulae determined by elemental analysis (Perkin-Elmer 240) were $C_{12}H_{7.99}Cl_{2.01}$ and $C_{12}H_{4.81}Cl_{5.19}$, respectively.

The purity of $O_2$ and $H_2$ gases purchased from Nippon Sanso LTD were 99.5% and 99.99999%, respectively.

*Procedure*

A few tenths of a gram of PCB's in a ceramic boat were put in a Pyrex discharge tube with an inner diameter of 10 mm. The pressure of the gas introduced to the vacuum line was controlled by adjusting a needle valve (Nupro 4BM metering valve). The PCB's were decomposed in a glow discharge plasma which was generated by a radio-frequency generator with a maximum power of 50 W. The temperature of the discharge tube in operation was about 200°C. The discharge gas flowed continuously through the discharge tube and then passed through two traps cooled to dry ice – acetone and liquid $N_2$ temperatures and was then pumped away by an oil-rotary pump with a capacity of 150 L/min.

*Product analysis*

The gaseous products in the dry ice – acetone and liquid $N_2$ traps were analysed with a Shimadzu 6APTF gas chromatograph with a thermal conductivity detector. A confirmation of products was performed using an Hitachi 063 gas chromatograph – mass spectrometer. For these analyses, 2 m stainless steel columns packed with Porapak Q (80–100 mesh) and 2,4-dimethylsulfolane (25% supported on Shimalite 60–80 mesh) were used.

The analysis for hydrogen chloride, chlorine, and chlorine oxides was done separately. In alkaline solution, chlorine and chlorides are converted to anions as follows:

$$Cl_2 \rightarrow Cl^- + ClO^-$$

$$HCl \rightarrow Cl^-$$

$$Cl_2O \rightarrow ClO^-$$

$$ClO_2 \rightarrow ClO_2^- + ClO_3^-$$

$$Cl_2O_6 \rightarrow ClO_3^- + ClO_4^-$$

[1]To whom all correspondence should be addressed.

0008-4042/82/222876-07$01.00/0

©1982 National Research Council of Canada/Conseil national de recherches du Canada

Can. J. Chem. Downloaded from www.nrcresearchpress.com by 210.87.254.40 on 09/06/12
For personal use only.

and

$$Cl_2O_7 \rightarrow ClO_4^-$$

Thus quantitative analyses of chlorine, hydrogen chloride, and chlorine oxides could be done by means of the Mohr method and redox titration methods (10, 11) after the gaseous products were dissolved in sodium hydroxide solution or potassium iodide and sodium hydrogencarbonate solutions. The analysis of $ClO_4^-$ was done by means of the Methylene Blue method (12).

*Emission spectra*

The emission spectra of plasmas were measured using a monochromator (Optech GM-N-250) equipped with a light chopper, photomultiplier (Hamamatsu TV, R-446), and lock-in amplifier (NF Circuit Design Block, LI-573). For the measurement of the emission spectra, the plasma was generated by a microwave generator (Ewig Shokai, MR-IIIS, 2450 MHz) with a cavity resonator. The radio-frequency generator could not be used because the noise from the generator was too high for compatibility with the lock-in ac detection.

## Results

*Oxygen plasma*

When 1/10 g of PCB's was subjected to an $O_2$ plasma operating at a pressure of 1.8 Torr (the flow rate is $3.15 \times 10^{-5}$ mol/s), they quickly decomposed into gaseous products in only 5 min. Temporary brownish liquid and solid products formed on the wall of the discharge tube also decomposed easily within 10 min. There was no time difference between KC-200 and KC-500 for their complete decomposition. The only product found in the dry ice – acetone cooled trap was water. The products in the liquid-$N_2$-cooled trap were analysed by gc and gc–ms. The products detected were carbon dioxide and hydrogen chloride. No carbonaceous compounds other than carbon dioxide were detected. On the average, 40% of the carbon content in PCB's was converted to carbon dioxide. The rest (60%) should be converted to carbon monoxide which can not be trapped by a liquid-$N_2$-cooled trap. A small amount of ozone, detected as an oxygen peak in a gas chromatogram, was also a gaseous product from the glow discharge in oxygen.

Chlorine and chlorine dioxide, which were not detected by the gas chromatograph owing to their high reactivities, were confirmed as reaction products by separate experiments as described in the previous section. The yields (mol%) of hydrogen chloride, chlorine, and chlorine dioxide for KC-200 and KC-500 decomposed in a 1.8 Torr $O_2$ plasma were 90, 9, 1 and 78, 21, 1, respectively. The total content of chlorine in these products corresponds almost exactly to that of the PCB sample. No $ClO_4^-$ ion was detected in an alkaline solution of decomposition products; i.e., the amounts of $Cl_2O_6$ and $Cl_2O_7$ were negligible as reaction products.

*Hydrogen plasma*

Contrary to the decomposition of PCB's in an $O_2$ glow discharge plasma, persistent brownish solid products were produced on the wall of the discharge tube when PCB's were subjected to a $H_2$ plasma. The solid products were found to decompose only very gradually but completely within a few hours under continuous stimulation by the $H_2$ plasma.

Figure 1 shows the gas chromatogram of the gaseous products from the decomposition of KC-200 in a plasma at a pressure of 1 Torr of hydrogen, obtained using an Hitachi 063 gc–ms. The gas chromatogram of the gaseous products from KC-500 was very similar to the one shown in Fig. 1. The most probable identification of peaks in Fig. 1 is given in its caption. In parentheses are shown the relative amounts (mol%) of each component. It is worth noting that no chlorinated compounds were detected in the chromatogram; i.e., the conversion of chlorine in PCB's to hydrogen chloride was very efficient (see below). In these experiments, hydrogen chloride, which does not appear in Fig. 1, was removed from the gaseous products by putting solid sodium hydroxide in the liquid-$N_2$-cooled trap in order to protect the apparatus from corrosion.

Figure 2 shows the $H_2$ pressure dependence of the yield of $Cl^-$ ion. The total content of chlorine in the PCB sample is designated to be 100%. In all runs shown in Fig. 2, no $ClO_n^-$ ($n = 1$) ions were detected; i.e., the yield of $Cl^-$ ion corresponds to that of hydrogen chloride. The yields of $Cl^-$ show maxima at about 1 Torr of $H_2$ pressure for both KC-200 and KC-500. The decrease of the yields at lower and higher pressure can be understood as follows. The solid products on the wall of the discharge tube below 1 Torr appeared as a firm deposit, and the lower the pressure, the harder it became to achieve complete decomposition of the solid products. At higher pressures, it was easier to decompose the solid products into gaseous products; however, the flow rate of the hydrogen gas inevitably became faster and some of the solid products were carried away downstream from the plasma region before suffering decomposition into gaseous products. The higher yield of $Cl^-$ for KC-500 than for KC-200 may be due to the slower rate of vaporization of the KC-500 sample. Although complete decomposition of solid products was difficult to attain and the stoichiometry of the conversion of chlorine in PCB's into products was far from adequate in this experiment, the conversion of chlorine in PCB's to hydrogen chloride could be considered very efficient because gaseous

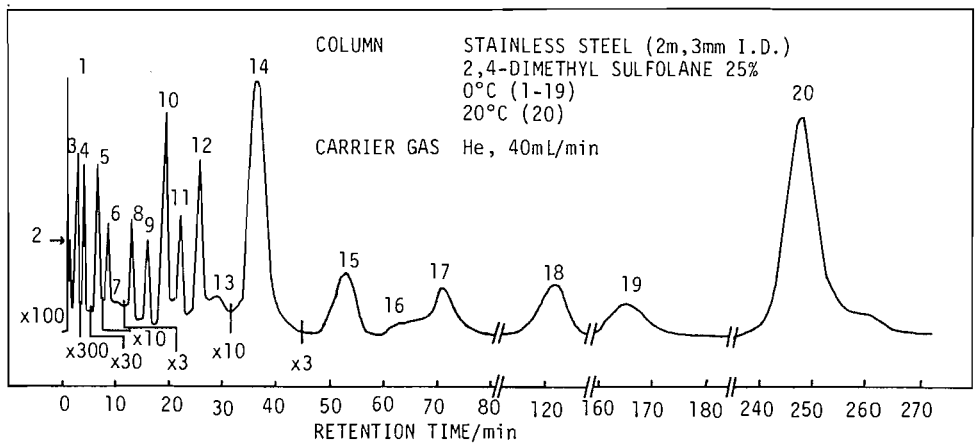


FIG. 1. Gas chromatogram of gaseous products from the decomposition of KC-200 in a plasma of 1 Torr hydrogen. The most probable identification of peaks is given below with the relative amount (mol%) of each component in parentheses: (*1*) ethane (18.0), (*2*) propane (3.6), (*3*) isobutane (7.6), (*4*) butane (43.0), (*5*) 1-pentene (5.8), (*6*) 2-methyl-1-butene (1.1), (*7*) 2-methyl-2-butene (0.1), (*8*) 4-methyl-1-pentene (0.5), (*9*) 1-butyne (0.6), (*10*) cyclopentene (1.2), (*11*) methylcyclopentane (0.6), (*12*) 3-methyl-2-pentene (1.3), (*13*) isopropenylcyclopropane (1.2), (*14*) 4,4-dimethyl-1-pentene (5.2), (*15*) 3-hexene (1.1), (*16*) cycloheptane (0.1), (*17*) 4-methyl-2-hexene (0.5), (*18*) not identified, (*19*) 1,3-butadiyne (2.4), (*20*) benzene (4.6).

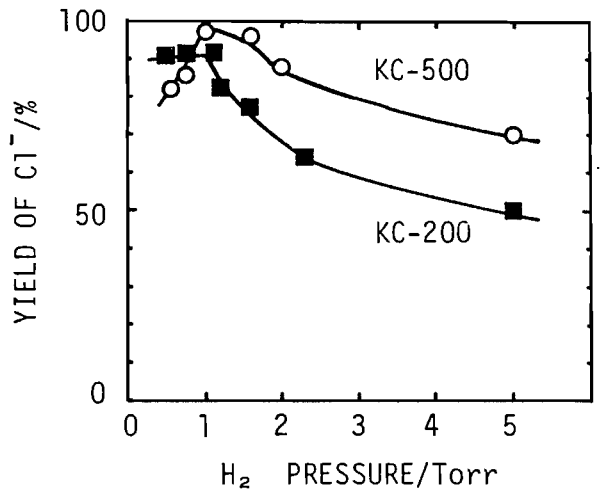


FIG. 2. The hydrogen pressure dependence on the yield of $Cl^-$ ion.

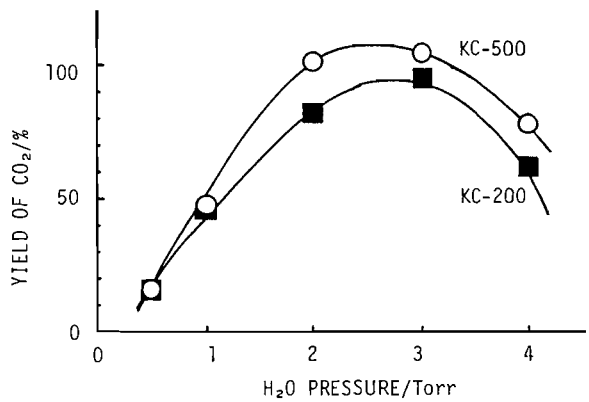


FIG. 3. The $H_2O$ pressure dependence on the yield of $CO_2$ produced from PCB's decomposed in a $H_2O$ plasma. ■: KC-200, ○: KC-500.

products detected by gc–ms did not contain chlorine atoms.

*Water vapor*

Brownish solid products were formed when ~100 mg of PCB's were decomposed in a $H_2O$ plasma as in the case of the $H_2$ plasma. However, it was much easier to decompose the solid products in a $H_2O$ plasma than in a $H_2$ plasma. The solid products could decompose completely within 60 min.

By gc and gc–ms analyses, the only products detected were $CO_2$ and HCl. The pressure dependence of the yield of $CO_2$ is shown in Fig. 3. The total carbon content in the PCB sample is designated to be 100%. Because no carbonaceous compounds other than $CO_2$ were detected by gc and gc–ms, all of the carbon in the PCB's must be converted to carbon monoxide and carbon dioxide.

In Fig. 4 is shown the $H_2O$ pressure dependence of the yield of $Cl^-$ ion. The total content of chlorine in the PCB sample is designated to be 100%. Because the conversion of the chlorine in PCB's to $Cl^-$ was found to be 100 + 2% for all pressures measured and no $ClO_n^-$ ($n \geqq 1$) was detected, almost all of the chlorine in the PCB's was converted to hydrogen chloride.

*Emission spectra*

The emission spectra of plasmas during the

Can. J. Chem. Downloaded from www.nrcresearchpress.com by 210.87.254.40 on 09/06/12
For personal use only.

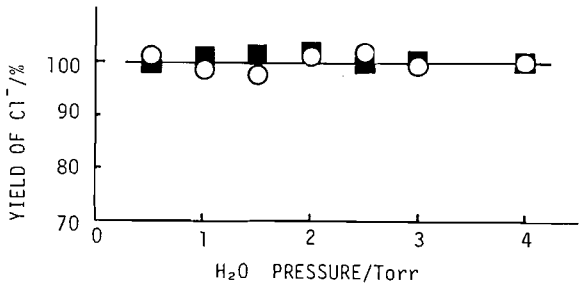


FIG. 4. The $H_2O$ pressure dependence on the yield of $Cl^-$ ion.

decomposition of KC-500 were measured. The wavelengths of the observed emission spectra of species which are the decomposition products from KC-500 are given below in Å units. The letters s, m, and w represent the relative emission intensities as being strong, medium, or weak.

*$O_2$ plasma*: CO(2665s, 2785w, 2833w, 2977s, 3134s, 3242w, 3305m, 3419w, 3680w, 4510s, 4661m, 4835s), OH(3064 system, $^2\Sigma \rightarrow {}^2\Pi$, s), CH(4312m), Cl(4526s, 4601w).

*$H_2$ plasma*: CH(4312s), $C_2$(5165m, 5540w, 5585w, 5635w).

*$H_2O$ plasma*: CH(4330m).

## Discussion

*Oxygen plasma*

As was mentioned previously, PCB's decomposed completely into gaseous products with a very high efficiency in an $O_2$ glow discharge plasma. The total quantity of oxygen flowed past the sample was only about three times the stoichiometric oxygen required for the perfect oxidation of PCB's. If a high-power radio-frequency generator were used and PCB's were fed continuously into a plasma, we think the present method could be technically applicable to the decomposition of PCB's. This high efficiency suggests that the direct decomposition of PCB's by high-energy electrons in a plasma was one of the major decomposition mechanisms of PCB's as well as the reaction of oxygen atoms with PCB's. In addition, ion/molecule reactions, whose rate constants are generally several orders of magnitude larger than those of neutral/neutral reactions, may play some roles for the dechlorination of PCB's. PCB's have positive electron affinities and thus electron capture by PCB molecules in a plasma would give a considerable concentration of negative molecular ions of PCB's in a plasma. Ion/molecule exchange reactions [1] and [2] involving $O_2$ and $O_2^-$,

[1] $MCl^- + O_2 = MO^- + ClO$

[2] $MCl + O_2^- = MO^- + ClO$

were found important in the negative ion/molecule reactions of chlorinated aromatic compounds and PCB's (13–15). The ClO radical, which can be also formed by the termolecular reaction [3],

[3] $Cl + O + M = ClO + M$

may be the precursor for the formation of $ClO_2$ (16):

[4] $ClO + ClO = ClO_2 + Cl$

Although rate constants have been measured for a number of oxygen atom reactions with aromatic molecules, the products of the elementary reactions are not well defined. Recently, Sloane identified the reaction products of $O(^3P)$ + benzene, toluene, and 1,3,5-trimethylbenzene collisions in molecular beams (17). He observed two product paths for O + benzene: (*1*) the O atom – benzene adduct, which is most likely phenol, and (*2*) carbon monoxide and a $C_5H_6$ hydrocarbon which is probably 3-penten-1-yne. The reactions of oxygen atoms with alkenes have been studied extensively, and CO has always been observed as one of the major products. The major product CO in this experiment must be formed by the reaction of oxygen atoms with various olefinic decomposition products which are formed by the primary reaction of O with PCB's and the dissociation of PCB's by electron impact in a plasma. The oxidation of CO to $CO_2$ must be ascribed mainly to the termolecular reaction [5],

[5] $CO + O + M = CO_2 + M$

where M represents the third-body or the wall.

In this experiment, it was found that the amount of solid products was relatively less than those formed in $H_2$ and $H_2O$ plasmas. As the solid products are formed mainly by the reactions of free radicals, the present experimental results suggest that the relative amount of reactive free radicals is less in an $O_2$ plasma than in $H_2$ and $H_2O$ plasmas. The ground state of an oxygen molecule is a triplet ($^3\Sigma_g^-$) and an $O_2$ molecule can act as a radical scavenger. Thus free radicals in an $O_2$ plasma could be scavenged by oxygen molecules (i.e. the formation of peroxides) and the formation of polymers by radical chain reactions or radical–radical recombination reactions must be more or less inhibited. This might explain why the $O_2$ plasma formed relatively less solid products than $H_2$ and $H_2O$ plasmas.

*Hydrogen plasma*

The efficiency of the decomposition of PCB's in a $H_2$ plasma was much lower than in $O_2$ and $H_2O$ plasmas. However, a gc–ms analysis showed that gaseous products from the decomposition of PCB's in a $H_2$ plasma did not contain chlorine atoms.

Can. J. Chem. Downloaded from www.nrcresearchpress.com by 210.87.254.40 on 09/06/12
For personal use only.

Can. J. Chem. Downloaded from www.nrcresearchpress.com by 210.87.254.40 on 09/06/12
For personal use only.

Almost all of the chlorine atoms in PCB's were converted to hydrogen chloride. This high yield of hydrogen chloride strongly suggests the very efficient dissociative electron attachment reactions of chlorinated compounds in the plasma.

[6] $MCl + e = M + Cl^-$

The produced $Cl^-$ ion would be rapidly converted to HCl in a hydrogen plasma by reaction [7],

[7] $Cl^- + H = HCl + e$

whose rate constant is very large ($0.96 \times 10^{-9}$ $cm^3$/molecule s) (18). We would like to suggest that the electron attachment reaction plays an important role for the dechlorination of PCB's in all of $O_2$, $H_2$, and $H_2O$ plasmas.

The optical radiation emitted by the $H_2$ plasma at a pressure of a few Torr contained an intense continuous spectrum in the ultraviolet region. The uv radiation may make some contribution to the decomposition of PCB's in a $H_2$ plasma. In addition, the uv radiation is strongly absorbed by solid products on the wall of the discharge tube where the polymer free radicals must be formed. The polymer free radicals are further cross-linked to form a three-dimensionally rigid solid. This may be the reason why the solid products formed in a $H_2$ plasma are quite stable against the continuous stimulation by a plasma.

*Water vapor plasma*

It was found that the decomposition of PCB's in a $H_2O$ plasma was quite efficient. The primary reactive radicals formed in a $H_2O$ plasma are OH and H. The recombination reaction [8] of two OH radicals produces an O atom.

[8] $OH + OH = H_2O + O$

Thus the major active species in a $H_2O$ plasma are considered to be H, OH, and O radicals. The decomposition of PCB's in a $H_2$ plasma was much slower than that in a $H_2O$ plasma. Thus the OH and O radicals must play important roles for the decomposition of PCB's in a $H_2O$ plasma. For the reactions with arenes, the rate constants of OH are one to two orders of magnitude larger than those of O. Perry *et al.* (19) suggested that the addition of the OH radical to the aromatic ring was a dominant path at low temperatures, and that hydrogen atom abstraction was more important at higher temperatures.

When PCB's were decomposed in plasmas of $H_2$ and $H_2O$, $Cl_2$ was not detected as a decomposition product. The $Cl_2$ molecule will be formed mainly by reaction [9].

[9] $Cl + Cl + M = Cl_2 + M$

One of the reactions which is a source of Cl radicals is the reaction of H with HCl; i.e., it consumes HCl.

[10] $H + HCl = H_2 + Cl$ (slow)

However, $Cl_2$ molecules when produced are quickly decomposed by the fast reaction [11].

[11] $H + Cl_2 = HCl + Cl$

As $Cl_2$ was one of the major products from PCB's decomposed in an oxygen plasma, the absence of $Cl_2$ for the case of $H_2$ and $H_2O$ plasmas must be due to the existence of hydrogen atoms in $H_2$ and $H_2O$ plasmas.

The strong $H_2O$ pressure dependence of the yield of $CO_2$ (Fig. 3) was not well understood. Because CO can be oxidized in a $H_2O$ plasma by reaction [12],

[12] $CO + OH = CO_2 + H$

the observed pressure dependence may be correlated with the relative concentration of OH radicals in the plasma.

The degradation of PCB's in water by ionizing radiation has been undertaken at several institutes (20). It was suggested that OH radicals in water play an important role for the decomposition of PCB's. The addition of a OH radical to the aromatic ring must be much more favorable than a hydrogen abstraction reaction in the liquid phase because the internal energy of adducts is efficiently absorbed by the medium. Thus low concentrations of PCB's in water can be made water soluble (i.e. less lipid-soluble) by the introduction of hydrophilic hydroxyl groups into PCB's — and consequently are unlikely to bioaccumulate — by bombardment with high-energy electrons.

*Wall effect*

The properties of polymeric films produced in various types of plasmas such as chemical inertness, good adhesion to the substrate, and ease and versatility of preparation could lead to important practical applications. However, the formation of nonvolatile polymeric solid films during the decomposition of PCB's in $O_2$, $H_2$, and $H_2O$ plasmas was apparently an undesirable result because the decomposition of solid films was the rate-controlling step for the complete decomposition of PCB's into gaseous products. In view of the large number of elementary reactions taking place in an electric discharge, the formulation of a mechanism for

Can. J. Chem. Downloaded from www.nrcresearchpress.com by 210.87.254.40 on 09/06/12
For personal use only.

polymer formation and the verification of this mechanism are very difficult tasks to accomplish. It is worth noting that the polymeric solid films were produced only on the part of the discharge tube *which was in contact with the plasma flame*. If the polymeric solids were formed in the gas phase, they should also deposit downstream from the plasma region because the flow rate of gas in the discharge tube was quite high (5–10 m $s^{-1}$). Therefore the wall itself must play a very important role for the formation of polymeric solid films on the wall of the discharge tube. Because the electron temperature is very much higher than the gas and ion temperatures in a low-temperature glow discharge plasma,[2] the wall which is in contact with the plasma becomes negatively charged under steady state conditions. The potential difference between the wall and the plasma (namely the ion sheath potential) keeps the net current (due to electrons and positive ions) to the wall zero. When the positive ions pass through the ion sheath,[3] they are accelerated and gain maximum kinetic energy corresponding to the sheath potential, which may be roughly estimated as 10 eV or even more (21) under the present experimental conditions. Some of this energy is dissipated through chemical effects such as the production of free radicals on the surface of the film. This leads to the continuous growth of polymers by the reactions of radicals with radicals and molecules. In brief, we think that the major process for the formation of polymeric solids is the bombardment of the solid surface by high-energy ions as well as electrons.

The rate of decomposition of solid products formed in an $O_2$ plasma was much faster than that in $H_2$ and $H_2O$ plasmas. This suggests the existence of chemical effects for the decomposition of solid products. If physical effects involving high-energy ions and electrons such as the ablation of solid products were important for the decomposition of solid products, the rate for the decomposition of solid products should not be very different amongst $O_2$, $H_2$, and $H_2O$ plasmas. When the temperature of the discharge tube was kept at room temperature by circulating water outside the discharge tube,[4] it took hours to decompose the solid products even in an $O_2$ plasma. This result clearly indicates that there is an activation energy for the decomposition reaction of solid products. This means that oxygen atoms play an important role for the decomposition of solid products in an $O_2$ plasma, because reactions of high-energy ions with solid products or an action of electrons should not show such a marked temperature dependence. From these results, we would like to conclude that for the formation of solid products, the high-energy ions and electrons play important roles, but for the decomposition of solid products, chemically reactive radicals play important roles.

According to the positive column theory (22), the electron temperature $T_e$ in a plasma is determined by the product of the radius of the discharge tube $r$ (or more appropriately the diffusion length $\Lambda$) and the gas pressure $p$; i.e., $T_e$ is a function of $pr$. The electron temperature will decrease with an increase in the value of $pr$; i.e., the plasma condition becomes milder with an increase in $pr$. Thus in order to suppress the formation of three-dimensionally cross-linked rigid products which are hard to decompose, a discharge tube with a larger radius and a higher gas pressure should be used because the ion sheath potential $V_s$ is a function of the electron temperature $T_e$,

$$[13] \quad V_s = \frac{kT_e}{2e} \ln \frac{T_e M}{T_p m}$$

where $k$ is the Boltzmann constant, $M$ the mass of an ion, $T_p$ the ion temperature, $m$ the electron mass, and $e$ the electron charge. With a decrease of the electric power of the generator, the electron and ion densities will decrease, but $T_e$ and $V_s$ stay almost constant because $T_e$ is only dependent on the value of $pr$.

[2]Under the present experimental conditions, the electron temperature may be around 4 eV. The ion temperature in a plasma is very close to the gas temperature (i.e. the temperature of the discharge tube). See ref. 21.

[3]The thickness of an ion sheath can be approximated as the same order of the Debye length under the present experimental conditions, which is of the order of $10^{-3}$ to $10^{-2}$ cm.

[4]For this experiment, a coaxial cylindrical discharge tube was used.

1. E. Ota, S. Inoue, and S. Otani. Nippon Kagaku Kaishi, 1407 (1977).
2. L. Karlson and E. Rosen. Chem. Script. **1**, 61 (1971).
3. M. Kondo *et al.* Nippon Koeishi, **22**, 271 (1975).
4. T. Sawai and Y. Shinozaki. Chem. Lett. 865 (1972).
5. S. Arai, M. Matsui, and M. Imamura. Rep. Inst. Phys. Chem. Res. **48**, 185 (1972).
6. T. Sawai, T. Shimokawa, and Y. Shinozaki. Bull. Chem. Soc. Jpn. **47**, 1889 (1974).
7. T. Sawai, T. Shimokawa, and T. Sawai. J. Nucl. Sci. Tech. **12**, 502 (1975).
8. T. Nishiwaki, J. Ninomiya, S. Yamanaka, and K. Anda. Nippon Kagaku Kaishi, 2225 (1972).
9. A. Oku, K. Yasufuku, S. Kato, and H. Kataoka. Nippon Kagaku Kaishi, 1577 (1978).
10. K. Nakamori, T. Takanashi, and R. Hirai. Kogyo Kagaku Zasshi, **59**, 22 (1956).

11. I. M. KOLTHOFF and R. BELCHER. Volmetric Anal. **III**, 262 (1957).
12. I. IWASAKI, S. UTSUMI, and C. KANG. Bull. Chem. Soc. Jpn. **36**, 325 (1963).
13. R. C. DOUGHERTY and J. D. ROBERTS. Anal. Chem. **47**, 54 (1975).
14. I. DZIDIC, D. I. CARROLL, R. N. STILLWELL, and E. C. HORNING. Anal. Chem. **47**, 1308 (1975).
15. D. F. HUNT, G. C. STAFFORD, JR., F. W. CROW, and J. W. RUSSELL. Anal. Chem. **48**, 2098 (1976).
16. M. A. A. CLYNE, D. MCKENNY, and R. T. WATSON. J. Chem. Soc. Faraday Trans. I, **71**, 332 (1975).
17. T. M. SLOANE. J. Chem. Phys. **67**, 2267 (1977).
18. C. J. HOWARD, F. C. FEHSENFELD, and M. MCFARLAND. J. Chem. Phys. **60**, 5086 (1974).
19. R. A. PERRY, R. ATKINSON, and J. N. PITTS, JR. J. Phys. Chem. **81**, 296 (1977).
20. A. SUESS and T. LESSEL. Radiat. Chem. **9**, 353 (1977); J. G. TRUMP *et al.* Radiation for a clean environment. Proc. Symp., 343, Munich; Chem. Eng. New, Jan. 9, 1978.
21. K. HIRAOKA and H. KAMADA. Jpn. J. Appl. Phys. **10**, 339 (1971).
22. A. VON ENGEL. Ionized gases. Oxford at the Clarendon Press, 1955.

Can. J. Chem. Downloaded from www.nrcresearchpress.com by 210.87.254.40 on 09/06/12
For personal use only.

# Temperature and concentration dependence of viscosity of $Mg(NO_3)_2$–$H_2O$ systems

S. MAHIUDDIN AND K. ISMAIL[1]

*Department of Chemistry, North-Eastern Hill University, Bijni Complex, Laitumkhrah, Shillong-793003, India*

Received January 7, 1982

S. MAHIUDDIN and K. ISMAIL. Can. J. Chem. **60**, 2883 (1982).

Densities and viscosities of aqueous magnesium nitrate solutions are measured as functions of temperature and composition. The temperature dependence of viscosity is described by the Vogel–Tammann–Fulcher (VTF) equation. By accounting quantitatively for the concentration dependences of all three parameters involved in the VTF equation an improved isothermal equation is obtained, it describes satisfactorily the concentration dependence of viscosity.

S. MAHIUDDIN et K. ISMAIL. Can. J. Chem. **60**, 2883 (1982).

On a mesuré, en fonction de la température et de la composition, les densités et les viscosités de solutions aqueuses de nitrate de magnésium. On décrit l'effet de la température sur la viscosité à l'aide de l'équation de Vogel–Tammann–Fulcher (VTF). En tenant compte quantitativement de l'effet de la concentration sur chacun des trois paramètres impliqués dans l'équation de VTF, on obtient une équation isotherme appropriée qui décrit d'une façon satisfaisante l'effet de la concentration sur la viscosité.

[Traduit par le journal]

Can. J. Chem. Downloaded from www.nrcresearchpress.com by 210.87.254.40 on 09/06/12
For personal use only.

## Introduction

It is known that in electrolyte solutions all empirical expressions (1–3) fail to explain the concentration dependence of viscosity at higher concentrations. At these concentrations, the viscosity data satisfactorily fit only Vand's (4) and similarly derived equations (5–8) but it is not clear why they work as well as they do.

One of the approaches being used to obtain an isothermal equation for explaining the concentration dependence of transport properties in glass-forming molten mixtures (9–11) is by substituting the empirical concentration dependences of the three parameters, $A$, $B$, and $T_0$, in the VTF equation (12)

$$[1] \quad \eta = AT^{1/2} \exp B/(T - T_0)$$

where $\eta$ is the viscosity and $T$ is the absolute temperature.

Angell and Bressel (13) extended this approach used in glass-forming molten mixtures to the $Ca(NO_3)_2$–$H_2O$ system and interestingly found that a Vand's type equation could be derived from eq. [1]. However, in getting the isothermal equation from [1] the concentration dependence of $A$ was completely ignored and that of $B$ was partly considered. Therefore, it is possible to improve the isothermal equation obtainable from eq. [1] by accounting appropriately for the concentration dependences of the $A$ and $B$ parameters of electrolyte solutions.

In an earlier paper (14) we derived eq. [1] from the Adam–Gibbs equation (15) after proper substitution for the temperature dependence of configurational heat capacity. Such a study has provided expressions for $A$ and $B$ according to which

$$[2] \quad A = A_0 \exp(-B_1/C_1T_0)$$

and

$$[3] \quad B = (B_1/C_1)(1 - C_2T_0/C_1)$$

$A_0$, $B_1$, $C_1$, and $C_2$ are all constant parameters for a particular system. $C_1$ is the difference in the heat capacities of glass and liquid at $T_0$. $C_2$ is the difference in the slopes of the plots of heat capacity versus $T$ for the glassy and liquid states. From eqs. [2] and [3] it is apparent that a quantitative description for the concentration dependences of $A$ and $B$ is possible.

In this paper we have studied the viscosities of aqueous magnesium nitrate solutions with concentration ranging from dilute to saturation point with a view to obtain an improved isothermal equation by incorporating, in light of eqs. [2] and [3], the concentration dependences of $A$ and $B$ also.

## Experimental

BDH(analar) grade magnesium nitrate hexahydrate was used in preparing all solutions. The water used was doubly distilled in a quartz distilling unit. The exact concentrations were volumetrically determined at 25°C by the EDTA titration method. Solutions having concentrations ranging between $0.0917m$ ($m$ = molality) and $6.3682m$ (nearly the saturation point at 50°C) were studied.

The viscosity measurements were made using a Hoppler BH-2 falling ball viscometer with an accuracy of 0.5%. In this viscometer, since the solution was sealed, the loss of water at high temperatures was prevented. The densities, $\rho$, of the solutions required for calculating their viscosities were measured accurate to 0.01% using a calibrated pycnometer.

All measurements were made in a thermostated water bath of stability ±0.02° (Ultra Thermostat type NBE) and at temperatures ranging from 17 to 89°C.

[1]To whom all correspondence should be addressed.

0008-4042/82/232883-06$01.00/0

©1982 National Research Council of Canada/Conseil national de recherches du Canada

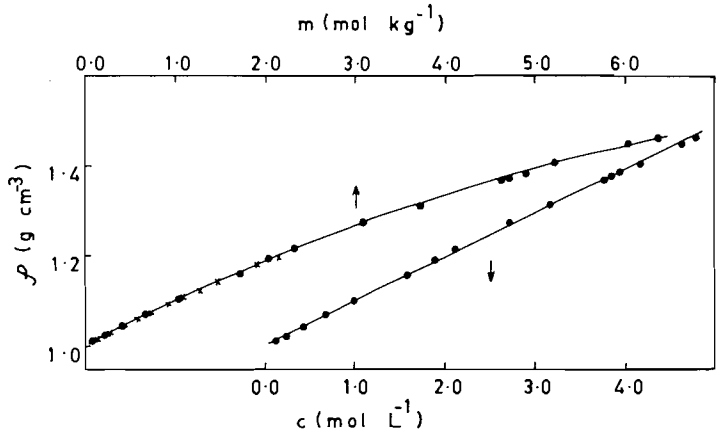


FIG. 1. Plots of densities of $Mg(NO_3)_2$–$H_2O$ systems at 20°C versus molality and molarity of $Mg(NO_3)_2$ (●, observed; ×, reported).

## Results and discussion

The measured densities of the magnesium nitrate solutions are found to be linear functions of temperature (Table 1) whereas their dependence on molality does not exhibit a linear relationship. Surprisingly, for the dependence of density on molarity, $c$ is found to be linear in the concentration range studied. Such dependences of ρ on concentration are illustrated in Fig. 1 by plotting ρ versus $m$ and ρ versus $c$ isotherms at 20°C. From Fig. 1 it may also be noted that the reported values (16) of densities of a few magnesium nitrate solutions at 20°C are in good agreement to within ±0.3% of the present values.

The measured viscosities of aqueous magnesium nitrate solutions are presented as Arrhenius plots in Fig. 2. The non-Arrhenius temperature dependences of η are therefore least-squares fitted to eq. [1]. The values of the parameters $A$, $B$, and $T_0$ so obtained are listed in Table 2.

TABLE 1. Parameters of the density equation $\rho = a - bt$(°C)

| $m$ (mol kg$^{-1}$) | $a$ | $b \times 10^4$ | Std. dev. in ρ, $\sigma \times 10^4$ |
|---|---|---|---|
| 0.0917 | 1.0214 | 4.6154 | 0.9282 |
| 0.2297 | 1.0346 | 4.3443 | 0.7162 |
| 0.4243 | 1.0559 | 4.5686 | 0.9182 |
| 0.6753 | 1.0816 | 5.1671 | 0.7699 |
| 1.0524 | 1.1170 | 5.2511 | 0.8032 |
| 1.7055 | 1.1714 | 5.2673 | 1.5334 |
| 2.0428 | 1.2047 | 5.4326 | 1.4241 |
| 2.3300 | 1.2310 | 5.7854 | 1.6654 |
| 3.1050 | 1.2884 | 5.9078 | 2.0046 |
| 3.7251 | 1.3289 | 6.2154 | 1.0309 |
| 4.6299 | 1.3828 | 6.0195 | 1.8120 |
| 4.7091 | 1.3906 | 6.1908 | 1.8578 |
| 4.8578 | 1.4002 | 5.8546 | 1.1534 |
| 5.2393 | 1.4227 | 6.4114 | 1.3185 |
| 6.0371 | 1.4671 | 8.0131 | 1.3727 |
| 6.3682 | 1.4801 | 8.1530 | 1.3131 |

It is clear from several studies (2, 8) that the viscosity of an electrolytic solution is governed by two types of interactions occurring in the solution, viz., ion–ion and ion–solvent. The contribution to viscosity from ion–ion interaction is described by a $c^{1/2}$ term and that due to ion–solvent or solute–solvent interaction shows an exponential dependence on concentration. It has been observed empirically that the contribution of the $c^{1/2}$ term is significant only at very low concentrations whereas at higher concentrations the exponential term due to the solute–solvent interaction dominates. Therefore, the variations occurring in the values of $A$, $B$, and $T_0$ as a function of concentration are considered to be governed predominantly by the solute–solvent interactions. Accordingly, an attempt has been made here to correlate first the variations produced in $T_0$ with the hydration phenomenon.

Hydration of the solute particles will cause the system to lose some of its configurational degrees of freedom, thereby resulting in a decrease of the configurational entropy, $S_c$, of the system. As the concentration increases $S_c$ will therefore keep on decreasing. Since $T_0$ is the temperature at which $S_c$ becomes zero, $T_0$ must increase with increase in concentration. Accordingly, $T_0$ can be related to the probability, $p$, of finding a solvent particle in the hydration shells of the solute particles which, of course, increases by increasing concentration because $p = nm/55.51$ where $n$ is the total hydration number of the solute. Consequently, the values of $T_0$ are drawn against $m$ and a linear plot is obtained (Fig. 3$a$), reflecting the dependence of $T_0$ on the hydration phenomenon of the solute. The observed

Can. J. Chem. Downloaded from www.nrcresearchpress.com by 210.87.254.40 on 09/06/12
For personal use only.

Can. J. Chem. Downloaded from www.nrcresearchpress.com by 210.87.254.40 on 09/06/12
For personal use only.

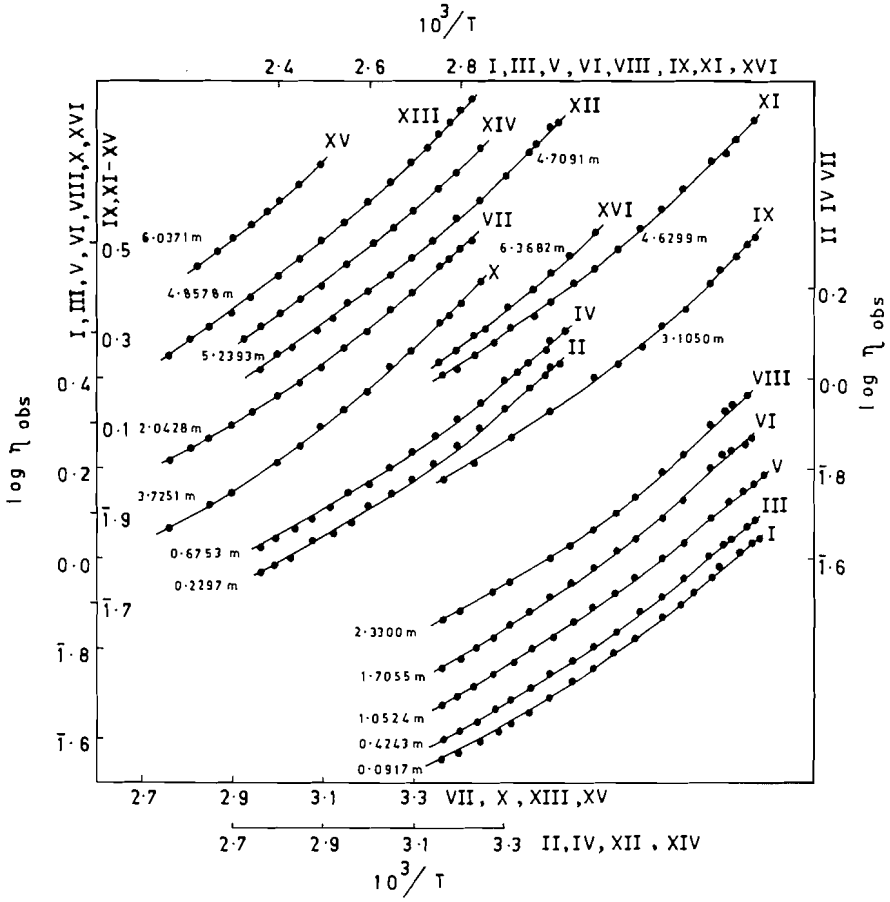


FIG. 2. Plots of log η versus $1/T$ for $Mg(NO_3)_2$–$H_2O$ systems.

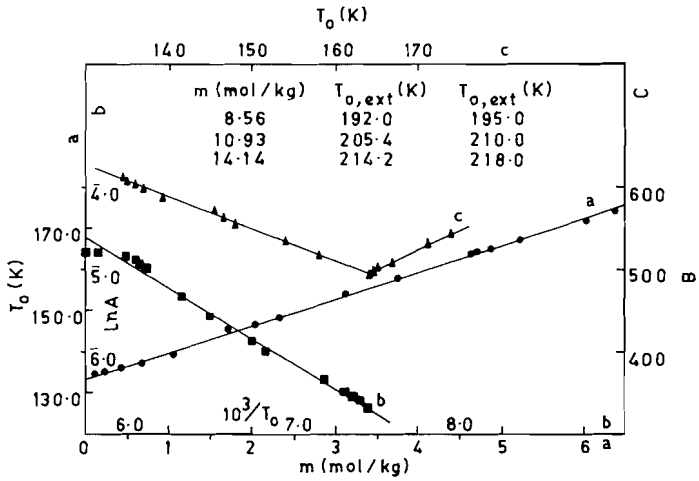


FIG. 3. Plots of ln $A$, $B$, and $T_0$ versus $1/T_0$, $T_0$, and $m$, respectively, for $Mg(NO_3)_2$–$H_2O$ systems.

Can. J. Chem. Downloaded from www.nrcresearchpress.com by 210.87.254.40 on 09/06/12
For personal use only.

TABLE 2. Parameters of eq. [1] for the viscosity of $Mg(NO_3)_2$–$H_2O$ systems (viscosity range in parentheses)

| $m$ (mol kg$^{-1}$) | Temperature range (°C) and viscosity range (cP) | $A \times 10^3$ | $B$ | $T_0$ (K) | Std. dev. in ln η |
|---|---|---|---|---|---|
| 0.0917 | 16.4–89.0 (1.11–0.36) | 1.2263 | 614.62 | 134.5 | $1.31 \times 10^{-3}$ |
| 0.2297 | 19.5–89.0 (1.08–0.37) | 1.3246 | 607.00 | 135.0 | $1.23 \times 10^{-3}$ |
| 0.4243 | 17.0–89.0 (1.22–0.39) | 1.4194 | 602.99 | 136.0 | $8.30 \times 10^{-4}$ |
| 0.6753 | 18.0–89.0 (1.28–0.42) | 1.5474 | 596.77 | 137.0 | $5.90 \times 10^{-4}$ |
| 1.0524 | 15.5–89.0 (1.53–0.47) | 1.7865 | 585.42 | 139.3 | $3.30 \times 10^{-4}$ |
| 1.7055 | 17.6–89.0 (1.87–0.57) | 2.0927 | 547.02 | 145.7 | $1.56 \times 10^{-3}$ |
| 2.0428 | 18.9–89.0 (2.04–0.66) | 2.4980 | 561.54 | 146.5 | $1.96 \times 10^{-3}$ |
| 2.3300 | 18.2–89.0 (2.31–0.72) | 2.7977 | 554.24 | 148.0 | $2.08 \times 10^{-3}$ |
| 3.1050 | 17.0–89.0 (3.26–0.94) | 3.7373 | 533.81 | 154.0 | $1.60 \times 10^{-3}$ |
| 3.7251 | 16.4–89.0 (4.11–1.16) | 4.7852 | 516.49 | 158.0 | $1.16 \times 10^{-3}$ |
| 4.6299 | 17.0–89.0 (5.91–1.61) | 7.0307 | 492.38 | 164.0 | $4.80 \times 10^{-4}$ |
| 4.7091 | 19.7–89.0 (5.82–1.68) | 7.2028 | 495.05 | 164.5 | $3.50 \times 10^{-4}$ |
| 4.8578 | 18.8–89.0 (6.58–1.79) | 7.4559 | 500.90 | 165.0 | $5.40 \times 10^{-4}$ |
| 5.2393 | 35.0–89.0 (5.16–2.06) | 7.9671 | 508.96 | 167.0 | $4.80 \times 10^{-4}$ |
| 6.0371 | 50.0–81.5 (4.73–2.81) | 8.1115 | 530.15 | 171.5 | $9.24 \times 10^{-4}$ |
| 6.3682 | 50.0–89.4 (5.32–2.74) | 7.9414 | 542.63 | 174.0 | $1.26 \times 10^{-3}$ |

concentration dependence of $T_0$ can therefore be written as

$$[4] \quad T_0 = T_0(0) + Q_1 m$$

where $T_0(0)$ refers to the $T_0$ value of the pure solvent and $Q_1$ is the slope. The least-squares fitted (standard deviation in $T_0$ = 0.64) values of $T_0(0)$ and $Q_1$ are found to be 133.48 K and 6.4441 K mol$^{-1}$ kg, respectively. It may be noted that the value 133.48 K for $T_0$ of water is in agreement with the glass transition temperature, $T_g$ (139 K) reported for amorphous solid water (17). Moreover, the reported (9) $T_0$ values of a few concentrated $Mg(NO_3)_2$–$H_2O$ systems based on their equivalent conductance data are in agreement to within ±5 K of the values of $T_0$ obtained by extrapolating the plot of $T_0$ versus $m$ (Fig. 3*a*) to the corresponding concentrations.

After accounting quantitatively for the concentration dependence of $T_0$, that of $A$ can easily be described in light of eq. [2]. A plot of ln $A$ versus $1/T_0$ is made (Fig. 3*b*) and it is found to be linear. The linearity of such a plot envisages the applicability of eq. [2] for describing the concentration dependence of $A$ and also reveals that the $B_1/C_1$ value is fairly constant in the concentration range studied. The least-squares fitted (standard deviation in ln $A$ = 0.09) values of ln $A_0$ and $B_1/C_1$ are found to be 2.3022 and 1208.2, respectively.

On the other hand, the $B$ parameter, without showing a monotonous variation, decreases initially with increase in concentration up to 4.63$m$ and

TABLE 3. Parameters of eq. [6] for the viscosity of $Mg(NO_3)_2$–$H_2O$ systems

| $T$ (K) | Concentration range (mol kg$^{-1}$) and viscosity range (cP) | $A_0'$ | $b'$ | $c' \times 10^3$ | Std. dev. in ln η |
|---|---|---|---|---|---|
| 298.0 | 0.0917–4.6299 (0.9086–4.8009) | 0.8775 | 0.3284 | 8.1356 | $1.14 \times 10^{-2}$ |
| | 0.0917–4.8578 (0.9086–5.5503) | 0.8820 | 0.3166 | 11.6670 | $1.56 \times 10^{-2}$ |
| 308.0 | 0.0917–4.6299 (0.7366–3.7642) | 0.7180 | 0.3106 | 10.4715 | $7.6 \times 10^{-3}$ |
| | 0.0917–5.2393 (0.7366–5.1554) | 0.7225 | 0.2967 | 14.3718 | $1.24 \times 10^{-2}$ |
| 323.0 | 0.0917–4.6299 (0.5692–2.7998) | 0.5581 | 0.2911 | 12.4280 | $1.03 \times 10^{-2}$ |
| | 0.0917–6.3682 (0.5692–5.3209) | 0.5476 | 0.3218 | 6.5556 | $2.71 \times 10^{-2}$ |

then increases (Table 2). The plot of $B$ versus $T_0$ is shown in Fig. 3*c*. According to eq. [3] the decrease in value of $B$ is attributable to the increase in value of $T_0$ as concentration increases. The linearity of the plot (Fig. 3*c*) implies that $C_2/C_1$ is almost constant up to $4.63m$. Both $C_1$ and $C_2$ have been found by Angell and Tucker (18) to decrease with increasing concentration for electrolyte solutions. Therefore, the constancy of $C_2/C_1$ must be due to the same rates of decrease of $C_1$ and $C_2$ up to $4.63m$, whereas the observed increase in $B$ beyond $4.63m$ appears to be attributable to the fact that, at these concentrations, the value of $C_2$ becomes very low. It may be governing the value of $C_2T_0/C_1$, causing a decrease in the value of this ratio with increase in concentration. These trends of $C_2/C_1$, viz., constancy up to $4.63m$ and then decrease, are also verified by calculating its values with the knowledge of $B$, $T_0$, and $B_1/C_1$ from the slope of Fig. 3*b*. This kind of behaviour of $B$ appears to imply a structural change around $4.63m$ which may be a transition to quasi-crystalline structure.

With the concentration dependences of $A$, $B$, and $T_0$ having been discussed, it is now possible to describe quantitatively the overall concentration dependence of η by the expression

$$[5] \quad \eta = A_0T^{1/2} \exp\left\{\frac{B_0[1 - Q_2(T_0(0) + Q_1m)]}{T - (T_0(0) + Q_1m)} - \frac{B_0}{T_0(0) + Q_1m}\right\}$$

where $B_0 = B_1/C_1$ and $Q_2 = C_2/C_1$. The values of $B_0$ and $Q_2$ are, of course, different below and above $4.63m$. By approximating $1/[T - T_0(0) - Q_1m]$ to $[1 + Q_1m/(T - T_0(0))]/(T - T_0(0))$ and $1/(T_0(0) + Q_1m)$ to $[1 - Q_1m/T_0(0)]/T_0(0)$, eq. [5] can be reduced to a simple isothermal expression of the form

$$[6] \quad \eta = A_0' \exp(b'm + c'm^2)$$

where $A_0'$, $b'$, and $c'$ are constants at a particular temperature. In fact, $A_0'$, $b'$, and $c'$ will have different values below and above $4.63m$. However, an attempt has been made to fit the viscosity data to eq. [6] in both concentration ranges $0.0917m$ to $4.6299m$ and $0.0917m$ to saturation point. It is apparent from Table 3 that in both concentration ranges the least-squares fittings are equally satisfactory. Moreover, the linearity of the plot of log η versus $b'm + c'm^2$ (Fig. 4) also reinforces the applicability of eq. [6] in explaining the concentration dependence of viscosity in the entire concentration range studied.

Finally, it is interesting to find that by neglecting the contribution of the $c'm^2$ term eq. [6] can be brought to the form of Vand's (4) as well as Angell

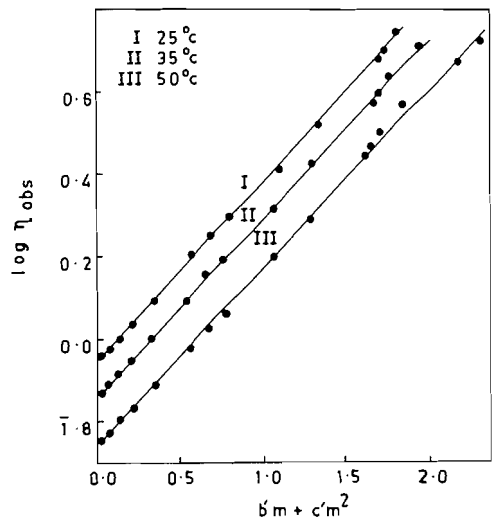


FIG. 4. Plots of log η versus $b'm + c'm^2$ for $Mg(NO_3)_2$–$H_2O$ systems (I: $b' = 0.3166$, $c' = 11.6670 \times 10^{-3}$; II: $b' = 0.2967$, $c' = 14.3718 \times 10^{-3}$; III: $b' = 0.3218$, $c' = 6.5556 \times 10^{-3}$).

Can. J. Chem. Downloaded from www.nrcresearchpress.com by 210.87.254.40 on 09/06/12
For personal use only.

and Bressels' (13) equations using the relations of $m$ with molarity and mol%. It may, therefore, be concluded that eq. [6] is an improved isothermal equation for describing the composition dependence of viscosity in aqueous solutions.

**Acknowledgment**

The financial assistance from the University to S.M. is gratefully acknowledged.

1. A. EINSTEIN. Ann. Phys. **19**, 289 (1906); **34**, 591 (1911).
2. G. JONES and M. DOLE. J. Am. Chem. Soc. **51**, 2950 (1929).
3. S. P. MOULIK. J. Phys. Chem. **72**, 4682 (1968).
4. V. VAND. J. Phys. Colloid Chem. **52**, 277 (1948); **52**, 300 (1948); **52**, 314 (1948).
5. E. MOONEY. J. Colloid Chem. **6**, 163 (1951).
6. J. PADOVA. J. Chem. Phys. **38**, 2635 (1963).
7. D. G. THOMAS. J. Colloid Sci. **20**, 267 (1965).
8. F. H. SPEDDING and M. J. PIKAL. J. Phys. Chem. **70**, 2430 (1966).
9. C. A. ANGELL. J. Phys. Chem. **70**, 3988 (1966).
10. C. A. ANGELL. J. Chem. Phys. **46**, 4673 (1967).
11. N. ISLAM and K. ISMAIL. J. Phys. Chem. **80**, 1929 (1976).
12. H. VOGEL. Physik. Z. **22**, 645 (1921); V. G. TAMMANN and W. HESSE. Z. Anorg. Allg. Chem. **156**, 245 (1926); G. S. FULCHER. J. Am. Chem. Soc. **8**, 339 (1925).
13. C. A. ANGELL and R. D. BRESSEL. J. Phys. Chem. **76**, 3244 (1972).
14. S. MAHIUDDIN and K. ISMAIL. To be published.
15. G. ADAM and J. H. GIBBS. J. Chem. Phys. **43**, 139 (1965).
16. J. A. DEAN (*Editor*). Lange's handbook of chemistry. 11th Ed. McGraw Hill, New York. 1973.
17. J. A. MCMILLAN and S. C. LOS. Nature, **206**, 806 (1965).
18. C. A. ANGELL and J. C. TUCKER. J. Phys. Chem. **84**, 268 (1980).

Can. J. Chem. Downloaded from www.nrcresearchpress.com by 210.87.254.40 on 09/06/12
For personal use only.

# Attraction and repulsion of floating particles

M. A. FORTES

*Departamento de Metalurgia, Instituto Superior Técnico; Centro de Mecânica e Materiais da Universidade Técnica de Lisboa, Av. Rovisco Pais, 1096 Lisboa Codex, Portugal*

Received March 17, 1982

M. A. FORTES. Can. J. Chem. **60**, 2889 (1982).

The horizontal force that has to be applied to floating cylinders to equilibrate the capillary force is calculated for a general geometry with cylindrical symmetry and for any wetting characteristics of the cylinders. The force on a cylinder can be related to a single parameter of each of the two menisci that contact the cylinder. It is found that the force between parallel vertical plates or parallelipipeds can be repulsive if one of the contact angles is acute and the other obtuse. The force on cylinders between fixed walls is also calculated and the results suggest that it may be possible to separate floating particles with different wetting properties by placing them between two walls with different contact angles.

M. A. FORTES. Can. J. Chem. **60**, 2889 (1982).

On a calculé la force horizontale que doit être appliquée à des cylindres flottants pour équilibrer les forces capillaires, pour une géométrie générale avec une symétrie cylindrique et pour n'importe quelle caractéristique de mouillage des cylindres. On peut relier la force sur un cylindre à un paramètre unique pour chacun des deux ménisques qui sont en contact avec le cylindre. On a trouvé que les forces entre les plaques verticales parallèles ou parallèlépipèdes peuvent être répulsives si un des angles de contact est aigu et l'autre obtu. On a également calculé la force qui s'exerce sur le cylindre entre deux parois fixes; les résultats suggèrent qu'il est possible de séparer des particules flottantes ayant des propriétés différentes de mouillage en les plaçant entre deux parois avec des angles de contact différents.

[Traduit par le journal]

## 1. Introduction

It is frequently observed that particles floating at the surface of a liquid at rest are submitted to forces which in most cases tend to produce clusters of particles. These may be either attracted to a wall or find an equilibrium position near the centre of the surface. These effects are due to the horizontal component of the capillary forces associated with the curved liquid surface. The calculation of such forces requires the determination of the equilibrium shape of the liquid surface (more generally of a fluid interface) by solving the Laplace differential equation submitted to the appropriate boundary conditions, for example, a constant contact angle of the liquid with the solid particles. When gravity is included, the only geometry for which the shape of the fluid interface can be determined in closed form is one with cylindrical symmetry. Gifford and Scriven (1) have analysed this situation for two "parallel" identical circular cylinders in free flotation and were able to determine the horizontal force as a function of separation by taking into account the vertical displacement experienced by the cylinders as their separation changes. They have assumed, however, that the arc wetted on each cylinder remained constant, instead of considering a constant contact angle; therefore they were not able to draw conclusions on the effect of wetting characteristics on the horizontal force. Under those conditions the (attractive) force was found to fall off nearly exponentially with separation. More recently, Chan *et al.* (2) found a similar variation for the case of two free floating spheres. They used approximate solutions for the Laplace equation, applicable to small Bond numbers (small particles). Again no special attention was given to the effect of the wetting properties of the floating bodies on the horizontal force.

The purpose of this paper is to analyse, for a cylindrical geometry, the effect of the wetting characteristics on the horizontal force between two or more floating bodies. The vertical component of the capillary forces will not be included in the analysis, that is, the positions of the floating bodies relative to some reference level are imposed by externally applied vertical forces. To simplify the treatment we shall assume frequently that the bodies are plates or prisms such that the wetted surfaces are planar and vertical. However, application to other geometries is straightforward. The analysis is a static one, as in previous treatments (1, 2), in that equilibrium of the bodies is always assumed; what is calculated is in fact the horizontal force that must be applied to the bodies to maintain equilibrium.

In section 2 we obtain the relevant equations for the fluid interface profile and in section 3 we derive general expressions for the horizontal force. It turns out that this force can be simply related to a single parameter of each of the two menisci contact-

0008-4042/82/232889-07$01.00/0

©1982 National Research Council of Canada/Conseil national de recherches du Canada

Can. J. Chem. Downloaded from www.nrcresearchpress.com by 210.87.254.6 on 09/06/12
For personal use only.

Can. J. Chem. Downloaded from www.nrcresearchpress.com by 210.87.254.6 on 09/06/12
For personal use only.

ing a floating cylinder. Examples of calculation of such forces between two cylinders or between a cylinder and the walls of a container are given in section 4, which show the effect of wetting properties. These calculations further suggest that in favourable cases it may be possible to separate floating particles of two different materials by placing them between two parallel walls with properly chosen contact angles.

## 2. Shape of the fluid interface

We use cartesian coordinates $x$, $z$, as in Fig. 1, with the origin at the point of contact of the fluid interface with the solid; $x$ is horizontal and $z$ vertical directed in such a way that the profile is in the region $x > 0$, $z > 0$ near the origin; therefore

$$\dot{z} = dz/dx > 0$$

in this region. There are four possibilities, indicated in Fig. 1, as regards the sign of $\ddot{z}$ near the origin and the direction of $z$ relative to that of $\boldsymbol{g}$ (the gravity acceleration). Let $\rho_0$ be the radius of curvature at the origin, with the sign of $\ddot{z}$ at or near the origin; $\gamma$ is the fluid interface tension and $\Delta\rho(> 0)$ is the difference between the densities of the two fluids. By noting the way the pressure difference across the interface varies with $z$, it is easy to conclude that the Laplace equation can be written as

$$[1] \quad \pm\gamma\frac{\ddot{z}}{(1+\dot{z}^2)^{3/2}} = \frac{\gamma}{\rho_0} + g\cdot\Delta\rho\cdot z$$

where the + sign applies to the profile region between the origin and the point (if it occurs) with $\dot{x} = dx/dz = 0$, and the − sign "after" this point. To integrate eq. [1] we first note that

$$[2] \quad \frac{\ddot{z}}{(1+\dot{z}^2)^{3/2}} = \mp\frac{\ddot{x}}{(1+\dot{x}^2)^{3/2}} = \mp\frac{d}{dz}\left[\frac{\dot{x}}{(1+\dot{x}^2)^{1/2}}\right]$$

where the − sign applies if $\dot{x} > 0$. Introducing the capillary constant, $a$, defined by

$$[3] \quad a^2 = \frac{\gamma}{g\cdot\Delta\rho}$$

and the adimensional quantities $X$, $Z$ (reduced cartesian coordinates) and $R$ (reduced radius of curvature of meniscus)

$$[4] \quad X = \frac{x}{a}; \quad Z = \frac{z}{a}; \quad R_0 = \frac{\rho_0}{a}$$

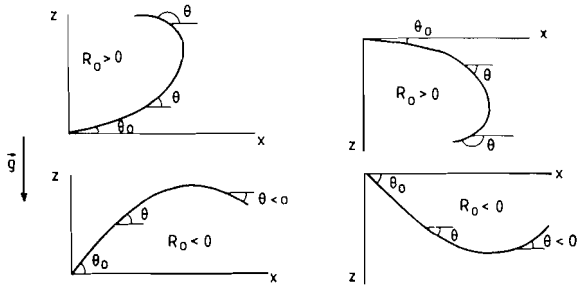


FIG. 1. Orientation of the coordinate system $x$, $z$ and definition of the angle $\theta$; $g$ is the gravity acceleration.

we may put [1] in the form

$$[5] \quad -\frac{d}{dZ}\left[\frac{\dot{X}}{(1+\dot{X}^2)^{1/2}}\right] = \frac{1}{R_0} + Z$$

applicable in the region with $\dot{X} > 0$. In other regions the − sign may have to be replaced by +. But

$$[6] \quad \frac{\dot{X}}{(1+\dot{X}^2)^{1/2}} = \cos\theta$$

where $\theta$ ($-\pi \le \theta \le \pi$) is the angle defined in Fig. 1 between the profile and the $X$-axis. If $\theta_0$ ($0 \le \theta_0 \le \pi/2$) is the value of this angle at the origin we obtain upon integration of [5]:

$$[7] \quad \cos\theta_0 - \cos\theta = \frac{Z}{R_0} + \frac{Z^2}{2}$$

It is easy to see that, with the definition of $\theta$ given above, this equation applies to the entire profile.

Equation [7] can be integrated to obtain $X(Z)$. Writing

$$[8] \quad \cos\theta = \cos\theta_0 - \frac{Z}{R_0} - \frac{Z^2}{2} = f(Z)$$

we obtain

$$[9] \quad X = \int_0^Z \frac{f(Z)}{(1-f^2(Z))^{1/2}}\,dZ$$

The integral may have to be decomposed if $\dot{X}$ changes sign. Introducing a new variable $\phi$ defined by

$$[10] \quad \phi = \frac{\pi}{2} - \frac{\theta}{2}$$

the integral [9] can be put in the form

$$[11] \quad \pm X = 2\int_{\phi_0}^{\phi}\sqrt{1-k^2\sin^2\phi}\,d\phi - (2-k^2)\int_{\phi_0}^{\phi}\frac{d\phi}{\sqrt{1-k^2\sin^2\phi}}$$

Can. J. Chem. Downloaded from www.nrcresearchpress.com by 210.87.254.6 on 09/06/12
For personal use only.

with the meniscus constant $k$ defined as

$$[12] \quad k = \left(\frac{2}{1 + \cos\theta_0 + 1/2R_0^2}\right)^{1/2} = \left(\frac{2}{2 + I}\right)^{1/2}$$

The + sign applies if $R_0 > 0$ ($\phi < \phi_0$ in the initial region) and the − sign if $R_0 < 0$ ($\phi > \phi_0$). Equation [11] is applicable in all cases. Introducing elliptic integrals of the first ($F$) and second ($E$) kind we obtain (3)

$$[13] \quad I > 0 \quad \pm kX = (2 - k^2)[F(\phi_0, k) - F(\phi, k)] - 2[E(\phi_0, k) - E(\phi, k)]$$

$$[14] \quad I < 0 \quad \pm X = F(\alpha_0, 1/k) - F(\alpha, 1/k) - 2[E(\alpha_0, 1/k) - E(\alpha, 1/k)]$$

where

$$[15] \quad \alpha = \arcsin(k \sin\phi)$$

For $I = 0$ ($k = 1$) the solution for $\theta > 0$ is

$$[16] \quad \pm X = G(\phi_0) - G(\phi)$$

where

$$[17] \quad G(\phi) = 2\sin\phi - \ln \operatorname{tg}\left(\frac{\phi}{2} + \frac{\pi}{4}\right)$$

For $\theta < 0$, $X$ is obtained as the sum of $X(\theta = 0)$ with $X(|\theta|)$.

Equation [12] incidentally shows that the quantity $\cos\theta + 1/(2R^2)$, where $\theta$, $R$ are the values at any point of a profile, is constant for each profile. This property is a direct consequence of eq. [2]. We may then introduce the quantity $I$ (cf. eq. [12]), the invariant of a meniscus, defined as

$$[18] \quad I = -1 + \cos\theta + \frac{1}{2R^2} = \text{constant}$$

and state that the various solutions form a one-parameter, $I$, family of curves. Since at the origin $\cos\theta_0 \geq 0$, the parameter $I$ may vary in the interval $[-1, +\infty]$. (As discussed below, for every $I$ there are in fact two solutions which are the mirror image of each other on a vertical or horizontal plane, according to the cases.)

We will now show that the solutions can be grouped into two types, which we term $a$-solutions (or $a$-menisci) and $i$-solutions (or $i$-menisci). The $a$-solutions have an apex (or $a$-point) $\dot{Z} = 0$, $\theta = 0$. (Note that all solutions have a point with $\dot{Z} = 0$, $\theta = \pi$ at the end of the region with $\dot{Z} < 0$.) The condition for an $a$-solution can be obtained from eq. [7], by making $\theta = 0$ and requiring that there is a solution for $Z$, with the result

$$[19] \quad I = \frac{1}{2R_0^2} + \cos\theta_0 - 1 \geq 0 \qquad (\dot{Z} = 0, \theta = 0)$$

The $i$-solutions have an inflection point ($i$-point), $\ddot{Z} = 0$. At this point $Z = -1/R_0$ (eq. [1]) and necessarily $0 < \cos\theta \leq 1$; eq. [7] then gives the following condition for an $i$-solution:

$$[20] \quad I = \frac{1}{2R_0^2} + \cos\theta_0 - 1 \leq 0 \qquad (\ddot{Z} = 0)$$

Both the $a$-point or the $i$-point may not be in the region with $Z > 0$. This will occur only for $R_0 < 0$.

The two types of solutions are schematically indicated in Fig. 2 up to the points with $\dot{Z} = 0$, $\theta = \pi$. Each $a$-solution can be characterized by the value, $R_a$, of the reduced radius of curvature at the apex; and each $i$-solution by the value of $\theta_i$ ($0 \leq \theta_i \leq \pi/2$), the slope at the $i$-point. Using the property [18] we have

$$[21] \quad I = -1 + \cos\theta_0 + \frac{1}{2R_0^2} = \frac{1}{2R_a^2} \quad (a\text{-solution})$$

$$[22] \quad I = -1 + \cos\theta_0 + \frac{1}{2R_0^2} = \cos\theta_i - 1 \quad (i\text{-solution})$$

For the purposes of computation it is convenient to place the origin at the $a$-point or $i$-point, as in Fig. 2, and obtain the curve $X(Z)$ from eqs. [7],

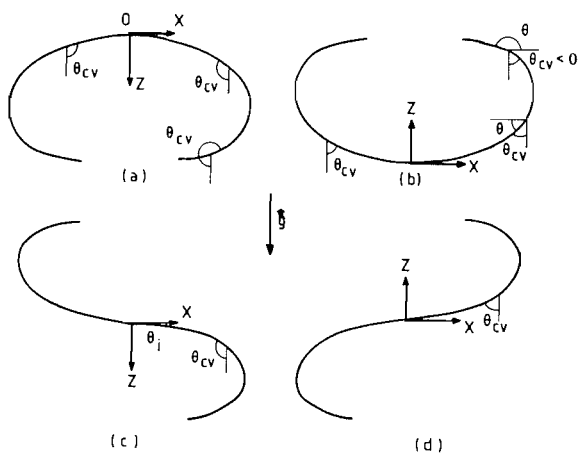


FIG. 2. Examples of $a$-solutions ($a$, $b$) and $i$-solutions ($c$, $d$). The coordinate system indicated is appropriate to the r.h.s. of the curves; the origin is at the $a$-point or $i$-point. The angle $\theta$ and the vertical contact angle $\theta_{cv}$ at various points are also indicated; $a$-solutions are even and $i$-solutions are odd.

Can. J. Chem. Downloaded from www.nrcresearchpress.com by 210.87.254.6 on 09/06/12
For personal use only.

[13], and [14], with θ in the interval 0, π. We note that $\phi_0 = \pi/2$ at an apex and $\alpha_0 = \pi/2$ at an *i*-point. For $I = 0$ the profile has a horizontal inflection point and is determined from eq. [16]. The two *a*-solutions in Fig. 2 are identical if they have the same $R_a$ (>0); and the two *i*-solutions in Fig. 2 are identical if they have the same $\theta_i$ (≥0).

### 3. Horizontal force

Consider a cylindrical body placed at a fluid interface with menisci on both sides 1, 2 of the body characterized by the values $\theta_{01}$, $R_{01}$ and $\theta_{02}$, $R_{02}$ at the lines of contact 1 and 2, respectively (Fig. 3). The horizontal force $F_{12}$ per unit length of the body, directed from side 1 to side 2, is the resultant of the horizontal components of the surface tension forces, γ, acting on the lines 1 and 2, and of the pressure difference forces, due to the curvature of the menisci, acting on the plane defined by the lines 1 and 2 (4). To keep equilibrium a force, $-F_{12}$, must be applied to the body.

Let *h* be the difference in the levels of the two contact lines ($h > 0$ if line 2 is above line 1). The pressure difference at the line of contact 1 is $\gamma/R_{01}$ and at line 2 it is $\gamma/R_{02}$. Equilibrium of pressure requires that

$$[23] \quad H = \frac{h}{a} = \frac{1}{R_{02}} - \frac{1}{R_{01}}$$

The horizontal resultant of the pressure difference forces on plane 12 is easily found to be

$$[24] \quad F_p = H\left(\frac{1}{R_{01}} + \frac{H}{2}\right) = H\left(\frac{1}{R_{02}} - \frac{H}{2}\right)$$

The horizontal force due to surface tension is

$$[25] \quad F_\gamma = \cos\theta_{02} - \cos\theta_{01}$$

Both these forces are expressed in γ units and refer to unit length of the cylinder. The total force is $F_p + F_\gamma$ which can be written, from eq. [23]

$$[26] \quad \frac{F_{12}}{\gamma} = \left(\cos\theta_{02} + \frac{1}{2R_{02}^2} - 1\right) - \left(\cos\theta_{01} + \frac{1}{2R_{01}^2} - 1\right)$$

or, using eq. [18],

$$[27] \quad F_{12}/\gamma = I_2 - I_1$$

This equation has a simple interpretation. Each meniscus exerts a horizontal force, directed to the side of the meniscus, with a value, in γ units and per unit length, equal to the invariant *I* of the meniscus profile. The net force is the resultant of the forces exerted by the two menisci. With this decomposition of $F_{12}$ in forces associated with each meniscus we may assign to an *a*-meniscus a force

$$[28] \quad F/\gamma = 1/2R_a^2$$

and to an *i*-meniscus a force

$$[29] \quad F/\gamma = \cos\theta_i - 1$$

The first is positive and vanishes for $R_a = \infty$. The other is negative and vanishes for $\theta_i = 0$. The special menisci for which $F = 0$ are of course free menisci connecting two distant cylinders or walls.

For two floating cylinders isolated at a liquid surface, the force between them is attractive if they are connected by an *a*-meniscus (Fig. 4*a*, *b*, *d*) and repulsive for an *i*-meniscus (Fig. 4*c*). This is true even if the *a*-point or *i*-point are not in the meniscus region. In the first case, if the free meniscus (side 1)

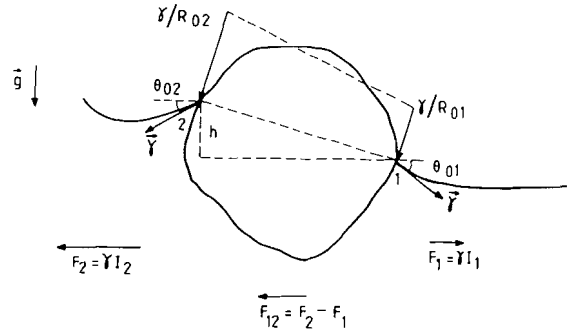


FIG. 3. Floating cylinder with menisci on both sides 1, 2. The horizontal force $F_{12}$ is the resultant of surface tension forces γ and pressure difference forces acting on the inclined plane 12 and varying from $\gamma/R_{01}$ to $\gamma/R_{02}$.

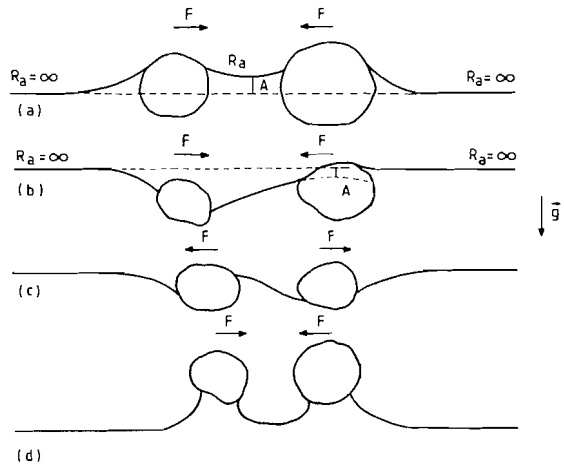


FIG. 4. Examples of menisci between two isolated floating cylinders. If the connecting meniscus is of the *a*-type (*a*, *b*, *d*) the force is attractive; if it is of the *i*-type (*c*) the force is repulsive.

is itself of the $a$-type (as in Fig. 4$a$, $b$), the radius of curvature at the apex of the connecting meniscus (side 2) must be equal to the height difference $A$ (in $a$ units) between the two apexes, so that

[30] $F_{12} = 1/2A^2$

The force is directed to side 2.

### 4. Force versus distance

In this section examples are given of the variation of the force $F$ with the width $X$ of a meniscus for fixed values of $\theta$ at the two ends of the meniscus. The results apply to any geometry of the solids, but in general the relation between the actual contact angle and the angle $\theta$ involves the slope angle of the solid surface at the line of contact. It is convenient to introduce what we term the vertical contact angle (v.c.a.) at the solid surface. This is the angle $\theta_{cv}$ defined in Fig. 2, between the fluid interface and a vertical half-plane below the line of contact, measured through the liquid phase (denser fluid). $\theta_{cv}$ can vary between $-\pi/2$ and $3\pi/2$. The relation between $\theta_{cv}$ and $\theta$ (as defined in Fig. 2) is

[31] $\theta_{cv} = \pi/2 \pm \theta$

where the + sign applies when the $z$-axis is parallel to $\boldsymbol{g}$.

Each meniscus can therefore be characterized by the values $\theta_{cv}$, $\theta_{cv}'$ of the v.c.a. at its ends and by the value of $X$, the horizontal reduced distance between the end points. The force due to the meniscus is, for the same $X$, equal to that due to a meniscus with v.c.a. $(\pi - \theta_{cv})$, $(\pi - \theta_{cv}')$ because of the identity of the menisci with the same $I$, as discussed above in relation to Fig. 2.

When two cylindrical bodies are connected by a meniscus such that the v.c.a.'s at each cylinder, respectively $\theta_{cv}$ and $\theta_{cv}'$, are both acute ($0 \leq \theta_{cv}$, $\theta_{cv}' < \pi/2$) or both obtuse, the meniscus is necessarily of the $a$-type and the force due to it is attractive. In all other cases, and in particular if one of the v.c.a. is acute and the other obtuse, the force may be repulsive or attractive depending on the type of meniscus, and therefore of distance.

In the following examples which illustrate these conclusions we shall consider only the interval 0, $\pi$ for the v.c.a. Note that the v.c.a. coincides with the actual contact angle if the solid surface is vertical at the region of contact. The examples then give directly the force on vertical plates or parallelipipeds placed at the fluid interface, with contact angles equal to the v.c.a.

Figures 5 and 6 show the horizontal capillary force, $F$, between two floating cylinders far from any other bodies, as a function of the horizontal

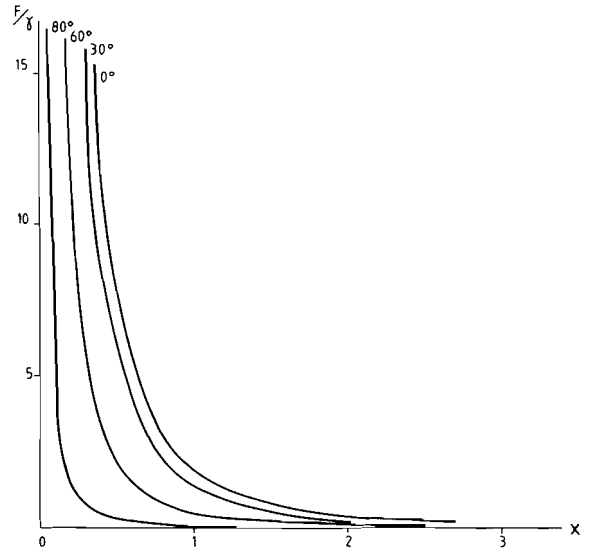


FIG. 5. Force versus separation for two floating cylinders with the same vertical contact angle $\theta_{cv}$. Each curve also applies to $\pi - \theta_{cv}$. Different curves do not intersect. All curves are asymptotic to the coordinate axes.

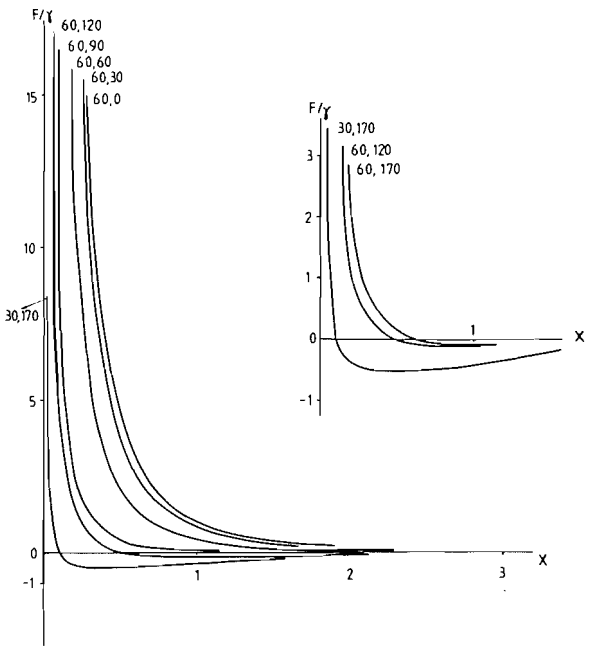


FIG. 6. Force versus separation for two floating cylinders with different vertical contact angles $\theta_{cv}$ and $\theta_{cv}'$ indicated in degrees. Each curve also applies to $(\pi - \theta_{cv})$, $(\pi - \theta_{cv}')$. The insert shows curves in a smaller scale; the continuation of the two top curves as $X \to \infty$, $F \to 0$, intersect each other. All curves are asymptotic to the coordinate axes.

Can. J. Chem. Downloaded from www.nrcresearchpress.com by 210.87.254.6 on 09/06/12
For personal use only.

Can. J. Chem. Downloaded from www.nrcresearchpress.com by 210.87.254.6 on 09/06/12
For personal use only.

distance $X$ between the lines of contact, for various combinations of $\theta_{cv}$, $\theta_{cv}'$. Each curve also applies to the complementary v.c.a.

In Fig. 5, the v.c.a.'s are the same at the two cylinders. The force is attractive at all separations ($F > 0$). The function $F(X)$ cannot be represented approximately by an exponential law, even at large distances. However, a power law, with $F$ proportional to $X^{-2}$, is a good approximation at small separations (see below).

Figure 6 applies to different angles. The curves for pairs acute–obtuse show the expected equilibrium position ($F = 0$) and a minimum (repulsive) force. At the equilibrium separation $I = 0$, and the corresponding value of $X$ can be obtained from eq. [16]. Figure 7 is a plot of the function $G(\phi)$ defined by eq. [17], from which the equilibrium position can be determined from the absolute value of the difference $G(\theta_{cv}) - G(\theta_{cv}')$. For example, for $\theta_{cv} = 0°$, $\theta_{cv}' = 120°$, the equilibrium

$$X = 0.533 - (-0.096) = 0.629$$

The equilibrium is unstable since the force is repulsive for separations larger than equilibrium separation and vice-versa. The value of the maximum repulsive force is $1 - |\sin\theta_{cv}|$, where $\theta_{cv}$ is the v.c.a. with smaller value of $|\sin\theta_{cv}|$. The repulsive force is at most equal to $\gamma$, per unit length.

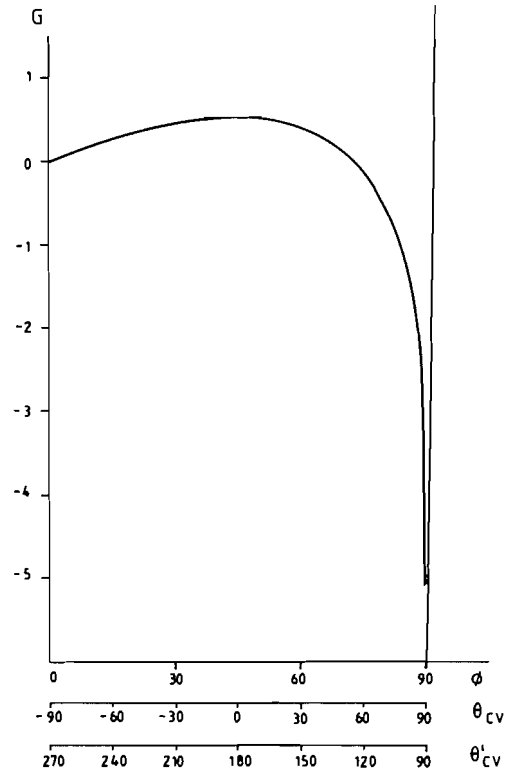


FIG. 7. The function $G(\phi)$ defined by eq. [17]. The equilibrium separation between two floating cylinders with vertical contact angles $\theta_{cv}$ and $\theta_{cv}'$ is the absolute value of $G(\theta_{cv}) - G(\theta_{cv}')$.

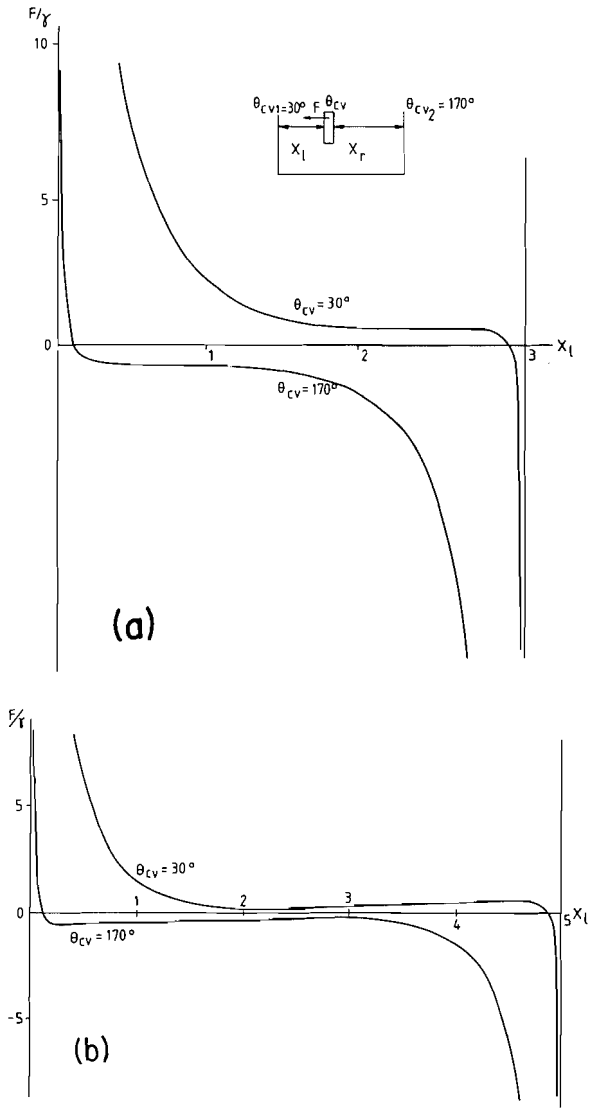


FIG. 8. The horizontal capillary force (in the direction of the left wall) on a floating prismatic particle placed between two walls as a function of the position. Wetting characteristics are indicated in the insert; (*a*) wall separation $X_l + X_r = 3a$; (*b*) wall separation $5a$.

The limiting behavior of $F(X)$ as $X \to 0$, $F \to \infty$ is easily found from eq. [11] by expanding the integrands in a power series of $k$. The result is

$$[32] \quad \frac{F}{\gamma} = \frac{2(\cos\theta_{cv} + \cos\theta_{cv}')^2}{X^2} \quad (X \to 0)$$

As $X \to \infty$, $F \to 0$, and the leading term in $X$ is

$F(\phi, k)$ for $\phi = \pi/2$, $k = 1$, which cannot be approximated by any simple function. The meniscus in this case contains an apex (with $R_a \to \infty$) or an inflection point (with $\theta_i \to 0$) between the two cylinders.

A different situation is that of a single cylindrical body between two walls at a given distance (Fig. 8, insert). The force on the cylinder as a function of its position between the walls can be obtained by combination of the curves, such as those in Figs. 5 and 6, for the appropriate v.c.a.'s at the walls ($\theta_{cv_1}$, $\theta_{cv_2}$) and at the cylinder ($\theta_{cv}$, assuming equal v.c.a. on both sides). Figures 8*a*, 8*b* apply to vertical parallelipipedic particles with contact angles 30° and 170°, respectively, for the left and right wall. In Fig. 8*a* the distance between the walls is $3a$ and in Fig. 8*b* it is $5a$. $F > 0$ indicates that the particle is attracted to the left wall. Note that the equilibrium position is stable.

## 5. Discussion

All the calculations were made on the assumption that the necessary forces are applied to keep the floating bodies at equilibrium. In addition to the horizontal force $-F_{12}$ that was calculated, a vertical force must also be applied if the bodies are to stay at equilibrium. This force must be varied as the relative position of the bodies changes, if their vertical positions relative to some reference level are to stay unchanged. Even in this case, the vertical contact angles may change as the bodies change their places, except for vertical solid surfaces. The situation is more complicated in free flotation (zero vertical applied force). When two free floating cylinders approach each other they may either tend to sink or to emerge depending on the geometry of their cross-sections. An analysis of this situation was undertaken by Gifford and Scriven (1) for free floating circular cylinders. The variation of the vertical contact angles implies that the function $F_{12}(X)$ will depend also on the geometry and densities, so that no general limiting laws are expected to hold.

The analysis of the horizontal force on a parallelipipedic particle between fixed vertical walls shows that there is a stable equilibrium position which depends on the wetting characteristics of the particle and walls. As the examples of Fig. 8 show it is in principle possible to separate particles with different wetting characteristics by placing the mixture between parallel walls of different contact angles. In the case of Fig. 8*a*, if the particles are placed at a distance $2.5a$ from the left wall ($\theta_{cv_1} = 30°$) the wettable particles ($\theta_{cv} = 30°$) will experience a small attractive force to the left wall, while the liquid repellent particles ($\theta_{cv} = 170°$) will be submitted to a larger force (approximately 12 times larger) in the opposite direction. The equilibrium positions of the two types of particles are approximately $2.8a$ apart.

Although the results of this paper apply exclusively to a cylindrical geometry, simple experiments show that the same type of effect of contact angles appears with particles of arbitrary noncylindrical shapes; in particular, the horizontal force between two such particles may be repulsive if their wetting characteristics are considerably different.

1. W. A. Gifford and L. E. Scriven. Chem. Eng. Sci. **26**, 287 (1971).
2. D. Y. C. Chan, J. D. Henry, Jr., and L. R. White. J. Colloid Interface Sci. **79**, 410 (1981).
3. I. S. Gradshteyn and I. M. Ryzhik. Table of integrals, series and products. Academic Press. 1980. p. 172.
4. M. A. Fortes. Rev. Port. Quím. In press.

Can. J. Chem. Downloaded from www.nrcresearchpress.com by 210.87.254.6 on 09/06/12
For personal use only.

# Mise en évidence de la formation d'hydrogène par la réaction de recombinaison bimoléculaire des radicaux $HO_2$. Réaction hétérogène de basse température des radicaux $HO_2$

KRIKOR A. SAHETCHIAN, ADOLPHE HEISS ET RENÉE RIGNY

*Laboratoire de Chimie Générale, Equipe de Recherche Associée au C.N.R.S. No 457, Université Pierre et Marie Curie, Tour 55, 4ème Etage, 4, Place Jussieu, 75230-Paris Cedex-05, France*

Reçu le 19 mars 1982

KRIKOR A. SAHETCHIAN, ADOLPHE HEISS et RENÉE RIGNY. Can. J. Chem. **60**, 2896 (1982).

On montre que les radicaux $HO_2$ ne réagissent pratiquement pas avec les parois de silice ou de verre Pyrex, traitées ou non à l'acide borique, aux températures supérieures à l'ambiante alors qu'aux températures inférieures à celle-ci ces radicaux disparaissent. Leur vitesse de disparition augmente avec la diminution de la température, contrairement à ce qui se passe à haute température ($t > 150$°C). Le coefficient apparent de recombinaison hétérogène peut être exprimé sous la forme $\gamma_a = 1{,}9 \times 10^{-11} \exp(11\,000/RT)$. L'utilisation, comme nouvelle source thermique de radicaux $HO_2$, du système $O_2$ + 10 ppm de $C_7H_{15}O—OC_7H_{15}$ (t 220–240°C, réacteur en silice recouvert de $B_2O_3$ puis traité par la réaction lente $H_2/O_2$, radicaux $HO_2$ formés par la réaction $C_7H_{15}O + O_2 \rightarrow HO_2$ + produit) a permis d'étudier la réaction de recombinaison bimoléculaire des radicaux $HO_2$. La formation d'hydrogène moléculaire ayant été mise en évidence dans ce système, nous en déduisons que cette réaction engendre $H_2O_2$ et $H_2$ suivant les deux voies parallèles suivantes:

$$HO_2 + HO_2 \begin{cases} \nearrow H_2O_2 + O_2 \\ \searrow H_2 + 2O_2 \end{cases}$$

KRIKOR A. SAHETCHIAN, ADOLPHE HEISS, and RENÉE RIGNY. Can. J. Chem. **60**, 2896 (1982).

It is shown that there is practically no reaction of $HO_2$ radicals on walls of quartz or Pyrex glass, coated or not with boric acid, at temperatures higher than the ambient one, whereas at lower temperatures these radicals disappear. The rate of disappearance increases with decreasing temperature, contrary to what occurs at high temperature ($t > 150$°C). The apparent coefficient of heterogeneous recombination may be expressed by $\gamma_a = 1.9 \times 10^{-11} \exp(11\,000/RT)$. By using, as a new thermal source of $HO_2$ radicals, the system $O_2$ + 10 ppm of $C_7H_{15}O—OC_7H_{15}$ (t 220–240°C, quartz vessel coated with $B_2O_3$ and treated by the slow reaction $H_2/O_2$, $HO_2$ radicals formed through the reaction $C_7H_{15}O + O_2 \rightarrow HO_2$ + product), it was possible to study the bimolecular recombination reaction of $HO_2$ radicals. The formation of molecular hydrogen was shown; we deduce from this that the recombination reaction produces $H_2O_2$ and $H_2$ by two competitive paths:

$$HO_2 + HO_2 \begin{cases} \nearrow H_2O_2 + O_2 \\ \searrow H_2 + 2O_2 \end{cases}$$

## Introduction

La réaction de recombinaison bimoléculaire en phase gazeuse des radicaux $HO_2$ joue un rôle important tant dans le domaine de la combustion que dans celui de la pollution atmosphérique. De nombreux travaux ont été consacrés à la détermination de ses caractéristiques cinétiques, mais les résultats sont incomplets et manquent d'une certaine cohérence.

En effet, cette réaction qui paraissait simple avec formation de peroxyde d'hydrogène (1)

[3*a*] $HO_2 + HO_2 \rightarrow H_2O_2 + O_2$

s'est révélée être beaucoup plus complexe (2–7).

Récemment, l'observation a été faite (4, 8) que les rendements en peroxyde d'hydrogène étaient inférieurs à ceux prévus par la réaction classique [3*a*].

La complexité des résultats obtenus peut être due *d'une part* à la complexité des mécanismes chimiques des méthodes utilisées, et *d'autre part* au processus hétérogène.

Lors des études de combustion, la réaction hétérogène des radicaux $HO_2$ est toujours envisagée. Elle peut être rendue négligeable en comparaison des réactions homogènes grâce à un recouvrement des parois, en particulier à l'acide borique, suivi d'un traitement par la réaction lente de l'hydrogène (9, 10).

Au cours de certaines déterminations de constantes de vitesse de réactions de radicaux $HO_2$, effectuées à des températures voisines de l'ambiante, différents recouvrements ont été utilisés (4, 7, 11, 12); il nous est apparu nécessaire d'étudier la réaction hétérogène des radicaux $HO_2$ parce qu'elle peut conduire à des complexités insoupçonnées.

Partant des considérations précédentes nous avons entrepris l'étude des réactions de recombi-

0008-4042/82/232896-07$01.00/0

©1982 National Research Council of Canada/Conseil national de recherches du Canada

Can. J. Chem. Downloaded from www.nrcresearchpress.com by 210.87.254.5 on 09/06/12
For personal use only.

Can. J. Chem. Downloaded from www.nrcresearchpress.com by 210.87.254.5 on 09/06/12
For personal use only.

naison, hétérogène et homogène, des radicaux $HO_2$.

Notre étude précédente (13) de la réaction hétérogène des radicaux, réalisée entre 300 et ~700 K, nous a incités à élargir le domaine vers les températures inférieures à l'ambiante. En fonction des résultats obtenus, nous avons choisi une plage de température où les réactions hétérogènes, de basse et de haute température, sont négligeables, pour étudier la recombinaison homogène des radicaux $HO_2$.

Comme nous l'avons montré ci-dessus, le grand nombre d'études, ne concordant pas toujours entre elles, réalisées à propos de la réaction [3*a*] nous a amenés à envisager la possibilité d'une nouvelle réaction [3*b*] en phase gazeuse, d'où le deuxième objet de cette étude:

[3*b*] $HO_2 + HO_2 \rightarrow H_2 + 2O_2$

Nous avons choisi les conditions expérimentales telles que les réactions hétérogènes soient rendues négligeables, et un mélange réactionnel où les radicaux $HO_2$ sont formés par une voie thermique (14) et où le mécanisme chimique est relativement simple.

## I. Réaction hétérogène des radicaux $HO_2$ de 230 à 300 K

Le dispositif expérimental est celui déjà décrit dans des études sur la décomposition de peroxydes (15).

Les radicaux $HO_2$ sont formés, en système dynamique (9), par la réaction lente de combustion de l'hydrogène à 510°C et sous une pression de 180 Torr, avec un mélange $2H_2 + 1O_2 + 0{,}03CO_2$, dans un réacteur préalablement traité à l'acide borique puis par cette même réaction lente (9, 10, 15). Une faible partie du flux réactionnel ($H_2$, $O_2$, $CO_2$ auxquels s'ajoutent les espèces $HO_2$, $H_2O_2$ et $H_2O$ formées dans la réaction) est extraite par la microfuite d'une sonde située dans l'axe du réacteur, en une position déterminée et pour un temps de séjour de 17 s. Ce flux extrait circule dans un tube de pyrex en U, sous une pression voisine de 0,2 Torr, puis les espèces condensables sont gelées sur le doigt, refroidi à l'azote liquide, d'un Dewar placé dans la cavité résonnante de l'appareil RPE (fig. 1) La fonction de $CO_2$ est de servir de matrice pour piéger les radicaux $HO_2$. La concentration des radicaux $HO_2$, dans le tube en U, avoisine $10^{10}$ particules/cm$^3$ et le temps de séjour est de l'ordre de quelques millisecondes. Pour rendre négligeable toute destruction aux parois des radicaux $HO_2$, les canalisations en Pyrex entre la sortie du réacteur et

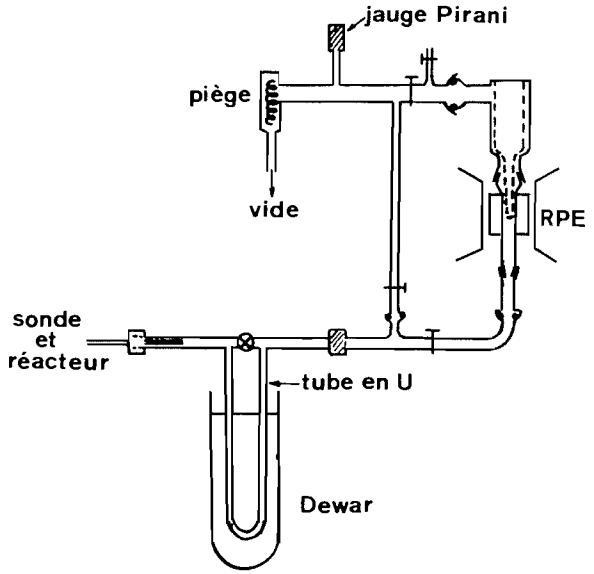


FIG. 1. Partie du montage expérimental.

le doigt froid ont également été traitées à l'acide borique. Le temps d'accumulation des radicaux sur le doigt froid est de 5 min, après quoi l'enregistrement RPE est effectué.

Les tubes de Pyrex en U ($\phi_{intérieur}$ = 5 mm, longueur ~ 21 cm), sont nettoyés avec un mélange sulfochromique, puis rincés à l'eau distillée. Ils sont: (*i*) soit plongés, à différentes profondeurs, dans un Dewar rempli d'éthanol et refroidi par de la Carboglace à une température $T$; en faisant varier la profondeur on suit l'évolution de la concentration des radicaux $HO_2$ en fonction du temps de séjour $t$ à cette température; (*ii*) soit plongés dans ce même Dewar à une profondeur déterminée, et en effectuant les expériences à des températures différentes; l'évolution de $[HO_2]$ est ainsi étudiée en fonction de la température, à temps de séjour constant; (*iii*) soit placés dans un four thermorégulé dont la température peut varier de l'ambiante à 600 K, mais le temps de séjour est fixé.

À tout moment existe la possibilité de vérifier que la concentration des radicaux $HO_2$, en fonction de la température $T$, provient bien de la réaction hétérogène sur les parois et non d'une modification des conditions de la combustion lente de l'hydrogène. Par conséquent, à l'entrée du tube en U, la concentration des radicaux $HO_2$ reste toujours constante et nous la considérerons comme la concentration initiale $[HO_2]_0$.

*Résultats*

Lorsque le flux gazeux circule par le tube en U,

Can. J. Chem. Downloaded from www.nrcresearchpress.com by 210.87.254.5 on 09/06/12
For personal use only.

nous constatons que, pour une immersion donnée de celui-ci et des conditions identiques (température, débit, longueur du tube), la concentration des radicaux diminue en fonction de la durée d'un essai, pour finir par se stabiliser à un état stationnaire. Chaque expérience a ensuite été réalisée une fois que cet état stationnaire est atteint et le temps nécessaire à son établissement est appelé temps de mise en équilibre $\tau$. Nous avons remarqué que ce temps $\tau$ est d'autant plus court que la température du tube est plus basse.

Nous avons suivi l'évolution de la concentration des radicaux $HO_2$, $[HO_2]_T$, en fonction de leur temps de séjour $t$ dans le tube en U, celui-ci étant à basse température (de 300 à 230 K). La figure 2*a* représente cette évolution à une température de $T$ = 263 K alors que la fig. 2*b*, représentant $\ln [HO_2]_T = f(t)$, montre que la cinétique de disparition des radicaux $HO_2$ est du premier ordre (le coefficient de corrélation de la droite des moindres carrés est $r^2$ = 0,98). Ces courbes sont valables pour des conditions de pression et de parois bien définies. En effet la disparition des radicaux $HO_2$ dépend non seulement du temps de séjour, mais aussi sans doute des produits formés au cours de la réaction de combustion de l'hydrogène, par exemple $H_2O$, $H_2O_2$. En particulier, l'eau formée et adsorbée sur les parois peut influencer le phénomène (4). A partir de la droite de la fig. 2*b*, une détermination de la constante de vitesse apparente de réaction hétérogène de basse température des radicaux $HO_2$ a été effectuée. La valeur trouvée, $k_a$ = 460 $s^{-1}$ à 263 K, constitue une estimation de cette constante de vitesse apparente.

A temps de séjour $t$ constant, l'évolution de la concentration des radicaux $HO_2$, $[HO_2]_t/[HO_2]_0$, en fonction de la température $T$ du tube a également été étudiée (fig. 3). Quand cette température change, le temps de séjour, à profondeur d'immersion constante, change lui aussi très légèrement, mais cette variation est négligeable en première approximation.

Pour des températures comprises entre 300 et 400 K, nous avons un palier (13), puis la concentration des radicaux $HO_2$ diminue quand $T$ continue à augmenter. Aux températures inférieures à 300 K, cette concentration diminue très fortement pour s'annuler vers 240 K. Pour des températures < 300 K et un tube traité à l'acide borique, la forme de la courbe est identique avec un très faible décalage de température. Cette rapide décroissance de concentration est à rapprocher de celle observée avec des parois traitées avec KCl, KBr, $BaBr_2$ quand la température augmente de 300 à 400 K (13).

Nous avons pu voir, dans nos expériences, que:

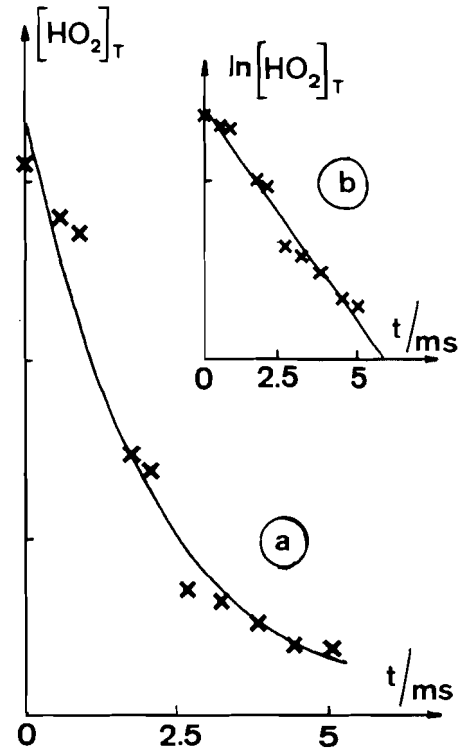


FIG. 2. (*a*) Evolution de $[HO_2]_T$ en fonction du temps de séjour $t$, à la température $T$ = 263 K, $[HO_2]_T$ en unités arbitraires. (*b*) Variation de ln $[HO_2]_T$ en fonction de $t$, à 263 K.

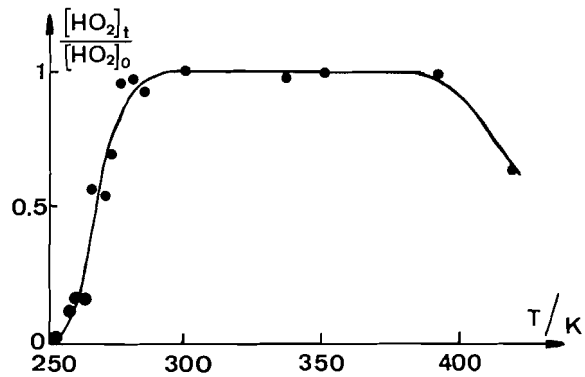


FIG. 3. Evolution de $[HO_2]_t/[HO_2]_0$ en fonction de la température absolue, pour un temps de séjour $t$ de 5 ms.

(*i*) la réaction de disparition des radicaux $HO_2$ obéit à une cinétique du premier ordre; (*ii*) la concentration de ces radicaux change très peu dans le domaine 298–400 K; (*iii*) la variation de concentration de ceux-ci à temps de séjour constant, peut être étudiée en fonction de $1/T$.

En supposant que le phénomène puisse être représenté par une équation de type Arrhénius, on obtiendra l'expression suivante, aux températures

Can. J. Chem. Downloaded from www.nrcresearchpress.com by 210.87.254.5 on 09/06/12
For personal use only.

$T < 298$ K:

$$\ln\left(\ln \frac{[HO_2]_0}{[HO_2]_{T,t}}\right) = -\frac{E_a}{RT} + \ln (A \times t)$$

où $E_a$ est l'incrément thermique de la réaction hétérogène de disparition des radicaux $HO_2$ et $A$ son facteur préexponentiel, $t$ représente le temps de séjour fixé. A partir du diagramme d'Arrhénius (fig. 4), la méthode des moindres carrés permet de déterminer $E_a$:

$$E_a = -11 \pm 3 \text{ kcal mol}^{-1} \text{ (erreur} = \pm 1 \text{ écart-type)}$$

Cette valeur de 11 kcal $mol^{-1}$ et l'observation expérimentale qu'il soit nécessaire de chauffer les parois pour revenir aux conditions initiales d'équilibre, permettraient de mettre en évidence une analogie entre ce phénomène et celui de la désorption de l'eau.

Bien que ce phénomène hétérogène soit différent de celui de haute température, nous estimons pouvoir lui appliquer la théorie des réactions hétérogènes de Semenov. Pour le domaine cinétique la valeur du coefficient apparent de recombinaison hétérogène $\gamma_a$ à 263 K est $\gamma_a = 2{,}3 \times 10^{-2}$. Pour nos conditions expérimentales, en tenant compte de l'énergie d'activation apparente déterminée ci-dessus, $\gamma_a$ peut être présenté sous la forme suivante:

$$\gamma_a = 1{,}9 \times 10^{-11} \exp \frac{11\,000}{RT}$$

Notons aussi que, en accord avec la référence 4, l'augmentation de la concentration en eau ou de celle d'autres produits présents dans le milieu, se traduirait par un accroissement de $\gamma_a$.

## II. Mise en évidence de la réaction $HO_2 + HO_2 \rightarrow H_2 + 2O_2$ [3*b*]

Les conditions expérimentales ayant été choisies pour rendre négligeable la réaction hétérogène des radicaux $HO_2$, nous avons entrepris une première étude de la recombinaison homogène de ces radicaux. Comme source propre thermique de radicaux $HO_2$, nous avons choisi le système oxygène + peroxyde de di-n heptyle $C_7H_{15}O—OC_7H_{15}$ (~ 10 ppm) précédemment étudié (14). La réaction en phase gazeuse, à une température comprise entre 150 et 240°C, de radicaux n-heptoxy (issus de la décomposition du peroxyde double ROOR précédent) et d'oxygène moléculaire engendre des radicaux $HO_2$. Le dispositif expérimental a déjà été décrit, mais quelques modifications lui ont été apportées.

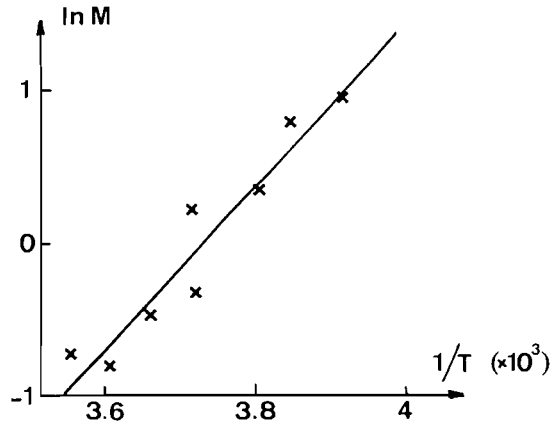


FIG. 4. Diagramme d'Arrhénius; ln $M = f(1/T)$ avec $M = \ln([HO_2]_0/[HO_2]_{T,5\text{ ms}})$ pour un temps de séjour de 5 ms.

Le peroxyde liquide ROOR est contenu dans une fiole à la température ambiante. Le flux d'oxygène passe par cette fiole et barbote dans le peroxyde liquide avant de traverser un réacteur en silice, à la pression atmosphérique. La possibilité existe d'envoyer directement le courant d'oxygène dans le réacteur sans passer par cette fiole. Le réacteur conicocylindrique (longueur 25 cm, diamètre de 1 à 4 cm) est traité à l'acide borique, puis par la réaction lente $H_2/O_2$ (10, 13, 15). Ce traitement a pour effet de rendre inertes, vis-à-vis des radicaux $HO_2$, les parois du réacteur. Celui-ci est placé dans un four à température uniforme et thermorégulée à $\pm$ 0,5°C. La sortie du réacteur est reliée à la boucle d'introduction (volume 3 $cm^3$) d'un chromatographe en phase gazeuse expérimental, conçu pour la détection de traces. Ce chromatographe a été élaboré, mis à notre disposition et manipulé par J. P. Nogier. La séparation est réalisée par une colonne garnie de tamis moléculaire 5 Å, longue de 6 m, avec l'argon N 60 (99,99990%) comme gaz porteur; la détection très sensible est réalisée dans un tube à décharge d'argon.

Le flux gazeux, à la sortie du réacteur, traverse en continu la boucle d'introduction du chromatographe pour être envoyé dans celui-ci au moment d'effectuer une analyse.

*Résultats*

Trois séries d'expériences ont été faites: (1) de l'oxygène pur (N 48 c'est-à-dire à 99,998% contenant moins de 0,1 ppm d'hydrogène, ou N 45 (99,995 avec $H_2 < 0{,}2$ ppm) est introduit dans le chromatographe, sans qu'aucun pic ne soit détecté (fig. 5*a*); (2) des mélanges d'oxygène N 45 ou d'azote N 48 contenant de faibles concentrations en hydrogène (40, 12,5 et 0,5 ppm) sont introduits

Can. J. Chem. Downloaded from www.nrcresearchpress.com by 210.87.254.5 on 09/06/12
For personal use only.

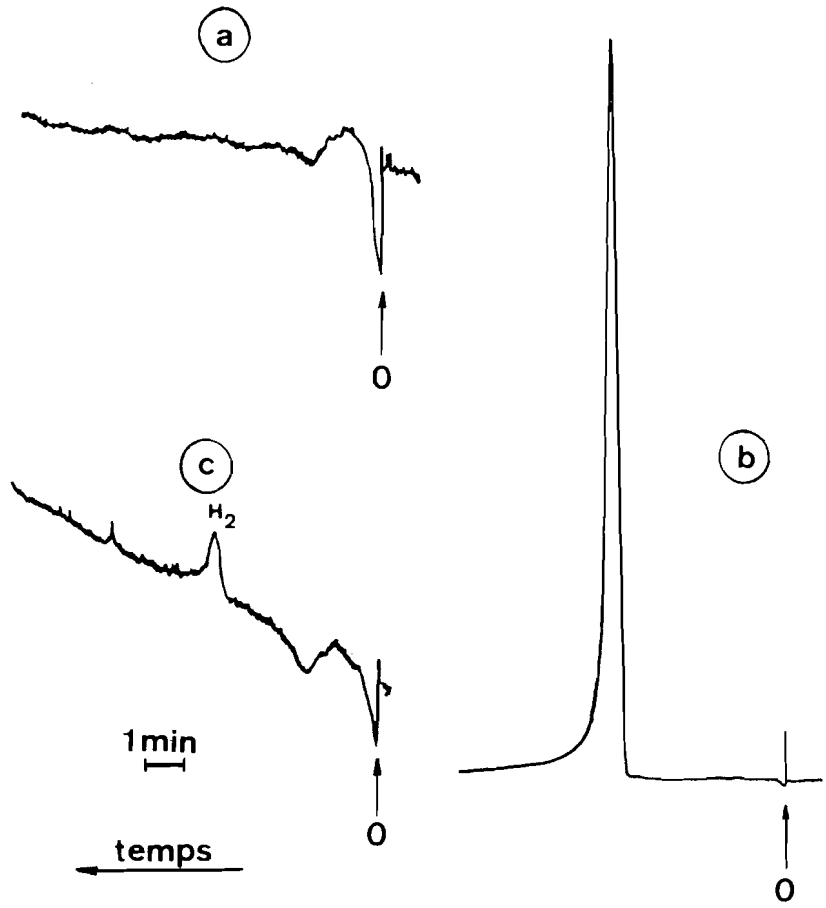


FIG. 5. Chromatogrammes en phase gazeuse. O: perturbation d'introduction. (*a*) oxygène N 45 seul; (*b*) pic obtenu avec 40 ppm. d'hydrogène dans l'oxygène N 45, sensibilité 10 fois plus faible qu'en (*a*) et (*c*); (*c*) pic d'hydrogène obtenu avec le mélange 10 ppm de ROOR dans l'oxygène N 45.

dans le chromatographe. Les chromatogrammes permettent de localiser $H_2$ (pic à 4 min) et de tester la sensibilité du détecteur vis-à-vis de ce gaz. Le pic obtenu pour une concentration de 40 ppm est représenté sur la fig. 5*b*; (3) des mélanges d'oxygène N 48 ou N 45 et de peroxyde ROOR (~ 10 ppm) avec des débits de 28 et 40 L $h^{-1}$, après passage par le réacteur à des températures de 238 ou 220°C, sont chromatographiés. Un des chromatogrammes est représenté sur la fig. 5*c*, où le pic correspond bien à celui de l'hydrogène moléculaire.

La bonne reproductibilité de ces expériences mérite d'être signalée. Plusieurs séries d'expériences complémentaires sont effectuées pour vérifier l'influence de divers facteurs.

(*i*) Après son passage dans le réacteur à 100°C, nous avons chromatographié le mélange $O_2$ + ROOR sans observer de formation d'hydrogène.

(*ii*) En opérant de même avec le mélange $O_2$ + $H_2O_2$ circulant dans le réacteur à 240°C, là aussi aucune formation de $H_2$ n'est détectée.

(*iii*) Pour des conditions identiques de température, pression, concentrations, des essais sont réalisés dans un réacteur en silice identique à celui décrit, mais avec la différence qu'il n'est pas traité à l'acide borique. Nous constatons que:

la décomposition de ROOR est pratiquement la même que dans le cas du réacteur traité; cela signifie que la décomposition se produit en phase gazeuse;

dans ces conditions, ni $H_2O_2$ (par chromatographie sur couches minces) ni $H_2$ (par chromatographie en phase gazeuse) ne sont mis en évidence.

## Discussion

Il est intéressant tout d'abord de remarquer que la formation d'hydrogène observée expérimentalement ne peut s'expliquer ni par des réactions hétérogènes, dont le rôle est négligeable aux températures auxquelles nous opérons grâce au traitement des parois effectué, ni par des réactions entre radicaux et peroxyde (ou des réactions telles que

Can. J. Chem. Downloaded from www.nrcresearchpress.com by 210.87.254.5 on 09/06/12
For personal use only.

décomposition, isomérisation etc ...) rendues négligeables par rapport à celle de RO avec $O_2$, grâce à la faible concentration en peroxyde ROOR et à la température des expériences relativement faible.

Les réactions principales se produisant dans le système $O_2$ + ROOR, avec nos conditions expérimentales, sont les suivantes (14).

[1] $\mathrm{ROOR} \xrightarrow{k_1} 2\mathrm{RO}$

[2] $\mathrm{RO} + \mathrm{O_2} \xrightarrow{k_2} \mathrm{HO_2} + \text{produit}$

[3] $\mathrm{HO_2} + \mathrm{HO_2} \xrightarrow{k_3} \mathrm{H_2O_2} + \mathrm{O_2}$

La réaction [2] peut aussi avoir lieu après isomérisation du radical RO. Dans les études des réactions concernant ces deux radicaux, la formation d'hydrogène atomique ou moléculaire n'est jamais mise en évidence. Pour le radical méthoxy $CH_3O$, la formation d'hydrogène atomique a été envisagée (16) alors que celle d'hydrogène moléculaire apparaît comme pratiquement très peu probable, d'après des calculs théoriques qui concluent à une barrière d'énergie très élevée pour la réaction $CH_3O \rightarrow CHO + H_2$ (17). Toutefois, même si de l'hydrogène atomique était susceptible de se produire, la vitesse de formation de $H_2$ par une réaction de H avec le peroxyde ou un produit de décomposition serait négligeable, en comparaison de la réaction $H + O_2 + M \rightarrow HO_2 + M$.

A partir des résultats expérimentaux, on observe que la présence d'hydrogène moléculaire est liée à celle des radicaux $HO_2$ et du peroxyde $H_2O_2$ dans le milieu en réaction. La formation d'hydrogène ne pouvant pas s'expliquer par les réactions [1] à [3] (et cherchant vainement dans la littérature une possible voie de formation de $H_2$ pendant la décomposition des radicaux RO), au vu des considérations précédentes, on en déduit que la réaction entre deux radicaux $HO_2$ engendre à la fois $H_2O_2$ et $H_2$. Ceci signifierait que la réaction [3] est en réalité complexe, ce qui expliquerait certaines incohérences entre la vitesse de formation de $H_2O_2$ et la disparition des radicaux $HO_2$ (4, 8). Il en résulte que la réaction de recombinaison se produirait suivant deux voies parallèles:

[3a] $\mathrm{HO_2} + \mathrm{HO_2} \rightarrow \mathrm{H_2O_2} + \mathrm{O_2}$

[3b] $\mathrm{HO_2} + \mathrm{HO_2} \rightarrow \mathrm{H_2} + 2\mathrm{O_2}$

La voie [3b] a été suggérée antérieurement (3, 5, 8).

Au cours de certaines expériences nous avons analysé le peroxyde d'hydrogène produit. A partir des chromatogrammes, une première estimation montre que le rapport $[H_2]/[H_2O_2]$ est de l'ordre de 10%. Bien que la probabilité du chemin réactionnel [3b] soit nettement plus faible que celle du chemin [3a] dans nos conditions, il peut jouer un rôle important, tant dans la chimie de la combustion que dans celle de l'atmosphère.

En effet, les radicaux $HO_2$ disparaissent par recombinaison bimoléculaire par les réactions [3a] et [3b]. Dans le domaine de la combustion, la voie [3b] constitue une rupture de chaîne alors que ce n'est pas toujours le cas pour la voie [3a], parce que le peroxyde d'hydrogène formé peut engendrer de nouvelles chaînes par suite de sa décomposition homogène ou hétérogène en radicaux. Il est bien connu que, dans la réaction d'oxydation des hydrocarbures, il se forme de l'hydrogène moléculaire; cette formation pourrait être expliquée par la réaction [3b].

En ce qui concerne la chimie de l'atmosphère, cette réaction de formation d'hydrogène n'a jamais été prise en considération. Pourtant elle pourrait jouer un rôle important dans les domaines où la concentration en radicaux $HO_2$ est relativement élevée, tels que la stratosphère ou la mésosphère. Son influence peut aussi être grande sur la teneur en eau de la stratosphère (elle serait peut-être une raison de la sécheresse inexpliquée de celle-ci), parce qu'elle diminue la formation de $H_2O_2$. Ajoutons, d'après Nicolet (18), qu'au voisinage de la mésopause, l'hydrogène atomique et l'hydrogène moléculaire doivent intervenir simultanément pour déterminer le comportement de l'hydrogène atomique dans l'exosphère.

## Conclusion

Cet article est constitué de deux parties décrivant chacune un phénomène nouveau lié aux radicaux perhydroxyles. La première se rapporte à la disparition hétérogène des radicaux $HO_2$ entre 230 et 300 K, alors que la seconde concerne une étude du mécanisme de la réaction de recombinaison bimoléculaire de ces radicaux.

La réaction hétérogène des radicaux $HO_2$ aux basses températures semble relever d'une adsorption physique de ceux-ci et cette réaction doit toujours être envisagée aux températures inférieures à l'ambiante. Elle ne dépendrait pas seulement de l'adsorption des radicaux $HO_2$, mais subirait aussi l'influence des produits formés en cours de réaction.

En ce qui concerne la réaction de recombinaison des radicaux $HO_2$ en phase gazeuse, elle s'effectuerait par les deux voies [3a] et [3b], la voie [3b] pouvant jouer un rôle non négligeable dans la chimie de la combustion, ainsi que dans celle de l'atmosphère. C'est pourquoi il est important de poursuivre l'étude de cette réaction.

## Remerciements

Les auteurs remercient vivement D. Delafosse et

M. Che pour leur discussion concernant la réaction hétérogène ainsi que J. P. Nogier pour avoir mis à notre disposition et manipulé un chromatographe en phase gazeuse conçu pour la détection de traces.

1. S. N. FONER et R. L. HUDSON. Adv. Chem. Ser. **36**, 34 (1962).
2. R. R. LII, R. A. GORSE JR., M. C. SAUER JR. et S. GORDON. J. Phys. Chem. **83**, 1803 (1979).
3. R. R. LII, R. A. GORSE JR., M. C. SAUER JR. et S. GORDON. J. Phys. Chem. **84**, 813 (1980).
4. R. A. COX et J. P. BURROWS. J. Phys. Chem. **83**, 2560 (1979).
5. E. J. HAMILTON et R. R. LII. Int. J. Chem. Kinet. **9**, 875 (1977).
6. J. P. BURROWS, R. A. COX et R. G. DERWENT. J. Photochem. **16**, 147 (1981).
7. B. A. THRUSH et J. P. T. WILKINSON. Chem. Phys. Lett. **66**, 441 (1979).
8. C. J. HOCHANADEL, T. J. SNORSKI et J. P. OGREN. J. Phys. Chem. **84**, 3274 (1980).
9. I. K. SHAKNAZARYAN, K. A. SAHETCHIAN (G. A. SACHYAN), A. G. PHILIPOSSYAN et A. B. NALBANDYAN. Int. J. Chem. Kinet. **6**, 693 (1974).
10. R. R. BALDWIN et L. MAYOR. Rev. Institut Français du Pétrole. Vol. 13. 1958. p. 397; Seventh Symposium (Internat.) on Combustion. 1959. p. 8.
11. W. B. DEMORE. J. Phys. Chem. **83**, 1113 (1979).
12. W. HACK, A. W. PREUSS, F. TEMPS et H. GG. WAGNER. Int. J. Chem. Kinet. **12**, 851 (1980).
13. I. A. VARDANYAN, K. A. SAHETCHIAN (G. A. SACHYAN) et A. B. NALBANDYAN. Combust. Flame, **17**, 315 (1971).
14. K. A. SAHETCHIAN, R. RIGNY, A. HEISS et R. I. BEN-AÏM. Chem. Phys. Lett. **87**, 333 (1982).
15. K. A. SAHETCHIAN, A. HEISS, R. RIGNY et R. I. BEN-AÏM. Int. J. Chem. Kinet. Sous presse.
16. L. BATT, J. P. BURROWS et G. N. ROBINSON. Chem. Phys. Lett. **78**, 467 (1981).
17. G. F. ADAMS, R. J. BARTLETT et G. D. PURVIS. Chem. Phys. Lett. **87**, 311 (1982).
18. M. NICOLET. Étude des réactions chimiques de l'ozone dans la stratosphère. Covos, Bruxelles, décembre 1977.

Can. J. Chem. Downloaded from www.nrcresearchpress.com by 210.87.254.5 on 09/06/12
For personal use only.

# Synthesis of *trans*(±)6-phenoxyacetamido-1-methylene-3,3-dicarboxymethyl-1-carbapenam

PIET HERDEWIJN, PAUL J. CLAES, AND HUBERT VANDERHAEGHE[1]

*Rega Institute and Pharmaceutical Institute, University of Leuven, 10 Minderbroedersstraat, B-3000 Leuven, Belgium*

Received April 16, 1982

PIET HERDEWIJN, PAUL J. CLAES, and HUBERT VANDERHAEGHE. Can. J. Chem. **60**, 2903 (1982).

Methyl 4-benzylidene-2-pyrroline-2-carboxylate and dimethyl-4-methylene-5-pyrroline-2,2-dicarboxylate were prepared by *N*-chlorination – dehydrochlorination starting from the corresponding 4-alkylidene- or 4-arylidene-pyrrolidine. Structure of the pyrroline compound was determined by spectrometry and by reaction with α-azidoacetyl chloride. The 2-carbomethoxy-4-benzylidene-$\Delta^2$-pyrroline compound gave, on reaction with α-azidoacetyl chloride, 2-benzylidene-5-carbomethoxy-6-azido-1-carbapenam. In the case of the 2,2-dicarbomethoxy-4-methylene-$\Delta^5$-pyrroline, *trans*-1-methylene-3,3-dicarbomethoxy-6-azido-1-carbapenam was formed. When *N*-chlorination – dehydrochlorination was carried out on 2-carbomethoxy-4-methylenepyrrolidine, double bond isomerization occurred with formation of 2-carbomethoxy-4-methylpyrrole.

PIET HERDEWIJN, PAUL J. CLAES et HUBERT VANDERHAEGHE. Can. J. Chem. **60**, 2903 (1982).

On a préparé le carboxylate-2 benzylidène-4 pyrroline-2 de méthyle et le dicarboxylate-2,2 méthylène-4 pyrroline-5 de méthyle au moyen d'une *N*-chloration – déhydrochloration en partant des alkylidène-4 ou arylidène-4 pyrrolidines correspondantes. On a déterminé la structure du composé pyrroline par spectrométrie et par la réaction avec le chlorure de l'α-azidoacétyle. Le composé carbométhoxy-2 benzylidène-4 $\Delta^2$-pyrroline réagit avec le chlorure d'α-azidoacétyle en donnant le benzylidène-2 carbométhoxy-5 azido-6 carbapénam-1. Dans le cas du dicarbométhoxy-2,2 méthylène-4 $\Delta^5$-pyrroline, on obtient le méthylène-1 dicarbométhoxy-3,3 azido-6 carbapénam-1 *trans*. Quand on effectue la *N*-chloration – déhydrochloration de la carbométhoxy-2 méthylène-4 pyrrolidine, il se produit une isomérisation de la double liaison avec la formation de carbométhoxy-2 méthyl-4 pyrrole.

[Traduit par le journal]

A number of penam and cefem analogs in which the sulfur atom has been replaced by other atoms have been described (1). Some of these compounds such as the 1-oxapenam, clavulanic acid (2) and the 1-carbapenem, thienamycin (3) are of therapeutic interest. The study of 1-alkylidene-1-carbapenams seemed to be of interest in this context. Certain 1-arylidene-5-alkylthio-1-carbapenams and 1-arylidene-6-alkylthio-1-carbacephams have been synthesized by Bose *et al.* (4). It should be noted that an acylamido side chain and a carboxyl group respectively in the 3- or 4-position are not present in these arylidene-β-lactams.

In the present work we investigated the preparation of methyl 4-alkylidene-5-pyrroline-2-carboxylates (**1***a–c*) and their conversion into bicyclic β-lactams by cycloaddition with azidoacetyl chloride according to Bose *et al.* (5). The synthetic approach examined for the preparation of the 4-alkylidene-5-pyrrolines (**1***a–c*) consists in *N*-chlorination of the corresponding methyl 4-alkylidene-pyrrolidine-2-carboxylates (**2***a–c*), followed by base-catalysed elimination of hydrochloric acid. A similar procedure is described by Schmidt and Poisel (6) for the preparation of racemic proline. The pyrrolidine **2***a* was obtained in five steps from 4-hydroxy-L-proline **3***a*.[2] In order to obtain a 1-methylene-1-carbapenam with the same configuration at C2 as in penicillins, 4-hydroxy-D-proline should be used as a starting material. However, in these experiments the more readily available *L*-enantiomer was used. Oxidation of *N-tert*-Boc-4-hydroxy-L-proline **3***b* with $CrO_3$/pyridine in $CH_2Cl_2$ gave the ketone **3***c* (60%), which was converted into the *N*-protected 4-methylenepyrrolidine **3***d* by condensation with methylenetriphenylphosphorane (4 equiv.) in THF (80% yield). When the Wittig reaction was carried out on the methyl ester instead of the acid **3***c*, only 5% of **3***e* was obtained. After esterification of the carboxyl group ($CH_2N_2$) and removal of the *N*-protecting group, the free base **2***a* was obtained as an unstable oil (85% yield based on **3***d*), which can be converted into a stable crystalline hydrochloride salt. When oxidation of **3***b* was attempted with DMSO–$Ac_2O$

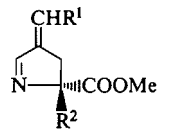


**1**

*a* $R^1 = H$, $R^2 = H$
*b* $R^1 = \phi$, $R^2 = H$
*c* $R^1 = H$, $R^2 = COOMe$

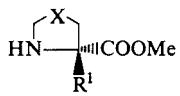


**2**

*a* $R^1 = H$, $X = >C = CH_2$
*b* $R^1 = H$, $X = >C = CH\phi$
*c* $R^1 = COOMe$, $X = >C = CH_2$

[1]Author to whom correspondence may be addressed.

[2]The D-configuration related to natural penicillin is given in all schemes, even when reactions were carried out with the L-enantiomer.

0008-4042/82/232903-05$01.00/0

©1982 National Research Council of Canada/Conseil national de recherches du Canada

Can. J. Chem. Downloaded from www.nrcresearchpress.com by 210.87.254.105 on 09/06/12
For personal use only.

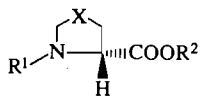

3

*a* $R^1 = R^2 = H$, X = $>C(OH)H$

*b* $R^1 = COOBu^t$, $R^2 = H$, X = $>C(OH)H$

*c* $R^1 = COOBu^t$, $R^2 = H$, X = $>C=O$

*d* $R^1 = COOBu^t$, $R^2 = H$, X = $>C=CH_2$

*e* $R^1 = COOBu^t$, $R^2 = Me$, X = $>C=CH_2$

*f* $R^1 = COOBu^t$, $R^2 = H$, X = $>C=CH\phi$

*g* $R^1 = COOBu^t$, $R^2 = Me$, X = $>C=CH\phi$

(7) the hydroxy group was converted into a methylthiomethyl ether. Oxidation of **3***b* with DMSO–DCCI–pyridine–$CF_3COOH$ gave the methylthiomethyl ester of **3***c* in a 93% yield. Removal of the methylthiomethyl ester with base or $HgCl_2/H_2S$ afforded the ketone **3***c* in low yield, due to degradation in the given reaction conditions.

The conversion of **2***a* into 5-pyrroline **1***a* was attempted by *N*-chlorination with *tert*-butylhypochlorite, followed by dehydrochlorination with $KO_2$/18-crown-6 polyether in $Et_2O$ (8). Since **1***a* contains a conjugated aldimine, one might expect that the pyrroline should be formed to some extent. However, the only compound isolated from the reaction mixture was the 2-carbomethoxy-4-methylpyrrole, which resulted from a migration of the exocyclic double bond into an *endo*-position, upon introduction of the aldimine function. Other dehydrohalogenating agents such as MeONa, pyridine, and $CH_3COOK$ gave similar results. Reaction mixtures, however, were more complex.

To avoid aromatization during the introduction of the aldimine function the *N*-chlorination – dehydrochlorination was repeated for methyl 4-benzylidene-pyrrolidine-2-carboxylate **2***b*. One might expect that the presence of the phenyl group would stabilize the exocyclic double bond and avoid to a certain extent its isomerization into an *endo*-position. Thus **3***c* was reacted with four equivalents of benzylidenetriphenylphosphorane in DMSO. The *N*-protected pyrrolidine **3***f* was isolated in a 82% yield as a 1:1 mixture of the *E*- and *Z*-isomers. Treatment of this mixture with $CH_2N_2$, followed by *N*-deprotection, afforded *E*- and *Z*-**2***b*, which were separated by fractional crystallization from ethanol–ether for further characterization. *N*-chlorination – dehydrochlorination conducted on the *E*,*Z*-mixture of **2***b* afforded 10% of the 2-carbomethoxy-4-benzylpyrrole and about 85% of an unstable pyrroline **4**, which was not isolated in a pure state. The structure **4** was based on the absence of an absorption band between 1560 and 1580 $cm^{-1}$, due to a C=N stretching vibration conjugated with an exocyclic carbon–carbon double bond (9), which excluded a 5-pyrroline structure. Absorptions at 1620 and 1630 $cm^{-1}$ (attributed to a C=C or a C=N bond conjugated with a phenyl or carbonyl group) are consistent with a methyl 2-pyrroline-2-carboxylate structure **4**. The formation of the latter results from proton abstraction in the 2-position during dehydrohalogenation. A further proof for the proposed structure was obtained by cycloaddition of azidoacetyl chloride to **4** (mixture of *E*- and *Z*-isomers) in benzene–cyclohexane containing $Et_3N$. The reaction product was found

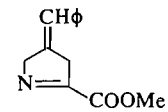

4

to be a bicyclic β-lactam, which was isolated by column chromatography in a 50% yield (based on **2***b*). Spectral data were consistent with the structure **5***a*. The ir spectrum showed the presence of a β-lactam carbonyl group (1780 $cm^{-1}$). The $^1$Hmr spectra showed two singlets at δ 4.56 and 4.59 ppm (due to the C6-protons), broad signals at δ 6.4 and 7.2 ppm for $C_6H_5CH{=}C<$, and the absence of a C5-proton. The interpretation of the $^1$Hmr spectrum of **5***a* was somewhat obscured by the fact that it was recorded on a mixture of *E*- and *Z*-isomers. To establish the relative configuration at C5 and C6 it is necessary to simplify spectral data by converting the *E*,*Z*-mixture into a single compound by ozonolysis of the exocyclic double bond. This was performed on **5***c*, which was obtained by reduction of the azide function ($H_2S/Et_3N$) followed by *N*-phenoxyacetylation. The *trans*-stereochemistry of the side-chain and the COOMe function in **5***d* was ascertained by comparison of its $^1$Hmr spectra

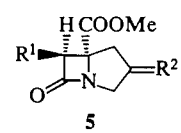

5

*a* $R^1 = N_3$, $R^2 = CH\phi$

*b* $R^1 = NH_2$, $R^2 = CH\phi$

*c* $R^1 = V$, $R^2 = CH\phi$

*d* $R^1 = V$, $R^2 = O$

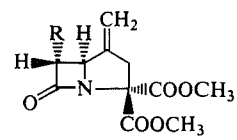

6

*a* R = $N_3$

*b* R = V

V = $\phi OCH_2CONH$

obtained in $CDCl_3$ and in $CDCl_3$ – DMSO-$d_6$. A solvent shift of 1.00 ppm was observed for the amide proton (from 7.82 ppm in $CDCl_3$ to 8.82 ppm in $CDCl_3$–DMSO), which is due to the formation of

Can. J. Chem. Downloaded from www.nrcresearchpress.com by 210.87.254.105 on 09/06/12
For personal use only.

Can. J. Chem. Downloaded from www.nrcresearchpress.com by 210.87.254.105 on 09/06/12
For personal use only.

a hydrogen bond between the amide proton and DMSO. This shift should not be expected for a *cis*-β-lactam in which both functions are presumed to form an intramolecular hydrogen bond. Further indication for the absence of an intramolecular hydrogen bond can be found in the sharp NH absorption (3420 $cm^{-1}$) in the ir spectrum and in the absence of an absorption between 3100 and 3375 $cm^{-1}$.

The experiments suggest that the conversion of pyrrolidine-2-carboxylates into the corresponding 5-pyrrolines by *N*-chlorination – dehydrochlorination is only feasible if the pyrroline has no hydrogen atom in the 2-position. To verify this hypothesis the pyrroline formation was studied for dimethyl 4-methylene-pyrrolidine-2,2-dicarboxylate (**2***c*). The latter was prepared (in a 25% yield) by reaction of dimethyl aminomalonate hydrochloride with 1 equivalent of 3-chloro-2-chloromethyl-1-propene in the presence of NaOMe (10). Introduction of the aldimine function by the *N*-chlorination – dehydrochlorination procedure gave an unstable reaction product, which was found to be the desired 5-pyrroline **1***c*. The structure was proven by cycloaddition with azidoacetyl chloride. This afforded the *trans*-6-azido-1-methylene-3,3-dicarboxymethyl-1-carbapenam **6***a* (15% yield based on **2***c*). Spectral data obtained for **6***a* were in agreement with the proposed structure. The ir spectrum showed the presence of a β-lactam carbonyl group at 1790 $cm^{-1}$. In the $^1$Hmr spectrum the C6 proton appears as a doublet ($J$ = 2.7 Hz) at 4.42 ppm, the 1-methylene- and C5-protons as multiplets, respectively, at 5.28 and 4.25 ppm. The coupling constant of 2.7 Hz for the C5- and the C6-protons suggested a *trans*-β-lactam (11). Reduction of the azide function of **6***a* and *N*-phenoxyacetylation gave the crystalline β-lactam **6***b*. 100 MHz $^1$Hmr and $^{13}$Cmr spectra confirmed the proposed structure and stereochemistry.

Epimerization of carbapenams at C-6 has not been reported hereto. Procedures worked out for epimerization of penicillins (12–14) are only successful to a certain extent in the parent cephalosporin series (15). Therefore it is not likely that these methods can be applied for the isomerization of 1-methylene-1-carbapenam nucleus. Thus conversion of **6***b* into a *cis*-β-lactam was not further investigated.

## Experimental

Melting points were determined with a Büchi–Tottoli apparatus and are uncorrected. Precoated Merck silica gel F 254 plates were used for tlc. Column chromatography was performed on silica gel (Merck, 0.040–0.063 mm). Infrared (ir) spectra were recorded on a Perkin Elmer 257 spectrometer. The $^1$Hmr spectra were recorded on a Hitachi–Perkin–Elmer R-24 60 MHz instrument in $CDCl_3$ with tetramethylsilane as internal standard unless stated otherwise. Mass spectra were determined with an AEI MS-12 apparatus. Elemental analyses were performed by Janssen Pharmaceutica, B-2340 Beerse, Belgium.

N-tert-*Boc-4-oxo-*L*-proline* **3***c*

$CrO_3$ (16.8 g, 168 mmol) was added to a stirred solution of pyridine (27 mL, 336 mmol) in anhydrous $CH_2Cl_2$ (350 mL) at 0°C. The reaction mixture was stirred for 5 min at 0°C and allowed to warm up to room temperature. A solution of *N-tert*-Boc-4-hydroxy-L-proline (16) (6.5 g, 28 mmol) in anhydrous $CH_2Cl_2$ (20 mL) containing pyridine (2.5 mL, 30 mmol) was added at once to the stirred suspension. After vigorous stirring for 4 h at room temperature, the solution was decanted and the black remaining solid was washed with acetone (3 × 100 mL). The combined organic solution was filtered and evaporated. The residue was taken up in a saturated NaCl solution (200 mL), acidified to pH 2.5 with 5*N* HCl, and extracted with EtOAc (5 × 100 mL). The EtOAc solution was dried over $MgSO_4$, Celite (150 g) was added, and the solvent was removed under reduced pressure. The adsorbed *N-tert*-Boc-4-oxo-L-proline was extracted with $Et_2O$ in a Soxhlet apparatus for 5 h. Evaporation afforded **3***c* (3.9 g, 60% yield) as an amorphous solid which can be used in the next step without further purification. Crystallization from $Et_2O$ gave analytically pure **3***c*, mp 148–150°C (dec.); ir ($CH_2Cl_2$): 1750 (ketone), 1650 (COOH) $cm^{-1}$. Compound **3***c* was converted into its benzyl ester (benzyl bromide/DMF/$Et_3N$) which was used for further spectrometric identification; ir ($CH_2Cl_2$): 1770 (ester), 1750 (ketone), 1703 (carbamate) $cm^{-1}$; $^1$Hmr δ: 1.4 (s, 9H, *t*-butyl), 2.70 (AB part of ABX pattern, 2H, $J_{ax}$ = 9 Hz, $J_{bx}$ = 4 Hz, $J_{ab}$ = 19 Hz, $CH_2CH$), 3.85 (s, 2H, $CH_2N$), 4.76 (X-part, 1H, CHN), 5.15 (s, 2H, $CH_2\phi$), 7.3 (s, 5H, phenyl) ppm. Oxidation of **3***b* in DMSO–benzene (1:1) containing pyridine (2 equiv.), $CF_3CO$-OH (1 equiv.), and dicyclohexylcarbodiimide (6 equiv.) afforded 93% of the crystalline methylthiomethylester of **3***c*, $^1$Hmr δ: 1.5 (s, 9H, *t*-butyl), 2.25 (s, 3H, SMe), 2.75 (AB part of ABX pattern, 2H, $J_{ax}$ = 9 Hz, $J_{bx}$ = 4 Hz, $J_{ab}$ = 19 Hz, $CH_2CH$), 3.87 (s, 2H, $CH_2N$), 4.77 (X-part, 1H, $CH_2N$), 5.2 (s, 2H, $CH_2S$) ppm.

N-tert-*Boc-methylene-*L*-proline* **3***d*

Methyltriphenylphosphonium bromide (17) (35.7 g, 100 mmol) was added to a stirred suspension of NaH (2.4 g, 100 mmol) in anhydrous THF (250 mL). The mixture was heated at 50°C for 4 h and a solution of *N-tert*-Boc-L-proline (5.7 g, 25 mmol) in anhydrous THF (50 mL) was added over a period of 30 min. After stirring overnight at 50°C, the suspension was cooled, poured into 500 mL 5% $NaHCO_3$, and washed twice with $Et_2O$. The aqueous solution was acidified to pH 3 with 2*N* HCl and extracted three times with EtOAc. The extract was dried over $Na_2SO_4$ and evaporated. The residual oil was chromatographed on a silica gel column using $C_6H_6$–$Me_2CO$–$CH_3COOH$ (87:12:1) as eluent to yield **3***d* (4.54 g, 80%) as an oil; $^1$Hmr δ: 1.42 (s, 9H, *t*-butyl), 2.83 (m, 2H, $CH_2CH$), 4.05 (m, 2H, $CH_2N$), 4.45 (m, 1H, CHN), 4.97 (m, 2H, $CH_2$=C), 10.4 (s, 1H, COOH) ppm.

*Methyl* N-tert-*Boc-4-methylene-*L*-proline* **3***e*

To a solution of **3***d* (3.4 g, 15 mmol) in anhydrous $CHCl_3$ (50 mL) was added an excess of $CH_2N_2$ (until the yellow color persisted). After removal of the solvent, the ester was obtained in a quantitative yield as an oil; ir ($CH_2Cl_2$): 1755 (ester), 1705 (carbamate), 1405, 1127, 900 (C=$CH_2$) $cm^{-1}$; $^1$Hmr δ: 1.42 (s, 9H, *t*-butyl), 2.75 (m, 2H, $CH_2CH$), 3.72 (s, 3H, $COOCH_3$), 4.07 (m, 2H, $CH_2N$), 4.44 (m, 1H, CHN), 4.98 (m, 2H, C=$CH_2$) ppm; ms *m/e*: 241 ($M^+$).

Can. J. Chem. Downloaded from www.nrcresearchpress.com by 210.87.254.105 on 09/06/12
For personal use only.

*Methyl 4-methylene-*L*-proline* **2**a

A solution of **3***e* (2.41 g, 10 mmol) in 98% HCOOH (50 mL) was kept at room temperature for 2.5 h and evaporated to dryness at a temperature below 30°C. The oily residue was partitioned between $Et_2O$ (100 mL) and 0.1 *N* HCl (100 mL). The aqueous layer was separated, made basic with 5% $NaHCO_3$, saturated with NaCl, and extracted with $CH_2Cl_2$ (3 × 100 mL). The $CH_2Cl_2$ extract was dried over $Na_2SO_4$ and evaporated to give **2***a* (1.2 g, 85%) as a light yellow oil. Analysis of the oil on tlc (10% MeOH/$CHCl_3$) showed a single spot. The compound was not stable as its free base and was converted into its hydrochloride for further characterization.

*Methyl 4-methylene-*L*-proline hydrochloride* **2**a·*HCl*

A solution of 1 *N* HCl in EtOH (5.5 mL) was added dropwise to a solution of **2***a* (705 mg, 5 mmol) in EtOH (20 mL). Addition of anhydrous $Et_2O$ afforded 820 mg of the title compound (92%) as colorless needles, mp 159–160°C (dec.) after recrystallization from EtOH/$Et_2O$; $[\alpha]_D^{25}$ −15.25° (*c* 1, $H_2O$); ir (KBr): 1750 (ester), 1677 ($CH_2$=CH) $cm^{-1}$; $^1$Hmr (360 MHz, DMSO-$d_6$) δ: 2.73 (m, 1H, $^2J_{3,3'}$ = 16.2 Hz, $^3J_{3,2}$ = 8 Hz, $^4J$ = 2 × 2.3 Hz, $^4J_{3,5}$ = 2.0 Hz, $^4J_{3,5'}$ = 0.6 Hz, H-3), 2.96 (m, 1H, $^2J_{3',3}$ = 16.2 Hz, $^3J_{3',2}$ = 8.4 Hz, $^4J$ = 2 × 2.1 Hz, $^4J_{3',5}$ = 0.95 Hz, $^4J_{3',5'}$ = 1.6 Hz, H-3'), 3.77 (s, 3H, COOMe), 3.81 (m, 1H, $^2J_{5,5'}$ = 15.2 Hz, $^4J$ = 2 × 2.2 Hz, $^4J_{5,3}$ = 2.0 Hz, $^4J_{5,3'}$ = 0.95 Hz, H-5), 3.88 (m, 1H, $^2J_{5',5}$ = 15.2 Hz, $^4J$ = 2 × 2 Hz, $^4J_{5',3}$ = 0.6 Hz, $^4J_{5',3'}$ = 1.6 Hz, H-5'), 4.56 (dd, 1H, $^3J_{2,3}$ = 8 Hz, $^3J_{2,3'}$ = 8.4 Hz, H-2), 5.15 (m, 2H, $^4J$ = 2 × 2.3 and 2 × 2.1 Hz, $^4J$ = 2 × 2.2 and 2 × 2 Hz, $CH_2$=C) ppm. *Anal.* calcd. for $C_7H_{11}O_2N$·HCl: C 47.31, H 6.82, N 7.88; found: C 47.20, H 6.71, N 7.70.

*Methyl 4-benzylidene-*N*-tert-Boc-*L*-proline* **3**g

Benzyltriphenylphosphonium bromide (21.65 g, 50 mmol) was gradually added to a solution of NaH (1.2 g, 50 mmol) in anhydrous DMSO (120 mL). The suspension was warmed up to 80°C and stirred for 1 h. The red color indicated the ylide formation. A solution of **3***c* (2.86 g, 12.5 mmol) in anhydrous DMSO (30 mL) was added dropwise over a period of 30 min to the stirred ylide solution. The reaction mixture was stirred for 6 h at 80°C, cooled to room temperature, poured into 500 mL 0.2 *N* HCl, and extracted with EtOAc (3 × 100 mL), which was then washed with water (3 × 100 mL). The organic solution was dried and the EtOAc removed. Purification of the residual oil by chromatography on a silica gel column using $C_6H_6$–$Me_2CO$–$CH_3COOH$ (89:10:1) yielded the acid **3***f*, which was converted into the methyl ester by reaction with $CH_2N_2$, as described in a previous section, yielding 3.25 g (82%) of the title compound as an oil. The $^1$Hmr spectrum showed that **3***g* was a mixture of two isomers: $^1$Hmr δ: 1.43 (s, 9H, *t*-butyl), 2.96 (m, 2H, $CH_2$CH), 3.65 and 3.67 (2 × s, 3H, $COOCH_3$), 4.15–4.65 (m, 3H, $CH_2N$ and CHN), 6.36 (m, 1H, CH=C), 7.23 (m, 5H, phenyl); ms *m/e*: 317 ($M^+$).

*Methyl 4-benzylidene-*L*-proline hydrochloride (***2***b·HCl)*

*N*-deprotection of **3***g* (3.17 g, 10 mmol) according to the procedure described for **3***e* gave **2***b* (1.93 g, 89%) as an oil, which was converted into the stable crystalline hydrochloride salt and isomers were separated by fractional crystallization from ethanol–water; ir (KBr): 1740 (ester), 1520, 1425, 1060, 910, 750, 700 (ϕ—CH=C) $cm^{-1}$. *E*-isomer, mp 164–167°C (dec.); $^1$Hmr (360 MHz, DMSO-$d_6$) δ: 2.95 (4 × d, 1H, $^2J_{3',3}$ = 17.2 Hz, $^3J_{3,2}$ = 7.4 Hz, $^4J$ = 2.6 Hz, H-3), 3.21 (4 × d, 1H, $^2J_{3',3}$ = 17.2 Hz, $^3J_{3',2}$ = 8.6 Hz, $^4J$ = 2.5 Hz, H-3'), 3.76 (s, 3H, COOMe), 3.95 (dd, 1H, $^2J_{5,5'}$ = 14 Hz, $^4J$ = 2.1 Hz, H-5), 4.05 (dd, 1H, $^2J_{5',5}$ = 14 Hz, $^4J$ = 1.7 Hz, H-5'), 4.57 (dd, 1H, $^3J_{2,3}$ = 7.4 Hz, $^3J_{2,3'}$ = 8.6 Hz, H-2), 6.57 (m, 1H, $^4J$ = 2.6 and 2.5 Hz, $^4J$ = 2.1 and 1.7 Hz, CH=C) ppm. *Anal.* calcd. for $C_{13}H_{15}O_2N$·HCl: C 61.52, H 6.37, N 5.52; found: C 61.22, H 6.36, N 5.39.

The Z-isomer has a mp of 157.5–159°C (dec.).

*2-Benzylidene-5-carbomethoxy-6-azido-1-carbapenam* **5**a

A mixture of the two geometric isomers of **2***b* was used in this reaction. To 10 mL of dry $Et_2O$ at 0°C were added separately **2***b* (2.17 g, 10 mmol) in dry $Et_2O$ (10 mL) and *tert*-butylhypochlorite (1.2 mL, 10 mmol) in dry $Et_2O$ (10 mL) over a period of 10 min. After stirring at 0°C for another 10 min, additional $Et_2O$ (50 mL) was added and the solution was washed with 0.1 *N* HCl (20 mL), with water (2 × 20 mL), dried ($Na_2SO_4$), and filtered. After cooling to −15°C, 18-crown-6 polyether (30 mg) and $KO_2$ (1.2 g) were added and the stirred reaction mixture was warmed up to room temperature over a period of 30 min. The precipitate was filtered off and the $Et_2O$ evaporated to give a pale yellow oil. Analysis of the oil by tlc ($CH_2Cl_2$–MeOH, 99:1) showed the presence of two compounds with $R_f$ 0.5 and 0.6. Partial decomposition during tlc of the more polar compound was observed. The residual oil was taken up in anhydrous benzene (100 mL) and cyclohexane (100 mL) containing $Et_3N$ (1.6 mL, 12 mmol). A solution of azidoacetyl chloride (18) (0.98 mL, 11 mmol) in cyclohexane (60 mL) was added over 1 h at room temperature. The mixture was stirred for another hour, diluted with benzene (400 mL), and washed successively with 0.5 *M* phosphate buffer pH 3 (100 mL), water (100 mL), and a saturated NaCl solution (100 mL). The organic layer was dried ($Na_2SO_4$) and concentrated to yield an oily residue, which afforded after chromatography on silica gel, using $C_6H_6$–$Me_2CO$ (99:1) as eluent, 1.5 g of **5***a* (50% yield); ir ($CH_2Cl_2$): 2130 (azide), 1780 (β-lactam), 1755 (ester) $cm^{-1}$; ms *m/e*: 298 ($M^+$). The $^1$Hmr spectrum showed two singlet signals at δ 3.72 and 3.75 ($COOCH_3$), two signals at δ 4.56 and 4.59 ($CHN_3$), and broad peaks at δ 6.4 and 7.2 ($C_6H_5CH$=C) due to the presence of two geometric isomers.

*2-Benzylidene-5-carbomethoxy-6-phenoxyacetamido-1-carbapenam* **5**c

A stream of dry $H_2S$ gas was bubbled through a solution of **5***a* (1.5 g, 5 mmol) and $Et_3N$ (0.91 mL, 6.55 mmol) in anhydrous $CH_2Cl_2$ (50 mL) at 0°C for a period of 30 min. The solution was evaporated and the crude amine **5***b* was taken up in anhydrous $CH_2Cl_2$ (50 mL). After cooling to 0°C in an ice bath, $Et_3N$ (0.71 mL, 5.05 mmol) in anhydrous $CH_2Cl_2$ (30 mL) and phenoxyacetyl chloride (920 mg, 5.4 mmol) in anhydrous $CH_2Cl_2$ (30 mL) were added simultaneously. The solution was stirred for 2 h at room temperature, washed with water (4×), dried ($Na_2SO_4$), and evaporated to yield an oil which was purified by chromatography on a silica gel column ($CH_2Cl_2$–$Me_2CO$, 98:2) to yield **5***c* (1.5 g, 75%); ir ($CH_2Cl_2$): 3415 (NH), 1775 (β-lactam), 1745 (ester), 1697 (amide) $cm^{-1}$; $^1$Hmr δ: 3.55 and 3.58 (2 × s, 3H, $COOCH_3$), 4.45 (s, 2H, $CH_2CO$), 5.38 (d, 1H, *J* = 9 Hz, H-6), 6.4 (m, 1H, CH=C), 7.75 (d, 1H, *J* = 9 Hz, NH) ppm.

*2-Oxo-5-carbomethoxy-6-phenoxyacetamido-1-carbapenam* **5**d

Ozonized oxygen containing 2.5 mmol of $O_3$ was bubbled through a solution of **5***c* (812 mg, 2 mmol) in EtOAc (50 mL) at −50°C over a period of 1 h. Excess $O_3$ was removed in a stream of $N_2$ and the reaction mixture was hydrogenated at room temperature under a pressure of 0.5 kg/$cm^2$ in the presence of 100 mg 5% Pd/$CaCO_3$ for a period of 20 min. The reaction mixture was filtered and evaporated. Chromatography on silica gel (eluent $CH_2Cl_2$–$Me_2CO$, 95:5) afforded **5***d* (478 mg, 72%) as an oil; ir ($CH_2Cl_2$): 1775 (β-lactam), 1755 and 1745 (ester and ketone), 1704 (amide) $cm^{-1}$; $^1$Hmr δ: 2.97 (m, 2H, H-1 and H-1'), 3.29 and 4.08 (AB pattern, 2H, *J* = 18 Hz, H-3 and H-3'), 3.64 (s, 3H, $COOCH_3$), 4.49 (s, 2H, $CH_2O$), 5.56 (d, 1H, *J* = 9 Hz, H-6), 6.78–7.5 (m, phenyl), 7.82 (d, 1H, *J* = 9 Hz, NH) ppm; ms *m/e*: 332 ($M^+$).

*2,2-Dicarbomethoxy-4-methylene-pyrrolidine* **2**c

3-Chloro-2-chloromethyl-1-propene (10 g, 80 mmol) was added dropwise to a stirred suspension of dimethyl aminomalonate

Can. J. Chem. Downloaded from www.nrcresearchpress.com by 210.87.254.105 on 09/06/12
For personal use only.

hydrochloride (14.68 g, 80 mmol) in anhydrous MeOH (200 mL) containing NaOMe (240 mmol). The mixture was refluxed for 6 h and the organic solvent was evaporated, leaving an orange slurry which was taken up in 1 *N* HCl (200 mL). The aqueous solution was washed with $Et_2O$ (2 × 100 mL), made alkaline with 2 *N* NaOH (pH 10), and extracted with $Et_2O$ (3 × 100 mL). The organic phase was dried ($Na_2SO_4$) and evaporated. Chromatography of the residual oil on a silica gel column, using $CH_2Cl_2$–EtOAc (98:2) as eluent, provided 3.34 g (25%) of **2***c*; $^1$Hmr δ: 2.77 (br s, 1H, NH), 3.03 (m, 2H, $CH_2$—C), 3.70 (m, 2H, $CH_2N$), 3.77 (s, 6H, $COOCH_3$), 4.95 (m, 2H, C=$CH_2$) ppm.

*1-Methylene-3,3-dicarbomethoxy-6-azido-1-carbapenam* **6**a

To 10 mL of dry $Et_2O$ at 0°C were added simultaneously **2***c* (2.09 g, 12.5 mmol) in dry $Et_2O$ (20 mL) and *tert*-butylhypochlorite (1.5 mL, 13.7 mmol) in dry $Et_2O$ (20 mL) over a period of 20 min. After stirring for 5 min the solution was washed with 0.1 *N* HCl (30 mL), with water (2 × 30 mL), dried ($Na_2SO_4$), and filtered. After cooling to 0°C, 18-crown-6 polyether (40 mg) and $KO_2$ (1.75 g) were added and the reaction mixture was stirred at 0°C for 15 min. The precipitate was filtered off and the $Et_2O$ evaporated to give an oily residue, which was taken up in anhydrous benzene (100 mL) and cyclohexane (100 mL) containing $Et_3N$ (2.07 mL, 15 mmol). A solution of azidoacetyl chloride (1.25 mL, 13.7 mmol) in cyclohexane (60 mL) was added over 40 min at room temperature and the mixture was stirred mechanically for another 40 min. The reaction mixture was worked up according to the procedure used for the synthesis of **5***a*, yielding 0.525 g of **6***a* (15%); ir ($CH_2Cl_2$): 2120 (azide), 1790 (β-lactam), 1755 (ester) cm$^{-1}$; $^1$Hmr δ: 3.28 (m, 2H, H-2), 3.78 and 3.81 (2 × s, 6H, $COOCH_3$), 4.25 (m, 1H, H-5), 4.42 (d, $J$ = 2.7 Hz, 1H, H-6), 5.28 (m, 2H, C=C$H_2$) ppm; ms *m/e*: 280 ($M^+$).

*1-Methylene-3,3-dicarbomethoxy-6-phenoxyacetamido-1-carbapenam* **6**b

Compound **6***b* was prepared as above by reduction with $H_2S$/$Et_3N$ and, subsequently, reaction with phenoxyacetyl chloride ($Et_3N$ at 0°C). After chromatography on a silica gel column (using $C_6H_6$–$Me_2CO$; 98:2 as eluent), there was obtained 270 mg (25%) of **6***b* (starting from 2 mmol of **6***a*) which was crystallized from $Et_2O$/hexane, mp 143–145°C (dec.); ir ($CH_2Cl_2$): 3425 (NH), 1790 (β-lactam), 1755 (ester), 1700 (amide), 1610, 1440, 910 (C=$CH_2$) cm$^{-1}$; $^1$Hmr (90 MHz, $CDCl_3$) δ: 3.31 (m, 2H, H-2), 3.78 and 3.80 (2 × s, 6H, $COOCH_3$), 4.30 (m, 1H, H-5), 4.53 (s, 2H, $CH_2O$), 5.07 (q, 1H, $J$ = 8.0 Hz, $J$ = 2.7 Hz, H-6), 5.36 (m, 2H, $CH_2$=C), 6.83–7.47 (m, 5H, phenyl), 7.6 (d, 1H, $J$ = 8 Hz, NH) ppm; $^{13}$Cmr ($CDCl_3$) δ: 44.3 (C2), 53.5 and 53.6 ($OCH_3$), 63.3 (C6), 65.2 (C5), 67.2 ($CH_2O$), 72.4 (C3), 112.2 (=$CH_2$), 114.9, 122.4 and 130 (phenyl), 142.5 (C1), 157.2 (*C*—$OCH_2$), 166.2, 168.6 and 171 (C=O) ppm; ms *m/e*: 388 ($M^+$). *Anal.* calcd. for $C_{19}H_{20}O_7N_2$: C 58.75, H 5.19, N 7.21; found: C 58.52, H 5.26, N 7.09.

## Acknowledgements

We are indebted to the Belgian Fonds voor Wetenschappelijk Geneeskundig Onderzoek for financial support, and to Dr. S. Toppet and Dr. F. Borremans for determination of $^{13}$C, $^1$H 90 MHz and 360 MHz nmr spectra. Thanks are due to Prof. G. Smets and Prof. M. Antheunis for providing these facilities. We also thank Dr. G. Janssen for mass spectrum determinations. P. Herdewijn is Aspirant of the Belgian Nationaal Fonds voor Wetenschappelijk Onderzoek.

1. (*a*) R. D. G. Cooper. *In* Topics in antibiotics. Vol. 3. *Edited by* P. Sammes. J. Wiley, New York. 1980. p. 41; (*b*) F. A. Jung, W. R. Pilgrim, J. P. Poyser, and P. J. Siret. *In* Topics in antibiotics. Vol. 4. *Edited by* P. Sammes. J. Wiley, New York. 1980. p. 51.
2. T. T. Howarth, A. G. Brown, and J. T. King. J. Chem. Soc. Chem. Commun. 226 (1976).
3. G. Albers-Schonberg, B. H. Arison, O. D. Hensen, J. Hirshfield, K. Hoogsteen, E. A. Kaczka, R. E. Rhodes, J. S. Kahan, F. M. Kahan, R. W. Ratcliffe, E. Walton, L. J. Ruswinkle, R. B. Morin, and B. G. Christensen. J. Am. Chem. Soc. **100**, 6491 (1978).
4. (*a*) A. K. Bose and J. L. Fahey. J. Org. Chem. **39**, 115 (1974); (*b*) A. K. Bose, W. A. Hoffman III, and M. S. Manhas. *In* Recent advances in the chemistry of β-lactam antibiotics. *Edited by* J. Elks. The Chemical Society, London. 1977. p. 269.
5. A. K. Bose, G. Spiegelman, and M. S. Manhas. J. Am. Chem. Soc. **90**, 4506 (1968).
6. U. Schmidt and H. Poisel. Angew. Chem. **89**, 824 (1977).
7. J. D. Albright and L. Goldman. J. Am. Chem. Soc. **87**, 4214 (1965); **89**, 2416 (1967).
8. F. E. Scully and R. C. Davis. J. Org. Chem. **43**, 1486 (1978).
9. A. I. Meyers. J. Org. Chem. **24**, 1233 (1959).
10. A. W. Burgsthaler, M. L. Trollope, and C. E. Aiman. Nature (London), **202**, 388 (1964).
11. S. M. Schmitt, D. B. R. Johnston, and B. G. Christensen. J. Org. Chem. **45**, 1135 (1980).
12. R. A. Firestone, N. S. Maciejewicz, R. W. Ratcliffe, and B. G. Christensen. J. Org. Chem. **39**, 439 (1974).
13. P. Claes, A. Vlietinck, E. Roets, H. Vanderhaeghe, and S. Toppet. J. Chem. Soc. Perkin Trans. I, 932 (1973).
14. A. Vlietinck, E. Roets, P. Claes, G. Janssen, and H. Vanderhaeghe. J. Chem. Soc. Perkin Trans. I, 937 (1973).
15. P. G. Claes, G. Decoster, L. A. Kerremans, and H. Vanderhaeghe. J. Antibiot. **32**, 820 (1979).
16. M. Itoh, D. Hagiwara, and T. Kamiya. Bull. Chem. Soc. Jpn. **50**, 718 (1977).
17. G. Wittig and U. Schöllkopf. Org. Synth. **40**, 66 (1960).
18. D. Hoppe and M. Kloft. Justus Liebigs Ann. Chem. 512 (1980).

# Low temperature carbon-13 magnetic resonance detection of axial conformers in vinyl- and formylcyclohexane: a deshielding γ–*gauche* effect

G. W. BUCHANAN

*Ottawa–Carleton Institute for Research and Graduate Studies in Chemistry, Carleton University, Ottawa, Ont., Canada K1S 5B6*

Received May 10, 1982

G. W. BUCHANAN. Can. J. Chem. **60**, 2908 (1982).

Using 50.3 MHz $^{13}C$ nmr at 173 K, distinct resonances for axial conformers of vinyl- and formylcyclohexane have been obtained. Substituent effects for axial and equatorial substitution of these groups have been derived. A deshielding γ–*gauche* effect was found for the axial substituent carbon of formylcyclohexane, a result attributed to the high preference for rotamers in which the formyl proton does not sterically interfere with *syn*-axial protons at C-3 and C-5 of the ring. Conformational free energies for the vinyl and formyl groups have been estimated to be 1.49 and 0.84 kcal/mol respectively.

G. W. BUCHANAN. Can. J. Chem. **60**, 2908 (1982).

En utilisant l'rmn de $^{13}C$ à 50.3 MHz et 173 K, on a trouvé des résonances pour la conformation axiale du vinyle- et formylecyclohexane. On a étudié les effets de la substitution axiale et equatoriale des deux groupements. Un déblindage γ–*gauche* a été trouvé pour le carbone axial du formylecyclohexane, un résultat attribué à la grande préférence pour les rotamères dans lesquels le proton formyle n'est pas dans une position près des protons *syn*-axiaux du cycle cyclohexanique. On a estimé les énergies conformationaux pour les groupements formyle et vinyle. Les valeurs sont 0.84 et 1.49 kcal/mol respectivement.

## Introduction

Low temperature $^{13}C$ nmr at high field is a powerful technique for measurement of low barrier conformational processes and detection of minor stereoisomers. Among the early applications in the latter area was the work of Anet *et al.* (1) in which the lowly populated axial conformer of methylcyclohexane was directly observed at 63.1 MHz.

Recently there has been renewed interest in determining the conformational preference of the vinyl group in substituted cyclohexanes (2). From low temperature $^{13}C$ nmr studies of *cis*-4-methyl-1-vinylcyclohexane, the conformational free energy of the vinyl group, $(-\Delta G^{0}_{CH=CH_2})$, has been determined to be $1.68 \pm 0.06$ kcal/mol, only slightly smaller than the currently accepted value of $1.75 \pm 0.06$ kcal/mol for the $CH_3$ group (3).

The use of 1,4-disubstituted derivatives, however, may suffer from the assumption of additivity of conformational free energies for the two substituents. Ideally one would prefer to have a direct measure of the conformational preference for a given functionality in the monosubstituted cyclohexane. In the recent report (2) it is stated that the conformational equilibrium in vinylcyclohexane is too one-sided to be measured directly. Considering the early success of high field $^{13}C$ nmr in studying methylcyclohexane (1), however, we deemed it worthwhile to search for the axial conformer of vinylcyclohexane using the same technique.

As a comparative system, we have chosen a conformationally less biased, but structurally related molecule, formylcyclohexane, for which the conformational free energy has already been directly determined via low temperature $^{1}H$ nmr (4).

## Results and discussion

### *Vinylcyclohexane*

$^{13}C$ chemical shifts for vinylcyclohexane (**1**) at room temperature in two solvent media and for individual conformers **1***A* and **1***E* at 173 K are presented in Table 1. Results for **1** in $CD_2Cl_2$–$CS_2$ are essentially identical to those reported by Eliel and Manoharan (2), for **1** in $CD_2Cl_2$.

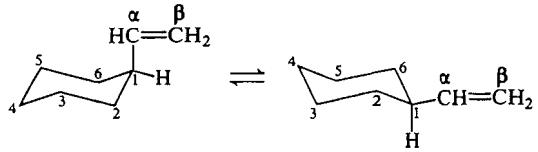


**1***A* **1***E*

At 173 K, five new resonances appeared for **1** which were not present at room temperature or at 203 K. Figure 1 shows a typical spectrum for the α-carbon of a 3.0 *M* solution of **1** in 1:1 $CD_2Cl_2$–$CS_2$ solution at 173 K. A new resonance has appeared at 141.54 ppm with an intensity ca. 1.5% of that for the peak at $\delta_c = 144.68$. New lines of this approximate intensity were observed near all resonances except that of C-4, where peak overlap presumably precludes identification of a resonance associated with C-4 of the axial conformer.

In order to provide satisfactory signal-to-noise ratios for resonances of the axial conformer, 2000 accumulations on the 3.0 *M* solutions of **1** were required. No substantial broadening of the equato-

0008-4042/82/232908-06$01.00/0

©1982 National Research Council of Canada/Conseil national de recherches du Canada

Can. J. Chem. Downloaded from www.nrcresearchpress.com by 210.87.254.6 on 09/06/12
For personal use only.

TABLE 1. $^{13}C$ chemical shifts of vinylcyclohexane conformers ($\delta_c \pm 0.01$)

| Compound | Solvent | C-1 | C-2,6 | C-3,5 | C-4 | C-α | C-β |
|---|---|---|---|---|---|---|---|
| **1** | $CD_2Cl_2$–$CS_2$ | 42.09 | 32.99 | 26.47 | 26.64 | 144.81 | 111.73 |
| **1*A*** | $CD_2Cl_2$–$CS_2$ | 37.28 | 30.51 | 21.43 | n.o.† | 141.54 | 114.17 |
| **1*E*** | $CD_2Cl_2$–$CS_2$ | 42.34 | 32.54 | 26.30 | 26.35 | 144.68 | 111.74 |
| **1** | $C_7D_8$ | 42.06 | 32.94 | 26.41 | 26.59 | 144.69 | 111.86 |
| **1*A*** | $C_7D_8$ | 36.97 | 30.49 | 21.72 | n.o.† | 141.47 | 114.01 |
| **1*E*** | $C_7D_8$ | 42.33 | 32.46 | 26.25 | 26.22 | 144.63 | 111.98 |

*At 173.0 ± 2.0 K.
†Abbreviation: n.o. ≡ not observable due to peak overlap.

Can. J. Chem. Downloaded from www.nrcresearchpress.com by 210.87.254.6 on 09/06/12
For personal use only.

rial resonances was noted as the bands for the axial form merged with them due to the high value of the equilibrium constant.

(a) *Chemical shifts*

Examination of data in Table 1 indicates that there is only a minor effect of solvent on shift values of individual conformers, with the maximum difference being 0.29 ppm (at C-1 and C-3,5 of the axial forms). There is however a general trend to slight upfield shifts in $C_7D_8$.

It is of particular interest to examine the steric effects on the chemical shifts of individual conformers. For the olefinic methine carbon (C-α), the axial carbon is *shielded* by an average of 3.15 ppm relative to its equatorial counterpart. This difference is somewhat smaller than that seen in stereochemically "rigid" molecules as shown below (5), but the trend is the same.

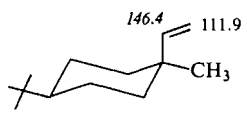


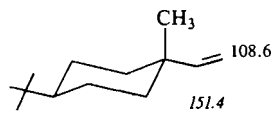


The average carbon chemical shift difference between axial and equatorial olefinic methylene groups of **1*A*** and **1*E*** is 2.23 ppm, with the equatorial methylene carbon being more shielded than its axial counterpart.

Data for the two conformers of *cis*-4-methyl-1-vinylcyclohexane (2) are also useful for comparison with **1*A*** and **1*E***, and these are presented below. The olefinic carbon shift differences between these conformers are within 0.3 ppm of those found in the present work.

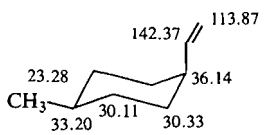


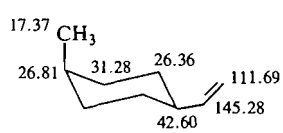


Data in Table 1 also indicate a substantial shift difference between C-1 resonances for **1*A*** and **1*E***, the axial conformer being shielded by an average of 5.21 ppm relative to its equatorial counterpart.

For C-3,5 of **1*A***, involved in a γ–*gauche* interaction with the vinyl methine carbon, the upfield shift is an average of 4.70 ppm relative to C-3,5 of **1*E***. In the case of C-2,6, the upfield shifts for **1*A*** relative to **1*E*** are somewhat smaller, ca. 2.00 ppm for results averaged over the two solvent media.

In general, the upfield shifts for the olefinic methine carbon, C-1, C-2,6, and C-3,5 of **1*A*** relative to **1*E*** are consistent with results for other pairs of monosubstituted cyclohexane conformers (1, 3, 6).

With these data in hand, combined with the cyclohexane chemical shift of 27.27 ppm at 173 K in $CD_2Cl_2$–$CS_2$, one can formulate a series of α, β, and γ substituent parameters for addition of axial and equatorial vinyl groups.

The values are as follows: $\alpha_{ax} = +10.01$, $\alpha_{eq} = +15.07$; $\beta_{ax} = +3.04$, $\beta_{eq} = +5.27$; $\gamma_{ax} = -5.84$ and $\gamma_{eq} = -0.97$. Of course these parameters will vary somewhat with solvent and solute concentration.

It is interesting to compare the above substituent effects with those for a methyl group (7), where $\alpha_{ax} = +1.1_0$, $\beta_{ax} = +5.15$, $\gamma_{ax} = -5.40$, $\alpha_{eq} = +5.6_5$, $\beta_{eq} = +8.9_0$, and $\gamma_{eq} = 0.00$.

The larger deshielding α effects of the vinyl

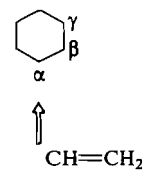


group (9–10 ppm more than $CH_3$) are clearly due to the β effect of the olefinic methylene group at C-1, below, an effect which is known to be deshielding (8).

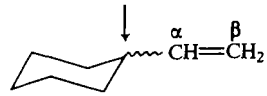


As noted previously (2), the deshielding effects for both axial and equatorial vinylcyclohexanes at C-2,6 are noticeably smaller than for the methyl-

Can. J. Chem. Downloaded from www.nrcresearchpress.com by 210.87.254.6 on 09/06/12
For personal use only.

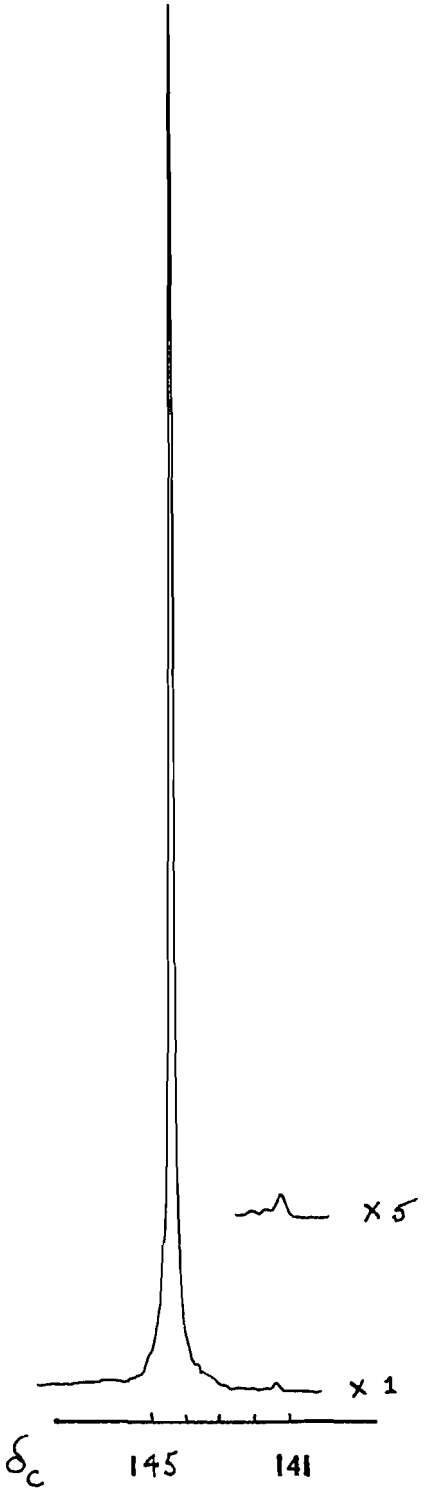


FIG. 1. C-α resonances for 1*A* and 1*E* at 173 K in 1:1 $CD_2Cl_2$–$CS_2$ (2000 accumulations on a 3.0 *M* solution).

cyclohexanes, which may be due to a contribution from a steric shielding effect of the terminal methylene group (below).

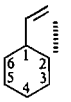

This result implies at least a minor population of the conformations of the vinyl group in which the double bond is eclipsed, or nearly so, with the C(1)—C(2) or C(1)—C(6) bond, rather than with the C(1)—H bond. A recent $^1H$ nmr study of couplings in vinylcyclohexane (9) supports this suggestion.

A further point of interest here is the upfield shift for the olefinic methylene carbon of 1*E* relative to 1*A*. The origin of this shielding may lie in an increased amount of double bond eclipsing with C(1)—C(2) or C(1)—C(6) in 1*E* compared to 1*A*.

Finally the $\gamma_{ax}$ shift for vinylcyclohexane is within 0.5 ppm of that found for methylcyclohexane (1, 7), which probably indicates a substantial preference for the bisecting conformation shown below. In view of the above evidence, we therefore suggest that this bisecting conformer dominates for 1*A*, with a minor contribution from conformers in which the double bond is nearly eclipsed with the C(1)—C(2) or C(1)—C(6) bond. For 1*E*, the degree of this type of eclipsing appears to exceed that present in 1*A*.

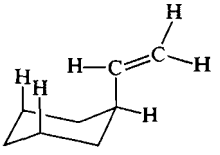

1*A*

(b) *Conformational free energy of the vinyl group*

For determination of *K*, the relative areas of the five distinguishable resonances for 1*A* (i.e. all except C-4) were measured relative to 1*E*, using graphical methods.

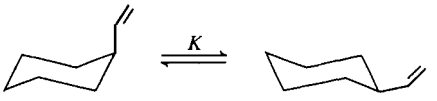


The average value of *K* (in $CD_2Cl_2$–$CS_2$) was 77.0, with values ranging from 95.0 to 50.1. Substitution into the equation $-\Delta G^0 = RT\ln K$ yields an average value of 1.49 kcal/mol as the conformational free energy of the vinyl group. Our limiting

TABLE 2. $^{13}C$ chemical shifts of formylcyclohexane conformers ($\delta_c \pm 0.01$)

| Compound | Solvent | C-1 | C-2,6 | C-3,5 | C-4 | C=O \| H |
|---|---|---|---|---|---|---|
| **2** | $CD_2Cl_2$–$CS_2$ | 49.99 | 26.10 | 25.25 | 26.16 | 204.10 |
| **2A*** | $CD_2Cl_2$–$CS_2$ | 46.87 | 24.97 | 22.99 | n.o.† | 206.49 |
| **2E*** | $CD_2Cl_2$–$CS_2$ | 50.45 | 25.98 | 25.62 | 26.14 | 205.45 |
| **2** | $C_7D_8$ | 49.87 | 26.16 | 25.32 | 26.27 | 202.47 |
| **2A*** | $C_7D_8$ | 46.36 | 24.47 | 23.07 | n.o.† | 204.33 |
| **2E*** | $C_7D_8$ | 49.85 | 25.70 | 25.45 | 25.99 | 203.12 |

*At 173.0 ± 2.0 K.
†Abbreviation: n.o. ≡ not observable due to peak overlap.

values are 1.56 kcal/mol (for $K = 95.0$) and 1.34 kcal/mol (for $K = 50.1$) respectively.

Based on results for *cis*-4-methyl-1-vinylcyclohexane, Eliel and Manoharan (2) have determined $-\Delta G^0_{CH=CH_2}$ to be 1.68 ± 0.06 kcal/mol. Due to the obvious difficulties in the present work of measuring $K$ precisely, our uncertainty is at least a factor of two higher than that quoted in the recent work (2). Nevertheless, it appears that direct determination of $-\Delta G^0_{CH=CH_2}$ leads to a smaller value than that obtained from a 1,4-disubstituted derivative. The present value of 1.49 kcal/mol is, however, larger than that of 1.39 kcal/mol obtained using 1-vinylcyclohexanol (10). We find no effect of solvent on $K$ within the limits of uncertainty.

*Formylcyclohexane*

$^{13}C$ chemical shifts for formylcyclohexane (**2**) at room temperature in two solvent media and for individual conformers **2A** and **2E** at 173 K are presented in Table 2.

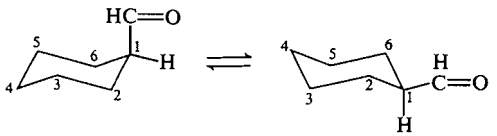

**2A** **2E**

The C-3,5 carbon resonance was distinguished from that for C-2,6 based on the totally coupled spectral appearance. At 173 K four new resonances appeared for **1** which were not present at 293 K or 203 K. Figure 2 shows a typical spectrum for the aldehyde carbon of a 1.5 *M* solution of **2** in 1:1 $CD_2Cl_2$–$CS_2$ solution at 173 K. A new resonance at $\delta_c = 206.49$ has appeared with an intensity ca. 10% of that at $\delta_c = 205.45$. Similarly, new lines were seen near all resonances except that of C-4, which was presumably obscured due to peak overlap.

(a) *Chemical shifts*

Data in Table 2 indicate that only the formyl carbon is substantially affected by a change in solvent, its resonance being shifted upfield by ca. 2 ppm in toluene-$d_8$ relative to the $CD_2Cl_2$–$CS_2$ solvent system. This upfield shift can be rationalized in terms of a solute–solvent collision complex as depicted below in which the electron deficient carbonyl carbon lies in the inner "shielding" region of the aromatic π cloud (11).

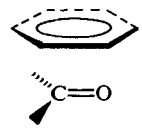

With regard to the steric effects on shifts of individual conformers, the most remarkable finding is that the *axial* aldehyde carbon is *deshielded* relative to its equatorial counterpart by ca. 1.1 ppm. To our knowledge, this is the first example of a case in which a carbon engaged in a γ-*gauche* interaction (i.e. with C-3,5 in **2A**) is deshielded relative to its equatorial counterpart **2E** which lacks this steric interaction.

Despite the fact that the aldehyde carbon is deshielded in the axial conformer, the resonances for C-1, C-2,6, and C-3,5 are all appreciably *shielded* in **2A** relative to **2E**. Using our shift of 27.27 ppm for cyclohexane in $CD_2Cl_2$–$CS_2$ at 173 K, one can obtain α, β, and γ shift parameters for the axial and equatorial formyl group substitution in the same way as was done for the vinyl function.

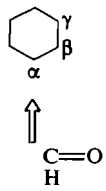

The results are as follows; $\alpha_{ax} = +19.60$, $\alpha_{eq} = +23.18$; $\beta_{ax} = -2.30$, $\beta_{eq} = -1.29$; $\gamma_{ax} = -4.28$, and $\gamma_{eq} = -1.65$.

It is interesting to compare these substituent induced shifts with those for butanol, below (12).

Can. J. Chem. Downloaded from www.nrcresearchpress.com by 210.87.254.6 on 09/06/12
For personal use only.

Can. J. Chem. Downloaded from www.nrcresearchpress.com by 210.87.254.6 on 09/06/12
For personal use only.

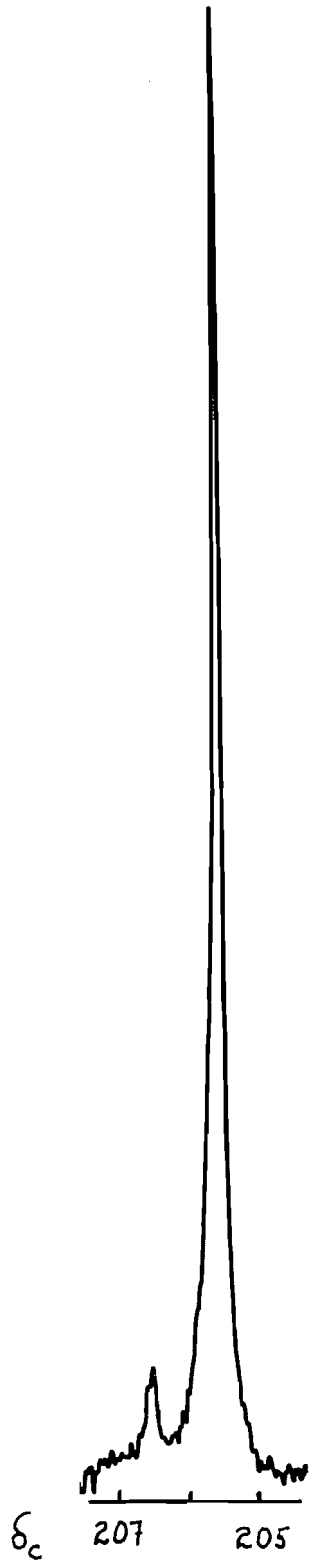


FIG. 2. Formyl carbon resonances for **2A** and **2E** at 173 K in 1:1 $CD_2Cl_2$–$CS_2$ (800 accumulations on a 1.5 *M* solution).

The attenuated deshielding α effect in the branched cyclohexanecarboxaldehyde relative to butanal is a normal result of chain branching and has ample precedent (8).

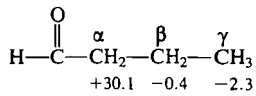


The *upfield* β shifts for butanal, **2A**, and **2E** are very likely a consequence of the presence of substantial amounts of rotamers in which the carbonyl oxygen is eclipsed with neighbouring C—C bonds. Thus, a shielding γ effect from the carbonyl oxygen becomes superimposed on a normally deshielding β effect. For butanal, it has been determined from $^1H$ nmr coupling constant analysis (13) that the eclipsed conformation (below) is present to an extent of ca. 60% at 20°C.

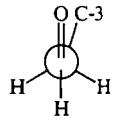


In the case of **2A** and **2E**, one can examine the relative upfield β shifts in terms of the conformer populations estimated from $^1H$ nmr (13, 14) for *cis*- and *trans*-4-*tert*-butylcyclohexanecarboxaldehydes. For **2A**, the probable conformers are shown below.

Conformer **2A**-i, or its mirror image, is deemed to be prevalent (93%) compared to a 7% population for **2A**-ii (14).

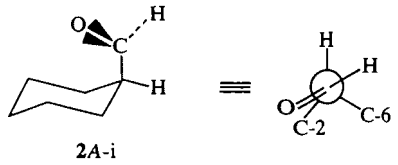


**2A**-i

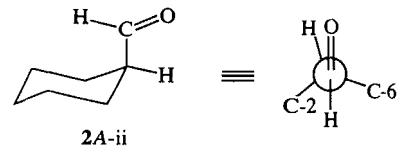


**2A**-ii

For **2E**, the probable conformers are depicted below.

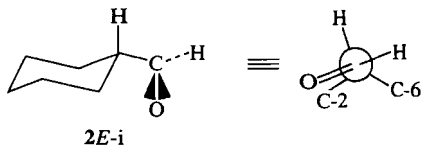


**2E**-i

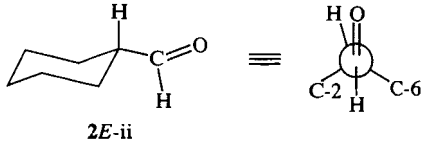


**2E**-ii

Can. J. Chem. Downloaded from www.nrcresearchpress.com by 210.87.254.6 on 09/06/12
For personal use only.

It was found (14) that **2***E*-i and its mirror image are favoured to the extent of 84% to 16% for **2***E*-ii. In the $^{13}C$ spectra, the β effect for **2***E* is −1.29 ppm, compared to −2.30 ppm for **2***A*. This seems consistent with the lower degree of preference for conformers having the C=O bond eclipsed with C-2 or C-6 in **2***E* than in **2***A*.

The γ effects involving $sp^3$ hybridized carbons are all shielding effects, even for **2***E*, where C-3,5 are *trans* to the formyl group. The $\gamma_{eq}$ value is only −1.65 ppm, however, compared to −4.28 ppm for $\gamma_{ax}$. One can rationalize the larger upfield γ effect at C-3,5 of **2***A* in terms of γ-*gauche* interactions between these carbons and the axial formyl carbon (below).

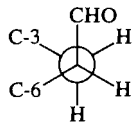


For the more freely rotating butanal, the magnitude of the γ shift is between those for **2***A* and **2***E*, but, as expected, considerably closer to that for **2***E*.

Finally, some comment on the *deshielded* formyl carbon in **2***A* relative to **2***E* is necessary. This appears to be the first example of an axial carbon, directly attached to a cyclohexane ring, being deshielded relative to its equatorial counterpart. The unique key feature of **2***A* is its highly preferred (93%) conformation **2***A*-i in which the formyl *proton* does not interfere spatially with the *syn*-axial protons at C-3 and C-5. One must infer, therefore, that when such an interaction is lacking, there is no reason to expect, a priori, an upfield shift for the attached axial carbon.

This phenomenon remains to be investigated for related systems, and work along these lines is in progress.

(b) *Conformational free energy of the formyl group*

From relative peak area measurements at 173 K, the average $-\Delta G^0_{CHO}$ was determined to be 0.84 ± 0.08 kcal/mol, in good accord with that determined previously (4) by $^1H$ nmr peak areas at the low temperature. No solvent dependence was evident.

## Experimental

(a) *Materials*

Vinylcyclohexane was obtained from Aldrich Chemical Corp. and distilled before use. Formylcyclohexane was purchased from Frinton Laboratories, South Vineland, New Jersey and used without further purification.

(b) *Spectra*

The $^{13}C$ nmr spectra were obtained at 50.3 MHz using a Varian XL-200 spectrometer. Sample concentrations were 3.0 *M* for **1** and 1.5 *M* for **2**, in 10 mm od tubes. Typically, spectra were obtained with complete $^1H$ noise decoupling. Normal conditions were as follows: sweep width = 10 000 Hz, number of data points = 32 000, pulse width = 7.0 μs (45°), acquisition time = 1.6 seconds, and repetition rate = 1.0 seconds. The number of accumulations for the low temperature spectra were typically 2000 for **1** and 800 for **2**.

## Acknowledgements

The continued financial support from the Natural Sciences and Engineering Research Council of Canada is gratefully acknowledged.

1. F. A. L. Anet, C. H. Bradley, and G. W. Buchanan. J. Am. Chem. Soc. **93**, 258 (1971).
2. E. L. Eliel and M. Manoharan. J. Org. Chem. **46**, 1959 (1981).
3. H. Booth and J. R. Everett. J. Chem. Soc. Chem. Commun. 278 (1976).
4. G. W. Buchanan and A. R. McCarville. Can. J. Chem. **50**, 1965 (1972).
5. B. L. Buckwalter, I. R. Burfitt, H. Felkin, M. Joly-Goudket, K. Naemura, M. F. Salomon, E. Wenkert, and P. M. Wovkulich. J. Am. Chem. Soc. **100**, 6445 (1978).
6. H.-J. Schneider and V. Hoppen. J. Org. Chem. **43**, 3866 (1978).
7. D. K. Dalling and D. M. Grant. J. Am. Chem. Soc. **89**, 6612 (1967).
8. J. B. Stothers. Carbon-13 nmr spectroscopy. Academic Press, New York, NY. 1972.
9. G. R. DeMare and S. Lapaille. Org. Magn. Reson. **13**, 75 (1980).
10. R. J. Ouellette, K. Liptak, and G. E. Booth. J. Org. Chem. **31**, 546 (1966).
11. J. Ronayne, M. V. Sargent, and D. H. Williams. J. Am. Chem. Soc. **88**, 5288 (1966).
12. E. Lippmaa and T. Pehk. Eesti NSV Tead. Akad. Toim. Keem. Geol. **17**, 210 (1968).
13. G. J. Karabatsos and N. Hsi. J. Am. Chem. Soc. **87**, 2864 (1965).
14. G. W. Buchanan, J. B. Stothers, and S.-T. Wu. Can. J. Chem. **45**, 2955 (1967).

# Thermolysis of 2-methoxy-2,5,5-trimethyl-$\Delta^3$-1,3,4-oxadiazoline

A. P. HITCHCOCK, S. ZWEEP, T. STEEL, M. BÉKHAZI, AND J. WARKENTIN
*Department of Chemistry, McMaster University, Hamilton, Ont., Canada L8S 4M1*

Received February 11, 1982

A. P. HITCHCOCK, S. ZWEEP, T. STEEL, M. BÉKHAZI, and J. WARKENTIN. Can. J. Chem. **60**, 2914 (1982).

The principal product of gas phase thermal decomposition of 2-methoxy-2,5,5-trimethyl-$\Delta^3$-1,3,4-oxadiazoline (methoxyoxadiazoline) was found to be 1-methoxy-1-[(1-methylethenyl)oxy]-ethane (vinyl ether). This arises from a selective 1,4-hydrogen shift in the carbonyl ylide intermediate. Fragmentation of the carbonyl ylide is the dominant process in the solution thermolysis of methoxyoxadiazoline. The phase and temperature dependence of this thermolysis is discussed in terms of the probable structure of the carbonyl ylide intermediate.

A. P. HITCHCOCK, S. ZWEEP, T. STEEL, M. BÉKHAZI et J. WARKENTIN. Can. J. Chem. **60**, 2914 (1982).

On a trouvé que le méthoxy-1 [(méthyléthenyl-1)oxy]-1 éthane (éther vinylique) est le produit principal de la décomposition thermique en phase gazeuse du méthoxy-2 triméthyl-2,5,5 $\Delta^3$ oxadiazoline-1,3,4 (méthoxyoxadiazoline). Ce produit provient d'un glissement sélectif 1,4 d'hydrogène dans l'intermédiaire ylure de carbonyle. La fragmentation de l'ylure de carbonyle est le processus dominant lors de la thermolyse de la méthoxyoxadiazoline en solution. On discute de l'influence de la température sur cette thermolyse en fonction de la structure probable de l'ylure de carbonyle intermédiaire.

[Traduit par le journal]

Can. J. Chem. Downloaded from www.nrcresearchpress.com by 210.87.254.6 on 09/06/12
For personal use only.

## Introduction

$\Delta^3$-1,3,4-Oxadiazolines (e.g. 2-methoxy-2,5,5-trimethyl-$\Delta^3$-1,3,4-oxadiazoline, **1**) undergo both thermal and photochemical decomposition to give a wide variety of products the nature of which depends on both the decomposition conditions and the nature of the substituents (1). In all cases the decomposition appears to involve the ejection of molecular nitrogen and the formation of a transient carbonyl ylide species, **2** (Fig. 1). The carbonyl ylide can then undergo a variety of intramolecular reactions (1) as outlined for **1** in Fig. 1. Thermolysis of **1** at 80°C in a variety of solvents (e.g. $C_6H_6$, $CCl_4$) yields primarily the fragmentation products (**4–7**) with little, if any, of the vinyl ether **8** (1-methoxy-1-[(1-methylethenyl)oxy]-ethane) or the epoxide **3**. Solution thermolysis of other substituted oxadiazolines (e.g. 2-aryl-2-methoxy analogs of **1**[1]) does yield the appropriate analogues of **8** and **3** in addition to the related fragmentation products. All of the product distribution evidence to date, from both thermolysis and photolysis of oxadiazolines, supports the hypothesis of the carbonyl ylide intermediate (1).

We have studied the gas phase thermolysis of **1** by photoelectron spectroscopy with the goal of obtaining direct spectroscopic evidence for the carbonyl ylide intermediate **3**.[2] Although bands attributable to the carbonyl ylide have not yet been detected in the photoelectron studies (probably due to lifetime limitations), it was discovered that **1** undergoes a qualitatively different thermal decomposition when isolated in the gas phase, with the principle final product resulting from a 1,4-hydrogen shift rather than fragmentation of the carbonyl ylide. The evidence for this alternative reaction pathway is presented.

Recently Houk *et al.* (2) have reported *ab initio* calculations of the geometric and electronic structure of substituted carbonyl ylides and have discussed their influence on the subsequent decomposition. These results provide a groundwork for our discussion of the phase dependence of the thermolysis of **1**.

## Experimental

Methoxyoxadiazoline (**1**) was prepared as described earlier (*1b*). In order to investigate the phase and temperature dependence, the gas phase thermolysis of **1** was carried out both at moderate (80°C) and elevated (300–450°C) temperatures. The higher temperature thermolyses were performed in the inlet to a lab-built HeI photoelectron spectrometer which has been described previously (3). It is based on the design of Frost *et al.* (4). The sample was passed at reduced pressure (ca. $10^{-2}$ Torr) through a 30 cm long quartz tube, the temperature of which was monitored by a thermocouple to within ± 10°C. For the trapping of products a Pyrex trap cooled with liquid nitrogen was installed at the outlet of the quartz tube. For the 80°C thermolysis a small amount of **1** was sealed in a flask sufficiently large for complete volatilization. The sample was then thermostatted at 80°C for one week. During this period essentially all of the starting material decomposed. The product distributions from the thermolysis reactions were determined by $^1$H nmr.

Compound **8** was isolated by preparative glpc from the material trapped following high temperature thermolysis: $^1$H nmr ($CDCl_3/Me_4Si$) δ: 1.35 (d, 3H, $CH_3CH$), 1.84 (s, 3H, $CH_3C{=}$), 3.33 (s, 3H, $OCH_3$), 3.95 (s, 2H, $=CH_2$), 5.10 (q, 1H, HC(O)O).

Products **4** and **6** were identified from their glpc retention times and from their $^1$H nmr spectra.

[1]M. Békhazi and J. Warkentin. Unpublished data.

[2]Details of the spectroscopic study will be published separately.

0008-4042/82/232914-04$01.00/0

©1982 National Research Council of Canada/Conseil national de recherches du Canada

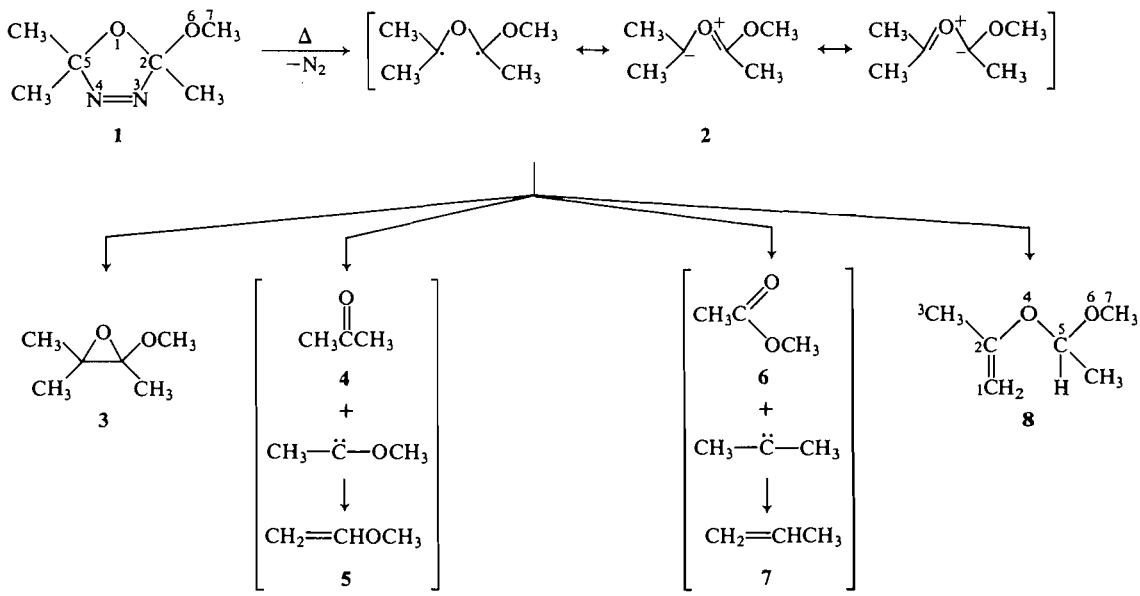

FIG. 1. Reaction pathways of methoxyoxadiazoline, **1**, following thermolysis.

## Results and discussion

Heating **1** as it entered the photoelectron spectrometer produced no detectable change in the spectrum until the furnace reached a temperature of 275°C. At this temperature the spectrum changed dramatically with the appearance of the sharp bands of molecular nitrogen. The transformation from reactant spectrum to thermolysis product spectrum occurred over a surprisingly small temperature range (ca. 25°C). This new spectrum of the thermal decomposition products remained essentially constant with increasing temperature up to 450°C, the highest temperature employed. Thus, the products of thermolysis of **1** are stable to 450°C during their residence time in the tube and essentially all of the starting material is destroyed at a temperature ≥ 300°C.

Following liquid nitrogen trapping the solidified 380°C thermolysis product mixture was warmed to room temperature (thereby losing volatile products) and analysed by gas chromatography and $^1$H nmr. Three decomposition products were positively identified: vinyl ether, **8** (ca. 70 mol% of the identified products), methyl acetate, **6** (ca. 20 mol%), and acetone, **4** (ca. 10 mol%). In addition, unidentified products gave rise to ca. 7% of the total nmr signal. The formation of methyl acetate and acetone imply the concomitant formation of propene and methyl vinyl ether **5** in equal amounts (1*a*, 1*b*) (Fig. 1). The $^1$H nmr yields listed above thus represent branching ratios in the thermal decomposition of **1** at 380°C. Signals due to **5** and **7** were not observed in the $^1$H nmr spectrum of the product mixture. Both are volatile and could have been partially lost by evaporation when the product mixture was warmed to room temperature. Vinyl ethers, such as **5** and **8**, are polymerizable and polymeric products may be responsible for some of the weak, unidentified lines in the nmr spectrum. We note that the vinyl ether **8** decomposed at room temperature in chloroform solution (open to the atmosphere) within hours after formation by thermolysis.

The possibility that catalysis by acidic sites on the walls of the quartz furnace tube is involved in the fragmentation processes was investigated by applying a passivation procedure to the quartz tube prior to one thermolysis run. The procedure consisted of washing the quartz tube with 0.1 *N* NaOH, coating with a 5% $(CH_3)_3SiCl$–toluene solution and rinsing with MeOH. Wall passivation had a negligible influence on the progress of the thermolysis as judged by the pe spectrum during decomposition and by the nmr spectrum of the trapped products. This suggests that wall reactions play a negligible role in the fragmentation.

The product distributions from gas phase thermolysis at high (380°C) and moderate (80°C) temperatures are compared in Table 1 to the product distributions from 80°C thermolysis of **1** in $CCl_4$ solution (1*a*). In contrast with solution thermolysis, where fragmentation dominates (1*a*, 1*b*), the

Can. J. Chem. Downloaded from www.nrcresearchpress.com by 210.87.254.6 on 09/06/12
For personal use only.

Can. J. Chem. Downloaded from www.nrcresearchpress.com by 210.87.254.6 on 09/06/12
For personal use only.

TABLE 1. Product yields (branching ratios) from gas phase and solution thermolysis of methoxyoxadiazoline, **1**

| | Yield (mol%) | | |
|---|---|---|---|
| | Gas phase | | Solution in $CCl_4$[a] |
| Species | $T$ = 380°C[b] | $T$ = 80°C | $T$ = 80°C |
| Vinyl ether, **8** | 69 (3)[c] | 50 (2)[c] | ≈0[d] |
| Acetone, **4** | 8 (2) | 28 (3) | 43 |
| Methyl acetate, **6** | 23 (3) | 22 (3) | 54 |
| Epoxide, **3** | 0 | 0 | 0 |

[a]The coproducts for acetone formation and for methyl acetate formation are $CH_3COCH_3$ and $CH_3CCH_3$. For the fate of these in $CCl_4$, see refs. 1*a*, 1*b*.
[b]This is the temperature of the quartz furnace. Due to the short residence time of the molecules ($10^{-2}$–$10^{-1}$ s) and limited numbers of collisions, the molecular temperature may be somewhat lower. However, the great difference in kinetics from the gas phase thermolysis (i.e. time constants of milliseconds instead of hours) is definitive evidence of a significantly higher molecular temperature.
[c]Average of three separate thermolyses. The numbers in brackets are the standard deviation in the last figure.
[d]Although **8** cannot be detected among the products, it is formed in low yield from thermolysis of **1** in other nonpolar solvents. We cannot rule out the possibility that **8** is a minor product in $CCl_4$ and that it does not survive the conditions.

1,4-H shift is the predominant route in the gas phase, even at 80°C. The relative yields of the 80°C and 380°C gas phase thermolyses are surprisingly similar, although the rates of decomposition are many orders of magnitude different, as expected.

There are several potential explanations of the dependence of the product ratio on the phase. As Table 1 shows, the yield of **8** is large in the gas phase and near zero in $CCl_4$, at 80°C. Mechanisms which account for this must either invoke a larger rate constant for H-transfer in the gas phase than in solution or lower rate constants for fragmentations in the gas phase than in solution, or both.

The 1,4-hydrogen shift is an allowed sigmatropic rearrangement which ought to be most facile if there is good conjugation, as is the case for the 0°,0° conformation of **2**.[3] That conformation, which is also the one with maximum diradical character and minimum polarity (2), is expected to be favoured in the gas phase. Since transition states for sigmatropic processes involving neutral species do not involve much charge separation, the system would appear to be set up for a facile 1,4-shift, probably requiring relatively little twisting to reach the transition state in the gas phase. Thermal fragmentations of carbonyl ylides, on the other hand, are not allowed from the 0°,0° conformation but are allowed from 0°,90° or 90°,0° conformations (2). The latter are thought to be much more zwitterionic than the 0°,0° conformation (2) and should therefore be relatively inaccessible in the gas phase as compared to a condensed phase. Thus, the 1,4-shift model appears to be adequate to explain the phase dependence.

In an alternative model,[4] the H-transfer which converts **2** to **8** is viewed as an intramolecular radical abstraction comparable to the H-transfer which occurs in the "ene" reaction, eq. [1].

[1] 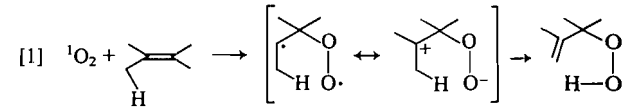

Harding and Goddard (5) have proposed that the "ene" reaction involves an intermediate which is predominantly a diradical in the gas phase and that the H-transfer from C to O (eq. [1]) is an intramolecular disproportionation. Some details of the "ene" reaction could be explained by assuming that the intermediate adopts more zwitterionic character (eq. [1]) in solution than in the gas phase (5). Although this model is an attractive alternative at first sight, there is an important difference between the transition states that are being compared. That for the "ene" reaction is six-membered while that for the process **2** → **8** is five-membered. Examination of a model suggests that the H-abstraction transition state (**9**) can involve reasonable distances and orbital alignments only if the

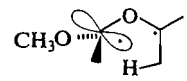

**9**

geometry is one approaching a 0°,90° conformation. Twisting away from the 0°,0° conformation permits the COC bond angle to decrease, because of reduced steric interactions, and brings the reacting sites closer together. At the same time, the "abstracting orbital" becomes better aligned with the reacting C—H bond. However, an increase in zwitterionic character would have to accompany the twisting (2). H-transfer should therefore be disfavoured in the gas phase, in contradiction of the experimental results.

Another alternative explanation would attribute the phase dependence to reactions of a "hot" intermediate. A vibrationally excited carbonyl ylide is a possibility because loss of nitrogen from the oxadiazoline is exothermic.[5] In the gas phase, at low pressure, such a nonequilibrated species might react before it could be deactivated to the ground

[3]In this labelling of the conformations of the ylide, each angle refers to the orientation of an X—C—X substituent plane with respect to the central C—O—C plane (2). For **2**, the first angle refers to the $CH_3$—C—$CH_3$ end while the second refers to the $CH_3O$—C—$CH_3$ end (arbitrary assignment).

[4]We thank a referee for suggesting this model.

[5]Using the following approximate bond energies (6), we estimate $\Delta H$ for $N_2$ loss to be at least −32 kcal mol$^{-1}$, neglecting the resonance energy of the ylide. Bond energies (kcal mol$^{-1}$): C—$N_{azo}$ (47), N=N (100), N≡N (226).

Can. J. Chem. Downloaded from www.nrcresearchpress.com by 210.87.254.6 on 09/06/12
For personal use only.

state through collisions. Although there are examples from the area of carbene chemistry of the dependence of final product composition on the rate of collisional deactivation (7), it is not clear in the present case that vibrational excitation should favour H-transfer over fragmentation. Although we cannot rule out this last alternative, we favour the first explanation for the phase dependence.

The temperature dependence of the product distribution in the gas phase is puzzling. There is no obvious explanation for it which is based on the intermediacy of oxirane **3**. That oxirane would have to open preferentially to ylide at high temperature and to carbenes and carbonyl compounds at low temperature. Since the fragmentations are expected to have entropies of activation at least as large as that of ring opening, such an explanation is unlikely to be correct. What is more, the known chemistry of similar oxiranes (8, 9) suggests that **3** would actually rearrange to a methoxy ketone, $CH_3COC(CH_3)_2OCH_3$. We are not aware of any precedent for conversion of **3** to **8** directly, without the intermediacy of **2**. If such a direct path is not available, then postulating equilibrium between **2** and **3** also cannot lead to a satisfactory explanation of the temperature dependence. Further studies, with other substituents, should help to establish whether or not the temperature dependence observed here is a general phenomenon in the chemistry of carbonyl ylides, whose fates are apparently very substituent dependent, as mentioned in the Introduction.

High temperature vapour phase thermolysis of **1** is a potentially useful synthetic procedure. Acetals in which one alkoxy function is enolic are rare and their synthesis by the usual avenues for acetals and ketals has not been reported. In the present thermolysis reaction the H-transfer process is quite selective in the sense that the hydrogen atom comes from the *gem*-dimethyl group and not from the other methyl group. The alternative product,

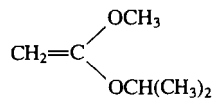

would have a vinyl signal near δ 3.0 in the $^1$H nmr spectrum, for $CH_2{=}C(OEt)_2$ absorbs at δ 3.01 (10). Since the $^1$H nmr spectra of our product mixtures have no appreciable absorption in that region, it is clear that little, if any, H-transfer occurs in the alternative sense.

**Acknowledgements**

The Natural Sciences and Engineering Research Council of Canada (NSERC) supported this work through research grants and NSERC summer studentships for S. Zweep and T. Steel. A. P. Hitchcock gratefully acknowledges the support of an NSERC University Fellowship.

1. (*a*) M. Békhazi. M.Sc. Thesis, McMaster University, 1979; (*b*) M. Békhazi and J. Warkentin. J. Am. Chem. Soc. **103**, 2473 (1981); (*c*) D. W. K. Yeung, G. A. MacAlpine, and J. Warkentin. J. Am. Chem. Soc. **100**, 1962 (1978). (*d*) N. Shimizu and P. D. Bartlett. J. Am. Chem. Soc. **100**, 4260 (1978).
2. K. N. Houk, N. G. Rondan, C. Santiago, C. J. Gallo, R. W. Gandour, and G. W. Griffin. J. Am. Chem. Soc. **102**, 1504 (1980).
3. A. P. Hitchcock, N. Hao, N. H. Werstiuk, M. J. McGlinchy, and T. Ziegler. Inorg. Chem. **21**, 793 (1982).
4. D. C. Frost, S. T. Lee, C. A. McDowell, and N. P. C. Westwood. J. Electron Spectrosc. **12**, 95 (1977).
5. L. B. Harding and W. A. Goddard III. J. Am. Chem. Soc. **102**, 439 (1980).
6. R. C. Weast (*Editor*). Handbook of chemistry and physics. 61st ed. Chemical Rubber Co. Press, Boca Raton, FL. 1980–1981.
7. H. M. Frey. J. Am. Chem. Soc. **82**, 5947 (1960).
8. R. W. Hoffmann and H. L. Luthardt. Tetrahedron Lett. 411 (1966).
9. R. W. Hoffmann and H. L. Luthardt. Chem. Ber. **101**, 381 (1968).
10. D. W. Cameron, M. J. Crossley, S. I. Feutrill, and P. G. Griffiths. Aust. J. Chem. **31**, 1335 (1978).

# The preparation of (*S*)-3,4-dehydroproline from (2*S*,4*R*)-4-hydroxyproline

HEINRICH RÜEGER AND M. H. BENN[1]

*Chemistry Department, The University, Calgary, Alta., Canada T2N 1N4*

Received June 1, 1982

HEINRICH RÜEGER and M. H. BENN. Can. J. Chem. **60**, 2918 (1982).

(2*S*,4*R*)-*N*-Benzyloxycarbonyl-4-tosyloxyproline methyl ester, readily prepared from commercially available (2*S*,4*R*)-*N*-benzyloxycarbonyl-4-hydroxyproline, was converted to (*S*)-3,4-dehydroproline of high enantiomeric purity by a process which involved a highly regioselective phenylselenoxide elimination to introduce the olefinic function.

HEINRICH RÜEGER et M. H. BENN. Can. J. Chem. **60**, 2918 (1982).

On a transformé l'ester méthylique de la *N*-benzyloxycarbonyltosyloxy-4 proline (2*S*,4*R*), provenant de la *N*-benzyloxycarbonylhydroxy-4 proline disponible commercialement, en déhydro-3,4 proline (*S*) d'une grande pureté énantiométrique. On a introduit la fonction oléfinique en utilisant une méthode qui fait intervenir une élimination très régiosélective par le sélénate de phényle.

[Traduit par le journal]

Seventy years ago Fischer and Gerlach (1) reported that the reduction of pyrrole-2-carboxamide with phosphonium iodide and fuming hydriodic acid yielded a product which they thought to be (±)-3,4-dehydroproline. Fifty years then passed until Robertson and Witkop (2) proved that, under carefully controlled conditions, this imino acid is indeed a product of the reaction.

Robertson and Witkop (2) obtained (*S*)-3,4-dehydroproline (**1**) of good optical purity by the action of hog acylase on (±)-3,4-dehydroproline amide, and provided the first report of its biological properties: saying *inter alia* that colleagues had found **1** to be a potent antimetabolite for some microorganisms, apparently as a consequence of its ability to act as an antagonist for (*S*)-proline. Subsequently, it has been shown (3) that **1** inhibits collagen synthesis in some mammalian cells, and that its introduction into peptides in lieu of (*S*)-proline can result (4) in modified biological properties, though not necessarily so (5).

Interest in the biological properties of **1** seems to have stimulated efforts to improve its availability. Various improvements in the Fischer–Witkop approach have been reported (5*b*, 6), culminating in those of Scott *et al.* (7).

As an alternative to these approaches, which require the resolution of racemic products, we were interested in preparing **1** from (2*S*,4*R*)-4-hydroxyproline (**2**). Although Robertson and Witkop (2) had noted that extensive efforts to convert 4-hydroxyproline to 3,4-dehydroproline had met with little success, it appeared to us that recent developments in synthetic methodology were encouraging: we were particularly impressed by the reported high-yield conversion of (2*S*,4*R*)-*N*-*tert*-butoxycarbonyl-4-hydroxyproline methyl ester via a Chugaev elimination (8), and thought that a selenoxide elimination might be even more regioselective in introducing the required 3-ene, i.e. we hoped that the sequence of reactions shown in Scheme 1 would provide a convenient route to (*S*)-3,4-dehydroproline.

We were guided in this plan by reports that selenoxide eliminations which could yield an olefin with or without oxygen (9) or sulphur (10) as a heteroatom substituent strongly favoured formation of the unsubstituted olefin. After we had completed our work, a publication describing the similar directive effects of amido groups appeared (11). We selected trimethylsilyl iodide for the final N-deblocking and ester cleavage reactions since it was known to effect these reactions under mild conditions (12), which an alkene survived (13).

As detailed in the Experimental section, these hopes were fulfilled: crystalline (*S*)-dehydroproline was obtained from the commercially available **3**, in 50% yield, with an optical rotation in accord with that reported for the enantiomerically pure amino acid.

## Experimental

Melting points were determined on a Leitz microscope hotstage melting point apparatus, and are uncorrected. The nmr data were collected on a Varian XL 200 instrument and chemical shifts are reported in parts per million relative to tetramethylsilane. In the case of the $^{13}C$ nmr spectrum of **1** the shifts are reported using 1,4-dioxane as an internal standard ($\delta$ = 66.6 ppm from TMS). Infrared spectra were recorded on a Perkin–Elmer 467 grating infrared spectrophotometer. Mass spectra were measured on a Varian MAT CH-5 spectrometer (*m*/*z* (relative intensity)) at 70 eV. The cd spectra were recorded with a Jasco J-500A instrument, $[\alpha]_D$ values with a Durrum–Jasco SS-20 machine. Combustion analyses were performed on a Perkin–

[1]Author to whom all correspondence should be addressed.

0008-4042/82/232918-03$01.00/0

©1982 National Research Council of Canada/Conseil national de recherches du Canada

Can. J. Chem. Downloaded from www.nrcresearchpress.com by 210.87.254.42 on 09/06/12
For personal use only.

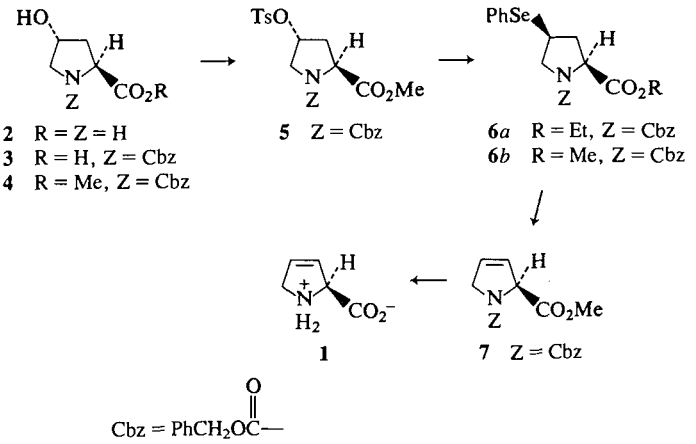


SCHEME 1

Elmer 240 elemental analyzer. All thin layer chromatography was performed using precoated Merck tlc plates: silica gel 60 F-254.

*(2S,4R)-N-Benzyloxycarbonyl-4-hydroxyproline methyl ester (4)*

To a stirred solution of (2*S*,4*R*)-*N*-carbobenzyloxy-4-hydroxyproline (Sigma) (99% pure by $[\alpha]_D$, homogeneous by tlc) (25 g, 94 mmol) in absolute EtOH (100 mL) was slowly added a cold solution of diazomethane (100 mmol) in $Et_2O$ (200 mL), the temperature being kept below 5°C. After 15 min the slight excess of diazomethane was decomposed with glacial acetic acid. The colorless solution was dried ($MgSO_4$), filtered, and concentrated to provide 25.0 g (99%) of **4** as a colorless oil (lit. oil (14), mp 82°C (15)), which was homogeneous on tlc, $R_f$ 0.57 (AcOEt/hexane 1:1); ir (film): 3450, 2960, 1745, 1700, 1495, 1425, 1360, 1210, 1170, 1125, 1090 $cm^{-1}$; nmr ($CDCl_3$) δ: 7.29 (5H, m), 5.10 (2H, m), 4.47 (2H, m), 3.74 + 3.54 (3H, s, two rotamers), 3.63 (2H, m), 2.62 (1H, br s), 2.28 (1H, m), 2.17 (1H, m); mass spectrum, *m/z*: 279 ($M^+$, 1.5), 220 (13), 176 (20), 92 (11), 91 (100), 65 (11), 44 (13).

*(2S,4R)-N-Benzyloxycarbonyl-4-tosyloxyproline methyl ester (5)*

To a solution of **4** (25.1 g, 90 mmol) in anhydrous pyridine (250 mL) was added *p*-toluenesulfonylchloride (18.9 g, 99 mmol) at 0–5°C, and the resulting mixture was refrigerated at that temperature for 1 week. The pyridine was removed under reduced pressure at 10–20°C, the residue dissolved in $Et_2O$ (400 mL), and this solution was then extracted with cold aqueous 5% HCl (3 × 30 mL) and $H_2O$ (5 × 30 mL). Evaporation of the dried $Et_2O$ layer gave an oil (40.2 g), which crystallized from $Et_2O$/pentane to give **5** (35.4 g, 91%): mp 74–75°C (lit. (14) mp 74–77°C); $[\alpha]_D^{27}$ −34.0° (*c* 5.0, $CHCl_3$); tlc, $R_f$ 0.51 (AcOEt/hexane 1:1); ir (KBr): 3060, 2990, 2950, 2870, 1735, 1690, 1425, 1355, 1275, 1180, 775, 765, 745, 710 695 $cm^{-1}$; nmr ($CDCl_3$) δ: 7.1–7.9 (9H, m), 5.10 (3H, m), 4.45 (1H, m), 3.73 + 3.51 (3H, s), 3.5–3.8 (2H, m), 2.45 + 2.43 (3H, s), 2.0–2.7 (2H, m); mass spectrum, *m/z*: 433 ($M^+$, 0.3), 158 (27), 91 (100), 65 (11). *Anal.* calcd. for $C_{21}H_{23}NO_7S$: C 58.18, H 5.35, N 3.23; found: C 58.41, H 5.39, N 3.30.

*(2S,4S)-N-Benzyloxycarbonyl-4-phenylselenoproline methyl ester (6)*

Diphenyldiselenide (8.58 g, 27.5 mmol) was dissolved in absolute EtOH (250 mL). $NaBH_4$ (2.08 g, 55 mmol) was then added in batches, while the reaction mixture was stirred under a $N_2$ atmosphere until the bright yellow solution turned colorless (9, 16). After addition of the tosylate **5** (19.1 g, 44 mmol) the reaction mixture was refluxed for 2.5 h. The solvent was removed *in vacuo*, the residue was diluted with $Et_2O$ (300 mL) and the resulting solution was washed with $H_2O$ (3 × 200 mL), then dried ($MgSO_4$), filtered, and concentrated to give a yellow oil (18.1 g). Thin-layer chromatography (AcOEt/hexane 1:2) revealed a single major product accompanied by two minor impurities. The mixture was purified by flash chromatography (17) on silica gel (300 g, 230–400 mesh, 30 × 5 cm). Petroleum ether/ethyl acetate 4:1 (500 mL), 3:1 (500 mL), and 2:1 (700 mL) eluted diphenyldiselenide (1.2 g), the ethyl ester[2] **6***a* (1.47 g, 8%), and the methyl ester **6***b* (14.97 g, 81%); **6***a* and **6***b* were homogeneous on tlc, $R_f$ 0.40, 0.34 (hexane/AcOEt 2:1) respectively, and crystallized on storage at 0°C. Recrystallization from $Et_2O$/pentane gave **6***a*, mp 46–47°C, and **6***b*, mp 53°C. The physical properties of **6***b* were as follows: $[\alpha]_D^{27}$ −25.7° (*c* 2.5, $CHCl_3$); ir (KBr): 3060, 2950, 2870, 1730, 1690, 1425, 1350, 1295, 1275, 1180, 1120, 1030, 775, 765, 745, 705, 665 $cm^{-1}$; nmr ($CDCl_3$) δ: 7.2–7.6 (10H, m), 5.12 (2H, m), 4.34 (1H, m), 4.0 (1H, m), 3.4–3.8 (2H, m), 3.71 + 3.54 (3H, s), 2.5–2.8 (1H, m), 1.95–2.2 (1H, m): mass spectrum, *m/z*: 419 ($M^+$, 1.6), 316 (9), 158 (8), 81 (100), 68 (15), 65 (19). *Anal.* calcd. for $C_{20}H_{21}NO_7Se$: C 58.33, H 5.36, N 3.24; found: C 58.45, H 5.35, N 3.22.

*(S)-N-Benzyloxycarbonyl-3,4-dehydroproline methyl ester (7)*

To a stirred solution of selenide **6***b* (8.36 g, 20 mmol) and pyridine (2.37 g, 30 mmol) in $CH_2Cl_2$ (100 mL) was gradually added 30% $H_2O_2$ (5.6 g, 50 mmol), while the reaction vessel was cooled in an ice bath (18). The reaction mixture was stirred vigorously at 25°C for an additional 1.5 h, then diluted with $CH_2Cl_2$ (100 mL) and extracted successively with aqueous 5% HCl (2 × 50 mL), saturated aqueous $Na_2CO_3$ solution (50 mL), and $H_2O$ (3 × 50 mL). The organic layer was dried ($MgSO_4$), the solvent removed under reduced pressure, and the residue purified by flash chromatography on silica gel (200 g, 230–400 mesh, 30 cm × 5 cm, AcOEt/petroleum ether 1:2), giving **7** as an oil (4.49 g, 87%); tlc, $R_f$ 0.64 (AcOEt/hexane 1:1); ir (film): 3085, 3060, 3030, 2950, 2900, 2865, 1750, 1710, 1620, 1498, 1415, 1355, 1310, 1260, 1205, 1180, 1125, 1105, 1000, 780, 770, 760, 700 $cm^{-1}$; nmr ($CDCl_3$) δ: 7.30 (5H, m), 5.97 (1H, m), 5.74 (1H, m), 5.0–5.3 (3H, m), 4.31 (2H, m), 3.74 + 3.50 (3H, s); mass spectrum, *m/z*:

[2]Formation of the ethyl ester could presumably be prevented by running the reaction in MeOH–THF.

Can. J. Chem. Downloaded from www.nrcresearchpress.com by 210.87.254.42 on 09/06/12
For personal use only.

261 ($M^+$, 0.3), 202 (25), 158 (36), 92 (19), 91 (100), 65 (21). We found no trace of the corresponding 4,5-dehydroproline, by tlc or $^1H$ nmr analysis of the crude reaction product, i.e. the selenoxide elimination must be very regioselective.

*(S)-Dehydroproline (1)*

To a solution of **7** (0.8 g, 3 mmol) in anhydrous $CH_3CN$ was added, via a syringe, trimethylsilyl iodide (1.3 mL, 9 mmol) under a nitrogen atmosphere (12, 13). The reaction mixture was then refluxed for 20 h. The mixture was then cooled to ca. 0°C and a mixture of EtOH/AcOH 1:1 (5 mL) was added quickly. After a further 20 min of stirring, the reaction mixture was further diluted with $H_2O$ (20 mL) and then extracted with $CH_2Cl_2$ (5 × 15 mL). The $H_2O$ layer was then poured onto a column of Dowex 50W-X8 (10 cm × 1.5 cm) cation exchange resin (100–200 mesh) (7). After washing the column with $H_2O$ (150 mL) until the eluates were neutral, the product was eluted with 0.5 *M* aqueous pyridine acetate solution (200 mL). The ninhydrin positive fractions were combined, and concentrated at <25°C. To remove traces of pyridine, the white residue was dissolved in $H_2O$ (20 mL) and reevaporated under the same conditions. This process was repeated once more. The wet solid residue (0.33 g) was dissolved in $H_2O$ (0.3 mL) and EtOH (3 mL), seeded, AcOEt (10 mL) added, and the solution refrigerated at −5°C overnight. The crystals which separated were filtered, washed with cold EtOH, $Et_2O$, and dried at 20°C/0.1 Torr, thus affording (*S*)-3,4-dehydroproline (**1**) (0.275 g, 80%): tlc, $R_f$ 0.22 (n-BuOH/AcOH/$H_2O$ 3:1:1); mp 242–243°C (dec.), $[\alpha]_D^{27}$ −404.6° (*c* 1.1, $H_2O$); e.e. 99.8%, (lit. (7) mp 244°C (dec.), $[\alpha]_D^{27}$ −403.1° (*c* 1.0, $H_2O$)); cd ($H_2O$): $\Delta\varepsilon_{202} = -25.4°$; ir (KBr): 3280, 3080, 2100–3300, 1620, 1600, 1360, 1330, 1280, 1270, 1230, 1195, 1065, 1005, 930, 830, 775, 740, 695; $^1H$ nmr ($CD_3COOD$) δ: 6.05 (1H, dddd, $J$ = 6.5, 2, 2, 2 Hz), 5.92 (1H, dddd, 6.5, 2.5, 2, 2 Hz), 5.15 (1H, m), 4.29 (2H, m) cf. lit. (19); $^{13}C$ nmr ($D_2O$, dioxane) δ: 172.2, 125.7, 125.4, 68.5, 52.4; mass spectrum, *m/z*: 111 ($M$ − 2, 12), 95 (12), 94 (12), 93 (12), 69 (17), 68 (70), 67 (100), 66 (16), 44 (59), 41 (100), 40 (34), 39 (59). *Anal.* calcd. for $C_5H_7NO_2$: C 53.06, H 6.24, N 12.39; found: C 53.11, H 6.36, N 12.44.

## Acknowledgements

This work was supported by an Alberta Heritage Foundation for Medical Research Studentship (to H.R.); and Grant A4547 of the Natural Sciences and Engineering Research Council of Canada (to M.H.B.).

1. E. Fischer and F. Gerlach. Chem. Ber. **45**, 2453 (1912).
2. A. V. Robertson and B. Witkop. J. Am. Chem. Soc. **84**, 1697 (1962).
3. S. S. Kerwar, A. M. Felix, R. J. Marcel, I. Tsai, and R. A. Salvador. J. Biol. Chem. **251**, 503 (1976).
4. S. Moore, A. M. Felix, J. Meienhofer, C. W. Smith, and R. Walter. J. Med. Chem. **20**, 495 (1977).
5. (*a*) A. M. Felix, M. H. Jimenez, R. Vergona, and M. R. Cohen. Int. J. Peptide Protein Res. **5**, 201 (1973); (*b*) A. M. Felix, C.-T. Wang, A. A. Liebman, C. M. Delaney, T. Mowles, B. A. Burghardt, A. M. Charnecki, and J. Meienhofer. Int. J. Peptide Protein Res. **10**, 299 (1977).
6. A. Corbella, P. Gariboldi, G. Jommi, and F. Mauri. Chem. Ind. London, 583 (1969).
7. J. W. Scott, A. Focella, U. O. Hengartner, D. R. Parrish, and D. Valentine, Jr. Synth. Commun. **10**, 529 (1980).
8. J.-R. Dormoy, B. Castro, G. Chappuis, U. S. Fritschi, and P. Grogg. Angew. Chem. Int. Ed. Engl. **19**, 742 (1980).
9. K. B. Sharpless and R. F. Lauer. J. Am. Chem. Soc. **95**, 2697 (1973).
10. K. C. Nicolaou, W. E. Barnette, and R. L. Magolda. J. Am. Chem. Soc. **100**, 2567 (1978).
11. A. Toshimitsu, H. Owada, T. Aoai, S. Uemura, and M. Okano. J. Chem. Soc. Chem. Commun. 546 (1981).
12. W. C. Groutas and D. Felker. Synthesis, 861 (1980), and references therein.
13. G. A. Olah, S. C. Narang, B. G. Balaram Gupta, and R. Malhotra. J. Org. Chem. **44**, 1247 (1979).
14. A. A. Patchett and B. Witkop. J. Am. Chem. Soc. **79**, 185 (1957).
15. T. Wieland, D. Schermer, G. Rohr, and H. Faulstich. Justus Liebigs Ann. Chem. 806 (1977).
16. K. B. Sharpless, M. W. Young, and R. F. Lauer. Tetrahedron Lett. 1979 (1973).
17. W. C. Still, M. Kahn, and A. Mitra. J. Org. Chem. **43**, 2923 (1978).
18. H. J. Reich, J. M. Renga, and I. L. Reich. J. Am. Chem. Soc. **97**, 5434 (1975).
19. L. F. Johnson, A. V. Robertson, W. R. J. Simpson, and B. Witkop. Aust. J. Chem. **19**, 115 (1966).

Can. J. Chem. Downloaded from www.nrcresearchpress.com by 210.87.254.42 on 09/06/12
For personal use only.

# The phosphorus-31 and metal nuclear magnetic resonance spectra of complexes of tin(II) and lead(II) with tricyclohexylphosphine oxide, sulfide, and selenide

PHILIP A. W. DEAN

*Department of Chemistry, University of Western Ontario, London, Ont., Canada N6A 5B7*

Received June 10, 1982

PHILIP A. W. DEAN. Can. J. Chem. **60**, 2921 (1982).

The new stannous and plumbous complexes $M(OP(C_6H_{11})_3)_n^{2+}$ ($n$ = 2 or 3, M = Sn or Pb) and $[M(SP(C_6H_{11})_3)_x(SeP(C_6H_{11})_3)_{3-x}]^{2+}$ (M = Sn or Pb) have been prepared in $SO_2$ solution and characterized by their reduced temperature slow-exchange $^{31}P$ and metal ($^{119}Sn$ or $^{207}Pb$) nmr spectra. No evidence could be found for complexes in which both $OP(C_6H_{11})_3$ and $EP(C_6H_{11})_3$ (E = S or Se) are coordinated to tin(II) or lead(II). The same pattern of chemical shifts is found in the $^{119}Sn$ and $^{207}Pb$ nmr spectra: $\delta_M(M(OP(C_6H_{11})_3)_2^{2+}) < \delta_M(M(OP(C_6H_{11})_3)_3^{2+} < \delta_M(M(SP(C_6H_{11})_3)_3^{2+}) < \delta_M(M(SeP(C_6H_{11})_3)_3^{2+})$ and a monotonic but non-linear variation of $\delta_M$ with $x$ for $[M(SP(C_6H_{11})_3)_x(SeP(C_6H_{11})_3)_{3-x}]^{2+}$. From $M(AsF_6)_2$ in $SO_2$ as reference, the range of the metal chemical shifts is 999–2079 ppm and 2407–7707 ppm in the $^{119}Sn$ and $^{207}Pb$ nmr spectra respectively. In the $^{31}P$ nmr spectra, all of the appropriate two-bond M—P couplings are observed, but the fine structure expected from coupling to $^{31}P$ could not always be observed in those metal nmr spectra which were measured at high field; it is suggested that these metal nmr spectra are "smeared out" by a combination of large temperature sensitivity of the metal chemical shifts and the small temperature variation allowed by the nmr spectrometer temperature controller and/or diffusion along any temperature gradients present along the length of the nmr sample.

PHILIP A. W. DEAN. Can. J. Chem. **60**, 2921 (1982).

On a préparé les nouveaux complexes stanneux et plombeux $M(OP(C_6H_{11})_3)_n^{2+}$ ($n$ = 2 ou 3, M = Sn ou Pb et $[(SP(C_6H_{11})_3)_x(SeP(C_6H_{11})_3)_{3-x}]^{2+}$ (M = Sn ou Pb) en solution dans le $SO_2$ et on les a caractérisés par leur spectre de rmn (du $^{119}Sn$ ou $^{207}Pb$) d'échange lent entre le $^{31}P$ et le métal à basse température. On ne peut prouver l'existence de complexes dans lesquels les deux groupes $OP(C_6H_{11})_3$ et $EP(C_6H_{11})_3$ (E = S ou Se) sont coordonnés à l'étain(II) ou au plomb(II). On trouve les mêmes types de déplacements chimiques dans les spectres de rmn du $^{119}Sn$ ou du $^{207}Pb$: $\delta_M(M(OP(C_6H_{11})_3)_2^{2+}) < \delta_M(M(OP(C_6H_{11})_3)_3^{2+} < \delta_M(M(SP(C_6H_{11})_3)_3^{2+}) < \delta_M(M(SeP(C_6H_{11})_3)_3^{2+})$ et une variation monotone mais non linéaire de $\delta_M$ avec $x$ pour le complexe $[M(SP(C_6H_{11})_3)_x(SeP(C_6H_{11})_3)_{3-x}]^{2+}$. A partir du $M(AsF_6)_2$ dans le $SO_2$ comme référence, l'ordre de grandeur des déplacements chimiques du métal se situe entre 999–2079 ppm et entre 2407–7707 ppm respectivement dans les spectres de rmn $^{119}Sn$ et du $^{207}Pb$. Dans les spectres du $^{31}P$, on observe tous les couplages appropriés M—P à travers deux liaisons mais on n'a pas toujours observé la structure fine attendue d'un couplage avec le $^{31}P$ dans les spectres de rmn du métal que l'on a mesurés à haut champ. On suggère que ces spectres de rmn de métal "sont étalés" par suite d'une combinaison de la grande sensibilité des déplacements chimiques à la température et de la faible variation de température que permet le contrôle de température du spectromètre et/ou la diffusion pour tout gradient de température présent dans l'échantillon de rmn.

[Traduit par le journal]

## Introduction

In a recent paper (1) we described, among other things, the slow exchange $^{31}P$ nmr spectra of complexes of divalent tin and lead with $Ph_3PO$ and some related polydentate phosphine oxides. Here we report an extension of this earlier work to stannous and plumbous complexes of $(C_6H_{11})_3PE$ (E = O, S, or Se) and mixtures of $(C_6H_{11})_3PS$ and $(C_6H_{11})_3PSe$,[1] the tricyclohexyl derivatives being chosen to give enhanced solubility. A variety of new tin(II) and lead(II) complexes have been characterized by their slow exchange $^{31}P$ and metal nmr spectra. This combination of nmr spectral measurements has let us obtain metal chemical shifts for a range of closely related complexes of tin(II) and lead(II) containing well-defined numbers and types of Group VIA donor atoms. Such metal nmr data are particularly helpful for heavy elements like tin and lead which have large chemical shift ranges; in these cases a knowledge of at least the approximate metal chemical shift to be expected in a particular situation can shorten appreciably the time taken to find the metal resonance. The approach used here, characterization of the complexes by $^{31}P$ nmr prior to measuring the metal nmr spectra, has been used earlier for a $^{113}Cd$ nmr study of cadmium complexes with a variety of phosphine oxides and chalcogenides (2–4).

Both $^{119}Sn$ and $^{207}Pb$ nuclei have been widely exploited in nmr studies (5). Probably reflecting the relative efforts which have been applied to the coordination chemistry of the metals in the +II and +IV oxidation states, most of the nmr studies have involved species in the +IV oxidation state. There does, however, seem to be an increasing interest in $^{119}Sn$ nmr spectroscopy of tin(II) complexes (e.g. refs. 6–8).

## Experimental

*Materials*

Isotopically-enriched yellow PbO (92.4 atom% $^{207}Pb$), ob-

[1]Hereafter, $C_6H_{11}$ will be abbreviated chx.

0008-4042/82/232921-06$01.00/0

©1982 National Research Council of Canada/Conseil national de recherches du Canada

Can. J. Chem. Downloaded from www.nrcresearchpress.com by 210.87.254.105 on 09/06/12
For personal use only.

Can. J. Chem. Downloaded from www.nrcresearchpress.com by 210.87.254.105 on 09/06/12
For personal use only.

tained from Oak Ridge National Laboratory, was dried under vacuum before use, as was isotopically natural yellow PbO (Fisher Scientific Co.). Stannous fluoride (Alfa, Ultrapure Grade), arsenic pentafluoride (Ozark-Mahoning, Inc.), and phosphorus pentafluoride (Matheson) were used as received. Antimony pentafluoride (PCR, Inc.) was purified by double distillation in a dry nitrogen atmosphere. The literature routes to $Sn(SbF_6)_2$ (9), and $Pb(SbF_6)_2$ and $Pb(AsF_6)_2.xSO_2$ (1) were used to prepare metal salts without isotopic enrichment. Tricyclohexylphosphine oxide, sulfide, and selenide were prepared during earlier work (3, 4, 10).

Sulfur dioxide (Canadian Liquid Air Ltd., Anhydrous Grade) was stored in the gas phase over Linde 3A Molecular Sieves for at least 12 h before use.

*General manipulative procedure*

Glove box and vacuum line manipulations, and preparations of sealed nmr samples were carried out as described in earlier publications from these laboratories (eg. refs. 2 and 10), except that for the nmr samples 8 mm od homemade sample tubes were used.

*Preparation of $Pb(AsF_6)_2$ from PbO*

The original preparation of $Pb(AsF_6)_2$ required anhydrous $PbF_2$ as a starting material (1). However, isotopically-enriched $PbF_2$ was not available, so $PF_5/AsF_5$ treatment of $^{107}$Pb-enriched PbO was used to prepare the $^{107}$Pb-enriched hexafluoroarsenate, following the procedure described recently for synthesis of $Cd(AsF_6)_2$ from CdO (4). *Anal.* (for an unenriched sample) calcd. for $As_2F_{12}Pb$: F 38.97, Pb 35.42; found: F 38.58, Pb 34.62. The hexafluoroarsenates prepared from PbO and $PbF_2$ show identical chemical behaviour.

*Nuclear magnetic resonance spectra*

Broad band proton decoupled 40.45 MHz $^{31}$P nmr spectra were measured using an XL-100-12 spectrometer system and referenced to external $OP(OMe)_3$ in $(CD_3)_2CO$ as reported earlier (10); the 8 mm sample tubes were held coaxially in 12 mm precision nmr tubes using a Teflon spacer. All $^{119}$Sn spectra were measured with a Bruker WH-400 spectrometer system operating at 148.93 without $^1$H decoupling. Typically, satisfactory spectra of ca. 0.075 *m* solutions in stationary 8 mm od tubes (held in a 10 mm precision nmr tube with a Teflon spacer) were obtained with several hundred 90° (35 μs) pulses at 30 $min^{-1}$ using a spectral window of 5 kHz, a 1.6 s acquisition time, and no lock. Spectra were referenced by sample interchange with a 0.075 *m* solution of $Sn(AsF_6)_2$ in $SO_2$ (prepared *in situ* from $SnF_2$:$AsF_5$ = 1:4; $Sn(AsF_6)_2$ is unstable to loss of $AsF_5$ (9)). An approximate conversion to $SnMe_4$ as reference is $\delta_{Sn(AsF_6)_2(SO_2,\ 213\ K)} = \delta_{SnMe_4(neat,\ 295\ K)} + 1898$ ppm.

Initial $^{207}$Pb nmr were obtained using a Varian XL-100 spectrometer system working at 20.89 MHz with no $^1$H decoupling. Several thousand transients were required using 90° (80 μs) pulses applied at 14 $min^{-1}$ with a 1 s acquisition time, a 12.5 kHz spectral window, and an annular $(CD_3)_2CO$ sample as a lock substance to obtain acceptable spectra from solutions containing ca. 0.075 *m* $^{207}$Pb in spinning 8 mm od tubes. The spectra of the same and additional samples were measured using the WH-400 spectrometer operating at 83.37 MHz. Typically, several hundred 90° (38 μs) pulses applied at 37 $min^{-1}$ with a 5 kHz spectral window, a 1.6 s acquisition time, and no lock were required to obtain a spectrum from stationary unlocked samples. The $^{207}$Pb nmr spectra were referenced to 0.075 *m* $^{207}$Pb-enriched $Pb(AsF_6)_2$ in $SO_2$ by sample interchange. An approximate conversion to 1.0 *M* $Pb(NO_3)_2$(aq) is $\delta_{Pb(AsF_6)_2(SO_2,\ 203\ K)} = \delta_{1\ M\ Pb(NO_3)_2(aq,\ 295\ K)} + 1105$ ppm. (Also $\delta_{1\ M\ Pb(NO_3)_2(aq)} \approx \delta_{PbMe_4(toluene)} + 2961$ ppm (5).)

*Elemental microanalysis*

Analyses were performed by Analytische Laboratorien, Elbach, W. Germany.

## Results and discussion

The salts $Sn(SbF_6)_2$ and $Pb(SbF_6)_2$ are insoluble in $SO_2$. However, addition of $(chx)_3PO$ causes their dissolution when L/M $\gtrsim$ 1.5, as has been observed for L = $Ph_3PO$ earlier (1). Similarly, addition of $(chx)_3PS$ or $(chx)_3PSe$, or mixtures of these two, causes dissolution when (total L)/M $\gtrsim$ 3. When L/M $\lesssim$ 3, the yellow colours characteristic of $(chx)_3PS$ and $(chx)_3PSe$ in $SO_2$ are blanched.

*$^{31}$P nmr spectra*

Slow exchange $^{31}$P nmr spectra of $(chx)_3PO$–$M(SbF_6)_2$ (M = Sn or Pb) mixtures in $SO_2$ can be obtained at reduced temperature when L/M $\lesssim$ 3, and for lead identical results can be obtained using $SO_2$-soluble $Pb(AsF_6)_2$. Excess ligand causes exchange-averaging (c.f. ref. 1). By observing the slow-exchange spectra as a function of L/M, the species $M(OP(chx)_3)_2^{2+}$ and $M(OP(chx)_3)_3^{2+}$ can be identified for both tin and lead, detection of the appropriate $^{117/119}$Sn and $^{207}$Pb satellites ($^{117}$Sn 7.76%, $^{119}$Sn 8.68%, $^{207}$Pb 21.11% natural abundance; all spin $I$ = 1/2) confirming the absence of intermolecular ligand exchange. The location of the $^{207}$Pb satellites was verified incidentally during $^{31}$P nmr measurements made on $^{207}$Pb-enriched samples prior to $^{207}$Pb nmr studies (see below). Details of the $^{31}$P nmr spectra of the $(chx)_3PO$ complexes of tin and lead are given in Tables 1 and 2, respectively. Particularly noteworthy in these spectra are the large complexation shifts which are typical of phosphine oxides (e.g. refs. 1, 2, 11, 12).

Slow exchange $^{31}$P nmr spectra of $SO_2$ solutions prepared from $M(SbF_6)_2$ (M = Sn or Pb) (or, for lead, $Pb(AsF_6)_2$) and $(chx)_3PS$ or $(chx)_3PSe$ or mixtures of the phosphine sulfide and selenide can be obtained provided (total L)/M $\gtrsim$ 3. When (total L)/M exceeds 3 fast exchange averages of the $M(EP(chx)_3)_3^{2+}$ and $EP(chx)_3$ spectra are observed at all temperatures; as with the phosphine oxide complexes (ref. 1 and see above) these results show that intermolecular exchange occurs associatively.

The species $M(EP(chx)_3)_3^{2+}$ (E = S or Se; M = Sn or Pb) give the anticipated slow exchange spectra consisting of a central singlet, flanked by metal satellites of the appropriate intensity and, for the $(chx)_3PSe$ complexes, $^{77}$Se satellites complete with their metal satellites ($^{77}$Se 7.58% natural abundance, spin $I$ = 1/2). In the spectra of the tin complexes separate $^{117}$Sn and $^{119}$Sn satellites were not resolved as they were in the spectra of the

Can. J. Chem. Downloaded from www.nrcresearchpress.com by 210.87.254.105 on 09/06/12
For personal use only.

TABLE 1. $^{31}P$ and $^{119}Sn$ nmr spectral parameters of tin(II) complexes of tricyclohexylphosphine oxide, sulfide, and selenide in liquid $SO_2$ at 213 K

| Complex[a] | $\delta_P$[b] (ppm) | $\Delta\delta_P$[c] (ppm) | $\delta_{Sn}$[d] (ppm) | $^2J(^{117/119}Sn—E—^{31}P)$ (Hz) | $^1J(^{31}P—^{77}Se)$ (Hz) | $\Delta^1J(^{31}P—^{77}Se)$ (Hz) |
|---|---|---|---|---|---|---|
| $[Sn(OP(chx)_3)_2]^{2+}$ | 75.4 | 15.2 | 999[g] | 251[h] | | |
| $[Sn(OP(chx)_3)_3]^{2+}$ | 72.3 | 12.2 | 1178[i] | 237[h] | | |
| $[Sn(SP(chx)_3)_3]^{2+}$ | 64.5 | 0.1 | 1992[j,k] | 11 | | |
| $[Sn(SP(chx)_3)_2(SeP(chx)_3)]^{2+}$ | 64.0<br>61.6 | −0.6<br>−0.7 | 2031[j,l] | 13<br>22 | 492 | 86 |
| $[Sn(SP(chx)_3)_3(SeP(chx)_3)_2]^{2+}$ | 63.6<br>61.1 | −1.0<br>−1.2 | 2059[m] | ~16<br>24 | 497 | 81 |
| $[Sn(SeP(chx)_3)_3]^{2+}$ | 60.6 | −1.6 | 2079[n] | 27 | 499 | 79 |

[a]chx = $C_6H_{11}$.
[b]Relative to external $OP(OMe)_3$ in $(CD_3)_2CO$; estimated error ±0.1 ppm or less; shifts to increasing frequency are taken as positive; $\delta_{OP(OMe)_3}$ (ext) ≈ $\delta_{H_3PO_4}$ (ext) − 0.7 ppm.
[c]$\Delta\delta$ = δ(complex) − δ(free ligand (at the same temperature)); $\Delta J$ = J(complex) − J(free ligand (at the same temperature)).
[d]Relative to external $Sn(AsF_6)_2$ in $SO_2$ at 213 K, for solutions in which the total tin concentration ≈ 0.075 *m*; estimated error ±1 ppm; shifts to increasing frequency are taken as positive; $\delta_{Sn(AsF_6)_2(SO_2\ 213\ K)} \approx \delta_{SnMe_4\ (neat,\ 295\ K)} + 1898$ ppm; $\nu_{1/2}(Sn(AsF_6)_2) \approx 25$ Hz.
[e]Measured in the $^{31}P$ nmr spectra; estimated error ±1 Hz.
[f]Separate $^{117/119}Sn$ satellite splittings were not resolved except where noted.
[g]Triplet splitting resolved.
[h]$^2J(^{119}Sn—O—^{31}P)$.
[i]Quartet splitting resolved.
[j]No fine structure resolved.
[k]$\nu_{1/2} \approx 45$ Hz.
[l]$\nu_{1/2} \approx 35$ Hz.
[m]Incompletely resolved symmetrical multiplet; $^1J(^{119}Sn—^{77}Se) \approx 650$ Hz.
[n]Poorly resolved quartet; $^1J(^{119}Sn—^{77}Se) = 570 \pm 10$ Hz.

TABLE 2. $^{31}P$ and $^{207}Pb$ nmr spectral parameters of lead(II) complexes of tricyclohexylphosphine oxide, sulfide, and selenide in liquid $SO_2$ at 203 K

| Complex[a] | $\delta_P$[b] (ppm) | $\Delta\delta_P$[c] (ppm) | $\delta_{Pb}$[d] (ppm) | Approx[e] $\nu_{1/2}$ (Hz) | $^2J(^{207}Pb—E—^{31}P)$[f] (Hz) | $^1J(^{31}P—^{77}Se)$[f] (Hz) | $\Delta^1J(^{31}P—^{77}Se)$ (Hz) |
|---|---|---|---|---|---|---|---|
| $[Pb(OP(chx)_3)_2]^{2+}$ | 70.9 | 10.3 | 2407 | 1400[g] | 50 | | |
| $[Pb(OP(chx)_3)_3]^{2+}$ | 68.5 | 7.9 | 2924 | [h] | 62 | | |
| $[Pb(SP(chx)_3)_3]^{2+}$ | 62.2 | −2.7 | 6523 | 170[i] | 31 | | |
| $[Pb(SP(chx)_3)_2(SeP(chx)_3)]^{2+}$ | 61.3<br>58.5 | −3.6<br>−4.1 | 6785 | 195 | 32<br>45 | 513 | −61 |
| $[Pb(SP(chx)_3)(SeP(chx)_3)_2]^{2+}$ | 60.5<br>57.4 | −4.4<br>−5.2 | 6967 | 200 | 38<br>47 | 517 | −57 |
| $[Pb(SeP(chx)_3)_3]^{2+}$ | 56.6 | −6.0 | 7077 | 200[j] | 50 | 520 | −54 |

[a,b,c]See footnotes *a*,*b*,*c* of Table 1.
[d]Relative to external $Pb(AsF_6)_2$ in $SO_2$ at 203 K, for solutions in which the total lead concentration ≈ 0.075 *m*; estimated error ±2 ppm; shifts to increasing frequency are taken as positive; $\delta_{Pb(AsF_6)_2(SO_2\ 203\ K)} \approx \delta_{1\ M\ Pb(NO_3)_2(aq,\ 295\ K)} + 1105$ ppm ($\delta_{1\ M\ Pb(NO_3)_2(aq)} \approx \delta_{PbMe_4(toluene)} + 2961$ ppm (5)); $\nu_{1/2}(Pb(AsF_6)_2) \approx 450$ Hz.
[e]The approximate linewidths in the table are those measured in the 83.4 MHz spectra; at this frequency the spectra showed no resolvable fine structure, except where noted (see text).
[f]See footnote *e* of Table 1.
[g]$\nu_{1/2} \approx 120$ Hz in the 20.9 MHz nmr spectrum.
[h]Quartet fine structure poorly resolved at 203 K, but quite clear at 223 K ($\nu_{1/2} \sim 40$ Hz; $\delta_{Pb} = 2914$ ppm); quartet fine structure ($\nu_{1/2} \approx 24$ Hz) observed in the 20.9 MHz nmr spectrum at 203 K.
[i]Quartet fine strueture ($\nu_{1/2} \approx 30$ Hz) observed in the 20.9 MHz nmr spectrum at 203 K.
[j]This resonance could not be observed in the 20.9 MHz spectrum because it fell in a region where interference was severe.

$OP(chx)_3$ complexes, for $^2J(^{117/119}Sn—E—^{31}P)$ is considerably smaller in magnitude for E = S or Se than for E = O. Again when $^{207}Pb$-enriched $Pb(AsF_6)_2$ was used as starting material the $^{207}Pb$ satellites in the spectra of the lead complexes showed the expected increase in intensity. The triligated species were the only ones present in measurable quantity even though the starting mixtures were metal-rich; no evidence was found for $M(EP(chx)_3)_2^{2+}$ when E = S or Se.

Nuclear magnetic resonance spectral details for $M(EP(chx)_3)_3^{2+}$ (E = S or Se) are included in Tables 1 and 2. The $^{31}P$ nmr complexation shifts of the $(chx)_3PS$ and $(chx)_3PSe$ complexes are small, as

Can. J. Chem. Downloaded from www.nrcresearchpress.com by 210.87.254.105 on 09/06/12
For personal use only.

has been found previously for the cadmium complexes of these ligands also (3). However, $^1J$(P—Se) is smaller in the phosphine selenide complex than in the free ligand, an effect characteristic of coordination through selenium (2, 3, 10, 13–17).

When mixtures of $(chx)_3PS$ and $(chx)_3PSe$ are used, and (total L)/M $\gtrsim$ 3, reduced temperature $^{31}P$ nmr indicates that a total of four species are formed in solution as the $(chx)_3PS/(chx)_3PSe$ ratio is varied. Evidently all four complexes of the series $[M(SP(chx)_3)_x(SeP(chx)_3)_{3-x}]^{2+}$ exist for both tin and lead, confirming that a maximum of three sulfur/selenium atoms can be bound. The $^{31}P$ nmr spectral parameters of the mixed complexes are included in Tables 1 and 2 for tin and lead respectively. As has been noted for similar mixed ligand complexes of cadmium (3), the various chemical shifts and coupling constants in the $^{31}P$ nmr spectra are not very sensitive to replacement of $(chx)_3PSe$ by $(chx)_3PS$ or vice-versa.

Attempts to obtain evidence for complexes with $(chx)_3PO$–$(chx)_3PS$ or $(chx)_3PO$–$(chx)_3PSe$ mixtures in their coordination shell were fruitless for both tin and lead as acceptors, as they had been earlier for cadmium as an acceptor (3). Samples with $((chx)_3PO + (chx)_3PE)/M \lesssim 3$ (E = S or Se) gave $^{31}P$ nmr spectra containing resonances from $M(EP(chx)_3)_3^{2+}$ and $M(OP(chx)_3)_3^{2+}$ and/or $M(OP(chx)_3)_2^{2+}$ (depending on the (total L)/M and $(chx)_3PO/(chx)_3PE$ ratios). Indeed, the mixed O—S or O—Se kernels do not seem to form readily even in intermediates (or transition states) in ligand exchange processes. In solutions in which $((chx)_3PO + (chx)_3PE)/M > 3$ but $(chx)_3PO/M < 3$, a slow exchange spectrum is observed for $M(OP(chx)_3)_3^{2+}$ while an exchange-averaged spectrum of $M(EP(chx)_3)_3^{2+}$ and $EP(chx)_3$ is seen, i.e. excess $EP(chx)_3$ causes ligand exchange of $M(EP(chx)_3)_3^{2+}$, suggesting that the $ME_4$ kernel forms transiently, but causes little or no ligand exchange of $M(OP(chx)_3)_3^{2+}$, suggesting that the $MO_3E$ kernel does not form. A recent interpretation (18) of this "antisymbiotic" (19) or "cooperative" (18) behaviour of ligands with "hard" and "soft" (20) ("class a" and "class b" (21)) donor atoms is that the true coordination numbers of the species which do not redistribute ($M(OP(chx)_3)_3^{2+}$ and $M(EP(chx)_3)_3^{2+}$ (E = S or Se; M = Sn or Pb) in the present case) differ. If this is so, perhaps the coordination sphere of "$M(OP(chx)_3)_3^{2+}$" includes $SO_2$, or fluorine(s) from the counter-ion, though the latter, if present, must be labile, for no coupling to $^{19}F$ is seen in the metal nmr spectra (see below).

*Metal nmr spectra*

Samples for $^{207}Pb$ nmr were prepared using $^{207}Pb$-enriched $Pb(AsF_6)_2$ (see Experimental Section) as starting material, so that spectra could readily be obtained at both 20.9 and 83.4 MHz. For $^{119}Sn$ nmr, natural $Sn(SbF_6)_2$ was the starting material, and spectra were measured at 148.9 MHz. Prior to measurement of the metal nmr spectra, the contents of the solutions at the appropriate reduced temperature were checked by $^{31}P$ nmr. Details of the $^{119}Sn$ and $^{207}Pb$ nmr spectra are given in Tables 1 and 2 respectively.

Complexation of $Pb(AsF_6)_2$ in $SO_2$ at 203 K induces shifts to lower shielding ranging from 2407 ppm for $Pb(OP(chx)_3)_2^{2+}$ to 7077 ppm for $Pb(SeP(chx)_3)_3^{2+}$. For the two $OP(chx)_3$ complexes the shifts are in the order $\delta_{3:1} > \delta_{2:1}$, while for the 3:1 complexes with different donor atoms the chemical shift sequence is $\delta_{Se} > \delta_S > \delta_O$ (analogous to the "inverse halogen dependence" (22)). The chemical shift sequence $\delta_{Se} > \delta_S$ was observed for solid PbE (23). Both the solid lead chalcogenides have smaller $^{207}Pb$ chemical shifts than the corresponding $Pb(EP(chx)_3)_3^{2+}$ complexes: relative to 1.0 *M* $Pb(NO_3)_2$(aq) shifts of PbE and $Pb(EP(chx)_3)_3^{2+}$ are approximately 3900 and 5410 and 5300 and 5970 ppm for E = S and Se, respectively (refs. 23 and 24, and Table 2). However, both the lead(II) calcogenides have the NaCl structure with six-coordinate lead ions (25*a*), in contrast to $Pb(EP(chx)_3)_3^{2+}$ in which trigonal pyramidal coordination about lead, with a stereochemically active lone pair, is anticipated. The increased coordination symmetry in the solid chalcogenides should result in a decreased paramagnetic contribution to the shielding and hence a smaller chemical shift (26).

Lead-207 data have also been reported for, *inter alia*, solid $PbZrO_3$ and red and yellow PbO (24). In $PbZrO_3$, the lead has flattened trigonal pyramidal coordination by oxygens (27), similar to the coordination geometry expected to occur in $Pb(OP(chx)_3)_3^{2+}$, and the lead chemical shifts of these two species are similar: approximately 1400 and 1820 ppm from 1.0 *M* $Pb(NO_3)_2$(aq) for $PbZrO_3$ and $Pb(OP(chx)_3)_3^{2+}$, respectively (ref. 24 and Table 2). The chemical shift of $Pb(OP(chx)_3)_2^{2+}$, ca. 1300 ppm for 1.0 *M* $Pb(NO_3)_2$(aq) (Table 2), also falls close to that of $PbZrO_3$, suggesting that its coordination geometry is close to trigonal pyramidal, perhaps with a coordinated $SO_2$ or anion occupying a coordination site. The similar magnitudes of $^2J(^{207}Pb—^{31}P)$ in $Pb(OP(chx)_3)_{2\text{ or }3}^{2+}$ (Table 2) also militate against a radical change in lead environment between the two $(chx)_3PO$ complexes. The coordination geometry about lead is square pyramidal and distorted 2 + 2 in red and yellow lead respectively (25*b*), and these two oxides have significantly larger chemical shifts than Pb(OP-

Can. J. Chem. Downloaded from www.nrcresearchpress.com by 210.87.254.105 on 09/06/12
For personal use only.

$(chx)_{3}{}_{2\text{ or }3}{}^{2+}$: approximately 2800 and 6600 ppm from $Pb(NO_3)_2$(aq) for red and yellow lead, respectively (24).

At 203 K, slow exchange $^{207}Pb$ nmr spectra were observed for equilibrium mixtures containing several members of the series $[Pb(SP(chx)_3)_x(SeP(chx)_3)_{3-x}]^{2+}$. For these complexes the $^{207}Pb$ chemical shifts increase monotonically but not linearly as $x$ decreases (Table 2). The chemical shifts can reasonably be accommodated using the concept of pairwise additivity (28) if each S–Se interaction produces a deshielding of 130 ppm from the chemical shift of $Pb(SP(chx)_3)_3{}^{2+}$ and each Se–Se interaction a deshielding of 185 ppm; these complexes presumably are trigonal pyramidal with a stereochemically active lone pair, but the sulfur – lone pair and selenium – lone pair interaction constants appear to be equal.

The chemical shifts measured in the 20.9 and 83.4 MHz $^{207}Pb$ nmr spectra did not differ significantly. However, there were noticeable differences in the extent to which the expected fine structure from two-bond $^{207}Pb$–$^{31}P$ scalar coupling was resolved (see Table 2). In the 203 K 20.9 MHz spectra, the resonances of $Pb(OP(chx)_3)_3{}^{2+}$ and $Pb(SP(chx)_3)_3{}^{2+}$ showed the expected quartet structure; there was no evidence for coupling of $^{207}Pb$ to the fluorine of any coordinated anion (see above). In contrast, and for reasons which are unclear, $Pb(OP(chx)_3)_2{}^{2+}$, though it gave a well-resolved 40.5 MHz $^{31}P$ nmr spectrum, showed a broad $^{207}Pb$ resonance with no observable fine structure. Unfortunately, instrumental limitations precluded measurement of the $^{207}Pb$ nmr spectrum of $Pb(SeP(chx)_3)_3{}^{2+}$ at 20.9 MHz. In the 203 K 83.4 MHz $^{207}Pb$ nmr spectrum of $Pb(OP(chx)_3)_3{}^{2+}$ the fine structure from $^2J(^{207}Pb—^{31}P)$ could barely be resolved, though it was better resolved at somewhat higher temperatures. At the higher field and 203 K, the signal from $Pb(OP(chx)_3)_2{}^{2+}$ was broader than at 20.9 MHz, and no fine structure could be resolved in the 83.4 MHz spectra of $Pb(EP(chx)_3)_3{}^{2+}$ (E = S or Se) at 203 K or higher temperatures. Relaxation via chemical shift anisotropy can be very important at high magnetic fields (see, for example, refs. 29 and 30) and may contribute to the broadness of the $^{207}Pb$ nmr lines observed at 83.4 MHz. However, a more mundane source of much of the linewidth is likely, for we found the $^{207}Pb$ chemical shifts of $Pb(OP(chx)_3)_3{}^{2+}$, $Pb(SP(chx)_3)_3{}^{2+}$, and $Pb(SeP(chx)_3)_3{}^{2+}$ (the only complexes for which this measurement was made) to have sizeable temperature coefficients (a decrease of ca. 10, and increases of ca. 3 and ca. 16 ppm, respectively, on changing the temperature from 203 to 223 K), and this significant temperature sensitivity (a phenomenon remarked on earlier for $^{207}Pb$ (31)), combined with the small temperature fluctuation allowed by the temperature controller (±0.3 K at the sample in the specifications for the WH-400) and/or diffusion along any temperature gradients present along the length of the sample,[2] must result in a "smearing out" of the spectrum which is more significant at the higher magnetic field, *ceteris paribus*.

The $^{119}Sn$ nmr data measured from the slow exchange 148.9 MHz spectra of the various tin(II) complexes studied at 213 K are given in Table 1. The pattern of $^{119}Sn$ chemical shifts observed is identical to that found for the analogous lead(II) complexes, leaving no doubt that tin(II), and not tin(IV) complexes, are being studied. There is a smooth but non-linear correlation between the $^{119}Sn$ and $^{207}Pb$ chemical shifts of analogous complexes. The overall range of the lead chemical shifts is 3.4 times that of the tin chemical shifts, though within the series of complexes $[M(SP(chx)_3)_x(SeP(chx)_3)_{3-x}]^{2+}$ the ratio is 6.4. A ratio of 3.0 has been noted previously for $\delta_{Pb}/\delta_{Sn}$ for a variety of organo-lead(IV) and -tin(IV) compounds (32).

The expected fine structure from $^2J(^{119}Sn—O—^{31}P)$ is observed in the $^{119}Sn$ nmr spectra of $Sn(OP(chx)_3)_n{}^{2+}$ ($n$ = 2 or 3). (There is no evidence for coupling to fluorine(s) of the anion.) However, in the spectrum of $Sn(SeP(chx)_3)_3{}^{2+}$ the quartet fine structure is barely resolved, and no fine structure would be seen in the spectrum of $Sn(SP(chx)_3)_3{}^{2+}$ for which the smallest value of the two-bond coupling to phosphorus is found by $^{31}P$ nmr (Table 1). The qualitative observation that the resolution of these spectra deteriorates with increasing spectral accumulation time at constant temperature suggests that, as for $^{207}Pb$ (see above), a combination of temperature sensitivity of $\delta_M$ and any small temperature variations within the samples smears the spectra out.

In the $^{119}Sn$ spectrum of $Sn(SeP(chx)_3)_3{}^{2+}$ the $^{77}Se$ satellites were clearly visible with intensity approximately that expected on statistical grounds for the Sn $^{77}SeSe_2$ kernel, i.e. 19.4% of the total intensity. The magnitude of the $^1J(^{119}Sn—^{77}Se)$, 570 ± 10 Hz, is smaller than that found in the tin(IV) compounds $Me_{4-n}Sn(SeR)_n$ (R = Me or Ph) (33) (e.g. 1520 ± 10 Hz for $Sn(SeMe)_4$) and somewhat smaller than the values of $^1J(^{199}Hg—^{77}Se)$ found in various complexes of $Bu^n{}_3PSe$ with mercuric halides and pseudohalides (17) (e.g. −751 ± 10 Hz for $Cl_2Hg(SePBu^n{}_3)_2$). Poorly resolved

[2]Thanks are due to a referee for suggesting the possible importance of lengthwise temperature gradients.

$^{77}$Se satellites (expected statistical intensity 14.0%) were observed for $[Sn(SP(chx)_3)(SeP(chx)_3)_2]^{2+}$; the value of $^1J(^{119}Sn—^{77}Se)$ was ca. 650 Hz. Unfortunately the $^{77}$Se satellites in the $^{119}$Sn spectrum of $[Sn(SP(chx)_3)_2(SeP(chx)_3)]^{2+}$ (expected intensity 7.58%) could not be observed, so it is not clear whether $^1J(^{119}Sn—^{77}Se)$ continues to increase with increasing substitution of $SP(chx)_3$ for $SeP(chx)_3$.

As for the analogous lead complexes (see above), monotonic but not linear changes in metal chemical shift with $x$ are found in the series $[Sn(SP(chx)_3)_x(SeP(chx)_3)_{3-x}]^{2+}$ (Table 1). The data can be accommodated by the approximate incremental pairwise additivity parameters $\Delta\delta_{S—Se} = 19$, $\Delta\delta_{Se—Se} = 29$ ppm.


## Acknowledgements

This work was made possible by an Operating Grant from the Natural Sciences and Engineering Research Council of Canada. The high field nmr spectra were obtained at the Southwestern Ontario NMR Centre, funded by a Major Installation Grant from the Natural Sciences and Engineering Research Council of Canada, with the expert technical assistance of Mr. Bruce MacDonald.



1. P. A. W. Dean, D. D. Phillips, and L. Polensek. Can. J. Chem. **59**, 50 (1981).
2. P. A. W. Dean and M. K. Hughes. Can. J. Chem. **58**, 180 (1980).
3. P. A. W. Dean and L. Polensek. Can. J. Chem. **58**, 1627 (1980).
4. P. A. W. Dean. Can. J. Chem. **59**, 3221 (1981).
5. R. K. Harris, J. D. Kennedy, and W. McFarlane. NMR and the periodic table. *Edited by* R. K. Harris and B. E. Mann. Academic Press, London. 1978. Chapt. 10 and references therein.
6. C. C. Hsu and R. A. Geanangel. Inorg. Chem. **19**, 110 (1980).
7. W.-W. du Mont and H.-J. Kroth. Z. Naturforsch. **35b**, 700 (1980).
8. H.-M. M. Yeh and R. A. Geanangel. Inorg. Chim. Acta, **52**, 113 (1981).
9. T. Birchall, P. A. W. Dean, and R. J. Gillespie. J. Chem. Soc. A, 1777 (1971).
10. P. A. W. Dean. Can. J. Chem. **57**, 754 (1979).
11. S. O. Grim and L. Satek. J. Coord. Chem. **6**, 39 (1976).
12. M. Zeldin, P. Mehta, and W. D. Vernon. Inorg. Chem. **18**, 463 (1979).
13. W. J. Stec, A. Okruszek, B. Uznanski, and J. Michalski. Phosphorus, **2**, 97 (1972).
14. C. Glidewell and E. J. Leslie. J. Chem. Soc. Dalton, 527 (1977).
15. S. O. Grim, E. D. Walton, and L. C. Satek. Inorg. Chim. Acta, **27**, L115 (1978).
16. S. O. Grim, E. D. Walton, and L. C. Satek. Can. J. Chem. **58**, 1476 (1980).
17. I. J. Colquhoun and W. McFarlane. J. Chem. Soc. Dalton, 658 (1981).
18. E. L. King. Abstr. 183rd ACS Natl. Meeting, Las Vegas, Nevada, March 1982. Abstr. INOR 185.
19. C. K. Jorgensen. Inorg. Chem. **3**, 1201 (1964).
20. R. G. Pearson. J. Am. Chem. Soc. **85**, 3533 (1963).
21. S. Ahrland, J. Chatt, and N. R. Davies. Q. Rev. Chem. Soc. **5**, 265 (1958).
22. R. G. Kidd and R. J. Goodfellow. NMR and the periodic table. *Edited by* R. K. Harris and B. E. Mann. Academic Press, London. 1978. Chapt. 8 and references therein.
23. I. Weinberg. J. Chem. Phys. **61**, 1112 (1962).
24. L. H. Piette and H. E. Weaver. J. Chem. Phys. **28**, 735 (1958).
25. A. F. Wells. Structural inorganic chemistry. 3rd ed. Oxford University Press, London, 1962. (*a*) p. 527, (*b*) p. 476, and references therein.
26. L. E. Orgel. Mol. Phys. **1**, 322 (1958).
27. F. Jona, G. Shirane, F. Mazzi, and R. Pepinsky. Phys. Rev. **105**, 849 (1957).
28. E. R. Malinowski. J. Am. Chem. Soc. **91**, 4701 (1969) and references therein.
29. J.-Y. Lallemond, J. Soulié, and J.-C. Chottard. J. Chem. Soc. Chem. Commun. 436 (1980).
30. R. E. Wasylishen, R. E. Lenkinski, and C. Roger. Can. J. Chem. **60**, 2113 (1982).
31. G. E. Maciel and J. L. Dallas. J. Am. Chem. Soc. **95**, 3039 (1973); O. Lutz and G. Stricker. Phys. Lett. **35**, 397 (1971).
32. J. D. Kennedy, W. McFarlane, and G. S. Pyne. J. Chem. Soc. Dalton, 2332 (1977).
33. J. D. Kennedy and W. McFarlane. J. Chem. Soc. Dalton, 2134 (1973).


Can. J. Chem. Downloaded from www.nrcresearchpress.com by 210.87.254.105 on 09/06/12
For personal use only.

# The influence of non-equilibrium transient effects on measurements of vibrational relaxation times and of dissociation rate constants

HESHEL TEITELBAUM

*Department of Chemistry, University of Ottawa, Ottawa-Carleton Centre for Graduate Studies, Ottawa, Ont., Canada K1N 9B4*

Received April 27, 1982

Can. J. Chem. Downloaded from www.nrcresearchpress.com by 210.87.254.105 on 09/06/12
For personal use only.

HESHEL TEITELBAUM. Can. J. Chem. **60**, 2927 (1982).

A semi-empirical analysis based on a rate law for vibrational relaxation of dissociating simple harmonic oscillators allows for a detailed study of measurements of vibrational relaxation times $\tau$ and of steady dissociation rate coefficients $k_0$. It is shown that non-equilibrium populations of vibrational energy levels prevent attainment of the thermodynamically expected equilibrium energy. Even under near-isothermal and mild conditions, $\tau \ll 1/k_0$, serious experimental errors result when the Bethe–Teller relaxation rate law is used. Closed form expressions are given which permit evaluation of these errors. Measurements should be analyzed using the rate law

$$-d\varepsilon/dt = (\varepsilon - \varepsilon_T)/\tau + k_d(\varepsilon_* + h\nu - \varepsilon)$$

where $\varepsilon$ is the vibrational energy per molecule, $\tau$ the relaxation time, $k_d$ the non-equilibrium rate coefficient, $\varepsilon_T$ the thermodynamically expected vibrational energy at temperature $T$, and $(\varepsilon_* + h\nu)$ the energy just above the dissociation limit. It is also shown that if

$$e^{-t_{inc}/\tau} \lesssim k_0\tau(4D'/5kT - 3)(5/2 + x_0)/e$$

a local minimum and maximum are predicted for measured density gradients in shock tube dissociations of diatomic molecules, where $t_{inc}$ is the incubation time, $D'$ the effective dissociation energy, and $x_0$ the mole fraction of dissociating molecules in an inert diluent. Expressions are given for extracting incubation times and rate constants from such studies when $x_0 \lesssim 0.3$. Analysis of experimental data actually showing such phenomena (J. Chem Phys. **55**, 4017 (1971)) is carried out. There are indications that any analysis which does not explicitly account for transient effects could result in errors in measured $k_0$'s of factors of 2 or more.

---

HESHEL TEITELBAUM. Can. J. Chem. **60**, 2927 (1982).

Une analyse semi-empirique basée sur la loi de vitesse de relaxation vibrationnelle des oscillateurs harmoniques simples de dissociation permet d'étudier en détail les mesures des temps de relaxation vibrationnelle $\tau$ et les coefficients $k_0$ de vitesse de dissociation stationnaire. On montre que le non-équilibre des populations des niveaux d'énergie vibrationnelle empêche d'atteindre l'énergie d'équilibre thermodynamiquement attendue. Même dans des conditions douces et presqu'isothermiques $\tau \ll 1/k_0$ il en résulte des erreurs expérimentales importantes quand on utilise la loi de vitesse de relaxation de Bethe–Teller. On donne des formes d'expressions rapprochées qui permettent d'évaluer ces erreurs. Les mesures doivent être analysées en utilisant la loi:

$$-d\varepsilon/dt = (\varepsilon - \varepsilon_T)/\tau + k_d(\varepsilon_* + h\nu - \varepsilon)$$

où $\varepsilon$ est l'énergie vibrationnelle par molécule, $\tau$ le temps de relaxation, $k_d$ le coefficient de vitesse de non-équilibre, $\varepsilon_T$ l'énergie vibrationnelle attendue thermodynamiquement à la température $T$ et $(\varepsilon_* + h\nu)$ l'énergie juste au-dessus de la limite de dissociation. On montre également que si

$$e^{-t_{inc}/\tau} \lesssim k_0\tau(4D'/5kT - 3)(5/2 + x_0)/e$$

on peut prévoir un minimum et un maximum locaux pour les gradients de densité mesurés lors des dissociations des molécules diatomiques dans des tubes blindés, où $t_{inc}$ est le temps d'incubation, $D'$ l'énergie effective de dissociation et $x_0$ la fraction molaire des molécules se dissociant dans un solvant inerte. On donne les expressions qui permettent de déduire les temps d'incubation et les constantes de vitesse à partir de telles études lorsque $x_0 \lesssim 0.3$. On effectue une analyse des données expérimentales qui montrent actuellement un tel phénomène (J. Chem. Phys. **55**, 4017 (1971)). Il y a des indications à l'effet que toute analyse qui ne tient pas explicitement compte des effets transitoires peut conduire à des facteurs d'erreurs de 2 ou plus sur les mesures de $k_0$.

[Traduit par le journal]

## Introduction

Recent theoretical studies of unimolecular reactions at the low pressure limit have shown that the dissociation process creates a non-equilibrium distribution of vibrational energy level populations (1–4), and that this is a major reason why measured rate coefficients are smaller than the rate constants predicted by theories assuming strong collisions, e.g., RRKM. In principle this non-equilibrium distribution can influence the vibrational relaxation process itself even for diatomic molecules. Expressions for the steady-state rate coefficient, transient rate coefficient, and incubation time have been obtained for cases where the density of vibrational energy levels were high (1, 2, 4), and numerical calculations done for diatomics (3, 5). Here we focus on obtaining an analytical expression for the vibrational relaxation time under conditions of non-equilibrium dissociation, particularly for diatomic molecules.

0008-4042/82/232927-16$01.00/0

©1982 National Research Council of Canada/Conseil national de recherches du Canada

Can. J. Chem. Downloaded from www.nrcresearchpress.com by 210.87.254.105 on 09/06/12
For personal use only.

**Rate law for vibrational energy**

We extend the Bethe–Teller model (6) which leads to the familiar rate law, valid only for non-dissociating molecules.

$$[1] \qquad -d\varepsilon/dt = (\varepsilon - \varepsilon_T)/\tau$$

Here $\varepsilon$ is the vibrational energy per molecule, and $\varepsilon_T$ is its value at thermal equilibrium at translational temperature $T$. We use the same model because of its success in predicting the observed rate law (7, 8) for the relaxation of vibrational energy when dissociation is not important. This model allows for single quantum transitions between vibrational levels of a harmonic oscillator effected by T–V energy transfer processes. The relaxing molecule may collide with itself or with an inert diluent. We ignore V–V energy transfer processes because they are resonant and will not affect the vibrational energy of harmonic oscillators. In order to represent the dissociation process somewhat realistically we truncate the harmonic oscillator potential at vibrational level $v_*$ just below the dissociation limit. If $N_v$ is the number of molecules in level $v$, the master equation is

$$[2] \qquad \frac{-dN_v}{dt} = k_{v,v+1}N_v + k_{v,v-1}N_v - k_{v-1,v}N_{v-1} - k_{v+1,v}N_{v+1}$$

where $k_{v,v'}$ is the rate coefficient for the transition $v \rightarrow v'$. For single quantum transitions dissociation occurs by transitions from $v_*$ to the continuum with a rate coefficient $k_{v_*,\infty}$. When recombination is ignored, only 3 terms including $N_{v_*}k_{v_*,\infty}$ appear in the expression for $-dN_{v_*}/dt$. For $v = 0$

$$-dN_0/dt = k_{0,1}N_0 - k_{1,0}N_1$$

According to the standard procedure eq. [2] is multiplied by $v$, and a summation over all $v$ is carried out:

$$[3] \qquad -\frac{d}{dt}\sum_0^{v_*} vN_v = -\sum_0^{v_*-1} k_{v,v+1}N_v + \sum_1^{v_*} k_{v,v-1}N_v + v_*k_{v_*,\infty}N_{v_*}$$

Use of the Landau–Teller scaling law

$$[4] \qquad \begin{aligned} k_{v+1,v} &= (v+1)k_{1,0} \\ k_{v,v+1} &= (v+1)k_{0,1} \end{aligned}$$

and detailed balancing, with $\theta = h\nu/k$

$$[5] \qquad k_{0,1} = k_{1,0}\, e^{-\theta/T}$$

and the constraints

$$\sum_0^{v_*} N_v = N$$

$$\sum_0^{v_*} (v + 1/2)h\nu N_v = E$$

lead to

$$[6] \qquad \frac{-d}{dt}\left(\frac{E}{h\nu} - \frac{N}{2}\right) = (k_{10} - k_{01})\left(\frac{E}{h\nu} - \frac{N}{2}\right) - k_{0,1}(N - N_{v_*} - v_*N_{v_*}) + v_*N_{v_*}k_{v_*,\infty}$$

Here $\nu$ is the fundamental frequency, and $E$ is the total vibrational energy of the $N$ molecules. The vibrational energy $E_T$ of the original $N^0$ undissociated molecules is given by

$$[7] \qquad E_T = N^0h\nu\left(\frac{1}{2} + \frac{e^{-\theta/T}}{1 - e^{-\theta/T}}\right)$$

A direct summation of eq. [2] gives

$$\sum_0^{v_*} \frac{dN_v}{dt} = -k_{v_*,\infty}N_{v_*} = \frac{dN}{dt}$$

Can. J. Chem. Downloaded from www.nrcresearchpress.com by 210.87.254.105 on 09/06/12
For personal use only.

But the phenomenological rate coefficient $k_d$ is defined as

$$k_d = \frac{-dN/dt}{N}$$

Thus

[8] $$k_{v_*,\infty} N_{v_*} = k_d N$$

and eq. [6] becomes

[9] $$\frac{-dE}{dt} = k_{1,0}(1 - e^{-\theta/T}) \frac{(E - NE_T)}{N^0} + k_{0,1} N_{v_*}(v_* + 1)h\nu + (v_* + 1/2)Nk_d h\nu$$

The combination $k_{1,0}(1 - e^{-\theta/T})$ is symbolized $\tau^{-1}$, and it is this value which one normally tries to extract from experiments. The second term on the right hand side is a truncation effect. The third term accounts for the decreasing number of molecules due to dissociation. More appropriate to this study is an expression for the rate of change of the vibrational energy per undissociated molecule, $\varepsilon(= E/N)$.

$$d\varepsilon/dt = N^{-2}(N dE/dt - E dN/dt)$$

Thus, if $\varepsilon_T = E_T/N^0$ and $\varepsilon_* = (v_* + 1/2)h\nu$, and $\varepsilon_0 = (1/2)h\nu$, then

[10] $$-d\varepsilon/dt = \tau^{-1}(\varepsilon - \varepsilon_T) + h\nu(N_{v_*}/N)(v_* + 1)k_{0,1} + k_d(\varepsilon_* - \varepsilon)$$

This is the correct rate law for a dissociating harmonic oscillator. The second term on the right hand side is a truncation effect; the third term appears because of non-equilibrium depletion of the vibrational energy levels. It prevents $\varepsilon$ from reaching its thermodynamic value $\varepsilon_T$. However, the second and third terms on the right hand side are generally small during the relaxation process, and eq. [10] is usually not distinguishable from eq. [1]. Nevertheless, it is clear that when $d\varepsilon/dt = 0$ during steady-state dissociation $\varepsilon = \varepsilon^\infty \neq \varepsilon_T$, and that even during vibrational relaxation the effective or phenomenological relaxation time $\tau' \neq \tau$, where

[11] $$\tau' \equiv -(\varepsilon - \varepsilon_T)/(d\varepsilon/dt)$$

In order to evaluate $\tau'$ we must first integrate eq. [10]. Noting eq. [8] and extrapolating eqs. [4] to include the continuum so that $k_{v_*,\infty} = (v_* + 1)k_{0,1}$,

[12] $$-d\varepsilon/dt = \tau^{-1}(\varepsilon - \varepsilon_T) + k_d(\varepsilon_* + h\nu - \varepsilon)$$

$\varepsilon^\infty$ is given by setting $d\varepsilon/dt = 0$. Thus

[13] $$\varepsilon^\infty = (\varepsilon_T/\tau - k_0[\varepsilon_* + h\nu])/(1/\tau - k_0)$$

Noting that $k_0$ (the steady-state rate constant) $\ll 1/\tau$,

$$\varepsilon^\infty \simeq \varepsilon_T - h\nu(v_* + 3/2)k_0\tau$$

During the steady-state dissociation when $k_d = k_0$, the solution to eq. [12] is:

$$\varepsilon = \varepsilon^\infty + (\varepsilon^0 - \varepsilon^\infty) \exp(-t[1/\tau - k_0])$$

where $\varepsilon^0$ is the initial vibrational energy per molecule at $t = 0$. If $\tau'$ were defined as the slope of a log-plot of $(\varepsilon^\infty - \varepsilon)$ vs. $t$, then $\tau' \approx \tau(1 + k_0\tau)$. However, $\varepsilon^\infty$ is usually not measurable, and so the phenomenological definition [11] is used. Since $\varepsilon^\infty \neq \varepsilon_T$ and $d\varepsilon/dt \to 0$, $\tau'$ defined by eq. [11] actually approaches infinity as time increases into the dissociation regime. Usually relaxation times are not measured under such conditions. Nevertheless because of current interest (9) in measuring incubation times $t_{inc}$, we must account for this, since such measurements rely on the interplay between relaxation and dissociation phenomena. Furthermore, it is not uncommon to measure late-stage relaxation times at temperatures where both processes become evident during a single experiment (9, 10). The error can be quite serious under such conditions (Fig. 1). Then it is crucial to use the correct rate law [12].

In integrating eq. [12] we note one further complication: during the incubation period, $k_d$ is a strong function of time. Forst (4) has derived an expression for the time variation valid for times $> (t_{inc} - \tau)$:

$$1 - k_d/k_0 = \exp[-(t - t_{inc} + \tau)/\tau]$$

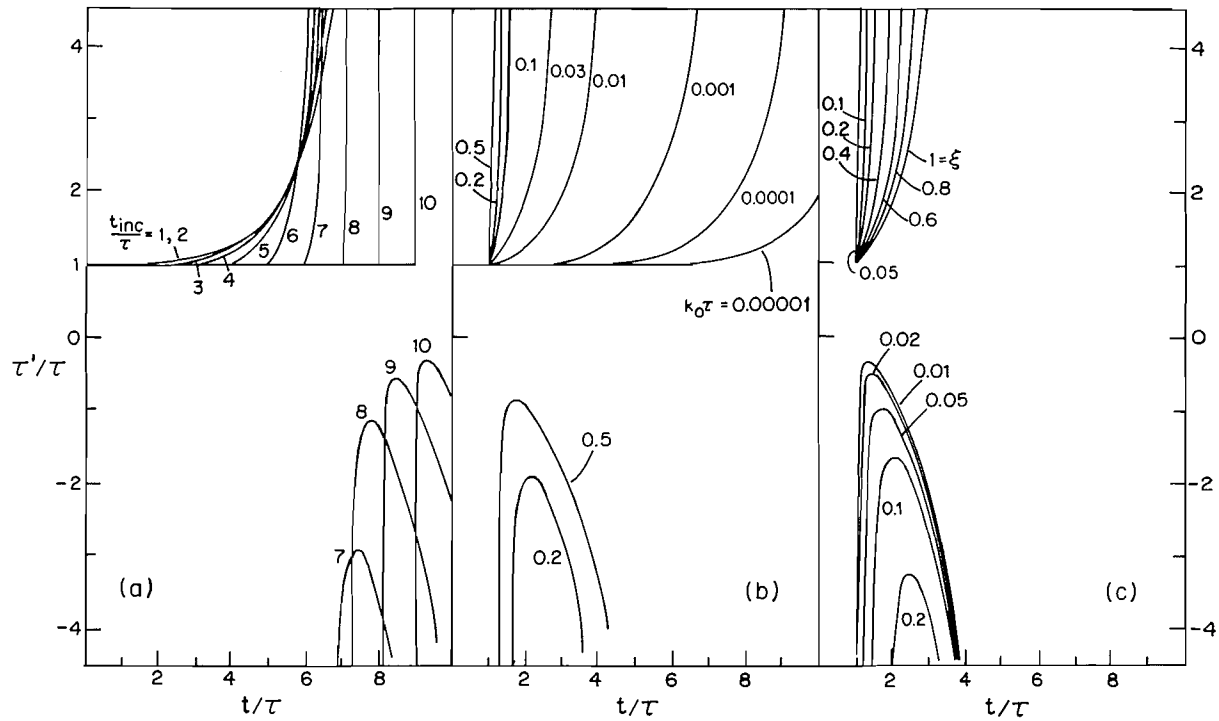


FIG. 1. Phenomenological isothermal relaxation times normalized by the simple harmonic oscillator time $k_{1,0}^{-1}(1-e^{-\theta/T})^{-1}$, as a function of reduced time, assuming no dissociation at $t \leq t_{inc} - \tau$; (*a*) dependence on incubation time; $k_0\tau = 0.001$; $\xi = 0.25$; (*b*) dependence on $k_0\tau$; $t_{inc}/\tau = 2$; $\xi = 0.25$; (*c*) dependence on $\xi = (\varepsilon_T - \varepsilon^0)/(\varepsilon_* + h\nu - \varepsilon_T)$; $t_{inc}/\tau = 2$; $k_0\tau = 0.1$. Note that if relaxation has proceeded sufficiently by $t = t_0$, then the vibrational energy overshoots its final value before equilibrating, during which time $\tau' < 0$.

where $t_{inc}$ is the incubation time necessary for the steady-state population of upper levels to evolve. At this point in time $k_d$ has reached within $e^{-1}$ of the steady dissociation constant, $k_0$. It is evident that $t_{inc}$ is larger than $\tau$, since $\tau$ is a measure of the time needed to redistribute energy among low vibrational levels only. (Figure 7 of ref. 11 shows a rare example of experiments where $\tau$, $t_{inc}$, and $k_0$ have all been measured. At low temperatures $\tau < t_{inc} \ll k_0^{-1}$.) At times earlier than $(t_{inc} - \tau)$ we set $k_d \simeq 0$. This approximation is not significant, since at early times $\tau' \approx \tau$ anyway, and at the times of interest eq. [14] is appropriate. Note that the transient behaviour of $k_d$ is determined by $t_{inc}/\tau$. At low temperatures $t_{inc} \gg \tau$, and the observed relaxation will be essentially complete before the incubation zone; however, at high temperatures when $t_{inc} \rightarrow 2$ to 4 times $\tau$, the incubation zone is one wherein a measurable portion of the relaxation takes place. Under near isothermal conditions the solution to eq. [12] is

$$[14] \qquad \frac{\varepsilon}{\varepsilon_T} = \frac{(\beta-1)k_0\tau(1-g\,e^{k_0\tau}) - (\beta k_0\tau - 1)f\,e^{k_0\tau} - \delta\,e^{-t_0/\tau}(1-k_0\tau)}{(1-k_0\tau)f e^{k_0\tau}}$$

where

$$\beta = (\varepsilon_* + h\nu)/\varepsilon_T$$

$$\delta = (\varepsilon_T - \varepsilon^0)/\varepsilon_T$$

$$t_0 = t_{inc} - \tau$$

$$f = u^{(k_0\tau - 1)}\,e^{-k_0\tau u}$$

$$u = e^{-(t-t_0)/\tau}$$

$$g = -(k_0\tau)^{-k_0\tau}[\gamma(k_0\tau, k_0\tau u) - \gamma(k_0\tau, k_0\tau)]$$

Can. J. Chem. Downloaded from www.nrcresearchpress.com by 210.87.254.105 on 09/06/12
For personal use only.

and $\gamma$ is the incomplete gamma function. With the use of eq. [12], the phenomenological relaxation time as defined by eq. [11] is given (for $\beta \neq 1$) by:

[15] $\tau'/\tau = \{1 - k_0\tau(1-u)(\varepsilon/\varepsilon_T - \beta)/(\varepsilon/\varepsilon_T - 1)\}^{-1}$

Figure 1 shows this relaxation time as a function of time. If measurements are made at times $\geq (t_{inc} - \tau)$, which are feasible especially when $t_{inc} \sim 2\tau$, then large errors can result. Note that the distortion to $\tau$ depends only on the parameters $k_0\tau$, $t_{inc}/\tau$, and $\xi = \delta/(\beta - 1) = (\varepsilon_T - \varepsilon^0)/(\varepsilon_* + h\nu - \varepsilon_T)$. The last parameter is the ratio of the maximum change in vibrational energy during the relaxation process to the excess energy of an average dissociating molecule. In principle these parameters are all determined by molecular properties and by temperature; however, since the theory of transient phenomena for diatomic molecules is not sufficiently developed to provide closed form expressions for $t_{inc}$ and $k_0\tau$, we treat the three parameters as independent. Distortion to $\tau'$ is largest at the highest temperatures when $k_0\tau \rightarrow 1$ and $t_{inc}/\tau \rightarrow 1$. In Fig. 1 we have evaluated $\tau'$ at times up to $10\tau$ or to the half-life for reaction ($k_0^{-1}$) whichever is smaller. Note that if relaxation has proceeded to such an extent at $t = t_0$ that $\varepsilon$ is already in excess of its final value $\varepsilon^\infty$, then the vibrational energy overshoots and the rate of relaxation becomes negative! This occurs when $1 - \delta\, e^{-t_0/\tau} > (1 - \beta k_0\tau)/(1 - k_0\tau)$. One further feature particularly noteworthy is the special case $\beta = 1$, for which $\varepsilon^\infty = \varepsilon_T$. Then $\tau'/\tau \rightarrow (1 - k_0\tau)^{-1}$.

## Incubation time measurements

Equally appropriate to such studies is an expression for the observable quantity in an experiment. The most sensitive technique to date for measuring vibrational relaxation times at high temperatures is shock tube densitometry. Here we obtain an expression for the rate of change of the gas temperature. In shock tube studies of relaxation–dissociation processes the temperature $T$ decreases monotonically, and this loss in thermal energy is taken up by the vibrational degree of freedom and by bond-breaking. The process occurs at constant pressure approximately, and the density is affected almost entirely by variations in the temperature and in the average molecular weight. The latter changes by the factor $(1 + \alpha x_0)$ where $x_0$ is the initial mole fraction of the dissociating molecule, and $\alpha$ is the degree of dissociation defined by $N = N^0(1 - \alpha)$. Thus we look for variation in the function $F = T(1 + \alpha x_0)$. In order to obtain $T$ we must solve an energy flux conservation equation involving the gas enthalpy $H$ and bulk flow kinetic energy. To a good approximation the shock process can be considered isenthalpic, so the temperature is determined by:

[16] $H = N_A(\bar{H}_A + \Delta_A) + N_B(\bar{H}_B + \Delta_B) + N_{AB}(\bar{H}_{AB} + \Delta_{AB}) + N_M\bar{H}_M = \text{constant}$

where $N_i$, $\bar{H}_i$, $\Delta_i$ are the number of moles, the molar heat content, and the molar heat of formation of species i respectively. M is an inert diluent (usually monatomic). In order to illustrate the phenomenon we have chosen the simple diatomic dissociation AB $\rightarrow$ A + B. It should be emphasized that for actual experiments the full solutions are routinely carried out (9, 10), but that we have made these reasonable approximations in order to eliminate flow variables yet retain the physics of the dissociation problem. The full solution does not significantly alter the result. Equation [16] becomes

$$[17]\quad x_0\alpha(\bar{H}_A + \bar{H}_B + D) + (1 - x_0)\bar{H}_M + (1 - \alpha)x_0\left[\int_0^T (\bar{C} - \bar{C}_v)_{AB}\,dT + \varepsilon\right] = (1 - x_0)\bar{H}_M(T_1) + x_0\left[\int_0^{T_1} (\bar{C} - \bar{C}_v)_{AB}\,dT + \varepsilon^0\right] = A$$

where $x_0 \equiv N_{AB}^0/(N_{AB}^0 + N_M)$, $D$ is the heat of reaction

[18] $D \approx \varepsilon_* + h\nu$

$T_1$ is the initial post-shock temperature, $T_0$ is the initial temperature, $\bar{C}_i$ is the molar heat capacity of species i, $\bar{C}$ is the total initial heat capacity, and $\bar{C}_v$ is the vibrational contribution to $\bar{C}$. Only AB vibrates and hence relaxes. Differentiation of eq. [17] with respect to gas-particle time and subsequent substitution of eqs. [12] and [18] lead to an expression for $dT/dt$ in terms of $d\alpha/dt$, $\bar{H}_i$, $\bar{C}_i$, and $\varepsilon$. The vibrational energy can be obtained from eq. [17] in terms of $\bar{H}_i$, $\bar{C}_i$, and $\alpha$. Thus

Can. J. Chem. Downloaded from www.nrcresearchpress.com by 210.87.254.105 on 09/06/12
For personal use only.

Can. J. Chem. Downloaded from www.nrcresearchpress.com by 210.87.254.105 on 09/06/12
For personal use only.

$$[19]\quad \frac{dT}{dt}\{\alpha x_0(\bar{C}_A + \bar{C}_B) + (1-x_0)\bar{C}_M + x_0(1-\alpha)(\bar{C} - \bar{C}_v)_{AB}\}$$
$$= \frac{d\alpha}{dt}\left\{\frac{1}{(1-\alpha)}\ [A - x_0\alpha(\bar{H}_A + \bar{H}_B + D) - (1-x_0)\bar{H}_M] - x_0(\bar{H}_A + \bar{H}_B + D)\right\}$$
$$- \frac{1}{\tau}\left[\alpha x_0(\bar{H}_A + \bar{H}_B - \bar{H}_{AB} + D) - \int_T^{T_1} \bar{C}\, dT - x_0\int_{T_1}^{T_0} \bar{C}_v\, dT\right]$$
$$+ k_d[Dx_0(1-\alpha) - A + x_0\alpha(\bar{H}_A + \bar{H}_B + D) + (1-x_0)\bar{H}_M]$$

The first term includes the effective heat capacity $\bar{C}$; the last term is the principal dissociation term which is constant at early times; the second term is a secondary dissociation term accounting for the disappearance of AB; the third term is the relaxation term which depends on $(T_1 - T)$ approximately. If the relaxation zone and dissociation zone are well separated, i.e. if $d[(1-\alpha)\varepsilon]/dt \approx (1-\alpha)d\varepsilon/dt$, then eq. [19] reduces approximately to the usual form

$$dT/dt \propto -x_0(\bar{H}_A + \bar{H}_B - \bar{H}_{AB} + D)d\alpha/dt - \bar{C}(T - T_e)/\tau$$

where $T_e$ is the temperature corresponding to thermal equilibrium prior to dissociation, were such a situation to occur: $\bar{C}(T_1 - T_e) = \bar{C}_v(T_1 - T_0)$. However, in the more general situation eq. [19] must be used. We can simplify it by noting the phenomenological definition of $k_d$, and of $\alpha$

$$[20]\quad d\alpha/dt = k_d(1-\alpha)$$

We treat $\bar{C}$ and $\bar{C}_v$ as essentially independent of temperature during reaction.

$$[21]\quad \bar{C}\, dT/dt \approx -k_d x_0(\bar{H}_A + \bar{H}_B)(1-\alpha) - \frac{1}{\tau}\{\bar{C}(T - T_1) + x_0\bar{C}_v(T_1 - T_0) + \alpha x_0(\bar{H}_A + \bar{H}_B - \bar{H}_{AB} + D)\}$$

where $\bar{H}_{AB}$ includes the true thermodynamic contribution of the vibrational energy at temperature $T$. The equation can be integrated numerically to obtain $T$ as a function of time, if one substitutes the Forst function for $k_d$ and the solution of eq. [20] for $\alpha$:

$$1 - \alpha = \exp[-k_0\tau(u - \ln u - 1)]$$

In this procedure we treat $k_0$, $\tau$, and $t_{inc}$ as being unaffected by the temperature changes. Note that $\xi$ depends on $\varepsilon_T$, $\varepsilon^0$, and $D$, i.e. on $T_1$, $T_0$, $D$, and $h\nu/kT$, basically. Thus aside from $k_0\tau$, $x_0$, $t_{inc}/\tau$, and $\xi$, a new parameter appears, $\theta/T = h\nu/kT$, which represents how classical the oscillator behaves. The observable

$$dF/dt = (1 + \alpha x_0)\, dT/dt + x_0 T\, d\alpha/dt$$

is shown in Fig. 2. Most notable is the pronounced minimum and subsequent maximum. This is to be expected, since $dT/dt$ depends on the rate of relaxation and the rate of dissociation. The former decreases as $\varepsilon^\infty$ is approached but the latter increases, after a delay time $t_0$, due to the dramatic increase in $k_d$. As the molecules begin to disappear all rates decrease. The position of the minimum and maximum can be found by setting $d^2F/dt^2$ to zero. We note that $(\bar{H}_A + \bar{H}_B - \bar{H}_{AB} + D) \equiv D' \approx D + kT/2 \simeq$ constant, at least with respect to the strongly varying $\alpha$. Thus

$$[22]\quad \bar{C}\, dT/dt = -Tf_1(t) - f_2(t)$$

where

$$f_1(t) = 5kx_0k_d(1-\alpha) + \bar{C}/\tau$$
$$f_2(t) = [x_0\bar{C}_v(T_1 - T_0) - \bar{C}T_1 + \alpha x_0(\bar{H}_A + \bar{H}_B - \bar{H}_{AB} + D)]/\tau$$

and $k$ is Boltzmann's constant. The temperature is a monotonically decreasing function of time with an initial decay constant $f_1/\bar{C}$. However, the observable depends on the rate of change of temperature, and the latter exhibits a minimum which is determined by the competition between decreasing $T$ and increasing $f_2$.

Under the most extreme conditions likely to be encountered in the laboratory $k_0\tau < 0.1$ (usually

Can. J. Chem. Downloaded from www.nrcresearchpress.com by 210.87.254.105 on 09/06/12
For personal use only.



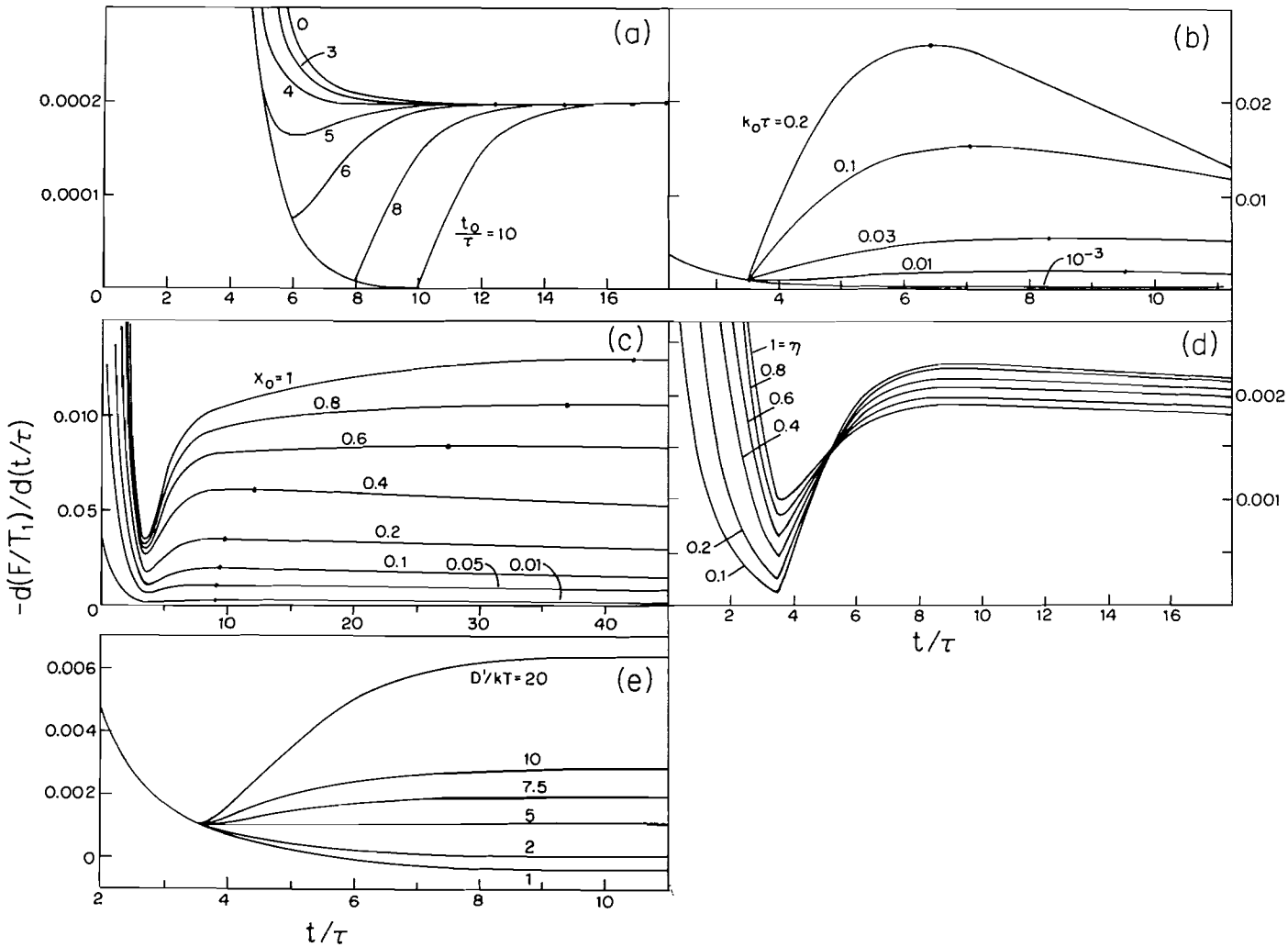


FIG. 2. Observed relaxation–dissociation rates (density gradient) as a function of reduced time. $d(F/T_1)/d(t/\tau) = (1 + \alpha x_0)d(T/T_1)/d(t/\tau) + x_0(T/T_1)d\alpha/d(t/\tau)$. Model assumes no dissociation prior to $t = t_0$. Products are each half as efficient as AB in dissociating AB. Figure shows influence of (*a*) dead time $t_0/\tau$; $k_0\tau = 0.001$; $x_0 = 0.1$; $\eta = 1.0$; $(1 - T_0/T_1) = 1.0$; $D/kT_1 = 7.5$. The extrema occur for $t_0/\tau \geq 3.9$; but the maxima are not very evident since dissociation proceeds on a time scale 1000 times longer than that for relaxation. They occur in the range $12.4 \rightarrow 18.8$ for $t_0/\tau = 4 \rightarrow 10$; (*b*) relative rates of dissociation and relaxation, $k_0\tau$. Here $t_0/\tau = 3.5$; $x_0 = 0.1$; $\eta = 1.0$; $(1 - T_0/T_1) = 1.0$; $D/kT_1 = 7.5$. The positions of the extrema are indicated by dots; (*c*) the mole fraction of dissociating gas, $x_0$. $k_0\tau = 0.01$; $t_0/\tau = 3.5$; $\eta = 1.0$; $(1 - T_0/T_1) = 1.0$; $D/kT_1 = 7.5$; (*d*) influence of closeness to classical oscillation, η; here $t_0/\tau = 3.5$; $x_0 = 0.1$; $k_0\tau = 0.01$; $(1 - T_0/T_1) = 1.0$; $D/kT_1 = 7.5$; (*e*) influence of bond strength $D/kT$. Here $t_0/\tau = 3.5$; $x_0 = 0.1$; $k_0\tau = 0.01$; $\eta = 1$; $(1 - T_0/T_1) = 1.0$. Note the change in sign at very high temperatures when molecular weight effects are more important than thermal effects.

$k_0\tau \ll 1$), and even if $t_{inc} \rightarrow \tau$ ($t_0 = t_{inc} - \tau \rightarrow 0$) under these circumstances, after one relaxation time beyond the dead-time ($t_0$), $\alpha$ is only 0.037. In order to obtain a simple expression for the position of the minimum, we set $\alpha \simeq k_0\tau(u - \ln u - 1)$ which is valid for $k_0\tau$ even as high as 0.3, and for $t < t_0 + 1.5\tau$. We can now integrate eq. [22] exactly:

$$[23] \quad \frac{dT}{dt} = -\frac{x_0\bar{C}_v}{\bar{\mathbb{C}}\tau}(T_1 - T_0)\,e^{-t/\tau_*} - \frac{x_0k_0}{(\bar{C} - \bar{\mathbb{C}})}[(5kT - D')\,e^{-v} - (5kT - D'\bar{\mathbb{C}}/\bar{C})\,e^{-\bar{C}_v/\bar{\mathbb{C}}}] - \frac{x_0k_0D'}{\bar{C}}$$

where $\tau_* = \tau(\bar{C} - \bar{C}_v)/\bar{C} \simeq \tau\bar{\mathbb{C}}/\bar{C}$ and $v = (t - t_0)/\tau$. The only further approximation made is that $k_0$, $\tau$, and $\bar{C}$ are not strongly time-dependent in the limited temperature range of a single dissociation experiment. We may now use eq. [23] to find the position of the minimum, given by $d(dF/dt)/dt = 0$, and $\alpha \simeq 0$:

$$[24] \quad \frac{d^2T}{dt^2} + 2x_0k_d\frac{dT}{dt} + x_0T\frac{dk_d}{dt} - x_0Tk_d^2 = 0$$

However, it is instructive to simplify eq. [23] for the special case $\bar{C} \simeq \bar{\mathbb{C}}$, i.e. for a dilute gas. Then

$$\frac{dT}{dt} = \begin{cases} -\dfrac{x_0\bar{C}_v}{\bar{\mathbb{C}}\tau}(T_1 - T_0)\,e^{-t/\tau} - \dfrac{x_0k_0D'(1 - e^{-v})}{\bar{\mathbb{C}}} & t \geq t_0 \\ -\dfrac{x_0\bar{C}_v}{\bar{\mathbb{C}}\tau}(T_1 - T_0)\,e^{-t/\tau} & t \leq t_0 \end{cases}$$

and we note that (*a*) $dT/dt \rightarrow -x_0k_0D'/\bar{\mathbb{C}}$ as expected for $t \gg \tau$, (*b*) the minimum occurs at exactly $t = t_0$, if (*c*) the relaxation has proceeded sufficiently by $t = t_0$ that

$$\bar{C}_v(T_1 - T_0)\,e^{-t_0/\tau_*} < k_0\tau_*D'$$

Were it not for the delay time, $dT/dt$ would vary monotonically with time, and not display a minimum.

For non-dilute gases the complete eq. [23] must be used. Since the time constant for decay of vibrational energy is slightly smaller than that for the growth of $k_d$, the true minimum will be at a time slightly beyond $t_0$, and the above criterion ought to be correspondingly modified. As written it is a conservative criterion. Equation [24] can be simplified with the use of eq. [23] and its derivative, to obtain an expression for $v = (t_{min} - t_0)/\tau$ at the minimum.

$$[25] \quad \frac{\bar{C}_v\bar{C}}{\bar{\mathbb{C}}^2\tau^2}(T_1 - T_0)\,e^{-t_0/\tau_*}\,e^{-\bar{C}_v/\bar{\mathbb{C}}} + \frac{k_0}{\tau}e^{-v}\left[\frac{5kT - D'}{\bar{C} - \bar{\mathbb{C}}} + T\right] - \frac{k_0}{\tau}e^{-\bar{C}_v/\bar{\mathbb{C}}}\frac{(5kT\bar{C}/\bar{\mathbb{C}} - D')}{(\bar{C} - \bar{\mathbb{C}})}$$
$$- (1 - e^{-v})^2k_0^2\left[\frac{T - 2x_0(5kT - D')}{\bar{C} - \bar{\mathbb{C}}}\right] - (1 - e^{-v})(1 - e^{-\bar{C}_v/\bar{\mathbb{C}}})2x_0k_0^2\frac{(5kT - D'\bar{\mathbb{C}}/\bar{C})}{(\bar{C} - \bar{\mathbb{C}})} = 0$$

An experimentalist would have to measure $k_0$, $\tau$, and $t_{min}$ (i.e. $v_{min}$), and then use eq. [25] to deduce $t_0$. However, since $k_0\tau \ll 1$, we may ignore terms in $(k_0\tau)^2$, and we obtain

$$[26] \quad \frac{t_{min}}{\tau} = \frac{t_0}{\tau} + \left(\frac{\bar{\mathbb{C}}}{\bar{C} - \bar{\mathbb{C}}}\right)\ln\left\{\frac{\bar{C}_v\bar{C}(T_1 - T_0)\,e^{-t_0/\tau_*}/\bar{\mathbb{C}}^2 - k_0\tau(5kT\bar{C}/\bar{\mathbb{C}} - D')/(\bar{C} - \bar{\mathbb{C}})}{-k_0\tau[(5kT - D')/(\bar{C} - \bar{\mathbb{C}}) + T]}\right\}$$

or $t_{min}/\tau = t_0/\tau$, whichever is greater. The latter is greater when

$$[5/2 + x_0(1 + \eta)]\eta(T_1 - T_0)\,e^{-t_0/\tau} < k_0\tau(25/4 - x_0^2)T$$

An accurate criterion for the existence of a minimum in $|dF/dt|$ is given by $d^2|dF/dt|/dt^2 > 0$. Thus, as long as

$$(5kT - D')/(\bar{C} - \bar{\mathbb{C}}) + T < 0$$

and

$$k_0\tau(5kT\bar{C}/\bar{\mathbb{C}} - D')\bar{\mathbb{C}}^2/(\bar{C} - \bar{\mathbb{C}}) < \bar{C}_v\bar{C}(T_1 - T_0)\,e^{-t_0/\tau_*}$$

then there will be a minimum; i.e. $kT$ must be less than $D'/(5 + x_0\eta)$ or $D'(\bar{\mathbb{C}}/5\bar{C})[1 - x_0\eta\bar{C}_v(1 - T_0/T_1)/(5\bar{\mathbb{C}}k_0\tau)e^{-t_0/\tau_*}]^{-1}$ whichever is more restrictive. Otherwise at high enough temperatures the effect of

Can. J. Chem. Downloaded from www.nrcresearchpress.com by 210.87.254.105 on 09/06/12
For personal use only.

changing mole number overcomes all thermal effects, and, as can be seen in Fig. 2*e*, the observable changes sign and simply decreases monotonically. Here we have used $\theta = h\nu/kT$, and $\eta = \bar{C}_v/k = (\theta/T)^2 \times e^{-\theta/T}(1 - e^{-\theta/T})^{-2}$ which is a measure of how classical an oscillator the molecule is. In obtaining these results we have set $\alpha \approx 0$, and therefore eq. [23] contains no information about the maximum, which occurs when the molecules begin to dissociate substantially. If this occurs so early that the observable has yet to decay to its expected minimum value, then no minimum (and subsequent maximum) will be observed. The condition for observing extrema is thus $t_{min} < t_{max}$. This will be discussed below.

The position of the maximum is determined primarily by the competition between an increasing $k_d$ and a decreasing $(1 - \alpha)$. The function $(1 - u)\exp[-k_0\tau(u - 1 - \ln u)]$ maximizes at a time $t_{max}$ given by

$$(t - t_0)/\tau = 2\ln(\{\sqrt{4 + 1/k_0\tau} + 1/\sqrt{k_0\tau}\}/2)$$

When $k_0\tau < 0.1$

$$(t - t_0)/\tau \approx -\ln k_0\tau > 2.3$$

At $t_{max}$

$$k_d \approx k_0(1 - k_0\tau) \approx k_0$$

and the corresponding $\alpha$ is only 0.131 or less. Thus in order to obtain a simple expression for $T(t)$ for use in eq. [24] we set

$$5kx_0k_d(1 - \alpha) \simeq 5kx_0k_0$$

and

$$\alpha \simeq 1 - \exp[-k_0(t - t_{inc})]$$

i.e.

$$u - 1 - \ln u \approx -1 - \ln u$$

and we solve eq. [22]. The temperature in the region of the maximum is given by:

$$[27]\quad T = T_1(\bar{C}/\bar{C}') - x_0(\bar{C}_v/\bar{C}')(T_1 - T_0)[1 - (\bar{C}'/\bar{C})\,e^{-(t-t_{inc})/\tau_{\neq}}\,e^{-t_{inc}/\tau_*}] + (1 - \bar{C}/\bar{C}')T_e\,e^{-(t-t_{inc})/\tau_{\neq}} - \frac{D'x_0}{\bar{C}'}\left[1 - \frac{e^{-k_0(t-t_{inc})}}{1 - k_0\tau_{\neq}} + \frac{k_0\tau_{\neq}}{1 - k_0\tau_{\neq}}\,e^{-(t-t_{inc})/\tau_*}\right] - x_0(k_0\tau/\bar{C})[(5kT_2 - D'\bar{\mathcal{C}}/\bar{C})(1 - 1/e) + D'/e]\,e^{-(t-t_{inc})/\tau_*}$$

where $\tau_{\neq} = \tau\bar{\mathcal{C}}/(\bar{C} + 5kx_0k_0\tau) \equiv \tau\bar{\mathcal{C}}/\bar{C}'$, and where we have used the boundary condition that at $t = t_{inc}$ (where $\alpha$ is still $\approx 0$) the temperature $T_2$ is given by the integral of eq. [23]. It was assumed that $T$ does not vary by more than 10%, so that factors involving $5kT$ could be considered constant. The maximum is found by setting $d^2F/dt^2 = 0$. This leads to the transcendental equation in $y$:

$$[28]\quad \frac{D'}{\bar{C}'T}\left(\frac{1}{1 - k_0\tau\bar{\mathcal{C}}/\bar{C}'}\right)\left\{k_0\tau - \frac{\bar{C}'}{\bar{\mathcal{C}}}e^{-\bar{C}'y/\bar{\mathcal{C}} + k_0\tau y} - 2x_0k_0\tau[1 - e^{-(y+1)}](e^{-k_0\tau y} - e^{-\bar{C}'y/\bar{\mathcal{C}}})\right\} + \frac{5k}{\bar{\mathcal{C}}}e^{-\bar{C}'y/\bar{\mathcal{C}}}\left\{\frac{\bar{C}'}{\bar{\mathcal{C}}}e^{k_0\tau y} - 2x_0k_0\tau[1 - e^{-(y+1)}]\right\} + e^{-(y+1)} - k_0\tau[1 - e^{-(y+1)}]^2 + e^{-\bar{C}'y/\bar{\mathcal{C}}}\,e^{k_0\tau y}\frac{\bar{C}}{\bar{\mathcal{C}}}\left\{\frac{\bar{C}_v\bar{C}'^2}{\bar{\mathcal{C}}\bar{C}^2}\left(1 - \frac{T_0}{T_1}\right)e^{-t_{inc}/\tau_*}\frac{1}{k_0\tau} - \frac{1}{e}\left[\left(\frac{5k}{\bar{\mathcal{C}}} - \frac{D'}{\bar{C}T}\right)(e - 1) + \frac{D'}{\bar{\mathcal{C}}T}\right]\right\} = 0$$

where $y = (t_{max} - t_{inc})/\tau$, and where we have made the approximations

$$(1 + \alpha x_0) \simeq 1; \quad T_1 \approx T_2 \approx T_e \approx T; \quad (1 - \alpha) \simeq e^{-k_0\tau y}$$

as before; and

$$x_0k_0\tau[1 - e^{-(1+y)}]\,e^{-k_0\tau y} \ll 1$$

Can. J. Chem. Downloaded from www.nrcresearchpress.com by 210.87.254.105 on 09/06/12
For personal use only.

which is true since $k_0\tau \ll 1$. The above equation can be simplified by setting $k_0\tau \ll 1$, i.e. $\bar{C}' \simeq \bar{C}$. We also note that $k_0\tau y$ can never be more than $\sim e^{-2}$. A glance at Fig. 2 confirms that $y > 1.3$, so that

$$e^{-(y+1)} \ll e^{-k_0\tau y}$$

Further simplification depends on how large $y$ is. If

$$2x_0k_0\tau\, e^{-k_0\tau y} \ll e^{-y}$$

i.e. if $y$ is at its lower limit $\sim 0$.

$$[29] \quad k_0\tau\, e^{\bar{C}y/\bar{\mathbb{C}}} \approx \frac{\dfrac{\bar{C}}{\bar{\mathbb{C}}}\left\{\dfrac{D'}{T}\left(\dfrac{1}{\bar{C}}+\dfrac{1}{\bar{\mathbb{C}}}\right)-\left(\dfrac{5k}{\bar{\mathbb{C}}}+1\right)-\dfrac{\bar{C}_v}{\bar{\mathbb{C}}}\dfrac{(1-T_0/T_1)}{k_0\tau}\,e^{-t_0/\tau_*}\right\}}{e[(1-2x_0)D'/\bar{C}T-1]}$$

The value of $y$ obtained from this expression is indeed small enough when

$$x_0 < \frac{(2D'/5kT-1)}{\left[\dfrac{2D'}{5kT}\left(\dfrac{2}{e}+1\right)-\dfrac{3}{e}\right]2}$$

In the allowed range of $D'/kT$, this particular value of $x_0$ ranges between 0.212 and 0.288. In obtaining this estimate we assumed that vibrational relaxation contributes little to the position of the maximum. The results of Fig. 2*c* are well predicted by eq. [29] in the mole fraction range < 0.3. Most experiments would in fact be carried out under such conditions. Nevertheless at higher mole fractions where

$$2x_0k_0\tau\, e^{-k_0\tau y} \gg e^{-y} \approx 0$$

eq. [28] reduces to

$$[30] \quad e^{k_0\tau y} \approx 2x_0D'/(D'-\bar{C}T)$$

Under the usual laboratory conditions of $k_0\tau < 0.1$, the dissociation rate constant is roughly within one tenth of its maximum value ($T = \infty$). Thus $D'/kT \gtrsim 2.3$. Actually, a maximum exists only if $D' \gtrsim 5kT$. Furthermore, if $\bar{C}T \ll D'$ then $k_0\tau \ll 1$ and eq. [30] approaches our rough estimate of $y \simeq -\ln k_0\tau$ very closely. Equation [30] overestimates the actual position of the maximum in Fig. 2*c* by factors ranging up to 4. Under these extreme conditions our approximation that the temperature is roughly constant and $T_0 \simeq T_2 \simeq T_1 \simeq T$ breaks down seriously. For such cases numerical simulation of the experiment is necessary.

We are now in a position to evaluate the second criterion for the existence of extrema, namely $t_{min} < t_{max}$, particularly for $x_0 \lesssim 0.3$. Use of eqs. [26] and [29] lead to

$$\frac{t_{min}}{\tau} = \begin{cases} \dfrac{t_0}{\tau}, & \text{if } \dfrac{\eta(1-T_0/T_1)\,e^{-t_0/\tau}}{k_0\tau} < \dfrac{(25/4-x_0^2)}{5/2+x_0(1+\eta)} \quad [31a] \\ \left(\dfrac{\bar{\mathbb{C}}}{\bar{C}-\bar{\mathbb{C}}}\right)\ln\left\{\dfrac{\dfrac{\bar{C}_v\bar{C}}{\bar{\mathbb{C}}^2}(T_1-T_0)\,e^{-t_0/\tau}-k_0\tau\left(\dfrac{5kT\bar{C}/\bar{\mathbb{C}}-D'}{\bar{C}-\bar{\mathbb{C}}}\right)}{-k_0\tau\left(\dfrac{5kT-D'}{\bar{C}-\bar{\mathbb{C}}}+T\right)}\right\}+\dfrac{t_0}{\tau}, \\ \quad \text{if } \dfrac{(25/4-x_0^2)}{5/2+x_0(1+\eta)} < \dfrac{\eta(1-T_0/T_1)\,e^{-t_0/\tau}}{k_0\tau} < \left(\dfrac{4D'}{5kT}-3\right)(5/2+x_0) \quad [31b] \end{cases}$$

There are no extrema if

$$\eta\frac{(1-T_0/T_1)\,e^{-t_0/\tau}}{k_0\tau} > \left(\frac{4D'}{5kT}-3\right)(5/2+x_0)$$

The value of $(\eta/k_0\tau)(1-T_0/T_1)e^{-t_0/\tau}$ is indicative of the extent to which vibrational relaxation has proceeded by the time dissociation has effectively begun.

Can. J. Chem. Downloaded from www.nrcresearchpress.com by 210.87.254.105 on 09/06/12
For personal use only.

In interpreting the extrema for a particular experiment it is worth noting that the position of the minimum is very sensitive to the value of $t_0/\tau$. $t_0/\tau$ also affects the position of the maximum; but the maximum is relatively broad and harder to locate. Thus the following procedure is suggested: Identify $t_0$ with $t_{min}$ and check the condition in eq. [31*a*]. If satisfied, then $t_0 = t_{min}$; if not, then $t_0$ is determined from eq. [31*b*] using precise measurements of $t_{min}$, $\tau$, and $k_0$ from the same experiment. Alternatively, if the maximum is well defined and if $x_0 < 0.3$, then $t_0/\tau$ can be determined by solving eq. [29] noting that $y = (t_{max}/\tau - t_0/\tau - 1)$. Furthermore, when conditions permit $t_{min} = t_0$, then $y = (t_{max} - t_{min})/\tau - 1$, and a measure of $(t_{max} - t_{min})$ will give $y$ directly, from which $t_0/\tau$ can be extracted using eq. [29]. This is sometimes preferable to using the simple expression $t_{inc} = t_{min} + \tau$ in cases where an *absolute* measure of $t_{min}$ is less accurate than that of $(t_{max} - t_{min})$ (i.e. when technical difficulties of the shock tube method near the time origin prevail). Nevertheless, as will be discussed below, interpretation of the maximum presents some problems, and use of $t_{inc} = t_{min} + \tau$ may yet lead to the most reliable measurements of incubation times.

## Discussion

The phenomena described above have actually been observed in shock tube dissociations of $H_2$ and $O_2$, although they have been attributed to other effects. Breshears *et al.* (BBK) have observed a curious "dip" in their densitometric studies (10) and gave the plausible explanation that catalytic dissociation by atoms was responsible for the sudden increase in $dF/dt$. The conditions of those experiments were exactly those necessary to observe incubation phenomena (12), and the form of the dip is exactly as predicted by Fig. 2. Nevertheless BBK assumed that at the minimum

$$k_0 = x_0(1 - \alpha)k_{AB-AB} + (1 - x_0)k_{M-AB}$$

and that at the maximum

$$k_0 = x_0(1 - \alpha)k_{AB-AB} + (1 - x_0)k_{M-AB} + x_0\alpha k_{A-AB} + x_0\alpha k_{B-AB}$$

where $k_{i-AB}$ is the quasi-first order rate coefficient for dissociation of AB by i, and where M is the inert-collider. Furthermore, it was supposed that at the minimum, relaxation was essentially complete ($k_0 \ll 1/\tau$) and that $k_d = k_0$. Under such conditions, our analysis, starting with eq. [17], could be repeated setting $\varepsilon = \varepsilon_T$; or alternatively eq. [27] with $\tau \to 0$, $t_0 \to 0$ could be used directly, and one would obtain

$$[32] \qquad \frac{dF}{dt} = -\frac{k_0 x_0 D'}{\bar{C}}(1 - \alpha)\left[1 - \frac{\bar{C}T}{D'(1 + \alpha x_0)}\right]$$

which is essentially the expression used by BBK with $\alpha = 0$ at the minimum. The maximum is supposed to occur because $k_0$ might increase faster than $(1 - \alpha)$ decreases. To simplify the discussion we make A = B, or at least $k_{A-AB} = k_{B-AB}$, i.e. the efficiencies of the two atoms in dissociating AB are similar. The maximum $\alpha_m$ is found by setting the derivative of $k_0(1 - \alpha)$ to zero. The result is

$$[33] \qquad 2\alpha_m x_0 = \frac{(1 - x_0)\phi_M + 2x_0(1 - \phi)}{1 - 2\phi}$$

where $\phi_M = k_{M-AB}/k_{AB-AB}$ is the relative efficiency of M:AB, and $\phi = k_{A-AB}/k_{AB-AB}$ is that of A:AB. A realistic solution ($0 < \alpha_m < 1$) occurs only if $\phi > 1 + (1 - x_0)\phi_M/2x_0$. BBK found $\phi_M \approx 0.1$ and $\phi \approx 6$; thus a maximum is indeed possible. However, the value of $\alpha_m$ lies in the range 0.37 to 0.45 for the mole fraction range 0.05 to 1.0, i.e. the reaction is almost half over by the time $t = t_{max}$: in other words the maximum caused by the incubation phenomenon has long passed before atom catalysis becomes important. Had $\alpha_m$ been less than that predicted by the incubation phenomenon's analysis: ($\alpha \ll 0.13$) one could say for certain that atom catalysis data could be extracted, although a modified procedure (see below) would have to be followed. However, in the present situation one is left with some doubt: either the maximum is due to an increase in $k_0$ because of $\phi$, $\phi_M$ or else it is due to transient phenomena in the dissociation of AB. In the former case the transient phenomenon occurs as well, but the possibility exists that it is unobserved and hidden in the shock front. However, our analysis showed that unless

$$\eta(1 - T_0/T_1)\, e^{-t_0/\tau} > (4D'/5kT - 3)(5/2 + x_0)k_0\tau$$

Can. J. Chem. Downloaded from www.nrcresearchpress.com by 210.87.254.105 on 09/06/12
For personal use only.

Can. J. Chem. Downloaded from www.nrcresearchpress.com by 210.87.254.105 on 09/06/12
For personal use only.

and $D'/kT \lesssim (5 + x_0\eta)$, the transient phenomena *will* manifest themselves as local minima if both the relaxation zone and the dissociation zone are evident in the same experiment. The actual position of the minimum[1] determined by BBK was $t_{min}/\tau = 3.22$ (for a 10% $O_2$ mixture in argon at 5811 K) and 3.20 (for a 10% $O_2$ mixture in Kr at 4942 K) (10*a*). The corresponding reported values of $k_0\tau$ were 0.021 and 0.012 respectively. Thus, under BBK's conditions $D'/kT_e$ were 10.72 and 12.51 respectively, while $t_0/\tau$ were 3.22 and 2.98 respectively. The necessary criteria are satisfied, and we therefore believe that at least some of BBK's experiments are excellent for determining incubation times, but not necessarily $k_0$.

In order to evaluate the BBK data it is convenient to first obtain an expression for $dF/dt$ at the extrema, i.e. for $(1 + \alpha x_0)dT/dt + x_0 T k_d(1 - \alpha)$.

At $t = t_{min}$, $\alpha \simeq 0$. Substituting $t_{min} = t_0$ (eq. [31*a*]) into

$$k_d = k_0[1 - \exp(-[t_{min} - t_0]/\tau)]$$

we obtain

$$[34a] \quad \left|\frac{dF}{dt}\right|_{min} = \frac{-x_0\bar{C}_v(T_1 - T_0)\, e^{-t_0/\tau_*}}{\bar{\mathcal{C}}\tau} \quad \text{for case } (a)$$

For the other possibility in eq. [31*b*] we note that the argument of the logarithm is $\sim 1$. Thus to a very good approximation

$$\frac{t_{min}}{\tau} \simeq \frac{t_0}{\tau} + \frac{\bar{C}/\bar{\mathcal{C}}}{D'/kT - (5 + x_0\eta)}\left[\frac{\eta(1 - T_0/T_1)\, e^{-t_0/\tau}}{k_0\tau} - \frac{(25/4 - x_0^2)}{5/2 + x_0(1 + \eta)}\right]$$

Using eq. [23] for $dT/dt$ and eq. [31*b*] to simplify:

$$\left|\frac{dF}{dt}\right|_{min} = x_0 k_0 T\left\{\left(\frac{D'}{\bar{C}T} - 1\right) - \left(\frac{D'/kT - [5 + x_0\eta]}{5/2 + x_0[1 + \eta]}\right) e^{-(t_{min} - t_0)/\tau}\right\}$$

where the above approximate expression for $(t_{min} - t_0)$ can be used. Evidently the further $(t_{min} - t_0)/\tau$ is from 0, the closer $dF/dt$ approaches a pure equilibrium dissociation value $x_0 k_0 T(D'/\bar{C}T - 1)$, and the less of an error is involved by assuming $|dF/dt|_{min}$ is a measure of $k_0$, but the less distinct the minimum becomes until the situation is reached when no extrema occur. However, if $t_{min}$ is not too different from $t_0$, then the exponential can be expanded to two terms, and thus

$$[34b] \quad \left|\frac{dF}{dt}\right|_{min} \simeq \frac{x_0\eta T}{(5/2 + x_0)\tau}\left\{(1 - T_0/T_1)\, e^{-t_0/\tau_*} - \frac{x_0 k_0\tau(5/2 - x_0)}{5/2 + x_0[1 + \eta]}\right\}$$

Secondly

$$k_d = k_0\,(1 - e^{-[t_{min} - t_0]/\tau}) \simeq k_0(t_{min} - t_0)/\tau$$

Therefore at the minimum, the effective rate coefficient is

$$k_d \approx \frac{\bar{C}/\bar{\mathcal{C}}}{D'/kT - (5 + x_0\eta)}\left[\frac{\eta(1 - T_0/T_1)\, e^{-t_0/\tau_*}}{\tau} - \frac{k_0(25/4 - x_0^2)}{5/2 + x_0(1 + \eta)}\right] \quad \text{for case } (b)$$

Setting $\alpha = 0$ in eq. [32] it is easy to see that if one did not suspect transient phenomena to be involved, one would deduce the measured rate coefficient by dividing the observable at the minimum by $[x_0 D'/\bar{C}] \times [1 - \bar{C}T/D']$. Therefore BBK measured $(\bar{C}/\bar{\mathcal{C}})\,(\eta/\tau)\,[kT/(D' - \bar{C}T)]\, e^{-t_0/\tau}$ in case (*a*) or approximately so in case (*b*) when $x_0 < 0.3$, i.e. BBK measured a value ranging somewhere between $k_d$ and $\sim\tau^{-1}\, e^{-t_0/\tau}$, but not $k_0$ as supposed! The question remains why those studies were apparently so successful in measuring not only rate coefficients, but also their temperature dependence and mole fraction dependence.

We note that case (*a*) ($t_{min} = t_0$) applies to most of the BBK experiments. For those few experiments to which case (*b*) applies the value of the observable at the minimum is not very far from the value at the maximum; i.e. the "dip" is not very distinct. Later it will be shown that the maximum is a good measure of $k_0$; thus Fig. 2*a* confirms that errors are <20% in such cases. Thus we restrict our discussion in the following to case (*a*) which is the more problematical situation.

It is clear that since a linear mixture rule was found to be obeyed, it is actually $\tau^{-1}\, e^{-t_0/\tau_*}$ that obeys

[1]There is some uncertainty in location of the absolute time origin of shock wave arrival, and the reported $t_{min}$ should be considered a lower limit.

this rule, and the observed relative efficiency $\phi_M$ is for relaxation and not for dissociation! Furthermore an estimate of $t_0/\tau$ can be made from theoretical studies of Dove and Troe (11), and of Forst and Penner (4). They both find (albeit strictly for polyatomic molecules at the low pressure limit) that $Z[M]t_{iyj} = -D/\langle\Delta\varepsilon\rangle$ roughly, where $\langle\Delta\varepsilon\rangle$ is the average energy transferred per collision, $Z$ is the collision frequency, and [M] is the gas concentration. If we use this expression to get an estimate of $t_{inc}$ for diatomic molecules, and use the fact that $\langle\Delta\varepsilon\rangle$ for the harmonic oscillator model is just $-h\nu p_{10}$ (13), where $Z[M]p_{10} = k_{10}$ for the transition $v = 1 \rightarrow 0$, then $k_{10}t_{inc} \approx D/h\nu$. Also $(k_{10} - k_{01}) = 1/\tau$. Thus $t_{inc}/\tau \approx (D/h\nu)(1 - e^{-h\nu/kT})$. At the temperatures of interest here $h\nu \ll kT$; thus $t_{inc}/\tau \simeq D/kT$; and it is therefore not surprising that the BBK measurement $\simeq (ekT/D'\tau)\, e^{-t_{inc}/\tau}$ would give roughly the correct temperature dependence! Using the values of $k_0\tau$, $t_0/\tau$, $D'/kT$ cited above, the measured $(\bar{C}/\bar{\mathbb{C}})(\eta/\tau)[kT/(D' - \bar{C}T)]\, e^{-t_0/\tau}$ is $0.24k_0$ at 5811 K, and $0.44k_0$ at 4942 K. The differences between the BBK results and the $k_0$'s reported by other workers, at least for $O_2$/Ar, are explicable in terms of these factors. We therefore believe that at least some of the BBK results are fortuitous. Similar considerations may apply to $H_2$ (10*b*).

The position of the BBK maximum ($t_{max}/\tau = 6.0$ at 5811 K and 5.7 at 4942 K) using the corrected BBK values for $k_0\tau$ are very well predicted from our eq. [29]. Since $(t_{max} - t_{inc})/\tau = -\ln(k_0\tau/a)$, $k_d = k_0(1 - k_0\tau/ae)$ at the maximum, where $a$ is given by the right hand side of eq. [29], and is of the order of unity. Also

$$\alpha = 1 - \exp[-k_0\tau_*(-\ln\{k_0\tau/a\} + k_0\tau/ae)] \simeq 1 - (k_0\tau/a)^{k_0\tau\bar{\mathbb{C}}/\bar{C}}$$

Thus

$$[35] \qquad \left|\frac{dF}{dt}\right|_{max} = \frac{k_0x_0D'}{\bar{C}}\left(\frac{k_0\tau}{a}\right)^{k_0\tau\bar{\mathbb{C}}/\bar{C}}\left\{1 - \frac{\bar{C}T}{D'(1+\alpha x_0)}\left[1 - \frac{1}{e}\left(\frac{k_0\tau}{a}\right)^{\bar{\mathbb{C}}/\bar{C}}\right] + \psi\right\}$$

where

$$\psi \approx k_0\tau\left[\frac{\bar{\mathbb{C}}}{\bar{C}} - \frac{\bar{C}}{\bar{\mathbb{C}}ae} - \frac{1}{ae}\left(1 - \frac{5kT}{D'}\frac{\bar{C}}{\bar{\mathbb{C}}}\right) + \frac{\bar{C}_v}{\bar{\mathbb{C}}}\left(\frac{\bar{C}T}{D'}\right)\frac{(1 - T_0/T_1)\, e^{-t_{inc}/\tau_*}}{a}\right] \ll 1$$

i.e.

$$\left|\frac{dF}{dt}\right|_{max} \simeq -\frac{k_0x_0D'}{\bar{C}}\left(\frac{k_0\tau}{a}\right)^{k_0\tau\bar{\mathbb{C}}/\bar{C}}\left\{1 - \frac{\bar{C}T}{D'(1+\alpha x_0)}\right\}$$

which is the same as eq. [32] with $\alpha$ evaluated at $t_{max}$. Since the rate coefficient is very close to $k_0$ at the maximum, we can consider $t_{max}$ to be the origin for dissociation with the value of the measured rate coefficient equal to an adjusted $k_0$, i.e., $k_0(k_0\tau/a)^{k_0\tau_*} \approx k_0$. Thereafter, one may analyze the measurements according to eq. [32]. Alternatively, one may consider the measured rate coefficient to be exactly $k_0$ only if one interprets the maximum as corresponding to a time slightly beyond the time origin for dissociation. This delay time $\Delta t$ is given by $1 - \alpha = (k_0\tau/a)^{k_0\tau_*}$, i.e., $e^{-k_0\Delta\tau} = (k_0\tau/a)^{k_0\tau_*}$, or $\Delta t/\tau_* = \ln(a/k_0\tau)$. Since $k_0\tau < 0.1$, very little error is induced by assuming an equilibrium dissociation process starting with time zero at the maximum. Unfortunately BBK did not use the maximum as a measure of the uncatalyzed $k_0$. They assumed that it is efficient atoms which are responsible for the relatively large observable at the maximum. With this assumption

$$k_0 = k_{AB-AB}[x_0(1 - \alpha) + (1 - x_0)\phi_M + 2x_0\alpha\phi]$$

where $\alpha$ (at $t_{max}$) is supposedly given by eq. [33]. Then at $t_{max}$

$$k_{max} = k_{AB-AB}[x_0\phi + (1 - x_0)\phi_M/2]$$

and the corresponding observable is $(k_{AB-AB}x_0D'/\bar{C})\,[x_0\phi + (1 - x_0)\phi_M/2]^2/(1 - 2\phi)x_0$. For small inert species' efficiencies ($\phi_M \ll 1$, as observed), the expression becomes $(k_{AB-AB}x_0^2D'/\bar{C})\phi^2/(1 - 2\phi)$, as long as $x_0$ is not too small. Evidently the quantity $\phi^2/(1 - 2\phi)$ can be estimated by dividing the maximum observable by $k_{AB-AB}x_0^2D'/\bar{C}$ which is determined from the minimum. The minimum is supposedly $\approx (k_{AB-AB}x_0D'/\bar{C})\,[x_0 + (1 - x_0)\phi_M]$, but in actual fact this expression closely approximates the true value at the maximum, whereas $(dF/dt)_{min}$ is given in reality by eq. [34]. Thus BBK measured

$$\left(\frac{\bar{\mathbb{C}}}{\bar{C}}\right)(k_0\tau/\eta)\frac{(D' - \bar{C}T)}{kT}e^{t_0/\tau}[x_0 + (1 - x_0)\phi_M]/x_0$$

Can. J. Chem. Downloaded from www.nrcresearchpress.com by 210.87.254.105 on 09/06/12
For personal use only.

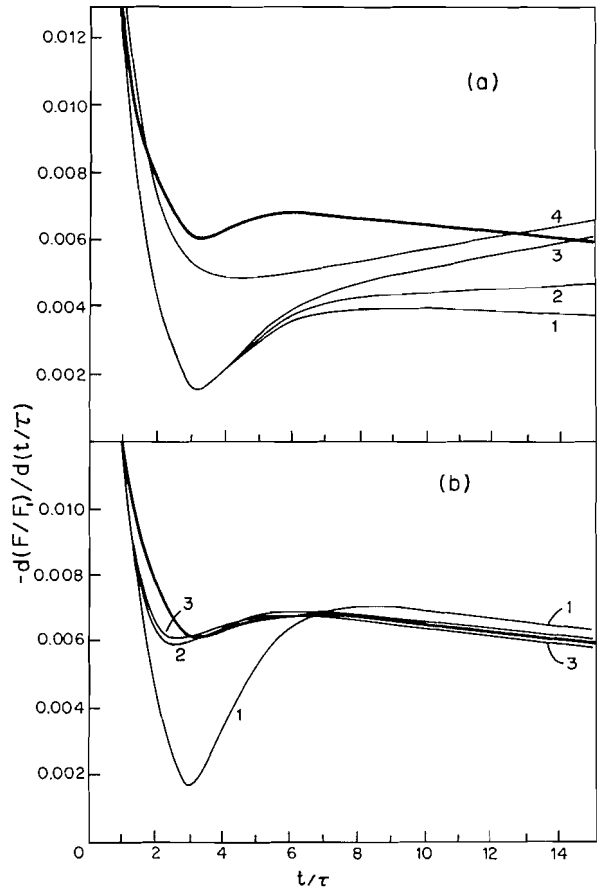


FIG. 3. Normalized density gradient as a function of reduced time for 10% $O_2$ in $K_r$ at 4942 K (= $T_e$). Thick lines are experimental results from Fig. 4 of ref. 10*a*, which has been converted from $d(\rho/\rho_0)/d(P\tau)$ to $-d(F/F_1)/d(t/\tau) = -d(F/T_1)/d(t/\tau)$ by multiplying by $P\tau/(\rho_1/\rho_0)$ under the approximation that $d\rho/\rho \simeq -dF/F$ (good to within 5% here). The gradient components due to vibrational relaxation match perfectly in scale, indicating a common time origin. $D/kT_1 = 11.6$. (*a*) Calculations with $k_0\tau = 0.012$ (as determined in ref. 10*a*) do not reproduce the dissociation portion of the gradient for any value of $t_0/\tau$ or $\phi$. Curve *1*: $t_0/\tau = 2.98$, $\phi = 0.5$ reproduces $t_{min}$, but the magnitude of the gradient and its subsequent decay rate are too small. Curves *1*, *2*, *3* show the effect of $\phi$. Curve *1*: $\phi = 0.5$; curve *2*: $\phi = 2.5$; curve *3*: $\phi = 5.0$. The maximum gradient is reproduced for $\phi = 4.5$, but $t_{max}$ is too large (28.0). Decreasing $t_0/\tau$ to 0 (curve *4*) does not decrease $t_{max}$ significantly. (*b*) Fit to experimental data using $k_0\tau \simeq 0.022$. Curve *1*: $\phi = 0.5$, $t_0/\tau = 2.98$, $k_0\tau = 0.022$. The maximum gradient and subsequent decay are reproduced exactly. Curve *2*: $\phi = 0.5$, $k_0\tau = 0.0213$, $t_0/\tau = 1.30$ additionally reproduces $t_{max}$ and the minimum gradient. Best fit (curve *3*) occurs for $t_0/\tau = 1.25$, $k_0\tau = 0.0217$, and $\phi$ in the range 0.05 to 0.55. Shown is $\phi = 0.05$. Thus the incubation time = 2.25 $\tau$.

For the conditions of ref. 10*a* (Figs. 3 and 4), this is 9.8 at 5811 K and 6.4 at 4942 K; and one inevitably extracts a large value for the relative atom efficiency regardless of what it really may be. (In Fig. 3 we estimate $\phi$ to be $0.30 \pm 0.25$ for one example.)

In summary, we have shown that the BBK experiments should not be interpreted in terms of atom catalysis, but rather in terms of non-equilibrium dissociation effects. It appears nevertheless that all the BBK results are fortuitously correct within a factor of 4. In view of the statement (10*b*) that had the maximum been used instead of the minimum in order to determine $k_{AB-AB}$ little change would have resulted, our conclusion is confirmed. Yet, it is not clear what the temperature and mole fraction dependence would be under those circumstances, nor at all clear what the atom efficiencies really are as a function of temperature.

In general when atom efficiencies play a role, the observed density gradient consists of a local minimum followed by an increase on a time scale $\sim\tau$ due to non-equilibrium effects. On a much longer time scale, the gradient would rise due to atom catalysis and then fall as the parent molecule disappears. Under rare circumstances with $k_0\tau \rightarrow 1$, atom catalysis might play a role in determining an early maximum.

Can. J. Chem. Downloaded from www.nrcresearchpress.com by 210.87.254.105 on 09/06/12
For personal use only.

This would necessitate reanalyzing the problem by replacing $k_0$ with $k_0\{1 + x_0\alpha(2\phi - 1)/[x_0 + (1 - x_0)\phi_M]\}$ which is a weak function of $\alpha$. Figure 3 shows $dF/dt$ obtained by solving eq. [21] with these changes for one example. Under the usual circumstances ($k_0\tau < 0.1$) $\phi$ has the effect of pushing the maximum out to times rather late in the dissociation. Although $\phi$ as large as 4.5 can predict the maximum gradient (using $k_0$ determined from the minimum gradient) $t_{max}$ is unsatisfactory (Fig. 3*a*). On the other hand, excellent agreement with experiment is obtained when the rate of dissociation is increased by almost doubling the uncatalyzed $k_0$, as suggested above, rather than introducing an unnecessarily large $\phi$. Even better agreement would result if the Forst function could be improved. Note, however, that a full analysis of such experiments is best done when the flow variables are included in the modelling.

Generally, if $\phi$ is smaller than the critical value, $[1 + (1 - x_0)\phi_M/2x_0]$, as it may be in the BBK studies, then a single early maximum appears which is interpreted entirely by non-equilibrium effects. Interpretation in terms of atom catalysis can lead to errors depending on the experimental conditions. Dissociation at the full equilibrium rate may be thought of as starting at a point in time just prior to the maximum. The value of the density gradient at the maximum leads to a very good estimate of initial dissociation rates. The location of the minimum and maximum are excellent measures of the incubation time for dissociation. The minimum in particular is valuable for this purpose because $t_{min} \simeq t_0$ even when atom catalysis is important, since it locates the point in time when the first molecules dissociate regardless of what species cause them to dissociate.

## Conclusion

We have used the truncated harmonic oscillator model to derive a rate law for the vibrational energy of a set of dissociating molecules. It shows that great care is needed when using the Bethe–Teller law as an approximation especially at high temperatures. Non-equilibrium effects such as the depletion of vibrational level populations cause overshoots of the vibrational energy, which does not reach its thermodynamically prescribed value. The resulting incubation time leads to measurable transient phenomena.

We have made a variety of approximations in order to show the relationship between observed local extrema and incubation times in dissociation experiments. The cumulative effect of all the approximations can be determined by comparing our analytical expressions [29] and [31] with the values of $t_{min}$ and $t_{max}$ in Fig. 2. In general the agreement is better than 5% for $x_0 < 0.3$. One can extend the range by solving the more exact transcendental equations [25] and [28] and by allowing the temperature to vary by more than a modest 10%. Further improvements to our analytical expressions require the inclusion of atom efficiencies and temperature-dependent $k_0$, $\tau$, $\eta$, $\bar{C}$, and $t_{inc}$. The use of the Forst function, valid only for $t > t_0$, introduced a discontinuity into our analysis. An improved function would smooth out Figs. 2 and 3 in the region of the minimum.

Although our analysis presents all possible values of the six parameters some are actually redundant: a given temperature automatically fixes $\eta$, $k_0$, $\tau$, $D/kT$, and $t_{inc}$ for a given molecule. Further advances in the theory of non-equilibrium dissociation of diatomic molecules should link the rate parameters and permit us *a priori* to evaluate the magnitude of the critical parameter $(\eta/k_0\tau)\, e^{-t_0/\tau}$ which determines whether a local minimum will appear in a given experiment or not. Work in this direction is now in progress. Whereas the present study indicates that the BBK experiments should be interpreted in terms of non-equilibrium kinetics, a definitive statement may have to await such theoretical advances. It is because of uncertainty concerning the participation of atoms in the dissociation that in the absence of theoretical advances one should use the local minimum (rather than the maximum) as a measure of incubation times, and the post-maximum rate of gradient decrease as a measure of the dissociation rate constant.

One major assumption explicitly made was that the molecular vibration in question could be treated as a harmonic oscillation. Clearly, molecules which dissociate cannot be well-described as harmonic oscillators. However, it must be emphasized that the present model is not used to calculate $k_0$, $\tau$, or $t_{inc}$ which are considered here to be experimentally determined. It is used to obtain an appropriate rate law for the relaxation of vibrational energy (eq. [12]) which *can* be well described in terms of harmonic oscillators. Modest corrections to the Bethe–Teller law account in a reasonable way for non-equilibrium effects. It may be argued that it is exactly these deviations which account for the whole experimental phenomena, and that it is therefore important that these deviations be treated accurately. Yet it is clear that no improvement in the relaxation model will change the conclusion that a local minimum occurs

Can. J. Chem. Downloaded from www.nrcresearchpress.com by 210.87.254.105 on 09/06/12
For personal use only.

roughly when dissociation precipitously begins, nor the conclusion that it is unwise to measure relaxation times even under relatively mild conditions such as $k_0\tau = 10^{-5}$ without accounting for the distortion to the equilibrium vibrational energy. Further work, now in progress, will determine the effect of anharmonicity.

Finally, the analysis presented here can be extended to include polyatomic molecules using the appropriate heat capacities and provided that the relaxation mechanism is known.

**Acknowledgements**

Support of the Natural Sciences and Engineering Research Council of Canada and discussions with J. E. Dove are gratefully acknowledged.

1. J. TROE. J. Chem. Phys. **66**, 4745 (1977).
2. D. C. TARDY and B. S. RABINOVITCH. Chem. Rev. 77, 369 (1977).
3. H. O. PRITCHARD. Acc. Chem. Res. **9**, 99 (1976).
4. W. FORST and A. P. PENNER. J. Chem. Phys. **72**, 1435 (1980).
5. D. G. TRUHLAR, N. C. BLAIS, J. C. J. HAJDUK, and J. H. KIEFER. Chem. Phys. Lett. **63**, 337 (1979).
6. (*a*) H. A. BETHE and E. TELLER. Ballistic Research Labs, Rept. X-117 (1941); (*b*) J. F. CLARKE and M. MCCHESNEY. The dynamics of real gases. Butterworths, London. 1964. p. 298.
7. R. W. LUTZ and J. H. KIEFER. Phys. Fluids, **9**, 1638 (1966).
8. J. E. DOVE and H. TEITELBAUM. Chem. Phys. **6**, 431 (1974).
9. J. E. DOVE, W. S. NIP, and H. TEITELBAUM. 15th Comb. Sym. 1974. p. 903.
10. (*a*) W. D. BRESHEARS, P. F. BIRD, and J. H. KIEFER. J. Chem. Phys. **55**, 4017 (1971); (*b*) W. D. BRESHEARS and P. F. BIRD. 14th Symposium (Internat.) on Combustion, The Combustion Institute, Pittsburgh. 1972. p. 211.
11. J. E. DOVE and J. TROE. Chem. Phys. **35**, 1 (1978).
12. H. TEITELBAUM. 14th Symposium (Internat.) on Combustion, The Combustion Institute, Pittsburgh. 1972. p. 217.
13. D. RAPP and T. KASSAL. Chem. Rev. **69**, 61 (1969).

Can. J. Chem. Downloaded from www.nrcresearchpress.com by 210.87.254.105 on 09/06/12
For personal use only.

# Alkaline oxidation of diastereoisomeric 4a,10a-dihydrofusarubins to norjavanicin, fusarubin, and a new antibiotic isofusarubin: nonenzymic formation of products in *Fusarium solani* cultures[1]

ARCHIBALD W. MCCULLOCH, A. GAVIN MCINNES,[2] AND DONALD G. SMITH

*Atlantic Research Laboratory, National Research Council of Canada, 1411 Oxford Street, Halifax, N.S., Canada B3H 3Z1*

AND

ITSUO KUROBANE[3] AND LEO C. VINING[2]

*Department of Biology, Dalhousie University, Halifax, N.S., Canada B3H 4J1*

Received June 2, 1982

Can. J. Chem. Downloaded from www.nrcresearchpress.com by 210.87.254.6 on 09/06/12
For personal use only.

ARCHIBALD W. MCCULLOCH, A. GAVIN MCINNES, DONALD G. SMITH, ITSUO KUROBANE, and LEO C. VINING. Can. J. Chem. **60**, 2943 (1982).

Conversion of two diastereoisomeric 4a,10a-dihydrofusarubins, produced by *Fusarium solani*, to fusarubin, norjavanicin, and a new compound, isofusarubin ((*E*)-6,7-dihydro-5,8-dihydroxy-2-methoxy-6-methylene-7-(2-oxopropylidene)-1,4-naphthalenedione), has been studied under a variety of culture conditions and in alkaline solution. Antibiotic and phototoxic activities of these compounds were determined and the structures of isofusarubin and of anhydroisofusarubin mono- and diacetates were elucidated by $^1H$ and $^{13}C$ nmr.

ARCHIBALD W. MCCULLOCH, A. GAVIN MCINNES, DONALD G. SMITH, ITSUO KUROBANE et LEO C. VINING. Can. J. Chem. **60**, 2943 (1982).

Utilisant plusieurs conditions différentes de culture en solution basique, on a étudié la transformation de deux dihydrofusarubines diastéréoisomères 4a,10a, produites par la *Fusarium solani* en fusarubine, en nojavanicine et en un nouveau composé la (*E*) dihydro-6,7 dihydroxy-5,8 méthoxy-2 méthylène-6 (oxo-2 propylidène)-7 naphtalènedione-1,4) isofusarubine. On a déterminé les activités antibiotique et phototoxique de ces composés et on a établi les structures des mono et diacétates de l'isofusarubine et de l'anhydroisofusarubine en faisant appel à la rmn du $^1H$ et du $^{13}C$.

[Traduit par le journal]

## Introduction

We have recently reported (1) that fusarubin **2** (2–8) is formed by nonenzymic oxidation of the diastereoisomeric 4a,10a-dihydrofusarubins **1***a* and **1***b* in alkaline cultures of *Fusarium solani*. Fusarubin has been dehydrated to anhydrofusarubin **3** by heating in glacial acetic acid (9); hydration of **3** under acidic conditions (4), or on standing in contact with the atmosphere (9), yielded **2**. The related metabolites javanicin **4** (2, 3), norjavanicin **5** (9), and bostrycoidin **6** (10) have also been obtained from *Fusarium* species. In this communication we report the isolation and structure of a new antibiotic and phototoxic compound **7** which was obtained from **1** by alkaline oxidation and to which we have given the trivial name isofusarubin. We provide evidence that **5** is also formed by nonenzymic oxidation of **1** in alkaline solutions and cultures.

## Materials and methods

*Organisms*

*Fusarium solani* strain 199 was obtained from Professor P. E. Nelson, Department of Plant Physiology, Pennsylvania State University, University Park, PA 16802, U.S.A.

*Culture medium*

One litre of medium had the following composition: maltose, 20–60 g; ammonium tartrate, 4.6–9.2 g; $KH_2PO_4$, 1 g; $MgSO_4 \cdot 7H_2O$, 0.5 g; NaCl, 0.1 g; $CaCl_2$, 0.1 g; $FeSO_4 \cdot 7H_2O$, 0.01 g; $ZnSO_4 \cdot 7H_2O$, 8.8 mg; $CuSO_4 \cdot 5H_2O$, 0.4 mg; $MnSO_4$, 0.06 mg; $H_3BO_3$, 0.06 mg; $(NH_4)_6Mo_7O_{24} \cdot 4H_2O$, 0.04 mg.

*Cultivation*

Spores from cultures grown on potato-dextrose agar for 2 weeks at 25°C were suspended in sterile distilled water and filtered through a cotton plug. The optical density of the filtrate at 640 nm was adjusted to 0.25. Each 50 mL aliquot of culture medium in a 250 mL Erlenmeyer flask was inoculated with 2.5 mL of the spore suspension and then incubated at 25°C on a rotary shaker (3.8 cm eccentricity, 220 rpm) for 2 to 6 days.

*Isolation of metabolites*

The mycelium was removed by filtration and washed with water until free of pigment. The filtrate, adjusted to about pH 3 with 1 *N* HCl, was extracted with an equal volume of ethyl acetate. The extract was washed with water, concentrated *in vacuo*, and chromatographed on a column of silicic acid using benzene – ethyl acetate mixtures for elution. Compound **3** was eluted with a 12:1, **4**, **5**, and **6** with a 6:1, **1***a* and **2** with a 3:1, and **1***b* with a 2:1 mixture. The physical constants as well as the ir, uv, and $^1H$ nmr spectral data of these compounds were indistinguishable from those reported in the literature (1, 9, 10, 11).

*Alkaline oxidation of* **1**a *and* **1**b

In preliminary experiments solutions of **1***a* and **1***b* in 0.1 *N* NaOH were sampled periodically and the formation of products was monitored by tlc. This established the following optimum conditions for producing **7**. Samples of **1***a* (708 mg) and **1***b*

[1]Issued as NRCC No. 20579.

[2]To whom correspondence should be directed.

[3]Present address: Hoechst Japan Ltd., Tokyo, Japan.

0008-4042/82/232943-07$01.00/0

©1982 National Research Council of Canada/Conseil national de recherches du Canada

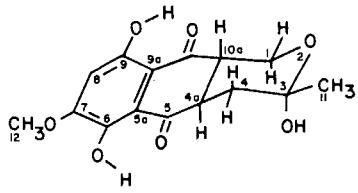

1a

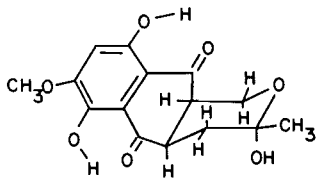

1b

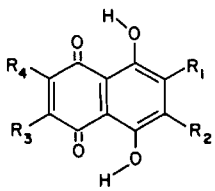

2 $R_1 + R_2 = CH_2OC(CH_3)(OH)CH_2$; $R_3 = OCH_3$; $R_4 = H$
3 $R_1 + R_2 = CH_2OC(CH_3)=CH$; $R_3 = OCH_3$; $R_4 = H$
4 $R_1 = CH_3$; $R_2 = CH_2COCH_3$; $R_3 = OCH_3$; $R_4 = H$
5 $R_1 = H$; $R_2 = CH_2COCH_3$; $R_3 = OCH_3$; $R_4 = H$
6 $R_1 = H$; $R_2 = OCH_3$; $R_3 + R_4 = CH=C(CH_3)N=CH$

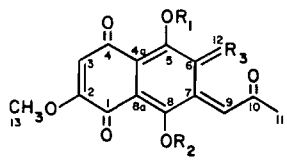

7 $R_1 = R_2 = H$; $R_3 = H_1, CH_2OH$
8 $R_1 = COCH_3$; $R_2 = H$; $R_3 = CH_2$
9 $R_1 = R_2 = COCH_3$; $R_3 = CH_2$

(168 mg) dissolved in 100 and 25 mL, respectively, of 0.1 *N* NaOH were aerated by stirring for 5 minutes at room temperature. After acidification with 0.2 *N* HCl the solutions were extracted with ethyl acetate. The extracts were washed with water, concentrated *in vacuo*, and chromatographed on columns of silicic acid. Reaction products **2** and **5** were eluted with the benzene – ethyl acetate mixtures already described above, whereas a 3:2 mixture gave isofusarubin **7**, mp 157–158°C (dark red prisms from ethanol); $[\alpha]_D^{20}$ +224 (*c* 0.051, acetone); $\lambda_{max}$ (95% ethanol): 224, 296, 475, 500, and 536 nm (log ε: 4.41, 3.93, 3.83, 3.85, and 3.64); $\nu_{max}$ (KBr): 3485, 3400, 1708, and 1595 $cm^{-1}$; $M^+$ at *m/e* 306.0752 (calcd. for $C_{15}H_{14}O_7$ 306.07396).

Acetylation of **7** with acetic anhydride in pyridine for 3 h at room temperature, and evaporation under reduced pressure, gave a brown gummy residue. Preparative tlc of this material on 2 mm thick Merck silica gel F254 precoated plates using ethyl acetate as developer gave a major band which on extraction with $CHCl_3$ gave anhydroisofusarubin monoacetate **8** in 47% yield, mp 168–172°C (bright yellow rosettes from ethyl acetate – petroleum ether or ethanol); $\nu_{max}$ (KBr): 3450, 1770, 1685, 1644, and 1613 $cm^{-1}$; $M^+$ at *m/e* 330.0725 (calcd. for $C_{17}H_{14}O_7$: 330.07396). In contrast, direct extraction of the gummy residue with $CHCl_3$ gave anhydroisofusarubin diacetate **9** in 80% yield, mp 133–134°C (yellow needles from 3:1 $CHCl_3$–hexane); $\lambda_{max}$ (95% ethanol): 220 and 226 nm (log ε: 4.37 and 4.36); $\nu_{max}$ (KBr): 1760 and 1618 $cm^{-1}$; $M^+$ at *m/e* 372.

*Nuclear magnetic resonance spectra*

Spectra were recorded in $CDCl_3$ solution (5 mm tubes) with TMS as internal reference. The $^1H$ nmr spectra of **7** and **9** at 100 MHz were obtained on a Varian HA-100D continuous-wave spectrometer, using the TMS signal for internal lock. The $^{13}C$ nmr spectra of **7** and **9** were recorded at 25.16 MHz with a Varian XL-100/15 Fourier transform spectrometer under the following conditions: sweep width (SW) 6016 Hz, acquisition time (AT) 1.6 s (data accuracy ±0.3 Hz), flip angle (FA) 35°, internal $^2H$ lock to solvent, temperature 29°C, $^1H$ irradiation at 100 MHz, (a) $\gamma H_2/2\pi \sim 3800$ Hz, broadband by 0 to 180° phase modulation at 150 Hz, or (b), as for (a), but irradiating only for 1.6 s between data acquisition periods to provide high resolution (HR) spectra with retained nOe.

The $^1H$ (80 MHz) and $^{13}C$ (20 MHz) nmr spectra of **7** and **8** were recorded on a Varian FT-80A spectrometer with internal $^2H$ lock to the solvent and a temperature of 35°C. Conditions for the $^1H$ spectra were SW 1000 Hz, AT 4.1 s (data accuracy ±0.1 Hz), FA 90°. The solution of **8** was degassed prior to nOe measurements. The $^{13}C$ spectra were acquired with SW 4132 Hz (**8**), 4505 Hz (**7**), AT 0.99, 0.91 or 1.98, 1.82 (data accuracy ±0.5 or ±0.3 Hz), FA 23° or 45°, $^1H$ irradiation at 80 Hz, (a) $\gamma H_2/2\pi \sim$ 4000 Hz, modulation bandwidth 2000 Hz (broadband decoupling), (b) as for (a) but irradiating for 2.0 s between data acquisitions only to retain nOe (HR spectra), and (c) as for (b) but with additional constant $^1H$ irradiation $\gamma H_2/2\pi$ 196 Hz at frequencies of individual $^1H$ resonances (single frequency decoupling with nOe retained at all resonances).

*Biological activity*

The method of Daniels (12) was used for the general assays with bacteria and yeasts, as described previously (13, 14). Duplicate cultures were incubated overnight after the discs containing 20 μg of compound were placed on them.

## Results

### *Production of 2, 5, and 7 from 1a and 1b*

Monitoring the reactions by tlc indicated that conversion of **1***a* and **1***b* to **2**, **5**, and **7** in 0.1 *N* NaOH at room temperature began immediately and

TABLE 1. Yields of **2**, **5**, and **7** produced from dihydrofusarubin in alkaline solution*

| | **1***a* | | **1***b* | |
|---|---|---|---|---|
| Compound | mg | % | mg | % |
| **2** | 331 | 46.8 | 89 | 53.0 |
| **5** | 70 | 9.8 | 47 | 28.6 |
| **7** | 274 | 38.7 | 21 | 12.5 |
| Total | 675 | 95.3 | 158 | 94.0 |

*Samples of **1***a* (708 mg) and **1***b* (168 mg) were dissolved in 0.1 *N* NaOH and the stirred solutions kept at room temperature for 5 min. Products were isolated as described in Materials and methods and crystallized once. Yields were calculated as a percentage by weight of the starting material. Value for **2** has been corrected for small amount of **3** produced during purification process.

Can. J. Chem. Downloaded from www.nrcresearchpress.com by 210.87.254.6 on 09/06/12
For personal use only.

TABLE 2. Antibiotic and phototoxic activities*

| | 1*a* | 1*b* | 2 | 3 | 4 | 5 | 6 | 7 |
|---|---|---|---|---|---|---|---|---|
| Yeast | | | | | | | | |
| *Candida albicans* | anti | anti | — | — | — | anti | anti | + |
| *Saccharomyces cerevisiae* | — | (anti) | anti | anti | — | (+) | NT | + |
| Gram positive bacteria | | | | | | | | |
| *Bacillus subtilis* | anti | anti | anti | anti | anti | anti | NT | anti |
| *Streptococcus faecalis* | anti | anti | anti | anti | anti | anti | NT | anti |
| *Streptomyces albus* | anti | anti | — | + | — | — | NT | — |
| Gram negative bacteria | | | | | | | | |
| *Escherichia coli* | — | — | — | — | — | — | NT | (anti) |
| *Proteus vulgaris* | — | (+) | — | — | — | — | NT | (+) |
| *Pseudomonas fluorescens* | — | — | — | — | — | — | NT | — |

*Assays were scored by the method of Towers *et al.* (13): + = phototoxic, — = inactive, ( ) = slightly active, anti = antibiotic, NT = not tested.

TABLE 3. $^1$H nuclear magnetic resonance data for isofusarubin (**7**), and the mono- and diacetate derivatives (**8**, **9**)*

| Compound | H-12 (t) | H-12 (g) | H-3 | H-6 | H-9 | H-13 | H-11 $CH_3CO_2$ | 5-OH | 8-OH | 12-OH |
|---|---|---|---|---|---|---|---|---|---|---|
| **7**† | 4.12 | 3.89 | 6.19(s) | 4.37 | 7.19(s) | 3.95(s) | 2.20(s) | 12.72(s), | 12.54(s) | 2.45(bs) |
| **8**‡ | 6.03(s), | 6.32(s) | 6.01(s) | | 7.21(d) | 3.86(s) | 2.38(s), 2.43(s) | | 10.71(d) | |
| **9** | 6.03(s), | 6.36(s) | 5.96(s) | | 7.28(s) | 3.85(s) | 2.32(s), 2.38(s), 2.42(s) | | | |

*Spectra were recorded (Varian HA-100-D (**7**, **9**) and FT-80A (**8**) spectrometers) in $C^2HCl_3$ with TMS as internal standard.
†H-12(t), H-12(g), and H-6 formed an ABC system in **7** (t = trans, g = gauche). Analysis of the system, with the Varian spin simulation program on a 620L computer, gave $J_{AB}$ 11.0, $J_{AC}$ 7.0, $J_{BC}$ 4.5 Hz. Signals for 5, 8, and 12-OH disappeared on addition of $^2H_2O$.
‡Signal for 8-OH in **8** disappeared on addition of $^2H_2O$ and that for H-9 (d, $^5J \sim 0.4$ Hz) became a singlet. The following nuclear Overhauser enhancements were observed (irradiated proton in parentheses): H-12, δ6.03 (H-12, δ6.32) 16%; H-3, H-9 (H-12, δ6.32) 0%; H-12's, H-3 (H-9) 0%.

was complete after 5 minutes. Yields at this time are given in Table 1. Over a 30 minute period **7** changed into many unidentified compounds and finally disappeared, whereas **5** was gradually degraded over 24 hours. On the other hand, **2** was relatively stable, with only a small amount being dehydrated to **3** over a 24 hour period.

*Production of* 1a, *1*b, *2, 4, 5, and 6 in cultures of* F. solani

Only **1***a*, **1***b*, and **4** were produced when the culture medium was rich in maltose (40 $gL^{-1}$ or above), irrespective of the ammonium tartrate concentration used (4.6–9.2 $gL^{-1}$). When maltose and ammonium tartrate were both low (20 and 4.6 $gL^{-1}$, respectively), **1***a*, **1***b*, and **4** could be isolated from a 2 day harvest and **2**, **4**, and **5** after 6 days. The production of metabolites was strongly inhibited when the medium was low in maltose (20 $gL^{-1}$) and high in ammonium tartrate (6.9–9.2 $gL^{-1}$), although some **2**, **4**, and **6** could be isolated after a 2 day interval.

*Antibiotic and phototoxic activities*

The results for **1***a* and **1***b*, their alkaline oxidation products, and related compounds isolated from *F. solani* are reported in Table 2. Compounds with phototoxic activity inhibit growth on exposure to uv irradiation only, whereas antibiotic activity is indicated if growth is inhibited in the dark also. The bioassay for **6** is incomplete because of lack of material.

## Discussion

*Structures of 7, 8, and 9*

The molecular formula $C_{15}H_{14}O_7$ obtained for **7** by accurate mass measurement is the same as that of **2** and the mass fragmentation patterns for the two compounds were similar. Thus **7** is formed, like **2** (1), by an autoxidation process involving the removal of a pair of hydrogens from **1***a* and **1***b*, the molecular skeleton probably remaining intact. Mass spectral measurements also indicated molecular formulae of $C_{17}H_{14}O_7$ for **8** and $C_{19}H_{16}O_8$ for **9**.

The characteristic singlet resonances obtained for methoxyl and quinone hydrogens in the $^1$H nmr spectra of **2**, **3** (9), and **4** (11) are also observed in the $^1$H nmr spectra of **7**, **8**, and **9** (see Table 3), suggesting that these three compounds contain the same substituted quinone ring system. Signals were present in the spectrum of **7** for an alcoholic and two phenolic hydroxyl hydrogens (chemical shifts temperature dependent and hydrogens exchangeable with deuterium), methyl hydrogens, an olefinic or aromatic hydrogen (δ 7.19), and hydroxymethyl hydrogens which are vicinally coupled to an aliphatic methine hydrogen. It was noteworthy

Can. J. Chem. Downloaded from www.nrcresearchpress.com by 210.87.254.6 on 09/06/12
For personal use only.

Can. J. Chem. Downloaded from www.nrcresearchpress.com by 210.87.254.6 on 09/06/12
For personal use only.





TABLE 4. $^{13}C$ nuclear magnetic resonance data ($\delta_C$ TMS; $^nJ_{CH}$, Hz) for isofusarubin (**7**), and the mono- and diacetate derivatives (**8**, **9**)*

| Compound | C-1 | C-2 | C-3 | C-4 | C-4a | C-5 | C-6 | C-7 | C-8 |
|---|---|---|---|---|---|---|---|---|---|
| **7** | 182.03(d)<br>$^3J$ 7.9 | 160.43(dq)<br>$^2J \sim {}^3J \sim 4.0$ | 110.01(d)<br>$^1J$ 164.4 | 187.02(m) | 109.85(m) | 156.52(ddd)<br>$^2J \sim 5$<br>$^3J \sim 5, 9$ | 53.31(m)<br>$^1J$ 130.7 | 135.98† | 156.52(ddd)<br>$^2J \sim 5$<br>$^3J \sim 5, 9$ |
| **8** | 185.00(d)<br>$^3J$ 8.1 | 159.05(dq)<br>$^2J \sim {}^3J \sim 3.9$ | 111.81(d)<br>$^1J$ 165.0 | 182.23(dd)<br>$^2J$ 1.2<br>$^5J$ 1.7 | 121.40(dd)<br>$^3J$ 5.4<br>$^5J$ 4.4 | 144.75(m) | 142.13(d)<br>$^3J$ 3.8 | 135.26(dd)<br>$^3J_t$ 10.6<br>$^3J_c$ 5.3 | 158.22(dd)<br>$^2J$ 4.7<br>$^3J$ 9.2 |
| **9** | 178.16(d)<br>$^3J$ 8.3 | 159.34(dq)<br>$^2J \sim {}^3J \sim 4.0$ | 110.28(d)<br>$^1J$ 165.3 | 182.51(dd)<br>$^2J$ 1.2<br>$^5J$ 1.7 | 123.94(dd)<br>$^3J$ 5.8<br>$^5J$ 4.7 | 144.05(m) | 146.89(d)<br>$^3J$ 4.5 | 139.77(dd)<br>$^3J_t$ 10.5<br>$^3J_c$ 5.4 | 145.45(d)<br>$^3J$ 9.3 |

| | C-8a | C-9 | C-10 | C-11 | C-12 | C-13 | $CH_3CO_2$ | $CH_3CO_2$ |
|---|---|---|---|---|---|---|---|---|
| **7** | 111.35(d)<br>$^3J$ 4.3 | 129.64(ddd)<br>$^1J$ 163.4<br>$^3J \sim {}^5J \sim 6.0$ | 206.98(dq)<br>$^2J \sim {}^2J \sim 6$ | 29.33(q)<br>$^1J$ 128.0 | 62.01(dt)<br>$^1J$ 146.5<br>$^2J$ 6.1 | 56.47(q)<br>$^1J$ 147.1 | | |
| **8** | 113.97(d)<br>$^3J$ 4.2 | 134.21(d)<br>$^1J$ 164.8 | 197.36† | 26.67(q)<br>$^1J$ 128.0 | 128.10(t)<br>$^1J$ 161.1 | 56.63(q)<br>$^1J$ 146.3 | 169.31(q)<br>$^2J$ 7.1 | 21.02(q)<br>$^1J$ 130.8 |
| **9** | 123.66(s) | 132.31(d)<br>$^1J$ 166.7 | 196.58(dq)<br>$^2J \sim {}^2J \sim 6$ | 26.63(q)<br>$^1J$ 128.2 | 129.13(t)<br>$^1J$ 161.8 | 56.57(q)<br>$^1J$ 146.9 | 168.45(q), 169.14(q)<br>$^2J$ 7.1 $^2J$ 7.2 | 20.71(q), 21.02(q)<br>$^1J$ 130.5 $^1J$ 130.4 |

*Pulse Fourier transform spectra recorded on Varian XL-100/15 and FT-80A spectrometers at 30°C in $C^2HCl_3$, with TMS as internal standard.
†Multiplicity not determined because of poor S/N.

Can. J. Chem. Downloaded from www.nrcresearchpress.com by 210.87.254.6 on 09/06/12
For personal use only.

that the resonances for the aliphatic methine hydrogens of **1***a* and **1***b* were absent from the spectrum of **7**.

Conversion of **7** to **8** and **9** resulted in one (**8**) or both (**9**) of the phenolic hydroxyl resonances in the $^1$H nmr spectrum being replaced by signals for acetoxyl methyl groups. Furthermore, the hydroxymethyl and aliphatic methine signals were absent from the spectra of **8** and **9**, singlet resonances for two olefinic hydrogens being observed instead. Nuclear Overhauser measurements (see footnote to Table 3) combined with the absence of an observable coupling (15) indicated that these olefinic hydrogens were geminal. Thus elimination of a molecule of water at C-6 and C-12 and acetylation of the phenolic hydroxyl groups appeared to be the only structural changes that had occurred during the formation of **8** and **9** from **7**. The phenolic hydrogen of **8** was long-range coupled to the unsaturated methine hydrogen designated H-9 and the coupling was removed when the hydroxyl hydrogen was exchanged for deuterium. This evidence suggests that the phenolic hydroxyl and unsaturated methine groups are on adjacent carbons.

Structures for **7**, **8**, and **9** were finally confirmed by $^{13}$C nmr studies including single $^1$H frequency decoupling experiments to correlate the $^1$H and $^{13}$C resonances.

The $^{13}$C chemical shifts for **7**, **8**, and **9** (Table 4) were, in some respects, reminiscent of our previously reported (16) and rigorously assigned data for anhydrofusarubin and its diacetate derivative, which possess 5,8-dihydroxy-2-methoxy-1,4-naphthalenedione ring systems. The close agreement between chemical shifts of corresponding carbons in these compounds is strong evidence for the presence of a structural fragment containing the quinone ring system plus C-5 and C-8 depicted in structures **7**, **8**, and **9**. Deuterium isotope chemical shifts in the spectrum of **7**-$d_3$ and one, two, and three bond $^{13}$C—H coupling data for **7**, **8**, and **9** provide further evidence for this fragment. The signs and magnitudes of the isotope chemical shifts for C-1 ($\Delta\delta_{2H}$ +0.09), C-4 ($\Delta\delta_{2H}$ +0.14), C-5 ($\Delta\delta_{2H}$ −0.40), and C-8 ($\Delta\delta_{2H}$ −0.40) indicated that the carbonyl and phenolic carbinol carbons were geminal[4] in **7** and therefore in **8** and **9**. Also H-3 was coupled to C-1, C-2, and C-3 in all three compounds and also to C-4 and C-4a of **8** and **9**, 5-OH was coupled to C-5 of **7**, and 8-OH to C-8 and C-8a of **7** and **8**. Thus the combined evidence for the common structural unit in **7**, **8**, and **9** is overwhelming and at the same time places the acetoxyl group in **8** at C-5.

Chemical shift considerations and multiplicities due to characteristic one bond $^{13}$C—H couplings indicated that the remaining resonances in the spectrum of **7** arose from the methyl (C-11) and carbonyl (C-10) carbons of an acetyl group, quaternary olefinic (C-7) and olefinic methine (C-9) carbons (which have to be adjacent from structural considerations), and the carbons of hydroxymethyl (C-12) and aliphatic methine (C-5) groups which also have to be adjacent on the basis of the $^1$H nmr evidence and the two bond coupling of H-6 to C-12. In addition, H-9 was two bond coupled to C-10 and three bond coupled to C-8, H-11 was two bond coupled to C-10, H-6 was three bond coupled to both C-9 and C-8, and H-12 was three bond coupled to C-5 (17). These observations established the molecular relationships depicted in structure **7**, except for the geometry of the C-7,C-9 double bond. Isotope chemical shifts in the spectrum of **7**-$d_3$ provided information on the latter. The sign of the isotope chemical shift for C-10 ($\Delta\delta_{2H}$ +0.17) indicates that this carbonyl group is hydrogen bonded to a hydroxyl group,[4] which must be 12-OH because the two phenolic hydroxyl groups are already known to be similarly bonded to the quinone carbonyl groups. This indicates that the C-7,C-9 double bond has an *E*-configuration. Molecular model studies also suggest that a *Z*-configuration would be difficult to attain because of severe steric interactions, whereas the *E*-configuration provides ample opportunity for the formation of a hydrogen bond between the C-10 carbonyl group and 12-OH. The isotope chemical shifts of $\Delta\delta_{2H}$ −0.20 observed for C-7 and C-9 are also consistent with the presence of a hydroxyl group at C-8 and hydrogen bonding of the C-10 carbonyl group to 12-OH although no attempt was made to determine their relative contributions.

From $^{13}$C chemical shift and $^{13}$C—H coupling considerations it was apparent that **8** and **9** had retained the $CH_3COCH{=}C\langle$ fragment present in **7** but that the hydroxymethyl and aliphatic methine groups had been replaced by a $\rangle C{=}CH_2$ group. Once again H-9 was three bond coupled to C-8. In addition it was three bond coupled to C-6 and, surprisingly, five bond coupled to C-4a. Moreover, both olefinic hydrogens bonded to C-12 were three bond coupled to C-7 and one of them, probably the one *trans* to C-5, was five bond coupled to C-4 (17). These observations place the C-12 exocyclic meth-

[4]Unpublished results on secalonic acids.

Can. J. Chem. Downloaded from www.nrcresearchpress.com by 210.87.254.6 on 09/06/12
For personal use only.

ylene group vicinal to the $CH_3COCH=$ and C-5 acetoxyl groups in both derivatives. The similarity of the $^{13}C$ chemical shifts for the $CH_3COCH=C$ carbons of **7**, **8**, and **9** strongly suggests that the double bond in all three compounds has the same *E*-configuration. This was also indicated by a careful nuclear Overhauser enhancement study which gave no enhancement of the H-12 resonances for **8** when H-9 was irradiated although a similar experiment involving the H-12 hydrogens had established that they were geminal (see footnote to Table 3). Retention of configuration at the C-7,C-9 double bond of **7** during acetylation in pyridine is not unexpected. Thus the combined evidence unequivocally established that isofusarubin and its acetate derivatives have the structures **7**, **8**, and **9**.

*Nonenzymic formations of 2, 5, and 7*

Although the mechanism of autoxidation in aqueous alkaline solution is not fully understood, it is probable that hydrogen loss from **1***a* and **1***b* involves the reaction of carbanions with molecular oxygen to furnish radicals and $\cdot O_2^-$ (18). Carbanion formation followed by electron abstraction at C-4a and C-10a would lead directly to **2** (Table 1) as illustrated in eq. [1]. Proton removal by base to

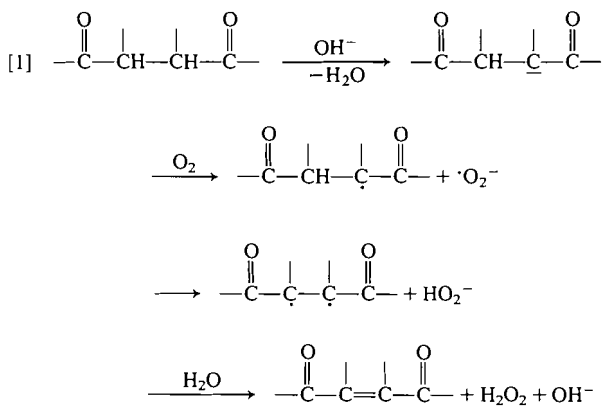

produce carbanions would obviously be promoted by the adjacent carbonyl groups. However, prior opening of the tetrahydropyran ring is required before **7** could be formed by removal of hydrogens from C-4 and C-4a. Moreover, production of **5** would also require prior opening of the tetrahydropyran rings of **1***a* and **1***b* and necessarily involves loss of formaldehyde via a retroaldol reaction at the resulting hydroxymethyl group to form 6,7-dihydronorjavanicin before autoxidation occurs. Differences in the rates of the retroaldol and autoxidation reactions probably account for the relative yields of **5** and **7** (Table 1). Formation of **2**, **5**, and **7** and their subsequent degradation in aqueous alkaline solution contrasts with the autoxidation of **1***a* and **1***b* which leads exclusively to **2** (1).

It is also noteworthy that **7** derived from both **1***a* and **1***b* had the same optical activity and therefore configuration at C-6. This can be explained if the dihydrofusarubins possess the same configuration at C-4a and **1***b* is converted through enolization to the more thermodynamically stable **1***a* (1) before conversion to **7**. The integrity of the chiral centers of **1***a* would be maintained because successive enolizations involving these sites would leave the molecule unchanged. Epimerization at C-6 of **7** would also be restricted because of the keto–enol tautomerism accompanying conversion of **1***a* to **7** and the steric interactions between the substituents at C-6 and C-7 which would hamper proton transfer from C-6 to C-4.

Cultures of *F. solani* produce only **1***a*, **1***b*, and **4** if maintained at ph $\approx$ 3 by providing a medium rich in maltose or by addition of acetic acid. When maltose and ammonium tartrate concentrations are low, **1***a*, **1***b*, and **4** are formed during the first two days when the pH is still low, but the amount of **1***a* and **1***b* decreases rapidly after 3 days. This loss is accompanied by a rapid increase in the pH of the medium (pH 8.2 after 6 days) and an increasing proportion of **2**, and to a lesser extent **5**, in the product. Addition of NaOH solution to cultures (pH $\approx$ 3) harvested after 2 days converts **1***a* and **1***b* to **2** and **5**. Thus the latter are produced nonenzymically in cultures of *F. solani* and by the same process as in 0.1 *N* NaOH. Loss of stability on prolonged exposure to basic conditions explains the low yield of **5** (5% of **2**) and the absence of **7** in the cultures.

**Acknowledgements**

The authors wish to thank Margaret Flack and John van Ingen for technical assistance, Professor P. E. Nelson for the culture of *Fusarium solani*, and Professor G. H. N. Towers for the bioassays.

1. I. KUROBANE, L. C. VINING, A. G. MCINNES, and D. G. SMITH. Can. J. Chem. **56**, 1593 (1978).
2. H. R. V. ARNSTEIN, A. H. COOK, and M. S. LACEY. Nature, **156**, 333 (1946).
3. H. R. V. ARNSTEIN and A. H. COOK. J. Chem. Soc. 1021 (1947).
4. H. W. RUELIUS and A. GAUHE. Ann. **569**, 38 (1950).
5. H. W. RUELIUS and A. GAUHE. Ann. **570**, 121 (1951).
6. G. P. ARSENAULT. Can. J. Chem. **43**, 2423 (1965).
7. E. HARDEGGER, K. STEINER, E. WIDMER, and A. PFIFFNER. Helv. Chim. Acta, **47**, 2027 (1964).
8. E. HARDEGGER, E. WIDMER, K. STEINER, and A. PFIFFNER. Helv. Chim. Acta, **47**, 2031 (1964).

9. W. S. CHILTON. J. Org. Chem. **33**, 4299 (1968).
10. G. P. ARSENAULT. Tetrahedron Lett. **45**, 4033 (1965).
11. E. WIDMER, J. W. MEYER, A. WALSER, and E. HARDEGGER. Helv. Chim. Acta, **48**, 538 (1965).
12. F. DANIELS. J. Invest. Dermatol. **44**, 259 (1965).
13. G. H. N. TOWERS, C-K. WAT, E. A. GRAHAM, R. J. BANDONI, G. F. Q. CHAN, J. C. MITCHELL, and J. LAM. Lloydia, **40**, 487 (1977).
14. C-K. WAT, R. K. BISWAS, E. A. GRAHAM, L. BOHM, and G. H. N. TOWERS. J. Nat. Prod. **42**, 103 (1979).
15. L. M. JACKMAN and S. STERNHELL. Applications of nuclear magnetic resonance in organic chemistry. 2nd ed. Pergamon Press, New York. 1969. p. 279.
16. I. KUROBANE, L. C. VINING, A. G. MCINNES, and J. A. WALTER. Can. J. Chem. **58**, 1380 (1980).
17. P. E. HANSEN. Prog. Nucl. Magn. Reson. Spectrosc. **14**, 175 (1981).
18. D. H. R. BARTON and D. W. JONES. J. Chem. Soc. 3563 (1965).

Can. J. Chem. Downloaded from www.nrcresearchpress.com by 210.87.254.6 on 09/06/12
For personal use only.

# Enzymes in organic synthesis. 28.[1] Reinvestigation of the horse liver alcohol dehydrogenase-catalyzed reductions of 2-alkylcyclohexanones. Identification of *cis*-alkylcyclohexanols as minor products

J. BRYAN JONES AND TETSUO TAKEMURA[2]

*Department of Chemistry, University of Toronto, Toronto, Ont., Canada M5S 1A1*

Received June 21, 1982

J. BRYAN JONES and TETSUO TAKEMURA. Can. J. Chem. **60**, 2950 (1982).

The formation of *cis*-2-alkylcyclohexanol products from horse liver alcohol dehydrogenase-catalyzed reductions of 2-alkylcyclohexanones has been detected for the first time. The *cis*-alcohols are minor (< 4%) products, with the isomeric *trans*-products being heavily predominant under all conditions. *cis*-Alcohol production can be suppressed by suitable manipulation of the reaction conditions. Exclusive formation of the *trans*-alcohols is favoured by operating in an appropriate buffer such as Tris-HCl at the lowest [E]/[S] and pH conditions possible, and by minimizing the reaction time. The results parallel the *cis*-alcohol formation observed previously with the analogous 3-alkyltetrahydrothiopyran-4-one substrates.

J. BRYAN JONES et TETSUO TAKEMURA. Can. J. Chem. **60**, 2950 (1982).

On a décelé pour la première fois la formation d'alkyl-2 cyclohexanols-*cis* lors des réductions d'alkyl-2 cyclohexanones catalysées par la déshydrogénase de l'alcool du foie de cheval. Les alcools *cis* sont des produits secondaires (<4%) tandis que les produits *trans* sont fortement majoritaires dans toutes les conditions. On peut éviter la formation d'alcool *cis* en jouant convenablement avec les conditions de réaction. On favorise la formation exclusive d'alcools *trans* en travaillant avec un tampon convenable tel le Tris-HCl aux plus faibles conditions possibles de [E]/[S] et de pH et en minimisant le temps de réaction. Les résultats sont identiques à ceux obtenus antérieurement lors de la formation d'alcools *cis* à partir des substrats analogues du type alkyl-3 tétrahydrothiopyranones-4.

[Traduit par le journal]

Horse liver alcohol dehydrogenase (HLADH)[3] is a commercially available NAD/H-dependent oxidoreductase that catalyzes highly stereoselective C=O ⇌ CH(OH) transformations for a broad structural range of aldehyde, ketone, and alcohol substrates (1, 2–9). As a result it is currently one of the most versatile and useful enzymes from the asymmetric synthetic point of view and many illustrations of its potential for the preparation of useful chiral synthons have been documented (2–9). Reductions of 2-alkylcyclohexanones were among the first of the preparative-scale HLADH-catalyzed reactions to be studied. Reductions of 2-methyl- and 2-ethylcyclohexanones ((±)-**1***a*,*b*) were reported to be stereospecific, with the (2*S*)-ketones being converted to the corresponding *trans*-alcohols (1*S*,2*S*)-**2***a*,*b* of 100% e.e., and the unreactive ketone enantiomers (2*R*)-**1***a*,*b* being recovered virtually optically pure (2–6). Subsequent work confirmed these results (5, 6). However, it was noted that in the reduction of 2-fluorocyclohexanone, a small (4%) amount of *cis*-2-fluorocyclohexanol of unrecorded chirality was formed in addition to the usual, predominant (96%), *trans*-product (6). Very recently, HLADH-catalyzed reductions of the related 3-alkyltetrahydrothiopyranone substrates (±)-**4***a*,*b* to the *trans*-alcohols **5***a*,*b* were also found to produce minor (2–3%) amounts of *cis*-alcohols **6***a*,*b*.

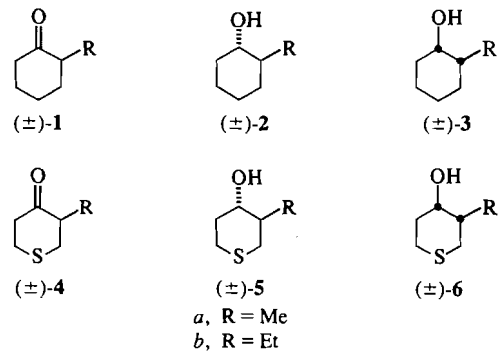


The formation, to whatever degree, of *cis*-alcohols during HLADH-mediated reductions of ketones such as **1** and **4** is of considerable interest with respect to delineating the possible active site orientations of such substrates (9*c*). Accordingly, we decided to reinvestigate the reductions of (±)-**1***a*,*b* since trace proportions of *cis*-alcohol products could well have escaped detection during the earlier studies. The results reported in this

[1]For Part 27, see ref. 1.

[2]On leave from the Department of Chemistry, Faculty of Science, Science University of Tokyo, Tokyo, Japan.

[3]Abbreviations used: HLADH, horse liver alcohol dehydrogenase; $NAD^+$, oxidized and reduced forms respectively of nicotinamide adenine dinucleotide; MTPA, (+)-2-methoxy-2-trifluoromethylphenylacetyl; $Eu(fod)_3$, tris(6.6.7.7.8.8-heptafluoro-2,2-dimethyl-3,5-octanedionato)europium(III).

0008-4042/82/232950-07$01.00/0

©1982 National Research Council of Canada/Conseil national de recherches du Canada

Can. J. Chem. Downloaded from www.nrcresearchpress.com by 210.87.254.6 on 09/06/12
For personal use only.

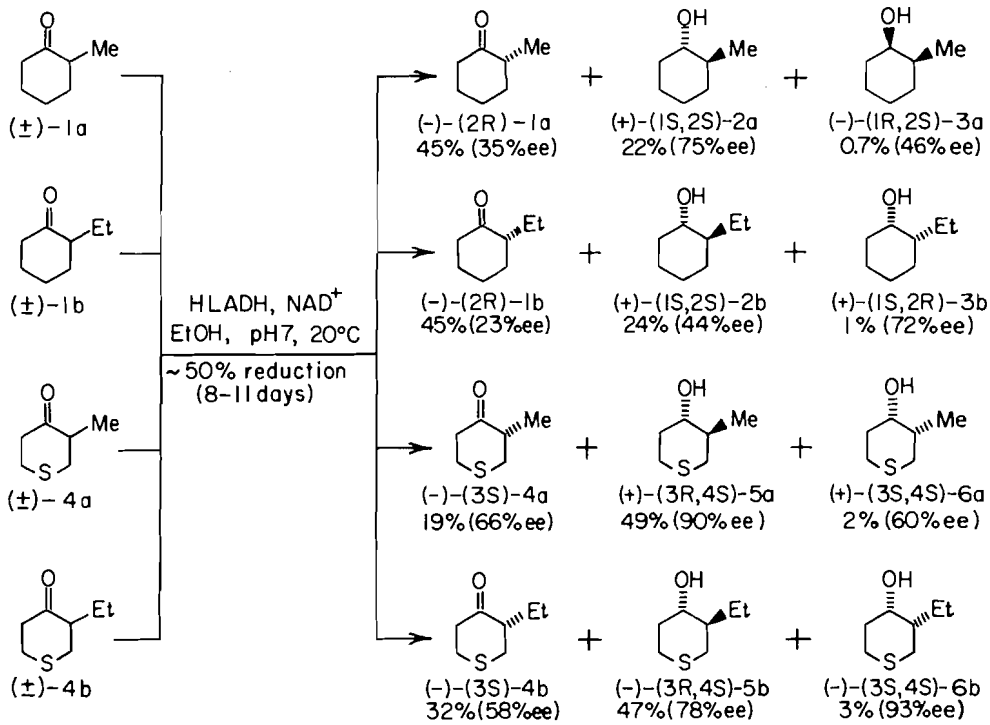


SCHEME 1

paper confirm that *cis*-alcohols can be produced in minor amounts during the reductions of all 2-substituted cyclohexanone and related substrates studied to date. Furthermore, the extent to which the *cis* compounds are formed is found to reflect the nature of the reaction conditions used. With the appropriate controls the formation of the *cis* by-products can be completely suppressed.

## Results

The racemic substrates and potential products **1**–**3***a*,*b* were all known compounds and were either purchased or prepared according to published procedures. Preparative-scale HLADH-catalyzed reductions of the alkylcyclohexanones (±)-**1***a*,*b* were carried out in phosphate buffer pH 7 on a 4-g scale. The results obtained are recorded in Scheme 1 together with the data obtained previously (1) on the 3-alkyltetrahydrothiopyranones (±)-**4***a*,*b*.

The unreacted ketones **1***a*,*b* and the product alcohols **2**,**3***a*,*b* were separated by mplc and their identities confirmed by comparison with their racemic counterparts. The e.e.'s of the ketones (−)-**1***a*,*b* were determined by their quantitative conversion to the corresponding ketals **7***a*,*b* with (−)-(2*R*,3*R*)-2,3-butanediol followed by $^{13}C$ nmr examinations of the diastereomeric ketal mixtures obtained (10). The corresponding ketals from the racemic ketones were used as reference standards. The $\Delta\delta$ values observed for the individual diastereotopic carbon atoms are recorded in Table 1. The e.e. values shown for (−)-**1***a*,*b* in Scheme 1 represent the averages of measurements on $^{13}C$ resonances of at least four different carbon atoms of **7***a*,*b*. The optical purities of the *trans*- and *cis*-alcohols **2**- and **3***a*,*b* of Scheme 1 were evaluated by $^1H$ nmr examination in the presence of Eu(fod)$_3$ of the methoxyl proton resonances of their MTPA-esters, **8***a*,*b* and **9***a*,*b* respectively (11). The $\Delta\Delta\delta$ values of the methoxyl peaks of the corresponding esters of the racemic alcohols used for comparison purposes are recorded in Table 2.

The absolute configurations of (−)-**1***a*, (+)-**2***a*, and (−)-**3***a* were assigned from the literature data (5, 12–14) and that of (−)-**1***b* by octant rule analysis (12, 15) of the Cotton effect of its cd spectrum. The absolute configurations of the *cis*- and *trans*-alcohols (+)-**3***b* and (+)-**2***b* were then established by their oxidation with pyridinium chlorochromate under neutral conditions (16) to (−)-(2*R*)-**1***b* and (+)-(2*S*)-**1***b* respectively.

The degree to which *cis*-alcohols are produced was found to be influenced by the reaction conditions and was studied in detail using (±)-**1***b* as the

Can. J. Chem. Downloaded from www.nrcresearchpress.com by 210.87.254.6 on 09/06/12
For personal use only.

TABLE 1. Enantiomeric shift differences in the $^{13}C$ nmr spectra of the diastereomeric ketals **7***a*,*b*[a]

| Ketal structure | Compound | Δδ, ppm | | | | | | | | | | |
|---|---|---|---|---|---|---|---|---|---|---|---|---|
| | | C-1 | C-2 | C-3 | C-4 | C-5 | C-6 | C-7 | C-8 | C-9 | C-10 | Other C |
| 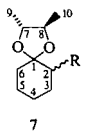 7 | **7***a* | 0 | 0.78[b] | 0.09 | 0 | 0.42[b] | 0.69[b] | 0.30 | 0.69[b] | 0.14 | 0 | 0.08 ($CH_3$) |
| | **7***b* | 0.27[b] | 0.67[b] | 0.07 | 0 | 0.49[b] | 0.67[b] | 0.13 | 0.33[b] | 0 | 0 | 0.09 ($CH_2CH_3$) |
| | | | | | | | | | | | | 0 ($CH_2CH_3$) |

[a]$^1H$ noise-decoupled spectra determined in $C^2HCl_3$. See ref. 1 for data on ketals of ketones **4***a*,*b*.
[b]Used for determining e.e. values shown in Scheme 1.

TABLE 2. Enantiomeric shift differences for the methoxyl protons of the MTPA esters **8**,**9***a*,*b*[a] from (±)-**2**,**3***a*,*b*

| Structures | Compound | $Eu(fod)_3$, equiv. | ΔΔδ, ppm |
|---|---|---|---|
| 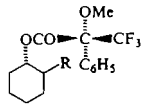 8 | **8***a* | 0.29 | 0.86 |
| | | 0.58 | 1.25 |
| | **8***b* | 0.30 | 1.22 |
| | | 0.75 | 1.80 |
| 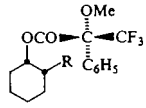 9 | **9***a* | 0.23 | 0.35 |
| | | 0.55 | 0.50 |
| | **9***b* | 0.27 | 0.78 |
| | | 0.65 | 0.98 |

[a]Determined at 60 MHz in $CCl_4$ solution. See ref. 1 for data on MTPA esters of **5**,**6***a*,*b*.

representative substrate. As shown in Table 3, the proportions of *cis*-alcohol **3***b* formed during HLADH-catalyzed reduction of 2-ethylcyclohexanone ((±)-**1***b*) can be minimized by working at lower pH's, and by appropriate choice of the buffer. Tris-HCl is a more suitable buffer in this regard than phosphate. The rate of the reaction is also an important parameter (Table 4). The amount of *cis*-alcohol formed increases steadily as the reaction period is extended and selection of a suitably short reaction time ensures that the *trans*-alcohol is the exclusive product. Formation of the *cis*-alcohol can also be suppressed by using a low [E]/[S] ratio. The yields of *cis*-alcohol isolated rise monotonically as the proportions of enzyme in the reaction mixture are increased, as illustrated by Table 5.

TABLE 3. Influence of buffer and of pH on *cis*-alcohol formation in HLADH-catalyzed reduction of (±)-**1***b*[a]

| pH | Buffer | Alcohol products (%)[b] | |
|---|---|---|---|
| | | *trans* (**2***b*) | *cis* (**3***b*) |
| 6 | Phosphate | 13.2 | 0 |
| 8 | Phosphate | 53.8 | 3.4 |
| 7 | Tris-HCl | 28.6 | <0.1 |
| 8 | Tris-HCl | 54.8 | 0.6 |
| 9 | Tris-HCl | 54.2 | 1.5 |

[a]Reactions carried out for 3 days at 20°C with [E]/[S] $3.1 \times 10^{-4}$ in 0.4 *M* buffer solutions.
[b]By glc.

## Discussion

The preparative-scale HLADH-catalyzed reductions summarized in Scheme 1 proceeded smoothly. Ethanol was used as the coupled substrate to recycle the catalytic quantity of the expensive $NAD^+$ coenzyme employed (17). The reductions of (±)-**1***a*,*b* were performed on a 4-g scale in order to ensure that sufficient quantities to permit complete and unequivocal characterization

TABLE 4. Effect of reaction time on *cis*-alcohol formation during HLADH-catalyzed reduction of (±)-**1***b*[a]

| Reaction period (h) | Alcohol products (%)[b] | |
|---|---|---|
| | *trans* (**2***b*) | *cis* (**3***b*) |
| 17 | 33 | 0 |
| 43 | 44.5 | 2.8 |
| 332 | 74 | 4.0 |

[a]In 0.4 *M* phosphate buffer pH 8, with [E]/[S] = $3.1 \times 10^{-4}$.
[b]By glc.

Can. J. Chem. Downloaded from www.nrcresearchpress.com by 210.87.254.6 on 09/06/12
For personal use only.

TABLE 5. Influence of [E]/[S] ratio on *cis*-alcohol formation in HLADH-catalyzed reduction of (±)-**1***b*[a]

| [E]/[S] (× $10^4$) | Reaction period | Extent of reduction % | Alcohol products (%)[b] | |
|---|---|---|---|---|
| | | | *trans* (**2***b*) | *cis* (**3***b*) |
| 4.9 | 26 h | 48 | 47.3 | 0.7 |
| 3.3 | 28 h | 43 | 42.5 | 0.5 |
| 0.65 | 9 days | 47 | 46.6 | 0.4 |
| 0.44 | 9 days | 49 | 48.9 | 0.1 |

[a]In 0.4 *M* Tris-HCl buffer pH 8, 20°C.
[b]By glc.

of the minor *cis*-alcohol products **3***a*,*b* were isolable from each reaction.

The direct $^1$H- and $^{13}$C-nmr based measurements of the e.e.'s of the alcohol products and recovered ketones isolated from the enzymic reactions presented no problems and the values cited in Scheme 1 are considered accurate to within ±3%. The peak assignments (Experimental section) and Δδ values recorded for the $^{13}$C resonances of the ketals **7***a*,*b* (Table 1) are in excellent agreement with those published recently by Meyers *et al.* (18), with the exception of the C-3 and C-4 assignments which are reversed. Our assignments are based on the substituent-induced shifts observed between the 2-methyl- and 2-ethyl-derivatives, and their analogy with the corresponding shifts in methyl and ethylcyclohexane (19). The low e.e.'s of the recovered ketones **1***a*,*b* are largely attributable to nonenzymic epimerization at C-2 during the lengthy reaction period.[4]

The absolute configuration determinations of the Scheme 1 cyclohexane derivatives were also straightforward, with the configurations of **1***a*, **2***a*, and **3***a* having been established previously (5, 9–11). The octant rule analysis (15) of the cd spectrum of (−)-**1***b* used to assign its C-2 chirality followed the well documented approach developed on the 2-methyl analogue (12). The configurations of (+)-**2***b* and (+)-**3***b* were then confirmed by their oxidation to (+)- and (−)-**1***b* respectively.

In the earlier studies on HLADH-catalyzed reductions of 2-alkylcyclohexanones, *trans*-alcohol products were obtained exclusively (5, 6). The absence of *cis*-alcohols in these previous reactions is in marked contrast to the present results. However, the Zürich (2, 3, 5) and Antwerp (6) groups effected their transformations under reaction conditions somewhat different from those employed in the Scheme 1 reactions. Recognition of this prompted an evaluation of the influence of various experimental parameters on *cis*-alcohol formation. As the data recorded in Tables 3–5 show, the reaction conditions employed are of prime importance in controlling the degree of *cis*-alcohol content.

If suppression of *cis*-alcohol production is desired, operating in Tris-HCl (6) rather than phosphate buffer and at pH's no higher than 7 is recommended (Table 3). While the use of phosphate buffer alone at pH > 7 does permit *cis*-alcohol formation, substitution of a glycine–arsenate-modified phosphate buffer of pH 8 once again appears to preclude the production of these minor by-products (5, 9*a*). Exclusive reduction to the *trans*-alcohol products can also be ensured by keeping the reaction time short (Table 4) and by operating with the [E]/[S] ratio at a minimum (Table 5). In the HLADH-mediated reductions of 2-alkylcyclohexanones performed by the Zürich and Antwerp groups, in which no *cis*-alcohols were produced, the [E]/[S] ratios employed were even lower, by factors of ~5 (5) and ~10 (6) respectively, than the lowest level of Table 5.

Both the diamond lattice (2, 4) and the cubic-section (9*c*) active-site models developed for predicting the stereochemistry of HLADH-catalyzed oxidoreductions are valid for kinetically controlled reactions only. Under such conditions, virtually exclusive *trans*-alcohol formation is predicted (2, 4, 9*a*, *c*). The Table 4 and 5 data support this view, with short reaction times and very high excesses of [S] over [E] favouring *trans*-, and minimizing *cis*-, alcohol accumulation.

For good substrates, HLADH-catalyzed reductions are rapid and no special precautions are needed to ensure that only the kinetically favoured products are formed (2, 4, 9). However, poor substrates are reduced slowly. As a result lengthy reaction periods are often required, thereby permitting products of pathways other than that of the initial, kinetically determined, direction to build up. The 2-alkylcyclohexanone **1***a*,*b* and 3-alkyl-

[4]The variations in the optical purities of the *trans*-alcohols **3***a*,*b* and **6***a*,*b* contrast the 100% e.e. levels cited previously for such HLADH-derived products (5, 6). These e.e. variations have now been found to be markedly influenced by the reaction conditions. A systematic study of the factors controlling product e.e.'s has been undertaken and will be reported shortly.

Can. J. Chem. Downloaded from www.nrcresearchpress.com by 210.87.254.6 on 09/06/12
For personal use only.

Can. J. Chem. Downloaded from www.nrcresearchpress.com by 210.87.254.6 on 09/06/12
For personal use only.

thiopyranone **4***a*,*b* reductions are in this latter category. In these cases, the *trans*-alcohol products of kinetic control are also thermodynamically favoured, having both substituents equatorial in the preferred chair conformations. However, in the presence of HLADH, the *trans*-alcohols **2***a*,*b* and **5***a*,*b* are also oxidized back to the parent ketones much more rapidly than the slowly accumulating *cis*-alcohols **3***a*,*b* and **6***a*,*b* (1). The reverse oxidation reaction can occur because, owing to the limitations of the NADH–coenzyme recycling procedure, there is always a small proportion of $NAD^+$ available to participate in an alcohol oxidation step. Accordingly, because the *trans*-alcohols are present in much higher concentrations, and are oxidized much faster than their *cis*-isomers, any *cis*-alcohols that do form accumulate.

The cubic-section model of the active-site region (9*c*) is in accord with the more rapid oxidation of the *trans*- than the *cis*-alcohols of a given series. Furthermore, it predicts that the *cis*-alcohols formed preferentially in the reduction mode will predominate in the enantiomers possessing the (1*S*) (or (4*S*) for the thioketones) absolute configurations. This is seen to be correct for (+)-**3***b*, (+)-**6***a*, and (+)-**6***b*. Disappointingly, favouring of the opposite (1*R*,2*S*) configuration is manifest in (−)-**3***a*.[5] However, since the model was formulated only for predicting the stereochemical outcome of kinetically controlled, preferred, oxidoreductions, this is not a significant discrepancy. Furthermore, use of the enzyme is clearly not preparatively viable for the preparation of *cis*-alcohols. In contrast, HLADH-catalyzed reduction of 2-alkylcyclohexanones and related substrates remains an excellent route to the corresponding optically active *trans*-alcohols, with pure products to be expected if phosphate buffer is avoided and the minimum amount of enzyme is used in solutions of the lowest practicable pH.

[5]The preferred stereochemistry of reduction of 2-alkylcyclohexanones has been analyzed in detail in cubic-section terms (9*c*). Only the (2*S*)-enantiomer of **1***a*,*b* (or (3*R*)-**4***a*,*b*) can form an allowed ES complex to lead to *trans*-(1*S*,2*S*)-**2***a*,*b* (or (3*R*,4*S*)-**5***a*,*b*). The allowed oxidation reactions follow the microscopic reverse paths. On the other hand, neither enantiomer of any *cis*-alcohol of Scheme 1 can bind to form an ES complex without the alkyl substituent violating either cube **E1** (e.g. 1*R*,2*S*-**3***b*) or cube **B1** (e.g. 1*S*,2*R*-**3***b*). All of **E1**, and half of **B1** are forbidden regions, and will not accommodate a substrate group. Formation of the *cis*-products is thus strongly disfavoured. However, the remaining half of cube **B1** will accept a small group and is thus less intolerant than **E1**. The configurations reflecting positioning of the alkyl substituents of the (2*R*)-**1** and (3*S*)-**4** ketones adjacent to, and in, the **B1** region should thus dominate any *cis*-alcohols that are formed. This agrees with the experimental data for (1*S*,2*R*)-**3***b* and (3*S*,4*S*)-**6***s*,*b*, but not for (1*R*,2*S*)-**3***a*. The formation of the latter stereoisomer cannot be explained at the current level of sophistication of the model. Interestingly, reduction of (±)-2-fluorocyclohexanone gives the highest proportion (4%) of *cis*-alcohol (of unspecified configuration) yet reported (6). This would be expected in terms of the above analysis since fluorine is a very small substituent and should, on steric grounds, be more easily accommodated in the open half of cube **B1** than any alkyl group.

## Experimental

The instrumentation and general purification and analytical procedures used were as described previously (9*d*). HLADH (EC 1.1.1.1) was 1× crystallized material purchased from Sigma. The activity of each batch of enzyme was determined (20) prior to use; amounts of HLADH quoted refer to milligrams of active enzyme. $NAD^+$ was obtained from Kyowa Hakko Kogyo, New York. The mplc separations were performed on silica (ICN 0.032–0.63 mm) with ethyl acetate – hexane (1:6) elution. Unless indicated otherwise, ir spectra were determined in $CCl_4$ and nmr spectra in $C^2HCl_3$. The Scheme 1 data on the tetrahydrothiopyrans **4***a*,*b*, **5***a*,*b*, and **6***a*,*b* are from ref. 1.

*Preparations of racemic ketone substrates and alcohol products*

*2-Methylcyclohexanone ((±)-1a)* was purchased from Aldrich and purified by Kugelrohr distillation, bp 162–163°C (lit. (21) bp 165–166°C); ir: 1714 $cm^{-1}$; $^1H$ nmr δ: 1.02 (3H, d, $J$ = 6 Hz) and 1.15–2.8 (9H, m) ppm.

cis- *and* trans-*2-Methylcyclohexanol* were prepared by $LiAlH_4$ reduction of 2-methylcyclohexanone. Separation of the mixture by mplc gave *cis*-2-methylcyclohexanol ((±)-**3***a*, 25% yield) bp 70°C (20 Torr) (lit. (13) bp 77–78°C (20 Torr)); ir (film): 3400 $cm^{-1}$; $^1H$ nmr δ: 0.97 (3H, d, $J$ = 6 Hz), 1.1–2.3 (9H, m), 1.86 (OH, s), and 3.80 (1H, m, $W_{\frac{1}{2}}$ = 8 Hz) ppm and *trans*-2-methylcyclohexanol ((±)-**2***a*, 44% yield) bp 74°C (27 Torr) (lit. (13) bp 78–79°C (20 Torr)); ir: 3640, 3380 $cm^{-1}$; $^1H$ nmr δ: 0.7–2.2 (12H, m), 2.70 (OH, s), and 3.10 (1H, m, $W_{\frac{1}{2}}$ = 20 Hz) ppm.

*2-Ethylcyclohexanone ((±)-1b)* was obtained in 90% yield by Jones oxidation of 2-ethylcyclohexanol (*cis*/*trans* mixture, purchased from Aldrich) bp 70°C (10 Torr) (lit. (22) bp 110°C (36 Torr)); ir: 1720 $cm^{-1}$; $^1H$ nmr δ: 0.9 (3H, t, $J$ = 7 Hz) and 1.1–2.5 (11H, m) ppm.

cis- *and* trans-*2-Ethylcyclohexanol*

The mplc separation of the commercial mixture (Aldrich) gave *cis*-2-ethylcyclohexanol ((±)-**3***b*, 29% yield) bp 82°C (10 Torr) (lit. (23) bp 180–182°C); ir: 3625, 3480 $cm^{-1}$; $^1H$ nmr δ: 0.92 (3H, t, $J$ = 6 Hz), 0.9–2.1 (11H, m), 1.77 (OH, s), and 3.92 (1H, m, $W_{\frac{1}{2}}$ = 8 Hz) ppm and *trans*-2-ethylcyclohexanol ((±)-**2***b*, 36% yield) bp 82°C (10 Torr) (lit. (24) bp 87–91°C (25 Torr)); ir: 3640, 3440 $cm^{-1}$; $^1H$ nmr δ: 0.87 (3H, t, $J$ = 6 Hz), 0.9–2.25 (11H, m), 2.10 (OH, s), and 3.15 (1H, m, $W_{\frac{1}{2}}$ = 20 Hz) ppm.

*HLADH-catalyzed reductions of (±)-1a,b*

The general procedure described previously (1, 9*e*) was used to reduce the ketone (4.0 g, ~35 mmol) with HLADH (300 mg), $NAD^+$ (6.0 g, 9.1 mmol), EtOH (11 mL) in 0.1 *M* potassium phosphate buffer pH 7 (1 L) at 20°C. The reactions were monitored by glc and terminated at the ~50% reduction point. The unchanged ketones and product alcohols were separated by mplc. The spectral properties of each compound were identical with those of the corresponding racemates characterized above. The individual reactions gave the following results after Kugelrohr distillation of each chromatographically purified product.

*Reduction of (±)-1a* (44% conversion) yielded (−)-2-methylcyclohexanone ((2*R*)-**1***a*, 1.8 g, 45% yield, 35% e.e.) bp 59°C (22

Can. J. Chem. Downloaded from www.nrcresearchpress.com by 210.87.254.6 on 09/06/12
For personal use only.

Torr) (lit. (12) bp 59–60°C (20 Torr)), $[\alpha]_D^{25}$ −3.39° (*c* 2.2, EtOH) (lit. (5) (2*S*)-**1***a* $[\alpha]_D^{25}$ +14.4° (*c* 1.03, EtOH)); (+)-*trans*-2-methylcyclohexanol ((1*S*,2*S*)-**2***a*, 881 mg, 22% yield, 75% e.e.), bp 70°C (15 Torr) (lit. (13) bp 78°C (20 Torr)), $[\alpha]_D^{25}$ +31.0° (*c* 2.2, EtOH) (lit. (5) $[\alpha]_D^{25}$ +40.8° (*c* 0.7, EtOH); and (−)-*cis*-2-methylcyclohexanol ((1*R*,2*S*)-**3***a*, 30 mg, 0.7% yield, 46% e.e.), bp 72°C (21 Torr) (lit. (13) bp 78–79°C (29 Torr)), $[\alpha]_D^{25}$ −10.2° (*c* 0.3, EtOH) (lit. (5) (1*S*,2*R*)-**3***a* $[\alpha]_D^{25}$ +15.7° (*c* 3.4, EtOH).

*Reduction of* (±)-*1*b (44% conversion gave (−)-2-ethylcyclohexanone ((2*R*)-**1***b*, 1.81 g, 45% yield, 23% e.e.), bp 82–85°C (22 Torr), $[\alpha]_D^{25}$ −4.75° (*c* 2.2, EtOH) (lit. (5) 18° (*c* 1.8, EtOH)); (+)-*trans*-2-ethylcyclohexanol ((1*S*,2*S*)-**2***b*, 960 mg, 24% yield, 44% e.e.), bp 80°C (18 Torr), $[\alpha]_D^{25}$ +26.6° (*c* 2.1, EtOH) (lit. (5) $[\alpha]_D$ 59.2° (*c* 1.45, EtOH); and (+)-*cis*-2-ethylcyclohexanol ((1*S*,2*R*)-**3***b*, 47 mg, 1.2% yield, 72% e.e.), bp 80°C (21 Torr), $[\alpha]_D^{25}$ +15.5° (*c* 0.54, EtOH).

*Enantiomeric excess determinations*

1. *Of ketones* **1**a,b

Each racemic (for reference) and optically active ketone **1***a*,*b* (1 mmol) was converted in quantitative yield to its ketal **7***a*,*b* with (−)-(2*R*,3*R*)-2,3-butanediol (1.3 mmol) as described previously (1). The e.e. values of the ketals from the optically active ketones of Scheme 1 were determined from the $^1$H-decoupled $^{13}$C nmr spectra of **7***a*,*b* by the method of Hiemstra and Wynberg (10). The Δδ values used are recorded in Table 1. The bp's (Kugelrohr) and nmr resonances of the ketals from the racemic ketones are recorded below.

*2-Methylcyclohexanone ketal* **7**a, bp 75°C (1 Torr), $^1$H nmr δ: 0.85 and 0.9 (3H, d of d, $J$ = 6 Hz), 1.25 (6H, d of d, $J$ = 6 Hz), 1.4–2.4 (9H, m), and 3.65 (2H, m, $W_{\frac{1}{2}}$ = 12 Hz) ppm; $^{13}$C nmr δ: 14.40 and 14.48 (C-2 $CH_3$), 16.16 and 16.30 (C-9), 17.82 (C-10), 23.84 and 24.26 (C-5), 25.00 (C-4), 32.17 and 32.26 (C-3), 36.59 and 37.28 (C-6), 39.73 and 40.51 (C-2), 77.48 and 77.78 (C-7), 79.14 and 79.83 (C-8), and 110.07 and 110.34 (C-1) ppm.

*2-Ethylcyclohexanone ketal* **7**b, bp 80°C (1.2 Torr), $^1$H nmr δ: 0.9 (3H, t, $J$ = 6 Hz), 1.2 (6H, d of d, $J$ = 4 Hz), 0.6–2.4 (11H, m), and 3.60 (2H, m, $W_{\frac{1}{2}}$ = 12 Hz) ppm; $^{13}$C nmr δ: 12.00 ($CH_2CH_3$), 16.28 (C-9), 17.89 (C-10), 20.85 and 20.94 ($CH_2CH_3$), 24.16 and 23.67 (C-5), 24.84 (C-4), 28.19–28.26 (C-3), 36.62 and 37.29 (C-6), 46.79 and 47.46 (C-2), 77.51 and 77.64 (C-7), 79.15 and 79.48 (C-8), and 110.07 and 110.34 (C-1) ppm.

2. *Alcohols* **2**a,b *and* **3**a,b

The racemic (for reference) and optically active alcohols **2**,**3***a*,*b* (20–30 mg) were each converted to their MTPA esters **8**,**9***a*,*b* in quantitative yields by the literature (1, 8) procedure using freshly prepared (+)-(2*R*)-2-methoxy-2-trifluoromethylphenylacetyl chloride (100 mg, ~2 equiv.), $[\alpha]_D^{25}$ 131.9°C (*c* 1, $CCl_4$) (lit. (8) $[\alpha]_D^{25}$ 129.0 ± 0.2° (*c* 5.17, $CCl_4$). The e.e.'s of the MTPA esters of the Scheme 1 alcohols were then determined from the 60 MHz $^1$H nmr methyl resonances in the presence of Eu(fod)$_3$. The bp's (Kugelrohr) and spectral data of the MTPA esters of the racemic alcohols **2**,**3***a*,*b* used to establish the ΔΔδ values summarized in Table 2 are as follows.

trans-*2-Methylcyclohexanol MTPA ester* **8**a, bp 90°C (0.2 Torr), ir: 1757 cm$^{-1}$; $^1$H nmr ($CCl_4$) δ: 0.73 and 0.96 (3H, d of d, $J$ = 6 Hz), 1.0–2.5 (9H, m), 3.53 (3H, s), 4.60 (1H, m, $W_{\frac{1}{2}}$ = 20 Hz), and 7.2–7.8 (5H, m) ppm.

cis-*2-Methylcyclohexanol MTPA ester* **9**a, bp 95°C (0.25 Torr), ir: 1762 cm$^{-1}$; $^1$H nmr ($CCl_4$) δ: 0.75 and 0.95 (3H, d of d, $J$ = 6 Hz), 1.05–2.40 (9H, m), 3.56 (3H, s), 5.12 (1H, m, $W_{\frac{1}{2}}$ = 8 Hz), and 7.15–7.75 (5H, m) ppm.

trans-*2-Ethylcyclohexanol MTPA ester* **8**b, bp 90°C (0.2 Torr), ir: 1757 cm$^{-1}$; $^1$H nmr ($CCl_4$) δ: 0.50–2.33 (14H, m), 3.56 (3H, s), 4.74 (1H, m, $W_{\frac{1}{2}}$ = 20 Hz), and 7.2–7.8 (5H, m) ppm.

cis-*2-Ethylcyclohexanol MTPA ester* **9**b, bp 95°C (0.25 Torr), ir: 1765 cm$^{-1}$; $^1$H nmr ($CCl_4$) δ: 0.90 (3H, t, $J$ = 5.5 Hz), 1.05–2.35 (11H, m), 3.50 (3H, s), 5.25 (1H, m, $W_{\frac{1}{2}}$ = 8 Hz), and 7.15–7.75 (5H, m) ppm.

*Absolute configuration determinations*

1. *Of the enzyme-derived ketones* **1**a,b

The (2*R*)-configuration of (−)-**1***a* was assigned from the literature data (5, 12–14). The configuration of (−)-**1***b* was established from octant rule analysis (12, 15) of its cd spectrum: cd (*c* 0.0149, EtOH, 20°C): $[\theta]_{329}$ 0°; $[\theta]_{292}$ −1350°; $[\theta]_{240}$ 0°, and comparison with that of the known (12) (−)-(2*R*)-**1***a*.

2. *Of the HLADH-derived alcohols* **2**,**3**a,b

The configurations of (+)-(1*S*,2*S*)-**2***a* and (−)-(1*R*,2*S*)-**3***a* were assigned from the literature data (5, 12–14). For the ethylcyclohexanols **2**,**3***b*, the relative configurations at C-1 and C-2 were established by their identification as *cis*- or *trans*-isomers from their $^1$H nmr spectra. The chiralities of the C-2 centres were then determined by oxidation of (+)-**2***b* and (+)-**3***b* to (+)-(2*S*)-**1***b* and (−)-(2*R*)-**1***b* respectively, and by comparison of the Cotton effect of the cd spectra of (+)-(2*R*)-**1***b* with that of (+)-(2*S*)-**1***a* established previously (12).

*Oxidation of* trans-*alcohol* (+)-**2**b *to* (+)-(2R)-*1*b

(+)-*trans*-2-Ethylcyclohexanol (**2***b*, 90 mg, 0.7 mmol, $[\alpha]_D^{25}$ +55.4° (*c* 0.9, EtOH)), pyridinium chlorochromate (335 mg, 1.55 mmol), and sodium acetate (17 mg, 0.21 mmol) in $CH_2Cl_2$ (5 mL) was stirred at 20°C for 1 day (16). Base-free work-up and purification gave 2-ethylcyclohexanone ((2*R*)-**1***b*, 70 mg, 79% yield) bp 80°C (7 Torr), $[\alpha]_D^{25}$ +21.3° (*c* 0.6, EtOH); cd (*c* 0.0123, EtOH, 20°C): $[\theta]_{330}$ 0°; $[\theta]_{293}$ +1870°; $[\theta]_{240}$ 0°.

*Oxidation of* cis-*alcohol* (+)-**3**b *to* (−)-(2S)-*1*b

Oxidation of (+)-*cis*-2-ethylcyclohexanol (**3***b*, 98 mg, 0.76 mmol, $[\alpha]_D^{25}$ +1.60° (*c* 1.2, EtOH)) with pyridinium chlorochromate (360 mg, 1.67 mmol) and sodium acetate (19 mg, 0.23 mmol) in $CH_2Cl_2$ (5 mL) for 12 h at 20°C, followed by base-free work-up, gave 2-ethylcyclohexanone ((2*S*)-**1***b*, 72 mg, 74% yield) bp 40°C (3 Torr), $[\alpha]_D^{25}$ −2.2° (*c* 1, EtOH).

*Influence of reaction conditions on* cis-*alcohol formation during HLADH-catalyzed reduction of* (±)-*1*b

The effects of buffer and pH were surveyed by following (by glc) the course of reduction of (±)-**1***b* (51 mg) with enzyme (10 mg), $NAD^+$ (79 mg), and EtOH (0.1 mL) in 0.4 *M* potassium phosphate, or Tris-HCl, buffer (10 mL) of pH 6 and 8, or 7, 8, and 9 respectively, at 20°C. The [E]/[S] ratio was 3.1 × 10$^{-4}$ for these studies. The results are summarized in Table 3. The dependence of *cis*-alcohol formation on reaction time was monitored in the same way under the same conditions in 0.4 *M* potassium phosphate buffer pH 8. The results are recorded in Table 4.

The influence of changes in the [E]/[S] ratio within the range 0.44–5.0 × 10$^{-4}$ was evaluated under the above conditions in 0.4 *M* Tris-HCl pH 8 (100 mL) using (±)-**1***b* (500 mg, 4 mmol), HLADH (14–159 mg, 0.175–2.00 μmol), $NAD^+$ (700 mg, 1.06 mmol), and EtOH (1 mL). The yields of *trans*- and *cis*-alcohols **2**,**3***b* observed are recorded in Table 5.

## Acknowledgements

We are grateful to the Natural Sciences and Engineering Research Council of Canada for their support of this work and to Hoffmann-La Roche, Nutley, New Jersey for additional financial aid. We are also indebted to Professor Keith Dorrington for the use of his cd machine, and to Dr. Lung-chi Yuan for her assistance in determining the absolute configuration of (+)-(1*S*,2*R*)**3***b*.

1. T. TAKEMURA and J. B. JONES. J. Org. Chem. In press.
2. V. PRELOG. Pure Appl. Chem. **9**, 119 (1964); V. RETEY. Ph.D. thesis 3409, ETH, Zürich, 1963.
3. M. NAKAZAKI, H. CHIKAMATSU, K. NAEMURA, T. SUZUKI, M. IWASAKI, Y. SASAKI, and T. FUJII. J. Org. Chem. **46**, 2726 (1981), and previous papers.
4. J. M. H. GRAVES, A. CLARK, and H. J. RINGOLD. Biochemistry, **4**, 2655 (1965); H. J. RINGOLD, T. BELLAS, and A. CLARK. Biochem. Biophys. Res. Commun. **27**, 361 (1967).
5. R. E. HELMCHEN-ZEIER. Ph.D. thesis 4991, ETH, Zürich, 1973.
6. T. A. VAN OSSELAER, G. L. LEMIERE, E. M. MERCKX, J. A. LEPOIVRE, and F. C. ALDERWEIRELDT. Bull. Soc. Chim. Belg. **87**, 799 (1978).
7. C. J. SUCKLING and K. E. SUCKLING. Chem. Soc. Rev. **3**, 387 (1974); I. MACINNES, D. C. NONHEBEL, S. T. ORSZULIK, and C. J. SUCKLING. Chem. Commun. 121 (1982).
8. O. ABRIL and G. M. WHITESIDES. J. Am. Chem. Soc. **104**, 1552 (1982).
9. (*a*) J. B. JONES and J. F. BECK. Tech. Chem. N.Y. **10**, 107 (1976); (*b*) J. B. JONES, I. J. JAKOVAC, H. B. GOODBRAND, and K. P. LOK. J. Am. Chem. Soc. **104**, 4659 (1982), and references therein; (*c*) J. B. JONES and I. J. JAKOVAC. Can. J. Chem. **60**, 19 (1982); (*d*) J. A. HASLEGRAVE and J. B. JONES. J. Am. Chem. Soc. **104**, 4666 (1982); (*e*) J. DAVIES and J. B. JONES. J. Am. Chem. Soc. **101**, 5405 (1979).
10. H. HIEMSTRA and H. WYNBERG. Tetrahedron Lett. 2183 (1977).
11. J. A. DALE, D. L. DULL, and H. S. MOSHER. J. Org. Chem. **34**, 2543 (1969).
12. C. DJERASSI and W. KLYNE. J. Chem. Soc. 4929 (1962); C. BEARD, C. DJERASSI, T. ELLIOTT, and R. C. C. TAO. J. Am. Chem. Soc. **84**, 874 (1962); C. J. CHEER and C. DJERASSI. Tetrahedron Lett. 3877 (1976).
13. G. A. GOUGH, H. HUNTER, and J. KENYON. J. Chem. Soc. 2052 (1926).
14. R. BAECKSTROEM and B. SJOEBERG. Ark. Kemi, **26**, 549 (1967).
15. W. MOFFITT, R. B. WOODWARD, A. MOSCOWITZ, W. KLYNE, and C. DJERASSI. J. Am. Chem. Soc. **83**, 4013 (1961).
16. E. J. COREY and J. W. SUGGS. Tetrahedron Lett. 2647 (1975).
17. B. ZAGALAK, P. A. FREY, G. L. KARABATSOS, and R. H. ABELES. J. Biol. Chem. **241**, 3028 (1966).
18. A. I. MEYERS, D. R. WILLIAMS, G. W. ERICKSON, S. WHITE, and M. DRUELINGER. J. Am. Chem. Soc. **103**, 3081 (1981).
19. J. B. STOTHERS. C-13 nmr spectroscopy. Academic Press, New York. 1972. pp. 64–67.
20. K. DALZIEL. Acta Chem. Scand. **11**, 397 (1957).
21. A. SKITA. Ber. **56**, 1016 (1923).
22. H. H. INHOFFEN, K. WEISSERMEL, G. QUINKERT, and D. BARTLING. Ber. **89**, 853 (1956).
23. H. Z. UNGNADE and A. D. MCLAREN. J. Am. Chem. Soc. **66**, 118 (1944).
24. P. D. BARTLETT and C. M. BERRY. J. Am. Chem. Soc. **56**, 2683 (1934).


Can. J. Chem. Downloaded from www.nrcresearchpress.com by 210.87.254.6 on 09/06/12
For personal use only.

# Structural studies of organoboron compounds. XII.[1] Crystal and molecular structures of (acetylacetonato)diphenylboron and (tropolonato)diphenylboron

STEVEN J. RETTIG AND JAMES TROTTER

*Department of Chemistry, University of British Columbia, 2036 Main Mall, Vancouver, B.C., Canada V6T 1Y6*

Received June 11, 1982

STEVEN J. RETTIG and JAMES TROTTER. Can. J. Chem. **60**, 2957 (1982).

There are two crystalline modifications of (acetylacetonato)diphenylboron: triclinic, $a = 8.3557(8)$, $b = 9.3519(8)$, $c = 9.6103(9)$ Å, $\alpha = 96.094(5)$, $\beta = 94.904(6)$, $\gamma = 93.489(6)°$, $Z = 2$, space group $P\bar{1}$, and monoclinic, $a = 11.6329(11)$, $b = 17.1628(8)$, $c = 7.6542(6)$ Å, $\beta = 97.669(4)°$, $Z = 4$, space group $P2_1/c$. Crystals of (tropolonato)diphenylboron are monoclinic, $a = 12.1596(5)$, $b = 10.2614(4)$, $c = 12.4883(6)$ Å, $\beta = 100.965(2)°$, $Z = 4$, space group $P2_1/c$. All three structures were solved by direct methods and were refined by full-matrix least-squares procedures to $R$ values of 0.046, 0.041, and 0.035 for 2465, 2124, and 1722 reflections with $I \geq 3\sigma(I)$ respectively. Each structure consists of discrete molecules containing tetrahedrally coordinated boron atoms, both the acetylacetonato and tropolonato moieties being delocalized and symmetric. The chelate rings in both forms of (acetylacetonato)-diphenylboron have distorted B-envelope conformations while the chelate ring in (tropolonato)diphenylboron is essentially planar. The mean B—O and B—C distances (corrected for libration) are: 1.543(4) and 1.605(4) Å in triclinic, 1.533(3) and 1.607(4) Å in monoclinic (acetylacetonato)diphenylboron, and 1.555(11) and 1.605(6) Å in (tropolonato)diphenylboron.

STEVEN J. RETTIG et JAMES TROTTER. Can. J. Chem. **60**, 2957 (1982).

L'(acétylacétonato)diphénylbore se présente sous deux formes cristallines: (*a*) une forme triclinique appartenant au groupe d'espace $P\bar{1}$ avec $a = 8{,}3557(8)$, $b = 9{,}3519(8)$, $c = 9{,}6103(9)$ Å, $\alpha = 96{,}094(5)$, $\beta = 94{,}904(6)$, $\gamma = 93{,}489(6)°$, $Z = 2$ et (*b*) une forme monoclinique appartenant au groupe d'espace $P2_1/c$ avec $a = 11{,}6329(11)$, $b = 17{,}1628(8)$, $c = 7{,}6542(6)$ Å, $\beta = 97{,}669(4)°$, $Z = 4$. Les cristaux du (tropolonato)diphénylbore sont monocliniques avec $a = 12{,}1596(5)$, $b = 10{,}2614(4)$, $c = 12{,}4883(6)$ Å, $\beta = 100{,}965(2)°$, $Z = 4$, groupe d'espace $P2_1/c$. On a résolu toutes les structures par des méthodes directes et on les a affinées par la methode des moindres carrés (matrice complète) jusqu'à des valeurs de $R$ de 0,046, 0,041 et 0,035 pour respectivement 2465, 2124 et 1722 réflexions avec $I \geq 3\sigma(I)$. Chaque structure comprend des molécules discrètes contenant des atomes de bore coordonnés de façon tétraédrique, les deux unités acétylacétonato et tropolonato étant symétriques et délocalisées. Les cycles du chélate dans les deux formes d'(acétylacétonato) diphénylbore ont des conformations du type enveloppe B déformées tandis que le cycle du chélate dans le (tropolonato) diphénylbore est essentiellement plan. Les distances moyennes B—O et B—C (corrigées pour la libration) sont de 1,543(4) et de 1,605(4) Å dans la forme triclinique et de 1,533 et 1,607(4) Å dans la forme monoclinique de l'(acétylacétonato) diphénylbore. Ces distances sont de 1,555(11) et de 1,605(6) Å dans le cas du tropolonato) diphénylbore.

[Traduit par le journal]

## Introduction

As part of a continuing study of the molecular structures of organoboron compounds (1–11) we now report the crystal and molecular structures of the acetylacetone and tropolone esters of diphenylborinic acid. Both (acetylacetonato)diphenylboron, **1**, and (tropolonato)diphenylboron, **2**, are stabilized by both intramolecular O → B interactions and by electron delocalization in the chelate rings. The chemical and physical properties of these compounds are well documented (12–17 and references therein).

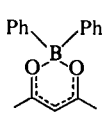


**1**

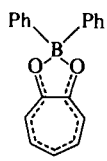


**2**

[1]References 1–11 list previous papers in this series.

## Experimental

The compounds were prepared by reacting (2-aminoethanolato)diphenylboron with the appropriate chelating agent in ethanol/acetone (1:1). With the exception of the solvent used, the procedure is identical to that previously reported for both **1** (12) and **2** (16). Two crystalline modifications of **1** were obtained. Colorless crystals of the triclinic form were isolated directly from the reaction mixture and recrystallization from acetone afforded colorless crystals of the monoclinic form. High-quality pale yellow crystals of **2** were isolated directly from the reaction mixture.

*Crystallographic studies*

*Triclinic (acetylacetonato)diphenylboron*

A crystal ca. 0.26 × 0.33 × 0.55 mm in size was mounted in a general orientation. Unit-cell parameters were refined by least-squares on 2 sin θ/λ values for 25 reflections measured on a diffractometer with Mo $K\alpha_1$ radiation ($\lambda = 0.70930$ Å). Crystal data at 22°C are:

$C_{17}H_{17}BO_2$ fw = 264.14

Triclinic, $a = 8.3557(8)$, $b = 9.3519(8)$, $c = 9.6103(9)$ Å, $\alpha = 96.094(5)$, $\beta = 94.904(6)$, $\gamma = 93.489(6)°$, $V = 742.1(1)$ Å$^3$, $Z = 2$, $\rho_c = 1.182$ g cm$^{-3}$, $F(000) = 280$, $\mu$(Mo Kα) = 0.70 cm$^{-1}$. Absent reflections: none, space group $P\bar{1}$ ($C_i^1$, No. 2, reduced cell) from structure analysis.

Intensities were measured with graphite-monochromated Mo

0008-4042/82/232957-08$01.00/0

©1982 National Research Council of Canada/Conseil national de recherches du Canada

Can. J. Chem. Downloaded from www.nrcresearchpress.com by 210.87.254.105 on 09/06/12
For personal use only.

TABLE 1. Final positional (fractional × $10^5$, H × $10^4$) and isotropic thermal parameters ($U \times 10^3$ Å$^2$) with estimated standard deviations in parentheses*

| Atom | $x$ | $y$ | $z$ | $U_{eq}/U_{iso}$ | Atom | $x$ | $y$ | $z$ | $U_{eq}/U_{iso}$ |
|---|---|---|---|---|---|---|---|---|---|
| | | | | Triclinic **1** | | | | | |
| O(1) | 37590(14) | 50537(10) | 17061(11) | 56 | B | 37236(20) | 66764(16) | 21428(17) | 45 |
| O(2) | 26821(12) | 68496(10) | 33915(10) | 50 | H(2) | 3023(24) | 3833(23) | 4528(22) | 84( 6) |
| C(1) | 36472(19) | 41454(15) | 26127(18) | 54 | H(5) | 6661(22) | 6047(22) | 1395(21) | 72( 5) |
| C(2) | 31724(22) | 45373(19) | 39275(20) | 63 | H(6) | 9217(30) | 6977(26) | 2160(26) | 103( 8) |
| C(3) | 26216(17) | 58822(17) | 42460(16) | 51 | H(7) | 9756(29) | 8900(23) | 4029(22) | 89( 6) |
| C(4) | 55169(17) | 73246(14) | 26798(15) | 46 | H(8) | 7562(26) | 9783(25) | 5017(24) | 96( 7) |
| C(5) | 68526(20) | 67963(20) | 20807(19) | 60 | H(9) | 4912(24) | 8847(20) | 4225(19) | 76( 5) |
| C(6) | 83993(24) | 73532(24) | 25390(23) | 74 | H(11) | 4002(23) | 9322(19) | 1126(19) | 67( 5) |
| C(7) | 86654(24) | 84630(23) | 36055(24) | 76 | H(12) | 2478(26) | 10385(25) | −571(23) | 97( 7) |
| C(8) | 73787(24) | 90201(21) | 42080(24) | 74 | H(13) | 415(24) | 8927(20) | −2052(21) | 77( 5) |
| C(9) | 58244(21) | 84577(17) | 37521(19) | 60 | H(14) | −118(24) | 6511(21) | −1746(22) | 84( 6) |
| C(10) | 28154(17) | 73580(14) | 8673(14) | 45 | H(15) | 1329(21) | 5554(21) | 195(18) | 68( 5) |
| C(11) | 31351(24) | 87733(17) | 5945(19) | 64 | H(16a) | 4935(41) | 2603(33) | 1679(34) | 139(13) |
| C(12) | 22722(27) | 93597(21) | −4767(22) | 77 | H(16b) | 3870(38) | 2145(35) | 2684(34) | 132(13) |
| C(13) | 10567(25) | 85527(23) | −12922(20) | 72 | H(16c) | 3159(42) | 2210(34) | 1334(37) | 144(11) |
| C(14) | 7200(22) | 71388(23) | −10730(19) | 69 | H(17a) | 2273(35) | 7196(34) | 5897(31) | 130(11) |
| C(15) | 15913(19) | 65554(19) | −98(17) | 56 | H(17b) | 650(35) | 6623(28) | 5253(28) | 122( 9) |
| C(16) | 39933(39) | 26434(22) | 20952(36) | 85 | H(17c) | 1761(28) | 5487(27) | 5993(26) | 105( 8) |
| C(17) | 18653(29) | 63016(31) | 55551(22) | 74 | | | | | |
| | | | | Monoclinic **1** | | | | | |
| O(1) | 11424(11) | 5789( 8) | 40338(17) | 59 | B | 23457(18) | 2897(13) | 37570(26) | 47 |
| O(2) | 29633(11) | 355( 7) | 55579(15) | 51 | H(2) | 1795(19) | 1250(15) | 7826(32) | 81( 7) |
| C(1) | 10454(18) | 9799(12) | 54495(27) | 58 | H(5) | 793(22) | −48(15) | 869(35) | 98( 8) |
| C(2) | 19027(21) | 9622(14) | 68721(29) | 65 | H(6) | 662(24) | −1030(17) | −1188(38) | 112(10) |
| C(3) | 28069(18) | 4436(11) | 69283(24) | 54 | H(7) | 1962(23) | −2078(19) | −841(41) | 116(10) |
| C(4) | 22182(15) | −4427(11) | 24598(23) | 47 | H(8) | 3476(24) | −2076(17) | 1485(38) | 114( 9) |
| C(5) | 13582(22) | −4607(17) | 10294(35) | 85 | H(9) | 3620(20) | −1066(14) | 3566(33) | 90( 8) |
| C(6) | 12556(25) | −10613(20) | −1858(40) | 100 | H(11) | 4693(17) | 609(12) | 4024(29) | 62( 6) |
| C(7) | 20219(26) | −16628(17) | −98(38) | 85 | H(12) | 5793(23) | 1590(14) | 2854(34) | 97( 9) |
| C(8) | 28960(26) | −16555(15) | 13641(37) | 85 | H(13) | 4821(22) | 2515(17) | 989(37) | 101( 8) |
| C(9) | 29853(20) | −10546(13) | 25861(30) | 66 | H(14) | 2731(20) | 2520(15) | 466(33) | 88( 8) |
| C(10) | 30574(16) | 9940(10) | 30348(21) | 46 | H(15) | 1679(21) | 1565(13) | 1660(32) | 81( 8) |
| C(11) | 42643(18) | 10167(12) | 33267(25) | 54 | H(16a) | −150(31) | 1652(20) | 6452(53) | 138(13) |
| C(12) | 49043(25) | 15773(14) | 25913(31) | 73 | H(16b) | −67(29) | 1870(25) | 4553(49) | 154(15) |
| C(13) | 43446(32) | 21427(15) | 15286(34) | 82 | H(16c) | −694(28) | 1122(18) | 4938(41) | 119(12) |
| C(14) | 31605(32) | 21445(14) | 12011(30) | 78 | H(17a) | 3503(27) | 610(20) | 9351(50) | 137(13) |
| C(15) | 25189(23) | 15793(13) | 19459(26) | 63 | H(17b) | 4371(33) | 349(23) | 8275(56) | 159(17) |
| C(16) | −433(27) | 14324(21) | 54073(50) | 85 | H(17c) | 3655(31) | −223(24) | 8780(51) | 150(15) |
| C(17) | 36447(32) | 2950(22) | 85392(31) | 78 | | | | | |
| | | | | **2** | | | | | |
| O(1) | 35069( 8) | 40572(10) | 78274( 8) | 48 | C(18) | 7964(19) | 72435(26) | 85407(18) | 76 |
| O(2) | 38158( 9) | 62490(10) | 74536( 9) | 52 | C(19) | 16606(16) | 69107(20) | 80178(15) | 61 |
| C(1) | 45117(12) | 44106(16) | 83103(12) | 43 | B | 28793(15) | 52267(18) | 71900(15) | 45 |
| C(2) | 46989(12) | 57596(17) | 80930(11) | 45 | H(3) | 5575(14) | 7421(20) | 8294(14) | 66( 5) |
| C(3) | 56401(15) | 65011(22) | 84762(14) | 61 | H(4) | 7182(16) | 6809(20) | 9290(16) | 79( 6) |
| C(4) | 66497(16) | 60914(26) | 90986(15) | 71 | H(5) | 7733(17) | 4797(19) | 9862(17) | 80( 6) |
| C(5) | 69727(17) | 48778(27) | 94994(16) | 75 | H(6) | 6713(17) | 2980(22) | 9786(18) | 92( 7) |
| C(6) | 63461(17) | 37567(24) | 94171(15) | 68 | H(7) | 4903(15) | 2675(21) | 8959(16) | 80( 6) |
| C(7) | 52479(14) | 35418(19) | 89177(13) | 55 | H(9) | 4175(17) | 5312(18) | 5574(16) | 71( 6) |
| C(8) | 26187(12) | 48830(15) | 59111(13) | 46 | H(10) | 3822(20) | 4766(22) | 3783(19) | 104( 8) |
| C(9) | 34291(16) | 49977(19) | 52692(16) | 63 | H(11) | 2060(17) | 3891(21) | 2942(21) | 93( 7) |
| C(10) | 32292(18) | 46454(23) | 41779(17) | 75 | H(12) | 662(17) | 3703(18) | 4003(16) | 77( 6) |
| C(11) | 22097(17) | 41577(22) | 36983(17) | 70 | H(13) | 986(16) | 4312(18) | 5799(15) | 68( 5) |
| C(12) | 13858(17) | 40419(21) | 42958(15) | 67 | H(15) | 1213(13) | 3770(18) | 7846(14) | 55( 5) |
| C(13) | 15865(14) | 44124(19) | 53852(14) | 57 | H(16) | −261(17) | 4358(20) | 8677(17) | 79( 6) |
| C(14) | 18488(13) | 56255(16) | 77418(12) | 47 | H(17) | −537(17) | 6552(22) | 9170(17) | 93( 7) |
| C(15) | 11021(14) | 47002(20) | 80068(14) | 56 | H(18) | 720(16) | 8124(23) | 8760(18) | 87( 7) |
| C(16) | 2250(16) | 50407(26) | 85171(16) | 68 | H(19) | 2176(15) | 7562(19) | 7871(15) | 65( 5) |
| C(17) | 835(18) | 63121(27) | 87905(17) | 76 | | | | | |

*$U_{eq}$ = (1/3) (trace $U$).

Can. J. Chem. Downloaded from www.nrcresearchpress.com by 210.87.254.105 on 09/06/12
For personal use only.

Can. J. Chem. Downloaded from www.nrcresearchpress.com by 210.87.254.105 on 09/06/12
For personal use only.

Kα radiation (λ = 0.71073 Å) on an Enraf-Nonius CAD4-F diffractometer. An ω–2θ scan at 0.96–10.06° min$^{-1}$ over a range of (0.65 + 0.35 tan θ) degrees in ω (extended by 25% on both sides for background measurement) was employed. Data were measured to 2θ = 60°. The intensities of three check reflections, measured every 3600 s throughout the data collection, remained constant to within 3%.

After data reduction, no absorption correction was made in view of the low value of μ. Of the 4297 independent reflections measured, 2465 (57.4%) had intensities greater than 3σ($I$) above background where $\sigma^2(I) = S + 2B + (0.04(S - B))^2$ with $S$ = scan count and $B$ = background count.

The centrosymmetric space group $P\bar{1}$ was indicated by the $E$-statistics. The structure was solved by direct methods, the coordinates of all non-hydrogen atoms being determined from an $E$-map. After full-matrix least-squares refinement of the non-hydrogen atoms with anisotropic thermal parameters to $R$ = 0.086, a difference map gave positions for all 17 hydrogen atoms which were refined with isotropic thermal parameters in subsequent least-squares cycles. The scattering factors of ref. 18 were used for non-hydrogen atoms and those of ref. 19 for hydrogen atoms. The weighting scheme, $w = 1/\sigma^2(F)$ where $\sigma^2(F)$ is derived from the previously defined $\sigma^2(I)$ gave uniform average values of $w(|F_o| - |F_c|)^2$ over ranges of both $|F_o|$ and sin θ/λ and was employed in the final stages of refinement. Convergence was reached at $R$ = 0.046 and $R_w$ = 0.061 for 2465 reflections with $I \geq 3\sigma(I)$. For all 4297 reflections $R$ = 0.087. The function minimized was $\Sigma w(|F_o| - |F_c|)^2$, $R = \Sigma||F_o| - |F_c||/\Sigma|F_o|$ and $R_w = (\Sigma w(|F_o| - |F_c|)^2/\Sigma w|F_o|^2)^{1/2}$.

On the final cycle of refinement the mean and maximum parameter shifts corresponded to 0.10 and 0.74σ respectively. The mean error in an observation of unit weight was 2.071. A final difference map showed no unusual features. The final positional and thermal parameters appear in Tables 1 and 2[2] respectively. Measured and calculated structure factors have been placed in the Depository of Unpublished Data.[2]

*Monoclinic (acetylacetonato)diphenylboron*

Experimental details are as above except where noted. Crystal dimensions were ca. 0.33 × 0.24 × 0.45 mm. Crystal data are:

$C_{17}H_{17}BO_2$ fw = 264.14

Monoclinic, $a$ = 11.6329(11), $b$ = 17.1628(8), $c$ = 7.6542(6) Å, β = 97.669(4)°, $V$ = 1514.5(2) Å$^3$, $Z$ = 4, $\rho_c$ = 1.158 g cm$^{-3}$, $F(000)$ = 560, μ(Mo Kα) = 0.68 cm$^{-1}$. Absent reflections: $h0l$, $l \neq 2n$ and $0k0$, $k \neq 2n$ uniquely indicate the space group $P2_1/c$ ($C_{2h}^5$, No. 14).

An ω–2θ scan at 0.96–10.06° min$^{-1}$ over a range of (0.70 + 0.35 tan θ)° in ω was employed. Of 3456 independent reflections measured (to 2θ = 55°), 2124 (61.5%) had intensities greater than 3σ($I$) above background.

The structure was solved by direct methods. After refinement of the non-hydrogen atoms with anisotropic thermal parameters to $R$ = 0.092, all H coordinates were determined from a difference map. In the final stages of refinement an isotropic Type I extinction correction (Thornley-Nelmes definition of mosaic anisotropy with a Lorentzian distribution) was applied (20–22). The final value of $g$ was 8.1(10) × 10$^4$. Convergence was reached at 0.041 and $R_w$ = 0.049 for 2124 reflections with $I \geq 3\sigma(I)$, for all 3456 reflections $R$ = 0.076. The mean and maximum parameter shifts on the final cycle of refinement corresponded to 0.07 and 0.36σ respectively and the mean error in an observation of unit weight was 1.076. A final difference map showed no unusual features.

*(Tropolonato)diphenylboron*

Crystal dimensions were ca. 0.15 × 0.28 × 0.48 mm. Crystal data are:

$C_{19}H_{15}BO_2$ fw = 286.14

Monoclinic, $a$ = 12.1596(5), $b$ = 10.2614(4), $c$ = 12.4883(6) Å, β = 100.965(2)°, $V$ = 1529.8(1) Å$^3$, $Z$ = 4, $\rho_c$ = 1.242 g cm$^{-3}$, $F(000)$ = 600, μ(Mo Kα) = 0.43 cm$^{-1}$. Absent reflections: $h0l$, $l \neq 2n$ and $0k0$, $k \neq 2n$ uniquely indicate the space group $P2_1/c$.

An ω–2θ scan at 0.96–10.06° min$^{-1}$ over a range of (0.70 + 0.35 tan θ)° was employed. Of 3497 independent reflections measured (to 2θ = 55°), 1722 (49.2%) had $I \geq 3\sigma(I)$. The structure was solved by direct methods. After refinement of the non-hydrogen atoms with anisotropic thermal parameters to $R$ = 0.080, the hydrogen atoms were located from a difference map. Convergence was reached at $R$ = 0.035 and $R_w$ = 0.040 for 1722 reflections with $I \geq 3\sigma(I)$, for all 3497 reflections $R$ = 0.100. The mean and maximum parameter shifts on the final cycle of refinement corresponded to 0.03 and 0.18σ respectively and the mean error in an observation of unit weight was 1.803.

*Analysis of thermal motion*

The thermal motion in each of the three molecules (shown in Figs. 1 and 2) has been analysed in terms of the rigid-body modes of translation, libration, and screw-motion (23). The rms errors in the $U_{ij}$ (derived from the least-squares analyses) are 0.0009, 0.0014, and 0.0010 Å$^2$ for triclinic **1**, monoclinic **1**, and **2** respectively. Analysis of the entire molecules in each case indicated significant independent motion of the phenyl groups and gave rms $\Delta U_{ij}$ values of 0.0062, 0.0068, and 0.0047 Å$^2$ for the three structures. The $C_6H_5B$ groups were separately analysed (rms $\Delta U_{ij}$ = 0.0015–0.0023 Å$^2$). For both forms of **1** the corrections to bonds in the chelate rings were based on the analyses of the whole molecule since the (acetylacetonato) $BC_2$ fragment of the monoclinic form gave a non-positive-definite libration tensor. For **2** the tropolonato-$BC_2$ moiety was separately analysed (rms $\Delta U_{ij}$ = 0.0023 Å$^2$). All rigid-body analyses employed gave physically reasonable results. The appropriate bond distances have been corrected for libration (23, 24), using shape parameters $q^2$ of 0.08 for all atoms involved. Corrected bond lengths appear in Table 3 along with the uncorrected values; corrected bond angles do not differ by more than 1σ from the uncorrected values given in Table 4. Intra-annular torsion angles defining the conformations of chelate rings are listed in Table 5. Bond lengths and angles involving hydrogen and a complete listing of torsion angles (Tables 6–8) are included as supplementary material.

## Results and discussion

Each of the three structures consists of discrete molecules separated by normal van der Waals distances, although in monoclinic **1** there is one unusually short H···H contact (H(5)···H(5)($-x$, $-y$, $-z$) = 2.13(5) Å). In each case $Ph_2B$ may be considered as a pseudo-metal (14) coordinated to fully delocalized acetylacetonato or tropolonato ligands resulting in distorted tetrahedral coordination about the boron atoms.

The most obvious difference between the molecules of **1** in the two different crystalline forms is the orientation of the pseudo-equatorial phenyl

[2]The structure factor table, Table 2 (anisotropic thermal parameters) and other material mentioned in the text are available, at a nominal charge, from the Depository of Unpublished Data, CISTI, National Research Council of Canada, Ottawa, Canada K1A 0S2.

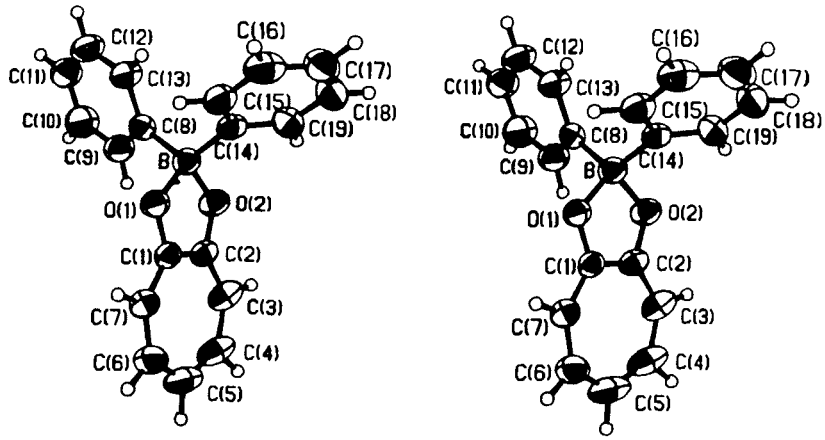


FIG. 1. Stereoscopic views of the triclinic (top) and monoclinic (bottom) forms of (acetylacetonato)diphenylboron. 50% probability thermal ellipsoids are shown for the non-hydrogen atoms. The monoclinic form shown is the mirror image of the molecule described by the coordinates in Table 1 for comparison with the triclinic form.

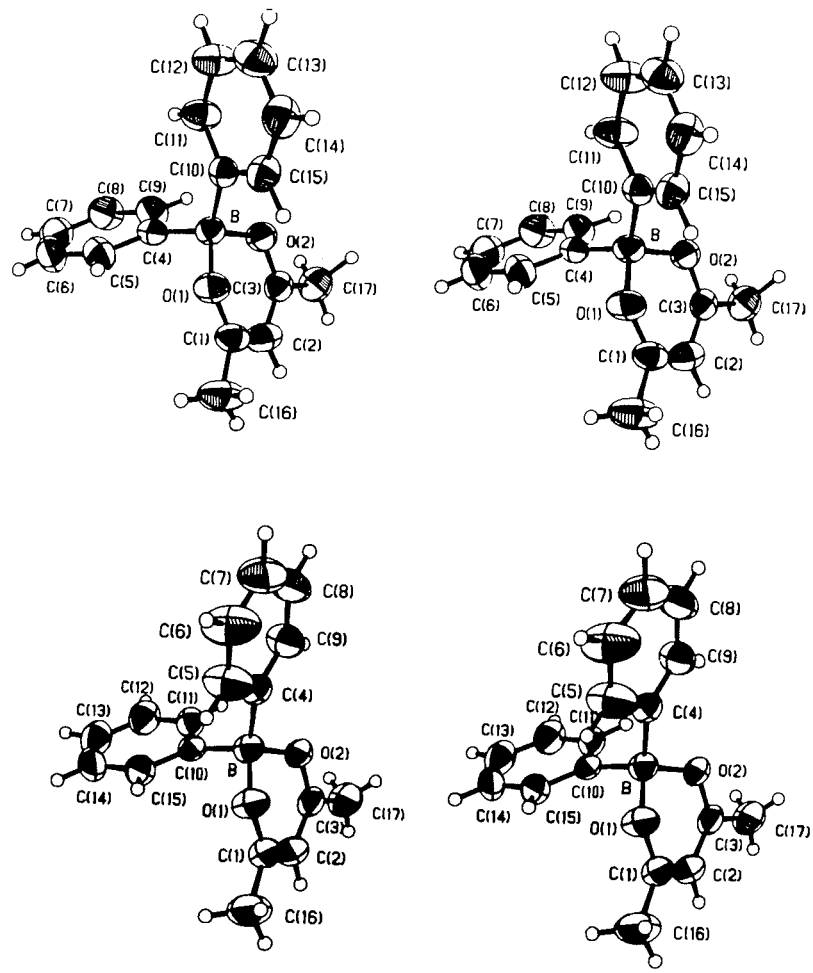


FIG. 2. Stereoscopic view of the (tropolonato)diphenylboron molecule. 50% probability thermal ellipsoids are shown for the non-hydrogen atoms.

Can. J. Chem. Downloaded from www.nrcresearchpress.com by 210.87.254.105 on 09/06/12
For personal use only.

TABLE 3. Bond lengths (Å) with estimated standard deviations in parentheses

| Bond | Length Uncorr. | Length Corr. | Bond | Length Uncorr. | Length Corr. |
|---|---|---|---|---|---|
| | | | Triclinic **1** | | |
| O(1)—C(1) | 1.284(2) | 1.287 | C(5)—C(6) | 1.381(3) | 1.386 |
| O(1)—B | 1.534(2) | 1.539 | C(6)—C(7) | 1.372(3) | 1.383 |
| O(2)—C(3) | 1.286(2) | 1.288 | C(7)—C(8) | 1.368(3) | 1.380 |
| O(2)—B | 1.541(2) | 1.547 | C(8)—C(9) | 1.388(2) | 1.393 |
| C(1)—C(2) | 1.375(2) | 1.381 | C(10)—C(11) | 1.391(2) | 1.403 |
| C(1)—C(16) | 1.493(2) | 1.497 | C(10)—C(15) | 1.394(2) | 1.406 |
| C(2)—C(3) | 1.378(2) | 1.383 | C(10)—B | 1.596(2) | 1.601 |
| C(3)—C(17) | 1.481(2) | 1.486 | C(11)—C(12) | 1.385(2) | 1.391 |
| C(4)—C(5) | 1.392(2) | 1.403 | C(12)—C(13) | 1.364(3) | 1.375 |
| C(4)—C(9) | 1.392(2) | 1.404 | C(13)—C(14) | 1.377(3) | 1.389 |
| C(4)—B | 1.603(2) | 1.608 | C(14)—C(15) | 1.382(2) | 1.387 |
| | | | Monoclinic **1** | | |
| O(1)—C(1) | 1.301(2) | 1.304 | C(5)—C(6) | 1.383(3) | 1.389 |
| O(1)—B | 1.526(2) | 1.530 | C(6)—C(7) | 1.359(4) | 1.380 |
| O(2)—C(3) | 1.294(2) | 1.297 | C(7)—C(8) | 1.362(4) | 1.379 |
| O(2)—B | 1.530(2) | 1.535 | C(8)—C(9) | 1.387(3) | 1.393 |
| C(1)—C(2) | 1.375(3) | 1.381 | C(10)—C(11) | 1.392(3) | 1.403 |
| C(1)—C(16) | 1.482(3) | 1.484 | C(10)—C(15) | 1.399(3) | 1.407 |
| C(2)—C(3) | 1.374(3) | 1.378 | C(10)—B | 1.604(3) | 1.610 |
| C(3)—C(17) | 1.488(3) | 1.488 | C(11)—C(12) | 1.382(3) | 1.388 |
| C(4)—C(5) | 1.381(3) | 1.399 | C(12)—C(13) | 1.373(4) | 1.380 |
| C(4)—C(9) | 1.373(3) | 1.394 | C(13)—C(14) | 1.367(4) | 1.377 |
| C(4)—B | 1.596(3) | 1.603 | C(14)—C(15) | 1.392(4) | 1.398 |
| | | | **2** | | |
| O(1)—C(1) | 1.307(2) | 1.311 | C(8)—B | 1.607(3) | 1.611 |
| O(1)—B | 1.557(2) | 1.565 | C(9)—C(10) | 1.386(3) | 1.390 |
| O(2)—C(2) | 1.310(2) | 1.315 | C(10)—C(11) | 1.365(3) | 1.374 |
| O(2)—B | 1.537(2) | 1.544 | C(11)—C(12) | 1.363(3) | 1.375 |
| C(1)—C(2) | 1.437(2) | 1.446 | C(12)—C(13) | 1.389(3) | 1.393 |
| C(1)—C(7) | 1.383(2) | 1.389 | C(14)—C(15) | 1.396(2) | 1.404 |
| C(2)—C(3) | 1.382(2) | 1.387 | C(14)—C(19) | 1.393(2) | 1.401 |
| C(3)—C(4) | 1.387(3) | 1.392 | C(14)—B | 1.594(2) | 1.599 |
| C(4)—C(5) | 1.371(3) | 1.379 | C(15)—C(16) | 1.387(3) | 1.392 |
| C(5)—C(6) | 1.373(3) | 1.380 | C(16)—C(17) | 1.368(3) | 1.376 |
| C(6)—C(7) | 1.380(3) | 1.385 | C(17)—C(18) | 1.366(3) | 1.373 |
| C(8)—C(9) | 1.389(2) | 1.400 | C(18)—C(19) | 1.381(3) | 1.386 |
| C(8)—C(13) | 1.388(2) | 1.397 | | | |

group (which contains C(10) in the triclinic form and C(4) in the monoclinic form). The asymmetric disposition of the phenyl rings in triclinic **1** (and in **2**) is that usually observed in $Ar_2B$ chelates (1–3, 6, 9) while the symmetric disposition observed in monoclinic **1** is less common (5, 11). Bond angles at B and O atoms, bond distances involving O, and chelate ring conformations differ significantly between the two modifications of **1** (see Tables 3–5). These differences presumably arise from steric effects and induced hybridization effects.

The acetylacetonato moiety in both forms of **1** is fully delocalized and symmetric, but unlike the planar chelate ring found for (benzoylacetonato)-difluoroboron, **3** (25), the six-membered chelate rings in **1** have distorted B-envelope conformations very similar to that observed in (salicylaldehydato)diphenylboron, **4** (5). The dihedral angles between the C(1)C(2)C(3) and the OBO planes are 31.9 and 41.1° for triclinic and monoclinic **1** respectively.

The mean[3] B—O distances in triclinic and monoclinic **1** are 1.543(4) and 1.533(3) Å (overall mean 1.538(7) Å). The B—O distance in **3** of 1.488(3) Å is shorter by 0.05 Å than those in **1**, this difference being the same as that between the B—O distances in *N*-methylacethydroxamato chelates of $F_2B$ (8) and $Ph_2B$ (11). The average B—O distance in **4** of 1.537 Å compares well with the mean for the two forms of **1**, although the individual values for **4** differ considerably (1.500(4) and 1.574(4) Å). The

[3]Here and elsewhere in this report mean values refer to weighted means with rms deviations from the mean in parentheses.

Can. J. Chem. Downloaded from www.nrcresearchpress.com by 210.87.254.105 on 09/06/12
For personal use only.

Can. J. Chem. Downloaded from www.nrcresearchpress.com by 210.87.254.105 on 09/06/12
For personal use only.

TABLE 4. Bond angles (deg) with estimated standard deviations in parentheses

| Bonds | Angle (deg) | Bonds | Angle (deg) |
|---|---|---|---|
| | Triclinic **1** | | |
| C(1)—O(1)—B | 120.89(12) | C(4)—C(9)—C(8) | 121.8(2) |
| C(3)—O(2)—B | 120.34(11) | C(11)—C(10)—C(15) | 116.25(14) |
| O(1)—C(1)—C(2) | 121.62(14) | C(11)—C(10)—B | 123.13(13) |
| O(1)—C(1)—C(16) | 114.7(2) | C(15)—C(10)—B | 120.57(13) |
| C(2)—C(1)—C(16) | 123.7(2) | C(10)—C(11)—C(12) | 121.9(2) |
| C(1)—C(2)—C(3) | 120.08(15) | C(11)—C(12)—C(13) | 120.2(2) |
| O(2)—C(3)—C(2) | 121.72(15) | C(12)—C(13)—C(14) | 119.7(2) |
| O(2)—C(3)—C(17) | 115.2(2) | C(13)—C(14)—C(15) | 119.9(2) |
| C(2)—C(3)—C(17) | 123.0(2) | C(10)—C(15)—C(14) | 122.0(2) |
| C(5)—C(4)—C(9) | 116.35(15) | O(1)—B —O(2) | 106.94(11) |
| C(5)—C(4)—B | 121.59(13) | O(1)—B —C(4) | 108.79(11) |
| C(9)—C(4)—B | 122.05(13) | O(1)—B —C(10) | 107.61(11) |
| C(4)—C(5)—C(6) | 121.8(2) | O(2)—B —C(4) | 108.20(11) |
| C(5)—C(6)—C(7) | 120.6(2) | O(2)—B —C(10) | 107.43(11) |
| C(6)—C(7)—C(8) | 119.3(2) | C(4)—B —C(10) | 117.42(12) |
| C(7)—C(8)—C(9) | 120.2(2) | | |
| | Monoclinic **1** | | |
| C(1)—O(1)—B | 118.07(15) | C(4)—C(9)—C(8) | 122.1(2) |
| C(3)—O(2)—B | 118.42(15) | C(11)—C(10)—C(15) | 115.9(2) |
| O(1)—C(1)—C(2) | 120.9(2) | C(11)—C(10)—B | 121.4(2) |
| O(1)—C(1)—C(16) | 115.3(2) | C(15)—C(10)—B | 122.4(2) |
| C(2)—C(1)—C(16) | 123.8(2) | C(10)—C(11)—C(12) | 122.7(2) |
| C(1)—C(2)—C(3) | 120.7(2) | C(11)—C(12)—C(13) | 119.7(3) |
| O(2)—C(3)—C(2) | 121.0(2) | C(12)—C(13)—C(14) | 119.8(3) |
| O(2)—C(3)—C(17) | 115.6(2) | C(13)—C(14)—C(15) | 120.4(2) |
| C(2)—C(3)—C(17) | 123.4(2) | C(10)—C(15)—C(14) | 121.5(2) |
| C(5)—C(4)—C(9) | 115.7(2) | O(1)—B —O(2) | 107.26(14) |
| C(5)—C(4)—B | 120.5(2) | O(1)—B —C(4) | 109.36(15) |
| C(9)—C(4)—B | 123.6(2) | O(1)—B —C(10) | 109.1(2) |
| C(4)—C(5)—C(6) | 122.6(2) | O(2)—B —C(4) | 109.22(15) |
| C(5)—C(6)—C(7) | 120.2(3) | O(2)—B —C(10) | 108.86(15) |
| C(6)—C(7)—C(8) | 118.8(2) | C(4)—B —C(10) | 112.85(15) |
| C(7)—C(8)—C(9) | 120.6(3) | | |
| | **2** | | |
| C(1)—O(1)—B | 110.26(12) | C(10)—C(11)—C(12) | 119.5(2) |
| C(2)—O(2)—B | 110.91(12) | C(11)—C(12)—C(13) | 120.1(2) |
| O(1)—C(1)—C(2) | 110.36(12) | C(8)—C(13)—C(12) | 122.2(2) |
| O(1)—C(1)—C(7) | 121.67(15) | C(15)—C(14)—C(19) | 116.1(2) |
| C(2)—C(1)—C(7) | 127.97(14) | C(15)—C(14)—B | 121.87(15) |
| O(2)—C(2)—C(1) | 110.08(12) | C(19)—C(14)—B | 121.98(15) |
| O(2)—C(2)—C(3) | 121.9(2) | C(14)—C(15)—C(16) | 121.9(2) |
| C(1)—C(2)—C(3) | 128.0(2) | C(15)—C(16)—C(17) | 119.9(2) |
| C(2)—C(3)—C(4) | 127.8(2) | C(16)—C(17)—C(18) | 119.7(2) |
| C(3)—C(4)—C(5) | 129.9(2) | C(17)—C(18)—C(19) | 120.5(2) |
| C(4)—C(5)—C(6) | 128.1(2) | C(14)—C(19)—C(18) | 121.8(2) |
| C(5)—C(6)—C(7) | 130.0(2) | O(1)—B —O(2) | 98.36(11) |
| C(1)—C(7)—C(6) | 127.9(2) | O(1)—B —C(8) | 108.89(13) |
| C(9)—C(8)—C(13) | 115.7(2) | O(1)—B —C(14) | 109.02(13) |
| C(9)—C(8)—B | 121.85(14) | O(2)—B —C(8) | 111.14(13) |
| C(13)—C(8)—B | 122.43(15) | O(2)—B —C(14) | 110.09(13) |
| C(8)—C(9)—C(10) | 122.3(2) | C(8)—B —C(14) | 117.60(13) |
| C(9)—C(10)—C(11) | 120.1(2) | | |

mean C—O distances, 1.288(1) and 1.301(4) Å for triclinic and monoclinic **1**, lie between the values of 1.304(2) Å for **3** and the mean of 1.274 Å for a number of metal complexes of acetylacetone (26). The mean chelate ring C—C distance of 1.381(2) Å is shorter than the values of 1.389(1) Å in **3** and 1.390 Å in the metal complexes. In the structure of **3** (determined at −180°C) the C—$CH_3$ bond was unusually short at 1.485(3) Å, this also being observed for **1**, the mean C—$CH_3$ distance being

Can. J. Chem. Downloaded from www.nrcresearchpress.com by 210.87.254.105 on 09/06/12
For personal use only.

TABLE 5. Intra-annular torsion angles (deg) standard deviations in parentheses

| Atoms | Value (deg) |
|---|---|
| Triclinic **1** | |
| B —O(1)—C(1)—C(2) | 13.3(2) |
| O(1)—C(1)—C(2)—C(3) | 7.6(2) |
| C(1)—C(2)—C(3)—O(2) | −7.0(2) |
| B —O(2)—C(3)—C(2) | −14.4(2) |
| C(3)—O(2)—B —O(1) | 30.5(2) |
| C(1)—O(1)—B —O(2) | −30.0(2) |
| Monoclinic **1** | |
| B —O(1)—C(1)—C(2) | −17.9(3) |
| O(1)—C(1)—C(2)—C(3) | −8.7(3) |
| C(1)—C(2)—C(3)—O(2) | 9.5(3) |
| B —O(2)—C(3)—C(2) | 16.4(3) |
| C(3)—O(2)—B —O(1) | −38.2(2) |
| C(1)—O(1)—B —O(2) | 38.8(2) |
| **2** | |
| B —O(1)—C(1)—C(2) | 0.1(2) |
| O(1)—C(1)—C(2)—O(2) | −1.2(2) |
| B —O(2)—C(2)—C(1) | 1.8(2) |
| C(2)—O(2)—B —O(1) | −1.56(15) |
| C(1)—O(1)—B —O(2) | 0.80(15) |

1.489(6) Å (libration corrected) compared to the average of 1.524 Å observed in the metal complexes (26).

The fused five- and seven-membered ring system in **2** is planar to within 0.06 Å, each of the rings being slightly but significantly non-planar (maximum deviations from the mean planes[4] being 0.006 and 0.012 Å for the 7- and 5-membered rings respectively). The tropolonato moiety is symmetric and fully delocalized; the unique C(1)—C(2) distance is 1.446(2) Å, mean C—O = 1.313(2) Å, and the remaining six C—C bonds are essentially equal (mean C—C = 1.385(5) Å). The two B—O distances in **2** are significantly different (1.565(2) and 1.544(2) Å), the average value of 1.555 Å being similar to the corresponding value of 1.550(2) Å observed in the structure of (*N*-methylacethydroxamato)diphenylboron (11) which also contains a planar five-membered chelate ring with two oxygen atoms bonded to boron. In 4,4-dimethyl-2,2-diphenyl-1,3-dioxa-4-azonia-2-boranatacyclopentane, **5** (3), which has a non-planar chelate ring, the B—O distances are 1.506(7) and 1.556(8) Å. The B—O distances in **1** and **2** are longer than the true single bonds in the tetrahedrally coordinated ethanolamine esters of diarylborinic acids which have a mean bond length of 1.477(5) Å (1, 2, 6) and in the related ethanolamine chelate spiro(9*H*-borepino-[2,3-*b*:7,6-*b*']dithiophene-9,2'-[1,3,2]oxazaborolidine) (27), in which B—O = 1.488(2) Å at 87 K.

In all three structures, the two B—C distances are somewhat different, this difference being significant only in the case of **2**. In both forms of **1** the pseudo-equatorial B—C distances are 0.007 Å shorter than the others, the overall mean being 1.606(4) Å compared with a mean of 1.605(6) Å in **2**. These values are both near the short end of the range 1.603(4) Å in **4** to 1.639(8) Å in **5** observed for $Ar_2B$ chelates (1–3, 5, 6, 9, 11). Differences between chemically equivalent B—C distances have been observed earlier (3, 5, 6, 28). The geometry of the B-substituted phenyl rings is as expected (28). With the exception of the C(10) ring in monoclinic **1** ($\chi^2 = 1.3$), all phenyl rings in **1** and **2** are significantly non-planar ($\chi^2 = 20.8$–$88.1$) although deviations from the mean planes are less than 0.012 Å in all cases (esd's of the deviations from the mean planes are 0.001–0.003 Å).

[4]Weighted least-squares mean planes via Hamilton method.

**Acknowledgments**

We thank the Natural Sciences and Engineering Research Council Canada for financial support and the University of British Columbia Computing Centre for assistance.

1. S. J. RETTIG and J. TROTTER. Can. J. Chem. **51**, 1288 (1973).
2. S. J. RETTIG and J. TROTTER. Acta Crystallogr. Sect. B, **30**, 2139 (1974).
3. S. J. RETTIG, J. TROTTER, and W. KLIEGEL. Can. J. Chem. **52**, 2531 (1974).
4. S. J. RETTIG and J. TROTTER. Can. J. Chem. **53**, 1393 (1975).
5. S. J. RETTIG and J. TROTTER. Can. J. Chem. **54**, 1168 (1976).
6. S. J. RETTIG and J. TROTTER. Can. J. Chem. **54**, 3130 (1976).
7. S. J. RETTIG, J. TROTTER, W. KLIEGEL, and H. BECKER. Can. J. Chem. **54**, 3142 (1976).
8. S. J. RETTIG, J. TROTTER, W. KLIEGEL, and D. NANNINGA. Can. J. Chem. **55**, 1 (1977).
9. S. J. RETTIG and J. TROTTER. Can. J. Chem. **55**, 958 (1977).
10. S. J. RETTIG and J. TROTTER. Can. J. Chem. **55**, 3071 (1977).
11. S. J. RETTIG, J. TROTTER, W. KLIEGEL, and D. NANNINGA. Can. J. Chem. **56**, 1676 (1978).
12. I. BALLY, A. ARSENE, M. BACESCU-ROMAN, and A. T. BALABAN. Tetrahedron Lett. 3929 (1965).
13. F. UMLAND and C. SCHLEYERBACH. Angew. Chem. **77**, 169 (1965); **77**, 426 (1965).
14. L. H. TOPORCER, R. E. DESSY, and S. I. E. GREEN. Inorg. Chem. **4**, 1649 (1965).
15. A. TRESTIANU, H. NICULESCU-MAJEWSKA, I. BALLY, A. BARABAS, and A. T. BALABAN. Tetrahedron, **24**, 2499 (1968).
16. I. BALLY, A. ARSENE, M. ROMAN, M. PARASCHIV, E. ROMAS, and A. T. BALABAN. Rev. Roum. Chim. **13**, 1225 (1968).

17. A. T. BALABAN, I. BALLY, V. I. MINKIN, and A. I. USACHEV. Tetrahedron, **33**, 3265 (1977).
18. D. T. CROMER and J. B. MANN. Acta Crystallogr. Sect. A, **24**, 321 (1968).
19. R. F. STEWART, E. R. DAVIDSON, and W. T. SIMPSON. J. Chem. Phys. **42**, 3175 (1965).
20. P. J. BECKER and P. COPPENS. Acta Crystallogr. Sect. A, **30**, 129 (1974); **30**, 148 (1974); **31**, 417 (1975).
21. P. COPPENS and W. C. HAMILTON. Acta Crystallogr. Sect. A, **26**, 71 (1970).
22. F. R. THORNLEY and R. J. NELMES. Acta Crystallogr. Sect. A, **30**, 748 (1974).
23. V. SCHOMAKER and K. N. TRUEBLOOD. Acta Crystallogr. Sect. B, **24**, 63 (1968).
24. D. W. J. CRUICKSHANK. Acta Crystallogr. **9**, 747 (1956); **9**, 754 (1956); **14**, 896 (1961).
25. A. W. HANSON and E. W. MACAULAY. Acta Crystallogr. Sect. B, **28**, 1961 (1972).
26. E. C. LINGAFELTER and R. L. BRAUN. J. Am. Chem. Soc. **88**, 2951 (1966).
27. I. CYNKIER and H. HOPE. Acta Crystallogr. Sect. B, **34**, 2990 (1978).
28. A. DOMENICANO, A. VACIAGO, and C. A. COULSON. Acta Crystallogr. Sect. B, **31**, 221 (1975); **31**, 1630 (1975).

Can. J. Chem. Downloaded from www.nrcresearchpress.com by 210.87.254.105 on 09/06/12
For personal use only.

# Five-membered ring annulation via thermal rearrangement of β-cyclopropyl α,β-unsaturated ketones. A formal total synthesis of the sesquiterpenoid (±)-zizaene

EDWARD PIERS, JACQUES BANVILLE, CHEUK KUN LAU, AND ISAO NAGAKURA

*Department of Chemistry, University of British Columbia, 2036 Main Mall, University Campus, Vancouver, B.C., Canada V6T 1Y6*

Received June 14, 1982

EDWARD PIERS, JACQUES BANVILLE, CHEUK KUN LAU, and ISAO NAGAKURA. Can. J. Chem. **60**, 2965 (1982).

Treatment of the β-iodo enones **7–10** with lithium (phenylthio)(cyclopropyl)cuprate provided excellent yields of the corresponding β-cyclopropyl α,β-unsaturated ketones **11–14**, respectively. When 3-isopropenyl-2-cyclohexen-1-one (**16**) was allowed to react with dimethyloxosulfonium methylide in dimethyl sulfoxide – tetrahydrofuran, 3-(1-methylcyclopropyl)-2-cyclohexen-1-one (**17**) was produced in 59% yield. Although thermal rearrangement (~425–450°C) of compounds **11** and **17** produced high yields of the annulation products **19** and **22**, respectively, similar reactions involving the β-cyclopropyl enones **12** and **13** were not efficient in terms of production of the corresponding bicyclic systems (**23**, **26**, and/or **27**, respectively). In these cases, predominant (**24** + **25** from **12**) or significant (**28** + **29** from **13**) amounts of monocyclic dienones were formed. The annulation product **22** served as a convenient starting material for a new formal total synthesis of the sesquiterpenoid (±)-zizaene (**30**). Conjugate addition of lithium divinylcuprate to **22** afforded the ketone **36** which was converted by standard methods (via **38** and **39**) into the enone **40**. Treatment of the latter substance with thiophenol in the presence of tetra-*n*-butylammonium fluoride gave **41**, which was transformed via ketalization (**41** → **42**), hydroboration (**42** → **43**), tosylation (**43** → **44**), and oxidation (**44** → **45**) into the sulfone **45**. When the latter compound was treated with potassium *tert*-butoxide in hexamethylphosphoramide, the tricyclic ketal sulfone **46** was produced in 85% yield. Reduction of **46** with sodium amalgam afforded the ketal **47**, which upon hydrolysis under mild conditions gave the ketone **32**. Treatment of the latter substance with sodium methoxide in methanol provided a 1:2 mixture of the epimeric ketones **31** and **32**, which had been converted previously by Coates and Sowerby into (±)-zizaene (**30**).

EDWARD PIERS, JACQUES BANVILLE, CHEUK KUN LAU et ISAO NAGAKURA. Can. J. Chem. **60**, 2965 (1982).

Les β-iodo énones **7–10** réagissent avec le (phénylthiocyclopropyl) cuprate de lithium en conduisant respectivement avec d'excellents rendements aux cétones α,β-insaturées, β-cyclopropyles correspondantes **11–14**. Si on laisse réagir l'isopropényl-3 cyclohexène-2 one-1 (**16**) avec le méthylure de diméthyloxosulfonium dans le diméthylsulfoxyde – tétrahydrofuranne, on obtient le (méthyl-1 cyclopropyl)-3 cyclohexèn-2 one-1 (**17**) avec un rendement de 59%. Bien que la transposition thermique (~425–450°C) des composés **11** et **17** donne avec de bons rendements respectivement les produits d'annellation **19** et **22**, les réactions analogues impliquant les β-cyclopropylenones **12** et **13** ne sont pas efficaces du point du vue de la formation des systèmes bicycliques correspondants (respectivement **23**, **26** et/ou **27**). Dans ces cas, il se forme des quantités majoritaires de diénones monocycliques (**24** + **25** à partir de **12**) ou des quantités significatives de ces mêmes composés (**28** + **29** à partir de **13**). Le produit d'annellation **22** sert de point de départ pour une nouvelle synthèse formelle et totale du sesquiterpène (±) zizaène (**30**). L'addition conjugué du divinylcuprate de lithium sur le composé **22** conduit à la cétone **36** que l'on transforme par des méthodes normales (via les composés **38** et **39**) en l'énone **40**. Cette dernière réagit avec le thiophénol en présence du fluorure de tétra-*n*-butylammonium pour donner le composé **41** que l'on transforme en sulfone **45** d'après la suite de réactions: la cétalisation (**41** → **42**), l'hydroboration (**42**→**43**), la tosylation (**43** → **44**) et l'oxydation en sulfone **45** à partir du composé **44**. Le sulfone en présence de *tert*-butylate de potassium dans l'hexaméthylphosphoramide conduit au sulfone cétal tricyclique **46** avec un rendement de 85%. La réduction du composé **46** par l'amalgame de sodium conduit au cétal **47** qui par hydrolyse dans des conditions douces fournit la cétone **32**. Cette dernière réagit avec le méthylate de sodium dans le méthanol en donnant un mélange 1:2 de cétones épimères **31** et **32** que Coates et Sowerby ont déjà transformé en (±) zizaène (**30**).

[Traduit par le journal]

## Introduction

The first examples of the thermal vinylcyclopropane to cyclopentene rearrangement, indicated in general terms by eq. [1], were reported more than

[1] 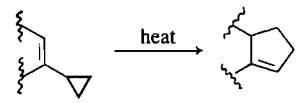


20 years ago (1, 2). Since that time, this interesting reaction has been studied quite extensively from a mechanistic point of view.[1] More recently, however, the synthetic utility of this type of transformation has received considerable attention, both in connection with methodology and natural product synthesis (10–24). In general, it has been found that, although successful execution of the rearrangement reaction often requires relatively high temperatures (typically in the range 400–600°C),[2] the products are, in many instances, formed cleanly and efficiently.

A recent report (25) from this laboratory de-

[1]For reviews, see refs. 3 and 4. For more recent studies, see refs. 5–9 and citations therein.

[2]An exception to this general statement can be found in the very interesting work of Danheiser and co-workers (20) who found that lithium salts of 2-vinylcyclopropanols rearrange to cyclopentenols at 25°C. For earlier work relating to the effect of substituents on the rate of the vinylcyclopropane to cyclopentene rearrangement, see ref. 21.

0008-4042/82/232965-11$01.00/0

©1982 National Research Council of Canada/Conseil national de recherches du Canada

Can. J. Chem. Downloaded from www.nrcresearchpress.com by 210.87.254.40 on 09/06/12
For personal use only.

Can. J. Chem. Downloaded from www.nrcresearchpress.com by 210.87.254.40 on 09/06/12
For personal use only.

scribed an efficient conversion of cyclic 1,3-diketones **1** into the corresponding β-halo α,β-unsaturated ketones **2** (X = Cl, Br, I). Work reported in a subsequent paper (26) revealed that the latter substances, particularly the bromo and iodo derivatives, react smoothly with a number of lithium (phenylthio)(alkyl)cuprate reagents to provide excellent yields of 3-alkyl- or 2,3-dialkyl-2-cycloalken-1-ones **3** (eq. [2]). Although these transfor-

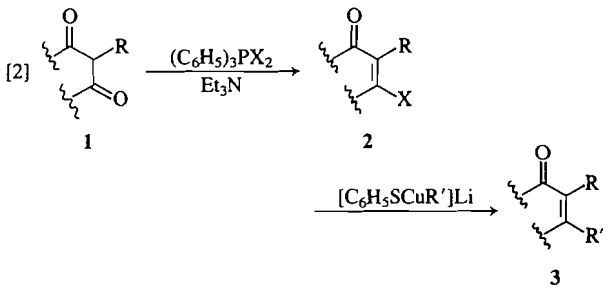


1 2 3

mations constitute a useful method for the overall conversion of **1** into **3**, we wished to extend this work to include the preparation of compounds **3** in which the R′ group would impart synthetically useful reactivity to these substances. For example, one possibility which we considered to be potentially interesting and useful is outlined in eq. [3].

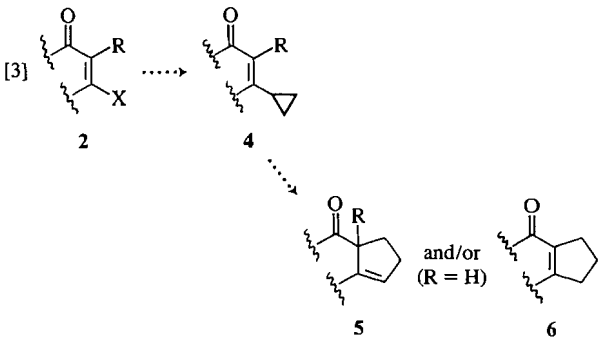


2 4 5 6

Thus, successful reaction of the β-halo enones **2** with a suitable (cyclopropyl)cuprate reagent would produce the β-cyclopropyl α,β-unsaturated ketones **4**. It is clear that the latter substances incorporate into their structures a vinylcyclopropane moiety and, if these materials were to be successfully subjected to thermal rearrangement, products **5** and/or **6** (if R = H) would be produced. In an overall sense, a new five-membered ring annulation sequence (**1** → **5** and/or **6**) would have been developed.

We report herein (a) the preparation of the β-cyclopropyl enones **11–14** and **17**, (b) the thermal rearrangement of four of these materials (**11–13, 17**), and (c) the use of one of the resultant annulated products (**22**) as a starting material for a new, formal total synthesis of the racemic modification of the tricyclic sesquiterpenoid (+)-zizaene (**30**).[3]

## Results and discussion

(a) *Preparation of the β-cyclopropyl α,β-unsaturated ketones 11–14 and 17 (see Chart 1)*

The β-cyclopropyl α,β-unsaturated ketones **11–14** were prepared conveniently by reaction of the corresponding β-iodo enones **7–10** (25) with lithium

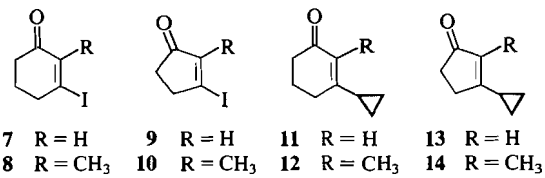

**7** R = H **8** R = $CH_3$ **9** R = H **10** R = $CH_3$ **11** R = H **12** R = $CH_3$ **13** R = H **14** R = $CH_3$

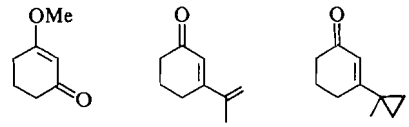

**15** **16** **17**

CHART 1

(phenylthio)(cyclopropyl)cuprate in ether–tetrahydrofuran (THF). A clear, light-brown solution of the latter reagent was produced by adding freshly prepared ethereal cyclopropyllithium (29)[4] (1 equivalent) to a slurry of phenylthiocopper (31, 32) in cold (−78°C) THF, and allowing the resultant mixture to stir at −20°C for 20 min.[5] Although the conversions **7** into **11** and **9** into **13** could be carried out efficiently (yields 82 and 97%, respectively) at −78°C (2.5 h) using 1.5 equivalents of the cuprate reagent, the transformations involving substrates containing an α methyl group (**8**, **10**) were, not unexpectedly, considerably more sluggish. In these cases, a higher reaction temperature (0°C) and more cuprate reagent (2 equivalents) were required to effect complete conversion of the starting material within the same length of time (2.5 h). However, these transformations were also clean and efficient (the yields of **12** and **14** were 88 and 84%, respectively) and, thus, the reaction of β-iodo enones with lithium (phenylthio)(cyclopropyl)-

[3]For preliminary reports regarding some of the work reported in this paper, see refs. 27 and 28.

[4]The cyclopropyllithium solution was standardized by the method of Gilman and Cartledge (30).

[5]To our knowledge, the first example of the use of a (cyclopropyl)copper reagent for the conjugate addition of a cyclopropyl group to an enone was reported by Hahn and Jones (33). For subsequent reports involving the use of these synthetically versatile reagents, see refs. 34–40.

Can. J. Chem. Downloaded from www.nrcresearchpress.com by 210.87.254.40 on 09/06/12
For personal use only.

cuprate appears to be an excellent method for the preparation of β-cyclopropyl enones.

With respect to the preparation of 3-(1-methylcyclopropyl)-2-cyclohexen-1-one (**17**) it is pertinent to point out that this compound was envisaged as being the starting material for a projected synthesis of (±)-zizaene (**30**) (*vide infra*). Therefore, we required fairly large quantities of this material and since we did not have a convenient source of 1-methylcyclopropyllithium, an alternative route to compound **17** was employed. Thus, treatment of 3-methoxy-2-cyclohexen-1-one (**15**) (41) with isopropenylmagnesium bromide, followed by acid hydrolysis of the resultant 1,2-addition product, provided 3-isopropenyl-2-cyclohexen-1-one (**16**) in 84% yield. The latter substance, when allowed to react with dimethyloxosulfonium methylide (42) in a mixture of dimethyl sulfoxide and THF, was converted into the desired β-(1-methylcyclopropyl) enone **17** (59% yield).

(b) *Thermal rearrangement of the β-cyclopropyl α,β-unsaturated ketones **11–13** and **17** (see Chart 2)*

A vertically held Pyrex tube (1.2 × 32 cm), filled with glass helices and surrounded by a vertical, tubular furnace, was washed thoroughly with saturated aqueous sodium bicarbonate, water, acetone, and *n*-hexane. The tube was then heated to 450°C for 3 h, during which time it was thoroughly purged with a stream of nitrogen. While a solution of 3-cyclopropyl-2-cyclohexen-1-one (**11**) in *n*-hexane was added dropwise to the top of the heated column, a slow stream of nitrogen (~3–5 mL/min) was passed through the tube and the thermolysate

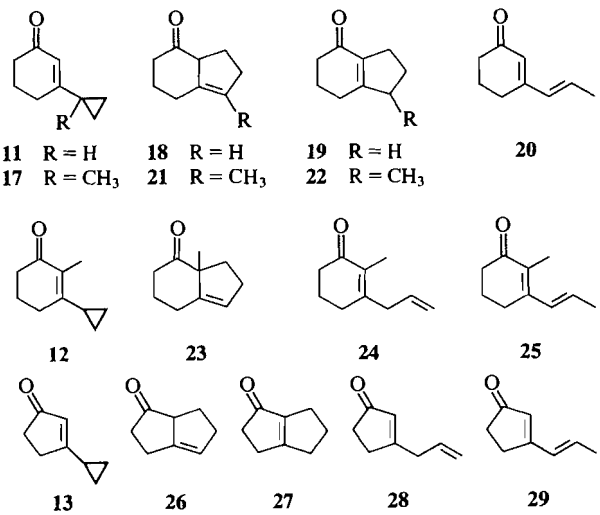


CHART 2

was collected in a two-necked flask equipped with a drying tube and immersed in a cold (−78°C) bath. Gas–liquid chromatographic analysis of the product, a colorless oil obtained in 78% yield, revealed that it consisted of three compounds, **18** (~3%), **19** (43) (~84%), and **20** (44) (~11%), along with a number of very minor unidentified components (~2%). A small sample of each of compounds **18**, **19**, and **20** was obtained by preparative glc and, in each case, the pure material exhibited spectral data in accord with the structural assignment. Furthermore, when a solution of **18** was passed through a short column of basic alumina, it was isomerized cleanly and efficiently to the conjugated enone **19**.

A brief study of the effect of thermolysis temperature on the rearrangement of compound **11** was carried out. For these experiments a longer thermolysis tube (100 cm), wrapped with a heating tape, was employed. The overall procedure used was very similar to that summarized above, although argon was employed as the "carrier gas" instead of nitrogen. The cyclopropyl enone **11** was subjected to thermolysis at 320, 400, 425, and 450°C. It was found that no rearrangement took place at 320°C, since starting material was recovered in essentially quantitative yield. At 400°C, the enone **11** was partially converted into a mixture of **18** and **19** (ratio ~2:1), but a considerable amount (~40%) of the starting material remained. The best result was obtained by carrying out the thermolysis at 425°C, under which conditions **11** was converted in high yield (98%) into an approximately 1:2 mixture of **18** and **19**, respectively, accompanied by < 5% of minor impurities. When a solution of this mixture was eluted through a column of basic alumina, the conjugated enone **19** could be obtained in 88% yield. Thermolysis of **11** at 450°C produced, in a yield (71%) significantly lower than that of the 425°C reaction, a mixture of compounds **18** (~5%), **19** (~90%), and minor impurities (~5%). This result was comparable to that obtained by rearrangement of **11** at ~450°C using the shorter thermolysis tube (*vide supra*), although the amount of the dienone **20** formed was diminished.

Thermolysis of 3-(1-methylcyclopropyl)-2-cyclohexen-1-one (**17**) at 450°C under conditions similar to those employed for compound **11** gave a mixture of two products, the ratio of which varied somewhat from one experiment to another. The spectral data derived from this mixture indicated that the two components were the positionally isomeric enones **21** and **22** and, therefore, these substances were not separated. Instead, a solution of this mixture in methanol containing sodium

Can. J. Chem. Downloaded from www.nrcresearchpress.com by 210.87.254.40 on 09/06/12
For personal use only.

methoxide was stirred at 0°C for 1 h. Under these conditions, compound **21** was completely converted into the conjugated enone **22**[6] and the latter substance was isolated in 87% yield. It should be noted that, in general, the thermal rearrangement of **17** was cleaner and less "temperamental" than that of the demethyl analog **11**. Furthermore, thermolysis of **17** could readily be carried out on preparative scale, thus providing a very convenient synthesis of appreciable quantities of the enone **22**.

An investigation of the thermal rearrangement of the cyclopropyl enones **12** and **13** showed that, with respect to the formation of annulated products, these reactions are not as synthetically useful as those employing compounds **11** and **17** as substrates. Not unexpectedly (3, 4), the presence of an α methyl substituent *cis* to the cyclopropyl group (substrate **12**) and the requirement of having to form a fairly strained bicyclo[3.3.0]octenone ring system **26** (rearrangement of **13**), have deleterious effects on the efficiency of ring formation. Thus, thermolysis of 3-cyclopropyl-2-methyl-2-cyclohexen-1-one (**12**) at 450°C (conditions similar to those employed for **11** and **17**) gave a mixture of products (73% yield) containing only a minor amount (~10%) of the desired annulation product **23**. The remainder of the mixture consisted of the dienones **24** (~20%) and **25** (~50%) along with a number of minor unidentified components (gas–liquid chromatographic analysis). Pure samples of compounds **23–25** were collected by preparative glc and, in each case, the substance exhibited spectral data in accord with the structural assignment.

Analysis (glc) of the product obtained (80% yield) from thermal rearrangement of the β-cyclopropyl cyclopentenone **13** showed that it consisted of four major components, **26** (~46%), **27** (~14%), **28** (~20%), and **29** (~18%), along with minor impurities (~2%). Again, a small sample of each of the major products, obtained by preparative glc, exhibited the expected spectral properties. Furthermore, the enone **26** and the dienone **28** were readily isomerized (basic alumina) into the corresponding conjugated isomers **27** and **29**, respectively.

Although the investigation summarized above was not extensive, it is clear that from a synthetic point of view, the results are mixed. Although thermolyses of the β-cyclopropyl enones **11** and **17** provide excellent methods for preparing the bicyclic enones **19** and **22**, similar reactions involving compounds **12** and **13** are, with respect to formation of annulation products, much less efficient. Finally, it is perhaps pertinent to point out that recent work, particularly that of Hudlicky and co-workers (16–19), has shown that product distribution in the vinylcyclopropane → cyclopentene rearrangement can vary considerably with reaction conditions and that this type of transformation can be carried out successfully on structurally quite complex substrates.

(c) *A formal total synthesis of (±)-zizaene (30)*

The structurally interesting sesquiterpenoid (+)-zizaene (**30**),[7] the parent hydrocarbon of a small number of zizaane-type natural products isolated from vetiver oil, contains the tricyclo[6.2.1.$0^{1,5}$]undecane carbon skeleton.[8] One possible route which might be employed for the total synthesis of (±)-zizaene is revealed by the retrosynthetic analysis outlined in Scheme 1. Thus, removal of the two methyl groups from C-7 of **30** and replacement of the exocyclic olefinic double bond at C-6 with a carbonyl group provides the tricyclic ketone **31**. In fact, at the time that we were planning our work, the latter substance (or an equilibrium mixture of **31** and the epimer **32**) had already been employed by Coates and Sowerby (49) as an intermediate in their total synthesis of racemic zizaene. Therefore, in our work, the ketones **31** and/or **32** became the synthetic targets.[9]

Heterolytic disconnection of the C-8—C-9 bond in **31** or **32** so as to leave C-8 as a donor atom and C-9 as an acceptor site gives the bicyclic synthon **33**. A synthetic equivalent to the latter species would have to contain functional groups at C-8 and C-9 which would render these positions nucleophilic and electrophilic, respectively. Since C-8 is β to the carbonyl group in **33**, it would, in terms of normal reactivity patterns, be considered as a potential electrophilic site and, therefore, reactivity umpolung[10] would have to be employed in effecting the synthetic conversion of **33** into **31** and/or **32**. Further disconnection involving the C-1—C-10 bond in **33** would provide the synthons **34** and **35**. It is clear that a potential synthetic equivalent to the synthon **34** would be the bicyclic enone **22**. Furthermore, on the basis of steric

[6]For an alternative preparation of this compound, see ref. 45.

[7]Other names for this natural product which can be found in the literature are tricyclovetivene, khusinene, and khusene.

[8]For previous synthetic work on zizaane-type sesquiterpenoids and for literature citations regarding the isolation and structural elucidation of members of this family of natural products, see refs. 46–52, inclusive.

[9]Very recently, an alternative preparation of (±)-**31** has been reported by Barker and Pattenden (53).

[10]For an excellent, stimulating article on methods of reactivity umpolung, see ref. 54.

Can. J. Chem. Downloaded from www.nrcresearchpress.com by 210.87.254.40 on 09/06/12
For personal use only.

considerations, conjugate addition of a suitable two-carbon species to the enone system in **22** would be expected to take place stereoselectively from the side opposite the adjacent secondary methyl group, thus producing a product which would be synthetically equivalent to **33**. Therefore, since a very convenient synthesis of the enone **22** was available (*vide supra*), we wished to investigate the possibility of employing this substance as the starting material in a projected synthesis of (±)-zizaene (**30**) via the general plan summarized in Scheme 1.

The reagent which served as a convenient source of the required two-carbon unit (cf. synthon **35**) was lithium divinylcuprate, readily prepared by addition of two equivalents of ethereal vinyllithium (55) to a solution of cuprous bromide – dimethylsulfide complex (56, 57) in a mixture of ether and dimethyl sulfide. Reaction of the enone **22** with 1.1 equivalents of the cuprate reagent afforded, after suitable work-up, a product which contained a number of minor, unidentified components with relatively short retention times (gas–liquid chromatographic analysis), along with two ketones in a ratio of ~98:2. Purification of this material by column chromatography on silica gel provided a small sample of the minor ketone and allowed for the isolation of the major product in 72% yield. As mentioned previously, the conjugate addition reaction was expected to be stereoselective in the desired sense, with transfer of the vinyl group occurring preferentially to the side of the enone opposite to the secondary methyl group. Therefore, with respect to the relative orientation of the vinyl and methyl groups, the major and minor ketonic products were assigned structures **36** and **37**, respectively (see Scheme 2). Furthermore,

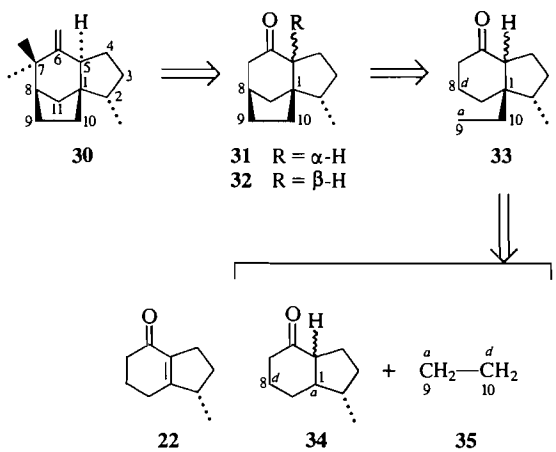


SCHEME 1

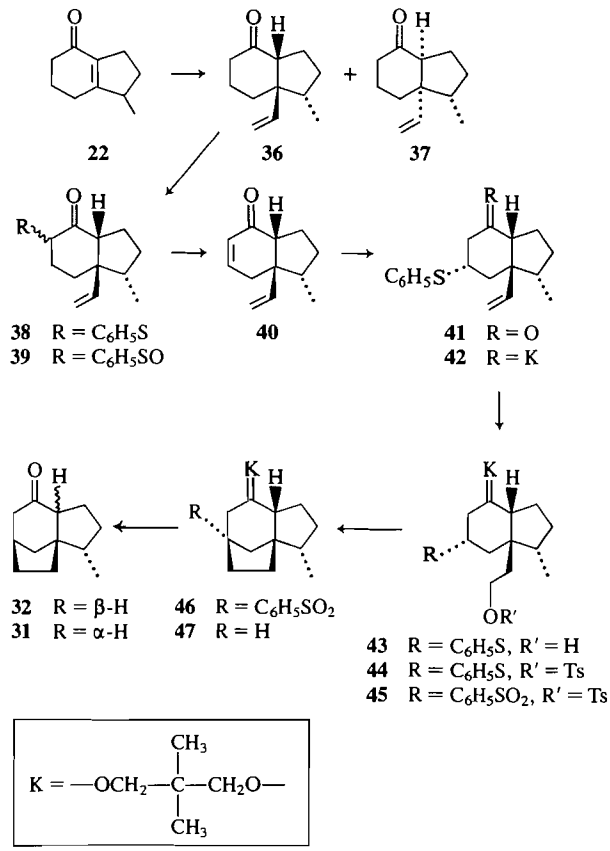


SCHEME 2

examination of molecular models, along with the knowledge that *cis*-hydrindan-4-one is more stable than the corresponding *trans* isomer (58), led to the conclusion that each of these compounds possesses a *cis*-fused ring system.[11] Although these latter assignments were not crucial in terms of the overall synthesis, the conclusion regarding the stereochemistry of the required isomer **36** was later shown to be correct.

When the keto olefin **36** was treated with three equivalents of lithium diisopropylamide in THF–hexamethylphosphoramide (HMPA) and the resultant enolate anion was trapped with diphenyl disulfide (59), the α-sulfenylated ketone **38** was obtained in 91% yield. The latter material, a mixture of epimers, was oxidized (sodium periodate in aqueous methanol) to the corresponding sulfoxide **39** which, upon heating (120°C/0.3 Torr) with direct distillation of the product, gave the enone **40** in 64% yield.

[11]Treatment of **36** and **37** with sodium methoxide in methanol showed that both were stable to epimerization conditions and that they were not interconvertible.

Can. J. Chem. Downloaded from www.nrcresearchpress.com by 210.87.254.40 on 09/06/12
For personal use only.

Bearing in mind the synthetic plan (Scheme 1), it was necessary at this stage of the synthesis to add an appropriate functional group to the β carbon atom of the α,β-unsaturated ketone system in **40**. The nature of this group had to be such that it would be capable of imparting nucleophilic character to the β carbon atom (cf. C-8 in synthon **33**), presumably by enhancing the acidity of the proton attached to this center. Furthermore, after having served its purpose, the group would have to be amenable to ready removal by a suitable chemical transformation. It appeared that a sulfur-containing moiety would adequately fulfil these requirements.

Treatment of the enone **40** with thiophenol in acetone containing tetra-*n*-butylammonium fluoride (60) afforded a single crystalline conjugate addition product in 95% yield. On the basis of an examination of molecular models of **40**, it seemed highly likely that the nucleophile would approach the β carbon of the enone system from the side opposite the angular vinyl group. Therefore, although conclusive evidence regarding this point was not sought, the conjugate addition product was assigned the stereochemistry shown in **41**. After ketalization of the latter substance, the vinyl group of the resultant product **42** was functionalized by hydroboration with borane – dimethyl sulfide (61). The crude product thus obtained consisted of a mixture of the starting material **42** and the desired ketal alcohol **43**. However, since the latter compound was quite unstable (interaction of the hydroxyl group and the ketal function?), this mixture was treated immediately with *p*-toluenesulfonyl chloride in pyridine. Separation of the resultant mixture by column chromatography on silica gel gave the desired tosylate **44** in 86% yield, based on unrecovered **42**.

Oxidation (*m*-chloroperbenzoic acid, dichloromethane, 0°C) of the sulfide linkage in **44** afforded a quantitative yield of the crystalline sulfone **45** and the stage was now set for effecting the closure of the five-membered ring to provide the required tricyclo[6.2.1.$0^{1,5}$]undecane ring system. Thus, when freshly prepared, dry potassium *tert*-butoxide was added to a solution of the sulfone tosylate **45** in HMPA, and the resultant solution was stirred at room temperature for 1.5 h, the crystalline tricyclic product **46** was produced in 85% yield. The phenyl sulfone moiety, having effectively served its required function, was removed cleanly and efficiently by reduction of **46** with sodium amalgam in methanol–benzene containing disodium hydrogen phosphate (62). The desired tricyclic ketal **47** was obtained in 90% yield. Treatment of compound **47** with oxalic acid in THF–methanol–water at room temperature gave the tricyclic ketone **32** (93% yield), containing none of the epimeric substance **31**. However, when a solution of **32** in methanol containing sodium methoxide was stirred at room temperature for 24 h, a 2:1 mixture of the epimers **32** and **31** was obtained. This mixture was spectrally identical[12] with a 2:1 mixture of the same two compounds which had been prepared previously by Coates and Sowerby (49) and which had been converted by these workers into (±)-zizaene (**30**). Therefore, the acquisition of this material completed, in a formal sense, a new total synthesis of the racemic sesquiterpenoid.

## Experimental

*General*

Melting points, which were taken on a Fisher–Johns melting point apparatus, and boiling points (or distillation temperatures) are uncorrected. Ultraviolet (uv) spectra were recorded on a Cary 15 spectrophotometer, while infrared (ir) spectra were taken on Perkin–Elmer models 710 or 710 B spectrophotometers. Proton magnetic resonance ($^1$H nmr) spectra (deuterochloroform solution unless otherwise noted) were measured using Varian Associates spectrometers, models T-60 and/or HA-100 or XL-100. Tetramethylsilane was employed as the internal standard. High resolution mass spectrometric measurements were recorded on a Kratos MS-50 mass spectrometer. Gas–liquid chromatography (glc) was carried out with a Hewlett–Packard model 5832 A gas chromatograph (analytical) or with a Varian Aerograph model 90-P instrument (preparative). Microanalysis were performed by Mr. P. Borda, Microanalytical Laboratory, University of British Columbia, Vancouver, B.C.

*3-Cyclopropyl-2-cyclohexen-1-one (11)*

To a cold (−78°C), stirred slurry of phenylthiocopper (32) (779 mg, 4.5 mmol) in dry THF (30 mL), under an atmosphere of argon, was added a solution of freshly prepared cyclopropyllithium (29, 30) (4.5 mmol) in ether. The mixture was warmed to −20°C and stirred at this temperature for 20 min. The resulting clear, light-brown solution was cooled to −78°C and a solution of 3-iodo-2-cyclohexen-1-one (7) (25) (666 mg, 3 mmol) in 6 mL of dry THF was added. After the reaction mixture had been stirred at −78°C for 2.5 h, methanol (2 mL) and ether (20 mL) were added, the mixture was allowed to warm to room temperature, and then was filtered through a short column of Florisil (30 g, 80–100 mesh). The column was eluted with a further 300 mL of ether. Removal of the solvent from the combined eluate, followed by distillation (air bath temperature 62–75°C/0.3 Torr) of the crude oil afforded 335 mg (82%) of the desired β-cyclopropyl enone **11** (33) as a colorless oil; uv (methanol) $\lambda_{max}$: 254 nm (ε 17100); ir (film): 1660, 1625, 1610 cm$^{-1}$; $^1$H nmr δ: 0.66–2.50 (m, 11H), 5.81 (s, 1H).

*3-Cyclopropyl-2-cyclopenten-1-one (13)*

The conversion of 3-iodo-2-cyclopenten-1-one (**9**) (25) into the corresponding β-cyclopropyl enone **13** was carried out via a procedure identical with that described above. From 624 mg (3 mmol) of **9** there was obtained 355 mg (97%) of crystalline product **13**; distillation temperature ~65°C (air bath)/0.2 Torr;

[12]We are very grateful to Professor R. M. Coates for his assistance in making this comparison.

Can. J. Chem. Downloaded from www.nrcresearchpress.com by 210.87.254.40 on 09/06/12
For personal use only.

mp 31–33°C; uv (methanol) $\lambda_{max}$: 244 nm (ε 16270); ir ($CHCl_3$): 1700, 1670, 1600 $cm^{-1}$; $^1H$ nmr δ: 0.74–1.22 (m, 4H), 2.00–2.68 (m, 1H), 3.26–3.60 (m, 4H), 5.88 (t, 1H, $J$ = 1.8 Hz). *Exact Mass* calcd. for $C_8H_{10}O$: 122.0731; found: 122.0733.

*3-Cyclopropyl-2-methyl-2-cyclohexen-1-one (12)*

The procedure used for the preparation of compound **12** was identical with that employed for the conversion of **7** into **11**, except that 2 equiv. (6 mmol) of lithium (phenylthio)(cyclopropyl)cuprate were used, and the reaction was carried out for 2.5 h at 0°C instead of at −78°C. From 708 mg (3 mmol) of 3-iodo-2-methyl-2-cyclohexen-1-one (**8**) (25) there was obtained 396 mg (88%) of an oil (distillation temperature 65–85°C (air bath)/0.35 Torr) which crystallized in a refrigerator. Recrystallization of a small sample of this material from ether–hexanes provided pure **12** (63); mp 36–37°C; uv (methanol) $\lambda_{max}$: 262 nm (ε 14950); ir ($CHCl_3$): 1660, 1610 $cm^{-1}$; $^1H$ nmr δ: 0.70–1.00 (m, 4H), 1.70–2.60 (m, 7H), 1.90 (s, 3H). *Exact Mass* calcd. for $C_{10}H_{14}O$: 150.1044; found: 150.1032.

*3-Cyclopropyl-2-methyl-2-cyclopenten-1-one (14)*

This compound was obtained via a procedure identical with that described for the preparation of the β-cyclopropyl enone **12** (see above). From 666 mg (3 mmol) of the iodo enone **10** (25) there was obtained a crude oil which upon distillation (air bath temperature ~50°C/0.1 Torr) gave 343 mg (84%) of the cyclopentenone **14** (63) as a colorless oil; uv (methanol) $\lambda_{max}$: 254 nm (ε 18580); ir (film): 1698, 1637 $cm^{-1}$; $^1H$ nmr δ: 0.80–1.15 (m, 4H), 1.77 (t, 3H, $J$ = 1.2 Hz), 1.90–2.40 (m, 5H). *Exact Mass* calcd. for $C_9H_{12}O$: 136.0887; found: 136.0888.

*3-Isopropenyl-2-cyclohexen-1-one (16)*

A stirred, cold (0°C) solution of isopropenylmagnesium bromide (29.04 g, 0.20 mol) in 50 mL of dry THF, under an atmosphere of nitrogen, was diluted with 75 mL of dry ether. A solution of 3-methoxy-2-cyclohexen-1-one (**15**) (41) (12.61 g, 0.10 mol) in 20 mL of dry ether was added dropwise and the resultant mixture was stirred at room temperature for 4 h. After the solution had been cooled to 0°C, 100 mL of 5% aqueous sulfuric acid was added slowly and the mixture was stirred for a few minutes. The organic phase was separated, washed successively with dilute aqueous sodium carbonate and water, and dried over anhydrous sodium sulfate. Removal of the solvent, followed by distillation of the residual oil gave 11.46 g (84%) of 3-isopropenyl-2-cyclohexen-1-one (**16**) as a clear colorless liquid; bp 60–63°C/0.3 Torr; uv (methanol) $\lambda_{max}$: 267 nm (ε 22000); ir (film): 2980, 1666, 1626, 1586, 1256, 878 $cm^{-1}$; $^1H$ nmr ($CCl_4$) δ: 1.77–2.60 (m, 6H), 1.97 (s, 3H), 5.17 (broad s, 1H), 5.33 (s, 1H), 5.83 (s, 1H). *Anal.* calcd. for $C_9H_{12}O$: C 79.39, H 8.88; found: C 79.53, H 9.04.

*3-(1-Methylcyclopropyl)-2-cyclohexen-1-one (17)*

A solution of dimethyloxosulfonium methylide (42) (0.082 mol) in 90 mL of dry dimethyl sulfoxide, kept under an atmosphere of nitrogen, was diluted with 40 mL of dry THF and cooled to 0°C. A solution of 3-isopropenyl-2-cyclohexen-1-one (11.0 g, 0.081 mol) in 10 mL of dry THF was added dropwise and the resultant reddish reaction mixture was stirred overnight at room temperature. The solution was poured into 500 mL of cold water and the resultant mixture was extracted with six 75 mL portions of ether. The combined extract was washed with water and brine and dried over anhydrous sodium sulfate. Removal of the solvent, followed by distillation of the residual oil, yielded 7.2 g (59%) of 3-(1-cyclopropyl)-2-cyclohexen-1-one (**17**) as a colorless oil which exhibited one peak by gas–liquid chromatographic analysis; bp 72–76°C/0.3 Torr; uv (methanol) $\lambda_{max}$: 253 nm (ε 16600); ir (film): 1665, 1610 $cm^{-1}$; $^1H$ nmr ($CCl_4$) δ: 0.4–1.08 (m, 4H), 1.15 (s, 3H), 1.67–2.35 (m, 6H), 5.70 (broad s, 1H). *Exact Mass* calcd. for $C_{10}H_{14}O$: 150.1044; found: 150.1039.

*Thermal rearrangement of 3-cyclopropyl-2-cyclohexen-1-one (11)*

(a) *Procedure A*

A vertically held Pyrex tube (1.2 × 32 cm), filled with glass helices and placed inside a vertical, tubular furnace, was washed successively with saturated aqueous sodium bicarbonate, water, acetone, and *n*-hexane. The tube was heated to 450°C and kept at this temperature for 3 h. During this time, the column was thoroughly purged with a stream of nitrogen. A solution of 3-cyclopropyl-2-cyclohexen-1-one (**11**) (200 mg) in *n*-hexane (20 mL) was added dropwise, over a period of 1.5 h, to the top of the heated tube. During this time, a slow flow of nitrogen (~3–5 mL/min) was passed through the column. The thermolysate was passed through a water condensor into a cold (−78°C) two-necked flask equipped with a drying tube. After the solution of **11** had been added, the hot tube was treated with an additional 30 mL of *n*-hexane. Removal of the solvent from the combined thermolysate, followed by distillation (air bath temperature ~110°C/16 Torr) of the residual material gave 156 mg (78%) of a colorless oil. Gas–liquid chromatographic analysis of this material showed that it consisted of a mixture of the ketones **18** (~3%), **19** (~84%), and **20** (~11%), along with a number of very minor unidentified components (~2%). A pure sample of each of compounds **18**, **19**, and **20** was obtained by preparative glc.

*Ketone* **18**: ir (film): 1718, 1665 $cm^{-1}$; $^1H$ nmr δ: 1.7–2.7 (diffuse m, 10H), 3.37 (m, 1H), 5.43 (m, 1H). When an ethereal solution of **18** was passed through a short column of basic alumina, compound **18** was isomerized cleanly into the conjugated isomer **19** (identification by glc, ir, and $^1H$ nmr).

*Ketone* **19**: ir (film): 1660, 1630 $cm^{-1}$; $^1H$ nmr δ: 1.7–2.8 (diffuse m). The 2,4-dinitrophenylhydrazone derivative exhibited mp 252°C (dec.) (lit. (43) mp 251.5°C (dec.)).

*Ketone* **20** (44): ir (film): 1670, 1642, 1590 $cm^{-1}$; $^1H$ nmr δ: 1.86 (d, 3H, $J$ = 5 Hz), 1.8–2.6 (diffuse m, 6H), 5.84 (s, 1H), 6.18 (m, 2H).

(b) *Procedure B*

This procedure was identical with that described above, except that the thermolysis tube was longer (100 cm), the tube was heated by means of a heating tape rather than a furnace, the "carrier gas" was argon instead of nitrogen, and the thermolysis temperature was 425°C rather than 450°C. From 200 mg of the β-cyclopropyl enone **11** there was obtained 196 mg (98%) of a distilled oil which, on the basis of analysis by glc, consisted very largely of the ketones **18** (~31%) and **19** (~67%). An ether solution of this mixture was passed through a short column of basic alumina, and the column was eluted with further volumes of ether. Removal of the solvent from the combined eluate, followed by bulb-to-bulb distillation of the residual oil, gave 176 mg (88%) of the enone **19**.

*Thermal rearrangement of 3-(1-methylcyclopropyl)-2-cyclohexen-1-one (17)*

Thermolysis of compound **17** was accomplished via a procedure very similar to that described under Procedure A, above, except that the thermolysis tube was 40 cm in length and the reaction was done on a much larger scale. Thus, from 12.3 g of **17** (added to the heated column as a solution in 30 mL of *n*-hexane) there was obtained a distilled oil which was shown by analysis (glc, ir, $^1H$ nmr) to consist of a mixture of the two ketones **21** and **22**, in a ratio of approximately 7:3, respectively.[13] This mixture was dissolved in 100 mL of methanol containing a small amount of sodium methoxide and the resultant solution was stirred at 0°C for 1 h. The methanol was removed under reduced pressure and the residue was taken up

[13]The ratio of the two products varied somewhat from one thermolysis experiment to another.

Can. J. Chem. Downloaded from www.nrcresearchpress.com by 210.87.254.40 on 09/06/12
For personal use only.

in ether. The ether solution was washed with brine and dried over anhydrous magnesium sulfate. Removal of the ether, followed by distillation of the residual material gave 10.7 g (87%) of the conjugated enone **22** as a clear oil which exhibited one peak by gas–liquid chromatographic analysis; bp 55–58°C/0.3 Torr; uv (methanol) $\lambda_{max}$: 247 nm (ε 12 100); ir (film): 1670, 1638 $cm^{-1}$; $^1H$ nmr δ: 1.08 (d, 3H, $J$ = 6.5 Hz), 1.1–1.7 (m, 2H), 1.7–3.0 (diffuse m, 9H). *Exact Mass* calcd. for $C_{10}H_{14}O$: 150.1044; found: 150.1032.

*Thermal rearrangement of 3-cyclopropyl-2-methyl-2-cyclohexen-1-one (12)*

Thermolysis of **12** was carried out via a procedure very similar to Procedure A, above. From 175 mg of **12** (added to the hot tube as a solution in 17.5 mL of *n*-hexane) there was obtained a crude thermolysate which upon distillation (air bath temperature ~110°C/12 Torr) gave 128 mg (73%) of a clear oil. Analysis of this material by glc showed that it consisted of a mixture of the ketones **23** (~10%), **24** (~20%), and **25** (~50%), along with a number of minor, unidentified components. A small sample of each of the major products was obtained by preparative glc.

*Ketone* **23**: ir (film): 1715, 1660 $cm^{-1}$; $^1H$ nmr δ: 1.23 (s, 3H), 1.4–2.8 (diffuse m, 10H), 5.30 (m, 1H). *Exact Mass* calcd. for $C_{10}H_{14}O$: 150.1044; found: 150.1039.

*Ketone* **24**: uv (methanol) $\lambda_{max}$: 243 nm (ε 9400); ir (film): 1665, 1635 $cm^{-1}$; $^1H$ nmr δ: 1.54–2.58 (diffuse m, 6H), 1.75 (t, 3H, $J \approx$ 1 Hz), 2.95 (d, 2H, $J$ = 6.5 Hz), 4.9–5.04 (m, 1H), 5.06–5.16 (m, 1H), 5.54–6.0 (m, 1H). *Exact Mass* calcd. for $C_{10}H_{14}O$: 150.1044; found: 150.1041.

*Ketone* **25**: uv (methanol) $\lambda_{max}$: 281 nm (ε 19 050); ir (film): 1660, 1630, 1585 $cm^{-1}$; $^1H$ nmr δ: ~1.8–2.08 (m, 2H), 1.86 (s, 3H), 1.91 (d, 3H, $J$ = 6 Hz), 2.32–2.58 (m, 4H), 5.96–6.36 (d of q, 1H, $J$ = 15, 6 Hz), 6.60 (broad d, 1H, J = 15 Hz). *Exact Mass* calcd. for $C_{10}H_{14}O$: 150.1044; found: 150.1038.

*Thermal rearrangement of 3-cyclopropyl-2-cyclopenten-1-one (13)*

From 200 mg of compound **13**, thermolyzed as described under Procedure A, above, there was obtained a crude mixture of products which, upon distillation (air bath temperature 100–110°C/16 Torr), gave 160 mg (80%) of a clear oil. Analysis of this material by glc showed that it consisted very largely of four components: **26** (~46%), **27** (~14%), **28** (~20%), and **29** (~18%). A pure sample of each of these compounds was obtained by preparative glc.

*Ketone* **26**: ir (film): 1740, 1660 $cm^{-1}$; $^1H$ nmr δ: 1.57–2.84 (diffuse m, 8H), 3.12–3.43 (m, 1H), 5.42–5.60 (m, 1H). *Exact Mass* calcd. for $C_8H_{10}O$: 122.0731; found: 122.0730. When an ethereal solution of **26** was eluted through a short column of basic alumina, it was isomerized to the α,β-unsaturated ketone **27**.

*Ketone* **27**: uv (methanol) $\lambda_{max}$: 237 nm (ε 11 370); ir (film): 1690, 1630 $cm^{-1}$; $^1H$ nmr δ: 2.20–2.90 (diffuse m). *Exact Mass* calcd. for $C_8H_{10}O$: 122.0731; found: 122.0734.

*Ketone* **28**: uv (methanol) $\lambda_{max}$: 226 nm (ε 14 090); ir (film): 1705, 1610 $cm^{-1}$; $^1H$ nmr δ: 2.2–2.8 (diffuse m, 4H), 3.12 (d, 3H, $J$ = 6.5 Hz), 5.00–5.12 (m, 1H), 5.14–5.26 (m, 1H), 5.64–6.08 (m, 1H), 5.93 (t, 1H, $J$ = 1.5 Hz). *Exact Mass* calcd. for $C_8H_{10}O$: 122.0731; found: 122.0728. When an ethereal solution of **28** was eluted through a short column of basic alumina, it was isomerized to the conjugated dienone **29**.

*Ketone* **29**: uv (methanol) $\lambda_{max}$: 268 nm (ε 18 630); ir (film): 1640, 1570 $cm^{-1}$; $^1H$ nmr δ: 1.89 (d, 3H, $J$ = 6 Hz), 2.2–2.8 (diffuse m, 4H), 5.91 (broad s, 1H), ~6.30 (d of q, 1H, $J$ = 16, 6 Hz), 6.56 (d, 1H, $J$ = 16 Hz). *Exact Mass* calcd. for $C_8H_{10}O$: 122.0731; found: 122.0732.

*Reaction of the enone 22 with lithium divinylcuprate*

A stirred solution of cuprous bromide – dimethyl sulfide complex (56, 57) (10.99 g, 53.4 mmol) in a mixture of dimethyl sulfide (53 mL) and ether (72 mL) was cooled to −60°C under an atmosphere of nitrogen. During this cooling, some of the complex crystallized from the solution. A solution of vinyllithium (55) in ether (121 mL, 0.92 *M*, 115 mmol) was added dropwise while the temperature of the reaction mixture was maintained at −50°C to −60°C. To the resulting dark-brown solution was added dropwise a solution of the bicyclic enone **22** (7.9 g, 49.3 mmol) in 30 mL of anhydrous ether. After the reaction mixture had been stirred at −50°C for 20 min and at room temperature for 1 h, it was diluted with ether (200 mL) and then treated with saturated aqueous ammonium chloride. The resulting mixture was filtered and the collected solid material was washed thoroughly with ether. The combined filtrate was washed successively with aqueous ammonium chloride and brine and dried over anhydrous magnesium sulfate. Removal of the solvent, followed by distillation (air bath temperature 60–70°C/0.3 Torr) of the residual oil, gave a clear liquid. Analysis of this material by glc showed that it contained, in addition to a number of minor unidentified components with very short retention times, two products in a ratio of about 98:2.

The distilled material was subjected to column chromatography on silica gel (400 g). Elution of the column with benzene gave a mixture of unidentified compounds which exhibited no carbonyl absorption in the ir spectrum. Further elution with benzene – ethyl acetate (9:1) gave the minor ketonic product **37**, contaminated with a small amount of the major product **36**. A small sample of **37** was obtained by preparative glc; ir (film): 3100, 1710, 1630, 900 $cm^{-1}$; $^1H$ nmr ($CCl_4$) δ: 0.77 (d, 3H, $J$ = 6.0 Hz), 2.56 (d of d, 1H, $J$ = 8, 5 Hz), 4.94 (d of d, 1H, $J$ = 18, 1.5 Hz), 5.07 (d of d, 1H, $J$ = 11, 1.5 Hz), 5.72 (d of d, 1H, $J$ = 18, 11 Hz). *Exact Mass* calcd. for $C_{12}H_{18}O$: 178.1358; found: 178.1369.

Further elution of the above chromatography column with benzene – ethyl acetate (9:1) gave the pure bicyclic ketone **36** (6.28 g, 72%) as a colorless oil which exhibited bp 65°C/0.1 Torr; ir (film): 3100, 1705, 1630, 910 $cm^{-1}$; $^1H$ nmr ($CCl_4$) δ: 0.90 (d, 3H, $J$ = 6.0 Hz), 4.89 (d of d, 1H, $J$ = 18, 1.5 Hz), 5.01 (d of d, 1H, $J$ = 11, 1.5 Hz), 5.67 (d of d, 1H, $J$ = 18, 11 Hz). *Anal.* calcd. for $C_{12}H_{18}O$: C 80.85, H 10.18; found: C 80.77, H. 10.20. *Exact Mass* calcd.: 178.1358; found: 178.1354.

Treatment of either of the two ketones **36** and **37** with sodium methoxide in methanol clearly showed that the two compounds were not interconvertible. In each case, only starting material was recovered.

*Preparation of the bicyclic α,β-unsaturated ketone 40*

To a cold (−25°C) solution of diisopropylamine (3.06 g, 30.2 mmol) in dry THF (40 mL) under an atmosphere of nitrogen was added a solution of *n*-butyllithium in hexane (11.6 mL, 2.6 *M*, 30.16 mmol) and the resulting solution was stirred for 30 min. A solution of the bicyclic ketone **36** (1.80 g, 10.1 mmol) in a mixture of dry THF (20 mL) and dry HMPA (20 mL) was added dropwise over a period of 10 min. After the reaction mixture had been stirred for 30 min at −25°C, for 1 h at 0°C, and for 15 min at room temperature, a solution of diphenyl disulfide (6.59 g, 30.18 mmol) in 20 mL of dry THF was added rapidly and the solution was stirred at room temperature for 2 h. Hydrochloric acid (10%) was added and the resultant mixture was extracted thoroughly with ether. The combined ether extract was washed successively with saturated aqueous sodium bicarbonate and brine and dried over anhydrous magnesium sulfate. Removal of the solvent afforded an oil which was subjected to column chromatography on silica gel (300 g). Elution of the column with benzene gave 2.634 g (91%) of the α-phenylthio ketone **38**.

Can. J. Chem. Downloaded from www.nrcresearchpress.com by 210.87.254.40 on 09/06/12
For personal use only.

Analysis of this material by tlc and $^1$H nmr showed that it was a mixture of two diastereomers. *Exact Mass* calcd. for $C_{18}H_{22}OS$: 286.1391; found: 286.1392.

To a cold (0°C) solution of the crude α-phenylthio ketone **38** (3.386 g, 11.8 mmol) in 50 mL of methanol was added dropwise a solution of sodium periodate (2.72 g, 12.7 mmol) in water (20 mL). After the resultant cloudy reaction mixture had been stirred at room temperature for 16 h, it was filtered and the solid collected material was washed with methanol. The combined filtrate was concentrated under reduced pressure and the residue was diluted with ether. The resultant solution was washed with brine and dried over anhydrous magnesium sulfate. Removal of the solvent gave the crude sulfoxide **39** as a yellow oil, to which was added ~20 mg of solid calcium carbonate. The resultant mixture was heated (air bath temperature 120°C) under reduced pressure (0.3 Torr) and the collected distillate was subjected to column chromatography on silica gel (100 g). Elution of the column with benzene–ether (95:5) afforded an oil which upon distillation (air bath temperature 80°C/0.3 Torr) gave 1.34 g (64%) of the pure bicyclic enone **40**; uv (methanol) $\lambda_{max}$: 228 nm (ε 7900); ir (film): 3100, 1670, 900 cm$^{-1}$; $^1$H nmr ($CCl_4$) δ: 0.89 (d, 3H, $J$ = 6.0 Hz), 1.12–2.64 (diffuse m, 8H), 4.91 (d of d, 1H, $J$ = 18, 1 Hz), 5.03 (d of d, 1H, $J$ = 11, 1 Hz), 5.69 (d of d, 1H, $J$ = 18, 11 Hz), 5.84 (broad d, 1H, $J$ = 10 Hz), 6.73 (d of d of d, 1H, $J$ = 10, 5, 3 Hz). *Anal.* calcd. for $C_{12}H_{16}O$: C 81.77, H 9.15; found: C 81.45, H 9.40. *Exact Mass* calcd.: 176.1202; found: 176.1207.

*Preparation of the phenylthio ketone **41***

To a stirred solution of the bicyclic enone **40** (0.17 g, 0.96 mmol) and tetra-*n*-butylammonium fluoride (0.013 g) in 1.5 mL of dry acetone under an atmosphere of nitrogen was added, dropwise, 0.117 g (1.06 mmol) of thiophenol. After the reaction mixture had been stirred for 3 h at room temperature, it was diluted with ether (100 mL) and the resultant solution was washed successively with saturated aqueous sodium bicarbonate and brine and then dried over anhydrous magnesium sulfate. Removal of the solvent gave 0.263 g (95%) of a crystalline material which was homogeneous by tlc. An analytical sample of the phenylthio ketone **41**, obtained by recrystallization of this material from pentane, exhibited mp 76–77°C; ir ($CHCl_3$): 3100, 1700, 1635, 1580, 915 cm$^{-1}$; $^1$H nmr δ: 0.86 (d, 3H, $J$ = 5.5 Hz), 1.4–2.2 (diffuse m, 7H), 2.45 (d, 2H, $J$ = 8 Hz), ~2.62 (m, 1H), 3.18–3.56 (m, 1H), 4.86 (d, 1H, $J$ = 17 Hz), 5.03 (d, 1H, $J \approx$ 11 Hz), 5.66 (d of d, 1H, $J$ = 17, 11 Hz), 7.30 (m, 5H). *Anal.* calcd. for $C_{18}H_{22}OS$: C 75.48, H 7.68; found: C 75.42, H 7.76. *Exact Mass* calcd.: 286.1391; found: 286.1368.

*Preparation of the ketal **42***

A solution of the phenylthio ketone **41** (0.247, 0.86 mmol) and 2,2-dimethyl-1,3-propanediol (0.269 g, 2.6 mmol) in 12 mL of benzene containing 0.01 g of *p*-toluenesulfonic acid was refluxed under a Dean–Stark water separator for 3 h. After a small amount of solid sodium bicarbonate had been added to the cooled solution, the latter was diluted with 100 mL of benzene and the resultant solution was washed successively with saturated aqueous sodium bicarbonate and brine and then dried over anhydrous magnesium sulfate. Removal of the solvent gave 0.317 g (99%) of the ketal **42** as a clear oil which was homogeneous by tlc; ir ($CHCl_3$): 3100, 1635, 1590, 1100, 910 cm$^{-1}$; $^1$H nmr δ: 0.69 (d, 3H, $J$ = 6.0 Hz), 0.80, 0.96 (s, s, 3H each), 1.06–1.96 (diffuse m, 8H), 2.19 (m, 1H), 2.57 (broad t, 1H), 3.2–3.6 (diffuse m, 5H), 4.74 (d of d, 1H, $J$ = 17, 1 Hz), 4.95 (d of d, 1H, $J$ = 11, 1 Hz), 5.58 (d of d, 1H, $J$ = 17, 11 Hz), 7.14–7.50 (m, 5H). *Exact Mass* calcd. for $C_{23}H_{32}O_2S$: 372.2123; found: 372.2149.

*Preparation of the ketal tosylate **44***

To a cold (0°C), stirred solution of the olefinic ketal **42** (0.96 g, 2.57 mmol) in 3 mL of dry THF was added 0.30 mL (3.0 mmol) of borane – dimethyl sulfide complex. The reaction mixture was stirred at 0°C for 2 h, slowly warmed to room temperature over a period of 1 h, and then stirred at this temperature for 1 h. After the mixture had been cooled to 0°C, it was treated successively with methanol (0.6 mL) 3 *N* sodium hydroxide (0.6 mL), and 30% hydrogen peroxide (0.6 mL). The resultant mixture was warmed to 45–50°C, maintained at this temperature for 1 h, diluted with 20 mL of aqueous sodium bicarbonate, and then extracted thoroughly with dichloromethane. The combined extract was washed with brine and dried over anhydrous magnesium sulfate. Removal of the solvent afforded a viscous oil which was dissolved immediately in dry pyridine (4 mL). The solution was treated with *p*-toluenesulfonyl chloride (0.54 g, 2.8 mmol), allowed to stand at room temperature overnight, and then poured into ice-cold water. The resultant mixture was extracted with dichloromethane. The combined extract was washed with brine and dried over anhydrous magnesium sulfate. Removal of the solvent gave a viscous oil which was subjected to column chromatography on silica gel (60 g). Elution of the column with benzene – ethyl acetate (97.5:2.5) gave 0.325 g (34%) of the starting material (olefinic ketal **42**) and 0.80 g (86%, based on unrecovered starting material) of the ketal tosylate **44**. The latter substance was obtained as a clear oil which was homogeneous by tlc and exhibited ir ($CHCl_3$): 1600, 1590, 1195, 1100, 955 cm$^{-1}$; $^1$H nmr δ: 0.70 (d, 3H, $J$ = 5.5 Hz), 0.79, 0.85, (s, s, 3H each), 1.1–2.5 (diffuse m, 12H), 2.38 (s, 3H), 3.04–3.46 (diffuse m, 5H), 3.86–4.30 (m, 2H), 7.12–7.44 (m, 7H), 7.74 (d, 2H, $J$ = 8 Hz). *Exact Mass* calcd. for $C_{30}H_{40}O_5S_2$: 544.2317; found: 544.2312.

*Preparation of the sulfone tosylate **45***

To a cold (0°C), stirred solution of the sulfide tosylate **44** (0.25 g, 0.46 mmol) in 3 mL of dry dichloromethane was added, over a period of about 2 min, 0.204 g of 85% *m*-chloroperbenzoic acid and the resultant solution was stirred at 0°C for 2 h. The solution was diluted with 50 mL of saturated aqueous sodium bicarbonate and the resultant mixture was extracted thoroughly with dichloromethane. The combined extract was washed with brine and dried over anhydrous magnesium sulfate. Removal of the solvent afforded a semicrystalline material which was subjected to column chromatography on silica gel (20 g). Elution of the column with benzene – ethyl acetate (9:1) gave 0.264 g (100%) of a crystalline compound which was homogeneous by tlc. An analytical sample of compound **45**, obtained by recrystallization of a small amount of this material from ether–hexane, exhibited mp 145–146°C; ir ($CHCl_3$): 1600, 1365, 1305, 1175, 1150, 1087, 960 cm$^{-1}$; $^1$H nmr δ: 0.75 (d, 3H, $J$ = 6 Hz), 0.82, 0.90 (s, s, 3H each), 1.10–2.56 (diffuse m, 12H), 2.44 (s, 3H), 2.94–3.54 (diffuse m, 5H), 3.94–4.32 (m, 2H), 7.30–8.00 (diffuse m, 9H). *Anal.* calcd. for $C_{30}H_{40}O_7S_2$: C 62.47, H 6.99, S 11.12; found: C 62.47, H 7.09, S 11.01.

*Preparation of the tricyclic ketal sulfone **46***

To a solution of the sulfone tosylate **45** (0.235 g, 0.41 mmol) in 3 mL of dry HMPA under an atmosphere of nitrogen was added, over a period of 2 min, freshly prepared dry potassium *tert*-butoxide (2.0 mmol) and the resultant solution was stirred at room temperature for 1.5 h. The reaction mixture was diluted with benzene (150 mL), washed 5 times with brine, and dried over anhydrous magnesium sulfate. Removal of the solvent, followed by column chromatography (10 g silica gel, elution of the column with 9:1 benzene – ethyl acetate) of the residue gave 0.139 g (85%) of the crystalline tricyclic sulfone **46**. An analytical

Can. J. Chem. Downloaded from www.nrcresearchpress.com by 210.87.254.40 on 09/06/12
For personal use only.

sample, obtained by recrystallization of a small amount of this material from ether, exhibited mp 168–169°C; ir ($CHCl_3$): 1305, 1150, 1110 $cm^{-1}$; $^1H$ nmr δ: 0.88 (d, 3H, $J$ = 6 Hz), 0.86, 0.88 (s, s, 3H each), 1.1–2.5 (diffuse m, 14H), 3.20–3.56 (diffuse m, 4H), 7.40–7.96 (diffuse m, 5H). *Anal.* calcd. for $C_{23}H_{32}O_4S$: C 68.28, H 7.97, S 7.92; found: C 68.06, H 8.09, S 7.80. *Exact Mass* calcd.: 404.2021; found: 404.2015.

*Preparation of the tricyclic ketal* **47**

To a stirred solution of the ketal sulfone **46** (0.130 g, 0.32 mmol) in a mixture of dry methanol (2.5 mL) and benzene (1.0 mL)[14] was added 0.91 g (6.4 mmol) of anhydrous disodium hydrogen phosphate and 2.4 g of pulverized 6% sodium amalgam and the resultant mixture was stirred at room temperature for 1.5 h. The reaction mixture was diluted with benzene and decanted. The residual solid material was washed with several portions of benzene. The combined organic phase was washed successively with aqueous sodium bicarbonate and brine and dried over anhydrous magnesium sulfate. Removal of the solvent gave an oil which was filtered through a short column of silica gel (2 g). Elution of the column with benzene – ethyl acetate (9:1) gave 0.076 g (90%) of the tricyclic ketal **47** which was homogeneous by tlc and glc. This material exhibited ir (film): 1470, 1100 $cm^{-1}$; $^1H$ nmr δ: 0.84 (d, 3H, $J$ = 6 Hz), 0.90, 0.97 (s, s, 3H each), 1.10–2.34 (diffuse m, 15H), 3.40, 3.52 (s, s, 2H each). *Anal.* calcd. for $C_{17}H_{28}O_2$: C 77.22, H 10.67; found: C 77.02, H 10.65.

*Preparation of the tricyclic ketone* **32**

To a solution of the ketal **47** (75 mg, 0.28 mmol) in a 5:3:2 mixture of THF, methanol, and water (2 mL) was added 76 mg (85 mmol) of oxalic acid and the resultant solution was stirred at room temperature for 45 min. The reaction mixture was diluted with 50 mL of benzene and then was washed successively with saturated aqueous sodium bicarbonate and brine. The organic phase was dried over anhydrous magnesium sulfate. Removal of the solvent, followed by distillation (air bath temperature 85°C/0.3 Torr) of the residual oil, afforded 47 mg (93%) of the ketone **32** as a clear colorless oil which was homogeneous by tlc and glc; ir (film): 1705 $cm^{-1}$; $^1H$ nmr δ: 0.89 (d, 3H, $J$ = 6 Hz), 1.16–2.58 (diffuse m, 15H). *Exact Mass* calcd. for $C_{12}H_{18}O$: 178.1357; found: 178.1366.

*Equilibration of the tricyclic ketone* **32**

A solution of the ketone **32** (12 mg) in methanol (1 mL) containing 20 mg of sodium methoxide was stirred at room temperature for 24 h. Ammonium chloride was added, the methanol was removed under reduced pressure, and the residual material was taken up in a mixture of ether and water. The aqueous layer was washed with additional volumes of ether and the combined extract was dried over anhydrous magnesium sulfate. Removal of the solvent, followed by distillation (air bath temperature 85–90°C/0.4 Torr) of the residual material, gave 10 mg of a clear colorless oil. Analysis of this oil by glc showed that it was a mixture of two compounds, ketones **31** and **32**, in a ratio of 1:2, respectively. The ir and $^1H$ nmr spectra of this mixture were identical with those of an equilibrated mixture of the same two compounds previously prepared by Coates and Sowerby (49).[12]

## Acknowledgements

We are grateful to the Natural Sciences and Engineering Research Council of Canada for financial support, for a postgraduate Scholarship (to C.K.L.), and for a Postdoctoral Fellowship (to J.B.).

[14]Compound **46** was quite insoluble in methanol. Therefore, benzene was added to increase the solubility.

1. N. P. Neureiter. J. Org. Chem. **24**, 2044 (1959).
2. C. G. Overberger and A. E. Borchert. J. Am. Chem. Soc. **82**, 4896 (1960).
3. C. D. Gutsche and D. Redmore. Carbocyclic ring expansion reactions. Academic Press, New York, NY. 1968. p. 163.
4. E. M. Mil'vitskaya, A. V. Tarakanova, and A. F. Plate. Russ. Chem. Rev. **45**, 469 (1976).
5. M. J. S. Dewar, G. J. Fonken, S. Kirschner, and D. E. Minter. J. Am. Chem. Soc. **97**, 6750 (1975).
6. G. D. Andrews and J. E. Baldwin. J. Am. Chem. Soc. **98**, 6705, 6706 (1976).
7. B. M. Trost and P. H. Scudder. J. Org. Chem. **46**, 506 (1981).
8. D. Brulé, J.-C. Chalchat, R.-P. Garry, B. LaCroix, A. Michet, and R. Vessière. Bull. Soc. Chim. Fr. II, 57 (1981).
9. W. R. Dolbier, Jr., B. H. Al-Sader, S. F. Sellers, and H. Koroniak. J. Am. Chem. Soc. **103**, 2138 (1981).
10. E. J. Corey and S. W. Walinsky. J. Am. Chem. Soc. **94**, 8932 (1972).
11. B. M. Trost and M. J. Bogdanowicz. J. Am. Chem. Soc. **95**, 5311 (1973).
12. S. A. Monti, F. G. Cowherd, and T. W. McAninch. J. Org. Chem. **40**, 858 (1975).
13. E. J. Corey and R. H. Wollenberg. J. Org. Chem. **40**, 2265 (1975).
14. B. M. Trost and D. E. Keeley. J. Am. Chem. Soc. **98**, 248 (1976).
15. B. M. Trost, Y. Nishimura, K. Yamamoto, and S. S. McElvain. J. Am. Chem. Soc. **101**, 1328 (1979).
16. T. Hudlicky, J. P. Sheth, V. Gee, and D. Barnvos. Tetrahedron Lett. 4889 (1979).
17. T. Hudlicky and F. J. Koszyk. Tetrahedron Lett. **21**, 2487 (1980).
18. T. Hudlicky, T. M. Kutchan, S. R. Wilson, and D. T. Mao. J. Am. Chem. Soc. **102**, 6351 (1980).
19. T. Hudlicky, F. J. Koszyk, T. M. Kutchan, and J. P. Sheth. J. Org. Chem. **45**, 5020 (1980).
20. R. L. Danheiser, C. Martinez-Davila, and J. M. Morin, Jr. J. Org. Chem. **45**, 1340 (1980); R. L. Danheiser, C. Martinez-Davila, R. J. Auchus, and J. T. Kadonaga. J. Am. Chem. Soc. **103**, 2443 (1981).
21. J. M. Simpson and H. G. Richey, Jr. Tetrahedron Lett. 2545 (1973).
22. T. Hudlicky, F. J. Koszyk, D. M. Dochwat, and G. L. Cantrell. J. Org. Chem. **46**, 2911 (1981).
23. L. A. Paquette, G. J. Wells, K. A. Horn, and T.-H. Yan. Tetrahedron Lett. **23**, 263 (1982).
24. T. Hudlicky and R. P. Short. J. Org. Chem. **47**, 1522 (1982).
25. E. Piers, J. R. Grierson, C. K. Lau, and I. Nagakura. Can. J. Chem. **60**, 210 (1982).
26. E. Piers, K. F. Cheng, and I. Nagakura. Can. J. Chem. **60**, 1256 (1982).
27. E. Piers, C. K. Lau, and I. Nagakura. Tetrahedron Lett. 3233 (1976).
28. E. Piers and J. Banville. J. Chem. Soc. Chem. Commun. 1138 (1979).
29. D. Seyferth and H. M. Cohen. J. Organomet. Chem. **1**, 15 (1963).
30. H. Gilman and F. K. Cartledge. J. Organomet. Chem. **2**, 447 (1964).

31. G. H. POSNER, C. E. WHITTEN, and J. J. STERLING. J. Am. Chem. Soc. **95**, 7788 (1973).
32. G. H. POSNER, D. J. BRUNELLE, and L. SINOWAY. Synthesis, 662 (1974).
33. R. C. HAHN and G. W. JONES. J. Am. Chem. Soc. **93**, 4232 (1971).
34. R. G. CARLSON and W. S. MARDIS. J. Org. Chem. **40**, 818 (1975).
35. J. P. MARINO and L. J. BROWNE. J. Org. Chem. **41**, 3629 (1976).
36. E. PIERS and I. NAGAKURA. Tetrahedron Lett. 3237 (1976).
37. E. PIERS, I. NAGAKURA, and J. E. SHAW. J. Org. Chem. **43**, 3431 (1978).
38. E. PIERS, I. NAGAKURA, and H. E. MORTON. J. Org. Chem. **43**, 3631 (1978).
39. E. PIERS and E. H. RUEDIGER. J. Chem. Soc. Chem. Commun. 166 (1979).
40. E. PIERS and H.-U. REISSIG. Angew. Chem. Int. Ed. Engl. **18**, 791 (1979).
41. H. STETTER. Chem. Ber. **85**, 61 (1952).
42. E. J. COREY and M. CHAYKOVSKY. J. Am. Chem. Soc. **87**, 1353 (1965); Org. Synth. **49**, 78 (1969).
43. R. T. CONLEY and B. E. NOWAK. J. Org. Chem. **26**, 692 (1961).
44. A. F. KLUGE and C. P. LILLYA. J. Org. Chem. **36**, 1977 (1971).
45. G. STORK and P. G. WILLIARD. J. Am. Chem. Soc. **99**, 7067 (1977).
46. F. KIDO, H. UDA, and A. YOSHIKOSHI. J. Chem. Soc. Perkin Trans. I, 1755 (1972).
47. D. F. MACSWEENEY and R. RAMAGE. Tetrahedron, **27**, 1481 (1971).
48. A. DELJAC, W. D. MACKAY, C. S. J. PAN, K. J. WIESNER, and K. WIESNER. Can. J. Chem. **50**, 726 (1972).
49. R. M. COATES and R. L. SOWERBY. J. Am. Chem. Soc. **94**, 5386 (1972).
50. N. HANAYAMA, F. KIDO, R. TANAKA, H. UDA, and A. YOSHIKOSHI. Tetrahedron, **29**, 945 (1973).
51. G. BUCHI, A. HAUSER, and J. LIMACHER. J. Org. Chem. **42**, 3324 (1977).
52. H. J. LIU and W. H. CHAN. Can. J. Chem. **57**, 708 (1979).
53. A. J. BARKER and G. PATTENDEN. Tetrahedron Lett. **22**, 2599 (1981).
54. D. SEEBACH. Angew. Chem. Int. Ed. Engl. **18**, 239 (1979).
55. D. SEYFERTH and M. H. WEINER. J. Am. Chem. Soc. **83**, 3583 (1961).
56. H. O. HOUSE, C. Y. CHU, J. M. WILKINS, and M. J. UMEN. J. Org. Chem. **40**, 1460 (1975).
57. P. G. M. WUTS. Synth. Commun. **11**, 139 (1981).
58. C. S. FOOTE and R. B. WOODWARD. Tetrahedron, **20**, 687 (1964).
59. B. M. TROST, T. N. SALZMANN, and K. HOROI. J. Am. Chem. Soc. **98**, 4887 (1976).
60. I. KUWAJIMA, T. MUROFUSHI, and E. NAKAMURA. Synthesis, 602 (1976).
61. C. F. LANE. J. Org. Chem. **39**, 1437 (1974).
62. B. M. TROST, H. C. ARNDT, P. E. STREGE, and T. R. VERHOEVEN. Tetrahedron Lett. 3477 (1976).
63. P. A. GRIECO and Y. OHFUNE. J. Org. Chem. **43**, 2720 (1978).

Can. J. Chem. Downloaded from www.nrcresearchpress.com by 210.87.254.40 on 09/06/12
For personal use only.

# A proton relaxation study of the conformations of some purine mononucleotides in aqueous solution

C. F. G. C. GERALDES[1]
*Chemistry Department, University of Coimbra, 3000 Coimbra, Portugal*
AND
H. SANTOS AND A. V. XAVIER
*Centro de Química Estrutural, I.S.T., 1096 Lisboa, Portugal*
Received May 28, 1982

C. F. G. C. GERALDES, H. SANTOS, and A. V. XAVIER. Can. J. Chem. **60**, 2976 (1982).

A method is described by which conformationally averaged interproton distances in mononucleotides are obtained from measured proton spin-lattice relaxation times and published crystal coordinates of selected mononucleotides. The glycosil conformations of adenosine in $D_2O$ and DMSO-$d_6$ and of 5'-AMP, 5'-GMP, 3'-AMP, and 2'-AMP in $D_2O$ are examined by quantitative analysis of the conformationally averaged interproton distances in terms of population distributions obtained from potential energy calculations. 5'-AMP strongly prefers a single glycosyl conformation in the *anti* range. Besides the *anti* conformation, 5'-GMP has a secondary minimum in the *syn* region. 3'-AMP, 2'-AMP, and adenosine have more latitude in their glycosyl torsion angle values, with both the *syn* and *anti* regions highly populated.

C. F. G. C. GERALDES, H. SANTOS et A. V. XAVIER. Can. J. Chem. **60**, 2976 (1982).

On décrit une méthode qui permet d'obtenir les distances conformationnelles moyennes interprotons des nucléotides, à partir de la mesure des temps de relaxation spin-réseau et des coordonnées des cristaux de mononucléotides choisis que l'on trouve dans la littérature. On a étudié les conformations du glycosyle de l'adénosine dans du $D_2O$, et du DMSO-$d_6$ et celles des composés suivants: AMP-5', GMP-5', AMP-3' et AMP-2' dans du $D_2O$, en faisant appel à l'analyse quantitative des distances conformationnelles moyennes interprotons en fonction de la distribution de population obtenue à partir des calculs d'énergie potentielle. Le composé AMP-5' adopte une conformation unique du glycosyle dans la région *anti*. En plus de la conformation *anti*, le composé GMP-5' a un minimum secondaire du côté *syn*. Dans le cas des composés AMP-3' et AMP-2' et de l'adénosine les valeurs de l'angle de torsion du glycosyle sont plus flexibles quand les régions *syn* et *anti* ont une forte population.

[Traduit par le journal]

## Introduction

The interpretation at molecular level of a wide range of biological phenomena involving nucleic acids or coenzymes containing nucleotidyl units relies on the conformation of their monomeric units in solution (1). One example of this situation is the different allosteric activator properties of 5'-AMP and of its chemical analogs for the catalytic action of phosphorylase b in the degradation of glycogen (2, 3). In order to define the mode of interaction of a small ligand (e.g. a nucleotide) with a macromolecule the knowledge of the conformation of the free ligand may be very important (4).

Most of the studies of nucleotide flexibility in aqueous solution, their preferred conformation and modes of internal motion using nuclear magnetic resonance (nmr) spectroscopy (5), have used methods like coupling constants analysis (6, 7), chemical shifts studies (6, 7), the lanthanide probe method (8–11), and the nuclear Overhauser effect (nOe) (12–15). Although this last method has proved to be very convenient in the study of the preferred orientation of the base around the glycosyl bond of mononucleotides, similar structural information has become available from $^{13}C$ and $^1H$ spin-lattice relaxation time ($T_1$) measurements (16–20) using pulsed Fourier transform (FT) nmr techniques (21). In this work we extend a previous conformational study of 5'-mononucleotides in aqueous solution using $^1H$ $T_1$ measurements (20) and more general conformational search methods than previously undertaken. The study is also extended to some 3'- and 2'-mononucleotides and to different conditions of concentration, temperature, and pH. The conclusions thus obtained are compared with conclusions from independent nmr methods (6–15) and theoretical potential energy calculations on these molecules (22–24, 31).

## Experimental

The mononucleotides, purchased from Sigma Chemical Comp., were lyophilized from $D_2O$ (from Norsk Hydro), redissolved in $D_2O$ (5–30 m*M* concentrations) and their pH adjusted with DCl or NaOD. Residual paramagnetic impurities were removed by addition of 1 m*M* EDTA and residual oxygen was removed by several freeze–pump–thaw cycles on a high vacuum line.

The proton nmr spectra were run on a 100 MHz JEOL JMN 100 PFT spectrometer, equipped with a JEOL 980A computer for Fourier transformation. The proton $T_1$ measurements were carried out by the inversion–recovery method (nonselective 180°–τ–90° pulse sequence).

[1]Author to whom correspondence should be addressed.

0008-4042/82/232976-08$01.00/0
©1982 National Research Council of Canada/Conseil national de recherches du Canada

Can. J. Chem. Downloaded from www.nrcresearchpress.com by 210.87.254.105 on 09/06/12
For personal use only.

Can. J. Chem. Downloaded from www.nrcresearchpress.com by 210.87.254.105 on 09/06/12
For personal use only.

Calculation of the $r_{ij}$ interproton distances was carried out using the Burlesk (8) program modified to give the various molecular conformations obtained by variation of the $\psi$ and $\chi$ angles with increments of 30° and 20° respectively. Two starting conformations were used, differing in the ribose ring conformation: one was $C_3'$ *endo* (*N*), the other $C_2'$ *endo* (*S*) (33). The crystal coordinates used were obtained from the literature (10, 24).

## Results and discussion

*Determination of the calculation parameters*

The use of spin-lattice relaxation times ($T_1$) in conformational studies relies on the following basic assumptions.

(1) Spin-lattice relaxation occurs dominantly through intramolecular dipolar interactions; this assumption is met for nonquadrupolar nuclei, like $^1H$ and $^{13}C$, in dilute nucleotide $^2H_2O$ solutions (where intermolecular stacking is absent) free of paramagnetic species (21, 25, 26), except for $H_2$ of adenine nucleotides, where intermolecular dipolar interactions are dominant (18).

(2) The molecule under study is rigid and its rotational motion can be considered to be isotropic, so that the motion of any proton–proton vector can be characterized by a single rotational correlation time $\tau_R$, which corresponds to the rotation of the whole molecule. This assumption does not hold in most flexible macromolecules, but in low molecular weight molecules, such as mononucleotides, it is supported by various observations: $\tau_R$ values obtained from $^{13}C$ $T_1$ values of nucleotide C—H groups agree with each other within experimental error, $\tau_R \sim 2 \times 10^{-10}$ s at 25°C (17–20); in 5'-AMP, $T_1$ minima of all protons occur at the same temperature, giving $\tau_R$ values in agreement with those obtained from $^{13}C$ $T_1$ values (18). Therefore it is concluded that the internal motions of mononucleotides (pseudorotation of the furanose ring, rotation about the $C_{4'}$—$C_{5'}$ bond, and base rotation about the glycosidic bond, $N_9$—$C_{1'}$) are much slower than the overall isotropic molecular motion (the rate constants for all internal motions $K \ll \tau_R^{-1} \sim 10^9$ s$^{-1}$). This means that these flexible molecules are rigid in the practical sense of relaxation effects.

(3) Differences in relaxation rate between lines split by spin–spin coupling are negligible, which is valid only for first-order spectra. As the theory of relaxation of spin–spin split lines is impractical at the moment (27), we take the average of the intensity over these lines as the proton magnetization.

Under these conditions, the longitudinal magnetization $\langle I_i(t)\rangle$ of proton $i$, at time $t$ after a nonselective 180° pulse at $t = 0$, in a multispin system subject to intramolecular dipolar relaxation, can be seen not to decay experimentally to the equilibrium value $I_0$, but to be a linear combination of $n$ exponential functions of time (25). This is basically due to the existence of cross-relaxation effects. However, considering an interval from $t = 0$ to $t = \Delta t$ ($\Delta t \ll T_1$, see ref. 19), it can be seen that the initial recovery of magnetization for any proton $i$ obeys a single exponential function of time, whose time constant $T_{1i}$, is the spin-lattice relaxation time of proton $i$, and is given by eq. [1] when the extreme narrowing condition ($\omega^2_H \tau^2_R \ll 1$) holds (at 100 MHz):

$$[1] \quad T_{1i}^{-1} \equiv R_i = \frac{3}{2}\gamma_H^4 \left(\frac{h}{2\pi}\right)^2 \tau_R \sum_{j \neq i} \langle r_{ij}^{-6}\rangle = 85.35 \times 10^{-6}\, \tau_R \rho_i$$

where the relaxation rate $R_i$ is given in s$^{-1}$, $\tau_R$ in $10^{-10}$ s, and

$$\rho_i = \sum_{j \neq i} \langle r_{ij}^{-6}\rangle = \sum_{j \neq i} \rho_{ij} \text{ is in nm}^{-6};$$

$\langle r_{ij}\rangle$ is the interproton distance averaged over all possible molecular conformers. This averaging procedure is valid because the relaxation rates are much smaller than the rate constants of the internal motions, $T_{1i}^{-1} \ll K$ (25) (see Table 1).

As the relaxation rates deviate from the initial rate progressively with time, the $T_1$ values were deduced by a least-squares approximation of the observed values of $\langle I_i(t)\rangle$ to $I_0[1 - 2\exp(-t/T_1)]$ up to 50% recovery of magnetization. The $T_1$ values obtained for the mononucleotides studied in this work and values from the literature are listed in Table 1, together with the ribose conformer *N* populations, obtained by analysis of vicinal coupling constants.

*Conformationally averaged $\overline{r_{8i}}$ distances.*

*Illustration of the method for 5'-AMP*

The experimental relaxation rates $R_i$ can be analysed in the following way in order to give conformationally averaged $\rho_i \equiv \langle r_{8i}^{-6}\rangle$ values. Calculated values of $\rho_i$ for the nucleotide protons as a function of the glycosidic $\chi$ angle for the *N* and *S* furanose ring conformations (Fig. 1) were obtained from the relevant computer measured $r_{ij}$ distances derived from the crystal coordinates for selected purine nucleotides available in the literature (19, 24). In these calculations we used an average conformation of the exocyclic group, given by the populations $P_{gg} = 0.7$, $P_{gt} = 0.2$, and $P_{tg} = 0.1$, obtained from coupling constants analysis. It was verified that the calculated $\rho_i$ values of most

TABLE 1. Proton spin-lattice relaxation times of various nucleotides in $^2H_2O$ in different solution conditions

| Nucleotide | Conditions | | | Proton $T_1$(s) | | | | | | | |
|---|---|---|---|---|---|---|---|---|---|---|---|
| | Concentration (m*M*) | *T*(°C) | pH | H(8) | H(1') | H(2') | H(3') | H(4') | H(5',") | %*N*[c] | Reference |
| 5'-AMP | 5 | 25 | 7.0 | 1.86 | 2.75 | [b] | [b] | [b] | [b] | | 30 |
| | 15 | 25 | 7.5 | 1.50 | 2.30 | 0.85 | 0.89 | 0.90 | 0.31 | | 20 |
| | 100 | 25 | 8.1 | 1.53 | 2.12 | 0.74 | 0.78 | [b] | [b] | 38 | 19 |
| | 5 | 5 | 7.0 | 1.73 | 1.30 | [b] | [b] | [b] | [b] | | 30 |
| | 30 | 25 | 2.0 | 1.50 | 2.34 | 0.84 | 0.88 | 1.0[a] | 0.30 | 42 | [a] |
| 5'-GMP | 15 | 25 | 7.5 | 1.80 | 2.00 | 0.85 | 0.80 | 0.90 | 0.32 | 38 | 20 |
| | 30 | 25 | 8.0 | 1.81 | 2.17 | 0.86 | 0.91 | 0.93 | 0.29 | | [a] |
| 3'-AMP | 30 | 25 | 8.0 | 0.75 | 0.98 | [b] | [b] | [b] | [b] | 34 | [a] |
| | 15 | 5 | 7.0 | 0.73 | 0.96 | [b] | [b] | [b] | [b] | | 30 |
| 2'-AMP | 30 | 25 | 2.0 | 0.75 | 0.95 | [b] | [b] | [b] | [b] | | [a] |
| | 15 | 5 | 7.0 | 0.73 | 0.91 | [b] | [b] | [b] | [b] | 33 | 30 |

[a]This work.
[b]Not observed.
[c]% *N* values from refs. 7 and 32.

protons are quite insensitive to these rotamer populations.

The value of the correlation time $\tau_R$ can be calculated from $\rho_{4'}$, which is the same for *N* and *S* puckers and independent of the glycosidic angle $\chi$ (Fig. 1). Insertion of the experimental $R_{4'}$ value and the calculated $\rho_{4'}$ in eq. [1] gives $\tau_R = 1.1 \times 10^{-10}$ s for 5'-AMP. This value is in good agreement with values determined by other methods (18, 20, 28). Insertion of the experimental $R_i$ values of Table 2 and of the calculated $\tau_R$ in eq. [1] gives the $\rho_i$ values also shown in Table 2.

Within the approximations of the pseudorotational model (33) and in the intermediate exchange region of internal motions ($K \ll \tau_R^{-1}$) (25) we can write

$$[2] \quad \rho_{ij} = |N|\,\rho_{ij}^N + |S|\,\rho_{ij}^S$$

where $|N|$ and $|S|$ are the *N* and *S* conformer populations (Table 1). Therefore

$$[3] \quad \rho_i = \rho_{8i} + \{|N| \sum_{n\neq i,8} \rho_{ni}^N + |S| \sum_{n\neq i,8} \rho_{ni}^8\} \qquad (i = 1', 2', 3', 4', 5', 5'')$$

Insertion in eq. [3] of the calculated $\rho_i$, $|N|$, $|S|$, $\rho_{ni}^N$, and $\rho_{ni}^S$ values allows the $\rho_{8i}$ values to be obtained, which give the average distance of $H_8$ to the ribose protons (Table 2), in reasonable agreement with DESERT distance data.

Once that

$$[4] \quad \rho_{8i} = |N|\,\rho_{8i}^N + |S|\,\rho_{8i}^S$$

and $\rho_{8i}^N$ and $\rho_{8i}^S$ depend on the $\Omega$ distributions of the glycosidic angles $\chi_N$ and $\chi_S$, such that

$$[5] \quad \rho_{8i}^{N,S} = \int_0^{360} \Omega(\chi_{N,S})\,\rho_{8i}\,(\chi_{N,S})\,d\chi_{N,S}$$

the problem of the conformational analysis of the nucleotide base is to obtain, from the calculated curves $\rho_{8i}$ ($\chi$) (Fig. 2), $\Omega$ distributions which give a good agreement between the calculated $\rho_{8i}$ values from eqs. [4] and [5] and those obtained from the relaxation rates (Table 2).

Two types of distributions were considered. The first consisted of discrete sets of $\chi$ values ($\chi_N$ and $\chi_S$) associated with *N* and *S* ribose puckers, and is based on the assumption that the base is confined to a narrow range of the *syn* or *anti* region. The $\chi$ values which give the best agreement between calculated and experimental $\rho_{8i}$ values are ($\chi_N$, $\chi_S$) = (20°, 150°) (Table 2), a *syn–anti* equilibrium showing an interesting correlation of ribose and base conformations (*N*, *anti* and *S*, *syn*) which has already been assumed in previous studies (29). This result is also in disagreement with a previous study on this system (20), the only one in the literature to claim that 5'-AMP has the base in a *syn* conformation. We believe that the conclusions of that work are a consequence of the method of analysis used, which restricts $\chi$ distributions to a single value $\chi = \chi_N = \chi_S$.

As far as continuous distributions of $\chi$ values are concerned, as it is clear that a number of angular distributions may lead to similar experimental results, we only tested the angular distribution derived from Boltzmann's statistics of potential energy curves computed by Sarma *et al.* (31) (Fig. 3). The values thus calculated (Table 2) show that this distribution is compatible with the experimental results. Therefore, while this method by itself does not allow us to define unequivocally the average base conformation of 5'-AMP, we can test potential energy calculations. However, its use together with independent methods (e.g. para-

Can. J. Chem. Downloaded from www.nrcresearchpress.com by 210.87.254.105 on 09/06/12
For personal use only.

Can. J. Chem. Downloaded from www.nrcresearchpress.com by 210.87.254.105 on 09/06/12
For personal use only.

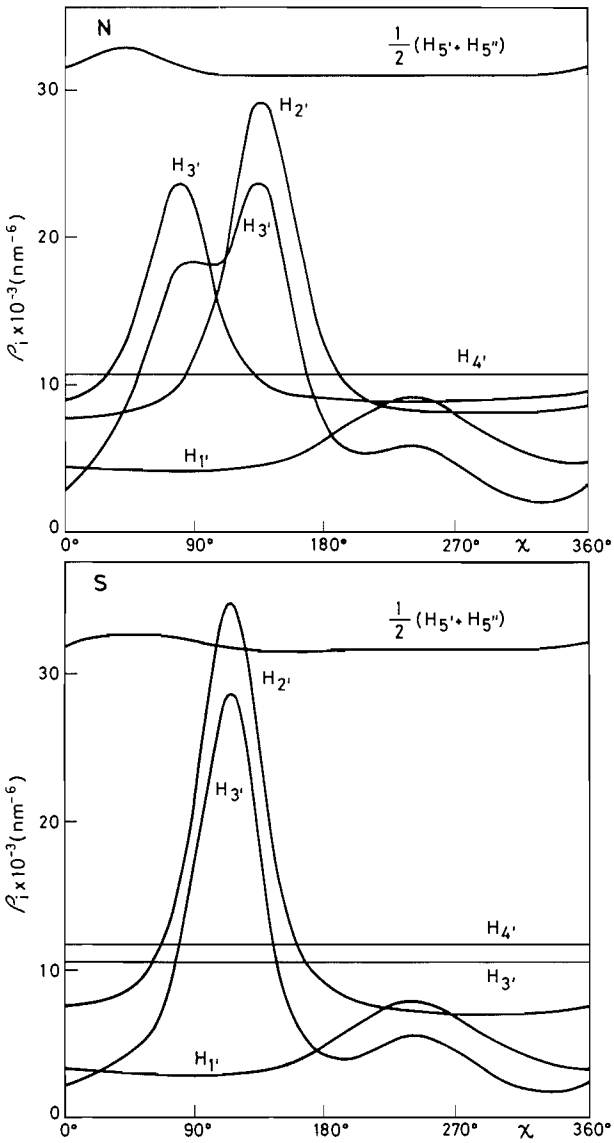


FIG. 1. $\rho_i$ as a function of $\chi$ for purine nucleotides with pure *N* and *S* puckers (see also ref. 29).

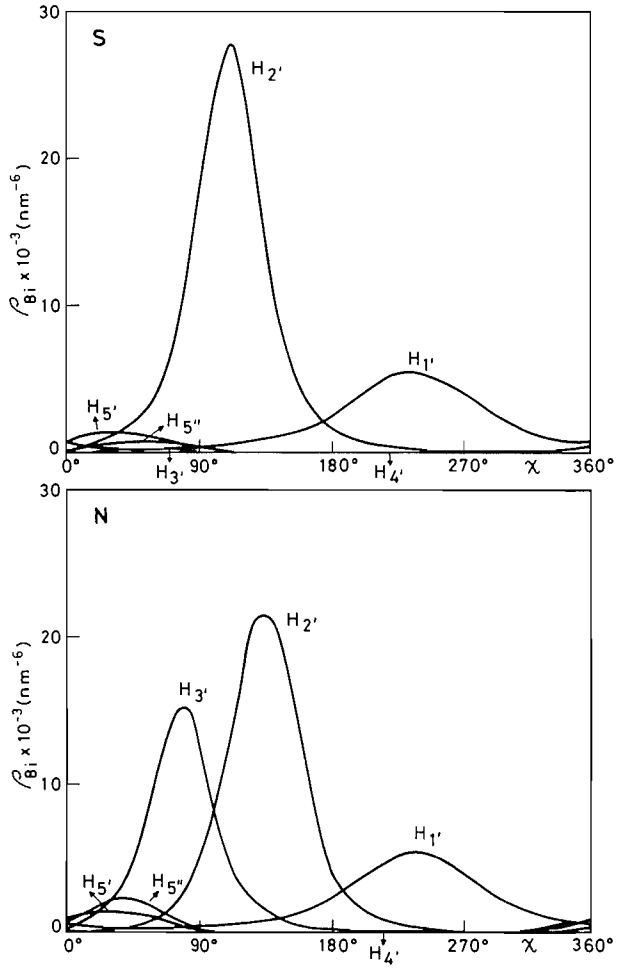


FIG. 2. $\rho_{8i}$ as a function of $\chi$ for pure *N* and *S* puckers.

magnetic probes (10)) allows us to conclude that the second distribution is in good agreement with all the experimental data.

Examination of $\rho_{8i}$ values for 5'-AMP (Table 3) in various experimental conditions shows that its base conformation is not significantly affected by pH or concentration. However a decrease of temperature to 5° C causes a decrease of $\rho_{81'}$ from 0.8 to 0.4. This is an indication of a more rigid *anti* conformation (see Fig. 2), possibly due to intermolecular base stacking, as was pointed out before (20).

### *Conformationally averaged $\overline{r_{8i}}$ distances for 5'-GMP, 3'-AMP, 2'-AMP, and adenosine*

Tables 1 and 3 present the measured proton spin-lattice relaxation times, and calculated conformationally averaged intermolecular distances for the above compounds. From the tabulated values of $\overline{r_{81'}}$ in Table 3, it is apparent that significant amounts of both *syn* and *anti* conformations exist about the glycosidic linkage in those molecules. The percentage of *syn* conformations increases in the order: 5'-AMP < 5'-GMP < 3'-AMP, 2'-AMP < adenosine.

A more quantitative interpretation of the $\overline{r_{8i}}$ values in terms of molecular conformation must include a statistical treatment over possible conformers. Angular distributions of $\chi$ values derived from several published potential energy curves were tested (22–24). In the case of 5'-GMP two possibilities were tested, corresponding respective-

TABLE 2. Glycosidic angle conformational analysis for 5'-AMP ($\tau_R = 1.1 \times 10^{-10}$ s)

| Proton | $T_{1i}$ (s) | $R_i$ (s$^{-1}$) | $\rho_i \times 10^{-3}$ (nm$^{-6}$) | $\rho_{8i} \times 10^{-3}$ (nm$^{-6}$) Measured[a] [1] | [2] | Calculated [3] | [4] |
|---|---|---|---|---|---|---|---|
| 8 | 1.50 | 0.67 | 7.1 | — | — | — | — |
| 1' | 2.30 | 0.43 | 4.6 | 1.3 | 0.8 | 0.6 | 0.9 |
| 2' | 0.85 | 1.18 | 12.6 | 4.9 | 4.1 | 4.1 | 4.1 |
| 3' | 0.89 | 1.12 | 11.9 | 1.2 | 0.8 | 0.8 | 1.0 |
| 4' | 0.90 | 1.11 | 11.8 | 0.3 | [b] | 0.3 | 0.3 |
| 5' + 5" | 0.31 | 3.23 | 34.4 | 2.0 | [b] | 1.2 | 1.2 |

[a][1] This work; [2] DESERT method (19); [3] two-state model, $\chi_N = 20°$, $\chi_S = 150°$; [4] distribution from potential energy curves (31) (see Fig. 3).
[b]Not determined.

TABLE 3. Measured $\rho_{8i} \times 10^{-3}$ (nm$^{-6}$) values and average distances $\overline{r_{8i}}$ (nm) for various nucleotides and adenosine

| Nucleotide | Experimental conditions: Concentration (m$M$) | $T$(°C) | pH | $\rho_{81'}(\overline{r_{81'}})$ | $\rho_{82'}(\overline{r_{82'}})$ | $\rho_{83'}(\overline{r_{83'}})$ | Reference |
|---|---|---|---|---|---|---|---|
| Ad ($D_2O$) | 100 | 51.5 | 7.0 | 3.2 (0.26) | 2.6 (0.27) | 1.4 (0.30) | 19 |
| Ad (DMSO-$d_6$) | 100 | 35 | — | 3.2 (0.26) | 3.2 (0.26) | 1.1 (0.31) | 19 |
| 5'-AMP | 100 | 28 | 8.1 | 0.8 (0.33) | 4.1 (0.25) | 0.8 (0.33) | 19 |
| | 15 | 25 | 7.5 | 1.3 (0.30) | 4.9 (0.24) | 1.2 (0.31) | [a] |
| | 5 | 5 | 7.0 | 0.4 (0.37) | [b] | [b] | 30 |
| | 30 | 25 | 2.0 | 0.8 (0.33) | 4.1 (0.25) | 0.8 (0.33) | [a] |
| 5'-GMP | 15 | 25 | 7.5 | 1.6 (0.29) | 4.9 (0.24) | 1.2 (0.31) | [a] |
| | 15 | 25 | 7.5 | 1.4 (0.30) | [b] | [b] | 20 |
| | 30 | 25 | 8.0 | 1.5 (0.30) | 4.9 (0.24) | 1.1 (0.31) | [a] |
| 3'-AMP | 30 | 25 | 8.0 | 2.6 (0.27) | [b] | [b] | [a] |
| | 15 | 5 | 7.0 | 2.6 (0.27) | [b] | [b] | 30 |
| 2'-AMP | 30 | 25 | 2.0 | 2.6 (0.27) | [b] | [b] | [a] |
| | 15 | 5 | 7.0 | 2.6 (0.27) | [b] | [b] | 30 |

[a]This work.
[b]Not observed.

ly to situations where (*i*) formation of a hydrogen bond between the O—H group of the phosphate and the $N_3$ atom of the base is possible, leading to a predominance of the *syn* base conformation, and (*ii*) a situation in which such a bond is impossible, leading to a predominance of the *anti* base conformation.

A good agreement between the calculated $\rho_{8i}$ values (Table 4) and the experimental values (Table 3) is obtained when a 1:1 equilibrium of *syn* and *anti* forms is considered (distribution 7), but this agreement no longer exists in the extreme *syn* and *anti* situations (distributions 5 and 6). Therefore the intermolecular bond POH...$N_3$ in 5'-GMP is not permanent. However, as the calculated $\rho_{82'}$ value is too small, the experimental $\chi$ angle distribution in the *anti* region goes to higher values (80°) than the calculated distribution implies (23).

In the case of 2'-AMP, various distributions were tested (distributions 16 to 19) based on potential energy calculations for 2'-GMP (23). The best agreement between experimental and calculated $\rho_{8i}$ values is obtained from distribution 16, which considers the existence of intramolecular bonds between POH and $N_3$ and between $O_5$·H and $N_3$. This distribution gives a predominantly *syn* ($\chi \sim 180°$ for $C_{3'}$ *endo* and $\chi \sim 220°$–$300°$ for $C_{2'}$ *endo* sugar conformations) over *anti* ($\chi \sim 40°$–$120°$ for $C_{2'}$ *endo* sugar conformation) base conformation.

In the case of 3'-AMP, as a phosphate group in the 3' position cannot have any direct effect on the glycosidic and exocyclic torsion angles, distributions based on potential energy calculations for adenosine (22) were used. These distributions were of course also used for the conformational analysis of adenosine in $D_2O$ and in DMSO-$d_6$. The best distributions for 3'-AMP and adenosine are, respectively, distributions 25 and 24, obtained by mixture of distributions 22 and 23 in different proportions. These assume no POH...$N_3$ intramolecular bond and the possibility of a $O_5$·H...$N_3$ intramolecular bond giving a *syn* base conforma-

Can. J. Chem. Downloaded from www.nrcresearchpress.com by 210.87.254.105 on 09/06/12
For personal use only.

Can. J. Chem. Downloaded from www.nrcresearchpress.com by 210.87.254.105 on 09/06/12
For personal use only.

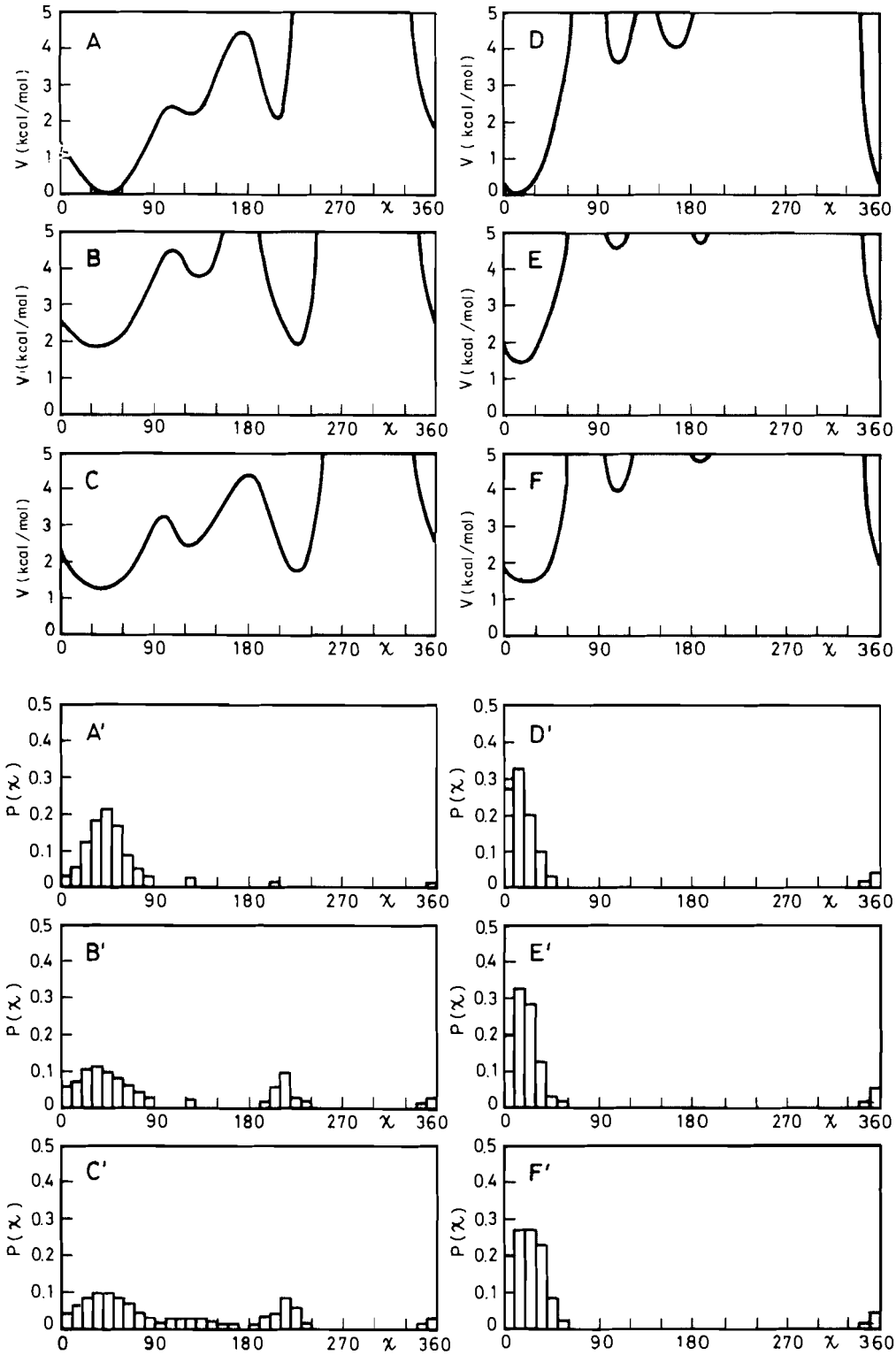


FIG. 3. Calculated potential energy curves for 5′-AMP from the literature (31) (A–F) and χ angle distributions derived from them by Boltzmann's statistics (A′–F′); A, B, C, A′, B′, C′ (*N* pucker); D, E, F, D′, E′, F′ (*S* pucker); A, D, A′, D′ (gg); B, E, B′, E′ (gt); C, F, C′, F′ (tg).

TABLE 4. Calculated $\rho_{8i}$ values for different nucleotides obtained from glycosidic angle distributions derived from published potential energy curves

| Nucleotide | Distribution | POH...$N_3$[b] | $O_{5'}$H...$N_3$[b] | $\chi$ angle | Sugar pucker | Reference | $\rho_{81'}$ | $\rho_{82'}$ | $\rho_{83'}$ |
|---|---|---|---|---|---|---|---|---|---|
| 5'-GMP | 1 | Y | N | *syn* | *N* | 23, 24 | 2.6 | 3.0 | 0.2 |
| | 2 | Y | N | *syn* | *S* | 23, 24 | 2.6 | 1.2 | 0.2 |
| | 3 | N | N | *anti* | *N* | 23 | 0.7 | 0.3 | 2.6 |
| | 4 | N | N | *anti* | *S* | 23 | 0.7 | 1.2 | 0.2 |
| | 5: 40% 1 + 60% 2 | Y | N | *syn* | *N/S* | [a] | 2.6 | 1.8 | 0.2 |
| | 6: 40% 3 + 60% 4 | N | N | *anti* | *N/S* | [a] | 0.7 | 1.0 | 1.2 |
| | 7: 50% 5 + 50% 6 | Y/N | N | *syn/anti* | *N/S* | [a] | 1.6 | 1.4 | 0.7 |
| 2'-AMP | 8 | Y | Y | *syn* | *N* | 23 | 1.8 | 2.0 | 0.2 |
| | 9 | Y | N | *anti* | *N* | 23 | 0.7 | 0.1 | 0.4 |
| | 10 | N | Y | *syn* | *N* | 23 | 2.6 | 2.8 | 0.1 |
| | 11 | N | N | *anti* | *N* | 23 | 1.2 | 2.3 | 3.6 |
| | 12 | Y | Y | *syn/anti* | *S* | 23 | 2.8 | 3.2 | 0.1 |
| | 13 | Y | Y | *syn/anti* | *S* | 23 | 1.7 | 5.4 | 0.1 |
| | 14 | N | N | *syn* | *S* | 23 | 4.8 | 0.1 | 0.1 |
| | 15 | N | N | *anti* | *S* | 23 | 0.7 | 13.8 | 0.1 |
| | 16: 30% 8 + 70% 12 | Y | Y | *syn/anti* | *N/S* | [a] | 2.5 | 2.8 | 0.2 |
| | 17: 30% 9 + 70% 13 | Y | N | *syn/anti* | *N/S* | [a] | 1.4 | 3.2 | 0.2 |
| | 18: 30% 10 + 70% 14 | N | Y | *syn* | *N/S* | [a] | 4.0 | 0.9 | 0.1 |
| | 19: 30% 11 + 70% 15 | N | N | *anti* | *N/S* | [a] | 0.9 | 10.2 | 1.2 |
| 3'-AMP, Ad | 20 | N | N | *anti* | *N* | 22 | 0.7 | 0.3 | 1.1 |
| | 21 | N | N | *syn/anti* | *S* | 22 | 1.9 | 6.0 | 0.2 |
| | 22 | N | Y | *syn* | *N/S* | 22 | 5.2 | 0.2 | 0.2 |
| | 23: 30% 20 + 70% 21 | N | N | *syn/anti* | *N/S* | [a] | 1.6 | 4.0 | 0.8 |
| | 24: 40% 22 + 60% 23 | N | Y/N | *syn/anti* | *N/S* | [a] | 3.2 | 2.6 | 0.7 |
| | 25: 30% 22 + 70% 23 | N | Y/N | *syn/anti* | *N/S* | [a] | 2.6 | 3.2 | 0.7 |

[a]This work.
[b]Y = Yes; N = No.

tion ($\chi \sim 230°$) (distribution 22) or no intramolecular $O_5$·H...$N_3$ bond giving an *anti* base conformation ($\chi \sim 300°$–$60°$) for a $C_{3'}$ *endo* sugar pucker (distribution 20) and a *syn/anti* mixture for a $C_{2'}$ *endo* sugar pucker (distribution 21).

## Conclusion

Conformationally averaged interproton distances in purine mononucleotides can be obtained by a new method based on measured proton spin-lattice relaxation times and published crystal coordinates of various mononucleotides. These distances compare reasonably well with values obtained from deuterium substitution effects on relaxation times (DESERT). Several published potential energy curves were tested and verified to be compatible with the experimental values. The variability of the glycosyl conformation of the purine mononucleotides increases in the order: 5'-AMP < 5'-GMP < 3'-AMP, 2'-AMP < adenosine.

## Acknowledgements

This work was subsidized by INIC, Portugal.

1. E. D. BERGMANN and B. PULLMAN (*Editors*). Conf. Biol. Molec. Polym., Jerusal. Symp. Quant. Chem. Biochem. Vol. V. Academic Press, New York. 1973.
2. J. MONOD, J. WYMAN, and J. P. CHANGEUX. J. Mol. Biol. **12**, 88 (1965).
3. W. BLACK and J. H. WANG. J. Biol. Chem. **234**, 5892 (1968).
4. A. S. V. BURGEN, G. C. K. ROBERTS, and J. FEENEY. Nature, **253**, 753 (1975).
5. D. B. DAVIES. Prog. Nucl. Magn. Reson. Spectrosc. **12**, 135 (1978).
6. D. B. DAVIES and S. S. DANYLUK. Biochemistry, **13**, 4417 (1974).
7. D. B. DAVIES and S. S. DANYLUK. Biochemistry, **14**, 543 (1975).
8. C. D. BARRY, J. A. GLASEL, R. J. P. WILLIAMS, and A. V. XAVIER. J. Mol. Biol. **84**, 471 (1974).
9. B. BIRDSALL, W. J. B. BIRDSALL, J. FEENEY, and J. THORNTON. J. Am. Chem. Soc. **97**, 2845 (1975).
10. C. F. G. C. GERALDES and R. J. P. WILLIAMS. Eur. J. Biochem. **85**, 463 (1978).
11. C. F. G. C. GERALDES. J. Magn. Reson. **36**, 89 (1979).
12. P. A. HART and J. P. DAVIS. J. Am. Chem. Soc. **93**, 753 (1971).
13. R. E. SCHIRMER, J. P. DAVIS, R. H. NOGGLE, and P. A. HART. J. Am. Chem. Soc. **94**, 2561 (1972).
14. T.-D. SON, W. GUSCHLBAUER, and M. GUÉRON. J. Am. Chem. Soc. **94**, 7903 (1972).
15. M. GUÉRON, C. CHACHATY, and T.-D. SON. Ann. N.Y. Acad. Sci. **222**, 307 (1973).
16. H. D. LÜDEMANN, E. WESTHOF, and O. RÖDER. Eur. J. Biochem. **49**, 143 (1974).
17. O. RÖDER, H. D. LÜDEMANN, and E. VON GOLDAMMER. Eur. J. Biochem. **53**, 517 (1976).
18. T. IMOTO, K. AKASAKA, and H. HATANO. Chem. Phys. Lett. **32**, 86 (1975).

Can. J. Chem. Downloaded from www.nrcresearchpress.com by 210.87.254.105 on 09/06/12
For personal use only.

19. K. AKASAKA, S. SHIBATA, T. IMOTO, and H. HATANO. J. Magn. Reson. **17**, 413 (1975); **18**, 328 (1975).
20. C. CHACHATY, T. ZEMB, G. LANGLET, T.-D. SON, H. BUC, and M. MORANGE. Eur. J. Biochem. **62**, 45 (1976); C. CHACHATY and G. LANGLET. FEBS Lett. **68**, 181 (1976).
21. T. C. FARRAR and E. D. BECKER. Pulse and Fourier transform NMR. Introduction to theory and methods. Academic Press, New York. 1971.
22. H. BERTHOD and B. PULLMAN. Biochim. Biophys. Acta, **232**, 595 (1971).
23. H. BERTHOD and B. PULLMAN. FEBS Lett. **30**, 231 (1973).
24. N. YATHINDRA and M. SUNDARALINGAM. Biopolymers, **12**, 297 (1973); **12**, 2075 (1973); **12**, 2261 (1973).
25. J. H. NOGGLE and R. E. SCHIRMER. The nuclear Overhauser effect, chemical applications. Academic Press, New York. 1971.
26. A. P. ZENS, T. J. WILLIAMS, J. C. WISOWATY, R. R. FISHER, R. B. DUNLAP, T. A. BRYSON, and P. D. ELLIS. J. Am. Chem. Soc. **97**, 2850 (1975).
27. I. D. CAMPBELL and R. FREEMAN. J. Magn. Reson. **11**, 143 (1973).
28. L. M. RHODES and P. R. SCHIMMEL. Biochemistry, **10**, 4426 (1971).
29. H. PLACH, E. WESTHOF, H.-D. LÜDEMANN, and R. MENGEL. Eur. J. Biochem. **80**, 295 (1977).
30. A. P. ZENS, T. A. BRYSON, R. B. DUNLAP, R. R. FISHER, and P. D. ELLIS. J. Am. Chem. Soc. **98**, 7559 (1976).
31. R. H. SARMA, C.-H. LEE, F. E. EVANS, N. YATHINDRA, and M. SUNDARALINGAM. J. Am. Chem. Soc. **96**, 7337 (1974).
32. C. M. DOBSON, C. F. G. C. GERALDES, G. RATCLIFFE, and R. J. P. WILLIAMS. Eur. J. Biochem. **88**, 259 (1978).
33. C. ALTONA and M. SUNDARALINGAM. J. Am. Chem. Soc. **94**, 8205 (1972); **95**, 2333 (1973).

Can. J. Chem. Downloaded from www.nrcresearchpress.com by 210.87.254.105 on 09/06/12
For personal use only.

Can. J. Chem. Downloaded from www.nrcresearchpress.com by 210.87.254.42 on 09/06/12
For personal use only.

COMMUNICATION

# Polymer supported enantioselective reactions. III. Protonation of lithioenamine derivatives of racemic 2-methylcyclohexanone

COLIN R. MCARTHUR,[1] JI-LONG JIANG, AND CLIFFORD C. LEZNOFF[1]

*Department of Chemistry, York University, Toronto, Ont., Canada M3J 1P3*

Received July 22, 1982

COLIN R. MCARTHUR, JI-LONG JIANG, and CLIFFORD C. LEZNOFF. Can. J. Chem. **60**, 2984 (1982).

Asymmetric protonations, with enantioselectivities ranging to 90%, were observed in reactions of lithioenamines derived from imines of racemic 2-methylcyclohexanone and insoluble cross-linked copolymers of polystyrene and divinylbenzene substituted with (*S*)-2-aminoalkoxymethyl groups.

COLIN R. MCARTHUR, JI-LONG JIANG et CLIFFORD C. LEZNOFF. Can. J. Chem. **60**, 2984 (1982).

On a observé des protonations asymétriques, avec des sélectivités énantiométriques allant jusqu'à 90%, lors de réactions de lithioénamines provenant des imines de la méthyl-2 cyclohexanone racémique avec un copolymère réticulé et insoluble de polystyrène et de divinylbenzène portant des groupes aminoalkoxyméthyle-2(*S*).

[Traduit par le journal]

Recently we reported the use of insoluble cross-linked copolymers of styrene and divinylbenzene with covalently bonded (*S*)-2-aminoalkoxy groups (**1**) in the asymmetric methylation of the lithioenamines derived from cyclohexanone and **1**. The polymeric system afforded higher enantioselectivities than were observed through the use of analogous systems, under comparable conditions, in solution (1).

We now report preliminary results in our study of asymmetric *protonations* of the lithioenamines derived from the polymer-bound ketimines **2** formed from reaction of **1** with racemic 2-methylcyclohexanone (pathway A).

Two examples of nonbiological systems involving asymmetric protonations, conducted in the solution phase, have been reported recently. Thus, amino-acids may be "deracemized" to 70% e.e. (2), and a bicyclobutane bridged enolate anion has been enantioselectively protonated to 48% e.e. (3).

In our studies, to distinguish between asymmetric protonation of the lithioenamines from **2** and a bias in the reaction of enantiomers during imine formation from racemic 2-methylcyclohexanone, imines **2** were subjected to direct hydrolysis (pathway B). The degree of resolution depends on the structure of **1**. Thus, 2-aminopropoxymethylated polystyrene (**1***a*) led to no apparent resolution, while the 3-phenyl derivative (**1***b*) afforded the 2-methylcyclohexanones with 50% excess of the (*S*)-enantiomer (Table 1). While **2***b*, then, must have (*S*)-2-methylcyclohexylidene moieties in 50% e.e., this chiral centre would be expected to be lost on deprotonation at the 2-position if a planar lithioenamine is assumed (see below).

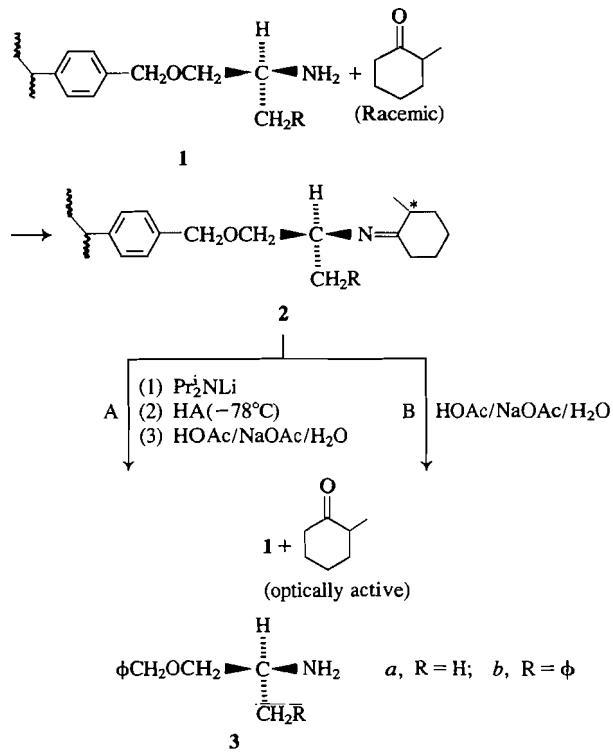


The enantioselectivity of pathway A was found to be highly dependent on both the structure of the asymmetric inducing moiety on the polymer, and on the structure of the protonating species (Table 1). Bias is moderately towards formation of excess

[1]Authors to whom correspondence may be addressed.

0008-4042/82/232984-02$01.00/0

©1982 National Research Council of Canada/Conseil national de recherches du Canada

TABLE 1. Enantiomeric excesses of product 2-methylcyclohexanone[a]

| | | Enantiomeric excess (*R*) or (*S*) (%)[b] | |
|---|---|---|---|
| | | R = H | R = ϕ |
| HA in Pathway A | HOAc | 20 (*R*) | 22 (*S*) |
| | $Et_3NHCl$ in THF | 36 (*R*) | — |
| | 2,6-Di-*t*-butyl *p*-cresol in THF | 8 (*R*) | — |
| | *t*-BuOH | — | 0 |
| | EtOH + $Et_3NHCl$ in THF | — | 82 (*S*) |
| | EtOH | 22 (*R*) | 90 (*S*) |
| Pathway B | | 0 | 50 (*S*) |

[a]Isolated as previously described (1); > 98% pure as determined by gc; yields 0.1–0.2 mmol per g of polymer.
[b]Based on optical rotation of pure (*R*)-2-methylcyclohexanone at −16.4°C (8).

(*R*)-2-methylcyclohexanone using **1***a*, but more strongly towards (*S*)-2-methylcyclohexanone using **1***b* (of the same chirality). It is noteworthy that, in the case of **1***b*, bond formation to the proton must have occurred on the side of the 2-position opposite to that in bond formation to carbon in the methylation reactions described earlier (1) in order for both to lead to (*S*)-2-methylcyclohexanone.

Most significant are two extremum results. (*S*)-2-Methylcyclohexanone was obtained in 90% e.e. when the lithioenamine from **2***b* was protonated using ethanol, but only racemic product was obtained using *tert*-butyl alcohol, after the resulting polymers were hydrolyzed under the same conditions. These observations are consistent with regioselective deprotonation of **2***b* at the 2-position to form a planar lithioenamine followed by highly diastereoselective *C*-protonation when ethanol is used, or nondiastereoselective selective protonation with *tert*-butyl alcohol. Predominant deprotonation at the more highly alkylated α-position has been observed in other ketimines (4, 5) including those of cyclohexanone imines (4) using alkylithium reagents. In view of the studies of Knorr and Löw (6) the *C*-protonation may be a result of a tautomerization[2] following an initial kinetically controlled *N*-protonation to form an enamine.

Another possibility may be deprotonation at the 6-position of the 2-methylcyclohexanone imine system, as observed by Meyers *et al.* (7) in reactions of lithium diisopropylamide on imines in solution, followed by a complex equilibration prior to hydrolysis.[2]

In any event, diastereoselective *C*-protonation at the 2-position ultimately must have occurred prior to hydrolysis by a mechanism that is highly influenced by the structure of the protonating species.

An analogous system in solution was investigated. The imine from racemic 2-methylcyclohexanone and (*S*)-2-aminopropyl benzyl ether (**3***a*) (1) was treated under the same conditions as those in pathway A for the polymeric system. The product exhibited no optical activity. We plan to examine the analogous system derived from (*S*)-2-amino-3-phenylpropyl benzyl ether (**3***b*).

Our result of 90% e.e. would appear to be unprecedented in enantioselective protonation reactions in nonbiological systems. These results are consistent with earlier observations (1) of enhancement of enantioselectivities through the use of polymer supported asymmetric inducing agents relative to analogous systems in solution. While mechanisms have been proposed to explain the predominant enantioselectivities in related reactions (9, 10) additional studies are required to rationalize the results that we report here. Studies in this area are continuing.

[2]We appreciate these alternative explanations suggested by one referee.

**Acknowledgements**

We thank the Natural Sciences and Engineering Research Council of Canada and the Faculty of Science, York University for financial support of this research.

1. (*a*) C. R. McArthur, P. M. Worster, J.-L. Jiang, and C. C. Leznoff. Can. J. Chem. **60**, 1836 (1982); (*b*) P. M. Worster, C. R. McArthur, and C. C. Leznoff. Angew. Chem. Int. Ed. Engl. **18**, 221 (1979).
2. L. Duhamel and J. C. Plaquevent. Tetrahedron Lett. **21**, 2521 (1980).
3. H. Hogeveen and L. Zwart. Tetrahedron Lett. **23**, 105 (1982).
4. A. Hosomi, Y. Araki, and H. Sakurai. J. Am. Chem. Soc. **104**, 2081 (1982).
5. J. K. Smith, D. E. Bergbreiter, and M. Newcomb. J. Org. Chem. **46**, 3157 (1981).
6. R. Knorr and P. Löw. J. Am. Chem. Soc. **102**, 3241 (1980).
7. A. I. Meyers, D. R. Williams, G. W. Erickson, S. White, and M. Druelinger. J. Am. Chem. Soc. **103**, 3081 (1981).
8. J. K. Whitesell and M. A. Whitesell. J. Org. Chem. **42**, 377 (1977).
9. A. I. Meyers, D. R. Williams, and M. Druelinger. J. Am. Chem. Soc. **98**, 3032 (1976); A. I. Meyers and D. R. Williams. J. Org. Chem. **43**, 3245 (1978).
10. R. R. Fraser, F. Akiyama, and J. Banville. Tetrahedron Lett. 3929 (1979).

Can. J. Chem. Downloaded from www.nrcresearchpress.com by 210.87.254.42 on 09/06/12
For personal use only.

# A carbon-13 nuclear magnetic resonance study of a series of 5-substituted benzimidazoles

BARRY J. BLACKBURN,[1] DOUGLAS W. ANKROM, AND HAROLD M. HUTTON[1]

*Chemistry Department, University of Winnipeg, Winnipeg, Man., Canada R3B 2E9*

Received December 21, 1981[2]

BARRY J. BLACKBURN, DOUGLAS W. ANKROM, and HAROLD M. HUTTON. Can. J. Chem. **60**, 2987 (1982).

Carbon-13 nmr chemical shift assignments are reported for a series of 5-substituted benzimidazoles, 2-methylbenzimidazole, and 5,6-dimethylbenzimidazole. By employing the three-parameter equation of Smith and Proulx, the chemical shifts of all the ring carbons of the 5-substituted compounds are correlated with $F$ and $R$ of Swain and Lupton and $Q$ of Schaefer; only the *ipso* carbon, C-5, has chemical shifts with a correlation coefficient less than 0.953. These correlations are compared with those obtained from the Swain–Lupton and Taft relationships; in general those from the latter two approaches are found to be less satisfactory. Correlations of the same chemical shifts with excess charge density values, calculated at the INDO level of approximation, are also presented.

BARRY J. BLACKBURN, DOUGLAS W. ANKROM et HAROLD M. HUTTON. Can. J. Chem. **60**, 2987 (1982).

On rapporte l'identification des déplacements chimiques en rmn du $^{13}C$ d'une série de benzimidazoles substituées en position 5, de la méthyl-2 benzimidazole et de la diméthyl-5,6 benzimidazole. En utilisant l'équation à trois paramètres de Smith et Proulx, on a pu établir une corrélation entre les déplacements chimiques de tous les carbones du cycle des composés substitués en position 5 avec les $F$ et $R$ de Swain et Lupton et le $Q$ de Schaefer; seul le carbone *ipso* C-5 a des dépacements chimiques avec un coefficient de corrélation inférieur à 0,953. On a comparé ces corrélation avec celles obtenues à partir des données de Swain–Lupton et Taft. Les corrélations de Swain–Lupton et Taft sont en général moins satisfaisantes. On présente également les corrélation des mêmes déplacements chimiques avec les valeurs de densité de charge en excès, au niveau d'approximation INDO.

[Traduit par le journal]

## Introduction

The carbon-13 nmr spectrum and carbon charge densities for benzimidazole, **1**, have been reported by Pugmire and Grant (1). The carbon-13 chemical shifts for some 5-substituted benzimidazoles have been published (2, 3); correlations were observed (2) for C-2 and C-8 using $\sigma_p$ and $\sigma_6$ substituent constants. For some other benzazoles, namely derivatives of benzimidazole (4), benzothiazole, **2** (5), and benzoxazole, **3** (6), with substitution only on C-2, reasonable correlations were reported for all ring carbon atoms using the $F$, $R$, and $Q$ substituent constants (7, 8) in the three-parameter equation of Smith and Proulx (9, 10).

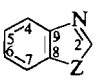

**1** Z = NH
**2** Z = S
**3** Z = O

Here we report the assignment of the carbon-13 resonances and the calculated carbon charge densities for a series of 5-substituted benzimidazoles with substituents ranging from strongly electron-releasing to strongly electron-withdrawing. We find benzene substituent-induced chemical shifts (SCS) do not always yield the correct assignment in benzimidazoles; thus the information presented regarding the coupled spectra should prove valuable in the assignment of other 5-substituted benzimidazoles and perhaps other benzazoles. The spectra of 2-methylbenzimidazole and 5,6-dimethylbenzimidazole were also examined as an aid to the assignments of the 5-substituted benzimidazoles. We present correlations for the chemical shifts of all the ring carbons of the 5-substituted compounds with both substituent constants and charge density values.

The results for 5-benzoylbenzimidazole are of particular interest due to the relationship of this compound to the well-known anthelmintic drug Vermox (11); Vermox differs by having a "methyl carbamate group" (carbomethoxyamino group, MeOOCNH—) in the 2 position. Work is in progress on the synthesis and carbon-13 nmr analysis of a series of these methyl (5-substituted-2-benzimidazolyl)carbamates.

## Experimental

Benzimidazole, 5-nitrobenzimidazole, and 5,6-dimethylbenzimidazole were purchased from Aldrich and used without further purification. No impurities were observed in the carbon-13 nmr spectra. The remainder of the compounds were prepared and purified by standard methods (12–15).

The carbon-13 nmr spectra were recorded on a Varian CFT-20 spectrometer at a temperature of 30°C. These compounds were run in dimethyl sulfoxide (DMSO) and, in some cases, methanol. For the protonation studies, weighed amounts of concentrated hydrochloric acid were added to the DMSO solutions. A coaxial tube containing $D_2O$ provided an external lock. Chemical shifts were referenced to TMS by setting the DMSO resonance at 40.5 ppm (16) and the methanol resonance at 49.9 (17).

Molecular orbital calculations at the INDO level of approxi-

[1]Authors to whom correspondence should be addressed.
[2]Revision received July 29, 1982.

0008-4042/82/242987-06$01.00/0
©1982 National Research Council of Canada/Conseil national de recherches du Canada

Can. J. Chem. Downloaded from www.nrcresearchpress.com by 210.87.254.5 on 09/06/12
For personal use only.

TABLE 1. The $^{13}C$ chemical shifts of substituted benzimidazoles

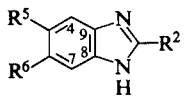

| Compound | $R^5$ | $R^6$ | $R^2$ | Solution | Chemical Shift in ppm from TMS* | | | | | | | |
|---|---|---|---|---|---|---|---|---|---|---|---|---|
| | | | | | C-2 | C-4 | C-5 | C-6 | C-7 | C-8 | C-9 | $CH_3$ |
| **4** | $NO_2$ | H | H | 2 *M* DMSO | 146.7 | 112.9 | 142.7 | 117.6 | 114.7 | 141.7 | 138.7 | |
| | | | | 0.5 *M* DMSO | 146.8 | 112.8 | 142.7 | 117.6 | 114.9 | 141.7 | 138.6 | |
| | | | | 0.17 *M* MeOH | 147.2 | 113.5 | 145.1 | 119.3 | 115.7 | 142.3 | 139.2 | |
| **5** | $COC_6H_5$ | H | H | 2 *M* DMSO | 144.9 | 119.0 | 131.2 | 124.1 | 115.2 | 141.1 | 138.3 | |
| **6** | Cl | H | H | 2 *M* DMSO | 143.8 | 115.6 | 126.8 | 122.6 | 116.8 | 136.8 | 139.5 | |
| | | | | 0.5 *M* DMSO | 143.5 | 115.3 | 126.3 | 122.1 | 116.5 | 136.7 | 139.4 | |
| | | | | 0.4 *M* MeOH | 143.9 | 116.0 | 129.4 | 124.3 | 117.0 | 137.2 | 139.5 | |
| **1** | H | H | H | 2 *M* DMSO | 142.2 | 115.5 | 122.0 | 122.0 | 115.5 | 138.3 | 138.3 | |
| | | | | 0.5 *M* DMSO | 142.0 | 115.4 | 121.8 | 121.8 | 115.4 | 138.1 | 138.1 | |
| **7** | $CH_3$ | H | H | 2 *M* DMSO | 141.8 | 114.8 | 131.2 | 123.5 | 115.5 | 137.0 | 138.1 | 21.4 |
| **8** | $OCH_3$ | H | H | 2 *M* DMSO | 141.9 | 97.8 | 156.0 | 111.9 | 116.7 | 133.8 | 138.2 | 55.7 |
| **9** | $NH_2$ | H | H | 2 *M* DMSO | 140.3 | 97.7 | 144.9 | 112.4 | 117.4 | 133.1 | 137.6 | |
| | | | | 0.5 *M* DMSO | 139.6 | 96.9 | 144.5 | 111.6 | 117.1 | 132.9 | 137.1 | |
| **10** | $CH_3$ | $CH_3$ | H | 1.4 *M* DMSO† | 141.2 | 115.5 | 130.3 | 130.3 | 115.5 | 136.9 | 136.9 | 20.0 |
| | | | | 0.5 *M* DMSO | 141.0 | 115.5 | 130.1 | 130.1 | 115.5 | 137.1 | 137.1 | 20.0 |
| **11** | H | H | $CH_3$ | 1.5 *M* DMSO† | 151.5 | 114.4 | 121.2 | 121.2 | 114.4 | 139.1 | 139.1 | 14.7 |

*Using the methyl resonance as 40.5 and 49.9 ppm for DMSO and MeOH, respectively.
†Approaching the limit of solubility.

mation (18, 19) were performed on an AMDAHL 470 Computer at the University of Manitoba. For the benzimidazole structure, a regular hexagon was added to the known geometry of imidazole (20). For the benzene ring portion a C—C distance of 1.378 Å and a C—H distance of 1.08 Å were used. Standard bond angles and bond lengths (18) were used for the substituents and, where rotation is possible, calculations were performed for all reasonable conformations and the results were averaged. In the amino compound the HNH angle and the angle between the $NH_2$ plane and the plane of the ring were taken to be 113° and 37.5°, respectively (21). The charge densities reported assume equal populations of the tautomeric forms.

## Results and discussion

The compounds studied are the following: the parent benzimidazole, **1**, the 5-substituted benzimidazoles, **4–9**, 5,6-dimethylbenzimidazole, **10**, and 2-methylbenzimidazole, **11**; their structures are indicated in Table 1 with their carbon-13 chemical shifts for the solvents and concentrations employed. The results indicate that there is little change in chemical shifts in going from 2 *M* to 0.5 *M* solutions in DMSO for the compounds studied; however, there are significant differences in going from DMSO to methanol solutions. For purposes of the correlations, the chemical shifts used were those obtained for 2 *M* solutions in DMSO. The carbon-13 nmr spectra for some of these compounds have been obtained previously (2, 3), but were redetermined in order to have constant experimental conditions and to be certain of the assignments (some discrepancies with the assignments in ref. 2 were found as discussed below).

### *Spectral assignment of the 5-substituted benzimidazoles*

For a preliminary assignment we applied benzene SCS values (22) to the shifts of the parent compound (1), but in examining the coupled spectra it was found that this was not always reliable in distinguishing $^{13}C$ resonances which are close together. With the exception of C-4 and C-6, all peak assignments were made on the basis of the coupled spectra. As expected, C-2 gives a doublet with a coupling of 205–210 Hz (23) due to the directly bonded proton, with no observable fine structure at the resolution obtained in these solutions (approximately 1 Hz). This large coupling serves to distinguish C-2 from the benzene ring carbon resonances which are split by 160–170 Hz. The nonprotonated carbons C-5, C-8, and C-9 can be identified by the $^3J_{(C,H)}$ values which are larger than $^2J_{(C,H)}$ values (24–27). As shown in Fig. 1 for 5-aminobenzimidazole, the *ipso* carbon, C-5, has one observable coupling, $^3J_{(C\text{-}5,H\text{-}7)}$, for the electron releasing substituents and hydrogen. For the electron-withdrawing substituents (5-nitro, 5-chloro, and 5-benzoyl) the *ipso* carbon exhibits, in addition, the two $^2J_{(C,H)}$ couplings. This increase in the two bond couplings is expected (28, 29) with electron-withdrawing substituents on the *ipso* carbon. For C-8, $^3J_{(C,H)}$ couplings are observed to H-2, H-4, and H-6; as shown in Fig. 1, the pattern is a doublet of triplets. For C-9, there is $^3J_{(C,H)}$ coupling to H-2 and H-7, giving a triplet or a doublet o

Can. J. Chem. Downloaded from www.nrcresearchpress.com by 210.87.254.5 on 09/06/12
For personal use only.

Can. J. Chem. Downloaded from www.nrcresearchpress.com by 210.87.254.5 on 09/06/12
For personal use only.

doublets depending on the relative magnitudes of these coupling constants. The origin of these patterns for C-8 and C-9 was confirmed by comparison to the coupled spectra for benzimidazole, 2-methylbenzimidazole, and 5,6-dimethylbenzimidazole. The resonance for C-7 is easily assigned as it has only a one bond C,H coupling, approximately 160–170 Hz. For C-4 and C-6, in addition to the directly bonded coupling, each has only a $^3J_{(C,H)}$; thus these resonances cannot be distinguished using only the coupled spectra. However, their large chemical shift difference permits easy assignment on the basis of the *ortho* SCS values, with C-6 always downfield of C-4 as in the parent compound. For 5-nitro- and 5-chlorobenzimidazole, we were able to confirm this on the basis of the work of Mathias and Overberger (2) who used compounds with 90% carbon-13 enrichment in the 2 position. Their assignment in methanol solution is certain for C-4 and C-6 because of the observed carbon–carbon couplings. A series of mixed solvents was used to ascertain that the order of the resonances does not change on going from methanol to DMSO. However, we do find serious discrepancies between our work and that of the above authors for 5-chloro- and 5-nitrobenzimidazole in methanol solution. Labelling of C-2 only provides an advantage in selecting the C-2, C-4, and C-7 resonances, and even at that does not distinguish between the latter two.

Pugmire and Grant (1) have shown that all the carbon resonances of the parent benzimidazole move upfield on protonation, with the exception of C-5 and C-6 which move downfield. In agreement with this, Mathias and Overberger (2) noted that, for the partial protonation of 5-chloro- and 5-nitrobenzimidazole in acetic acid, C-8 and C-9 move upfield and C-5 and C-6 move downfield. We have found that the observations for the parent benzimidazole apply to the carbon chemical shifts of 5-substituted benzimidazoles in general, except for C-7 in compounds which contain electron-withdrawing groups. For 5-nitro-, C-7 moved downfield with protonation while for 5-chloro- and 5-benzoylbenzimidazole there was little change in shift with protonation. Thus protonation studies are useful as an aid for chemical shift assignment in benzimidazoles. In this present study our assignments of C-4 and C-6 are further substantiated by protonation studies in DMSO solutions.

*Correlation of the chemical shifts with substituent parameters*

Methods (30) for the correlation of chemical shifts with substituent constants other than that of Smith and Proulx (9, 10) do not give good correlations for even the majority of carbon atoms in aromatic systems; therefore we have used the latter approach, which utilizes eq. [1], as our initial method of correlating the chemical shifts of the 2 *M*

$$[1] \quad \delta = aF + bR + cQ + d$$

DMSO solutions of the 5-substituted benzimidazoles. In [1], $F$ and $R$ are the Swain and Lupton substituent constants and $Q$ is a semi-empirical parameter defined by Schaefer and co-workers (8). To determine if the inclusion of $Q$ resulted in a significant improvement for all carbon atoms, correlations were also attempted with eq. [2] which

$$[2] \quad \delta = aF + bR + d$$

uses the Swain and Lupton constants only. As the Taft equation, [3], using $\sigma_I$ and $\sigma_R^0$ (31) for the polar

$$[3] \quad \delta = \rho_I\sigma_I + \rho_R\sigma_R^0 + d$$

and resonance substituent constants, sometimes gives better results than eq. [2], correlations with these parameters were also tried. The numerical values of the substituent constants were taken from the original articles (7, 10, 31). The coefficients obtained by multiple linear regression analysis are presented in Table 2. (The chemical shifts of the benzoyl compound were not used in these numerical analyses as all the required substituent constants are not available.) As well, in Table 2, the correlation coefficient $r$ and the $F$ test of the variance are given.

The values of the correlation coefficients for eq. [1] indicate that these results compare favorably with those obtained for other benzazole systems (4, 5, 6, 10). For the *ipso* carbon, C-5, the correlation is not quite as good; this is consistent with the results observed for the 2-substituted benzimidazoles (4). Thus chemical shifts of 5-substituted benzimidazoles can be satisfactorily predicted for compounds having substituent groups for which $F$, $R$, and $Q$ values are available. In principle, the results from Table 2 could be used to generate the $F$, $R$, and $Q$ values for the benzoyl substituent; however, we believe that the data from several systems should be used to obtain these parameters.

It can be seen from the calculations with eq. [2] that the absence of $Q$ decreases the quality of the correlation, as measured by the correlation coefficient, for all chemical shifts. Surprisingly, for the chemical shifts of the *ortho* carbon C-4, $Q$ does not seem to be statistically significant; for the *ipso* carbon, C-5, $Q$ appears to be of marginal significance. (The correlation coefficient $r$ almost inevitably gets better as more variables are added to a

Can. J. Chem. Downloaded from www.nrcresearchpress.com by 210.87.254.5 on 09/06/12
For personal use only.

TABLE 2. Linear regression analysis for the 5-substituted benzimidazoles

| | $\delta = aF + bR + cQ + d$ | | | | | | $\delta = aF + bR + d$ | | | | | | $\delta = \rho_I\sigma_I + \rho_R\sigma_R^0 + d$ | | | | | |
|---|---|---|---|---|---|---|---|---|---|---|---|---|---|---|---|---|---|---|
| Carbon | $a$ | $b$ | $c$ | $d$ | $r$* | $F$† | $a$ | $b$ | $d$ | $r$* | $F$† | $\rho_I$ | $\rho_R$ | $d$ | $r$* | $F$† |
| C-2 | 3.29 ±0.17 | 4.10 ±0.48 | −0.26 ±0.11 | 142.9 | 0.9991 | 363 | 3.37 ±0.26 | 3.13 ±0.39 | 142.3 | 0.9965 | 215 | 5.63 ±0.50 | 4.97 ±0.55 | 142.3 | 0.9947 | 140 |
| C-4 | 3.18 ±3.75 | 9.4 ±10.6 | 5.04 ±2.44 | 105.5 | 0.9713 | 11 | 1.76 ±3.14 | −23.8 ±4.2 | 112.6 | 0.9590 | 17 | −4.93 ±10.9 | 30.1 ±11.9 | 115.9 | 0.8275 | 3.3 |
| C-5 | 12.5 ±10.2 | 3.0 ±29.0 | −10.0 ±6.7 | 146.9 | 0.8943 | 2.7 | 16.1 ±11.9 | −34.4 ±17.6 | 124.0 | 0.7580 | 2.0 | 21.3 ±20.9 | −32.5 ±22.7 | 126.0 | 0.6741 | 1.2 |
| C-6 | −3.95 ±2.84 | 0.13 ±8.02 | 4.14 ±1.85 | 114.2 | 0.9525 | 6.5 | −5.43 ±4.22 | 15.6 ±6.3 | 123.7 | 0.8213 | 3.1 | −6.85 ±8.01 | 15.1 ±8.71 | 122.8 | 0.7169 | 1.6 |
| C-7 | 0.50 ±0.36 | −5.53 ±1.03 | 0.65 ±0.24 | 113.8 | 0.9801 | 16 | 0.27 ±0.63 | −3.11 ±0.93 | 115.3 | 0.9009 | 6.5 | 0.29 ±0.75 | −3.93 ±0.81 | 115.3 | 0.9434 | 12 |
| C-8 | 0.87 ±0.50 | 12.4 ±1.4 | −0.96 ±0.33 | 140.5 | 0.9960 | 83 | 1.21 ±0.92 | 8.79 ±1.37 | 138.3 | 0.9783 | 33 | 2.48 ±0.06 | 11.56 ±0.06 | 138.3 | 1.0000 | $22\times10^3$ |
| C-9 | 1.01 ±0.04 | −2.13 ±0.12 | 0.73 ±0.03 | 136.6 | 0.9993 | 476 | 0.75 ±0.63 | 0.60 ±0.94 | 138.3 | 0.7252 | 1.7 | 1.39 ±1.05 | 0.56 ±1.14 | 138.2 | 0.6767 | 1.3 |

*Correlation coefficient.
†$F$ test of the variance.

correlation, whereas the $F$ test only improves if the additional variable results in a statistically significant improvement, e.g. see ref. 32.) Even for C-2, where the correlation coefficients are similar, the $F$ test of the variance increases on including $Q$, indicating that its inclusion is statistically significant. Only for C-8 is there a good single parameter correlation with $R$ of Swain and Lupton ($r = 0.966$, $F$ test = 55); this is not unexpected at the *para* position.

The correlations of the chemical shifts with the Taft parameters $\sigma_I$ and $\sigma_R^0$ (eq. [3]) are not as good as those with either eq. [1] or eq. [2], except for that of C-8. The single parameter correlation of the chemical shift of C-8 with $\sigma_R^0$ ($r = 0.9782$, $F = 89$) is less satisfactory than the dual parameter correlation; the enormous decrease in the $F$ test of the variance indicates that $\sigma_I$ does make a significant contribution. (A single parameter correlation of the chemical shift of C-8 with $\sigma_I$ was very poor.) It is noteworthy that use of eq. [3] indicates that, while resonance is the most important contribution, the field effect is also significant, whereas use of eq. [2] suggests that the field effect is not statistically significant. This discrepancy is not surprising if criticism (33) that the Swain–Lupton approach does not satisfactorily separate field and resonance effects is well founded.

### *Correlation of the chemical shifts with charge densities*

The excess charge density with respect to the neutral atom, calculated at the INDO level of approximation, is given in Table 3 for each carbon atom. It is possible to test the correlation between the experimental chemical shifts and the total excess charge density (see Fig. 2) on the carbon atoms by making use of eq. [4] (34). Using all ring

$$[4] \quad \delta = Aq_{\sigma+\pi} + B$$

carbons of benzimidazole and the five 5-substituted benzimidazoles, we found that $A = -133 \pm 24$ ppm/electron and $B = 119 \pm 3$ ppm with a correlation coefficient $r = 0.870$ and $\psi = 0.51$ (where $\psi^2 = 2(1 - r)$). The standard deviation of charge density values is 0.091 and that of the chemical shifts is 13.9 ppm. Jaffe (35) has stated that $r$ must be over 0.96 and Exner (36) that $\psi$ must be less than 0.20 for a good correlation. If the correlation analysis is restricted to the 36 phenyl carbons there is a slightly better correlation, with $A = -183 \pm 30$ ppm/electron and $B = 118 \pm 2$ ppm ($r = 0.903$, $\psi = 0.44$); standard deviations of charge densities and chemical shifts

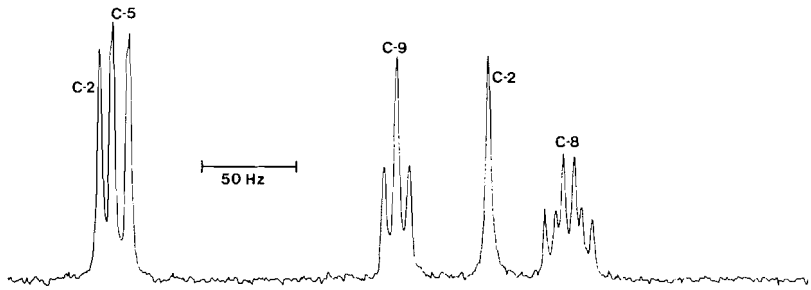


FIG. 1. The low field portion of the coupled $^{13}C$ nmr spectrum of 2 *M* 5-aminobenzimidazole in DMSO.

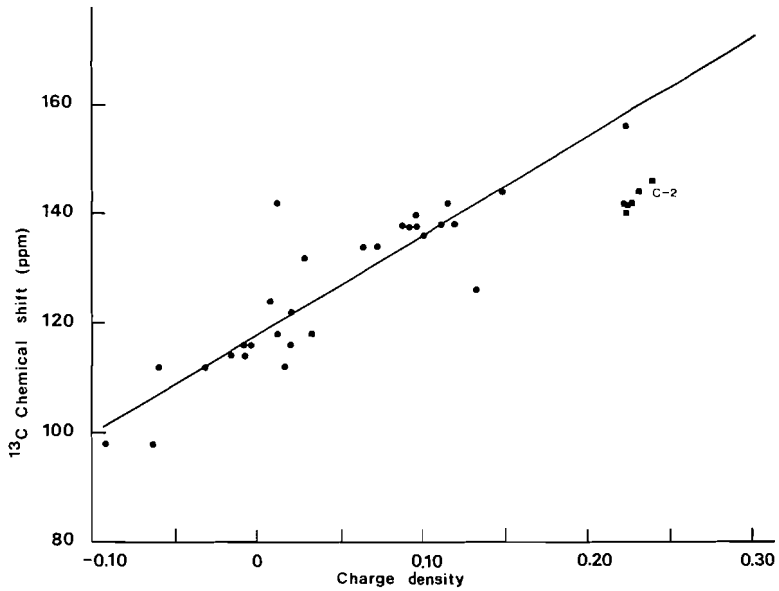


FIG. 2. A plot of the $^{13}C$ chemical shifts (ppm) vs. calculated excess charge densities for a series of 5-substituted benzimidazoles. The C-2 carbons are represented by ■.

TABLE 3. Calculated excess charge densities for the 5-substituted benzimidazoles

| Compound | R5* | Carbon | | | | | | |
|---|---|---|---|---|---|---|---|---|
| | | C-2 | C-4 | C-5 | C-6 | C-7 | C-8 | C-9 |
| **4** | $NO_2$ | 0.238 | 0.015 | 0.011 | 0.033 | −0.007 | 0.114 | 0.094 |
| **6** | Cl | 0.233 | −0.003 | 0.131 | 0.020 | −0.003 | 0.100 | 0.097 |
| **1** | H | 0.228 | −0.007 | 0.018 | 0.018 | −0.007 | 0.093 | 0.093 |
| **7** | $CH_3$ | 0.227 | −0.018 | 0.028 | 0.008 | −0.003 | 0.089 | 0.095 |
| **8** | $OCH_3$ | 0.226 | −0.091 | 0.224 | −0.059 | 0.020 | 0.064 | 0.118 |
| **9** | $NH_2$ | 0.225 | −0.064 | 0.149 | −0.034 | 0.013 | 0.070 | 0.112 |
| *r*† | | 0.9782 | 0.9145 | 0.6396 | 0.7992 | 0.7342 | 0.9384 | 0.9953 |

*Designation as in Table 1.
†Correlation coefficient from the linear regression analysis.

are 0.067 ppm/electron and 13.6 ppm, respectively. These results show that there is only fair agreement for these correlations. In Table 3 the correlation coefficient for chemical shift versus excess charge density is given for each carbon atom. As can be seen, the correlations for the individual carbon atoms are not satisfactory overall; a poor correlation is not unexpected (22, 37) for carbons other than the *para*. However the correlation for the *para* carbon is not too good; this could be due to

Can. J. Chem. Downloaded from www.nrcresearchpress.com by 210.87.254.5 on 09/06/12
For personal use only.

unequal tautomer populations for these benzimidazoles. This will be tested by a similar study on a series of 5-substituted benzoxazoles where tautomerism involving two positions on the 5-membered ring is not possible.


## Acknowledgements

We thank Dr. Ted Schaefer of the University of Manitoba for the use of his INDO MO program, our colleague Dr. Rod Wasylishen for helpful discussions, and the University of Winnipeg for financial assistance. We also thank the referees for useful suggestions.



1. R. J. PUGMIRE and D. M. GRANT. J. Am. Chem. Soc. **93**, 1880 (1971).
2. L. J. MATHIAS and C. G. OVERBERGER. J. Org. Chem. **43**, 3526 (1978).
3. A. FRUCHIER, L. PAPPALARDO, and J. ELGUERO. Anal. Quim. **76**, 79 (1980).
4. V. A. LOPYREV, L. I. LARINA, T. I. VAKUL'SKAYA, M. F. LARIN, O. B. NEFEDOVA, E. F. SHIBANOVA, and M. G. VORONKOV. Org. Magn. Reson. **15**, 219 (1981).
5. R. FAURE, J. ELGUERO, E. J. VINCENT, and R. LAZARO. Org. Magn. Reson. **11**, 617 (1978).
6. J. LLINARES, J. P. GALY, R. FAURE, E. J. VINCENT, and J. ELGUERO. Can. J. Chem. **57**, 937 (1979).
7. C. G. SWAIN and E. C. LUPTON. J. Am. Chem. Soc. **90**, 4328 (1968).
8. F. HRUSKA, H. M. HUTTON, and T. SCHAEFER. Can. J. Chem. **43**, 2392 (1965).
9. W. B. SMITH and T. W. PROULX. Org. Magn. Reson. **8**, 205 (1976).
10. W. B. SMITH and T. W. PROULX. Org. Magn. Reson. **8**, 567 (1976).
11. P. N. PRESTON. Chem. Rev. **74**, 279 (1974).
12. L. F. FIESER and K. L. WILLIAMSON. Organic experiments. 3rd ed. D. C. Heath and Company, Lexington, Mass. 1975. p. 324.
13. D. J. RABIGER and M. M. JOULLIE. J. Org. Chem. **29**, 476 (1964).
14. D. J. RABIGER and M. M. JOULLIE. J. Chem. Soc. 915 (1964).
15. M. STAUBLE. Helv. Chim. Acta, **32**, 135 (1949).
16. G. C. LEVY and G. L. NELSON. Carbon-13 nuclear magnetic resonance for organic chemists. Wiley–Interscience, New York. 1972. p. 23.
17. E. BREITMAIER, G. HAAS, and W. VOELTER. Atlas of carbon-13 nmr data. Vol. 1. Heyden, London. 1975. p. ix.
18. J. A. POPLE and D. L. BEVERIDGE. Approximate molecular orbital theory. McGraw–Hill, New York. 1970.
19. G. E. MACIEL, J. W. MCIVER, JR., N. W. OSTLUND, and J. A. POPLE. J. Am. Chem. Soc. **92**, 1 (1970).
20. B. M. CRAVEN, R. K. MCMULLAN, J. D. BELL, and H. C. FREEMAN. Acta Crystallogr. Sect. B, **33**, 2585 (1977).
21. D. CHRISTEN, D. DAMIANI, and D. G. LISTER. J. Mol. Struct. **41**, 315 (1977).
22. D. F. EWING. Org. Magn. Reson. **12**, 499 (1979).
23. J. B. STOTHERS. Carbon-13 nmr spectroscopy. Academic Press, New York. 1972. p. 343.
24. A. R. TARPLEY, JR. and J. H. GOLDSTEIN. J. Phys. Chem. **76**, 515 (1972).
25. J. P. JACOBSEN and K. SCHAUMBURG. Mol. Phys. **28**, 1505 (1974).
26. M. HANSEN and H. J. JAKOBSEN. J. Magn. Reson. **20**, 520 (1975).
27. L. ERNST, E. LUSTIG, and V. WRAY. J. Magn. Reson. **22**, 459 (1976).
28. D. F. EWING. *In* Annual reports on nmr spectroscopy. Vol. 6A. *Edited by* E. F. Mooney. Academic Press, New York. 1975. p. 389.
29. C. J. JAMESON and M. C. DAMASCO. Mol. Phys. **18**, 491 (1970).
30. D. F. EWING. *In* Correlation analysis in chemistry: recent advances. *Edited by* N. B. Chapman and J. Shorter. Plenum, New York. 1978. p. 357.
31. S. EHRENSON, R. T. C. BROWNLEE, and R. W. TAFT. *In* Progress in physical organic chemistry. Vol. 10. *Edited by* A. S. Streitwieser, Jr. and R. W. Taft. Wiley–Interscience, New York. 1973. p. 1.
32. W. F. REYNOLDS. J. Chem. Soc. Perkin Trans. II, 985 (1980).
33. J. SHORTER. *In* Correlation analysis in chemistry: recent advances. *Edited by* N. B. Chapman and J. Shorter. Plenum, New York. 1978. p. 119.
34. J. A. POPLE and G. A. SEGAL. J. Chem. Phys. **44**, 3289 (1966).
35. H. H. JAFFE. Chem. Rev. **53**, 191 (1953).
36. O. EXNER. Coll. Czech. Chem. Commun. **31**, 3222 (1966).
37. G. L. NELSON, G. C. LEVY, and J. D. CARGIOLI. J. Am. Chem. Soc. **94**, 3089 (1972).


Can. J. Chem. Downloaded from www.nrcresearchpress.com by 210.87.254.5 on 09/06/12
For personal use only.

# Arylallyl cations and their stereospecific cyclization to bicyclic trienylic cations

D. M. DYTNERSKI, K. RANGANAYAKULU, B. P. SINGH, AND T. S. SORENSEN
*The Department of Chemistry, University of Calgary, Calgary, Alta., Canada T2N 1N4*

Received June 3, 1982

D. M. DYTNERSKI, K. RANGANAYAKULU, B. P. SINGH, and T. S. SORENSEN. Can. J. Chem. **60**, 2993 (1982).

A series of arylallyl alcohols, where aryl = 2,6-dimethylphenyl, mesityl, duryl, or pentamethylphenyl, was prepared. On addition to strong acid, these generate arylallyl cations. In some cases these allyl cations are observable and were characterized as *in situ* solution species by nmr spectroscopy. In other cases, an immediate cyclization takes place, leading stereospecifically to a series of bicyclic trienyl cations, which were also thoroughly characterized. The stereochemistry of this cyclization reaction, which was initially expected to follow the "rules" for electrocyclic ring closures, was probed in some detail. It is tentatively concluded that the stereochemistry in the products is not that expected from a conrotatory ring closure. Two diarylmethyl cations were also prepared. However, these did not cyclize.

D. M. DYTNERSKI, K. RANGANAYAKULU, B. P. SINGH et T. S. SORENSEN. Can. J. Chem. **60**, 2993 (1982).

On a préparé une série d'alcools arylallyliques où le groupe aryl = diméthyl-2,6 phényle, mésityle, duryle ou pentaméthylphényle. Ces alcools en présence d'acides forts produisent des cations arylallyles. Dans certains cas on observe ces cations allyles et on les caractérise *in situ* en solution par la spectroscopie de rmn. Dans d'autres cas il se produit immédiatement une cyclisation, qui conduit de façon stéréospécifique à des séries de cations triényles bicycliques que l'on a entièrement caractérisés. On a établi de façon détaillée la stéréochimie de cette réaction de cyclisation, qui pensait-on devait suivre les règles de fermeture électrocyclique de cycles. On conclut que la stéréochimie des produits n'est pas celle attendue d'une fermeture conrotatoire de cycle. On a également préparé deux cations diarylméthyles. Toutefois ces cations ne se cyclisent pas.

[Traduit par le journal]

## Introduction

The pentadienyl → cyclopentenyl (I → II) cation ring closure was first observed nearly 20 years ago (1), subsequently classified as an "electrocyclic" closure by Woodward and Hoffmann (2) and then, using methyl-substituted derivatives of I of fixed geometry, shown (3) to follow the predicted conrotatory mode.

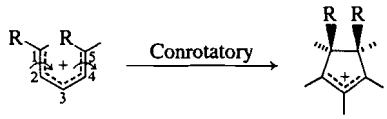


I II

This closure is irreversible, i.e. II is much more stable than I. The net bond energy changes involved in this can be very simply summarized:

[1] Pentadienyl resonance energy (R.E.) + π-bond → allyl R.E. + σ-bond

Thus, the main driving force is the favorable formation of a σ-bond from a π-bond (about 15–25 kcal/mol), the difference in the two R.E.'s expected to be small in comparison.

The present study involves extensions of the basic I framework, incorporating one and then two aromatic rings in place of the 1,2 and 4,5 "double bonds" of the pentadienyl unit. The possibility of a ring closure, analogous to I → II, can again be considered from two separate viewpoints, viz. is the open or closed cation the more stable and, secondly, in the event that ring closure does occur, what is the stereochemical outcome? The possible reactions are summarized below, the numbers in brackets referring to the above questions:

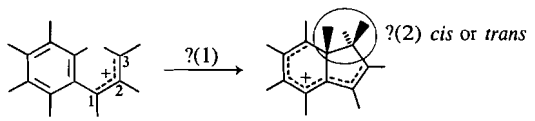


III IV

[2] Aryl R.E. + allyl R.E. + π-bond $\xrightarrow{?}$ trienyl R.E. + σ-bond

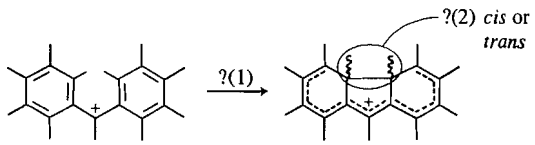


VI VII

[3] 2 × Aryl R.E. + π-bond $\xrightarrow{?}$ pentaenylic R.E. + σ-bond

Examples of diarylmethyl cations VI are numerous (4), but only a few arylallyl cations III have been studied (5–8). No previous stereochemical work on these cyclizations has been reported.

## Results and discussion

### *The arylallyl cation III case*

Our approach to studying a possible III → IV cyclization had to deal first with preventing the facile rearomatization of IV, a cation species previously unknown because of this. As it turned

0008-4042/82/242993-12$01.00/0
©1982 National Research Council of Canada/Conseil national de recherches du Canada

Can. J. Chem. Downloaded from www.nrcresearchpress.com by 210.87.254.6 on 09/06/12
For personal use only.

Can. J. Chem. Downloaded from www.nrcresearchpress.com by 210.87.254.6 on 09/06/12
For personal use only.

out, this was easily done by using aryl rings with both *ortho*-positions methyl-substituted. As implied, the cyclization of III to IV does occur in most of these cases, i.e. IV is thermodynamically more stable than III, in spite of the loss of aryl R.E. (see eq. [2]).

The first systems looked at were based on a mesitylene ring with the incipient allyl cation portion having either one or two methyl substituents, the one on C-3 being necessary to create the potential stereochemistry in IV. The starting alcohols **1**–**4** were prepared from mesitaldehyde and the corresponding vinyl lithium or from mesityl lithium and the α,β-unsaturated aldehyde.

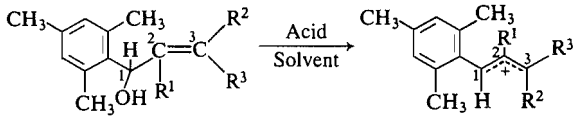


**1** $R^1 = R^2 = H$, $R^3 = CH_3$
**2** $R^1 = R^3 = H$, $R^2 = CH_3$
**3** $R^1 = R^2 = CH_3$, $R^3 = H$
**4** $R^1 = R^3 = CH_3$, $R^2 = H$

III-1 $R^1 = R^2 = H$, $R^3 = CH_3$
III-2 $R^1 = R^3 = H$, $R^2 = CH_3$
Not directly observed
Not directly observed

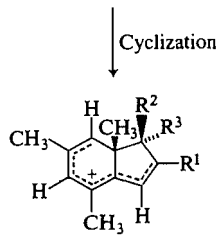


IV-1 Not directly observed
IV-2 Not directly observed
IV-3 } $R^1 = R^2 = CH_3$, $R^3 = H$
or
IV-4 } $R^1 = R^3 = CH_3$, $R^2 = H$

Alcohols **1** and **2**, on addition to $FSO_3H$–$SO_2ClF$ (1:4) at −120°C, yield the corresponding allylic cations III-1 and III-2, although III-2 was never obtained pure. At about −100°C, III-2 rearranges to the more stable III-1 geometry and this facile process no doubt occurs to some extent in the preparation of III-2. At much higher temperatures (35°C), cation III-1 cyclizes, but a rearranged indanyl cation V-1 was the first observed species (5) (destroying any stereochemistry inherent in IV).

There are indications from previous literature examples (6) that substituting a methyl group at C-2 in III would increase the cyclization rate. This indeed was the case here and, on addition of alcohols **3** or **4** to the acid, only the cyclized ion (IV-3 or IV-4) was observed, even at temperatures as low as −120°C. The cyclized ion, by $^{13}C$ and $^1H$ nmr, appears to be a *single* stereoisomer and it is significant and disquieting that both alcohols should give the same cyclized ion.

Ideally, one would like to directly observe both cation structures III and IV *in the same system*. One possibility for the nonobservation of IV-1 might be that this ion is actually less stable than III-1. The corresponding durene-substituted alcohols **5** and **6** (analogous to **1** and **4**) were therefore prepared. Note that IV-5 and IV-6, compared to IV-4 (or a possible IV-1), have two extra methyl groups in stabilizing positions on the trienylic cation framework (denoted above in IV by ●). In any event, ionization of **5** leads cleanly to III-5 and this in turn cyclizes very cleanly to IV-5 at −70°C. Alcohol **6** (like **4**) yields only the cyclized ion IV-6, on ionization at −120°C. Both IV-5 and IV-6 appear to be *single* stereoisomers.

All of the observable III and IV ions were characterized as *in situ* solution species by $^1H$ and $^{13}C$ nmr spectroscopy and the data are given in Tables 1 and 2. Data for the further rearranged indanyl cations have been presented elsewhere (13).

*Thermodynamic aspects (question 1 in the Introduction)*

Obviously IV-4, IV-5, IV-6 (and a pentamethyl species IV-8 to be discussed subsequently) are all more stable than the open arylallyl cations III. The situation with III-1 is less clear since the cyclization here proceeds directly to a rearomatized indanyl cation V-1. However, the observation that III-5 cyclizes to IV-5 at −70°C, whereas III-1 forms the indanyl cation V-1 only at +35°C, is a strong indication that III-1 is more stable than the unseen IV-1, since there is little kinetic reason why these very similar ions should not have cyclized (III →

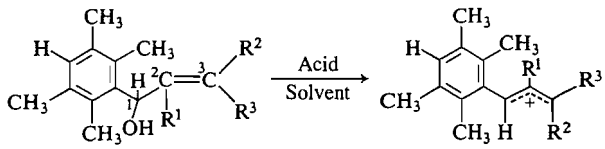


**5** $R^1 = R^2 = H$, $R^3 = CH_3$
**6** $R^1 = R^3 = CH_3$, $R^2 = H$

III-5 $R^1 = R^2 = H$, $R^3 = CH_3$
Not directly observed

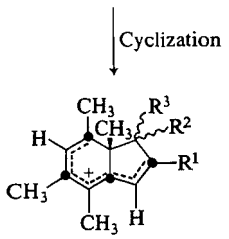


IV-5 $R^1 = R^2 = H$, $R^3 = CH_3$
IV-6 $R^1 = R^3 = CH_3$, $R^2 = H$

TABLE 1. $^1H$ nuclear magnetic resonance spectra of arylallyl cations III and trienylic cations IV

| Cation | Solvent | Temperature °C | Position[a] ortho | meta | para | 1 | 2 | 3 |
|---|---|---|---|---|---|---|---|---|
| III-1 | $FSO_3H$–$SO_2ClF$ | −60 | 2.60<br>2.68 | 7.16[b] | 2.41 | 9.00[c] | 7.73[d] | 8.21[e]<br>2.49[f] |
| III-2 | $FSO_3H$–$SO_2ClF$ | −90 | [g] | [g] | [g] | 9.90[h] | [g] | [g] |
| III-5 | $FSO_3H$–$SO_2ClF$ | −100 | 2.51[i] | 2.21 | 7.61 | 9.21[d] | 7.84[c] | 8.34[e]<br>2.51[i] |
| III-7 | $FSO_3H$ | −28 | 2.66 | 7.27[j] | 7.75[k] | 9.22[d] | 7.78[c] | 8.47[l]<br>2.55[f] |

| | | | Proton or methyl on carbon position 1 | 2 | 4 | 5 | 6 | 7 | 8 | 9 |
|---|---|---|---|---|---|---|---|---|---|---|
| IV-3 | $FSO_3H$–$SO_2ClF$ | −80 | 2.40 | 7.12 | 2.06* | 7.46* | 2.19* | 7.54* | 1.25 | 1.35[m]<br>3.02[n] |
| IV-5 | $FSO_3H$–$SO_2ClF$ | −50 | 7.70[o] | 7.20[p] | 2.19* | 2.40 | 6.95* | 2.49* | 1.24 | 1.40[q]<br>3.12[r] |
| IV-6 | $FSO_3H$–$SO_2ClF$ | −30 | 2.29* | 7.00 | 2.12 | 2.29* | 6.71 | 2.38 | 1.23 | 1.38[m]<br>2.98[n] |
| IV-8 | 96% $H_2SO_4$ | 0 | 2.19* | 6.90 | 1.95* | 2.19* | 2.08* | 2.32* | 1.10 | 1.32[m]<br>2.94[n] |

[a] Referenced indirectly to internal TMS in $SO_2ClF$ = δ 0.00, except for IV-8, which is referenced to TMS/$CDCl_3$ = δ 0.00. Tentative assignments indicated by *.
[b] Broad, two peaks in some spectra.
[c] d, d, $J$ = 13.6 and 13.6.
[d] d, $J$ = 13.6.
[e] d, q, $J$ = 13.6 and 6.5.
[f] d, $J$ = 7.
[g] Peaks are overlapped with ion III-1 peaks.
[h] d, $J$ = 14.
[i] Broad.
[j] d, $J$ = 7.2.
[k] t, $J$ = 7.2.
[l] d, q, $J$ = 13.6 and 7.0.
[m] d, $J$ = 7.0.
[n] q, $J$ = 7.0.
[o] d, d, $J$ = 5.50 and 1.80.
[p] d, d, $J$ = 5.50 and 1.90.
[q] d, $J$ = 7.3.
[r] q, $J$ = 7.3, also coupled to H-1 and H-2.

IV) at rather similar rates. This possible situation is presented diagrammatically in Fig. 1. Note that III-1 contains an extra *p*-Me stabilizing group, compared to III-5, while IV-5 has two extra stabilizing methyl substituents compared to the unseen IV-1.

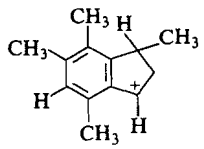

V-1

In an attempt to find a possible case where III and IV might be in observable equilibrium (and thereby obtain proof for the Fig. 1 conjecture), the *m*-xylene system was prepared, starting with alcohol **7**. Cation III-7 should be similar in stability to III-5, but IV-7 should be less stable than IV-5 because the additional methyl groups in IV-5 are stabilizing (see IV-5 structure). However, addition of **7** to the acid solvent gave III-7, but this only yields an indanyl cation mixture on cyclization (+20°C). In spite of this negative result, we still believe that ions III and IV are similar in energy. This point is significant in our rationalization of the stereochemistry involved in the cyclization.

Cation IV is a benzenonium ion, normally considered a high energy intermediate in Friedel–Crafts alkylations. However, intermediates like IV always have a vanishly small concentration in normal alkylations *for kinetic reasons*, and one should not conclude anything about the actual thermodynamics of the benzenonium ion without some other kind of evidence.

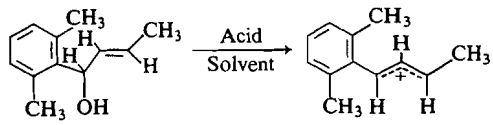

7 III-7

Cyclization

Cation IV-7
not observed

Can. J. Chem. Downloaded from www.nrcresearchpress.com by 210.87.254.6 on 09/06/12
For personal use only.

Can. J. Chem. Downloaded from www.nrcresearchpress.com by 210.87.254.6 on 09/06/12
For personal use only.



TABLE 2. $^{13}C$ nuclear magnetic resonance spectra of arylallyl cations III and trienylic cations IV

| Cation | Solvent | Temperature °C | Position[a] | | | | | | | | | |
|---|---|---|---|---|---|---|---|---|---|---|---|---|
| | | | *ortho* | *meta* | *para* | *ipso* | C-1 | C-2 | C-3 | Methyls | | |
| III-1[b] | $FSO_3H$–$SO_2ClF$ | −50 | 156.2<br>161.0 | 133.5<br>135.2 | 168.3 | 133.5 | 193.2 | 137.1 | 184.8 | 21.1, 23.4, 24.6, 25.5 | | |
| III-5 | $FSO_3H$–$SO_2ClF$ | −110 | 153.1<br>158.5 | 140.2*<br>141.2* | 155.1 | 138.1* | 197.5 | 139.5 | 189.8 | 17.9, 20.7, 21.1<br>22.4, 26.6 | | |
| III-7 | $FSO_3H$ | −50 | 155.9<br>160.6 | 132.1<br>133.4 | 150.0 | 134.6 | 199.9 | 138.1 | 188.9 | 20.9, 25.3(×2) | | |
| | | | C-1 | 2 | 3 | 4 | 5 | 6 | 7 | 8 | 9 | Methyls |
| IV-3 | $FSO_3H$–$SO_2ClF$ | −80 | 210.3 | 133.6 | 214.0 | 136.2* | 160.5* | 135.7* | 162.7* | 71.3 | 58.0 | 10.5, 16.7, 20.1, 21.7, 36.3[c] |
| IV-5 | $FSO_3H$–$SO_2ClF$ | −50 | 190.3 | 132.5* | 207.8 | 133.7 | 177.1* | 131.2* | 182.4* | 69.0 | 52.0 | 12.5, 13.1, 22.8, 23.9, 37.8 |
| IV-6 | $FSO_3H$–$SO_2ClF$ | −60 | 198.4 | 131.6* | 209.0 | 132.3 | 178.7* | 130.8* | 184.8* | 68.4 | 54.7 | 12.3, 13.8, 20.2, 23.0, 24.2, 38.1 |
| IV-8 | $FSO_3H$ | −57 | 197.1 | 131.4* | 207.7 | 132.4* | 179.8* | 135.4* | 180.3* | 68.7 | 55.1 | 12.7, 14.9(×2), 19.7, 19.9, 21.9, 38.3 |

[a] δ ppm, relative to internal $CFCl_3$ = δ 117.9. All multiplicities have been confirmed by off-resonance decoupling but a definitive assignment of closely spaced peaks of similar multiplicity is impossible. The tentative assignments are indicated by *.
[b] Line-broadening, described in the text, occurs at higher temperatures.
[c] A low field methyl carbon is present in all cases and is probably the methyl at C-8.

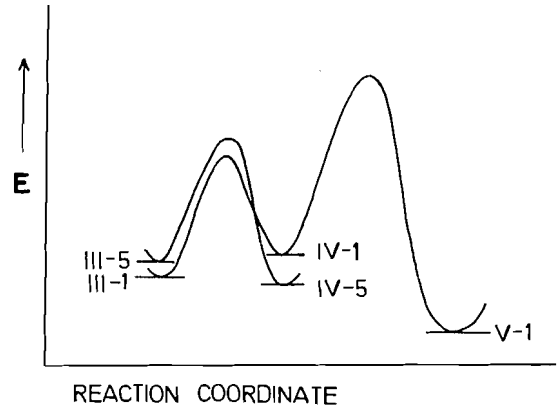


FIG. 1. This diagram is based on the assumption that the kinetics for III-1 → [IV-1] → V-1 would be similar to those observed for III-5 → IV-5 and that thermodynamic factors are responsible for the nonobservation of IV-1. III-1 is placed lower than III-5 because of the favorable *p*-Me group of the former. IV-5 is placed lower than IV-1 because of the two extra favorable methyl substituents.

*Structure of the arylallyl cations*

In cations III-1, III-5, and III-7, all three vicinal protons on the allyl unit have a 13.6 Hz coupling constant characteristic of a mutual *trans*-orientation. This leaves the aryl ring in the expected *anti*-orientation, as shown below:

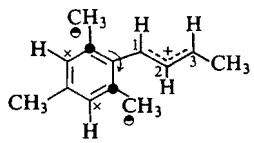

⊖, ●, and × become equivalent by 180° rotation of the aryl ring

III-1

Cation III-2 likewise has a *trans*-orientation about C-1,C-2. The *cis*-orientation for H-2,H-3 in this ion follows because of the stereochemistry present in alcohol **2**, but the actual peaks for H-2 and H-3 are overlapped with others from ion III-1 and no $J_{2,3}$ constant could be obtained. The rearrangement of III-2 to III-1 is expected on stability grounds (9).

The bulky mesityl and duryl rings in III may not be entirely coplanar with the allyl part, but there is nevertheless a sizeable barrier for rotation about the C-1–aryl bond. This barrier can be determined for III-1, based on the line-broadening observed for the *ortho* and *meta* carbons ($^{13}C$ nmr) or the *ortho*-methyl groups ($^{13}C$ nmr). A barrier of 14 kcal/mol was estimated from the coalescence temperature of the aryl *meta* carbon peaks.

*The cyclization of III to IV*

Before discussing the cyclization of the arylallyl cations, one should comment briefly on the conformational requirements.

As in the pentadienyl cation case, the ring closure presumably proceeds via a geometric isomer of the arylallyl cation in which 180° rotation has occurred around the C-1,C-2 "bond" of the ground-state conformation (eq. [4]).

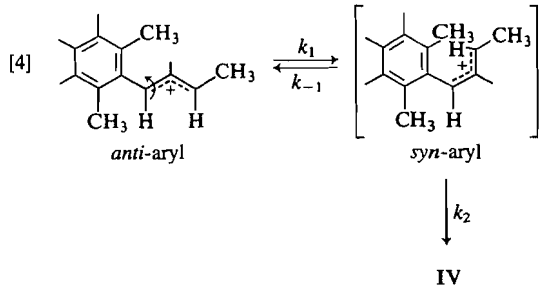

[4]

*anti*-aryl *syn*-aryl

IV

This high energy *syn*-arylallyl cation cannot be planar, but this need not affect the chances for an electrocyclic ring closure, i.e. one governed by electronic rather than steric factors, since the previously-studied pentamethylpentadienyl cation cyclizations (which are nearly stereospecific) have very similar steric interactions in their "U" (reactive) conformations (3).

The arylallyl cations involving a 2-methyl substituent, e.g. from alcohols **3**, **4**, **6**, and **8**, could not be observed because of the enormous rapidity of the cyclization rate. For example, one can estimate that this substitution in the case of alcohols **5** and **6** is responsible for a minimum $10^3$ increase in cyclization rate. The major source of this rate gain must involve a destabilization of the *anti*-arylallyl cation because it is now impossible to have a planar conjugated system, as illustrated below:

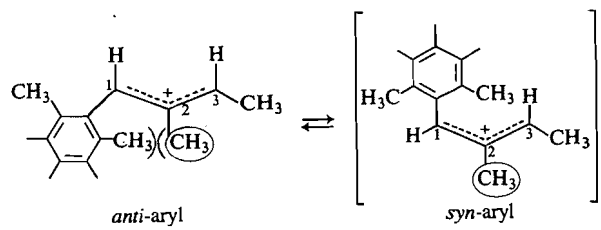

*anti*-aryl *syn*-aryl

The corresponding *syn*-arylallyl conformation is much less affected by this methyl group substitution and the overall effect is to reduce the energy difference between these ions. In this connection it should be noted that the present experiments do not tell one whether $k_1$ or $k_2$ in eq. [4] is rate-determining.

Alcohol **5**, where one can "see" both the arylallyl cation III-5 and the cyclized product IV-5, is the only case where the cyclization rate could be directly measured. The rate is first order and was experimentally measured by monitoring the loss of

Can. J. Chem. Downloaded from www.nrcresearchpress.com by 210.87.254.6 on 09/06/12
For personal use only.

Can. J. Chem. Downloaded from www.nrcresearchpress.com by 210.87.254.6 on 09/06/12
For personal use only.

$^1$H nmr peaks due to III-5 and the formation of IV-5 peaks, giving $k_{overall} = 5 \times 10^{-4}\,s^{-1}$ in $FSO_3H$ at $-70°C$, $\Delta G^{\neq} = 15.6$ kcal/mol.

Although there is no direct evidence in these cyclizations that the *syn*-isomers exist as discrete species, we do have direct evidence for these from a *ring-opening* reaction to be discussed later in this paper.

*Structural evidence for cations IV*

In the $^1$H nmr, the cyclized cations IV all show one high field (saturated) quaternary methyl and a high field methyl doublet. In IV-5, the two low field protons are coupled, $J = 5.5$ Hz, indicating a *cis*-orientation. The $^{13}$C spectra are also very diagnostic, showing seven low field carbons. The four carbons formally sharing the positive charge

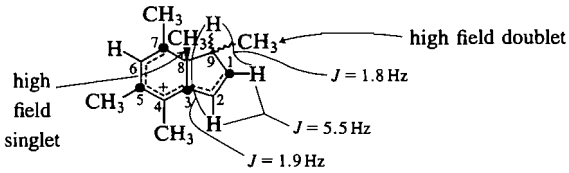


IV-5

(● in the structure above) form one group and the other three a higher field group. In the specific case of IV-5, three of the lower field group are quaternary and one is CH, while the upper field group has one quaternary and two CH carbons (see Tables 1 and 2).

The visible spectrum of IV-8 has $\lambda_{max} = 483$ nm, $\varepsilon_{max} = 9400$, as the longest wavelength absorption, in good agreement with 473 nm for an acyclic trienylic cation (10).

*Stereochemistry of cyclized ions IV (question 2 – Introduction)*

As previously noted, the $^{13}$C nmr spectra of IV-4, IV-5, IV-6, and IV-8 are consistent with the initial formation of a *single* stereoisomer. To try to determine this stereochemistry, the following methods were tried.

1. Assuming the product was one of kinetic control, we tried to equilibrate the ion at C-9 to at least produce *both* stereoisomers. This kind of equilibration works for the simple cyclopentenyl cations (11), e.g. 1,2,3,4,5-pentamethylcyclopentenyl cation eventually forms a *trans*/*cis* ratio of 3.9, starting from either relatively pure isomer. The usual equilibration mechanism would involve deprotonation–reprotonation at C-9 and the rate for such reactions becomes faster the weaker the acid solvent (stronger bases present) (12).

However, cation IV-6 resolutely refused to do anything, even when acids as weak as aqueous trifluoroacetic acid were used. That an acid–base equilibration reaction *was not* occurring was clear, because when $CF_3COOD$–$D_2O$ mixtures were used, no D appeared at C-9 in the ion. Eventually, if one weakens the acid solvent too much, degradation occurs but with no sign of any second equilibration partner.

2. Nuclear Overhauser enhancement nmr experiments were attempted on ion IV-6; the two possible geometries are shown below:

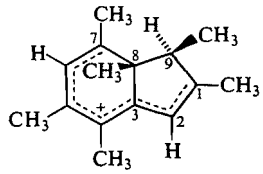

IV-6A

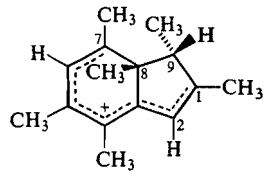

IV-6B

In IV-6B, the C-7 and C-9 methyl groups are quite close in space. However, using degassed samples of IV-6 in $D_2SO_4$ solvent (or IV-4 in $DSO_3F$ solvent), no measurable nOe effects were found for these methyls. A subsequent $T_1$ measurement on several of the ions revealed that the methyl groups in question have very short relaxation times (shown below for IV-4).

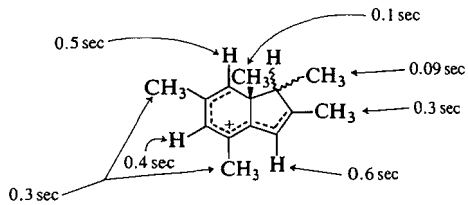


IV-4 $T_1$ relaxation times (−55°C, $DFSO_3$)

The usual nOe effects could be obtained on protonated DMF in $D_2SO_4$ or $DSO_3F$ and these protons also have much longer $T_1$'s, for example 1.3, 1.2 s for the high and low field methyls and 0.8 s for the methine proton in $D_2SO_4$ at 22°C. At the same temperature in $DSO_3F$, $T_1$ values are 3.1, 2.8, and 5.0 s. The short $T_1$ problem in IV-4 likely stems from the large size of the ion, resulting in correlation times very suitable for $T_1$ relaxation. It is significant in this regard that the quaternary methyl has a very short relaxation time and this protrudes from the top of the nearly planar surface formed by the remaining atoms.

3. Attempts to obtain crystalline salts of IV-8, suitable for X-ray work, were unsuccessful. The ion solutions are highly colored, making visual observation of crystal formation difficult. The usual material obtained was amorphous.

*Cation IV quenching studies*

Quenching sulfuric acid solutions of IV-6 in

Can. J. Chem. Downloaded from www.nrcresearchpress.com by 210.87.254.6 on 09/06/12
For personal use only.

$H_2O$–$(CH_2OH)_2$–NaOH at ca. −20°C results in a near quantitative yield of proton-elimination products, obtained as an oil. This material (from $^1H$ and $^{13}C$ nmr) is mainly a mixture of two compounds. The major isomer is a 3aH-indene **9**, involving proton loss at C-9 in the ion. This unfortunately destroys the stereochemistry inherent in the system and is thus of no use to us. The spectral and chemical properties of **9**, as well as synthetic possibilities, are discussed elsewhere (13).

The minor component is the more interesting since it shows both the high field quaternary methyl *and* the high field doublet methyl which were present in the ion. In principle, one can eliminate a proton from the termini of IV-6 in two ways, viz. conjugated tetraenes **10** or **11**, respectively. However, a detailed analysis of the $^1H$ spectrum, particularly the coupling constants, favours **10**. This is discussed more fully in the "pentamethylbenzene" analog (ion IV-8).

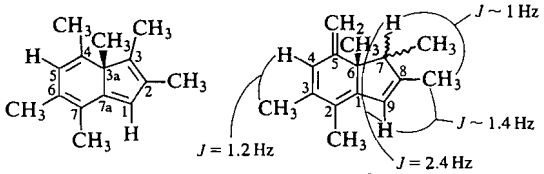

**9** **10**

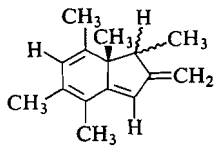

**11**

Attempts to separate **9** and **10** were unsuccessful because both compounds are very sensitive. Some chemical degradation studies were attempted on the mixture but no useful results were obtained. One can convert **9** into a ring-opened ketone (13), while leaving **10** at least partly untouched. This helps in assigning the nmr spectrum of **10**, but the isolation of pure **10** still proved impossible in our hands. We also sought quenching procedures designed to get better yields of **10**, but to no avail. However, it was discovered that the pentamethylbenzene analog, cation IV-8, could be quenched to give mainly the exocyclic tetraene component. Cation IV-8 is produced very cleanly from alcohol **8**.

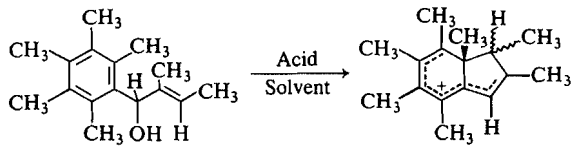

**8** IV-8

Quenching IV-8 leads to a mixture which is mainly an exocyclic tetraene, together with a smaller amount of the 3aH-indene **12** (13). The exocyclic tetraene was assigned the structure **13** rather than **14** on the basis of the $^1H$ nmr coupling constants observed (also applied to the assignment of **10** vs. **11**).

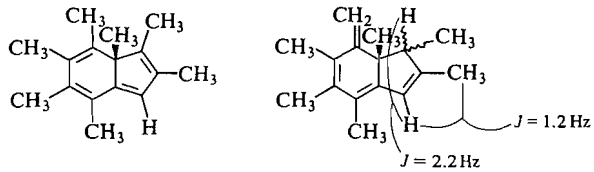

**12** **13**

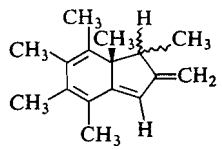

**14**

Compounds **12** and **13** were obtained as an oil and attempts to separate these sensitive substances by chromatography or low temperature crystallization were unsuccessful. The apparently ready conversion of **13** to **12** makes chemical degradation studies difficult. The primary attempt in these degradation studies was to first convert the $=CH_2$ in **13** to $=O$, which could perhaps be obtained crystalline itself or as an adduct (then X-ray analysis). Numerous ozonolysis and periodic acid – $OsO_4$ reactions always led to crude mixtures in which the saturated

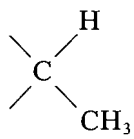

functionality was very weak or missing in the $^1H$ nmr spectra of the crude products. In attempts to convert $=CH_2$ to $-CH_2OH$, 9-BBN proved unreactive. The major problem is probably that the $=CH_2$ group is well-shielded by the other methyl substituents and reactions at other sites or **13** → **12** rearrangements intervene.

*Attempts to determine the stereochemistry in IV by kinetically-controlled protonation of 3aH-indenes 9 or 12*

With pentamethylcyclopentadiene **15** (11) or 1,3-diphenyl-2-methylindene **16** (6), protonation occurs under kinetic control and results predominantly in that cation isomer in which the proton approaches from the least hindered side, giving in these cases the less-stable *cis*-isomer. In the case of **9**, it is not immediately obvious which side is the more hindered, but the protonation in $H_2SO_4$ should defi-

Can. J. Chem. Downloaded from www.nrcresearchpress.com by 210.87.254.6 on 09/06/12
For personal use only.

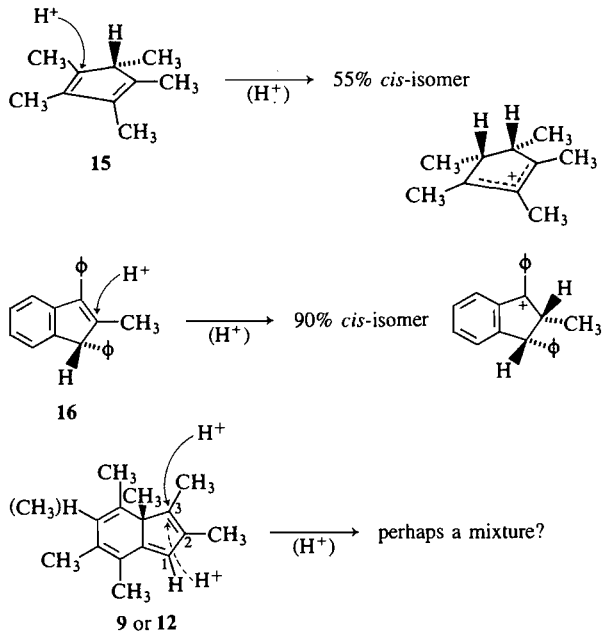


15 16 9 or 12

nitely be kinetically controlled (earlier in this paper it was remarked that no H–D exchange occurs in any of the acid solvents). However, protonation in $H_2SO_4$ results in only one cation being formed, the *same* one as produced in the original cyclization reaction. Protonation does occur at C-3 because, in $CF_3COOD$, the high field methyl doublet of IV-6 is at least partially collapsed.

*Possible stereochemical differentiation by nOe and $T_1$ studies on the tetraene* ***13***

$T_1$ values (in seconds) for degassed samples of **13**

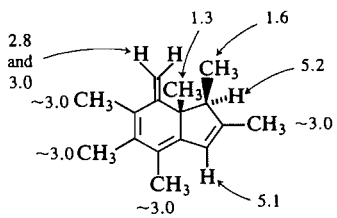


**13**

in $CDCl_3$ are given below. Both aliphatic methyl groups are seen to have rather short $T_1$'s. The nOe experiments were tried at both 200 and 400 MHz $^1H$ fields. At 400 MHz, there is virtually no enhancement of the quaternary methyl on irradiation of the methyl doublet and vice versa. Conversely, there is no nOe effect (200 MHz) between the methyl doublet and either of the $=CH_2$ protons.

*Molecular orbital calculations*

Further to our attempts to assign the stereochemistry to these ions, semiempirical MINDO/3 calculations were performed on the model cations IV-9A and IV-9B (corresponding to IV-5 with removal of C-4 and C-5 methyl groups). The geometries were fully optimized except for hydrogen dihedral angles in methyl groups. In addition, all methyl C—H bonds were made equal and, separately, all $C_{sp^2}$—H bonds were kept equal. These calculations are relevant if one assumes that the observed IV-cations might be products of thermodynamic rather than kinetic control (see Discussion). The total energies (in kcal/mol) for IV-9A and IV-9B are given next to the structure.

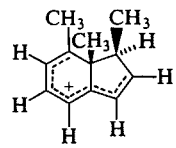

IV-9A 217.87 kcal/mol

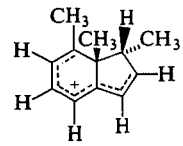

IV-9B 217.91 kcal/mol

Structure IV-9A is shown in Fig. 2. These calculations suggest the two ions to be essentially of equal energy and are of no use, in a total energy sense, in helping one assign the unknown stereochemistry. However, the optimized geometries do offer some help in interpreting the H-9,H-1 coupling constant in ion IV-5.

*The H-9,H-1 vicinal coupling constant in ion IV-5*

The H-1,H-2 coupling in ion IV-5 is 5.5 Hz, typical of *cis* double bond coupling in five-membered rings, and this value can be used to calibrate the Karplus curve. The observed H-9,H-1 coupling of 1.8 Hz corresponds to a dihedral angle of about 52°. The calculated dihedral angles in IV-9A and IV-9B are 79 and 47°, respectively. Clearly, ion IV-9B is favored on this basis.

The Karplus relationship generally cannot be used to any degree of "exactness" but the two dihedral angles calculated in this case are sufficiently

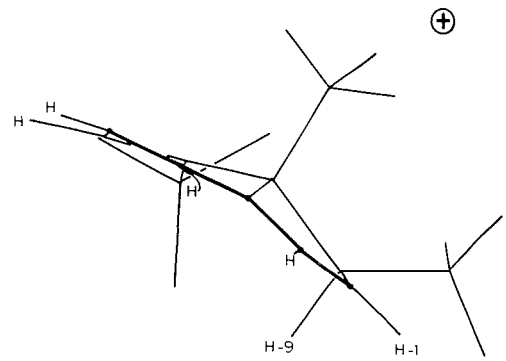


FIG. 2. Computed structure (MINDO/3) for the model cation IV-9A. Note that the H-9,H-1 dihedral angle of 79° is not consistent with the experimental nmr data, and thus the IV-9B structure is favored.

Can. J. Chem. Downloaded from www.nrcresearchpress.com by 210.87.254.6 on 09/06/12
For personal use only.

different that one has some confidence in the assignment.

*Ring-opening reaction of tetraene 13*

This reaction is not relevant to the stereochemistry problem, but is very relevant to the cyclization mechanism shown in eq. [4]. The tetraene mixture from the quench of ion IV-8 (mainly **12** and **13**), on standing in dilute aqueous acid (ca. pH = 1), is fairly rapidly converted to the alcohol **17**, whose structure has been proven (13).

[5]

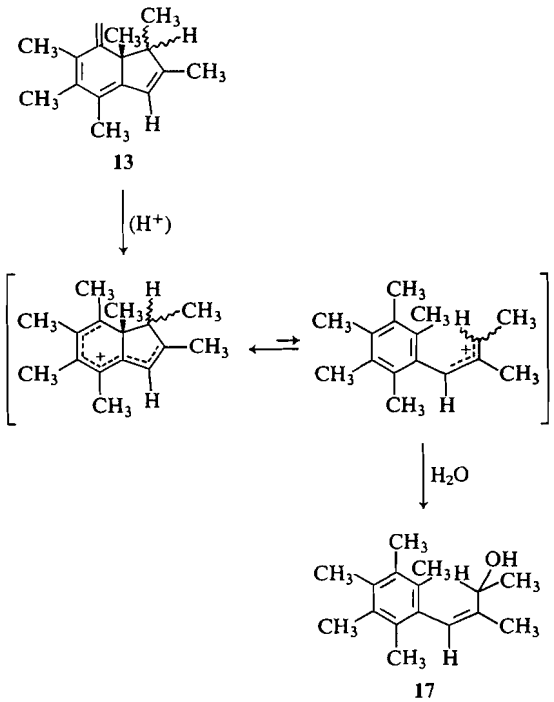


Two points are significant here: (1) the *syn*-arylallyl cation is the obvious precursor of **17**, and thus the existence of this intermediate is confirmed, and (2) the energy separation between the closed and open ions is likely small, a conclusion also reached on other grounds.

*Discussion of the arylallyl cation results*

Simple HMO theory predicts a conrotatory closure for the aryallyl cations. With a ground-state *anti*-methyl substituent as a marker, this leads to a predicted *cis*-dimethyl geometry (eq. [6]) in the cyclized ions.

Experimentally, one finds only one isomer being produced. We assume that this single isomer probably has the same stereochemistry in all of the IV-ions, although there is no complete proof that this is so. In addition, the evidence for a single ion is based on the premise that the $^{13}C$ and $^{1}H$ nmr

[6]

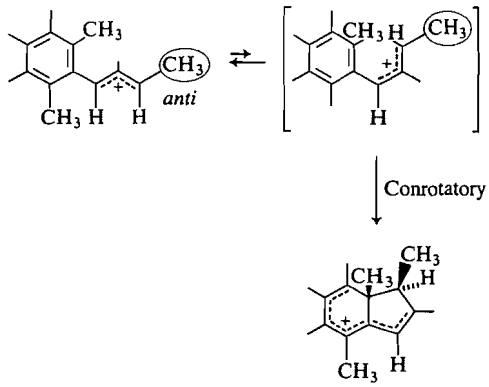


spectra would not be absolutely identical for the two stereoisomers.

The argument against a conrotatory ring closure in our examples is that both alcohols **3** and **4**, which have *syn*- and *anti*-methyl substituents, respectively, give the same single cyclic ion IV product. It is possible of course that III-3 and III-4 are rapidly interconverted before cyclization, since neither ion is directly observed. However, the stable isomer of the two is III-4 and this should produce the *cis*-dimethyl geometry. In the case of ions III-1 and III-2, the corresponding *syn* → *anti* rate is measurable and is indeed relatively fast.

All in all, it seems most probable that, in spite of the MO calculations, one stereoisomer, probably the *trans*-dimethyl isomer, is significantly more stable than the other and that the stereochemistry of our cyclization reaction is governed by this thermodynamic factor.

Even allowing for the above, there are excellent precedents for expecting a kinetically controlled protonation of the isoindenes **9** and **12**, which should have given a IV mixture containing both stereoisomers. Any possible isomerization of one stereoisomer to the other has already been shown not to involve a deprotonation–reprotonation mechanism, but the mechanism shown in eq. [7] could conceivably allow a rapid equilibration to the more stable IV-isomer and is illustrated for the case where the *trans*-dimethyl isomer is assumed to be the more stable. The key feature is that the "open" and "closed" ions be similar in energy, a conclusion already reached from several pieces of evidence.

*The diarylmethyl cations*

The diduryl- and dimesitylmethyl cations VI-1 and VI-2 were produced from the known alcohols (14, 15) and chemical shift data ($^{1}H$ and $^{13}C$) are given in Tables 3 and 4. In $CF_3COOH$, the cations have $\lambda_{max}$ = 510 and 526 nm, $\varepsilon_{max}$ = 23 300 and 35 700, respectively. These ions show no indication

[7] 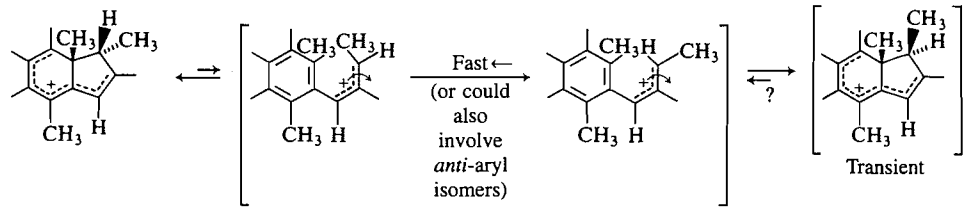


of cyclizing, even after prolonged storage at 20°C. In view of the previous conclusions regarding arylallyl cations, one would confidently predict that the cyclized ions VII would be of high energy relative to VI.

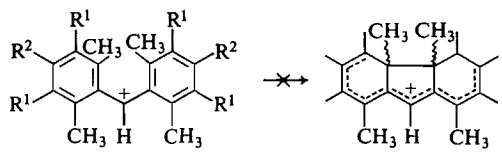

VI-1 $R^1 = CH_3$, $R^2 = H$
VI-2 $R^1 = H$, $R^2 = CH_3$

VII

*Discussion of the diarylmethyl cation results*

Only when rearomatization of VII can readily occur would it be possible to carry out a cyclization of VI (via VII as a high-energy intermediate). An example of this is the well-known conversion of triphenylmethanol into 9-phenylfluorene (16), carried out in strong acid. Photochemical cyclizations of triarylmethyl cations are also known (17). A mass-spectral study (18) of diphenylmethyl bromide has been interpreted in terms of a diphenylmethyl cation cyclization, to give an analog of VII, which subsequently loses $H_2$. On this basis, the cyclization stereochemistry was postulated to be the *cis* di-H analog of VII (a disrotatory cyclization), since the concerted loss of $H_2$ from the *trans* isomer was considered unlikely. However, these results are very indirect and interpretation in terms of specific structures is conjectural.

## Conclusions

With respect to the questions asked in the Introduction: (1) the cyclization of arylallyl cations is generally favorable, but there is evidence that the *energy differences are small*; (2) the cyclization product consists of only *one stereoisomer*, most probably the *trans*-dimethyl structure IV-B. However, there are still a number of unanswered mechanistic questions in this connection and (3) diarylmethyl cations VI do not cyclize to cation VII and are undoubtedly thermodynamically more stable than VII.

TABLE 3. $^1H$ nuclear magnetic resonance spectra of diarylmethyl cations

| Cation | Solvent | Temperature °C | Position[a] *ortho* | *meta* | *para* | $\overset{+}{C}H$ |
|---|---|---|---|---|---|---|
| VI-1 | $FSO_3H$ | 25 | 2.65 | 2.65 | 8.00 | 10.66 |
| VI-2 | $FSO_3H$ | 25 | 2.73 | 7.53 | 2.83 | 10.20 |

[a]Chemical shifts in δ ppm relative to external TMS in TMS-$d_{12}$.

## Experimental

The nmr spectra were obtained on Varian models HA-100 and XL-200 and Bruker model WH-90 spectrometers. Electronic spectra were obtained in 96% $H_2SO_4$ solution on a Cary 219 spectrophotometer. Constant temperature runs (and kinetic measurements) were obtained on the Bruker instrument using a previously described calibration procedure (19). The nmr spectra of all neutral compounds were measured in $CDCl_3$ or $CFCl_3$ solutions and are quoted relative to internal TMS (δ = 0.00).

All lithium reactions were carried out under a nitrogen or argon atmosphere. Boiling points and melting points are uncorrected.

*Ion preparations* ($FSO_3H$–$SO_2ClF$, $FSO_3H$, 96% $H_2SO_4$, $CF_3COOH$)

For $^1H$ nmr work, the alcohol (50 mg) in a small amount of $CFCl_3$ was added by pipette to 0.5 mL of 1:4 v/v $FSO_3H$–$SO_2ClF$ solutions contained in a 5 mm nmr tube and cooled to ca. −125°C using a pentane–$N_2$ slush bath. The solution was stirred with a Pt wire during the alcohol addition. All of the ions in this work are very highly colored. For $^{13}C$ nmr spectra, about 200 mg of alcohol was used (10 mm tubes) in ca. 2 mL of the acid solution. About 6000 accumulations were needed for good signal-to-noise spectra, usually employing a sweep width of 9000 Hz on the Bruker WH-90. Off-resonance spectra were also obtained to aid in the assignments. For pure $FSO_3H$ solvent, the alcohol, in a very small amount of $CDCl_3$, was added with stirring to the $FSO_3H$, the latter in an nmr tube and cooled at ca. −80°C in a Dry Ice bath. Sulfuric acid solutions were prepared by adding the acid and an equal volume upper pentane layer to a 5 mL flask. To the stirred mixture at −10 to 0°C was added dropwise the alcohol dissolved in a small amount of pentane. After a few minutes, the lower layer ion solution was removed by pipette and transferred to nmr tubes. For $CF_3COOH$ solutions, the solid alcohol was added directly in small portions to the stirred acid at 0°C.

For $FSO_3H$–$SO_2ClF$ solutions, the $^{19}F$ signal of $SO_2ClF$ was used as a lock. For $FSO_3H$ solutions, a 2 mm ($^1H$) or 5 mm ($^{13}C$) insert of TMS-$d_{12}$ was used as lock. For sulfuric acid solutions, either the TMS-$d_{12}$ or a dimethylether-$d_6$ insert was used for locking, while $CF_3COOH$ solutions were locked to the $^{19}F$ of the acid. In $FSO_3H$–$SO_2ClF$ solutions, $CFCl_3$ serves as an internal $^{13}C$ reference (δ 117.9), while in the $^1H$ spectra, a small amount of TMS in the TMS-$d_{12}$ served as a reference. The dimethyl ether-$d_6$ insert also contained a small amount of TMS. The δ positions of the various references, relative to TMS in $CDCl_3$ or $SO_2ClF$, have been determined for both iron magnet and supercon field configurations.

Can. J. Chem. Downloaded from www.nrcresearchpress.com by 210.87.254.6 on 09/06/12
For personal use only.

TABLE 4. $^{13}C$ nuclear magnetic resonance spectra of diarylmethyl cations

| Cation | Solvent | Temperature °C | Position[a] | | | | | | | |
|---|---|---|---|---|---|---|---|---|---|---|
| | | | *ortho* | *meta* | *para* | *ipso* | *o*-$CH_3$ | *m*-$CH_3$ | *p*-$CH_3$ | $\overset{+}{C}H$ |
| VI-1 | $CF_3COOH$ | 25 | 148.5 | 140.5 | 142.6 | 142.6 | 18.9* | 17.5* | — | 193.0 |
| VI-2 | $CF_3COOH$ | 25 | 151.9 | 133.7 | 163.6 | 139.3 | 20.7 | — | 22.7 | 187.6 |

[a]In ppm relative to external TMS = δ 0.0, * indicates tentative assignments.

For the acid–base exchange attempts, deuterated acids $CF_3COOD$ and $CF_3COOD$–$D_2O$ solvents were used ($^1H$ nmr spectra), employing the same experimental techniques.

For the reprotonation studies on the **9**, **10** or **12**, **13** mixtures (attempted kinetic protonation), $FSO_3H$ or $H_2SO_4$ solvents were used, the former using a $CDCl_3$ solution, the latter using the pentane extraction method. The deuterated acid used in these studies was $CF_3COOD$.

The arylallyl alcohols were prepared by adding known aldehydes to known aryl or vinyl lithium compounds (prepared *in situ*). The crude alcohols were purified by vacuum distillation or recrystallization, or both. The $^1H$ nmr characterization does not include the OH proton.

E-*1-Mesityl-2-buten-1-ol* ***1***

From mesityl lithium and crotonaldehyde, the crude product directly recrystallized from pentane, 96% yield, mp 57–58°C; $^1H$ nmr: 1.66 (d, $J$ = 7, C-3 methyl), 2.19 (*p*-$CH_3$), 2.32 (*o*-$CH_3$), 5.3–5.9 (complex, protons on C-1, 2, and 3), 6.76 (*m*-H); $^{13}C$ nmr: 17.7 (C-3 methyl), 20.6 (*o*-$CH_3$), 20.7 (*p*-$CH_3$), 71.6 (C-1), 126.5 (C-3), 130.0 (*meta*), 131.7 (C-2), 135.7 (*ipso*), 136.3 (*ortho*), 136.7 (*para*). *Anal.* calcd. for $C_{13}H_{18}O$: C 82.1, H 9.5; found: C 81.9, H 9.3.

Z-*1-Mesityl-2-buten-1-ol* ***2***

Mesitaldehyde was added to the lithium reagent from *Z*-1-bromo-1-propene. The crude solid product could not be further purified since all attempts to recrystallize the alcohol from pentane resulted in an allylic rearrangement. However, the $^1H$ and $^{13}C$ nmr spectra of the crude alcohol indicated that it was nearly pure. Yield 88%, mp 45–46°C; $^1H$ nmr: 1.62 (d, $J$ = 7, C-3 methyl), 2.18 (*p*-$CH_3$), 2.35 (*o*-$CH_3$), 5.51 (complex, H-3), 5.82 (complex H-1 and H-2), 6.74 (*m*-H); $^{13}C$ nmr: 13.2 (C-3 methyl), 20.7 (*o*- and *p*-$CH_3$'s), 67.1 (C-1), 126.1 (C-3), 130.1 (*meta*), 132.1 (C-2), 136.1 (*ipso*), 136.2 (*ortho*), 136.7 (*para*). *Anal.* calcd. for $C_{13}H_{18}O$: C 82.1, H 9.5; found: C 82.2, H 9.5.

Z-*1-Mesityl-2-methyl-2-buten-1-ol* ***3***

Mesitaldehyde was added to the lithium reagent from *Z*-2-bromo-2-butene, 75% yield, bp 95–98°C/0.05 Torr. The nmr spectrum (see below) indicates that ca. 10% of the *E*-isomer is present, $^1H$ nmr: 1.54 (d, $J$ is hidden, C-3 methyl), 1.56 (C-2 methyl), 2.18 (*p*-$CH_3$), 2.28 (*o*-$CH_3$), 5.33 (quart., $J$ = 7, H-3), 5.70 (H-1), 6.71 (*m*-H); $^{13}C$ nmr: 14.2 (C-3 methyl), 21.5 (*o*-, *p*-, and C-2 methyls), 71.9 (C-1), 123.1 (C-3), 130.7 (*meta*), 136.6, 137.1, 137.3 (*ortho*, *para*, *ipso*, C-2). *Anal.* calcd. for $C_{14}H_{20}O$: C 82.3, H 9.9; found: C 82.0, H 9.8.

E-*1-Mesityl-2-methyl-2-buten-1-ol* ***4***

Tiglaldehyde was added to mesityl lithium, the crude product directly recrystallized, from pentane, 94% yield, mp 63–64°C; $^1H$ nmr: 1.56 (d, $J$ = 7, C-3 methyl), 1.48 (C-2 methyl), 2.16 (*p*-$CH_3$), 2.22 (*o*-$CH_3$), 5.32 (H-1), 5.37 (quart., $J$ = 7, H-3), 6.68 (*m*-H). Considerable long range coupling is present in the C-1, 2, and 3 methyls and protons; $^{13}C$ nmr: 13.0 and 13.6 (C-2 and C-3 methyls), 20.5 (*o*-$CH_3$), 20.7 (*p*-$CH_3$), 74.0 (C-1), 118.4 (C-3), 129.9 (*meta*), 135.3 (C-2), 135.4 (*para*), 136.7 (*ipso*), 137.1 (*ortho*). *Anal.* calcd. for $C_{14}H_{20}O$: C 82.3, H 9.9; found: C 82.3, H 9.9.

E-*1-Duryl-2-buten-1-ol* ***5***

Crotonaldehyde was added to duryl lithium and the residue purified by vacuum distillation, bp 120–122°C/0.05 Torr, mp 79–80°C, yield 83%; $^1H$ nmr: 1.60 (d, $J$ = 7, methyl on C-3), 2.15 (*m*-$CH_3$), 2.20 (*o*-$CH_3$), 5.26–5.94 (multiplet, H-1, 2, 3), 6.80 (*p*-H); $^{13}C$ nmr: 16.2 (*m*-$CH_3$), 17.7 (C-3 methyl), 20.5 (*o*-$CH_3$), 71.8 (C-1), 126.6 (C-3), 131.2 (*para*-H), 132.2 (C-2), 132.4 (*ortho*), 134.5 (*meta*), 138.8 (*ipso*). *Anal.* calcd. for $C_{14}H_{20}O$: C 82.3, H 9.9; found: C 81.9, H 9.8.

E-*1-Duryl-2-methyl-2-buten-1-ol* ***6***

Tigaldehyde was added to duryl lithium and the residue purified by vacuum distillation, bp 128–131°C/0.15 Torr, mp 45–46°C, yield 85%; $^1H$ nmr: 1.54 (d, $J$ = 7, C-3 methyl), 1.55 (C-2 methyl), 2.13 (*o*- and *m*-$CH_3$'s), 5.32 (quart., $J$ = 7, H-3), 5.52 (H-1), 6.83 (*p*-H). Considerable long range coupling is present in the C-1, 2, and 3 methyls and protons; $^{13}C$ nmr: 13.1 and 13.7 (C-2 and C-3 methyls), 16.1 (*m*-$CH_3$), 20.5 (*o*-$CH_3$), 74.5 (C-1), 118.6 (C-3), 131.0 (*p*-H), 133.1 (C-2), 134.3 (*meta*), 136.0 (*ortho*), 138.6 (*ipso*). *Anal.* calcd. for $C_{15}H_{22}O$: C 82.5, H 10.2; found: C 82.0, H 10.0.

E-*1-[1-(2,6-Dimethylphenyl)]-2-buten-1-ol* ***7***

Crotonaldehyde was added to the lithium reagent from 2-bromo-*m*-xylene. The crude solid was recrystallized from pentane, mp 49–50°C, yield 88%; $^1H$ nmr: 1.65 (d, $J$ = 7, C-3 methyl), 2.35 (*o*-$CH_3$), 5.30–5.90 (mult., H-1, 2, 3), 6.82–7.00 (mult., *m*-H, and *p*-H); $^{13}C$ nmr: 17.7 (C-3 methyl), 20.8 (*o*-$CH_3$), 71.6 (C-1), 125.9 and 127.4 (C-3 and *para* C), 129.5 (*meta*), 132.4 (C-2), 136.6 (*ortho*), 139.1 (*ipso*). *Anal.* calcd. for $C_{12}H_{16}O$: C 81.8, H 9.2; found: C 81.9, H 9.3.

E-*1(1-Pentamethylphenyl)-2-buten-1-ol* ***8***

Tiglaldehyde was added to the lithium reagent from pentamethylbromobenzene. The latter required 24 h reflux (diethyl ether solvent) to form. Distillation of the crude residue, bp 148–149°C/0.05 Torr and recrystallization from pentane gave 52% yield of the pure alcohol, mp 82–83°C; $^1H$ nmr: 1.55 (d, $J$ = 7, C-3 methyl), 1.61 (C-2 methyl), 2.20 (*o*-, *m*-, and *p*-methyl), 5.1–5.75 (H-1 and H-3); $^{13}C$ nmr: 13.1, 13.6 (C-2 and C-3 methyls), 16.6 and 17.1 (*o*- and *m*-$CH_3$), 16.9 (*p*-$CH_3$), 74.7 (C-1), 118.3 (C-3), 132.8, 133.0 (*meta* and C-2), 133.7 (*para*), 136.9, 137.0 (*ortho* and *ipso*). *Anal.* calcd. for $C_{16}H_{24}O$: C 82.75, H 10.3; found: C 82.7, H 10.6.

*2,3,6,7,8-Pentamethyl-5-methylenebicyclo[4.3.0]nona-1,3,8-triene* ***10***

This compound, in a mixture together with isoindene **9** (ca. 1:2–3 of **10**/**9**), was obtained as an oil. It was characterized by $^1H$ nmr spectroscopy: 6.09 (1H, mult., H-9), 5.82 (1H, mult., H-4), 4.69 and 4.80 (each 1H), singlets, $=CH_2$), 2.56 (1H, broad quart., $J$ = 7, H-7), 1.74 (3H) and 1.80 (6H), ($CH_3$'s at C-2, 3, and 8), 1.05 (3H, doublet, $J$ = 7, $CH_3$ at C-7), 0.89 (3H, singlet, $CH_3$ at C-6). The nmr assignments are aided by being able to convert **9** into a ketone while leaving **10** intact (13). Long range coupling

Can. J. Chem. Downloaded from www.nrcresearchpress.com by 210.87.254.6 on 09/06/12
For personal use only.

constants were obtained by decoupling studies and are shown on structure **10**.

*2,3,4,6,7,8-Hexamethyl-5-methylenebicyclo[4.3.0]nona-1,3,9-triene* ***13***

This compound, in a mixture with isoindene **12** (ca. 2–3:1 of **13**/**12**), was obtained as an oil and characterized by $^1$H nmr spectroscopy: 6.07 (1H, mult., H-9), 4.94 and 4.89 (each 1H, singlets, $=CH_2$), 2.6 (1H, broad quart., $J$ = 7, H-7), 1.82 and 1.81 (9H, $CH_3$'s at C-2, 3, 4), 1.74 (3H, $CH_3$ at C-8), 1.09 (3H, doublet, $J$ = 7.2, $CH_3$ at C-7), 0.85 (3H, singlet, $CH_3$ at C-6). Long range coupling constants were obtained by decoupling studies and are shown on structure **13**.

*Quenching experiments*

Several experiments in which $CF_3COOH$, 96% $H_2SO_4$, and $FSO_3H$ were employed as acid solvents for preparing the ions showed that 96% $H_2SO_4$ is the most convenient of these for quenching in base to give neutral products. Cations IV-6 and IV-8 were employed in these quenching studies. The only drawback to using 96% $H_2SO_4$ is the relatively high melting point. Cation IV-4, for example, is stable only up to about −30°C and therefore cannot be prepared in 96% $H_2SO_4$. The best quenching procedure was to add the sulfuric acid solution (typically 1 g of ion/10 mL of acid solvent) dropwise at 0°C to a vigorously stirred mixture of 60 g of sodium carbonate in 200 mL of water, 200 mL of ethylene glycol, and 200 mL pentane, cooled to −20°C. After warming to 20°C, the pentane layer was separated, a further pentane extraction made, and the combined layers washed with sodium carbonate solution and then water, and dried over anhydrous $K_2CO_3$. Removal of the solvent gave >90% recovery of organic material. In some cases, the main product is an alcohol (by nmr) but this alcohol is very unstable and readily dehydrates to the alkene material which is more often the direct first observed product. Other quenching procedures using $NH_2^-/NH_3$, a $CH_2Cl_2/Na_2CO_3$ suspension, or aqueous pyridine as bases were unsatisfactory.

*Molecular orbital calculations*

The standard MINDO/3 procedure of Dewar and co-workers was used (20). A PLUTO plotting routine (21) was used to construct the diagram in Fig. 2.

*Nuclear Overhauser effect experiments*

The 400 MHz measurements were performed at the University of Alberta on a Bruker WH-400 spectrometer using a subtraction routine to plot only difference spectra. The 200 MHz experiments were carried out on a Varian XL-200 using the subtraction routine No. 28 from the Varian library of pulse sequences for this instrument.

$T_1$ *experiments*

The inversion–recovery method was used, with automatic data processing by the XL-200 nmr spectrometer. Standard deviations were usually less than ±10%. Samples were deoxygenated by nitrogen purging for several hours.

*Crystalline salt attempts*

The alcohol **8** was treated for several hours at 0°C with an excess of $PCl_5$. The solid was filtered off and to the resulting solution was added a suspension of $AlCl_3$ in $CH_2Cl_2$ (1:1 molar ratio of presumed organic chloride/$AlCl_3$). An immediate reddish-black color developed and the solution was filtered under nitrogen. Partial evaporation of the $CH_2Cl_2$ usually gave a dark amorphous solid.

## Acknowledgements

We thank the Natural Sciences and Engineering Research Council of Canada for generous financial support. The University of Alberta is thanked for the 400 MHz nmr spectra. Miss B. Odell and Dr. K. Rajeswari are thanked for some preliminary experiments.

1. (*a*) N. C. Deno and C. U. Pittman, Jr. J. Am. Chem. Soc. **86**, 1871 (1964); (*b*) T. S. Sorensen. Can. J. Chem. **42**, 2768 (1964).
2. R. B. Woodward and R. Hoffmann. J. Am. Chem. Soc. **87**, 395 (1965).
3. (*a*) P. H. Campbell, N. W. K. Chiu, K. Deugau, I. J. Miller, and T. S. Sorensen. J. Am. Chem. Soc. **91**, 6404 (1969); (*b*) N. W. K. Chiu and T. S. Sorensen. Can. J. Chem. **51**, 2776 (1973).
4. N. C. Deno and W. L. Evans. J. Am. Chem. Soc. **79**, 5804 (1957).
5. N. C. Deno, C. U. Pittman, Jr., and J. O. Turner. J. Am. Chem. Soc. **87**, 2155 (1965).
6. C. U. Pittman, Jr. and W. G. Miller. J. Am. Chem. Soc. **95**, 2947 (1973).
7. G. A. Olah and R. J. Spear. J. Am. Chem. Soc. **97**, 1539 (1975).
8. F. A. Olah, G. Asensio, and H. Mayr. J. Org. Chem. **43**, 1518 (1978).
9. P. von R. Schleyer, T. M. Su, M. Saunders, and J. C. Rosenfeld. J. Am. Chem. Soc. **91**, 5174 (1969).
10. T. S. Sorensen. J. Am. Chem. Soc. **87**, 5075 (1965).
11. T. S. Sorensen, I. J. Miller, and C. M. Urness. Can. J. Chem. **48**, 3374 (1970).
12. N. W. K. Chiu and T. S. Sorensen. Can. J. Chem. **51**, 2783 (1973).
13. D. M. Dytnerski, K. Ranganayakulu, B. P. Singh, and T. S. Sorensen. J. Org. Chem. In press.
14. J. Coops, W. Th. Nauta, M. J. E. Ernsting, and A. C. Faber. Recl. Trav. Chim. Pays-Bas, **59**, 1109 (1940).
15. E. P. Kohler and R. Baltzly. J. Am. Chem. Soc. **54**, 4015 (1932).
16. R. A. Benkeser and W. Shroeder. J. Org. Chem. **23**, 1059 (1958).
17. (*a*) E. E. van Tamelen, T. M. Cole, Jr., R. H. Greeley, and H. Schumacher. J. Am. Chem. Soc. **90**, 1372 (1968); (*b*) D. M. Allen and E. D. Owen. J. Chem. Soc. Chem. Commun. 848 (1971); (*c*) E. E. van Tamelen and T. M. Cole, Jr. J. Am. Chem. Soc. **93**, 6158 (1971).
18. R. A. Johnstone and S. D. Ward. J. Chem. Soc. C, 1805 (1968).
19. R. P. Kirchen and T. S. Sorensen. J. Am. Chem. Soc. **100**, 1487 (1978).
20. R. C. Bingham, M. J. S. Dewar, and D. H. Ho. J. Am. Chem. Soc. **97**, 1285 (1975).
21. S. Motherwell. A program for plotting molecular and crystal structures. Univ. Chem. Lab., Cambridge, England.

Can. J. Chem. Downloaded from www.nrcresearchpress.com by 210.87.254.6 on 09/06/12
For personal use only.

# Biologically active acyclonucleoside analogues. II. The synthesis of 9-[[2-hydroxy-1-(hydroxymethyl)ethoxy]methyl]guanine (BIOLF-62)

KELVIN K. OGILVIE,[1] UKKEN O. CHERIYAN, AND BRUNO K. RADATUS
*Department of Chemistry, McGill University, Montreal, P.Q., Canada H3A 2K6*
AND
KENDALL O. SMITH, KAREN S. GALLOWAY, AND WIEBKE L. KENNELL
*Department of Microbiology, The University of Texas Health Science Center at San Antonio, San Antonio, TX 78282, U.S.A.*
Received June 4, 1982

KELVIN K. OGILVIE, UKKEN O. CHERIYAN, BRUNO K. RADATUS, KENDALL O. SMITH, KAREN S. GALLOWAY, and WIEBKE L. KENNELL. Can. J. Chem. **60**, 3005 (1982).

The chemical synthesis of 9-[[2-hydroxy-1-(hydroxymethyl)ethoxy]methyl]guanine is described. This compound, known as BIOLF-62, is active against herpesviruses. This compound is a member of a novel class of nucleoside analogues which lack a rigid carbohydrate ring, but which possess all of the functional groups of naturally occurring deoxynucleosides.

KELVIN K. OGILVIE, UKKEN O. CHERIYAN, BRUNO K. RADATUS, KENDALL O. SMITH, KAREN S. GALLOWAY et WIEBKE L. KENNELL. Can. J. Chem. **60**, 3005 (1982).

L'auteur décrit la synthèse chimique du 9-[[2-hydroxy-1 (hydroxyméthyle)éthoxy]méthyl]guanine. Ce composé, connu comme le BIOLF-62, est actif contre les virus de l'herpès. Ce composé fait partie d'une nouvelle classe d'analogues nucléosides à qui il manque un anneau rigide d'hydrates de carbone, mais qui possèdent tous les groupes fonctionnels des déoxynucléosides formés naturellement.

[Traduit par le journal]

Can. J. Chem. Downloaded from www.nrcresearchpress.com by 210.87.254.42 on 09/06/12
For personal use only.

The search for biologically active molecules has focused a great deal of attention on modified nucleosides (1–3). For several years we have been developing a nucleoside analogue structure intended to interfere with viral and bacterial systems. The structure was designed to lack the rigid conformational feature (*syn–anti*) of natural nucleosides but at the same time retain the essential chemical features of natural nucleosides (e.g., purine or pyrimidine ring, $O^{3'}$, $O^{4'}$, and $O^{5'}$ oxygen functionalities). In a preliminary report (4) we described the synthesis of the adenine analogue 9[[2-hydroxy-1-(hydroxymethyl)ethoxy]methyl]adenine. This compound was neither a substrate nor an inhibitor for adenosine deaminase, a key enzyme in animal systems that inactivates in vivo most adenine derivatives that show promising biological activity in vitro. In this report we wish to describe the synthesis of another member of this series, the potent antiviral compound 9[[2-hydroxy-1-(hydroxymethyl)ethoxy]methyl]guanine (**5**) which is known as BIOLF-62.

## Results and discussion

The first route fully explored for the synthesis of BIOLF-62 involved the condensation of 6-chloroguanine[2] (**2**) with 1,3-dibenzyloxy-2-chloromethoxypropane (**1**, ref. 4). The procedure was based on the mercuric cyanide – silylated base procedure (5). Thus, 6-chloroguanine was silylated with HMDS and coupled with **1** in refluxing benzene using $Hg(CN)_2$ and ammonium sulfate as catalysts. The condensation was generally complete within 3 h. Yields were in the 80% range for both small and large scale reactions.

Tetrabutylammonium iodide has been proposed (6) as a mild catalyst in coupling reactions of this type. Thus when **1** and **2** were condensed in acetonitrile using a catalytic amount of $(n\text{Bu})_4\text{NI}$ a fairly rapid reaction occurred. The desired product **3** was isolated in 38% yield. Finally, the Hilbert–Johnson coupling method (as elaborated by Niedballa and Vorbuggen (7)) using stannic chloride gave very low yields of desired product.

The 6-chloroguanine derivative **3** was converted into the desired guanine derivative **4** by a standard procedure (5). These conditions employ sodium methoxide, mercaptoethanol, and a trace of water in methanol at reflux for 2 to 3 h. After work-up the product **4** was obtained in 70% yield.

The removal of the benzyl groups was easily accomplished by either of two routes. In the first

[1]Author to whom correspondence may be addressed. Part I is ref. 4.

[2]Proper name is 2-amino-6-chloropurine but is sold commercially as 6-chloroguanine.

0008-4042/82/243005-06$01.00/0
©1982 National Research Council of Canada/Conseil national de recherches du Canada

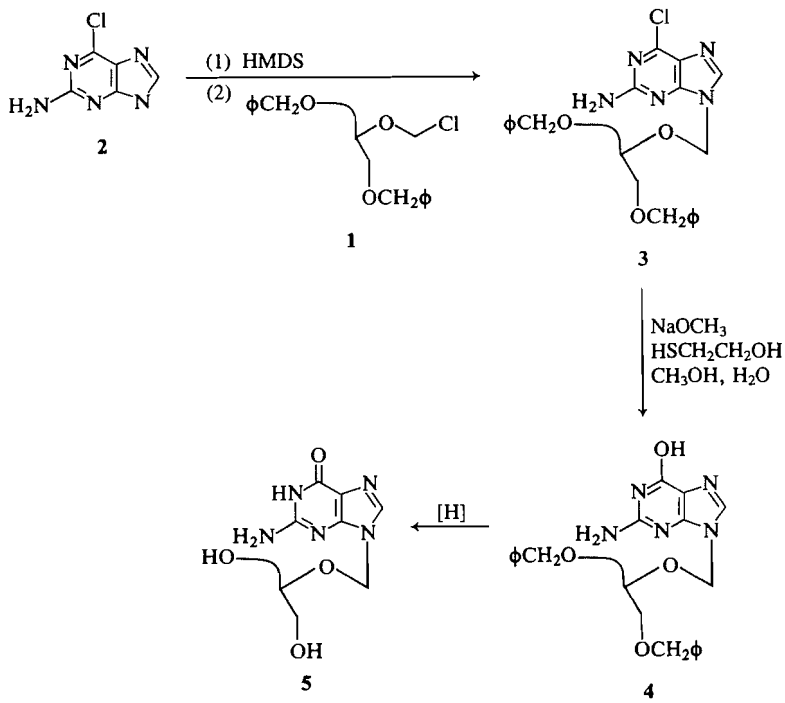


case, catalytic transfer reduction (8) using palladium black and cyclohexene in refluxing ethanol gave an 84% yield of **5** after 18 h. The alternate procedure used was a Birch reduction which produced **5** in similar yields. The Birch reduction has the advantage of being a faster procedure (~ 15 min).

The synthesis of **5** from 6-chloroguanine proved to be straightforward and easy to carry out. However, it suffers from the fact that 6-chloroguanine is very expensive and sometimes difficult to obtain. Alternate routes to **5** were sought and these included the condensation of *N*-acetylguanine with **1**. Several standard condensation procedures were investigated including the use of TBAI, molecular sieves, stannic chloride, and mercuric cyanide as condensation catalysts. The TBAI reaction gave the best results with 28% yields each for the N-9 isomer **7** and the N-7 isomer **8***a*.

In another experiment, guanine was condensed

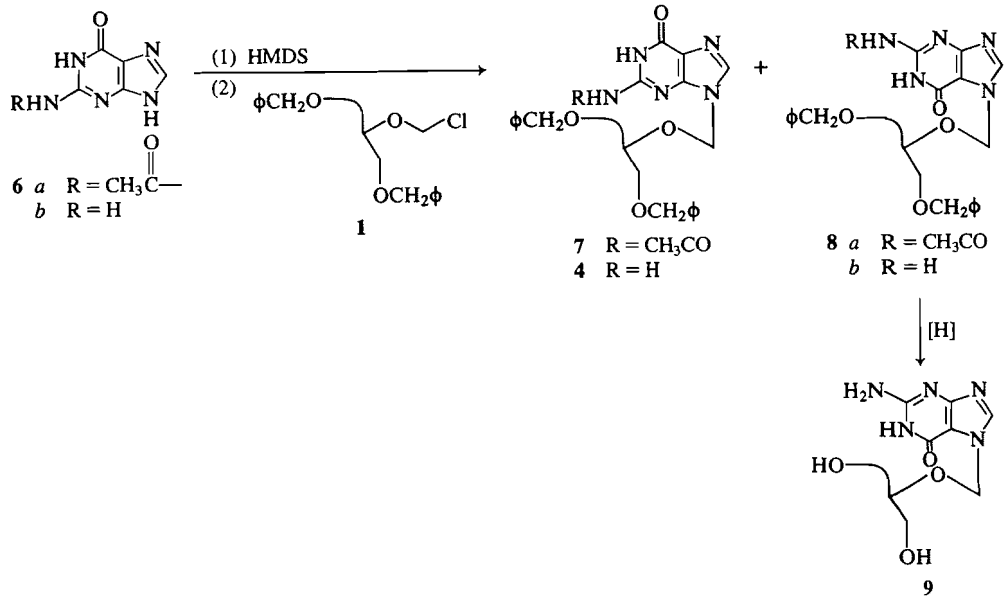


Can. J. Chem. Downloaded from www.nrcresearchpress.com by 210.87.254.42 on 09/06/12
For personal use only.

TABLE 1. Physical properties of guanine derivatives

| Compound | Melting point (°C) | $R_f$* | λ max† pH 1 | pH 7 | pH 13 |
|---|---|---|---|---|---|
| **3** | 70–75 | 0.25(a) | 246, 312 | 246, 310 | 246, 309 |
| **4** | 181–183 | 0.40(b) | 256, 275(s) | 252, 270(s) | 258, 266 |
| **5** | > 285 (dec.) | 0.42(c) | 255, 275(s) | 253, 270(s) | 258, 266 |
| **7** | 143–145 | 0.37(d) | 262 | 258, 281(s) | 263 |
| **8***a* | 133–135 | 0.55(d) | 264 | 264, 274(s) | 268 |
| **8***b* | 235–238 | 0.40(b) | 250, 273 | 248, 282 | 279 |
| **9** | > 290 (dec.) | 0.44(c) | 252, 270(s) | 243, 287 | 282 |
| 7-Methylguanine | | | 250, 271(s) | 248, 285 | 280 |
| $N^2$-methylguanine | | | 258, 275 | 256, 270 | 253, 268 |
| Guanosine | | | 256, 273(s) | 252, 270(s) | 259, 266 |

*Thin-layer chromatography, Merck analytical sheets #5735. Solvents used were: (a) EtOAc–hexane (3:1); (b) EtOAC–MeOH (3:1); (c) iPrOH–$NH_4OH$–$H_2O$ (7:1:2); (d) $CHCl_3$–MeOH (9:1).
†Samples dissolved in methanol–water (1:1) except for 5 where water was the solvent.

TABLE 2. $^{13}C$ nuclear magnetic resonance data* (δ ppm)

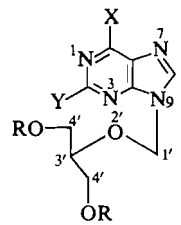


**3**, X = Cl, Y = $NH_2$, R—$CH_2\phi$
**4**, X = OH, Y = $NH_2$, R = $CH_2\phi$
**5**, X = OH, Y = $NH_2$, R = H

| Compound | C-2 | C-4 | C-5 | C-6 | C-8 | C-1′ | C-3′ | C-4′ | —$\overset{*}{C}H_2\phi$ |
|---|---|---|---|---|---|---|---|---|---|
| **3** | 154.19 | 149.55 | 123.33 | 160.01 | 143.24 | 70.19 | 77.04 | 69.65 | 72.19 |
| **4** | 153.96 | 151.43 | 116.69 | 156.93 | 138.37 | 71.69 | 76.60 | 69.75 | 72.29 |
| **5** | 153.96 | 151.43 | 116.52 | 157.04 | 137.89 | 71.64 | 80.16 | 60.96 | |

*$^{13}C$ Spectra were recorded in DMSO-$d_6$ on a Bruker WP90 spectrometer.

directly to **1** using TBAI as catalyst. The slow step in this route was the silylation of guanine which required 4 days. The condensation proceeded smoothly giving a high yield in the initial condensation. However, the product was largely a 7:3 mixture of **4** and **8***b* which had similar chromatographic properties in all solvents investigated. Fortunately it was found that a mixture containing only **4** and **8***b* could be separated by fractional crystallization from ethanol. The N-7 isomer **8***b* precipitates fairly rapidly and can be separated. The N-9 isomer **4** begins to crystallize after the N-7 isomer has been removed. In this way a 41% overall yield of **4** was obtained.

The N-9 isomers were fairly easy to characterize by direct (5) comparison of their properties to known N-9 alkylated guanines including the natural nucleoside guanosine. The assignment of the N-7 isomers is also based on the spectroscopic properties. The physical properties of all compounds are collected in Tables 1 to 4.

*Sensitivity of various viruses to BIOLF-62*

Eight different herpesviruses from six animal species were tested for their susceptibility to BIOLF-62. Four of these viruses, equine herpesviruses 1 and 3 and human herpesviruses 1 and 2, were extremely sensitive to the drug, all being inhibited by 50% (effective dose, 50%) at concentrations between 0.03 and 0.3 μg/mL. Swine and bovine herpesviruses (pseudorabies and infectious bovine rhinotracheitis virus) were slightly sensitive, being 50% inhibited at 5–6 μg/mL. Feline and canine herpesviruses were insensitive, requiring 32 or more μg/mL for inhibition. Several other viruses were tested and were found resistant (human cytomegaloviruses, herpes zoster virus, vaccinia virus, and human adenovirus (9).

Can. J. Chem. Downloaded from www.nrcresearchpress.com by 210.87.254.42 on 09/06/12
For personal use only.

TABLE 3. Proton magnetic resonance data for guanine derivatives* (δ ppm)

| Compound | H-8 | $NH_2$ | H-1′ | H-3′ | H-4′ | $—CH_2\phi$ | Aromatic |
|---|---|---|---|---|---|---|---|
| **3** | 8.24 | | 5.54 | 4.04 | 3.38 | 4.34 | 7.20 |
| **4** | 7.80 | 6.50 | 5.46 | 4.02 | 3.38 | 4.20 | 7.24 |
| **5** | 7.80 | 6.50 | 5.44 | 3.40 (m, 5H) | | | |
| **7** | 8.10 | | 5.56 | 4.00 | 3.38 | 4.40 | 7.20 |
| **8***a* | 8.36 | | 5.74 | 4.10 | 3.34 | 4.36 | 7.24 |
| **8***b* | 8.10 | 6.20 | 5.68 | 4.10 | 3.34 | 4.40 | 7.24 |
| **9** | 8.13 | 6.20 | 5.72 | 3.37 | | | |

*Spectra were recorded in DMSO-$d_6$ (TMS as internal standard) on a Varian XL-200 spectrometer. Chemical shifts are reported in ppm downfield from TMS. The $NH_2$ protons were exchangeable with $D_2O$. For compounds **5** and **7** the OH protons appeared at δ = 4.60. For compound **7** the acetyl protons appeared at δ = 2.14. The numbering system is as described in Table 2.

TABLE 4. Elemental analyses

| Compound | Formula | Calculated (%) | | | Found (%) | | |
|---|---|---|---|---|---|---|---|
| | | C | H | N | C | H | N |
| **3** | $C_{23}H_{24}N_5O_3Cl$ | 60.86 | 5.33 | 15.43 | 60.91 | 5.37 | 15.32 |
| **4** | $C_{23}H_{25}N_5O_4$ | 63.43 | 5.79 | 16.08 | 63.43 | 5.75 | 16.14 |
| **5** | $C_9H_{13}N_5O_4 \cdot H_2O$ | 39.56 | 5.53 | 25.63 | 39.41 | 5.30 | 25.69 |

## Experimental

*Preparation of 9-[[2-benzyloxy-1-(benzyloxymethyl)ethoxy]-methyl]-6-chloroguanine (**3**)*

*Method A*

6-Chloroguanine (15 g, 0.088 mol) was suspended in 1,1,1,3,-3,3-hexamethyldisilizane(HMDS, 200 mL). Ammonium sulfate (1.5 g) was added and the mixture was heated at reflux with exclusion of moisture for 2 h. The, by now clear, solution was concentrated at reduced pressure to leave a pale yellow solid. Mercuric cyanide (24 g, 0.095 mol) and benzene (250 mL) were added and the system was heated to reflux. To the refluxing solution was added compound **1** (29.93 g, 0.093 mol) dissolved in benzene (250 mL). The system was heated at reflux under a nitrogen atmosphere for a period of 3 h. The benzene was removed at reduced pressure and the residue was stirred with 1.5 L of dichloromethane. The solution was collected by filtration and washed twice with a 30% aqueous solution of potassium iodide (300 mL), twice with 10% aqueous potassium carbonate solution (300 mL), twice with water (300 mL), and finally with saturated sodium chloride solution (300 mL). The solution was then dried over sodium sulfate and evaporated at reduced pressure to leave 55 g of crude product.

The crude product was dissolved in a minimum volume of dichloromethane and applied to a silica gel column (8.5 × 30 cm) prepared in EtOAc–hexane (2:3). The column was eluted first with 2L of EtOAc–hexane (2:3) followed by 3 L of EtOAc–hexane (75:25). The desired product was eluted by the more polar solvent. A total of 32 g (80%) of compound **3** was obtained in this manner. Physical properties are collected in Tables 1–4.

*Conversion of **3** into 9-[[2-benzyloxy-1-(benzyloxymethyl)-ethoxy]methyl]guanine (**4**)*

Compound **3** (24 g, 0.05 mol) was dissolved in dry methanol (500 mL) and an additional 200 mL of methanol containing 4.6 g of sodium were added, followed by mercaptoethanol (16 mL) and water (1 mL). The resulting solution was refluxed under nitrogen for 1.5 h. At this point an additional 3 g of sodium in 50 mL of methanol was added and refluxing was continued for 1 h. The solution was concentrated at reduced pressure to approximately 70 mL and poured into water (400 mL). The pH of the solution was adjusted to pH 6 with glacial acetic acid. A yellow precipitate, which was collected by filtration and washed thoroughly with water and then ether, formed immediately. The solid was dried under vacuum (22 g). The nmr spectrum of the crude product indicated the presence of a major and minor (~ 20%) component. The solid was therefore stirred with warm ethyl acetate, collected by filtration, and crystallized from absolute ethanol to give 16 g (70%) of pure compound **4**. Physical properties are collected in Tables 1 to 4.

*Method B*

6-Chloroguanine (1.8 g, 10.6 mmol) was heated at reflux in HMDS (40 mL) containing ammonium sulfate (200 mg) until it became clear (2 h). The solvents were removed at reduced pressure and the residue was dissolved in dry acetonitrile (60 mL). To this solution was added tetra-*n*-butyl ammonium iodide (TBAI, 40 mg) followed by compound **1** (11 mmol) dissolved in acetonitrile (40 mL). The resulting solution was heated at reflux under a nitrogen atmosphere for 2 h. The solvents were then removed at reduced pressure and the residue was dissolved in methanol (100 mL) and the solution was stirred for 2 h. Again solvents were removed and the residue was dissolved in dichloromethane (300 mL) and the solution was filtered through Celite. After removal of solvents, 5.5 g of a viscous liquid was obtained. Pure **3** was isolated from the above liquid by flash chromatography on silica gel (Merck silica gel 60, 5 × 15 cm). The residue was dissolved in the minimum amount of dichloromethane and applied to the column which was eluted with hexane – ethyl acetate (1:3, 1 liter). Fractions of 50 mL were collected and fractions #13–19 contained the desired compound **3** (1.83 g, 38%).

*Condensation of* N*-acetylguanine (**6**a) and **1***

*Method A*

*N*-Acetylguanine (1.08 g, 5.65 mmol) was heated at reflux for 16 h in HMDS (50 mL) containing ammonium sulfate (50 mg). Solvents were removed at reduced pressure and the residue was dissolved in acetonitrile (75 mL) along with compound **1** (6 mmol) and TBAI (50 mg) and the solution was heated at reflux overnight. A mixture of methanol (40 mL) and water (10 mL)

Can. J. Chem. Downloaded from www.nrcresearchpress.com by 210.87.254.42 on 09/06/12
For personal use only.

Can. J. Chem. Downloaded from www.nrcresearchpress.com by 210.87.254.42 on 09/06/12
For personal use only.

was added and the solution was stirred for 1 h. Solvents were removed at reduced pressure and the products were isolated by silica gel column chromatography (20 × 5.5 cm) using methanol – ethyl acetate (7:93) as eluant. Fractions of 20 mL were collected every 20 min. Fractions 10 to 30 were combined and gave 1 g of a mixture of compounds that were further separated on silica thick-layer plates developed in 5% methanol in dichloromethane. Three bands were obtained containing 490 mg, 204 mg, and 250 mg, respectively. The latter material was the 7-alkylated isomer (**8***a*) and the others were unidentified. Fractions 30 to 50 were combined to give 500 mg of the 7-alkylated derivative (**8***a*) for a total yield of 750 mg (28%, Tables 1 and 3). The $^{13}C$ spectra showed important peaks at δ 173.23 (C=O), 23.53 ($CH_3$), 74.78 (C-1'), 76.45 (C-3'), 69.60 (C-4'), and 72.08 (—$\overset{*}{C}H_2\phi$)). Fractions 52 to 85 were combined to give 750 mg of the desired N-9 product **7** (28%, Tables 1 and 3). The $^{13}C$ spectra showed important peaks at δ 173.34 (C=O), 23.69 ($CH_3$), 72.19 (C-1'), 76.83 (C-3'), 69.65 (C-4'), and 72.19 (—$\overset{*}{C}H_2\phi$).

*Method B*

This procedure was similar to method A, except that the condensation between **1** and **6***a* was carried out in dichloroethane (75 mL) at reflux for 4 h over molecular sieves (4 Å). On work-up the product distribution was found to be virtually the same as that for method A.

*Method C*

This procedure was similar to method B, except that freshly distilled stannic chloride (1 mL) was used as catalyst and the reaction (in dichloroethane) was allowed to stand overnight at room temperature. The solution was poured into aqueous sodium bicarbonate solution and the products were extracted into chloroform. On work-up the product distribution was found to be 0.15 g (3%) of the 7-isomer (**8***a*), and 0.43 g (9%) of the 9-isomer (**7**).

*Method D*

This procedure was similar to method C, except that the solvent was benzene (90 mL) and the catalyst was mercuric cyanide. After refluxing for 1½ h the products were isolated as before to give 1.03 g of the 7-isomer (**8***a*, 22%), and 0.68 g (14%) of the 9-isomer (**7**).

*Conversion of* **7** *into* **4**

Compound **7** (1.3 g, 2.7 mmol) was dissolved in pyridine (1.5 mL) and concentrated ammonium hydroxide (6 mL) was added. The solution was heated at 55°C in a tightly stoppered flask for 15 h. The product **4** crystallized from solution as it was produced and 1.18 g (99%) was collected in this manner.

*Conversion of* **8**a *into* **8**b

This procedure was identical to that described above for **7** and the product **8***b* was obtained in 95% yield.

*Conversion of* **4** *into 9[[2-hydroxy-1-(hydroxymethyl)ethoxy]-methyl]guanine* **5**

*Method A. Catalytic transfer hydrogenation*

Compound **4** (15.6 g, 36 mmol) was dissolved in refluxing ethanol (800 mL). Cyclohexene (400 mL) and palladium black (15 g) were added and refluxing was continued for 18 h. The solution was collected by filtration and the palladium catalyst was extracted five times with hot DMF (200 mL, 100°C). The filtrate and washings were combined and evaporated to leave a residue which was dissolved in hot ethanol–water (200 mL each) and filtered through Celite containing 0.5 g of activated charcoal. The solvent was removed at reduced pressure and the residue crystallized from ethanol–water (4:1). A total of 7.72 g (84%) of **5** was recovered.

*Method B. Birch reduction*

A two-liter three-necked flask fitted with a Dry Ice condenser was cooled in an acetone – Dry Ice bath under a stream of nitrogen. About one liter of liquid ammonia was collected in the flask by condensing dry ammonia gas. A slurry of the compound **4** (20 g, 45.7 mmol) in dry THF (100 mL) was added with stirring. The temperature of the bath was then allowed to rise to −45° to −40°C. Sodium was then added in small quantities until a permanent blue colour was obtained. The stirring was continued for 15 min. The blue colour was then discharged by the addition of ammonium chloride in small quantities. (Note: All the above operations were carried out under nitrogen.) The ammonia and THF were then evaporated off under a stream of nitrogen. The white residue obtained was agitated with benzene (300 mL) and filtered. The solid left behind was dissolved in water (500 mL) and extracted with benzene (3 × 200 mL). The aqueous layer was acidified with acetic acid (pH 5–6) and left overnight. The white precipitate obtained was collected by filtration. It was dissolved in boiling water (700 mL). Norite (neutral) was then added and filtered. The filtrate on standing gave 7.6 g of white crystals. The mother liquors on concentration yielded another crop of crystals (1.4 g) for a total yield of **5**, 9.0 g (77%).

*Conversion of* **8**b *into* **9**

Compound **8***b* was converted by catalytic transfer hydrogenation into **9** by a procedure identical to that described under method A for the conversion of **4** into **5**. Compound **9** was crystallized from ethanol and obtained in an 89% yield.

*Condensation of guanine* **6**b *with* **1** *to give* **4**

Guanine (3.1 g, 20.5 mmol) and ammonium sulfate (250 mg) were weighed into a 500 mL round-bottom flask. 1,1,1,3,3,3-Hexamethyldisilazane (150 mL) was added and the mixture was heated under reflux with the exclusion of moisture. After 2 days an additional 150 mg of ammonium sulfate was added and reflux was continued. After two days (total 4 days) the solution was clear.

The solvent was removed at reduced pressure and the residue was dissolved in 120 mL of freshly distilled acetonitrile. Tetra-*n*-butylammonium iodide (80 mg) was added, followed by 21.2 mmol of the chloromethylether (compound **1**) in acetonitrile (50 mL). The resulting solution was heated at reflux under nitrogen for 15 h. A thin-layer chromatogram in ethyl acetate – methanol (4:1, v/v) showed a major band at $R_f$ 0.30 and a minor band at the origin. The band at 0.30 contains the desired product and the N-7 isomer in a ratio of 7:3 (nmr determination).

The solvents were removed at reduced pressure and the residue was dissolved in 800 mL of dichloromethane. This solution was washed successively with potassium carbonate solution (10% in water, 200 mL) and water (200 mL). The dichloromethane solution was then evaporated to a small volume. Methanol (50 mL) was added and the solvents were removed at reduced pressure. The residue (10 g) was dissolved in dichloromethane (200 mL) and applied directly to a silica gel column (8.5 × 17 cm, 500 g). Elution was carried out using ethyl acetate – methanol (4:1, v/v). Fractions of 20 mL were collected every 15 min. The desired product was contained in fractions 21 to 130. The material contained in these fractions was washed with hot ethyl acetate and then crystallized from ethanol. The N-7 isomer (**8***b*) selectively crystallizes first, followed by a slower crystallization of **4**. In this way 3.64 g of **4** (41%) was obtained. The yield of the N-7 isomer was 1 g (11%).

## Acknowledgement

We gratefully acknowledge financial support from Bio Logicals Inc.

1. B. Goz. Pharmacol. Rev. **29**, 249 (1978).
2. M. Privat de Garilhe and J. de Rudder. C.R. Acad. Sci. **259**, 2725 (1964).
3. H. J. Schaeffer, L. Beauchamp, P. de Miranda, G. B. Elion, D. J. Bauer, and P. Collins. Nature, **272**, 583 (1978).
4. K. K. Ogilvie and M. F. Gillen. Tetrahedron Lett. **21**, 327 (1980).
5. W. W. Lee, A. P. Martinez, L. Goodman, and D. Henry. J. Org. Chem. **37**, 2923 (1972).
6. A. Matsuda, Y. Kurasawa, and K. A. Watanabe. Synthesis, 748 (1981); Z. Tocik, R. A. Earl, and J. Beranek. Nucleic Acids Res. **8**, 4755 (1980).
7. B. U. Niedballa and H. Vorburggen. Angew. Chem. Int. Ed. Engl. **9**, 461 (1970).
8. E. A. Braude, R. P. Linstead, P. W. Mitchell, and K. R. H. Woolridge. J. Chem. Soc. 3595 (1954); V. S. Rao and A. S. Perlin. Carbohydr. Res. **83**, 175 (1980); S. Hanessian, T. J. Liak, and B. Vanasse. Synthesis, 396 (1981).
9. K. O. Smith, K. S. Galloway, W. L. Kennell, K. K. Ogilvie, and B. K. Radatus. Antimicrob. Agents Chemother. **22**, 55 (1982).

Can. J. Chem. Downloaded from www.nrcresearchpress.com by 210.87.254.42 on 09/06/12
For personal use only.

# Thermochemical parameters for organic radicals and radical ions. Part 2.[1] The protonation of hydrocarbon radicals in the gas phase

A. MARTIN DE P. NICHOLAS, RUSSELL J. BOYD, AND DONALD R. ARNOLD[2]

*Department of Chemistry, Dalhousie University, Halifax, N.S., Canada B3H 4J3*

Received June 3, 1982

A. MARTIN DE P. NICHOLAS, RUSSELL J. BOYD, and DONALD R. ARNOLD. Can. J. Chem. **60**, 3011 (1982).

A thermochemical cycle is used to estimate the gas phase acidity of several hydrocarbon radical cations: hydrocarbon radical cation ($pK_a$), methane ($\geq 86.5 \pm 1$), ethane ($101 \pm 1$, $102 \pm 1$), ethylene ($\geq 125 \pm 2$), acetylene ($118 \pm 3$, $122 \pm 1$), propene ($124 \pm 1$, $122 \pm 1$), cyclopropane ($\geq 134$, $\geq 131$), benzene ($147 \pm 1$), and toluene ($139 \pm 1$, 140). Similarly, proton affinities of the conjugate base, the hydrocarbon radical, are estimated.

An estimate of the proton affinity is obtained using *ab initio* MO calculations. A Hartree–Fock proton affinity, $PA_{HF(R^{\bullet})g}$ is defined as the difference in the computed energies of a radical cation and its conjugate base at the Hartree–Fock level. Calculations at the SCF level are carried out using both the minimal (STO-3G) and extended basis sets, without (3-21G, 4-31G, and 6-31G) and with (4-31G* and 6-31G*) polarization functions on carbon.

The agreement between the thermochemical and *ab initio* estimates of the proton affinity is satisfactory.

A. MARTIN DE P. NICHOLAS, RUSSELL J. BOYD et DONALD R. ARNOLD. Can. J. Chem. **60**, 3011 (1982).

On a utilisé un cycle thermochimique pour évaluer l'acidité en phase gazeuse de plusieurs cations radicalaires hydrocarbonés; cation radicalaire hydrocarboné ($\geq 86{,}5 \pm 1$), éthane ($101 \pm 1$, $102 \pm 1$), éthylène ($\geq 125 \pm 2$), acétylène ($118 \pm 3$, $122 \pm 1$), propène ($124 \pm 1$, $122 \pm 1$), cyclopropane ($\geq 134$, $\geq 131$), benzène ($147 \pm 1$) et toluène ($139 \pm 1$, 140). On a évalué de la même façon les affinités des différentes bases conjuguées pour le proton, ainsi que le radical hydrocarboné.

On a obtenu une évaluation de l'affinité pour le proton en utilisant les calculs de MO "*ab initio*". On définit une affinité pour le proton de type Hartree–Fock, $PA_{HF(R^{\bullet})g}$ comme étant la différence des énergies calculées du cation radicalaire et de sa base conjuguée au niveau Hartree–Fock. On a fait des calculs au niveau SCF en utilisant les deux ensembles de base (STO-3G) sous la forme la plus simple et la plus complete sans les ensembles (3-21G, 4-31G et 6-31G) et avec les fonctions de polarisation sur le carbone (4-31G* et 6-31G*). L'accord est satisfaisant entre les évaluations de l'affinité du proton faites thermochimiquement et celles faites d'après le calcul *ab initio*.

[Traduit par le journal]

## Introduction

Radical cations are formed by the protonation of radicals in the gas phase (reaction [1]). This is

[1] $\quad R^{\bullet}_{(g)} + H^{+}_{(g)} \rightarrow RH^{+\bullet}_{(g)}$

usually a facile process and in the absence of solvent all protonation reactions are highly exergonic. This results from the relative instability of the unsolvated proton, which attaches to any radical with which it collides. The basicity of hydrocarbon radicals in solution is a subject of considerable interest. These radicals show little or no tendency to protonate even in strongly acidic solutions and, therefore, direct determination of radical basicity is difficult (1, 2).

The energy change involved in the gas phase protonation reaction (reaction [1]) provides a direct measure of the intrinsic basicity of a radical. Recently experimental determinations of the proton affinity of hydrocarbon radicals have been reported (3, 4). The occurrence of a proton transfer reaction, reaction [2], has been used to bracket the proton affinity of a radical relative to standard bases. The limitation on the accuracy of this technique does not permit direct measurements of absolute proton affinities.

[2] $\quad RH^{+\bullet}_{(g)} + B_{(g)} \rightarrow R^{\bullet}_{(g)} + BH^{+}_{(g)}$

Thermochemical cycles recently have been used to establish an absolute scale of proton affinities for radicals (3), and to estimate the $pK_a$'s of radical cations in the gas phase and in solution (5). The relationship between the acidities of radical cations in the gas phase and in solution involves the solvation of $RH^{+\bullet}$, $R^{\bullet}$, and $H^{+}$. In our previous paper we have shown that the determination of the gas phase acidity of a radical cation provides a method of estimating its $pK_a$ in solution (5). The deprotonation of radical cations, an important reactive pathway in the oxidation of hydrocarbons (6, 7), has been shown to occur even in strongly acidic solutions (2, 8). Thus, establishing an absolute scale of gas phase acidities for radical cations will be useful in understanding the behaviour of these reactive species in solution.

The prediction of equilibrium geometries and relative energies of small neutral molecules, radicals, and radical ions is one of the promising areas for the application of molecular orbital (MO) theory (9). *Ab initio*, single determinant, self-consistent

[1]Part 1, ref. 5.

[2]To whom all correspondence should be addressed.

0008-4042/82/243011-08$01.00/0

©1982 National Research Council of Canada/Conseil national de recherches du Canada

Can. J. Chem. Downloaded from www.nrcresearchpress.com by 210.87.254.40 on 09/06/12
For personal use only.

Can. J. Chem. Downloaded from www.nrcresearchpress.com by 210.87.254.40 on 09/06/12
For personal use only.

field (SCF) theory can be used to estimate the energy change of eq. [1], $\Delta E_1$, at 0 K. $R^{\bullet}$ and $RH^{+\bullet}$ have the same number of electrons and multiplicity, which minimizes the difference in their correlation energies. If this difference is neglected $\Delta E_1$ can be obtained directly using Hartree–Fock (SCF) wave functions (*vide infra*).

In the present work, the $pK_a$ of hydrocarbon radical cations ($RH^{+\bullet}$) and the proton affinity of the corresponding radicals ($R^{\bullet}$) are estimated using a thermochemical cycle described previously (5). The thermochemical proton affinities are then compared with the Hartree–Fock proton affinities obtained from *ab initio* MO calculations using three types of basis functions.

This study was undertaken as part of our continuing interest in the properties of radicals and radical ions (5). The purpose of this work was to study the thermodynamics of the protonation of hydrocarbon radicals and to ascertain the feasibility of using *ab initio*, single determinant, MO calculations to determine the proton affinities of these radicals. Radicals can be classified according to the type of orbital the unpaired electron occupies and in this paper the protonation of representative p, σ and π (aliphatic), and σ and π (aromatic) radicals is described.

## Method

*Thermochemical calculations*

The gas phase acidity of a radical cation ($RH^{+\bullet}$) can be expressed in terms of the free energy change, $\Delta G_3$, for its deprotonation in the gas phase, eq. [4].

[3] $$RH^{+\bullet}{}_{(g)} \rightarrow R^{\bullet}{}_{(g)} + H^{+}{}_{(g)}$$

[4] $$pK_{a(RH^{+\bullet})g} = \Delta G_3/2.303RT$$

We have shown that the quantity $\Delta G_3$ can be calculated for many radical cations using existing thermochemical data (eq. [5]).

[5] $$\Delta G_3 = -F(\mathrm{IP(adiabatic)}_{RH}) + \Delta G^0{}_{BDE(RH)g} + \Delta G^0{}_{f(H^+)g} - \Delta G^0{}_{f(H)g}$$

where $\mathrm{IP(adiabatic)}_{RH}$ is the adiabatic ionization potential in electron volts. The changes in entropy and heat capacity on ionization of RH to the radical cation $RH^{+\bullet}$ have been shown to be small and are neglected in this work (10); $F$ is the Faraday constant and $\Delta G^0{}_{BDE(RH)g}$ is the standard free energy change associated with the homolytic cleavage of the R—H bond in the gas phase.

The proton affinity of a radical $R^{\bullet}$ in the gas phase ($PA_{(R^{\bullet})g}$) is equal to the enthalpy change for eq. [3], $\Delta H_3$, and is given by eq. [6].

[6] $$PA_{(R^{\bullet})g} = \Delta H_3 = -F(\mathrm{IP(adiabatic)}_{RH}) + \Delta H^0{}_{BDE(RH)g} + \Delta H^0{}_{f(H^+)g} - \Delta H^0{}_{f(H)g}$$

$\Delta H^0{}_{BDE(RH)g}$ is the standard enthalpy change associated with the homolytic cleavage of the R—H bond in the gas phase. $\Delta H^0{}_{f(H^+)g} - \Delta H^0{}_{f(H)g}$ is usually assumed to be equal to the ionization potential of H. This simplifies eq. [6] to eq. [7].

[7] $$PA_{(R^{\bullet})g} = -F(\mathrm{IP(adiabatic)}_{RH} - \mathrm{IP}_H) + \Delta H^0{}_{BDE(RH)g}$$

Ab initio *MO calculations*

The energy difference between $R^{\bullet}{}_{(g)}$ and $RH^{+\bullet}{}_{(g)}$, ($\Delta E_3$), at 0 K has been related to the gas phase proton affinity of $R^{\bullet}$, $PA_{(R^{\bullet})g}$, by eq. [8] (11).

[8] $$PA_{(R^{\bullet})g} = \Delta E_3 - \Delta\mathrm{ZPE} + (5/2)RT$$

The term ΔZPE is the difference in the zero point energies of $R^{\bullet}{}_{(g)}$ and $RH^{+\bullet}{}_{(g)}$, and $(5/2)RT$ is a thermodynamic temperature correction term. The term $\Delta E_3$ includes both the dominant Hartree–Fock energy difference and any correlation energy corrections. We define the Hartree–Fock energy contribution to the proton affinity of a radical as the Hartree–Fock proton affinity and denote it by $PA_{HF(R^{\bullet})}$.

[9] $$PA_{HF(R^{\bullet})} = E_{HF(R^{\bullet})} - E_{HF(RH^{+\bullet})} + (5/2)RT$$

where $PA_{HF(R^{\bullet})g}$ can be expressed under standard conditions at any temperature, $T$, eq. [9]. Due to the large computational (CPU) time required in using near Hartree–Fock basis sets, basis sets of limited size have been used in this work. However, a fair estimate of the energy difference between two species, at the Hartree–Fock level, can be obtained using basis sets of limited size. Thus, eq. [10] has been assumed, where the Hartree–Fock energy ($E_{HF}$) in eq. [9] is replaced by $E_{SCF}$, the energy

[10] $$PA_{HF(R^{\bullet})} = E_{SCF(R^{\bullet})} - E_{SCF(RH^{+\bullet})} + (5/2)RT$$

computed using an *ab initio*, single determinant, self-consistent field procedure.

Standard single determinant MO theory was used. The *ab initio* MO calculations described were obtained by the use of the GAUSSIAN 76 program (12). The open-shell, spin-unrestricted (UHF) procedure was employed (13) to compute the energies of all the radicals and radical cations. The six basis sets used have been previously described in the literature (14–18). The minimal STO-3G (14), and extended basis sets of two types (15–18) were used. These were the split-valence

Can. J. Chem. Downloaded from www.nrcresearchpress.com by 210.87.254.40 on 09/06/12
For personal use only.

basis sets, without (3-21G (15), 4-31G (16), and 6-31G (17)) and with (4-31G* and 6-31G* (18)) polarization functions on carbon. The variation of $PA_{HF(R^{\cdot})}$ (eq. [10]), with basis sets, was studied while constraining the radical cations and their conjugate bases to their STO-3G optimized geometries. The 3-21G $PA_{HF(R^{\cdot})}$ values for the methyl, ethyl, vinyl, and ethynyl radicals were also computed using 3-21G optimized geometries.

*Geometries*

Geometry optimizations, subject only to the imposed symmetry constraints, were carried out at the STO-3G level. Complete optimizations at the STO-3G level were performed for the radical cations of propene ($C_s$ symmetry) and benzene ($D_{6h}$ symmetry). Complete optimizations were carried out at the 3-21G level, for the radical cations of ethane, acetylene, and ethylene. The STO-3G geometry of the cyclopropane radical cation was computed in our laboratory as part of another program.[3] All other optimized geometries at the STO-3G and 3-21G levels used in this work were obtained from the work of Pople and co-workers (9, 19). Due to the large CPU time requirements only partial optimization of the phenyl and benzyl radicals, and the toluene radical cation, were performed.

*Propene radical cation*

Rotation around the C—C single bond indicated that the lowest energy with $C_s$ symmetry was obtained when the molecule was oriented as shown in Fig. 1.

*Benzene radical cation*

$C_6H_6^{+\cdot}$ is obtained by the removal of a π electron from a $(1a_{2u})^2(1e_{1g})^4$ electronic configuration. The Jahn–Teller theorem states that in such a situation the molecule distorts from a $D_{6h}$ symmetry such that the degeneracy of the $e_{1g}$ orbitals is removed. However, a $D_{6h}$ symmetry was assumed in this work. Optimization at the STO-3G level lead to the following structure $D_{6h}$, $r_{CC}$ = 1.417 Å and $r_{CH}$ = 1.089 Å.

*Phenyl radical*

A $C_{2v}$ symmetry was assumed, together with the further constraint that the carbon skeleton $C_2$—$C_3$—$C_4$ and the hydrogens $H_2$, $H_3$, and $H_4$ were fixed in the same positions as in the optimized STO-3G structure of benzene (19). Optimization of the remaining parameters, assuming $r(C_1H_1)$ = 1.083 Å, $r(C_5H_5)$ = 1.083 Å, and $\angle H_1C_1C_2$ = 120°, and $\angle H_5C_5C_4$ = 120°, lead to the structure given in Fig. 2*a*.

*Benzyl radical*

The geometrical parameters of the $CH_2^{\cdot}$ group attached to a standard phenyl ring[4] were optimized (Fig. 2*b*).

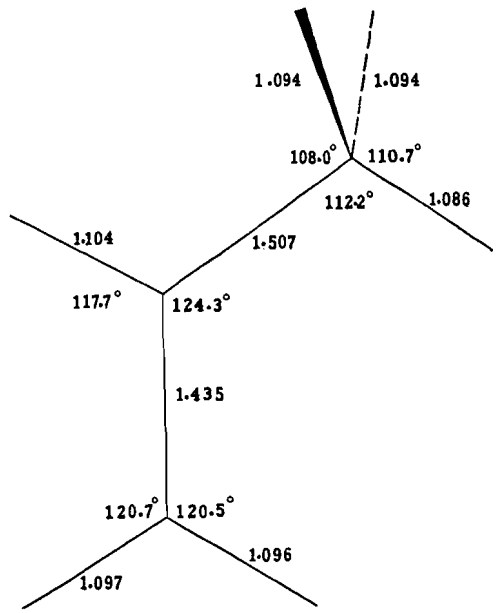


FIG. 1. Completely optimized STO-3G structure of the propene radical cation ($C_s$).

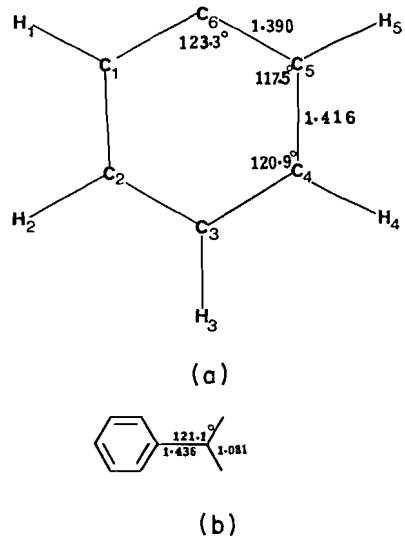


FIG. 2. Partially optimized STO-3G structures of (*a*), the phenyl radical ($C_{2v}$), (*b*), the benzyl radical ($C_{2v}$).

[3]D. D. M. Wayner. Unpublished results.

[4]$r_{CC}$ = 1.38669 Å and $r_{CH}$ = 1.08258 Å (STO-3G values for benzene ref. 19).

Can. J. Chem. Downloaded from www.nrcresearchpress.com by 210.87.254.40 on 09/06/12
For personal use only.

TABLE 1. The adiabatic ionization potential (IP) and gas phase bond dissociation data of RH at 300 K

| RH | IP/kcal mol$^{-1}$ [a] | $\Delta H^0_{BDE}$/kcal mol$^{-1}$ | $\Delta S^0_{BDE}$/cal mol$^{-1}$ K$^{-1}$ [b] | $\Delta G^0_{BDE}$/kcal mol$^{-1}$ |
|---|---|---|---|---|
| Methane | ≤290.9±0.2 | 104.4±0.7[c] | 29.3±1.0 | 95.6±0.8 |
| Ethane | 265.4±0.2 | 98.8±1.5[b] | 30.5±1.0 | 89.7±1.5 |
| | | 100.3±1.0[d] | | 91.2±1.0 |
| Ethylene | 242.4±0.7 | ≥109±2[b,e] | 31.3±1.0 | ≥99.6±2 |
| Acetylene | 263.1±0.2 | 120±3[b] | 29.0±1.0 | 111±3 |
| | | 125±1[e] | | 116±1 |
| Propene | 224.6±0.2 | 87.8±1.5[b] | 25.7±1.0 | 80.1±1.5 |
| | | 86.3±1.5[f] | | 78.6±1.5 |
| | | 86.6±1.5[g] | | 78.9±1.5 |
| Cyclopropane (i) | ≤226[h] | 105±3[b] | 31.0±1.0 | 96±3 |
| | | 101±1[e] | | 91.7±1 |
| Cyclopropane (ii)[i] | ≤226[h] | 80.0±1.5[b,j] | 32.7±1.0[j] | 70.2±1.5[j] |
| Benzene | 213.2±0.05 | 111±1.5[b] | 32.5±1.0 | 101±1.5 |
| Toluene | 203.4±0.2 | 87.9±1.5[g] | 26.1±1.0 | 80.1±1.5 |
| | | 88.9[h,j] | | 81.1[h] |

[a]Reference 21.
[b]Reference 22c.
[c]Reference 22a.
[d]Reference 22b.
[e]Reference 23.
[f]Reference 24.
[g]Reference 25.
[h]Error limits not defined.
[i]Energetics involving the formation of the allyl radical have been considered. $\Delta H^0_{BDE} = \Delta H^0_{f(allyl)g} + \Delta H^0_{f(H)g} - \Delta H^0_{f(c\text{-}C_3H_6)g}$. $\Delta S^0_{BDE} = S^0_{(allyl)g} + S^0_{(H)g} - S^0_{(c\text{-}C_3H_6)g}$.
[j]Reference 3.

TABLE 2. The gas phase acidity of radical cations ($RH^{+\cdot}$) and the proton affinity of their conjugate bases ($R^{\cdot}$) at 300 K

| RH | $\Delta G_3$/kcal mol$^{-1}$ [a] (eq. [5]) | p$K_a(RH^{+\cdot})g$ [b] (eq. [4]) | $PA_{(R^{\cdot})g}$ [c]/kcal mol$^{-1}$ (eq. [6]) |
|---|---|---|---|
| Methane | ≥118.7±0.8 | ≥86.5±0.6 | ≥127±1 |
| Ethane | 138±1.5 | 101±1 | 147±1.5 |
| | 140±1 | 102±1 | 149±1 |
| Ethylene | ≥171±2 | ≥125±2 | ≥180±2 |
| Acetylene | 162±3 | 118±3 | 171±3 |
| | 167±1 | 122±1 | 176±1 |
| Propene | 170±1.5 | 124±1 | 177±1.5 |
| | 168±1.5 | 122±1 | 175±1.5 |
| | 168±1.5 | 122±1 | 176±1.5 |
| Cyclopropane (i) | ≥184[d] | ≥134[d] | ≥193[d] |
| | ≥180[d] | ≥131[d] | ≥188[d] |
| Cyclopropane (ii)[e] | ≥158[d] | ≥115[d] | ≥168[d] |
| Benzene | 202±1.5 | 147±1 | 211±1.5 |
| Toluene | 191±1.5 | 139±1 | 198±1.5 |
| | 192[d] | 140[d] | 199[d] |

[a]Calculated using $\Delta G^0_{f(RH^{+\cdot})g} - \Delta G^0_{f(H)g} = 314.0$ kcal mol$^{-1}$ (21).
[b]p$K_a(RH^{+\cdot})g = 0.7286$, $\Delta G_3$/kcal mol$^{-1}$ at 300 K.
[c]Calculated using $\Delta H^0_{f(RH^{+\cdot})g} - \Delta H^0_{f(H)g} = 313.6$ kcal mol$^{-1}$ (21).
[d]Error limits not defined.
[e]Data calculated for the ($c$-$C_3H_6^{+\cdot}$/allyl radical) acid–base system. However, note that for the deprotonation of $c$-$C_3H_6^{+\cdot}$ the kinetically controlled product is the cyclopropyl radical (ref. 4).

*Toluene radical cation*

A hydrogen of the STO-3G optimized structure of $C_6H_6^{+\cdot}$ ($D_{6h}$) was replaced by a model $CH_3$ group ($r_{CH}$ = 1.09 Å and ∠HCH = 109.5°) at an optimized C—C bond distance ($C_s$ symmetry, $r_{CC}$ = 1.525 Å).

## Applications

Tables 1 and 2 show that the p$K_a$ of a radical cation ($RH^{+\cdot}$) is not directly correlated to either the ionization potential or the bond dissociation free energy of RH. Similarly, the variation of $PA_{(R^{\cdot})g}$ for the series of radicals studied in this work must be discussed in terms of both $IP_{RH}$ and $\Delta H_{BDE}$ of RH. From Table 2, it is seen that the radical cation of methane is the strongest acid (p$K_a$ = 86.5) and the benzene radical cation the weakest acid (p$K_a$ = 147) of the radical cations studied.

Compared to benzene, saturated hydrocarbons have higher IP values and lower $\Delta H_{BDE}$ and $\Delta G_{BDE}$ values which make their radical cations stronger acids than the benzene radical cation. Molecules

TABLE 3. The computed UHF total energies ($E$) of open-shell species at the STO-3G geometry

| Species (symmetry) | $-E$/au STO-3G | $-(E - E_{STO\text{-}3G})$/au 3-21G[a] | 4-31G | 6-31G[a] | 4-31G*[a] | 6-31G*[a] |
|---|---|---|---|---|---|---|
| $CH_3^{\bullet}(C_{3v})$ | 39.07701[b] | 0.26473 | 0.42692[b] | 0.46861 | 0.44176 | 0.48138 |
| $CH_4^{+\bullet}(D_{2d})$ | 39.29386[b] | 0.23402 | 0.39971[b] | 0.44069 | 0.41651 | 0.45516 |
| $C_2H_5^{\bullet}(C_s)$ | 77.66300[b] | 0.50009 | 0.82229[b] | 0.90486 | 0.85577 | 0.93368 |
| $C_2H_6^{+\bullet}(D_{3d})$ | 77.94048[b] | 0.47139 | 0.79308[b] | 0.87428 | 0.82907 | 0.90647 |
| $C_2H_3^{\bullet}(C_s)$ planar | 76.43573[b] | 0.52595 | 0.84644[b] | 0.92941 | 0.87493 | 0.95350 |
| $C_2H_4^{+\bullet}(D_{2h})$ | 76.79755[b] | 0.47123 | 0.79834[b] | 0.88102 | 0.83460 | 0.91213 |
| $C_2H^{\bullet}(C_{\infty v})$ | 75.19609[b] | 0.53581 | 0.85099[b] | 0.93238 | 0.87605 | 0.95386 |
| $C_2H_2^{+\bullet}(D_{\infty h})$ | 75.53549[b] | 0.48995 | 0.81230[b] | 0.89336 | 0.84853 | 0.92546 |
| Allyl ($C_{2v}$) | 115.05429[c] | 0.76802 | 1.25051[a] | 1.37467 | 1.29623 | 1.41327 |
| $C_3H_6^{+\bullet}(C_s)$ | 115.40747[a] | 0.70691 | 1.19357[a] | 1.31722 | 1.24757 | 1.36345 |
| Cyclopropyl ($C_s$) | 115.01383[c] | 0.74212 | 1.22487[a] | 1.34975 | 1.28466 | 1.40124 |
| $c$-$C_3H_6^{+\bullet}(C_{2v})$ | 115.38241[d] | 0.70308 | 1.18689[a] | 1.31094 | 1.24756 | 1.36383 |
| Phenyl ($C_{2v}$) | 227.23946[a] | 1.54261 | 2.48241[a] | 2.74763 | — | — |
| $C_6H_6^{+\bullet}(D_{6h})$ | 227.65759[a] | 1.46186 | 2.42691[a] | 2.67063 | — | — |
| Benzyl ($C_{2v}$) | 265.87734[a] | — | — | — | — | — |
| Toluene radical cation ($C_s$) | 266.25329[a] | — | — | — | — | — |

[a]Obtained in this work.
[b]Reference 9.
[c]Reference 19.
[d]D. D. M. Wayner, unpublished results.

containing π-electrons and/or heteroatoms with unshared electron pairs usually have IP values lower than those of saturated compounds. Among these molecules the aromatics usually have lower IP values relative to the aliphatics. In general, aliphatic hydrocarbon radical cations are stronger acids than are aromatic hydrocarbon radical cations. However, the acidity of the radical cations of such electron-rich molecules will also depend on the nature of the conjugate base. For example, the IP values of propene and toluene are lower than those of ethylene and benzene respectively; but, the radical cations of propene and toluene are stronger acids than the radical cations of ethylene and benzene respectively. This is because the radical cations of propene and toluene are π-acids and on deprotonation yield resonance stabilized radicals, while the radical cations of ethylene and benzene are σ-acids.

*Ab initio* calculations show that the STO-3G results yield higher values for $PA_{HF(R^{\bullet})}$ compared to the extended basis sets. The difference between the Hartree–Fock and thermochemical proton affinities of radicals will not be expected to be greater than 10 kcal mol$^{-1}$ (20). Of the basis sets used in this work, the 3-21G basis set, at the STO-3G geometry, yields $PA_{HF(R^{\bullet})}$ closest to the corresponding thermochemical values. The energies of $RH^{+\bullet}$ and $R^{\bullet}$ are lowered to a greater extent by increasing the number of primitives that describe the core rather than by adding polarization functions on carbon (Table 3). The addition of polarization functions on carbon to the 4-31G and 6-31G split-valence basis sets had a greater effect on the energy of $RH^{+\bullet}$; while, increasing the number of Gaussian functions describing the core in the 4-31G and 4-31G* basis sets lowered the energy of $R^{\bullet}$ by a greater amount. Consequently, the $PA_{HF(R^{\bullet})}$ value was increased by the addition of polarization functions, and decreased by increasing the number of primitives describing the core. Complete optimization at the 3-21G level did not significantly change the $PA_{HF(R^{\bullet})}$ values (Table 4). Thus, single point calculations using larger basis sets at the STO-3G geometry can yield useful information about the effects of basis set size on $PA_{HF(R^{\bullet})}$.

In the next section the thermochemical and Hartree–Fock proton affinities of $R^{\bullet}$ in each of the acid–base pairs ($RH^{+\bullet}/R^{\bullet}$) are compared. The uncertainty of the results obtained is also discussed. Comparison with experimental determinations of $PA_{(R^{\bullet})g}$ is made in the few cases where data is available.

*Methyl ($CH_3^{\bullet}/CH_4^{+\bullet}$)*

For closed-shell species ΔZPE in eq. [8] is expected to be positive and the correlation energy usually small (20). Thus, $PA_{HF(R^{\bullet})g}$ is expected to be larger than the thermochemical value. However, the $PA_{HF(CH_3^{\bullet})g}$ values obtained for all the extended basis sets are lower than the thermochemical value.[5] This may be due to the weakening of the C—H bonds in methane on ionization to an extent such that the zero-point energy of $CH_4^{+\bullet}$ is smaller

[5]UHF calculations using a Van Duijnevelt CGTO (C⟨4*s*, 3*p*⟩ and H⟨3*s*⟩ basis set (26) also yielded $PA_{HF(R^{\bullet})g}$ values lower than the thermochemical value. $PA_{HF(CH_3^{\bullet})CGTO//STO\text{-}3G}$ = 120.0 kcal mol$^{-1}$.

Can. J. Chem. Downloaded from www.nrcresearchpress.com by 210.87.254.40 on 09/06/12
For personal use only.

TABLE 4. The effect of complete optimization at the 3-21G level on total energies and proton affinities

| RH | $\Delta E_{R^\bullet}$/au[a] | $\Delta E_{RH^{+\bullet}}$/au[a] | $\Delta PA_{HF(R^\bullet)g}$[b]/kcal mol$^{-1}$ | $PA_{HF(R^\bullet)g}$[c]/kcal mol$^{-1}$ |
|---|---|---|---|---|
| Methane[d] | −0.00087 | −0.00103 | 0.1 | 118.4 |
| Ethane | −0.00055 | −0.00569 | 3.2 | 160.8 |
| Ethylene | −0.00111 | −0.00268 | 1.0 | 195.2 |
| Acetylene[e] | −0.00016 | −0.00010 | 0.0 | 185.7 |

[a] $\Delta E = E_{3\text{-}21G//3\text{-}21G} - E_{3\text{-}21G//STO\text{-}3G}$. $E_{R^\bullet(3\text{-}21G//3\text{-}21G)}$ was obtained from ref. 19.
[b] $\Delta PA_{HF(R^\bullet)g} = PA_{HF(R^\bullet)g\ 3\text{-}21G//3\text{-}21G} - PA_{HF(R^\bullet)g\ 3\text{-}21G//STO\text{-}3G}$.
[c] $PA_{HF(R^\bullet)g} = PA_{HF(R^\bullet)g\ 3\text{-}21G//3\text{-}21G}$.
[d] Complete optimization at the 4-31G and 6-31G* levels also does not significantly change the computed $PA_{HF(R^\bullet)g}$ for these basis sets (Table 5) at the STO-3G geometry. $PA_{HF(CH_3^\bullet)g\ 4\text{-}31G//4\text{-}31G} = 120.9$ kcal mol$^{-1}$; $PA_{HF(CH_3^\bullet)g\ 6\text{-}31G^*//6\text{-}31G^*} = 121.6$ kcal mol$^{-1}$.
[e] Complete optimization at the 6-31G* level does not significantly change $PA_{HF(R^\bullet)g}$ (Table 4). $PA_{HF(C_2H^\bullet)g\ 6\text{-}31G^*//6\text{-}31G^*} = 197.8$ kcal mol$^{-1}$; $PA_{HF(C_2H^\bullet)g\ 6\text{-}31G^*//STO\text{-}3G} = 196.6$ kcal mol$^{-1}$.

Can. J. Chem. Downloaded from www.nrcresearchpress.com by 210.87.254.40 on 09/06/12
For personal use only.

than that of $CH_3^\bullet$. We intend to consider this point in detail in our future work. The thermochemical method gives only a lower limit of $PA_{(R^\bullet)g}$ because the IP(adiabatic) has been reported as an upper limit of the true value (21). The $\Delta H_{BDE}$ used in this work is based on recent experimental results and a critical review of earlier data and is the currently recommended value (22).

*Ethyl* ($C_2H_5^\bullet/C_2H_6^{+\bullet}$)

As expected, all computed $PA_{HF(R^\bullet)g}$ values are larger than the thermochemical $PA_{(R^\bullet)g}$ value. The error in the thermochemical proton affinity largely depends on the uncertainty in $\Delta H_{BDE}$ because the error in IP(adiabatic) is small (21). The proton affinity of the ethyl radical is ~20 kcal mol$^{-1}$ greater than that of the methyl radical. This indicates that replacing a H in $CH_3^\bullet$ by a methyl group results in a greater stabilization of $RH^{+\bullet}$ relative to $R^\bullet$.

*Vinyl* ($C_2H_3^\bullet/C_2H_4^{+\bullet}$)

The thermochemical method gives only a lower limit of the $PA_{(R^\bullet)g}$ value, because $\Delta H_{BDE}$ has been reported as a lower limit of the true value (23). There is a fair agreement between the experimental (4) and thermochemical proton affinities. The difference between the thermochemical and the computed Hartree–Fock proton affinities is larger than that usually expected from ΔZPE and correlation energy contributions. The proton affinity of the vinyl radical is ~30 kcal mol$^{-1}$ greater than that of ethyl radical. This results from the ease of ionization and the greater $\Delta H_{BDE}$ value of ethylene relative to ethane.

*Ethynyl* ($C_2H^\bullet/C_2H_2^{+\bullet}$)

There is a large variation between the $\Delta H_{BDE}$ values of acetylene that have been used in this work to estimate the thermochemical proton affinity (Table 1). No experimental determination is available to assess the accuracy of the thermochemical values. There is a large difference between the computed Hartree–Fock and thermochemical proton affinities; the uncertainty in the $\Delta H_{BDE}$ values precludes a discussion of the reasons for this difference. The estimated proton affinity of the ethynyl radical is lower than that of the vinyl radical, because the difference in IP(adiabatic) values ($\Delta IP \sim 20$ kcal mol$^{-1}$) more than offsets the difference in the bond dissociation enthalpies ($\Delta(\Delta H_{BDE}) \sim 15$ kcal mol$^{-1}$).

*Allyl* ($C_3H_5^\bullet/C_3H_6^{+\bullet}$)

The allyl radical can, in principle, be formed by the deprotonation of the radical cations of both propene and cyclopropane. We have estimated the proton affinity of the allyl radical in forming both of its conjugate acids. The thermochemical proton affinity for the formation of the propene radical cation is lower than the experimental value. The error in the thermochemical value is largely dependent on the accuracy of the $\Delta H_{BDE}$ value. The accuracy of the experimental determination is also limited to ±2 kcal mol$^{-1}$ by the bracketing technique used (3, 4). As expected, the $PA_{HF(R^\bullet)g}$ values are greater than the thermochemical proton affinity.

*Cyclopropyl* (c-$C_3H_5^\bullet$/c-$C_3H_6^{+\bullet}$)

There is a large variation between $\Delta H_{BDE}$ values of cyclopropane reported in the literature (4, 22*c*, 23). We have used two of these values to estimate $PA_{(R^\bullet)g}$. The thermochemical method gives a lower limit to $PA_{(R^\bullet)g}$ (Table 2). One of the estimated thermochemical proton affinities agrees well with the experimental value (Table 5). The difference between $PA_{HF(R^\bullet)g}$ and the thermochemical values is larger than in the propene system. As in the ethynyl system this difference cannot be explained by the absence of a reliable thermochemical proton affinity. The cyclopropyl radical has a proton affinity larger

Can. J. Chem. Downloaded from www.nrcresearchpress.com by 210.87.254.40 on 09/06/12
For personal use only.



TABLE 5. A comparison of the proton affinities of radicals

| | $PA_{HF(R^{\bullet})g}$/kcal mol$^{-1}$[a] | | | | | | $PA_{(R^{\bullet})g}$/kcal mol$^{-1}$ | |
|---|---|---|---|---|---|---|---|---|
| Radical | STO-3G//STO-3G | 3-21G//STO-3G | 4-31G//STO-3G | 6-31G//STO-3G | 4-31G*//STO-3G | 6-31G*//STO-3G | Thermochemical eq. [6] | Experimental |
| Methyl | 137.6 | 118.3 | 120.5 | 120.0 | 121.7 | 121.1 | ≥127±1 | — |
| Ethyl | 175.6 | 157.6 | 157.3 | 156.4 | 158.9 | 158.5 | 147±1.5 | |
| | | | | | | | 149±1 | — |
| Vinyl | 228.5 | 194.2 | 198.4 | 198.2 | 203.2 | 202.6 | ≥180±2 | 182.6±2[b] |
| | | | | | | | 171±3 | — |
| Ethynyl | 214.5 | 185.7 | 190.2 | 190.0 | 197.2 | 196.6 | 176±1 | |
| Allyl (i) | 223.1 | 184.8 | 187.4 | 187.1 | 192.6 | 191.9 | 177±1.5 | |
| | | | | | | | 175±1.5 | |
| | | | | | | | 176±1.5 | 180.2±2[b] |
| Allyl (ii)[c] | 207.4 | 166.6 | 167.5 | 167.4 | 176.8 | 176.4 | ≥168[d] | |
| Cyclopropyl | 232.8 | 208.3 | 208.9 | 208.4 | 209.5 | 209.3 | ≥193[d] | 187.5±2[b] |
| | | | | | | | ≥188[d] | |
| Phenyl[e] | 263.9 | 213.2 | 229.1 | 215.6 | — | — | 211±1.5 | — |
| Benzyl[e] | 237.4 | — | — | — | — | — | 198±1.5 | 198.3±2[b] |
| | | | | | | | 199 | 199.2[d,f] |

[a]Following Pople and co-workers (15) we use A//B to indicate calculations which have been performed at level A using a geometry which is optimum for level B.
[b]Reference 4.
[c]Data calculated for the ($c$-$C_3H_6^{+\bullet}$/allyl) acid–base system.
[d]Error limits not defined.
[e]Only a partial optimization at the STO-3G level was performed (see text).
[f]Reference 3.

Can. J. Chem. Downloaded from www.nrcresearchpress.com by 210.87.254.40 on 09/06/12
For personal use only.

than that of the vinyl and allyl radicals. This is largely due to the relatively low IP(adiabatic) of cyclopropane.

*Phenyl ($C_6H_5^{\cdot}/C_6H_6^{+\cdot}$)*

Attempts to experimentally determine $PA_{(R^{\cdot})g}$ have thus far failed (4). One of the reasons has been the absence of a suitable reference base with a proton affinity greater than 210 kcal $mol^{-1}$. The thermochemical approach provides a method of obtaining the $PA_{(R^{\cdot})g}$ value. The IP(adiabatic) of benzene has been determined with a negligible error (21). Consequently, the uncertainty in the $PA_{(R^{\cdot})g}$ estimated in this work depends on the accuracy of the $\Delta H_{BDE}$ value. Only a partial optimization was carried out to obtain the STO-3G equilibrium geometries for $C_6H_5^{\cdot}$ and $C_6H_6^{+\cdot}$. Thus, the slight difference between the Hartree–Fock and thermochemical proton affinities obtained in this work may be due to a fortuitous cancellation of errors.

*Benzyl ($C_6H_5CH_2^{\cdot}/C_6H_5CH_3^{+\cdot}$)*

The thermochemical $PA_{(R^{\cdot})}$ values agree well with the experimental determinations. In fact, one of the reported experimental values is a thermochemical value, because it was established by the use of a thermochemical cycle (3). The error in the IP(adiabatic) value and $\Delta H_{BDE}$ is small; it has been suggested that the thermochemical proton affinity of the benzyl radical is suitable to be used to establish an absolute scale of proton affinities (3).

## Conclusion

It has been demonstrated that a thermochemical approach can be used to obtain reliable proton affinities of free radicals, and to establish an absolute scale of $PA_{(R^{\cdot})g}$ values. Except for the ethynyl radical, the trend in the *ab initio* and thermochemical proton affinities agree. Thus, the *ab initio* self-consistent field MO method can be used to obtain relative values of proton affinities in the absence of accurate thermochemical data.

## Acknowledgements

This work was supported by a grant from the Natural Sciences and Engineering Research Council of Canada. D.R.A. is grateful for a Fellowship from the Guggenheim Foundation and A.M.N. for the award of an Izaac Walton Killam Memorial Scholarship. The authors are grateful to the Dalhousie University Computer Centre for generous amounts of computing time.

1. (*a*) P. H. Plesch and I. Sestàkovà. J. Chem. Soc. B, 87 (1970); (*b*) P. H. Plesch and I. Sestàkovà. J. Chem. Soc. B, 1337 (1971).
2. K. Sehested and J. Holcman. J. Phys. Chem. **82**, 651 (1978).
3. M. Meot-Ner. J. Am. Chem. Soc. **104**, 5 (1982).
4. D. G. DeFrees, R. T. McIver, and W. J. Hehre. J. Am. Chem. Soc. **102**, 3334 (1980).
5. A. M. de P. Nicholas and D. R. Arnold. Can. J. Chem. **60**, 2165 (1982).
6. (*a*) P. J. Andrulis, Jr., M. J. S. Dewer, R. Dietz, and R. L. Hunt. J. Am. Chem. Soc. **88**, 5473 (1966); (*b*) E. I. Heiba, R. M. Dessau, and W. J. Koehl, Jr. J. Am. Chem. Soc. **91**, 6830 (1969).
7. (*a*) A. J. Bard, A. Ledwith, and H. J. Shine. Adv. Phys. Org. Chem. **13**, 156 (1976); (*b*) L. Eberson, L. Jönsson, and L.-G. Wistrand. Acta Chem. Scand. B**32**, 520 (1978).
8. B. G. Gilbert, R. O. C. Norman, and P. S. Williams. J. Chem. Soc. Perkin II, 1402 (1981).
9. W. A. Lathan, L. A. Curtiss, W. J. Hehre, J. B. Lisle, and J. A. Pople. Prog. Phys. Org. Chem. **11**, 175 (1974).
10. (*a*) M. Meot-Ner and F. H. Field. Chem. Phys. Lett. **44**, 484 (1976); (*b*) S. G. Lias and P. Ausloos. J. Am. Chem. Soc. **100**, 6027 (1978).
11. R. A. Eades, K. Scanion, M. R. Ellenberger, D. A. Dixon, and D. S. Marynick. J. Phys. Chem. **84**, 2840 (1980).
12. J. S. Binkley, R. A. Whitehead, P. C. Hariharan, R. Seeger, and J. A. Pople. QCPE, **11**, 368 (1978).
13. J. A. Pople and R. K. Nesbet. J. Chem. Phys. **22**, 571 (1954).
14. W. J. Hehre, R. F. Stewart, and J. A. Pople. J. Chem. Phys. **51**, 2657 (1969).
15. J. S. Binkley, J. A. Pople, and W. J. Hehre. J. Am. Chem. Soc. **102**, 939 (1980).
16. R. Ditchfield, W. J. Hehre, and J. A. Pople. J. Chem. Phys. **54**, 724 (1971).
17. W. J. Hehre, R. Ditchfield, and J. A. Pople. J. Chem. Phys. **56**, 2257 (1972).
18. P. C. Hariharan and J. A. Pople. Theoret. Chim. Acta, **28**, 213 (1973).
19. R. A. Whiteside, J. S. Binkley, R. Krishnan, D. J. Defrees, H. B. Schlegel, and J. A. Pople. Carnegie-Mellon Quantum Chemistry Archive (1980).
20. A. C. Hopkinson. Applications of MO theory in organic chemistry. Progress in theoretical organic chemistry. Vol. 2. *Edited by* I. G. Csizmadia. Elsevier, New York. 1977. p. 174.
21. H. M. Rosenstock, K. Draxl, B. W. Steiner, and J. T. Herron. J. Phys. Chem. Ref. Data, Suppl. 1, **6** (1977).
22. (*a*) J. C. Traeger and R. G. McLoughlin. J. Am. Chem. Soc. **103**, 3647 (1981); (*b*) A. L. Castelhano, P. R. Marriott, and D. Griller. J. Am. Chem. Soc. **103**, 4262 (1981); (*c*) S. W. Benson. Thermochemical kinetics. 2nd ed. Wiley Interscience, New York. 1976.
23. R. C. Weast (*Editor*). CRC Handbook of Chemistry and Physics. 62nd ed. CRC Press. 1982. p. F-191.
24. M. Rossi, K. D. King, and D. M. Golden. J. Am. Chem. Soc. **101**, 1223 (1979).
25. M. Rossi and D. M. Golden. J. Am. Chem. Soc. **101**, 1230 (1979).
26. R. B. Van Duijnevelt. IBM RJ, 945 (1971); J. Pacansky. J. Phys. Chem. **86**, 485 (1982).

# Studies on reaction kinetics and on $^{82}Br$ exchange in the solvolysis of triphenylvinyl bromide or trianisylvinyl bromide in 70% HOAc – 30% $H_2O$

CHOI CHUCK LEE AND CRAIG A. OBAFEMI

*Department of Chemistry, University of Saskatchewan, Saskatoon, Sask., Canada S7N 0W0*

AND

ZVI RAPPOPORT

*Department of Organic Chemistry, Hebrew University of Jerusalem, Jerusalem 91904, Israel*

Received June 16, 1982

CHOI CHUCK LEE, CRAIG A. OBAFEMI, and ZVI RAPPOPORT. Can. J. Chem. **60**, 3019 (1982).

Studies were carried out on the kinetics of solvolysis of triphenylvinyl bromide (**1**-Br) or trianisylvinyl bromide (**2**-Br) in 70% HOAc – 30% $H_2O$ in the presence of added $Et_4NBr$, NaOAc, or $LiClO_4$ and on the degree of incorporation of $^{82}Br$-labeled bromide into **1**-Br or **2**-Br during the solvolysis. Common ion rate depression and $^{82}Br$ exchange were observed for both substrates, indicating the involvement of the dissociated triphenylvinyl and trianisylvinyl cations. For both substrates, a normal salt effect was found for NaOAc and $LiClO_4$. With NaOAc, there was also a steeper rise in rate at low concentrations of added salt, but this initial rate enhancement was only 11 and 13%, respectively, for **1**-Br and **2**-Br, and the fact that $LiClO_4$ showed only a normal salt effect suggested that probably there was no special salt effect for NaOAc. These results, considered in conjunction with previous scrambling data, led to the suggestion that the previously observed insensitivity of the extent of isotopic scrambling in the solvolysis of **1**-Br-2-$^{14}C$ may be due to a low selectivity for the less stable triphenylvinyl cation.

---

CHOI CHUCK LEE, CRAIG A. OBAFEMI et ZVI RAPPOPORT. Can. J. Chem. **60**, 3019 (1982).

On a étudié les cinétiques de la solvolyse du bromure de triphénylvinyle (Br-**1**) ou du bromure de trianisylvinyle (Br-**2**) dans un mélange de AcOH–$H_2O$ à 70:30 en présence de $Et_4NBr$, NaOAc ou $LiClO_4$, et le degré d'incorporation du bromure marqué $^{82}Br$ dans le Br-**1** ou le Br-**2** au cours de la solvolyse. On a observé une diminution de la vitesse de l'ion commun et un échange de $^{82}Br$ pour les deux substrats. Ceci indique une participation des cations dissociés de triphénylvinyle et de trianisylvinyle. On a trouvé, pour les deux substrats, un effet de sel normal dans le cas du NaOAc et du $LiClO_4$. Dans le cas du NaOAc il y a également une augmentation plus rapide de la vitesse à de faibles concentrations de sel ajouté; mais cette l'augmentation de la vitesse initiale est respectivement de 11 et de 13% seulement pour le Br-**1** et le Br-**2** et l'effet normal de sel du $LiClO_4$ suggère que probablement le NaOAc n'a pas d'effet de sel spécial. Ces résultats joints aux données antérieures de mélange, suggèrent que la constance du taux de mélange isotopique observée antérieurement au cours de la solvolyse de Br-**1** $^{14}C$-2, peut être due à une faible sélectivité envers le cation triphénylvinyle moins stable.

[Traduit par le journal]

In an early study on vinyl cations, Jones and Miller (1) reported that the decomposition in HOAc of 1-phenyl-2,2-di-*p*-tolylvinylphenyltriazene gave 80% of the unrearranged 1-phenyl-2,2-di-*p*-tolylvinyl acetate and 20% of the rearranged 2-phenyl-1,2-di-*p*-tolylvinyl acetate, the latter being derived from the rearrangement of the 1-phenyl-2,2-di-*p*-tolylvinyl cation to the more stable 2-phenyl-1,2-di-*p*-tolylvinyl cation. In the presence of 10 molar equivalents of added KOAc, however, the formation of the rearranged product was completely suppressed. Similarly, Lee and Ko (2) have found that the trianisylvinyl cation generated from the decomposition in HOAc of trianisyl[2-$^{14}C$]vinylphenyltriazene showed about 38% scrambling of the $^{14}C$-label from C-2 to C-1 arising from 1,2-anisyl shifts. When the reaction was carried out in the presence of 1.7 molar equivalents of NaOAc, the extent of scrambling was decreased to about 17%. These findings were considered to be consistent with the formation of the dissociated "free" triarylvinyl cation, the 1,2-aryl shifts in which would be decreased by the presence of the more nucleophilic acetate ion (1, 2).

In the solvolysis of triphenyl[2-$^{14}C$]vinyl triflate (**1**-OTf-2-$^{14}C$) in HOAc, HCOOH, or $CF_3COOH$, it was found that the extent of isotopic scrambling arising from 1,2-phenyl shifts was not significantly affected by the presence of 1.1 molar equivalents of the conjugate base of the solvent (3). Moreover, in the solvolysis of triphenyl[2-$^{14}C$]vinyl bromide (**1**-Br-2-$^{14}C$) in 70% HOAc – 30% $H_2O$ (by volume) (to be designated 70% HOAc), the presence of about 3 molar equivalents of NaOAc or NaBr also did not materially change the extent of scrambling (4). It was, therefore, suggested (3, 4) that in the triphenylvinyl cationic system, the degenerate rearrangement arising from 1,2-phenyl shifts likely took place in the ion pair, and at this stage of ionization, the process could be insensitive to the presence of externally added nucleophiles.

With 1–3 molar equivalents of added nucleophile, the molar ratio of solvent to nucleophile was still quite high. Hence there was the possibility that

0008-4042/82/243019-07$01.00/0

©1982 National Research Council of Canada/Conseil national de recherches du Canada

Can. J. Chem. Downloaded from www.nrcresearchpress.com by 210.87.254.6 on 09/06/12
For personal use only.

Can. J. Chem. Downloaded from www.nrcresearchpress.com by 210.87.254.6 on 09/06/12
For personal use only.

with the triphenylvinyl cationic system, rather than involving ion pairs, the insensitivity of the extent of scrambling to the presence of added nucleophiles could be due to a predominant product formation from capture of the free ion by the excess solvent. In an attempt to resolve such conflicting possibilities, a recent study was made on the effects of relatively large amounts of added NaOAc or $Et_4NBr$ on the extent of scrambling in the solvolysis of triphenyl[2-$^{14}$C]vinyl bromide (**1**-Br-2-$^{14}$C) or trianisyl[2-$^{14}$C]vinyl bromide (**2**-Br-2-$^{14}$C) in 70% HOAc (5). It was found that in the solvolysis of **1**-Br-2-$^{14}$C in 70% HOAc, there was no significant variation in the extent of scrambling when the reaction was carried out in the presence of 25 molar equivalents of added $Et_4NBr$ or up to 30 molar equivalents of added NaOAc. The conditions of the latter experiment, 25 m*M* **1**-Br-2-$^{14}$C and 750 m*M* NaOAc, were of such high concentrations that some of the reactant, **1**-Br-2-$^{14}$C, was salted out of solution, and yet the extent of scrambling in the reaction product was not significantly affected. On the other hand, in the solvolysis of **2**-Br-2-$^{14}$C in 70% HOAc, the scrambling of the label from C-2 to C-1 observed in the reaction product was found to decrease with increasing amounts of added NaOAc (5). These findings thus appeared to be consistent with the earlier proposal that in the solvolysis of **1**-Br-2-$^{14}$C, the 1,2-phenyl shifts occurred in the ion pair stage, while in the solvolysis of **2**-Br-2-$^{14}$C, the 1,2-anisyl shifts took place in the dissociated "free" trianisylvinyl cation.

Some anomalies were noted, however, in the solvolysis of **1**-Br-2-$^{14}$C or **2**-Br-2-$^{14}$C in 70% HOAc in the presence of added NaOAc and/or $Et_4NBr$ (5). While no accurate rate constants were measured in these studies, estimates of the % reaction for individual experiments suggested that the reaction rates were decreased by the presence of added $Et_4NBr$. Such a common ion rate depression has usually been attributed to external ion returns from dissociated ions to covalent reactant (6). Moreover, in both the solvolyses of **1**-Br-2-$^{14}$C and **2**-Br-2-$^{14}$C in 70% HOAc, selected experiments showed very low extents of scrambling in the recovered unconsumed reactant, except in the reaction of **2**-Br-2-$^{14}$C in the presence of very large amounts of $Et_4NBr$. The occurrence of returns from dissociated ions to give a common ion rate depression would be consistent with an absence of scrambling in the recovered reactant only if the capture of the free ion is faster than its internal rearrangement through 1,2-shifts. In order to obtain more information to clarify such possibilities, we have carried out more detailed kinetic studies on the solvolysis of **1**-Br or **2**-Br in 70% HOAc and we have also investigated the degree of incorporation through isotopic exchange of added [$^{82}$Br]-bromide ion into the organic substrate, **1**-Br or **2**-Br, under some of the conditions previously employed in the scrambling studies (5).

## Results and discussion

In the isotopic scrambling studies with **1**-Br-2-$^{14}$C or **2**-Br-2-$^{14}$C in 70% HOAc (5), experiments were carried out with 15 or 25 m*M* **1**-Br-2-$^{14}$C in the presence of added acetate or bromide ions at 150 ± 2°C, while such experiments with **2**-Br-2-$^{14}$C mostly involved a substrate concentration of 6.0 m*M* and a reaction temperature of 120 ± 1°C. Similar, but not identical, conditions were employed in the present kinetic studies involving the presence of added NaOAc, $Et_4NBr$, or $LiClO_4$. The results are given in Tables 1 and 2 and the effects of added NaOAc or $LiClO_4$ on the specific rate constants are shown in Figs. 1 and 2.

In the exchange studies, experiments were carried out in the presence of added $^{82}$Br-labeled bromide ions, usually as $Et_4NBr$, again under conditions similar to those used in some of the scrambling studies (5). These experiments were carried to roughly 50% completion and the incorporations of $^{82}$Br-activity into the recovered **1**-Br or **2**-Br were determined. The extents of exchange in the recovered substrate were then calculated, an illustration of the calculation being given in the

TABLE 1. Specific rate constants for the solvolysis of 15 m*M* triphenylvinyl bromide (**1**-Br) in 70% HOAc – 30% $H_2O$ at 150 ± 0.2°C

| | Added salt | | | |
|---|---|---|---|---|
| Expt. | [NaOAc] (m*M*) | [$Et_4NBr$] (m*M*) | [$LiClO_4$] (m*M*) | $10^6k$ ($s^{-1}$) |
| TP-1 | — | — | — | 4.30±0.03 |
| TP-2 | — | 45.0 | — | 3.90±0.02 |
| TP-3 | — | 75.0 | — | 3.83±0.03 |
| TP-4 | — | 150.0 | — | 3.68±0.04 |
| TP-5 | 2.0 | — | — | 4.32±0.02 |
| TP-6 | 5.0 | — | — | 4.36±0.02 |
| TP-7 | 10.0 | — | — | 4.47±0.03 |
| TP-8 | 15.0 | — | — | 4.54±0.04 |
| TP-9 | 20.0 | — | — | 4.62±0.02 |
| TP-10 | 30.0 | — | — | 4.75±0.03 |
| TP-11 | 45.0 | — | — | 4.90±0.02 |
| TP-12 | 75.0 | — | — | 4.98±0.04 |
| TP-13 | 120.0 | — | — | 5.08±0.02 |
| TP-14 | 150.0 | — | — | 5.14±0.03 |
| TP-15 | — | — | 15.0 | 4.42±0.04 |
| TP-16 | — | — | 75.0 | 5.23±0.04 |
| TP-17 | — | — | 150.0 | 6.00±0.03 |

Can. J. Chem. Downloaded from www.nrcresearchpress.com by 210.87.254.6 on 09/06/12
For personal use only.

TABLE 2. Specific rate constants for the solvolysis of 6.0 m*M* trianisylvinyl bromide (**2**-Br) in 70% HOAc – 30% $H_2O$ at 116 ± 0.2°C

| | Added salt | | | |
|---|---|---|---|---|
| Expt. | [NaOAc] (m*M*) | [$Et_4NBr$] (m*M*) | [$LiClO_4$] (m*M*) | $10^3k$ ($s^{-1}$) |
| TA-1 | — | — | — | 1.35±0.01 |
| TA-2 | — | 6.0 | — | 1.04±0.03 |
| TA-3 | — | 60.0 | — | 0.59±0.02 |
| TA-4 | — | 180.0 | — | 0.46±0.02 |
| TA-5 | 2.0 | — | — | 1.38±0.02 |
| TA-6 | 4.0 | — | — | 1.43±0.01 |
| TA-7 | 6.0 | — | — | 1.46±0.03 |
| TA-8 | 8.0 | — | — | 1.50±0.02 |
| TA-9 | 10.0 | — | — | 1.54±0.03 |
| TA-10 | 20.0 | — | — | 1.56±0.03 |
| TA-11 | 40.0 | — | — | 1.60±0.02 |
| TA-12 | 60.0 | — | — | 1.63±0.03 |
| TA-13 | 80.0 | — | — | 1.69±0.01 |
| TA-14 | 120.0 | — | — | 1.77±0.02 |
| TA-15 | 150.0 | — | — | 1.83±0.03 |
| TA-16 | — | — | 30.0 | 1.44±0.02 |
| TA-17 | — | — | 60.0 | 1.60±0.02 |
| TA-18 | — | — | 100.0 | 1.74±0.02 |

Experimental section. The pertinent data are summarized in Table 3. It is of interest to point out that 100% exchange in the recovered substrate involved a complete mixing of the bromine atoms in both the added bromide and the organic bromide. Thus with a higher concentration of added labeled bromide and the same relatively low concentration of the substrate, the acutal % incorporation of $^{82}Br$ activity into the recovered substrate may become lower even though there may be a greater extent of exchange. In Expts. 2 and 3 (Table 3), for example, the concentrations of the added [$^{82}Br$]$Et_4NBr$ were 45 and 375 m*M*, respectively, while the concentration of **1**-Br was 15 m*M* in both cases. Although the % incorporation in Expt. 3 of the 375 m*M* [$^{82}Br$]-$Et_4NBr$ was lower than the % incorporation in Expt. 2 of the 45 m*M* labeled bromide, the actual amount of $^{82}Br$ incorporated into the recovered substrate, and hence the extent of $^{82}Br$ exchange, was higher in Expt. 3 than in Expt. 2. Similar trends were noted in Expts. 5 and 6 and in Expts. 7 and 8.

In discussing the present results in conjunction with the previously observed scrambling data (5), one may consider the solvolytic scheme of Winstein *et al.* (6, 7) involving progressively more dissociated ionic intermediates from covalent substrate I to intimate ion pair II to solvent-separated ion pair III to dissociated ions IV (reaction [1]). In a

[1] $\underset{\text{I}}{RX} \rightleftarrows \underset{\text{II}}{R^+X^-} \rightleftarrows \underset{\text{III}}{R^+||X^-} \rightleftarrows \underset{\text{IV}}{R^+ + X^-}$

comprehensive review on ions and ion pairs in solvolysis reactions by Raber, Harris, and Schleyer (6), it was pointed out that whenever a common ion rate depression has been observed, it has invariably also been possible to demonstrate exchange. The present results are in agreement with this conclusion. The data from Expt. TP-1 to TP-4 and TA-1 to TA-4 in Tables 1 and 2 show that there is a common ion rate depression for both **1**-Br and **2**-Br, confirming the previous indication of such rate depressions from rough estimates based on single point determinations of % reaction (5). Moreover, Table 3 shows that there is also exchange between the added labeled bromide ion and **1**-Br or **2**-Br. The observation of both the mass-law effect and $^{82}Br$ exchange thus strongly suggests the involvement of dissociated ions IV in the solvolysis in 70% HOAc of both **1**-Br and **2**-Br.

From Figs. 1 and 2 showing the effects of added NaOAc or $LiClO_4$, it is seen that the shapes of the lines for the changes in specific rate constants for the solvolysis of **1**-Br or **2**-Br with increasing amounts of NaOAc resemble those customarily observed for a "special salt effect" (6–8), i.e., a steep increase at low salt concentrations followed by a moderate increase at higher salt concentrations. A formal interpretation of such a special salt effect would indicate the intermediacy of the solvent-separated ion pair III in the present reactions with **1**-Br and **2**-Br. However, such an interpretation seems to be unlikely for two reasons. Firstly, the rate enhancement in the steep region as measured by $k_{ext}^0/k_t^0$, where $k_t^0$ is the titrimetric rate constant in the absence of added salt and $k_{ext}^0$ is the extrapolated value to zero salt concentration for that portion of the graph which shows the normal salt effect at higher salt concentrations, is only 4.79/4.30 or 1.52/1.35, equalling 1.11 or 1.13, respectively, for **1**-Br or **2**-Br. These values are much smaller than such rate enhancements in other systems showing the special salt effect which usually gave $k_{ext}^0/k_t^0$ in the order of about 2–3 (6). Secondly, a similar plot for $LiClO_4$ shows only a normal salt effect (Figs. 1 and 2) and since $LiClO_4$ is a much more efficient special salt than other salts including NaOAc, it is unlikely that in the present cases with **1**-Br and **2**-Br, $LiClO_4$ would act only as a normal salt while NaOAc would act as a special salt. While it is probable that NaOAc did not cause a special salt effect, at present we do not have an explanation for the initial 11–13% rise in the rate constants at low concentrations of added NaOAc. More experimentation will be required in order to probe the generality of this behavior.

The normal salt effect for $LiClO_4$ and for NaOAc

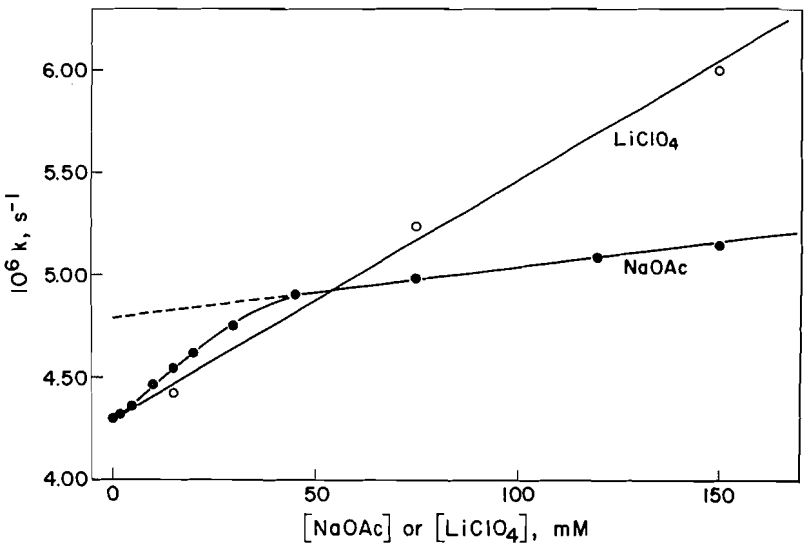


FIG. 1. Effects of added NaOAc or $LiClO_4$ on the specific rate constant in the solvolysis of triphenylvinyl bromide (1-Br) in 70% HOAc – 30% $H_2O$.

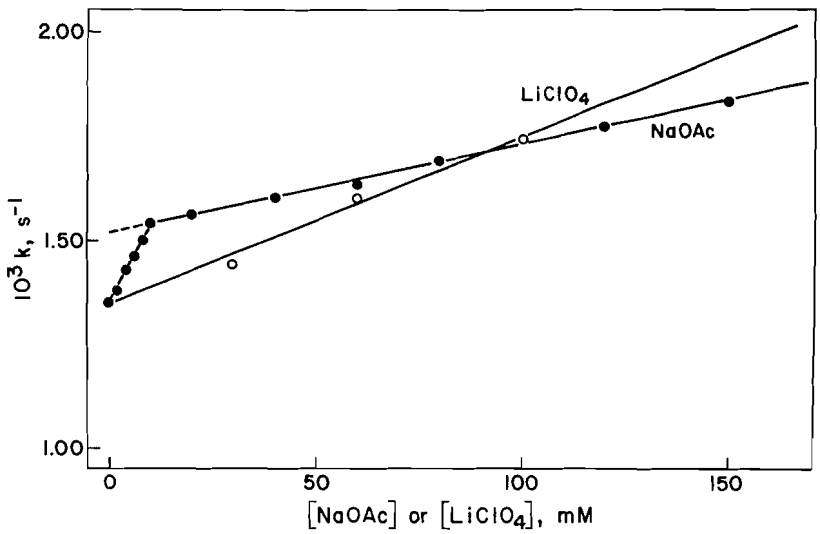


FIG. 2. Effects of added NaOAc or $LiClO_4$ on the specific rate constant in the solvolysis of trianisylvinyl bromide (2-Br) in 70% HOAc – 30% $H_2O$.

in the present reactions can be treated in terms of eqs. [2] and [3], respectively (6).

$$[2] \quad k_t = k_t^0(1 + b[\text{salt}])$$

$$[3] \quad k_t = k_{ext}^0(1 + b[\text{salt}])$$

Using eqs. [2] and [3] and data from Figs. 1 and 2, the $b$ values for the solvolysis in 70% HOAc of **1**-Br and **2**-Br, respectively, were found to be 2.5 and 3.0 for $LiClO_4$, and 0.51 and 1.4 for NaOAc. Since there is a normal salt effect, the actual rate depression due to the added common ion should be larger than the simple difference between the observed rate constant with no added salt ($k_t^0$) and the rate constant with added $Et_4NBr$ ($k_{dep}$) as given in Tables 1 and 2. The normal salt effect due to the added $Et_4NBr$ should be taken into account and this was done by calculating corrected $k_t^0$ values, $k_{corr}^0$, using eq. [2]. Since no $b$ value was obtained for $Et_4NBr$, the $b$ values for both NaOAc and $LiClO_4$ were utilized to approximate the normal salt effect of $Et_4NBr$. The results are summarized in Table 4. Since common ion rate depression arose from external ion returns from free ion IV to

Can. J. Chem. Downloaded from www.nrcresearchpress.com by 210.87.254.6 on 09/06/12
For personal use only.

TABLE 3. Data from exchange reactions in 70% HOAc – 30% $H_2O$ between [$^{82}$Br]$Et_4NBr$ and triphenylvinyl bromide (1-Br) or trianisylvinyl bromide (2-Br)[a]

| Expt. | RBr | [RBr] (m$M$) | [$Et_4NBr$*] (m$M$) | [NaOAc] (m$M$) | % Reaction[b] | $^{82}$Br Activity added (dpm × $10^{-7}$) | $^{82}$Br Incorporated in recovered RBr (%) | Extent of $^{82}$Br exchange in recovered RBr (%) |
|---|---|---|---|---|---|---|---|---|
| 1[c] | 1-Br | 25 | 75[d] | — | 55 | 5.39 | 1.0 | 9.1 |
| 2 | 1-Br | 15 | 45 | — | 43 | 1.72 | 0.99 | 7.0 |
| 3[c] | 1-Br | 15 | 375 | — | 57[e] | 1.34 | 0.28 | 17 |
| 4[f] | 2-Br | 6.0 | 60 | — | 50 | 1.84 | 2.3 | 51 |
| 5[f] | 2-Br | 6.0 | 180 | — | 42 | 1.83 | 0.99 | 53 |
| 6[f] | 2-Br | 6.0 | 500 | — | 44 | 1.77 | 0.44 | 65 |
| 7[f] | 2-Br | 6.0 | 60 | 60 | 55 | 1.73 | 1.2 | 29 |
| 8[f] | 2-Br | 6.0 | 177 | 178 | 50 | 1.85 | 0.68 | 42 |

[a]The reactions with 1-Br or 2-Br, respectively, were carried out at 150 ± 0.2°C for 2 days or at 120 ± 0.2°C for 12 min.
[b]From titration of the liberated $Br^-$ ions in parallel control experiments.
[c]The conditions of Expts. 1 and 3, respectively, approximated those of Expts. 3 and 10 in Table 1 or ref. 5.
[d]Added as [$^{82}$Br]NaBr.
[e]The reaction time was 4 days.
[f]The conditions of Expts. 4–8, respectively, approximated those of Expts. 3, 4, 6, 12, and 15 in Table 2 or ref. 5.

TABLE 4. Extents of common ion rate depression after correction for the normal salt effect

| Substrate | [$Et_4NBr$] (m$M$) | $k_{dep}$[a] ($s^{-1}$) | Corrected $k_t^{0}$[b] ($s^{-1}$) A[c] | Corrected $k_t^{0}$[b] ($s^{-1}$) B[d] | $1-(k_{dep}/k_{corr}^{0})$ A | $1-(k_{dep}/k_{corr}^{0})$ B |
|---|---|---|---|---|---|---|
| 1-Br | 45 | $3.90\times10^{-6}$ | $4.40\times10^{-6}$ | $4.77\times10^{-6}$ | 0.13 | 0.18 |
| 1-Br | 75 | $3.83\times10^{-6}$ | $4.46\times10^{-6}$ | $5.12\times10^{-6}$ | 0.14 | 0.25 |
| 1-Br | 150 | $3.68\times10^{-6}$ | $4.63\times10^{-6}$ | $5.91\times10^{-6}$ | 0.21 | 0.38 |
| 2-Br | 6 | $1.04\times10^{-3}$ | $1.36\times10^{-3}$ | $1.37\times10^{-3}$ | 0.24 | 0.24 |
| 2-Br | 60 | $0.59\times10^{-3}$ | $1.46\times10^{-3}$ | $1.59\times10^{-3}$ | 0.60 | 0.63 |
| 2-Br | 180 | $0.46\times10^{-3}$ | $1.69\times10^{-3}$ | $3.20\times10^{-3}$ | 0.73 | 0.86 |

[a]Titrimetric rate constants from Expts. TP-2, TP-3, and TP-4 of Table 1 and from Expts. TA-2, TA-3, and TA-4 of Table 2.
[b]Corrected for the expected increase in the observed $k_t^{0}$ of $4.30\times10^{-6}$ and $1.35\times10^{-3}$ $s^{-1}$, respectively, for 1-Br and 2-Br due to the normal salt effect of the added $Et_4NBr$.
[c]Using the $b$ value from NaOAc of 0.51 or 1.4 for 1-Br or 2-Br, respectively.
[d]Using the $b$ value from $LiClO_4$ of 2.5 or 3.0 for 1-Br or 2-Br, respectively.

TABLE 5. Isotopic scrambling data from the solvolysis in 70% HOAc – 30% $H_2O$ for tripheny|[2-$^{14}$C]vinyl bromide (1-Br-2-$^{14}$C] at 150 ± 1°C for 4 days and for trianisyl-[2-$^{14}$C]vinyl bromide (2-Br-2-$^{14}$C) at 120 ± 1°C for 12 min

| RBr | [RBr] (m$M$) | [$Et_4NBr$] (m$M$) | Scrambling in product (%) | Scrambling in recovered reactant (%) |
|---|---|---|---|---|
| 1-Br-2-$^{14}$C | 15 | 375 | 14.9 | 0.7 |
| 1-Br-2-$^{14}$C | 15 | 375 | 14.8 | 0.6 |
| 1-Br-2-$^{14}$C | 5.0 | 500 | 13.8 | 1.1 |
| 1-Br-2-$^{14}$C | 5.0 | 500 | 13.9 | 0.9 |
| 2-Br-2-$^{14}$C[a] | 5.9 | 500 | 28.0 | 2.0 |
| 2-Br-2-$^{14}$C[a] | 5.9 | 1000 | 19.4 | 5.0 |
| 2-Br-2-$^{14}$C[a] | 6.0 | 2000 | 17.6 | 9.0 |

[a]Data from ref. 5.

covalent substrate, $1-(k_{dep}/k_{corr}^{0})$ would be a measure of the fraction of free ions that had undergone the return process. In theory, if still higher concentrations of $Br^-$ were present in the reaction mixture, further decrease in rate could result. However, from the experiments that were actually carried out to give the data in Table 4, it may be concluded that the minimum fraction of the reaction involving free ion IV (9) would be 38% and 86%, respectively, for 1-Br and 2-Br, if the $b$ value for $Et_4NBr$ were similar to that of $LiClO_4$.

In the isotopic scrambling studies with 1-Br-2-$^{14}$C (4, 5), it was found that for solvolysis in 70% HOAc in the absence of added salt or in the presence of 3 equivalents of added NaOAc or NaBr, the recovered unconsumed reactant showed what was believed to be a negligible amount of scrambling of 0.5% or less. Similarly, in the solvol-

Can. J. Chem. Downloaded from www.nrcresearchpress.com by 210.87.254.6 on 09/06/12
For personal use only.

Can. J. Chem. Downloaded from www.nrcresearchpress.com by 210.87.254.6 on 09/06/12
For personal use only.

ysis of 2-Br-2-$^{14}$C (5) in 70% HOAc in the presence of up to 30 equivalents of NaOAc and 30 equivalents of $Et_4NBr$, the recovered substrate showed isotopic scramblings of only 1% or less. In the presence of very large amounts of added $Et_4NBr$, however, significant extents of scrambling in the recovered unconsumed reactant were observed in the reactions with 2-Br-2-$^{14}$C (5) and these results are reproduced in Table 5. In order to obtain data for comparison from the triphenylvinyl system under conditions of high concentrations of added bromide ions, 1-Br-2-$^{14}$C was solvolyzed in 70% HOAc under such conditions to give the results recorded in Table 5, showing that in the presence of large amounts of $Et_4NBr$, the scramblings in the recovered reactant are indeed more than the previously reported 0.5% or less. Thus all the results discussed so far suggest a considerable degree of similarity in the behaviors of 1-Br and 2-Br during solvolysis in 70% HOAc. The previously observed scramblings of about 0.5% or 1% in the recovered reactant, although small, were probably real. The small extent of scrambling in the recovered reactant apparently is due to a high rate of the return process compared to a relatively low rate of the 1,2-shift process.

One significant difference that was observed in the solvolysis of 1-Br-2-$^{14}$C and 2-Br-2-$^{14}$C in 70% HOAc was the effect of added NaOAc on the extents of isotopic scrambling (5). In the solvolysis of 15 or 25 m*M* 1-Br-2-$^{14}$C in the presence of up to 30 equivalent of added NaOAc, the scramblings observed in the reaction product were $14.7 \pm 0.7\%$. Since the precision in measuring $^{14}$C scramblings of this type could show variation as large as $\pm 1\%$, the only conclusion that could be drawn was that added NaOAc had little effect on the extent of scrambling in the solvolysis of 1-Br-2-$^{14}$C. On the other hand, in the solvolysis of 2-Br-2-$^{14}$C in 70% HOAc, the extent of scrambling in the product was decreased by the presence of added NaOAc (5). Since exchange does not occur in the intimate ion pair II (6), II may be the least sensitive to externally added nucleophiles. Thus it was suggested (3, 4) that in the solvolysis of 1-Br, if the rearrangement from internal 1,2-shifts occurred in an ion pair stage, the presence of added NaOAc may show little effect on the extent of scrambling.

The results from the present work, however, have shown that, similar to 2-Br, the solvolysis of 1-Br in 70% HOAc also proceeds to the dissociated ion IV. If the $14.7 \pm 0.7\%$ scrambling that was observed in the solvolysis of 1-Br-2-$^{14}$C were due to 1,2-shifts in the intimate ion pair II, upon further ionization of II to IV, IV would also have already been scrambled to the extent of about 14.7% and external ion returns from such a scrambled IV should give a recovered reactant showing a much greater extent of scrambling than the approximately 0.5% that was observed. The previously suggested role for ion pairs in accounting for the insensitivity of the extent of scrambling for 1-Br-2-$^{14}$C to added NaOAc must, therefore, be reconsidered. Probably, the triphenylvinyl cation, being less stable than the trianisylvinyl cation, would react rapidly once it is formed and would show a low selectivity or low ability to discriminate between different nucleophiles (10). Thus the presence of even 30 molar equivalents of NaOAc did not significantly affect the extent of scrambling in the solvolysis of 1-Br-2-$^{14}$C in 70% HOAc (5). The finding from the present work that the degree of $^{82}$Br exchange (Table 3) and the extent of common ion rate depression (Table 4) are lower for 1-Br than 2-Br would also be consistent with a less selective cation from 1-Br.

## Experimental

*Kinetic studies*

Individual samples of 15 m*M* 1-Br or 6.0 m*M* 2-Br in 70% HOAc – 30% $H_2O$ (by volume) containing various amounts of $Et_4NBr$, NaOAc, or $LiClO_4$ as given in Tables 1 and 2 were placed in sealed tubes. The reaction mixtures were heated for various lengths of time at $150 \pm 0.2$°C or $116 \pm 0.2$°C, respectively, for 1-Br or 2-Br. At least 6 points were obtained for each experiment listed in Tables 1 and 2, the reaction being followed to at least 80% completion. The liberated $Br^-$ ions were determined by potentiometric titration with $AgNO_3$. The specific rate constants and their standard errors were then obtained from a computer program designed for the treatment of the experimental data by the method of least squares.

*$^{82}$Br exchange studies*

Individual solvolysis experiments with 1-Br or 2-Br in the presence of added $^{82}$Br-labeled bromide ions were carried out in sealed tubes under the conditions given in Table 3. After the desired length of reaction time, each tube was cooled in an ice bath before it was opened and an appropriate amount of 1-Br or 2-Br was added as carrier. The mixture was then extracted with $CHCl_3$ and from the extract, 1-Br or 2-Br was recovered and purified by passage through an alumina column. The $^{82}$Br activity incorporated into the recovered 1-Br or 2-Br was then measured using a γ-ray counter in the laboratory of the radiation safety officer, University of Saskatchewan. The added [$^{82}$Br]-$Et_4NBr$ and the recovered 1-Br and 2-Br were counted as solutions in 70% HOAc. A sample containing a known amount of $^{82}$Br was used as a reference standard and the standard was counted immediately before and after the counting of a sample to provide the correction for the decay of $^{82}$Br.

As an illustration of the treatment of the experimental data, the details for Expt. 4, Table 3 (the first entry for 2-Br) are described. In this experiment, a solution of 25.5 mg (0.060 mmol) of 2-Br and 126 mg (0.600 mmol) of [$^{82}$Br]$Et_4NBr$ in 10 mL of 70% HOAc was heated in a sealed tube at $120 \pm 0.2$°C for 12 min. Upon work up of the reaction mixture after the addition of 100.7 mg of 2-Br as carrier, 85.6 mg of 2-Br was recovered. From a parallel experiment under the same conditions except

that ordinary $Et_4NBr$ without the label was utilized, titration of the liberated bromide ion showed that the extent of the reaction was 50%.

Thus after the reaction, the original substrate remaining was $0.50 \times 25.5 = 12.8$ mg. Together with the 100.7 mg of carrier, the total 2-Br present was $12.8 + 100.7 = 113.5$ mg.

The total $^{82}Br$ activity introduced as $Et_4NBr$ was $1.84 \times 10^7$ dpm.

The $^{82}Br$ activity in the 85.6 mg of recovered 2-Br was $3.16 \times 10^5$ dpm.

Hence the $^{82}Br$ activity in the unconsumed 2-Br was $(113.5/85.6) \times 3.16 \times 10^5 = 4.19 \times 10^5$ dpm.

Therefore, the incorporation of $^{82}Br$ into the recovered unconsumed reactant was $[(4.19 \times 10^5)/(1.84 \times 10^7)] \times 100 = 2.3\%$.

For 100% exchange, there would be a complete mixing of 100% of the $^{82}Br$ in the 0.060 mmol of substrate and the 0.600 mmol of added bromide, and the $^{82}Br$ incorporation in the recovered reactant would be $100/0.660 = 152\%$ $^{82}Br$/mmol 2-Br.

The observed incorporation in the recovered reactant was 2.3% of the $^{82}Br$ in $(0.50 \times 0.060)$ mmol of 2-Br or $2.3/0.030 = 77\%$ $^{82}Br$/mmol 2-Br.

Therefore, the extent of exchange in the recovered reactant was $(77/152) \times 100 = 51\%$.

## Acknowledgments

Valuable comments by Professor P. v. R. Schleyer, Universität Erlangen Nürnberg, the assistance of S. D. Choubal, radiation safety officer, in the measurement of $^{82}Br$ activity, and the financial support given by the Natural Sciences and Engineering Research Council of Canada are sincerely acknowledged.

1. W. M. Jones and F. W. Miller. J. Am. Chem. Soc. **89**, 1960 (1967).
2. C. C. Lee and E. C. F. Ko. Can. J. Chem. **54**, 3041 (1976).
3. C. C. Lee, A. J. Cessna, B. A. Davis, and M. Oka. Can. J. Chem. **52**, 2679 (1974).
4. C. C. Lee and E. C. F. Ko. Can. J. Chem. **56**, 2459 (1978).
5. C. C. Lee, E. C. F. Ko, and Z. Rappoport. Can. J. Chem. **58**, 2369 (1980).
6. D. J. Raber, J. M. Harris, and P. v. R. Schleyer. *In* Ions and ion pairs in organic reactions. Vol. 2. *Edited by* M. Szwarc. John Wiley and Sons, New York. 1974. Chapt. 3.
7. S. Winstein, E. Clippinger, A. H. Fainberg, and G. C. Robinson. J. Am. Chem. Soc. **76**, 2597 (1954).
8. S. Winstein, P. E. Klinedinst, Jr., and G. C. Robinson. J. Am. Chem. Soc. **83**, 885 (1961).
9. Z. Rappoport, P. Shulman, and M. Thuval (Shoolman). J. Am. Chem. Soc. **100**, 7041 (1978).
10. J. Hine. Physical organic chemistry. 2nd ed. McGraw-Hill, New York. 1962. p. 271; J. March. Advanced organic chemistry. 2nd ed. McGraw-Hill, New York. 1977. p. 271.

Can. J. Chem. Downloaded from www.nrcresearchpress.com by 210.87.254.6 on 09/06/12
For personal use only.

# A $^1H$ and $^{13}C$ nuclear magnetic resonance study of nucleosides with methylated pyrimidine bases

FRANK E. HRUSKA AND WAYNE J. P. BLONSKI

*Chemistry Department, University of Manitoba, Winnipeg, Man., Canada R3T 2N2*

Received July 9, 1982

FRANK E. HRUSKA and WAYNE J. P. BLONSKI. Can. J. Chem. **60**, 3026 (1982).

Alkylated pyrimidine bases are of interest from the viewpoint of mutagenesis and carcinogenesis. $^1H$ nuclear magnetic resonance data are presented for a series of ribosides and arabinosides alkylated at the O2, O4, N3, and C5 positions of the pyrimidine base. The data provide information about the stereochemical effects of base methylation. The $J(5—6)$ proton coupling constants show that O-alkylation leads to a decrease in the $\pi$-bond order of the C5—C6 bond. The $^{13}C$ chemical shifts are related to the tautomeric changes effected by O-alkylation.

FRANK E. HRUSKA et WAYNE J. P. BLONSKI. Can. J. Chem. **60**, 3026 (1982).

Les bases alkylées du type pyrimidine présentent un intérêt du point de vue de la mutagénèse et de la carcinogénèse. On présente les données de la rmn du $^1H$ relatives à une série de ribosides et d'arabinosides alkylées en positions O2, O4, N3 et C5 de la pyrimidine. Les données fournissent des informations sur les effets stéréochimiques de la méthylation de la base. Les constantes de couplage du proton $J(5–6)$ révèlent que l'O-alkylation conduit à une diminution dans l'ordre de la liaison $\pi$ de la liaison C5—C6. On a relié les déplacements chimiques du $^{13}C$ aux changements tautomériques occasionnés par la O-alkylation.

[Traduit par le journal]

## Introduction

The alkylation of nucleic acid bases is of considerable interest from the viewpoint of mutagenesis and carcinogenesis (1–8). Following the early interest in N-7 alkylation of guanine (9, 10), much attention was shifted to O-alkylation when Loveless (11) identified $O^6$-methylguanine as a minor alkylation product and proposed that the resulting tautomeric shift could lead to mispairing of bases. An extensive array of O- and N-alkylated purine and pyrimidine bases has now been detected in nucleic acids treated with alkylating agents (12).

To continue our studies on modified nucleosides (13), we have carried out complete analyses of the $^1H$ nmr spectra of a series of uracil ribonucleosides methylated at the C5, N3, O2, and O4 positions of the base (Fig. 1). We have also obtained the $^1H$ nmr spectra of $O^4$-methylarabinouridine, an analogue of arabinocytidine. The data provide information about the stereochemical and electronic effects of base alkylation. To further characterize these molecules we report their $^{13}C$ chemical shift data obtained in aqueous solution.

## Experimental

*Materials*

The $m^2U$ was prepared according to Kimura *et al.* (14), the $m^4U$ according to Robins and Naik (15), and $m^3U$ according to Miles (16). The $m^4aU$ was prepared according to the procedure described for $m^4U$ (15). The products were purified by recrystallization or by chromatography (Whatman 3MM paper; solvent system n-butanol – ethanol–water = 80:10:25 volume ratio). U, C, $m^5U$, aU, and aC were purchased from the Sigma Chemical Co.

*$^1H$ nuclear magnetic resonance experiments*

The $^1H$ nmr spectra were obtained on either a Nicolet NT360 (Purdue University) or a Bruker WP-400 (University of Alberta, Edmonton). All samples were examined in 5 mm (od) tubes at concentrations of 2–5 mg/mL in $D_2O$ containing 0.1 mg/mL of sodium 3'-trimethylsilylpropionate-2,2,3,3-$d_4$ (TSP) as internal reference. Treatment with dithizone according to Cozzone and Jardetzky (17) removed paramagnetic metal ions. The pH was 7.0 ± 0.3 in each case (uncorrected for the deuterium isotope effect). The temperature was maintained at 298 K (400 MHz

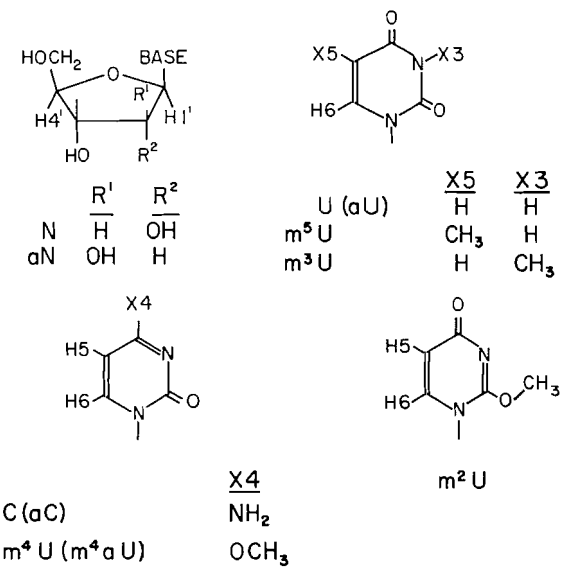


FIG. 1. (a) Structure of ribonucleosides (N): uridine (U), cytidine (C), 5-methyluridine or thymidine ($m^5U$ or T), $N^3$-methyluridine ($m^3U$), $O^4$-methyluridine ($m^4U$), and $O^2$-methyluridine ($m^2U$). (b) Structure of arabinonucleosides (aN): arabinocytidine (aC), arabinouridine (aU), $O^4$-methylarabinouridine ($m^4aU$). As oriented the bases would be in the *anti* conformer range; a 180° rotation about the N1—C1' bond would make them *syn*.

0008-4042/82/243026-07$01.00/0

©1982 National Research Council of Canada/Conseil national de recherches du Canada

Can. J. Chem. Downloaded from www.nrcresearchpress.com by 210.87.254.105 on 09/06/12
For personal use only.

Can. J. Chem. Downloaded from www.nrcresearchpress.com by 210.87.254.105 on 09/06/12
For personal use only.

TABLE 1. $^1$H chemical shifts (δ) and $^1$H—$^1$H coupling constants ($J$) for a series of pyrimidine ribose and arabinose nucleosides in aqueous solution[a,b]

| Parameter[c] | U | C | m$^5$U | m$^3$U | m$^2$U | m$^4$U | Um | aU | aC | m$^4$aU |
|---|---|---|---|---|---|---|---|---|---|---|
| δ6 | 7.92 | 7.89 | 7.70 | 7.88 | 8.08 | 8.17 | 7.95 | 7.87 | 7.83 | 8.10 |
| 5 | 5.91 | 6.08 | — | 5.96 | 6.17 | 6.25 | 5.94 | 5.89 | 6.06 | 6.26 |
| 1′ | 5.93 | 5.94 | 5.93 | 5.94 | 5.96 | 5.93 | 6.02 | 6.20 | 6.22 | 6.23 |
| 2′ | 4.37 | 4.35 | 4.35 | 4.34 | 4.38 | 4.33 | 4.09 | 4.43 | 4.43 | 4.47 |
| 3′ | 4.25 | 4.25 | 4.25 | 4.22 | 4.23 | 4.20 | 4.38 | 4.16 | 4.15 | 4.14 |
| 4′ | 4.16 | 4.17 | 4.12 | 4.14 | 4.18 | 4.18 | 4.15 | 4.02 | 4.04 | 4.07 |
| 5′ | 3.94 | 3.97 | 3.92 | 3.93 | 3.99 | 3.98 | 3.96 | 3.94 | 3.94 | 3.93 |
| 5″ | 3.83 | 3.86 | 3.82 | 3.82 | 3.86 | 3.85 | 3.85 | 3.86 | 3.86 | 3.86 |
| $CH_3$ | — | — | 1.90 | 3.33 | 4.06 | 3.95 | 3.55 | — | — | 3.96 |
| $J$1′2′ | 4.8 | 4.0 | 5.0 | 4.1 | 3.4 | 3.1 | 4.0 | 5.1 | 4.9 | 4.6 |
| 2′3′ | 5.2 | 5.2 | 5.3 | 5.4 | 5.3 | 5.0 | 5.4 | 4.5 | 4.0 | 3.9 |
| 3′4′ | 5.4 | 6.0 | 5.3 | 5.9 | 6.4 | 6.4 | 5.9 | 5.5 | 5.3 | 5.3 |
| 4′5′ | 2.9 | 2.8 | 3.0 | 2.9 | 2.8 | 2.5 | 2.9 | 3.2 | 3.2 | 3.4 |
| 4′5″ | 4.4 | 4.3 | 4.3 | 4.5 | 4.3 | 4.1 | 4.3 | 5.6 | 5.7 | 5.7 |
| Σ | 7.3 | 7.3 | 7.3 | 7.4 | 7.1 | 6.5 | 7.3 | 8.8 | 8.9 | 9.1 |
| 56 | 8.1 | 7.6 | — | 8.1 | 7.6 | 7.5 | 8.0 | 8.1 | 7.6 | 7.5 |

[a]δ(ppm) from TSP, $J$ in Hz. Abbreviations defined in Fig. 1.
[b]Data at 360 MHz (m$^5$U, m$^3$U, m$^2$U, m$^4$U) (25°C) and 400 MHz (m$^4$aU) (20°C); 220 MHz (U, C, aU, aC) (18°C) (Refs. 19–21); 100 MHz (Um) (25°C). Data at 100 MHz and 220 MHz with internal DSS reference; corrected to TSP by δ(TSP) = δ(DSS) + 0.04 ppm.
[c]$J_{5',5''}$ not included; −12.7 ± 0.2 Hz. Σ = $J$(4′–5′) + $J$(4′–5″).

TABLE 2. $^{13}$C chemical shifts for a series of pyrimidine ribose and arabinose nucleosides in aqueous solution[a,b]

| Parameter | U | C | m$^5$U | m$^3$U | m$^2$U | m$^4$U | aU | aC | m$^4$aU |
|---|---|---|---|---|---|---|---|---|---|
| δ4 | 168.7 | 167.4 | 167.7 | 166.7 | 176.1 | 174.2 | 167.5 | 167.4 | 174.1 |
| 2 | 153.9 | 158.8 | 153.1 | 153.3 | 158.4 | 158.9 | 152.7 | 158.6 | 156.6 |
| 6 | 142.9 | 142.9 | 138.7 | 140.9 | 141.4 | 145.1 | 144.3 | 144.0 | 146.3 |
| 5 | 103.6 | 97.4 | 112.7 | 102.7 | 108.3 | 98.5 | 102.4 | 96.5 | 97.7 |
| 1′ | 90.7 | 91.6 | 90.2 | 91.7 | 92.3 | 92.3 | 86.5 | 87.2 | 88.0 |
| 2′ | 74.9 | 75.3 | 74.8 | 75.1 | 75.7 | 75.6 | 76.8 | 76.8 | 76.8 |
| 3′ | 70.8 | 70.6 | 70.7 | 70.6 | 70.2 | 70.3 | 76.2 | 76.8 | 76.7 |
| 4′ | 85.4 | 85.0 | 85.4 | 85.3 | 85.5 | 85.1 | 84.3 | 84.5 | 85.0 |
| 5′ | 62.1 | 62.1 | 62.0 | 62.0 | 61.7 | 61.8 | 61.8 | 62.1 | 62.1 |
| C-$CH_3$ | — | — | 12.8 | — | — | — | — | — | — |
| O(N)-$CH_3$ | — | — | — | 29.0 | 57.6 | 56.1 | — | — | 56.1 |

[a]Carbon data (297 K) at 22.63 MHz relative to TMS; measured relative to internal dioxane at 67.86 ppm.
[b]Symbols in Fig. 1.

data) or at 293 K (360 MHz data). Spectral analysis was carried out using LAME (18) and computer-simulated spectra were generated as a final test of the chemical shifts (δ) and coupling constants ($J$) (Table 1). The uncertainties in δ and $J$ are estimated to be about ± 0.001 ppm and ± 0.1 Hz, respectively. For comparison, literature data for U (19), Um (20), and aU (21) are included. Um is 2′-O-methyluridine, i.e. the 2′-OH of the sugar has been methylated.

### *$^{13}$C nuclear magnetic resonance experiments*

Proton-decoupled $^{13}$C nmr spectra were obtained on a Bruker WH-90DS spectrometer (22.63 MHz), according to described procedures (22). The nucleoside samples were contained in 10 mm (od) tubes at concentrations of 25–50 mg/mL in $D_2O$, containing 1% dioxane as internal reference. Following a suggestion by Dr. D. W. McBride of our department, we removed paramagnetic ions by shaking the sample with an acetylacetone–toluene mixture (equal volumes) and separating the phases. The pH was adjusted to 7.0 ± 0.2 (uncorrected for the deuterium isotope effect). The probe temperature was regulated at 297 K. The $^{13}$C chemical data (Table 2) are reported in ppm downfield from external TMS by setting internal dioxane equal to 67.86 ppm.

## Results and discussion

### *Assignment of the spectra*

The $^1$H spectral assignments were initiated with literature data for U (19), C (20), and aU (21). Also useful were data for C-, N-, and O-methylated pyrimidine bases (23) and the partial analysis of the 5′-monophosphate of m$^3$U (24). The H5′, H5″ assignment followed from the literature (25, 26). The $^{13}$C nmr assignments were made by comparison with literature data for pyrimidine bases and nucleosides (24, 27, 28). For the arabinosides, the relative chemical shifts of C2′ and C3′ are 0.6 ppm or less; the assignments here are arbitrary.

### *Conformation about the* N*-glycosyl bond*

Crystallographic studies have revealed the *anti*

Can. J. Chem. Downloaded from www.nrcresearchpress.com by 210.87.254.105 on 09/06/12
For personal use only.

conformation (Fig. 1) for U (29), C (30), m$^5$U (31), and aC (32) in the solid state. For pyrimidine ribosides and 2′-deoxyribosides in solution a test for the *anti* and *syn* conformers (Fig. 1) is based on chemical shift comparisons, particularly for H2′ which experiences a large deshielding (0.5–0.6 ppm) in the *syn* form due to the magnetic anisotropy of the 2-keto oxygen (33). Table 1 shows that methylation at the O2, N3, O4, and C5 positions of the uracil ring has little influence on the ribose chemical shifts and hence on the *anti*, *syn* blend. In particular, δ(H2′) lies in the narrow range (4.33–4.38 ppm) expected for a preferred *anti* conformation (33). (An exception is Um (δ(H2′) = 4.09 ppm). This upfield shift can be attributed to a direct effect of the O2′-alkylation (34) rather than changes in the *anti*, *syn* blend.) In the case of m$^2$U, methylation has converted the 2-keto to a methoxyl group whose shielding effects in a *syn* pyrimidine nucleoside have not been evaluated. (This could be accomplished with, say, the 6-methyl derivative of m$^2$U.) However, the overall trends in the ribose chemical shifts and steric considerations suggest the *anti* form for m$^2$U.

Solid state (32) as well as solution data (35) point to a preference for the *anti* forms of aU and aC. The remarkable similarity in the ribose chemical shift data of aU, aC, and m$^4$aU indicates that O4-methylation of a pyrimidine arabinoside does not influence the *anti–syn* distribution and hence m$^4$aU prefers the *anti* conformation in solution as well.

Further support for the *anti* conformation in the ribosides and arabinosides is provided as follows.

(a) The presence of a 0.3–0.5 Hz five-bond coupling between H5 and H1′ is consistent with the "zig-zag" coupling path between the two protons (33, 36). (A four-bond coupling (0.2–0.3 Hz) between H6 and H1′ was also apparent in the spectra of, in particular, the O2- and O4-methylated molecules.)

(b) Methylation does not lead to the destabilization of the g$^+$(ψ) conformer expected for a *syn* pyrimidine nucleoside (13, 33). (See below.)

*Conformation of the sugar ring*

For the ribose derivatives the *cis* $J$(2′—3′) couplings (Table 1) fall in the narrow range 5.0–5.4 Hz, consistent with uniform pseudorotational parameters ($P$, $\tau_m$) (37) and typical of "normal" ribose rings (33). The *trans* couplings, $J$(1′—2′) and $J$(3′—4′), show a greater variation and the generally observed inverse correlation (33, 38). In terms of the *N* (3′-*endo*), *S* (2′-*endo*) blend, a near balance is indicated for U (53% *N*) and m$^5$U (51% *N*), while increases in *N* are evident for C (60%), Um (60%), m$^3$U (59%), m$^2$U (65%), and m$^4$U (67%) (Table 3). Theoretical treatments have linked electronic changes due to C5 substitution to changes in sugar pucker (39). Ultimately the electronic effects of O2-, O4-, and N3-methylation are responsible for the changes in pucker of the modified nucleosides, but these effects have not yet been considered with theoretical calculations.

TABLE 3. Calculated population (%) of the g$^+$(ψ), t(ψ) and g$^-$(ψ) rotamers about the C(4′)—C(5′) bond and the contribution (%) of 3′*endo* (*N*) to the $N \rightleftharpoons S$ blend

| Nucleoside | *N* | g$^+$ | t | g$^-$ |
|---|---|---|---|---|
| U | 53 | 62 | 32 | 5 |
| C | 60 | 63 | 32 | 4 |
| m$^5$U | 51 | 63 | 31 | 6 |
| m$^3$U | 59 | 61 | 33 | 5 |
| m$^2$U | 65 | 64 | 32 | 4 |
| m$^4$U | 67 | 69 | 30 | 0 |
| Um | 60 | 63 | 31 | 5 |
| aU | 54 | 47 | 44 | 8 |
| aC | 53 | 46 | 46 | 8 |
| m$^4$aU | 54 | 44 | 45 | 11 |

[a] $\%N = 100\% J_{3'4'}/(J_{1'2'} + J_{3'4'})$ for ribosides; for arabinosides: following ref. 21.
[b] $\%g^+(\psi)$, etc., from $J_{4'5'}$ and $J_{4'5''}$ following Haasnoot *et al.* (40).

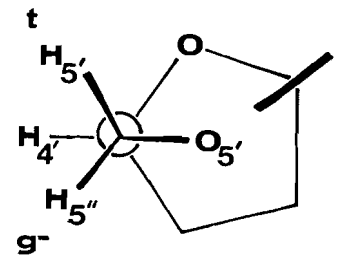


FIG. 2. Newman projection viewed along the C5′—C4′ (ψ) bond. The g$^+$ conformer is shown. t and g$^-$ give the location of Θ5′ in the t and g$^-$ conformers, respectively.

For the three arabinosides, the small variation (< 0.7 Hz) in the $J$(1′—2′), $J$(2′—3′), and $J$(3′—4′) coupling constants indicates that the sugar pucker is little affected by the modifications to the base (estimated[1] $\%N \approx 54\%$).

*Conformation about the C4′—C5′ bond*

Table 3 contains the g$^+$(ψ), t(ψ), and g$^-$(ψ) populations (Fig. 2) calculated from the $J$(4′—5′) and $J$(4′—5″) data using the parameterization of Haasnoot *et al.* (40). For the ribosides, the %g$^+$(ψ) lies in the range 61–69% while t(ψ) lies in the range 30–34%. Minimal contribution (<6%) is made by g$^-$(ψ), the conformer least often seen in crystalline ribosides (41). The m$^4$U shows both the largest

[1] According to ref. 21.

Can. J. Chem. Downloaded from www.nrcresearchpress.com by 210.87.254.105 on 09/06/12
For personal use only.

%$g^+(\psi)$ and the largest %$N$, in line with a correlation already seen in pyrimidine ribosides (33, 38, 42).

Relative to the ribosides, a sizeable shift in the arabinosides occurs from the $g^+(\psi)$ to the $t(\psi)$ conformer which are now equally populated. No drastic change occurs upon O4-methylation of the uracil base of arabinouridine. The shift to the $t(\psi)$ conformer provides further evidence that the 2′,5′-hydrogen bonds noted in some crystalline arabinosides (32, 43) and predicted by theory (44) are unimportant in aqueous solution.

*J(5—6) and base tautomerism*

Methylation of a uracil base at the O4 position causes a tautomeric shift from the diketo to the 4-lactim form which resembles the cytosine base (Fig. 1). Methylation at the O2 position leads to a quininoidal structure while methylation at C5, C6, and N3 leaves the uracil in the diketo form. These differences in hybridization of the ring are reflected in the magnitude of the vicinal $J(5—6)$ coupling constants (Table 1) which fall into two narrow ranges: 8.0–8.1 Hz for the diketo molecules (U, aU, $m^3U$, Um) and 7.5–7.6 Hz for the cytosine-like (C, aC, $m^4U$, $m^4aU$) and quininoidal ($m^2U$) molecules. In line with these trends is the $J(5—6)$ coupling (7.4 Hz) in 2,2′-anhydro-(1-β-D-arabinofuranosyl)-uracil in which the quininoidal uracil structure is formed by the anhydro link between the C2 position of the base and the C2′ position of the sugar (45). Also relevant is that, upon formation of the anionic form of U and dU by ionization of the N3-H at pH 9.5, $J(5—6)$ decreases to 7.6–7.7 Hz (36). This decrease in $J(5—6)$ relative to the unionized base seems reasonable since the anion (Fig. 3a) can be represented by a combination of the cytosine and quininoid resonance structures (Figs. 3b and 3c, respectively (46)). Based on work by Veillard (47) we conclude that the π-bond orders of the C5—C6 bond of the cytosine-type and quininoidal molecules, and the anionic uracils, are similar, and smaller than the π-bond orders of the C5—C6 bonds of the diketo molecules. This view is in line with calculations (48) on cytosine, uracil, and its 4-enol-2-keto tautomer (which is isoelectronic with $m^4U$).

*Trends in the base $^1H$ chemical shifts*

Using Table 1 we have constructed Fig. 4 which shows more clearly how the proton shifts, δ(H6) and δ(H5), are affected by base alkylation. In addition to the riboside and arabinoside data, we included data for the corresponding 2′-deoxyribosides whose study is in progress ($m^2dU$, $m^4dU$,

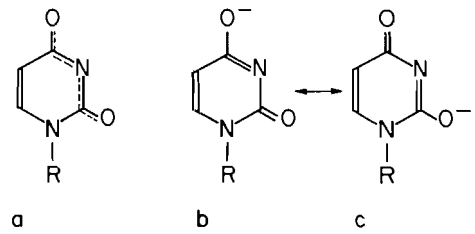


FIG. 3. (a) Standard representation of the uracil anion formed by dissociation of the N3 proton. Cytosine-like (b) and quininoidal (c) representations of the anion.

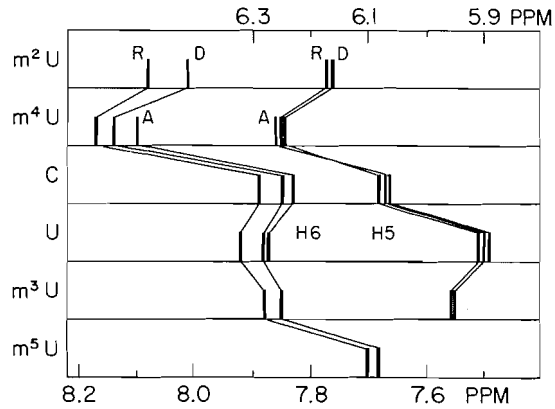


FIG. 4. Chemical shifts (ppm relative to internal TSP) of the H6 (bottom scale) and H5 protons (top scale) for a series of base-methylated ribosides, arabinosides (Table 1), and 2′-deoxyribosides (work in progress). The symbols for the *ribo*-nucleosides (U etc.) are on the vertical axis. Data for the corresponding arabinosides (aU, etc.) and 2′-deoxyribonucleosides (dU, etc.) are on the same levels. The connected δ(H6) and δ(H5) data for the riboses, arabinoses, and deoxyriboses are labelled R, A, D, respectively.

dC, dU, $m^3dU$, $m^5dU$(dT)). The following are some trends which should be useful for purposes of identification.

1. The H6 and the H5 chemical shifts show parallel behaviour for the three series of molecules, indicating that the nature of the sugar moiety does not significantly modulate the effect of the base modification.

2. For a particular base the dependence on the nature of the sugar is greater for δ(H6) than for δ(H5), in line with the relative separation of these protons from the sugar. (Compare, for example, U, aU, dU.) The largest variation for δ(H6) is 0.07 ppm ($m^2$ base), but only 0.02 ppm for δ(H5).

3. N3-methylation which does not alter the tautomeric form of the base has a small effect on δ(H5) and δ(H6) (≤ 0.05 ppm).

4. Methylation at C5 increases the shielding of H6 by 0.15–0.18 ppm, in line with the observed shielding increments for olefinic protons effected

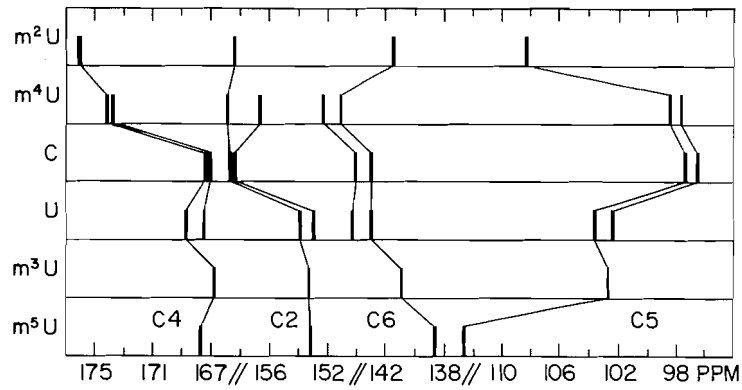


FIG. 5. Correlation diagram showing the effect of methylation on the pyrimidine ring carbon chemical shifts (in ppm) relative to TMS (Table 2). The symbols for the ribonucleosides (U, etc.) are given on the vertical axis (see Fig. 1 for definitions). The arabinoside data is given on the same level as the corresponding riboside (U-aU, C-aC, $m^4U$-$m^4aU$).

by *cis* alkylation (49). (Compare U with $m^5U$ and dU with $m^5dU$.)

5. Upon O4-methylation, H6 and H5 are deshielded by 0.25 ppm and 0.35 ppm, respectively; upon O2-methylation, H6 and H5 are deshielded by ~0.16 ppm and 0.26 ppm, respectively. This suggests that O-methylation is reflected in the electronic properties of the C5—C6 bond. In the cytosine (C) base H5 is also deshielded relative to the U base, but to a lesser extent (~0.17 ppm) than in the isoelectronic $m^4U$ base. However, relative to U, the H6 proton of C is *shielded* slightly (0.03 ppm), in contrast with the large deshielding of H6 in the $m^4U$ base.

6. The methyl proton shifts lie in the range 1.9–4.1 ppm (Table 1) with the order of increasing shielding (O2-Me < O4-Me < O2′-Me < N3′-Me < C5-Me).

### $^{13}C$ *chemical shifts*

Using the data in Table 2 we have constructed the correlation diagram (Fig. 5) which illustrates how base alkylation influences the $^{13}C$ chemical shifts of the pyrimidine base carbon atoms. In this section we discuss qualitatively some of the shielding trends, bearing in mind the attempts which have been made to relate $^{13}C$ chemical shifts to electronic properties of the bases (27, 28, 50, 51).

1. C5-methylation has a large deshielding effect on C5 (9 ppm) and a large shielding effect on C6 (4 ppm). Similar trends have been seen for U and $m^5U$ (and the parent bases) in DMSO solution (27, 28, 50, 51). In their $^{13}C$ nmr study, Ellis *et al.* (51) have found that, insofar as the $^{13}C$ shieldings of C5 and C6 are concerned, the 5-substituted uracils may be considered as either a set of trisubstituted ethylenes or of monosubstituted benzenes.

2. Since replacement of the N3 hydrogen by an alkyl group is not expected to significantly perturb the electronic structure of the base, it is not surprising that N3-methylation has the smallest effect overall on the $^{13}C$ chemical shifts. (Compare U and $m^3U$.) The largest effects are seen at C4 (+2.0 ppm) and at C6 (+2.1 ppm). It is interesting that the carbon most distant from the substituent (C6) is the most strongly affected. Comparable trends have been seen by Still *et al.* in the study of methylated pyrimidines in DMSO solution (27).

3. The largest effects are due to O2- and O4-methylation, consistent with the tautomeric changes which accompany these modifications. Methylation of either O2 or O4 leads to a large deshielding of *both* of the carbonyl carbons, C2 and C4 (3.9 to 7.4 ppm relative to U or to aU). It is interesting that C4 is more strongly affected than C2 by both O2- and O4-methylation. These observations provide further evidence for the strong conjugation of the O2—C2—N3—C4—O4 fragment. On the other hand, C5 is shielded by O4-methylation but deshielded to a comparable extent by O2-methylation (5—6 ppm). In contrast, C6 is deshielded by O4-methylation (≃2 ppm) but shielded by O2-methylation (≃3 ppm). We are not able to provide a simple rationale for all of these changes. However, they do suggest that O-methylation causes a polarization throughout the pyrimidine ring.

It is also interesting to compare the $^{13}C$ shifts of the O-methyl derivatives ($m^4U$ or $m^4aU$) with those of the corresponding cytosine derivatives (C or aC). Their C2, C5, and C6 shifts are identical to within about 2 ppm, in line with the isoelectronic nature of the $m^4U$ and C bases, and suggesting similar electronic effects of the methoxy and amino groups on these carbons. However, the C4 resonances of the $m^4U$ bases are shifted significantly downfield from the C base (≃7 ppm). This difference may simply reflect that an O-atom has greater electronegativity than a N-atom.

Can. J. Chem. Downloaded from www.nrcresearchpress.com by 210.87.254.105 on 09/06/12
For personal use only.

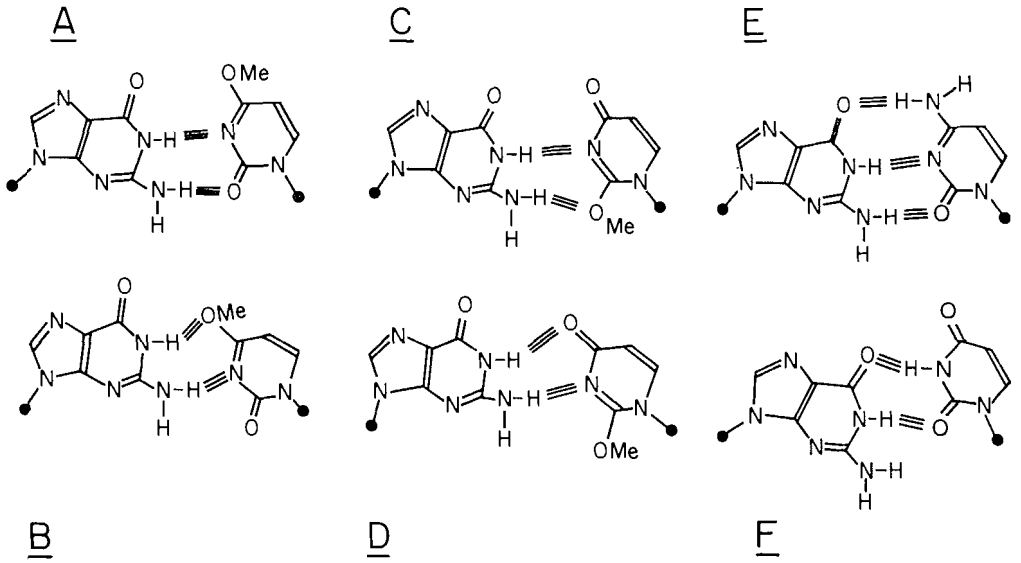


FIG. 6. Hydrogen bonded base pairs. A and B: G–m$^4$U; C and D: G–m$^2$U; E: Watson–Crick G–C; F: G–U (wobble). In A to D the methoxy group is rotated to a conformer which allows the approach of interacting groups.

4. The methyl carbon shifts are in the range 13–57 ppm. The order of increasing shielding (O2-Me < O4-Me < N3-Me < C5-Me) parallels that of the methyl proton shifts. The shifts of the sugar carbon atoms are relatively invariant to the base. The largest effect (+1.6 ppm at C1′) is due to O2- and O4-methylation and suggests some polarization of the N1—C1′ bond.

*Base pairing*

Mispairing of purine and pyrimidine bases has been invoked in attempts to rationalize the changes in the information encoded in nucleic acids which are elicited by alkylation (2, 8), but no direct experimental evidence has so far been provided for these mispairs. Both m$^2$U (or m$^2$T) and m$^4$U (or m$^4$T) can form at most one hydrogen bond with A (adenine), the normal base complement of U (or T) (2). The G–m$^4$T complex with two hydrogen bonds (Fig. 6A) was the first postulated mispair for an O-alkylated thymine base (6). Its geometry would resemble that of the Watson–Crick G–C base pair (Fig. 6E), except for the noninvolvement of the 4-methoxy and the 6-keto groups. This structure, however, overlooks any steric effects of the 4-methyl group in *syn*, planar conformation which places the methyl hydrogens near to the N3 atom. (Calculations by Psoda *et al.* on O$^6$-methylguanine (52) lead us to think that the *syn*, planar conformer is favoured in m$^4$U(m$^4$T) as well as in m$^2$U(m$^2$T), but our nmr data provide no direct information about this matter.) If we continue to overlook steric effects, we can visualize a second G–m$^4$T complex with two hydrogen bonds (Fig. 6B) which requires a "wobble" of the pyrimidine base. Similarly we can conceive of two G–m$^2$T complexes, each with a pair of hydrogen bonds. The first (Fig. 6C) would have an overall geometry resembling the G–C and G–m$^4$T base pairs while the second (Fig. 6D) requires a wobble of the pyrimidine to align the hydrogen donating and accepting groups. The wobble of the pyrimidine base (Fig. 6B, D) is opposite in direction to the G–T(U) wobble base pair (Fig. 6F) which exists in tRNA acceptor stems (53).

The base pairs (Fig. 6A–D) raise the important question whether the 2- and 4-methoxy oxygens are capable of acting as hydrogen acceptors and whether the out-of-plane conformations of the methoxyl groups which would permit hydrogen bonding are energetically not too unfavorable. We have constructed space-filling models of right-handed and left-handed (Z-DNA) double helices, and found that the four base pairs (Fig. 6A–D) can be accommodated with only small adjustments in the conformation of the ribose phosphate backbone. We are hoping to extend our present work to synthetic oligonucleotides containing O-methylated pyrimidines in order to assess their ability to enter into ordered structures.

## Summary and conclusion

The $^1$H and $^{13}$C nmr data are presented for a series of ribosides and arabinosides with O-methylated pyrimidine bases. The $^1$H nmr data demonstrate that large changes in sugar conformation do not accompany methylation at the O2, N3, O4, or C5 positions of the base. The aberrant

Can. J. Chem. Downloaded from www.nrcresearchpress.com by 210.87.254.105 on 09/06/12
For personal use only.

biological behaviour of the O- and N-methylated molecules must be linked most closely to their altered hydrogen bonding (and perhaps base stacking) properties. The $J(5—6)$ proton couplings suggest a decreased $\pi$-bond order in the C5—C6 bonds of the O-methylated uracil bases. The $^{13}C$ chemical shifts indicate a general polarization of the base due to O-methylation.


## Acknowledgements

This work was funded by the Natural Sciences and Engineering Research Council of Canada. We acknowledge discussions with Drs. Hunter, McKinnon, McBride, Sadana, and Schaefer. We are grateful to Dr. J. L. Markley, The Biochemical Magnetic Resonance Laboratory, Purdue University (NIH Grant RR-01077) for 360 MHz spectra and Dr. D. L. Rabinstein, University of Alberta, Edmonton, for the 400 MHz spectrum of $m^4aU$. We thank L. Davies for some of the initial synthesis. We are especially grateful to Mr. K. Marat for his help in acquiring the $^{13}C$ nmr data and to Dr. W. P. Niemczura for acquiring the 360 MHz data.



1. B. Singer and M. Kroger. Prog. Nucleic Acid Res. Mol. Biol. **23**, 151 (1979).
2. B. Singer. *In* Carcinogenesis: fundamental mechanisms and environmental effects. *Edited by* B. Pullman, P. O. P. Ts'O, and H. Gelboin. D. Reidel Publishing Co., Dordrecht, The Netherlands. 1980. p. 91.
3. M. F. Rajewsky, R. Muller, J. Adamkiewicz, and W. Drosdziok. *In* Carcinogenesis: fundamental mechanisms and environmental effects. *Edited by* B. Pullman, P. O. P. Ts'O, and H. Gelboin. D. Reidel Publishing Co., Dordrecht, The Netherlands. 1980. p. 207.
4. M. Kroger and B. Singer. Biochemistry, **18**, 3493 (1979).
5. B. Pullman, D. Perahia, and C. Didier. Nucleic Acid Res. **6**, 3821 (1979).
6. R. Saffhill and P. J. Abbott. Nucleic Acid Res. **5**, 1971 (1978).
7. B. Singer, H. Fraenkel-Conrat, and J. T. Kusmierek. Proc. Natl. Acad. Sci. U.S.A. **75**, 1722 (1978).
8. P. J. Abbott and R. Saffhill. Nucleic Acid Res. **4**, 761 (1977).
9. P. Brookes and P. D. Lawley. Biochem. J. **80**, 495 (1961).
10. H. Fraenkel-Conrat. Biochim. Biophys. Acta, **49**, 169 (1961).
11. A. Loveless. Nature (London), **223**, 206 (1969).
12. B. Singer. Prog. Nucleic Acid Res. Mol. Biol. **15**, 219 (1975).
13. W. P. Niemczura, F. E. Hruska, K. L. Sadana, and P. C. Loewen. Biopolymers, **20**, 1671 (1981), and references therein.
14. J. Kimura, Y. Fujisawa, T. Sawada, and O. Mitsunobu. Chem. Lett. 691 (1974).
15. M. J. Robins and S. R. Naik. Biochemistry, **10**, 3591 (1971).
16. H. T. Miles. Biochim. Biophys. Acta, **22**, 247 (1956).
17. P. J. Cozzone and O. Jardetzky. Biochemistry, **15**, 4860 (1976).
18. C. W. Haigh and J. M. Williams. J. Mol. Spectrosc. **32**, 398 (1969).
19. T. Schleich, B. J. Blackburn, R. D. Lapper, and I. C. P. Smith. Biochemistry, **11**, 137 (1972).
20. F. E. Hruska, A. Mak, H. Singh, and D. Shugar. Can. J. Chem. **51**, 1099 (1972).
21. J. G. Dalton, A. L. George, F. E. Hruska, T. N. McCaig, K. K. Ogilvie, J. Peeling, and D. J. Wood. Biochim. Biophys. Acta, **478**, 261 (1977).
22. W. P. Niemczura and F. E. Hruska. Can. J. Chem. **58**, 472 (1980).
23. J. L. Wong and D. S. Fuchs. J. Org. Chem. **35**, 3786 (1970).
24. C.-G. Lee and C.-J. Chang. J. Carbohydr. Nucleosides Nucleotides, **5**, 343 (1978).
25. M. Remin and D. Shugar. Biochem. Biophys. Res. Commun. **48**, 636 (1972).
26. R. G. S. Ritchie and A. S. Perlin. Carbohydr. Res. **55**, 121 (1977).
27. I. W. J. Still, N. Plavac, D. M. McKinnon, and M. S. Chauhan. Can. J. Chem. **56**, 725 (1978).
28. A. J. Jones, D. M. Grant, M. W. Winkley, and R. K. Robbins. J. Phys. Chem. **74**, 2684 (1970).
29. E. A. Green, R. Shiono, R. D. Rosenstein, and D. J. Abraham. Chem. Commun. **53**, 1973.
30. S. Furberg, C. S. Peterson, and C. Romming. Acta Crystallogr. **18**, 313 (1965).
31. D. J. Hunt and E. Subramanian. Acta Crystallogr. Sect. B, **25**, 2144 (1969).
32. A. K. Chwang and M. Sundaralingam. Nature, **243**, 79 (1973).
33. D. B. Davies. Prog. Nucl. Magn. Reson. Spectrosc. **12**, 135 (1978).
34. C. R. Narayanan and K. N. Iyer. Tetrahedron Lett. 3741 (1965).
35. W. Guschlbauer and M. Privat de Garilhe. Bull. Soc. Chim. Biol. **51**, 10 (1969).
36. F. E. Hruska. Can. J. Chem. **49**, 2111 (1971).
37. C. Altona and M. Sundaralingam. J. Am. Chem. Soc. **95**, 2333 (1973).
38. F. E. Hruska. Jerusalem Symp. Quantum Chem. Biochem. **5**, 345 (1973).
39. E. Egert, H. J. Lindner, W. Hillen, and M. C. Bohm. J. Am. Chem. Soc. **102**, 3707 (1980).
40. C. A. G. Haasnoot, F. A. A. M. de Leeuw, H. P. M. de Leeuw, and C. Altona. Recl. Trav. Chim. Pays-Bas, **98**, 576 (1980).
41. M. Sundaralingam. Jerusalem Symp. Quantum Chem. Biochem. **5**, 417 (1973).
42. S. Yokoyama, F. Inagaki, and T. Miyazawa. J. Am. Chem. Soc. **20**, 2981 (1981).
43. P. Tollin, H. R. Wilson, and D. W. Young. Acta Crystallogr. Sect. B, **29**, 1641 (1973).
44. A. Saran, B. Pullman, and B. Perahia. Biochim. Biophys. Acta, **349**, 189 (1974).
45. F. E. Hruska, J. G. Dalton, and M. Remin. Can. J. Chem. **57**, 2191 (1979).
46. J. S. Kwiatkowski and B. Pullman. Adv. Heterocycl. Chem. **18**, 199 (1975).
47. A. Veillard. J. Chim. Phys. 1056 (1962).
48. B. Pullman and A. Pullman. Quantum biochemistry, John Wiley and Sons, New York, NY. 1963. p. 679.
49. U. E. Matter, C. Pascual, E. Pretsch, A. Pross, W. Simon, and S. Sternhell. Tetrahedron, **25**, 691 (1969).
50. A. R. Tarpley, Jr. and J. H. Goldstein. J. Am. Chem. Soc. **93**, 3773 (1971).
51. P. D. Ellis, R. B. Dunlap, A. L. Pollard, K. Seidman, and A. D. Cardin. J. Am. Chem. Soc. **95**, 4398 (1973).
52. A. Psoda, B. Kierdaszuk, A. Pohorille, M. Geller, J. T. Kusmierek, and D. Shugar. Int. J. Quantum Chem. **20**, 543 (1981).
53. M. Sundaralingam. Int. J. Quantum Chem. **4**, 11 (1977).


Can. J. Chem. Downloaded from www.nrcresearchpress.com by 210.87.254.105 on 09/06/12
For personal use only.

# Metal ion – biomolecule interactions. IV.[1] Methylmercury(II) complexes of 1-methylimidazoline-2-thione (methimazole), a potentially useful protective agent in organomercurial intoxication

ERWIN BUNCEL,[2] ALBERT R. NORRIS, AND SPENCER E. TAYLOR[3]
*Department of Chemistry, Queen's University, Kingston, Ont., Canada K7L 3N6*
AND
WILLIAM J. RACZ
*Department of Pharmacology, Queen's University, Kingston, Ont., Canada K7L 3N6*

Received June 8, 1982

ERWIN BUNCEL, ALBERT R. NORRIS, SPENCER E. TAYLOR, and WILLIAM J. RACZ. Can. J. Chem. **60**, 3033 (1982).

Two 1:1 methylmercury(II)-1-methylimidazoline-2-thione (methimazole, MeImSH) complexes, [MeHg(MeImSH)]$NO_3$ and [MeHg(MeImS)], have been isolated from aqueous solution under acidic and basic conditions, respectively. $^1H$ nmr and ir spectroscopy, as well as analytical data, were used to characterize the complexes. The nmr data, in particular, lead to the conclusion that the principal binding mode under both sets of conditions involves the sulfur atom at $C_2$. However, under conditions of 2:1 ($MeHg^{II}$:MeImSH) stoichiometry, binding to $N_3$ is also found to occur. These interpretations have necessitated a reexamination of the $^1H$ nmr spectrum of the free ligand, in particular with respect to assignment of NH and SH resonances corresponding to the two possible tautomeric forms. It has been found in this work that 1-methylimidazoline-2-thione shows a high affinity for $MeHg^{II}$ binding, which may be pertinent with respect to a previous report concerning the protective nature of this compound in organomercurial intoxication.

ERWIN BUNCEL, ALBERT R. NORRIS, SPENCER E. TAYLOR et WILLIAM J. RACZ. Can. J. Chem. **60**, 3033 (1982).

On a isolé deux complexes de type 1:1 de méthylmercure(II) mercapto-2 méthyl-1 imidazole (méthimazole, MeImSH) [MeHg(MeImSH]$NO_3$ et [MeHg(MeImS)] à partir de solutions aqueuses dans des conditions acides et basiques respectivement. On a fait appel à la rmn du $^1H$ à la spectroscopie ir aussi bien qu'aux données analytiques pour caractériser ces complexes. Les données de la rmn en particulier font penser que le mode principal de liaison dans les deux conditions implique l'atome de soufre au niveau du carbone en position 2. Cependant, dans les conditions stochioemétrique 2:1 de ($MeHg^{II}$:MeImSH) la liaison impliquant l'azote en position 3 s'établit également. Ces interprétations font ressentir la nécessité d'examiner de nouveau le spectre de rmn du $^1H$ du ligand libre, en particulier en ce qui à trait à l'attribution des résonances du NH et du SH correspondant aux deux formes tautomères possibles. On a trouvé, dans ce travail, que le méthimazole montre une grande affinité pour la liaison $MeHg^{II}$, laquelle peut être intéressante compte tenu des données antérieures relatives à la nature protectrice de ce composé dans les cas d'intoxication par les organomercures.

[Traduit par le journal]

## Introduction

In previous papers in this series, we have investigated the binding of methylmercury(II) towards a number of nucleoside and imidazole systems, and found the involvement of both nitrogen and carbon centers in complex formation (1–3). The present paper is concerned with the $MeHg^{II}$ binding characteristics of the 1-methylimidazole system modified by the introduction of a sulfur function at $C_2$, viz. 1-methylimidazoline-2-thione, hereafter referred to by its trivial name, methimazole, and abbreviated as MeImSH. (Formally, the $C_2$—H in 1-methylimidazole is replaced by SH; see, however, the discussion on thione–thiol tautomerism.)

Methimazole is known to have several chemotherapeutic applications, particularly in the treatment of thyroid disorders (4). Our interest in this particular imidazole derivative was initiated by the report (5) that the use of methimazole (and other sulfur-containing thyroid hormone inhibitors) afforded a significant degree of protection against the effects of dimethylmercury and diphenylmercury intoxication in laboratory animals.

The interaction of heavy metal ions with methimazole has to date received little attention. Dehand and Jordanov (6), in synthesizing $Pt^{II}$ and $Pd^{II}$ complexes for antitumor screening purposes (7), deduced on the basis of ir spectroscopy that $N_3$ was the preferred binding site under acidic conditions, while the sulfur atom was implicated under basic conditions. $^1H$ nmr spectroscopy was used to confirm the previous ir assignments (6). Unexpectedly, during the course of the present study, we were unable to reproduce the spectrum of methimazole as previously reported in $(CD_3)_2SO$ solution (6). Since many of the deductions regarding binding sites in the present study relied heavily on $^1H$ nmr analyses, a reexamination of the spectral

[1]Part III is ref. 3.
[2]To whom all correspondence should be addressed.
[3]Present address: Inorganic Chemistry Laboratory, University of Oxford, South Parks Road, Oxford, 0X1 3QR, U.K.

0008-4042/82/243033-06$01.00/0
©1982 National Research Council of Canada/Conseil national de recherches du Canada

Can. J. Chem. Downloaded from www.nrcresearchpress.com by 210.87.254.105 on 09/06/12
For personal use only.

Can. J. Chem. Downloaded from www.nrcresearchpress.com by 210.87.254.105 on 09/06/12
For personal use only.

characteristics of methimazole is included in the present paper.

## Experimental

Methimazole was purchased from the Sigma Chemical Co. and recrystallized from ethanol before use, mp 144–146°C, lit. (8) 142°C. *Anal.* calcd. for $C_4H_6N_2S$: C 42.11, H 5.26, N 24.56; found: C 42.17, H 5.39, N 25.07.

$^1$H nmr spectra were recorded at 60 MHz on a Varian EM 360 or Bruker HX-60 instrument and referenced with respect to internal $(CH_3)_4Si$. Infrared spectra were recorded as 1% KBr discs on Perkin-Elmer 180 or 598 spectrophotometers.

Microanalyses were performed by the Guelph Chemical Laboratory. Melting points were taken on a Mel-temp melting point apparatus and are uncorrected.

*Methimazole–MeHg$^{II}$ complex formation*

An equimolar mixture of methimazole (0.183 g) and methylmercuric nitrate (0.445 g) in distilled water (7 mL) resulted in the formation of a white, gelatinous precipitate. Upon heating the precipitate dissolved, affording a neutral solution, which was set aside to crystallize. After one day, white crystals of a substance **A** appeared; these were removed by filtration, washed quickly with water, and dried *in vacuo*, mp 142–143°C (decomp.). Yield = 0.454 g. *Anal.* calcd. for [MeHg(MeImSH)]$NO_3$: C 15.32, H 2.30, N 10.73, S 8.17; found: C 15.38, H 2.34, N 10.84, S 8.26.

Under more basic conditions, but still retaining 1:1 stoichiometry, a solution (10 mL) containing methimazole (0.183 g) and sodium hydroxide (1.60 mL of a 1 *M* stock solution) was added slowly with stirring to a methylmercuric nitrate solution (0.444 g in 5 mL distilled water). During the addition a faint cloudiness was apparent which, on complete addition, yielded a white precipitate. After continuing to stir for 1–2 min, the precipitate transformed into a yellow oil. The volume of the resultant mixture was then doubled by the addition of an equal volume (15 mL) of absolute ethanol, and it was stirred vigorously for ca. 15 min, after which time the mixture still retained its two-phase nature. However, on standing, the yellow oil solidified to give a pale yellow solid ($\mathbf{B}_1$) and, almost simultaneously, small white needles ($\mathbf{B}_2$) appeared in the bulk of the solution. The apparent pH of the resultant solution was ca. 8. The total product was removed by filtration and washed with water. Separation of $\mathbf{B}_1$ and $\mathbf{B}_2$ was easily effected by the ready removal of the solid mass of the former. Yield of $\mathbf{B}_1$ = 0.133 g (mp 83–84°C). *Anal.* $\mathbf{B}_1$. calcd. for [MeHg(MeImS)]: C 18.26, H 2.43, N 8.52, S 9.74; found: C 18.15, H 2.51, N 8.71, S 9.94. Yield of $\mathbf{B}_2$ = 0.251 g (mp 76–77°C). *Anal.* $\mathbf{B}_2$. calcd. for [MeHg(MeImS)]: (as above); found: C 18.15, H 2.50, N 8.77, S 9.89.

The ir as well as the nmr spectra of $\mathbf{B}_1$ and $\mathbf{B}_2$ were identical, within experimental error. In view of this fact, and the identity within experimental error of the analytical data for $\mathbf{B}_1$ and $\mathbf{B}_2$, it is concluded that these represent the same compound, having the molecular formula [MeHg(MeImS)]. In the ensuing discussion (vide infra) this compound will be denoted by **B**.

Under conditions of 2:1 MeHg$^{II}$–methimazole stoichiometry, binding to both $N_3$ and sulfur was envisaged. To this end, an aqueous solution (5 mL) of methimazole (0.065 g, 0.57 mmol) and sodium hydroxide (0.57 mL of a 1 *M* solution, 0.57 mmol) was added to a stirred solution of methylmercuric nitrate (0.314 g, 1.13 mmol) in distilled water (5 mL). During the addition, a light-brown oil, **C**, collected at the bottom of the vessel; unlike the case of the 1:1 reaction (above), on subsequent treatment with ethanol this did not solidify. On solvent evaporation, a small quantity of a crystalline material formed and was removed. This is believed to be $NaNO_3$ by virtue of the lack of detectable protons in the $^1$H nmr spectrum and the presence of $NO_3^-$ in the ir. The $^1$H nmr spectrum of **C** showed 2:1 MeHg$^{II}$:methimazole stoichiometry, as expected, and as such **C** was formulated as being [$(MeHg)_2$(MeImS)]$NO_3$.

## Results and discussion

*Possible binding sites and tautomerism in methimazole*

At the outset of this study it was envisaged that the sulfur atom at $C_2$ would modify the MeHg$^{II}$ binding characteristics of the 1-methylimidazole system, studied previously (3). In the "parent" substrate, both $N_3$ and $C_2$ have been identified as binding sites (3). In methimazole, the sulfur bound to $C_2$ clearly prevents the possibility of direct MeHg$^{II}$ binding to $C_2$, although $N_3$ is still available. The preference of MeHg$^{II}$ for soft donor atoms such as sulfur, however, would be expected to result in this being a more likely binding site than $N_3$. In their study of binding of metal ions to methimazole, Dehand and Jordanov (6) made inferences concerning the sites of binding of Pd$^{II}$ and Pt$^{II}$, on the basis of ir and $^1$H nmr evidence. However, we were unable to reproduce the published spectrum (6) of methimazole, for which correct assignment of NH and SH resonances is crucial in assigning metal ion binding sites.

Mercaptoazole derivatives such as methimazole are capable of existing in two tautomeric forms, **1**

[1] 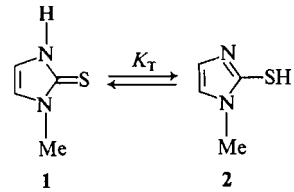


**1** **2**

and **2** (reaction [1]) (9). In $(CD_3)_2SO$ solution, we find the $^1$H nmr spectrum of methimazole to consist of four resonances (Fig. 1). The signals due to the

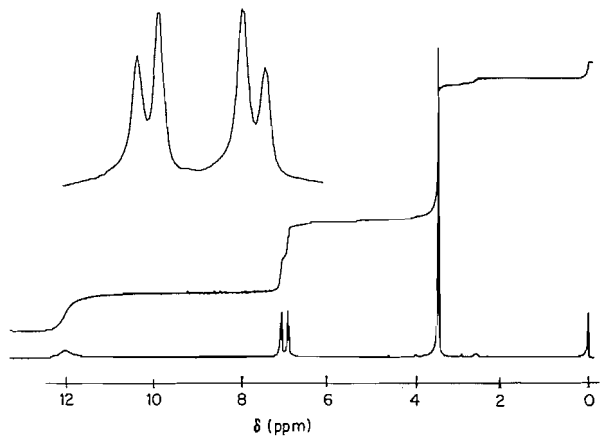


FIG. 1. Proton magnetic resonance spectrum of methimazole in $(CD_3)_2SO$. (Inset $H_4$, $H_5$ quartet on expanded scale.)

TABLE 1. $^1$H nmr spectra at 60 MHz of methimazole in various solvents at 22 ± 1°C

| Solvent | Chemical shift[a,b] | | | |
|---|---|---|---|---|
| | $H_4$ | $H_5$ | $CH_3$ | NH[d] |
| $(CD_3)_2SO$ | 6.87±0.01(d) | 7.05±0.01(d) | 3.45±0.01(s) | 12.0±0.2(br) |
| $CDCl_3$ | 6.71±0.04(s) | 6.71±0.04(s) | 3.60±0.03(s) | 12.1±0.2(br) |
| $CD_3CN$ | 6.84±0.01(d) | 6.73±0.01(d) | 3.49±0.01(s) | 10.70±0.08(br) |
| $(CD_3)_2CO$ | 7.01±0.01(d) | 6.93±0.01(d) | 3.54±0.01(s) | 11.2±0.2 (br) |
| $CD_3NO_2$[c] | 6.87(s) | 6.87(s) | 3.53(s) | 10.9(br) |
| $C_5D_5N$ | 7.00±0.02(d) | 6.89±0.02(d) | 3.58±0.02(s) | 11.4±0.3(v.br) |

[a]Where indicated, the quoted uncertainties take into account a concentration range from 0.3–1.0 *M*.
[b]δ(ppm) from internal $(CH_3)_4Si$; s = singlet, d = doublet ($J$ = 2.5 Hz), br = broad.
[c]For a saturated solution.
[d]The relative integral height of this signal corresponds to < 1 proton (see text).

methyl group, $H_4$ and $H_5$ (δ 3.45, 6.87 (d), and 7.05 (d)), are as quoted by Dehand and Jordanov (6), but we observe an additional (broad) resonance at low field (~δ 12) which we ascribe to NH, by analogy with other azole NH functions (e.g. imidazole, δ(NH) 11.6 (3)). This is in marked contrast with the previous report (6) of a resonance at δ 5.40, assigned to the NH proton of **1** and a signal at δ 3.80 assigned to the SH proton of **2** in the same solvent. These signals, at δ 5.40 and 3.80 were not found in our system. In the published spectrum (6) it is also evident that the total integral due to "NH" and "SH" signal is >1 proton.

We find that the position of the NH resonance appears to be concentration- and solvent-dependent, varying between δ 10.7 and 12.1, and integrates to <1 proton, the difference presumably being accounted for by the **2** (SH) tautomer (10). Solvent dependences of the $^1$H nmr spectral parameters at 60 MHz, shown in Table 1, have been averaged over the concentration range 0.3–1 *M*. In none of the solvents examined was a signal at δ 3.8, previously assigned to SH, apparent. This contrasts with the case of thiomorpholin-3-thione in which both NH and SH signals appear in $CDCl_3$, at δ 8.36 and 1.88 respectively (10), such that $K_T$ (reaction [1]) ≈ 0.25 at 28°C. In the case of methimazole, as in the case of thiamorpholin-3-thione (10), the NH signal is observed to shift to higher field on decreasing the substrate concentration. Such spectral features are a consequence of self-association and solvation of the substrate (9). In methimazole, the higher concentration serves to stabilize the thioketo structure, through a dimerization equilibrium (reaction [2]) (9). The dimeric structure **1**-D is presumably the structure reflected in the solid-state ir spectrum of methimazole, as well as in the $^1$H nmr spectra of concentrated solutions of methimazole in weakly-coordinating solvents.

[2] 2(**1**) ⇌ 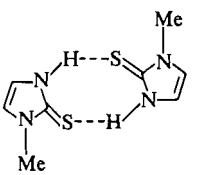

**1**-D

*Sites of metal ion binding in methimazole: N- versus S-methylmercuration*

In light of the above discussion concerning tautomerism in the methimazole system, we can view the deprotonation of **1** and **2** as giving rise to the delocalized anion **3**, according to reaction [3].

[3] **1** ⇌ 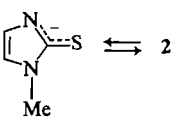 ⇌ **2**

**3**

One can then envisage **3** as having the potentiality of an ambidentate ligand with respect to metal ion coordination (i.e. $N_3$ versus S binding). This may serve as the basis for the structural assignment of the complexes **A**, **B**, and **C**, which have been obtained under different conditions of pH and stoichiometry (see Experimental).

The tendency for heavy metal ions such as $Hg^{II}$ to favour sulfur over nitrogen donor atoms would seem to suggest S as the most probable $MeHg^{II}$ binding site in the product **B** prepared under conditions in which deprotonation of methimazole would occur, i.e. at high initial pH ($pK_a$ for deprotonation of methimazole is 11.6 (11)). The complex **B** is found by microanalysis to correspond to the formula [MeHg(MeImS)] and this formulation is supported by the $^1$H nmr spectrum. Thus the structure of this complex can be represented by either **4** or **5**. Evidence in favour of structure **4** derives from the low value (Table 2) of $^2J(^{199}Hg$—

Can. J. Chem. Downloaded from www.nrcresearchpress.com by 210.87.254.105 on 09/06/12
For personal use only.

TABLE 2. $^1H$ nmr spectral data for the methimazole systems

| Compound | Chemical shifts[a] [$^2J(^{199}Hg—^1H)$][b] | | | | |
|---|---|---|---|---|---|
| | $H_4$[c] | $H_5$[c] | NH | $CH_3$ | $CH_3Hg^{II}$ |
| Methimazole (**1** ⇄ **2**) | 6.87 | 7.05 | 12.0[d,e] | 3.45 | — |
| **4**, [MeHg(MeImS)] | 6.67 | 6.99 | — | 3.48 | 0.72(184.6) |
| **6**, [MeHg(MeImSH)]$NO_3$ | 7.46 | 7.56 | 13.77[d] | 3.72 | 0.78(204.2) |
| **9**, [$(MeHg)_2$(MeImS)]$NO_3$ | 7.20 | 7.46 | — | 3.72 | 0.78(207.8) |

[a]δ(ppm) obtained in $(CD_3)_2SO$ solution referenced to internal $(CH_3)_4Si$.
[b]$[^2J(^{199}Hg—^1H)]$ values (in parentheses) given in Hz; the signs of the coupling constants have not been determined.
[c]Doublets ($J$ ~2–3 Hz).
[d]Broad resonances.
[e]Concentration dependent (see Table 1).

$^1H$), 184.6 Hz in $(CD_3)_2SO$, which is characteristic of *S*-bonded $MeHg^{II}$ (14).

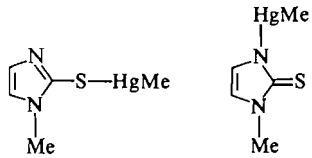


**4** **5**

Assignment of *S* bonding in methimazole complexes has generally been based on ir spectral considerations (6, 13). Thus $Pd^{II}$, $Pt^{II}$ (6), $Co^{II}$, and $Zn^{II}$ (13) binding to S have been identified by noting changes in intensities and positions of certain assigned bands, as compared with the free ligand. However, this type of analysis, in the case of methimazole, may lead to uncertain inferences since the ir spectrum of the free ligand corresponds to the hydrogen-bonded dimer **1**-D (9), whereas metal ion complexation removes the ability for hydrogen bonding. In addition, an examination of the literature reveals that there is little agreement in the band assignments of methimazole. The various assignments given to the major bands within the range 1600–300 $cm^{-1}$ are listed in Table 3. This overall disagreement, coupled with the fact that the ir spectrum of methimazole does not correspond to that of "free" methimazole, suggests that ir spectroscopy is not a reliable method of assigning metal ion binding sites in such systems. Indeed, if the criteria used in the past (6, 13) for identifying *S* bonding were applied to the present system (i.e. a decrease in frequency of band *1* and decreases in frequency and intensity of bands *2*, *8*, and *18* (6), or a decrease in frequency (by 20–25 $cm^{-1}$) of band *16* (13)), this would lead to the conclusion that (apart from the behaviour of bands *1* and *2*) this complex is *not* *S*-bonded. However, the $^1H$ nmr and other evidence cited above provide strong support for an S-bonded structure for **B**, i.e. structure **4**.

Complex **A**, formed under acidic conditions, corresponds to the formula [MeHg(MeImSH)]-$NO_3$, and can be considered as derived from a similar ambidentate system (i.e. N vs. S, as in **6** and **7**). In solution, the $^1H$ nmr spectrum of **A** reveals a broad resonance, centered at δ 13.77 (Table 2),

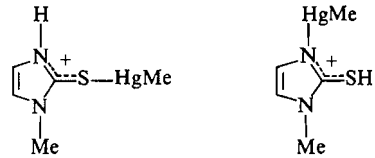


**6** **7**

integrating to ca. 1 proton, and ascribable to NH. Of the two possible structures for **A**, that is **6** and **7**, it appears that **6**, containing *S*-bound $MeHg^{II}$, is the more likely possibility in solution. The ir spectrum of **A** is also in accord with the formulation in **6**. The presence of nitrate is indicated (band *4*), and the positions of the ν(Hg—C) and ν(Hg—ligand) bands (*19* and *21*, respectively) are very similar to their positions in **B** where *S*-bonding (**4**) was assigned above. The positions of the latter band in **A** and **B** (~336 $cm^{-1}$) compares very well with the ν(Hg—S) stretching frequencies in $MeHg^{II}$ complexes with a number of thiols (15), whilst the ν(Hg—C) vibration (~550 $cm^{-1}$) is more typical of *S*-bonding than *N*-bonding (16).

A notable feature in the $^1H$ nmr spectrum of **A** is that the coupling constant $^2J(^{199}Hg—^1H)$ of 204.2 Hz (Table 2) is higher than the value (184.6 Hz) found for *S*-bonding in **B** (**4**). This probably reflects the fact that protonation of $N_3$ has taken place in **A** (**6**), thereby decreasing the basicity of the sulfur donor atom. It is also pertinent that $N_3$ coordination by $MeHg^{II}$ in 1-methylimidazole, which gives rise to **8**, leads to a coupling constant of 222.1 Hz (3), significantly higher than that observed for **A** (6). In addition, the ir spectrum of **8** shows no bands in

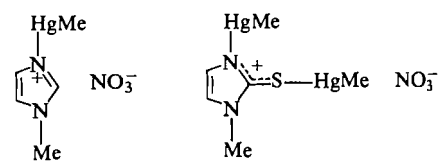


**8** **9**

Can. J. Chem. Downloaded from www.nrcresearchpress.com by 210.87.254.105 on 09/06/12
For personal use only.

TABLE 3. Main ir spectral bands of methimazole and its 1:1 methylmercury(II) complexes in the region 1600–300 $cm^{-1}$ [a,b]

| | Band number and assignment | MeImSH[c] | [MeHg(MeImSH)]$NO_3$(**6**)[d] | [MeHg(MeImS)](**4**)[d] |
|---|---|---|---|---|
| *1* | ν(C═C)[ν(C═N) + ν(N—C═S)][e] | 1569s | 1577s | 1510m |
| *2* | δNH + ν(C⋯N), [ν(C═N) + ν(N—C═S)][e,f] | 1460s | 1475m | 1450s |
| *3* | [g] | 1396m | 1419m,sh | 1410m |
| *4* | ν($NO_3^-$) | — | 1390s | — |
| *5* | — | — | — | 1382m–w |
| *6* | — | — | 1360sh | 1360s |
| *7* | ν(C⋯N) + δNH | 1332m | 1305s | 1319m |
| *8* | [g][ν(C—S)][e,h] | 1272s | 1264m | 1278s |
| *9* | Ring mode | 1245m | — | — |
| *10* | ν(C═S) | 1146m | 1150m | 1143m |
| *11* | — | — | — | 1115m |
| *12* | δCH[i] | 1083m | 1086vw | 1086w |
| *13* | [g] | 1014m | 1034m | — |
| *14* | Ring mode | 910w | 916w | 914w |
| *15* | γCH | 844w | 850vw | 860w |
| *16* | γNH[j] | 765s | 780w–m | 779m,sh |
| *17* | γCH | 740s | 740m | 759s |
| *18* | Ring mode, [ν(C—S)][e] | 670m | 670m | 680s |
| *19* | ν(Hg—C)[k] | — | 544w | 554w |
| *20* | δ(C═S) or ring mode + ν(C═S) | 525m | 500w | 532w |
| *21* | ν(Hg—ligand)[k] | — | 336m | 337m |

[a]Spectra recorded as 1% KBr discs.
[b]s, m, and w are strong, medium, and weak intensity bands respectively; sh = shoulder.
[c]Assignments are from ref. 12 unless otherwise indicated.
[d]See Experimental for designation.
[e]Assignments from ref. 6.
[f]Thioamide band I from ref. 13.
[g]Bands unassigned in ref. 12.
[h]Thioamide band II from ref. 13.
[i]Thioamide band III from ref. 13.
[j]Thioamide band IV from ref. 13.
[k]Present assignments.

the region 500–300 $cm^{-1}$, suggesting that the band observed at 336 $cm^{-1}$ for **A** is *not* due to *N*-coordination. Thus the sum of the evidence is in accord with the assignment of structure **6** to compound **A**.[4]

Under conditions of 2:1 $MeHg^{II}$:methimazole stoichiometry, a further replacement of the $N_3$ proton in **6** occurs, giving rise to complex **C**, to which structure **9** is assigned. Not surprisingly in this case, the coupling constant in **9**, 207.8 Hz, is found to be approximately intermediate between the value obtained previously (3) for **8** (222.1 Hz) and the value (184.6 Hz) for **4**, indicating rapid exchange of $MeHg^{II}$ between the two environments.

## Concluding remarks

We have found in the present study that 1:1 $MeHg^{II}$–methimazole complexes involve binding via the sulfur atom (i.e. **4** and **6**), which contrasts with the report by Dehand and Jordanov (6) that binding of $Pd^{II}$ and $Pt^{II}$ to methimazole occurs via $N_3$ at low pH, and via $N_3$ and S at high pH. In our system, under acidic conditions, S was found to be the $MeHg^{II}$ binding site, with $N_3$ protonated. Under basic conditions, S remained the donor atom, with deprotonation of $N_3$ taking place, and giving rise to the neutral complex **4**. The resulting increase in strength of the Hg—S bond is reflected in the magnitude of the $^2J(^{199}Hg—^1H)$ coupling constants. Thus methimazole shows different coordination behaviour to its parent, 1-methylimidazole (3), with $N_3$ no longer being the primary donor atom. This is in accord with the preference of $Hg^{II}$ for soft (class *b*) donor atoms such as sulfur (17).

Extrapolating to biological systems, the significance of these results is that any purine carrying a thiol (or thioketo) substituent would presumably bind $Hg^{II}$ primarily through the sulfur atom; such characteristics have previously been demonstrated by Lippard and co-workers (18) using $^{13}C$ nmr spectroscopy with sulfur-containing nucleosides. Only when the sulfur atom is blocked by alkylation or prior coordination, do other (nitrogen) sites become important.

Although the effectiveness of methimazole in protecting against organomercurial intoxication is believed to be by virtue of its action on the thyroid

[4]An X-ray crystal structure determination of **6** has been performed (A. L. Beauchamp) and will be reported in due course.

Can. J. Chem. Downloaded from www.nrcresearchpress.com by 210.87.254.105 on 09/06/12
For personal use only.

gland (5), it can be envisaged that methimazole would also be effective in competing with sulfur-containing bio-ligands for $Hg^{II}$.


## Acknowledgements

We thank the Natural Sciences and Engineering Research Council of Canada for support of the work via the Strategic Grants Program in Environmental Toxicology. Helpful discussions with Dr. B. K. Hunter are also acknowledged.



1. E. Buncel, A. R. Norris, W. J. Racz, and S. E. Taylor. J. Chem. Soc. Chem. Commun. 562 (1979); Inorg. Chem. **20**, 98 (1981).
2. S. E. Taylor, E. Buncel, and A. R. Norris. J. Inorg. Biochem. **15**, 131 (1981).
3. A. R. Norris, E. Buncel, and S. E. Taylor. J. Inorg. Biochem. **16**, 279 (1982).
4. A. Taurog. Endocrinology, **98**, 1031 (1976).
5. S. Szabo, P. Kourounakis, K. Kovacs, B. Tuchweber, and B. D. Garg. Toxicol. Appl. Pharmacol. **30**, 175 (1974).
6. J. Dehand and J. Jordanov. Inorg. Chim. Acta, **17**, 37 (1976).
7. J. Dehand, J. Jordanov, and J. P. Beck. Chem.-Biol. Interactions, **11**, 605 (1975).
8. Dictionary of organic compounds. Vol. 4. Eyre and Spottiswoode, London. 1965. p. 2100.
9. E. Gentric, J. Lauransan, C. Roussel, and J. Metzger. J. Chem. Soc. Perkin Trans. **II**, 1015 (1977).
10. D. De Filippo, A. Lai, E. F. Trogu, and G. Verani. J. Inorg. Nucl. Chem. **36**, 73 (1974).
11. H. Sakurai and S. Takeshina. Trans. Met. Chem. **2**, 103 (1977).
12. G. Mille, J. Kister, G. Assef, and J. Chouteau. C.R. Acad. Sc. Paris, Ser. C, **286**, 477 (1978).
13. E. S. Raper and J. L. Brookes. J. Inorg. Nucl. Chem. **39**, 2163 (1977).
14. D. L. Rabenstein. Acc. Chem. Res. **11**, 100 (1978).
15. A. J. Canty and R. Kishimoto. Inorg. Chim. Acta, **24**, 109 (1977).
16. Y.-S. Wong, A. J. Carty, and P. C. Chieh. J. Chem. Soc. Dalton Trans. 1157 (1977).
17. S. Ahrland, J. Chatt, and N. R. Davies. Q. Rev. Chem. Soc. **11**, 265 (1958).
18. K. W. Jennette, S. J. Lippard, and D. A. Ucko. Biochim. Biophys. Acta, **402**, 403 (1975).


Can. J. Chem. Downloaded from www.nrcresearchpress.com by 210.87.254.105 on 09/06/12
For personal use only.

# Kinetics of the reaction $C_2H_5 + H_2 \rightarrow C_2H_6 + H$ from 1111–1200 K

J.-R. CAO AND M. H. BACK

*Chemistry Department, University of Ottawa, Ottawa, Ont., Canada K1N 9B4*

Received June 16, 1982

J.-R. CAO and M. H. BACK. Can. J. Chem. **60**, 3039 (1982).

A system for the measurement of the rate constant for the elementary reaction

$$C_2H_5 + H_2 \rightarrow C_2H_6 + H$$

in the temperature range 1111–1200 K is described and is based on the thermal production of an equilibrium concentration of hydrogen atoms. In a mixture of hydrogen with about 10 ppm ethylene this reaction is the rate-controlling step in the hydrogenation of ethylene. The product ethane undergoes rapid secondary dissociation and the final product is methane. The values obtained in the present work, which are represented by the following expression,

$$\log k \text{ (L mol}^{-1} \text{ s}^{-1}) = 10.6 - 23000/2.3RT$$

($R$ = 1.987 cal mol$^{-1}$ deg$^{-1}$) are compared to those obtained at lower temperature (820–350 K) and to those calculated from measurements of the reverse reaction.

---

J.-R. CAO et M. H. BACK. Can. J. Chem. **60**, 3039 (1982).

On décrit un système de mesure de la constante de vitesse de la réaction élémentaire

$$C_2H_5 + H_2 \rightarrow C_2H_6 + H$$

dans l'intervalle de température allant de 1111 à 1200 K. Ce système se base sur la formation thermique d'une concentration à l'équilibre des atomes d'hydrogène. Dans un mélange d'hydrogène avec environ 10 ppm d'éthylène, cette réaction constitue l'étape déterminante de la réaction d'hydrogénation de l'éthylène. L'éthane obtenu subit une dissociation secondaire rapide et conduit au méthane comme produit final. On a comparé les valeurs obtenues que l'on représente par l'expression suivante

$$\log k \text{ (L mol}^{-1} \text{ s}^{-1}) = 10{,}6 - 23000/2{,}3RT$$

($R$ = 1,987 cal mol$^{-1}$ deg$^{-1}$), avec celles obtenues à plus basse température (820–350 K) et avec celles calculées à partir des mesures de la réaction inverse.

[Traduit par le journal]

Can. J. Chem. Downloaded from www.nrcresearchpress.com by 210.87.254.5 on 09/06/12
For personal use only.

## Introduction

There has been much interest in recent years in extending measurements of rate constants for elementary reactions of hydrocarbon radicals into a high-temperature region. Few rate constants for these radicals have been measured at temperatures above 1000 K, yet many thermal reaction systems involving these radicals have been studied at these temperatures and higher. In order to understand the mechanisms of these reactions it is essential to have reliable measurements of the rate constants for the elementary reactions involved, many of which are obtained by extrapolation from measurements made at much lower temperatures. Serious errors may be introduced in this procedure by the non-Arrhenius behavior observed for the reactions of hydrogen atoms and small radicals (1). This behavior, which is not unexpected over a wide temperature range, is of theoretical as well as practical importance in the understanding of reaction mechanisms and the details of reaction pathways (2).

A new system for the measurement of rate constants for radical reactions at temperatures above 1000 K has been explored in this laboratory. The method is based on the premise that at these temperatures and moderate pressures of hydrogen an equilibrium concentration of hydrogen atoms can be maintained in the system. A small quantity of reactant, in our studies, ethylene, in concentrations of a few ppm, is added to the hydrogen and the rate of consumption of ethylene and appearance of the products is measured. The assumption is made, and tested by the kinetics, that the equilibrium between hydrogen molecules and atoms is not significantly perturbed by the addition of the reagent. In the present study, it is shown that as well as the equilibrium concentration of hydrogen atoms, an equilibrium concentration of ethyl radicals is attained by addition of hydrogen atoms to ethylene and the rate-controlling step is the abstraction reaction of ethyl radicals with hydrogen.

$$C_2H_5 + H_2 \rightarrow C_2H_6 + H$$

Measurements of the rate of disappearance of ethylene thus lead to values for the rate constant for this reaction over the temperature range 1111–1200 K. Only four measurements of this rate constant have been reported (3–6), all of which are below

0008-4042/82/243039-10$01.00/0

©1982 National Research Council of Canada/Conseil national de recherches du Canada

820 K. New measurements should therefore be valuable in establishing this rate constant in the high temperature region. Many measurements of the rate constant for the reverse reaction have been reported (7) and it is of interest to compare these values with those of the forward reaction through the equilibrium constant. It will be shown that agreement between the forward and reverse rate constants can be achieved only if the heat of formation of the ethyl radical is somewhat larger than has previously been accepted (8).

## Experimental

The reaction was studied in a static system with provision for storage, mixing, introduction, and sampling of the reactants and products. The reaction vessel was a quartz cylinder with diameter 4.4 cm and volume 182 $cm^3$, and was placed in the center of a Lindberg three-zone tubular furnace. A second vessel of similar dimensions and packed with quartz tubes to give a S/V ratio of 7.5 $cm^{-1}$ was used to test for the importance of surface reactions. Mixtures were prepared in a 2-L spherical flask with minimum dead space by introducing first the small pressure of ethylene and then filling with hydrogen. After a mixing period of 12 h the composition of the mixture was homogeneous and invariant. Ethylene was Research Grade (99.98%) obtained from Matheson of Canada, Whitby, Ont. Hydrogen was purified by passage through a Molecular Sieve 5A column at liquid nitrogen temperature with a residence time of 1–2 s. Such treatment is usually sufficient to reduce the oxygen impurity to less than 1 ppm (9), although the present analysis system, using gas chromatography with a thermal conductivity detector, could not detect less than 6 ppm.

The products were analyzed by expansion into a Toepler pump from which duplicate samples were taken for analysis. Analyses were made on a Hewlett-Packard model 5750 with FID detector, using a 1.2 m column of Durapak (phenylisocyanate on Porasil) maintained at 30°C. The reactant ethylene and the products methane and ethane were measured for reaction times from 1–40 min.

## Results

The rate of hydrogenation of ethylene in the unpacked vessel was measured at 1111 K for five concentrations of ethylene in hydrogen ranging from 9–36 ppm. At each concentration the rate was measured at four or five total pressures ranging from 100–300 Torr. These data allowed the determination of the order with respect to each reactant. The rate was also measured at five temperatures over the range 1111–1192 K. In addition, at 1192 K, the total order of the rate with respect to both reactants was measured.

The primary product of the hydrogenation was ethane, but at the temperature of the reaction, secondary decomposition was rapid and the final product was methane. The yields as a function of time at 1111 K are shown in Figs. 1, 2, and 3. It is clear that ethane is an intermediate product and even at the lowest temperature its yield is small. It gradually became undetectable as the temperature

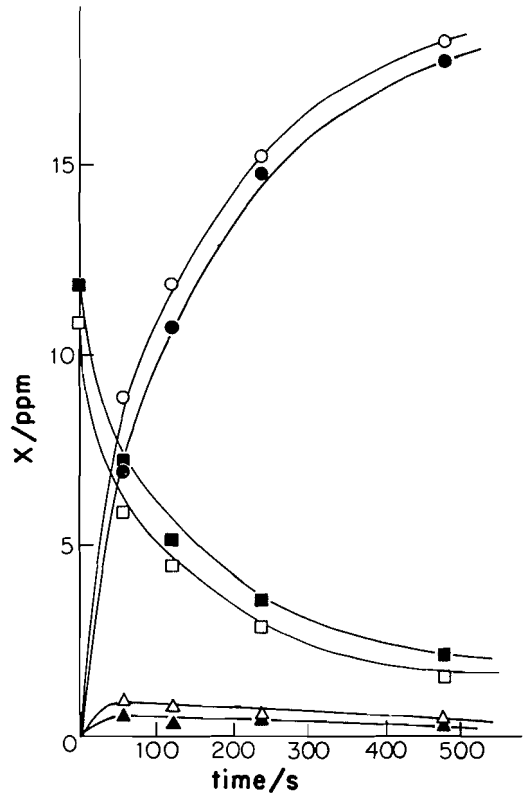


FIG. 1. Variation in mole fraction of reactant and products at 1111 K and total pressure of 182 Torr. □, $C_2H_4$; ○, $CH_4$; △, $C_2H_6$. Open symbols refer to unpacked vessel (S/V ~ 1 $cm^{-1}$) and filled symbols refer to packed vessel (S/V ~ 7 $cm^{-1}$).

was increased. It should be noted that equilibrium in this system corresponds to almost complete conversion of ethylene to methane. The reaction was therefore followed by the disappearance of ethylene and the appearance of methane.

The measurement of the initial rates from the data involved a search for an equation giving the best linear extrapolation. Integrated equations for orders of 0.5, 1, 1.5, and 2 were tested and the best extrapolation was obtained with the function $1/x$ against time. A summary of the measurements is given in Table 1. In fact, these initial rates were within about 25% of those estimated directly from the yield–time plots or from the function log $x$ against time. It should be emphasized that the function used to estimate the initial rates is not particularly significant in terms of the mechanism of the reaction during the initial stages.

The dependence of the rate on the initial concentration of the reactant is the characteristic of most importance to the mechanism. The rate of disappearance of ethylene may be written as

$$-R_{C_2H_4} = k[H_2]^m[C_2H_4]^n$$

Can. J. Chem. Downloaded from www.nrcresearchpress.com by 210.87.254.5 on 09/06/12
For personal use only.

Can. J. Chem. Downloaded from www.nrcresearchpress.com by 210.87.254.5 on 09/06/12
For personal use only.

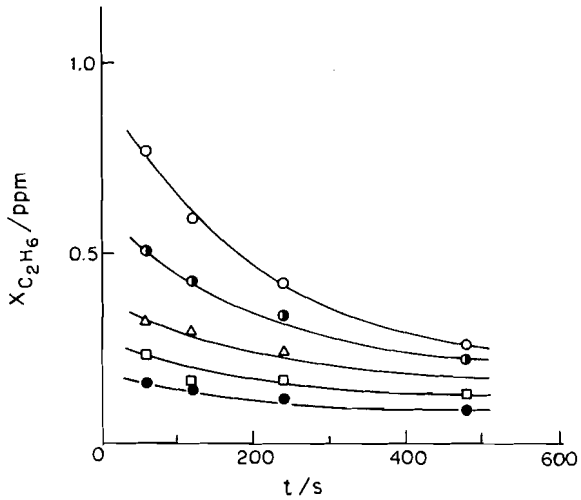


FIG. 2. Mole fraction of ethane as a function of time at various temperatures. Initial concentration of ethane: 9.33 ppm; total pressure: 182 Torr. ○, 1111 K; ◑, 1131 K; □, 1171 K; ●, 1192 K; △, 1151 K. Open symbols refer to unpacked vessel (S/V ~ 1 $cm^{-1}$) and filled symbols refer to packed vessel (S/V ~ 7 $cm^{-1}$).

where $k$ represents an over-all rate constant and $m$ and $n$ represent the order of the rate with respect to hydrogen and ethylene, respectively. Designating the mole fraction of each reactant by $X$ and making the approximation that $X_{H_2} = 1$,

$$-R_{C_2H_4} = kP^{m+n}X_{C_2H_4}{}^n$$

where $P$ is the total pressure.

A log–log plot of the initial rate as a function of $X_{C_2H_4}$ is shown in Fig. 4 for four total pressures. Since the concentration of hydrogen is essentially constant for each total pressure, the slope of these plots gives a value for $n$ of $1.0 \pm 0.1$. The initial rate as a function of the total pressure for each of the concentrations of ethylene is given in Fig. 5. The slope of these plots, all equal to $2.4 \pm 0.1$, gives the total order, $m + n$. A similar plot using the data obtained at 1192 K (Table 1) gives a value for $m + n = 2.5$. The value of $m$ is therefore $1.5 \pm 0.1$. An Arrhenius plot of the initial rate gives an activation energy of 33 kcal/mol.

In the packed vessel, rates were measured at total pressures of 116, 182, 274, and 325 Torr for each of three mixtures, 12, 18.5, and 28 ppm ethylene at 1111 K. The results are given as the corresponding filled symbols in Figs. 1, 2, and 4. The results show that heterogeneous processes are not important in the rate-determining steps of the reaction except to a slight extent at the highest pressures.

These results suggest that the hydrogenation of ethylene may occur through a simple set of reactions where the H-atom concentration in the

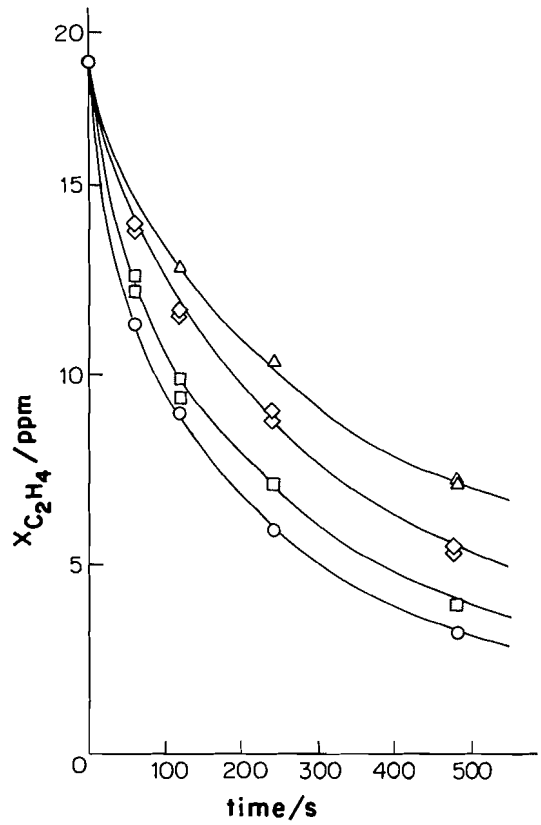


FIG. 3. Mole fraction of ethylene as a function of time at 1111 K with initial concentration of ethylene of 19.2 ppm. Total pressure: △, 85.5 Torr; ◇, 117 Torr; □, 149 Torr; ○, 182 Torr.

system is determined by the equilibrium between molecules and atoms.

[1] $H_2 \rightleftarrows 2H$

[2] $H + C_2H_4 + M \rightleftarrows C_2H_5 + M$

[3] $C_2H_5 + H_2 \rightarrow C_2H_6 + H$

[4] $C_2H_6 \rightarrow 2CH_3$

[5] $CH_3 + H_2 \rightarrow CH_4 + H$

[6] $C_2H_5 + H \rightarrow C_2H_6$

Considering only the reactions occurring in the initial stages,

$$[7] \quad -R_{C_2H_4} = R_{C_2H_6} = \frac{k_3k_2[M]^xK_1{}^{1/2}[H_2]^{3/2}[C_2H_4]}{k_{-2}[M]^x + k_3[H_2]}$$

where $x$, having values between 1 and 0, represents the dependence of the rates [2] and [−2] on the concentration of third body.

The characteristics of the rate depend critically on the ratio of rates $k_{-2}[C_2H_5][M]^x$ and $k_3[C_2H_5][H_2]$.

*Case 1*: If $k_{-2}[M]^x \gg k_3[H_2]$ and the concentration

TABLE 1. Initial rates of reaction of ethylene and values for $k_3$

| $T$/K | Pressure/ Torr | $X_{C_2H_4}$/ ppm | $-\frac{d}{dt}[CH_4]$/ mol $L^{-1}$ $s^{-1}$ × $10^{-10}$ | $K_1^{1/2}$/ $(mol\ L^{-1})^{1/2}$ × $10^{-9}$ | $K_2$/ $(mol\ L^{-1})^{-1}$ × $10^4$ | $k_3$/ $L\ mol^{-1}\ s^{-1}$ × $10^{-6}$ |
|---|---|---|---|---|---|---|
| 1071 | 182 | 10.84 | 2.64 | 1.51 | 3.19 | 1.31 |
| 1111 | 117 | 10.84 | 1.42 | 3.48 | 1.72 | 1.91 |
| | | 19.2 | 1.75 | | | 1.32 |
| | | 27.3 | 2.65 | | | 1.42 |
| | | 36.6 | 4.26 | | | 1.70 |
| | 182 | 9.33 | 2.82 | | | 1.39 |
| | | 10.84 | 3.49 | | | 1.56 |
| | | 19.2 | 5.23 | | | 1.32 |
| | | 27.3 | 8.37 | | | 1.49 |
| | | 36.6 | 11.0 | | | 1.46 |
| | 308 | 10.84 | 14.8 | | | 1.73 |
| | | 19.7 | 19.3 | | | 1.24 |
| | | 27.3 | 28.9 | | | 1.34 |
| | | 36.6 | 39.3 | | | 1.36 |
| 1131 | 182 | 9.33 | 3.44 | 4.89 | 1.39 | 1.64 |
| 1151 | 182 | 9.33 | 4.59 | 7.00 | 0.966 | 2.05 |
| | | 10.84 | 5.89 | | | 2.18 |
| 1171 | 182 | 9.33 | 6.26 | 10.02 | 0.729 | 2.62 |
| 1181 | 182 | 10.84 | 8.28 | 12.8 | 0.640 | 2.84 |
| 1192 | 119 | 9.33 | 3.18 | 18.1 | 0.556 | 3.31 |
| | 182 | 9.33 | 8.97 | | | 2.98 |
| | 248 | 9.33 | 19.5 | | | 3.22 |
| | | | Packed reaction vessel S/V = 7.0 $cm^{-1}$ | | | |
| 1111 | 116 | 11.85 | 1.91 | 3.48 | 1.72 | |
| | | 18.46 | 2.03 | | | 1.61 |
| | | 27.9 | 2.33 | | | 1.22 |
| | 182 | 11.85 | 3.63 | | | 1.49 |
| | | 18.46 | 4.10 | | | |
| | | 27.9 | 7.17 | | | 1.26 |
| | 274 | 11.85 | 7.60 | | | 1.09 |
| | | 18.46 | 8.63 | | | |
| | | 27.9 | 15.8 | | | 0.97 |
| | 325 | 11.85 | 11.4 | | | 1.07 |

of ethyl radicals is controlled by the equilibrium reaction [2],

[8] $$-R_{C_2H_4} = k_3K_2K_1^{1/2}[H_2]^{3/2}[C_2H_4]$$

*Case 2*: If $k_{-2}[M]^x \ll k_3[H_2]$

[9] $$-R_{C_2H_4} = k_2[M]^xK_1^{1/2}[H_2]^{1/2}[C_2H_4]$$

The order of the rate is consistent with either case if $x$ is close to 1. The activation energy of the rate, 33 kcal/mol, is, however, consistent only with the first case where an equilibrium concentration of ethyl radicals is maintained. Taking $\Delta H_2 = -41.0$ kcal/mol (see Appendix) and $\Delta H_1 = 104.2$ kcal/mol, case 1 gives $E_3 = 22$ kcal/mol. It will be shown later that this is a reasonable value at temperatures in the region of 1100 K. On the other hand, from eq. [9] describing case 2, and using a value of $E_2$ of about 4 kcal/mol (7), the activation energy of the rate wil be about 56 kcal/mol, far outside the measured value. A calculation of the relative magnitude o $k_{-2}$ and $k_3[H_2]$ is not conclusive (although ar estimate gives $k_{-2}$ about five times greater thar $k_3[H_2]$) because rather long extrapolations are required in both cases and for $k_{-2}$ both the value o the rate constant and its pressure-dependence mus be obtained. It may be concluded that the mecha nism is best described by the conditions imposed by case 1 and that eq. [8] adequately expresses the rate of disappearance of ethylene in the system.

The order with respect to hydrogen and the activation energy of the rate strongly suggest tha hydrogen atoms are maintained at an equilibrium

Can. J. Chem. Downloaded from www.nrcresearchpress.com by 210.87.254.5 on 09/06/12
For personal use only.

Can. J. Chem. Downloaded from www.nrcresearchpress.com by 210.87.254.5 on 09/06/12
For personal use only.

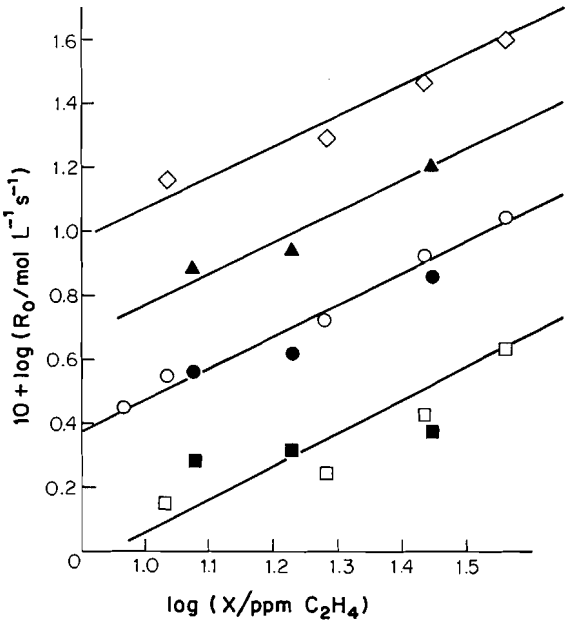


FIG. 4. Logarithm of the initial rate of reaction of ethylene as a function of the logarithm of the initial mole fraction of ethylene for various total pressures at 1111 K. ◇, 307 Torr, slope = 0.95; ▲, 274 Torr, slope = 0.97; ○, 183 Torr; slope = 0.98; □, 117 Torr, slope = 1.03. Open symbols refer to unpacked vessel (S/V ~ 1 $cm^{-1}$) and filled symbols refer to packed vessel (S/V ~ 7 $cm^{-1}$).

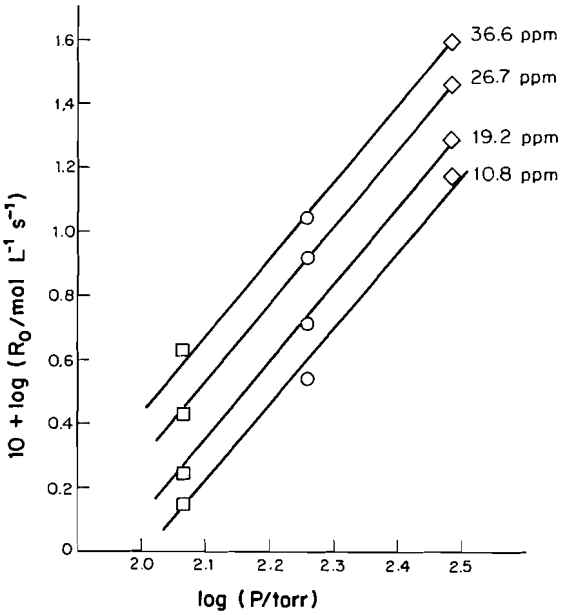


FIG. 5. Logarithm of the initial rate of reaction of ethylene as a function of the logarithm of the total pressure at 1111 K for various initial concentrations of ethylene.

concentration. It may be questioned, however, that the homogeneous rate of dissociation of hydrogen is sufficiently fast to produce the equilibrium concentration in the short times of these reactions. Calculations based on the value of the rate constant for combination of hydrogen atoms measured at room temperature (10) (an upper limit) and the equilibrium constant at the temperature of the reaction, show that homogeneous dissociation is indeed too slow by at least a factor of $10^2$. It must be concluded that dissociation is catalyzed by the quartz surface. The fact that the rate was not affected by an increase in S/V ratio of the reaction vessel further suggests that an equilibrium concentration of hydrogen atoms is rapidly attained in both vessels.

Some comments concerning the importance of other reactions which might affect the concentration of radicals in the system may clarify the mechanism. The occurrence of reaction [6] could reduce the concentration of hydrogen atoms below equilibrium. At 1111 K and a pressure of hydrogen of 182 Torr, the equilibrium concentration of hydrogen atoms is $1.7 \times 10^{-10}$ mol $L^{-1}$. Under the same conditions, with 10 ppm $C_2H_4$, the equilibrium ratio of $C_2H_5/H$ equals $1 \times 10^{-3}$. Taking again the value of $k_{-1}$ measured at room temperature (10) and a value of $1 \times 10^{10}$ L $mol^{-1}$ $s^{-1}$ for $k_6$, the homogeneous rates of reaction [−1] and [6] are comparable. We have, nevertheless, argued that the dissociation of hydrogen and the combination of hydrogen atoms must occur on the surface much more rapidly than in the gas phase. The measurements by Sepehrad, Marshall, and Purnell (19) of the rate of combination of hydrogen atoms on the surface show that this is the case. In their system hydrogen atoms disappeared at the wall in a first-order process,

[W] $H \rightarrow \frac{1}{2}H_2$

and a value of $k_w$ of $20 \pm 15$ $s^{-1}$ was obtained at temperatures in the region of 800 K. In the present system wall recombination is probably slower since the steady-state concentration of hydrogen atoms is less than in the flow system of Sepehrad *et al.* Nevertheless use of their value for $k_w$ provides an upper limit to the rate of removal of hydrogen atoms. The ratio of the rates of reactions [W] and [6] may be expressed as follows:

$$R_w/R_6 = k_w/k_6K_2[H][C_2H_4]$$

and with the conditions described above ($K_2$ at 1111 K = $1.7 \times 10^4$ L $mol^{-1}$),

$$R_w/R_6 = 2.6 \times 10^4$$

Can. J. Chem. Downloaded from www.nrcresearchpress.com by 210.87.254.5 on 09/06/12
For personal use only.

Therefore termination by reaction [6] is probably not sufficiently important to reduce the concentration of hydrogen atoms significantly below equilibrium. Furthermore, this reaction probably requires collisional stabilization, without which the ethane molecule will dissociate into two methyl radicals which will rapidly convert to methane, returning hydrogen atoms to the system.

A possible initiation process is the reaction of ethylene with hydrogen to give an ethyl radical and a hydrogen atom,

[10] $C_2H_4 + H_2 \rightarrow C_2H_5 + H$

If termination occurs by reaction [6], then, under steady-state conditions,

$$[C_2H_5] = k_{10}[C_2H_4][H_2]/k_6[H]$$

The rate constant for reaction [10] may be estimated from values of $\Delta H$ and $\Delta S$ and may be expressed as

$$\log k_{10}\ (\text{L mol}^{-1}\ \text{s}^{-1}) = 9.8 - 65300/2.3RT$$

At 1111 K, $k_{10} = 9.6 \times 10^{-4}$ L mol$^{-1}$ s$^{-1}$. Taking again the conditions of 182 Torr hydrogen and 10 ppm $C_2H_4$ and assuming $k_6 \sim 1 \times 10^{10}$ L mol$^{-1}$ s$^{-1}$ (an upper limit),

$$[C_2H_5] \sim 3 \times 10^{-14}\ \text{mol L}^{-1}$$

This value, although only approximate, is lower than the equilibrium concentration of ethyl radicals of $\sim 2 \times 10^{-13}$ estimated under the same conditions. Reaction [10] may therefore be neglected as a significant source of ethyl radicals. Furthermore, a contribution by ethylene to the initiation process would increase the order of the rate with respect to the concentration of ethylene.

It can also be shown that reaction [10] cannot itself account for the disappearance of ethylene. According to reaction [10] the rate of disappearance of ethylene may be written as

$$-R_{C_2H_4} = k_{10}[C_2H_4][H_2]$$

Taking the same conditions as an example, the rate of disappearance of ethylene may be estimated as $6 \times 10^{-14}$ mol L$^{-1}$ s$^{-1}$, while the observed rate is $3 \times 10^{-10}$ mol L$^{-1}$ s$^{-1}$ (Table 1). One further possibility for consumption of ethylene is the unimolecular dissociation,

[11] $C_2H_4 \rightarrow C_2H_3 + H$

This reaction has been observed and measured in the shock-tube pyrolysis of ethylene (11, 12) as a second-order process. A reasonable value for the unimolecular dissociation is

$$\log k_{11}\ (\text{s}^{-1}) = 16 - 104000/2.3RT$$

and at 1111 K, $k_{11} = 3.5 \times 10^{-5}$ s$^{-1}$. Taking the same conditions as above,

$$-R_{C_2H_4} = k_{11}[C_2H_4] = 8.8 \times 10^{-13}\ \text{mol L}^{-1}\ \text{s}^{-1}$$

This must be an upper limit since the dissociation will undoubtedly be partly pressure-dependent at the temperature of these experiments. Therefore neither reaction [11] nor reaction [10] are sufficiently fast to account for the rate of disappearance of ethylene.

The rates of reactions [10] and [11] may also be compared to the rate of dissociation of hydrogen, in order to compare the rate of production of hydrogen atoms in the system. A value for the rate of dissociation of hydrogen on the surface may be obtained from the equilibrium represented by reaction [W], and again represents an upper limit.

$$K_w = k_{-w}/k_w = (K_{H_2})^{1/2}$$

Using the value for $k_w$ as already discussed,

$$k_{-w} = 7.0 \times 10^{-8}\ (\text{mol/L})^{1/2}\ \text{s}^{-1}$$

The ratio of rates may be expressed as follows:

$$\frac{R_{-w}}{R_{10}} = \frac{k_{-w}[H_2]^{1/2}}{k_{10}[C_2H_4][H_2]} = 5.8 \times 10^4$$

$$\frac{R_{-w}}{R_{11}} = \frac{k_{-w}[H_2]^{1/2}}{k_{11}[C_2H_4]} = 4.2 \times 10^3$$

Even though this represents an upper limit to the rate of formation of hydrogen atoms from hydrogen, it is unlikely that reactions [10] or [11] are important in the present system.

*Rate of formation of methane*

The rate of formation of methane may be equated to the rate of disappearance of ethane if all methyl radicals react by reaction [5].

$$R_{CH_4} = 2k_4[C_2H_6]$$

The maximum concentration of ethane is given as follows,

$$[C_2H_6]_m = \frac{k_3[C_2H_5][H_2]}{k_{-3}[H] + k_4}$$

If the concentration of both the ethyl radical and the hydrogen atom are given by the relevant equilibrium constant the maximum rate of formation of methane is

[12] $$R_{CH_4} = \frac{2k_4k_3K_2K_1^{1/2}[H_2]^{3/2}[C_2H_4]}{k_{-3}K_1^{1/2}[H_2]^{1/2} + k_4}$$

since $k_{-3} = k_3/K_3$ the rate constant $k_3$ may be expressed as

TABLE 2. Initial rate of formation of methane and values for $k_3$, total pressure: 182 Torr; $X_{C_2H_4}$: 9.33 ppm

| $T$/K | $\frac{d}{dt}[CH_4]$/ mol $L^{-1}$ $s^{-1}$ × $10^{-10}$ | $K_3/10^{-3}$ | $k_4/s^{-1}$ | $k_3$/L $mol^{-1}$ $s^{-1}$ × $10^6$ |
|---|---|---|---|---|
| 1111 | 2.50 | 3.87 | 0.0676 | 1.10 |
| 1131 | 3.96 | 4.06 | 0.151 | 1.46 |
| 1151 | 4.92 | 4.21 | 0.282 | 1.76 |
| 1171 | 6.42 | 4.37 | 0.525 | 2.27 |
| 1192 | 8.62 | 4.54 | 1.00 | 2.29 |

$$[13]\quad k_3 = \frac{R_{CH_4}k_4}{K_1^{1/2}[H_2]^{1/2}\left[2k_4K_2[H_2][C_2H_4] - \frac{R_{CH_4}}{K_3}\right]}$$

Since the product ethane achieves its maximum concentration at a very short time of reaction, the maximum rate of formation of methane may be obtained by an extrapolation procedure similar to that used to obtain the initial rate of disappearance of ethylene. In other words, a maximum rate will be indistinguishable from an initial rate on the time scale of the present experiments. These rates of formation of methane are shown in Table 2.

The relative importance of the terms in the denominator of eq. [12] may be deduced from the measured activation energy of the rate of formation of methane, which was 38 kcal/mol. If $k_4 \gg k_{-3}K_1^{1/2}[H_2]^{1/2}$ and ethane is removed primarily by dissociation, the rate of formation of methane becomes

$$[14]\quad R_{CH_4} = 2k_3K_2K_1^{1/2}[H_2]^{3/2}[C_2H_4]$$

which is exactly twice the rate of disappearance of ethylene. Since the activation energies for the rate of disappearance of ethylene and the rate of formation of methane were similar, it may be concluded that the simplified expression, eq. [14], closely describes the mechanism for formation of methane. The other situation, in which $k_4$ may be neglected in the denominator, would predict a much higher activation energy, about 63 kcal/mol. Nevertheless, the initial rate of formation of methane was not exactly twice the initial rate of disappearance of ethylene, indicating that some ethane may be lost by the reverse of reaction [3]. The complete eq. [13] was therefore used to calculate $k_3$.

*Calculation of* $k_3$

Using eqs. [8] and [13] values of $k_3$ were calculated from the rate of disappearance of ethylene and from the rate of formation of methane. The results together with the values of $k_4$, $K_2$, and $K_3$ used in the calculations, are included in Tables 1 and 2. The fall-off in $k_4$ was estimated by extrapolation of the results of Lin and Back (13). Other data are given in the Appendix. An Arrhenius plot of $k_3$ is given in Fig. 6. The activation energy measured for $k_3$ is 23 ± 2 kcal/mol. These results are shown together with the four other sets of measurements previously reported at lower temperatures as the filled points in Fig. 7. Also on this graph are values of $k_3$ calculated from the measurements of $k_{-3}$, and the equilibrium constant $K_3$. The points given represent the limits of the temperature range for each set of data and the lines represent the values reported for $A$ and $E$. The thermodynamic quantities used in the calculation are given in the Appendix.

The measurements of $k_3$ derived from $k_{-3}$ are somewhat lower than the direct measurements of $k_3$, but may be considered in reasonable agreement. Two points concerning the calculations should be noted. The four measurements of $k_3$ were

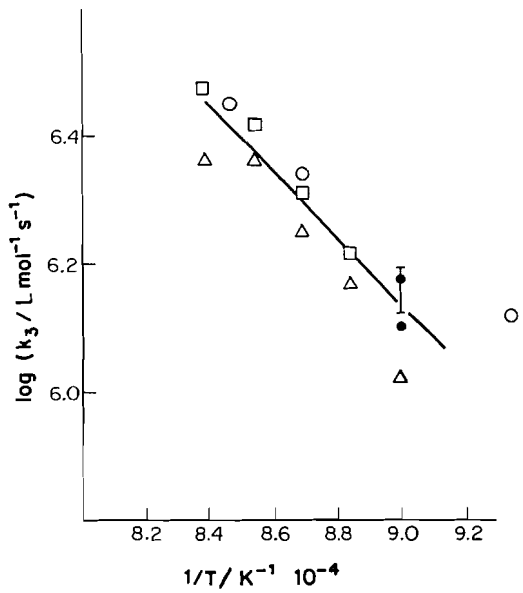


FIG. 6. Arrhenius plot for $k_3$ measured in the present experiments. □, 9.3 ppm $C_2H_4$; ○, 10.8 ppm $C_2H_4$; △, calculated from the yield of $CH_4$; I, range of values at 1111 K for five concentrations of $C_2H_4$; filled symbols: packed vessel.

Can. J. Chem. Downloaded from www.nrcresearchpress.com by 210.87.254.5 on 09/06/12
For personal use only.

Can. J. Chem. Downloaded from www.nrcresearchpress.com by 210.87.254.5 on 09/06/12
For personal use only.

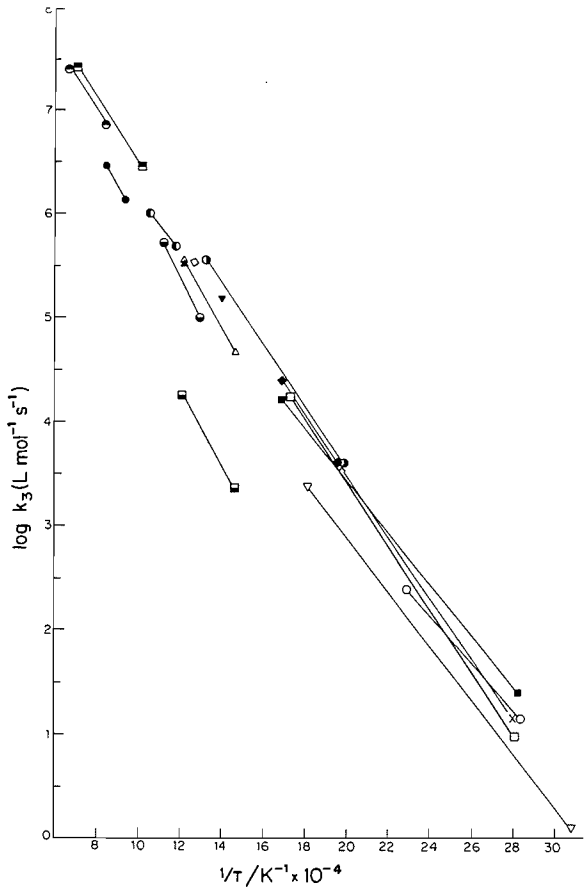


FIG. 7. Arrhenius plot for $k_3$. Filled symbols represent direct measurements of $k_3$. Other symbols represent measurements of $k_{-3}$ converted to $k_3$ using the calculated values of $K_3$. ■, ref. 3; ◆, ref. 4; ●, present work; ▲, ref. 5; ▼, ref. 6; □, ref. 27; ◑, ref. 32; ×, ref. 29; ○, ref. 21; ▽, ref. 26; △, ref. 24; ◇, ref. 30 and 31; ◒, ref. 22; ◒, ref. 23; ◐, ref. 28; ◓, ref. 25; ◓, ref. 33.

all made relative to the rate constant for the combination of ethyl radicals, $k_c$, which in each case was taken as $2.2 \times 10^{10}$ L mol$^{-1}$ s$^{-1}$. More recent work indicates that $k_c \sim 1 \times 10^{10}$ L mol$^{-1}$ s$^{-1}$ (14, 15) and these values were therefore lowered by $\sqrt{2.2}$. The equilibrium constant, $K_3$, was calculated using a value of 28 kcal/mol for $\Delta H_f(C_2H_5)$. Although this value is given in most references (8, 16) as 26 kcal/mol, $k_3$ calculated with this value is considerably lower than the direct measurements of $k_3$. Recent measurements of the heat of formation of the ethyl radical relative to that of the methyl radical using a radical buffer system in an isooctane solution (17) have given a value of 28 kcal/mol, using $\Delta H_f(CH_3) = 34.4$ kcal/mol. The fact that the independent measurements of $k_3$ and $k_{-3}$ are in reasonable agreement using the value of $\Delta H_f(C_2H_5) = 28$ kcal/mol suggests that the higher value may be preferable. The difference of 2 kcal/mol increases the calculated values of $k_3$ by a factor of two. A similar comparison between forward and reverse rate constants for the reaction of methyl radicals with hydrogen led to the acceptance of a higher value (at that time) for the heat of formation of the methyl radical (18). In a recent discussion of this system, the authors concluded that the independent measurements of the forward and reverse rate constants were in agreement within a factor of 2 or 3 (19, 20). A similar agreement is indicated in the present comparison of the system involving ethyl radicals.

The present measurements are in good agreement with the values of $k_3$ calculated from measurements of $k_{-3}$. They appear somewhat below an extrapolation of the values measured below 820 K but are within the limits of error encompassed by both sets of measurements. Most of the measured rate constants are within a factor of two of an average value. On the other hand, values for the Arrhenius parameters are often very different, as can be observed from the variation in slopes of the lines in Fig. 7.

The activation energy of $k_3$ obtained in the present results appears at first unusually high, although there are no other data for $k_3$ above about 820 K. It has been observed that the activation energy of similar abstraction reactions rises gradually but substantially above 900 K. For example, in their discussion of non-Arrhenius behaviour in some simple abstraction reactions Clark and Dove (2) showed that the literature data on reaction [−3] can be fitted by a smooth curve giving a continuously increasing activation energy with increasing temperature. From this curve, $E_{-3}$ was about 14 kcal/mol in the temperature range 1100–1200 K. Since $\Delta H_3$ at this temperature is 4.5 kcal/mol (see Appendix), $E_3$ should be 18.5 kcal/mol, in reasonable agreement with the present results. Closer examination of the combined sets of measurements may, however, throw some doubt on the magnitude of the change in activation energy over the whole temperature range. The results could, in fact, be fitted reasonably well by a linear relation. This was the conclusion reached by Sepehrad, Marshall, and Purnell (19) in a comparison of measurements reported for $k_{-5}$. Nevertheless, the best fit probably indicates a change in activation energy from 12 kcal/mol in the range 350–550 K to about 17 kcal/mol from 800–1200 K, which is a smaller increase than previously supposed. The comparison of these two sets of data shows the magnitude of error which can be expected in values for rate constants for radical abstraction reactions. It also illustrates

Can. J. Chem. Downloaded from www.nrcresearchpress.com by 210.87.254.5 on 09/06/12
For personal use only.

the danger in the use of extrapolated values and the need to acquire a consistent set of data.

*Evaluation of the method*

A possible source of error in the present measurements which would lead to an underestimate of $k_3$ is an overestimate of either the hydrogen atom concentration or the ethyl radical concentration. It seems unlikely that the hydrogen atom concentration is much below equilibrium since the large increase in surface area had no effect on the rate. It is known that hydrogen atoms are strongly adsorbed on quartz surfaces, leading to heterogeneous reactions, but the absence of a perturbing effect of the surface is easily explained if atoms and molecules are in equilibrium. The concentration of ethyl radicals, on the other hand, may be reduced below the equilibrium value under conditions where $k_3[H_2]$ may become comparable in rate to the dissociation reaction, [−2]. Estimates of the relative magnitude of these two rates suggests they may be comparable, but the over-all activation energy of the rate was incompatible with the exclusion of reaction [−2] as the rate-controlling removal of ethyl radicals. This factor could cause an underestimate of $k_3$ by perhaps a factor of two. The estimate of the initial rate also involves some uncertainty, but it seems unlikely that this could be more than 30 or 40%. The system is kinetically simple and offers a well-controlled concentration of atoms. Further studies on other systems should prove useful in providing data on the region above 1000 K.

**Acknowledgements**

The authors wish to thank the Natural Sciences and Engineering Research Council of Canada for financial support of this work. J.-R. Cao also thanks the government of the People's Republic of China for financial support during the course of this work. The authors are also grateful to Dr. R. A. Back for reading the manuscript.

1. W. C. Gardiner. Acc. Chem. Res. **10**, 326 (1977).
2. T. C. Clark and J. E. Dove. Can. J. Chem. **51**, 2147 (1973).
3. P. J. Boddy and E. W. R. Steacie. Can. J. Chem. **39**, 13 (1961).
4. L. E. Reid and D. J. LeRoy. Can. J. Chem. **46**, 3275 (1968).
5. M. P. Halstead and C. P. Quinn. Trans. Far. Soc. **64**, 1560 (1968).
6. R. R. Baldwin, D. H. Langford, M. J. Matchan, R. W. Walker, and D. A. Yorke. 13th Int. Symp. Comb. Combustion Institute, Pittsburgh. 1971. p. 251.
7. J. A. Kerr (*Editor*). CRC handbook of bimolecular and termolecular gas reactions. CRC Press, Boca Raton, FL. 1981.
8. H. E. O'Neal and S. W. Benson. Thermochemistry of free radicals. *In* Free radicals. Vol. 2. *Edited by* J. K. Kochi. Wiley, New York. 1973. p. 275.
9. C. R. Baker and R. S. Paul. Chem. Eng. Prog. **59**, 61 (1963).
10. J. E. Bennett and D. R. Blackmore. 13th Int. Symp. Comb. Combustion Institute, Pittsburgh. 1971. p. 51.
11. T. H. Just, P. Roth, and R. Damm. 16th Int. Symp. Comb. Combustion Institute, Pittsburgh. 1977. p. 961.
12. T. Tanzawa and W. C. Gardiner. Comb. Flame, **39**, 241 (1980).
13. M. C. Lin and M. H. Back. Can. J. Chem. **44**, 505 (1966); **44**, 2357 (1966). M. C. Lin. Ph.D. thesis. University of Ottawa, Ottawa, Canada. 1966.
14. D. M. Golden, K. Y. Choo, M. J. Perona, and L. W. Piszkiewicz. Int. J. Chem. Kinet. **8**, 381 (1976).
15. H. Adachs, N. Basco, and D. G. L. James. Int. J. Chem. Kinet. **11**, 995 (1979).
16. S. W. Benson. Thermochemical kinetics. 2nd ed. John Wiley, New York. 1976.
17. A. L. Castelhano, P. R. Marriott, and D. Griller. J. Am. Chem. Soc. **103**, 4262 (1981).
18. R. W. Walker. J. Chem. Soc. A, 2391 (1968).
19. A. Sepehrad, R. M. Marshall, and J. H. Purnell. J. Chem. Soc. Faraday Trans. 1, **75**, 835 (1979).
20. R. M. Marshall and G. Shahkar. J. Chem. Soc. Faraday Trans. 1, **77**, 2271 (1981).
21. M. R. Berlie and D. J. LeRoy. Discuss. Faraday Soc. **14**, 50 (1953).
22. N. I. Gorban and A. B. Nalbandyan. Dokl. Akad. Nauk SSSR, **132**, 1335 (1960).
23. V. V. Voevodsky and V. N. Kondratiev. Progress in reaction kinetics. Pergamon Press, Oxford, **1**, 41 (1961).
24. N. I. Gorban and A. B. Nalbandyan. Russ. J. Phys. Chem. **36**, 946 (1962).
25. C. P. Fenimore and G. W. Jones. 9th Int. Symp. Comb. Academic Press, New York. 1963. p. 597.
26. K. Yang. J. Phys. Chem. **67**, 562 (1963).
27. B. de B. Darwent and R. Roberts. Discuss. Faraday Soc. **14**, 55 (1953).
28. N. I. Parsamyan, E. A. Arakelyan, V. V. Azatyan, and A. B. Nalbandyan. Izv. Akad. Nank. SSSR, Ser. Khim. 496 (1968).
29. V. V. Azatyan, S. B. Filippov, A. B. Nalbandyan, and L. B. Ramanovich. Arm. Khim. Zh. **22**, 193 (1969).
30. R. R. Baldwin, D. E. Hopkins, and R. W. Walker. Trans. Faraday Soc. **66**, 189 (1970).
31. R. R. Baldwin and A. Melvin. J. Chem. Soc. 1785 (1964).
32. P. Camilleri, R. M. Marshall, and J. H. Purnell. J. Chem. Soc. Faraday Trans. 1, **70**, 1434 (1974).
33. J. N. Bradley. Proc. R. Soc. London, A**337**, 199 (1974).

## Appendix

*Thermodynamic data*

| | $\Delta H_f(298)$/kcal mol$^{-1}$ | $S^0(298)$/cal deg$^{-1}$ mol$^{-1}$ |
|---|---|---|
| H | 52.1 | 27.4 |
| $C_2H_4$ | 12.5 | 52.4 |
| $C_2H_5$ | 28.0 | 59.0 |
| $C_2H_6$ | −20.2 | 54.9 |

*Equilibrium constants*

(*a*) $H + C_2H_4 \rightleftharpoons C_2H_5$

| $T$/K | $\Delta H_T$/kcal mol$^{-1}$ | $\Delta S_T$/cal mol$^{-1}$ deg$^{-1}$ | $K$/(mol L$^{-1}$)$^{-1}$ × $10^4$ |
|---|---|---|---|
| 1000 | −38.7 | −24.5 | 10.7 |
| 1100 | −39.0 | −24.7 | 2.03 |
| 1200 | −39.2 | −24.9 | 0.50 |

(*b*) $C_2H_5 + H_2 \rightleftharpoons C_2H_6 + H$

| $T$/K | $\Delta H_T$/kcal mol$^{-1}$ | $\Delta S_T$/cal mol$^{-1}$ deg$^{-1}$ | $K/10^{-3}$ |
|---|---|---|---|
| 1000 | 4.28 | −7.24 | 3.03 |
| 1100 | 4.39 | −7.10 | 3.80 |
| 1200 | 4.45 | −6.98 | 4.61 |

Can. J. Chem. Downloaded from www.nrcresearchpress.com by 210.87.254.5 on 09/06/12
For personal use only.

# Halogenation of 1,6-diazaphenalene. Theoretical and experimental results

ROBERT W. WEBER, SHIEU-JEING LEE, SAMUEL MILOSEVICH, WALTER B. ENGLAND,[1] AND JAMES M. COOK[1]

*Department of Chemistry and Laboratory for Surface Studies, University of Wisconsin–Milwaukee, Milwaukee, WI 53201, U.S.A.*

Received April 14, 1982

ROBERT W. WEBER, SHIEU-JEING LEE, SAMUEL MILOSEVICH, WALTER B. ENGLAND, and JAMES M. COOK. Can. J. Chem. **60**, 3049 (1982).

Bromination of 1,6-diazaphenalene **1** yields a mixture of mono-, di-, and tri-bromo derivatives, while bromination of the conjugate acid **2** provides the 7-bromo isomer **7** in 81% yield. Charge densities and localization energies have been calculated, and are found to be in agreement with the orientation pattern observed during electrophilic substitution. These observations have been employed to develop several routes to 7-substituted 1,6-diazaphenalenes.

ROBERT W. WEBER, SHIEU-JEING LEE, SAMUEL MILOSEVICH, WALTER B. ENGLAND et JAMES M. COOK. Can. J. Chem. **60**, 3049 (1982).

La bromation du diaza-1,6 phénalène **1** donne un mélange de dérivés mono-, di- et tri-bromés tandis que la bromation de l'acide conjugué **2** conduit à l'isomère bromé en position 7, **7** avec un rendement de 81%. On a calculé les densités de charge et les énergies de localisation. Les valeurs obtenues sont en accord avec le mode d'orientation observé lors d'une substitution électrophile. On a utilisé ces observations pour développer plusieurs voies d'accès aux diaza-1,6 phénalènes substitués en position 7.

[Traduit par le journal]

Can. J. Chem. Downloaded from www.nrcresearchpress.com by 210.87.254.105 on 09/06/12
For personal use only.

The heterocyclic base 1,6-diazaphenalene **1** was first reported in 1978 (1). This compound is of interest from both a chemical and electronic point of view for proton transfer from **1***a* to **1***b* would generate a species **1***b* identical in structure with **1***a*.

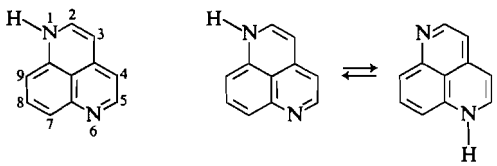

**1** **1***a* **1***b*

This process is more rapid than the nmr time scale and results in a simplified nmr spectrum analogous to the case of imidazole (2), and it has been suggested that many of the properties of **1** are imidazole-like (1). In this vein, the reaction of **1** with various electrophiles has been studied under conditions reported to provide substituted imidazoles (3, 4). These studies have dealt primarily with halogenation and nitration reactions under neutral and acidic conditions. Moreover, experiments have generally been carried out with one mole (or less) of the electrophile to more accurately determine the most reactive site for electrophilic substitution.

In order to compare the experimental results with the reactivity predicted by molecular orbital theory, INDO calculations (5) were carried out on the base **1**, conjugate acid **2**, and the anion **3**. The geometries required for the calculations were obtained using standard bond lengths (6). The neutral species **1** was considered as an enamine fused to a quinoline system. A symmetrical structure was chosen for the protonated form **2** based on nmr data (7). Similarly, removal of two hydrogen atoms from the nitrogens of **2** yielded the geometry used for the anion **3**.

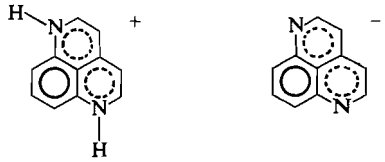

**2** **3**

The total charge densities obtained for these compounds are given in Table 1. The HOMO and LUMO electron densities are given in Table 2, and

TABLE 1. Total electron densities for 1,6-diazaphenalene **1**, conjugate acid **2**, anion **3**, 3-chloro-1,6-diazaphenalene **10**, and 2,3-dichloro-1,6-diazaphenalene **11**

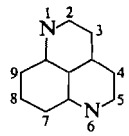

| Atom | 1 | 2 | 3 | 10 | 11 |
|---|---|---|---|---|---|
| N1 | 5.1252 | 5.0544 | 5.3671 | 5.1218 | 5.1382 |
| C2 | 3.8233 | 3.7933 | 3.8235 | 3.8593 | 3.7987 |
| C3 | 4.1101 | 4.0883 | 4.1562 | 4.0286 | 4.0589 |
| C4 | 4.0784 | 4.0883 | 4.1562 | 4.0719 | 4.0755 |
| C5 | 3.8245 | 3.7933 | 3.8235 | 3.8259 | 3.8241 |
| N6 | 5.2547 | 5.0544 | 5.3671 | 5.2605 | 5.2633 |
| C7 | 4.0671 | 4.0671 | 4.1498 | 4.0670 | 4.0659 |
| C8 | 3.9340 | 3.8929 | 3.9285 | 3.9336 | 3.9340 |
| C9 | 4.0766 | 4.0671 | 4.1498 | 4.0754 | 4.0744 |

[1]Author to whom correspondence should be addressed.

0008-4042/82/243049-06$01.00/0

©1982 National Research Council of Canada/Conseil national de recherches du Canada

TABLE 2. Calculated densities and virtual densities of frontier electrons for electrophilic (HOMO) and nucleophilic (LUMO) reactions on 1,6-diazaphenalene **1**, conjugate acid **2**, anion **3**, 3-chloro-1,6-diazaphenalene **10**, and 2,3-dichloro-1,6-diazaphenalene **11**

| | 1 | | 2 | | 3 | | 10 | | 11 | |
|---|---|---|---|---|---|---|---|---|---|---|
| Atom | HOMO | LUMO | HOMO | LUMO | HOMO | LUMO | HOMO | LUMO | HOMO | LUMO |
| N1 | 0.384 | 0.170 | 0.348 | 0.239 | 0.361 | 0.334 | 0.399 | 0.169 | 0.342 | 0.163 |
| C2 | 0.078 | 0.212 | 0.024 | 0.382 | 0.001 | 0.244 | 0.120 | 0.215 | 0.117 | 0.208 |
| C3 | 0.266 | 0.001 | 0.273 | 0.002 | 0.314 | 0.021 | 0.273 | 0.002 | 0.313 | 0.000 |
| C4 | 0.242 | 0.088 | 0.273 | 0.002 | 0.314 | 0.021 | 0.215 | 0.094 | 0.221 | 0.090 |
| C5 | 0.017 | 0.213 | 0.024 | 0.382 | 0.001 | 0.244 | 0.012 | 0.211 | 0.001 | 0.211 |
| N6 | 0.326 | 0.328 | 0.348 | 0.239 | 0.361 | 0.334 | 0.277 | 0.335 | 0.282 | 0.326 |
| C7 | 0.277 | 0.163 | 0.300 | 0.003 | 0.323 | 0.028 | 0.241 | 0.156 | 0.219 | 0.165 |
| C8 | 0.023 | 0.116 | 0.000 | 0.088 | 0.000 | 0.157 | 0.016 | 0.111 | 0.014 | 0.133 |
| C9 | 0.238 | 0.041 | 0.300 | 0.003 | 0.323 | 0.028 | 0.217 | 0.041 | 0.200 | 0.044 |

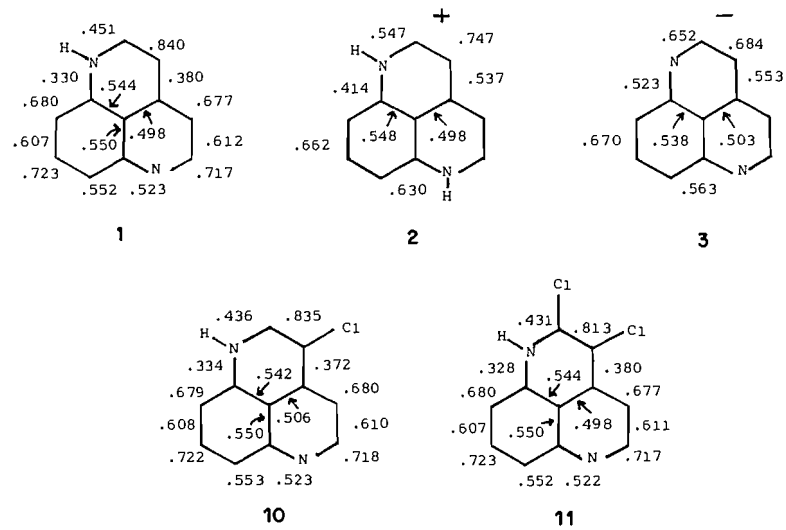


FIG. 1. Calculated bond orders ($\pi$) for 1,6-diazaphenalene **1**, the cation **2**, and anion **3**, 3-chloro-1,6-diazaphenalene **10**, and 2,3-dichloro-1,6-diazaphenalene **11**.

the calculated bond orders are listed in Fig. 1. The total charge densities in the neutral molecule **1** predict a reactivity to electrophilic substitution in the order of positions 3 > 4 > 9 > 7. In the symmetrical ions 2 and 3 the same trend (3(4) > 7(9)) is apparent. According to the frontier orbital theory of Fukui *et al.* (8), reactivity with electrophiles is governed by the electron densities of the highest occupied molecular orbital (HOMO), while the lowest unoccupied molecular orbital (LUMO) determines orientation in reactions with nucleophiles. From the HOMO densities a reactivity pattern of 7 > 3 > 4 > 9 is predicted for **1**, and this trend (7 > 3) continues for the charged species **2** and **3**. The virtual LUMO densities for all three species indicate that nucleophilic attack should occur at positions 2 and 5.

For comparison with experimental results the neutral molecule **1** will be considered first. The products obtained from the bromination of **1** under analogous conditions to those reported for the bromination of imidazole are given in Scheme 1 (9). The reactions were carried out in acetic acid – sodium acetate solution with one equivalent or less of bromine (4). Since significant amounts of di- and tri-substituted diazaphenalenes were formed in this process, yields were low due to recovery of unreacted **1**, as well as difficulties encountered during separation; however, the relative amounts of the isomers present are quite representative. When a large excess of sodium acetate was employed (40:1 ratio) the major product was the 3,4,7-tribromo derivative **4**, followed by the 2,3,4-tribromodiazaphenalene **5** and the 2,3-dibromo compound **6** (4). Upon reducing the amount of sodium acetate to 24 equivalents, the 2,3,4-tribromo derivative **5** now became the major product, followed by the 2,3-dibromodiazaphenalene **6**. At this point the 7-bromo-

Can. J. Chem. Downloaded from www.nrcresearchpress.com by 210.87.254.105 on 09/06/12
For personal use only.

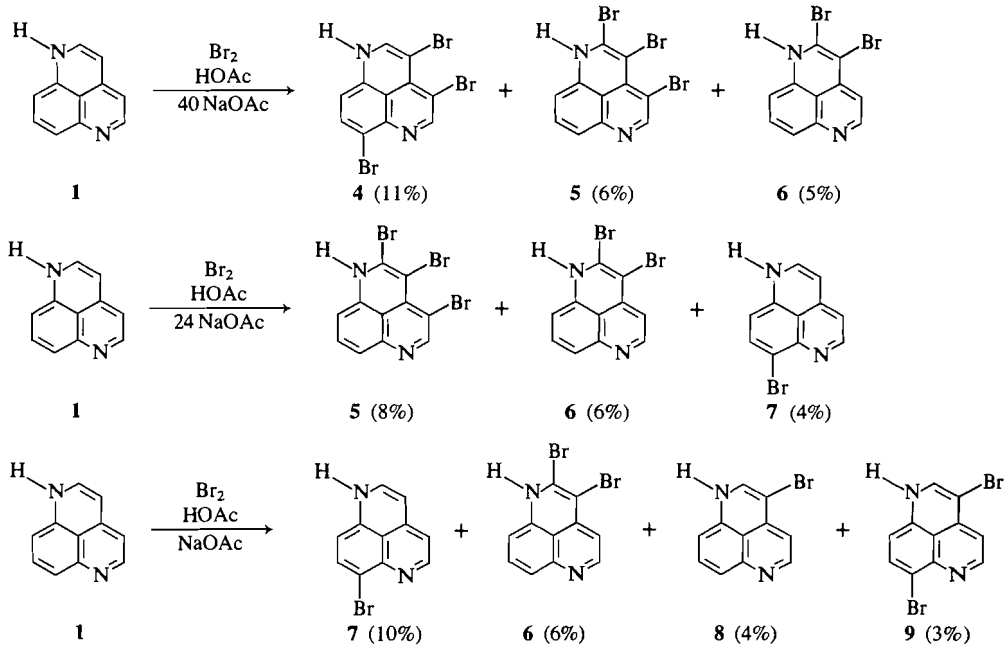


SCHEME 1

diazaphenalene **7** was also obtained. Upon further reduction of the amount of sodium acetate to one equivalent, the 7-bromo derivative **7** now became the major product, followed by the 2,3-dibromo compound **6**, the 3-bromodiazaphenalene **8**, and the 3,7-dibromodiazaphenalene **9**. At this point a trend appeared clear. The more acidic reaction medium (less sodium acetate) favored formation of the 7-bromo-1,6-diazaphenalene **7** in preference to the other isomers and the amount of 2,3-dibromo-1,6-diazaphenalene **6** remained relatively constant. Similarly the pH dependence of the relative rates of bromination of imidazole has been reported (10).

While it is difficult to ascertain the order of addition in the polyhalogenated compounds, the positions substituted correspond to those of high electron density with the exception of the products having bromine in the 2 position. This is unusual for the 2 position would be the expected site of nucleophilic substitution, based on the calculated electron densities. To examine this further, INDO calculations were carried out on 3-chloro-1,6-diazaphenalene **10** and 2,3-dichloro-1,6-diazaphenalene **11** using the third row reparameterizations of Gordon *et al.* (11); we assume here that chlorine and bromine affect the molecule similarly. The total charge densities obtained are listed in Table 1, the HOMO and LUMO densities in Table 2, and the calculated bond orders are illustrated in Fig. 1. Placing the chlorine atom at position 3 alters the order of decreasing electron density from 3 > 4 > 9 > 7 to 9 > 4 > 7; however, in the 2,3-dichloro compound **11** this sequence returns to 4 > 9 > 7. The HOMO densities in the 3-chloro derivative **10** again favor substitution in the 7 position. In the dichloro derivative **11**, however, attack at the 4 position is now favored for the first time in the series.

Two pathways for the formation of the 2,3-dibromo isomer **6** are shown in Scheme 2. The path **1**

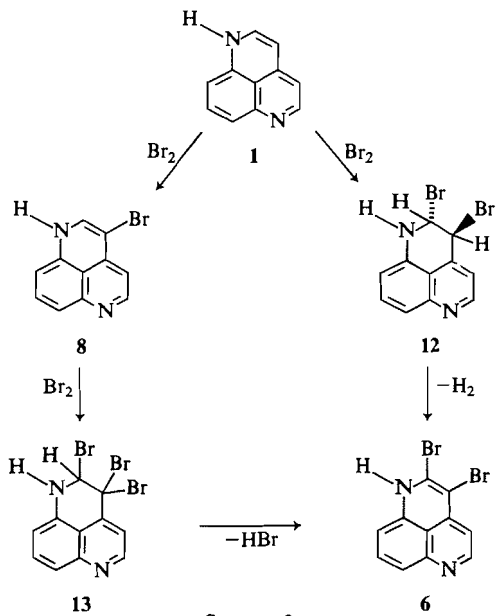


SCHEME 2

Can. J. Chem. Downloaded from www.nrcresearchpress.com by 210.87.254.105 on 09/06/12
For personal use only.

Can. J. Chem. Downloaded from www.nrcresearchpress.com by 210.87.254.105 on 09/06/12
For personal use only.

→ **8** → **13** → **6** first involves substitution of bromine at position 3, followed by addition of $Br_2$ across the 2–3 double bond. Elimination of HBr would then generate **6**. At this point an additional experiment needs to be discussed. When the base **1** was treated with half an equivalent of bromine, the major product was 3-bromo-1,6-diazaphenalene **8**, which was not isolated in substantial quantities when one equivalent of bromine was used. The other major product was the 7-bromo isomer **7**, as shown below. Since bromine is an oxidizing agent, the lesser concentration of this reagent may have impeded conversion of **12** to **6**; however, at no time was a dihydro intermediate related to **12** or **13** isolated from the reaction.

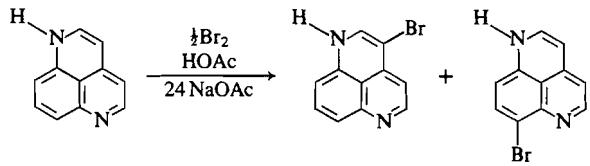


**1** **8** (11%) **7** (8%)

The INDO calculations indicate that the 2–3 bond contains the most double bond character in the molecule ($\pi$ bond order of 0.840, see Fig. 1) and substitution of a chlorine atom at the 3 position only decreases this slightly ($\pi$ bond order of 0.835). The highest degree of polarization in the molecule, considering both total electron densities and HOMO densities, is between the carbon atoms in the 2 and 3 positions. These factors should favor the addition of $Br_2$ across the 2–3 double bond. A 2,3,3-tribromo diazaphenalene such as **13** has never been observed; however, the lack of stability for such a species would be expected to prevent isolation.

The alternate pathway, **1** → **12** → **6** involves addition of $Br_2$ across the 2–3 double bond, followed by loss of $H_2$. While the 2,3-dihydro-1,6-diazaphenalene **14** slowly (3) reverts to **1** upon standing for several weeks as shown below, one might expect loss of HBr to be a more favorable process in the case of the dibromide **12** (3). If indeed this were the case, one would expect to isolate both the 2-bromo and 3-bromo isomers generated from the loss of HBr from **12**. It is important to note here that the 2-bromo-1,6-diazaphenalene has never been observed in work carried out to date, and the only compounds obtained that bear a bromine atom in the 2 position were also substituted with bromine at the 3 position. Since both pathways appear feasible, however, the exact nature of the formation of **6** must remain, for the moment, a matter for further experiments.

In terms of synthetic utility, it is desirable to

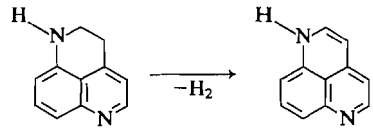


**14** **1**

obtain one product in preference to all other possible isomers. Because 7-substituted 1,6-diazaphenalenes are important intermediates for the synthesis of potential antimalarial agents (1, 7), conditions were sought under which the 7-substituted derivatives would be the major or exclusive product. From the results previously discussed it was known that increased acidity favored the formation of the 7-substituted product. It had also been shown that 1,6-diazaphenalene was protonated to yield the cation **2** in trifluoroacetic acid (4); therefore, reactions were attempted in this medium and the result with bromine is presented below.

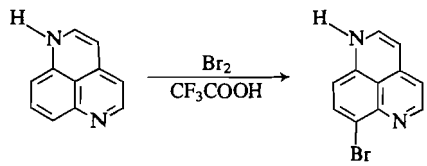


**1** **7** (81%)

Without exception brominations carried out in this medium resulted in the almost exclusive formation of the 7-substituted product. However, in the case of the protonated diazaphenalene **2** the comparable electron densities of the 3 and 7 positions argue against exclusive substitution. We therefore utilized the Wheland model of the transition state (12) to calculate $\pi$ localization energies ($\pi$ bonding between the atom undergoing substitution and the rest of the molecule is cut off). Since the conjugate acid **2** of 1,6-diazaphenalene was symmetrical, calculations were only carried out for substitution at the 2, 3, 7, and 8 positions. The resulting localization energies indicate that the lowest energy $\sigma$ complex is reached for substitution at the 2 position, followed by substitution at positions 7(9), 8, and 3(5) in that order. Since electrophilic attack at the 2 position is electrostatically unlikely, the result that substitution at position 7(9) is favored over the other possibilities is in complete agreement with the experimental observations. The localization energies relative to substitution at position 7 are given below.

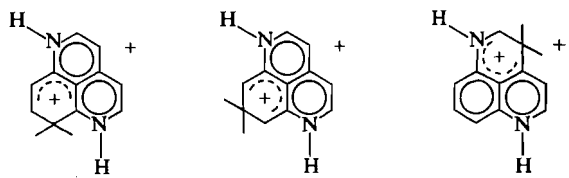

0 kcal/mol 7 kcal/mol 21 kcal/mol

Can. J. Chem. Downloaded from www.nrcresearchpress.com by 210.87.254.105 on 09/06/12
For personal use only.

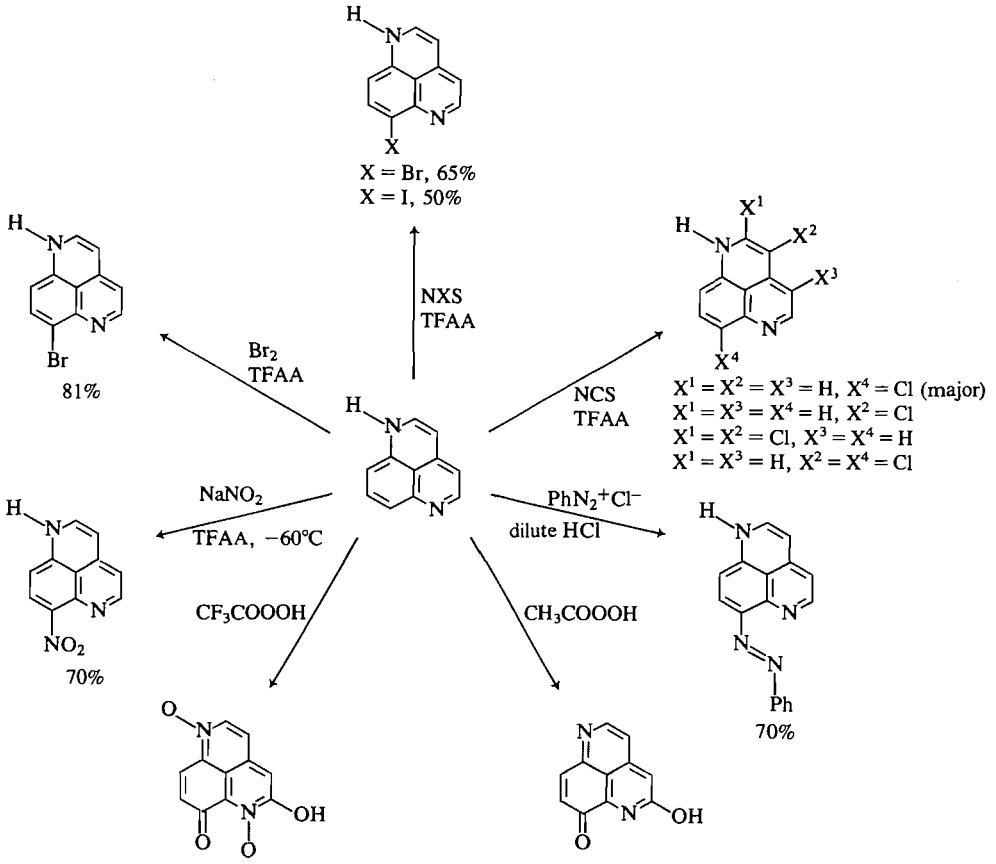


SCHEME 3

The ability to predict that protonated species **2** will react with electrophiles preferentially at the 7 position has been recently employed to design and execute a number of experiments. Outlined in Scheme 3[2] are a series of reactions in which the protonated diazaphenalene **2** has been treated with a variety of electrophiles such as chloronium, iodonium, diazonium, and nitronium ions, as well as peroxy acids. In all cases in which electrophilic substitution has been performed in acidic media, reaction occurred predominantly at the 7 position. These results correlate well with theoretical predictions; advantage will be taken of this phenomenon to prepare potential antimalarial agents.

## Experimental

Microanalyses were performed on a F and M Scientific Corp. Model 185 carbon, hydrogen, and nitrogen analyzer. Some analyses were carried out at the National Institutes of Health, Bethesda, Maryland. Melting points were taken on a Thomas–Hoover melting point apparatus and are not corrected. Nuclear magnetic resonance spectra were recorded on Varian T-60 and JEOL FX-90 spectrometers. Infrared spectra were taken on a Beckman Acculab-1 instrument, and mass spectra were recorded on a Hewlett–Packard 5855 GC/MS. High performance liquid chromatography (hplc) was carried out on a Waters Preparative LC-500 system. The preparation of **1** has been described elsewhere (see ref. 1*b*).

*General procedure for bromination of 1 in acetic acid*

The 1,6-diazaphenalene **1** (1.68g, 0.01 mol) was dissolved in glacial acetic acid (180 mL) and the appropriate amount of sodium acetate added. To the stirred mixture, bromine (0.51 mL, 0.01 mol) dissolved in acetic acid (3.3 mL) was added dropwise. After stirring for 2 hours, the solvent was removed under reduced pressure. The residue was washed with water and dried overnight. The resulting mixture was separated by hplc ($SiO_2$, 10% ethyl acetate in benzene).

*3,4,7-Tribromo-1,6-diazaphenalene 4*

Melting point >300°C; ir (KBr): 3250 (s), 1584 (s), 1340 (s), 1262 (s), 1236 (s), 1178 (s), 1080 (m), 790 (m), and 684 (m) $cm^{-1}$; nmr (DMSO-$d_6$) δ: 6.20 (1H, d, $J$ = 8 Hz), 7.42 (1H, d, $J$ = 8 Hz), 7.88 (1H, s), 8.26 (1H, s); mass spectrum (CI, $CH_4$): 406 (P + 1, 100%), 326 (34). *Anal.* calcd. for $C_{11}H_5N_2Br_3$: C 32.63, H 1.24, N 6.92; found: C 32.49, H 1.46, N 7.01.

*2,3,4-Tribromo-1,6-diazaphenalene 5*

Melting point >300°C; ir (KBr): 3325 (b), 1585 (s), 1340 (s), 1265 (s), 1235 (s), 790 (s), 765 (s), and 685 (s) $cm^{-1}$, nmr (DMSO-$d_6$) δ: 6.22 (1H, d, $J$ = 8 Hz), 7.40 (1H, t, $J$ = 8 Hz), 7.58 (1H, d, $J$ = 8 Hz), 8.02 (1H, s); mass spectrum (CI, $CH_4$): 406 (P + 1, 32%). *Anal.* calcd. for $C_{11}H_5N_2Br_2$: C 32.63, H 1.24, N 6.92; found: C 32.98, H 1.12, N 7.03.

[2]S. J. Lee, K. Avasthi, J. C. Chang, and J. M. Cook. Unpublished results.

Can. J. Chem. Downloaded from www.nrcresearchpress.com by 210.87.254.105 on 09/06/12
For personal use only.

*2,3-Dibromo-1,6-diazaphenalene* **6**

Melting point >300°C; ir (KBr): 3065 (b), 1592 (s), 1338 (s), 1262 (s), 1239 (s), 804 (s), 785 (s), and 760 (s) $cm^{-1}$; nmr ($CF_3COOH$) δ: 6.22 (1H, d, $J$ = 7 Hz), 6.98 (1H, d, $J$ = 9 Hz), 7.54 (1H, t, $J$ = 7 Hz), 7.65 (1H, d, $J$ = 7 Hz), and 8.14 (1H, d, $J$ = 9 Hz); mass spectrum (CI, $CH_4$): 327 (P + 1, 100%). *Anal.* calcd. for $C_{11}H_6N_2Br_2$: C 40.53, H 1.86, N 8.59; found: C 39.82, H 2.01, N 8.19.

*7-Bromo-1,6-diazaphenalene* **7**

Melting point >300°C; ir (KBr): 2800 (b), 1850 (b), 1615 (s), 1565 (s), 1465 (s), 1322 (s), 1200 (s), 1100 (s), 862 (s), and 780 (s) $cm^{-1}$; nmr (DMSO-$d_6$) δ: 6.15 (1H, d, $J$ = 7 Hz), 6.35 (1H, d, $J$ = 5 Hz), 6.60 (1H, d, $J$ = 8 Hz), 7.40 (1H, d, $J$ = 7 Hz), 7.64 (1H, d, $J$ = 8 Hz), and 8.20 (1H, d, $J$ = 5 Hz); mass spectrum (CI, $CH_4$): 248 (P + 1, 100%). *Anal.* calcd. for $C_{11}H_7N_2Br$: C 53.47, H 2.86; found: C 53.69, H 2.72.

*3-Bromo-1,6-diazaphenalene* **8**

Melting point >300°C; ir (KBr): 2860 (b), 1605 (s), 1550 (s), 1450 (s), 1283 (s), 1190 (s), 790 (s), and 760 (s) $cm^{-1}$; nmr (DMSO-$d_6$) δ: 5.83 (1H, d, $J$ = 7 Hz), 6.72 (1H, d, $J$ = 8 Hz), 7.00 (1H, d, $J$ = 8 Hz), 7.36 (1H, d, $J$ = 7 Hz), 7.41 (1H, t, $J$ = 7 Hz), and 8.15 (1H, s); mass spectrum (CI, $CH_4$): 248 (P + 1, 100%). *Anal.* calcd. for $C_{11}H_7N_2Br$: C 53.47, H 2.86, N 11.34; found: C 52.86, H 2.71, N 11.20.

*3,7-Dibromo-1,6-diazaphenalene* **9**

Melting point >300°C; ir (KBr): 3050 (b), 1580 (s), 1320 (s), 1230 (s), 1162 (m), 1068 (m), and 750 (m) $cm^{-1}$; nmr (DMSO-$d_6$) δ: 6.42 (1H, d, $J$ = 7 Hz), 7.21 (1H, d, $J$ = 8 Hz), 7.55 (1H, d, $J$ = 8 Hz), 8.04 (1H, d, $J$ = 7 Hz), and 8.61 (1H, s); mass spectrum (CI, $CH_4$): 327 (P + 1, 100%). *Anal.* calcd. for $C_{11}H_6N_2Br_2$: C 40.53, H 1.86; found: C 40.82, H 1.85.

*Bromination of* **1** *in trifluoroacetic acid*

The 1,6-diazaphenalene **1** (1.68 g, 0.01 mol) was suspended in dry methylene chloride (100 mL) and trifluoroacetic acid (24.5 mL) was added. After cooling the solution to −60°C (chloroform/Dry Ice), bromine (0.51 mL, 0.01 mol) in methylene chloride (50 mL) was added dropwise. The mixture was kept at −60°C for 1 hour followed by stirring at room temperature for 30 min. After removal of the solvent under reduced pressure, the residue was neutralized (aqueous KOH) and the resulting orange precipitate was filtered, washed with water, and dried overnight. Column chromatography ($Al_2O_3$, tetrahydrofuran – ethyl acetate gradient) yielded **7**, 2.0 g, 81% (see above).

## Acknowledgement

We are grateful to Prof. M. S. Gordon for providing us with his third row INDO programs. This paper has been designated as Contribution No. 1651 to the Army Research Program on Antiparasitic Drugs.

1. (*a*) M. I. El-Sheikh, J. C. Chang, and J. M. Cook. Heterocycles, **9**, 1561 (1978); (*b*) J. C. Chang, M. I. El-Sheikh, A. Harmon, K. Avasthi, and J. M. Cook. J. Org. Chem. **46**, 4188 (1981).
2. C. Pouchert and J. R. Campbell. The Aldrich library of nmr spectra. Vol. VIII. 1974. p. 127.
3. K. Avasthi, S. J. Lee, J. M. Cook, J. D. Pickett, and H. H. Wasserman. Heterocycles, **16**, 1453 (1981).
4. S. J. Lee and J. M. Cook. Heterocycles, **16**, 2125 (1981).
5. J. A. Pople, D. P. Santry, and G. A. Segal. J. Chem. Phys. **43**, S129 (1965); J. A. Pople and G. A. Segal. J. Chem. Phys. **43**, S136 (1965); J. A. Pople, D. L. Beveridge, and P. A. Dobosh. J. Chem. Phys. **47**, 2026 (1967).
6. R. C. Weast (*Editor*). Handbook of chemistry and physics. 52nd ed. Chemical Rubber Co. 1971. p. F173.
7. J. C. Chang. M.S. Thesis, University of Wisconsin–Milwaukee, Milwaukee, Wisconsin. 1979.
8. K. Fukui, T. Yonezawa, and C. Nagata. Bull. Chem. Soc. Jpn. **27**, 423 (1954).
9. K. E. Stensio, K. Wahlberg, and R. Wahren. Acta Chemica. Scand. **27**, 2197 (1973).
10. B. E. Boulton and B. A. W. Coller. Aust. J. Chem. **27**, 2331 (1974).
11. M. S. Gordon, M. D. Bjorke, F. J. Marsh, and M. S. Korth. J. Am. Chem. Soc. **100**, 2670 (1978).
12. G. W. Wheland. J. Am. Chem. Soc. **64**, 900 (1942).

# Synthesis of (−)- and (+)-2-hydroxy-6-keto-*N*-methylmorphinans, their *O*-methyl ethers, and 2-deoxy congeners

HELMUT SCHMIDHAMMER AND ARNOLD BROSSI[1]

*Section on Medicinal Chemistry, Laboratory of Chemistry, Institute of Arthritis, Diabetes, and Digestive and Kidney Diseases, National Institutes of Health, Bethesda, MD 20205, U.S.A.*

Received June 7, 1982

HELMUT SCHMIDHAMMER and ARNOLD BROSSI. Can. J. Chem. **60**, 3055 (1982).

Bischler–Napieralski cyclization of the known phenylacetamide **1**, followed by selective ether cleavage of the 3,4-dihydroisoquinoline **2** and sodium borohydride reduction, afforded the tetrahydroisoquinoline **4**. Optical resolution of **4** with tartaric acid gave the optical isomers **4***a*, *b*, which were converted into the 6-ketomorphinans **9***a*, *b* and their *O*-methyl ethers **10***a*, *b* by the following reaction sequence: Birch reduction, *N*-formylation of the dihydro bases, Grewe cyclization, removal of the *N*-formyl protecting groups, reductive *N*-methylation, and *O*-methylation. The 2-deoxy congeners **12***a*, *b* were obtained from **9***a*, *b* by phenyltetrazolylation, and catalytic removal of the heterocyclic ether function. The (−)-enantiomer **12***a* obtained by this synthesis was identical with material prepared from natural morphine, and exhibited the high antinociceptive potency already reported.

HELMUT SCHMIDHAMMER et ARNOLD BROSSI. Can. J. Chem. **60**, 3055 (1982).

La réaction de cyclisation de Bischler–Napieralski de la phénylacétamide **1** suivie du clivage sélectif de l'éther de la dihydro-3,4 isoquinoléine **2** et de la réduction par le borohydrure de sodium, conduit à la tétrahydroisoquinoléine **4**. La résolution optique du composé **4** avec l'acide tartrique permet d'obtenir les isomères optiques **4***a*,*b* que l'on transforme en céto-6 morphinans **9***a*,*b* et en leurs éthers *O*-méthyliques **10***a*,*b* selon les réactions suivantes: la réduction de Birch, la *N*-formylation des bases dihydro, la cyclisation de Grewe, le clivage des groupes protecteurs *N*-formyle, la *N*-méthylation réductive et l'*O*-méthylation. On obtient les congénères déoxy-2 **12***a*,*b* à partir d'une phényltétrazolylation de **9***a*,*b* et de l'élimination catalysée de la fonction éther hétérocyclique. L'énantiomère (−) **12***a* obtenue de cette façon est identique au produit préparé à partir de la morphine naturelle et exhibe le même pouvoir antinociceptif déjà rapporté.

[Traduit par le journal]

The aromatic unsubstituted 6-keto-*N*-methylmorphinan **12***a*, first prepared from natural morphine, showed high antinociceptive potency in the hot-plate assay in mice (1). This result was astonishing, since it was assumed that the presence of a phenolic hydroxy group at C-3 (2) or a methyl ether group at C-4 (3) were essential to manifest good analgetic activity in this group of compounds. The little known pharmacological profiles of the (+)-enantiomers of 6-keto-morphinans suggested that a total synthesis of **12***a* be conceived, which would allow at the same time the preparation of its optical isomer **12***b*. The Grewe cyclization of appropriately substituted octahydroisoquinolines, chosen as the key reaction in the synthesis of **12***a*, *b*, is greatly facilitated by the presence of an electron withdrawing group on the amine nitrogen (4), and a hydroxy group *para*-positioned at the point of ring closure (5). It seemed therefore advisable to first attempt the synthesis of 2-hydroxy substituted 6-ketomorphinans, also needed for our SAR studies, and to eliminate the phenolic 2-hydroxy group afterwards. Elimination of phenolic hydroxy groups has been carried out in several alkaloidal systems and was not expected to give rise to any difficulties (6). This plan has now been accomplished and afforded, as expected, an easy entry into the groups of optically active 2-hydroxy-6-keto-*N*-methylmorphinans and their 2-deoxy congeners.

The synthesis of **9***a*, *b* by the route suggested had precedent in Beyerman's synthesis of 3-hydroxy-6-keto-*N*-methylmorphinan (7), and proceeded as follows. Bischler–Napieralski cyclization of the known amide **1** (8, 9), readily available from *m*-methoxybenzaldehyde, afforded the 3,4-dihydroisoquinoline (DIQ) **2**. The DIQ **2** underwent smooth *O*-demethylation at C-3′ with 48% HBr to afford the phenolic DIQ **3** (10). Reduction of **3** was carried out with $NaBH_4$ and afforded the tetrahydroisoquinoline (TIQ) **4**. Optical resolution of **4** with *d*- and *l*-tartaric acid afforded the optical isomers **4***a*, *b*. Their optical purity was determined by $^1H$ nmr analysis of the methylbenzyl urea derivatives, obtained from both isomers and optically active 1-methylbenzyl isocyanate (11). The individual diastereomers obtained showed little diastereomeric contamination and proved that **4***a*, *b* were optically > 99% pure.

The synthesis of **9***a*, *b* was carried through with the optical isomers **4***a*, *b*, employing identical reaction conditions. Since **12***a* prepared from **4***a* via **9***a* proved to be identical with material prepared from natural morphine (1), only the *a*-series will be discussed in detail. The physical data of the com-

[1]Author to whom correspondence should be addressed.

0008-4042/82/243055-06$01.00/0

©1982 National Research Council of Canada/Conseil national de recherches du Canada

Can. J. Chem. Downloaded from www.nrcresearchpress.com by 210.87.254.40 on 09/06/12
For personal use only.

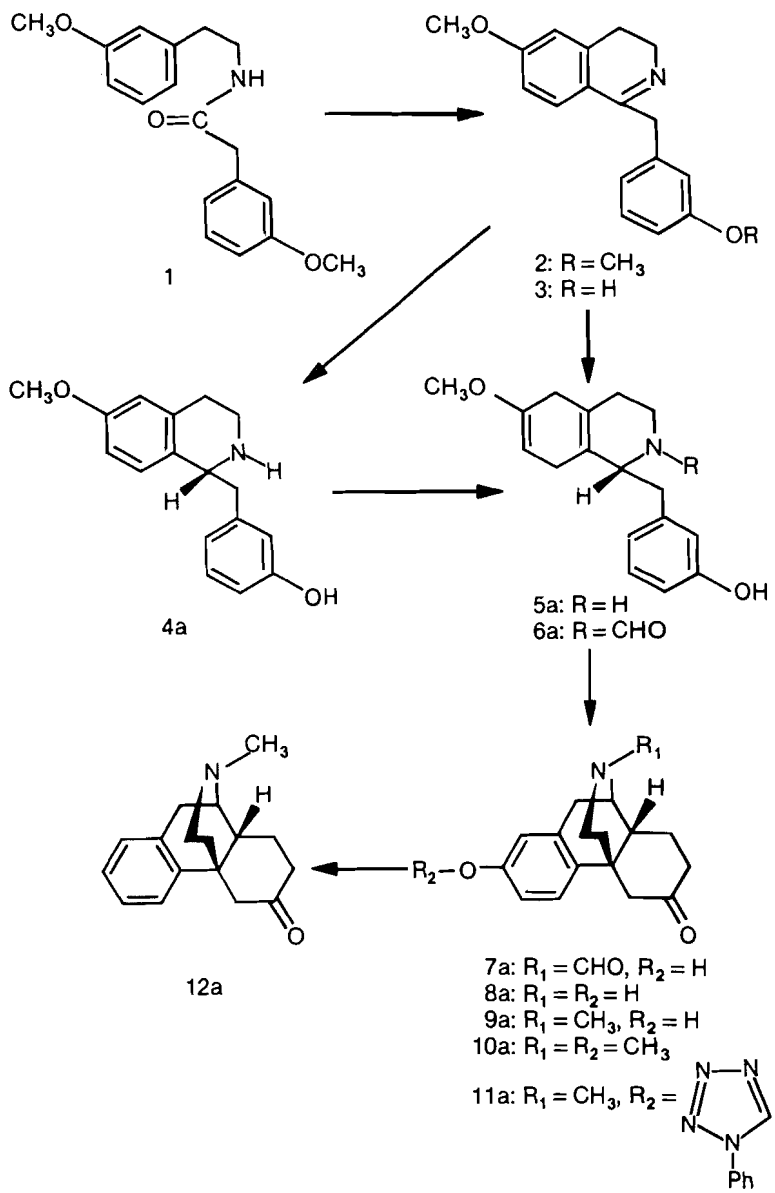


The compounds of the a-series shown above belong to the natural series of 6-ketomorphinans.

SCHEME 1

pounds belonging to the *b*-series and the data for **4**, **5**, **6**, **7**, **8**, and **9** of the racemic series will be listed in the experimental part.

Birch reduction of **4***a* afforded the dihydro base **5***a*, which was *N*-formylated with ethyl formate prior to cyclization. The Grewe cyclization proceeded best in 80% sulfuric acid at 25°C and afforded the *N*-formyl-2-hydroxy-6-ketomorphinan (**7***a*) in 82% yield. The isomeric 4-hydroxy-6-ketomorphinans could only be detected as trace impurities by tlc analysis. This material proved to be a mixture of rotamers, already encountered in other series of *N*-formylated TIQ (12) and morphinans (13). Acid hydrolysis of **7***a* afforded **8***a*, which was converted into **9***a* by a reductive *N*-methylation, and into the *O*-methyl ether **10***a* with phenyltrimethylammonium chloride in DMF. Wolff–Kishner reduction of **8***b*, the optical anti-

Can. J. Chem. Downloaded from www.nrcresearchpress.com by 210.87.254.40 on 09/06/12
For personal use only.

Can. J. Chem. Downloaded from www.nrcresearchpress.com by 210.87.254.40 on 09/06/12
For personal use only.

pode of **8***a*, afforded (+)-2-hydroxy-*N*-methylmorphinan identical by mp and optical rotation with material prepared by a different procedure (4). Phenyltetrazolylation of **9***a* afforded the ether **11***a*, which after catalytic hydrogenation over Pd/C in acetic acid gave the aromatic unsubstituted ketomorphinan **12***a*, identical in every respect with material prepared from morphine (1). This characterizes the TIQ **4***a* as the *R*-isomer and **9***a* and **12***a* as the isomers belonging to the series of (−)-morphinans originating from natural morphine (1, 14). The enantiomers **9***b* and **12***b*, prepared similarly from **4***b*, showed the expected opposite optical behaviour and belong to the series of (+)-morphinans similarly related to (+)-morphine. The analgesic activity of the ketomorphinans prepared here was measured in mice after sc injection by the hot-plate assay. The 2-OH ketone **9***a* ($ED_{50}$ 20.7 mg/kg) was found to be about 20 times and the *O*-methyl ether **10***a* ($ED_{50}$ 8.6 mg/kg) about 10 times less potent than morphine ($ED_{50}$ 0.87 mg/kg). The aromatic unsubstituted ketone **12***a* ($ED_{50}$ 0.33 mg/kg), however, was found to be about 3 times more potent than morphine. It is thus clearly demonstrated that the position of the aromatic oxygenation in oxygenated 6-ketomorphinans is critical for antinociception. Details concerning the biological properties of 6-ketomorphinans are reported elsewhere (15).

## Experimental

Melting points (corrected) were determined with a Fisher–Johns apparatus. Elemental analyses were performed by the Section on Microanalytical Services and Instrumentation of this laboratory. Infrared spectra were recorded on a Beckman IR 4230 spectrometer. Optical rotations were measured by using a Perkin–Elmer Model 241 MC polarimeter with the solvents and concentrations specified. Nuclear magnetic resonance spectra were determined by using a Varian HR-220 spectrometer or a JEOL JNM-FX 100 spectrometer with TMS as internal reference (s = singlet, d = doublet, dd = doublet of doublets, m = multiplet). Chemical ionization mass spectra (ci ms) were obtained by using a Finnigan 1015 D spectrometer with a Model 6000 data collection system. Electron ionization mass spectra (ei ms) were obtained with a Hitachi Perkin–Elmer RMU-6E spectrometer (70 eV).

*1-(3-Methoxybenzyl)-6-methoxy-3,4-dihydroisoquinoline hydrogen bromide (**2**·HBr)*

To a solution of 97.6 g (328 mmol) of **1** in 400 mL acetonitrile were added 50 mL (0.53 mol) of $POCl_3$. At room temperature argon was passed through this mixture during 30 min. Then the mixture was refluxed for 1.0 h under argon, evaporated, cooled to 0–5°C and basified with concentrated NaOH. Extraction with $CH_2Cl_2$, followed by washings with $H_2O$ and brine, drying, and evaporation gave 91.4 g of an oily residue, which was dissolved in 60 mL MeOH. To this solution sufficient 48% HBr (55 mL) was added to give a pH of 1. Addition of $Et_2O$ and cooling to 4°C overnight yielded 91.8 g of **2**·HBr (77%). An analytical sample of **2**·HBr was provided by recrystallization from MeOH/$Et_2O$; mp 221–223°C; nmr ($CDCl_3$) δ: 3.77, 3.88 (2s, 6H, $2OCH_3$), 4.58 (s, 2H, exchanges with $D_2O$, benzylic H), 6.70–7.16 (m, 6H, ArH), 7.84 (d, 1H, ArH, $J$ = 8 Hz); ei ms *m/e*: 281 ($M^+$). *Anal.* calcd. for $C_{18}H_{19}NO_2$·HBr: C 59.67, H 5.57, N 3.82, Br 22.06; found: C 59.82, H 5.56, N 4.03, Br 22.34.

*1-(3-Hydroxybenzyl)-6-methoxy-3,4-dihydroisoquinoline (**3**)*

A solution of 85 g (235 mmol) of **2**·HBr in 200 mL of 48% HBr was refluxed for 50 min, evaporated, and the residue dissolved in 50 mL MeOH. After addition of $Et_2O$ the resulting mixture was kept at 4°C overnight to yield 67.1 g (82%) of **3**·HBr, mp 106–108°C. A portion of this material was converted to the free base **3**; mp 132–134°C (EtOH); ir ($CHCl_3$): 3600 (OH) $cm^{-1}$; nmr ($CDCl_3$) δ: 2.68, 3.62 (2t, 4H, $2CH_2$, $J$ = 8Hz), 3.82 (s, 3H, $OCH_3$), 4.01 (s, 2H, exchanges with $D_2O$, benzylic H), 6.66–7.50 (m, 7H, ArH); ei ms *m/e*: 267 ($M^+$). *Anal.* calcd. for $C_{17}H_{17}NO_2$: C 76.38, H 6.41, N 5.24; found: C 76.11, H 6.48, N 5.15.

*(±)-1-(3-Hydroxybenzyl)-6-methoxy-1,2,3,4-tetrahydroisoquinoline (**4**)*

A stirred solution of 52 g (149 mmol) of **3**·HBr in 400 mL EtOH was treated with 8 g (211 mmol) $NaBH_4$ in small portions during 20 min while maintaining the temperature at 20–30°C with an ice bath. After the addition of $NaBH_4$ was complete, the mixture was stirred for 15 min at room temperature, then cooled to 0–5°C and the excess $NaBH_4$ was destroyed with 30% AcOH to give a final pH of 5. After evaporation, the residue was dissolved in $H_2O$, rendered alkaline with concentrated aqueous $NH_3$, and extracted with $CHCl_3$/2-propanol (2:1). The organic layer was washed with brine, dried, and evaporated to yield 39.4 g (98%) crystalline product. This crude **4** was used for optical resolution. A sample was recrystallized from MeOH to give pure **4**; mp 155–156°C; ir ($CHCl_3$): 3600 (OH) $cm^{-1}$; nmr (DMSO-$d_6$) δ: 3.66 (s, 3H, $OCH_3$), 6.48–6.76 (m, 5H, ArH), 6.96–7.14 (m, 2H, ArH), 9.20 (s, broad, 1H, OH); ci ms *m/e*: 270 ($M^+$ + 1), 162 ($M^+$ − 3-hydroxybenzyl). *Anal.* calcd. for $C_{17}H_{19}NO_2$: C 75.81, H 7.11, N 5.20; found: C 75.93, H 6.98, N 5.47.

*Optical resolution of (±)-1-(3-hydroxybenzyl)-6-methoxy-1,2,3,4-tetrahydroisoquinoline (**4**)*

A mixture of 38.0 g (141 mmol) of **4** and 22.2 g (148 mmol) of *d*-tartaric acid was dissolved in 90 mL MeOH at the boiling point. This mixture was kept at 4°C for 15 h. Then the formed crystals were collected to give 17.8 g nearly pure **4***b*·*d*-tartrate. This material was recrystallized from 40 mL MeOH to yield 12.5 g of pure **4***b*·*d*-tartrate. From combined mother liquors another 14.3 g of pure **4***b*·*d*-tartrate were obtained. Together 26.8 g (91%) of optically > 99% pure **4***b*·*d*-tartrate were obtained;[2] mp 183–185°C; $[\alpha]_D^{26}$ −10.4° (*c* 0.92, $H_2O$). *Anal.* calcd. for $C_{21}H_{25}NO_8$: C 60.13, H 6.01, N 3.34; found: C 59.77, H 5.86, N 3.25.

Compound **4***b*·*d*-tartrate was converted to the free base in the usual way (described below). After recrystallization from MeOH, 16.1 g of *(−)-1-(3-hydroxybenzyl)-6-methoxy-1,2,3,4-tetrahydroisoquinoline* (**4***b*) were obtained; mp 179–180°C; $[\alpha]_D^{26}$ −35.6° (*c* 0.84, 95% EtOH).

The mother liquor of the first crystallization of **4***b*·*d*-tartrate was evaporated, dissolved in $H_2O$, rendered alkaline with concentrated aqueous $NH_3$, and extracted with $CHCl_3$/2-propanol (2:1). The organic layer was washed with brine, dried, and evaporated to give 29.1 g of a solid. Following this, 17.0 g (113 mmol) l-tartaric acid and 60 mL MeOH were added. This

[2]The optical purity was determined by reaction of the bases **4***a*, *b* with (*R*)-(+)-α-methylbenzyl isocyanate in deuteriochloroform followed by 220 MHz nmr analysis of the resulting diastereomeric urea derivatives (11).

Can. J. Chem. Downloaded from www.nrcresearchpress.com by 210.87.254.40 on 09/06/12
For personal use only.

mixture was stirred at the boiling point until a clear solution was obtained. After 18 h at 4°C, 21.9 g of nearly pure **4***a*·l-tartrate could be collected. This material was recrystallized from 50 mL MeOH to give 16.7 g pure **4***a*·l-tartrate. From combined mother liquors another 11.2 g of pure **4***a*·l-tartrate were obtained. Together 27.9 g (94%) of optically > 99% pure **4***a*·l-tartrate·$H_2O$ were obtained;[2] mp 174–176°C; $[\alpha]_D^{24}$ +10.3° (*c* 0.86, $H_2O$). *Anal.* calcd. for $C_{21}H_{25}NO_8 \cdot H_2O$: C 57.66, H 6.22, N 3.20; found: C 57.84, H 6.13, N 3.13.

Compound **4***a*·l-tartrate was converted to the free base in the usual way. Recrystallization from MeOH yielded 15.8 g of *(+)-1-(3-hydroxybenzyl)-6-methoxy-1,2,3,4-tetrahydroisoquinoline* (**4***a*); mp 179–180°C; $[\alpha]_D^{26}$ +35.4° (*c* 0.98, 95% EtOH).

*(±)-1-(3-Hydroxybenzyl)-6-methoxy-1,2,3,4,5,8-hexahydroisoquinoline (5)*

To 500 mL distilled $NH_3$ were added 5.5 g (0.79 mol) Li metal and 250 mL of a 1:1 mixture of dry *t*-BuOH/dry $Et_2O$ at −70°C. Into this well stirred mixture a solution of 13.5 g (50 mmol) of **3** in 400 mL dry *t*-BuOH/dry $Et_2O$ (1:1) was dropped during 30 min. This mixture was stirred at −70°C for 1 h, then 100 mL MeOH were added dropwise. The mixture was allowed to warm up slowly and was then kept at room temperature overnight. After evaporation the resulting solid was dissolved in $H_2O$ and an aqueous solution of 45 g (0.84 mol) $NH_4Cl$ was added. The precipitate was collected and washed with MeOH and n-hexane to yield 12.3 g (90%) of **5**. An analytical sample of **5** was obtained by recrystallization from MeOH; mp 183–185°C; ir (KBr): 3400 and 3300 (OH, NH), 1700 and 1670 (C=C) $cm^{-1}$; nmr ($CDCl_3$) δ: 3.58 (s, 3H, $OCH_3$), 4.66 (s, 1H, C7—H), 6.64 (m, 3H, ArH), 7.12 (dd, 1H, ArH, *J* = 8, 8 Hz); ci ms *m/e*: 272 ($M^+$ + 1). *Anal.* calcd. for $C_{17}H_{21}NO_2$: C 75.24, H 7.80, N 5.16; found: C 74.92, H 7.90, N 5.11.

*(+)-1-(3-Hydroxybenzyl)-6-methoxy-1,2,3,4,5,8-hexahydroisoquinoline (5a)*

To 400 mL distilled $NH_3$ were added 7.0 g (1.0 mol) Li metal and 400 mL of a 1:1 mixture of dry *t*-BuOH/dry $Et_2O$ at −70°C. To this well stirred mixture 15.0 g (56 mmol) of powdered **4***a* were added at once. This mixture was stirred at −70°C for 1 h, then 100 mL MeOH were added dropwise. The mixture was allowed to warm up slowly and was then kept at room temperature overnight. After evaporation the resulting solid was dissolved in $H_2O$ and an aqueous solution of 60 g (1.12 mol) $NH_4Cl$ was added. The precipitate was collected, washed subsequently with $H_2O$, MeOH, and petroleum ether to yield 14.5 g (96%) of **5***a*, mp 190–193°C. Recrystallization of a portion of this material from MeOH afforded an analytical sample of **5***a*; mp 195–196°C; $[\alpha]_D^{25}$ +101.9° (*c* 0.95, 95% EtOH). *Anal.* calcd. for $C_{17}H_{21}NO_2$: C 75.24, H 7.80, N 5.16; found: C 75.11, H 7.56, N 5.07.

*(−)-1-(3-Hydroxybenzyl)-6-methoxy-1,2,3,4,5,8-hexahydroisoquinoline (5b)*

Preparation of this compound from **4***b* on the same scale and essentially as described above for the enantiomer afforded 14.6 g (97%) of **5***b*, mp 192–194°C. Recrystallization from MeOH afforded the analytical sample; mp 195–196°C; $[\alpha]_D^{26}$ −102.0° (*c* 1.10, 95% EtOH). *Anal.* calcd. for $C_{17}H_{21}NO_2$: C 75.24, H 7.80, N 5.16; found: C 75.23, H 7.71, N 5.06.

*(+)-N-Formyl-1-(3-hydroxybenzyl)-6-methoxy-1,2,3,4,5,8-hexahydroisoquinoline (6a)*

To a solution of 14.0 g (51.6 mmol) of **5***a* in 120 mL dry DMF were added 180 mL dry ethyl formate at 90°C (bath temperature) during 30 min. The resulting solution was refluxed for 60 h under argon. Evaporation yielded a crystalline solid, which was treated with 50 mL MeOH to give 14.6 g (95%) of **6***a*, mp 225–228°C. An analytical sample was prepared by recrystallization of a portion of this material with 2-propanol; mp 226–229°C; $[\alpha]_D^{24}$ +3.5° (*c* 1.03, DMSO); ir (KBr): 3180 (OH), 1705 and 1675 (C=C), 1640 (NCHO) $cm^{-1}$; nmr (DMSO-$d_6$) δ: 3.47 (s, 3H, $OCH_3$), 4.70 (s, 1H, C7—H), 6.56 (m, 3H, ArH), 7.00 (dd, 1H, ArH, *J* = 8, 8 Hz), 7.35 (s, 1H, CHO), 9.24 (s, 1H, OH); ci ms *m/e*: 300 ($M^+$ + 1). *Anal.* calcd. for $C_{18}H_{21}NO_3$: C 72.21, H 7.07, N 4.68; found: C 72.12, H 6.89, N 4.41.

*(−)-N-Formyl-1-(3-hydroxybenzyl)-6-methoxy-1,2,3,4,5,8-hexahydroisoquinoline (6b)*

Preparation of this compound from **5***b* on the same scale and exactly as described above for the enantiomer afforded 14.8 g (96%) **6***b*, mp 223–227°C. Recrystallization from 2-propanol gave an analytical sample; mp 227–229°C; $[\alpha]_D^{25}$ −0.6° (*c* 0.93, DMSO). *Anal.* calcd. for $C_{18}H_{21}NO_3$: C 72.21, H 7.07, N 4.68; found: C 72.08, H 7.11, N 4.57.

*(±)-N-Formyl-1-(3-hydroxybenzyl)-6-methoxy-1,2,3,4,5,8-hexahydroisoquinoline (6)*

This compound was prepared from 5.5 g of **5** essentially as described above to afford 5.5 g (91%) of **6**, mp 201–204°C. An analytical sample was obtained by recrystallization from 2-propanol; mp 204–206°C. *Anal.* calcd. for $C_{18}H_{21}NO_3$: C 72.21, H 7.07, N 4.68; found: C 72.01, H 6.96, N 4.44.

*(−)-N-Formyl-2-hydroxymorphinan-6-one (7a)*

To a well stirred mixture of 14.0 g (46.8 mmol) **6***a* and 500 mL $Et_2O$ were added dropwise 300 mL 80% $H_2SO_4$ at 0°C under an argon atmosphere during 3.5 h. The resulting solution was then kept at room temperature for 20 h, poured on 1.0 L ice water, and the organic solvent was evaporated. The aqueous solution was extracted with 6 × 200 mL $CHCl_3$/2-propanol (3:1). The organic layer was washed with water, dried, and evaporated to give 10.9 g (82%) **7***a* as a foam, which was used for the next step without further purification. An analytical sample was prepared by crystallization with MeOH; mp 259–261°C; $[\alpha]_D^{24}$ −219.1° (*c* 0.82, DMSO); ir (KBr): 3260 (OH), 1705 (CO), 1650 and 1620 (NCHO); nmr (DMSO-$d_6$) δ: 4.58 (m, 1H, C9—H), 6.52 (m, 2H, ArH), 7.04 (d, 1H, ArH, *J* = 8 Hz), 7.95 (s, 1H, CHO), 9.20 (s, 1H, OH); ei ms *m/e*: 285 ($M^+$). *Anal.* calcd. for $C_{17}H_{19}NO_3$: C 71.56, H 6.71, N 4.91; found: C 71.49, H 6.47, N 4.79.

*(+)-N-Formyl-2-hydroxymorphinan-6-one (7b)*

Preparation of this compound from **6***b* on the same scale and essentially as described above for the enantiomer afforded 11.2 g (84%) **7***b* as a foam, which was used for the next step without further purification. Crystallization with MeOH gave an analytical sample; mp 260–262°C; $[\alpha]_D^{24}$ +222.5° (*c* 0.87, DMSO). *Anal.* calcd. for $C_{17}H_{19}NO_3$: C 71.56, H 6.71, N 4.91; found: C 71.34, H 6.64, N 4.68.

*(±)-N-Formyl-2-hydroxymorphinan-6-one (7)*

This compound was prepared in a similar manner as described for both enantiomers, from 4.3 g **6** to give 3.5 g (85%) **7** as a foam, which was used for the next step without further purification. Crystallization with MeOH afforded an analytical sample; mp 244–247°C; *Anal.* calcd. for $C_{17}H_{19}NO_3 \cdot 0.5H_2O$: C 69.37, H 6.85, N 4.76; found: C 69.70, H 6.74, N 4.66.

*(−)-2-Hydroxymorphinan-6-one (8a)*

A solution of 8.0 g (28.0 mmol) **7***a* in 81 mL MeOH and 9 mL concentrated HCl was refluxed for 16 h and then evaporated. The oily residue was dissolved in $H_2O$, basified with concentrated aqueous $NH_3$, and extracted with a total amount of 250 mL $CHCl_3$/2-propanol (3:1). The organic layer was washed with brine, dried, and evaporated to give a crystalline residue, which yielded after treatment with MeOH 6.1 g (85%) of **8***a*. An analytical sample was recrystallized with MeOH; mp 282–286°C (dec.); $[\alpha]_D^{25}$ −116.9° (*c* 0.95, DMSO); ir (KBr): 3400 (broad,

Can. J. Chem. Downloaded from www.nrcresearchpress.com by 210.87.254.40 on 09/06/12
For personal use only.

OH), 3280 (NH); nmr (DMSO-$d_6$) δ: 6.48 (m, 2H, ArH), 6.96 (d, 1H, ArH, $J$ = 8 Hz); ei ms *m/e*: 257 ($M^+$). *Anal.* calcd. for $C_{16}H_{19}NO_2$: C 74.68, H 7.44, N 5.44; found: C 74.40, H 7.65, N 5.36.

*(+)-2-Hydroxymorphinan-6-one (**8**b)*

Preparation of this compound from **7***b* in the same scale and manner as described above afforded 6.2 g (86%) of **8***b*. An analytical sample was obtained by recrystallization from MeOH; mp 281–284°C (dec.); $[\alpha]_D^{25}$ +117.6° (*c* 1.03, DMSO). *Anal.* calcd. for $C_{16}H_{19}NO_2$: C 74.68, H 7.44, N 5.44; found: C 74.40, H 7.63, N 5.68.

*(±)-2-Hydroxymorphinan-6-one (**8**)*

Preparation of this compound from 3.5 g **7** in the same manner as described above afforded 2.45 g (78%) of **8**. An analytical sample was obtained by recrystallization from MeOH; mp > 270°C (dec.). *Anal.* calcd. for $C_{16}H_{19}NO_2 \cdot 0.5H_2O$: C 72.15, H 7.57, N 5.26; found: C 72.29, H 7.28, N 5.31.

*(−)-2-Hydroxy-*N*-methylmorphinan-6-one (**9**a)*

A mixture of 5.5 g (21.4 mmol) of **8***a*, 5.5 g (40.4 mmol) of $NaOAc \cdot 3H_2O$, 17.6 mL of 37% formaline, and 1.5 g 10% Pd/C catalyst was hydrogenated in 150 mL 2 *N* AcOH at 50 psi and room temperature for 2 h. The mixture was filtered, washed with 2 *N* AcOH, the filtrate was basified with concentrated aqueous $NH_3$ and extracted with a total amount of 200 mL $CHCl_3$/2-propanol (3:1). The organic layer was washed with $H_2O$, dried, and evaporated to give a foam, which after crystallization from MeOH yielded 5.4 g (93%) **9***a*. An analytical sample was formed by recrystallization from MeOH; mp 115–117°C; $[\alpha]_D^{24}$ −130.2° (*c* 0.89, DMF); ir (KBr): 3400 (OH), 1705 (CO) $cm^{-1}$; nmr (DMSO-$d_6$) δ: 2.24 (s, 3H, $NCH_3$), 6.48 (m, 2H, ArH), 6.92 (d, 1H, ArH, $J$ = 8 Hz), 8.92 (s, 1H, OH); ci ms *m/e*: 272 ($M^+ + 1$). *Anal.* calcd. for $C_{17}H_{21}NO_2 \cdot CH_3OH$: C 71.25, H 8.31, N 4.62; found: C 71.26, H 8.73, N 4.43.

*(+)-2-Hydroxy-*N*-methylmorphinan-6-one (**9**b)*

Preparation of this compound from **8***b* on the same scale and manner as described above afforded 5.3 g (91%) **9***b*. An analytical sample was recrystallized from MeOH; mp 115–117°C; $[\alpha]_D^{24}$ +130.9° (*c* 0.95, DMF). *Anal.* calcd. for $C_{17}H_{21}NO_2 \cdot CH_3OH$: C 71.25, H 8.31, N 4.62; found: C 70.83, H 8.31, N 4.50.

Wolff–Kishner reduction of this material carried out in the usual way afforded the known (+)-2-hydroxy-*N*-methylmorphinan (4); mp 182–184°C (MeOH); $[\alpha]_D^{25}$ +40.8° (*c* 0.92, MeOH) (lit. (4) mp 181–183°C ($Et_2O$); $[\alpha]_D^{25}$ +41.4° (*c* 0.45, MeOH)).

*(±)-2-Hydroxy-*N*-methylmorphinan-6-one (**9**)*

Preparation of this compound from 2.5 g **8** essentially as described above yielded 2.2 g (83%) **9**. An analytical sample was prepared by recrystallization from 2-propanol; mp 240–242°C (dec.). *Anal.* calcd. for $C_{17}H_{21}NO_2$: C 75.24, H 7.80, N 5.16; found: C 74.93, H 7.85, N 5.11.

*(−)-2-Methoxy-*N*-methylmorphinan-6-one (**10**a)*

A mixture of 300 mg (1.1 mmol) of **9***a*, 300 mg (2.2 mmol) of anhydrous $K_2CO_3$, and 380 mg (2.2 mmol) of phenyltrimethylammonium chloride in 20 mL anhydrous DMF was stirred at 80°C (bath temperature) under argon for 6 h. The mixture was filtered, washed with $CHCl_3$, and the filtrate was evaporated. The residue was dissolved in $CH_2Cl_2$, washed with 1 *N* NaOH and brine, dried, and evaporated to give a crystalline solid, which was recrystallized from isopropyl ether to yield 210 mg (67%) of **10***a*. An analytical sample was recrystallized from MeOH; mp 149–151°C; $[\alpha]_D^{24}$ −125.8° (*c* 0.97, $CHCl_3$); ir (KBr): 1705 (CO) $cm^{-1}$; nmr ($CDCl_3$) δ: 2.44 (s, 3H, $NCH_3$), 3.74 (s, 3H, $OCH_3$), 6.66 (m, 2H, ArH), 7.14 (d, 1H, ArH, $J$ = 8 Hz); ei ms *m/e*: 285 ($M^+$). *Anal.* calcd. for $C_{18}H_{23}NO_2$: C 75.75, H 8.12, N 4.91; found: C 75.51, H 8.09, N 4.89.

*(+)-2-Methoxy-*N*-methylmorphinan-6-one (**10**b)*

Preparation of this compound from **9***a* on the same scale and essentially as described above yielded 200 mg (63%) of **10***b*. An analytical sample was prepared by recrystallization from MeOH; mp 150–152°C; $[\alpha]_D^{24}$ +126.0° (*c* 1.08, $CHCl_3$). *Anal.* calcd. for $C_{18}H_{23}NO_2$: C 75.75, H 8.12, N 4.91; found: C 75.93, H 8.19, N 4.89.

*(−)-2-[(1-Phenyl-1*H*-tetrazol-5-yl)oxy]-*N*-methylmorphinan-6-one (**11**a)*

A mixture of 3.7 g (13.6 mmol) of **9***a*, 3.7 g (26.8 mmol) of anhydrous $K_2CO_3$, and 2.6 g (14.4 mmol) of 5-chloro-1-phenyl-1*H*-tetrazole in 40 mL anhydrous DMF was stirred at room temperature under argon atmosphere for 18 h. The mixture was filtered, washed with $CHCl_3$, and the filtrate was evaporated. The residue was dissolved in $CH_2Cl_2$ and extracted with 10% aqueous tartaric acid. The aqueous layer was washed with $Et_2O$, rendered alkaline with concentrated NaOH, and extracted with $CH_2Cl_2$. The organic layer was washed with brine, dried, and evaporated to give 5.4 g (95%) of **11***a* as an oil, which was used for the next step without further purification. An analytical sample was obtained by crystallization with AcOEt; mp 133–134°C; $[\alpha]_D^{24}$ −80.1° (*c* 1.03, $CHCl_3$); ir (KBr): 1705 (CO) $cm^{-1}$; nmr ($CDCl_3$) δ: 2.38 (s, 3H, $NCH_3$), 7.04–7.78 (m, 8H, ArH); ei ms *m/e*: 415 ($M^+$). *Anal.* calcd. for $C_{24}H_{25}N_5O_2$: C 69.38, H 6.07, N 16.85; found: C 69.66, H 6.25, N 16.68.

*(+)-2-[(1-Phenyl-1*H*-tetrazol-5-yl)oxy]-*N*-methylmorphinan-6-one (**11**b)*

This compound was prepared from 2 g of **9***b* essentially as described above, yielded 2.8 (91%) of **11***b* as an oil, which was used for the next step without further purification. An analytical sample was obtained by crystallization with AcOEt; mp 132–134°C; $[\alpha]_D^{24}$ +80.4° (*c* 1.15, $CHCl_3$). *Anal.* calcd. for $C_{24}H_{25}N_5O_2$: C 69.38, H 6.07, N 16.85; found: C 69.51, H 5.93, N 17.08.

*(−)-*N*-Methylmorphinan-6-one (**12**a) (1)*

To a solution of 4.0 g (9.6 mmol) of crude **11***a* in 50 mL of glacial acetic acid were added 8.0 g 10% Pd/C catalyst. This mixture was hydrogenated at 50 psi at room temperature for 24 h. The catalyst was filtered off, washed with glacial acetic acid, and the filtrate was evaporated. The residue was dissolved in $H_2O$, rendered alkaline with concentrated NaOH, and extracted with $CH_2Cl_2$. The organic layer was washed with brine, dried, and evaporated to give a crystalline solid, which was treated with isopropyl ether to yield 1.9 g (77%) of **12***a*. An analytical sample was recrystallized with isopropyl ether; mp 165–167°C (lit. (1) mp 164–166°C); $[\alpha]_D^{25}$ −135.8° (*c* 0.86, $CHCl_3$) (lit. (1) $[\alpha]_D^{26}$ −137.8° (*c* 0.92, $CHCl_3$)); ir and nmr were identical with an authentic sample.

*(+)-*N*-Methylmorphinan-6-one (**12**b)*

This compound was prepared from 2.7 g of crude **11***b* essentially as described above, yielded 1.2 g (72%) of **12***b*. An analytical sample was recrystallized with isopropyl ether; mp 165–167°C; $[\alpha]_D^{24}$ +136.1° (*c* 1.01, $CHCl_3$). *Anal.* calcd. for $C_{17}H_{21}NO$: C 79.96, H 8.29, N 5.49; found: C 79.93, H 8.32, N 5.36.

## Acknowledgement

We thank Dr. A. E. Jacobson and L. Atwell for having provided us with the biological data of the compounds described here.

1. H. Schmidhammer, A. E. Jacobson, and A. Brossi. Heterocycles, **17**, 391 (1982).
2. J. Hellerbach, O. Schnider, H. Besendorf, and B.

PELLMONT. *In* Synthetic analgesics. Part II, a monograph in Organic chemistry. Vol. 8, Pergamon Press, New York. 1966. pp. 74–75.
3. A. E. JACOBSON, F.-L. HSU, M. D. ROZWADOWSKA, H. SCHMIDHAMMER, L. ATWELL, A. BROSSI, and F. MEDZIHRADSKY. Helv. Chim. Acta, **64**, 1298 (1981); A. MANMADE, H. C. DALZELL, J. F. HOWES, and R. K. RAZDAN. J. Med. Chem. **24**, 1437 (1981).
4. E. MOHACSI and W. LEIMGRUBER. U. S. Patent No. 3,914,234 (1975), assigned to Hoffmann-La Roche Inc.
5. R. GREWE and A. MONDON. Chem. Ber. **81**, 279 (1948); R. GREWE, H. FISCHER, and W. I. FRIEDRICHSEN. Chem. Ber. **100**, 1 (1967); H. HENECKA. Ann. **583**, 110 (1949); W. S. JOHNSON. *In* Organic reactions. Vol. II. John Wiley & Sons, New York. 1944. pp. 118–120.
6. A. BROSSI, M. F. RAHMAN, K. C. RICE, M. GERECKE, R. BORER, J. O'BRIEN, and S. TEITEL. Heterocycles, **7**, 277 (1977); J. REDEN, M. REICH, K. C. RICE, A. E. JACOBSON, A. BROSSI, R. A. STREATY, and W. KLEE. J. Med. Chem. **22**, 256 (1979).
7. C. OLIEMAN, PH. NAGELHOUT, A. D. DEGROOT, L. MAAT, and H. C. BEYERMAN. Recl. Trav. Chim. Pays-Bas, **99**, 353 (1980).
8. J. JIRKOWSKY and M. PROTIVA. Collect. Czech. Chem. Commun. **29**, 400 (1964).
9. S. N. CHAKRAVATI, R. D. HAWORTH, and W. H. PERKIN, JR. J. Chem. Soc. 2270 (1927).
10. A. BROSSI and S. TEITEL. Helv. Chim. Acta, **53**, 1779 (1970).
11. K. C. RICE and A. BROSSI. J. Org. Chem. **45**, 592 (1980).
12. K. C. RICE, W. C. RIPKA, J. REDEN, and A. BROSSI. J. Org. Chem. **45**, 601 (1980); A. BROSSI. Proceedings of the 4th Asian Symposium on Medicinal Plants and Spices, Bangkok, Thailand. Unesco Publication. September 1980. p. 261; C. SZÁNTAY, G. BLASKÓ, M. BÁRCZAI-BEKE, and G. DÖRNYEI. Heterocycles, **14**, 1127 (1980); H. VAN KONINGSFELD and C. OLIEMAN. Cryst. Struct. Commun. **10**, 541 (1981).
13. K. C. RICE. J. Org. Chem. **45**, 3135 (1980).
14. A. BROSSI. Proceedings First Int. Conference on Chemistry and Biotechnology of Biologically Active Nat. Products. Vol. 1. *Edited by* Bulgarian Academy of Sciences, Varna. October 1981. p. 114.
15. H. SCHMIDHAMMER, A. E. JACOBSON, and A. BROSSI. Med. Res. Rev. 1983. Submitted.

Can. J. Chem. Downloaded from www.nrcresearchpress.com by 210.87.254.40 on 09/06/12
For personal use only.

# Mechanistic studies in strong acids. VIII.[1] Hydrolysis mechanisms for some thiobenzoic acids and esters in aqueous sulfuric acid, determined using the excess acidity method[2]

ROBIN A. COX AND KEITH YATES

*Department of Chemistry, University of Toronto, 80 St. George St., Toronto, Ont., Canada M5S 1A1*

Received July 6, 1982

ROBIN A. COX and KEITH YATES. Can. J. Chem. **60**, 3061 (1982).

The excess acidity method has been applied to hydrolysis rate data, obtained as a function of medium composition, for four thiobenzoic acids, thioacetic acid, eight ethyl thiolbenzoates, and eight ethyl thionbenzoates in aqueous sulfuric acid. The mechanistic behaviour thus revealed has both similarities to and differences from that of a typical ester like ethyl benzoate, which gives benzoic acid by an A-2 reaction involving two water molecules in weak acid, and by A-1 acylium ion formation in strong acid. The thioacids follow this behaviour, except that the A-2 process involves three water molecules, and that the mechanistic changeover occurs in 60% rather than 80% acid. The A-2 process for the ethyl thiolbenzoates is slow; the major hydrolysis mechanism is acylium ion formation, not in an A-1 reaction but by a concerted A–$S_E2$ process involving both proton transfer to sulfur and carbon–sulfur bond breaking. The major proton transfer agent is the undissociated sulfuric acid molecule. The thionbenzoate esters, in contrast, undergo very fast A-2 hydrolysis; so fast, in fact, that the initial protonation of sulfur is the rate-determining step in acids more dilute than about 62% w/w. It appears that proton transfer to sulfur is a comparatively slow process.

ROBIN A. COX et KEITH YATES. Can. J. Chem. **60**, 3061 (1982).

On a appliqué la méthode d'acidité en excès aux données de vitesse d'hydrolyse, obtenues en fonction de la composition du milieu, de quatre acides thiobenzoiques, à l'acide thioacétique, à huit thiolbenzoates d'éthyle et à huit thionbenzoates d'éthyle dans l'acide sulfurique aqueux. Le mécanisme ainsi révélé ressemble et diffère à la fois de celui d'un ester typique tel le benzoate d'éthyle qui conduit à l'acide benzoique selon une réaction de type A-2 qui implique deux molécules d'eau en présence d'un acide faible et selon une formation d'ion acylium de type A-1 en présence d'un acide fort. Les thioacides ont ce même comportement à l'exception du fait que le mécanisme de type A-2 implique trois molécules d'eau et que ce changement de mécanisme se produit dans un milieu acide à 60% plutôt qu'à 80%. Le processus A-2 est lent dans le cas des thiolbenzoates d'éthyle. Le mécanisme principal d'hydrolyse est la formation de l'ion acylium, non pas selon une réaction de type A-1 mais selon un mécanisme concerté du type A–$S_E2$ qui implique à la fois un transfert de proton sur le soufre et une rupture de la liaison carbone–soufre. Le principal agent de transfert du proton est la molécule d'acide sulfurique non dissocié. Les esters thionbenzoates au contraire, subissent une hydrolyse très rapide du type A-2. Cette hydrolyse est si rapide qu'en fait la protonation initiale du soufre est l'étape déterminante dans un milieu acide dont la dilution est supérieure à 62% w/w environ. Il semble que le transfert de proton sur le soufre est comparativement un processus lent.

[Traduit par le journal]

## Introduction

The excess acidity method has proved to be of considerable value in determining the details of mechanistic behaviour for reactions in aqueous acid media, particularly sulfuric acid (1–4). To date it has been applied to acid-catalyzed enolizations (2), to the hydrolyses of some crowded benzoate esters (3), to aromatic nitrations (5), and to benzamide, methylbenzimidatium ion, and lactam hydrolyses (4). In this paper the method is applied to the hydrolysis reactions undergone by four thiobenzoic acids (**1**), by thioacetic acid (**2**), by eight ethyl thiolbenzoates (**3**), and by eight ethyl thionbenzoates (**4**), in aqueous sulfuric acid.

All of these compounds give the parent carboxylic acid as product, and previous studies (6–8), using the *r*-parameter (9) and transition-state activity coefficient (10) methods, have suggested that, following a pre-equilibrium protonation step, they probably all hydrolyze either via an $A_{Ac}2$ mechanism involving water (preferred by **4**), or by acylium ion formation (preferred by **3**), depending on the acid concentration (6–8).

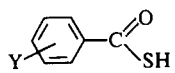

**1***a*, Y = 4-OMe
**1***b*, Y = 4-Me
**1***c*, Y = H
**1***d*, Y = 4-Cl

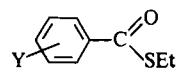

**3***a*, Y = 4-OMe
**3***b*, Y = 4-Me
**3***c*, Y = 3-Me
**3***d*, Y = H
**3***e*, Y = 4-Cl
**3***f*, Y = 3-Br
**3***g*, Y = 3-$NO_2$
**3***h*, Y = 4-$NO_2$

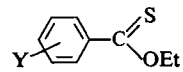

**4***a*, Y = 4-OMe
**4***b*, Y = 4-Me
**4***c*, Y = 3-Me
**4***d*, Y = H
**4***e*, Y = 4-Cl
**4***f*, Y = 4-Br
**4***g*, Y = 3-Br
**4***h*, Y = 4-$NO_2$

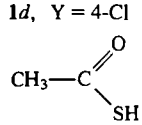

**2**

## Experimental

The protonation $pK_{SH^+}$ and $m^*$ values for **1***b*, **1***c*, and **3***c*–**3***h* were obtained from ionization ratio (*I*) data (7, 8) using eq. [1];

$$[1] \quad \log I - \log C_{H^+} = m^*X + pK_{SH^+}$$

values of *X* and log $C_{H^+}$ were available (11), and these were corrected to the measurement temperature, 5°C or 10°C (7, 8), as

[1]Parts I–VII are refs. 16–18 and 1–4.

[2]Presented at the 65th Chemical Conference of the Chemical Institute of Canada, Toronto, Ont., June 1982, No. OR10-3.

0008-4042/82/243061-10$01.00/0

©1982 National Research Council of Canada/Conseil national de recherches du Canada

Can. J. Chem. Downloaded from www.nrcresearchpress.com by 210.87.254.6 on 09/06/12
For personal use only.

Can. J. Chem. Downloaded from www.nrcresearchpress.com by 210.87.254.6 on 09/06/12
For personal use only.

described previously (3). log $I$ data could not be obtained for **1***a*, **1***d*, **3***a*, and **3***b* (7, 8); for these p$K_{SH^+}$ was obtained from p$\sigma$ plots by extrapolation, and $m^*$ was assumed to be the averages of the **1***b*–**1***c* and **3***c*–**3***h* slopes. These were used to calculate the required protonation correction terms, log $[C_S/(C_S + C_{SH^+})]$, see eqs. [5], [7], [10], and [13]; p$K_{SH^+}$ was corrected to the reaction temperature, if necessary, by assuming that $\Delta G^0 = \Delta H^0$ for the protonation process, as before (3, 4). The 25°C values given in Tables 2 and 3 have been corrected in this way. For **4** p$K_{SH^+}$ and $m^*$ had previously been derived (11); thioacetic acid **2** was assumed to be unprotonated, which is reasonable on the basis of the very small protonation correction terms found for thiobenzoic acid, **1***c*.

Observed rate constants as a function of sulfuric acid concentration at 25°C, $k_\psi$, were available for **3** and **4** (6, 7), as were data at 50°C and two other temperatures for **1** and **2** (8). Temperature-corrected log water activities and log bisulfate ion concentrations in molarity units were those used before (3, 4); log sulfuric acid activities at 25°C were obtained from Giauque *et al.* (12) and converted to molarity units. The computer program used to separate individual processes, in those cases where mixed mechanisms were found, was that used previously (3, 4). Straight lines were fitted using standard least-squares analysis techniques. The $\sigma$ and $\sigma^+$ values were taken from Hammett (13). $\sigma^+$ was used in correlations except for the methoxy substituent, where an average of $\sigma$ and $\sigma^+$ was used, previous experience having found this to be the best compromise for sulfuric acid solutions (14).

## Kinetic analysis

*A-2 Mechanism*

For a typical $A_{Ac}2$ hydrolysis (1, 3), reaction [2],[3]

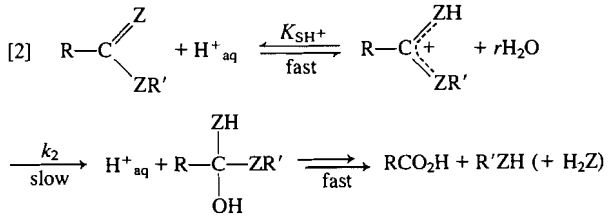

[3] $$k_\psi(C_S + C_{SH^+}) = k_2 a_{SH^+} a_{H_2O}{}^r / f_\ddagger$$

the observed pseudo-first-order rate constant $k_\psi$ is given by eq. [3], if the nucleophile is water; $a$ = activity, $C$ = molar concentration, $f$ = molar activity coefficient, and $r$ is the number of water molecules involved in bond making/breaking processes at the transition state (1, 4, 9). Substituting $a_{SH^+} = a_S a_{H^+}/K_{SH^+} = C_S C_{H^+} f_S f_{H^+}/K_{SH^+}$ into eq. [3], gathering terms and taking logs gives eq. [4] (1).

[4] $$\log k_\psi - \log [C_S/(C_S + C_{SH^+})] - \log C_{H^+} = \log (k_2/K_{SH^+}) + r \log a_{H_2O} + \log (f_S f_{H^+}/f_\ddagger)$$

It has been shown previously that the assumption $\log (f_S f_{H^+}/f_\ddagger) = m^\ddagger \log (f_S f_{H^+}/f_{SH^+})$ is valid (1), and since $\log (f_S f_{H^+}/f_{SH^+}) = m^* \log (f_{B^*} f_{H^+}/f_{B^*H^+}) =$ $m^*X$, where $X$ is the excess acidity for a standard base B* (11, 15), eq. [4] becomes eq. [5]. For A-2 reactions $m^\ddagger{}_2 \simeq 1$ is typical (1).

[5] $$\log k_\psi - \log [C_S/(C_S + C_{SH^+})] - \log C_{H^+} = \log (k_2/K_{SH^+}) + r \log a_{H_2O} + m^\ddagger{}_2 m^* X$$

*A-1 Mechanism*

Similar reasoning to the above results in eq. [7] for an $A_{Ac}1$ hydrolysis, reaction [6]. Protonation is

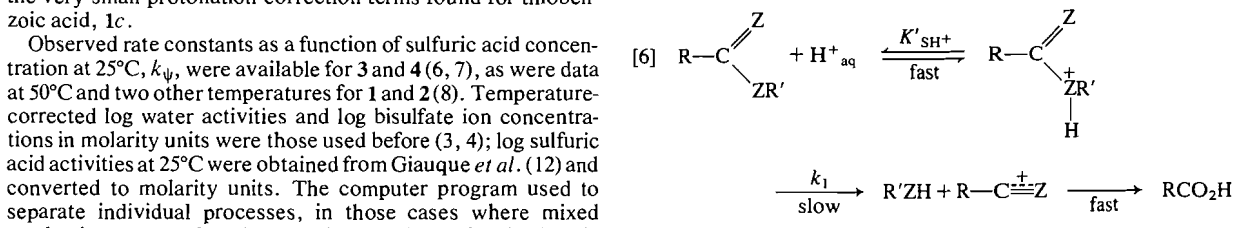

[7] $$\log k_\psi - \log [C_S/(C_S + C_{SH^+})] - \log C_{H^+} = \log (k_1/K'_{SH^+}) + m^\ddagger{}_1 m^{*\prime} X$$

at the ester Z rather than the carbonyl Z, represented by $K'_{SH^+}$ and $m^{*\prime}$ rather than $K_{SH^+}$ and $m^*$; however, the latter is still the most favoured protonation site (1, 3, 6, 7), and the amount of substrate "locked up" in the carbonyl- or thiocarbonyl-protonated form is accounted for by the protonation correction term, log $[C_S/(C_S + C_{SH^+})]$. For A-1 reactions $m^\ddagger{}_1 > 1$ is typical, values of 2–3 not being uncommon (1).

*A–$S_E2$ Mechanism*

If the initial protonation in reaction [2] is slow, $k_0$, reaction [8] can easily be derived (1). If the protonation in reaction [6] is involved in the rate-determining step, as shown in reaction [9], then eq. [10] is the result. For both of these $m^\ddagger{}_0 < 1$

[8] $$\log k_\psi - \log C_{H^+} = \log k_0 + m^\ddagger{}_0 m^* X$$

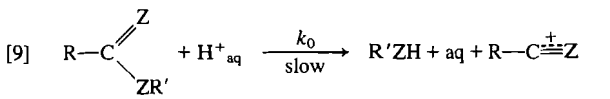

[10] $$\log k_\psi - \log [C_S/(C_S + C_{SH^+})] - \log C_{H^+} = \log k_0 + m^\ddagger{}_0 m^{*\prime} X$$

(1), which is a useful criterion for distinguishing eq. [8] or eq. [10] (A–$S_E2$) from eq. [7] (A-1). Distinguishing these from A-2 mechanisms is straightforward insofar as the water or bisulfate ion activity is not involved (1–4).

However, A–$S_E2$ mechanisms involve general acid catalysis, and protonated water is not the strongest acid in concentrated sulfuric acid solutions (16). Catalysis by undissociated $H_2SO_4$ molecules (16–18), and even by $H_3SO_4{}^+$ in really strong

[3]In reaction [2] and subsequent reactions R = substituted phenyl (or methyl), Z = O or S, and ZR′ = OEt, SEt, or SH.

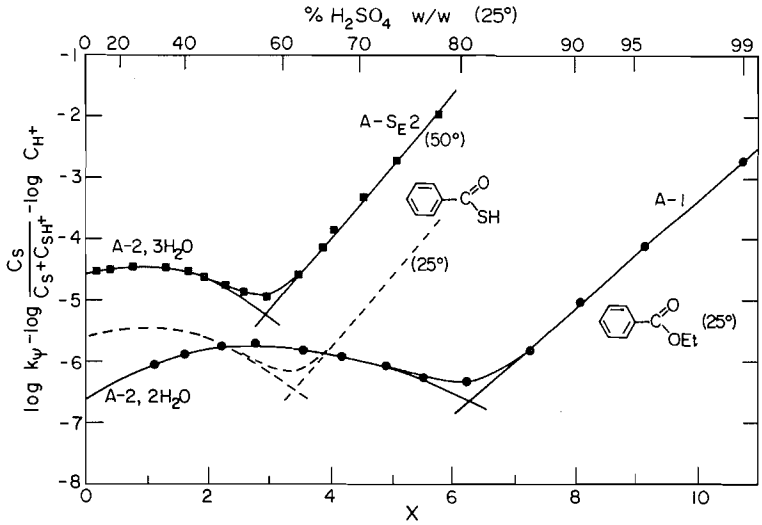


FIG. 1. Excess acidity plots for the hydrolyses of ethyl benzoate at 25°C (6) and thiobenzoic acid at 50°C (with an extrapolation to 25°C), in aqueous $H_2SO_4$.

acid (16), has been observed before, and deserves consideration here. From reaction [11] derivation

[11] 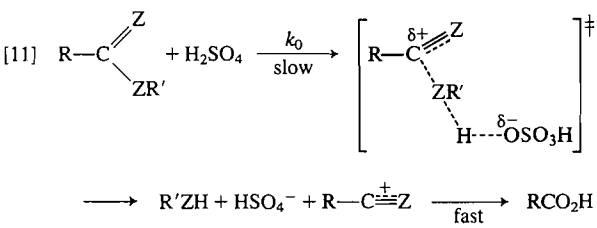

of eq. [12] with the activity coefficient term log

$$[12]\quad \log k_\psi - \log [C_S/(C_S + C_{SH^+})] - \log a_{H_2SO_4} = \log k_0 + \log (f_S/f_\pm)$$

$(f_S/f_\pm)$ is straightforward. Regarding the latter, since $\log (f_S f_{H^+}/f_\pm) = m^\pm m^* X$, if $\log f_{H^+}$ is linear in $X$ then $\log (f_S/f_\pm)$ is too. Values of $a^*_{H^+}$, obtained (19) on making the Boyd assumption (20),[4] are available as a function of acid molarity for several acid systems (19). From these, $\log f^*_{H^+}$ (= $\log a^*_{H^+}$ − $\log C_{H^+}$) was derived and plotted against $X$. This graph was accurately linear, 0.9998 over 22 points with slope 2.10 ± 0.01, over the 5–70% $H_2SO_4$ range in which $\log a^*_{H^+}$ has been measured. Thus the assumption that $\log (f_S/f_\pm)$ is also linear in $X$ is very reasonable, and eq. [12] becomes eq. [13].

$$[13]\quad \log k_\psi - \log [C_S/(C_S + C_{SH^+})] - \log a_{H_2SO_4} = \log k_0 + mX$$

[4]The Boyd assumption is that $\log f_{TEA^+}$ is invariant with acidity, $TEA^+$ being the tetraethylammonium cation; $\log f^*_{H^+} = \log (f_{H^+}/f_{TEA^+})$.

## Results

A typical ester like ethyl benzoate hydrolyzes according to reaction [2] in acid more dilute than, and reaction [6] in acid more concentrated than, 80% $H_2SO_4$, as we have shown elsewhere (1, 3). The A-2 reaction involves two water molecules (3). Ethyl benzoate hydrolysis rate data (1, 6) are plotted according to eqs. [5] and [7] in Fig. 1; $k_\psi$ was separated into its components according to $k_\psi = k_{A\text{-}2} + k_{A\text{-}1}$ using an available computer program (3).

The thioacids **1** and **2** (8) exhibited very similar behaviour to this, except that three rather than two water molecules were found to be involved in the A-2 process (e.g. $r = 3.3 \pm 0.4$ for thiobenzoic acid, taken as a fixed value of 3 in subsequent calculations). Also the switchover to the acylium ion mechanism occurred in more dilute acid, about 60%. This behaviour is illustrated for thiobenzoic acid at 50°C in Fig. 1, together with an extrapolation to 25°C for direct comparison with ethyl benzoate.

Data at several temperatures were available for **1***c* and **2** (8), and this permitted calculation of standard-state activation parameters (i.e. values in water at 25°C) as described previously (3, 4). These are given in Table 1, together with the previously obtained methyl benzoate numbers (3), for comparison; included in Table 1 are the $m^\pm$ and $m^*$ slopes. Where possible $m^\pm_2$ and $\Delta H^\pm$ (i.e. $k_2$ in eq. [5]) are separated from $m^*$ and $\Delta H^0$ ($K_{SH^+}$ in eq. [5]); independent measurements of $pK_{SH^+}$ could be made in most cases (see Experimental section), which gave $m^*$ and enabled estimation of $\Delta H^0$ on

Can. J. Chem. Downloaded from www.nrcresearchpress.com by 210.87.254.6 on 09/06/12
For personal use only.

Can. J. Chem. Downloaded from www.nrcresearchpress.com by 210.87.254.6 on 09/06/12
For personal use only.

TABLE 1. Standard state activation parameters for **1***c*, **2**, and methyl benzoate

| Quantity[a] | Thiobenzoic acid | Thioacetic acid | Methyl benzoate (3) |
|---|---|---|---|
| *A-2 reaction* | | | |
| $\Delta G^0 = \Delta H^{0\,b}$ | −7.720±0.094 | — | −9.57±0.14 |
| $\Delta H^{\ddagger} - \Delta H^0$ | 17.9±1.1 | 15.60±0.46 | 22.62±0.27 |
| $\Delta S^{\ddagger}$ | −48.1±3.6 | −47.9±1.6 | −30.01±0.92 |
| $\Delta H^{\ddagger}$ | 10.2±1.1 | — | 13.05±0.30 |
| $m^*$ | 0.677±0.010 | — | 0.842±0.016 |
| $m^{\ddagger}{}_2 m^*$ | 0.620±0.014 | 0.538±0.011 | 0.8508±0.0071 |
| $m^{\ddagger}{}_2$ | 0.917±0.025 | — | 1.010±0.021 |
| *A-1 or A–$S_E$2 reaction*[c] | | | |
| $\Delta H$ | 31.0±1.1 | 26.39±0.78 | 40.33±0.68 |
| $\Delta S$ | −2.3±3.6 | −6.1±2.8 | +10.5±2.6 |
| $m$ | 1.168±0.015 | 0.905±0.044 | 1.241±0.036 |

[a]$\Delta H$ in kcal/mol, $\Delta S$ in entropy units, all at 25°C. Superscript 0 refers to the protonation, see text.
[b]$\Delta S^0 = 0$ is assumed for the pre-equilibrium protonation.
[c]See text. Probably A–$S_E$2 for the thioacids, with $\Delta H = \Delta H^{\ddagger}$, $\Delta S = \Delta S^{\ddagger}$, and $m = m^{\ddagger}{}_0 m^{*\prime}$; reaction [9] and eq. [10]. Probably A-1 for methyl benzoate, with $\Delta H = \Delta H^{\ddagger} - \Delta H^{0\prime}$, $\Delta S = \Delta S^{\ddagger}$ $(-\Delta S^{0\prime})$, and $m = m^{\ddagger}{}_1 m^{*\prime}$; reaction [6] and eq. [7].

the reasonable assumption that $\Delta S^0 \simeq 0$ for the protonation (3, 4). The other thioacids were only studied at 50°C; Table 2 gives the $pK_{SH^+}$ and $m^*$ values of **1***a*–**1***d*, together with the results of applying the various rate equations to the hydrolysis data obtained for them (8).

The question arises as to whether the acylium ion reaction for these substrates is A-1 (reaction [6]) or A–$S_E$2 (reaction [9]). Although $m^*$ for protonation at SH could not be measured, $m^*$ for known sulfur protonations averages 1.3 (11). Thus $m^{\ddagger}$ for the acylium ion reaction would be less than one, in three out of four cases for the thiobenzoic acids **1** (Table 2), and for thioacetic acid as well (Table 1). This is indicative of A–$S_E$2 rather than A-1 reaction according to the criteria given above. Also the activation entropies for **1***b* and **2** are negative (Table 1), as compared to methyl benzoate, which gives the positive value typical of an A-1 process (3, 4).[5]

The rate data obtained for the ethyl thiolbenzoates **3** are plotted as a function of $X$ in Fig. 2. Comparison of Figs. 1 and 2 shows that the A-2 reaction is far less important for **3**. However, the dominant reaction is not an A-1 process, since the right-hand parts of the Fig. 2 curves are not linear in $X$. Neither is it an A-2 reaction; no water or bisulfate ion mechanism could be found which fitted the data on the basis of equations similar to eq. [5].

The only remaining possibility is an A–$S_E$2 rate-determining proton transfer, and transfer from protonated water can be ruled out, at least over most of the acidity region covered by Fig. 2, as the above kinetic analysis shows that the Fig. 2 plots should be linear in $X$ in this case too. Thus the proton transfer must be from undissociated $H_2SO_4$ molecules, reaction [11] above, and eq. [13] should apply. This was in fact found to be the case for **3** in the strong acid region, as can be seen from Fig. 3.

The slopes and intercepts of the Fig. 3 graphs, together with the basicities of **3**, are given in Table 3.

The choice of medium for a reaction rate LFER was not straightforward; the Table 3 intercepts refer to pure water, which contains no free $H_2SO_4$ and in which the preferred hydrolysis mechanism is reaction [2] rather than reaction [11]. Extrapolation to 100% $H_2SO_4$ is not possible because $X$ is not known at this point (11), and in any case the strongest catalyzing acid in pure $H_2SO_4$ is $H_3SO_4^+$ rather than $H_2SO_4$ (16). Accordingly, an arbitrary value of 90% $H_2SO_4$ was chosen for the LFER, as indicated in Fig. 3; the resulting $\rho$ was $-3.95 \pm 0.13$ (0.997, 8 compounds).

From Figs. 2 and 3, it is apparent that, although the reaction [11] mechanism applies over most of the acidity range, other mechanisms are important in the weak acid region. The parent compound **3***d* has sufficient data points in this region to permit their evaluation. It was found that two additional mechanisms were required to fit the experimental data, an A-2 reaction involving two water molecules in the aqueous acid region (the reaction [2] mechanism above), and an A–$S_E$2 reaction with protonated water as the catalyzing acid in the 50-70% $H_2SO_4$ region, reaction [9]. Separation of the various mechanisms was again possible, and their contribution to the overall hydrolysis rate data for ethyl thiolbenzoate is illustrated in Fig. 4. Some evidence is apparent from Fig. 3 for additional low acidity mechanisms for **3***a*–**3***c* also, but the data were insufficient for adequate quantification.

The rate data obtained for **4**, the ethyl thionbenzoates (6, 7), are plotted against $X$ in Fig. 5.[6] These graphs curve downward, typical of A-2 reactions involving water (1, 4); a reaction [2] mechanism seems reasonable and eq. [5] should apply. In Fig. 6[6] the data are plotted according to eq. [5] assuming the involvement of two water molecules. Good linearity is apparent for the acidity region above

[5]A referee has commented that determination of the kinetic solvent isotope effect should enable these two possibilities to be more clearly distinguished.

[6]In Figs. 5 and 6 the $y$-axis numbers refer to the curve for the parent compound (H) only. The other curves are displaced by one log unit from the preceding one, in order to avoid superimposition.

TABLE 2. Basicities, and slope and intercept data, for the hydrolyses of some thiobenzoic acids at 50°C

| | Value for substituent | | | |
|---|---|---|---|---|
| | 4-$OCH_3$ | 4-$CH_3$ | H | 4-Cl |
| *Basicities* | | | | |
| $pK_{SH^+}$ (25°C) | (−4.9)[a] | −5.19±0.18 | −5.659±0.073 | (−5.8)[a] |
| $m^*$ | (0.67)[b] | 0.654±0.026 | 0.677±0.010 | (0.67)[b] |
| *A-2 reaction* | | | | |
| log $(k_2/K_{SH^+})$[c] | −9.968±0.031 | −9.815±0.035 | −9.800±0.016 | −9.896±0.028 |
| $m^{\neq}{}_2 m^*$ | 0.537±0.037 | 0.588±0.027 | 0.620±0.014 | 0.668±0.016 |
| log $k_2$[c] | −5.47±0.13 | −5.02±0.18 | −4.58±0.08 | −4.52±0.13 |
| $m^{\neq}{}_2$ | 0.81±0.04 | 0.899±0.055 | 0.917±0.025 | 1.00±0.04 |
| *A–$S_E2$ reaction* | | | | |
| log $k_0$ | −6.56±0.17 | −8.90±0.15 | −8.687±0.058 | −9.14±0.20 |
| $m^{\neq}{}_0 m^{*\prime}$ | 0.672±0.049 | 1.418±0.038 | 1.168±0.015 | 1.108±0.047 |

[a]Extrapolated using ρσ relationship (Table 5).
[b]Average of 1*b* and 1*c* values.
[c]Intercept in 1 *M* $H_2O$ (values in pure water can be obtained by adding 3 × log (54.85) to these).

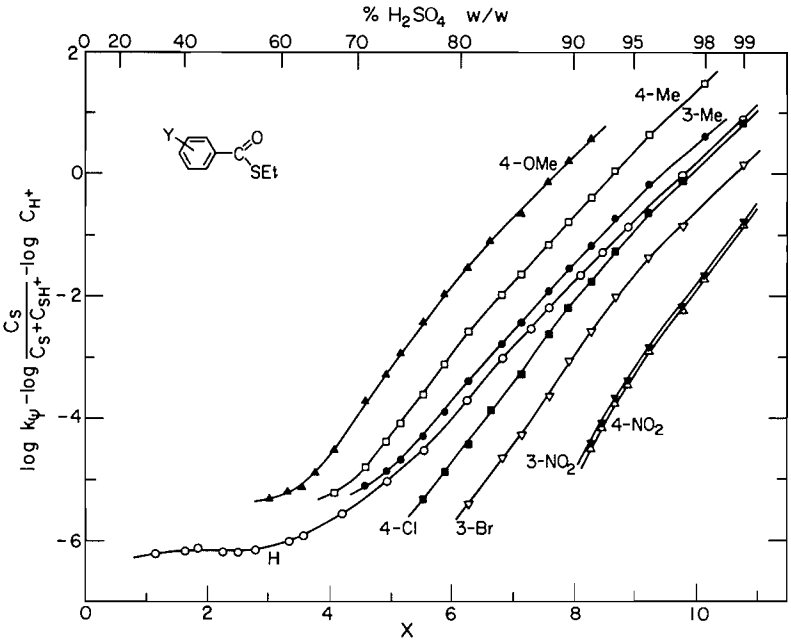


FIG. 2. Excess acidity plots for the hydrolyses of some ethyl thiolbenzoates in aqueous $H_2SO_4$ at 25°C (6, 7).

62% $H_2SO_4$, which is evidence for the applicability of the reaction [2] mechanism in this region; the reaction is fast for **4**, as compared to **1** and ethyl benzoate.

All of the Fig. 6 curves deviate somewhat at low acidity. However, the deviant points in Fig. 6 all show good linearity in $X$, as can be seen from Fig. 5. This means that, below 62% in acidity, the rate-determining process is no longer an A-2 reaction, but an A-1 or A–$S_E2$ one. For the parent compound **4***d* the slope against $X$, $m^{\neq}{}_0 m^*$, is 0.82 ± 0.02; using the known $m^*$ of 1.39 (11) $m^{\neq}{}_0 = 0.58$ is obtained. The other compounds evidently behave similarly. This number is quite typical for an A–$S_E2$ reaction with protonated water as the catalyzing acid (1). The most obvious explanation is that the A-2 reaction for these compounds is sufficiently fast that the initial protonation on sulfur becomes rate-determining at acidities well below the $pK_{SH^+}$ of the substrate (equivalent to 73% $H_2SO_4$ for **4***d* (11)), see reaction [2], and that the rate equation that applies is eq. [8]. The rate constants obtained for **4** according to eqs. [5] and [8] are given in Table 4.

Can. J. Chem. Downloaded from www.nrcresearchpress.com by 210.87.254.6 on 09/06/12
For personal use only.

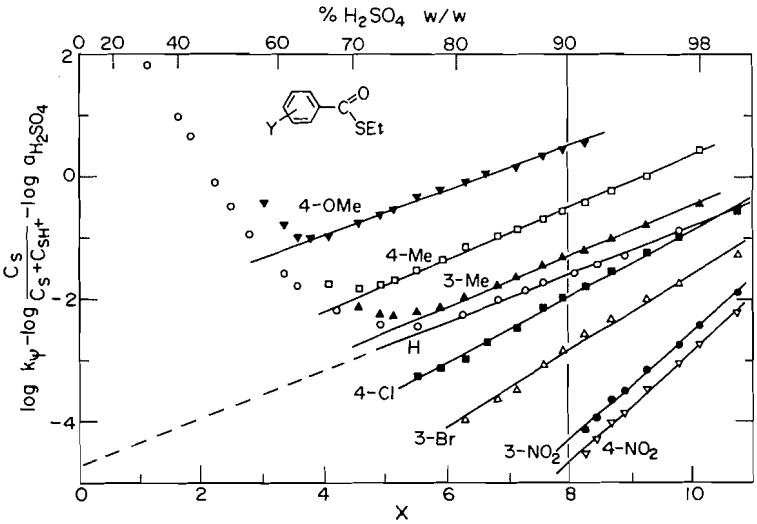


FIG. 3. Plots on the basis of eq. [13] for the hydrolyses in Fig. 2. The line for the 3-$NO_2$ substituent is offset upwards by 0.3 log units for clarity.

TABLE 3. Basicity and rate data for the hydrolyses of some ethyl thiolbenzoates (3) in sulfuric acid

| | $pK_{SH^+}$ (25°C) | $m^*$ | log $k_0$ (25°C)[a] | Slope[b] |
|---|---|---|---|---|
| 4-OMe | (−3.77)[c] | (0.683)[d] | −2.42±0.06 | 0.367±0.010 |
| 4-Me | (−4.20)[c] | (0.683)[d] | −3.92±0.06 | 0.428±0.008 |
| 3-Me | −4.77±0.14 | 0.675±0.024 | −4.68±0.06 | 0.423±0.008 |
| H | −4.81±0.08 | 0.647±0.014 | −4.74±0.08 | 0.394±0.009 |
| 4-Cl | −5.02±0.10 | 0.663±0.016 | −6.29±0.08 | 0.542±0.011 |
| 3-Br | −5.53±0.13 | 0.655±0.018 | −7.84±0.18 | 0.625±0.021 |
| 3-$NO_2$ | −6.25±0.21 | 0.721±0.028 | −11.69±0.18 | 0.886±0.020 |
| 4-$NO_2$ | −6.47±0.35 | 0.737±0.045 | −11.97±0.20 | 0.911±0.022 |

[a]Intercept of eq. [13].
[b]Assuming log ($f_S/f_{\neq}$) is linear in $X$, see text and eq. [13].
[c]Extrapolated from ρσ relationship (Table 5).
[d]Average of measured values in this column.

The curve for the parent compound **4***d* also deviates at high acidity (above 90% $H_2SO_4$), see Fig. 6. This could be due to the onset of a thioacylium ion mechanism, or to bisulfate ion taking over from water in the reaction [2] A-2 mechanism, as has been observed in the hydrolysis of benzamide (4). With only two points available deciding between these two is difficult, but the observed $m^{\neq}$ values offer a clue, being ~0.9 for the A-1/A–$S_E2$ and ~1.2 for the A-2/$HSO_4^-$ processes. The latter mechanism seems the most reasonable.

Comparison between the various basicities and rates is facilitated by the summary Table 5, which mainly concerns the unsubstituted parent compounds. Also given are the intercept and slope data for ethyl benzoate (1, 6), together with that extrapolated to 25°C for thiobenzoic acid, see Fig. 1. Included are the data for the other two hydrolysis mechanisms for ethyl thiolbenzoate, illustrated in Fig. 4; the more sophisticated treatment in this paper supercedes that previously given for ethyl thiolbenzoate and ethyl thionbenzoate (1). Table 5 also contains the several ρ values obtained using data for the substituted compounds; the data are rather sparse for the thioacids, but reasonable values could be obtained in most other instances.

## Discussion

The rate constants and basicities provided by the excess acidity method can be usefully compared, e.g. in deriving ρ values, since they are all extrapolated to the same standard state, the hypothetical ideal 1 *M* acid solution in water which is also the standard for pH measurements (11). The $m^*$ and $m^{\neq}$ slopes can also provide useful information (1).

Looking first at the substrate basicities, the stability of the protonated form is seen to decrease in the series PhCOSEt > PhCOSH > PhCOOEt > PhCSOEt, as shown by the more negative $pK_{SH^+}$ values in Table 5. In the same series the decreasing

Can. J. Chem. Downloaded from www.nrcresearchpress.com by 210.87.254.6 on 09/06/12
For personal use only.

Can. J. Chem. Downloaded from www.nrcresearchpress.com by 210.87.254.6 on 09/06/12
For personal use only.

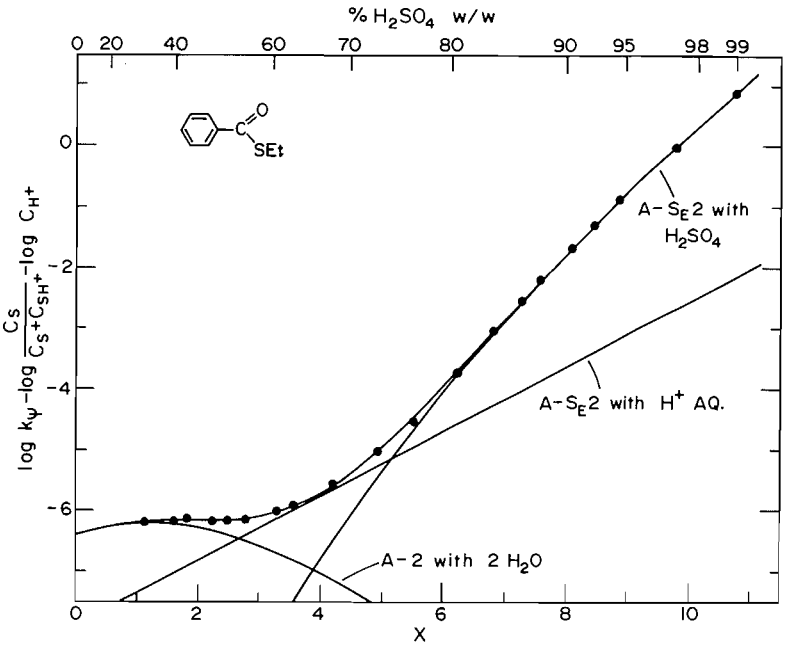


FIG. 4. Excess acidity plot for the hydrolysis of ethyl thiolbenzoate in aqueous $H_2SO_4$ at 25°C, showing the contribution of the different mechanisms.

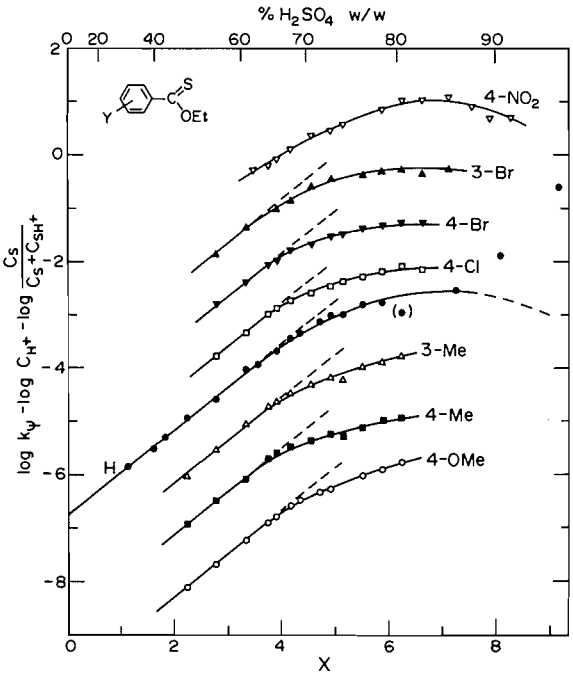


FIG. 5. Excess acidity plots for the hydrolyses of some ethyl thionbenzoates in aqueous $H_2SO_4$ at 25°C (6, 7).[6]

TABLE 4. Rate data for the hydrolyses of some ethyl thionbenzoates (**4**) in sulfuric acid at 25°C

| Substituent | log $k_0$[a] | log $k_2$[b] | $m^*_2$[b] |
|---|---|---|---|
| 4-OMe | −6.93 | −3.55±0.11 | 1.073±0.018 |
| 4-Me | −6.74 | −2.61±0.14 | 1.013±0.021 |
| 3-Me | −6.79 | −2.38±0.15 | 1.025±0.021 |
| H | −6.78 | −2.83±0.17 | 1.131±0.026 |
| 4-Cl | −7.02 | −2.70±0.17 | 1.128±0.029 |
| 4-Br | −7.09 | −2.67±0.20 | 1.126±0.032 |
| 3-Br | −7.09 | −2.52±0.21 | 1.190±0.035 |
| 4-$NO_2$ | [c] | −2.46±0.08 | 1.338±0.012 |

[a]Intercepts of Fig. 5, see eq. [8]. Only the parent compound had sufficient data points to enable proper statistical evaluation; log $k_0$ = −6.784±0.047, $m^*_0 m^*$ = 0.810±0.019. This slope was then assumed to apply to all the other compounds.
[b]Obtained from the Fig. 6 slopes and intercepts using known $m^*$ and $pK_{SH^+}$ values (11); see eq. [5]. Values in 1 *M* $H_2O$.
[c]Could not be evaluated.

ρ values show that the degree of internal resonance in the carbonyl/thiocarbonyl system increases, i.e. stabilization from the phenyl ring becomes less important, so that the latter would seem to be the more important acid weakening/base strengthening effect of the two. Carbonyl oxygen protonation has the characteristic $m^* = 0.6$–$0.7$ (1, 11), compared to 1.4 for thiocarbonyl sulfur protonation.

The A-2 reaction [2] which these substrates undergo has the reactivity order thionesters > thioacids > esters > thiolesters (Table 5). Deferring the thioacids for later consideration, this order is reasonable on the basis of substrate basicity, the most difficult to protonate (thionesters) being the most reactive, presumably on the basis of enhanced carbon electrophilicity caused by the decreased positive charge dispersal into the phenyl ring noted above. Esters, thionesters, and thiolesters all react with two water molecules ($r = 2$) as

Can. J. Chem. Downloaded from www.nrcresearchpress.com by 210.87.254.6 on 09/06/12
For personal use only.

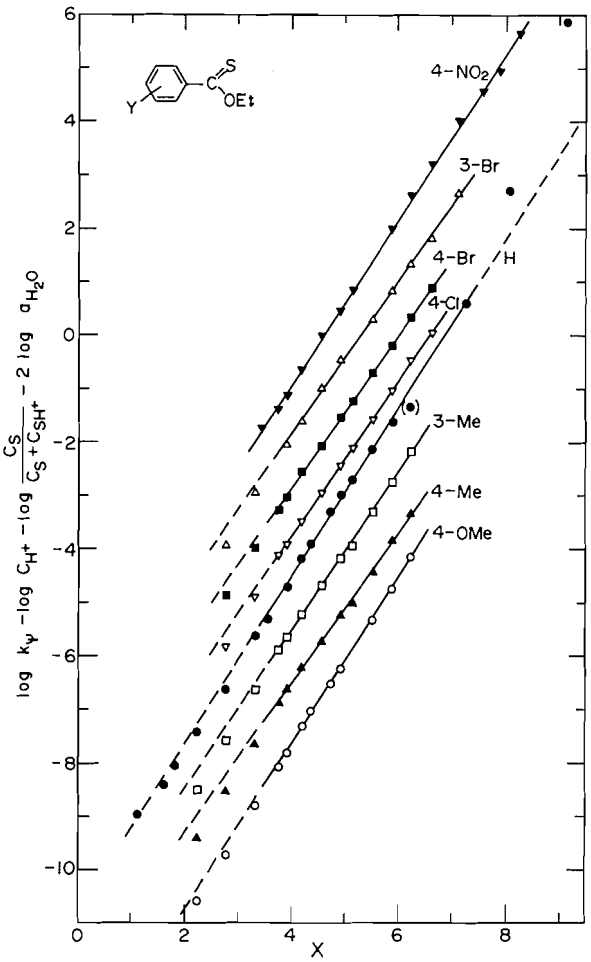


FIG. 6. Plots on the basis of eq. [5] for the hydrolyses in Fig. 5.[6]

shown in reaction [14] (3). Support for the charge dispersal into the medium indicated by reaction [14] comes from the small positive ρ values. $m^{+}{}_{2}$ encompasses the range 0.8–1.3 (Tables 1, 2, 4, and 5) typical of A-2 reactions (1); ethyl thiolbenzoate

[14]

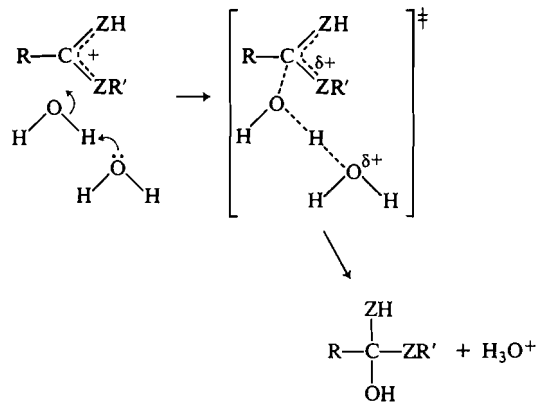

seems slightly low at 0.74 (Table 5), but since this value was derived using few measurements on only one compound (see Fig. 4) it should not perhaps be taken too seriously.

The thioacid A-2 reactions, however, are different. They involve three water molecules rather than two, the reactions are faster than the basicities would predict and the hydrolysis is characterized by a large positive ρ (1.6). Their activation enthalpies are lower than that for methyl benzoate (Table 1) and the entropies of activation are more negative at −48 eu. The cyclic 3 $H_2O$ mechanism previously suggested for amide hydrolysis has activation entropies of about this magnitude (4), but that is a positive species → positive species reaction which is not likely to produce a large ρ. Also, in the tetrahedral intermediate sulfur will not be so basic as nitrogen, which becomes protonated in the mechanism cited (4). One possibility that suggests itself for the thioacids is mechanism [15]. This would give a larger positive ρ, reflecting increased positive charge dispersal in the transition state, and would give enhanced reactivity (low $\Delta H^{\ddagger}$'s) since the entity reacting with the carbon electrophile is more negative in character. Also, the thioacids are the only substrates in the study which do not have a bulky ethyl group, perhaps providing "room" for the third water molecule to act and serving to explain why the thioacids react in this way and the thiolesters, for instance, do not. If this mechanism is correct the product of mechanism [15] would

[15]

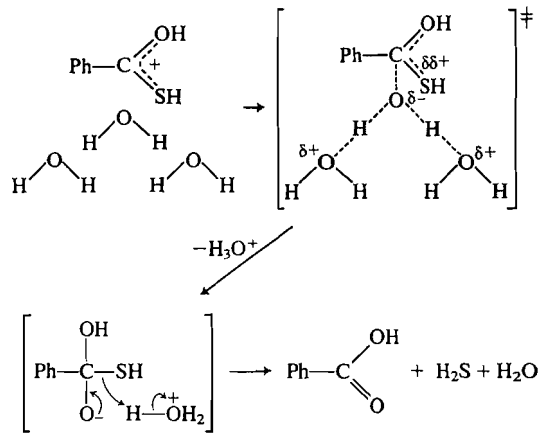

react very quickly, as shown, and presumably the reaction would be essentially irreversible. Thus $^{18}O$ exchange into the substrate would not be predicted to occur. Evidence, however, is lacking.

Acylium ion formation, the mechanism favoured in stronger acid media, can involve either stepwise or concerted proton transfer, reaction [16]. The stepwise path is the familiar $A_{Ac}1$ ester hydrolysis

TABLE 5. Comparison data for the unsubstituted compounds in water at 25°C

| Parameter | Value | | | |
|---|---|---|---|---|
| | Ph—C(=O)—OEt | Ph—C(=O)—SH | Ph—C(=O)—SEt | Ph—C(=S)—OEt |
| *Basicities* | | | | |
| $pK_{SH^+}$ | −6.00±0.14[a] | −5.66±0.07 | −4.81±0.08 | −7.99±0.13[a] |
| $m^*$ | 0.72±0.02[a] | 0.68±0.01 | 0.65±0.01 | 1.39±0.03[a] |
| ρ | 0.9−1.1[b] | 1.4(2)[c] | 2.20±0.09 | 1.02±0.06[d] |
| *A-2 reaction*[e] | | | | |
| $\log (k_2/K_{SH^+})$ | −6.62±0.02[f] | −5.62±0.06[f] | −6.40±0.07[g] | −7.33±0.10 |
| $m^{\neq}{}_2 m^*$ | 0.82±0.01 | 0.62±0.01 | 0.48±0.05 | 1.58±0.02 |
| $r$[h] | 2[a] | 3 | 2 | 2 |
| $\log k_2$ | −0.62±0.14[a] | 0.04±0.09 | −1.58±0.11 | 0.66±0.17 |
| $m^{\neq}{}_2$ | 1.14±0.03[a] | 0.92±0.02 | 0.74±0.08 | 1.13±0.03 |
| ρ | ~0.1[i] | 1.6(4)[c] | — | 0.16±0.12 |
| *A-$S_E$2 reaction*[j] | | | | |
| $\log k_0$ | −12.15±0.09[a,f,k] | −10.45±0.19[f] | −7.88±0.19[g] | −6.78±0.05[l] |
| $m^{\neq}{}_0 m^{*\prime}$ | 0.88±0.01[a,m] | 1.17±0.02[n] | 0.53±0.05[n] | 0.81±0.02[o] |
| ρ | −3 to −4[p] | −4.1(3)[c] | −3.95±0.13[q] | −0.29±0.18 |

[a] Data from ref. 1. All errors quoted are standard deviations.
[b] 1.1, measured for benzoic acids; 0.9, estimated for ethyl benzoates (14).
[c] Parentheses enclose the number of points.
[d] Obtained using data from ref. 11.
[e] In 55.34 *M* water, not 1 *M*.
[f] Intercept of Fig. 1 (25°C).
[g] Intercept of Fig. 4.
[h] Number of water molecules in the transition state.
[i] Reference 21. Combined; refers to $\log (k_2/K_{SH^+})$.
[j] Proton transfer from protonated water, not $H_2SO_4$.
[k] $\log (k_1/K_{SH^+})$ for A-1 reaction, see eq. [7].
[l] Intercept of Fig. 5.
[m] $m^{\neq}{}_1 m^{*\prime}$; protonation at ester oxygen.
[n] Protonation at sulfur, eqs. [9], [10].
[o] Equation [8].
[p] Reference 21.
[q] Reaction with undissociated $H_2SO_4$ molecules in 90% $H_2SO_4$, eqs. [11], [12]; see text.

mechanism (3), characterized by positive entropies of activation and $m^{\neq} > 1$, see Table 1. However, the thiolesters and thioacids prefer the concerted pathway, with small negative entropies of activation, see above; either "$H^+$" or $H_2SO_4$ can be the general acid, depending on the medium. Both pathways have large negative ρ values, −3 to −4 (Table 5), indicative of concentration of positive charge at the acylium centre in the transition state in both cases, which suggests the concerted nature of the proton transfer/bond breaking process in the A-$S_E$2 reaction. Not much information can be obtained from the slopes of eq. [13] quoted in Table 3, as there is nothing with which to compare them. They are all, however, less than one.

Acylium ion formation is much faster for those substrates with —SH and —SEt groups: see the activation enthalpies in Table 1, the relative rates in Table 5, the earlier switchover to acylium ion formation illustrated in Fig. 1, and the dominance of this process for the thiolesters in Figs. 2 and 4. Thus the kinetic basicity of sulfur seems much higher than that of oxygen, which is reasonable on the basis of the polarizable or "soft" nature of sulfur as compared to oxygen. Most of the activation energy for the stepwise path is probably the energy required for the initial unfavourable protonation on the ether oxygen.

Thioacylium ions were not observed in this work. The thionesters are potentially capable of

[16] 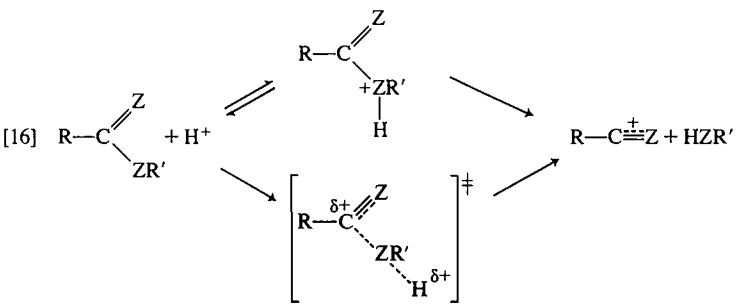

Can. J. Chem. Downloaded from www.nrcresearchpress.com by 210.87.254.6 on 09/06/12
For personal use only.

reacting in this way, but in fact react by the A-2 mechanism, with two water molecules up to about 85% $H_2SO_4$, and probably with one bisulfate ion after that point. These substrates are so reactive towards nucleophilic addition that the initial protonation at sulfur becomes rate-determining at acidities below 62%; compare $\log k_0 = -6.78$ with $\log (k_2/K_{SH^+}) = -7.33$ in Table 5. This reaction has a $\rho$ of $-0.3 \pm 0.2$ (Table 5), compared to the $\rho$ for equilibrium protonation of 1.0, i.e. rather less than half a positive charge is present at the transition state. This is in passable agreement with the observed $m^{\neq}_0$ of $0.58 \pm 0.02$, indicating approximate half-transfer of the proton at this point (1). It is interesting that proton transfer to sulfur is involved in the slow step of the reaction at least some of the time, for all three types of sulfur-containing substrate in the study.

**Acknowledgement**

Financial support of this research is by the Natural Sciences and Engineering Research Council of Canada.

1. R. A. Cox and K. Yates. Can. J. Chem. **57**, 2944 (1979).
2. R. A. Cox, C. R. Smith, and K. Yates. Can. J. Chem. **57**, 2952 (1979).
3. R. A. Cox, M. F. Goldman, and K. Yates. Can. J. Chem. **57**, 2960 (1979).
4. R. A. Cox and K. Yates. Can. J. Chem. **59**, 2853 (1981).
5. P. G. Traverso, N. C. Marziano, and R. C. Passerini. J. Chem. Soc. Perkin Trans. II, 845 (1977); N. C. Marziano, P. G. Traverso, and G. G. Cimino. J. Chem. Soc. Perkin Trans. II, 574 (1980).
6. J. T. Edward and S. C. Wong. J. Am. Chem. Soc. **99**, 7224 (1977).
7. J. T. Edward, S. C. Wong, and G. Welch. Can. J. Chem. **56**, 931 (1978).
8. J. T. Edward, G. Welch, and S. C. Wong. Can. J. Chem. **56**, 935 (1978).
9. K. Yates. Acc. Chem. Res. **4**, 136 (1971).
10. K. Yates and T. A. Modro. Acc. Chem. Res. **11**, 190 (1978).
11. R. A. Cox and K. Yates. J. Am. Chem. Soc. **100**, 3861 (1978).
12. W. F. Giauque, E. W. Hornung, J. E. Kunzler, and T. R. Rubin. J. Am. Chem. Soc. **82**, 62 (1960).
13. L. P. Hammett. Physical organic chemistry. 2nd. ed. McGraw-Hill, Toronto. 1970. p. 356.
14. R. Stewart and K. Yates. J. Am. Chem. Soc. **80**, 6355 (1958); K. Yates and R. Stewart. Can. J. Chem. **37**, 664 (1959); R. Stewart and K. Yates. J. Am. Chem. Soc. **82**, 4059 (1960); K. Yates. Ph.D. Thesis, University of British Columbia. 1959.
15. R. A. Cox and K. Yates. Can. J. Chem. **59**, 2116 (1981).
16. R. A. Cox. J. Am. Chem. Soc. **96**, 1059 (1974).
17. R. A. Cox and E. Buncel. J. Am. Chem. Soc. **97**, 1871 (1975).
18. R. A. Cox, A. J. Dolenko, and E. Buncel. J. Chem. Soc. Perkin Trans. II, 471 (1975).
19. T. A. Modro, K. Yates, and J. Janata. J. Am. Chem. Soc. **97**, 1492 (1975).
20. R. H. Boyd. J. Am. Chem. Soc. **85**, 1555 (1963).
21. M. F. Goldman. Ph.D. Thesis, University of Toronto. 1975. pp. 159–177.

Can. J. Chem. Downloaded from www.nrcresearchpress.com by 210.87.254.6 on 09/06/12
For personal use only.

# L'enrobage moléculaire: complexation du cation sodium par le dibenzo-24-couronne-8[1,2]

MICHEL BISNAIRE, CHRISTIAN DETELLIER[3] ET DOMINIQUE NADON

*L'Institut Ottawa–Carleton de recherche et d'études avancées en chimie, Campus de l'université d'Ottawa, Ottawa, Ont., Canada KIN 9B4*

Reçu le 9 juillet 1982

MICHEL BISNAIRE, CHRISTIAN DETELLIER et DOMINIQUE NADON. Can. J. Chem. **60**, 3071 (1982).

Nous avons étudié la structure et la microdynamique en solution du complexe dibenzo-24-couronne-8 – perchlorate de sodium par rmn du Na-23 et du C-13. Dans l'ensemble des solvants étudiés (acétone, acétonitrile, pyridine, nitrométhane, carbonate de propylène et chloroforme-*d*) ainsi que dans les mélanges binaires acétone/pyridine, acétonitrile/nitrométhane, carbonate de propylène/méthanol, la couronne entoure le cation sodium, expulsant de sa couche de coordination anion conjugué ou molécules de solvant. La mesure des temps de relaxation quadripolaire en Na-23 et dipôle–dipôle en C-13 nous a permis de calculer le temps de corrélation effectif du complexe en solution dans le chloroforme-*d* ($65 \pm 11$ ps) et la constante de couplage quadripolaire du Na-23 dans tous ces solvants et mélanges de solvant (0.8–1.2 MHz). La couche de coordination du sodium est complètement figée un laps de temps supérieur au temps de corrélation réorientationnel.

MICHEL BISNAIRE, CHRISTIAN DETELLIER, and DOMINIQUE NADON. Can. J. Chem. **60**, 3071 (1982).

Structure and microdynamics in solution of the dibenzo-24-crown-8 – sodium perchlorate complex have been studied by Na-23 and C-13 nmr. In all solvents (acetone, acetonitrile, pyridine, nitromethane, propylene carbonate, and chloroform-*d*) and in the binary mixtures acetone/pyridine, acetonitrile/nitromethane, propylene carbonate/methanol, the crown wraps around the sodium cation and expels the conjugate anion and the solvent molecules from the cation coordination sphere. Measurements of Na-23 quadrupolar and C-13 dipole–dipole relaxation times give the effective correlation time of the complex in $CDCl_3$ solution ($65 \pm 11$ ps) and the Na-23 quadrupolar coupling constant in all those solvents and binary mixtures (0.8–1.2 MHz). The sodium coordination shell is completely frozen during a time superior to the reorientational correlation time.

## Introduction

Voilà maintenant quinze années, depuis la classique étude de Pedersen (1), que la classe de composés appelée éthers-couronne connaît une vogue importante, tant pour ses applications en chimie organique que pour ses propriétés de transport ionique membranaire. Ces molécules, complexant sélectivement les cations alcalins, les dissimulent aux yeux de l'anion conjugué, augmentant d'autant ses potentialités réactives. C'est l'activation anionique, et en dérive l'application de ces composés aux réactions organiques, tant en solution homogène (3), qu'en catalyse par transfert de phase (4–6).

Pourtant, ces ligands macrocycliques, n'offrant au cation qu'une cavité bi-dimensionnelle, lui laissent tout loisir de s'apparier à l'anion conjugué, d'un côté ou l'autre de la couronne. C'est là un écueil majeur à l'utilisation vraiment efficace des éthers-couronne en activation anionique (5). Les cryptands (7) surmontent cet écueil en offrant au cation la possibilité de se nicher au creux d'une molécule macrobicyclique, l'isolant parfaitement du reste de la solution. Les structures cristallographiques de quelques complexes entre cations alcalins et grands éthers-couronne ont montré que ceux-ci peuvent aussi se replier à l'entour du cation, le séparant de l'anion conjugué, à l'instar des cryptands. C'est le cas de l'assemblage entre le dibenzo-30-couronne-10 et KSCN (8) ou KI (9) où le composé couronne s'enroule autour du cation dans une conformation du type "balle de tennis" de symétrie $C_2$ (10). Nous nous intéressons à cerner la structure et la microdynamique en solution des complexes entre cations alcalins et grands éthers-couronne.

La rmn du noyau métallique lui-même est une sonde très utile pour déterminer l'environnement immédiat du cation en solution (11). Popov et ses collaborateurs ont étudié récemment, par la mesure des déplacements chimiques des noyaux Na-23 ou Cs-133, la complexation de ces cations par de grands éthers-couronne (12, 13). Le système formé par le tétraphénylborate de sodium et le dibenzo-24-couronne-8 (DB24C8) (**1**) a retenu notre atten-

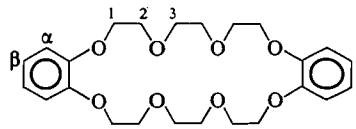


**1**

[1]Nous avons choisi d'employer tout au long de l'article l'appellation usuelle initialement formulée par Pedersen (1), au lieu de l'appellation officielle 2,3,14,15-dibenzo-1,4,7,10,13,16,-19,22-octaoxacyclotétraeicosa-2,14-diène, peut-être un peu lourde, ou de l'appellation suggérée récemment par Weber et Vögtle (2).

[2]Présenté en partie au 50e Congrès de l'Association Canadienne Française pour l'Avancement des Sciences (ACFAS), Montréal, 12–14 mai 1982.

[3]Auteur à qui adresser la correspondance.

0008-4042/82/243071-06$01.00/0

©1982 National Research Council of Canada/Conseil national de recherches du Canada

Can. J. Chem. Downloaded from www.nrcresearchpress.com by 210.87.254.42 on 09/06/12
For personal use only.

Can. J. Chem. Downloaded from www.nrcresearchpress.com by 210.87.254.42 on 09/06/12
For personal use only.

tion: les déplacements chimiques, qui montrent la formation d'un complexe de stoéchiométrie 1:1, sont peu sensibles à la nature des trois solvants étudiés (13), suggérant l'enveloppement du cation par la couronne.

## Partie expérimentale

Le dibenzo-24-couronne-8 a été obtenu chez Parish Chem. Co. ou synthétisé selon la procédure de Pedersen (1) et a été séché sous vide à 60°C pendant plusieurs heures. Le perchlorate de sodium (Aldrich 99 + %) a été séché à 70°C sous 1 Torr pendant une vingtaine d'heures. Les solvants ont été séchés selon des procédures publiées (13, 16) et stockés sur tamis moléculaire 4 Å.

Les spectres rmn ont été obtenus à l'aide d'un spectromètre Varian FT-80 opérant à 21.04 MHz pour le Na-23 et à 20.0 MHz pour le C-13. Les déplacements chimiques du Na-23 ont été mesurés par rapport à une solution de NaCl 3 *M* dans $D_2O$, et le verrouillage assuré soit par du benzène-$d_6$ dans un tube coaxial, soit par du $D_2O$ externe. Dans tous les cas, les déplacements chimiques sont exprimés par rapport à NaCl à dilution infinie dans $H_2O$, après correction pour la concentration en chlorure de sodium de la référence et pour la différence éventuelle du solvant deutéré de verrouillage. Les raies observées étaient toutes de forme lorentzienne.

La mesure des temps de relaxation $T_1$ en C-13 a été effectuée sur des échantillons dégazés, à l'aide de la séquence d'inversion–recouvrement 180°–τ–90°, le temps de recyclage étant supérieur dans tous les cas à quatre fois le temps de relaxation à mesurer. L'effet nucléaire Overhauser a été mesuré par la technique du découplage en retenue.

La solution du complexe dans le chloroforme deutéré a été préparée par dissolution de quantités stoéchiométriques de DB24C8 et de perchlorate de sodium dans l'acétone, évaporation de ce solvant et dissolution du complexe dans $CDCl_3$.

Les viscosités des solutions ont été mesurées à l'aide d'un viscosimètre de type Desreux–Bishoff (14) sous enceinte thermostatée à 297 K, la température de la sonde rmn. Le volume du complexe DB24C8–sodium a été mesuré par le volume d'eau déplacé par un modèle moléculaire de type CPK, enrobé parfaitement de Parafilm pour garantir son étanchéité. Conway et Ayranci (15) ont montré que cette méthode, simple et astucieuse, se révèle très puissante dans la détermination des volumes moléculaires de molécules neutres, auxquelles nous pouvons assimiler ce complexe. Le volume moléculaire du complexe ainsi mesuré vaut 1.9 ± 0.1 nm³.

## Résultats et discussion

Les déplacements chimiques en Na-23 caractéristiques du cation sodium complexé par le dibenzo-24-couronne-8 dans une série de solvants sont présentés dans le tableau 1. Dans toute la gamme des solvants étudiés le déplacement chimique reste compris dans une fourchette de 1 ppm, à l'exception du mélange binaire méthanol – carbonate de propylène, de fraction molaire 0.15 en carbonate de propylène, qui s'en écarte légèrement. Les paramètres caractérisant la basicité de ces solvants, et particulièrement le nombre de donicité (20), balaient une large gamme allant d'un solvant de nombre de donicité (DN) nul, tel le chloroforme, à un solvant bon donneur tel la pyridine (DN = 33). Il est à noter pourtant que la constante de formation du complexe est très faible dans d'autres solvants bons donneurs tels le diméthylsulfoxyde ou la *N*,*N* diméthylformamide (13).

Comme il a été montré que le déplacement chimique du sodium-23 est relié linéairement au nombre de donicité du solvant dans lequel est dissous le perchlorate ou le tétraphénylborate de sodium (21), l'incorporation ne fut ce que d'une molécule de solvant dans la première couche de coordination du cation devrait provoquer une variation de déplacement chimique nettement plus conséquente que celle expérimentalement observée. D'autre part, le déplacement chimique est insensible à la nature de l'anion. Ainsi, lors de la complexation, toutes les molécules de solvants sont expulsées de la couche de coordination du sodium. Les largeurs de raie à mi-hauteur caractéristiques du cation sodium complexé par le DB24C8 sont également indiquées dans le tableau 1. Elles se rangent d'une quarantaine de Hz (AN, Ac) à plus de deux cents Hz (PC). Dans des conditions de rétrécissement extrême, la largeur de raie d'un noyau quadripolaire est fournie par l'équation [1]

$$[1]\quad \frac{1}{T_q} = \pi \nu_{\frac{1}{2}} = \frac{3}{40}\,\frac{2I+3}{I^2(2I-1)} \times \left(1+\frac{\eta^2}{3}\right)\left(\frac{e^2qQ}{\hbar}\right)^2 \tau_c$$

où $T_q$ est le temps de relaxation quadripolaire, $I$ le nombre de spin, $\eta$ un paramètre d'asymétrie, $q$, le gradient de champ au site du noyau, $Q$ le moment quadripolaire et $\tau_c$ le temps de corrélation caractéristique de la relaxation quadripolaire. Dans le cas du Na-23 ($I = 3/2$), pour un paramètre d'asymétrie nul, la relation devient (22):

$$[2]\quad \frac{1}{T_q} = \pi \nu_{\frac{1}{2}} = \frac{2\pi^2}{5}\chi^2 \tau_c$$

où

$$\chi = \frac{e^2qQ}{\hbar}$$

$\chi$ peut donc être calculé à partir de la largeur de raie expérimentale en Na-23, si le temps de corrélation $\tau_c$ est connu. Si ce temps de corrélation, caractéristique de la fluctuation du gradient du champ, prend son origine dans un mouvement purement réorientationnel, c'est-à-dire si le temps de vie d'une couche de coordination bien définie du cation sodium est long vis-à-vis du temps caractéristique

Can. J. Chem. Downloaded from www.nrcresearchpress.com by 210.87.254.42 on 09/06/12
For personal use only.

TABLEAU 1. Déplacements chimiques et largeurs de raie Na-23 du complexe DB24C8–sodium

| Solvant[a,b] | Anion[c] | δ(ppm)[d] | $\nu_{\frac{1}{2}}$(Hz)[e] |
|---|---|---|---|
| NM | $ClO_4^-$ | −7.9 | 65(±3) |
| NM | $B\phi_4^-$ | −7.7 | |
| AN | $ClO_4^-$ | −8.8 | 39(±2) |
| AN | $B\phi_4^-$ | −8.4 | |
| AC | $ClO_4^-$ | −8.4 | 38(±2) |
| Py | $ClO_4^-$ | −8.9 | 109(±4) |
| Py | $B\phi_4^-$ | −8.8 | |
| Py/THF | $ClO_4^-$ | −7.9 | 102(±4) |
| PC | $ClO_4^-$ | −8.0 | 225(±8) |
| MeOH/PC | $ClO_4^-$ | −7.0 | 66(±3) |
| $CDCl_3$ | $ClO_4^-$ | −8.0 | 123(±4) |

[a]NM = nitrométhane, AN = acétonitrile, Ac = acétone, Py = pyridine, Py/THF: mélange pyridine–tétrahydrofuranne, de fraction molaire 0.60 en pyridine, PC = carbonate de propylène, MeOH/PC = mélange méthanol – carbonate de propylène de fraction molaire 0.15 en méthanol.

[b]Dans ces solvants, seul un complexe de stoéchiométrie 1:1 se forme, avec une constante de formation supérieure ou égale à $10^3$ (13, 16), ce que nous avons vérifié dans le cas du perchlorate par une étude de la variation du déplacement chimique et de la largeur de raie du Na-23 en fonction du rapport [couronne]/[$Na^+$] dans NM, AN, Py/THF, Py et Ac (17). Dans tous les cas, un rapport 2:1 en [couronne]/[sodium] conduit à l'obtention de plus de 99% de sodium complexé.

[c]$ClO_4^-$: ce travail, $B\phi_4^-$: tétraphénylborate (réf. 13).

[d]Mesuré par rapport à NaCl dans $H_2O$ à dilution infinie, toutes corrections effectuées: voir partie expérimentale; ±0.1 ppm.

[e]Largeur de raie à mi-hauteur du signal Na-23 du cation sodium complexé par le DB24C8.

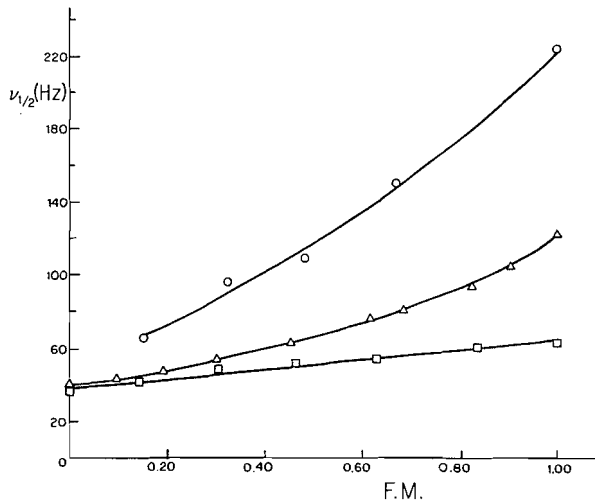


FIG. 1. Largeurs de raie à mi-hauteur ($\nu_{\frac{1}{2}}$) du sodium-23 pour le complexe $Na^+$–DB24C8 en fonction de la fraction molaire des mélanges binaires acétonitrile/nitrométhane (□), acétone/pyridine (△) et méthanol/carbonate de propylène (○). La trop faible solubilité du complexe dans le méthanol explique l'absence de points expérimentaux dans la zone des fractions molaires en méthanol de 0 à 0.15. La concentration en $NaClO_4$ est de 0.010 *M*, celle en DB24C8 de 0.020 *M*, dans tous les cas.

de la réorientation moléculaire, le temps de corrélation obéit à la relation de Debye–Stokes–Einstein, fournie par l'equation [3]

$$[3] \quad \tau_c = \frac{4}{3}\pi a^3 \frac{\eta}{kT} f_r$$

où $a$ est le rayon moléculaire, $\eta$ la viscosité du milieu[4] et $f_r$ le coefficient de microviscosité (23). La symétrie de la couche de coordination du cation se reflétant dans $\chi$, sa constance au long des solvants étudiés permettra à la largeur de raie d'être proportionnelle à la viscosité du solvant, uniquement (24–26). Effectivement, c'est ce que l'on observe. Les solvants peu visqueux (AN, $\eta$ = 0.335 cP; Ac, $\eta$ = 0.343 cP) fournissent une raie fine (40 Hz), les solvants plus visqueux (Py, $\eta$ = 0.955 cP, PC, $\eta$ = 2.41 cP) une raie large. Nous avons testé davantage cette invariance de $\chi$: lorsque le complexe est plongé dans un mélange binaire de deux solvants comportant des sites donneurs différents, tels la pyridine et l'acétone, le maintien de molécules de solvant dans la couche de coordination du cation produira un gradient de champ très dissymétrique, la variation de la constante de couplage quadripolaire au long du mélange binaire et la non-linéarité de $\nu_{\frac{1}{2}}$ avec $\eta$. La figure 1 montre la variation de la largeur de raie du Na-23 en fonction de la composition de mélange binaire pour trois paires de solvants: acétone et pyridine, nitrométhane et acétonitrile, carbonate de propylène et méthanol. Quant au test, il est concluant: on obtient d'excellentes relations linéaires entre la largeur de raie et la viscosité de ces solutions dans tous les cas (Fig. 2). La régression linéaire est même excellente pour l'ensemble des points expérimentaux ($\rho$ = 0.989 pour les 22 points). Une conclusion en découle: dans tous ces environnements, soumise à des pressions internes diverses, à la présence de solvants de donicités différentes, la couche de coordination du cation sodium reste remarquablement constante. Qui plus est, elle est rigide dans le domaine de temps de la réorientation moléculaire: l'orientation de chaque interaction $Na^+$ .... O, figée dans ce domaine de temps, ne fluctue que par la réorientation globale de la supramolécule. Quelle est la valeur de $\chi$? La connaissance de $\tau_c$ dans l'équation [2] nous permettrait son calcul. Puisque, comme nous venons de le montrer, $\tau_c$ est d'origine purement réorientationnelle, il peut être égalé aux temps de corrélation réorientationnels mesurés sur d'autres noyaux de la supramolécule, comme les C-13 du ligand. Cette approche a été décrite par Kintzinger et Lehn (27), et leur avait permis de calculer les constantes de couplage quadripolaires $\chi$ du cation sodium encagé

[4]Ne pas confondre $\eta$, la viscosité, avec le paramètre d'asymétrie de l'équation [1], malencontreusement nommé habituellement $\eta$, lui aussi.

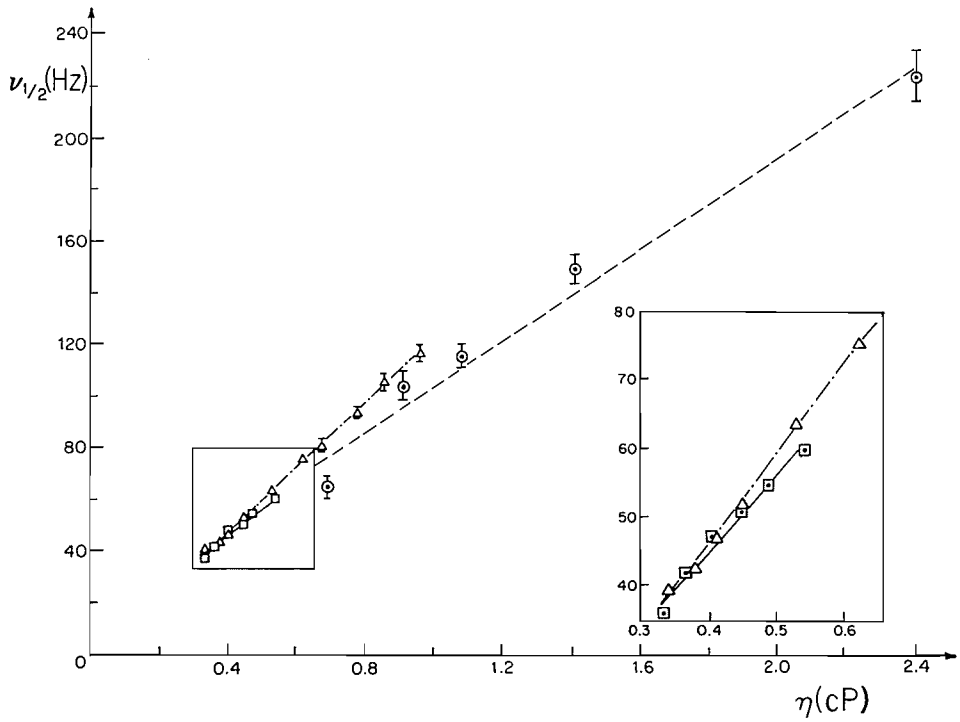


FIG. 2. Largeurs de raie à mi-hauteur ($\nu_{\frac{1}{2}}$) du sodium-23 en fonction de la viscosité ($\eta$) pour le complexe sodium - dibenzo-24-couronne-8 en solution dans divers mélanges binaires: –○–: mélange carbonate de propylène/méthanol (le coefficient de corrélation linéaire, $\rho$, est égal à 0.994 pour 5 points); –.–.△–.–: mélange acétone/pyridine ($\rho$ = 0.999 pour 10 points); –□–: mélange acétonitrile/nitrométhane ($\rho$ = 0.984 pour 7 points). Pour plus de clarté, la portion de graphique correspondant au mélange acétonitrile/nitrométhane est agrandie. La droite de régression sur l'ensemble des points expérimentaux, correspondant aux 6 solvants, n'est pas indiquée. Son équation est $\nu_{\frac{1}{2}} = 93.7\ \eta + 11.4$ ($\rho$ = 0.989 pour 22 points).

dans des cryptands. La vitesse de relaxation dipôle–dipôle de noyaux C-13 suit la relation [4]

$$[4]\quad \frac{1}{T_1^{DD}} = N_H\ \gamma_C^2\ \gamma_H^2\ \hbar^2\ r_{CH}^{-6}\ \tau_{eff}$$

où $N_H$ est le nombre d'hydrogène directement attachés au C-13, $\gamma_C$ et $\gamma_H$ sont les rapports gyromagnétiques des noyaux C-13 et H-1 et $r_{CH}$ est la longueur de la liaison C—H, dans le cas de carbones protonés où les contributions provenant d'hydrogènes non directement liés peuvent être ignorées (28). Pour des molécules de la taille du complexe étudié, la contribution dominante au temps de relaxation mesuré est d'origine dipolaire. En fait, c'est le cas à 80–90% comme nous l'avons vérifié par la mesure de l'effet nucléaire Overhauser (nOe) (tableau 2), et $T_1^{DD}$ a été calculé par l'équation [5] (27)

$$[5]\quad T_1^{DD} = T_1^{obs} \cdot \frac{1.98}{(nOe)_{obs}}$$

Compte tenu des erreurs de mesure, le temps de corrélation réorientationnel effectif, $\tau_{eff}$ est pratiquement constant pour les différents carbones (tableau 2). La différence notée entre les carbones aromatiques et les carbones éthérés, à la limite de l'erreur expérimentale, peut provenir de la réorientation anisotrope de la supramolécule. Il est à noter également que les valeurs de $T_1$ que nous mesurons sont en bon accord avec des valeurs précédemment publiées (18, 19) pour les complexes formés entre KSCN et le DB30C10 ou le DB18C6, où il apparaissait également une rigidité de la couronne après la complexation. Le temps de corrélation moyen obtenu est de 65 ± 11 ps, et, grâce à l'équation [2], la valeur de $\chi$ en dérive: 1.2 MHz dans $CDCl_3$. Nous avons déterminé le volume moléculaire du complexe (1.9 ± 0.1 nm$^3$) (voir partie expérimentale). L'équation [3] fournit ainsi une valeur pour le coefficient de microviscosité (23) égale à 0.24. Lorsque les molécules de solvant et de soluté sont de même taille, ce coefficient est égal à 0.17 (23). Pour des solutés de rayon moléculaire 0.5 nm, Kintzinger et Lehn trouvaient un coefficient de 0.20 (27). Dans le cas du complexe étudié le rayon moléculaire égale 0.77 nm et un coefficient de 0.24 est logique. L'équation [3] nous a ainsi permis de calculer $\chi$ pour l'ensemble des solvants étudiés. Le

Can. J. Chem. Downloaded from www.nrcresearchpress.com by 210.87.254.42 on 09/06/12
For personal use only.

TABLEAU 2. δ, $T_1$, nOe et $\tau_{eff}$ en C-13

| Complexe | | C(1) | C(2) | C(3) | α | β |
|---|---|---|---|---|---|---|
| DB24C8–$NaClO_4$[a] | δ(ppm)[b,c] | 68.70 | 67.47 | 67.15 | 116.88 | 123.59 |
| | $T_1^{obs}$(s)[d] | 0.33 | 0.36 | 0.35 | 0.54 | 0.48 |
| | nOe[e] | 1.59 | 1.78 | 1.84 | 1.66 | 1.68 |
| | $\tau_{eff}$(ps)[f] | 55 | 57 | 60 | 71 | 80 |
| DB30C10–KSCN[g,h] | $T_1^{obs}$(s) | 0.82 | 0.77 | 0.73 | 1.40 | 1.40 |
| DB18C6–KSCN[i] | $T_1^{obs}$(s) | 0.50 | 0.50 | | 0.90 | 1.00 |

[a] Ce travail.
[b] Les déplacements chimiques sont exprimés en ppm, par rapport au tétraméthylsilane interne (±0.05 ppm).
[c] Le déplacement chimique du carbone aromatique non protoné est 148.05.
[d] L'estimation de l'erreur sur $T_1^{obs}$ est de ±10%.
[e] Erreur: ±5%.
[f] Calculé à l'aide de l'équation [4], en utilisant une valeur de $r$ égale à 0.1085 ± 0.0005 nm. L'erreur estimée sur $\tau_{eff}$ est de ± 15%. La moyenne de $\tau_{eff}$ sur les cinq valeurs est 65 ± 11 ps (voir discussion).
[g] Référence 18; solvant $CDCl_3$ à 320 K.
[h] La numérotation des carbones du DB30C10 est analogue à celle utilisée pour **1**.
[i] Référence 19; solvant $CD_2Cl_2$.

TABLEAU 3. Constantes de couplage quadripolaire du $Na^+$-23 complexé

| Solvants[a] | NM | AN | Ac | Py | Py/THF | PC | MeOH/PC | $CDCl_3$ |
|---|---|---|---|---|---|---|---|---|
| χ (MHz)[b] | 0.8 | 0.9 | 0.9 | 0.9 | 1.1 | 0.8 | 0.8 | 1.2 |

[a] Signification des abréviations: voir tableau 1.
[b] Calculé selon l'équation [3] sauf pour $CDCl_3$ où χ a été calculé selon l'équation [2] (voir texte); l'estimation de l'erreur sur χ est 20%.

tableau 3 fournit ces valeurs pour les solvants purs. Il est à noter que χ est constant également dans toute la gamme de chaque mélange binaire étudié. Cette valeur de χ est à comparer à celle déterminée dans le cas du cryptand 2,2,2 (1.0 MHz) où le cation sodium est niché dans une cavité tapissée de 6 atomes d'oxygène. Les cryptands 2,2,1 ou 2,1,1 fournissaient au sodium un environnement moins symétrique, reflété par la valeur de χ (1.4 et 2.2 MHz, respectivement) (27). De plus, les déplacements chimiques sont comparables: −8 et −11 ppm respectivement pour le DB24C8 et le cryptand 2,2,2: un argument étayant la théorie de Deverell (29, 30) de la proportionalité de la constante de couplage quadripolaire à la partie paramagnétique de la constante d'écran $\sigma_p$. Il a été récemment montré, dans une série de solvants aminés, une corrélation similaire confirmant cette théorie très peu testée jusqu'à présent (26).

En somme, le DB24C8 s'enroule autour du cation sodium, excluant de la couche de coordination du cation anion ou molécules de solvant. L'agrégat supramoléculaire sodium–DB24C8 a une structure bien définie, figée un laps de temps supérieur à $10^{-10}$ s, régie par des facteurs configurationnels et conformationnels (31). La détermination de la constante de couplage quadripolaire du sodium en solution et sa relation au déplacement chimique par une approche du type de celle que nous avons suivie, en immergeant l'ion dans une structure moléculaire le protégeant de tout autre environnement nous promettent d'avoir accès aux paramètres de solvatation et de complexation d'une manière nette et précise (32).

## Remerciements

Nous remercions le Conseil de Recherches en Sciences Naturelles et en Génie du Canada (CRSNG) pour son soutien financier. L'un de nous (D.N.) remercie également le CRSNG pour l'octroi d'une bourse de recherche d'été. Nous remercions le Dr R. R. Fraser pour des discussions stimulantes et M[r] Raj Capoor pour son experte assistance technique.

1. C. J. PEDERSEN. J. Am. Chem. Soc. **89**, 7017 (1967).
2. E. WEBER et F. VÖGTLE. Inorg. Chim. Acta, **45**, C65 (1980).
3. G. W. GOKEL et H. D. DURST. Synthesis, 168 (1976).
4. P. VIOUT. J. Mol. Catal. **10**, 231 (1981).
5. D. LANDINI, A. MAIA, F. MONTANARI et F. M. PIRISI. J. Chem. Soc. Perkin Trans. II, 46 (1980).
6. P. E. STOTT, J. S. BRADSHAW et W. W. PARISH. J. Am. Chem. Soc. **102**, 4810 (1980).
7. J. M. LEHN. Acc. Chem. Res. **11**, 49 (1978).
8. J. HASEK, D. HLAVATA et K. HUML. Acta Crystallogr. Sect. B, **36**, 1782 (1980).
9. M. A. BUSH et M. R. TRUTER. J. Chem. Soc. Perkin Trans. II, 345 (1972).
10. J. DALE. Isr. J. Chem. **20**, 3 (1980).
11. P. LASZLO. Angew. Chem. Int. Ed. Engl. **17**, 254 (1978).
12. M. SHAMSIPUR et A. I. POPOV. J. Am. Chem. Soc. **101**, 4051 (1979).
13. M. SHAMSIPUR, G. ROUNAGHI et A. I. POPOV. J. Solution Chem. **9**, 701 (1980).
14. V. DESREUX et J. BISCHOFF. Bull. Soc. Chim. Belg. **59**, 93 (1950).
15. B. CONWAY et E. AYRANCI. J. Chem. Soc. Faraday Trans. I. Sous presse.

Can. J. Chem. Downloaded from www.nrcresearchpress.com by 210.87.254.42 on 09/06/12
For personal use only.

16. Y. TAKEDA, H. YANO, M. ISHIBASHI et H. ISOUZUMI. Bull. Chem. Soc. Jpn. **53**, 72 (1980).
17. M. BISNAIRE. Thèse de Baccalauréat, Université d'Ottawa, 1982.
18. D. LIVE et S. I. CHAN. J. Am. Chem. Soc. **98**, 3769 (1976).
19. M. C. FEDARKO. J. Magn. Reson. **12**, 30 (1973).
20. U. MAYER et V. GUTMANN. Struct. Bonding, **12**, 113 (1972).
21. R. H. ERLICH et A. I. POPOV. J. Am. Chem. Soc. **93**, 5620 (1971).
22. A. ABRAGAM. The principles of nuclear magnetism. Clarendon Press, Oxford. 1961. Chapt. 8.
23. A. GIERER et K. WIRTZ. Z. Naturforsch. Teil A, **8**, 532 (1953).
24. C. DETELLIER et P. LASZLO. Bull. Soc. Chim. Belg. **84**, 1087 (1975).
25. A. DELVILLE, C. DETELLIER, A. GERSTMANS et P. LASZLO. J. Am. Chem. Soc. **102**, 6558 (1980).
26. A. DELVILLE, C. DETELLIER, A. GERSTMANS et P. LASZLO. J. Magn. Reson. **42**, 14 (1981).
27. J. P. KINTZINGER et J. M. LEHN. J. Am. Chem. Soc. **96**, 3313 (1974).
28. G. C. LEVY, R. L. LICHTER et G. L. NELSON. Carbon-13 nuclear magnetic resonance spectroscopy. J. Wiley & Sons, New York. 1980. Chap. 8.
29. J. KONDO et J. YAMASHITA. J. Phys. Chem. Solids, **10**, 245 (1959).
30. C. DEVERELL. Prog. Nucl. Magn. Reson. Spectrosc. **4**, 235 (1969).
31. A. C. COXON, D. A. LAIDLER, R. B. PETTMAN et J. F. STODDART. J. Am. Chem. Soc. **100**, 8260 (1978).
32. C. DETELLIER et P. LASZLO. Studies of ion–molecule interactions by nmr spectroscopy. *In* Molecular interactions. Vol. 5. *Edited by* H. Ratajczak and W. J. Orville-Thomas. J. Wiley & Sons, New York. Sous presse.

Can. J. Chem. Downloaded from www.nrcresearchpress.com by 210.87.254.42 on 09/06/12
For personal use only.

# The influence of crown ethers on the kinetics of E1cB and E2 β-elimination reactions of di(4-nitrophenyl)fluoroethanes with sodium methoxide in methanol

KENNETH T. LEFFEK AND GRZEGORZ SCHROEDER[1]
*Chemistry Department, Dalhousie University, Halifax, N.S., Canada B3H 4H6*
Received March 23, 1982

KENNETH T. LEFFEK and GRZEGORZ SCHROEDER. Can. J. Chem. **60**, 3077 (1982).

The addition of crown ethers 1,4,7,10,13-pentaoxacyclopentadecane (15C5) and 1,4,7,10,13,16-hexaoxacyclooctadecane (18C6) in quantities equimolar to the base, to β-elimination reactions of 1,1,1-trifluoro-2,2-di(4-nitrophenyl)ethane and 1-fluoro-2,2-di(4-nitrophenyl)ethane promoted by sodium methoxide in methanol, has been investigated. In the E2 reaction of the monofluoro compound, the crown ethers caused no change in the kinetic order and only small changes in the second-order rate constants and activation parameters. The primary deuterium isotope effect was also unaltered by the presence of crown ethers.

For the $(E1cB)_R$ reaction of the trifluoro compound, no change in kinetic order was found, but slightly larger rate constant changes and an increase in the isotope effect from $k_H/k_D$ = 1.0 to 1.25 at 25°C was observed. This is interpreted as an alteration in mechanism from $(E1cB)_R$ towards $(E1cB)_I$.

KENNETH T. LEFFEK et GRZEGORZ SCHROEDER. Can. J. Chem. **60**, 3077 (1982).

On a étudié l'addition d'éthers couronnes pentaoxa-1,4,7,10,13 cyclopentadécane (15C5) et hexaoxa-1,4,7,10,13,16 cyclooctadécane (18C6) en quantités équimoléculaires à la base lors des réactions d'élimination β du trifluoro-1,1,1 di(nitrophényl-4)-2,2 éthane et du fluoro-1 di(nitrophényl-4)-2,2 éthane favorisées par le méthylate de sodium dans le méthanol. Dans le cas de la réaction de type E2 du composé monofluoré, les éthers couronnes ne changent pas l'ordre cinétique et ne provoquent que de faibles variations des constantes de vitesse d'ordre deux et des paramètres d'activation. La présence des éthers couronnes n'affecte pas l'effet isotopique primaire du deutérium.

On n'a pas trouvé de changement dans l'ordre cinétique de la réaction de type $(E1cB)_R$ du composé trifluoré, mais on a observé des variations légèrement plus prononcées de la constante de vitesse et une augmentation de l'effet isotopique de $k_H/k_D$ = 1,0 à 1,25 à 25°C. On interprète ceci comme étant une évolution du mécanisme de $(E1cB)_R$ vers $(E1cB)_I$.

[Traduit par le journal]

## Introduction

The effect of crown ethers as additives to alkoxide promoted β-elimination reactions is emerging as an additional tool for the elucidation of the character of the transition states of these reactions (1–8). Recently Alunni *et al.* (1) concluded, from the effect of the addition of dicyclohexyl-18-crown-6 ether to 1-chloro and 1-bromo-1,2-diphenylethane eliminations induced by potassium *tert*-butoxide in *tert*-butanol, that the nonassociated $t\text{BuO}^-$ reacted via a transition state which had smaller bond breaking of the carbon–halogen bond and the same carbon–hydrogen bond breaking as the transition state for the associated base, $t\text{BuO}^-\text{K}^+$. The smaller carbon–halogen bond breaking was at variance with earlier work (3, 5). It was noted (1) that the crown ether may give rise to differences between the associated and dissociated base–solvent systems other than simply increasing the base strength.

In a previous study (9), we attempted to define the general effect, including solvation changes, of crown ethers on β-elimination reactions by studying the addition of 1,4,7,10,13-pentaoxacyclopentadecane (15C5) and 1,4,7,10,13,16-hexaoxacyclooctadecane (18C6) to reactions of some *p*-chlorophenylethanes promoted by sodium ethoxide and *tert*-butoxide in the corresponding alcohol solvents. In these reactions the crown ethers produced various effects, in some cases increasing the second-order rate constant and in other cases decreasing it. Similarly, the changes in the activation parameters, $\Delta H^{\ddagger}$ and $\Delta S^{\ddagger}$ followed no simple pattern.

It is to be expected that, in addition to bringing about a dissociation of the alkoxide base ion-pairs, crown ethers might affect the mechanism of β-elimination reactions in different ways depending upon the mechanism of the reaction in the absence of crown ethers. We have, therefore, investigated the influence of crown ethers for two β-elimination reactions, one which follows the $(E1cB)_R$ mechanism and another which has a symmetrical E2 state. The base sodium methoxide in methanol was chosen in order that the effect of crown ether on base association would be minimized, since $\text{Na}^+\text{OCH}_3^-$ is largely dissociated in dilute solution (10), so that we could observe the influence of crown ethers other than their base dissociation effect. This type of control experiment does not seem to have been performed, but it is important in the interpretation of rate constant and isotope effect changes induced by crown ethers in reac-

[1]Postdoctoral Fellow 1980–1981.

0008-4042/82/243077-04$01.00/0
©1982 National Research Council of Canada/Conseil national de recherches du Canada

Can. J. Chem. Downloaded from www.nrcresearchpress.com by 210.87.254.40 on 09/06/12
For personal use only.

TABLE 1. Rate constants and isotopic rate ratios for the reaction of $(4\text{-}NO_2C_6H_4)_2CHCF_3$* and $(4\text{-}NO_2C_6H_4)_2CDCF_3$* and methoxide in methanol with added crown ethers

| Temperature (°C) | $10^3$ [$\bar{O}CH_3$] ($M$) | $10^4k_H$ ($s^{-1}$) | $10^4k_D$ ($s^{-1}$) | $k_{2H}$ ($L\,mol^{-1}\,s^{-1}$) | $k_{2D}$ ($L\,mol^{-1}\,s^{-1}$) | $k_{2H}/k_{2D}$ |
|---|---|---|---|---|---|---|
| (a) Sodium methoxide | | | | | | |
| 20.0 | 0.5–5.0 | 0.55– 8.6 | 0.52– 7.9 | $0.17_8$ | $0.16_5$ | $1.0_8$ |
| 25.0 | 0.5–5.0 | 0.90– 14.5 | 0.89– 14.3 | $0.30_1$ | $0.30_5$ | $0.9_9$ |
| 30.0 | 0.5–5.0 | 1.55– 24.8 | 1.40– 24.1 | $0.51_2$ | $0.51_9$ | $0.9_9$ |
| 35.0 | 0.5–5.0 | 4.8 – 50.6 | 4.60– 49.1 | 1.01 | 0.99 | $1.0_2$ |
| 40.0 | 0.5–5.0 | 5.0 – 75.2 | 4.90– 74.9 | 1.56 | 1.55 | $1.0_1$ |
| (b) Sodium methoxide with equimolar 15-crown-5 ether | | | | | | |
| 20.0 | 0.5–5.0 | 1.4 – 17.2 | 0.81– 13.5 | $0.35_2$ | $0.28_2$ | $1.2_6$ |
| 25.0 | 0.5–5.0 | 2.7 – 30.2 | 2.3 – 24.5 | $0.6_1$ | $0.49_3$ | $1.2_4$ |
| 30.0 | 0.5–5.0 | 4.1 – 48.8 | 3.2 – 40.1 | $0.99_5$ | $0.82_1$ | $1.2_1$ |
| 35.0 | 0.5–5.0 | 8.4 – 81.8 | 7.2 – 70.0 | 1.63 | 1.40 | $1.1_6$ |
| 40.0 | 0.5–5.0 | 10.1 –127. | 8.8 –110. | 2.59 | 2.25 | $1.1_5$ |
| (c) Sodium methoxide with equimolar 18-crown-6 ether | | | | | | |
| 20.0 | 0.5–5.0 | 1.0 – 15.9 | 0.59– 12.4 | $0.33_3$ | $0.26_4$ | $1.2_6$ |
| 25.0 | 0.5–5.0 | 2.0 – 28.2 | 1.7 – 23.2 | $0.58_7$ | $0.48_0$ | $1.2_2$ |
| 30.0 | 0.5–5.0 | 3.3 – 46.1 | 2.3 – 39.1 | $0.96_0$ | $0.81_9$ | $1.1_7$ |
| 35.0 | 0.5–5.0 | 6.9 – 79.6 | 5.8 – 68.7 | 1.63 | 1.41 | $1.1_6$ |
| 40.0 | 0.5–5.0 | 10.1 –126. | 8.5 –113. | 2.58 | 2.33 | $1.1_1$ |

*Initial concentration of substrates $5 \times 10^{-5}$ $M$.

tions involving alkoxide bases which are highly associated in the absence of crown ethers.

## Results and discussion

1,1,1-Trifluoro-2,2-di(4-nitrophenyl)ethane was shown to react with sodium methoxide in methanol by the $(E1cB)_R$ mechanism (11) and in a recent reinvestigation (12) 1-fluoro-2,2-di(4-nitrophenyl)-ethane was found to follow a concerted E2 mechanism with a symmetrical transition state with the same base–solvent system. Pseudo first-order rate constants were determined for the β-elimination of HF from these two substrates and their $1d_1$ deuterated analogues promoted by a large excess of sodium methoxide in methanol, in the presence of the crown ethers 15C5 and 18C6 in concentrations equal to that of the methoxide. The second-order rate constants were calculated from plots of the first-order constants vs. base concentration. In all cases these plots were linear, indicating a kinetic order of unity in methoxide for the reaction in the presence of crown ethers. The rate constant measurements for the trifluoro compound in the absence of crown ethers were repeated and the present work gave values about 15% lower than those previously determined (11). The present measurements were made by following the increase in absorbance at 338 nm, the isobestic point for the subsequent reaction of the olefin, whereas the earlier measurements were made at 325 nm, the absorbance maximum of the olefin product. The activation parameters are also slightly different from our previously published results, but by amounts less than the experimental uncertainties. The rate constants are shown in Tables 1 and 2 and the activation parameters in Table 3.

The ion-pair dissociation constant for sodium methoxide in methanol is about $0.02_5$ mol $L^{-1}$ (10), from which it can be calculated that the degree of dissociation of the base in these reactions varies from 83% at $5 \times 10^{-3}$ $M$ to 98% at $0.5 \times 10^{-3}$ $M$ sodium methoxide. For a carbenium ion reacting with sodium methoxide, it was shown (10) that the active base is the free methoxide ion. Also, for some β-elimination reactions with sodium ethoxide, McLennan determined (13) the rate constant for the free ethoxide ion to be more than 4 times greater than that for the sodium ethoxide ion-pair in ethanol. From these studies and the fact that our plots of $k_{2H}$ and $k_{2D}$ vs. base concentration are linear, it may be deduced that the elimination reactions proceed via the dissociated methoxide ion. Therefore, the rate change which may be expected if the crown ethers merely result in the complete dissociation of the base is an increase of about 25%.

The results in Tables 1 and 2 show that both crown ethers have very similar effects on the second-order rate constants, giving an increase of about 100% for the $(E1cB)_R$ reaction of the trifluoro compound and a small decrease (30% or less) for the E2 reaction of the monofluoro compound. For the trifluoro compound a small isotope effect, $k_H/k_D \sim 1.25$ at 25°C, is introduced by the crown ethers, but for the E2 reaction of the monofluoro compound the crown ethers have no effect at all on the

Can. J. Chem. Downloaded from www.nrcresearchpress.com by 210.87.254.40 on 09/06/12
For personal use only.

TABLE 2. Rate constants and isotopic rate ratios for the reaction of $(4\text{-}NO_2C_6H_4)_2CHCH_2F$* and $4NO_2C_6H_4\text{-}CDCH_2F$* and methoxide in methanol with added crown ethers

| Temperature (°C) | $10^3$ [$\bar{O}CH_3$] ($M$) | $10^4k_H$ ($s^{-1}$) | $10^4k_D$ ($s^{-1}$) | $k_{2H}$ (L $mol^{-1}$ $s^{-1}$) | $k_{2D}$ (L $mol^{-1}$ $s^{-1}$) | $k_{2H}/k_{2D}$ |
|---|---|---|---|---|---|---|
| (a) Sodium methoxide† | | | | | | |
| 25.0 | 0.5–5.0 | 12.8–33.8 | 1.01– 5.50 | $0.48_3$ | $0.09_9$ | $4.8_8$ |
| 30.0 | 0.5–5.0 | 13.8–42.9 | 1.74– 7.70 | $0.64_2$ | $0.13_6$ | $4.7_2$ |
| 35.0 | 0.5–5.0 | 15.1–58.4 | 2.1 –11.5 | $0.95_4$ | $0.21_0$ | $4.5_2$ |
| (b) Sodium methoxide with equimolar 15-crown-5 ether | | | | | | |
| 20.0 | 0.5–5.0 | 5.0–21.1 | — | $0.35_7$ | — | — |
| 25.0 | 0.5–5.0 | 7.8–28.3 | 0.65– 4.9 | $0.45_4$ | $0.09_3$ | $4.8_8$ |
| 30.0 | 0.5–5.0 | 8.5–33.6 | 1.2 – 6.4 | $0.56_0$ | $0.11_6$ | $4.8_3$ |
| 35.0 | 0.5–5.0 | 10.6–42.5 | 2.9 – 9.7 | $0.71_0$ | $0.15_0$ | $4.7_3$ |
| 40.0 | 0.5–5.0 | 13.0–49.4 | 3.2 –11.1 | $0.81_0$ | $0.17_5$ | $4.6_3$ |
| 45.0 | 0.5–5.0 | — | 3.9 –13.3 | — | $0.20_9$ | — |
| (c) Sodium methoxide with equimolar 18-crown-6 ether | | | | | | |
| 20.0 | 0.5–5.0 | 8.1–20.5 | — | $0.27_5$ | — | — |
| 25.0 | 0.5–5.0 | 11.5–26.8 | 1.4 – 4.5 | $0.33_6$ | $0.06_9$ | $4.8_7$ |
| 30.0 | 0.5–5.0 | 13.9–35.1 | 1.6 – 6.0 | $0.46_9$ | $0.10_0$ | $4.6_9$ |
| 35.0 | 0.5–5.0 | 15.7–45.3 | 2.1 – 8.7 | $0.66_8$ | $0.14_7$ | $4.5_4$ |
| 40.0 | 0.5–5.0 | 16.6–54.8 | 2.3 –10.8 | $0.84_7$ | $0.19_0$ | $4.4_6$ |
| 45.0 | 0.5–5.0 | — | 4.1 –14.6 | — | $0.23_3$ | — |

*Initial concentration of substrates $5 \times 10^{-5}$ $M$.
†Reference 12.

TABLE 3. Activation parameters for the β-elimination reactions of di(4-nitrophenyl)-fluoroethane and sodium methoxide with added crown ethers

| Reaction | $\Delta H^{\ddagger}$ (kcal $mol^{-1}$) | $\Delta S^{\ddagger}$ (cal $mol^{-1}$ $deg^{-1}$) |
|---|---|---|
| $(4NO_2C_6H_4)_2CHCF_3 + \bar{O}CH_3$ | 19.6±0.7 | 5.0±2.3 |
| $(4NO_2C_6H_4)_2CDCF_3 + \bar{O}CH_3$ | 20.0±0.5 | 6.4±1.7 |
| $(4NO_2C_6H_4)_2CHCF_3 + \bar{O}CH_3$/15C5 | 17.5±0.2 | −0.7±0.5 |
| $(4NO_2C_6H_4)_2CDCF_3 + \bar{O}CH_3$/15C5 | 18.4±0.2 | 1.6±0.4 |
| $(4NO_2C_6H_4)_2CHCF_3 + \bar{O}CH_3$/18C6 | 18.0±0.2 | 0.9±0.7 |
| $(4NO_2C_6H_4)_2CDCF_3 + \bar{O}CH_3$/18C6 | 19.2±0.2 | 4.4±0.5 |
| $(4NO_2C_6H_4)_2CHCH_2F + \bar{O}CH_3$* | 9.9±0.7 | −26.6±2.3 |
| $(4NO_2C_6H_4)_2CDCH_2F + \bar{O}CH_3$* | 10.6±0.8 | −27.6±2.8 |
| $(4NO_2C_6H_4)_2CHCH_2F + \bar{O}CH_3$/15C5 | 7.0±0.3 | −36.6±1.1 |
| $(4NO_2C_6H_4)_2CDCH_2F + \bar{O}CH_3$/15C5 | 7.0±0.3 | −39.6±1.1 |
| $(4NO_2C_6H_4)_2CHCH_2F + \bar{O}CH_3$/18C6 | 10.1±0.6 | −26.7±2.0 |
| $(4NO_2C_6H_4)_2CDCH_2F + \bar{O}CH_3$/18C6 | 11.0±0.8 | −28.8±2.5 |

*Reference 12.

isotopic rate ratio of 4.7 to 4.8 at 25°C. This latter observation confirms a similar one by Alunni *et al.* for E2 reactions (1). Thus, the crown ethers do not affect the transition state of the E2 reaction with respect to the C—H bond breaking, but give rate constants about 50% less than would be predicted for complete dissociation of the alkoxide base. This is a very small change compared to the rate enhancements by factors of up to 250 found when crown ethers are added to reactions involving highly associated bases (1, 3). The small decrease in rate is probably due to changes in the solvation of the transition state around the C—F bond, brought about by the complexing of the sodium cation with the crown ether, which inhibits the C—F bond breaking process. The 18-crown-6 ether has practically no effect at all on the activation parameters of the E2 reaction of the monofluoro compound, but the 15-crown-5 produces a compensating decrease in $\Delta H^{\ddagger}$ and an increase in negative $\Delta S^{\ddagger}$.

For the $(E1cB)_R$ mechanism, shown in eq. [1], the inequality $k_{-1}[BH] \gg k_2$ is assumed for the steady-state approximation for $S^-$ to yield the rate

$$[1] \quad B^- + SH \underset{k_{-1}}{\overset{k_1}{\rightleftharpoons}} S^- + BH \xrightarrow{k_2} P + F^-$$

equation [2]. Since BH is the solvent methanol, the

$$[2] \quad \frac{d[P]}{dt} = \frac{k_1k_2}{k_{-1}} \frac{[B^-][SH]}{[BH]}$$

Can. J. Chem. Downloaded from www.nrcresearchpress.com by 210.87.254.40 on 09/06/12
For personal use only.

$(ElcB)_R$ mechanism shows no primary deuterium isotope effect.

At the other extreme, when $k_2 \gg k_{-1}[BH]$, the mechanism $(ElcB)_I$ operates and the rate equation is [3]. For this mechanism the magnitude of $k_H/k_D$

$$[3] \quad \frac{d[P]}{dt} = k_1[B^-][SH]$$

is predicted (14) to be between 2 and 8.

A small isotope effect of 1.25 could appear if the added crown ethers changed the relative magnitudes of $k_{-1}[BH]$ and $k_2$. If $k_2$ is increased relative to $k_{-1}[BH]$ the mechanism would change from $(E1cB)_R$ towards $(E1cB)_I$ introducing an isotope effect.

Normally the carbanion is probably appreciably associated with sodium ions in ion-pairs, but in the presence of crown ethers where the $Na^+$ ions are complexed, the carbanion would be in the form of free ions and thereby both $k_{-1}[BH]$ and $k_2$ would be increased. However, the overall activation energy is decreased (Table 3) by 1.5 to 2 kcal $mol^{-1}$. Thus, the height of the energy barrier for loss of $F^-$ from the carbanion is decreased and $k_2$ is, therefore, increased to a greater extent than $k_{-1}[BH]$, altering the mechanism from $(E1cB)_R$ towards $(E1cB)_I$. The source of the decrease in $\Delta H^{\ddagger}$ may be that there is no energy requirement to break up the carbanion ion-pair to allow the negative charge to transfer to a fluorine atom.

It is presumed that the magnitude of $k_1$ would not be altered by the crown ethers, since we have seen from the E2 case that C—H bond breaking is unaffected by crown ether addition.

It is concluded that crown ethers added to an E2 β-elimination have only a small effect, other than the change in the dissociation of the alkoxide base. In the $(E1cB)_R$ case, however, crown ethers can bring about a change of mechanism to some extent, towards the $(E1cB)_I$ mechanism. It is, therefore, a kinetic tool which should be used with care at this extreme of the spectrum of β-elimination mechanisms.

## Experimental

The fluoroethanes were prepared as described previously (11, 12). The 15-crown-5 ether (Aldrich) was purified by distillation at reduced pressure and the 18-crown-6 ether (Aldrich) was recrystallized from hexane, mp 39–40°C.

The kinetic runs were carried out with a Unicam SP800 spectrophotometer, using the technique previously described (11).

## Acknowledgement

The authors are grateful for financial support by the Natural Sciences and Engineering Research Council of Canada.

1. S. Alunni, P. Perucci, and R. Ruzziconi. Gazz. Chim. Ital. **110**, 261 (1980).
2. S. Alunni, E. Baciocchi, and P. Perucci. J. Org. Chem. **42**, 2170 (1977).
3. S. Alunni, E. Baciocchi, and P. Perucci. J. Org. Chem. **41**, 2636 (1976).
4. R. A. Bartsch, G. M. Pruss, O. M. Cook, E. L. Buswell, B. A. Bushan, and K. E. Wiegers. J. Am. Chem. Soc. **95**, 6745 (1973).
5. R. A. Bartsch, E. A. Mintz, and R. M. Parlman. J. Am. Chem. Soc. **96**, 4249 (1974).
6. M. Svoboda, J. Hapala, and J. Zavada. Tetrahedron Lett. 265 (1972).
7. J. Zavada, M. Pankova, and M. Svoboda. Collect. Czech. Chem. Commun. **41**, 3778 (1976).
8. R. A. Bartsch and J. Zavada. Chem. Rev. **80**, 4531 (1980).
9. A. Jarczewski, G. Schroeder, and K. T. Leffek. J. Chem. Soc. Perkin Trans. II 866 (1979).
10. K. T. Leffek and A. Suszka. Can. J. Chem. **53**, 1537 (1975).
11. J. Kurzawa and K. T. Leffek. Can. J. Chem. **55**, 1696 (1977).
12. K. T. Leffek and G. Schroeder. Can. J. Chem. **60**, 1696 (1982).
13. D. J. McLennan. J. Chem. Soc. Perkin Trans. II 1577 (1972).
14. F. G. Bordwell. Acc. Chem. Res. **5**, 374 (1972).

Can. J. Chem. Downloaded from www.nrcresearchpress.com by 210.87.254.40 on 09/06/12
For personal use only.

# Phosphonodipeptides: synthesis and separation of diastereoisomers

PAWEŁ KAFARSKI, BARBARA LEJCZAK, AND PRZEMSŁAW MASTALERZ

*Institute of Organic and Physical Chemistry, Technical University of Wrocław, Wybrzeże Wyspiańskiego 27, 50-370 Wrocław, Poland*

AND

JERZY SZEWCZYK AND CZESŁAW WASIELEWSKI

*Department of Organic Chemistry, Technical University of Gdańsk, Majakowskiego 11/12, 80-951 Gdańsk, Poland*

Received March 15, 1982

PAWEŁ KAFARSKI, BARBARA LEJCZAK, PRZEMSŁAW MASTALERZ, JERZY SZEWCZYK, and CZESŁAW WASIELEWSKI. Can. J. Chem. **60**, 3081 (1982).

Diastereoisomeric mixtures of phosphonodipeptides, prepared from racemic dialkyl 1-aminoalkanephosphonates, were separated by ion-exchange column chromatography. Phosphonodipeptides were found to be much more readily available from dialkyl 1-aminoalkanephosphonates than from the corresponding free acids and the mixed carboxylic – carbonic anhydride method was found to be the most effective one.

PAWEŁ KAFARSKI, BARBARA LEJCZAK, PRZEMSŁAW MASTALERZ, JERZY SZEWCZYK et CZESŁAW WASIELEWSKI. Can. J. Chem. **60**, 3081 (1982).

On a séparé des mélanges disastéroisomères de phosphonodipeptides, préparés à partir d'amino-1 alcanephosphonates de dialkyles racémiques, par chromatographie sur colonnes échangeuses d'ions. On a trouvé que les phosphonodipeptides sont plus facilement accessibles à partir des amino-1 alcanephosphonates de dialkyles qu'à partir des acides libres correspondants et on a trouvé que la méthode des anhydres mixtes de l'acide carbonique est la plus efficace.

[Traduit par le journal]

Can. J. Chem. Downloaded from www.nrcresearchpress.com by 210.87.254.5 on 09/06/12
For personal use only.

Peptides of aminoalkanephosphonic acids are now receiving considerable interest because some representatives of this class were found to repress bacterial growth at very low concentration levels (1–5).

Although the mechanism of molecular action of phosphonopeptides is quite well established (1, 3, 6, 7), their biochemistry is little known and several important metabolic aspects await elucidation. Progress in this field should be facilitated by increased availability of pure diastereoisomers of phosphonodipeptides.

We wish to report a simple and effective method for the separation of diastereoisomeric phosphonodipeptides by means of ion-exchange column chromatography. Since literature data on the synthesis of dipeptides containing *P*-terminal aminoalkanephosphonic acids are scarce (8–15), we have also described the routes for their preparation followed in this study.

*Synthesis of phosphonodipeptides*

We have prepared the peptides **1** by condensation of *N*-phthaloyl-, *N*-formyl-, or preferably *N*-benzyloxycarbonylamino acids **2** with 1-aminoalkanephosphonic acids as well as with their dialkyl esters.

The literature data and our observations on the preparation of phosphonodipeptides from free 1-aminoalkanephosphonic acids indicate that the yields of the coupling step are usually low or moderate. Moreover the use of bulky *N*-protected amino acids drastically decreases the reaction yield. Thus, following the methods of Martell and co-workers (11), we were unable to prepare dipep-

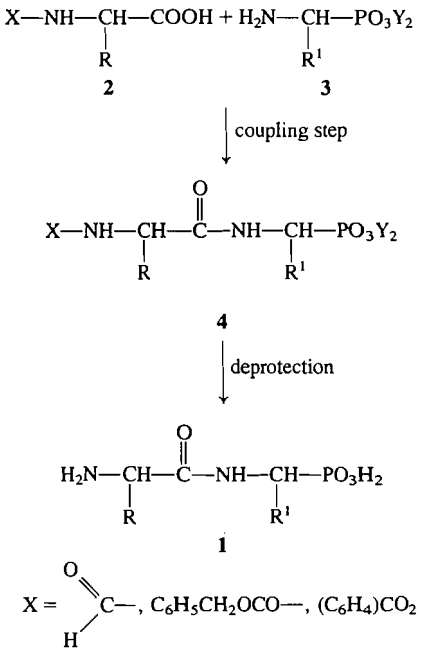


Y = H, $CH_3$, $CH_3CH_2$, $(CH_3)_2CH$

R = H, $CH_3$, $(CH_3)_2CH$, $(CH_3)_2CHCH_2$, $C_6H_5CH_2$, $CH_3SCH_2CH_2$, $H_2NCH_2CH_2CH_2CH_2$ and **2** was also proline

$R^1$ = $CH_3$, $CH_3CH_2$, $(CH_3)_2CH$, $(CH_3)_2CHCH_2$

0008-4042/82/243081-04$01.00/0

©1982 National Research Council of Canada/Conseil national de recherches du Canada

TABLE 1. Phosphonodipeptides:[a] A—NH—CH(R¹)—$PO_3H_2 \cdot xH_2O$

| A | R¹ | x | Yield (%) method | | | Melting point (°C) | $[\alpha]_{578}^{20}$ ($c$ = 1%, $H_2O$) |
|---|---|---|---|---|---|---|---|
| L-Ala | $CH_3$ | 1.5 | 61 A | 56 C | 65 D | 278–286 dec. | +12° |
| L-Val | $CH_3$ | 1.5 | 72,5 A | | | 251–257 dec. | +38° |
| L-Leu | $CH_3$ | 2 | 59 A | 66 C | | 247–251 dec. | +30° |
| L-Met | $CH_3$ | 1.5 | 46 A | | | 208–213 dec. | +23° |
| Gly | $CH_3CH_2$ | 1.5 | 66 A | 52 B | | 269–272 dec. | — |
| L-Ala | $CH_3CH_2$ | 0.5 | 81 A | | | 271–275 dec. | +18° |
| L-Leu | $CH_3CH_2$ | 1.5 | 65 A | | | 254–256 dec. | +25° |
| L-Val | $(CH_3)_2CH$ | 2 | 78 A | 59 B | | 253–255 dec. | +37° |
| L-Leu | $(CH_3)_2CH$ | 0.5 | 69 A | | | 260–263 dec. | +26° |
| L-Phe | $(CH_3)_2CH$ | — | 60 A | 45 C | | 261–265 dec. | +55°[b] |
| L-Val | $(CH_3)_2CHCH_2$ | 3 | 82 A | | | 262–266 dec. | +29° |
| L-Leu | $(CH_3)_2CHCH_2$ | 2 | 80 A | | | 266–268 dec. | +28° |
| L-Ala | $C_6H_5$ | 0.5 | 54 B | 50 D | | 272–273 dec. | +6° |
| L-Pro | $C_6H_5$ | 0.5 | 63 A | 50 D | | 279–281 dec. | −53° |
| L-Lys | $C_6H_5$ | 2.5 | 75 A | | | 265–268 | +17° |

[a]The microanalyses were in satisfactory agreement with the calculated values: N, ±0.34; P, ±0.33.
[b]$c$ = 2%, 1 $N$ NaOH.

tides containing *N*-terminal valine or leucine, while the peptides of phenylalanine were obtained in 5–10% yield.

Also, the active ester method gave low yields of the desired products (10–15). Our studies with *p*-nitrophenyl and cyanomethyl esters of *N*-phthaloylamino acids confirmed the observations that free aminoalkanephosphonic acids are particularly unsuitable as substrates for the synthesis of phosphonodipeptides.

We were able to obtain much better results using the dialkyl 1-aminoalkanephosphonates (16) instead of free acids. Thus, the desired peptides were prepared by condensation of *N*-protected amino acids **2** with dialkyl 1-aminoalkanephosphonates **3** (the methyl, ethyl, and isopropyl esters can be used interchangeably without noticeable effect on yields or purity of products) by means of the dicyclohexylcarbodiimide (DCC) or, preferably, the mixed carboxylic – carbonic anhydride (MCA) method. The DCC method often gave the corresponding *N*-acylureas, the side products of the reaction, in relatively high yields (about 30%). Conventional removal of the blocking groups yielded the peptides listed in Table 1.

*Separation of diastereoisomeric phosphonodipeptides*

Using ion-exchange column chromatography for purification of the phosphonodipeptides **1**, we have observed a separation of diastereoisomers. There appears to be no evidence for preparative separation of diastereoisomeric dipeptides in the literature, although there are reports describing analytical separation of carboxylic peptides (17, 18). Diastereoisomeric phosphonodipeptides have never been separated by ion-exchange chromatography.

Thus, mixtures of diastereoisomeric phosphonodipeptides, prepared from racemic 1-aminoalkanephosphonates, were placed on a Dowex 50W ($H^+$ form) 100–200 mesh column and simple elution with water yielded quantitatively the pure diastereoisomers (Table 2). Using a 200 × 20 mm column

Can. J. Chem. Downloaded from www.nrcresearchpress.com by 210.87.254.5 on 09/06/12
For personal use only.

TABLE 2. Diastereoisomers of phosphonodipeptides **1**

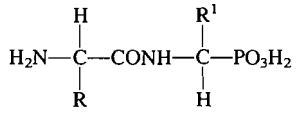

*S,S*-dipeptide
**1***a*

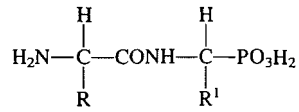

*S,R*-dipeptide
**1***b*

| | | Tentative configuration of phosphonodipeptide | | | |
|---|---|---|---|---|---|
| | | *S,S*-dipeptide | | *S,R*-dipeptide | |
| R | $R^1$ | $[\alpha]_{578}^{20}$ ($c$ = 1%, $H_2O$) | $R_f$[a] | $[\alpha]_{578}^{20}$ ($c$ = 1%, $H_2O$) | $R_f$[a] |
| $CH_3$ | $CH_3$ | +75°[b] | 0.08 | −49°[c] | 0.06 |
| $(CH_3)_2CH$ | $CH_3$ | +84° | 0.15 | −9°[d] | 0.10 |
| $(CH_3)_2CHCH_2$ | $CH_3$ | +73° | 0.23 | −13°[e] | 0.17 |
| $CH_3$ | $CH_3CH_2$ | +75° | 0.11 | −53° | 0.09 |
| $(CH_3)_2CHCH_2$ | $CH_3CH_2$ | +83° | 0.26 | −22° | 0.20 |
| $(CH_3)_2CH$ | $(CH_3)_2CH$ | +66° | 0.38 | +7° | 0.31 |
| $(CH_3)_2CHCH_2$ | $(CH_3)_2CH$ | +51° | 0.30 | +1° | 0.26 |
| $(CH_3)_2CH$ | $(CH_3)_2CHCH_2$ | +87° | 0.30 | −23° | 0.26 |

[a]Silica-gel, Merck 60F 254, *n*-butanol – acetic acid – water 12:3:5, spots visualized by ninhydrin reagent.
[b]Literature (23) for *N*-(*S*)-alanyl-(*S*)-1-aminoethanephosphonic acids: $[\alpha]_D^{20}$ +84° ($c$ = 1%, $H_2O$).
[c]Literature (4, 22) for *N*-(*S*)-alanyl-(*R*)-1-aminoethanephosphonic acid: $[\alpha]_D^{20}$ −45.4° or −46.3° ($c$ = 1%, $H_2O$).
[d]Literature (22) for *N*-(*S*)-valyl-(*R*)-1-aminoethanephosphonic acid: $[\alpha]_D^{20}$ −9.3° ($c$ = 1%, $H_2O$).
[e]Literature (22) for *N*-(*S*)-leucyl-(*R*)-1-aminoethanephosphonic acid: $[\alpha]_D^{20}$ −14.2° ($c$ = 1%, $H_2O$).

we were able to separate 0.7 to 2.0 g portions of the mixture of diastereoisomers.

Specific rotation values shown in Table 2 indicate that there is a correlation of relative rotation for the pairs of diastereoisomers and the retention factor, the isomers of higher positive rotation being eluted faster. According to the general rule (19, 20), validated recently also for phosphonopeptides (21), the peptides which are eluted faster may be considered as possessing *S,S* (L,D) configuration. The tentative configurations proposed in Table 2 result from relative mobilities of the diastereoisomers on the Dowex column as well as on tlc plates.

In the case of peptides of 1-aminoethanephosphonic acid, our assignments are in accordance with those reported by the La Roche group (4, 22, 23) for *N*-L-alanyl-, *N*-L-valyl-, and *N*-L-leucyl-1-aminoethanephosphonic acids (see footnotes to Table 2).

## Experimental

The melting points were determined on a Koeffler apparatus and are uncorrected. The structure of the prepared peptides was confirmed by means of ir and nmr spectroscopy.

*Preparation of phosphonodipeptides by means of the MCA method*

*From* N-*benzyloxycarbonylamino acids (Method A)*

A solution of 0.01 mol of *N*-benzyloxycarbonylamino acid and 1.5 cm³ of triethylamine in 30 cm³ of dry chloroform was cooled to about −5°C and treated with 1.0 cm³ (0.011 *M*) of ethyl chloroformate. After 30 min, 0.011 mol of ester **3** was added and the solution was left to reach room temperature, then the solution was slowly heated to the boiling point. The resulting solution was washed successively with water, 5% hydrochloric acid, water, saturated solution of sodium bicarbonate, and water. Finally it was extracted with brine and dried over sodium sulphate. The solvent was distilled off and the oily residue representing crude peptide **4** was dissolved in 20 cm³ of 40% hydrogen bromide in glacial acetic acid solution and left overnight. Then acetic acid and excess of hydrogen bromide were removed under reduced pressure, the oily residue was dissolved in water and extracted with ether to remove benzyl bromide, and the solvent was stripped off under the reduced pressure. The residue was then dissolved in absolute ethanol and the crude peptide was precipitated with propylene oxide or pyridine.

Chromatographically pure products were obtained upon crystallization from water–ethanol or water–acetone mixtures.

*From* N-*phthaloylamino acids (Method B)*

The condensation of phthaloylamino acids with esters **3** and isolation of phthaloylated peptides **4** was carried out as described for crude *N*-benzyloxycarbonylpeptides **4**. The crude phthaloylated peptides were first dephthaloylated by boiling for 1 h with hydrazine hydrate in ethanol and *P*-alkyl groups were then removed with hydrogen bromide in acetic acid. Pure peptides were isolated as described above.

*From* N-*formylamino acids (Method C)*

The procedure for the preparation of *N*-formylpeptides **4** was identical as described for *N*-benzyloxycarbonylpeptides. Crude peptides were first deformylated with hydrogen chloride in methanol and then *P*-alkyl groups were removed with hydrogen bromide in glacial acetic acid solution. Pure peptides were isolated by standard procedure.

*Preparation of phosphonodipeptides by the DCC method (Method D)*

*N*-Protected amino acid **2** (0.005 mol) and 0.8 cm³ of triethylamine were dissolved in 20 cm³ of dry chloroform and 0.005 mol of diethyl 1-aminoalkanephosphonate was added. Then 0.005

Can. J. Chem. Downloaded from www.nrcresearchpress.com by 210.87.254.5 on 09/06/12
For personal use only.

mol, i.e. 1.03 g, of dicyclohexylcarbodiimide was added and the mixture was left overnight. After filtration of the formed dicyclohexylurea the peptide was obtained as in Method A.

*Separation of diastereoisomers – a typical example*

Crude (without crystallization) *N*-L-valyl-1-aminoethanephosphonic acid (1.0 g) was chromatographed on a 200 × 20 mm Dowex 50W X8 ($H^+$ form) 100–200 mesh column with water as eluent. The elution was monitored by ninhydrin reaction. Fractions of 16 $cm^3$ were collected. The *S*,*S*-dipeptide was obtained from fractions 106–200 and weighed 420 mg. The *S*,*R*-diastereoisomer was eluted from 225 up to 700 fractions; 460 mg of this isomer was obtained. The yield of pure diastereoisomers was 88%.

## Acknowledgement

This work was supported by grant R.1.9.

1. E. Bayer, K. H. Gugel, H. Hägele, H. Hagenmaier, S. Jessipow, W. A. König, and H. Zähner. Helv. Chim. Acta, **55**, 224 (1972).
2. B. K. Park, A. Mirota, and H. Sakai. Agric. Biol. Chem. **40**, 1905 (1976).
3. J. G. Allen, F. R. Atherton, M. J. Hall, C. H. Hassall, S. W. Holmes, R. W. Lambert, L. J. Nisbet, and P. S. Ringrose. Nature **272**, 56 (1978).
4. F. R. Atherton, M. J. Hall, C. H. Hassall, R. W. Lambert, and P. S. Ringrose. Antimicrob. Agents Chemother. **15**, 677 (1979).
5. F. R. Atherton, M. J. Hall, C. H. Hassall, S. W. Holmes, R. W. Lambert, W. J. Lloyd, and P. S. Ringrose. Antimicrob. Agents Chemother. **18**, 897 (1980).
6. H. Diddens, H. Zähner, E. Kraas, W. Göhring, and G. Jung. Eur. J. Biochem. **66**, 11 (1976).
7. F. R. Atherton, M. J. Hall, C. H. Hassall, R. W. Lambert, W. J. Lloyd, and P. S. Ringrose. Antimicrob. Agents Chemother. **15**, 696 (1979).
8. K. T. Poroshin and V. K. Buritchenko. Dokl. Akad. Nauk SSSR, **156**, 386 (1964).
9. V. K. Buritchenko, K. T. Poroshin, S. B. Davidyant, and L. S. Kuzyat. Dokl. Akad. Nauk Tad. SSR, **9**, 17 (1966); Chem Abstr. **66**, 18852 (1967).
10. S. Bajusz, A. Z. Ronai, J. I. Szekely, A. Turan, A. Juhasz, A. Patty, E. Miglecz, and I. Berzetti. FEBS Lett. **117**, 308 (1980).
11. M. Hariharan, R. J. Motekaitis, and A. E. Martell. J. Org. Chem. **40**, 470 (1975).
12. P. Kafarski and P. Mastalerz. Rocz. Chem. **51**, 433 (1977).
13. W. F. Gilmore and M. A. McBride. J. Pharm. Sci. **63**, 1087 (1974).
14. J. W. Huber III, W. F. Gilmore, and L. W. Robertson. J. Med. Chem. **18**, 106 (1975).
15. V. B. Taurusova, I. A. Gandurina, Y. N. Zhukov, G. M. Yakovleva, and R. M. Khomutov. Izv. Akad. Nauk SSSR Ser. Khim. 1596 (1979).
16. J. Kowalik, L. Kupczyk-Subotkowska, and P. Mastalerz. Synthesis, 57 (1981).
17. N. Izumiya and M. Muracka. Peptides, 347 (1970).
18. J. M. Manning, A. Marglin, and S. Moore. Progress in peptide research. Vol. II. *Edited by* Saul Lande, New York. 1972. Proceedings of the 2nd American Peptide Symposium, August 17–19, 1970. p. 173.
19. T. Sokołowska and J. F. Biernat. J. Chromatogr., **13**, 269 (1964).
20. A. Arendt, A. Kołodziejczyk, and T. Sokołowska. Chromatographia, **9**, 123 (1976).
21. Cz. Wasielewski and A. Sobczak. 5th Polish Conference on Amino Acid and Peptide Chemistry. Łódź, 1979. p. 69.
22. F. R. Atherton, M. J. Hall, C. H. Hassall, R. W. Lambert, and P. S. Ringrose. German Patent No. 26.02.193 (1976).
23. F. R. Atherton, M. J. Hall, C. H. Hassall, R. W. Lambert, and P. S. Ringrose. German Patent No. 27.21.761 (1977).

## ADDITIONS AND CORRECTIONS/AJOUTS ET CORRECTIONS

Vol. 60, 1982

**John W. ApSimon, Alfred S. Chau, Robin Sampson, Hung Tze, and Alain Fruchier.** The reaction of heptachlor on alumina impregnated with sulfuric acid in the presence of various aromatic compounds.

Page 2002. The structure for compounds **1–7** is missing a chlorine atom, which has been corrected as shown here.

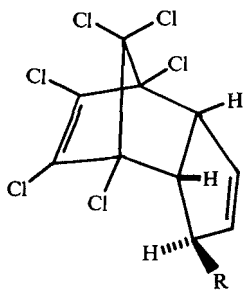


**1** R = Cl
**2** R = ϕ
**3** R = *p*-tolyl
**4** R = *o*-hydroxyphenyl
**5** R = 2′,3′-dichlorophenyl
**6** R = —O-3-*exo*-chlordene
**7** R = H

Can. J. Chem. Downloaded from www.nrcresearchpress.com by 210.87.254.5 on 09/06/12
For personal use only.